Petroleum Geology: From Mature Basins to New Frontiers

Proceedings of the 7th Petroleum Geology Conference

Edited by
B. A. Vining and S. C. Pickering

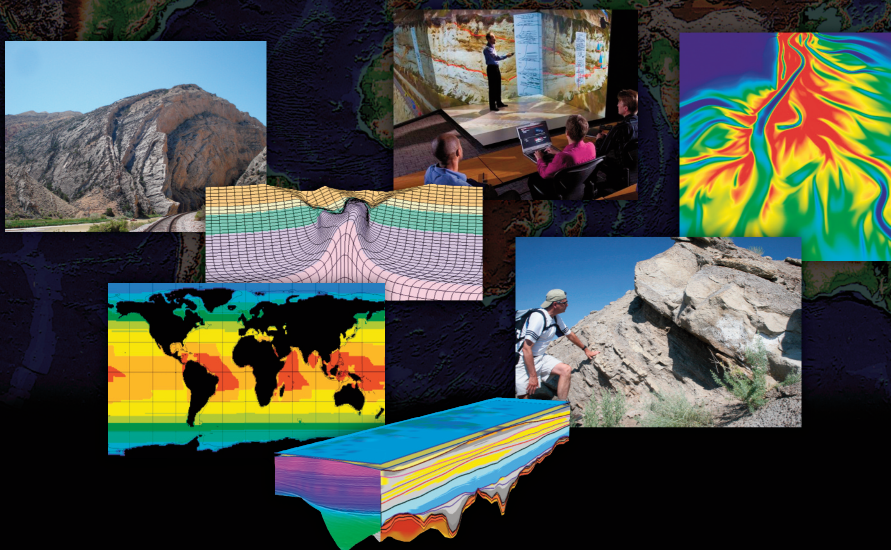

Published by The Geological Society

THE GEOLOGICAL SOCIETY

The Geological Society of London (GSL) was founded in 1807. It is the oldest national geological society in the world and the largest in Europe. It was incorporated under Royal Charter in 1825 and is Registered Charity 210161.

The Society is the UK national learned and professional society for geology with a worldwide Fellowship (FGS) of 10 000. The Society has the power to confer Chartered status on suitably qualified Fellows, and about 2000 of the Fellowship carry the title (CGeol). Chartered Geologists may also obtain the equivalent European title, European Geologist (EurGeol). One fifth of the Society's fellowship resides outside the UK. To find out more about the Society, log on to www.geolsoc.org.uk.

The Geological Society Publishing House (Bath, UK) produces the Society's international journals and books, and acts as European distributor for selected publications of the American Association of Petroleum Geologists (AAPG), the American Geological Institute (AGI), the Indonesian Petroleum Association (IPA), the Geological Society of America (GSA), the Society for Sedimentary Geology (SEPM) and the Geologists' Association (GA). Joint marketing agreements ensure that GSL Fellows may purchase these societies' publications at a discount. The Society's online bookshop (accessible from www.geolsoc.org.uk) offers secure book purchasing with your credit or debit card.

To find out about joining the Society and benefiting from substantial discounts on publications of GSL and other societies worldwide, consult www.geolsoc.org.uk, or contact the Fellowship Department at: The Geological Society, Burlington House, Piccadilly, London W1J 0BG: Tel. +44 (0)20 7434 9944; Fax +44 (0)20 7439 8975; E-mail: enquiries@geolsoc.org.uk.

For information about the Society's meetings, consult Events on www.geolsoc.org.uk. To find out more about the Society's Corporate Affiliates Scheme, write to enquiries@geolsoc.org.uk.

Published by The Geological Society from:
The Geological Society Publishing House
Unit 7, Brassmill Enterprise Centre
Brassmill Lane
Bath BA1 3JN, UK

(*Orders*: Tel. +44 (0)1225 445046
Fax +44 (0)1225 442836)
Online bookshop: http://www.geolsoc.org.uk/bookshop

British Library Cataloguing in Publication Data

A catalogue record for this book is available from the British Library.

ISBN 978-1-86239-298-4

Typeset by Techset Composition Ltd, Salisbury, UK

Printed by The Charlesworth Group, Wakefield, UK

Distribution

USA
AAPG Bookstore
PO Box 979
Tulsa
OK 74101-0979
USA
(*Orders*: Tel. +1 918 584-2555
Fax +1 918 560-2652
E-mail: bookstore@aapg.org

India
Affiliated East-West Press Private Ltd
Marketing Division
G-1/16 Ansari Road, Darya Ganj
New Delhi 110 002
India
(*Orders*: Tel. +91 11 2327-9113/2326-4180
Fax +91 11 2326-0538
E-mail: affiliat@vsnl.com

Japan
Kanda Book Trading Company
Cityhouse Tama 204
Tsurumaki 1-3-10
Tama-shi, Tokyo 206-0034
Japan
(*Orders*: Tel. +81 (0)423 57-7650
Fax +81 (0)423 57-7651
E-mail: geokanda@ma.kcom.ne.jp)

Contents

Session: Passive Margins

The Technical and Editorial Committee

Bernie Vining
Baker Hughes, UK
Conference Chair and
Joint Editor-in-Chief

Alastair Fraser
Imperial College London, UK
Convenor and Session Editor,
Russia, Former Soviet Union and
the Circum-Arctic

Steve Pickering
Schlumberger, Gatwick, UK
Conference Deputy Chair and
Joint Editor-in-Chief

Scot Fraser
BHP Billiton, Houston, USA
Convenor, Passive Margins

Mark Allen
Durham University, UK
Co-convenor and Session Editor,
Russia,
Former Soviet Union and
the Circum-Arctic

Graham Goffey
PA Resources, London, UK
Convenor and Session Editor
Europe

John Argent
BG Group, Reading, UK
Convenor and Session Editor,
Passive Margins

Gary Hampson
Imperial College London, UK
Convenor, Core Workshop

Jonathan Craig
Eni Exploration & Production, Milan,
Italy
Convenor and Session Editor
North Africa and Middle East

Howard Johnson
BGS Edinburgh, UK
Convenor and Session Editor,
Unconventional Hydrocarbon
Resources

Tony Dore
Statoil, Houston, USA
Convenor and Session Editor,
Passive Margins and
Unconventional Hydrocarbon
Resource

Ken McCaffrey
Durham University, UK
Convenor, Virtual field trips

James Maynard
ExxonMobil International,
Leatherhead, UK
Convenor and Session Editor,
Russia, Former Soviet Union and
the Circum-Arctic

Robert Scott
CASP, Cambridge, UK
Convenor and Session Editor, Russia,
Former Soviet Union and the Circum-Arctic

Jonathan Redfern
University of Manchester, UK
Convenor and Session Editor,
North Africa and Middle East

John Underhill
University of Edinburgh, UK
Convenor, Geocontroversies

Bryan Ritchie
BP Houston, USA
Poster Chair and Session Editor,
North Africa and Middle East

Session editors and other technical contributors:

Matthew Allen, Stewart Clark, Richard Davies, Sergey Drachev, Steve Garrett, Jon Gluyas, Mark Lappin, Adam Law, Bruce Levell, Kevin McLachlan, Julian Rush, John Smallwood, Michael Thomas, Ian Walker

The Petroleum Geology Conferences Board Members:

Chris Bulley (Petroleum Exploration Society of Great Britain), Jerry Chessell (Petroleum Exploration Society of Great Britain), Roger Cooper (Energy Institute), Andy Fleet (The Geological Society of London), Louise Kingham (Energy Institute), John Martin (Energy Institute), Edmund Nickless (The Geological Society of London)

Organising Committee:

Marian Scutt (Petroleum Exploration Society of Great Britain), Jacqueline Warner (Energy Institute), Georgina Worrall (The Geological Society of London)

And with thanks to:

Malcolm Brown (BG Group) PGC VII Sponsorship Chairman

For help with the core workshop:

British Sedimentological Research Group (BSRG), British Geological Survey (BGS)

Grateful thanks are extended to the following companies for their generous sponsorship of the conference:

BG Group
BGS
BP
Centrica Energy
Chevron
ConocoPhillips
ExxonMobil
Hardy Oil and Gas plc
Hess
Maersk
MND Exploration & Production
Nexen
Petro-Canada
PA Resources
Schlumberger
Serica Energy
Sonangol Gas Natural
StatoilHydro
Venture Production plc

Preface

The Seventh Petroleum Geology Conference (PGC VII) was the latest in a prestigious series dating back to 1974. Over the years, this conference series and the associated proceedings volumes, commonly known as the 'Barbicans', have provided an important reference to NW Europe exploration and production, from its early life as an emerging world class petroleum province, through to its current mature stage. The previous conference opened the door to embracing selected other areas of the world, while still maintaining the tradition of the former five preceding conferences. The seventh conference, entitled: 'Petroleum Geology: from Mature Basins to New Frontiers', while also staying true to its roots, was a truly international conference, with sessions encompassing many of the petroleum provinces of the world, that is: Europe; Russia, the Former Soviet Union (FSU) and the circum Arctic; North Africa and the Middle East; and Passive Margins worldwide. As the world seeks new energy sources, it was most appropriate to have a session dedicated entirely to unconventional hydrocarbon resources. Regular features such as a core workshop were present. In addition, innovative new features, such as the geocontroversies debates and virtual field trips, both of which are described below, enhanced what was already a well established conference format.

The conference series has been distinguished by its high scientific quality; PGC VII is no exception. We are confident that these proceedings volumes will continue to be the standard reference for successive generations of petroleum geoscientists. The proceedings, in general, will follow the thematic format of the conference itself, and the majority of the papers presented in the conference appear as scientific contributions in the proceedings volumes. This preface attempts to provide an insight into the unifying themes of the conference.

The scene was set by a plenary address on 'Global Petroleum Systems' to place the various geographic-based sessions into their mega-regional plate perspective.

The geocontroversies debates, mentioned above, were designed to address certain broader challenges facing society and the petroleum industry today, in contrast to the highly scientific nature of the presentations in the other sessions. The format of the geocontroversies debates was one whereby two expert protagonists presented their case: one for and one against a motion. The three motions, one of which was presented on each of the three days of the conference, were entitled: 'This House believes that the North Sea is finished'; 'This House believes that National Oil Companies (NOCs) are the future of the petroleum industry'; and 'This House believes "Peak Oil" is no longer a concern'. Each debate was concluded with a poll in which the audience raised a yellow or red card to indicate their support or opposition to the motion. The results were, respectively, that the North Sea is not finished; NOCs are the future of the petroleum industry; and that 'Peak Oil' is indeed with us! The debates were a great success, enjoyed by all, and set a benchmark for the future.

The virtual field trips transcended all aspects of petroleum geoscience, using a medium whereby delegates could 'return to the rocks' and go on a field trip to various exotic parts of the world, but without leaving London. Significant advances over recent years in geoscience data acquisition, visualization and analysis now permit the construction of detailed digital outcrop models. In a visualization environment, these outcrop models can be viewed sequentially in 3D to simulate a geological field trip. While it is recognized that virtual field trips will not surpass the benefits of undertaking actual field work, they clearly have their place in the petroleum geoscientists' tool-kit. For example, digital outcrop mapping techniques, showing lateral and vertical facies associations and the distribution of fracture networks, can be transformed into a static geocellular model, the forerunner for reservoir simulation. Eight case studies are provided as video-clips on the accompanying DVD. The various localities visited include Ireland, France, Norway, Egypt, Greece and the USA. More widespread use of these technologies, and associated new developments, are undoubtedly a future trend in petroleum geoscience, as the keen interest in this session demonstrated.

The core workshop has been a successful regular feature of recent 'Barbican' conferences, enabling petroleum geoscientists to 'get their hands on the rocks'. This has, in large part, been due to the enthusiasm and dedication of Dr Colin Oakman. Colin sadly passed away at the time of preparing for PGC VII. It is most appropriate that this core workshop bears his name. Colin would have been duly proud. The core workshop focussed on reservoir sedimentology of the North Sea Basin and featured presentations by PhD students, academics and consultants that placed the reservoirs, as shown by the cores, into context. The cores illustrated a diverse range of 'classic' North Sea reservoirs. Cores were presented from the alluvial and fluvial clastics and carbonate turbidites of the Carboniferous of the southern North Sea. The central North Sea was represented by cores from Triassic aeolian and fluvial clastics, Jurassic (Fulmar Formation) shoreface sandstones and Cretaceous deepwater fan deposits. The northern North Sea was represented by cores from the deltaic sequences of the Jurassic (Brent group). In summary, the core workshop provided an impressive display of reservoirs of various ages, facies and geography across the North Sea Basin to complement the papers and posters of the Europe session.

Europe, in particular the North Sea, has been the cornerstone of the 'Barbican' conferences over the past 35 years, as summarized in the Europe section of these proceedings volumes. This conference confirmed that a high interest in Europe continues, manifesting itself as the most extensive session of the conference. This is depicted in the proceedings by the themes of exploration, field development and production, and new techniques in exploration and exploitation. The key issues addressed include small pool and high-pressure, high-temperature exploration, late-stage field exploitation, and field redevelopment. In addition, the North Sea has, for many years, provided copious high-quality, multidisciplinary subsurface datasets that permit tracking of plays and fields from discovery through to late life and, in some cases, rehabilitation; it is truly a world class 'laboratory' for future exploration and production activities around the world. This aspect is complemented by the pioneering of emerging technologies that also have applicability around the world.

The exploration theme has papers, regional, local and of a detailed case-study nature, that describe current exploration activity for small, deep pool, and complex structural and stratigraphic prospects in mature and frontier plays. The detailed integration of seismic, well and analogue-derived technologies to better understand structural evolution and sequence stratigraphic-based depositional systems are illustrated by case examples. The field development and production theme contains papers that describe the petroleum industry's responses to the challenges of low-permeability reservoirs and reservoir prediction. Finally, the theme on new techniques in exploration and exploitation contains papers that emphasize the need for integration across the spectrum of geoscience and petroleum engineering disciplines. Papers pertaining to recent advances in petrophysics, 3D and 4D seismic applications, and the targeting of drilling and completion technologies within integrated reservoir models complete this most rewarding section in the proceedings. For those readers searching for Atlantic margin papers in this section, these are placed more appropriately in the Passive Margins section. In this regard, we would encourage readers to look throughout the proceedings, as their particular subject of interest may be in a different section.

The Russia, FSU and circum-Arctic session covered vast, diverse regions, with some complex petroleum systems, ranging in age from the Neoproterozoic to the Cenozoic. These regions have attracted considerable interest from the petroleum industry over the past 20 years. The offshore Arctic, in particular, is perceived as a possible future world-class petroleum province with the likelihood of some new giant fields. It has, however, significant technological challenges in addition to important environmental considerations and its remoteness from markets. The series of regional papers addresses the geology of the Arctic basins, including their tectonic origin, and proposes models for their genetic evolution. It is truly a circum-Arctic regional section, with papers from Russia, Norway, Greenland, USA and Canada. In contrast, at a field scale, this section hosts two field development papers from the north Caspian Basin: the giant Karachaganak and Kashagan fields.

The North Africa and Middle East session is also strongly represented by papers addressing the regional geology. However, in this region, the emphasis was on the search for new older and deeper plays in known areas, and conventional plays in the frontiers. The North Africa petroleum systems of the Ghadames and Kufra basins are featured, including discussion of the glacio-eustatic controls on facies patterns. The impact of recent advances in seismic technology, in providing a step-change improvement in our understanding of basins, and their possible deeper potential, was demonstrated by papers from the comparatively well known Gulf of Suez and northern Red Sea areas. Moving to a field scale, a case study of the appraisal of the Taq Taq field in northeast Iraq provides insights into the technological approaches used to model fracture systems.

The session on Passive Margins was highly popular with delegates. Passive Margins have been the mainstay of global exploration success and fast-track field development over the past 25 years. Deepwater production now exists from Passive Margins as diverse as Angola, Nigeria, Brazil, US Gulf of Mexico, Egypt and India. A generation of petroleum geoscientists have now spent a significant part of their careers exploring Passive Margins using methodologies mostly based on direct hydrocarbon indicators.

It is welcoming now to see a more holistic approach to our understanding of Passive Margins, this being a key feature of the conference and proceedings. New insights are presented and old dogmas questioned. The evolution of Passive Margins is examined using exciting new information on the deeper structure of continental margins. New models are being developed that propose, for example, multiphase rifting events and a better understanding of the role and implications of volcanics. This diverse nature of Passive Margin geodynamics has resulted in different views regarding genetic basin evolution and architecture. This impacts our understanding of thermal history and subsequently the predicted level of maturation of source rocks. Further examples of a more holistic approach include discussion and integration of 'source to sink' concepts that address geomorphology, drainage systems, sediment supply and the influence of palaeoclimate. A principal benefit of these new approaches is a better understanding of the potential of a variety of play types, for example, deltaic depocentres, slope by-pass systems, carbonate platforms and margins, deepwater fold-belts, and pre-rift and syn-rift sections. Technology will continue to play a vital role. Papers were presented that demonstrate that improved seismic imaging techniques are having a profound effect in our understanding of the pre-salt plays offshore Angola. Will the latter mirror the conjugate margin offshore Brazil, the scene of many exciting, world class discoveries in recent years? The comprehensive Atlantic Margin section addresses new results in understanding the sub-volcanic geology of this extensive region. We are confident that further applications of these new approaches will breathe further life into Passive Margins worldwide and unlock new, deeper play potential.

Since the last conference in 2003, there has been a significant increase in interest in unconventional hydrocarbon resources to address, in part, the world's future energy needs. This has been particularly apparent in North America. It therefore appeared appropriate for this conference to address this important topic, and to assign a separate session devoted exclusively to unconventional oil and gas resources. These resources include oil sands, oil shale, shale gas, basin-centred gas, coal bed methane and gas hydrates. Unconventional oil and gas resources are commonly described as continuous or regionally pervasive and, although in-place volume estimates may be large, overall recovery is relatively low. These accumulations certainly challenge the paradigms associated with conventional resources, for example trap delineation is often problematic; reservoirs are developed in rocks formerly considered as sources and seals; and many unconventional oil and gas resources lack hydrocarbon–water contacts.

Pioneering research and technological innovation is underway. Many initiatives are focussed on North America, although other areas of the world are emerging. Aspects of this research are highlighted and complemented by some initial studies in Europe.

A spectrum of different examples from various parts of the world were presented. These include: the Bakken petroleum system, a tight oil play of the Williston Basin in North America; the basin-centred gas plays of the Western Canada Foreland Basin and the Pannonian Basin, Hungary; and the heavy oil deposits of the Athabasca Oil Sands in Canada.

The geological storage of carbon dioxide is rapidly gaining recognition as an important potential method for reducing carbon dioxide greenhouse gas emissions in the near future. These developments are driven by concerns to address climate change. However, these technologies are expected to also have future application to the petroleum industry and other parts of the energy sector. Recent findings from current commercial carbon capture and storage projects in the North Sea and North Africa are presented, and are complemented by major research programmes in North America.

The 'Seventh Petroleum Geology Conference; from Mature Basins to New Frontiers', and these proceedings, owed their success to the efforts of many dedicated individuals over a considerable period of time. We take this opportunity to thank each of them for their contributions, energy and enthusiasm, which have resulted in a complex job well done. We fully recognize that this success has been achieved at the same time as other competing demands for their skills and expertise. The willingness of many companies to release proprietary datasets and concepts, a hallmark of an up-to-date conference and scientific publication, is also gratefully acknowledged. We believe that the highest scientific standards have been attained in line with the tradition of the 'Barbican' conferences and proceedings of the past. In particular, we thank all members of the PGC VII Board, Organizing Committee, and Technical Committee, the latter as convenors for the conference, and subsequently as authors, referees and editors for the proceedings volumes. It has been an honour and a privilege to work with them. We also thank all our sponsor companies and universities for their support, whether this has been through direct funding, or indirectly through the provision of their staffs' valuable time. Finally, we thank the staff of The Geological Society Publishing House for preparation of a publication that will stand the test of time. We hope and trust that you, the reader, will enjoy the proceedings and use them extensively as a scientific standard reference, both as a book on your bookshelf and digitally on your desktop, in the global search for, and exploitation of, future energy resources.

Bernie Vining and Stephen Pickering
London, 2010

Global petroleum systems in space and time

S. MAY,[1] R. KLEIST,[2] E. KNELLER,[1] C. JOHNSON[1] and S. CREANEY[2]

[1]*ExxonMobil Upstream Research Co., P.O. Box 2189, Houston, TX 77252, USA (e-mail: steve.may@exxonmobil.com)*
[2]*ExxonMobil Exploration Co., P.O. Box 4778, Houston, TX 77210, USA*

Abstract: Each of the Earth's approximately 900 sedimentary basins is a unique result of geologic, hydrologic, atmospheric and biologic processes. The interaction of these processes results in complex histories that are palaeogeographically linked within tectonic provinces. Process-based genetic analysis provides the fundamental framework for predicting the distribution and character of petroleum systems. New technologies enable the exploitation of this predictability and are themselves the origin of new ideas and improved systems understanding. Petroleum geoscience embraces both forward modelling of processes as well as observation, calibration and inverse modelling. This approach of forward and inverse modelling promotes a general scientific methodology of simulation, prediction, testing and learning that allows us to describe the genetics of sedimentary basins. Genetic analysis can be applied to the spectrum of resource types from hydrocarbon to groundwater to mineral systems and across the range of scales from regional to play to prospect. Like the study of evolution through the fossil record, fundamental characteristics of petroleum systems can be recovered from the patterns of their distribution within the framework provided by plate motion, palaeogeography and palaeoclimate. These fundamental drivers control regional tectonics, subsidence, fill history and deformation that result in the phenotypic expression of individual basins and their fluid systems. Genetic analysis results in a taxonomic hierarchy that facilitates prediction and guides resource exploration. Although genetic analysis provides a framework for understanding the distribution and nature of petroleum systems, that framework itself is insufficient to address the challenges now facing the petroleum industry. New technologies are required to enable exploration in frontier settings, to identify new opportunities in mature basins, to maximize recovery from existing fields, and to unlock the potential of unconventional resources. Future success in all of these areas is fundamentally dependent on our ability to conceptualize new ideas.

Keywords: basin, petroleum system, palaeogeography, plate reconstruction, play element, genetic, tectonics, hydrocarbon

The objectives of this paper are threefold. Firstly, to provide a perspective on global petroleum systems including the global experience base and genetic thinking at a variety of scales from plates to pores. Secondly, to address the role of technology both in supporting identification of new opportunities and in maximizing value of existing assets, and thirdly to introduce the themes of the 7th Petroleum Geology Conference.

Our industry is currently facing a number of challenges. In the spring of 2008, the price for a barrel of oil was approximately US$90. By midsummer, it had exceeded US$140 and by March of 2009 it had dropped below US$40. The impact of such dramatic price fluctuation is clearly reflected in the news headlines. During the summer of 2008, many companies were announcing major new projects in what had been economically challenged opportunities such as Canadian tar sands. In the past few months, many of these same companies have announced decisions to delay or defer these same projects.

The asset portfolio of many major international oil companies is evolving through the inclusion of new asset types and a changing distribution of asset classes. To some degree, this has always been the case in our industry. For example, the same comments were made when the industry evolved from dominantly onshore in the 1940s–1950s to including significant offshore operations in the 1960s. The move into very deep water in offshore West Africa, Gulf of Mexico and elsewhere in the 1980s is another example. Now, as exploration for conventional hydrocarbons becomes increasingly challenged, the asset portfolio includes more and more hydrocarbon resources associated with what a decade ago were largely considered economically and technically unattractive opportunities.

The primary objective for most exploration activities is profitable acquisition of the best quality resources available. Recognizing both the difficulty in prediction of the price environment and the long-term nature of our projects, our industry has always relied on the development of new technology to make these resources profitable. Technology itself, however, presents an increasingly demanding challenge. Lienhard (1979) and others have demonstrated that the rate of technology change is exponential given that two criteria are met: (1) incentive/motivation exists to improve the technology; and (2) the technology is not limited by basic laws of science. Although Moore's law related to the exponential increase in the number of transistors placed on an integrated circuit is the most commonly cited example, many technologies exhibit this behaviour. Examples in our industry include LNG train capacity, heavy oil recovery, and controlled source electromagnetic imaging performance. The pace of technology development demands that companies are actively engaged in technology innovation just to keep up with the rapidly changing technology landscape.

A large number of organizations within our industry are now facing a demographic challenge that has been referred to as the 'crew change'. The experience profile of these organizations includes a large population of staff nearing retirement age, followed by an underrepresented population of 32–45 year olds, and then a population of young staff with limited experience. This has led to significant activity associated with efforts to capture and transfer knowledge within organizations.

Our industry has always faced challenges such as these and will continue to be faced with new challenges in the future. Success in

VINING, B. A. & PICKERING, S. C. (eds) *Petroleum Geology: From Mature Basins to New Frontiers – Proceedings of the 7th Petroleum Geology Conference*, 1–9. DOI: 10.1144/0070001

the face of such challenges depends in part on a few simple principles. From a business perspective, these principles might include such things as profitable volumes growth, operations integrity, effective knowledge transfer and commitment to research and development.

In addition to these extrinsic challenges, we are continually faced with the intrinsic challenges associated with sedimentary basins and their petroleum systems. All basins are unique. They represent complex systems with long histories involving multiple agents, numerous non-linear processes, feedback and emergent behaviour. Our ability to image, sample and measure these systems is limited, yet business success is dependent on our ability to predict the distribution and characteristics of these systems and, most importantly, how they will produce. In addition, especially in basins where we have our most mature knowledge through a history of exploration and production, the realization is increasingly common that future opportunities will be more subtle. Our ability to identify opportunities associated with new hydrocarbon resources as well as to maximize the value of existing resources also relies on fundamental principles such as genetic basin analysis and improvements in technology capability.

Genetic basin analysis

Genetic basin analysis has a long and colourful history. The Rover Boys are representative of an early phase of genetic analysis. They were a group of geologists who, during the 1940s through the 1960s, were sent out by Standard Oil management into the unknown basin areas in the world to make a quick assessment of hydrocarbon prospectivity. They developed an impressive understanding of global geology and hydrocarbon potential based on their widespread travels and fundamental field observations. Describing the history of the Rover Boys, Dave Kingston wrote: ‘By the mid-1960s, the best-looking onshore basins worldwide had been examined and surface field work had given way to a new frontier – the offshore. ... The roving days were over by the end of the 1960s’.

Although the quote from Dave Kingston carries more than a hint of sadness, the Rover Boys would reinvent themselves through a series of global studies groups and projects that were fundamentally based on genetic analysis. A report by Dave Kingston and others from 1973 on basin classification identified a series of ‘prime genetic parameters’ including basement composition (oceanic or continental), the type of past plate movement involved in basin formation (divergent, convergent), the present day plate position, the number of structural or subsidence events and the number of changes in the latter. This eventually became the Kingston basin classification that was published in 1983 and used by many geologists for a number of years (Kingston *et al.* 1983).

Similarly, some organizations within our industry were very early adopters of plate tectonic theory and quickly translated it into implications for understanding and predicting basin history. For example, in 1968 Temple and Nelson wrote a report entitled ‘Origin and Evolution of the Continental Margins’ that concluded: ‘Based on the hypothesis of sea floor spreading and continental drift, a model for the origin and evolution of continental margins is proposed. ... The type of margin and its predictable characteristics ... should lead to a better assessment of their petroleum potential’. This was 1968! Remember, the classic paper by Le Pichon on seafloor spreading was only just published in 1968 (Le Pichon 1968).

Within just a few years of the emergence of the plate tectonic paradigm, it was becoming common practice within regional studies groups to generate plate reconstructions as base maps for palaeogeography and to convolve that framework with models of subsidence and eustasy to predict the accommodation history, sedimentary fill patterns and play element distribution in frontier basins. This was genetic basin analysis being used as a framework to understand petroleum systems in space and time. Interestingly, even early on, the approach often addressed the entire Phanerozoic as recognition of inheritance associated with basin evolution and included more than just the region of interest as recognition of the necessity to look broadly within genetically related tectonostratigraphic provinces.

During the 1980s and 1990s, major advances were made in petroleum systems analysis that, when linked with genetic basin analysis, provided the foundation for modern approaches to understanding and predicting the time–space distribution of petroleum systems. For example, Waples (1980) drawing from the earlier work of Lopatin (1971) described the time–temperature behaviour of conversion of kerogen into liquid hydrocarbon and showed how this could be predicted from burial history. Welte & Yukler (1981) described what they called the ‘3D deterministic dynamic model’, which was essentially an early basin model that coupled descriptions of maturation and fluid migration within a 3D cellular model that evolved through time. Demiason & Huizinga (1994) defined an approach to genetic classification of petroleum systems based on consideration of charge, migration and trap characteristics. Magoon & Dow (1994) outlined an approach for integrated petroleum systems analysis, bringing clarity to the definition of petroleum systems, their constituent elements and the importance of understanding their temporal and spatial relationships.

Genetic basin analysis: overview

Now, genetic analysis embraces a full systems approach that addresses the fundamental processes associated with how basins form, fill and evolve (Fig. 1). This evolution includes both the rock and fluid systems and the goal is to identify the simple patterns that underlie fundamental relationships that in turn provide predictability. The process of genetic analysis causes one to move from a collection of observations such as simply listing the ages of play elements on a single chart to a systems-level understanding of the dependencies, feedback loops and inherent non-linearity. This increased ability to utilize complexity provides increased insight and ability to be predictive.

In addition to these aspects, genetic basin analysis also provides a framework for knowledge capture, which has been described as one of the key challenges facing our industry today and over the decade. The fundamental process relationships provide an architecture for both understanding and predicting the behaviour of basins and their associated petroleum systems. They also imply a structure for knowledge organization that is reflected in the hierarchy from tectonostratigraphic provinces, to terranes, to basins, to basin phases, to second and higher order accommodation cycles. Data and knowledge organized this way logically supports the notion of an integrated Earth model, reinforces the lessons learned through genetic analysis, and therefore transfers data, knowledge and understanding (Loutit 1996).

All basins are unique yet the processes that control how basin form, fill, deform and evolve fluids are common and predictable. These processes are ordered in a natural hierarchy that ranges from plate motion to pore and grain evolution. Plate interaction and interplate events drive intraplate deformation. Intraplate deformation creates both mountains and basins and provides a large-scale control on accommodation history. Intraplate deformation also controls the timing and style of some trap types and orogenic fluid movement. Accommodation space for sediment accumulation is modified by sea-level and climate process and influences the depositional systems and stratal geometry as expressed through local palaeogeography. Stratal geometry and

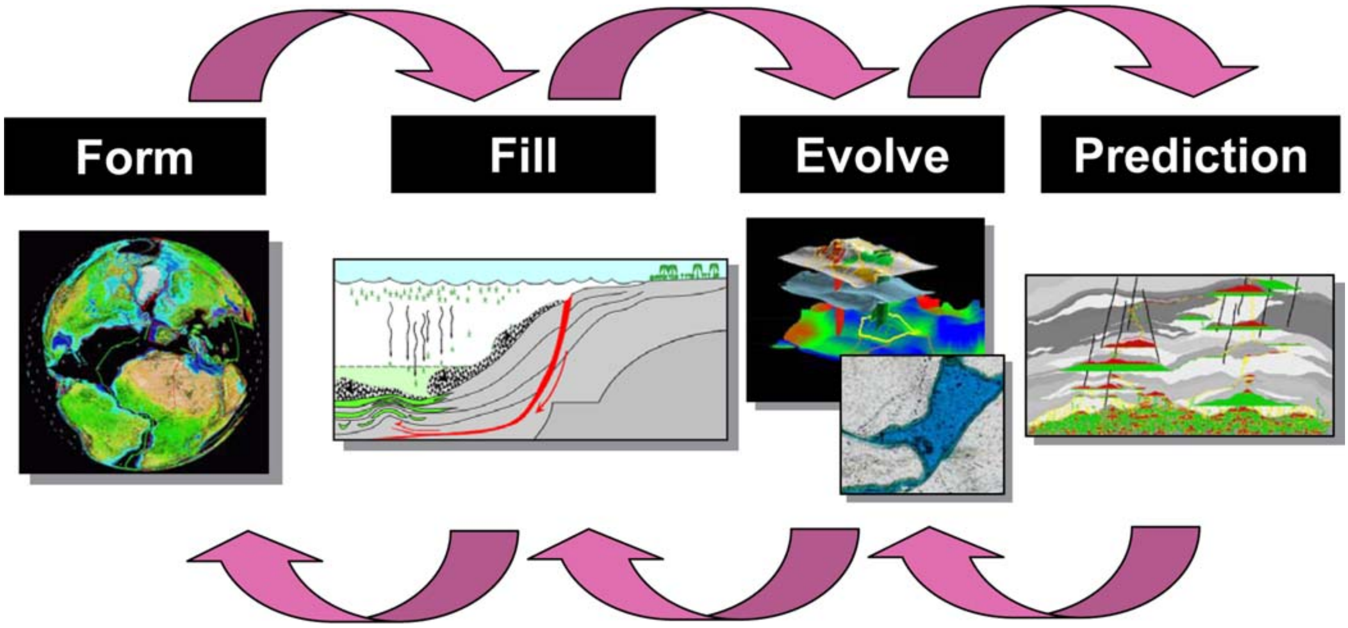

Fig. 1. Genetic basin analysis is a full-systems approach based on the fundamental processes of how basins form, fill and evolve, including both rock and fluid systems in order to make predictions about the distribution and character of global petroleum systems in space and time.

sediment distribution control the gross distribution and timing of petroleum system elements such as source, reservoir and seal. Post-depositional evolution associated with process such as burial, compaction, fluid expulsion and deformation can modify the previously developed elements and control HC migration (Fig. 2).

This hierarchy of process provides the fundamental underpinning of genetic analysis and is supported by an evolving suite of concepts, methods and tools. These include software for modelling plate motion, lithospheric deformation, subsidence, palaeogeography, sediment deposition, maturation, migration, fluid flow and diagenesis. These also include concepts and methods related to how basement architecture can provide controls on subsequent deformational behaviour, or how production, preservation and dilution control the distribution of organic-rich sediment in space and time. These also include analytical tools such as petroleum geochemistry, fluid inclusion analysis, microscopy and rock mechanics experiments. The value of genetic basin analysis is enhanced through advanced visualization and informatics technology and though a commitment to knowledge capture and knowledge organization as described previously.

As a basin forms and fills it is influenced by a variety of Earth processes and 'inherits' characteristics from all stages of its development. These stages are commonly expressed as basin phases that can be recognized or characterized by key attributes such as plate position, subsidence mechanism/rate and basin geometry. Even though all basins are unique due to the complex combination of these inherited characteristics, the Earth processes are common and therefore predictable. They possess characteristics that permit recognition with incomplete local data because of their predictability from global and regional patterns.

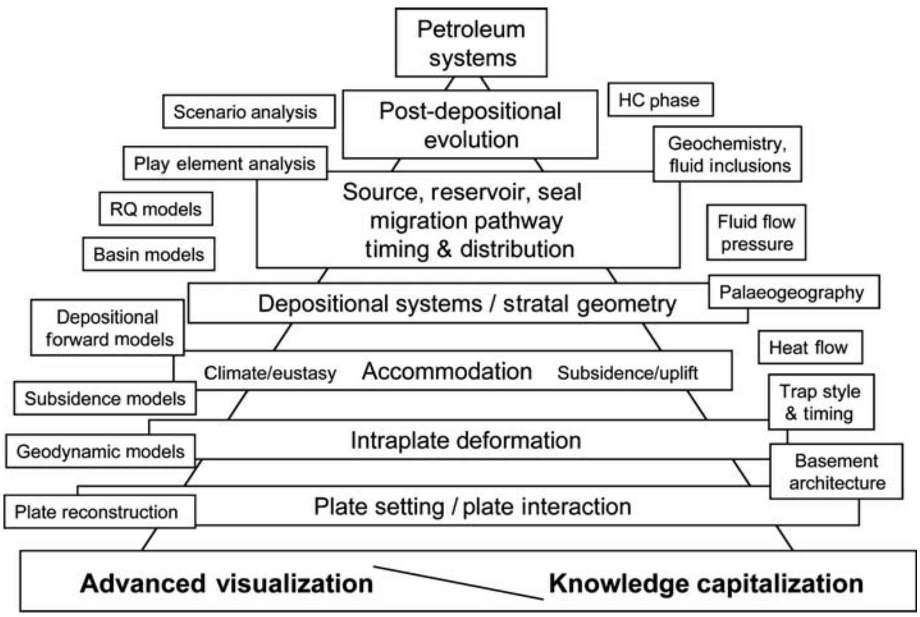

Fig. 2. Hierarchy of processes associated with genetic basin analysis.

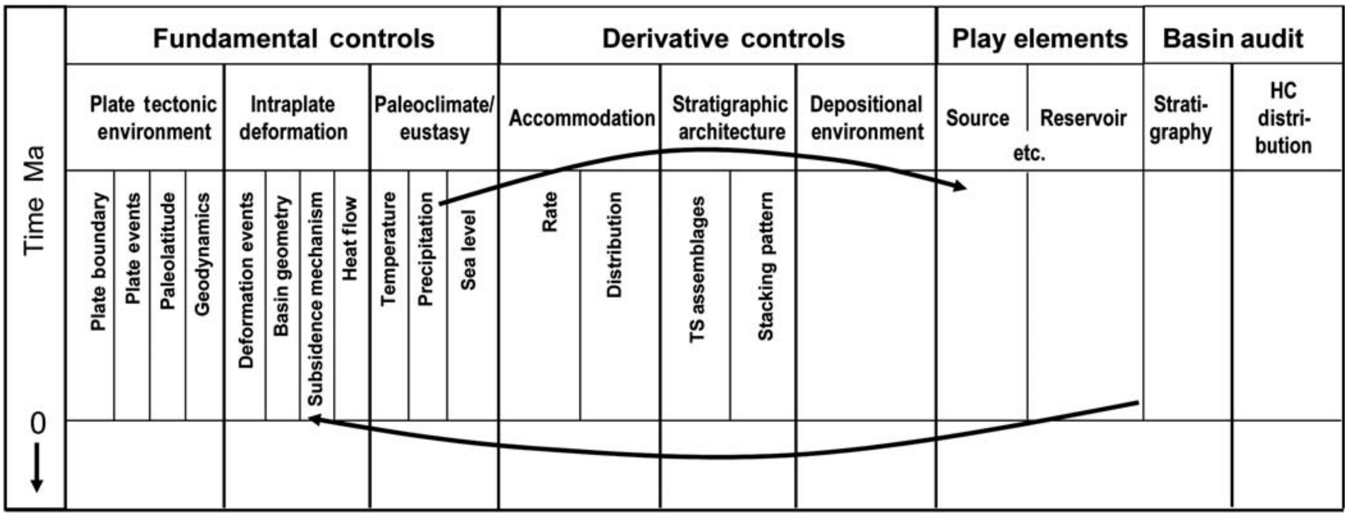

Fig. 3. Genetic analysis summary chart.

The viability of petroleum systems is a result of the combinations through time and space of these fundamental processes. A genetic analysis summary chart as shown in Figure 3 is one tool for capturing data and knowledge to assess and predict play element distribution, quality and hydrocarbon potential. This chart is organized to reflect the hierarchy of processes represented through fundamental controls such as plate tectonic environment, intraplate deformation and palaeoclimate, then the derivative controls of accommodation, stratigraphic architecture and depositional environment, then the timing of known play elements and finally the details of stratigraphy and hydrocarbon distribution. In this view, the latter are treated as an audit of the predictions from genetic analysis.

Building a summary chart in this way from left to right forces the mindset of genetic analysis and involves investigation of interactions between processes, feedback, non-linearity and emergent behaviours. This is a fundamental difference between genetic analysis and petroleum systems analysis as described by other authors where the summary chart is a series of columns for play elements against time (e.g. Magoon & Dow 1994) or the other common approach that shows stratigraphy on the left, play elements through the centre and tectonic events on the far right, as an afterthought.

Taking the analogy with genetics a step further, the basin or petroleum system genotype is expressed through the temporal convolution of processes such as palaeolatitude v. time, tectonic setting v. time, subsidence style v. time, palaeoclimate v. time, etc. The phenotype, or the material expression of this genetic sequence, is expressed through such attributes as play element distributions, field size distributions, hydrocarbon type distributions and creaming curves. For example, the Gippsland Basin offshore Australia is a basin with relatively simple genetics, and the creaming curve was nearly vertical in the late 1960s as the large structures with good top seal were all drilled over a short period of time. The main plays in the basin were tested and developed in a relatively efficient manner with about 350 total wells for a cumulative in-place volume of about seven billion oil equivalent barrels (GOEB). This is in sharp contrast to the Gulf of Mexico, with a creaming curve that climbed more or less steadily from 1950 to 2005, capturing about 60 GOEBs though about 50 000 cumulative wells. This is a basin with a complex genetic history, including multiple basin phases, a complex distribution of stacked play elements and salt tectonics. The continued exploration success in this basin has been enabled by numerous technology advances in both the geoscience and engineering domains.

Genetic basin analysis: global data and global plate motion

Genetic analysis of global basins and petroleum systems is now supported by a variety of global data sets some of which are publicly available and some of which have been developed by individual organizations. These include DEM/bathymetry, global geology, global tectonics, age of ocean crust, crustal thickness, total sediment fill and genetic analysis summary charts. The global data sets also include volume data such as seismic tomography (Van der Hilst *et al.* 1997). Advances in computer hardware including graphics and visualization tools allow these types of data to be manipulated and utilized for various kinds of analysis and at a variety of scales from global plate reconstruction to local basin geology.

Global plate motion models and associated palaeogeographic reconstructions provide a useful framework for understanding global petroleum systems in space and time. Global data sets can be integrated with the global plate model to illustrate the distribution of key petroleum system elements such as source, reservoir and seal (Fig. 4). Global plate motion models provide the foundation for a genetic framework that drives understanding and prediction of intraplate deformation, palaeogeography, palaeoclimate, basin history, play element distribution and quality. Plate reconstructions have long provided base maps for palaeogeographic models, but genetic analysis also requires an understanding of plate motion. Plate events can represent relatively instantaneous changes in plate motion or they can represent longer intervals of time during which a new plate boundary is organized. Changes in plate velocity, direction and boundary conditions correspond temporally and spatially with events of basin subsidence.

It is important to utilize global plate models that are internally consistent, but that also capture alternative scenarios. Given the common uncertainties associated with data used to constrain plate reconstructions (e.g. palaeomagnetic data, potential fields data, biogeographic data, etc.), alternative scenarios are almost always possible.

As an example of global genetic analysis, the Late Cretaceous (Turonian) is a time of widespread organic rich rocks including marine shales of the Cretaceous Interior Seaway in North America, the Gulf of Mexico, the North American Arctic, South America, West and South Africa, the Arabian Peninsula, Europe and East Central Australia. By this time, Pangea had been largely dismembered and most modern major ocean basins were growing

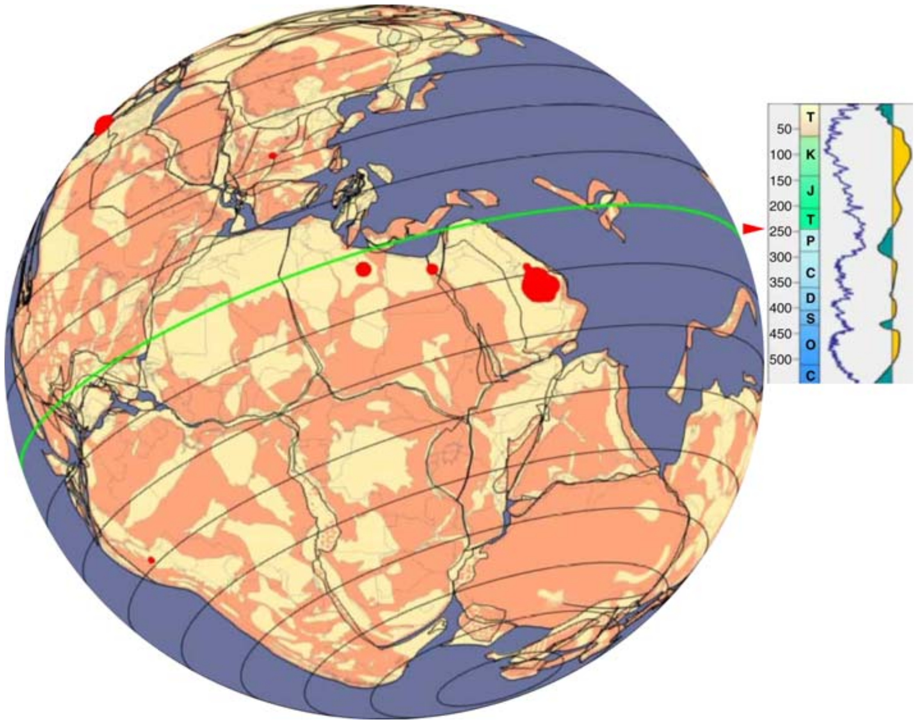

Fig. 4. Global plate reconstruction in the Late Jurassic illustrating plate geometry and basin location providing a time–space framework for genetic analysis of petroleum systems.

through seafloor spreading. Sea level was at its highest stand in the Phanerozoic and global climate was in a greenhouse period with very warm and equable conditions, including relatively low equator-to-pole gradients. Broad flooded shelves support deposition of reef building carbonates that become important reservoirs and the lack of polar ice is expressed through relatively low amplitude, high-frequency eustatic fluctuation. Palaeoclimate modelling predicts areas of significant marine upwelling and also significant restriction in the northern South Atlantic, the North American Interior Seaway, the North Atlantic, West Siberia and associated areas of the Arctic. The ability to analyse global datasets within a plate tectonic reference frame linked to other fundamental controls like eustasy and climate is essential for genetic analysis of petroleum systems in space and time.

Patterns emerge from this type of analysis that reflect fundamental controls on these elements and their interaction in space and time resulting in petroleum systems. For example, at the largest scales, there are clear relationships between global plate motion, eustasy, climate, the evolution of plant forms and the distribution of widespread source intervals. By the early 1990s, Klemme & Ulmishek (1991) and others recognized large-scale patterns controlling the distribution of key source rocks and parameters such as eustasy, subsidence and climate by generating global source rock distribution and type maps on plate reconstructions. Major periods of widespread, marine source rocks are correlated with first-, second- and third-order eustatic rises and periods of widespread basin formation associated with global plate tectonics. During these periods of widespread deposition, the organic characteristics, thickness and distribution of source rocks are controlled by regional palaeogeographic factors including the degree of oceanic circulation restriction, the evaporation–precipitation balance in each basin, and the degree of dilution associated with clastic influx in marginal marine settings.

Identification of these patterns that describe known petroleum system elements is only the first step towards what really matters – that is to utilize these patterns and fundamental relationships to identify new opportunities.

Genetic basin analysis: example

As a brief example of genetic analysis at the regional to basin scale, we will consider the Bighorn Basin in Wyoming. The Bighorn Basin contains more than 8 km of preserved Phanerozoic sediments that were deposited on Archaean crystalline basement of the Wyoming Craton (Snoke 1993). In the Early Palaeozoic, the basin is located in a proximal passive margin location in equatorial latitudes. By the Late Palaeozoic, that margin had become much more complex and was evolving into a convergent margin initially associated with the collision of offshore arcs and also probably influenced by the South America–North American collision to the south. By the Jurassic–Cretaceous, the Bighorn Basin was located in a proximal retroarc foreland setting with the arc to the west above a dominantly east-dipping subduction system. This foreland was disrupted during the Late Cretaceous–Early Cenozoic Laramide Orogeny that has been linked to a variety of convergent margin geometries or events with the currently favoured being flat-slab subduction during increased convergence rates (DeCelles 2004).

Plate events associated with the transition from passive to convergent margin temporally coincided with two events of intraplate deformation expressed as tectonic subsidence in the late Palaeozoic. In conjunction with second-order eustatic trends, these intraplate events controlled the timing of accommodation events that influenced the deposition of key reservoirs (carbonate and clastic). Later, after the convergent margin became better organized, the Bighorn Basin area was part of a broad retroarc foreland system that stretched from the Gulf of Mexico to Alaska. Tectonic subsidence, associated with this basin phase in conjunction with first- and second-order eustatic rises, resulted in deposition of source, seal and reservoir elements during the Cretaceous. Finally, the primary phase of rapid subsidence and sediment accumulation during the Laramide Orogeny drove all local source rocks into the oil generation window and produced the local basement-involved compressional structures that represent the major traps in the basin. The four main intervals identified by prediction from plate motion to intraplate deformation to accommodation do, in fact, control much of the distribution of hydrocarbons within the Bighorn Basin as well as the timing of key events such as trap formation and local maturation.

Application of genetic analysis over decades on a global scale reveals patterns of relationships as just described for the Bighorn Basin. For example, genetic analysis of numerous basins that include a foreland phase late in their evolution reveals that stacked source intervals commonly include both widespread pre-kinematic elements that are often oil-prone and somewhat more restricted syn-kinematic elements that can be both oil- and gas-prone. The foreland phase of subsidence and filling often drives maturation of the pre-kinematic source. Migration often includes both long-distance lateral migration and cross-stratal migration associated with encroaching compressional deformation. Such systems often include the potential for stratigraphic traps, hotelling and remigration.

Technology

Although genetic analysis provides a framework for understanding the distribution and nature of petroleum systems, that framework itself is insufficient to address the challenges now facing the petroleum industry. New technologies, including concepts, methods and tools, are required to enable exploration in frontier settings, to identify new opportunities in mature basins, to maximize recovery from existing fields, and to unlock the potential of unconventional resources. Future success in all of these areas is fundamentally dependent on our ability to conceptualize new ideas.

Concepts

Extensional systems

New concepts for extension of the lithosphere provide new ideas for the evolution of passive margins and the petroleum systems associated with them, especially in hyper-extended regions of outer continental margins. For many years, the pure shear model for lithospheric extension was the dominant model used for interpreting subsidence and heat flow on passive margins (McKenzie 1978). This 'classic' view led to a model of uniform thinning of the lithosphere from the hinge zone out to the continent–ocean boundary. A variety of alternative models including those of Wernicke (1985) and Lister *et al.* (1986) proposed that other mechanisms such as simple shear associated with major detachment faults and asymmetry may be important. Whereas these were largely kinematic models, advances in dynamical modelling that include realistic boundary conditions (e.g. strain rate), rheology and behaviour (e.g. strain softening) provide insights into the genetic processes that control architecture, subsidence and heat flow in extensional systems.

Most recently Manatschal and others (e.g. Manatschal 2004; Peron-Pinvidic *et al.* 2007) have proposed new models to describe the mechanisms by which continental lithosphere is thinned during formation of passive margins. These models have been driven by a combination of field work in the Swiss Alps, ODP drilling off the Iberian margin and geodynamic modelling. Removal of the entire crust is explained by a model where deformation is partitioned in the lithosphere and fault geometry changes as a function of the rheological evolution of the extending material. Initial stretching is accommodated by brittle deformation in the crust (e.g. North Sea). Crustal thinning evolves through deep faulting below a mid-crustal decoupling zone (e.g. Ivrea zone, Alps) and wholesale removal of the crust occurs after strain is localized on through-going detachment faults as sub-continental mantle rocks are exhumed. The continent–ocean transition is being redefined on the basis of these ideas and new observations from outcrop, drilling and reflection and refraction seismic data. On the Iberian margin, the zone of exhumation is >100 km wide and contains organized magnetic anomalies apparently related to serpentenization during extension rather than seafloor spreading (Sibuet *et al.* 2007).

The genetic implications of such models range from alternative reconstruction of conjugate margins, to reinterpretation of syn-rift and post-rift tectonostratigraphic assemblages, to alternative models for heat flow. The recognition of syn-extensional sag associated with preferential thinning of the lower crust without brittle upper-crustal deformation is a critical observation. These alternative models may result in new ideas about play element distribution and quality and associated hydrocarbon systems.

Methods

Detrital zircon geochronology

In addition to new concepts, there are a variety of new methods being developed that will impact our understanding of genetic controls on petroleum systems. U–Pb ages from detrital zircons are providing useful data for a variety of geoscience applications including plate reconstructions, regional tectonic models, palaeogeography, palaeodrainage evolution and sandstone composition. Although detrital zircon geochronology has been used for a number of years, recent advances in analytical techniques have improved the robustness and utility of this method. Modern laboratories utilize micromass isoprobe multicollector (ICP-MS) with a laser ablation system to date individual zircon grains that can be selected to represent all sizes and morphologies present in a sample (Miller *et al.* 2006). Some laboratories can now process more than 500 analyses per day, making it possible to efficiently and cost-effectively produce robust characterizations of the zircon age spectra for sediment samples.

Recent examples have demonstrated the value of this technique for characterizing source terrains for sandstones (e.g. Gehrels *et al.* 2008*a*). These authors sampled a large number of sediments from various terranes in the Tibetan region. Comparison of the zircon age spectra from these sediments suggests that the commonly accepted locations for major sutures separating terranes of different affinity and palaeogeographic proximity may be suspect. These new methods and the new data they produce can result in alternative plate reconstructions which, in turn, yield alternative palaeogeographies and potentially new models for play element distribution and quality.

A collaborative effort between the University of Arizona, the University of Kansas and ExxonMobil is developing a global database for detrital zircon dates that will be accessible to the global community to evaluate plate reconstructions and palaeogeography (Gehrels *et al.* 2008*b*).

Tools

Representation of genetic analysis in Bayesian Belief Networks

'New' tools are also impacting the genetic analysis of basins and petroleum systems. 'New' is used in quotes, because the fundamental theorem for the tool referenced here was published by Bayes in 1763. Nevertheless, a new application of this old theorem was recently published by Heins & Kairo (2007) as a model called SandGEM for predicting sand character through integrated genetic analysis. Although geoscientists have agreed on the fundamental processes that control sand generation for many years (Sorby 1880), the work of Heins and Kairo provides the first systematic approach to applying genetic analysis. To codify the relationships between genetic controls, they utilize a Bayesian Belief Network (BBN). In this approach, the primary genetic factors include tectonic setting and weathering processes, hinterland controls and erosion/transport processes, as well as basin controls including depositional processes. The BBN provides a useful technique for concatenating a web of conditional probabilities that represents the genetic relationships in the system. Relatively complex cause and effect relationships including single causes with multiple effects or even contradictory effects can be accommodated.

In SandGEM, as proposed by Heins & Kairo (2007), there are seven input nodes representing climate and weathering potential, climate flushing potential, regional topographic gradient, hinterland transport distance, basin subsidence rate, basin fluvial transport distance and depositional facies. The three output nodes include deposited sand composition, deposited grain size and sorting, and deposited matrix abundance. The SandGEM model has been calibrated in modern systems where the genetic factors are well constrained. In a series of validation studies in modern systems from South America and Australia, Heins & Kairo (2007) conclude that the BBN approach accurately predicts sand composition and texture across a range of different environments. SandGEM is just one example of how genetic analysis can be applied through probabilistic tools to understand and predict the behaviour of complex systems.

Similar approaches are being developed and tested for a variety of other petroleum system elements such as organic-rich rock. Genetic analysis of the controls on distribution and quality of source rocks has been an area of research for many years. Process-based models are now able to incorporate factors that control production such as in the case of marine upwelling, preservation such as in areas of palaeogeographic restriction and dilution such as is related to the inverse of clastic sediment supply (Bohacs & Heins 2007). As in the previous example for prediction of sandstone composition, BBNs are proving a useful approach for capturing complex relationships and generating probabilistic predictions about the likelihood of occurrence in time and space of organic-rich sediments.

Forward modelling

A variety of new tools are emerging for forward modelling of key genetic processes. These tools are enabled by advances in computing and visualization as well as the creative investigation of fundamental physics and geology.

For example, Miller *et al.* (2008) have reported on new approaches to develop full physics depositional models based on numerical description of fluid flow and sediment transport. Because these models can be developed to utilize multi-processor architecture, the time to run an interestingly large (space and time) model is becoming reasonable. There is a range of potential applications for such process-based models, from developing new insights into stratigraphic processes, to extraction of patterns and statistics for rule-based and geostatistical modelling, to full physics simulation of the erosion and deposition of a reservoir.

Other applications of new forward modelling capabilities include geodynamic modelling for improved understanding of lithospheric scale processes (e.g. Huismans & Beaumont 2007), mechanical modelling of crustal deformation in compressional settings, and models that attempt to incorporate deformation, development of topography through landscape evolution algorithms and sedimentation all within a single integrated model that includes feedback between the various processes (Braun & Yamato 2008). This is a glimpse of a future that will eventually evolve full-physics forward models of coupled Earth processes in order to simulate and test the fundamental controls on how basins form, fill and evolve – that is, genetic analysis.

Forward modelling is essential to calibrate and test process-based understanding and it provides a quantitative methodology to predict away from empirical data and evaluate alternatives. However, forward modelling is not a ‘silver bullet’ and model integrity is completely dependent on the validity of process description and the fidelity of input data.

Forward modelling provides an approach to predicting the subsurface through simulation of Earth history. Such predictions must be tested against and calibrated with our empirical understanding of the present state of the Earth through inversion of geophysical and well bore detection technologies and data. The return loop of test and learn is critical for the continuous evolution of the models. Both sides of this methodology must feed the integrated Earth Model that provides the common environment for the ‘simulate, predict, test, and learn’ process, for capturing our knowledge, and for identifying new opportunities (Fig. 5).

Opportunities

For a number of our organizations, offshore West Africa provides an example of how both genetic analysis and technology have supported a very successful series of ventures. Various West African basins including those offshore Angola, Nigeria and Equatorial Guinea, enjoy robust petroleum systems resulting in a prolific hydrocarbon province. The relatively rapid and efficient exploration was driven by continuing genetic analysis and by technology developments. Improvements in genetic understanding of deep water depositional processes and associated reservoir styles were key. Many intra- and extra-basinal variables and controls contribute to the development of a particular reservoir architectural style. Depositional styles observed in offshore West Africa include distributary systems, weakly confined systems, confined systems and bypass systems. The genetics of each of these styles influences reservoir architecture and performance.

Prediction from genetic models was effectively coupled with new technologies to image or detect the current subsurface state in offshore West Africa. Improvements in seismic data quality and DHI/AVO analysis played a significant role. For a robust suite of prospects, economic success rate increased from about 36% to over 60% for prospects with DHI support (Rudolph 2008).

Another opportunity where genetic analysis and technology are playing a key role is associated with unconventional resources, including heavy oil, tight gas, shale gas, coal bed methane and others. These types of resources are becoming increasingly important contributors to the asset portfolios of many organizations. Given experience with assets like Cold Lake heavy oil, we often think of these unconventional resources as requiring a long start-up time but also with a long asset life, heightened need for close integration of subsurface characterization, exploitation technology and commercial considerations and for their operational intensity. Conversely, the emergence of the unconventional gas play in the Barnett Shale has been dramatic, increasing from about 0.5 billion cubic feet per day (GCFPD) in 2002 to about 4.7 GCFPD at the end of 2007. The evolution of the Barnett play has been supported by improved genetic understanding of shale gas plays (Pollastro *et al.* 2007) and the controls on rock mechanics and gas distribution as well as a number of technology advancements primarily related to well architecture and reservoir stimulation.

Even though many of the unconventional resources require a different mindset when it comes to development and production strategies, they are still conducive to genetic analysis. Key

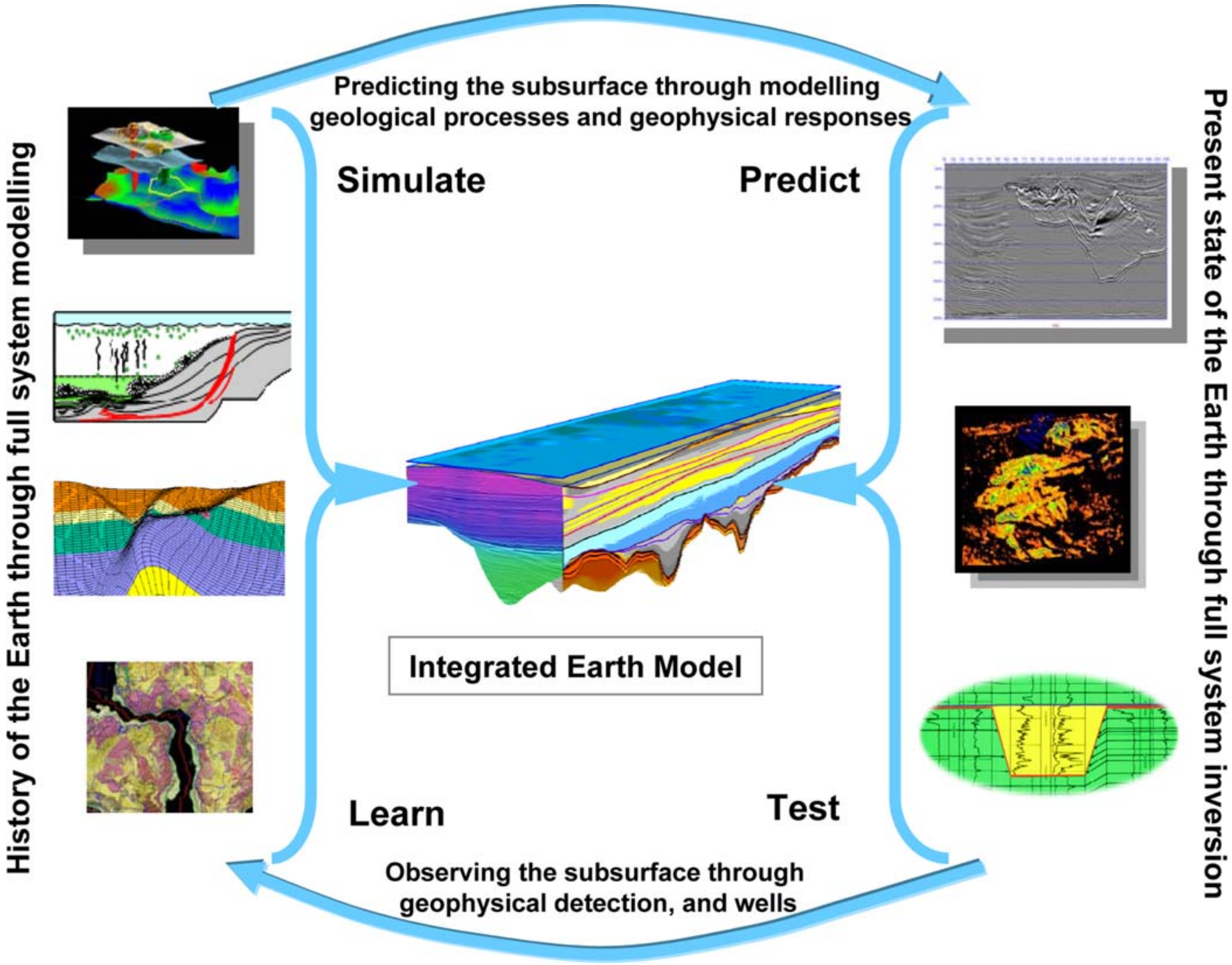

Fig. 5. Both forward and inverse models calibrated with appropriate data support the process of simulate, predict, test and learn that is fundamental to genetic analysis.

questions about the fundamental controls on sweet spots are now being studied with a genetic approach that spans plate-to-pore scales.

Summary

Genetic analysis encourages us to embrace systems thinking and complexity, to be aware that opportunities are often more unique than similar and to be very careful when attempting to use analogues. This is wise as the subsurface is almost always more complex than we initially predict. A case from the Gulf of Mexico illustrates this point. At the time of the development funding decision for this particular case, a simple model was based on a couple of exploration and delineation wells, poor quality seismic and a depositional model. The result was the pre-development cross-section with widespread 'sheet' sands and only modest variability. The narrow range of scenarios carried at this time did not include the potential for a highly channelized reservoir. With additional wells and improved seismic, a revised model now includes a highly channelized reservoir, with significantly more complex connectivity architecture demonstrated by well logs, higher resolution seismic, geochemistry and engineering data. Failure to embrace the potential complexity and failure to consider fundamental relationships, like the fact that continuous sheet sands are uncommon in this setting, can lead us down unfortunate paths.

As geoscientists, there is an easy way to reinforce the truism of the discussion above, and that is to spend as much time as possible observing the rocks. Getting on the rocks either in the field, in the core laboratory, or in the CAVE to make observations, develop interpretations and models and then test those models against the next outcrop or the next structure or the next core is always an educational and often a humbling experience. The complexity is what keeps it fascinating and discovering the patterns that underlie the genetic relationships is what keeps it rewarding.

References

Bayes, T. 1763. An essay towards solving a problem in the doctrine of chances. *Philosophical Transactions Royal Society London*, **53**, 370–418.

Bohacs, K. M. & Heins, W. 2007. Genetic basin analysis and paleoenvironmental reconstructions of the Mesozoic and Cenozoic strata of the Libya region. *Libya 2007, 3rd North African/Mediterranean Petroleum and Geosciences Conference & Exhibition*, Tripoli, Libya, 26–27 February 2007, Presentation A10.

Braun, J. & Yamato, P. 2008. Multi-scale couplings between surface processes and deformation of a three-dimensional orogenic wedge. Third International Geomodelling Conference, Firenze, Italy. *Bollettino di Geofisica*, **49**, 442–446.

DeCelles, P. G. 2004. Late Jurassic to Eocene evolution of the Cordilleran Thrust Belt and Foreland Basin System, western USA. *American Journal of Science*, **304**, 105–168.

Demiason, G. & Huizinga, B. J. 1994. Genetic classification of petroleum systems using three factors: charge, migration and entrapment. *In*: Magoon, L. B. & Dow, W. G. (eds) *The Petroleum System – from Source to Trap*. American Association Petroleum Geology, Tulsa, OK, Memoirs, **60**, 73–89.

Gehrels, G., Kapp, P., Pullen, A. & Ding, L. 2008*a*. U–Pb basement and detrital zircon geochronology of the Southern Tibetan Plateau and Tethyan Himalaya. *Geological Society of America Abstracts with Programs, National Meeting*, Abstract 234–238.

Gehrels, G., Walker, D., Bowring, J., Bowring, S. & May, S. 2008*b*. Tripoli, U–Pb_Redux, DZdatabase, and EarthChem: components of an integrated system for archiving, analyzing, and portraying U–Th–Pb geochronologic data. *5th Biennial Geochemical SIMS Workshop*, Madison, WI.

Heins, W. A. & Kairo, S. 2007. Predicting sand character with integrated genetic analysis. *In*: Arribas, J., Critelli, S. & Johnsson, M. J. (eds) *Sedimentary Provenance and Petrogenesis: Perspectives from Petrography and Geochemistry*, Geological Society of America, Boulder, CO, Special Papers, **420**, 345–379.

Huismans, R. S. & Beaumont, C. 2007. Roles of lithospheric strain softening and heterogeneity in determining the geometry of rifts and continental margins. *In*: Karner, G. D., Manatschal, G. & Pinhein, L. M. (eds) *Imaging, Mapping and Modelling Continental Lithosphere Extension and Breakup*. Geological Society, London, Special Publications, **282**, 111–138.

Kingston, D. R., Dishroon, C. P. & Williams, P. A. 1983. Global basin classification system. *American Association of Petroleum Geologists Bulletin*, **67**, 2175–2193.

Klemme, H. D. & Ulmishek, G. F. 1991. Effective petroleum source rocks of the world: stratigraphic distribution and controlling depositional factors. *American Association of Petroleum Geologists Bulletin*, **75**, 1809–1851.

Le Pichon, X. 1968. Sea-floor spreading and continental drift. *Journal of Geophysical Research*, **73**, 3661–3697.

Lienhard, J. 1979. The rate of technological improvement before and after the 1830s. *Technology and Culture*, **20**, 515–530.

Lister, G. S., Etheridge, M. & Symonds, P. 1986. Detachment faulting and the evolution of passive continental margins. *Geology*, **14**, 246–250.

Lopatin, N. V. 1971. Temperature and geologic time as factors in coalification. *Akademii Nauk SSSR. Bulletin De L'Academie Des Sciences De L'URSS. Serie Geologique*, **3**, 95–106.

Loutit, T. S. 1996. Australian petroleum research and development: an example of problem-driven geoscience research management. *APPEA Journal*, **36**, 500–515.

Magoon, L. B. & Dow, W. G. 1994. The petroleum system. *In*: Magoon, L. B. & Dow, W. G. (eds) *The Petroleum System – from Source to Trap*. American Association Petroleum Geology, Tulsa, OK, Memoirs, **60**, 3–24.

Manatschal, G. 2004. New models for evolution of magma-poor rifted margins based on a review of data and concepts from West Iberia and the Alps. *International Journal of Earth Science*, **93**, 432–466.

McKenzie, D. 1978. Some remarks on the development of sedimentary basins. *Earth and Planetary Science Letters*, **40**, 25–32.

Miller, E. L., Toro, J. *ET AL*. 2006. New insights into Arctic paleogeography and tectonics from U–Pb detrital zircon geochronology. *Tectonics*, **25**, TC3013.

Miller, J. K., Sun, T., Li, H. & Stewart, J. 2008. Process-based modeling of reservoirs: why do it? *American Association Petroleum Geology International Conference and Exhibition*, Cape Town, South Africa, 26–29 October 2008, http://www.searchanddiscovery.com/abstracts/html/2008/intl_capetown/abstracts/471682.htm.

Peron-Pinvidic, G., Manataschal, G., Minshull, T. & Sawyer, D. 2007. Tectonosedimentary evolution of the deep Iberia-Newfoundland margins: evidence for a complex breakup history. *Tectonics*, **26**, TC2011.

Pollastro, R. M., Jarvie, D. M., Hill, R. J. & Adams, C. W. 2007. Geologic framework of the Mississippian Barnett Shale, Barnett–Paleozoic total petroleum system, Bend Arch–Fort Worth Basin, Texas. *American Association of Petroleum Geologists Bulletin*, **91**, 405–436.

Rudolph, K. W. 2008. Learning by the bit: 15 years of West Africa deepwater exploration, development, and production. *American Association Petroleum Geology International Conference and Exhibition*, Cape Town, South Africa, 26–29 October 2008, http://www.searchanddiscovery.com/abstracts/html/2008/intl_capetown/abstracts/471355.htm.

Sibuet, J.-C., Srivastava, S. & Manatschal, G. 2007. Exhumed mantle-forming transitional crust in the Newfoundland–Iberia rift and associated magnetic anomalies. *Journal of Geophysical Research*, **112**(B6), NIL_84–NIL_106.

Snoke, A. W. 1993. Geologic history of Wyoming within the tectonic frame work of the North American Cordillera. *In*: Snoke, A. W., Steidtmann, J. R. & Roberts, S. M. (eds) *Geology of Wyoming*. Geological Survey of Wyoming, Memoirs, **5**, 2–56.

Sorby, H. C. 1880. On the structure and origin of non-calcareous stratified rocks. *Geological Society, London, Quarterly Journal*, **36**, 46–92.

van der Hilst, R. D., Widyantoro, S. & Engdahl, E. R. 1997. Evidence for deep mantle convection from global tomography. *Nature*, **386**, 578–584.

Waples, D. 1980. Time and temperature in petroleum formation: application of Lopatin's method to petroleum exploration. *American Association of Petroleum Geologists Bulletin*, **64**, 916–926.

Welte, D. H. & Yukler, M. A. 1981. Petroleum origin and accumulation in Basin Evolution – a quantitative model. *American Association of Petroleum Geologists Bulletin*, **65**, 1387–1396.

Wernicke, B. 1985. Uniform-sense normal simple shear of the continental lithosphere. *Canadian Journal of Earth Science*, **22**, 108–125.

The GeoControversies debates

J. R. UNDERHILL

Grant Institute of Geology, The School of Geosciences, The King's Buildings, University of Edinburgh, West Mains Road, Edinburgh EH9 3JW, UK (e-mail: jru@staffmail.ed.ac.uk)

Abstract: An opportunity to discuss and publically debate three critical issues of concern to oil company geologists was introduced into the Petroleum Geology Conference (PGC) programme for the first time in 2009. The debates selected focused on whether "peak oil" was already upon us; the relative role of National Oil Companies (NOCs) versus that of International Oil Companies (IOCs) and whether North Sea Exploration was finished. In each case, the arguments were delivered by two experts, who presented the case for and against each motion before answering questions and facing a vote by the audience, who showed coloured cards to indicate their support for what they had heard. All three debates proved to be extremely popular and were very well attended for all three days. The novel concept was deemed a great success and added significant value to the PGC.

Keywords: GeoControversy debates, peak oil, National Oil Companies, North Sea exploration

The Petroleum Geology Conference (PGC) – organized by the Geological Society, Petroleum Exploration Society of Great Britain (PESGB) and the Energy Institute – has a rich tradition of furthering the understanding of the geology of the North Sea basin. The series of seven conferences that have been held over the past 30 years or so have stressed the basin's important place in global oil and gas exploration and development through the delivery of technical presentations and poster displays. At the most recent PGC7, three innovative, hour-long debates were added to the conference programme, at which two expert protagonists presented their views for and against the three following motions of direct relevance to the petroleum industry:

- 'This House believes "peak oil" is no longer a concern'.
- 'This House believes that National Oil Companies (NOCs) are the future of the petroleum industry'.
- 'This House believes that the North Sea is finished'.

Each of the PGC debates ended with a poll at which the audience raised a yellow or red card (Fig. 1) to indicate their support for or opposition to the motions. The conclusions of the polls were that 'peak oil' was indeed with us; that oil power increasingly lay with NOCs; and the companies' North Sea exploration days were not yet numbered.

Debate 1: 'This house believes "peak oil" is no longer a concern'

'Peak oil' was a term originally coined in the mid-1950s by M. King Hubbert, a US Shell geologist, to describe the inflection point at the top of a production curve at which peak production is achieved and after which the rate of oil extraction inextricably declines. Whilst the term could arguably be applied to individual wells and fields, it is most commonly used in the evaluation of prospective sedimentary basins, countries and, more especially, in geopolitical circles to describe global production. 'Hubbert's Peak', as it has become known, was surpassed in the US in 1971 and in the late 1990s in the North Sea as major fields discovered in the 1970s entered a phase of terminal decline. However, controversy surrounds whether the balance and offset between the cumulative effect of basin maturity and exploration success in new frontier basins has already been achieved or will soon be reached.

The following section summarizes the debate, which focused upon whether 'peak oil' is already upon us. Whilst David Jenkins, a former Technical Director and Board Member at BP, argued that 'peak oil' is not of immediate concern, Jeremy Leggett of Solarcentury spoke against the motion.

For the motion: David Jenkins

"Historically the concerns about 'peak oil' have focused on the inability of supply to meet progressively increasing demand. The time of peaking relates to the degree of cumulative production from the resource base and, once it is passed, declining production is inevitable. 'Peak oil' concerns are entwined in a wistful recall for the days when cheap energy underpinned the Organization for Economic Cooperation and Development's (OECD) rapid economic growth. Those days are now over and will never return. The world needs to become accustomed to expensive energy. If the present concerns about carbon dioxide (CO_2) persist, the concomitant requirement to decarbonize carbon-based fuels will mean a further significant increase in costs. In fact, rather than the supply peak around which commentators have fretted, high energy prices could even engender a demand peak for oil, something which the environmental movement would applaud.

It is important to recognize that there is no near-term resource peak for oil, nor gas or coal. That is quite clear from the 2005 International Energy Agency's (IEA's) *World Energy Outlook*. This gave an assessment of 'available oil resources' at over 3.5 trillion barrels, and did not include any contribution from gas-to-liquid or coal-to-liquid technologies, which could become significant sources of liquid petroleum at prices above $100 per barrel.

The question of whether or when we experience peaks in production is fundamentally about market forces and definitely not related to a resource peak, as exemplified in the classic King Hubbert model. We had a production peak in 2008. It was caused by a very sharp speculative run up in price and led to the inevitable cut back in demand. Although the price has since come back, it remains high in historic terms and demand is continuing to decline. Investment, though, has also been cut back dramatically and we can certainly expect a supply shortfall sometime in the next four to seven years. This shortfall will also not be related to peak oil, but it will cause a further spike in price as occurred in 2008 and then, as last year, demand will again drop. The pattern

VINING, B. A. & PICKERING, S. C. (eds) *Petroleum Geology: From Mature Basins to New Frontiers – Proceedings of the 7th Petroleum Geology Conference*, 11–17. DOI: 10.1144/0070011

Fig. 1. The PGC7 audience were asked to raise a yellow or red card to indicate their support or opposition to each debated motion, the novelty of which was evidently enjoyed by all participants.

in the future is likely to be one of an extended irregular production plateau, punctuated by abrupt swings in prices leading to abrupt changes in demand.

Although at the moment we rely almost exclusively on liquid petroleum for road, marine and air transport fuels, and because mobility is so fundamental to our way of life and standard of living, we cannot conceive how we could change. This perceived dependence has underpinned our worries about global oil supply peaking. Decarbonizing energy because of the fear of climate change, however irrational that fear may actually prove to be, would have the effect of forcing such change. Moving away from the internal combustion engine to an electric drive train, associated with greatly increased production of biofuels, is soon to become technically feasible and could very plausibly produce a scenario that eliminated further growth in global demand for oil. Combine this with the production capacity available from the global resource base and a future world of expensive carbon-free energy, and then 'peak oil' clearly becomes an artefact of a prior economic world. In this somewhat bleak future it will definitely not be one of our many concerns."

Against the motion: Jeremy Leggett

"'Early peakers' like me fear that the oil industry has lapsed into a culture of over-exuberance about both the remaining oil reserves and prospects of oil yet-to-be-discovered, and about the industry's ability to deliver capacity to the market even if enough resources exist. In the corporate world, early peakers include the recently formed UK Industry Taskforce on Peak Oil and Energy Security (ITPOES), members of which include Virgin, Arup, Foster and Partners, Scottish and Southern Energy, Solarcentury, Stagecoach and Yahoo.

The first report of the ITPOES group of companies, released in November 2008 at the London Stock Exchange, presented evidence that total global oil production will begin declining early in the next decade. The main argument is that new capacity flows coming onstream from discoveries made by the oil industry over the preceding decade will begin dropping at that time. This problem will be compounded by other issues, including the accelerating depletion of the many old oil fields that prop up much of global oil production today, the probable exaggeration by OPEC countries of their reserves, and the failure of the 'price-mechanism' assumption that higher prices will lead to increased exploration and expanding discoveries.

In the same week as the ITPOES report was released, the IEA published its latest weighty annual report, the *World Energy Outlook*. In 2008, for the first time, the IEA conducted an oilfield-by-oilfield study of the world's existing oil reserves. It revealed that the fields currently in production are running out alarmingly fast. Crude oil production from all the world's existing fields climbs unevenly from just below 60 million barrels per day in 1990 to a peak – more exactly a brief plateau – of just over 70 million barrels per day between 2005 and 2008. In 2009, however, crude production begins a steep descent, falling steadily all the way below 30 million barrels per day by 2030. To meet the projected demand figure by 2030, up to 64 million barrels per day of totally new production capacity would be needed onstream within 22 years. That, the IEA points out, is fully six times the production of Saudi Arabia today.

The oil industry is not discovering giant oil fields at anything like the rate it did in the 1960s – the peak decade for discoveries. This is the case despite much better equipment for exploration today, and even after four years of rising oil prices from 2004 into 2008, when exploration was not hampered by lack of funds for investment. When the oil companies do make big discoveries, the lead times from discovery to first new oil delivered to market are long – often more than 10 years. In addition, the oil industry has profound infrastructure problems, and major issues with under-skilling and under-investment.

Many drilling rigs, pipelines, tankers and refineries were built more than 30 years ago, and according to some insider experts the physical state of the global oil infrastructure is a major problem even at current rates of oil production, much less the significantly higher levels anticipated in the future. The average age of personnel in the oil industry is 49, with an average retirement age of 55 – little less than a human-resources time-bomb.

To add to the challenges, the industry's overall exploration budget has actually fallen in real terms in recent years. The ITPOES fears that these issues will synergize to compound the 'peak oil' crisis, thus gravely impairing society's collective ability to respond.

In conclusion, this debate is all about the risk of a mighty global industry having its asset assessment systemically overstated, due to an endemic culture of over-optimism, with potentially ruinous economic implications. That couldn't possibly happen could it?"

Debate 2: 'This house believes that National Oil Companies are the future of the petroleum industry'

Whilst the UK has long since lost its very own national oil company (BNOC) and even its private successor, Britoil, NOCs have become increasingly important around the globe. This has happened rapidly; as recently as the mid-1970s the seven oil majors controlled around 80% of the world's oil supplies. Today, the five majors that remain control just 5% of reserves and national interests prevail in most of the petroleum producing nations.

The following article summarizes the debate which focused on whether the rise of the NOCs were a threat or an opportunity. Whilst Marlan Downey, an American Association of Petroleum Geologists (AAPG) past President and former Technical Director and Board Member at Arco, argued that NOCs are the reality and future, Peter Gaffney of the Society of Petroleum Engineers (SPE) and co-founder of the consultancy Gaffney, Cline & Associates (GCA) spoke against the motion.

For the motion: Marlan W. Downey

"For me, as someone whose career was mainly as a representative of the international oil companies (IOCs), it's like speaking at a funeral. I mourn the weakening of the IOCs to a point where they are near-to-death. Once, they controlled nearly 100% of all oil produced. Now, ExxonMobil, the world's largest IOC, controls only about 1% of the world's oil reserves. The hydrocarbon energy business (exploration and production) has shifted into the hands of the NOCs. Things have changed forever.

Once, the IOCs and their clients, the great powers, imposed their will on the penniless, powerless countries where oil was found. The great powers, economically allied with the IOCs, divided much of the world up into 'spheres of influence' and agreed not to compete with one another. British Petroleum was formed to give the UK government control of Persian oil via the 60-year D'Arcy concession.

Once, the IOCs boycotted oil producing countries that asked to retain a share of their oil. Shell refused the strange new concept of production-sharing contracts when they were introduced in Indonesia. In other words, the IOCs controlled the production, transportation, refining and marketing of nearly all the oil in the world, outside the United States. Now their share of that production has shrunk to total less than 10%.

Once, the IOCs alone had the capital, the technology and the project management skills to undertake large oil development projects. They provided all the capital, the technology, the project management skills and, fairly enough, took most of the oil.

Once, oil producing countries courted IOCs, rolling out the red carpet for international investors. Now, IOCs are coming (hat-in-hand) to plead to work with NOCs in oil producing countries.

Once, oil importing countries closely supported the interests of the IOCs – no longer. The UK won't do battle on the part of BP. NOCs, in contrast, are totally supported by their host countries. Now, we see a total asymmetry of contract sanctity. A producing country can abrogate its oil production contract, citing such legal fictions as 'the doctrine of changing circumstances', and face no consequences.

Once, IOCs were *needed*; now they are, sometimes, reluctantly *accepted* – accepted to do the difficult and risky projects that are on the bottom of the value order list of NOCs. We see an extraordinary shift in relationships – IOCs are no longer needed, only accepted, to supply low-cost risk capital. That's dangerous. During the 1990s I declined many opportunities to invest in the Former Soviet Union (FSU), as it was clear that they did not *need* my staff, my technology – they only wanted me to bring capital.

Once, NOCs were simply a local politician's dream, a way to provide costless patronage and thousands of jobs to kith and kin, with cities, hospitals and schools clustered like satellites around the oil fields. They siphoned off a tiny bit of the oil field's revenue as it was transmitted to the uses of the producing state. They had no real or useful function. These embryonic NOCs were staffed with civil servants, functionaries and accountants, and had few or no qualified engineers, geologists or geophysicists.

Today, the NOCs, two generations old, are benefiting from staff that have had 50 years of training on the job, and are making use of wise graduates from the greatest universities of the world. Now, the negotiating power, the control of oil, belongs to the NOCs in oil producing countries. Now, and in the future, producing nations and their petroleum operating arms, the NOCs, are awash with capital, possessed of great staff and rich in technology. That is the current status of relationships – where will it take us in the future?

Wisdom is recognizing life as it is – not as it once was. The IOCs gave up their dominance in technology by gutting their laboratories and research staffs in the 1980s and 1990s to save a few dollars. How stupid was that? Today, Petrobras doesn't need any help from Shell to develop in the deepwater. Saudi Aramco doesn't need any help from Chevron to manage large oil field projects in Saudi Arabia.

There is a golden rule for international business that needs to be kept in mind; I saw it expressed recently in the *Financial Times*: 'Them that has the gold makes the rules'. IOCs have been relegated to the leavings of exploration and production, and (should they ever approach success) are likely to have the prize taken from them. The exporting countries, with their surrogate NOCs, with an abundance of capital, manpower and technology, will make the rules.

Forget the myth of contractual third party arbitration. Does anyone doubt that courts in the FSU will rule on petroleum contract disputes in a manner favourable to the FSU? Does anyone doubt that Abu Dhabi can purchase whatever technology they need from service companies?

Now the future exploration and production business belongs to the NOCs – we taught them well . . . as foster parents and former partners, we wish them well. NOCs are the future of the hydrocarbon energy business – it *is* their century."

Against the motion: Peter Gaffney

"We originally agreed to this debate over a year ago when the oil price was $130 per barrel and increasing, and the world economy hadn't yet heard the bad news. On the day of the debate – 1 April 2009, April Fools' Day! – the price was about $50 per barrel, the Henry Hub gas price was down at $4/million cubic feet (mn cf) and we remain in the worst recession since the 1930s if not before. So, perhaps the question addressed in this debate has become less relevant as many governments fight to mitigate unemployment and economic security by pumping billions of dollars into, among other things, alternative fuels and possibly eventually changing the relative importance of petroleum at some point in the foreseeable future.

The NOCs themselves can be divided into two groups – the producers and the consumers, with almost equal and opposite objectives. While they often work together, the consumers are always looking to both reduce their import costs and secure their long-term sources across as wide a variety of suppliers as is reasonably practical.

The exporting NOCs themselves are facing much of the same suffering as the rest of the industry. Indeed, for the first time in several years, they are looking for partners on a broader front than previously, also curbing their plans for new plants and/or production capacity. The last few months have clearly shown that the market is a more powerful influence than the exporting NOCs – as much as they wished to stem the price fall tide, they were largely powerless to stop it.

I believe that, regardless of how important petroleum is to the world economy, particularly as a basic transportation fuel, it is still a commodity and as such will continue to oscillate in price through its foreseeable life. Commodity prices tend to be determined by a combination of perception and reality – and that perception is largely that expressed by the consumers.

Part of the basis of the belief that the NOCs are the future of the industry is linked to the concerns that many larger companies have regarding their ability to work with today's NOCs. The reality is that many of the larger companies have found it difficult to accept the realities of the modern day world – that is, that NOCs have matured and graduated into worthy competitors in their own right and that the deals available today need to be structured in today's real world, not that of the 1950s.

The NOCs themselves are widening their net to be international competitors across a broad front and look to work with others to mitigate their own risks. It is perhaps relevant to quote one of the renowned earlier petroleum industry experts – A. I. Levorsen, who wrote *Geology of Petroleum* many years ago: 'The petroleum geologist is the centre piece in the foundation of the petroleum industry. The industry is completely dependent upon a continuing discovery of new pools, or extension of old pools, for maintenance of its supply of crude oil and thereby of itself; and most certainly the discovery and production of oil is a geological enterprise'. This is still true today and the centre and fountain of such thoughts and ideas is not necessarily in the NOCs but exists, and will continue to exist, in the challenging minds of the professionals in our industry throughout the world – be it in NOCs or elsewhere.

However, let us consider this position in another context. China and India are key driving forces in the world economy today. In the future they will also be substantial and growing consuming nations and, as such, have a capability to influence the market from a very different perspective from that of the exporting countries.

Returning to the current situation, the industry already has spare capacity in excess of some 7 million barrels per day. Even with the expected declines in existing production sources, with possibly even lower operating levels we can anticipate that it will take some considerable time to take up this spare capacity to the point where capacity alone – rather than sentiment, hedge funds and/or politics – encourages significant increases in the price of oil and gas.

Peter Tertzakian, in his 2006 book *A Thousand Barrels a Second*, forecast the 'coming breakpoint', as he called it, in petroleum's tightening supply demand environment and he suggested that such a breakpoint may come about in different ways. What we have seen in the recent economic turndown is the very sort of event that helps to realize the breakpoint that he anticipated. Perhaps fortunately we will get a softer landing than might have been anticipated previously, as the supply limitations will now not materialize quite as early as it looked like they would just one year ago.

New technology itself is changing our situations too. Who could have imagined 10 years ago the huge new resources of natural gas that have become available in the United States through coal bed methane and the very successful shale gas developments? These natural gas developments alone are likely to materially change the energy dynamics not only of North America but also that of the rest of the world's energy position over the decades ahead. So, yet another factor which is completely independent of the effects of the NOCs has provided and will continue to provide a level of alternative investment opportunities.

To summarize, it is likely that whereas the NOCs will continue to have an effect on the way the petroleum industry addresses the future, there are many other factors which will also have a significant impact – as they have repeatedly done in the past. While I remain extremely optimistic about the opportunities for the oil and gas business, I remain enough of a realist to believe that no one group of organizations holds the key to the future and that people in general, the professionals within our business, including those in the NOCs, happenstance will continue to fashion our industry to provide the lowest cost supplies to meet the demands of the future."

Debate 3: 'This house believes that the North Sea is finished'

North Sea oil and gas provided the financial basis for Britain's economic recovery in the 1980s and 1990s. Phenomenal exploration success boosted Treasury income and provided the platform for stable government and prosperity. Recent years, however, have seen many changes with mergers and acquisitions leading to new mega-nationals seeing the North Sea as a less attractive exploration province now that the most obvious large structures have been drilled and the very largest fields have been exploited. Given those changes, the debate centred upon whether the North Sea had any form of future or not.

The following summarizes the debate, which focused upon determining whether the end of North Sea exploration is nigh. Whilst Richard Hardman, Director and Technical Adviser to the Board of FX Energy and former North Sea Exploration Manager of Amerada Hess, argued that North Sea exploration was in terminal decline, Jim Hannon, a Managing Director at HannonWestwood, spoke against the motion (Fig. 2).

For the motion: Richard Hardman

"One of the most successful companies of recent years, OILEXCO, has filed for bankruptcy despite having a 40% interest in Huntington, perhaps a 150 million barrel field and the biggest discovery for some time. Was it just bad luck, bad timing, bad management or is it a feature of the North Sea today? I will leave it to you the audience to decide after you have heard the arguments for and against the proposition.

Some years ago at an art fair I bought a large slate engraved with the words 'For he has hold not of an image but reality' – an apt aspiration for an oil and gas explorer. Only when the drill bit hits the horizon where pay should be found do we know if our ideas are based on reality. Explorers are true artists and, like artists, the only test is 'do their dreams make money?' A pessimistic explorer is a contradiction in terms – an oxymoron. One without creativity is like an artist who only paints pictures by numbers. To explore satisfactorily you have to think creatively, use ideas based on all the knowledge available and then take the risk you may have got it all wrong. Keeping this in mind there is always a risk the creative mind wanders off into the fictional domain, particularly as by trade, training and inclination we are optimists. And it is my contention that this is what is happening with the North Sea today.

An analysis of risk in exploration has shown that the biggest risk an explorer faces is not failing to find oil or gas but the risk of losing the job. Looking at the North Sea as a whole it is difficult to find disinterested parties who can appraise its merits clinically. The other day the UK Oil Minister, Mike O'Brien, joined in the optimism. On the *Today* programme, referring to the latest round of licensing, he said the undiscovered resources in the UK offshore

Fig. 2. The GeoControversies debates led to robust questioning and lively debate chaired superbly by Julian Rush (on the left), as exemplified here, where Jim Hannon was put on the spot in 'the North Sea is finished' debate.

amounted to 20 billion boe. He did not mention the risk and seemed to assume that this was the bounty to be found. He had no choice but to be up-beat.

The thought that these riches are at an end is unbearable at a time of the greatest economic downturn since the 1930s, and it is better politically to be unrealistic than tell a sober truth. Where many people's livelihoods and several political futures depend on a mature basin, its potential will always be overstated.

To recap today's presentations [at PGC7], the biggest single item in this analysis is the basins and their capacity to contain additional reserves. In the UK, new plays are either of moderate risk and small, or large and very risky involving new and untested ideas. Only west of Shetland is there running room – and costs are so high that this is a big company playground and is not the North Sea. Norway is over red-taped – attractive for exploration when you have qualified, but procedures are cumbersome and the authorities never allow speed to be of the essence. Meanwhile, Denmark has too small a prospective area and is largely explored out. The Netherlands still has potential, but how much of an open door policy is pursued is debateable. It is a very complex area and, hence, as new technology develops more subtle traps are identified.

Consequently, as far as exploration goes, the North Sea is finished – at least for anything except the very smallest of companies. I wish it were otherwise."

Against the motion: Jim Hannon

"The UK continental shelf (UKCS) was projected to hold some 60 billion boe, of which perhaps 35 billion have been produced – leaving some 20–25 billion boe potentially available. But can it be recovered and is there the technical, political and business resolve to pursue the remaining opportunity?

The key components to consider are, first, the geology – the remaining resource potential; secondly, recent drilling activity and results; third, the commercial hurdle; and fourth, the present structure of the industry – the number and composition of oil companies that are currently participators on the UKCS.

A review of the North Sea's remaining resource potential suggests that there are around 430 undeveloped discoveries with a total unrisked potential of 8 billion boe – giving an average discovery size of 21 million boe. The database also contains details on over 1500 prospects, with total unrisked potential of 65 billion boe, an average prospect having around 40 million boe.

In the past five years, around 60 exploration and appraisal wells have been drilled in each year – a total of over 250 wells. Hannon-Westwood have calculated a success rate of 86% for appraisal wells and, for exploration wells, 42% discovered oil or gas. The planned well database contains some 190 wells in planning for the remainder of 2009 until 2011, suggesting that enthusiasm for the basin remains undiminished. It is worth noting that, although the average discovery size has been around 20 million boe, the majors have access to west of Shetland and central North Sea high pressure/high temperature prospectivity, enabling them to drill prospects well in excess of 60 million boe.

Using economic models tailored to test the quality of the undeveloped discoveries and undrilled prospects, and taking conservative parameters, numbers were reduced by 10% for discoveries and by 25% for prospects, while capex and opex were inflated. A discounted profitability index was calculated to measure the capital efficiency of each project at a range of oil and gas prices. The results show that at $40 per barrel only 18 of the undeveloped discoveries are commercial – being just 4% of the total, but at $60 per barrel around 200 discoveries become viable. On analysing the prospects, a similar outcome unfolds.

At $40 per barrel, only some 85 prospects would be fit for consideration for drilling – representing about 6% of the population, but at $60 per barrel, the number rises to 700 prospects (45% of the total). In total, at $60 per barrel, some 900 structures merit drilling, targeting 9 billion boe and potentially delivering a business net present value of $100 billion after a capital investment of $105 billion. A low commercial hurdle and a very substantial business opportunity, by any measure. However, is the industry optimally structured to seize this opportunity?

HannonWestwood consider that the scale of the resource outlined is optimally fit for a licensee population of perhaps 40–50 companies, but there are currently 168 licensees on the UKCS. While the weakest players will go, funding has to be secured for the best of the prospects developed by the Promote licensees; their expectations, if realistic, have to be met. Economic success is more likely to be delivered through a significant drilling programme, scheduled in a cost-effective way, than through participation in one or two wells per year with a likely 80% failure rate. Companies need a good business plan to recognize the risk and to be able to tolerate the North Sea cost base. The majors will continue to target high value prospects; for others, the key for success will be some consolidation and the innovative alignment of funding to talent."

Summary: Julian Rush

"It was a privilege to chair the well attended debates. The idea had always been to challenge and to provoke discussion (Fig. 2). That the GeoControversies debates succeeded in doing that, and more, with rigour and good humour, is a tremendous tribute to the organizing skill and hard work of all concerned and to the way in which the conference embraced the concept and engaged in the discussion.

During the first debate on 'peak oil' between Jeremy Leggett and David Jenkins, I was reminded of the furore surrounding *The Limits to Growth* from the *Club of Rome* in the early 1970s. It was published while I was an undergraduate studying Engineering and Economics, and I recall it prompted considerable debate. Much maligned for predictions it didn't actually make, not least the infamous 'forecast' that oil would run out in 1992, it did serve to start a debate that continues to this day about the way Earth's growing human population uses and exploits the planet's resources.

The discussion is rightly wider now than the narrow issue of supply and demand, as both speakers in the 'peak oil' debate implicitly recognized. It is no longer a debate based on the assumption that resources are infinite and demand enduring and inflexible, but one coloured by the realization that peak oil must happen; it is a necessary precondition for the successful adaptation of humanity to climate change.

The issue, then, is not a matter of if, but when? And the timing is critical, especially if you accept the latest warnings from IPCC (Intergovernmental Panel on Climate Change) scientists of the need for greenhouse gas emissions cuts way beyond those currently contemplated in international negotiations.

Can 'peak oil' be managed so there is a smooth transition to replacement technologies or fuel sources with urgency but without excessive societal disruption? Both contributors agreed oil prices will rise in the next few years; the trick for the world's leaders is to put in place timely policy responses to use such rising prices so they act as a driver to accelerate the switch to a low-carbon economy and infrastructure. Arguably, they have been dismally slow to do so. Or will unfettered market forces drive up oil prices so quickly, as oil companies seek to recover the costs of extraction from increasingly difficult environments like the deep sea or tar sands, that wealthy western societies, at least, are left with difficult choices about unaffordable lifestyles? For the politicians, that is a distinctly uncomfortable scenario, one likely to be made of their own reluctance to act. The problem is, as both David Jenkins and Jeremy Leggett make clear, particularly acute when it comes to transport.

Then there are the oil companies. 'Business as usual' is a superficially attractive option for those unwilling or unable to adapt. Already we see many of the majors retrenching to their core businesses. But by adopting strategies designed to delay peak oil in order to protect their short-term vested interests, they risk not only exacerbating climate change – for which they are unlikely to be forgiven – but their very survival as well when their bluff is eventually called.

As for the second NOC debate, I found it interesting to see an audience largely comprising individuals dependent in one way or another upon private sector IOCs willingly persuaded their benefactor's time was up.

As someone whose job is to report for a daily TV news programme, it is rare to get the opportunity to step back from the immediate to consider a bigger, strategic picture. The changing financial and corporate structure of a global industry is pretty dry stuff – not, I'll admit, the bread and butter of a jobbing hack, unless, like the banking sector, it suddenly implodes. Not that the NOC debate was dry – far from it. This PGC debate offered that opportunity and both speakers and the audience embraced it vigorously.

The world's oil and gas industry has clearly changed in the last three decades as it has evolved to meet new global political realities as wealth, power and influence ebb and flow across the planet. Geopolitics is an ecosystem and at the heart of this debate was a question about which structure – NOC or international private sector oil company – is best fitted to evolve further. A company is like an organism, and it fights for its survival. (How else to view the millions of dollars spent by the fossil fuel industry lobbying against action to limit the effects of climate change?) The 21st century will see huge changes in the geopolitical ecosystem as the economies of China, India, Brazil and others grow to equal and surpass the western economies.

NOCs, both speakers agreed, are now the dominant life-form in the petroleum industry. By their very nature they are intimately bound to their political masters, masters whose ambition is the growth of their economies, a symbiotic relationship that currently benefits both. But will they survive to be the future of the petroleum industry? To my surprise the audience thought they would – Marlan Downey's was overwhelmingly voted the more persuasive argument. That assumes, of course, that the NOCs' political masters see oil and gas as part of their plans for growth. Is there a future of any kind for the petroleum industry in the sort of low-carbon geopolitical ecosystem that may evolve if developed and developing countries do actually agree action to limit the effects of climate change? One was left pondering the key question as to whether all oil companies, both private and national, face extinction before the first half of the 21st century is out.

It was a brave challenge in the final, North Sea debate to ask a conference of petroleum geologists to look over the edge of the abyss and ask them to consider if they still had a purpose. There can't have been many in the auditorium at the QEII Centre who had not looked out over the grey waters of the North Sea at some stage in their career as they pondered what lay beneath. The North Sea has been the nursery of a generation of geologists, their geo-playground and their workplace. They looked over the edge in the North Sea debate though and decided the explorers' days were not yet numbered. But, reflecting on the debate between Richard Hardman and Jim Hannon, I wonder if they reached the right answer for the wrong reasons.

The debate, of course, was about exploration for oil and gas – were the glory days of the past over yet? But we are heading into a low-carbon future, one that seeks not to praise carbon, but to bury it. The North Sea is routinely promoted as the ideal location to store carbon dioxide (CO_2) when it is eventually captured from power stations and industry.

Carbon capture technology is in its infancy, but the engineering problems are not insurmountable. I have little doubt it will succeed – it has to. Storage, though, is usually taken for granted; where there was methane, so there can be CO_2. It may not be that easy – CO_2 is not CH_4. Their geochemistry is different. While CO_2 has been successfully sequestered for over a decade in Statoil's Sleipner field, or used to enhance oil recovery in depleted oil fields in Canada, it cannot be taken for granted that formations that stored methane for millennia will do the same for CO_2. Finding the reservoirs where CO_2 can be safely sequestered for the significant time-scales required, in formations that don't leak, is a geological challenge of a different kind that will need considerable 'exploration'.

North Sea exploration, then, does have a future, as the audience decided – but I would not be surprised if the young geologists in the audience who will be doing the exploring find themselves using their considerable skills and knowledge as petroleum geologists to look for something other than petroleum products."

Conclusion

The introduction of the novel new series of debates was a huge success, being well attended and a subject of lively debate and discussion long after the lunchtime sessions were concluded. The debates spawned articles in *Petroleum Review* and *GeoEnergy*, and have even led to the instigation of Petroleum Group GeoControversy debates at Burlington House on subjects like the formation of the 'Silverpit Crater' and the like. In so doing, the PGC has demonstrated flexibility and yet again led the way to leave a legacy for the geoscientific community. Hopefully, when PGC8 comes around, it will be ripe for a new series of debates on those GeoControversies of the moment.

I wish to acknowledge the help and support of Bernie Vining, Graham Goffey and Al Fraser, whose enthusiasm for the notion of the GeoControversies Debates and unstinting enthusiasm for the concept materially contributed to their success. Thanks are given to the conference photographer for providing the photos used in the paper.

Virtual fieldtrips for petroleum geoscientists

K. J. W. McCAFFREY,[1] D. HODGETTS,[2] J. HOWELL,[3] D. HUNT,[4] J. IMBER,[1] R. R. JONES,[5] M. TOMASSO,[6] J. THURMOND[4] and S. VISEUR[7]

[1]*Department of Earth Sciences, Durham University, Durham DH1 3LE, UK (e-mail: k.j.w.mccaffrey@durham.ac.uk)*
[2]*Department of Earth Sciences, University of Manchester, Manchester M13 9PL,UK*
[3]*Centre for Integrated Petroleum Research, University of Bergen, Bergen N5007, Norway*
[4]*Statoil Research Centre Bergen, Sandsliveien 90, 5020 Bergen, Norway*
[5]*Geospatial Research Ltd, Earth Sciences, Durham University, Durham DH1 3LE, UK*
[6]*Enhanced Oil Recovery Institute, University of Wyoming, 1000 E. University Ave, Dept 4068, Laramie, WY 82071, USA*
[7]*Géologie des Systèmes Carbonatés, EA 4234, Université de Provence Aix-Marseille 1, Centre de Sédimentologie-Paléontologie, case 673, place Victor Hugo, 13331 Marseille, cedex 03, France*

Abstract: Significant advances in geosciences data acquisition, visualization and analysis now allow highly detailed outcrop models to be constructed for a range of petroleum industry purposes. From a given field locality, a virtual outcrop is created from a centimetre-scale digital elevation model and colour photographs with geological information overlaid as appropriate. In a visualization environment, these datasets can be viewed sequentially to simulate undertaking a fieldtrip. These *virtual fieldtrips* allow geoscientists to improve and expand the traditional fieldwork experience in a number of ways, ranging from planning and health and safety considerations for management, to providing live supplemental technical content on a mobile device to the fieldtrip participant. The fieldtrips are easily archived and content can be reviewed in the office to provide analogue information during technical work. Examples of virtual fieldtrips are provided on the DVD that accompanies this volume.

Keywords: virtual outcrops, fieldwork, laser scanning, lidar, analogue model

Over the last 10 years there have been significant advances in geoscience data acquisition and visualization techniques. These advances have revolutionized geological fieldwork, primarily with the emergence of the *virtual outcrop* (VO), where a high-resolution copy of the outcrop is recreated on a computer in 3D. While 'virtual fieldwork' is unlikely to surpass the experience gained during real fieldwork, it is now clear that digital outcrops can provide significant insights that can supplement the traditional field experience.

Despite high costs and an increasingly stringent health and safety culture, the petroleum industry still sees clear benefits from subsurface technical personnel undertaking fieldwork and spending time at outcrops. There are a number of different types of fieldwork that geoscientists working in the petroleum industry may carry out, including:

(1) Multidisciplinary excursions, typically involving all the technical staff (geoscientists, reservoir engineers, drillers, etc.) within an asset. Such trips will normally be to outcrops that are analogous to a particular licence block or field and will be designed to increase understanding of the subsurface challenges faced by the team.
(2) High-level training for expert geoscientists to increase knowledge of geological processes and products, especially in sedimentology, stratigraphy and structural geology. Such trips may also include a component of fieldwork in which data are collected to address specific challenges (e.g. Dreyer *et al.* 1993; van Wagoner & Bertram 1995 and numerous other examples).
(3) Geoscience training for non-geologists, typically reservoir engineers and geophysicists, in order to improve understanding of geology and how it impacts their respective disciplines.
(4) Collection of field data to build analogue models for reservoir flow or forward seismic modelling. Such work is commonly focused on collecting data to address a specific reservoir or exploration-related issue (e.g. Howell *et al.* 2005).
(5) Pioneering field survey in frontier petroleum provinces, where fundamental new data from the outcropping part of a basin are collected to support petroleum exploration (e.g. Reynolds *et al.* 1998).
(6) Calibration and validation of numerical modelling of reservoir processes (e.g. Jones *et al.* 2008).

In this paper we explore the way in which VO datasets can be utilized in almost all of these different types of fieldwork setting. This paper also serves as an introduction to the eight case study examples that are provided as video clips on the accompanying DVD. These have been selected to communicate different aspects of the data capture, visualization and the range of applications that are being developed for virtual fieldwork datasets.

Creation of virtual fieldtrips

Virtual reality technology allows the user to interact with an artificial computer-simulated 3D environment. In the context of geological fieldwork, this generally means a geoscientist being able to interact with a digital representation of a field-site projected onto a screen or series of screens. A minimum requirement would be that the user can change their vantage point and gain a different view of an object as opposed to a fixed vantage point that is gained from viewing a photograph. This means that the digitized field-site or outcrop must be embedded in a 3D world and that the user has a means of moving around it in a virtual sense.

VINING, B. A. & PICKERING, S. C. (eds) *Petroleum Geology: From Mature Basins to New Frontiers – Proceedings of the 7th Petroleum Geology Conference*, 19–26. DOI: 10.1144/0070019

The basis for virtual fieldwork is a VO. These are models which are created from raw data acquired using a combination of satellite positioning, remote sensing and laser-based mapping survey (see McCaffrey *et al.* 2005; Pringle *et al.* 2006 for a summary of these technologies). The VO is generated in vector formats, generally georeferenced to global or local coordinate systems and viewed using 3D visualization hardware and software. In geology, the first VO datasets were created by Xu *et al.* (2000) and quickly followed by many others (e.g. Pringle *et al.* 2001; Pringle 2004*a*, *b*; Jones *et al.* 2004; Hodgetts *et al.* 2004; Bellian *et al.* 2005; Clegg *et al.* 2005; Trinks *et al.* 2005; Tomasso *et al.* 2006; Enge *et al.* 2007; Redfern *et al.* 2007; Janson *et al.* 2007; Buckley *et al.* 2008; Fabuel-Perez *et al.* 2009; Wilson *et al.* 2009). In addition to the VO, most virtual fieldtrips will also include other data that supplement the basic outcrop, including sedimentary logs, structural measurements, projected bedding and fault surfaces and even geocellular models of the outcrops (Pringle *et al.* 2006; Labourdette & Jones 2007).

The basic workflow to create a virtual fieldtrip is summarized in Figure 1. Underlying all other components is the topography digitized as a detailed digital elevation model (DEM). The resolution of a DEM is dependant on how the underlying data were acquired. There is worldwide coverage at 90 m resolution (size of each pixel) created from the Shuttle Radar Topography Mission (SRTM) and freely available to download (http://srtm.csi.cgiar.org/). Increasingly, 30, 25 and 10 m data is available in many countries. The large scale (100×100 km) of the San Rafael Swell in central Utah included in this publication was built entirely from free, publicly available data including the USGS 10 m DEM and 1 m resolution aerial photo from the Utah Geological Survey. Similar image resolution can commonly be found in Google Earth and other free GIS applications and has been used for the Lofoten and western Ireland models summarized later. For higher-resolution topography, a bespoke capture process is usually undertaken. This usually involves a ranging device, generally a laser, being scanned across the target, although photogrammetric methods can be used for the same purpose (e.g. Pringle *et al.* 2001, 2004*b*). Airborne laser scanner or lidar (light detection and ranging) topography datasets have a resolution of 50 cm^{-1} m and are flown over areas in the region of 10 s km^2. For topographic models of individual outcrops a ground-based (terrestrial) laser scanner is generally used (Fig. 1) and these systems have the capability to generate centimetre resolution topography over distances up to a kilometre. These systems are coupled with high-resolution digital cameras and together manage to capture the type of micro-topographic features that are found in outcrops such as bedding, sedimentary and tectonic structures.

Once the topography has been captured the next step is to create a VO, also called a digital outcrop model (DOM) (Bellian 2005). This generally involves creating a meshed patch from the DEM and rendering it with images from the fieldsite (see Bonnaffé *et al.* 2007; Buckley *et al.* 2008 for reviews of the process). These images are derived from satellite images, aerial photographs or high-resolution digital outcrop photographs depending on the resolution required. These surface patches provide a good virtual representation of the field site or outcrop when inspected from various vantage points in a 3D viewer. At this stage other related data can be added as point, line or polygon features (Fig. 2). For example, orientation data could be plotted as a 3D symbol inclined in the correct direction or the results from geochemical analysis of samples as a proportional symbol. Lines are used to represent the traces of logs, bedding planes or other structural features and polygons to define areas on outcrops. Georeferencing is critical and field data that are to be included in the VO will ideally be mapped with a GPS (global positioning system) receiver and the location coordinates converted to the same scheme as the topographic model.

The paucity of geoscientific interpretation software for virtual models has made it difficult to unlock the full power of a VO. Many of the existing software packages for lidar data are designed for land surveying or civil engineering purposes, and so do not provide the tools needed by geologists. Recently a variety of software has been developed by different groups to aid visualization, interpretation and modelling of lidar data. These new software approaches have allowed better use of lidar, DEM and satellite image data in a variety of applications (Redfern *et al.* 2007; Bates *et al.* 2008; Fabuel-Perez *et al.* 2009; Wilson *et al.* 2009). The objective is to place points onto the 3D surface of the outcrops and to build those interpretations into surfaces. These interpretations can be guided by traditional field measurements, such as orientation data or existing boundary correlations, in either an algorithmic or a heuristic manner. The interpreted surfaces can then be constructed into data volumes using geomodelling tools designed for subsurface work (e.g. Petrel, RMS, Gocad, etc.).

The final step is to assemble the fieldtrip so that the outcrop models can be viewed in a logical and pedagogical manner. A number of software packages are emerging that support participation in the virtual fieldtrip. Typically it has been the practice to load separate models sequentially in the preferred viewer. More recently, systems such as Google Earth allow a large-scale overview, with individual localities nested inside, allowing the entire multiscale virtual fieldtrip to be undertaken from a single platform. These systems have the advantage that they are already widely used, intuitive and freely available. The VO models and interpretations for each outcrop can be assembled and loaded individually as Google Earth KML (Keyhole Markup Language) files. They can then be successively viewed by selecting in the 'My Places' listing and the software will move automatically between locations, preserving the geographical context and giving a real 'trip experience'. An exciting result is that multiple fieldtrip itineraries to address specific issues can be constructed using the same base of fundamental data.

Applications in the petroleum industry

There are a number of ways in which the virtual fieldtrip can add value to the industry (see Table 1 for specific examples and references).

As an additional training tool on a traditional fieldtrip

Virtual fieldtrips can supplement real fieldtrips by providing easily digestible technical content such as orientation context before and during a real excursion and opportunities for customized follow-up work afterwards. In this case the virtual fieldtrip may be used to show the participants where they will visit prior to going on the trip and also can act as a refresher on return. A morning or evening classroom session with a virtual fieldtrip can provide opportunities on the day to expand the discussion to encompass other datasets such as synthetic seismic, geocellular models and flow simulation results.

To provide additional field time outside scheduled fieldtrips

While real fieldtrips happen once or twice a year and involve significant logistics and travel time, the virtual fieldtrip can happen at any time. This enables the geoscientist working on a reservoir model to be able to take a 20 min virtual trip to an analogue without leaving his/her desk. Another example is a seismic interpreter trying to understand which model to push through a data volume. Here, having easy access to analogue material can be an invaluable aid to encourage interpreters to consider a range of

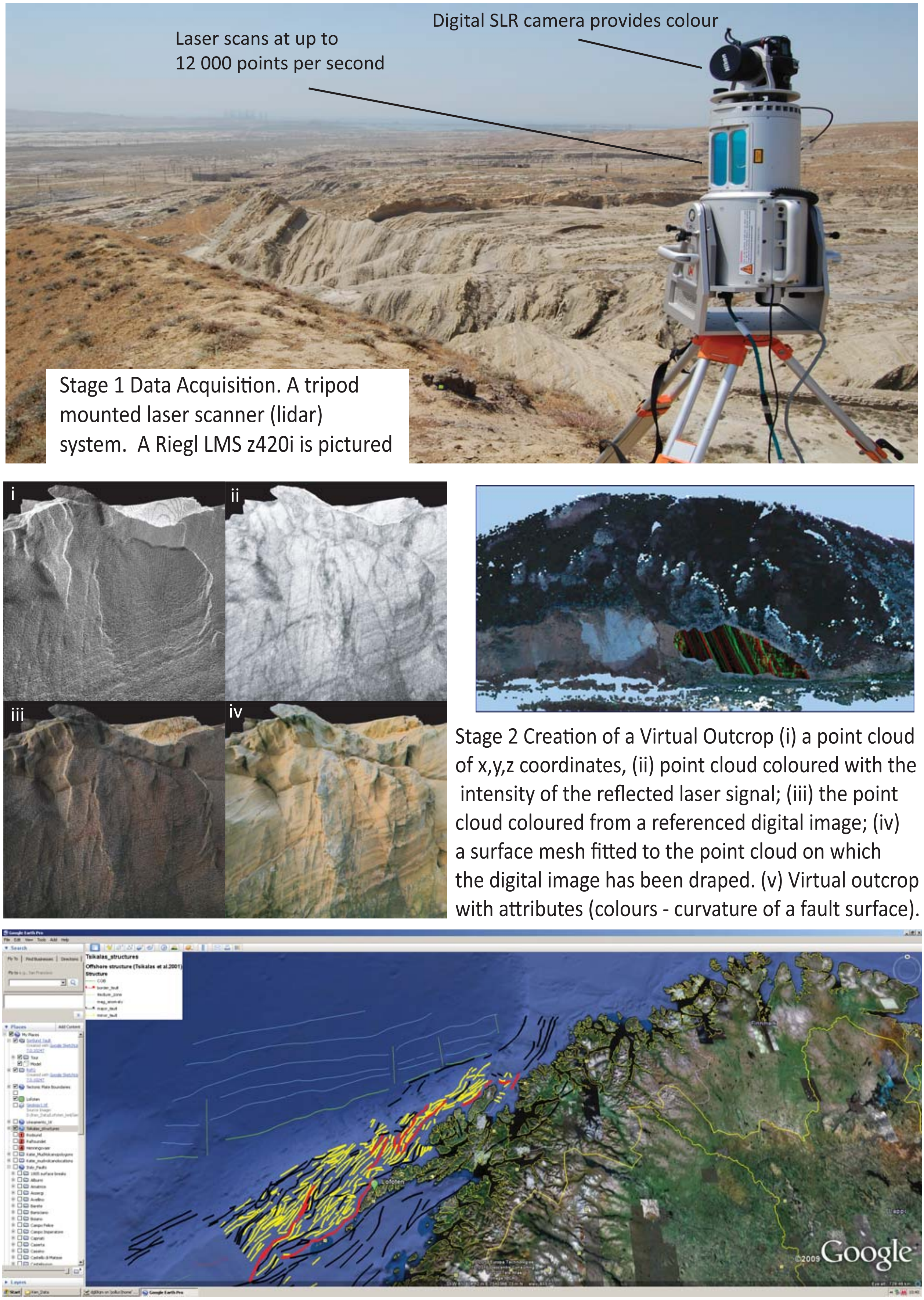

Fig. 1. Virtual fieldtrips workflow.

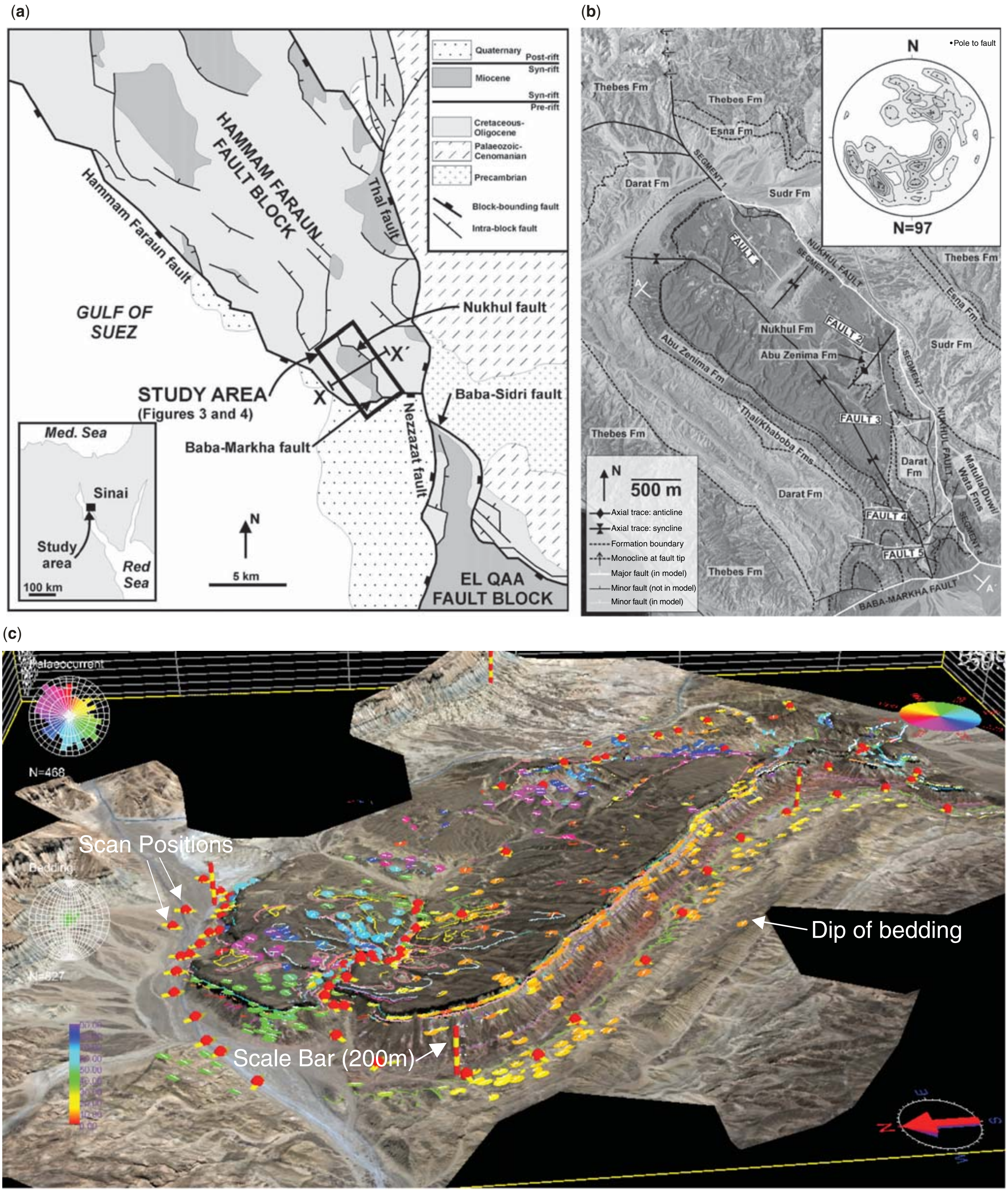

Fig. 2. (**a**) Location map of the Nukhul syncline dataset (adapted from Jackson *et al.* 2006; Sharp *et al.* 2000). (**b**) Simplified structural map of the Nukhul Syncline showing the stereonet of poles to fault planes from Wilson *et al.* (2009). (**c**) Lidar-derived DEM overlain by Quickbird Satellite image showing bedding orientation, horizon interpretations and scan positions in the VRGS software.

possible models. Virtual fieldtrips can also be used to illustrate specific points in meetings between partners and between disciplines.

Multiscale model context

Our understanding of the way in which some geological processes operate across a wide range of scales remains relatively poor. For example, processes operating in rifted margin and foreland fold/thrust belts can span up to eight orders of magnitude in length. The main advantage is the facility for researchers to view individual outcrops in their correct relative position at a variety of zoom settings, allowing simultaneous appreciation of fine-scale structure and overall geometry of the feature of interest.

Table 1. Use of virtual fieldwork in petroleum geosciences

Use	Detail	Study
Exploration	Multiscale model context images	Jones *et al.* (2009*b*), Clegg *et al.* (2005), McCaffrey *et al.* (2005)
Reservoir management	Geobody dimensions, geometry and properties, forward seismic modelling	Bellian *et al.* (2005), Pringle *et al.* (2004*a*, *b*, 2006), Hodgetts *et al.* (2004), Pearce *et al.* (2006), Tomasso *et al.* (2006), Enge *et al.* (2007), Janson *et al.* (2007), Pyles *et al.* (2010), Tomasso *et al.* (2010), Rotevatn *et al.* (2009), Enge *et al.* (2007)
	Discontinuity dimensions, geometry, attributes	Ahlgren & Holmlund (2003), Kokkalas *et al.* (2007), Trinks *et al.* (2005), Renard *et al.* (2006), Olariu *et al.* (2008), Sagy *et al.* (2007), Jones *et al.* (2009*a*)
Knowledge and training	Support or alternative for a traditional fieldtrip HSE for fieldtrips	—
	3D visualization/spatial awareness	McCaffrey *et al.* (2003, 2008)
Resources – including geoconservation	Capturing important outcrops for future study	Bates *et al.* (2008)

Constraints on geobody dimensions, geometry and properties

Outcrop analogue studies are a key way of improving understanding of reservoir facies architecture, geometry and facies distributions. Subtle surfaces with very low bedding dip that are very difficult to measure in the field can be mapped and correlated over large areas. The VO also provides a very efficient method of producing quantitative data on subseismic scale facies and reservoir architecture. Bed geometries that are below seismic resolution can be measured very quickly, providing large volumes of tightly constrained data, often from inaccessible cliff sections. These data can be used to populate subsurface models with facies objects away from the borehole and also to model the outcrop directly and test the impact of heterogeneities on flow.

The integration of lidar technology with standard outcrop data collection techniques has led to a step-change in the analysis of 3D outcrops, enabling workers to interrogate the outcrop in much more detail (e.g. Pyles *et al.* 2010). Three-dimensional reservoir models generated from these outcrops, populated with petrophysical parameters from analogue producing reservoirs, enable issues such as connectivity to be studied. To bridge the gap in scale between the outcrop resolution and subsurface data collection, forward seismic models can be generated, in either 2D (e.g. Sullivan *et al.* 2000; Bakke *et al.* 2008) or 3D (e.g. Tomasso *et al.* 2006; Janson *et al.* 2007). Forward seismic models can be generated at specific frequencies, or the frequency spectrum tailored to a specific subsurface seismic image (Tomasso *et al.* in press). Seismic architectures can then be compared back to the known outcrop architecture, and the forward seismic model investigated for attribute combinations that can increase the resolution and interpretability of the stratigraphic architecture.

Constraints on discontinuity dimensions and geometry

Building fractured reservoir models has in the past involved laborious digitizing work on remote sensed images and outcrop photographs and the resulting models are usually dimensionally limited by the original input media (2D images). VO datasets provide input data that has a 3D component gained from the intersection of fracture surfaces with the microtopography. The development of automated fracture picking methods allows the geologist to better focus on the interpretation and analysis of outcrop analogue data and to extract parameters for the building of discrete fracture network models. If the fractures define the topography, as is often the case in an opencast pit or quarry, automated surface fitting algorithms can be used to build a fracture model. Where the fractures intersect the topography edge, detection methods used with seismic data may be employed.

Knowledge and training

VOs and fieldtrips can offer an efficient way to provide training for personnel. The training for many specialist disciplines involves fieldwork and virtual datasets can assist with pre-fieldwork preparation, presenting supplementary data during a course and post-excursion follow-up exercises (e.g. forward seismic models draped on to the outcrop). VOs could offer a useful mechanism to provide orientation for non-geoscientists and a vehicle for improving communication between disciplines. Finally, pre-fieldwork health and safety requirements can also be addressed using a virtual fieldtrip.

Planning and logistics

Virtual fieldtrips are also valuable for planning and logistics for fieldtrips in the real world. The amount of time a petroleum industry geologist spends in the field is typically limited by time or budget constraints, and making the most of that time is essential. Virtual models are frequently used in seismic survey planning, where understanding topography, surface obstructions and surficial geology is essential for a successful field campaign. Additionally, they are an increasingly essential part of planning fieldwork campaigns and keeping track of personnel working in a field area via the use of real-time GPS tracking devices. This means that health and safety issues are addressed through the use of virtual models both by shifting some ‘fieldwork’ back to the office, and also by adding to the safety of individuals while in the field.

Examples on DVD

In the accompanying DVD there will be short video clips to illustrate the following eight virtual fieldtrips.

1. Shannon Basin, West of Ireland (Thurmond et al.*)*

The Carboniferous Shannon Basin in western Ireland is approximately 100 km wide and filled with a sedimentary succession of up to 2200 m thick. The fill is an overall deepening to shallowing-upwards succession from shallow-water clastics to deepwater carbonates through a source-rock quality deep basinal shale (Clare Shale), followed by a 460 m thick sand-rich turbidite unit (the Ross Formation), a 550 m thick overall fine-grained, complex slope succession (the Gull Island Formation) and capped by a 900 m thick succession of deltaic cyclothems of the Central Clare Group.

Outcrops of the Shannon Basin have been extensively studied, and provide both a testing ground for new ideas and a frequently visited location for fieldtrips and schools. There have been several studies aimed at collecting 3D data from the better-exposed outcrops, and these data have been used for various types of analyses, including sedimentological interpretation, structural measurement and construction of synthetic seismic profiles. The virtual fieldtrip provides an overview of Statoil's efforts in the Shannon Basin, including integration of several 3D outcrop models (photorealistic models), interpretations and advanced synthetic seismic within the framework of Google Earth and proprietary extensions to it. This illustrates how a wide variety of scales can be visualized simultaneously – from centimetre-scale features on a VO to basin-wide synthetic seismic lines and cross-sections.

2. Grès d'Annot Formation, SE France (Tomasso et al.*)*

Salt withdrawal minibasins contain significant petroleum reservoirs in many petroleum provinces around the world, such as the deep northern Gulf of Mexico and offshore Brazil. These minibasins are typically connected by large canyon-like channels that serve as conduits for sediment gravity flows bypassing from proximal basins into adjacent distal basins. The Grand Coyer sub-basin of the Eocene–Oligocene Grès d'Annot Formation of the southwestern French Alps provides an excellent outcrop analogue of an interbasinal conduit that connects the proximal southern Annot sub-basin to the distal northern Trois Evéchês sub-basin. Stratigraphic columns, palaeocurrent, photomosaic and lidar data were collected to address the stratigraphy of the conduit.

This virtual fieldtrip visits several of the key exposures around the Grand Coyer sub-basin, illustrating and analysing the stratigraphic packaging moving from lower to upper fill, from axis to margin, and from proximal to distal deposition. Using a detailed, outcrop-based geological model of the conduit, large (field) scale forward seismic models are used to contrast the geometries that we see in the outcrop with those that we would resolve on seismic images. Lessons learned from these exposures could be used to better predict sand distribution and reservoir geometry within interbasinal conduits.

3. Nukul syncline, Gulf of Suez (Hodgetts et al.*)*

The authors have developed bespoke software called Virtual Reality Geological Studio (VRGS) which can be used for the interpretation and integration of traditional forms of data with the lidar scan data (Fig. 2). The development of this software was driven by the lack of geoscience-specific software that allows full use of the scan data. In outcrop data it is often difficult to constrain geometries in 3D. Data is usually high-density in some areas, and sparse in others, leading to increased uncertainty. This may be the case for sediment bodies, faults or surfaces. In order to constrain these geometries as much information from the outcrop must be used as possible. In this study a large lidar dataset (over 100 linked and georeferenced scan positions) is used to derive information in addition to traditional fieldwork to help constrain hanging wall morphology (Fig. 2) in a syn-rift fault block comprising early Miocene strata in the Gulf of Suez. The resulting integrated dataset of both lidar and field-based observations has been used to build and condition a reservoir model in Petrel.

4. Deltaic reservoir analogues from central Utah (Howell et al.*)*

This virtual fieldtrip illustrates the utilization of outcrops and VOs to build geometrically accurate geocellular models that have been used to address oilfield production challenges at a variety of scales. VOs from two Cretaceous deltaic units, the Panther Tongue sandstone and the Ferron Sandstone that crop out in the northern Book Cliffs and the San Rafael Swell, are presented. This involved creating a large-scale VO covering 10 000 km^2 from publicly available DEM and aerial photo data. This was used to build a geocellular model that captures the very large-scale stratigraphic architecture of the Mesaverde Group clastic wedge, including the Panther Tongue and Ferron sandstones. Detailed lidar studies of selected outcrops from the Panther Tongue and Ferron Sandstone have captured the detail of individual delta front clinothems and bedsets. The data have been used to capture statistics that describe clinothem bed thickness and downdip bed thinning trends. The VOs have also been used as the basis for a series of geocellular models that were flow-simulated to investigate the effects of shale-draped clinoforms as barriers in deltaic reservoirs.

5. Lofoten, Norway (McCaffrey et al.*)*

The Lofoten–Vesterålen offshore continental margin is a narrow shelf with a relatively steep slope and crustal thickness up to *c.* 30 km. The area has a prolonged post-Caledonian history of intermittent extension and basin formation documented from the Devono-Carboniferous to Cenozoic times (Bergh *et al.* 2007). The Lofoten archipelago is composed mainly of high-grade metamorphic Precambrian rocks which have been uplifted in the footwall to a Mesozoic normal fault (west Lofoten boundary fault). The exposed rocks are mainly Palaeoproterozic migmatitic gneisses that have been intruded by mangeritic and charnockitic plutons. Using a combination of Google Earth and laser scanned outcrops, the Lofoten virtual fieldtrip provides an opportunity to examine Mesozoic faulting in crystalline basement and allows us to directly study faults and fractures onshore, placing kinematic constraints on the early evolution of parts of the margin that are located in the subsurface offshore. In addition the fieldtrip provides an opportunity to study faults/fractures developed in basement crystalline rocks which are generally not well imaged in seismic data sets. Thus this virtual fieldtrip can provide a potential analogue for basement-hosted reservoirs, for example, Clair field, Faero-Shetland basin where Mesozoic faults cut crystalline basement rocks.

6. Arkitsa fault, Greece (Jones et al.*)*

This VO dataset shows complex fault geometries developing in an area of active extension, and also illustrates how an enhanced view of the outcrop can be presented by superimposing quantitative geometrical analyses on top of the VO topography. The outcrop is an important analogue for studying the development of 3D fault zones and associated fault damage, and the likely effects on connectivity and reservoir performance. It is located on the eastern shore of Gulf of Evia in central Greece, an area that is currently undergoing active north–south to NE–SW regional extension, with rates on the order of 1–2 mm/year, in response to the complex tectonic interplay between subduction beneath the Hellenic Arc, back-arc extension in the Aegean, and the westward movement of the Anatolian plate. The Arkitsa fault has a throw of >500 m and is part of an array that extends for over 100 km along-strike. The footwall rocks are Upper Triassic–Jurassic platform carbonates and the hanging-wall rocks are Pliocene to Quaternary sediments. The Arkitsa fault is best exposed in an outcrop 450 m south of the main Athens–Lamia national road, where recent quarrying activity during the last 20 years has removed hanging-wall colluvium to reveal clean, fresh exposures of the upper 65–70 m of three large fault panels.

This virtual fieldtrip, created using a terrestrial laser scanning (lidar) workflow, shows that it is a powerful and versatile tool that is highly suitable for acquisition of very detailed, precise measurements of slip-surface geometry from well exposed faults (Kokkalas *et al.* 2007; Jones *et al.* 2009*a*). Quantitative analysis of the lidar data, combined with 3D visualization software, allows the spatial variation in various geometrical properties across the fault surface to be clearly shown. Properties such as variation in orientation and curvature (normal, mean and Gaussian) allow culminations and depressions, fault corrugations, and fault splays and bifurcations to be easily identified.

7. Moab fault, Utah (Imber et al.*)*

The Moab Fault is a steep normal fault which cuts and exposes a sequence of interbedded sands and argillaceous units ranging from Late Permian to Mid Cretaceous age. Throws of up to 960 m are observed in surface exposures. The footwall and hanging-wall strata are deformed into a series of long-wavelength normal drag folds of variable amplitude that trend NW, approximately parallel to the strike of the Moab Fault. The Moab virtual fieldtrip has been created using terrestrial laser scanning methods to illustrate the sizes and shapes of normal drag zones and the effect of normal drag on fault throw distributions and juxtapositions. From the fieldtrip we can quantify the along-strike variability which places constraints on how to model in flow simulators. In the Moab fault example, drag accounts for *c*. 30–50% of total throw with a steep inner drag zone (bed dip $< 50^\circ$) up to 150 m wide, and a more gently dipping outer drag zone (bed dip $< 15^\circ$) up to 350 m wide. The along-strike 'drag wavelength' of at least 800 m is larger than the grid cell size of a typical flow simulator, implying that normal drag zones should be modelled explicitly to capture their effect on across-fault juxtapositions.

8. Carbonates, Alpine foreland (Viseur et al.*)*

Carbonate architectures can be complex, reflecting spatial and temporal changes and the interaction between biological, physical and sedimentary processes. In such cases, it can be difficult to characterize the 3D geometry of sedimentary or diagenetic bodies at a range of different scales. Laser scanning technology offers a new approach to determine these geometries from outcrops. We present a case study located near Marseilles (France) and corresponding to the 'La Marcouline' formation. These deposits are particularly interesting to model as: (1) they are located in the transition zone between the northern Provence platform and the South Provence Trough; (2) the passage between the carbonate platform deposits (north to south prograding) and the clastic deposits ranging from marginal to deeper marine sediments can be easily followed thanks to continuous outcrops. This study shows how it has been possible to combine classical field data with digital outcrop data in order to construct a high-resolution model of carbonate architectures. The workflow involved (1) data acquisition and building and construction of a VO model; (2) the integration of logs and maps; and (3) the use of automated pattern extraction for the picking of geological strata. The virtual fieldtrip shows the application of the automated tools for the detection of geological information from the VO. Finally, the 3D model of the 'la Marcouline' carbonate architecture, built from the outcrop interpretations and our evolutionary 4D model displaying the carbonate bodies in chronological order, is shown.

Future trends

- VOs and fieldtrips technologies are not yet standard tools for the industry geoscientist but we expect their widespread adoption in the next 5–10 years. A combination of hardware and software advances, both on the acquisition and also on the visualization side will ease the transition into mainstream activities.
- A variety of custom software tools are being created to interpret VO data. These will continue to be developed with particular emphasis on intuitive interpretation and quantitative data extraction.
- The latest generation of smart mobile devices (such as the iPhone) are powerful enough to be visualization platforms in their own right. This means that virtual fieldtrips can be made 'portable', and therefore be used directly in conjunction with real-world field excursions. Many of these devices also have integrated GPS systems, allowing a fieldtrip participant to more actively follow a virtual field guide, and also have direct access to a wide variety of data to provide context to what they are seeing in real time.
- More sophisticated laser scanners are moving beyond simple ranging devices, the latest instruments offering full-waveform capabilities that will allow surface characteristics (e.g. water content) to be determined. On-board inertial systems mean that instruments can be used from boats and helicopters, increasing the range and size of outcrops that can be captured.
- Google Earth is the obvious platform to deliver seamless virtual fieldtrips that will be available to a range of users.
- We expect increasing use of standards in VOs datasets. The Open Geospatial Consortium (http://www.opengeospatial.org/) has recently added KML to their list of approved formats – thereby making it easier to construct virtual fieldtrips that comply with open standards for use and interchange.
- We finish by calling for access to shared datasets to avoid groups/companies having to acquire the same primary datasets and welcome the development of databases and repositories with the support of industry.

The authors thank Tony Reynolds for reviewing an earlier draft of this paper. Production of the video clips on the DVD was sponsored by Statoil. K. J. W. McCaffrey acknowledges receipt of a Royal Society Industry Fellowship.

References

Ahlgren, S. & Holmlund, J. 2003. Using 3-D outcrop laser scan for fracture analysis. American Association of Petroleum Geologists (AAPG) Search and Discovery Article 40099. World Wide Web Address: http://www.searchanddiscovery.net/documents/geophysical/2003/ahlgren/index.htm.

Bakke, K., Gjelberg, J. & Petersen, S. A. 2008. Compound seismic modelling of the Ainsa II turbidite system, Spain: application to deep-water channel systems offshore Angola. *Marine and Petroleum Geology*, **25**, 1058–1073.

Bates, K. T., Rarity, F. *et al*. 2008. High-resolution LIDAR and photogrammetric survey of the Fumanya dinosaur tracksites (Catalonia): implications for the conservation and interpretation of geological heritage sites. *Journal of the Geological Society, London*, **165**, 115–127; doi: 10.1144/0016-76492007-033.

Bellian, J. A., Kerans, C. & Jennette, D. C. 2005. Digital outcrop models: applications of terrestrial scanning lidar technology in stratigraphic modelling. *Journal of Sedimentary Research*, **75**, 166–176.

Bergh, S. G., Eig, K., Kløvjan, O. S., Henningsen, T., Olesen, O. & Hansen, J. A. 2007. The Lofoten-Vesterålen continental margin: a multiphase Mesozoic–Palaeogene rifted shelf as shown by offshore–onshore brittle fault-fracture analysis. *Norwegian Journal of Geology*, **87**, 29–58.

Bonnaffé, F., Jennette, D. & Andrews, J. 2007. A method for acquiring and processing ground-based lidar data in difficult-to-access outcrops for use in three-dimensional, virtual-reality models. *Geosphere*, **3**, 501–510.

Buckley, S., Howell, J., Enge, H. & Kurz, T. 2008. Terrestrial laser scanning in geology: data acquisition, processing and accuracy considerations. *Journal of the Geological Society*, **165**, 625–638.

Clegg, P., Trinks, I. *et al*. 2005. Towards the virtual outcrop. *Geoscientist*, **15**, 8–9.

Dreyer, T., Falt, L., Høy, T., Knarud, R., Steel, R. & Cuevas, J.-L. 1993. Sedimentary architecture of field analogues for reservoir information (SAFARI): a case study of the fluvial Escanilla Formation, Spanish Pyrenees. *In*: Flint, S. S. & Bryant, I. D. (eds) *The Geological Modelling of Hydrocarbon Reservoirs and Outcrop Analogues*. International Association of Sedimentologists, Special Publications, Blackwell Scientific Publications (Oxford, Boston), **15**, 57–79.

Enge, H. D., Buckley, S. J., Rotevatn, A. & Howell, J. A. 2007. From outcrop to reservoir simulation model: workflow and procedures. *Geosphere*, **3**, 469–490; doi: 10.1130/GES00099.1.

Fabuel-Perez, I., Hodgetts, D. & Redfern, J. 2009. A new approach for outcrop characterization and geostatistical analysis of a low-sinuosity fluvial-dominated succession using digital outcrop models: Upper Triassic Oukaimeden Sandstone Formation, central High Atlas, Morocco. *American Association of Petroleum Geologists Bulletin*, **93**, 795–827.

Hodgetts, D., Drinkwater, N. J., Hodgson, D. M., Kavanagh, J., Flint, S., Keogh, K. & Howell, J. 2004. Three-dimensional geological models from outcrop data using digital data collection techniques: an example from the Tanqua Karoo depocentre, South Africa. *In*: Curtis, A. & Wood, R. (eds) *Geological Prior Information: Informing Science and Engineering*. Geological Society, London, Special Publications, **239**, 57–75.

Howell, J., Schwarz, E., Spalleti, L. & Veiga, G. D. 2005. An overview of the Neuquen Basin. *In*: Veiga, G. D., Spalletti, L. A., Howell, J. A. & Schwarz, E. (eds) *The Neuquen Basin, Argentina: A Case Study in Sequence Stratigraphy and Basin Dynamics*. Geological Society, London, Special Publications, **252**, 1–14.

Jackson, C. A. L., Gawthorpe, R. L., Leppard, C. W. & Sharp, I. R. 2006. Rift-initiation development of normal fault blocks: insights from the Hammam Faraun fault block, Suez Rift, Egypt. *Journal of the Geological Society, London*, **163**, 165–183.

Janson, X., Kerans, C., Bellian, J. A. & Fitchen, W. 2007. Three-dimensional geological and synthetic seismic model of Early Permian redeposited basinal carbonate deposits, Victorio Canyon, west Texas. *American Association of Petroleum Geologists Bulletin*, **91**, 1405–1436.

Jones, R. R., McCaffrey, K. J. W., Wilson, R. W. & Holdsworth, R. E. 2004. Digital field data acquisition: towards increased quantification of uncertainty during geological mapping. *In*: Curtis, A. & Wood, R. (eds) *Geological Prior Information*. Geological Society, London, Special Publications, **239**, 43–56.

Jones, R. R., McCaffrey, K. J. W. *et al*. 2008. *Calibration and Validation of Reservoir Models: the Importance of High Resolution, Quantitative Outcrop Analogues*. Geological Society, London, Special Publications, **309**, 87–98; doi: 10.1144/SP309.7.

Jones, R. R., Kokkalas, S. & McCaffrey, K. J. W. 2009*a*. Quantitative analysis and visualisation of non-planar fault surfaces using terrestrial laser scanning ('LIDAR') – the Arkitsa Fault, Central Greece as a case study. *Geosphere*, **5**, 465–482; doi: 10.1130/GES00216.1.

Jones, R. R., McCaffrey, K. J. W. *et al*. 2009*b*. Integration of regional to outcrop digital data: 3D visualisation of multi-scale geological models. *Computers & Geosciences*, **35**, 4–18.

Kokkalas, S., Jones, R. R., McCaffrey, K. J. W. & Clegg, P. 2007. Quantitative fault analysis at Arkitsa Central Greece, using terrestrial laser-scanning (LiDAR). *Bulletin of Geological Society Greece*, **660**, 1959–1972.

Labourdette, R. & Jones, R. R. 2007. Characterization of fluvial architectural elements using a three dimensional outcrop dataset: Escanilla braided system – South-Central Pyrenees, Spain. *Geosphere*, **3**, 422–434.

McCaffrey, K. J. W., Holdsworth, R. E., Clegg, P., Jones, R. R. & Wilson, R. 2003. Using digital mapping and 3D visualization to enhance and modernise undergraduate fieldwork experience. *Planet Magazine Special Edition*, **5**, 34–36.

McCaffrey, K. J. W., Jones, R. R. *et al*. 2005. Unlocking the spatial dimension: digital technologies and the future of geoscience fieldwork. *Journal of the Geological Society, London*, **162**, 927–938.

McCaffrey, K. J. W., Feely, M., Hennessey, R. & Thompson, J. 2008. Visualization of folding in marble outcrops, Connemara, western Ireland. An application of virtual outcrop technology. *Geosphere*, **4**, 588–599.

Olariu, M. I., Ferguson, J. F., Aitken, C. L. V. & Xu, X. 2008. Outcrop fracture characterization using terrestrial laser scanners: deep-water Jackfork sandstone at Big Rock Quarry, Arkansas. *Geosphere*, 247–259; doi: 10.1130/GES00139.1.

Pearce, M. A., Jones, R. R., Smith, S. A. F., McCaffrey, K. J. W. & Clegg, P. 2006. Numerical analysis of fold curvature using data acquired by high-precision GPS. *Journal of Structural Geology*, **28**, 1640–1646.

Pringle, J. K., Clark, J. D., Westerman, A. R., Stanbrook, D. A., Gardiner, A. R. & Morgan, B. E. F. 2001. Virtual outcrops: 3-D reservoir analogues. *In*: Ailleres, L. & Rawling, T. (eds) *Animations in Geology. Journal of the Virtual Explorer*, **3**.

Pringle, J. K., Westerman, A. R. & Gardiner, A. R. 2004*a*. Virtual geological outcrops – fieldwork and analysis made less exhausting? *Geology Today*, **20**, 67–72; doi: 10.1111/j.1365–2451.2004.00450.x.

Pringle, J. K., Westerman, A. R., Clark, J. D., Drinkwater, N. J. & Gardiner, A. R. 2004*b*. 3D high-resolution digital models of outcrop analogue study sites to constrain reservoir model uncertainty: an example from Alport Castles, Derbyshire, UK. *Petroleum Geoscience*, **10**, 343–352.

Pringle, J. K., Howell, J. A., Hodgetts, D., Westerman, A. R. & Hodgson, D. M. 2006. Virtual outcrop models of petroleum reservoir analogues: a review of the current state-of-the-art. *First Break*, **24**, 33–42.

Pyles, D. R., Jennette, D. C., Tomasso, M., Beaubouef, R. T. & Rossen, C. 2010. Process-related concepts learned from a 3D outcrop of a sinuous slope channel complex: Beacon Channel, Brushy Canyon Formation, west Texas. *Journal of Sedimentary Research*, **80**, 67–96.

Redfern, J., Hodgetts, D. & Fabuel-Perez, I. 2007. Digital analysis brings renaissance for petroleum geology outcrop studies in North Africa. *First Break*, **25**, 81–87.

Renard, F., Voisin, C., Marsan, D. & Schmittbuhl, J. 2006. High resolution 3D laser scanner measurements of a strike-slip fault quantify its morphological anisotropy at all scales. *Geophysical Research Letters*, **33**, L04305; doi: 10.1029/2005GL025038.

Reynolds, A. D., Simmons, M. D. *et al*. 1998. Implications of outcrop geology for reservoirs in the Neogene Productive Series: Apsheron Peninsula, Azerbaijan. *American Association of Petroleum Geologists Bulletin*, **82**, 25–49.

Sagy, A., Brodsky, E. E. & Axen, G. J. 2007. Evolution of fault-surface roughness with slip. *Geology*, **35**, 3, 707, 283–286; doi: 10.1130/G23235A.1.

Sharp, I. R., Gawthorpe, R. L., Underhill, J. R. & Gupta, S. 2000. Fault-propagation folding in extensional settings: examples of structural style and synrift sedimentary response from the Suez rift, Sinai, Egypt. *Geological Society of America Bulletin*, **112**, 1877–1899.

Sullivan, M., Jensen, G., Goulding, F., Jennette, D., Foreman, L. & Stern, D. 2000. Architectural analysis of deep-water outcrops: implications for exploration and development of the Diana Sub-Basin, western Gulf of Mexico. *In*: Weimer, P., Slatt, R. M. *et al*. (eds) *Deep-Water Reservoirs of the World: 20th Annual GCSSEPM Foundation Bob F. Perkins Research Conference*, 3–6 December 2000, 1010–1031.

Tomasso, M., Bonnaffé, F. L., Pyles, D. R., Bouroullec, R. & Jennette, D. C. 2006. Outcrop versus seismic architecture of deep-water deposits: use of lidar along a slope-to-basin transect of the Brushy Canyon Formation, west Texas. *In*: Slatt, R., Rosen, N. C. *et al*. (eds) *Reservoir Characterization: Integrating Technology and Business Practices: 26th Annual GCSSEPM Foundation Bob F. Perkins Research Conference*, 3–6 December 2006, 755–770.

Tomasso, M., Bouroullec, R. & Pyles, D. R. 2010. The use of spectral recomposition in tailored forward seismic modeling of outcrop analogs. *American Association of Petroleum Geologists Bulletin*, **94**, 457–474.

Trinks, I., Clegg, P. *et al*. 2005. Mapping and analysing virtual outcrops. *Visual Geosciences*, **10**, 13–19; doi: 10.1007/s10069-005-0026-9.

van Wagoner, J. C. & Bertram, G. T. 1995. Sequence Stratigraphy of Foreland Basin Deposits. *American Association of Petroleum Geologists*, Tulsa, OK, Memoirs, **64**.

Wilson, P., Hodgetts, D., Rarity, F., Gawthorpe, R. L. & Sharp, I. R. 2009. Structural geology and 4D evolution of a half-graben: new digital outcrop modelling techniques applied to the Nukhul half-graben, Suez rift, Egypt. *Journal of Structural Geology*, **31**, 328–345.

Xu, X., Aiken, C. *et al*. 2000. Creating virtual 3-D outcrop: leading edge. *Society of Exploration Geophysicists*, **19**, 197–202; doi: 10.1190/1.1438576.

Colin Oakman core workshop

G. J. HAMPSON,[1] J. D. COLLINSON[2] and P. GUTTERIDGE[3]

[1]*Department of Earth Science and Engineering, Imperial College London, South Kensington Campus, London SW7 2AZ, UK (e-mail: g.j.hampson@imperial.ac.uk)*
[2]*John Collinson Consulting, Delos, Knowl Wall, Beech, Staffordshire ST4 8SE, UK*
[3]*Cambridge Carbonates Ltd, Meadow Barn, Mill Lane, Brailsford, Ashbourne, Derbyshire DE6 3BB, UK*

The core workshop followed the format of the three core events at previous Petroleum Geology Conferences (e.g. Oakman & Martin 1993), although it was smaller in scale and its focus was on the reservoir sedimentology of the North Sea. The workshop was organized by the British Sedimentological Research Group (BSRG) with the cooperation of the Petroleum Exploration Society of Great Britain (PESGB) and British Geological Survey (BGS), who provided and transported all of the cores on display. BSRG exists to promote and support the work of young researchers in sedimentary geology (including stratigraphy, diagenesis, process sedimentology and geochemistry), many of whom go on to successful careers in the oil industry. Within this context, the workshop featured presentations by PhD students, academics and consultants that put the reservoirs illustrated by the cored intervals into context, from both a depositional and a commercial standpoint.

Fig. 1. Colin Oakman (1955–2008).

Colin Oakman (Fig. 1), a leading force in organizing core workshops at previous Petroleum Geology Conferences, sadly died prior to the conference. The workshop was dedicated to Colin's memory in appreciation of his enthusiasm and hard work.

Sedimentology is a key component in understanding the character and distribution of hydrocarbon reservoirs, and its application continues to play a major role in exploration and production activities in the North Sea. Despite new and ever more sophisticated remote-sensing technologies, cores continue to provide the direct rock samples that are critical to many aspects of reservoir geology, and ultimately to the efficient extraction of hydrocarbon resources. On display were about 320 m of core from 15 wells, selected to illustrate a diverse range of reservoirs and plays, including the 'classic' reservoir intervals that have been the engine of North Sea production over the last 30 years, and less conventional, emerging plays that may sustain future development. The cored intervals represented Lower Carboniferous shelfal and resedimented carbonates, Upper Carboniferous deltas and alluvial plains, Permian brecciated carbonates, Permo-Triassic marginal aeolian and dryland river deposits, a range of Middle–Upper Jurassic deltaic and shallow-marine systems, and Cretaceous–Cenozoic deepwater fans (Table 1). The workshop highlighted the challenges of interpreting sedimentary processes and environments from core data and emphasized the role that core sedimentology has played, and continues to play, in reservoir characterization, development and management.

During the conference, over 300 delegates attended the scheduled presentations for each of the cores and associated posters, and many more delegates browsed the core displays outside of these presentations. Both presenters and visitors appreciated the opportunity to discuss geological concepts and models against

VINING, B. A. & PICKERING, S. C. (eds) *Petroleum Geology: From Mature Basins to New Frontiers – Proceedings of the 7th Petroleum Geology Conference*, 27–28. DOI: 10.1144/0070027

Table 1. Summary of core intervals displayed

Well	Age	Summary	Geographical area	Presenters and contributors
Somerton 1	Lower Carboniferous	Mineralized and dolomitized cyclical shelf carbonates	Norfolk, onshore UK	Peter Gutteridge (Cambridge Carbonates Ltd)
Roddlesworth 1	Lower Carboniferous	Resedimented carbonate turbidites and debris flows	Lancashire, onshore UK	Peter Gutteridge (Cambridge Carbonates Ltd)
43/27-1	Upper Carboniferous	Fluvial-dominated deltaic cycles (Millstone Grit Fm.)	Johnston Field, UK Southern North Sea	John Collinson (John Collinson Consulting) and Gary Hampson (Imperial College)
43/25a-2X	Upper Carboniferous	Semi-arid alluvial plain deposits (Ketch Fm.)	West Boulton area, UK Southern North Sea	John Collinson (John Collinson Consulting) and Gary Hampson (Imperial College)
48/10b-3	Lower Permian	Aeolian erg margin, fluvial and sabkha deposits (Rotliegend Gp.)	Saturn Field, UK Southern North Sea	Samantha Taggart, Gary Hampson and Matthew Jackson (Imperial College)
30/24-20, 30/24-26	Upper Permian	Collapse-brecciated carbonates (Zechstein Gp.)	Ardmore Field, UK Central North Sea	Peter Gutteridge (Cambridge Carbonates Ltd)
110/2b-9	Lower Triassic	Aeolian erg margin, fluvial and playa deposits (Sherwood Sandstone Gp.)	Dalton Field, UK East Irish Sea	Joanne Venus, Nigel Mountney (University of Leeds) and Neil Meadows (Redrock Associates International Ltd)
22/24d-10	Upper Triassic	Semi-arid fluvial and terminal splay deposits (Skagerrak Fm.)	Egret Field, UK Central North Sea	Gary Hampson (Imperial College) and Tom McKie (Shell UK)
3/4a-12	Middle Jurassic	Wave-dominated delta front and delta plain (Brent Gp.)	Strathspey Field, UK Northern North Sea	Gary Hampson (Imperial College)
21/18a-2A	Upper Jurassic	Bioturbated shoreface-shelf (Fulmar Fm.)	Kittiwake Field, UK Central North Sea	Gary Hampson (Imperial College)
16/8a-4	Upper Jurassic	Syn-rift deepwater fan deposits (Ling Sandstone Mbr, Heather Fm.)	Kingfisher Field, UK Northern North Sea	Rachel Kieft, Gary Hampson and Christopher Jackson (Imperial College)
16/26-B01, 16/26-B04	Lower Cretaceous	Confined deepwater fan deposits (Britannia Sandstone Fm.)	Britannia Field, UK Central North Sea	Graham Blackbourn (Blackbourn Geoconsulting), Joris Eggenhuisen (University of Leeds) and John Collinson (John Collinson Consulting)
9/23b-24	Paleocene	Deepwater sandstone injections (Sele Fm.)	Harding Field, UK Northern North Sea	Evelina Dmitrieva, Greg Seymour, Lidia Lonergan and Gary Hampson (Imperial College)

the backdrop of the rocks themselves; this approach stimulated much feedback and discussion.

We would like to thank all of the presenters and contributors, and the companies who provided access to material for poster displays to accompany the cores (Blackbourn Geoconsulting, BP, Cambridge Carbonates Ltd, ConocoPhillips, E.On Ruhrgas, Fairfield Energy, GDF Suez, Ichron Ltd, John Collinson Consulting, Redrock Associates International Ltd, Shell UK). The support of the BSRG, PESGB and BGS is gratefully acknowledged, and in particular the efforts of the following individuals: Jon Noad (BSRG), John Ludden, Robert Gatliff, Richard Sutherland, Michael Howe, Scott Renshaw (BGS), Jerry Chessell, Jon Gluyas, Barrie Wells (PESGB) and Georgina Worrall (Geological Society).

Reference

Oakman, C. D. & Martin, J. H. 1993. Core workshop and discussion forum. *In*: Parker, J. R. (ed.) *Petroleum Geology of Northwest Europe: Proceedings of the 4th Conference*. Geological Society, London, 1541–1542; doi: 10.1144/0041541.

Session: Europe

Europe overview

G. GOFFEY

PA Resources UK Limited, 4th Floor Waterfront, Winslow Road, Hammersmith, London, UK (e-mail: ggoffey@paresources.uk.com)

Abstract: Over 35 years, the Petroleum Geology Conference series has been the leading UK conference dedicated to making public the scientific advances and findings of some four decades of NW European hydrocarbon exploration and production. Leading edge issues in the NW European province after four decades include small pool and high pressure high temperature (HPHT) exploration, late-stage field exploitation and field redevelopment. The rich subsurface datasets and pioneering of emerging technologies provide a stream of valuable models, lessons, techniques and ideas which have both local and international applicability. Papers grouped under the exploration theme contain regional, local and detailed studies which illustrate the nature of current exploration activity for small, deep and complex structural and stratigraphic prospects. Closer and more comprehensive integration of seismic-derived understanding of structural evolution and seismic, well and analogue-derived depositional and sequence stratigraphic constraints are probably the most fruitful approaches and are shown by a number of papers. Papers on field development and production themes describe the industry's response to challenges such as low permeability and reservoir prediction through the use of multiple 3D and 4D seismic datasets and the exploitation of advances in drilling, well logging and completion technologies to drain progressively smaller per well reserves. Again, integration is the watchword, here between interpretations and analyses of subsurface data with well planning and construction. Finally, a number of papers describe current techniques in petrophysics, 3D and 4D seismic applications and remote sensing approaches.

History of the Petroleum Geology Conference series from 1974 to date: from NW Europe to international

The first conference in 1974 was described in the foreword to the proceedings as 'the most important and significant geological conference ever presented in the European area, and possibly in the world, in view of the great importance of the North Sea development in the total world energy picture'. The conference was seen as unique because most of the presentations were previously unpublished findings of the oil industry, rather than from academia. Publication of the proceedings of the conference (Woodland 1975) initiated a series that have become essential reference works for geoscientists working the NW European hydrocarbon basins.

The second conference was held in 1980 (Illing & Hobson 1981) and more than 1000 delegates from 12 countries listened to papers describing the emergence of the North Sea as a major oil province. The Right Honourable David Howells, then UK Secretary of State for Energy, commented on how the discovery of new oil reserves would depend on new ideas and a fresh approach. His talk anticipated the licensing of previously unexplored deepwater areas west of the UK and highlighted the need for new discoveries to sustain UK hydrocarbon self-sufficiency into the 1990s.

The third conference (Brooks & Glennie 1987) took place in 1986 in arguably the first major downturn experienced by the modern petroleum industry. In his opening address, the Right Honourable Alick Buchanan-Smith, UK Minister of State for Energy, presciently observed the cost in human terms of the industry downturn, with the great loss of skilled personnel from the industry.

The fourth conference was held in 1992 (Parker 1993) and attracted 1230 delegates including 350 from 15 overseas countries. This was the first event to feature a Core Workshop displaying some 600 m of cored rocks. Conference Chairman Jim Brooks observed in his introduction that whilst the *major* companies had dominated in the early days of North Sea exploration, *independents* were increasingly involved in the exploration, development and production of offshore fields.

Held in 1997, the fifth conference (Fleet & Boldy 1999) was the last to be focused exclusively on NW Europe. Highlights of this conference were the increasing integration of disciplines within the geosciences and of geosciences with other disciplines, the development of reservoir modelling and 3D/4D seismic techniques, and the ongoing refinement of sequence stratigraphic approaches.

The sixth conference in 2003 (Doré & Vining 2005) was the first to explicitly broaden its perspective to encompass international activities. Entitled *North West Europe and Global Perspectives*, the conference aimed to both import ideas and concepts from the international arena as well as exporting to other parts of the world ideas and concepts developed in the North Sea 'laboratory'. New themes for the NW Europe industry were infrastructure-led exploration, tail-end production and field rejuvenation. The emergence of gas as a fuel for the future was marked by a section dedicated entirely to gas.

The Right Honourable John Smith, then UK Under-Secretary of State for Energy, commented in his opening address to the First Conference in 1974 that 'the successful exploitation of North Sea hydrocarbon resources with the new data and technological innovation it will produce, will lead ... to worldwide development of offshore petroleum in waters that have until now seemed impossible to work'. In 2009, the seventh conference was inspired by Smith's prescient observations to build upon the NW European roots of the series to develop into a truly international conference, sharing insights, techniques and success stories on a global basis 'from mature basins to new frontiers'.

Overview of the Europe proceedings

The NW European province continues to mature and break new ground, particularly in small pool exploration, development

VINING, B. A. & PICKERING, S. C. (eds) *Petroleum Geology: From Mature Basins to New Frontiers – Proceedings of the 7th Petroleum Geology Conference*, 31–33. DOI: 10.1144/0070031 © Petroleum Geology Conferences Ltd. Published by the Geological Society, London.

and exploitation. The extensive subsurface datasets prevalent in NW Europe and the response of the industry to the challenges it faces provide a rich stream of valuable models, lessons, techniques and ideas which have both local and international applicability. Equally, the importance of new ideas and a fresh approach as noted in 1980 are as important as ever and the industry needs to look to the international arena as a source of such ideas and approaches.

The Europe session at the 7th Petroleum Geology Conference was the most extensive session at the conference and, in addition, the core workshop contained core exclusively from reservoirs of the North Sea and adjacent petroliferous basins. Given the history of the conference series as a NW Europe conference, this emphasis on Europe was to be expected. Papers and posters contained within this proceedings volume have been grouped into three sub-themes: exploration; field development and production; and techniques in exploration and production.

Exploration

A number of authors contributed regional-level papers on European petroleum provinces, represented here by papers from Erratt, Milton-Worsell *et al.*, Petersen, Knutz and Bertello. Erratt draws attention to the interplay between tectonics and sedimentation in hydrocarbon play development. Whilst Milton-Worsell uses an extensive regional dataset of well and in particular long-offset seismic data to draw attention to a potential Palaeozoic basin in an underexplored area of the Central North Sea flanks, Knutz examines the development of Mio-Pliocene ‘channel’ features in the main body of the rift and their linkage to deeper structure, hydrocarbon leakage and potential contourite depositional processes. Further south, a poster by Petersen examines the controlling influence on exploration outcomes of source rock quality in the NW Danish Central Graben. Finally Bertello provides an overview of hydrocarbon occurrence in fold belt to foreland settings in Italy – by a considerable degree the most important hydrocarbon province in southern Europe and not widely appreciated by northern European geoscientists.

The depositional, sedimentological and sequence stratigraphic setting of Middle and Upper Jurassic reservoirs is explored in papers and posters by Johannesen *et al.*, Kieft and Sansom. Johannessen *et al.* draw together a revised palaeogeographic understanding of Late Jurassic deposition in the Danish Central Graben utilizing recent exploration results, whilst the poster of Johannesen *et al.* develops a Recent analogue for the depositional architecture of a deep Upper Jurassic barrier and shoreface sandstone reservoir in the Danish offshore. A poster from Kieft explores the use of an extensive core database to understand reservoir development within an overall transgressive interval of marine and marginal marine sandstones of the Middle Jurassic Hugin Formation in the Norwegian South Viking Graben. Finally Sansom constructs a detailed understanding of the shallow marine, Late Jurassic Fulmar reservoir and highlights the previously unrecognized controlling role of intra-Volgian tectonic reconfiguration events on basin morphology and reservoir distribution and preservation. Taken together, these papers illustrate the insights possible in the data-rich North Sea setting when reservoir models are built or critically challenged through analysis at various levels from detailed regional reviews, through to core-based studies and the use of Recent analogues.

Several papers look at recent discoveries and soon to be drilled prospects. Hollywood and Olsen examine the Paleocene and Upper Jurassic Fulmar discoveries at Huntington in the UK Central North Sea, where the oil columns discovered exceeded the pre-drill predictions due to stratigraphic trapping elements. Similarly, Ward *et al.* review the HPHT Jasmine discovery, also in the UK Central North Sea, and where again the discovered hydrocarbon column exceeded pre-drill predictions, in this case by some 1100 feet, for reasons not yet fully understood but assumed to relate to fault seal. Rodriguez described the extensive de-risking of what was at the time an undrilled seismic anomaly/stratigraphic prospect West of Shetlands.

These papers and several unpublished oral presentations at the Conference illustrate the nature of exploration activity after four decades of North Sea exploration. Structural traps tend to be small and larger finds tend to occur in stratigraphic traps and complex or deep structural traps. The rich North Sea database lends itself to reworking and to the generation of new insights from comprehensive regional evaluation and the development of models which better integrate seismic-derived understanding of structural evolution and seismic, well and analogue-derived depositional and sequence stratigraphic constraints. It is not clear that such work is undertaken with the frequency, perspicacity and creativity that are justified.

Field development and production

Several papers typified the techniques which have been evolved to understand and tackle the reservoir complexities which pose challenges in the appraisal and development of North Sea fields in the fourth decade of activity in the basin. Challenges include low permeability, reservoir development and prediction, and modelling and understanding of the dynamic behaviour of the reservoir to permit continued commercial development.

Seismic methods including improved 3D data and the use of AVO techniques during appraisal and in a 4D sense during production have become routine and are substantial value drivers. Similarly, drilling, well logging and completion technologies are allowing new field development and the exploitation of progressively smaller per well reserves. The careful evaluation of all subsurface data and integration with well planning and construction are fundamental in realizing the value offered by these technologies.

The value of seismic methods is shown by Gordon *et al.* in the evaluation of gas-condensate reservoirs in Laggan and Tormore Fields, West of Shetlands, aided by the use of AVO techniques to reduce uncertainty on reservoir development. Witt *et al.* report on the start-up of the naturally fractured Clair Field, West of Shetlands, the drainage and completion strategies adopted and the use of permanent ocean bottom cables to assess the 4D response of the reservoir and improve production history matching.

Drilling and completion techniques are fundamental to the papers of Tringham *et al.* and Purvis *et al.*, who both describe the use of long-reach horizontal wells with multistage hydraulic fracturing to dramatically improve reservoir deliverability in low permeability gas-bearing sandstones in the Southern North Sea. Hampson and Walden provide an update on the two large producing heavy oil fields, Alba and Captain. Here intensive data gathering through multiple 3D surveys, the drilling of pilot holes and logging while drilling (LWD) techniques have allowed long horizontal development wells to be carefully placed to optimize recovery and commercially drain small in-field targets of the order of 1 to 2×10^6 bbl.

Several additional papers examined the continued exploitation of some of the North Sea’s largest fields. Gill and Shepherd describe the geological and reservoir management workflows used to identify field infill drilling targets and optimize field management in Nelson Field, themes continued by Brook *et al.* in their description of late stage infill drilling in the Scott–Telford field complex. Ray *et al.* describe the evolved geological understanding of the Buzzard Field sediment gravity flow reservoir and the insights achieved through integration of core, log and dynamic field data.

The challenges of HPHT field appraisal and development are elegantly captured in papers by Kape *et al.* and Quin *et al.* The former highlight the importance of careful geological evaluation and modelling given the inevitably under-appraised nature of HPHT fields. This carrying through of risk to the development phase is exemplified by Quin *et al.*'s paper, which demonstrates how the excellent reservoir encountered in appraisal drilling in Kristin Field on the Halten Terrace, NCS, was found through development and production to be unrepresentative of the appreciably poorer reservoir away from the appraisal wells.

Finally, and in a sense coming full circle, Reekie *et al.* review the redevelopment of Donan Field and the way that many of the field development techniques which have evolved in the last 20 years have allowed commercial redevelopment of a prematurely abandoned field.

Techniques in exploration and exploitation

This section covers a suite of papers which describe the use of a variety of geological, petrophysical, seismic and remote sensing techniques in exploration and production applications. The role of careful petrophysical evaluation is underlined by papers by Worthington and by Fabricius and Rana. Worthington describes a modus operandi for the recognition of bypassed pay, whilst Fabricius and Rana provide a case history evaluation of the post-fill tilted oil–water contact in the Danish chalk field, Tyra, through analysis of capillary pressure data. Staying with the chalk, Hampton *et al.* illustrate the development and use of a fully calibrated biostratigraphic zonation with particular intra-field applicability to aid well placement and reservoir management.

O'Connor *et al.* explore the use of well-derived pressure profiles to predict overpressure distribution and development and infer the development of topseal capacity whilst Purves *et al.* use 3D seismic data to map fault damage zones as a contribution to the assessment of fault-sealing potential.

With the rich North Sea datasets, seismic techniques continue to be instrumental in field exploitation in particular. A number of papers provide illustrations of current seismic applications. Rushmere *et al.* analyse the relative impact of acquisition and particularly processing improvements in increasing 4D signal-to-noise ratios, whilst Herwanger *et al.* examine the application of 4D techniques and their integration into dynamic field models at South Arne Field in Denmark. Abramowitz *et al.* expand the use of 3D integrated with well data and 2D seismic inversion into a regional study of intra-chalk porosity variations.

Finally, in the remote sensing domain, Hardy and Jones show how deepwater seismic data has unexpectedly revealed temperature and salinity stratification on the water column, whilst Olesen *et al.* publish results of the Geological Survey of Norway's aeromagnetic data acquisition and modelling, constrained by some 40 000 measurements of magnetic susceptibility and remnance to increase the utility and insight available through the modelling of magnetic data.

References

Brooks, J. & Glennie, K. W. (eds) 1987. *Petroleum Geology of North-West Europe*. Graham & Trotman, London.

Doré, A. G. & Vining, B. A. (eds) 2005. *Petroleum Geology: North-West Europe and Global Perspectives: Proceedings of the 6th Petroleum Geology Conference*. Geological Society, London.

Fleet, A. J. & Boldy, S. A. R. (eds) 1999. *Petroleum Geology of Northwest Europe: Proceedings of the 5th Conference*. Geological Society, London.

Illing, L. V. & Hobson, G. D. (eds) 1981. *Petroleum Geology of the Continental Shelf of North-West Europe*. Heyden, London.

Parker, J. R. (ed.) 1993. *Petroleum Geology of Northwest Europe: Proceedings of the 4th Conference*. Geological Society, London.

Woodland, A. W. (ed.) 1975. *Petroleum and the Continental Shelf of North West Europe*. Applied Science, London.

Session: Europe

Exploration

North Sea hydrocarbon systems: some aspects of our evolving insights into a classic hydrocarbon province

D. ERRATT,[1] G. M. THOMAS,[1] N. R. HARTLEY,[2] R. MUSUM,[3] P. H. NICHOLSON[1] and Y. SPISTO[1]

[1]*ExxonMobil International Ltd, ExxonMobil House, Ermyn Way, Leatherhead, Surrey KT22 8UX, UK (e-mail: duncan.erratt@exxonmobil.com)*
[2]*ExxonMobil Development Company, 12450 Greenspoint Drive, Houston, TX 77060 USA*
[3]*ExxonMobil Exploration and Production Norway AS, PO Box 60, 4064 Stavanger, Norway*

Abstract: A review is given of the development of the understanding of the structure and stratigraphy of a classic petroleum province through 35 years of NW European Petroleum Geology Conferences, using new examples to illustrate the interplay between tectonics and sedimentation in the development of some of the major hydrocarbon plays. Cimmerian tectonics is discussed, with regard to the evidence for regional-scale truncation beneath the Mid Cimmerian unconformity, and the stratal motifs characteristic of rifting associated with the Early and Late Cimmerian events. New data revealing the structural geometries associated with polyphase rifting in the East Shetland Basin are presented. The seismic and sequence stratigraphy of Jurassic and Cenozoic sequences are reviewed and new data presented, with a discussion of generic play controls in North Sea Jurassic deepwater reservoirs. The development of integrated hydrocarbon system studies is reviewed, and the remaining challenges to predictive capabilities discussed. The impact of advances in geoscience and technology on North Sea creaming curves is discussed.

Keywords: North Sea, hydrocarbon systems, Jurassic, Cenozoic, tectonics, seismic and sequence stratigraphy

The exploration of the North Sea has spanned over 40 years, and has paralleled significant advances not only in the quality and quantity of subsurface data, but also in the Earth sciences generally. Many aspects of North Sea geology we now take for granted developed as a result of the application of new and sometimes controversial geological concepts, the pioneering application of new technologies and many years of passionate debate.

This paper discusses the development of key geological concepts underpinning our understanding of North Sea geology in the 34 years since the publication of the first NW European Conference volume (Woodland 1975), illustrating the part played by the North Sea in the development of our understanding of fundamental geological processes and rift basins, specifically the structural and stratigraphic consequences of polyphase Mesozoic extension and uplift (the 'Cimmerian' tectonic pulses), and parallels in the sequence stratigraphic context of shallow to deepwater reservoir transitions in the Jurassic and Palaeogene. Developments in basin modelling studies are discussed. Throughout the paper, historical references to earlier North West European/'Barbican'/'PGC' conferences are made by way of reference to the date, editor or position of the conference in the sequence.

Regional setting

The geological evolution and exploration history of the North Sea has been comprehensively documented elsewhere, most notably in the precursors to this volume (Woodland 1975; Illing & Hobson 1981; Brooks & Glennie 1987; Parker 1993; Fleet & Boldy 1999; Doré & Vining 2005) and the North Sea Millennium Atlas (Evans *et al.* 2003). Figures 1 and 2 summarize the tectonic and stratigraphic architecture of the North Sea rift system, and highlight the location of the examples drawn on in this paper. The rift basin results principally from several phases of extension commencing in the Permian, climaxing in the Late Jurassic (the principal trap-forming event), with minor, more localized reactivation in the Albo-Aptian. Permian extension was superimposed on Carboniferous and Devonian strata subcropping the Base Permian 'Saalian Unconformity'. Coal-bearing Carboniferous provides the source to the Southern North Sea Gas Province, and both Carboniferous and Devonian reservoirs occur in traps on the rift flanks. Regional subsidence was punctuated by early Mid Jurassic uplift. Varying degrees of mild regional compressive pulses result in local basin inversion, most notably in the Late Campanian, and salt diapirism throughout the Cenozoic. With regards to the basin fill, a broad continental to marine transition occurs from Triassic to Late Jurassic. Reservoir-prone Triassic and Jurassic sequences are pervasive throughout the rift system, with the Triassic becoming shale prone in its lower parts towards the south. The Jurassic reservoirs give way to widespread Jurassic shales with generally increasing organic content towards the Jurassic–Cretaceous boundary, culminating in the world-class Kimmeridge Clay source rock. With the cessation of rifting at the end of the Jurassic, effective Cretaceous seals to much of the future hydrocarbon system were deposited across the abandoned rift topography. Locally developed Albo-Aptian sandstones were deposited basinally in response to hinterland rejuvenation resulting from extension switching to the proto-Atlantic margin. This critical phase in the history of the NW European margin was responsible for leaving the pre-Cretaceous plays of the North Sea largely intact. Widespread Late Cretaceous chalk deposition preceded the influx of significant quantities of Cenozoic coarse clastics in response to the emplacement of the Iceland plume and the corresponding uplift of the Scottish mainland. Post Palaeogene deposition is predominantly shale prone into a gently subsiding thermal sag basin.

North Sea tectonics, main themes and historical milestones

'Cimmerian' events and the North Sea Dome

The rift basin architecture of the North Sea rift was apparent on early vintages of seismic data, although not prior to the First

VINING, B. A. & PICKERING, S. C. (eds) *Petroleum Geology: From Mature Basins to New Frontiers – Proceedings of the 7th Petroleum Geology Conference*, 37–56. DOI: 10.1144/0070037

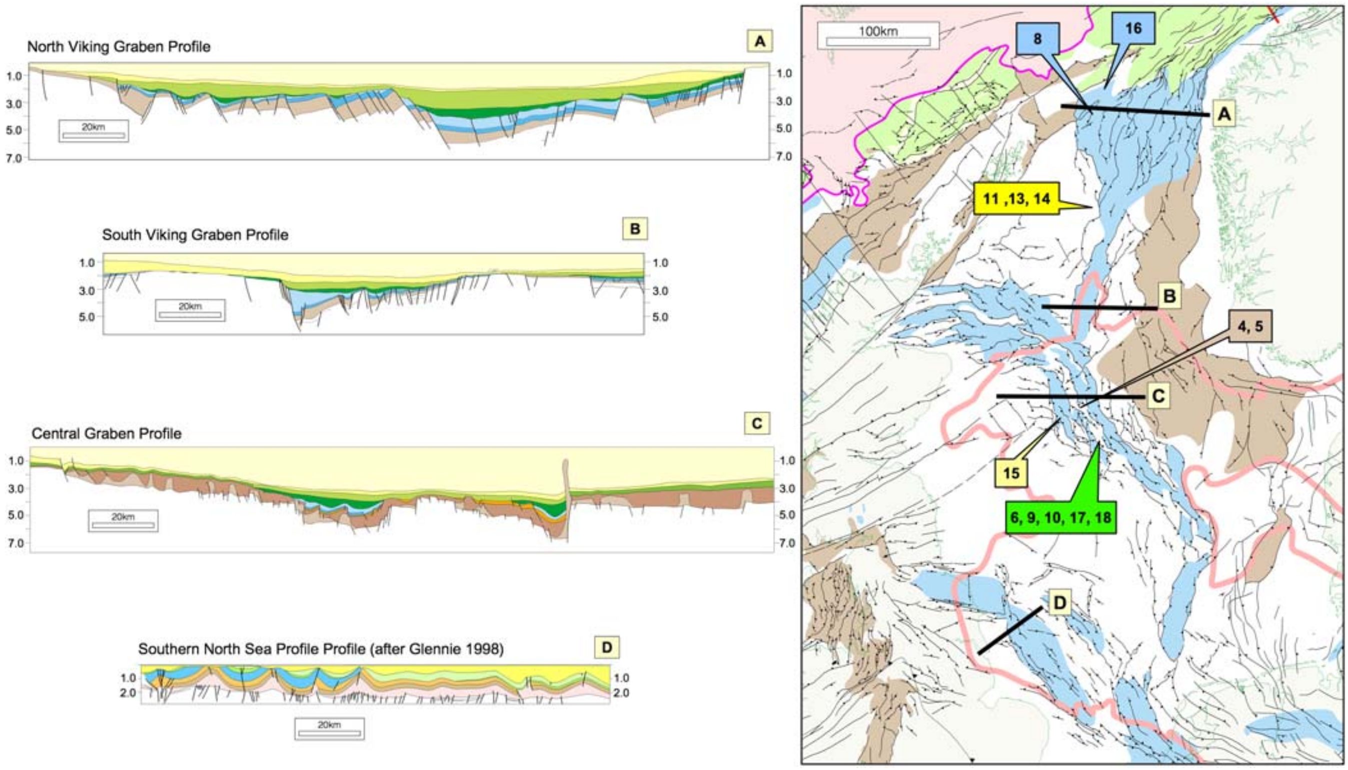

Fig. 1. Structural elements of the North Sea Rift. Map shows principal fault trends at the Base Cretaceous. Colour scheme on map shows timing of principal rift events, migrating westward towards ultimate Atlantic break-up in the early Cenozoic. Colour scheme for map corresponds to cross-sections. Predominantly Triassic rifting, brown; Jurassic, blue; Cretaceous, green; Cenozoic, yellow. Pink on map represents geology obscured by Cenozoic igneous extrusives. Zechstein salt on sections C and D in light pink. Locations of figures in text are numbered.

Licence Round in 1964 (e.g. Erratt *et al.* 2005), at which time only the Cenozoic sag basin was imaged. Ultimately, the major rift-related unconformity acquired a varied nomenclature, the terms Base Cretaceous, Late Cimmerian or 'X' becoming largely synonymous and interchangeable. The use of the term 'Cimmerian' was the subject of some debate, as evidenced by the discussion of P. Ziegler's paper in the proceedings of the first conference (Woodland 1975). The early regional syntheses of the Ziegler brothers led to the development of a model of a regional strain ellipse to describe the regional context of the Jurassic rift (Ziegler W. H. 1975*b*), and eventually to the appreciation of regional-scale uplift during the early Jurassic, Peter Ziegler's 'mid Cimmerian dome' (Ziegler 1981). In time, these studies were to prove prescient, demonstrating the importance of understanding regional-scale tectonics to provide rational models of rift evolution and play development (Fig. 3).

The 'Mid Cimmerian' and controls on effective Triassic reservoir distribution

The absence of Lower Jurassic strata via regional truncation led to Ziegler's interpretation of the regional 'Mid Cimmerian' unconformity, centred on the Rattray igneous province, as described in the 1981 volume (Illing & Hobson 1981). Detailed correlation and mapping of the truncation and onlap patterns by Underhill & Partington (1993) documented the areal extent of the dome. They considered the amount of uplift associated with the transient mantle plume to have been in the region of 400–500 m, somewhat less than earlier estimates. Davies *et al.* (1999) highlighted the minimal impact of the deflating dome on the stratigraphic architecture of the succeeding Late Jurassic rift.

Underhill and Partington's (1993) detailed stratigraphic correlations and analyses demonstrated the regional overstep of the Middle and Late Jurassic across the unconformity, truncation patterns to the north and west, facilitated by the well-constrained stratigraphies of the Viking Graben and Inner Moray Firth respectively. The progressive subcrop of the Mid Cimmerian Unconformity towards the dome centre from the south was not as extensively documented as those from the north and west, hampered by the lack of deep well data from the Central Graben, the absence via truncation of a readily correlatable Liassic sequence, and the lack of a sufficiently detailed Triassic stratigraphy in the Central Graben to facilitate recognition of a regional subcrop pattern.

At the first conference, a review of the Triassic by Brennand (1975) shows a heavily truncated Triassic section present across the Central Graben region, comprising only the basal Triassic Bunter Shales (later named Smith Bank Formation). This interpretation reflected both the paucity of well control and the inevitable bias introduced by wells drilled on eroded structural highs (see comparison in Fig. 5).

The field of Triassic stratigraphy has witnessed one of the more notable advances in our understanding of North Sea geology. The work of Phil Goldsmith (e.g. Goldsmith *et al.* 2003) showed that in the Central North Sea, in particular, sequences are correlatable over a wide area, in spite of being deposited in a continental setting in which bio-stratigraphic control is scarce, and where active basement extension and accompanying salt tectonics resulted in significant lateral thickness variations. Nonetheless, climatically controlled signals represented by repeated lacustrine transgressions still enable a relatively high degree of confidence in well correlation.

Following Brennand's initial foray into the Triassic, further drilling in the Central North Sea area, especially in the high pressure/high temperature domain (McKie & Audretsch 2005; Erratt *et al.* 2005) revealed a sand-prone section of regional

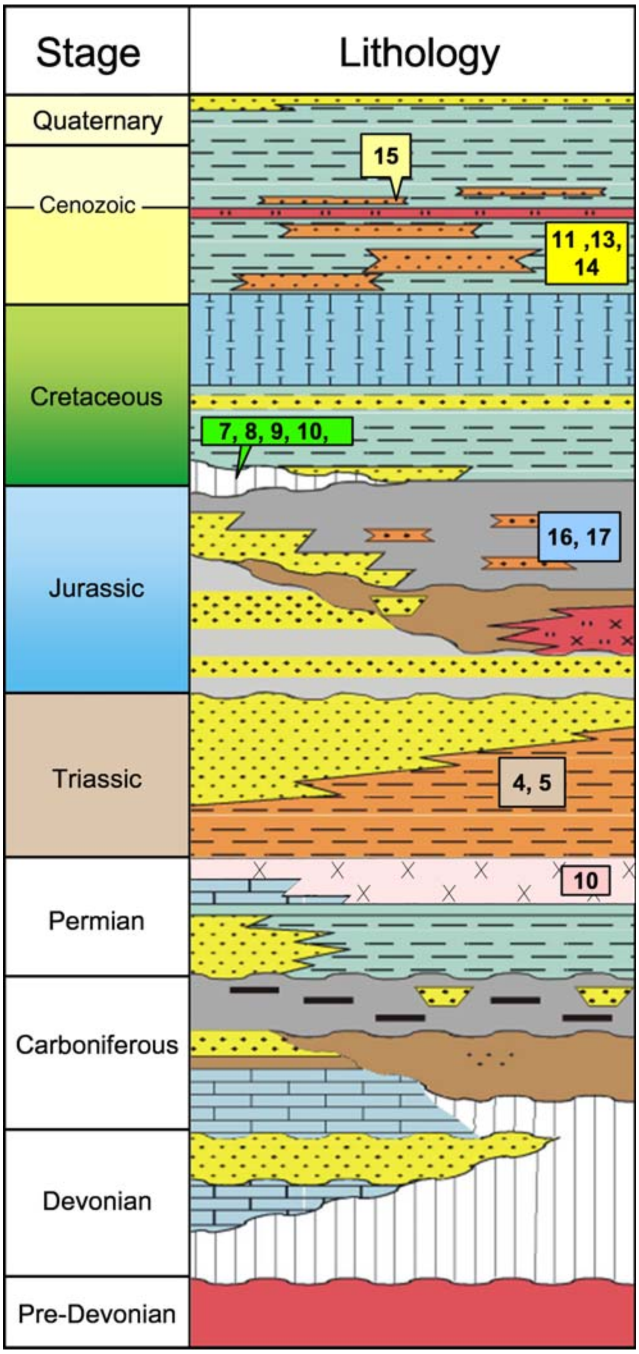

Fig. 2. Generalized stratigraphy of the North Sea Rift (after Vining *et al.* 2005). Location of figures in text are numbered.

extent succeeding the Smith Bank/Bunter shales (the Skagerrak Sandstones), and a regionally extensive unconformity at the base of the Middle Jurassic which cuts progressively further downsection towards the north and the centre of the mid Cimmerian 'dome'. The Triassic stratigraphy of the North Sea Rift is summarized in Figure 4. The refinement of the standard two-fold nomenclature of the Smith Bank Shale and Skagerrak Sandstone Formations into a regionally correlatable section based on the 'J' Ridge area (Goldsmith *et al.* 1995, 2003) moved the stratigraphy of the Central North Sea closer to the classic Germanic three-fold subdivision of the Bunter, Muschelkalk and Keuper. Coupled with improved regionally extensive 3D seismic data, the resulting higher resolution litho and seismic stratigraphy (Fig. 5), enabled the recognition of a subcrop pattern of the Triassic beneath the Mid Cimmerian unconformity to the south of the dome, further reinforcing the models of Ziegler (1981) and Underhill & Partington (1993). This regional truncation, which on structural highs is further accentuated by the later Base Cretaceous/Late Cimmerian unconformity, controls the northern limit of high quality Triassic reservoirs of the upper units of the Judy Member of the Skagerrak Formation. Tests north of this truncation line are uniformly disappointing until younger section re-occurs on the northern flank of the 'dome'.

Late Cimmerian tectonics and fault geometries

Since the initial 1975 volume, the application of the 'Cimmerian' nomenclature to the North Sea, the precise timing of the multiple phases of extension associated with Mid Jurassic to earliest Cretaceous tectonics, and the origin of the structural events in terms of the dominant structural processes have been the subject of extensive and long running debate (see discussion of Ziegler's 1975 paper). Subsequent accounts describe the complexities of the stratigraphy of the Jurassic/Cretaceous boundary in the North Sea, particularly Rawson & Riley (1982), Partington *et al.* (1993) and Rattey & Hayward (1993). All of these have run alongside the development of the paradigm established by McKenzie (1978) in the evolution of sedimentary basins, and failed rifts of the North Sea type in particular, which ushered in a parallel debate about the quantitative modelling of subsidence, thermal history and the evolution of hydrocarbon systems.

The single most telling factor in the advancement of our collective understanding of the dominant structural processes has been the acquisition of a regionally extensive blanket of 3D seismic data. Interpretation of these data, combined with dense high-quality well control and detailed quantitative structural analyses, eventually resulted in a regionally coherent picture of the structural evolution of the North Sea Rift, reconciled with the tectonic evolution of NW Europe and the European Atlantic Margin. For the purposes of the following account, the terms Mid Cimmerian will refer to the Base Mid Jurassic unconformity as described by Ziegler (1981) and Underhill & Partington (1993), whilst the Late Cimmerian will be used synonymously with the Base Cretaceous seismic event and group of related surfaces forming the regional surface of passive onlap.

Crustal scale deformation: pure and simple shear, basin forming mechanisms

Early contributions to the debate on the structural evolution of the North Sea rift built on the early regional syntheses by the Zieglers, describing the interaction of the predominantly extensional tectonic regime with the pre-existing Palaeozoic structural fabrics (e.g. Threlfall 1981). By the mid 1980s the acquisition of deep reflection profiles around the UK Continental shelf, in particular the BIRPS programme (e.g. McGeary *et al.* 1987), had been extended to the North Sea, and ushered in a new debate around the role of crustal scale detachments (e.g. Wernicke 1985) in the formation of the basin. The third conference (Brooks & Glennie 1987) contained significant contributions from Gibbs (1987) and Beach (1987) which interpreted the crustal scale structural development of the basin in light of these new models. By the 1990s models invoking both pure and simple shear were emerging (e.g. Kusznir *et al.* 1991). The debate expanded by the time of the fourth conference to encapsulate the observations by a number of workers (e.g. Ziegler 1983) that extension measured from fault heaves or the dip of fault blocks could not be reconciled with that predicted by subsidence analysis (see discussion in Roberts *et al.* 1993). The difficulties in applying their techniques were highlighted at the time, in particular those associated with halokinesis in the Central Trough region of the North Sea. These may present issues to revisit given both the extent and quality of the regional 3D coverage

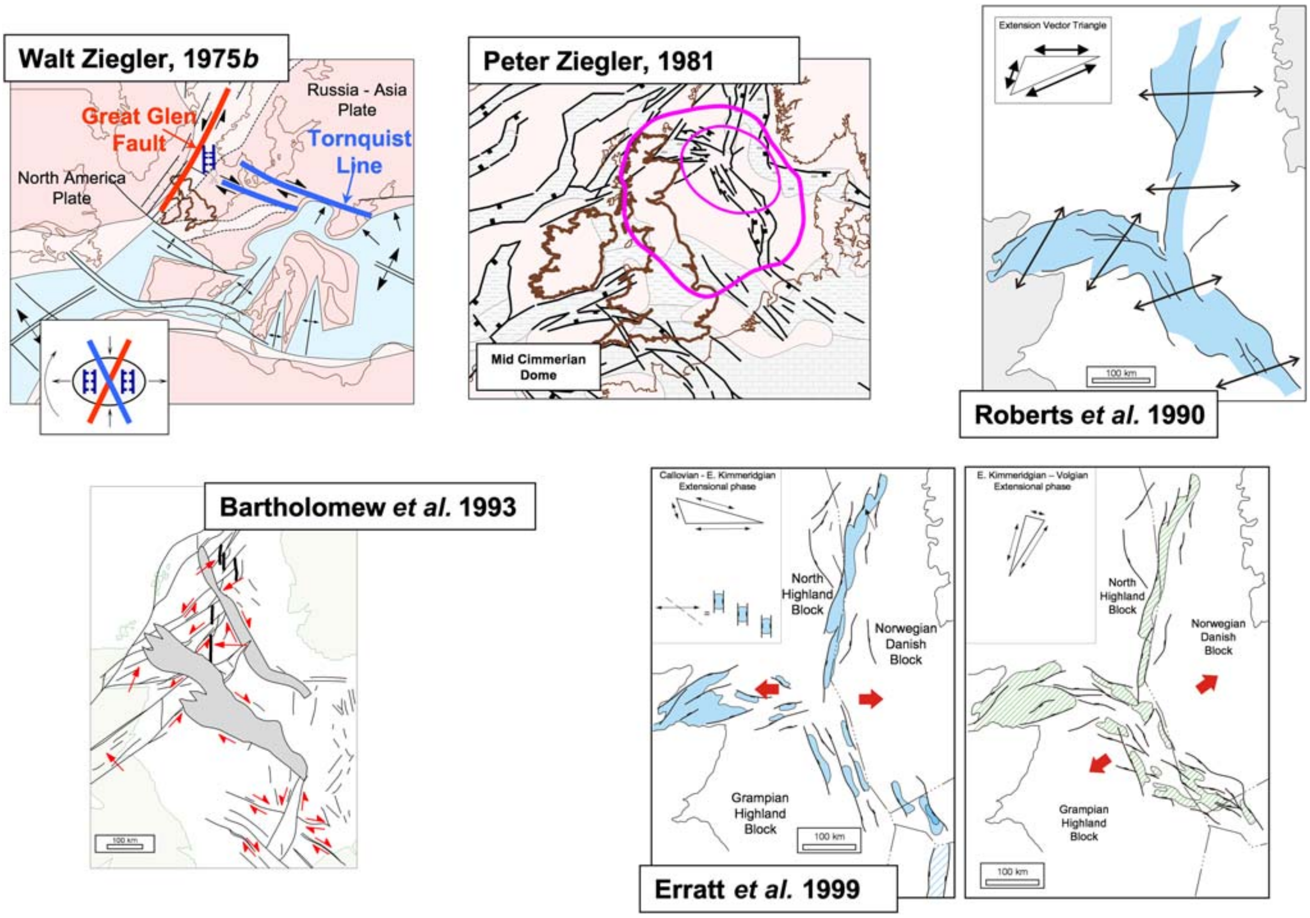

Fig. 3. The evolution of North Sea tectonic models. A regional strain ellipse to describe the regional context of the rift (after Ziegler 1975*b*), Peter Ziegler's 'mid Cimmerian dome' (after Ziegler 1981; Underhill & Partington 1993). Extensional models (e.g. Roberts *et al.* 1990; Erratt et al. 1999) competed with strike-slip (e.g. Bartholomew *et al.* 1993) as databases and imaging improved.

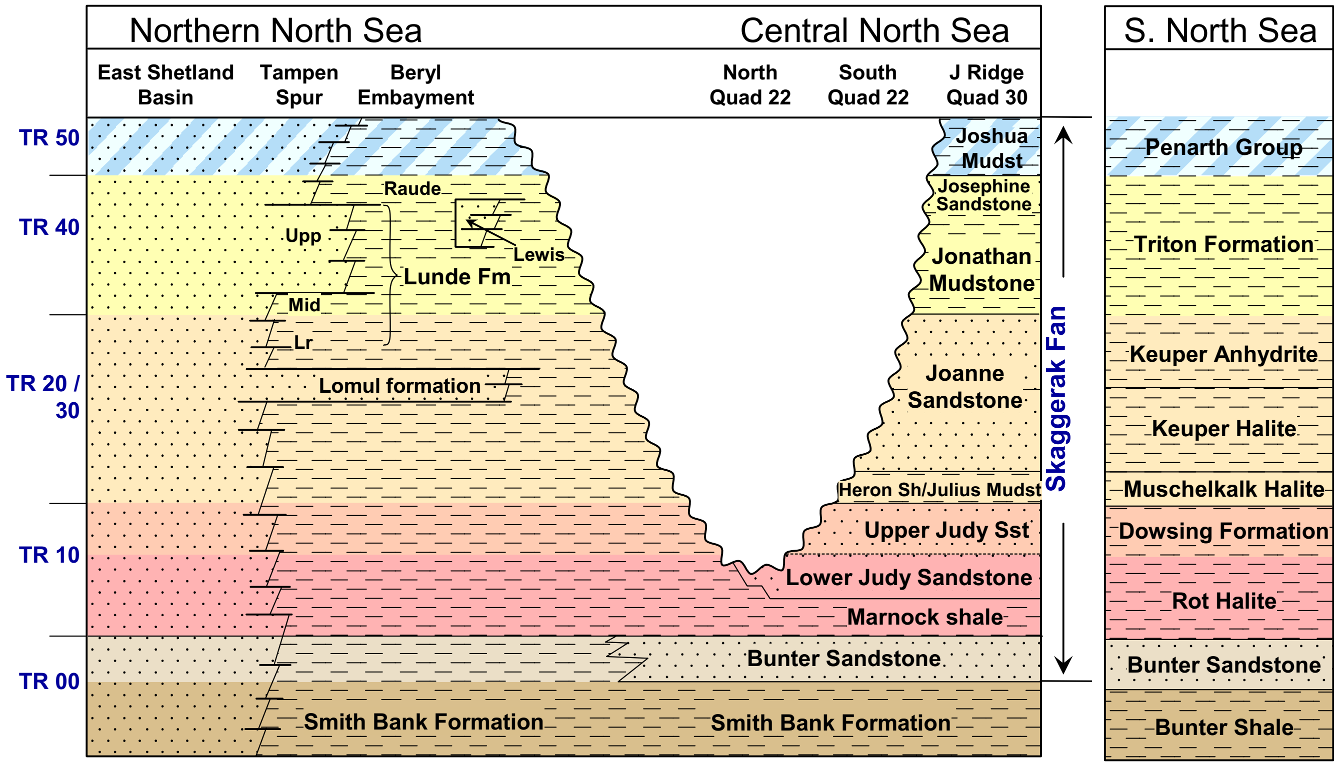

Fig. 4. The Triassic stratigraphy of the North Sea Rift (after Goldsmith *et al.* 2003).

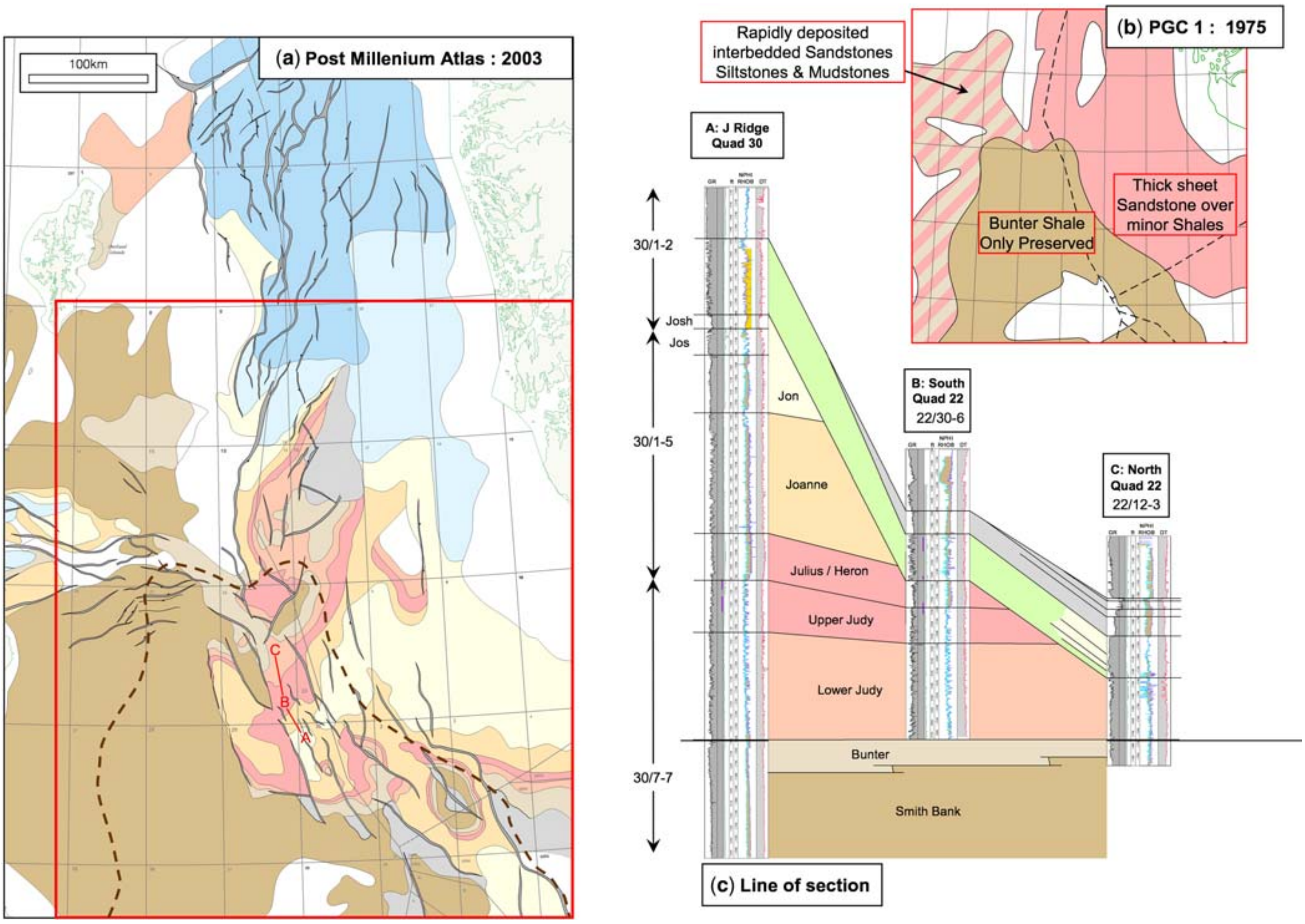

Fig. 5. (**a**) Truncation of Triassic strata beneath the 'Mid Cimmerian' unconformity in the Central North Sea, and the Jurassic subcrop of the unconformity in the Viking Graben. (**b**) A comparison with early models based on considerably less well data (after Brennand 1975). (**c**) Well data from the Central North Sea illustrating truncation of the Triassic beneath Middle Jurassic. Colour code for Triassic as in Figure 4. Light blue areas on map denote Lower Jurassic subcrop; dark blue denotes no truncation beneath the correlative conformity. White areas are structural highs with no presumed deposition; cross-hatched areas interpreted as Triassic eroded beneath Base Cretaceous Unconformity.

now available and new interpretations of the kinematics of Jurassic rifting. The relative merits of the pure shear and simple shear models are captured by Zanella *et al.* (2003), and as indicated by them, the application of new insights resulting from concepts of depth-dependent extension (e.g. Karner & Kusznir 2007) suggests potentially important developments in understanding the history of North Sea extension and subsidence.

Structural processes at a trap scale: strike- v. dip-slip and salt tectonics

Addressing the linkage between the deep crustal structure and the prevailing structural style in the prospective Mesozoic basin fill required 3D data of regional extent. Its arrival ushered in an alternative pervasive regional control for structural geometries on a trap scale, in the form of strike-slip tectonics. One of the main talking points of the fourth conference (Parker 1993) was the debate surrounding the merits of this model, largely superceding the discussions of pure v. simple shear and large-scale basin geometries in the context of the PGC conferences.

Basement-involved strike-slip faulting had been invoked as a dominant process in the Southern North Sea/Zechstein basin. In this basin, two dominant fault orientations are apparent, with localized inversions along the WNW trend. The pattern of two dominant fault trends with a preferential inversion of the WNW trend is repeated in the Central Trough area of the main North Sea rift, and was documented by Erratt *et al.* (1999). Jurassic age strike-slip faulting as the dominant structural process in the main rift system, however, was somewhat more contentious. Possible examples of strike-slip-related structures were presented from a number of North Sea domains. Whilst all were drawn from 3D seismic data, two prevailing issues required reconciliation. Firstly, in the Central Trough, were structural geometries the result of pervasive strike-slip faulting (e.g. Bartholomew *et al.* 1993), or the interplay between salt tectonics and basement extension? Secondly, how were structural geometries throughout the North Sea impacted by the multi-phase extensional history recorded across the entire region?

Polyphase rifting

The interaction of the multiple phases of Mesozoic extension on a regional scale was persuasively demonstrated by Doré *et al.* (1999). This regional-scale overprinting placed the evolution of the North Sea structural fabrics in a consistent regional framework, and with the availability of regionally extensive 3D coverage within the North Sea, was able to place some of the more problematic 2D structural and stratigraphic geometries in an appropriate context (Fig. 6). The 3D coverage provided the necessary vertical and areal resolution to overcome difficulties in fault aliasing and reliable seismic stratigraphic correlation. Much of the debate in the 1990s revolved around the Central Trough. However, data from elsewhere in the North Sea does not suffer from the ambiguities presented by the overprint of salt tectonics. Figure 7 illustrates

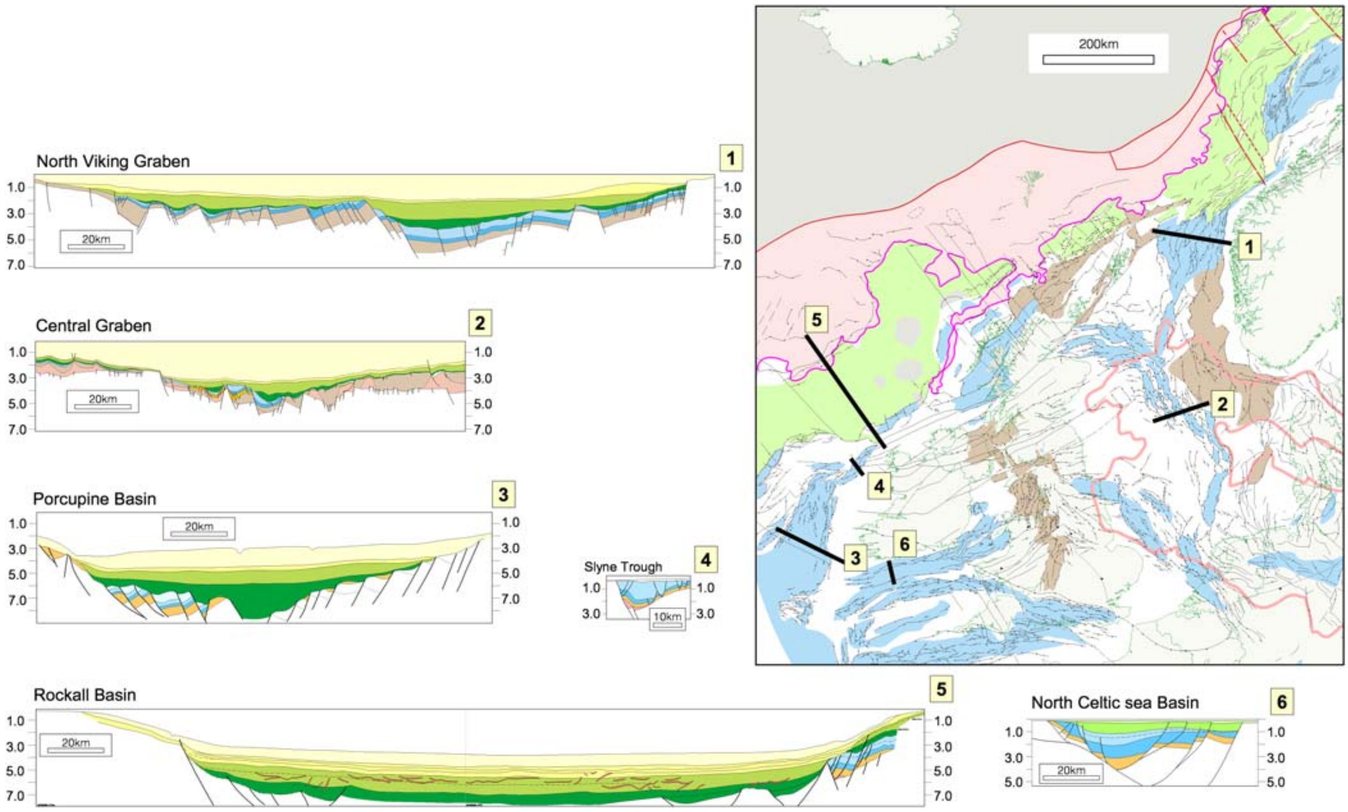

Fig. 6. Comparative NW European basin architectures illustrating regional-scale polyphase rifting. Colour scheme for map and sections as in Figure 1.

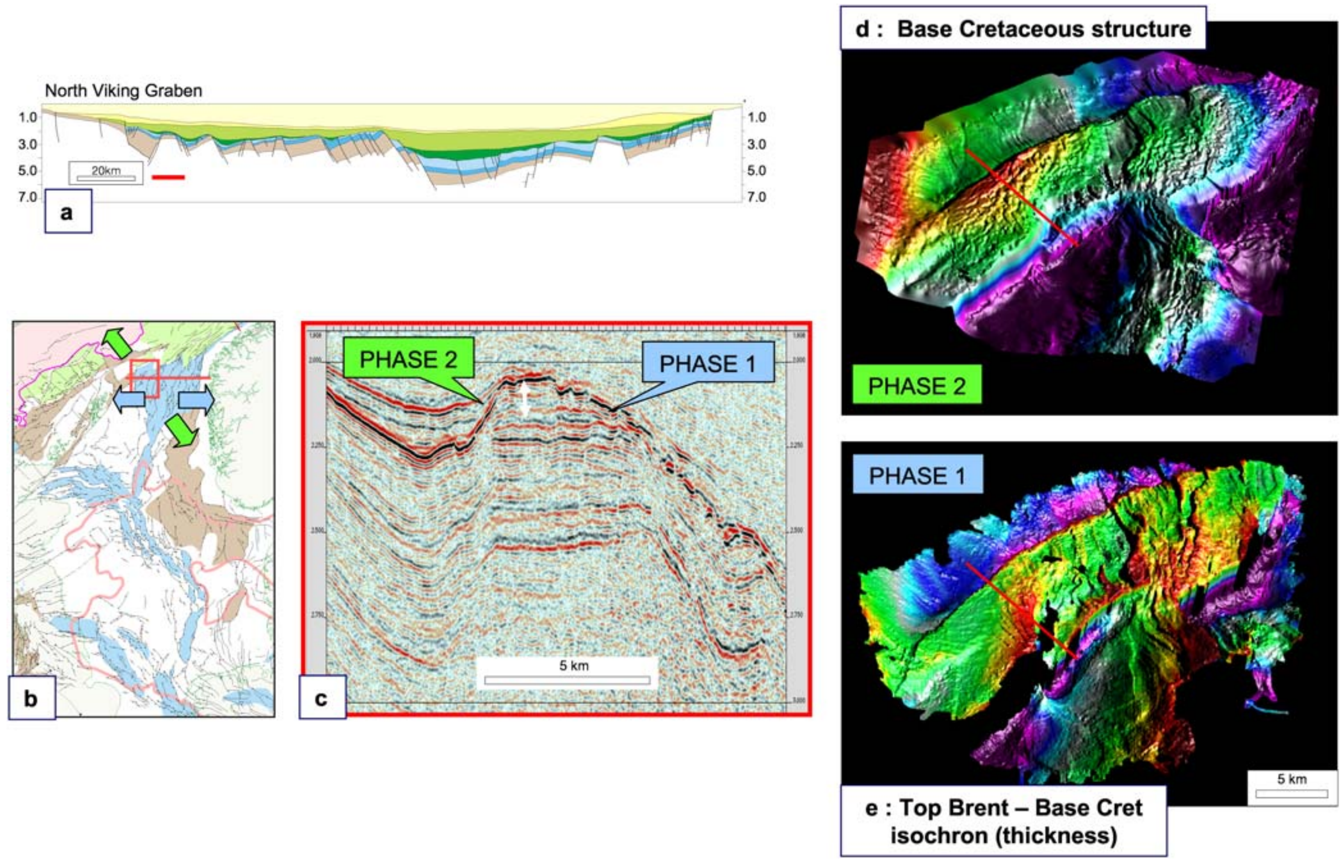

Fig. 7. The interplay of multiple phases of Late Jurassic extension in the evolution of the Tern Horst, ESB, UK Quad 210. Seismic line (**c**) is located on regional cross-section (**a**) and shaded relief images (**d** and **e**) by red lines. Shaded relief images illustrate the two phases of rotation of the feature, resulting in the unusual erosional profile of the feature beneath the Late Cimmerian. Upper image (d) is TWT structure to Base Cretaceous (red, highs; purple, lows), lower (e) is Base Cretaceous to Top Brent TWT thickness (red, thins; purple, thicks, arrowed on seismic section) draped on the Top Brent time surface. Two phases of rotation denoted by green and red arrows and cross-referenced to extension directions shown on structural elements map (**b**).

the interplay of multiple phases of Late Jurassic extension in the evolution of the Tern Horst, a prominent feature towards the western margin of the East Shetland Basin (ESB) in UK Quad 210. The seismic section illustrates a long-observed peculiarity of the Tern Field. The crest of the structure at Base Cretaceous/Late Cimmerian level is underlain by a section of Upper Jurassic Kimmeridge and Heather Shale, which thins downflank towards the east, towards the axis of the Viking Graben. The thinning is clearly the result of truncation at a horizon at or just beneath the Late Cimmerian surface. This trend is counter to the more commonly observed thinning towards the crest of a westerly dipping structure, which dips away from the axis of the graben at all pre- and syn-rift stratigraphic levels, exemplified by structures such as the Brent Field. A shaded relief image of the Late Cimmerian surface shows two main fault trends, a NE–SW trend defining the Tern Horst, and a lesser north–south trend superimposed on top of the horst and extending beyond it. Coupled with the stratal relationships evident on seismic, the horst block can be seen to be the result of at least two phases of extension post-deposition of the Brent reservoir section. The first rotated structures along north–south faults away from the axis of the graben, resulting in truncation of a structural crest on the east side of the present day horst. The second event, resulting in faults along the NE–SW trend, re-orientates and overprints the earlier fabric and rotates structures away from the axis of the proto-Atlantic rift. The re-utilization during Late Jurassic rifting ('Late Cimmerian') of earlier Triassic faults ('Early Cimmerian') in the ESB is sporadic, a characteristic also illustrated by the Tern Horst and the interplay between the Jurassic margin of the ESB and the Triassic Unst Basin (Fig. 7). The eastern bounding fault of the Unst Basin constitutes the northwestern bounding fault of the Tern Horst as the former continues on a northeasterly trend beneath the Jurassic fault block terrane of the ESB. This fault is reactivated as described above and forms a receiving half-graben to Upper Jurassic deep-water sands, broadly equivalent in the context of the first-order tectono-stratigraphic evolution of the basin to the reservoirs at the Magnus Fields. These sands, like those at Magnus, are themselves rotated and truncated by end Jurassic/earliest Cretaceous movement along the northerly trending western margin of the ESB.

Examples of poly-phase rifting in the Central North Sea and Moray Firth have been documented elsewhere (e.g. Hibbert & Mackertich 1993; Erratt *et al.* 1999), which built on the work of Roberts *et al.* (1990), and continued to compile a compelling body of data in support of dip-slip models. By the time of the fifth conference, the completion of the emerging regional blanket of 3D seismic data, and the appearance of the elegant reconciliation of basement extension and salt withdrawal by Helgeson (1999), had gone a long way to resolving the questions raised by the strike-slip v. dip-slip debate of the fourth conference (Figs 8 & 9).

Implications of trap scale salt-related geometries for regional tectono-stratigraphy

The role of salt tectonics in determining the structural fabric of the Mesozoic section of the Central Trough, and the platform areas in particular, surfaced during the 1980s, partly in response

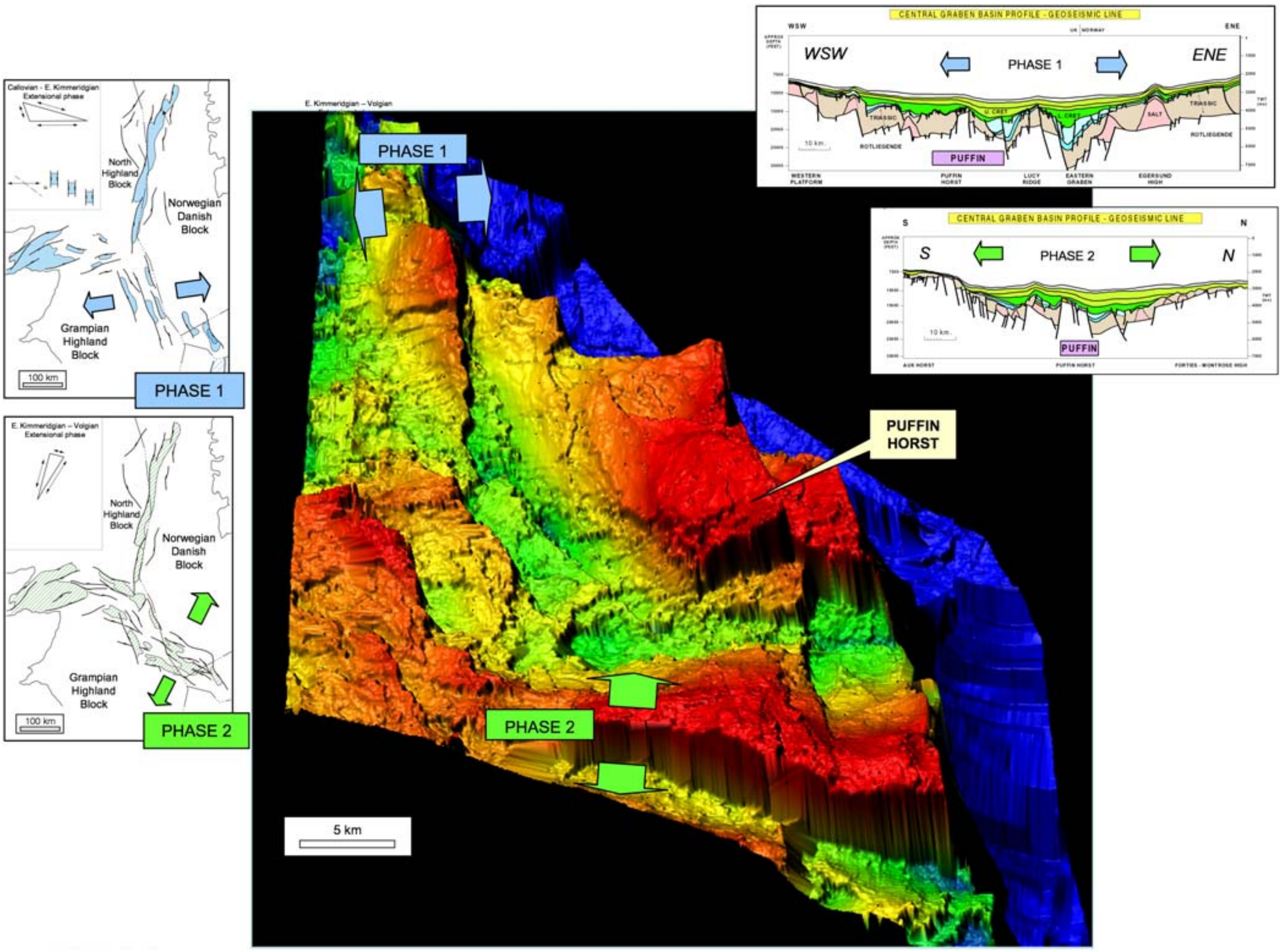

Fig. 8. Shaded relief image of the Base Zechstein surface on the Puffin Horst area of the Central North Sea (red, highs; blue, lows). Two dominant fault trends are apparent, corresponding to the polyphase model of Erratt *et al.* (1999) as shown on maps. The regional sections locate the horst within the wider graben area.

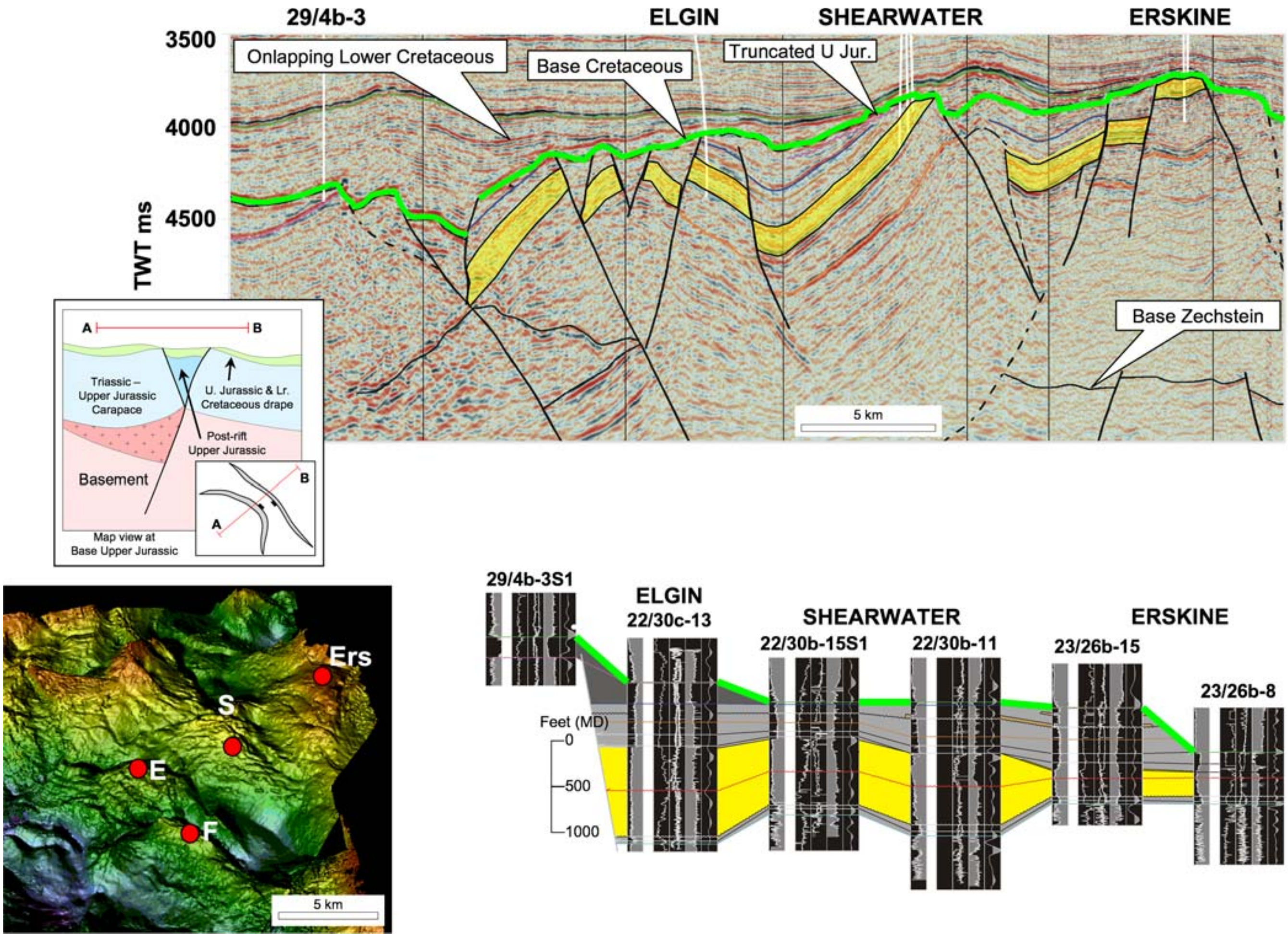

Fig. 9. Seismic line illustrating Helgeson's (1999) model of interaction between pre- and post-salt sections during Cimmerian rifting and the impact of polyphase rifting on the stratal relationships above and below the Base Cretaceous surface.

to structural models invoking gravity driven processes (e.g. Gibbs 1984). Smith (1987) in the third, and Wakefield *et al.* (1993) and Erratt (1993) in the fourth conferences illustrated the alternative salt withdrawal hypothesis, the latter introducing the 'pod'/'interpod' terminology to describe areas of complete salt withdrawal and grounding of the Triassic section, and areas of preserved Zechstein salt respectively. Stewart (1993) described similar features from the Norwegian sector (e.g. the Ula Field), whilst Stewart & Clark's (1999) paper in the fifth conference was a thorough synthesis of the previous studies in the light of new examples. These debates took place against a backdrop of considerable uncertainty in the amount of Zechstein salt underpinning the Mesozoic section of the Central Trough, apparently acting as a regional-scale decollement between the Mesozoic carapace and the underlying rifted basement. Initial models of the basin, and resulting regional transects (e.g. Glennie 1998) indicate a relatively thick, continuous salt section across the main graben areas (Fig. 10). Conversely, the platform areas, having given rise to the development of the pod–interpod model and consequent total salt withdrawal, point to a pattern of frequent welding of the Triassic section with the Palaeozoic of the rift floor. Stewart & Clark (1999) demonstrated that much of the salt withdrawal had taken place as early as the Triassic. Regional considerations of poly-phase rifting indicated that, for the most part, the main locus of Triassic rifting was offset relative to the main Jurassic graben (e.g. Erratt *et al.* 1999). As such, it was unlikely that the thick salt invoked in earlier models would be accommodated by an age model invoking Permian rifting providing the necessary accommodation for the thick Zechstein sequence. Helgeson's model, which invoked frequent welding of the pre- and post-salt section, pointed towards a much thinner regional salt layer beneath the graben, and for the first time provided consistency in interpretation of the structural fabrics of graben and platforms.

The Late Cimmerian: fundamental change in rift architecture and stratal geometries

The debate over the applicability of the 'Cimmerian' nomenclature to some extent clouds the fundamental observation that the Late Cimmerian event in the North Sea rift marks a fundamental change in rift architecture and accompanying structural geometries relative to earlier rift events.

Sinclair *et al.* (1994) drew attention to the changing stratal geometries throughout the Jurassic in their consideration of the Jean d'Arc, Outer Moray Firth and Porcupine Basins. The stratal patterns described in the Porcupine Basin, in the sequences onlapping the Late Cimmerian unconformity, mimic those in the North Sea, showing passive onlap, which contrasts markedly with the classic 'syn-rift', fanning stratal geometries of the bulk of the Upper Jurassic section (e.g. Figs 7 & 9). The polyphase rift model of Erratt *et al.* (1999) describes the overprint of the latter by the former, although their account does not explicitly describe this fairly obvious phenomenon. Similarly, their published cross-sections show the overprint of the two basin types in both the ESB (Fig. 7), where the Late Cimmerian 'Tern Horst' overprints the Triassic Unst Basin and earlier Late Jurassic structures, and in the Central North Sea, where the 'strike lines' to the earlier phase rifts become 'dip lines' to the last ('Late Cimmerian') phase as

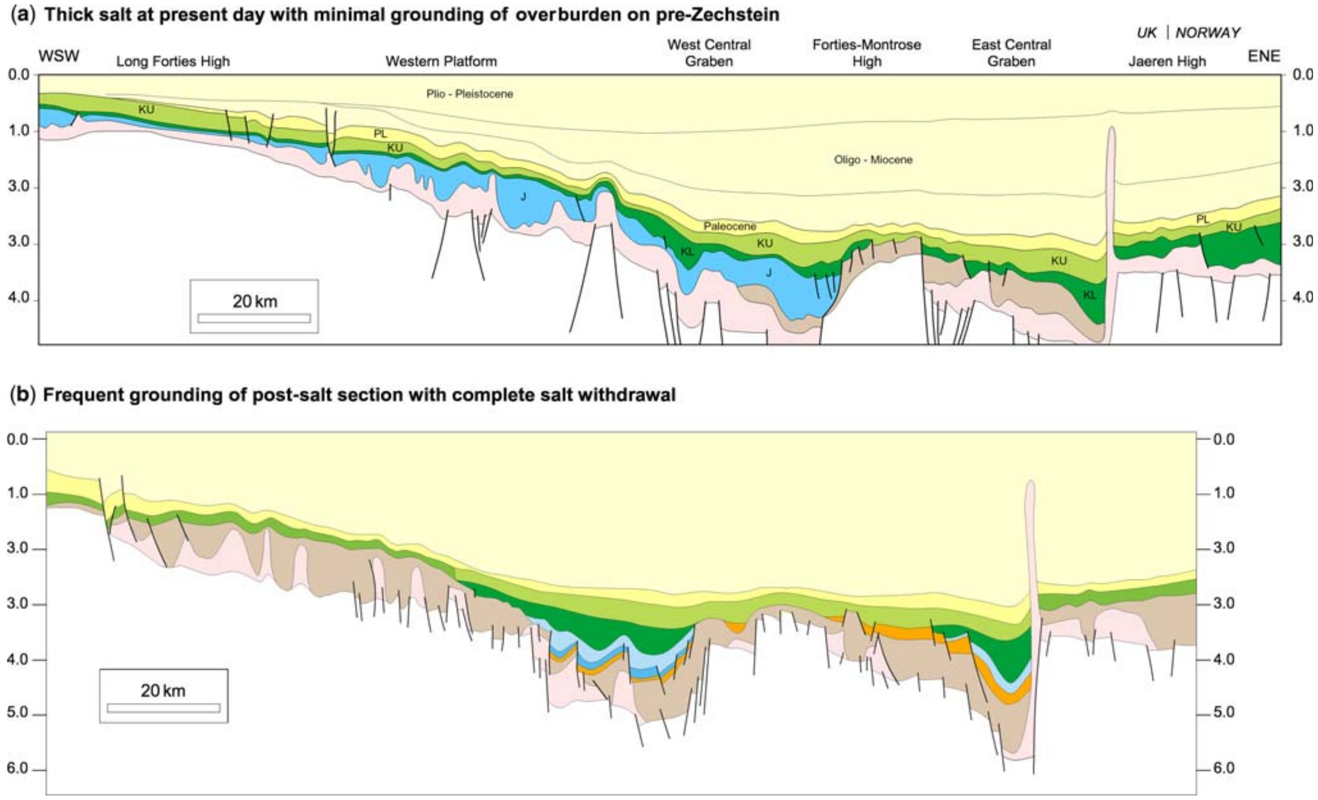

Fig. 10. Comparison regional traverses. (**a**) Early models (e.g. after Glennie) of the basin indicate a relatively thick, continuous salt section across the main graben areas. Later models (**b**) indicate a hard linkage via a thinner initial salt thickness. Colour scheme as in Figure 1.

extension vectors change (see figures in Erratt *et al.* 1999). New perspectives on basin architecture and rift timing, coupled with the application of robust sequence stratigraphic models, leads to an appreciation of the spatial distribution of Jurassic basin floor reservoirs. A possible explanation for the relative lack of success in this play in certain parts of the rift system results, and is discussed in a subsequent section.

North Sea deepwater reservoirs: some comparisons between the Palaeogene and Late Jurassic

The ground-breaking regional studies published by geoscientists from BP in the fourth conference (Parker 1993) marked a major milestone in the wider understanding of the interplay between North Sea tectonics and stratigraphy, and more generally, the application of sequence stratigraphy in a syn-rift setting (e.g. Partington *et al.* 1993; Rattey & Hayward 1993; Underhill & Partington 1993). The early seismic stratigraphic analysis by Vail & Todd (1981) of the Northern North Sea Jurassic sequences appeared in the proceedings of the second conference, the landmark 1977 AAPG Memoir 26 (see Fig. 12) having appeared between the first and second conferences. Data quality and limited seismic resolution were barriers to the application of the technique throughout much of the Brent province and the Jurassic sequences of the entire rift. Subsequently, however, the Upper Jurassic 'Troll delta' presented some well-imaged progradational geometries, and these are presented and discussed in the Millennium Atlas (Fraser *et al.* 2003).

Cenozoic examples and play considerations

Cenozoic sequences in the North Sea present better subjects for seismic stratigraphic analysis than their Jurassic counterparts, being thicker, shallower and preserving complete, largely undeformed shelf to basin transitions, as evidenced by the early examples published by Vail and his co-workers in the aforementioned AAPG memoir. The stratal relationships typical of progradational highstand sequences can be observed even on the earliest vintages of 2D seismic coverage. Subsequently, regional-scale 3D seismic coverage revealed a higher-order stratal architecture internal to the shelfal, highstand sequences, as well as a detailed picture of the distribution and architecture of basin floor, lowstand reservoir sequences (e.g. Fig. 11). Figure 13 illustrates the higher-order architecture of the Late Paleocene ('Sele/Hermod') shelf. Well 9/18-30 penetrated a thick sandstone section, with a distinctive blocky gamma ray signature. Seismic data indicates a high-amplitude planar, gently basinward dipping reflector at the base of this sequence. This unit is interpreted as an example of a lowstand 'shelf margin wedge'; the basal reflector marks a sequence boundary, possibly an example of the early 'Type 2 Sequence Boundary' of the type described by the Exxon group in their early publications. This represents a basinward shift in facies without significant bypass of the shelf and corresponding deposition of sand on the basin floor. The blocky signature of the sandstone section in 9/18-30 shows a predominantly aggradational stacking pattern, itself indicative of deposition during a relative lowstand of sea-level (e.g. Van Wagoner *et al.* 1990). The association of these phenomena in a relatively subtle manifestation of the sequence stratigraphic model may serve as a template for certain aspects of Upper Jurassic shallow marine depositional systems in other parts of the North Sea which do not benefit from direct seismic imaging of stratal geometries by virtue of depth and consequent limited seismic resolution. The application of this template to the Upper Jurassic is discussed in a subsequent section.

The latest Paleocene shelfal 'Hermod' sequences are succeeded by isolated, mounded deepwater basin floor sands of the Early Eocene Balder Formation. These are very well sorted sands

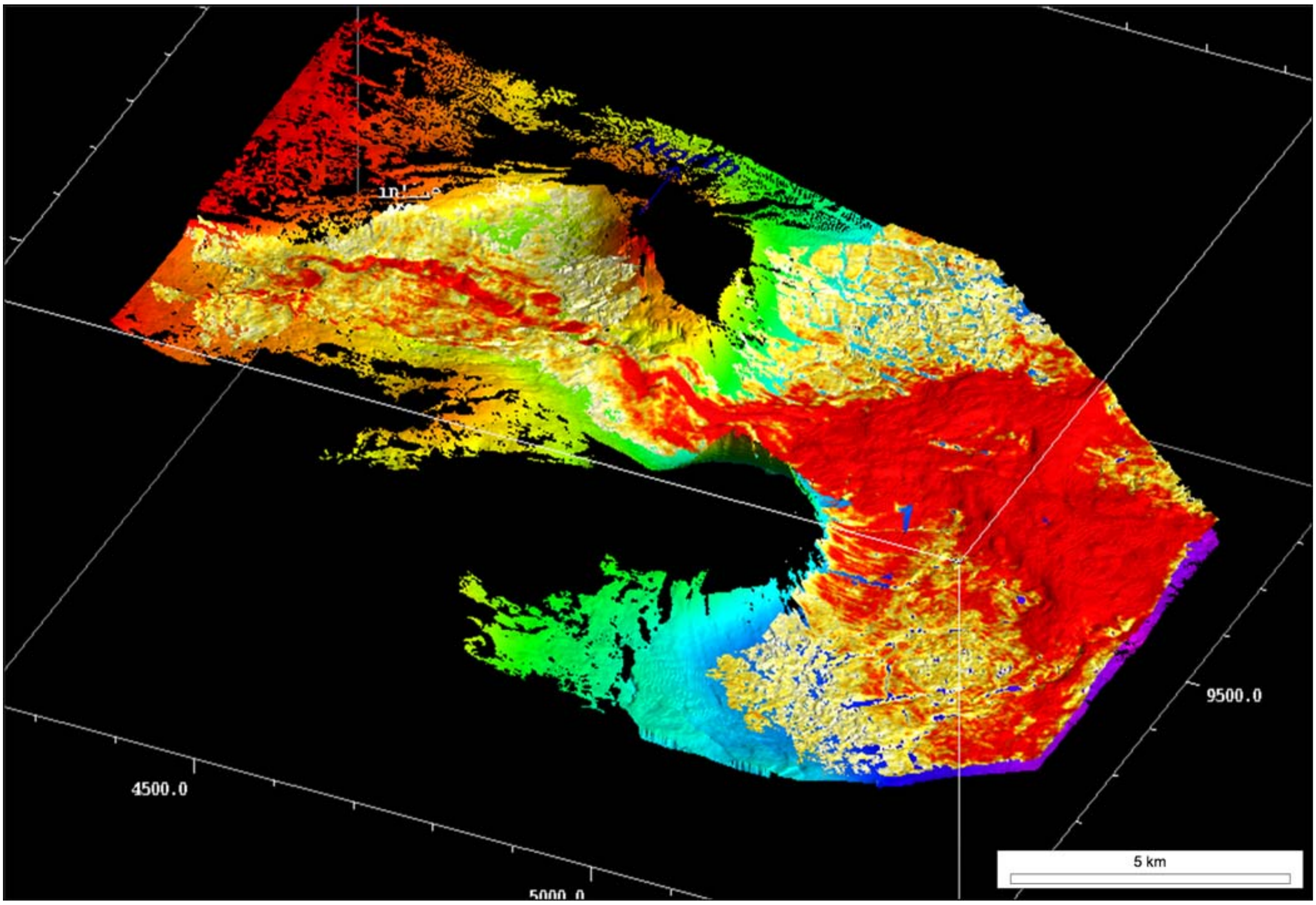

Fig. 11. Eocene Tay formation fan system, Gannet Area, Central North Sea. The distribution of Eocene sands is shown in red derived from seismic amplitudes, draped on the top Paleocene time structure (red, high; purple, low). The shorter face of the reference box is 10 km wide.

re-deposited from a shallow marine setting (e.g. Dixon & Pearce 1995), probably indicating the widespread collapse of a shelf margin system similar to the underlying Hermod system.

Sandstone injectites

Before turning to Jurassic depositional systems, the Cenozoic sequences of the Northern North Sea and their high-quality seismic images merit further attention with regards to the definition of play fairways and the role of sandstone injectites.

Our understanding of the importance of sandstone remobilization in modifying the configuration of North Sea Cenozoic reservoirs has evolved dramatically since the availability of 3D seismic data (e.g. Lonergan *et al.* 2000) and was discussed by Hurst *et al.* (2005) at the sixth conference. The Cenozoic basin floor sequences of the Northern North Sea area display large, mounded geometries, typified by the Eocene Harding/Gryphon fields of the UK Beryl Embayment area, and the Paleocene/Eocene Balder Field in the Norwegian sector. Although occurring in different parts of the stratigraphy, and in markedly different locations, these fields have in common their location above the flanks of underlying westerly dipping rift elements, counter to the regional west–east sediment input direction of the Cenozoic sequences.

On a first-order scale these opposing dips account for the location of the two principal fairways in the Cenozoic play in this sector of the North Sea. The example of the Balder trend against the eastern flank of the underlying rift shoulder is repeated further south in the Sleipner and Everest complexes. The block diagrams of the UK Quad 9 play area in Figure 14a illustrate this setting.

The Balder Field and Harding/Gryphon complexes are further characterized by injectite complexes, occurring at all scales from core to seismic. Injectite complexes on a field scale present opportunities for near-field exploration. However, the relative lack of exploration success in many apparent four-way top reservoir closures, amongst mounded basin floor features away from the main play fairways, is probably due to the regional-scale effects of sandstone injections. Such areas are typified by failure to encounter hydrocarbon columns in the main massive reservoir sequences in structures displaying apparent four-way dip closure, and the occurrence of hydrocarbons in overlying injectites (e.g. 9/15-3 in Fig. 14b). This suggests that closure height at base of the ultimate top seal, effectively at the crest of the injectite 'swarm', is the key element in defining the relationship between closure height and the likelihood of encountering hydrocarbons in the massive 'primary depositional' reservoir section. Structures in the two main play fairways described above benefit from the inherited 'counter-depositional' dip relative to regional facies trends, allowing the build-up of hydrocarbon columns through the injectite swarm and into the massive reservoirs.

Upper Jurassic deepwater depositional systems

The Upper Jurassic depositional systems of the North Sea have been the subject of extensive regional studies, and multiple generations of stratigraphic schemes, summarized by Fraser *et al.* (2003) in the Millennium Atlas. In the BP studies published in the proceedings of the fourth conference, Partington *et al.* (1993) referenced the Upper Jurassic deepwater reservoirs of the Central North Sea as one of the remaining underexplored exploration plays of the

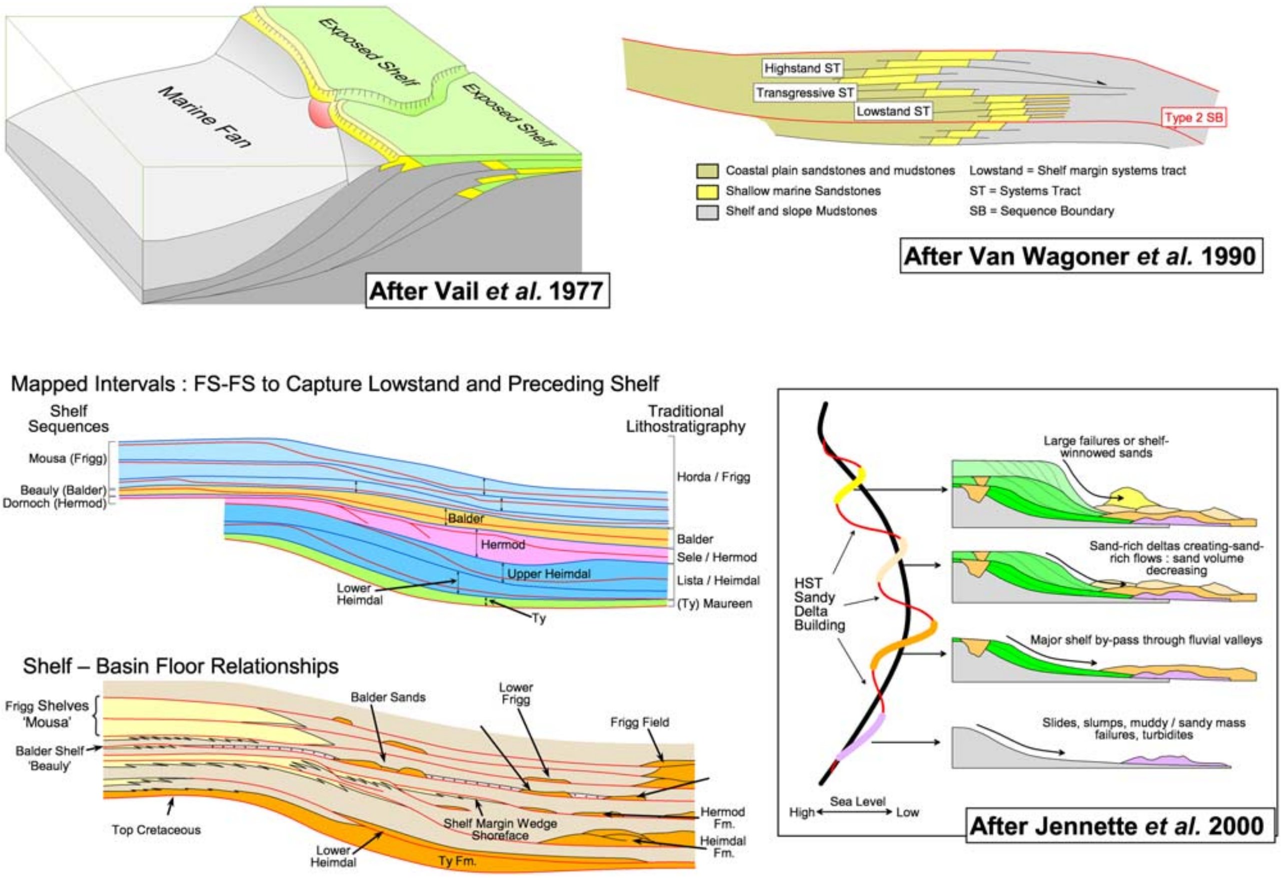

Fig. 12. Classic sequence stratigraphic models and the stratigraphic architecture of the Paleocene/Eocene sequences in the UK Quad 9/Norway Quad 26 area. See text for discussion.

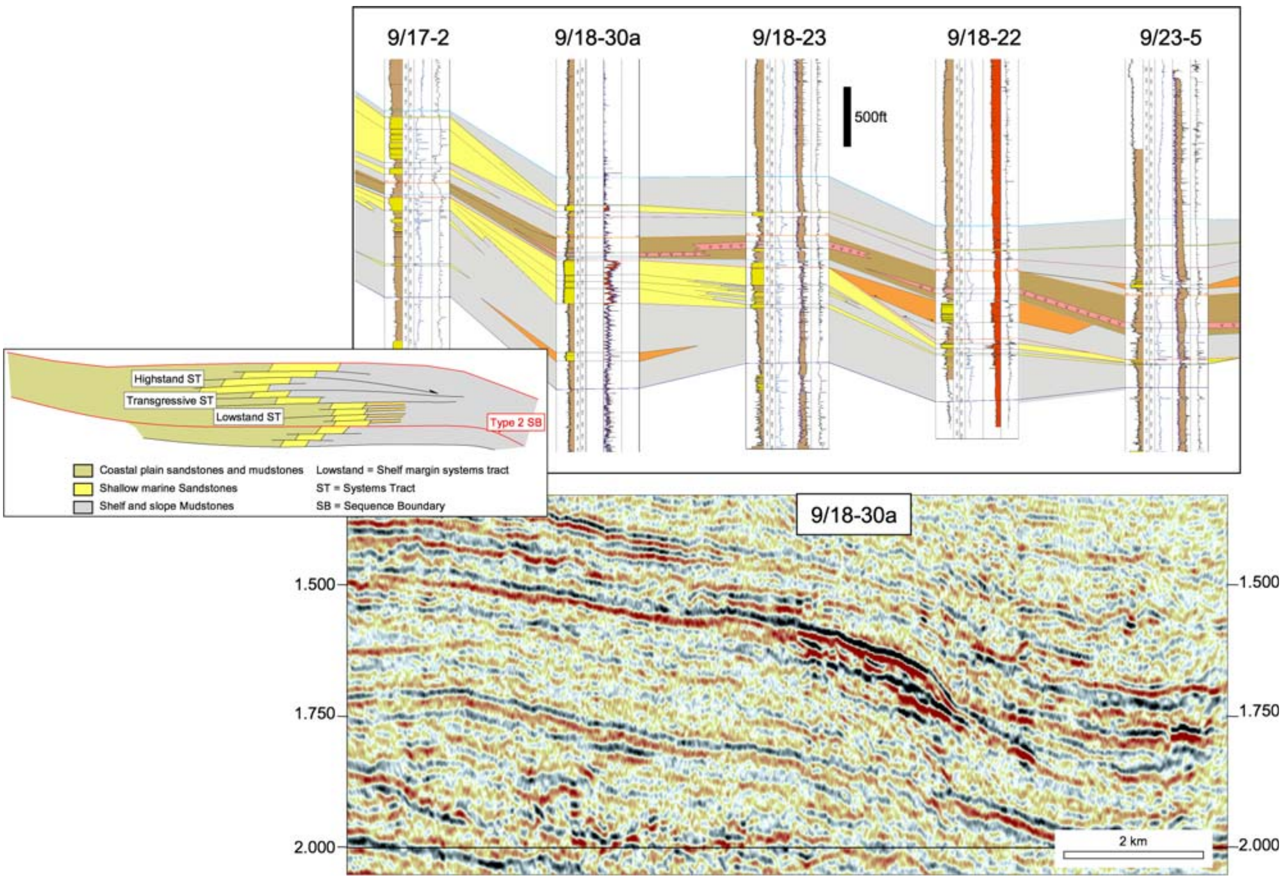

Fig. 13. Seismic and well log expression of the higher-order architecture of the Late Paleocene ('Sele/Hermod') shelf, UK Quad 9, and a type 2 sequence. Red and blue horizons reference the type 2 sequence boundary at the top and base of the 'shelf margin wedge'.

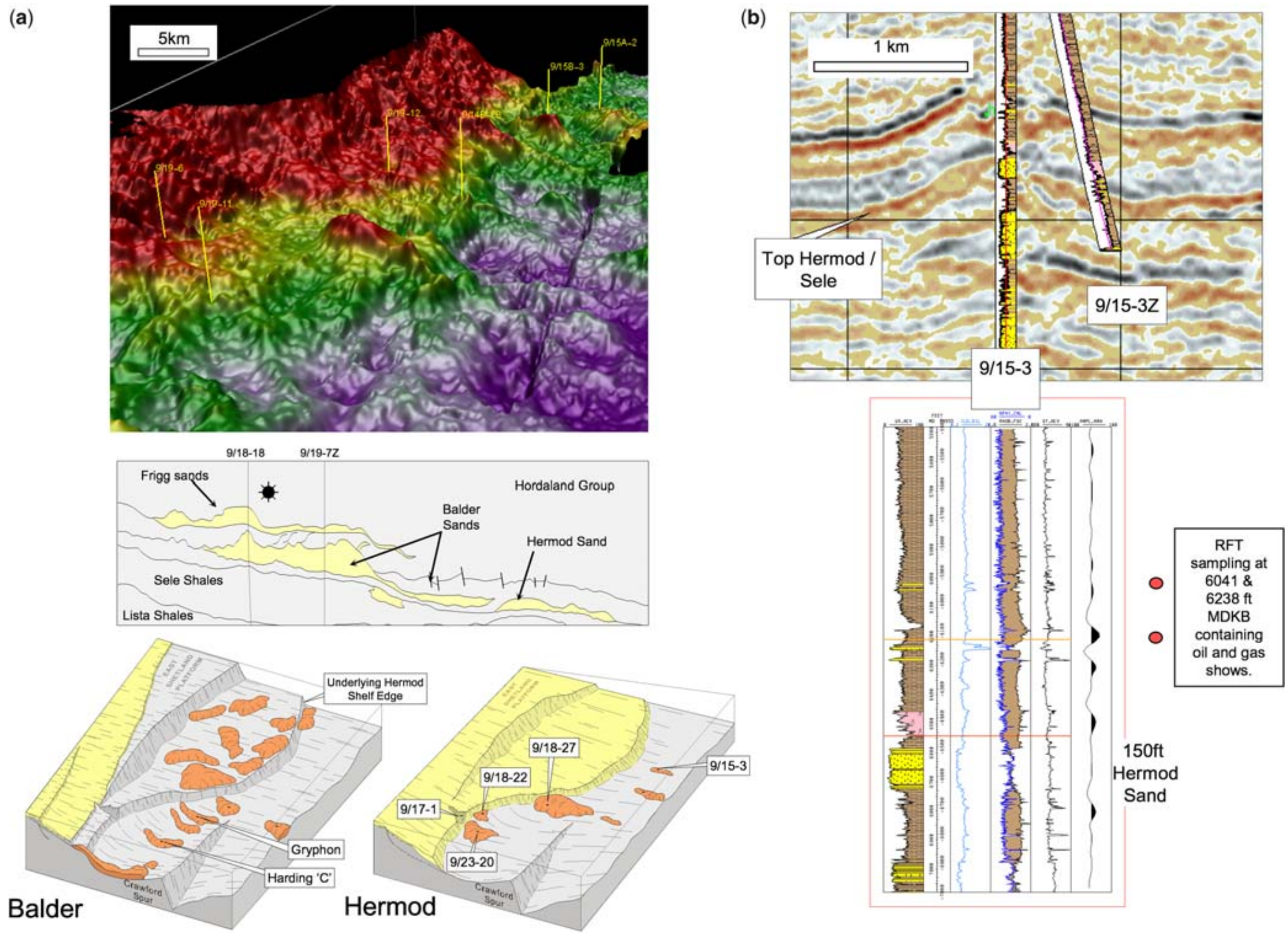

Fig. 14. The importance of basement structure in overcoming the risk posed by regional sand connectivity to effective trapping of hydrocarbons in compaction drape closures on the basin floor. Success cases exemplified by Gryphon (block diagram in **a**). Failure cases exemplified by the cross-section in (a) (9/19-7 well) and the 9/15-3 well (**b**). The shaded relief image is of the Top Hermod surface, UK blocks 9/14 and 15 (red, high; purple, low). Seismic line courtesy of Lundin.

North Sea. Some 16 years later, this play (especially in the Kimmeridgian/Volgian of the Central North Sea) remains enigmatic, in spite of success in the Moray Firth in the form of the Buzzard discovery in 2001 (Doré & Robbins 2005). The Moray Firth and the South Viking Graben are the two principal fairways for the Upper Jurassic deepwater play and have been the subject of numerous detailed accounts of their stratigraphy and depositional processes. Less widely discussed in the literature are the Upper Jurassic reservoirs of the ESB in the Northern North Sea, the Magnus Sandstone and its equivalents. In spite of this, Magnus, with production in excess of 750 mmboe (MacGregor *et al.* 2005), was the last giant field to be brought on stream in the UK North Sea. These three areas stand in marked contrast to the Central North Sea with regards to the Upper Jurassic deepwater reservoir play, in spite of a proven Upper Jurassic shoreface play in the latter (the Fulmar and Ula Formation reservoirs). This section compares and contrasts these systems to address the relative lack of success in the Central North Sea.

Sandstone provenance and reservoir fairway development

The deepwater systems of the South Viking Graben and Moray Firth owe their origin principally to the prolific sediment provenance areas of the Fladen Ground Spur and the Scottish mainland. Here, first cycle Devonian sediments derived from the denudation of the Caledonides subcrop extensively around the basin margins and provide a significant sediment source for Jurassic basin fill.

The ESB and Central Trough do not show similar occurrences of such prolific coarse clastic successions in their Upper Jurassic sections, with perhaps the exception of the Tail End Graben. However, deepwater Magnus Sands of the ESB constitute the reservoir section for the Magnus and Penguin Fields. The Magnus Sandstone reservoir is considered to be the lateral equivalent of the thick Upper Jurassic reservoirs drilled on the western flank of the basin in blocks 210/19 and 20 in the 1970s.

In spite of its inclusion in the regional accounts of North Sea Jurassic stratigraphy by the BP group in the fourth conference (e.g. Partington *et al.* 1993; Rattey & Hayward 1993), the significance of this fairway as an analogue for deepwater exploration has perhaps been lost due to being overshadowed by its illustrious counterparts in the Cenozoic, and the more prolific Jurassic fairways. 3D seismic coverage completed during the 1990s displays a network of amplitude phenomena associated with the development of the Upper Jurassic reservoirs along this flank of the basin. Reservoirs on the Magnus Field are similarly derived from the west (De'Ath & Schuyleman 1981), the depositional architecture of the complete basin floor system having been disrupted by faulting along a SW–NE proto-Atlantic trend described in an earlier section (Fig. 15). Published accounts by Surlyk (1987) of the Jameson Land Upper Jurassic outcrops reveal similar sand body geometries to those imaged west of Magnus.

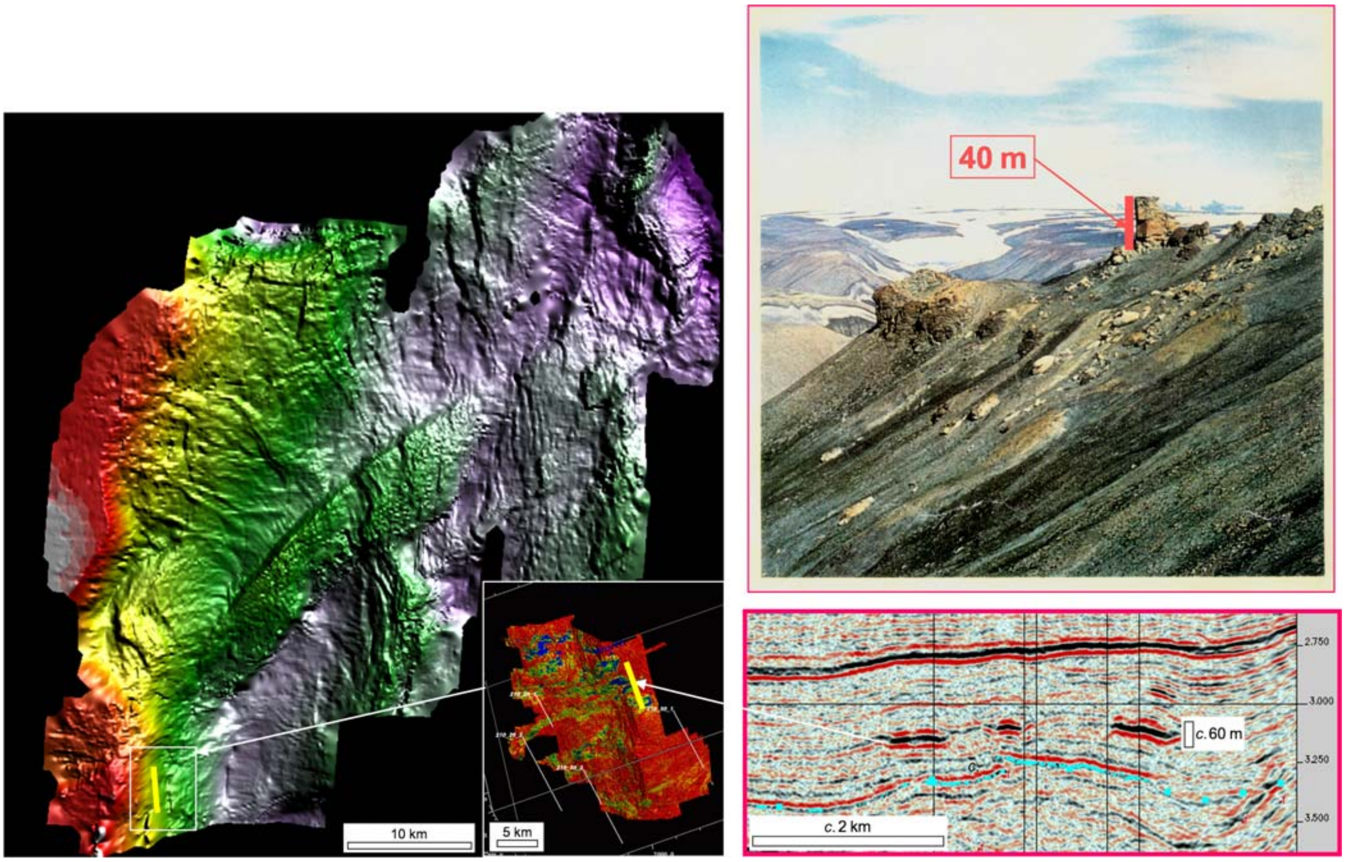

Fig. 15. Upper Jurassic deepwater reservoirs of the ESB and Jameson Land, East Greenland. Shaded relief image is of the Base Cretaceous, illustrating compaction drape over basin floor fans and feeder systems. Amplitude extraction is of events illustrated in the seismic line A–A′, of a comparable scale to 'gully sandstones' described by Surlyk (1987) in the Hareelv Formation of Jameson Land. Photograph courtesy of Finn Surlyk, seismic courtesy of Schlumberger.

Bio-stratigraphic data reveals that the Magnus sands were probably derived from a re-worked shallow marine section. In this respect they are analogous to the Cenozoic Hermod and Balder sands. These observations point towards a key control in delivery of sand to the basin floor in the absence of a significant, proximal first-order provenance, namely the oversupply of sand to the shelf and the collapse of shelf margin sequences to be re-deposited in deeper water, a mechanism similar to that already described in relation to the Eocene Balder Sand Formation of the UK Quad 9 area (see Figs 12 & 13, e.g. Jennette *et al.* 2000).

Comparing the Upper Jurassic of the Central Trough

The Fulmar and Ula Formations of the Upper Jurassic of the Central Trough (Fig. 16) are significant plays in the UK and Norwegian sectors respectively, and developed in shallow marine facies. They occur in fields in both deep graben settings, where the reservoirs are predominantly Oxfordian in age, and the marginal platforms, where they are largely Kimmeridgian to Volgian (e.g. Donovan *et al.* 1993; Partington *et al.* 1993; Wakefield *et al.* 1993; Jeremiah & Nicholson 1999; Fraser *et al.* 2003).

Although hydrocarbon-bearing deepwater equivalents have been encountered in the Oxfordian at the Jacqui discovery, Kimmeridgian at Shearwater, Erskine and Fulmar (the Ribble Member), and still younger at the Selkirk discovery, none are as significant as their counterparts in the Jurassic or Cenozoic sections in either the Central North Sea or elsewhere. Indeed, even comparing the Central North Sea Jurassic to the relatively minor Magnus play described above, there are no comparable occurrences of the seismic signatures associated with this fairway in the UK sector of the Central Trough. Consideration of the likely controlling mechanisms of these counterparts may point to an explanation of these significant differences.

Provenance/hinterland

Howell *et al.* (1996) offered a convincing account of the relationship between Fulmar Formation depocentres and the hinterland, with shoreface fairways forming at entry points in the relays in the graben system. This model offered a compelling fit with the recognition that the Oxfordian fairways were in turn located at the northern and southern limits of a series of en-echelon graben developing during the Oxfordian, with gradual retreat of these fairways away from the basin centres and ultimately onto the platforms in the Kimmeridgian (Erratt *et al.* 1999; Jeremiah & Nicholson 1999). Heavy mineral analysis of the Fulmar sands indicates a progressive un-roofing of the hinterland, with sediments derived from finer-grained and mixed lithologies in Triassic and Middle Jurassic sequences, indicating a less effective reservoir provenance than those feeding the South Viking Graben and Moray Firth systems.

Basin setting/response to sea-level

The early Oxfordian fairways are considered to have been deposited in a ramp-type setting. Fulmar sand reservoir log signatures are characteristically blocky, indicating deposition during relative sea-level lowstand conditions. The predominance of this log signature in the Fulmar Fm. suggests that much of the sediment deposited during the lowstands was in fact captured in the shallow marine shore-face realm, with relatively little by-pass to the offshore. Such a setting would be comparable to the Late Paleocene 'Hermod' system described earlier, in which sea-level falls result in large-scale exposure and incision of the shelf, with a basinward

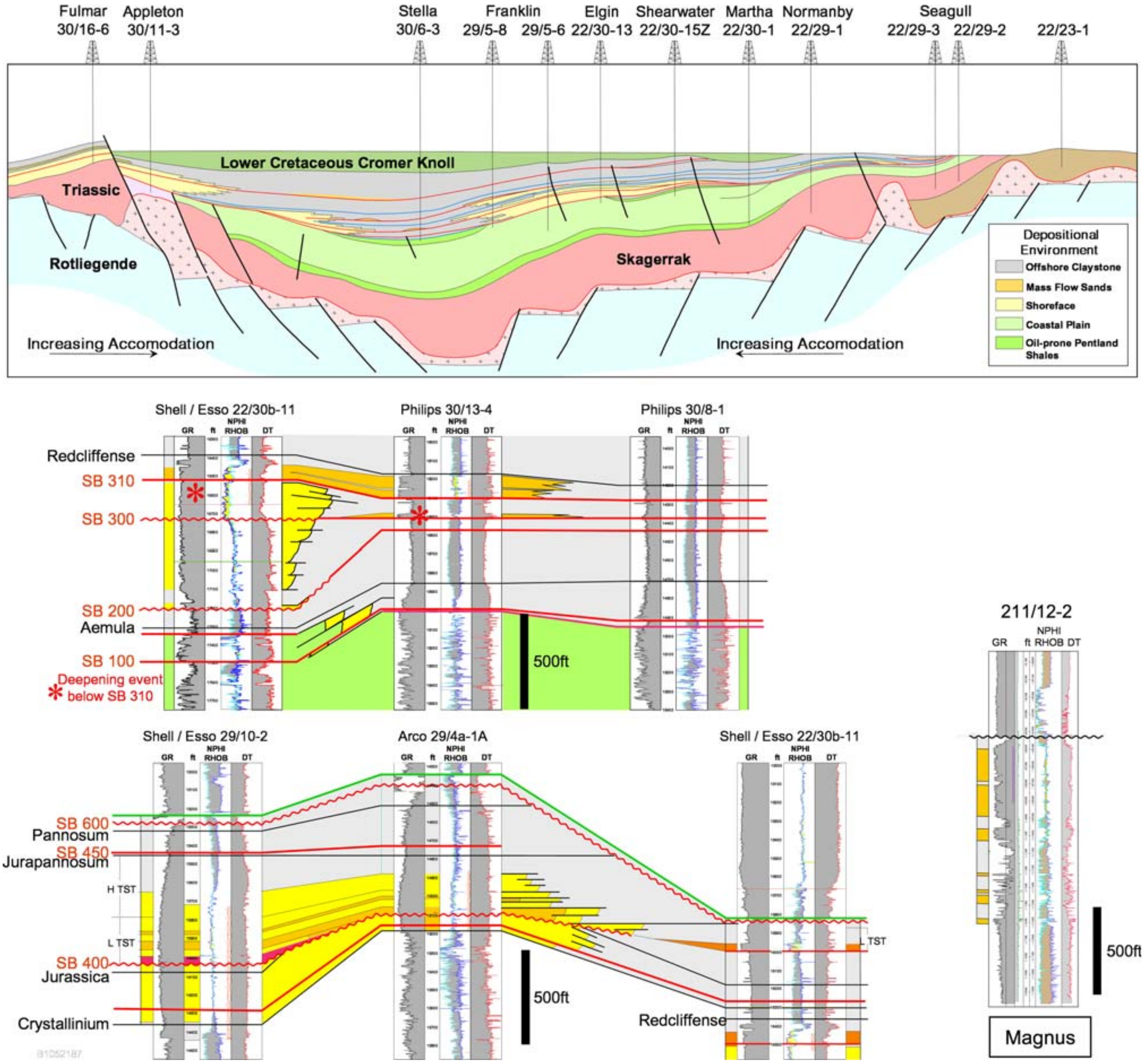

Fig. 16. Upper Jurassic deepwater reservoirs in the Central North Sea (well log sections after Jeremiah & Nicholson 1999). These reservoirs are relatively thin compared with their ESB counterparts (Magnus Field well log for comparison). Sands are likely to have remained stored in or close to the shallow marine environment in type 2 sequences, illustrated on the accompanying schematic cross-section (see also Fig. 13 for cross-reference to Cenozoic example.)

shift in facies above a 'Type 2 Unconformity' (Van Wagoner *et al.* 1990). Type 2 unconformities are considered to be typical of ramp-type shelf-basin transitions.

Basin architecture

The comparison of profiles from the Central Trough and South Viking Graben (Fig. 1) demonstrates a significant first-order difference in basin architectures, which, given that the Upper Jurassic is a syn-rift succession deposited during the formation of these basins, should be expected to have exerted a significant control on sediment dispersal and fairway development.

The South Viking Graben is essentially a single half-graben with the formation of one principal depocentre, with major footwall uplift across its main bounding fault resulting in significant erosion of the Palaeozoic floor of the rift, in this instance coincident with a Devonian basin containing the key first-order products of Caledonide denudation. The receiving basin is relatively narrow. This compares closely to the sub-basins of the Moray Firth, and both display significant vertical stacking of lowstand reservoirs (e.g. Partington *et al.* 1993; Fraser *et al.* 2003). Although lacking the spectacular half-graben geometry of the South Viking Graben, the Moray Firth benefits from close proximity to the Scottish mainland and significant sources of Palaeozoic sediments. By comparison with these close neighbours, the Central Trough comprises a number of smaller sub-basins. With extension effectively dissipated across a network of en-echelon bounding faults, the corresponding footwall uplift in these locations is reduced, such that occurrences of truncation sufficient to expose the Palaeozoic to erosion at these locations are relatively rare (e.g. Embla High adjacent to the Feda Graben).

The role of salt withdrawal

A further factor inhibiting the delivery of sand to deeper water environments may be salt withdrawal during the deposition of the Fulmar Fm. sequences, forming local sediment traps, thereby reducing the potential for sediment bypass.

Hydrocarbon systems

Comprehensive accounts of source rock development, maturation and migration appear in the Millennium Atlas (Kubala *et al.* 2003; Moss *et al.* 2003), and in particular, Cornford (1990). Relative to the fields of tectonics and reservoir stratigraphy, source rocks and the dynamic aspects of the North Sea hydrocarbon system were relatively under-represented in the early conferences, perhaps as a consequence of the realization that Kimmeridge Clay and its equivalent is a highly effective source rock throughout the basin (e.g. Barnard & Cooper 1981). This is not altogether surprising, since it is generally the case that, once proven, marine source rocks tend to be relatively widespread in lightly structured basins. Consequently, the search for new hydrocarbons in the maturing North Sea tended to focus on the search for new reservoir targets and subtle stratigraphic traps. By comparison with its NW European counterparts, the North Sea was already proven as a 'forgiving' hydrocarbon system with plays from the Palaeozoic to the Neogene.

The development of our predictive capabilities with regard to the more dynamic aspects of hydrocarbon systems, such as the maturation and migration of hydrocarbons, diagenesis and overpressure has, perhaps not surprisingly, tracked the development of computing technology in a fashion not dissimilar to the field of seismic technology.

As such it was only by the time of the fifth and sixth conferences in 1997 and 2003, well into the era of 3D seismic and routine, desk-top computer-based petroleum geoscience, that quantitative and computationally intensive basin modelling studies started to appear. [Compare the discussions of Fleet & Cordey (1993), Burley & Scotchman (1999) and Fries *et al.* (2005) from the fourth, fifth and sixth conference proceedings, respectively.] However two authors in particular, Goff (1983) and Cayley (1987), pre-empted this era with seminal papers on the maturation and migration of hydrocarbons in the Viking and Central Grabens, respectively. Cayley's paper drew attention to the dynamic aspects of the highly prospective multi-tiered hydrocarbon system of the Central North Sea, which by virtue of the development of drilling technology and demonstrated prospectivity in the deep overpressured parts of the graben (in contrast to the Northern North Sea), was taking exploration activity into the high pressure/high temperature domain (Erratt *et al.* 2005). This paper was the first to present a basin-wide map of overpressure at Cenozoic and Mesozoic levels, and ushered in a new generation of hydrocarbon system studies that addressed the important aspects of overpressure, top seal integrity and, most importantly, operational imperatives in this challenging subsurface environment. Gaarenstrom *et al.* (1993) built on the work of Cayley and his co-workers to provide an attempt at a quantitative analysis of top seal failure in the Central North Sea, a significant aspect of migration into Upper Cretaceous chalk reservoirs. This seal failure permitted formation of the vertical migration pathways, without which this locally prolific interval would have failed due to its normally poor regional horizontal permeability. As data quality and density increased, Cayley and Gaarenstrom's early maps gave way to more detailed descriptions of discrete pressure cells in the deep graben areas, with cell boundaries capable of leading to differences in overpressure of up to 2000 psi (e.g. Nicholson & Cayley 1998; Erratt *et al.* 2005; Winefield *et al.* 2005) (Fig. 17). On a first-order scale, the 'Golden Zone' concept of Nadeau *et al.* (2005) provides an integrated perspective on the temperature and pressure controls on the distribution of the bulk of the world's recoverable hydrocarbons. Meanwhile, in basins such as the North Sea where the, albeit relatively high-risk, high-pressure, domains remain prospective, predicting overpressure remains challenging, given the various contributing mechanisms in its generation: rapid Cenozoic burial, late gas generation and oil to gas cracking (Swarbrick *et al.* 2005). These factors, coupled with the limits to resolution in the mapping of the critical facies distributions and fault juxtaposition relationships, will continue to make overpressure prediction challenging, along with its dependent risks of top seal integrity and reservoir quality. Inevitably, studies in this realm have encapsulated efforts to predict the occurrence of the high-quality reservoirs at depths beyond those commonly encountered in the Northern North Sea and Moray Firth (see discussions in Fries *et al.* 2005, and Erratt *et al.* 2005). Here again, prediction remains challenging with the various controlling mechanisms operating across the scales from basin-wide (e.g. rapid Cenozoic burial leading to disequilibrium compaction; Moss *et al.* 2003; Jones *et al.* 2005) to pore-scale (chlorite and micro-crystalline quartz grain coats as inhibitors to quartz cementation; e.g. Paxton *et al.* 1995; Ajdukiewicz *et al.* 2001). Whilst the former might lend itself to some relatively high degree of predictability, the latter, being critically dependent on a detailed understanding of facies distributions, will remain a challenge in the face of insufficient well control or seismic resolution. Recent wells in the UK Central Trough have been at the limits of predictive capabilities with regards to pore pressure, deep reservoir quality and trap integrity (both with regards to top seal integrity and fault seal). Results in what is by now a mature exploration setting have been mixed, and these elements remain difficult to reliably predict. Erratt *et al.* (2005) and Winefield *et al.* (2005) presented the results of some of these wells with regards to top seal integrity.

A retrospective view of the petroleum geology of the North Sea

The ultimate goal in the exploration of conventional hydrocarbon resources in the subsurface is reliable remote sensing of hydrocarbons and the accurate estimation of their recoverable volumes. In the absence of reliable remote sensing either of hydrocarbons directly, or of any of the component parts of a working hydrocarbon system, we have to rely on forward models based on our understanding of the available data and the fundamentals of geology. The latter is largely dictated by the prevailing paradigms of the day. This is the wider context of any consideration of our progress in understanding the petroleum geology of the North Sea and in our predictive capabilities. It seems reasonable therefore to assess advances in the understanding of North Sea hydrocarbon systems in the context of three factors: data, technology and fundamental geological principles.

Two fundamental paradigm shifts in geological thought have broadly paralleled the exploration of the North Sea which dates from the early 1960s, namely plate tectonics and sequence stratigraphy. Plate tectonics provided a predictive framework for regional syntheses such as those of the Zieglers and their contemporaries, and set the stage for decades of constructive development of regional models and new play concepts. To appreciate the impact, one need look no further than the parallel and contemporaneous new models of the evolution of orogenic belts, and the revolution in thought (e.g. Dewey & Bird 1970) ushered in by plate tectonics. Furthermore, it provided a unifying framework within which the parallel disciplines of structural mapping and subsidence analysis would ultimately lead to predictive models of the evolution of heat flow through time (McKenzie 1978). These would in turn underpin the development of hydrocarbon system analysis and quantitative basin modelling.

In the fields of stratigraphy and sedimentology, the impacts of first seismic and subsequently sequence stratigraphy (Vail *et al.* 1977; Van Wagoner *et al.* 1990) were no less dramatic. These disciplines, again evolving in parallel with the exploration of the North

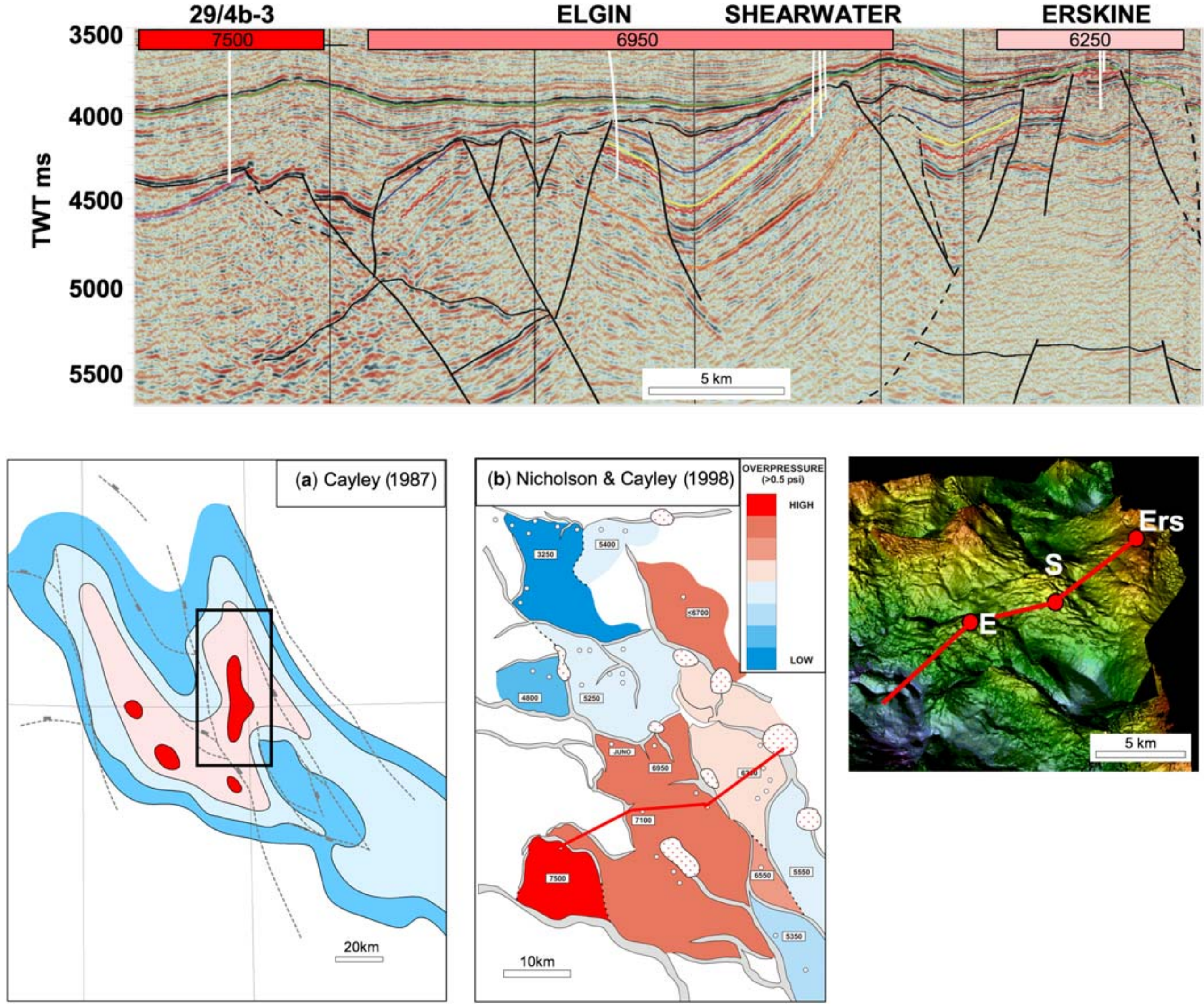

Fig. 17. Pressure distribution in the Central North Sea. Early mapping of pressure distribution (after Cayley 1987) based on 2D seismic, compared with Nicholson & Cayley's (1998) mapping based on closer well spacing and 3D seismic mapping (location shown on map **a**). The pressure cells are illustrated on the seismic traverse repeated from Figure 9.

Sea and the availability of increasingly high-resolution multi-channel seismic data, moved stratigraphy away from a largely descriptive discipline based on *ad hoc* local models towards a unifying, predictive theory. Despite early and widespread resistance, based largely around concerns that sequence stratigraphic models developed for the most part in the relatively unstructured Cretaceous Interior seaway of the USA were inappropriate in active rift settings, by the early 1990s and the fourth conference the discipline was firmly cemented at the core of North Sea geoscience (Donovan *et al.* 1993; Partington *et al.* 1993). Furthermore, seismic and sequence stratigraphy shifted the emphasis of stratigraphic and sedimentological research to outcrops that could be readily compared with standard seismic reflection data. This trend started in the Book Cliffs of Utah in the shallow marine domain and continued through to the Karoo Group of South Africa in deepwater settings. Importantly, Surlyk's work on North Sea analogues in East Greenland was a pioneering effort in this regard (Fig. 15).

With regards to technological advances, in the seismic realm the advent of multi-channel data, increasingly sophisticated processing algorithms, and ultimately of large-scale 3D surveys, have directly improved our ability to accurately describe and map stratigraphy and move structural analysis from the qualitative to quantitative. This transition has been driven to a great extent by advances in computing technology allowing the processing of huge seismic datasets. The same advances have facilitated the use of computationally intensive 3D basin modelling algorithms to enable prediction of the dynamic elements of the hydrocarbon system. All three subdisciplines – structural geology and tectonics, stratigraphy and sedimentology, and hydrocarbon systems analysis – have advanced on the back of regional-scale high-resolution subsurface imaging, to a degree unimaginable in the late 1970s and early 1980s. No less significant have been the advances in drilling technology that have enabled effective exploration and data gathering from high-pressure, high-temperature domains, largely off limits prior to the 1980s.

All of the advances described above pose the questions: 'What was the impact of these revolutions on the success or otherwise of the North Sea exploration venture?' and 'What are the implications for future exploration?' A review of the creaming curves presented by Vining *et al.* (2005) and Erratt *et al.* (2005) is an appropriate backdrop against which to address this question (Fig. 18). Removing the steep part of the curves prior to 1980

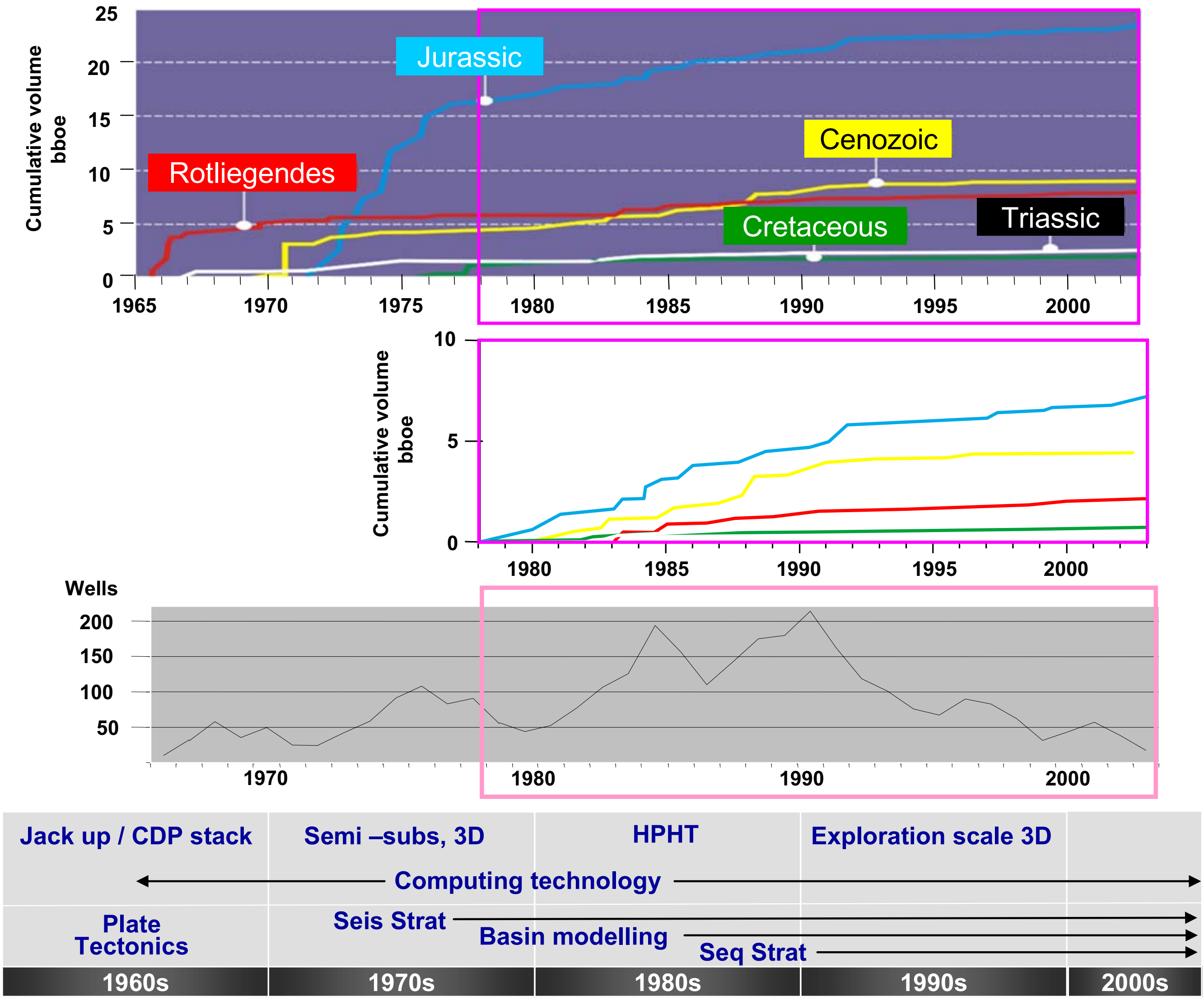

Fig. 18. Creaming curves (after Vining *et al.* 2005), drilling activity and milestones in geology and exploration technology. The arrested flattening of the Jurassic curve is illustrated by the expanded cumulative volume scale, and explained by high levels of activity in high pressure/high temperature domains. The approximate coincidental jump in the Cenozoic curve marks the discovery of the Nelson Field.

provides a more realistic perspective on the impact of these factors. Clearly, the breakthrough in high-pressure, high-temperature drilling technology opened up significant new fairways in the deep grabens. Intriguingly, most of the discoveries in this domain came before the advent of exploration-scale 3D seismic. Indeed, the significant impacts of the application of both 3D seismic data and sequence stratigraphy in the North Sea have tended to be in the production realm, with the widespread application of sequence stratigraphic techniques post-dating the bulk of the exploration success. It can be reasonably argued that in the 1980s and early 1990s, the advances in drilling technology in a forgiving hydrocarbon system were the trigger for any kick in the creaming curve. The historical tendency in the North Sea has been that readily identifiable structural traps are likely to be drilled, and, only after repeated failures with a clearly identifiable fatal flaw will structures in a trend remain undrilled (e.g. Triassic Smith Bank Pods on platform areas; Fig. 1). Stratigraphic trapping concepts have been and will continue to be pursued, especially when in the shallower, less operationally challenging subsurface environments. An example of such a play that indeed owed much to the availability of exploration-scale 3D is the Albo-Aptian Kopervik Sandstone trend of the Outer Moray Firth (Wilson *et al.* 2005). The value of reprocessing 3D data to help mature a sound geologically based play model was highlighted by Doré & Robbins (2005) on the Buzzard Field. It might be reasonably argued that the Alba/Chestnut Eocene discoveries would have been quickly revealed even on conventional low-fold 3D, and mapping of the play would not have been subject to the confusion that reigned following their discovery (see Bain 1993). However, the development of new trapping concepts in future will almost certainly depend heavily on continued improvements in seismic imaging technology, as will advances in basin modelling given its critical dependency on the fidelity of the input models.

On a concluding note, the impact of advances in technologies, data and paradigms, developed in part or in whole in the North Sea, is difficult to overestimate. The quality of North Sea datasets now widely available to both industry and academia alike is likely to keep the region at the forefront of geoscience research for the foreseeable future.

We would like to thank the management of ExxonMobil International Ltd and Shell UK for permission to publish this paper. Thanks to Graham Muckle and Finola Williams for assistance in drafting the figures, and Mike Thomas and Tom McKay for their constructive reviews of the paper.

References

Ajdukiewicz, J. M., Paxton, S. T., Jennette, D. C., Nicholson, P. H. & Erratt, D. 2001. Reservoir quality controls in the deep Fulmar Formation, Central North Sea. *In*: *Abstracts of the American Association of Petroleum Geologists Annual Convention, Denver 2001*.

Bain, J. S. 1993. Historical overview of exploration of Tertiary plays in the UK North Sea. *In*: Parker, J. R. (ed.) *Petroleum Geology of Northwest Europe: Proceedings of the 4th Conference*. Geological Society, London, 5–13; doi: 10.1144/0040005.

Barnard, P. C. & Cooper, B. S. 1981. Oils and source rocks of the North Sea area. *In*: Illing, L.V. & Hobson, G. D. (eds) *Petroleum Geology of the Continental Shelf of North-West Europe*. Heyden, London, 169–175.

Bartholomew, I. D., Peters, J. M. & Powell, C. M. 1993. Regional structural evolution of the North Sea, oblique slip and the reactivation of basement lineaments. *In*: Parker, J. R. (ed.) *Petroleum Geology of Northwest Europe: Proceedings of the 4th Conference*. Geological Society, London, 1109–1122; doi: 10.1144/0041109.

Beach, A. 1987. A regional model for linked tectonics in north-west Europe. *In*: Brooks, J. & Glennie, K. W. (eds) *Petroleum Geology of North West Europe*. Graham & Trotman, London, 43–48.

Brennand, T. P. 1975. The Triassic of the North Sea. *In*: Woodland, A. W. (ed.) *Petroleum and the Continental Shelf of North West Europe*. Applied Science, London, 285–310.

Brooks, J. & Glennie, K. W. (eds) 1987. *Petroleum Geology of North West Europe*. Graham & Trotman, London.

Burley, S. D. & Scotchman, I. C. 1999. Basin modelling applications in reducing risk and maximizing reserves. Introduction and review. *In*: Fleet, A. J. & Boldy, S. A. R. (eds) *Petroleum Geology of Northwest Europe: Proceedings of the 5th Conference*. Geological Society, London, 1309–1311; doi: 10.1144/0051309.

Cayley, G. T. 1987. Hydrocarbon migration in the Central North Sea. *In*: Brooks, J. & Glennie, K. W. (eds) *Petroleum Geology of North West Europe*. Graham & Trotman, London, 549–555.

Cornford, C. R. 1990. Source rocks and hydrocarbons of the North Sea. *In*: Glennie, K. W. (ed.) *Introduction to the Petroleum Geology of the North Sea*, 3rd edn. Blackwell Science, Oxford, 294–361.

Davies, R. J., O'Donnell, D. *et al*. 1999. The origin and genesis of major Jurassic unconformities within the triple junction area of the North Sea, UK. *In*: Fleet, A. J. & Boldy, S. A. R. (eds) *Petroleum Geology of Northwest Europe: Proceedings of the 5th Conference*. Geological Society, London, 117–132; doi: 10.1144/0050117.

De'Ath, N. G. & Schuyleman, S. F. 1981. The geology of the Magnus Oilfield. *In*: Illing, L. V. & Hobson, G. D. (eds) *Petroleum Geology of the Continental Shelf of North-West Europe*. Heyden, London, 342–351.

Dewey, J. F. & Bird, J. M. 1970. Mountain belts and the new global tectonics. *Journal of Geophysical Research*, **75**, 2625–2647.

Dixon, R. J. & Pearce, J. 1995. Tertiary sequence stratigraphy and play fairway definition, Bruce–Beryl Embayment, Quadrant 9, UKCS. *In*: Steel, R. J., Felt, V. L., Johannessen, E. P. & Mathieu, C. (eds) *Sequence Stratigraphy of the Northwest European Margin*. Norwegian Petroleum Society, Special Publications, **5**. Elsevier, Amsterdam, 443–469.

Donovan, A. D., Djakic, A. W., Ioannides, N. S., Garfield, T. R. & Jones, C. R. 1993. Sequence stratigraphic control on middle and upper Jurassic reservoir distribution within the UK Central North Sea. *In*: Parker, J. R. (ed.) *Petroleum Geology of Northwest Europe: Proceedings of the 4th Conference*. Geological Society, London, 251–269; doi: 10.1144/0040251.

Doré, G. & Robbins, J. 2005. The Buzzard Field. *In*: Doré, A. G. & Vining, B. A. (eds) *Petroleum Geology: North-West Europe and Global Perspectives – Proceedings of the 6th Petroleum Geology Conference*. Geological Society, London, 241–252; doi: 10.1144/0060241.

Doré, A. G. & Vining, B. A. (eds) 2005. *Petroleum Geology: North-West Europe and Global Perspectives – Proceedings of the 6th Petroleum Geology Conference*. Geological Society, London.

Doré, A. G., Lundin, E. R., Jensen, L. N., Birkeland, O., Eliassen, P. E. & Fichler, C. 1999. Principal tectonic events in the evolution of the northwest European Atlantic Margin. *In*: Fleet, A. J. & Boldy, S. A. R. (eds) *Petroleum Geology of Northwest Europe: Proceedings of the 5th Conference*. Geological Society, London, 41–61; doi: 10.1144/0050041.

Erratt, D. 1993. Relationships between basement faulting, salt withdrawal and Late Jurassic rifting, UK Central North Sea. *In*: Parker, J. R. (ed.) *Petroleum Geology of Northwest Europe: Proceedings of the 4th Conference*. Geological Society, London, 1211–1219; doi: 10.1144/0041219.

Erratt, D., Thomas, G. M. & Wall, G. R. T. 1999. The evolution of the Central North Sea Rift. *In*: Fleet, A. J. & Boldy, S. A. R. (eds) *Petroleum Geology of Northwest Europe: Proceedings of the 5th Conference*. Geological Society, London, 63–82; doi: 10.1144/0050063.

Erratt, D., Nicholson, P. H., Winefield, P., Milton-Worssell, R. J., Cayley, G. T. & Arter, G. 2005. Exploration history of the high-pressure, high-temperature plays: UK Central North Sea. *In*: Doré, A. G. & Vining, B. A. (eds) *Petroleum Geology: North-West Europe and Global Perspectives – Proceedings of the 6th Petroleum Geology Conference*. Geological Society, London, 253–267; doi: 10.1144/0060253.

Evans, D., Graham, C., Armour, A. & Bathurst, P. (eds) 2003. *The Millennium Atlas: Petroleum Geology of the Central and Northern North Sea*. Geological Society, London.

Fleet, A. J. & Boldy, S. A. R. (eds) 1999. *Petroleum Geology of Northwest Europe: Proceedings of the 5th Conference*. Geological Society, London.

Fleet, A. J. & Cordey, W. G. 1993. Fluids: migration, overpressure and diagenesis. Introduction and review. 1993. *In*: Parker, J. R. (ed.) *Petroleum Geology of Northwest Europe: Proceedings of the 4th Conference*. Geological Society, London, 1293; doi: 10.1144/0041293.

Fraser, S. I., Robinson, A. M. *et al*. 2003. Upper Jurassic. *In*: Evans, D., Graham, C., Armour, A. & Bathurst, P. (eds) *The Millennium Atlas: Petroleum Geology of the Central and Northern North Sea*. Geological Society, London, 157–189.

Fries, G., Nadeau, P. H. & Scotchman, I. C. 2005. Understanding petroleum systems: an overview. *In*: Doré, A. G. & Vining, B. A. (eds) *Petroleum Geology: North-West Europe and Global Perspectives – Proceedings of the 6th Petroleum Geology Conference*. Geological Society, London, 1235–1236; doi: 10.1144/0061235.

Gaarenstrom, L., Tromp, R. A. J., de Jong, M. C. & Brandenburg, A. M. 1993. Overpressure in the Central North Sea: implications for trap integrity and drilling safety. *In*: Parker, J. R. (ed.) *Petroleum Geology of Northwest Europe: Proceedings of the 4th Conference*. Geological Society, London, 1305–1313; doi: 10.1144/0041305.

Gibbs, A. D. 1984. Clyde Field secondary growth fault detachment above basement faults in North Sea. *AAPG Bulletin*, **68**, 1029–1039.

Gibbs, A. D. 1987. Deep seismic profiles in the northern North Sea. *In*: Brooks, J. & Glennie, K. W. (eds) *Petroleum Geology of North West Europe*. Graham & Trotman, London, 1025–1028.

Glennie, K. W. (ed.) 1998. *Petroleum Geology of the North Sea. Basic Concepts and Recent Advances*, 4th edn. Blackwell, Oxford.

Goff, J. C. 1983. Hydrocarbon generation and migration from Jurassic source rocks in the East Shetland Basin and Viking Graben of the northern North Sea. *Journal of the Geological Society of London*, **140**, 445–474.

Goldsmith, P. J., Rich, B. & Standring, J. 1995. Triassic correlation and stratigraphy in the South Central Graben, UK North Sea. *In*: Boldy, S. A. (ed.) *Permian and Triassic Rifting in Northwest Europe*. Geological Society, London, Special Publications, **91**, 123–143.

Goldsmith, P. J., Hudson, G. & Van Veen, P. 2003. Triassic. *In*: Evans, D., Graham, C., Armour, A. & Bathurst, P. (eds) *The Millennium Atlas: Petroleum Geology of the Central and Northern North Sea*. Geological Society, London, 105–207.

Helgeson, D. E. 1999. Structural development and trap formation in the Central North Sea HP/HT play. *In*: Fleet, A. J. & Boldy, S. A. R. (eds) *Petroleum Geology of Northwest Europe: Proceedings of the 5th Conference*. Geological Society, London, 1029–1034; doi: 10.1144/0051029.

Hibbert, M. J. & Mackertich, D. S. 1993. The structural evolution of the eastern end of the Halibut Horst, Block 15/21, Outer Moray Firth, UK North Sea. *In*: Parker, J. R. (ed.) *Petroleum Geology of Northwest Europe: Proceedings of the 4th Conference*. Geological Society, London, 1179–1188; doi: 10.1144/0041179.

Howell, J. A., Flint, S. S. & Hunt, C. 1996. Sedimentological aspects of the Humber Group (upper Jurassic) of the south Central Graben, UK North Sea. *Sedimentology*, **43**, 89–114.

Hurst, A., Cartwright, J. A., Duranti, D., Huuse, M. & Nelson, M. 2005. Sand injectites: an emerging global play in deep water clactic environments. *In*: Doré, A. G. & Vining, B. A. (eds) *Petroleum Geology: North-West Europe and Global Perspectives – Proceedings of the 6th Petroleum Geology Conference*. Geological Society, London, 133–144; doi: 10.1144/0060133.

Illing, L. V. & Hobson, G. D. (eds) 1981. *Petroleum Geology of the Continental Shelf of North-West Europe*. Heyden, London.

Jennette, D. C., Garfield, T. R., Mohrig, D. C. & Cayley, G. T. 2000. The interaction of shelf accommodation, sediment supply and sea level in controlling the facies, architecture and sequence stacking patterns of the Tay and Forties/Sele basin-floor fans, Central North Sea. *In*: Weimer, P., Slatt, R. M., Coleman, J., Rosen, R. C., Nelson, H., Bouma, A. H., Styzen, M. J. & Lawrence, D. T. (eds) *Deep Water Reservoirs of the World. Gulf Coast Section of the Society of Economic Palaeontologists and Mineralogists Foundation, 20th Annual Bob F. Perkins Research Conference*. Houston, TX.

Jeremiah, J. M. & Nicholson, P. H. 1999. Middle Oxfordian to Volgian sequence stratigraphy of the greater Shearwater area. *In*: Fleet, A. J. & Boldy, S. A. R. (eds) *Petroleum Geology of Northwest Europe: Proceedings of the 5th Conference*. Geological Society, London, 153–170; doi: 10.1144/0050153.

Jones, A. D., Auld, H. A., Carpenter, T. J., Fetkovitch, E., Palmer, I. A., Rigatos, E. N. & Thompson, M. W. 2005. Jade Field: an innovative approach to high-pressure, high temperature field development. *In*: Doré, A. G. & Vining, B. A. (eds) *Petroleum Geology: North-West Europe and Global Perspectives – Proceedings of the 6th Petroleum Geology Conference*. Geological Society, London, 269–283; doi: 10.1144/0060269.

Kubala, M., Bastow, M., Thompson, S., Scotchman, I. & Oygard, K. 2003. Geothermal regime, petroleum generation and migration. *In*: Evans, D., Graham, C., Armour, A. & Bathurst, P. (eds) *The Millennium Atlas: Petroleum Geology of the Central and Northern North Sea*. Geological Society, London, 289–315.

Kusznir, N. J. & Karner, G. D. 2007. Continental lithospheric thinning and breakup in response to upwelling divergent mantle flow: application to the Woodlark, Newfoundland and Iberia margins. *In*: Karner, G. D., Manatschal, G. & Pinheiro, L. M. (eds) *Imaging, Mapping, and Modelling Continental Lithosphere Thinning and Break up*. Geological Society, London, Special Publications, **282**, 389–419.

Kusznir, N. J., Marsden, G. & Egan, S. S. 1991. A flexural cantilever simple-shear/pure shear model of continental lithosphere extension: applications to the Jeanne d'Arc Basin, Grand Banks and Viking Graben, North Sea. *In*: Roberts, A. M., Yielding, G. & Freeman, B. (eds) *The Geometry of Normal Faults*. Geological Society, London, Special Publications, **56**, 41–60.

Lonergan, L., Lee, N., Johnson, H. D., Cartwright, J. A. & Jolly, R. J. H. 2000. Remobilization and injection in deepwater depositional systems: implications for reservoir architecture and prediction. *In*: Weimer, P., Slatt, R. M., Coleman, J., Rosen, R. C., Nelson, H., Bouma, A. H., Styzen, M. J. & Lawrence, D. T. (eds) *Deep Water Reservoirs of the World. Gulf Coast Section of the Society of Economic Palaeontologists and Mineralogists Foundation, 20th Annual Bob F. Perkins Research Conference*. Houston, TX.

MacGregor, A. G., Trussell, P., Lauver, S., Bedrock, M., Bryce, J. & Moulds, T. 2005. The Magnus Field: extending field life through good reservoir management and enhanced oil recovery. *In*: Doré, A. G. & Vining, B. A. (eds) *Petroleum Geology: North-West Europe and Global Perspectives – Proceedings of the 6th Petroleum Geology Conference*. Geological Society, London, 469–475; doi: 10.1144/0060469.

McGeary, S., Cheadle, M. J., Warner, M. R. & Blundell, D. J. 1987. Crustal structure of the continental shelf around Britain derived from BIRPS deep seismic profiling. *In*: Brooks, J. & Glennie, K. W. (eds) *Petroleum Geology of North West Europe*. Graham & Trotman, London, 33–41.

McKenzie, D. 1978. Some remarks on the development of sedimentary basins. *Earth and Planetary Science Letters*, **40**, 25–32.

McKie, T. & Audretsch, P. 2005. Depositional and structural controls on Triassic reservoir performance in the Heron cluster, ETAP, Central North Sea. *In*: Doré, A. G. & Vining, B. A. (eds) *Petroleum Geology: North-West Europe and Global Perspectives – Proceedings of the 6th Petroleum Geology Conference*. Geological Society, London, 285–298; doi: 10.1144/0060285.

Moss, B., Barson, D., Rakhit, K., Dennis, H. & Swarbrick, R. 2003. Formation pore pressures and formation waters. *In*: Evans, D., Graham, C., Armour, A. & Bathurst, P. (eds) *The Millennium Atlas: Petroleum Geology of the Central and Northern North Sea*. Geological Society, London, 317–329.

Nadeau, P. H., Bjorkum, P. A. & Walderhaug, O. 2005. Petroleum system analysis: impact of shale diagenesis on reservoir fluid pressure, hydrocarbon migration and biodegradation risks. *In*: Doré, A. G. & Vining, B. A. (eds) *Petroleum Geology: North-West Europe and Global Perspectives – Proceedings of the 6th Petroleum Geology Conference*. Geological Society, London, 1267–1274; doi: 10.1144/0061267.

Nicholson, P. H. & Cayley, G. T. 1998. Ultra high pressure: implications for prospectivity and drilling. *American Association of Petroleum Geologist Bulletin*, **82**, 1883–1984.

Parker, J. R. (ed.) 1993. *Petroleum Geology of Northwest Europe: Proceedings of the 4th Conference*. Geological Society, London.

Partington, M. A., Mitchener, B. C., Milton, N. J. & Fraser, A, J. 1993. Genetic sequence stratigraphy for the North Sea late Jurassic and early Cretaceous: distribution and prediction of Kimmeridgian–late Ryazanian reservoirs in the North Sea and adjacent areas. *In*: Parker, J. R. (ed.) *Petroleum Geology of Northwest Europe: Proceedings of the 4th Conference*. Geological Society, London, 371–386; doi: 10.1144/0040371.

Paxton, S. T., Wehr, F. L., Ajdukiewicz, J. M. & Cayley, G. T. 1995. Assessment of reservoir quality potential; a synthesis of observations from different geological settings. *In*: *AAPG 1995 Annual Convention*, Texas, Abstracts, AAPG Bulletin, **79**, 75.

Rattey, P. & Hayward, A. B. 1993. Sequence stratigraphy of a failed rift system: the middle Jurassic to early Cretaceous basin evolution of the Central and Northern North Sea. *In*: Parker, J. R. (ed.) *Petroleum Geology of Northwest Europe: Proceedings of the 4th Conference*. Geological Society, London, 215–249; doi: 10.1144/0040215.

Rawson, P. F. & Riley, L. A. 1982. Latest Jurassic–Early Cretaceous events and 'Late Cimmerian' in the North Sea area. *American Association of Petroleum Geologists Bulletin*, **66**, 2628–2648.

Roberts, A. M., Yielding, G. & Badley, M. 1990. A kinematic model for the orthogonal opening of the late Jurassic North Sea rift system. Denmark–Mid Norway. *In*: Blundell, D. J. & Gibbs, A. D. (eds) *Tectonic Evolution of the North Sea Rifts*. Oxford University Press, Oxford, 180–199.

Roberts, A. M., Yielding, G., Kusznir, N. J., Walker, I. & Dorn-Lopez, D. 1993. Mesozoic extension in the North Sea: constraints from flexural backstripping, forward modelling and fault populations. *In*: Parker, J. R. (ed.) *Petroleum Geology of Northwest Europe: Proceedings of the 4th Conference*. Geological Society, London, 1123–1136.

Sinclair, I. K., Shannon, P. M., Williams, B. P. J., Harker, S. R. & Moore, J. G. 1994. Tectonic control on sedimentary evolution of three North Atlantic borderland Mesozoic basins. *Basin Research*, **6**, 193–217.

Smith, R. L. 1987. The structural development of the Clyde field. *In*: Brooks, J. & Glennie, K. W. (eds) *Petroleum Geology of North West Europe*. Graham & Trotman, London, 523–531.

Stewart, I. J. 1993. Structural controls in the Late Jurassic age shelf system, Ula trend, Norwegian North Sea. *In*: Parker, J. R. (ed.) *Petroleum Geology of Northwest Europe: Proceedings of the 4th Conference*. Geological Society, London, 469–483; doi: 10.1144/0040469.

Stewart, S. A. & Clark, J. A. 1999. Impact of salt on the structure of the Central North Sea hydrocarbon fairways. *In*: Fleet, A. J. & Boldy, S. A. R. (eds) *Petroleum Geology of Northwest Europe: Proceedings of the 5th Conference*. Geological Society, London, 179–200; doi: 10.1144/0050179.

Surlyk 1987. Slope and Deep Shelf Gully Sandstones, Upper Jurassic, East Greenland. *American Association of Petroleum Geologists Bulletin*, **71**, 464–475.

Swarbrick, R. E., Seldon, B. & Mallon, A. J. 2005. Modelling the Central North Sea pressure history. *In*: Doré, A. G. & Vining, B. A. (eds) *Petroleum Geology: North-West Europe and Global Perspectives – Proceedings of the 6th Petroleum Geology Conference*. Geological Society, London, 1237–1245; doi: 10.1144/0061237.

Threlfall, W. H. 1981. Structural framework of the central and northern North Sea. *In*: Illing, L. V. & Hobson, G. D. (eds) *Petroleum Geology of the Continental Shelf of North-West Europe*. Heyden, London, 98–103.

Underhill, J. R. & Partington, M. A. 1993. Jurassic thermal doming and deflation in the North Sea: implications of the sequence stratigraphic evidence. *In*: Parker, J. R. (ed.) *Petroleum Geology of Northwest Europe: Proceedings of the 4th Conference*. Geological Society, London, 337–345; doi: 10.1144/0040337.

Vail, P. R. & Todd, R. G. 1981. Northern North Sea Jurassic unconformities, chronostratigraphy and sea-level changes from seismic stratigraphy. *In*: Illing, L. V. & Hobson, G. D. (eds) *Petroleum Geology of the Continental Shelf of North-West Europe*. Heyden, London, 216–235.

Vail, P. R., Mitchum, R. M., Jr. & Thompson, S., III 1977. Seismic stratigraphy and global changes of sea level from coastal onlap. *In*: Payton, C. E. (ed.) *Seismic Stratigraphy – Applications to Hydrocarbon Exploration*. American Association of Petroleum Geologists, Tulsa, OK, Memoirs, **26**, 63–81.

Van Wagoner, J. C., Mitchum, R. M., Campion, K. M. & Rahmanian, V. D. 1990. *Siliciclastic Sequence Stratigraphy in Well Logs, Cores, and Outcrops: Concepts for High Resolution Correlation of Time and Facies*. American Association of Petroleum Geologists, Tulsa, OK.

Vining, B. A., Mabillard, J. B. & Van Rijssen, P. 2005. UK North Sea exploration: a future? *In*: Doré, A. G. & Vining, B. A. (eds) *Petroleum Geology: North-West Europe and Global Perspectives – Proceedings of the 6th Petroleum Geology Conference*. Geological Society, London, 35–39; doi: 10.1144/0060035.

Wakefield, L. L., Droste, H., Giles, M. R. & Janssen, R. 1993. Late Jurassic plays along the western margin of the Central Graben. *In*: Parker, J. R. (ed.) *Petroleum Geology of Northwest Europe: Proceedings of the 4th Conference*. Geological Society, London, 459–468; doi: 10.1144/0040459.

Wernicke, B. 1985. Uniform sense simple shear of the continental lithosphere. *Canadian Journal of Earth Sciences*, **22**, 108–215.

Wilson, J., Wall, G., Kloosterman, H. J., Coney, D., Cayley, G., Walker, J. & Linskaill, C. 2005. The discovery of Goldeneye: Kopervik prospect and play mapping in the South Halibut of the Moray Firth. *In*: Doré, A. G. & Vining, B. A. (eds) *Petroleum Geology: North-West Europe and Global Perspectives – Proceedings of the 6th Petroleum Geology Conference*. Geological Society, London, 199–216; doi: 10.1144/0060199.

Winefield, P., Gilham, R. & Elsinger, R. 2005. Plumbing the depths of the Central Graben: towards an integrated pressure, fluid and charge model for the Central North Sea HPHT play. *In*: Doré, A. G. & Vining, B. A. (eds) *Petroleum Geology: North-West Europe and Global Perspectives – Proceedings of the 6th Petroleum Geology Conference*. Geological Society, London, 1301–1315; doi: 10.1144/0061301.

Woodland, A. W. (ed.) 1975. *Petroleum and the Continental Shelf of North-West Europe*. Applied Science, London.

Zanella, E., Coward, M. P. & McGrandle, A. 2003. Crustal structure. *In*: Evans, D., Graham, C., Armour, A. & Bathurst, P. (eds) *The Millennium Atlas: Petroleum Geology of the Central and Northern North Sea*. Geological Society, London, 35–43.

Ziegler, P. A. 1975*a*. North Sea Basin history in the tectonic framework of North-Western Europe. *In*: Woodland, A. W. (ed.) *Petroleum and the Continental Shelf of North-West Europe*. Applied Science, London, 131–148.

Ziegler, W. H. 1975*b*. Outline of the geological history of the North Sea. *In*: Woodland, A. W. (ed.) *Petroleum and the Continental Shelf of North-West Europe*. Applied Science, London, 165–187.

Ziegler, P. A. 1981. Evolution of sedimentary basins in North-west Europe. *In*: Illing, L. V. & Hobson, G. D. (eds) *Petroleum Geology of the Continental Shelf of North-West Europe*. Heyden, London, 1–39.

Ziegler, P. A. 1983. Discussion on: Crustal thinning and subsidence in the North Sea. *Nature*, **304**, 561.

The search for a Carboniferous petroleum system beneath the Central North Sea

R. MILTON-WORSSELL,[1] K. SMITH,[2] A. MCGRANDLE,[3] J. WATSON[3] and D. CAMERON[2]

[1]*Department of Energy and Climate Change, 3 Whitehall Place, London SW1A 2HD, UK (e-mail: Richard.Milton-Worssell@decc.gsi.gov.uk)*
[2]*British Geological Survey, Murchison House, West Mains Road, Edinburgh EH9 3LA, UK*
[3]*ARKeX Ltd., 1 Mercers Manor Barns, Sherington, Newport Pagnell MK16 9PU, UK*

Abstract: This paper integrates interpretations of modern long-offset seismic datasets with potential field anomalies derived from dense grids of 2D gravity and magnetic data to present a regional-scale synthesis of Devonian, Carboniferous and Early Permian basin development beneath the UK Central North Sea. The 95 000 km^2 study area has had little modern exploration for petroleum systems beneath the Upper Permian. Seismic interpretation and potential field modelling confirm that along the southern fringe of the Central North Sea, as in northern England, Lower Carboniferous basin development was strongly influenced by the disposition of granite-cored Lower Palaeozoic basement blocks – Farne Block, Dogger Block and Devil's Hole High. This study adds a previously unidentified WNW–ESE trending pre-Devonian basement block, the Auk–Flora Ridge, that exerted a profound control on Late Devonian to Mesozoic structural evolution of the south-Central North Sea. From the Flora Field, where it is overlain by relatively thick mid-Devonian to earliest Permian strata, the sub-Permian relief of this block becomes progressively shallower towards the NW. On its southern flank lies a parallel half-graben, akin to the Stainmore Trough in northern England, and interpreted as also containing several thousand feet of Lower Carboniferous strata. As indicated by the coal measures section in well 39/7-1, these strata are likely to include prolific source rocks, which have been modelled as being fully mature for oil generation in Quadrant 29. Potential field modelling extends this interpretation beyond the current seismic coverage, and suggests that Carboniferous to earliest Permian basin development in the Central North Sea was strongly influenced by an underlying Scottish–Norwegian SW–NE trending Caledonoid structural fabric. An earliest Permian, Lower Rotliegend unit thickens southwards towards the Auk–Flora Ridge, and rests unconformably on one or more undrilled NE–SW trending Carboniferous basins. Red-bed fluvial facies akin to those at Flora are likely to dominate the substantial post-Dinantian fill of these basins, but significant thicknesses of Westphalian coal-measure source rocks may also be present locally. As in central Scotland, the Dinantian strata underlying a widespread mid-Carboniferous unconformity in these basins are likely to contain further coal-measure intervals and local developments of oil-shale source rocks. These Westphalian and Dinantian source rocks are key elements of a Carboniferous petroleum system that remains largely untested across large areas of the Central North Sea.

Keywords: Central North Sea, Devonian, Carboniferous petroleum system, Rotliegendes, basin morphology, potential field modelling

This paper presents a regional-scale synthesis of Devonian to Early Permian basin development beneath the UK Central North Sea. The Carboniferous of the Central North Sea is one of the last remaining underexplored play fairways on the UK North Sea. It has been probed by only 25 exploration wells, of which 11 confirmed the potential for source rock intervals within both Dinantian and Westphalian-age coal measures. Until the recent advent of long-offset seismic data acquisition, it has remained poorly imaged on conventional seismic data. Nevertheless, an Exploration of Unproven Plays study (Hay *et al.* 2005) highlighted the possibility for expulsion of significant volumes of gas from these coal measures, where mature, into intra-Carboniferous, Lower Permian and Mesozoic traps remote from the traditional Central Graben Jurassic source kitchen. This hypothesis is supported by their recognition of prominent gas chimneys in the Mesozoic and Cenozoic strata of southern Quadrant 29 (Fig. 1), up to 50 km SW of the Jurassic source kitchen, but directly overlying a Dinantian coal-measure basin interpreted by Hay *et al.* (2005) and modelled by them as being fully mature for gas generation.

This study is based on interpretation of modern long-offset 2D and 3D seismic data of 2003–2008 vintage (Fig. 1), tied to the 117 wells that have drilled through the base of the Permian, and integrated with and validated by 3D inversion of potential field anomalies derived from dense grids of BGS and government-released industry 2D gravity and magnetic data. The interpretation of pre-Permian basin morphology has been made largely by analogy with the structural framework of the equivalent, more clearly imaged strata in onshore Britain. In England, the Carboniferous strata are now known to be disposed about a mosaic of clearly defined ramps, tilted blocks and half-graben structures (Grayson & Oldham 1987; Kirby *et al.* 1987; Smith & Smith 1989; Fraser & Gawthorpe 1990; Fraser *et al.* 1990). By contrast, the Midland Valley of Scotland was a tectonically complex area of Late Palaeozoic rifting, strike-slip faulting and prolonged volcanism (Ritchie *et al.* 2003).

Sub-Zechstein well sections

Unlike in onshore England and the Southern North Sea, the majority of deep Central North Sea wells have proved Upper Devonian continental red-bed facies rather than Carboniferous strata directly beneath a regional base Permian unconformity. We acknowledge that Upper Devonian and Late Carboniferous red-bed sections are not easily distinguished in all wells. Thirty-four of the interpreted Upper Devonian well penetrations are near or beneath the Auk and Argyll oil fields in the south of Quadrant 30 (Fig. 2). Six wells in this area proved Middle Devonian shallow-marine limestones, evaporites and mudstones of the Kyle Group,

VINING, B. A. & PICKERING, S. C. (eds) *Petroleum Geology: From Mature Basins to New Frontiers – Proceedings of the 7th Petroleum Geology Conference*, 57–75. DOI: 10.1144/0070057

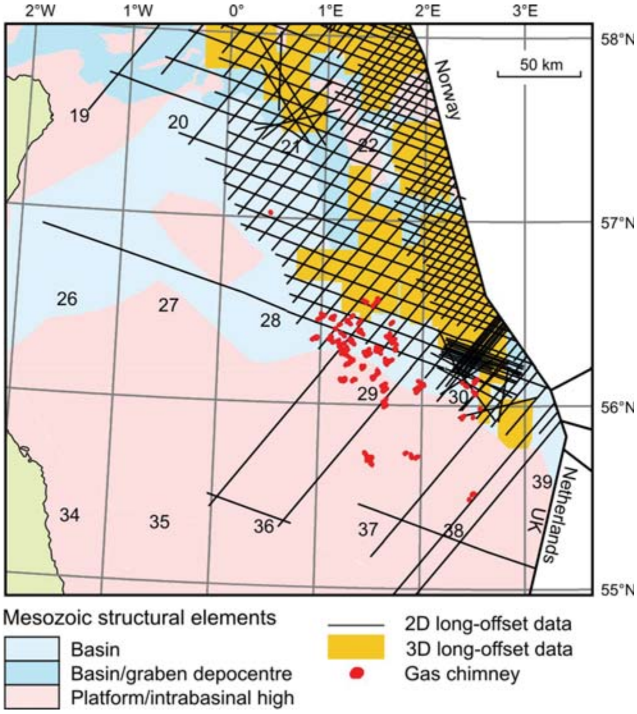

Fig. 1. Location of long-offset seismic data used in the study and of gas chimneys mapped in the Cenozoic section by Hay *et al.* (2005).

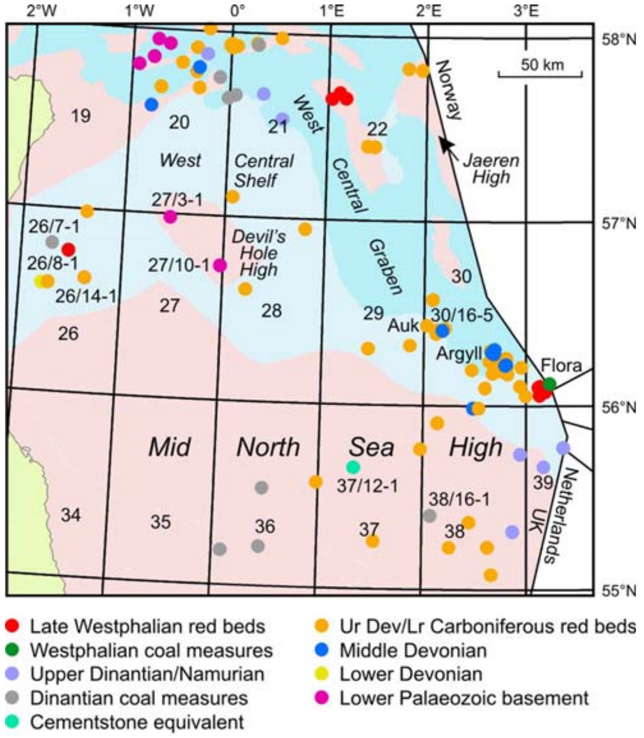

Fig. 2. Pre-Permian stratigraphy recorded in Central North Sea wells (Mesozoic structural elements as in Fig. 1).

subcropping the base Permian unconformity in four wells and lying below the Upper Devonian in two. Key well 30/16-5 (Fig. 2) drilled through the base of the Middle Devonian strata into mildly metamorphosed Lower Palaeozoic basement of Scottish Southern Uplands affinity. A summary of Permian and pre-Permian lithostratigraphy and of potential source rock and reservoir intervals in the region is shown in Figure 3. Initial indications from the well data are that pre-Middle Devonian strata may rise to relatively shallow levels beneath much of the Auk–Argyll region.

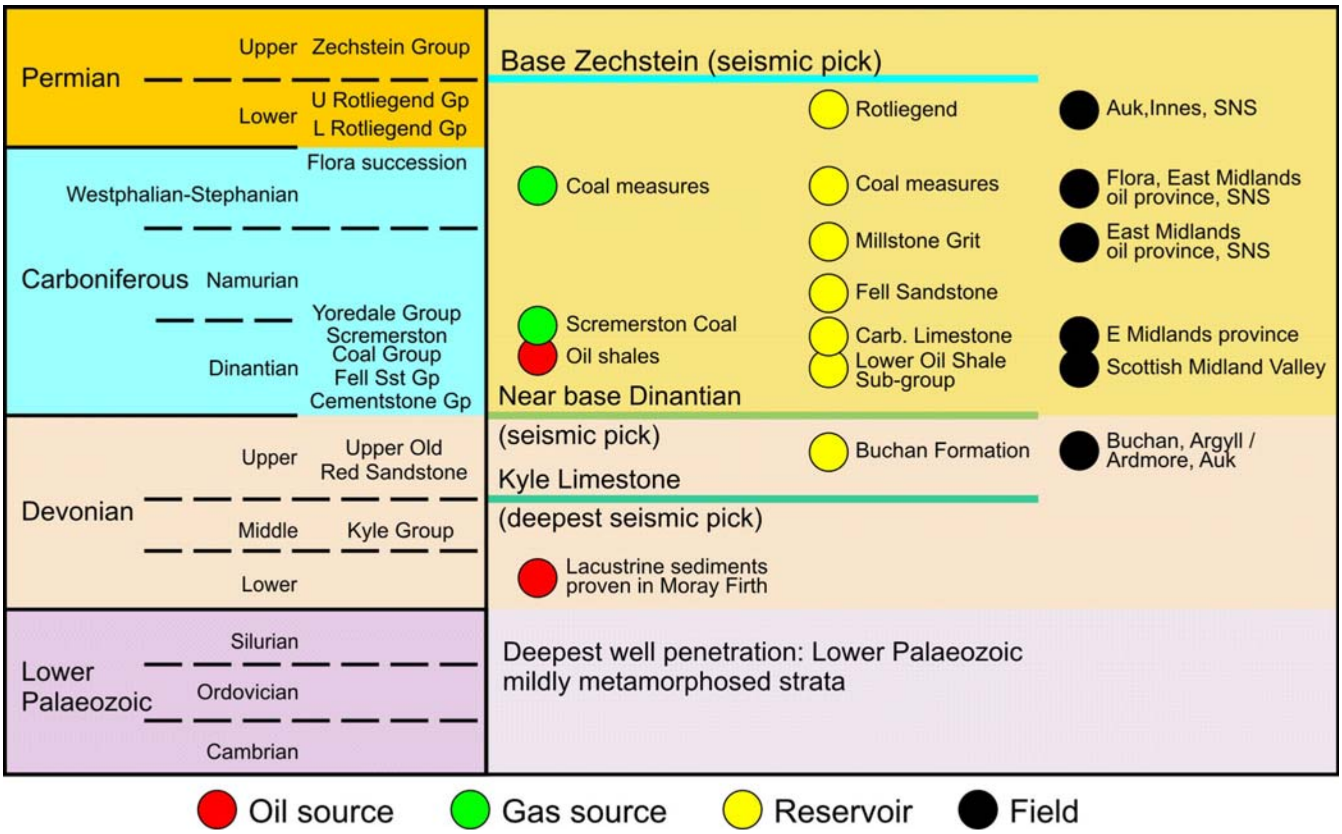

Fig. 3. Summary of Permian and pre-Permian lithostratigraphy and of potential source rock and reservoir succession in the region. The lithostratigraphy is after Cameron (1993*a*, *b*).

Drilling has revealed that the Mid North Sea High was not a uniformly positive feature in Carboniferous times. Directly beneath the Permian, nine of its wells proved Upper Devonian strata, whereas another five wells encountered Lower Carboniferous strata of Northumberland Trough affinity (Fig. 2). These wells include 37/12-1, which drilled 476 m of unfossiliferous mudstones, limestones and minor anhydrites in a succession resembling the largely Courceyan (Tournaisian)-age Cementstone Group in Northumberland. The three wells in Quadrant 36 and well 38/16-1 drilled Dinantian strata, including coal measures, which we correlate with Northumberland's Scremerston Coal Group.

In and adjacent to the Flora Field on the eastern fringes of the Mid North Sea High, six wells have provided key information on Upper Carboniferous to Lower Permian stratigraphic relationships. Westphalian B to Stephanian age Lower and Upper Flora Sandstone units here (Fig. 3) are separated by a Lower Volcanic unit, 250 m thick in Flora well 31/26a-12. The sandstone units show close lithological affinity to Late Westphalian red-bed sequences in the Southern North Sea (Martin *et al.* 2002). These strata are unconformably overlain by an argillaceous Grensen Formation and an Upper Volcanic unit, radiometrically dated as Stephanian or Asselian (basal Permian) in age. Correlated by Martin *et al.* (2002) with the Lower Rotliegend Group of onshore Europe, these strata have no equivalents in the UK Southern North Sea. Hence two regional base Upper Rotliegend Group (base Auk Formation equivalent) and base Lower Rotliegend Group unconformities are represented in these wells. The extent of the latter unconformity and of the Lower Rotliegend Group in the Central North Sea has been poorly reported up to now.

The Devil's Hole High wells 27/3-1 and 27/10-1, along with well 26/14-1, terminated in Lower Palaeozoic mildly metamorphosed basement. Well 26/7-1 drilled 1090 m of Holkerian to Chadian-age Lower Carboniferous coal measures that have closer affinity with equivalent sediments in the Midland Valley of Scotland than with the Scremerston Coal Group of the Northumberland Trough. In nearby well 26/8-1 these coal measures and the Lower Permian Auk Formation are separated by 899 m of dominantly arenaceous red beds. At least the lowest 306 m of these red beds were ascribed to the Westphalian. If correct, this provides the possibility for another significant unconformity within the Carboniferous section that is perhaps equivalent to the unconformity separating Late Namurian and younger from Early Namurian and older strata in the Midland Valley of Scotland.

Four wells in the NW of Quadrant 20 proved shallow-buried Caledonian granite beneath the base of the Permian. Remaining wells in this region record a progression from Late Devonian to earliest Carboniferous continental red-bed facies (Buchan Formation) through a transitional unit comprising cyclic alternations of sandstone and mudstone units (Tayport Formation) to Dinantian coal measures (Firth Coal Formation). The boundaries between these units are demonstrably diachronous (Cameron 1993*a*, *b*), suggesting that palaeorelief may have influenced facies development at least in this region during early Carboniferous times.

Seismic interpretation

In the Central North Sea the quality of information on sub-Zechstein geology that can be derived from seismic interpretation is influenced strongly by the structural complexity of its Zechstein to Cenozoic overburden. The information is best imaged on seismic profiles in the Auk–Argyll area, where the top of the Middle Devonian Kyle Limestone forms a conspicuous, high-amplitude and continuous reflector between and beyond the six wells that have drilled this unit. To the north, the Forties–Montrose High and Jaeren High provide windows of good-quality sub-Zechstein information also, showing many features in common with the Auk–Argyll area, but with limited well control. By contrast, the seismic data yield little or no information on the Middle Devonian to Lower Permian section beneath the Mesozoic Central Graben of the North Sea, but this section is inferred to have undergone significant stretching during creation of the Graben in any case.

Beyond the limit of the Kyle Limestone reflector, the seismic interpretation of Lower Carboniferous strata relies heavily on comparison of seismic facies with the equivalent drilled strata on the southern flank of the Mid North Sea High and in the Northumberland Trough in northern England (Chadwick *et al.* 1995). This is necessary because of the scarcity of deep Carboniferous wells in the Central North Sea. The deepest reliable reflector in this region has been taken by analogy with the Northumberland Trough as representing the downward transition from Late Devonian continental red-bed deposits to Early Dinantian Cementstone Group-equivalent strata and labelled as near base Dinantian. Two relatively transparent and stripey reflector packages above this have been interpreted as probably equivalent to the Fell Sandstone Group and Scremerston Coal Group of the Northumberland Trough, respectively, and their boundary picked as a mid-Dinantian event. The areas in which Kyle Limestone and intra-Dinantian reflectors have been picked are not mutually exclusive. Nevertheless, on Figure 4 the isopachs from the base of the Zechstein to near base Dinantian reflector provide a first impression of the potential thickness of Middle Devonian to Lower Permian strata

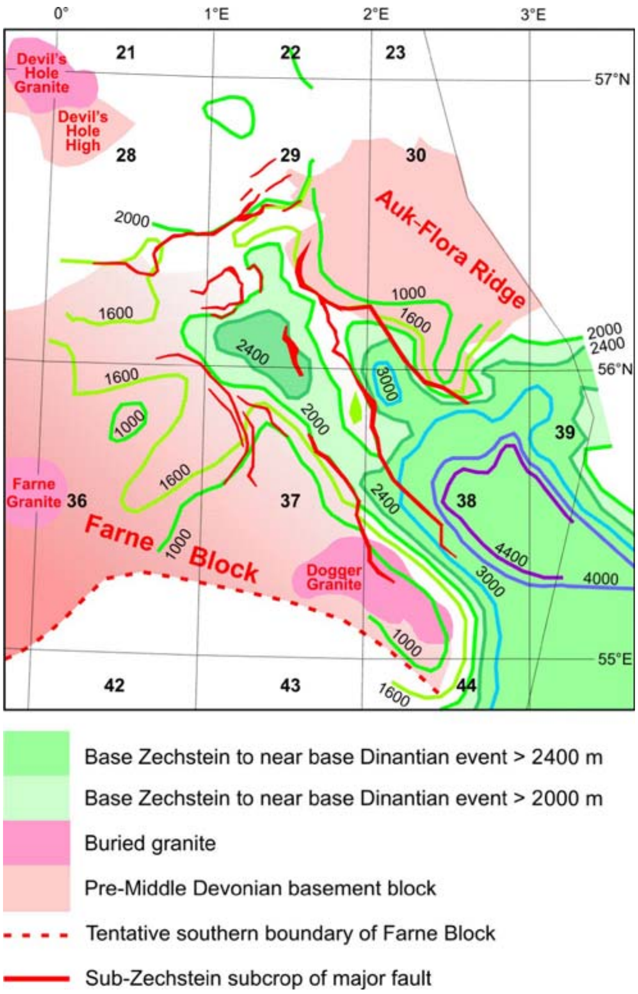

Fig. 4. Approximate thickness of pre-Zechstein Upper Palaeozoic (base Zechstein Group to near base Dinantian); isochrons converted to thickness assuming a standard interval velocity of 4 km s^{-1}.

in the region, as derived from the seismic interpretation. In the following sections we describe key long-offset seismic profiles and link them to known onshore geological analogues.

Sub-Zechstein seismo-stratigraphic relationships in the Auk–Argyll–Flora area

All of the principal sub-Zechstein stratigraphic relationships of the Central North Sea can be observed on seismic profiles from between the Auk and Flora oil fields. On Figure 5, acquired close to the west of the Flora Field, a prominent deep reflector that correlates with the drilled Middle Devonian Kyle Limestone at the Argyll Field is overlain successively by seismic units correlated with continental red-bed facies of the Upper Old Red Sandstone and overlying Cementstone Group and Fell Sandstone Group. Another prominent mid-Dinantian reflector is correlated with the base of the Scremerston Coal Group equivalent coal measures, which were drilled nearby in well 39/7-1. A regional mid-Carboniferous unconformity separates remaining Dinantian to early Namurian strata from an overlying succession that includes the Westphalian A coal measures drilled in well 31/27-1 and the Late Westphalian to Stephanian red-bed and volcanic units proved at the Flora Field. In structural terms, the relatively simple relationships depicted on this profile are broadly comparable with the east Pennine Basin of eastern England, in which thick sections of Upper Carboniferous strata are preserved in broad, open gently synclinal features.

The whole of this sub-Permian section is strongly condensed on a second example seismic profile (Fig. 6), located north of the previous example west-northwestwards towards the Auk Field. The entire Dinantian section is missing, with Upper Devonian continental red-bed facies subcropping the mid-Carboniferous unconformity on this profile. Upper Carboniferous strata are also completely eroded beneath the base Permian unconformity along much of its length. The Middle Devonian Kyle Limestone is at relatively shallow depths beneath the Permian, and it becomes even shallower to come close to subcropping the base of the Permian in nearby Auk Field well 30/16-5 (Trewin *et al.* 2003). Lower Palaeozoic strata of Southern Uplands affinity have been drilled in the same well, indicating that the seismic profile depicts part of an uplifted block of pre-Middle Devonian basement, which we term the Auk–Flora Ridge. Comparable uplifted blocks overlain by deeply eroded Upper Devonian and/or Carboniferous strata are widespread in onshore Britain, and include the Pentland Hills Inlier in the Midland Valley of Scotland and the Southern Uplands Lower Palaeozoic massif. Comparable English uplifted Lower Palaeozoic basement blocks include the Cross Fell Inlier alongside the Alston Block and parts of the East Midlands, where some Carboniferous anticlines are underlain by uplifted Lower Palaeozoic basement blocks.

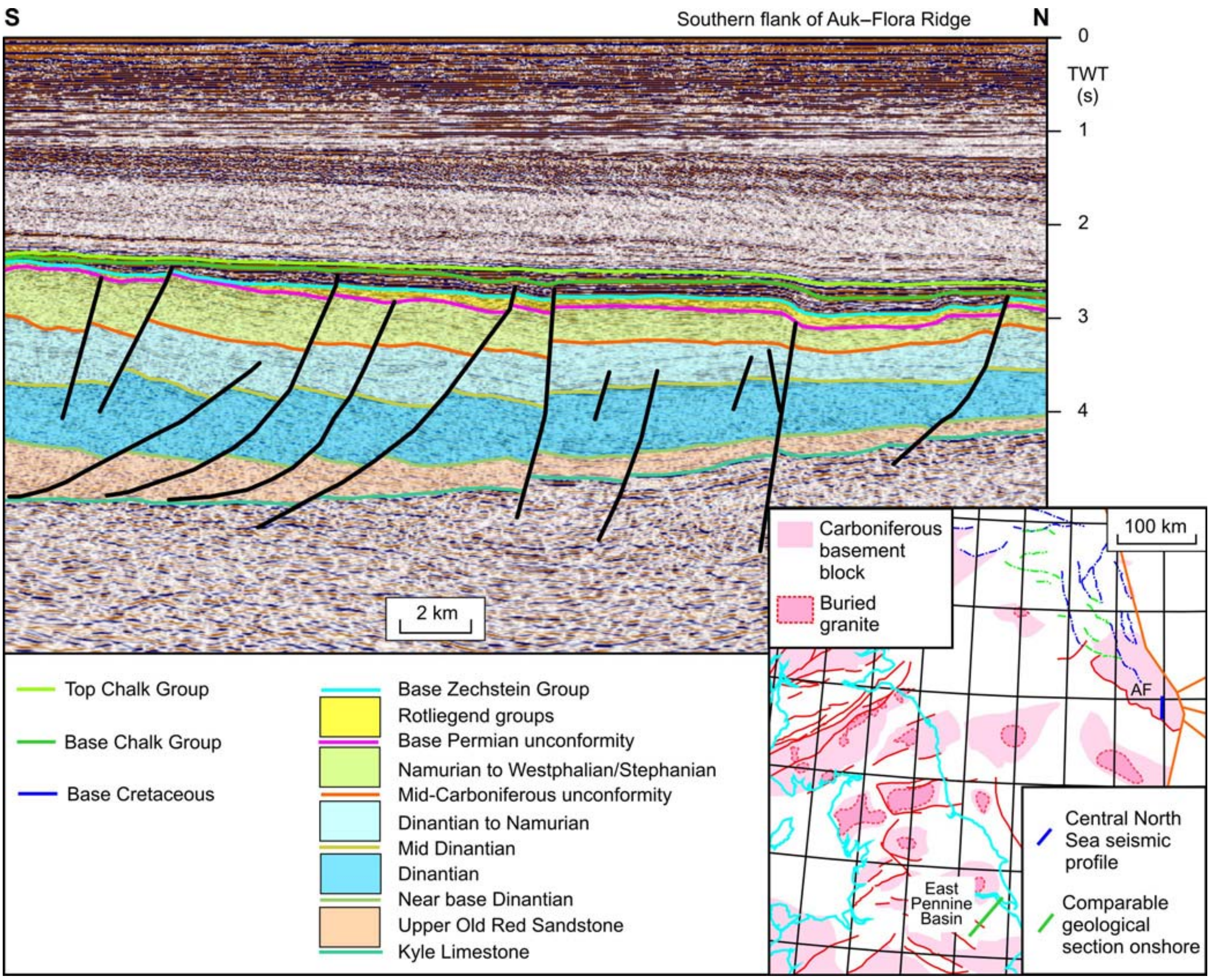

Fig. 5. Interpretation of example seismic profile from the southern flank of the Auk–Flora Ridge (AF); data courtesy of CGGVeritas.

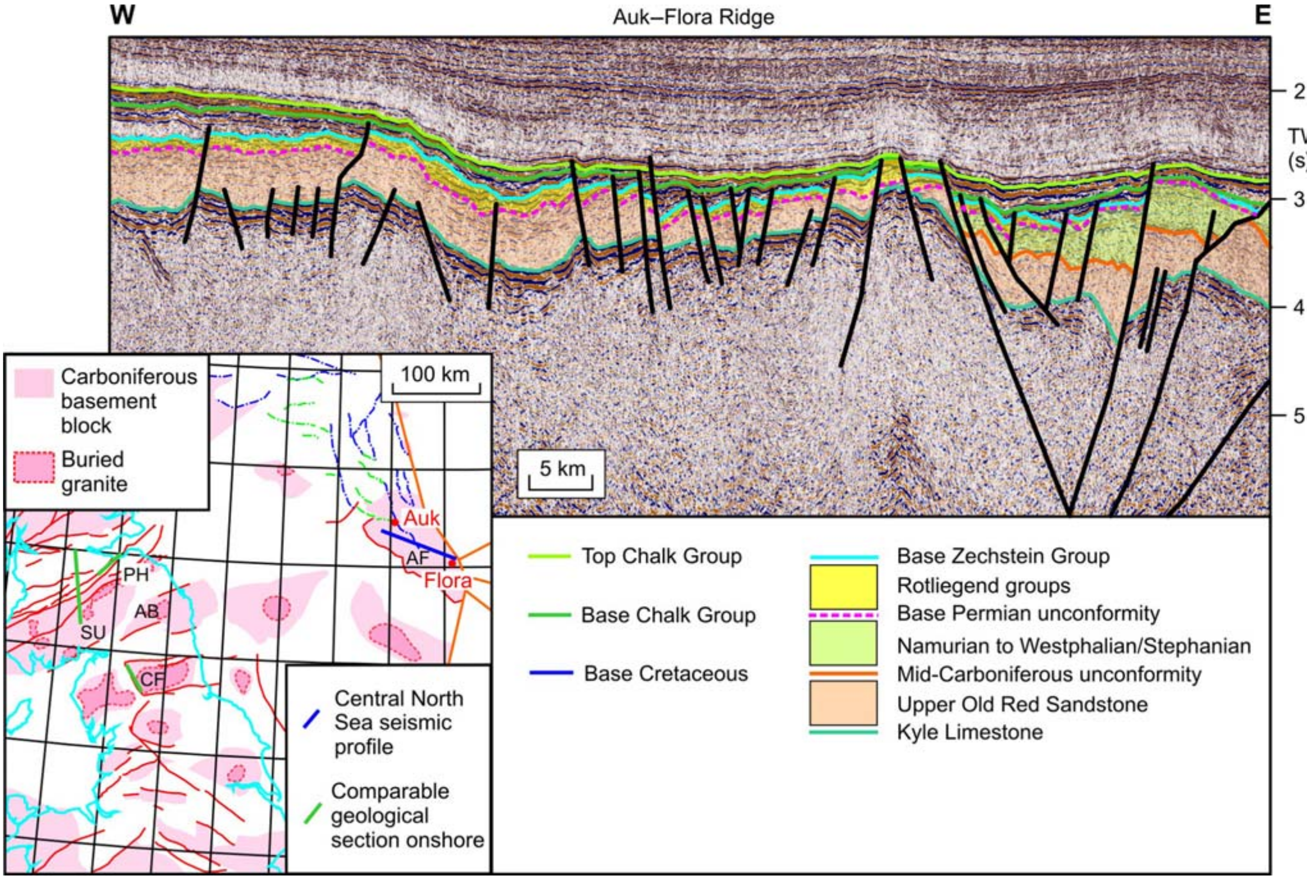

Fig. 6. Interpretation of example seismic profile along the crest of the Auk–Flora Ridge (AF); data courtesy of TGS NOPEC Geophysical Co. (UK) Ltd. PH, Pentland Hills Inlier; SU, Southern Uplands; AB, Alston Block; CF, Cross Fell Inlier.

All of the onshore examples of Lower Palaeozoic basement blocks are bounded by one or more prominent oblique-slip, reverse or normal fault systems (e.g. Askrigg Block, Underhill *et al.* 1988; East Midlands, Smith *et al.* 2005), and there is evidence on the seismic profile shown on Figure 7 that the northern flank of the Auk–Flora Ridge is also delimited by a major reverse fault system. The Auk–Flora Ridge is represented by the seismically transparent sub-Rotliegend feature in the southern third of this profile, and is interpreted to be composed largely or entirely of pre-Middle Devonian basement here. This pre-Middle Devonian basement block is cut in the south by the boundary fault of the Mesozoic West Central Graben, which has a substantially thicker Lower Permian section preserved on its hanging wall. At the intra-grabenal high near the centre of the profile this Lower Permian section can be divided by a prominent reflector into seismic units that most likely correlate with the Upper and Lower Rotliegend units of the Flora area. Our interpretation suggests that this intra-grabenal high lies near the depocentre for the combined Upper and Lower Rotliegend units in the Central North Sea.

The reflective section beneath the intra-grabenal high on the same profile (Fig. 7) appears to extend to the northern boundary fault of the Auk–Flora Ridge, and has been interpreted by analogy with seismic facies in the Southern North Sea and Northumberland Trough to include folded Dinantian strata that are absent over the crest of the Ridge. High-amplitude events deeper in the section are perhaps imaging igneous intrusives such as those modelled in this area by Lyngsie & Thybo (2007). Local reduction in thickness of and unconformable relationships between the Upper Cretaceous Hod and Tor formations directly above the Auk–Flora Ridge boundary fault system (S. J. Stoker, pers. comm.) suggest a component of subsequent reverse reactivation in its movement history.

Sub-Zechstein seismo-stratigraphic relationships in the Mid North Sea high area

On the southern flank of the Auk–Flora Ridge (Figs 4 & 8), there is compelling evidence for the preservation of up to 5.5 km of Upper Devonian to Dinantian strata in an approximately half-graben feature within what is conventionally regarded as the Mid North Sea High. This conclusively demonstrates that the Mid North Sea High is at least in part a post-Carboniferous feature. Notably, the fill of this basin could potentially include a significant thickness of Scremerston Coal Group-equivalent gas-prone source rocks, although thermal modelling (Hay *et al.* 2005) suggests that such may be only marginally mature here. Below these, its fill also includes a unit of high-amplitude reflections similar to that equated by Chadwick *et al.* (1995) with an anhydrite-rich sabkha interval of earliest Dinantian age within the Northumberland Trough in northern England. Notably, the interval above these high-amplitude reflections appears to thicken onto the hanging walls of the half-graben controlling faults, suggesting an element of rifting in this early Carboniferous basin, perhaps of broadly comparable age to active pre-Asbian faulting recorded in the east Pennine area by Fraser & Gawthorpe (1990).

The southern flank of this Upper Devonian to Dinantian basin is constrained by a prominent Lower Palaeozoic basement block that was structurally elevated persistently through Carboniferous times. Our potential field modelling confirms and refines the interpretation by Donato *et al.* (1983) that this Lower Palaeozoic basement block contains a Caledonoid granite core. Comparable granite-cored Lower Palaeozoic basement blocks in England include the Askrigg Block; hence the half-graben on the profile can be regarded as an analogue of the early Carboniferous Stainmore Trough of northern England.

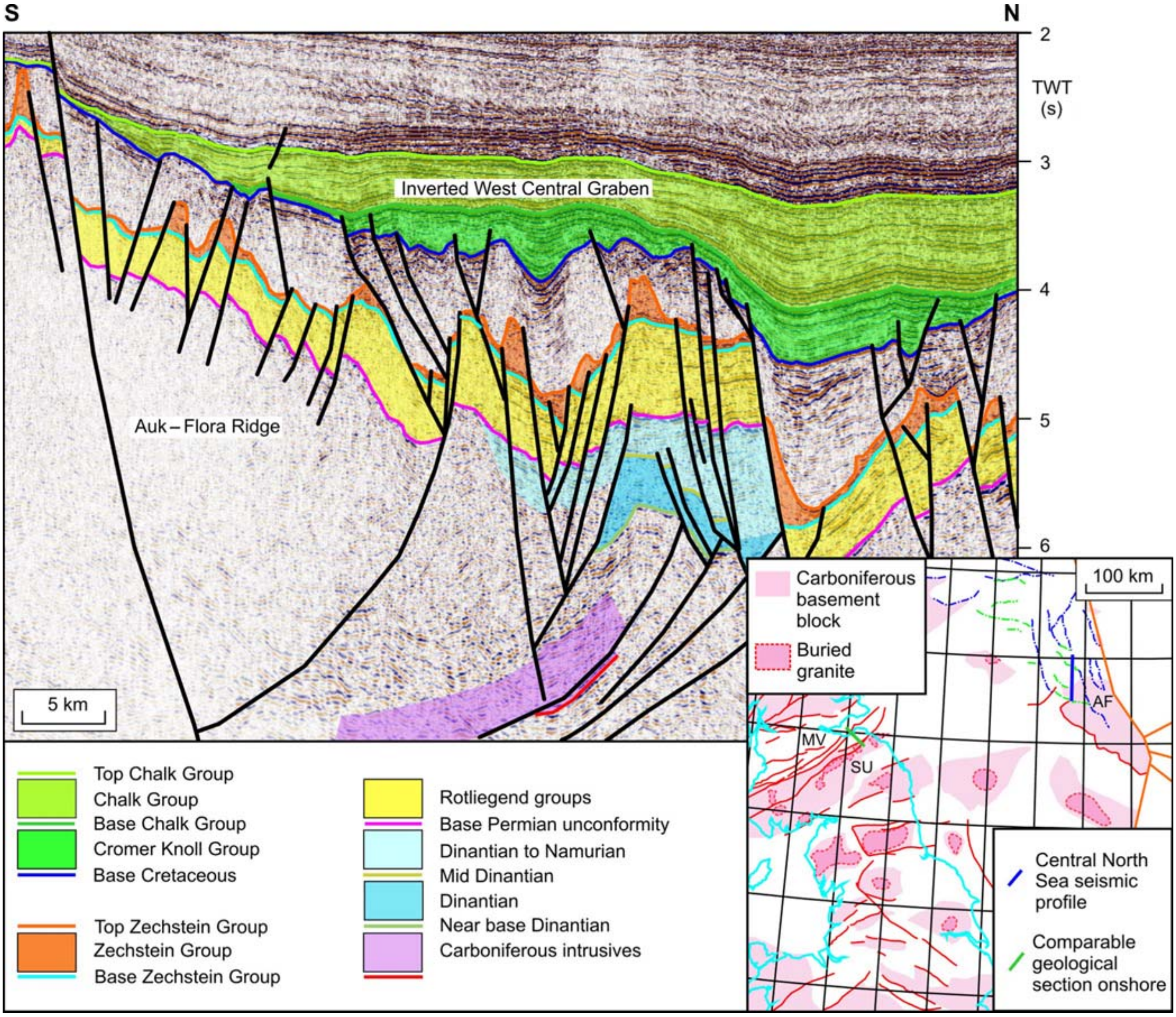

Fig. 7. Interpretation of example seismic profile crossing the northern flank of the Auk–Flora Ridge (AF); data courtesy of CGGVeritas. MV, Midland Valley of Scotland; SU, Southern Uplands.

Sub-Zechstein seismo-stratigraphic relationships in the Jaeren high area

The seismo-stratigraphic relationships established in the drilled Auk–Flora area can be extrapolated to enable interpretation of undrilled sub-Zechstein sections in other parts of the Central North Sea. On the illustrated seismic profile crossing the Jaeren High (Fig. 9), a uniform thickness of Upper Rotliegend strata overlies a northward-thinning unit, which is interpreted to be equivalent to the Lower Rotliegend unit of the Flora area because it rests on a truncation surface that is most likely to be the base Permian unconformity. Imaged only at the northern end of the profile, the faulted, high-amplitude reflector at the base of the underlying steeper-dipping strata is interpreted to be a continuation of the Kyle Limestone event of the Auk–Argyll area. By extrapolation from the Mid North Sea High profile (Fig. 8), these steeper-dipping strata are interpreted to also include Upper Devonian, Lower Carboniferous and Upper Carboniferous seismo-stratigraphic units.

The relative thicknesses of Upper Carboniferous and Lower Carboniferous strata might appear to be anomalous on this profile. However, similar relationships are well known from onshore. For instance, Figure 10 illustrates that, along the southern margin of the Craven Basin, the Upper Carboniferous interval has been completely eroded from the inverted Craven Basin (Evans & Kirby 1999), but is thickly preserved above a condensed Lower Carboniferous shelfal sequence across a Lower Palaeozoic basement block, the Central Lancashire High. The southern part of the Jaeren High Mesozoic footwall block is inferred to overlie a shallow pre-Carboniferous basement block.

Sub-Zechstein seismo-stratigraphic relationships on the West Central Shelf

In an example seismic profile from the West Central Shelf (Fig. 11), the Rotliegend strata are again composed of two discrete seismo-stratigraphic units, although the Upper Rotliegend interval oversteps the Lower Rotliegend beyond the western end of the profile. The most striking feature on this profile is a strongly erosional intra-Carboniferous unconformity that appears to have been dissected into a seismic facies of discontinuous high-amplitude reflectors that may be indicative of coal measures. A lenticular seismic package is imaged directly overlying the deepest notch in the unconformity surface. The lenticular package is interpreted to represent the fill of an erosional channel. In 3D, both the channel

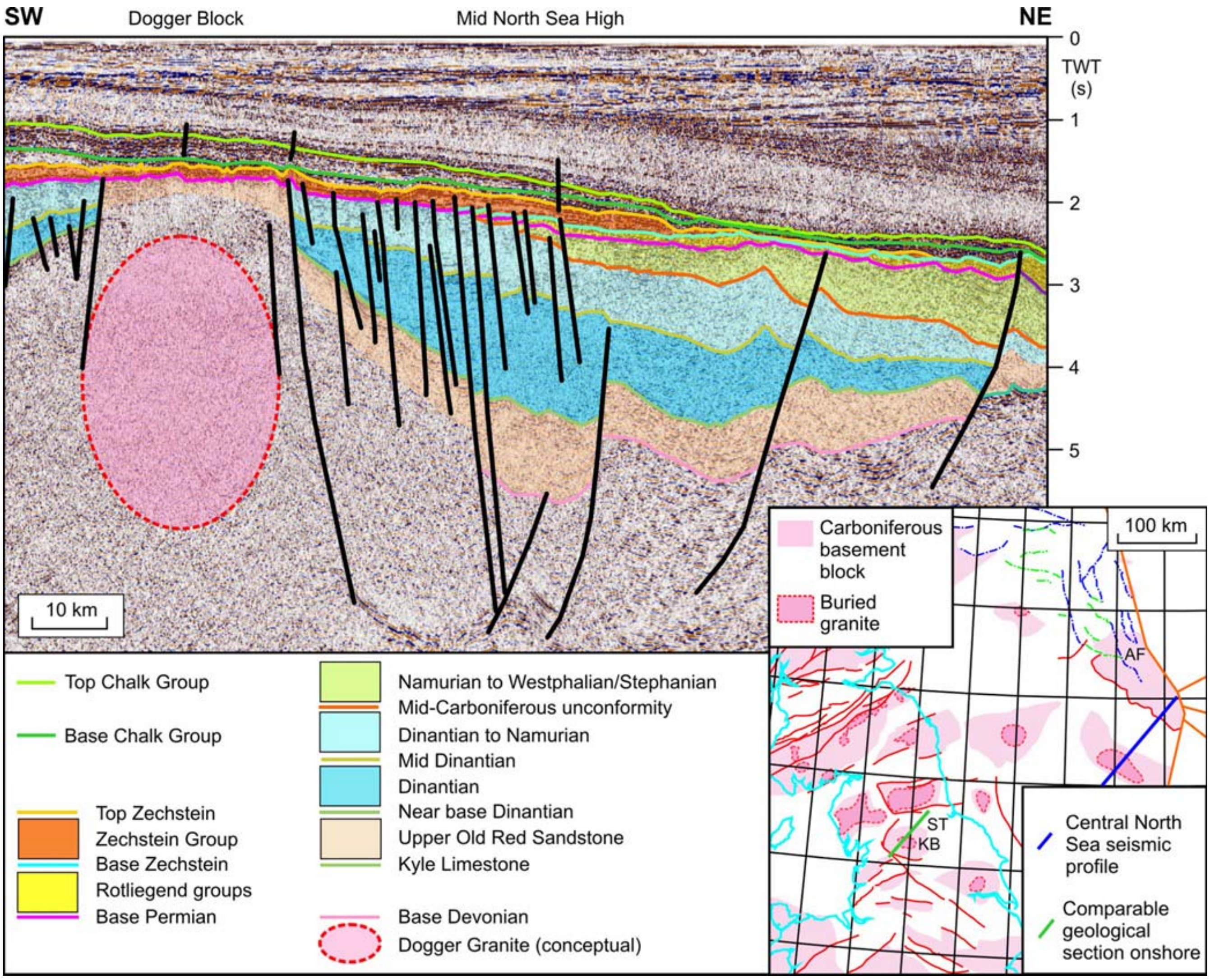

Fig. 8. Interpretation of example seismic profile from the Dogger Granite to the southern flank of the Auk–Flora Ridge (AF); data courtesy of TGS NOPEC Geophysical Co. (UK) Ltd. KB, Askrigg Block; ST, Stainmore Trough. The top of the Dogger Granite cannot be resolved on the seismic data.

and its infill body trend roughly west–east and are up to 2 km wide. Their scale and trend are comparable with mapped mid-Namurian channel features associated with an influx of coarse detritus in the Midland Valley of Scotland (Read 1990).

North of this, another seismic profile (Fig. 12) provides an illustration of a simple pre-Permian syncline, bounded to the west by a westerly-dipping reverse fault, and comparable in style and orientation if not in scale to the Midlothian Syncline in the Midland Valley of Scotland. The latter developed in the Late Carboniferous as syn-sedimentary folding superseded extension in front of a Lower Palaeozoic basement block (Ritchie *et al.* 2003; Underhill *et al.* 2008). These two profiles suggest that large parts of the Carboniferous tectonic style beneath the West Central Shelf have more in common with the Midland Valley of Scotland than with the tectonic style of the Auk–Flora area and the eastern part of the Mid North Sea High.

Potential field modelling

The aim of our potential field modelling has been to separate the gravity response of the crystalline (sub-Lower Palaeozoic) basement from the gravity responses of its overlying Lower Palaeozoic, Devono-Carboniferous, Permian and post-Permian sedimentary basins. It is worth emphasizing that the end result of the 3D modelling is a depth surface to high-density or crystalline basement – this surface defines the base of the accommodation space to be filled by the Lower Palaeozoic and overlying sedimentary basins.

Three-dimensional forward and inverse modelling – modelling technique

A 3D-forward and inversion modelling technique has been used to derive the crystalline basement and other surfaces, combining the methodologies of Parker (1972) and Oldenburg (1974). The user has full control over the spatial wavelengths being inverted, thereby allowing the physical properties of specific horizons to be targeted. The modelling software uses an iterative method to calculate layer depths in such a way that the computed potential field response of the final model provides best fit to the geological data observed from the seismic interpretation.

The 3D inversion involves two principal stages: (i) construction of an input earth model, including 3D inversion for deep crustal surfaces, and (ii) 3D inversion for structure of the crystalline basement to minimize the difference grid, defined by the difference between calculated and observed gravity response. In this study the model was a complex seven-layer model comprising a combination of sedimentary and crystalline basement layers, most with laterally varying densities. The top crystalline basement is usually the

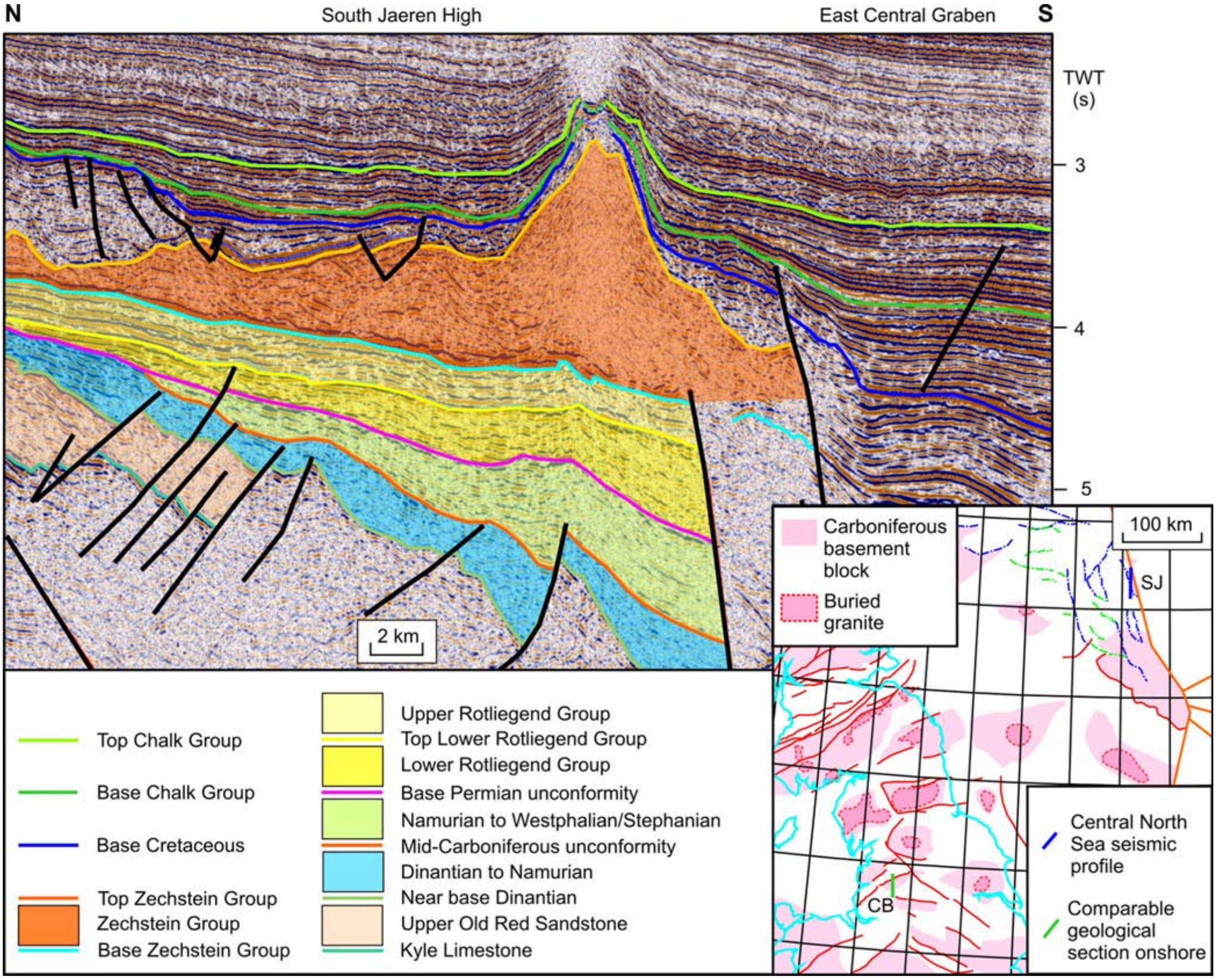

Fig. 9. Interpretation of example seismic profile from the south Jaeren High (SJ); data courtesy of CGGVeritas. CB, Craven Basin.

'seed' horizon which is modified during the inversion. For this project, a filtered version of the base Zechstein surface derived from seismic interpretation was used as the seed crystalline basement horizon.

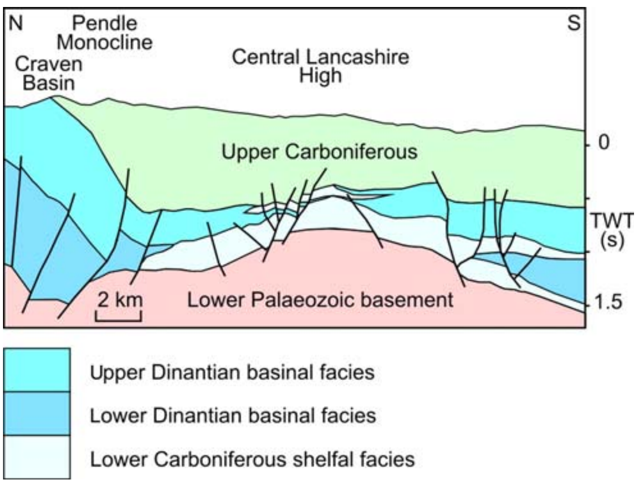

Fig. 10. Analogue from the southern margin of the Craven Basin (interpretation after Evans & Kirby 1999) for the sub-Permian stratigraphic relationships observed beneath the southern Jaeren High.

Construction of the input model: data input considerations

The regional control depth horizons were derived principally from the PGS 'North Sea Digital Atlas' time horizons, providing a more comprehensive data coverage than is currently available from the long-offset seismic data. Depth conversion of the input time surfaces was achieved by trendform gridding of interval velocities obtained from all exploration and appraisal wells in the study area. Initial inversions suggested considerable errors in the thickness of interpreted Permian salt in the Digital Atlas in the Central Graben. The top Permian salt horizon was therefore revised across the Central Graben using modern 3D seismic datasets. Further constraints included the results from preliminary 2D modelling of key seismic lines and selected magnetic crystalline basement depth estimates.

The Moho beneath the area was derived from an inversion of a surface obtained from the results of a refraction seismic study by Kelly *et al.* (2007). The gravity inversion for the Moho surface was constrained to the long-wavelength gravity signal only.

Lateral horizon density variations are difficult to represent adequately in a potential field model. In many studies the model is kept as simple as possible by applying single value densities to individual layers. Initial test inversions indicated that this approach is inappropriate in the Central North Sea, generating significant deviations with the depths derived from the seismic interpretation,

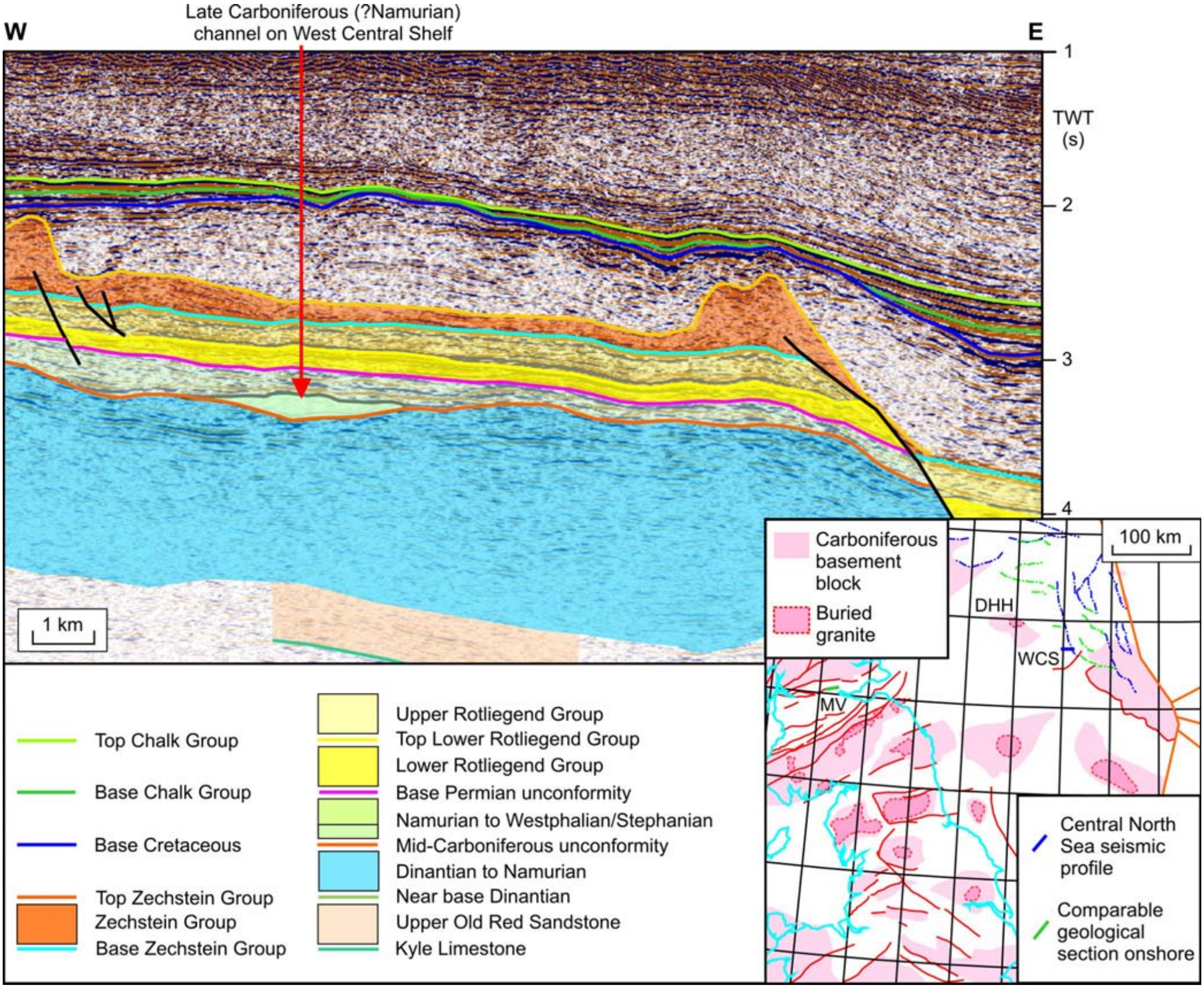

Fig. 11. Interpretation of example seismic profile from the West Central Shelf (WCS); data courtesy of CGGVeritas. DHH, Devil's Hole Horst; MV, Midland Valley of Scotland.

for instance on the western flank of the Central Graben. The solution applied was to derive grids of variable densities for all of the post-Permian layers (Table 1) from the grids of interval velocities that had been used for depth conversion of the seismic data – essentially producing a 'density cube' from the seismically derived 'velocity cube' over the entire project area. The final 3D input model is summarized in Figure 13.

Three-dimensional inversion solution

Top crystalline basement depths were computed by 3D inversion of the free air gravity. Predicted crystalline basement relief was computed by perturbing the top crystalline basement surface until the updated forward response of the model closely matched the observed gravity data. The inversion algorithm was then used to adjust this surface until the observed and computed responses matched within acceptable limits. The wavelengths are controlled during the inversion, allowing the longer wavelengths (deeper structure) to be targeted first, and gradually reducing the wavelengths to target the shallower structure. This is an iterative process, with the results examined at each stage. As most of the long-wavelength anomalies had been accounted for during the construction of the input model and the associated inversion processes to create the Moho/Lower Crustal surface, and since there was a fairly high degree of confidence in the starting surface, the input residual gravity grid did not contain many long-wavelength features. Hence the starting wavelength in the final inversion was 50 km, and this was successively iterated down to 2 km. The initial crystalline basement result, masked back to the limit of the study, is shown in Figure 14.

Three concentric 'lows' modelled within the initial crystalline basement surface were interpreted to be artefacts related to granitic intrusions (Fig. 15). The Farne and the Dogger granites within the Mid North Sea High have been described by Donato *et al.* (1983) and the third, the Devil's Hole Granite within the Devil's Hole High, by Hay *et al.* (2005). The morphology of these granitic bodies was projected downwards from the initial crystalline basement surface to a depth of 10 km. A further iteration of the 3D model (Fig. 16) produced a final crystalline basement surface (Fig. 17). The associated gravity error grid suggests that the crystalline basement depth surface has accounted for the appropriate anomaly wavelengths, and that most of the remaining errors can be attributed to post-crystalline basement geology or small-scale data anomalies.

Observations on sub-Permian basin architecture from the potential field model

In this study we have attempted to image the top of the crystalline basement from the gravity data as a first step towards deriving sub-Zechstein isopachs, which in turn should provide indications for the

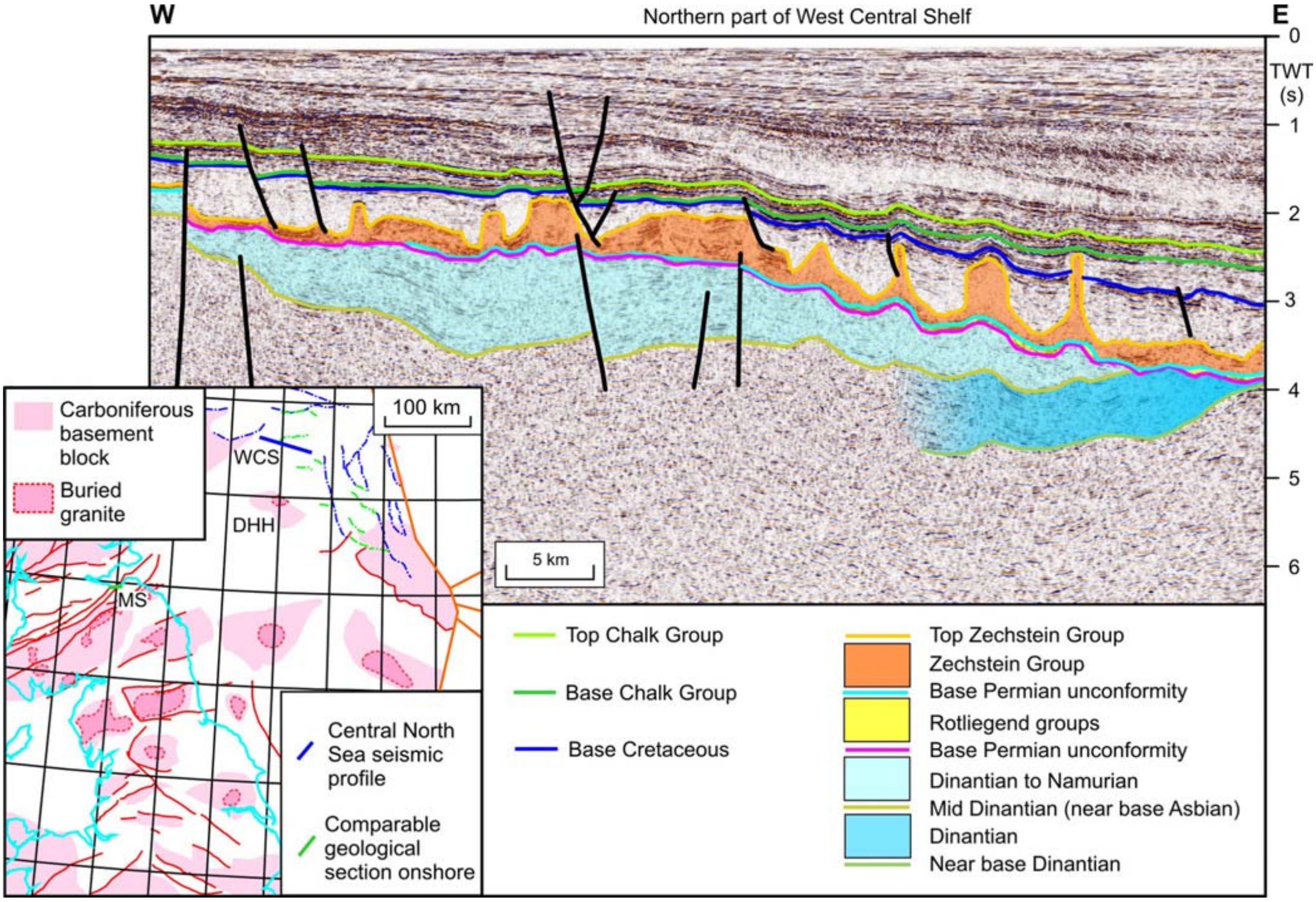

Fig. 12. Interpretation of example seismic profile from the West Central Shelf (WCS); data courtesy of TGS NOPEC Geophysical Co. (UK) Ltd. DHH, Devil's Hole Horst; MS, Midlothian Syncline, Midland Valley of Scotland.

locations of candidate Devono-Carboniferous basins in the subsurface.

Isopachs derived from the gravity modelling for the '*composite layer*' between the base of the Zechstein Group and the top of crystalline basement are shown in Figure 18. This '*composite layer*' includes the Rotliegend Group sediments that have been mapped from seismic interpretation as ranging between 0.1 and 1.8 km thick (Fig. 19). It also includes the underlying Devonian and Carboniferous strata, and at least in the offshore continuation of the Southern Uplands, it may also contain substantial thicknesses of Lower Palaeozoic rocks. This '*composite layer*' is up to 3.8 km thick, but it is modelled as being patchily thin or absent beneath the Mesozoic graben. In these patchily thin or absent areas, the 3D inversion has pushed the crystalline basement surface all the way up to the base of the Zechstein Group in order to match with the observed (survey) gravity. Density variation within the crystalline basement is likely to be small, so a more likely cause is lateral density variation within the composite Lower Palaeozoic to Rotliegend layer. It might be expected, for instance, that the stretched and hence condensed sub-Zechstein sections beneath the Mesozoic graben might have significantly higher density than laterally equivalent sections elsewhere in the region. Similarly, where the layer is dominated by Lower Palaeozoic strata it should have higher density than where it contains significant thicknesses of Rotliegend or Devono-Carboniferous sediments. It is possible to subdivide the composite layer in areas where there may be patchy seismic or well control, but the reliability of that subdivision derived purely from the 3D model would decrease rapidly further from the control points.

The potential errors in the modelled thickness of the composite sub-Zechstein layer, interpreted as resulting from lateral density variations, are calculated to be of the order of 0.3–0.4 km. We also recognize that Lyngsie *et al.* (2006), Lyngsie (2007) and Lyngsie & Thybo (2007) suggest a possible explanation involving a contrast in lower crustal density across the suture between Laurentia and Baltica crystalline basement, which they trace approximately beneath the northern flank of the Auk–Flora Ridge, and continuing northwestward below the western margin of the Central Graben. Bearing these two caveats in mind, the

Table 1. Summary of layer density values input to the 3D inversion model; where a density range is specified this represents lateral variation in density as derived from the velocity cube

Bounding horizon names for layers	Density ($g\ cm^{-3}$)
Sea-level to sea bed	1.03
Seabed to top Chalk Group	1.99–2.16
Top Chalk Group to base Chalk Group	2.20–2.50
Base Chalk Group to base Cretaceous	2.09–2.57
Base Cretaceous to top Permian (top Zechstein Group)	1.99–2.54
Top Permian to top Rotliegend Group (base Zechstein Group)	2.16
Top Rotliegend Group to top crystalline basement	2.55
Top crystalline basement to Moho	2.80
All sub-Moho section	3.20

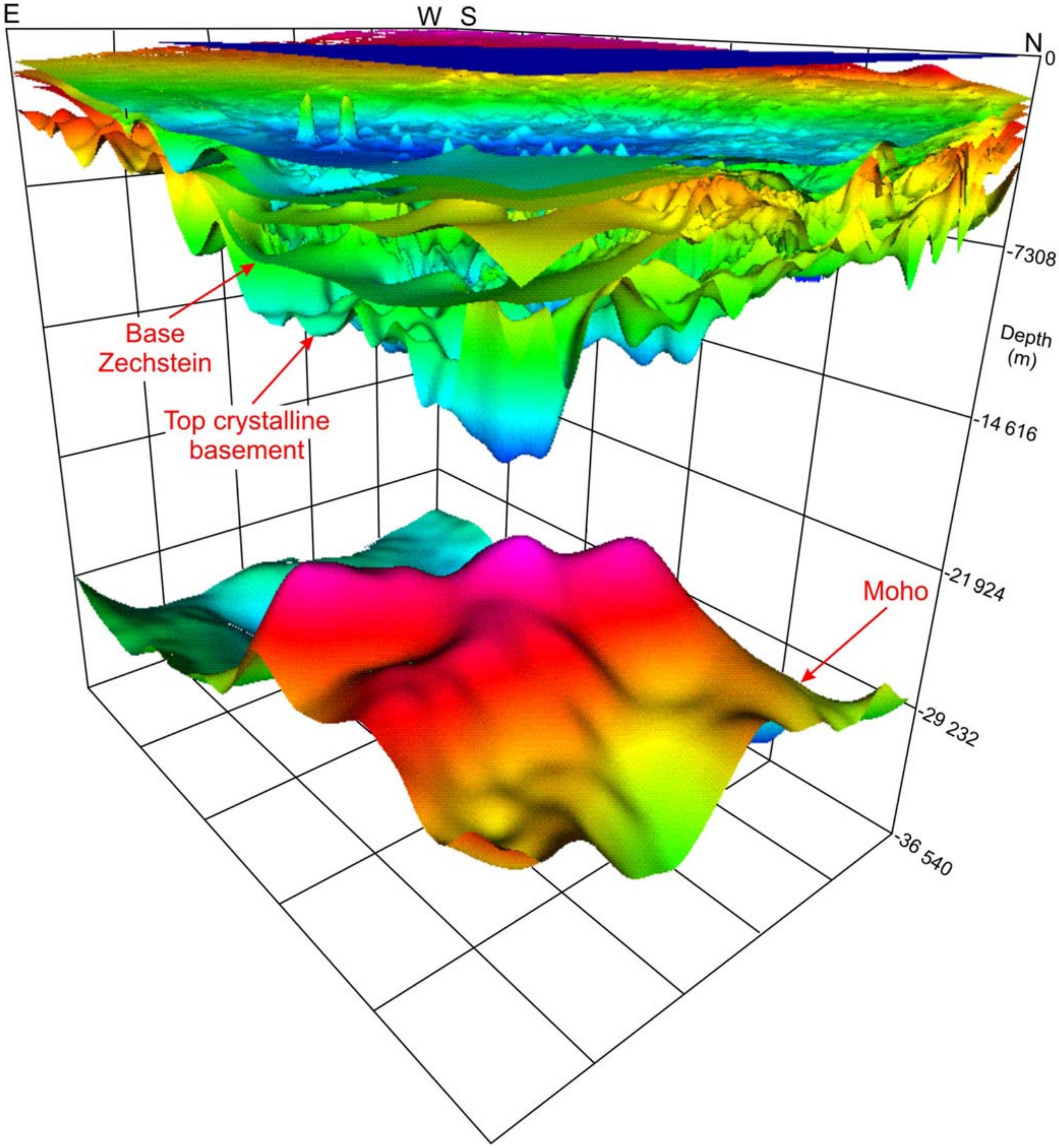

Fig. 13. Starting 3D model with the crystalline basement depth seed surface prior to inversion, viewed from the NE.

sub-Zechstein isopach map (Fig. 19) does provide encouraging indications for the presence of substantial sedimentary basins beneath the Zechstein Group. Also, bearing in mind the thickness of Rotliegend strata derived from the seismic interpretation (Fig. 19), these are the most likely locations for candidate Devono-Carboniferous basins as derived from the gravity data.

The fit of the modelled top of crystalline basement to the long-offset seismic data is demonstrated in Figure 20, which traverses the West Central Shelf, the West Central Graben, the Forties–Montrose High, the East Central Graben, and ends on the Jaeren High with its Devono-Carboniferous core. The sub-Zechstein 'composite layer' is uncoloured on the seismic profile; see Figure 18 for location of the profile.

Synthesis of the geophysical methods

The seismic interpretation has provided indications that many of the basement controls that defined the architecture of the onshore UK Lower Carboniferous basins also operated across the UK Central North Sea. In the SE Central North Sea where the seismic imaging is clearest, it contains elements comparable with the Askrigg Block (Dogger Block) and Stainmore Trough (Mid North Sea High Carboniferous Basin) (Figs 4 & 21–23). The up-thrust Auk–Flora Ridge intra-basinal Lower Palaeozoic basement block resembles the Pentland Hills Inlier within the Midland Valley of Scotland and the Cross Fell Inlier in northern England. We recognize that in one area just south of the Devil's

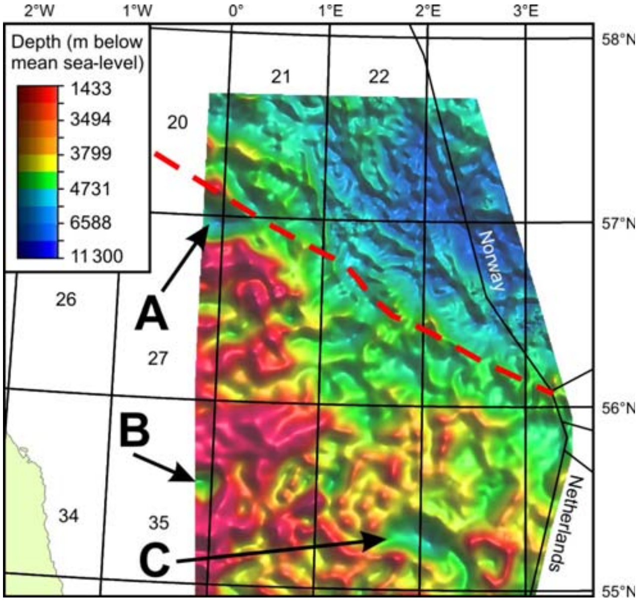

Fig. 14. Initial output of the crystalline basement surface showing the anomalies associated with granites. A, Devil's Hole Granite; B, Farne Granite; C, Dogger Granite.

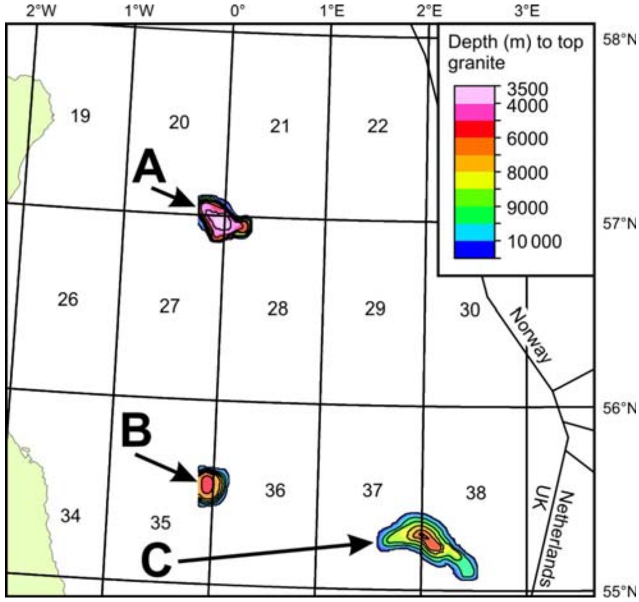

Fig. 15. Depth contours (1000 m interval) at the top of granites A to C. A, Devil's Hole Granite; B, Farne Granite; C, Dogger Granite.

Hole High there is a discrepancy between the gravity & seismic results, which suggest relatively thin and thick sub-Zechstein strata respectively, and this requires further investigation.

On a regional scale, the seismic interpretation has been used to provide a preliminary indication of Lower Carboniferous basin distribution in the east-Central North Sea (Fig. 24). In addition to Lower Carboniferous basins proven by drilling on the eastern Mid North Sea High and in northern Quadrant 21, undrilled Lower Carboniferous basins have also been interpreted in southern Quadrant 29, and to the north and NW of the Auk–Flora Ridge.

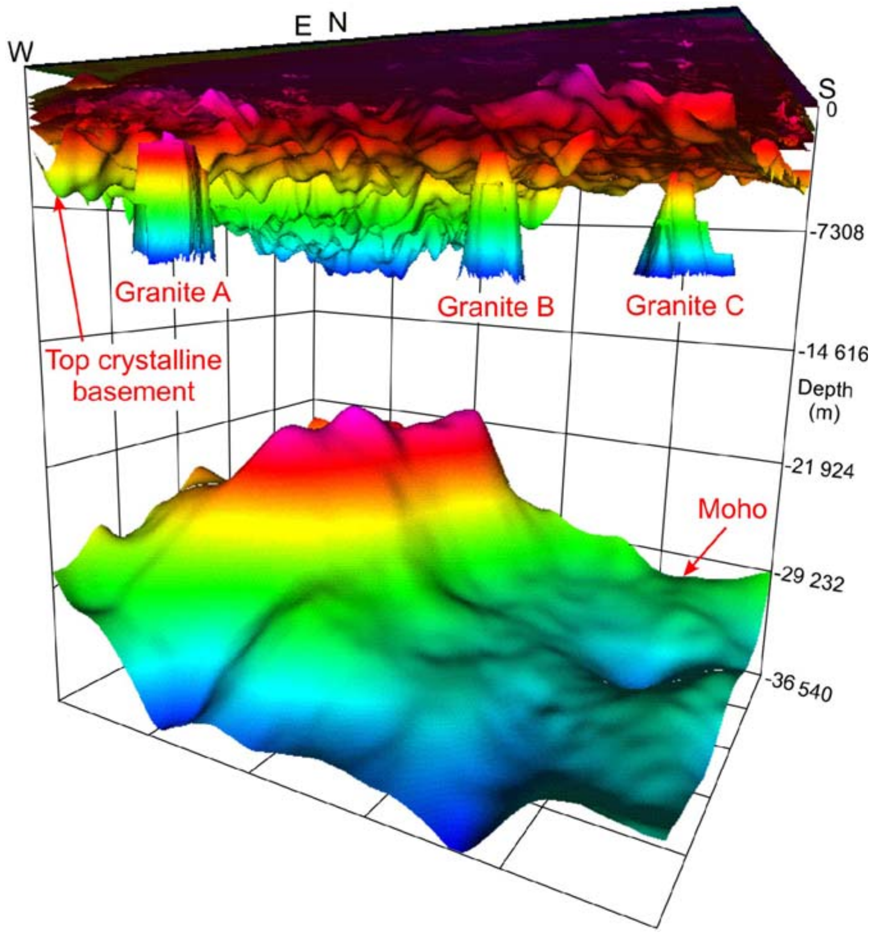

Fig. 16. Modified 3D model showing the detailed morphologies of granites A–C prior to inversion, viewed from SW. A, Devil's Hole Granite; B, Farne Granite; C, Dogger Granite.

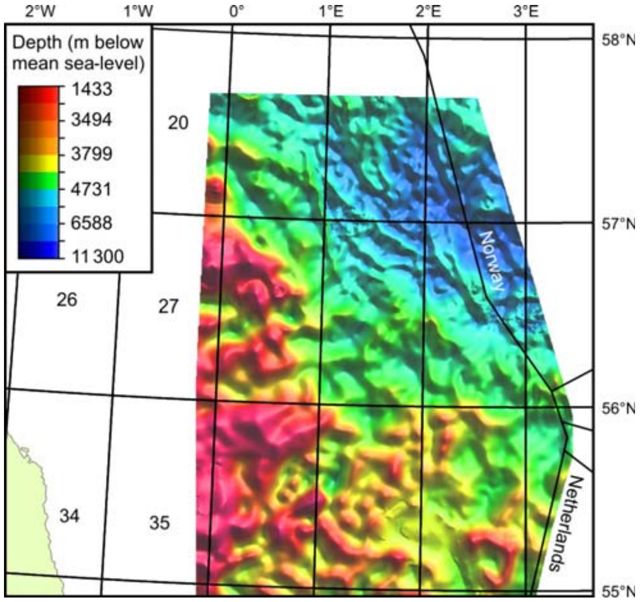

Fig. 17. Final output of the crystalline basement surface.

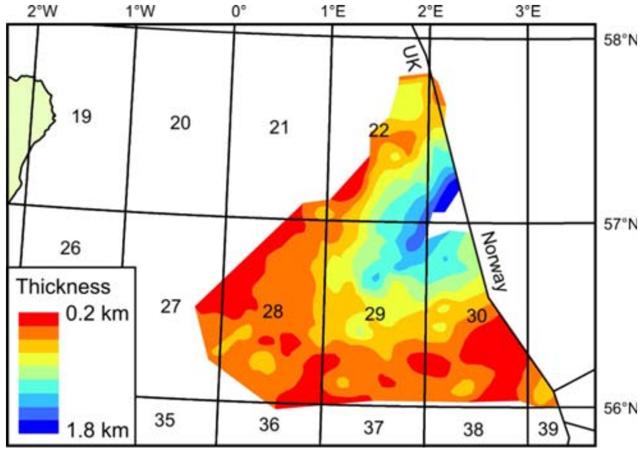

Fig. 19. Approximate thickness of combined Upper and Lower Rotliegend Groups; isochrons converted to thickness assuming a standard interval velocity of 4 km s^{-1}.

Based on the seismic interpretation, these are the regions that are most likely to contain significant volumes of coal-measure source rocks within the sub-Permian section.

The locations of candidate Devono-Carboniferous basins as deduced from gravity modelling do show some features in common with the seismic interpretation (Fig. 25). Encouragingly, both methods provide indications for the undrilled Devono-Carboniferous basin in the south of Quadrant 29, here shown on the contoured crystalline basement surface (Fig. 26) and on a 3D representation of this (Figs 27 & 28). This lends support for a working petroleum system in the south of Quadrant 29, based on the possible presence of significant volumes of mature Carboniferous source rocks. The gravity modelling suggests a NW-trending chain of apparent sub-Zechstein sediment thicks underlying and extending NW of the Auk–Flora Ridge of relatively thin Middle Devonian to Carboniferous strata based on the seismic interpretation. If this observation is derived from a low density unit within the upper crust, then it indicates the Auk–Flora Ridge is possibly underlain by an inverted Lower Devonian basin.

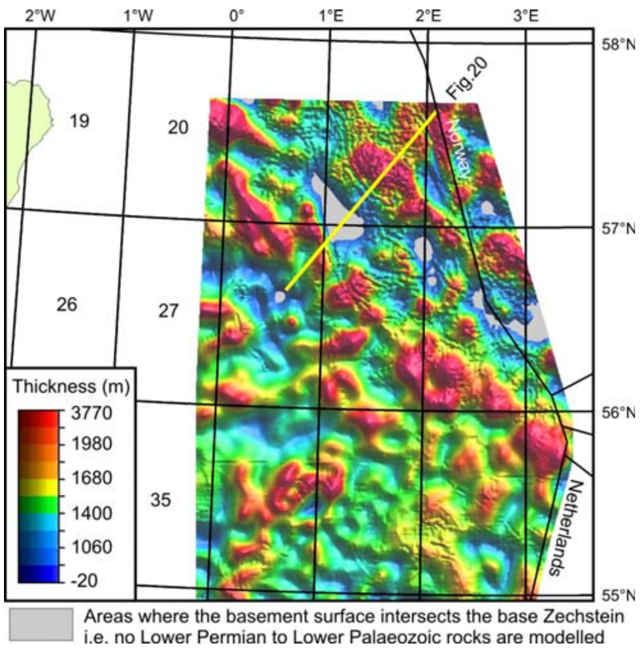

Fig. 18. Isopachs of the sub-Zechstein 'composite layer'.

The Rotliegend strata are divisible into Upper and Lower Rotliegend seismic units in the Flora area, on the Jaeren High and on parts of the West Central Shelf, but are not divisible consistently on a regional scale. Where they can be distinguished, the Upper Rotliegend unit is of relatively uniform thickness, and it oversteps the Lower Rotliegend unit at the basin margins. On some seismic profiles there are indications that thickness variation within the Lower Rotliegend unit is partly a result of penecontemporaneous Early Permian fault activity. This unit is largely composed of volcanic rocks in the Flora area and further east in the North Sea (Heeremans & Faleide 2004), but it may be predominantly composed of continental red-bed facies in the remainder of the UK sector, where it remains relatively undrilled. Isopachs of the combined Upper and Lower Rotliegend units follow a concentric pattern about a NE-trending depocentre that intersects the UK/Norway median line at 57°N (Fig. 19).

Hydrocarbon prospectivity implications

Source rocks

Potential source rocks of the Central North Sea's Carboniferous petroleum system have been poorly sampled by exploration drilling. Only 25 wells have drilled through the base of the Permian into Carboniferous strata in an area of 95 000 km^2 (Fig. 2), with the majority of these wells located around the periphery of the area. Despite this, 11 of the wells have drilled sections of Dinantian and/or Westphalian coal measures. From analyses of these coal measures in well 26/8-1, Hay *et al.* (2005) confirmed their potential for significant hydrocarbon-generating capacity where these are thermally mature. Geochemical analyses indicate that oil within Rotliegend sandstone fluid inclusions in well 29/20-1 has been most likely derived from Carboniferous lacustrine source rocks (PA Resources UK 2010).

Dinantian to Namurian palaeogeography in the onshore UK was dominated by the progressive southwards advance of a major fluvio-deltaic system across the region (Fraser & Gawthorpe 1990; Fraser *et al.* 1990). In the northernmost basins that were overwhelmed earliest by the fluvio-deltaic influx, potential pre-Westphalian source rocks are limited to the mid-Dinantian coal measures of the Scremerston Coal Group or to the thick non-marine oil shales developed within volcanic terrain in the Midland Valley of Scotland. Notably absent from the northern onshore basins are substantial thicknesses of Late Dinantian to Early Namurian

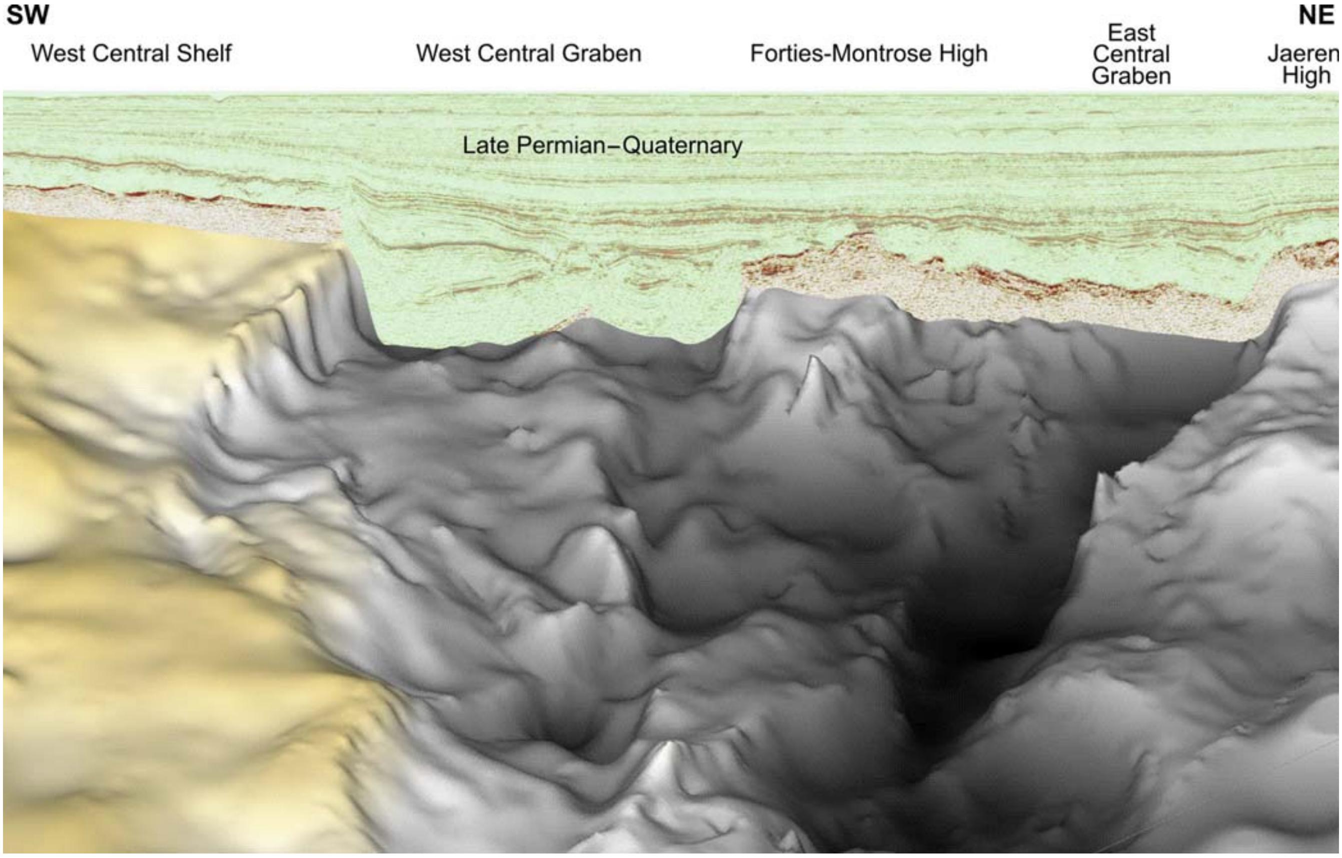

Fig. 20. Three-dimensional view from SE of modelled top crystalline basement surface intersecting a 2D long-offset seismic profile across the northern part of the study area, which traverses the West Central Shelf, the West Central Graben, the Forties–Montrose High, the East Central Graben, and ends on the Jaeren High with its Devono-Carboniferous core. The sub-Zechstein 'composite layer' is uncoloured on the seismic profile; see Figure 18 for location of the profile. Data courtesy of TGS NOPEC Geophysical Co. (UK) Ltd.

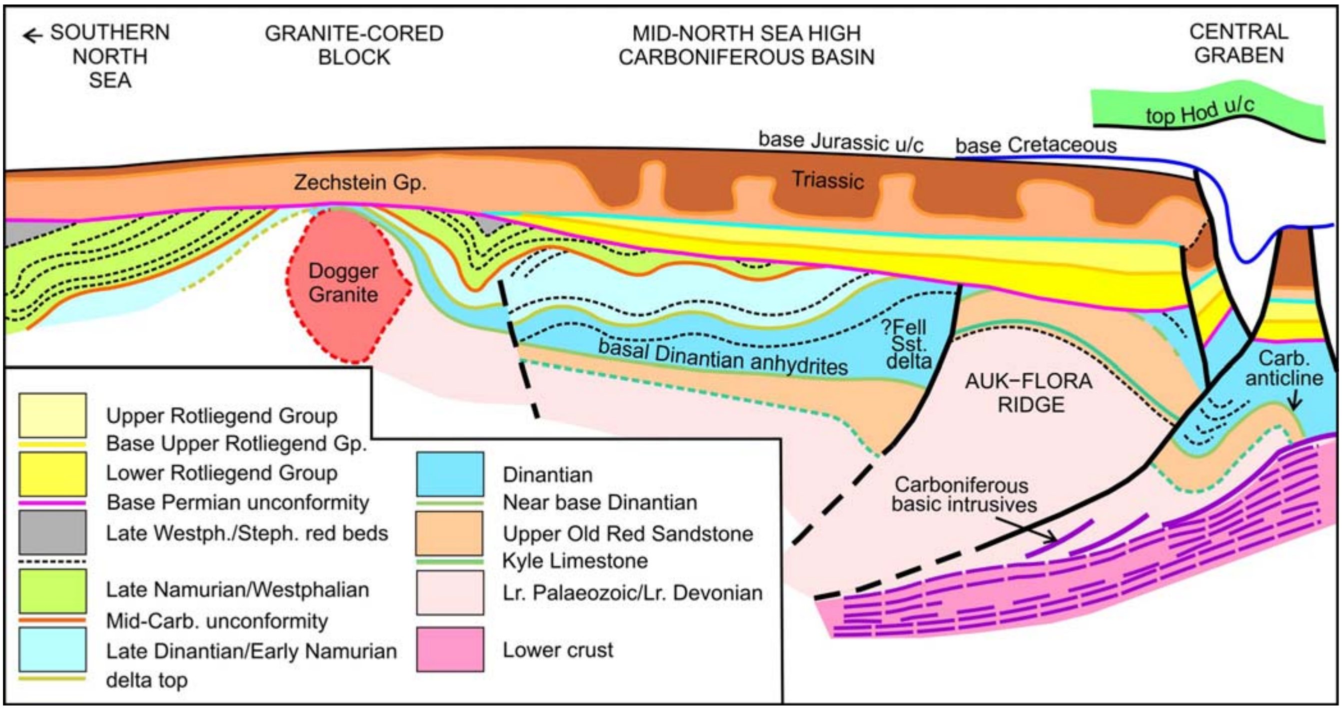

Fig. 21. Schematic profile showing generalized structural and stratigraphic relationships across the Mid North Sea High, from south of the Dogger Block to the Central Graben.

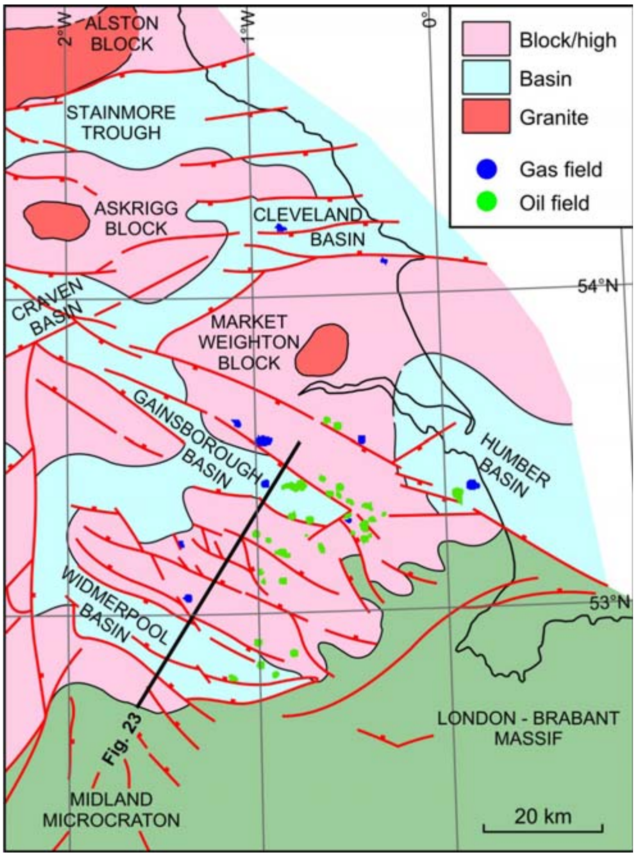

Fig. 22. Map of the Carboniferous block and basin structure of northern England, showing the onshore oil and gas fields and their structural setting; adapted from Fraser *et al.* (1990).

organic-rich marine shales such as those that accumulated in sediment-starved basins beyond the advancing deltas to form the principal source rocks for the oil and gas fields of the East Midlands of England and the East Irish Sea Basin.

For this reason, mid-Dinantian coal measures or oil shales are considered to provide the best opportunity for significant volumes of source rocks in the east-Central North Sea. This is because the seismic mapping indicates that Westphalian coal measures, the principal source rocks in the Southern North Sea, have been largely removed by pre-Permian erosion. The Dinantian sections drilled in wells 38/16-1 and 39/7-1 provide encouragement for potentially significant volumes of source rocks in the southern Devono-Carboniferous basins – the latter well proved coal seams up to 4.5 m thick, constituting 16% of an 87 m-thick coal-measure unit. Bruce & Stemmerik (2003) recorded likely oil shales with TOC values as high as 15–24% within 500 m of Late Dinantian to earliest Namurian strata drilled in well 20/10a-3.

Underhill *et al.* (2008) noted that Carboniferous source rocks at elevated structural locations in the eastern Midland Valley of Scotland and in offshore well 25/26-1 lie close to the oil window. They inferred from burial history modelling that deeper-buried sections became mature for oil generation in the Late Carboniferous, and following end-Carboniferous, Variscan uplift re-entered the oil window during the Mesozoic. Much of the Midland Valley was elevated out of the oil window once more by Palaeogene uplift, but petroleum generation may be continuing in the deepest-buried strata today.

Offshore, Hay *et al.* (2005) concluded from burial history modelling that mid-Dinantian coal-measure source rocks that they interpreted beneath south-central Quadrant 29 are also mature for oil generation, and may even have entered the gas window locally. They estimated that up to 28 billion barrels of oil and 156 tcf of gas could have been expelled from this area alone. Their modelling suggests that most of this hydrocarbon expulsion has been since the Paleocene, hence post-dating all reservoir and trap development in the region. However, Hay *et al.* (2005) predicted that any Dinantian strata preserved in Mid North Sea High Carboniferous basins are only marginally mature for oil generation.

Play types and traps

On a local scale, the ranges of Central North Sea play types that can be invoked from thermally mature Carboniferous source-rock kitchens are largely dependent on the efficiency of the regional Zechstein Group evaporite seal. Where this seal is intact, hydrocarbon charge will be limited to reservoirs and traps within the sub-Zechstein section, in a block and basin setting similar to northern England (Fig. 22). Where this seal has been breached in areas of Zechstein Group salt withdrawal, there are also opportunities for charging reservoirs in the post-Permian section. Hay *et al.* (2005) have used the occurrence of gas chimneys within the Mesozoic section as indicators of relatively widespread Zechstein seal breach in the south of Quadrant 29. Modern long-offset seismic

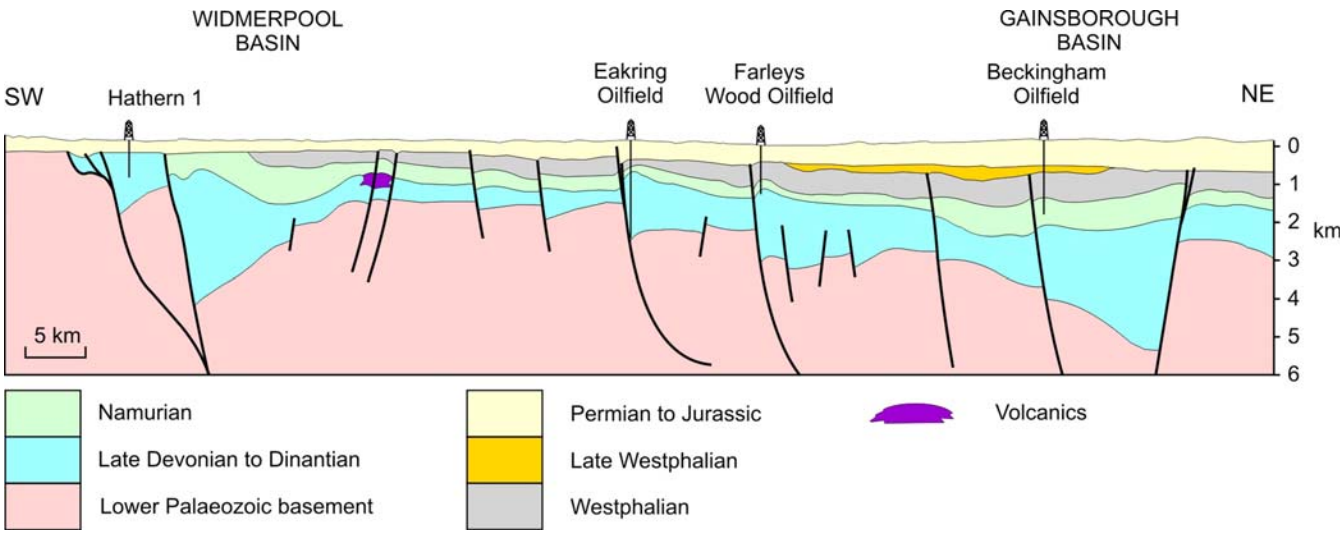

Fig. 23. Cross-section of the Carboniferous block and basin structure of northern England, showing the structural setting of several onshore oil fields; from Fraser *et al.* (1990).

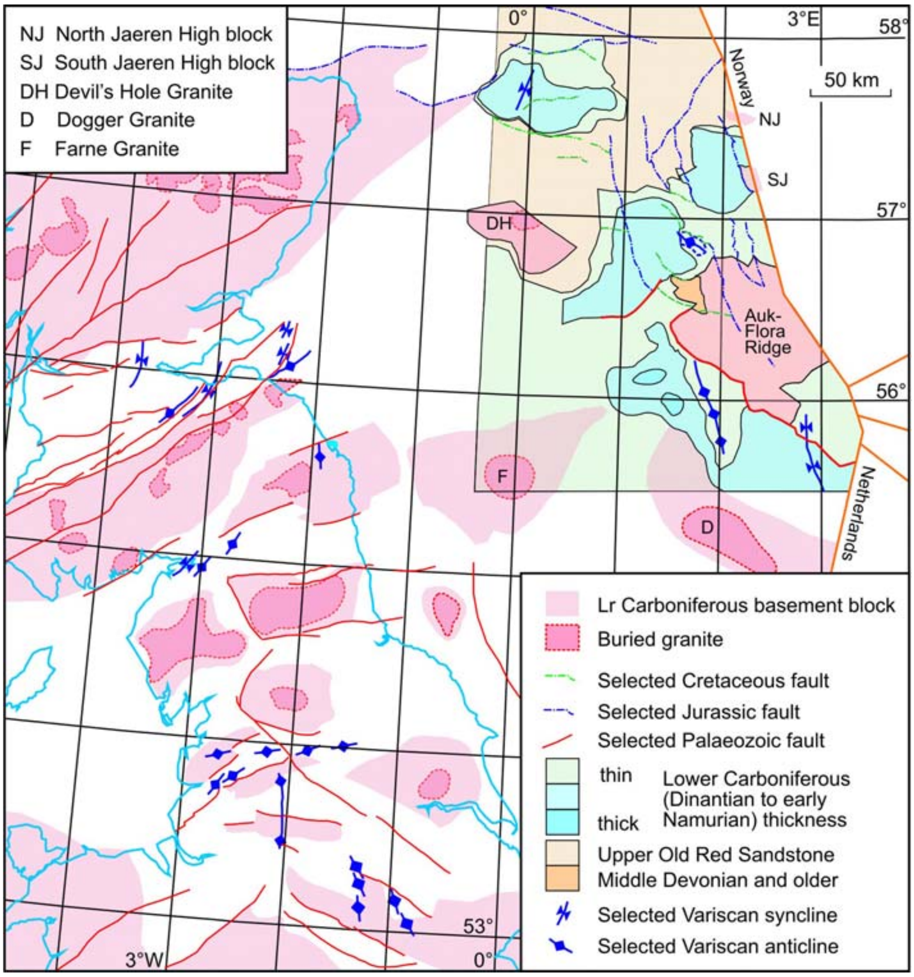

Fig. 24. Lower Carboniferous basin configuration in the Central North Sea, based on the seismic interpretation, with selected Palaeozoic structural elements; onshore interpretation adapted from Fraser & Gawthorpe (1990).

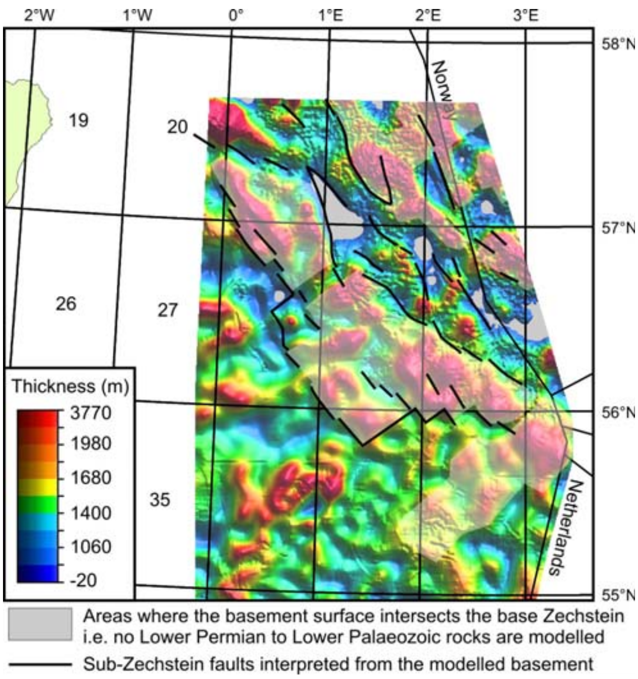

Fig. 25. Isopach map of the sub-Zechstein 'composite layer' and candidate Devono-Carboniferous basin outlines.

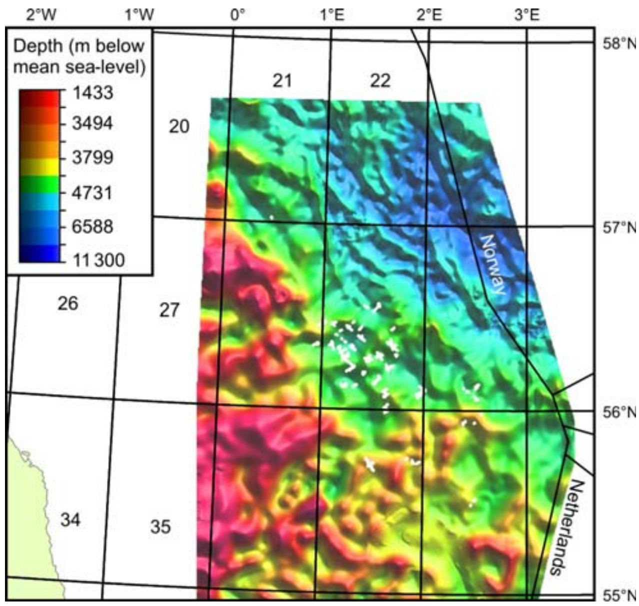

Fig. 26. Shaded relief crystalline basement surface overlain with the gas chimneys (white polygons).

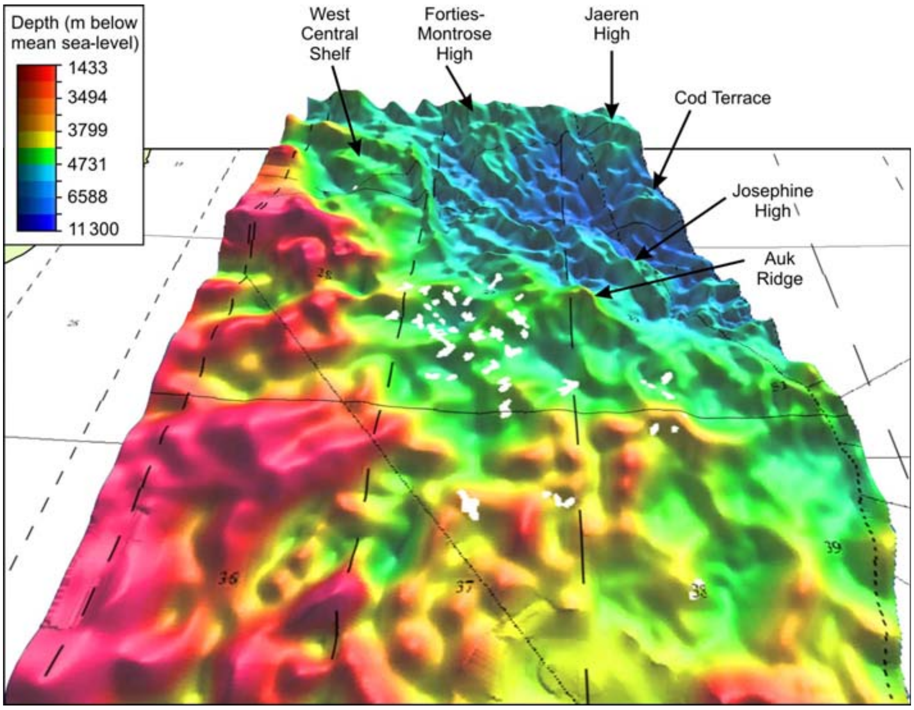

Fig. 27. Three-dimensional display of the crystalline basement surface overlain with the gas chimneys.

coverage is sparse in this area, but is sufficient to verify that some of these gas chimneys are genuine and likely to be thermogenic, whereas others relate to amplitude anomalies confined to the Quaternary section and may be indicators of biogenic gas. Gas chimneys are uncommon above all other candidate Carboniferous source rock basins (Fig. 26), indicating that, if mature, their Zechstein topseal is intact. Where the Zechstein topseal is breached, hydrocarbons could potentially migrate into Triassic to Cenozoic play fairways, which are equally underexplored to the west of the Central Graben's Jurassic source kitchen.

Rotliegend Group desert sandstones have been the primary focus of Central North Sea sub-Zechstein exploration to date, with the Auk, Argyll/Ardmore and Innes fields sourced from the Upper Jurassic kitchen of the Central Graben. Less well appreciated has been the potential for Rotliegend Group targets above thermally mature Carboniferous source-rock basins, either in structurally constrained traps or in updip pinchout traps around the margin of the Rotliegend basin.

Potential sub-Rotliegend targets fall into three categories – Zechstein subcrop traps beyond the limit of the Rotliegend

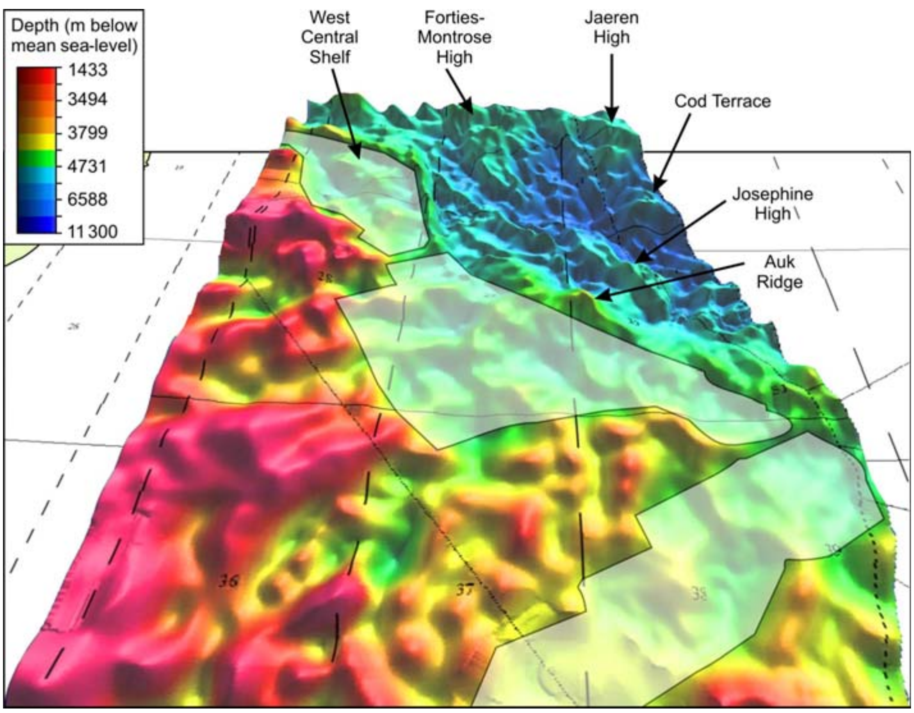

Fig. 28. Three-dimensional display of the crystalline basement surface and candidate Devono-Carboniferous basins, which predominantly underlie the gas chimneys mapped by Hay *et al.* (2005).

fairway, Lower Rotliegend subcrop traps, and intra-Carboniferous traps. Prime examples of the first two categories are the Upper Devonian producing reservoir in the Argyll/Ardmore Field (Robson 1991) and the Upper Carboniferous, Upper Flora Sandstone producing reservoir in the Flora Field (Martin *et al.* 2002). Both of these discoveries were made by serendipity, with Rotliegend reservoirs being their primary targets, but both were sourced from the Jurassic source kitchen.

In summary, our paper reaffirms the likely existence of the overlooked Carboniferous petroleum system proposed by Hay *et al.* (2005). This petroleum system has the potential for extending the geographic distribution of valid exploration targets, in all of the principal play fairways of the Central North Sea, with potential Carboniferous drilling objectives as shallow as 8500 feet.

Conclusion

Our interpretation has revealed a Devono-Carboniferous basin architecture for the Central North Sea, which exhibits many features in common with the contemporary basins of northern England and southern Scotland. By analogy with these basins, their Central North Sea equivalents are likely to contain significant volumes of coal-measure and perhaps also oil-shale source rocks. Where thermally mature, these source-rock intervals are key elements of an underexplored Carboniferous petroleum system, potentially extending far to the west of the Jurassic source kitchen, which has been the focus of almost all Central North Sea exploration to date. The recognition by Hay *et al.* (2005) of gas chimneys above the Zechstein layer stretching from block 21/27 through southern Quadrant 29 to the Mid North Sea High suggests that postulated underlying Carboniferous source rocks may be thermally mature in many of the Devono-Carboniferous basins imaged in this study (Figs 2 & 24–28). We conclude that exploration opportunities associated with this petroleum system occur both in Devonian to Lower Permian plays beneath the regional Zechstein evaporite seal and, where halokinetic thinning has enabled seal breach, in the underexplored Mesozoic and Cenozoic plays above.

This paper is published with the permission of the Head, Oil & Gas Licensing, Exploration & Development, Department of Energy and Climate Change (DECC), and the Executive Director, British Geological Survey (NERC). The views expressed in the paper are the views of the authors, and not necessarily those of the DECC/BGS/ARKeX. Our grateful thanks are extended to colleagues for their contributions and debate, and for providing scientific rigueur to challenge our assumptions as the study evolved. The authors gratefully acknowledge permission to publish seismic data owned by TGS-Nopec Geophysical Co. UK Ltd and CGGVeritas.

References

Bruce, D. R. S. & Stemmerik, L. 2003. Carboniferous. *In*: Evans, D., Graham, C., Armour, A. & Bathurst, P. (eds) *The Millennium Atlas: Petroleum Geology of the Central and Northern North Sea*. Geological Society, London, 83–89.

Cameron, T. D. J. 1993*a*. Triassic, Permian and pre-Permian of the Central and Northern North Sea. *In*: Knox, R. W. O'B. & Cordey, W. G. (eds) *Lithostratigraphic Nomenclature of the UK North Sea*. British Geological Survey, Nottingham.

Cameron, T. D. J. 1993*b*. Carboniferous and Devonian of the Southern North Sea. *In*: Knox, R. W. O'B. & Cordey, W. G. (eds) *Lithostratigraphic Nomenclature of the UK North Sea*. British Geological Survey, Nottingham.

Chadwick, R. A., Holliday, D. W., Holloway, S. & Hulbert, A. G. 1995. *The Structure and Evolution of the Northumberland-Solway Basin and Adjacent Areas*. Subsurface Memoirs of the British Geological Survey. HMSO, London.

Donato, J. A., Martindale, W. & Tully, M. C. 1983. Buried granites within the Mid North Sea High. *Journal of the Geological Society, London*, **140**, 825–837.

Evans, D. J. & Kirby, G. A. 1999. The architecture of concealed Dinantian carbonate sequences over the Central Lancashire and Holme highs, northern England. *Proceedings of the Yorkshire Geological Society*, **52**, 297–312.

Fraser, A. J. & Gawthorpe, R. L. 1990. Tectono-stratigraphic development and hydrocarbon habitat of the Carboniferous in northern England. *In*: Hardman, R. F. P. & Brooks, J. (eds) *Tectonic Events Responsible for Britain's Oil Reserves*. Geological Society, London, Special Publications, **55**, 49–86.

Fraser, A. J., Nash, D. F., Steele, R. P. & Ebdon, C. C. 1990. A regional assessment of the intra-Carboniferous play of northern England. *In*: Brooks, J. (ed.) *Classic Petroleum Provinces*. Geological Society, London, Special Publications, **50**, 417–440.

Grayson, R. F. & Oldham, L. 1987. A new structural framework for the northern British Dinantian as a basis for oil, gas and mineral exploration. *In*: Miller, J., Adams, A. E. & Wright, V. P. (eds) *European Dinantian Environments*. Wiley, Chichester, 33–59.

Hay, S., Jones, C. M., Barker, F. & He, Z. 2005. Exploration of unproven plays; Mid North Sea High. World Wide Web Address: https://www.og.decc.gov.uk/UKpromote/posters/expl_unp_plays.htm.

Heeremans, M. & Faleide, J. I. 2004. Late Carboniferous–Permian tectonics and magmatic activity in the Skagerrak, Kattegat and the North Sea. *In*: Wilson, M., Neumann, E.-R., Davies, G. R., Timmerman, M. J., Heeremans, M. & Larsen, B. T. (eds) *Permo-Carboniferous Magmatism and Rifting in Europe*. Geological Society, London, Special Publications, **223**, 157–176.

Kelly, A., England, R. W. & Maguire, P. K. H. 2007. A crustal seismic velocity model for the UK, Ireland and surrounding seas. *Geophysical Journal International*, **171**, 1172–1184.

Kirby, G. A., Baily, H. E. *et al*. 1987. *The Structure and Evolution of the Craven Basin and Adjacent Areas*. Subsurface Memoirs of the British Geological Survey. HMSO, London.

Lyngsie, S. B. 2007. *Continental sutures and their influence on rifting in the North Sea*. PhD thesis, University of Copenhagen.

Lyngsie, S. B. & Thybo, H. 2007. A new tectonic model for the Laurentia Avalonia Baltica sutures in the North Sea: a case study along MONA LISA profile 3. *Tectonophysics*, **429**, 201–227.

Lyngsie, S. B., Thybo, H. & Rasmussen, T. M. 2006. Regional geological and tectonic structures of the North Sea area from potential field modelling. *Tectonophysics*, **413**, 147–170.

Martin, C. A. L., Stewart, S. A. & Doubleday, P. A. 2002. Upper Carboniferous and Lower Permian tectonostratigraphy on the southern margin of the Central North Sea. *Journal of the Geological Society, London*, **159**, 731–749.

Oldenburg, D. W. 1974. The inversion and interpretation of gravity anomalies. *Geophysics*, **39**, 526–536.

PA Resources UK. 2010. Relinquishment Report Licence P1318 23rd Round Promote UKCS Blocks 29/19a, 29/20b, 29/24 and 29/25. World Wide Web Address: https://www.og.decc.gov.uk/UKpromote/relinqs/UKPrelinqs.htm.

Parker, R. L. 1972. The rapid calculation of potential anomalies. *Geophysical Journal of the Royal Astronomical Society*, **42**, 315–334.

Read, W. A. 1990. The interplay of sedimentation, volcanicity and tectonics in the Passage Group (Arnsbergian, E2, to Westphalian A) in the Midland Valley of Scotland. *In*: Arthurton, R. S., Gutteridge, P. & Nolan, S. C. (eds) *The Role of Tectonics in Devonian and Carboniferous Sedimentation in the British Isles*. Geological Society, London, 143–152.

Ritchie, J. D., Johnson, H., Browne, M. A. E. & Monaghan, A. A. 2003. Late Devonian–Carboniferous tectonic evolution within the Firth of Forth, Midland Valley; as revealed from 2D seismic reflection data. *Scottish Journal of Geology*, **39**, 121–134.

Robson, D. 1991. The Argyll, Duncan and Innes Fields, Blocks 30/24, 30/25a, UK North Sea. *In*: Abbotts, I. L. (ed.) *United Kingdom Oil and Gas Fields, 25 Years Commemorative Volume*. Geological Society, London, Memoirs, **14**, 219–225.

Smith, N. J. P., Kirby, G. A. & Pharaoh, T. C. 2005. *The Structure and Evolution of the South-West Pennine Basin and Adjacent Areas*.

Subsurface Memoirs of the British Geological Survey. HMSO, London.

Smith, K. & Smith, N. J. P. 1989. Deep geology. *In*: Plant, J. A. & Jones, D. G. *Metallogenic Models and Exploration Criteria for Buried Carbonate-hosted ore Deposits – A Multidisciplinary Study in Eastern England*. British Geological Survey, Keyworth/Institute of Mining and Metallurgy, London, 53–64.

Trewin, N. H., Fryberger, S. G. & Kreutz, H. 2003. The Auk field, block 30/16, UK North Sea. *In*: Gluyas, J. G. & Hichens, H. M. (eds) *United Kingdom Oil and Gas Fields, Commemorative Millennium Volume*. Geological Society, London, Memoirs, **20**, 485–496.

Underhill, J. R., Gayer, R. A., Woodcock, N. H., Donnelly, R., Jolley, E. J. & Stimpson, I. G. 1988. The Dent Fault System, northern England – reinterpreted as a major oblique-slip fault zone. *Journal of the Geological Society, London*, **145**, 303–316.

Underhill, J. R., Monaghan, A. A. & Browne, M. A. E. 2008. Controls on structural styles, basin development and petroleum prospectivity in the Midland Valley of Scotland. *Marine and Petroleum Geology*, **25**, 1000–1022.

Channel structures formed by contour currents and fluid expulsion: significance for Late Neogene development of the central North Sea basin

P. C. KNUTZ

Geological Survey of Denmark and Greenland, Geophysics Department, Øster Voldgade 10, 1350 Copenhagen, Denmark (e-mail: pkn@geus.dk)

Abstract: Channel horizons, delimiting a major Pliocene sedimentary prism in the central North Sea basin, have been investigated in the context of oceanographic, climatic and tectonic controls, using 3D seismic and well data from the UK and Norwegian sector. Aggrading channel structures, forming 700–2500 m wide and 75–150 m deep linear to arcuate troughs, superimpose the truncated distal part of the prism in the northern Central Graben. The origin of the aggradational channel and prism complex is related to differential deposition and erosion by contour currents that intensified as tectonic subsidence formed a deep marine basin (>600 m) with open connections to the Atlantic and Norwegian Sea. The largest channel troughs appear to be filled with consolidated sediments and emerge from areas where the Neogene strata is pierced by salt diapir chimneys. From Early Pleistocene (*c*. 2.5 Ma) the channels were subject to progressive burial by rapid clinoform progradation. Based on the seismic observations, a depositional model is proposed that relates contourite channel development to fluid expulsion from salt diapir structures and fracture zones extending from lower Miocene strata. The sedimentary prism accumulated over a Late Miocene/Early Pliocene Unconformity marked by incised channels that are reminiscent of a northward diverging drainage system. This erosive low-stand development is probably related to late Alpine compression, which promoted uplift in the British Isles and the Channel region. The ensuing subsidence of the central North Sea, associated with concomitant uplift of the Norwegian–Danish Basin, generated the present southwestward dip of 0.5–0.8° of the basal unconformity. The Late Miocene compressional phase followed by rapid basin depending during Pliocene to early Pleistocene suggests that present concepts of North Sea basin development have to be re-evaluated.

Keywords: North Sea, neogene basin, pliocene, 3D seismic, aggradational prism, contour current, salt diapir leakage, tectonic subsidence

The Late Cenozoic succession forms an integral part of the North Sea petroleum system by sustaining overpressure in the deeper stratigraphic sections and preventing prolific hydrocarbon leakage from Cretaceous and Early Cenozoic reservoir accumulations (Cayley 1987; Thrasher *et al.* 1996). The infill history of the 1500 m deep Late Neogene basin (i.e. last 15 Ma) is manifest by a succession of Upper Miocene, Pliocene and Quaternary depositional units, formed in response to tectonically induced subsidence, sediment supply, eustatic sea-level changes and oceanographic currents (Nielsen *et al.* 1986; Kooi *et al.* 1991; Galloway *et al.* 1993; Michelsen *et al.* 1995). 2D and 3D seismic studies of this package have demonstrated the presence of buried geomorphic features, representing channels, pockmarks and sedimentary extrusion, as well as fluid-flow anomalies generated by hydrocarbon leakage from structural reservoirs (Cartwright 1995; Heggland 1998; Fichler *et al.* 2005; Andresen *et al.* 2008). These lateral and vertical heterogeneities in the Late Cenozoic overburden have received modest attention despite the relevance for evaluating remaining hydrocarbon prospects in the mature North Sea province. Moreover, an assessment of velocity anomalies induced by these features is important for identifying drilling hazards and achieving precise depth conversion of deeper target horizons (Armstrong *et al.* 2001). Also, recognition of geomorphic elements associated with palaeo-surfaces may further new understandings of how depositional patterns and processes are related to changes in basin configurations. The objective of this study is to investigate complex channel structures in the Late Neogene section of the Central Graben (UK and Norwegian sector) based on 3D seismic interpretation using the PGS Central North Sea MegaSurvey. The seismic–stratigraphic framework is mainly defined by major unconformities tied to geophysical log parameters from key wells, and correlation to biostratigraphic records in the southern Central Graben. The origins of the channel systems are discussed in context of the depositional and tectonic development of the Neogene North Sea basin.

Regional background

The North Sea Central Graben is an epicontinental basin formed by lithospheric extension during the Permo-Triassic and Late Jurassic–Early Cretaceous (Ziegler 1992). Its present structural configuration of intra-basinal lows and highs is the result of multiple tectonic inversion phases that ceased during Paleocene to Early Eocene (Gatliff *et al.* 1994). From Eocene to Late Pleistocene, a succession of up to 2800 m of mainly undercompacted marine mudstone filled the North Sea basin (Jordt *et al.* 1995; Michelsen *et al.* 1995). A phase of rapid aggradational and progradational infill occurred during the Late Neogene with more than 1000 m of sediments accumulating in the Central Graben depocentre, mainly by transport from NW and west (Michelsen *et al.* 1995; Sorensen *et al.* 1997). The southern North Sea basin was infilled by progressive westward expansion of deltaic sedimentation that was active until Early–Mid Pleistocene (Cameron *et al.* 1993; Overeem *et al.* 2001; Kuhlmann & Wong 2008). In the northern North Sea (south Viking Graben) mounded sand accumulations of the Late Miocene–Early Pliocene Utsira Fm. (Gregersen *et al.* 1997; Eidvin & Rundberg 2007) were probably formed in a deep shelf setting (water depths of 200–300 m) with sediment transport predominated by strong ocean currents (Galloway 2002). In this region Neogene chronology has been established by foraminifer

VINING, B. A. & PICKERING, S. C. (eds) *Petroleum Geology: From Mature Basins to New Frontiers – Proceedings of the 7th Petroleum Geology Conference*, 77–94. DOI: 10.1144/0070077 © Petroleum Geology Conferences Ltd. Published by the Geological Society, London.

biostratigraphy from key wells, Sr isotope dating and multiple well log correlation (Head *et al.* 2004; Eidvin & Rundberg 2007). In the southern and eastern North Sea, the age of Neogene units is construed primarily by application of dinocyst biostratigraphy (Kuhlmann *et al.* 2006; Dybkjær & Piasecki 2008), assisted by marine-to-onshore correlations using an extensive 2D seismic and borehole database (Rasmussen *et al.* 2005).

Basin modelling suggests that periods of anomalous subsidence, deviating from predicted post-rift thermal subsidence, are required to explain the Cenozoic sedimentary architecture of the North Sea (Kyrkjebø *et al.* 2000; Faleide *et al.* 2002). The causes of intraplate tectonic movements are not fully understood, but may involve crustal flexuring, associated with changes in the regional stress field produced by Mid-Atlantic Ridge dynamics and the African–Eurasian plate collision (Kooi *et al.* 1991; Dore & Lundin 1996). Long-wave geodynamic movements, associated with the Neogene Alpine collision, exercised a primary control on the palaeogeography in NW Europe and sediment fluxes to the southern North Sea basin (Ziegler 1992; van Vliet-Lanoë *et al.* 2002; Hillis *et al.* 2008). Late Miocene (i.e. Messinian) compression is associated with a major transgressional phase in the southern North Sea region, resulting in by-pass of river systems and peat development in the central parts (Vandenberghe *et al.* 1998; Rasmussen 2004). The complex development of Neogene strata, resulting from interaction between subsidence, erosion and deposition, has attracted opposing views with respect to primary controls on basin development. In the eastern North Sea over the Norwegian–Danish Basin, an exhumed section (500–1000 m) of post-Mid-Miocene sediments has been a principle argument for a Pliocene phase of active tectonic uplift (Japsen *et al.* 2007). Others have disputed this concept, giving preference to Late Cenozoic progressions in climate-induced weathering and sediment isostacy as an explanation for incongruent sedimentation patterns (Huuse 2002; Nielsen *et al.* 2002). From an E&P perspective, an important consequence of Neogene subsidence was the westward tilting of strata along the eastern basin margin, promoting updip movement of Jurassic hydrocarbon fluids via Cenozoic formations into structural traps of the Danish chalk fields (Rasmussen *et al.* 2005; Vejbæk *et al.* 2005).

The Cenozoic package is pierced by salt diapirs that protrude from Triassic salt ridges through deep-seated structural faults (Jackson & Seni 1984; Bishop 1996). In the east Central Graben, salt domes form prominent structural traps by the wedging of Upper Cretaceous and sand-prone Paleocene units against their downturned crests (Davison *et al.* 2000*b*). The majority of these salt structures have been drilled, encountering hydrocarbon columns ranging from 600 to 1300 m within Upper Cretaceous and Paleocene formations. The salt diapirs are commonly associated with gas chimneys, that extend into the younger Cenozoic succession as a product of vertical fluid-flow from deeper stratigraphic horizons (Thrasher *et al.* 1996; Løseth *et al.* 2008). Hydrocarbon leakage is observed above several producing fields in the Central Graben (e.g. Machar, Medan and Tommeliten), by the presence of seabed pockmarks and traces of thermogenic gas (Heggland 1998).

A 2D seismic study of the Late Neogene package by Cartwright (1995) revealed a series of ridge–trough sedimentary structures in the NW part of the Central Graben (UK quadrant 22). In compliance with the restricted resolution and geographical extent of the data, Cartwright suggested the features could have formed as a result of downslope sediment transfer from a deltaic system, or, alternatively, alongslope oceanic currents flowing through the North Sea basin. Over the last decade, the increasing availability of commercial 3D seismic data has endorsed a process-based understanding of spatial depositional and erosional patterns within the strata column (Gregersen 1997; Praeg 1997; Hansen *et al.* 2004; Kuhlmann & Wong 2008; Andresen *et al.* 2009).

Geophysical data and methods

The study area is located within the UK and Norwegian Central Graben and includes UK quads 22, 23 and 29, and Norwegian quads 1, 2 and 7 (Fig. 1). The seismic interpretation, based on PGS Central North Sea MegaSurvey (version 2006), covers approximately 25 000 km^2 with a bin spacing (line and trace) of 12.5 m. The record length is 7000 ms and the sample rate is 4 ms. The dominant frequencies extracted from the seismic data at well positions varied from 15 to 40 Hz. With checkshot velocities of 1.8–2.0 km s^{-1} recorded in the Neogene interval, this yields a vertical resolution ranging from 10 to 33 m. The seismic data was converted to zero phase and is in reverse SEG standard (a positive pulse corresponds to a downward decrease in acoustic impedance). The regional mapping was based on a decimated dataset with a line and trace spacing of 37.5 m.

The MegaSurvey is constructed from many individual 3D survey volumes, allowing a consistent tracing of prominent reflectors over a wide region, with only a few limited areas missing. The seismic data patches still mirror the original sampling and processing parameters, which differ from area to area, visible on time slice maps as significant amplitude changes. In some areas the amplitudes in neighbouring survey patches change phase, suggesting different phase rotations or time shifts between individual surveys. Because of these edge effects, care was required in the mapping of seismic horizons and the use of autopicking utilities. In addition to these data and processing artefacts, the seismic image quality is influenced by velocity anomalies in the overburden caused by infilled Quaternary valleys and shallow gas accumulations.

Following seismic stratigraphic principles based on geometries and terminations of strata (Mitchum *et al.* 1977), six seismic horizons, representing major depositional or erosional boundaries, were identified within the Late Neogene package. Detailed mapping was performed on the northern sections of horizons 4 and 6 to capture sub-kilometre scale channel features. A regional seismic interpretation of all horizon was carried out, in order to relate the channel features to major depositional phases in the central basin, and establish seismic–stratigraphic (e.g. chronological) ties southward into the Danish sector, where the biostratigraphic framework is based on dinocyst zonations (Rasmussen *et al.* 2005; Dybkjær & Piasecki 2008). As part of the regional seismic interpretation, TWT thickness (isochron) maps, based on a 5×5 km grid, were produced for the Late Neogene mega-units. The horizons have been tied to selected wells using log traces of gamma-ray (GR), deep resistivity (ILD), sonic (DT), density (RHOB) and calliper (depending on the availability and quality of borehole data from the Neogene interval).

Results

Seismic-stratigraphy of the Late Neogene succession

The interpreted horizons are demonstrated on three regional seismic sections with ties to selected wells (Figs 2–4). Table 1 summarizes information on horizon reflection character, well log response and stratigraphic correlation. A regional well log correlation and stratigraphic time scale are shown in Figure 5. Late Neogene depositional changes in the Central Graben are illustrated by isochron maps of three major horizon intervals (Fig. 6).

Horizon 1 is equivalent to the Mid Miocene Unconformity (MMU) that forms the base boundary of the Late Neogene basin (Fig. 1) (Clausen & Korstgaard 1993). It is defined by a negative (red) high-amplitude pulse, corresponding to a downward decrease in acoustic impedance from normally compacted sediments to overpressured sediments (Figs 2–4). The horizon is modified by small-scale polygonal faulting related to shale dewatering during

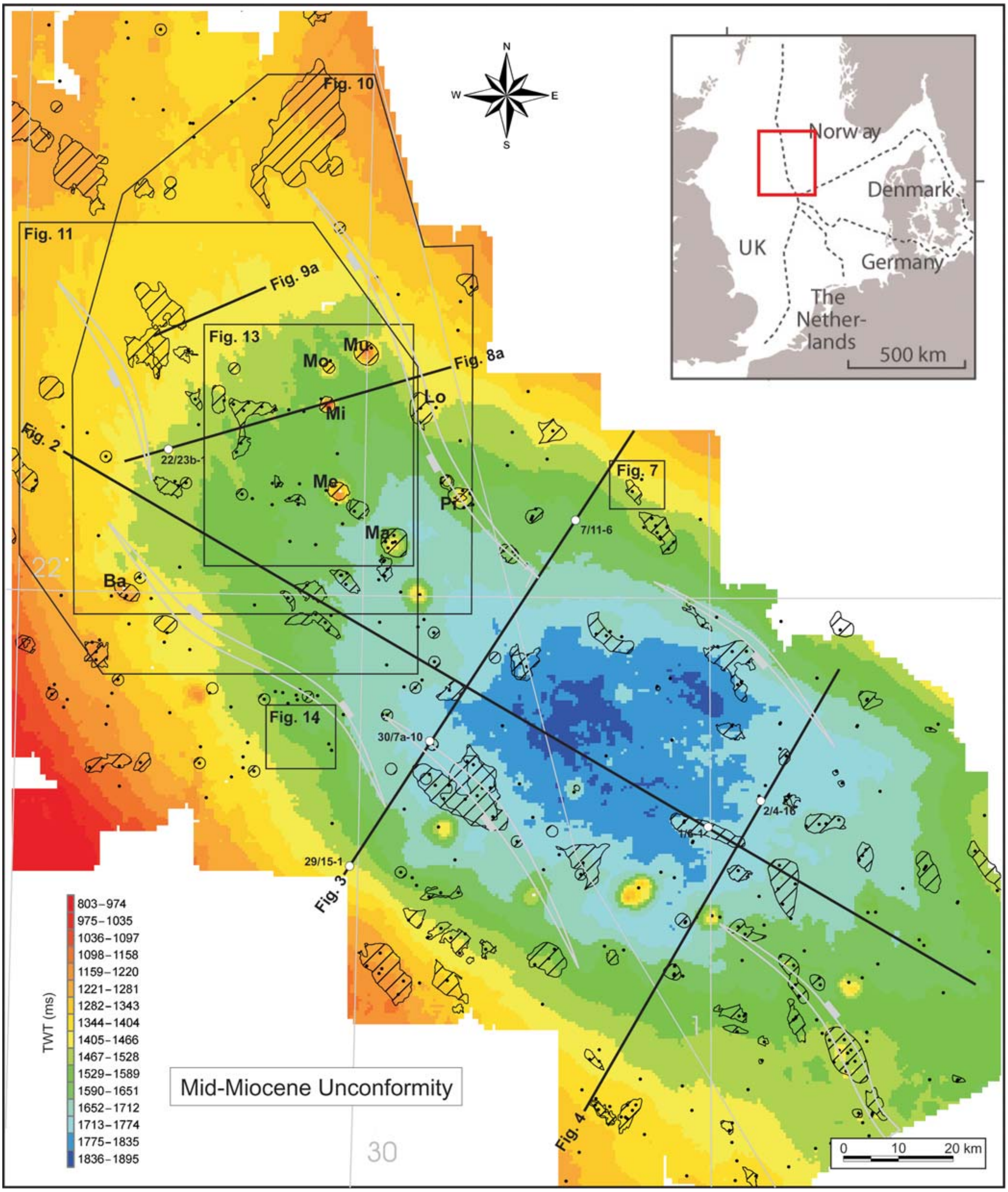

Fig. 1. TWT structure map of the Mid Miocene Unconformity across the UK and Norwegian sector of the Central Graben. Positions of seismic lines, wells and 3D horizon maps in subsequent figures are indicated. Hydrocarbon fields/discoveries are outlined (cross-hatch). Concentric salt diapirs within the detailed mapping area are indicated: Banff (Ba), Lomond (Lo), Machar (Ma), Merganser (Me), Mirren (Mi), Monan (Mo), Mungo (Mu) and Pierce (Pi). Major bounding faults delimit the Central Graben from Jæren High and Sørvestlandet High to the NE, and the West Central Shelf and Mid North Sea High to the SW.

the early burial stage (Cartwright & Dewhurst 1998). These features become more pronounced in the basin centre where the MMU attains a maximum depth of 1800 m. Horizon 2 marks the upper boundary of a parallel stratified unit that drapes across the basin topography, displaying a maximum TWT thickness of *c.* 0.2 s in the central parts and onlap onto the basin margin toward west and SW (Figs 3 & 4). As such, it is conformable to the MMU horizon, except over salt diapir structures where the entire sequence is truncated (Figs 1 & 8). On the SE flank of the basin, Horizon 2 forms a prominent downlap surface for the overlying succession (Fig. 4). A strong and regionally consistent GR log response, often seen as an upper and lower peak, indicates a

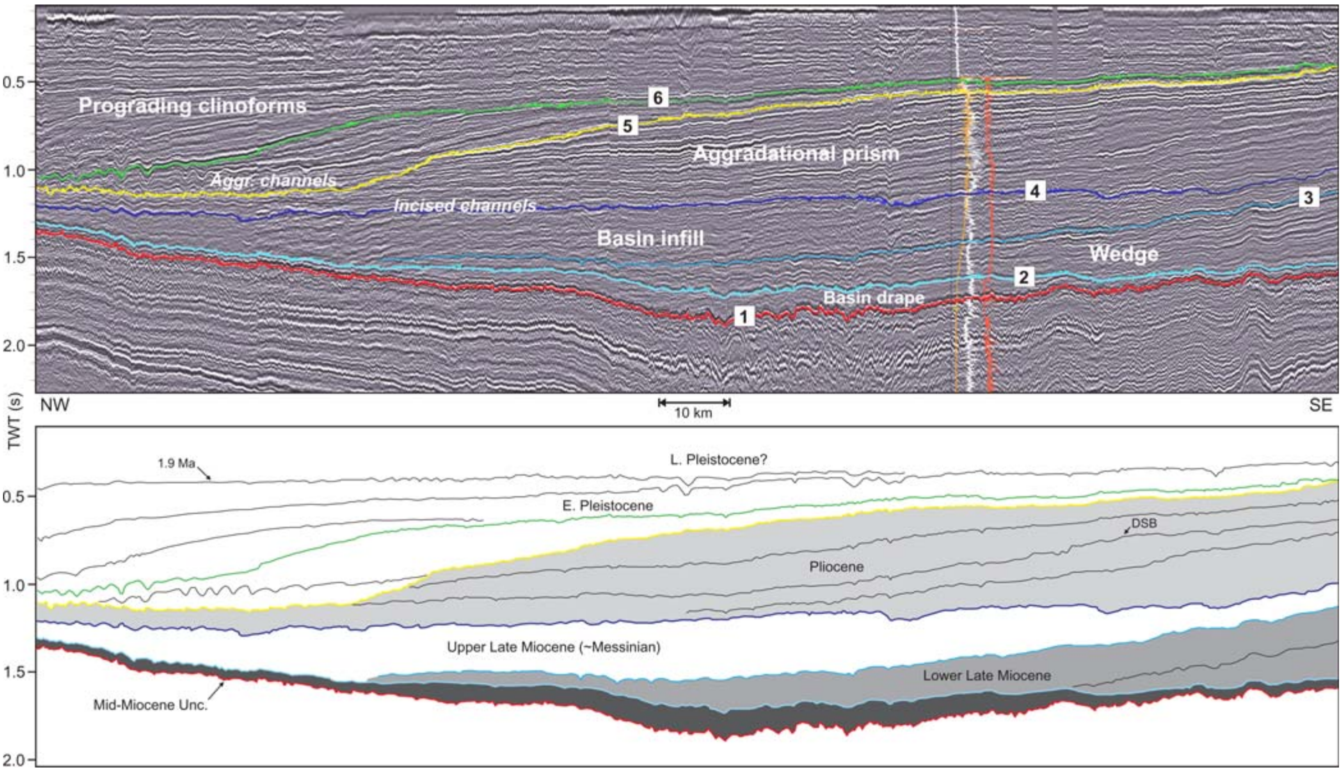

Fig. 2. Regional seismic profile and corresponding interpretation along the NW–SE axis of the Central Graben (line position shown in Fig. 1). Seismic character, well log signature and stratigraphic correlation of horizons are summarized in Table 1. An age of 1.9 Ma at the top marker of the progradational succession is based on chronological results from the southern Central Graben (Kuhlmann & Wong 2008). Position of well 1/6–1 is shown with log traces representing resistivity (orange), GR (white) and sonic (red). Position of a DSB within the Pliocene prism is interpreted from a shift in dip above a series of truncated wedge-shaped units. Total line length: 185 km. Data courtesy of PGS Ltd.

mica-rich shale composition. The unit is interpreted as a hemipelagic transgressive deposit, representing a maximum flooding surface that is time-equivalent with the Hodde Formation in western Denmark (Michelsen *et al.* 1995).

The ensuing Late Miocene succession, delimited by horizons 2 and 4, displays progressive infill of the central basin by two major depositional units. The lower unit (horizons 2–3) forms a wedge package that extends over the southeastern Central Graben and thins over the western margin towards west and SW (Figs 2 & 6a) (Michelsen *et al.* 1995). The upper unit of the Late Miocene succession (horizons 3–4) fills the distal accommodation space of the central basin. Internally, the unit is weakly reflective,

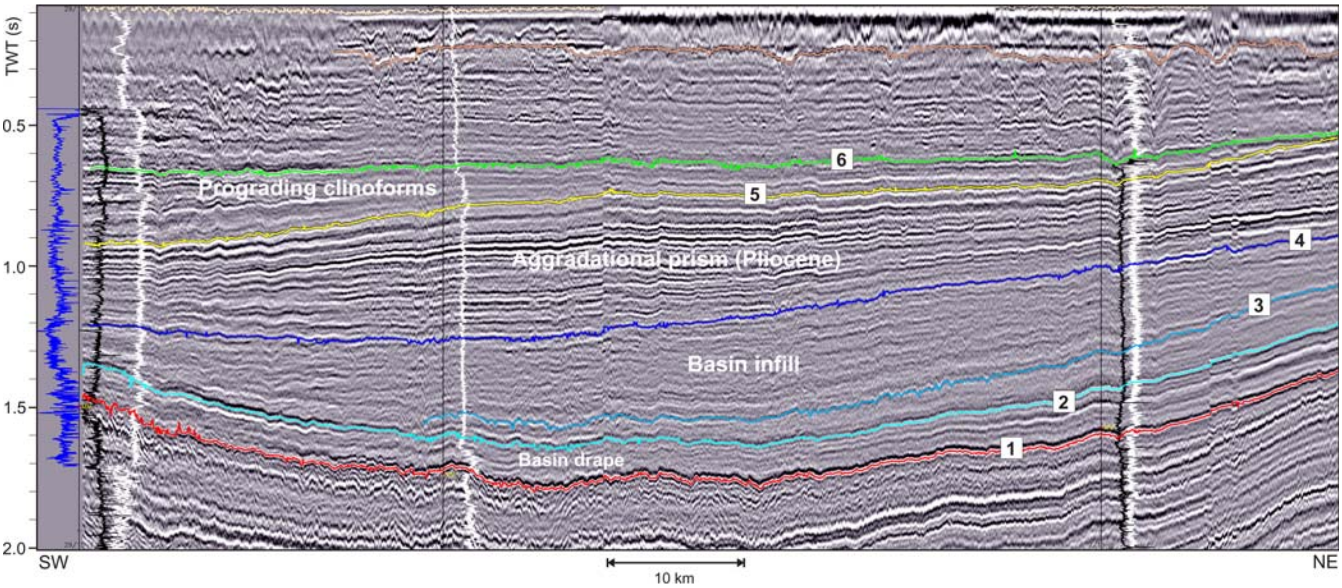

Fig. 3. Regional seismic profile perpendicular to the basin axis (line position shown in Fig. 1). Seismic character, well log signature and stratigraphic correlation of horizons are summarized in Table 1. Position of wells 29/15–1, 30/7a-10 and 7/11–6 are shown with log traces representing calliper (blue), density (black) and GR (white). Note thickening of the Pliocene prism over the central part of the basin. Truncation formed by glacial valley systems is observed in the shallow interval (brown horizon). Total line length: 93 km. Data courtesy of PGS Ltd.

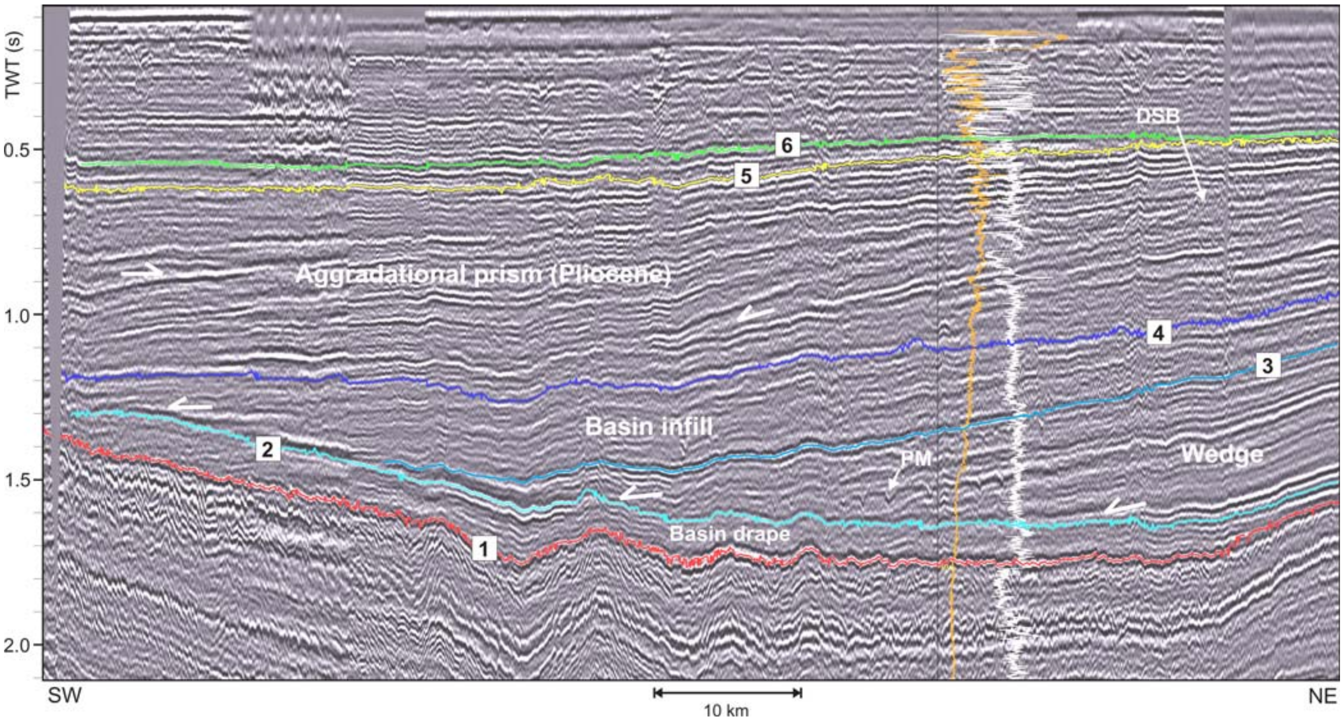

Fig. 4. Regional seismic profile perpendicular to the basin axis (line position shown in Fig. 1). Seismic character, well log signature and stratigraphic correlation of horizons are summarized in Table 1. Position of well 2/4–16 is shown with log traces representing resistivity (orange) and GR (white). Notice the internal strata complexity of the Pliocene succession, manifest by a series of coarsening-upward depositional units that appear to onlap a concave dipping and truncating reflector, interpreted as a DSB. Pockmark (PM) features are observed below Horizon 3. Total line length: 90 km. Data courtesy of PGS Ltd.

displaying a discontinuous and hummocky seismic facies with elements of progradation toward NW (Fig. 2). The erosional character of Horizon 4 is best defined in the northern and western part of the basin, where it is clearly marked by incised channel features (see detailed description detail below). The unconformity can be traced into the southern basin (Feda Graben), but becomes less distinctive as the horizon enters a more conformable package updip eastwards. Along the northeastward basin margin Horizon 4

Table 1. Summary of horizon characteristics and inferred ages

Horizons	Seismic reflection character	Log response	Correlation	Stratigraphic age*
H6	Strong, continuous reflector (N in basin section); part of conformable prograding succession	GR decrease (or sharp transition); DT trough	Intra CSS-9 (1) Condensed interval above Unit 7.4 (2) and Seq. I (3)	Early Pleistocene (2.2–2.5 Ma)
H5	Strong, continuous reflector (P) over sediment prism; truncated and poorly traceable on northward downdip section	GR and DT trough; ILD peak	Top CSS-8 (1) Top Unit 7.4 (2) Top Sequence I (3)	Late Pliocene (*c*. 2.6 Ma)
H4	Moderate to weak response (P) with low lateral continuity; displays incised unconformity with low-angle downlap above	GR minima; ILD culmination after gradual increase; CALIP decrease	Top CSS-7 (1) Top Unit 7.1 (2) Top Sequence F (3)	Miocene/Pliocene transition (5–6 Ma)
H3	Moderate, semi-continuous reflector (N) with onlap termination or distal pinchout toward N and W	Base of GR peak; ILD trough	Intra CSS-7 (1) Intra Unit 7.1 (2) Top sequence E (3)	Upper Late Miocene (7–8 Ma)
H2	Moderate, continuous reflector (N); prominent downlap surface in the Central Graben, distal onlap over the western basin margin	GR and CALIP increase; DT and RHOB decrease	Intra CSS-7 (1) Intra Unit 7.1 (2) Base Sequence E (3)	Upper Mid Miocene (11–12 Ma)
H1	Strong continuous response (N); unconformable horizon marked by polygonal faulting	Base of GR peak; DT and RHOB low; minor ILD decrease	Top CSS-6 (1) Top Unit 6 (2) Top Sequence D (3)	Lower Mid Miocene (15–16 Ma)

*ICS International Stratigraphic Chart, 2009.

Summary of reflection character, well-log response, correlation to previously defined units, and stratigraphic ages of seismic horizons 1–6. P, positive phase ('hard kick'); N, negative phase ('soft kick'). Bracketed numbers in correlation column refer to (1) Jordt *et al.* (1995), (2) Michelsen *et al.* (1995) and (3) Rasmussen *et al.* (2005). Approximate stratigraphic ages are based on Dybkjær & Piasecki (2008), although with the Pliocene/Pleistocene boundary defined at 2.59 Ma, equivalent to Top Piacenzian, following the International Stratigraphic Chart, version 2009 (www.stratigraphy.org/upload/ISChart2009.pdf).

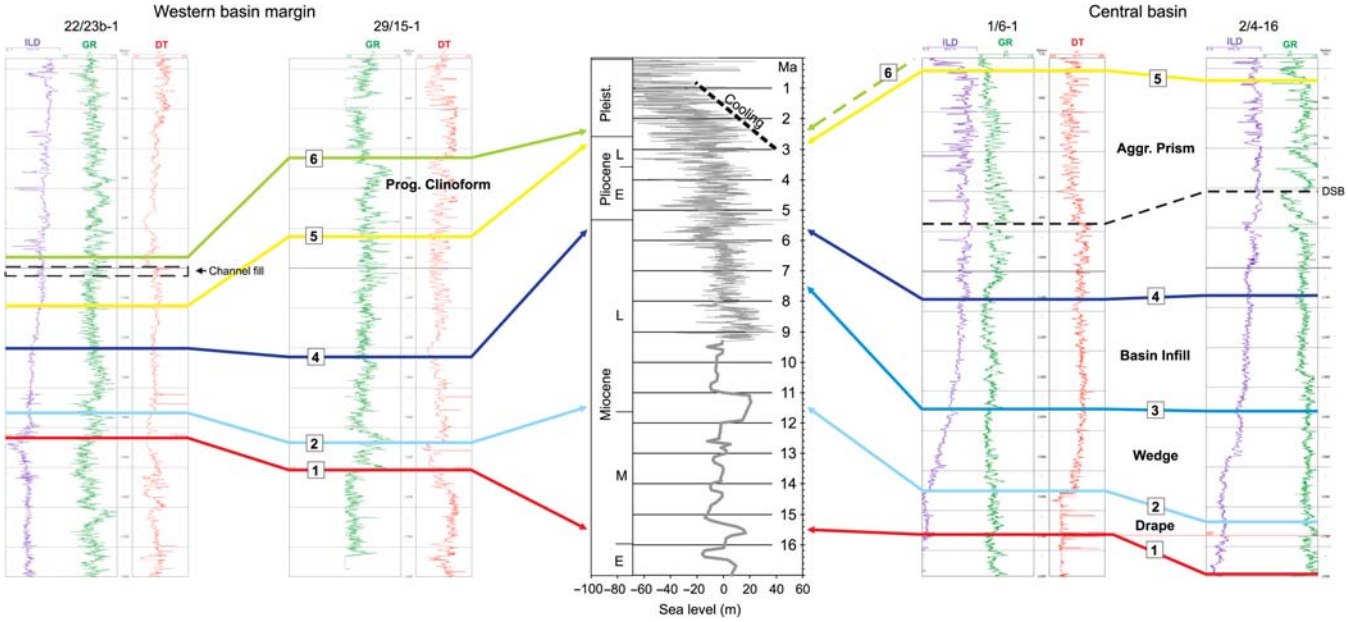

Fig. 5. Correlation of interpreted horizons between four wells forming a SE–NW transect through the Central Graben (see Fig. 1 for well locations). The horizons are projected onto a time-scale of global sea-level fluctuations over the last 17 Ma (Miller *et al.* 2005) using the inferred stratigraphic ages in Table 1. Hatched line between wells 1/6-1 and 2/4-16 demarcates the base of the mounded prism component that correlates updip to a DSB (Figs 2 & 4).

displays a southwesterly dip of 0.5–0.8° (Figs 3 & 4). On log motifs the horizon is characterized by the culmination of a steady increase in resistivity (Fig. 5).

The Pliocene succession, bounded by horizons 4 and 5, forms a wedge-shaped sedimentary prism constructed by progradational and aggradational units that build out towards the NW from a main depocentre over the Feda Graben (Figs 2–4, 6b). The aggradational component of the prism, occupying the central basin, is characterized by convex, high-amplitude reflectors forming individual units that thin toward the margins of the prism body (Fig. 3). In the southwestern sector of the basin the base of the succession thickens into a separate package of westward dipping units. This package is bounded above by a positive phase reflector, displaying a marked change in dip interpreted as a depositional shore-line break (DSB) (Van Wagoner *et al.* 1988) (Figs 2 & 4). On well log motifs, the mounded aggrading component of the prism is characterized by high-frequency GR variations and distinct saw-tooth patterns, indicative of upward-coarsening cycles (Fig. 5) (see also Sorensen *et al.* 1997). Internal strata configurations of the sedimentary prism have been noted, but a detailed analysis of these features has not been completed as part of this study. Toward NW, the gross geometry of the prism is determined by thinning and apparent truncation of strata underneath the dipping section of Horizon 5 (Fig. 2). Along its deep basinward position in the northern basin, Horizon 5 is superimposed by hummocky reflectors representing aggradational channel formations encapsulated by a progradational clinoform unit (see detailed description below). Further north, the horizon becomes a downlap surface for younger progradational units. The relief assumed from the internal depositional break amounts to 400 m, while the maximum relief of the prism, from topset strata to its basinward unconformity, is *c*. 700 m (based on average V_{seis} of 2000 m s^{-1}). Correlating

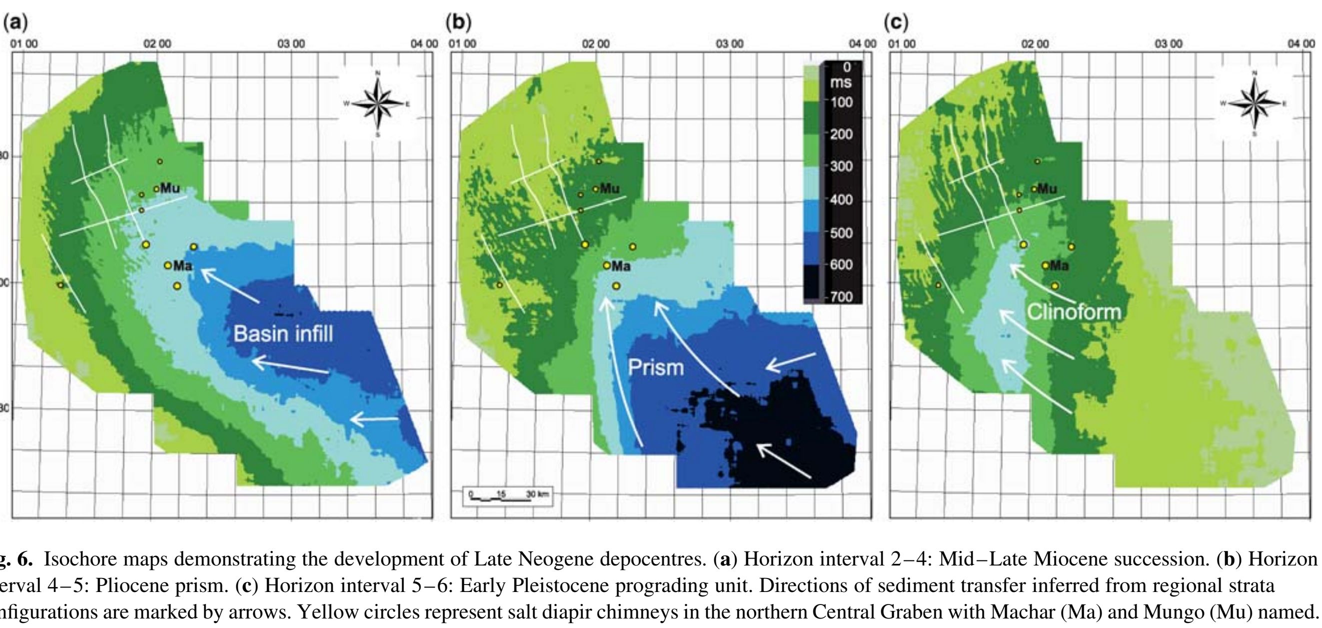

Fig. 6. Isochore maps demonstrating the development of Late Neogene depocentres. (**a**) Horizon interval 2–4: Mid–Late Miocene succession. (**b**) Horizon interval 4–5: Pliocene prism. (**c**) Horizon interval 5–6: Early Pleistocene prograding unit. Directions of sediment transfer inferred from regional strata configurations are marked by arrows. Yellow circles represent salt diapir chimneys in the northern Central Graben with Machar (Ma) and Mungo (Mu) named. Positions of seismic sections in Figures 8, 9 and 12 are shown.

Horizon 5 to the Lone-1 well in the Danish sector suggests a biostratigraphic age of 2.4–2.6 Ma (Piasecki, pers. comm.). Assuming a Pliocene age for the entire sediment prism (2.6–5.3 Ma) yields average sediment rates of 0.1–0.2 m ka^{-1}. However, the northward depocentre progression of the prism, and hence asynchronous development along the graben axis, implies that true sedimentation rates were higher.

Horizon 6 defines the top of a clinoform within a progradational system above the sedimentary prism. The clinoform unit contains the geomorphic elements of an aggrading channel system (see detailed description below) and demarcates a 400 m thick, north–south elongated depocentre across the northern Central Graben (Fig. 6c). Horizon 6 can be traced from a basinward position at the northern end of the survey and southward updip, where it converges to a near-horizontal position above Horizon 5 (Figs 2 & 3). Here, thinning and apparent truncation of topset strata is observed within the condensed interval over the prism succession (Fig. 7). There is no evidence of channel incision or patterns associated with fluvial-deltaic point sources for the progradational complex, but signatures of iceberg scouring in the 40–60 ms interval above H6 suggests that shallow glacial-marine conditions were introduced during deposition of subsequent progradational units (Fig. 7). Iceberg grooves at this level may possibly reflect the onset of major glaciations in the North Sea. A minimum age of 1.9 Ma of the progradational package is suggested by correlation of Horizon 6 southward along the condensed section into the Danish sector.

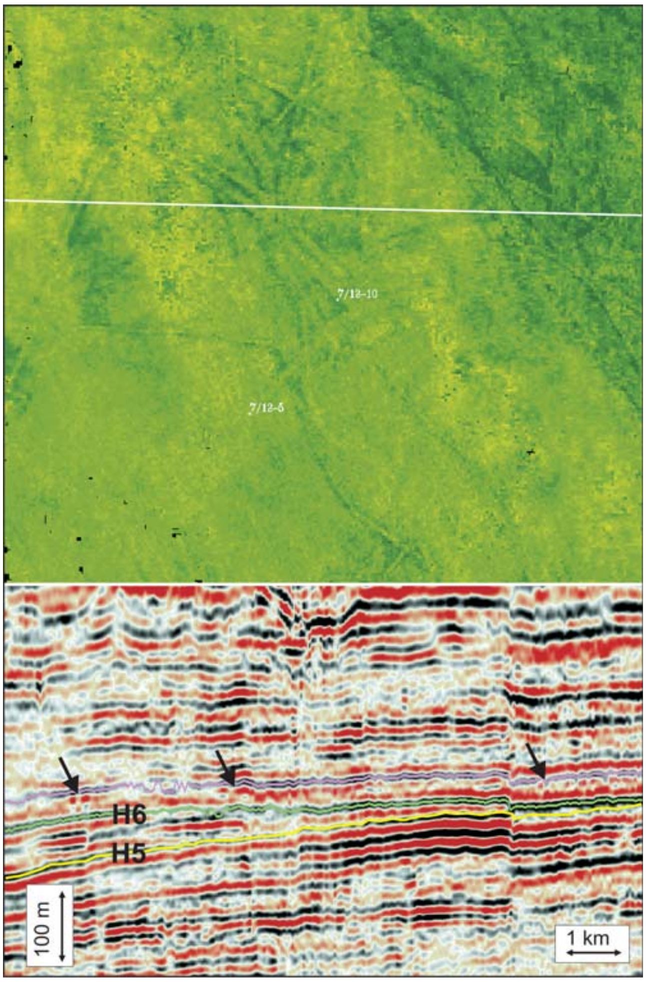

Fig. 7. Randomly interlaced furrows related to iceberg keel erosion along the condensed section of the Early Pleistocene progradational system (location of map shown in Fig. 1). The map was derived from amplitude extraction between Horizon 6 and the reflector located 40–60 ms above. In the seismic profile the iceberg furrows are seen as very subtle features (indicated by arrows) and thus are difficult to indentify without 3D attribute mapping. Vertical discontinuity to the right represents survey boundary.

The sigmoidal clinoform package (Fig. 2) is related to a rapid phase of deltaic progradation, infilling the remaining western part of the North Sea basin in a general direction from east to west. Previous work in the southern North Sea basin (Cameron *et al.* 1993) has established the seismic-stratigraphy with ties to Dutch reference wells (Kuhlmann & Wong 2008). These results date the progradational units to between 2.6 and 1.9 Ma, thus supporting the inferred minimum age. As far as a near-synchronous basin-wide development of the progradational complex can be assumed, the initial clinoform defined by Horizon 6 was probably deposited during the earliest Pleistocene (2.2–2.5 Ma) with very high sedimentation rates in excess of 0.80 m ka^{-1} (Fig. 5). The clinoform may correlate with the 'mudstone drape' capping the Utsira Sand north of the study area (Head *et al.* 2004).

Observations from detailed mapping of channel features

Incised channels on Horizon 4. The erosional character of Horizon 4 is clearly displayed on the seismic sections across the northern Central Graben (Figs 8 & 9). Incisional features form a network of cross-cutting channels, which can be traced from the central parts of the basin and northwards following a main trend along the inclined NE section of Horizon 4 (Fig. 10). The channel network disappears toward south (approximately defined by seismic line in Fig. 3), or becomes untraceable due to scale resolution and processing quality. The TWT structure of Horizon 4 demonstrates a complex morphology, representing two generations of erosional events (Fig. 10). Linear channel-ridge features, manifest by a low relief (<30 ms TWT) along a 330° strike, are superimposed by segments of cross-cutting curvature channels displaying depths of 40–70 ms and widths of 600–1200 m. Infilling of the incised channels occurs predominantly by lateral accretion, on a scale approaching the limit of seismic resolution (Fig. 10, seismic insert). On the eastward basin margin, incised channels are observed to pass alongside concentric zones above major salt diapirs. The channel pathways, however, do not appear to be determined or influenced by these features, suggesting that they commenced prior to salt piercement of the Late Neogene sediment package.

Seismic facies of lateral accretion, covering the incised channels, is indicative of a high-energy setting dominated by bedload transport, representing a fluvial-deltaic or possibly shallow marine (e.g. intertidal) environment (Collinson 1996). The channel pattern is reminiscent of a drainage system, following the central axis of the basin and diverging towards the north. A high proportion of non-cohesive sediments in the Upper Late Miocene interval, below Horizon 4, is suggested by low GR and calliper log values, combined with a gradual and consistent increase in resistivity (e.g. wells 29/15-1 and 1/6-1) (Fig. 5). Formation of the incised channels at base sea-level is supported by the presence of freshwater flora and increased levels of reworked dinocysts in the corresponding Messinian interval in Danish wells Lone-1 and Tove-1 (Piasecki, pers. comm.).

Aggrading channels below Horizon 6. The TWT structure of Horizon 6 (Fig. 11a, b) illustrates the morphology of channels at a stage of progradational infill below the clinoform unit (Fig. 8). Laterally, two different types of channel geometry are recognized: (1) curved and discontinuous (i.e. segmented) channels with a variable spacing of 3–8 km, extending from the NE section of the lower slope; (2) linear, but likewise discontinuous, channels with a more regular spacing of 2–3 km in the NW part of the basin.

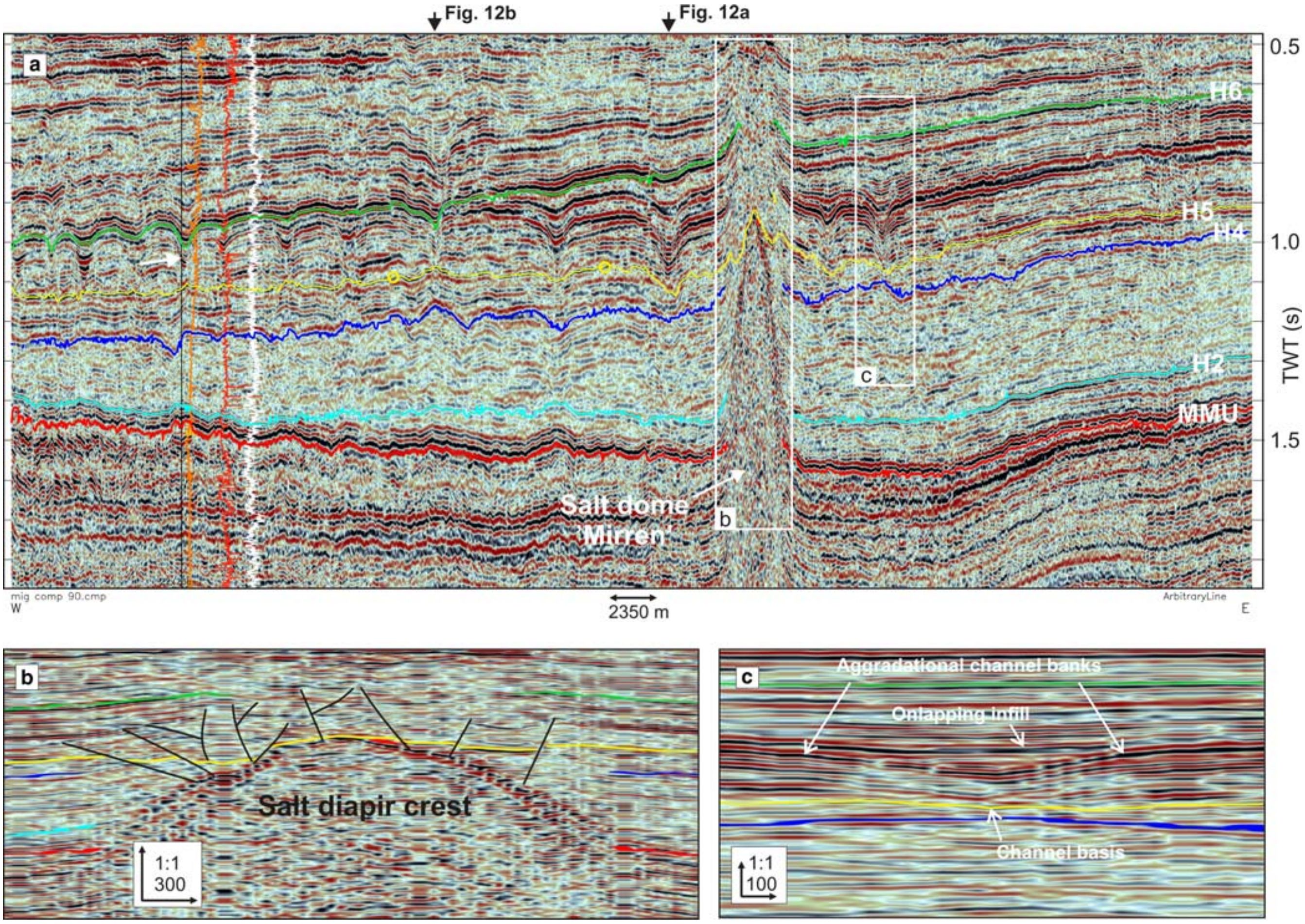

Fig. 8. (**a**) Seismic cross-section of channel features in vicinity of the 'Mirren' salt dome (line position shown in Figs 1, 10 & 11). Horizon 4 (blue) is marked by erosion and incised channelization (compare with Fig. 10). Aggradational channels build up from a stratigraphic level close to Horizon 5 (yellow) and are subject to progressive downdip burial within the clinoform below Horizon 6 (green). Notice the incongruent infill patterns of adjacent channels east of the 'Mirren' dome. Well log traces represent GR (white), sonic (red) and resistivity (orange). Strong reflection at the base of aggradational channel corresponds to sonic velocity peaks (marked by arrow). Abrupt shifts on Horizon 5 reflect survey patches. (**b**, **c**) Detailed zoom-in on specific sections displayed with 1:1 aspect ratios (ms v. m) approaching a true scale. (**b**) Top of the 'Mirren' structure illustrating thinning and extensional faulting of Horizon 5 over the diapir crest. (**c**) Detailed structure of channel profile indicating aggradational channel banks and onlapping infill within a 100 ms deep trough. Data courtesy of PGS Ltd.

The channel widths range from 700 to 2500 m, with type 1 troughs showing the largest cross-sections. The discontinuity of type 1 channels occurs in a manner where troughs die out and re-appear in a slightly offset position, resulting in en-echelon geometries on Horizon 6 (Fig. 11). Type 1 channels are oriented almost due north while type 2 are aligned NNW (330°). It is noteworthy that the channels are orientated at an oblique angle to the general strike of the clinoform slope.

The architecture of the aggrading channel (Figs 8 & 9) demonstrates consecutive stages of development. The base of the channel thalwegs apparently corresponds to Horizon 5, although a precise definition of the deepest stratigraphic level is difficult due to acoustic distortion (e.g. seismic pull-up) below the troughs, intrabed multiples and possible tuning artefacts. Truncation of Horizon 5 is generally observed below the deepest channel troughs, suggesting that the initial channel pathway was generated by erosion (Fig. 9b). Basal truncation occasionally coincides with incision on Horizon 4, below, although a regular superposition of the two channel morphologies is not observed (Figs 8 & 9). The erosive stage is associated with formation of low-relief channel banks. Subsequently, the channel profile deepens by preferential deposition over interchannel regions, forming mounded and generally symmetric structures that tend to be marked by erosion along steep channel flanks (Fig. 9c). Channel depths measured by the height from aggrading flanks to the incised base are in the range of 60–120 ms TWT, while apparent dips across the steep flanks are within 5–15°. The deepest parts of the troughs are characterized by parallel onlap and occasionally lenticular infill facies (Figs 8c & 9b). The channel morphology is gradually reduced and buried as younger clinoforms prograde northwestward (Fig. 8a). The asynchronous development implies that the channel sections furthest to the south, underneath the depocentre of the clinoform, are completely buried at a time when channels further north are still active, in agreement with observations by Cartwright (1995). Channel segments further into the basin experience burial at a later stage during deposition of younger clinoform units above Horizon 6.

Type 1 channels are associated with marked acoustic pull-ups on the MMU below. These seismic anomalies of up to 25–30 ms TWT are clearly visible on the MMU structure map (Fig. 11c), and correspond vertically to the deepest segments of the aggradational channel network (compare with Fig. 11b). A time–depth conversion study by Armstrong *et al.* (2001) indicates that these anomalies are generated by P-wave velocity contrasts between *intra*channel deposits and the juxtaposed *inter*channel aggradational regions. A difference in V_{seis} of 400–600 m s^{-1} is required to explain the pull-up on the MMU level, suggesting that the infill represents consolidated sandstone, presumably formed by early diagenetic calcite precipitation (Hovland *et al.* 1987; Schulz-Rojahn *et al.* 1998).

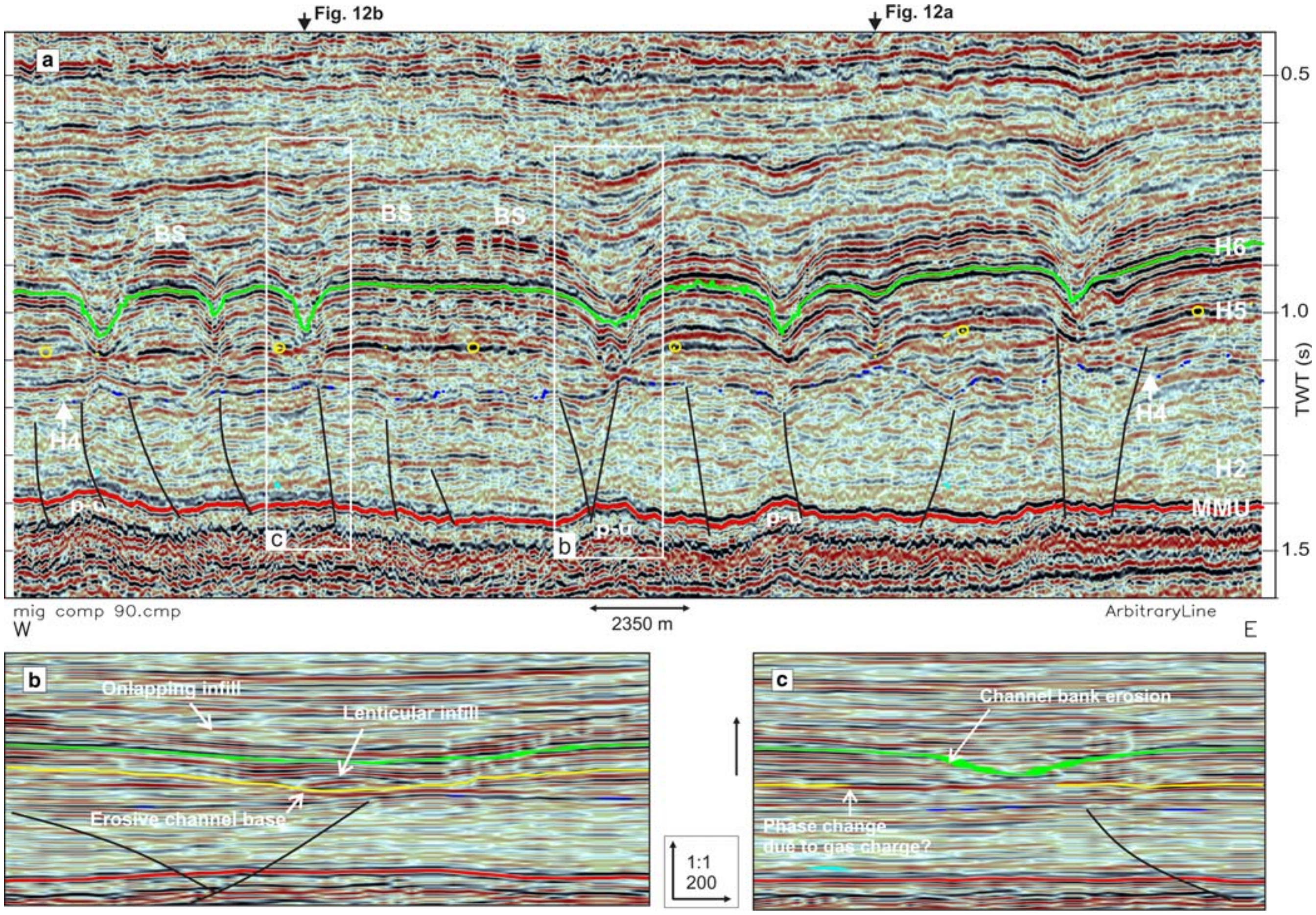

Fig. 9. (**a**) Seismic cross-section of channel formations in the northern part of the basin (line position shown in Figs 1, 10 & 11) with indications of faults extending from the MMU. Horizon 4 (blue) is marked by erosion and incised channelization (compare with Fig. 10). Aggradational channels build up from a stratigraphic level immediately below Horizon 5 (yellow). At this location active channel troughs are time-correspondent with Horizon 6 (compare with Fig. 11). Notice bright spots (BS) over interchannel regions and prominent acoustic pull-up (p-u) of the MMU below channel troughs. (**b**, **c**) Detailed architecture of the aggradational channels is shown in zoom-in sections with 1:1 aspect ratios (ms v. m) approaching a true scale. The channel trough in (**b**) displays a lenticular infill above an erosional base. A local amplitude phase shift along Horizon 5 (**c**) suggests presence of gas charged sediments below the channel trough (notice lack of pull-up). Data courtesy of PGS Ltd.

An average V_{seis} of 2500 m s^{-1} for the infill facies implies that actual trough depths are likely to be in the range 75–150 m. Well verification of inferred channel sands was limited to a single borehole penetrating a type 2 channel trough (Figs 5 & 8a). The base of this channel is marked by a 'hard-kick' that correlates with two sharp but minor peaks on the sonic log. It is noteworthy that some of the channels lack a distinctive pull-up response despite the presence of deeply infilled troughs. This may possibly be explained by a more fine-grained channel infill (e.g. less intense cementation), or the presence of gas charged sediments, as suggested in Figure 9c.

The extent and geometry of the channel segments buried below the clinoform is illustrated by axial seismic profiles (Fig. 12) and channels traces on time-slice sections (Fig. 13). The axial profiles highlight the discontinuous channel pathways and noticeable lack of gradient along thalwegs. Some of the channels terminate at accumulations of hummocky or mounded depositional features which resemble contourites (Nielsen *et al.* 2008). A migrating seismic facies of these deposits suggests a northward sediment transport (Fig. 12c).

Relationship between channels and salt diapir leakage zones

Type 1 channels tend to commence from a position at (or in vicinity of) concentric chimney features related to fluid-escape over the major salt diapirs, henceforth abbreviated SLZ, Salt diapir Leakage Zones (Fig. 13). A prominent example is the channel beginning at 'Merganser' SLZ, which is infilled by a 200 m thick succession of downlapping wedge-formed units that thicken toward the steeply inclined reflectors of the chimney (Fig. 12a). The two channel segments commencing north of the 'Machar' SLZ appear to coalesce as they by-pass three SLZ further to the north (Fig. 13b). The diachronous infill structure of these adjacent channels (Fig. 8a) implies abrupt, localized shifts in sediment flux or hydrodynamic conditions. The youngest channel elements commence north of the clinoform depocentre, apparently time-equivalent with Horizon 6 (Fig. 11). The east Central Graben diapirs protrude into Late Neogene strata (post-MMU), while protrusion into the Pleistocene interval is observed for the 'Pierce' structures, located over the main eastern boundary fault (Fig. 1) (Davison *et al.* 2000*b*). Over the salt crests the unit below Horizon 5 is marked by thinning and extensional faulting (Fig. 8b). Mapping of these features and determination of their stratigraphic relationship is limited by the seismic resolution and sediment deformation caused by subsequent fluid leakage.

Type 2 channels generally commence at the base of the clinoform unit (Horizon 6) and are not associated with concentric leakage zones. In the western basin linear pathways of type 2 channels are seen to pass through the 'Banff' SLZ, suggesting that the channels formed prior to major fluid expulsion at this site

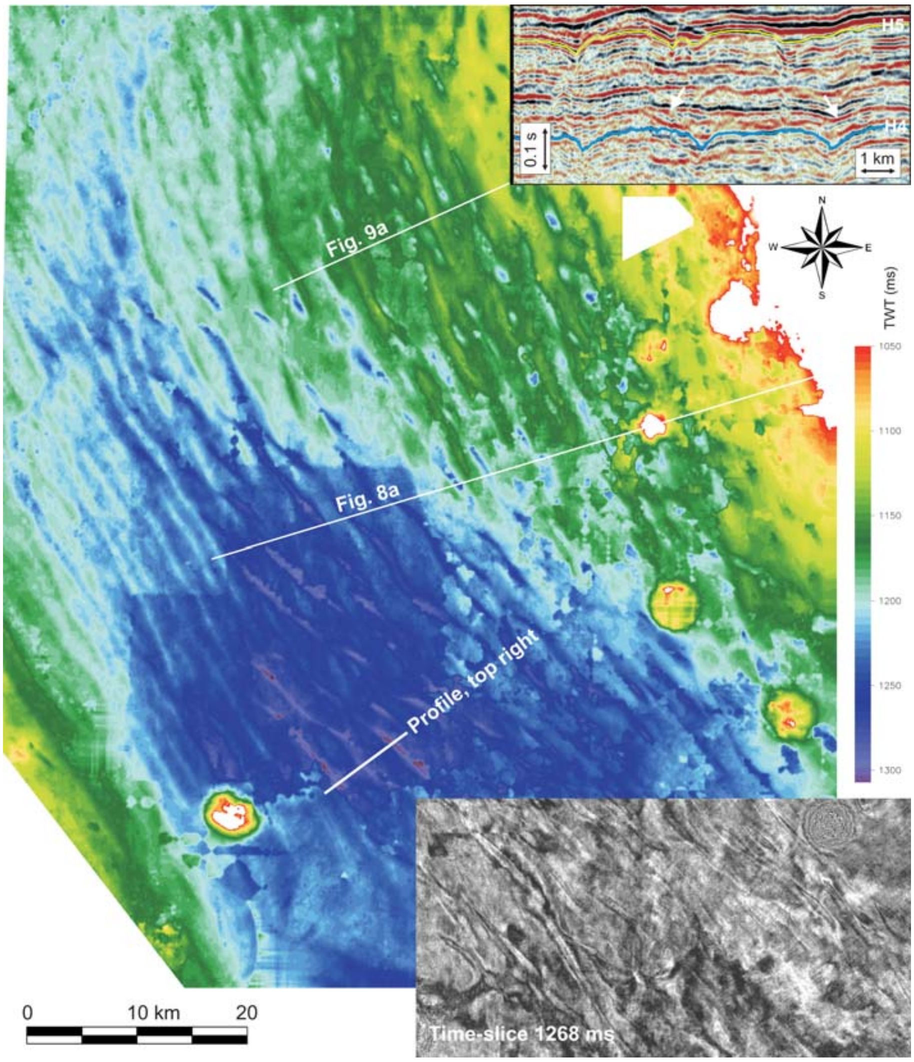

Fig. 10. TWT structure map of Horizon 4, displaying multiple incised channels that appear to cut across a former relief of ridge-trough elements. Insert, lower right, shows a seismic time-slice revealing the channel network in more detail. Channel pathways are apparently unaffected by concentric salt diapirs. The detailed seismic section (insert, top right) demonstrates seismic facies interpreted as lateral accretionary units (arrows) that infill and bury the incised channels. Notice the regional westward dip (*c.* 0.5°) across the eastern basin margin.

(Fig. 11). Potential linkages to minor (i.e. non-diapiric) gas chimneys that punctuate the Cenozoic overburden in numerous places (Fig. 12) have not been explored as part of this study, since it would require seismic attribute analyses based on individual 3D volumes. Nonetheless, it is noticeable that some of the channel elements initiate from positions close to leakage zones, marked by seismic pull-down and bright anomalies (Figs 12 & 14).

Discussion

Evidence for a contour current depositional setting

Cartwright (1995) proposed that the aggrading channels form the downslope component of a deltaic system prograding westward from the eastern North Sea (Skaggerak region). Alternatively, it was suggested that the channel features could be related to oceanic contour currents that inundated the basin at a time when a southern connection to the North Atlantic became established. Observations extracted from the present 3D seismic analyses favour a contour current mechanism, rather than gravity-driven sediment transport, for these features: firstly, the channel banks build up from a basal unconformity, which lacks a regional inclination for gravity-driven transport and updip connection to a major sediment source, for example, a fluvio-deltaic distributary system. Secondly, the channels are not continuous but display linear or arcuate segments, oriented at an oblique angle to the slope of the clinoform unit. Finally, mounded-elongate sedimentary bodies at channel terminations (Fig. 12) display asymmetric geometries and a base-disconcordant relationship that are characteristic of contourites (Faugeres *et al.* 1999; Nielsen *et al.* 2008).

The semi-parallel to arcuate pattern of channel troughs expressed by Horizon 6 (Fig. 11) displays a close resemblance to contourite ridges, channels and furrows, generated by geostrophic bottom currents (i.e. driven by horizontal pressure gradients balanced by the Coriolis effect), as observed in the Faroe–Shetland Channel (Knutz & Cartwright 2004) and Gulf of Cadiz (Hernandez-Molina *et al.* 2006). A noticeable difference is the gross symmetric shape of interchannel regions compared with the typical upslope migrating character of contourite bedforms (Nielsen *et al.* 2008). This may be attributed to the modest slope gradient in the North Sea basin and a high sediment flux focussed along the basin axis. Despite the abundance of contourites described from continental margins, modern analogues formed in semi-enclosed marginal basins are sparsely documented (Rebesco & Camerlenghi 2008). Moreover, a detailed morphological definition of these deep marine deposits rests on the availability of 3D acoustic imaging. Analogue comparisons may be considered from the pre-Neogene depositional record

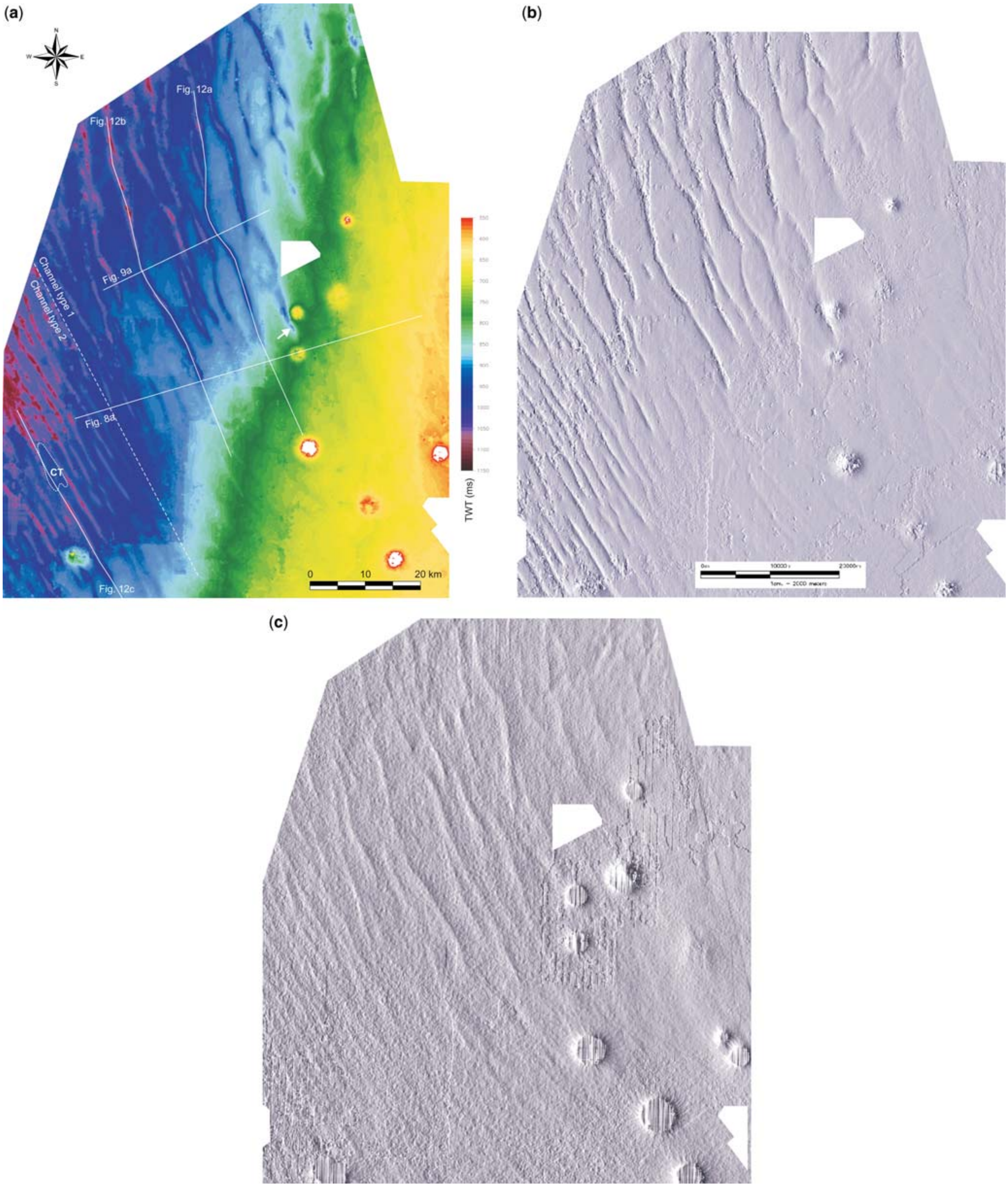

Fig. 11. (**a**) TWT structure map of Horizon 6 (position shown in Fig. 1), displaying aggradational channel elements and concentric leakage zones protruding from salt diapirs. Two types of channel geometries are recognized: curved channels with a variable en-echelon style spacing (type 1), and linear channels with a more regular spacing of 2–3 km (type 2). The channel pathways generally extend updip into the clinoform unit below the horizon, except one channel commencing from the slope break of Horizon 6 (marked by arrow). The slightly bulging character of the slope section towards the south corresponds to the northern fringe of the clinoform depocentre (compare with Fig. 6a). Position of contourite (CT) deposit inferred from the profile in Figure 12c is outlined. Delineations of seismic data patches are visible. (**b**, **c**) 3D differential maps of Horizon 6 (b) and MMU (c), enhancing the detailed topology of the seismic surfaces. The ridge-like features on the MMU horizon (c) are interpreted as artefacts representing seismic pull-up from high-velocity infill of the channel troughs, presumably carbonate cemented sand (compare with seismic cross-sections in Figs 8 & 9).

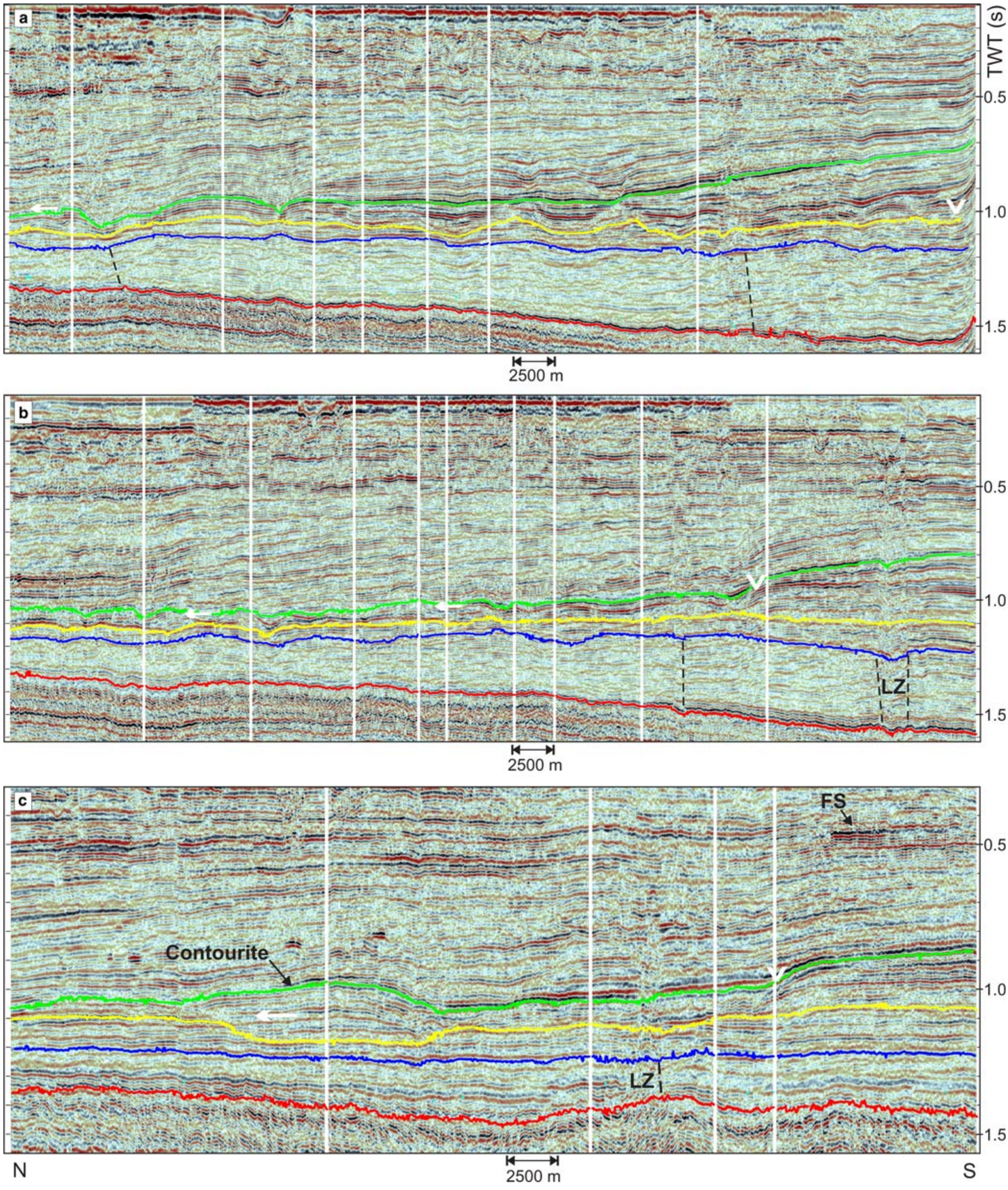

Fig. 12. Multipanel seismic sections (**a**–**c**) tracing the through axis along three channel pathways (line positions shown in Fig. 11). Notation of colour-coded horizons as in Figure 8. V-marks demarcate points of channel commencement below Horizon 6. Notice the initiation point of channel in (a) is located in the clinoform package below downlapping wedge units extending from the 'Merganser' leakage zone. In contrast, channels (b) and (c) commence at the base-of-slope defined by Horizon 6. Channel (b) is located downdip from a diffuse leakage zone (LZ), indicated by amplitude dimming, bright anomalies and seismic pull-down. Channel (c) terminates at a mounded, asymmetric depositional unit interpreted as a contourite deposit. Direction of apparent sediment migration is indicated by arrows. Data courtesy of PGS Ltd.

of the North Sea basin. Interestingly, the initial erosive stage of channelization (Figs 8 & 9) resembles low-relief channel elements recognized in the Upper Cretaceous Hod Formation, conceivably generated by geostrophic bottom-currents traversing the epieric Chalk Sea (Esmerode *et al.* 2008). This may suggest a non-cohesive character of the erosive precursor channels in contrast to the subsequent aggradational build-up, presumably requiring a high flux of clay-rich sediments.

The mounded geometry of the prism and internal high-amplitude reflection character, displaying downflank thinning/erosion

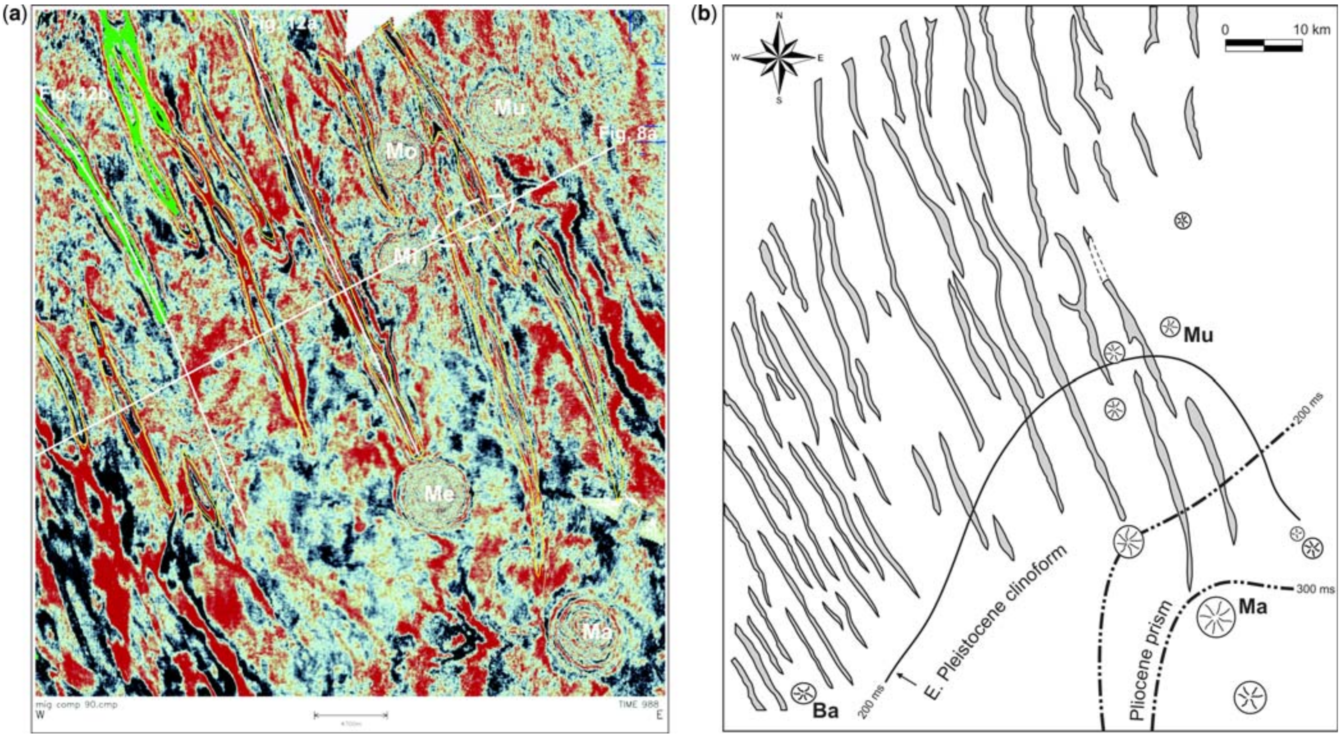

Fig. 13. (**a**) Time-slice map (988 ms TWT), cross-cutting the concentric leakage zones and aggrading channels within the clinoform unit (position is shown in Fig. 1). The leakage zones are named according to underlying salt structure: Ma, Machar; Me, Merganser; Mi, Mirren; Mo, Monan; Mu, Mungo. Position of diachronously infilled channels east of 'Merganser' is highlighted (Fig. 8a). (**b**) Traces of channel troughs based on Horizon 6 (Fig. 11a, b) and time-slice maps. The large aggradational channels (type 1) extend below the clinoform, where they appear to converge toward the concentric leakage zones. Depocentre limits of the Pliocene sediment prism (hatched lines) and Early Pleistocene clinoform (full line) are demarcated by isochrons obtained from Figure 6.

(Figs 2 & 3), represents features common to giant sediment drifts shaped along continental margins by geostrophic boundary currents (McCave & Tucholke 1986; Faugeres *et al.* 1999; Nielsen *et al.* 2008). The configuration of the erosive base of channel features juxtaposed to the aggradational prism implies that oceanographic currents were a controlling factor for sediment dispersal throughout the Pliocene. The situation of the prism, north of the main Late Neogene depocentre (Fig. 6b; see also Michelsen *et al.* 1995), is suggestive of a fan–drift contourite system (Faugeres *et al.* 1999; Knutz 2008) constructed by muddy sediments dispersed from fluvio-deltaic sources and subsequently carried alongslope by northbound oceanic currents. A potential sediment source for the Pliocene prism is the giant Baltic River (or 'Eridanos') system that drained into the German Bight until commencement of major glaciations (Zagwijn 1989; Overeem *et al.* 2001). The progradational complex of the 'southern embayment' outlined by Sorensen *et al.* (1997) appears to form the deltaic component of this drainage system. It is conceivable that sediment transport was enhanced by tidal forces but, even so, the scale and configuration of depositional elements suggests that persistent unidirectional currents were operative, similar to the geostrophic meridional flow of intermediate water masses along the NE Atlantic margin (Kenyon 1986; McCave & Tucholke 1986). For oceanographic currents to winnow and transport silt-size sediments, persistent currents of 0.15–0.20 m s^{-1} would be necessary, while currents in excess of 0.40 cm^{-1} are required for bedload movement of quartz sand (McCave 1995). Thus, construction of the aggradational channels involved steep hydrodynamic gradients, from near-quiescence over interchannel regions to high-competence flow speeds in the deep troughs. The parallel stratified channel-fill is comparable to modern environments of contourite sands, generated by strong bottom-currents in confined moat-channel settings, developed along continental slopes or circumventing sea mounts (Viana *et al.* 1998; Akhmetzhanov *et al.* 2007).

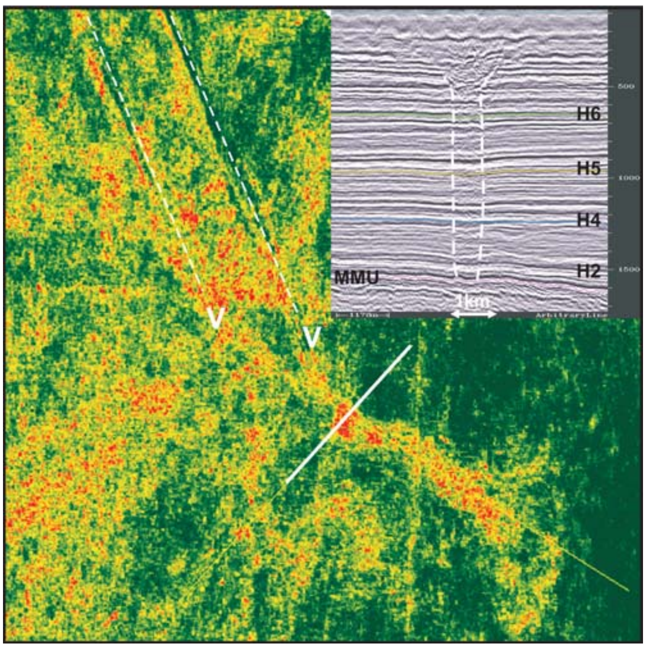

Fig. 14. Coherency map, extracted from a 100 ms interval above Horizon 4, illustrating the southernmost limit of two linear channels (type 2). The channels commence downdip from an area of low coherency (bright colours) and low-velocity pull-down below a glacial tunnel-valley (see seismic insert).

Geological controls on aggrading channels

The convergence between type 1 channels and the SLZ (Fig. 13b) alludes to a mechanistic linkage between focussed fluid-flow and bottom-current sediment transport. Previous studies have associated fluid leakage over the salt diapirs with the main phase of hydrocarbon migration into structurally confined closures along the flanks (Heggland 1998). Accordingly, fluid leakage must have succeeded peak oil maturity of Upper Jurassic source rocks, estimated to Mid–Late Miocene (Kubala *et al.* 2003). Observations by Davison *et al.* (2000*a*) of tensile fracturing, brecciation and abundant calcite cementation in chalk units above salt diapir crests, suggest that the concentric chimneys of the eastern Central Graben were conducive for pressurized fluids from older units. Episodic fluid expulsion, promoted by the buoyancy effects of the large hydrocarbon columns, is also indicated by underfilling of diapir traps (Davison *et al.* 2000*b*). Previous studies have identified Neogene sediment loading as a primary factor for development of a regional SE-to-NW pore-pressure gradient in Upper Cretaceous–Early Cenozoic formations (Japsen 1998; Vejbæk *et al.* 2005). Likewise, it is possible that fluid expulsions from the salt diapir structures may have been triggered by the northward progressing sedimentary prism (Figs 6, 13b & 15).

The structural observations and likely timing of hydrocarbon charge suggest that the formation of aggradational channels was promoted by fluid expulsion from leakage zones, positioned upstream in the bottom-current flow. This scenario is illustrated by the depositional model in Figure 15. Intense fluid escape from the seabed would facilitate mobilization of fine-grained sediments passing through the progradational system, thus making it available for suspension-transport by contour currents. It is plausible that extrusion of sediments from deeper stratigraphic intervals contributed to the channel architecture, by forming a point source for coarse-grained channel infill. Extrusive processes are presently observed over leakage zones in Gulf of Mexico, supplying an allochtonous Miocene foraminifer assemblage to the modern seabed (Kohl & Roberts 1994). Seismic results from the Norwegian–Danish Basin suggest that pressurized fluids from Paleocene formations are capable of injecting sand-prone sediments through 1 km of overburden, resulting in extrusive mounds at Mid-Miocene level (Andresen *et al.* 2009).

The previous discussion has focussed on the aggradational stage of channel formation. An important question remains as to what mechanism promoted the initial erosive trace along the channel base (Fig. 9). It is difficult to explain the segmented pattern of primary incision and bank accretion as driven exclusively by self-organizing ocean current dynamics, without an element of geological control. A more plausible scenario is that current erosion occurred preferentially along corridors of low sediment strength, promoted by fluid-flow from faults and fracture zones (Fig. 15). An early stage of this process may be represented by elongate pockmarks, observed as common phenomena in the Miocene interval of the central basin (Andresen *et al.* 2008, p. 1270) and in the present North Sea (Skaggerak) (Bøe *et al.* 1998). Also, it is pertinent to note a striking resemblance between type 1 channel styles and extensional fault patterns in the Cenozoic section west of the Central Graben (UK quad 20) (Bishop 1996). The similarity includes the arcuate en-echelon geometry scale dimension as well as the NNW–SSE orientation of these features. An inherited structural control on channel pathways is insinuated by small-scale faults that extend from the polygonally faulted lower Miocene interval to positions below the channel troughs (Fig. 9). Complete recognition of insidious faults and fracturing underneath the channels is hampered by prominent seismic pull-ups, acoustic distortion below thalwegs, and abundant seismic data boundaries. These issues stipulate the need for more research based on dedicated seismic processing. Nevertheless, enhanced fluid-flow into the channel troughs, along fracture zones connected to the MMU, would promote carbonate cementation of channel sands (Schulz-Rojahn *et al.* 1998), thus explaining the high-velocity infill (Fig. 15).

Conceivably, the concept of enhanced seabed erosion induced by fluid escape could also apply to the formation of the linear aggrading channels (type 2). However, since their spacing and NNW alignment is very similar to the antecedent incised channels, developed on the Late Miocene/Early Miocene unconformity (Horizon 4), an inherited morphological control cannot be ruled out (Cartwright 1995). Commencement of linear channels in the vicinity of fluid anomalies and velocity pull-down may suggest enhanced sediment mobility generated by hydrocarbon leakage (Fig. 14). These low-velocity zones are commonly associated with buried Pleistocene valleys formed by melt-water drainage, thus affording a potential linkage between subglacial erosion and zones of fluid expulsion (Fichler *et al.* 2005).

Implications for Late Neogene basin development

The morphological expressions of the channel horizons and the regional mapping of major depositional units in the central basin add new constraints on the Late Cenozoic development of the North Sea basin. The seismic geometry of the Late Miocene/Early Pliocene low-stand unconformity (Horizon 4) and the overlying aggradational sediment prism demonstrate rapid basin subsidence, with 600–700 m of accommodation space generated over less than 3 Ma. The development of the basal unconformity also corresponds to a 50 m eustatic sea-level fall during the Messinian, lasting *c.* 0.7 Ma (Miller *et al.* 2005), but clearly the contribution of sea-level dictated by global ice-volume is insignificant compared with the observed changes (Fig. 5). The Late Cenozoic subsidence history of the North Sea basin has been related to changes in intra-plate stress regimes (Kooi *et al.* 1991), invoking a response to the last tectonic cycle of the Eurasian–African plate collision, which culminated during Late Miocene (Ziegler 1992). Palaeo-records from NW Europe indicate a Late Miocene sea-level regression and exposure of the Dover Strait associated with compression along the Variscian deformation front (van Vliet-Lanoë *et al.* 2002). According to Hillis *et al.* (2008), crustal compression during the Miocene was the main cause of uplift in the British Isles and southern North Sea, evident by widespread exhumation of older Cenozoic strata, notably in the Wessex–Weald Basin. A Mid to Late Miocene compressional phase has also been advocated for the British–Norwegian Atlantic margin (Ritchie *et al.* 2003; Løseth & Henriksen 2005), suggesting that tectonic stress-fields developed by a combination of Mid-Atlantic oceanic ridge-push and Late Alpine collision (Dore & Lundin 1996).

As discussed earlier, formation of aggrading channels and the prism complex appears to have evolved under the influence of geostrophic currents, implying an open connection to the Atlantic Ocean via the Channel strait. Such a current system would probably require water depths of more than 300 m (Kenyon 1986; New & Smythe-Wright 2001), unless hydrographic conditions specific to the Pliocene palaeoceanography (Raymo *et al.* 1996) permitted a shallower mode of circulation. Palaeogeographic reconstructions, based on the shelly ‘Crag’ and ‘Red Sand’ formations in NW Europe, indicate that a broad seaway to the Atlantic existed during Late Pliocene, 3.75–2.55 Ma (Zagwijn 1989; Funnell 1996; van Vliet-Lanoë *et al.* 2002). The elevated position, up to 180 m above datum in eastern England, and the marine fauna assemblage of these deposits, suggests that sea-levels were substantially higher than present (Funnell 1996). The palaeobathymetric configuration of the Channel is difficult to ascertain but seismic signatures of bottom-current erosion in the southern North Sea basin, at palaeo water depths of at least 250–300 m, support the presence of a Late Pliocene–Early Pleistocene intermediate water passage (Kuhlmann & Wong 2008). From *c.* 2.4 Ma (pre-Tiglian) the Channel seaway closed as the southern North Sea basin became

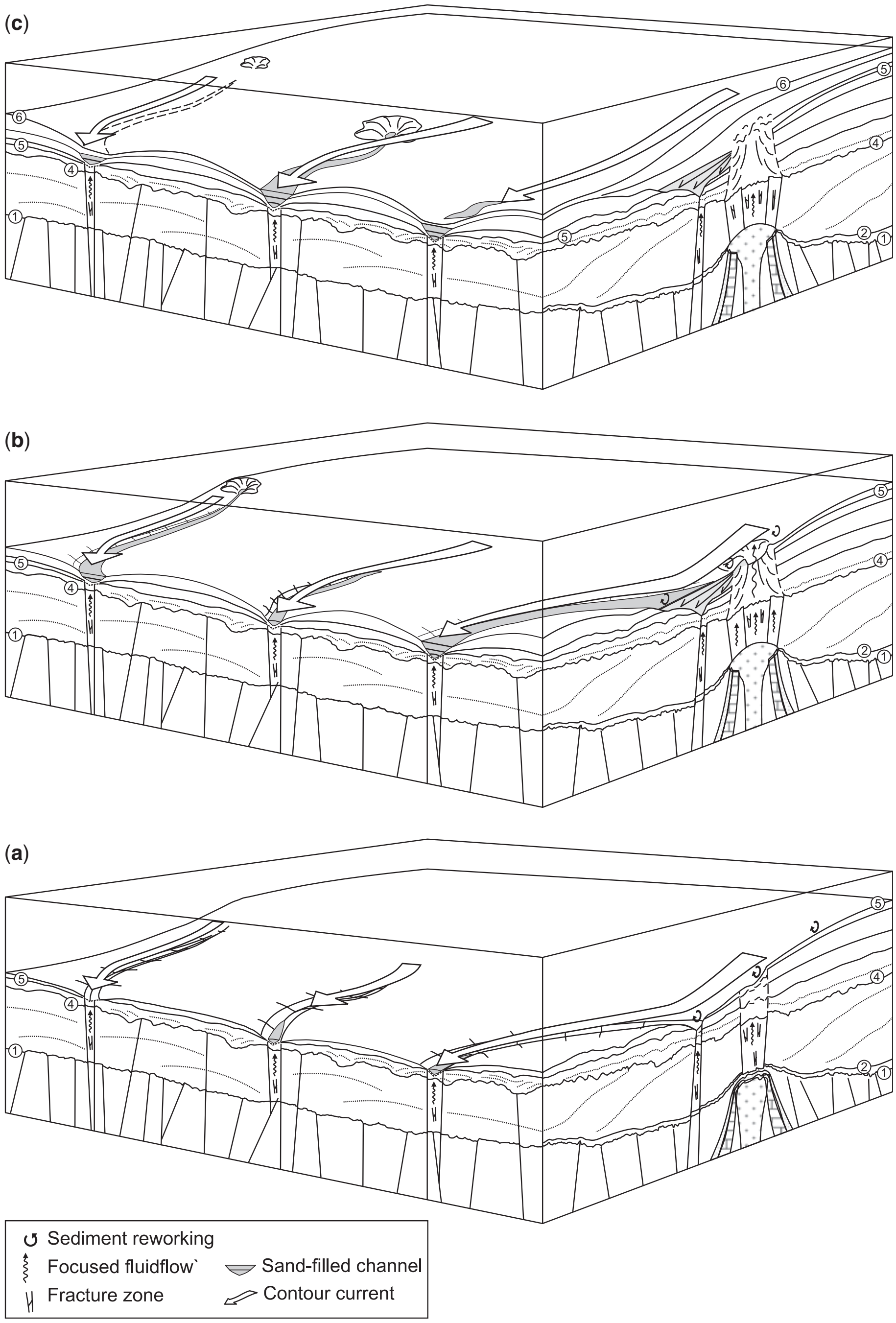

Fig. 15. Depositional model illustrating development stages for the aggradational channels. (**a**) Erosional stage: initial channel trace is formed by strong contour currents, eroding and winnowing the seabed, preferentially along corridors of low sediment strength related to fault/fracture zones. A primordial thalweg is formed by accretion of low-relief banks along the flanks of channel pathways. At this stage, fluid-flow activity over SLZ is low but increasing due to gravitational loading of the sediment prism. (**b**) Aggradational and infilling stage: channels are confined by high fine-clastic accumulation rates over interchannel regions. Hydrographic conditions at the seabed are augmented by the relief of the channel profiles (60–120 m deep, 700–2500 m wide), causing erosion in the deepest troughs. Deepening of the channels is succeeded by infill of non-cohesive silt and sand. A principle source for this material is related to extrusive sediments, derived from intense fluid expulsion over SLZ and subsequently distributed into the channel network by northward bottom-currents. The leakage zones formed pockmarks or mud-volcanoes on the seabed, similar to modern features observed in Gulf of Mexico (Milkov 2006), east Atlantic margins (Berndt 2005; Gay *et al.* 2007) and Mediterranean (Geletti *et al.* 2008). The dynamic linkage to SLZ point sources upstream means that infilling of troughs tends to proceed diachronously (e.g. infill history may differ between adjacent channel). (**c**) Burial stage: rapid burial by progradational units eventually terminates the channel formations and SLZ fluid-flow activity. This occurs progressively so that, when channels and SLZ to the south are completely buried by the clinoform unit (Horizon 6), channel profiles in basinward positions to the clinoform depocentre continue to be maintained by contour currents. Consolidation of channel infill by carbonate cementation commences during early burial stage. Horizons are numbered according to Figure 2 and Table 1. The model is not to scale although a vertical exaggeration of 1:5 may be assumed for the channel profiles.

progressively infilled by the Ur–Frisia delta complex (Cameron *et al.* 1992).

The Late Miocene/Early Pliocene unconformity is a key horizon for understanding the Late Neogene basin development of the Central Graben. The regional tilt expressed by this horizon has previously been associated with the most recent exhumation phase of the Norwegian–Danish Basin, attributed to active uplift of Scandinavia (Overeem *et al.* 2001; Japsen *et al.* 2007). The alignment of incised channels along the graben axis suggests that the SW dip of Horizon 4 (Fig. 10) was introduced subsequent to the erosive formation of these channels. Basin subsidence probably commenced during the Early Pliocene as the prism complex accumulated northward, in response to accommodation space. The oceanographic response to this bathymetric deepening was the development of south-to-north geostrophic currents, intensifying along the eastern margin of the basin. Depositional breaks within the prism package (Figs 1 & 3) suggest that during the first stage of subsidence increase in sea-level was balanced by high sediment fluxes. As subsidence progressed, the depositional system appears to have drowned, resulting in the mounded aggradational geometry of the prism. Post-depositional modification of deltaic units in the Danish sector suggests that the basin continued to tilt into the Early Pleistocene (Gelasian) (Japsen *et al.* 2007), which may explain the shift in geometries from the prism wedge to clinoform development (Fig. 6).

Gravitational loading by the succeeding late Neogene depositional units would sustain subsidence in the central parts of the basin (Fig. 1) by an amount depending on flexural rigidity of the lithosphere and bulk density of overburden (Thorne & Watts 1989). However, a passive subsidence model relying on intensified weathering induced by glaciations (Huuse 2002) is incompatible with the interpretation of the prism and abounding channels as elements of North Atlantic upper-intermediate circulation during the Pliocene climate optimum (Haywood *et al.* 2000). On the other hand, the mechanism(s) for active tectonic uplift of large intra-continental regions and corresponding basin subsidence are enigmatic and remain to be identified (Stoker *et al.* 2005). In the present case, the development of a deep seaway through the central North Sea, subsequent to late Miocene compression, suggests that mechanisms alternative to recent concepts of intraplate tectonics should be explored (Wees & Cloethingh 1996). The detailed basin stratigraphy and depositional patterns presented in this study provide a relevant comparison for future work on basin analysis.

Conclusions

Aggrading channels, 700–2500 m wide and 75–150 m deep, developed over the basinward condensed section of a Pliocene sedimentary prism in the northern Central Graben. The seismic architecture indicates that they evolved in consecutive stages of basal erosion, aggradational build-up, infilling and burial by clinoform progradation during the Early Pleistocene (from *c.* 2.6 Ma). The channels are oriented north to NNW with a geometric style that changes laterally from linear, closely spaced ridge-trough structures *sensu* (Cartwright 1995) to arcuate channel shapes.

The channel formations are related to a contour current depositional regime that commenced subsequent to rapid basin subsidence during the Pliocene. Observations in favour of this interpretation include a lack of a consistent slope gradient along thalwegs and the presence of migrating depositional mounds at channel terminations. A contour current mechanism is also implied by the mounded wedge geometry of the contiguous aggradational prism that extends northward from its main depocentre in the south Central Graben, reminiscent of a fan-drift depositional system (Faugeres *et al.* 1999). The relief of the Pliocene sediment prism suggests that water depths reached 600 m or more in the northern Central Graben, promoting the development of the prism complex by northbound geostrophic currents. The sediment source for the prism is probably related to the large Baltic River system that drained into the German Bight.

A striking character of the aggradational channels is the seismic pull-up they generate on the MMU, suggesting a coarse-grained and carbonate cemented infill. Also, it is noticeable that the largest of the arcuate channel elements commence in the vicinity of concentric chimneys related to leakage zones above salt diapirs. At these locations, troughs tend to deepen with infill displaying downlap away from the leakage zones. A geological control on the initial formation of channel pathways (erosional stage) is suggested by the presence of faults approaching seismic resolution below the troughs. Based on the 3D seismic observations, a depositional model is presented that links channel development stages to fluid expulsion from salt diapir structures and fracture zones extending from the MMU. It is recommended that geological factors for channel development, involving extensional faults and fluid leakage, are investigated in future studies.

The sedimentary prism accumulated over a Late Miocene/Early Pliocene low-stand unconformity, marked by numerous incised channels infilled by accretionary units. The erosive development of this horizon, reminiscent of a drainage system, is associated with Late Alpine compression related to uplift in the British Isles and the Channel region (Hillis *et al.* 2008). The southwestward inclination of the basal unconformity (0.5–0.8°) is related to rapid basin subsidence, facilitating successive stages of aggradational and progradational build-up of the prism complex.

The onset of basin subsidence and modification of the Late Miocene/Early Pliocene unconformity is linked to concomitant uplift of the Norwegian–Danish Basin, thus highlighting a first-order tectonic control on accommodation space and sediment supply. However, the underlying mechanism for active tectonic uplift over large intra-continental regions is presently unknown, and recent basin modelling of intraplate flexure cannot explain the observed late Neogene depositional record of the central North Sea.

PGS Ltd and EON UK are thanked for allowing access to the 3D seismic volume and North Sea well data. The chronology of the seismic stratigraphy has benefitted from helpful comments and information provided by E. S. Rasmussen and S. Piasecki. The manuscript was improved by the helpful comments from two reviewers. This work is supported by GEUS and a stipend from the Inge Lehmann foundation.

References

Akhmetzhanov, A., Kenyon, N. H., Habgood, E., Van Der Mollen, A. S., Nielsen, T., Ivanov, M. & Shashkin, P. 2007. North Atlantic contourite sand channels. *In*: Viana, A. R. & Rebesco, M. (eds) *Economic and Palaeoceanographic Significance of Contourite Deposits*. Geological Society, London, Special Publications, **276**, 25–47.

Andresen, K. J., Huuse, M. & Clausen, O. R. 2008. Morphology and distribution of Oligocene and Miocene pockmarks in the Danish North Sea – implications for bottom current activity and fluid migration. *Basin Research*, **20**, 445–466.

Andresen, K. J., Clausen, O. R. & Huuse, M. 2009. A giant [5.3 × 10(7) m(3)] middle Miocene (*c.* 15 Ma) sediment mound (M1) above the Siri Canyon, Norwegian–Danish Basin: origin and significance. *Marine and Petroleum Geology*, **26**, 1640–1655.

Armstrong, T., McAteer, J. & Connolly, P. 2001. Removal of overburden velocity anomaly effects for depth conversion. *Geophysical Prospecting*, **49**, 79–99.

Berndt, C. 2005. Focused fluid flow in passive continental margins. *Philosophical Transactions of the Royal Society A – Mathematical Physical and Engineering Sciences*, **363**, 2855–2871.

Bishop, D. J. 1996. Regional distribution and geometry of salt diapirs and supra-Zechstein Group faults in the western and central North Sea. *Marine and Petroleum Geology*, **13**, 355–364.

Bøe, R., Rise, L. & Ottesen, D. 1998. Elongate depressions on the southern slope of the Norwegian Trench (Skagerrak): morphology and evolution. *Marine Geology*, **146**, 191–203.

Cameron, T. D. J., Crosby, A., Balson, P. S., Jeffery, D. H., Lott, G. K., Bulat, J. & Harrison, D. J. 1992. *United Kingdom Offshore Regional Report: the Geology of the Southern North Sea*. HMSO for the British Geological Survey, London.

Cameron, T. D. J., Bulat, J. & Mesdag, C. S. 1993. High-resolution seismic profile through a late Cenozoic delta-complex in the southern North-Sea. *Marine and Petroleum Geology*, **10**, 591–599.

Cartwright, J. A. 1995. Seismic-stratigraphical analysis of large-scale ridge-through sedimentary structures in the Late Miocene to early Pliocene of the central North Sea. *In*: Plint, G. A. (ed.) *Sedimentary Facies Analysis; a Tribute to the Research and Teaching of Harold G. Reading*. Special Publication no. 22 of the International Association of Sedimentologists. Oxford, Blackwell, 285–303.

Cartwright, J. & Dewhurst, D. N. 1998. Layer-bound compaction faults in fine-grained sediments. *GSA Bulletin*, **110**, 1242–1257.

Cayley, G. T. 1987. Hydrocarbon migration in the Central North Sea. *In*: Brooks, J. & Glennie, K. W. (eds) *Petroleum Geology of Northwest Europe*. London, Graham and Trotman, 549–555.

Clausen, O. R. & Korstgard, J. A. 1993. Small-scale faulting as an indicator of deformation mechanism in the Tertiary sediments of the northern Danish Central Trough. *Journal of Structural Geology*, **15**, 1343–1357.

Collinson, J. D. 1996. Alluvial sediments. *In*: Reading, H. G. (ed.) *Sedimentary Environments: Processes, Facies and Stratigraphy*. Blackwell, Oxford, 37–82.

Davison, I., Alsop, G. I., Evans, N. G. & Safaricz, M. 2000*a*. Overburden deformation patterns and mechanisms of salt diapir penetration in the Central Graben, North Sea. *Marine and Petroleum Geology*, **17**, 601–618.

Davison, I., Alsop, I. *et al*. 2000*b*. Geometry and late-stage structural evolution of Central Graben salt diapirs, North Sea. *Marine and Petroleum Geology*, **17**, 499–522.

Dore, A. G. & Lundin, E. R. 1996. Cenozoic compressional structures on the NE Atlantic margin: Nature, origin and potential significance for hydrocarbon exploration. *Petroleum Geoscience*, **2**, 299–311.

Dybkjær, K. & Piasecki, S. 2008. A new Neogene biostratigraphy for Denmark. *Geological Survey of Denmark and Greenland Bulletin*, **15**, 29–32.

Eidvin, T. & Rundberg, Y. 2007. Post-Eocene strata of the southern Viking Graben, northern North Sea; integrated biostratigraphic, strontium isotopic and lithostratigraphic study. *Norwegian Journal of Geology*, **87**, 391–450.

Esmerode, E. V., Lykke-Andersen, H. & Surlyk, F. 2008. Interaction between bottom currents and slope failure in the Late Cretaceous of the southern Danish Central Graben, North Sea. *Journal of the Geological Society*, **165**, 55–72.

Faleide, J. I., Kyrkjebø, R., Kjennerud, T., Gabrielsen, R. H., Jordt, H., Fanavoll, S. & Bjerke, M. D. 2002. Tectonic impact on sedimentary processes during Cenozoic evolution of the northern North Sea and surrounding areas. *In*: Doré, A. G., Cartwright, J., Stoker, M. S., Turner, J. P. & White, N. (eds) *Exhumation of the North Atlantic Margin: Timing, Mechanisms and Implications for Petroleum Exploration*. Geological Society, London, Special Publications, **196**, 235–269.

Faugeres, J. C., Stow, D. A. V., Imbert, P. & Viana, A. 1999. Seismic features diagnostic of contourite drifts. *Marine Geology*, **162**, 1–38.

Fichler, C., Henriksen, S., Rueslaatten, H. & Hovland, M. 2005. North Sea Quaternary morphology from seismic and magnetic data: indications for gas hydrates during glaciation? *Petroleum Geoscience*, **11**, 331–337.

Funnell, B. M. 1996. Plio-Pleistocene palaeogeography of the southern North Sea basin (3.75–0.60 Ma). *Quaternary Science Reviews*, **15**, 391–405.

Galloway, W. E. 2002. Paleogeographic setting and depositional architecture of a sand-dominated shelf depositional system, Miocene Utsira formation, North Sea Basin. *Journal of Sedimentary Research*, **72**, 476–490.

Galloway, W. E., Garber, J. L., Liu, X. & Sloan, B. J. 1993. Sequence stratigraphy and depositional framework of the Cenozoic fill, Central and Northern North Sea Basin. *In*: Parker, J. R. (ed.) *Petroleum Geology of Northwest Europe: Proceedings of the 4th Conference*. Geological Society, London, 33–43; doi: 10.1144/0040033.

Gatliff, R. W., Richards, P. C. *et al*. 1994. *United Kingdom Offshore Regional Report: The Geology of the Central North Sea*. HMSO for the British Geological Survey, London.

Gay, A., Lopez, M., Berndt, C. & Seranne, M. 2007. Geological controls on focused fluid flow associated with seafloor seeps in the Lower Congo Basin. *Marine Geology*, **244**, 68–92.

Geletti, R., Del Ben, A., Busetti, M., Ramella, R. & Volpi, V. 2008. Gas seeps linked to salt structures in the Central Adriatic Sea. *Basin Research*, **20**, 473–487.

Gregersen, U. 1997. The depositional significance of 3-D seismic attributes in the Upper Cenozoic of the Central North Sea. *Petroleum Geoscience*, **3**, 291–304.

Gregersen, U., Michelsen, O. & Sorensen, J. C. 1997. Stratigraphy and facies distribution of the Utsira formation and the Pliocene sequences in the northern North Sea. *Marine and Petroleum Geology*, **14**, 893–914.

Hansen, J. P. V., Clausen, O. R. & Huuse, M. 2004. 3D seismic analysis reveals the origin of ambiguous erosional features at a major sequence boundary in the eastern North Sea: near top Oligocene. *In*: Davies, R. J., Cartwright, J., Stewart, S. A., Lappin, M. & Underhill, J. R. (eds) *3D Seismic Technology: Application to the Exploration of Sedimentary Basins*, Geological Society, London, Memoirs, 83–89.

Haywood, A. M., Sellwood, B. W. & Valdes, P. J. 2000. Regional warming: Pliocene (3 Ma) paleoclimate of Europe and the Mediterranean. *Geology*, **28**, 1063–1066.

Head, M. J., Riding, J. B., Eidvin, T. & Chadwick, R. A. 2004. Palynological and foraminiferal biostratigraphy of (Upper Pliocene) Nordland Group mudstones at Sleipner, northern North Sea. *Marine and Petroleum Geology*, **21**, 277–297.

Heggland, R. 1998. Gas seepage as an indicator of deeper prospective reservoirs. A study based on exploration 3D seismic data. *Marine and Petroleum Geology*. **15**, 1–9.

Hernandez-Molina, F. J., Llave, E. *et al*. 2006. The contourite depositional system of the Gulf of Cadiz: A sedimentary model related to the bottom current activity of the Mediterranean outflow water and its interaction with the continental margin. *Deep-Sea Research Part II*, **53**, 1420–1463.

Hillis, R. R., Holford, S. P. *et al*. 2008. Cenozoic exhumation of the southern British Isles. *Geology*, **36**, 371–374.

Hovland, M., Talbot, M. R., Qvale, H., Olaussen, S. & Aasberg, L. 1987. Methane-related carbonate cements in pockmarks of the North Sea. *Journal of Sedimentary Research*, **57**, 881–892.

Huuse, M. 2002. Late Cenozoic palaeogeography of the eastern North Sea Basin: climatic v. tectonic forcing of basin margin uplift and deltaic progradation. *Bulletin of the Geological Society of Denmark*, **49**, 145–170.

Jackson, M. P. A. & Seni, S. J. 1984. *Atlas of Salt Domes*. Report of Investigations no. 140.

Japsen, P. 1998. Regional velocity-depth anomalies, North Sea Chalk: a record of overpressure and neogene uplift and erosion. *AAPG Bulletin*, **82**, 2031–2074.

Japsen, P., Green, P. F., Nielsen, L. H., Rasmussen, E. S. & Bidstrup, T. 2007. Mesozoic-Cenozoic exhumation events in the eastern North Sea Basin: a multi-disciplinary study based on paleothermal data, paleoburial, stratigraphic and seismic data. *Basin Research*, **10**, 1–40.

Jordt, H., Faleide, J. I., Bjorlykke, K. & Ibrahim, M. T. 1995. Cenozoic sequence stratigraphy of the central and northern North-Sea Basin – tectonic development, sediment distribution and provenance areas. *Marine and Petroleum Geology*, **12**, 845–879.

Kenyon, N. H. 1986. Evidence from bedforms for a strong poleward current along the upper continental slope of NW Europe. *Marine Geology*, **72**, 187–189.

Knutz, P. C. 2008. Palaeoceanographic significance of contourite drifts. *In*: Rebesco, M. & Camerlenghi, A. (eds) *Contourites*. Elsevier, Oxford, 511–535.

Knutz, P. C. & Cartwright, J. 2004. 3D anatomy of late Neogene contourite drifts and associated mass flows in the Faeroe-Shetland Basin. *In*: Davies, R. J., Cartwright, J., Stewart, S. A., Lappin, M. & Underhill, J. R. (eds) *3D Seismic Technology: Application to the Exploration of Sedimentary Basins*. Geological Society, London, Memoirs, 63–71.

Kohl, B. & Roberts, H. H. 1994. Fossil foraminifera from 4 active mud volcanos in the Gulf-of-Mexico. *Geo-Marine Letters*, **14**, 126–134.

Kooi, H., Hettema, M. & Cloetingh, S. 1991. Lithospheric dynamics and the rapid Pliocene-Quaternary subsidence phase in the southern North Sea Basin. *Tectonophysics*, **192**, 245–259.

Kubala, M., Bastow, M., Thompson, S., Scotchman, I. & Øygard, K. 2003. Geothermal regime, petroleum generation and migration. *In*: Evans, D., Armour, A., Bathurst, P., Gammage, J., Swallow, J., Graham, C. & Stewart, H. (eds) *The Millennium Atlas: Petroleum Geology of the Central and Northern North Sea*. Geological Society, London, 289–315.

Kuhlmann, G. & Wong, T. E. 2008. Pliocene paleoenvironment evolution as interpreted from 3D-seismic data in the southern North Sea, Dutch offshore sector. *Marine and Petroleum Geology*, **25**, 173–189.

Kuhlmann, G., Langereis, C., Munsterman, D., van Leeuwen, R. J., Verreussel, R., Meulenkamp, J. & Wong, T. 2006. Chronostratigraphy of late Neogene sediments in the southern North Sea Basin and paleoenvironmental interpretations. *Palaeogeography Palaeoclimatology Palaeoecology*, **239**, 426–455.

Kyrkjebø, R., Hamborg, M., Faleide, J. I., Jordt, H. & Christiansson, P. 2000. Cenozoic tectonic subsidence from 2D depositional simulations of a regional transect in the northern North Sea Basin. *In*: Nøttvedt, A. (ed.) *Dynamics of the Norwegian Margin*. Norsk Hydro Research Centre, Berge, Norway. Geological Society, London, Special Publications, **167**, 273–294.

Løseth, H. & Henriksen, S. 2005. A Middle to Late Miocene compression phase along the Norwegian passive margin. *In*: Doré, A. G. & Vining, B. A. (eds) *Petroleum Geology: North-West Europe and Global Perspectives: Proceedings of the 6th Petroleum Geology Conference*. Geological Society, London, 845–859; doi: 10.1144/0060845.

Løseth, H., Gading, M. & Wensaas, L. 2008. Hydrocarbon leakage interpreted on seismic data. *Marine and Petroleum Geology*, **26**, 1304–1319.

McCave, I. N. 1995. Sedimentary processes and the creation of the stratigraphic record in the Late Quaternary North Atlantic Ocean. *Philosophical Transactions of the Royal Society of London, B*, **348**, 229–241.

McCave, I. N. & Tucholke, B. E. 1986. Deep current-controlled sedimentation in the western North Atlantic. *In*: Vogt, P. R. & Tucholke, B. E. (eds) *The Geology of North America*. Geological Society of America, Boulder, CO, 451–468.

Michelsen, O., Danielsen, M., Heilmann-Clausen, C., Jordt, H., Laursen, G. V. & Thomsen, E. 1995. Occurrence of major sequence stratigraphic boundaries in relation to basin development in Cenozoic deposits of the southeastern North Sea. *In*: Steel, R. J., Felt, V. L., Johannessen, E. P. & Mathieu, C. (eds) *Sequence Stratigraphy of the Northwest European Margin*. Norwegian Petroleum Society Special Publication no. 5. Amsterdam, Elsevier, 415–427.

Milkov, A. 2006. Global distribution of mud volcanoes and their significance in petroleum exploration as a source of methane in the atmosphere and hydrosphere and as a geohazard. *Mud Volcanoes, Geodynamics and Seismicity*, 29–24.

Miller, K. G., Kominz, M. A. *et al*. 2005. The Phanerozoic record of global sea-level change. *Science*, **310**, 1293–1298.

Mitchum, R. M., Vail, P. R. & Sangree, J. B. 1977. Seismic stratigraphy and global changes of sealevel, Part 6: Stratigraphic interpretation of seismic reflection in depositional sequences. *Application of Seismic Reflection Configuration to Stratigrapic Interpretation Memoir*, **26**, 117–133.

New, A. L. & Smythe-Wright, D. 2001. Aspects of the circulation in the Rockall Trough. *Continental Shelf Research*, **21**, 777–810.

Nielsen, O. B., Sorensen, S., Thiede, J. & Skarbo, O. 1986. Cenozoic differential subsidence of North-Sea. *AAPG Bulletin*, **70**, 276–298.

Nielsen, S. B., Paulsen, G. E. *et al*. 2002. Paleocene initiation of Cenozoic uplift in Norway. *In*: Doré, A. G., Cartwright, J., Stoker, M. S., Turner, J. P. & White, N. (eds) *Exhumation of the North Atlantic Margin: Timing, Mechanisms and Implications for Petroleum Exploration*. Geological Society, London, Special Publications, **196**, 45–65.

Nielsen, T., Knutz, P. C. & Kuijpers, A. 2008. Seismic expression of contourite depositional systems. *In*: Rebesco, M. & Camerlenghi, A. (eds) *Contourites*. Elsevier, Oxford, 301–321.

Overeem, I., Weltje, G. J., Bishop-Kay, C. & Kroonenberg, S. B. 2001. The Late Cenozoic Eridanos delta system in the Southern North Sea Basin: a climate signal in sediment supply? *Basin Research*, **13**, 293–312.

Praeg, D. 1997. Buried tunnel-valleys: 3D-seismic morphostratigraphy. *In*: Davies, T. A., Bell, T., Cooper, A. K., Josenhans, H., Polyak, L., Solheim, A., Stoker, M. S. & Stravers, J. A. (eds) *Glaciated Continental Margins: an Atlas of Acoustic Images*. Chapman & Hall, London, 68–69.

Rasmussen, E. S. 2004. Stratigraphy and depositional evolution of the uppermost Oligocene–Miocene succession in western Denmark. *Bulletin of the Geological Society of Denmark*, **51**, 89–109.

Rasmussen, E. S., Vejbæk, O. V., Bidstrup, T., Piasecki, S. & Dybkjær, K. 2005. Late Cenozoic depositional history of the Danish North Sea Basin: implication for the petroleum systems in the Kraka, Halfdan, Siri and Nini fields. *In*: Doré, A. G. & Vining, B. A. (eds) *Petroleum Geology: North-West Europe and Global Perspectives: Proceedings of the 6th Petroleum Conference*. Geological Society, London, 1347–1358; doi: 10.1144/0061347.

Raymo, M. E., Grant, B., Horowitz, M. & Rau, G. H. 1996. Mid-Pliocene warmth: stronger greenhouse and stronger conveyor. *Marine Micropalaeontology*, **27**, 313–326.

Rebesco, M. & Camerlenghi, A. 2008. *Seismic Expression of Contourite Depositional Systems*. Elsevier, Oxford.

Ritchie, J. D., Johnson, H. & Kimbell, G. S. 2003. The nature and age of Cenozoic contractional deformation within the NE Faroe-Shetland Basin. *Marine and Petroleum Geology*, **20**, 399–409.

Schulz-Rojahn, J., Ryan-Grigor, S. & Anderson, A. 1998. Structural controls on seismic-scale carbonate cementation in hydrocarbon-bearing Jurassic fluvial and marine sandstones from Australia: a comparison. *Special Publications of the International Association of Sedimentologists*, **26**, 327–362.

Sorensen, J. C., Gregersen, U., Breiner, M. & Michelsen, O. 1997. High-frequency sequence stratigraphy of Upper Cenozoic deposits in the central and southeastern North Sea areas. *Marine and Petroleum Geology*, **14**, 99–123.

Stoker, M. S., Praeg, D. *et al*. 2005. Neogene evolution of the Atlantic continental margin of NW Europe (Lofoten Islands to SW Ireland): anything but passive. *In*: Doré, A. G. & Vining, B. A. (eds) *Petroleum Geology: North-West Europe and Global Perspectives: Proceedings of the 6th Petroleum Geology Conference*. Geological Society, London, 1057–1076; doi: 10.1144/0061057.

Thorne, J. A. & Watts, A. B. 1989. Quantitative analysis of North Sea subsidence. *AAPG Bulletin*, **73**, 88–116.

Thrasher, J. A., Fleet, A. J., Hay, S. J., Hovland, M. & Düppenbecker, S. 1996. Understanding geology as the key to using seepage in exploration: spectrum of seepage styles. *In*: Schumacher, D. & Abrams, A. M. (eds) *Hydrocarbon Migration and its Near-Surface Expression*. AAPG Memoir, **66**, 223–241.

Vandenberghe, N., Laga, P., Steurbaut, E., Hardenbol, J. & Vail, P. 1998. Tertiary sequence stratigraphy at the southern border of the North Sea Basin in Belgium. *In*: Graciansky, P., Hardenbol, J., Jacquin, T. & Vail, P. (eds) *Mesozoic and Cenozoic Sequence Stratigraphy of European Basins*. SEPM Society for Sedimentary Geology, Tulsa, Oklahoma, 119–153.

van Vliet-Lanoë, B., Vandenberghe, N. *et al*. 2002. Palaeogeographic evolution of northwestern Europe during the Upper Cenozoic. *Geodiversitas*, **24**, 511–541.

Van Wagoner, J. C., Posamentier, H. W. *et al*. 1988. An overview of the fundamentals of sequence stratigraphy and key definitions. *In*: Wilgus, C. K., Hastings, B. S. *et al*. (eds) *Sea-level Changes: An Integrated Approach*. Society of Economic Paleontologists and Mineralogists, Tulsa, OK, Special Publications, **42**, 39–45.

Van Wees, J. D. & Cloetingh, S. 1996. 3D Flexure and intraplate compression in the North Sea Basin. *Tectonophysics*, **266**, 343–359.

Vejbæk, O. V., Frykman, P., Bech, N. & Nielsen, C. M. 2005. The history of hydrocarbon filling of Danish Chalk fields. *In*: Doré, A. G. & Vining, B. A. (eds) *Petroleum Geology: North-West Europe and Global Perspectives: Proceedings of the 6th Petroleum Geology Conference*. Geological Society, London, 1331–1346; doi: 10.1144/0061331.

Viana, A. R., Faugeres, J.-C. & Stow, D. A. V. 1998. Bottom-current-controlled sand deposits – a review of modern shallow- to deep-water environments. *Sedimentary Geology*, **115**, 53–80.

Zagwijn, W. H. 1989. The Netherlands during the Tertiary and the Quaternary: a case history of Coastal Lowland evolution. *Geologie en Mijnbouw*, **68**, 107–120.

Ziegler, P. A. 1992. European Cenozoic rift system. *Tectonophysics*, **208**, 91–111.

Source rock quality and maturity and oil types in the NW Danish Central Graben: implications for petroleum prospectivity evaluation in an Upper Jurassic sandstone play area

H. I. PETERSEN, H. P. NYTOFT, H. VOSGERAU, C. ANDERSEN, J. A. BOJESEN-KOEFOED and A. MATHIESEN

Geological Survey of Denmark and Greenland (GEUS), Øster Voldgade 10, DK-1350 Copenhagen K, Denmark (e-mail: hip@geus.dk)

Abstract: The principal exploration targets in the northwestern part of the Danish Central Graben have been Upper Jurassic sandstone reservoirs. The presence and effectiveness of the oil-generating rocks of the Upper Jurassic–lowermost Cretaceous marine shales of the Farsund Formation has generally not been considered as a significant risk. This study provides an evaluation of the source rock quality, maturity and distribution and of the oils in this area. The kerogen in the Farsund Formation is algal-derived, and kerogen type ranges from Type II to Type III. Generally the source rock quality is fair to excellent, but the petroleum generation potential varies considerably. In most wells the uppermost part of the Farsund Formation (Bo Member) consists of highly oil-prone shales. However, the presence of oil-prone kerogen may be masked by kerogen of poorer source quality. Favourable conditions for oil-prone kerogen preservation were present during the time of deposition of upper parts of the Farsund Formation, but exceptions are not unusual. Similar vitrinite reflectance gradients indicate a uniform thermal regime over the area. The oil window occurs from *c.* 3800–4000 to 4800 m, i.e. spanning approximately 800–1000 m. A general decrease in the generation potential from the top towards the base of the formation is caused by both generation and deterioration of kerogen quality. The Gertrud Graben and Feda Graben constitute the main kitchen areas, and oil compositions indicate sourcing from marine shales. In the shallow parts of the Outer Rough Basin the shales are mostly immature and the sourcing is dependent on kitchen areas outside the area or on Palaeozoic rocks. Mature Zechstein is indicated by a minor oil show probably locally sourced.

Keywords: source rock, maturity, petroleum potential, oil, Upper Jurassic, Danish Central Graben, North Sea

The Danish Central Graben (DCG) is part of the Jurassic North Sea Central Graben rift complex and consists of a system of NW–SE trending halfgraben (Fig. 1). Three main hydrocarbon reservoirs occur in the DCG: Middle and Upper Jurassic sandstones and Upper Cretaceous–Danian chalk. In the study area situated in the northwestern part of the DCG bordering the Norwegian, British and German sectors the exploration targets have mainly been Kimmeridgian back-barrier and shoreface sandstones belonging to the Heno Formation, located on tilted fault blocks (Johannessen 2003). Exploration results have been less successful compared with the chalk fairway further south due to large variations in reservoir quality. A number of discoveries have been made, and two fields have been declared commercial, although not yet in production. These are the Freja Field on the Gert Ridge, and the Hejre Field in the Gertrud Graben (Fig. 1). Both accumulations are deep at about 5000 m and characterized by high temperatures (154–163°C) and overpressure in the order of 7000 psi. On the flanks of the Mid North Sea High the primary target has been Volgian shallow marine sandstones. Similar sands are known from the nearby Fife and Fergus Fields in the UK sector (Fig. 1).

The Upper Jurassic to lowermost Cretaceous marine shales of the Farsund Formation, including the organic-rich Bo Member, are the principal source rocks (Damtoft *et al.* 1992; Ineson *et al.* 2003). They correspond to the Kimmeridge Clay Formation and equivalents elsewhere in the North Sea (Cornford 1998). The presence and effectiveness of the source rocks has not been considered a significant exploration risk. However, a better understanding of source rock distribution and maturity, lateral and vertical variations in kerogen quality, and oil composition may play an important role in the exploration success.

The present study aims to provide a comprehensive evaluation of (i) the variations in source quality, maturity and distribution of the Farsund Formation in the northwestern part of the DCG, and (ii) the composition of oils encountered in the area.

Methods

Source rock data from 966 samples from the Farsund Formation in 21 wells were obtained by pyrolysis using Rock-Eval instruments and more recently using a Humble Source Rock Analyzer. Total organic carbon (TOC) contents were determined by combustion in LECO induction furnaces. Samples with TOC contents of <0.5 wt% and/or S_2 pyrolysis yields of <0.2 mg HC g^{-1} rock were omitted as these give an unreliable hydrogen index (HI). Samples from wells drilled with oil-based mud (OBM) were extracted with dichloromethane–methanol (93:7 v/v) before analysis to avoid contamination and flawed S_2 yields. Vitrinite reflectance (VR) measurements (random) were performed on dispersed organic matter by means of a Leitz MPV-SP system. Oils from the Mona-1, Gert-1, Rita-1, Olaf-1, Wessel-1, Saxo-1 and Tordenskjold-1 wells were analysed together with source rock extracts from the Farsund Formation in the Rita-1 well (11 samples), the Tordenskjold-1 well (three samples) and the Wessel-1 well (four samples). Four of the samples from the Rita-1 well were from the Bo Member. Four Permian (Zechstein Z2) carbonate samples (3134.0–3142.5 m) from the Wessel-1 well were also analysed. The gas chromatography–mass spectrometry (GC–MS and GC–MS–MS) analyses were carried out using an Agilent 6890N gas chromatograph connected to a Waters (Micromass) Quattro Micro GC tandem quadropole

VINING, B. A. & PICKERING, S. C. (eds) *Petroleum Geology: From Mature Basins to New Frontiers – Proceedings of the 7th Petroleum Geology Conference*, 95–111. DOI: 10.1144/0070095

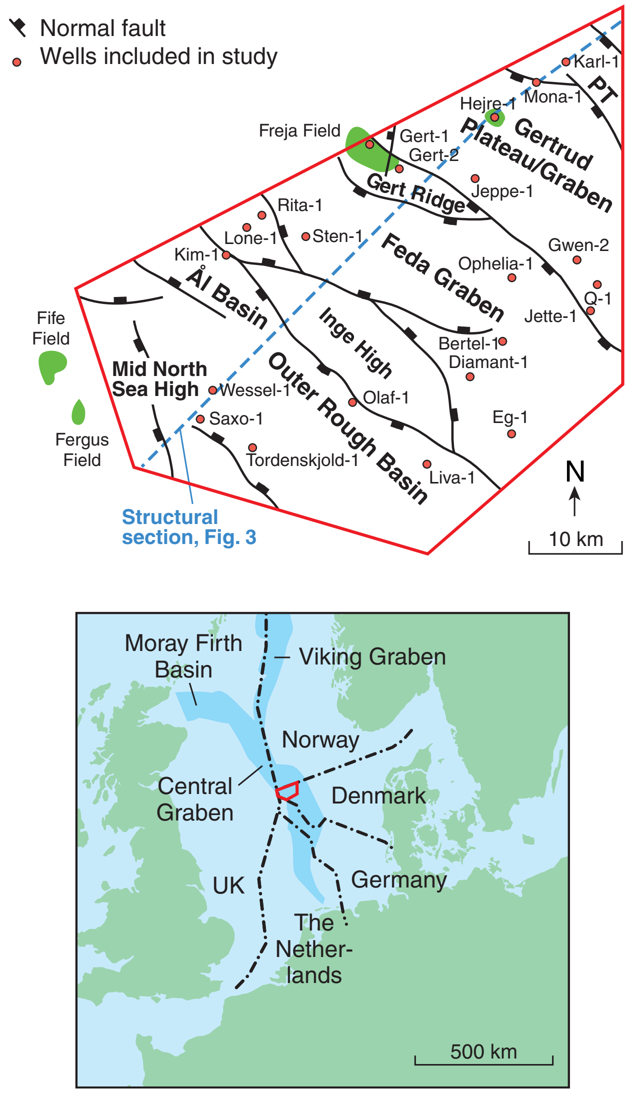

Fig. 1. Map showing the study area (red frame: northwestern part of the DCG) in the Central Graben rift system. Enlargement shows the Jurassic structural elements in the study area and the wells included in the study. The Olaf-1 well did not drill into the U. Jurassic and only an oil sample has been analysed from the well. PT: Piggvar Terrace.

mass spectrometer. A Phenomenex ZB-5 capillary column (30 m × 0.25 mm i.d., film thickness 0.10 μm) was used. The injection temperature was 70°C (2 min hold). The temperature program was 30°C/min from 70 to 100°C and 4°C/min from 100 to 308°C followed by 8 min at 308°C. Argon was used as collision gas for MS–MS experiments.

Regional setting

The DCG consists of a system of generally NW–SE trending half-graben bounded by the Coffee Soil Fault to the east, and by the Mid North Sea high in the west (Japsen *et al.* 2003) (Fig. 1). Jurassic rifting commenced during Bajocian in the east. During the Kimmeridgian, the depocentre shifted westward and deposition gradually coved larger areas reaching the flanks of the Mid North Sea High during the Volgian (Johannessen *et al.* 2010). In the overall extensional regime, compressional features also occur, resulting from oblique-slip movements between different graben segments. The structure of the study area is illustrated by depth structure maps of the top and base of the Upper Jurassic section, the Upper Jurassic isochore and a simplified structural profile through the northwestern part of the DCG (Figs 2 & 3). The Piggvar Terrace in the NE is located between the Mandal High and the northeastward tilted Gertrud Graben, which is separated from the southwestward dipping Feda Graben by the Gert Ridge. In both graben segments the thickness of Upper Jurassic strata locally exceeds 1500 m. The Ål Basin and the shallow Outer Rough Basin, which has a thin Upper Jurassic section, are located west of the Inge High, on which Jurassic strata are thin or absent.

The syn-rift sedimentary fill in the northwestern part of the DCG is dominated by the shales of the Kimmeridgian to Ryazanian Farsund Formation (Figs 2 & 3; Table 1). Widespread shallow to marginal marine sandstones of the Heno Formation were deposited over an erosion surface associated with a cessation or slowdown of subsidence during the Late Kimmeridgian (Andsbjerg & Dybkjær 2003). In the west, shallow marine sandstones of Volgian age have been encountered on the flanks of the Mid North Sea High (Johannessen *et al.* 2010).

Source rock maturity and quality

The organic richness and source rock quality of the shales of the Farsund Formation are known to show lateral and stratigraphical variations (Damtoft *et al.* 1992). These variations in TOC and HI suggest that several factors, such as variations in oxygen content in the bottom waters, organic matter production and sediment input, determined composition and preservation of kerogen in the rocks. The shales in the upper levels of the Farsund Formation are generally 'hot' and were previously referred to as the informal 'Hot Unit' because of high levels of radioactivity recorded by the γ-ray logs (Jensen *et al.* 1986; Ineson *et al.* 2003). These shales are referred to as the Bo Member (Volgian–Ryazanian). The member is partly equivalent to the Clay Deep Member and Mandal Formation from the Dutch and Norwegian North Sea sectors, respectively, and it is defined by significantly higher gamma-ray (GR) levels than the underlying and overlying shales (Michelsen *et al.* 2003) (Fig. 4). It is normally assumed that the HI values and TOC content increase and the kerogen becomes more oil-prone through the Farsund Formation, particularly in the Bo Member, which generally is considered to possess the best source potential (Damtoft *et al.* 1992). In the northwestern part of the DCG the Bo Member is present in the Piggvar Terrace, the Gertrud and Feda Grabens and the Ål Basin, whereas it is thin to absent on the Gert Ridge and seems to be absent on the Inge High and in the Outer Rough Basin (Table 1). The member is anomalously thick in a few wells (*c.* 100 m), but in most wells the thickness is between 20 and 50 m.

Thermal maturity and the oil window

VR gradients for the Outer Rough Basin/Ål Basin, Feda Graben/Gert Ridge and Gertrud Graben/Piggvar Terrace areas show largely similar and relatively well defined maturity trends (Fig. 5). The similar maturity gradients indicate a uniform thermal regime for the northwestern part of the DCG. If a VR of 0.6%R_o is used as the start of the oil window, the VR trends suggest a burial depth of approximately 4000 m for the start of the oil window. The occurrence of oils with low-maturity biomarker signatures elsewhere in the DCG may suggest that petroleum generation in some cases may take place at modest levels of thermal maturation (about 0.5%R_o or less). In the Piggvar Terrace, Gertrud Graben, Feda Graben, Ål Basin and partly on the Gert Ridge, the entire or part of the Farsund Formation seems to be buried to 4000 m or deeper, indicating that the source rocks are within the oil window (Fig. 6a, b; Table 1). On the Inge High

Table 1. Depth range, thickness and petroleum generation potential of the Farsund Formation and Bo Member

Area	Well	Farsund Formation (total; incl. Bo Member)					Bo Member			
		Depth range (m)	Thickness (m)	T_{max} (°C)	HI range (mg HC/g TOC)	$HI_{average}$ (mg HC/g TOC)	Thickness (m)	T_{max} (°C)	HI range (mg HC/g TOC)	$HI_{average}$ (mg HC/g TOC)
Ål Basin	Kim-1	4107.4–4607.6	500	446	39–300	132	100	441	39–300	153
Outer Rough Basin	Liva-1	4225.7–4265.3	40	436	11–266	139	Absent	—	—	—
Outer Rough Basin	Saxo-1	3032.0–3040.0	8	427	160–385	285	Absent	—	—	—
Outer Rough Basin	Tordenskjold-1	3403.5–3532.0	128	436	235–541	366	Absent	—	—	—
Outer Rough Basin	Wessel-1	3028.6–3040.9	12	428	513–544	526	Absent	—	—	—
Feda Graben	Bertel-1	4324.0–4659.0	335	443	94–369	210	22	439	299–369	329
Feda Graben	Diamant-1	3704.8–3829.1	124	431	185–649	468	?3	431	185	185
Feda Graben	Eg-1	4130.0–4383.0	253	440	138–551	261	20	437	322–541	446
Feda Graben	Lone-1	3521.6–3797.1	276	439	107–552	217	36	436	135–297	225
Feda Graben	Ophelia-1	4456.5–4851.0	395	445	116–618	205	33	442	303–342	316
Feda Graben	Rita-1	3750.9–4509.5	759	439	19–552	240	65	434	179–552	438
Feda Graben	Sten-1	4047.3–4114.7	67[a]	431	177–291	235	Absent	—	—	—
Gert Ridge	Gert-1	4014.4–4732.2	718	443	68–324	152	Absent	—	—	—
Gert Ridge	Gert-2	4006.6–4778.1	771	434	126–459	240	18	427	404–459	429
Gertrud Graben	Gwen-2	4066.6–4223.5	157	442	26–166	85	?8	—	—	—
Gertrud Graben	Hejre-1	4310.0–5098.0	788	438	107–497	294	102	439	188–451	361
Gertrud Graben	Jeppe-1	4386.0–4941.0	555	442	11–543	104	27	441	169–543	453
Gertrud Graben	Jette-1	4083.0–4174.0	91	441	261–385	328	Absent	—	—	—
Gertrud Graben	Q-1	4004.7–4093.7	89	446	50–108	84	Absent	—	—	—
Piggvar Terrace	Karl-1	4265.9–4422.9	157	445	87–294	143	Absent	—	—	—
Piggvar Terrace	Mona-1	4023.3–4241.5	218[a]	440	72–359	185	44	439	72–359	196

[a]Base Farsund Formation not reached.

and in large parts of the Outer Rough Basin, the top of the Farsund Formation is buried to less than about 3600 m, implying immaturity of the source rocks (Fig. 6a, b; Table 1). This renders the Outer Rough Basin dependent on kitchen areas located outside the area, or on Palaeozoic source rocks. However, in the Liva-1 well, which was drilled on an anticlinal structure in the Outer Rough Basin close to the bounding fault of the Inge High, the Farsund Formation is buried below 4000 m depth and a local kitchen with mature source rocks may be present immediately NW of the well (Fig. 6a, b). Thermally mature shales of the Farsund Formation occur mainly in the Feda Graben and Gertrud Graben (Fig. 6a, b). The highest maturities (VR $>1\%R_o$) have been reached in depocentres in these graben. A VR of $1.02\%R_o$ at the base of the Farsund Formation at *c.* 5000 m burial depth in the Hejre-1 well is low, which could be due to retardation of VR caused by the overpressure (Carr 2000) in the well.

A decrease in HI and an increase in the production index ($PI = S_1/S_1 + S_2$) below *c.* 3800–4000 m, supports the top of the oil window as defined by VR ($0.6\%R_o$), and suggests that the decrease in HI is related to generation (Fig. 7a, b). Generally PI increases from approximately 0.1–0.4 from the onset of oil generation and through the oil window (Espitalié *et al.* 1985, 1986). Many of the studied wells were drilled with OBM, and the samples from these wells were solvent-extracted before analysis in order to avoid unreliable geochemical data caused by contamination. However, in nine wells samples were not contaminated by OBM and for these samples the PI was calculated (Fig. 7b). In the majority of the samples PI reached 0.1 at *c.* 3800–4000 m and increased gradually to 0.35–0.4 at about 4700 m. The observed variation in PI may be due to differences in kerogen composition (Hunt 1996), but some of the very high PI values between 3900 and 4000 m may indicate migrated hydrocarbons. Below *c.* 4800 m

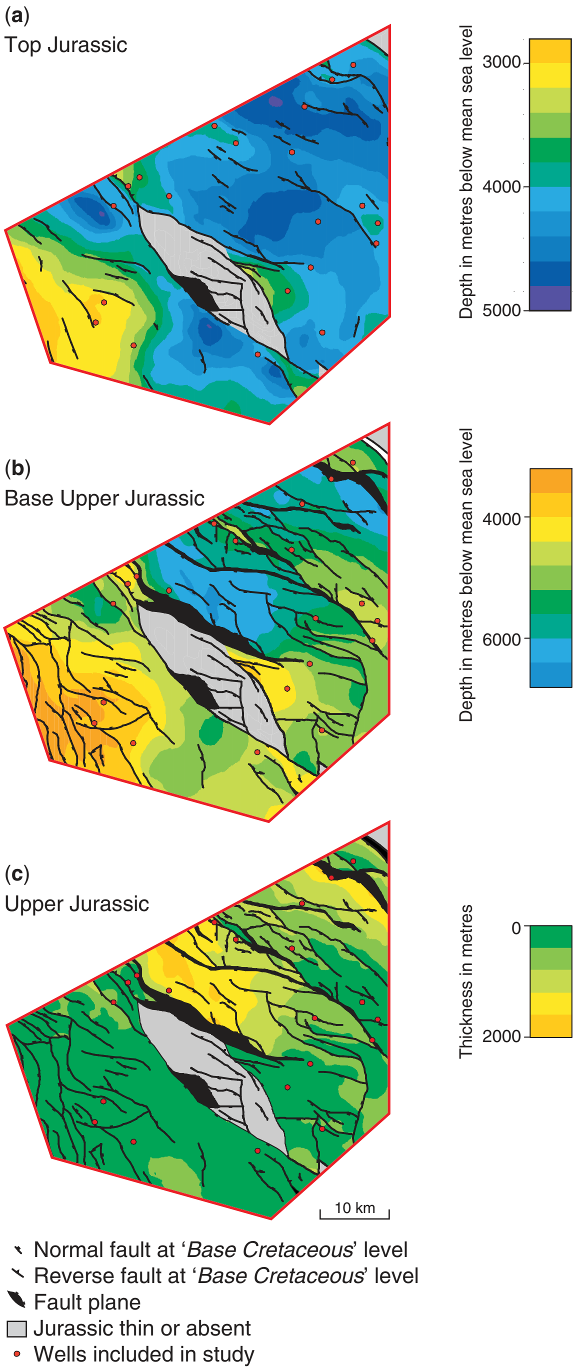

Fig. 2. (**a**) Depth map showing depth to the top of the Upper Jurassic units (top of the Farsund Formation). (**b**) Depth map showing depth to the base of the Upper Jurassic units. (**c**) Isochore map showing the thickness of the Upper Jurassic units. Maps modified from Japsen *et al.* (2003).

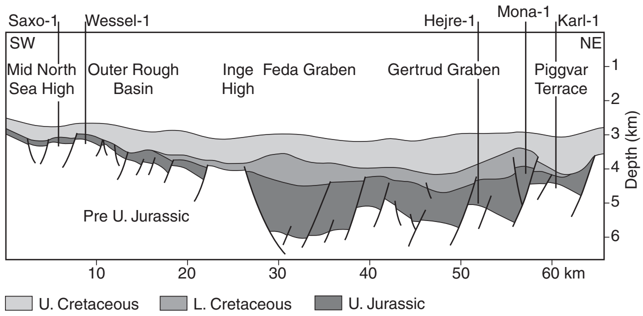

Fig. 3. Simplified structural section through the northwestern part of the DCG showing distribution of Upper Jurassic and Cretaceous sediments (see Fig. 1 for location).

the HI values are generally less than 200–300 mg HC/g TOC, indicating that mainly a gas-potential remains. The oil window thus occurs from *c*. 3800–4000 to 4800 m, i.e. spanning approximately 800–1000 m (Fig. 7a). However, HI values also fluctuate through the Farsund Formation, reflecting organic facies variations. This issue is discussed below.

Kerogen composition and source rock quality

The organic matter in the marine shales of the Farsund Formation is dominated by algal-derived fluorescent amorphous organic matter (AOM), and alginite with *Leiosphaerida* and *Tasmanites* morphology (Fig. 8). Immature to early mature samples from four wells show variations in kerogen composition from Type II to Type III (Fig. 9). The kerogen in the Farsund Formation (excluding the Bo Member) is classified as Type III in the Jeppe-1 well, Type II/III in the Gert-1 and Rita-1 wells, and Type II in the Diamant-1 well. The kerogen in Diamant-1 is of better quality than the Type II kerogen in the Bo Member in both Jeppe-1 and Rita-1 (Fig. 9).

The shales of the Farsund Formation show a large range in HI in the different graben and basins, which is partly controlled by maturity, but also by variations in kerogen quality (Figs 7a & 10a, c). The source rock quality can generally be classified as fair to excellent (Fig. 10b, d). In the Jeppe-1, Gwen-2 and Q-1 wells, however, many samples of the Farsund Formation (excluding the Bo Member) are classified as poor source rocks. The range in HI and average HI values indicates petroleum generation potential from non-generative/gas-prone (e.g. Jeppe-1, Gwen-2 and Q-1 wells) to highly oil-prone (Jette-1, Diamant-1, Tordenskjold-1 and Wessel-1 wells) (Table 1). Hence, in the Gertrud Graben and Piggvar Terrace area, the Farsund Formation (excluding the Bo Member) is a less oil-prone source rock. Only the Jette-1 and Hejre-1 wells contain shales with an enhanced oil-generating potential (Table 1). The oil-prone nature in Hejre-1 is present despite the higher thermal maturity of the shales, where VR values from approximately 0.75 to 1.0%R_o indicate depletion of the generation potential. The oil potential of the Farsund Formation is better developed in the Feda Graben and Gert Ridge, where the shales mostly are gas/oil prone (Table 1). The thick Farsund Formation in the Kim-1 well in the Ål Basin is gas-prone (Table 1). In the Outer Rough Basin, the shales of the Farsund Formation are rich oil-prone source rocks in a number of wells, but the formation is generally thin and in all wells the shales are immature (Fig. 6a, b; Table 1).

The Bo Member is traditionally considered to be the most oil-prone part of the Farsund Formation, and in the studied wells the HI values and TOC contents show a significant increase in the member (Fig. 11). In the majority of the wells the Bo Member has average HI values from 316 to 453 mg HC g^{-1} TOC, indicating a potential for oil and gas generation (Fig. 10c; Table 1). In the Mona-1 and Kim-1 wells the shales are gas- or gas/oil-prone. Hence, although the Bo Member has high GR values, it is not necessarily oil-prone (Fig. 4). The source rock quality of the Bo Member seems to be best developed in the deeper parts of the Feda and Gertrud Grabens (Fig. 6c, d). The Norwegian Hod and Valhall oilfields immediately north of the Danish sector occur on trend with the Feda Graben, which makes it likely that the good generation potential in the Feda Graben continues northward into the Norwegian sector. The Danish Freja Field (Gert wells) and

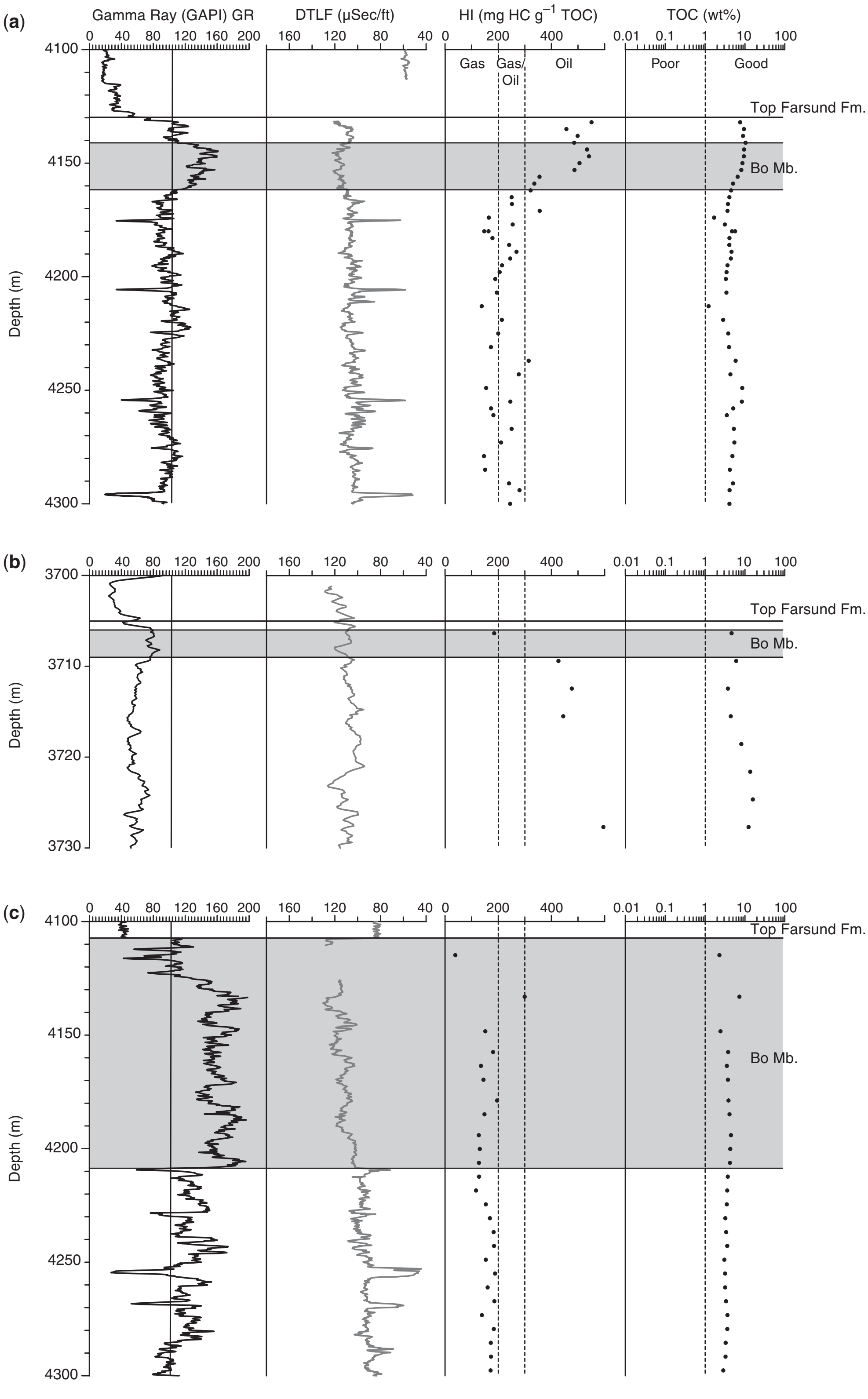

Fig. 4. GR and sonic logs of three wells showing (**a**) high GR, TOC and HI values in the Bo Member in the Eg-1 well, (**b**) low GR values in both the Farsund Formation and the Bo Member but high TOC and HI values in the Farsund Formation in the Diamant-1 well, and (**c**) high GR values but low TOC and HI values in the Bo Member in the Kim-1 well.

the Hejre oil discovery are likewise derived from areas predicted to have good source quality in the Gertrud and Feda Grabens. High HI values seem overall to coincide with high TOC contents. The apparent decline in TOC content closer to structural highs, such as the Inge High, may be caused by dilution from siliciclastics, whereas the decline in generation potential may be caused by a higher input of terrestrial organic matter and/or more oxygenated conditions (e.g. Damtoft *et al.* 1992) (Fig. 6c, d). In areas where the Bo Member is either poorly developed or absent to very thin, the shales of the remaining Farsund Formation may be rich source rocks (encircled wells Jette-1, Diamant-1, Wessel-1 and Tordenskjold-1 in Fig. 6c).

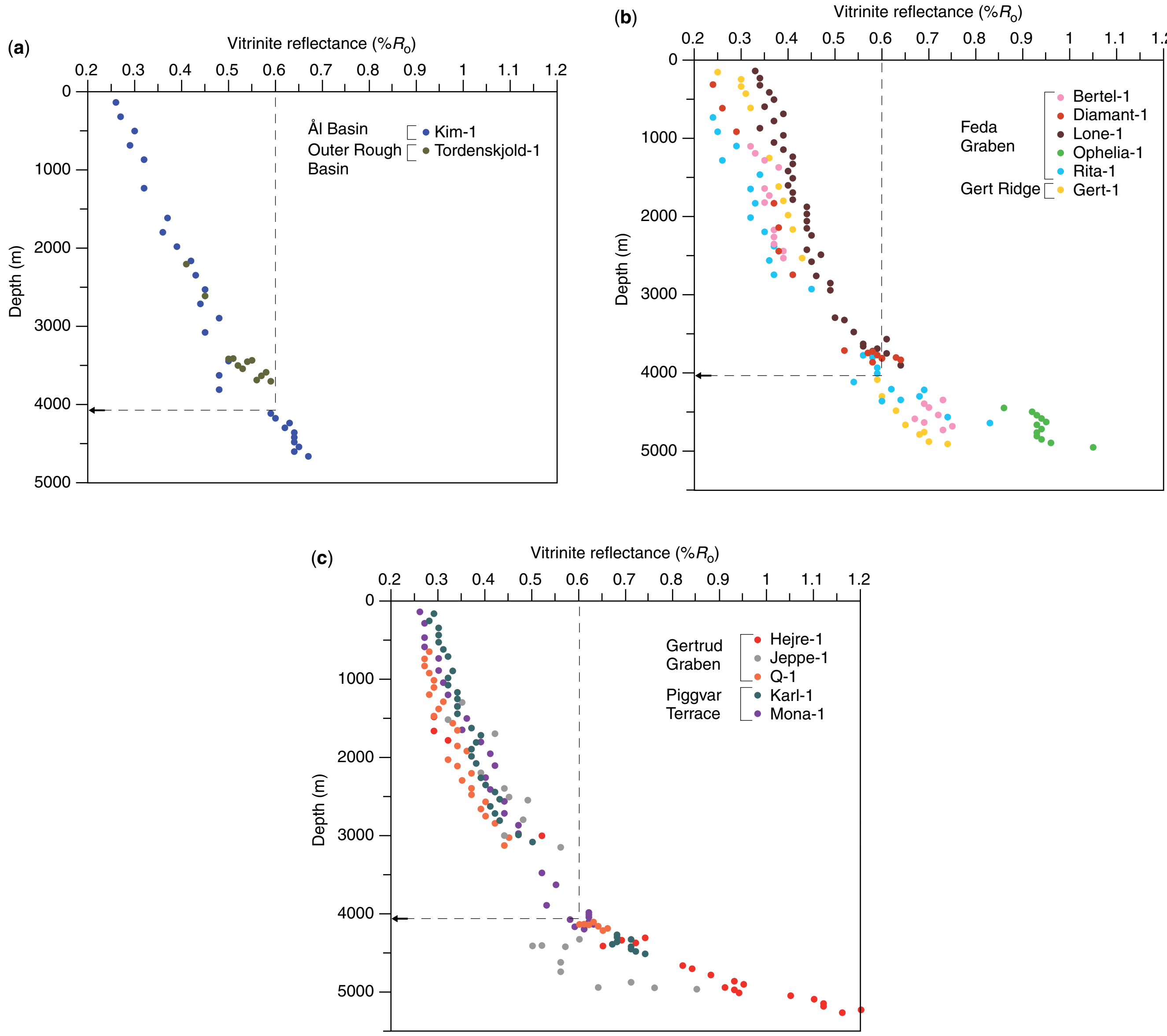

Fig. 5. VR trends of the wells in the (**a**) Outer Rough and Ål Basins, (**b**) Feda Graben and Gert Ridge, and (**c**) Gertrud Graben and Piggvar Terrace. Using a VR of 0.6%R_o the top of the oil window is at about 4000 m depth.

Although HI decreases with burial below 3800 m due to maturation, HI and TOC fluctuate throughout the Farsund Formation, and intervals within the formation may be considerably richer than suggested by the average HI. For example the Gert-2 and Hejre-1 wells contain about 300 and 200 m, respectively, thick oil-prone intervals in the lower–middle part of the Farsund Formation. The Gert-2 and Bertel-1 wells have a pronounced TOC-peak in the lowermost part of the Farsund Formation (Fig. 11). These variations in TOC and HI are consistent with the subtle facies changes observed in a core spanning a minor part of the Farsund Formation and the base of the Bo Member in the Jeppe-1 well (Ineson *et al.* 2003). A gradual decrease in HI with depth in the Farsund Formation of the Ophelia-1 well and the Gert-2 well may thus result from maturation but also deterioration in kerogen quality with depth (Fig. 11). For example, the lower (4632 m; TOC = 5.77 wt%, HI = 200 mg HC g^{-1} TOC) and upper (4344 m; TOC = 8.13 wt%, HI = 321 mg HC g^{-1} TOC) part of the Farsund Formation in the Bertel-1 well show variations in kerogen composition. The upper sample is characterized by fluorescing AOM, alginite, liptodetrinite and abundant pyrite, whereas the lower sample is characterized by less and weaker fluorescing AOM, more vitrinite and inertinite, and non-fluorescing organic matter. The weaker fluorescence intensity could be caused by higher maturity, but the higher vitrinite and inertinite content and lower TOC suggests stronger terrestrial influence and higher oxygen availability. More favourable conditions for preservation of oil-prone kerogen appear to have existed during deposition of the upper parts of the Farsund Formation, including the Bo Member, although exceptions occur. The kerogen quality is, for example, excellent (average HI = 468 mg HC g^{-1} TOC) through the entire Farsund Formation in the Diamant-1 well where the Bo Member is absent or may be very thin (?3 m). In the Upper Jurassic Draupne Formation in the North Viking Graben of Norway, similar lateral and stratigraphical organic facies variations with significant variations in source potential have been identified (Keym *et al.* 2006). Kerogen composition ranges from Type II to Type II/III with more gas- and condensate-prone kerogen containing a higher proportion of terrestrial organic matter occurring in the lower parts of the formation.

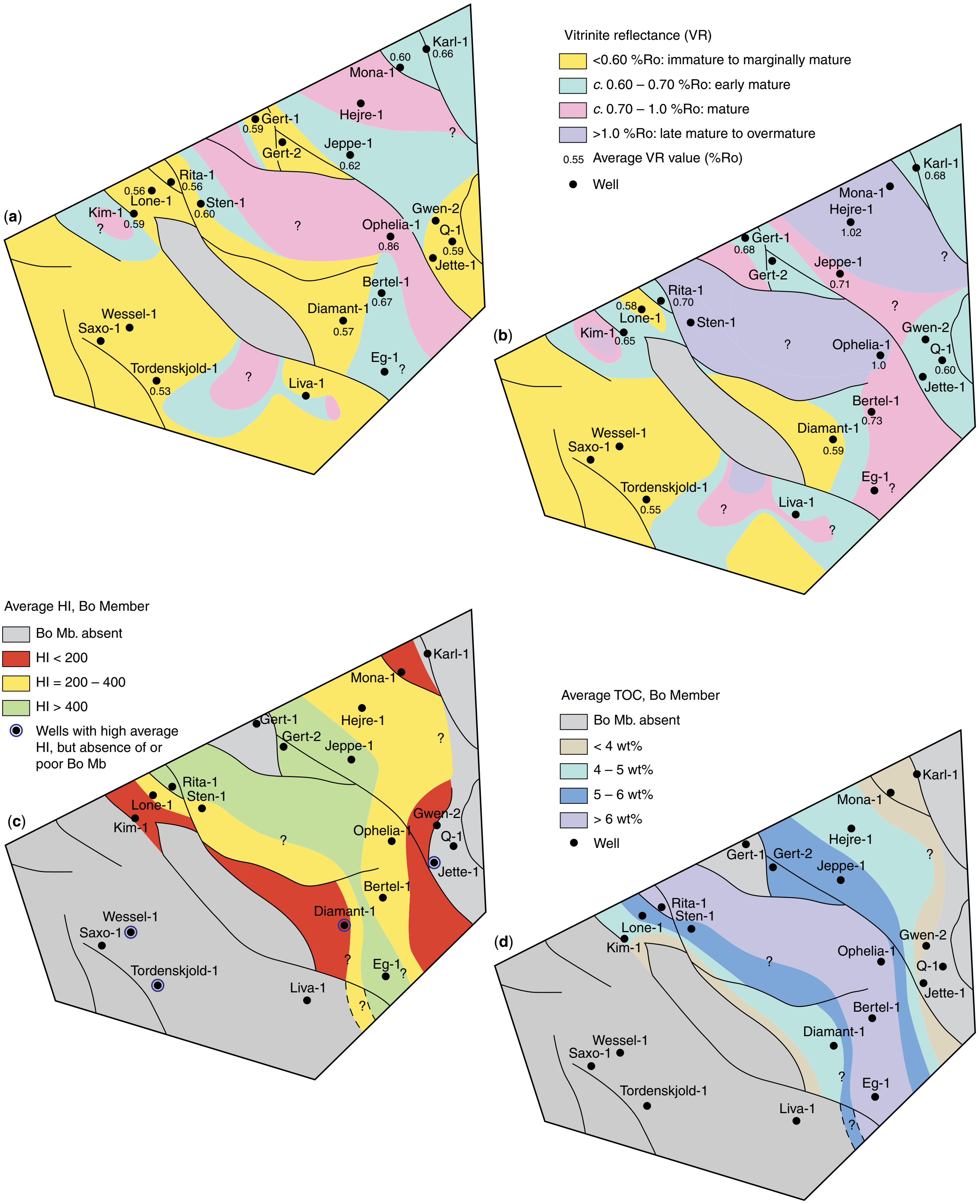

Fig. 6. (**a**) Thermal maturity map of the 'top Farsund Formation', (**b**) thermal maturity map of the 'base Farsund Formation', and (**c**) map showing the average HI of the Bo Member. Wells with high average HI values (>300 mg HC g^{-1} TOC) but with an absent or only very thin Bo Member are encircled. (**d**) Map showing the average TOC content of the Bo Member.

Estimation of HI of the generative kerogen

The measured HI is a measure of the current bulk petroleum generation potential of the kerogen present in the source rock. The kerogen may be a mixture of oil-prone (sapropelic), gas-prone and inert organic material, and the HI value is an average of the source potential. It is, however, possible to estimate the HI for the generative (or 'live') kerogen (HI_{live}). The intercept TOC

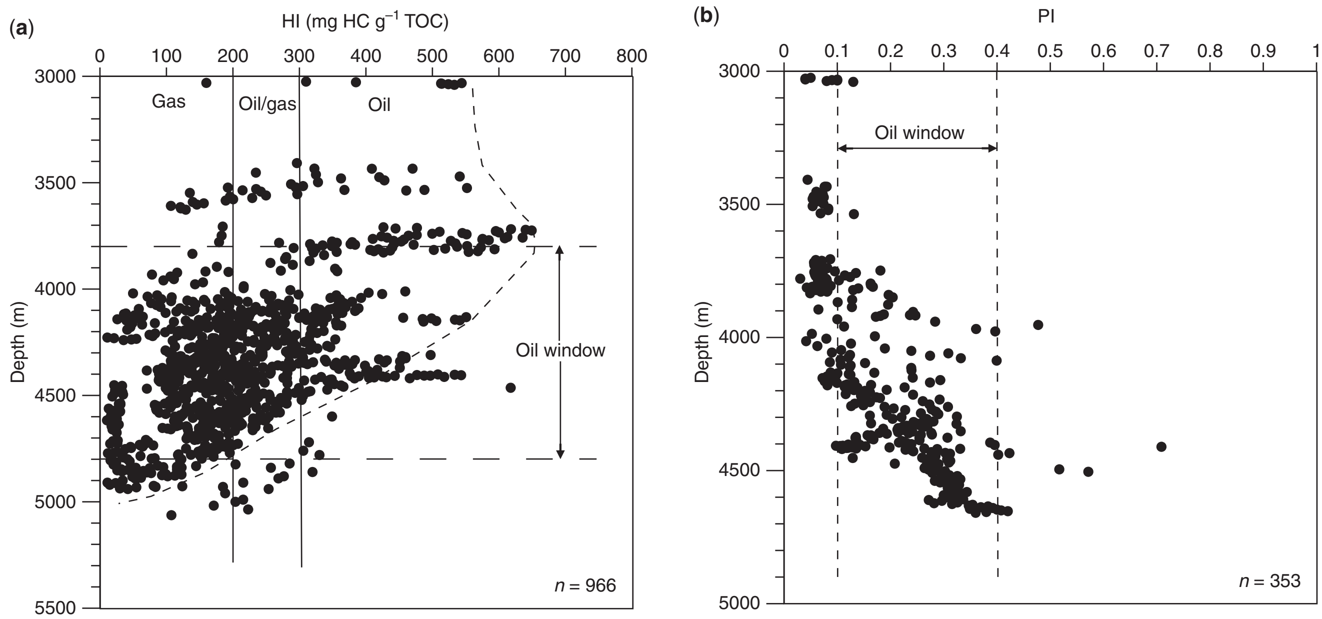

Fig. 7. (**a**) HI v. depth plot for all studied wells. HI shows a gradual decrease through the Farsund Formation at depths greater than *c*. 3800 m, which is caused by generation as the shales pass through the oil window with increasing burial depth. At *c*. 4800 m HI is generally less than 200–300 mg HC/g TOC. (**b**) PI v. depth plot for nine wells not contaminated by oil-based drilling mud. PI is generally 0.1 or higher at about 3800–4000 m and increases to 0.35–0.4 at *c*. 4700 m. The oil window is thus spanning about 800–1000 m.

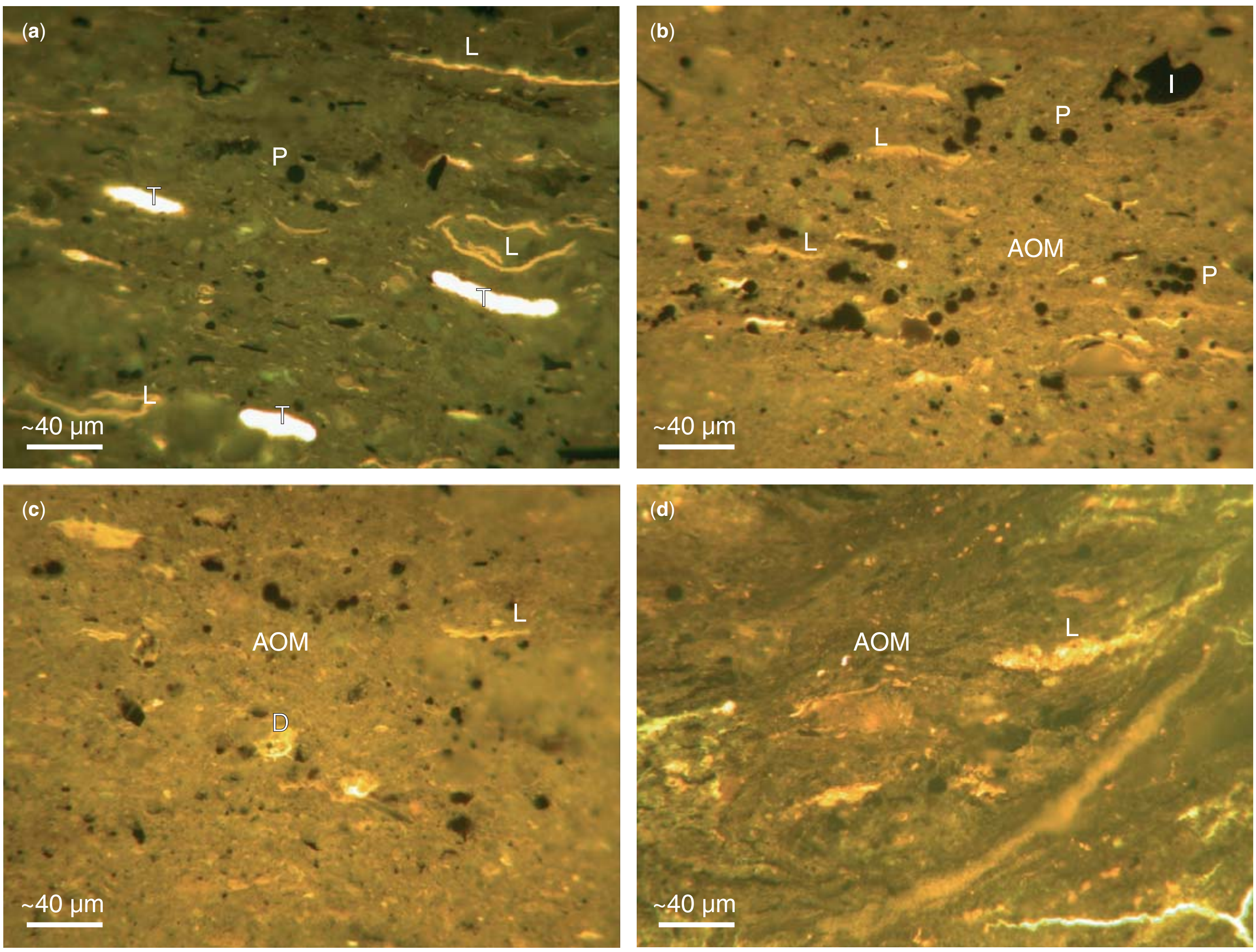

Fig. 8. Photomicrographs in fluorescing-inducing blue light and oil immersion of highly sapropelic kerogen in the (**a**) Jeppe-1 well, Bo Member, 4406.96 m (plug); (**b**) and (**c**) Diamant-1 well, Farsund Formation, 3727.70 m (SWC), (**d**) Bertel-1 well, Bo Member, 4344 m (cuttings). AOM: amorphous organic matter; D: dinoflagelate; I: inertinite; L: *Leiosphaerida*-type alginite; P: framboidal pyrite; T: *Tasmanites*-type alginite.

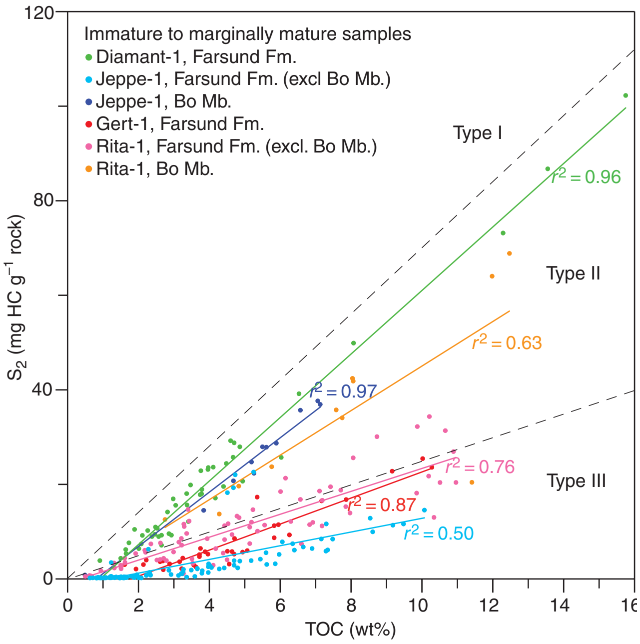

Fig. 9. S_2 v. TOC plot of immature to marginally mature samples from the Farsund Formation and Bo Member in four selected wells. The regression lines show the variation in kerogen type (cf. Langford & Blanc-Valleron 1990) between wells but also between the Farsund Formation and Bo Member in individual wells.

value of the gradient in a S_2 v. TOC cross-plot may be absorptive capacity of the mineral matrix (Langford & Blanc-Valleron 1990), or dead organic carbon, i.e. non-generative kerogen (Cornford *et al.* 1998). Dahl *et al.* (2004) used the equation $HI_{live} = 100 \times S_2/(TOC_{measured} - TOC_{dead\ carbon})$ to estimate the average HI for the generative kerogen. This method has been used to calculate the HI_{live} for immature to early mature samples from the Bo Member and Farsund Formation (excluding the Bo Member) in a number of wells (Fig. 12; Table 2). In the Farsund Formation 39–83% of the measured TOC contents are 'live', whereas 64–82% of the measured TOC contents in the Bo Member are 'live' (Table 2). Using this correction in the Diamant-1 and Jette-1 wells the organic matter in the Farsund Formation is mostly composed of oil-prone kerogen, while in the Eg-1 and Gert-1 wells less oil-prone kerogen is present. Calculation of HI_{live} indicates the presence of substantial proportions of oil-prone kerogen, which is masked by kerogen with a poorer source quality. In the Gert-1 well, the Farsund Formation is rated gas-prone from an average HI of 152 mg HC g^{-1} TOC, but using the correction a HI_{live} of 317 mg HC g^{-1} TOC_{live} is obtained, albeit with a lower richness ($TOC = 4.56$ wt% $\rightarrow$ $TOC_{live} = 2.41$ wt%) (Tables 1 & 2). This suggests that areas considered to be gas-prone based on average HI values may be more oil-prone than previously assumed from Rock-Eval data alone.

Oils: composition and source

Hydrocarbons have been encountered in a number of wells in the northwestern part of the DCG, but only two discoveries have hitherto been declared commercial, the Freja Field and the Hejre discovery (Fig. 1). Biomarker analyses of oils indicate a marine shale source, but there are also indications of a Palaeozoic source in the Outer Rough Basin. Oils from the Mona-1 well (Fig. 13) and Olaf-1 well show the typical biomarker characteristics of the Bo Member of the Farsund Formation as exemplified by the four uppermost Rita-1 well extracts (Table 3). These characteristics include the presence of 28,30-bisnorhopane and higher carbon number 28-norhopanes, a high C_{35} homohopane index, and a high proportion of C_{30} steranes (Table 3). Sterane maturity parameters such as C_{29} 20S/(20S + 20R) and the relative proportions of $\beta\beta$-steranes and diasteranes indicate, however, generation from a more mature Bo Member than in the Rita-1 well (Table 3). Oils from the Gert-1, Lone-1 and Rita-1 wells contain virtually no 28,30-bisnorhopane. The C_{35} homohopane index and the proportion of C_{30} steranes is low, and in that way they are more similar to extracts from the deeper part of the Farsund Formation in the Rita-1 well. The relative proportion of rearranged steranes and hopanes (diasteranes, neohopanes, diahopanes and the early eluting series of rearranged hopanes) is related to both source facies and thermal maturity. An increase with depth in the relative abundances of these compounds can be seen in the Rita-1 well around 3900 m (Table 3). This is partly related to the transition from the Bo Member to the deeper part of the Farsund Formation, which probably was deposited under more oxic conditions. However, the rearranged steranes and hopanes are more stable than regular counterparts. At high maturities the latter are preferentially destroyed giving an increase in all ratios involving the rearranged compounds (Farrimond *et al.* 1998). Also deeper in the well there is a decrease in the hopane:sterane ratio. In the Rita-1 well this happens below 4200 m (Table 3). The hopane:sterane ratio, the diasterane:reg. sterane ratio, and the various rearranged hopane ratios for oils from the Gert-1 and Rita-1 wells are similar to those of the source rock extract from 4474 m in the Rita-1 well, suggesting that the oils were generated from a source of the same thermal maturity.

Oils from the Saxo-1 well and to some extent also the Tordenskjold-1 well, both reservoired in Zechstein intervals, have the same biomarker characteristics as extracts from Permian (Zechstein Z2) samples from the Wessel-1 well. These indicate a carbonate/marly source rock, deposited under conditions of high salinity, which received only minor contributions from higher land plants (Fig. 13; Table 3). These biomarker characteristics include a very high hopane/sterane ratio, abundant 30-norhopanes including 29,30-bisnorhopane, high proportions of $\alpha\beta\beta$-steranes, low proportions of diasteranes and rearranged hopanes, high proportions of homohopanes $>C_{30}$ (e.g. as reflected in the C_{35} homohopane index), and the presence of significant gammacerane, which indicates water-column stratification (by salinity gradient) (Sinninghe Damsté *et al.* 1995). The extracts have lower $C_{30}/(C_{27}–C_{30})$ sterane ratios than samples from oils and source rock extracts from the Farsund Formation (open marine). C_{30} steranes (24-*n*-propylcholestanes) in crude oils are indicators of input of marine organic matter to source rocks (Moldowan *et al.* 1990). One of the two oil samples from the Saxo-1 well (3208 m) has a very high content of β-carotane which, like gammacerane, is associated primarily with anoxic, saline lacustrine or highly restricted marine settings (Hall & Douglas 1983). Oil traces extracted from Upper Jurassic sandstones in the Wessel-1 well show a few of the same characteristics, such as the presence of gammacerane and a high C_{35} homohopane index, whereas most other biomarker ratios including the 24-nordiasterane ratio (NDR, age-related; Fig. 13, Table 3; Holba *et al.* 1998) suggest a Jurassic source.

Discussion

Highly organic-rich and oil-prone shales of the Bo Member are largely restricted to the depocentres of the Feda and Gertrud Grabens (Fig. 6c, d). Outside of these areas the Bo Member constitutes a poor source rock or is absent, but the rest of Farsund

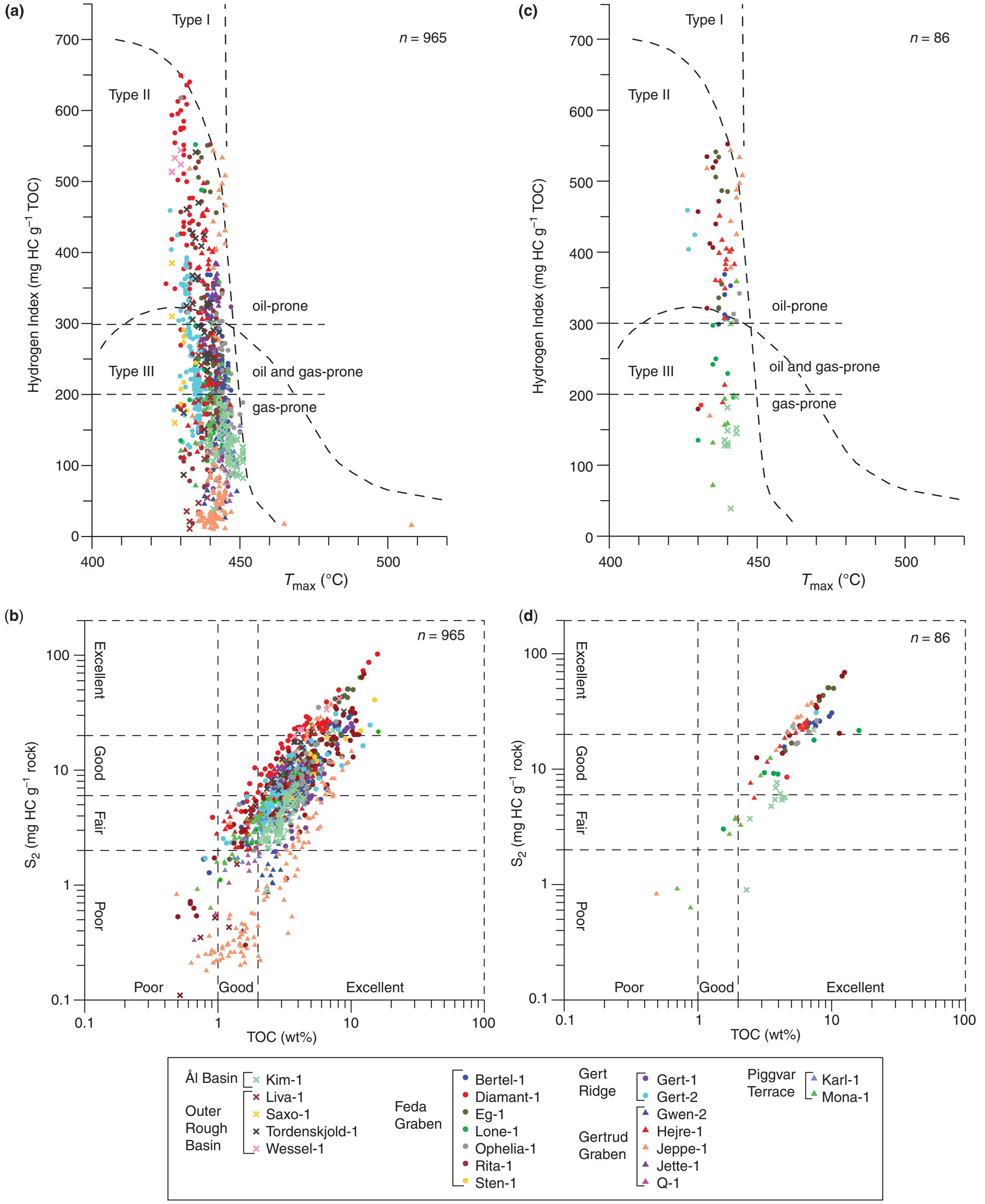

Fig. 10. Source rock potential and quality of the Upper Jurassic–lowermost Cretaceous marine shales in the study area shown by HI v. T_{max} and S_2 v. TOC plots. (**a**) and (**b**) Farsund Formation including the Bo Member, (**c**) and (**d**) only Bo Member.

Formation may be a good source (e.g. Diamant-1, Jette-1, Tordenskjold-1, Wessel-1; Fig. 6c). The HI values of the Farsund Formation are generally highly variable in the wells. Although the average HI value of the Farsund Formation in a well may indicate minor potential, intervals in the formation can be highly oil-prone (Fig. 11). In addition, estimation of HI_{live} values suggests that the shales may contain higher proportions of oil-prone kerogen, which can be 'masked' by the presence of dead carbon (e.g.

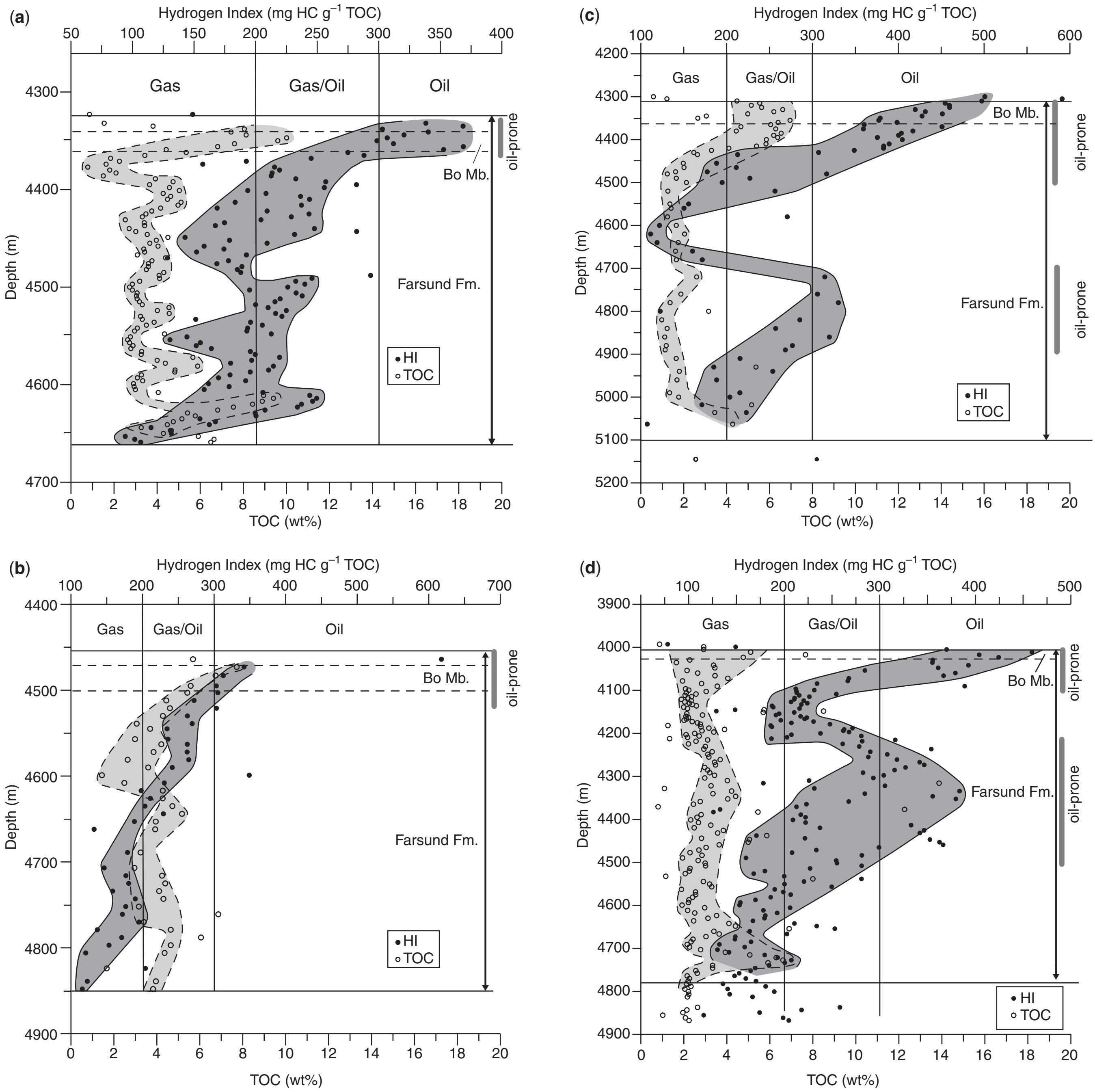

Fig. 11. Variability in TOC content and HI through the Farsund Formation in the (**a**) Bertel-1 well, (**b**) Ophelia-1 well, (**c**) Hejre-1 well and (**d**) Gert-2 well. A general increase in both values is recorded in the upper part towards the Bo Member.

Gert-1 well; Table 2). This indicates that the oil generation potential in some areas may be underestimated by using average HI values. It has generally been assumed that the oil-prone organofacies declines from top to base of the Farsund Formation (Damtoft *et al.* 1992), owing to more oxic depositional conditions. Geochemical data and petrographical observations from this study support this assumption. However, it is obvious that the gradual decrease in HI and associated increase in PI at depth greater than *c*. 3800–4000 m in all wells is caused by increasing maturity as the shales pass through the oil window (Fig. 7a, b). Lower HI values in the lower part of the Farsund Formation are thus mainly a function of higher maturity. The Farsund Formation is mature in the depocentres of the Feda Graben, Gertrud Graben and Ål Basin and possibly in a deep between the Tordenskjold-1 and Liva-1 wells in the Outer Rough Basin (Fig. 6a, b). However, in the deepest parts of the Feda Graben and Gertrud Graben the lower Farsund Formation is probably overmature due to burial depths of 6000 m or more (Fig. 2b). The Farsund Formation is early mature on the Piggvar Terrace, whereas only the lower part of the formation is early mature on the Gert Ridge and in the area around the Gwen-2, Q-1 and Jette-1 wells. By superimposing the areas with oil-prone source rocks (HI >300 mg HC g^{-1} TOC; Bo Member and/or Farsund Formation) with areas where the source rocks are thermally mature, kitchen areas can be delineated (Fig. 14). The Feda and Gertrud Grabens constitute potential kitchen areas. The main kitchen areas probably occur in the Gertrud Graben, including the area around the Hejre discovery, and in the Feda Graben from the area around Ophelia-1 and

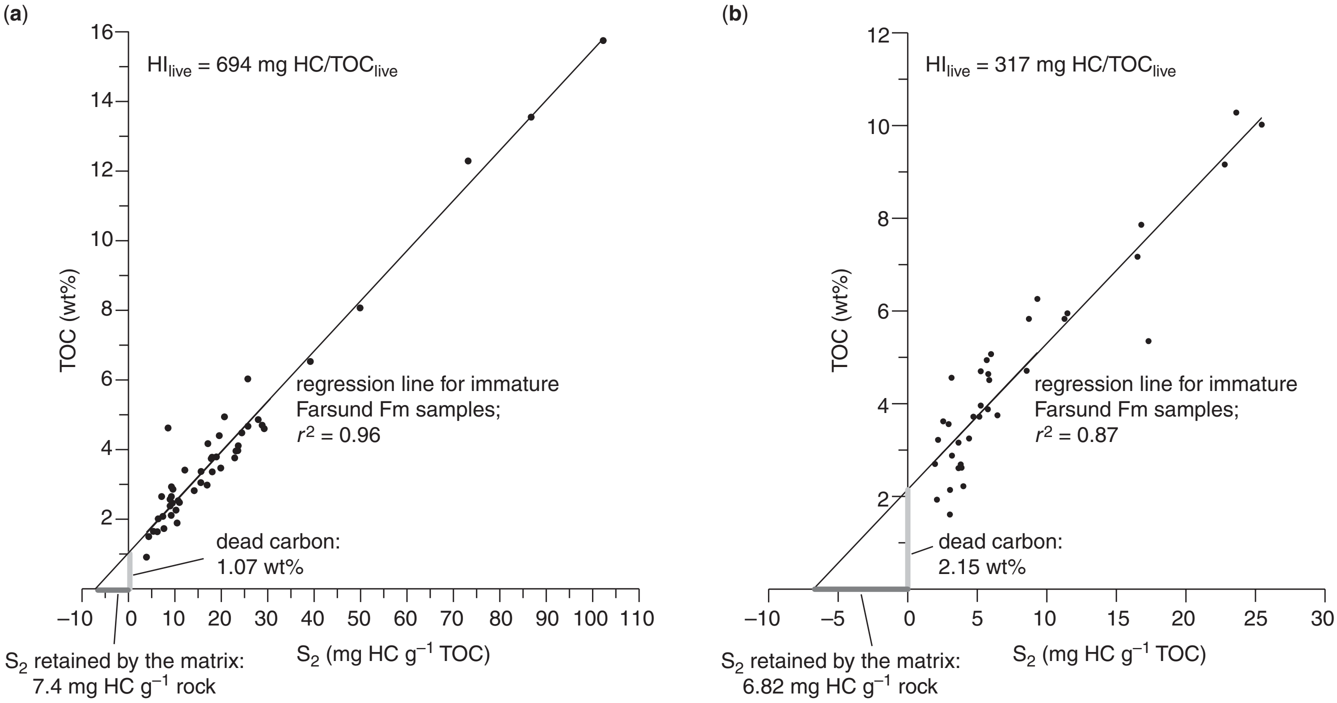

Fig. 12. Estimation of the average proportion of dead carbon and average HI_{live} for the Farsund Formation in the (**a**) Diamant-1 well and (**b**) Gert-1 well.

northwards, continuing into the Norwegian sector (Fig. 14). A small kitchen may be present in the deep close to the Liva-1 well in the Outer Rough Basin, which may source the hydrocarbons encountered in Cretaceous chalk of the Olaf-1 well, located up-dip from the kitchen.

The vast majority of hydrocarbons encountered have geochemical characteristics that are typical for oils sourced from the Upper Jurassic–lowermost Cretaceous marine shales. The distribution of C_{27}–C_{30} steranes was analysed by principal component analysis (Fig. 15). Most extracts from the Farsund Formation shales in the Rita-1 and Tordenskjold-1 wells, and tested crude oils (Lone-1, Mona-1, Olaf-1, Rita-1 and Gert-1 wells), plot on a diagonal line, mainly reflecting a similar source but increasing maturity (from the upper left corner towards lower right corner; Fig. 15). The extracts from the Farsund Formation in Wessel-1 well are atypical, and the biomarker composition does not resemble that of the oil shows in this well. Despite excellent source potentials recorded in the Farsund Formation in the Wessel-1 and Tordenskjold-1 wells, thermal immaturity of the shales indicates that generation from Farsund Formation is highly unlikely in the shallow parts of the Outer Rough Basin. This suggests that the Outer Rough Basin is dependent on migration from outside the area, or on deeper buried Palaeozoic source rocks. Oil show samples from the Saxo-1 well resemble the extracts from the Zechstein section in the Wessel-1 well (Fig. 15), and the geochemical signature indicates that they were sourced from carbonate/marly source rocks, suggesting the presence of mature Zechstein source rocks in Outer Rough Basin.

Conclusions

The Upper Jurassic–lowermost Cretaceous marine shales of the Farsund Formation are present regionally in the northwestern part of the DCG. In the Outer Rough Basin the formation is relatively thin, and on the Inge High it is thin or absent. The generally organic-rich Bo Member ('Hot Unit') in the upper part of the Farsund Formation is present in the Piggvar Terrace, the Gertrud

Table 2. Proportion of reactive kerogen in selected wells

Well	HI_{live} (mg HC g^{-1} TOC)		TOC_{live} (wt%)		HI (mg HC g^{-1} TOC)		TOC (wt%)	
	Farsund Fm.[a]	Bo Mb.	Farsund Fm.[a]	Bo Mb.	Farsund Fm.[a]	Bo Mb.	Farsund Fm.[a]	Bo Mb.
Diamant-1	697	n.d.	2.98 (74%)	n.d.	474	185	4.05	4.62
Eg-1	644	731	1.75 (39%)	4.95 (64%)	248	446	4.55	7.75
Gert-1	317	—	2.41 (53%)	—	152	—	4.56	—
Jeppe-1	n.d.	595	n.d.	4.25 (82%)	94	453	3.43	5.20
Jette-1	394	—	2.74 (83%)	—	328	—	3.31	—

[a]Bo Member not included.
n.d.: Not detected.
In brackets: percentage TOC_{live} of original TOC.

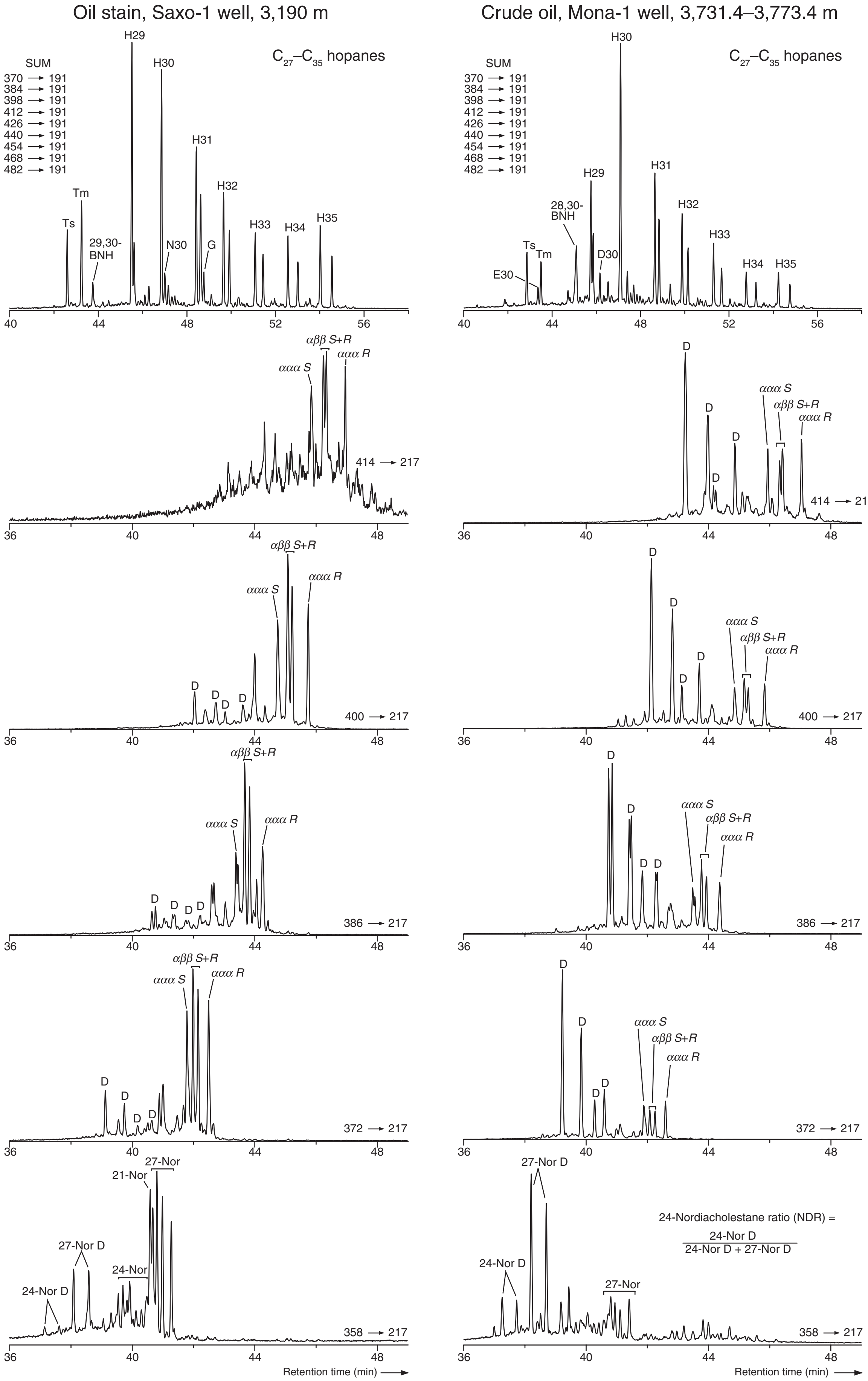

Fig. 13. C_{27}–C_{35} hopanes and C_{26}–C_{30} steranes in the oil sample from the Saxo-1 well, possibly sourced from Permian (Zechstein Z2) carbonate/marly source rocks and in a typical crude oil (Mona-1 well, 3731–3773 m) sourced from the shales of the Bo Member. Ts: 22,29,30-trisnorneohopane; Tm: 22,29,30-trisnorhopane; 28,30-BNH: 28,30-bisnorhopane; 29,30-BNH: 29,30-bisnorhopane; H: $17\alpha,21\beta$(H)-hopanes; E30: 'early eluting rearranged hopane'; D30: diahopane; N30: 30-norhomohopane; G: gammacerane; $\alpha\alpha\alpha$ S: $5\alpha,14\alpha,17\alpha$(H) 20S steranes; $\alpha\beta\beta$ S + R: $5\alpha,14\beta,17\beta$(H) 20S + 20R steranes; $\alpha\alpha\alpha$ R: $5\alpha,14\alpha,17\alpha$(H) 20R steranes; D: diasteranes; 21-Nor: 21-norcholestanes; 24-Nor: 24-norcholestanes; 27-Nor: 27-norcholestanes; 24-Nor-D: 24-nordiacholestanes; 27-Nor-D: 27-nordiacholestanes.

Table 3. Biomarker ratios for oils and source rocks in the NW part of the DCG.

Sample type	% C_{27} ster.	% C_{28} ster.	% C_{29} ster.	% C_{30} ster.	$S/(S+R)$	$\beta\beta$	Dst	NDR	Ts	29,30-BNH	28,30-BNH	29Ts	H29/H30	E30/H30	D30/H30	G/H30	HHI	HOEP	Ho/St
Mona-1, 3731–3773 m, oil	36.2	29.3	34.6	9.3	0.52	0.51	0.69	0.21	0.56	0.01	0.32	0.37	0.47	0.066	0.107	0.01	0.103	1.05	0.27
Gert-1, oil	35.1	26.0	38.9	5.2	0.55	0.62	0.81	0.24	0.83	0.00	0.00	0.66	0.45	0.233	0.434	0.00	0.038	1.00	0.12
Lone-1, oil	37.7	29.3	33.0	8.3	0.44	0.51	0.66	0.20	0.63	0.01	0.04	0.35	0.55	0.041	0.093	0.01	0.069	1.12	0.36
Rita-1, 3773 m, sr	36.2	31.6	32.1	9.2	0.45	0.38	0.40	0.18	0.51	0.02	0.16	0.24	0.69	0.009	0.045	0.02	0.089	1.18	0.33
Rita-1, 3780–3786 m, sr	36.5	31.4	32.1	9.5	0.47	0.39	0.43	0.16	0.41	0.03	0.10	0.18	0.67	0.007	0.033	0.10	0.097	1.24	0.42
Rita-1, 3804 m, sr	33.9	32.3	33.8	8.7	0.46	0.39	0.41	0.19	0.32	0.03	0.10	0.15	0.68	0.006	0.025	0.13	0.084	1.19	0.48
Rita-1, 3819–3822 m, sr	36.4	31.8	31.8	10.1	0.46	0.38	0.50	0.18	0.46	0.02	0.04	0.22	0.59	0.014	0.044	0.07	0.090	1.15	0.34
Rita-1, 3916 m core, sr	37.7	30.4	31.9	7.6	0.49	0.45	0.51	0.19	0.66	0.01	0.00	0.38	0.43	0.017	0.062	0.01	0.048	1.10	0.48
Rita-1, 3918 m core, sr	34.8	29.6	35.6	8.2	0.48	0.40	0.51	0.20	0.62	0.01	0.00	0.37	0.43	0.019	0.052	0.00	0.044	1.30	0.46
Rita-1, 3919 m core, sr	38.2	26.6	35.2	7.1	0.49	0.42	0.60	0.21	0.55	0.01	0.00	0.37	0.49	0.029	0.066	0.01	0.037	1.35	0.48
Rita-1, 4042 m, sr	36.3	31.8	31.9	8.5	0.54	0.55	0.58	0.16	0.66	0.01	0.01	0.37	0.42	0.015	0.063	0.01	0.069	1.03	0.39
Rita-1, 4215 m, sr	40.6	27.0	32.4	5.9	0.55	0.64	0.61	0.23	0.76	0.01	0.02	0.47	0.44	0.024	0.099	0.03	0.046	1.04	0.52
Rita-1, 4325 m, sr	39.5	27.2	33.2	5.2	0.55	0.65	0.75	0.22	0.84	0.01	0.01	0.59	0.39	0.056	0.176	0.04	0.055	0.95	0.30
Rita-1, 4474 m, sr	41.2	24.9	33.9	4.7	0.51	0.66	0.85	0.25	0.92	0.00	0.00	0.76	0.39	0.276	0.476	0.07	0.058	0.85	0.19
Rita-1, 4651 m, oil	34.6	25.1	40.3	5.4	0.57	0.63	0.77	0.25	0.90	0.00	0.00	0.68	0.34	0.220	0.467	0.05	0.054	0.93	0.19
Olaf-1, oil	36.4	31.4	32.2	8.9	0.49	0.59	0.73	0.23	0.69	0.01	0.15	0.39	0.44	0.057	0.111	0.01	0.084	1.08	0.26
Saxo-1, 3190 m, oil	28.1	24.5	47.4	1.6	0.55	0.57	0.15	0.12	0.43	0.10	0.00	0.16	1.09	0.002	0.030	0.11	0.159	0.97	1.55
Saxo-1, 3208 m, oil	26.4	29.9	43.7	2.3	0.46	0.40	0.44	0.17	0.38	0.05	0.01	0.19	0.53	0.002	0.034	0.42	0.191	0.70	4.33
Tordenskjold-1, 3434.55 m, sr	33.6	31.5	35.0	7.4	0.37	0.30	0.55	0.24	0.48	0.01	0.01	0.31	0.54	0.055	0.074	0.01	0.063	1.19	0.28
Tordenskjold-1, 3474 m, sr	36.9	29.0	34.1	7.8	0.40	0.32	0.55	0.24	0.47	0.02	0.02	0.30	0.61	0.053	0.073	0.01	0.070	1.23	0.31
Tordenskjold-1, 3537 m, sr	36.5	30.1	33.5	7.3	0.43	0.35	0.54	0.22	0.49	0.02	0.01	0.31	0.57	0.037	0.069	0.03	0.072	1.10	0.31
Tordenskjold-1, 3648 m, oil	31.3	25.2	43.5	3.6	0.51	0.53	0.49	0.10	0.48	0.11	0.01	0.17	1.29	0.018	0.051	0.05	0.158	1.00	1.27

Wessel-1, 3031.9 m, sr	35.2	32.9	31.9	8.7	0.22	0.26	0.46	0.17	0.49	0.02	0.01	0.34	0.40	0.033	0.057	0.04	0.156	1.27	0.08
Wessel-1, 3035.0 m, sr	41.2	28.6	30.2	8.4	0.28	0.29	0.53	0.18	0.45	0.02	0.01	0.30	0.65	0.060	0.080	0.07	0.221	1.43	0.14
Wessel-1, 3037.0 m, sr	37.7	30.8	31.5	9.0	0.25	0.29	0.52	0.19	0.52	0.02	0.00	0.29	0.75	0.043	0.068	0.06	0.221	1.34	0.17
Wessel-1, 3040.2 m, sr	40.9	27.9	31.1	6.9	0.31	0.29	0.55	0.16	0.42	0.02	0.01	0.31	0.61	0.052	0.078	0.03	0.210	1.22	0.11
Wessel-1, 3041.5 m, oil	38.7	28.5	32.8	7.5	0.54	0.56	0.60	0.18	0.50	0.02	0.01	0.29	0.46	0.019	0.053	0.05	0.171	0.94	0.45
Wessel-1, 3042.5 m, oil	40.1	28.5	31.5	7.5	0.52	0.56	0.59	0.19	0.49	0.02	0.01	0.29	0.33	0.011	0.037	0.07	0.173	0.96	0.54
Wessel-1, 3043.5 m, oil	39.7	28.2	32.1	7.2	0.51	0.56	0.60	0.19	0.50	0.03	0.01	0.30	0.52	0.019	0.058	0.04	0.176	0.95	0.49
Wessel-1, 3044.5 m, oil	39.4	28.1	32.5	7.3	0.51	0.56	0.60	0.18	0.50	0.03	0.01	0.30	0.50	0.017	0.055	0.04	0.175	0.95	0.48
Wessel-1, 3134.7 m, sr Zechst	32.8	23.5	43.7	1.7	0.54	0.58	0.18	0.09	0.40	0.07	0.00	0.23	0.88	0.002	0.021	0.08	0.213	1.07	3.07
Wessel-1, 3135.5 m, sr Zechst	32.9	23.9	43.2	1.6	0.54	0.58	0.16	0.10	0.41	0.06	0.00	0.21	0.90	0.002	0.022	0.07	0.207	1.09	2.92
Wessel-1, 3136.5 m, sr Zechst	33.0	23.6	43.5	1.6	0.54	0.58	0.18	0.10	0.41	0.07	0.00	0.22	0.95	0.002	0.027	0.08	0.201	1.09	2.93
Wessel-1, 3141.0 m, sr Zechst	27.7	22.7	49.7	1.2	0.54	0.59	0.22	0.09	0.39	0.09	0.01	0.17	1.03	0.002	0.030	0.12	0.223	1.04	2.71

sr: source rock extract from Farsund Formation shale; sr Zechst: extract from Permian (Zechstein Z2) samples.
%C_{27} ster: 100 × (C_{27} steranes + C_{27} diasteranes)/(C_{27-29} steranes + C_{27-29} diasteranes).
%C_{28} ster: 100 × (C_{28} steranes + C_{28} diasteranes)/(C_{27-29} steranes + C_{27-29} diasteranes).
%C_{29} ster: 100 × (C_{29} steranes + C_{29} diasteranes)/(C_{27-29} steranes + C_{27-29} diasteranes).
%C_{30} ster: 100 × (C_{30} steranes + C_{30} diasteranes)/(C_{27-30} steranes + C_{27-30} diasteranes).
S/(S + R): C_{29} regular sterane isomerisation ratio, 20S/(20S + 20R).
$\beta\beta$: C_{29} regular steranes, ratio of $\beta\beta$-epimers to total, $\beta\beta/(\alpha\alpha + \beta\beta)$.
Dst: C_{29} diasteranes/(C_{29} diasteranes + C_{29} reg. steranes).
NDR: 24-Nordiacholestane ratio, 24-nor-D/(24-nor-D + 27-nor-D).
Ts: Ts/(Ts + Tm).
29Ts: 29Ts/(29Ts + H29).
29,30-BNH: 29,30-bisnorhopane/H30.
28,30-BNH: 28,30-bisnorhopane/H30.
H29/H30: Norhopane/hopane.
D30/H30: C_{30} 17α-diahopane/H30.
E30/H30: C_{30} "early eluting rearranged hopane"/H30.
G/H30: Gammacerane/H30.
HHI: C_{35} homohopane index, $H_{35}/(H_{31-}H_{35})$.
HOEP: $(H_{31} + 6 \times H_{33} + H_{35})/(4 \times H_{32} + 4 \times H_{34})$.
Ho/St: Sum C_{27-35} hopanes (19)/Sum C_{27-30} diasteranes + C_{27-30} reg. steranes (32).

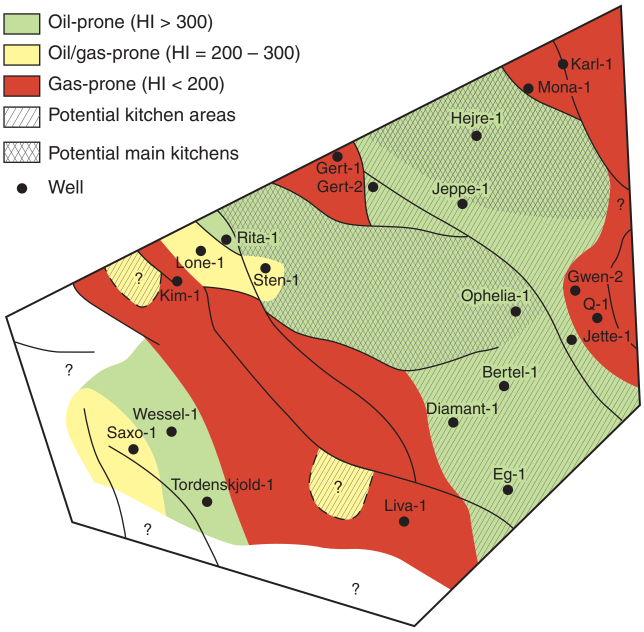

Fig. 14. Potential kitchen areas in the northwestern part of the DCG based on the presence of rich and thermally mature shales of the Bo Member and/or the Farsund Formation. Main kitchens are defined where the shales are rich, thick and mature, which is restricted to the depocentres of the Gertrud and Feda Grabens.

and Feda Grabens and the Ål Basin, but is thin to absent on the Gert Ridge and absent on the Inge High and in the Outer Rough Basin.

The kerogen composition varies from Type II to Type III. The kerogen is principally algal-derived material consisting of fluorescing AOM and alginite with *Leiosphaerida* and *Tasmanites* morphology. Organic richness (TOC) and HI show lateral and stratigraphical variations, with a significant improvement in the Bo Member. The variations indicate shifts in kerogen quality from non-generative through gas-prone to highly oil-prone. The source quality can be classified as fair to excellent, and in most wells the shales of the Bo Member are oil-prone with average HI values ranging from 316 to 453 mg HC g^{-1} TOC. The presence of oil-prone kerogen delineated by HI alone may be masked by kerogen of poorer quality. Hence, areas considered to be gas-prone based on average HI values may be more prolific than initially interpreted. The start of the oil window occurs at *c.* 3800–4000 m depth and the oil window spans 800–1000 m. The decrease in HI and associated increase in PI at depth greater than *c.* 3800–4000 m in all wells is caused by increasing maturity as the shales pass through the oil window. An overall deterioration of kerogen quality with depth in the Farsund Formation probably contributes to the decreasing HI. Potential main kitchen areas with rich, mature and thick source rock units occur in the Gertrud Graben and the Feda Graben.

Oils analysed were generated from the highly oil-prone shales mainly present in the upper part of the Farsund Formation, including the Bo Member, and from the more mature and slightly poorer

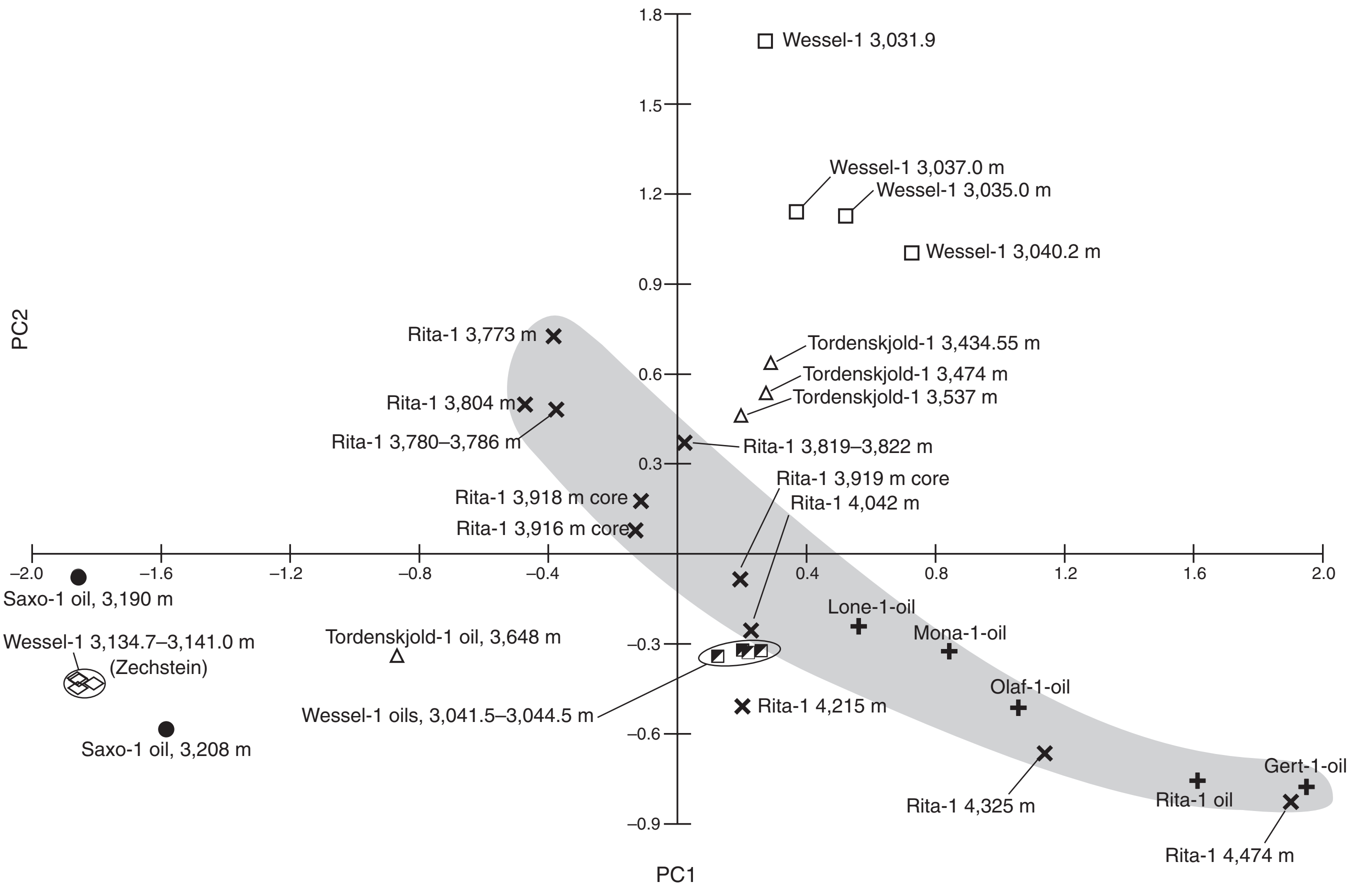

Fig. 15. Principal component analysis of C_{27}–C_{30} steranes in oils and source rocks in the northwestern part of the DCG (see also Table 3). Shaded area shows trend of extracts from the Farsund Formation in the Rita-1 well.

quality lower part of the Farsund Formation. A probable Zechstein-sourced oil-show on the flanks of the Mid North Sea High indicates the presence of mature Palaeozoic source rocks in the Outer Rough Basin.

J. Halskov and S. Sølberg (GEUS) are thanked for drafting the figures. The paper benefited from constructive reviews by J. Miles and A. Law.

References

Andsbjerg, J. & Dybkjær, K. 2003. Sequence stratigraphy of the Jurassic of the Danish Central Graben. *In*: Ineson, J. R. & Surlyk, F. (eds) *The Jurassic of Denmark and Greenland*. Geological Survey of Denmark and Greenland Bulletin, **1**, 265–300.

Carr, A. D. , 2000. Suppression and retardation of vitrinite reflectance, Part 1. Formation and significance for hydrocarbon generation. *Journal of Petroleum Geology*, **23**, 313–343.

Cornford, C. 1998. Source rocks and hydrocarbons of the North Sea. *In*: Glennie, K. W. (ed.) *Petroleum Geology of the North Sea. Basic Concepts and Recent Advances*. Blackwell Science, Oxford, 376–462.

Cornford, C., Gardner, P. & Burgess, C. 1998. Geochemical truths in large data sets. I: geochemical screening data. *Organic Geochemistry*, **29**, 519–530.

Dahl, B., Bojesen-Koefoed, J. A., Holm, A., Justwan, H., Rasmussen, E. & Thomsen, E. 2004. A new approach to interpreting Rock-Eval S_2 and TOC data for kerogen quality assessment. *Organic Geochemistry*, **35**, 1461–1477.

Damtoft, K., Nielsen, L. H., Johannessen, P. N., Thomsen, E. & Andersen, P. R. 1992. Hydrocarbon plays of the Danish Central Trough. *In*: Spencer, A. M. (ed.) *Generation, Accumulation and Production of Europe's Hydrocarbons II*. Special Publication of the European Association of Petroleum Geoscientists, **2**. Springer, Berlin, 35–58.

Espitalié, J., Deroo, G. & Marquis, F. 1985. La pyrolyse Rock-Eval et ses applications. Part II. *Revue de l'Institut Français du Pétrole*, **40**, 755–784.

Espitalié, J., Deroo, G. & Marquis, F. 1986. La pyrolyse Rock-Eval et ses applications. Part III. *Revue de l'Institut Français du Pétrole*, **41**, 73–89.

Farrimond, P., Taylor, A. & Telnæs, N. 1998. Biomarker maturity parameters: the role of generation and thermal degradation. *Organic Geochemistry*, **29**, 1181–1197.

Hall, P. B. & Douglas, A. G. 1983. The distribution of cyclic alkanes in two lacustrine deposits. *In*: Bjorøy, M. *et al*. (eds) *Advances in Organic Geochemistry 1981*. Wiley, Chichester, 576–587.

Holba, A. G., Dzou, L. I. P. & Masterson, W. D. 1998. Application of 24-norcholestanes for constraining source age of petroleum. *Organic Geochemistry*, **29**, 1269–1283.

Hunt, J. M. 1996. *Petroleum Geochemistry and Geology*. W. H. Freeman, New York.

Ineson, J. R., Bojesen-Koefoed, J. A., Dybkjær, K. & Nielsen, L. H. 2003. Volgian–Ryazanian 'hot shales' of the Bo Member (Farsund Formation) in the Danish Central Graben, North Sea: stratigraphy, facies and geochemistry. *In*: Ineson, J. R. & Surlyk, F. (eds) *The Jurassic of Denmark and Greenland*. Geological Survey of Denmark and Greenland Bulletin, **1**, 403–436.

Japsen, P., Britze, P. & Andersen, A. 2003. Upper Jurassic–Lower Cretaceous of the Danish Central Graben: structural framework and nomenclature. *In*: Ineson, J. R. & Surlyk, F. (eds) *The Jurassic of Denmark and Greenland*. Geological Survey of Denmark and Greenland Bulletin, **1**, 233–246.

Jensen, T. F., Holm, L., Frandsen, N. & Michelsen, O. 1986. Jurassic–Lower Cretaceous lithostratigraphic nomenclature for the Danish Central Graben. *Danmarks og Grønlands Geologiske Undersøgelse Serie A*, **12**, 65pp.

Johannessen, P. N. 2003. Sedimentology and sequence stratigraphy of paralic and shallow marine Upper Jurassic sandstones in the northern Danish Central Graben. *In*: Ineson, J. R. & Surlyk, F. (eds) *The Jurassic of Denmark and Greenland*. Geological Survey of Denmark and Greenland Bulletin, **1**, 367–402.

Johannessen, P. N., Dybkjær, K., Andersen, C., Kristensen, L., Hovikoski, J. & Vosgerau, H. 2010. Upper Jurassic reservoir sandstones in the Danish Central Graben: new insights on distribution and depositional environments. *In*: Vining, B. A. & Pickering, S. C. (eds) *Petroleum Geology: From Mature Basins to New Frontiers – Proceedings of the 7th Petroleum Geology Conference*. Geological Society, London, 127–143; doi: 10.1144/0070127.

Keym, M., Dieckmann, V. ET AL. 2006. Source rock heterogeneity of the Upper Jurassic Draupne Formation, North Viking Graben, and its relevance to petroleum generation studies. *Organic Geochemistry*, **37**, 220–243.

Langford, F. F. & Blanc-Valleron, M.-M. 1990. Interpreting Rock-Eval pyrolysis data using graphs of pyrolizable hydrocarbons vs. total organic carbon. *American Association of Petroleum Geologists Bulletin*, **74**, 799–804.

Michelsen, O., Nielsen, L. H., Johannessen, P. N., Andsbjerg, J. & Surlyk, F. 2003. Jurassic lithostratigraphic and stratigraphic development onshore and offshore Denmark. *In*: Ineson, J. R. & Surlyk, F. (eds) *The Jurassic of Denmark and Greenland*. Geological Survey of Denmark and Greenland Bulletin, **1**, 147–216.

Moldowan, J. M., Fago, F. J. ET AL. 1990. Sedimentary 24-*n*-propylcholestanes, molecular fossils diagnostic of marine algae. *Science*, **247**, 309–312.

Sinninghe Damsté, J. S., Kenig, F. ET AL. 1995. Evidence for gammacerane as an indicator of water column stratification. *Geochimica et Cosmochimica Acta*, **59**, 1895–1900.

From thrust-and-fold belt to foreland: hydrocarbon occurrences in Italy

F. BERTELLO, R. FANTONI, R. FRANCIOSI, V. GATTI, M. GHIELMI and A. PUGLIESE

Eni Exploration & Production Division, via Emilia, 1-20097 San Donato Milanese, Italy (e-mail: francesco.bertello@eni.it)

Abstract: Italy is the most hydrocarbon endowed country of southern Europe, with total discovered reserves (produced + remaining) of 1840 million barrels of oil and 30 trillion ft^3 of gas. The production of oil amounts to 43.2 million barrels per year, about 75% of which comes from the Val d'Agri Field in the southern Apennines. The production of gas is 340 billion ft^3 per year, most of it coming from the northern Adriatic Sea. Hydrocarbon occurrences derive from a variety of petroleum systems which are the result of a complex geological history. At least five important source rocks have been recognized which are distributed in age from Mesozoic through Pleistocene. Three of them were deposited during Mesozoic crustal extension and are mainly oil-prone. Hydrocarbon occurrences associated with these sources are usually found in complex carbonate structures along the Apennines thrust-and-fold belt and in the foreland. Villafortuna–Trecate (Po Plain), Val d'Agri/Tempa Rossa (southern Apennines) and Gela (Sicily) fields represent the largest oil accumulations pertaining to these systems. Two other important sources rocks were deposited in the foredeep terrigenous units of the foreland basins which formed during the Cenozoic orogenesis. The older source is thermogenic gas-prone and is found in the highly tectonized Oligo-Miocene foredeep wedges: gas occurrences associated with this source are mainly concentrated along the northern Apennines margin (e.g. Cortemaggiore Field), in Calabria (e.g. Luna Field) and Sicily (e.g. Gagliano Field). The younger source is biogenic gas-prone and is situated in the outer Plio-Pleistocene foredeeps. The most important gas fields of Italy, located in the eastern Po Plain and northern Adriatic sea (Barbara and other gas fields), have originated from this source. Hydrocarbon exploration in Italy is overall mature, especially for gas, whose residual potential is estimated to be 6.0 trillion ft^3 of reserves. The remaining potential of oil is estimated to be 800 million barrels.

Keywords: Alps, Apennines, Cenozoic compression, foreland, hydrocarbon occurrences, Italy, Mesozoic extension, gas fields, oil fields, thrust-and-fold belt

Geological framework

The Italian landscape is largely dominated by the Southern Alps and Apennines mountain chains. The Alps bound Italy on the north, whilst the Apennines traverse the entire peninsula and form the backbone of the country. These mountains constitute two thrust-and-fold belts which arose during Cenozoic times as a result of the interaction between the European and the Adriatic–African tectonic plates.

The Southern Alps have a southward vergence and constitute the antithetic retrobelt of the Alpine orogen which started to develop from Cretaceous times and went through the main collisional phase from Eocene to Pliocene times. The Apennines have an orogenic polarity towards the East and developed mostly after the Oligocene (Carminati *et al.* 2004). The two chains are bordered in their outer margins by foreland basins (with foredeep and piggyback basins), which are well developed, especially along the Adriatic sectors, and by relatively wide foreland areas (i.e. Po Plain, Adriatic Sea and Hyblean Basin). The Po Plain is unusual in that it represents the common foreland of the Southern Alps and the northern Apennines (Fantoni & Franciosi 2008). The Tyrrhenian Sea and the western sectors of the Apennines are considered a back-arc basin system developed in response to the counterclockwise rotation of the Apennines (Carminati *et al.* 2004).

The formation of the two orogens was preceded by a lengthy crustal stretching and extension episode which lasted for most of the Mesozoic and was generally characterized by carbonate type sedimentation (e.g. Bertotti *et al.* 1993 and references therein, for the Southern Alps). Most of the carbonate structures were later rejuvenated and involved in the Cenozoic orogenesis.

In this geological framework several petroleum systems have developed, some of which are of paramount economic importance and make Italy the most endowed hydrocarbon province in southern Europe.

The simplified geological map of the country and the schematic cross-section in Figure 1 illustrate the general location of oil and gas accumulations in Italy. Hydrocarbons are found in the thrust belt, along the foreland basins and in the foreland. In particular, oil and associated natural gas are present in the stratigraphically deeper – mainly Mesozoic – successions of the foreland regions and in the outermost sectors of the Southern Alps and Apennines belts, while thermogenic gas is found in the Oligo-Miocene tectonized sediments of the Apennines. Biogenic gas is abundant in the Plio-Pleistocene successions of the foreland basins (mostly in the foredeeps). No hydrocarbons have been discovered to date in the back-arc tectonic zone.

Historical perspective

Entrepreneurial exploration for hydrocarbons in Italy is thought to have started in 1860 when in Ozzano, near the city of Parma, the Achille Donzelli company drilled two wells to depths of 32 and 45 m, obtaining 25 kg of oil per day (Magini 1937; Eni S.p.A. 2009). In the following decades until the close of the century, several shallow wells were drilled by small enterprises along the southern margin of the Po Plain and in central Italy (around the cities of Pescara and Frosinone), leading to small volumes of oil production, which were used mainly for public lighting purposes. During the first three decades of the 1900s other small discoveries were made in the same areas and in Sicily. Gas also started to be used for domestic purposes or to fuel lights.

In 1926 AGIP (Azienda Generale Italiana Petroli) was founded by the government as an attempt to break the market for petroleum

VINING, B. A. & PICKERING, S. C. (eds) *Petroleum Geology: From Mature Basins to New Frontiers – Proceedings of the 7th Petroleum Geology Conference*, 113–126. DOI: 10.1144/0070113

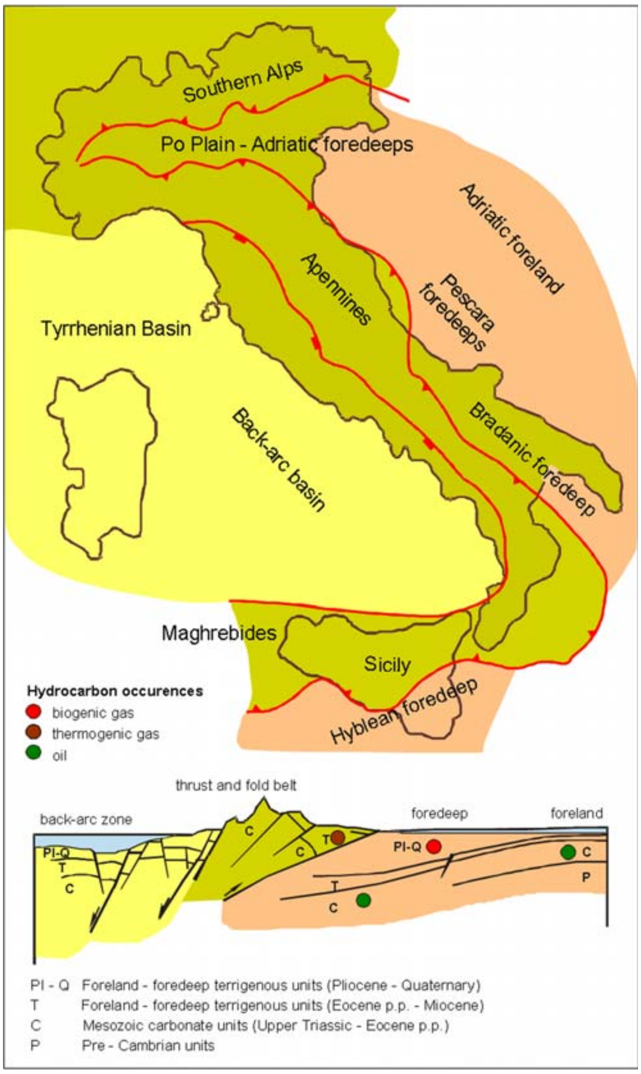

Fig. 1. Geological framework and hydrocarbon occurrences.

products which, in Italy, had fallen under the control of branches of multinational oil companies. AGIP, later incorporated in Eni (Ente Nazionale Idrocarburi), was soon to become the principal player in the oil and gas business of the country.

The search for hydrocarbons rose to an industrial level of activity during the 1940s. The exploration moved from the hills of the northern Apennines to the Po Plain: Caviaga was here discovered in 1944 and turned out to be the largest gas field in western Europe of that time. Gas was to become the backbone of the Italian energy policy. During those years the first natural gas pipeline network was also built to convey gas from the fields of the Po Plain to the cities of Lodi and Milan. In the following decades successful exploration campaigns were also carried out all along the peri-Adriatic foredeeps, in Calabria and Sicily, both onshore and offshore. Besides Eni, other major companies, such as Edison, Enterprise, Elf, Esso, Fina, Gulf, Shell and Total, greatly contributed to these successes. Subsequently, the national gas pipeline network was much increased (up to 30 000 km) and, because of the growing demand, import lines from outside the country were also laid. In the early 1970s international pipelines from the Netherlands and the Soviet Union were opened, and in 1983 the 2500 km-long Transmediterranean pipeline, transporting gas from the Hassi-R-Mel Field in Algeria to the Po Plain, was inaugurated. More recently, in 2004, the Green Stream, a gas pipeline connecting Libya to Sicily, was opened.

During the almost 150 years of exploration and production activity in Italy, the following records were attained:

- 1944 – Caviaga, the largest gas field in the western Europe at the time, is discovered.
- 1959 – Agip's 'Gela Mare 21', the first offshore well in Europe, is drilled offshore Sicily.
- 1976 – the first remote-controlled platform in Italy for crude oil production is put in place at Perla 1, offshore Sicily.
- 1977 – Agip drills to a record depth of 5500 m in the Malossa Field (near Milan) and discovers a new oil pool.
- 1984 – Villafortuna, the largest onshore oil field in Europe, is discovered in northern Italy at a new record depth of 6000 m. Its size will be superseded by the giant Monte Alpi Field (Val d'Agri), discovered in 1988.
- 1990s – Aquila oil field (Otranto Channel) is put into production. The field is in 800 m of water, the deepest in Europe.

Today, the Italian petroleum acreage comprises 86 exploration permits and 195 development leases covering more than 53 000 km^2. The licences are distributed mainly in the Po Plain, in the peri-Adriatic foredeeps, in the southern Apennines and in Sicily (Fig. 2). More than 250 000 km of 2D seismic lines and 35 000 km^2. of 3D seismic surveys have been acquired, and more than 7000 wells have been drilled for hydrocarbon exploration and production (Fig. 3).

In terms of petroleum endowment, Italy is the fourth richest country of western Europe, after Norway, the UK and the Netherlands. According to the Italian Ministry of Economic Development (UNMIG 2009) and the Italian Association of Oil Companies (Unione Petrolifera Italiana 2009), 140 million tonnes (1040 MMbbl) of oil and 700 billion m^3 (24.7 Tcf) of gas have been produced so far in the country. The production of oil is

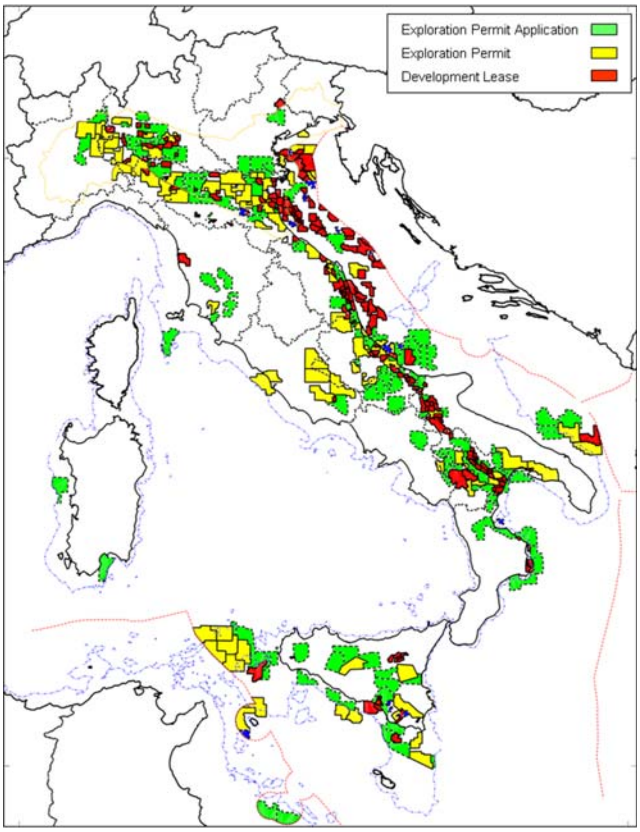

Fig. 2. Petroleum acreage.

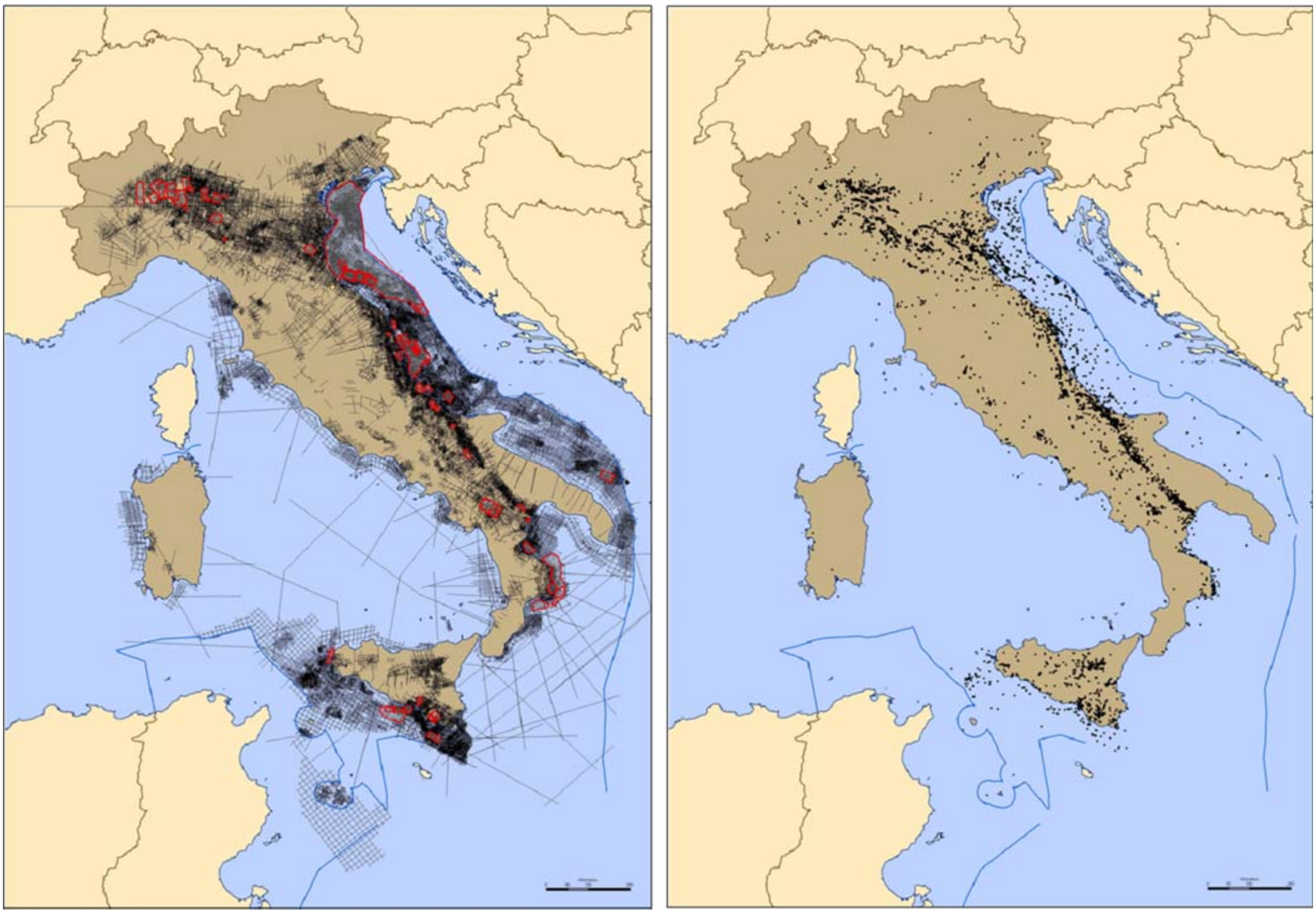

Fig. 3. Two-/three-dimensional (red areas) seismic surveys (left) and wells (right).

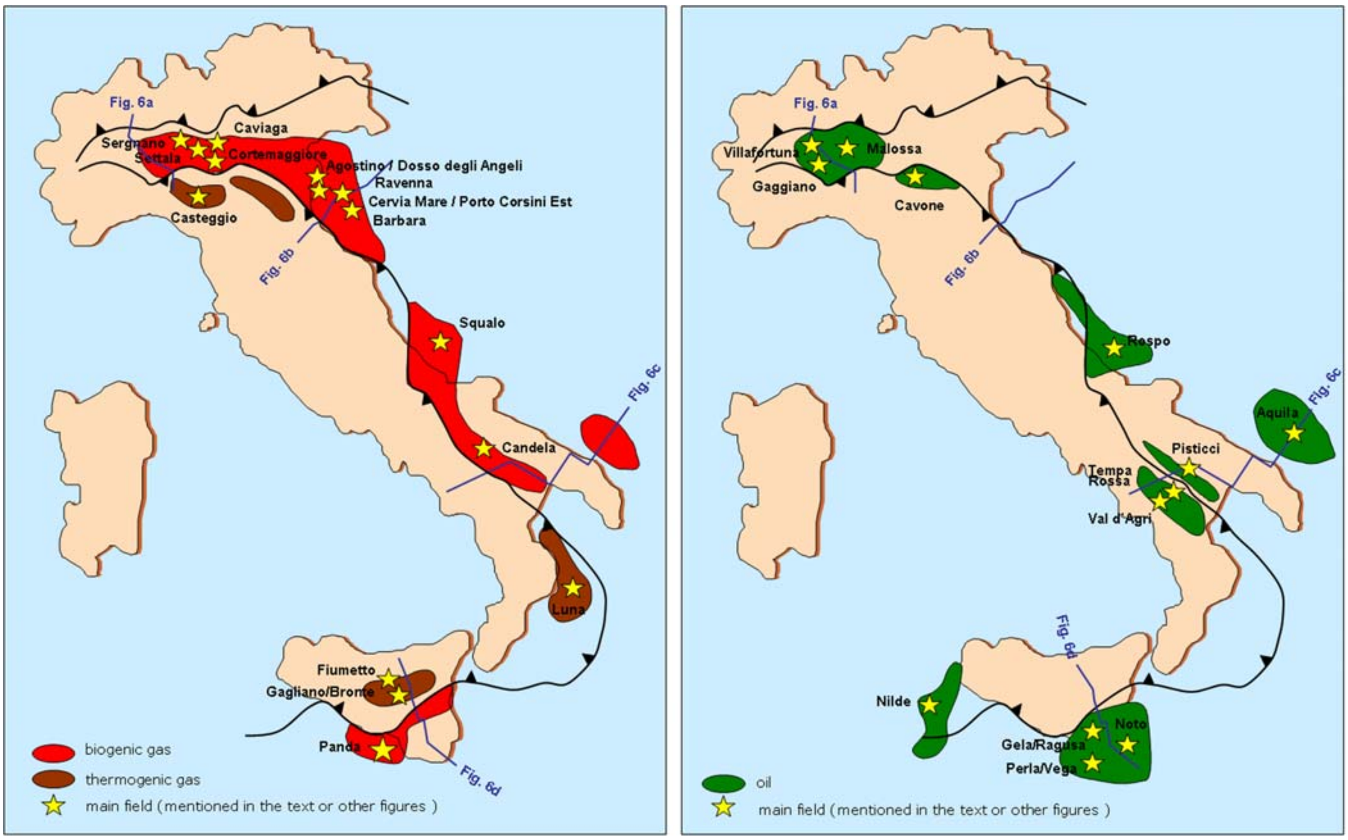

Fig. 4. Gas provinces (left) and oil provinces (right). Location of the geological sections of Figure 6.

5.8 MMtonne per year (43.2 MMbbl/year) (2007), about 75% of which comes from the Val d'Agri Field. The production is expected to increase slightly in the next few years due to new development wells of Val d'Agri coming on stream and the start of production in the nearby Tempa Rossa Field.

The production of gas in 2007 was 9.7 billion m^3 per year (340 Bcf/year), continuing the declining trend from the peak of 20.6 Bcm (730 Bcf/year) attained in 1994. Today's production comes from more than 100 fields, the largest ones being located in the Adriatic Sea.

Overall, Italian hydrocarbon production accounts for less than 10% of the energy demand, and the country therefore has to rely on large oil and gas imports. At the end of 2006 remaining hydrocarbon reserves (proven + 50% of the probable + 20% of the possible reserves) amounted to 110 MMtonne (800 Mbbl) of oil and 150 Bcm (5.3 Tcf) of gas, with an expected residual life of 20 and 14 years respectively. According to UNMIG (2009), the yet-to-be-discovered reserves are estimated to be 110 MMtonne (800 MMbbl) of oil and 170 Bcm (6.0 Tcf) of gas.

Hydrocarbon occurrences

The hydrocarbon occurrences of Italy tend to concentrate in oil and gas provinces as illustrated in Figure 4, where the names of the major fields are also indicated. Oil is found principally in the western Po Plain, in the southern Apennines and in Sicily, while gas accumulations are mainly concentrated in the Po Plain and northern Adriatic Sea (Anelli *et al.* 1996; Casero 2004). Three groups of hydrocarbon occurrences have been identified (Bertello *et al.* 2008*a*, *b*):

- oil and thermogenic gas in the carbonate Mesozoic substratum;
- thermogenic gas in the thrusted terrigenous Oligo-Miocene foredeep sedimentary wedges; and
- biogenic gas in the terrigenous Plio-Pleistocene foredeep wedges.

At the origin of these different hydrocarbon types is a variety of petroleum systems (Fig. 5). The Mesozoic carbonate units mostly contain oil and thermogenic gas in different geological scenarios due also to the fact that, as will be illustrated later, three main Mesozoic source rocks exist and were effective in generating hydrocarbons. The Oligo-Miocene tectonized terrigenous foredeeps host only thermogenic gas with subordinated quantities of condensate, derived from widespread but poorly effective type III source rocks. The terrigenous units of the Plio-Pleistocene foredeeps accommodate large quantities of biogenic gas which are at the origin of the largest and most productive fields, notably in the eastern Po Plain and northern Adriatic sea.

The stratigraphic position and structural domain of the Italian hydrocarbon occurrences is also illustrated in the geological sections of Figure 6, where the locations of some important fields are indicated as well.

Oil and thermogenic gas in the Mesozoic carbonate substratum

In the Mesozoic carbonate successions three different petroleum systems are present, of Middle Triassic, Late Triassic/Early Jurassic and Cretaceous age (Zappaterra 1994; Fantoni *et al.* 2008).

Middle Triassic petroleum system (Villafortuna–Trecate Field). The Middle Triassic petroleum system is linked to the earliest stage of the Tethyan fragmentation. Because of its depth it can

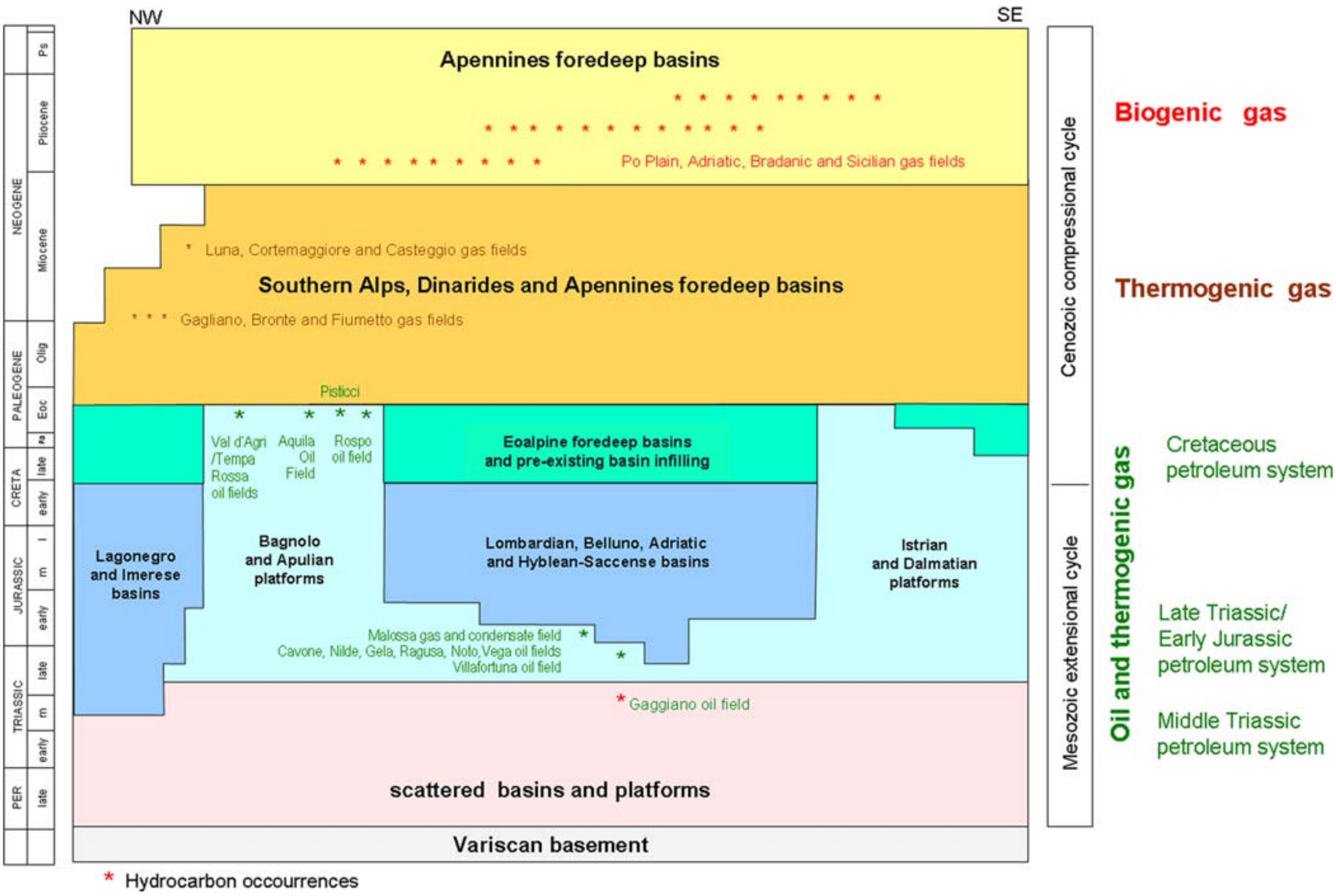

Fig. 5. Tectono-stratigraphic cycles and hydrocarbon occurrences.

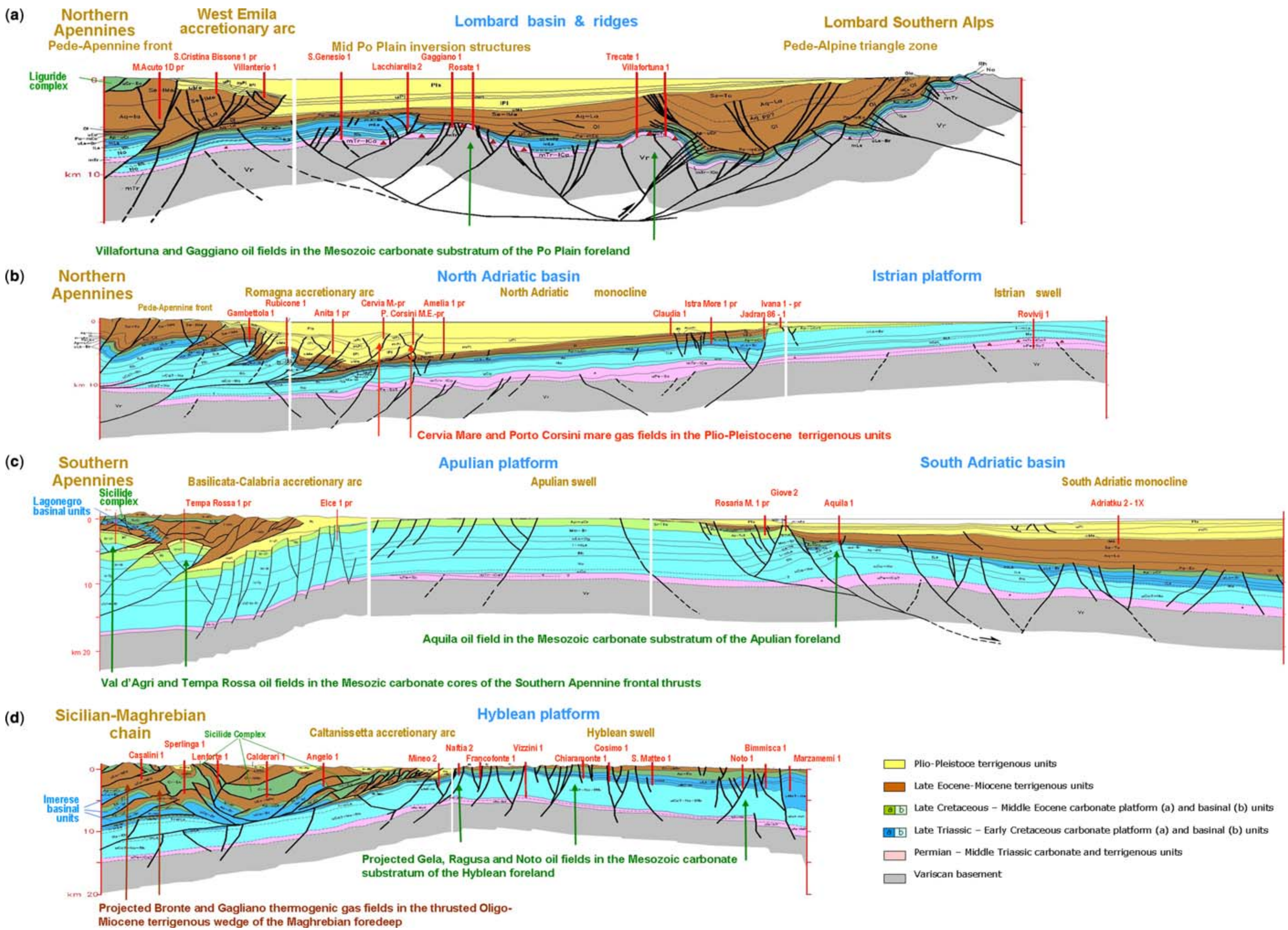

Fig. 6. Geological sections and major hydrocarbon occurrences (vertical exaggeration 2:1). Location in Figure 4.

be pursued only in the outer sector of the foredeeps and in foreland regions, whereas along the thrust belt it is generally too deep and overcooked. It involves dolomitized platform units of Late Triassic–Early Jurassic which were charged by Middle Triassic carbonate source rocks deposited in the confined basins created by the rifting. Traps are mostly provided by Mesozoic structures locally inverted by the Cenozoic compression (Fig. 6a).

The Villafortuna Field, discovered in 1984 in northern Italy, and its Trecate extension constitute the largest oil accumulation pertaining to this play (Fantoni *et al.* 2001; Bello & Fantoni 2001; Fig. 7). The trap consists of a buried alpine fold involving a pre-existing Mesozoic extensional relief. The structural high of the Mesozoic carbonate succession has a vertical relief of about 3000 m relative to the adjacent northern zone, and is bordered by an alpine southerly dipping backthrust forming a triangle zone. Mesozoic extensional features are also present which consist of blocks of a smaller hierarchical order, rotated and bordered by NNW trending faults.

The petroleum system is wholly developed inside the Triassic succession, and consists of two main reservoirs, made from dolomitized carbonate platform rocks, and a set of source rocks deposited in the adjacent anoxic intra-platform basins. All these rocks have important outcrop analogues in the western sector of the Southern Alps which have allowed a detailed study of their characteristics. The lower reservoir is represented by the Anisian (Middle Triassic) Monte San Giorgio Dolomite, which was deposited in a peritidal to subtidal environment and is today entirely dolomitized. The porous system is represented by a few small vugs, moulds and rarely by intercrystalline porosity. The porosity and permeability values are generally low, the reservoir producing from a fracture network that provides a certain degree of permeability and improved porosity. Fractures are locally enlarged by dissolution. The overlying shaly and tuffaceous Besano Shales (Anisian/Ladinian, Middle Triassic) provide the seal and are at the same time a source rock. The upper reservoir consists of three carbonate platform units of Norian (Late Triassic) to Hettangian (Early Jurassic) age: the Dolomia Principale, the Campo dei Fiori Limestone and the Conchodon Dolomite. They are characterized by different petrophysical properties due to their different original textures and subsequent diagenesis. The Dolomia Principale and Campo dei Fiori Limestone formations exhibit similar petrophysical properties, with low porosity and permeability values, locally increased by the presence of a network of fractures. A red palaeosoil, originating from a temporary subaerial exposure, separates the Campo dei Fiori Dolomite from the Conchodon Dolomite. The latter formation shows great variations in the porous system, as a result of an intense diagenesis, including deep burial dolomitization and various steps of recrystallization and dissolution. The petrophysical characteristics of the Conchodon Dolomite make it the most productive reservoir interval of this play. The overlying shaly limestone of the Medolo Group (Lower Liassic) constitutes the regional seal for these three reservoirs.

The hydrocarbons were generated from Middle Triassic source rock formations, namely the previously mentioned Besano Shales (Anisian/Ladinian) and the Meride Limestone (Ladinian). In the Villafortuna–Trecate area the maturity of the kerogen in these rocks is high and only the residual naphthogenic properties can be measured; therefore the original properties have been estimated by considering the geochemical data of immature outcrop samples. The two source rocks are characterized by type II kerogen content. The Besano Shales comprise dark laminated dolostones and black shales with very high TOC. The Meride Limestone has lower TOC values, but the formation has a very significant thickness (up to 500 m). The main hydrocarbon expulsion phase in the drainage area of Villafortuna–Trecate occurred very recently, during the Plio-Pleistocene strong burial (Fantoni & Scotti 2009), and after the last structuring age (Oligocene to Messinian) (Fantoni *et al.* 2004 and references therein).

Late Triassic–Early Jurassic petroleum system (Gela Field). The Late Triassic–Early Jurassic petroleum system is linked to the main phase of the Tethyan rifting and is the most explored of the three systems, both in the foreland and in the thrust belt, and from Lombardy to Sicily. The source rocks are terrigenous or mixed carbonate/terrigenous, and were deposited during the anoxic stage that preceded the extension of the Jurassic basins. Because of the discontinuity of the regional and local seals, the reservoirs are located in a wide chronostratigraphic range, from the coeval platform units up to the topmost carbonate units, and even in the overlying terrigenous sequences (Nilde Field, Miocene, Sicily). The related hydrocarbon accumulations mainly occur in the reactivated structures of the foreland margin: Malossa and other Po Plain gas and condensate fields (Mattavelli & Margarucci 1992); northern Appennines (Cavone Field); all Apulian (Pisticci) and mid and south Adriatic oil fields (e.g. Aquila Field: Fig. 6c); Gela and all the other Sicilian oil fields (Fig. 6d).

The Gela heavy oil field, discovered in 1956, is a remarkable example of the Late Triassic–Early Jurassic system, its geological framework being illustrated in Figure 8. The field is located in the Ragusa Basin, in the southern part of Sicily, and extends both onshore and offshore. It is the largest oil accumulation of this petroleum system. The trap is a gentle NE–SW trending asymmetric faulted anticline. The structure formed during the Mesozoic as an extensional feature and was subsequently inverted and folded during the Miocene–Pliocene compressive/transpressive phase.

The reservoirs are located in the Upper Triassic to Early Jurassic succession. The main reservoir is the Upper Triassic Sciacca Formation, consisting of dolomitized carbonate platform rocks. This formation is overlain by the Upper Rhaetian Noto Formation, which is made from alternating laminated carbonates and euxinic shales, the carbonate layers having poor to moderate reservoir characteristics. On top of the Noto Formation lies the shale and shaly limestone Hettangian Streppenosa Formation, which constitutes a regional seal and has moderate source rock characteristics as well (Frixa *et al.* 2000).

The origin and distribution of porosity in the Sciacca Formation are controlled by a complex diagenetic history. The original sediment was partly cemented in peritidal environments. This early diagenetic phase produced extensive meteoric dissolution, followed by pervasive cementation. Carbonate cements subsequently filled primary fenestral, sheet-crack and mouldic porosities. Dolomite cements and internal sediments occur in fenestral cavities, reflecting early phases of diagenesis. Coarse dolomite fabrics are very common in the reservoir and could be considered to be the result of a successive diagenetic phase controlled by fractures.

The porosity and permeability values are usually low, but are locally improved by fracture networks that connect vugs and porous layers and support the production of the field.

The heavy oil of the Gela Field was generated by the anoxic marls and marly limestones of the Noto Formation and by the overlying black shales of the Streppenosa Formation (Brosse *et al.* 1988). These source rocks have a type II kerogen and are of predominantly marine origin. The heavy oil gravity (less than 20° API) is thought to be related to the carbonate origin, notably of the Noto Formation, and to the low degree of maturation reached by the sources. The Noto Formation has the highest TOC, while the Streppenosa Formation has somewhat poorer geochemical characteristics which are nevertheless compensated for, in terms of hydrocarbon generation effectiveness, by the greater formation thickness (>3000 m in the depocentre of the Ragusa Basin). The source rock's maturation was probably reached during the

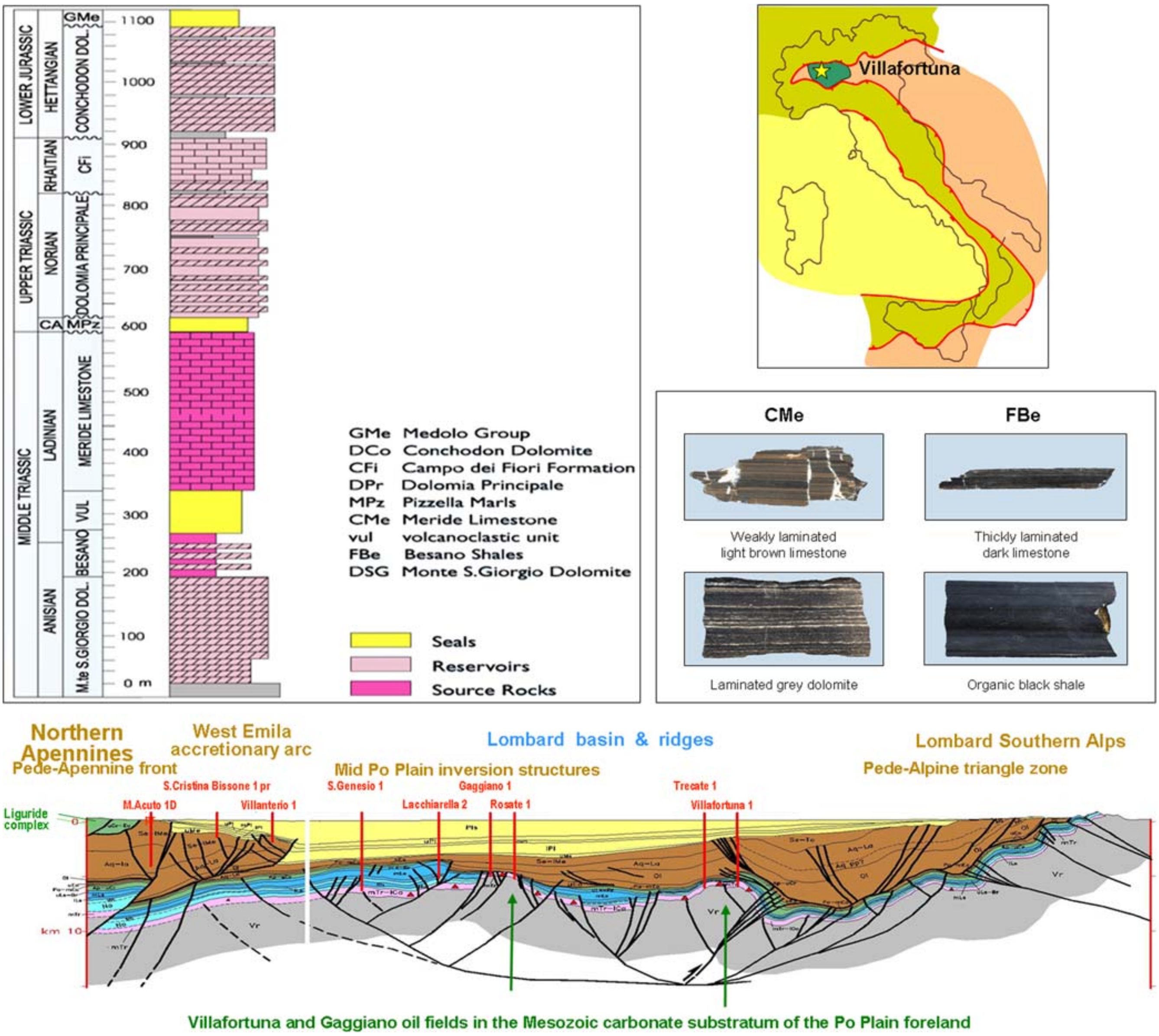

Fig. 7. Villafortuna–Trecate oil field.

Plio-Pleistocene, that is, when the allochtonous Gela Nappe was emplaced in the area.

Cretaceous petroleum system (Val d'Agri Field). This system lies in the Mesozoic carbonate substratum of the foredeep/foreland area and of the external thrust belt of the southern Apennines, and bears the largest oil and gas accumulations of Italy, namely the oil fields of Val d'Agri (composed by the Monte Alpi, Monte Enoc and Cerro Falcone culminations) and Tempa Rossa.

Long-lasting carbonate platforms were deposited, the largest ones being the Apulian (southern Apennines) (Mostardini & Merlini 1986), the Bagnolo (northern Apennines) and the Dalmatian (Croatia, Montenegro and Albania) platforms. Within these platforms, extension created new accommodation space in which thick shallow-water carbonate successions accumulated and a major anoxic event occurred during Albian–Cenomanian times, leading to the formation of the main source rock. During the Miocene and Pliocene, the Apulian Platform, sitting on the Ionian–Adriatic lithosphere, was strongly involved in several thrusts and backthrusts. It was also overlain by earlier allochthonous ENE-ward verging tectonic units (Allochthonous Complex) composed of Mesozoic–Cenozoic mostly deepwater marine sediments deposited along the Adriatic passive margin, and by Lower–Middle Miocene turbidite successions. The accretionary prism was eventually cross-cut by normal faults, formed during the extensional phase, active to the present.

Because of the low permeability of its reservoirs, the Cretaceous play is most successfully explored in the highly fractured frontal structures of the thrust belt (e.g. Val d'Agri and Tempa Rossa oil fields: Fig. 6c). The Val d'Agri giant oil field, discovered in 1988, is the largest oil accumulation of the Cretaceous petroleum system and is briefly described in Figure 9. The reservoir is represented by the Cretaceous to Miocene limestone and dolostone of the Apulian Platform. The sedimentary evolution of this succession is complex and can be summarized, from the bottom to the top, as follows. The Early Cretaceous (Neocomian and Aptian) is characterized by a thick succession of shallow-water dolomitic limestones deposited in a restricted platform environment. The deposition of a less restricted Albian platform facies precedes the formation of intra-platform basins that developed during the Cenomanian within the Apulian Platform as a result of an important phase of extensional/trans-tensional tectonics (Carannante *et al.*

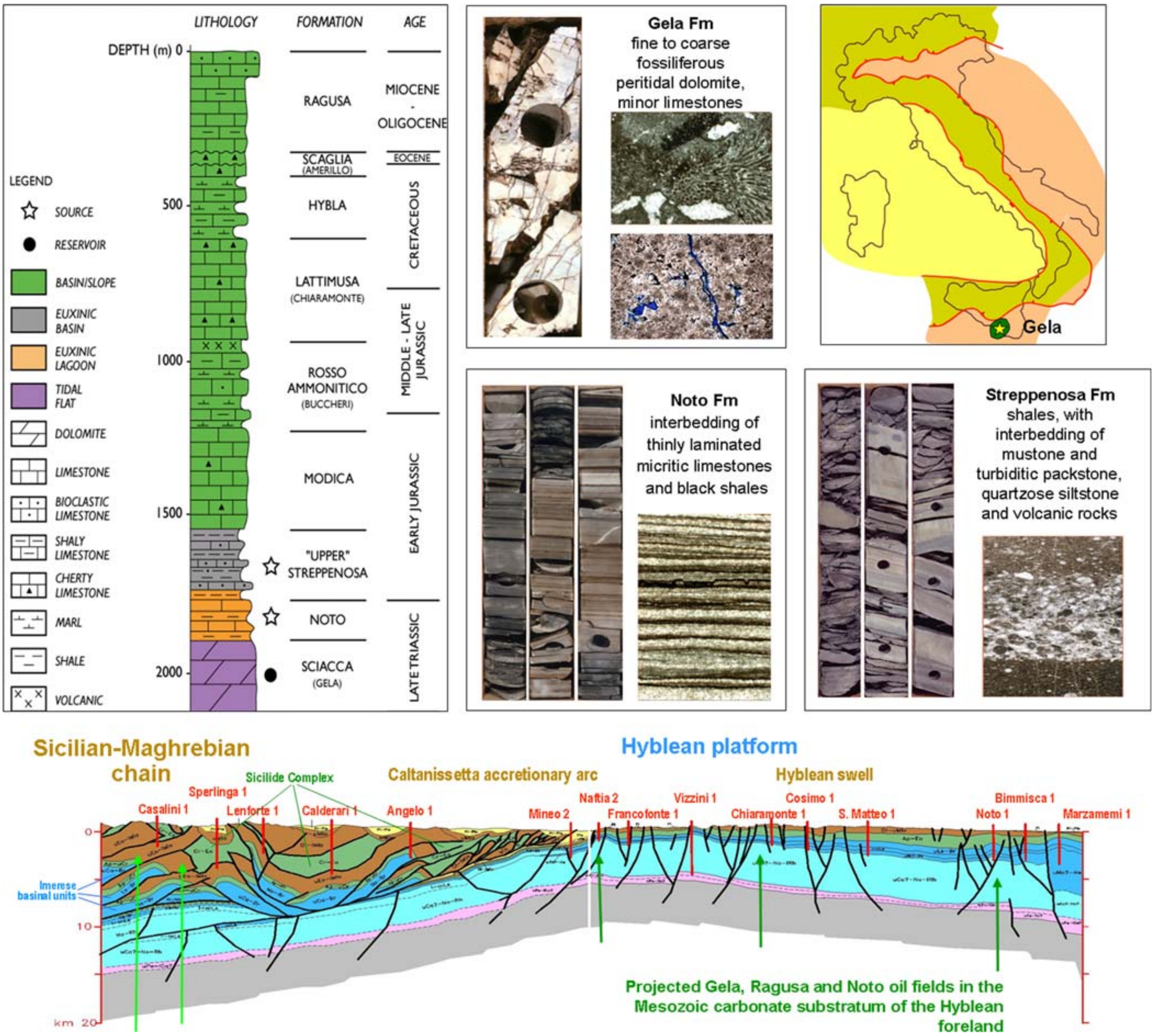

Fig. 8. Gela oil field.

2009). These basins were probably NW–SE oriented and hosted the deposition of organic-rich laminites that constitute the source rock of this petroleum system. The Early Senonian is characterized by a shallow-water limestone succession related to a carbonate ramp pervasively populated by rudists. An outer ramp facies with planktonic organisms rests on top of the rudist limestone and testifies to the first platform drowning episode. During the Late Senonian, the deposition of pelagic limestone (Scaglia Formation) defines the final platform drowning.

The petrophysical characteristics of the Val d'Agri reservoir are strongly dependent on the type of depositional facies. The Albian–Cenomanian sequence is generally characterized by low intercrystalline porosity, but reservoir quality can improve where karst-fractures (fractures enlarged by dissolution) are present. The Senonian shallow-water limestone generally exhibits low porosity, of intragranular and mouldic type. In contrast, the layers containing rudist fossils have relatively good properties due to intrafossil porosity.

The Lower Pliocene shales and marls overlying the Apulian Platform constitute the main seal of the Cretaceous play. Top and lateral seals of the Val d'Agri Field are locally made also by the thick Miocene shaly and marly sequence of the Allochthonous Complex.

The hydrocarbons of the Val d'Agri Field originated from an Albian–Cenomanian marine source-rock. This sequence is characterized by laminated dolomitic limestone (500–600 m of thickness) deposited on a shallow-water carbonate ramp during episodes of restricted water circulation and anoxic conditions. It is a fair to good quality source rock. The kerogen is a sulphur-rich type II. The source-rock entered the oil window during the Pliocene, when the Apennines accretionary prism involved the field area and the Allochthonous Complex built up.

The trap of the field is represented by a large-scale pop-up bounded by NW–SE high-angle reverse faults. The structure is a result of the intense Apennines transpressive deformation that affected the area during the Middle–Late Pliocene and Early Pleistocene (van Dijk *et al.* 2000; Shiner *et al.* 2004). The vertical throw exceeds 1000 m.

The Cretaceous Apulian Platform succession of the Val d'Agri Field is considered a single-layer reservoir. The main hydrocarbon phase is light oil with associated gas. Gas and condensate (gas-cap) and heavy oil are also represented.

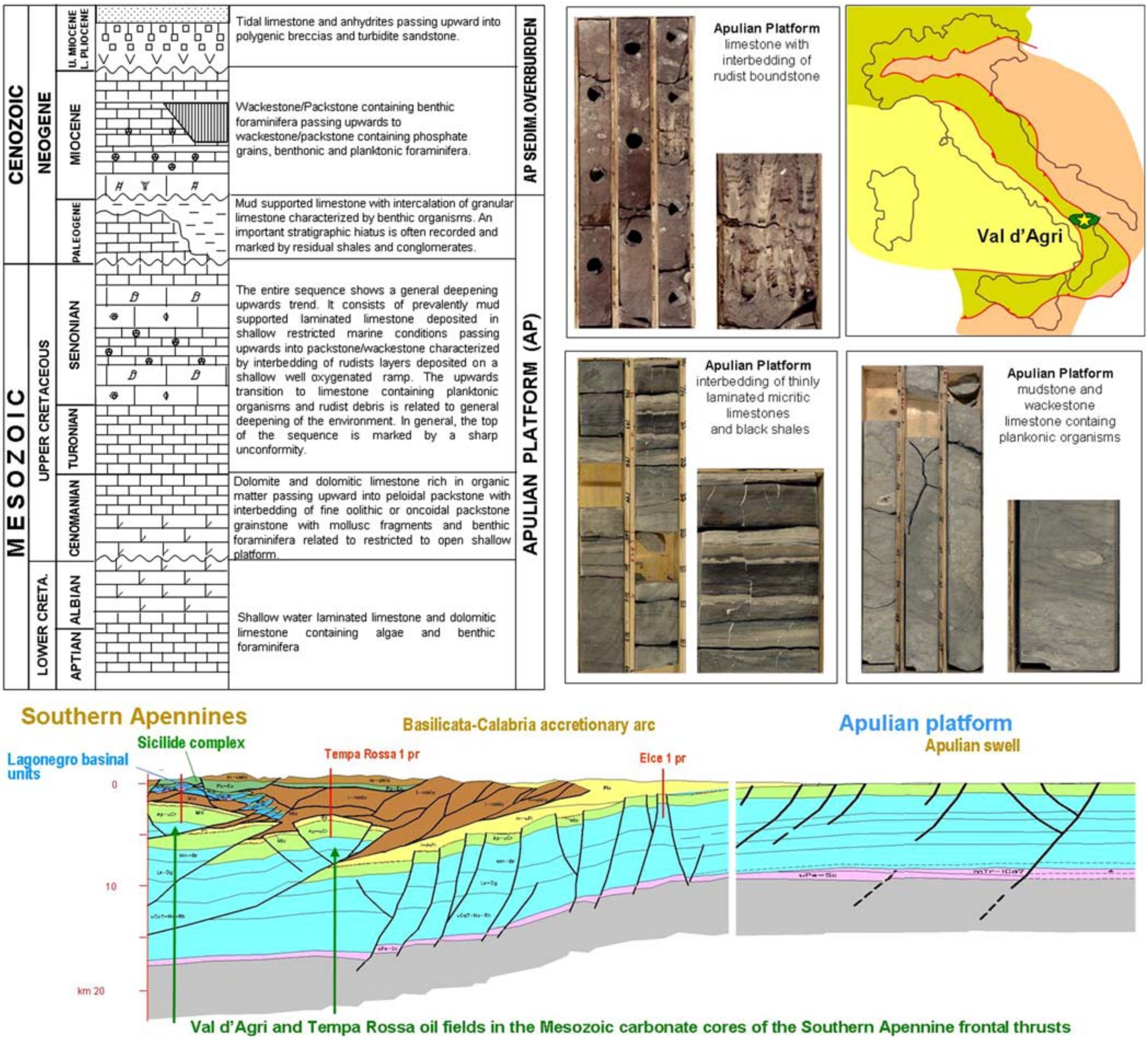

Fig. 9. Val d'Agri oil field.

Thermogenic gas in the thrusted terrigenous Oligo-Miocene foredeep sedimentary wedges

This system includes the Oligo-Miocene turbidite foredeep sedimentary wedges of the Southern Alps and of the Apennines, whose successions have been tectonically involved in the thrust belts of the two chains (Fig. 5). The turbidite reservoirs are mostly represented by type I thick-bedded sandstone lobes and thin-bedded, fine-grained basin plain/lobe fringe deposits (Ricci Lucchi 1986; Dalla *et al.* 1992). The deep burial of these sediments allowed an early thermogenic generation from the shales interbedded in the successions. The organic matter is of terrestrial origin (gas-prone kerogen type III) with very low average TOC. The main hydrocarbon phase is thermogenic gas with minor amounts of condensate and light oil.

The traps are usually structural. Gas occurrences related to this petroleum system have been found in the Southern Alps and the northern Apennines (e.g. Cortemaggiore and Casteggio fields), but the most important discoveries were made in the southern Apennines, namely in Calabria (Luna Field) and in Sicily (Gagliano, Bronte and Fiumetto fields: Fig. 6d). The exploration of this play is made difficult by generally poor seismic imaging, a result of the structural complexity of the related geological framework. Exploration can also be of little reward in terms of amount of gas in place (small traps) and reservoir quality (low porosity and permeability due to diagenesis).

Biogenic gas in the terrigenous Plio-Pleistocene foredeep wedges

Several biogenic gas fields have been discovered in the Plio-Pleistocene successions of the late Apennine foredeep depocentres and in the outer fronts of the Apennine thrust belt, namely in the Po Plain, in the northern and central Adriatic Sea, in southern Italy and in Sicily (Fig. 5). These successions mainly consist of some thousands of metres of sand-rich turbidites. As in the older Oligo-Miocene foredeeps, the high-efficiency type I turbidite systems with longitudinal palaeocurrents are largely predominant (Minervini *et al.* 2008; Ghielmi *et al.* 2008*b*). Thick-bedded sand lobes and thin-bedded, fine-grained basin plain/lobe fringe deposits are the main facies associations of the turbidite reservoirs. The

Plio-Pleistocene clays interbedded in the turbidite successions are both the source-rock and the effective vertical seal. Also in this case, the organic matter is of terrestrial origin (kerogen type III) and the average TOC is usually very low. The derived hydrocarbon phase is biogenic gas. The gas generation and expulsion started immediately after deposition. Exceptionally, the reservoirs may consist either of Messinian conglomerates and sandstones sealed by Lower Pliocene clay (e.g. Sergnano Field, Po Plain area) or of Cretaceous Apulian Platform carbonates (e.g. Cupello and Ferrandina fields, Bradanic Foredeep). In these reservoirs the biogenic gas is mixed with minor amounts of thermogenic gas generated by older and deeper source-rocks.

Traps are most commonly structural and range from thrust propagation folds of the inner foredeep margins (e.g. Cervia Mare and Porto Corsini East: Fig. 6b) to gentle folds draping the underlying morphology of the pre-Pliocene substratum in the outer foredeep margins, the substratum being represented by Miocene or older terrigenous sediments or by the Mesozoic–Cenozoic carbonate platforms (e.g. Barbara Field). Stratigraphic traps also occur and are mainly related to turbidite reservoir onlaps on the flanks of the thrust propagation folds or on the foreland ramp.

The exploration of the biogenic play started during the late 1940s in the central Po Plain and progressively moved southeastward and offshore. From the early 1980s, the seismic DHI technologies became the key support for any successful exploration in this play. The most important discoveries occurred in the Adriatic Sea, where hundreds of seismic bright spots were successfully tested and put into production. Among them the Barbara gas field stands out for its giant size.

Today the exploration of the biogenic play is very mature and limited to the search of small accumulations near the existing fields. Some potential is also left in thin-bedded reservoirs below the seismic resolution.

Two examples of biogenic gas accumulations, the Porto Corsini East and the Settala fields, are illustrated.

The Porto Corsini East Field is one of the largest biogenic gas fields of the northern Adriatic Sea (Fig. 10). The trap is structural: a clear four-way closure in a NE-verging fault-propagation fold (Ghielmi *et al.* 2008*a*). The fold shows a regular and elongated shape and is affected by a system of frontal thrust planes and by one major NW–SE trending back-thrust. The trap was generated during the Late Pliocene and the Early Pleistocene as a response

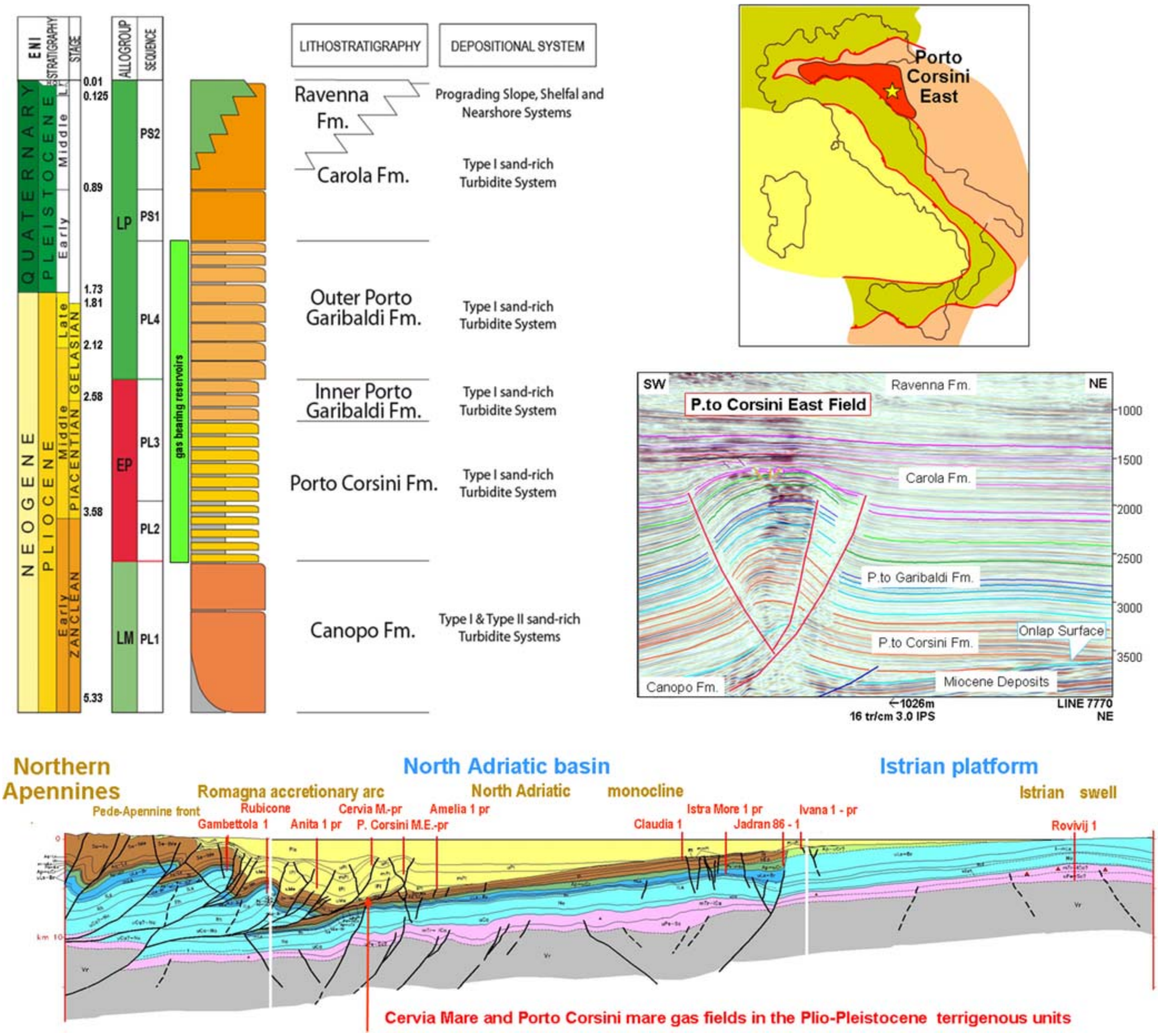

Fig. 10. Porto Corsini East gas field.

to the Apennine compressive deformation. The vertical displacement can reach 800–1000 m for some layers.

The gas field consists of several independent superimposed pools (single layer or multilayer). The target is represented by a thick sequence of Lower Pliocene to Lower Pleistocene foredeep turbidites of the Porto Corsini, Porto Garibaldi and Carola Formations. Thick-bedded turbidite proximal and distal sand lobes are the prevailing facies associations (Bettazzoli & Visentin 1998; Ghielmi *et al.* 2008*b*). Thin-bedded fine-grained turbidite basin plain deposits are also present but are subordinate. The turbidite sequence was deposited by high-efficiency large-scale type I turbidite systems (*sensu* Mutti *et al.* 1999) in the Po Plain–Adriatic Foredeep (Ghielmi *et al.* 2008*b*). The palaeocurrents are from the NW and are parallel to the foredeep main axis. The pelitic layers interbedded with the sandy reservoirs provide the multiple vertical seals. The source-rock for the biogenic gas is mainly represented by the interbedded Plio-Pleistocene clays. The presence of biogenic gas is associated with clear DHIs: superimposed bright spots, flat spots reflecting the gas–water contact and pull-down (Fig. 10).

The Settala Field is a remarkable example of a mixed structural–stratigraphic trap (Fig. 11). It was discovered in 1977 in the central Po Plain close to Milan. The target is represented by the Middle–Upper Pliocene turbidite sands of the Asti Formation deposited in the central part of the west–east oriented western Po Plain Foredeep (Minervini *et al.* 2008). The reservoir mostly consists of amalgamated thick-bedded medium-grained sand, which is referred to distal sand lobes deposited by a high-efficiency type I turbidite system. The palaeocurrents, parallel to the foredeep main axis, were from west. The mixed trap is represented by a stratigraphic closure (onlap) of the turbidite reservoirs towards the northeast onto a quite steep foreland ramp. A clear angular unconformity is due to the basinward tilting of the former foreland area during Messinian and Pliocene. The lateral closures (towards NW and SE) are provided by the draping of an erosional Messinian high, while the closure towards the foredeep depocentre is due to dip. The vertical and lateral seals are made by the interbedded turbidite clay of Asti Formation and by the foreland and foreland ramp Lower Pliocene clay of the Santerno Formation respectively. Also in this case, the biogenic gas accumulation is associated with recognizable seismic DHI: amplitude anomaly with a clear flat spot at the base (Fig. 11). Because of the amalgamation of the sand beds, no intermediate clay seals are present and the field consists of a 100 m-thick single layer reservoir.

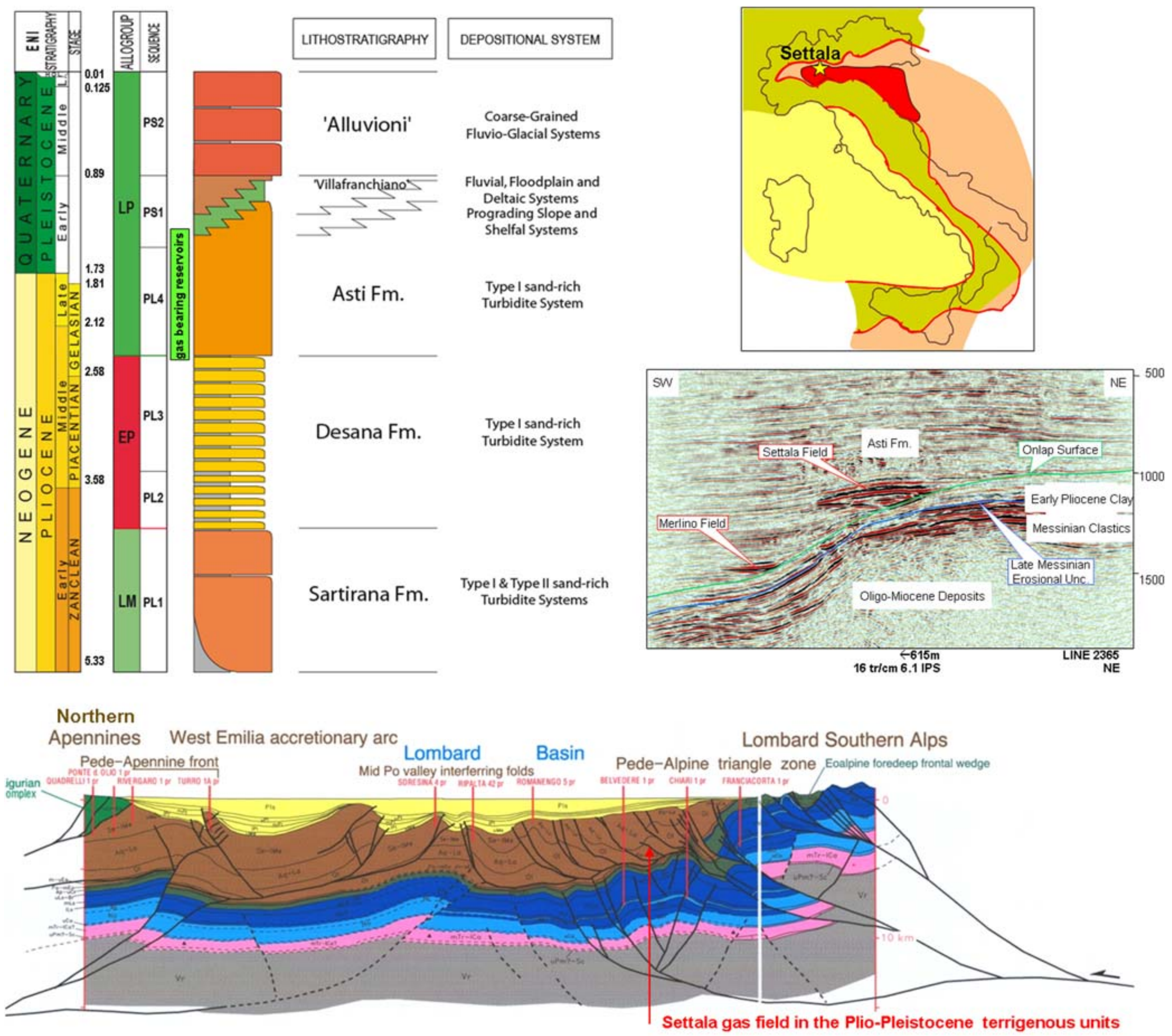

Fig. 11. Settala gas field.

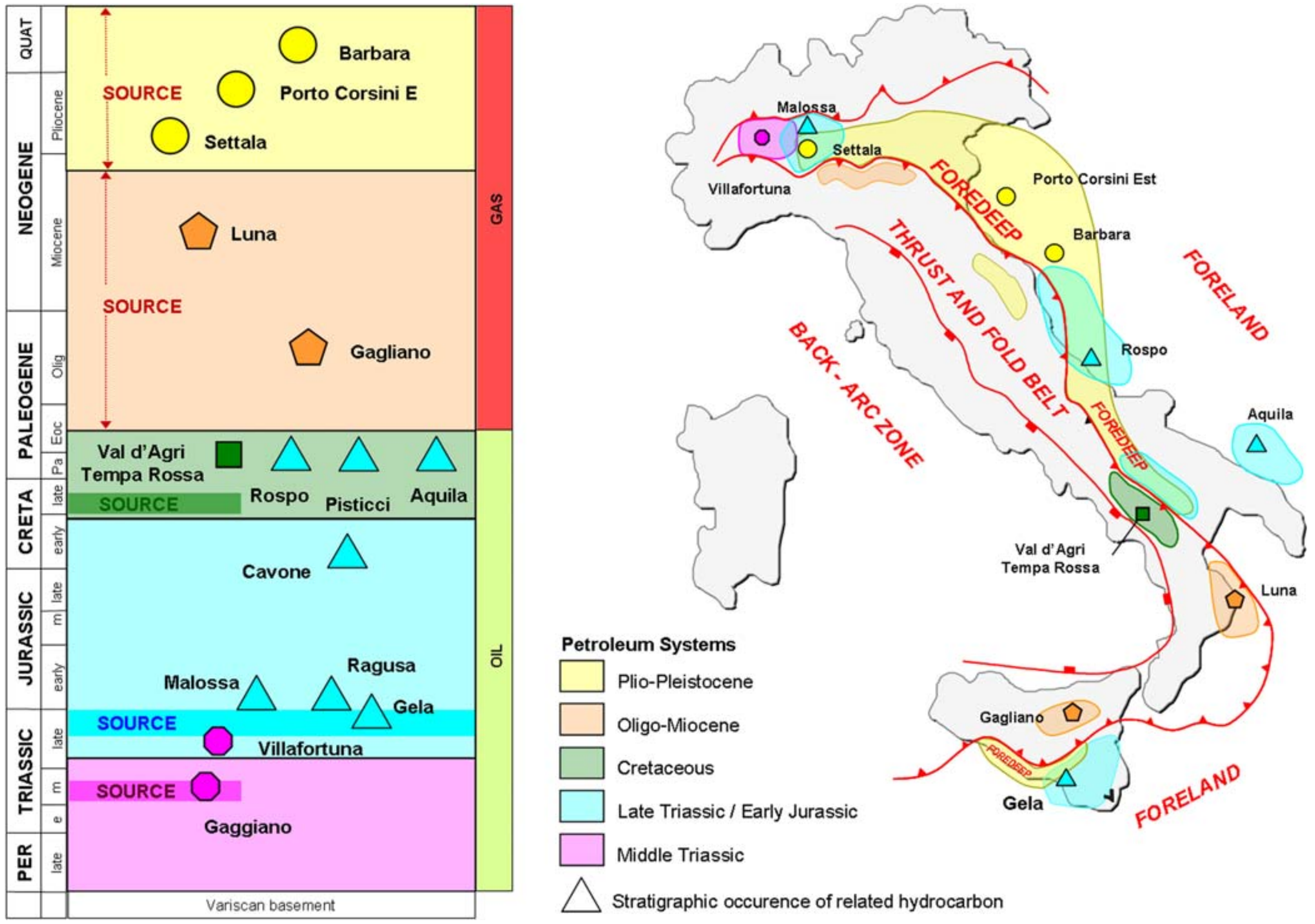

Fig. 12. Stratigraphic and geographic location of the Italian petroleum systems.

Conclusions

A variety of petroleum systems are present in Italy as a result of a complex geological history. At least five important hydrocarbon source rocks have been recognized which are distributed from Mesozoic through Pleistocene.

Three of these (Besano Shales – Meride Limestone, Streppenosa and Noto Formations and Albian–Cenomanian units) were deposited during Mesozoic crustal stretching and extension and are mainly oil-prone. Hydrocarbon occurrences associated with these sources are found in complex geological scenarios along the Apennines belt, both in sub-thrust and thrusted units and in the foreland. Villafortuna–Trecate (Po Plain), Val d'Agri/Tempa Rossa (southern Apennines) and Gela (Sicily) fields represent the largest oil accumulations pertaining to these systems and rank among the largest onshore fields of western Europe.

Two other important source rocks (Oligo-Miocene terrigenous units and Plio-Pleistocene terrigenous units) were deposited in the foredeep basins which formed during the Alpine and Apennine orogenesis. The first source rock is thermogenic gas-prone and occurs in the Oligo-Miocene foredeep basins, which were later involved in the tectonic compression. Gas occurrences associated with this source are mainly concentrated along the northern Apennine margin (e.g. Cortemaggiore Field), in Calabria (e.g. Luna Field) and Sicily (e.g. Gagliano Field). The second source is biogenic gas-prone and is found in the recent undeformed (or slightly deformed) Plio-Pleistocene foredeeps. The most important gas fields of Italy, located in the eastern Po Plain and northern Adriatic (Barbara et alia), have originated from this source.

Figure 12 summarizes the stratigraphic and structural location of the Italian petroleum systems. It clearly shows the geographic limitation of the oil prolific Villafortuna–Trecate Middle Triassic and Val d'Agri/Tempa Rossa Cretaceous systems, as opposed to the wide distribution of the oil-prone Late Triassic–Early Jurassic and of the biogenic gas-prone Plio-Pleistocene systems. The Late Triassic–Early Jurassic system is also peculiar in that, due to a general lack of regional seals in the section overlying the source rock, oil accumulations can be found in a variety of stratigraphic intervals of the Mesozoic and Early Cenozoic carbonate succession.

The results of the exploration history of Italy can be summarized in the creaming curves. The curve (Fig. 13) for the gas has a moderate slope until the late 1950s, when exploration and discoveries were limited to the northern Apennines and the Po Plain (Caviaga, Cortemaggiore). Then the curve becomes very steep, reflecting a series of successes in the Adriatic Sea (Agostino and Dosso degli Angeli, Barbara), in the Pescara and Bradanica foredeeps (Squalo and Candela respectively), in Calabria (Luna) and Sicily (Gagliano). From the early 1980s onward the curve becomes much less steep, indicating that the gas exploration in Italy is mature and activities are mainly conducted near the existing fields.

The creaming curve for the oil discoveries (Fig. 13) is remarkably different. After an initial boost with the discoveries in Sicily in the late 1950s (Ragusa, Gela), no significant successes were attained until the early 1970s, when discoveries were made in the deepest carbonate succession of the Po Plain (Malossa) and in the Pescara offshore (Rospo). Two other significant boosts occurred in the 1980s (Villafortuna–Trecate, Aquila, Vega) and in the late

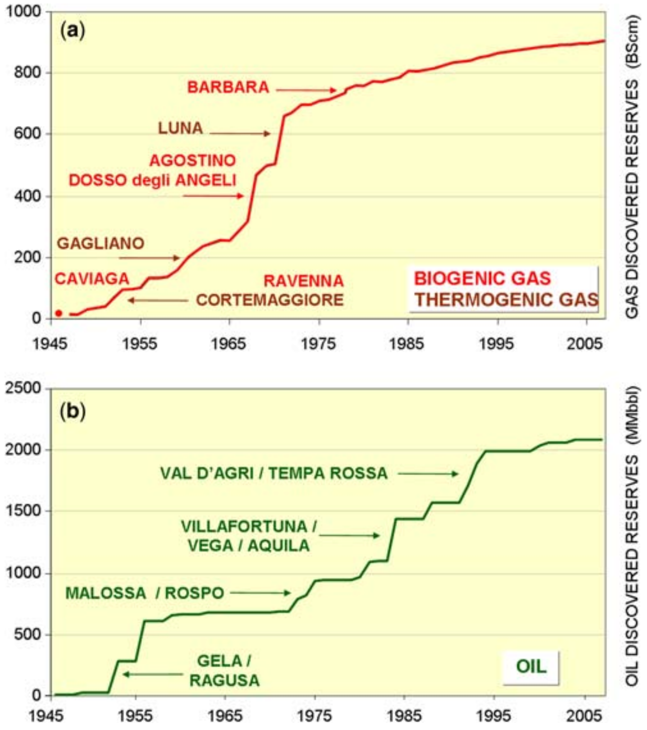

Fig. 13. Cumulative discovered reserves: (**a**) gas in the terrigenous foredeep wedges; (**b**) oil and thermogenic gas occurrence in the carbonate Mesozoic substratum).

1980s/early 1990s (Val d'Agri, Tempa Rossa). The curve seems to indicate that oil exploration in Italy has probably not reached as mature a stage as gas. Some further potential is believed to be left in more complex and deep structural scenarios along the Apennine thrust belt.

In terms of petroleum endowment, Italy is the fourth richest country of western Europe, after Norway, the UK and the Netherlands. About 1040 MMbbl of oil and 24.7 Tcf of gas have been produced so far in the country. Nowadays the production of oil is 43.2 MMbbl per year (2007), about 75% of which comes from the Val d'Agri Field. The production of gas is 340 Bcf/year, continuing the declining trend from the peak of 730 Bcf/year attained in 1994, the largest producing fields being located in the Adriatic Sea. The yet-to-be-discovered reserves are estimated to be rather limited (800 MMbbl of oil, 6.0 Tcf of gas) and in the next decades the country will become more and more dependent on oil and gas imports.

The authors would like to thank C. Doglioni for his kind review of this manuscript. Comments and suggestions by Mike Thomas and Enzo Zappaterra also helped improve the clarity of the text. The authors are grateful to all Eni colleagues who contributed with data, ideas and useful discussions to the preparation of these notes. They acknowledge Shell Italia E&P S.p.A. for the permission to publish an outline of the Val d'Agri Field and a regional geological section where the location of the Val d'Agri and Tempa Rossa fields is shown. They also acknowledge Stogit S.p.A. for the permission to publish an outline of the Settala Field.

References

Anelli, L., Mattavelli, L. & Pieri, M. 1996. Structural–stratigraphic evolution of Italy and its petroleum systems. *In*: Ziegler, P. A. & Horvath, F. (eds) *Peri-Tethys Memoir 2*, Memoirs of the Museum of Natural History and Materials, **170**, 455–483.

Bello, M. & Fantoni, R. 2002. Deep oil play in Po Valley. Deformation and hydrocarbon generation in a deformed foreland. *AAPG Hedberg Conference: 'Deformation History, Fluid Flow Reconstruction and Reservoir Appraisal in Foreland Fold and Thrust Belts'*, 14–18 May 2002, Palermo, Abstracts book, 1–4.

Bertello, F., Fantoni, R. & Franciosi, R. 2008*a*. Exploration country focus: Italy. AAPG–ER Newsletter, June 2008, 5–9.

Bertotti, G., Picotti, V., Bernoulli, D. & Castellarin, A. 1993. From rifting to drifting: tectonic evolution of the Southalpine upper crust from the Triassic to the Early Cretaceous. *Sedimentary Geology*, **86**, 53–76.

Bettazzoli, P. & Visentin, C. 1998. 3D architecture of the Porto Garibaldi turbidite complex (Northern Apennines Foreland Basin – Italy). *15th International Sedimentology Congress*, 13–17 April 1998, Alicante.

Brosse, E., Loreau, J. P., Huc, A. Y., Frixa, A., Martellini, L. & Riva, A. 1988. *The Organic Matter of Interlayered Carbonates and Clay Sediments. Trias/Lias, Sicily. In*: Mattavelli, L. & Novelli, L. (eds) *Advances in Organic Geochemistry*. Pergamon, Oxford, 433–443.

Carannante, G., Pugliese, A., Ruberti, D., Simone, L., Vigliotti, M. & Vigorito, M. 2009. Evoluzione cretacica di un settore della piattaforma apula da dati di sottosuolo e di affioramento (Appennino campano-molisano). *Bollettino Società Geologica Italiana*, **128**, 3–31.

Carminati, E., Doglioni, C. & Scrocca, D. 2004. Alps vs Apennines. *In*: Crescenti, V., D'Offizi, S., Merlino, S. & Sacchi, L. (eds) *Geology of Italy*. Special Volume of the Italian Geological Society for the IGC 32 Florence-2004. *Società Geologica Italiana*, 141–151.

Casero, P. 2004. Structural setting of petroleum exploration plays in Italy. *In*: Crescenti, V., D'Offizi, S., Merlino, S. & Sacchi, L. (eds) *Geology of Italy*. Special Volume of the Italian Geological Society for the IGC 32 Florence 2004. *Società Geologica Italiana*, 189–199.

Dalla, S., Rossi, M. *et al*. 1992. Late Eocene–Tortonian Tectono–Sedimentary Evolution in the Western part of the Padan basin (Northern Italy). *Paleontologia I Evoluciò (Spain)*, **24–25**, 341–362.

Eni, S.p.A. 2009. *The Italian Petroleum Research History*. World Wide Web Address: www.eni.it

Fantoni, R. & Franciosi, R. 2008. 8 geological sections crossing Po Plain and Adriatic foreland. *Rendiconti Società Geologica Italiana, 3/1, Riassunti dell'84th Congresso Nazionale Sassari*, 15–17 September 2008, Italy, 367–368.

Fantoni, R. & Scotti, P. 2009. Time of hydrocarbon generation vs trap forming age in Mesozoic oil play in Po Plain. *Rendiconti Società Geologica Italiana, 5, Convegno Annuale Gruppo di Geologia Strutturale*, 25–28 February 2009, Udine, 89–92.

Fantoni, R., Bello, M., Ronchi, P. & Scotti, P. 2002. Po Valley oil play: from the Villafortuna–Trecate field to South-Alpine and Northern Apennine exploration. *EAGE Conference*, Florence, Extended Abstracts Book.

Fantoni, R., Bersezio, R. & Forcella, F. 2004. Alpine structure and deformation chronology at the Southern Alps – Po Plain border in Lombard. *Bollettino Società Geologica Italiana*, **123**, 463–476.

Fantoni, R., Bertello, F. & Franciosi, R. 2008. Reservoirs and source rocks in Mesozoic carbonate units of Italy. *Rendiconti Società Geologica Italiana, 3/1, Nazionale Sassari*, 15–17 September 2008, Italy, 365–366.

Frixa, A., Bertamoni, M., Catrullo, D., Trincianti, E. & Miuccio, G. 2000. Late Norian–Hettangian paleogeography in the area between wells Noto 1 and Polpo 1, S-E Sicily. *Memorie Società Geologica Italiana*, **55**, 279–284.

Ghielmi, M., Nini, C. *et al*. 2008*a*. Modern Po Plain–Adriatic foredeep (Italy): geological framework and hydrocarbon exploration. *70th EAGE Conference & Exhibition – Workshop no. 3: Hydrocarbon Plays and Future Potential of the Circum-Mediterranean Region*, May 2008, Rome.

Ghielmi, M., Nini, C., Rogledi, S., Minervini, M. & Rossi, M. 2008*b*. Tectono-stratigraphic framework of the Pliocene-to-Pleistocene succession in the Po-Plain–Adriatic Foredeep (Italy). *Rendiconti Società Geologica Italiana, 3/1, Riassunti dell'84th Congresso Nazionale Sassari*, 15–17 September 2008, Italy, 365–366.

Magini, M. 1937. L'Italia e il petrolio tra storia e cronologia. Mondadori.

Mattavelli, L. & Margarucci, V. 1992. Malossa field – Italy. *In*: *Treatise of Petroleum Geology, Atlas of Oil and Gas Fields, Structural Traps.* American Association of Petroleum, **VII**, 119–133.

Minervini, M., Ghielmi, M., Rogledi, S. & Rossi, M. 2008. Tectono-Stratigraphic Framework of the Messinian-to-Pleistocene

Succession in the Western Po-Plain Foredeep (Italy). *Rend. Soc. Geol. It, 3/1, Riassunti dell'84th Congresso Nazionale Sassari*, 15–17 September 2008, Italy, 365–366.

Mostardini, F. & Merlini, S. 1986. Appennino centro-meridionale: sezioni geologiche e proposta di modello strutturale. *AGIP, 73th Congresso della Società Geologica Italiana*, Roma.

Mutti, E., Tinterri, R., Remacha, E., Mavilla, N., Angella, S. & Fava, L. 1999. An introduction to the analysis of ancient turbidite basins from an outcrop perspective. AAPG Continuing Education Course Note Series 39.

Ricci Lucchi, F. 1986. The Oligocene to Recent foreland basins of the Northern Apennines. *In*: Allen, P. A. & Homewood, P. (eds) *Foreland Basin*. International Association of Sedimentologists, Special Publications, **8**, 105–139.

Shiner, P., Beccacini, A. & Mazzoli, S. 2004. Thin-skinned structural models for Apulian carbonate reservoir: constraints from the Val d'Agri Fields, S. Apennines, Italy. *Marine and Petroleum Geology*, **21**, 805–827.

Unione Petrolifera Italiana 2009. Data Book 2009, Energia e Petrolio. World Wide Web Address: www.unionepetrolifera.it, 132 pp.

UNMIG – Ufficio Nazionale Minerario per gli Idrocarburi e la Geotermia (Ministero dello Sviluppo Economico) 2009. *Statistiche dell'Energia*. World Wide Web Address: http://unmig.sviluppoeconomico.gov.it

Van Dijk, T. P., Bello, M., Toscano, C., Bersani, A. & Nardona, S. 2000. Tectonic model and three-dimensional fracture network analysis of Monte Alpi (southern Apennines). *Tectonophysics*, **324**, 203–237.

Zappaterra, E. 1994. Source-rock distribution model of the Periadriatic Region. *AAPG Bulletin*, **78**, 333–354.

Upper Jurassic reservoir sandstones in the Danish Central Graben: new insights on distribution and depositional environments

P. N. JOHANNESSEN, K. DYBKJÆR, C. ANDERSEN, L. KRISTENSEN, J. HOVIKOSKI and H. VOSGERAU

Geological Survey of Denmark and Greenland (GEUS), Øster Voldgade 10, DK-1350 Copenhagen K, Denmark (e-mail: pjo@geus.dk)

Abstract: Recently available well data from the northern part of the Danish Central Graben have been analysed to further understand the basin development, biostratigraphy, depositional models and palaeogeography of Upper Jurassic reservoir sandstones, which are the primary exploration targets in this basin. Notably, the discovery of the Hejre accumulation in 2001, where oil has been encountered in Upper Jurassic good reservoir quality sandstones at a depth of more than 5000 m, triggered renewed interest in the Upper Jurassic High Temperature–High Pressure sandstone play in the area.

Overall the Danish Central Graben was transgressed from east to west during the Late Jurassic. During the Late Kimmeridgian, marginal and shallow marine sandstones assigned to the Heno Formation were deposited at the margin of the Feda Graben, and on the Gertrud and Heno Plateaus and constitute the reservoirs in the Freja and Hejre discoveries. The sandstones are analogues to the UK Fulmar and Norwegian Ula Formations encountered in several hydrocarbon fields.

During the Early Volgian, the transgression continued westwards across the Outer Rough Basin along the margin of the Mid North Sea High, where shoreface sandstones with excellent porosities and permeabilities were deposited close to similar sandstones of the Fulmar Formation in the British Fergus, Fife and Angus fields.

During this overall westward transgression, the eastern and central parts of the Danish Central Graben continued to subside and offshore mudstones accumulated, locally intercalated with gravity-flow sandstones. In the easternmost Danish Central Graben, in the Tail End Graben, Upper Kimmeridgian gravity-flow sandstones of the Svane-1 well have proved the presence of gas at *c.* 6 km depth.

Hydrocarbon-bearing Upper Jurassic sandstone reservoirs at significant depths (deeper than 5 km) may form the future exploration targets in the northern part of the Danish Central Graben.

Keywords: reservoir sandstones, sedimentology, biostratigraphy, basin development, palaeogeography, Upper Jurassic, Danish Central Graben, North Sea

Compared with neighbouring areas in Norwegian and UK waters, where production takes place from shallow marine Ula and Fulmar Formations (Fraser *et al.* 2003), the Upper Jurassic sandstone play in the Danish sector has historically been less successful, due mainly to large variations in reservoir quality. A number of technical discoveries have been made and two accumulations have been declared commercial although not yet in production. These are the Freja Field on the Gert Ridge, located near the Norwegian border with reservoirs in Upper Kimmeridgian back-barrier and shoreface sandstones of the Heno Formation, and the Elly Gas Field located in the south close to the German sector hosted in Upper Kimmeridgian shoreface sandstones of the Heno Formation (Figs 1 & 2) (Hemmet 2005).

In 2001, oil was encountered in sandstones of the Heno Formation in the Hejre-1 well located on a tilted fault block in the Gertrud Graben area at a depth below 5000 m. The discovery was appraised down-flank by the Hejre-2 well in 2005, where good production rates of oil and associated gas were recorded (Danish Energy Agency 2005). The Svane-1 well located in a High Temperature–High Pressure (HTHP) environment in the northern part of the Tail End Graben was drilled in 2002 to a total depth of 5865 m. Four sandstone-bearing successions of presumed gravity-flow origin of Upper Kimmeridgian to Lower Volgian age were found below 5300 m with high gas saturations. The net sand thickness is about 150 m but individual sandstones are thin (up to 15 m). The recent deep-seated Hejre and Svane discoveries have triggered renewed interest in the Upper Jurassic HTHP sandstone plays in the area.

The aim of this paper is to present an updated overview of the stratigraphy, sand distribution, depositional environments and reservoir characteristics of the Upper Jurassic potential reservoir sandstones in the northern part of the Danish Central Graben. A series of palaeogeographic maps illustrates the basin evolution during the Late Kimmeridgian to Ryazanian.

Structural setting

The northern Danish Central Graben study area forms part of the Jurassic North Sea rift complex (Fig. 1). The basin consists of a system of NNW–SSE trending half-grabens bounded by the Coffee Soil Fault to the east (western margin of the Ringkøbing–Fyn High), and by the Mid North Sea High to the west (e.g. Japsen *et al.* 2003; Møller & Rasmussen 2003). Rifting took place from Middle Jurassic times and persisted into the Early Cretaceous. The syn-rift sedimentary fill is mudstone-dominated, rich in organic matter at certain intervals and with subordinate amounts of sandstones (Petersen *et al.* 2010). The early development was characterized by fault-controlled subsidence and deposition in the eastern part, especially along north–south segments of the Coffee Soil Fault (Korstgaard *et al.* 1993; Bruhn & Vagle 2005). During the Kimmeridgian, the tectonic trend shifted to a dominant NW–SE trend; the depocentres shifted westwards and deposition

VINING, B. A. & PICKERING, S. C. (eds) *Petroleum Geology: From Mature Basins to New Frontiers – Proceedings of the 7th Petroleum Geology Conference*, 127–143. DOI: 10.1144/0070127

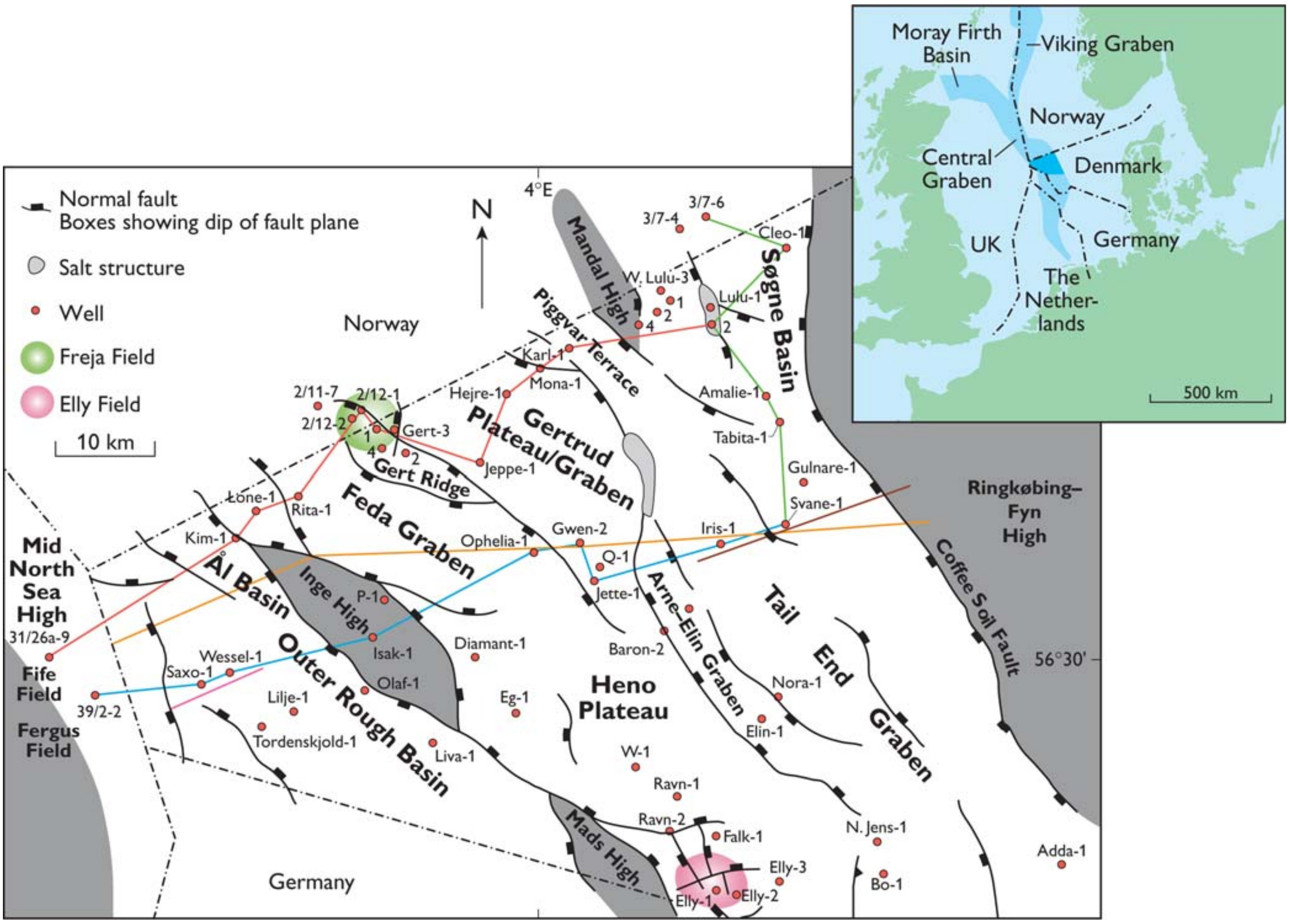

Fig. 1. Structural map of the Danish Central Graben. Location of all wells comprising Upper Jurassic deposits is shown. Position of the geotraverse in Figure 4 is shown in yellow, while the positions of the seismic lines shown in Figures 14 and 15 are shown in red-brown and pink, respectively. The positions of the log-panels shown in Figures 6–8 are shown in red, blue and green, respectively. Inserted map shows the Central Graben, Viking Graben and Moray Firth Basin.

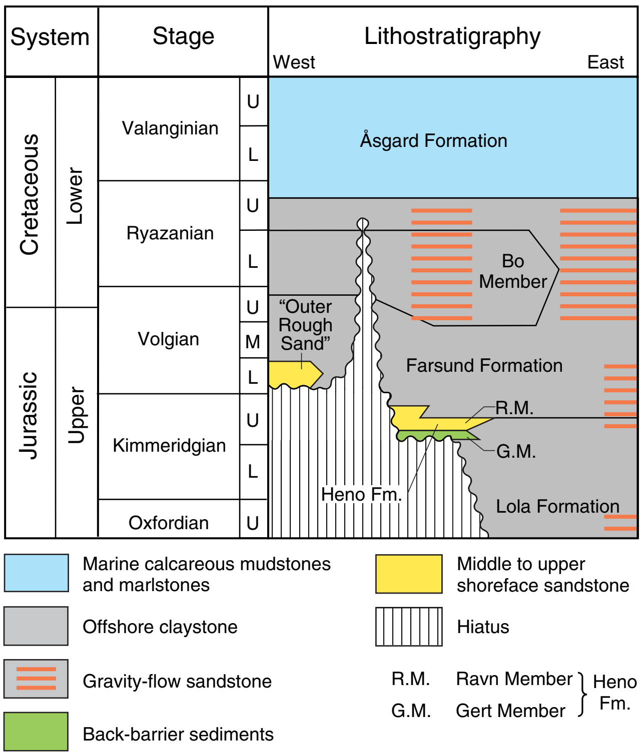

Fig. 2. Time stratigraphic chart covering the Upper Jurassic and Lower Cretaceous succession in the Danish Central Graben.

gradually covered larger areas, reaching the flanks of the Mid North Sea High during the Early Volgian. Despite the overall extensional tectonic regime, compressional features occur, caused by oblique-slip movements along different graben segments.

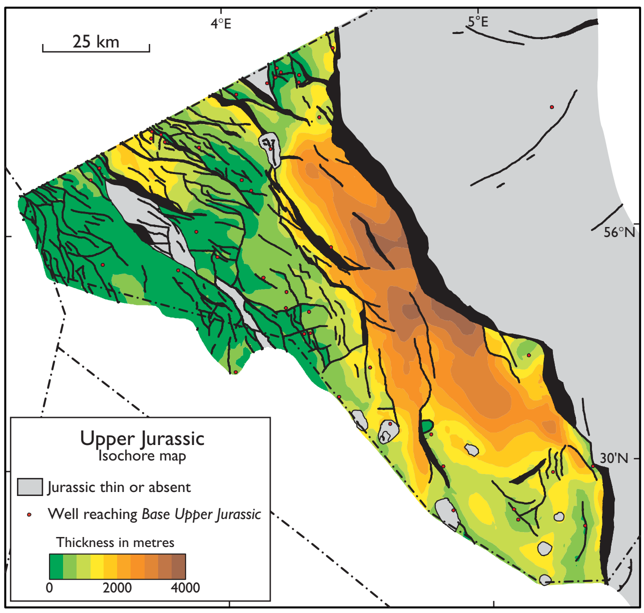

Fig. 3. Upper Jurassic isochore map of the Danish Central Graben (Britze *et al.* 1995).

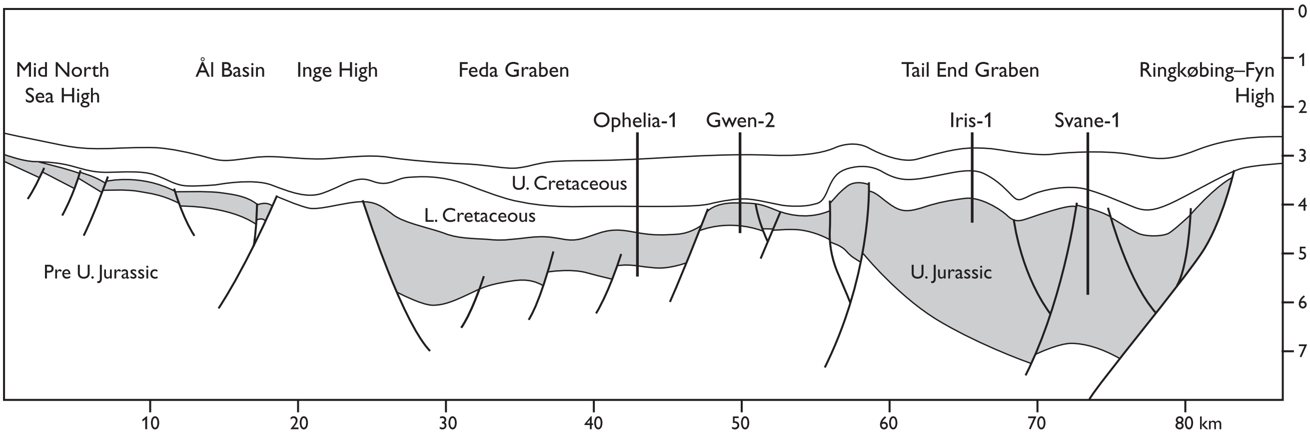

Fig. 4. Simplified structural profile across the northern part of the Danish Central Graben. For location see Figure 1.

The structural control on deposition is illustrated by the Upper Jurassic isochore map in Figure 3 (Britze *et al.* 1995) and by the simplified structural profile across the northern part of the study area (Fig. 4). The dominant Jurassic structural element is the Tail End Graben in the east containing up to 3600 m of Upper Jurassic sediments dominated by claystones. It grades into the Søgne Basin in the north with reduced sediment thicknesses. Towards the west, the Tail End Graben is separated from the Heno Plateau with westward thinning Jurassic cover by the Arne–Elin Graben (Fig. 1). The Heno Plateau passes northwards into the Gertrud Plateau/Graben, which is separated from the southwestward dipping Feda Graben by the Gert Ridge. In both graben segments, the thickness of Upper Jurassic strata locally exceeds 1500 m. The Early Cretaceous Ål Basin and the shallow Outer Rough Basin are located west of the Inge High in which Jurassic strata are thin or absent (Figs 1, 3 & 4) (Britze *et al.* 1995).

Methods

The chronostratigraphic framework for the studied succession is primarily based on first and last occurrences of dinoflagellate cyst (dinocyst) species (Fig. 5). Each bioevent has been given a number in order to be able to show the location of that specific bioevent in the wells included in the log panels (Figs 6–8). The biostratigraphic data have been compiled from published papers (Johannessen *et al.* 1996; Dybkjær 1998; Andsbjerg & Dybkjær 2003; Ineson *et al.* 2003), unpublished data and service company reports. Spores and pollen were included in the Rita-1 and Gwen-2 wells to support the stratigraphic interpretations. In addition, new biostratigraphic and palynofacies investigations have been carried out on cuttings and core samples for the present study. In the present study we have not correlated the studied succession with the 'genetic stratigraphic sequences' defined by Partington *et al.* (1993*a*, *b*), although this subdivision is used by several companies operating in the Danish Central Graben. The biostratigraphic events used for dating the sequences (and especially the maximum flooding surfaces) by Partington *et al.* (1993*b*) was mainly based on data from the Outer Moray Firth (pers. comm. M. Partington 1995). In many cases the biostratigraphic events used by Partington *et al.* (1993*b*) are acmes of specific species and these acmes do not occur in the same stratigraphic levels and the same order in the Danish Central Graben. Furthermore, the last occurrences ('species top' by Partington *et al.* 1993*b*) in some occasions occur in a different order in the Danish Central Graben than are indicated by Partington *et al.* (1993*b*).

The sedimentology of the cores has been studied in detail, focussing particularly on trace fossil assemblages, because most primary sedimentary structures are not preserved due to intensive bioturbation. The interpreted depositional environments from the core studies have been extrapolated via petrophysical well logs above and below the cored sections. Utilizing the new sedimentological and biostratigraphical data, an updated time stratigraphic chart has been constructed to show the overall depositional history of the northern Danish Central Graben (Fig. 2).

Log-correlation panels have been constructed to show the interrelations and distribution of depositional environments within the basin (Figs 6–8) and schematic palaeogeographical summary maps are created (Fig. 9). Note that the term 'shoreface' is used in this paper in a broad sense to cover various wave-influenced and wave-dominated shallow marine environments. Porosity–permeability plots are presented from cores and compared with poroperm data from the nearby Fergus and Fife fields of the UK sector.

Upper Jurassic reservoir sandstones

Initial subsidence along the Coffee Soil Fault, the eastern boundary of the Danish Central Graben, during the Middle Jurassic resulted in deposition of paralic to shallow marine sandstones in the Søgne Basin and in the Tail End Graben (Andsbjerg 2003; Andsbjerg & Dybkjær 2003). Westward propagation of active NW–SE trending normal faults occurred during the Late Jurassic. This was coeval with a eustatic sea-level rise and resulted in an overall stepwise transgression towards the west (Fig. 9a–g) (Andsbjerg & Dybkjær 2003; Johannessen 2003).

The overall depositional environments, the distribution and the reservoir characteristics of the different Upper Jurassic sandstones in the Danish Central Graben will be presented chronologically in the following sections, based on published literature and unpublished data from new wells.

Upper Kimmeridgian paralic and shoreface sandstones

Distribution and stratigraphy. The sandstones referred to as the Gert Member of the Heno Formation (Fig. 2) (Michelsen *et al.* 2003) were deposited in the marginal areas of the Feda Graben and on the Gertrud and Heno Plateaus during the Late Kimmeridgian (Fig. 9a, b) (Johannessen *et al.* 1996; Andsbjerg & Dybkjær 2003; Johannessen 2003). The succession is represented by cores in the Gert-1, Rita-1 and 2/12-1 wells in this paper (Fig. 6).

Depositional environments. The cored succession in the Gert-1 well, situated at the margin of the Feda Graben up against the Gertrud Plateau (Fig. 1), is composed of sandstones interbedded with thin claystone and coal beds often underlain by rootlets.

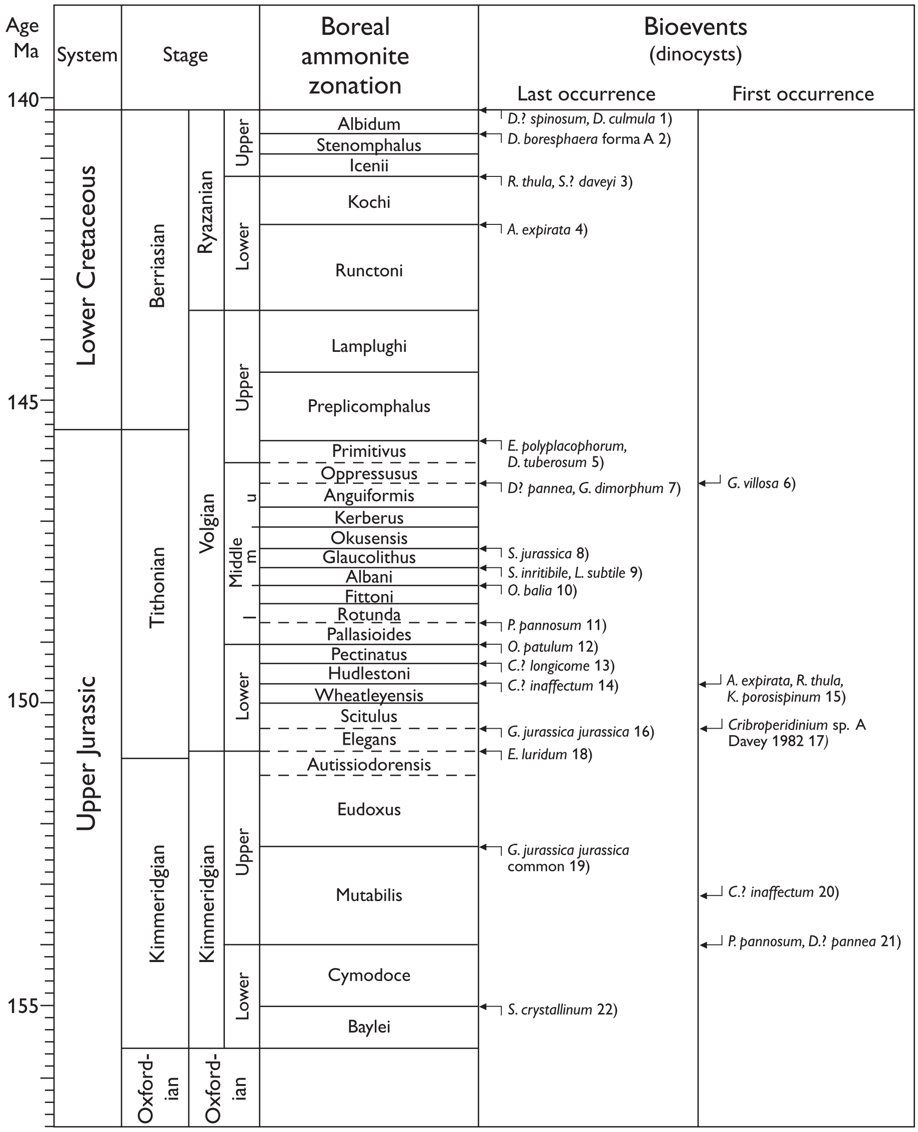

Fig. 5. Chronostratigraphic scheme showing the correlation between the bioevents (first and last occurrences of dinocyst species) recorded in the studied wells, the boreal ammonite zonation and the chronostratigraphy. Ages after Gradstein *et al.* (2004). The correlation is based on Davey (1979, 1982), Cox *et al.* (1987), Heilmann-Clausen (1987), Riding (1987), Poulsen (1991), Poulsen & Riding (1992), Riding & Thomas (1992) and Costa & Davey (1992). Note that each bioevent has been given a number in order to be able to show the location of that specific bioevent in the wells included in the log panels (Figs 6–8).

Spores and pollen are abundant, and numerous burrows of *Ophiomorpha* are observed but dinoflagellate cysts are scarce; together these features suggest deposition in a back-barrier setting (Johannessen *et al.* 1996; Johannessen 2003). Cross-bedded sandstones that overlie claystones and are capped by claystones or coal beds (sometimes with rootlets) were probably deposited by washover fans (Fig. 10a) (Schwartz 1982). The gamma-ray (GR) and sonic log motif is highly serrated (Fig. 11). Above the cored section, the log motif is non-serrated, suggesting that a cleaner sandstone unit abruptly overlies the back-barrier sediments, indicating deposition during high energy levels on the shoreface. The uppermost part of the sandy section shows a fining-upward, backstepping shoreface sandstone succession which fines upwards to offshore claystones of the Lola Formation, indicating an overall transgressive succession (Fig. 6) (Johannessen 2003).

It is very unusual to develop and preserve such *c.* 60 m thick back-barrier sediments as seen in the Gert-1 well. This thick accumulation resulted firstly because there was a sand surplus and secondly because they were accumulated at the steep margins of the Feda Graben towards the plateau areas during a transgression, forcing the back-barrier sediments and the shoreface sandstones to stack vertically (Johannessen *et al.* 2008, 2010). The sandstones of the Gert Member were probably derived from local sediment sources during the transgression, such as the exposed Carboniferous sediments in the Gert Ridge area and sediments on the Heno and Gertrud Plateaus (Johannessen *et al.* 1996).

The Norwegian 2/12-1 well, situated 2.5 km NW of the Gert-1 well, farther out in the Feda Graben, comprises an equally thick Gert Member sandstone succession but one that is dominated by shoreface sandstones (Fig. 6). Only the lowermost part was deposited in a back-barrier environment (Bergan *et al.* 1989; Söderström *et al*. 1991; Johannessen 2003).

In the Rita-1 well, situated at the western margin of the Feda Graben (Fig. 1), the cored interval of the Gert Member consists of alternating mudstones, mud-draped sandstones and conglomeratic intervals. Recurring sedimentary successions consist of 1–3 m thick units of diminutive, (pyritized) *Chondrites*-bearing massive organic-rich mudstones that grade upward into mud-crack-bearing heterolithic bedding, which is interpreted to reflect a gradation from an oxygen-deficient lagoonal environment to an intertidal setting.

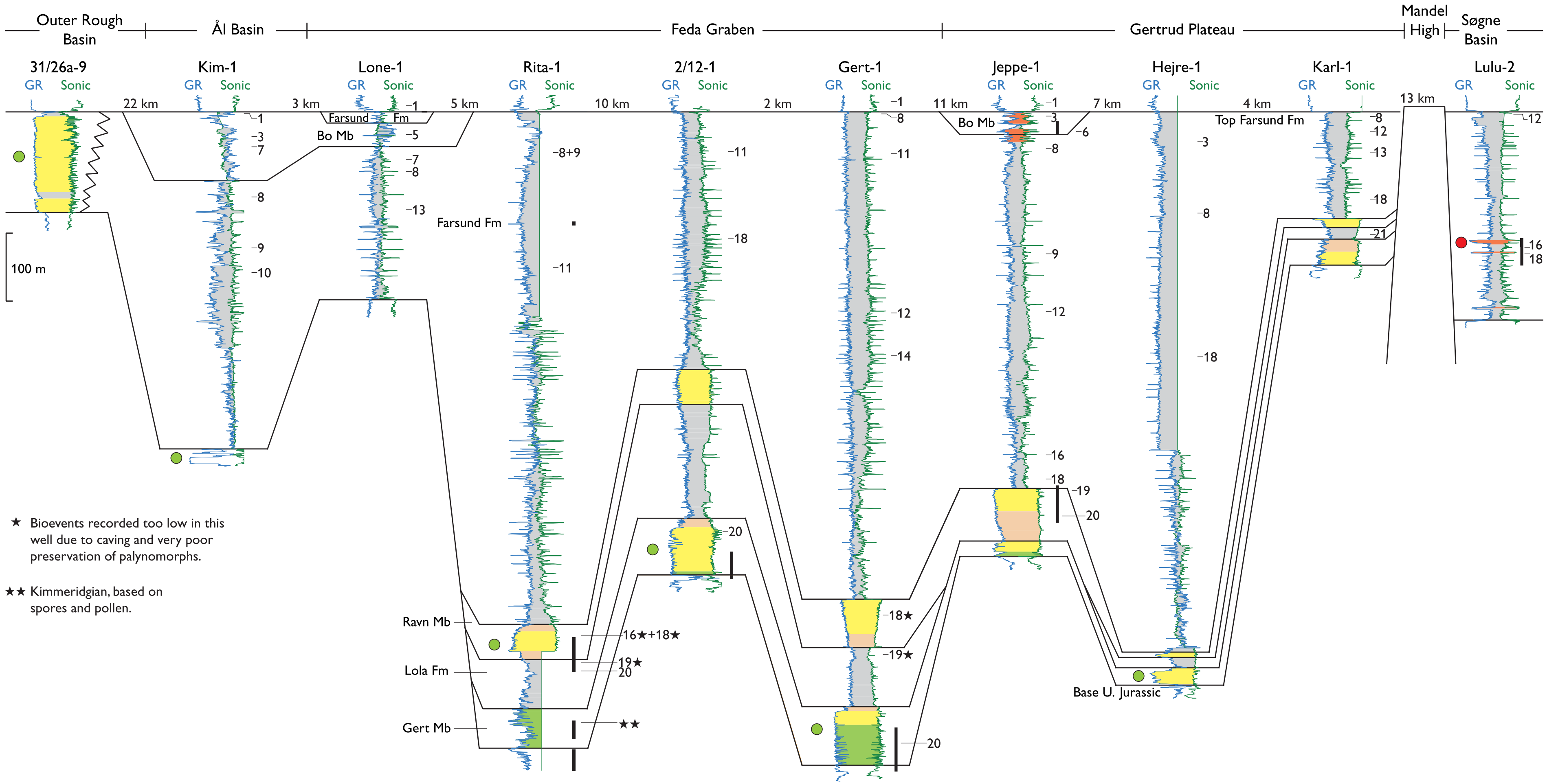

Fig. 6. Log correlation panel. The numbers shown refer to specific bioevents recorded in the wells, see Figure 5. Position of line is shown in Figure 1. For legend see Figure 7.

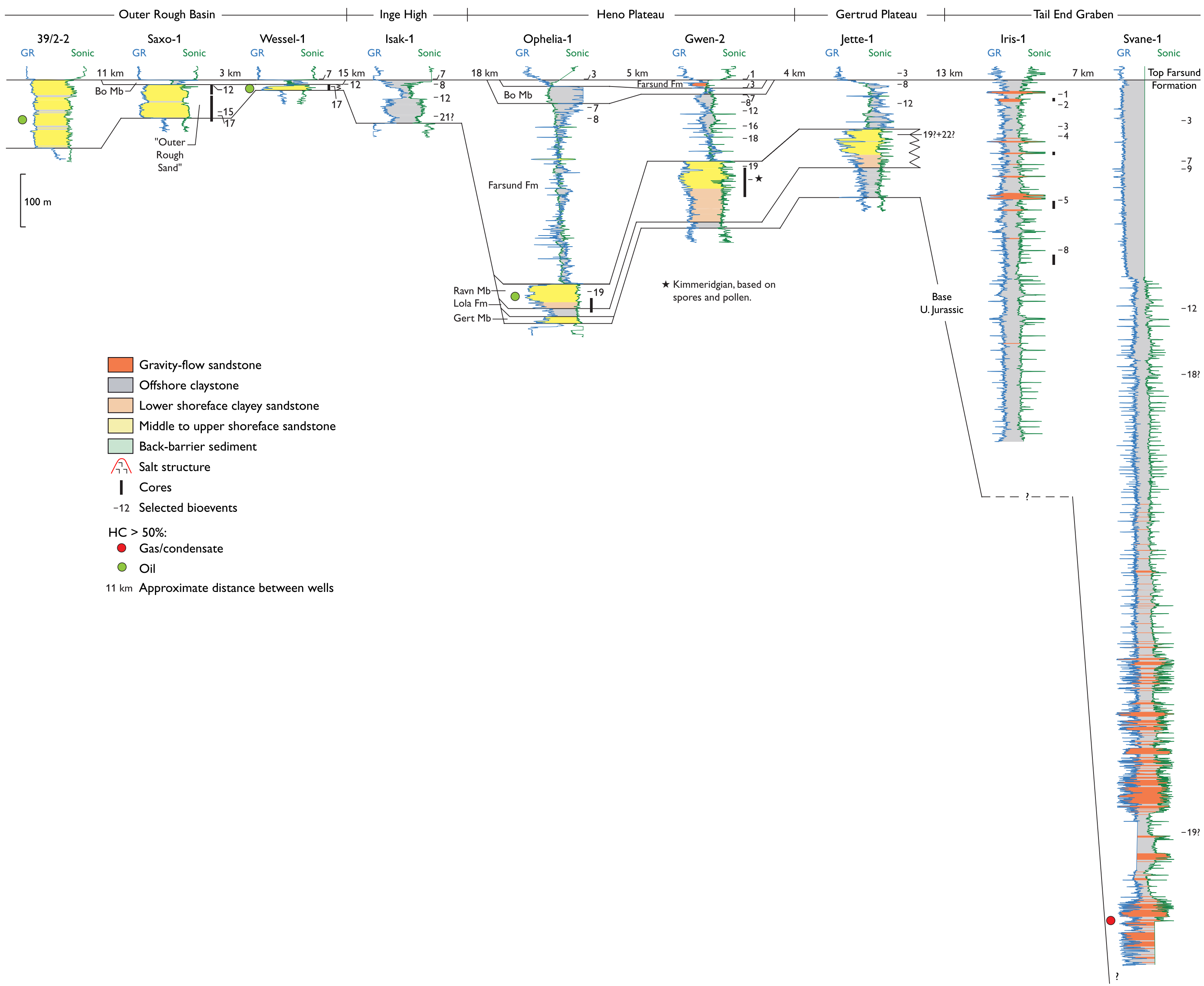

Fig. 7. Log correlation panel. The numbers shown refer to specific bioevents recorded in the wells, see Figure 5. Position of line is shown in Figure 1.

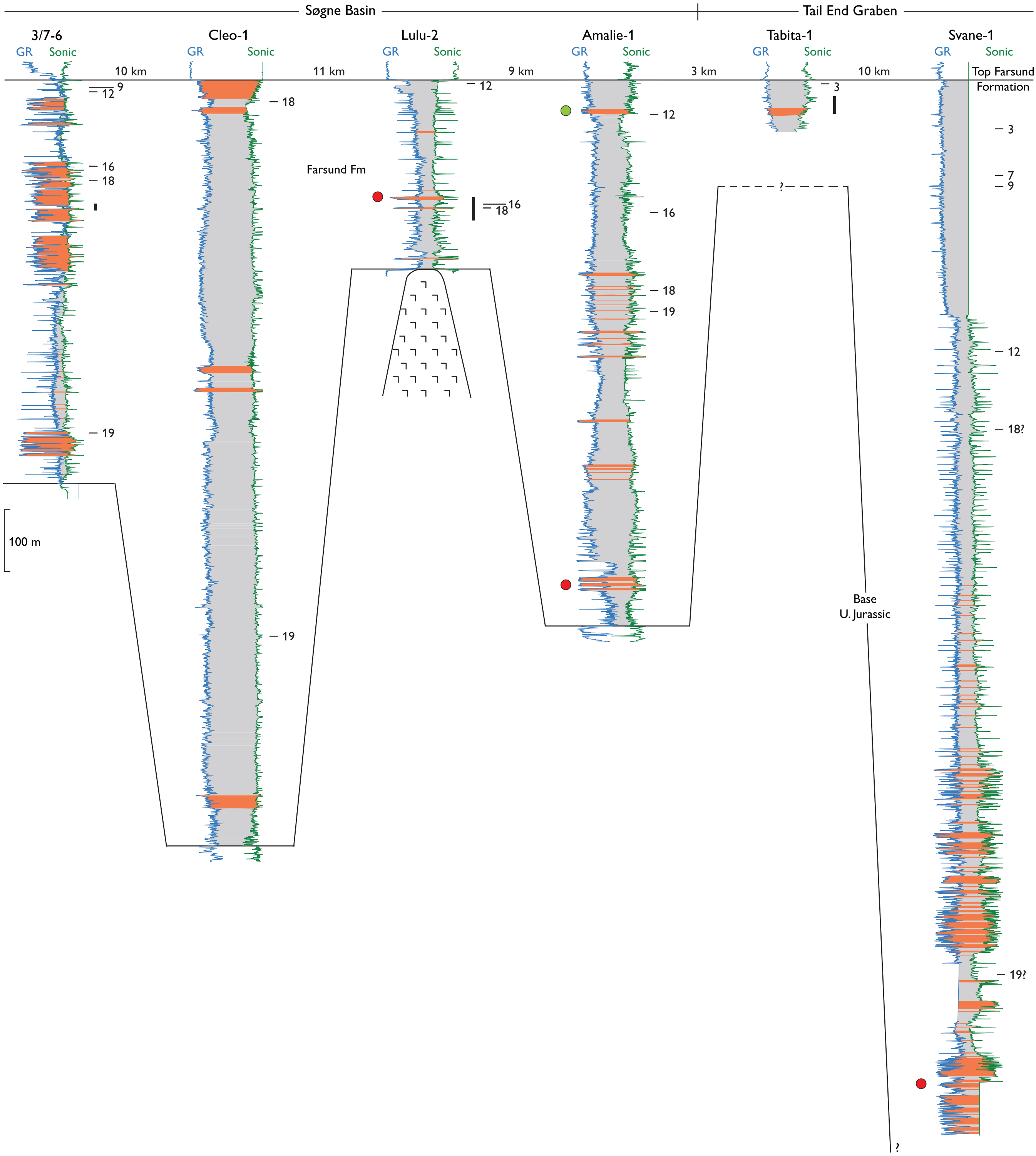

Fig. 8. Log correlation panel. The numbers shown refer to specific bioevents recorded in the wells, see Figure 5. Position of line is shown in Figure 1. For legend see Figure 7.

Locally, these successions are further overlain by root-bearing mudstone intervals, or are truncated by 1–2 m thick rhythmically cross-stratified heterolithic sandstone successions interpreted as tidal channel and bar deposits. The base of the channel units typically contains interbedded or mixed conglomerates and highly deformed, carbonaceous mudstone beds pointing to high-energy conditions and formation of abundant fluid mud in the depositional system. The channel units are mainly unburrowed, but toward the top of the cored interval, local occurrences of *Asterosoma, Cylindrichnus* and *Ophiomorpha* were observed, suggesting increasing marine influence, and thus transgressive setting for the upper-most part of the core. In concert, the observed lagoonal, tidal and marsh sub-environments are consistent with the overall interpretation of a back-barrier and paralic setting for the Gert Member (Fig. 6).

Reservoir characteristics. Despite reservoir depths of *c.* 5 km, the sandstone reservoir of the Gert Member contains producible volumes of oil in the Freja Field, herein represented by the Gert-1 and 2/12-1 wells (Fig. 11) (Hemmet 2005; Danish Energy Agency 2008). The Gert Member consists of clean sandstones with good reservoir quality and reaches a thickness up to *c.* 90 m in both the Gert-1 and the 2/12-1 wells. Sandstone thickness

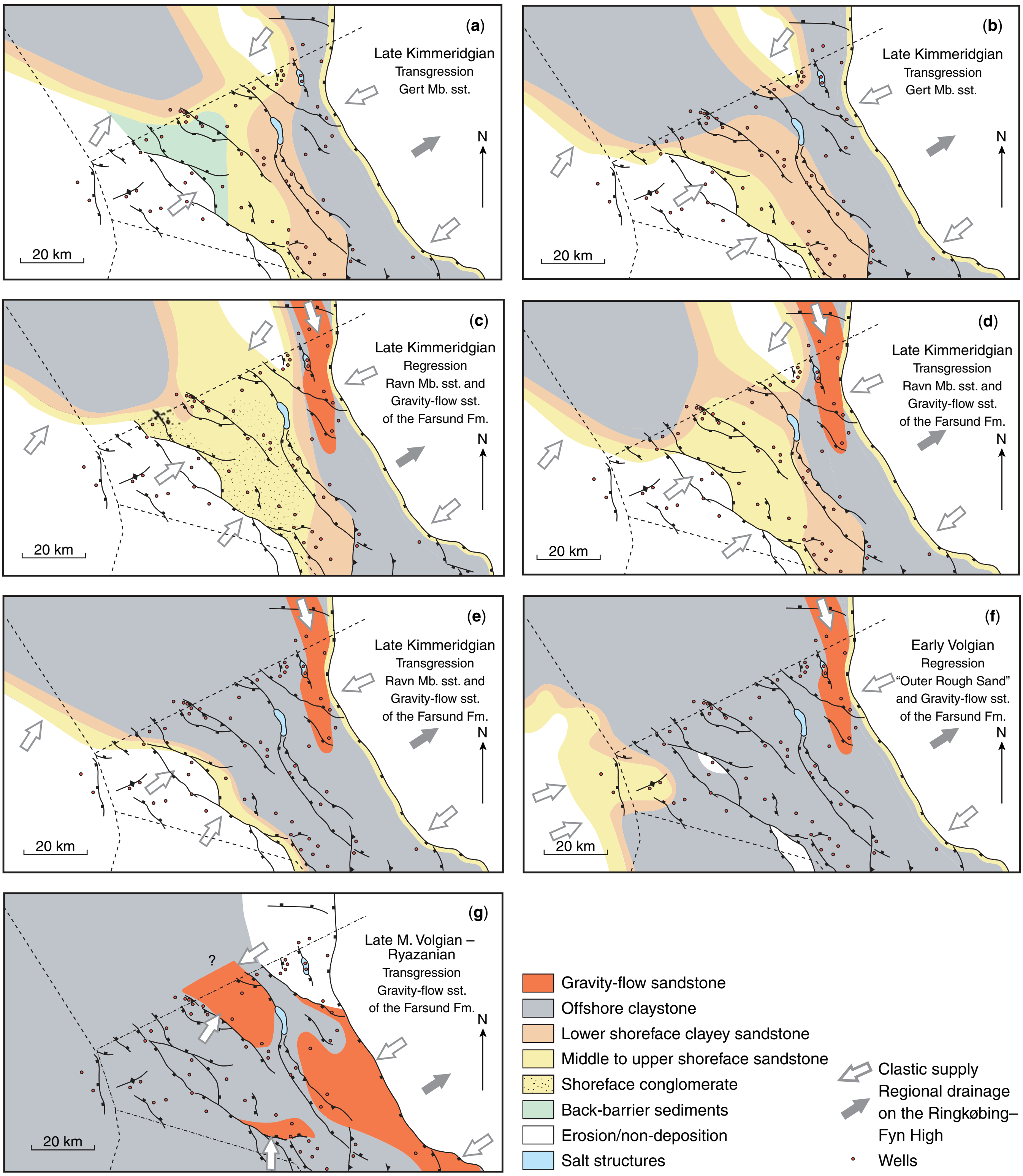

Fig. 9. Series of palaeogeographic maps illustrating facies distributions and basin evolution during the Late Kimmeridgian to Ryazanian.

decreases in a southerly and easterly direction, and in the Hejre-1 well, for example, the net sand thickness is less than 25 m (Fig. 6). Porosities are generally in the range 15–20%. The presence of high porosity sandstones of the Hejre-2 is caused by dissolution and illite replacement of detrital feldspars and early authigenic K-feldspar cement, thus creating secondary porosity (Weibel & Keulen 2008). Oil saturations up to 80% are recorded in the Gert-1, 2/12-1 and Hejre-1 wells (Fig. 11). In spite of overall good reservoir quality, core data from the Gert-1 well do not show a well defined relationship between porosity and permeability. The permeability varies considerably at a given porosity value. Generally the sandstone permeability is less than 100 mD in Gert-1, but occasionally the permeability may exceed 100 mD provided that the porosity is fairly high (Fig. 12). In the Rita-1, Ophelia-1 and Jeppe-1 wells, the reservoir sandstones are characterized by poorer reservoir quality than seen in Gert-1, Hejre-1 and 2/12-1. The reservoir quality sandstones of the Hejre-1 and Gert-1 wells are situated in a HTHP environment with overpressures of 7020 and 6800 psi, respectively (Table 1).

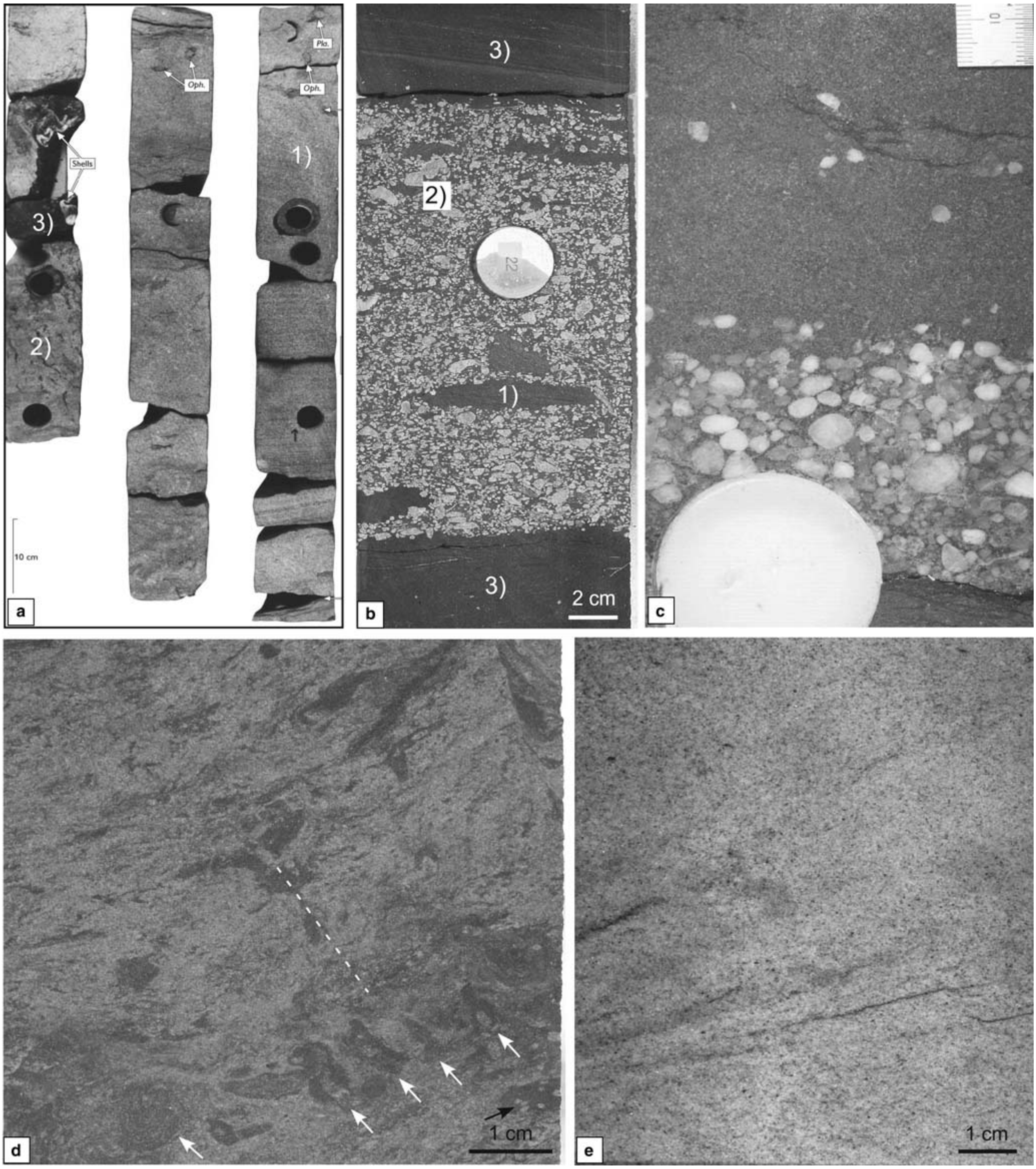

Fig. 10. Core photos of selected facies. (**a**) A sediment succession consisting of cross-stratified sand (1) grading upward into root-bearing sand (2) and further into a coal-layer (3). This succession overlies organic rich mudstones and is interpreted to represent a washover fan in a back-barrier setting. Gert Member, Gert-1 well. (**b**) Intra- and extraformational clast (1 and 2, respectively) bearing conglomeratic bed interbedded with laminated claystones (3). Farsund Formation, Tabita-1 well. (**c**) A sharp-based gravel bed interbedded with massive appearing fine-grained sandstone. The sandstone facies bear common outsized clasts and mud-drapes. Ravn Member, Ophelia-1 well. (**d**) Bioturbated muddy sandstone. Characteristic trace fossils include abundant *Asterosoma* (white arrows), which is re-burrowed with *Chondrites* (black arrow). Dashed white line indicates the location of a central vertical tube. Ravn Member, Rita-1 well. (**e**) Tangentially cross-stratified sandstone. 'Outer Rough Sand', Saxo-1 well.

Palaeogeography. The Heno and Gertrud Plateaus formed a positive north–south trending area between the Mandal High to the NE and the Mid North Sea High to the SW (Fig. 9a–d). The back-barrier and shoreface sandstones of the Gert Member were deposited during the Late Kimmeridgian, when the transgression started in the deep part of the Feda Graben and moved towards the Heno and Gertrud Plateau margins and ultimately drowned the plateau areas (Fig. 9a, b). As the regional gradient on the plateau areas was low, the transgression was rapid, leaving only a thin section of back-barrier sediments overlain by thin shoreface sands and topped by offshore claystones (Fig. 6, Jeppe-1) (Johannessen *et al.* 1996; Johannessen 2003).

The upper parts of the shoreface sandstones are back-stepping and are overlain by offshore claystones of the Lola Formation in the

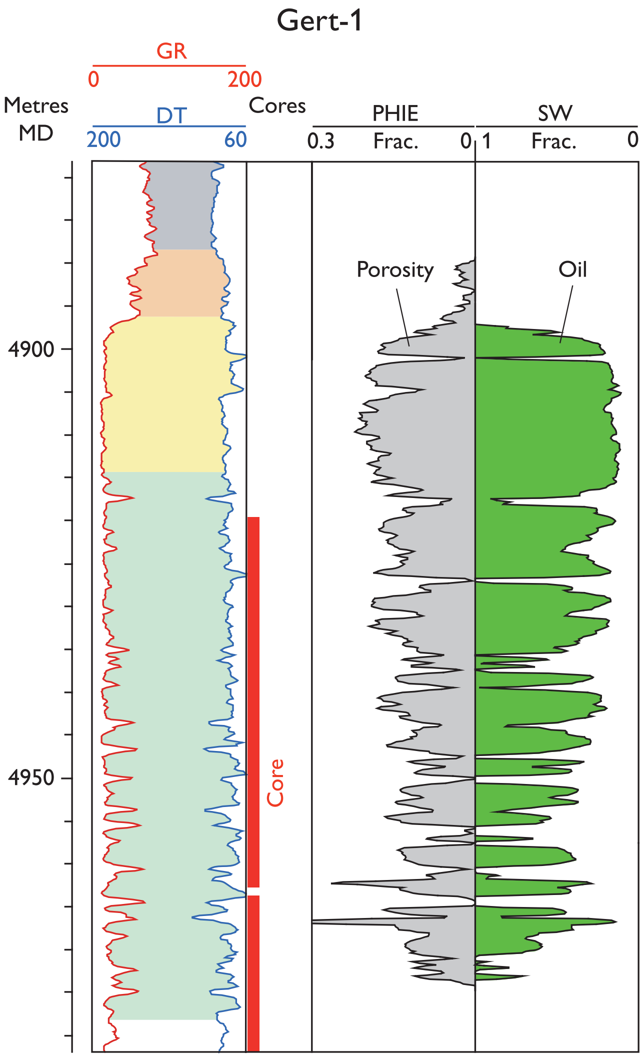

Fig. 11. Porosity and oil saturation plot for back-barrier and shoreface sandstones of the Gert Member in the Gert-1 well. PHIE is the effective porosity (highlighted by grey colour fill) as interpreted from the well log data. SW is the water saturation estimated on the basis of the porosity evaluation, resistivity log data and a set of petrophysical parameters representing the sandstone layers. The oil saturation (green colour fill) is calculated as 1-SW. For legend see Figure 7.

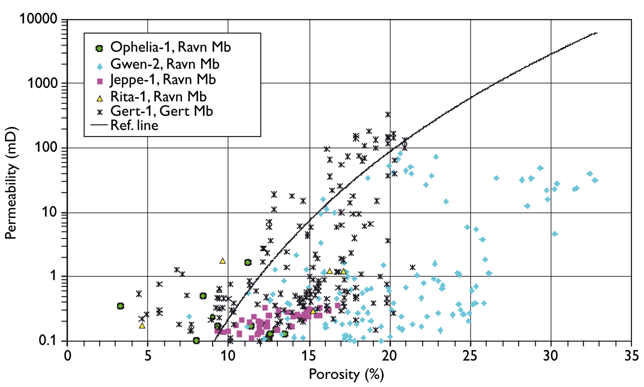

Fig. 12. Porosity–permeability relationship: shoreface to paralic sandstones of the Heno Formation (Gert and Ravn Members), cored in selected wells. The plot is based on conventional core analysis data from the wells Gert-1 (Gert Mb); Ophelia-1, Gwen-2, Jeppe-1 and Rita-1 (Ravn Mb). The trend line is from Figure 17 and plotted for reference.

Table 1. Formation pressures of the Svane-1, Hejre-1 and Gert-1 well

Well	Approximate depth (m)	Formation pressure (psi)	Hydrostatic pressure (psi)	Overpressure (psi)	Temperature (°C)
Svane-1	5350	16 530	7900	8630	180
Hejre-1	5100	16 740	7530	7020	165
Gert-1	4900	14 000	7200	6800	155

basin areas (Figs 6 & 7). On the higher plateaus, the water depth was too shallow and energy levels too high for deposition of clay and thus sandstones were deposited here, for example, Jeppe-1 (Fig. 6).

Upper Kimmeridgian shallow marine sandstones

Distribution and stratigraphy. The sandstones referred to the Ravn Member (Fig. 2) (Michelsen *et al.* 2003) were deposited in the same areas as the Gert Member, later during the Late Kimmeridgian (Fig. 9c–e) (Johannessen *et al.* 1996; Andsbjerg & Dybkjær 2003; Johannessen 2003). The succession is represented by cores in the Rita-1, Ophelia-1, Jeppe-1 and Gwen-2 wells in this paper (Figs 6 & 7).

Depositional environment. Deposition of the regressive shoreface and deltaic sandstones of the Ravn Member followed the transgression during which the paralic and shoreface sandstones of the Gert Member were deposited (Fig. 9c–e). In general, they consist of intensely bioturbated shallow marine sandstones. The lowest part is prograding whereas the uppermost part is retrograding (Johannessen *et al.* 1996; Johannessen 2003). This vertical trend is also seen in the Norwegian and UK sectors in the time equivalent Ula and Fulmar Formations, respectively (Bergan *et al.* 1989; Howell *et al.* 1996; Mackertich 1996). A conglomerate bed, 0.2–2 m thick, marks the maximum regression which can be mapped over a large area (Fig. 9c). The shoreface sandstones are often thick and very widespread. The best reservoir sands are developed on the Heno and Gertrud Plateaus and shale out towards the Feda and Tail End Grabens.

The 50 m long core in the Rita-1 well, situated at the SW margin of the Feda Graben, covers much of the Ravn Member interval (Figs 6 & 13). At the base it consists of a 25 m thick coarsening upward claystone to clayey sandstone succession, which represents a distal offshore to offshore-shoreface transition from the Lola Formation to the Ravn Member. This succession is truncated by a prominent erosion surface in the middle of the core, above which the deposits grade into a succession of stacked, variably developed, coarsening upward, 1–4 m thick parasequences. Figure 13 illustrates a section of the core, which contains many of the characteristic features for these sediments: the base of a parasequence typically consists of sporadically bioturbated interlaminated mud and sand, which grades upward into bioturbated heterolithic bedding and further into clayey and pebbly sand at the top of the parasequences (Figs 10d & 13). The dominance of elements of distal and archetypal *Cruziana* ichnofacies (Fig. 10d) (MacEachern *et al.* 2008) coupled with high clay content even in high-energy facies in these successions is interpreted to reflect a downdrift offshore–lower shoreface setting.

Ophelia-1, located on the Heno Plateau, has a 27 m thick core consisting typically of variably developed 1–6 m thick parasequences (Fig. 13). Some typical recurring features of these sediments are shown in Figure 13, and include the following elements: the lower part of a sequence may contain interlaminated clay and sand or heterolithic climbing combined-flow ripple cross-stratification. The heterolithic intervals display occasional double

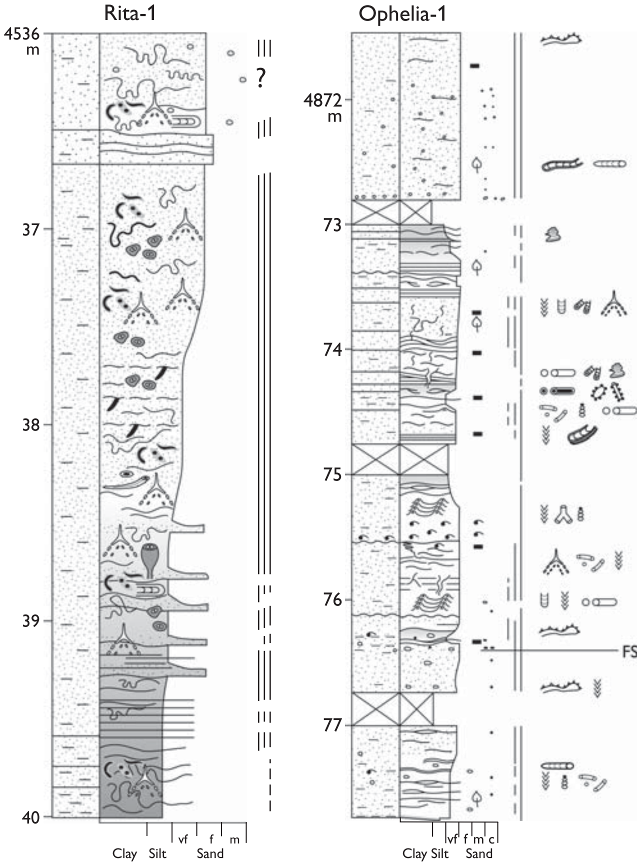

Fig. 13. Detailed sedimentological core logs of Ravn Member intervals in Rita-1 and Ophelia-1 wells. The Rita-1 interval demonstrates an intensively bioturbated coarsening upward parasequence. The sediments are characterized by abundant soft sedimentary deformation structures, relict sand–clay couplets, and pervasive deposit feeding trace fossils such as *Asterosoma* and *Chondrites*. The succession is interpreted to reflect a downdrift offshore–lower shoreface setting. The illustrated Ophelia-1 interval is interpreted to show, for example, common tempestite intervals interbedded with tidal and wave-influenced, heterolithic fair weather facies. The interval is interpreted as mixed-influenced delta front. See Figure 16 for symbols.

mud-drapes and subdued trace fossil diversity, which is interpreted to indicate tidal and possibly local brackish water influence. Upwards, these deposits begin to alternate with erosionally based, planar-laminated and low-angle cross-stratified, decimetre-scale sandstone intervals, which are interpreted as tempestites. On the top of the parasequence, the sediments further grade or are abruptly overlain by a 1–3 m thick succession of sporadically bioturbated, massive, graded and parallel-laminated sandstone beds, which contain locally thick mud-drapes and dispersed conglomerates. In general, Ophelia-1 sediments are interpreted to represent various storm-, wave- and tide-influenced deltaic and proximal offshore environments (Figs 10c & 13).

Reservoir characteristics. Porosities exceeding 15% are interpreted from log data acquired in the Jette-1 and Gwen-2 wells, located on the Gertrud Plateau (Fig. 1). Highly porous sandstone beds, having porosities in the range 20–30%, are interpreted in the upper part of the Ravn Member in Jette-1. The net sand thickness is *c.* 40 m, but despite good reservoir quality it is not hydrocarbon bearing. Similarly in Gwen-2, the presence of *c.* 20 m net sand with porosities exceeding 20% is verified by log and core data, and it is noteworthy that the permeability range is large (0.1–100 mD) (Fig. 12). This range is presumably related to varying clay content and the presence of cement in the sandstone matrix.

In a large number of wells situated on the Gertrud Plateau and in the Feda Graben, the Ravn Member is characterized by rather poor reservoir properties, as the sandstones may be cemented by calcite and, moreover, the pores are to some extent filled with diagenetic clay (illite). In such tight Ravn Member reservoirs, the porosity is generally below 15% and the permeability is in the range 0.1–1 mD, as observed in the cores from Ophelia-1, Jeppe-1 and Rita-1 (Fig. 12). A low-porosity Ravn Member has also been encountered in the 2/12-1, Gert-1 and Hejre-1 wells. Despite such low porosities in the Ravn Member reservoir, oil has been encountered in both the Ophelia-1 and Rita-1 wells. It appears that the back-barrier and shoreface sandstones of the Gert Member in general have a better reservoir potential than the shoreface sandstones of the Ravn Member.

Palaeogeography. Regressive to transgressive shoreface sandstones of the Ravn Member were deposited during the Late Kimmeridgian on the Gertrud and Heno Plateaus and cover a large area of the northern Central Graben (Fig. 9c–e). The plateaus were flanked by two deep, broad graben areas: the Feda Graben to the NW and the Tail End Graben to the SE. The basal regressive shoreface sandstones were probably formed due to a pause in fault activity and subsidence (Andsbjerg & Dybkjær 2003). Subsequently, the shoreface sandstones back-stepped during renewed subsidence (Fig. 9d). The shoreface sandstones of the Ravn Member are comparable to Upper Jurassic sandstones of the UK Fulmar and Norwegian Ula Formations (Fraser *et al.* 2003). At this time, the Mid North Sea High reached as far east as the Inge and Mads Highs and contributed much of the sand to the Heno and Gertrud Plateaus, although sand was probably also derived from the Mandal High, NE of the Gertrud Plateau (Fig. 9c–e). Farther out in the basins, claystones of the Farsund Formation were deposited.

In the latest Kimmeridgian, the previously positive Heno and Gertrud Plateaus were transgressed both from the NW from the Feda Graben and from the SE from the Tail End Graben. Later the Gertrud Plateau began to subside and was thus transformed into a graben (henceforth the Gertrud Graben) (Japsen *et al.* 2003; Møller & Rasmussen 2003).

Upper Kimmeridgian to Lower Volgian gravity-flow sandstones

Distribution and stratigraphy. Thin sandstone units, 0.1–5 m thick, are interbedded with the offshore claystones of the Farsund Formation in the Tail End Graben (Svane-1 and Amalie-1) and the Søgne Basin (Lulu-2, Cleo-1 and 3/7-6) (Figs 6–8 & 9c–f). The sandstones are probably of Late Kimmeridgian to Early Volgian age, but are poorly dated.

Depositional environment. In the Lulu-2 well, two sandstone beds (2 and 5 m thick respectively) are encountered. A 36 m long core shows that the sandstones are fine-grained and interbedded with parallel laminated, mostly non-bioturbated claystones. The two sandstones are mostly structureless, but cross-lamination has been observed locally. Thin siltstone and very fine-grained sandstone laminae are often slumped. Partial Bouma sequences occur. The siltstones and fine-grained sandstones were probably deposited from turbidity currents while anoxic conditions prevailed at the sea-bottom. The sediments have also undergone slump processes (Johannessen 1997).

In the Svane-1 well in the Tail End Graben, the GR and sonic logs show four sandy units, *c.* 40–125 m thick. The log patterns are very serrated and blocky and are similar to those in the

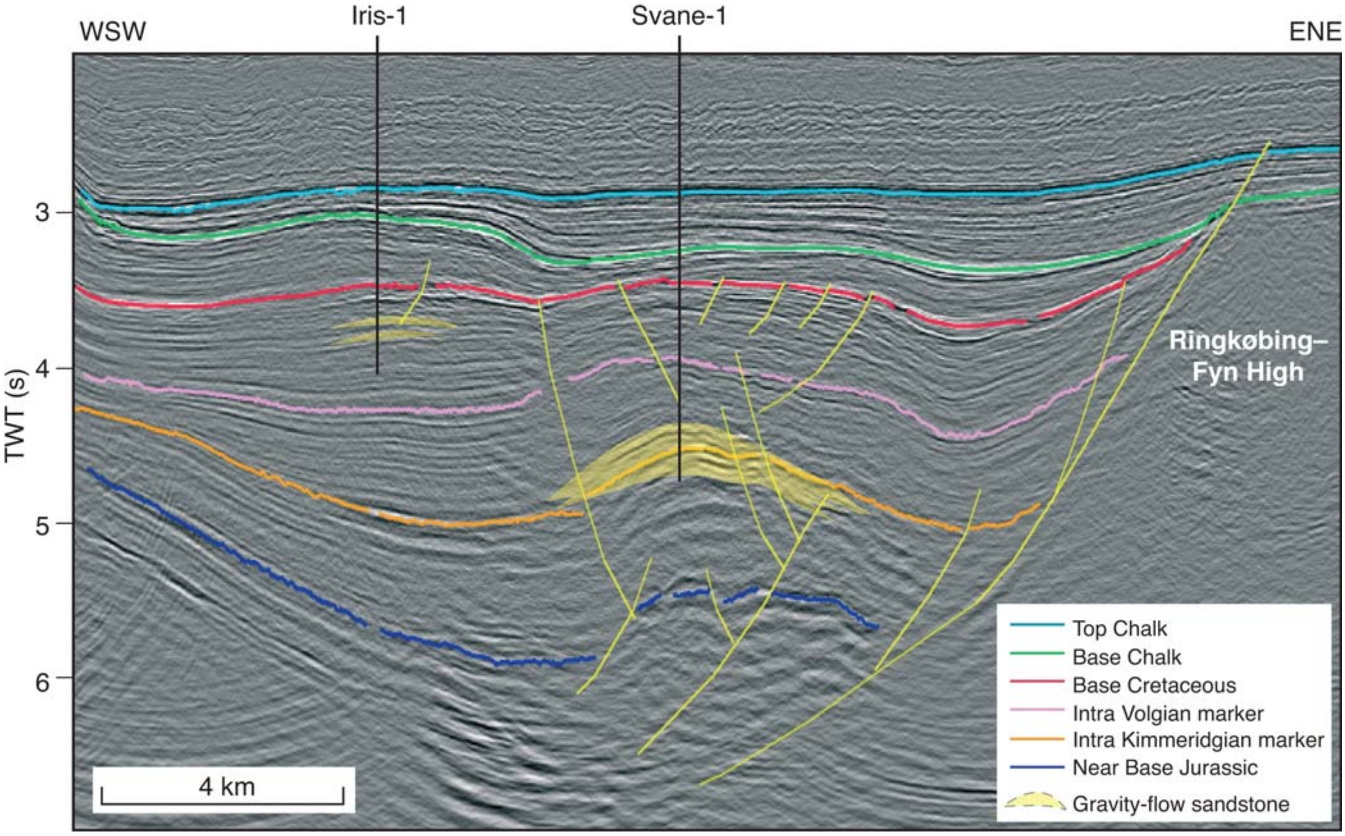

Fig. 14. Seismic section across the Tail End Graben through the Iris-1 and Svane-1 locations highlighting the location of the gravity-flow sandstones. For location see Figure 1.

Norwegian 3/7-6 well in the Søgne Basin (Fig. 8). A 10.5 m long core from the 3/7-6 well shows thin centimetre-scale sandstone beds within offshore claystones of the Farsund Formation (Oljedirektoratet 2009). The clay and sandstones are non-bioturbated and were probably deposited from turbidity currents. Thus it is assumed that the sandstones in the Svane-1 also were deposited from turbidity currents. The Svane-1 well is almost 6000 m deep and located on a four-way dip closed structure with seismic amplitude anomalies encountering the sandstone-bearing successions below 5300 m (Fig. 14).

In the Amalie-1 and Cleo-1 wells, lying between the Svane-1 and 3/7-6 locations, thin sandstone beds of inferred turbidite origin occur interbedded within claystones of the Farsund Formation (Fig. 8). This could imply that the turbidite sandstones of the Svane-1 may well have been derived from the north, from the Søgne Basin (Fig. 9c–f). The sandstones could alternatively have been derived from the east, from the Ringkøbing–Fyn High.

The lowermost part of the Upper Jurassic section in the Amalie-1 well encounters three gas-bearing massive sandstone beds, 5–8 m thick, with no upward coarsening or fining grain-size trends, probably deposited by gravity-flow processes (Figs 2 & 8). They are Oxfordian in age (Andsbjerg & Dybkjær 2003).

Reservoir characteristics. The Svane-1 well has proved the presence of gas in sandstones at *c*. 6 km depth. The net sand thickness is greater than 150 m in the Svane-1 and the 3/7-6 wells. No core data are available from the Svane-1 well, but locally relatively high porosities up to 15–20% at a depth of almost 6000 m have been interpreted from log data in certain intervals. The reservoir sandstones are gas-charged and a DST conducted in the lower part of the well flowed 2.3 MMscf of gas per day; the DST tested a net sand interval of *c*. 100 m. The reservoir quality sandstones of the Svane-1 well are situated in a HTHP environment with overpressures of 8600 psi (Table 1). The substantial overpressures at a depth of 5350 m signify that the pore pressure is close to the fracture pressure.

The thin gas-bearing cored sandstone interval in Lulu-2, located at a depth of 3500 m, shows porosities up to 23% and permeabilities up to 100 mD, but these data may not be representative of the turbidite sandstones in general in this area.

Palaeogeography. During the Late Kimmeridgian to Early Volgian the Tail End Graben and Søgne basin subsided and thick offshore mudstones of the Farsund Formation were locally intercalated with gravity-flow sandstones (Fig. 9c–f). Sand may have been derived from the Ringkøbing Fyn High to the east, forming marginal fans, and from the north, from the Søgne Basin and Mandal High, producing basin-axial gravity-flow systems.

Lower Volgian shoreface sandstones

Distribution and stratigraphy. Shoreface sandstones, informally termed the 'Outer Rough Sand', were deposited in the Early Volgian on the eastern part of the Mid North Sea High, where the Outer Rough Basin began to subside. The 'Outer Rough Sand' is documented by the Saxo-1 and Wessel-1 wells in the Danish sector (Figs 2 & 9f). The wells are located on separate tilted fault blocks on the flanks of the Mid North Sea High about 3 km apart (Fig. 15). The shoreface sandstones of the Saxo-1 and Wessel-1 wells have now been very precisely dated to Early Volgian (Scitulus to Pectinatus Zones), deposited within a period no longer than 1.4 million years (Fig. 5). At this time the sand source area of the Mid North Sea High was situated in the easternmost part of the UK sector (Fig. 9f).

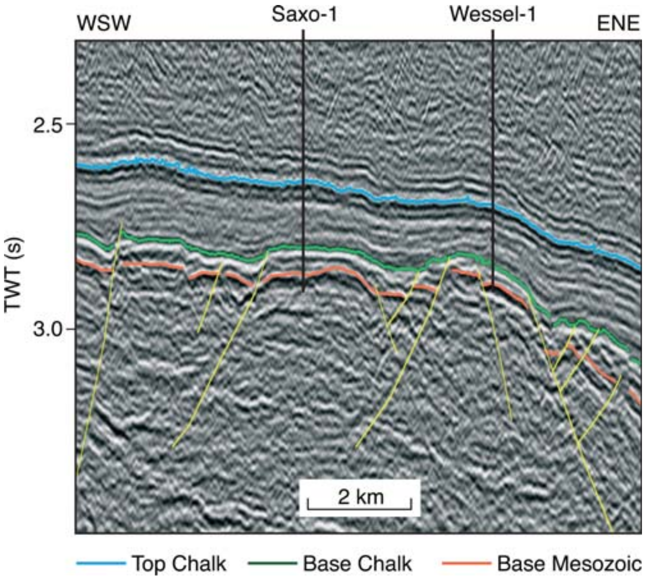

Fig. 15. Seismic section through the Saxo-1 and Wessel-1 locations on the flank of the Mid North Sea High. The Volgian sandstone intervals are close to seismic resolution. For location see Figure 1.

Depositional environment. The Saxo-1 core records a 65 m thick succession of moderately to well sorted, fine- to medium-grained sandstones (Fig. 16). The sandstones are organized into variably developed, 2–12 m thick, coarsening upward or aggrading parasequences that are generally interpreted to represent shoreface complexes. This interpretation is supported by abundant elements of the *Skolithos* ichnofacies, occurrences of *Macaronichnus* in the top parts of the parasequences, well-sorted sandstones and local tangentially cross-stratified intervals, which in concert are consistent with a high-energy, wave-dominated shoreface setting (Figs 10e & 16).

The Wessel-1 core records a 8 m thick succession of fully bioturbated, fine- to medium-grained sandstones, which are locally intercalated with few centimetre- to decimetre-thick (extraformational) pebble rich intervals. These deposits are organized into sharp-based *c.* 1 m thick aggrading parasequences, which are typically burrowed with abundant *Macaronichnus* burrows. Elements of *Skolithos* ichnofacies (e.g. *Diplocraterion*, *Palaeophycus*, vertical shafts) are also present in several parasequences, but their occurrence is limited to certain intervals (brief colonization windows for suspension feeders). At the top, the parasequences are capped by prominent erosive hiatal surfaces. The hiatal surfaces are typically burrowed with spreite-bearing trace fossils and locally of passively filled vertical burrows forming *Glossifungites* ichnofacies demarcated surfaces. The deposits are interpreted to represent low-accommodation space shoreface successions in a tectonically complex setting.

The reservoir thickness decreases rapidly from 65 m in the Saxo-1 well to less than 10 m in Wessel-1, 3 km towards the NE (Fig. 7). Towards the west (11 km) to the UK well 39/2-2 of the Fergus Field and towards the NW (15 km) to the UK Fife Field, the shoreface sandstones increase in thickness (*c.* 125 m thick) and are dated to be of Late Kimmeridgian to Middle Volgian age (Figs 1 & 7) (Fraser *et al.* 2003). This indicates that the regional sand source area and most of the accommodation space was located to the west on the Mid North Sea High and that shoreface sands prograded towards the east into the Outer Rough Basin (Fig. 9f). Detailed studies of shoreface sandstones in the British Fife Field area shows that they prograded four times: twice towards the SW and twice towards the SE (Currie *et al.* 1999).

No sandstone was encountered in the remaining wells in the Danish part of the Outer Rough Basin. The offshore claystones of the Farsund Formation in the Liva-1, Tordenskjold-1 and Lilje-1 wells were deposited at the same time as the prograding shoreface sandstones in the Saxo-1 and Wessel-1 wells (Fig. 9f).

In the Ål Basin area and the area north of the Inge High and the SW margin of Feda Graben, the Kim-1, Lone-1 and Rita-1 wells show an upward coarsening succession overlain by an upward fining succession in the Lower Volgian claystones of the Farsund Formation (Fig. 6). This regressive–transgressive trend in the claystone successions may reflect the distal signal of a shoreface sand progradation and retrogradation from west, but not reaching these wells.

Parts of the Inge High must have been submerged, as Lower Volgian claystones of the Farsund Formation are recorded in the Isak-1 well (Figs 7 & 9f). As Permian Rotliegend strata are unconformably overlain by Upper Cretaceous sediments in the P-1 well, Jurassic sediments were either not deposited or later eroded in this part of the high.

Reservoir characteristics. The 'Outer Rough Sand' is generally characterized by good to excellent reservoir properties. The porosity range is 19–31% in the two UK oil fields, but they differ with respect to permeability; in the Fergus Field the average permeability of the sandstones is about 500 mD whereas in the Fife Field it is less than 100 mD (Fig. 17) (Shepherd *et al.* 2003). The sandstones of the Saxo-1 well display porosities as high as 22–33% and the average permeability is about 1000 mD (range 500–2500 mD) but it is not oil-bearing (Fig. 17). The average permeability of the reservoir sandstone in Saxo-1 is thus higher than observed in the Fergus Field. The reservoir properties of the 'Outer Rough Sand' deteriorate in an easterly direction.

Palaeogeography. During the Early Volgian, the Outer Rough Basin (eastern margin of the Mid North Sea High) probably began to subside and shoreface sandstones ('Outer Rough Sand') were deposited while the rest of the Danish Central Graben was subsiding and offshore claystones were deposited except the Inge and Mads Highs, which probably formed sub-aerial intra-basinal highs (Fig. 9f). The sand was derived from the Mid North Sea High and the shoreline was located farther west in the eastern part of the UK sector. The 'Outer Rough Sand' was probably in connection with the shoreface sandstones of the Fulmar Formation in the UK sector (Fig. 9f).

Upper Middle Volgian to Ryazanian gravity-flow sandstones

Distribution and stratigraphy. After deposition and drowning of Lower Volgian shoreface sandstones on the eastern margin of the Mid North Sea High offshore, claystones of the Farsund Formation, locally intercalated with gravity-flow sandstones, were deposited in the Danish Central Graben (Fig. 9g). Gravity-flow sandstones have been recorded in the Tail End Graben, Arne-Elin Graben, Poul Plateau, Gertrud Graben, and the southern part of the Heno Plateau NE of the Mads High (Figs 1 & 9g) (Damtoft *et al.* 1992; Johannessen 1997; Andsbjerg & Dybkjær 2003; Michelsen *et al.* 2003). No shallow marine sandstones were deposited.

Depositional environment. Cores from the Tabita-1 well in the Tail End Graben include a 20 cm thick quartz clast-supported conglomerate bed with clast sizes up to *c.* 1 cm and also contain several claystone clasts up to 4 cm in length (Fig. 10b). The conglomerate has a sharp boundary at the base and top to the non-bioturbated claystones of the Farsund Formation. Abundant outsized quartz

Fig. 16. Sedimentological core log of 'Outer Rough Sands' in the Saxo-1 well. The deposits are interpreted to represent stacked shoreface complexes. Note the common occurrence of elements of the *Skolithos* ichnofacies (e.g. *Ophiomorpha, Diplocraterion* and *Skolithos*) and *Macaronichnus*, which are all consistent with high-energy wave-dominated settings.

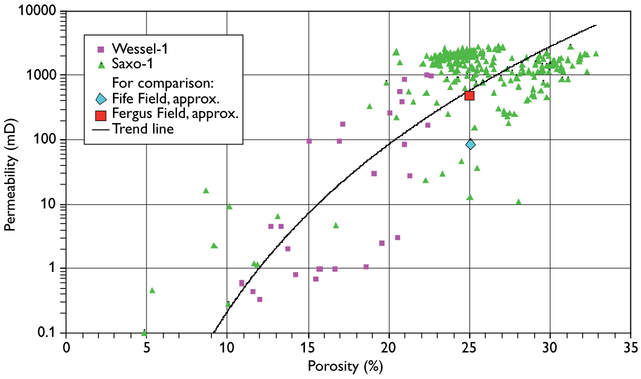

Fig. 17. Porosity–permeability relationship for shoreface sandstones of the 'Outer Rough Sand' on the eastern flank of the Mid North Sea High. The plot is based on conventional core analysis data from the Wessel-1 and Saxo-1 wells supplemented with average values applying to the Fife and Fergus Fields in the UK sector (Shephard *et al.* 2003). The solid trend line represents the assumed porosity–permeability relation.

clasts, up to 1.5 cm, are often seen in the claystones in different concentrations, sometimes clast-supported and sometimes matrix-supported. The relatively large amount of outsized quartz clasts indicates that coarse-grained sediments were available in or at the margins of the basin, thus it may be possible to find thick coarse-grained reservoir sandstones in the basin. The clay clast conglomerates in cores show at least four types of claystone lithologies which may have been derived from different areas and may represent different ages. The conglomerates were deposited by a range of gravity-flow processes. Amalie-1, situated *c.* 3 km north of the Tabita-1 well, contains thin sandstone beds probably also of gravity-flow origin and of similar age (Figs 8 & 9g).

Sandstones and siltstones deposited by gravity-flows are also represented in cores in the upper part of the Farsund Formation in the Iris-1 well located in the axis of the Tail End Graben (Figs 7, 9g & 14) (Damtoft *et al.* 1992; Johannessen 1997). Quartz conglomerate beds, 5 cm thick, with clast size of up to 2 cm, occur within the claystones of the Farsund Formation. In addition, large claystone clasts up to 6 cm have been observed.

The sandy succession within the organic-rich claystones of the Bo Member in the Jeppe-1 well is cored and is dominated by packets of thin non-bioturbated sandstone–mudstone turbidites interbedded with hemi-pelagic laminae and beds (Figs 6 & 9g) (Ineson *et al.* 2003). Medium-grained sandstone turbidites and debris flows 5–20 cm thick, and sandstone-mudstone slump sheets 10–15 cm thick are also seen. Small-scale, 1–10 cm, sand injections is the main post depositional modification of the sandstones (Ineson *et al.* 2003). The slump sheets and debris flow sandstones and mudstones were deposited on intra-basinal slopes in the vicinity of Jeppe-1 and were probably derived from the Gert Ridge, 2 km west of Jeppe-1. Here locally exposed, uplifted fault slices of shoreface sandstones of the Heno Formation may have been eroded and transported into the basin (Ineson *et al.* 2003). Sandstones, *c.* 10 m thick, are recorded above the claystones of the Farsund Formation and the organic-rich shales of the Bo Member in the Gwen-2 well (Figs 7 & 9g). They were probably deposited by gravity-flows (Johannessen *et al.* 1996).

High-amplitude seismic horizons with high acoustic impedance values have been interpreted to represent sand-rich turbidites preserved in hanging-wall blocks in the depocentres of the Gertrud Graben and are correlated to the turbidites in Jeppe-1 (Fig. 9g) (Rasmussen *et al.* 1999; Gregersen & Rasmussen 2000). Thus these turbidite sandstones may have derived from the Gert Ridge as the turbidite sandstones of the Jeppe-1 well.

Reservoir characteristics. In both in the Jeppe-1 and Tabita-1 cores, oil shows have been encountered in the gravity-flow sandstones.

Palaeogeography. Deposition of offshore claystones of the Farsund Formation completely dominated the Danish Central Graben in Late Middle Volgian to Ryazanian times (Fig. 9g) (Ineson *et al.* 2003). The wells in the Danish part of the Søgne Basin do not encounter Middle to Upper Volgian and Ryazanian sediments (Andsbjerg & Dybkjær 2003; Møller & Rasmussen 2003). This may indicate a Middle to Late Volgian inversion and erosion of the Søgne Basin and Mandal High areas, which may have given rise to gravity-flow sandstones towards south in the Tail End Graben and SW in the eastern side of the Gertrud Graben. Sand may also have been shed from the Ringkøbing–Fyn High from the east forming marginal fans. Organic-rich claystones of the Ryazanian Bo Member of the Farsund Formation were deposited over most of the Danish Central Graben with the exception of the easternmost part along the Ringkøbing Fyn High, probably because of large sediment input diluting the organic matter (Figs 2 & 9g) (Dybkjær 1998; Ineson *et al.* 2003).

Conclusions

New released wells and detailed sedimentological studies of new cores, together with new biostratigraphic datings, have added to our understanding of the depositional history of the Upper Jurassic succession in the northern part of the Danish Central Graben. The depositional model has been re-evaluated and summarized as a series of palaeogeographic maps covering the Late Kimmeridgian to Ryazanian interval. New wells drilled on the Heno and Gertrud Plateaus during the last 5–8 years overall confirm the earlier published interpretations of the depositional environments and distribution of paralic to shallow marine sandstones of the Upper Kimmeridgian Heno Formation (Gert and Ravn Member) and thus prove the general applicability of the depositional model. However, new core data has revealed that the shoreface sandstones of the Heno Formation are more heterogeneous than previously considered, displaying substantial variability in claystone content. This variability is interpreted to be caused by the interplay between shoreface sandstones, location of deltas and long-shore current directions. The down-drift shoreface sandstones may show particularly diminished vertical permeability comparing to their up-drift counterparts due to abundant clay-drapes characteristic for these deposits. Moreover, as much of the mudstones are derived from a continental setting in the down-drift examples, the quantity of TOC may be variable in these strata. Further work in the area should include mapping of the river mouth locations so that these reservoir quality controlling factors could be predicted. The discovery of the Freja and Hejre Fields proves that Upper Jurassic reservoir quality sandstones of the Gert Member exist at great depths (5000 m or even deeper). In particular, the discovery of the Hejre accumulation triggered renewed interest in Upper Jurassic HTHP sandstone plays in the area.

Thick, porous shoreface sandstones of the Lower Volgian 'Outer Rough Sand' in the Danish Outer Rough Basin at the margin of the Mid North Sea High are documented east of the equivalent sandstones of the UK Fulmar Formation. The palaeogeographic understanding of this westernmost Danish area may help to a more focused exploration of the reservoir potential in the Outer Rough Basin.

Gravity-flow sandstones intercalated in offshore claystones were mainly deposited during two periods: (1) Late Kimmeridgian to Early Volgian in the Tail End Graben and the Søgne Basin; and (2) Late Middle Volgian to Ryazanian in the central part of the Tail End Graben and along the Ringkøbing–Fyn High, in the

Gertrud Graben and in the southern part of the Heno Plateau NE of the Mads High. In some cases these gravity-flow sandstones are situated within or near the organic-rich offshore shales of the upper Middle Volgian–Ryazanian Bo Member, which is an excellent source rock. Surprisingly good reservoir quality of the gravity-flow sandstones at almost 6000 m of depth has been encountered in the Svane-1 well.

The frequent occurrence of gravel- to pebble-sized quartz clasts throughout the Upper Jurassic in shoreface sandstones, gravity-flow sandstones and in the offshore mudstones all over the Danish Central Graben shows that there were coarse clastic sediment source areas nearby. The challenge is to predict where these coarse-grained sediments have been deposited in thick successions where they probably will constitute good reservoirs.

Jon R. Ineson is thanked for stimulating discussions, critical reading of an early version of the text and major improvements to the English. We also thank Lars Hamberg and two anonymous reviewers for their constructive comments.

References

Andsbjerg, J. 2003. Sedimentology and sequence stratigraphy of the Bryne and Lulu Formations, Middle Jurassic, northern Danish Central Graben. *In*: Ineson, J. R. & Surlyk, F. (eds) *The Jurassic of Denmark and Greenland*. Geological Survey of Denmark and Greenland Bulletin, **1**, 301–348.

Andsbjerg, J. & Dybkjær, K. 2003. Sequence stratigraphy of the Jurassic of the Danish Central Graben. *In*: Ineson, J. R. & Surlyk, F. (eds) *The Jurassic of Denmark and Greenland*. Geological Survey of Denmark and Greenland Bulletin, **1**, 265–300.

Bergan, M., Tørudbakken, B. & Wandås, B. 1989. Lithostratographic correlation of Upper Jurassic sandstones within the Norwegian Central Graben: sedimentological and tectonic implications. *In*: Collinson, J. D. (ed.) *Correlation in Hydrocarbon Exploration*. Norwegian Petroleum Society (NPF), Graham & Trotman, London, 243–251.

Britze, P., Japsen, P. & Andersen, C. 1995. Geological map of Denmark. 1:200 000. The Danish Central Graben. 'Base Upper Jurassic' and the Upper Jurassic (two-way traveltime and depth, interval velocity and isochore). *Danmarks Geologiske Undersøgelse Kortserie*, **50**, 7 pp.

Bruhn, R. & Vagle, K. 2005. Relay ramp evolution and mass flow deposition (Upper Kimmeridgian-Lower Volgian) in the Tail End Graben, Danish North Sea. *Basin Research*, **17**, 551–567.

Costa, L. I. & Davey, R. J. 1992. Dinoflagellate cysts of the Cretaceous System. *In*: Powell, A. J. (ed.) *A Stratigraphic Index of Dinoflagellate Cysts*. British Micropalaeontological Society Publication Series, Chapman & Hall, London, 99–153.

Cox, B. M., Lott, G. K., Thomas, J. E. & Wilkinson, I. P. 1987. Upper Jurassic stratigraphy of four shallow cored boreholes in the U.K. sector of the Northern North Sea. *Proceedings of the Yorkshire Geological Society*, **46**, 97–109.

Currie, S., Gowland, S., Taylor, A. & Woodward, M. 1999. The reservoir development of the Fife Field. *In*: Fleet, A. J. & Boldy, S. A. R. (eds) *Petroleum Geology of Northwest Europe: Proceedings of the 5th Conference*. Geological Society, London, 1135–1145; doi: 10.1144/0051135.

Damtoft, K., Nielsen, L. H., Johannessen, P. N., Thomsen, E. & Andersen, P. R. 1992. Hydrocarbon plays of the Danish Central Through. *In*: Spencer, A. M. (ed.) *Generation, Accumulation and Production of Europe's Hydrocarbons II*. Special Publications of the European Association of Petroleum Geoscientists, **2**, Springer, Berlin, 35–58.

Danish Energy Agency, 2005. Press release 01-03-05: Hejre-2 boringen fandt olie.

Danish Energy Agency, 2008. Oil and Gas Production in Denmark 07. World Wide Web Adress: http://www.ens.dk/graphics/Publikationer/Olie_Gas_UK/Energistyrelsen%20UK_LOW.pdf.

Davey, R. J. 1979. The stratigraphic distribution of dinocysts in the Portlandian (latest Jurassic) to Barremian (early Cretaceous) of the Northwest Europe. *American Association of Stratigraphic Palynologists, Contribution Series*, **5B**, 48–81.

Davey, R. L. 1982. Dinocyst Stratigraphy of the latest Jurassic to Early Cretaceous of the Haldager No. 1 borehole, Denmark. *Geological Survey of Denmark*, **B6**, 57 pp.

Dybkjær, K. 1998. Palynological dating of the Mandal Formation (uppermost Jurassic–lowermost Cretaceous, Norwegian Central Graben) and correlation to organic-rich shales in the Danish sector. *Marine and Petroleun Geology*, **15**, 495–503.

Fraser, S. I., Robinson, A. M., Johnson, H. D., Underhill, J. R., Kadolsky, D. G. A., Connell, R., Johannessen, P. N. & Ravnås, R. 2003. Upper Jurassic. *In*: Evans, D., Graham, C., Armour, A. & Bathurst, P. (eds) *The Millennium Atlas: Petroleum Geology of the Central and Northern North Sea*. The Geological Society, London, 157–189.

Gradstein, F. M., Ogg, J. G. & Smith, A. G. 2004. *A Geological Time Scale 2004*. Cambridge University Press and International Commission on Stratigraphy, Cambridge.

Gregersen, U. & Rasmussen, E. S. 2000. The subtle play-potential of Upper Jurassic–Lower Cretaceous block-faulted turbidites in the Danish Central Graben, North Sea. *Marine and Petroleum Geology*, **17**, 691–708.

Heilmann-Clausen, C. 1987. Lower Cretaceous dinoflagellate biostratigraphy in the Danish Central Trough. *Geological Survey of Denmark Series A*, **17**, 87 pp.

Hemmet, M. 2005. The hydrocarbon potential of the Danish Continental Shelf. *In*: Doré, A. G. & Vinning, B. A. (eds) *Petroleum Geology: North-West Europe and Global Perspectives: Proceedings of the 6th Petroleum Geology Conference*. Geological Society, London, 85–97; doi: 10.1144/0060085.

Howell, J. A., Flint, S. S. & Hunt, C. 1996. Sedimentological aspects of the Humber Group (Upper Jurassic) of the South Central Graben, UK North Sea. *Sedimentology*, **43**, 89–114.

Ineson, J., Bojesen-Koefod, J. A., Dybkjær, K. & Nielsen, L. H. 2003. Volgian-Ryazanian 'hot shales' of the Bo Member (Farsund Formation) in the Danish Central Graben, North Sea: stratigraphy, facies, and geochemistry. *In*: Ineson, J. R. & Surlyk, F. (eds) *The Jurassic of Denmark and Greenland*. Geological Survey of Denmark and Greenland Bulletin, **1**, 403–436.

Japsen, P., Britze, P. & Andersen, C. 2003. Upper Jurassic–Lower Cretaceous of the Danish Central Graben: structural framework and nomenclature. *In*: Ineson, J. R. & Surlyk, F. (eds) *The Jurassic of Denmark and Greenland*. Geological Survey of Denmark and Greenland Bulletin, **1**, 233–246.

Johannessen, P. N. 1997. Upper Jurassic back-barrier and shoreface reservoir sandstones and thin turbidite sandstones in the Danish Central Trough, North Sea. *In*: Oakman, C. D., Martin, J. H. & Corbett, P. W. M. (eds) *Cores from the Northwest European Hydrocarbon Province: An Illustration of Geological Applications from Exploration to Development*. The Geological Society, London, 11–20.

Johannessen, P. N. 2003. Sedimentology and sequence stratigraphy of paralic and shallow marine Upper Jurassic sandstones in the northern Danish Central Graben. *In*: Ineson, J. R. & Surlyk, F. (eds) *The Jurassic of Denmark and Greenland*. Geological Survey of Denmark and Greenland Bulletin, **1**, 367–402.

Johannessen, P. N., Dybkjær, K. & Rasmussen, E. S. 1996. Sequence stratigraphy of Upper Jurassic reservoir sandstones in the northern part of the Danish Central Trough, North Sea. *Marine and Petroleum Geology*, **13**, 755–770.

Johannessen, P. N., Nielsen, L. H. *et al*. 2008. Sedimentary facies and architecture of the Holocene to Recent barrier island in the Danish Wadden Sea. *Geological Survey of Denmark and Greenland Bulletin*, **15**, 49–52.

Johannessen, P. N., Nielsen, L. H., Nielsen, L., Møller, I., Pejrup, M. & Andersen, T. J. 2010. Architecture of an Upper Jurassic barrier island sandstone reservoir, Danish Central Graben: implications of a Holocene–Recent analogue from the Wadden Sea. *In*: Vining, B. A. & Pickering, S. C. (eds) *Petroleum Geology: From Mature Basins to New Frontiers – Proceedings of the 7th Petroleum Geology Conference*. Geological Society, London, 145–155; doi: 10.1144/0070145.

Korstgaard, J. A., Lerche, I., Mogensen, T. E. & Thomsen, R. O. 1993. Salt and fault interactions in the northeastern Danish Central Graben: observations and inferences. *Bulletin of the Geological Society of Denmark*, **40**, 197–255.

MacEachern, J. A., Bann, K. L., Pemberton, S. G. & Gingras, M. K. 2008. The ichnofacies paradigm: high-resolution paleoenvironmental interpretation of the rock record. *In*: MacEachern, J. A., Bann, K. L., Gingras, M. K. & Pemberton, S. G. (eds) *Applied Ichnology: SEPM, Short Course Notes*. SEPM, Tulsa, Oklahoma, **52**, 27–64.

Mackertich, D. 1996. The Fife Field, UK Central North Sea. *Petroleum Geoscience*, **2**, 373–380.

Michelsen, O., Nielsen, L. H., Johannessen, P. N., Andsbjerg, J. & Surlyk, F. 2003. Jurassic lithostratigraphy and stratigraphic development onshore and offshore Denmark. *In*: Ineson, J. R. & Surlyk, F. (eds) *The Jurassic of Denmark and Greenland*. Geological Survey of Denmark and Greenland Bulletin, **1**, 147–216.

Møller, J. J. & Rasmussen, E. S. 2003. Middle Jurassic–Early Cretaceous rifting of the Danish Central Graben. *In*: Ineson, J. R. & Surlyk, F. (eds) *The Jurassic of Denmark and Greenland*. Geological Survey of Denmark and Greenland Bulletin, **1**, 247–264.

Oljedirektoratet, 2009. Norwegian Petroleum Directorates fact page for well 3/7–6. World Wide Web Address: http://www.npd.no/engelsk/cwi/pbl/en/wdss_index.htm.

Partington, M. A., Mitchener, B. C., Milton, N. J. & Fraser, A. J. 1993*a*. A genetic stratigraphic sequence stratigraphy for the North Sea Jurassic and Early Cretaceous: stratigraphic distribution and prediction of Kimmeridgian–Late Ryazanian reservoirs in the Viking Graben and adjacent areas. *In*: Parker, J. R. (ed.) *Petroleum Geology of Northwest Europe: Proceedings of the 4th Conference*. Geological Society, London, 347–370; doi: 10.1144/0040347.

Partington, M. A., Copestake, P., Mitchener, B. C. & Underhill, J. R. 1993*b*. Biostratigraphic calibration of genetic stratigraphic sequences in the Jurassic–lowermost Cretaceous (Hettangian to Ryazanian) of the North Sea and adjacent areas. *In*: Parker, J. R. (ed.) *Petroleum Geology of Northwest Europe: Proceedings of the 4th Conference*. Geological Society, London, 371–386; doi: 10.1144/0040371.

Petersen, H. I., Nytoft, H. P., Vosgerau, H., Andersen, C., Bojesen-Koefoed, J. A. & Mathiesen, A. 2010. Source rock quality and maturity and oil types in the NW Danish Central Graben: implications for petroleum prospectivity evaluation in an Upper Jurassic sandstone play area. *In*: Vining, B. A. & Pickering, S. C. (eds) *Petroleum Geology: From Mature Basins to New Frontiers – Proceedings of the 7th Petroleum Geology Conference*. Geological Society, London, 95–111; doi: 10.1144/0070095.

Poulsen, N. E. 1991. Upper Jurassic dinocyst stratigraphy in the Danish Central Trough. *In*: Michelsen, O. & Frandsen, N. (eds) *The Jurassic of the Southern Central Trough*. Danmarks Geologiske Undersøgelse Serie B, **16**, 7–15.

Poulsen, N. E. & Riding, J. B. 1992. A revision of the Late Jurassic dinoflagellate cysts *Ambonosphaera*? *staffinensis* (Gitmez 1970) comb. Nov. and *Senoniasphaera Jurassica* (Gitmez & Sarjeant 1972) Lentin & Williams 1976. *Palynology*, **16**, 25–34.

Rasmussen, E. S., Jepsen, A. M. & Maver, K. G. 1999. Upper Jurassic basin axial turbidites within the Gertrud Graben, Danish Central Graben. *In*: Fleet, A. J. & Boldy, A. R. (eds) *Petroleum Geology of Northwest Europe: Proceedings of the 5th Conference*. Geological Society, London, 897–906; doi: 10.1144/0050897.

Riding, J. B. 1987. Dinoflagellate cyst stratigraphy of the Nettelton Botton Borehole (Jurassic: Hettangian to Kimmeridgian), Lincolnshire, England. *Proceedings of the Yorkshire Geological Society*, **46**, 231–266.

Riding, J. B. & Thomas, J. E. 1992. Dinoflagellate cysts of the Jurassic System. *In*: Powell, A. J. (ed.) *A Stratigraphic Index of Dinoflagellate Cysts*. British Micropalaeontological Society Publication Series. Chapman & Hall, London, 7–97.

Schwartz, R. K. 1982. Bedform and stratification characteristics on some modern small-scale washover sand bodies. *Sedimentology*, **29**, 835–849.

Shepherd, M., MacGregor, A., Bush, K. & Wakefield, J. 2003. The Fife and Fergus Fields, Block 31/26a, UK North Sea. *In*: Gluyas, J. G. & Hichens, H. M. (eds) *United Kingdom Oil and Gas Fields, Commemorative Millennium Volume*. Geological Society, London, *Memoirs*, **20**, 537–547.

Söderström, B., Forsberg, A., Holtar, E. & Rasmussen, B. A. 1991. The Mjølner Field, a deep Jurassic oil field in the Central North Sea. *First Break*, **9**, 156–171.

Weibel, R. & Keulen, N. 2008. Diagenesis influencing the porosity of Upper Jurassic reservoir sandstones, Danish North Sea. *Geological Survey of Denmark and Greenland Bulletin*, **15**, 9–12.

Architecture of an Upper Jurassic barrier island sandstone reservoir, Danish Central Graben: implications of a Holocene–Recent analogue from the Wadden Sea

P. N. JOHANNESSEN,[1] L. H. NIELSEN,[1] L. NIELSEN,[2] I. MØLLER,[1] M. PEJRUP[2] and T. J. ANDERSEN[2]

[1]*Geological Survey of Denmark and Greenland (GEUS), Øster Voldgade 10, DK-1350 Copenhagen K, Denmark (e-mail: pjo@geus.dk)*
[2]*Institute for Geography and Geology, University of Copenhagen, Øster Voldgade 10, DK-1350 Copenhagen K, Denmark*

Abstract: An unusually thick (*c.* 88 m), transgressive barrier island and shoreface sandstone succession characterizes the Upper Jurassic Heno Formation reservoir of the Freja oil field situated on the boundary of Denmark and Norway. The development and preservation of such thick transgressive barrier island sands is puzzling since a barrier island typically migrates landwards during transgression and only a thin succession of back-barrier and shoreface sands is preserved. Investigation of the development and geometry of the Freja reservoir sandstones is problematic since the reservoir is buried *c.* 5 km and seismic resolution is inadequate for architectural analysis. Description of the reservoir sandstone bodies is thus based on sedimentological interpretation and correlation of seven wells, of which five were cored. Palaeotopography played a major role in the position and preservation of the thick reservoir sandstones. Using the nearest maximum flooding surface above the reservoir as a datum for well-log correlations, the base of the barrier island succession in the wells is reconstructed as a surface with steep, seaward-dipping palaeotopography. The relief is *c.* 270 m over a distance of *c.* 8 km and dips WNW.

As a complementary approach to investigation of the reservoir architecture, a Holocene–Recent barrier island system in the Danish part of the NW European Wadden Sea has been studied and used as an analogue. The barrier island of Rømø developed during a relative sea-level rise of *c.* 15 m during the last *c.* 8000 years and is up to 20 m thick. To unravel the internal 3D facies architecture of the island, an extensive ground penetrating radar (GPR) survey of 35 km line length and seven cores, *c.* 25 m long, was obtained. Although the barrier island experienced a rapid relative sea-level rise, sedimentation kept pace such that the island aggraded and even prograded seawards and became wider and longer due to the large surplus of sand.

Keywords: barrier island sandstones, Central Graben, Upper Jurassic palaeotopography, Freja–Mjølner Field, modern analogue

Back-barrier and shoreface sandstones (88 m thick in the Gert-1 well) constitute the reservoir in the Freja commercial oil field, which lies on the border between Denmark and Norway in the northern part of the Danish Central Graben (Fig. 1) (Johannessen 2003; Johannessen *et al.* 2010). The Freja discovery is expected to contain oil reserves of about 1 000 000 m^3 (Danish Energy Agency 2008). Oil saturations are up to 80% in the Gert-1 well where the sandstone permeability is generally less than 100 mD and the porosity is 10–20% (Figs 2 & 3). Feldspar dissolution has increased the porosity. The depth of the reservoir is *c.* 4900 m. Formation pressure is *c.* 14 000 psi; hydrostatic pressure is 7200 psi and overpressure is 6800 psi. Reservoir temperature is 155°C.

The Norwegian part of the discovery is called the Mjølner Field. The Norwegian 2/12-1 well encounters a 71 m thick primarily shoreface sandstone succession at a depth of 4600 m containing oil (Söderström *et al.* 1991). The porosity is higher than normal at such depths, probably because of the high pressure in the reservoir (Söderström *et al.* 1991).

Well-constrained reservoir models are mandatory for effective drainage of trapped hydrocarbons. As the sandstone reservoir of the Freja discovery is situated in a structurally complex area at great depths, the seismic resolution is low, *c.* 50 m (Rasmussen 1995). Consequently, it is necessary to make a sedimentological and stratigraphical interpretation based on cores and well logs to make a model of the sand distribution in the Freja discovery.

Unusually thick back-barrier sediments, 70 m thick, are encountered in the Gert-1 well. Normally barrier island systems are considered to migrate landwards during transgressions, mainly by washover events breaching the subaerial barrier during storm episodes and depositing washover fans in the back-barrier lagoon (Elliott 1986). Storm-induced erosion also transports barrier island sand seaward where the sand is deposited as storm sand beds. With continued sea-level rise, the barrier–lagoonal system moves in a landward direction leaving only a relatively thin sand succession behind, owing to transgressive erosion.

How then were such thick transgressive back-barrier sandstones developed and preserved in the Freja discovery? To answer this question two studies have been carried out, an analogue study of the Holocene–Recent barrier island of Rømø and an analysis of the palaeotopography of the Freja discovery area.

Ongoing well documented studies of the Rømø barrier island show that it has aggraded during a relative sea-level rise of *c.* 15 m during the last *c.* 8000 years and consists of 10–15 m thick barrier island and back-barrier sediments (Johannessen *et al.* 2008). The present-day physiographic setting and depositional processes are well known (Lumborg & Pejrup 2005; Madsen *et al.* 2007; Johannessen *et al.* 2008). Rømø is thus an ideal place for direct analogue studies which can be used in the Freja discovery area.

Although the barrier island experienced a rapid relative sea-level rise, sedimentation kept pace and the island aggraded and even prograded seawards and also became wider and longer due to the large surplus of sand. The internal architecture has been characterized using cores from seven wells and 35 km of GPR lines (Nielsen *et al.* 2009).

VINING, B. A. & PICKERING, S. C. (eds) *Petroleum Geology: From Mature Basins to New Frontiers – Proceedings of the 7th Petroleum Geology Conference*, 145–155. DOI: 10.1144/0070145

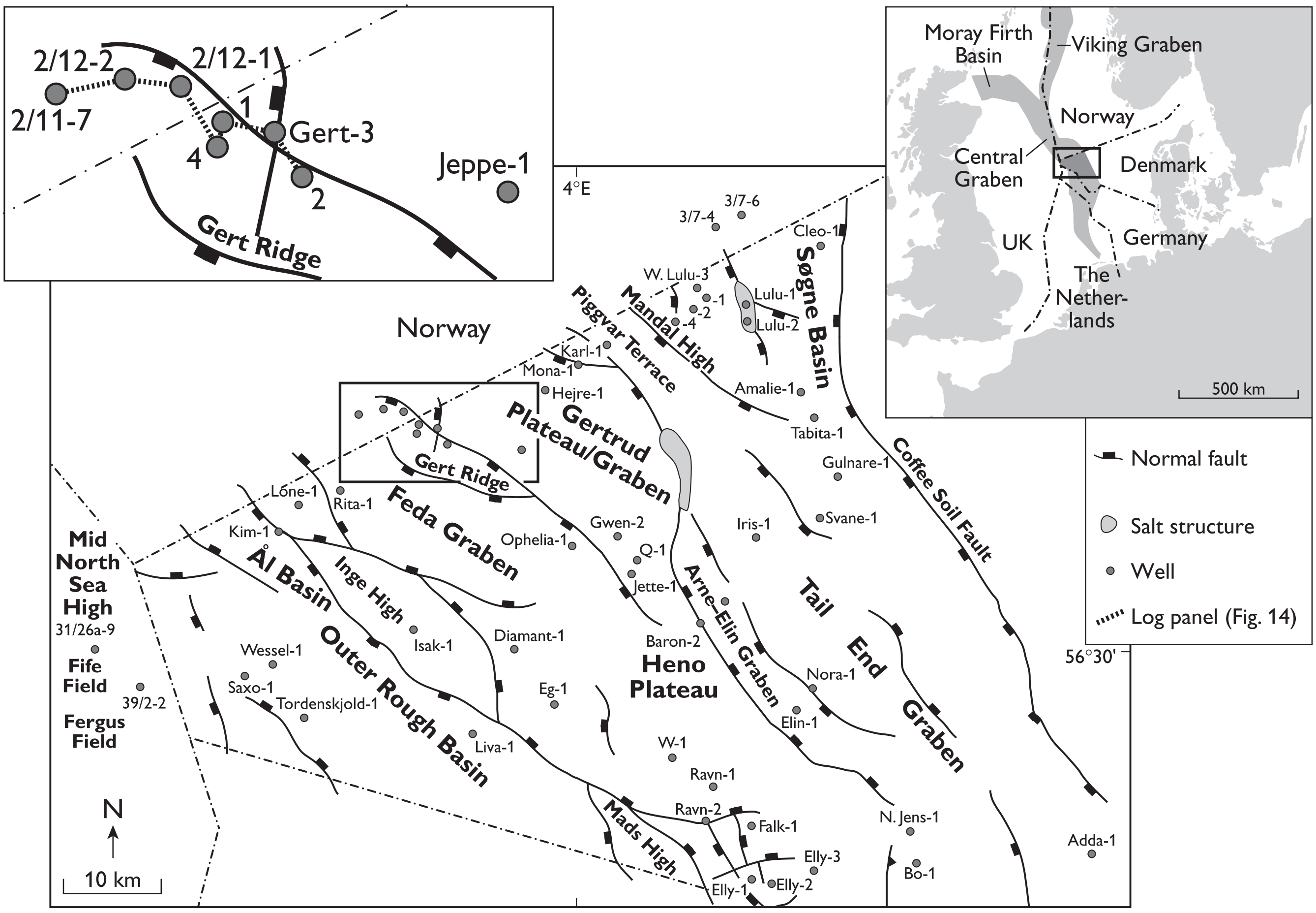

Fig. 1. Map of the Danish Central Graben showing structural elements and location of wells in the Freja–Mølner Field. Major Upper Jurassic to Lower Cretaceous faults are shown.

To explain the thick barrier island sandstones in the Freja discovery, it is also necessary to consider the palaeotopography which was inundated during the Late Jurassic transgression. A steep topography would have forced the stacking of thick barrier island and shoreface sandstones and lagoonal sediments if large amounts of sediment were available. Using the nearest maximum flooding surface above the reservoir as a datum line for well-log correlations, the base of the barrier island succession in the wells outlines a surface with steep, seaward-dipping palaeotopography.

The Holocene–Recent Rømø barrier island system

The Holocene–Recent Rømø barrier island situated in the Danish part of the Wadden Sea in the SE part of the North Sea developed on a gently westward dipping Weichselian outwash plain of fluvial sand that was transgressed by the sea due to the rapid Holocene sea-level rise (Fig. 4). A hiatus (*c.* 13 000–8000 BP) separates the Holocene marine sediments from the underlying fluvial sand.

Morphology and depositional environments

The advantage of using the micro-tidal Rømø barrier island as a reservoir analogue is that modern sedimentary processes and environments, geomorphology and historical development are very well known (Fig. 5) (e.g. Bartholdy & Pejrup 1994; Lumborg & Pejrup 2005). The island is *c.* 14 km long, *c.* 4 km wide and up to 20 m thick and separated from the mainland by a *c.* 8 km wide lagoon (Fig. 5). Tidal inlets, *c.* 1 km across and up to 30 m deep, occur at the northern and southern tips of the island. The inlets continue as tidal channels into the lagoon where shallow creeks cut sand flats and mixed flats. Subtidal ebb-deltas are located where the tidal inlets terminate in the North Sea (Fig. 5). The NE and SE part of the Rømø lagoonal coast consists of salt marsh up to 2 km wide. The NW and SW parts of the island are characterized by sandflats, up to 2.7 km wide, with four broad (0.8–1.6 km) swash bars separated by three tidal troughs (up to *c.* 50 m wide) migrating towards the island (Fig. 6). Aeolian dunes are found on large parts of the island. The spring tidal range is 2 m. Westerly winds with a fetch of *c.* 800 km dominate and, during strong wind setup, the water level increases considerably, up to 5 m above mean sea-level. Storm surges break through beach ridges and aeolian dunes and, in the initial stages of island development, when the island was narrow, numerous washover fans were deposited in the back-barrier lagoon. During the last 3000–5000 years, the island has been too wide to be fully breached and thus washover deposits accumulated between old beach ridges.

Methods

To investigate the internal 3D facies architecture of the *c.* 8000-year-old Rømø barrier island, seven cores, each up to *c.* 25 m long, were taken (Figs 6 & 7). Sedimentary units were defined and interpreted on the basis of sediment texture and structures, bedding, organic content, macrofauna and palynomorphs. To facilitate correlations between the cored wells, a survey of 35 km of GPR profiles was carried out (Fig. 6) (Johannessen *et al.* 2008; Møller *et al.* 2008; Nielsen *et al.* 2009). Maximum signal penetration is *c.* 15 m with a resolution of 0.2–0.3 m. The interpreted sedimentary environments based on the entire dataset are compared with the recent environments of the barrier island. This full-scale ‘natural laboratory’ gives a unique dataset which may be used as an analogue for deeply buried hydrocarbon reservoirs where data are limited.

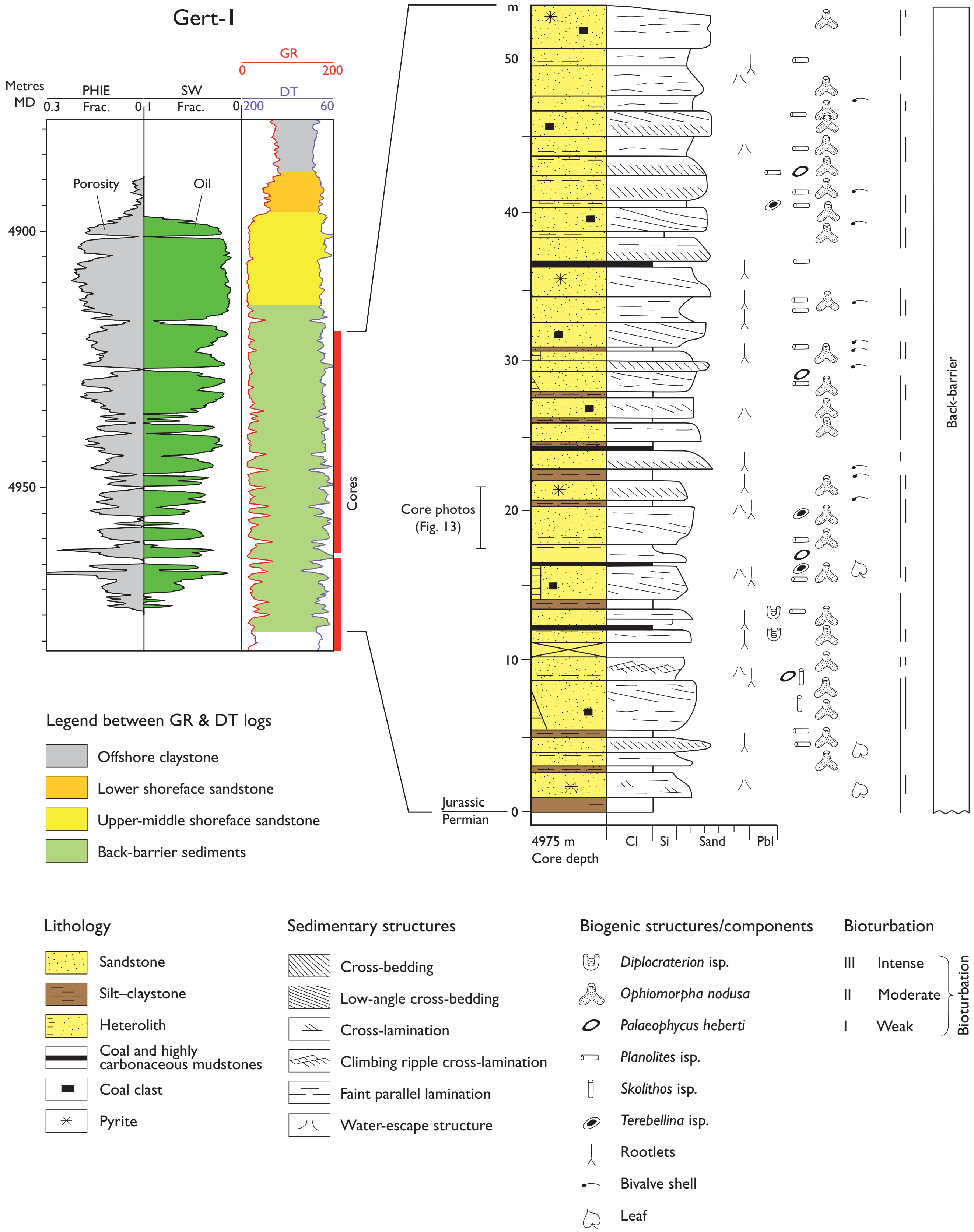

Fig. 2. Sedimentological core log and porosity–oil saturation plot in the Gert-1 well (Fig. 1). The cored sediments were deposited in a back-barrier environment. Many of the cross-bedded sandstones were probably deposited by washover fans.

Vertical section through the Rømø barrier island

The barrier island sediments are up to 20 m thick, including the aeolian dune sands. The island originated on a local palaeohigh on the Pleistocene outwash plain while lagoonal sedimentation was initiated in a palaeolow directly landward of the barrier (Fig. 7). The Holocene succession of the easternmost cores, Rømø-1 and Rømø-2, drilled in the present lagoon, consists entirely of lagoonal sand and mud flat deposits (Fig. 7). The Holocene succession of the easternmost core on the barrier island of Rømø

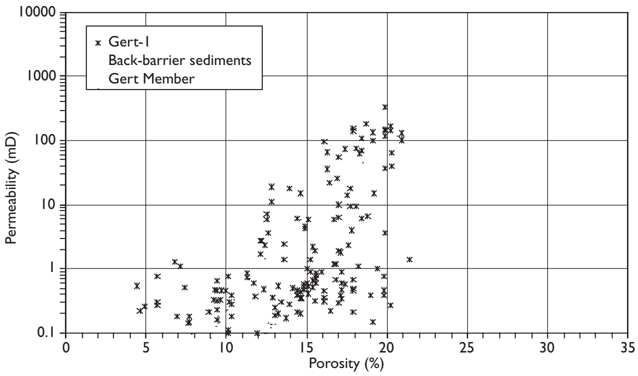

Fig. 3. Porosity–permeability plot of the back barrier sediments of the Gert Member in the Gert-1 well (Fig. 2).

(Rømø-3) is composed mostly of washover fan sand, minor salt marsh and lagoonal sediments topped by aeolian sand (Fig. 7). Lagoonal sediments are not found in the central and western parts of the Rømø barrier island, where the Holocene is composed of prograding shoreface sands.

A series of beach ridges up to 2.5 m high, often with fine-grained swales in between, are observed on GPR sections from the central part of the island beneath the modern aeolian dune sands (Fig. 8) (Møller *et al.* 2008; Nielsen *et al.* 2009). The beach ridges are often characterized by steep erosional seaward flanks and more gently dipping landward flanks. Cross-bedded sets, up to 2.5 m thick, with eastward dipping foresets are shown by the GPR sections immediately east of the beach ridges and can be followed for up to 1 km eastwards (Fig. 8). These cross-bed sets typically rest on weakly eastward (lagoon-ward) dipping surfaces and are interpreted as washover fans. As washover fans constitute a major part of the barrier island sand, a modern example of a washover fan is shown from the Skallingen peninsula, situated in the northernmost part of the Danish Wadden Sea (Fig. 9). During a storm in 1990, storm surges broke through beach ridges and aeolian dunes at peak sea-level 4.12 m above m.s.l. and a washover fan, 250 m long and wide, was deposited in the lagoon within a few hours; this fan displayed a steep slipface, indicating that internally it comprised a steep cross-bedded set *c.* 0.5 m thick (Fig. 9) (Nielsen & Nielsen 2006).

Fig. 4. The Wadden Sea situated in the SE part of the North Sea. The study area is located in the Danish part of the Wadden Sea.

Within the Rømø barrier island complex gently westward dipping sandy shoreface clinoforms can be followed upward and eastward to beach ridges (Fig. 8). Cross-bed sets, up to 125 m long, with eastward dipping foresets are occasionally seen on the westward-dipping shoreface clinoforms close to the beach ridges and are interpreted as swash bars that migrated towards the beach (Fig. 8). Channel fills, *c.* 2 m deep and 20 m wide, cutting into the upper part of the shoreface sands and located landward of the swash bars are interpreted as filled troughs (Fig. 8). As sand from the landward moving swash bars filled the troughs, the troughs moved towards the east (Fig. 8). Today such swash bar–trough systems are seen on the NW and SW coast of Rømø.

The number of beach ridges decreases towards the north and south. In the northern and southern parts of the island, the GPR sections are dominated by co-sets with westerly and easterly dipping foresets with reactivation surfaces, indicating bipolar current directions (Fig. 10) (Møller *et al.* 2008). These sediments were probably deposited in deep, broad tidal inlets at both ends of the barrier island, similar to those observed today. The Rømø cross-section clearly shows that all of the various facies packages have both aggraded and prograded (Fig. 7).

Palaeogeographic reconstruction of the Rømø barrier island from 8000 years BP–Recent

The core and GPR data in combination with the Recent morphology allow a detailed palaeogeographic interpretation of the barrier island through time. The oldest part of the barrier island formed *c.* 8000 years BP and since then the island has aggraded and prograded towards the west, north and south during a sea-level rise of *c.* 15 m (Fig. 7). During the last 3500 years, progradation has accelerated due to decreased rates of relative sea-level rise. Only very minor back-stepping into the lagoon is seen, despite the sea-level rise, demonstrating that there has been a large surplus of sand compared with the accommodation space, which allowed the barrier island to aggrade and prograde seaward. The dominance of sand is also evident from the sandy back-barrier environment. The sand was supplied by longshore drift and onshore transport.

The Rømø barrier island thus shows that barrier islands do not necessarily back-step, preserving only a thin transgressive sand unit. On the contrary, the Rømø case shows that, if there is a surplus of sand, a barrier island can aggrade and prograde during a sea-level rise, creating thick barrier island, shoreface and lagoonal successions.

The Upper Jurassic barrier island system of the Freja discovery

The Upper Jurassic (Upper Kimmeridgian) barrier island and shoreface sandstones of the Freja discovery are situated in the northernmost part of the Danish Central Graben in the North Sea, straddling the boundary between Denmark and Norway (Fig. 1) (Johannessen 2003; Johannessen *et al.* 2010). Barrier island and shoreface sandstones were deposited at the head of a NW–SE trending, *c.* 375 km long and 65 km broad marine basin extending from the northern Central Graben northwards to the Outer Moray Firth (Fig. 11) (Fraser *et al.* 2002). The southern part of this basin coincided with the Feda Graben and narrowed in a SE direction, terminating at the Heno and Gertrud Plateaus in the Freja area (Fig. 11) (Johannessen 2003). During the Late Kimmeridgian, the northernmost part of the Danish Central Graben and the southernmost part of the Norwegian Central Graben were characterized by two prominent highs: the Mandal High NE of the Freja structure and the Mid North Sea High SW of the Freja structure (Fig. 11). Large amounts of sand were probably transported to this area by

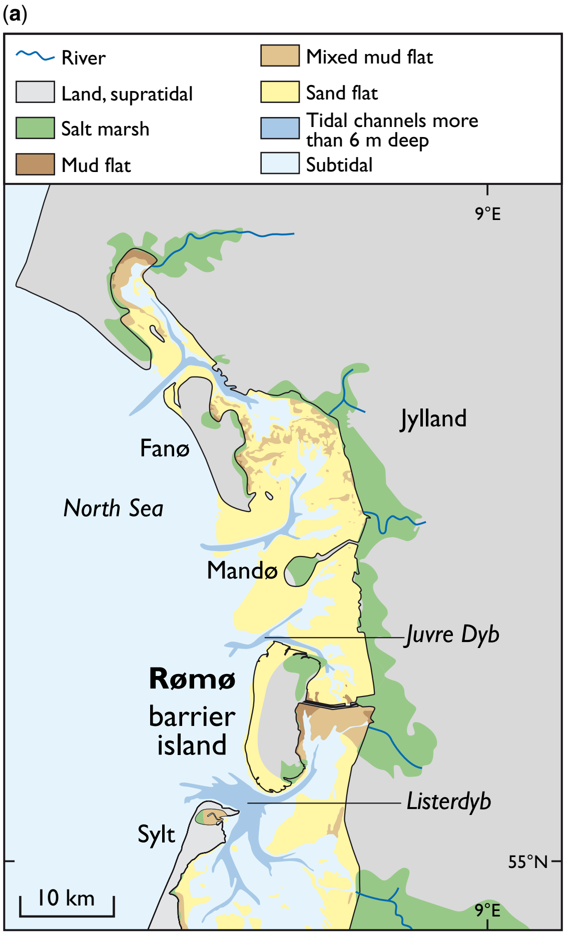

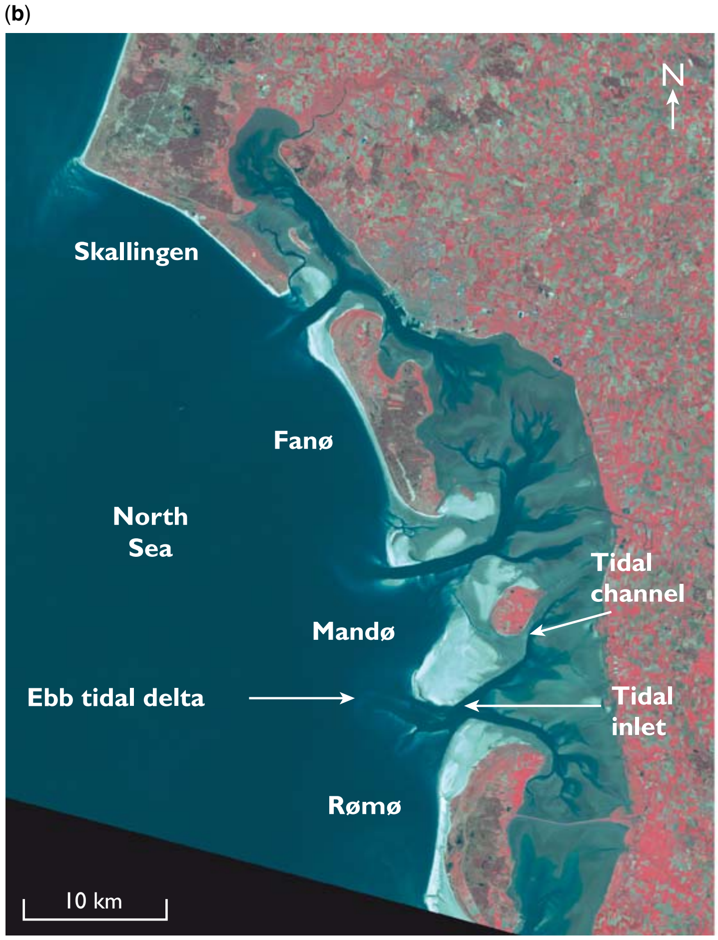

Fig. 5. The Danish Wadden Sea. (**a**) The distributions of sediment types and subtidal channels are shown. The mainland of Jylland east of the lagoon consists mainly of sandy glacial deposits. Modified from Pejrup (2006) and Sørensen *et al.* (2006). (**b**) Landsat photo (+ETM 9 May 2001) of the Danish tidal area with distinct tidal sand flats and subtidal channels. Note the subtidal ebb-deltas where the main channels terminate in the North Sea.

rivers from the plateau areas in the north, south and east with subsequent longshore transport and reworking by waves. The large thickness of reservoir sandstones in the Freja area (88 m in Gert-1 and 71 m in 2/12-1) indicates it was a sand-rich system.

Stratigraphy

The westernmost part of the Heno Formation overlies the Base Upper Jurassic unconformity (Andsbjerg & Dybkjær 2003; Johannessen 2003; Michelsen *et al.* 2003; Johannessen *et al.* 2010). The formation consists of back-barrier and shoreface sandstones of the Gert Member succeeded by shoreface sandstones of the Ravn Member (Fig. 12). In the Freja discovery area, offshore claystones of the Lola Formation separate the reservoir sandstones of the Gert and Ravn Members, but claystones are absent on the plateau areas where the Gert Member is directly overlain by the Ravn Member (Fig. 12). The present study focuses on the reservoir sandstones of the Gert Member.

Depositional environments

As the vertical seismic resolution at the reservoir depth of *c.* 5 km is only *c.* 50 m and the post-depositional structural development is very complex, the construction of a reservoir model relies on sedimentological and stratigraphical interpretations based on cores and well logs.

Back-barrier sediments. Interpretation of depositional environments is based on all cores and well logs from the Freja discovery (Damtoft *et al.* 1992; Johannessen *et al.* 1996; Johannessen 1997, 2003). In the cores from the Gert-1 well, the back-barrier sediments are characterized by interbedded, fine-grained sandstones and claystones with coal beds up to 15 cm thick (Fig. 2). Rootlets are abundant and often associated with coal or claystone beds. The organic matter is dominated by continentally derived particles such as black wood, spores and pollen. There are also remnants of leaves. Only a few marine dinoflagellate cysts are present and the dominance amongst these of a single genus (*Sentusidinium*) indicates a low salinity, highly-stressed environment (e.g. Noe-Nygaard *et al.* 1987; Smelror & Leereveld 1989). Numerous burrows of *Ophiomorpha*, *Planolites*, *Skolithos*, *Diplocraterion*, *Phycosiphon* and *Terebellina* are recognized. Cross-bedded sandstones, up to 2 m thick, overlying claystones and topped by claystones or coal beds with underlying rootlets are interpreted as washover fan sandstones deposited in the lagoon (Fig. 13). The association of the identified sedimentary structures, ichnofacies and fossils indicates that the sediments were deposited within a back-barrier setting (Johannessen 2003). The back-barrier section of the Gert-1 well is characterized by a serrated gamma-ray (GR) log pattern (Fig. 2). It is overlain abruptly by an 18 m thick section characterized by consistently low and uniform GR readings, which suggests cleaner and probably coarser sandstones than in the lagoonal deposits below, and that probably were deposited in the upper-to-middle shoreface above a ravinement surface (Fig. 2) (Johannessen 2003). A 6 m thick succession of very fine-grained sandstones overlies the upper-to-middle shoreface sandstones and is in turn overlain by offshore claystones; these deposits represent back-stepping lower shoreface sandstones (Fig. 2). The whole vertical section from back-barrier sediments at the base through

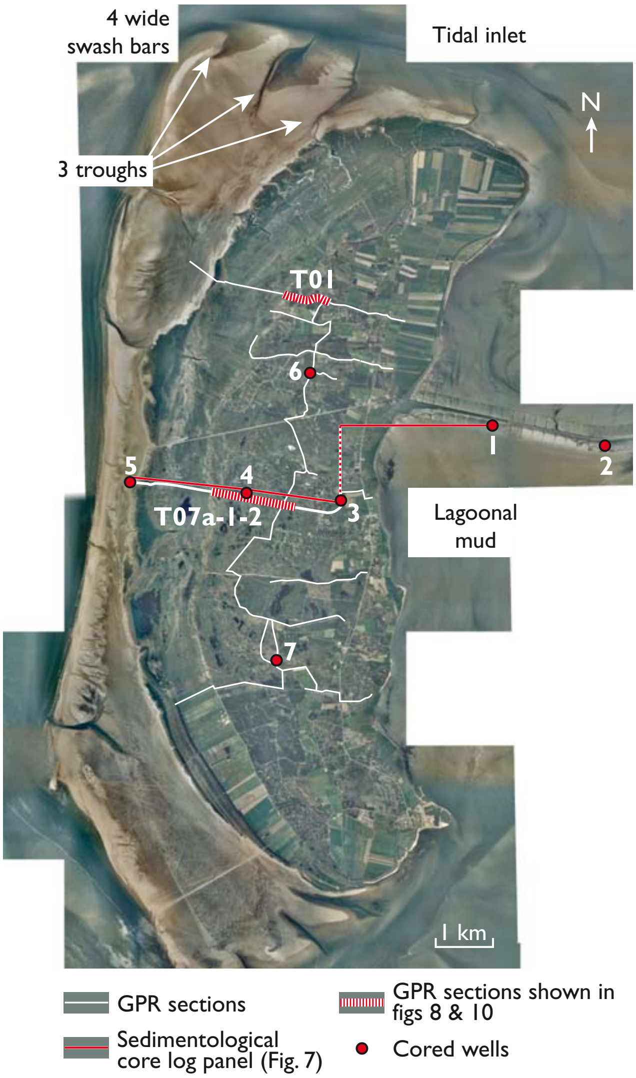

Fig. 6. Ortho photo of the Rømø barrier island showing the distribution of GPR reflection profiles and position of the seven cored wells. Very wide tidal flat sands characterize the NW and SW end of Rømø. The island is dominated by aeolian dune sand. Copyright Scankort.

back-stepping shoreface sandstones, to offshore claystones indicates that this succession was deposited during a transgression. All wells in the area show the same overall facies trend as the Gert-1 well, indicating an overall transgression which came from the NW and spread to the SE from the Feda Graben to the Gertrud Plateau (Fig. 14). Aeolian sandstones are lacking between the back-barrier sandstones and the shoreface sandstones, probably due to erosion during the transgression.

Shoreface sandstones. The Upper Jurassic very fine- to medium-grained sandstone reservoir in the Norwegian well 2/12-1 farther palaeoseaward in the Feda Graben consists of a thin (2 m) basal back-barrier mudstone unit overlain by a very thick (69 m) section of shoreface sandstones (Fig. 14) (Söderström *et al.* 1991); the lower half of this reservoir sandstone section is cored. The lowermost 20 m of the shoreface sandstone section is organized into thin (1–6 m) stacked cycles. Each cycle is characterized by an erosional base that is often overlain by a transgressive lag. The overlying sandstones in a cycle are either massive or cross-bedded; some mud-drapes are present. The degree of bioturbation is most often high to moderate and burrows of *Skolithos*, *Teichichnus*, *Terebellina* and *Asterosoma* are identified. The upper 10–40 cm of individual cycles are often penetrated by rootlets (Söderström *et al.* 1991).

Thick stacked Upper Jurassic barrier island sandstones

In order to reconstruct the palaeotopography over which the Late Jurassic barrier island system retreated, the first maximum flooding surface above the reservoir is chosen as a datum that is assumed to approximate to a horizontal surface at the time of the deposition (Fig. 14). This is of course a misrepresentation, as the seabed probably was dipping weakly seaward. As the claystone succession becomes thinner and sandier from the Feda Graben towards the Gertrud Plateau, the claystones are decompacted by a factor of 1.3 in order to obtain a more correct sediment thickness for the reconstruction of the palaeotopography. It is clear that the 2/11-1, 2/12-2, 2/12-1, Gert-4 and Gert-1 wells are located at the margin of the Feda Graben, whereas the Gert-3, Gert-2 and Jeppe-1 wells are located on the margin of the Gertrud Plateau (Fig. 14). The overall sandstone architecture is reconstructed by applying the simple principle that back-barrier sediments, shoreface sandstones and offshore claystones were deposited at the

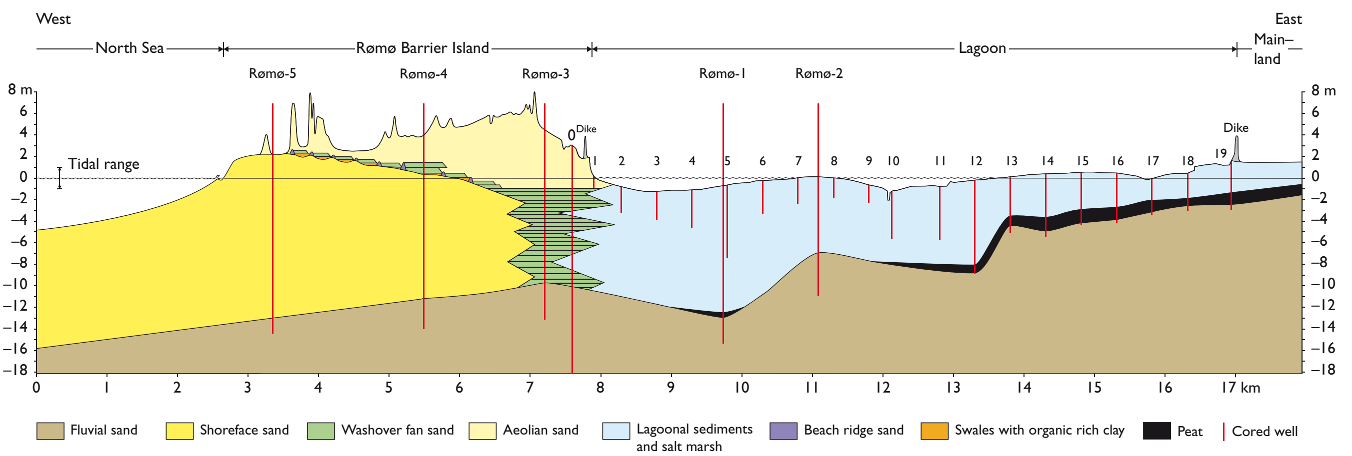

Fig. 7. West–east cross-section across the Rømø barrier island system from the North Sea to the west coast of Jylland, based on the Rømø-5 to Rømø-1 cores. Shoreface sands dominate the western part of the island and washover fans and salt marsh sediments dominate the easternmost part of the island. Lagoonal sediments are only seen in the absolute easternmost part of the island and further to the east in the lagoonal area. Aeolian dune sands dominate the topmost part of Rømø barrier island. Information from the 19 wells in the lagoon is taken from Betænkning angaaende Dæmning mellem Rømø og Fastlandet og Landvindingsarbejder i Vadehavet indenfor Rømø (1938).

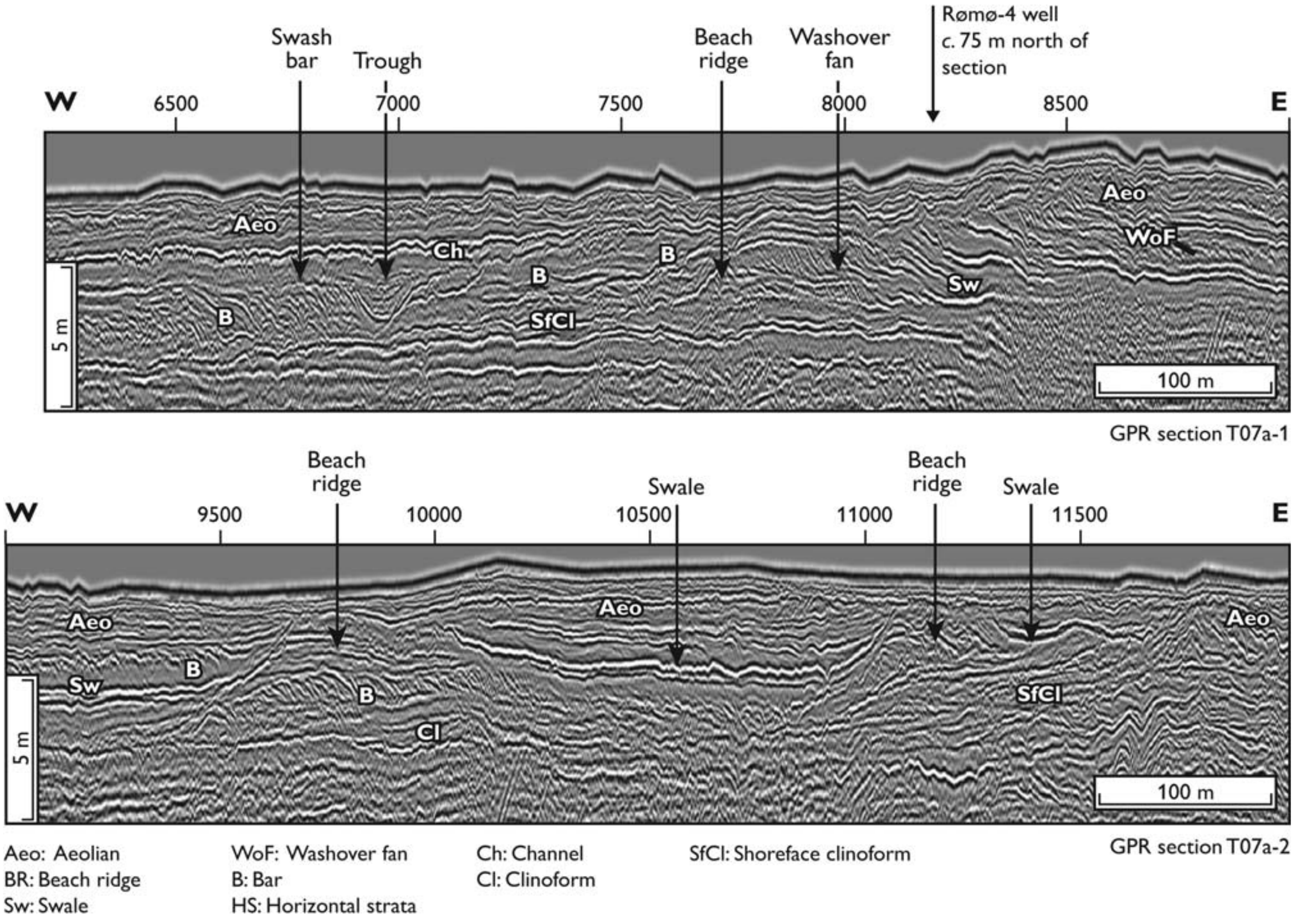

Fig. 8. GPR profile on Rømø barrier island oriented west–east. Sections T07a-1 (upper) and T07a-2 (lower) form a continuous line across the centre of the island (Fig. 6). The succession of beach ridges show shoreface progradation towards the west. The upper part of the section consists of aeolian sand. For location see Figure 6.

same time in laterally extensive, virtually horizontal packages bounded by minor flooding surfaces. Thus, based on core and log data, the sediments are grouped into a series of thin (4–7 m) parasequences that form the fundamental building blocks in the reconstruction (Fig. 14). Furthermore the depositional facies interpreted from cores and petrophysical logs are honoured, and it is assumed that these parasequences onlap the palaeotopography towards the SE.

Although the aggradational sandy successions are nearly similar in thickness, the entire back-barrier succession is much thicker in

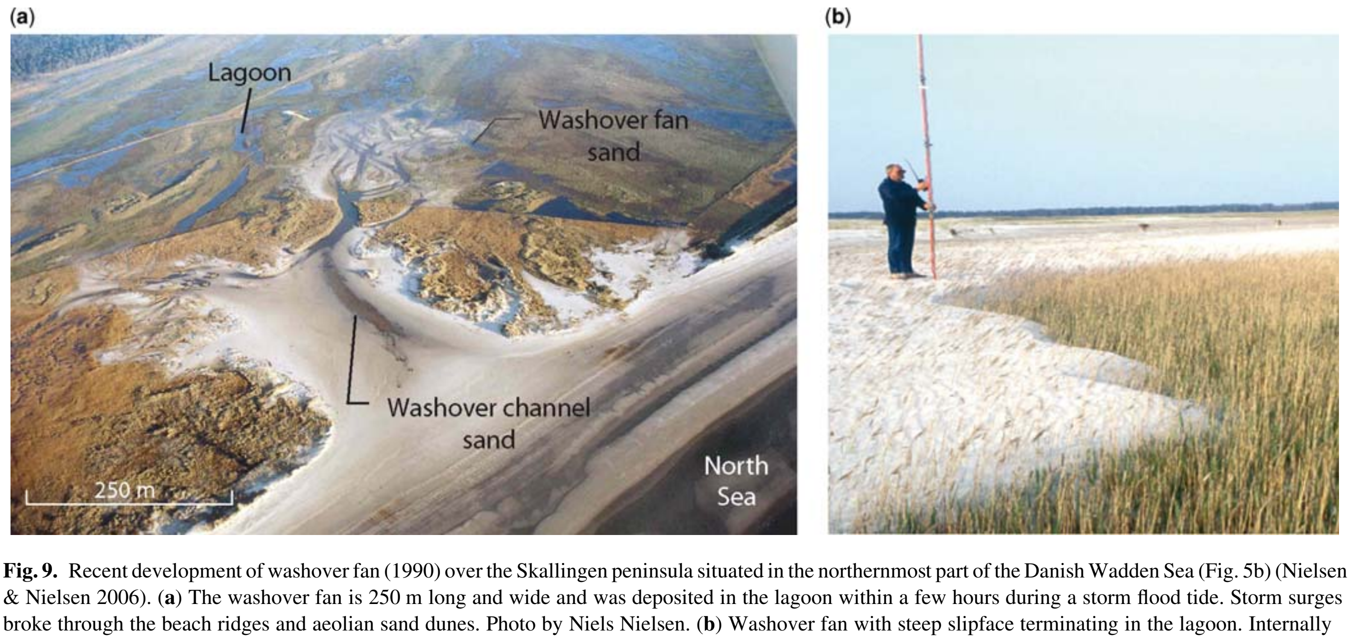

Fig. 9. Recent development of washover fan (1990) over the Skallingen peninsula situated in the northernmost part of the Danish Wadden Sea (Fig. 5b) (Nielsen & Nielsen 2006). (**a**) The washover fan is 250 m long and wide and was deposited in the lagoon within a few hours during a storm flood tide. Storm surges broke through the beach ridges and aeolian sand dunes. Photo by Niels Nielsen. (**b**) Washover fan with steep slipface terminating in the lagoon. Internally the *c*. 0.5 m thick washover fan is characterized by steep foresets. The washover fan was deposited several metres above mean sea-level as it formed during a storm when the storm peak sea-level was elevated by more than 4 m due to the combined effect of high tide and storm surge. Photo by Niels Nielsen.

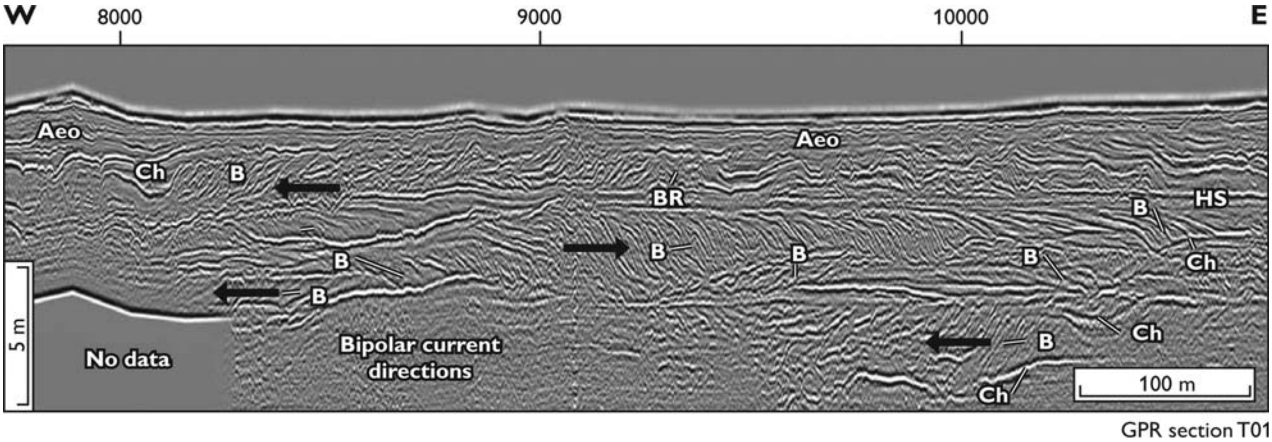

Fig. 10. GPR profile on Rømø barrier island oriented west–east. Section T01 is from the northern part of the island, which contains abundant tidal inlet sands. For location see Figure 6. Abbreviations annotated on reflector packages are the same as in Figure 8.

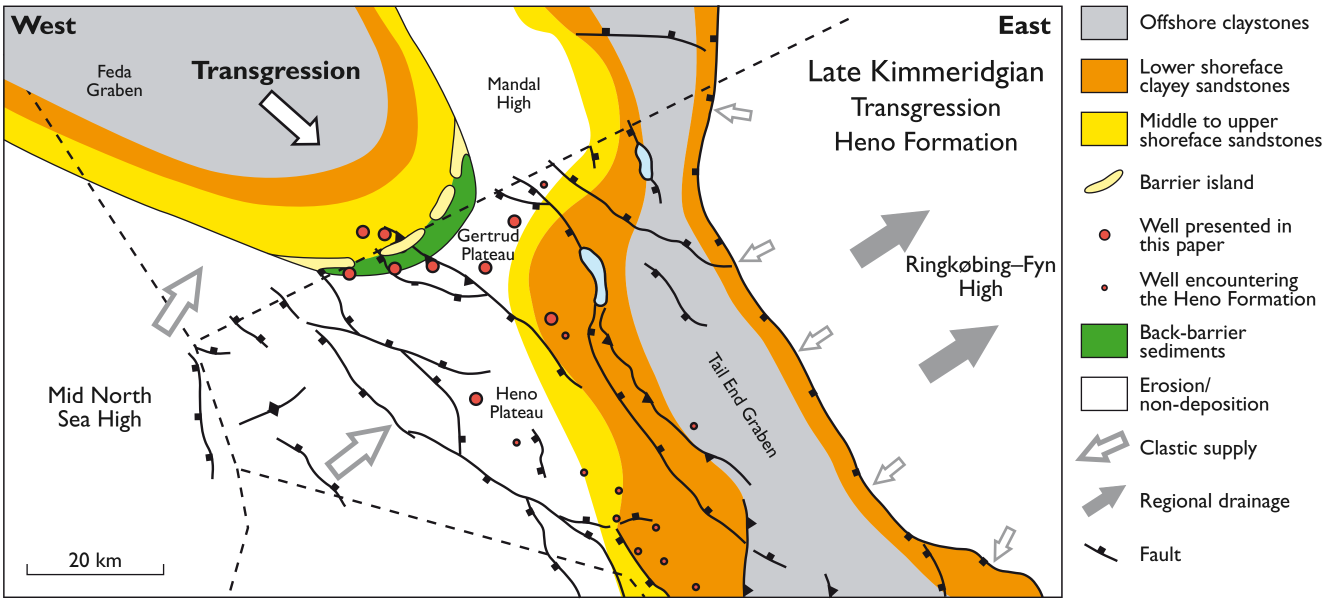

Fig. 11. Late Kimmeridgian palaeogeographic map from the northern part of the Danish Central Graben where the Freja oil field is located (Fig. 1).

Gert-1 than in 2/12-1, indicating that the sandy successions were accumulating vertically and that Gert-1 is situated palaeolandward of 2/12-1 (Fig. 14). The Gert-1 well may thus have been situated in a position similar to the Rømø-3 core close to the back-barrier

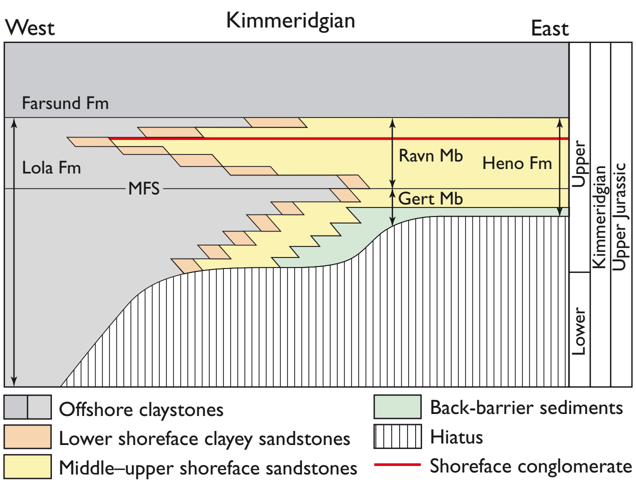

Fig. 12. Late Kimmeridgian time stratigraphic scheme.

area, whereas the 2/12-1 well was probably situated in a position similar to the Rømø-4 or Rømø-5 cores on the seaward shoreface (Fig. 7).

By applying these relatively simple principles in combination with the detailed sedimentary facies analyses, a model of the deeply buried Upper Jurassic Freja discovery is established. The model acknowledges realistic sedimentary processes and the response of a barrier island–lagoonal system to a significant relative sea-level rise. This fairly simple geological model of rising sea-level meeting a high relief palaeotopography that halted the overall transgression and leads to a vertical stacking of thick reservoir sandstones adequately explains the distribution of the reservoir sandstone facies in the Freja Field area as presented here.

This model facilitates estimates of high, mean and low case reservoir volumes, by shifting the position of the seaward and landward termination of the shoreface sandstones within each parasequence between the wells, while honouring the information at each well (Fig. 14). These sandstones are probably the most porous part of the reservoir.

The modern analogue of the Rømø barrier island in the Danish part of the Wadden Sea shows clearly that barrier islands can aggrade and even prograde during a rise in relative sea-level, as Rømø has experienced over the last 8000 years as sea-level has

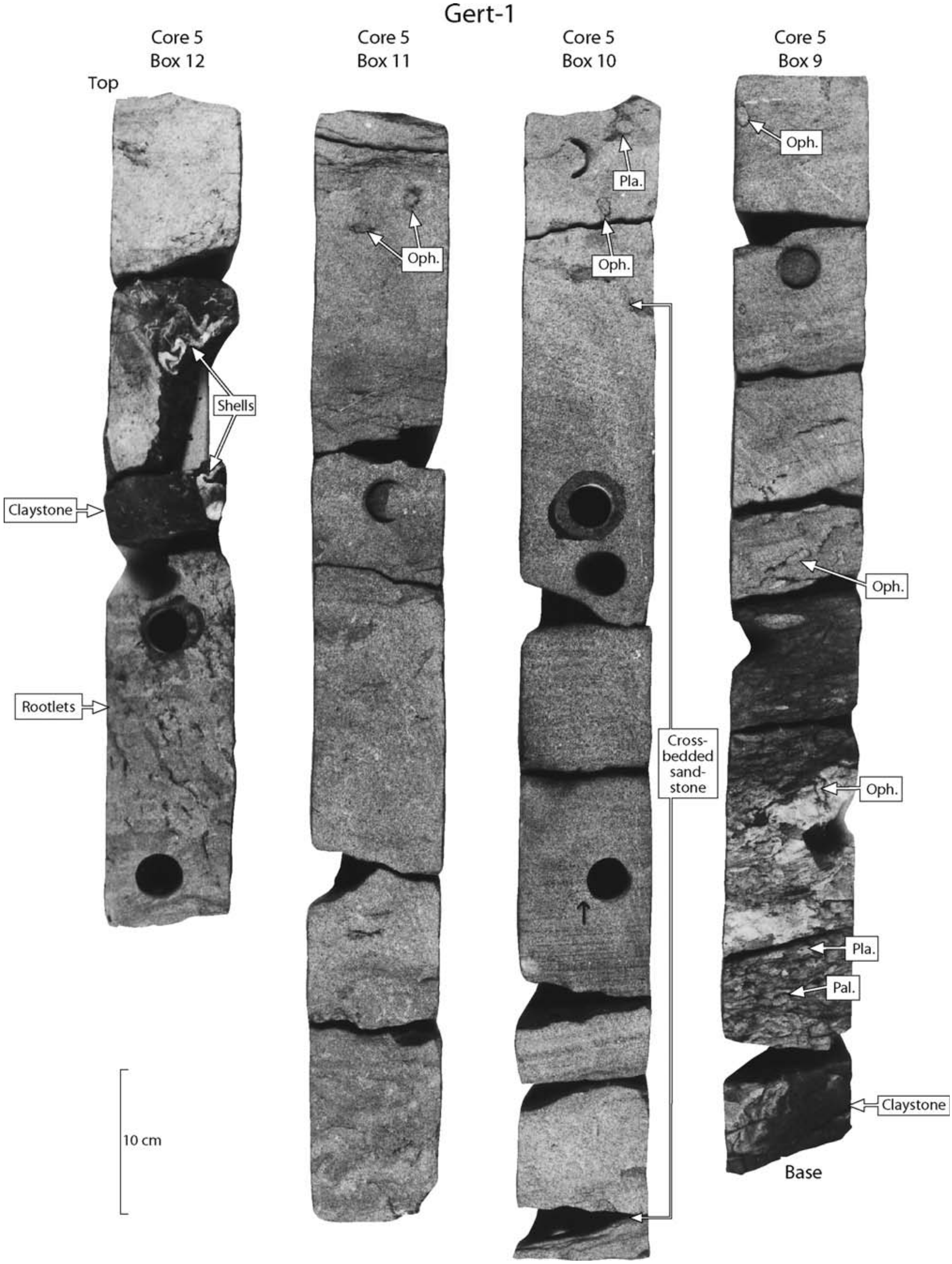

Fig. 13. Core photographs of an interpreted washover fan in the Gert-1 well. For position of core photographs see Figure 2 on sedimentary core log.

risen 15 m. In sand-rich systems, sedimentation can easily keep pace with sea-level rise.

As the top and bottom defining the thickness of the Gert Member is very difficult to define on seismic sections at these depths, it is impossible to show growth strata in the hanging walls indicating syn-depositional normal fault activity. Thus normal faults in Figure 14 may have been syn-depositional, but are not needed to explain these unusual thick back-barrier sediments.

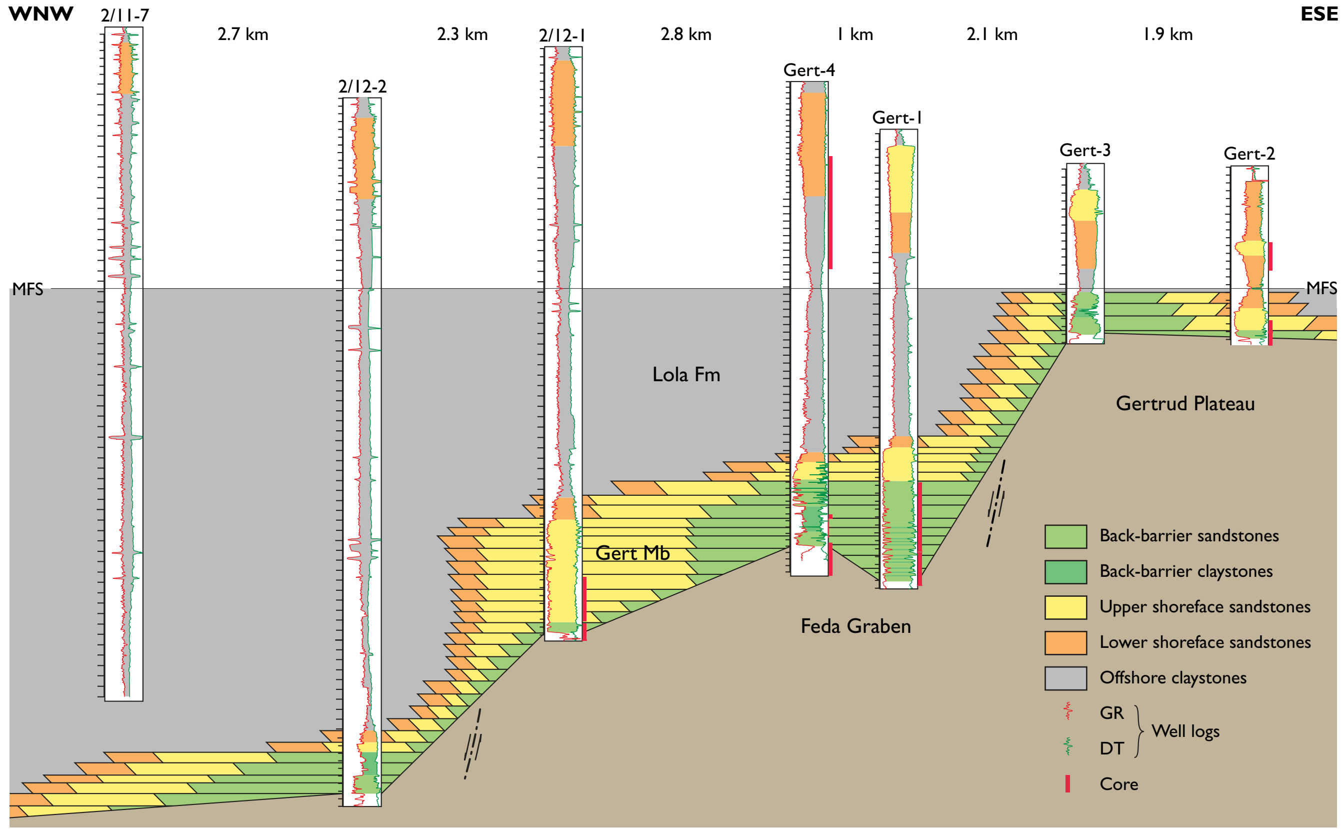

Fig. 14. Well log panel through the wells of the Freja oil field, showing distribution of reservoir facies within the basic stratigraphic building blocks (parasequences) which define the reservoir geometry. Discrimination between back-barrier sandstones and claystones is only indicated between the log curves for each well. Pre-Jurassic to Kimmeridgian faults are shown. They may have been active when the reservoir sandstones were deposited.

Conclusions

The thick back-barrier and shoreface sandstones of the Freja commercial oil field can be explained on the basis of simple sedimentological principles using depositional mechanisms, palaeotopography and rising sea-level. The Rømø barrier island analogue shows that, if there is a large surplus of sand, a barrier island may aggrade and even prograde during a sea-level rise. The reconstruction of the palaeotopography in the Upper Jurassic Freja discovery area shows that barrier island sandstones may have aggraded during a sea-level rise if the underlying, seaward-dipping palaeotopography was sufficiently steep to retard the transgression. Both mechanisms have probably contributed to the accumulation of the thick barrier island sandstone successions in the Freja discovery. Syn-sedimentary normal fault activity is not needed to explain these thick back-barrier sediments.

The resulting depositional model, built on detailed facies analysis of cores and well logs from the reservoir combined with modern analogue data, allow the construction of a reliable reservoir model that can be used for volumetric calculations and field development plans.

Jon R. Ineson is thanked for critical reading of the text and major improvement of the English. Finn Jakobsen is thanked for very helpful discussions. The Danish Natural Science Research Council (grant no. 272-05-0278) and Geocenter Copenhagen Foundation (grant no. 603-00003) are thanked for financial support. We also thank Gary Hampson and two anonymous reviewers for their very constructive comments.

References

Andsbjerg, J. & Dybkjær, K. 2003. Sequence stratigraphy of the Jurassic of the Danish Central Graben. *In*: Ineson, J. R. & Surlyk, F. (eds) *The Jurassic of Denmark and Greenland*. Geological Survey of Denmark and Greenland Bulletin, **1**, 265–300.

Bartholdy, J. & Pejrup, M. 1994. Holocene evolution of the Danish Wadden Sea. *Senckenbergiana Maritima*, **24**, 187–209.

Betænkning angaaende Dæmning mellem Rømø og Fastlandet og Landvindingsarbejder i Vadehavet indenfor Rømø, 1938. 127.

Damtoft, K., Nielsen, L. H., Johannessen, P. N., Thomsen, E. & Andersen, P. R. 1992. Hydrocarbon plays of the Danish Central Trough. *In*: Spencer, A. M. (ed.) *Generation, Accumulation and Production of Europe's Hydrocarbons II*. Special Publications of the European Association of Petroleum Geoscientists, **2**, Springer, Berlin, 35–58.

Danish Energy Agency, 2008. Oil and Gas Production in Denmark 07. World Wide Web Address: http://www.ens.dk/graphics/Publikationer/Olie_Gas_UK/Energistyrelsen%20UK_LOW.pdf.

Elliott, T. 1986. Siliciclastic shorelines. *In*: Reading, H. G. (ed.) *Sedimentary Environments and Facies*, 2nd edn. Blackwell Scientific, Oxford, 615.

Fraser, S. I., Robinson, A. M., Johnson, H. D., Underhill, J. R., Kadolsky, D. G. A., Connell, R., Johannessen, P. N. & Ravnås, R. 2002. Upper Jurassic. *In*: Evans, D., Graham, C., Armour, A. & Bathurst, P. (eds) *The Millennium Atlas: Petroleum Geology of the Central and Northern North Sea*. The Geological Society, London, 157–189.

Johannessen, P. N. 1997. Upper Jurassic back-barrier and shoreface reservoir sandstones and thin turbidite sandstones in the Danish Central Trough, North Sea. *In*: Oakman, C. D., Martin, J. H. & Corbett, P. W. M. (eds) *Cores from the Northwest European Hydrocarbon Province: An Illustration of Geological Applications from Exploration to Development*. The Geological Society, London, 11–20

Johannessen, P. N. 2003. Sedimentology and sequence stratigraphy of paralic and shallow marine Upper Jurassic sandstones in the northern Danish Central Graben. *In*: Ineson, J. R. & Surlyk, F. (eds) *The Jurassic of Denmark and Greenland*. Geological Survey of Denmark and Greenland Bulletin, **1**, 367–402.

Johannessen, P. N., Dybkjær, K. & Rasmussen, E. S. 1996. Sequence stratigraphy of Upper Jurassic reservoir sandstones in the northern part of the Danish Central Trough, North Sea. *Marine and Petroleum Geology*, **13**, 755–770.

Johannessen, P. N., Nielsen, L.H. *et al*. 2008. Sedimentary facies and architecture of the Holocene to Recent Rømø barrier island in the Danish Wadden Sea. *Geological Survey of Denmark and Greenland Bulletin*, **15**, 49–52.

Johannessen, P. N., Dybkjær, K., Andersen, C., Kristensen, L., Hovikoski, J. & Vosgerau, H. 2010. Upper Jurassic reservoir sandstones in the Danish Central Graben: new insights on distribution and depositional environments. *In*: Vining, B. A. & Pickering, S. C. (eds) *Petroleum Geology: From Mature Basins to New Frontiers – Proceedings of the 7th Petroleum Geology Conference*. Geological Society, London, 127–143; doi: 10.1144/0070127.

Lumborg, U. & Pejrup, M. 2005. Modelling of cohesive sediment transport in a tidal lagoon – an annual budget. *Marine Geology*, **218**, 1–16.

Madsen, A. T., Murray, A. S. & Andersen, T. J. 2007. Optical dating of dune ridges on Rømø, a barrier island in the Wadden Sea. Denmark. *Journal of Coastal Research*, **23**, 1259–1269.

Michelsen, O., Nielsen, L. H., Johannessen, P. N., Andsbjerg, J. & Surlyk, F. 2003. Jurassic lithostratigraphy and stratigraphic development onshore and offshore Denmark. *In*: Ineson, J. R. & Surlyk, F. (eds) *The Jurassic of Denmark and Greenland*. Geological Survey of Denmark and Greenland Bulletin, **1**, 147–216.

Møller, I., Nielsen, L., Johannessen, P. N., Nielsen, L. H., Pejrup, M., Andersen, T. J. & Korshøj, J. S. 2008. Creating the framework of sedimentary architecture of a barrier island in the Danish Wadden Sea. *Proceedings of 12th International Conference on Ground Penetrating Radar, Birmingham*, UK, 8 pp.

Nielsen, L., Møller, I., Nielsen, L. H., Johannessen, P. N., Pejrup, M., Andersen, T. J. & Korshøj, J. S. 2009. Integrating ground-penetrating radar and borehole data from a Wadden Sea barrier island. *Journal of Applied Geophysics*, **68**, 47–59.

Nielsen, N. & Nielsen, J. 2006. Development of a Washover Fan on a transgressive Barrier, Skallingen, Denmark. *Journal of Coastal Research, Special Issue*, **39**, 107–111.

Noe-Nygaard, N., Surlyk, F. & Piasecki, S. 1987. Bivalve mass mortality caused by toxic dinoflagellate blooms in a Berriasian–Valanginian lagoon, Bornholm, Denmark. *Palaios*, **2**, 263–273.

Pejrup, M. 2006. Det danske vadehav og store landvindingsprojekter. *In*: Fenchel, T. (ed.) *Naturen i Danmark: Havet*. Gyldendal, Copenhagen, 433–415.

Rasmussen, E. S. 1995. Structural evolution of the Gert-Mjølner area. *Marine and Petroleum Geology*, **12**, 377–385.

Smelror, M. & Leereveld, H. 1989. Dinoflagellate and acritarch assemblages from the Late Bathonian to Early Oxfordian of Montagne Crussol, Rhone Valley, southern France. *Palynology*, **13**, 121–141.

Söderström, B., Forsberg, A., Holtar, E. & Rasmussen, B. A. 1991. The Mjølner Field, a deep Jurassic oil field in the Central North Sea. *First Break*, **9**, 156–171.

Sørensen, T. H., Bartholdy, J., Christiansen, C. & Pedersen, J. B. T. 2006. Intertidal surface type mapping in the Danish Wadden Sea. *Marine Geology*, **235**, 87–99.

Sedimentology and sequence stratigraphy of the Hugin Formation, Quadrant 15, Norwegian sector, South Viking Graben

R. L. KIEFT,[1,2] C. A.-L. JACKSON,[1] G. J. HAMPSON[1] and E. LARSEN[3,4]

[1]*Department of Earth Science and Engineering, Imperial College London, South Kensington Campus, London SW7 2AZ, UK (e-mail: rachel.kieft@uk.bp.com)*
[2]*Present address: BP Exploration, Chertsey Road, Sunbury-on-Thames, Middlesex TW16 7LN, UK*
[3]*Statoil, Grenseveien 21, N-4035 Stavanger, Norway*
[4]*Present address: Rocksource ASA, Box 994 Sentrum, Olav Kyrres gate 22, N-5808 Bergen, Norway*

Abstract: The Middle Jurassic Hugin Formation has been the target of exploration within Quadrant 15 of the Norwegian South Viking Graben since the 1960s. The Hugin formation comprises shallow-marine and marginal-marine sediments deposited during the overall transgression and southward retreat of the 'Brent Delta' systems. Sedimentological analysis of cores across the quadrant has identified six facies associations: bay-fill, shoreface, mouth bar, fluvio-tidal channel-fill, coastal plain and offshore open marine. These facies associations are arranged in a series of parasequences bounded by flooding surfaces, several of which are correlated regionally using biostratigraphic data. Within this stratigraphic framework, facies association distributions and stratigraphic architectures are complicated, reflecting the spatial and temporal interaction of various physical processes (e.g. waves and tides) with an evolving structural template produced by rift initiation and salt movement. The overall transgression was highly diachronous, becoming younger from north to south. The northern part of the study area (Sigrun–Gudrun area) is characterized by a series of backstepping, linear, north–south-trending barrier shorelines and sheltered bays. The central part of the study area (Dagny area) contains stacked, backstepping strandplain shorelines that fringed syn-depositional topographic highs. Local angular unconformities are developed around these highs, implying that they formed above fault-block crests and salt-cored structures. The southern part of the study area (Sleipner area) contains stacked deltaic shorelines that were modified by both waves and tides. Sandbody geometry is closely related to depositional regime and syn-depositional tectonic setting within the basin; a robust understanding of both is critical to successful exploration of Hugin Formation reservoirs.

Keywords: Hugin Formation, South Viking Graben, shallow marine, transgression, Jurassic

The Middle Jurassic Hugin Formation has been the subject of exploration efforts in the South Viking Graben, northern North Sea, since the 1960s. The Hugin formation forms part of the Vestland Group, and comprises shallow-marine and marginal-marine deposits that interfinger with the continental deposits of the underlying Sleipner Formation and the offshore marine shales of the overlying Heather Formation (Vollset & Dore 1984; Partington *et al.* 1993). Despite the discovery of the Sleipner Vest and Øst Fields in 1974 and 1981, respectively (Milner & Olsen 1998; Isaksen *et al.* 2002), exploration has been hampered by the absence of a regional sequence stratigraphic framework supported by depositional models that allow prediction of reservoir distribution and quality within specific stratigraphic intervals. The development of an integrated sedimentological and stratigraphic understanding of the formation is complicated by two factors. Firstly, shallow-marine and marginal-marine deposits in the formation exhibit a mixed regime of physical processes (i.e. waves, tides and riverine) that varies laterally within the South Viking Graben (e.g. Richards 1991; Folkestad & Satur 2008), suggesting that a single depositional model is inappropriate for the area as a whole. Secondly, the construction of a stratigraphic framework is complicated by syn-depositional rift-related faulting and halokinesis (Kessler *et al.* 1995; Sneider *et al.* 1995; Milner & Olsen 1998). The resulting syn-depositional structural template was complex and dynamic. In similar rift- or salt-basin settings, an evolving structural template controls the local development of accommodation, topography and sediment routing, which in turn influence facies distributions, architectures and character (e.g. Gawthorpe & Leeder 2000; Shelley & Lawton 2005). The aims of this paper are to present an updated regional depositional model and sequence stratigraphic framework for the Hugin Formation within Quadrant 15 (Fig. 1). Additional wells and new biostratigraphical analyses have been used to update previous studies (e.g. Varadi *et al.* 1998). This study is aiding current exploration within the region, as well as providing generic insights into the relationship between sedimentology, sequence stratigraphy and structural development that may be applicable to other rift basins and areas of halokinesis.

Previous studies

The Hugin Formation is an overall transgressive unit that was deposited during rift-related subsidence and subsequent flooding of the South Viking Graben during north-to-south retreat of the 'Brent Delta' megasequence (e.g. Rattey & Hayward 1993; Husmo *et al.* 2003). The Hugin Formation is Late Bajocian to Oxfordian in age, but transgression of the graben was diachronous and the formation becomes younger from north to south (Fig. 2; Mitchener *et al.* 1992; Partington *et al.* 1993; Rattey & Hayward 1993; Richards *et al.* 1993). Several other names have been used to describe the same lithostratigraphic interval, including the Beryl Formation and 'Bruce Group sands' in the Bruce–Beryl embayment of the UK sector (Mitchener *et al.* 1992; Richards *et al.* 1993; Husmo *et al.* 2003). Time-equivalent deep-marine turbidites in the basin axis have been referred to as the Ling Sandstone Member of the Heather Formation (Cockings *et al.* 1992; Husmo *et al.* 2003) or as part of the Bruce or Heather Sandstones

VINING, B. A. & PICKERING, S. C. (eds) *Petroleum Geology: From Mature Basins to New Frontiers – Proceedings of the 7th Petroleum Geology Conference*, 157–176. DOI: 10.1144/0070157

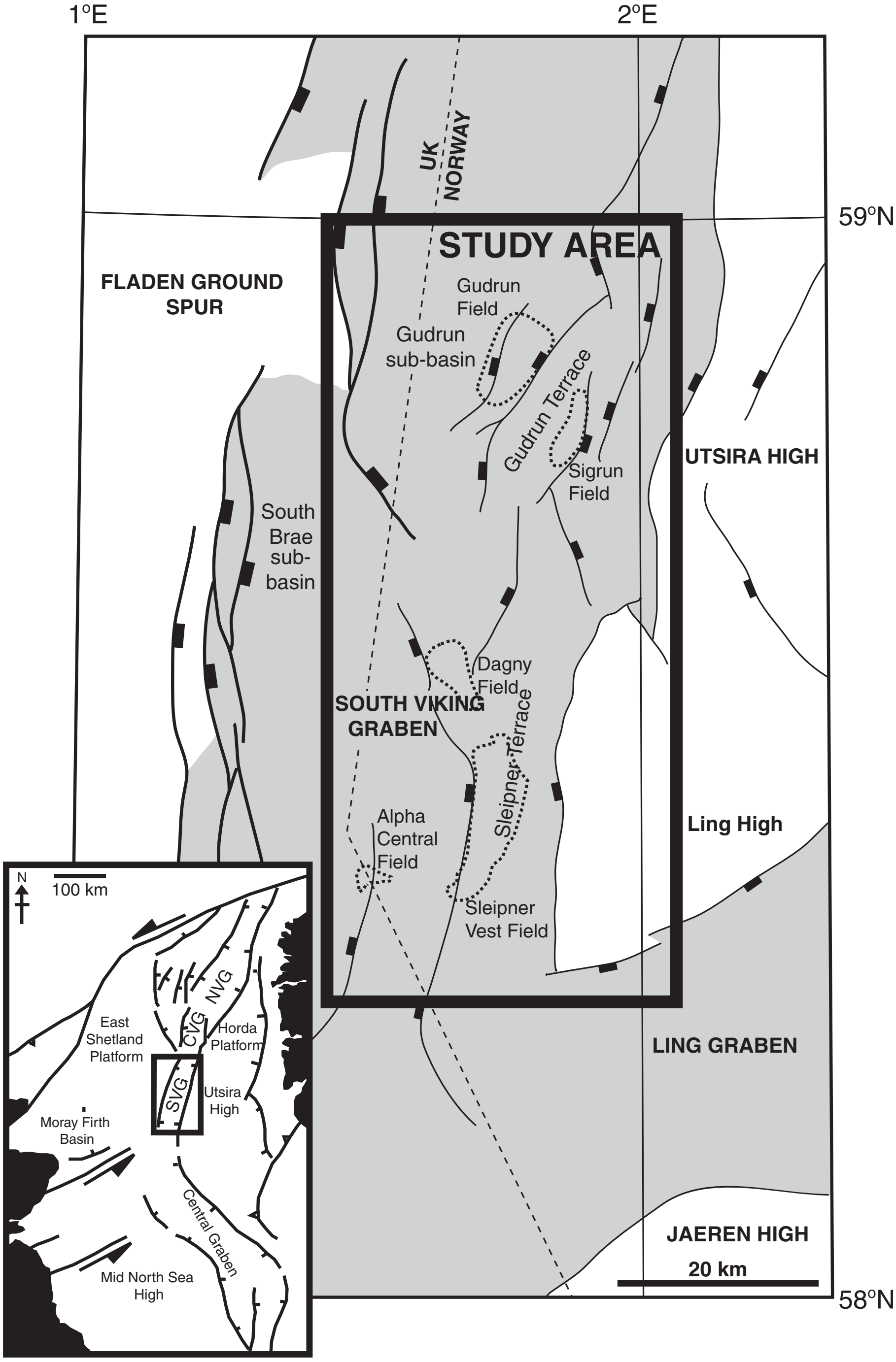

Fig. 1. Present-day structural setting of the study area. Abbreviations used: SVG, South Viking Graben; CVG, Central Viking Graben; NVG, North Viking Graben. Modified from Zanella & Coward (2003).

(Richards *et al.* 1993; Spence & Kreutz 2003). Rift-related faulting and associated localized tectonic subsidence within the South Viking Graben have influenced sediment routing, gross thickness, facies distributions and facies belt orientations within the Hugin Formation (Sneider *et al.* 1995; Milner & Olsen 1998; Varadi *et al.* 1998).

The Hugin Formation was first described from the Sleipner Vest Field to the south of the study area (well 15/9-2; Vollset & Dore 1984) to comprise a stacked succession of nearshore-to-shallow-marine sandstones and coals with some fluvio-deltaic influence. A wave-dominated barrier shoreline was interpreted from well data distributed more regionally in the South Viking Graben (Harris & Fowler 1987). Sequence stratigraphic analysis (Varadi *et al.* 1998) resulted in recognition of regional flooding surfaces and sequence boundaries that divide the succession into a series of cycles, each recording shoreline progradation and subsequent retrogradation. More detailed studies on the Sleipner Vest and Øst fields have defined several facies associations within such cycles: alluvial plain, coastal swamp, barrier-shoreline complex (including shoreface, mouth bar, tidal channel, tidal dune and tidal flat deposits), lagoon and/or bay, and offshore deposits, with the last corresponding to the shelfal Heather Formation (Milner & Olsen 1998; Folkestad & Satur 2008). The best quality reservoir units occur within shoreface deposits whilst the worst occur within lagoon and/or bay deposits (Harris & Fowler 1987; Milner & Olsen 1998). The strong tidal signatures recognized

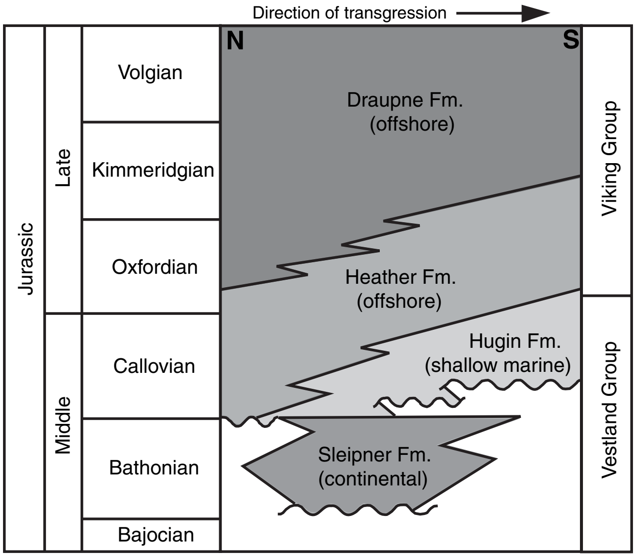

Fig. 2. Jurassic lithostratigraphy of the study area.

throughout the Hugin Formation are interpreted to be the result of wave suppression within the narrow (*c*. 30 km), elongate (*c*. 100–120 km) graben during deposition (Richards 1991; Folkestad & Satur 2008).

Tectonic setting

Since the Cambrian, four major tectonic events have influenced the area now defined as the South Viking Graben: (1) Late Ordovician–Early Silurian collision of the Caledonian Orogeny; (2) Carboniferous to Permian rifting and basin formation; (3) Mesozoic rifting and graben formation; and (4) Late Cretaceous to Early Cenozoic inversion (Ziegler 1990; Lyngsie *et al.* 2006). The South Viking Graben is a NNE–SSW trending half-graben, bounded to the west by a series of ESE-dipping faults and the Palaeozoic high of the Fladen Ground Spur (Thomas & Coward 1996; Husmo *et al.* 2003). To the east, the graben shallows onto the Utsira High, a structurally complex area of localized faulting, tilting and erosion (Thomas & Coward 1996; Husmo *et al.* 2003). This study focuses on Norwegian Quadrant 15, which is located on the hanging-wall dipslope of the South Viking Graben (Fig. 1).

The study area is dissected by a series of intra-graben, NNE–SSW-trending normal faults that predominantly detach on the Upper Permian Zechstein Supergroup salt layer (Thomas & Coward 1996; Jackson & Larsen 2008). These faults are antithetic to the main graben-bounding fault array that lies to the west of the study area. In the north of the study area, these faults developed in response to gravity-driven sliding of units above the mobile Zechstein Supergroup salt (Thomas & Coward 1996; Jackson & Larsen 2008). Towards the south, salt-related structures become more prominent, with the occurrence of salt-cored anticlines, diapirs and salt-withdrawal basins. Differential subsidence across these faults and salt-cored features was superimposed on the overall westward-rotation of the hanging-wall dipslope, leading to complex interaction between these local and regional tectonics, eustasy and drainage patterns. Locally, compressional anticlines and growth folds are associated with reverse reactivation of older extensional faults (e.g. Thomas & Coward 1996; Knott 2001; Jackson & Larsen 2008). These structures are interpreted to have developed during the Late Jurassic (Thomas & Coward 1996; Jackson & Larsen 2008) and they therefore post-date Hugin Formation deposition.

Dataset and methodology

Almost 600 m of Hugin Formation core from 16 regional wells (Fig. 3) has been logged for this study. Wireline-logs were available for all of the cored wells and new, high-resolution biostratigraphic analyses were available for 13 of the wells. Sedimentological analysis involved recording grain size, sorting and sphericity of matrix and clasts, colour variations, sedimentary structures, bed thickness, the nature of bounding contacts and macro-fauna type and preservation state. The degree of bioturbation is recorded using the bioturbation index (BI) scheme of Taylor & Goldring (1993), which is based on a visual assessment of the amount of 'bioturbated' v. 'unbioturbated' texture and ranges from 0 (no bioturbation) to 6 (complete bioturbation). Wireline-log character and cross-plot analyses (sonic (DT) v. gamma ray (GR); density (RHOB) v. neutron porosity (NPHI)) have been used to identify distinctive wireline-log responses for each facies identified in core. The characteristic wireline-log responses were then used to qualitatively interpret uncored intervals within the studied wells.

Sedimentology of the Hugin Formation

Fifteen facies have been recognized within the Hugin Formation (Table 1). These facies have been grouped into six facies associations, which are discussed below and summarized in Figures 4–6.

Bay-fill facies association: A

Complete, well-developed successions of the bay-fill facies association occur in the northern part of the study area (wells G–L; Fig. 3). Incomplete successions of the association, comprising individual facies, are also recognized interbedded with fluvio-tidal channel and shoreface facies associations (described below) in the south of the study area (well A; Fig. 3).

Description. Units of this facies association are typically composed of a coarsening-upwards succession that comprises, from base to top, facies A1, A2, A3 and A4 (Figs 4a & 5a). Parallel-laminated mudstones and siltstones at the base of the succession (facies A1) locally contain beds of densely packed, disarticulated bivalve shells. This facies passes gradationally upward into interbedded heteroliths (facies A2). Very fine-grained sandstones in these heteroliths occur as non-parallel or wavy laminae and lenticular, trough and low-angle (hummocky?) cross-stratified beds. Sandstone beds thicken and coarsen upwards in the succession, until mudstones occur only as thin laminae and drapes (facies A3). Bioturbation is variable in intensity, although *Diplocraterion* is occasionally identified in the lower, finer-grained parts of the facies association. Wavy bedding, high-angle cross-bedding and occasional wave ripples are preserved where bioturbation intensity is low. Locally this facies is truncated by sharp-based successions of coarse-grained sandstones with rare wispy lamination, ripples and sparse bioturbation (facies A4). Although shells and shell fragments are common throughout these sharp-based successions, they are typically concentrated towards the base. Successions of this facies association are commonly capped by thin deposits of the coastal plain facies association (described below).

Interpretation. The coarsening-upwards successions that typify this facies association imply a shallowing-upward or progradational trend, with increasing proximity to the source of sand towards the top of the succession. Parallel-laminated mudstones record deposition from suspension, while sandstone laminae and beds contain structures that record episodic deposition from suspension or tractional currents. Quasi-rhythmical interbedding of mudstone and sandstone (facies A2 and A3) suggest regular and

Table 1. Summary of facies in the Hugin Formation. Thickness and lateral extent reflect the observed thickness from core and the interpreted lateral extent based on well correlations. Bioturbation fabric is described using the Bioturbation Index (BI) scheme of Taylor & Goldring (1993)

Facies	Description	Thickness (t) and (l) lateral extent	Bioturbation	Wireline-log character	Interpretation
A1	Parallel-laminated mudstone with rare siltstone laminae, locally sideritic. Monospecific assemblage of disarticulated bivalves oriented parallel to bedding and concentrated into thick (60–205 cm) bioclastic-rich beds. Rare gastropods	t = 30–425 cm l = <6 to >29 km	BI = 0–2 (Pl)	GR 41–308 API DT 225–355 μs m^{-1} NPHI 0.167–0.464 v/v RHOB 2280–2820 g cm^{-3}	Restricted marine shale
A2	Interbedded claystone and very fine-grained sandstone. Non-parallel and wavy lamination, trough cross-stratification and hummocky cross-stratification in sandstone beds. Rare disarticulated bivalve shells oriented parallel to bedding	t = 10–725 cm l = <8 km to >13 km	BI = 2–3 (Te, Sk, Pl, Ar, Pa, Op)	GR 17–65 API DT 189–268 μs m^{-1} NPHI? RHOB 2280–2820 g cm^{-3}	Muddy shallow bay-fill
A3	Fine- to medium-grained sandstone. Moderately to well sorted. Wavy bedding, high-angle cross-bedding and occasional wave ripples. Calcite cement and soft sediment deformation locally observed. Disarticulated bivalves throughout, sometimes concentrated in thin beds (<10 cm)	t = 60–370 cm l = <8 km to >8 km	BI = 0–4 (Pa, Dip, Ro/Cy?, Pl, Op)	GR 18–46 API DT 199–314 μs m^{-1} NPHI 0.077–0.518 v/v RHOB 1690–2745 g cm^{-3}	Sandy shallow bay-fill
A4	Coarse- to fine-grained sandstone with fining- and coarsening-upward motifs. Moderately to well sorted with sub-rounded grains. Sparse sedimentary structures include ripples and mudstone drapes. Disarticulated bivalves and shell fragments common, concentrated into thin beds (<40 cm). Locally contains calcite-cemented nodules. Sharp, possibly erosive contacts at individual bed bases	t = 250–500 cm l = <1.8 km to >4.2 km	BI = 1–3 (Op, ET)	GR 7–35 API DT 175–230 μs m^{-1} NPHI 0.038–0.146 v/v RHOB 2280–2820 g cm^{-3}	Marine channel-fill sandstone
B1	Upward-coarsening, siltstone to very fine-grained, moderately sorted sandstone. Shell debris, quartz granules and angular carbonaceous fragments throughout. Primary sedimentary structures are poorly preserved, but contains rare thin (30–75 cm), sharp-based, very fine- to fine-grained cross-laminated sandstone beds	t = 30–480 cm l = <2 km	BI = 4–5 (Pa, Ch, Op, Pl, Ter, As?)	GR 18–80 API DT 168–291 μs m^{-1} NPHI 0.038–0.191 v/v RHOB 2322–2723 g cm^{-3}	Distal lower shoreface
B2	Very fine- to fine-grained, moderately to well sorted sandstone. Fine-grained, carbonaceous laminae throughout. Dominantly low-angle cross-bedding, with subordinate parallel lamination. Carbonate-cemented nodules	t = 130–440 cm l = 1.7 km (min) to 12 km (max)	BI = 3–4 (Op)	GR 20–56 API DT 179–277 μs m^{-1} NPHI 0.048–0.168 v/v RHOB 2314–2696 g cm^{-3}	Proximal lower shoreface
B3	Fine- to medium-grained, well sorted, coarsening-upwards, cross-laminated sandstone. Discrete laminae of coarser sediment, carbonaceous fragments and shell fragments occur throughout	t = 425–800 cm l = <1.7 km (min) to 8 km (max)	BI = 0* (crypto/Mac?)	GR 15–25 API DT 250–275 μs m^{-1} NPHI 0.094–0.113 v/v RHOB 2271–2342 g cm^{-3}	Upper shoreface
C1	Highly bioturbated siltstone to very fine-grained sandstone with stringers and thin (5–20 cm) beds of rounded granules	t = 175–1010 cm l = <7.2 km (min) to <19.6 km (max)	BI = 4–5 (Pa, Ch, Op, P)	GR 20–80 API DT 230–260 μs m^{-1} NPHI 0.084–0.169 v/v RHOB 2327–2521 g cm^{-3}	Distal mouth bar
C2	Very fine- to fine-grained sandstone with low-angle cross-bedding. Stringers and thin (5–15 cm) beds of rounded granules occur throughout. Monospecific trace fossil assemblage (*Ophiomorpha*)	t = 290–775 cm l = <5 km	BI = 0–2 (Op)	GR 12–58 API DT 167–397 μs m^{-1} NPHI 0.051–0.595 v/v RHOB 1612–2705 g cm^{-3}	Proximal mouth bar
D1	Fining-upward very coarse- to fine-grained sandstone with possible bidirectional cross-sets and swaley cross-stratification. Stacked fining-upward beds with sparse coarse-grained stringers. Sharp, possibly erosive contacts at individual bed bases	t = 740–820 cm l = <2 km	BI = 0–1 (Sk, ET)	GR 8–134 API DT 235–335 μs m^{-1} NPHI 0.140–0.469 v/v RHOB 2284–2570 g cm^{-3}	Tidally influenced fluvial channel-fill sandstone

(*Continued*)

Table 1. *Continued*

Facies	Description	Thickness (t) and (l) lateral extent	Bioturbation	Wireline-log character	Interpretation
D2	Fining-upward coarse- to medium-grained sandstone with unidirectional cross-bedding, carbonaceous laminae and fragments throughout. Sharp, possibly erosive contacts at individual bed bases	t = 580 cm l = <2 km to >2 km	BI = 0–1 (ET)	GR 9–34 API DT 241–297 μs m^{-1} NPHI 0.140–0.289 v/v RHOB 2168–2447 g cm^{-3}	Fluvial channel-fill sandstone
E1	Coal and carbonaceous shale. Basal contact typically parallel although may be undulose. Diagenetic pyrite nodules are recognized	t = 30–520 cm l = <6 km to >19.6 km	BI = 0	GR 8–56 API DT 313–427 μs m^{-1} NPHI 0.2405–0.529 v/v RHOB 1930–2225 g cm^{-3}	Coal
E2	Interbedded dark grey mud/claystone and siltstone to very fine-grained sandstone. Wavy to non-parallel lamination penetrated and disrupted by roots	t = 60 cm l = <2 km to >2 km	BI = 3–4 (roots)	GR 32–60 API DT 358–415 μs m^{-1} NPHI 0.4225–0.4993 v/v RHOB 1994–2148 g cm^{-3}	Coastal plain fines
F	Mudstone with rare siltstone beds. Parallel lamination, soft sediment deformation developed locally at bed tops. Rare thin (<100 cm), finely laminated, unbioturbated beds of very fine-grained sandstone	t = complete section not penetrated l = <1.7 km to >37.6 km	BI = 3–5, occ. 0 (Pl, Op, Ch, Zo, Tae, As. Te)	GR 4–134 API DT 187–450 μs m^{-1} NPHI 0.114–0.618 v/v RHOB 1730–2925 g cm^{-3}	Open marine shale

*Note that the bioturbation scheme cannot be used to describe cryptobioturbation, where sediment is pervasively bioturbated with little to no distortion of primary structures (e.g. facies B3). Individual trace fossils, listed in brackets, are abbreviated as follows: Te, *Teichichnus*; Sk, *Skolithos*; Ar, *Arenicolites*; Pa, *Palaeophycus*; Op, *Ophiomorpha*; Dip, *Diplocraterion*; Ros, *Rosselia*; Cy, *Cylindrichnus*; Pl, *Planolites*; Ch, *Chondrites*; Ter, *Terebellin*a (*Schaubcylindrichnus Fria*); As, *Asterosoma*; Mac, *Macaronichnus*; ET, escape traces; crypto, cryptobioturbation.

repeated fluctuations in energy regime, which implies tidal action (e.g. Nio & Yang 1991). Wave and storm influence is also present, indicated by rare wave ripples and low-angle cross-stratification, interpreted as hummocky cross-stratification on the basis of its occurrence only in very fine- to fine-grained sandstone (e.g. Dott & Bourgeois 1982; Duke *et al.* 1991). Sharp-based sandstones that occur locally in the upper part of the successions are interpreted as channel fills (facies A4). The occurrence of shell fragments in lags and dispersed through these sandstones, together with rare mudstone drapes, has been recorded as a common feature in tidal inlet channel-fill deposits (e.g. Moslow & Tye 1985; Israel *et al.* 1987; Simms *et al.* 2006). The occurrence of a monospecific shell assemblage and low-to-moderate intensity bioturbation by a restricted trace fossil assemblage indicates deposition in a restricted marine environment (Pemberton *et al.* 1992; MacEachern & Bann 2008). This interpretation is supported by the common occurrence of low-diversity dinocyst assemblages. Successions of this facies association are therefore interpreted to record periodic infilling of restricted marine embayments and/or lagoons that were locally contiguous with tidal inlet channels. The restricted marine character of these successions may be explained by deposition in sheltered lagoons and/or embayments that either lay behind coeval barriers and spits fronted by wave-dominated shorefaces (Harris & Fowler 1987; Hampson *et al.* 2009) or were protected by rift-generated islands and shoals. The pervasive tidal signature in this facies association may simply reflect the absence of wave reworking in the sheltered lagoons and/or embayments, although the narrow, elongate shape of the South Viking Graben may have locally amplified tidal currents and further suppressed wave activity (Husmo *et al.* 2003; Folkestad & Satur 2008).

Sequence stratigraphy. At the base of successions of this facies association, lagoonal and/or bay-fill mudstones (facies A1) representing relatively deep water (4–45 m based on thickness of associated parasequences; see below) are typically juxtaposed directly above coastal plain coals. The bases of these successions are therefore interpreted as flooding surfaces (*sensu* Van Wagoner *et al.* 1988), although they may have formed in response to allogenic or autogenic changes in relative sea-level and sediment supply. An increase in bioturbation intensity is typically observed at these flooding surfaces, combined with the occurrence of *Diplocraterion*, an indicator of more marine conditions (Taylor & Goldring 1993). Some flooding surfaces are also associated with a lag deposit of fine- to medium-grained sandstone. Where flooding surfaces are underlain by tidal inlet channel-fill deposits (facies A4), the basal erosion surfaces of the channels may record tidal erosion during transgression (i.e. tidal ravinement surfaces, *sensu* Swift 1968). This interpretation is supported by the occurrence of winnowed, coarse-grained and/or bioclastic lags at the bases of some channels. In one instance, a lagoonal and/or bay-fill succession is erosively overlain by upper shoreface sandstones (facies B3, described below); the base of this sandstone is interpreted to record wave erosion during transgression (i.e. a wave ravinement surface, *sensu* Swift 1968). Each of the upward-shallowing, flooding surface-bound successions is termed a parasequence (*sensu* Van Wagoner *et al.* 1990). Individual parasequence thickness varies from 4 to 45 m, and the duration of each parasequence is approximately 500–600 ka, based on high-resolution biostratigraphy (Hampson *et al.* 2009). The thickest parasequences occur in the western part of the study area, where subsidence and accommodation space are greatest due to activity on the basin-bounding fault zone.

Wireline-log character. Gamma ray (GR) logs through successions of this facies association show an upward-decreasing trend as they become more sandstone-rich towards their tops (Fig. 4a). Facies A1 and A2 exhibit high GR values and a serrate pattern, reflecting their heterolithic character, whereas sandstone-dominated facies A3 has a smoother, funnel-shaped GR profile. Facies A4 has the lowest GR values and a sharp-based blocky log character, consistent with its association with channel-fill sandstones. The four constituent facies also have distinctive

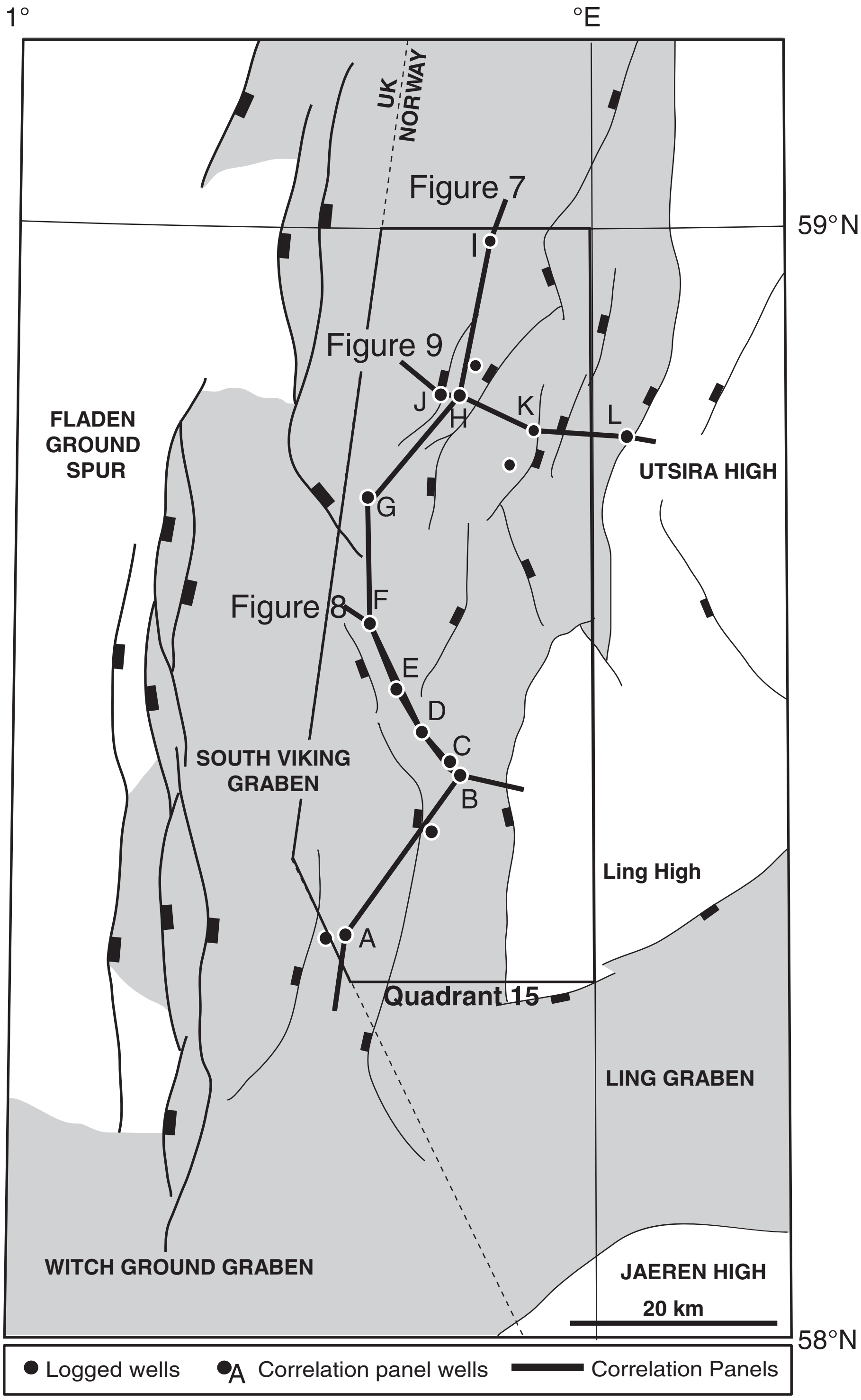

Fig. 3. Map showing the distribution of cored wells, correlation panels and seismic lines used in this study (Figs 4 & 7–9).

signatures when wireline-log cross-plots are generated (Fig. 6a); their wireline-log characteristics are summarized in Table 1.

Shoreface facies association: B

Complete, well-developed successions of the shoreface facies association are developed in the central and southern parts of the study area (wells A–E, Fig. 3). Several stacked shoreface successions are recognized within the central portion of the study area (e.g. wells C & E, Fig. 3), whilst to the south they interfinger in vertical successions with facies of the bay-fill, coastal plain, mouth bar and fluvio-tidal channel associations (e.g. well A, Fig. 3).

Description. Units of this facies association are typically composed of upward-coarsening and cleaning successions. Complete successions comprise, from base to top, facies B1, B2 and B3; incomplete successions of B1 to B2 facies and B2 to B3 facies are more typical of the central part of the study area (Figs 4b & 5b). Highly bioturbated siltstone to very fine-grained sandstone at the base of a succession (facies B1) passes gradationally upwards into moderately to well-sorted, very fine- to fine-grained sandstones (facies B2) and then well-sorted, fine- to medium-grained sandstones (facies B3). Sharp-based beds of very fine- to fine-grained, unbioturbated, low-angle cross-laminated sandstone (30–75 cm thick) occur within facies B1 and B2, and cross-lamination is

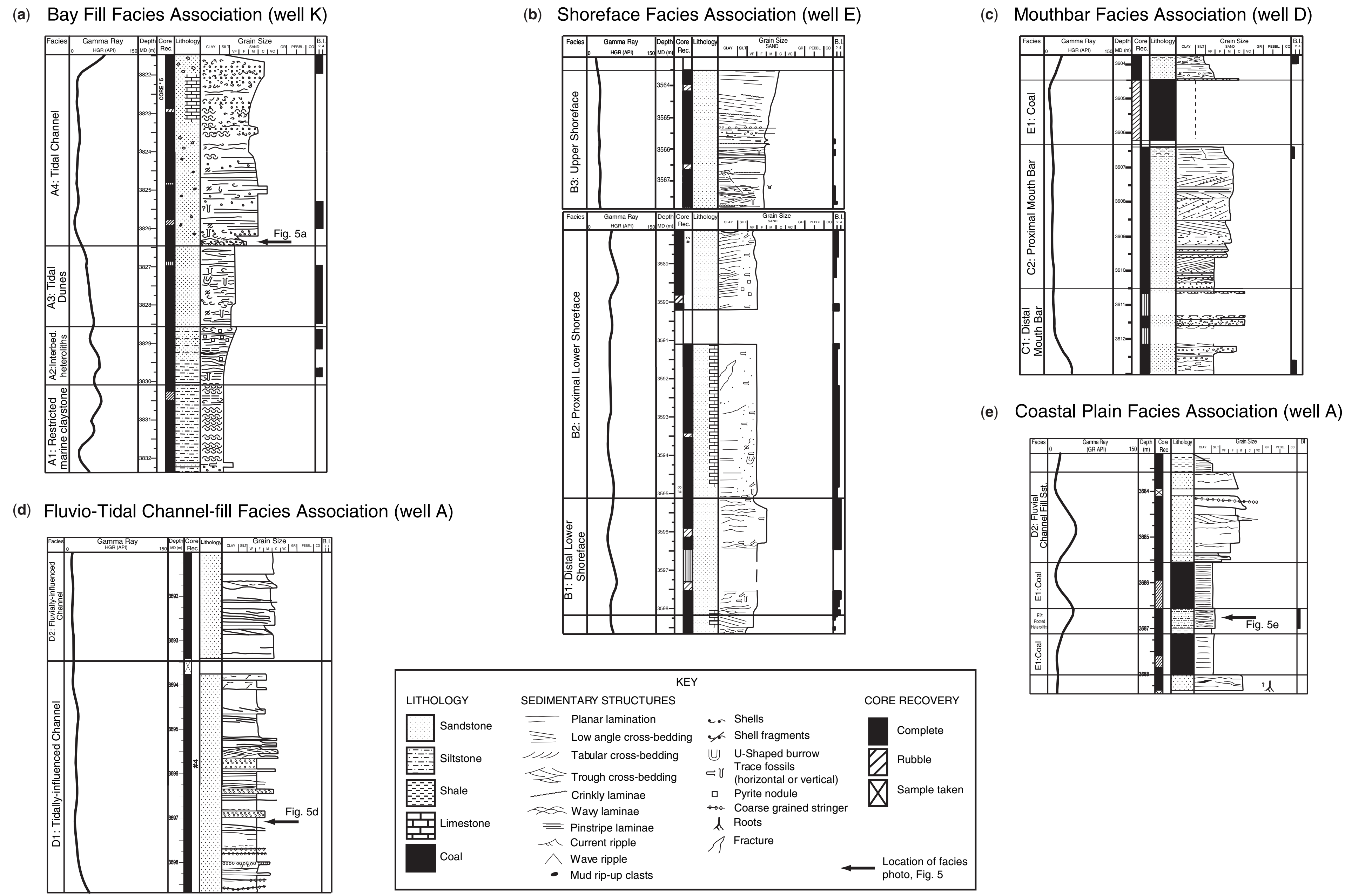

Fig. 4. Core descriptions and GR log characteristics of successions illustrating the principal facies associations in the Hugin Formation: (**a**) bay-fill; (**b**) shoreface; (**c**) mouth bar; (**d**) fluvio-tidal channel-fill; and (**e**) coastal plain.

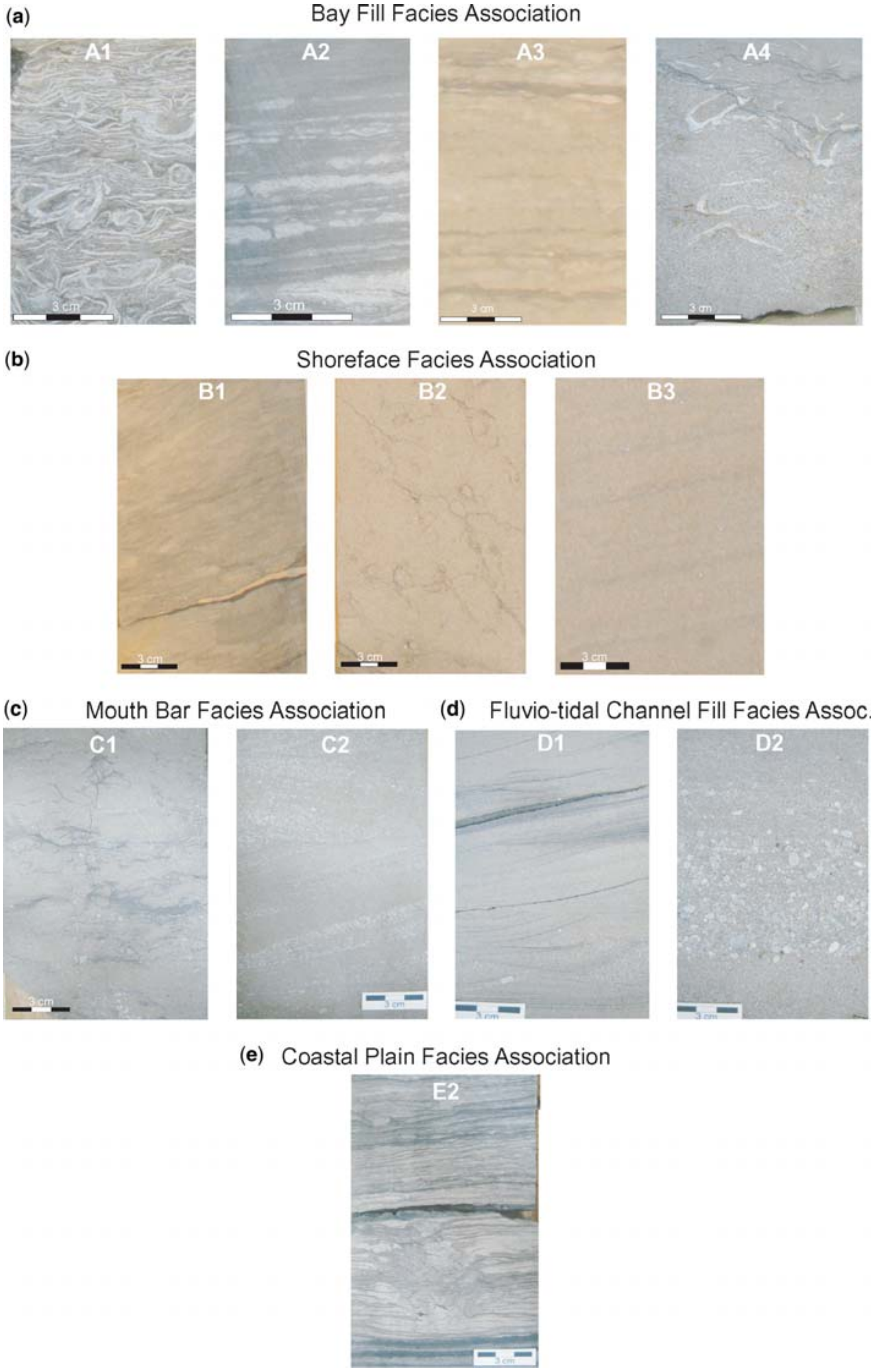

Fig. 5. Core photographs illustrating the selected facies in the principal facies associations of the Hugin Formation: (**a**) bay-fill; (**b**) shoreface; (**c**) mouth bar; (**d**) fluvio-tidal channel-fill; and (**e**) coastal plain. Photographs are located in the successions illustrated in Figure 4 where possible. Photos from: (a) A1, well K, 3838.70 cm; A2, well K, 3836.80 m; A3, well K, 3836.00 m; A4, well K, 3826.35 m; (b) B1, well D, 3599.70 m; B2, well D, 3584.25 m; B3, well D, 3581.10 m; (c) C1, well K, 3615.30 m; C2, 3608.30 m; (d) D1, well A, 3698.6 m; D2, well A, 3661.25 m; (e) E2, well A, 3687 m. Depths given are core depths and have not been shifted to wireline-log depths.

pervasive in facies B3. Bioturbation decreases in intensity and diversity from the base to top of the successions, allowing increasing preservation of cross-lamination. A monospecific assemblage of *Ophiomorpha* characterizes facies B2, whereas the ‘fuzzy’ appearance of some laminae in facies B3 may indicate cryptobioturbation or *Macaronichnus*.

Interpretation. The coarsening-upward trend in grain size and upward decrease in bioturbation intensity within the successions implies an upward increase in energy due to shallowing. The high intensity and diversity of bioturbation within fine-grained sediments is typical of the *Cruziana* ichnofacies indicating a low-energy and low-stress fully marine environment of deposition (MacEachern & Pemberton 1992; MacEachern & Bann 2008), whilst monospecific bioturbation by resilient *Ophiomorpha* burrows is typical of the *Skolithos* ichnofacies and is indicative of a loose substrate or higher energy setting such as middle or upper shoreface (MacEachern & Pemberton 1992; Martin 1993). Sharp-based, sparsely bioturbated sandstone beds within facies B1 and B2 are interpreted to record storm events (e.g. Pemberton

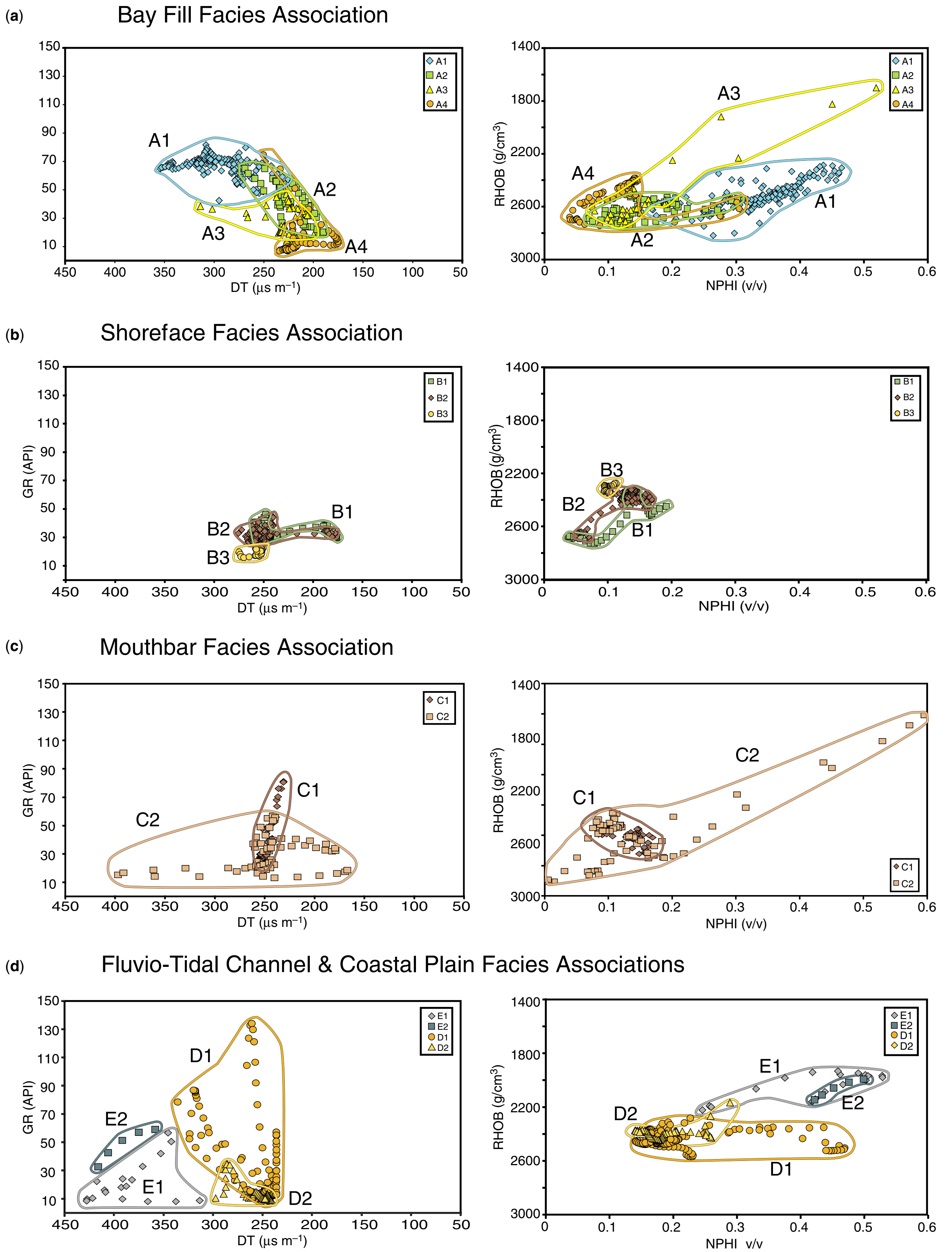

Fig. 6. Wireline-log cross-plots of, in the left-hand column, GR v. DT data and, in right-hand column, RHOB v. NPHI data. These cross-plots illustrate the quantitative log character of the principal facies associations of the Hugin Formation: (**a**) bay-fill (well H); (**b**) shoreface (well E); (**c**) mouth bar (well D); and (**d**) fluvio-tidal channel-fill and coastal plain (well A). The cross-plots are compiled with data from logged core intervals within the named wells.

et al. 1992). Well-sorted cross-laminated sandstones with low levels of bioturbation or cryptobioturbation (facies B3) are typical of upper shoreface-to-foreshore settings (Pemberton *et al.* 2008). This facies association is interpreted to have been deposited within a prograding shoreface with variable storm influence, as part of a strandplain, barrier-island or spit shoreline.

Sequence stratigraphy. At the base of successions of this facies association, distal or proximal lower shoreface deposits (facies B1 and B2) representing relatively deep-water marine deposition below the fair-weather wave base are juxtaposed directly above coastal plain coals or, less typically, fluvio-tidal channel-fill sandstones. The bases of these successions are therefore interpreted as flooding surfaces (*sensu* Van Wagoner *et al.* 1988). Some such flooding surfaces occur coincident with coarse-grained, locally carbonaceous or bioclastic lag deposits 5–15 cm thick. The stratigraphic context of these lags records transgression, and they are thus interpreted as wave ravinement surfaces (*sensu* Swift 1968), which suggests erosion of the uppermost part of the underlying succession during shoreface retreat. A few of these flooding surfaces are also associated with a calcite-cemented interval that may represent re-precipitation of bioclastic material (e.g. within a transgressive lag). In the central part of the study area, shoreface parasequences are rarely complete, comprising successions of facies B1–B2 only. The shoreline may not have prograded far enough into the basin to deposit upper shoreface deposits (facies B3) in this location, or they may have been deposited and subsequently removed by transgressive erosion during shoreline retreat. Alternatively, the deep *Ophiomorpha* that are characteristic of facies B2 may have intensely bioturbated remnant upper shoreface sandstones after flooding, giving the appearance of facies B2. Parasequence thickness varies from 10 to 23 m, and the duration of each parasequence is approximately 500 ka to over 1 Ma based on high-resolution biostratigraphy. To the south of the study area, shoreface parasequences comprise complete facies successions (B1–B3) that pass upwards into coal and coastal plain deposits, recording continued progradation of the shoreline without a sequence stratigraphic discontinuity.

Wireline-log character. The GR log character of successions of this facies association shows an upward-decreasing trend as they become more sandstone-rich towards their tops (Fig. 4b). The gradational contacts between facies can make recognition of distinct facies boundaries in wireline-log data difficult, although typically facies B1 is represented by a serrate, sometimes funnel-shaped GR curve, whilst facies B2 and B3 have lower GR values and are more blocky in character. Cross-plotting GR against DT and NPHI against RHOB (Fig. 6b) shows extensive overlap between facies B1 and B2, which makes distinguishing these facies difficult away from core control, whilst facies B3 plots as a distinctly separate group on both graphs.

Mouth bar facies association: C

This facies association is developed in the central part of the study area, where it interfingers with shoreface deposits. Deposits of this association are similar to the mouth bar facies association described in the Sleipner Vest Field by Folkestad & Satur (2008).

Description. Units of this facies association comprise either a complete upward-coarsening succession of C1 and overlying C2 facies, or individual beds of C1 and/or C2 facies that interfinger with shoreface deposits (Figs 4c & 5c). The lower part of complete successions consists of moderately to highly bioturbated siltstones and very fine-grained sandstones that coarsen upward to medium- through very coarse-grained sandstones (facies C1). Cross-bedding, including coarse-grained stringers, and mudstone laminae are preserved at bed tops and as drapes along cross-bed foresets where bioturbation intensity is lowest. Complete successions are more sand-rich in their upper parts, which corresponds with a decrease in bioturbation intensity and the loss of very coarse-grained sandstone stringers (facies C2). Successions of this facies association are commonly capped by a coal, although some are truncated by overlying shoreface deposits.

Interpretation. The upward-coarsening grain-size trend of successions of this facies association implies a progradational trend, with increasing proximity to the source of coarse sand and granules towards the top. The intensity and diversity of bioturbation suggests a marine depositional setting, whilst poorly sorted, coarse-grained sandstones and stringers are indicative of fluvial input (e.g. Fielding *et al.* 2005) and mudstone drapes and laminae may imply tidal action (e.g. Nio & Yang 1991). Preservation of indicators of fluvial sediment influx suggests deposition in mouth bars and signifies low wave reworking of fluvially supplied sediment, which may support wave suppression within the narrow graben (Folkestad & Satur 2008).

Sequence stratigraphy. Distal mouth bar deposits (facies C1) at the base of the succession are seen juxtaposed directly above both coastal plain coals and upper shoreface sandstones, implying a flooding surface (*sensu* Van Wagoner *et al.* 1988) at their base. A sharp increase in bioturbation, locally coupled with coarse-grained sandstone, carbonaceous and bioclastic beds, marks this surface. Where this facies association occurs interfingered with units of the shoreface facies association, autogenic lateral migration of the fluvial system is inferred to drive this stratigraphic relationship rather than a relative sea-level change.

Wireline-log character. The GR log character of this facies association is variable with upward-decreasing profiles and, less commonly, upward-increasing, blocky and funnel-shaped profiles recognized. Wireline-log cross-plots (Fig. 6c) show significant overlap between facies C1 and C2, although facies C2 exhibits a broader range of values. The wireline-log character of the mouth bar facies association (particularly facies C1) is very similar to that of the shoreface facies association, making it difficult to differentiate between the two facies associations away from core control.

Fluvio-tidal channel-fill facies association: D

Identified in the southern part of the study area, this facies association occurs closely associated with mouth bar and coastal plain deposits. Facies D1 is broadly equivalent to the tidal channel facies association previously described from the Sleipner Vest Field (Folkestad & Satur 2008).

Description. Facies D1 and D2 both comprise sharp-based, upward-fining successions of coarse- to medium-grained, cross-bedded sandstones (Figs 4d & 5d). In facies D1, the sandstones contain bi-directional cross-bed sets and/or swaley cross-stratification, and asymmetrical ripple forms preserved by mudstone drapes. Bioturbation intensity is low to zero, with rare escape traces present within finer-grained intervals. The sandstones in facies D2 contain unidirectional cross-bed sets which lack bioturbation and mud drapes, although carbonaceous fragments and laminae are common. Some successions of facies D2 exhibit a weak upward-coarsening trend in grain size in their lower parts. Units of facies D1 pass vertically and laterally into units of facies D2, but are also overlain by bay-fill, shoreface, mouth bar and offshore deposits. Units of facies D2 are commonly overlain by coals and coastal plain deposits.

Interpretation. The sharp, possibly erosive, bases and upward-fining character of successions of this facies association indicate deposition within channels under conditions of gradually decreasing energy, which may record channel migration or abandonment. Bi-directional cross-bed sets and mud drapes in facies D1 are indicative of tidal influence (e.g. Nio & Yang 1991), whilst the absence of such features in facies D2 suggests less tidal and marine influence. These interpretations imply that facies D2 is the updip equivalent of facies D1. Alternatively, the lack of tidal influence within facies D2 could represent deposition in rivers that lacked tidal amplification near their mouths and were associated with linear-to-lobate, deltaic shorelines; facies D1 would then represent deposition within funnel-shaped estuaries that locally amplified tidal currents. The overall depositional setting of this facies association is interpreted to be variably marine-influenced fluvial channel fills.

Sequence stratigraphy. The basal surfaces of successions of this facies association may not necessarily have sequence stratigraphic importance, but instead record autogenic channel migration and avulsion. However, where a unit of marine-influenced facies D1 directly overlies coastal plain deposits, a tidal ravinement surface is interpreted at its base, as the precursor or updip correlative to a flooding surface. Where such units overlie bay-fill deposits, they are difficult to distinguish from tidal inlets that formed as part of a barrier island and associated shoreface (facies A4, Table 1); inlet channel-fills pinch out landward into bay-fill deposits, whereas fluvio-tidal channel-fills extend up depositional dip into fluvial channels in the coastal plain. Sequence stratigraphic interpretation and correlation of channel-fill sandstones that overlie bay-fill deposits are therefore uncertain, particularly in the absence of core.

Wireline-log character. This facies association is generally represented by low GR values and a blocky GR profile (Fig. 4d), although rare upward-decreasing and upward-increasing GR profiles are also noted. Wireline cross-plots (Fig. 6d) highlight variation in the GR, RHOB and NPHI response of the facies (Table 1).

Coastal plain facies association: E

Thin accumulations of this facies association occur throughout the study area, although the thickest and best developed examples are closely associated with fluvio-tidal channel-fill deposits in the southern part of the study area.

Description. This facies association predominantly comprises coal (facies E1) with associated heterolithic deposits of interbedded mudstone, siltstone and very fine-grained sandstone (facies E2) (Figs 4e & 5e). Preserved root traces are common throughout the heteroliths, disrupting lamination below coal beds. Wood fragments occur within coal beds, and angular carbonaceous fragments from the coal beds are reworked into overlying sediments. Units of this facies association are locally eroded by fluvio-tidal channel-fill deposits and pass laterally into bay-fill and shoreface deposits. The units are abruptly overlain by offshore, shoreface, mouth bar and bay-fill deposits. Coal beds and thin successions of facies E2 cap upward-coarsening shoreface, mouth bar and bay-fill successions.

Interpretation. Coal deposition can occur in a wide range of depositional environments; however, the context of coals (facies E1) in the Hugin Formation suggests a coastal plain environment. Roots beneath the coal beds indicate that they developed *in situ*. The interbedding of sandstones and siltstones with mudstones in facies E2 suggests a regularly fluctuating energy regime, most likely related to variations in discharge and sediment load in adjacent fluvio-tidal channels. The association of facies E2 with coals (facies E1), bay-fill, shoreface, mouth-bar and fluvio-tidal channel-fill deposits supports a coastal plain environment of deposition.

Sequence stratigraphy. Thin intervals of the coastal plain facies association that cap upward-coarsening shoreface, mouth bar and bay-fill successions are interpreted to record subaerial deposition in response to shoreline progradation, and they thus form the upper part of shallow-marine and marginal-marine parasequences. Where these coastal plain intervals are abruptly overlain by offshore, shoreface, mouth bar and bay-fill deposits, their upper bounding surfaces are interpreted as flooding surfaces that record increases in water depth. Coal fragments reworked from the coastal plain intervals into overlying deposits imply erosion during transgression.

Wireline-log character. This facies association is typically represented by a low GR, blocky to serrate log curve (Fig. 4e), although funnel shaped patterns are also observed. This facies association is characterized by high DT values combined with low GR values (Fig. 6d). Coal units (facies E1) are distinctive throughout the study area with low GR, very slow sonic and low density values, allowing them to be easily identified away from core control.

Offshore open-marine facies association: F

This facies association is equivalent to the shales of the Heather Formation, and interfingers with shoreface, mouth bar and bay-fill deposits in the southern part of the study area.

Description. This facies association comprises highly bioturbated mudstones and siltstones that constitutes a single facies (F). Bioturbation ranges from moderate to high in intensity, and is highly diverse. Trace fossil assemblages are similar to the archetypal *Cruziana* ichnofacies (cf. MacEachern & Bann 2008). Unbioturbated, coarse-grained siltstone to very fine-grained sandstone beds occur locally, and contain parallel lamination and soft sediment deformation. Units of facies F are gradationally overlain by upward-coarsening shoreface and mouth bar deposits, and they pass laterally into bay-fill, shoreface and mouth bar deposits. These units abruptly overlie shoreface, bay-fill, fluvio-tidal channel-fill and coastal plain deposits.

Interpretation. The fine-grained character of these deposits, combined with their parallel laminated character where not bioturbated, suggests deposition by fall-out from suspension. The high degree of bioturbation by a fully marine trace fossil suite of the *Cruziana* ichnofacies implies deposition in an open-marine setting, below fair weather wave base. Sharp-based, coarser-grained beds that lack bioturbation are interpreted to have been deposited during major storm events. Soft-sediment deformation within and below these beds is attributed to loading and water escape.

Sequence stratigraphy. This facies association represents the deepest fully marine setting observed within the studied interval. Where units of the facies association are juxtaposed directly above shoreface, bay-fill, fluvio-tidal channel-fill or coastal plain deposits, their bases represent abrupt deepening across a flooding surface (*sensu* Van Wagoner *et al.* 1990). The gradational upper contacts of the units represent gradual shallowing into shoreface and mouth bar deposits.

Wireline-log character. Units of this facies association have consistently high GR values, with bed-scale variations in grain size represented by a slightly serrate GR-log character.

Sequence stratigraphic framework

The facies associations described above and their bounding sequence stratigraphic surfaces have been correlated to construct a regional sequence stratigraphic framework for the Hugin Formation within the study area. Correlation between the wells has been constrained by a newly revised, high-resolution biostratigraphic and chronostratigraphic scheme that is based on the Statoil ASA biostratigraphic framework for Jurassic strata in the North Sea. Although fine biostratigraphic resolution (*c.* 500 ka) was achieved within the marine Hugin and Heather formations, the long-ranging character of pollen and spores within the Sleipner Formation precludes a similarly detailed zonation of this unit. As a result, correlation of sequence stratigraphic surfaces between the Hugin and Sleipner formations is difficult. Regionally extensive flooding surfaces have been identified where marine microfossil assemblages with high diversity and abundance occur associated with distinctive GR profiles. Where possible, these regional extensive flooding surfaces have been tied into the widely used nomenclature of Partington *et al.* (1993) and are, therefore, referred to as maximum flooding surfaces. One additional regional maximum flooding surface has been identified, referred to below as MFS A; this surface is slightly older than MFS J42 (Partington *et al.* 1993). Higher-order flooding surfaces of sub-regional and local extent have been identified by facies interpretation of core and wireline-log data, and their correlation constrained by distinct palynological events and zones. The sequence stratigraphic framework and associated facies distributions are illustrated below using three correlations through the study area (Figs 3 & 7–9) and two gross palaeogeographic reconstructions that represent early Hugin deposition (MFS A) and mid to late Hugin deposition (MFS J44) (Fig. 10). The presented maps reflect snapshots in time recording final shallow-marine deposition within the parasequence that precedes the transgression associated with the named MFS.

The highly variable nature of interpreted subsidence rates and sediment supply across the study area, which is typical of both rift basins and salt-influenced provinces, makes it both scientifically unsound and impractical to apply systems-tract terminology. Stratigraphic architectures are demonstrably different in the northern, central and southern parts of the study area (Figs 7–9), and they are also likely to have varied around actively growing structures such as rift-related fault blocks (e.g. Gawthorpe *et al.* 1994; Gawthorpe & Leeder 2000) and salt diapirs and walls (e.g. Giles & Lawton 2002; Aschoff & Giles 2005). Although alternating highstand and transgressive systems tracts have been interpreted in the rapidly, but laterally uniformly subsiding Sleipner Vest Field (Folkestad & Satur 2008), it is more appropriate over much of the study area to apply descriptive sequence stratigraphic schemes that do not assume cyclical relative sea-level changes of at least sub-regional extent. Such descriptive schemes include the terminology of parasequence stacking patterns (Van Wagoner *et al.* 1988) and shoreline trajectory analysis (Helland-Hansen & Martinsen 1996; Helland-Hansen & Hampson 2009). We refer to sequence stratigraphic surfaces of various types and lateral extents below, without forcing the intervening stratigraphic packages into an inappropriate systems-tract template.

Regional correlation along basin axis

The studied strata are subdivided into five intervals bounded by regional maximum flooding surfaces that can be correlated along the axis of the South Viking Graben (Figs 3 & 7). Within the first, lowermost interval (below MFS J36), shallow marine deposition (Hugin Formation) was confined to the northern part of the study area within restricted marine bays and/or lagoons which pass to the south into coastal plain deposits (Sleipner Formation). In the second interval (between MFS J36 and MFS A), bay-fill deposition persisted in the north and passed towards the central part of the study area into coastal plain deposits (Sleipner Formation) overlain locally by shoreface deposits (Hugin Formation) and offshore mudstones (Heather Formation). These offshore mudstones are penetrated within the most basinward (i.e. westwards) well (well F, Figs 3 & 7) and imply that locally irregular shoreline trends were developed as a result of early flooding of the graben. Further south, shoreface deposits pass updip into coastal plain (Sleipner Formation) deposits. In the third interval (between an MFS A and MFS J44), offshore mudstone (Heather Formation) deposition dominated the study area with shoreface deposition (Hugin Formation) locally restricted to the central and northernmost parts of the study area. Interpretation of the age and depositional setting of sandstones in the northernmost well (well I, Fig. 7) is, however, poorly constrained by biostratigraphic and core data. Similarly, the fourth interval (between MFS J44 and MFS J46) is dominated by offshore mudstone (Heather Formation) deposition across the study area, with two exceptions. Firstly, shoreface sandstones persist in the central part of the study area (well E, Fig. 7). Secondly, a series of parasequences comprising fluvio-tidal channel-fill, bay-fill, mouth bar and coastal plain deposits build out from the south (well A, Fig. 7), as part of a major delta system present in the vicinity of the Sleipner Vest Field (Vollset & Dore 1984; Milner & Olsen 1998; Folkestad & Satur 2008). This depositional pattern persists into the fifth, uppermost interval (between MFS J46 and MFS J52), with both shoreface and fluvio-deltaic deposits being capped by offshore mudstones (Heather Formation) in the upper part of this interval.

The intervals defined by regional maximum flooding surfaces can be further subdivided by flooding surfaces of sub-regional and local extent. The limited extent of these flooding surfaces most likely reflects variations in sediment supply and accommodation creation that were caused by rift-fault initiation and linkage and/or by the growth of salt-cored highs (e.g. Figs 7b & 9b). Candidate sequence boundaries of local extent are interpreted in the southernmost part of the study area (well A, Fig. 7), based on vertical facies juxtapositions that suggest abrupt basinward facies dislocations. These sequence boundaries can be traced into and through the Sleipner Vest Field (corresponding to the surfaces of maximum regression of Folkestad & Satur 2008), but cannot be correlated more widely. Their limited extent is typical of net-transgressive strata, within which sequence boundary expression is suppressed (e.g. Nummedal & Swift 1987; Sneider *et al.* 1995), and also of rift basins, where sequence boundary development is enhanced by uplift in marginal areas and suppressed by increased subsidence in axial depocentres (e.g. Mitchener *et al.* 1992; Gawthorpe *et al.* 1994).

Axis-perpendicular sub-regional correlation, Sigrun–Gudrun area

In the northern part of the study area, near the Sigrun and Gudrun fields, thick (up to 200 m) successions of up to 12 stacked bay-fill and shoreface parasequences are defined by localized flooding surfaces (Fig. 8). Most of this succession occurs within the second regionally mapped interval (between MFS J36 and MFS A). The underlying regionally mapped interval (below MFS J36) lies below the interval penetrated in the westward-lying wells (well J, Fig. 8) and is represented by coastal plain (Sleipner Formation) deposits or an unconformity in the eastern part of the Sigrun–Gudrun area. The bay-fill parasequences thicken markedly

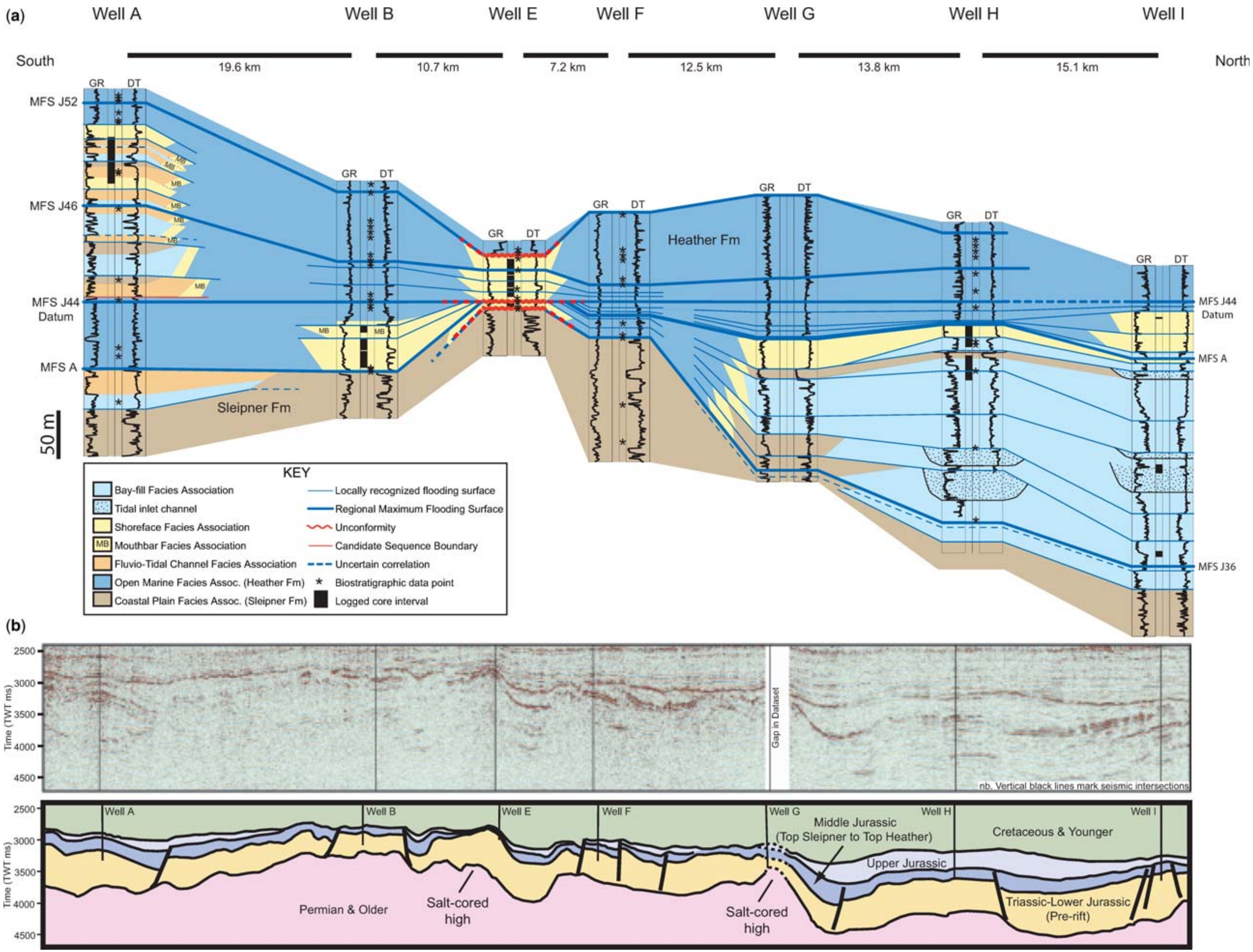

Fig. 7. (**a**) Regional north–south-oriented well-log correlation panel and (**b**) corresponding seismic section along the axis of the South Viking Graben (see Fig. 3 for location). In general, the Hugin Formation becomes younger towards the south. Well-log correlation is constrained by a combination of seismically mapped thicknesses and biostratigraphic data in wells A, B, E, F and H (biostratigraphic sample points are marked by asterisks).

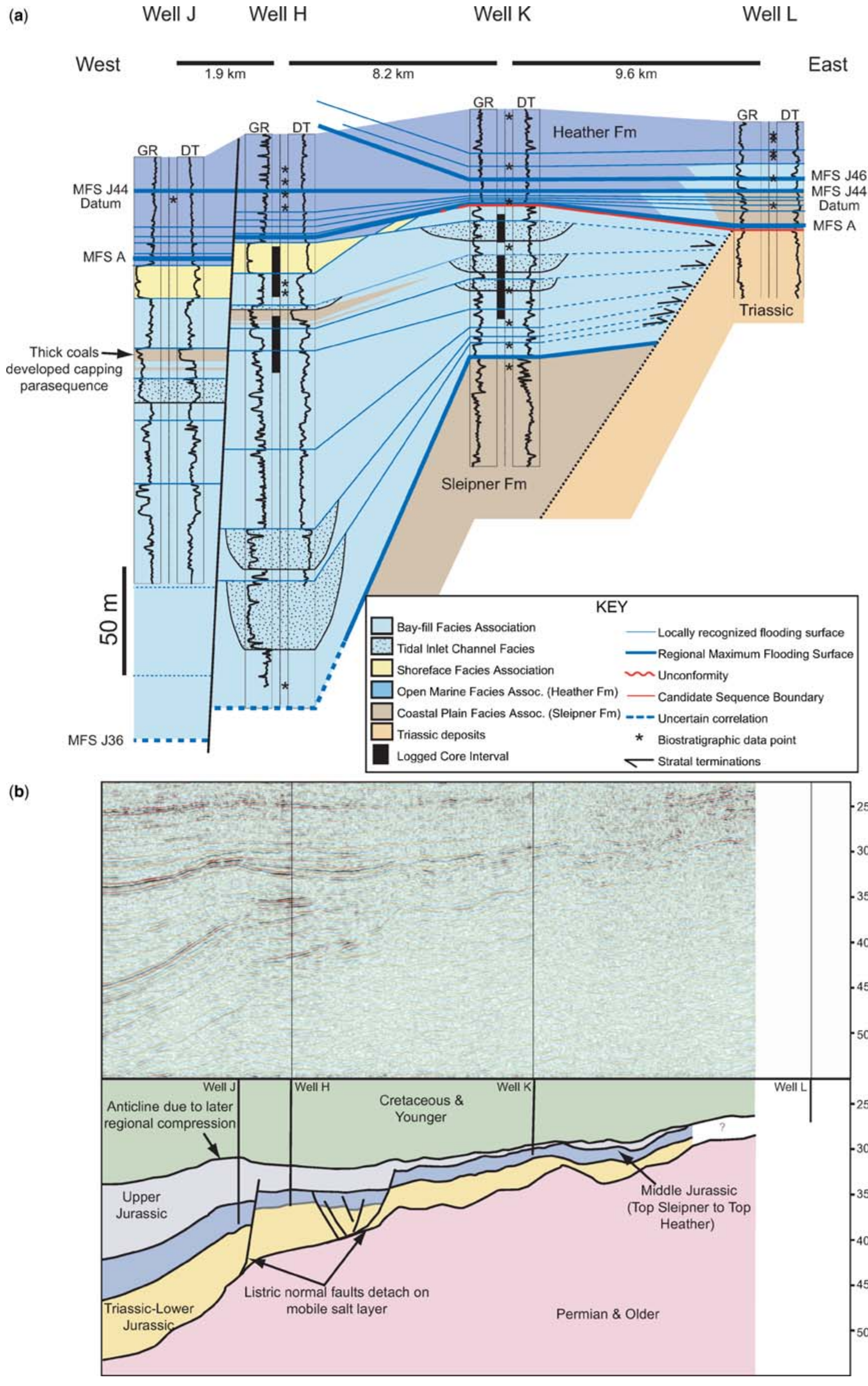

Fig. 8. (**a**) Regional west–east-oriented well-log correlation panel and (**b**) corresponding seismic section perpendicular to the axis of the South Viking Graben in the Sigrun–Gudrun area (see Fig. 3 for location). The Hugin Formation becomes younger towards the east. Well-log correlation is constrained by a combination of seismically mapped thicknesses, which indicate that the fault between wells H and J was active during Hugin Formation deposition, and biostratigraphic data in wells H, J, K and L (biostratigraphic sample points are marked by asterisks). The key is the same as for Figure 7.

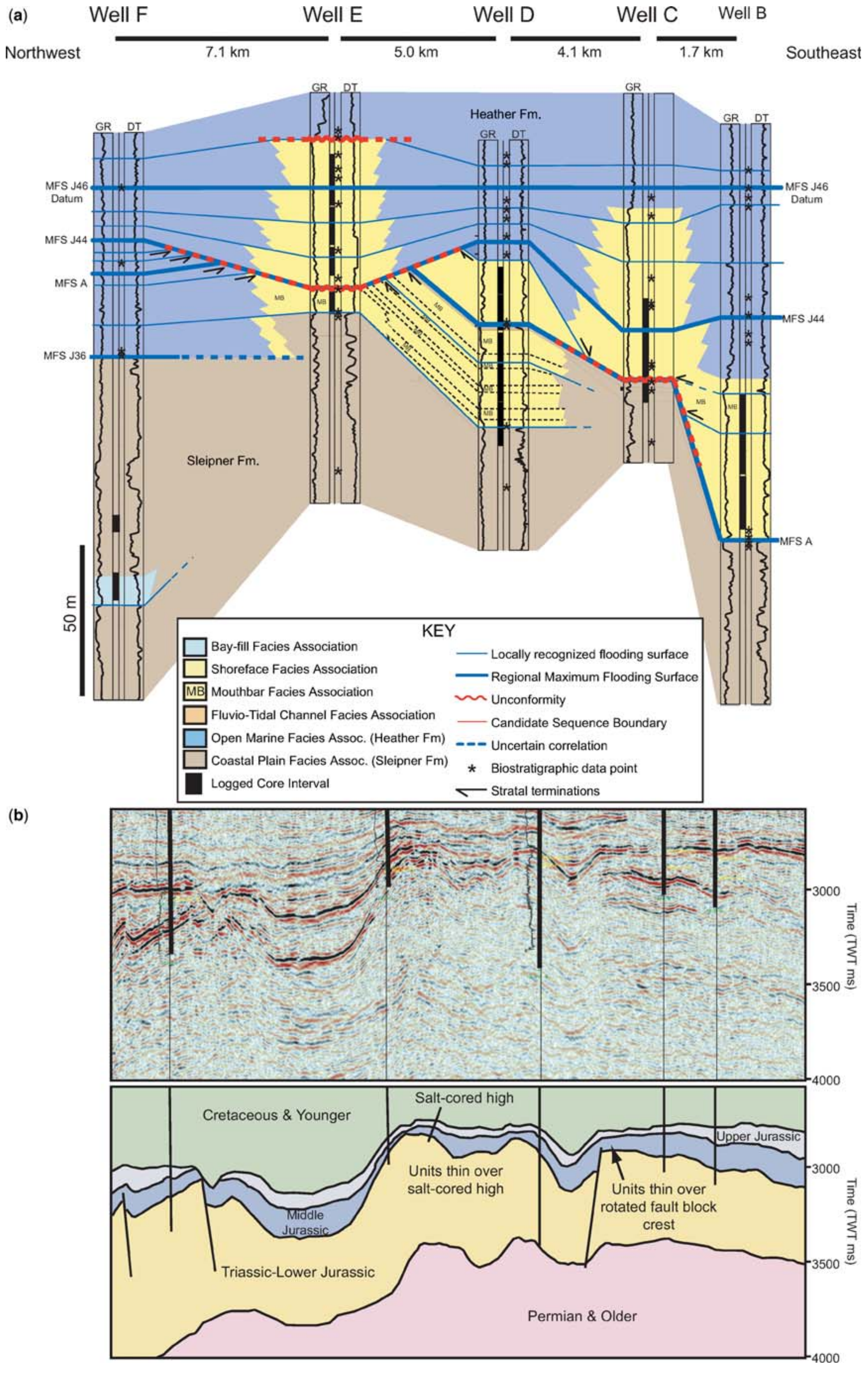

Fig. 9. (**a**) Regional NW–SE-oriented well-log correlation panel and (**b**) corresponding seismic section oblique to the axis of the South Viking Graben in the Dagny area (see Fig. 3 for location). The Hugin Formation is highly diachronous and exhibits large local thickness variations, including across syn-depositional faults. Well-log correlation is constrained by a combination of seismically mapped thicknesses and biostratigraphic data in wells B, C, D, E and F (biostratigraphic sample points are marked by asterisks). The key is the same as for Figure 7.

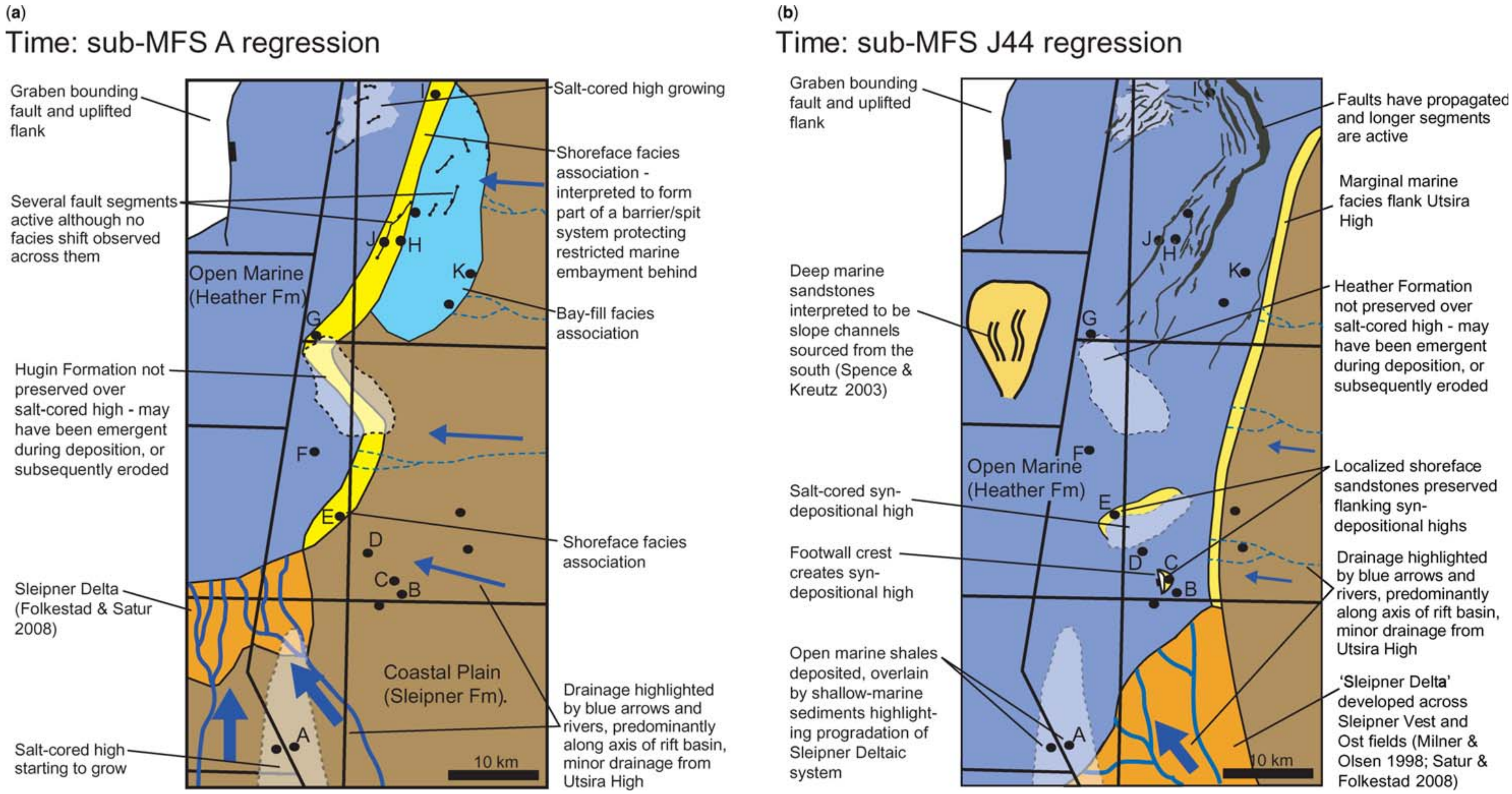

Fig. 10. Palaeogeographic reconstructions of deposition in the study area during (**a**) Early Callovian (MFS A) and (**b**) Middle Callovian (MFS J44) times.

towards the west and thin to the east, where they are interpreted to onlap Triassic strata. Westward thickening also occurs in the hanging wall of a normal fault in the western part of the Sigrun–Gudrun area, but this thickening is not accompanied by a noticeable facies shift. Several of the bay-fill parasequences are truncated by thick (up to 45 m) channel-fill sandstones that are not cored. These sandstones are interpreted as tidal inlet channel-fill deposits (facies A4), based on their clean, low GR character, which is consistent with marine reworking, and the occurrence of shoreface sandstones in overlying strata. Alternatively, these sandstones may alternatively represent fluvio-tidal channel-fill deposits (facies D1, D2). Shoreface sandstones occur in the uppermost Hugin Formation, above the stacked bay-fill parasequences, in the western part of the Sigrun–Gudrun area. These shoreface deposits pass eastward into bay-fill deposits. Prior to formation of regional flooding surface MFS A, most of the Sigrun–Gudrun area had been covered by offshore mudstones (Heather Formation). Above this surface, in the third and fourth regionally mapped intervals (between MFS A and MFS J46), coastal plain deposits (Sleipner Formation) unconformably overlie Triassic strata and pass westward into bay-fill deposits and offshore mudstones (Heather Formation). The entire Sigrun–Gudrun area was flooded during the fifth regionally mapped interval (between MFS J46 and MFS J52).

Flooding of the Sigrun–Gudrun area was diachronous, becoming younger from west to east. The relatively low-energy, restricted-marine character of the bay-fill parasequences implies the presence further west of coeval barriers and spits fronted by wave-dominated shorefaces (Harris & Fowler 1987; Hampson *et al.* 2009) or rift-generated islands and shoals. The local occurrence of wave-dominated shoreface deposits above the bay-fill parasequences supports the former interpretation, although the latter cannot be discounted. In any case, aggradational stacking of the bay-fill parasequences indicates that sediment supply and accommodation generated by tectonic subsidence were roughly in balance during deposition of the second regionally mapped interval (between MFS J36 and MFS A).

Axis-perpendicular sub-regional correlation, Dagny area

In the centre of the study area, around the Dagny Field, localized flooding surfaces subdivide the five regionally mapped intervals into 11 parasequences (Figs 3 & 9), which cannot be correlated to those in the Sigrun–Gudrun area (Fig. 8). Coastal plain (Sleipner Formation) deposition occurred across the Dagny area in the lowermost regionally mapped interval (below MFS J36). Marine flooding of the Dagny area commenced during deposition of the second regionally mapped interval (between MFS J36 and MFS A). Within this interval, offshore mudstones (Heather Formation) in the NW pass to the south through mouth bar and shoreface deposits (Hugin Formation) into coastal plain deposits (Sleipner Formation). Within the overlying regionally mapped interval (between MFS A and MFS J44), marine flooding occurred over the whole of the Dagny area, with shoreface sandstones and offshore mudstones being deposited. The base and top of this interval are marked by local unconformities, interpreted due to missing or significantly thinned biostratigraphic zones. Observation of seismic reflection event geometries suggests these surfaces are angular unconformities developed towards the crest of salt-cored structural highs or rotated fault blocks. The lower unconformity correlates to a thick shoreface succession (well B, Fig. 9), which is interpreted to onlap or downlap the underlying shoreface parasequences (well C, Fig. 9). Biostratigraphic data indicate that the upper unconformity is marked by significant missing sections, implying deep erosional truncation of underlying shoreface parasequences that may have been deposited coevally with those observed to the SE (well D, Fig. 9), while correlative offshore mudstones occur towards the NW (in well E, Fig. 9). The fourth regionally mapped interval (between MFS J44 and MFS J46) is present across the Dagny area and contains laterally discontinuous shoreface sandstones (in wells C and E, Fig. 9) that pinch out to the NW and SE into offshore shales (Heather Formation). The entire Dagny area was flooded prior to deposition of regional maximum flooding surface MFS J46, with the exception of well E (Fig. 9), in which shoreface sandstones were deposited. Biostratigraphic data indicate that these sandstones are capped by another locally developed Early to Middle Oxfordian unconformity, which lies within the fifth regionally mapped interval (between MFS J46 and MFS J52) and is overlain by offshore mudstones (Heather Formation).

The mouth bar deposits interpreted within the second and third regionally mapped intervals (between MFS J36 and MFS J44) in the northwestern part of the Dagny area pass updip into coastal plain deposits (Sleipner Formation) (Fig. 9), suggesting that they are linked to either the delta system in the Sleipner Vest area to the south or to small rivers draining the eastern graben margin. This subtle fluvial signature is absent in younger units, corresponding to the fourth and fifth regionally mapped intervals (between MFS J44 and MFS J52). In these younger intervals, the complex and highly localized distribution of shoreface deposits suggest that they were geographically detached from the Sleipner Vest delta system to the south and potentially from the shoreline along the eastern graben margin. The resulting shoreface sandstone distribution is interpreted to have been controlled by syn-depositional development of salt-cored highs and rotated fault-block crests that formed islands and shoals whilst deeper water depositional conditions prevailed elsewhere in the Dagny area. These 'isolated' shoreface sandstones may have been deposited by in-place reworking of older sandstones that were eroded at angular unconformities, or they may have been fed by southward-directed longshore currents that nourished spit systems connected to the Utsira High, on the eastern graben margin (Figs 1 & 10b). The rapid facies transitions from syn-depositional topographic highs, marked by angular unconformities, into adjacent areas of expanded stratigraphy indicate that sediment supply was not sufficient to keep pace with accommodation generated by rift-fault development and salt movement.

Palaeogeographic reconstruction, sub-MFS A regression

The well correlations described above highlight the diachroneity and complex spatial distribution of flooding within the South Viking Graben during the Middle Jurassic. These patterns become clearer in palaeogeographic reconstructions described below.

Prior to transgression and development of regional maximum flooding surface MFS A (Figs 7–9), coastal plain deposition (Sleipner Formation) was prevalent throughout much of the study area, with shallow-marine sedimentation limited to the NW, in the Sigrun–Gudrun area (Fig. 10a). Barrier islands fronted by wave-dominated shorefaces are interpreted to have been the predominant shoreline type in the northern part of the study area. These barrier islands sheltered a restricted marine embayment to the east, on the western flank of the Utsira High. The barrier islands are inferred to have developed initially during parasequence-bounding transgressions, but may have been maintained during subsequent regressions by southward-directed sand transport via longshore currents, as occurs in approximately one-third of modern barrier island systems (Stutz & Pilkey 2001). Minor river systems are interpreted to have drained from the Utsira High down the hanging-wall dipslope towards the main graben-bounding fault and into this embayment. The barrier island system may have been supplied with sediment by southward-directed longshore drift generated by oblique wave approach from the north or NW, or by transgressive reworking of underlying bay-fill deposits during barrier retreat. The former mechanism appears more likely, because the shoreface sandstones are significantly coarser grained than the bay-fill deposits. The ultimate source of such coarse sand was most likely the Utsira High (Fig. 1), where Cretaceous and Cenozoic sediments directly overlie eroded granitic basement (e.g. Zanella & Coward 2003), although potential drainage systems that supplied this sediment to the shoreline are not resolved in seismic and well data.

A salt-cored high is mapped in seismic data to the south of the restricted marine embayment, in an area lacking well control in between the Sigrun–Gudrun and Dagny areas; Middle Jurassic strata are absent over this structure. This absence implies either non-deposition or subsequent erosion of the Middle Jurassic section; the former interpretation would indicate that the structure formed a syn-depositional topographic high that may have defined the southern limit of the restricted marine embayment.

To the south of this salt-cored high, in the Dagny area, shoreface sandstones abut directly against coastal plain deposits, implying a wave-dominated strandplain shoreline. Further south, in the area around the Sleipner Vest Field, fluvial–deltaic deposition occurred. The deposits of the 'Sleipner Delta' were influenced by both waves and tides (Folkestad & Satur 2008). Although the limited wave energy in these deposits appears to contradict the interpretation of strong wave-generated longshore currents in the Sigrun–Gudrun area, the discrepancy can be explained by the more enclosed and sheltered location of the Sleipner Vest area at the southern limit of the embryonic South Viking Graben. Folkestad & Satur (2008) argue that the narrow geometry of the graben in this area would have suppressed wave action and amplified tidal currents. Dominant fluvial drainage into the South Viking Graben is interpreted to have been from the south, along the basin axis, and the 'Sleipner Delta' deposits form a small component of the regional back-stepping Middle-to-Upper Jurassic 'Brent Delta' systems (Rattey & Hayward 1993; Milner & Olsen 1998; Husmo *et al.* 2003).

Palaeogeographic reconstruction, sub-MFS J44 regression

Prior to transgression and development of regional maximum flooding surface MFS J44 (Figs 7–9), the majority of the study area was flooded and offshore mudstone deposition (Heather Formation) was prevalent (Fig. 10b), with deepwater fan sandstones (Ling Member, Heather Formation) deposited in the basin axis within the UK sector (e.g. in well 16/8A-4; Cockings *et al.* 1992). The distribution of these deepwater fan sandstones is poorly defined, but they are interpreted to have been axially sourced from the south (Spence & Kreutz 2003). Coastal plain deposits (Sleipner Formation) lay in the SE of the study area and are interpreted to have been fringed by shoreline deposits that are not penetrated by wells. These deposits are inferred to be shoreface sandstones rather than bay-fill heteroliths due to the wider, more open geometry of the basin at this time. 'Isolated' shoreface sandstones are locally developed within the Dagny area, most likely fringing syn-depositional topographic highs formed by fault-block crests and salt-cored structures. Fluvial–deltaic deposits are not present in the study area at this time but occur further south in the area of the Sleipner Vest and Ost fields (Folkestad & Satur 2008). The 'Sleipner Delta' system later prograded to the north and west, to deposit younger fluvio-deltaic units within the study area (between MFS J44 and MFS J52 in well A, Fig. 7).

Summary and implications for exploration

The Hugin Formation was deposited during a tectonically driven transgression that flooded the South Viking Graben. Biostratigraphic data permit robust correlation of regional maximum flooding surfaces over distances of several tens of kilometres, and these correlations indicate overall younging of the unit up the hanging wall to the east, and along the main basin axis to the south. Relatively early flooding (Middle Callovian, MFS A) of the southernmost wells, however, implies that open marine conditions may have existed within the basin axis at this time. Biostratigraphically driven correlations also indicate that each of the main facies associations was developed within a different structural location and therefore had local stratigraphic development controlled by markedly different tectonic styles. In addition, distance from the main fluvial sediment supply system into the basin axis from the south was also a key control on facies development and distribution. Parasequence-bounding flooding surfaces and candidate sequence boundaries are also recognized and correlated locally; they cannot, however, be confidently correlated throughout the area. This is interpreted to be a function of the overall transgressive nature of the succession and, more importantly, significant spatial variations in fault- and halokinesis-controlled subsidence across the basin. Differential subsidence restricted sequence boundary development to the basin flanks and these surfaces are interpreted to pass into correlative conformities or flooding surfaces in more basinal settings.

The complex spatial variations in facies within the Hugin Formation have significant implications for regional exploration within the South Viking Graben. The more prospective reservoir intervals are likely to be in the upper part of the unit where shallow-marine rather than restricted-marine deposits are best developed. Potential reservoir sandstones occur in four locations:

(1) North–south-trending belts of shoreface sandstone occur in northern parts of the study area, together with more laterally restricted, tidal inlet channel-fill sandstones that erode into bay-fill deposits of marginal reservoir quality. These potential reservoir sandstones, although deposited during active growth faulting, do not appear to have had their location or areal extent determined by syn-depositional tectonic features. Therefore, predicting their occurrence based on structural location is problematic.
(2) Shoreface sandstones with complex plan-view geometries and rapid lateral pinchouts occur in central parts of the study area. These sandstones fringe or overlie growing halokinesis-related structures and other palaeo-topographic highs.
(3) North–south-trending, channelized and lobate mouth-bar sandstones of the 'Sleipner Delta' remained relatively fixed in their overall location within southern parts of the study area. The gross distribution of these sandstones is caused by high fluvial sediment supply from the south, focussed along the main axial drainage pathway.
(4) Axially fed deepwater fan deposits of the Ling Sandstone Member (Heather Formation) occur in the basin centre. These deepwater sandstones may have been genetically linked to the broadly coeval shallow-marine and coastal-plain deposits of the 'Sleipner Delta', although the details of this linkage are unclear in the absence of more data to further constrain their age and palaeogeographic distribution.

The stratigraphic and palaeogeographic reconstructions presented here indicate that the geometry and distribution of these various potential reservoir sandstones is closely related to both depositional regime (i.e. shoreface, river-dominated delta, barred lagoons) and structural location. Therefore, a robust understanding of temporal and spatial variation in depositional system type and tectonically driven, syn-depositional basin geometry is critical to successful exploration of reservoirs in the Hugin Formation and coeval strata.

Statoil ASA are thanked for funding this research project, and together with their partners within licence PL303 are thanked for permission to publish this work. We also thank A. Tjemsland for biostratigraphic analysis and related discussions, and K. Kane for help with seismic interpretation and drafting of some figures. Landmark Graphics are gratefully acknowledged for provision of OpenWorks software through the Academic Licence Agreement with Imperial College.

References

Aschoff, J. L. & Giles, K. A. 2005. Salt diapir-influenced, shallow-marine sediment dispersal patterns: insights from outcrop analogs. *Bulletin of the American Association of Petroleum Geologists*, **89**, 447–469.

Cockings, J. H., Kessler, L. G., Mazza, T. A. & Riley, L. A. 1992. Bathonian to mid-Oxfordian sequence stratigraphy of the South Viking Graben, North Sea. *In*: Hardman, R. F. P. (ed.) *Exploration Britain; Geological Insights for the Next Decade*. Geological Society, London, Special Publications, **67**, 65–105.

Dott, R. H. & Bourgeois, J. 1982. Hummocky stratification: significance of its variable bedding sequences. *Bulletin of the Geological Society of America*, **93**, 663–680.

Duke, W. L., Arnott, R. W. C. & Cheel, R. J. 1991. Shelf sandstones and hummocky cross-stratification; new insights on a stormy debate. *Geology*, **19**, 625–628.

Fielding, C. R., Trueman, J. D. & Alexander, J. 2005. Sharp-based, flood-dominated mouth bar sands from the Burdekin River delta of northeastern Australia; extending the spectrum of mouth-bar facies, geometry, and stacking patterns. *Journal of Sedimentary Research*, **75**, 55–66.

Folkestad, A. & Satur, N. 2008. Depositional model and sedimentary partioning of the Middle Jurassic Hugin Formation, Southern Viking Graben, North Sea. *Sedimentary Geology*, **207**, 1–21.

Gawthorpe, R. L. & Leeder, M. R. 2000. Tectono-sedimentary evolution of active extensional basins. *Basin Research*, **12**, 195–218.

Gawthorpe, R. L., Fraser, A. J. & Collier, R. E. L. 1994. Sequence stratigraphy in active extensional basins: implications for the interpretation of ancient basin-fills. *Marine and Petroleum Geology*, **11**, 642–658.

Giles, K. A. & Lawton, T. F. 2002. Halokinetic sequence stratigraphy adjacent to the El Papalote Diapir, northeastern Mexico. *Bulletin of the American Association of Petroleum Geologists*, **86**, 823–840.

Hampson, G.J., Sixsmith, P. J., Kieft, R. L., Jackson, C. A.-L. & Johnson, H. D. 2009. Quantitative analysis of net-transgressive shoreline trajectories and stratigraphic architectures: Mid-to-Late Jurassic of the North Sea rift basin. *Basin Research*, **21**, 528–558.

Harris, J. P. & Fowler, R. M. 1987. Enhanced prospectivity of the Mid–Late Jurassic sediments of the South. *In*: Brooks, J. & Glennie, K. W. (eds) *Petroleum Geology of North West Europe*. Graham & Trotman, London, 879–898.

Helland-Hansen, W. & Hampson, G. J. 2009. Trajectory analysis: concepts and applications. *Basin Research*, **21**, 454–483.

Helland-Hansen, W. & Martinsen, O. J. 1996. Shoreline trajectories and sequences: description of variable depositional-dip scenarios. *Journal of Sedimentary Research*, **B66**, 670–688.

Husmo, T., Hamar, G., Hoiland, O., Johannsessen, E. P. & Romuld, A. 2003. Lower and Middle Jurassic. *In*: Evans, D., Graham, C., Armour, A. & Bathurst, P. (eds) *The Millennium Atlas; Petroleum Geology of the Central and Northern North Sea*. Geological Society, London, 129–155.

Isaksen, G. H., Patience, R., van Graas, G. & Jenssen, A. I. 2002. Hydrocarbon system analysis in a rift basin with mixed marine and nonmarine source rocks; the South Viking Graben, North Sea. *Bulletin of the American Association of Petroleum Geologists*, **86**, 557–591.

Israel, A. M., Ethridge, F. G. & Estes, E. L. 1987. A sedimentological description of a microtidal, flood-tidal delta, San Luis Pass, Texas. *Journal of Sedimentary Petrology*, **57**, 288–300.

Jackson, C. A.-L. & Larsen, E. 2008. Temporal constraints on basin inversion provided by 3D seismic and well data: a case study from the South Viking Graben, offshore Norway. *Basin Research*, **20**, 397–417.

Kessler, L. G., II, Cockings, J. H. & Mazza, T. A. 1995. Sedimentological nature and tectonic implications of marine flooding surfaces and their basinward equivalents: examples from Middle Jurassic, South Viking Graben, North Sea and Middle Ordovician, Williston Basin, western North America. *In*: Steel, R. J., Felt, V. L., Johannesson, E. P. & Mathieu, C. (eds) *Sequence Stratigraphy on the Northwest European Margin*. Norwegian Petroleum Society, Trondheim, Special Publications, **5**, 167–197.

Knott, S. D. 2001. Gravity-driven crustal shortening in failed rifts. *Journal of the Geological Society, London*, **158**, 193–196.

Lyngsie, S. B., Thybo, H. & Rasmussen, T. M. 2006. Regional geological and tectonic structures of the North Sea area from potential field modelling. *Tectonophysics*, **413**, 147–170.

MacEachern, J. A. & Bann, K. L. 2008. The role of ichnology in refining shallow marine facies models. *In*: Hampson, G. J., Steel, R. J., Burgess, P. M. & Dalrymple, R. W. (eds) *Recent Advances in Models of Siliciclastic Shallow-Marine Stratigraphy*. Society of Economic Paleontologists and Mineralogists, Special Publications, Tulsa, Oklahoma, **90**, 73–116.

MacEachern, J. A. & Pemberton, S. G. 1992. Ichnological aspects of Cretaceous shoreface successions and shoreface variability in the Western Interior Seaway of North America. *In*: Pemberton, S. G. (ed.) *SEPM Core Workshop No. 17*. SEPM, Calgary, 57–84.

Martin, M. A. 1993. *Trace fossil analysis and sequence stratigraphy of the Upper Jurassic Fulmar Formation, Western Central Graben (U.K.C.S.)*. PhD thesis, University of Manchester, UK.

Milner, P. S. & Olsen, T. 1998. Predicted distribution of the Hugin Formation reservoir interval in the Sleipner Øst field, South Viking Graben; the testing of a three-dimensional sequence stratigraphic model. *In*: Gradstein, F. M., Sandvik, K. O. & Milton, N. J. (eds) *Sequence Stratigraphy, Concepts and Applications*. Norwegian Petroleum Society, Trondheim, Special Publications, **8**, 337–354.

Mitchener, B. C., Lawrence, D. A., Partington, M. A., Bowman, M. B. J. & Gluyas, J. 1992. Brent Group: sequence stratigraphy and regional implications. *In*: Morton, A. C., Hazeldine, R. S., Giles, M. R. & Brown, S. (eds) *Geology of the Brent Group*. Geological Society, London, Special Publications, **61**, 45–80.

Moslow, T. F. & Tye, R. S. 1985. Recognition and characterization of Holocene tidal inlet sequences. *Marine Geology*, **63**, 129–151.

Nio, S.-D. & Yang, C. 1991. Diagnostic attributes of clastic tidal deposits: a review. *Canadian Society of Petroleum Geologists, Memoirs*, **16**, 3–27.

Nummedal, D. & Swift, D. J. P. 1987. Transgressive stratigraphy at sequence-bounding unconformities: some principles derived from Holocene and Cretaceous examples. *In*: Nummedal, D., Pilkey, O. H. & Howard, S. D. (eds) *Sea Level Fluctuation and Coastal Evolution*. Society for Economic Paleontologists and Mineralogists, Special Publications, Tulsa, Oklahoma, **41**, 241–260.

Partington, M. A., Copestake, P., Mitchener, B. C. & Underhill, J. R. 1993. Biostratigraphic calibration of genetic stratigraphic sequences of the Jurassic-lowermost Cretaceous (Hettangian to Ryazanian) of the North Sea and adjacent areas. *In*: Parker, J. R. (ed.) *Petroleum Geology of Northwest Europe: Proceedings of the 4th Conference*. Geological Society, London, 347–370; doi: 10.1144/0040347.

Pemberton, S. G., MacEachern, J. A. & Frey, R. W. 1992. Trace fossil facies models: environmental and allostratigraphic significance. *In*: Walker, R. G. & James, N. P. (eds) *Facies Models: Response to Sea Level Change*. Geological Association of Canada, Newfoundland, 47–72.

Pemberton, S. G., MacEachern, J. A., Gingras, M. K. & Saunders, T. A. 2008. Biogenic chaos: cryptobioturbation and the work of sedimentologically friendly organisms. *Palaeogeography, Palaeoclimatology, Palaeoecology*, **270**, 273–279.

Rattey, R. P. & Hayward, A. B. 1993. Sequence stratigraphy of a failed rift system; the Middle Jurassic to Early Cretaceous basin evolution of the central and northern North Sea. *In*: Parker, J. R. (ed.) *Petroleum Geology of Northwest Europe: Proceedings of the 4th Conference*. Geological Society, London, 215–249; doi: 10.1144/0040215.

Richards, P. C. 1991. An estuarine facies model for the Middle Jurassic Sleipner Formation; Beryl Embayment, North Sea. *Journal of the Geological Society, London*, **148**, 459–471.

Richards, P. C., Lott, G. K., Johnson, H., Knox, R. W. O'B. & Riding, J. B. 1993. Jurassic of the central and northern North Sea. *In*: Knox, R. W. O'B. & Cordey, W. G. (eds) *Lithostratigraphic nomenclature of the UK North Sea*. British Geological Survey, Nottingham, 219.

Shelley, D. C. & Lawton, T. F. 2005. Sequence stratigraphy of tidally-influenced deposits in a salt-withdrawal minibasin: upper sandstone member of the Potrerillos Formation (Paleocene), La Popa basin Mexico. *Bulletin of the American Association of Petroleum Geologists*, **89**, 1157–1179.

Simms, A. R., Anderson, J. B. & Blum, M. 2006. Barrier island aggradation via inlet migration; Mustang Island, Texas. *Sedimentary Geology*, **187**, 105–125.

Sneider, J. S., Clarens, P. & de Vail, P. R. 1995. Sequence stratigraphy of the Middle to Upper Jurassic, Viking Graben, North Sea. *In*: Steel, R. J., Felt, V. L., Johannesson, E. P. & Mathieu, C. (eds) *Sequence Stratigraphy on the Northwest European Margin*. Norwegian Petroleum Society, Trondheim, Special Publications, **5**, 167–197.

Spence, S. & Kreutz, H. 2003. The Kingfisher Field, block 16/8a, UK North Sea. *In*: Gluyas, J. G. & Hichens, H. M. (eds) *United Kingdom Oil and Gas Fields Commemorative Millennium Volume*. Geological Society, London, Memoirs, **20**, 305–314.

Stutz, M. L. & Pilkey, O. H. 2001. A review of global barrier island distribution. *Journal of Coastal Research*, **34**, 15–22.

Swift, D. J. P. 1968. Coastal erosion and transgressive stratigraphy. *Journal of Geology*, **76**, 444–456.

Taylor, A. M. & Goldring, R. 1993. Description and analysis of bioturbation and ichnofabric. *Journal of the Geological Society*, **150**, 141–148.

Thomas, D. W. & Coward, M. P. 1996. Mesozoic regional tectonics and South Viking Graben formation; evidence for localised thin-skinned detachments during rift development and inversion. *Marine and Petroleum Geology*, **13**, 149–177.

Van Wagoner, J. C., Mitchum, R. M., Campion, K. M. & Rahmanian, V. D. 1990. Siliciclastic sequence stratigraphy in well logs, cores, and outcrops; concepts for high-resolution correlation of time and facies. Methods in Exploration Series. *American Association of Petroleum Geologists*, **7**.

Van Wagoner, J. C., Posamentier, H. W., Mitchum, R. M., Jnr., Vail, P. R., Sarg, J. F., Loutit, T. S. & Hardenbol, J. 1988. An overview of the fundamentals of sequence stratigraphy and key definitions. *In*: Wilgus, C. K., Hastings, B. S., Ross, C. A., Posamentier, H. W., Van Wagoner, J. & Kendall, C. G. St. C. (eds) *Sea-level Changes; an Integrated Approach*. Society of Economic Paleontologists and Mineralogists, Special Publications, Tulsa, Oklahoma, **42**, 39–45.

Varadi, M., Antonsen, P., Eien, M. & Häger, K. 1998. Jurassic genetic sequence stratigraphy of the Norwegian block 15/5 area, South Viking Graben. *In*: Gradstein, F. M., Sandvik, K. O. & Milton, N. J. (eds) *Sequence Stratigraphy – Concepts and Applications*. Norwegian Petroleum Society, Trondheim, Special Publications, 373–401.

Vollset, J. & Dore, A. G. 1984. A revised Triassic and Jurassic lithostratigraphic nomenclature for the Norwegian North Sea. *NPD Bulletin, Oljedirektoratet*, **3**, 53.

Zanella, E. & Coward, M. P. 2003. Structural framework. *In*: Evans, D., Graham, C., Armour, A. & Bathurst, P. (eds) *The Millenium Atlas: Petroleum Geology of the Central and Northern North Sea*. Geological Society, London, 45–59.

Ziegler, P. A. 1990. Tectonic and palaeogeographic development of the North Sea rift system. *In*: Blundell, D. J. & Gibbs, A. D. (eds) *Tectonic Evolution of the North Sea Rifts*. Oxford University Press, New York, 1–36.

Reappraisal of the sequence stratigraphy of the Humber Group of the UK Central Graben

P. J. SANSOM

BG Group, Thames Valley Park, Reading, Berkshire RG6 1PT, UK (e-mail: pamela.sansom@bg-group.com)

Abstract: Deposition of the Callovian–Ryazanian Humber Group of the UK Central Graben occurred during rifting and long-term relative sea-level rise, which acted to suppress the formation of eustatically forced Exxon-type sequence boundaries. The superposition of highly variable halokinetically controlled subsidence means that classic, passive-margin derived sequence stratigraphic models are not appropriate to describe stratigraphic evolution in this rift setting. The sequence stratigraphy of the Humber Group has been re-evaluated using a transgressive–regressive sequence model, where maximum regressive surfaces are employed as sequence bounding surfaces. The Humber Group comprises two megasequences which reveal distinct phases of evolution of the basin. The latest Callovian–Kimmeridgian megasequence comprises a conformable sequence stack which lacks significant internal unconformities and records progressive marine flooding and overall backstepping onto the basin flanks during a phase of active rifting. The Volgian–Ryazanian megasequence is condensed and highly fragmentary due to punctuation by a number of unconformities which are consistently recognizable throughout the basin. The onset of this change in architectural style corresponds to the oldest unconformity at the base of the Volgian–Ryazanian succession, termed the Base Volgian–Ryazanian Unconformity, of latest Kimmeridgian to earliest Volgian age. The patterns of erosion of the Callovian–Kimmeridgian megasequence and the intra Volgian–Ryazanian unconformities record the effects of dramatic redistribution of underlying salt accompanied by probable uplift of the Forties–Montrose High and J Ridge, resulting in major modification of the basin morphology and the severing of possible earlier links with the Fisher Bank Basin. The kinematics of this event are equivocal, but it is possible that restricted Volgian–Ryazanian depocentres resulted from localized salt collapse rather than basement extension. Widespread erosion of Callovian–Kimmeridgian Humber Group sediments may have occurred in some areas where Volgian–Ryazanian Kimmeridge Clay deposits now overlie pre-Jurassic strata, and exploration models must incorporate the effects of Volgian reconfiguration in order to accurately predict reservoir distribution.

Keywords: Central Graben, Fulmar Sandstone, Humber Group, sequence stratigraphy, tectonic reconfiguration, Upper Jurassic

The Upper Jurassic succession of the UK Central Graben is a well studied interval which is considered relatively mature from an exploration perspective (see Erratt *et al.* 2005 for a review of exploration history). The shallow-marine Fulmar Sandstone and its equivalents comprise the primary reservoir, and significant fields include Fulmar and the high-pressure high-temperature (HPHT) Elgin, Franklin, Shearwater and Erskine trend (Fig. 1). The presence of Permian Zechstein salt below the Triassic and Jurassic sequences has resulted in major halokinesis, which has given rise to a complex structural and depositional history throughout much of the basin. Despite the long history of exploration, significant uncertainties remain, especially around the prediction of both the original depositional extent and the subsequent post-depositional preservation of reservoirs. This complexity and inherent uncertainty mean that further potential remains within the Upper Jurassic and drilling continues to deliver some surprising results.

Background

Understanding and predicting the stratigraphic architecture of the Upper Jurassic interval in the Central Graben relies upon the integration of three main areas of geological study: the sequence stratigraphic framework within the evolving rift system, the depositional model for the paralic, shallow marine and offshore deposits and the structural model linking extension, halokinetic movements of the underlying salt and deposition of the intervening Triassic–Jurassic sequences (see Fraser *et al.* 2002 for a summary of the petroleum geology of the Upper Jurassic of the North Sea). The 1990s marked a significant advance in the understanding of these elements with the publication of key work, including: biostratigraphically-calibrated sequence stratigraphic schemes (Partington *et al.* 1993*a*, *b*; Price *et al.* 1993; Duxbury *et al.* 1999; Jeremiah & Nicholson 1999); the shoreface depositional model and the use of detailed ichnofabric analysis to construct sedimentological and sequence stratigraphic models (Taylor & Gawthorpe 1993; Gowland 1996; Martin & Pollard 1996); models describing the influence of salt movements on Triassic and Jurassic deposition (Hodgson *et al.* 1992; Erratt 1993; Wakefield *et al.* 1993; Penge *et al.* 1999; Stewart & Clark 1999); and basin-scale structural evolution models (Underhill & Partington 1993; Erratt *et al.* 1999).

Much of the uncertainty in Upper Jurassic interpretation stems from the difficulty of acquiring good data on which to base predictive models (e.g. summary in Price *et al.* 1993). Probably the most significant of these is the thermal maturity of deeply buried (>10 000 ft) sediments, causing degradation of the palynomorphs (dinocysts) on which the biostratigraphic dating schemes are largely based. Dating of reservoir intervals is further compromised by poor recovery from sandstones, and reservoir correlation is further complicated by the similarity of shallow marine facies across wide areas and through time. The regional seismic interpretation was enhanced by the release in 2001 of the PGS 3D Mega-Survey seismic dataset covering the whole basin, but resolution is generally poor below the Base Cretaceous Unconformity (BCU) and may be affected by BCU multiples in the critical Upper Jurassic interval, although quality is improving with the latest long-offset

VINING, B. A. & PICKERING, S. C. (eds) *Petroleum Geology: From Mature Basins to New Frontiers – Proceedings of the 7th Petroleum Geology Conference*, 177–211. DOI: 10.1144/0070177

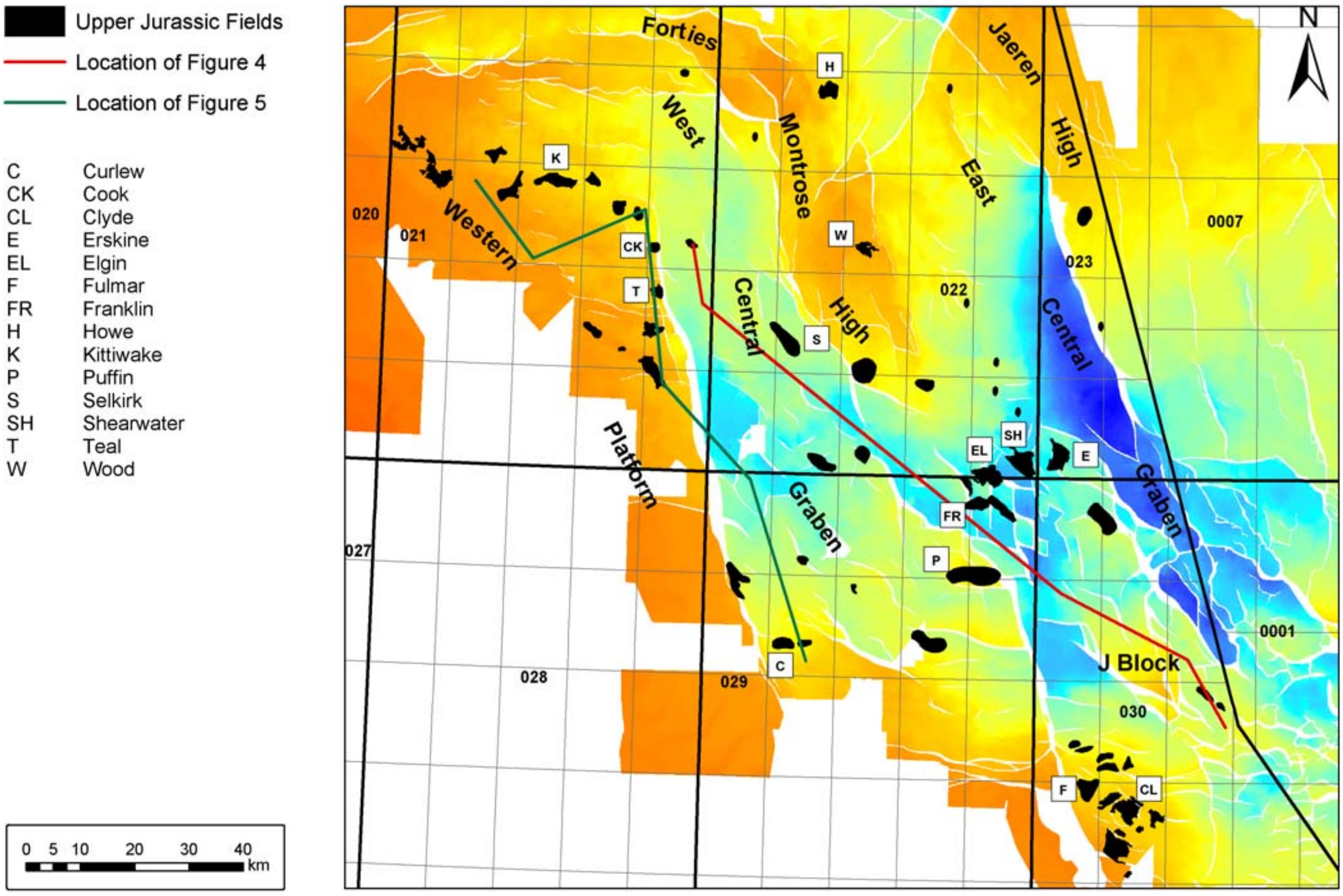

Fig. 1. Map of the study area showing the main structural features defined by the Top Rotliegend TWT structure map (yellow, high; blue, low), together with the Jurassic fields and discoveries referenced in the text and location of well correlations shown in Figures 4 and 5.

surveys. However, a lack of impedance contrast between shallow marine Fulmar sandstones or turbidite sandstones and the associated Heather and Kimmeridge Clay shales means that reservoir intervals and intra-Jurassic unconformities can often not be mapped directly. There is limited potential for seismic sequence stratigraphy as the Upper Jurassic sequences are mostly below seismic resolution. Furthermore much of the study area lies within the HPHT province of the Central Graben, and drilling problems, often related to high overpressure and high temperature, have resulted in failed logs (e.g. 21/25-11, 22/21-2, 22/25-1, 22/27a-1) or failure to reach target reservoirs (e.g. 21/20b-4y, 29/2a-4), reducing the data value of some wells in key locations. The key outstanding uncertainties are summarized below:

- Inconsistency exists between the various sequence stratigraphic models and the interpretations based on them.
- The relative importance of eustatic, tectonic and sediment supply controls on sequence architecture and facies distribution is equivocal.
- The dating of rift events is complicated by the difficulty of distinguishing between halokinetically induced and basement extension-related subsidence and their respective influences on accommodation space.
- The age and origin of erosional unconformities within the Kimmeridge Clay Formation (KCF) and their impact on the prediction of reservoir distribution and preservation have not been studied in detail.
- The presence of a significant unconformity within the Pentland Formation is equivocal due to poor biostratigraphic control, and the extent to which shallow marine Fulmar and Heather deposition was coeval and/or conformable with deposition of the Pentland Formation can be ambiguous.
- The shallow marine bioturbated shoreface model is well established for the Fulmar Sandstone, but does not account for the deposition of mass flow sands which occur both intercalated with and laterally equivalent to shoreface deposits.

Alternative stratigraphic models can be constructed which are valid within the relatively loose biostratigraphic and seismic control, and this is manifested by the variation seen between Central North Sea (CNS) Upper Jurassic palaeogeographic maps and correlation models from published work (Price *et al.* 1993; Rattey & Hayward 1993; Jeremiah & Nicholson 1999; Fraser *et al.* 2002), non-proprietary consultant reports and in-house company studies. The first part of this paper attempts to address these issues through the revision of the sequence stratigraphic framework and development of an updated basin-wide correlation model. In the second part of this study, the model is employed to investigate the timing, effects and implications of tectonic reconfiguration of the graben system.

Study methodology

This study involved stratigraphic analysis of the Humber Group interval in over 300 wells in the Central Graben, in an area comprising parts of Quads 21, 22, 23, 29 and 30 (Fig. 2). The study interval is loosely referred to as the Upper Jurassic, but in fact comprises the latest Middle Jurassic (Callovian) to earliest Cretaceous (Ryazanian) succession. A database was compiled from released and proprietary well logs, biostratigraphic reports and core descriptions together with published studies. However, no new analyses were

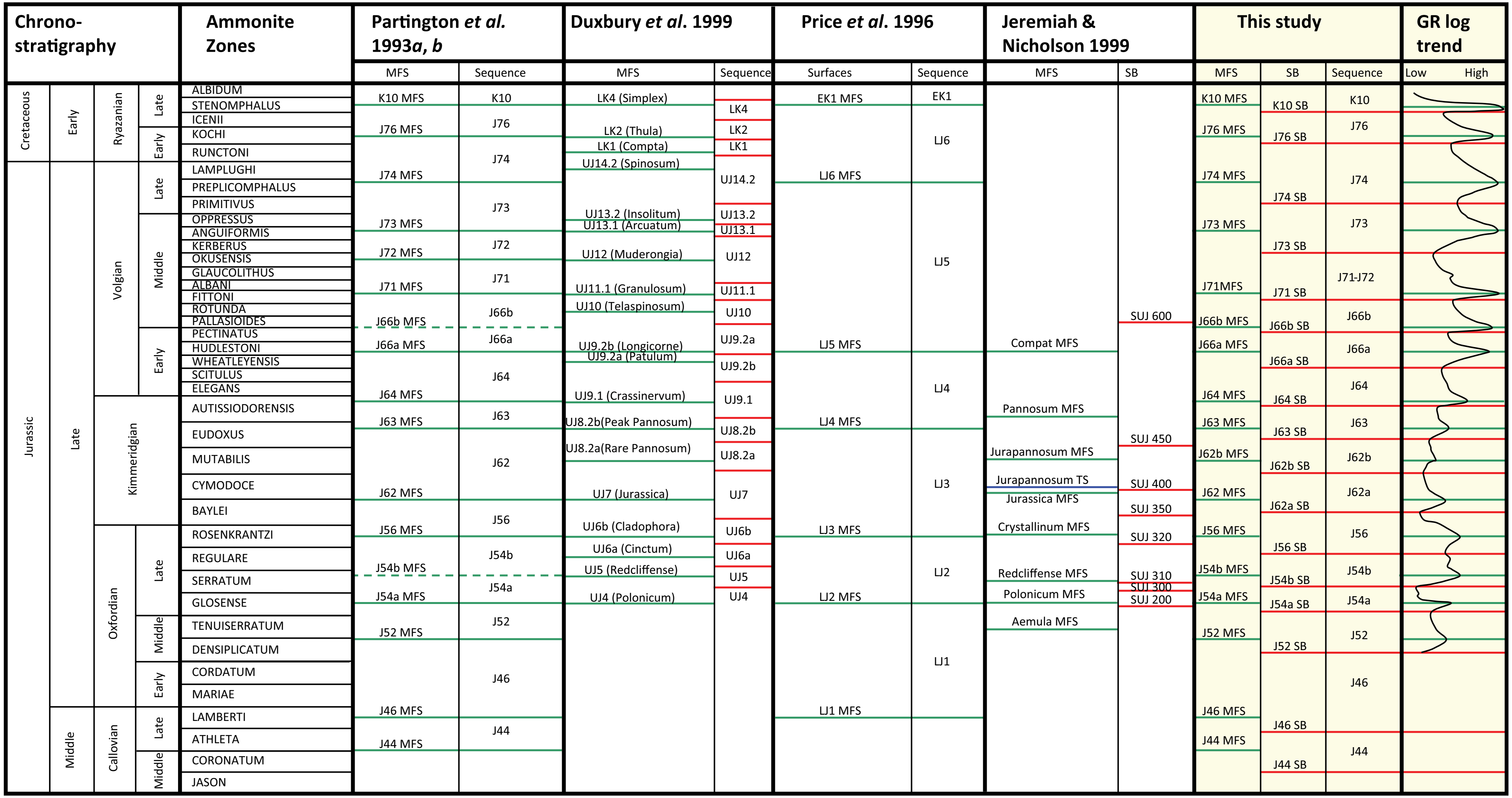

Fig. 2. Comparison of published sequence stratigraphic schemes for the Callovian–Ryazanian interval of the Central Graben with the scheme used in this study.

carried out and the age and quality of the biostratigraphic data in particular is highly variable. A sequence stratigraphic interpretation was made for each well containing an Upper Jurassic succession. Maximum flooding surfaces (MFSs), maximum regressive surfaces (MRSs) and unconformities were identified from log character and core descriptions and dated using the available biostratigraphic data. Where the biostratigraphic data was poor or absent, interpretations were made based on log character motifs and comparison with adjacent better-dated wells. MFSs and sequence boundaries (SBs) (MRSs and unconformities) were identified and correlated to produce a stratigraphic framework, which describes the thickness and facies variations of the Upper Jurassic interval. This was integrated with seismic data to provide an understanding of the relationship between structural history and stratigraphic architecture. Because of the limited biostratigraphic control, particularly in the Late Oxfordian to Early Kimmeridgian section, the correlation is necessarily model-driven and it is accepted that alternative models may be valid within the data constraints.

Geological setting

Structurally, the West Central Graben (WCG), East Central Graben (ECG) and 30/6 Graben form part of a series of en-echelon rift basins (Erratt *et al.* 1999) which are well defined at the Top Rotliegend structural level (Fig. 1). The platform areas (Western Platform, Jaeren High) and intrabasinal highs (Forties–Montrose High, J Ridge) are defined by major north–south to NNW–SSE trending faults at Top Rotliegend level, which pass into terrace areas in the transfer zones between the major graben (e.g. Puffin Terrace, Fulmar–Clyde Terrace). The Permian Rotliegend 'basement' is overlain by variable thicknesses of mobile Upper Permian Zechstein salt, which is believed to have been initially thicker in the basinal areas and thinner over the platforms and highs (Smith *et al.* 1993, fig. 4). Early Triassic rifting initiated salt movements and deposition of the succeeding fluvio-lacustrine deposits of the Smith Bank Formation shales and fluvial deposits of the Skagerrak Formation sandstones led to the differentiation of sediment mini-basins, or 'pods', and intervening salt highs (Hodgson *et al.* 1992).

The region experienced uplift and erosion during the Early Jurassic as a result of thermal doming centred on the North Sea triple junction to the north (Underhill & Partington 1993) so that latest Triassic and Early Jurassic sediments are only rarely preserved in isolated salt-withdrawal depocentres. Collapse of the thermal dome led to the establishment of fluvial and then fluvio-deltaic conditions and the deposition of the Pentland Formation sediments during the Middle Jurassic. Coincident localized volcanic activity led to the accumulation of lavas and tuffaceous sediments of the Rattray Formation in the north (Forties Volcanic Province) and south (Puffin Centre) of the study area (Smith & Ritchie 1993).

Callovian to Early Oxfordian subsidence and/or relative sea-level rise led to marine flooding of the Pentland depocentres in the grabens and the transition from coastal plain to shallow marine shoreface deposits of the Fulmar Formation sandstones and shelf shales of the Heather Formation. During the Kimmeridgian to Ryazanian these shallow marine systems backstepped onto exposed Triassic sediments on the platforms and highs as anoxic marine shales of the Kimmeridge Clay Formation were deposited in the graben centres. Isolated turbidite sandstones, such as the informally named Freshney, Erskine and Selkirk members, were deposited within the Heather and Kimmeridge Clay shales. Anoxic conditions were terminated in the Late Ryazanian as the North Sea rift was abandoned and extension switched to the Atlantic Margin (Rattey & Hayward 1993). Within the Central Graben, the Triassic and Jurassic sequences are affected by complex structural and sedimentary architectures resulting from the superposition of rift events onto an area with varying thicknesses of Zechstein halite, both within the grabens and on the marginal platforms and highs. It is important to understand the effects of halokinesis on the Jurassic section because it affects both the initial distribution of the Fulmar sandstones and their subsequent preservation. Models for the development of complex salt structures and their impact on Fulmar sand distribution during the Upper Jurassic are summarized in Fraser *et al.* (2002).

The relationship between the salt and basin architecture provides a fundamental and relatively predictable control on the location of Humber Group depocentres. On platform areas such as the Western Platform, Forties–Montrose High (FMH) and Jaeren High, the salt layer was relatively thin, short-wavelength Smith Bank pods had grounded and deformation of the supra-salt cover and the subsalt 'basement' became coupled from Triassic time onwards. Dissolution or extensional collapse of salt wall areas provided accommodation space for Triassic Skagerrak and Jurassic Fulmar sandstones, so that salt highs and Humber Group depocentres were mostly co-located throughout the Upper Jurassic. In contrast, deformation remained largely decoupled in the basinal areas containing thick salt, at least until the late Kimmeridgian. Late Callovian–Kimmeridgian depocentres were located in the axes of larger wavelength basins which had been subsiding between the salt highs throughout the Triassic and Middle Jurassic. The salt walls, whilst covered, were areas of low accommodation space. Pod grounding, coupled with possible changes in stress regime in the Volgian (Erratt *et al.* 1999), led to widespread collapse of the basinal salt walls so that depocentres shifted into new, often highly asymmetrical salt withdrawal synclines between the pods. Hence the location of Callovian–Kimmeridgian sediment thicks and Volgian–Ryazanian thicks is commonly mutually exclusive in the graben centres.

The involvement of salt modifies the basin geometries and loci of accommodation space development which controlled Fulmar sand distribution compared with a salt-free rift model. In salt-free rift models, surface faulting is hard-linked to basement displacement (e.g. at the graben bounding fault). The creation of maximum accommodation space is localized in the immediate hanging wall of the active fault and the syn-depositional sequence thickens into the active fault (fig. 10b of Howell *et al.* 1996). Where salt is involved and basement faulting is decoupled from surface deformation, the displacement is spread over a wider area and extends into the footwall of the active fault (Dooley *et al.* 2003, fig. 3). This produces a ramp margin without the obvious thickening of syn-rift packages into the hanging wall. The syn-rift deposits extend onto the footwall and may be thickest some distance outboard of the fault in the centre of an actively subsiding mini-basin. During the Oxfordian to Kimmeridgian it is considered more likely that salt acted to produce a complex pattern of differential accommodation space, with basin margins comprising gentle ramps and intrabasinal highs forming low-relief emergent areas, rather than active faults extending to the surface to produce areas of high differential relief (as is suggested in fig. 11.34, Diagram H of Fraser *et al.* 2002; Howell *et al.* 1996).

Previous sequence stratigraphic studies

The 4th Petroleum Geology Conference (1993) saw the publication of several regional sequence stratigraphic syntheses of the Upper Jurassic of the North Sea (Donovan *et al.* 1993; Partington *et al.* 1993*a*, *b*; Price *et al.* 1993; Rattey & Hayward 1993, 'BP Scheme'), which represented a major advance over the previously lithostratigraphically-dominated approach. These were followed by others during the late 1990s (Shell scheme of Jeremiah & Nicholson 1999 for the Greater Shearwater area; Duxbury *et al.* 1999 for the Outer Moray Firth), together with a number of field specific

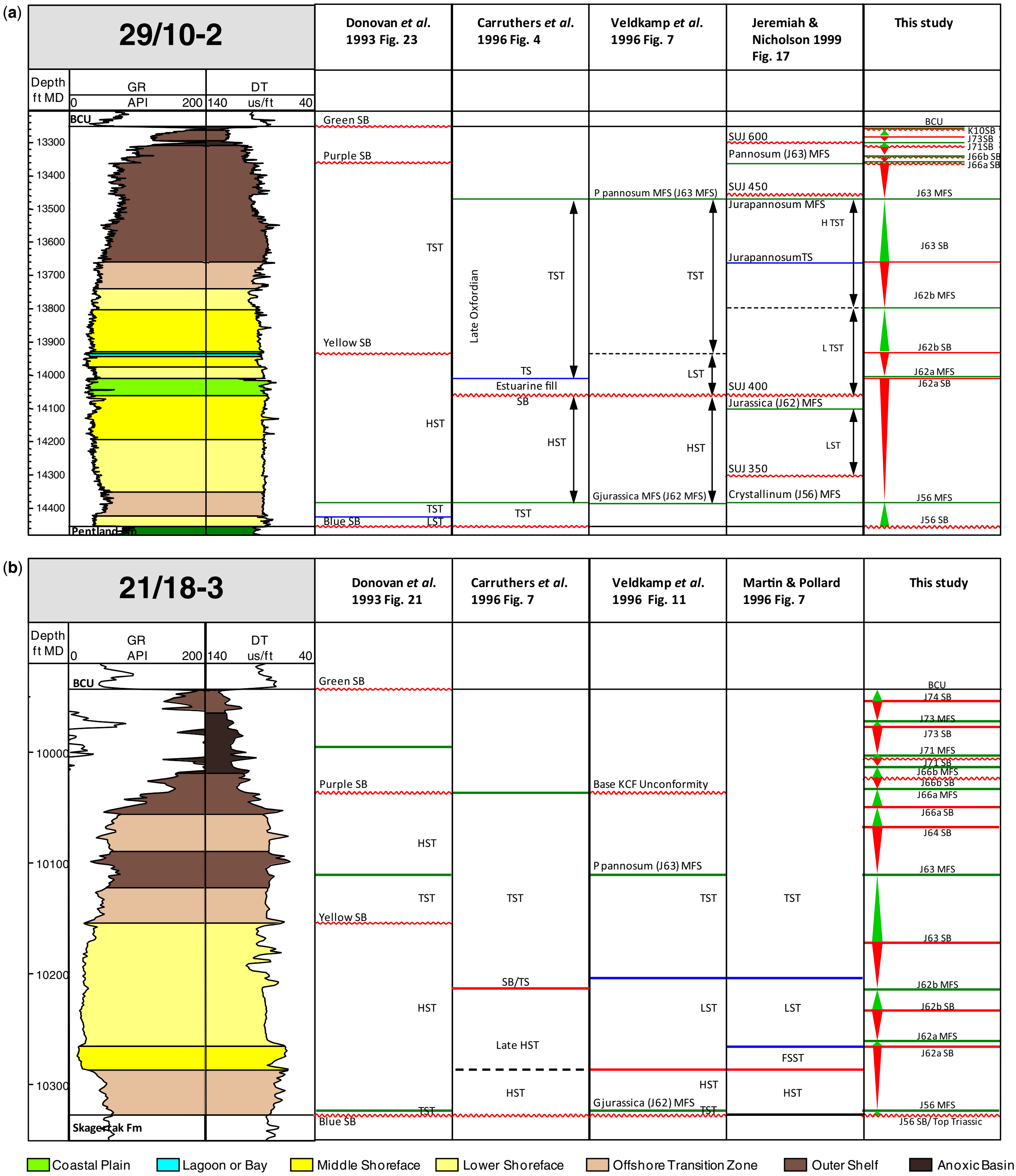

Fig. 3. Comparison of published sequence stratigraphic interpretations of (**a**) well 29/10-2 and (**b**) well 21/18-3 with the interpretation of this study.

reservoir layering schemes (Kittiwake, Martin & Pollard 1996; Elgin–Franklin, Lasocki *et al.* 1999; Erskine, Coward 2003; Fulmar, Kuhn *et al.* 2003; Clyde, Turner 1993). As a result, a variety of published (Fig. 2) and unpublished stratigraphic schemes is currently in use in the North Sea industry at the exploration and reservoir scales, but there is disagreement on the calibration of some key bioevents between schemes, as demonstrated by Hesketh and Underhill (2002, fig. 16). The lack of a consistent scheme and terminology is problematical for industry users looking to compare interpretations and reflects both the inherent uncertainties and data deficiencies highlighted above but also variations in the use of the sequence stratigraphic method, specifically the definition of sequence boundaries.

Genetic stratigraphic schemes have been the most widely used, because of the relative ease of picking and correlating MFSs using wireline log data. Sequence stratigraphic schemes based on the definition of unconformity-bounded units (Donovan *et al.* 1993; Rattey & Hayward 1993) have not been adopted due to the lack of well developed Exxon-type SBs in the Upper Jurassic succession and the difficulty of picking the equivalent surfaces in the basin. Rattey & Hayward (1993) outlined the Middle Jurassic to Early Cretaceous evolution of the North Sea by describing a series of regional, seismically mappable tectonostratigraphic sequences (J20–J70), where SBs were defined as regional unconformities or hiatuses. However, the basal 'sequence boundaries' of sequences J50, J60 and J70 described in the Central Graben area are flooding events causing deepening in basinal areas and/or onlap onto older unconformities at the basin margins, rather than widespread erosive events.

The BP J sequence scheme of Partington *et al.* (1993*a*, *b*) has become the most widely adopted framework due to the detailed publication of the biostratigraphic calibration of the MFSs that bound the sequences, although it was proposed as a 'preliminary subdivision' and updates have not been published. There is general agreement between most of the MFSs in this scheme and similar biostratigraphically-calibrated schemes of Price *et al.* (1993), Jeremiah & Nicholson (1999) and Duxbury *et al.* (1999) (Fig. 2). Palynological (dinocyst) zonation provides the primary means of dating the Upper Jurassic marine sequences, but recovery can be poor due to high thermal maturity. The preservation of radiolaria and foraminifera is unaffected and micropalaeontological zonation, although of lower resolution, can provide control where palynology is lacking (Partington *et al.* 1993*b*; Price *et al.* 1993). However, the use of agglutinating forams in particular was challenged by Veldkamp *et al.* (1996) due to facies dependency.

The term 'sequence boundaries' has been used variably in previous studies. Partington *et al.* (1993*a*), Price *et al.* (1993) and Carruthers *et al.* (1996) use the term to refer to subaerial unconformities and their correlative (start of base level fall) conformities, rather than to mean the surfaces that bound their sequences, which are MFSs in their genetic schemes. This has led to variation in the nomenclature between schemes where the 'sequence boundary' is younger than the MFS with the same name (e.g. Partington *et al.* 1993*a*) and others where it is older than the MFS with the same name (e.g. Duxbury *et al.* 1999). Jeremiah & Nicholson (1999) avoided this by presenting a 'hybrid' scheme with MFSs following a dinocyst naming convention and 'Exxon-type' (start of base level fall) SBs following a numerical scheme.

Most of the published studies place candidate Exxon-type SBs at the base of submarine fan deposits and at the base of shoreface sandstones. Partington *et al.* (1993*a*) proposed candidate SBs at the base of turbidite deposits laid down following their 'tectonically enhanced maximum flooding surfaces' J63, J71 and J73. Carruthers *et al.* (1996) and Jeremiah & Nicholson (1999) placed SBs at the base of intra-Heather Formation turbidite deposits also at the base of some shoreface packages marked by an abrupt reduction in GR response, interpreted as representing a basinward shift in facies. Embry *et al.* (2007) criticized this method of defining the SB since the start of mass flow deposition may not coincide with the onset of base level fall, and the base of a shoreface sandstone is a diachronous surface, constituting either a 'within-trend facies change' or a regressive surface of marine erosion. Veldkamp *et al.* (1996) discussed the different options for picking the SB in Kimmeridgian shoreface successions in the Central Graben and noted that in core from well 21/18-2Az the sharp GR reduction correlated to a gradational facies change rather than an abrupt surface.

Turner (1993) subdivided the Fulmar Sandstone of the Clyde Field into progradational and retrogradational units using MFSs and MRSs. Kuhn *et al.* (2003) placed the Fulmar field reservoir within the sequence stratigraphic scheme of Duxbury *et al.* (1999). The SBs in this example correspond to MRSs at the top of prograding shoreface packages. The intervening MFSs divide each sequence into a transgressive and a regressive portion. Kuhn *et al.* (2003) referred to the regressive portion as the highstand systems tract (HST). Folkestad & Satur (2008) is the only example of the application of a true transgressive–regressive model to a comparable succession in the North Sea. They defined eight depositional sequences bounded by MRSs, each comprising a transgressive systems tract (TST) and a regressive systems tract (RST), in the Callovian–Oxfordian Hugin Formation of the Sleipner area of the South Viking Graben and highlighted the difference between stratigraphic architecture in rapidly subsiding basins and sequence stratigraphic models developed for passive margins.

Most of the previous work has attempted to pick an unconformity or correlative conformity corresponding to the start of base level fall as the SB (Exxon-type SB) and differentiate the regressive deposits into HST and lowstand systems tract (LST). Whilst there is general agreement on the placement and correlation of MFSs, there is much less agreement on the location of SBs. The difficulty of picking a start of base level fall SB within the conformable regressive packages of the Upper Jurassic succession has resulted in a wide variety of sequence stratigraphic models based on the same dataset for some wells (Fig. 3). There is some evidence for forced regression in the current well (wireline log and core) dataset of the Central Graben (e.g. well 21/18-3, Martin & Pollard 1996), but its expression appears to be very sensitive to the local balance of subsidence and sediment supply and it is not generally possible to differentiate between a prograding succession deposited during rising relative sea-level rise (HST) and one deposited after the onset of base level fall (forced regressive systems tract) or shortly after the end of base level fall (LST). It is argued therefore that the use of the Exxon-type passive margin sequence stratigraphic model is inappropriate for the Upper Jurassic of the Central Graben and it is much more practical to pick the MRS (start of base level rise) as the SB in this setting.

Revised sequence stratigraphic model

In this study, a transgressive–regressive (T–R) sequence stratigraphic scheme (Fig. 2) was derived from the BP genetic sequence scheme of Partington *et al.* (1993*a*, *b*) by recognizing SBs at MRSs and/or unconformities between the MFSs. A regional correlation of wells with the most complete Oxfordian–Kimmeridgian succession using this scheme is shown in Figure 4, and a correlation demonstrating the most complete Volgian–Ryazanian successions is shown in Figure 5. The Partington *et al.* (1993*a*, *b*) scheme gives MFSs both a number and an ammonite zone name (e.g. J62 MFS/baylei MFS). There has been subsequent argument against the use of onshore-derived ammonite zones for naming MFSs because of the uncertainty in the calibration of the ammonite and microfossil data sets, with dinocyst names used in preference (Duxbury *et al.* 1999; Jeremiah & Nicholson 1999). In this study the use of a numerical scheme for MFSs and SBs is preferred because the relative age of the sequences is inherent in the nomenclature. Also, picks for these surfaces are made on log character alone where biostratigraphic data are lacking, and the use of a numerical scheme avoids the implication that diagnostic taxa were identified. An additional MFS has been designated to aid subdivision of the thick Kimmeridgian sequences of the Central Graben, and is named J62b MFS in this study. It equates to the Jurapannosum MFS of Jeremiah & Nicholson (1999) and the UJ8.2a (Rare Pannosum) MFS of Duxbury *et al.* (1999), although biostratigraphic calibration differs between these two schemes, with the Jurapannosum MFS defined as lying below the last down-hole occurrence of *Perisseiasphaeridium pannosum* and the LJ8.2a MFS defined as lying above the deepest (rare) occurrence of *P. pannosum*. This degree of sequence resolution is believed to be necessary to capture both the main stages of expansion of the Callovian–Kimmeridgian

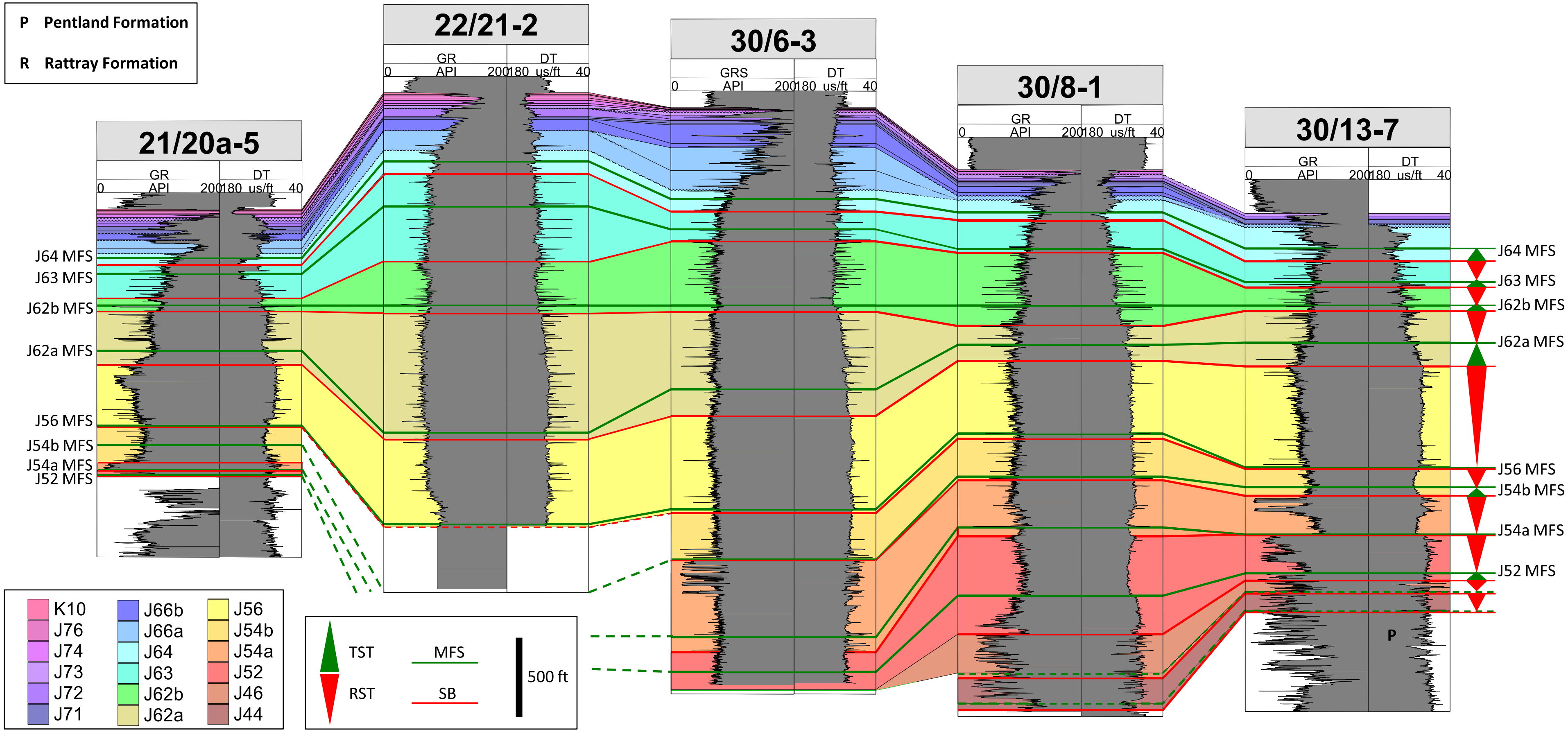

Fig. 4. Regional sequence stratigraphic correlation of wells with the most complete Callovian–Kimmeridgian megasequence succession. Note the relatively consistent log trends, particularly the thick, progradational sequence that defines the J56 RST, and the change from more strongly progradational (RST dominated) sequences J52–J62a to dominantly aggradation in J62b and J63 and overall regression at the J64 SB, which defines the top of the Callovian–Kimmeridgian megasequence. Note also the high degree of condensation of sequences J64–K10 compared with the older succession. See Figure 1 for location.

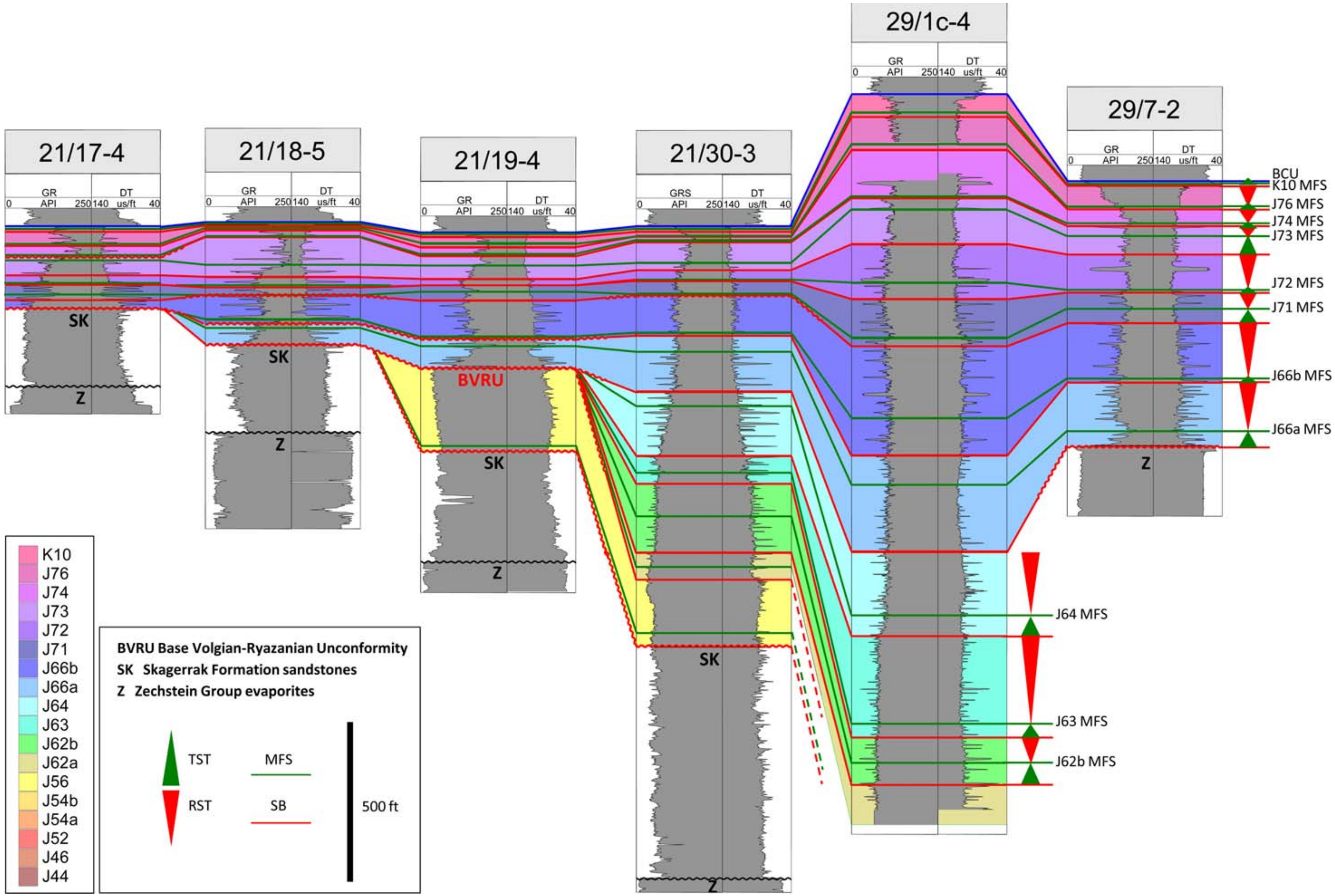

Fig. 5. Regional sequence stratigraphic correlation of wells with a more complete Volgian–Ryazanian megasequence succession. Note the thick, well-defined TSTs of sequences J64 and J66a and the characteristic GR-SONIC bow between the J71 MFS and the J73 MFS. Most of these wells are located over relatively shallow salt, and late salt withdrawal is interpreted to have created accommodation space for more complete preservation of the Volgian–Ryazanian megasequence, although the Late Volgian–Ryazanian sequences remain relatively thin and condensed.

megasequence and the significant unconformities in the Volgian–Ryazanian megasequence.

Sequence stratigraphic surfaces are more difficult to define in coastal plain settings lacking marine flooding events and in transitional marine environments where a complex embayed deltaic coastline characterized by rapid lateral facies changes is envisaged. In this study, MFSs have been correlated to widespread lacustrine shales or coal horizons within the upper Pentland Formation and candidate SBs are placed at the top of sandy units underlying coals, which is taken to represent the MRS of the fluvial system prior to base level rise and swamp development. Where a coal lies at the interface of coastal plain and marine deposits, it is placed at the base of the TST. However, it is recognized that, without biostratigraphic control, the picking of these surfaces is much more subjective than their marine equivalents. In the absence of core it is difficult to differentiate between lagoonal or restricted bay mudstones and shelf shales. Even where clear coal-bearing coastal plain deposits occur between shoreface sandstones (e.g. 29/10-2, Fig. 3a), it is not always easy to determine if these lie beneath the MRS at the top of a regressive sequence capped by a normal marine ravinement surface, or overlie the subaerial unconformity at the base of a transgressive systems tract, although there are obvious implications for the amount of erosion and potential for downdip reservoirs between the two interpretations.

The decision on whether to propose a T–R sequence scheme, or the inverse genetic or R–T (regressive–transgressive) scheme with sequences bounded by the MFSs is not trivial. The appeal of a T–R sequence scheme is that the higher-order sequences are components of, and share boundaries with, the major lower-order tectonostratigraphic units that define the large-scale basin history such as the Aalenian unconformity and the BCU. Furthermore, the Upper Jurassic succession records progressive marine flooding and expansion of the basin and it seems appropriate to think of each sequence beginning with transgression rather than regression following the MFS. The disadvantages of choosing a depositional sequence scheme here are that subaerial unconformities are not well developed within the Upper Jurassic succession, so that most SBs would be defined by MRSs. The disadvantage of MRSs is that they may have a strong local sediment supply control, so that the MRS of a low-order sequence may occur within different higher-order component sequences in different areas of the basin if, for example, delta lobe or fan lobe switching occurs. MRSs are also difficult to identify in deepwater mass flow deposits and Embry *et al.* (2007) suggest picking the MRS at the interface between thickening-up and thinning-up deposits. The MRS can also be difficult to define consistently in thick aggradational packages. Furthermore, the MRSs are not biostratigraphically calibrated in the published schemes so that their position in relation to key bioevents is uncertain.

Unconformities in the Central Graben

Significant unconformities of varying areal and temporal extent have been recognized both bounding and within the Callovian–Ryazanian interval in the North Sea. Over much of the CNS, the Pentland and Rattray Formations are absent and the base of the study interval is clearly defined where it unconformably overlies Triassic sediments. This has been termed the Mid-Cimmerian or Aalenian Unconformity and records thermal doming centred on the North Sea triple-junction during the Early Jurassic (Underhill & Partington 1993; Davies *et al.* 1999). This resulted in the non-deposition or erosion of virtually all Lower Jurassic deposits, except for rare isolated occurrences preserved in salt-withdrawal accommodation space, so that Middle Jurassic and younger deposits rest unconformably on the Triassic. Deposition of the Middle Jurassic Pentland Formation deposits and Upper Jurassic marine deposits resulted in the gradual onlap and burial of this unconformity, so that at any one location it is a compound subaerial unconformity forming the SB at the base of the overlying sequence, although the bulk of the erosion occurred during the Early Jurassic.

Where the Pentland Formation is present, it is not clear whether a significant pre-Callovian intra-Pentland unconformity exists. The Middle Jurassic fluvial deposits of the Pentland Formation have not been investigated in detail for this study and their dating and correlation is difficult due to poor recovery of diagnostic palynomorphs, rapid lateral facies variation of the fluvial channel and lacustrine deposits and lack of marine incursions throughout most of the succession. Several workers have interpreted a significant unconformity between Pentland deposits and the Upper Jurassic marine succession, such as the Lavender SB of Donovan *et al.* (1993). Rattey & Hayward (1993) state that 'much of the CNS that was covered by coastal plain in J30 [latest Bajocian–Middle Callovian] has no recognized J40 [Middle Callovian–Middle Oxfordian] cover' although their figures 14 and 15 imply continued deposition in the East and West Central Graben axes. Davies *et al.* (1999) interpreted an intra-Callovian unconformity separating Bathonian–Bajocian aged Pentland deposits from younger Fulmar and Heather deposits in West Central Graben blocks 21/15, 21/20, 22/16 and 22/22. However, no firm dating of the Pentland Formation in this area was available for this study. The similar thickness and facies consistency of the coastal plain deposits in block 21/15 suggests that the Pentland facies may be genetically related to the overlying Fulmar shallow marine sandstones, representing base level rise and onlap during the early stages of flooding of the West Central Graben during the Middle Oxfordian, with an unconformity existing between the Rattray Formation and the base of the Pentland Formation here. In this study, some released well reports in the 22/13 area provide evidence for a Bathonian age for the upper Pentland Formation deposits (presence of *Quadraeculina anellaeformis*) and indicate an unconformity between the Bathonian and the Upper Callovian. It is therefore likely that an unconformity spanning at least the Middle and Early Callovian exists in the area, although it cannot be picked reliably from log data within Pentland successions. In the Danish sector, Andsbjerg (2003) documents a regional erosional unconformity of Late Bathonian to Early Callovian age that separates floodplain deposits of the Lower Bryne Formation (Pentland Formation equivalent) from estuarine deposits of the Upper Bryne Formation.

Throughout much of the WCG and ECG a high-amplitude reflector corresponds to low-density/slow-sonic shale units associated with coals near the top of the Pentland Formation, and the consistency of this 'near Top Pentland' marker suggests that no significant erosion of the upper Pentland has occurred and that the upper Pentland and Fulmar/Heather formations are conformable here (Price *et al.* 1993; Erratt *et al.* 1999; Jeremiah & Nicholson 1999). Jeremiah & Nicholson (1999) reported increased marine affinities in the micropalaeontological association in the upper parts of the Pentland Formation in the Shearwater area. Coward (2003) reported marine palynomorphs from the uppermost Pentland Formation in the Erskine field and suggested that it was deposited in a marginal marine setting and is conformable with the overlying Heather Formation shales. This study supports the conclusion that the Pentland Formation, at least in the deeper parts of the basin characterized by the near Top Pentland seismic marker and where marine incursion occurred by sequence J52 or earlier, is conformable with the basal Fulmar or Heather Formation deposits. The increased presence of coals in the uppermost part of the Pentland Formation and the common occurrence of coal at the contact between the Pentland and Fulmar/Heather deposits suggest a gradual rise in base level and widespread development of swampy delta plain conditions characterized by mouthbars, tidally influenced lagoons and lakes in response to marine incursion in other parts of the basin. Isolated and locally thick occurrences of Pentland facies occur on some terrace areas, such as the Puffin Terrace, and Veldkamp *et al.* (1996) report Kimmeridgian-age Pentland deposits from the Western Platform (well 21/18-6). It is therefore envisaged that coastal plain deposition occurred in restricted lows on platform and intrabasinal high areas related to Oxfordian–Kimmeridgian shoreface deposition in the basin. In general, however, there is only limited evidence for Fulmar age-equivalent coastal plain deposits, which is surprising considering the thick aggradational packages of Fulmar sandstone seen in some areas. This may be because the combination of the rift setting and the controlling influence of the salt walls on accommodation space resulted in relatively narrow coastal plain margins in comparison to passive margin settings.

The upper boundary to the Callovian–Late Ryazanian tectonostratigraphic succession is the so-called ‘Base Cretaceous Unconformity’, although this comprises a conformable facies change from anoxic claystones of the Kimmeridge Clay Formation to oxic marls and claystones of the Cromer Knoll Group in some areas where the latest Upper Jurassic depocentres continued into the Lower Cretaceous (Rattey & Hayward 1993). Elsewhere Cretaceous deposits onlap remnant topography so that a significant angular unconformity is developed, with Lower or Upper Cretaceous deposits commonly overlying Triassic sediments.

Significant unconformities are also apparent within the Upper Jurassic interval (Rawson & Riley 1982, Base Kimmeridge Clay unconformity of Veldkamp *et al.* 1996, figs 8 & 12 and the Intra Kimmeridgian unconformity of Kuhn *et al.* 2003, fig. 5). These are manifested by sharp truncation of Fulmar or Heather successions which are unconformably overlain by high gamma ray (GR) claystones of the Kimmeridge Clay Formation. Rawson & Riley (1982) describe a number of intra-Volgian unconformities from the onshore Upper Jurassic of the UK and the offshore North Sea, which they attribute to a major phase of uplift and erosion across Europe during Volgian to Ryazanian time. These may equate to unconformities seen at the J66a, J66b, J71, J73 or J74 SBs in this study. Davies *et al.* (1999, fig. 8) showed a localized unconformity of latest Kimmeridgian to earliest Volgian age in the Puffin and Shearwater–Erskine area, but it was not discussed further. In general, however, the focus has been on describing reservoir intervals, and detailed studies of the age and extent of intra-Humber Group unconformities in the UK Central Graben area have not been published.

Callovian–Kimmeridgian megasequence (J44–J63)

The Callovian–Kimmeridgian megasequence comprises sequences J44–J63 in the study area and is interpreted as a conformable stack of composite transgressive and regressive packages that lacks significant internal unconformities. Proximal–distal trends are maintained from sequence to sequence, and there is a clear consistency to the sequence trends, manifested by characteristic basin-wide GR motifs (Fig. 4). This aids correlation where biostratigraphic data is lacking and indicates a regional tectonic and/or eustatic control on accommodation space, which is modified by local halokinesis and sediment supply variations.

Sequences J44 (Callovian)

Sequence J44 is believed to be entirely represented by coastal plain deposits of the Pentland Formation within both the WCG and ECG. The nearest marine sediments at this time comprise marginal marine barrier and lagoon deposits at the southern end of the Fisher Bank Basin (FBB) in blocks 22/12 and 22/13, and support subsequent northerly marine flooding of the West Central Graben, as suggested by Jeremiah & Nicholson (1999). The boundaries of sequence J44 cannot be defined with any certainty within the fully continental succession. However, it is believed to be present at least in areas of the basin which saw the onset of marine conditions in sequences J46 and J52 (axis of the WCG, Elgin–Franklin–Shearwater–Erskine trend, axis of the ECG). In other areas of the basin, older Middle Jurassic Rattray deposits were exposed (northern block 21/15), whilst older Pentland Formation deposits were possibly exposed on flanks of the basin bounding platforms and intrabasinal highs. Triassic sediments remained exposed on the Western Platform, Puffin Terrace, the J Ridge and the Clyde–Fulmar Terrace. The FMH is believed to have been mostly exposed at this time, although Pentland facies may have traversed the high in the 22/11–22/12 area as a precursor to later northerly marine incursion into the WCG.

Sequence J46 (Late Callovian–Early Oxfordian)

The presence of sequence J46 deposits in the WCG records the establishment of fully marine conditions south of the FBB (Fig. 6). This sequence comprises outer shelf shales (wells 22/21-4, 22/21-7 and 22/22b-2y, Fig. 7) with possible tidal flat deposits recorded from a short core in well 22/27a-2. Coastal plain environments are interpreted to either have continued conformably from sequence J44 or to have been established for the first time in the south of the graben in the 29/2 and 29/7 areas. The J46 SB is picked as an MRS at the interface of non-marine shales and a transgressive marine shale package. Where a coal is present at this interface it is placed at the base of the J46 TST. This sequence records rapid flooding of a low-relief swampy coastal plain in a narrow zone possibly restricted to the eastern side of the WCG. Probable bar-barrier sandstones were deposited at the southern end of the FBB and may extend into the northern part of the WCG (wells 21/15a-6 and 22/11-4), although there is no supporting age data. In the ECG swampy delta plain conditions are interpreted to have developed throughout the Elgin–Franklin–Shearwater–Erskine trend and down into the 30/8 and 30/13 areas, with possible tidal influence suggesting a link to marine conditions in the WCG, and also possibly to the southern FBB via the northern end of the ECG. Here, the J46 SB is interpreted to lie at the base of the near-Top Pentland shale marker with the MFS lying within the shale.

Sequence J52 (Middle Oxfordian)

Sequence J52 records the onset of marine flooding of a large part of the ECG (Jeremiah & Nicholson 1999), although it is unclear whether this occurred from the FBB to the north or WCG to the west, or even via the Feda Graben to the east. In the WCG, marine conditions remained restricted to the east side of the graben (Fig. 8), but Pentland deposits in the 21/15 and 21/20 areas are interpreted as recording onlap of coastal plain sediments onto the exposed Triassic land surface. Probable mouthbar deposits accumulated in the Curlew embayment at the southern end of the WCG, suggesting establishment of deltaic conditions and proximity to a significant fluvial input point. Again shoreface sandstones are not widely developed, suggesting widespread drowning of low-gradient sediment source areas. The exceptions to this are areas surrounding the Puffin High where J52 sandstones of shoreface or equivocal marginal marine facies are seen in wells 29/2a-2, 29/2b-5, 22/27a-2 and the Elgin and Franklin fields (e.g. 22/30c-10, 29/5b-6z), suggesting a significant sediment source in this area. A 125 ft-thick sandstone package of possible turbidite origin may lie in sequence J52 in well 22/21-7. Elsewhere sequence J52 comprises shelf shales. In the Erskine area, Jeremiah & Nicholson (1999) interpreted the Fulmar Sandstone to be a composite body comprising the equivalent of J52 and J54 sequences, with the

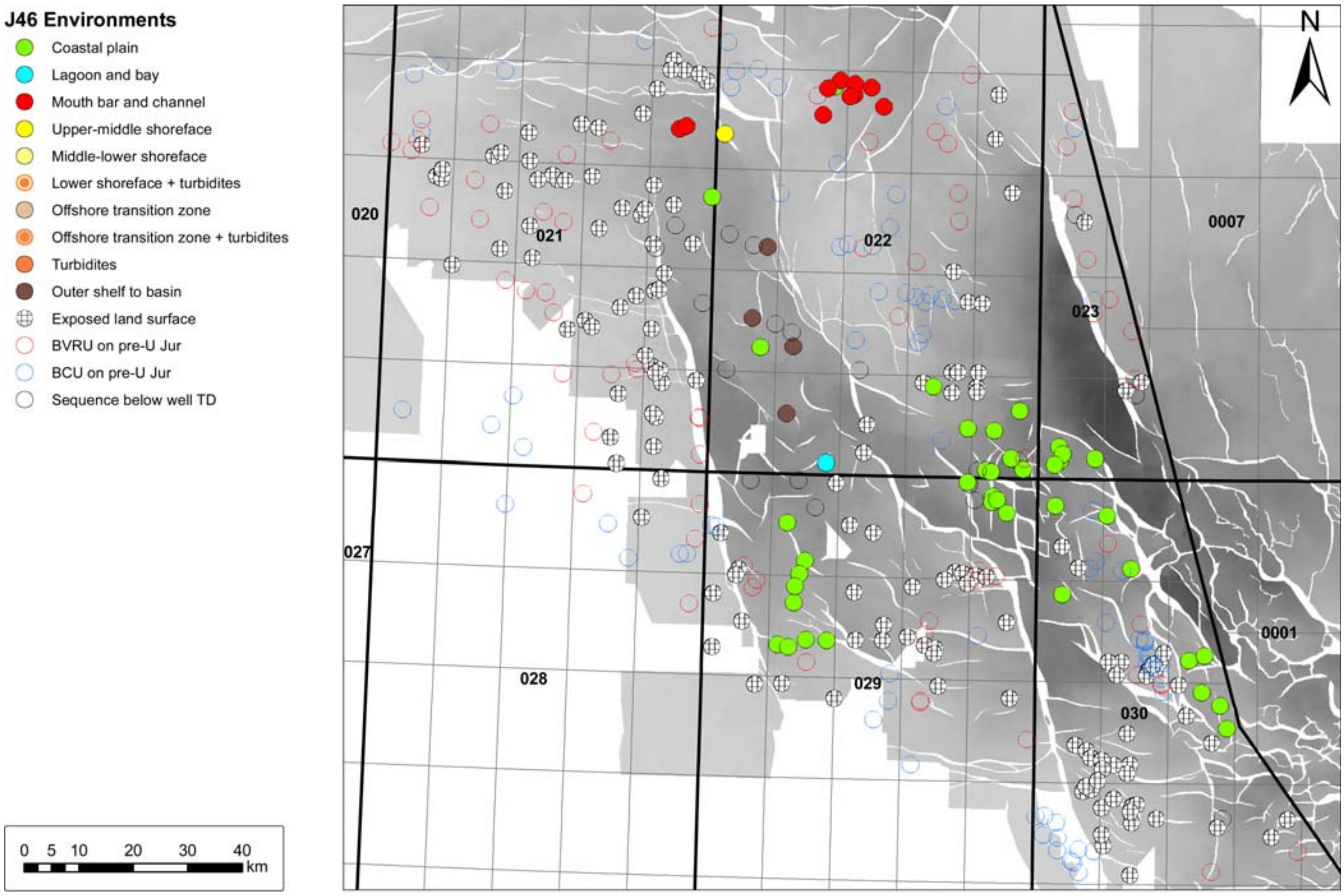

Fig. 6. Sequence J46 depositional environments. Marine conditions were established in the WCG, possibly linking to barrier and lagoon deposits at the southern end of the FBB. Swampy coastal plain conditions are interpreted to have developed in the axis of the East Central Graben as a precursor to marine transgression in sequence J52.

equivalent of the J54a MFS (Polonicum MFS of Jeremiah & Nicholson 1999) cut out by the SJU300 SB. This study interprets J52 sandstones as present here, but there is insufficient biostratigraphic control to confirm the interpretation. In the Shearwater area, Jeremiah & Nicholson (1999) also interpreted the coal-rich deposits at the top of the Pentland to represent 'the initial part of the Middle Oxfordian transgression'. These deposits are here interpreted to comprise the J52 TST which culminates in the J52 MFS at or near the base of the overlying Heather Formation marine shales.

Sequence J54a (Late Oxfordian)

Despite the importance of sandstones of sequence J54a as productive reservoirs in the Elgin–Franklin–Shearwater–Erskine trend (Fig. 9), this sequence is poorly biostratigraphically constrained. Within the available biostratigraphic dataset, it is not possible to differentiate with certainty between sequences J54a, J54b and J56 because of the lack of palynological distinction between these units coupled with commonly poor microfossil and palynomorph recovery. Thus the definition and correlation of these sequences, especially in marginal marine facies, is often subjective and alternative interpretations are possible. The correlations proposed here are constrained largely by working upwards from good J52 sequence dating and downwards from good J62 sequence control.

The J54a SB conforms to a MRS at the top of the J52 RST over most of the basin, although this may only be weakly developed where sequence J52 comprises Heather Formation shales with a dominantly aggradational trend. Where the J54a sequence oversteps J52 coastal plain deposits the SB is picked as a MRS at the base of coals immediately underlying the first marine deposits (e.g. 21/20-1, 21/20a-5). The J54a TST records continued flooding of the basin and limited overstepping of the Pentland basin for the first time onto Triassic deposits (e.g. 30/7a-P12), where the SB comprises an unconformable shoreline ravinement surface. The flooding culminates in the J54a MFS.

The J54a RST records a major progradation of sandy shoreface deposits into the basin coupled with the deposition of locally thick mass-flow sandstones as a result of the re-establishment of major sand supply systems to the basin following the J46–J52 (Late Callovian to Middle Oxfordian) transgressions. In the Curlew (29/7) area, deltaic conditions prevailed, characterized by mouthbar, barrier, lagoon and coal swamp deposition. The interpretation favoured here places the shoreface sandstones of both wells 21/20-1 and 22/16a-2z in the J54a RST. This differs from the more complex interpretation of Donovan *et al.* (1993), which interprets the shoreface package of well 22/16a-2z as a HST and the shoreface package of 21/20-2 as the following LST, despite the fact that 22/16a-2z appears to lie in a more basinal location.

The regressive shoreface sandstones of sequence J54a show a considerable variation in thickness from around 200 ft in WCG wells 21/20-1, 21/20a-5 and 22/16a-2z to over 600 ft thick in the Elgin depocentre (e.g. 22/30c-13), attributed to differential halokinetic control of accommodation space. The presence of salt highs and withdrawal basins disrupts the assumption of the basic sequence stratigraphic model that accommodation space and water depth increase with increasing distance from shore. Jeremiah & Nicholson (1999) attribute the lack of Fulmar

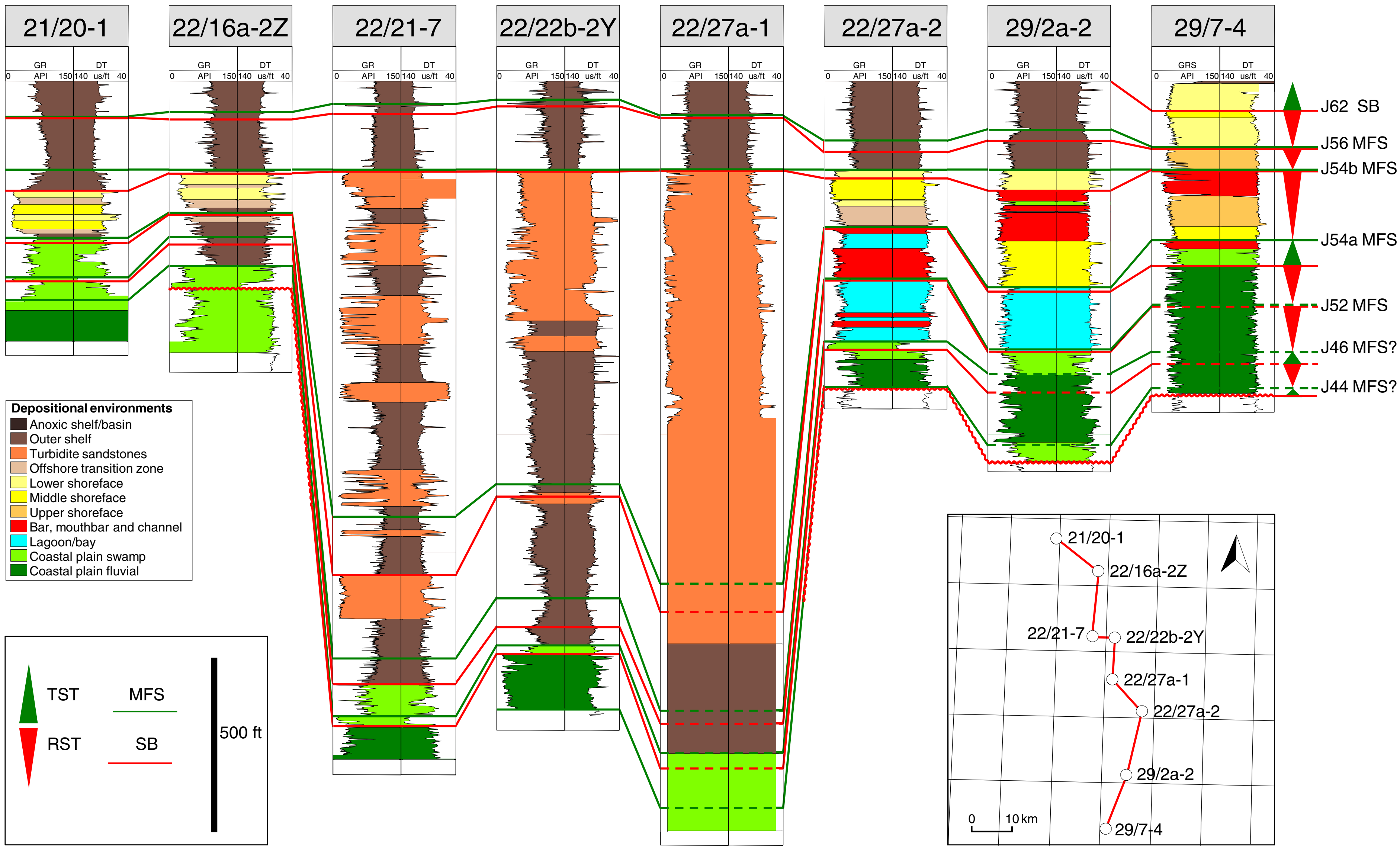

Fig. 7. Well correlation of sequences J46–J54b along the axis of the West Central Graben. The thick turbidite sandstones of sequence J54a indicate both high accommodation space and high sediment supply and are interpreted to indicate an area of enhanced salt withdrawal. The turbidite deposits are interpreted as being coeval with shoreface deposits in the north of the basin and shoreface and deltaic (mouthbar and/or tidal deposits) in the south of the graben.

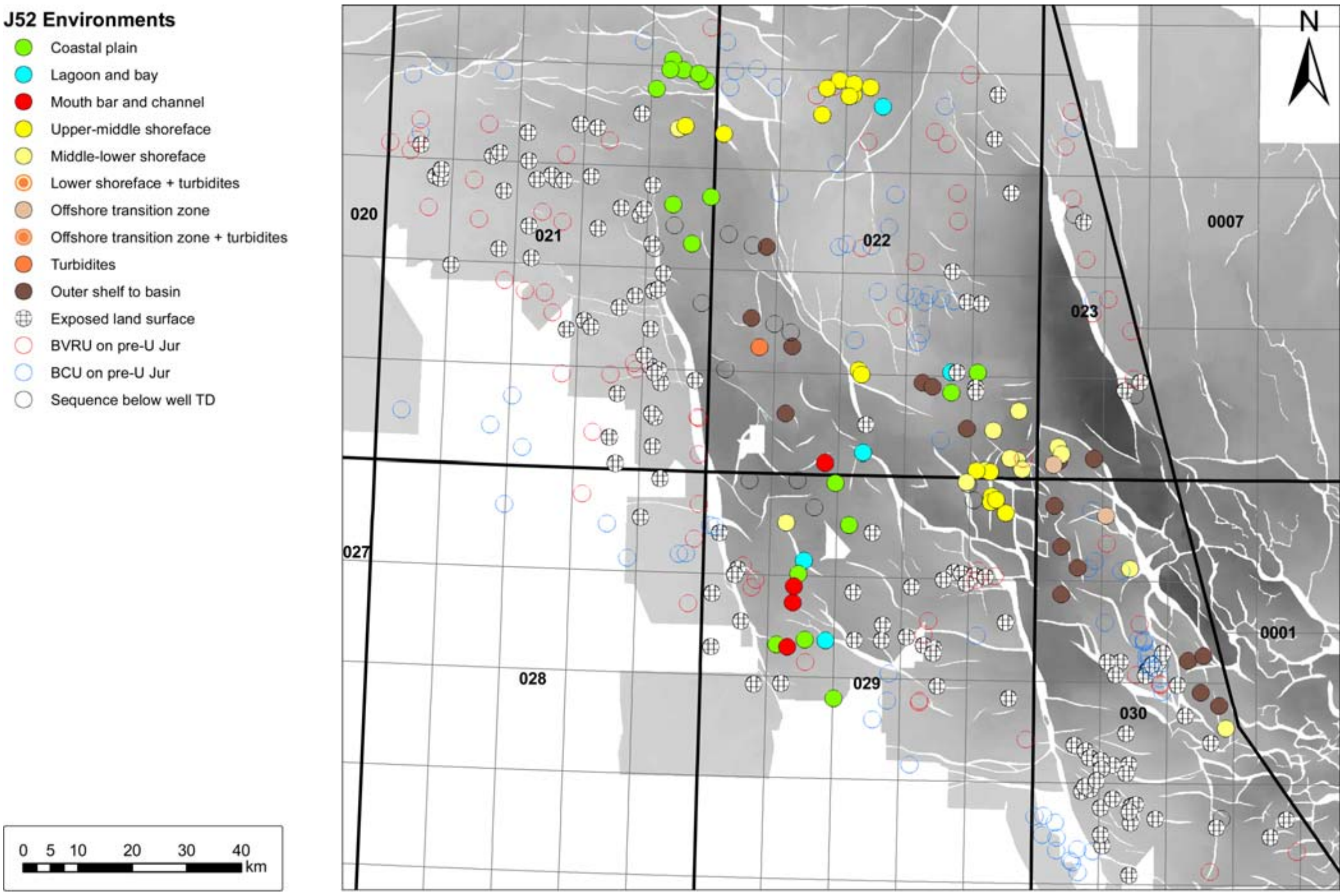

Fig. 8. Sequence J52 depositional environments. Marine conditions were established in the East Central Graben together with shoreface deposition in the Elgin–Franklin area (ECG) and the Howe area (southern end of the FBB). A marine link is believed to have been established between the West and East Central Graben.

sandstones on the Kessog high (well 30/1c-3) to a forced regression above their SJU200 SB, which translated the shoreline into the basin in the Shearwater (22/30) area (their fig. 9). This would imply the formation of a subaerial unconformity in the 30/1c-3 area. However, the succession in 30/1c-3 can be interpreted as complete, although condensed and shale-prone.

Sequence J54a contains the best-developed Humber Group turbidite deposits in the study area. The thickest J54a mass-flow sandstones are found in the centre of the WCG in wells 22/21-7, 22/22b-2z and 22/27a-2 (Fig. 7), with thinner successions also present in the 30/6 graben and 30/13 area of the southern ECG (Fig. 9). Gravity flow deposits are seen in core in the topmost part of the sequence in well 22/27a-2 where they correspond to a characteristic blocky log character and are interpreted on the basis of this log character in uncored wells. The detailed relationship of the turbidite deposits to the shoreface sandstones is unclear, although they occur both interbedded with offshore transition zone sediments (e.g. well 22/30-1) and more basinal shales (e.g. 30/13-4). Jeremiah & Nicholson (1999) attribute turbidite deposits overlying shoreface sandstones at the top of the Fulmar Sandstone in well 22/30b-11 to a distinct tectonic pulse resulting in the emplacement of mass flow sands within the lower shoreface to offshore environment above their SJU310 SB. However, the thick succession of turbidites in the WCG (Fig. 7) is interpreted as demonstrating that mass flow sandstones were being deposited throughout the duration of sequence J54a and are coeval with the shoreface deposits, rather than comprising separate lowstand deposits. The correlations of Jeremiah & Nicholson (1999, their figs 12 & 17) imply that turbidite deposition is mutually exclusive with shoreface deposition and occurs as a result of erosion and bypass of the shoreface during forced regression. This study proposes that turbidite deposition occurred synchronously with shoreface progradation and also potentially during transgression as a result of erosive ravinement of the shoreface. It is possible that the turbidite sandstones are sourced by bypass of sediment through the low-accommodation space areas of condensed shoreface deposition (e.g. 21/20, 22/28) or they may have been sourced more directly from marginal platforms and intrabasinal highs, so that they are laterally interfingering with distal shoreface sediments. The mechanism for putting sufficient sediment into suspension to generate the turbidity currents in this setting remains unclear. Pattison & Hoffman (2008) describe shelf turbidite deposits from the Campanian Blackhawk Formation of the Book Cliffs, Utah, which are detached from their coeval shorefaces and deposited below fair-weather wavebase. They proposed that turbidity currents, generated by storm waves, river flood events (hyperpycnal flows), high rates of sedimentation or earthquakes, cut channels across the shelf that allowed sediments to bypass the shoreface and be deposited on the outer shelf. In this outcrop analogue, mass-flow sandstones were deposited in both shelf channel and lobe settings. The location of the best-developed turbidite deposits in wells 22/21-7, 22/22b-2 and 22/27-1 (although lower section is not logged) may suggest proximity to a major fluvial input, to the west (Western Platform), south (Curlew embayment) or east (FMH). Seismic data indicates that wells 21/25-11 and 22/21-2 both terminate above the base of the Upper Jurassic and just penetrate possible J54a sandstones, although their depositional environment is unknown and logs failed in the basal sections of both wells. It is therefore possible that well developed J54a shoreface or turbidite deposits are

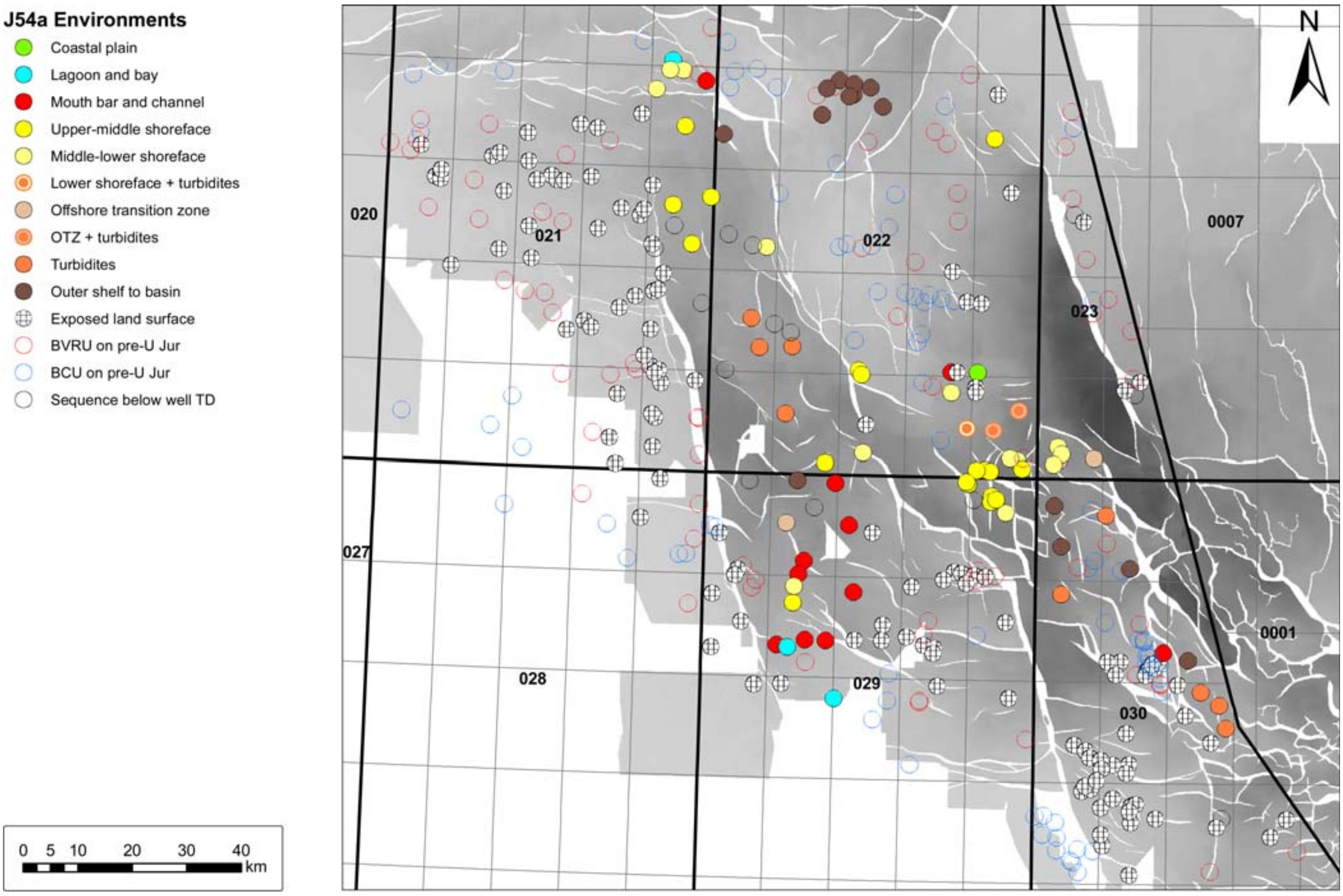

Fig. 9. Sequence J54a depositional environments. Widespread shoreface deposition was established in both the WCG and ECG, together with the deposition of turbidite sandstones in the graben axes, during a period of high sand supply. Deltaic conditions were established in the Curlew Embayment at the southern end of the WCG.

present on the western side of the WCG, sourced from erosion of Skagerrak sandstones on the Western Platform.

Sequence J54b (Late Oxfordian)

The J54b SB is picked at the uppermost MRS of sequence J54a (equivalent to the Redcliffense TS of Jeremiah & Nicholson 1999, fig. 7). The onset of transgression at the base of the J54b TST is an important event that terminated shoreface deposition across the Shearwater and Erskine fields (Jeremiah & Nicholson 1999) and across most of the West and East Central Grabens. This transgressive event significantly overstepped the Pentland Basin (as defined by the extent of the near-top Pentland seismic marker) and initiated flooding of exposed Triassic sediments on the margin of platform areas such as the Teal embayment (21/25, Fig. 10). In many wells, the TST is very thin or virtually absent, suggesting that transgression was rapid and possibly erosive. Thin turbidite deposits are seen at this flooding event in well 22/23b-6 and transgression may have initiated the turbidite deposition described by Jeremiah & Nicholson (1999) in well 22/30b-11. In basinal areas, sequence J54b is characterized by shales with an aggradational GR log signature. J54b shoreface sandstones are limited, but where present in the Elgin and Franklin fields, Turnstone discovery (22/23b-5 and -6) and Teal embayment wells, they exhibit a characteristic log profile commonly showing two or more prograding packages. In the Curlew (29/7) area deltaic and marginal marine environments of sequence J54a were succeeded by fully marine shoreface conditions. In these locations, higher rates of sediment supply were able to compete with the pulses of relative sea-level rise and re-establish shorefaces, and this may indicate the location of major sediment input points into the basin.

J56 (Late Oxfordian–earliest Kimmeridgian)

The J56 SB is very weakly defined within the aggradational J54b shales. The J56 MFS is again poorly controlled by the available biostratigraphic dataset, but is clear on logs at the base of a characteristic, thick, upward-decreasing (prograding) GR profile which characterizes the J56 RST (Fig. 4). This culminates in a clear MRS which constitutes the J62a SB. The J56 MFS is equivalent to the Crystallinum MFS of Jeremiah & Nicholson (1999), which records the widespread flooding of Triassic platform areas such as the Puffin Terrace, eastern part of the Western Platform, J Block/J Ridge and Fulmar–Clyde Terrace (Fig. 11). Prior to this, J Block and the J Ridge were exposed and acted to separate the 30/6 graben and southern ECG. Widespread flooding of the FMH is also envisaged to have occurred at this time, although the evidence has been subsequently eroded. Across most of the graben areas, the J56 sequence is shale prone and the TST is usually thin. Where it transgresses Triassic sediments, the basal SB corresponds to an unconformable shoreline ravinement surface and a glauconitic transgressive sandstone is commonly developed. On J Block and the J Ridge, transgression appears to have cut off the sand supply so that shelf shales were deposited above the initial transgressive sandstone. However, sandy shoreface deposition became established on the Western Platform, Puffin Terrace, Fulmar–Clyde Terrace and Curlew Embayment.

An important observation of the J56 MRS in basinal areas is that it marks the most proximal (lowest GR) shales seen following the

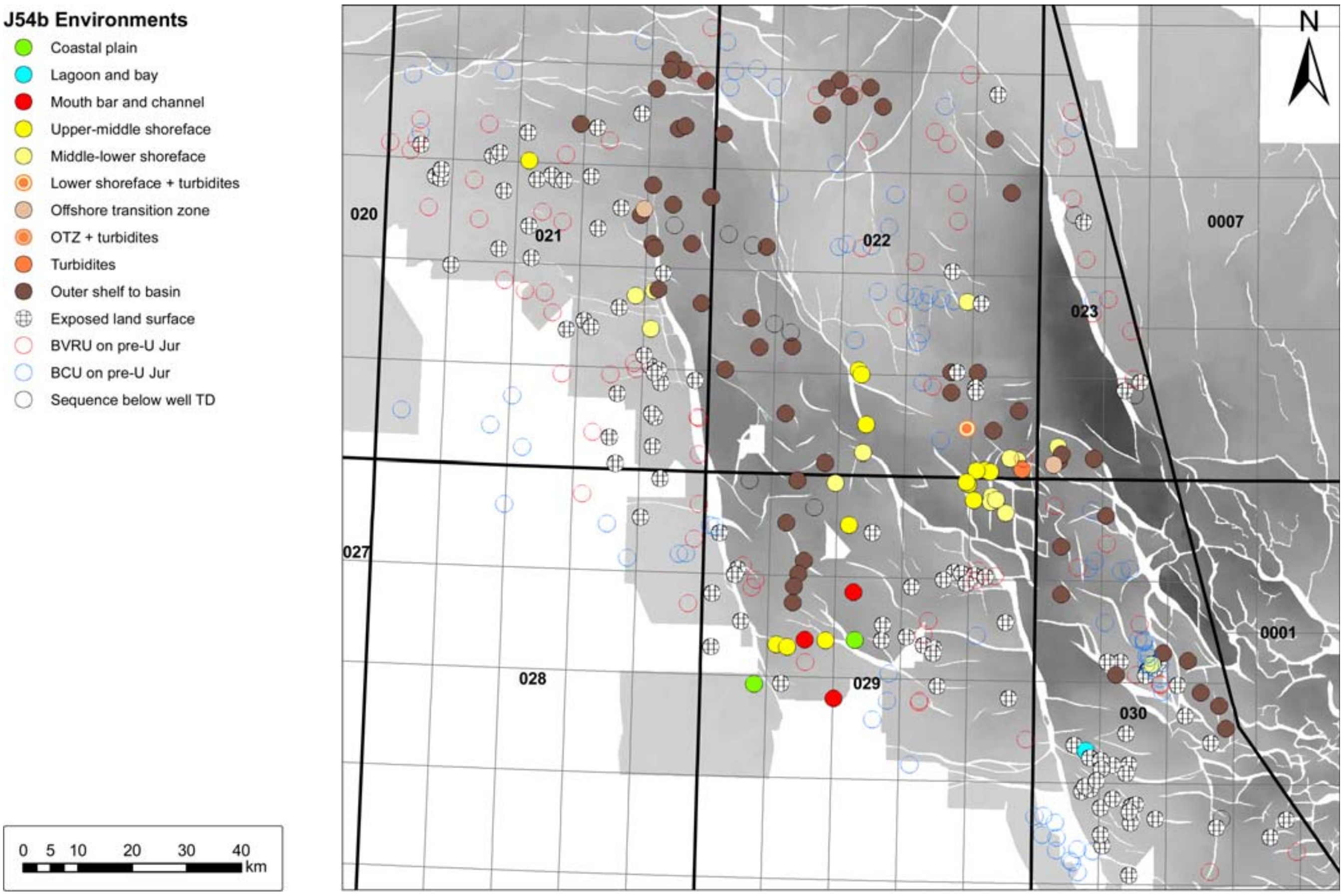

Fig. 10. Sequence J54b depositional environments. Shallow marine environments stepped outside the Pentland basin onto exposed Triassic strata on the Western Platform (Teal embayment) and J Block. Shoreface deposition was established in the Curlew Embayment, but shoreface sandstones are reduced compared with sequence J54a, possibly reflecting the drowning of sediment source areas.

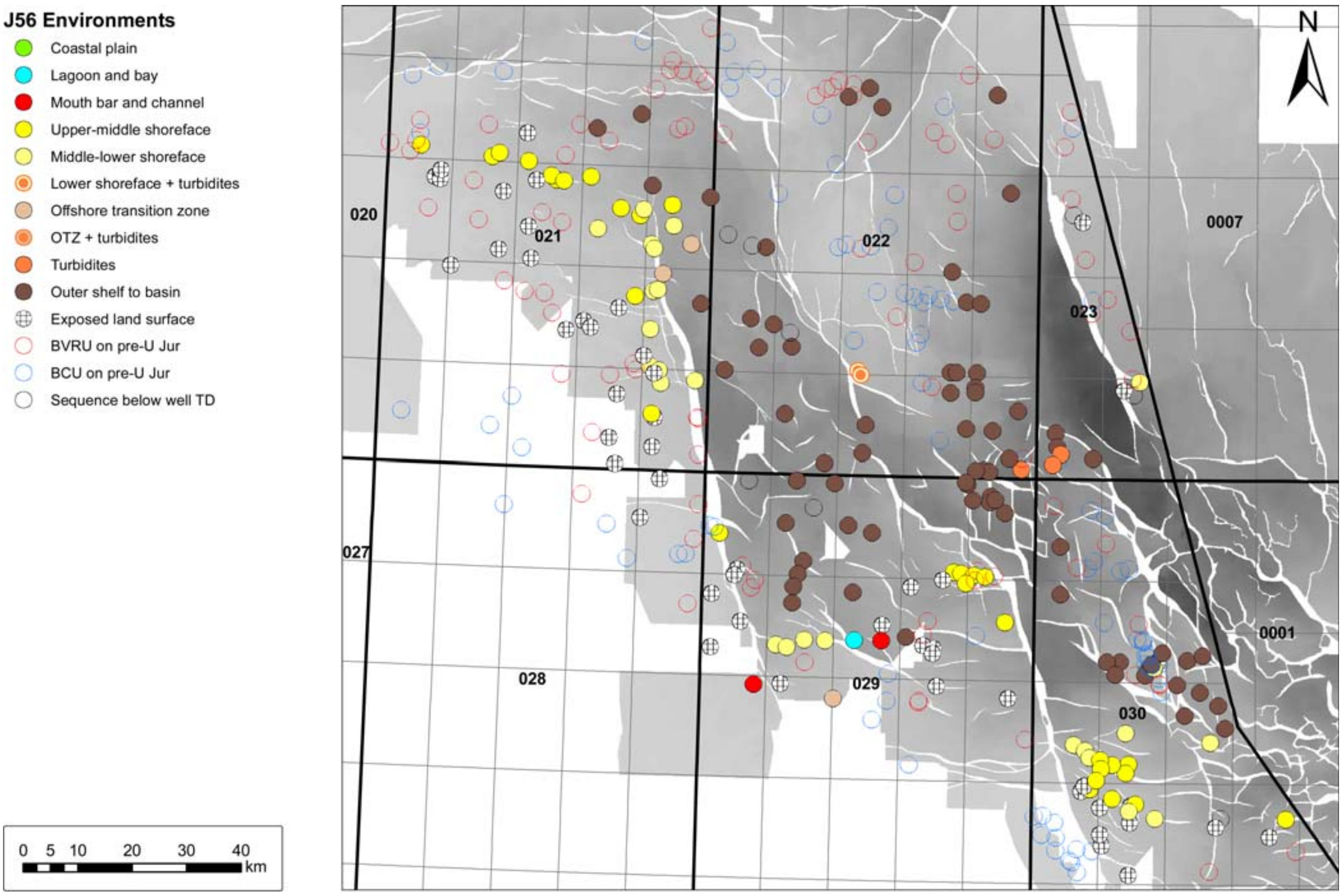

Fig. 11. Sequence J56 depositional environments. Widespread flooding of the marginal platforms and highs occurred, together with limited turbidite deposition in the Shearwater and Erskine areas. Shoreface environments were established on the Western Platform, Puffin Terrace and Fulmar–Clyde Terrace.

J54b MFS, and marks the change from overall progradation of the Humber Group system to aggradation and retrogradation. The RST culminates in the deposition of shoreface sands in the western parts of the WCG (wells 21/20b-4, 21/20a-5, 21/20b-6z), and suggests both the presence of an increased sand supply to the west or NW of the WCG and possibly also the occurrence of a forced regression towards the end of sequence J56. Mass-flow sandstones seen in Shearwater (22/30b-11) and Erskine (23/26b-15) are interpreted to lie within sequence J56, rather than J62 as proposed by Jeremiah & Nicholson (1999, above their Jurassica MFS and SJU400 SB), because they lie within a clearly progradational shale trend characteristic of the J56 RST elsewhere. These turbidite deposits could have been derived from sequence J56 shorefaces on the Puffin Terrace to the SE, southern end of the FMH to the north or the edge of the Jaeren High to the east.

The observation that the J56 RST contains the most proximal post-J54b MFS sediments in the graben is followed through to the analysis of shoreface sandstones on the platform and terrace areas and leads to a different interpretation of sequences J56 and J62 in these areas from that of previous authors (Fig. 3a). Well 29/10-2 on the Puffin Terrace lies in an area of enhanced accommodation space where a thick Pentland-facies coastal plain sequence, which may be partially equivalent to the thick J54a–J54b shoreface sandstones in the Elgin and Franklin fields, is overlain by the J56 TST (Fig. 12). This is succeeded by a thick J56 progradational shoreface sequence (J56 RST), which is cored and capped by coal-bearing coastal plain deposits. Markedly different sequence stratigraphic interpretations of this well have been made by several authors (Fig. 3a; Donovan *et al.* 1993; Carruthers *et al.* 1996; Veldkamp *et al.* 1996; Jeremiah & Nicholson 1999), with most suggesting that the coastal plain deposits overlie a subaerial unconformity constituting a SB that post-dates and may cut out the J62 MFS (Jurassica MFS of Jeremiah & Nicholson 1999). The coastal plain deposits seen in 29/10-2 are the most proximal facies seen in the well post the J56 MFS, and an alternative interpretation suggested here is that this deposit represents the maximum progradation of the J56 RST, so that the J62 SB lies at the top of the coastal plain package, where it is either a MRS or an unconformable shoreline ravinement surface. Alternatively the coastal plain package could form the J62 TST so that the J62 SB is a subaerial unconformity at the base package. In both cases, the J62 MFS is interpreted as lying in a higher GR shoreface unit just above the coastal plain deposits. The J62 RST is then interpreted as comprising a relatively thin unit of proximal shoreface deposits capped by a further thin coal.

Well 21/18-3 has also been subject to a range of different interpretations (Fig. 3b), but this succession can be interpreted in a very similar way to 29/10-2. The J56 TST is limited to a thin transgressive lag (Veldkamp *et al.* 1996) overlying the top Triassic surface. The J56 RST is a shallowing-upwards succession which commences with offshore transition zone deposits and culminates in a strongly prograding middle to upper shoreface package which may represent a forced regression (Martin & Pollard 1996). The MRS at the top of this package corresponds to the J62a SB, which is closely followed by the J62a MFS. This relationship becomes clearer towards the basin in wells 21/20a-2 and 21/20a-5, where increased accommodation space has resulted in a clearer separation of the systems tracts (Fig. 13).

Sequences J62a and J62b (Kimmeridgian)

Sequences J62a and J62b contain the bulk of the productive reservoirs in a number of fields including Fulmar, Clyde, Kittiwake and Cook (Fig. 1). Sequences J62a and J62b have been defined based on the recognition of the Jurapannosum MFS of Jeremiah & Nicholson (1999), which is termed the J62b MFS in this study. The J62a SB conforms to the clear MRS at the top of sequence J56 and the J62a TST is moderately to well developed above this. The J62a and J62b MFSs record further backstepping of the shallow marine system onto the surrounding platform areas (Figs 14 & 15), although they are not as marked as the J56 transgression, except on the western part of the Puffin Terrace (29/8 area) where the Fulmar shorefaces bypassed the 29/8 area as a result of rapid transgression of a low-relief area (Jeremiah & Nicholson 1999). Sequences J62a and J62b commonly exhibit an overall aggradational trend, with only weakly developed progradational and retrogradational profiles, indicating equilibrium between sediment supply and accommodation space. The accumulation of thick aggradational shoreface deposits in the Fulmar and Clyde areas has been suggested to indicate a link between sediment supply and accommodation space controlled by salt withdrawal (Kuhn *et al.* 2003; Turner 1993). The J62b MFS is interpreted as corresponding to the UJ8.2a MFS in the Fulmar Field (Kuhn *et al.* 2003) and the MFA1 MFS in the Clyde Field (Turner 1993). SBs are difficult to define consistently in these sequences where only a small change in the sediment supply/accommodation space relationship can change the position of the MRS defining the J62b SB between the two MFSs, and the proportion of each sequence represented by TST and RST appears variable. In some cases sequence J62a appears thin where the MRS lies only a short distance above the J62a MFS (e.g. wells 21/18-3 and 29/10-2), whilst in others it is much thicker where the MRS occurs much closer to the J62b MFS (e.g. 21/20b-4y, 21/20a-5 and 21/20b-6z). This suggests that the J62b SB as picked in this study is likely to be time transgressive in some areas. In most areas, however, the J62b RST is thin, recording the overall reduction in sediment supply relative to accommodation space.

In this study, significant sequence J62a turbidite sandstones have only been recognized in well 21/20b-4y, with possible stringers extending into well 21/20a-5, despite the extensive development of J62 shorefaces. This contrasts markedly with the widespread turbidite deposition in sequence J54a, and may reflect the overall aggradation rather than progradation of the J62a shorefaces.

Sequence J63 (late Kimmeridgian)

Sequence J63 is mostly represented by anoxic shales and is dominated by a well developed TST, again reflecting the long-term relative sea-level rise. The J63 SB comprises a coincident MRS and transgressive surface. The overlying TST terminates Fulmar shoreface deposition on the eastern side of the Western Platform (e.g. Kittiwake) and across the Puffin Terrace (e.g. 29/10-2), and as the shoreline stepped back to the west and south, shoreface environments were developed for the first time further west on the Western Platform (e.g. 21/17-3) and on the southern margin of the Puffin Terrace (e.g. 29/2b-2, 29/9b-9, 29/14b-1A). In the Fulmar Field, the Auk Terrace continued as a sediment source but also limited the extent of transgression so that J62b shoreface deposition (Mersey Sands) continued into sequence J63. The J63 SB is interpreted at the change from an aggradational to a retrogradational trend in the lower part of reservoir unit U3.2 of Kuhn *et al.* (2003, fig. 8). The thick TST culminated in the J63 MFS, which was followed by the rapid, but short-lived progradation that characterizes the thin J63 RST, which was rapidly overwhelmed by the ongoing relative sea-level rise.

Volgian–Ryazanian megasequence (J64–K10)

The Volgian–Ryazanian megasequence comprises sequences J64–K10 and is mostly represented by warm to hot shales of the Kimmeridge Clay Formation, with subordinate turbidite and shoreface deposits (Fig. 16). Where the megasequence unconformably

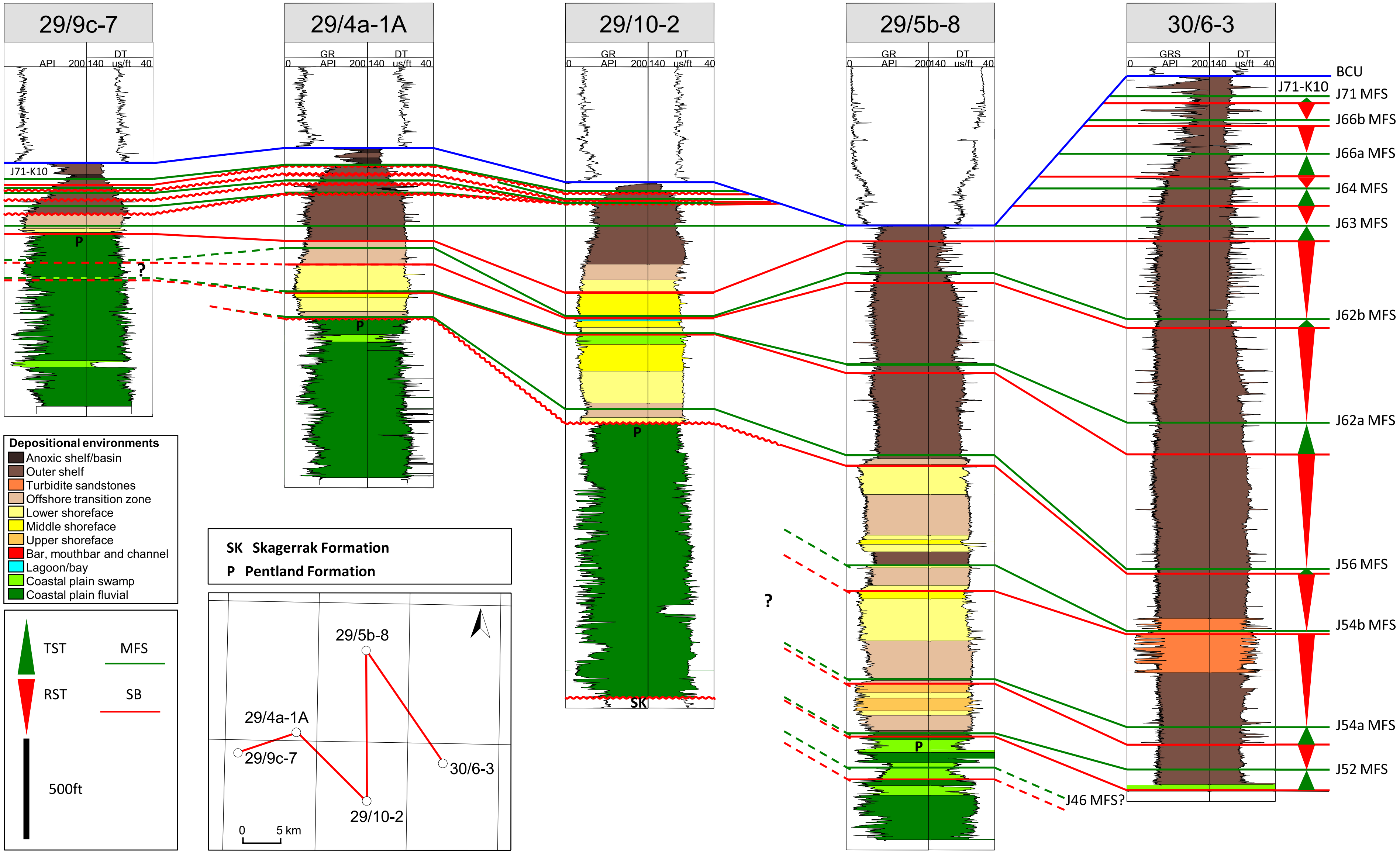

Fig. 12. Well correlation showing back-stepping of the shallow marine system from the 30/6 graben onto the Puffin Terrace in sequence J56. Biostratigraphic data are lacking to confirm whether the upper part of the Pentland succession represents the landward equivalent of the thick aggradational Fulmar Sandstone deposits seen in sequences J52–J54b in the Elgin and Franklin fields.

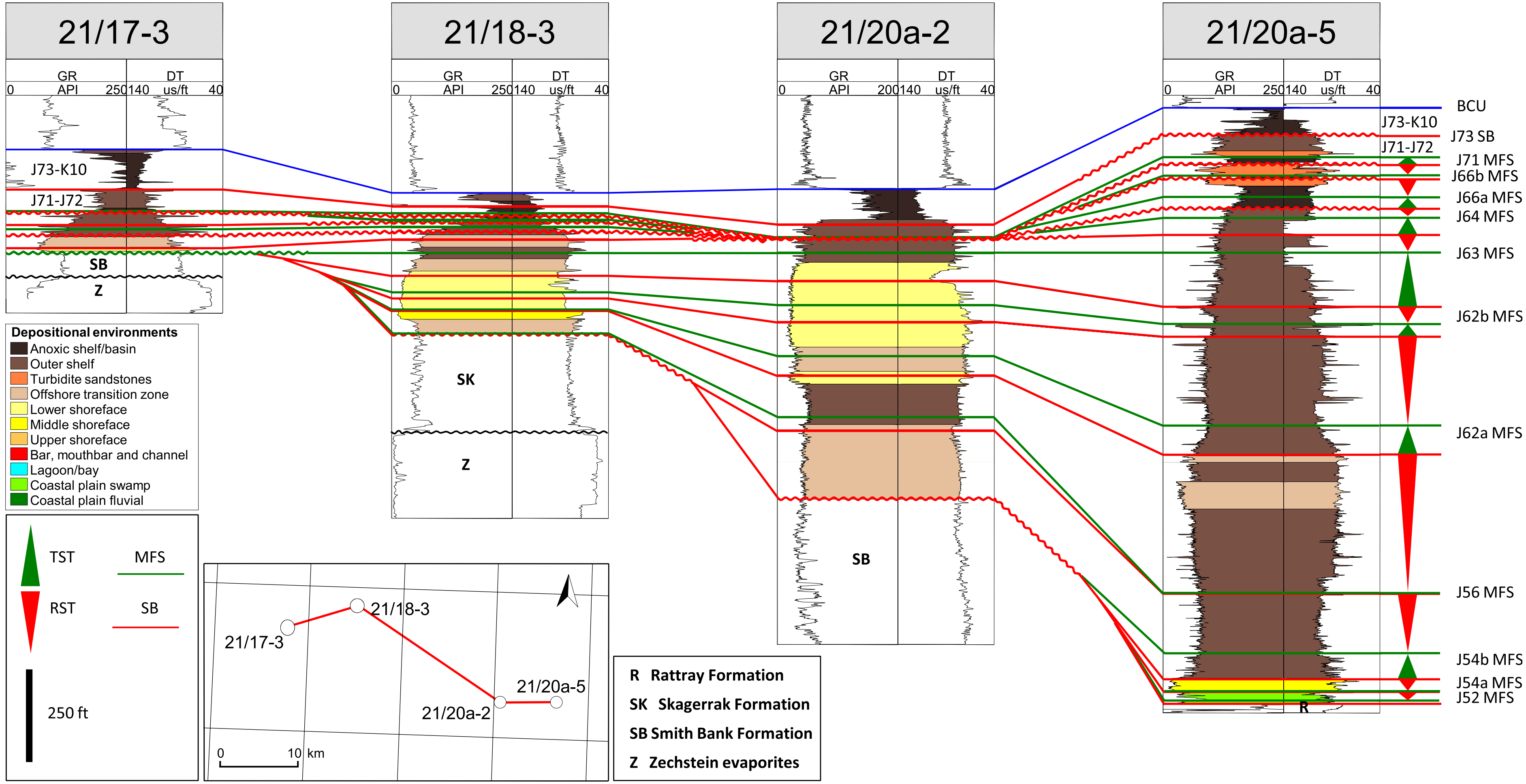

Fig. 13. Well correlation illustrating the back-stepping of the shallow marine system from the WCG onto the Western Platform in sequences J54b and J56 and illustrating the relationship between sequence J56 deposits on the platform area and the graben. A marked increase in progradation is seen at the top of sequence J56 in wells 21/20a-5, 21/20a-2 and 21/18-3. This trend is seen across the basin and may record a forced regression.

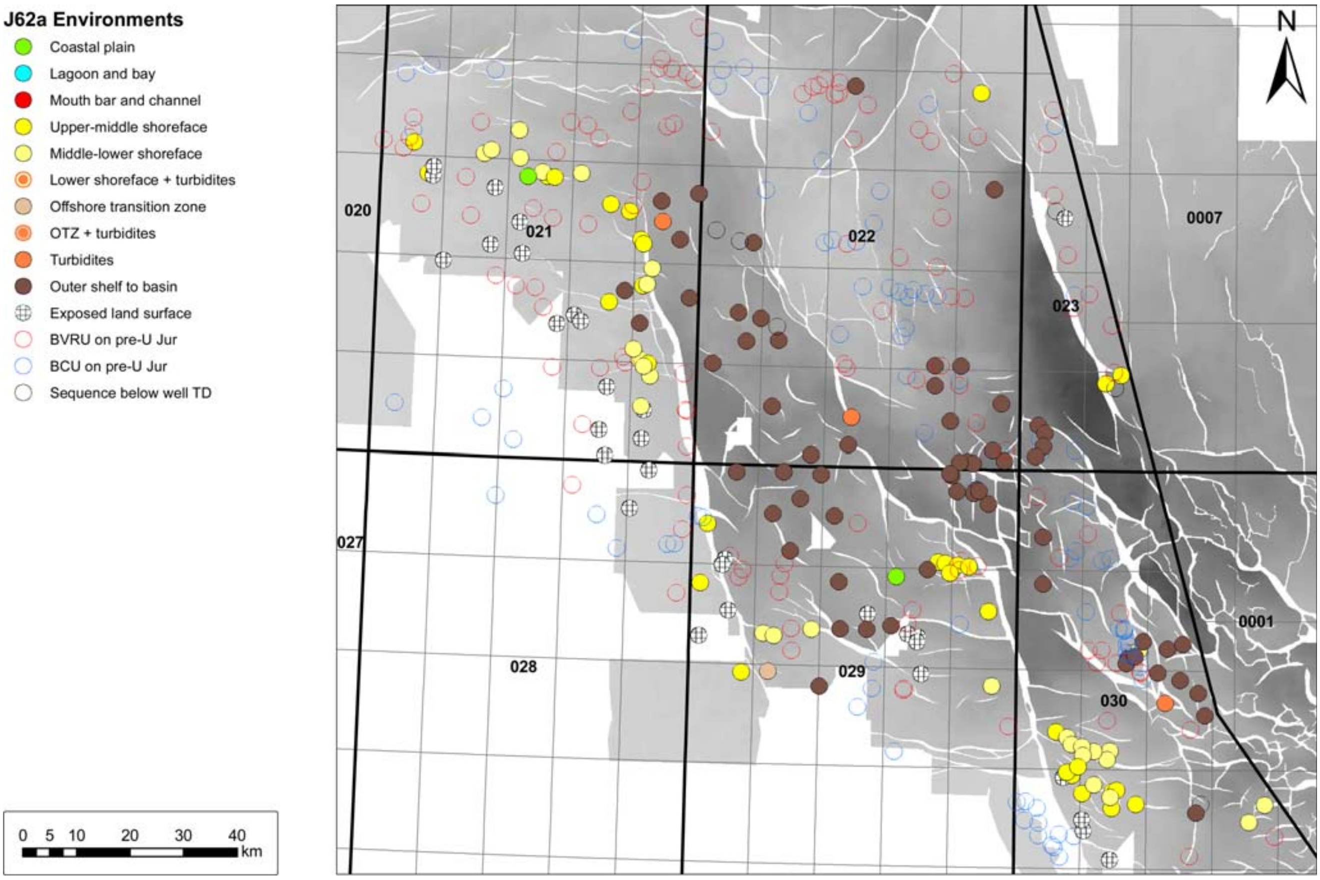

Fig. 14. Sequence J62a depositional environments. Deposition of thick, aggradational shoreface successions occurred on the Western Platform, Puffin Terrace and Fulmar–Clyde Terrace, accompanied by limited turbidite deposition in the basinal areas.

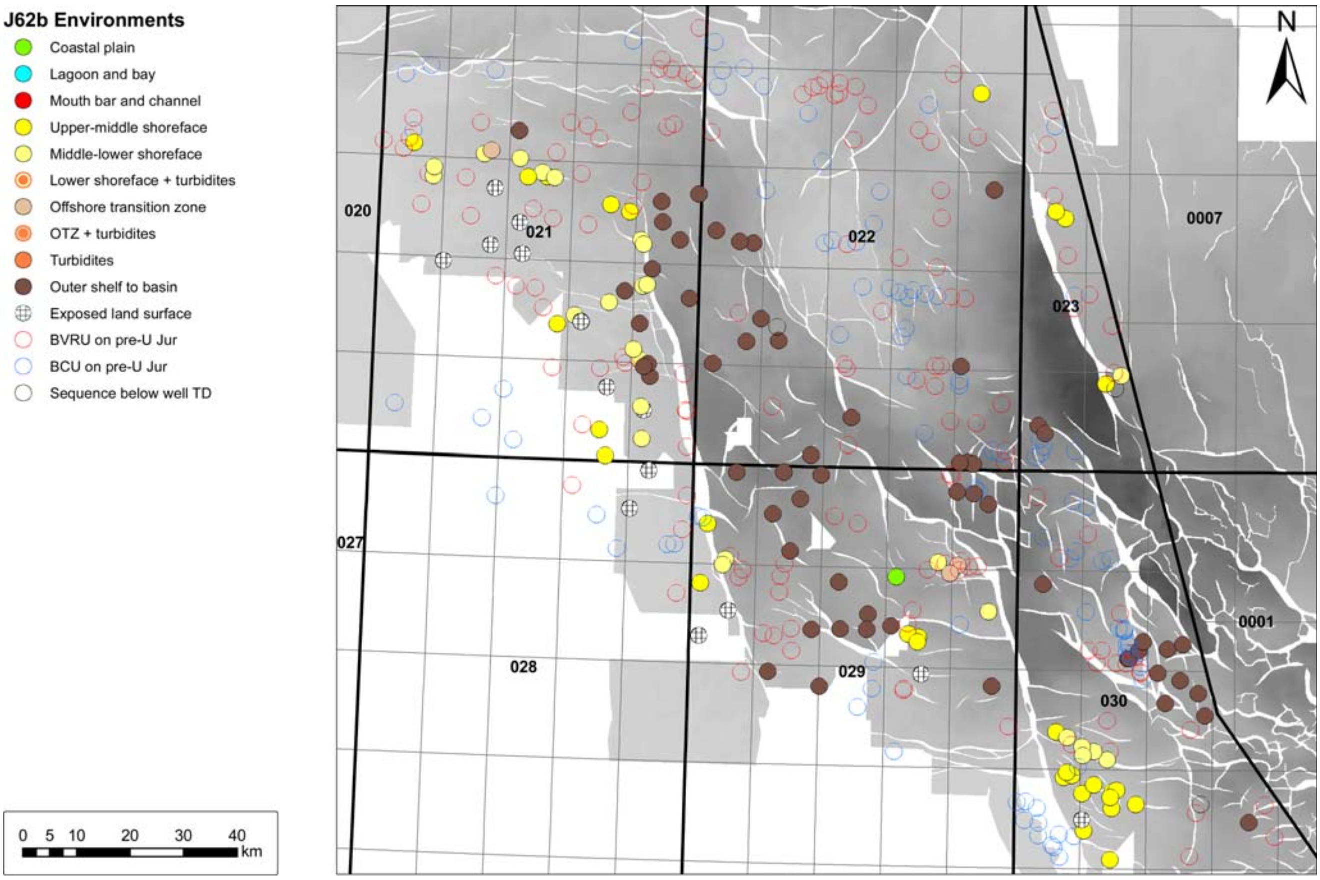

Fig. 15. Sequence J62b depositional environments. Aggradational to retrogradational shoreface deposition continued on the terrace areas with limited expansion of the marine basin.

overlies deposits of the Callovian–Kimmeridgian megasequence, a basal Volgian–Ryazanian megasequence unconformity (BVRU) can be defined. Most of the SBs within the megasequence are also commonly unconformities and the succession is usually highly incomplete in the majority of wells, owing to a combination of internal time-gaps and missing section at the BCU. The BVRU is commonly a composite unconformity, representing erosion and/or non-deposition at two or more of the J64–K10 SBs. The dominance of incomplete successions is due to the preferential location of wells on the structural highs. The unconformities are interpreted as being of dominantly tectonic origin, formed by block rotation and break-up during Volgian–Ryazanian salt collapse. The Volgian salt-withdrawal depocentres are rarely penetrated as they represent present-day lows, but are likely to contain a more complete succession. An element of eustatic control is, however, suggested by consistent log profiles within the more complete successions (Fig. 5), which aids the recognition of incomplete sequences. In the incomplete successions, retrogradational packages dominate over progradational packages and abrupt GR increases occur within composite retrogradational packages which are interpreted as representing stacked TSTs with the RSTs missing at the unconformities.

Where the BVRU is present, determination of the exact timing of the erosional event is complicated by poor biostratigraphic control, and once the unconformity is recognized, the potential for reworking and further blurring of the biostratigraphic resolution becomes apparent. If an unconformity is not recognized and reworking is not correctly identified, then deposits overlying the unconformity may be mis-dated as older than their true age. This is a particular problem where biostratigraphic analyses are based on cuttings, or the original core and sidewall core derived datasets are not available, so that it is difficult to distinguish reworking of older forms from caving of younger forms. Jeremiah & Nicholson (1999) attributed the formation of their SJU600 SB to the tectonic reconfiguration event of Erratt *et al.* (1999), which they dated as latest Early Volgian to basal Middle Volgian based on the occurrence of the marker dinocysts *Muderongia* sp. A Davey 1979 (*Muderongia c.f. simplex* of Duxbury *et al.* 1999) in conjunction with rare *Oligosphaeridium patulum* in sediments immediately overlying older, truncated sequences in the Greater Shearwater area. However, this study has identified wells with a significant interval of older KCF sediments between the BVRU and the characteristic cool KCF facies interval containing the above palynomorphs, suggesting an older age for the onset of reconfiguration. Within the dataset available for this study, the oldest unconformity at the base of the Volgian–Ryazanian megasequence is interpreted as corresponding to the J64 SB, dating the onset of the structural reconfiguration event as latest Kimmeridgian to earliest Early Volgian. This can be demonstrated by tracing the progressive truncation of sequences from wells with a complete succession into wells with a truncated profile. On the western side of the WCG, a complete, although condensed, succession is interpreted in well 21/20a-5, and the basal Volgian–Ryazanian unconformity can be seen progressively down-cutting towards the north, resulting in the complete removal of sequences down to J54b in well 21/15a-6 (Fig. 17). In the Curlew area at the southern end of the WCG, the BCU lies shallower at around 7900–12 300 ft TVDss and biostratigraphic control is relatively good (Fig. 18). Complete condensed, or possibly slightly truncated, successions are

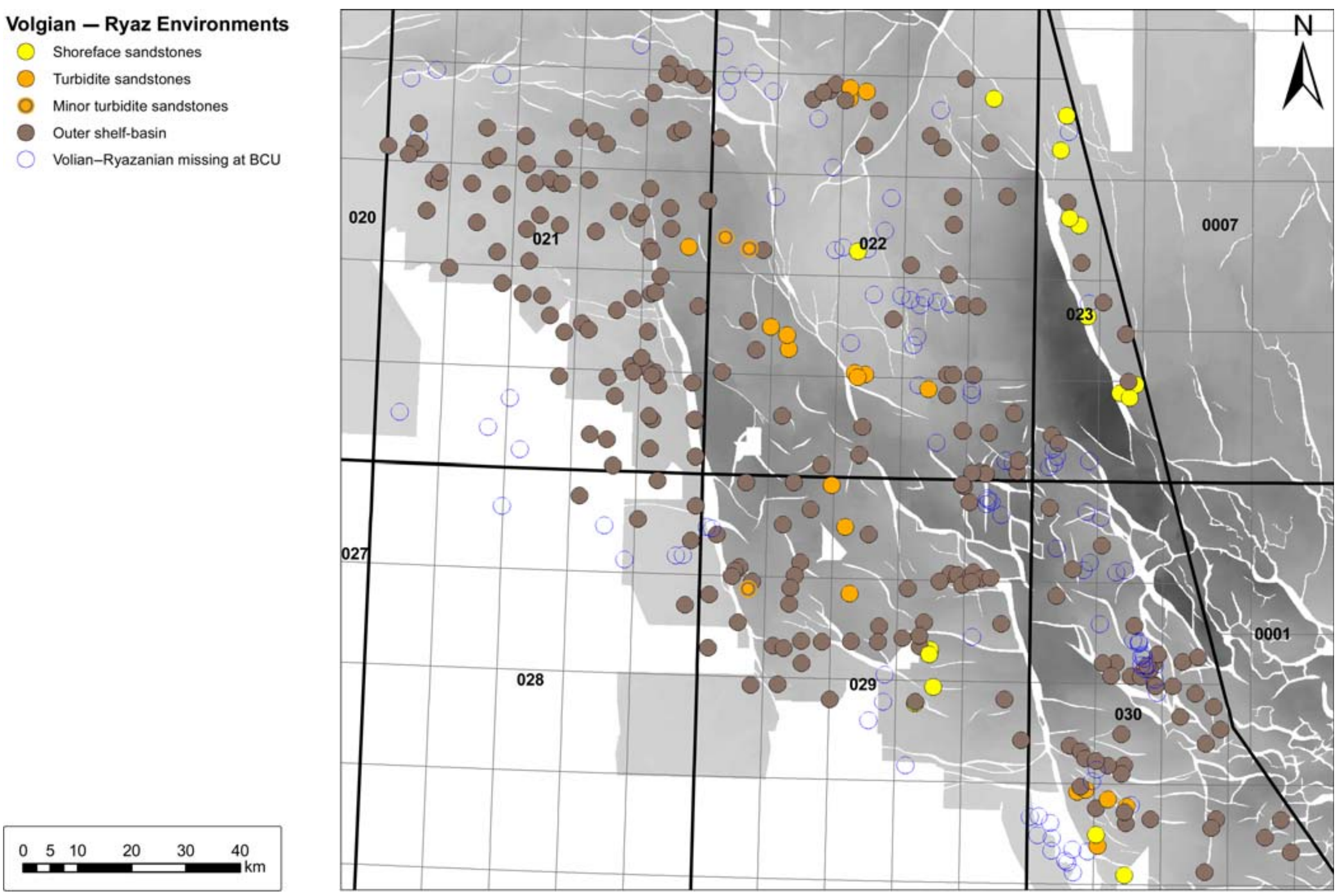

Fig. 16. Summary of environments in the Volgian–Ryazanian megasequence. Shoreface and turbidite sandstones are mostly restricted to sequences J64 and J66a. The shoreface sandstones represent back-stepping onto the remnant topography of the Auk Terrace in the south of the area and Jaeren High in the east, whilst turbidite deposition is interpreted to represent increased sediment supply resulting from block rotation, uplift and erosion.

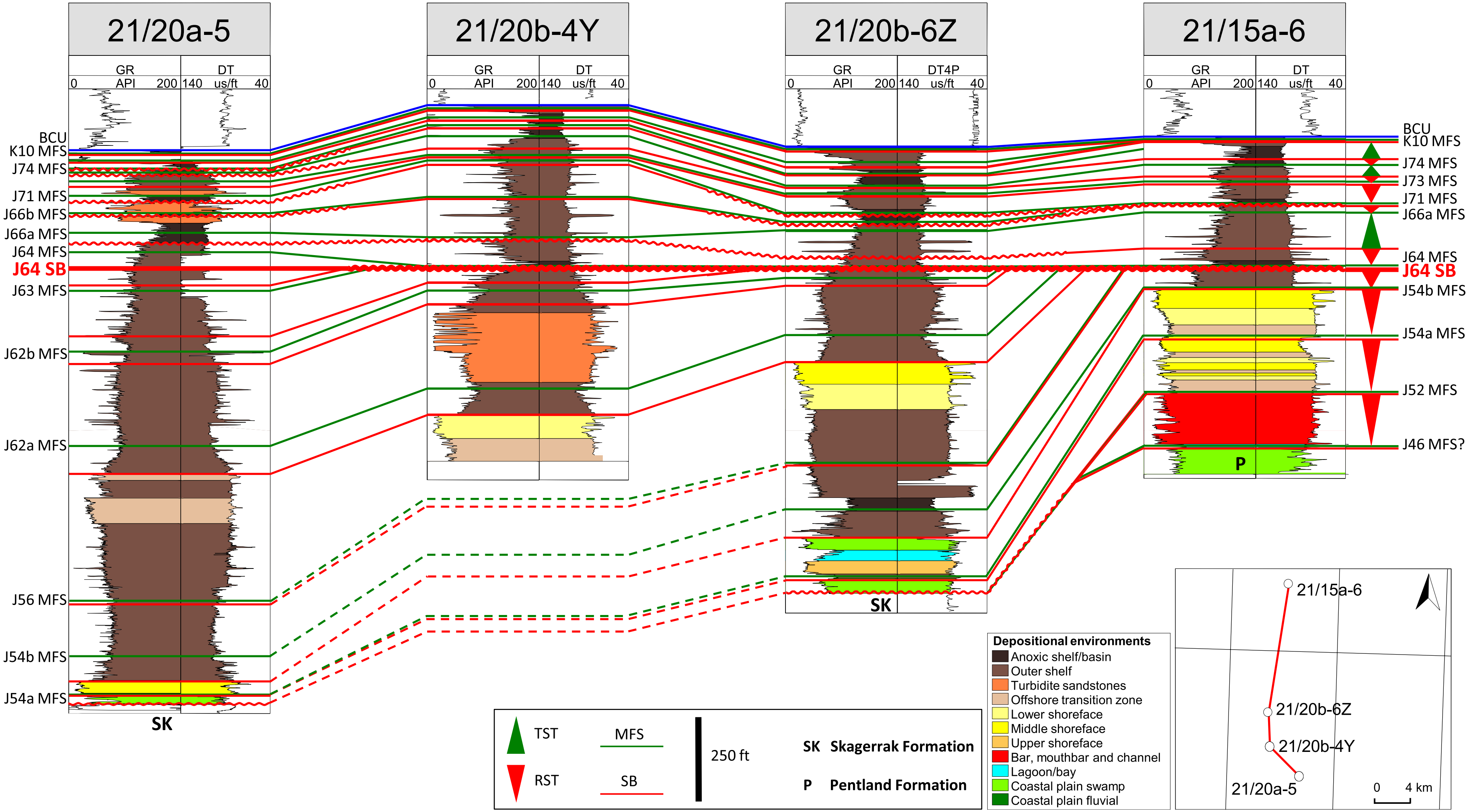

Fig. 17. Well correlation from the WCG showing progressive truncation below the BVRU, which correlates to the J64 SB in the more complete succession in well 21/20a-5. The BVRU is interpreted as cutting down into sequence J63 in 21/20b-4, sequence J62b in 21/20b-6 and sequence J54b in 21/15a-6.

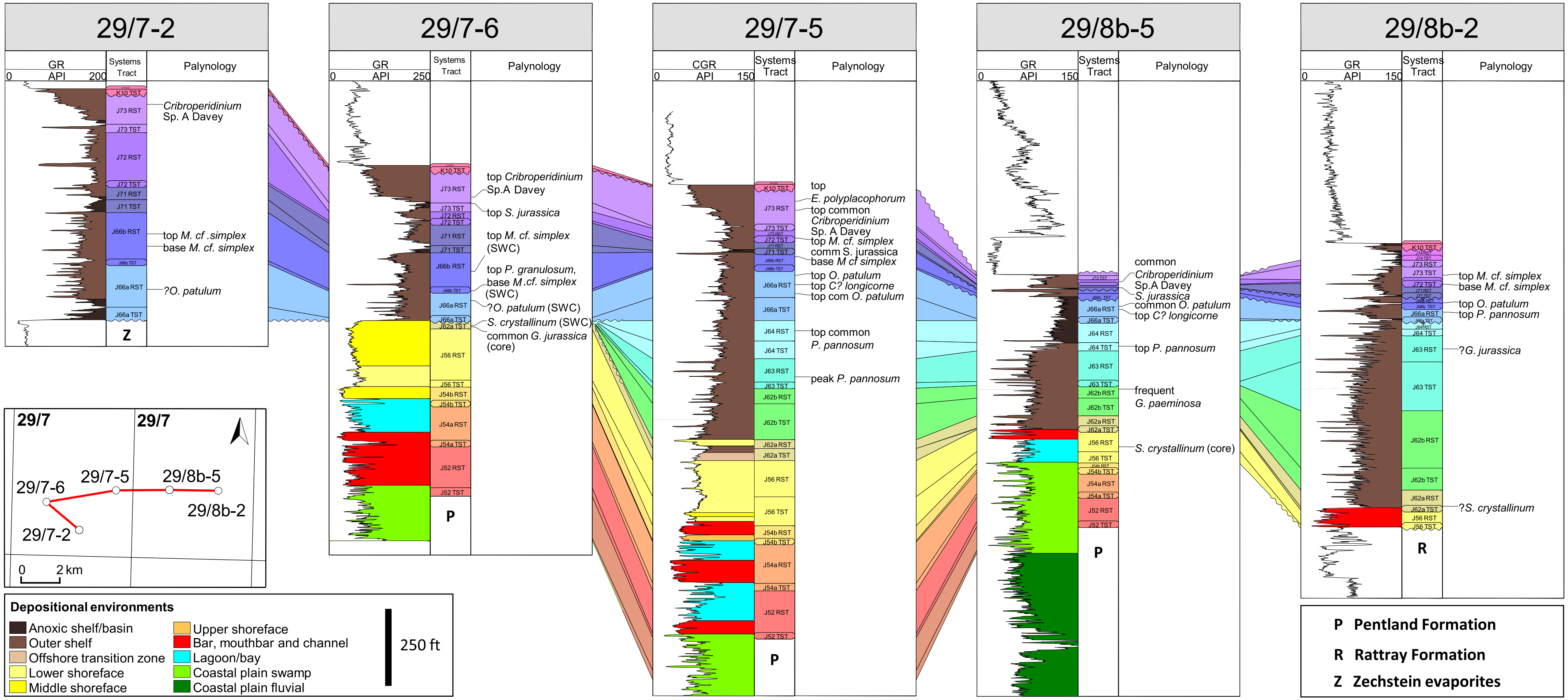

Fig. 18. Well correlation showing biostratigraphic calibration of the sequences and the BVRU in the Curlew area. Complete condensed, or possibly slightly truncated, successions are interpreted in wells 29/7-5 and 29/8b-2, whilst the J66a SB is interpreted as having cut down to sequence J62a TST in 29/7-6. The base occurrence of *M.c.f. simplex* is taken to calibrate sequence J66b, although the top occurrence is interpreted to be depressed in 29/7-2 and 29/7-6 by comparison to adjacent wells.

interpreted in wells 29/7-5 and 29/8b-2, whilst the J66a TST is interpreted as overlying the basal unconformity in 29/7-6, where erosion has cut down to the J62a TST, dating the unconformity as late Kimmeridgian to Early Volgian. The complex Heather and Kimmeridge Clay relationships seen across the Curlew field are attributed to differential erosion and onlap on to the BVRU rather than the rapid lateral facies changes envisaged by Eneyok *et al.* (2003).

The expression of the BVRU and overlying Volgian–Ryazanian megasequence can be grouped into three broad log character motifs. 'Expanded' successions are relatively complete and conformable with the underlying sequence J63. They usually comprise thick sequences of Kimmeridge Clay, which show weak to rarely strong development of the J64 RST. 'Condensed' successions show a marked convex shoulder on GR logs, where the GR increases sharply and sequences J64 and J66 appear either complete and condensed relative to the older sequences in the well and the expanded wells, or the J64 and J66a RSTs are absent, resulting in stacking of the J64 and J66a TSTs, culminating in the J66a MFS. In these wells where sequence J64 overlies sequence J63, the J64 SB corresponds to a MRS at the top of a thin J63 RST, and in some cases the shift to high GR KCF facies above the MRS may be very abrupt so that it is difficult to ascertain whether this represents simply a very sudden tectonically forced deepening (a tectonically enhanced MFS in the sense of Partington *et al.* 1993*a*) or whether some erosion is involved. In 'truncated' successions, the BVRU is clearly an erosional unconformity representing a significant time gap and high-GR sequence J64 or younger Kimmeridge Clay deposits unconformably overlie J63 or older deposits. An extreme end member of this type of succession occurs where sequences J64–K10 overlie pre-Upper Jurassic (typically Triassic) deposits. Whilst this may simply record the final stages of onlap of the Humber Group onto pre-existing topography, there is also the potential that older Humber Group sediments have been eroded at these locations.

Sequence J64 (Early Volgian)

Sequence J64 is commonly missing at the BVRU, with J66a or younger sequences overlying pre-J64 deposits. Where present, the J64 TST is characterized by a marked upward increase in GR values above the J63 RST, indicating rapid deepening culminating in the J64 MFS. The J64 RST is commonly truncated by the J66a SB. However, in some expanded intervals, the J64 RST is well developed and contains sandy turbidite deposits, as seen in the Selkirk discovery (22/22b-2 and -4). Rarely, well developed progradational shoreface deposits are present, as in the Wood field (22/18-6) on the FMH, at the southern edge of the Puffin Terrace (29/9 and 29/14 area) and on the western margin of the Jaeren High, which are equivalent to the thick J64 shoreface sandstones of the Norwegian Gyda field (Partington *et al.* 1993*a*, fig. 13). Both the deposition of the turbidites and the renewed shoreface progradation may be indicative of structural uplift and rejuvenation of sediment source areas.

Sequence J66a (Early Volgian)

Sequence J66a is characterized by a thick transgressive shale package with an upwardly increasing GR profile which commonly overlies Kimmeridgian or older sequences on the BVRU. The J66a MFS is commonly characterized by higher GR values than the older J64 MFS. The J66a RST is variably truncated by the J66b SB unconformity, but where present, it is represented by lower GR shales with occasional sandy turbidite deposits, and rarely shoreface sandstones (22/18-6).

Sequence J66b (latest Early–earliest Middle Volgian)

Sequence J66b is also commonly highly truncated or missing below the J71 SB. It comprises Kimmeridge Clay Formation shales and is similar in log character to sequence J66a so that the two can be difficult to distinguish in the absence of biostratigraphic control. The differentiation of the J66b sequence is necessary, however, to differentiate the Early Volgian erosional events.

Sequence J71–J72 (Middle Volgian)

Sequences J71 and J72 are characterized throughout the study area by a well-developed and diagnostic GR-SONIC bow between the J71 and J73 MFSs, and recording a major influx of cooler Kimmeridge Clay facies into the basin (Fig. 5). The sequences themselves can be difficult to distinguish due to only weak development of the J72 MFS. The J71 MFS is readily identified throughout the study area as a well defined GR peak that marks the culmination of the overall transgressive trend seen throughout sequences J63–J66b and the development of anoxic conditions throughout the basin. The J71 TST is usually thin and the base is commonly marked by an abrupt GR log break at the top of sequence J66b, which suggests that the J71 SB is an unconformity. The J71 MFS is widely recognized even in highly incomplete Volgian–Ryazanian successions, suggesting it represents widespread flooding of topography and fault blocks created during the Early Volgian tectonic reconfiguration. This may suggest that it represents a regional eustatically-controlled sea-level rise.

The J71 and J72 RSTs comprise the lower part of the GR-SONIC bow, with the lowest GR values probably occurring at the top of sequence J72 and defining the J72 MRS/J73 SB. This records a significant pulse of progradation, but sands are limited to rare, thin turbidite stringers, probably reflecting the regional drowning of source areas by the J71 MFS. The first downhole and top common occurrences of *M. simplex* (*Muderongia* sp. A Davey) occur between the J73 and J71 MFSs, providing good dating constraint.

Sequences J73–J76 (latest Middle Volgian–Early Ryazanian)

The J73 TST is commonly thick and comprises the upper part of the well-defined Middle Volgian GR-SONIC bow, representing renewed relative sea-level rise culminating in the J73 MFS. In highly incomplete Volgian–Ryazanian intervals, the lower part of the GR-SONIC bow may be absent above the J71 MFS, representing a significant missing section at the J73 SB. The J73 RST is commonly either very thin or missing at the J74 SB, so that the J73 and J74 TSTs are commonly stacked into a composite transgressive sequence culminating in very high GR anoxic shales that characterize the J74 MFS. Sequences J74 and J76 are poorly defined in the study area, owing to a combination of condensation, onlap and erosion at either the K10 SB or the BCU. Where identified, they are characterized by thin, abrupt TSTs. The K10 SB is commonly underlain by a thin but well-defined cool shale package that may represent the J76 RST. The lack of accommodation space and sediment supply during the Late Volgian and Early Ryazanian contrasts with the Moray Firth Basin, which was a site of significant turbidite deposition at this time (Fraser *et al.* 2002, fig. 11.17).

Sequence K10 (Late Ryazanian)

Although it is thin (typically 10 ft), sequence K10 is usually easily recognized by a characteristic GR log couplet just below the 'BCU' (base of the Cromer Knoll Group). Lower GR values at the base of the sequence define the SB, which is overlain by highly condensed Kimmeridge Clay deposits that are characterized by very high GR values. Sequence K10 is also easily recognized in the available micropalaeontological datasets by the presence of *Tricolocapsa* species 1. The K10 SB is an unconformity which commonly cuts out Early Ryazanian and Late Volgian (J74–J76) deposits. However, the sequence may be conformable with the basal deposits of the Cromer Knoll Group. The very high GR values suggest that relative sea-level rise contributed to further restriction of water circulation and stagnation in conditions of very low sediment supply.

Evidence for and implications of tectonic reconfiguration of the Central Graben

Salt redistribution and block rotation

The formation of the basal Volgian and intra Volgian–Ryazanian unconformities and relationship between wells showing expanded, condensed and truncated log profiles can be attributed to the wells being located on different parts of a fault block that was undergoing rotation from sequence J64 times onwards (Fig. 19). Erosion and deep truncation takes place on the crest of the block updip of the pivot point as illustrated by Davies *et al.* (1999, fig. 11). Truncation becomes progressively less downdip, passing into a zone of omission then condensation around the pivot point, before expanding further downdip into a syn-rotational growth sequence in the hanging wall to the active fault. Within the Central Graben, this situation arose during redistribution of the underlying salt in response to the change of kinematic regime proposed by Erratt *et al.* (1999). This had a dramatic and sudden effect, inducing lateral movements of the salt along the salt walls, causing some areas to rise and others to collapse, with new Volgian faults forming at the interface. This broke up the Triassic–Jurassic mini-basins and the new fault blocks rotated into the evolving Volgian depocentres located over falling salt structures. The CNS diapirs are envisaged to have been initiated at this time by these movements.

The seismic line in Figure 20 from the West Central Graben illustrates this process. The Upper Jurassic section is shown thickening westward into a basin-margin salt-withdrawal depocentre which persisted into the Lower Cretaceous. Grounding of the Triassic pod onto a Rotliegend horst in the centre of the basin and collapse of the marginal salt highs caused dissection of the depocentre into two smaller Volgian basins and collapse of the basin margins. On the western margin, a Triassic Smith Bank pod is interpreted to have rotated into the basin due to deflation of the basin margin salt wall. On the eastern side, the turbidite deposits which form the Selkirk reservoir (wells 22/22b-2 and -4) are placed within the J64 RST (Fig. 21). These sandstones are interpreted as providing further evidence of the timing of uplift, erosion and reworking of Fulmar and/or Skagerrak sandstones on the FMH as a result of the tectonic reconfiguration of the basin.

Evidence for basement uplift

Whilst the pattern of erosion associated with the formation of the BVRU is obviously biased by the location of most wells on the structural highs and not in the Volgian depocentres, consideration of this pattern suggests that pod grounding and fault block rotation due to salt redistribution alone may not be sufficient to account for the degree of erosion seen in some areas. Figure 22 shows the sequence age of the subcrop to the BVRU (J64 SB or younger SBs). This shows a pattern of deep truncation of the pre-Volgian succession down to sequences J52–J56 on the flanks of the FMH and along the SE-trending axis between the West and East Central Graben which terminates in J Block and the J Ridge. Deep truncation of the succession down to sequences J56–J62a is also seen at the northern end of the Western Platform (border of blocks 21/19 and 21/20) and in the south of the WCG in the Curlew (29/7) area. This correlates with the areas of uplift and subsidence observed by Erratt *et al.* (1999), who documented uplift of the Auk Terrace and J Ridge together with collapse of the Puffin Terrace and dissection of the Jacqui (30/8) graben. Along the crest of the Forties–Montrose, Kessog and J-Block highs, Upper Jurassic sediments are either completely absent, so that Cretaceous strata overlie predominantly Triassic (less commonly Middle

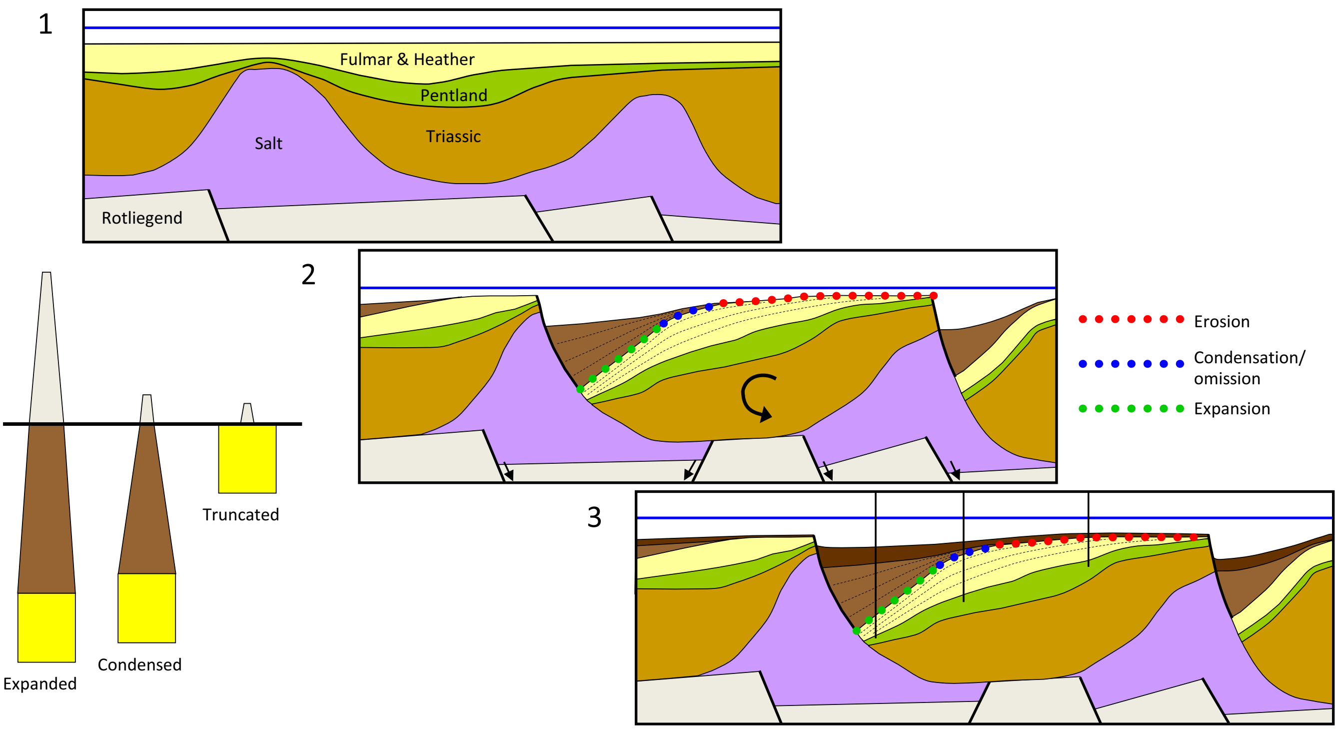

Fig. 19. Conceptual model illustrating the process of formation of truncated, condensed and expanded Volgian–Ryazanian (J64–K10) successions during pod breakup and rotation resulting from partial collapse of the adjacent salt walls.

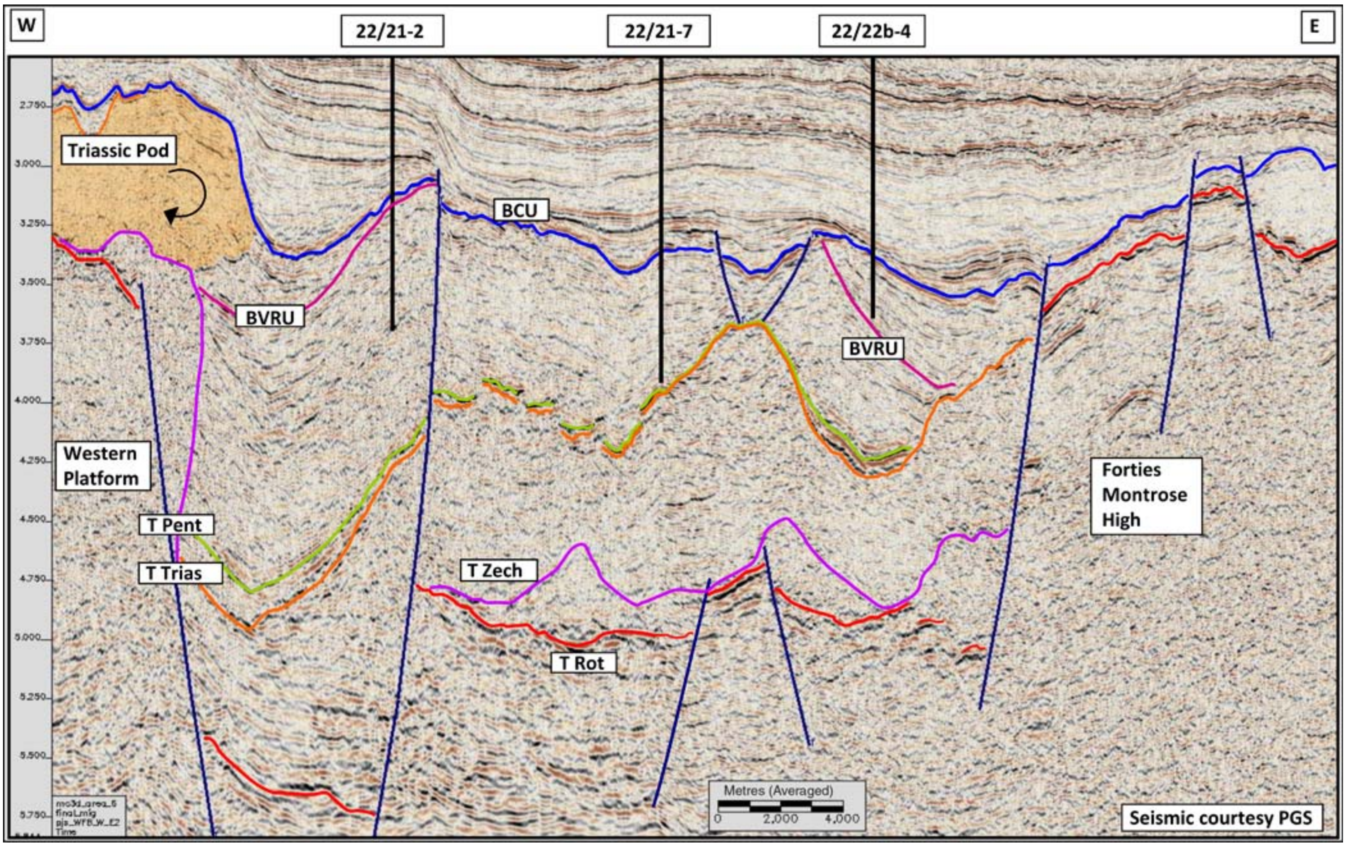

Fig. 20. Seismic line across the WCG showing a large, grounded Triassic pod in the centre of the basin and the development of Volgian depocentres at the basin flanks due to deflation of salt walls at the basin margin. The removal of salt has caused a Triassic pod to rotate into the graben from the Western Platform.

Jurassic or Permian) sediments, or are represented by sequence J64–K10 (Volgian–Ryazanian) KCF only. At first glance, the pattern of wells containing only a Volgian to Ryazanian Upper Jurassic succession, or where the Upper Jurassic is absent, could be explained by the simple onlap of the Upper Jurassic sequences onto the intrabasinal highs as rifting progressed, with the Volgian shoreface deposits representing the final stages of backstepping of the Fulmar system. However, the recognition of the BVRU allows the possibility that some, if not all, of these areas were drowned prior to tectonic reconfiguration, and that widespread uplift and erosion of the highs has occurred.

Figure 23 shows a north–south seismic line along the northern axis of the West Central Graben. This demonstrates northward thinning of the Upper Jurassic succession, as might be expected due to onlap onto the FMH. However, a well correlation along this line (Fig. 24) indicates that this thinning is in large part due to truncation within the Upper Jurassic interval by the J64 SB and/or younger SBs and onlap of this surface by successively younger Kimmeridge Clay sequences to the north. This implies that uplift of the FMH and tilting of the West Forties basin occurred as a result of the tectonic reconfiguration.

Timing and style of tectonic events

There is considerable variation in the interpreted ages and kinematics of the Late Jurassic rift events in the Central Graben. Price *et al.* (1993) suggested that rifting was largely confined to the Late Oxfordian to Early Kimmeridgian, since this was when the major sand influxes occurred. Rattey & Hayward (1993) and Partington *et al.* (1993*a*) favoured a younger late Kimmeridgian to Early Volgian (J63–J66) age for the onset of the main rift phase in the Central Graben. Rattey & Hayward (1993) concluded that the change from rifting to thermal subsidence occurred at the base of sequence J70, owing to an apparent absence of J70 and younger unconformities. Davies *et al.* (1999) distinguished an intra-Callovian unconformity and a Middle Oxfordian unconformity, both generated by extension-related uplift, from the older intra-Aalenian (Mid Cimmerian) unconformity generated above the North Sea thermal dome. Significantly they noted changes in the geometry of the rift system at these events and attributed the switch to a NW–SE orientated depocentre in Kimmeridgian–Volgian times in the Witch Ground Graben to a third phase of re-orientated rifting.

Erratt *et al.* (1999) attributed the overprinting of the Oxfordian–Kimmeridgian basin fabric to a change in the extension direction from west–east to SW–NE, resulting from rotation of the kinematic axes of the Central Graben in the Middle to Late Volgian, although Jeremiah & Nicholson (1999) interpreted a latest Early Volgian to basal Middle Volgian age for this event. Erratt *et al.* (1999) attributed the reactivation of the Auk margin and J Ridge to footwall uplift associated with a pulse of basement extension and suggested that some structures of apparent strike-slip origin could be attributed to the superposition of rift events with differing orientations. Conversely, Jones *et al.* (1999) argued that the apparently conflicting extension directions presented in earlier work could be explained by a phase of relatively weak Callovian to early Kimmeridgian NW–SE extension, succeeded by a phase of sinistral shear between the Tornquist Zone and the Trans-European Fault Zone in the Kimmeridgian to Ryazanian, during which the Central Graben experienced transpression along NW–SE faults and extension across west–east faults. They argued that no change in the regional extension vector was necessary to explain the observed structures. Alternatively, Stewart & Clark (1999)

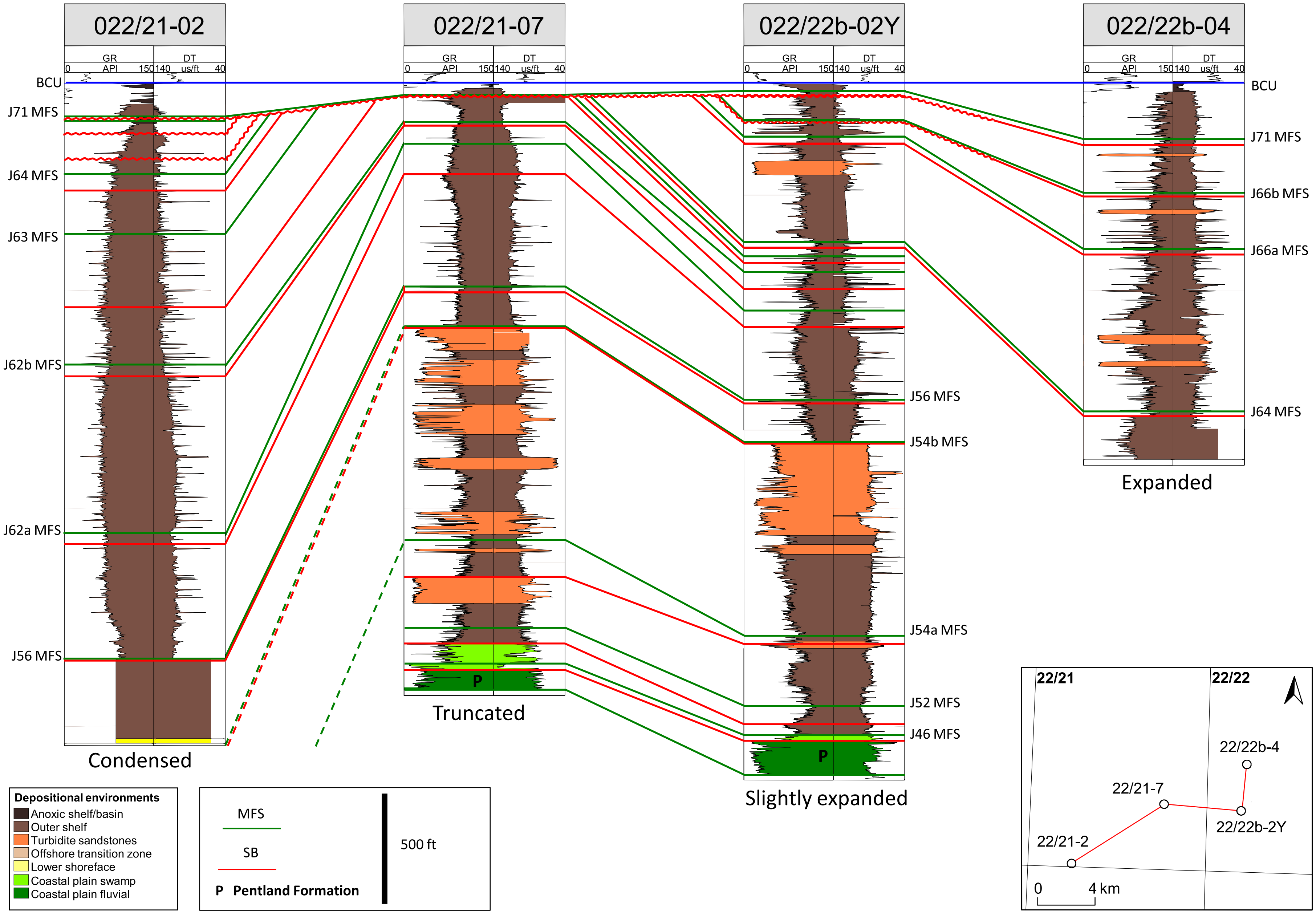

Fig. 21. Well correlation showing marked truncation below the BVRU in the centre of the WCG and expansion of the Volgian section (sequences J64–J66b) into the marginal depocentre, where the Selkirk turbidites were deposited during sequences J64 and J66a in wells 22/22b-2Y and 22/22b-4. Note, however, that Late Volgian–Ryazanian sequences are missing in these wells despite their increased accommodation space during the Volgian, possibly recording progressive grounding of the underlying pod flank.

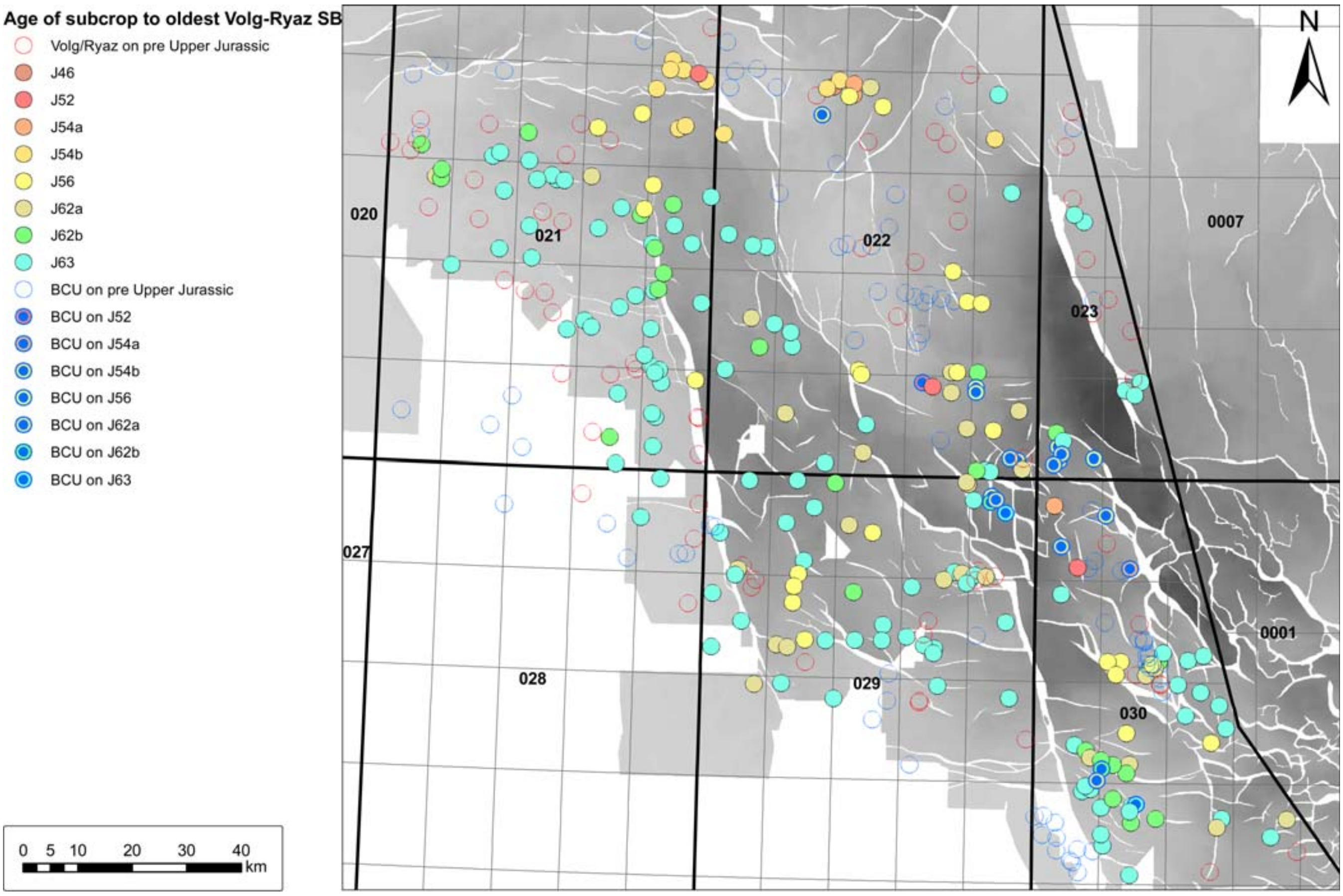

Fig. 22. Subcrop to the oldest Volgian–Ryazanian SB by sequence age. Note the deep truncation down to sequences J52–J56 on the flanks of the FMH and J Ridge. Areas where the Callovian–Kimmeridgian megasequence (e.g. Shearwater–Erskine area) or pre-Upper Jurassic deposits now subcrop the BCU may also have been deeply truncated at this time, but the evidence has been removed by subsequent erosion.

proposed that the late Upper Jurassic and Lower Cretaceous isopachs were a function of salt redistribution controlled by thin-skinned, gravity-driven tectonics rather than basement extension. Stewart (1993) proposed that the geometry of the Ula Trend in the Norwegian Central Graben resulted from a combination of dip-slip and sinistral oblique-slip on deeper Early Permian faults, and that halokinesis played only a minor role in controlling deposition of the Upper Jurassic succession.

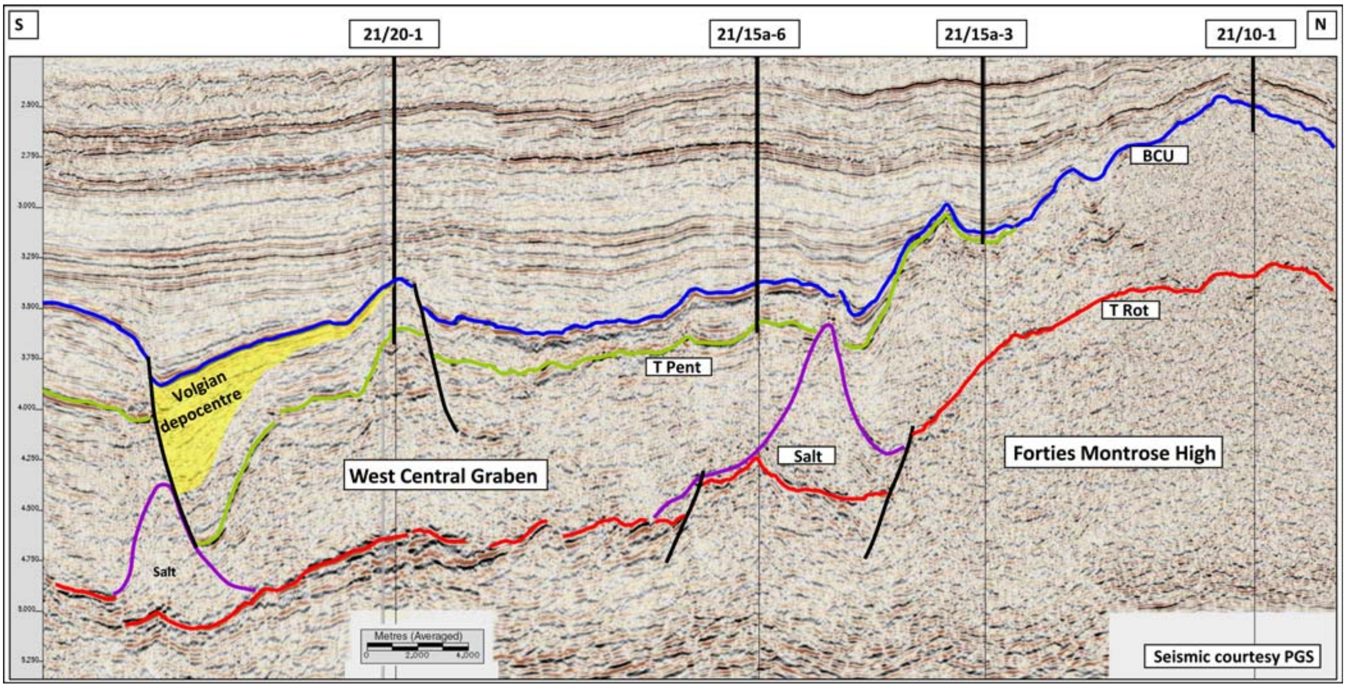

Fig. 23. Seismic line from the northern axis of the WCG showing northward thinning of the Humber Group succession on to the FMH and the location of a Volgian depocentre downdip from well 21/20a-1.

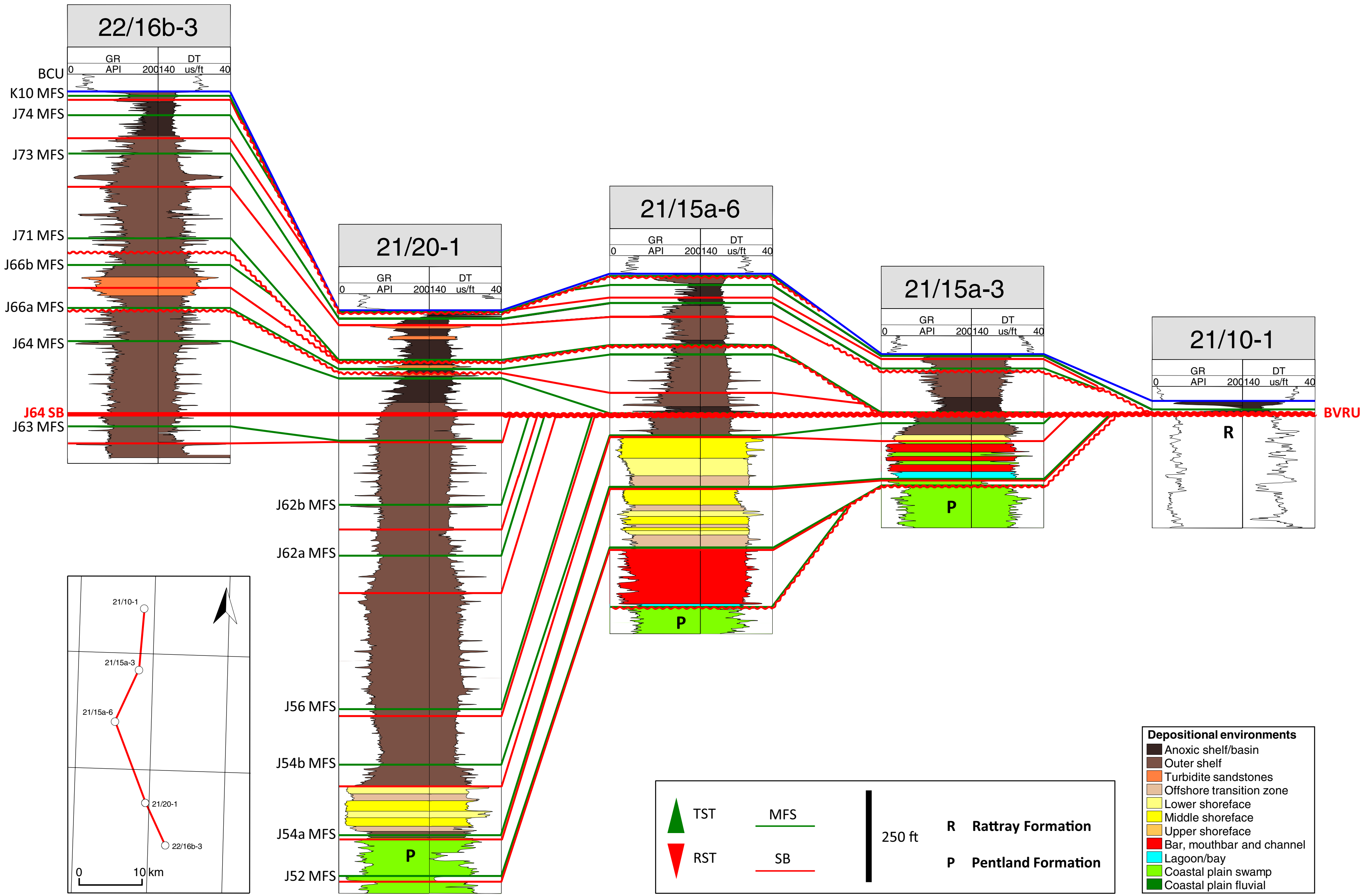

Fig. 24. Well correlation showing the progressive truncation of the Callovian–Kimmeridgian megasequence beneath the BVRU, which is interpreted as recording reactivation of the FMH during the latest Kimmeridgian to earliest Volgian. Section is missing both as a result of truncation below and onlap onto the BVRU.

The sequence stratigraphic interpretation presented here clearly records a major change in the factors controlling sequence architecture during the deposition of the Humber Group and favours a latest Kimmeridgian to earliest Early Volgian age for the onset of this event. Prior to this, the regionally consistent nature of log motifs and sequence stacking patterns and lack of obvious unconformities seen within the component sequences of the Callovian–Kimmeridgian megasequence indicates basin-wide controls on relative sea-level, which could be eustatic or tectonic, but were most likely a combination of both. Jeremiah & Nicholson (1999) favoured rifting-induced tectonic events as the main control on sequence geometry and flooding events. Alternatively, rifting could have been relatively weak, as suggested by Jones *et al.* (1999) so that salt acted very effectively to decouple basement extension from surface displacement and the effects of basement extension were distributed more widely across the basin, masking the movement on individual faults and giving the appearance of more areally uniform subsidence.

It is unclear to what extent the redistribution of salt and the breakup of the Callovian–Kimmeridgian basin required, or was indicative of, a major rift pulse, and whether the rejuvenation of the FMH and other elements was simply due to footwall uplift, or reflects a more regional uplift event. It is possible that the development of Volgian–Ryazanian depocentres can be attributed to the redistribution of salt, as suggested by Stewart & Clark (1999), triggered by relatively minor basement extension. Whilst the Volgian was a time of rapid creation of accommodation space and turbidite deposition in the Moray Firth Witch Ground Graben (Davies *et al.* 1999; Erratt *et al.* 1999), it largely resulted in a reduction of accommodation space and erosion in the WCG and ECG, except in the relatively localized areas undergoing salt collapse. It is suggested that the BVRU may effectively record the end of major basement extension in this part of the Central Graben, with the rifting largely transferring to other areas, and the overprinting of the earlier basin fabric, due to a combination of basement uplift and halokinesis resulting from a changing stress regime.

Implications of Early Volgian reconfiguration for exploration models

From a petroleum exploration perspective, the most important implication arising from recognition of the BVRU and younger unconformities is that the present-day structure of the Central Graben does not reflect the architecture of the basins in which the bulk of the Fulmar Sandstone and subordinate Oxfordian–Kimmeridgian turbidite sandstone reservoirs were deposited. It is therefore necessary to remove the effects of the Volgian reconfiguration and reconstruct the Callovian–Kimmeridgian basin morphology to predict the original extent and likely depositional facies and produce effective predictive models. No structural restorations of the Central Graben using the ability of modern software to effectively model salt movements and incorporating the latest Kimeridgian–earliest Volgian reconfiguration have been published, and the older published models tend to treat the Upper Jurassic interval as a single time-step, showing the Upper Jurassic thickening as a simple wedge into the basin bounding faults (e.g. Price *et al.* 1993; Rattey & Hayward 1993).

Basin-scale palaeogeographic reconfiguration

At the basin scale, Early Volgian reactivation of the FMH and J Ridge trend is believed to have been responsible for major reconfiguration of the connections between the ECG and WCG and between both these areas and the FBB (Erratt *et al.* 1999; Jeremiah & Nicholson 1999). The presence of older Callovian to Early Oxfordian (J44–J46) barrier, lagoon and shoreface deposits in the Howe area (22/12 and 22/13) at the transition between the FMH and the FBB suggests that marine incursion of the West Central Graben could have occurred from the north, across the present-day FMH through blocks 22/12 and 22/11. This implies that a structural low connecting the WCG and FBB in the Early Oxfordian was inverted to become a structural high by the end of the Upper Jurassic, resulting in complete erosion of Jurassic sediments so that Lower Cretaceous successions now rest on Triassic strata. If this interpretation is correct, it indicates the potentially large amounts of uplift and erosion that accompanied the formation of the BVRU.

Similarly, Early Volgian uplift is interpreted to have formed the structural arch between the FMH and the Jaeren High, along the trend of the Montrose–Jaeren transfer fault of Penge *et al.* (1999). Volgian Kimmeridge Clay, interpreted as representing onlap onto the BVRU, now overlies Triassic strata in this area (southern part of block 22/14 and northern part of block 22/19). This uplift may have severed an earlier connection between the FBB and the northern end of the East Central Graben, and it is possible that Early Oxfordian shallow marine deposition occurred in the deep parts of the ECG in the hanging wall of the Jaeren High bounding fault, where the Upper Jurassic has not been penetrated (SW block 23/16, N blocks 23/26 and 23/27). Early Volgian uplift in the 22/29 area between the southern end of the FMH and the Puffin Terrace is also interpreted to have removed the connection between the WCG and ECG, which had probably existed since Middle or Late Oxfordian times.

In published palaeogeographic maps, the FMH is shown as a subaerially exposed ridge and therefore a potential sediment source, throughout most of the Upper Jurassic (Rattey & Hayward 1993, figs 16 & 17; Erratt *et al.* 1999; Fraser *et al.* 2002, fig. 11.18), although Rattey and Hayward (1993) interpret drowning by the Ryazanian (their fig. 19). Recognition of the potentially large degree of uplift of the FMH suggests that the high could have been drowned much earlier. Sequence J56 shoreface sandstones are interpreted on the margins of the FMH, indicating that it was exposed at this time (wells 22/23-5 and -6). Younger pre-Volgian shoreface sandstones (sequences J62a–J63) have not been found here to date. The FMH could possibly have been mostly drowned as early as the early Kimmeridgian J62a MFS, so that it did not act as a significant sediment source again until re-exposure and rejuvenation in the Early Volgian. It is suggested here that the Volgian (J64 and J66) shoreface sandstones of the Wood discovery (22/18-6) could have been deposited as a result of this rejuvenation and erosion of Skagerrak and possibly older Fulmar source areas, rather than simply representing the final stages of backstepping of the Fulmar system onto a quiescent high. It remains possible that further J54a and possibly J54b–J62 Fulmar shoreface sandstones exist in undrilled interpod areas on the FMH, preserved in salt-withdrawal depocentres that subsided below the level of Volgian–Ryazanian erosion.

Modification of the palaeovalley model

Taking this interpretation a stage further, a modification is suggested to the model of Wakefield *et al.* (1993) which ascribes the distribution of Kimmeridgian Fulmar sandstones on the Western Platform to deposition in salt-cored palaeovalleys between exposed Smith Bank pods. In this area, Fulmar Sandstones of sequences J56–J62b are preserved in the interpod areas between grounded Smith Bank pods, whilst only Volgian Kimmeridge Clay units are typically found on the pods themselves. Sequences J56–J62b show a very similar architecture across the area from Kittiwake (e.g. 21/18-3) in the north to Guillemot (e.g. 21/30-3) in the south (Wakefield *et al.* 1993; Veldkamp *et al.* 1996) and this pattern continues on the Puffin Terrace (e.g. 29/9a-5 and 29/10-2).

Transgressive sandstones associated with the J56 basal flooding event are commonly characterized by the presence of glauconite, suggesting fully open marine conditions and widespread winnowing during transgression. On the Western Platform, precursor Oxfordian marginal marine facies are absent, and Fulmar marine deposits directly overlie the Top Triassic unconformity with no lateral variation in the environment of the basal units (Wakefield *et al.* 1993). Well 21/18-6, however, contains a basal succession of Kimmeridgian-aged Pentland facies (Veldkamp *et al.* 1996). Wakefield *et al.* (1993) attribute the lack of preserved coastal plain facies to erosional ravinement during the J56 transgression. However, it seems unlikely that so little facies variation and the widespread evidence of relatively high-energy winnowing would be seen if the Fulmar sandstones had been deposited in narrow palaeovalleys with the complex and sinuous plan-form morphology of the salt-cored interpods. Much more evidence of coeval marginal marine facies, such as that seen in 21/18-6, might be expected in embayments and terminations of the palaeovalley system, and it is unlikely that transgressive ravinement would have been efficient enough to remove all evidence of precursor coastal plain sediments across such a complex topography.

Thickness variations in sequences J56–J62b and onlap onto Smith Bank pods (Veldkamp *et al.* 1996; Stewart *et al.* 1999) support the existence of variations in accommodation space and palaeotopography on the Triassic exposure surface. However, it is suggested that palaeotopography might not have been great and that the Fulmar sand deposition could have originally been more widespread, extending further over the Smith Bank pods. Differential syn- and post-depositional subsidence of the salt-cored interpod areas during the Kimmeridgian, driven by extension or gravity sliding, created additional accommodation space so that Fulmar sands were preserved there and eroded from the crests of the grounded Smith Bank highs by the BVRU. Deep truncation seen at the base Volgian unconformity in wells such as 21/19-4 and 21/25-9 indicates that a significant amount of Fulmar Sandstone may have been eroded in some areas. Deposition of the Kimmeridge Clay resumed with rising sea-levels across both the interpods containing Fulmar deposits and the exposed Smith Bank highs.

Volgian turbidites

Volgian (dominantly sequence J64 and J66a) turbidite sandstones, attributed to erosion on the BVRU, occur scattered throughout the Central Graben (Fig. 16), but are generally thin and of limited areal extent. Early Volgian uplift of the FMH and J Block, together with fault block rotation and crestal erosion, resulted in the rejuvenation or creation of new sand source areas in the basin. The subcrop to the base Volgian–Ryazanian megasequence (J64 or younger SBs) is shown by formation, as a proxy for lithology, in Figure 25. Mostly the BVRU erodes into Kimmeridge Clay or Heather shales in the graben areas, but it can be seen cutting into Fulmar sandstone in several areas such as Curlew (block 29/7) and the updip (eastern) portions of Fulmar and Clyde (blocks 30/16 & 17). Along the crest of the FMH and on J Block, Volgian Kimmeridge Clay overlies Triassic sediments and the BVRU is interpreted to have eroded most pre-Volgian Upper Jurassic sediments, including potentially large areas of Fulmar sandstone, re-exposing Skagerrak Sandstone source areas. Locations where Cretaceous deposits directly overlie pre-Upper Jurassic successions were either never onlapped, or any evidence of Jurassic sediments and Volgian–Ryazanian erosion has been removed by younger unconformities.

In a modification of the Fulmar Field evolution model of Kuhn *et al.* (2003), the Ribble turbidite deposits that constitute the shallowest reservoir in the Fulmar Field are here assigned to the J64 RST and interpreted as representing the best developed of the J64 turbidite deposits discovered to date in the Central Graben. The Fulmar Field stratigraphy records the westward migration of the Fulmar sandstone onlap onto the Auk Terrace. The Fulmar Sandstone thickens dramatically across a NW–SE orientated hinge line, which Kuhn *et al.* (2003) interpret as recording the enhancement of accommodation space due to withdrawal of the underlying salt resulting in thick, aggradational deposition of sequence UJ8.2a (sequence J62b of this study) in the central and western parts of the field. Kuhn *et al.* (2003) state that biostratigraphic evidence clearly calibrates the UJ8.2b (J63) MFS within the Avon shale, between the top of the Fulmar Sandstone and the Ribble turbidite sandstones, although the supporting data are not presented. The current study proposes an alternative correlation model (Fig. 26) to that of Kuhn *et al.* (2003, fig. 8), where the J63 MFS is placed just below the top of the Fulmar sandstone, at the top of a gradually retrograding package that corresponds to layer U3.2 (interpreted as the J63 TST in this study). The J64 SB and virtually coincident J64 MFS are placed at the interface of the Fulmar sandstone and Avon shale (Fig. 26). The J64 SB may be conformable to only slightly erosive in the west of the field, but in contrast to the model of Kuhn *et al.* (2003), it is interpreted as cutting down deeply into sequence UJ8.2a (J62b) sandstones to the east of the hinge line, so that the eastward thinning of the Fulmar reservoir is due to erosional truncation in addition to westward expansion into a salt withdrawal depocentre. Whilst some syn-depositional thickening of the Fulmar sandstone due to depositional loading of the salt may have occurred, the main salt withdrawal event is envisaged to have been triggered by the tectonic reconfiguration, and to have terminated Fulmar Sandstone deposition through rapid deepening. Breakup and rotation of the underlying Triassic pod caused uplift of the eastern part of the field, resulting in erosion of considerable thicknesses of Fulmar sandstone to the east of the hinge line, which was potentially reworked into the Ribble turbidites. The biostratigraphic data is not available to test this alternative interpretation, but the apparent discrepancy in age interpretation between this study and Kuhn *et al.* (2003) may be accounted for by their *sensu lato* use of sequence UJ8.2b, as Kuhn *et al.* state that the Shell sequence stratigraphic scheme does not recognize the UJ9.1 (J64) MFS, and/or may reflect reworking of Kimmeridgian biostratigraphic markers into the Early Volgian. The Ribble Turbidites are shown as occurring in sequences UJ9.1 and UJ9.2a in Fraser *et al* (2002, fig. 11.17), mostly above the J64 MFS.

Despite the evidence for Early Volgian to Ryazanian erosional events, contemporaneous turbidite deposits are limited compared with the well developed reservoirs of the Moray Firth. This is probably due to the combination of the poor development of contemporaneous shorefaces to concentrate and winnow the sand and the highly dissected nature of the salt-collapse depocentres, so that relatively small volumes of sand were redeposited locally rather than being delivered to a single depocentre. The distribution of the turbidite deposits does not conform to any relationship with the overall thickness of the Volgian succession, or location of the depocentres, and they are often not visible on seismic, making them a challenging exploration target. In some cases, turbidites are seen directly overlying the BVRU on deeply truncated Oxfordian successions, which may represent penetration of slope channel systems (e.g. 22/13a-1z and -2).

Prospect-scale models

Recognition of erosion at the BVRU has a large impact on the prediction of reservoir presence in undrilled prospects. If the unconformity is not recognized and the Fulmar–Kimmeridge Clay relationship is interpreted as depositional facies change,

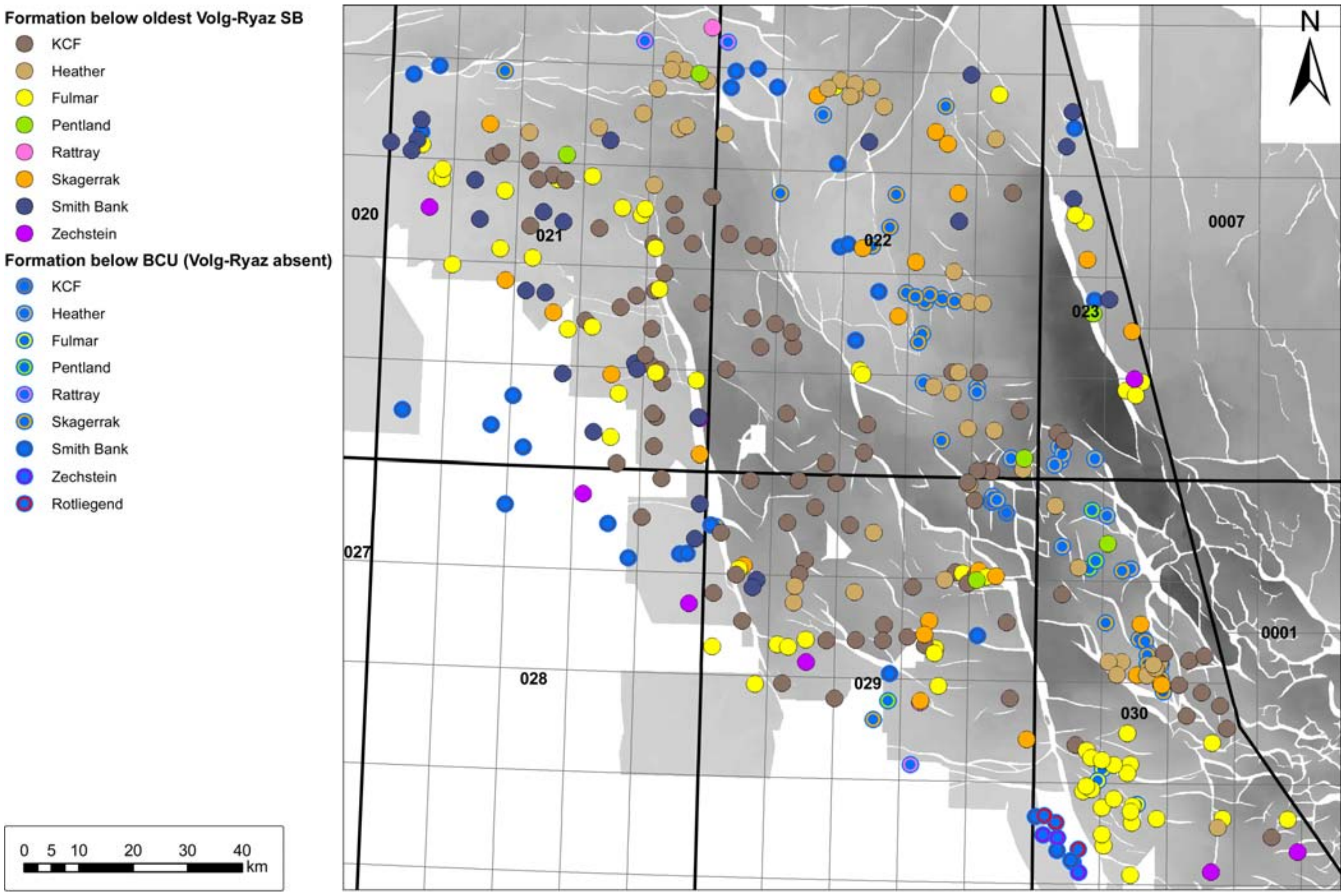

Fig. 25. Subcrop to the J64 SB or younger SBs by formation (lithology). Note areas where the Fulmar and Skagerrak sandstones are eroded, providing a possible sediment source for Volgian turbidites.

then the potential for downdip prospectivity may be limited (Fig. 27a), compared with a model where the unconformity is interpreted and the potential for increased preservation of the reservoir downdip is seen (Fig. 27b). Some exploration models have used a simple formula to predict the thickness of the Fulmar Sandstone as a percentage of the total Humber Group thickness. Although this appears to work locally (e.g. Hollywood 2009, Huntingdon discovery), consideration of the effects of late Kimmeridgian–Early Volgian reconfiguration and salt remobilization implies that this should only hold true where the BVRU forms the top of the Fulmar sandstone across the fault block, as the degree of truncation of the pre-Volgian interval would increase towards the block crest (Fig. 27c). However, this relationship will not work where the Fulmar sandstone does not fill the entire space under the base Volgian unconformity and some of the Heather Formation is preserved. In this case, the Fulmar may be thickest near the crest of the fault block, especially if the Volgian fault has broken through the centre of a pod where accommodation space was greatest during Fulmar deposition (Fig. 27d).

Pre-drill seismic interpretation of Fulmar fault block crest or pinch-out prospects is always challenging due to the difficulty of distinguishing thinning and onlap of sequences that are below seismic resolution, particularly when affected by BCU multiples. In the case of three-way dip and stratigraphic traps, the BVRU can further complicate the interpretation of the reservoir pinchout. For example, well and seismic data can show the pinchout of the Upper Jurassic below the BCU, but erosion on the unconformity may mean that the Fulmar pinchout is further downdip than expected (Fig. 27e). On the positive side, the Upper Jurassic succession may not pinch out, but the BVRU may provide an element of trapping that either produces a stratigraphic trap (Fig. 26f) or enhances the closure of a primarily structural trap.

Conclusions

- Subdivision and correlation of the Humber Group sediments of the Central Graben are poorly constrained biostratigraphically, due to poor palynomorph recovery and, seismically, due to the sub-seismic nature of the sequences. Correlation is therefore largely based on well log data and there is considerable scope for variations in interpretation.
- The widely differing sequence stratigraphic interpretations of some wells demonstrate the difficulty of applying an 'Exxon-type' model for SB and system tract definition in this setting. A T–R model, where transgressive and regressive systems tracts are defined on the basis of MFSs and SBs which comprise unconformities and MRSs, is a more effective means of subdividing and correlating the Humber Group. A T–R model has been derived from the J sequence scheme of Partington *et al.* (1993*a*) and results in a more robust and objective sequence stratigraphic framework for the Humber Group. Whilst it is recognized that there are some difficulties with defining consistent MRSs, the uncertainty associated with this approach is considered to be much less than that involved in picking SBs that are correlative conformities relating to the start of base level fall and using these to assign lowstand and highstand tracts.
- The Humber Group comprises two megasequences which record distinct phases of evolution of the Central Graben Upper Jurassic rift. The Late Callovian–Kimmeridgian

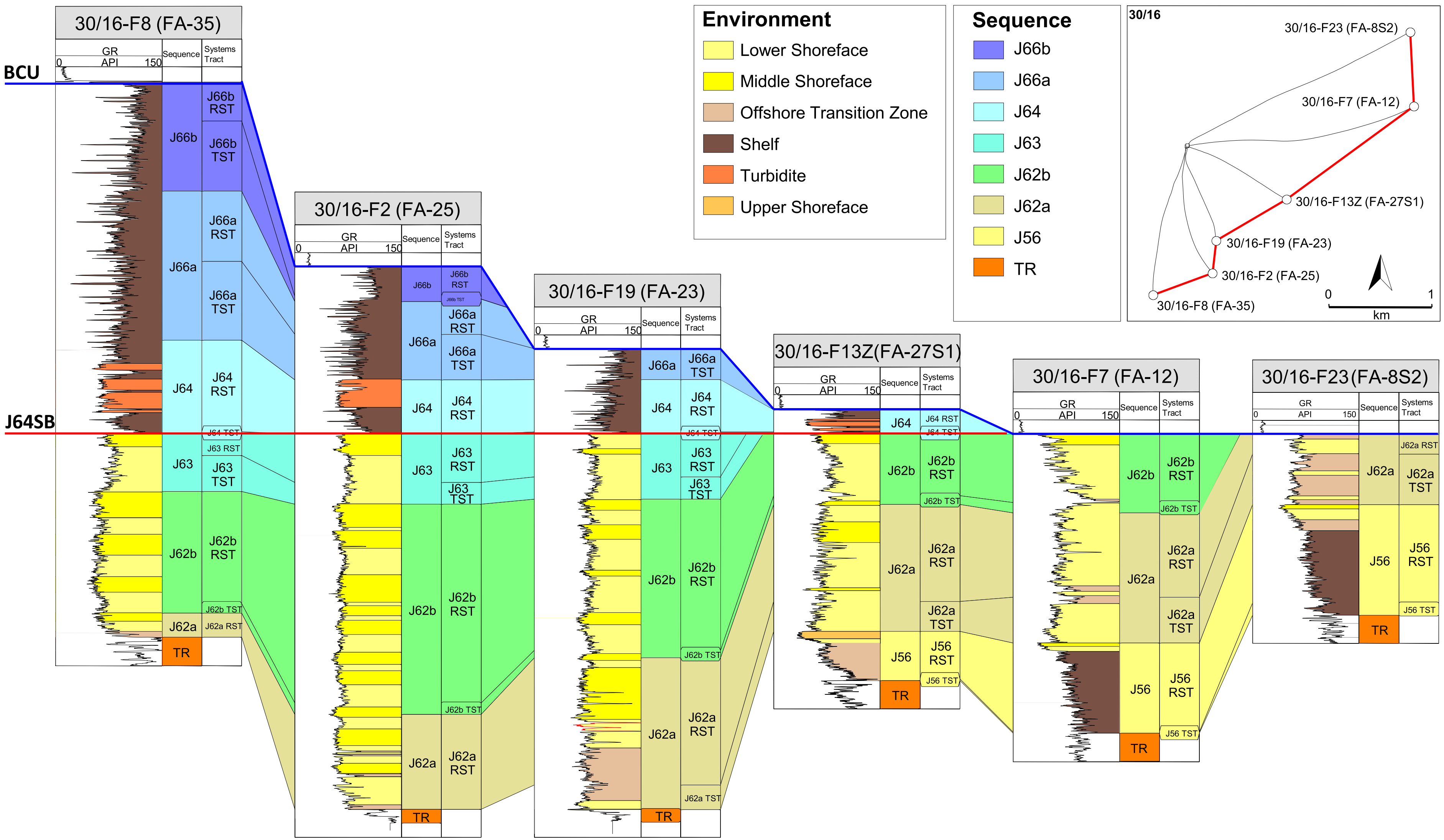

Fig. 26. Alternative correlation model for the Fulmar Field, attributing eastward thinning of the succession to erosion beneath the J64 SB/BVRU. The Ribble Turbidites are assigned to sequence J64 RST.

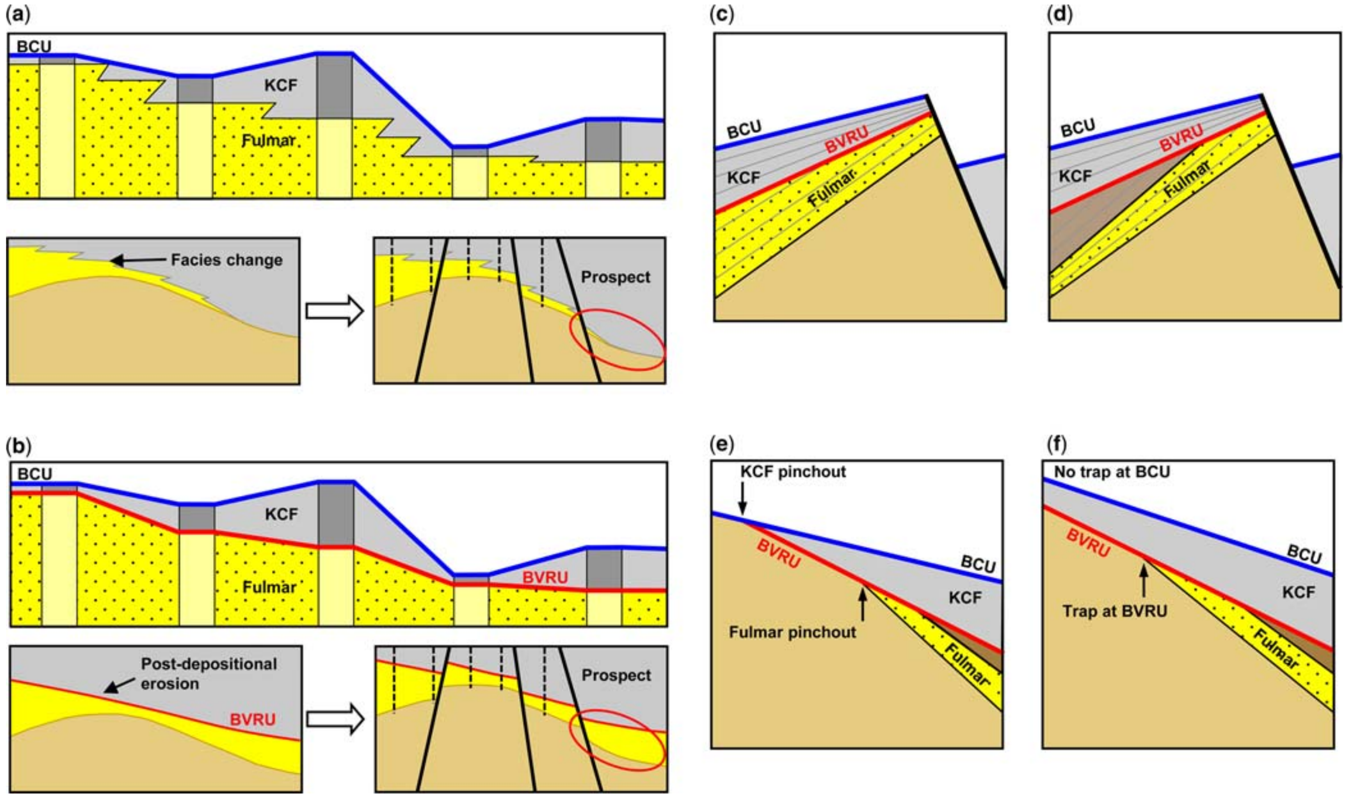

Fig. 27. Implications of the BVRU and tectonic reconfiguration event for prospect models.

megasequence (J44–J63) records the progressive back-stepping of the shallow marine system onto the basin margin platforms and intrabasinal highs. Erosional unconformities are not significant and individual sequences show a consistent architecture throughout the study area, reflecting regional tectonic or eustatic control, but vary significantly in thickness, reflecting local variations in halokinetically controlled accommodation space and sediment supply. Some sequences can be recognized by their characteristic log profiles where biostratigraphic dating evidence is lacking. The Volgian–Ryazanian megasequence is fragmentary and punctuated by unconformities which record erosion on rotating fault block crest and probable basement uplift. However, sequences again show a consistent log character reflecting regional controls on relative sea-level.

- The onset of tectonic reconfiguration is marked by an unconformity at the base of the Volgian–Ryazanian megasequence, termed the Base Volgian–Ryazanian Unconformity, on fault block crests and the influx of cool shales with subordinate turbidite sandstones into the evolving salt-collapse depocentres. The apparent age of this unconformity varies depending on degree of truncation below and onlap above the surface. However, the oldest unconformity is consistently underlain by J63 or older deposits and overlain by J64 or younger deposits. This event is therefore considered to correspond to the J64 SB in more complete successions and is dated as latest Kimmeridgian to Early Volgian.
- Shelf turbidite deposits are recognized as being an integral part of the Upper Jurassic shoreface system. They are believed to have been initiated during 'normal' progradation by storm and/or river flood events and do not necessarily require or indicate a base-level fall. Turbidite deposits are abundant in sequence J54a and are also present in sequence J56 and rarely in sequence J62a.
- Three characteristic log profiles, termed expanded, condensed and truncated, can be recognized within the Volgian–Ryazanian megasequence and reflect the position of wells on the fault blocks created during the latest Kimmeridgian–earliest Volgian reconfiguration. The pattern of truncation and erosion of pre-Volgian sequences reflects both fault block formation and rotation due to salt distribution and basement uplift of areas such as the FMH and J Ridge.
- Basement uplift resulted in significant dissection and modification of the basin architecture and potentially widespread erosion of Callovian–Kimmeridgian (sequences J46–J63) Humber Group sediments in areas where Volgian Kimmeridge Clay deposits now overlie Triassic strata. This erosion resulted in the localized deposition of turbidite sandstones.
- The effects of basement extension and eustasy cannot be clearly distinguished in the Callovian–Kimmeridgian megasequence and regional consistency of component sequences points to basin-wide controls on relative sea-level. The tectonic reconfiguration event may record salt distribution and basement uplift although the kinematics of this event are uncertain.
- Exploration models must take account of the effects of tectonic reconfiguration and erosion on the BVRU in order to accurately predict the original depositional extent of Fulmar Sandstone and associated turbidite reservoirs and the likelihood of their preservation.
- Further work is required across the entire Upper Jurassic rift system to help distinguish between the relative importance of basement extension, halokinesis and eustasy in controlling accommodation space. However, whilst prediction of the age and likely component sequences of the Upper Jurassic succession can be made based on the structural position in the basin, the limited understanding of factors controlling sediment supply remains the biggest unknown for the prediction of reservoir presence, particularly for the turbidite sandstone

play. More detailed regional mapping of unconformities is required to differentiate areas with differing structural history and to better inform the discussion on the timing, magnitude, effects and kinematics of tectonic events.

This paper is published with the permission of BG Group. The views expressed are those of the author and not necessarily those of BG Group. This work draws on a large amount of unpublished data and much use was made of the non-proprietary reports of Geostrat Ltd, IHS Energy Inc. (formerly IEDS Ltd) and sedimentological interpretations of Ichron Ltd. Neil Grant, Heather Auld and Mike Martin are thanked for constructive reviews.

References

Andsbjerg, J. 2003. Sedimentology and sequence stratigraphy of the Bryne and Lulu Formations, Middle Jurassic, northern Danish Central Graben. *Geological Survey of Denmark and Greenland Bulletin*, **1**, 301–347.

Carruthers, A., McKie, T., Price, J., Dyer, R., Williams, G. & Watson, P. 1996. The application of sequence stratigraphy to the understanding of Late Jurassic turbidite plays in the Central North Sea, UKCS. *In*: Hurst, A., Johnson, H. D., Burley, S. D., Canham, A. C. & Mackertich, D. S. (eds) *Geology of the Humber Group: Central Graben and Moray Firth, UKCS*. Geological Society, London, Special Publications, **114**, 29–45.

Coward, R. N. 2003. The Erskine Field, Block 23/26, UK North Sea. *In*: Gluyas, J. G. & Hichens, H. M. (eds) *United Kingdom Oil and Gas Fields, Commemorative Millennium Volume*. Geological Society, London, Memoir, **20**, 523–536.

Davies, R. J., O'Donnell, D. *et al*. 1999. The origin and genesis of major Jurassic unconformities within the triple junction area of the North Sea, UK. *In*: Fleet, A. J. & Boldy, S. A. R. (eds) *Petroleum Geology of Northwest Europe: Proceedings of the 5th Conference*. Geological Society, London, 117–131; doi: 10.1144/0050117.

Donovan, A. D., Djakic, A. W., Ioannides, N. S., Garfield, T. R. & Jones, C. R. 1993. Sequence stratigraphic control on middle and upper Jurassic reservoir distribution within the UK Central North Sea. *In*: Parker, J. R. (ed.) *Petroleum Geology of Northwest Europe: Proceedings of the 4th Conference*. Geological Society, London, 251–269; doi: 10.1144/0040251.

Dooley, T., McClay, K. R. & Pascoe, R. 2003. 3D analogue models of variable displacement extensional faults; applications to the Revfallet fault system, offshore mid-Norway. *In*: Nieuwland, D. A. (ed.) *New Insights into Structural Interpretation and Modelling*. Geological Society, London, Special Publications, **212**, 151–167.

Duxbury, S., Kadolsky, D. & Johnson, S. 1999. Sequence stratigraphic subdivision of the Humber group in the Outer Moray Firth area (UKCS, North Sea). *In*: Jones, R. & Simmons, M. (eds) *Biostratigraphy in Production and Development Geology*. Geological Society, London **152**, 23–54.

Embry, A., Johannessen, E., Owen, D., Beauchamp, B. & Gianolla, P. 2007. *Sequence stratigraphy as a 'concrete' stratigraphic discipline*. Report of the ISSC Task Group on Sequence Stratigraphy. World Wide Web Address: http://strata.geol.sc.edu/PDF-Files/SeqStrat-Refs/Formal_Sequ_Strati_Feb_2007.pdf

Eneyok, G., Bussink, P. & Maan, A. 2003. The Curlew Field, Block 29/7, UK North Sea. *In*: Gluyas, J. A. & Hichens, H. M. (eds) *United Kingdom Oil and Gas Fields, Commemorative Millennium Volume*. Geological Society, London, Memoir, **20**, 509–522.

Erratt, D. 1993. Relationships between basement faulting, salt withdrawal and Late Jurassic rifting, UK Central North Sea. *In*: Parker, J. R. (ed.) *Petroleum Geology of Northwest Europe: Proceedings of the 4th Conference*. Geological Society, London, 1211–1220; doi: 10.1144/0041211.

Erratt, D., Thomas, G. M. & Wall, G. R. T. 1999. The evolution of the Central North Sea Rift. *In*: Fleet, A. J. & Boldy, S. A. R. (eds) *Petroleum Geology of Northwest Europe: Proceedings of the 5th Conference*. Geological Society, London, 63–82; doi: 10.1144/0050063.

Erratt, D., Nicholson, P. H., Winefield, P., Milton-Worssell, R. J., Cayley, G. T. & Arter, G. 2005. Exploration history of the high-pressure, high-temperature plays: UK Central North Sea. *In*: Doré, A. G. & Vining, B. A. (eds) *Petroleum Geology: North-West Europe and Global Perspectives: Proceedings of the 6th Petroleum Geology Conference*. Geological Society, London, 253–267; doi: 10.1144/0060253.

Folkestad, A. & Satur, N. 2008. Regressive and transgressive cycles in a rift basin: depositional and sedimentary partitioning of the Middle Jurassic Hugin Formation, Southern Viking Graben, North Sea. *Sedimentary Geology* **207**, 1–21.

Fraser, S. I., Robinson, A. M. *et al*. 2002. Upper Jurassic. *In*: Evans, D., Graham, C., Armour, A. & Bathurst, P. (eds) *The Millennium Atlas: Petroleum Geology of the Central and Northern North Sea*. Geological Society, London, 157–189.

Gowland, S. 1996. Facies characteristics and depositional models of highly bioturbated shallow marine siliciclastic strata: an example from the Fulmar formation (Late Jurassic), UK Central Graben. *In*: Hurst, A., Johnson, H. D. & Mackertich, D. S. (eds) *Geology of the Humber Group: Central Graben and Moray Firth, UKCS*. Geological Society, London, Special Publications, **114**, 185–214.

Hesketh, R. A. P. & Underhill, J. R. 2002. The biostratigraphic calibration of the Scottish and Outer Moray Firth Upper Jurassic successions: a new basis for the correlation of Late Oxfordian–Early Kimmeridgian Humber Group reservoirs in the North Sea Basin. *Marine and Petroleum Geology*, **19**, 541–562.

Hodgson, N. A., Farnsworth, J. & Fraser, A. J. 1992. Salt-related tectonics, sedimentation and hydrocarbon plays in the Central Graben, North Sea, UKCS. *In*: Hardman, R. F. P. (ed.) *Exploration Britain: Geological Insights for the Next Decade*. Geological Society, London, Special Publications, **67**, 31–64.

Hollywood, J. 2009. The Huntington Discoveries: efficient exploration in the UK Central North Sea. Oral presentation, Seventh Petroleum Geology Conference: from Mature Basins to New Frontiers.

Howell, J. A., Flint, S. S. & Hunt, C. 1996. Sedimentological aspects of the Humber Group (Upper Jurassic) of the South Central Graben, UK North Sea. *Sedimentology*, **43**, 89–114.

Jeremiah, J. M. & Nicholson, P. H. 1999. Middle Oxfordian to Volgian sequence stratigraphy of the Greater Shearwater area. *In*: Fleet, A. J. & Boldy, S. A. R. (eds) *Petroleum Geology of Northwest Europe: Proceedings of the 5th Conference*. Geological Society, London, 153–170; doi: 10.1144/0050153.

Jones, G., Rorison, P., Frost, R., Knipe, R. & Colleran, J. 1999. Tectonostratigraphic development of the southern part of UKCS Quadrant 15 (eastern Witch Ground Graben): implications for the Mesozoic-Tertiary evolution of the Central North Sea Basin. *In*: Fleet, A. J. & Boldy, S. A. R. (eds) *Petroleum Geology of Northwest Europe: Proceedings of the 5th Conference*. Geological Society, London, 133–151; doi: 10.1144/0050133.

Kuhn, O., Smith, S. W., Van Noort, K. & Loiseau, B. 2003. The Fulmar Field, blocks 30/16, 30/11b, UK North Sea. *In*: Gluyas, J. G. & Hichens, H. M. (eds) *United Kingdom Oil and Gas Fields, Commemorative Millennium Volume*. Geological Society, London, Memoir, **20**, 563–585.

Lasocki, J., Guemene, J. M., Hedayati, A., Legorjus, C. & Page, W. M. 1999. The Elgin and Franklin fields: UK Blocks 22/30c, 22/30b and 29/5b. *In*: Fleet, A. J. & Boldy, S. A. R. (eds) *Petroleum Geology of Northwest Europe: Proceedings of the 5th Conference*. Geological Society, London, 1007–1020; doi: 10.1144/0051007.

Martin, M. A. & Pollard, J. E. 1996. The role of trace fossil (ichnofabric) analysis in the development of depositional models for the Upper Jurassic Fulmar Formation of the Kittiwake Field (Quadrant 21 UKCS). *In*: Hurst, A., Johnson, H. D. & Mackertich, D. S. (eds) *Geology of the Humber Group: Central Graben and Moray Firth, UKCS*. Geological Society, London, Special Publications, **114**, 163–183.

Partington, M. A., Mitchener, B. C., Milton, N. J. & Fraser, A. J. 1993*a*. Genetic sequence stratigraphy for the North Sea Late Jurassic and Early Cretaceous: distribution and prediction of Kimmeridgian–Late Ryazanian reservoirs in the North Sea and adjacent areas. *In*: Parker, J. R. (ed.) *Petroleum Geology of Northwest Europe: Proceedings of the 4th Conference*. Geological Society, London, 347–370; doi: 10.1144/0040347.

Partington, M. A., Copestale, P., Mitchener, B. C. & Underhill, J. R. 1993*b*. Phase rift history biostratigraphic calibration of genetic stratigraphic sequences in the Jurassic–lowermost Cretaceous (Hettangian to Ryazanian) of the North Sea and adjacent areas. *In*: Parker, J. R. (ed.) *Petroleum Geology of Northwest Europe: Proceedings of the 4th Conference*. Geological Society, London, 371–386; doi: 10.1144/0040371.

Pattison, S. A. & Hoffman, T. A. 2008. Sedimentology, architecture, and origin of shelf turbidite bodies in the Upper Cretaceous Kennilworth Member, Book Cliffs, Utah, USA. *In*: Hampson, J., Steel, R. J., Burgess, P. M. & Dalrymple, R. W. (eds) *Recent Advances in Models on Siliciclastic Shallow-marine Stratigraphy*. SEPM, Tulsa, OK, Special Publications, **90**, 391–420.

Penge, J., Munns, J. W., Taylor, B. & Windle, T. M. 1999. Rift-raft tectonics: examples of gravitational tectonics from the Zechstein Basins of northwest Europe. *In*: Fleet, A. J. & Boldy, S. A. R. (eds) *Petroleum Geology of Northwest Europe: Proceedings of the 5th Conference*. Geological Society, London, 201–213; doi: 10.1144/0050201.

Price, J., Dyer, R., Goodall, I., McKie, T., Watson, P. & Williams, G. 1993. Effective stratigraphical subdivision of the Humber Group and the Late Jurassic evolution of the UK Central Graben. *In*: Parker, J. R. (ed.) *Petroleum Geology of Northwest Europe: Proceedings of the 4th Conference*. Geological Society, London, 443–458; doi: 10.1144/0040443.

Rattey, P. & Hayward, A. B. 1993. Sequence stratigraphy of a failed rift system: the Middle Jurassic to Early Cretaceous basin evolution of the Central and Northern North Sea. *In*: Parker, J. R. (ed.) *Petroleum Geology of Northwest Europe: Proceedings of the 4th Conference*. Geological Society, London, 215–249; doi: 10.1144/0040215.

Rawson, P. F. & Riley, L. A. 1982. Latest Jurassic–Early Cretaceous events and the 'Late Cimmerian Unconformity' in North Sea area. *Bulletin of the AAPG*, **66**, 2628–2648.

Smith, K. & Ritchie, J. D. 1993. Jurassic volcanic centres in the Central North Sea. *In*: Parker, J. R. (ed.) *Petroleum Geology of Northwest Europe: Proceedings of the 4th Conference*. Geological Society, London, 519–531; doi: 10.1144/0040519.

Smith, I. R., Hodgson, N. & Fulton, M. 1993. Salt control on Triassic reservoir distribution, UKCS Central North Sea. *In*: Parker, J. R. (ed.) *Petroleum Geology of Northwest Europe: Proceedings of the 4th Conference*. Geological Society, London, 547–557; doi: 10.1144/0040547.

Stewart, I. J. 1993. Structural controls on the Late Jurassic age shelf system, Ula Trend, Norwegian North Sea. *In*: Parker, J. R. (ed.) *Petroleum Geology of Northwest Europe: Proceedings of the 4th Conference*. Geological Society, London, 469–483; doi: 10.1144/0040469.

Stewart, S. A. & Clark, J. A. 1999. Impact of salt on the structure of the Central North Sea hydrocarbon fairways. *In*: Fleet, A. J. & Boldy, S. A. R. (eds) *Petroleum Geology of Northwest Europe: Proceedings of the 5th Conference*. Geological Society, London, 179–200; doi: 10.1144/0050179.

Stewart, S. A., Fraser, S. I., Cartwright, J. A., Clark, J. A. & Johnson, H. D. 1999. Controls upon Upper Jurassic sediment distribution in the Durward-Dauntless area, UK blocks 21/11, 21/16. *In*: Fleet, A. J. & Boldy, S. A. R. (eds) *Petroleum Geology of Northwest Europe: Proceedings of the 5th Conference*. Geological Society, London, 879–896; doi: 10.1144/0050879.

Taylor, A. M. & Gawthorpe, R. L. 1993. Application of sequence stratigraphy and trace fossil analysis to reservoir description: examples from the Jurassic of the North Sea. *In*: Parker, J. R. (ed.) *Petroleum Geology of Northwest Europe: Proceedings of the 4th Conference*. Geological Society, London, 317–335; doi: 10.1144/0040317.

Turner, P. J. 1993. Clyde: reappraisal of a producing field. *In*: Parker, J. R. (ed.) *Petroleum Geology of Northwest Europe: Proceedings of the 4th Conference*. Geological Society, London, 1503–1512; doi: 10.1144/0041503.

Underhill, J. R. & Partington, M. A. 1993. Jurassic thermal doming and deflation in the North Sea: implications of the stratigraphic evidence. *In*: Parker, J. R. (ed.) *Petroleum Geology of Northwest Europe: Proceedings of the 4th Conference*. Geological Society, London, 337–345; doi: 10.1144/0040337.

Veldkamp, J. J., Gaillard, M. G., Jonkers, H. A. & Levell, B. K. 1996. A Kimmeridgian time-slice through the Humber Group. *In*: Hurst, A., Johnson, H. D., Burley, S. D., Canham, A. C. & Mackertich, D. S. (eds) *Geology of the Humber Group: Central Graben and Moray Firth, UKCS*. Geological Society, London, Special Publications, **114**, 1–28.

Wakefield, L. L., Droste, H., Giles, M. R. & Janssen, R. 1993. Late Jurassic plays along the western margin of the Central Graben. *In*: Parker, J. R. (ed.) *Petroleum Geology of Northwest Europe: Proceedings of the 4th Conference*. Geological Society, London, 459–468; doi: 10.1144/0040459.

The Huntington discoveries: efficient exploration in the UK Central North Sea

J. M. HOLLYWOOD and R. C. OLSON

Carrizo Oil & Gas Inc., 1000 Louisiana Street, Suite 1500, Houston, Texas, USA (e-mail: jim.hollywood@crzo.net)

Abstract: The Huntington discoveries are an unusual exploration success in that two oil accumulations were tested in separate syn- and post-rift reservoirs with a single well. The discoveries are located 205 km east of Aberdeen in the East Central Graben some 35 km east of Forties Field in 300 ft of water. The 22/14-5 discovery well, drilled in May 2007, encountered a 122 ft oil column in the Paleocene Forties Sandstone and also a 136 ft oil column in the Upper Jurassic Fulmar Sandstone. Both the Forties and the Fulmar contain high-quality oil, 41 and 39° api gravity, respectively. Aggregate flow rates from the two zones exceeded 11 000 boepd on test. Appraisal drilling of the Forties was completed in late 2007 with first oil targeted for 2011. The Fulmar appraisal programme is currently in progress. The Forties reservoir is a high net to gross sandstone containing stacked channel sequences deposited in a submarine fan system. The Fulmar reservoir also contains a thick sand package deposited in a shallow marine shelf setting. Pre-drill mapping based on reprocessed 3D seismic indicated a structural closure on both horizons at the location tested by the well. At both the Forties and Fulmar targets, however, the oil column height exceeded the pre-drill prognosis. This overview will focus on pre-drill perceptions of the prospect relative to actual drilling results.

Keywords: Huntington, North Sea, Paleocene, Jurassic, exploration

The Huntington discoveries lie in the northern part of the East Central Graben in block 22/14b (Fig. 1). Carrizo Oil & Gas Inc. acquired Traditional Licence P. 1114 (blocks 22/14b and 22/19b) in the UK 21st Round of licensing in 2003. The area was selected for application by Carrizo as it contained the 22/14b-3 and 22/14b-4 discoveries made in Triassic Skagerrak Sandstones in 1988 and 1992, respectively. Although only the 22/14b-3 well was tested with subcommercial flow rates of 113 barrels of oil per day (bopd), the wells demonstrated the presence of a large, oil-bearing trap. Reservoir potential was also seen in the Paleocene Forties, Andrew and Maureen Sandstones and the Upper Jurassic Fulmar Sandstone (Fig. 2).

Following award of the licence, Carrizo conducted a technical evaluation of well and 3D seismic data to identify prospects, assess technical risk and estimate potential resources in the event of a discovery. This work highlighted the Huntington prospects (Paleocene and Fulmar) as the best opportunity on the acreage, given reservoir and trap potential at two separate horizons. Throughout this period, Carrizo was also attempting to farmout the licence to reduce project risk during the drilling phase. Notwithstanding the multi-zone reservoir potential at Huntington, the farmout required three years to complete with the prospects being shown to more than 40 companies. Ultimately, Carrizo was joined in blocks 22/14b, 19b and the Huntington prospects by Oilexco (40% and operator), E.ON Ruhrgas UK Ltd (25%) and Denerco (20%), with the latter interest subsequently being acquired in corporate acquisitions by first Altinex and finally Noreco. The Huntington 22/14-5 well spudded in April 2007 after the partner group was finalized.

This paper will focus on the technical work and pre-drill predictions underpinning the farmout effort, some of the perceptions of the farmout companies and finally, the well results. We believe this comparison of project perception and outcome is interesting and provides encouragement for further exploration of the UKCS.

Pre-discovery exploration

Exploration of the Paleocene Forties Sandstone in this area kicked off in the late 1960s with the discovery of Arbroath Field (1969) in block 22/18 (Fig. 1). One year later the supergiant Forties Field (1970) was discovered which further increased interest in the area. These early discoveries were followed by a series of Paleocene discoveries in the area at: Montrose (1971), Fleming (1982), Everest (1985), Nelson (1987) Mungo (1989) and Arkwright (1990). By 1990, all significant Forties structural closures had been tested and from 1990 to 2007 only five exploration wells were drilled for the Paleocene in this area.

Following the early successes in the Paleocene Forties Sandstone, considerable effort was focused on evaluating the Upper Jurassic Fulmar Sandstone in the middle to late 1980s. Fulmar discoveries at Howe (1987) and Bardolino (1988) which tested 1781 bopd and an aggregate 16 721 bopd from Upper Jurassic reservoirs, respectively, triggered a wave of exploration and appraisal drilling in the area. Unfortunately, the Fulmar is not as uniformly distributed as the Forties and about 50% of the wells targeting the Fulmar did not encounter the reservoir. The disappointing drilling outcomes discouraged further exploration in the area and no wells targeting the Fulmar were completed from 1997 until Huntington was tested in 2007.

The Triassic Skagerrak Sandstone also represented a reservoir objective in the 22/14-3 well. This well encountered a 139 ft gross oil column in the Skagerrak and tested 33° api oil at a rate of 113 bopd. An appraisal well drilled four years later targeting both Fulmar and Skagerrak reservoirs established a 389 ft gross oil column in the Skagerrak but was not tested. No Fulmar section was present in the well. Notably, both of these oil-bearing zones occur within the Base Cretaceous Unconformity (BCU) closure that the 22/14-5 Huntington discovery was drilled in.

Previous drilling results significantly shaped the perceived technical risks in the area. Historically, Forties discoveries were made

VINING, B. A. & PICKERING, S. C. (eds) *Petroleum Geology: From Mature Basins to New Frontiers – Proceedings of the 7th Petroleum Geology Conference*, 213–223. DOI: 10.1144/0070213

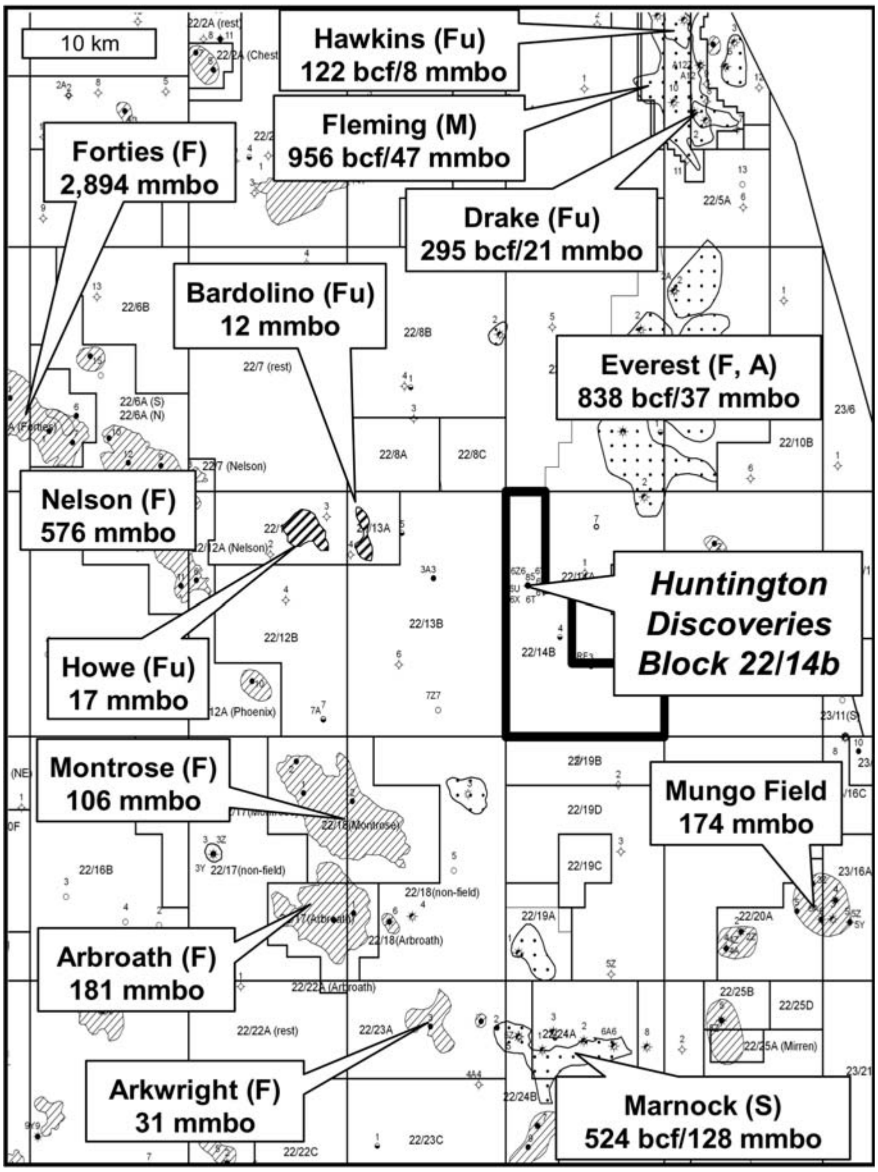

Fig. 1. Location map. Oil and gas fields indicated with cross-hatch and stipple patterns, respectively. Fields are labelled with reserves and productive reservoir. Reservoirs are abbreviated as follows: Paleocene Forties (F); Andrew (A); Maureen (M); Jurassic Fulmar (Fu); and Triassic Skagerrak (S). The primary producing reservoirs in the Huntington area are Paleocene sandstones but there is also production from the Jurassic and Triassic nearby.

largely on structural closures, although stratigraphic elements often alter reservoir distribution and connectivity within any given feature. Stratigraphic trapping potential with possible reserves upside, however, was not seen to add incremental volume to Forties structural closures. The mixed results in pursuing the Fulmar and the poor seismic resolution of the Fulmar reservoir led many to regard it as too risky for further drilling. Also, the poor flow rates obtained from the Skagerrak in the 22/14-3 well discouraged others from pursuing Triassic reservoirs in the area.

Technical evaluation

Block 22/14b is located on the SE flank of the Jurassic Fisher Bank basin (Fig. 3). The SW, downthrown extension of the Jaeren High transects the block, separating the Fisher Bank basin in the north from the East Central Graben basin, another major Jurassic depocentre, to the SE. These basins were filled with thick Upper Jurassic sandstone and claystone deposited in response to rifting and coeval with an overall rise in eustatic sea-level (Erratt *et al.* 1999). During post-rift thermal subsidence, significant thicknesses of Cretaceous, Paleocene and Eocene sediments in-filled the area.

The Upper Jurassic Kimmeridge Clay Formation (KCF) is the primary source rock for oil and gas in the area. The KCF is thermally mature to generate oil over most of block 22/14b and several adjacent blocks to the west, south and SE (Kubala *et al.* 2003). To the north in the Fisher Bank basin and to the south in the East Central Graben, it lies within the gas window. Triassic and Jurassic reservoirs within the BCU closure at Huntington lie in an ideal location to receive migrating hydrocarbons generated from downdip kitchens surrounding the structure on all sides but the NE. Reconstructions show this area has been high since the Triassic. Indeed, the presence of substantial oil columns in the Triassic Skagerrak Formation in the 22/14-3 and 22/14-4 wells on the Huntington structure confirms the charge model for the Jurassic and older sections. At the 22/14-3 well, the oil also contains a significant contribution from woody–coaly source rocks in the Middle Jurassic Pentland Formation (Isaksen 2004).

Oil migration from Jurassic source rocks to Paleocene reservoirs requires buoyant movement through several thousand feet of low

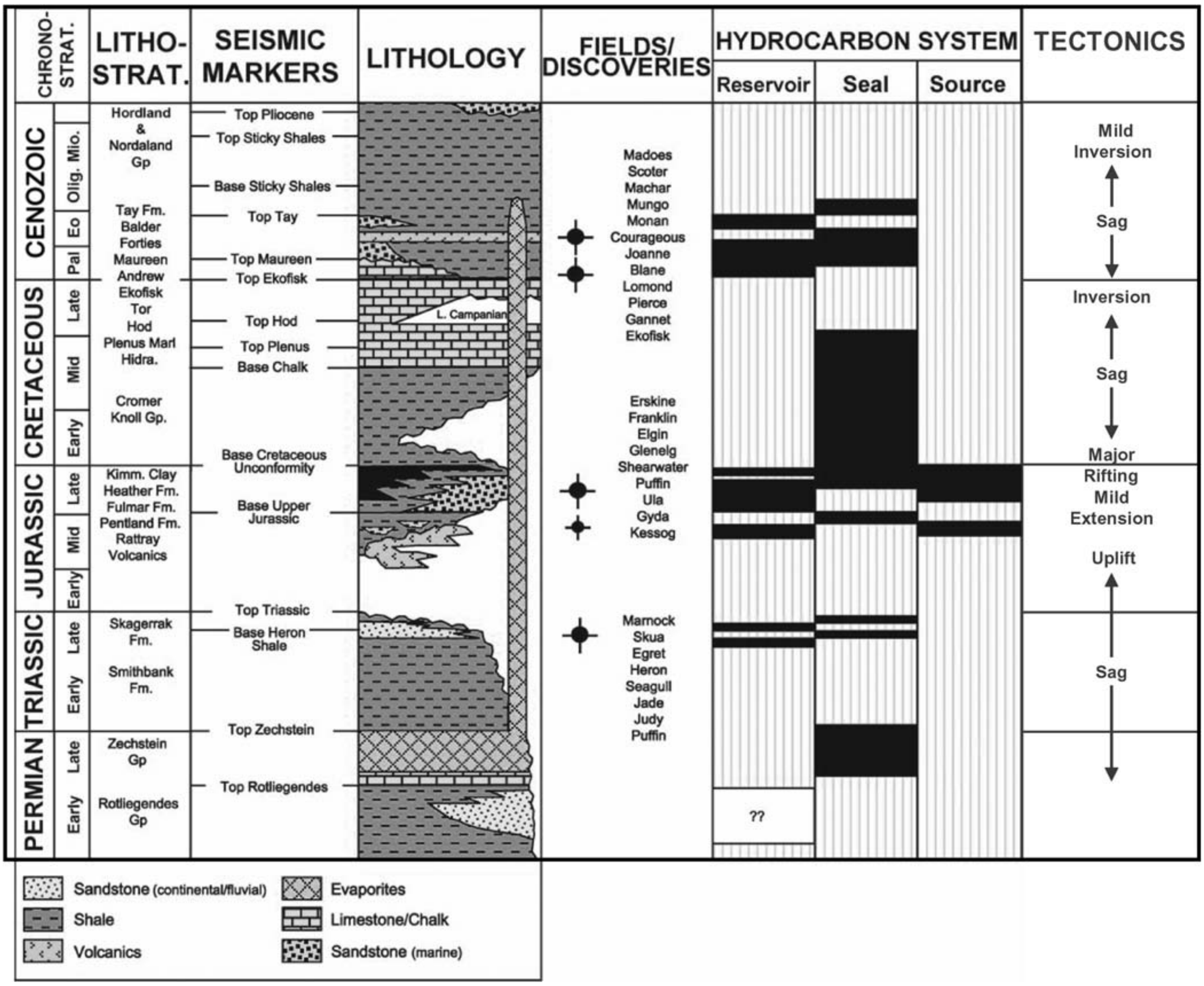

Fig. 2. Stratigraphic framework, modified from Winefield *et al.* (2005). Reservoir potential at Huntington was seen in the Paleocene Forties and Upper Jurassic Fulmar with source potential in the Upper Jurassic Kimmeridge Clay. The main tectonic phases are shown at the right, with the Fulmar being deposited during active rifting and the Forties being deposited during a later sag phase. Modified after Winefield *et al*. (2005).

permeability sediments. Biomarker analysis shows this is possible in the region as oil samples from the Forties and Montrose Fields have been correlated to Kimmeridge source beds. It is not clear, however, where vertical migration is occurring in the immediate vicinity of Huntington. The presence of oil and gas in the Forties in numerous closures on all sides of the Huntington prospect suggests that hydrocarbon charge is working in this area.

Two primary reservoir intervals were studied for the Huntington prospect: the Paleocene Forties Sandstone Member and the Upper Jurassic Fulmar Sandstone. The Forties Sandstone is the primary producing interval at nearly all the nearby fields, that is, Forties, Nelson, Montrose, Arbroath, Arkwright, Everest, Monan and Mungo. The Forties is a sand-rich turbidite system deposited by SE trending currents. In this portion of the turbidite fan, the Forties reservoir is dominated by channel sandstones and associated channel margin and levee facies (Hempton *et al.* 2005). The Forties Sandstone isopach illustrates the channelized nature of the major sand bodies in the area (Fig. 4). Within the channel fairways, net to gross ratios can be as high as 85% while inter-channel facies may have net to gross ratios as low as 25%. Under certain conditions, these inter-channel facies may provide permeability baffles or barriers between channels as seen at several nearby fields such as Everest, Nelson and Montrose and Arbroath.

The average porosity range of the Forties Sandstone in fields near blocks 22/14b is 20–26% with average permeability in the range of 30–300 mD. Recoveries from this reservoir can be excellent. As an example, the first 16 wells on the Forties Field collectively produced 10^6 barrels of oil (Leonard *et al.* 2000) and it is estimated the field may ultimately produce 70% of original oil in place (Hempton *et al.* 2005).

A second reservoir objective at Huntington was the Upper Jurassic Fulmar Sandstone on the western flank of the Huntington BCU structure. Although the 22/14-3 and 22/14-4 wells confirmed the presence of an oil-bearing Triassic Skagerrak reservoir, the challenge was to find a reservoir that could produce at commercial flow rates within the BCU structural closure. The Fulmar is well developed on the west side of the Fisher Bank basin and immediately west of Huntington at the 22/13-1, 2, 3 and 5 wells. On the east side of the basin, the Fulmar reservoir is commonly absent where it has been eroded from the crest of structures during Late Jurassic faulting and block rotation. The schematically restored Fulmar isopach map (Fig. 5) is an attempt to illustrate the thickness of the Fulmar in the Huntington area at the time of deposition. Fulmar thickness is highly variable across the region, attaining a maximum value of 898 ft at the 22/5-2 well to the north while being

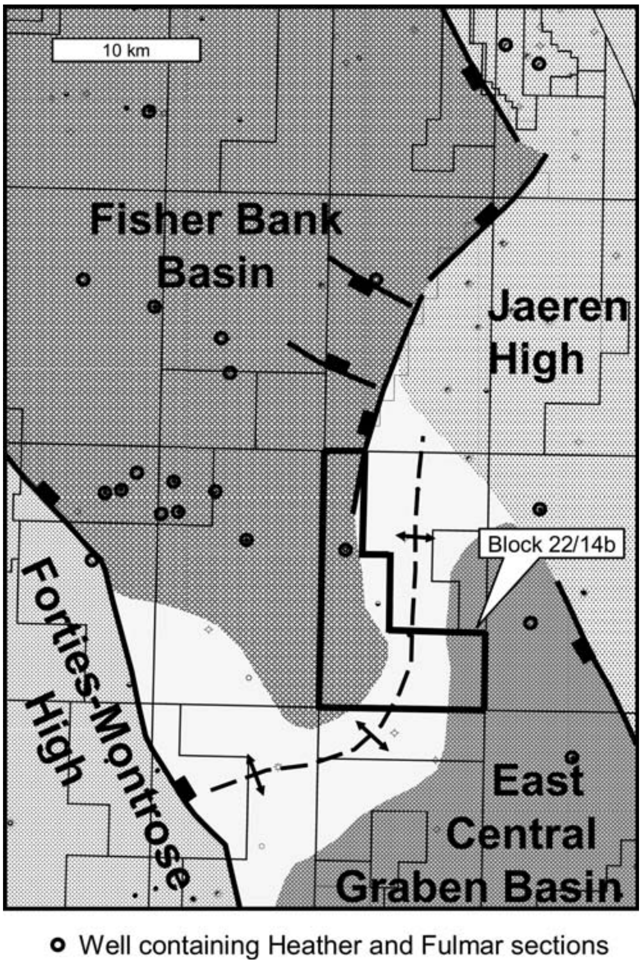

Fig. 3. Structural elements. Jurassic basins are indicated with grey shading while high blocks with little or no Jurassic sedimentation are shown with a stipple pattern. Wells containing both Upper Jurassic Heather and Fulmar sections lie primarily within two Jurassic basins: the Fisher Bank basin to the north and East Central Graben basin to the south.

absent in many locations to the west and east. As a result, isopach contours are simplified and honour the thickest values only to provide an indication of the primary Fulmar depocentre. The restored palaeo-isopach map suggests the Fulmar once covered much of the area except prominent basement features such as the Jaeren and Forties–Montrose Highs with thickening into the basin.

The Fulmar reservoir is highly productive at Fulmar, Kittiwake, Shearwater, Elgin, Franklin and Ula Fields to the south and east of block 22/14b. It also produces at Drake, Hawkins and Howe Fields to the west and north of Huntington. At Howe Field in block 22/12, the initial production from a single well is reported to have exceeded 12 000 bopd. The Fulmar is fine-grained, bioturbated sandstone deposited in a shallow marine setting in the Fisher Bank basin. Typically the interval thickens down-structure within individual fault blocks and within the basin in general. A plot of the gross Upper Jurassic thickness v. gross Fulmar Sandstone thickness for individual wells is illustrated in Figure 6. The best-fit linear relationship from this dataset can be used in conjunction with the Upper Jurassic gross isopach determined from 3D seismic mapping to predict the thickness of Fulmar Sandstone in this area. A Fulmar thickness of 100 ft was predicted for the Huntington 22/14-5 location using this approach. Reservoir quality is variable depending mainly on depositional facies. Surrounding fields have an average porosity range of 17–23% and permeabilities of 5–700 mD.

The initial seismic interpretation was based on the PGS Mega Survey using 3D data acquired with a relatively short cable: 3000–3500 m. The data quality allowed a detailed interpretation of the key horizons within the Cenozoic and Cretaceous sections. The Balder, Sele, Forties, Ekofisk and BCU structure interpretations (time and depth) provided the initial key horizons for evaluation of the Forties, Fulmar and Skagerrak exploration potential. The pre-Cretaceous section interpretation was less reliable due to poorer data quality, but it was possible to create Base Upper Jurassic, Upper Permian Zechstein (top salt) and Lower Permian Rotliegend structure maps in certain areas. A near-top Fulmar was later interpreted and subsequently used to evaluate the Fulmar structure/stratigraphic trap potential at the Huntington prospect. Numerous time to depth sensitivities were calculated primarily to see if there were any significant changes to the low-relief Forties depth structural closure. In the end, a layer cake time to depth conversion using constant interval velocities was used for the Forties, BCU and Jurassic depth structures and this approach provided the best fit to the well control. Essentially the time and depth structures and closures are similar for each of the Fulmar, BCU and Forties interpretations.

While data quality was good to acceptable from the licensed PGS Mega survey data, it was recognized that reprocessing would be essential to acquire an improved image of the subsurface. Carrizo therefore reprocessed the entire 3D dataset surrounding block 22/14b in 2004 and 2005 to produce a modern Pre-Stack Time Migration (PreSTM) image of the subsurface. The reprocessed seismic provided: (1) a seamless, zero-phased (North Sea convention-impedance increase is represented as a trough) 3D dataset between four different seismic surveys; (2) improved data quality in the Paleocene and pre-Cretaceous sections; and (3) AVO products including near (0–20°), mid (20–30°) and far (30–40°) angle volumes for the assessment of reservoir properties and fluid content in the Cenozoic section.

The BCU depth structural closure covers approximately 6000 acres and encompasses the 22/14-3 and 4 discoveries and the Huntington 22/14-5 location within independent four-way dip closure (Fig. 7). The closure lies on the west side of a large north-trending Zechstein salt wall which could act as a stratigraphic seal and provide greater downdip closure. The Fulmar reservoir was interpreted to be preserved along the western flank of the BCU structure with dip closure to the north, west and south and truncation to the east beneath the BCU/Kimmeridge shale with potential lateral and bottom seal with the Triassic Smith Bank shale and Zechstein salt. Both the 22/14-3 and 4 wells proved oil in the Triassic Skagerrak with oil-down-tos (ODT) of 11 980 and 12 517 ft subsea, respectively. Both wells penetrated a thin Upper Jurassic section lying directly on the Skagerrak. The 22/14-5 well targeted the Fulmar downdip of these wells, but above the Skagerrak ODT seen in 22/14-4 (Fig. 8).

The Forties time and depth structural closure based on the PreSTM 3D was the same as that interpreted from the original PGS Mega Survey 3D. The Forties prospect remained a small structural closure with approximately 35 ft maximum relief and 1000 acres of closure (Fig. 9). If the charge to the structure exceeded trap volume, it was expected to spill towards the 22/14-1 dry hole to the NW. The low-relief structural closure limited possible reserves volumes at Huntington unless a stratigraphic barrier could be identified to separate the prospect from the 22/14-1 well.

The PreSTM 3D AVO products proved valuable in the interpretation and prediction of fluid content in the Forties. These AVO products were used to calibrate the offset response of a Forties oil well, gas well and dry hole (Fig. 10). The 22/18-2 oil well on Montrose Field exhibits a trough at Top Forties on the near offset changing to a peak with increasing amplitude on the far offsets using North Sea polarity convention. Thus, an

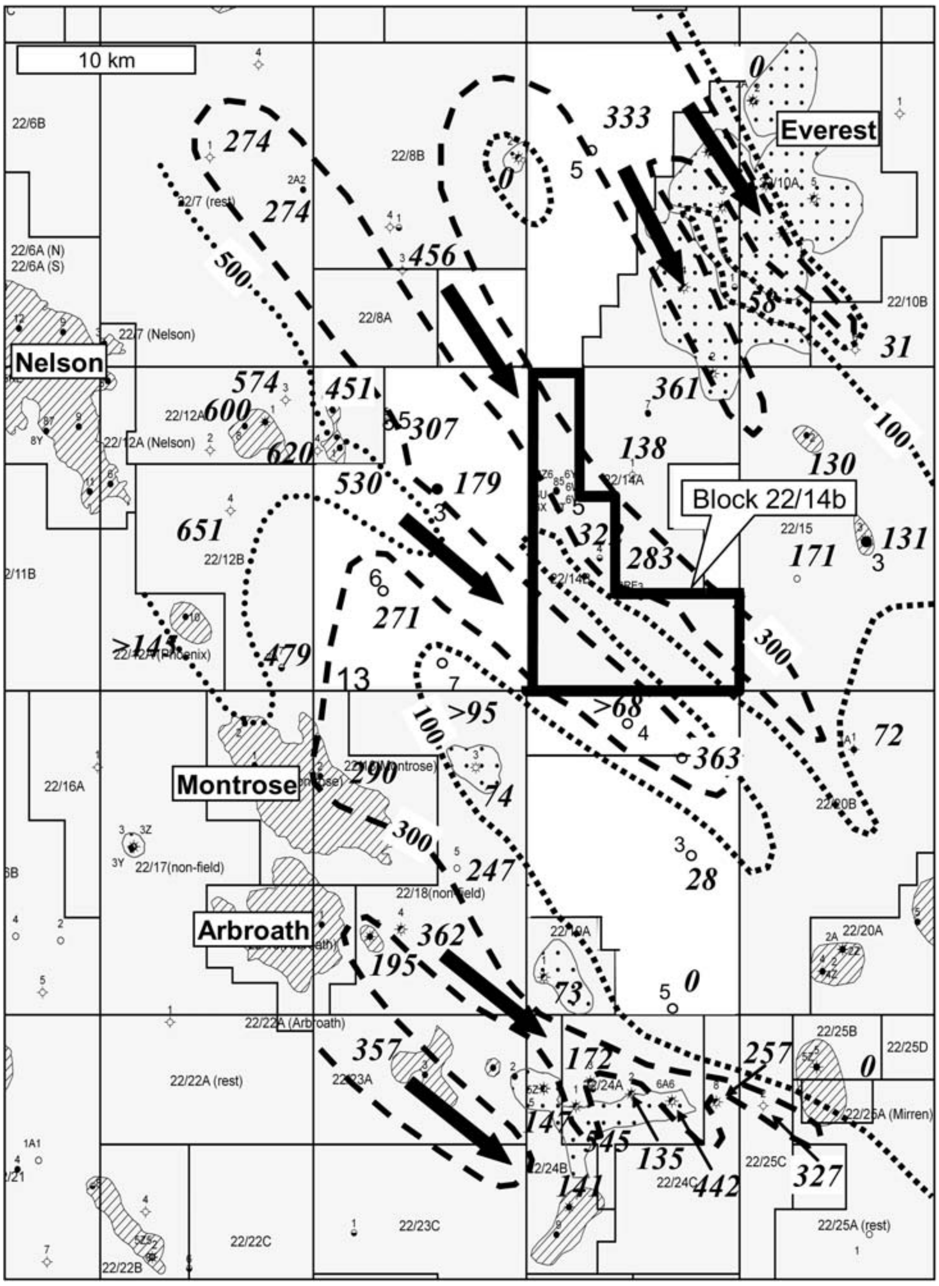

Fig. 4. Paleocene Forties Sandstone isopach map. This isopach has been constructed using only well data. Thickness is in feet as determined using a 45° api gamma ray (GR) cutoff. The contour interval is 200 ft. Areas of thick sandstone are indicated with a black arrow and are believed to correspond to channel complexes which exhibit a SE trend. The Huntington location appears to be in a favourable position for channel axis development.

oil-bearing Forties section yields a Class IIp response on the gathers as a result of the phase change with increasing offset. The gas case was calibrated using the 22/14-2 well from Everest Field. Here the top Forties event is a peak on the near offset going to a stronger peak on the far offsets, resulting in a Class II AVO response. The 22/14-4 well provided the wet reservoir calibration which exhibits a trough on the near and far offsets with little change in amplitude. At the Huntington prospect location, the top Forties event is a trough on the near offset data going to a peak on the far offset data. Huntington was interpreted to be most similar in offset response to the Montrose example and therefore expected to be an oil prospect.

The AVO products from the PreSTM 3D were also used to predict the Forties channel fairway and the likelihood of a stratigraphic component separating Huntington from the 22/14-1 well dry hole. Using the far-angle stack, two reflectors, the 'A' event at the top Forties and 'B' event within the Forties interval were picked and displayed as amplitude intensity. The highest A-amplitude values appeared to correlate to the Forties structural closure with a noticeable shift to the NW of the closure (Fig. 11). This shift of the amplitude anomaly beyond structural closure implied a possible stratigraphic trapping element to the prospect. The B-amplitude did not correspond to structure but instead showed lateral terminations of seismic reflectors along a curvilinear trend extending from the 22/8-3 well south through the Huntington location continuing south to the 22/14-4 well (Fig. 12). It was proposed that this feature might be an erosional scour at the base of a multi-channel complex since the 22/8-3 and 22/14-4 wells both have a thick Forties channel sequence. This feature extended across the Huntington Forties structural closure and it was concluded that a Forties channel sequence would be present at the 22/14-5 well location.

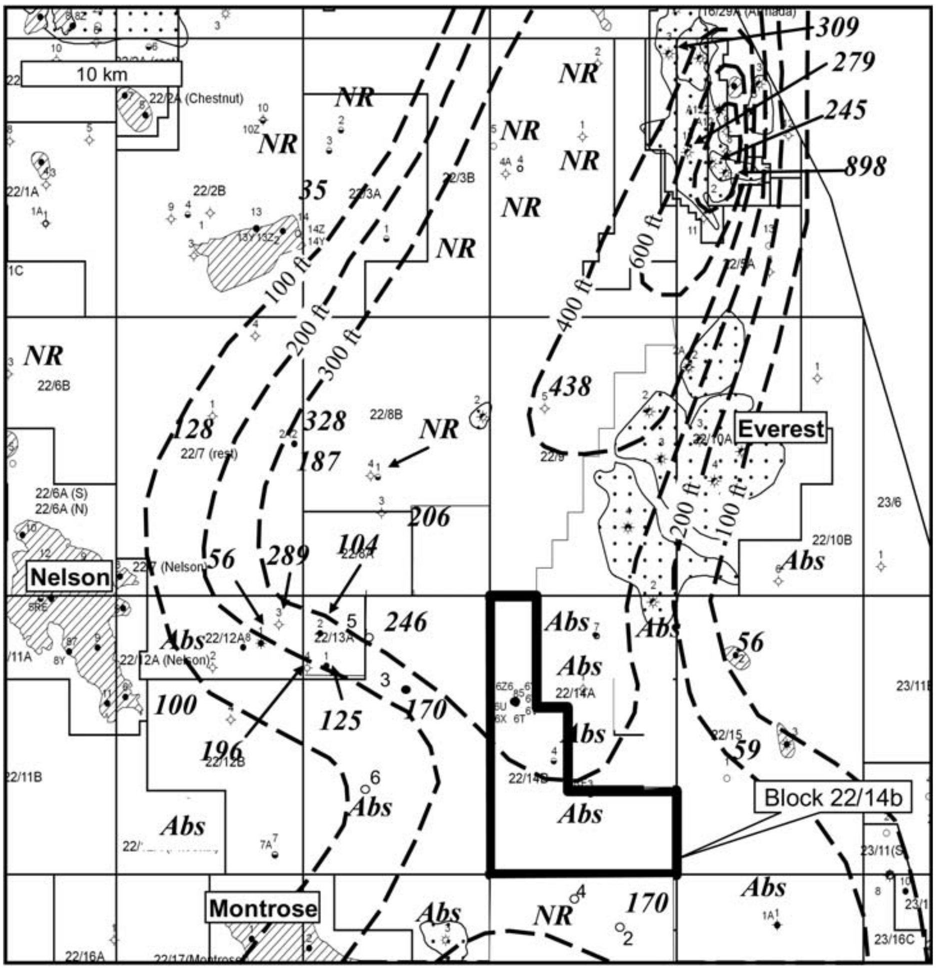

Fig. 5. Upper Jurassic Fulmar Sandstone schematically restored isopach map. This restored isopach has been constructed using only well data. Thickness is in feet as determined using a 50° api GR cutoff. The contour interval is 100 ft. Wells that did not reach the Fulmar are marked 'NR' and those marked 'Abs' are where the Fulmar was absent. The map is a restored isopach in the sense that it contours only the thickest values while ignoring the thinner values.

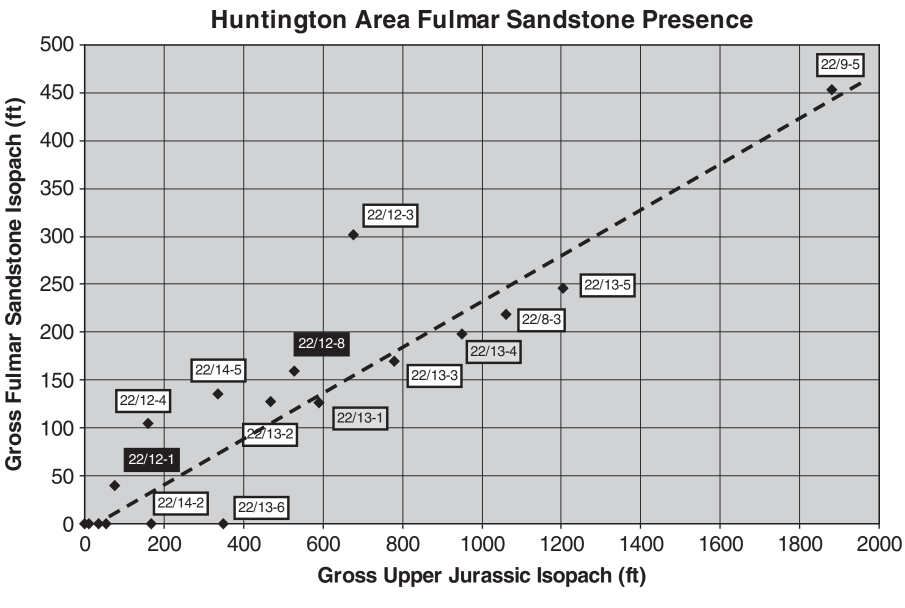

Fig. 6. Plot of the gross Upper Jurassic isopach v. the gross Fulmar Sandstone isopach for wells in the Fisher Bank basin. Wells drilled in the same fault block such as 22/13-1 and 22/13-4 or 22/12-1 and 22/12-8 are highlighted in similar font. Gross Fulmar thickness appears to vary directly with gross Upper Jurassic thickness in a linear manner in this area.

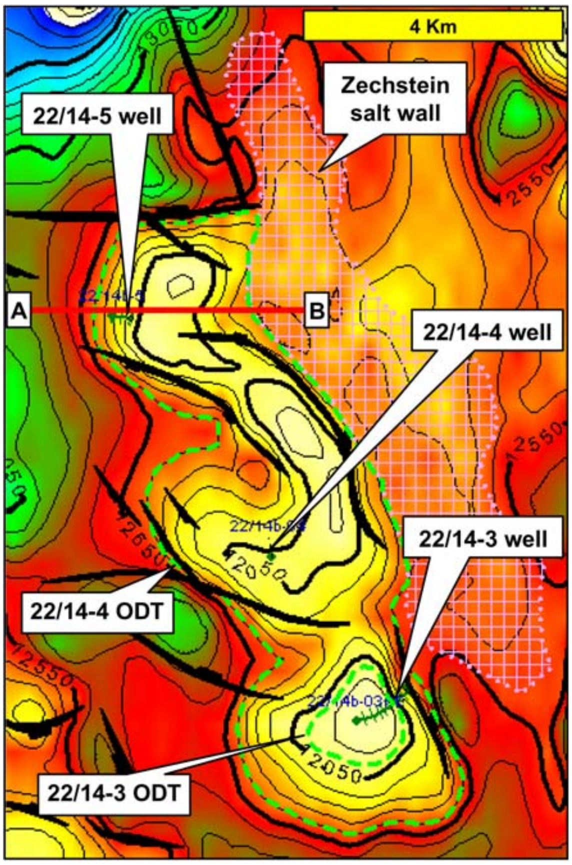

Fig. 7. BCU depth structure map. Huntington 22/14-5 well is located on the west flank of the northern culmination within the closure tested by the 22/14-3 and 4 Skagerrak oil discoveries. Well 22/14-5 was located to evaluate the Fulmar reservoir above the ODT seen in the 22/14-4 well. The BCU closure is flanked by a Zechstein salt wall to the east. Contour interval is 50 ft. The location of the seismic line in Figure 8 is shown here by the line 'AB'.

Pre-drill predictions

Prior to drilling and based on the technical evaluation and observations, Carrizo made the following predictions for the Forties reservoir: (1) it would be oil-bearing, from AVO analysis; (2) it would have a high net-to-gross reservoir section, also from AVO analysis; and (3) the AVO amplitude anomaly suggested that there might be a stratigraphic element to the trap since the anomaly extended beyond structural closure, particularly to the NW.

The key predictions for the Fulmar were: (1) the reservoir was expected to be about 100 ft thick at the well location; (2) it was likely to be oil-bearing based on the charge analysis; and (3) given there is no Fulmar in the 3 and 4 wells a stratigraphic trapping element might exist against the Smith Bank and possibly the Zechstein salt wall flanking the structure to the east. This stratigraphic component was supported both from seismic interpretation and pressure data, which indicated the 22/14-3 and 4 wells both required much higher mud weights to drill the Triassic section than the 22/14-1 well located on the updip side of the salt wall.

Market perceptions

As mentioned earlier, Carrizo conducted an extensive farmout effort in order to spread the risk during the exploration drilling phase. During this process, many companies commented on various aspects of the technical evaluation of the prospects, particularly the technical risks. It is instructive to reflect on these technical concerns in the context of the outcome of the well.

Initially, most companies thought reprocessing the short-cable 3D seismic would not provide the offsets needed to improve data quality in the pre-Cretaceous section or give the angles needed for AVO products to evaluate the Forties interval. Many companies regarded the Paleocene Forties prospect as having a high probability of success but very small reserves potential with limited economic value. Few companies seemed to believe there was upside potential for a stratigraphic trap. Many evaluated the

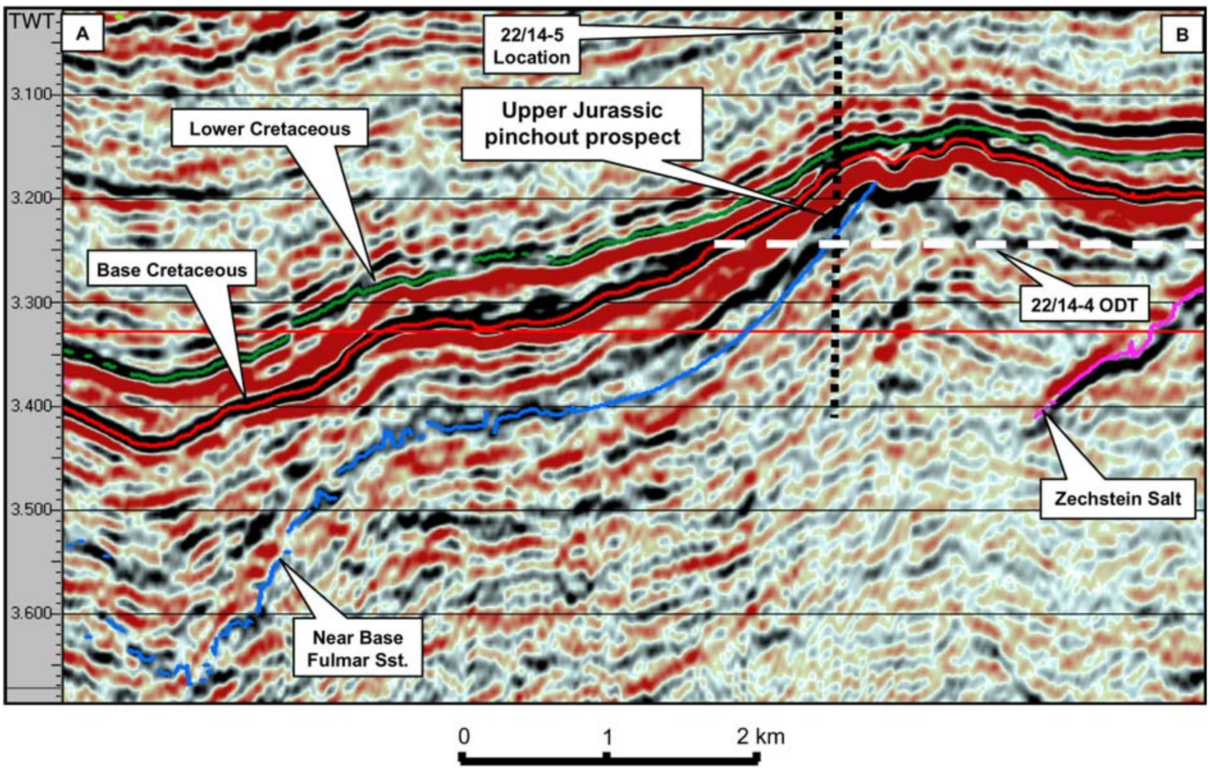

Fig. 8. West to east 3D seismic line (PreSTM) through Huntington Fulmar well location 22/14-5. The Fulmar reservoir is poorly imaged on 3D seismic data in this area. Courtesy of PGS.

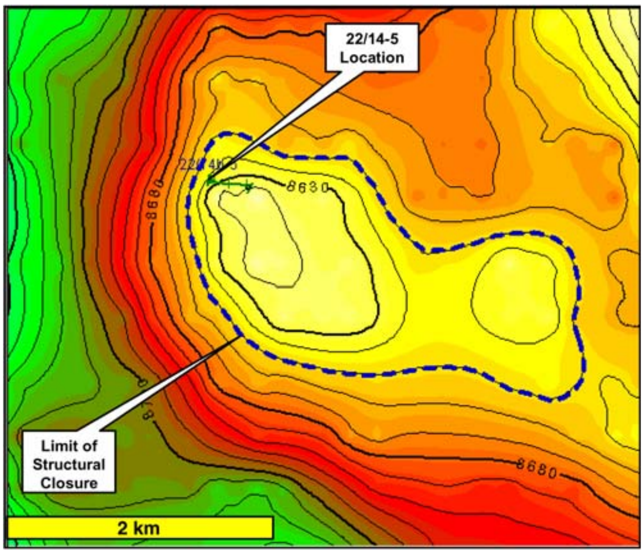

Fig. 9. Huntington Forties depth structure map. Blue dashed contour represents independent four-way dip closure separate from the 22/14-1 dry hole to the NE. Contour interval is 10 ft.

prospect as a gas opportunity rather than an oil prospect due to its proximity to Everest Field. Ultimately, these issues are related to the AVO analysis. Companies could see that the Huntington amplitude response did not look like the nearest offset well at Everest Field. Many companies did not seem to accept the more subtle amplitude response as indicative of oil in the Forties. As a result, they attributed the amplitude response to factors other than fluid and were unable to attribute additional reserves potential associated with a stratigraphic trap to the prospect.

The reaction to the Fulmar prospect was quite different as most companies seemed to believe that it should be possible to image a top Fulmar seismic reflector in this area and that the inability to do so meant the Fulmar may not be present. Others were concerned that if the Fulmar could not be seismically resolved, then its distribution in the area was unknown. Also, some companies rigorously applied the pod concept and thought the well should be drilled on top of the salt wall in order to find the Fulmar Sandstone.

Similar perceptions are likely when evaluating prospects in any mature basin. First, existing well control limits our ability to add ‘romance’ or large upside reserves potential to prospects. In the case of Huntington, there were two deep wells, which proved

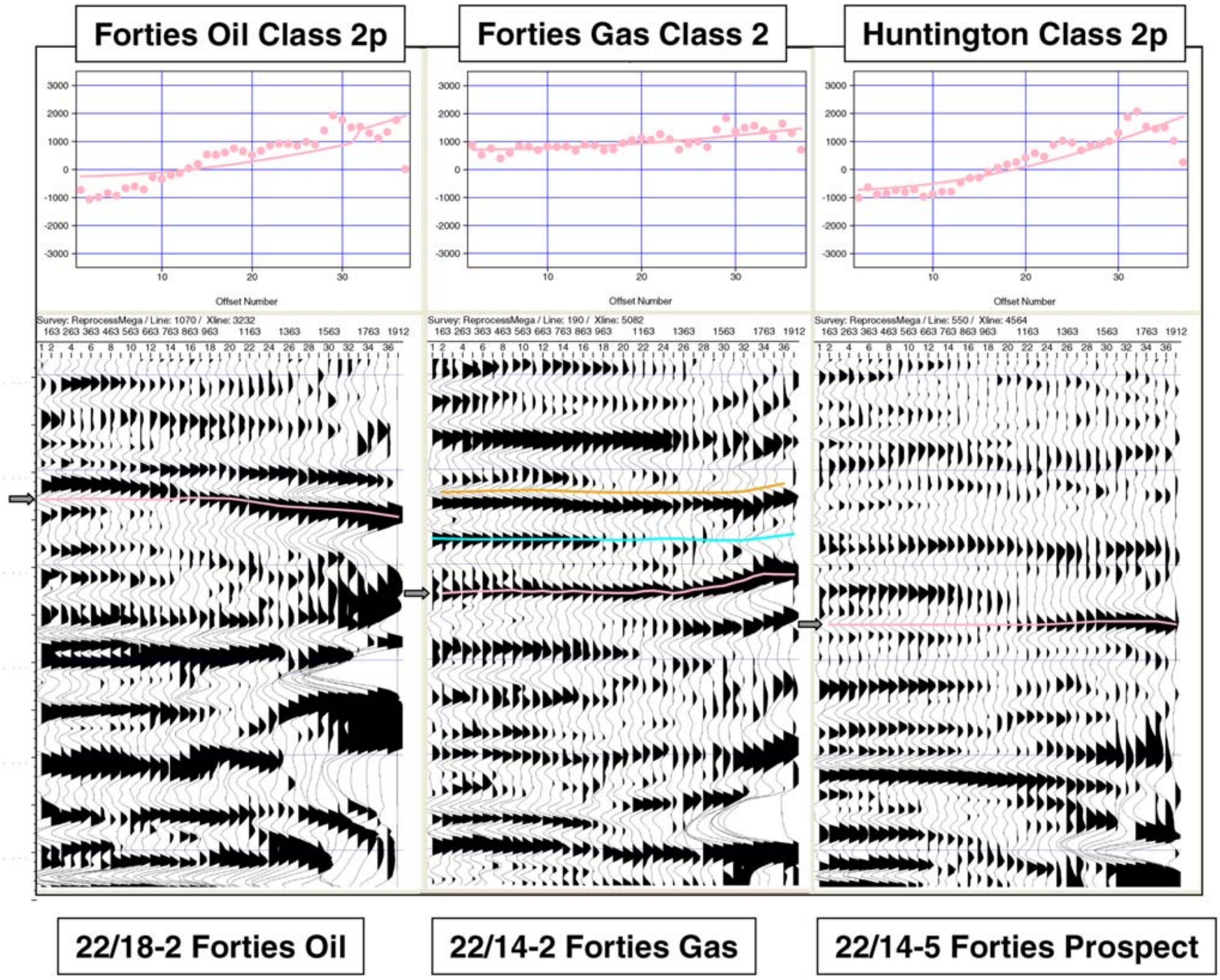

Fig. 10. Forties AVO response, gas v. oil. Three gathers with amplitude v. offset response for wells 22/18-2 Montrose oil (Class IIp AVO), 22/14-2 Everest gas (Class II AVO) and 22/14-5 Huntington (Class IIp AVO). The Top Forties Sandstone event is highlighted with a small grey arrow at the left edge of each panel of gathers. A plot of amplitude strength v. offset is shown at the top of each gather panel for the Top Forties Sandstone event.

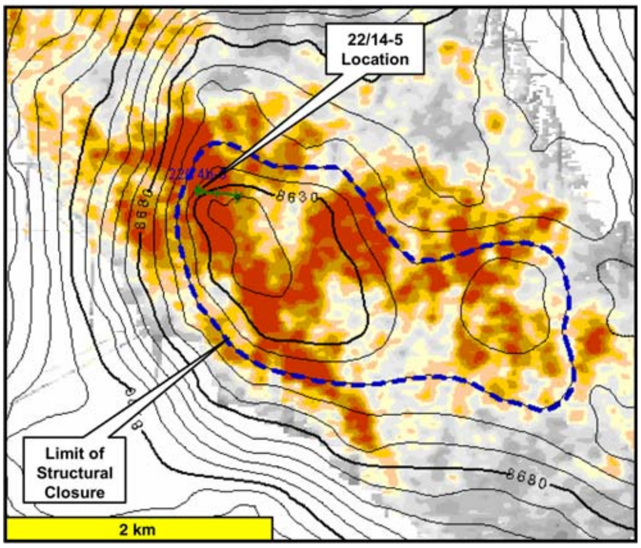

Fig. 11. Forties depth structure with far-offset (30–40°) A-amplitude anomaly. Amplitude extends beyond independent structural closure shown by blue dashed contour. Contour interval is 10 ft.

oil within the BCU closure, and one well, which proved water within the Forties closure, previously drilled. Second, the seismic amplitude response at Huntington did not neatly fit into pre-existing categories and is in fact a fairly subtle response. If the 3D seismic had exhibited an obvious amplitude response at Huntington, the prospect would have been drilled long ago. In general, prospects in mature areas are likely to be fairly subtle with ambiguous responses. Finally, there seems to be reluctance to invest in prospects left behind by other companies unless there is a convincing case for large reserves potential.

Drilling results

The 22/14-5 well penetrated a sand-rich Forties reservoir section containing a gross 122-ft oil column (Fig. 13). Net pay was 82.5 ft, implying a net to gross ratio of 67% with average porosity of 19.7% and average water saturation of 46.5%. A drill stem test over the upper 50 ft of the reservoir yielded maximum flow rates of 5577 bopd. Oil gravity was 41° api and there is no evidence for a free gas cap. The actual gross oil column height is about four to five times the structural relief at the drilling location. This discrepancy implies there is a stratigraphic element to the trap. It is believed that the channel sandstone complex drilled at Huntington shales out to the NE to provide stratigraphic separation from the 22/14-1 dry hole. The small structural closure at Huntington may result from differential compaction of the Huntington channel complex relative to the more shale-rich section in the saddle to the NE.

The Huntington well also drilled a 136 ft gross oil column in the Fulmar Sandstone (Fig. 14). This interval has net pay of 72 ft, indicating a net to gross ratio of 53% with average porosity of 16.1% and average water saturation of 47%. This interval was also tested, yielding a flow rate of 4624 bopd from a 120 ft perforated interval. Oil gravity was 39° api. The ODT in the Fulmar is 56 ft deeper than the ODT in the Skagerrak at the 22/14-4 well. The column height also exceeds closure at the BCU, suggesting a stratigraphic component to this trap. It is believed that the Smith Bank and the Zechstein salt wall to the NE of the Huntington structure provide bottom and lateral sealing components to the Fulmar discovery.

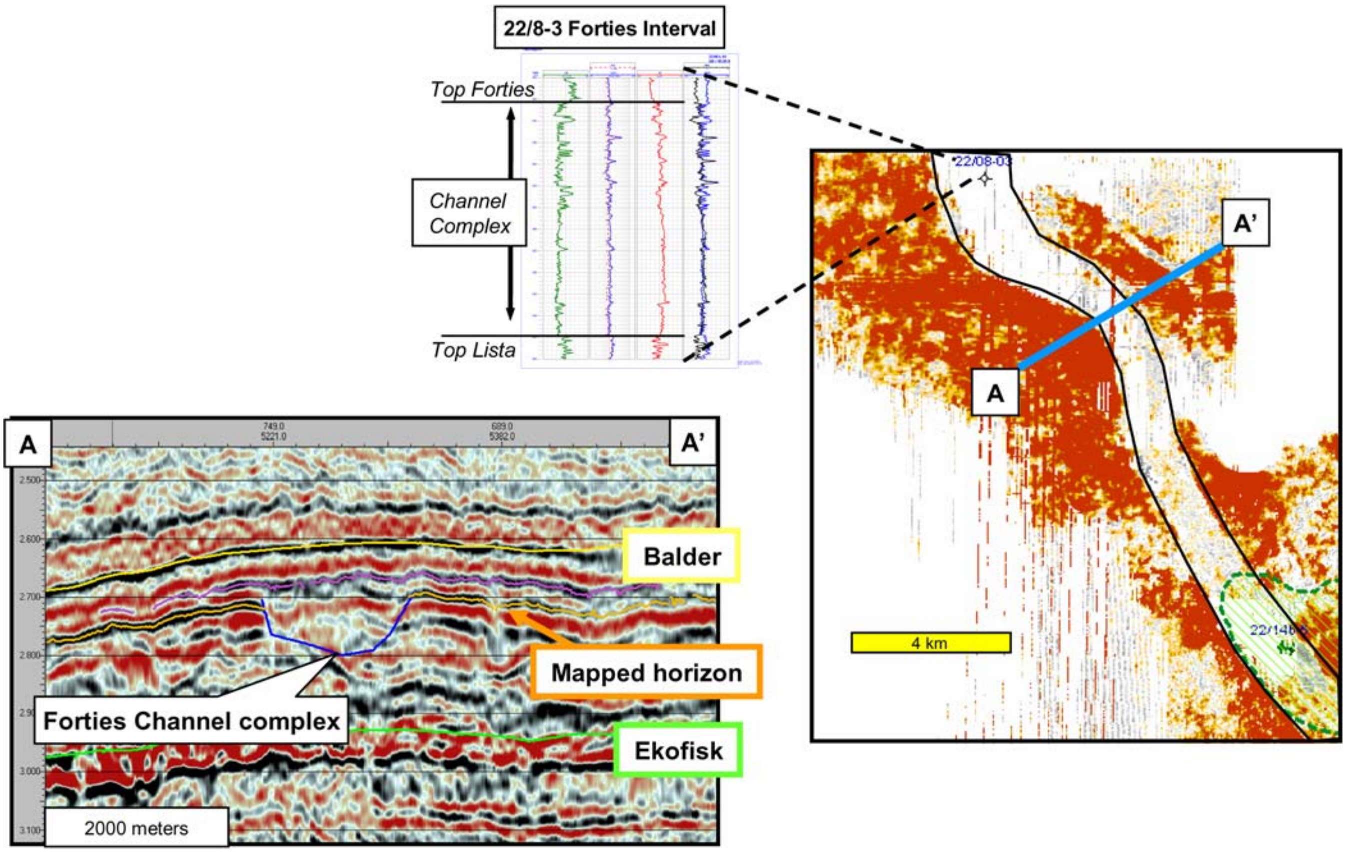

Fig. 12. Forties sandstone reservoir prediction. The far-offset (30–40°) seismic line illustrates a possible channel complex where the mapped horizon is absent. The map on the right displays amplitude on the mapped horizon (B-amplitude). The dim amplitude trending SE from the 22/8-3 is interpreted to represent a channel sandstone. A channel complex was therefore predicted for the 22/14-5 Huntington location. Courtesy of PGS.

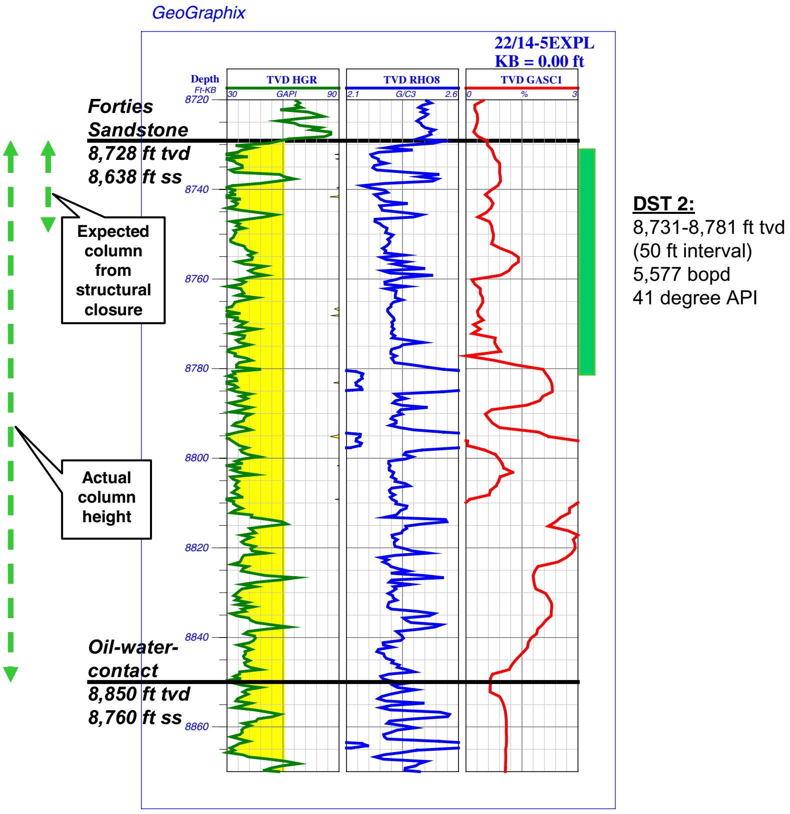

Fig. 13. 22/14-5 Forties well log section. The log display includes GR, density and mud log total gas curves from left to right. The gross column height was 122 ft with 83 ft of net pay. Average porosity was 19.7% and average water saturation 46.5%. The perforated interval is indicated by the green bar at the right edge of the log plot. The expected column height on the left side above was much smaller than the actual column height.

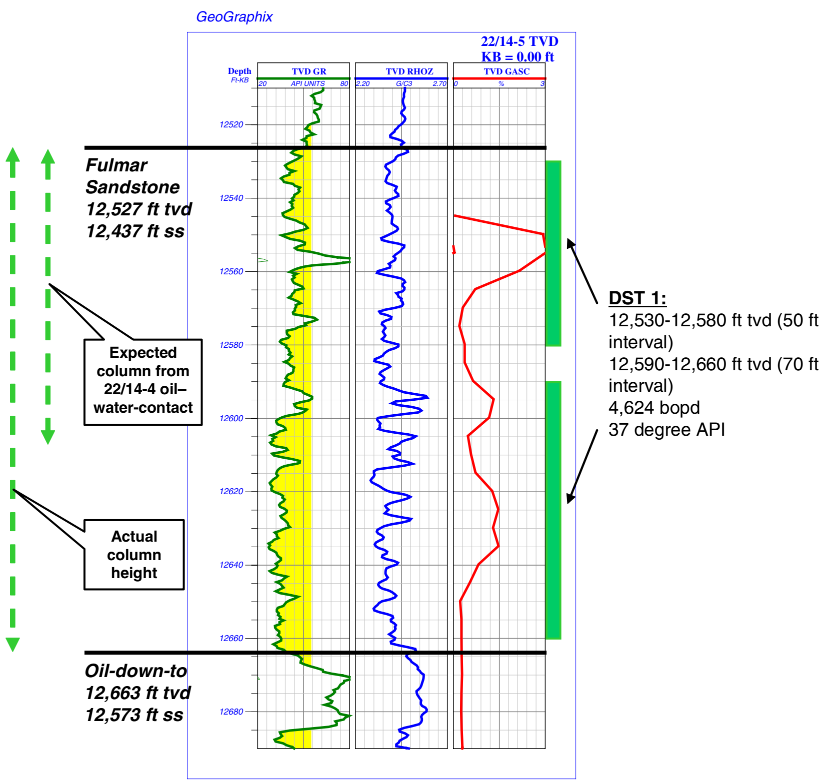

Fig. 14. 22/14-5 Fulmar well log section. The log display includes GR, density and mud log total gas curves from left to right. The gross column height was 136 ft with 72 ft of net pay. Average porosity was 16.1% and average water saturation 47%. The perforated interval is indicated by the green bar at the right edge of the log plot. The expected column height on the left side above was smaller than the actual column height.

Table 1. Comparison of prognosed and actual results for the 22/14-5 Huntington discoveries

	Prognosed	Actual
Forties sandstone		
Depth to top	8640 ft ss	8638 ft ss
Hydrocarbon phase	Oil	Oil
Reservoir pressure	3950 psi	3900 psi
Column height	20 ft	122 ft
Fulmar sandstone		
Depth to top	12 335 ft ss	12 437 ft ss
Hydrocarbon phase	Oil	Oil
Reservoir thickness	100 ft	136 ft
Oil-down-to	12 517 ft ss	12 573 ft ss

The pre-drill predictions were quite accurate except for the oil column heights (Table 1). In an unusually favourable coincidence, the column heights exceeded expectations in both the Forties and Fulmar reservoirs. It is believed that stratigraphic components to the trap increased the height, areal extent and reserves potential for each discovery. While this potential had been foreseen prior to drilling, it was not regarded as the most likely outcome.

The authors wish to thank Carrizo Oil & Gas, Inc. and in particular S. P. Johnson IV, J. Greene, G. Uhland, G. Evans, B. Fisher, J. Lund and J. Thompson for their continued support of this project. We are also grateful to the P1114 co-venturers, E.ON Ruhrgas UK Exploration and Production Ltd, Norwegian Energy Company UK Ltd and Oilexco North Sea Ltd for permission to present and publish this paper. However, the views expressed here are those of the authors and do not necessarily reflect those of the P1114 co-venture group. PGS is thanked for allowing reproduction of several seismic lines. We also acknowledge the technical contributions of R. Gassett for his work in AVO analysis and fluid substitution and E. Pasternack for petrophysical analysis. Finally, we are particularly grateful for the support of M. Stockwell, C. Møller and R. Christensen, who enabled this prospect to be drilled.

References

Erratt, D., Thomas, G. M. & Wall, G. R. T. 1999. The evolution of the Central North Sea Rift. *In*: Fleet, A. J. & Boldy, S. A. R. (eds) *Petroleum Geology of Northwest Europe: Proceedings of the 5th Conference*, Geological Society, London, 63–82. doi: 10.1144/0050063.

Hempton, M., Marshall, J., Sadler, S., Hogg, N., Charles, R. & Harvey, C. 2005. Turbidite reservoirs of the Sele Formation, Central North Sea: geological challenges for improving production. *In*: Doré, A. G. & Vining, B. A. (eds) *Petroleum Geology: North-West Europe and Global Perspectives: Proceedings of the 6th Petroleum Geology Conference*, Geological Society, London, 449–459. doi: 10.1144/0060449.

Isaksen, G. H. 2004. Central North Sea hydrocarbon systems: generation, migration, entrapment, and thermal degradation of oil and gas. *AAPG Bulletin*, **88**, 1545–1572.

Kubala, M., Bastow, M., Thompson, S., Scotchman, I. & Oygard, K. 2003. Geothermal regime, petroleum generation and migration. *In*: Evans, D., Graham, C., Armour, A. & Bathurst, P. (eds) *The Millennium Atlas: Petroleum Geology of the Central and Northern North Sea*. Geological Society, London, 289–315.

Leonard, A., Jolley, L., Carter, A., Mills, C., Jones, N. & Bowman, M. 2000. Lessons Learned from the Management of Basin Floor Submarine Fan Reservoirs in the UKCS. *In*: Weimer, P., Slatt, R. *et al*. (eds) *Deep-water Reservoirs of the World, Gulf Coast Section Society of Economic Paleontologists and Mineralogists Foundation 20th Annual Research Conference*, Houston, Texas, 478–501.

Winefield, P., Gilham, R. & Elsinger, R. 2005. Plumbing the depths of the Central Graben: towards an integrated pressure, fluid and charge model for the Central North Sea HPHT play. *In*: Doré, A. G. & Vining, B. A. (eds) *Petroleum Geology: North-West Europe and Global Perspectives: Proceedings of the 6th Petroleum Geology Conference*, Geological Society, London, 1301–1315. doi: 10.1144/0061301.

The Jasmine discovery, Central North Sea, UKCS

S. ARCHER,[1] S. WARD,[2] S. MENAD,[3] I. SHAHIM,[4] N. GRANT,[2] H. SLOAN[2] and A. COLE[2]

[1]*Department of Geology and Petroleum Geology, Meston Building, Kings College, Aberdeen AB24 3UE, UK*
[2]*ConocoPhillips Petroleum Company UK Limited, Rubislaw House, Anderson Drive, Aberdeen AB15 6FZ, UK (e-mail: Simon.Ward@conocophillips.com)*
[3]*ConocoPhillips Pty Ltd, 53 Ord St, Perth 6005, Australia*
[4]*ConocoPhillips Company, Subsurface Technology Group, North Dairy Ashford, Houston, TX 77079, USA*

Abstract: The Jasmine Field is located in blocks 30/06 and 30/07a on the J Ridge, the southeastern extension of the Forties–Montrose High, which separates the eastern and western basins of the UK Central North Sea. The field was discovered in 2006 and is close to two ConocoPhillips producing fields, Jade and Judy, which serve as useful local analogues. The main *West Limb* structure is a turtle-back faulted anticline NW of the Joanne salt pillow. The primary reservoir is Triassic in age and consists of stacked fluvial sandstones of the Joanne Member of the Skagerrak Formation. The HPHT exploration wells 30/06-6 and geological sidetrack 30/06-6Z discovered a rich gas condensate column of 2300 ft, some 1100 ft deeper than the mapped independent structural closure of the prospect, and achieved good flow rates on test. To appraise the discovery and assess the potential for significant additional volumes in an adjacent downfaulted terrace, a programme comprising a main well and two sidetrack wells was initiated in 2007. Appraisal well 30/06-7 discovered a 550 ft hydrocarbon column in the *Northern Terrace* with a hydrocarbon–water contact shallower than that observed in the West Limb, thereby proving structural compartmentalization between the two fault blocks. Good flow rates were achieved from a drill stem test in mechanical sidetrack well 30/06-7Z. Sidetracks 30/06-7Y and 30/06-7X were drilled to confirm the northwestern extension of the West Limb discovery and to test the northern extent of the Northern Terrace accumulation, respectively. This programme has reduced volumetric uncertainty but the trapping mechanism and the ultimate extent of the Jasmine accumulation remain unknown. Comprehensive data acquisition throughout the exploration and appraisal phases, including drill stem testing, core recovery and seismic data reprocessing, has facilitated a detailed reservoir characterization programme. Jasmine represents a significant new high pressure/high temperature resource in the mature Central North Sea and is currently undergoing development planning.

Keywords: Jasmine Field, Central North Sea, high pressure/high temperature (HPHT), Skagerrak, Triassic, condensate

Location and aims

The Jasmine Field was discovered in 2006 by exploration well 30/6-6. The field straddles blocks 30/06 and 30/07 of the UK sector of the Central North Sea, 270 km east of Aberdeen and is located 9 km west of the Judy Field and 16 km south of the Jade Field (Fig. 1). The aim of this paper is to document the discovery and appraisal history of the Jasmine accumulation and outline the ongoing reservoir characterization programme. The Jasmine Field represents one of the most significant discoveries made in the North Sea in recent years.

Licence and exploitation history

The ConocoPhillips-operated Judy, Joanne and Jasmine fields are located primarily in Block 30/07a with southern and western flanks extending into adjacent blocks 30/12a, and 30/06. Phillips Petroleum UK Ltd acquired operatorship of Licence P.032, which includes blocks 30/07a and 30/12a, from Gulf Oil in 1972, and part of P.011 (30/06) from Shell in 1993.

The *J Block* area is a prolific hydrocarbon-rich region which straddles the J Ridge, a large intra-basinal horst within the Central Graben. The J Block assets comprise a number of hydrocarbon fields with reservoirs in the Triassic Skagerrak Fm., the Upper Jurassic Fulmar Fm., the Upper Cretaceous chalk and Paleocene Andrew sandstone. The Joanne Field was discovered in 1981 by well 30/07a-1, which encountered hydrocarbons in both the Paleocene Andrew ('A1') sands and the Cretaceous chalk Tor Formation. It was appraised by a further four wells including 30/07a-5 (1985), which targeted the western flank of the field terminating in the Lower Cretaceous Cromer Knoll Group *c.* 500 ft above a structure now known to be the Jasmine Field. An opportunity to deepen the well was not taken on account of predicted poor reservoir quality based on the earlier 30/07a-3 well results, and the poor quality of the seismic image of the underlying section.

The Judy Field was discovered in 1985 by well 30/07a-4A, which encountered hydrocarbons in both Upper Jurassic and Triassic sections (Keller *et al.* 2005). It was appraised by five further wells and project sanction was achieved in 1992. The Judy platform and the connected Joanne (Chalk) subsea manifold were installed in 1993, with first production in 1995. Total cumulative production to end 2008 is 160 MMBOE with peak production of 79 MBOE per day being achieved in Q3 2006. Average production rates in 2008 were 41 MBOE per day.

The Jade Field was discovered in 1996 by well 30/02c-3 and appraised by well 30/02c-4 (Jones *et al.* 2005). The field is tied back to the Judy platform and has been on production since 2001 with cumulative production to end 2008 of 107 MMBOE. Peak rates of 58 MBOE per day were achieved during the period 2002–2005 while average rates in 2008 were 31 MBOE per day.

The Jasmine Field was discovered in 2006 on the western flank of the J Ridge (Fig. 2) by a coventurer group comprising three companies: ConocoPhillips (Operator, 36.5%), Eni UK (33.0%) and BG Group (30.5%). The geology of the Jasmine Field is in many ways analogous to that of the other local Skagerrak accumulations and has benefited from both the static and dynamic knowledge

VINING, B. A. & PICKERING, S. C. (eds) *Petroleum Geology: From Mature Basins to New Frontiers – Proceedings of the 7th Petroleum Geology Conference*, 225–243. DOI: 10.1144/0070225

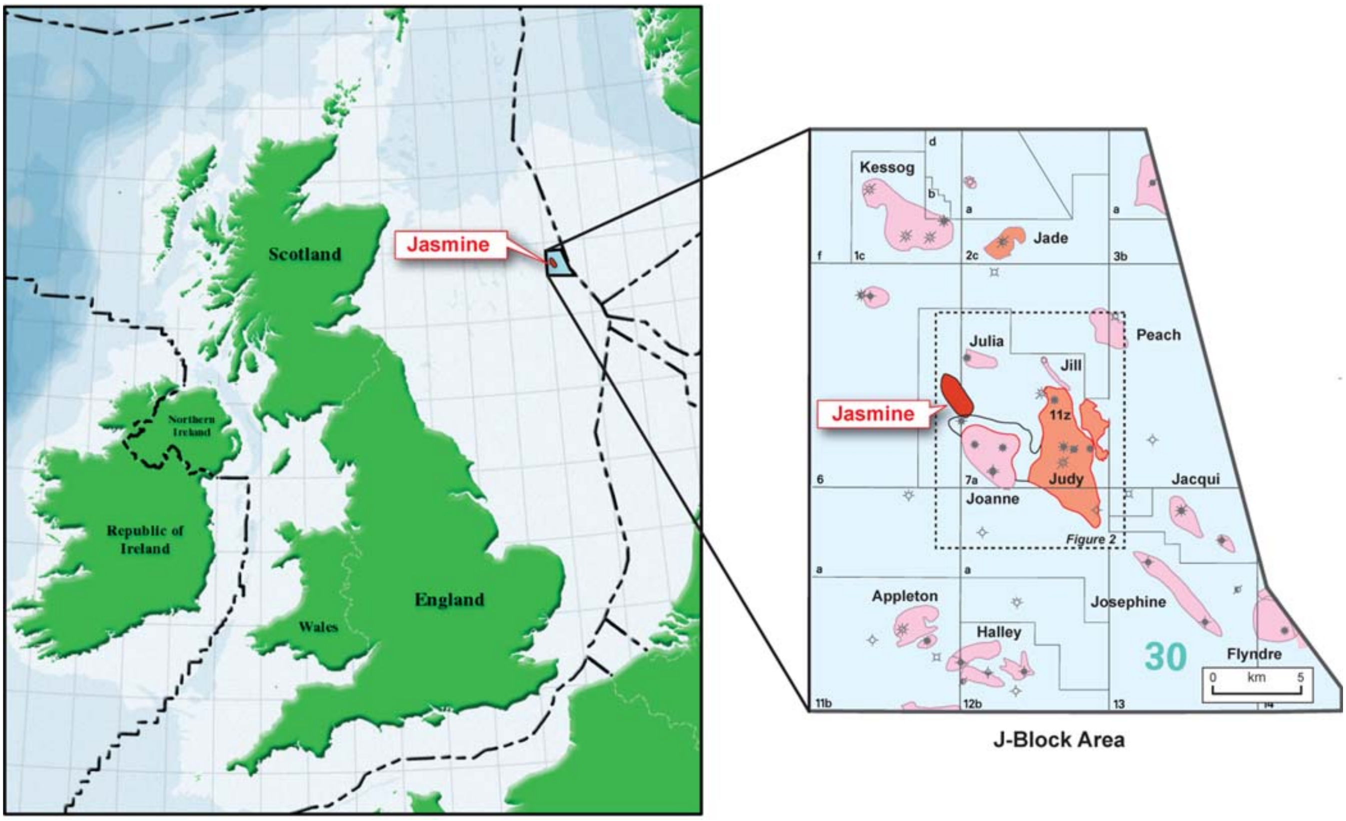

Fig. 1. Jasmine Field location. Figure 2 area shown as dotted outline.

compiled on these reservoirs since their discovery. The Jasmine Field lies at a current burial depth which is intermediate between the shallower Judy and the deeper Jade fields (Fig. 3). These two assets therefore provide useful local analogues as to Jasmine's likely dynamic behaviour, particularly in terms of bracketing pressure, temperature, fluid type and well performance parameters.

Stratigraphic and structural setting

A stratigraphic nomenclature for the Triassic of the Central Graben was proposed by Goldsmith *et al.* (1995). It was based on biostratigraphic and lithostratigraphic methods, including wireline log correlations, and established a stratigraphic framework which introduced the J Member terminology within the Skagerrak Formation, whereby female names represent reservoir sandstone intervals and male names represent thick intervening sealing mudstones (Fig. 4).

The Skagerrak Formation is a sequence of continental sediments, deposited on a wide alluvial plain which extends throughout much of the Central North Sea. The primary reservoir in the Jasmine Field consists of a succession of stacked moderate net to gross fluvial deposits which comprise the Joanne Sandstone Member of the Skagerrak Formation. The average reservoir thickness for Judy and Joanne Sandstone members is *c.* 1000 ft each in the Jasmine area. The fluvial sandstone reservoir facies include both confined, channelized and unconfined, sheet flood and crevasse splay components. Mudstones constitute non-reservoir floodplain, playa and lacustrine facies, although the degree and style of fluvio-lacustrine interaction is still much debated.

The top seal to the Joanne reservoir is provided by the Jonathan Mudstone Member and the base seal by the Julius Mudstone Member (Fig. 4). The Julius mudstone varies between 200 and 300 ft in thickness and the Jonathan mudstone can achieve up to 900 ft thickness where fully preserved. These exceptionally thick mudstone intervals, in addition to the Lower Triassic Smith Bank Formation, are a characteristic yet enigmatic feature of the Skagerrak.

The Skagerrak succession most probably accumulated in a semi-arid terminal basin without direct oceanic connection. The sands were probably shed from hinterlands to the NW and NE, that is, the Scottish and Scandinavian Caledonian Highlands. The Skagerrak reservoirs accumulated in a series of salt-withdrawal mini basins (e.g. Hodgson *et al.* 1992; Smith *et al.* 1993; Barde *et al.* 2002; Matthews *et al.* 2007). The rate of generation of halokinetic accommodation space is thought to play a major role in controlling reservoir architecture and stacking patterns by governing channel location and degree of channel amalgamation (lateral and vertical net to gross).

Structurally, the Jasmine Field sits on the western edge of the J Ridge, a Jurassic age intra-basinal horst block, situated medially within the Central Graben. The horst plunges to the NNW and is bound by deep Late Jurassic aged graben, the Harrier sub-basin to the west and the Eastern Central Graben to the east.

The J Ridge has had a protracted structural evolution. Evidence exists for early Triassic-age fault movements which contributed to the creation of variable accommodation space for deposition of the Smith Bank Formation. This early Mesozoic extension episode combined with sediment loading contributed to early mobilization of the Zechstein salt. The deposition of the Smith Bank Formation was confined to mini-basins flanked by resultant salt walls and larger salt stocks (Goldsmith *et al.* 2003). The Jasmine field occupies one such mini-basin and is a distinct Triassic depocentre from that associated with the Jade and Judy Fields on the eastern side of the J Ridge. Growth of the salt walls and pillows during Triassic deposition led to the broadening of the early mini-basins such that the maximum mini-basin extent occurred during deposition of the Joanne Sandstone Member of the Skagerrak Formation. The eventual grounding of the salt may have led to the

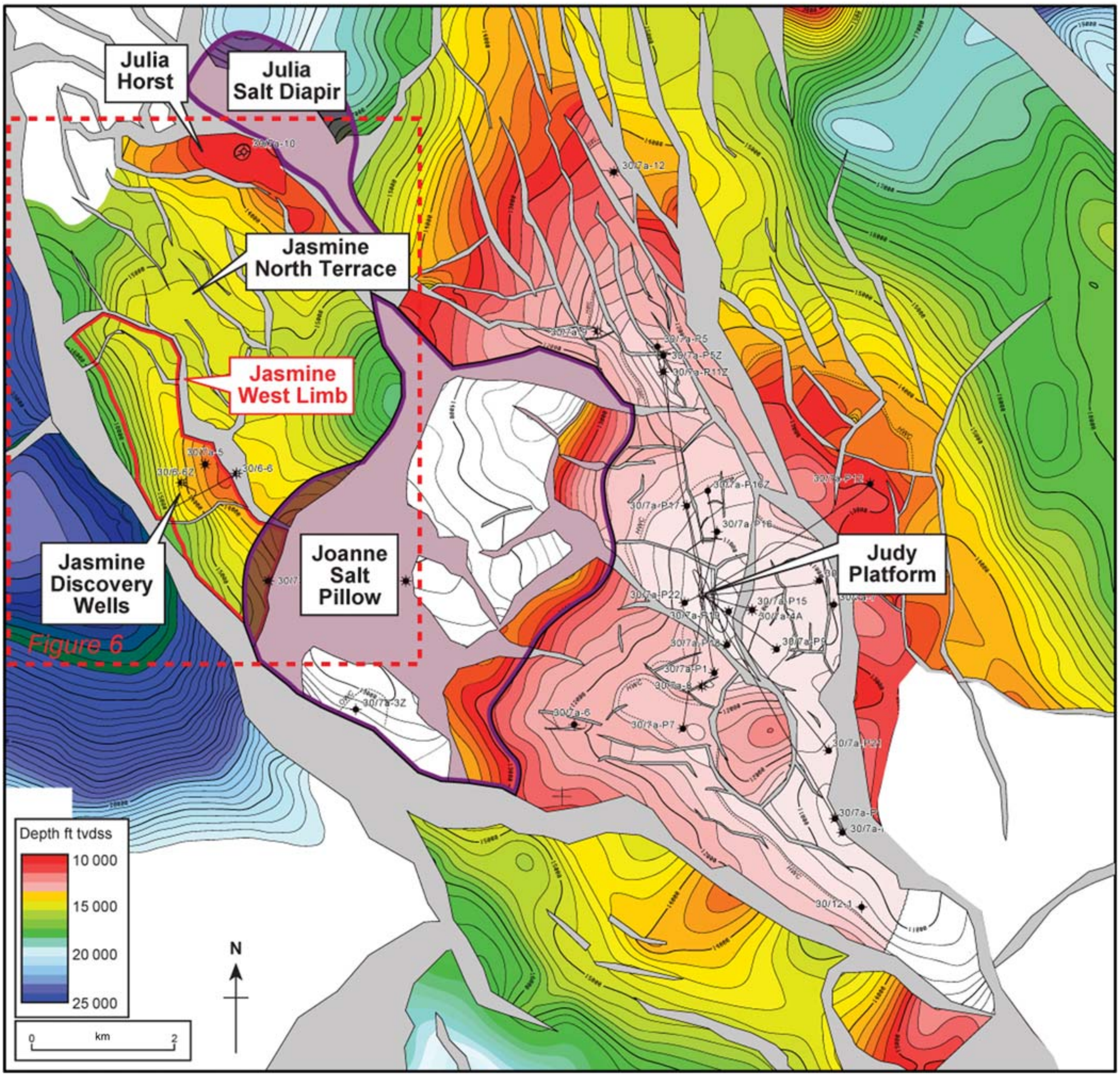

Fig. 2. J Ridge Top Triassic Unconformity structure map.

formation of intra-basinal highs and the development of multiple unconformities. An episode of Late Triassic (Late Joanne/Early Jonathan) faulting is evident, although not easily discernible, within the Northern Terrace area of the Jasmine Field (Fig. 5).

Middle Jurassic uplift and erosion led to the creation of the Mid-Cimmerian unconformity. During Late Jurassic rifting the J Ridge formed as a large intra-basinal horst block. The residual salt bodies suffered extension and collapse during this extensional event, creating localized depocentres both on the flanks and on top of the ridge. Salt collapse and continued extension also resulted in the dismemberment of the Triassic mini-basin fills into a series of faulted, turtle-back anticlines. These form the main trapping structures for the Jade and Judy Fields.

The Jasmine West Limb faulted anticline also owes its formation to this Late Jurassic rifting episode and salt withdrawal. The structure is perched above the western J Ridge boundary fault and is a steeply rotated fault block which evolved from a turtle-back anticline into a forced fold as displacement accumulated on the boundary fault during Late Jurassic rifting.

The Jasmine Northern Terrace area forms a foundered saddle region between the main Jasmine West Limb discovery to the SW and the water-saturated Julia horst block (30/7a-10) to the NE (Figs 2 & 5). The Northern Terrace is characterized by a set of northeasterly dipping domino-style fault blocks where the faulting appears multi-phase with Triassic and Upper Jurassic age structures dominating in different areas. The Northern Terrace saddle area relies heavily on fault seal to be an effective trap. There may also be a stratigraphic seal element provided by the Middle Joanne shale-prone interval, suggesting the possibility of a complex sealing mechanism involving both structural and stratigraphic seal components.

Exploration phase

Pre-drill prospect evaluation

The original Jasmine prospect was perceived to require a lateral side-seal to the SE against the Joanne salt pillow, which was a

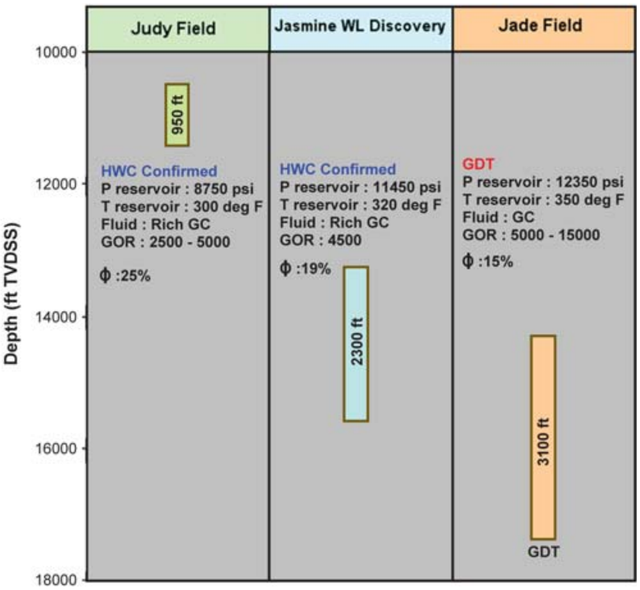

Fig. 3. Jasmine and local producing field analogues.

concept not previously proven in the immediate area. The northern end of the structure was assumed to be a simple spill point toward the NW at a depth of *c.* −14 600 ft tvdss which gave a three-way structural closure of *c.* 1200 ft elevation.

Semi-regional seismic mapping integrated with knowledge of the local analogue fields led to the prognosis that the reservoir comprised Joanne and Judy Member fluvial sandstones of the Triassic Skagerrak Formation. The prognosed fluid type was gas condensate with hydrocarbon charge modelled as being sourced from a kitchen to the SW involving fluid migration across the major Upper Jurassic J Ridge western boundary fault. Although source quantity is abundant in this part of the Central Graben due to the thickness and richness of the Upper Jurassic Kimmeridge Clay Fm. and Heather Fm. shales, the effectiveness of the charge in migrating across the poorly imaged boundary fault was considered a major pre-drill uncertainty.

Discovery well results

30/06-6. Exploration well 30/06-6 was drilled into the crest of the west limb footwall to test the independent structural closure which abutted the Joanne salt pillow (Fig. 6a). The well was successful in discovering a significant, *c.* 1000 ft thick, column of rich gas condensate within the Joanne Sandstone Member of the Skagerrak Formation. The column extended down to the Julius Mudstone and the well terminated in the underlying Judy Sandstone which was water-saturated, confirming hydrocarbons-down-to (HDT) the base of the Joanne Sandstone. Figure 6b shows the mapped extent of the accumulation consistent with the HDT proven by the well.

A comprehensive suite of wireline logs was run which confirmed the Joanne Sandstone interval to have good porosity (average 17%) and a moderate net to gross (average 60%) (Fig. 7). A drill stem test (DST) was conducted and encouraging flow rates of gas and associated condensate were achieved with an estimated production potential consistent with the adjacent producing assets had the well been completed as a typical J Block production well.

Even more encouraging were the pressure data results (see Fig. 12). Modular dynamics tester (MDT) data points from the water-saturated Judy Sandstone interval lay on the same trend as those from the water-saturated Julia horst well (30/07a-10), implying a common regional aquifer. Pressure data acquired in the hydrocarbon leg gave a trend whose projection suggested a FWL of *c.* −15 800 ft tvdss, 1300 ft deeper than the proven HDT and some 1200 ft deeper than the lowest closing contour (LCC) of the Jasmine West Limb structure (Fig. 6c).

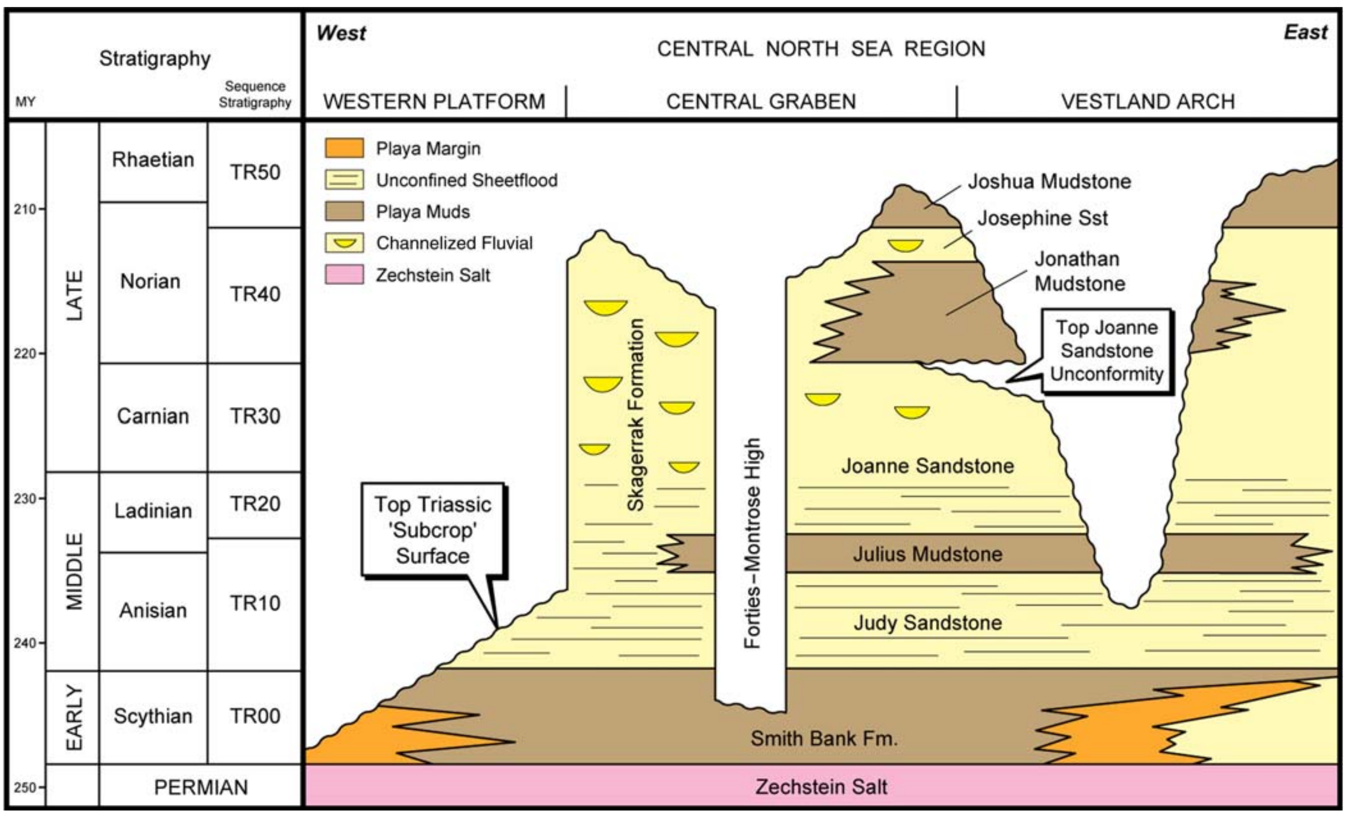

Fig. 4. Triassic stratigraphic framework (modified after Goldsmith *et al.* 1995).

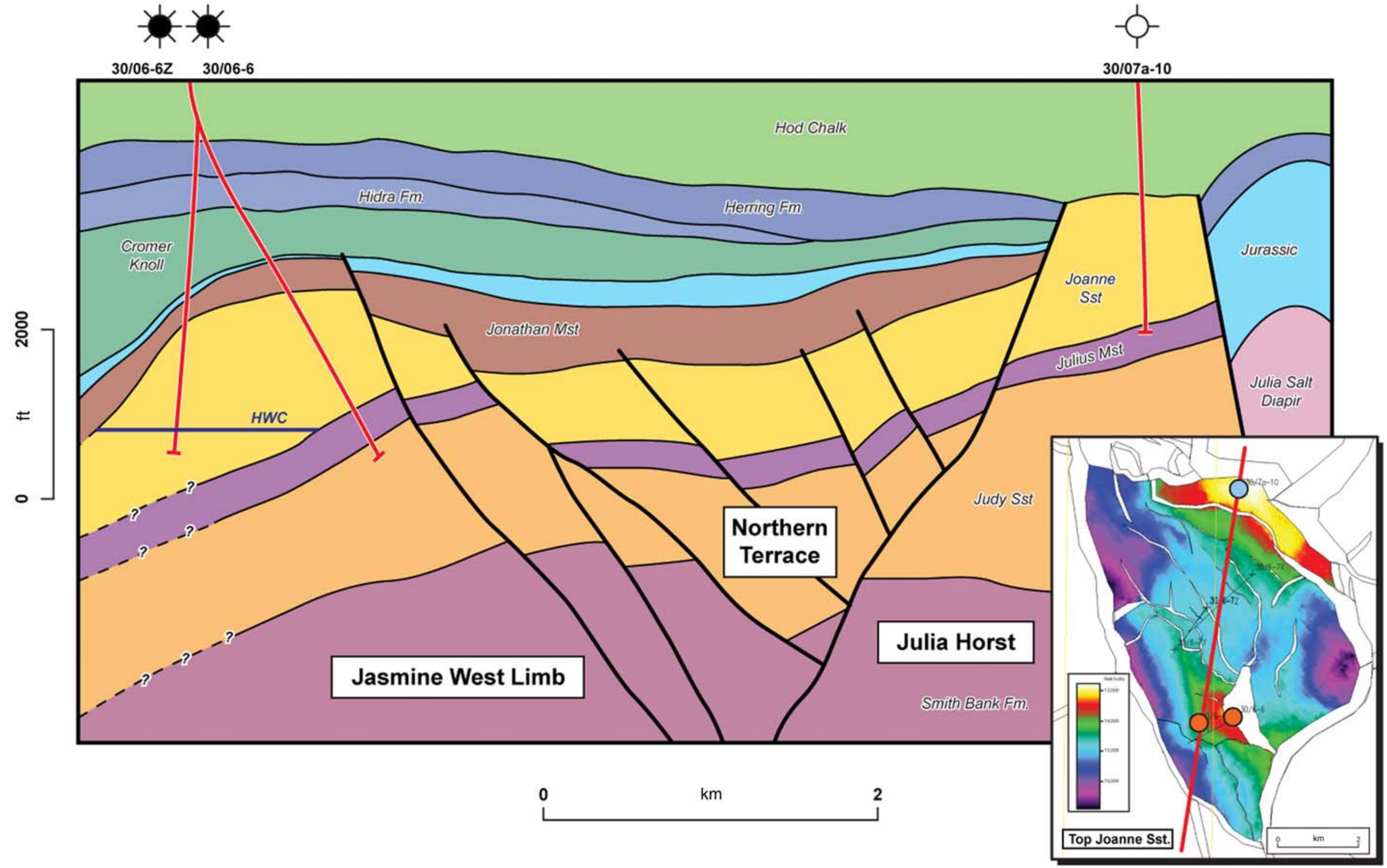

Fig. 5. Jasmine–Julia structural cross section.

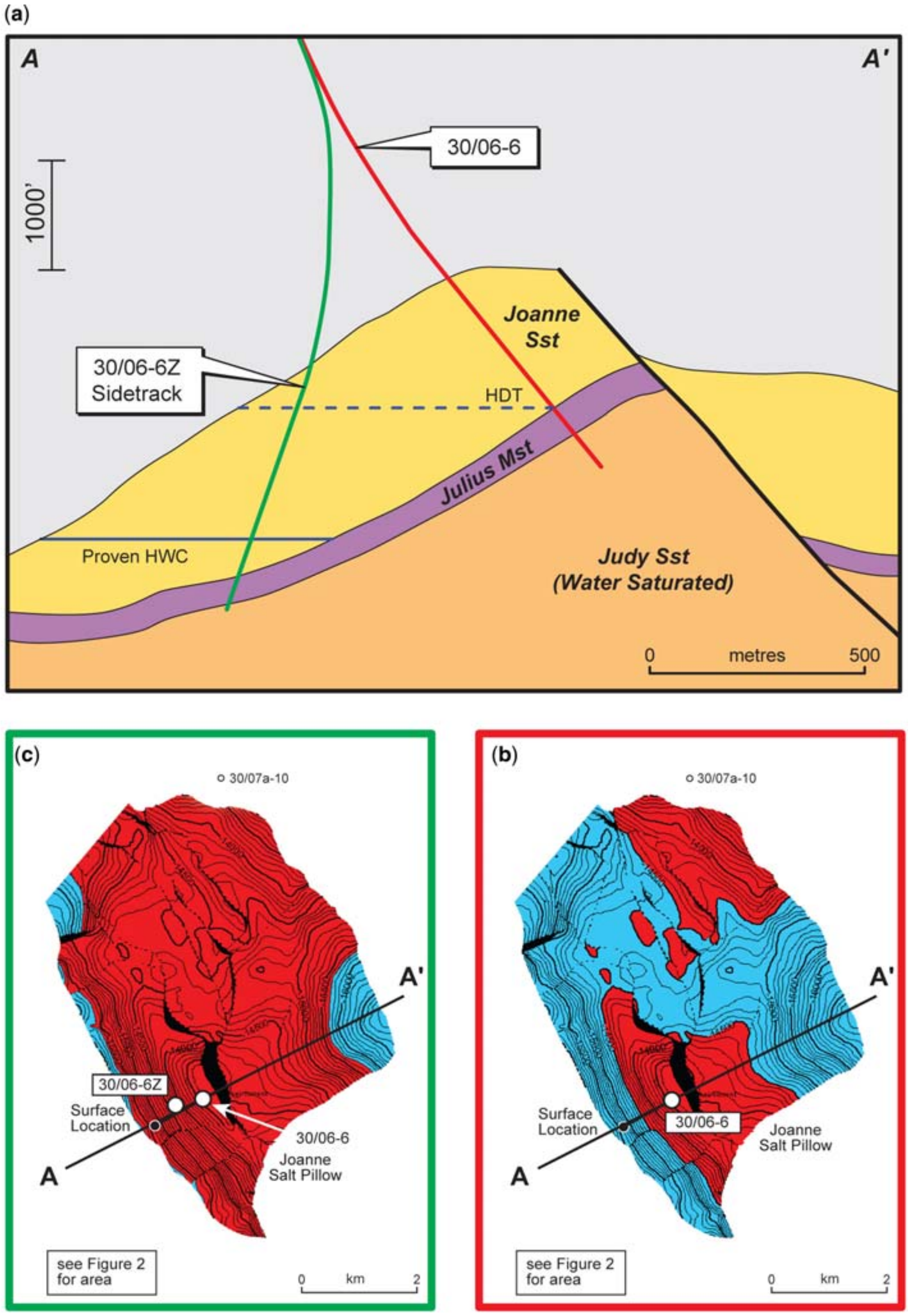

Fig. 6. Exploration drilling phase summary. (**a**) Cross-section through West Limb showing 30/06-6 and -6Z wells. (**b**) Accumulation extent consistent with HDT in 30/06-6 discovery well. (**c**) Accumulation extent consistent with HWC in 30/06-6Z sidetrack well.

30/06-6Z. A geological sidetrack was drilled in order to test the predicted deeper contact suggested by the pressure gradients and potentially prove up a very sizeable accumulation indeed. Geological sidetrack 30/6-6Z was planned to intersect the prognosed hydrocarbon–water contact (HWC) by targeting a downdip location such that the contact would be observed within the Joanne Sandstone reservoir. In order to avoid any ambiguity in contact definition, and to allow for depth uncertainty at Top Julius Mudstone, a deviated well path back towards the WSW was necessary (Fig. 6a).

The sidetrack successfully proved a HWC within the Joanne reservoir at the predicted level of *c.* −15 600 ft tvdss. The hydrocarbon-bearing interval in the 30/06-06Z sidetrack was *c.* 1600 ft TVD in gross thickness and the two wellbores therefore confirmed a hydrocarbon column of *c.* 2300 ft, with a HWC some 1000 ft deeper than the LCC. They conclusively proved the effectiveness of the Julius Mudstone as the bottom seal to the accumulation.

The fact that the HWC was encountered deeper than the spill point and that there was a lack of obvious closure or sealing mechanism at the northwestern extent of the West Limb (Fig. 6c) pointed to the very real possibility that the accumulation may extend into the adjacent Northern Terrace area. The uncertainty in the trapping mechanism was referred to as the ‘Jasmine discovery sealing conundrum’ and the issue is summarized in Figure 8.

Appraisal phase

Appraisal programme

In 2007, an appraisal programme was planned to achieve two main goals: test for volumetric upside in the Northern Terrace and

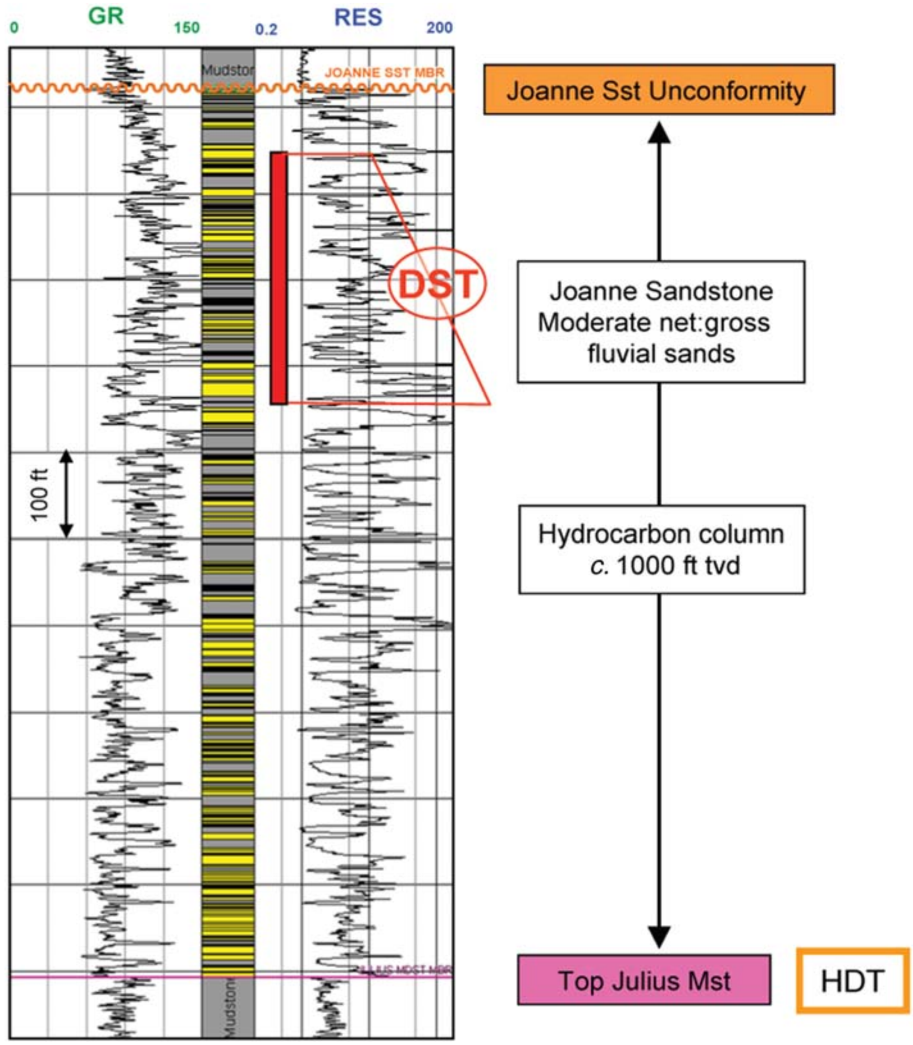

Fig. 7. 30/06-6 wireline log data.

undertake an additional penetration of the Jasmine West Limb to prove lateral continuity of the accumulation along-strike to the NW of the discovery well. A range of well designs and potential locations were considered before deciding on a three-well appraisal programme. The appraisal wellbores were to be drilled from a single top hole location positioned above the NE segment of the West Limb (Figs 9 & 10).

The main bore (30/06-7) was planned to test for the presence of hydrocarbons in the adjacent compartment of the Northern Terrace and, if present, to establish any continuity with the West Limb. A deep sidetrack was planned to drop back to the northern end of the West Limb to further appraise the main structure. A second shallow sidetrack was planned as a longer stepout well, targeting the ultimate northeasterly extent of any accumulation but contingent on success in the main bore (30/06-7).

The Northern Terrace is a poorly imaged, complexly faulted, foundered saddle area which separates the Jasmine West Limb accumulation from the water-saturated Julia horst, 6 km to the NE (see Fig. 2). This area's structural complexity is accentuated by a switch in fault polarity which occurs towards the NW, where two fault arrays with opposing-dip tip out in a transfer–wrench system. The faults can be interpreted on seismic data to terminate along-strike, resulting in a series of relay ramps. In the event that they are non-sealing then the area could conceivably represent a single, large contiguous trap (see Fig. 6c). Even in a sealing fault scenario hydrocarbons could potentially follow migration routes around fault tips, depending on the column heights involved (see Fig. 2).

The quality of the seismic image from the existing seismic datasets was considered inadequate for detailed well planning and control whilst drilling. Hence, early in 2007, a fast-track reprocessing programme was undertaken in order to provide data of sufficient quality. This work comprised several phases designed to deliver early results in a timeframe to support the drilling programme whilst permitting later stage refinements to produce an optimized dataset for reservoir characterization purposes. The reprocessing programme is discussed in detail under 'Reservoir characterization programme'.

The wellpaths were planned using the early products from the reprocessing programme. Key objectives were to target panels of coherent seismic data avoiding the seismically resolvable faulting whilst achieving well trajectories which could be logged using wireline tools (Fig. 10).

Appraisal drilling results

30/06-07 and -07Z. The main bore well targeted the nearest fault block of the Northern Terrace and spudded in October 2007. The well encountered hydrocarbons in both the primary Triassic Joanne Sandstone Member and in an overlying secondary Middle Jurassic Pentland Formation reservoir.

Within the Joanne interval, the well found hydrocarbons down to the top of a distinctive red-coloured shale-prone section (informally termed the Middle Joanne sub-member) at −15 300 ft tvdss, which is 300 ft shallower than the HWC discovered in the West Limb.

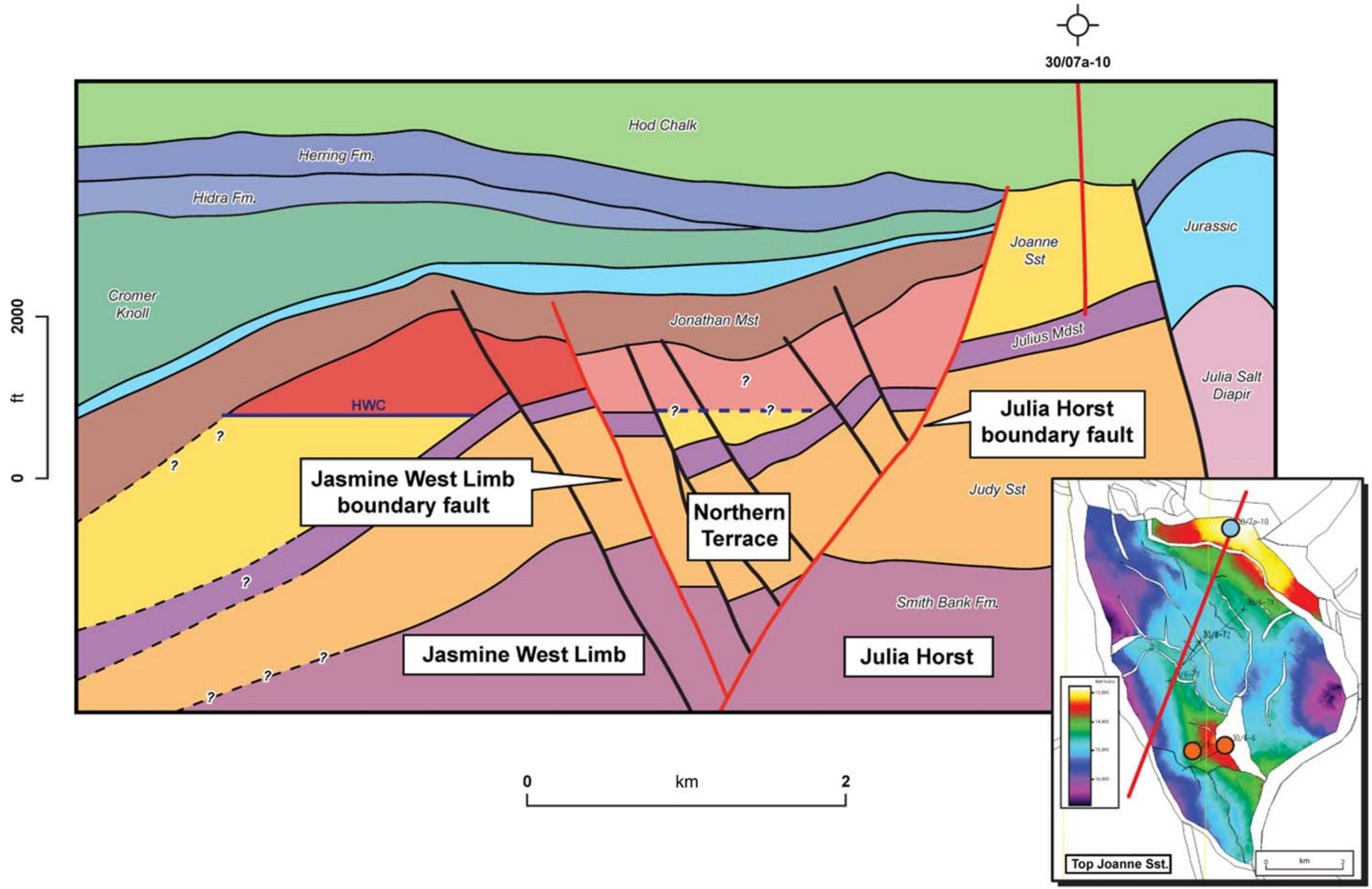

Fig. 8. Jasmine discovery sealing conundrum. What is the sealing mechanism which allows Jasmine West Limb to have an accumulation significantly deeper than the structural spill point and downdip from the water-wet Julia horst? Three candidate options for the sealing mechanism are: (i) West Limb Boundary Fault; (ii) Julia Horst boundary fault; and (iii) intermediate fault or other mechanism?

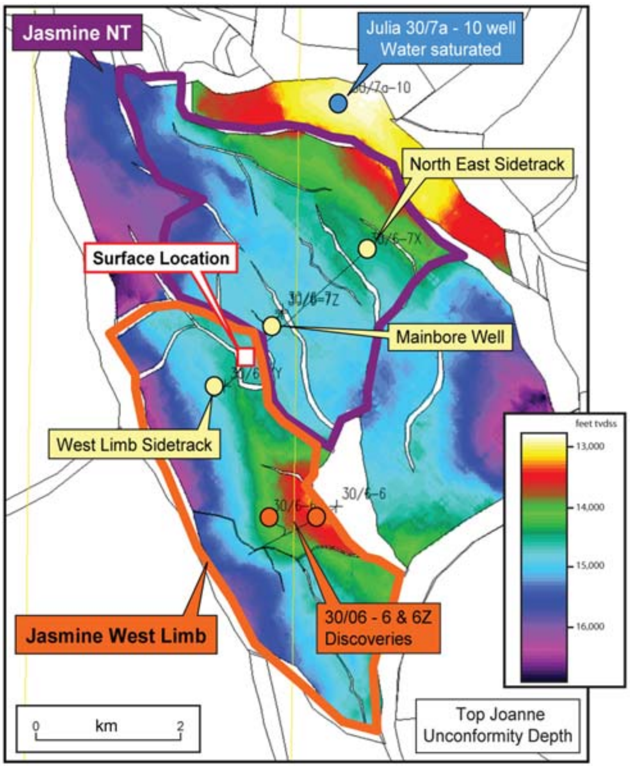

Fig. 9. Appraisal drilling locations.

The underlying Middle Joanne sandstones were water-saturated and the well was terminated within the Lower Joanne. The pressure data and the position of the HWC indicated that the Jasmine Northern Terrace is not in communication with the Jasmine West Limb core area.

In order to better characterize the Jasmine reservoir, a conventional core was taken in this first appraisal well. No core had been obtained in the 30/06-6 or -6Z exploration wells and it was recognized that on account of its down-faulted, deeper structural position, reservoir quality in the Northern Terrace was a significant uncertainty. A 128 ft core was recovered in two coring runs from the Upper Joanne Sandstone section.

A comprehensive logging programme was undertaken and petrophysical analysis revealed the hydrocarbon-bearing Joanne Sandstone to be *c.* 600 ft MD in gross thickness. Porosities of *c.* 16% were better than prognosed given the greater depth compared with the West Limb whilst net to gross was slightly poorer at *c.* 50%. A necessary mechanical sidetrack 30/06-7Z was drilled close to the original borehole to enable a DST to be performed. The DST confirmed that the reservoir could flow at commercial rates.

The fluid type proved to be a volatile oil and hence slightly heavier than the rich gas condensate discovered previously in the West Limb core area at the same depth. The most likely interpretation for the difference in composition is that the same source rock provided both charges at different maturity states with slightly later charge timing to the West Limb compared with the Northern Terrace. The well data has conclusively proven that the master fault separating the Jasmine West Limb from the Northern Terrace acts as a sealing fault over geological time scales.

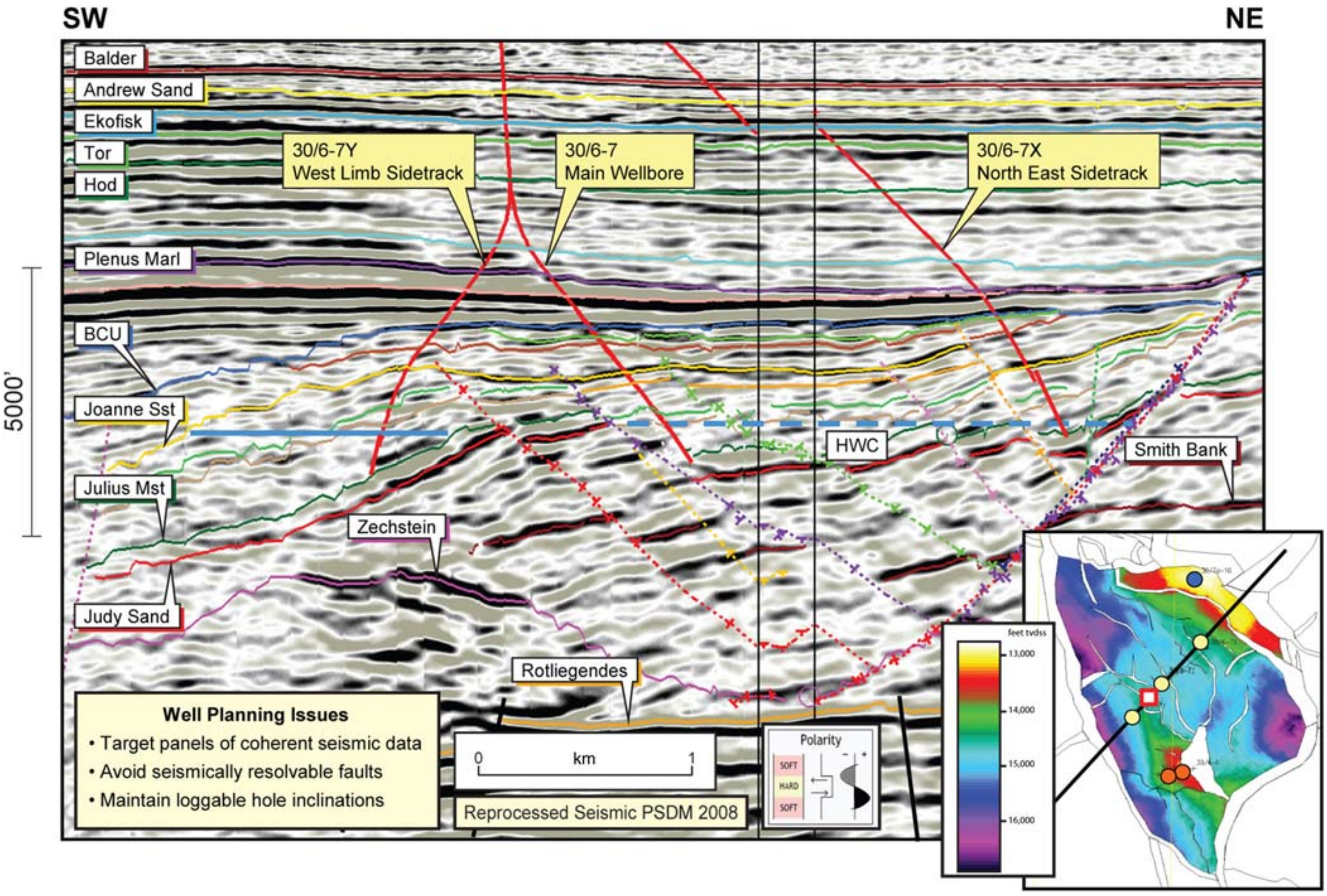

Fig. 10. Appraisal wells on seismic depth section.

Secondary reservoirs had been anticipated in the interval between Base Cretaceous Unconformity (BCU) and Top Joanne Sandstone. Well 30/06-7 encountered hydrocarbon-bearing Middle Jurassic Pentland Formation sandstones (90 ft thick) and thin (15 ft thick) Triassic intra-Jonathan Member sandstones. The Pentland sandstone is in a higher pressure regime than the underlying Joanne Sandstone interval. Therefore the thick Jonathan Mudstone Member acts as an effective top seal to the Joanne accumulation.

30/06-7Y. The 30/06-7Y well was sidetracked from within the Hod Formation SW into the northern area of the West Limb with the aim of reducing uncertainty in the resource volume in Jasmine's core area. Lateral variations in reservoir quantity or quality and the potential for along-strike compartmentalization were the key pre-drill uncertainties (Figs 9 & 10).

The well encountered hydrocarbons in the Triassic Joanne Sandstone Member and also in a secondary Triassic reservoir, the younger Josephine Sandstone Member. The well terminated in the Lower Joanne Sandstone Member immediately above the Julius Mudstone Member. The Joanne Sandstone penetrated by the 30/06-7Y well is *c.* 1500 ft MD in gross thickness with reservoir properties on trend with those from the 30/06-6 and 30/06-6Z discovery wells. The Josephine Sandstone Member in the 30/06-7Y well is *c.* 250 ft MD in gross thickness. Pressure data confirmed that the entire West Limb is within the same pressure regime. No DST was performed in this well.

30/06-7 and -07Y VSP programme. The geometric configuration of the 30/6-07 and the 30/6-07Y sidetrack wells in the same azimuthal plane afforded the opportunity to acquire high-resolution vertical seismic profiling (VSP) control either side of the boundary fault zone separating the West Limb from the Northern Terrace. Data were acquired via a rig-source survey in 30/6-07 and a walkabove survey in 30/6-07Y. The datasets were processed both individually and later migrated together to produce a contiguous high-resolution image across the complex boundary zone (Fig. 11).

The VSP products were compared with the reprocessed seismic volume and the most significant improvement in image quality was noted to occur in the Upper Triassic section. This gave rise to a change in the Top Joanne Sandstone seismic interpretation in 30/06-7 which was now interpreted on a deeper event with the original pick correlated as the top of the Lower Jonathan mudstone. This revision was incorporated into the geological model and into the planning for the long step-out appraisal sidetrack to the NE (30/06-7X).

30/06-7X. The encouraging results from the 30/06-7 and -7Z wells led to the step-out geological sidetrack to the most north-easterly fault block in the Northern terrace to test the extent of the accumulation (see Figs 9 & 10). A shallow kick-off (Mid-Miocene) sidetrack well from the 30/06-7 main bore commenced in April 2008. The well encountered reservoir-quality sandstones in the Middle Jurassic Pentland Formation, the Triassic Josephine Sandstone Member and the Triassic Joanne Sandstone Member, but none showed any indications of the presence of hydrocarbons. The well, combined with the water leg data from the other 30/06 and 30/07 wells, confirmed the presence of a common aquifer within the greater Jasmine area (Fig. 12).

The ultimate trapping mechanism for the Northern Terrace discovery is still not fully understood. Intriguingly the HDT discovered in the 30/06-7 and -7Z wells is coincident with a 60 ft thick red shale unit which may be acting as a stratigraphic bottom seal. Pressure data supports the interpretation that the HWC resides within the depth interval of the shale unit. The mid Northern Terrace area remains untested and the remaining uncertainty in the northern extent of the accumulation will be carried into the development phase of the project. The relative roles and potential interaction between fault seal and thick shales that may act as stratigraphic seals will be an important topic for future investigation. Hence the 'Jasmine sealing conundrum' postulated pre-appraisal drilling has been reduced but not entirely solved (Fig. 13).

Secondary reservoirs summary

Each of the appraisal wells encountered at least one 'secondary' reservoir in the overlying Base Cretaceous to Top Joanne Sandstone interval and these are summarized below.

- 30/06-7 and 30/06-7Z encountered hydrocarbon-bearing Middle Jurassic, Pentland Formation sands;
- 30/06-7Y encountered hydrocarbon-bearing Upper Triassic, Skagerrak Fm., Josephine Member sands;
- 30/06-7X encountered Pentland Fm. and Josephine Member sands which were both water-saturated.

These stratigraphic intervals are not easily resolved seismically and therefore biostratigraphy, chemostratigraphy, cuttings descriptions and the correlation of wireline log signatures have been instrumental in their correlation and dating. No secondary reservoirs were encountered during the drilling of the exploration wells (30/06-6 and 30/06-6Z) due to their crestal position on the West Limb.

Any tectono-stratigraphic model which attempts to explain the distribution of the Pentland Formation has to account for both local and regional erosive events. Local processes have been superimposed on the regional scale effects of the mid-Cimmerian unconformity which cuts out Late Triassic and Early Jurassic strata in all wells. The actual amount of missing section varies considerably from well to well due to variable degrees of erosion/incision and the age of the overlying Jurassic supra-crop. The degree of Late Jurassic incision into the Pentland Formation is difficult to assess, but exerts an additional local control on preserved Pentland thickness. The resource potential presented by these secondary reservoirs will be addressed during field development.

Reservoir characterization programme

An active reservoir characterization programme followed the discovery of the Jasmine accumulation and has progressed significantly with the appraisal drilling and associated data acquisition. Activities have included seismic reprocessing and interpretation, LWD (logging while drilling) and wireline logging (including the acquisition of image logs), core analysis, geomodelling and numerous in-house and contractor/university studies. The key lessons from this integrated reservoir characterization phase are discussed below.

Seismic reprocessing

The existing datasets used in earlier interpretations of the Jasmine area comprised two surveys:

- proprietary Phillips 'JBlock99' survey (1999) acquired in dip (NE–SW) orientation centred on the Judy and Joanne fields and processed as a pre-stack time migration (PSTM);
- non-proprietary regional 'CNS Cornerstone' survey (2003) acquired north–south and reprocessed as a pre-stack depth migration (PSDM) in 2006.

Both surveys suffered from several limitations including poor top reservoir imaging, indistinct fault plane and salt flank definition

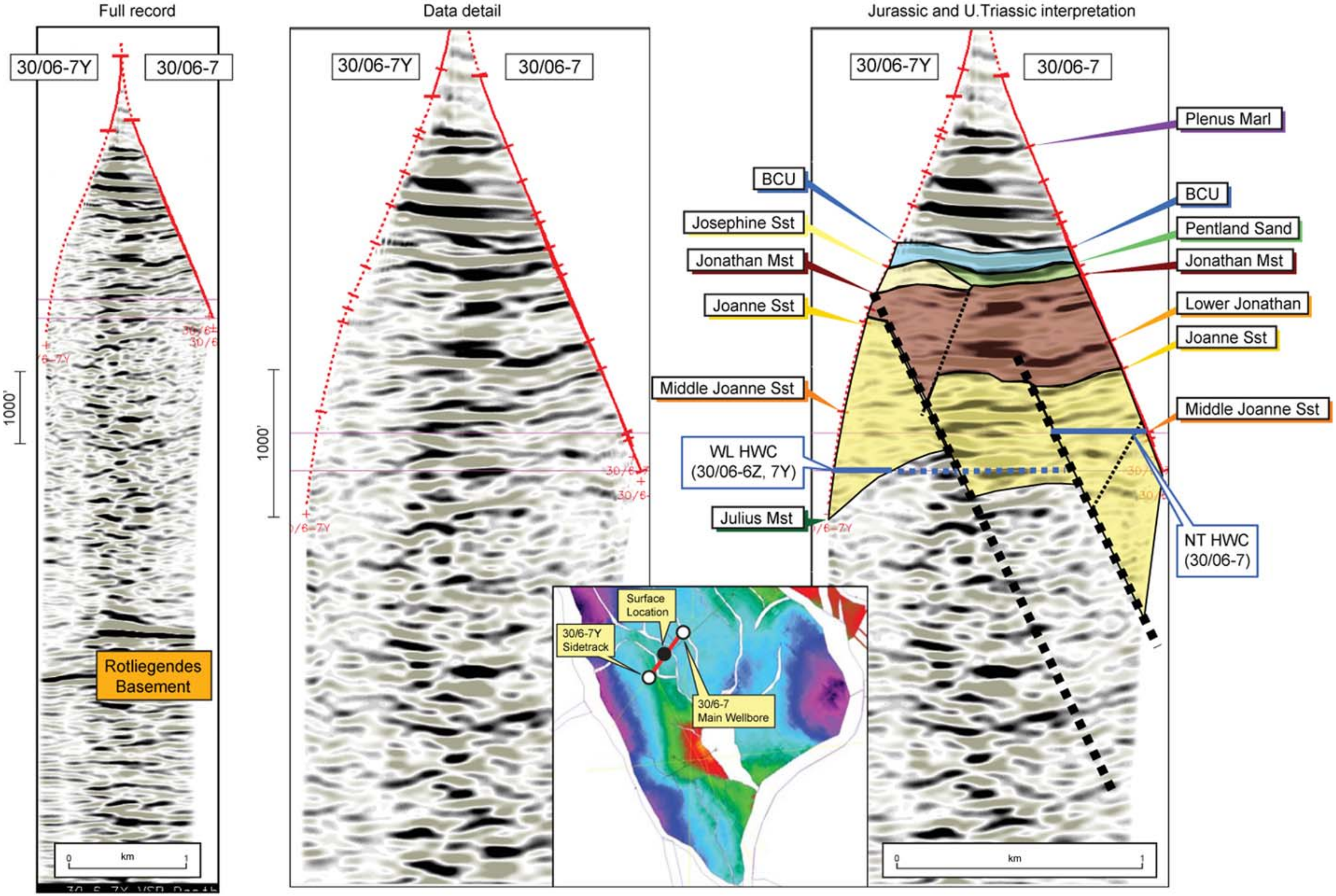

Fig. 11. 30/06-7–30/06-7Y migrated VSP image.

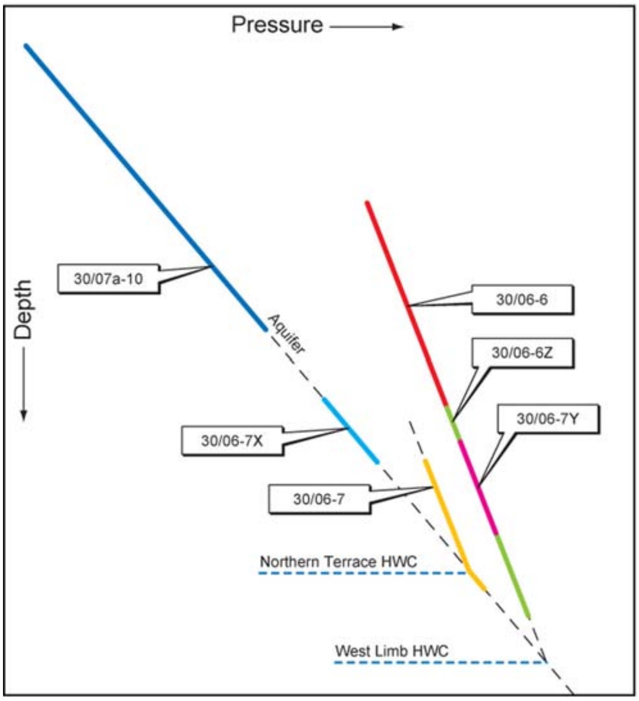

Fig. 12. Jasmine and Julia wells pressure data.

and persistent multiple overprinting, which particularly obscured the internal character of the reservoir interval (see Fig. 15a, c). These factors hindered confident seismic interpretation and the ability to support the planned programmes for the appraisal and development of the Jasmine Field. Hence the need was recognized for a significant improvement in quality of the seismic image across the area.

It was decided that both the above surveys should be processed with a common velocity model in order to utilize their respective advantages in coverage and orientation and then combined post-stack in order to benefit from the dual azimuth illumination (Fig. 14a–c).

The main areas of focus of the reprocessing effort were as follows:

- Noise removal – improvement of signal-to-noise ratio throughout the data using 3D attenuation tools.
- Multiple attenuation – identification of multiple generators through forward modelling and VSP analysis. Attenuation using state-of-the-art demultiple algorithms including surface-related multiple elimination (SRME).
- Model building – dedicated velocity model building project which made major improvements to the existing model, particularly in the high-velocity chalk intervals.
- Imaging – Kirchoff and wave equation anisotropic imaging algorithms.

A theme of the reprocessing project was to take an image-based approach to making key decisions and parameter optimization. This necessitated the output of a series of intermediate PSDM data volumes at key stages during the processing workflow. These products provided the additional benefit of enabling the geological interpretation to be improved and thereby to better support the well planning process. A total of eight iterations of PSDM volumes were output during the processing workflow. Throughout the sequence, verification was maintained on the position of the seismic events in PSDM depth relative to the well control. This was achieved using a combination of well VSPs, synthetic seismograms and a cross-check by converting time domain PSDM (time) and PSTM datasets to depth using a well-based layered velocity model. This enabled the PSDM products to be used in the depth domain, greatly facilitating both operational and geological model building tasks. Significant uplift in image quality was achieved and specific areas of improvement are highlighted in Figure 15b, d.

Structural model

The structural history of the Jasmine area is discussed under ‘Stratigraphic and structural setting’. A more detailed model is currently being reconstructed at both semi-regional and field scales in order to provide a quantitative analysis of fault seal and compartmentalization factors for inclusion in the Jasmine static and dynamic geomodels.

Depositional model

The Central Graben probably constituted an internally draining basin during the Triassic and in the absence of eustatic control, tectonics and climate were the key allogenic controls on sedimentation. Although broadly semi-arid in character, the Triassic climate is thought to have been variable at a number of temporal and geographic scales (McKie & Williams 2009). Long-timescale fluctuations in hinterland climate are thought to be the controlling factor in the generation of the sandstone and mudstone cyclicity observed at the member scale within the Skagerrak Formation (Goldsmith *et al.* 1995, 2003).

A previously published curve of climatic cyclicity (Goldsmith *et al.* 2003) suggests that the thick mudstone members of the Skagerrak Formation represent relatively wet, lacustrine or swamp depositional environments and that the intervening sandstone members represent a fluvial system that progrades and extends basinward during relatively drier climatic phases.

Goldsmith *et al.*’s (2003) interpretation would require that, during lacustrine (humid) phases when mudstones were developing in the basin centre, the fluvial system would retrograde back to the lake margins due to lake expansion, resulting in large-scale Jonathan or Julius age lake margin deltas and lacustrine shoreface facies being supplied by these high discharge (humid climate) streams. These facies types have not been observed. In summary, the logical sequence stratigraphic extension of the Goldsmith *et al.* (2003) interpretation cannot be matched with current observations and knowledge of facies types and their distributions.

The preferred interpretation outlined here advocates a reversal of the Goldsmith *et al.* (2003) climatic curve in order to better match the facies observations from core, cuttings and wireline log data as evidenced by the following:

(1) Core from the Jonathan Mudstone Member in Jade well 30/02c-J07 contains mudstone interbedded with evaporites and there is no evidence for the development of lacustrine laminites.
(2) Cuttings from the Joshua Mudstone Member in Jasmine well 30/06-07Y and from the Julius Mudstone Member on Jade both contain anhydrite.

The commonly observed symmetrical nature of the Julius Mudstone wireline log character, where the central portion is more resistive, denser and sonically faster, is highly suggestive of a more evaporite-rich, drier phase during Middle Julius times than during the transitional periods with Judy and Joanne Sandstone times.

This climatic re-interpretation invokes a semi-arid playa lake environmental interpretation for the Julius and Jonathan Mudstones, during which times the fluvial system retrogrades and is

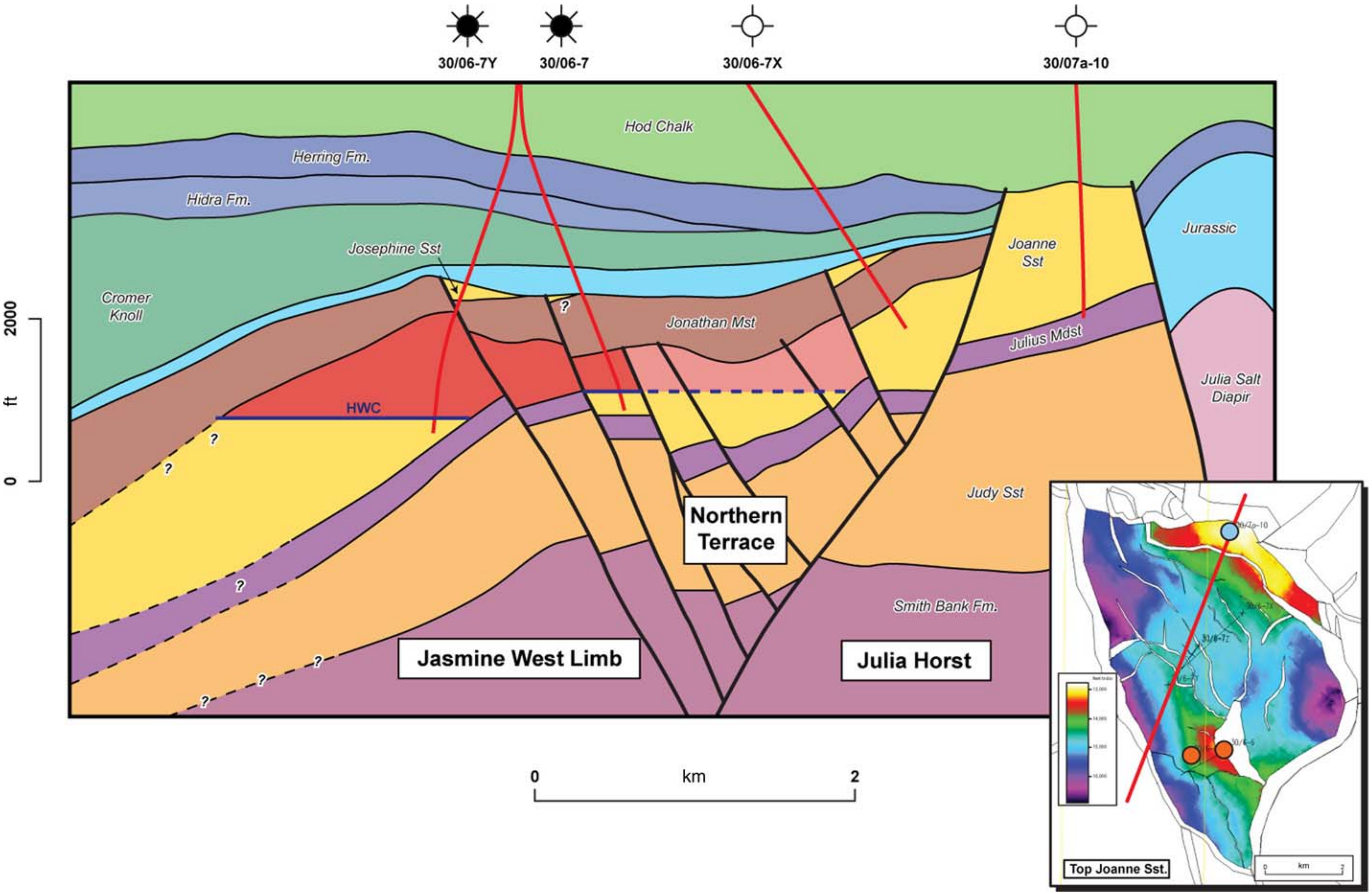

Fig. 13. Jasmine appraisal sealing conundrum.

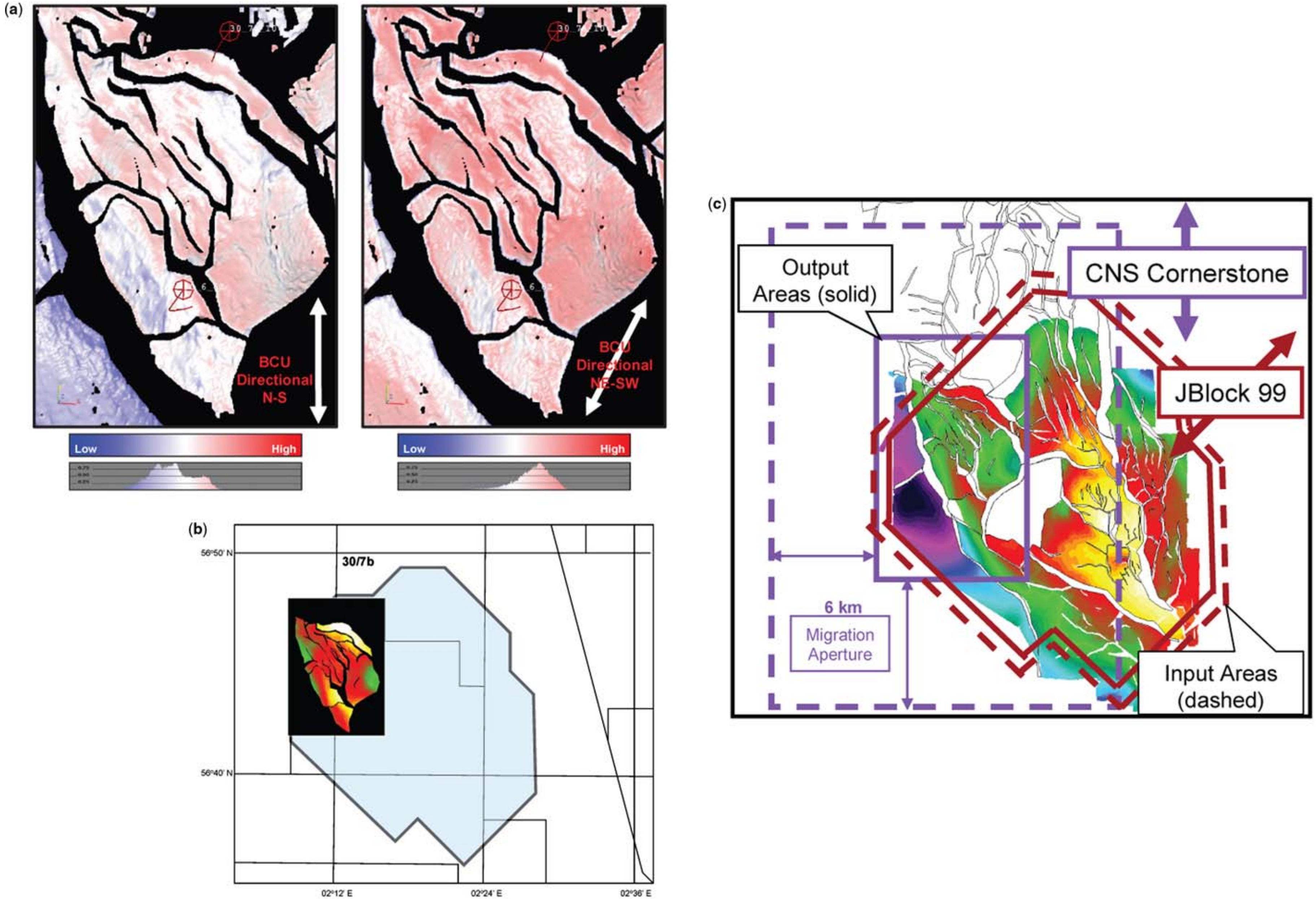

Fig. 14. Seismic reprocessing strategy. (**a**) Seismic illumination study; (**b**) J Block 99 survey acquisition area; (**c**) seismic reprocessing areas.

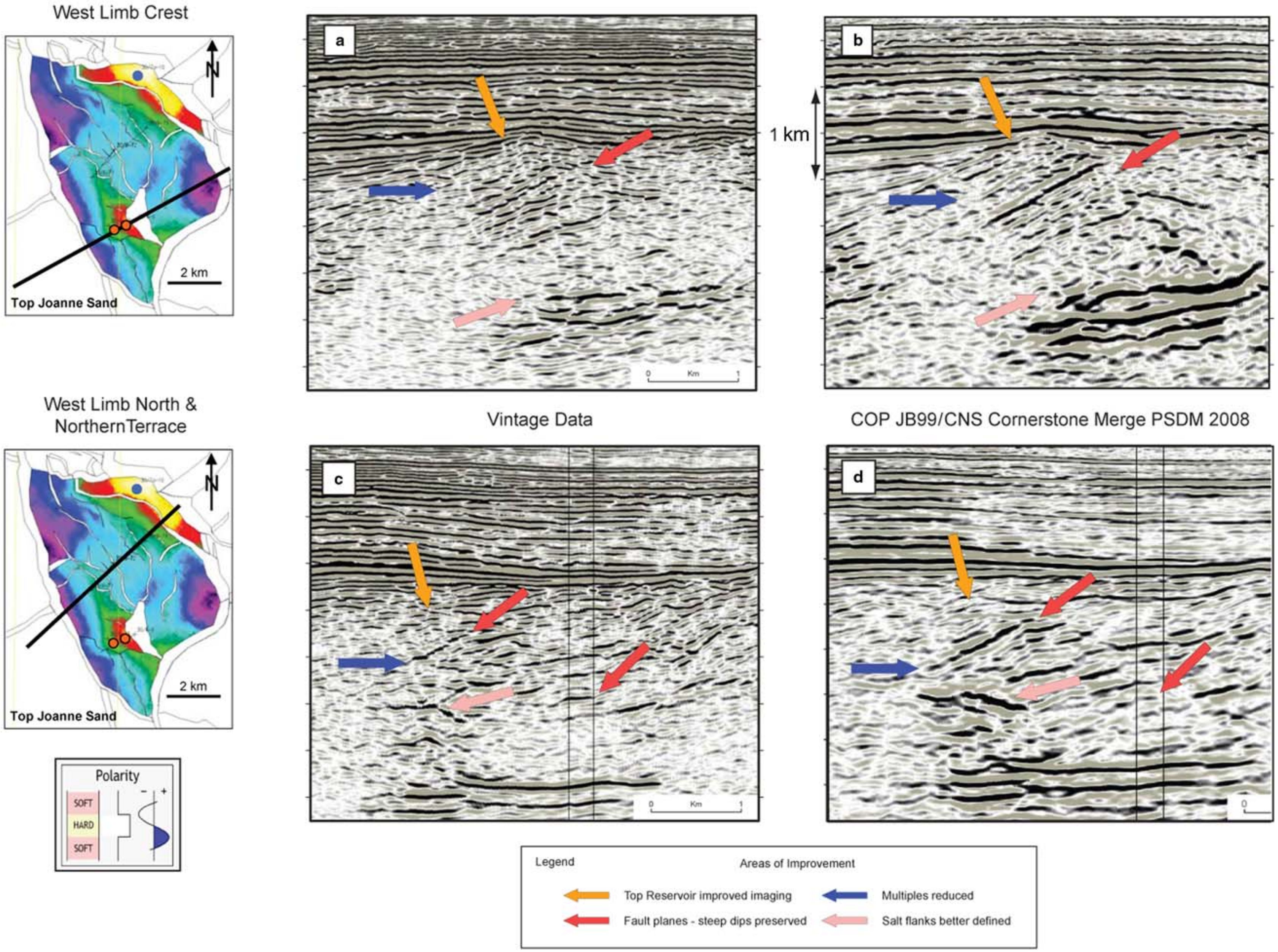

Fig. 15. Seismic reprocessing results. (**a**) Reprocessed data: dip line across West Limb crest highlighting areas of improved imaging. (**b**) Reprocessed data: interpreted dip line across West Limb. (**c**) Reprocessed data: dip line across West Limb and Northern Terrace highlighting areas of improved imaging. (**d**) Reprocessed data: interpreted dip line across West Limb and Northern Terrace.

relatively inactive and incapable of long distance sand transport. In contrast to this semi-arid climatic interpretation for the deposition of thick mudstone members, a wetter sub-humid climate for the Judy, Joanne and Josephine Sandstone Members is envisaged, where higher discharges activate and sustain a competent fluvial system during pluvial climatic phases (Fig. 16). This climatic re-interpretation introduces the possibility that the major switch on of sand supply at the base of the Skagerrak Formation (base Judy Sandstone Member) was, in part, controlled by climatic change to wetter conditions rather than being solely a progradational response to the cessation of active faulting. This major, progradation-driven, basinward shift in fluvial facies strongly suggests that the basal Judy and basal Joanne surfaces represent climatically controlled sequence boundaries.

Intra-reservoir correlation

As standard practice, both biostratigraphic and chemostratigraphic analyses have been performed. There is good agreement between the correlations made independently by the two techniques and this has given increased confidence to the presence and correlatability of the Joanne reservoir in general and, in particular, the 'Middle Joanne' shalier interval shown on the stratigraphic correlation panel (Fig. 17). The Middle Joanne unit is an informal zone that has the stratigraphic status of sub-member. The biostratigraphic pick intimately associated with the middle of the mudstone interval was made in wells 30/06-6 and -6Z. It represents the Carnian–Carnian/Norian boundary and is associated with the *Triadispora* spp. palynological occurrence.

The Middle Joanne shalier interval is only recognized within the Jasmine Field and cannot be readily correlated in a lithostratigraphic sense to either the Jade or Judy Fields. This lack of correlation between the Jasmine and Jade/Judy mini-basins is believed to have significance, and the local nature of this low net/gross interval guides the interpretation of its cause. Rather than appealing to regional scale climate or tectonics, its origin is most likely due to a local change in halokinetic accommodation space (increased rate of salt withdrawal) within the Jasmine pod. The likely controls on sedimentation within the Jasmine reservoir are summarized in Figure 16.

Reservoir zonation scheme

The Jasmine reservoir zonation scheme subdivides the Joanne Sandstone Member into three sub-members, Upper, Middle and Lower, in order to distinguish the Middle Joanne shalier interval from the higher net to gross Upper and Lower Joanne. These informal reservoir sub-divisions are shown in Figure 17.

Top Joanne. The top reservoir surface is a late Joanne age unconformity and the erosion surface is one of the key seismically observable surfaces within the Jasmine mini-basin. Reflector

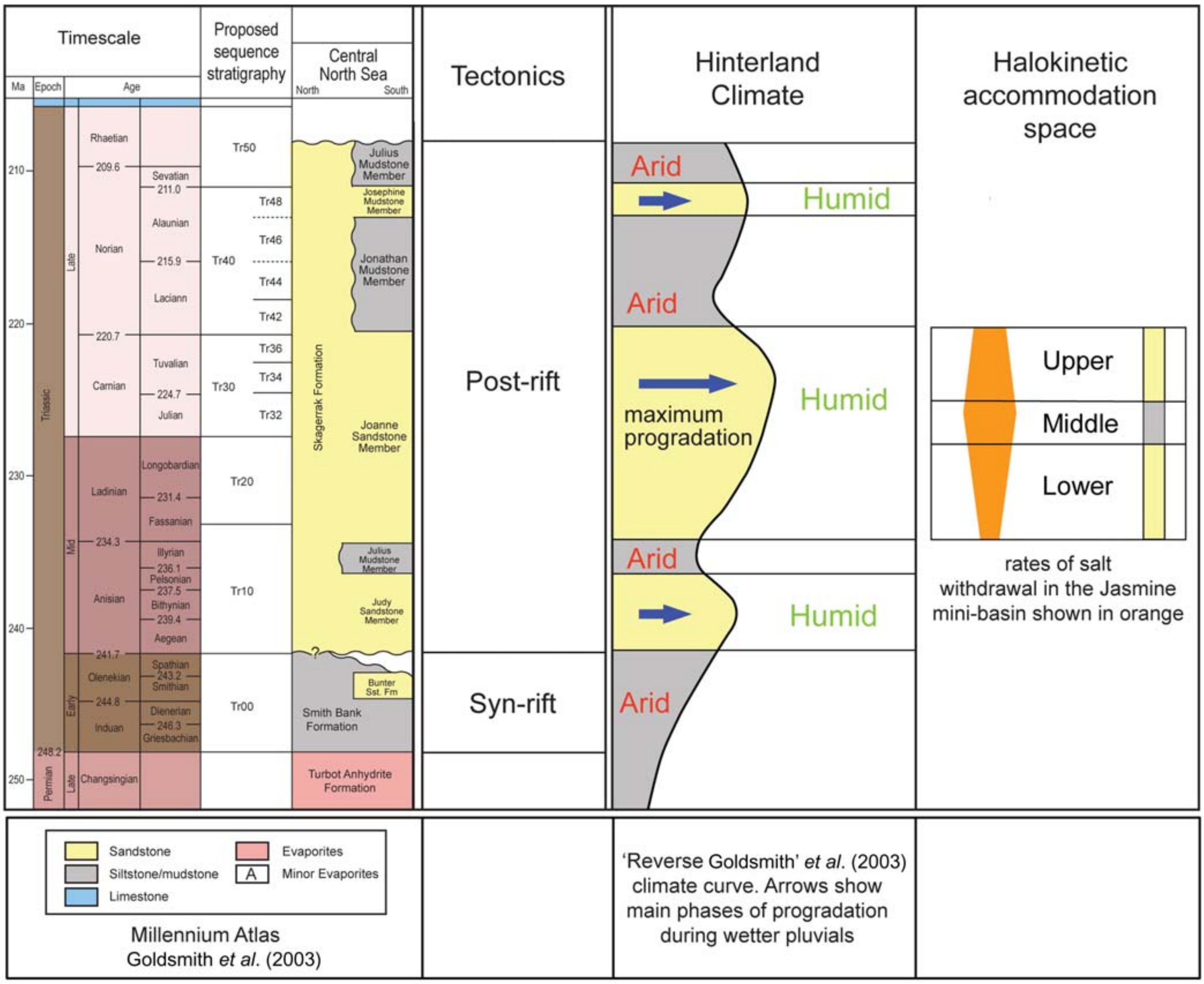

Fig. 16. Summary of controls on Skagerrak sedimentation.

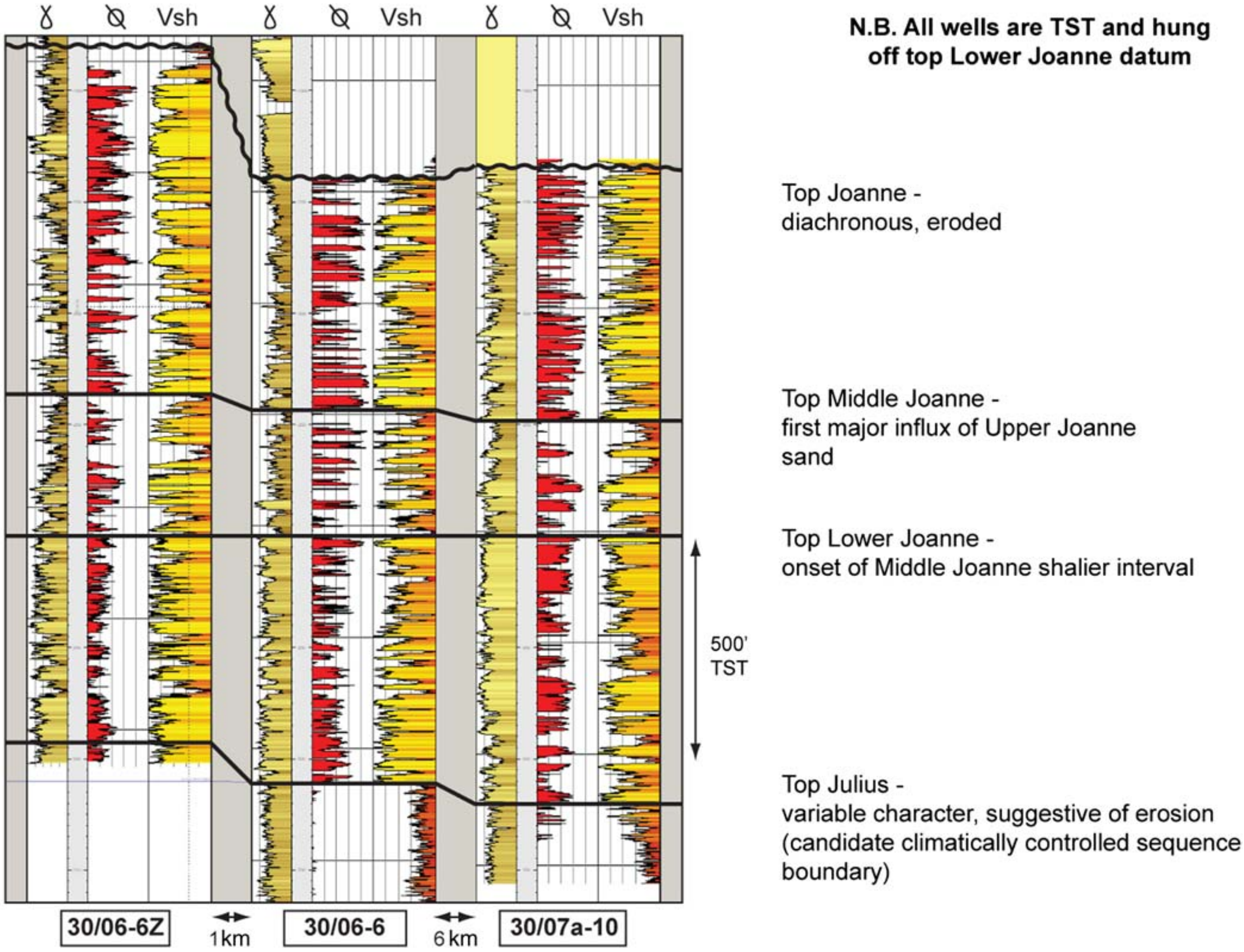

Fig. 17. 30/06-6, 30/06-6Z, 30/07a-10 well correlation panel.

truncation and the angularity of the unconformity are now imaged with increased clarity on the reprocessed seismic data. The causal mechanism behind this erosive pulse is currently not well understood, but one possible interpretation is that erosion was initiated by the grounding of the Jasmine pod. Zechstein salt, thought to have been *c.* 1500 ft thick (Goldsmith *et al.* 2003), may have evacuated sufficiently to ground the Smith Bank Formation on to the Rotliegendes. The initial weld point may have occurred locally in the area of the West Limb crest, allowing the Northern Terrace to continue subsiding, reducing the amount of missing time and ultimately allowing the development of a thicker Jonathan Mudstone.

This interpretation opens up the possibility that the initial grounding point of the pod is coincident spatially with the central, thickest part of the mini-basin, which may have the highest concentration of fluvial channels. This would lead to a predominance of high-quality channel facies within the crestal part of the field, following grounding in the Late Triassic and the Late Jurassic extension and rotation of the turtle back anticline.

In addition to the seismically observed unconformity, chemostratigraphy demonstrates that erosion has truncated the top Joanne, and that this is particularly pronounced at the crest of the West Limb core area. Erosion is less pronounced in the down-flank positions of 30/06-6Z and 30/06-7Y.

The least erosion, and therefore the most conformable relationship, between the Joanne Sandstone and the Jonathan Mudstone, is thought to exist at the 30/06-7 well. The location of this well suggests that the Northern Terrace, in contrast to the grounded West Limb, had already foundered as a relative topographic low at end Joanne times and therefore was not as prone to the end Joanne erosional pulse. The preservation of a ratty, low-porosity, Joanne/Jonathan facies transition zone at the 30/06-7 well location substantiates this model.

Top Middle Joanne. The top Middle Joanne seismic marker has been utilized in the reservoir zonation scheme and the building of the geomodel. In sequence stratigraphic terms, the top Middle Joanne surface is interpreted to be a sequence boundary. This key stratigraphic surface is characterized in wells by a sharp based fluvial channel or amalgamated channel complex, associated with cleaner, high-porosity facies and hails a return to higher net to gross. It is likely that there has been minor erosion across this surface due to a relative decrease in accommodation space. The reworking and migration of the fluvial system into and across itself has apparently increased its reservoir potential.

Top Lower Joanne. The top Lower Joanne stratigraphic surface represents the onset of Middle Joanne sand and shale deposition. The Lower Joanne interval appears to have a log character which is unique within the area. Sand bodies are blockier exhibiting box-car gamma ray (GR) motifs, slightly lower absolute GR API values and higher net to gross in general, possibly due to a greater degree of amalgamation.

Top Julius Mudstone. The Julius Mudstone generates a strong seismic response which has been interpreted with a high degree of confidence and is a key horizon in defining the Jasmine structure (see Fig. 10). The top of the mudstone defines the base of the Joanne reservoir and has been used in the Jasmine geomodel. Figure 17 shows the position of the key stratigraphic surfaces and notes the differences in wireline log character between the Upper, Middle and Lower Joanne.

Reservoir quality

The Jasmine porosity and permeability (poroperm) data broadly overlie the Jade core data from well 30/02c-4. Although not quite matching the highest porosities and permeabilities in Jade (even though Jasmine core was cut roughly 150 ft shallower than the Jade core), permeabilities of up to *c.* 800 mD are observed in the Jasmine core data. The Joanne reservoir sands encountered in the 30/06-7 core are of better quality than the reservoir sands at the same depth in 30/06-6 and 30/06-6Z discovery wells in the West Limb, as determined from wireline log data.

Reservoir quality is known to deteriorate with depth at two scales of observation. A regional trend of degradation in average porosity with depth is observed throughout the analogous fields. Additionally, there is a deterioration with depth down through the hydrocarbon column. A porosity loss gradient of *c.* 5 pu per 1000 ft occurs in sandstones in West Limb wells 30/06-6, 30/06-6Z and 30/06-7Y. This is thought to reflect increased compaction as a function of greater effective stress combined with the diagenetic effects of increasing temperature with depth.

Compartmentalization

Structural compartmentalization plays a significant role in the Jasmine Field as demonstrated by the HWC and pressure differences between the West Limb and the Northern Terrace. There is also a sealing compartment boundary between the 30/06-7 well and the 30/06-7X dry hole but it is not yet known whether this is due to structural or stratigraphic compartmentalization and trapping (the ‘Jasmine sealing conundrum’). Studies are currently ongoing to develop a predictive fault seal model.

The ‘Middle Joanne’ shalier interval may represent an important intrareservoir baffle or barrier due to a subtle increase in the volume of shale. From a reservoir performance standpoint, recognition of this lower net to gross interval is an important element to retain in the static and dynamic reservoir models used to plan the field development. Historical information regarding the lack of vertical communication within Skagerrak reservoirs of the Heron cluster was documented by McKie & Audretsch (2005) and demonstrates from the completion strategy employed that the shales were barriers to vertical flow.

The MDT pressure gradients from the hydrocarbon leg above and below the Middle Joanne in the West Limb are aligned, proving that over geological timescales the interval did not seal two separate fluid compartments. However, it is highly likely that stratigraphic compartmentalization due to the presence of the Middle Joanne shalier interval will be of importance over production timescales. This is a key issue being addressed in development well planning.

Drill stem tests

DSTs were conducted on wells 30/06-6 and 30/06-7Z. In order to reduce the risk of formation damage, both wells were perforated underbalanced.

30/06-6. The planned test programme comprised three main flow periods. A very brief post-perforation cleanup flow and initial shut-in period confirmed the reservoir pressure. This was then followed by a 12 h cleanup flow, an 18 h shut-in period, and finally a 24 h main flow followed by a 36 h shut-in period. Surface and bottom-hole fluid samples were successfully collected during cleanup and main flow periods. No water was produced during any of the production tests.

The analytical results of these data have been used to calibrate the reservoir simulation model. The pressure buildup behaviour in 30/06-6 is similar to that from other J Block wells.

Summary

The Jasmine West Limb discovery (30/06-6 and -6Z) is a major find in a mature area of the Central North Sea adjacent to existing infrastructure. Appraisal drilling (30/06-7Y) on the West Limb has reduced uncertainty of the resource estimate in the core area.

A successful appraisal test (30/06-7 and -7Z) has proven hydrocarbon presence in the adjacent Northern Terrace area. A dry hole penetration (30/06-7X) to the NE has confirmed a single drill centre development concept.

Comprehensive data acquisition has facilitated a detailed reservoir characterization programme, including seismic reprocessing, VSP acquisition, core analysis, biostratigraphy, chemostratigraphy, geomodelling, DST and MDT analyses.

Jasmine is a large and exciting discovery and is one of the most significant discoveries made on the UKCS in recent years. It represents an important resource addition for the Jasmine coventurers and the UK.

The authors wish to thank the Jasmine Coventurer Group for permission to publish this paper: ConocoPhillips (UK) Ltd, ENI UK, BG Group. Seismic data examples are courtesy of CGGVeritas. The views and interpretations contained within this paper are those of ConocoPhillips. Thanks are also due to our numerous colleagues who have worked on and helped steer the Jasmine discovery and appraisal project, including: Aberdeen – Mark Brown, Tim Carpenter, Ron Divine, Nigel Evans, Iain Mearns, Simon Phipps, Gill Ratcliffe, Andy Scott, Qing Shen, Keren Simpkin, Bob Sneddon, Colin Stevenson; Houston – Chuck Mosher, Kirk Wallace, Stephen Longshaw.

References

Barde, J. P., Chamberlain, P. *et al*. 2002. Sedimentation during halokinesis: Permo-Triassic reservoirs of the Saigak Field, Precaspian Basin, Kazakhstan. *Petroleum Geoscience*, **8**, 177–187.

Goldsmith, P. J., Rich, B. & Standring, J. 1995. Triassic stratigraphy in the South Central Graben, UK North Sea. *In*: Boldy, S. A. R. (ed.) *Permian and Triassic Rifting in Northwest Europe*. Geological Society, London, Special Publications, **91**, 123–143.

Goldsmith, P. J., Hudson, G. & Van Veen, P. 2003. Triassic. *In*: Evans, D., Graham, C., Armour, A. & Bathhurst, P. (eds) *The Millennium Atlas: Petroleum Geology of the Central and Northern North Sea*. Geological Society, London, 105–127.

Hodgson, N. A., Farnsworth, J. & Fraser, A. J. 1992. Salt-related tectonics, sedimentation and hydrocarbon plays in the Central Graben, North Sea, UKCS (United Kingdom Continental Shelf). *In*: Hardman, R. F. P. (ed.) *Exploration Britain: Geological Insights for the Next Decade*. Geological Society, London, Special Publications, **67**, 31–63.

Jones, A. D., Auld, H. A. *et al*. 2005. Jade Field: an innovative approach to high-pressure, high-temperature field development. *In*: Doré, A. G. & Vining, B. A. (eds) *Petroleum Geology: North-West Europe and Global Perspectives: Proceedings of the 6th Petroleum Geology Conference*. Geological Society, London, 269–283; doi: 10.1144/0060269.

Keller, T., Bayes, R., Auld, H. & Lines, M. 2005. Judy Field: rejuvenation through a second phase of drilling. *In*: Doré, A. G. & Vining, B. A. (eds) *Petroleum Geology: North-West Europe and Global*

Perspectives: Proceedings of the 6th Petroleum Geology Conference. Geological Society, London, 651–661; doi: 10.1144/0060651.

Matthews, W. J., Hampson, G. J., Trudgill, B. D. & Underhill, J. R. 2007. Controls on fluviolacustrine reservoir distribution and architecture in passive salt-diapir provinces: insights from outcrop analogues. *AAPG Bulletin*, **91**, 1367–1403.

McKie, T. & Audretsch, P. 2005. Depositional and structural controls on Triassic reservoir performance in the Heron Cluster, ETAP, Central North Sea. *In*: Doré, A. G. & Vining, B. A. (eds) *Petroleum Geology: North-West Europe and Global Perspectives: Proceedings of the 6th Petroleum Geology Conference*. Geological Society, London, 285–297; doi: 10.1144/0060285.

McKie, T. & Williams, B. 2009. Triassic palaeogeography and fluvial dispersal across the northwest European Basins. *Geological Journal*, **44**, 711–741.

Smith, R. I., Hodgson, N. & Fulton, M. 1993. Salt control of Triassic reservoir distribution, UKCS (UK Continental Shelf) Central North Sea. *In*: Parker, J. R. (ed.) *Petroleum Geology of NW Europe: Proceedings of the 4th Conference*. Geological Society, London, 547–557; doi: 10.1144/0040547.

Prospectivity of the T38 sequence in the Northern Judd Basin

J. M. RODRIGUEZ,[1] G. PICKERING[1] and W. J. KIRK[2]

[1]*OMV (UK) Limited, 14 Ryder Street, London SW1Y 6QB, UK (e-mail: jean.rodriguez@omv.com)*
[2]*OMV New Zealand Ltd, Level 10, Deloitte House, 10 Brandon Street, Wellington, New Zealand*

Abstract: A seismic amplitude anomaly has been identified at the Upper Paleocene T38 level in the northern Judd Basin and will be tested by the drillbit in 2009. Prospectivity at shallower levels has been largely ignored due to the fact that the main regional seal in the area was recognized to be the T35/T36 mudstones below the Kettla Tuff. Seismo-stratigraphic analysis of the T38 sequence directly above the tuff marker has identified the potential for a new play type, especially adjacent to fault zones where these mudstones are breached, allowing hydrocarbons to migrate from the Upper Jurassic source kitchen into any traps identified above the seal. In this area, the T38 is represented by a series of northerly prograding low-angle clinoforms representing the final marine infill of sediments into the basin from the south. Erosion of top sets in a more marginal setting is observed, along with deposition of basin floor fans at the toe of the prograding clinoforms. The overlying seals are basinal sediments as well as mudstones and siltstones of subsequent progradational sequences. Mild structural modification of potential stratigraphic traps in the Judd Basin occurred during the Oligo-Miocene inversion associated with continued opening of the North Atlantic. Drilling seismic amplitude anomalies in the West of Shetlands area has often been unsuccessful. Therefore, a fully integrated geophysical and geological evaluation was carried out on the T38 anomaly comprising rock physics, amplitude variation with offset analysis, fault seal analysis and the acquisition of a CSEM survey which, supported by a valid geologic model, have reduced the risk from high to moderate. The results indicate that the anomaly has the potential to be sand-bearing and contain oil and gas. It is proposed that an integrated evaluation can reduce the level of uncertainty associated with an anomaly much more effectively and so improve the chance of exploration success.

Keywords: Paleocene, Judd Basin, T38 prospectivity, seismic amplitude anomaly, rock physics, CSEM

The Judd Basin is situated to the west of the Shetland Isles and lies in the southernmost part of the Faroe–Shetland Basin. It is delineated by the Westray Fault to the north, the southern extent of the Rona Ridge to the east and the Judd High to the south. Its western limits lie close to the UK–Faroese border (Fig. 1). Water depths range from 300 to 1000 m and drilling to date has concentrated predominantly in the shallower southern and eastern areas of the basin (Smallwood & Kirk 2005).

Prospectivity in the Judd Basin has mainly focussed on sands within the Paleocene Vaila Formation, specifically the T31 through to T35 (Ebdon *et al.* 1995; Fig. 2), which are the main producing reservoirs in the area (Lamers & Carmichael 1999). These sands produce oil from the Foinaven, Loyal and Schiehallion Fields (Cooper *et al.* 1999; Leach *et al.* 1999) and are the reservoir in the Suilven discovery (Fig. 3). Both Foinaven and Schiehallion fields have stratigraphic and structural elements and are associated with strong amplitude anomalies, which have an amplitude variation with offset (AVO) response. To date, production in the basin has been from below the main sealing mudstones of the upper Vaila and lower Lamba Formations (T35 and T36), the top of which is well represented by the Kettla Tuff marker on 3D seismic data. A new potential play has been identified by the OMV-led partnership above the Kettla Tuff within the T38 clinoforms of the upper Lamba Formation and is defined by a strong seismic anomaly believed to be associated with a toe of slope fan that is hydrocarbon filled.

Many amplitude anomalies previously drilled in the area have been unsuccessful (Smallwood & Kirk 2005; Loizou *et al.* 2008). The object of this paper is to discuss the T38 play identified in the northern Judd Basin and the various studies which were undertaken in order to reduce the risk on prospectivity.

Stratigraphy

The stratigraphy of the Judd Basin is shown in Figure 2 (Ebdon *et al.* 1995). Many of the wells drilled in the area only penetrated Cenozoic sediments. A few wells which have drilled deeper into the Jurassic and basement were located on structural highs. Well 204/15-2 drilled into Basement on the southern part of the Nave High and identified 234 m of Upper Jurassic shales, silts and sands with shows indicating the presence of an Upper Jurassic source rock in the eastern part of the area. Well 204/19-1 drilled into the Westray Ridge and encountered basement and thick Jurassic sands with oil shows. In the south of the basin, to the west of Foinaven, there are two wells (204/23-1 and 204/22-1), which encountered basement with oil and gas shows as well as Upper Jurassic shales (Fig. 3).

During the Cretaceous, extension and deposition appear to have been directed NE, away from the Judd area, towards the main part of the Faroe–Shetland Basin. As a result the Cretaceous is relatively thin. However, by the Cenozoic, extension and sedimentation had also migrated westward. Strongly influenced by the underlying Cretaceous topography, the basin had become a focus for thick aggradational sequences from the Scottish-Shetland mainland, which was undergoing uplift due to extensive volcanism. The geometry of the Judd Basin was asymmetric with the main depocentre located in the west, affected by significant syn-sedimentary growth on the hanging wall of the Westray Fault within the Faroese sector. Early deposition was focussed in this area with deep water marine sediments (T10–T30s) sourced from the Judd High to the south as well as from the Rona Ridge further to the east. This is reflected in the distribution of coarser clastic deposits in the western part of the basin with predominantly

VINING, B. A. & PICKERING, S. C. (eds) *Petroleum Geology: From Mature Basins to New Frontiers – Proceedings of the 7th Petroleum Geology Conference*, 245–259. DOI: 10.1144/0070245

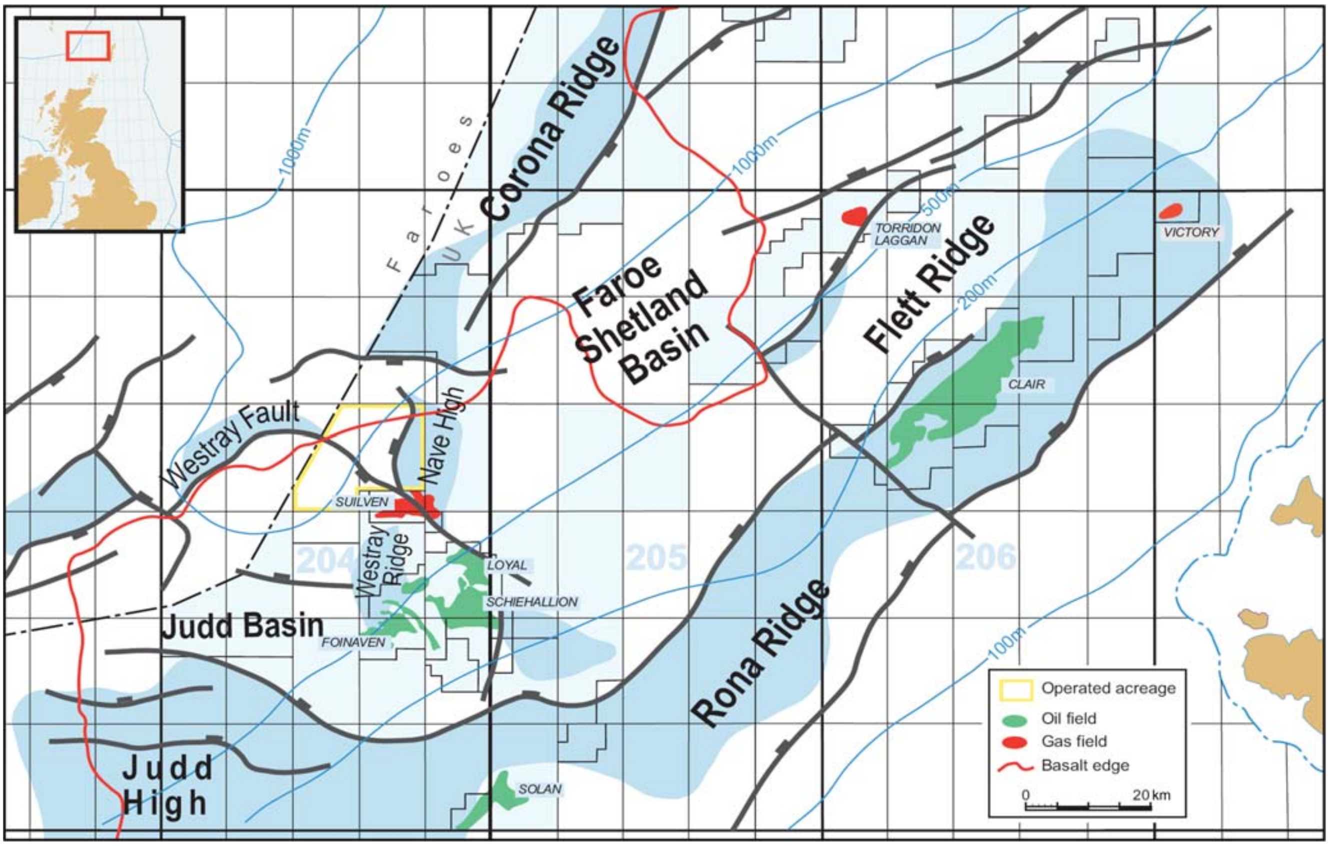

Fig. 1. West of Shetlands area structural elements.

finer-grained sediments laid down further east in a more slope setting.

By the T35, thick mudstones were deposited in the eastern part of the basin, providing the main top seal for the Foinaven and Schiehallion oil producing fields. During the T36 interval, several thick sandy fans, sourced from the south, were deposited into the basin in response to renewed uplift. In the area of interest (North Judd Basin) the Kintail fan is observed thickening towards the NW and pinching out eastwards towards the Westray Ridge. Above the Kintail fan lies the key seismic marker of the Kettla Tuff (T36 Andrew Tuff equivalent). This marks a major change from aggradational infilling to the onset of progradation as additional sediment continues to be shed from the Scottish mainland to the east. In this part of the Judd Basin, progradation is from the south/SE and the T38 interval is represented by a series of predominantly mud-prone, low-angled clinoforms. Several local rises and falls of relative sea-level are recorded during this time as topsets, where preserved, appear to lie at slightly varying heights. The height of the clinoforms indicates that the palaeowater depth was a minimum of 200 m. Toe of slope sands are also observed within the progradational sequences in response to the various relative sea-level falls, for example, 204/18-1, probably as a result of local pulses in sediment input and minor activity along the Westray Fault.

In the northern Judd Basin, erosion of the T38 top sets (204/18-1, Fig. 4) heralds the onset of a more deltaic/paralic environment of deposition represented by sand, mudstone and lignite sediments of the T45-50 sequence (Fig. 2), as the basin progressively fills from the south/SE. Further west, sedimentation interfingers with volcanic lava flows, which take advantage of any topographic lows. After the T50 interval, the basin becomes once again inundated with marine sediments as the basin subsided following ongoing extension further to the NW in response to continued opening of the North Atlantic.

Structure

The main structural trend in the Faroe–Shetland Basin is dominantly NE/SW, derived from an earlier Late Cretaceous rifting phase (Dean *et al.* 1999; Fig. 1). Aeromagnetic data show clearly the main basins and highs within the Faroe Shetland area and the main NE/SW trend of these structures, such as the Corona Ridge and the Rona Ridge (Fig. 5).

In the Judd Basin, the structural grain becomes increasingly east–west, where the NE/SW trend is offset dextrally by the Judd High and Westray Ridge during the Paleocene (Dean *et al.* 1999). These east–west faults not only impact sediment direction into the basin but are also fundamental to trap formation of the Foinaven and Schiehallion fields (Smallwood & Kirk 2005). The NE/SW trend in the northern part of the Judd Basin is also broken up orthogonally by NW/SE lineaments, such as the eastern extent of the Westray Fault. Here it offsets the Westray Ridge to the south from the Nave High to the north (Fig. 1). Close to the Faroes border the fault system becomes increasingly broken up and subsequently alters direction to become SW/NE trending in its western part within the Faroes area. These faults were reactivated transtensionally throughout the Paleocene (Doré *et al.* 1999) and overprint the pre-existing tectonic fabric by modifying and offsetting earlier faulting.

Paleocene lava flows and accompanying sills and dykes are found in the westernmost part of the Judd Basin within the Flett Formation (T40-45) and were emplaced in response to the extensional breakup of the North Atlantic. Finally, inversion of the basin occurred during the Oligo-Miocene along the Westray and Judd Faults in response to extension switching further westwards and to a lesser extent the buttressing effect caused by the impact, on a larger scale, of Alpine compression in western Europe (Doré *et al.* 1999). Plio-Pleistocene effects can also be observed in the

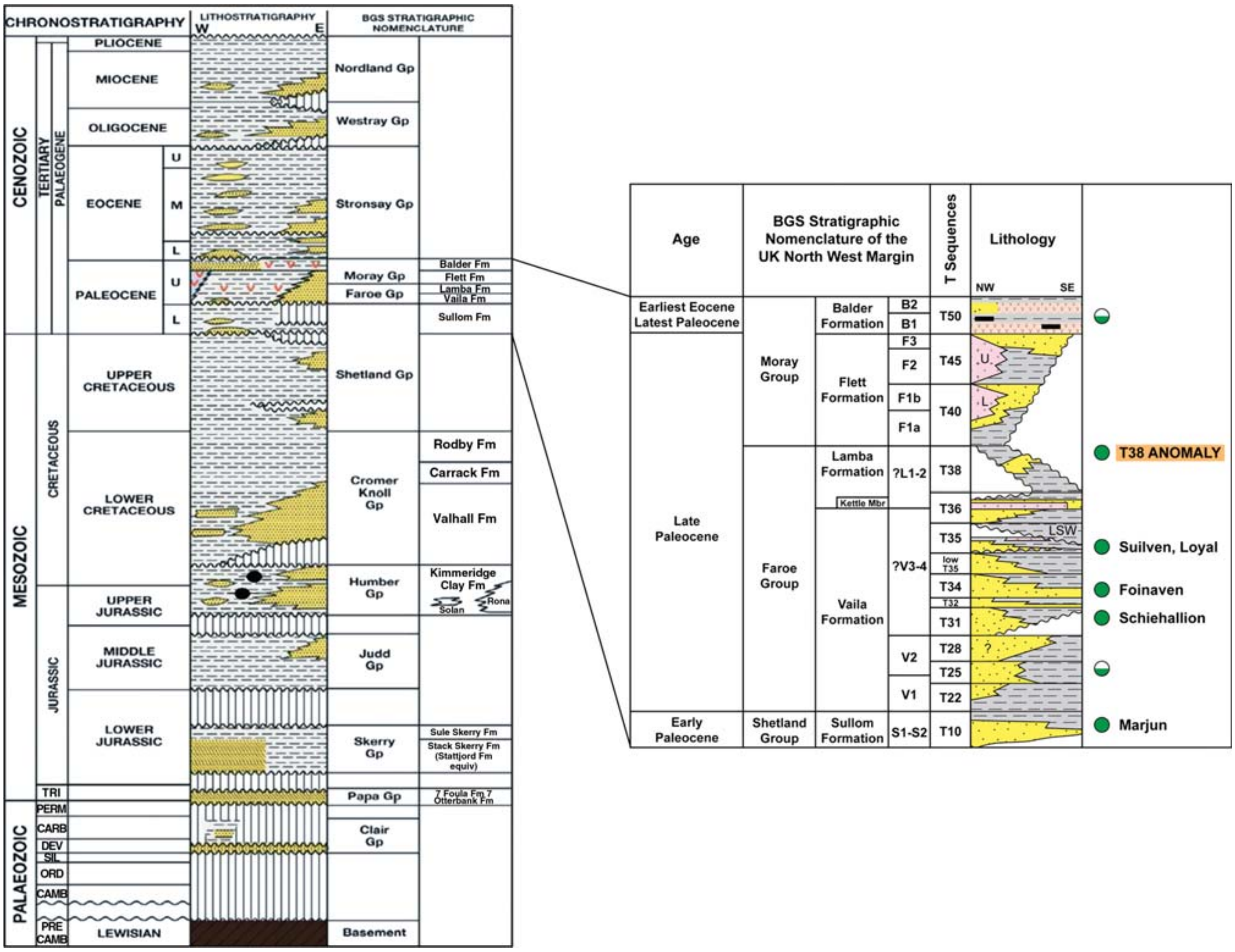

Fig. 2. Stratigraphic column of the Judd Basin. After Smallwood & Kirk (2005).

area at the sea bed attributed to glacial erosion and isostatic adjustment (Fig. 6).

Main prospectivity in the Judd Basin

The main prospectivity in the Judd Basin to date has been within the aggradational sequences of the T31 to T35 (Foinaven, Schiehallion). Lying at depths of approximately 2000–2200 m below the seabed and capped by the main seal in the area (the T35/T36 mudstones), prospectivity has predominantly targeted the pre-Kettla Tuff (T36) sediments. Most wells in the basin contain sand with shows only below this level, with the exception of 204/25a-2, a south Schiehallion exploration well, which has recorded oil from the T50/T45 (Fig. 3) and, more significantly,

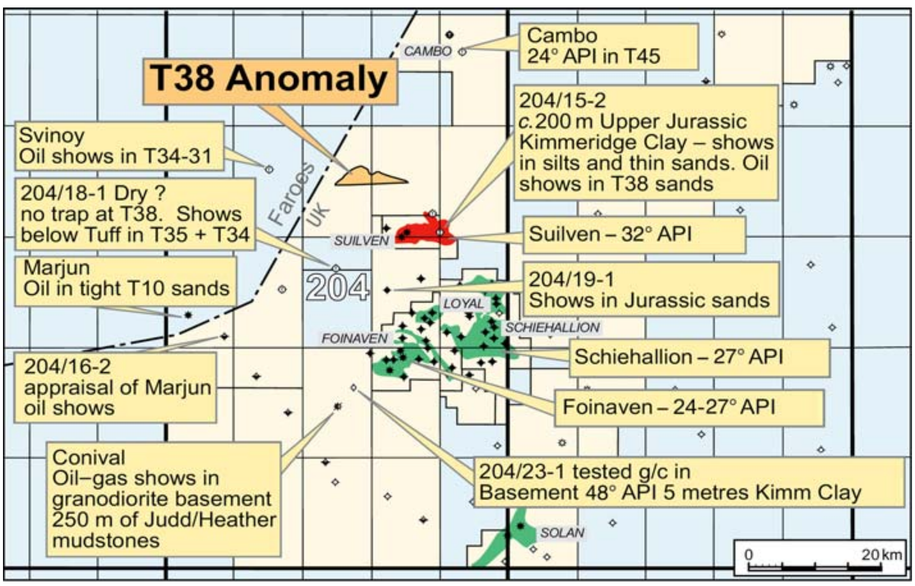

Fig. 3. Hydrocarbon occurrences in the Judd Basin.

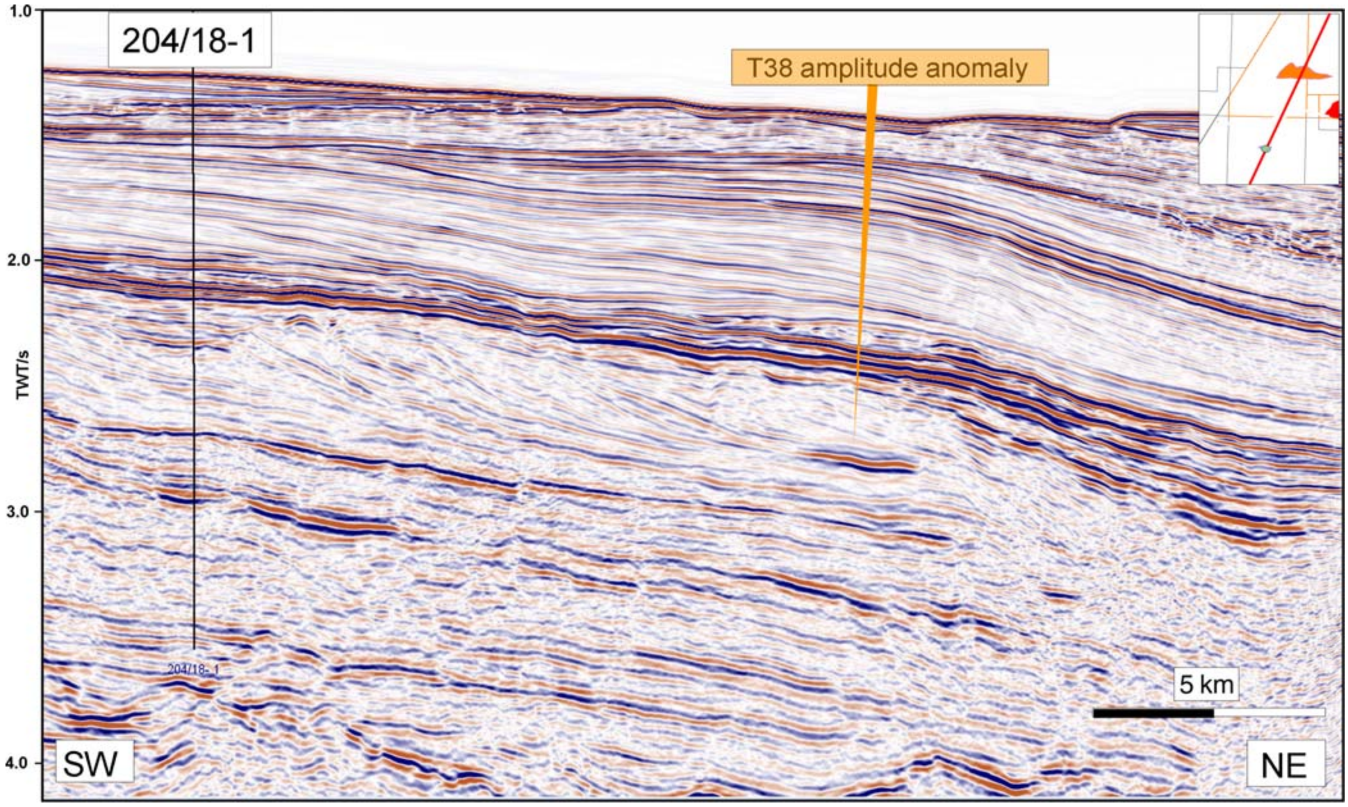

Fig. 4. SW/NE seismic 2D line through the T38 anomaly and well 204/18-1. Red, negative; black, positive.

204/15-2, which has oil shows in thin T38 sands. Both Foinaven and Schiehallion fields are combined structural/stratigraphic traps. Trapping is aided by a general easterly pinchout of the Paleocene sands and by the fact that, during the T25–T35 interval, sands were being deposited in a slope environment, sometimes within confined channels. These fields are represented by amplitudes on seismic which demonstrate a Class 3 AVO effect (i.e. a brightening with offset) in response to the fluid content (and more commonly related to a gas effect) within the reservoir sands. The eastern flank of Schiehallion is defined by the amplitude shutoff and represents the sand pinchout edge. An amplitude shutoff is also clearly observed in parts of the western limit of the field where

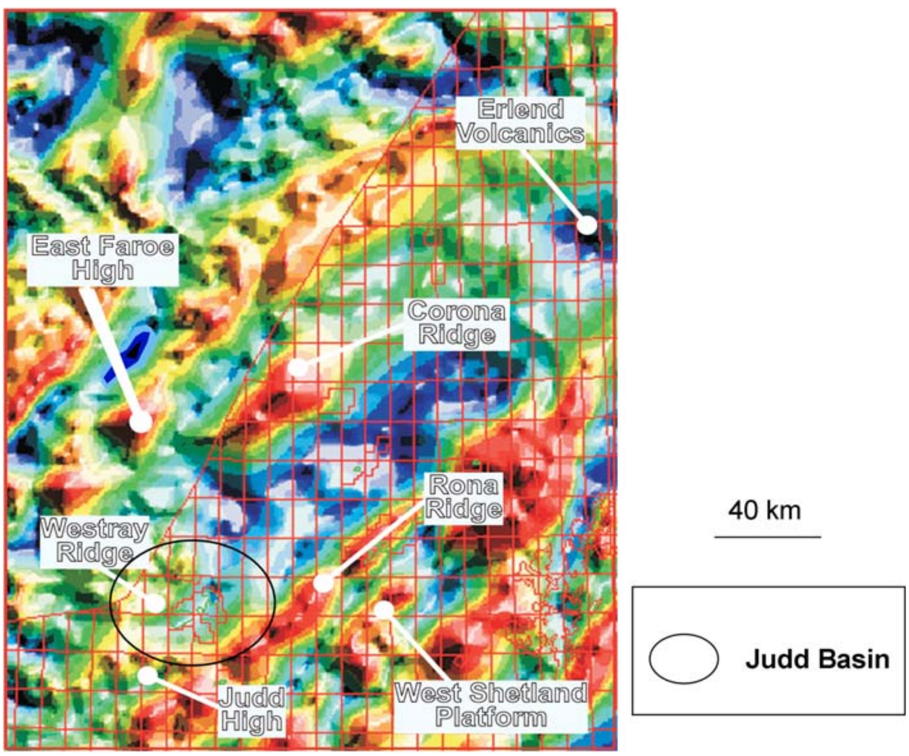

Fig. 5. Aeromagnetic map over the southern part of the West of Shetlands Area. Red, high; blue, low.

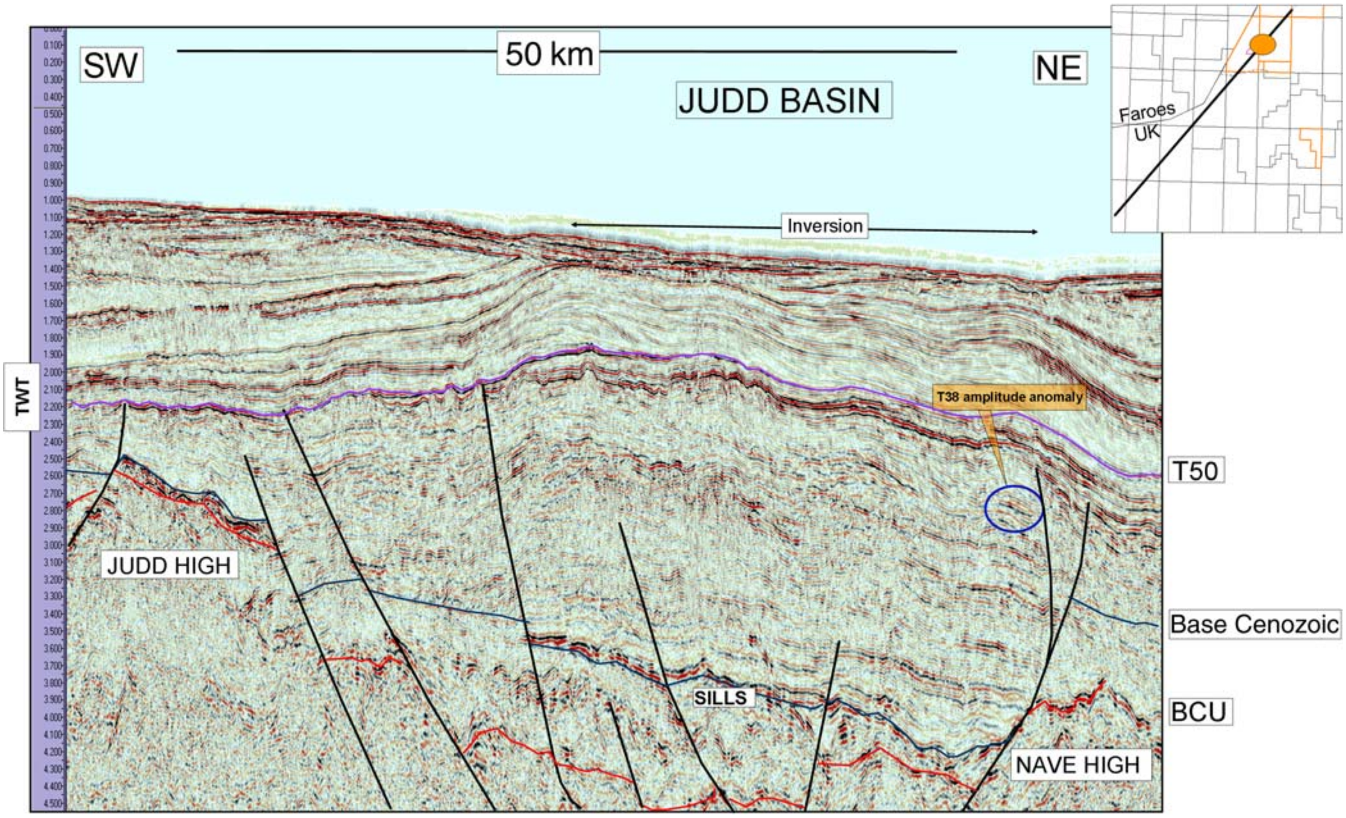

Fig. 6. SW/NE regional seismic line over the Judd Basin showing the basin inversion and the T38 seismic anomaly. Red, negative; black, positive. Courtesy of CGGVeritas.

the T31 sands pass below the oil water contact, confirming the transition from oil to water (Fig. 7).

These oil-producing fields lie in the SE part of the Judd Basin with Foinaven located above the Westray Ridge and Schiehallion further to the east. Understanding the structure as well as the depositional history is key to understanding the prospectivity of the area, especially the sealing, trapping and migration potential within the Judd Basin.

T38 prospectivity within the Lamba formation and reducing the level of uncertainty

Within the T38 sequence of the northern Judd Basin, a significant seismic amplitude anomaly has been identified which has been studied and observed for a number of years by previous operators in the area. Straddling two licences and previously lying mostly within the former ‘White Zone’ (Faroe/UK disputed area) in water depths of over 1000 m, it is only within the last couple of years that this anomaly has been fully licensed to the OMV-led partnership.

Seismic coverage over the area is good, with a 3D seismic survey shot by CGGVeritas in 1998, which has since been reprocessed several times, most recently in 2008. In addition a proprietary 2D 6 km cable seismic survey was shot in 2005 by OMV, which was aimed specifically at the anomaly and tied directly into wells, which lay upslope to the south (204/18-1), and SE (204/14-2).

In the West of Shetlands area, several wells have drilled seismic amplitude anomalies but failed to find hydrocarbons. These were found to be due to a variety of reasons such as the presence of seismic artefacts (such as multiples and tuning effects), tight sands, high-porosity water-wet sands, shale velocity anisotropy and igneous rocks (Smallwood & Kirk 2005; Loizou *et al.* 2008). As a result, several studies have been undertaken to better understand the amplitude anomaly in an attempt to reduce the risk before going ahead to drill in an area of deep water and harsh environmental conditions. It is considered that a more integrated approach to the evaluation of such an amplitude anomaly should reduce the chance of encountering some of these pitfalls.

This paper does not attempt to discuss the techniques but will concentrate on the value the results have had in reducing the level of uncertainty associated with the T38 seismic amplitude anomaly. The following summarizes the results and inferences based on the studies carried out.

Reservoir

As a new play, understanding the environment of deposition is a major key to identifying reservoir presence. The paucity of wells within the northern Judd Basin and the distances away of the few wells from the anomaly imply that the stratigraphy is not fully defined and the possibility of encountering tuffs and intrusives within the target zone is still a concern. However, an attempt has been made to place the anomaly within a recognizable stratigraphic framework.

The analogue well for the prospect is 204/18-1, which lies approximately 12 km to the south of the amplitude anomaly in a marginally more updip location. At the well, there is a 118 m (gross) T38 sand interval, which has an average porosity of 26% and a net to gross (N/G) of 0.8 (Fig. 8), that is interpreted as a base of slope fan at the toe of a series of prograding clinoforms (G. Bertram, pers. comm. 2006). Figure 4 shows a 2D line passing through well 204/18-1 and the T38 anomaly, and demonstrates clearly the similarity in its depositional setting, although the anomaly is slightly younger. The seismic line also demonstrates that the water-wet sands in the well are barely visible on the reflection data.

Regional mapping suggests that the sand is sourced from the south and west from channels which cut down into the top sets of

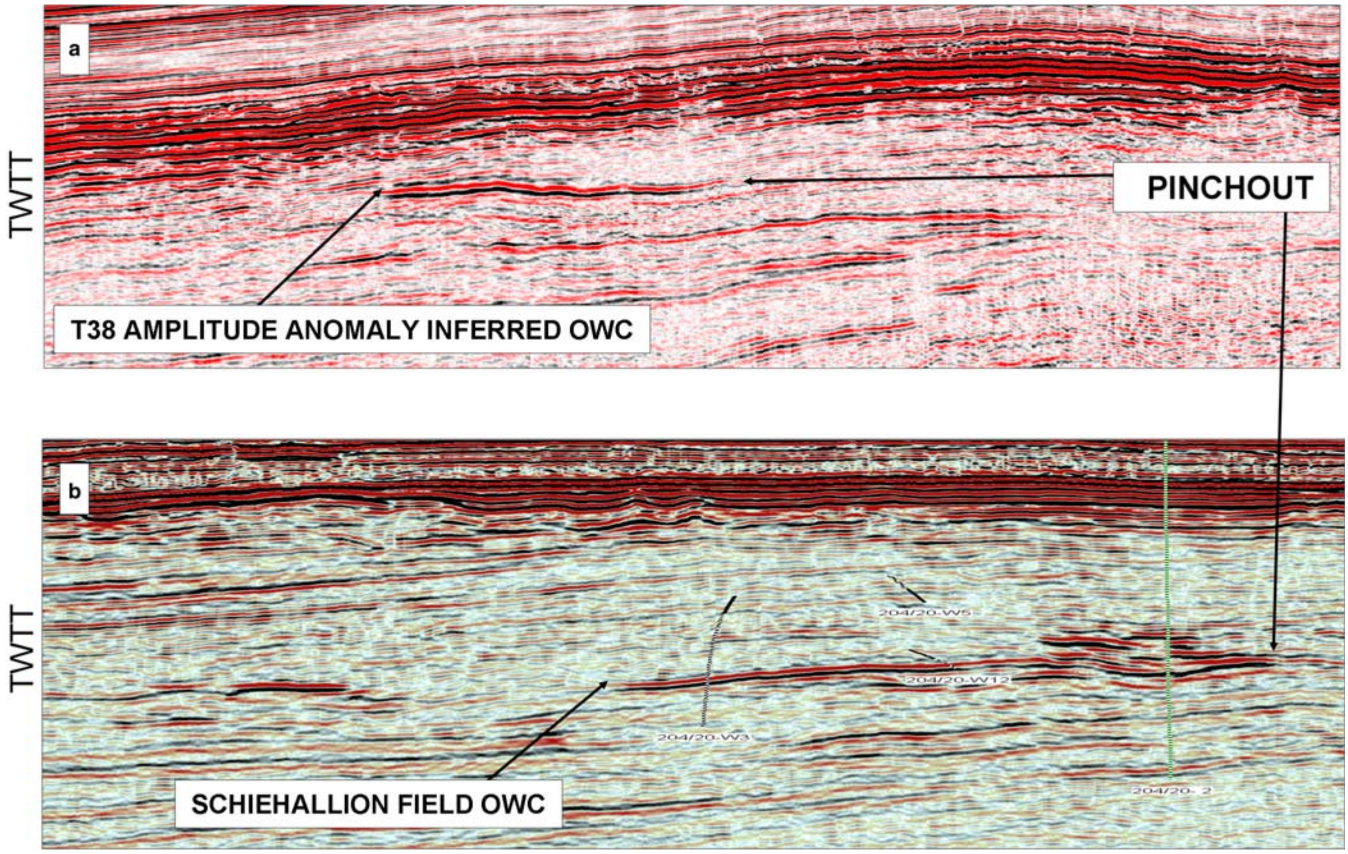

Fig. 7. 3D seismic lines showing the amplitude shutoff at the OWC and pinchout edge. Comparison of (**a**) the T38 anomaly with (**b**) the Schiehallion Field. Red/brown, negative; black, positive. Depths are comparable at approx 2500 m tvdss.

the progrades (such as the one observed in 204/18-1, illustrated in Fig. 4). The interpretation indicates the presence of a sand channel trending NW–SE from the shelf, cutting down into the top sets of the clinoforms. These sands flow into an embayment where its eastern limits are defined by the structural expression of the Nave High and are reworked from the west at the toe of slope (Fig. 9) by basin floor currents. Similar aged sands within a comparable depositional setting have also been observed at the Svinoy well

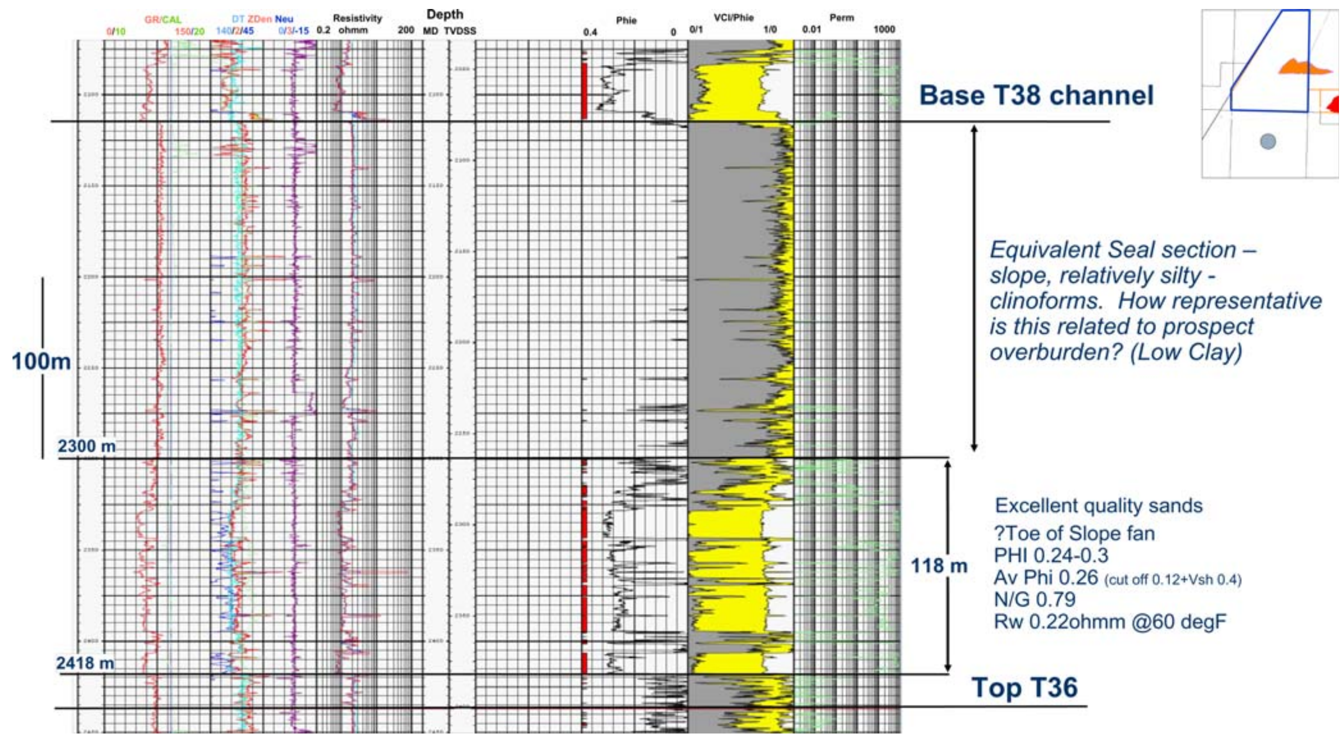

Fig. 8. Well 204/18-1 (reservoir analogue for the T38 anomaly).

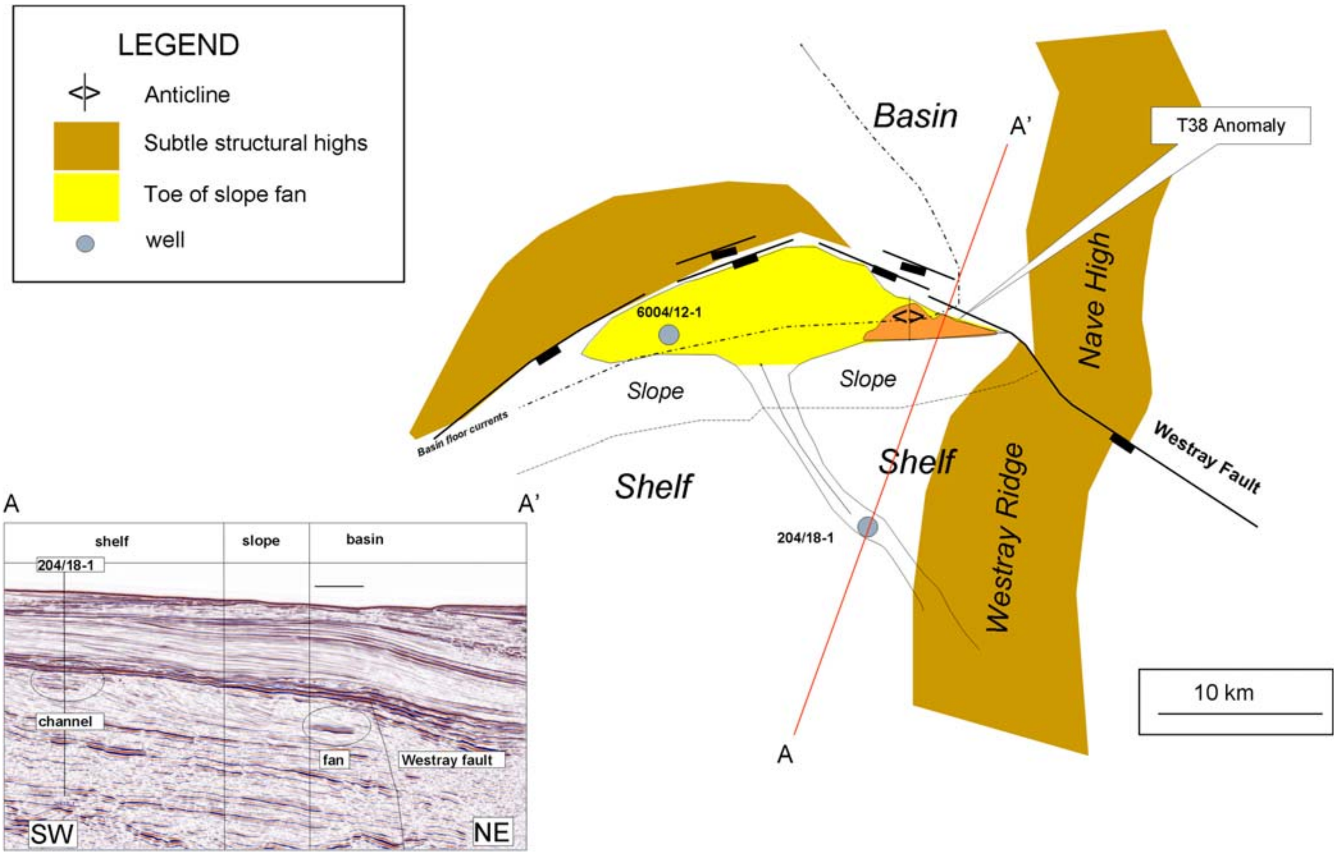

Fig. 9. Depositional concept.

(6004/12-1) further to the west in the Faroes sector. Both the sand in the 204/18-1 well and the amplitude anomaly (or prospect) lie at comparable depths and, therefore, it is considered that the quality of the reservoir will be similar.

The risk that the prospect could be predominantly shale-prone still remains (Johannessen & Steel 2005). However, the Judd Basin is observed to be predominantly sandy away from the slope. The presence of the T38 sand in the 204/18-1 well, in a similar depositional setting, and at Svinoy, as well as the observation of significant later T38 channels downcutting into the top sets, supports the presence of sand input at this time. The top sets also appear to be relatively flat, suggesting that the shelf would not have acted as a barrier to these sands being deposited into the basin.

Trap

The prospect can be mapped as a seismic event which has a soft kick, as demonstrated by detailed wavelet extraction and well-to-seismic ties from nearby wells. Identified as a combination trap, the prospect has a three-way dip closure with a stratigraphic pinchout to the south.

The seismic amplitude anomaly is strongly conformable with structure to the west, where the sand is interpreted to be thicker. This is consistent with a model of sands originating from a westerly direction (Fig. 10). The anomaly conformance with structure is not as evident to the north and east. There are several explanations for this. Surface channels over the anomaly may cause the amplitude event to break up to some degree. However, it is believed that the main cause is due to the sands pinching out in response to the presence of the Nave High – the northerly extension of the Westray Ridge. Comparisons with Schiehallion, approximately 30 km to the SE, can be made with respect to the pinchout of the sands and the resulting amplitude switchoff (Fig. 7), as well as a clear amplitude with depth shutoff observed in the NW segment of the field, where sheet/amalgamated channel sands pass below the oil–water contact (Leach *et al.* 1999).

Seismic amplitudes hint at the presence of the possible sand below the oil–water contact towards the west of the anomaly. This is consistent with the assumption that the source for the sands is controlled from a channel further to the west of the anomaly.

The southerly limit is abrupt. Although it may be possible to invoke a minor southern fault over part of the anomaly, the amplitude shutoff against the toe of the clinoforms is predominantly stratigraphic. The low-angle progrades imply the presence of fine-grained sediments, which act as side and base seals to the inferred sand body.

Hydrocarbon sourcing

Although there are some minor hydrocarbon shows identified below the regional T35/T36 seal, the T38 analogue sands in the 204/18-1 well were found to be dry. Figure 3 shows hydrocarbon occurrences of released wells in the Judd Basin. From the distribution of hydrocarbon shows, it can be demonstrated clearly that there is an extensive petroleum system working within the whole of the Judd Basin. As discussed, the majority of the hydrocarbon occurrences are reservoired within sandstones below the regional seal (the T35/T36 mudstones). However, as mentioned earlier, there are a few wells where hydrocarbons have migrated up into shallower reservoirs, such as in the 204/25a-2 exploration well, which was drilled in the southern part of the Schiehallion field. Most importantly, well 204/15-2, which drilled through the Westray Fault, encountered a thin 5 m T38 sand with significant oil shows and supports the model of charging proposed in this paper.

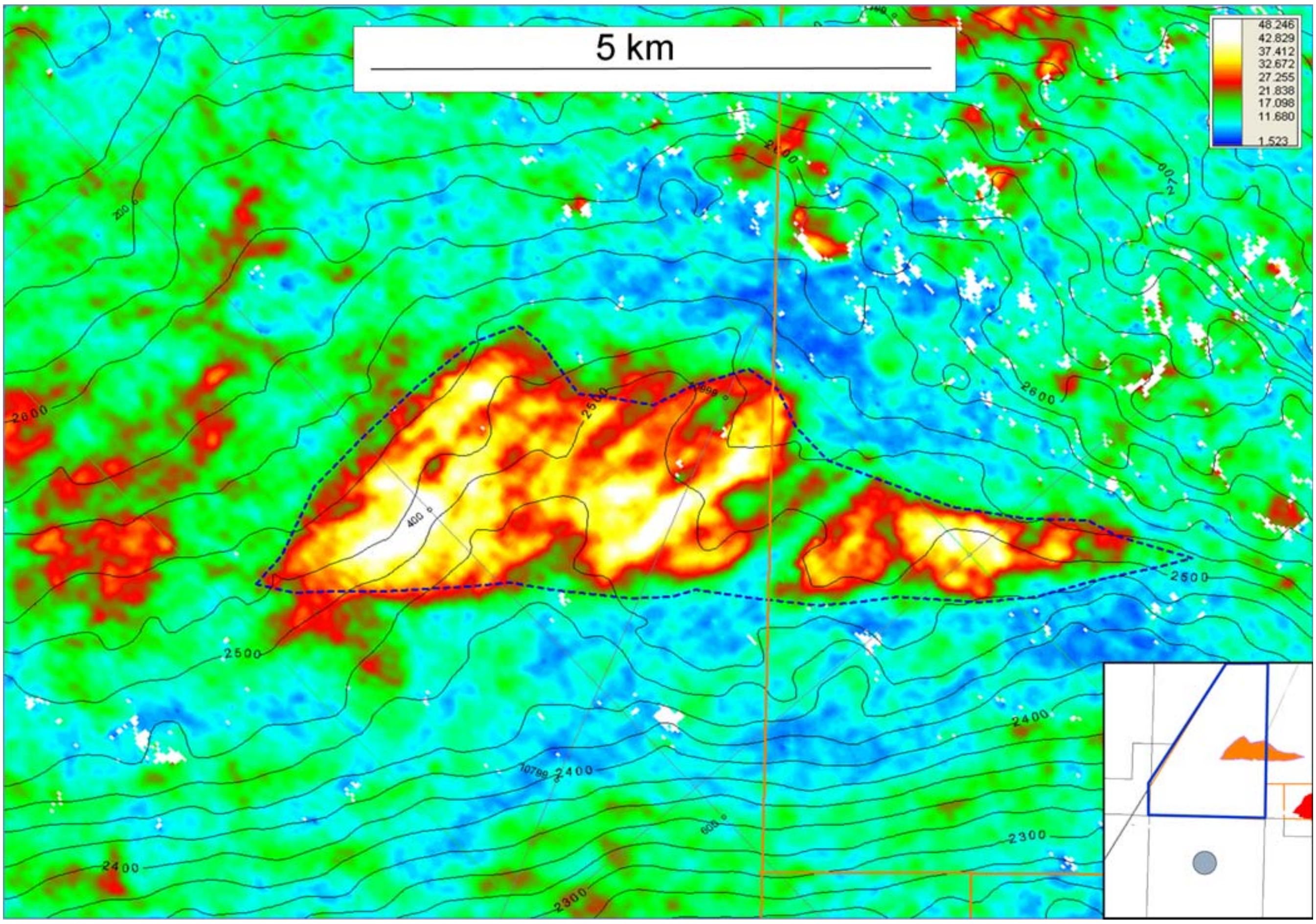

Fig. 10. T38 seismic anomaly: map showing amplitude variation and depth. Contour interval: 20 m. Courtesy of CGGVeritas.

A study undertaken in order to understand the potential sourcing of hydrocarbons into the anomaly focused specifically on how the Westray Fault system could impact migration. The main Westray Fault lies directly to the north and east of the prospect. An important difference between the T38 prospect and the T38 sand body at the 204/18-1 well is that the latter does not appear to be plumbed in to a fault system, which has broken through the regional seal. Additionally, minor antithetic faults associated with the Westray Fault can be observed clearly on seismic to penetrate the prospect without apparently breaching up into the overlying T45 sediments (Fig. 11). It is inferred from observation that the equivalent sands within the 204/18-1 well are either not plumbed in to a migration system and the regional seal is effective, or the sands have no updip seal. However, without further investigation, it is uncertain why these sands failed to trap hydrocarbons.

The Judd Basin is a predominantly oil-prone basin, unlike the Flett Basin further to the NE, which is gas-prone due to the greater depth of burial of the Upper Jurassic Kimmeridge Clay source rock. However, there have been various studies that have tried to accommodate the overwhelming presence of oil discoveries and the occasional presence of gas chimneys in the Judd Basin to one which has been modelled to be predominantly generating gas. The *motel* (Lamers & Carmichael 1999) and the *whoopee-cushion* (Iliffe *et al.* 1999) models are two which have tried to resolve this conundrum. Other models (Carr & Scotchman 2003; Carr *et al.* 2009) have tried varying the amount of overpressure as well as the temperature in response to basin history and the effects of extension, volcanism and inversion. A modelled pseudo-well just to the south of the T38 anomaly in block 204/13 predicts the Kimmeridge Clay source rock to be late mature for oil generation (Carr & Scotchman 2003) based on extensive retardation caused by highly overpressured source rocks.

Suilven, an oil and gas discovery in the T35 interval, also lies directly south of the Westray Fault but unlike the T38 anomaly is situated close to the eastern part of the Nave High. Normally, hydrocarbons require sand-to-sand juxtaposition against the fault in order to migrate into the highest sand below the regional seal (Clarke *et al.* 2005). It was modelled that hydrocarbons could readily migrate into the T35 reservoir by this process, as the Paleocene sediments below are predominantly sandy.

Conversely, it was found that, although the fault system penetrated the base of the T38 amplitude anomaly, it appeared that the regional seal was not breached. There was insufficient throw to provide potential sand-to-sand juxtaposition for hydrocarbon migration based on this model. However, by modelling parallel flow, that is, an open Westray Fault system which acts as a conduit to flow, the T38 anomaly could be charged. The history of this fault system is complex, but it is not inconceivable that part of the network could become capable of allowing parallel flow during the transtensional–transcompressional phases associated with the Oligo-Miocene inversion of the basin. The presence of oil in thin T38 sands in well 204/15-2 (Fig. 3) supports this model.

Interestingly, it was also observed that Suilven located just to the SW of the Faroe–Shetland Basin was in a favourable position to be additionally sourced from the NE. This could explain why the discovery is one of the few accumulations in the area that is predominantly gas with oil, where hydrocarbons are sourced not only from the gas-prone Flett area but also from the oil-prone Judd Basin.

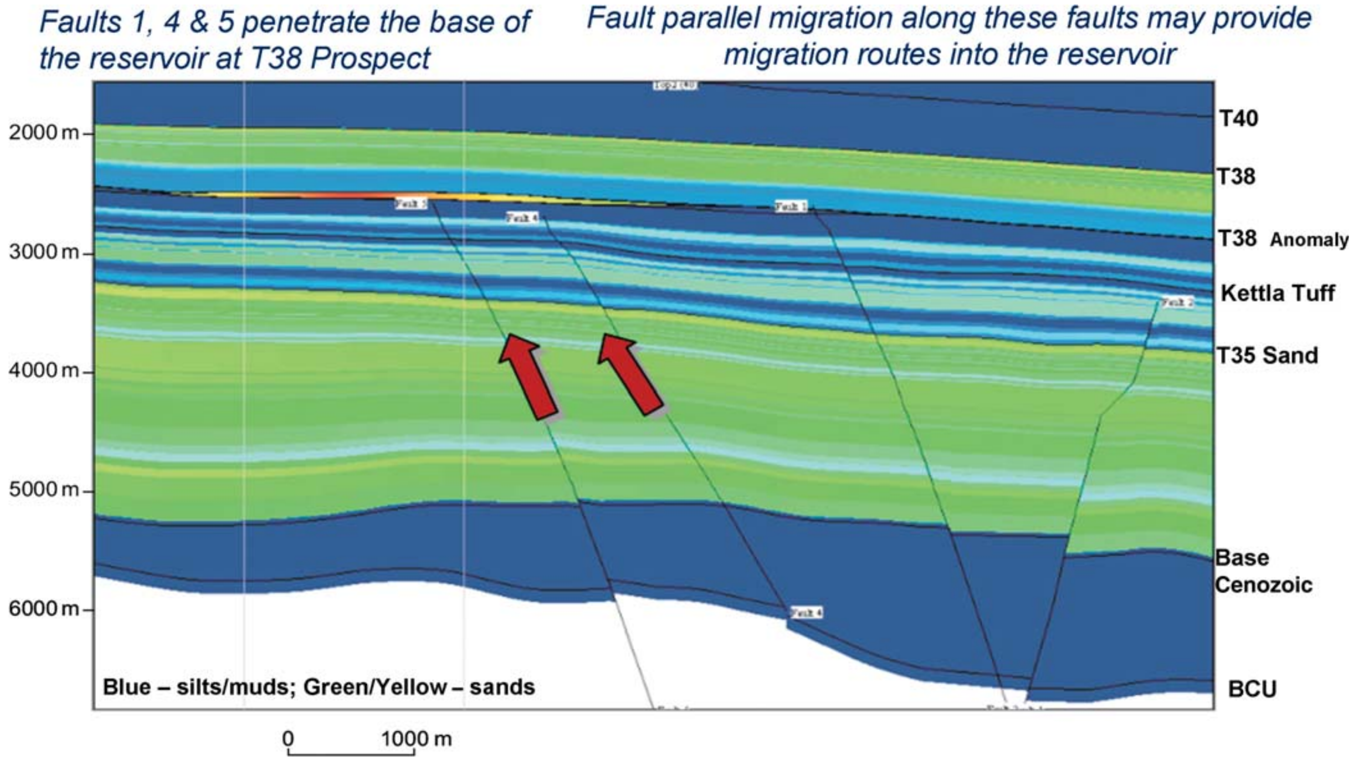

Fig. 11. Oil Migration model: fault parallel migration into the T38 anomaly along the Westray Fault system.

One observation from the study was that, if the fault system became open, then the anomaly could easily be charged by the faults that penetrated its base. It is also possible that the regional seal may be breached to the north of the prospect, for example, downdip from the anomaly in an area not covered by the study. One point that appears to tie in with the rock physics work was that, if the anomaly was no longer plumbed in to the migration system, then the likelihood of the fluid phase being oil was greater.

Seal

The sealing capacity of the overburden comprising the clinoforms and the integrity of the pinchout edge were considered major risks to the success of the prospect. A further study was undertaken on the overburden based on cuttings and sidewall cores from three local wells, 204/18-1, 204/14b-1 and 204/14b-2. In addition, a core from comparable mudstones was used to calibrate the rock strength as some of the sidewall cores had degenerated and cuttings were not suitable. The lithology of the clinoforms from cuttings and sidewall cores was a mixture of siltstone with minor mudstone. Very few silty sands were observed, which supported the assumption made from the seismic that the clinoforms were predominantly composed of finer grained sediment (G. Bertram, pers. comm. 2006).

The results of the study were encouraging. Two clay types were modelled: low clay (predominantly siltstone) and high clay (predominantly mudstone). In the case of the cap rock comprising predominantly silt or low clay, the model indicated that a 150 m column of relatively heavy oil (*c.* 25° API) or a 40 m column of gas could be trapped at the T38 anomaly. In a mudstone or high clay case, the column height increased to a 1000 m column of heavy oil or 270 m column of gas. This latter case is unlikely as the column mapped from the crest to the interpreted shutoff is in the order of 90 m and the crude is anticipated to be relatively heavy, of the order of around 25° API, similar to the Foinaven and Schiehallion fields, which lie at comparable depths below the seafloor. Therefore, the results of the analysis indicate that the top seal could provide sufficient sealing potential for the T38 anomaly and these results can be supported by the column represented by the anomaly observed on the seismic. Furthermore, it was also observed that none of the samples analysed reached the critical brittle index of 2, indicating that the cap rock is unlikely to be subject to brittle fracture and thus be less likely to continually leak hydrocarbons through fractures.

Rock physics analysis

As the interest in this prospect was initially driven by the existence of the seismic amplitude anomaly, it is critical to understand the nature of the seismic response and to try and match it with possible lithological and fluid scenarios. The methods used for this can be characterized as either inversion – using the seismic reflectivity data to create attribute volumes, which can then be related to likely geological cases – or forward modelling – taking a geological case and modelling seismic data and comparing the results to the real seismic. The two approaches have been used for the area, on both re-processed 3D seismic and the longer offset 2D data acquired by OMV. It is beyond the scope of this paper to discuss all the work in detail; however the key results can be summarized:

(1) the seismic amplitude anomaly is present on both the 3D and 2D data and is maintained in the re-processing, so the risk that it is an artefact of either acquisition or processing is very low;
(2) the AVO behaviour of the seismic anomaly is similar on all the datasets; this is an anomaly that has weak near-stack response and strong far-stack response, with any downdip extension of the 'body' having a weak seismic response on both stacks;
(3) the polarity of the anomaly is best modelled by a decrease in impedance with a low Poisson ratio, thus reducing the risk that the cause is either volcanic (high impedance) or a coal (high Poisson ratio).

With these properties in mind, a sand body, probably hydrocarbon-filled, seems a reasonable explanation. A key aspect is whether the anomaly represents the entirety of the sand body, or whether it extends downdip as an aquifer, which appears to be more likely from both the seismic evidence and geological context. If the anomaly represents the entire body then the nature of the fluid is more difficult to determine. If the body extends downdip then the body must give rise to low amplitude when water-filled, with a high far-stack response only when hydrocarbon-filled. This makes conventional gas saturation less likely, as this would have a high (soft kick) near-stack response if the water response is weak in the same sand, but does not preclude a low saturation (*c*. 10–15%) gas. However, a low saturation gas accumulation would not give rise to any resistivity anomaly on the controlled-source electromagnetic (CSEM) survey (see next section). The proposed model of an oil-filled sand body would produce a CSEM anomaly and fits with the seismic observations.

More detailed modelling of such an oil-filled sand body was carried out to try to match the more detailed amplitude variations. These suggested that there were some tuning effects, due to both thinning sands updip and with the contact proposed as the cause of the amplitude 'shut-off' downdip. They are shown in Figure 12, with the background properties extrapolated from the 204/14-2 well and the prospect geobody based on the previous inversion outputs adjusted to optimize the match with the seismic response. A contact was created in the geobody to provide an oil and water leg using standard fluid substitution techniques. The principal seismic used was the OMV 2-D data, which both tied the 204/14-2 well and provided better offset data due to the longer cable used in the acquisition. The modelled and real data from near- and far-angle stacks are shown in Figures 13–17. This shows that the model correctly predicts the low near-stack response in both the oil and water legs of the geobody, with an increase in the far-stack response for the oil leg. The more detailed amplitude match was improved by varying the thickness of the geobody within the oil leg to create a larger degree of tuning. This gave the increased far-stack amplitude approaching the crest of the geobody, and also the secondary increase near the contact where tuning with the OWC occurs. It was also confirmation that a variable sand thickness was present over the structure and that resource estimates needed to take this into account.

CSEM survey

A two-line CSEM survey was acquired over the T38 anomaly with one of the lines passing through the Suilven discovery. To optimize the results, these lines were positioned over the widest part of the anomaly to get the best coverage of data. The method used to analyse the results required that a background model be first built based on the lithology and general structure along the lines chosen. Resistivity values for the expected lithologies were input into the model and, therefore, some assumptions had to be made, especially in the shallower sections where no well data were available. The structure is also quite complex and the model had to deal with shallow seafloor wedging as well as the anticline in the northern part of the Judd inversion. Any resistive anomalies obtained from the CSEM-acquired data which were not part of the background model were highlighted and investigated.

Results from the CSEM line, which also passes through the Suilven discovery, are shown in Figure 18. The results indicate an anomaly at the T38 prospect and to a lesser extent over Suilven. It is possible to observe an effect from Suilven, but this is quite weak due to the fact that the analysis was focussed on the T38 seismic anomaly, which lies approximately 600 m shallower. In addition, the T35 oil- and gas-bearing sands at Suilven have relatively low resistivity readings, not getting much above 20 Ω m and reflect poorer quality reservoirs with correspondingly higher water saturations.

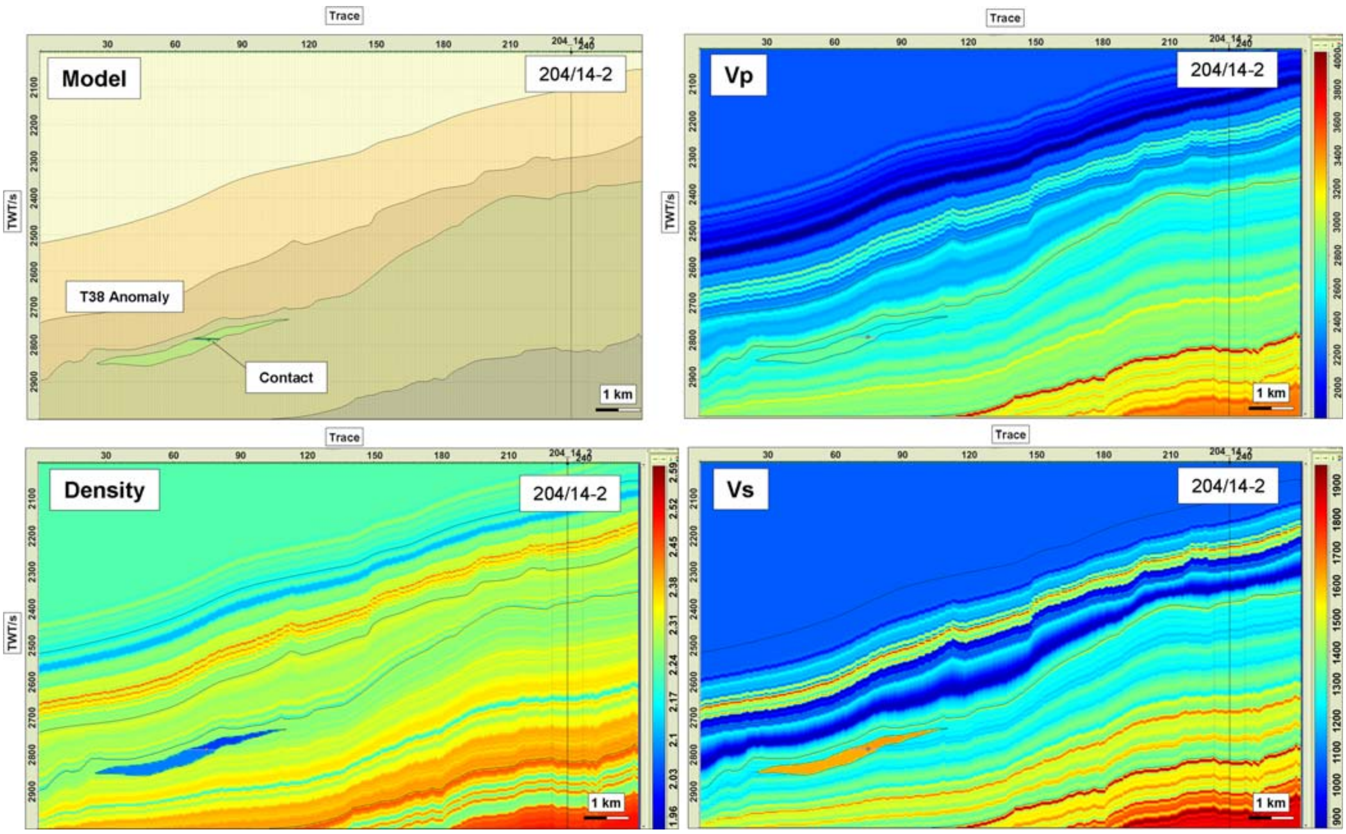

Fig. 12. T38 seismic model also showing VP, VS and density.

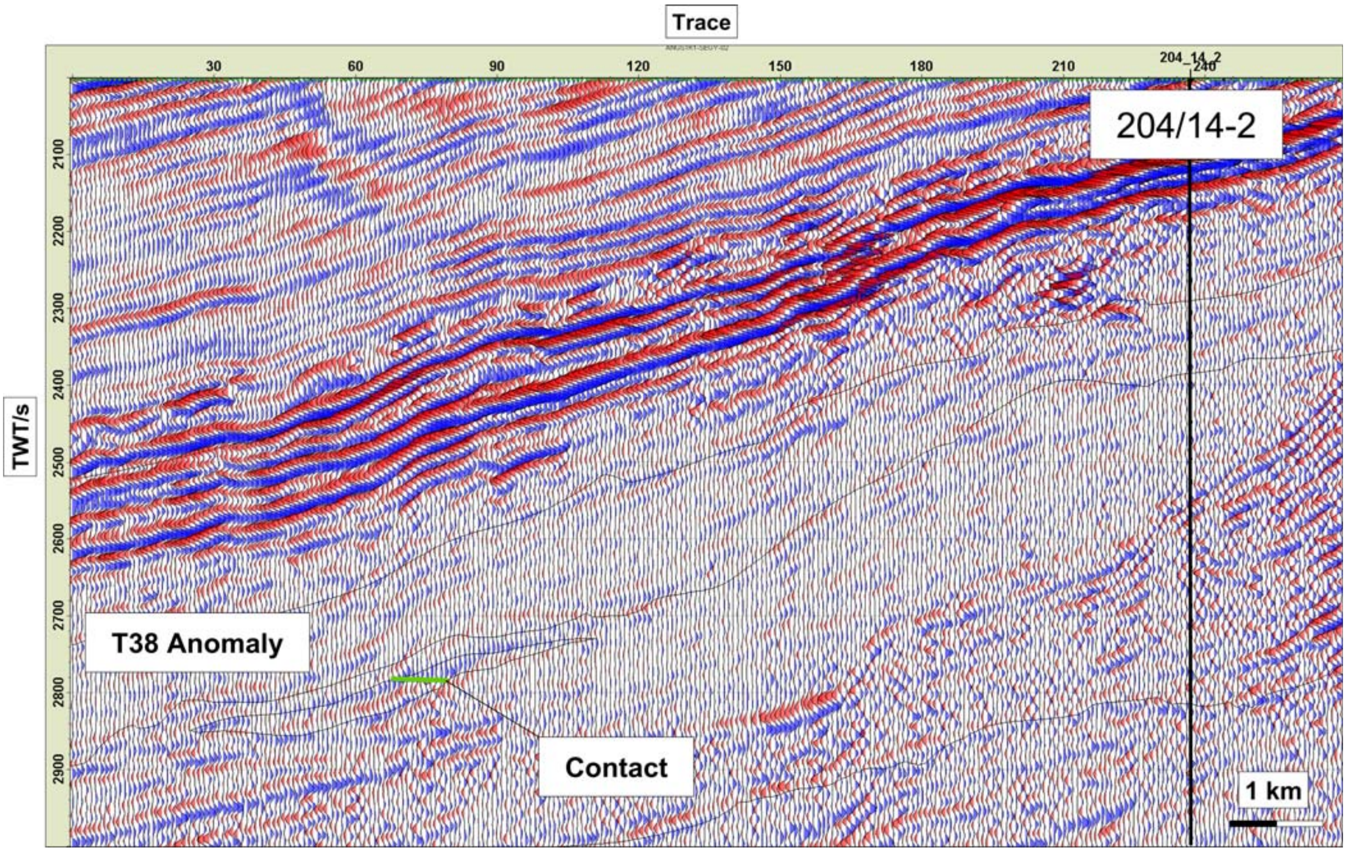

Fig. 13. OMV05-2 near-stack 3–13°.

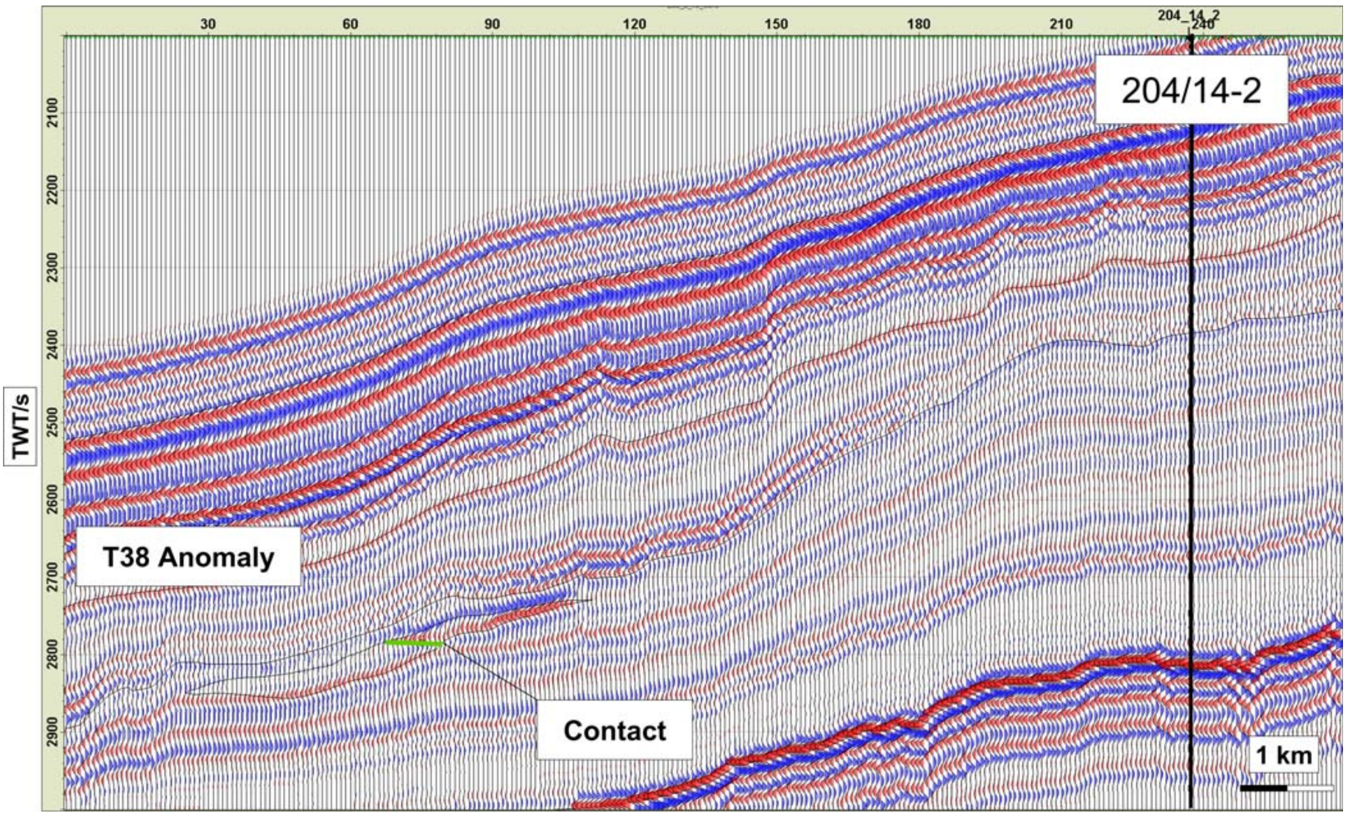

Fig. 14. Model near-stack (oil).

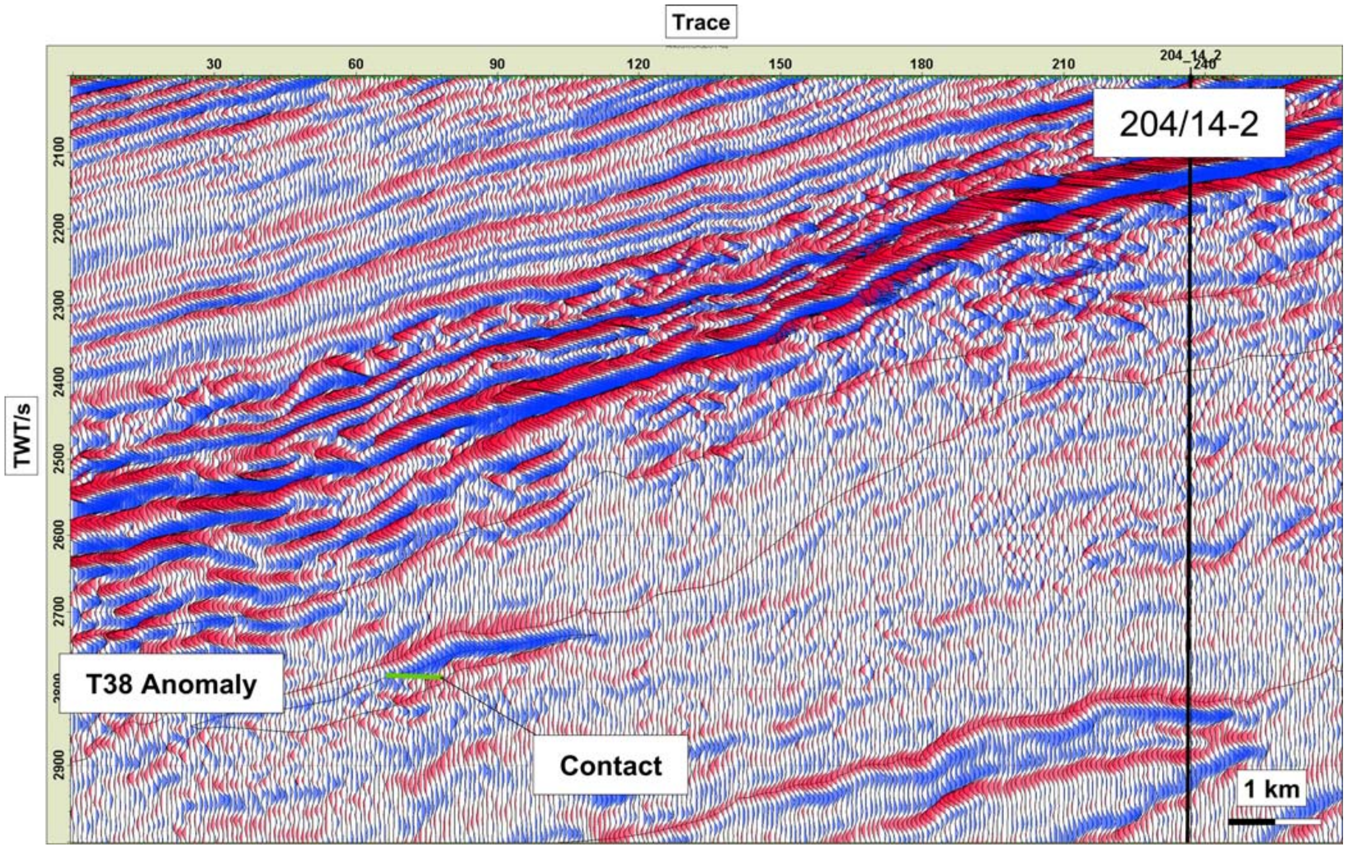

Fig. 15. OMV05-2 far-stack 25–35°.

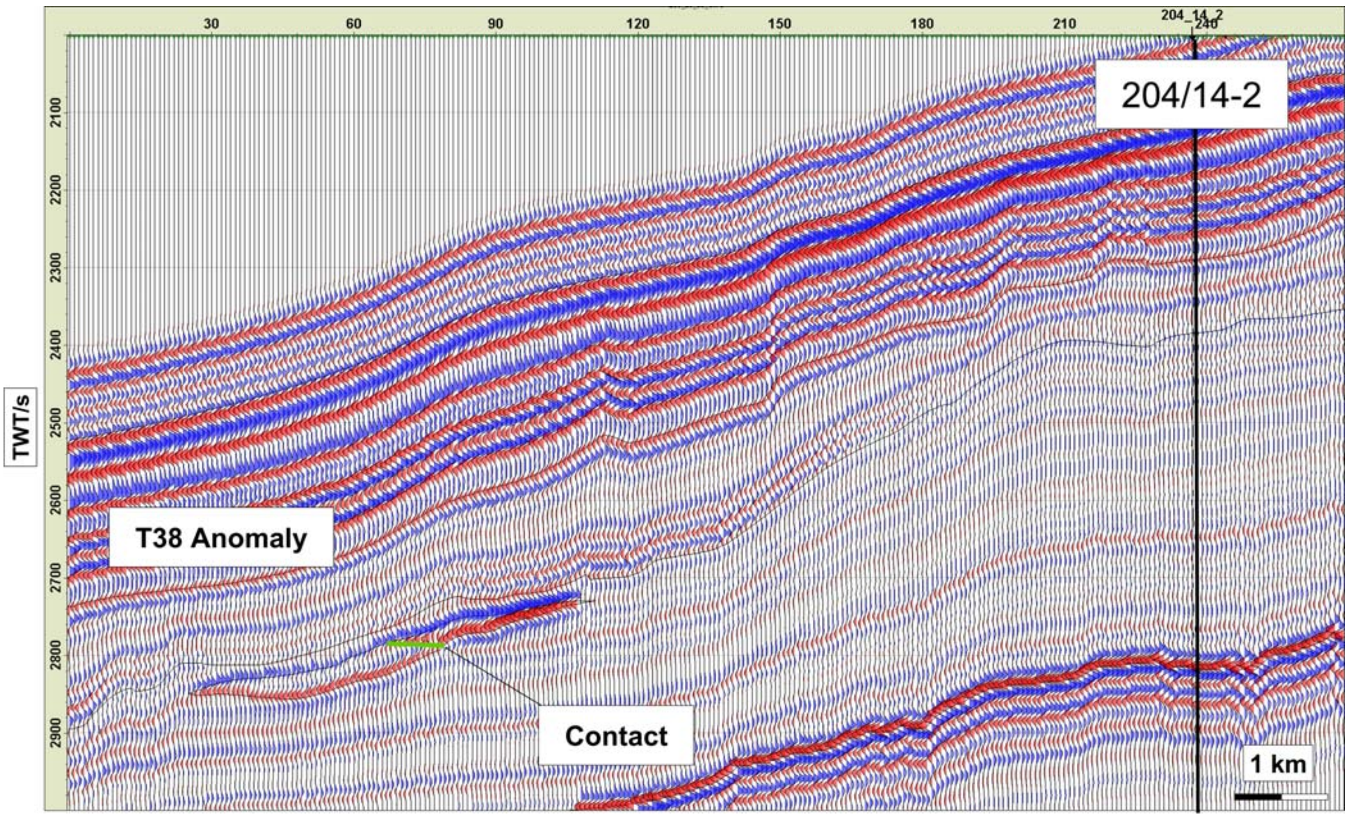

Fig. 16. Model far-stack (oil).

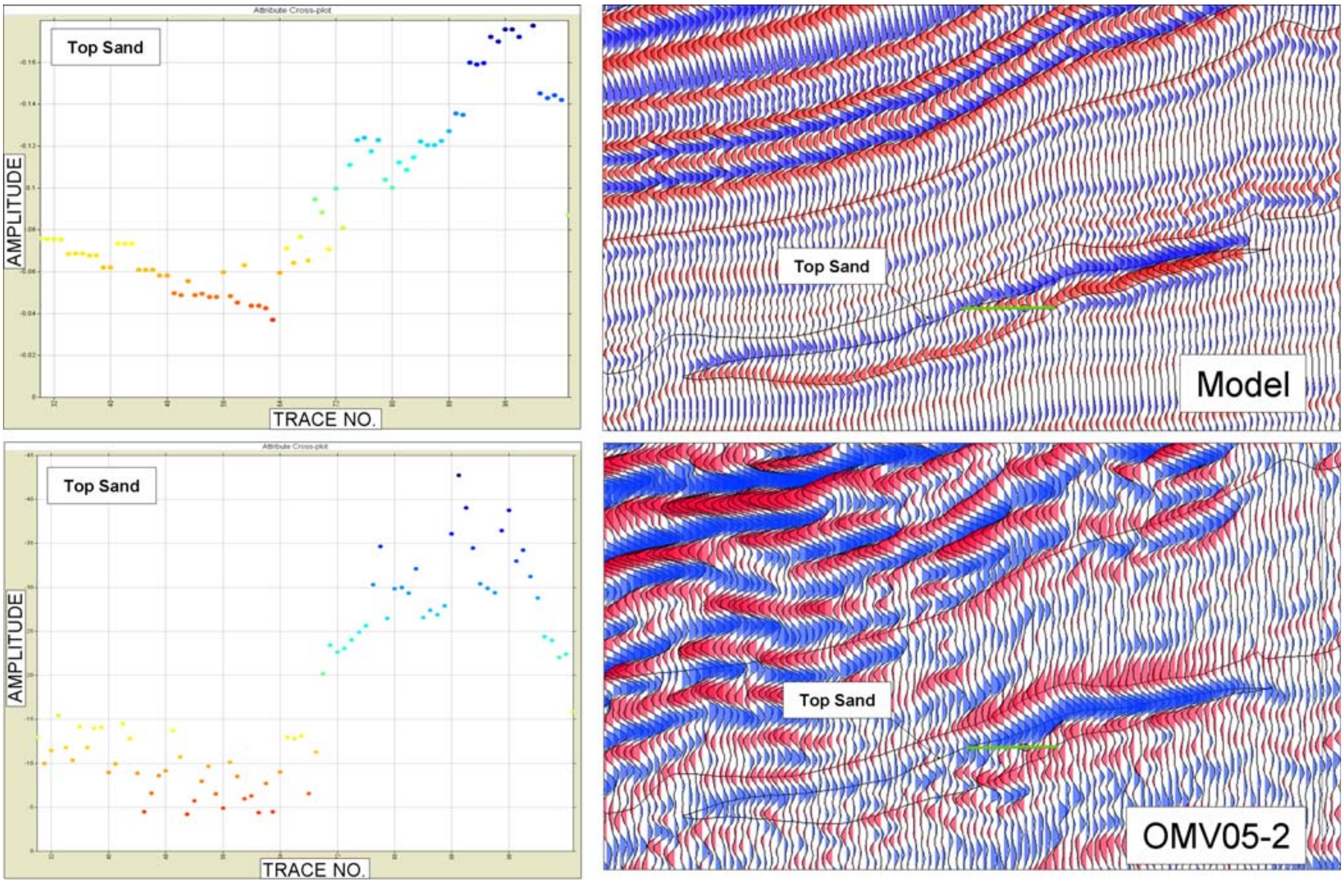

Fig. 17. Top sand amplitude – far stack; optimized thickness model.

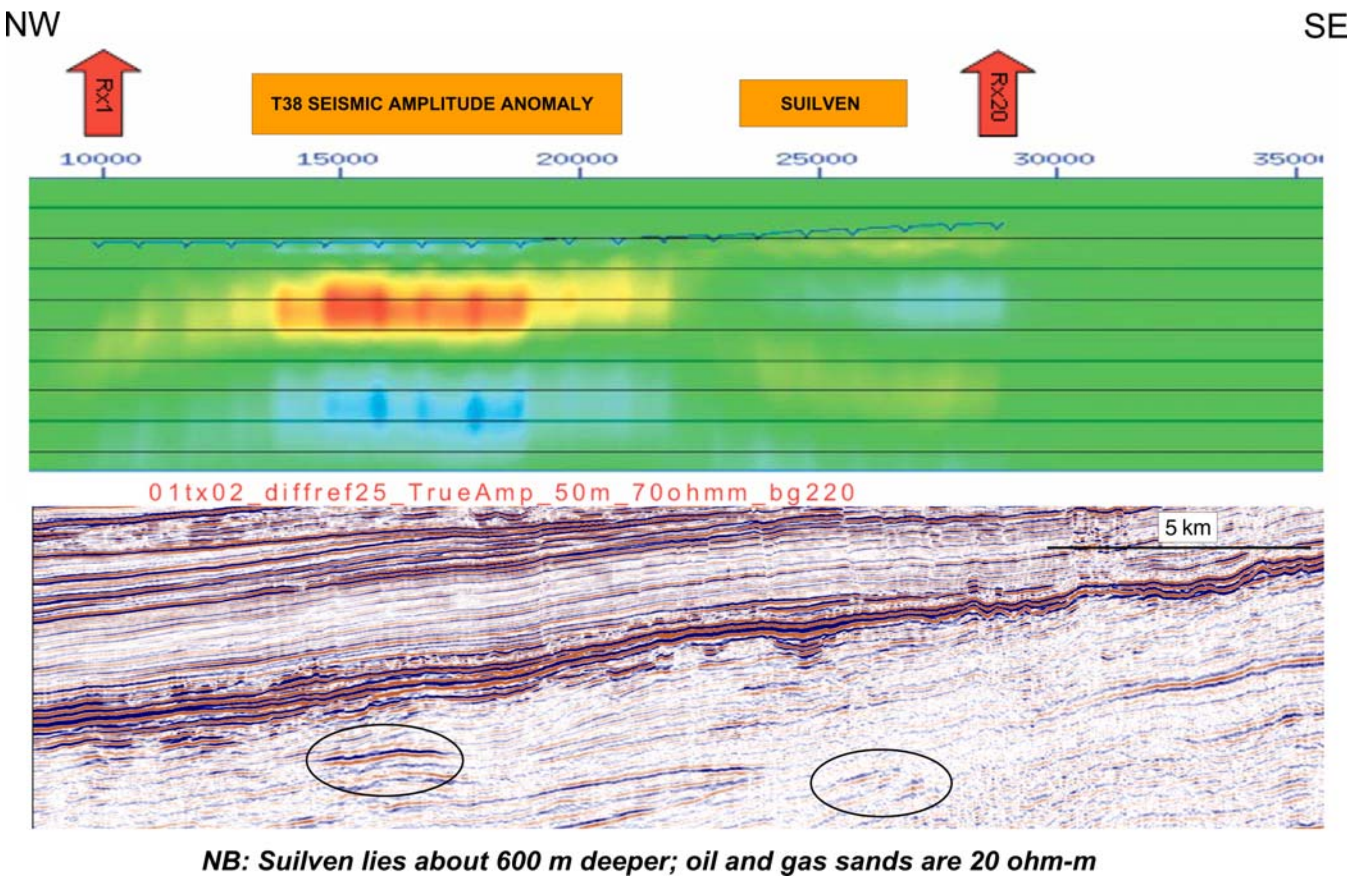

Fig. 18. NW/SE CSEM line over T38 anomaly also showing Suilven. Courtesy of CGGVeritas.

The results from the CSEM analysis are encouraging and may indicate the presence of a highly resistive, hydrocarbon-bearing sandstone with a thickness of 50 m and a resistivity in the order of 70 Ω m. A thicker hydrocarbon-bearing sand with a lower resistivity would also be a valid result from this analysis.

Discussion

The various studies discussed in this paper each appear to support the possibility that there are hydrocarbons present within a T38 sand body and that the hydrocarbon phase is most likely to be oil with the potential for a gas cap. Interestingly, none of these studies has yielded an absolute negative result.

If the phase is not oil, as expressed in the rock physics evaluation as the alternative model, then there is the possibility that the anomaly could be low-saturation gas-bearing sands. Although the Judd Basin is known to be a predominantly oil-bearing province, gas in the Suilven discovery may be sourced today from the gas-prone Faroe–Shetland Basin to the NE via the Westray Fault. In addition, the results from the CSEM survey indicate that the anomaly is associated with a 70 Ω m resistive body, which may be 50 m thick and therefore unlikely to be low-saturation gas, which generally loads to significantly lower resistivity.

The Westray Fault is instrumental in providing the conduit for sourcing the prospect and, although the anomaly lies above the main T35/T36 shales (the regional seal), it can be seen that smaller faults associated with the main Westray Fault system are cutting up through to the base of the anomaly. This fault has been instrumental in the inversion of the Judd Basin throughout the Oligo-Miocene and defines its northernmost extent. It is possible that fault parallel migration into the prospect and into the T38 sands in well 204/15-2 occurred at this time.

There are examples where base of slope fans have been prognosed as sand only to find that the sediment proven by the drill was predominantly mudstone (Johannessen & Steel 2005). However, in this instance, there is an analogue sandstone identified in a very similar depositional setting relatively close by. Additionally, channels can be observed on the 3D seismic data cutting down into the topsets of the clinoforms at well 204/18-1. It is possible that these could be age equivalent to the T38 anomaly.

The top seal for the prospect consists of slope sediments from the overlying clinoforms and the side seal is defined by the change in lithology from a sandy toe of slope fan to the distal mudstones of the toe itself. The toe appears on seismic to be near-horizontal, suggesting the presence of mudstone (coarser clastics would produce a steeper gradient). However, the slope may contain thief sands, which could release hydrocarbons upslope and away from the prospect. While there were silts identified within the cuttings of the adjacent wells, these appear to be capable of retaining a column of relatively heavy oil comparable to the column invoked from the seismic.

The trap lies at the base of the slope and is believed to be unique within the Judd Basin. However, both major fields in the area are known to be partly stratigraphic and, therefore, it is shown that combination traps in this area are successful.

The T38 seismic amplitude anomaly is a new and probably unique play in the Judd Basin – lying above the regional seal and also lying at the base of a set of clinoforms. Although the play was unsuccessful in well 204/18-1, this is thought to be due to the lack of trap at the location and the fact that the sands were not plumbed in to a migration route.

Conclusions

The history of previous seismic anomalies which have been drilled and proved to be unsuccessful in the quest for hydrocarbons has led the OMV group to carry out a series of investigations on the T38 amplitude anomaly. A fully integrated geophysical and geological evaluation comprising rock physics, AVO analysis, fault seal analysis and the acquisition of a CSEM survey supported by a valid geologic model have, together, led to a reduction in the risk from high to moderate. The results of the analyses indicate that the seismic amplitude anomaly has the potential to be sand-bearing and to contain oil. The well will be drilled later this year and the results will be eagerly awaited.

The authors would like to thank the management of OMV (UK) Limited and partners, Dana Petroleum Plc, Faroe Petroleum plc and Idemitsu E&P UK Ltd, for permission to publish this paper, CGGVeritas for allowing us to publish their 3D and 2D seismic data, the Schiehallion group for allowing us to publish a 3D seismic line over the field, RDR, BGS (S. Clarke), EMGS and G. Bertram for their studies and support together with present and past workers, B. Richardson, R. Koehazy from OMV Vienna and R. Robertson now at Fairfield Energy Limited. Further thanks are given to P. Krois, S. Hannke, M. Scherer, J. Parry and J. Austin as well as the conference reviewers for their helpful comments and improvements to the manuscript.

References

Carr, A. D. & Scotchman, I. C. 2003. Thermal history modelling in the southern Faroe–Shetland Basin. *Petroleum Geoscience*, **9**, 333–345.

Carr, A. D., Snape, C. E., Meredith, W., Uguna, C., Scotchman, I. C. & Davis, R. C. 2009. The effects of water pressure on hydrocarbon generation reactions: some inferences from laboratory experiments. *Petroleum Geoscience*, **15**, 17–26.

Clarke, S. M., Burley, S. D. & Williams, G. D. 2005. Dynamic fault seal analysis and flow pathway modelling in three dimensional basin models. *In*: Doré, A. G. & Vining, B. A. (eds) *Petroleum Geology: North-West Europe and Global Perspectives: Proceedings of the 6th Petroleum Geology Conference*. Geological Society, London, 1275–1288; doi: 10.1144/0061275.

Cooper, M. M., Evans, A. C., Lynch, D. J., Neville, G. & Newley, T. 1999. The Foinaven Field: managing reservoir development uncertainty prior to start-up. *In*: Fleet, A. J. & Boldy, S. A. R. (eds) *Petroleum Geology of Northwest Europe: Proceedings of the 5th Conference*. Geological Society, London, 675–682; doi: 10.1144/0050675.

Dean, K., McLachlan, K. & Chambers, A. 1999. Rifting and the development of the Faroe–Shetland Basin. *In*: Fleet, A. J. & Boldy, S. A. R. (eds) *Petroleum Geology of Northwest Europe: Proceedings of the 5th Conference*. Geological Society, London, 533–544; doi: 10.1144/0050533.

Doré, A. G., Lundin, E. R., Jensen, L. N., Birkeland, O., Eliassen, P. E. & Fichler, C. 1999. Principal tectonic events in the evolution of the northwest European Atlantic margin. *In*: Fleet, A. J. & Boldy, S. A. R. (eds) *Petroleum Geology of Northwest Europe: Proceedings of the 5th Conference*. Geological Society, London, 41–61; doi: 10.1144/0050041.

Ebdon, C. C., Granger, P. J., Johnson, H. D. & Evans, A. M. 1995. Early Tertiary evolution and sequence stratigraphy of the Faroe–Shetland Basin: implications for hydrocarbon prospectivity. *In*: Scrutton, R. A. *et al*. (eds) *The Tectonics, Sedimentation and Palaeoceanography of the North Atlantic Region*. Geological Society, London, Special Publications, **90**, 51–69.

Iliffe, J. E., Robertson, A. G., Ward, G. H. F., Wynn, C., Pead, S. D. M. & Cameron, N. 1999. The importance of fluid pressures and migration to the hydrocarbon prospectivity of the Faroe–Shetland White Zone. *In*: Fleet, A. J. & Boldy, S. A. R. (eds) *Petroleum Geology of Northwest Europe: Proceedings of the 5th Conference*. Geological Society, London, 601–611; doi: 10.1144/0050601.

Johannessen, E. P. & Steel, R. J. 2005. Shelf-margin clinoforms and prediction of deepwater sands. *Basin Research*, **17**, 521–550.

Lamers, E. & Carmichael, S. M. M. 1999. The Paleocene deepwater sandstone play West of Shetland. *In*: Fleet, A. J. & Boldy, S. A. R.

(eds) *Petroleum Geology of Northwest Europe: Proceedings of the 5th Conference*. Geological Society, London, 645–659; doi: 10.1144/0050645.

Leach, H. M., Herbert, N., Los, A. & Smith, R. L. 1999. The Schiehallion development. *In*: Fleet, A. J. & Boldy, S. A. R. (eds) *Petroleum Geology of Northwest Europe: Proceedings of the 5th Conference*. Geological Society, London, 683–692; doi: 10.1144/0050683.

Loizou, N., Liu, E. & Chapman, M. 2008. AVO analyses and spectral decomposition of seismic data from four wells West of Shetland, UK. *Petroleum Geoscience*, **14**, 355–368.

Smallwood, J. R. & Kirk, W. J. 2005. Paleocene exploration in the Faroe–Shetland Channel: disappointments and discoveries. *In*: Doré, A. G. & Vining, B. A. (eds) *Petroleum Geology: North-West Europe and Global Perspectives: Proceedings of the 6th Petroleum Geology Conference*. Geological Society, London, 997–991; doi: 10.1144/0060997.

Can stratigraphic plays change the petroleum exploration outlook of the Netherlands?

F. F. N. VAN HULTEN

Energie Beheer Nederland B.V., PO Box 6500, 6401JH, Heerlen, The Netherlands (e-mail: Fran_Hulten@compuserve.com)

Abstract: Fifty years after the discovery of the giant Groningen gas field, good insight into the remaining hydrocarbon exploration potential of the Netherlands is of great interest due to the aging infrastructure. In a review of prospective areas, the stratigraphic element of Dutch play areas has been summarized for conventional and unconventional formations. This is to answer the question of whether stratigraphic traps can contribute to future exploration. Complex faulting, very common in the Dutch subsurface, makes structural definition generally the highest prospect risk. With increase in 3D coverage over the country, many structures have now been drilled successfully. The success of structural traps has left the stratigraphic plays and prospects under-explored. Most hydrocarbon reserves in the Netherlands have been discovered in Permian Rotliegend and Triassic Bunter sandstone reservoirs, which are not prone to much stratigraphic trapping as a consequence of very gradual facies changes. Other prospective horizons and hydrocarbon reservoirs in the country range in age from Carboniferous to Cenozoic and can be found in clastic and carbonate rocks. They share an overall comparable basin setting but the varying interplay at basin margins creates varying stratigraphic elements. Rifting creates new facies variation during the Mesozoic. Salt movement is another factor that creates stratigraphic components in trapping. The various erosional events create other possibilities for stratigraphic trapping. This, combined with varying relative sea-levels through time, creates very distinct stratigraphic intervals often correlatable over large distances. The very limited contribution of stratigraphic traps to present-day gas finds may change in the future because of improved seismic. Risking of prospects needs better understanding of stratigraphic elements in various plays. This includes the stratigraphic aspects of reservoir sealing in dominantly structural traps and the nature of source horizons.

Keywords: the Netherlands, stratigraphic traps

The Netherlands (Fig. 1) is an important hydrocarbon-producing province in NW Europe. Exploration drilling and good seismic coverage have contributed to good knowledge of the deeper geology of the country and the surrounding area (for a comprehensive overview, see Glennie 1998; Wong 2007; Doornenbal & Stevenson 2010). The giant Groningen gas field and Schoonebeek, the largest onshore oil field in Western Europe, were found underneath the Dutch territory. Fifty years after the landmark giant Permian Rotliegend Groningen gas field discovery, about 350 gas and oil fields have been found and petroleum exploration remains successful. Energie Beheer Nederland B.V. (EBN) was founded to represent the national interest in the management of petroleum reserves after the Groningen discovery and today participates in more than 300, mainly gas, fields for the Dutch state. EBN is actively studying the remaining exploration potential because activity is declining and aging infrastructure, in particular offshore, will make exploration less attractive in the foreseeable future. Timing is essential, as relatively small prospects will be increasingly less feasible. The depth of most fields and prospects generally exceeds 3500 m (ranging between 2000 and over 4000 m). This, combined with often heterogeneous shallower layers, makes good seismic coverage a necessity for prospect evaluation. Part of the exploration success of the last 30 years is due to extensive 3D coverage. The ‘sub salt’ Rotliegend exploration target, the most prolific gas-producing horizon, makes it necessary to solve very complicated structural problems. Complex faulting at the prospect level, added to the often complex overburden geology, as a result of salt movements and rifting with associated inversion, makes structural definition generally the highest prospect risk. Within classic play areas increased 3D coverage means that most larger structures have been drilled.

The emphasis of a typical prospect evaluation has remained on structural aspects of the seismic interpretation. Stratigraphic elements are often less researched. Pure stratigraphic plays also gained by 3D seismic, but were at a disadvantage due to higher risk. With improved seismic acquisition and processing power, during the last 15 years amplitude information (Hoetz & Watters 1992) has increasingly become a tool for better field and prospect evaluation. Amplitude information can now in many cases be used for sub salt Rotliegend reservoir assessment, yet it has not delivered the successes the 3D delivered for the structural trap. Stratigraphic plays were also less popular as log and other well information was often not available. A change in mining legislation has changed this. Log data is publicly available now via the TNO/NLOG website (Geological Survey of the Netherlands). This opens up new possibilities for stratigraphic research. A new look at subtle stratigraphic variations in prospective formations can reduce risk and improve prospectivity. In-house EBN data supplemented with the additional log resources have been used in this study. Owing to EBN’s participation in so many hydrocarbon fields, sedimentological settings of reservoirs could be studied across licence boundaries and the trapping of over 300 fields investigated. With the new information, play maps of the various prospective formations could be adjusted.

Structural v. stratigraphic traps

A stratigraphic trap is defined by Levorson (1936) as: A trap in which a variation in the stratigraphy is the chief confining element in the reservoir which traps the hydrocarbons. Examples include wedging out, lateral facies change or truncation of the

VINING, B. A. & PICKERING, S. C. (eds) *Petroleum Geology: From Mature Basins to New Frontiers – Proceedings of the 7th Petroleum Geology Conference*, 261–275. DOI: 10.1144/0070261 © Petroleum Geology Conferences Ltd. Published by the Geological Society, London.

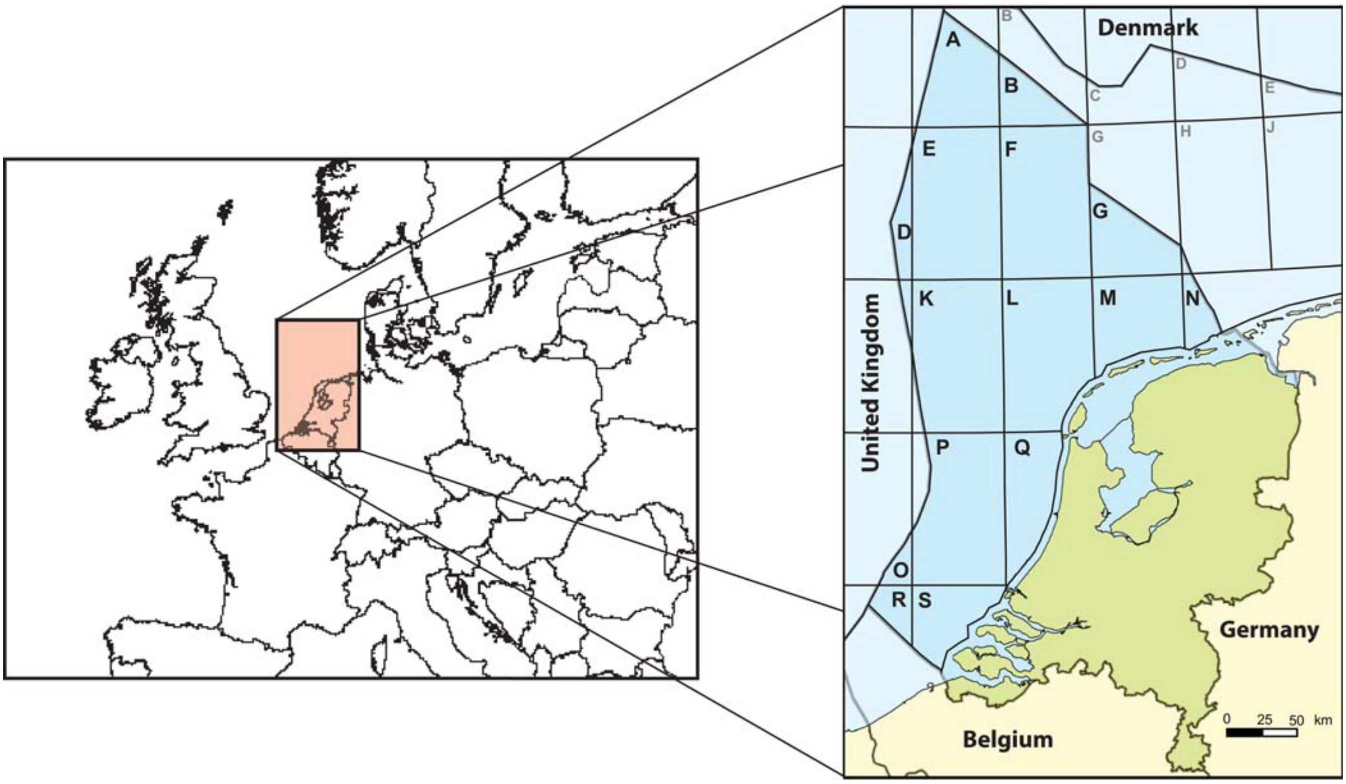

Fig. 1. Index map of the Netherlands. When the Netherlands are discussed it concerns the on- and offshore.

reservoir. When looking for stratigraphic elements that play a major role in the trapping of hydrocarbon accumulations in the Netherlands the following features are important:

- truncation at unconformities;
- other traps related to erosion at unconformities;
- facies change traps;
- facies changes related to salt movement;
- diagenetic traps.

Unconformities are an important element in several traps in combination with faults. A stratigraphical log (Fig. 2) of the Netherlands displays two major unconformities and several minor ones (Van Adrichem Boogaert & Kouwe 1997; Wong *et al.* 2007). Traps associated with unconformities are found in several fields. The truncation is never the main trapping element – there is always faulting as well. Salt movement also causes facies changes and salt dissolution creates accommodation that is filled with good reservoir sands for a number of fields.

There is no good example of a field that displays diagenetic trapping; however, there are (Lower Germanic) Triassic Bunter fields that are partly salt filled, which seems to contribute to trapping of the gas accumulation (Fontaine *et al.* 1993). Salt-plugging can be present in the reservoir several hundred metres from salt-domes (Dronkert & Remmelts 1996).

The survey of over 300 Dutch fields demonstrates that most known producing hydrocarbon accumulations are structurally trapped. The dominance of the Permian Upper Rotliegendes Group reservoirs is the reason why the stratigraphic trap has not been very critical for the Netherlands. Trapping in the Rotliegend Slochteren Formation, being relatively uniform in thickness and reservoir quality, rarely requires a stratigraphic explanation. Fault definition in that formation is often the essential prospect risk. Most Rotliegend as well as Bunter fields can be described as a dip-closure with three or more faults.

A small number of fields have significant stratigraphic elements in their trapping. Quantification is not very meaningful because of large uncertainties. For example, in a number of cases the current interpretation of a fault may turn out to be a facies change after more study.

Some stratigraphy plays a role in all traps, even in structural traps. In almost all cases the stratigraphy creates some kind of permeability barrier (no connections between the pores) needed for the trap:

- Most fields have at least one stratigraphic element due to the top seal. Little has been published on seal quality or regional seals. An exception is the study of late Triassic seals (Spain & Conrad 1997).
- Most Permian and Triassic traps are faulted dip closures. The stratigraphy of down-thrown or up-thrown block determines the sealing.
- Shallower formations are less brittle compared to Palaeozoic Rotliegend and Zechstein and have a lower fault frequency. Facies changes have a higher chance of sealing the reservoir.
- Unconformity traps at the Saalian unconformity are very common in Carboniferous-age reservoirs. At the other unconformities also stratigraphic trapping has been observed. Triassic reservoirs close to saltdomes often show such traps.
- Clastics are the dominant reservoir rock of the Netherlands. In carbonate accumulation a strong stratigraphic element is present. There is no lack of carbonates in the Dutch subsurface. Carbonate gas field reservoirs are mainly found in the Permian Zechstein. Seismic suggests that there are significant buildups of Mississippian age, but they are still exploration leads. Thin Late Triassic Muschelkalk carbonate reservoirs are very marginal and the Chalk is largely disappointing as an exploration target in the Netherlands, with only 1–3 finds.
- Well spacing can obscure stratigraphic trapping. Since most wells are drilled for gas, spacing is rather wide. Therefore it is easy to overlook stratigraphic elements of a trap.

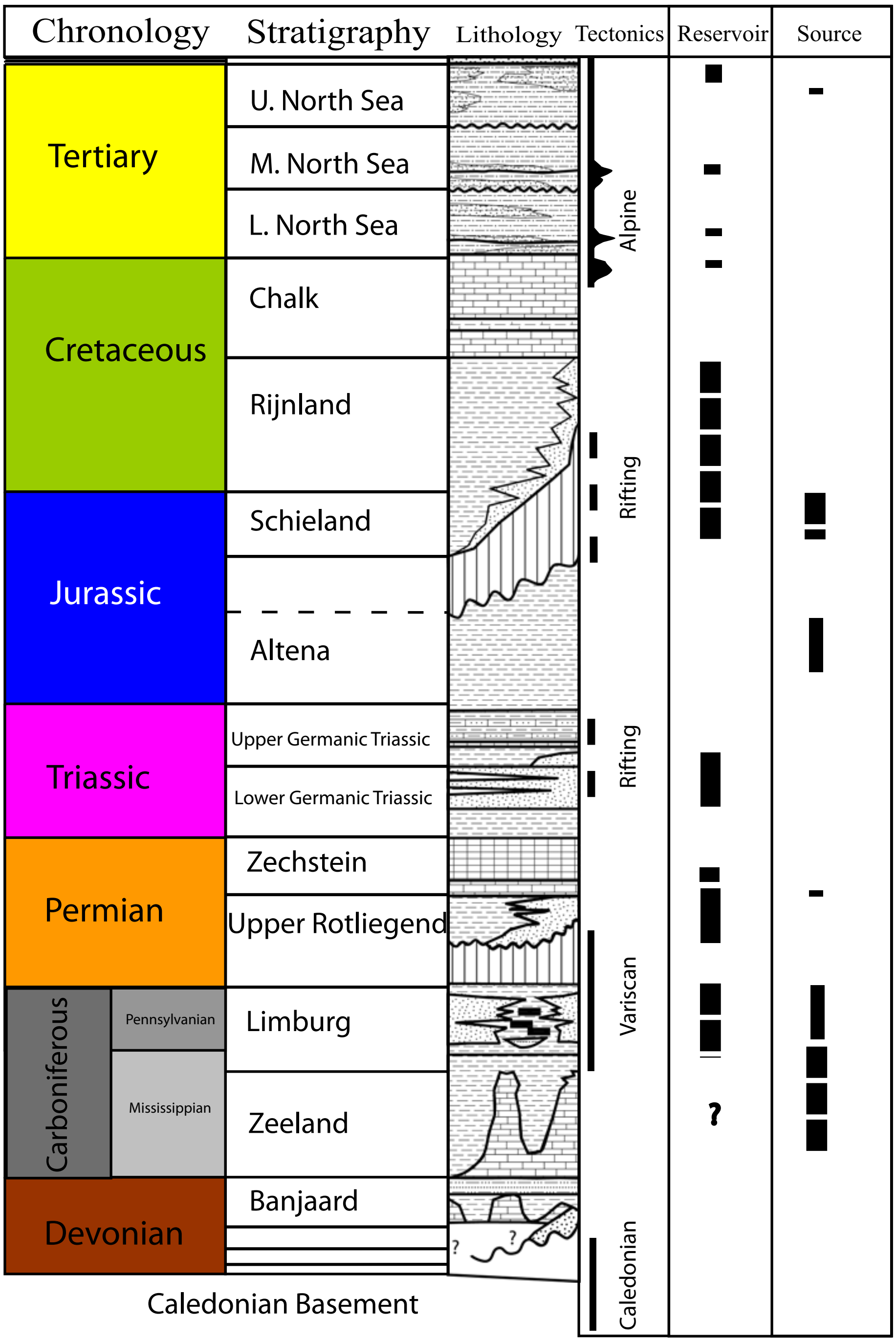

Fig. 2. Stratigraphic column.

Plays in the Netherlands

To understand stratigraphic plays in the Netherlands it is important to give a summary of the major plays. In all plays some stratigraphic element plays a role. In the following a quick review is given of the main source rocks and the structural setting.

Based on source rock a number of play groups can be distinguished (Spencer & Leckie 1996). The most important groups of source rocks are listed below.

Late Carboniferous gas

The main family of plays is associated to charge from coals of Late Carboniferous age. Most gas reservoirs in the Netherlands have been found in the Permian Rotliegend, with 80% of reserves of the country contained in these Permian sandstones. Triassic Bunter sandstone reservoirs hold significant amounts of gas as well and gas is found in other reservoirs of Pennsylvanian, Permian and Cretaceous age. It is generally assumed that most of these gas accumulations are charged by the gas-prone Type III source rocks of the Pennsylvanian age coal measures of the Limburg Group, which underlie almost the entire Netherlands (Wong *et al.* 2007). About 3% of the more than 1000 m section contains coals and organic-rich shales. The cumulative thickness, of several tens of metres, could have charged the basin many times over.

Early Jurassic Posidonia shale

Sixty years ago, oil fields in Cretaceous-age sands were discovered in the vicinity of The Hague and Rotterdam. They belong to a family of play types related to the presence of Early Jurassic Type II source rocks. These marine Late Triassic and Early Jurassic shales contain a few kerogen-rich intervals. The richest bituminous interval is the 15–30 m thick Posidonia with an average TOC of 5%. The Mesozoic oil-generating shale is geographically restricted to basin areas. In the southern part of the Drenthe province, Schoonebeek, the largest onshore oilfield (lbbl bls) of Western Europe, was discovered in an Early Cretaceous reservoir (see Fig. 2). It has been charged by a local lagoonal or lacustrine Ryazanian source rock (Wong *et al.* 2007) and has no significance for a regional play study.

Geverik shale

Gerling *et al.* (1999) noted, based on isotope data, that gas from many Rotliegend and Late Carboniferous gas fields in the Southern Permian Basin area originates from marine source rock. As most Late Carboniferous coal is of terrestrial origin, the marine Mississippian Geverik Type II hot shale, with a TOC of about 8%, is a likely candidate as source (Van Adrichem Boogaert & Kouwe 1997). Few wells have drilled this Geverik black shale. The black shale was deposited during or at the end of the Mississippian, under anoxic conditions which restricted circulation. It is assumed that the basin areas are at least 200 m deeper than the surrounding areas. Based on the overall palaeogeographical setting during the Mississippian (Van Hulten & Poty 2008) it is assumed that the hot shale is present in all deep Mississippian basin areas and has a wide geographical extent with considerable charge potential.

Biogenic gas

Last year production started from offshore Cenozoic-age reservoirs. These and many other shallow gas accumulations are filled with biogenic gas. It is composed exclusively of methane and isotope data indicate a bacterial origin. Schroot & Schüttenhelm (2003) note that methane concentrations near the sediment surface are very low but increase below the sulphate–methane transition zone. At the sulphate-containing zone there is a rapid increase in methane concentration. These authors note that locally thermogenic gas can leak into the shallow formations.

The first three source rock intervals and other less important source rocks like the Permian Kupfershiefer (Wong *et al.* 2007) and the Late Jurassic Kimmeridgian (Clay Deep Formation, Van Adrichem Boogaert & Kouwe 1997) were all deposited during relative sea-level high stands. It is interesting to note that the sediments deposited during the major Late Cretaceous high stand are devoid of source potential (Glennie 1998).

These relatively high stands also have another effect on viable prospects. They provide the regional seals key to prospect risking. The interplay of these major sealing and source horizons in the Netherlands is an important element in play analysis.

Basin evolution: the structural framework

The initial structural setting is comparable to adjacent parts of the Southern North Sea area in the UK. With the Netherlands it shares a general setting along a NW–SE strike. To understand the overall basin setting, two bounding highs have to be considered, the London Brabant Massif in the south and the Mid North Sea High in the north (Fig. 3), that share a Caledonian (Late Silurian) origin. Both highs were hardly a source of sediment but they provide a logical basin termination because erosion and non-deposition show on most maps. They also acted as some kind of

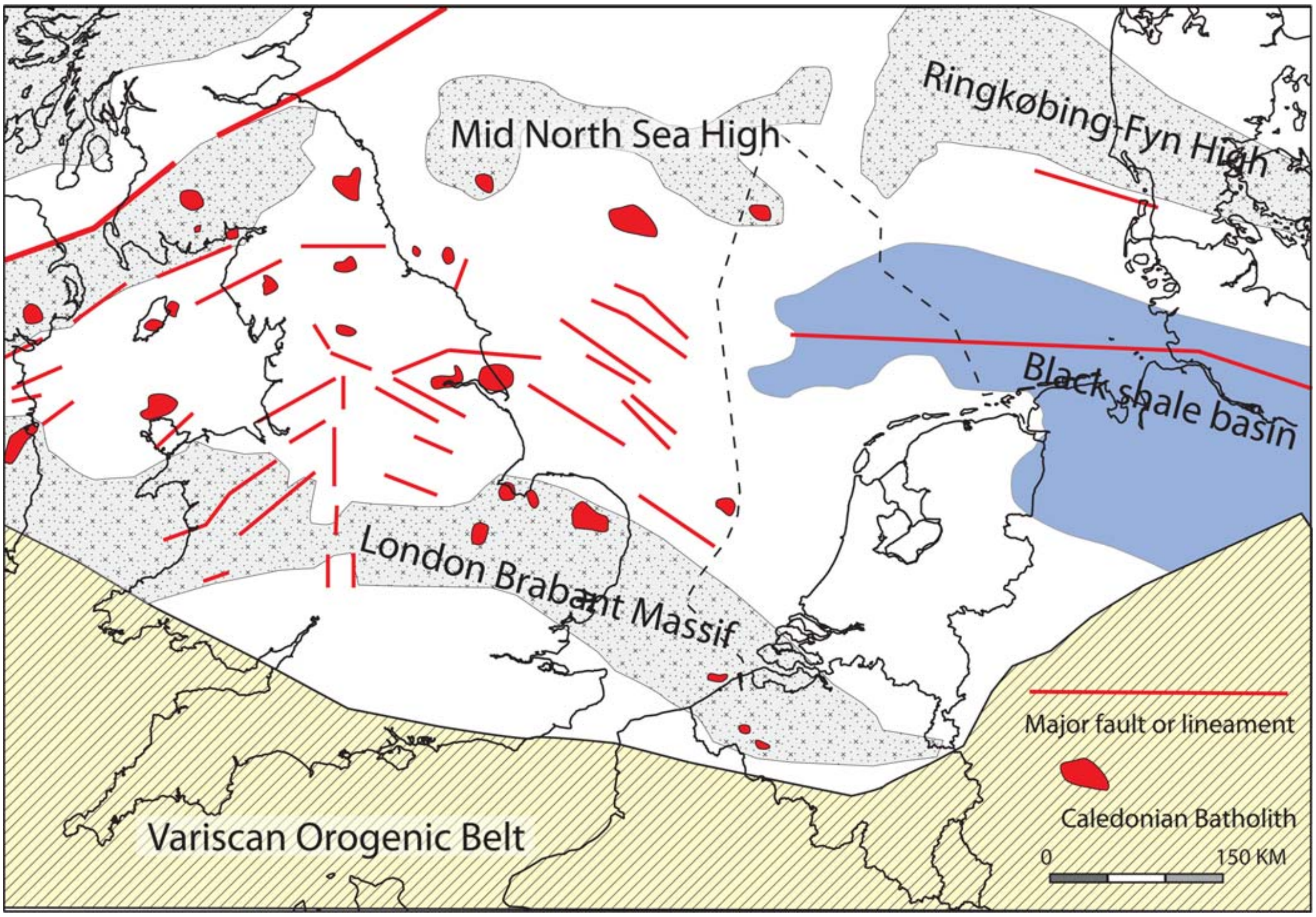

Fig. 3. Structural elements, Palaeozoic.

threshold for the area from sedimentation originating from the Caledonian in the north and later the Variscan southern highlands as well. The northern offshore half of the Netherlands displays a low topography trough time. The southern half with the onshore Texel-IJsselmeer High and the surrounding areas are generally much shallower. This results in asymmetric basin geometry over the Netherlands, which is essential for understanding facies trends in various time intervals.

This geometry is the result of continental scale collision during the Caledonian orogeny. The Netherlands are part of the micro continent Avalonia that amalgamates with Baltica in the Early Silurian when the Tornquist Ocean was closed. Deep seismic shows a shallow Moho in the northern part of the Dutch offshore. This can be explained by the presence of a slice of non-subducted oceanic crust (Abramovitz *et al.* 1998). Sinking ocean crust is also an explanation of why the northern Dutch offshore is a major depocentre. This Silurian–Devonian basin is the predecessor of the Post Variscan Southern Permian Basin. It differs significantly from the latter as it is bordered by a major ocean in the SE.

The Iapetus closure during the Late Silurian occurred outside the Netherlands, but the collision is central to the forming of the London Brabant Massif (Wong *et al.* 2007) and many granite plutons, for example on the Mid North Sea High. In the Devonian and Mississippian, half-grabens formed in the southern part of the Netherlands in an extensional tectonic regime thereafter. The structural grain is more or less NW–SW. The NE strike is parallel to the Thor suture, the boundary between the continents Baltica and Avalonia. The Dutch on- and offshore was largely peripheral to the Variscan orogeny until its latest phases. It resulted in an unconformity between the Carboniferous strata and the overlying Permian Rotliegend and is often clearly visible on newer vintage seismic. Erosion may in places remove more than 1000 m of Carboniferous (Wong *et al.* 2007). A period with relative minor tectonic movements followed and lasted until the mid Triassic.

During the Mesozoic a number of rifting events (Fig. 4) occurred related to the break-up of Pangaea (Glennie 1998). They were of great importance for forming hydrocarbon traps. Also salt tectonics had a severe effect on structuration of shallower layers and generated many traps.

Late Triassic rifting is active in the Dutch Central Graben area. It is also known as the Early Kimmerian tectonic phase (see Van Adrichem Boogaert & Kouwe 1997; Wong *et al.* 2007). Regional uplift and erosion over most of the Netherlands occurred during the Late Jurassic, lasting in some areas until the Early Cretaceous. The major Dutch tectonic elements formed during the Mid and Late Kimmerian tectonic phase, in the later part of the Jurassic. It affects almost the whole country.

The Alpine collision adds a compressional element to rifting tectonics. The soft sediments in newly formed grabens are inverted in at least three major inversion periods. The Sub Hercynian (Late Cretaceous), the Laramide (Early Paleocene) and Pyrenean (Eocene–Oligocene) inversions are recognized widely and have a profound but not always understood effect on traps, hydrocarbon generation and migration. It is not clear if the Mid Miocene unconformity is caused by a tectonic event (Savian phase) or a dramatic sea-level drop or both.

Plays based on basin evolution and depositional model

Beside the structural framework, the source rock mapping and the regional seals, the depositional model of the reservoir rock constrains the play mapping. The general facies development of prospective horizons has been well described (for a more detailed description refer to Glennie 1998; Wong *et al.* 2007). There are a few key periods which most affected the development of the bulk of the petroleum finds and have received most study (Wong *et al.* 2007). Deposits from the different time periods share comparable characteristics since the overall basin setting has been similar over long periods. In the country, plays with a stratigraphic component are frequently associated with basin margins. Insight in facies development at basin fringes yielded some very good gas and oil fields (e.g. Van de Sande *et al.* 1996 for Zechstein; Geluk 2005 for Triassic).

During the Mesozoic rifting new facies variation was created in rift areas. Perhaps more important for trapping of hydrocarbons is

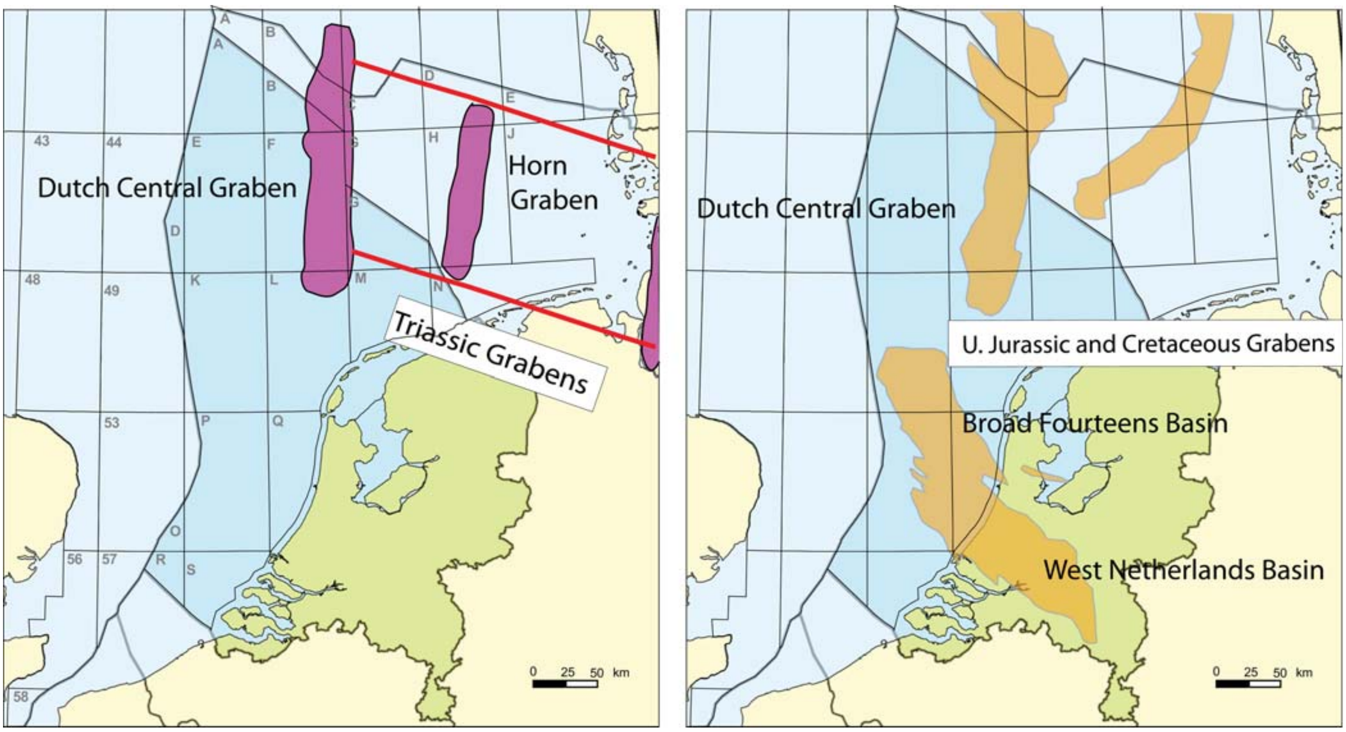

Fig. 4. Structural elements, Mesozoic and Cenozoic.

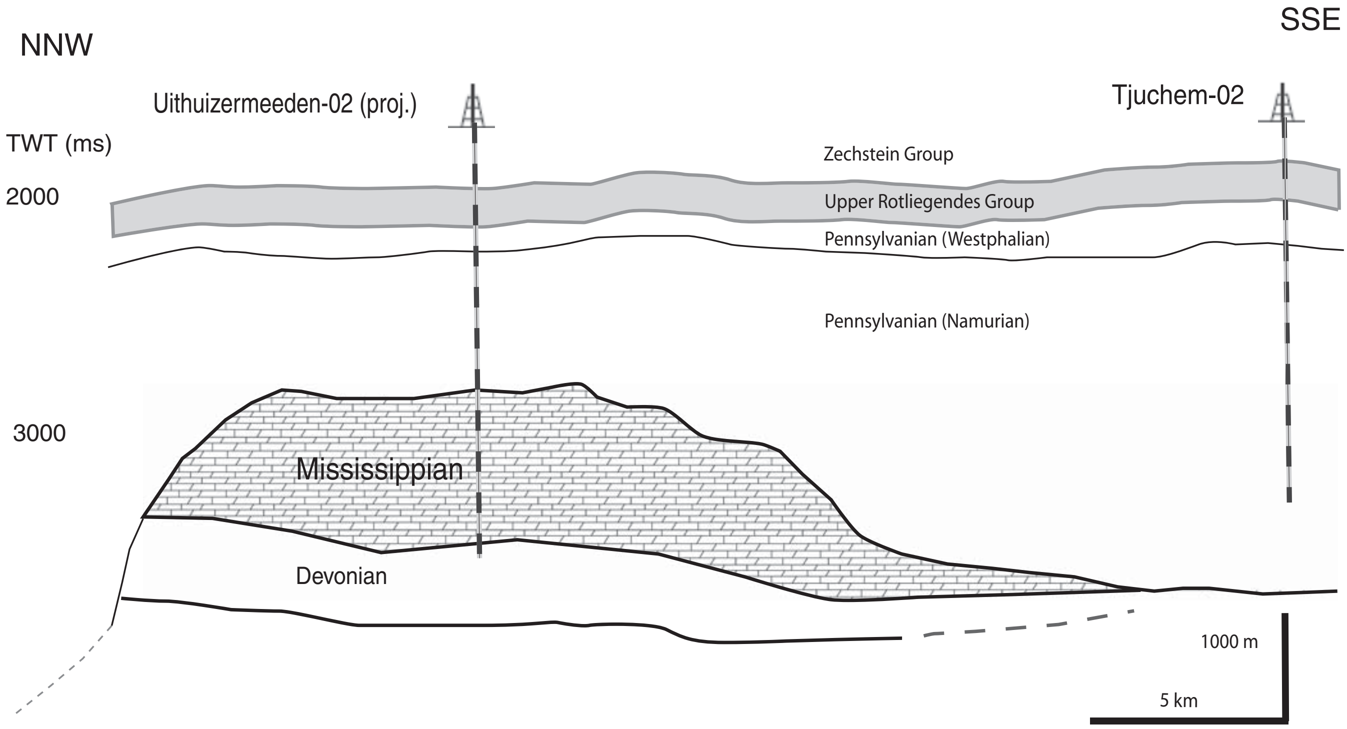

Fig. 5. Sedimentological model of Mississippian reefs. Modified after Kombrink (2008).

the widespread salt movement over large parts of the country after the Mid Triassic.

In the following, a brief summary of play areas based on stratigraphy is given.

Devonian and Mississippian

Recently new information has become available in basin areas on carbonate buildups of Mississippian age (Kombrink 2008; Van Hulten & Poty 2008). These Mississippian reef leads, with no hydrocarbon shows in the Netherlands so far, have a very strong stratigraphic component because their morphology suggests that mounded closures can be expected. In this stage of exploration it is uncertain if reservoir rock is present at the depth of 3000–6000 m where these reefs have been detected. Very few wells in the country go deeper than the Upper Carboniferous, with the exception of some wells close to the London Brabant Massif and a few wells on the Mid North Sea High. Seismic interpretation has shown that large carbonate platforms (Fig. 5) may exist and may form a perfect stratigraphic trap as they are encased in very thick Carboniferous shale. The tallest reefs are in the Groningen Friesland area (Kombrink 2008). Reefs are also seen in the southwestern Dutch Offshore (Van Hulten & Poty 2008). Subcrop information at the Saalian unconformity indicates that a shallow platform area (Fig. 6) is present to the south and a deep basin in the north comparable to Northern Germany (Van Hulten & Poty 2008).

The major reefs as seen on the recently published seismic are most likely of Mississippian age and it is unclear to what extent Devonian carbonates may form traps. Information on the Middle Devonian or older rocks is rarely present in the Netherlands. Devonian of Givetian or Frasnian age in parts of the Netherlands may be developed in carbonate facies. Based on palaeo-wind considerations with trade winds not coming from the (present day) east as in the Mississippian (Van Hulten & Poty 2008), but from the south, reefal buildups may be present in the southern part of the country and in particular on the Mid North High. The assumption is based on a tropical palaeo-position of the area during the Mid Devonian below the equator.

Pennsylvanian

The very thick almost uniform repetition of sand and shale with coals of Late Carboniferous (Pennsylvanian) age are well known in NW Europe in the UK, Belgium and Germany (Glennie 1998; Wong *et al.* 2007). In the Netherlands the more than 1000 m-thick clastic section is called the Limburg Group. Considering its nature, with sands interbedded in shale beds, it is surprising that almost no stratigraphic traps have been found. Major intra-Carboniferous shale intervals like the Maurits coal Formation or even the marine bands may form intra-Carboniferous seals. At this moment it does not form a widely accepted play idea. The facies analysis suggests that the relief is very low due to high sedimentation rate (Wong *et al.* 2007). The Saalian subcrop map, which shows the erosion at the Late Carboniferous to Early Permian Carboniferous unconformity (Van Hulten & Poty 2008), suggests that the deepest part of the basin is situated to the north, in the offshore area off the Frisian Islands. This is supported by observations that suggest prograding sedimentation toward the north in the southern part of the basin and toward the south or SW direction in the northern part of the basin (Wong *et al.* 2007). Almost all known fields (Fig. 7) are traps against the important Saalian unconformity. The Limburg Group displays mostly an angular unconformity with overlying Permian age formations. Channel fills are common reservoir facies type but facies changes are not commonly the main trapping element. Fields are bounded by faults not unlike fields of the Rotliegend Group. In literature the possibility of intra-Pennsylvanian stratigraphic traps is mentioned owing to the presence of incised channels (Hampson *et al.* 1999; Kosters & Donselaar 2003). No gas accumulations have been found that have such trapping configuration.

Rotliegend

The Rotliegend Slochteren sand is the most prospective reservoir unit in the Netherlands (Wong *et al.* 2007). Its geology and depositional setting have been well described (George & Berry 1993,

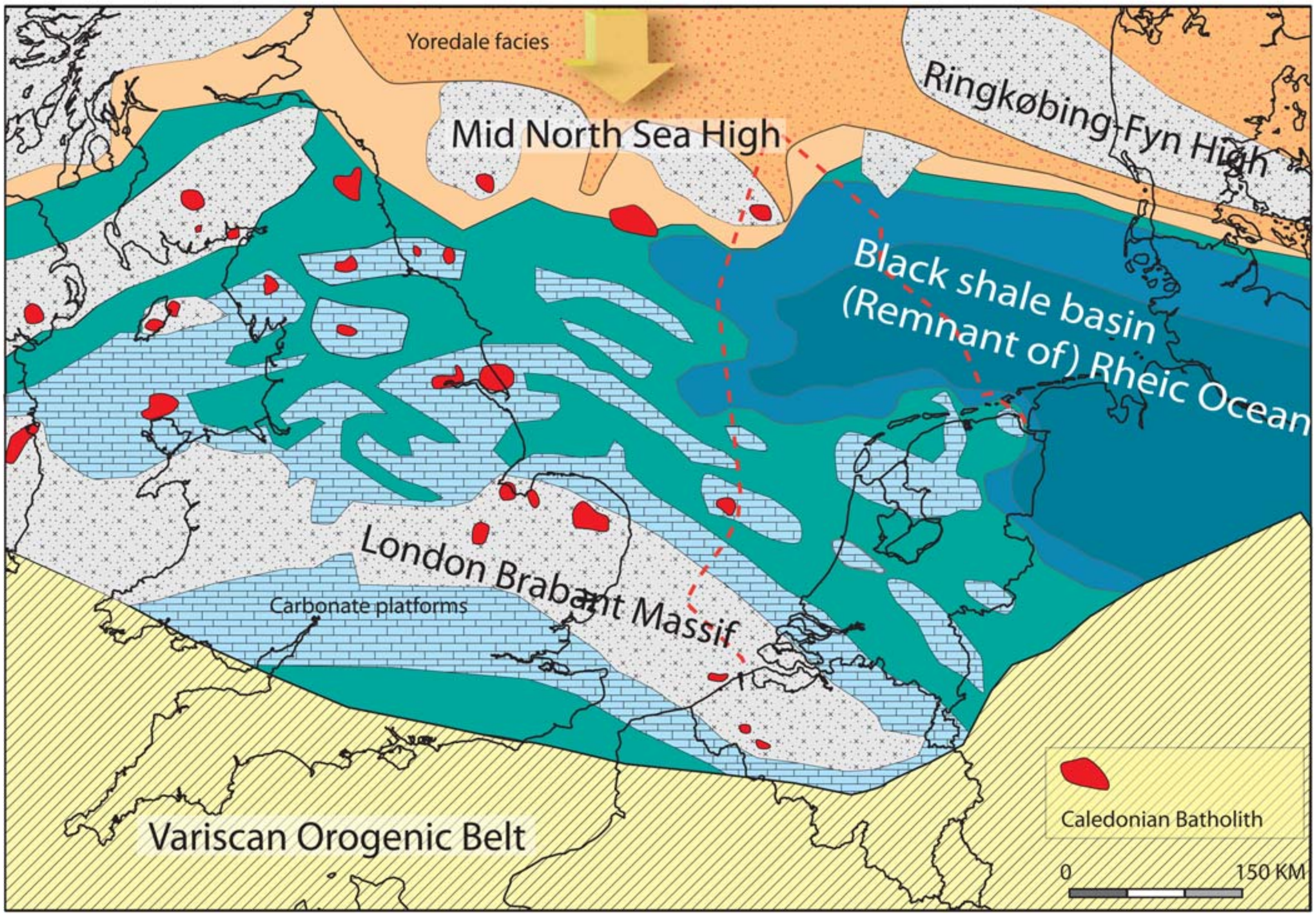

Fig. 6. Facies map, Mississippian.

1994; Verdier 1996; Glennie 1998; Geluk 2005). The deepest part of the basin is found again in the Dutch offshore area and most reservoirs are found at the southern basin margin. The reservoir that is dominated by desert fluviatile and aeolian facies can be subdivided in an Upper and Lower Slochteren stratigraphic unit. Facies changes in reservoir sands are very gradual and large scale compared to the frequency of faulting (Wong *et al.* 2007). This causes most, if not all, Rotliegend gas fields (Fig. 8) to be structural traps. Despite the structural nature of their trapping, studying stratigraphic elements may contribute to reducing exploration risk. There are two stratigraphic elements that are important for exploration. The northern sand limit is a target for exploration. Here it is important to distinguish between Upper and Lower Slochteren Units. They have a different sedimentation history. The other element is the interaction of sedimentation with palaeo-topography. This is key to understanding thickness variations in the Lower Slochteren sands. Sands can be thicker in depressions or be missing on highs. New emphasis on the interaction of palaeo-topography and depositional models (Maynard & Gibson 2001) shows that these models can help understand the trapping and reservoir distribution.

Zechstein

The Zechstein sediments are dominantly evaporitic and are not only known as reservoirs but also have cap rock qualities. Seven evaporitic cycles can be distinguished, of which five are recognized in the Netherlands. The various salt members of the last Zechstein cycles are seals for most Permian and Pennsylvanian traps. The mobile salt often forms structures of the shallower hydrocarbon traps. The first petroleum plays in Western Europe were related to traps associated with salt domes in the Hannover area. Also in the Netherlands, many traps above the salt are related to salt movement.

The basin configuration, essential for facies distribution, is comparable to the earlier formations. The deepest part is again the northern offshore and for play studies the various Zechstein coast lines have to be mapped. For reservoirs in the Zechstein Group the facies distribution plays an important role. Despite the importance of the stratigraphy for the reservoir, all fields (Fig. 9) seem to be structurally trapped. The reservoir rocks are peri-marine carbonates. The early reservoir cycles (Ze2, Ze3) form significant reservoirs. The later cycles have reservoirs in a few exceptional cases. To determine the prospectivity of the Zechstein carbonates, the stratigraphic element is a key element. For example, the main productive Zechstein horizon, the Zechstein Ze2, is prospective over a narrow east–west geographical zone. A time map can be very helpful to map the reef edge (Van de Sande *et al.* 1996).

Most fields were found more than 10 years ago, but near-field exploration or play extension outside known areas may revive the play. The lateral changes of other Zechstein horizons is also less researched.

Triassic

The Triassic Main Buntsandstein Formation is the second important hydrocarbon-producing formation for the Netherlands. The facies development in a desert environment is comparable to the Rotliegend. The fringe facies are now close to the London Brabant Massif in the south. Due to its sedimentological setting

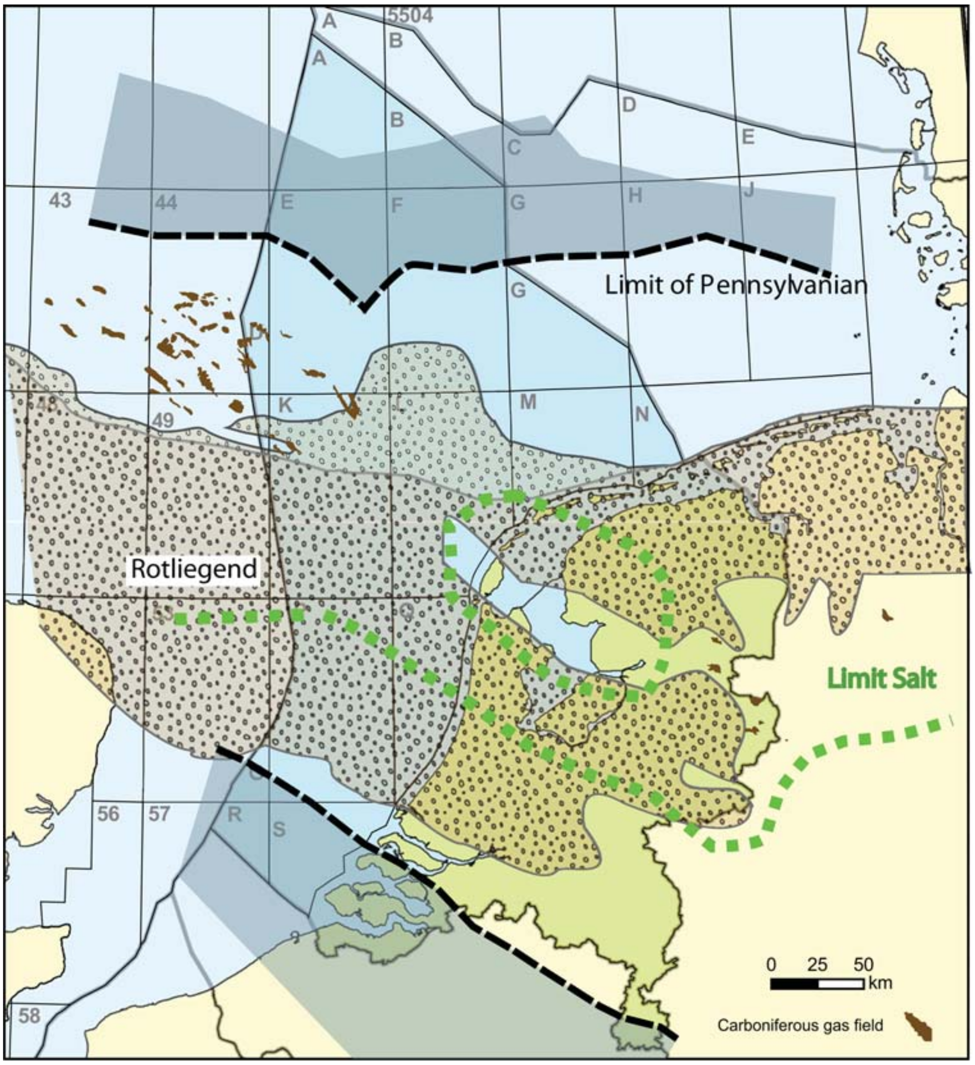

Fig. 7. Play map, Pennsylvanian.

in a desert lake environment (Fontaine *et al.* 1993; Ames & Farfan 1996; Geluk 2005), the formation is remarkably constant over large distances. The basin configuration with erosional highs in the southern half of the country can be seen during minor erosional episodes (Fig. 10). Subtle erosion during the so-called Detfurth and Solling unconformity created some thickness differences and pinchouts (Geluk 2005).

Initial rifting commenced during the Triassic. The combination of the rifting with the first salt movement changes the sedimentation pattern dramatically. Marine conditions were again established in the basin, but it did little to create good reservoir conditions. The only exception is the Solling 'Fatsands' (De Jager & Barrio 2003) deposited in salt dissolution depressions.

The other formations of late Triassic age rarely display good reservoirs. The Muschelkalk displays significant facies changes (Borkhtaria *et al.* 2005; Pöppelreiter *et al.* 2005) and may be a target for stratigraphical trapping, for example the Triassic Muschelkalk age back shoal facies in the Coevorden field. The best reservoir facies are believed to exist towards the east in Germany.

From the Late Triassic section potential reservoirs have been described in Germany, but are not known to trap hydrocarbons like the Shilf sandstone of the Keuper (Geluk 2005). Due to later erosion, the upper Triassic sediments are mainly found in basin areas. This is also the case for deposits of Early Jurassic age.

Early Jurassic

The Early Jurassic section contains mainly shale and is more important as source rock than as reservoir. The shale of this period contains the important Posidonia unit, the most productive oil source rock of the Netherlands (Fig. 11). The Posidonia is only found in basin areas, so the original lateral extent is uncertain. At the top part of the Early Jurassic section, sandstones (Van Adrichem Boogaert & Kouwe 1997) can be found, close to the Mid or Late Kimmerian unconformity, and can create an unconformity trap.

Late Jurassic and Early Cretaceous

After the subsiding of the Mid Jurassic rift dome in the Northern North Sea and coupled to relative rapid rise in sea-level, the erosion stopped and full marine conditions returned to large parts of the Netherlands (Glennie 1998). Late Jurassic geological history is complicated because of erosion, in Cretaceous and Cenozoic times. Its lateral extent is uncertain. Even more than Triassic sediments, most Jurassic sediment has been found in basin areas only (Fig. 12). Outside these rift basins, Late Jurassic sediments are rare and are associated with salt withdrawal or faulting (Van Adrichem Boogaert & Kouwe 1997). The rupturing of the Central Graben rift started in the north and progressed towards the Broad Fourteens Basin. A step-by-step north to south marine

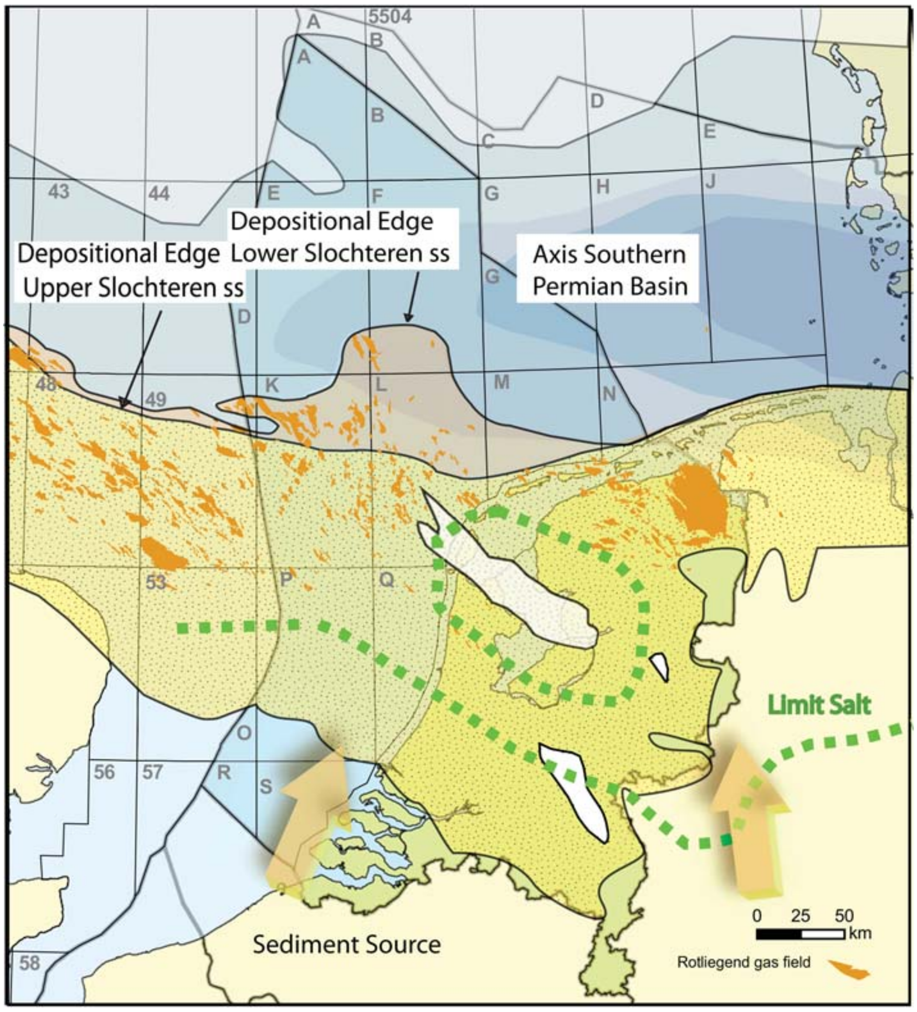

Fig. 8. Play map, Permian Upper Rotliegend.

transgression started during the Callovian and continued into the Lower Cretaceous. A stacked prograding coastal-barrier complex of Callovian age forms, for example, the F3-FB field (Van Adrichem Boogaert & Kouwe 1997). Periods of transgression alternate with periods of terrestrial progradation. This very complex clastic basin fill is the perfect setting for stratigraphic traps; however, the various inversion events turned many potential stratigraphic traps into structural traps.

Halokinetic activity of Zechstein salts complicates trapping in some areas. The reservoir sands are mostly fine-grained. The Jurassic and Cretaceous basin shales are good seals (e.g. the Vlieland shale).

An example of possible stratigraphic traps is given by Abbink *et al.* (2006) for the Dutch Central Graben. A Late Jurassic play in deltaic facies is comparable to the model for the Delfland (Late Jurassic–Early Cretaceous) in the SW part of the Dutch onshore (Den Hartog Jager 1996). Delfland oil reservoirs are stratigraphically trapped and generally very small.

Another example of a play with a stratigraphic component is the spiculite reef play in sands of Late Jurassic age (Abbink *et al.* 2006). Dissolved sponge spicules are creating pore space and its silica enhances reservoir properties. Two fields produce from this reservoir and the thickness trends in buildups suggest a sponge bioherm.

The sands of the Lower Cretaceous Vlieland Formation are one of the prime candidates for stratigraphic traps. For example, the Vlieland Leeuwarden Field and its satellite fields Rauwerd and Grouw (Figs 13 & 14) are some of the few, if not the only, fields described in the literature (Cottençon *et al.* 1975), which have dominant stratigraphic trapping. Zechstein salt dissolution in the subsurface creates accommodation space at the unconformity. The Vlieland reservoir sands pinch out against 'bald zones' with no sand.

The Rijswijk oil province and reservoirs in the Broad Fourteens Basin (Bodenhausen & Ott 1981; Roelofsen & De Boer 1991; Racero-Baena & Drake 1996; Den Hartog Jager 1996) show synsedimentary facies change at faults. Later inversion creates largely structural traps.

Late Cretaceous Chalk

The uniform cover of the cream-colored micritic limestone of the marine Late Cretaceous Chalk Group is present underneath large parts of the country (see Van der Molen 2004; Wong *et al.* 2007). The lithology is dominantly a pelagic bioclastic friable limestone, the autochthonous chalk, with green sands present at the southern fringes of the West Netherlands Basin. With the exception of a few inverted areas near the Dutch Central Graben and the central Netherlands, a 500 m-thick Chalk section is very common. Highs like the London Brabant Massif almost never flooded in geological history. During the Upper Cretaceous they are submerged due to high global sea-level. Average water depth is estimated at a few hundred metres. Near highs the depth is much shallower and locally much deeper. In some areas over 1500 m of Chalk has been deposited (Wong *et al.* 2007). Wireline correlations indicate several intra-formational unconformities. Redeposition of

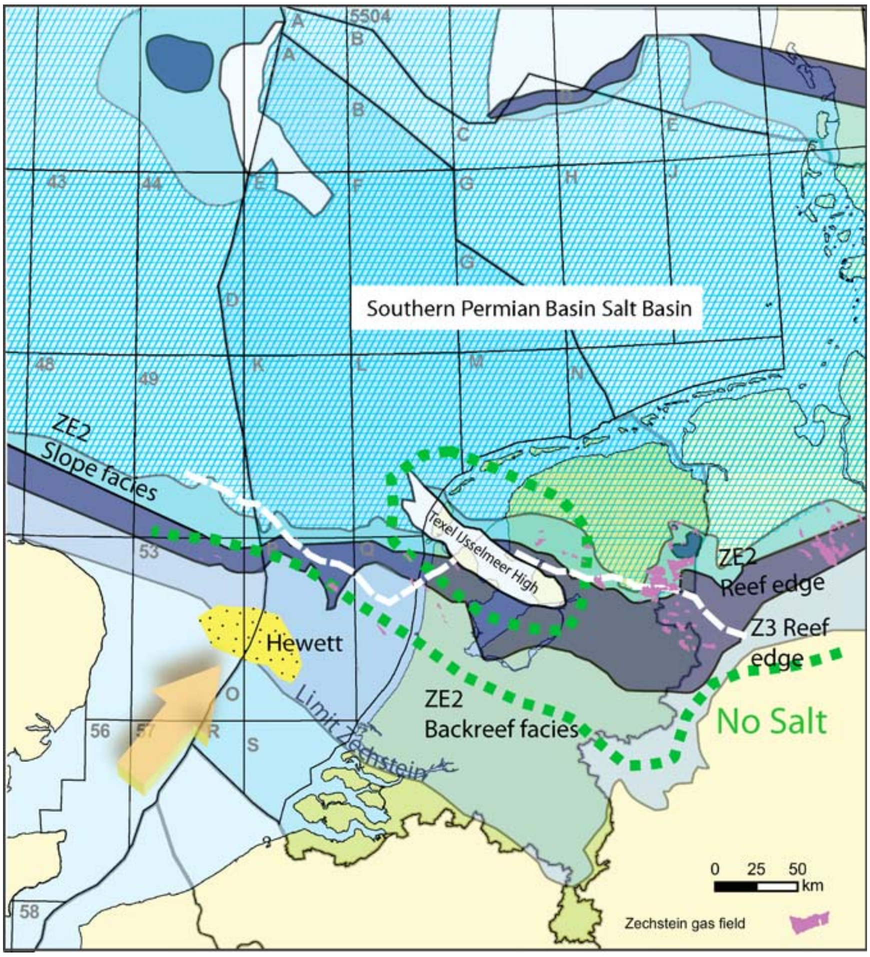

Fig. 9. Play map, Zechstein Group.

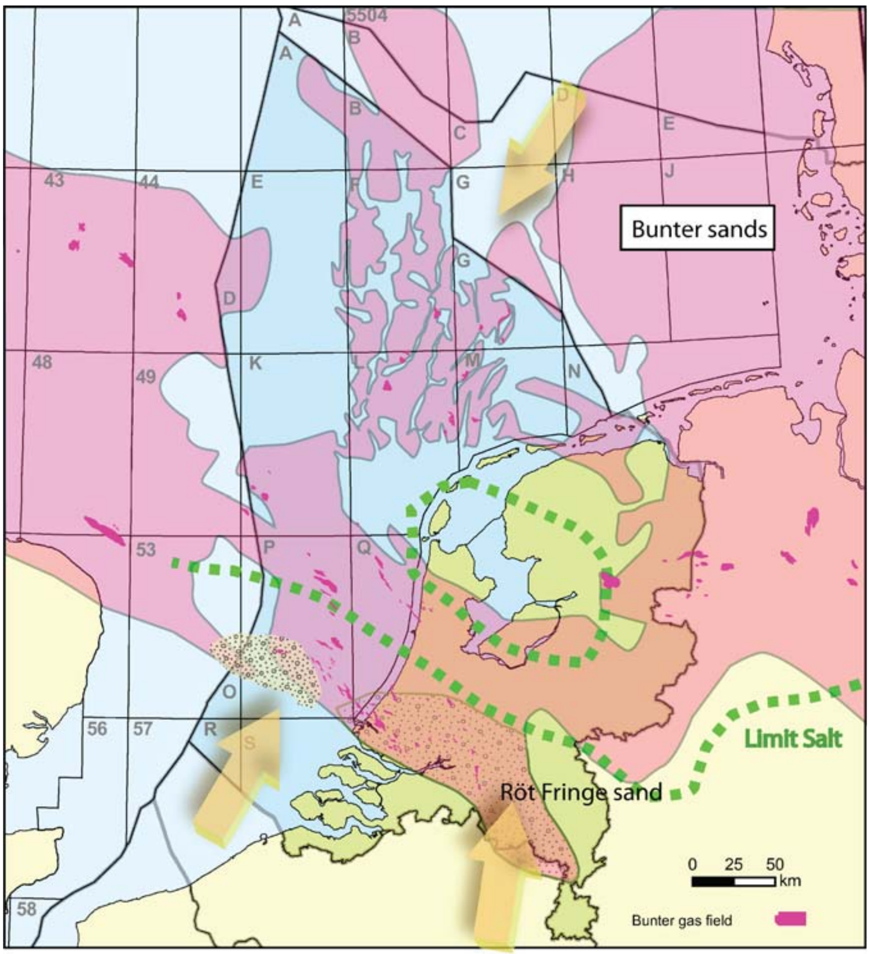

Fig. 10. Play map, Triassic Bunter.

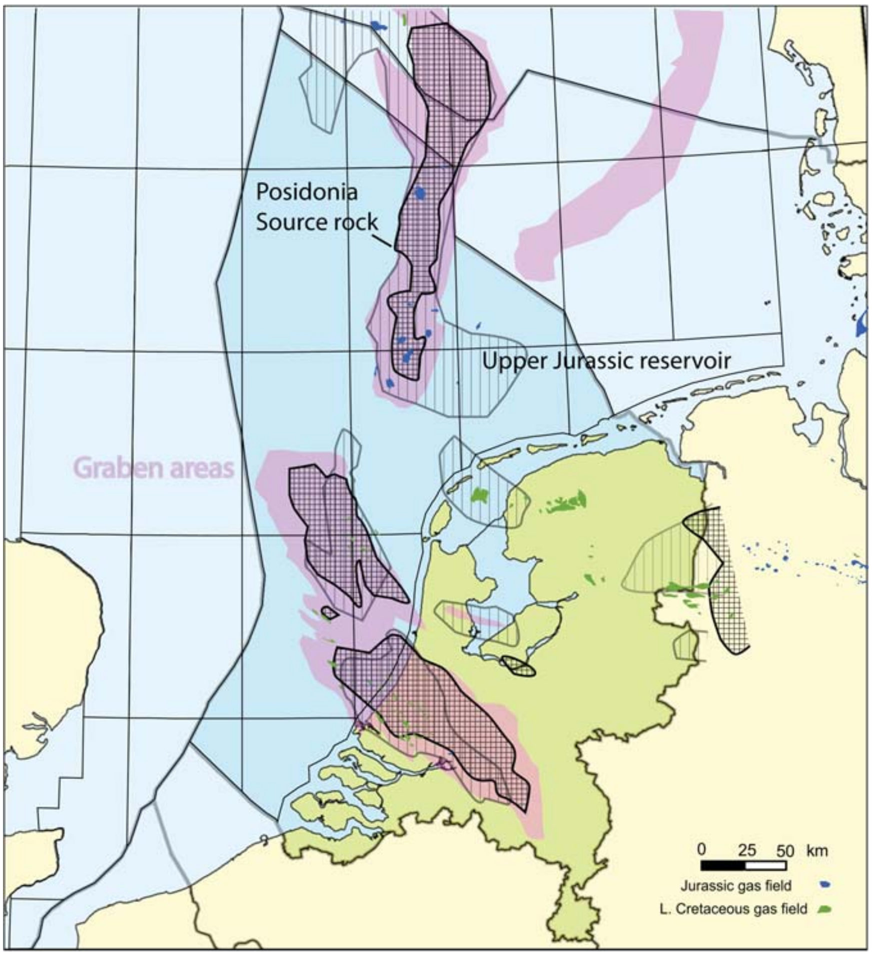

Fig. 11. The Early Jurassic source rock.

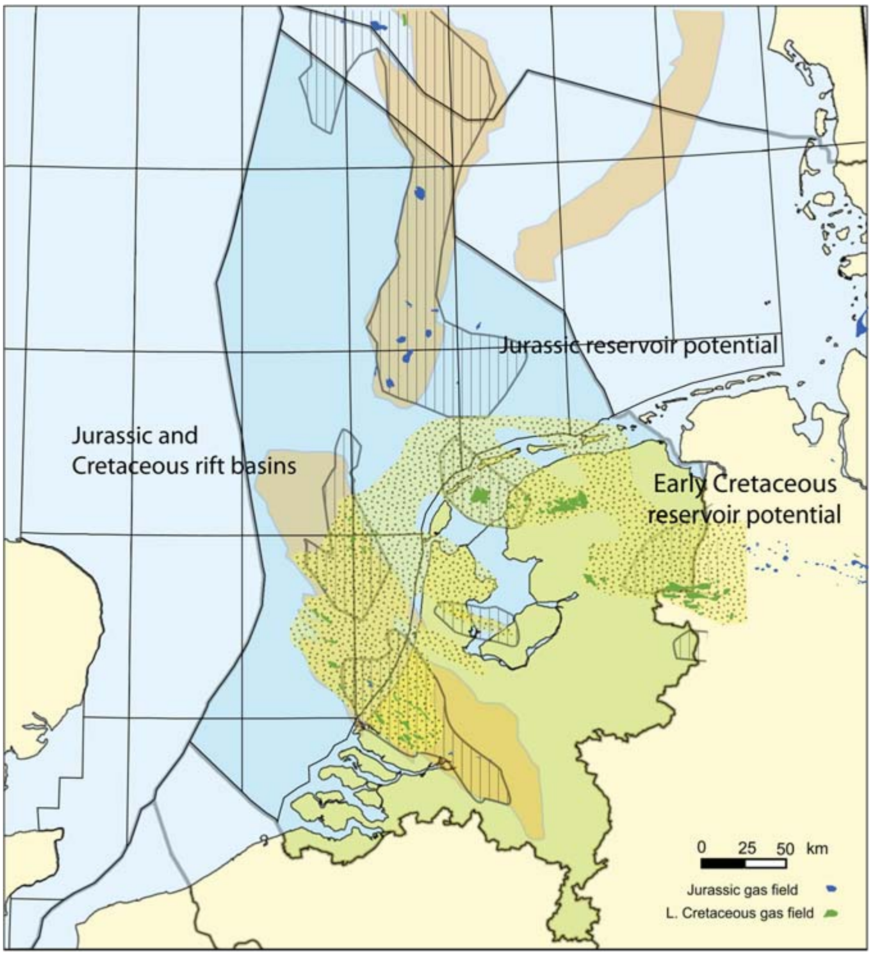

Fig. 12. Play map, Late Jurassic and Early Cretaceous.

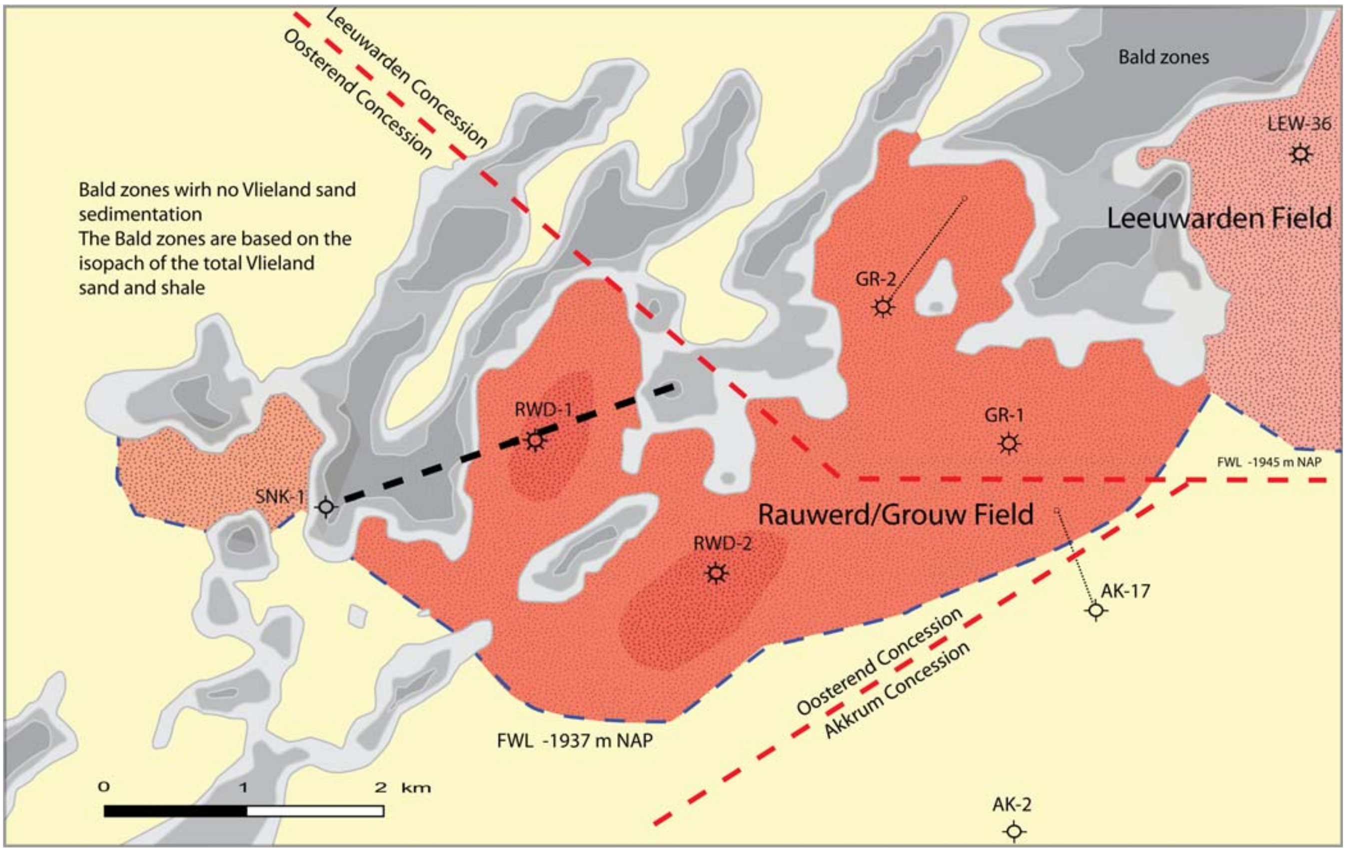

Fig. 13. Stratigraphic trapping of the Lower Cretaceous Rauwerd, Grouw and Leeuwarden Field area because of thinning of the sands against highs at the unconformity. The lows and highs have been created by salt solution.

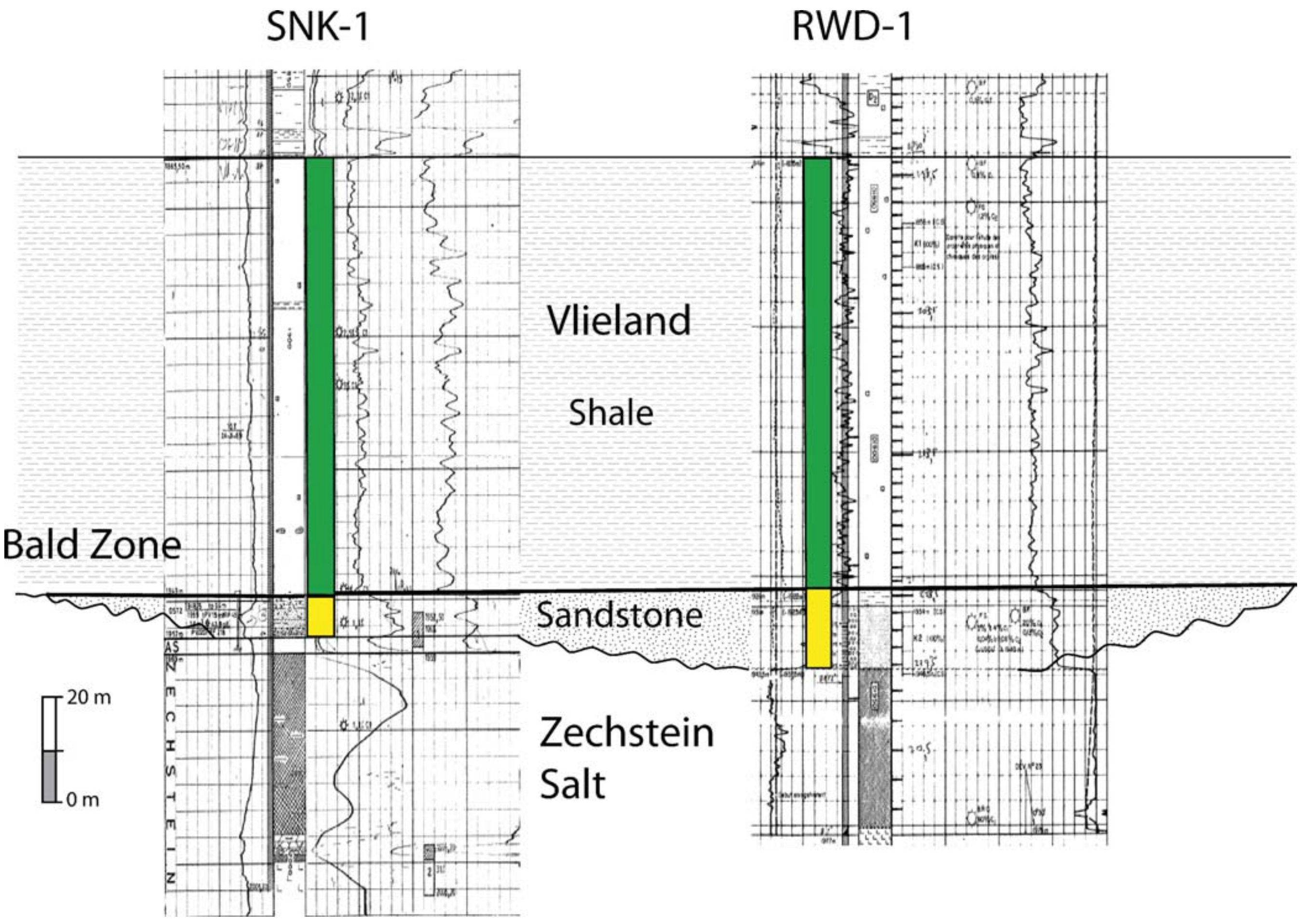

Fig. 14. Cross section Rauwerd-1–Sneek-1 showing the thinner sands in the area with thinner Vlieland section. In Rauwerd, full sand section.

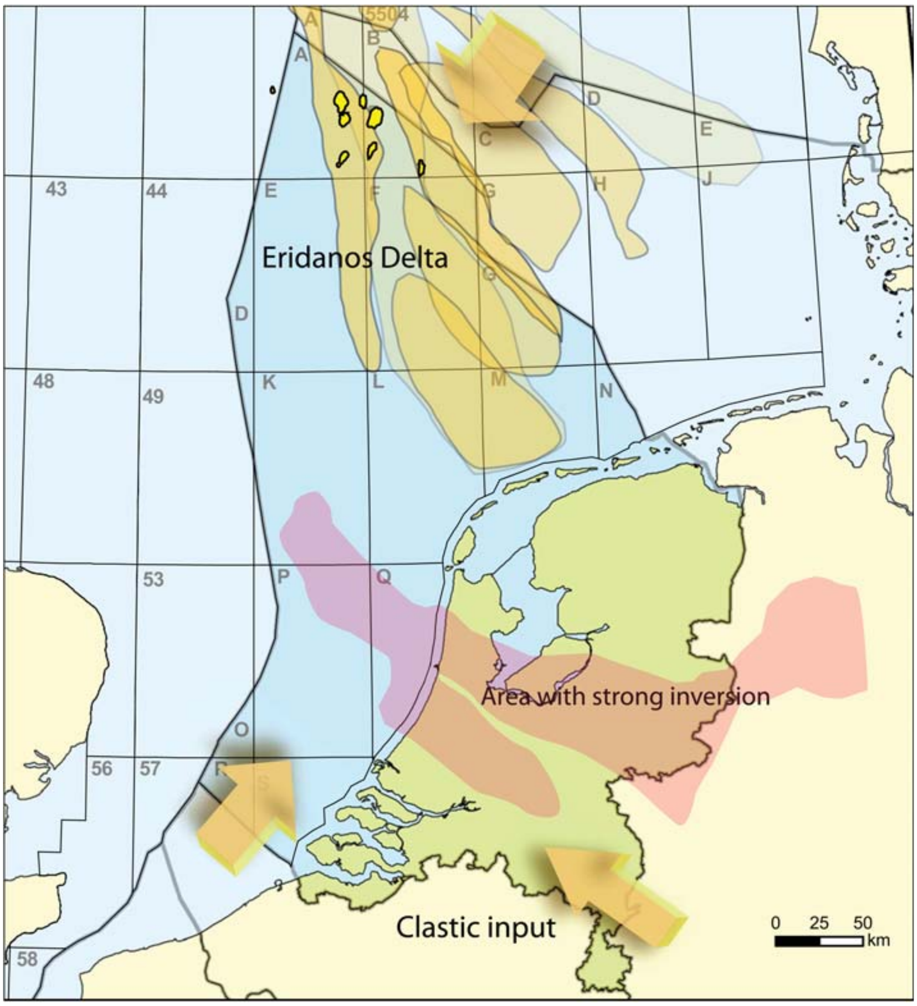

Fig. 15. Cenozoic fields and the main clastic input into the basin.

autochthonous Chalk can be seen on the seismic (Van der Molen 2004). The Chalk Group is an important hydrocarbon producing formation in countries outside the Netherlands like Norway, the UK and Denmark. Thousands of wells have been at least drilled to the Chalk group in the Netherlands. Compared with Denmark (Vejbæk *et al.* 2005) which has Chalk fields on the east side of the Central Graben not too far from the Dutch offshore, the results are very disappointing. One oil field on the west side of the Central Graben and one gas field onshore have been discovered. The poor results may be due to lack of charge. The important Kimmeridge Clay source rock, imperative to charge in many North Sea Chalk fields (Glennie 1998) is not well developed further south. It is not a lack of traps. Salt movements may provide structural traps and the unconformities can create stratigraphic traps.

Cenozoic

The Cenozoic age sediments are called the North Sea Group which is almost present below the whole country. Over large areas the thickness of the dominantly siliciclastic sediments reaches over 1000 m. In the northern offshore area the thickness reaches 2000 m. The North Sea sediments are dominated by marine or near-shore facies (Van Adrichem Boogaert & Kouwe 1997; De Lugt *et al.* 2003; Kuhlmann *et al.* 2006). A number of breaks are created by tectonic events and sea-level low stands. The tectonic inversion caused widespread erosion. The Mid North Sea Group base is defined on a major break at the Late Eocene. The Base of the Upper North Sea Group is the Mid Miocene unconformity. A lowstand as well as a tectonic event have been proposed for the explanation of severe erosion (Wong *et al.* 2007). Shale is dominant, but the section contains various sands linked to the tectonic events and sedimentation breaks (De Lugt *et al.* 2003; Wong *et al.* 2007) that can contain gas. Often the gas is clearly visible on the seismic owing to a bright amplitude effect. The shallow gas in various sands in the North Sea is generally not seen as a prospect and is considered a drilling hazard. Gas production started last year from North Sea accumulations in the northern A and B blocks (Fig. 15). Coastal sands from the late Pliocene Eridanos delta trapped gas in low relief structures created by salt doming. The sediments build out from the east (Sørensen *et al.* 1997; Kuhlmann *et al.* 2006). As a result of rapid facies changes in the delta, there is also a stratigraphic component in trapping. The presence of active salt domes causes most North Sea gas sands to have a strong structural component in their trapping. Facies change in sands also can provide stratigraphic traps.

Conclusions

The success of structural traps for Dutch hydrocarbon exploration prospectivity left the stratigraphic plays and prospects with less attention. Stratigraphic trapping is rarely confirmed and is limited to a few horizons. Stratigraphic aspects of plays are significant to more than the top seal only. Good sedimentological models make it possible to differentiate play areas. In the structural setting of the Netherlands, the stratigraphical trap will be rare in the Rotliegend since facies changes are relatively gradual compared with the high frequency of faulting. The shallow marine Late Jurassic and Early Cretaceous play areas have a number of proven accumulations with strong stratigraphic aspects. Trapping in carbonates has a strong stratigraphic element due to rapid facies changes in most carbonates found in the Dutch subsurface. Mississippian carbonate leads deserve more attention because they may give a new stimulus to exploration, hopefully even more than many high-ranking prospects based on structural trapping. With the improvement of the seismic, acquisition and processing, the search for stratigraphic traps should get a higher priority.

The author thanks Energie Beheer Nederland B. V. for permission to publish this paper. Anonymous reviewers are thanked for their constructive editing.

References

Abbink, O. A., Mijnlieff, H. F., Munsterman, D. K. & Verreussel, R. M. C. H. 2006. New stratigraphic insights in the 'Late Jurassic' of the Southern Central North Sea Graben and Terschelling Basin (Dutch Offshore) and related exploration potential. *Geologie en Mijnbouw/Netherlands Journal of Geosciences*, **85**, 221–238.

Abramovitz, T. & Thybo, H. 1998. Seismic structure across the Caledonian deformation front along MONA LISA profile 1 in the southeastern North Sea. *Tectonophysics*, **288**, 153–176.

Ames, R. & Farfan, P. F. 1996. The environment of deposition of the Triassic Main Buntsandstein Formation in the P and Q quadrants, offshore the Netherlands. *In*: Rondeel, H. E., Batjes, D. A. J. & Nieuwenhuijs, W. H. (eds) *Geology of Gas and Oil under the Netherlands*. Royal Geological and Mining Society of the Netherlands, Kluwer Academic, Dordrecht, 167–178.

Bodenhausen, J. W. A. & Ott, W. F. 1981. Habitat of the Rijswijk oil province, onshore, the Netherlands. *In*: Illing, L. V. & Hobson, G. D. (eds) *Petroleum Geology of the Continental Shelf of North-West Europe: Proceedings of the 2nd Conference*. Institute of Petroleum, London, 301–309.

Borkhataria, R., Aigner, T., Pöppelreiter, M. C. & Pipping, J. C. P. 2005. Characterisation of epeiric 'Layer-cake' carbonate reservoirs: Upper Muschelkalk (Middle Triassic), The Netherlands. *Journal of Petroleum Geology*, **28**, 119–146.

Cottençon, A., Parant, B. & Flaceliçre, G. 1975. Lower Cretaceous gas fields in Holland. *In*: Woodland, A. W. (ed.) *Petroleum and the Continental Shelf of North-West Europe*. Applied Science, Barking, **1**, 403–412.

De Jager, J. & Barrio, C. 2003. The 'Fat Sand' play – a new Triassic play in the Southern Permian Basin. *In*: Doré, A. G. & Vining, B. A. (eds) *Petroleum Geology: North-West Europe and Global Perspectives: Proceedings of the 6th Petroleum Geology Conference*. Geological Society, London, 105; doi: 10.1144/0060105.

De Lugt, I. R., Van Wees, J. D. A. M. & Wong, T. E. 2003. The tectonic evolution of the Southern Dutch North Sea during the Palaeogene: basin inversion in distinct pulses. *Tectonophysics*, **373**, 141–159.

Den Hartog Jager, D. G. 1996. Fluviomarine sequences in the Lower Cretaceous of the West Netherlands Basin: correlation and seismic expression. *In*: Rondeel, H. E., Batjes, D. A. J. & Nieuwenhuijs, W. H. (eds) *Geology of Gas and Oil under the Netherlands*. Royal Geological and Mining Society of the Netherlands, Kluwer Academic, Dordrecht, 229–242.

Doornenbal, J. C. & Stevenson, A. G. (eds) 2010. *Petroleum Geological Atlas of the Southern Permian Basin Area*. European Association of Geoscientists and Engineers Publications BV., Houten, The Netherlands.

Dronkert, H. & Remmelts, G. O. 1996. Influence of salt structures on reservoir rocks in Block L2, Dutch continental shelf. *In*: Rondeel, H. E., Batjes, D. A. J. & Nieuwenhuijs, W. H. (eds) *Geology of Gas and Oil under the Netherlands*. Royal Geological and Mining Society of the Netherlands, Kluwer Academic, Dordrecht, 159–166.

Fontaine, J. M., Guastella, G., Jouault, P. & de la Vega, P. 1993. F15-A: a Triassic gas field on the eastern limit of the Dutch Central Graben. *In*: Parker, J. R. (ed.) *Petroleum Geology of Northwest Europe: Proceedings of the 4th Conference*. Geological Society, London, 583–593; doi: 10.1144/0040583.

Geluk, M. C. 2005. *Stratigraphy and tectonics of Permo-Triassic basins in the Netherlands and surrounding areas*. Ph.D. thesis, University of Utrecht.

George, G. T. & Berry, J. K. 1993. A new lithostratigraphy and depositional model for the Upper Rotliegend of the UK sector of the Southern North Sea. *In*: North, C. P. & Prosser, D. J. (eds) *Characterisation of Fluvial and Aeolian Reservoirs*. The Geological Society, London, Special Publications, **73**, 291–319.

George, G. T. & Berry, J. K. 1994. A new palaeogeographic and depositional model for the Upper Rotliegend, offshore The Netherlands. *First Break*, **12**, 147–158.

Gerling, P., Geluk, M. C., Kockel, F., Lockhorst, A., Lott, G. K. & Nicholson, R. A. 1999. 'NW European Gas Atlas' – new implications for the Carboniferous gas plays in the western part of the Southern Permian Basin. *In*: Fleet, A. J. & Boldy, S. A. R. (eds) *Petroleum Geology of Northwest Europe: Proceedings of the 5th Conference*. Geological Society, London, 799–808; doi: 10.1144/0050799.

Glennie, K. W. (ed.) 1998. *Petroleum Geology of the North Sea, Basic Concepts and Recent Advances*. Blackwell Science, London.

Hampson, G. J., Davies, S. J., Elliott, T., Flint, S. S. & Stollhoven, H. 1999. Incised valley fill sandstone bodies in Upper Carboniferous fluvio-deltaic strata: recognition and reservoir characterization of Southern North Sea analogues. *In*: Fleet, A. J. & Boldy, S. A. R. (eds) *Petroleum Geology of Northwest Europe: Proceedings of the 5th Conference*. Geological Society, London, 771–788; doi: 10.1144/0050771.

Hoetz, H. L. J. G. & Watters, D. G. 1992. Seismic horizon attribute mapping for the Annerveen Gasfield, the Netherlands. *First Break*, **10**, 41–51.

Kombrink, H. 2008. The Carboniferous of the Netherlands and surrounding areas; a basin analysis. *Geologica Ultraiectina*, **294**. Ph.D. thesis, University of Utrecht.

Kosters, M. & Donselaar, M. E. 2003. Syn-sedimentary faulting and the formation of localized reservoir sands: Carboniferous examples from the Campine Basin, Belgium and the Dutch offshore. *Petroleum Geoscience*, **9**, 309–319.

Kuhlmann, G., Langereis, C. G., Munsterman, D., Leeuwen, R. J., van Verreussel, R., Meulenkamp, J. E. & Wong, T. E. 2006. Chronostratigraphy of Late Neogene sediments in the southern North Sea Basin and paleoenvironmental interpretations. *Palaeogeography, Palaeoclimatology, Palaeoecology*, **239**, 426–455.

Levorson, A. I. 1936. Stratigraphic versus structural accumulation. *American Association of Petroleum Geologists Bulletin*, **20**, 521–530.

Maynard, J. R. & Gibson, J. P. 2001. Potential for subtle traps in the Permian Rotliegend of the UK Southern North Sea. *Petroleum Geoscience*, **7**, 301–314.

Pöppelreiter, M. C., Borkhataria, R., Aigner, T. & Pipping, K. 2005. Production from Muschelkalk carbonates (Triassic, NE Netherlands): unique play or overlooked opportunity. *In*: Doré, A. G. & Vining, B. A. (eds) *Petroleum Geology: North-West Europe and Global Perspectives: Proceedings of the 6th Petroleum Geology Conference*. Geological Society, London, 299–315; doi: 10.1144/0060299.

Racero-Baena, A. & Drake, S. J. 1996. Structural style and reservoir development in the West-Netherlands oil province. *In*: Rondeel, H. E., Batjes, D. A. J. & Nieuwenhuijs, W. H. (eds) *Geology of Gas and Oil under the Netherlands*. Royal Geological and Mining Society of the Netherlands, Kluwer Academic Publishers, Dordrecht, 211–227.

Roelofsen, J. W. & De Boer, W. D. 1991. Geology of the Lower Cretaceous Q/1 oil-fields, Broad Fourteens Basin, the Netherlands. *In*: Spencer, A. M. (ed.) *Generation, Accumulation and Production of Europe's Hydrocarbons, Proceedings. First Conference EAPG, 30 May to 2 June*. Special Publications of the European Association of Petroleum Geoscientists, West Berlin, **1**, 203–216.

Schroot, B. M. & Schüttenhelm, R. T. E. 2003. Expressions of shallow gas in the Netherlands North Sea. *Geologie en Mijnbouw/Netherlands Journal of Geosciences*, **82**, 91–105.

Sørensen, J. C., Gregersen, U., Breiner, M. & Michelsen, O. 1997. High-frequency sequence stratigraphy of Upper Cenozoic deposits in the central and southeastern North Sea areas. *Marine and Petroleum Geolgy*, **14**, 99–123.

Spain, D. R. & Conrad, C. P. 1997. Quantitative analysis of top-seal capacity: offshore Netherlands, southern North Sea. *Geologie en Mijnbouw*, **76**, 217–226.

Spencer, A. M., Leckie, G. G. & Chew, K. J. 1996. North Sea hydrocarbon plays and their resources. *First Break*, **14**, 345–357.

Van Adrichem Boogaert, H. A. & Kouwe, W. F. P. [comp.] 1997. *Stratigraphic Nomenclature of the Netherlands, Revision and Update by RGD and NOGEPA*. Mededelingen Rijks Geologische Dienst, nieuwe serie, **50**, sections a–j.

Van der Molen, A. S. 2004. Sedimentary development, seismic stratigraphy and burial compaction of the Chalk Group in the Netherlands North Sea area. *Geologica Ultraiectina*, **248**, Ph.D. thesis, University of Utrecht.

Van de Sande, J. M. M., Reijers, T. J. A. & Casson, N. 1996. Multidisciplinary exploration strategy in the northeast Netherlands Zechstein 2 Carbonate play, guided by 3D seismics. *In*: Rondeel, H. E., Batjes, D. A. J. & Nieuwenhuijs, W. H. (eds) *Geology of Gas and Oil under the Netherlands*. Royal Geological and Mining Society of the Netherlands, Kluwer Academic, Dordrecht, 125–142.

Van Hulten, F. F. N. & Poty, E. 2008. Geological factors controlling Early Carboniferous carbonate platform development in the Netherlands. *Geological Journal*, **43**, 175–196.

Vejbæk, O. V., Frykman, P., Bech, N. & Nielsen, C. M. 2005. The history of hydrocarbon filling of Danish Chalk fields. *In*: Doré, A. G. & Vining, B. A. (eds) *Petroleum Geology: North-West Europe and Global Perspectives: Proceedings of the 6th Petroleum Geology Conference*. Geological Society, London, 1331–1345; doi: 10.1144/0061331.

Verdier, J. P. 1996. The Rotliegend sedimentation history of the southern North Sea and adjacent countries. *In*: Rondeel, H. E., Batjes, D. A. J. & Nieuwenhuijs, W. H. (eds) *Geology of Gas and Oil under the Netherlands*. Royal Geological and Mining Society of the Netherlands, Kluwer Academic, Dordrecht, 45–56.

Wong, T. E., Batjes, D. A. J. & de Jager, J. (eds) 2007. *Geology of the Netherlands*. Royal Netherlands Academy of Arts and Sciences, Amsterdam.

Session: Europe

Field Development and Production

Laggan; a mature understanding of an undeveloped discovery, more than 20 years old

A. GORDON,[1] T. YOUNIS,[1] C. BERNARD-GRAILLE,[1] R. GRAY,[2] J.-M. URRUTY,[2] L. BEN-BRAHIM,[2] J.-C. NAVARRE,[3] B. PATERNOSTER[4] and G. EVERS[2]

[1]*Total SA, Tour Coupole, 2, Place Jean Millier, 92078, La Defense 6, France (e-mail: andy.gordon@total.com)*
[2]*Total E & P Ltd, Crawpeel Road, Altens Industrial Estate, Aberdeen AB12 3FG, UK*
[3]*Total Upstream Nigeria Ltd, 35 Kofo Abayomi St., Victoria Island, Lagos, Nigeria*
[4]*Total SA, CSTJF, Avenue Larribau, Pau 64018, France*

Abstract: Laggan, located in the west of Shetland, was discovered in 1986. There is now an improved understanding of Laggan, thanks to innovative and fully integrated geoscience studies and a successful appraisal campaign. Development studies are well advanced, with the discovery of Tormore in 2007 providing the potential for a combined development project. Laggan and Tormore are Paleocene gas condensate discoveries in approximately 600 m water depth. The traps are both mixed, stratigraphic with updip closure against bounding faults. The reservoir comprises sand-rich turbidite channelized lobes and lobes. Reservoir properties are good (permeability range 30–300 mD) due to the presence of chlorite and pre-sorting on the shelf. The geoscience evaluation of Laggan has matured over the last four years with the help of fully integrated studies using 3D seismic and well data. The depositional model has been defined on the basis of an evaluation of cores and seismic and supported by analogue studies. Seismic inversion studies have also helped constrain the reservoir architecture. Of particular value has been the application of AVO to quantify net gas sand, recognized as the principal static uncertainty. The main dynamic uncertainty is the risk of compartmentalization. This risk has been reduced through an improved definition of the fault configuration by re-processing the seismic and detailed seismic attribute analysis. The potential of Tormore was recognized by applying the geoscience understanding of Laggan to help de-risk the prospect. In particular, it was recognized that Laggan could be used as an analogue for the Tormore trapping configuration and reservoir potential and that AVO could be used to help define the Gas–Water Contact. The exploration well, drilled in 2007, was successful in finding a similar reservoir to that encountered in Laggan. The fluid encountered was a gas condensate, approximately three times richer than Laggan.

Keywords: undeveloped gas condensate discovery, turbidites, chlorite, AVO, uncertainty analysis

Laggan and Tormore are Paleocene gas condensate discoveries in approximately 600 m water depth, in blocks 206/1a and 205/5a respectively in the Flett Sub-Basin of the UKCS Faroe–Shetland Basin (Figs 1 & 2). Laggan and Tormore are situated approximately 35 km to the NW of the Clair Field and 120 km to the NW of the Shetland Islands (Fig. 1).

The traps are both mixed, stratigraphic with updip closure against bounding faults. The reservoir comprises sand-rich turbidite channelized lobes and lobes. Reservoir properties are good (permeability range is 30–300 mD) due to the presence of chlorite and pre-sorting on the shelf.

There are four exploration and appraisal wells in Laggan (Fig. 3). Laggan was discovered in 1986 by the 206/1–2 well which contained lean gas condensate. In 1996, the second well 206/1–3 targeted an amplitude shut-off downdip. The well encountered the gas–water contact (GWC) and confirmed that there was no oil rim. Well 206/1a–4a was drilled in 2004 to appraise the crest of the structure and then side-tracked downdip (as well 206/1a–4z). The 2004 appraisal well programme confirmed the updip potential of Laggan and in particular, the hypothesis that the gas saturations updip were significantly improved relative to the downdip wells, thanks to a long transition zone related to the presence of chlorite.

The Tormore exploration well, located 12 km to the SW of Laggan (Fig. 4) was drilled in 2007 and was successful in finding a similar reservoir to that encountered in Laggan. The fluid encountered was a gas condensate, approximately three times richer than that of Laggan.

Depositional model

The depositional model has been defined on the basis of an integrated study of cores, seismic and analogue studies. Seismic inversion studies have also helped to constrain the reservoir architecture.

The Laggan sands were deposited in a deep water environment. They are very well sorted, with a notable absence of very coarse grained sandstones, pebbly sandstones or conglomerates (Fig. 5). This supports a model of a sand supply that has been sorted on a shelf, prior to being transported and re-deposited in the basin as amalgamated turbidites.

A 'Low Reflectivity Seismic Package', developed in the SW of Laggan with chaotic seismic facies, pre-dates the Laggan sands (location, Fig. 6). This interval was cored in the 206/1–3 well and comprises debris flows and thin-bedded turbidites with poor reservoir potential (maximum permeability 0.17 mD). The conclusion that the interval has poor potential is supported by the absence of an amplitude variation with offset (AVO) response, in contrast to the Laggan sands. The onlap of the Laggan sands to the SW onto the depositional relief associated with the Low Reflectivity Package is evident from seismic data.

The more channelized/confined form of the Laggan sands on the flank of the Low Reflectivity Package is recognized in particular along the trend of the bounding fault, which may have been active prior to the Laggan sands to create a topographic low. The Laggan sands are interpreted to be absent or very thin (less than 10 m) on the depositional relief created by the low reflectivity

VINING, B. A. & PICKERING, S. C. (eds) *Petroleum Geology: From Mature Basins to New Frontiers – Proceedings of the 7th Petroleum Geology Conference*, 279–297. DOI: 10.1144/0070279

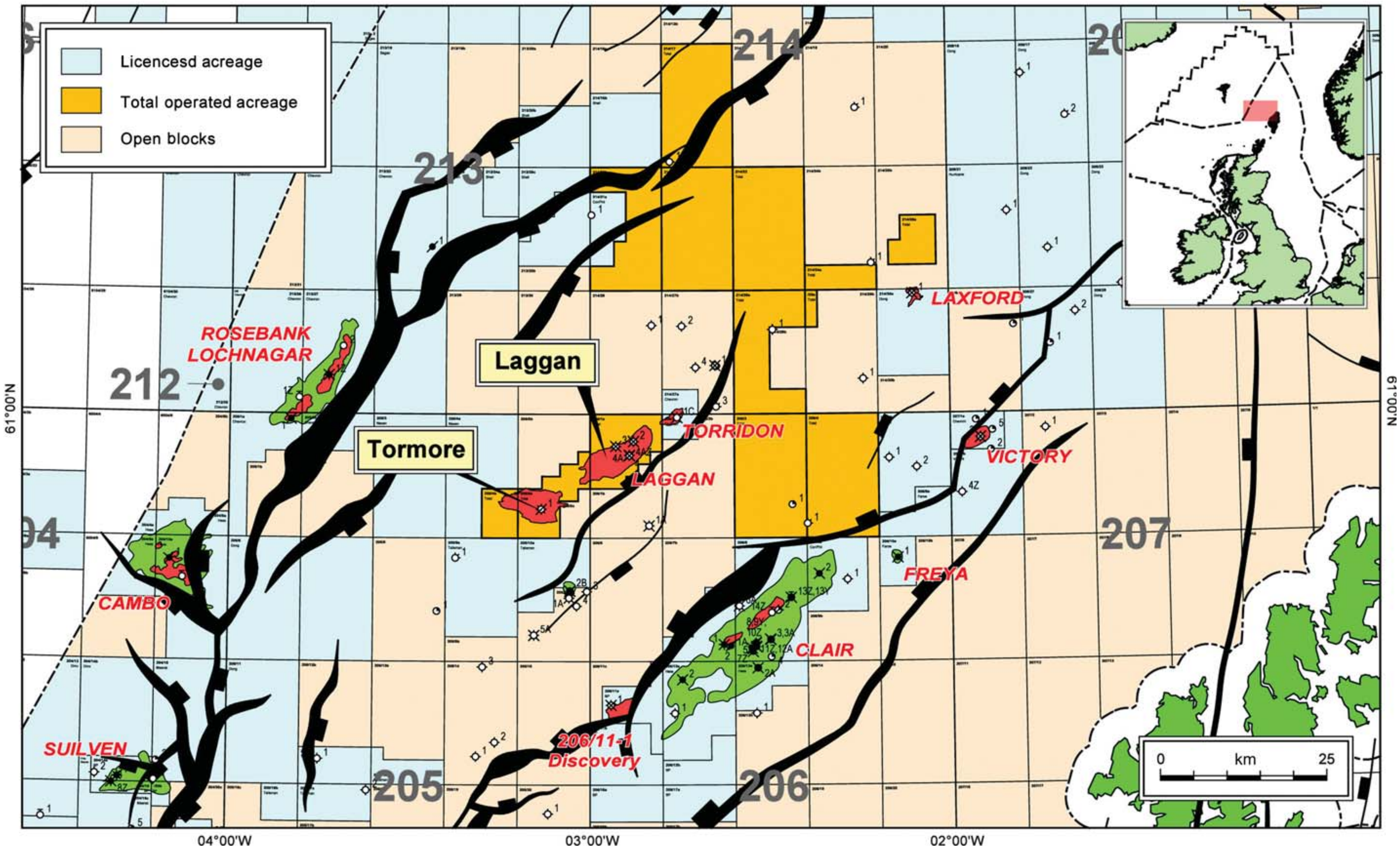

Fig. 1. Location map of Laggan and Tormore. Laggan and Tormore lie in the Flett Sub-Basin of the UKCS Faroe–Shetland Basin.

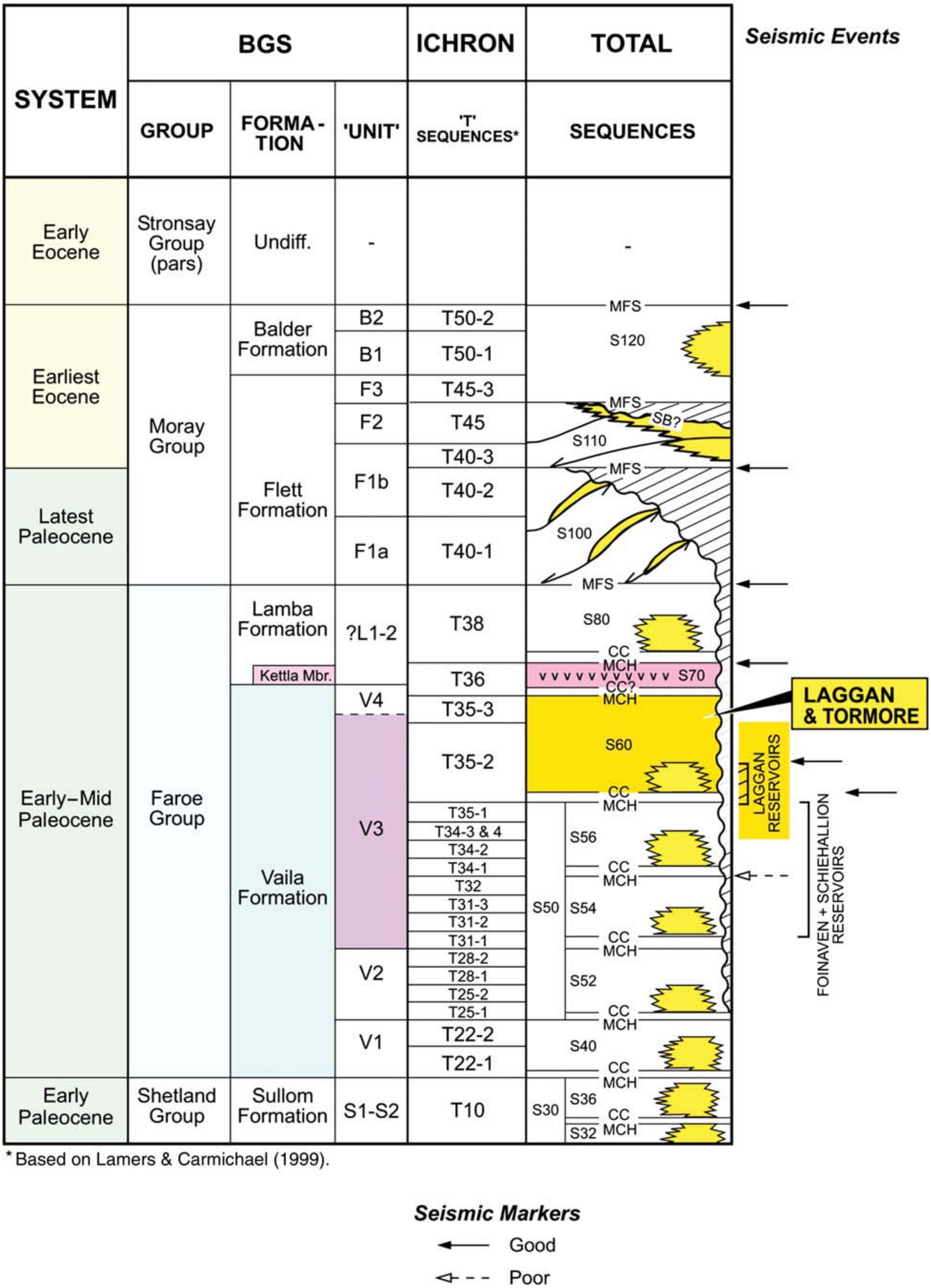

Fig. 2. Faroe Shetland Paleocene stratigraphy with a comparison of the schemes utilized in the West of Shetland Area. The Laggan sands are part of the V3 unit of the Vaila Formation.

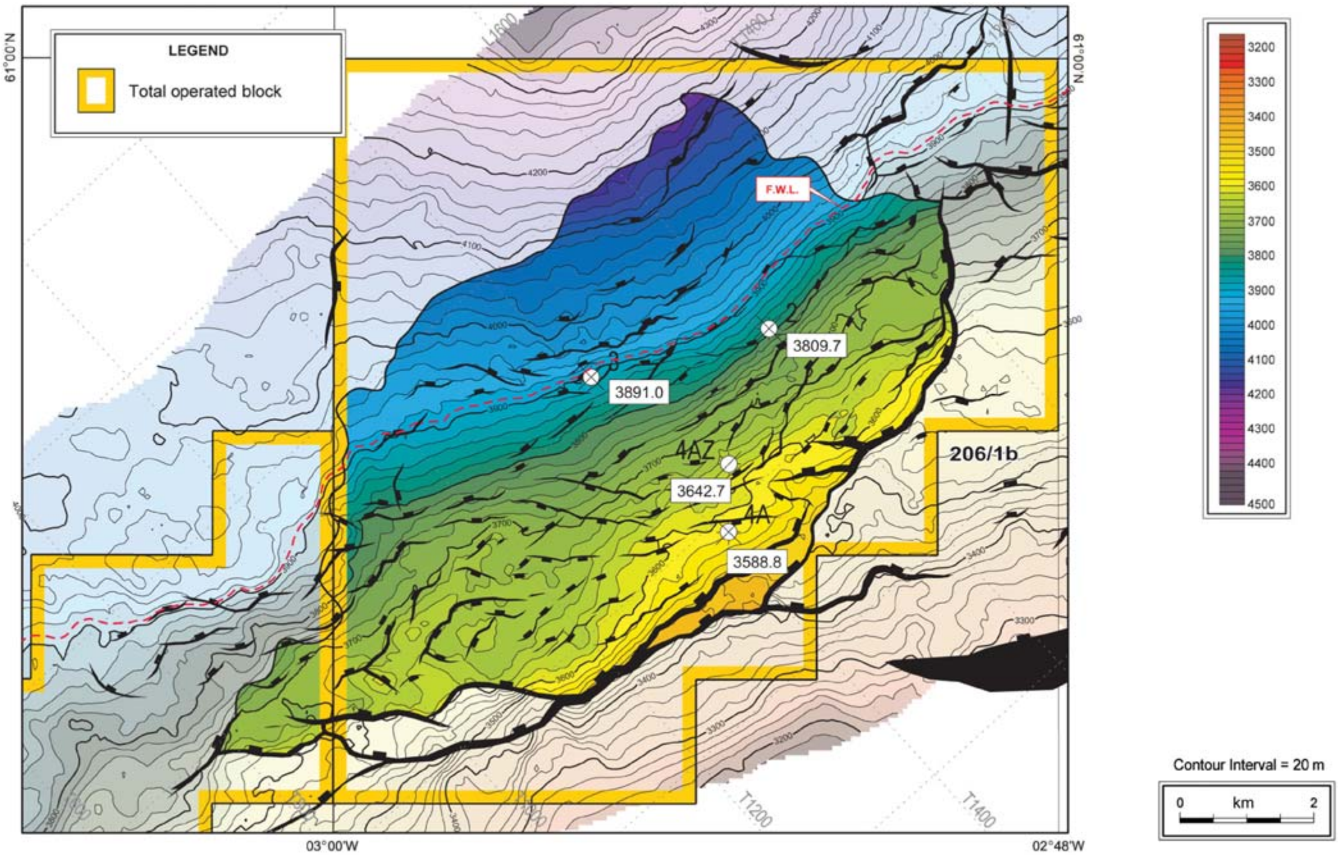

Fig. 3. Laggan, Top Reservoir depth structure map showing the outline of the field and the location of the four exploration and appraisal wells. The Laggan trap is mixed, stratigraphic with updip closure against bounding faults.

mound. The Laggan sands are interpreted to be more lobate/less confined in the main depocentre of Laggan (Fig. 6). This hypothesis is supported by the subtle but recurring coarsening upward pattern noted in the Laggan cores.

The Laggan reservoir is subdivided into three units (A, B and C). The depositional model for the Laggan C sand (lowermost reservoir unit) is also constrained by the seismic interpretation of a near-top C sand seismic event. The C sands were deposited in the initial topographic lows that were related to faulting (Fig. 7). It is noted that the C sand has a greater thickness in the depocentre to the NW of 206/1a–4z than tested by any of the four wells.

The BC shales represent a phase when the sand sedimentation supply was shut off and hemi-pelagites and mud and silt turbidites draped the C sand. Thickening of the BC shales is interpreted basinward towards the NNW and is supported by the trends in the well data (Figs 7 & 8).

The seismic impedance (IP) data shows clearly the mechanism of compensation in response to depositional relief and differential compaction; the B sand depocentres are located on the flank of the C sand depocentre (Fig. 7). Progressive onlap of the margins by the B sand is proposed, noting that the C sand extension is more limited than the B sand.

The AB shales represent another phase of hemi-pelagite mud fall-out or mud to silt turbidites and drape the B sands. Thickening of the AB shales is interpreted basinward towards the NNW and is supported by trends in the well data.

Although the resolution of the seismic data is insufficient to delineate the A and B sands individually, the well data suggests that compensation plays a role in the A sand architecture, similar to the B sand, with the A sand for example being notably thicker in the 206/1a–4a well (with a thin B sand) in comparison to the 206/1a–4z well (with a thick B sand). Thin A sands are therefore expected over the B/C sand depocentres in response to compensation (Fig. 7). The A sand distribution is more widespread than the B sand, in line with a model of progressive onlap onto the basin margins. The A sand deposition was terminated, prior to a high stand period, with no significant sand supply in the Laggan area.

The main implications of the depositional model are as follows:

- In terms of reservoir quality and heterogeneity, the reservoir comprises mature, very well sorted sands and no significant heterogeneity is expected (thin inter-bedded turbidites are likely to be rare).
- In terms of connectivity, there is an inferred low erosion potential associated with these mature, fine sand turbidite flows. The Laggan A, B and C sands are disconnected on a pure stratigraphic basis and therefore for intra-reservoir juxtaposition faults are required.

Laggan sands sediment supply and palaeo-transport direction

On the basis of the analysis of seismically derived isopach maps, amplitude extractions, well correlations, biostratigraphy and heavy mineral analysis, the following depositional scheme is proposed. The Laggan feeder system is not preserved, but is interpreted to be dip-orientated, controlled by bathymetry lows on the slope, possibly associated with deep transfer fault zones. Active faulting at the time of deposition and compensation could have controlled the change in transport direction of the turbidite flows in the Laggan area towards the east/NE and parallel to the trend of the main Laggan faults (Figs 6 & 7). The Laggan sands correspond to turbiditic channelized lobes/lobes deposited at the base of slope as ponded turbidites, controlled by normal faults. The regional basin bathymetry also controlled the distribution of the turbidite lobes.

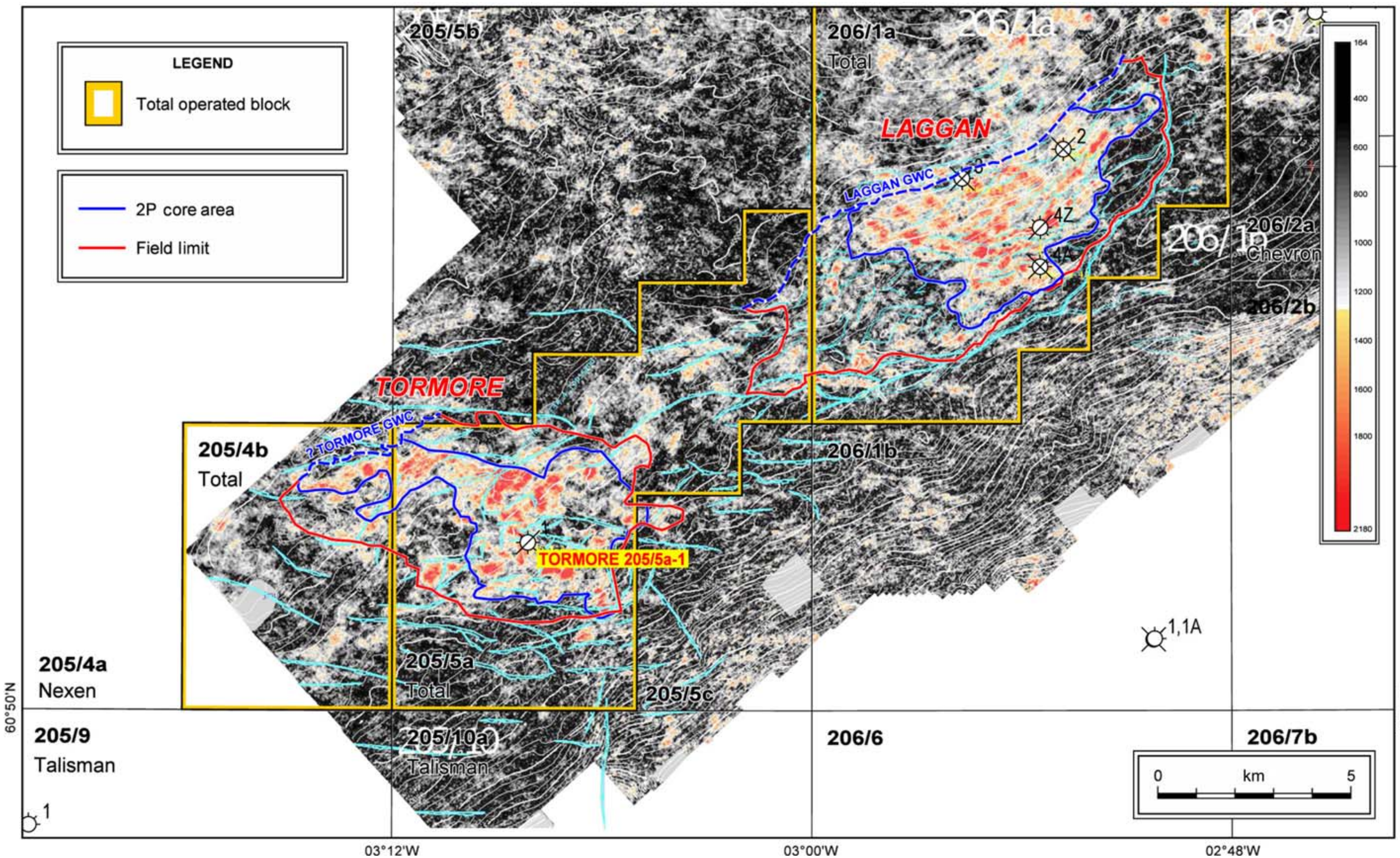

Fig. 4. Laggan, Tormore AVO and structural map. The Tormore exploration well is located 12 km to the SW of Laggan and was successful in finding a similar HC bearing reservoir as Laggan. The Laggan GWC corresponds to the AVO amplitude shut-off and it is assumed the same relationship applies for Tormore.

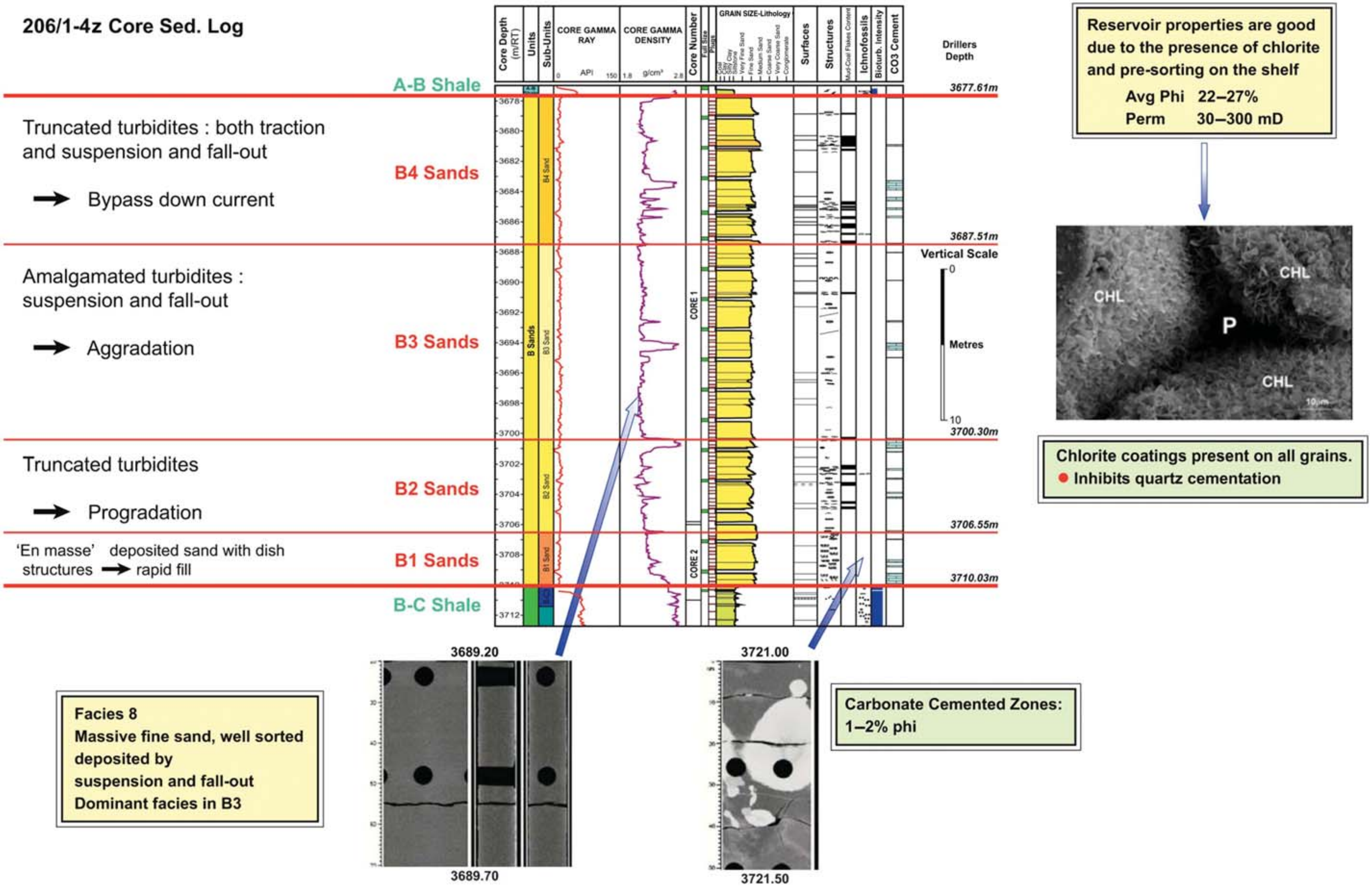

Fig. 5. Laggan reservoir characterization, with the interpretation of the 206/1a–4z cored interval shown. Reservoir properties are good due to pre-sorting on the shelf and the presence of chlorite.

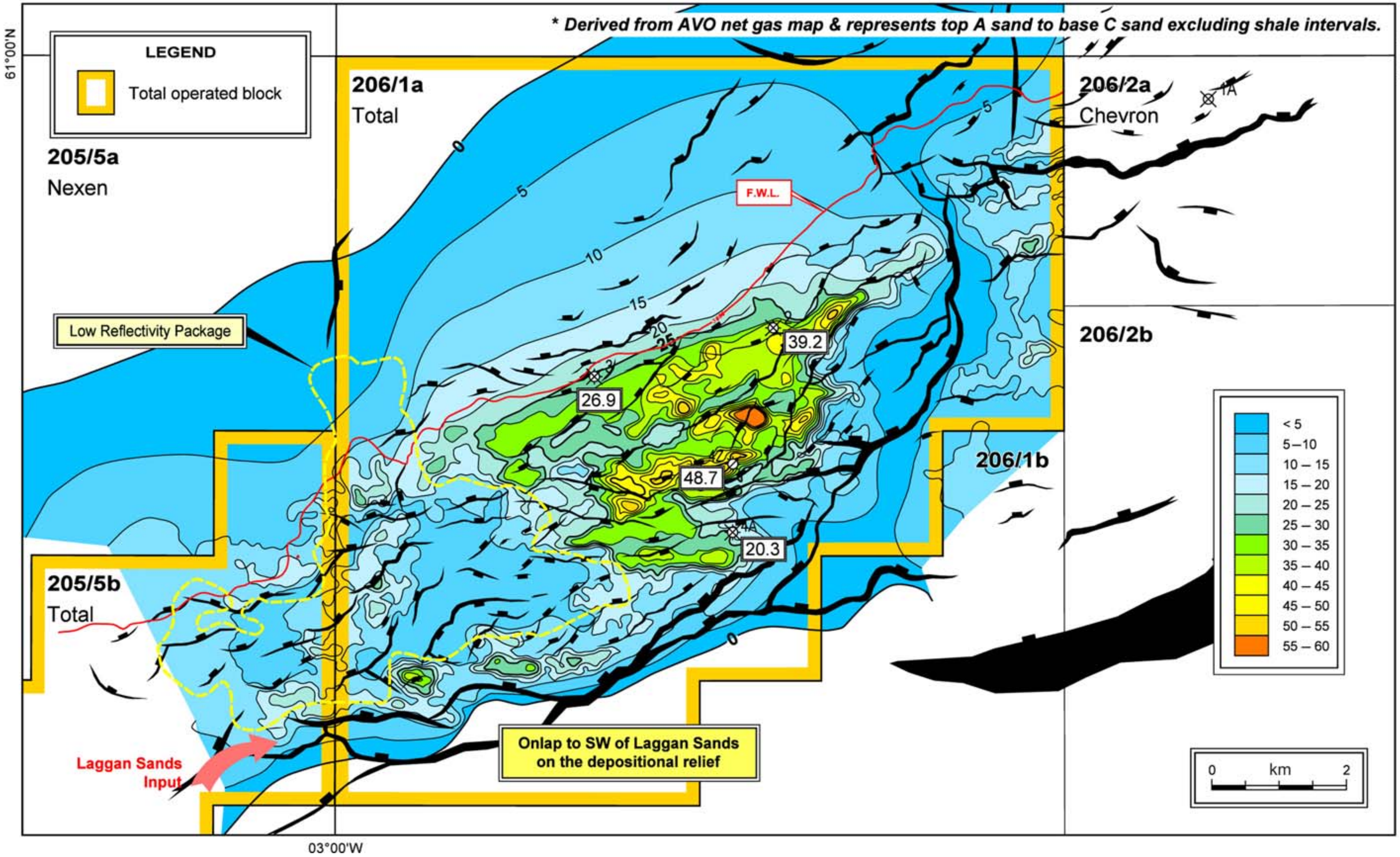

Fig. 6. Laggan sands, total gross sand isochore map. The map was derived from the Laggan AVO net gas sand map. The Laggan sands are interpreted to be more channelized/confined to the SW and more lobate/less confined in the main depocentre of Laggan, where the four wells have been drilled.

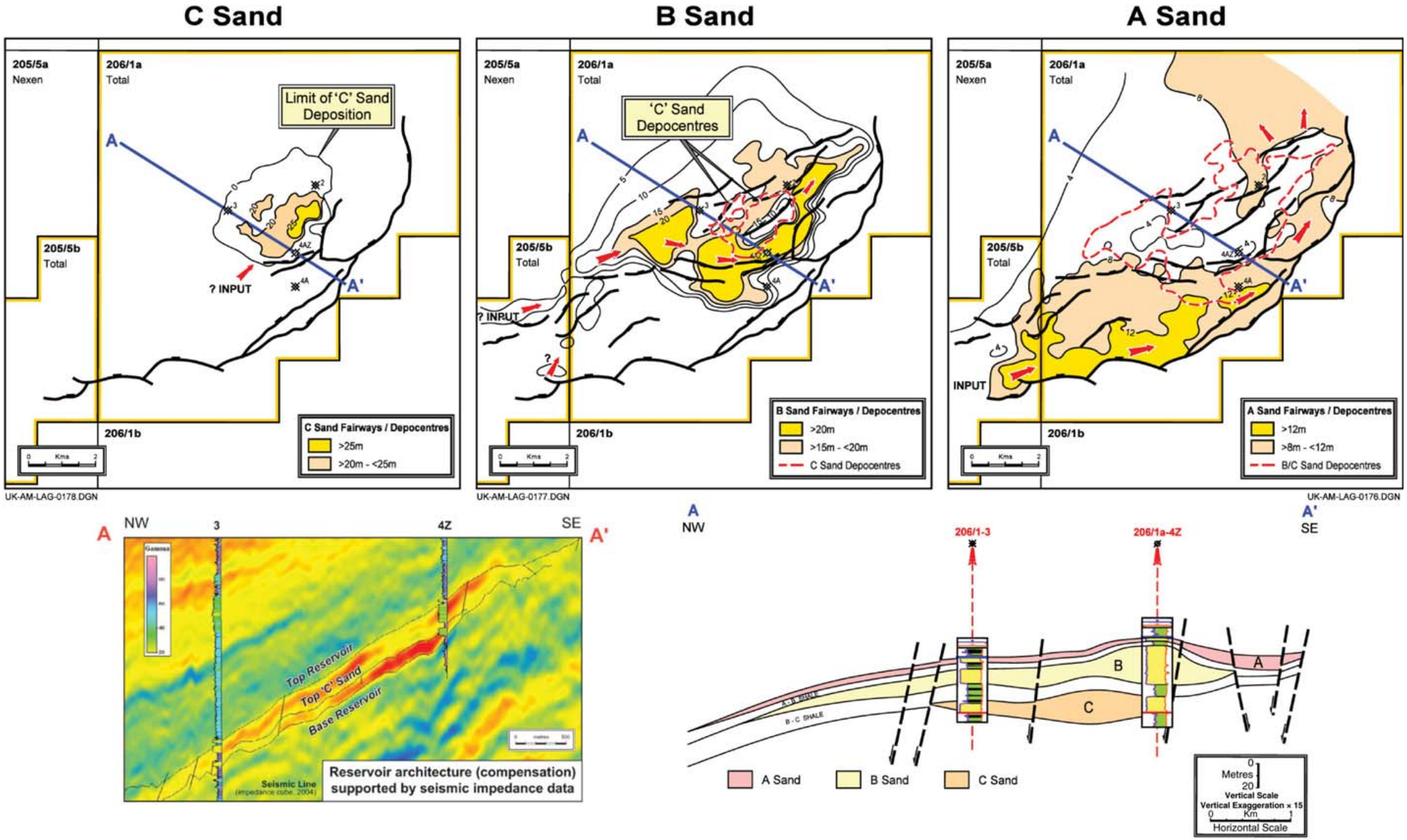

Fig. 7. Laggan depositional model for A, B and C sands. The role of compensation is inferred from seismic IP and well data. The B sand depocentres are located on the flank of the C sand depocentre. The A sand fairway is on the flank of the B sand fairway.

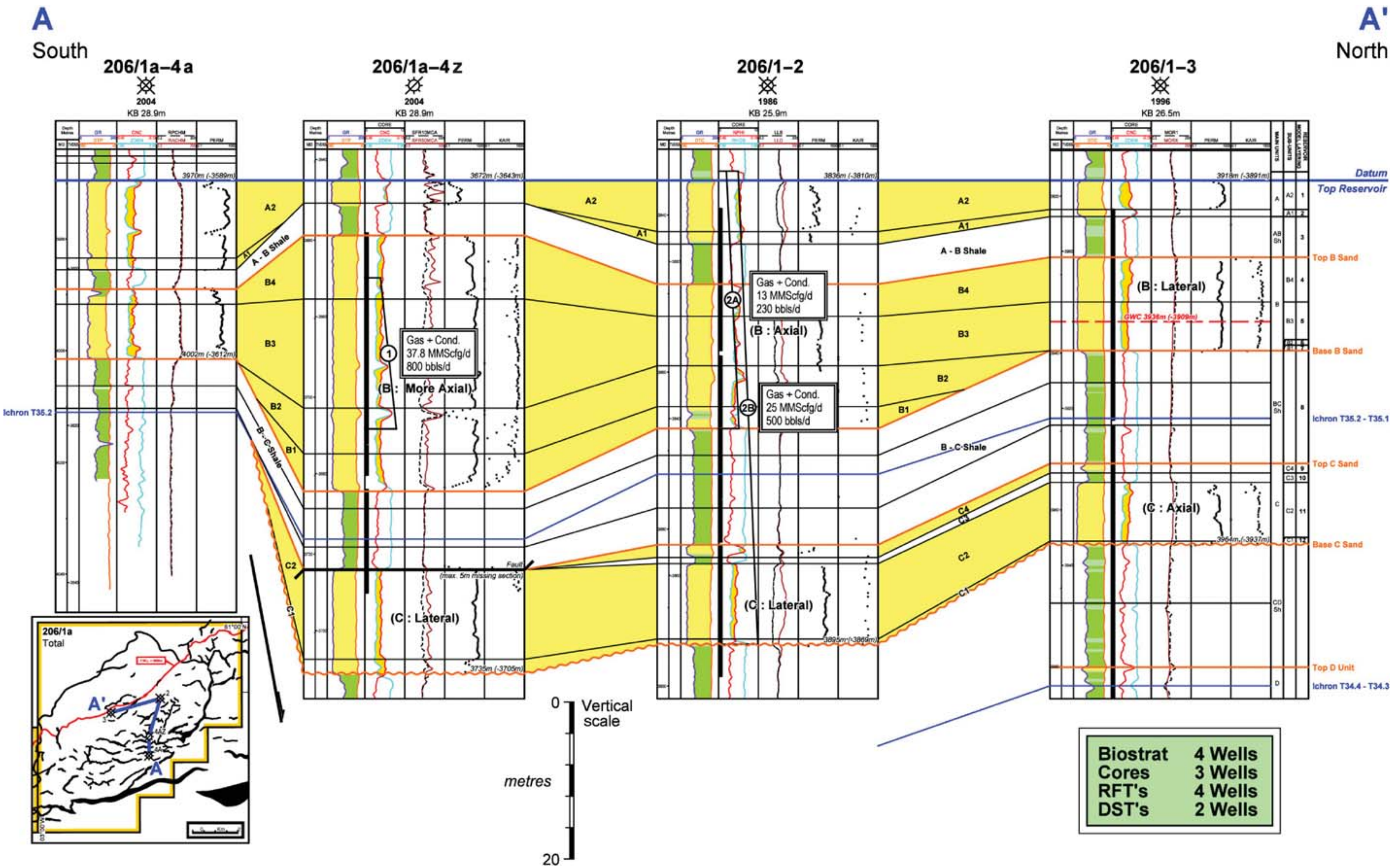

Fig. 8. Laggan Reservoir correlation. The sub-division of the reservoir into three main sand units (A, B, C sands), inter-bedded with two field-wide correlatable shales, is supported by biostratigraphic, seismic and sedimentological evidence.

Reservoir correlation

The sub-division of the reservoir into three main sand units (A, B and C sands), inter-bedded with two field-wide correlatable and predominantly hemi-pelagic shales is supported by the integrated geological scheme; in particular biostratigraphic, seismic and sedimentological evidence (Fig. 8).

A biostratigraphic study was completed by Ichron on the four Laggan wells. Correlatable biostratigraphic zones were identified and defined where possible on downhole occurrence, but influxes and base occurrences, along with trends in assemblage composition, were also used. The palynological and micropalaeontological zonations follow an internal Ichron scheme, which has been used widely in the West of Shetland Basin (Fig. 2 and Lamers & Carmichael 1999). Two key biostratigraphic markers have been identified which provide a framework for the reservoir correlation: first, Ichron T6 event (T35.2 to 35.1 sequence) within the B–C shales and notably absent in the 206/1a–4a well; and second, Ichron T5.4 event (T34.4 to 34.3 sequence) below the base reservoir (Figs 2 & 8).

The seismic interpretation also supports the model that the C sand is absent in the 206/1a–4a well, with the southern limit of the C sands controlled by a fault lying to the north of the 206/1a–4a well (Fig. 7). The more limited reservoir distribution of the C sands (present in only three of the four wells) in comparison with the overlying A and B sands (present in all four Laggan wells) is also compatible with the interpretation of the Laggan sands as ponded turbidites. C sand deposition comprised the initial infilling of the fault-controlled basin topography. It is therefore not surprising that the subsequent deposits of the A and B sands were more widespread.

Petrographic overview

In terms of the petrographic analysis of the three cored Laggan wells, the Laggan sands comprise arkosic sandstones with an average porosity from thin section analysis of 16% (10% primary, 6% secondary) for the calcite-free samples. Calcite cements occur in nodules, which make up about 10% of the thickness of the cored sands and have typically 1–2% porosity (Fig. 5). These nodules are not expected to form continuous layers. Non-calcite cemented samples have about 1–2% quartz cement and 3% clay cement (mainly illite and kaolinite). Although chlorite is a minor component (3–7 wt%), it occurs as a thin, continuous coat on all grains. Chlorite plays a key role in porosity and permeability preservation by inhibiting quartz cementation. Analysis of the chlorite indicates an Fe/Fe + Mg ratio of around 0.6 (Sullivan *et al.* 1999). This is a lower ratio than that found in chlorite from shallow marine sandstones (normally around 0.7–0.8, Hillier 1994). The current preferred mechanism for the origin of chlorite in the Laggan sands is related to the post-depositional infiltration of alteration products from tuffaceous material. Tuffs have been identified and analysed in cores in the interval below the Laggan sands and they contain trace elements, including rare earth elements similar to the chlorite analysed in the Laggan sands.

Petrophysical interpretation

Average porosity for the reservoir sands per Laggan well ranges between 19 and 23%. Net-to-gross values are between 90 and 100% for the reservoir sands. Wells 206/1a–4a and 206/1a–4z were drilled with the aim of confirming irreducible levels beyond the transition zones and both wells found irreducible water levels of around 16–18%.

A GWC of 3909 m TVDSS was encountered in the 206/1–3 well. This conclusion can be confidently drawn from reprocessed resistivity log data which supports the reservoir pressure data in defining the GWC.

Water salinity remains the single most important uncertainty for the Laggan petrophysical analysis. Well 206/1–3 sampled water with a salinity in the order of 6000 ppm in the aquifer. Derived water salinity values to match extensive core saturation height modelling and NMR log determined saturations indicate, however, that water salinity levels are of the order of 38 000 ppm NaCl equivalent in the updip 206/1a–4a and 4z wells. This implies a possible salinity gradient of approximately 150 ppm NaCl per metre, or a step change between the aquifer and the hydrocarbon leg. This uncertainty cannot be resolved with current data and requires additional sampling of the formation waters.

Extensive core-based capillary pressure experiments were conducted to evaluate the water saturation v. height in the Laggan sands. The reservoir material that was tested can, regardless of the sand interval, be seen as one coherent unit, as all capillary pressure experiments collapsed on one another after Leverett-*J* dynamic normalization. The resulting saturation height function by porosity classes is displayed in Figure 9 with the large transition zone effects of up to 200 m clearly seen.

As noted above, chlorite forms a ubiquitous grain coating within the fine to medium grained Laggan sands and has a fundamental effect on the petrophysical characteristics. Firstly, the chlorite at the reservoir depth preserves porosity as well as permeability by restricting potential quartz overgrowths. Secondly, the high surface area of the chlorite and its grain coating morphology result in high surface-bound water, which can provide an explanation for the extensive transition zone that is observed from capillary pressure experiments. The extensive transition zone is extraordinary given the fact that the reservoir is filled with lean gas condensate.

The current uncertainty on the Laggan water saturations determined from the integration of core and log measurements has been estimated as approximately $\pm 5\%$ saturation units.

Seismic interpretation

The 3D seismic dataset over Laggan comprises several different datasets acquired in 1995 and 1996. Unfortunately no single dataset covers Laggan. A marked improvement in data quality has been achieved through re-processing the data several times between 2002 and 2006. The current 3D seismic interpretation of Laggan was based on a combination of the 2005 PreSTM re-processed seismic dataset, which covers only the central part of the field and the 2002/2003 PreSTM reprocessed dataset for the rest of the field.

A semi-regional PreSTM seismic re-processing study was also performed in 2006 comprising six different surveys covering an area of 2044 km^2. The purpose of this study was to provide a regionally continuous dataset covering Laggan and surrounding blocks, and this was used to interpret Tormore.

A new 3D seismic acquisition campaign is planned in 2009 over Laggan and Tormore. The primary objective is to provide a modern, consistent 3D dataset to help optimize the location and often complex trajectories of the planned Laggan and Tormore development wells and provide a viable baseline for any future 4D project.

A seismic section through the Laggan wells is shown in Figure 10. The Laggan sands, being of lower IP than the overlying shales, correspond to a peak at the top of the reservoir, while the base corresponds to a trough (North Sea polarity). The black peak that can be observed between top and base reservoir in the 206/1–4z can be considered as near Top C sand. None of the individual sand layers (A, B and C sands with thickness variations from 3 to 33 m) is seismically resolved. The tuning thickness is estimated

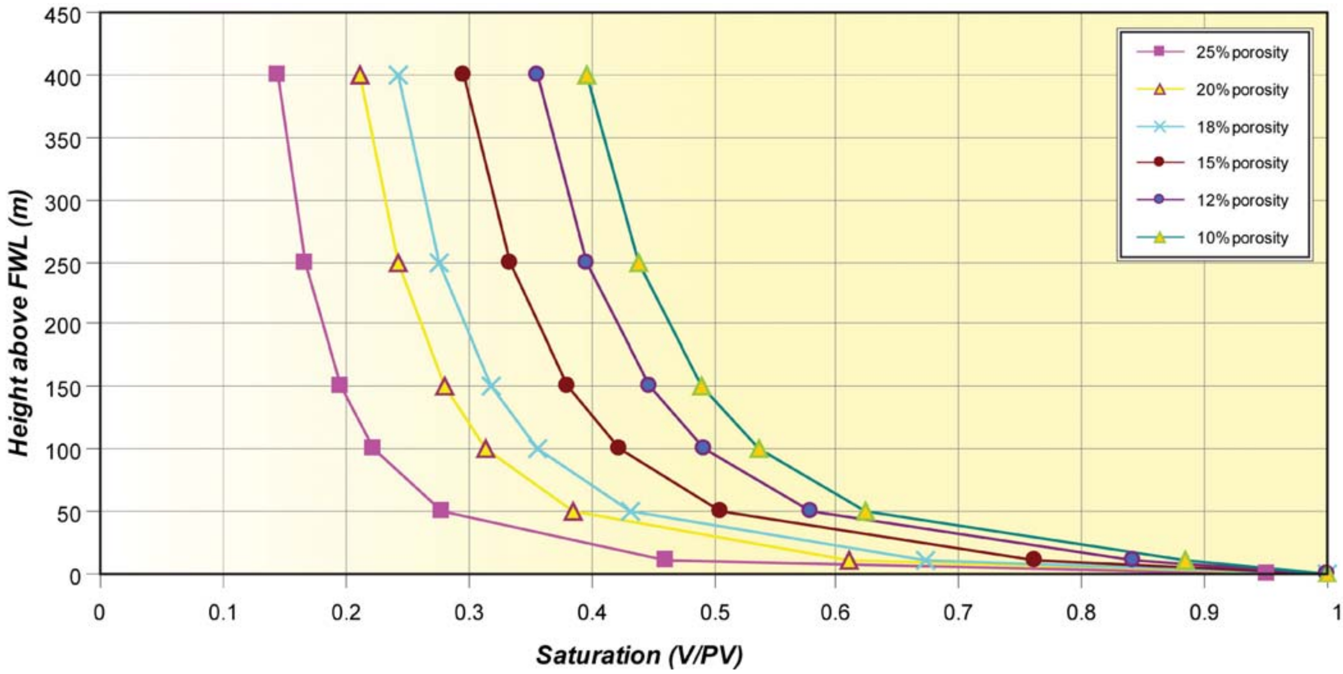

Fig. 9. Laggan *J*-function derived SW height relationship. Large transition zone effects of up to 200 m are clearly seen and are related to the presence of chlorite.

from the tuning curve to be between 16 and 20 ms, depending on which seismic dataset is considered. The Laggan sands gross reservoir thickness is below tuning thickness over the major part of Laggan.

Seismic inversion

A seismic acoustic inversion was completed in 2006. The resolution of the inversion dataset is, however, not enough to resolve the individual sand layers (Fig. 7). Furthermore, it is difficult to distinguish sand from shale layers using the inversion alone. The idea of using these inversion data to derive reservoir thickness was therefore quickly abandoned. The inversion data was mainly used for fine tuning the picking of the top and base of the reservoir, constraining the depositional model (reservoir architecture) and assessing aquifer size.

AVO analysis

The principle for Total's AVO analysis simply relates to the observation that Poisson's ratio (equivalent to V_p/V_s) contrast is the key driver for differences in the far angle reflectivities at identical near-angle reflectivities (Ostrander 1984).

In the west of Shetland, pre-stack data analysis needs to cope with imperfect data. The acquisition conditions are known to be harsh and the locally complex sedimentary overburden hampers seismic propagation. Seismic resolution and amplitude fidelity are therefore limited. Total's proprietary AVO analysis methodology is particularly suited for this challenging task (Paternoster *et al.* 2008). It relies first on a suite of seismic data quality assessments and is designed to robustly enhance AVO anomalies derived from the AVO 'Seismofacies' volume. Seismic data is taken into account as they are and not as they should be. Well data is not used to generate this AVO volume. It is used as an independent control and validation. The impact of frequency harmonization and data scaling on relative difference is a key factor in the analysis.

Net pay estimation

In the Laggan evaluation, AVO Seismofacies was used as a direct estimation of the cumulated (total) net pay of the Laggan sands. It should be noted that AVO enhances the contribution of Poisson's ratio to seismic attributes (Castagna & Swan 1997). Gas sands are enhanced relative to other lithological contrasts in the AVO volume. Filtering the higher frequency content of the seismic data increases the interference between the tops and bases of the various sand bodies. The resulting tuned AVO response can therefore be expected to be linearly related to the cumulated reservoir thickness. Interferences from internal contrasts simply discount the non-reservoir from the overall responses. These two characteristics are particularly suited to Laggan's blocky sand bodies and thickness ranges. As a result, the AVO Seismofacies response is found to be very well correlated with Net Pay thickness at the four Laggan well penetrations (Fig. 11). This crossplot gives a much improved correlation co-efficient relative to cross plotting net pay v. filtered amplitude data (0.96 v. 0.50).

Compartmentalization

The risk of compartmentalization is identified as the main dynamic uncertainty. This risk has been reduced through an improved definition of the fault configuration, by re-processing the 3D seismic and detailed seismic attribute analysis.

Pressure data (RFT and DST) from the 206/1–2 well indicates a possible disconnection within the reservoir (Fig. 12). The mapped faults from the seismic interpretation do not, however, form isolated panels within the reservoir. The possibility of field-wide compartments (potentially under seismic resolution) was therefore considered.

A DST was performed in the B sand in the 206/1a–4z well. The well was tested at a rate of 37.8 MMscfg/day and 800 bbls/day of condensate through a 1 inch choke. It is difficult to explain the transient depletion observed and mobility reduction seen on the pressure build up (PBU) derivative based on the depositional model. The Laggan sands are interpreted to have no significant lateral heterogeneity on the basis of the depositional model. A

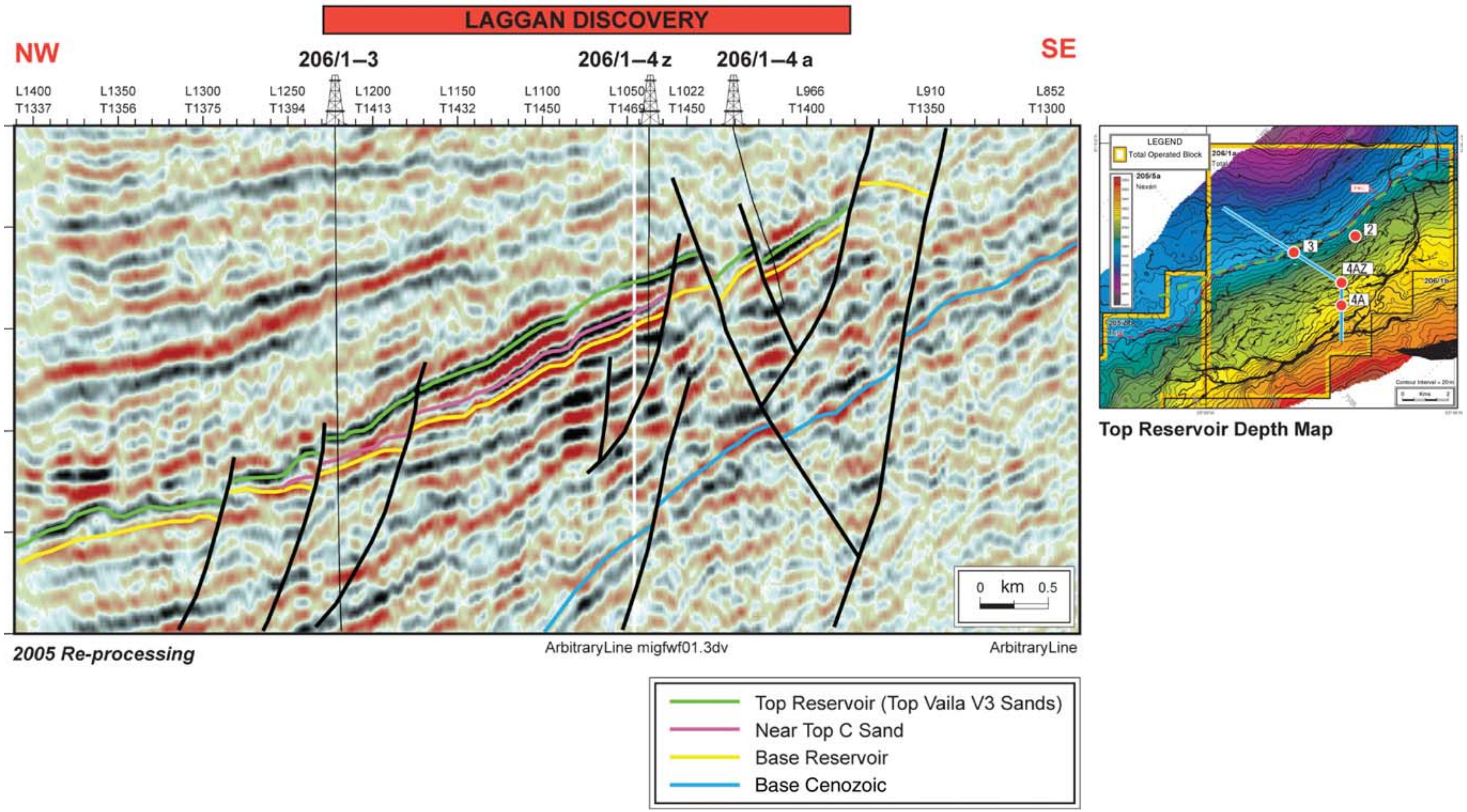

Fig. 10. Arbitrary seismic line through Laggan wells 206/1–3, 4a and 4z. The updip limit of the Laggan discovery is a significant fault downthrowing to the NW. None of the individual sands (A, B and C) are seismically resolved and the Laggan gross reservoir thickness is below tuning thickness over the major part of Laggan.

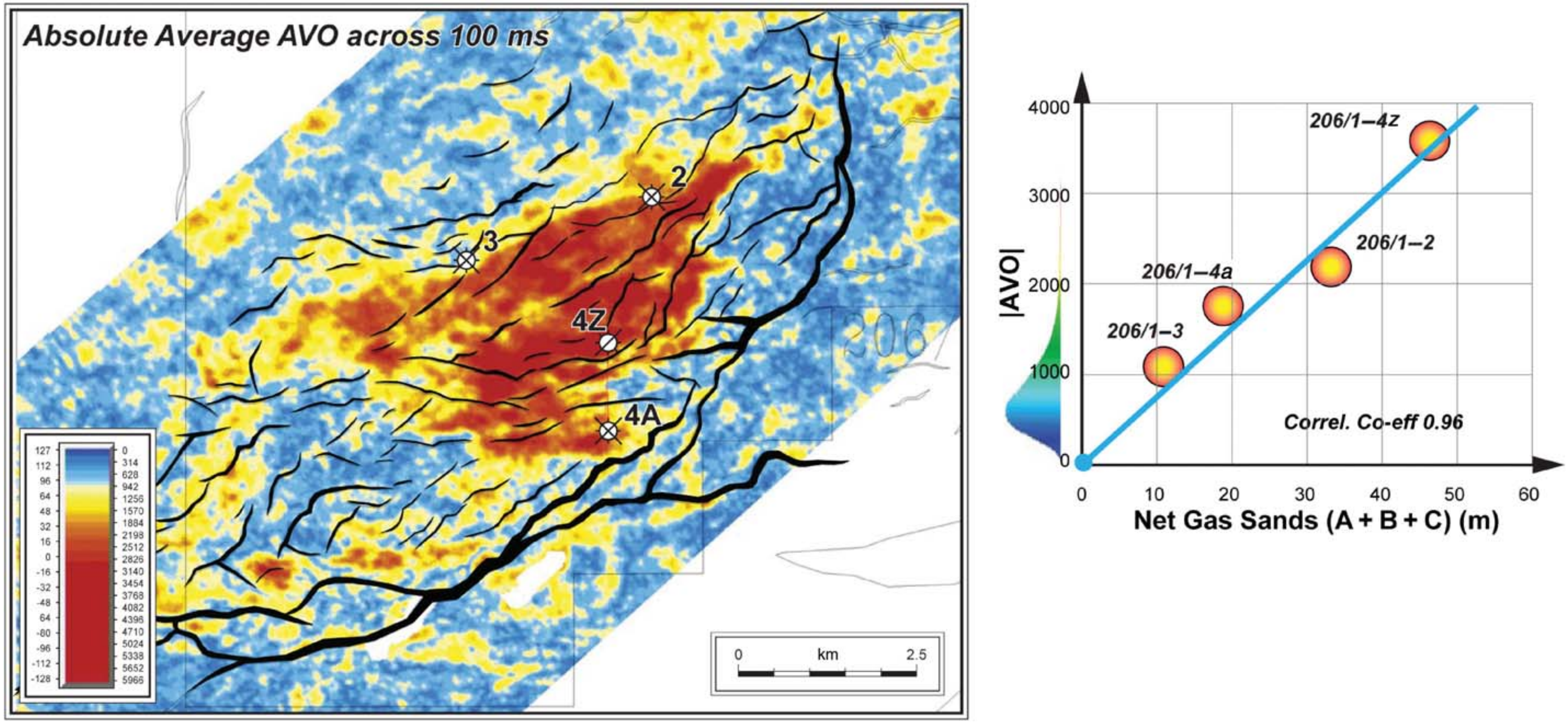

Fig. 11. Calculating net gas sand on Laggan using AVO. A very good correlation is observed between AVO and net gas sand. The relationship was applied to reduce the main static uncertainty, that is, predicting reservoir thickness away from well control.

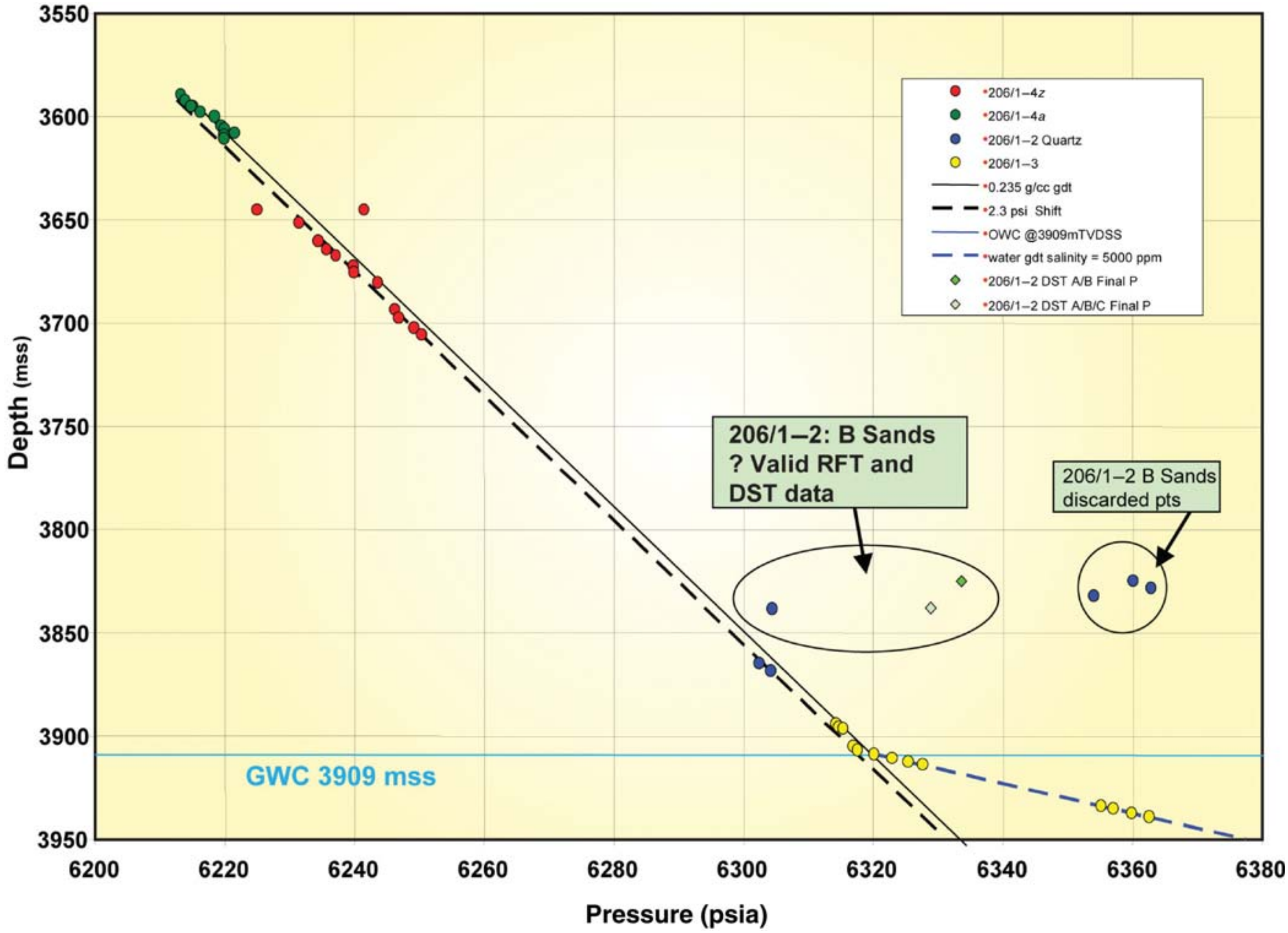

Fig. 12. Laggan pressure v. depth plot. Pressure data (RFT and DST) from the 206/1–2 well suggests a disconnection within the reservoir.

more likely concept is to explain the PBU characteristics based on sub-seismic faulting.

A complimentary fault seal evaluation study was performed involving the analysis of cores and fault juxtapositions (Fig. 13). The review of the Laggan cores indicated several cataclastic bands. These cataclastic bands have the potential to seal by the formation of finer particles by grain crushing with the destruction of chlorite coatings and consequently significant permeability reduction. The fault juxtaposition analysis using a 1D approach of Laggan well data indicated the potential to have both cataclasis and shale smearing with small throws (less than 25 m). No faults are evident from dipmeter logs, although it is recognized that cataclastic bands are below the resolution of the tool.

The analysis of seismic attribute data suggested a large number of relay zones. These zones could represent potential pathways for fluid flow, if they were not affected by cataclasis. The identification of potential compartments was based on the analysis of the following data with an iterative approach applied (Fig. 14). The mapped fault polygons were the starting point to define compartments and then it was assessed how far the faults could be realistically extended and whether they could realistically form compartments. Another consideration was the fault throw, with a simple concept applied; the larger the throw, the more likely the fault is to seal. Seismic attribute maps were analysed, with combined dip, azimuth and fault cubes proving to be particularly useful. The available dynamic data was also integrated in the study (pressure data from the four Laggan wells and DSTs performed in Laggan wells 206/1–2 and 4z).

An additional degree of complexity was, however, required to match the DST data with the introduction of segments, representing partially sealing panels. Segments are simply less well defined panels, with poor evidence of fault continuity relative to compartments, given the available data. The 206/1a–4z PBU was matched using first a 2D numerical model (in Saphir). A match was obtained using a variable transmissibility of the segments and by extending an existing fault. A second match was then performed using the Eclipse model, where the PBU was simulated (Fig. 15). A uniform reduction of transmissibility along the segments (transmissibility multiplier of 0.005) was used to match the transient depletion.

Finally, three different scenarios were defined to reflect the uncertainty and capture potential downside and upside cases, relative to the base case, as follows. Eight compartments were defined for the downside scenario within the main field area (Fig. 14). Two compartments were defined for the base case scenario within the main field area, compatible with a possible interpretation of the 206/1–2 RFT and DST data (Fig. 12). For the upside scenario, there were no compartments, reflecting the uncertainty with the 206/1–2 pressure data interpretation. For all three cases, partially sealing segments were defined with reduced transmissibility, in order to match the dynamic data.

Static uncertainty study

An uncertainty study (using ALEA/JACTA software) was completed to quantify the static uncertainties and in particular to

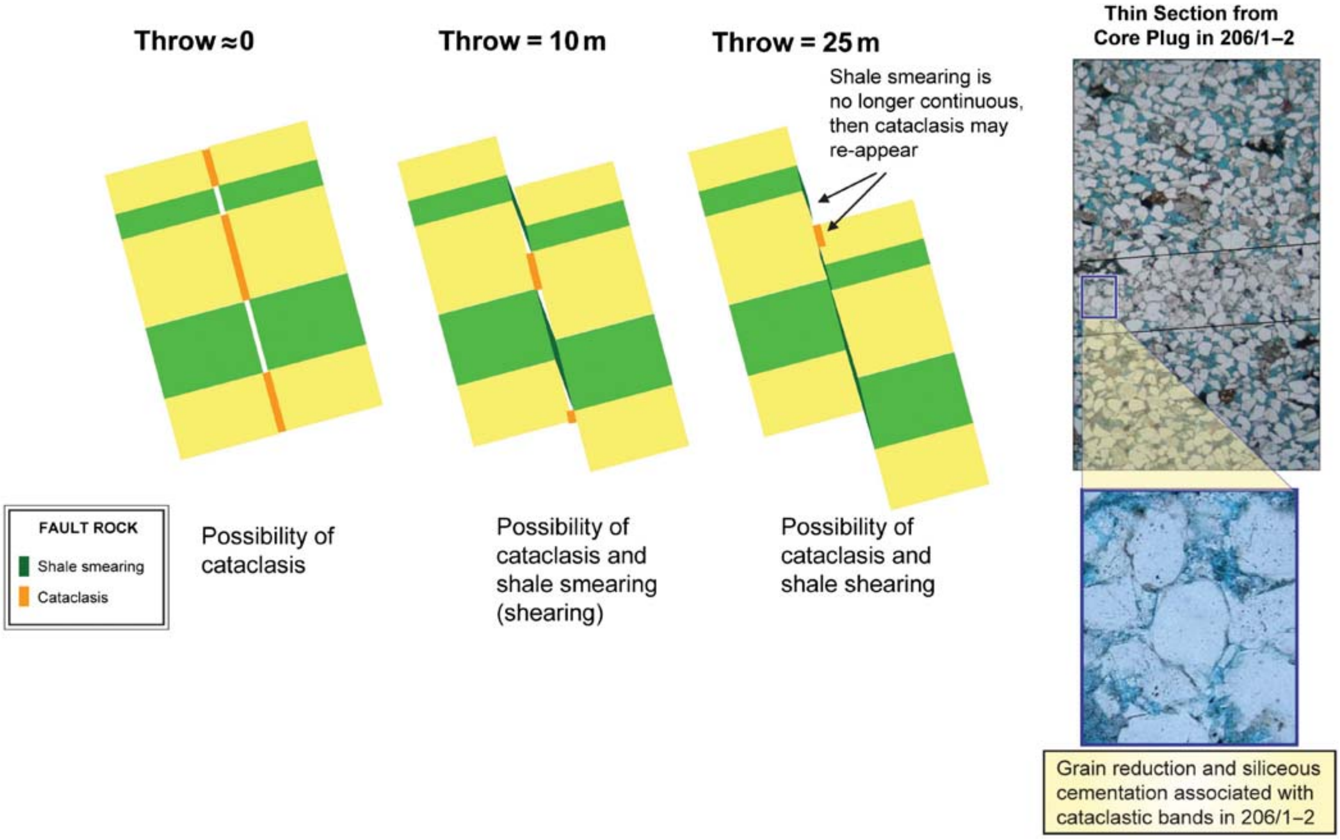

Fig. 13. Fault juxtaposition analysis and cataclastic bands in well 206/1–2. Fault juxtaposition analysis indicated the potential to have both cataclasis and shale smearing with faults with small throw (below seismic resolution).

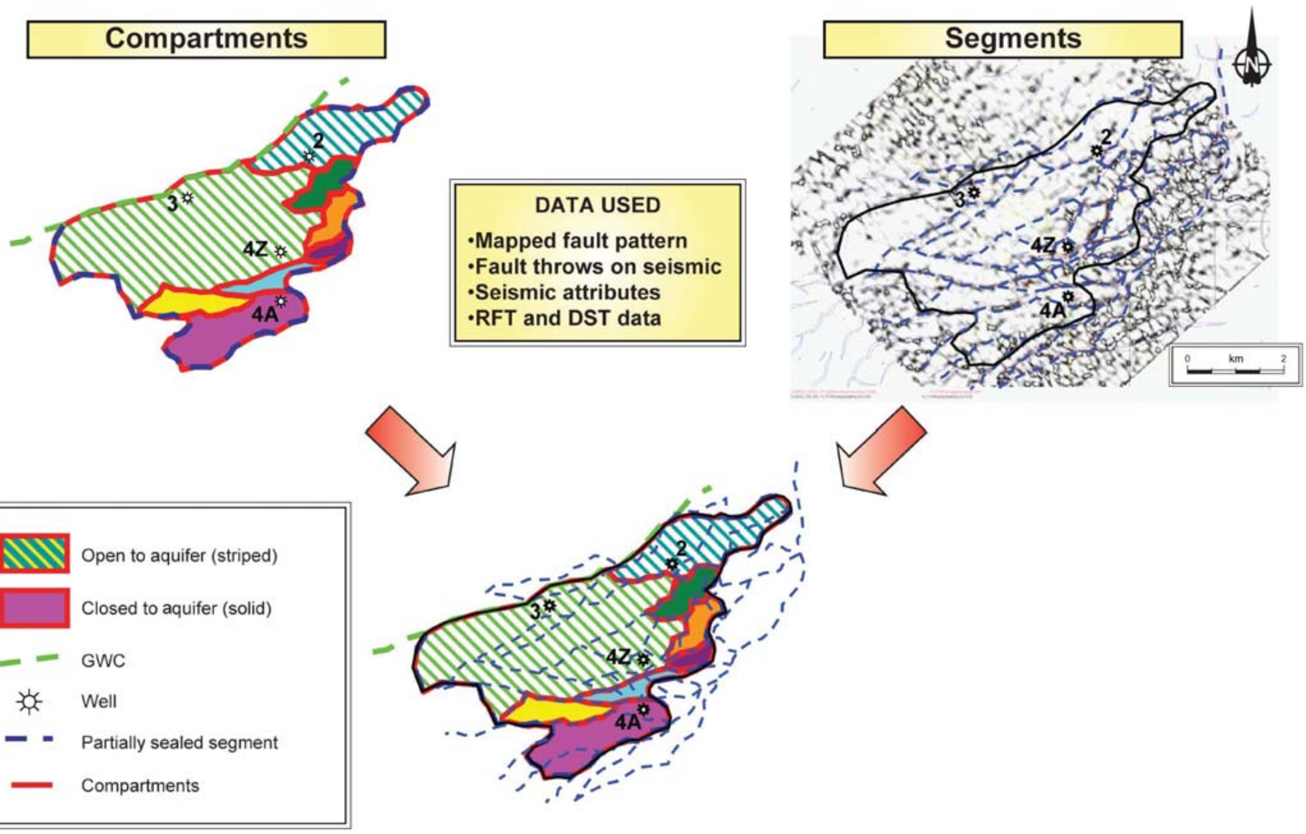

Fig. 14. Definition of compartments and segments. In order to match the dynamic data, a combination of isolated compartments and partially sealing segments was used in the reservoir simulation studies.

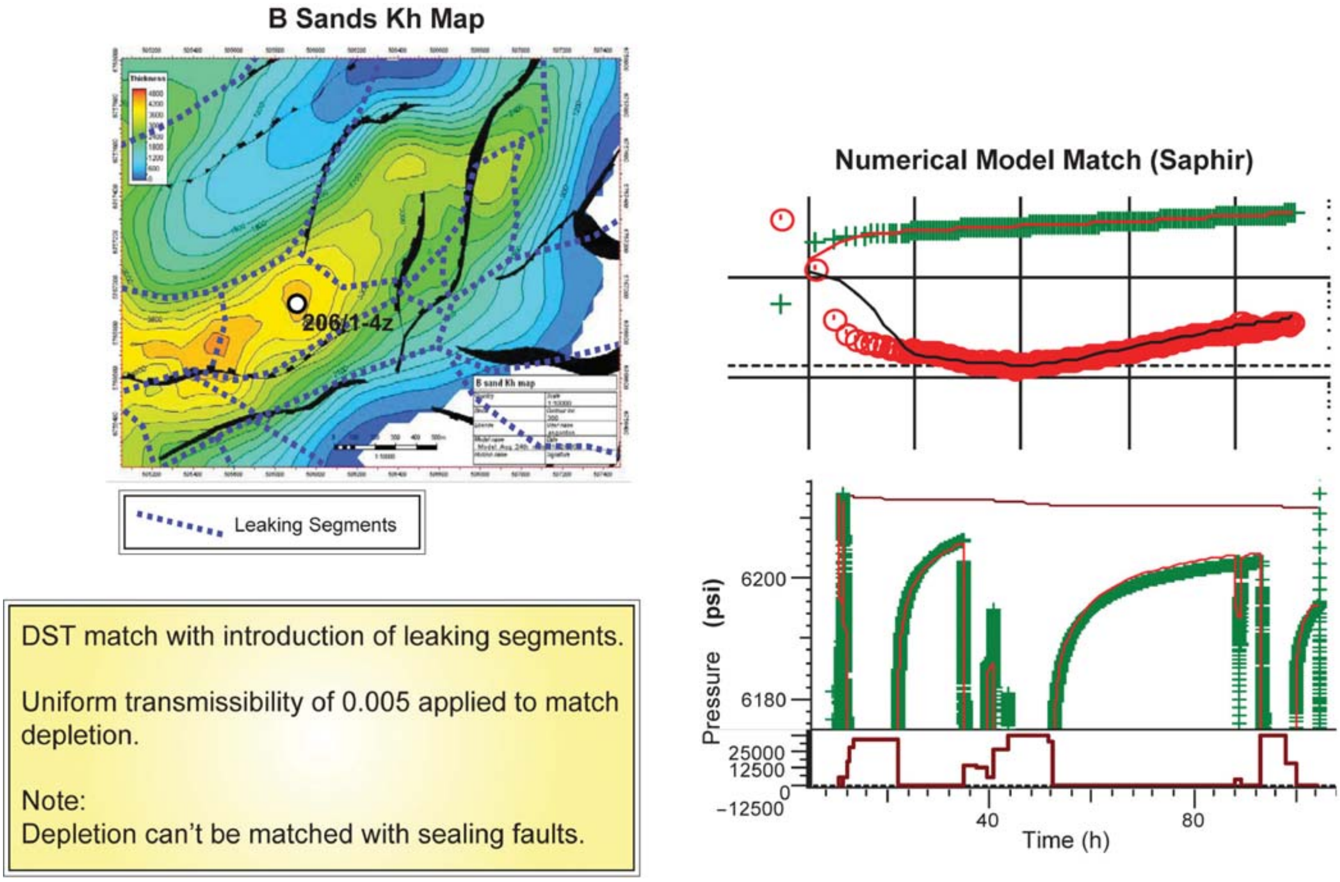

Fig. 15. 206/1a–4z match with leaking segments. The transient depletion and mobility reduction seen on the PBU was matched by partially sealing faults (in part sub-seismic).

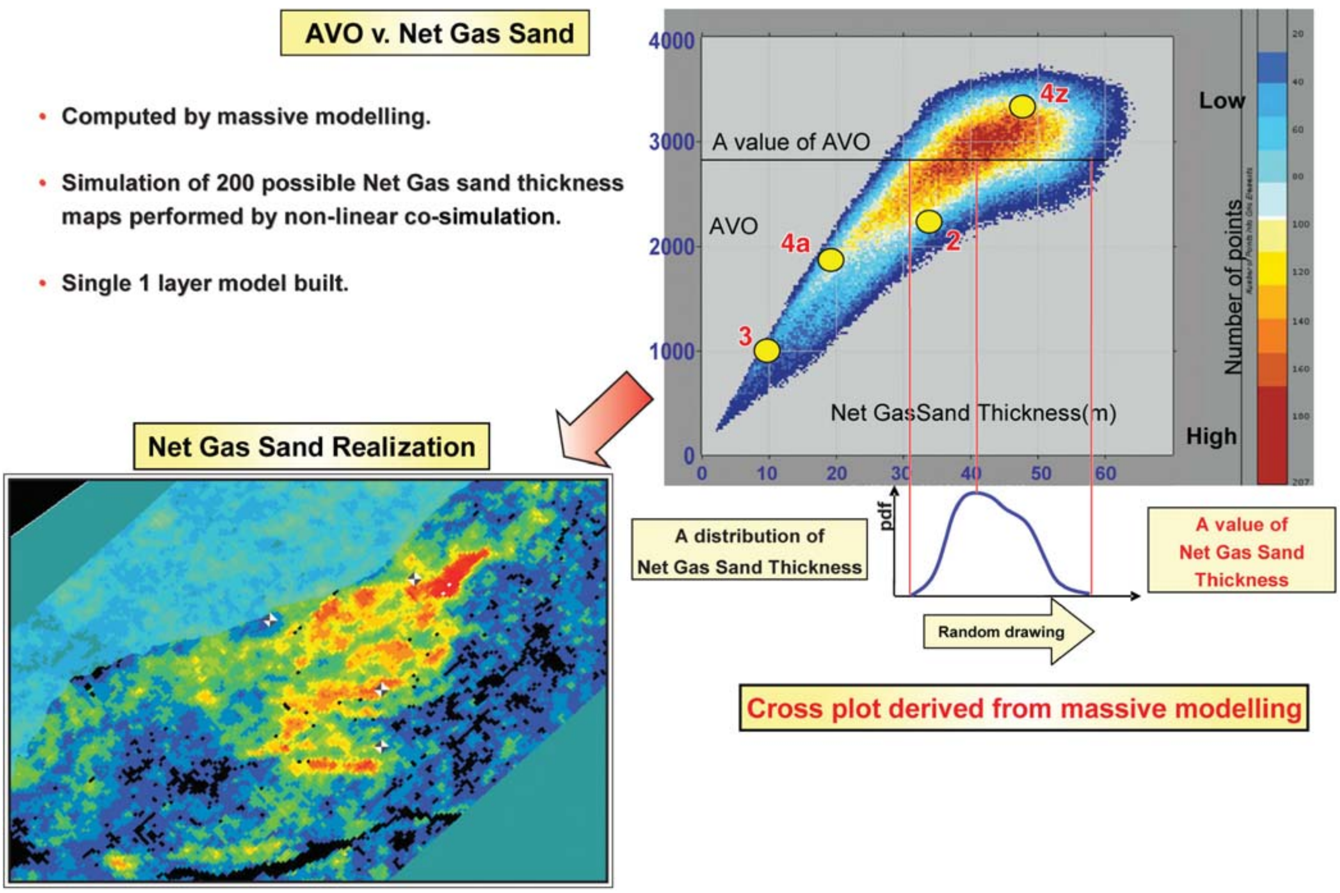

Fig. 16. Uncertainty on net gas sand thickness from AVO. The uncertainty was computed by massive modelling. Two hundred possible net gas sand thickness maps were generated by non-linear co-simulation.

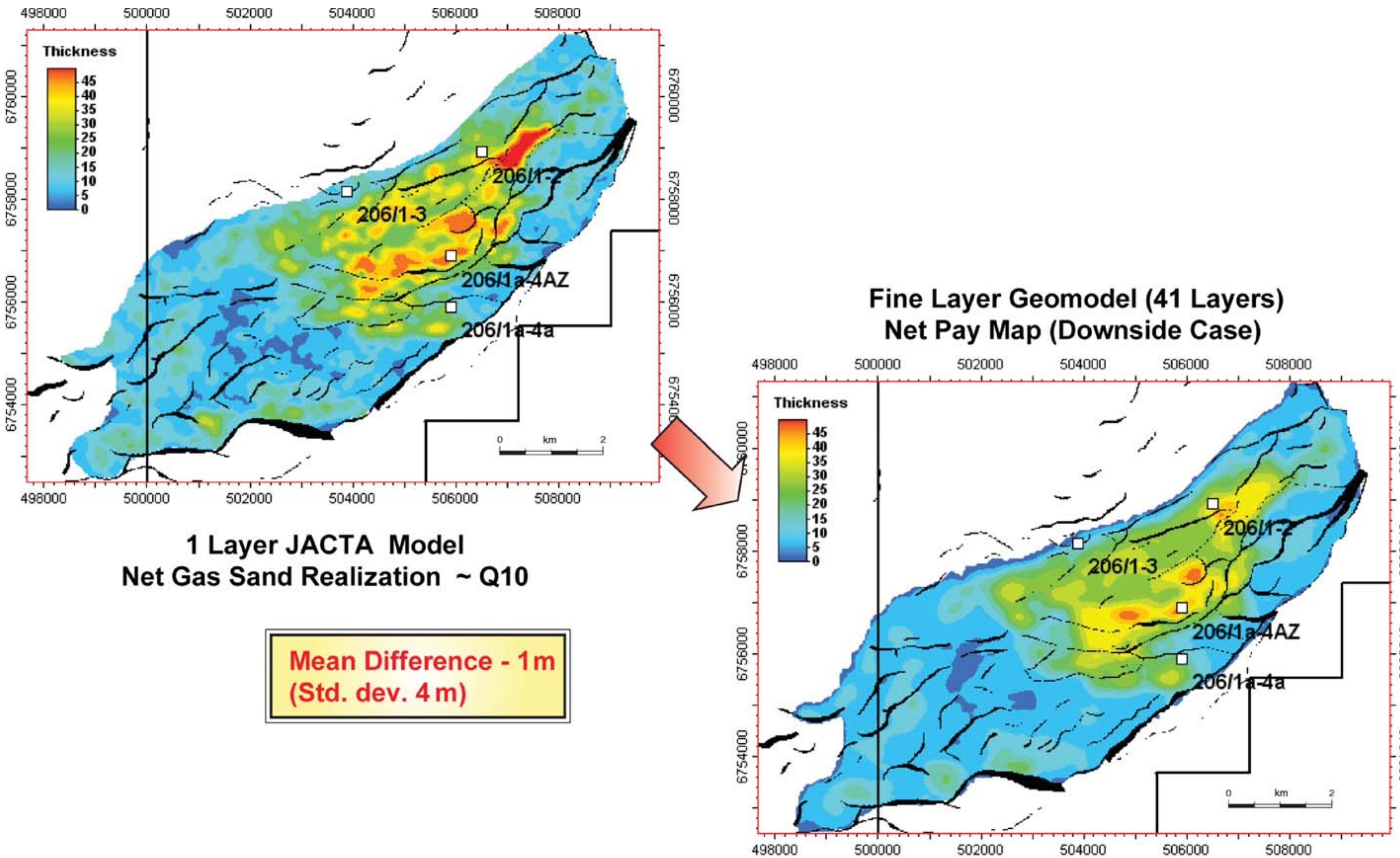

Fig. 17. Net pay v. net gas sand map (downside case). The challenge was to build fine-layer 3D geological models, which were broadly compatible with results of the one-layer JACTA models.

address the uncertainty on the relationship between AVO and net gas sand (Guemene *et al.* 2006). Static uncertainties evaluated in the study were:

(a) depth of top reservoir (from seismic picking) and depth conversion uncertainties;
(b) depth of the GWC;
(c) net gas sand derived from the AVO map;
(d) porosity modelling;
(e) water saturation evaluation.

The study was performed in three steps. First, an evaluation of the structural uncertainties was performed using ALEA software. The uncertainty in depth at top reservoir was assessed as ranging from 0 to 50 m, and 200 possible maps at top reservoir were simulated.

Second, the uncertainty on net sand from AVO was addressed. The dispersion was estimated using Massive Modelling, with the following workflow. Log elastic properties (Rho, V_p, V_s) were upscaled for each reservoir (A, B and C sands) to generate a distribution of parameter values at sand layer scale. Then millions of 1D models were generated, sampling the parameter distributions with sand and shale layer thicknesses representing the plausible variations across Laggan. Thereafter, massive seismic modelling of randomly sampled models (hundreds of thousands) was performed to generate AVO 'Seismofacies' traces. AVO attribute extraction was performed, as per real seismic data. The AVO v. net gas sand thickness (Net Gas column) was then cross plotted (Fig. 16).

The third step was the geological in-filling, using JACTA software. Two hundred possible net gas sand thickness maps were generated by non-linear co-simulation. A single 1 m-thick layer model was built. The porosity uncertainty was defined by the mean uncertainty affecting two average porosity maps derived from the Geomodel. The mean uncertainty was assessed as approximately 1 standard deviation corresponding to approximately ± 1 porosity unit.

The GWC was randomly sampled with the uncertainty range, based on the interpretation of the pressure data. The uncertainty was assessed as ranging from -3 to $+1$ m. The water saturation transition zone was defined by a J function and the associated uncertainty was modelled with an uncertainty range of approximately $\pm 5\%$.

Sensitivity analysis was performed to identify the key sources of uncertainty. The principal uncertainty was identified as the one related to the application of AVO to define net gas sand. Uncertainties relating to porosity and saturation are secondary. Structural uncertainties (top reservoir and GWC) are the least important, as expected with a significant hydrocarbon column of approximately 400 m and well-defined GWC from pressure and log data.

3D geological models

Three different 3D geological models were built to reflect the downside, base case and upside scenarios, which broadly reflected the results of the uncertainty study and the integrated geological scheme. As noted previously, the major static uncertainty is the sand thickness distribution and prediction, particularly in areas where the gross reservoir is below seismic tuning thickness.

In the 3D geological model for the base case scenario, the sand isochores were guided by the AVO total net gas sand map (primarily in the seismically tuned area), the seismic isochores (primarily in the non-tuned area) and the depositional model (e.g. Fig. 7). The fine layers in the base case geomodel were proportionally built, with the aim of having approximately 1–2 m-thick sand layers. The Net to Gross grids were generated by sequential Gaussian simulation (SGS) of upscaled well logs with azimuth trends compatible with the geological scheme. The porosity grids were also generated by SGS of upscaled well logs, with the seismic IP cube applied as external drift. A strong correlation between IP and porosity ($R = 0.95$) in the aquifer was demonstrated by a fluid substitution study using Gassmann modelling. The permeability grids were generated by permeability/porosity transforms for the individual sands, based on the Laggan core data. The water saturation grids were derived from the saturation height function, based on end face corrected capillary pressure data from the 206/1–3 and 4z wells. The free water level for Laggan was defined from RFT and log data in the 206/1–3 well at 3909 mss, as previously noted.

The construction of the downside and upside geomodels was broadly similar to the methodology applied in the base case scenario. The challenge was to build fine-layered 3D geological models, which were broadly compatible in terms of gas initially in place (GIIP) distribution with the corresponding 1 layer JACTA models (i.e. realizations which represented approximately Q10 and Q90 in terms of GIIP). The sand isochores in the downside and upside 3D geological models were based in particular on approximately Q10 and Q90 net gas sand realizations from JACTA (example Fig. 17). In the downside geomodel, a more pessimistic approach to porosity modelling was also applied relative to the most likely model, that is, SGS with no external trend applied and a more pessimistic saturation height function was also applied. In the upside geomodel, a more optimistic approach to porosity modelling was applied relative to the most likely model, that is, increased correlation coefficient applied with the seismic IP data as external drift, re-sampled in the geomodel. A more optimistic saturation height function was also applied.

The geomodels were then exported for reservoir simulation studies, including the optimization of the planned development wells for Laggan and reserves evaluations.

Tormore

The potential of Tormore was recognized, by applying the geoscience understanding of Laggan to help de-risk the prospect. In particular, it was recognized that Laggan could be used as an analogue for the Tormore trapping configuration and reservoir potential and that AVO could be used to help define the GWC. The exploration well was successful in finding a similar reservoir as was encountered in Laggan.

The Tormore discovery well, 205/5a-1 was drilled and tested in 2007 (Fig. 4). The well was tested at a rate of 28.3 MMscfg/day and 1975 bbls/day of condensate from the C sand. The condensate gas ratio (CGR) is approximately 70 stb/MMscf, that is, more than three times richer than Laggan.

The main static and dynamic uncertainties on Tormore are similar to Laggan, that is, sand thickness distribution and water saturation (long transition associated with chlorite) and the degree of compartmentalization.

Conclusions

The geoscience evaluation of Laggan has matured over the last four years, with the help of fully integrated studies using seismic and well data. The depositional model has been defined on the basis of an integrated study of cores, seismic and analogue studies. Seismic inversion studies have also helped constrain the reservoir architecture. Of particular value has been the application of AVO to quantify net gas sand, recognized as the principal static uncertainty. The main dynamic uncertainty is the risk of compartmentalization. This risk has been reduced through an improved definition of the fault configuration, by re-processing the seismic and detailed seismic attribute analysis.

Way forward

Development studies are now well advanced, with the discovery of Tormore in 2007 providing the potential for a combined development project. A new seismic acquisition campaign is planned in 2009 over Laggan and Tormore. The primary objective is to help optimize the location and often complex trajectories of the planned Laggan and Tormore development wells. An improved understanding of the Laggan and Tormore geological scheme should also hopefully arise, with an expected improvement in seismic imaging.

The authors would like to thank DONG, ENI and Chevron for their permission to publish this paper, as well as their invaluable contribution to the project. We would like also to acknowledge with many thanks the contributions of numerous colleagues who have also studied Laggan, including H. Declerck, H. van Dongen, J. Gerard, J. P. Gomez, J. M. Guemene, R. Rebut, S. Hillier and T. Whitbread.

References

Castagna, J. & Swan, H. W. 1997. Principles of AVO crossplotting. *The Leading Edge*, **16**, 337–342.

Guemene, J. M., Paternoster, B., Toinet, S., Biver, P., Gordon, A. & Declerck, H. 2006. A new approach to quantifying uncertainties, from seismic characterisation to hydrocarbon in place. *EAGE 68th Conference and Exhibition*, Vienna, 12–15 June 2006.

Hillier, S. 1994. Pore filling chlorites in siliclastic reservoir sandstones: electron microprobe, SEM and XRD data and implications for their origin. *Clay Minerals*, **29**, 665–679.

Lamers, E. & Carmichael, S. M. M. 1999. The paleocene deepwater sandstone play of west of Shetland. *In*: Fleet, A. J. & Boldy, S. A. R. (eds) *Petroleum Geology of Northwest Europe: Proceedings of the 5th Conference*, 645–659; doi: 10.1144/0050645.

Ostrander, W. J. 1984. Plane-wave reflection coefficients for gas sands at non normal angles of incidences. *Geophysics*, **49**, 1637–1648.

Paternoster, B., Ben Brahim, L., Gordon, A., Whitbread, T., Achilli, F., Urruty, J.-M. & Younis, T. 2008. Using AVO for exploration in the West of Shetlands. *PETEX Conference*, London, 2008.

Sullivan, M., Coombes, T., Imbert, P. & Ahamdach-Demars, C. 1999. Reservoir quality and petrophysical evaluation of Paleocene sandstones in the West of Shetland area. *In*: Fleet, A. J. & Boldy, S. A. R. (eds) *Petroleum Geology of Northwest Europe: Proceedings of the 5th Conference*, 627–633; doi:10.1144/0050627.

Managing the start-up of a fractured oil reservoir: development of the Clair field, West of Shetland

A. J. WITT, S. R. FOWLER, R. M. KJELSTADLI, L. F. DRAPER, D. BARR and J. P. MCGARRITY

BP Exploration Operating Company Ltd, 1 Wellheads Avenue, Dyce, Aberdeen AB21 7PB, UK (e-mail: andrew.witt@uk.bp.com)

Abstract: The Clair oilfield was discovered in 1977 and began production in 2005. It is a heterogeneous fractured sandstone reservoir with an estimated STOIIP of *c.* 1.5 billion barrels in the Phase 1 development area. An extended appraisal programme was required to assess reservoir deliverability, which is controlled by the distribution of natural fractures. Development drilling increased the understanding of the fracture system, through acquisition of conventional core, open-hole logging, drilling mud-loss recording, production logging and well test transient analysis. These data revealed a complex fracture system of conductive faults and background joints. Post-production formation pressure measurements showed greater lateral and vertical connectivity than would be expected from matrix and fluid properties alone. However, large pressure differences were encountered close to or across features mappable at a seismic scale. Closed fractures or sealing faults can form baffles between compartments, and conductive faults or fractures allow rapid pressure communication. In some cases the connection path or barrier can be identified with seismically mapped features. When the field was put onto water injection, one year after start-up, a key concern was the degree of imbibition of water from the fractures to the matrix. Despite the observed pressure connectivity, water breakthrough did not take place until 2007. Most producers have completions designed to permit zonal water shut-off. A successful intervention was carried out in early 2008, after a production logging run had demonstrated water entry at the toe of a high-angle well. The crestal Core segment of the development benefits from a permanent 4D seismic array of ocean-bottom cables. In 2007 the first permanent monitor survey was acquired and processing gave indications of a 4D response. These 4D data are improving the dynamic reservoir understanding and providing valuable spatial context to the well results.

Keywords: 4D seismic, Clair field, fractured reservoir, Old Red Sandstone, reservoir management

The Clair oilfield lies 75 km west of the Shetland Islands in UKCS blocks 206/7a (Production Licence P.168), 206/8 (P.165), 206/9a (P.170), 206/11a (P.168), 206/12a (P.169) and 206/13a (P.169), all awarded in the fourth licensing round of 1972. The current ownership is: BP 28.6015% (Operator), ConocoPhillips 24.0029%, Chevron 19.4225%, Shell 18.6831% and Hess 9.2900%. It was discovered in 1977 and in 1989 the field co-venturers entered into a 'Joint Appraisal Agreement' which resulted in the first 3D seismic survey being shot over the area, paving the way for the future appraisal campaign. After a successful extended well test the 'Clair Unitization and Field Operating Agreement' was approved in 1997. A field development plan was submitted and development consent was received in 2001. Production commenced in February 2005. From initial discovery to first oil the field was appraised by a total of 23 wells. Twelve development wells have subsequently been drilled from a fixed platform. Clair lies in a water depth of 140 m, and production is transported via the West of Shetland pipeline and on to the Sullom Voe terminal.

Pre-production modelling (Barr *et al.* 2007 and references therein) was designed to understand the range of uncertainty associated with production from the fracture network, and its interaction with the matrix where most of the oil is stored. As development continued the models were continually updated with new static and dynamic field data. This paper documents the first three years of field life, with reference to the original field development plan, and outline decisions that were taken as a response to the changing understanding of dynamic reservoir behaviour.

Structure and stratigraphy

The geology of the Clair oilfield has been described by Coney *et al.* (1993) and Barr *et al.* (2007). The hydrocarbon trap is a four-way dip closure, extending over *c.* 220 km^2. It is located in the extensional Faroe–Shetland Basin, which is of Devonian to Cretaceous age and has a predominantly NE–SW trending fault network (Fig. 1). The oilfield itself is situated on the crest and downflank terrace of the Rona Ridge, a basement high formed in the Devonian. The reservoir comprises late to mid Devonian Old Red Sandstone and contains an extensive natural fracture network. The whole Greater Clair closure is estimated to have a stock tank oil initially in place (STOIIP) in excess of 5 billion barrels.

Clair was discovered in 1977 when exploration well 206/8-1A penetrated 568 m of oil-bearing Devonian sandstones, which tested 25.2° API oil at 1502 BOPD from Unit V and 1415 BOPD from Unit VI (Ridd 1981). Appraisal continued with drill-out of the large structural blocks that comprise the closure, each demonstrating the lateral continuity of the Old Red Sandstone with similar reservoir properties.

The stratigraphy of the Clair Group (Fig. 2) was first described by Allen & Mange-Rajetzky (1992) and more recently by Nichols (2005). The Clair Group is a fluvial succession, with a thickness related to the amount of accommodation space preserved in the relict topography formed by Lewisian Gneiss basement. The Devonian Lower Clair Group forms the main hydrocarbon reservoir; the overlying Upper Clair Group (Carboniferous) contains abundant smectite and is not targeted by the current development. The Lower Clair Group is divided into six reservoir units; Unit VI, Unit V and Unit III have the highest reservoir quality. They are distinguished by correlation of conventional log suites (gamma-ray, resistivity, density); variation in heavy mineral assemblages (Morton *et al.* 2003) complements the log correlation. The Devonian–Carboniferous stratigraphy is unconformably overlain by the Upper Cretaceous Shetland Group, which forms the cap rock.

VINING, B. A. & PICKERING, S. C. (eds) *Petroleum Geology: From Mature Basins to New Frontiers – Proceedings of the 7th Petroleum Geology Conference*, 299–313. DOI: 10.1144/0070299

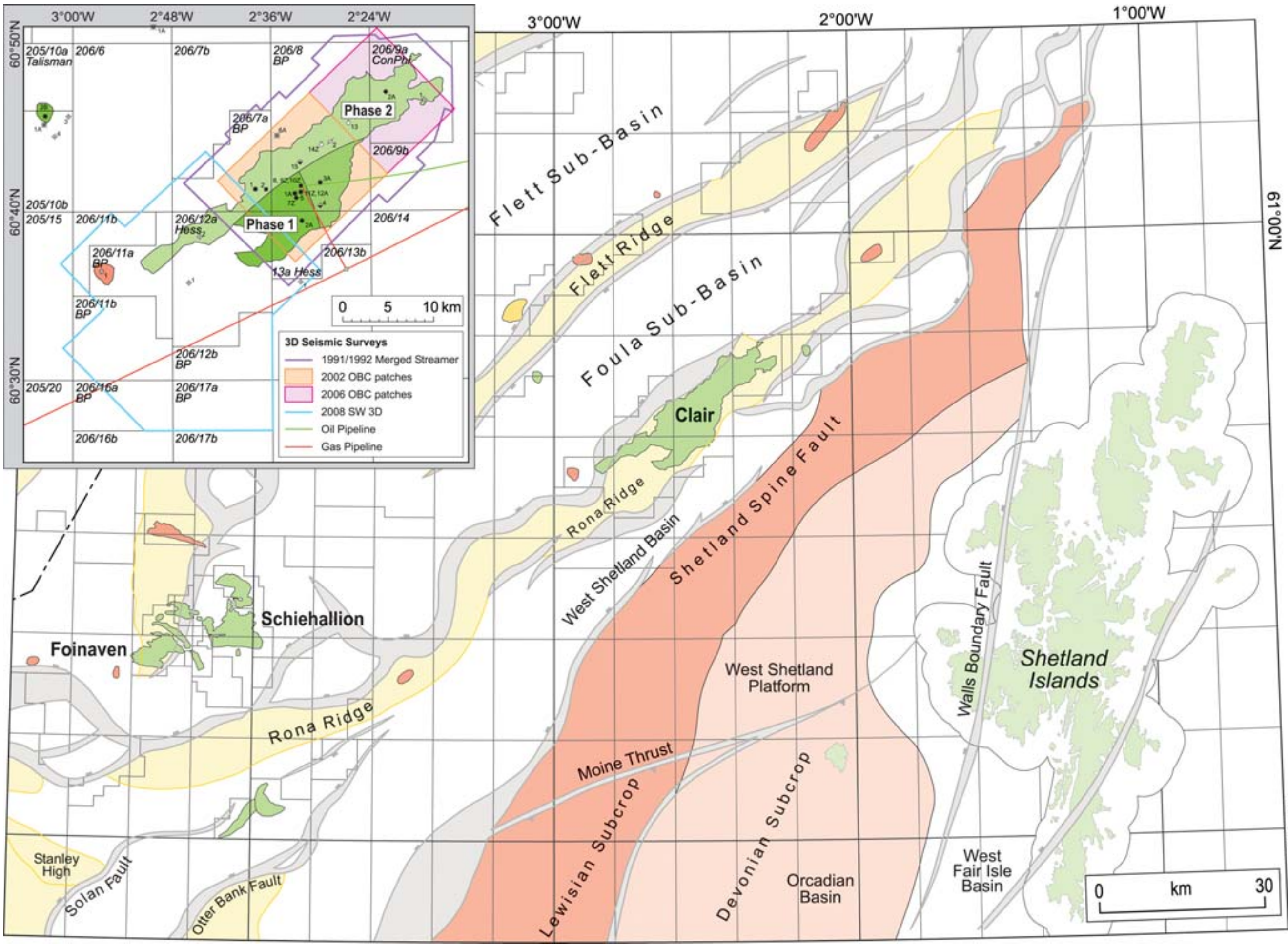

Fig. 1. Structural features of the Faroe–Shetland Basin, with Clair field location and seismic data coverage.

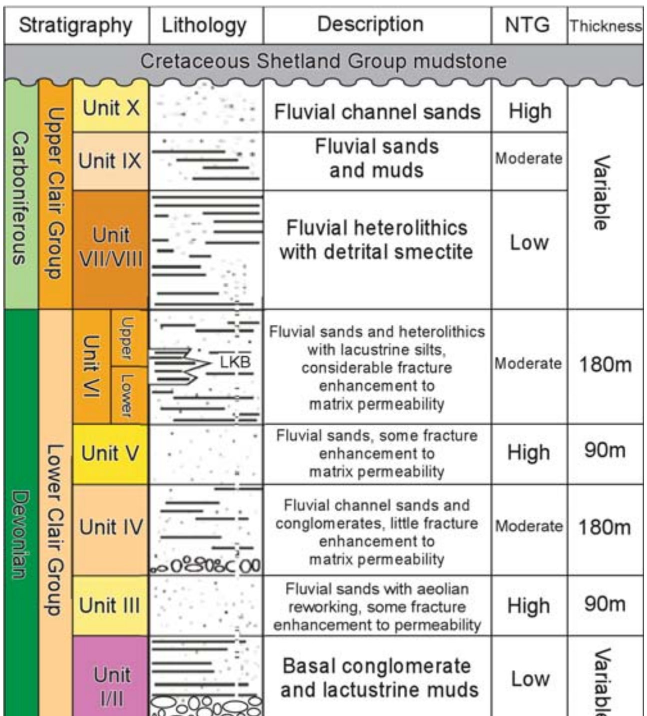

Fig. 2. Clair Group stratigraphy and matrix properties summary.

Development drilling to date has targeted two units of the Lower Clair Group, Unit V and Unit VI. Unit V (*c*. 90 m thick) is a homogeneous, high net-to-gross interval of fine- to medium-grained sandstone, representing the deposits of high energy fluvial channels and sheets. Reservoir quality is primarily controlled by grain size, with variable degradation caused by calcite cementation. Unit VI (*c*. 180 m thick) is a heterogeneous interval of fine grained sandstone and siltstone, representing the deposits of fluvial channels and channel abandonment facies. Unit VI is divided into upper and lower sub-units by the Lacustrine Key Bed (LKB), a pervasive mudstone present across much of the field. Typical reservoir matrix properties of the net sands are slightly poorer than in Unit V and the proportion of net sand is much lower. Within Unit VI the net to gross ratio varies widely across the field from non-net to good quality intervals in an unsystematic fashion. Unit III is similar to Unit V but with a higher proportion of aeolian facies. As in Unit V, the best matrix reservoir quality is found in the coarsest fluvial sands. Unit IV represents a more proximal, less well-sorted fluvial facies with a higher proportion of heterolithic and shaly sands, with poor reservoir properties.

Fractures are developed in all units to varying degrees (Barr *et al.* 2007, p. 209, Fig. 4b), controlled by mechanical stratigraphy, location within the field and proximity to faults. Brittle fractures dominate over granulation seams in the lower-porosity, fine-grained or cemented facies; however, many of these are occluded by calcite cement and do not contribute to fluid flow (Barr *et al.* 2007, p. 211, Fig. 6). Granulation seams are common in clean, high-permeability sands, but their baffling effect within the reservoir is diminished by a tendency for uncemented brittle fractures. Shaly sands and mudstones are weakly fractured and those which are present tend to be cemented. The net effect of these controls is that (in fractured parts of the field), fractures subtly enhance matrix permeability in Unit III and Unit V (but where dominant, granulation seams may degrade it), considerably enhance matrix permeability in Unit VI and make little or no contribution in Unit IV and in the LKB mudstone (Fig. 2). The Upper Clair Group is less well constrained but conductive fractures appear to be relatively unimportant.

Since early project planning the Greater Clair closure has been segmented into two areas: Phase 1 and Phase 2, named to reflect possible future phasing of the development (Fig. 1). The Phase 1 area consists of the Core, Graben and Horst segments, which have an estimated STOIIP of *c.* 1.5 billion barrels and are currently under development (Fig. 3). The Phase 2 area is the large SW–NE striking dip closure above the Rona Ridge, known locally as the Clair Ridge. The Ridge is currently under appraisal; recent well 206/8-13Z was abandoned with a downhole gauge that could transmit pressure data to the surface. The well is situated 8.5 km from the fixed production platform. Data from this gauge shows pressure decline over a time interval consistent with the overall pressure profile in the Core segment. This indicates that the Ridge Fault, dividing Phase 1 from Phase 2, could be transmissible or that pressure is being transmitted through conduits in the fractured basement. Closure of the Clair Ridge continues to the SW; this area was awarded in the 25th licensing round of 2008 as a traditional seaward licence (P.1570), comprising blocks 206/11b, 206/12b, 206/16a and 206/17a.

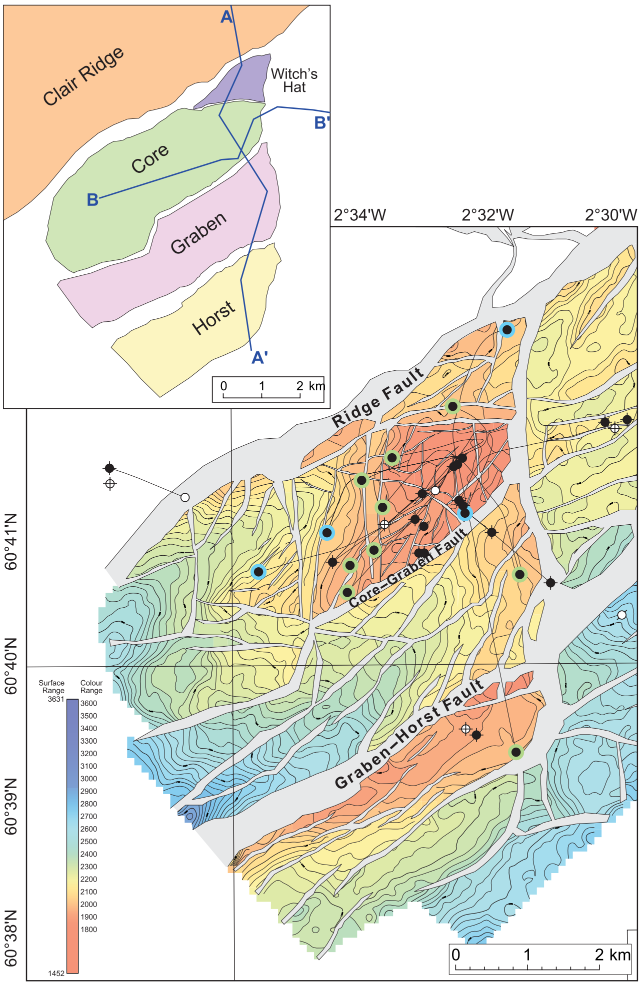

Fig. 3. Top Unit V map derived from OBC dataset, 2008. This map shows the field as developed in March 2009. Green circle represents a production well and blue circle represents a water injection well.

Within the Phase 1 area the Core, Graben and Horst segments (Fig. 4) are formed by significant NE–SW extensional faulting inherited from the Devonian–Carboniferous basin. Within the Core faults trend predominantly NE–SW, with some orientated north to south and east to west. The NE–SW trend is orthogonal to the main extension direction of the segment bounding Ridge Fault. The Core, Graben and Horst form a faulted roll-over structure in the hanging wall of the fault, with the Graben segment forming a crestal-collapse feature. Extension on the Graben-bounding faults primarily took place during deposition of Carboniferous Upper Clair Group sediments, indicated by significant thinning of the Upper Clair Group in the footwalls of the bounding faults. As a result of subsequent inversion, the Clair Group structural crest (the Base Cretaceous Unconformity) is located above the Graben.

Basement topography in the Core of the field is more irregular than in the Graben or on most of the Horst. The lowermost reservoir units thin significantly onto local basement highs. The thinner Lower Clair Group succession appears to be more intensely fractured than the thicker sections. Fault throws within the Core display displacements of the order of 25 m when mapped on seismic data. Larger faults within the area have throws in the range 50–75 m. Development drilling has demonstrated that mapped faults within the reservoir are generally transmissible, but some baffling occurs across larger faults, especially where different units are juxtaposed. Abundant faulting in the Core segment may be due to the proximity of the Ridge Fault.

The Graben contains fewer faults than the Core. The faults generally have a small throw in the up-dip area of the segment, increasing in throw to the SW. Two production wells have been drilled into the Graben, the second in 2009. Development drilling in the Graben has shown that the segment bounding Core–Graben Fault (Fig. 3) is partially transmissive, as depletion was observed in the Graben Lower Clair Group due to production from the Core. Maximum depletion was observed in Upper Unit VI (which is juxtaposed against Core segment Unit V); depletion decreases with distance from the fault.

As of 2008 the Horst was undeveloped. One production well was drilled and brought online in early 2009. In the up-dip area of the Horst there are relatively few faults compared with the Core. The SE edge of the structure is cut by a number of normal NE–SW trending faults which typically have displacements of 50–100 m. Displacement along the segment bounding Graben–Horst Fault is typically 200 m in the NE, but increases rapidly to the SW as the Graben deepens relative to the Horst.

This paper describes the most recent (2008) subsurface understanding of the Core segment of the Phase 1 development area only, where the majority of production and injection wells have been drilled.

Pre-development appraisal

After discovery by well 206/8-1A, the Core segment was appraised in 1980 with well 206/8-5 (Fig. 1). Upper Unit VI was tested at 1050 BOPD, following stimulation by hydraulic fracturing. In 1985 a further stimulation was planned in 206/8-7, but following mechanical problems the well was side-tracked and the programme was not completed. Allen & Mange-Rajetzky (1992) described the stratigraphy of the Clair Group with reference to the fully cored 206/8-7. Post-well heavy mineral analysis showed that the well penetrated the Core–Graben fault, resulting in a thinned and unrepresentative section.

Well 206/8-8 marked a turning point in the development of Clair. Drilled in 1991, facilitated by the 'Joint Appraisal

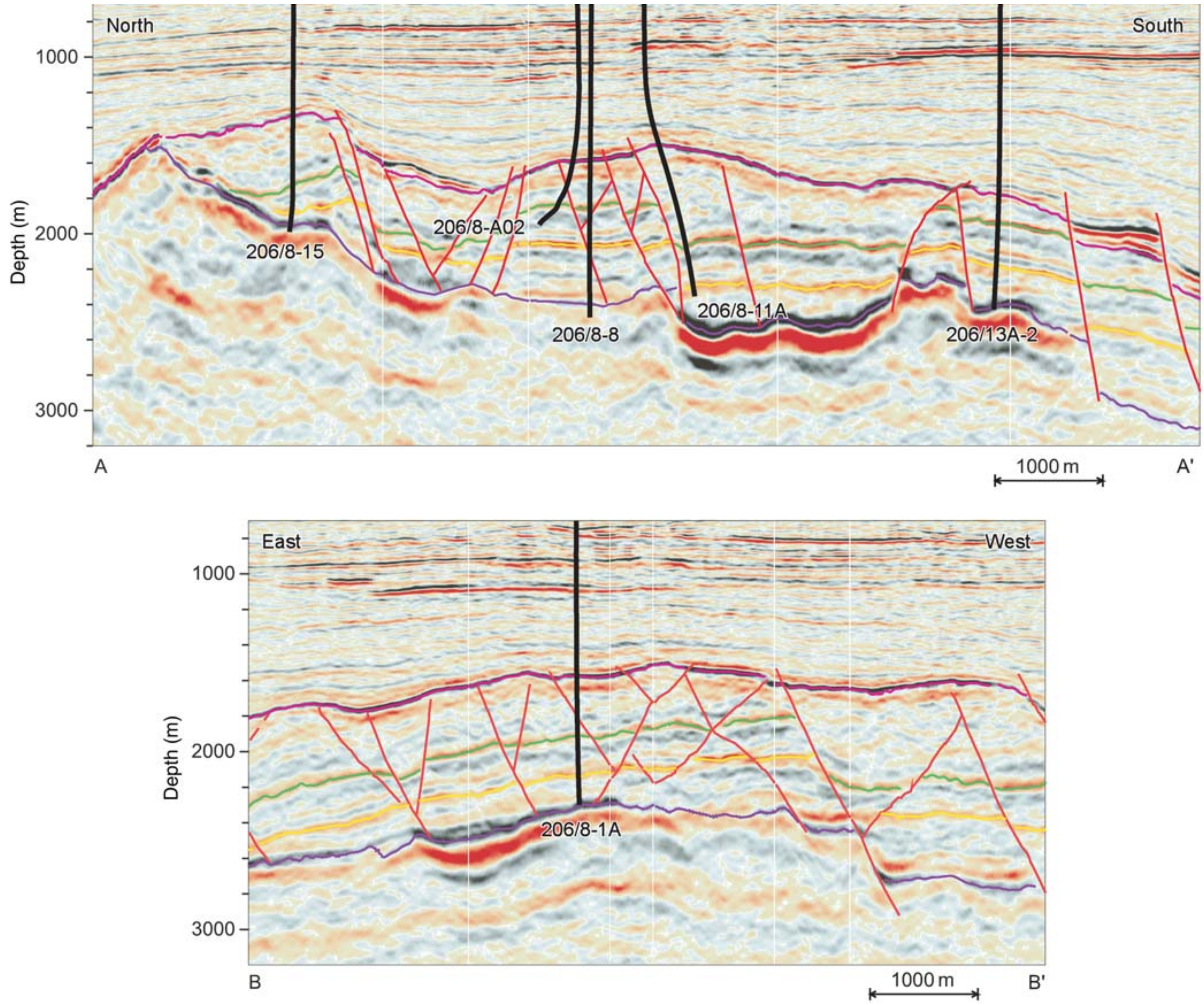

Fig. 4. Seismic line and cross-line through the Clair field from 2006 OBC data, line locations shown on Figure 3. Horizons are Base Cretaceous Unconformity (magenta), Top Unit V (green), Top Unit III (yellow) and Basement (purple).

Agreement', its aim was to demonstrate commercial flow rates from the Core, the central 'roll-over' area of Coney *et al.* (1993). The well was situated at the structural crest of the Core and penetrated a full succession. Fully cored and logged sedimentologically and structurally, it is now considered to be the Lower Clair Group reference section. Unit V tested at 3100 BOPD, which was maintained for the full six-day flow period. Unit VI was tested at 1850 BOPD, which increased to 3250 BOPD following hydraulic fracturing and was sustained for another six-day flow period. Permeability-height was an order of magnitude greater than that expected from the core plug data (Barr *et al.* 2007), clearly demonstrating the benefits of accessing the existing natural fracture network. The post-stimulation test also demonstrated that connection into the natural fracture network could be achieved with hydraulic fracturing. Well 206/8-8 was the last vertical appraisal well. Subsequent wells were deviated to target natural fractures, with increased length in specific reservoir units.

Well 206/8-9Z was drilled the following year with the objective of testing a high-angle section of Unit V, targeted to intersect the dominant open fracture orientation observed in 206/8-8 and to maximize reservoir length in Unit V. The high angle section in Unit V and Unit VI flowed at 7306 BOPD which was sustained for 9.5 hours. A large contribution to this flow was interpreted to be from the existing natural fracture network.

Well 206/8-10Z (1996) was the final appraisal well drilled in the Core segment; following the success of 206/8-9Z it targeted another naturally fractured section interpreted from seismic data. During a 50-day extended well test the horizontal section of Unit V and Unit VI produced at an average rate of 10,200 BOPD. This element of appraisal was instrumental in unlocking the commerciality of the development, demonstrating that a second well planned to intersect mapped fractured sections yielded another high production rate (Smith *et al.* 1995). This gave confidence that high production rate development wells could be planned by targeting similarly fractured areas (Smith & McGarrity 2001), providing a robust technical case from which further commercial and project planning could proceed. The sustained rate demonstrated the ability of natural fractures in the vicinity of the wellbore to link into the wider fracture network (Barr *et al.* 2007). Well 206/8-9Z was re-entered after the extended well test and side-tracked as observation well 206/8-9Y. It encountered depleted Lower Clair Group and material balance calculations indicated that a STOIIP of *c*. 500–600 MMBBL had been contacted by the extended well test. This volume was too large to be purely held in fracture aperture alone suggesting communication out into the wider matrix, reducing the uncertainty relating to segmentation and compartmentalization. Well 206/8-10Z was suspended for subsequent tie-back to the future development.

Original field development plan

After the successful appraisal campaign the Clair co-ventures sanctioned the project for development. Early on a decision was made to not pre-drill the field; this was intended to allow time for dynamic reservoir data from early wells to impact the later well sequence. The original development plan contained 23 wells (15 producers and eight water injectors), including the suspended 206/8-10Z (Fig. 5). The early producers were planned to target Unit V with a horizontal section; later wells had Unit VI targets. Early water injection was seen as critical as the aquifer was not expected to provide pressure support. Within the original field development plan the Core segment was to be the focus of the initial drilling sequence of 10 wells, including four water injectors. The field development plan concentrated on what were perceived to be the key uncertainties of the development at the time, specifically the dynamic response of the reservoir to production. These uncertainties were related to how the field would respond to water flood, controlled by the compartmentalization and connectivity of the fracture network and the degree of matrix imbibition. Development wells were expected to water out within 1–3 years, so the facilities were designed to handle large quantities of produced water.

Initial 3D seismic data over the development area was a streamer seismic survey, acquired in 1990. Data quality was poor despite reprocessing and, after a successful 2D ocean-bottom cable (OBC) trial in 2000, a 3D OBC was acquired in 2002, which led to a step change in data quality due to higher-fold, richer offset-azimuth distribution and improved multiple attenuation (Kommedal *et al.* 2005). This was subsequently reprocessed in 2006 along with additional OBC acquisition over the Clair Ridge, leading to further improvement and interpretation detail compared to the initial 3D streamer data (Fig. 6). The OBC data significantly helped well planning before start-up. The initial well sequence was planned, honouring the development plan strategy of maximizing

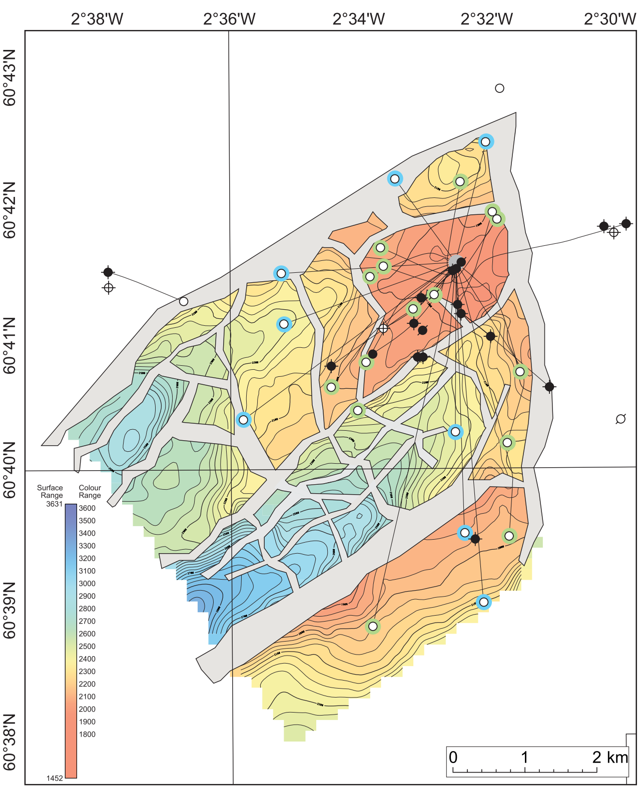

Fig. 5. Top Unit V map derived from streamer dataset, 2001. Green circle represents planned production well, blue circle represents planned water injection well and grey circle represents planned cutting re-injection well.

learning through careful phasing of the wells (the Plan–Do–Measure–Learn–Plan loop of Clifford *et al.* 2005).

Managing field start-up

The original field development plan called for early water injection wells to support offtake at 206/8-10Z. These injectors were planned to the SW of the Core segment, down the flank of the structure with the intention of initiating water drive up to the producing well stock at the crest (Fig. 5). The first new development well was planned to be a dedicated cuttings re-injector, with the second a downflank water injector. However, during the well design phase of the development well completions were changed to allow cuttings to be injected down the annulus and into the Cenozoic and Cretaceous overburden, removing the need for the dedicated well.

Producer-led start-up

As the project matured the well sequence evolved. There was an obvious desire for a fast production ramp-up, but this was at odds with the original field development plan of early water injection. Clair fluid produced from the 206/8-10Z extended well test was undersaturated, and at the end of the test reservoir pressure was 300–400 psi above bubble point. Therefore there was the possibility of safely producing for a period before water injection without inducing gas breakout. Clair had not been pre-drilled so dynamic reservoir data could be taken into account when planning future wells. The main uncertainties pertaining to well placement were related to how the reservoir would deplete and if mapped faults would be conductive or behave as baffles. A well sequence was developed to maximize depletion in the Core, through the placement of early producers. To manage offtake within the safety window above bubble point each well would be completed with a downhole pressure gauge, used to calculate reservoir pressure during regular pressure build-up tests. Formation pressure data acquired in the wells would address the main uncertainty of dynamic reservoir communication, establishing communication pathways across the field. Using this rationale a water injector could be optimally placed as understanding of the reservoir developed, giving flexibility to the future water flood pattern. This strategy also reduced the risk of directly connecting a producer and injector pair through a conductive fault, by only placing injectors in areas not deemed to be in direct communication with producers.

To ensure the delivery of high-rate early producers a similar well design to 206/8-10Z was adopted; horizontal Unit V sections targeting faults mapped on the OBC data. Production logging during the extended well test had demonstrated that the majority of the production was from Unit V, with most of the inflow occurring around the intersection with seismically mappable fault lineaments. The earlier horizontal well 206/8-9Z had demonstrated a similar pattern, but with a strong influx from a Unit VI interval which saw significant mud losses and is presumably fractured (Clifford *et al.* 2005, p. 8, Fig. 7). A suite of pre-production fracture models, built using conditioning maps based upon seismic edge-detection and other methods (Barr *et al.* 2007), had been used to model horizontal and vertical (Barr *et al.* 2007, p. 222, Fig. 15) well test production log profiles. Cored vertical wells provided constraints on small-scale joint conductivity, and horizontal wells crossing mappable faults or lineaments constrained fault-zone conductivity. The 206/8-10Z observations were consistent with a conductive-fault model, with a fault conductivity (fault aperture multiplied by permeability) of *c.* 7000 mDm. This proved to be a reasonable value for full-field history matching of the extended well test. However the pressure build-up and

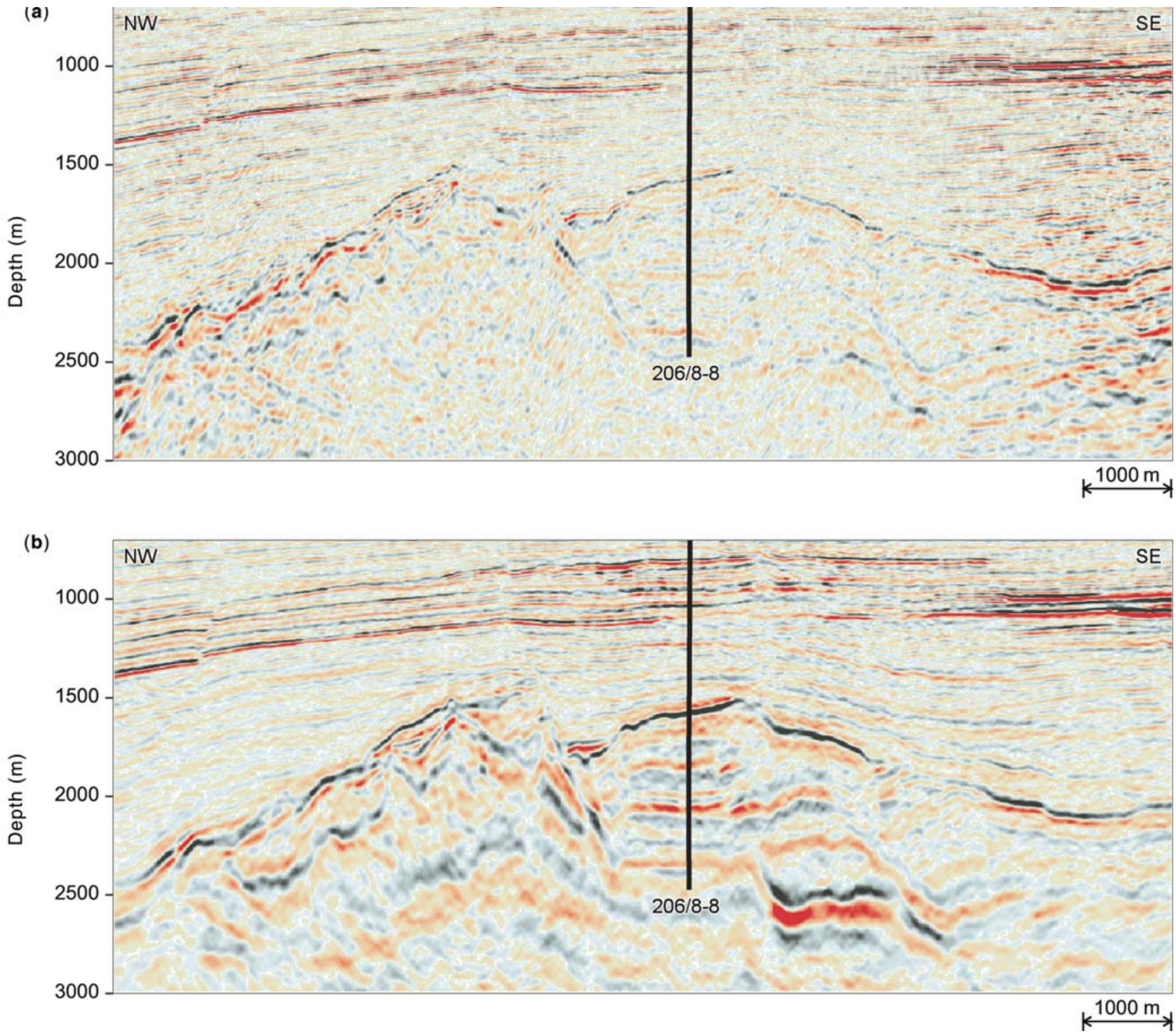

Fig. 6. Comparison of uninterpreted seismic data displayed in depth between (**a**) 1992 streamer data and (**b**) OBC data reprocessed in 2006. Well 206/8-8 is located approximately at the structural crest of the field. The Base Cretaceous Unconformity is visible at 1550 m at the well location and Top Unit V is at 1800 m.

material balance observations could also be matched by models with an intensely developed set of small-scale joints, all that was necessary was that contacted volume had the right overall permeability and oil in place. Production logging data supported the hypothesis that the well had produced from narrow, discrete fractured zones, or 'fracture clusters' related to the seismically mappable features. The averaging effect of a single, centrally placed well observation became apparent during subsequent development drilling, which found some wells much more fractured than 206/8-10Z and others less fractured. The observation of Barr *et al.* (2007) that most of the pre-production fracture models could be matched to the extended well test data is perhaps not surprising, given that the conductivity and spacing or frequency of their individual elements had been calibrated at or in the vicinity of the extended well test well. They anticipated that the percentage of models which matched would reduce as more wells were drilled, with most models failing by the second or third production well and all models failing to predict water breakthrough times from the fourth well (and first water injector).

Data acquisition strategy

An extensive static database had been built up over the years of appraisal, including over 5000 m of recovered core, conventional formation evaluation logs, image logs and mud loss data. The strategy for the early development wells was to have intensive data acquisition programmes to establish links between static data, dynamic data and reservoir performance. These data would be used to develop predictive models for matrix properties and fracture character, and help in understanding reservoir communication. Later infill wells had less intensive data acquisition as reservoir understanding developed. The first horizontal well of the development would provide a calibration point for future wells in the field. All planned wells crossed seismic features interpreted as faults, consistent with the successful horizontal appraisal wells. A core across one of these features was planned as a key reference dataset, to analyse fracture distribution and the lateral changes observed in the reservoir properties of the matrix.

To improve fracture characterization outside the cored interval, micro-resistivity and acoustic image logs were planned across the

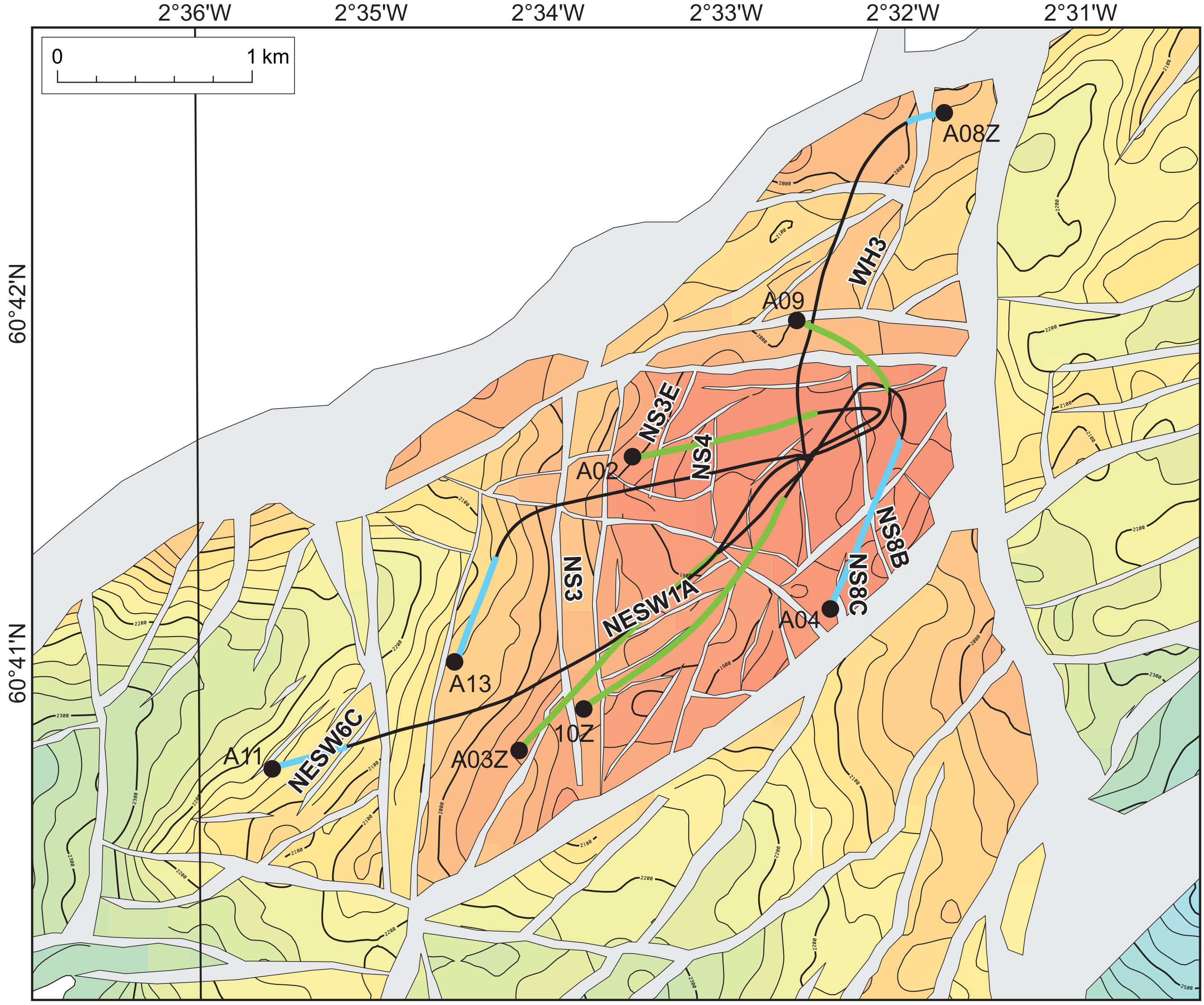

Fig. 7. Detailed map of the Top Unit V in Core segment. Producing and injecting completed sections are coloured green and blue respectively. Wells and faults referred to in the text are located.

whole reservoir section. This was the lynch-pin of the forward data acquisition plan: having confident calibration of the image logs to the core in the first well would enable interpretation of image logs in future uncored wells. For wells drilled with a water-based mud system, micro-resistivity tools can determine whether a fracture is open or closed at the wellbore: closed or cemented fractures will typically be resistive whereas open fractures filled with water-based mud will be conductive. Clay-plugged fractures also appear conductive but these were known from core observations to be relatively few in number. In an oil-based mud system an open fracture filled with oil will appear resistive. However, a calcite cemented fracture will also appear resistive. Acoustic image logs should in principle be best able to determine whether a fracture is open, with open fractures returning a low impedance signal, particularly if there has been some spalling of material at the wellbore. However, the acoustic logs have somewhat lower resolution and in Clair have proved to be more prone to acquisition-related problems such as stick-slip or (in the appraisal wells) baffling of the reflected signal by thick mud-cake. Azimuthal density and gamma logs have still lower resolution but can be recorded while drilling, giving them an advantage in making real-time drilling decisions. Although the density log can directly measure the porosity in an open fracture, only the largest fractures are detected because the response is dominated by the surrounding matrix.

Micro-resistivity and acoustic logs run over the same section identify different features, and fracture interpretation must consider both hole conditions and the strengths and weaknesses of each tool. Acoustic and density tools have full circumferential coverage; fractures cutting the wellbore at a low angle are readily interpreted. Micro-resistivity tools are pad-based, and the gaps created can complicate fracture identification. Running both tools in early wells established which method worked best within the Clair reservoir. To date, micro-resistivity tools in water-based mud have proven the best for both fracture and sedimentological characterization.

To establish the azimuth of fractures logged in core it is necessary to scribe upon acquisition. Scribing involves scouring a reference line of known orientation onto the core as it is acquired, but can lead to difficulties with recovery. Acquiring image logs over the cored section removes the need for scribing. Image logs are acquired with azimuthal data, providing a reference against which a core can be orientated. As fracture distribution was a key element of the core acquisition programme the core barrels were designed to be transported in large sections to minimize saw cuts to the fractured intervals. The barrels were opened onshore for description where matrix samples for special core analysis could be picked from unfractured sections of core. In past wells the usefulness of such samples had often been limited by the frequent occurrence of fractures and granulation seams, typically several per metre in 206/8-8 (Barr *et al.* 2007) in all but a few short, sparsely fractured sections.

Measurement of formation pressure enables an assessment of the degree of reservoir communication. The virgin pressure gradient of the reservoir had been established during appraisal. The near-vertical 206/8-9Y observation well recorded depletion from the top of Unit VI to near the base of Unit IV, despite extended well test offtake mainly from Unit V (Barr *et al.* 2007, p. 209; Fig. 4a), demonstrating vertical connectivity. In a fully homogeneous system uniform depletion would be expected, but the baffling and focussing nature of the fracture and matrix manifests as variable depletion along the well length. By measuring depletion at numerous points along a horizontal well it was hoped that direct comparisons could be made with fracture logs, building up the detailed picture of lateral connectivity within the reservoir desired for effective water injector placement.

All wells were planned to have a baseline production log run at time of start-up. This was to establish which units of the stratigraphy were producing and the relative contributions of fracture and matrix. To facilitate the production logging, and envisaging the need for continual production logs throughout field life, the platform facilities were designed with a dedicated intervention deck allowing simultaneous operations with drilling.

The data acquisition packages were designed to reduce over field life, so that just key data was subsequently collected, with confidence in the calibration having been previously established. For example, the core and image logs acquired in the original well would reduce to a single image log in later wells. The technology of logging while drilling (LWD) was used to move away from dedicated wireline or pipe-conveyed logging runs. As the development commenced and technology developed, all elements of the original package (with the exception of core) became available through the use of LWD technology. This does entail some loss of resolution in production wells drilled with oil-based mud, such that only the general proportion of fracturing along the well is determined, and relies on linkage to more sensitive core and wireline or pipe-conveyed logs in nearby wells.

Early well results

As originally planned the appraisal well 206/8-10Z was the first well to come into production, tied back as 206/8-A01. Well 206/8-A02 was the first well to be drilled from the fixed platform, a horizontal Unit V well crossing a fault of similar scale to that crossed by 206/8-10Z (Fig. 7). The well was cored across the targeted fault as planned. Core analysis demonstrated that the matrix properties of Unit V were consistent with those observed in other wells in the Core segment. The bed parallel core proved invaluable when assessing lateral heterogeneity of the fluvial channel systems and interpreting channel widths from cross-bedding dimensions. Palaeocurrent analysis suggests sand dispersal broadly towards the south. These interpretations are consistent with similar measurements made across the entire reservoir section from image log analysis, and with other wells support the gross depositional environment interpretation proposed by Nichols (2005) for the Clair field area and the wider basin. As planned, image log calibration with the cored section gave confidence that it was possible to resolve natural fractures in the logs.

Well 206/8-A02 (Fig. 8) crossed mapped fault NS4 at 2660 m measured depth (MD), and cores were acquired on both sides of the fault. A fault interpreted from wireline image logs corresponds to 2.4 m of unrecovered core between runs, representing the location of NS4. Fracture intensity is interpreted as the abundance of fractures per metre of logged core or image log, corrected for borehole orientation bias. Curves are calculated at a 1 and 20 m

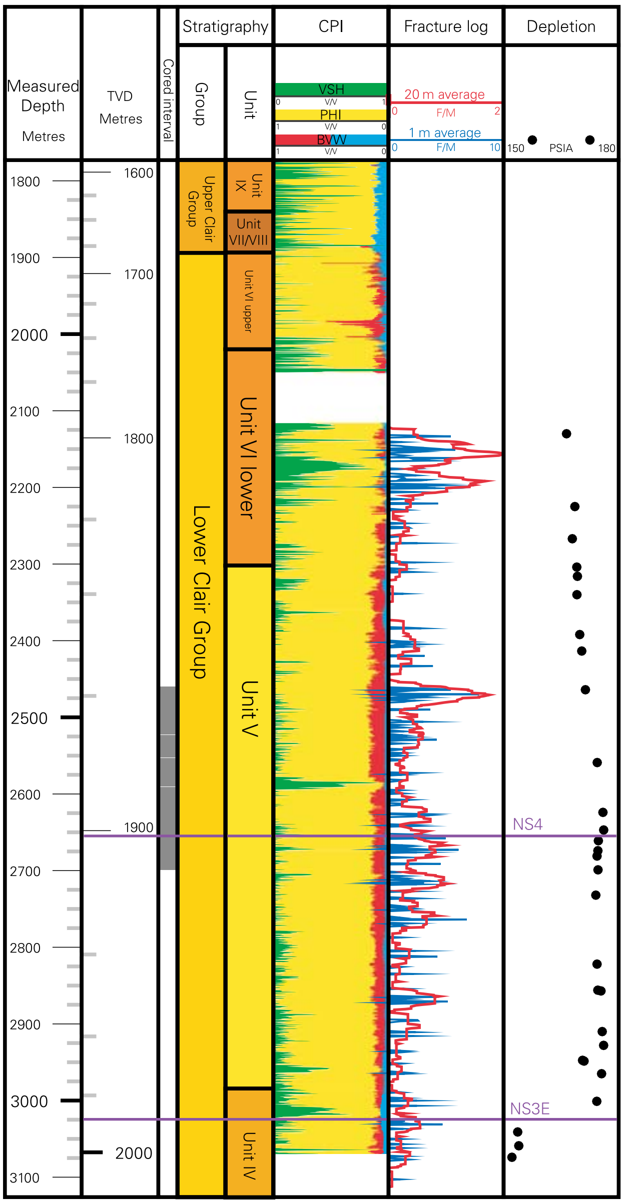

Fig. 8. Well data from 206/8-A02, displayed in measured depth. Fracture logs are derived from image log interpretation, corrected for borehole bias. Depletion is calculated from formation pressure measurements with respect to virgin pressure. Recovered core and interpreted faults are located.

moving average; the 20 m curve is commonly used within the Clair reservoir. Within the well fracture intensity was highest within the top of the logged section, within lower Unit VI, with intensities typically over one fracture per metre. In contrast to predrill expectations Unit V was relatively less fractured, with intensities typically under one fracture per metre, with no clear 'fracture cluster' visible around the fault. Depletion due to production from 206/8-10Z was observed along the length of 206/8-A02. A uniform depletion profile was observed throughout Unit VI and Unit V, indicating good vertical communication through fractures. Maximum depletion occurred as the well crossed fault NS4, but production logging showed that *c.* 80% of the inflow was occurring within Unit VI lower. The depleted Unit V contributed relatively little, although it was not possible to lift the drilling mud out of that section of the well so it is possible that the toe would have flowed had it been 'cleaned up'. The zone of high fracture density in Unit VI was interpreted to be related to a series of small mapped faults connecting down into Unit V. The zone of maximum depletion near fault NS4 did not correspond with the best matrix quality or with the highest fracture frequency observed on the image log. It perhaps reflects the presence of a narrow, conductive fault core as was seen on image logs in some subsequent wells. With pervasive fracturing over the whole of Unit V, uniform depletion except at the fault and no 'fracture cluster', the well is interpreted to be an example of joint-like behaviour in Unit V but fault-dominated in Unit VI. The toe of the well crosses NS3E and depletion significantly reduces by *c.* 30 psi. At the time of drilling it was thought that this could reflect the deterioration of matrix quality within Unit IV, although it seems equally likely that there could be reservoir quality degradation around the mapped fault (see below).

Well 206/8-A02 commenced production at a rate of 12 500 BOPD, consistent with estimates from pre-drill simulation. Measurements from permanent downhole gauges installed in the first two development wells showed that the pressure drop in the reservoir was slower than expected, possibly suggesting a larger contribution from the aquifer or a flux from outside the development area. Pressure support had also been indicated by repressurization of 206/8-10Z by the time it was re-entered, 8.5 years after the extended well test. In line with the producer-led start-up a third production well, 206/8-A03Z, was drilled. In order to maximize production in a known area, the well was drilled parallel to the 206/8-9Z well trajectory, crossing fault NESW1A that had contributed a significant amount of the inflow during the extended well test. The well path descends through Unit VI and becomes horizontal within Unit V (Fig. 7). It crosses from the footwall to the hanging wall of fault NESW1A (Fig. 9) at 2743 m MD, jumping up stratigraphy to the Unit VI/V boundary before repenetrating Unit V. Fracture analysis was complicated by acquisition issues but the fracture logs record relatively higher fracturing in Unit VI than Unit V. Within Unit V, high fracture counts correlate well to the crossing of fault NESW1A and NS3.

Formation pressure tests proved the most valuable data and recorded a much wider range of depletion than observed in 206/8-A02. The highest depletion was observed at fault NESW1A within Unit V. As in 206/8-A02, maximum depletion cannot be exactly matched to fracture-frequency maxima perhaps because the most conductive features are not clearly imaged. For example, in a highly-fractured zone or breccia it may be impossible to pick individual fractures, and the image may be degraded due to hole washout and enlargement. Alternatively depletion may be associated with a few long, well-connected fractures which present a similar aperture and hence image log appearance to the more abundant, shorter fractures. The decline rate in depletion away from the fault is similar in Units V and VI, despite the much better matrix quality in Unit V, indicating that more abundant or better connected fracture are present in Unit VI and serve to equalize the two units' overall permeability. It also indicates that fault NESW1A is unique in this well either in absolute conductivity or in connectedness to well 206/8-10Z, because the other fracture frequency peaks (some of which correspond to mapped faults or coherency lineaments) do not interrupt the uniform along-hole decline in depletion. Wells 206/8-10Z and 206/8-A03Z show some interference, suggesting that these wells are linked, but not directly by a single conductive fault. This favours the first interpretation, that it is the fault properties which are distinctive and not a fortuitous well-to-well connection. The well was brought on production at 8000 BOPD with no adverse affects to the existing two producing wells.

Injector positioning and timing

With three production wells in the Core segment and the reservoir undergoing primary depletion, no significant increase in gas–oil ratio (GOR) had been recorded but pressure data from the downhole

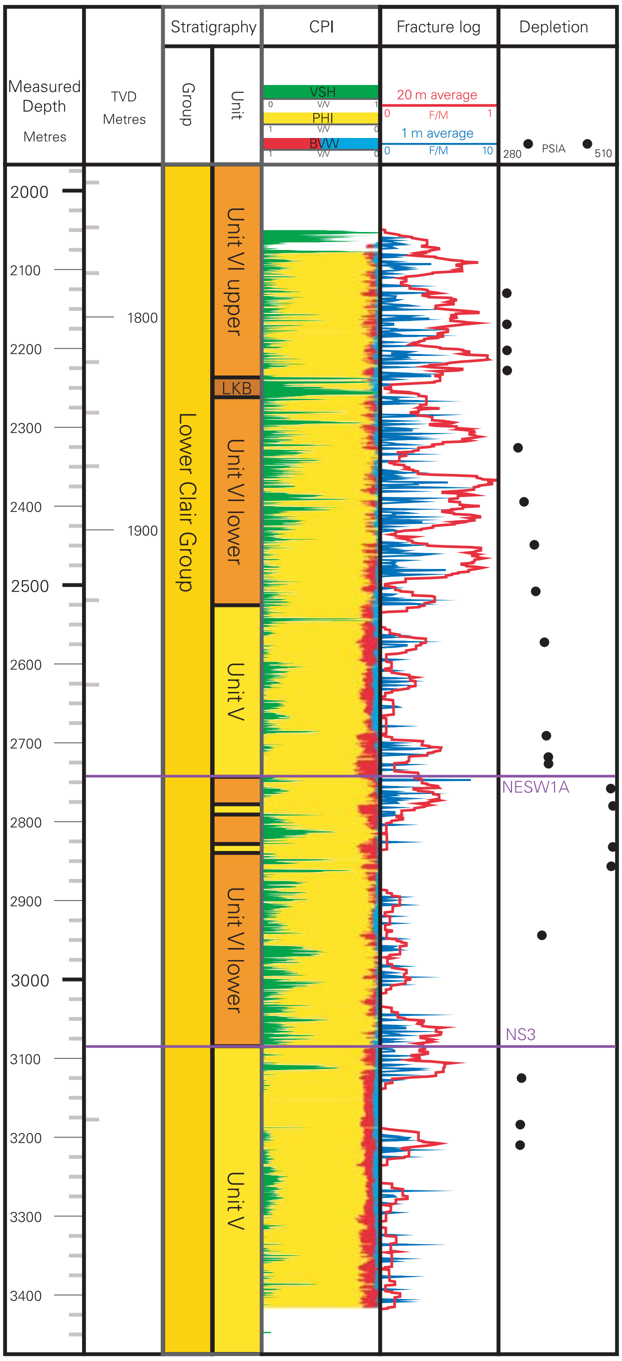

Fig. 9. Well data from 206/8-A03Z, displayed in measured depth. The well crosses fault NESW1A and cuts up stratigraphy along the Unit VI/Unit V boundary before crossing fault NS3 and re-entering Unit V.

gauges confirmed that pressure support would soon be required (Fig. 10). The goal of the producer-led start-up, to maximize depletion within the reservoir in order to optimally place water injecting wells, had been achieved. While the development drilling programme had continued, several water injector targets had been planned in parallel. The location of the first water injector was therefore not fixed at this stage (Clifford *et al.* 2005), and there were several attractive targets. Originally the first injector was planned to be located downflank. However, there was concern that the distance between that planned location and the pressure sink in the crestal Core (1.3 km) was too great to effectively support the producers. Pressure support could have taken too long to arrive. To mitigate this risk a crestal target was chosen, closer to the three producers (Fig. 7). As well as direct support to

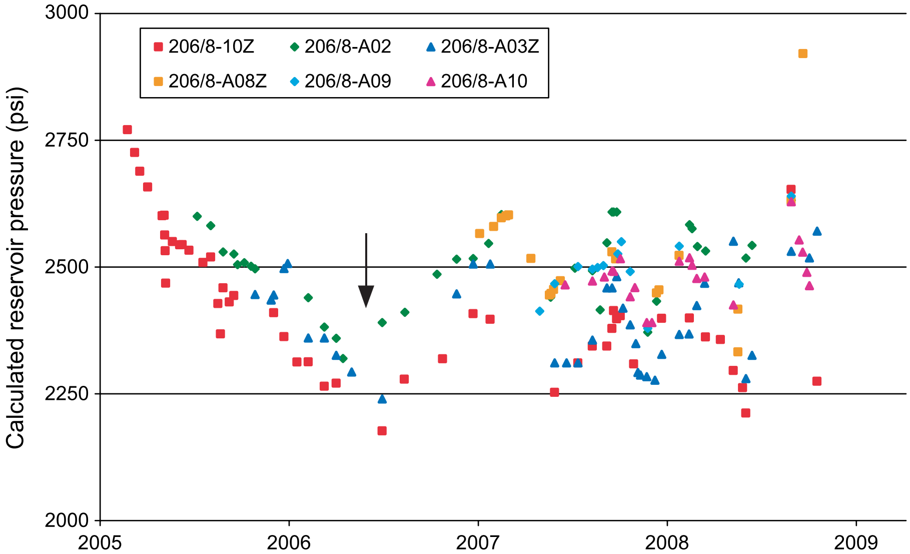

Fig. 10. Field pressure decline graph. Reservoir pressure is calculated from pressure measurements made at downhole gauges during pressure build-up tests. Arrow indicates start-up of water injection in June 2006.

the producers, the crestal injector also allowed for sweep of attic volume at the crest of the field.

The 206/8-A04 injector (Fig. 11) was drilled in the oil leg with water-based mud, which allowed for accurate fracture characterization using a micro-resistivity image log. In contrast to the previous two producers Unit VI is relatively less fractured than Unit V, with the greatest abundance of fractures being within the top of Unit V. The well crosses fault NS8B at 2605 m MD. Towards the toe of the well logged fractures become less abundant, presumably with distance away from the mapped fault. This behaviour is more akin to 206/8-A03Z with discrete fractured zones, and led to concern that injected water would preferentially flow into these fractures and not uniformly along the whole length of the well.

High depletion was observed throughout Unit V, demonstrating good communication with the producing wells. The highest depletion was observed at the toe of the well, just after fault NS8C was crossed. At this point the well was closest to the main producing interval logged in 206/8-10Z, further supporting a model of 'fracture clusters' around faults providing key communication pathways within the reservoir. After completion, an injection log was acquired over the reservoir. The temperature profile measured during a 12-hour shut-in pass yielded valuable insight into how the injector was performing. As cool sea water was injected the high reservoir temperature was cooled along the length of the wellbore; assuming that the degree of cooling was proportional to the amount of injection, interpretations can be made as to where the injection water is entering the formation. Temperature began to reduce in lower Unit VI and remained cool throughout the length of Unit V, over the highly fractured section, increasing marginally over the relatively less fractured toe section. This suggested good uniform injection across the whole of the completed length, not just the most fractured sections, which had been the original concern. This well has a very high total fracture count so it might be supposed that the uniform spread of injected water reflects a highly connected fracture set, such that even relatively unfractured sections are still above the percolation threshold and adding more fractures does not substantially increase the effective permeability. However, other aspects of the well behaviour contradict this interpretation: for example, well test pressure fall-off interpretation yields a relatively low *kh* (permeability multiplied by height), consistent with only moderate enhancement of matrix permeability. Together with evidence for matrix-like sweep of the water away from this well (see below), this suggests that the fractures, although frequent, are relatively poorly connected and most 'dead-end' in matrix. This data was the first evidence that water could imbibe into relatively unfractured matrix, increasing the sweep efficiency and ultimately leading to higher recovery.

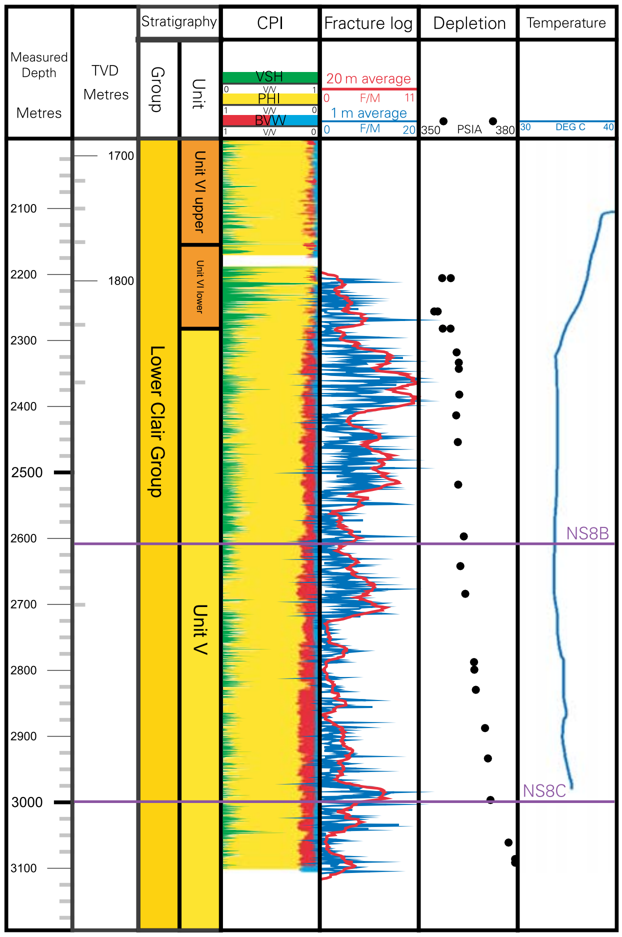

Fig. 11. Well data from first water injector 206/8-A04, displayed in measured depth. Note temperature profile from shut-in pass of production log; consistent cooling is observed, suggesting uniform injection.

The initial injection rate of 206/8-A04 was over 35 000 barrels of water per day (BWPD), consistent with pre-drill expectations, 18 months after first production from the field.

Well interference testing demonstrated that 206/8-A04 strongly supported 206/8-A02 (600 m away), and also provided pressure support to 206/8-10Z and 206/8-A03Z. Reservoir pressure rose in response to water injection (Fig. 10) but, despite their close proximity and pressure communication, 206/8-A02 did not experience early water breakthrough. Dry production was sustained for 20 months after the onset of water injection (Fig. 12). The volume of water injected by 206/8-A04 before water breakthrough occurred within 206/8-A02 was *c.* 6.5 million barrels. This indicates that the field does not consist solely of a fully connected network of conductive faults or ‘fracture clusters’. Some conductive elements must terminate in matrix so that flow is forced through both matrix and fractures. This enabled some of the more extreme models considered by Barr *et al.* (2007) to be ruled out. For example, those with all mapped faults conductive (Barr *et al.* 2007, p. 217; Fig. 10) or those with all the permeability enhancement provided by a dense, well-connected joint set (Barr *et al.* 2007, p. 220; Fig. 14) and points to the limitations of an extended well test in predicting water flood behaviour. Reasonable matches were obtained by combining disconnected subseismic fault models (Barr *et al.* 2007, p. 218; Fig. 12) with a scaled-down version of a relatively bland joint set model, just sufficient to explain the pressure equalization away from conductive faults and vertically in Unit VI. Matrix block size (which in the simulation model controls imbibition of water from fractures to matrix) was treated as a tuneable history-matching parameter and was best matched with values in the 5–10 m range. This is much larger than the tens of centimetres which would be inferred from conductive fracture spacing in 206/8-A04, supporting the view that most of those fractures are disconnected and only the larger ones link together to form a fracture network. Subsequent discrete fracture modelling used only the largest joints with along-hole spacings of several metres as conditioning input (fortuitously, this approximates to the detection limit of the medium resolution acoustic and micro-resistivity image logs).

Reservoir pressure was restored in the Core segment and successful surveillance had enabled learning to be maximized from three high-rate producers before the need for water injection. However, downflank injectors were required to assist in peripheral sweep and improve recovery. Well 206/8-A11 was drilled to the SW of the Core segment, as a high-angle well penetrating deep into the Lower Clair Group (Fig. 7). The well was drilled with a step out of *c.* 3 km from the fixed platform, outboard of major north–south trending faults, intersecting fault NESW6C at 4000 m MD. It was hoped that the fault would effectively diffuse the injection water along its length, providing the opportunity for uniform imbibition into the matrix and effective sweep up dip to the crest of the field. The well penetrated the standard Lower Clair Group succession (Fig. 13); fractures were most abundant in lower Unit VI (one to three fractures per metre), with counts dropping off to under 0.5 fractures per metre in Unit V. To date all previous wells had demonstrated a good degree of pressure communication throughout the reservoir. The well data demonstrated reasonable reservoir quality but no depletion within Unit V, implying no Unit V communication with the producers. This was probably the largest surprise since the field start-up, as until then only the segment bounding the Core–Graben Fault had proved to be a pressure baffle and even the fault separating the Core from the ‘Witch’s Hat’ segment, with over 100 m throw, had been open to flow. Also surprising was that Unit III, in the water leg, was depleted. All offtake in the development area is from Unit V and Unit VI so the observed depletion suggests that some faults are acting as vertical pressure conduits, allowing communication across low-permeability and relatively unfractured Unit IV to Unit III. This had actually been considered as an alternative interpretation of the 206/8-9Z production log data (Clifford *et al.* 2005, p. 8; Fig. 7). A strong Unit V matrix contribution was required to sustain flow from the toe of the well, where mud losses and open fractures were scarce. If no matrix contribution was assumed, the one conductive fault in that interval required pressure support from Unit III to match its inflow performance. This interpretation was considered less likely at the time, in light of the lack of Unit III depletion following the extended well test. In retrospect the well may have been connected into down-dip Unit III, which is poorly connected to updip Unit III at the observation well 206/8-9Y.

During injectivity testing 206/8-A11 quickly built pressure locally due to a lack of connection to the producers. The injection pressure was increased in an attempt to hydraulically fracture down into the undepleted Unit V. As sustainable injectivity rates of over 30 000 BWPD were achieved, the well clearly injected into a large

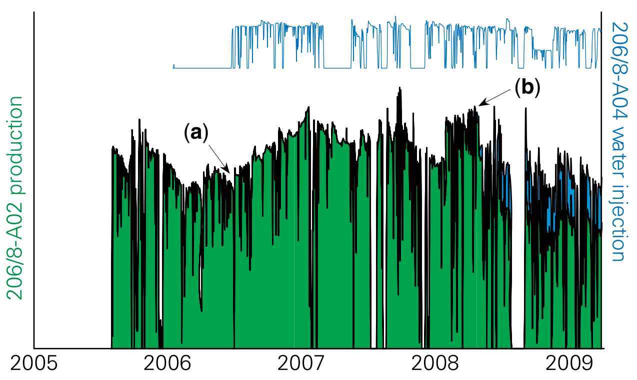

Fig. 12. Oil (green) and water (blue) production data from 206/8-A02 plotted with injection data from 206/8-A04 (upper blue line); distance between wells is *c.* 600 m. (**a**) Increase in production rate at time of injection start-up in June 2006; (**b**) water breakthrough in March 2008.

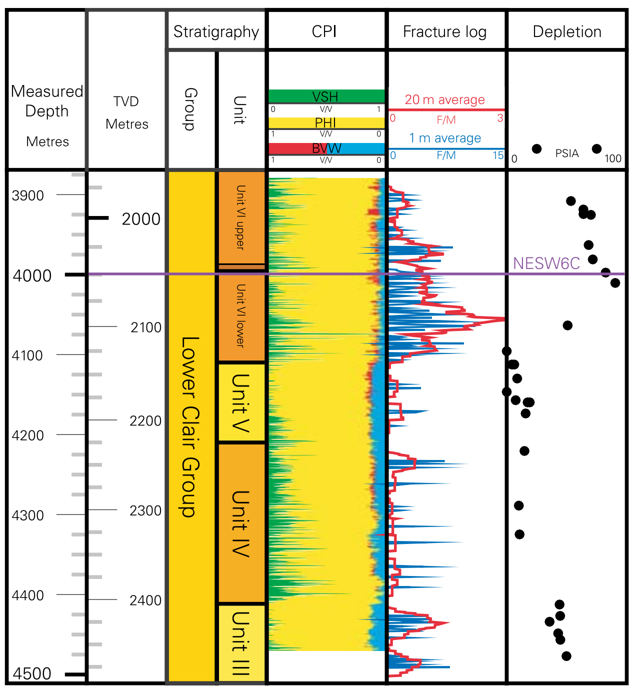

Fig. 13. Well data from water injector 206/8-A11, displayed in measured depth. Note lack of depletion within Unit V; Unit III appears depleted below.

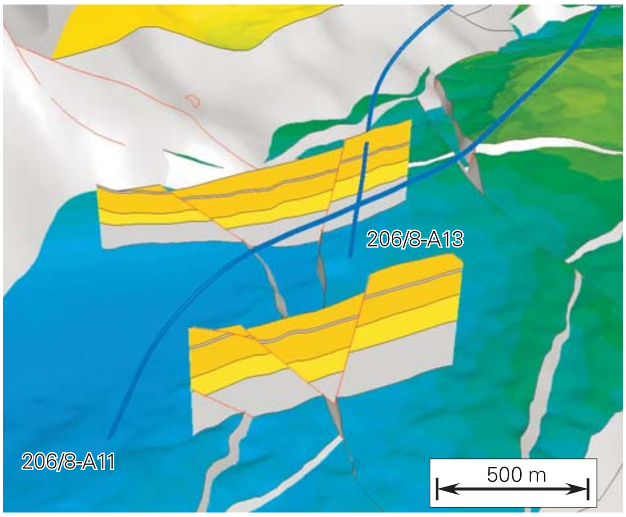

Fig. 14. North-facing perspective view of fault juxtaposition in the downdip Core segment; cross-sections are projected at both well locations. Orange stratigraphy represents Unit VI and yellow stratigraphy represents Unit V. At both locations fault offsets alone are not large enough to completely offset Unit V.

storage volume, it was concluded that it was better connected to the downflank aquifer (estimated at several billion barrels) than to the producing area. The well was completed as a Unit VI-only injector, with future plans to side-track up-dip.

The lack of depletion was difficult to explain by fault juxtaposition alone (Fig. 14) as the offsets are not great enough to completely isolate Unit V in this area, implying a degree of fault sealing. A second injector had been planned to the north of the 206/8-A11 well location, but as the previous well had demonstrated little or no communication to the crestal Core the target became much less attractive. The reason for the compartmentalization remains unclear, but there seemed significant risk that a second well in the same area may be prone to similar issues. As a direct result of these concerns the second downflank injector 206/8-A13 was moved east, closer to the producers to mitigate the risk of any baffling around the mapped fault. Reservoir quality in this well is significantly degraded in lower Unit V. A modest fault offset could juxtapose the good reservoir in the 206/8-A11 area against poor reservoir in 206/8-A13. This model could explain the undepleted pressure in 206/8-A11.

Across the field petrographic analysis of downhole samples of poor quality reservoir have indicated that the matrix has been pervasively cemented by calcite, and more rarely quartz, which occludes almost the entire pore network. Reservoir quality degradation could be related to local cementation around faults. Zones of cemented matrix had been observed during the appraisal programme, both within the Core and the other segments. Petrographic analysis of appraisal cores confirms the same pervasive calcite cementation seen in these development wells. The factors controlling the distribution of these cemented zones could relate to primary depositional fabric (with the proportion of calcrete varying across the field) and fluid movement through the fault system. At present it has not been possible to reliably map these cemented zones at a field scale, although they clearly can act as baffles within the reservoir.

It is also possible that the granulation seams which make up *c*. 50% of logged fractures also act as baffles, although it is unclear whether they form a connected network outside of fault damage zones. The calcite cemented fractures invariably show cavity-filling rather than crack-seal textures, and so are thought to represent filled open fractures rather than primary veins. As there is abundant dynamic evidence for a connected open fracture network, it is reasonable to assume that cementation of such a network would give rise to well connected barriers. One could take two extreme views of the impact of faults on Clair reservoir connectivity: on the one hand, granulation seams are pervasive, connected and therefore all faults are barriers except where breached by open fractures; alternatively, the primary fault and granulation seam fabric has been disrupted by multiple brittle reactivation events and all faults are open except where sealed by late cement. Either model would predict a patchwork of sealed, open and conductive faults, difficult to distinguish from dynamic data alone.

In light of these well results the production-led start-up is justified. If the original field development plan had been followed and downflank water injectors drilled at the start of the development (Fig. 5), there would have been no production offtake so lack of depletion in the downflank area would have been no indication of poor connectivity. This would have resulted in the completion of a well like 206/8-A11 across all reservoir units, and possibly other outboard injectors in similar positions. The strategy of maximizing depletion (within the safety window above bubble point) clearly showed that some downflank areas are not in pressure communication with the crestal Core, and as a result has helped to effectively place water injection wells.

As the development has progressed, production wells continue to target mapped faults. Two of the more recent producers in the Core segment have demonstrated particularly high production rates of up to 20 000 BOPD. Recent wells have marked a strategic shift as dedicated Unit VI-only producers, cutting a number of mapped faults. These wells access significantly poorer matrix but exploit the high fracture intensity seen in Unit VI in the early producing wells (Fig. 9).

Water breakthrough

A key uncertainty in the development was the timing of water breakthrough. This had been predicted to be relatively early in pre-development models, and this had greatly influenced the original field development plan. First water production occurred in September 2007 in the ‘Witch’s Hat’ fault block to the north of the main Core segment (Fig. 3). The ‘Witch’s Hat’ is a small downthrown segment directly to the south of the Ridge Fault, in a structurally complex area north of the fixed platform. The segment was developed in early 2007 with a producer–injector pair. The injector, 206/8-A08Z, was located in the northern corner of the segment, adjacent to the Ridge Fault, and was drilled first to provide additional support to the Core producers. It was drilled into a damage zone of what was later mapped as a north to south trending fault WH3 (Fig. 7). The well was initially planned based on a time migrated seismic dataset; there was significant improvement in the fault imaging with pre-stack depth migration that became available after the well was drilled. Reservoir quality was poorer than expected, but pressure data confirmed good connectivity to the rest of the Core. Despite the poor matrix properties the well achieved an injection rate of 35 000 BWPD and provided excellent pressure support to the Core. Dynamic data indicates that the poor matrix quality extends hundreds of metres from the fault (or at least that flow is confined within the fault, perhaps by a sealing damage zone), but reservoir pressure near the well has not increased dramatically so the fault must connect into a region of good-quality matrix (or more likely, matrix and fractures) which is being drained by the Core producers. This contrasts with 206/8-A04, where water was dispersed very close to the well in good quality matrix.

Well 206/8-A09 was drilled into the faulted terrace separating the Core segment from the ‘Witch’s Hat’ (Fig. 7). During drilling

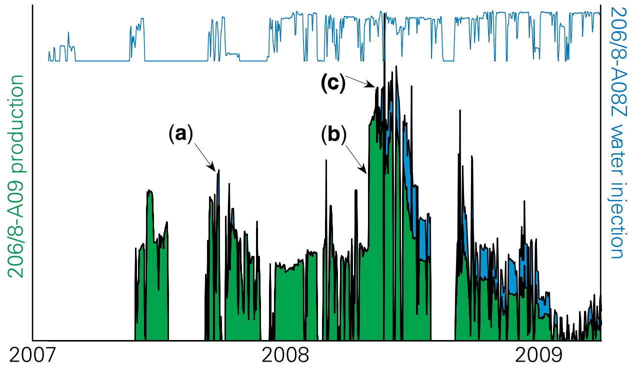

Fig. 15. Oil (green) and water (blue) production data from 206/8-A09 plotted with injection data from 206/8-A08Z (upper blue line), distance between wells is *c*. 1200 m. (**a**) Water breakthrough in September 2007; (**b**) rate increase in May 2008 after water shut-off; (**c**) continued water cut development.

of the reservoir section over 4500 barrels of drilling mud were lost, giving an early indication of large open fractures in this area. Subsequent image log interpretation confirmed a highly fractured section where individual fractures could not be distinguished due to the highly fractured nature of the reservoir. The well achieved an initial rate of over 5000 BOPD, with rapid interference (*c*. 1 hour) with its paired injector 206/8-A08Z, 1200 m to the north. At the time the well had the highest productivity index of any in the field, with its rate limited only by the platform's capacity to deal with the large amount of drilling solids (loss control material) which flowed back. At the time of completion in May 2007 there was no water production from the field, despite the beginning of water injection in June 2006. Shortly after 206/8-A09 was brought into production, water breakthrough occurred (Fig. 15). Testing the well showed that the water cut was strongly rate dependent (at 3000 barrels per day (BPD) the well produced dry, at 5000 BPD it produced at 30% water cut). The two wells within the 'Witch's Hat' segment appear to be in direct communication through the mapped conductive fault.

The risk of early water breakthrough had been recognized during the well design phase, and to mitigate against this the completion was designed to allowed for zonal isolation. A production log confirmed water entering at the toe section and the interval was successfully plugged back, restoring dry oil production. The well rate was successfully increased following the intervention but after two weeks the water-cut began to develop once again; the point of water entry had re-established at a shallower depth in response to the changed completion. The well was choked back to manage the increasing quantities of produced water and was listed as a candidate for a future side-track campaign. This experience demonstrated the risk of injector and producer directly connecting into the same fault system.

Water flood development

After the success of the permanent Life of Field Seismic (LoFS) system on Valhall (van Gestel *et al.* 2008) a small permanent system was installed in 2006 to monitor the 4D seismic response in the central Core segment (Foster *et al.* 2008). It had the objectives of monitoring the developing water flood front and identifying areas of gas breakout, enabling the optimization of development drilling locations and water injection management. As the 4D seismic response at Clair was predicted to be small (1–2% acoustic impedance change), the initial installation was a test to confirm if a response could be recognized. The plan was to acquire three surveys and then assess the results before deciding on future acquisition. Three annual surveys have now been acquired (2006, 2007 and 2008).

4D seismic data has helped in the understanding of water movement in the Core segment. Comparison of the first LoFS survey in 2006 to the original OBC data acquired before start-up has proved challenging due to high noise levels (low reproducibility between different receiver installations). Comparisons using the LoFS on LoFS surveys with the same permanently installed array have proved valuable in understanding the water flood pattern. For example the 4D difference map of 2006–2007 for the upper part of Unit V shows an acoustic hardening or dimming of the reservoir consistent with an increase of water saturation around the 206/8-A04 water injector (Fig. 16b). The area of inferred increased water saturation is concentrated at the heel section of the well with less pronounced changes at the toe. This correlates well to the temperature log (Fig. 11), which established that injection was occurring relatively uniformly across the completed section, but dropping off at the toe (also consistent with logged fracture distribution). Four-dimensional seismic data shows dimming is concentrated in the upper part of Unit V, which has the highest reservoir quality. Locally, where the water signature crosses a fault, there is a response in lower Unit V. Away from the fault the 4D change reverts back to upper Unit V. This could indicate vertical water movement along mapped fault planes.

The 4D difference map (Fig. 16a) shows that the area of dimming extends to the NW of the heel of 206/8-A04 towards the heel of 206/8-A02. The injector is drilled close to the intersection of two faults, and the 4D response to water is strongest at the intersection.

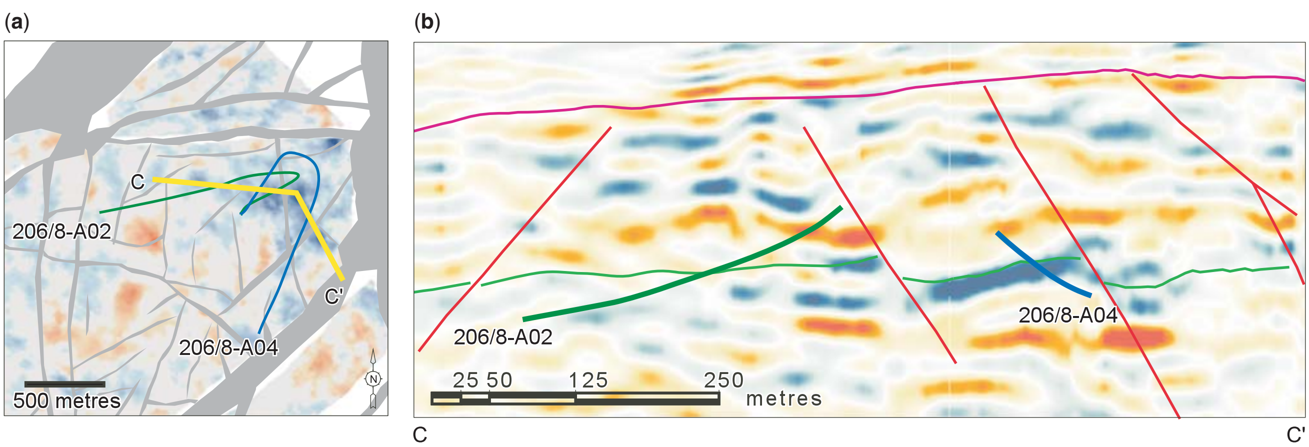

Fig. 16. (**a**) Core segment 2006–2007 4D difference map based upon Top Unit V; blue is inferred as water saturation increase. (**b**) Cross-section between injector 206/8-A04 and producer 206/8-A02. Horizons are Base Cretaceous Unconformity (magenta) and Top Unit V (green).

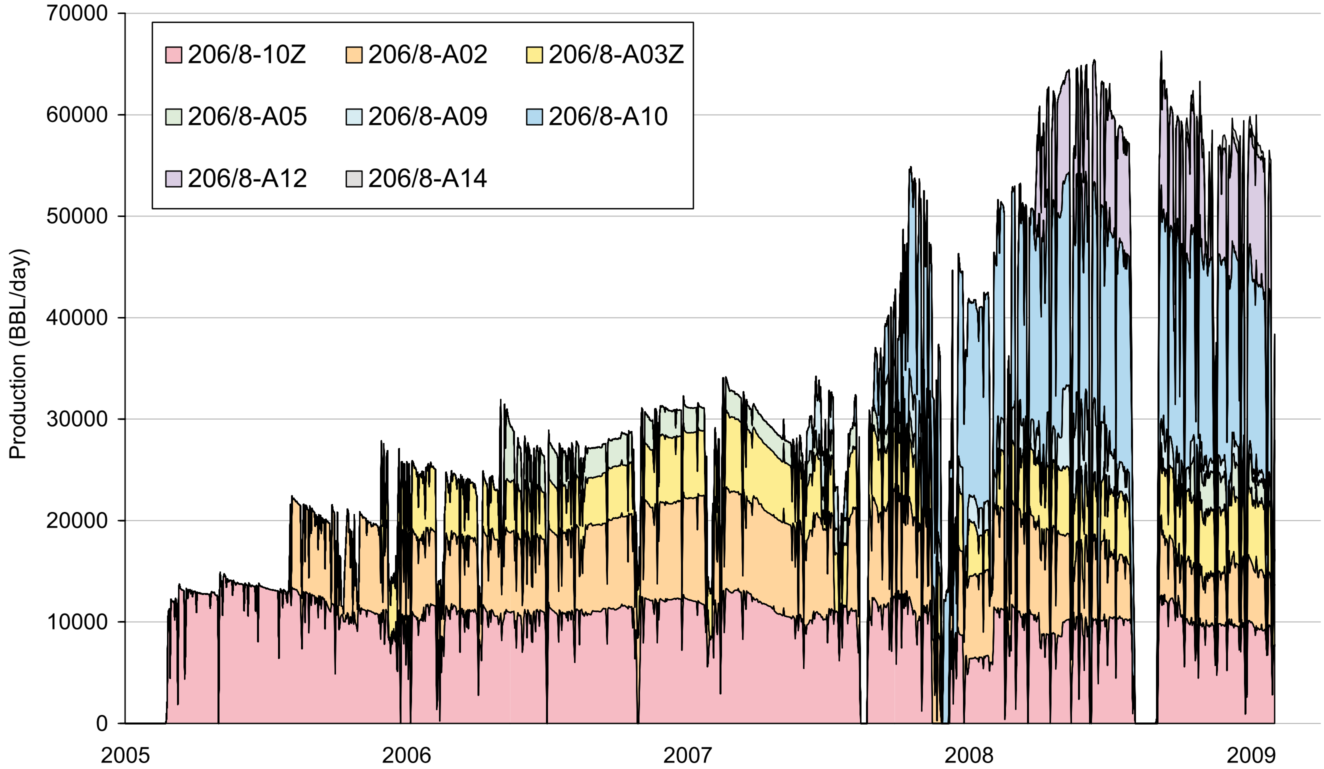

Fig. 17. Clair field start-up, oil production profile.

Well 206/8-A02 was the second well to see increased water production. Water breakthrough occurred 20 months after injection start-up in March 2008 (Fig. 12), suggesting that the two wells are not in direct communication. This is supported by the mapped area of dimming suggesting that the reservoir pressure in the area around the injector is much higher than the pressure around the producer.

Pressure support was provided to the all Core wells, with some seeing more direct support than others. This has created lateral and vertical differences in depletion, and probably small amounts of free gas in some areas when the reservoir pressure was near the bubble point. At low gas saturation the mobility of the gas is low or immobile, and no increased GOR has been seen in any of the production wells. At 206/8-A02 the 4D response is characterized by a brightening or acoustic softening, suggesting a small increase in gas saturation in the reservoir as a result of production. This can be tied to wells which have seen the highest pressure depletion. A similar brightening is also seen at other production wells in the Core segment and also in the Graben (Fig. 3), which is partly covered by LoFS 4D data and has been producing without pressure support since 2006.

The production capacity of the facilities was reached in mid-2008, three years after the first well was brought online (Fig. 17). In the Core segment the primary well targets have now been drilled or are currently being planned. Most future targets are likely to be accessed by side-tracking existing wells. In this complex reservoir, a detailed and integrated understanding is required to ensure that these side-track locations are successful. Four-dimensional seismic data will have a key role to play in identifying successful target areas, away from water and from areas of secondary gas development.

Conclusion

Early appraisal well data demonstrated the complex nature of the reservoir, which resulted in a 28 year gap between initial discovery and development start-up. During this period the appraisal campaign collected a wealth of static data, highlighting the main uncertainties and barriers to an earlier development. Initial vertical appraisal well rates were low; successive penetrations established the Clair Group stratigraphy and the influence of fractures. As seismic technology developed the natural fracture network was targeted, initially vertically with 206/8-8, demonstrating the potential of the reservoir to deliver increased rates from fractured intervals. With the ability to drill horizontal wells, and the developing knowledge of the fracture network, the appraisal campaign culminated in the successful drilling and testing of 206/8-10Z. The extensive appraisal well database allowed for a clear static description, highlighting the remaining dynamic uncertainties in the original field development plan.

Prior to production start-up the key decision was taken not to pre-drill, giving the opportunity to respond to dynamic changes within the reservoir with a flexible well sequence. A suite of fracture models attempted to capture the range of pre-production uncertainty. These models controlled the distribution of fractures within the reservoir, ranging from relatively densely fractured joints models to models with discrete ‘fracture clusters’ around mapped faults. This suite of models underpinned the future development, allowing data from subsequent wells to be analysed within an already established framework. At this time the degree of matrix imbibition was unknown and all planning included significant measures to handle large quantities of produced water.

To address the range of uncertainty, flexibility was seen as key to the development. Analysis of appraisal well data demonstrated that a producer-led start-up could be adopted, in a safety window above reservoir bubble point. This decision emphasized the importance of data acquisition in the early wells and all were completed with extensive datasets to fully characterize both fractures and matrix. Regular monitoring of pressure data allowed for the delay in water injection and an initial period to analyse the results from the first development wells. Early well results were in line with pre-drill simulation estimates. Key observations were made using reservoir pressure data, noting the contrasting styles of uniform depletion (206/8-A02) and depletion concentrated around interpreted 'fracture clusters' (206/8-A03Z). These observations allowed the pre-drill models to be refined while water injector targets were planned at multiple locations. The integration of all static and dynamic data underpinned the decision to drill the first water injector at a crestal position, in a change from the original field development plan.

The delay in the onset of water breakthrough after injection start-up was evidence that matrix imbibition was occurring and some downside pre-drill models could finally be eliminated. Core segment water breakthrough occurred 20 months after water injection start-up. Effective matrix imbibition has been inferred from the timing of water breakthrough and from the 4D seismic response. An injector inadvertently drilled within a fault damage zone in the 'Witch's Hat' segment is interpreted to have connected directly to a producer through the conductive fault system, highlighting one of the key pre-drill risks documented by the field development plan.

Data from later development wells continues to surprise, most notably with the lack of depletion observed downdip in the Core segment within well 206/8-A11. This reinforces the importance of the producer-led start-up, maximizing depletion in the Core to highlight communication pathways within the reservoir. As the development continues, 4D seismic data is improving the dynamic reservoir understanding and providing valuable spatial context to the well results. It may be possible to map these communication pathways and their associated barriers, and as the development continues, 4D seismic data will prove valuable in identifying future side-track targets.

The producer-led start-up created an opportunity to learn from the rapidly growing well stock and, crucially, influence the development based upon the observations made. The complex nature of the reservoir highlighted the need for the rapid, early data integration that defined the early years of the development of the Clair field.

This paper is published with kind permission of BP Exploration Operating Company Ltd and the Clair field co-venturers: ConocoPhillips (U.K.) Ltd, Chevron Upstream Europe, Shell UK Ltd and Hess Ltd. The development of the Clair field stands as a testament to the work of our predecessors throughout appraisal and pre-development, and more recently our colleagues within the Clair Reservoir Management Team. The authors would like to thank M. Kidd for cartography, and the manuscript has benefited significantly from reviews by W. Narr, R. Knipe and an anonymous reviewer.

References

Allen, P. A. & Mange-Rajetzky, M. A. 1992. Devonian–Carboniferous sedimentary evolution of the Clair area, offshore northwestern UK: impact of changing provenance. *Marine and Petroleum Geology*, **9**, 29–52.

Barr, D., Savory, K., Fowler, S., Arman, K. & McGarrity, J. P. 2007. Predevelopment fracture modeling in the Clair Field, West of Shetland. *In*: Lonergan, L., Jolly, R. J., Sanderson, D. J. & Rawnsley, K. (eds) *Fractured Reservoirs*. Geological Society, London, Special Publications, **270**, 199–219.

Clifford, P., O'Donovan, A., Savory, K., Smith, G. & Barr, D. 2005. *Clair Field – Managing Uncertainty in the Development of a Waterflood Fractured Reservoir*. SPE, **96316**.

Coney, D., Fyfe, T. B., Retail, P. & Smith, P. J. 1993. Clair appraisal: benefits of a co-operative approach. *In*: Parker, J. R. (ed.) *Petroleum Geology of Northwest Europe: Proceedings of the 4th Conference*. Geological Society, London, 1409–1420. doi: 10.1144/0041409.

Foster, D., Fowler, S., McGarrity, J., Riviere, M., Robinson, N., Seaborne, R. & Watson, P. 2008. Building on BP's large-scale OBC monitoring experience – the Clair and Chirag-Azeri projects. *The Leading Edge*, **27**, 1632–1637.

Kommedal, J. H., Fowler, S. & McGarrity, J. P. 2005. Improving P-wave imaging with 3D OBS data from the Clair field. *First Break*, **23**, 51–54.

Morton, A. C., Spicer, P. J. & Ewen, D. 2003. Geosteering of high-angle wells using heavy-mineral analysis: the Clair field, west of Shetland, U.K. *In*: Carr, T. R., Mason, E. P. & Feazel, C. T. (eds) *Horizontal Wells: Focus on the Reservoir*. AAPG, Tulsa, OK, Methods in Exploration, **14**, 249–260.

Nichols, G. J. 2005. Sedimentary evolution of the Lower Clair Group, Devonian, West of Shetland: climate and sediment supply controls on fluvial, aeolian and lacustrine deposition. *In*: Doré, A. G. & Vining, B. A. (eds) *Petroleum Geology: Northwest Europe and Global Perspectives: Proceedings of the 6th Petroleum Geology Conference*. Geological Society, London, 957–967. doi: 10.1144/0060957.

Ridd, M. F. 1981. Petroleum geology west of the Shetlands. *In*: Illing, L. V. & Hobson, G. D. (eds) *Petroleum Geology of the Continental Shelf of North-West Europe*. The Institute of Petroleum, London, 414–425.

Smith, P. J., Daly, M. & Stump, M. 1995. *The Paradox of a New Oil Province – Foinaven and Clair*. SPE, **30354**.

Smith, R. L. & McGarrity, J. P. 2001. Cracking the fractures – seismic anisotropy in an offshore reservoir. *The Leading Edge*, **20**, 18–26.

van Gestel, J. P., Kommedal, J. H., Barkved, O. I., Mundal, I., Bakke, R. & Best, K. D. 2008. Continuous seismic surveillance of Valhall Field. *The Leading Edge*, **27**, 1616–1621.

Overcoming multiple uncertainties in a challenging gas development: Chiswick Field UK SNS

R. NESBIT[1] and K. OVERSHOTT[2]

[1]*Schlumberger, 256 St Georges Terrace, Perth, WA 6000, Australia*
[2]*Venture Production plc, Kings Close, 62 Huntly Street, Aberdeen AB10 1RS, UK*
(e-mail: katie.overshott@centrica.com)

Abstract: Twenty-three years after BP discovered the Chiswick Field in 1984, first gas production was achieved by Venture Production. During its long period of appraisal and development, this asset has passed between five different operators and a large number of co-venturers. Prior to development, the field represented one of the largest undeveloped gas volumes present in the UK Southern North Sea. Key uncertainties include reservoir compartmentalization, low net/gross ratios and poor reservoir permeability, uncertainties in structural mapping and gas–water contact depths, as well as a widely varying Carboniferous subcrop and significant lateral changes in fluviatile sandstone architecture. Drilling and completion during the first phase of development were a significant challenge, with ambitious long and deep fracture-stimulated horizontal wells. The installation comprised a five-slot minimum facilities well-head platform with production tied back via the Venture-operated Markham J6A Platform with gas landed in Den Helder, Holland. As part of Phase II development a further three wells are being planned to accelerate recovery and access the remaining undeveloped reserves in both the primary Carboniferous and secondary Rotliegend reservoirs in the Chiswick Field.

Keywords: Carboniferous, hydraulic fracturing

The Chiswick Field is located in block 49/4a, UK Southern North Sea (SNS), approximately 160 km NE of Great Yarmouth (Fig. 1). The reservoir is primarily of Upper Carboniferous Westphalian A and B age with Permian Rotliegend as a secondary reservoir target. The field is a slightly elongate faulted anticline lying on the same dominant Hercynian NW–SE trend as the Markham Field to the SE and the Ketch Field to the NW and covers an area of some 37 km^2. The field is subdivided into five main fault compartments named Alpha, Beta, Gamma, Delta and Epsilon (Fig. 2). Depth to the top reservoir is around 3300 m TVDss at the crest of the structure and the volume of gas-in-place is estimated to be in the region of 600 BCF. BP discovered the field in 1984 with the well 49/4-1, which encountered gas within the Carboniferous Westphalian A and B channel sandstones.

Chiswick remained one of the largest undeveloped gas accumulations in the SNS for more than 20 years predominantly as a consequence of the significant number of uncertainties associated with the field. Reservoir distribution is recognized as the primary uncertainty, particularly in undrilled fault blocks. The Carboniferous is erosionally truncated below the Hercynian unconformity; therefore, predicting whether Westphalian A or B reservoir is present at the subcrop away from well control is difficult and this is exacerbated by the channelized nature of the reservoir sands. The porosity and permeability of these sands is low and they are part of an overall low net to gross sequence. This introduces uncertainty with respect to the connectivity of individual channel sands and also in terms of production and the connection of sufficient quantities of sand to the wellbore to achieve economic flow rates. Further uncertainties exist in the form of potential reservoir compartmentalization and structural elevation as a result of depth conversion, which is made more challenging due to a complex overburden.

Field history

Block 49/4a has a complicated history beginning in 1965 when it was first awarded to Gulf Oil during the second licensing round. Since then, more than ten different licensees have been involved in 49/4a. Venture Production's involvement began in June 2006 when they acquired the entire share capital of CH4, giving a 95% interest in Chiswick. In March 2008 Venture purchased the remaining 5% equity from Wintershall. The number of equity swaps and licensees involved in the block has undoubtedly played a role in the length of time it has taken to develop the Chiswick Field.

Prior to Venture Production's involvement, four wells were drilled on the Chiswick structure. The first was in 1984 when BP drilled the discovery well 49/4-1, which encountered a 130 m gas column within the Westphalian A and B. Total net pay in this well is around 30 m with an average porosity of 8% and permeability of 2 mD. After a 10 000 lb mini fracture the well flowed at a maximum rate of 8.5 MMscf per day with a 690 psig flowing tubing head pressure (FTHP); the well was subsequently plugged and abandoned.

In 1986 BP drilled an appraisal well, 49/4-2A, in the fault block adjacent to the 49/4-1 well. The well was drilled in a down-dip location and, although a good quality interval of sands was encountered within the Westphalian A and B, much of it was in the water leg with only 5 m of net pay present. A DST failed to produce gas to surface.

BP's third well on the field, 49/4-3, was drilled in 1989 in the same fault block as 49/4-2A and encountered a 168 m gas column in the Westphalian A with net pay of around 30 m. After a 418 000 lb hydraulic fracture, the well flowed at 17.5 MMscf per day compared with a pre-stimulation flow rate of just 5.8 MMscf per day. Detailed analysis of the treatment suggested that the fracture design was not optimal and the well was not fully cleaned up prior to testing; nonetheless, the concept of hydraulically fracturing a vertical well was clearly a positive step towards a viable development strategy.

LASMO drilled well 49/4a-5 in 1999 in order to further appraise the reservoir in the 49/4-1 block. This sub-horizontal well was designed to penetrate multiple channel sands above the gas water contact. The well encountered 150 m of net pay within the Westphalian A and B, although true vertical thickness (TVT) was only 18 m, with porosity and permeability similar to that of the 49/4-1

Vining, B. A. & Pickering, S. C. (eds) *Petroleum Geology: From Mature Basins to New Frontiers – Proceedings of the 7th Petroleum Geology Conference*, 315–323. DOI: 10.1144/0070315

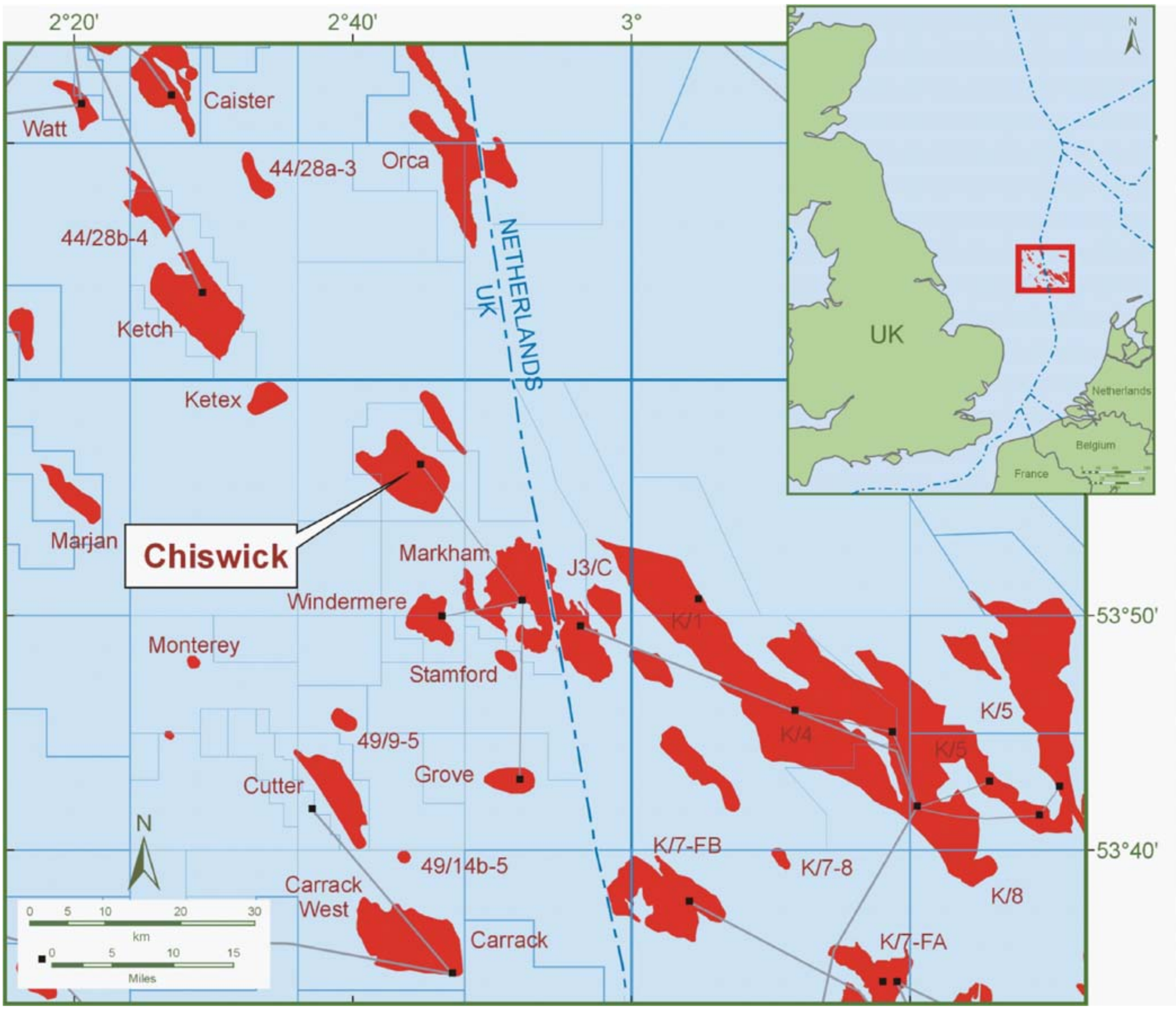

Fig. 1. Chiswick Field location map.

well. A drill stem test was performed which achieved a maximum flow rate of 13 MMscf per day through a slotted liner. Although this sub-horizontal well ultimately failed to produce a commercial flow rate, it was certainly more effective than the previous unstimulated vertical wells (Table 1).

Structural history and stratigraphy

Structure

This Chiswick Field lies in a region of structural complexity owing to multiple phases of tectonic activity which also controlled the preservation of the Carboniferous sediments. The area is dominated by a pre-Zechstein NW–SE structural grain which can be attributed to the Late Silurian Caledonian Orogeny. During the Early Carboniferous, north–south extension took place involving major normal and oblique slip reactivation of pre-existing faults trends forming tilted fault blocks. This episodic rifting allowed thick Lower Carboniferous packages to accumulate. In the late Carboniferous, the Variscan Orogeny resulted in transpressional fault reactivation and gentle folding of strata along the pre-existing NW–SE fault trend. Uplift and erosion followed, creating a major unconformity between the Carboniferous and overlying Permian sediments, commonly referred to as the Base Permian Unconformity (BPU). Further reactivation of Carboniferous faults occurred as a result of extensional episodes in the Jurassic (Cimmerian) and compressive inversional episodes in the Cretaceous and early Cenozoic (Glennie & Underhill 1998).

The Chiswick structure is defined at Top Carboniferous as a broad NW–SE-trending faulted anticline and was formed during the Variscan Orogeny. It is located on the southern edge of the Caister–Murdoch ridge which continues SE to the Markham Field. Pre-Permian NE–SW-trending faults with strike lengths much shorter than the major NW–SE faults cross-cut the structure, dividing it into three main sub-blocks, Alpha, Beta and Gamma.

Stratigraphy

The Carboniferous rocks present within the Chiswick Field are of Westphalian age and can be divided into two zones: the Westphalian A (Langsettian) and the younger Westphalian B (Duckmantian) (modified from Ritchie & Pratsides 1993). These two zones are divided by the *A. Vanderbeckei* marine band, which is a regionally extensive marker horizon (Fig. 3). The Carboniferous is erosionally truncated at the BPU and overlain by the Lower Permian Rotliegend. The Rotliegend contains thin Leman sands and silts overlain by thicker Silverpit shales/silts and sands. The Zechstein

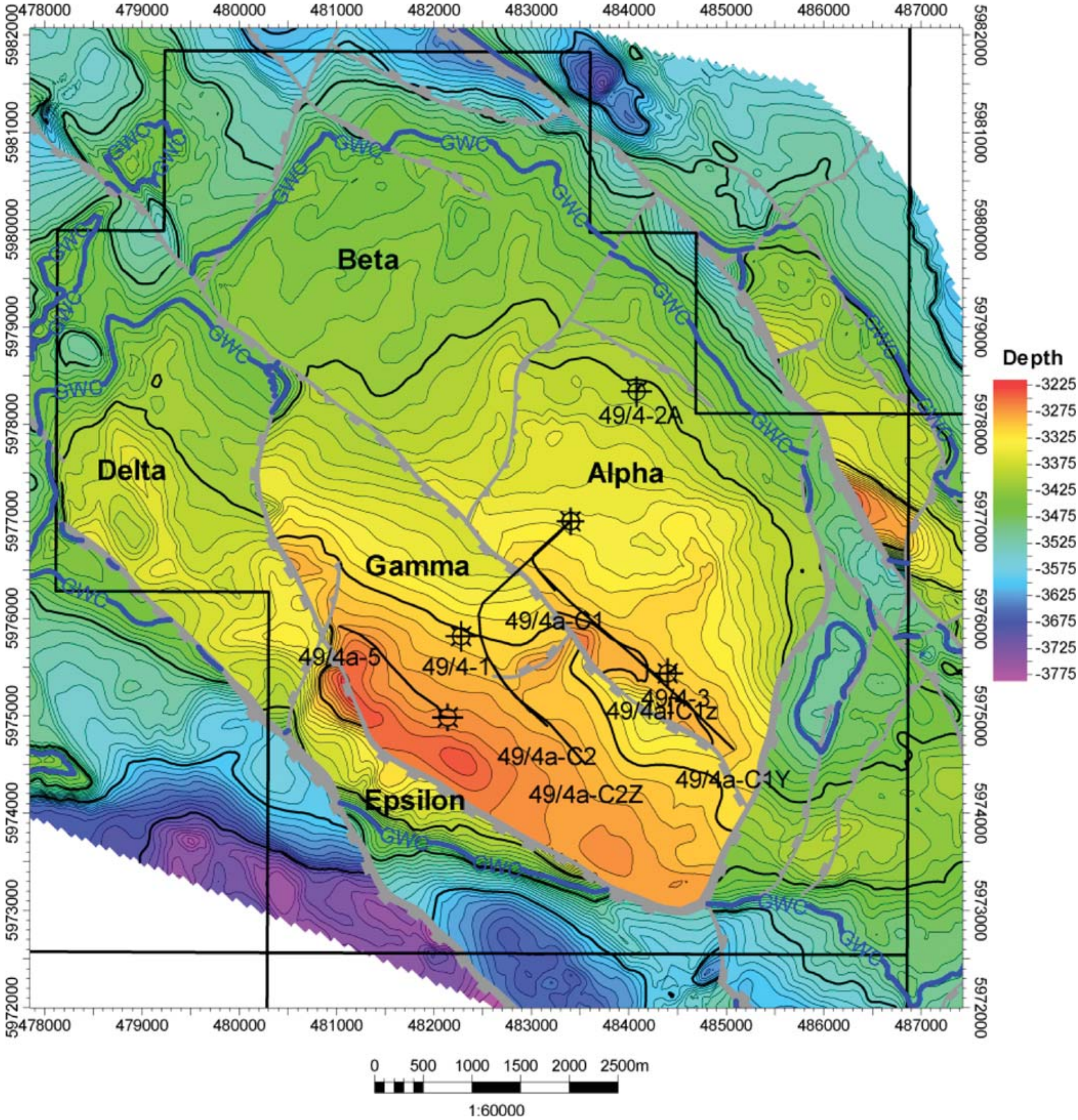

Fig. 2. Top Carboniferous depth structure map highlighting Chiswick Field sub-blocks.

Table 1. Chiswick appraisal well results

Well	Year	Operator	Maximum flow rate (MMSCF per day)		Comments
			Pre-fracture	Post-fracture	
49/4-1	1984	BP	0.2	8.5	10 000 lb mini fracture
49/4-2A	1986	BP	–	–	431 BWPD
49/4-3	1989	BP	5.8	17.7	418 000 lb fracture
49/4a-5	1999	Lasmo	13.0	–	Sub-horizontal well – slotted liner

evaporates act as a seal over the field. Overlying the Permian are the Triassic continental sandstones and shales with Jurassic sediments being absent in this area. The Early Cretaceous is dominated by mudstone facies and the Upper Cretaceous is represented by the Chalk group (Ritchie & Pratsides 1993). Clastic deposition resumed in the Early Cenozoic and is approximately 200 m thick over Chiswick.

Carboniferous reservoir

All Chiswick wells penetrate the Silverpit, Leman and the Westphalian A interval. Five out of the eight wells on the field encounter the Westphalian B depending on the extent of the truncation of the BPU in a given area. The Alpha block is predominantly eroded

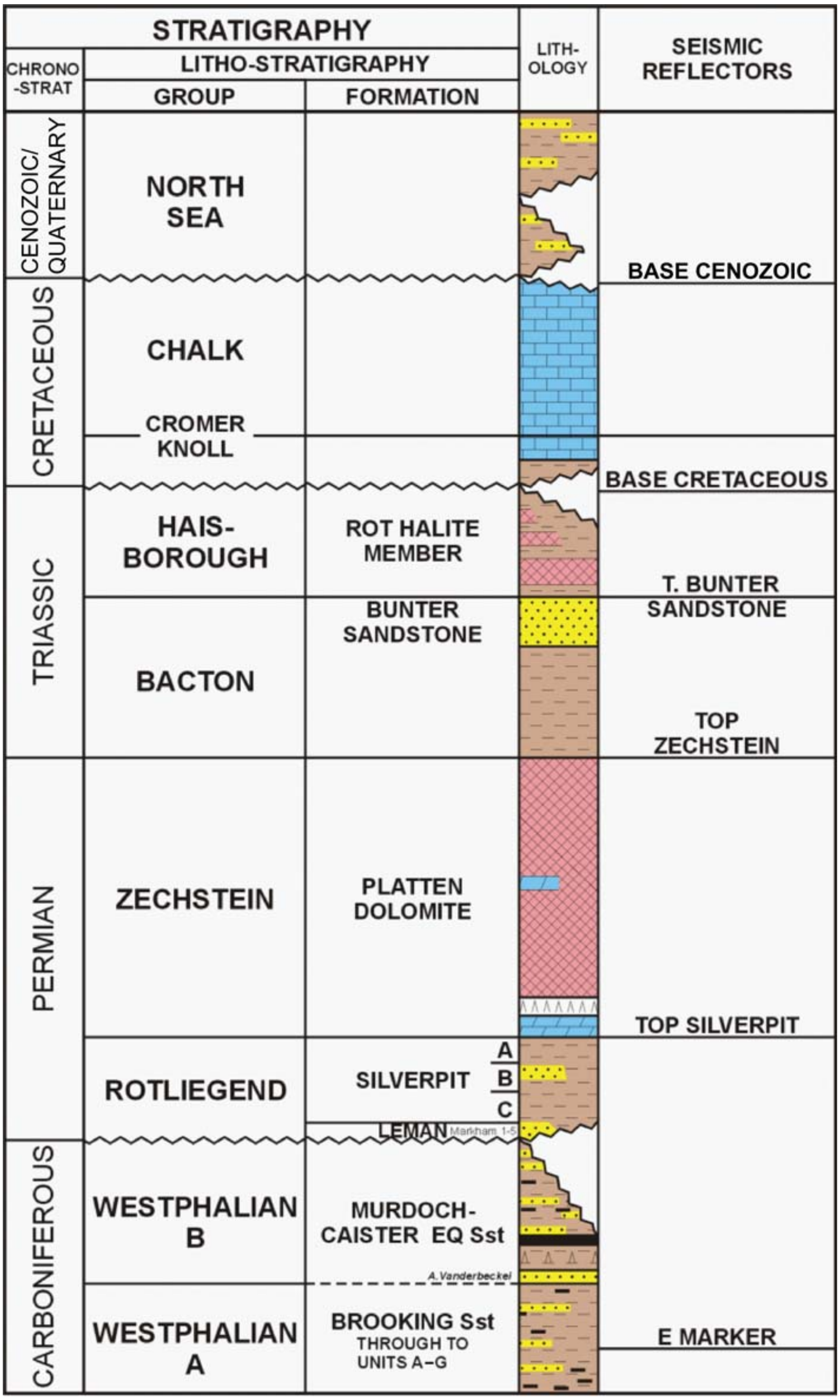

Fig. 3. Chiswick Field stratigraphic column.

down to Top Westphalian A, with the Gamma block preserving both the Westphalian A and part of the Westphalian B, which contains the Murdoch–Caister equivalent sands. The other three blocks, Beta, Delta and Epsilon Carboniferous subcrop, can be prognosed by interpreting on seismic the E coal marker of Westphalian A age, which is a laterally continuous coal horizon over the Chiswick Field and can be isopached to the unconformity (Fig. 3).

During the Carboniferous the Chiswick Field was situated within a low relief delta plain which contained fluvial, crevasse splays, flood plain and swamp deposits in an overall humid environment. The presence of organic matter resulted in the formation of coal seams within the field which represent marker beds that can be correlated and provide the basis of the nomenclature for the layers within the field. These coals also create barriers/baffles within the field and reduce vertical connectivity. One of these markers (E) was used for seismic interpretation as mentioned earlier. The Westphalian is highly variable both laterally and vertically and one of the main controls on deposition was sea level. A sea-level rise resulted in aggradation of the delta plain, leading to an overall poorly drained environment where marsh/lacustrine environments were present (Quirk 1993). This is compared with progradation of the delta plain associated with a sea-level drop. Within the Chiswick Field the channel sands are the main reservoir with the best reservoir quality within low sinuosity fluvial channels which are laterally extensive. The distribution, size and connectivity of these channel sands remain a major uncertainty within the field with regards to effective gas-in-place.

Westphalian A. The Westphalian A has been divided into units from Brooking through to A–G on the basis of a coal palynology correlation (Fig. 3). The net-to-gross of the Westphalian A is 38% with net porosities of 11% and net permeabilities of 32 mD from core and log analysis. The best reservoir quality lies within the E2 sands which have a net-to-gross of 43%, average net porosity of 12%. Interpretation of the core from wells 49/4-1, 49/4-2A and 49/4-3 shows the presence of low to moderate sinuosity fluvial channels sands with associated facies of crevasse splay, mouth bars and floodplain shales, silts and coals. The channel sands are upward-fining, vertically stacked and are thought to be laterally extensive based on well data and correlations. Interpretation of dipmeter data shows that most of the fluvial channel sands within the field originated from the north, which is consistent with the regional interpretation of Westphalian channel sands flowing from north to south from the Mid North Sea High (Bailey *et al.* 1993).

Westphalian B. The Westphalian B is separated from the Westphalian A by the *A. Vanderbeckei* marine band, which reflects the drowning of the coastal/delta plain. This marine band has been identified in 49/4-1, 49/4-2A, 49/4a-5 and the recent Gamma block well 49/4a-C2Z. At the base of Westphalian B and predominantly within the Gamma block lie the Murdoch–Caister equivalent channel sands. These sands are vertically stacked and represent low sinuosity, coarse-grained fluvial channels with an average net-to-gross of 55%, average net porosity of 13%. These sands were probably deposited during a relative drop in sea-level and sediment source rejuvenation from the Mid North Sea High where Devonian sediments were exposed (Bailey *et al.* 1993). They represent the best reservoir quality sands within the Chiswick Field and the porosity and permeability of these sands may have been enhanced by sub-BPU leaching of feldspars (Ritchie & Pratsides 1993).

Rotliegend reservoir

The Chiswick Field lies on the edge of the Silver Pit Lake where the Silverpit is represented by lacustrine claystone, siltstone and occasional sands (Fig. 3). Underlying the Silverpit and lying directly over the BPU are the Leman sands and siltstones which grade into aeolian facies towards the south as seen in the Venture-operated Markham Field, where this interval forms the main reservoir. The Silverpit and the Leman of the Rotliegend together have a relatively constant thickness of 220 m over Chiswick. The post-Hercynian topography influenced the distribution of sands, with aeolian sands being thin or absent over the structural highs and preserved downwind of these highs (Bailey *et al.* 1993). The low net-to-gross of 16% within the Leman sands in the Chiswick Field suggests that it was structurally higher than the Markham Field during the Lower Permian.

Over Chiswick the Leman thickness varies between 18 and 44 m with an average net porosity of 11%. The overlying Silverpit has a thickness between 185 and 200 m with a substantially lower net-to-gross of 8%, average net porosity of 11%.

Seismic interpretation

Database

Prior to the acquisition of 3D data, mapping had been based on 1700 km of 2D seismic from 14 different surveys. Interpretation was challenging owing to phase shifts, time shifts and differing migration velocities giving inconsistent imaging and variable data quality. In 1994 LASMO North Sea contracted Geco-Prakla to acquire and process 440 km^2 of 3D seismic data over block 49/4a covering the Chiswick Field and the surrounding area. The result was a high-quality pre-stack time-migrated volume on which key reflectors and faults could be mapped with confidence across the field, which undoubtedly reduced uncertainty in terms of structural and stratigraphic mapping. The data was reprocessed by Centrica in 2005 using a common reflection surface technique which resulted in improved signal-to-noise ratio, subtle enhancement of the intra-Carboniferous reflectors and sharpened fault definition. Improvements in the overburden can also be seen with superior imaging of steeply dipping chalk and intra-Zechstein events.

Interpretation

A number of key seismic horizons were picked in order to generate accurate depth structure maps of the field (Fig. 4):

(1) Top Chalk
(2) Top Red Chalk
(3) Top Zechstein
(4) Base Zechstein
(5) BPU
(6) Intra Carboniferous E Marker

The Top Chalk pick is generally unambiguous owing to a strong seismic event resulting from a large increase in acoustic impedance at the onset of the Cretaceous. Top Red Chalk is also quite consistent with a strong decrease in acoustic impedance going from the Upper Cretaceous Chalk into the clay rich Red Chalk of the Cromer Knoll group. Top Zechstein is another relatively clear seismic event with a positive impedance contrast going from the Bunter claystones into the Zechstein halite. Difficultly arises in areas where the salt is steeply dipping and the image is degraded. Mapping the Top Zechstein reveals pronounced NW–SE trending synclines and anticlines resulting from dramatic salt swells. Within the salt itself, very high amplitude discontinuous events can be seen. These represent high-velocity carbonate rafts which are abundant in the area and distort the image beneath, particularly when lying close to the base of the Zechstein. Top Rotliegend is a strong decrease in impedance going from Zechstein salt into Silverpit claystones and can be mapped with relative confidence in the area. This pick can be ambiguous when Zechstein carbonate rafts appear to touch down on the Top Rotliegend surface, causing interference. A marked difference in structure is noted at Top Rotliegend, where heavy faulting with a strong NW–SE trend is clearly visible. The interpretation of the BPU is quite problematic as the Carboniferous subcrop varies over the area, generating an inconsistent and often weak seismic response. The well data shows that the Rotliegend show little variation in thickness over the area. The thickness of the Rotliegend is quite consistent and shows a gradual change over the study area. Consequently a BPU surface was created using a Rotliegend isochore from the well data and adding this to the Top Rotliegend depth surface. The intra Carboniferous E Marker corresponds to the top of a Westphalian A coal band and was picked as it defines the structure of the Carboniferous below the unconformity. This horizon also defines the base of the main reservoir sands and is therefore important

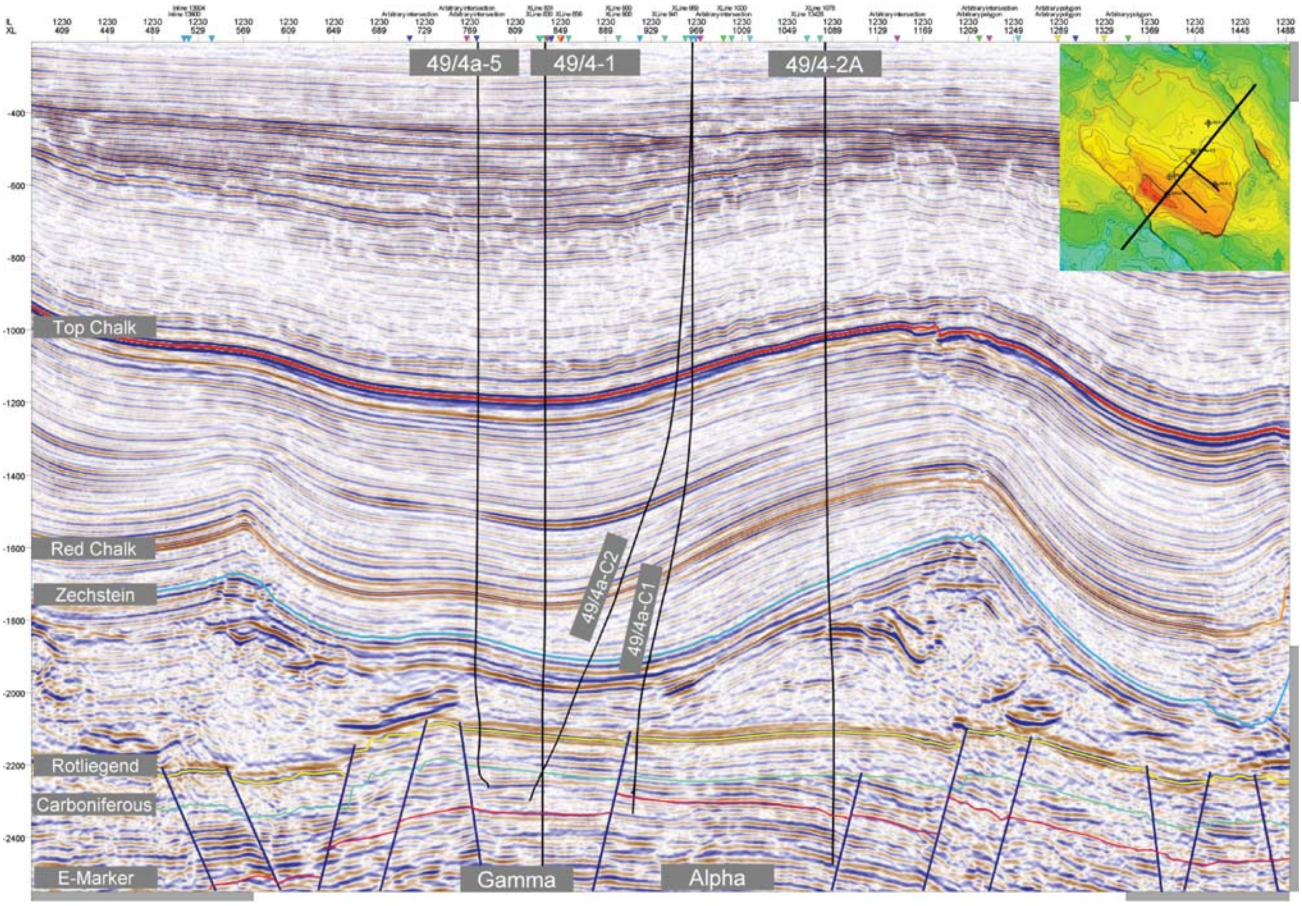

Fig. 4. Seismic section orientated SW–NE through the Chiswick Field.

for building the internal layering of the Carboniferous in the static reservoir model. Individual sands within the Carboniferous are not readily identifiable on seismic; they tend to have a similar acoustic impedance to the shales and thus show little seismic response. Much of the reflectivity within the Carboniferous is thought to be generated by coals. Seismic data gives only a generalized impression of the erosional character and subcrop at the Hercynian unconformity, which is highly dependent on data quality.

Depth conversion

The Chiswick Field shows considerable distortion in the time domain and this is primarily due to the variation in the thickness of the Zechstein salt; therefore accurate mapping and depth conversion are essential in understanding the configuration of the field (Fig. 5). Fortunately this is aided by comprehensive well coverage over the structure and surrounding area. Time grids were converted to depth using a vertical layer cake method with layers defined by the key seismic horizon already discussed. Instantaneous velocity v. depth functions were calculated for each of the layers down to Top Rotliegend using calibrated velocity logs from almost thirty wells. BPU was generated by using the Rotliegend well isochore added to the Top Rotliegend depth grid. E Marker was calculated using a constant velocity of 4250 m s^{-1} below the BPU. Residual depth errors at Top Rotliegend lie within the range of $\pm$10 m.

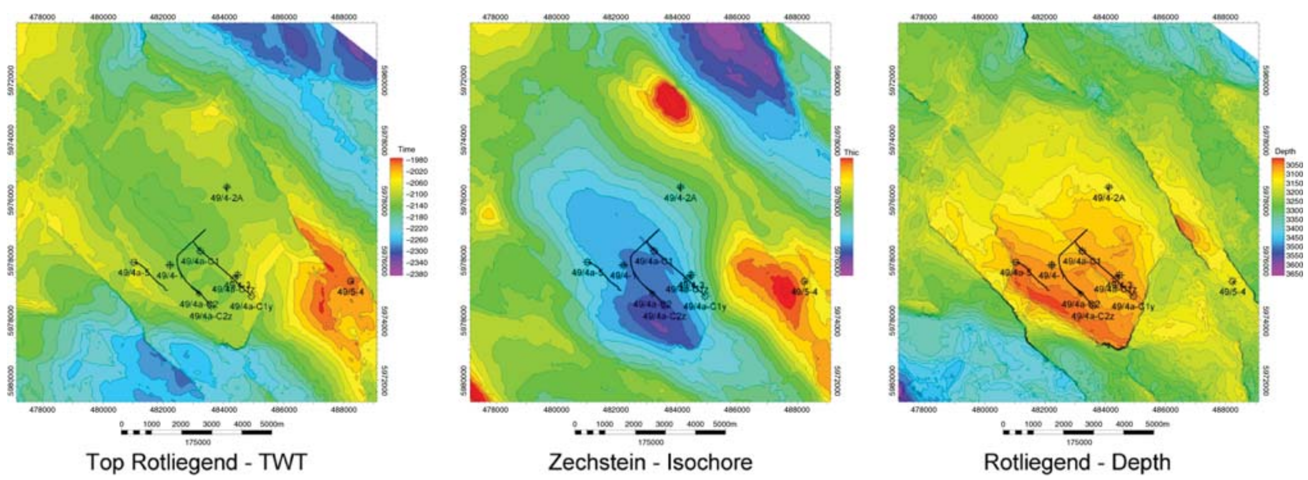

Fig. 5. Comparison of Top Rotliegend two-way time and depth maps with Zechstein isochore.

Phase I field development

Development plan

The Chiswick Field Development Plan and Environmental Statement were submitted to the DTI (Department of Trade and Industry) in April 2006 and approved in July that year. The proposed development plan was to drill two long reach horizontal wells, completed with conventional $5\frac{1}{2}$ inch cemented liners and stimulated with multiple propped hydraulic fractures. The development concept was based on reservoir engineering and hydraulic fracturing studies commissioned by CH4 and was designed to address the key concerns of reservoir connectivity and deliverability. With planned horizontal sections of more than 2000 m and up to five hydraulic fractures per well, the wells were designed to connect as many channel sands to the wellbore as possible and improve initial well productivity.

Hydraulic fracturing is a method of creating artificial fractures extending from the borehole into the reservoir formation, which provide a pathway for gas to flow more easily into the well. The fractures are formed by pumping fluid down the wellbore in order to increase downhole pressure to a level which exceeds the fracture gradient of the reservoir formation. The fluid is then forced into the fracture causing it to propagate further into the formation. A propping material is usually added to the fracture fluid in order to hold the fractures open once the operation has stopped and the fracturing fluid dissipated. Hydraulic fracturing has been an enabling technology in developing tight gas reservoirs around the world and has been used extensively in the North Sea to develop oil bearing Chalk reservoirs; however, Chiswick was the first UKCS gas field to be developed using this technique in horizontal wells.

Both wells were designed with the horizontal sections orientated such that they are in line with the regional maximum principle stress at reservoir level, thus encouraging the development of longitudinal fractures. The optimum fracture design was to place 400 000 lb of 12/18 resin-coated proppant with a borate cross-linked gel system, which according to fracture modelling studies would give a fracture half length of 200 m and a height of 75 m.

The first well was planned to target the reservoirs of the Alpha fault block and was to spud at the end of 2006, with a second well targeting the Gamma fault block in 2007. Both wells were drilled with the Noble Kolskaya jack-up rig and were operated by Wintershall, who had a 5% interest in the block at the time. Development of the field is through a normally unmanned five slot MFP (minimum facilities platform). This is tied back to the Markham J6A platform via a 17 km 10 inch pipeline where fluid processing was carried out before delivery onshore to the NAM-operated Den Helder gas terminal via the K13 extension and WGT (Westgastransport) pipeline.

Drilling results

Alpha well. The Chiswick Alpha well, 49/4a-C1, was spudded in December 2006 and presented a number of considerable technical challenges. Since the depths of individual sands cannot be accurately prognosed by geological or geophysical means, a pilot hole was drilled to allow accurate targeting of the reservoir sands. The pilot hole was then plugged back before kicking off the 49/4a-C1z horizontal reservoir section below the 9 5/8 inch casing shoe. Unfortunately, whilst drilling the horizontal section the hole began to pack off and, whilst attempting to work through the blockage, it was accidentally side-tracked. It was decided that drilling would continue and the new side-track became 49/4a-C1y. TD was reached in April 2007, having drilled 6073 mMD. The well had penetrated Westphalian A sands with a total gross thickness of 2415 m, of which 594 m was net pay with average porosities of 10–11%, and permeabilities in the order of 1–2 mD.

The well was suspended at this stage for just over 2 months until a stimulation vessel could be mobilized. Five separate zones within the C, D and E sands were subsequently fractured into which a total of 2 000 000 lb of proppant was pumped along with 600 000 gallons of fluid. Clean-up was performed over a period of 17 days, after which a maximum flow rate of approaching 50 MMscf per day was achieved. The well was brought on stream in September 2007 (Fig. 6).

Gamma well. The second Chiswick development, 49/4a-C2 well was spudded in June 2007. A pilot hole was not used in this instance owing to the proximity of the 49/4-1 well. Drilling again proved to be a challenge and, whilst attempting to drill through the Carboniferous at 4914 mMD, the well began to collapse. A number of days were spent reaming though coal layers, but eventually the well had to be side-tracked and became 49/4a-C2z. The side-track was kicked off at 4370 mMD in the Carboniferous Brooking B sandstone and was geosteered, using an azimuthal gamma log to stay within the main reservoir sands until TD. However, low rate of penetration (ROP) and multiple bottom hole assembly (BHA) failures slowed progress and, with the stimulation vessel timing in mind, TD was called in November 2007 having drilled 5485 mMD out of a planned 6000 mMD. The well had successfully penetrated a gross reservoir thickness of 1218 m, of which 353 m was net pay.

Hydraulic fractures were placed in four zones, one within the Caister Murdoch sands and three within the Brooking sandstones. In total, almost 1 000 000 lb of proppant was pumped along with around 420 000 gallons of fluid. Additionally, thin sands within the secondary Permian Silverpit and Leman reservoirs were perforated. Having spent 24 days cleaning up the well, a maximum flow rate of more than 62 MMscf per day was achieved with facilities constraints. The well then commenced production in March 2008 (Fig. 7).

Discussion

Despite considerable subsurface uncertainties, Phase I drilling on the Chiswick Field has resulted in two successful gas producers. Careful stratigraphic correlation based on palynological studies combined with detailed mapping has reduced the uncertainty in terms of reservoir distribution. This has greatly improved the understanding of the field and enabled better prediction of the Carboniferous subcrop across the Alpha and Gamma fault blocks, giving the ability to target specific reservoir units with improved accuracy. The two horizontal development wells were successfully geosteered using an azimuthal gamma ray (GR) tool to target specific reservoir units. These wells were hydraulically fractured to reduce some of the uncertainties surrounding sand-to-sand and sand-to-wellbore connectivity, the result of which has been excellent flow rates in both wells.

However, drilling the Phase I development wells on Chiswick has also highlighted a number of issues, particularly concerning optimum well design and fracture placement. Recent simulation work based on Phase I well results has attempted to understand well performance and the effectiveness of the hydraulic fractures, and in particular which zones are contributing to flow. The study shows that the two producing wells in the Alpha and Gamma blocks behave quite differently. The Alpha well exhibits a lower productivity than the Gamma well; however, the Alpha well is thought to be connected to a much larger reservoir volume which appears to drain most of the Chiswick Field. Conversely the Gamma well appears to drain a single highly permeable unit within the Gamma block.

Therefore the second phase of development will use sub-horizontal wells to improve vertical drainage of the field with a

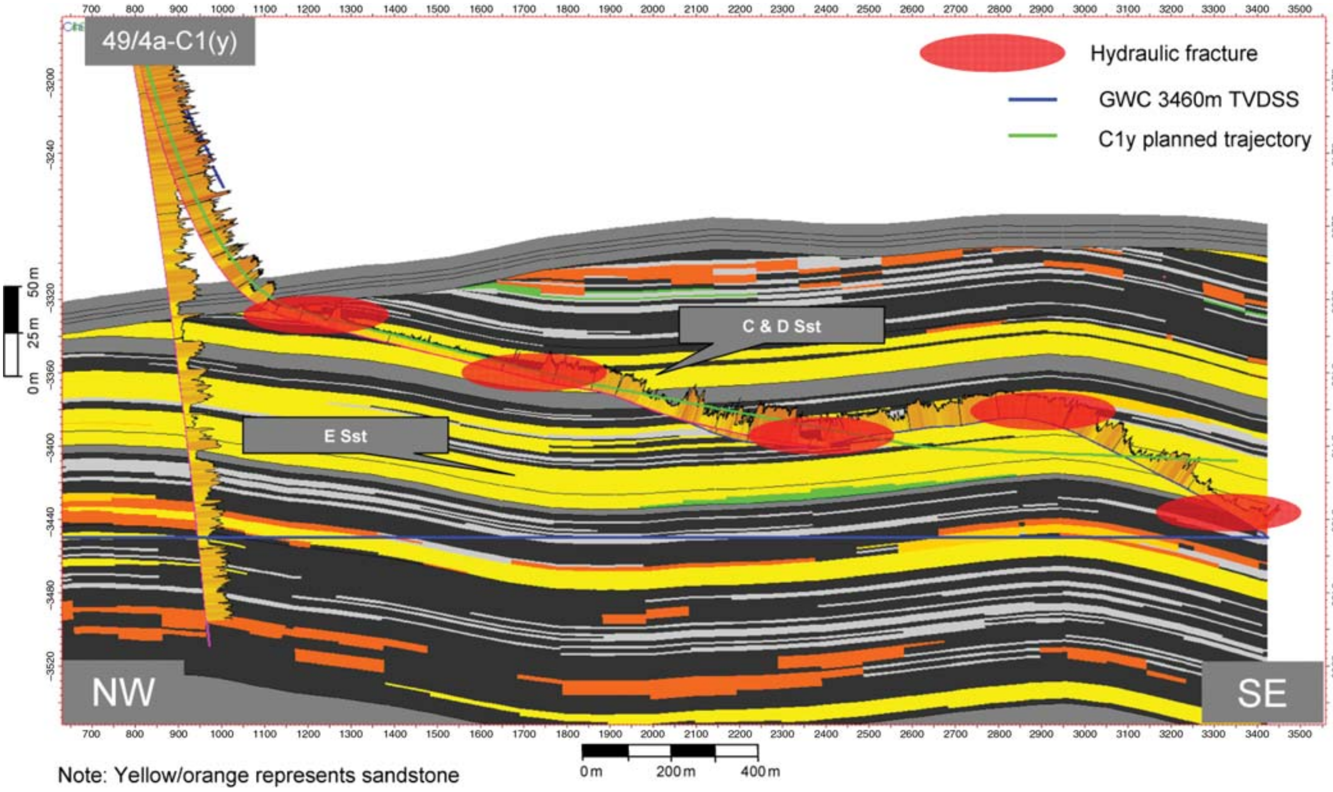

Fig. 6. Geological well section for 49/4a-C1 (Alpha) through pre-drill model showing hydraulic fracture locations.

single hydraulic fracture targeting each individual sand rather than multiple fractures within one sand unit. This approach is considered to be optimal, particularly in the case of the untested Beta block where uncertainty over Carboniferous subcrop and sand distribution remains the greatest.

Phase II field development

Venture plan to drill at least two additional wells on the Chiswick Field in the near future in order to add additional reserves and accelerate production. A new Chiswick geocellular model was created

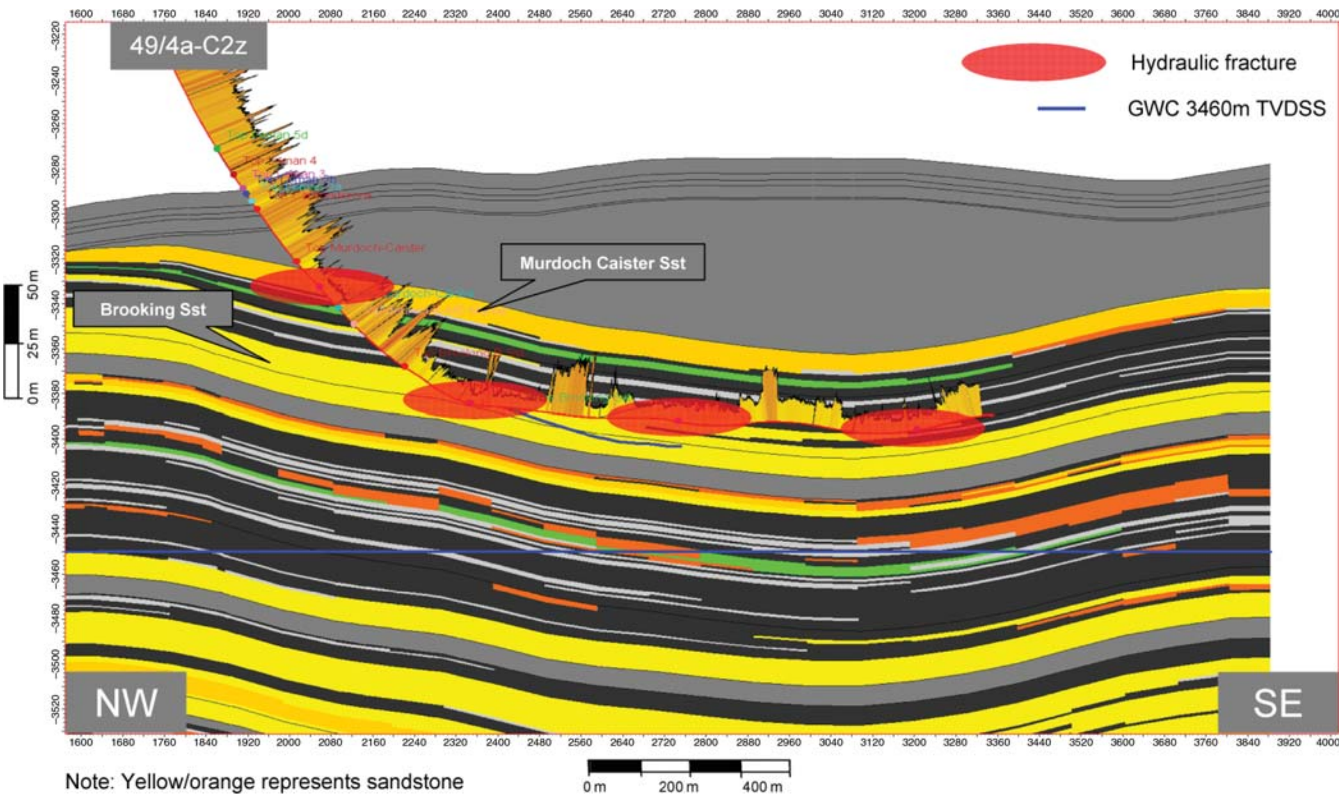

Fig. 7. Geological well section for 49/4a-C2 (Gamma) through pre-drill model showing hydraulic fracture locations.

based on the interpretation of the reprocessed seismic data and updated petrophysical analysis from Phase I drilling results.

This model was then simulated in an attempt to understand the performance of the two producing wells and to determine optimum areas for Phase II wells to be placed. Phase II development wells will incorporate the lessons learnt from Phase I in terms of well trajectory design, drilling practices and hydraulic fracturing strategy.

Conclusion

The Chiswick Field was brought on stream in September 2007 – 23 years after the discovery well was drilled with two wells producing at rates in excess of initial expectations. Subsurface uncertainties have been addressed with a comprehensive technical work programme and also through the use of appropriate technology in the form of hydraulically fractured long reach horizontal wells, a first for a North Sea gas development. Phase II of the Chiswick development is currently scheduled to commence late in 2009, when the first of at least two additional wells will be drilled.

Thanks are extended to M. Tringham for his significant contribution to the project and also to B. Stevens for his comprehensive reservoir engineering study. CH4 and Senergy (RML) are thanked for their work in progressing the project to development drilling phase, as are Wintershall's operations team for drilling the Alpha and Gamma wells. I. Bartholomew and K. Purvis are thanked for their helpful input as reviewers.

References

Bailey, J. B., Arbin, P., Daffinotic, O., Gibson, P. & Ritchie, J. S. 1993. Permo-carboniferous plays of the Silver Pit Basin. *In*: Parker, J. R. (ed.) *Petroleum Geology of North West Europe; Proceedings of the 4th Conference*. The Geological Society, London, 707–715. doi: 10.1144/0040707.

Glennie, K. W. & Underhill, J. R. 1998. Origin, development and evolution of structural styles. *In*: Glennie, K. W. (ed.) *Petroleum Geology of the North Sea*, 4th edn. Blackwell, Oxford, 42–84.

Quirk, D. G. 1993. Interpreting the Upper Carboniferous of the Dutch Cleaver Bank High. *In*: Parker, J. R. (ed.) *Petroleum Geology of North West Europe; Proceedings of the 4th Conference*. The Geological Society, London, 697–706. doi: 10.1144/0040697.

Ritchie, J. S. & Pratsides, P. 1993. The Caister Fields, Block 44/23a, UK North Sea. *In*: Parker, J. R. (ed.) *Petroleum Geology of Northwest Europe; Proceedings of the 4th Conference*. The Geological Society, London, 759–769. doi: 10.1144/0040759.

The Ensign enigma: improving well deliverability in a tight gas reservoir

K. PURVIS, K. E. OVERSHOTT, J. C. MADGETT and T. NIVEN

Venture Production plc, Kings Close, 62 Huntly Street, Aberdeen AB10 1RS, UK (e-mail: katie.overshott@centrica.com)

Abstract: The Ensign Gas Field is located in the Sole Pit basin in the Southern North Sea. The reservoir is the Rotliegend Group Leman Sandstone Formation of Lower Permian age and comprises sediments deposited in an arid continental environment. The main gas-bearing interval in the field consists of sabkha, waterlain and minor aeolian sands, reflecting deposition in an erg margin/lake margin setting. The poor primary reservoir quality of these sands has been severely reduced by extensive illite cementation resulting in average air permeabilities of <1 mD. Attempts to develop the field economically utilizing fracture-stimulated vertical wells has met with mixed results, with flow rates of 14 MMscf per day and lower being measured during testing. The most recent appraisal well drilled on the field was a long horizontal well that was stimulated with five hydraulic fractures resulting in an economic flow rate of 44 MMscf per day. Analysis of the core and log data acquired during the appraisal of the field has shown that the reservoir contains a heterogeneous distribution of fractures, faults and micro-faults. The fracture population is dominated by conductive north–south striking fractures, with subordinate NNW–SSE resistive fractures and NE–SW mixed fractures that are arranged in clusters, with zones of high and low fracture density. Well results to date suggest that the NE–SW open and partially open fractures observed in core do not improve reservoir productivity, but those orientated north–south that are conductive appear to improve well deliverability.

Keywords: Rotliegend, Leman Sandstone, illite cementation, fracture stimulation

The Ensign Field is located 90 km NE of the Norfolk coast in the Sole Pit area of the Southern North Sea (Fig. 1). The field is located 10 km east of the Shell-operated Barque Field and 15 km west of the Venture-operated Audrey Field. Ensign is an elongated NW–SE trending field 2 km wide and 8 km in length (Fig. 2). The water depth over the field is 90 ft, and the top reservoir is *c*. 8450 ft TVDSS at its crest.

The reservoir is the Leman Sandstone of the Lower Permian Rotliegend Group, and is *c*. 800 ft thick, but only partially gas-filled, owing to the depth of the spill point. The gas is very dry, containing 96% methane and small amounts of CO_2 (0.5%) and N_2 (1%). The gas in place volume for the Ensign field is *c*. 350 BCF.

The Ensign Field name was assigned while under the ownership of Shell and Esso, and reflects the practice of naming gas fields in the SNS after vessels and nautical terms from maritime history. The ensign is the flag or colour of a ship and came into use on the ships of Queen Elizabeth I in the 1570s, and imitated regimental flags, which at that time were called ensigns.

Field history

The Ensign Field is located in Blocks 48/14a and 48/15a that are covered by the P008 and P130 Licences respectively. The P008 licence was awarded to Shell and Esso in 1964 as part of the first licensing round, while P130 was a fourth round award to Conoco in 1972. Venture acquired 100% equity in the Ensign Field as a consequence of two separate transactions involving Shell UK Limited, Esso Exploration and Centrica Resources Limited in 2005.

The Ensign Field wells are listed in Table 1 along with information on well operator and well type. The field was discovered in 1986 by the Shell-operated 48/14-2 vertical well that encountered a 542 ft gas column in the poor quality Lower Permian Rotliegend sandstone reservoir (Fig. 2). Although the reservoir failed to flow during initial testing, after stimulation by hydraulic fracturing the well flowed at a sustained rate of *c*. 14 MMscf per day. This rate was not economic at the prevailing gas prices and consequently the field was not developed. In 1988 Conoco drilled a well 48/15a-6 in the eastern portion of the field, but the reservoir was encountered deep to prognosis predominantly in the water leg and was consequently not tested. The next appraisal well to be drilled was the Venture-operated well 48/14-5 that spudded in September 2006. This well was planned to appraise the reservoir and consequently had a full logging suite including borehole image logs and was cored. After fracture stimulation the well tested at rates of up to 20 MMscf per day, but this declined to 12 MMscf per day and the well was suspended as a potential future production well. The last well drilled in the field was spudded in September 2007 and was as a horizontal production well. The well encountered over 4500 ft of net sand, was stimulated by five hydraulic fractures and flowed at a facilities-constrained rate of 44 MMscf per day. The well has been suspended as a future production well.

Structure and tectonic setting

The Ensign Field is situated in the Southern Permian Basin in the NW–SE trending Sole Pit Basin (Fig. 1). The area has been subjected to a number of tectonic events, with the Hercynian orogeny in the Late Carboniferous resulting in the pervasive NW–SE structural grain (Glennie & Underhill 1998). The main phase of development of the Sole Pit Basin occurred in the Permian, when thermal subsidence occurred. During this period the Lower Permian Rotliegend continental sediments were deposited that form the reservoir of the Ensign Field. Basin subsidence continued from the Triassic to Late Cretaceous times by which time the reservoir of the Ensign Field would have been buried to a depth of $>13\,000$ ft TVDSS. The next stage of the structural history was successive periods of uplift during the early Cenozoic with a major phase of inversion in the Miocene related to the Alpine orogeny. The inversion in the Sole Pit during this period removed approximately 5000 ft of post-Liassic sediments and has resulted in the Ensign reservoir being at its current depth of *c*. 8500 ft TVDSS.

Vining, B. A. & Pickering, S. C. (eds) *Petroleum Geology: From Mature Basins to New Frontiers – Proceedings of the 7th Petroleum Geology Conference*, 325–336. DOI: 10.1144/0070325

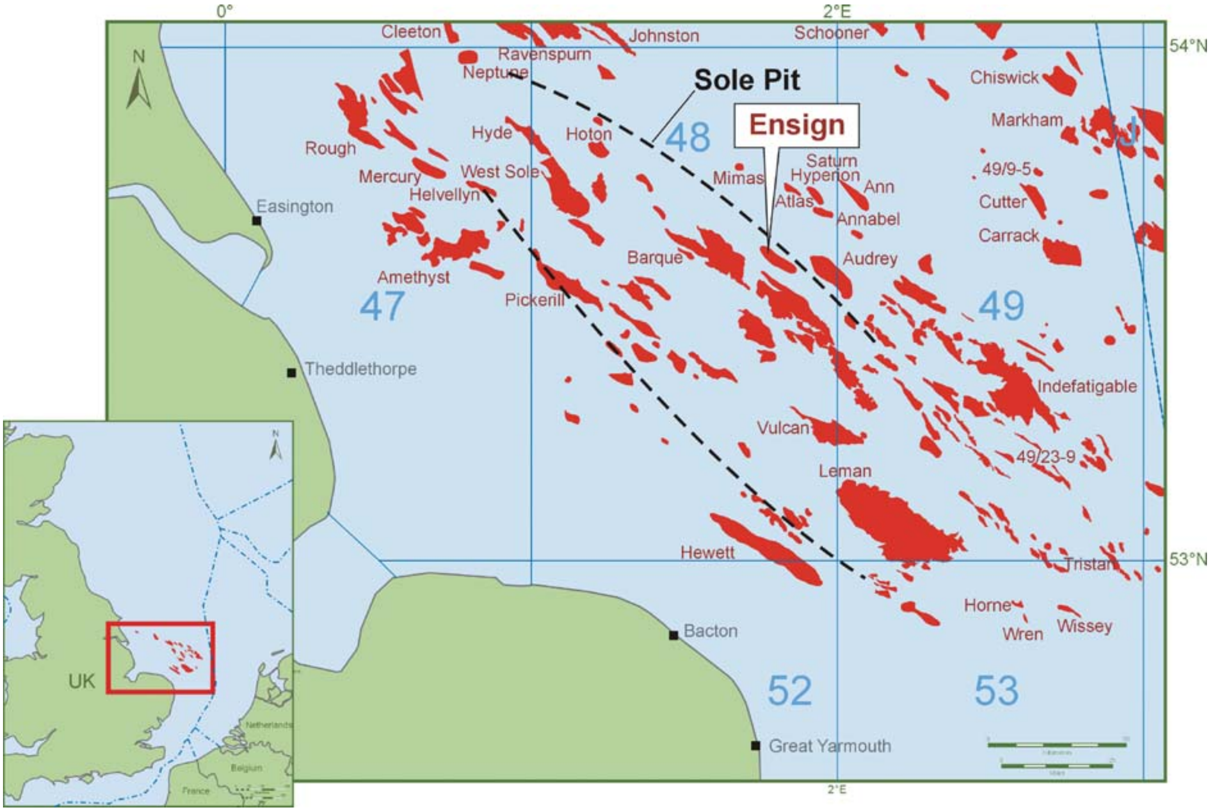

Fig. 1. Map showing the location of the Ensign Field and Sole Pit area.

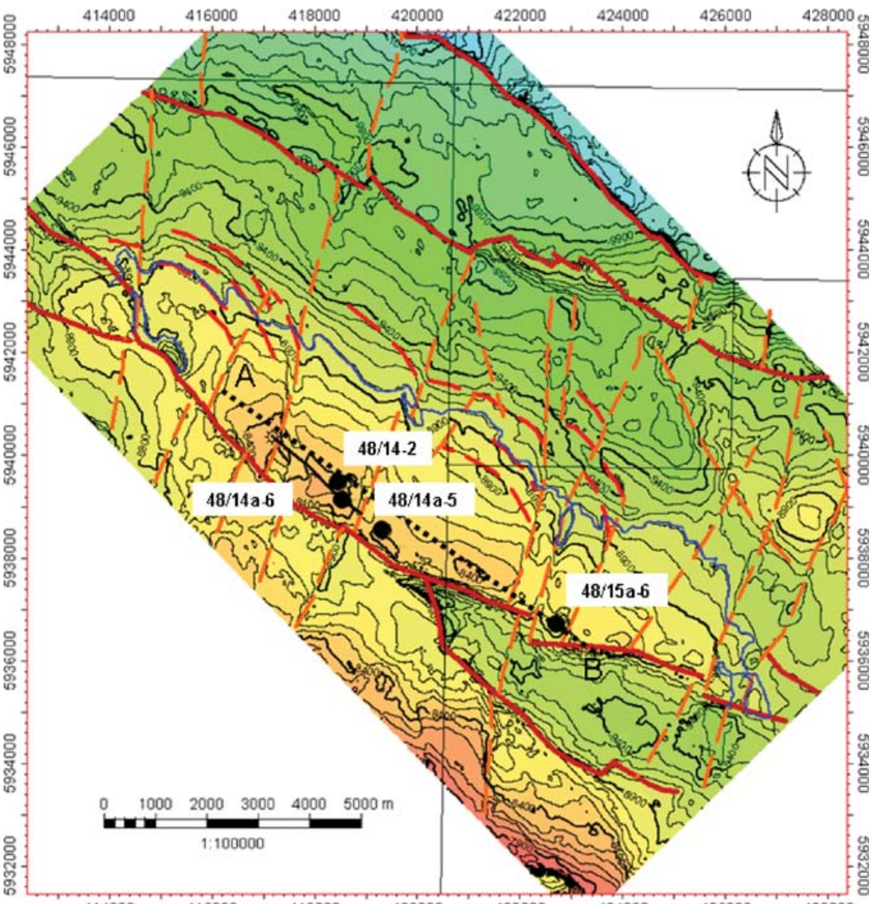

Fig. 2. Ensign Field top Leman Sandstone depth map based upon 3D data showing major faults and NNE–SSW lineaments. Line A–B shows the location of the seismic section in Fig. 4.

Table 1. Ensign well data

Well	Year drilled	Operator	Well type*	Stimulation	Core
48/14-2	1986	Shell	EV	Single fracture	Yes
48/14a-5	1988	Conoco	AV	None	Yes
48/14a-5	2006	Venture	AV	Single fracture	Yes
48/14a-6	2007	Venture	ADH	Multiple fracture	No

*Well type: E, exploration; A, appraisal; D, development; V, vertical; H, horizontal.

Stratigraphy

The stratigraphic sequence encountered in the Ensign Field is shown in Fig. 3. The oldest rocks penetrated by any of the Ensign Field wells are sands, silts and shales of Carboniferous age.

The Lower Permian Leman Sandstone rests unconformably on the Carboniferous and consists of a variety of facies associations, which have been interpreted as the products of deposition in fluvial (wadi), aeolian, sabkha and lacustrine environments (Glennie 1972). The Leman sandstones are overlain by a *c*. 550 ft thick Zechstein sequence comprising cyclic evaporites and carbonates that acts as the seal for the Ensign Field. The Zechstein deposits reflect the marine transgression into the Southern Permian Basin (Glennie & Buller 1983). Overlying the Zechstein are the three units of the Triassic Bacton Group: the Brockelschiefer, Bunter Shale and Bunter Sandstone that represent a return to continental sedimentation. In total the Bacton Group is *c*. 2000 ft thick over the Ensign Field. Subsequent deposition of the Middle and Upper Triassic Haisborough Group marks a return to marginal and fully marine environments with the occurrence of *c*. 2800 ft of evaporites and mudstones. Overlying the Triassic is a *c*. 2500 ft section of Lower Jurassic Lias shales with a thin veneer of Quaternary–Recent deposits beneath the sea bed. The absent Jurassic–Cenozoic section was removed during the Cenozoic inversion of the Sole Pit area.

Reservoir sedimentology

The Leman Sandstone reservoir of the Ensign Field was deposited in a continental desert environment (Glennie *et al.* 1978) and has

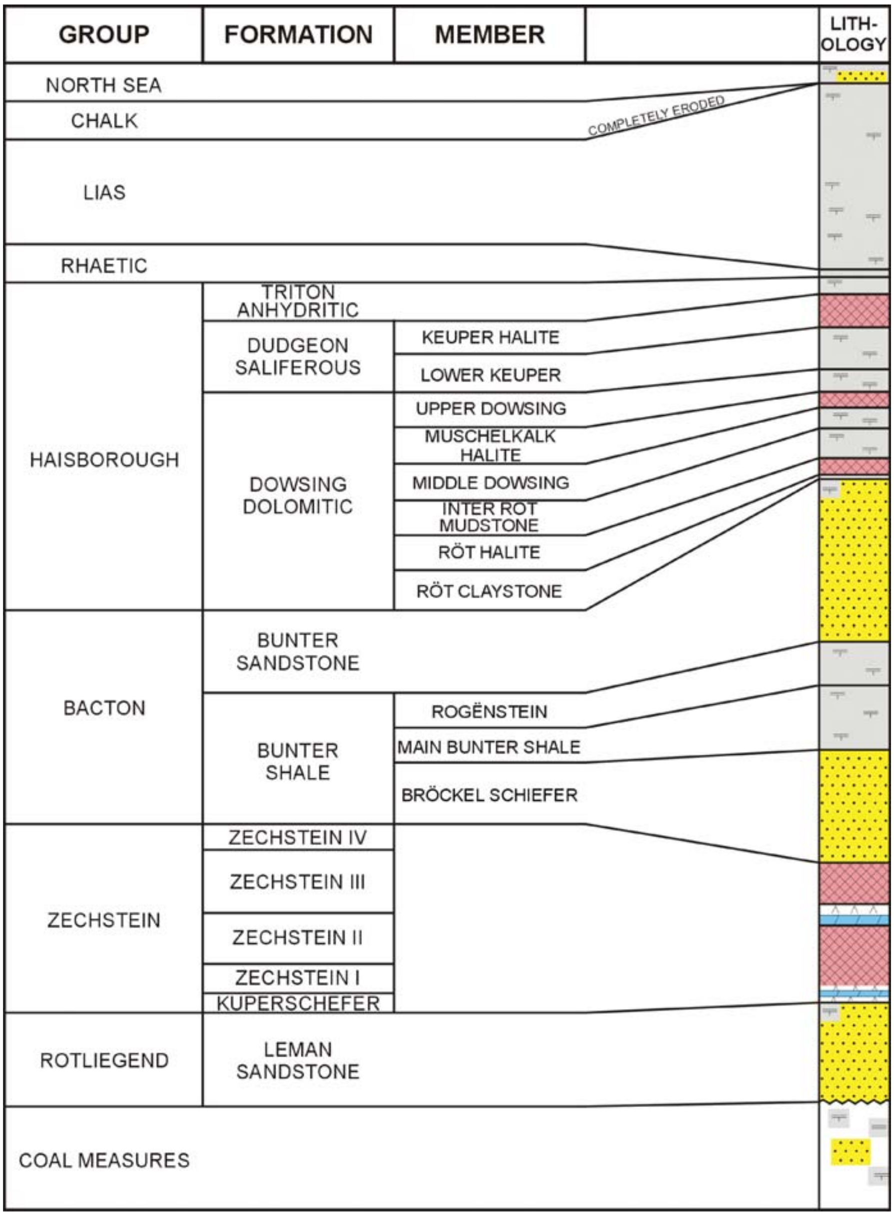

Fig. 3. Ensign Field stratigraphic sequence.

been divided by Venture into six reservoir zones (A–F) that can be correlated across the field.

The Upper A unit has been further subdivided into the A000 unit that corresponds to the Weissliegend at the very top of the Rotliegend. This unit comprises massive sands that were reworked as a result of the Zechstein marine transgression (Glennie & Buller 1983). In the Ensign Field this unit is extensively cemented and of very poor reservoir quality. The A100 lies below the Weissliegend and is dominated by sabkha, sandsheet and waterlain sandstones that were deposited in an erg margin–lake margin environment.

The B unit sandstones are of slightly better reservoir quality, reflecting the presence of more fluvial deposits, less sabkha sands and occasional aeolian units. The B unit sandstones represent the deposits of a less humid environment with less lacustrine influence.

The C unit underlies the B unit and is composed of 10–20 ft thick muddy sabkha sandstones and siltstones, and playa lake claystones. This unit is correlatable across the Ensign Field and over several kilometres in the Barque Field (Sarginson 2003). The C unit represents an expansion of the Silverpit lake, with the muddy sabkha deposits reflecting a more humid climate. The C unit is an important unit in the Ensign Field as it occurs just above the GWC in the central part of the field and acts as a natural barrier to the propagation of any hydraulic fractures owing to its high clay content.

The D and E units are characterized by large-scale cross-bedded aeolian sandstone units thought to have been deposited in a drier erg interior setting. These units have the best reservoir properties, with average porosities of 15–20%, although in the Ensign Field these units are predominantly located in the water leg.

The lowermost F unit comprises sandsheet, sabkha and waterlain sandstones deposited in an erg margin setting. This unit is entirely in the water leg.

Although the reservoir quality of the Leman Sandstone units can be related to their primary environment of deposition, with the aeolian units having higher porosities than the sabkha sands, extensive illite cementation has greatly reduced the permeability of the sandstones. In the A and B units, the main gas-bearing intervals in the Ensign Field, the average net pay core porosity is 9.8% and the average permeability is 0.15 mD.

Reservoir structure

The Ensign Field is situated at the crest of a NW–SE trending dip-closed anticline that is fault-bound to the SW (Fig. 2). The anticline was formed by transpressive tectonic stresses during the Cenozoic, which resulted in the widespread inversion of the basin (Glennie & Underhill 1998). The field is cross-cut by NNE–SSW trending lineaments that may be faults, but have not been cored and show no offsets on seismic data. These lineaments have been recognized in the nearby Barque Field (Sarginson 2003) and by analogy it is likely that cataclasis and mineralization may have resulted in these becoming permeability barriers, potentially compartmentalizing the reservoir.

Seismic interpretation

The original seismic volume used for the seismic interpretation of the Ensign Field area was the Galleon 3D that had been acquired by Shell in 1992. Analysis of the data revealed that the quality of this 3D data was not suitable for the planned appraisal and development of the field. It was therefore decided to undertake a PreSDM reprocessing exercise over the field and surrounding area utilizing the input from five different seismic volumes. The resulting 3D

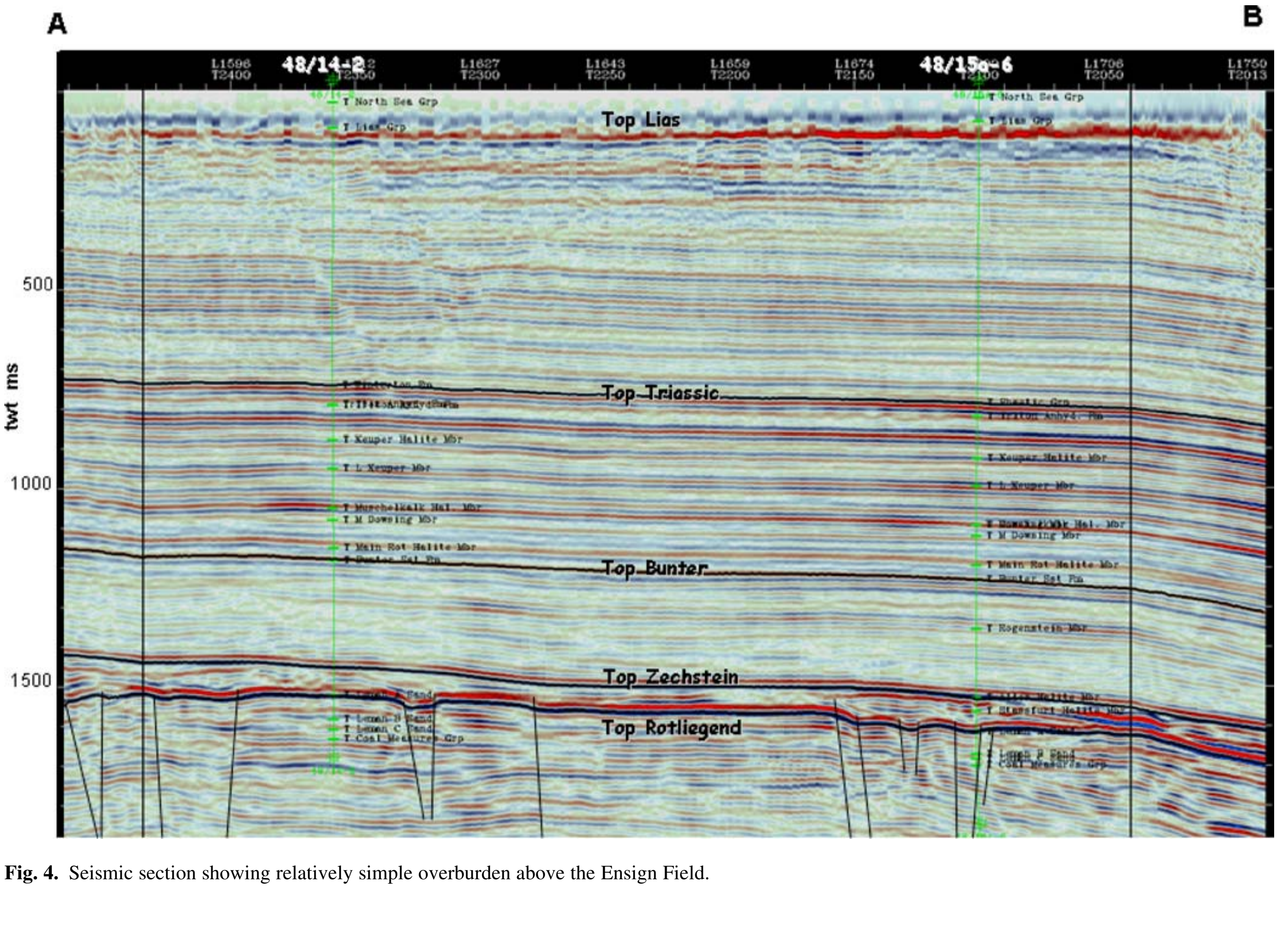

Fig. 4. Seismic section showing relatively simple overburden above the Ensign Field.

volume allowed a more detailed and coherent structural interpretation to be undertaken.

The overburden interval over the Ensign Field is relatively simple (Fig. 4). The Sole Pit inversion has removed the Cenozoic and Chalk units, resulting in the Lias being the first pre-Quaternary interval encountered below the sea bed. The Triassic section is very continuous and devoid of any large faults that occur in other parts of the Ensign–Audrey Field area to the NE. The Zechstein section is significantly thinner than the regional average which has been caused by halite withdrawal that fed the Audrey salt wall to the east. Consequently, the Zechstein over Ensign is dominated by a dolomite and anhydrite rich sequence that creates a higher than normal interval velocity.

Utilizing the initial discovery and appraisal wells to constrain the depth conversion, and the benign nature of the overburden, the subsequent appraisal wells have encountered the reservoir on prognosis.

Field appraisal Phase I

After acquiring the Ensign Field, Venture began an extensive data gathering and interpretation exercise in order to determine the best method of appraising and developing the field as quickly as possible. As mentioned above, part of this exercise involved the re-processing of the 3D seismic over the field that was part of a larger project that covered most of the acreage in the Venture-operated Audrey Field area. It was realized that the seismic reprocessing would take a significant amount of time and that this should not hold up the appraisal of the field. Consequently the results of the previous wells were reviewed in order to arrive at a better understanding of the controls on reservoir quality and deliverability. Key to unlocking the Ensign Field were the results of the Shell-operated discovery well 48/14-2 drilled 20 years previously. Although the well failed to flow when first tested, it flowed at a sustained rate of *c*. 14 MMscf per day after stimulation by a single hydraulic fracture. It was deemed that, with the prevailing gas price (2006), this type of well would form the basis of an economic development. In comparison it was felt that the Conoco well 48/15a-6 had less impact on the field appraisal as this well appeared to have been drilled into a complex fractured zone, was extensively fracture-cemented, and occurred in a portion of the field with a thinner gas column that would not form a part of the Ensign Field core development area.

48/14-2 well evaluation

The Ensign Discovery well encountered a 542 ft gas column predominantly in the upper A and B units of the Rotliegend sequence (Fig. 5). Unlike the neighbouring Shell-operated Barque gas field (Sarginson 2003), the lower units, which typically comprise

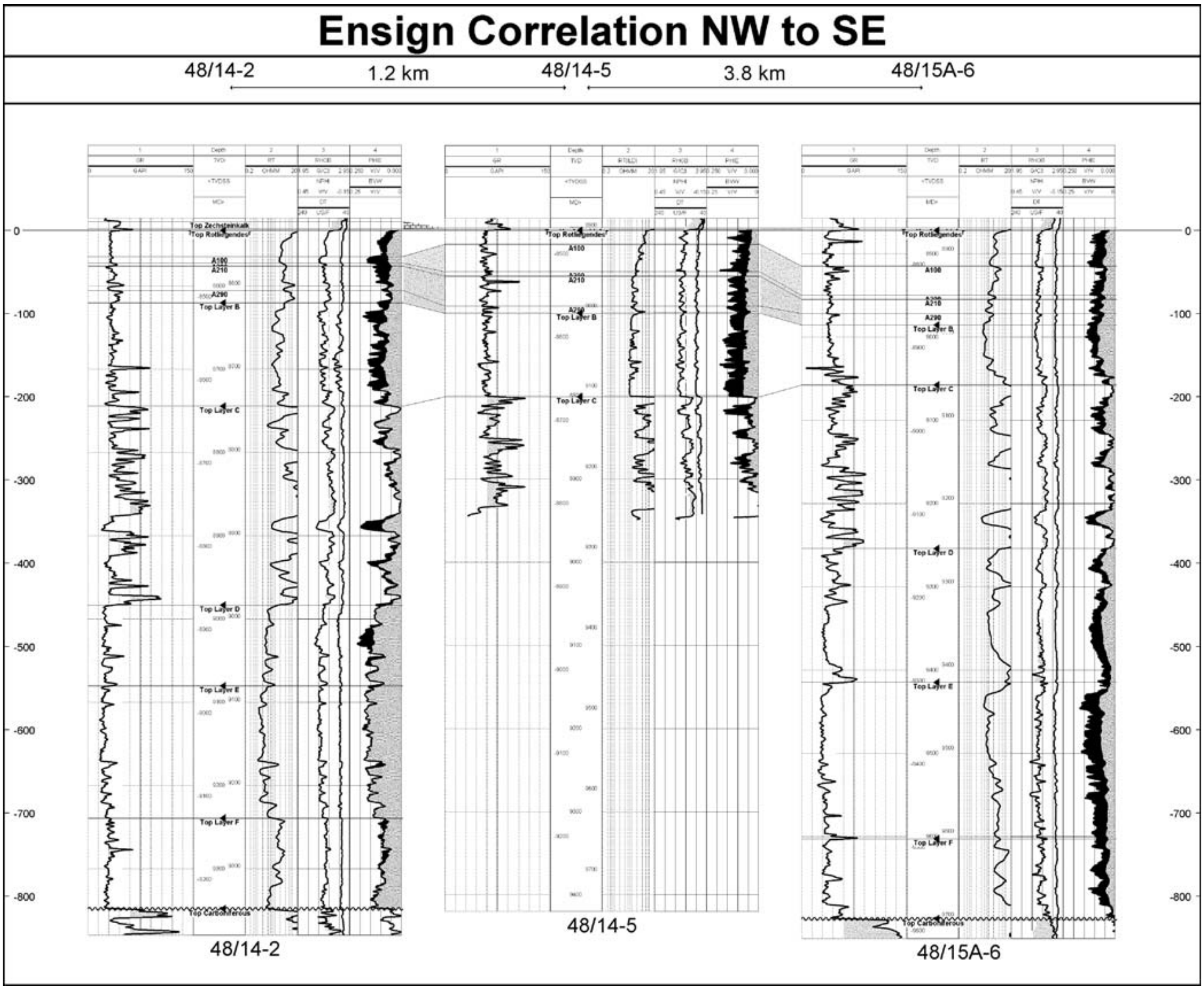

Fig. 5. Correlation panel of the Leman Sandstone in the discovery and appraisal wells of the Ensign Field.

better quality aeolian units, were below the GWC. The entire Rotliegend interval was cored (*c*. 800 ft), which provided a detailed facies and reservoir database.

Examination of the core acquired shows that the A–C units are dominated by sands interpreted as having been deposited in a damp sand flat (44%) and fluvial environment (23%) with very limited aeolian sands (5% dune facies and 2% dry sand flat). The core-derived porosity and permeability data (Fig. 6) show that these upper units of the reservoir are of very poor quality (<1 mD permeability) and scanning electron microscope (SEM) analysis confirms that this was primarily as a consequence of pore-lining illite that reduced the permeability (Fig. 7a). Although the aeolian units have slightly better reservoir quality, the average permeability of dune facies is 0.27 mD compared with the average damp sand flat permeability of 0.13 mD; it should be noted that the highest overall permeabilities were measured in the damp sand flat facies (0.82 mD). The low permeabilities measured in the aeolian sands, despite their larger grain size, better sorting and low detrital clay component, confirms the detrimental impact of the development of the authigenic fibrous illite on reservoir permeability.

Detailed examination of the core also showed that it was almost devoid of any fractures over its entire 800 ft. Analysis of the core photographs, core descriptions and the core itself revealed only four fractures in the *c*. 350 ft upper gas-bearing interval above the C unit. The fractures were either filled with anhydrite cement (2) or were small cataclastic shear fractures (2). Only one rubble zone was encountered at the base of one cored interval that appears not to be fracture-related. Core recovery of the A–C units was very good, with 100% recovery in five of the six cores and the one core with 97% recovery. The lack of any open or partially open fractures suggested that the productivity of the discovery well after fracture stimulation had not been enhanced by a naturally occurring fracture network.

The hydraulic fracture stimulation parameters for this well have been reviewed and interpreted in order to determine the size and

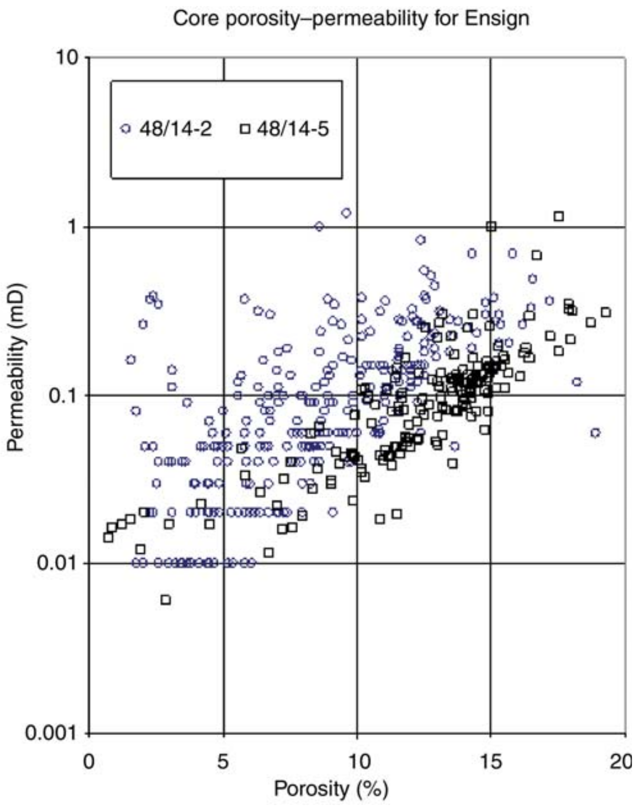

Fig. 6. Porosity–permeability cross plot of core recovered from the A–C units in wells 48/14-2 and 48/14-5.

effectiveness of the fracture induced. Table 2 shows the type and amount of proppant and fluids utilized. The initial fracture modelling results, whilst not unique, point to a fracture with a height of 160 ft, half length of 600 ft (i.e. the fracture extends 600 ft on either side of the well bore) and a width of *c*. 0.25 in. Utilizing these parameters and the resultant flow rates on test supports a productivity index (PI) of 11.5 Mscf day^{-1} psi^{-1} and a permeability height (Kh) of 51.2 mDft. It should be noted that the Kh of the perforated interval was significantly lower than this (*c*. 20 mDft), and consequently it would appear that the hydraulic fracture encountered a better quality reservoir away from the well bore.

Although it had previously been thought that the hydraulic fracture had connected into a naturally occurring open fracture network system, evaluation of the data acquired during and after the fracture stimulation did not support this view. Analysis of the well test data supported the view that there was only weak support for a fracture network connected to the well. The relatively low flow rates of *c*. 14 MMscf per day are in line with the overall poor quality reservoir.

Collation of all the available data (core, log, fracture stimulation, test results) supported the view that the Ensign Field could be developed utilizing fracture-stimulated sub-vertical wells. In order to test this theory and move the field towards development, an appraisal well (48/14a-5) was drilled into the fault block adjacent to the discovery well (Fig. 2). This well was designed with an extensive data acquisition program, including image log and core, as well as a fracture stimulation programme that was designed to create a larger, more effective fracture than that created in the discovery well 20 years previously.

The appraisal well was drilled in 2006 and targeted the upper reservoir intervals (units A and B) in order to minimize the risk of the planned hydraulic fracture extending into the water leg below the C unit. The well encountered the reservoir on prognosis and was successfully fracture-stimulated. In comparison to the 48/14-2 well, 730 000 lb of proppant were emplaced, 40% more than in the discovery well (Table 2). Despite the larger fracture developed, the well failed to flow at the sustained rates of the discovery well. The initial gas rates of 20 MMscf per day declined to below 12 MMscf per day, and failed to stabilize; that is, the gas rate was still falling when the well test was concluded. The poor well deliverability was unexpected and resulted in a detailed examination of the data acquired in the 48/14-5 well in order to understand the reason for the underperformance.

48/14a-5 well evaluation

Analysis of the core showed that the interval comprised similar facies to the 48/14-2 well, but with a higher proportion of waterlain sands. Aeolian dry sand flat deposits were more common than in the discovery well (14 v. 2%) but dune sands were less prevalent (1 v. 2%). However, the reservoir quality was very poor with low permeabilities (Fig. 6). Initially there were concerns that the permeabilities were lower than the discovery well, but this proved to be an analytical artefact as a consequence of the 48/14a-5 samples having been analysed at 800 psi confining pressure compared with the discovery well samples that were analysed at 230 psi confining pressure. It is believed that the lower measured permeabilities at the higher confining pressures are a consequence of the reduction in gas slippage and bypass during the permeability measurement. To confirm this to be the case, samples from the discovery well were re-analysed at 800 psi confining pressure, resulting in permeabilities similar to the 48/14a-5 well. SEM analysis confirmed that the cause of the very low permeabilities was extensive illite cementation (Fig. 7b) that was blocking the pore throats. Although no age dating was undertaken on the illites from this well, K–Ar dating of the illite fraction from the 48/14-2 and 48/15a-6

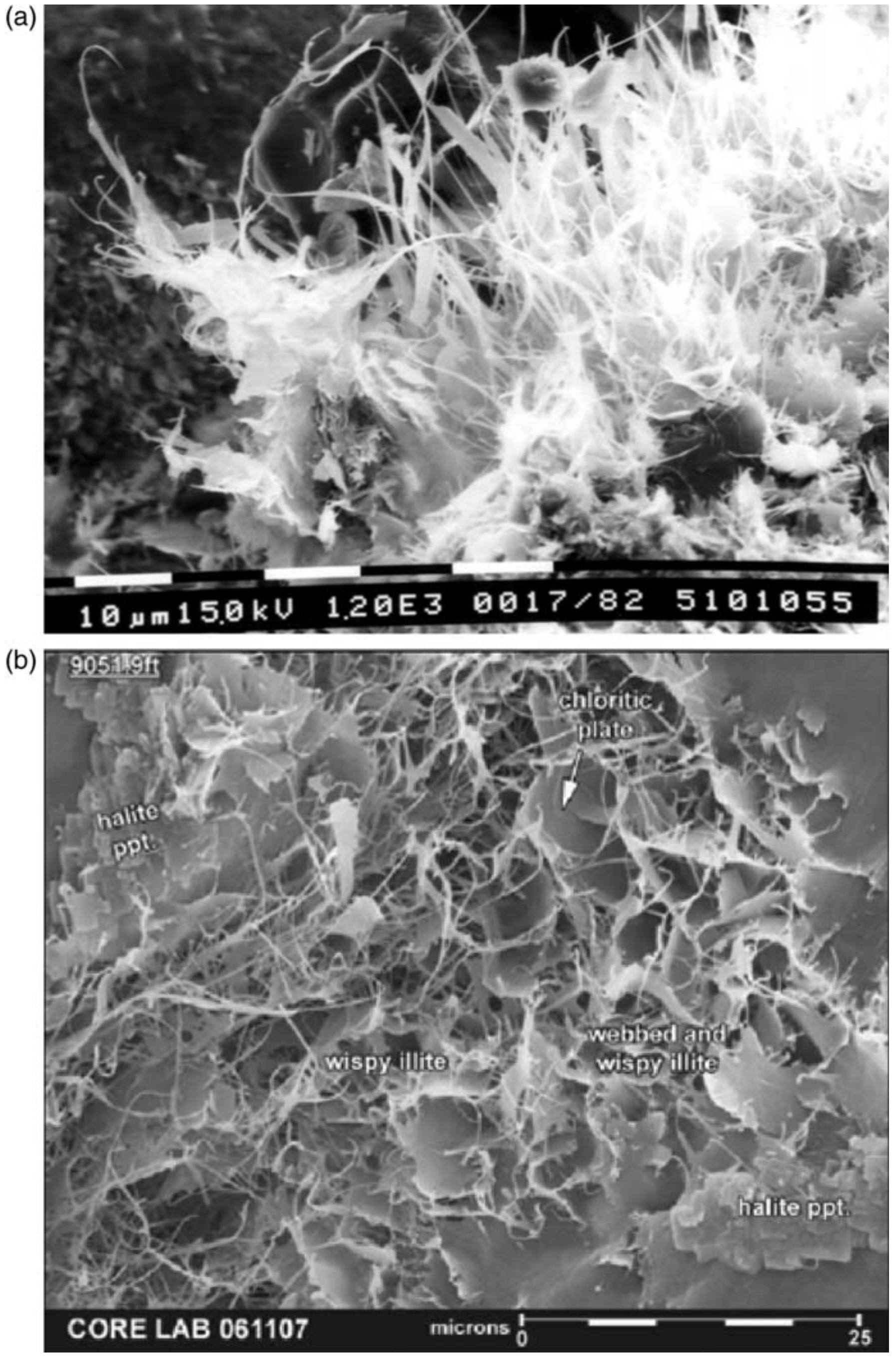

Fig. 7. (**a**) Scanning electron photomicrograph of fibrous illite from reservoir sample in well 48/14-2. (**b**) Scanning electron photomicrograph plate of fibrous illite from reservoir sample in well 48/14a-5.

Table 2. Hydraulic fracture proppant size and volumes utilized in the Ensign Field

Well	Proppant size*	Proppant type	Proppant volume
48/14-2	20/40	Ottawa Sand and Interprop	520 000 lb
48/14a-5	12/18	Resin-coated proppant	730 000 lb
48/14a-6 Fracture 1	12/18	Resin-coated proppant	380 000 lb
48/14a-6 Fracture 2			515 000 lb
48/14a-6 Fracture 3			500 000 lb
48/14a-6 Fracture 4			520 000 lb
48/14a-6 Fracture 5			500 000 lb

*Proppant size is measured in standard US sieve size.

wells produced a Late Jurassic age range of 147–167 Ma. This age of illite growth is comparable to other illite age dates in the Sole Pit Basin (Robinson *et al.* 1993).

In comparison to the core from well 48/14-2 that was almost devoid of fractures, the 48/14a-5 core contained a number of open and partially open fractures (Fig. 8), as well as a major drilling-induced axial tension fracture that ran for several metres along the core. The open and partially open fractures were observed in the core as high-angle features with minor amounts of vertical displacement, typically 4–5 mm, that were partially cemented by dolomite and anhydrite. Fracture widths were 0.5–6 mm, but predominantly 2–4 mm. No cataclastic shear zones were observed in the *c.* 193 ft of core recovered. In total, excluding drilling-induced fractures, 22 open, partially open and cemented fractures were observed in the *c.* 193 ft of core, that is, a fracture density of 8.7 ft per fracture, compared with the 48/14-2 fracture density of 87 ft per fracture. It was hoped that the open and partially open fractures could contribute to flow after fracture stimulation, but the well test results suggest that these fractures had no impact on well deliverability.

The acquisition of Schlumberger Full-bore Micro-Imager log data (FMI) over the reservoir interval allowed calibration of the fractures observed in core and the identification of additional fractures in the uncored intervals. It should be noted that, while fractures observed in the core can be described as open, partially open or closed and these fractures can be correlated directly with the FMI log, in the uncored intervals the fracture types can only be inferred from the FMI log data. It is assumed that as the FMI log produces resistivity images of the borehole, fractures that are electrically conductive are open, whilst those that are electrically resistive are closed or cemented (Serra 1989). The images showed the well to be extensively naturally fractured, with 83 fractures identified over an interval of 391 ft. The dominant orientation of the open and partially open fractures was NE–SW with dips of *c.* 65° towards the NW (Fig. 9), while the drilling-induced axial tension fractures were orientated NW–SE, reflecting the current stress environment in the SNS (World Stress Map 2008). It should be noted that any hydraulic fracture stimulation in the 48/14a-5 well would be perpendicular to the direction of minimum stress and hence be aligned parallel to the drilling-induced fractures. Consequently it is assumed that the hydraulic fracture in the 48/14a-5 well will have cross-cut the open and partially open fractures observed in the core and FMI. The poor performance of this well suggested that there was not a significant amount of flow from the naturally occurring fractures and that this orientation of fractures may not have any impact on reservoir deliverability. Owing to the poor and declining flow rates, no production logging was undertaken on this well, so it is not possible to determine where exactly in the perforated and hydraulically fractured interval any flow was coming from.

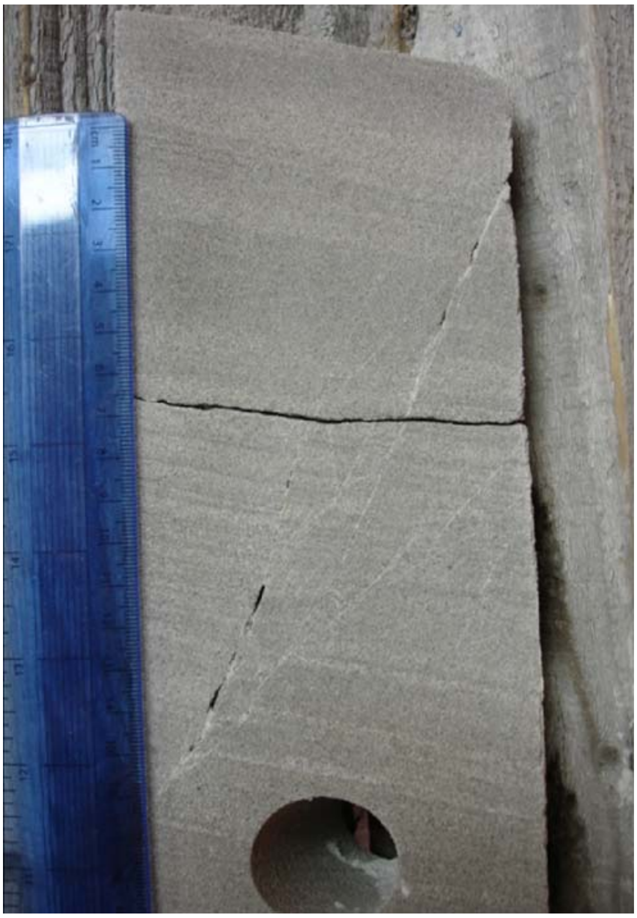

Fig. 8. Photograph of core taken from 48/14a-5 showing an open and partially open fracture network.

Appraisal Phase II

The results of the first appraisal well drilled by Venture suggested that the preferred option of developing the field utilizing fracture-stimulated near vertical wells would not be economic given the flow rates measured. Consequently the next appraisal well was planned as a long horizontal well that would be fracture stimulated with five hydraulic fractures. The successful development of the Venture-operated Chiswick Field utilizing multiple fractured horizontal wells proved this to be a viable approach to improving recovery in low productivity reservoirs (Nesbit & Overshott 2010).

The second Venture appraisal well (48/14a-6) targeted the NE portion of the field and had a trajectory such that it passed within 330 ft of the successfully fracture-stimulated discovery well (Fig. 2). The long horizontal length of the well (*c.* 5900 ft) was designed to allow the gas in several fault blocks to be accessed, as well as increasing the chance of encountering areas of better reservoir quality with the planned hydraulic fractures.

The well was successfully drilled in 2007 to a total measured depth of 15 275 ft, and encountered over 4800 ft of net sand (Fig. 10). The well was fracture stimulated over five intervals after the production liner was run. Each fracture was designed to emplace 500 000 lb of 12/18 proppant, that is, five times the volume of the original fracture stimulation of the 48/14-2 discovery well. When the well was tested it flowed at a rate of 44 MMscf per day that was limited by facilities constraints. The absolute open flow (AOF) of the well was calculated at 80 MMscf per day, at the high end of expectations. The well has been suspended and is planned for use as a production well.

48/14a-6 well evaluation

As the 48/14a-6 well was drilled within 330 ft of the fully cored discovery well 48/14-2, no core was taken. The reservoir interval was logged both using real-time MWD data and subsequent pipe-conveyed open hole logging, including an FMI. Analysis of the log data showed that the well penetrated the A100 and B units and had reservoir properties similar to the other wells drilled in the central portion of the field (Table 3). Analysis of the FMI data showed that the well had encountered a variable set of fractures that included faults, drilling-induced fractures as well as conductive, resistive and 'mixed' fractures with a distinct range of orientations. These findings were in marked contrast to previous observations that included the low number of fractures observed in the core from the discovery well 48/14-2, and the dominance of a single orientation of open and partially open fractures observed

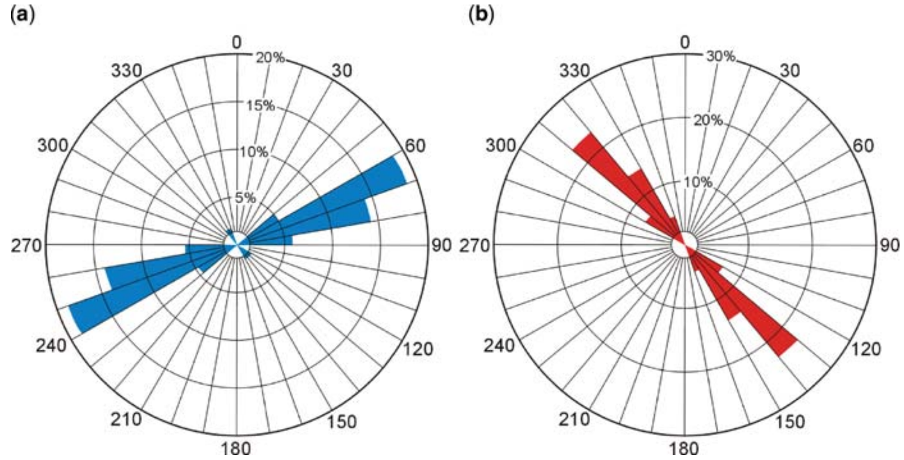

Fig. 9. Rose diagram showing strike orientation of (**a**) open and partially open fractures ($n = 53$) and (**b**) drilling-induced axial tension fractures ($n = 22$) in the FMI log acquired in well 48/14-5.

both in the core and FMI acquired in the 48/14a-5 appraisal well. It was hoped that, by studying the results of the FMI in the horizontal well, a unified theory could be derived to account for the well deliverability observed in the Ensign Field, which could aid the placement of future wells and optimize the field development.

Drilling induced fractures. Five drilling induced axial tension fractures were observed in the reservoir interval, with a NW–SE strike. These fractures are parallel to the direction of maximum horizontal stress, and are of the same orientation as the drilling-induced fractures observed in the 48/14-5 appraisal well.

Faults. 18 faults were observed in the FMI data, with the majority dipping to the east. A large conductive, north–south orientated fault was observed on the FMI with an associated conductive fracture network (Fig. 11).

Fractures. A total of 806 fractures were identified on the FMI log of which 665 were conductive, 115 resistive and 42 mixed, that is, partially conductive and partially resistive. By analogy to the 48/14a-5 well it is assumed that the electrically conductive fractures are open, and those that are resistive are closed or cemented. The different types of fracture also have a preferred orientation, with the conductive fractures striking north–south (dip east and west), the resistive fractures NNW–SSE (dip ENE and WSW), and the mixed fractures striking NE–SW (dip NW and SE) (Fig. 12). It was also noticed that the fractures are not spaced homogeneously along the well path, but appear in clusters, with zones of high fracture density and low fracture density. Given the well trajectory, the likely laterally extensive nature of the sand bodies and the lack of any obvious facies control on the fracture distribution observed in the 48/14a-5 core, it is unlikely that the zones of high fracture density observed in the 48/14a-6 well are related to variations in lithology.

It should be noted that a horizontal well provides a much denser sampling of rock heterogeneity than a vertical well, especially with respect to fractures that are typically high angle, and which may be undersampled by a vertical well. In addition, although an FMI image acquired in a vertical well may intersect fewer fractures, it does not impart any directional bias. In comparison, in a horizontal well the identification of fractures is strongly affected by borehole orientation and consequent sampling bias. The probability that a

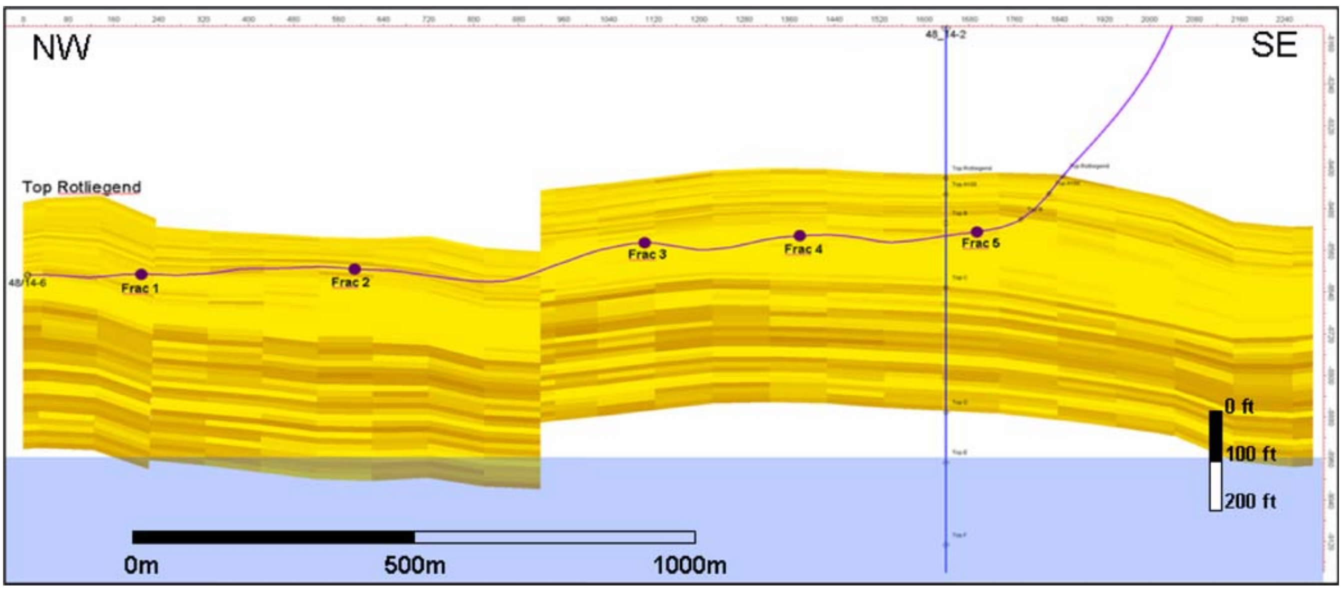

Fig. 10. Geological cross section showing the 48/14a-6 well path through the upper Leman Sandstone interval and the location of the hydraulic fracture-stimulated intervals.

Table 3. Average reservoir properties of the Upper Leman interval by unit

Well	Unit	Porosity (%)	Net/gross (%)	SW (%)
48/14-2	A000	10.9	90	56
	A100	11.3	90	61
	B	11.5	77	69
48/14a-5	A000	10.2	82	38
	A100	10.9	96	55
	B	13.4	99	55
48/14a-6*	A&B	11.4	75	48

*Owing to the well trajectory, it was not always possible to determine if the well was in the upper part of the B unit or the lower part of the A100 unit, hence for 48/14a-6 the reservoir quality has been averaged over all the units intersected. The low net/gross reflects the cemented fault zones that the well intersected.

fracture is identified on an FMI image in a horizontal well is dependent on the angle of intersection between the fracture and the well orientation. Fractures that are parallel to the well bore will be strongly undersampled, while those that are perpendicular to the well will be well sampled. This sampling bias can be corrected for and weighted fracture density distributions derived (Terzaghi 1965). The main impact with regards to the fracture distribution observed in the 48/14a-6 is that a Terzaghi weighted fracture distribution suggests that there are more resistive NNW–SSE fractures than imaged on the FMI log.

As well as the fracture type and orientation recorded in the FMI data, additional reservoir data was gathered after the well had been fracture stimulated. During the well flow testing a temperature log was acquired to observe whether the zones that had been fracture stimulated were actually contributing to flow. The observed temperature profile in the vicinity of the fracture-stimulated zones confirmed that they are contributing to flow, although it was not possible to quantify the relative flow contributions from each zone. Owing to operational constraints it was not possible to run

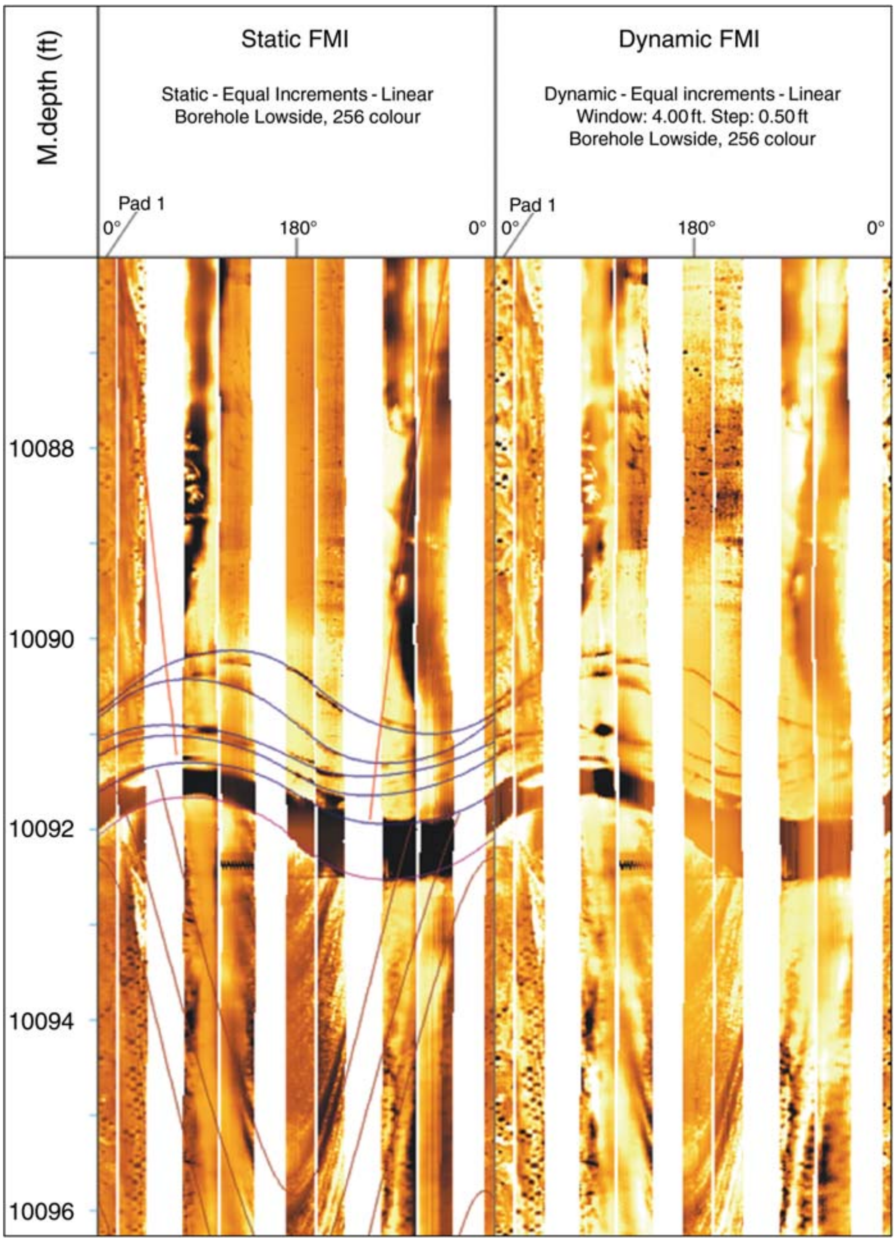

Fig. 11. FMI image of conductive fault and associated conductive fractures observed in the FMI log from well 48/14a-6. The fault is the dark (conductive) sinusoid at 10 092 ft on the FMI image.

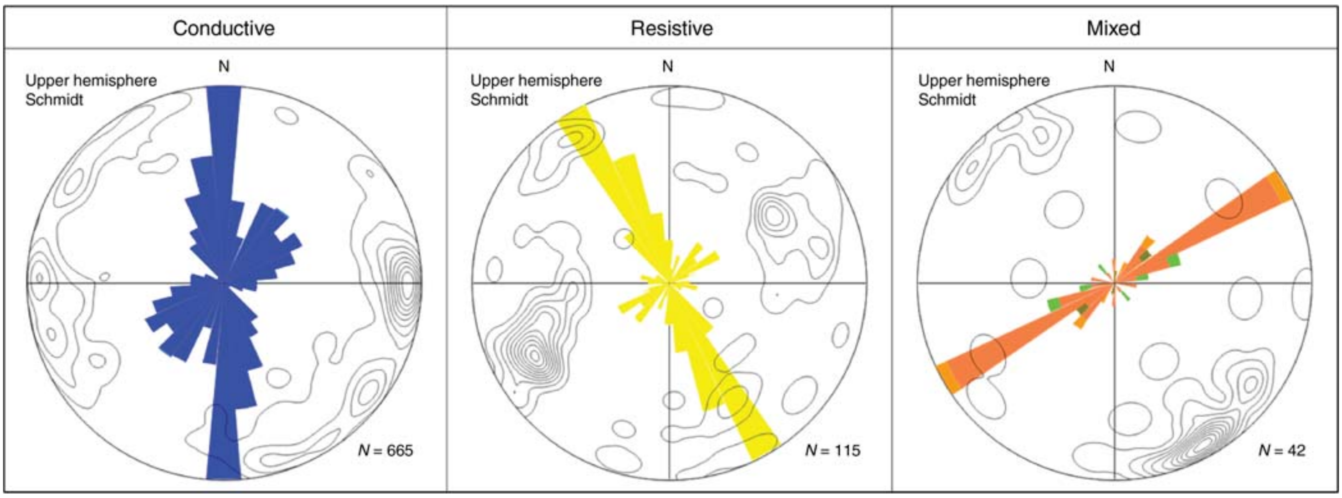

Fig. 12. Upper hemisphere Schmidt stereoplots showing the orientation of conductive, resistive and mixed fractures interpreted from the FMI acquired in the 48/14a-6 horizontal well.

a production log that may have quantified the contributions to flow from each zone.

Discussion: the potential role of naturally occurring fractures on productivity in tight gas reservoirs

The Ensign Field has proven more enigmatic than expected. The successful development of the central and northern portion of the field utilizing a multiple fracture-stimulated horizontal well has unlocked its potential, but a number of questions remain. For example: (1) why did the discovery well contain few fractures throughout its cored interval, although the FMI in this fault block shows a number of fractures and faults? (2) Why did the discovery well flow better than anticipated given its very poor reservoir quality? (3) Why did the 48/14a-5 well not flow better given that it encountered open and partially open fractures? Given the data acquired during Venture's appraisal campaign on Ensign, it is hoped that we can answer the critical question which is 'Is there an overriding control on reservoir deliverability that will help optimize the future development of the field?'

One conclusion that can be drawn from the observed fracture distribution is that different fracture types appear to have different effects on well deliverability. The open and partially open NE–SW striking fractures encountered in the 48/14a-5 appraisal well do not appear to have any impact on well deliverability. Although these fractures are observed to be open in core, they do not appear to enhance reservoir productivity, possibly because in the subsurface under the present stress regime they are closed, although partial mineralization of the fractures would tend to inhibit this. The only interval in the 48/14a-6 horizontal well that contained a significant proportion of these NE–SW striking mixed fractures was in the most northern fault block near the toe of the well. Unfortunately this interval was not accessed by the temperature log, and consequently may or may not be contributing to flow. It should be noted, however, that this interval also had the smallest induced fracture based upon the amount of proppant emplaced (Table 3).

Analysis of the fracture orientation in the fault block containing the discovery well shows a preponderance of the north–south striking conductive, potentially open, fractures. In addition, a large conductive north–south striking fault with associated conductive fractures was observed in the FMI log (Fig. 11) in the portion of the well that passed close to the discovery well. A plot of the 48/14a-6 well path showing the location and orientation of the fractures and the location of the 48/14-2 well bore at top reservoir (Fig. 13) suggests that the discovery well is located in a relatively fracture-free zone, between a series of fracture corridors. This may account for why the 48/14-2 well core contains few fractures and why on fracture stimulation the well performed better than expected given the very poor quality of the reservoir. It is likely that the induced hydraulic fracture would have extended across the north–south trending fracture corridors and 'tapped into' the natural fracture network. It should be noted, however, that the potential connection of the well bore with a network of natural fractures

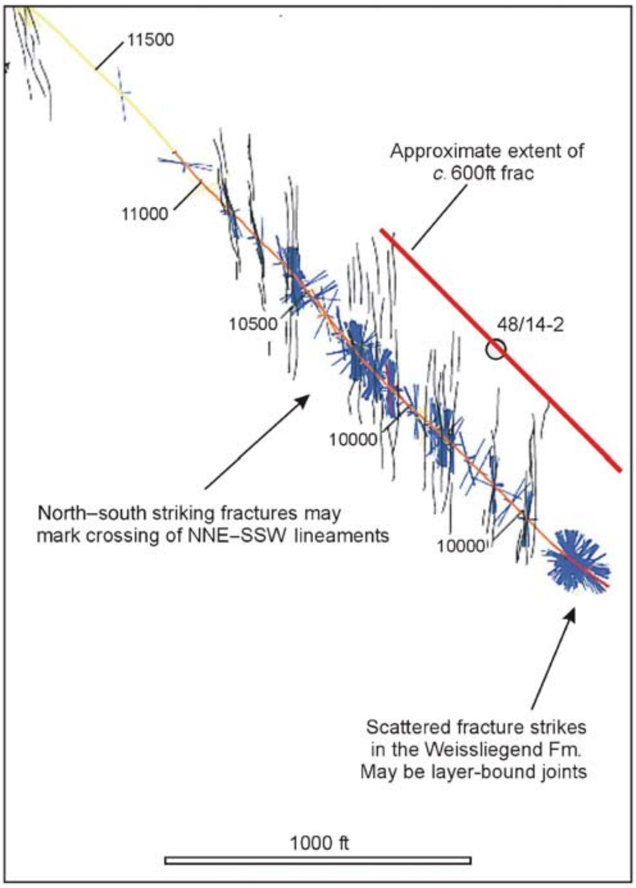

Fig. 13. Diagram showing the 48/14a-6 well path in the vicinity of the 48/14-2 discovery well annotated with the interpreted fractures and likely extent and orientation of the hydraulic fracture.

in both the 48/14-2 and 48/14a-6 wells does not appear to result in the response typical of a classic open fracture network. In both wells there does not appear to have been a sudden loss of fluids and proppant into the fracture system during the fracture stimulation process. It is more as if the natural fractures are acting as an improved matrix rather than a large-scale open fracture system.

Based on the observations and well results to date on Ensign it appears that: (1) the NE–SW striking open and partially open fractures do not appear to improve well deliverability; (2) the north–south striking conductive fractures appear to improve well deliverability; and (3) it is assumed that the resistive fractures that strike NW–SE have no impact upon well delivery.

The varying style and orientation of the fracture networks suggest that they may have formed under different stress and tectonic regimes during the structural development of the Ensign Field. At present the unifying theory of fracture formation, orientation and improvement in well deliverability has not been tested further in the Ensign Field. Ongoing technical work will hopefully improve our understanding on this matter. The model proposed for fracture style and orientation accounts for the well results to date and will be evaluated as the Ensign Field is developed further.

Conclusions

The Leman Sandstone reservoir of the Ensign Field comprises sabkha, fluvial and aeolian sandstones deposited in an arid continental environment. The sediments were deposited in a variety of erg margin–lake margin settings that have resulted in units that are correlatable across the field. In the Ensign Field the gas-bearing interval is dominated by sabkha and waterlain deposits with only minor aeolian sandstones.

Reservoir quality in the gas-bearing interval is universally very poor, in part owing to the poor primary depositional facies, but predominantly as a consequence of extensive illite cementation. The average core-derived permeability in the gas leg is <1 mD.

Core and FMI analysis shows that the Ensign Field has a heterogeneous distribution of fractures and faults. The fracture population is dominated by conductive (probably open) north–south striking fractures, with subordinate NNW–SSE resistive (probably closed) fractures and NE–SW mixed fractures. Analysis of the FMI data from the long horizontal well 48/14a-6 shows that the fractures are arranged in clusters, with zones of high and low fracture density.

Well results to date suggest that the NE–SW open and partially open fracture observed in core do not improve reservoir productivity, but those orientated north–south that are conductive appear to improve well deliverability.

The uncertainty in fracture type and distribution in the very tight gas reservoir of the Ensign Field has been overcome by utilizing a multiple fracture-stimulated long horizontal well. Although this technology has moved the field towards economic development, further technical work will be undertaken to reduce the uncertainty in the controls on well deliverability and optimize the field's future development.

The authors would like to thank the SNS gas asset team for their work that has resulted in the successful development of the Ensign Field. Sami Haidar at Fracture Technologies is thanked for early input into this work, and Schlumberger and Task Geoscience are acknowledged for the original FMI interpretations undertaken. The authors would also like to thank constructive reviews by Graham Goffey and Jon Gutmanis.

Delegate questions

Delegate: Ian Lisseter, Challenger Minerals Inc.

Question: Is there a density of FMI identified fracturing below which a multi-frac might not be attempted?

Answer: Owing to the uncertainty in the contribution of the fractures in the Ensign Field and the very low matrix permeability, horizontal wells that are stimulated by a number of hydraulic fractures is the base plan, irrespective of natural fracture density.

Question: What direction do the induced fractures have?

Answer: The induced fractures have the same orientation as the drilling-induced axial tension fractures that are parallel to S_{hmax}, and consequently are orientated approximately NW–SE.

References

Glennie, K. W. 1972. Early Permian (Rotliegendes) Palaeowinds of the North Sea. *Sedimentary Geology*, **34**, 245–265.

Glennie, K. W. & Buller, A. T. 1983. The Permian Weissliegend of NW Europe: the partial deformation of aeolian dune sands caused by the Zechstein transgression. *Sedimentary Geology*, **35**, 43–81.

Glennie, K. W. & Underhill, J. R. 1998. Origin, development and evolution of structural styles. *In*: Glennie, K. W. (ed.) *Petroleum Geology of the North Sea: Basic Concepts and Recent Advances*. Blackwell Scientific, Oxford, 42–84.

Glennie, K. W., Mudd, G. C. & Nagtegaal, P. J. C. 1978. Depositional environment and diagenesis of Permian Sandstones in Leman Bank and Sole Pit Areas of the UK southern North Sea. *Journal of the Geological Society, London*, **135**, 25–34.

Nesbit, R. & Overshott, K. 2010. Overcoming multiple uncertainties in a challenging gas development: Chiswick Field UK SNS. *In*: Vining, B. A. & Pickering, S. C. (eds) *Petroleum Geology: From Mature Basins to New Frontiers – Proceedings of the 7th Petroleum Geology Conference*. Geological Society, London, 315–323; doi: 10.1144/0070315.

Robinson, A. G., Coleman, M. L. & Gluyas, J. G. 1993. The age and cause of illite cement growth, Village Fields area, Southern North Sea: evidence from K-Ar ages and $^{18}O/^{16}O$ ratios. *American Association of Petroleum Geologist Bulletin*, **77**, 68–80.

Sarginson, M. J. 2003. The Barque Field, 48/13a, 48/14, UK North Sea. *In*: Gluyas, J. G. & Hichens, H. M. (eds) *United Kingdom Oil and Gas Fields, Commemorative Millennium Volume*. Geological Society, London, Memoirs, **20**, 663–670.

Serra, O. 1989. *Formation Microscanner Image Interpretation*. Schlumberger Educational Services, Texas.

Terzaghi, R. D. 1965. Sources of error in joint surveys. *Geotechnique*, **15**, 287–304.

World Stress Map. 2008. *The World Stress Map Project*. World Wide Web Address: http://www.world-stress-map.org.

Maximizing production and reserves from offshore heavy oil fields using seismic and drilling technology: Alba and Captain Fields, UKNS

J. M. HAMPSON, S. F. WALDEN and C. BELL

Chevron Upstream Europe, Chevron House, Hill of Rubislaw, Aberdeen AB15 6XL, UK (e-mail: johnhampson@chevron.com)

Abstract: Chevron North Sea Limited operates Alba and Captain, two large, mature, heavy oil fields in blocks 16/26 and 13/22a of the UK sector of the North Sea, respectively. Although the fields are structurally and stratigraphically different, their development schemes have been similar. Common components to both fields are that they are marine sandstone reservoirs; have one steel jacket, plus subsea templates; are under water injection for pressure support; utilize long horizontal development wells; use pilot holes and logging while drilling (LWD) geosteering tools to optimize well locations; and have seismic resolution issues. New technologies and techniques have been developed and adopted to maximize production and reserves from the fields. The benefits to both Alba and Captain of previous and new technologies are reviewed below.

Keywords: Alba, Captain, 4D seismic, fault, pilot hole, geosteering

Field history and background

Alba Field

The Alba Field is a mature (15 years on production), heavy oil (19° API) asset located in block 16/26 in the Outer Moray Firth, Central North Sea, 225 km NE of Aberdeen (Fig. 1). It was discovered in 1984 by a Britannia Field appraisal well (16/26-5), which encountered oil-bearing sands in the Eocene age Nauchlan and Brioc Sandstones and has been on stream since 1994. It is currently producing from 26 platforms and 10 subsea horizontal wells and has seven water injector wells (Fig. 2). Cumulative oil production reached 350×10^6 bbl in 2008 of a field STOIIP (stock tank oil initially in place) of 1000×10^6 bbl. Average daily oil production is currently 35 000 bopd with field water cut of 87% (Fig. 3).

The field overlies the Mesozoic Witch Ground Graben with the Fladen Ground Spur to the North and Renee Ridge to the South. The Alba reservoir is an elongate, Mid–Late Eocene, turbidite channel fill, deposited in a pre-existing erosional slope scar. The poorly consolidated sands were subjected to significant remobilization and injection shortly after deposition and burial. The reservoir facies is a quite simple, almost binary system of sand and intra-reservoir shale bodies; reservoir properties range from 30–35% porosity and 2–4 Da horizontal permeability.

The Alba reservoir level is affected by significant faulting (Lonergan & Cartwright 1999), which has strongly influenced reservoir architecture. Two fault families have been identified on various seismic datasets. Polygonal faults have developed in the surrounding shales as a result of de-watering and where they cut into the reservoir (laterally or into the top) seems to coincide with the location of major sand injectites. These faults only cut through the entire reservoir where it is relatively thin and have been mainly interpreted on compressional (P-wave or PP) seismic data. Sub-vertical faults are present mainly at reservoir level and form a dense network. These faults can be best observed on shear (S-wave or PS) seismic data and their generation mechanism is probably compaction-related.

Despite the importance of faulting, the poor imaging of the pre-production 1989 3D seismic data (P-wave streamer survey) did not permit detailed fault mapping. It was not until the acquisition of the 1998 4C (four component) OBC (Ocean Bottom Cable) survey and subsequent 2008 4D survey that interpretation of the faults improved (Fig. 4). Although these fault sets have been known in the past, their transmissibility character and impact on flow were previously unclear. A few early wells had shown evidence of possible fault baffling with oil- and water-filled sand found on either side of faulted shale breaks. However, elsewhere, faults may act as conduits, locally concentrating flow and causing point inflow in wells and significantly influencing fluid movement within the reservoir.

Alba Field development

Alba Field development has been driven by technology step-changes that have resulted in significant improvements in the understanding of static geology and dynamic reservoir conditions. Two key areas that have resulted in major changes are seismic and drilling.

Seismic technology. Prior to the first 3D survey, all that could be identified of what was subsequently to become Alba on 2D data was the oil–water contact (OWC) in the 12 Area of the field, a strong amplitude, flat seismic event. Alba now has had the benefit of five 3D seismic surveys, together with reprocessing of some datasets. These are shown in Table 1 (abbreviated name in parentheses).

The 1989 pre-production P-wave survey provided the first 3D seismic interpretation of the field. Early geological models suggested the field was a ‘tank of sand’ with discontinuous intra-reservoir shales, which were interpreted to have little or no impact on fluid movement and production (Fig. 5a). This interpretation was largely driven by the very poorly imaged top and base reservoir, but clearly identifiable OWC.

The first step-change in understanding of the field occurred following acquisition of the third seismic dataset in 1998 (MacLeod *et al.* 1999). This OBC survey recorded *S* (shear) wave energy, converted from P waves that provided the first image of top and base reservoir due to the large shear impedance contrast of the reservoir with the surrounding shale (Fig. 6). *PZ*, the recorded P-wave energy, was also acquired with the OBC and was used in the well planning process.

The shear impedance inversion of this dataset also provided the first image of sand/shale distribution within the reservoir. It was also following interpretation of these data that large-scale

VINING, B. A. & PICKERING, S. C. (eds) *Petroleum Geology: From Mature Basins to New Frontiers – Proceedings of the 7th Petroleum Geology Conference*, 337–347. DOI: 10.1144/0070337

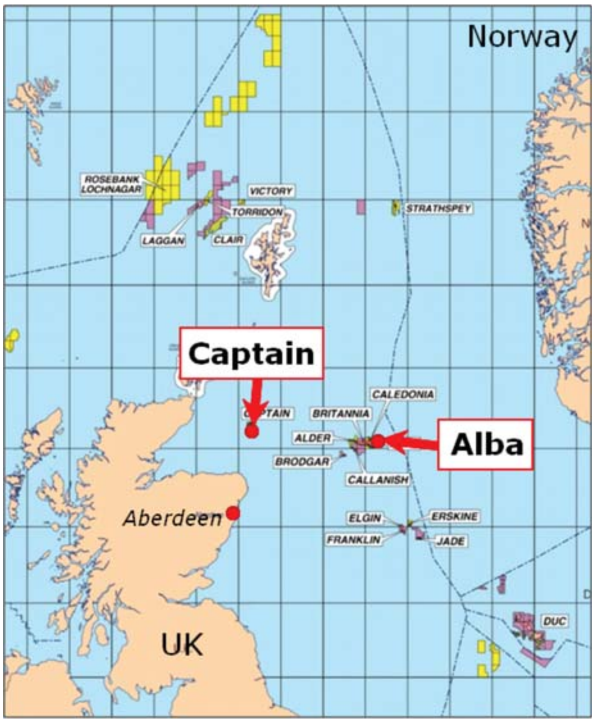

Fig. 1. Location map.

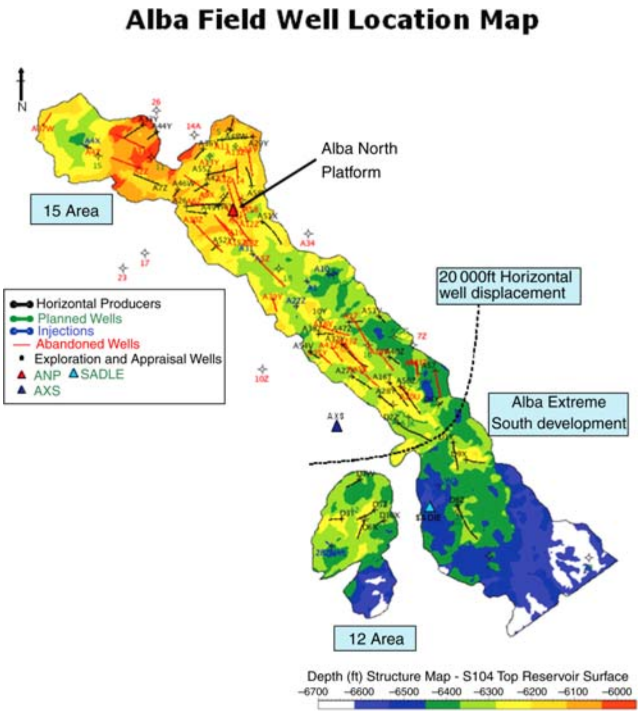

Fig. 2. Alba Field location map.

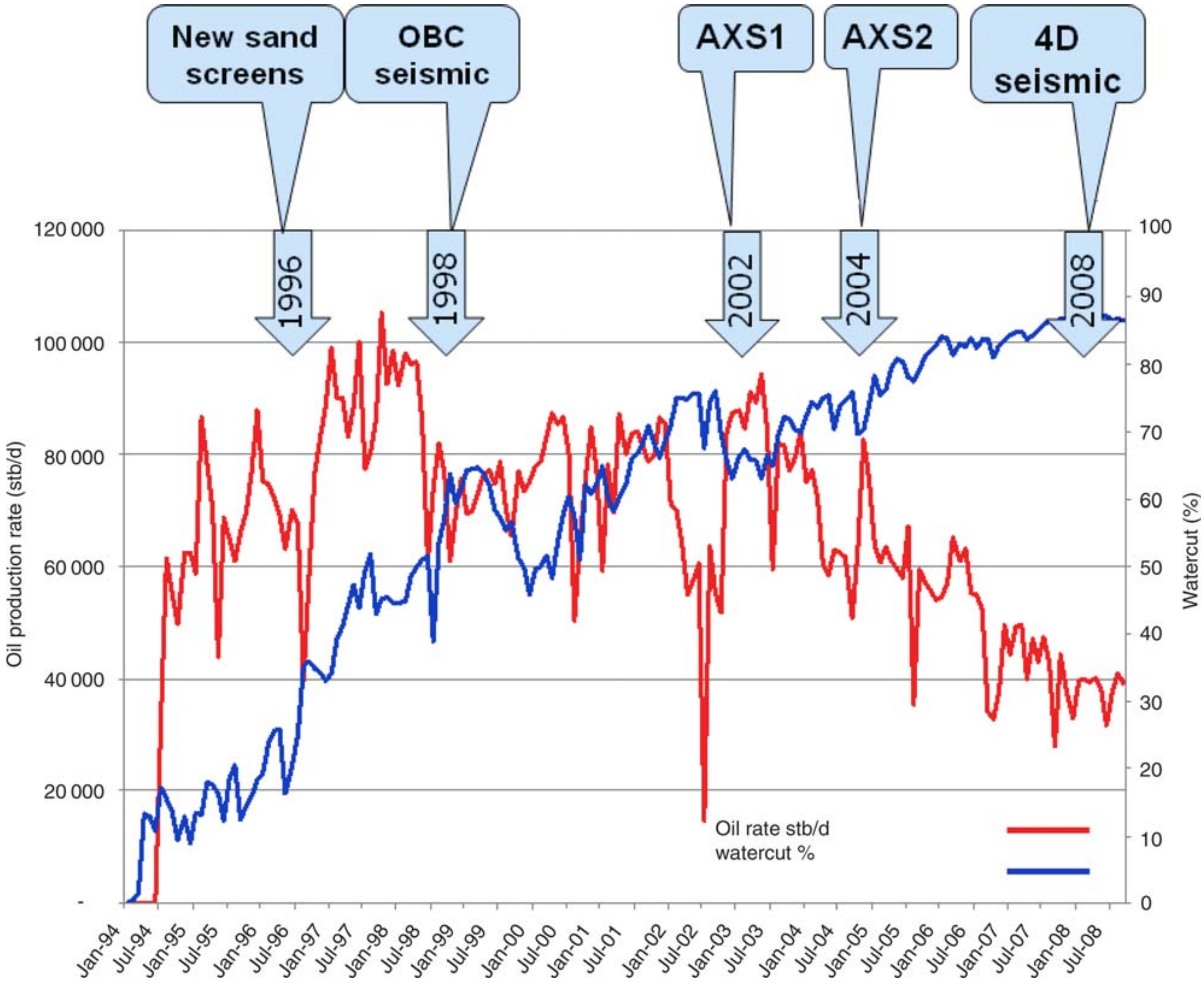

Fig. 3. Alba Field production.

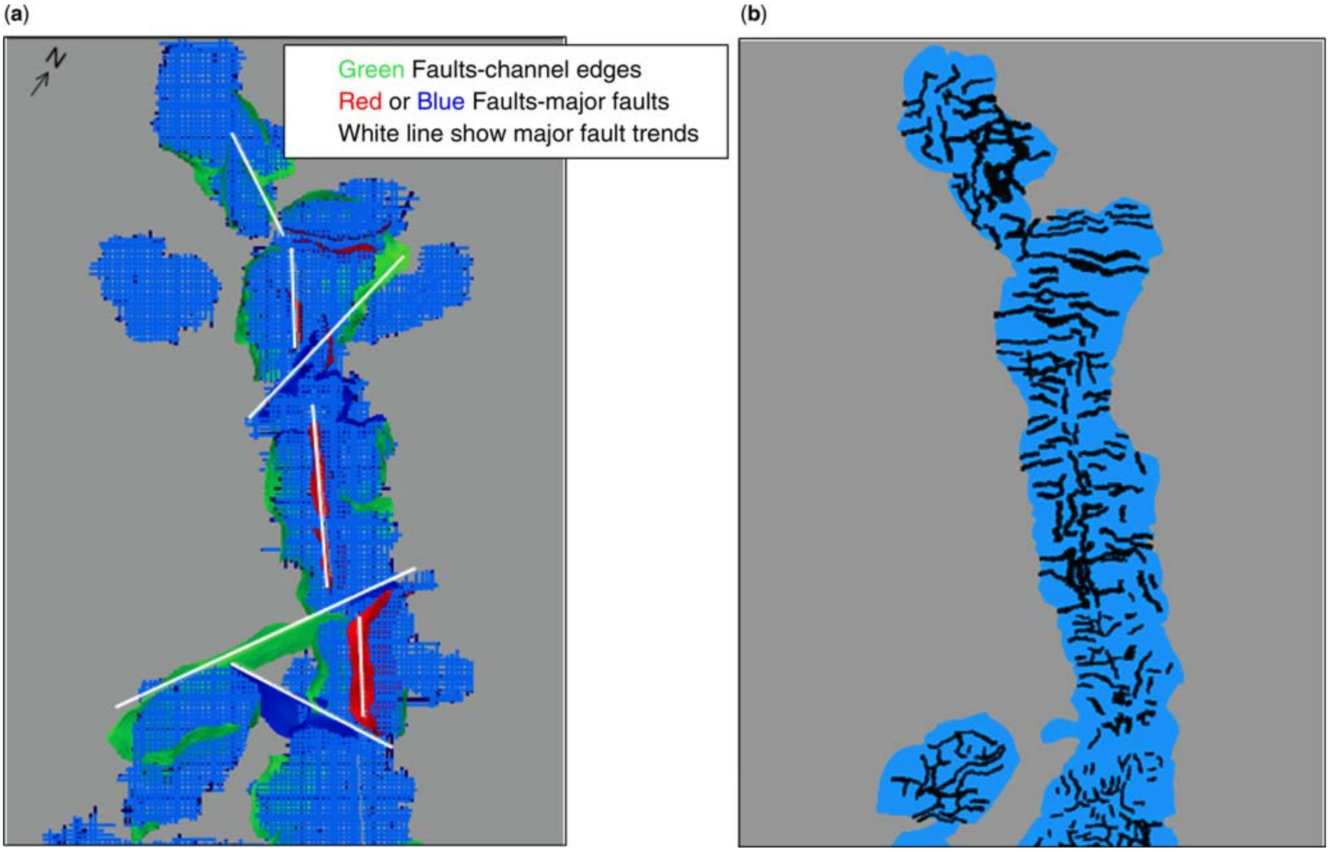

Fig. 4. Alba fault interpretations. (**a**) Early interpretation had few faults influencing fluid movement. (**b**) Current interpretation much more complex: enabled by joint interpretation of PP, PS & 4D; latest 3D interpretation application.

injected sands at the field margins ('wings') and above the main field were first recognized (Fig. 5b). They had previously been considered to be relatively small-scale features (Newton & Flanagan 1993), but the PS data quality enabled significant subsequent research.

In 2002 a non-proprietary P-wave seismic dataset was acquired primarily to image the deeper Britannia reservoir, not as a designed 4D dataset. The 2002 survey was recorded at a similar north–south azimuth to the 1991 survey. As a result, after some delay due to a feasibility study and other development priorities, the 2002 and 1991 datasets were co-processed together (PP05). This PP05 dataset has only been used qualitatively in target maturation due to the poor repeatability; comparing this dataset with the 2008 dedicated 4D acquisition highlights the fact that co-processing can only go so far in resolving acquisition-related 4D noise.

Table 1. Alba Field – seismic data history

1989	Alba streamer survey (not currently used because of poor imaging)
1991	Britannia streamer survey (Alba pre-production survey – PP91)
1998	Alba OBC 4C survey; PS and PZ recorded; not designed for 4D (PS99)
2002	Q15 streamer survey; not designed for 4D (PP02)
2004	Reprocessing of 1998 OBC survey (PS04)
2005	Parallel processing of Britannia and Q15 surveys (PP05)
2008	Alba streamer dedicated 4D (PP08)

Reprocessing of 1998 OBC that included a pre-stack, anisotropic migration (PS04) in 2004 provided an alternative image of the field. This dataset is somewhat lower frequency, but gives a useful alternative model when risking well targets.

Alba's viscous oil (19° API, 6–10 cP) properties together with the high poroperm sands result in a strong seismic fluid response, which makes it very suitable for 4D technology. Multiple feasibility studies have confirmed a very strong 4D signal on Alba due almost entirely to saturation changes because the field pressure has been maintained by full-voidage water injection over the field life. In order to locate the remaining oil after 14 years of production, a dedicated 4D survey was acquired in 2008 which provided the fourth time step after the 1991 Baseline, 1998 OBC PZ and 2002 Monitor surveys. Key components of the business case developed for a new 'dedicated' 4D were capturing incremental production, de-risking existing targets and reducing drilling costs by optimizing wellpath design. There were also several intangibles such as an improved reservoir model. The Alba drilling programme has been driven by the reservoir model built from the 1998 OBC seismic survey and the targets are now approaching the resolution of these reservoir models. The 2008 4D provides an independent constraint on reservoir history matching.

Alba is using new workflows to extract value from the survey. High noise levels in the previous 2002/1991 co-processed 4D data limited its use to a 'soft' constraint in prior history matching. However, with the data quality of the dedicated acquisition, interpreted oil–water contacts are being combined with traditional well-related history matching parameters as 'hard' data constraints in the simulation model history match (Fig. 7).

The re-interpretation of all three datasets, completed over the past 12 months, is providing new insights into the reservoir geology and, in particular, the way faults affect fluid flow. There

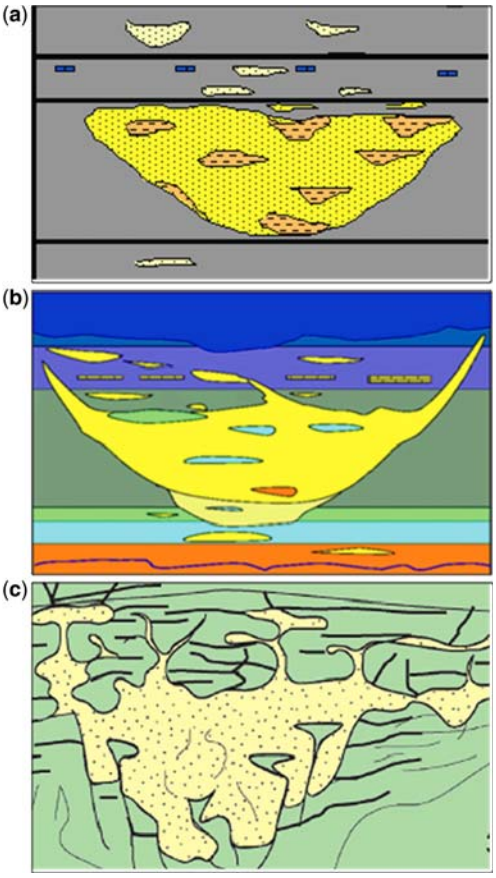

Fig. 5. Alba cartoon geological models. (**a**) At field development: simple, lensoid shape; PP seismic imaged OWC only. (**b**) After 1998 OBC seismic: imaged top/base; injected sands, wings and crest. (**c**) Probable complexity: multiple injectites, small- and large-scale faults (Surlyk *et al.* 2007).

are indications that water cones beneath producers are sharper than previously modelled, providing opportunities for inter-cone infill targets (Fig. 8). In addition, the impact of fault baffling on fluid movement has been noted in several areas of the field.

Injected sands and field edge. The presence of injected sands in Alba has been well documented (Duranti *et al.* 2002 and others). However the location, size and shape of the injectites was difficult to predict from seismic data and some early attempts to produce from them proved difficult as a result of early completion failures due to shale fines migration and sand screen hot-spotting. Work on seismic tuning (Fig. 9) showed a predictable relationship between amplitude decay and reservoir sand thickness. This changed the previous Alba edge of field 'cliff' model to the current more predictable thinning model and enabled more confident targeting of field edge drilling targets. Wells drilled on the eastern and western edges of the main field in 2005 confirmed the new thinning model predictions. The current view of likely field complexity is illustrated by the diagram in Figure 5c (Surlyk *et al.* 2007).

Alba drilling technology. Alba (and Captain) Field would not have been successfully developed without advances in horizontal drilling and completion technology that occurred during the 1990s because of the unconsolidated nature of the reservoir sand and the long (>500 ft) production intervals located close to the roof that are required to effectively capture the oil reserves.

Whilst rotary steerable systems (RSS) enabled long horizontal wells to be drilled, gravel-packed sand screens provided the necessary solids control required to prevent production of the fine-grained, poorly consolidated sand. The first of a new generation of sand screens was used in 1996 to combat early well failures and, together with gravel-packing, these have continued to provide effective sand control combined with long well life.

When field development was first sanctioned, two platforms had been planned. Only Alba Northern Platform (ANP) was ever commissioned. Before the second platform was built, advances in drilling technology meant that a significantly larger portion of the field could be reached by long horizontal wells. The first extended reach drilling (ERD) wells in 1997 hinted at difficulties to come in exploiting extreme southern reserves. Well lengths were originally 15 000 ft MD, but this limit was subsequently extended to the current 20 000 ft MD by the use of improved technology and drilling practices.

However, this still left significant reserves in the extreme south and 12 Area of the field. To produce this oil, the more cost-effective

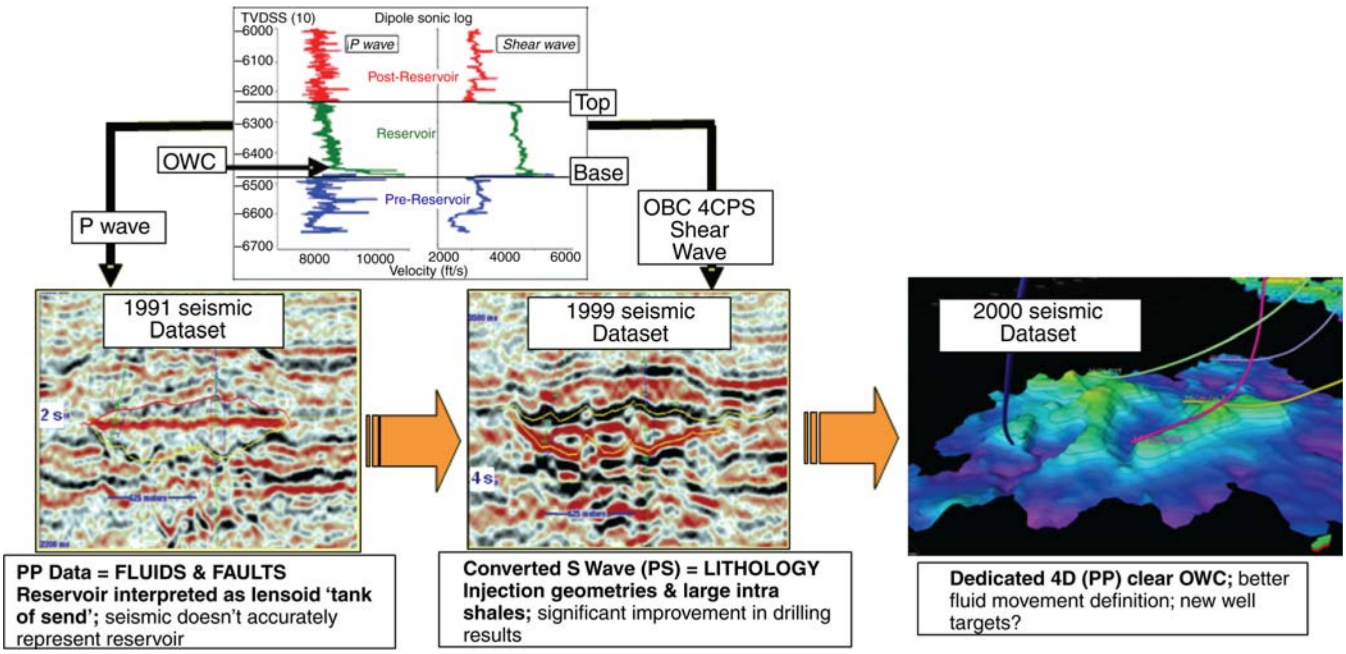

Fig. 6. Alba seismic datasets.

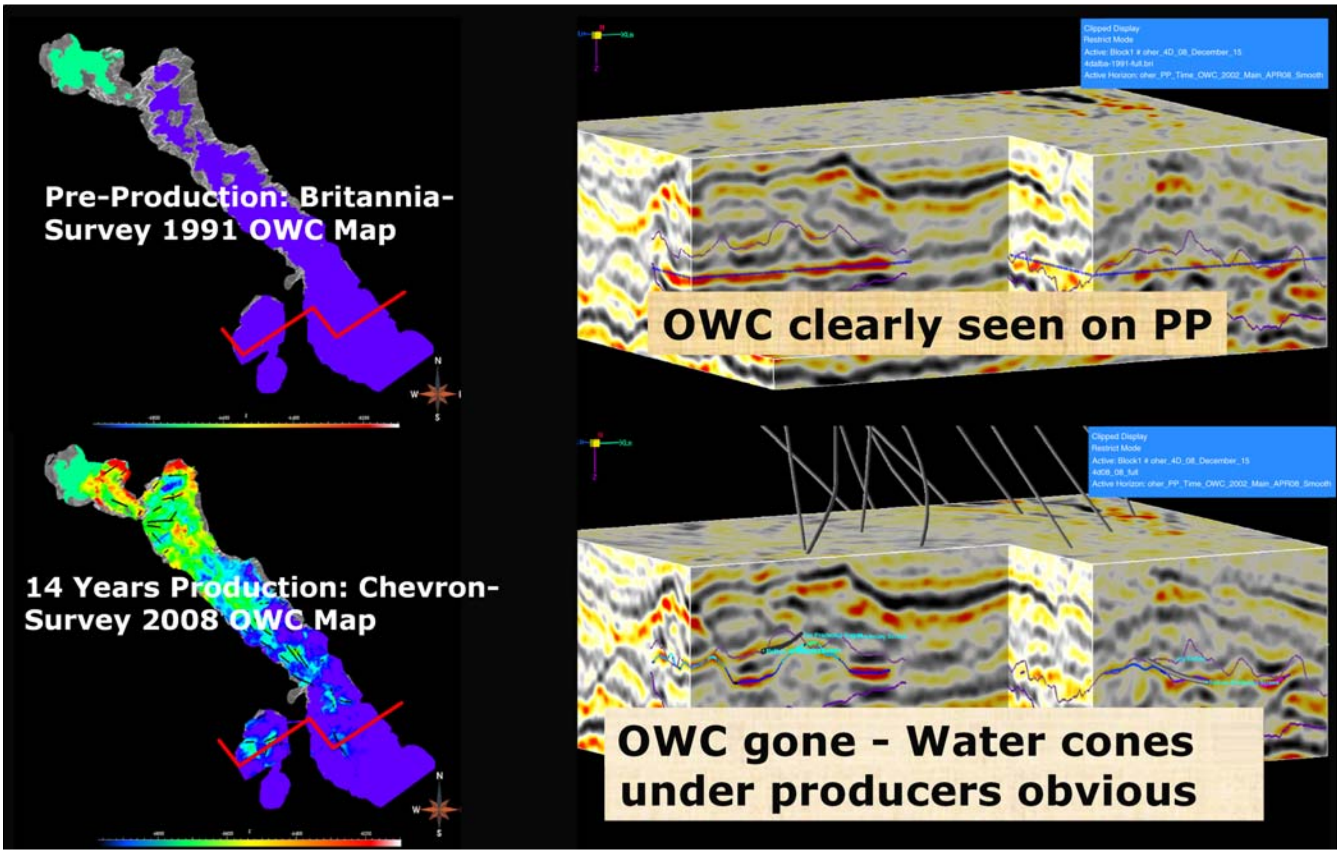

Fig. 7. Alba 4D seismic showing OWC movement.

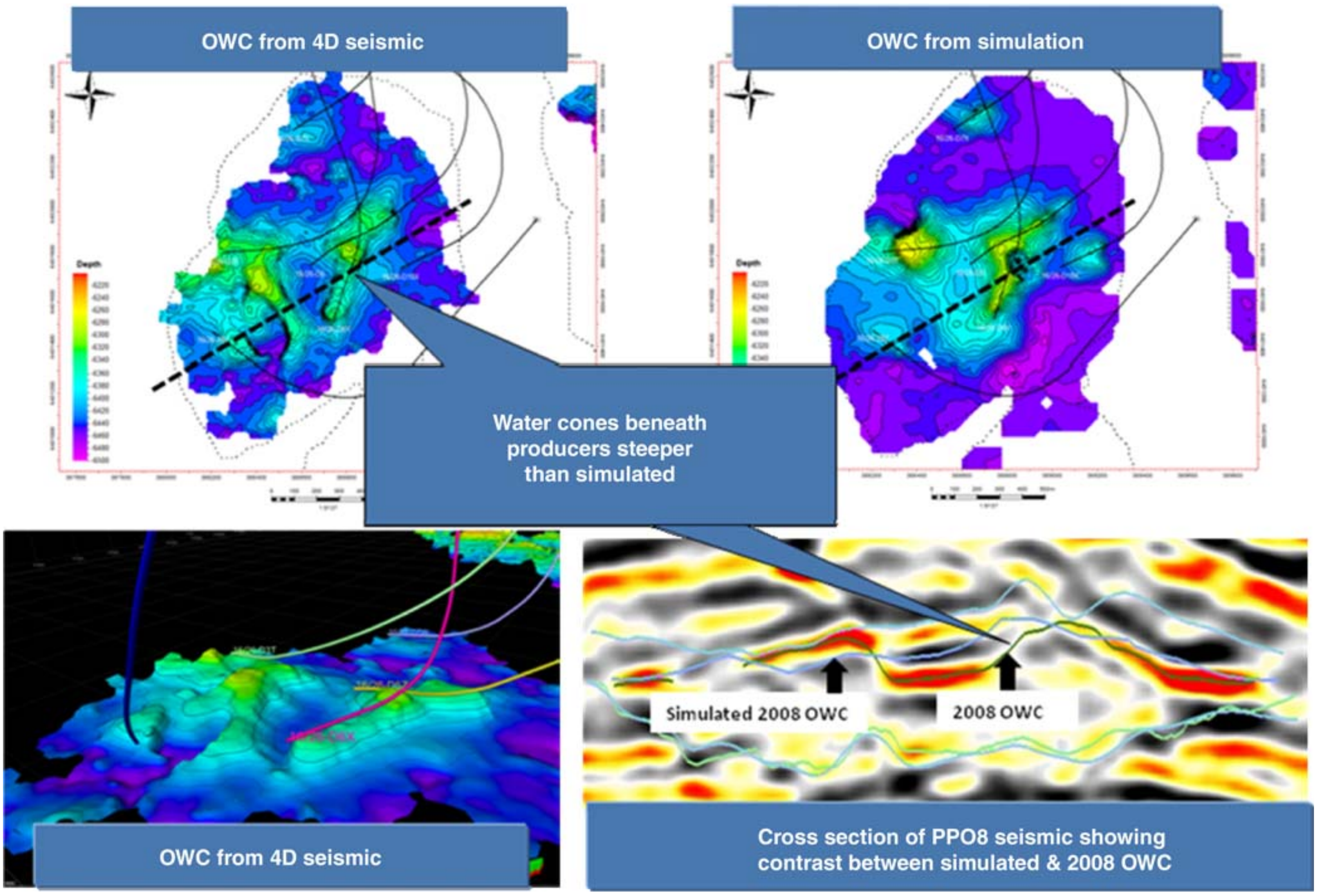

Fig. 8. Alba 4D data showing water cones beneath producers.

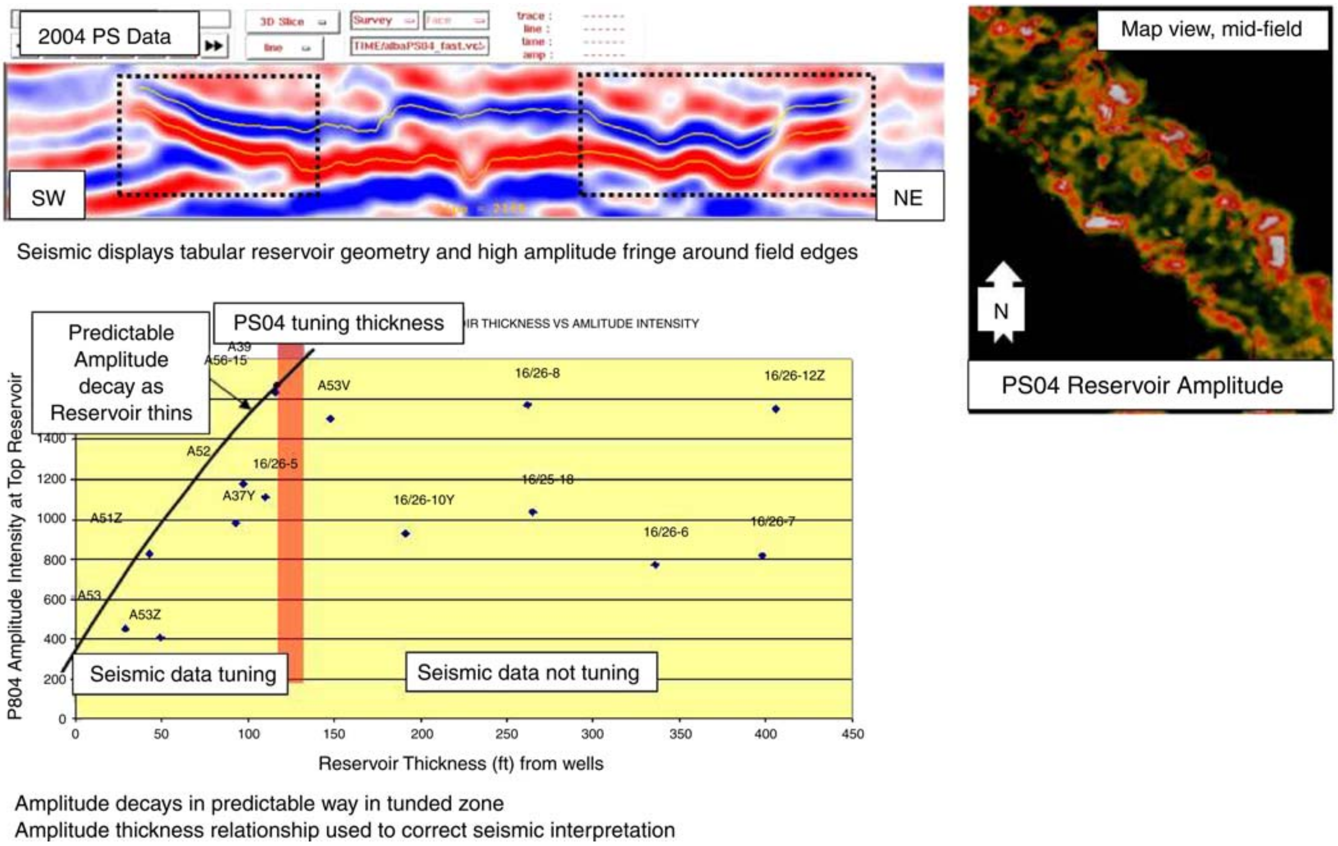

Fig. 9. Alba – field edge seismic tuning.

alternative of subsea manifolds and pipeline tie-back to ANP was utilized, starting in 2002 with AXS (Alba eXtreme South) phase 1 and continuing in 2004 and 2006 with additional producers.

ANP was built with 24 drilling slots, but currently has 31 wells. This was achieved by splitting seven slots in 2000. With 12 subsea wells, Alba has the capacity for 43 active wells. In fact the 59th platform well is being drilled in 2009 and this has been achieved by recovering failed well slots. A well failure rate of 5% per annum has meant that Alba has not been slot constrained.

In an attempt to reduce well costs, deep sidetrack slot recovery, where the production casing is exited in 8.5 ft hole size by means of a whipstock, instead of the previously used method of cutting and retrieving the 9.625 ft casing and drilling a new 12.25 ft hole, was successfully tested in 2006. This required the use of different well construction techniques in order to maintain minimum production hole size requirements. This is now the preferred well construction on Alba, wherever slot–target combinations are appropriate.

Alba pilot holes. The first pilot holes drilled on Alba were mostly sub-horizontal and were drilled to locate top reservoir and completion hole landout points. As a result, many early Alba wells were not located optimally in the reservoir and often left significant attic oil above the well. However, after acquiring the OBC data in 1998 (PS99), which completely changed the field understanding, sub-horizontal pilot holes were no longer required to locate the top reservoir. The very rugose top reservoir surface, resulting from sand remobilization and injection, necessitates horizontal pilot holes to be used to optimize completion hole locations, but the advent of geosteering LWD tools has reduced that need. The first geosteering using a deep-reading azimuthal resistivity LWD tool was tested in 2005, and quickly provided significant benefits in capturing attic oil by drilling close to top reservoir (Fig. 10). Geosteering using wellsite palaeontology and LWD had been used from well A2 onwards, but the dip direction of the shale was unknown and this technique was later abandoned. Drop trajectory pilot holes are drilled at key locations in order to calibrate the seismic data and reservoir models, by locating top and base reservoir and the producing OWC, which aids 4D seismic and reservoir model calibration.

Horizontal pilot holes have added $>1 \times 10^6$ stb oil by optimizing a single producer well location. Thus, seismic technology has been a key enabler to optimizing field development, increasing production and reserves. Improved imaging of reservoir geometry, lithology distribution and fault position has provided the means to locate additional production wells. Pilot holes have added significant additional recovery and are important for reservoir surveillance. Rotary steerable drilling systems and LWD geosteering tools have provided the mechanisms to optimally locate these wells and completion technology has enabled longer, higher, sand-free production rates and well life. Typical infill targets are $2-4 \times 10^6$ bbl recoverable, so the potential additional $0.5-1.5 \times 10^6$ bbl achieved using these technologies proves significant.

Captain Field

The Captain Field is a large (>1 Bbbl STOIIP) heavy oil accumulation located in block 13/22a of the Inner Moray Firth area of the UK sector of the North Sea, approximately 130 km NE of Aberdeen (Fig. 1).

The Captain Field was discovered in 1977 and developed in 1997 after a significant period of appraisal. It is a combined structural and stratigraphic closure that overlies the east–west trending Captain Ridge (Rose *et al.* 2000). Within this structure, relatively heavy (13–21° API) and extremely viscous oil (49–150 cP) and gas is trapped within largely unconsolidated sandstone reservoirs. The field is being developed with long horizontal wells (some

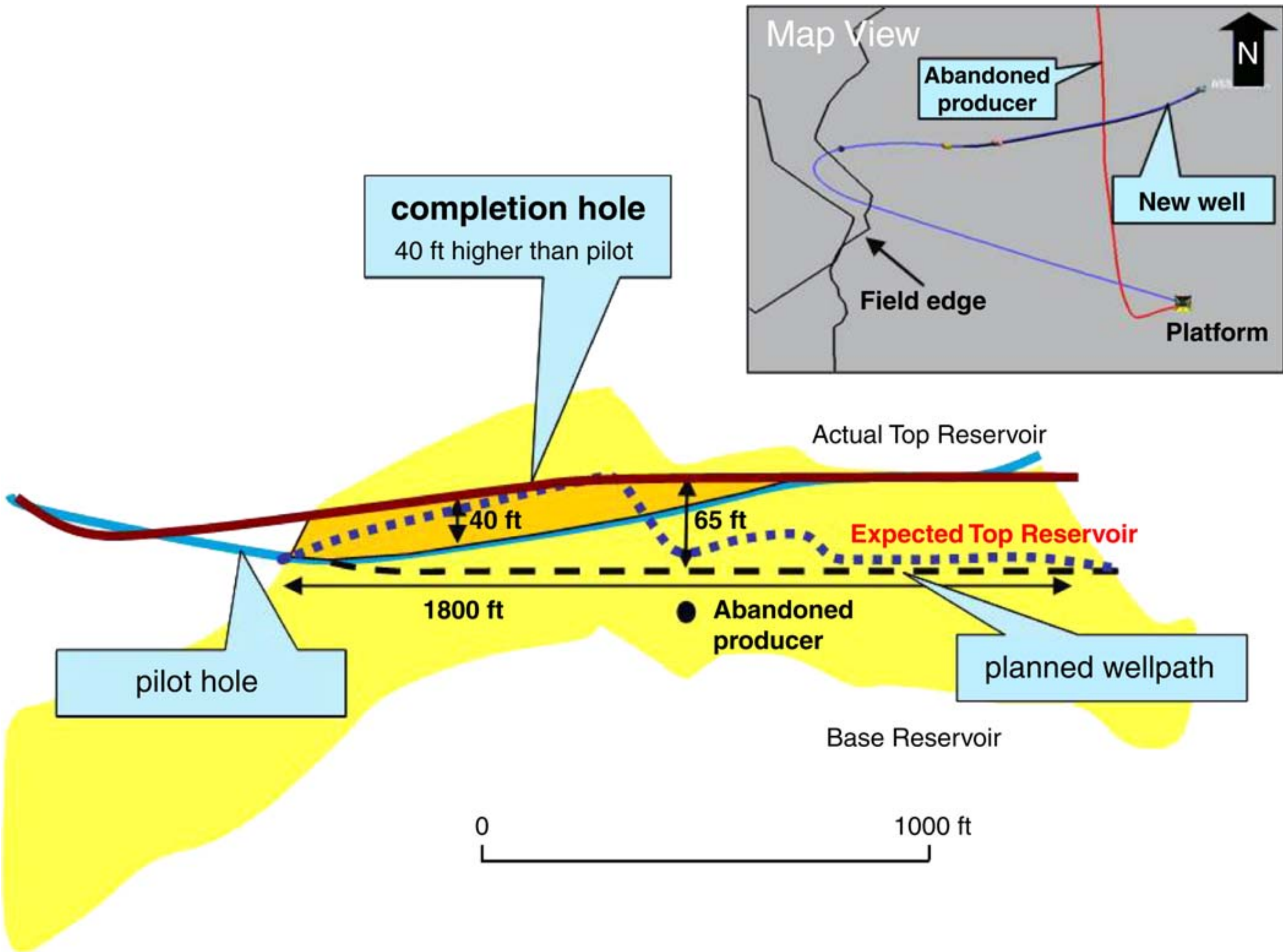

Fig. 10. Alba pilot hole – attic oil capture.

completions intervals greater than 8000 ft MD) at very shallow subsea depths (less than 3200 ft), is currently under water flood and has produced 240×10^6 bbl oil to date.

Captain reservoirs

The Captain Field has two main producing Lower Cretaceous reservoirs; the sheet-like deep-water Upper Captain Sandstone and the channelized Lower Captain Sandstone. In the eastern part of the Field, the Upper Jurassic, Heather Formation, faulted, marginal marine Ross Sand member is an important reservoir.

The Lower Cretaceous aged Upper Captain Sand (UCS) directly underlies 1300 ft of Cretaceous chalk (Figs 11 & 12) and contains the bulk of the reserves in the Field. The UCS lies between 0 and 50 ft below the base Chalk and the top reservoir is not resolvable on seismic. The reservoir is remarkably massive and lacks any internal architecture. Laterally, the reservoir is very continuous, as observed in horizontal wells, is highly porous (31% average) and permeable (5 Da average). The Upper Captain Sandstone hydrocarbon accumulation is a combined structural and stratigraphic trap. In general, the reservoir has the form of a gently northward dipping wedge of massive, sheet-like sandstone. An extensive aquifer lies along the northern margin of the accumulation and a large gas cap is present to the north central part of the field. Small, isolated gas caps are also present towards the updip pinchout and erosion edges.

The Lower Captain Sand (LCS) is interpreted to be a weakly confined, channelized reservoir with poorer reservoir quality (net-to-gross, porosity, permeability) than the UCS. The trapping mechanism is structural/stratigraphic in nature, the same as the UCS. There are a few production wells in the reservoir, but production performance is poorer than the UCS, and is not currently a focus of development. There can be erosion of the top reservoir surface, sometimes leading to 10–20 ft deep scours, which can make it difficult to drill close to the roof with horizontal wells.

The Jurassic (Oxfordian) age, Ross Sand member is between 60 and 120 ft thick, averaging 90 ft. It has fairly uniform thickness and good porosity (27% average) and permeability (2 Da average) in the eastern part of the Captain Field.

There are two vintages of 3D seismic data acquisition at Captain Field. The latest is a Q-Marine survey acquired in 2003 (Fig. 12). A test 2D 4C survey was acquired in 1997, but the results did not improve the imaging in the reservoir intervals.

The seismic imaging of the reservoirs is poor due to (1) the thick, relatively high velocity chalk interval that overlies the reservoirs, and (2) the close proximity of the strong base Chalk reflector to the main reservoir. This difficult imaging and low GOR preclude the use of 4D seismic monitoring. The Q-Marine survey is currently being reprocessed to improve overall imaging of the sub-chalk reservoirs.

Captain Field development

Drilling technology. Similarly to Alba Field, Captain Field would not have been successfully developed without advances in horizontal drilling technology that occurred during the 1990s.

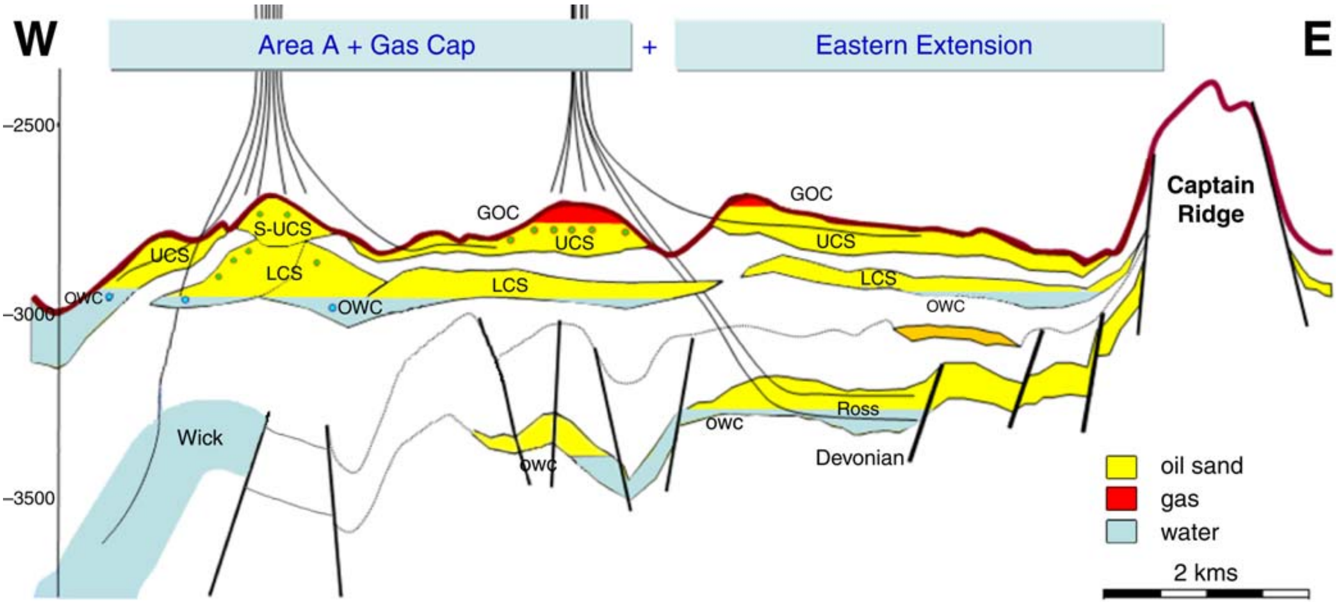

Fig. 11. Captain Field schematic cross section showing reservoirs.

This shallow reservoir with high viscosity oil cannot be produced at commercial rates from vertical wells. Early horizontal production wells were placed near the top third of the reservoir to minimize the chance of penetrating shales that are detrimental to gravel pack completions by risking the placement of the gravel along the entire wellbore as a result of washouts or blockage due to pack-offs. In 2005, Captain Field went exclusively with wire-wrapped screen completions that were more tolerant of shales. This allowed new wells to be placed near the top of the sand, producing the previously stranded attic oil.

Additional reserves are found out of reach of the platform (Fig. 13) and these are being produced via two subsea templates installed in 2000 and 2005. Technologies have been developed and employed to drill and complete long horizontal wells from these templates.

Captain pilot holes. To best capture attic oil, the elevation of the roof of the reservoir needs to be known. The top and base UCS reservoir is poorly imaged on seismic data. Since the top structure is poorly known away from well control, attic oil is left behind; since the base reservoir is also poorly known away from well control, water movement is very difficult to predict and model (Fig. 14). Thus, the best way to gather definitive information about the structure of the top and base UCS reservoir is to drill pilot holes that intersect both horizons. Pilot holes were first used on Captain in early 2004. Pilot holes are either horizontal S shaped – to penetrate top and base reservoir at multiple points along the well bore – or vertical drop pilots to gather information on deeper reservoirs. This appraisal method is clearly cost effective, as placing wells nearer the roof of the formation recovers significant incremental oil. The current estimate of the height of attic

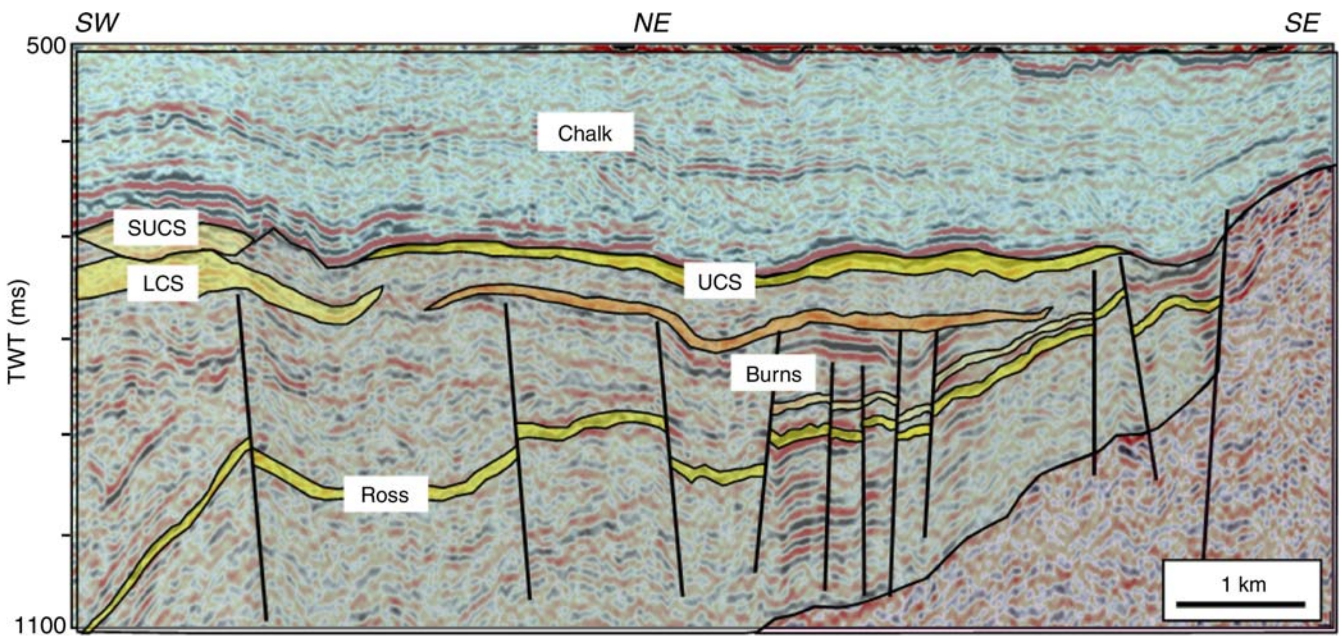

Fig. 12. Captain Field seismic, showing main reservoir intervals.

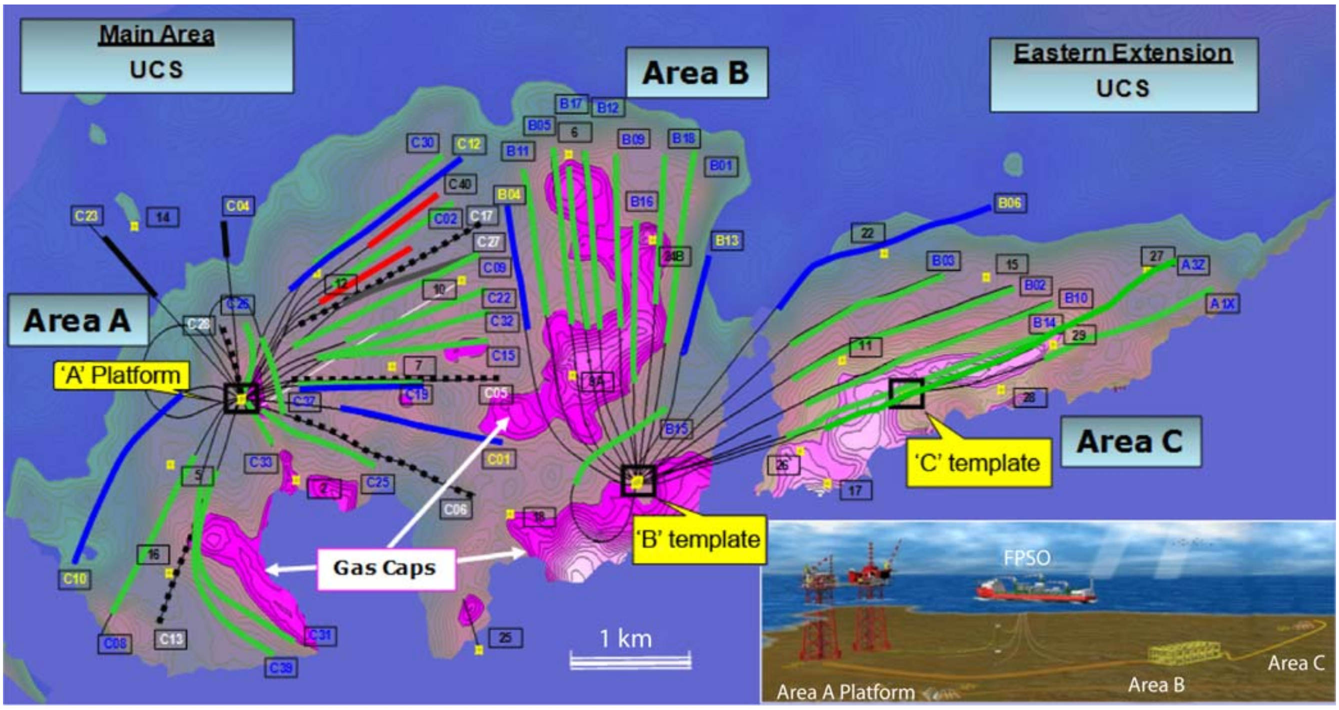

Fig. 13. Captain Field UCS map showing phased development areas.

oil above the producing intervals is shown in Figure 15. A key reason for the pilot holes is to reduce uncertainty and recognize upside in future well locations. This has been demonstrated in Area 'C' and the C39 well, southern lobe strategy that has accessed additional reserves to the south and west of the platform, previously thought to be too thin to develop. Horizontal and vertical pilot holes continue to be used on Captain to assess current targets and to appraise for future targets. As on Alba, the advent of azimuthal, deep reading resistivity geosteering LWD tools has reduced the need for drilling pilots to place wells at the top. The first true geosteering (deep-reading azimuthal resistivity) LWD tool used in 2005 provided significant benefits in capturing attic oil by drilling close to top reservoir. However, pilot holes are still required to assess reservoir thickness greater than 30 ft, and to gather information about deeper targets. Additionally, drop pilot holes are used at key locations to calibrate the seismic data and reservoir models.

Pilot well example. The A3 well was a subsea, horizontal well planned for the UCS in the eastern part of the field (Figs 13 & 16). This well was drilled because an earlier pilot hole had recognized upside in the area. The Ross/Burns reservoirs lie directly below the UCS and LCS. A drop pilot was planned for the Ross/Burns to test the OWC and reservoir continuity and communication between the Ross and minor Burns reservoir. The drop pilot was successfully completed. A new LKO (Lowest Known Oil) was found from the drop pilot, but no OWC. Pressure information proved that the LCS, Burns and Ross reservoirs were not in communication. After the drop pilot was completed, the horizontal well bore was drilled in the UCS. However, the dip in the top of the reservoir was not as expected and the pilot well dropped into a zone with higher water saturation. The well was steered up to find the top reservoir, which was encountered 40 ft higher than expected. A side track was then planned to follow the top reservoir and the final production well path was on average 25 ft higher in the reservoir than the original prognosed path. Reservoir simulation estimates indicate that an additional 1×10^6 bbl oil of reserves is expected from the final well path, a significant add to this target, since typical infill target size is approximately $2-3 \times 10^6$ bbl oil. It only took an extra day to drill the final well path and so the incremental cost was economically justified. Another key success of this well was the ability to generate a real-time rebuild of the reservoir model using distance to bed boundary calculation, enabling real-time simulation and informed decision making.

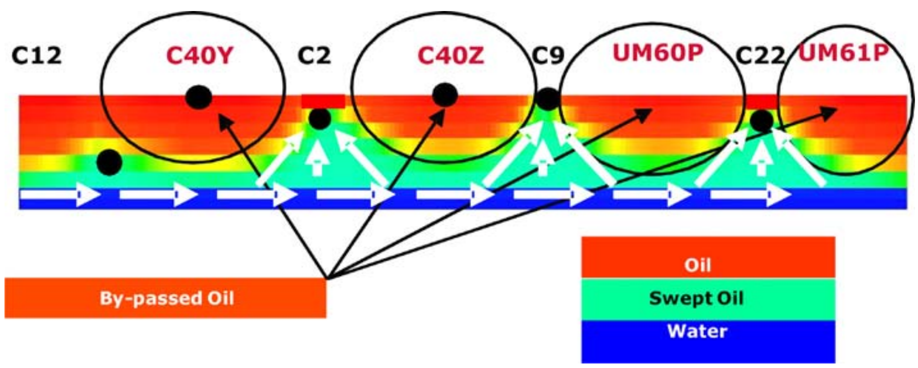

Fig. 14. Captain Field drainage schematic.

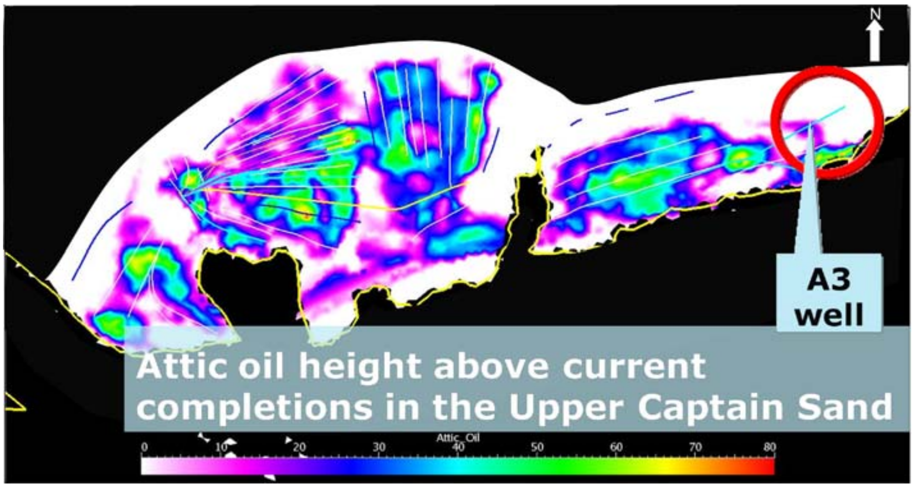

Fig. 15. Captain Field, attic oil map.

Future opportunities

Alba. The operator envisages that Alba Field has potential to produce 500×10^6 bbl oil (10% greater than currently estimated) through lower-cost drilling and target de-risking using the 4D seismic results. Although not currently slot constrained, due to a 5% annual well failure rate, Alba has many more, smaller targets than available slots. However, not all of them are currently economic, so alternative well construction techniques are under evaluation, including lower completions for increased shale tolerance and TTD (through tubing drilling). Additionally, multi-lateral wells, as recently drilled on Captain Field, are being investigated, allowing multiple targets to be drilled from one platform slot.

To allow targets further from the platform to be reached, managed pressure drilling (MPD) is planned. MPD is a method of regulating the bottom-hole drilling fluid pressure via a closed system of surface valves. This enables the 8.5 ft completion holes to be drilled with lower mud weights, overcoming the effective circulating density limitations currently experienced. This is because in smaller diameter ERD wells it is not possible to maintain sufficient overbalance to control reservoir pressure during connections, while also preventing fracturing of the overlying shale, without MPD.

Enhanced oil recovery (EOR) mechanisms are a potential alternative to the drill bit but are not currently attractive from a capital efficiency perspective. The most technically promising, polymer chemical flooding, works by wetting the reservoir sandstones to increase residual water saturation, thereby enabling additional oil to be produced. However, significant cost and logistical issues are associated with this technology.

Captain

The Captain Field vision is to recover 50% of the oil in place. Conventional field development options (close infill drilling and water flood) are forecast to recover 32% of the original oil in place. EOR mechanisms will be necessary to go beyond the expected recovery from conventional development and these are currently being investigated. High-resolution reservoir models are being used to predict polymer flood performance using different reservoir sensitivities. A pilot flood has been approved that will address flood performance, costs and logistical issues.

Two dual-lateral wells have been drilled on Captain Field and more are planned. Advantages are the ability to reach additional targets in areas of slot constraints, and economic advantages – dual lateral well costs have been 1.5 times those of a single well. Production challenges are being worked in long horizontal dual lateral wells in this highly viscous oil reservoir.

Both Alba and Captain continually evaluate new technology as appropriate. Seismic data is currently being reprocessed on Captain to better image the reservoirs and delineate future targets. Captain will test deep sidetrack well designs. Using existing trees, a sidetrack from the 9–5/8 ft casing will be attempted to replace a well with a lower completion failure and will optimally place the well higher to recover attic oil. Other improvements to

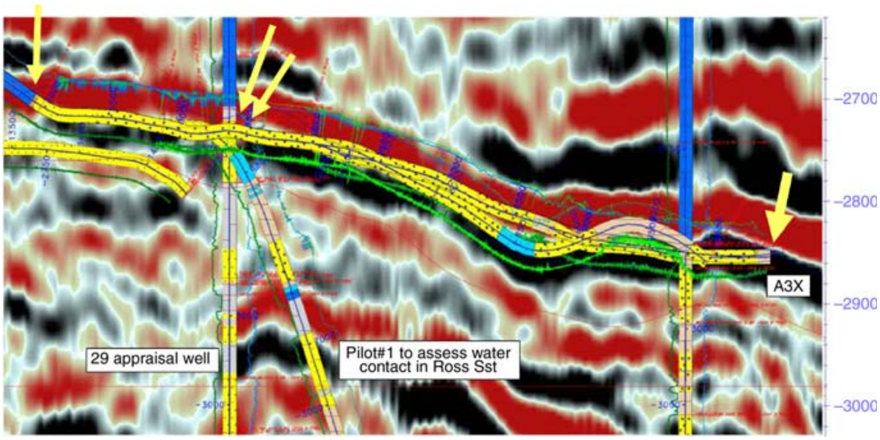

Fig. 16. Captain Field, Well A3 pilot holes, with seismic backdrop.

drilling and completion technology employed include placing cement in new wells higher to provide the option and flexibility to drill workover laterals.

Lessons learnt

Numerous lessons have been learnt during the ongoing development of Alba and Captain Fields. Their similarities have enabled these lessons to be shared to the mutual benefit of both assets and their owners. Some key lessons are listed below:

Seismic. Predicting water movement in a viscous oil system can prove challenging, particularly if the base reservoir and faults are poorly defined. Thus it is necessary to ensure that appropriate data acquisition and surveillance programmes are developed both before and during field development. Each new survey on Alba has improved reservoir understanding.

Maximum value must be extracted from seismic by processing and interpreting as quickly as possible. If reservoir image is a key uncertainty then reprocessing should be considered. Seismic processing techniques are continually being improved, so the value gained from reprocessed data will probably significantly outweigh the cost.

If the reservoir is suitable, it should be planned to acquire 4D data early in and throughout field life. The potential value of 4D data should not be underestimated and, if acquired early on, may change development plans and reduce Capex spend by optimally locating wells. Even the fast-track processed 4D Alba data has provided insights into fluid flow and water coning beneath producers.

Drilling/pilot holes. Early adoption of new drilling technology should always be considered. It can quickly add value. Rotary steerable systems and sand screen technology quickly opened up distant targets on both Alba and Captain.

Pilot holes, when appropriately used, can provide a cost-effective way to maximize value in a mature asset. As shown above, pilot holes can add significant oil volumes, establish current fluid contacts, minimize attic oil and lead to recognition of new target opportunities, thus increasing both production and reserves.

One should not always be driven by well costs, as a few extra days drilling can add significant value. Pilot holes on both Alba and Captain can be drilled in a few days, with costs being less than £0.5 mm.

Summary and conclusions

Alba and Captain Fields both have a number of subsurface similarities, including approximately 1 Bn barrels STOIIP; heavy oil (19° API), which is difficult to produce by conventional methods; very fine to medium grained, marine, mass flow sandstone reservoirs with good poroperm characteristics; and seismic resolution issues (but for differing reasons).

Development similarities include water flood for pressure support; one steel jacket, plus subsea templates; long horizontal development wells; pilot holes and LWD geosteering tools to optimize well locations; and production of more than original recoverable oil estimates.

Technology has provided three key enablers to help maximize production and reserves in these fields. These are 1) seismic technology – conventional and shear wave, streamer and OBC, 4D; 2) drilling technology – rotary steerable systems; long horizontal completion intervals; ERD; sand screens with gravel-packs; multilaterals; 3) pilot holes and geosteering technology – low cost, high benefit; LWD azimuthal geosteering tools.

Future technologies that may provide opportunities to further increase production and reserves include alternative well construction techniques, such as multi-lateral, slim-hole and managed pressure drilling, and enhanced oil recovery.

The benefits and business impact of these technologies include increased production and recovery potential, more wells from existing facilities, improved reservoir understanding and longer potential field life.

The authors would like to thank the Alba and Captain Subsurface teams for their valuable contributions and editorial advice. Thanks also to Chevron, the Alba co-owners (ConocoPhillips, StatoilHydro, BP, Total, Cieco and Endeavour) and Captain co-owner (KCCL) for their continued support and permission to publish this paper.

References

Duranti, D., Hurst, A., Bell, C., Groves, S. & Hanson, R. 2002. Injected and remobilised eocene sandstones from the Alba Field, UKCS; core and wireline log characteristics. *Petroleum Geoscience*, **8**, 141–149.

Lonergan, L. & Cartwright, J. A. 1999. Polygonal faults and their influence on deep-water sandstone reservoir geometries, Alba Field, UK Central North Sea. *AAPG Bulletin*, **83**, 410–432.

MacLeod, M. K., Hanson, R. A., Bell, C. R. & McHugo, S. 1999. The Alba Field ocean bottom cable seismic survey: impact on development. *The Leading Edge*, November, 1306–1312.

Newton, S. K. & Flanagan, K. P. 1993. The Alba Field: evolution of the depositional model. *In*: Parker, J. R. (ed.) *Petroleum Geology of Northwest Europe: Proceedings of the 4th Conference*. Geological Society, London, 161–171; doi: 10.1144/0040161.

Rose, P. T. S., Manighetti, A., Regan, K. J. & Smith, T. 2000. Sand body geometry, constrained and predicted during a horizontal drilling campaign in a Lower Cretaceous turbidite sand system, Captain Field, UKCS Block 13/22a. *Petroleum Geoscience*, **6**, 255–263.

Surlyk, F., Gjelberg, J. & Noe-Nygaard, N. 2007. The Upper Jurassic Harleev Formation of East Greenland: a giant sedimentary injection complex. *In*: Hurst, A. & Cartwright, J. (eds) *Sand Injectites: Implications for Hydrocarbon Exploration and Production*. AAPG Memoirs, **87**, 141–149.

Locating the remaining oil in the Nelson Field

C. E. GILL and M. SHEPHERD

Shell UK Ltd, 1 Altens Farm Road, Nigg, Aberdeen AB24 5DG, UK (e-mail: Caroline.Gill@shell.com)

Abstract: The Nelson Field has been in production since 1994 and is at the mid-mature stage of field life. The current management strategy has focussed on identifying infill well locations with the aim of recovering bypassed oil. An increasingly detailed reservoir description is required in order to locate these opportunities and to help screen them for their economic viability. A systematic workflow has been followed through to localize those areas of the Nelson Field where the target oil volumes are most likely to be found. This workflow is given the name 'locate the remaining oil' within Shell. The aim of this workflow is to understand the relationship between sweep and the geological framework of the reservoir. On this basis, drainage cells are defined within the reservoir. Rather than behaving as a single 'tank' of oil with a common rising oil–water contact, the Nelson Field produces from nine discrete drainage volumes, each with separate producing oil–water contacts. The drainage cells have been defined on the basis of sedimentology, oil and water geochemistry in combination with quantitative volumetric analysis. Screening of the nine drainage cells in the reservoir has identified four cells that contain significant remaining volumes of mobile oil. These have then been investigated in further detail with a view to locating any stranded oil volumes that are unlikely to be produced by the existing well stock, and to determine if these are large enough to justify infill well drilling.

Keywords: bypassed oil, channelized turbidites, drainage cells, infill wells, Nelson Field

Many of the mature fields in the North Sea have been in production since the 1970s and the early 1980s. Nelson started production in 1994 and is one of the more recent of the large fields in the North Sea to come on stream. Yet by 2010, the Nelson Field has been producing for 16 years and is already at the mid-mature phase of its field life. At this stage, the reservoir is showing complex sweep patterns caused by the influx of both aquifer and injection water to replace the large volume of oil that has been produced. The result is a patchwork configuration of largely swept production fairways interspersed vertically and laterally with numerous bypassed oil pockets of various shapes and sizes.

A common theme in the management of offshore assets at this point in field life is the intent to maximize recovery by drilling new infill wells in order to target any bypassed oil volumes. In light of these difficulties, this paper describes pragmatic methods of predicting the location of remaining oil volumes in a mature producing offshore field. New offshore wells are deliberately targeted at locations where the high cost of drilling can be justified on the basis that the expected incremental oil reserves will be large enough to make the project economic. The task of defining new well opportunities can be challenging. As offshore fields age, it becomes increasingly difficult to establish with a high degree of certainty that any of the remaining oil pockets are big enough to justify drilling.

The basic difficulties involved in the practice of reservoir management of mature fields offshore can be summarized as follows:

(1) There are limits to the ability to map the detailed heterogeneity within a reservoir where there are so few well control points.
(2) It is not easy to detect the presence and location of the large target volumes, particularly in reservoirs with complex sedimentological-controlled heterogeneity.
(3) Locating the bypassed oil volumes is problematic in a reservoir with complex sweep patterns.
(4) It is hard to confidently estimate the range in target oil volumes given the uncertainty involved.
(5) Justifying the large expense of drilling wells is a challenge given an uncertain outcome.

The use of predictive models to plan infill wells

Predictive models of both the geology and sweep are required to plan infill wells. Given the sparseness of well control data offshore, these models tend to approximate to a first-order understanding of the reservoir character. Mapping at the macroscopic (inter-well) scale is used to establish both the main production fairways and those areas of the field where the geology is more complex. Cores and wireline logs in the wells will give a sense of the geological heterogeneity on a finer scale, and these provide an understanding of the detailed flow complexity, particularly with reference to sedimentological analogues at the outcrop scale. This level of analysis is usually sufficient to allow wells to be drilled with confidence in those areas of the field where they are likely to be in contact with large economic volumes of oil. These 'slam-dunk' wells tend to be identified and drilled early in field life. After field start-up, the intention is to keep a field on plateau for as long as possible and the drilling of low-risk targets will help to produce oil at sufficient rates to do this. This was the case with the Nelson Field, where the first production wells tended to be drilled in the thick sandy channel complexes rather than in the more heterogeneous areas of the reservoir. Once the more obvious targets have been drilled, then attention will be given to the medium- and high-risk volumes in the rest of the field. It is these types of targets that are commonly drilled in North Sea fields at the start of the 21st century.

There are three basic approaches that have been adopted by subsurface teams to define targets for drilling in mature fields offshore: (1) the reservoir engineering-led approach uses reservoir simulation models with the geological model at its core as the focus of defining remaining oil targets; (2) the geophysical-led approach uses 4D seismic data as the main basis for defining bypassed oil volumes in mature producing fields where the image quality is reasonable; and (3) the geology-led approach uses a predictive conceptual model which combines the reservoir geology framework and production data to help locate the remaining oil volumes. The task of locating the remaining oil, via a geologically led model, is the subject of this paper.

VINING, B. A. & PICKERING, S. C. (eds) *Petroleum Geology: From Mature Basins to New Frontiers – Proceedings of the 7th Petroleum Geology Conference*, 349–368. DOI: 10.1144/0070349

A workflow for locating the remaining oil

The workflow, which the geologist uses to evaluate infill potential in mature fields, has been called ‘Locate The Remaining Oil’ by Shell and ‘Target the Remaining Oil’ by Statoil (Wetzaeler *et al.* 1996; Hansen *et al.* 2002). It is based on techniques which were developed in the early days of production geology. Later, in the 1990s, the conceptual framework for locating the remaining oil volumes in mature fields was established when a number of important papers were published by staff from both the Bureau of Economic Geology at The University of Texas at Austin in the United States and Shell in Europe (e.g. Bryant & Livera 1991; Hamilton *et al.* 1998; Holtz & Hamilton 1998; Weber 1999).

The main steps in the workflow are as follows (Table 1):

Step 1: The reservoir geology is characterized within the context of a sequence stratigraphic subdivision. The sedimentological scheme is represented as lithofacies maps for each sequence and these show the major macroforms present. Macroforms are sediment bodies which are found at the macroscopic level of heterogeneity, that is, at a scale of hundreds of metres. The structural framework is also mapped and any faults delineated.

Step 2: The second stage involves understanding how the fluid flow within the reservoir is influenced by the geological framework. In a producing field, a basic analysis of reservoir performance will focus on determining the main production fairways accessed by the production wells, the location of volumes of ‘slow oil’ in low permeability rock and where oil is trapped in large dead-end volumes. There are two ways insights can be gained on how the reservoir geology influences fluid flow. The first involves the use of analogue data, either from producing fields with similar geology or from appropriate field outcrops. For example, if a nearby field producing from the same stratigraphic interval is known to show specific production patterns related to the reservoir architecture, then these are features that are worth looking for in the field under review. Outcrops with a similar environment of deposition to the reservoir in question can also be used to give insights as to how the geology may influence production behaviour. The second approach uses data integration techniques. Data integration is the main method for co-analysing geology and production data (Bryant & Livera 1991). The analysis focuses on understanding both the controls on vertical flow and the controls on areal flow within the reservoir. By combining production data with the geological interpretation, common patterns may be observed that show how the reservoir architecture is influencing the production pathways within the field. The method mainly involves graphical overlays of the two data types.

Step 3: Once the vertical and lateral controls on flow have been mapped out, these features are combined to define drainage cells (compartments) within the field. This is an important step, as it allows the production performance of the reservoir to be framed and localized within the field. Quantitative volumetric analysis of volumes in place v. the cumulative oil production at the drainage cell level will indicate those areas of the field where the larger volumes of remaining oil are more likely to be found.

Step 4: The next step involves looking for individual targets within each drainage cell, particularly those cells with significant remaining oil volumes. Specific trapping styles are looked for as a means of identifying target volumes.

Table 1. Workflow for locating the remaining oil in mature fields

1. The geological conceptual model is established for both the sedimentological and structural framework.
2. An analysis is made as to how the geological framework influences fluid flow.
   - 2.1 Analogue producing fields and outcrops are analysed to get insights into the producing characteristics of the review field.
   - 2.2 Data integration techniques are used to try to understand how the reservoir performs. This involves identifying the major permeability barriers to vertical and lateral flow.
3. Drainage cells (self-contained tanks) are defined within the reservoir. The remaining oil volumes are quantified for each drainage cell.
4. The trapping style within each drainage cell is established with view to defining target oil volumes for infill wells.

Background information on the Nelson Field

The Nelson Field is located in blocks 22/11, 22/6a and 22/12a in the UK Central North Sea. The field shows an elongate dip-closed structure and is one of several Paleocene-age oil fields located above the Forties Montrose High (Fig. 1).

The reservoir interval comprises sandstones of the Paleocene Forties Sandstone Member. The Forties Sandstone Member overlies the Lista Formation in a conformable relationship and is itself overlain by shales of the Sele Formation. The latter forms the seal for the field (Fig. 2).

The Nelson Field is developed with a 36-slot minimum facilities platform with a four-well subsea template to the south which is tied back to the platform (Fig. 3). The production facilities have a peak daily capacity of 160 000 barrels of oil and 65 million ft^3 of gas. Total liquid capacity is 250 000 barrels of fluid. The hydrocarbon type is a light 40° API oil with a gas–oil ratio of 555 scf/bbl. Live crude is exported by pipeline via the Forties Field to Cruden Bay on the east coast of Scotland. The oil originally in place is estimated at 790×10^6 bbl. Current cumulative oil production is approximately 430×10^6 bbl. Maximum production rates were approximately 160 000 barrels of oil per day in 1995 and the current rate is 20 000 barrels of oil per day.

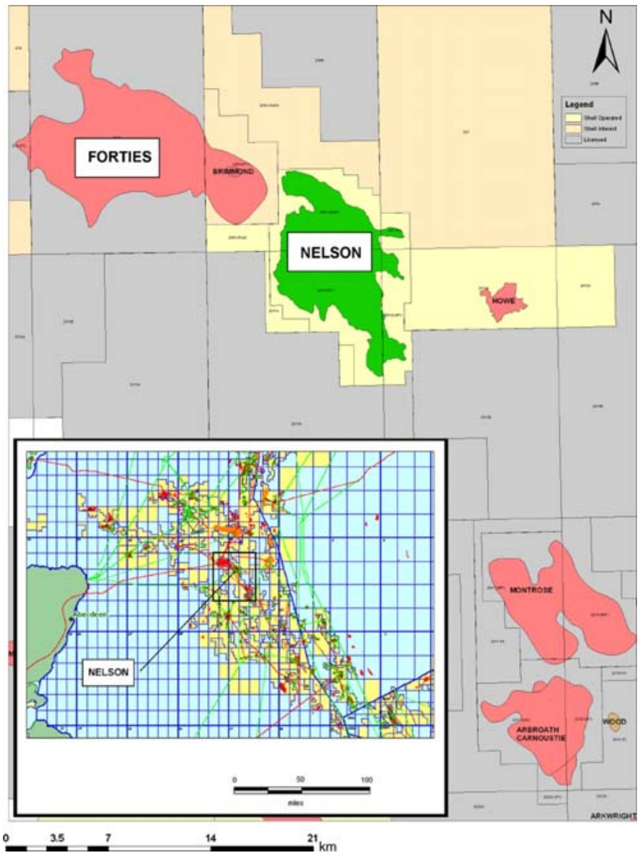

Fig. 1. Location of the Nelson Field in the Central North Sea.

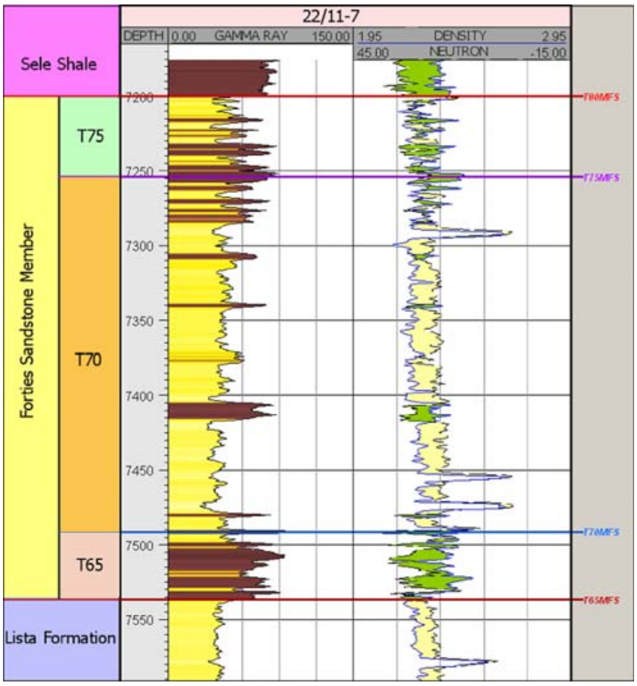

Fig. 2. Type well for the Nelson Field, well 22/11-7. The Paleocene Forties Sandstone Member comprises the reservoir interval for the Nelson Field. The T65, T70 and T75 sequences provide the stratigraphic framework for reservoir characterization.

Oil is produced from two main reservoir units in the Nelson Field; the stratigraphically younger unit is the T75 sequence, which is underlain by the T70 sequence. The principal areas of oil production are from three NW–SE trending sandstone-filled channel complexes, termed hereafter the western, central and eastern channels (Figs 4–6). The reservoir quality is excellent with overall net to gross in the main channel fairways averaging 70%, porosity averaging 23% and zonal average permeabilities ranging from 150 to 300 mD (Kunka *et al.* 2003).

The turbidite channel complexes are genetically linked to and flanked by channel margin deposits. These sediments comprise low net to gross (average 45%) interbedded shale and sandstone intervals. The turbidite channel complexes follow topographically low areas and show incision of the basal surface into underlying marine shales or pre-existing turbidite channels.

Pods of marine shales with thinner overbank/splay deposits lie in the areas between the channel complexes. These areas represent interchannel sediments.

The central channel complex (T70 sequence)

The central channel is in the older T70 sequence, which is separated from the younger T75 sequence by shales representing the T75 maximum flooding surface (MFS; Fig. 4). The overbank and splay deposits are thick and laterally extensive.

The western channel complex (T75 sequence)

The western channel complex is the stratigraphically youngest of the Nelson channel macroforms and was deposited to the west of the bathymetric high formed by the sediments of the older central channel complex (Fig. 4). The lower section shows an onlap relationship onto the basal surface, indicating that these sediments have ponded into a pre-existing channel feature. The upper portion is more tabular, and extends beyond the area of ponded channel fill sediments. It connects into a series of splay sands in the margin and interchannel area above the central channel complex (Fig. 7).

The eastern channel complex (T75 sequence)

The eastern channel complex was deposited on the margin of the topographic high left by the sediments of the central channel complex (Fig. 4). The eastern channel complex is more proximal than the western channel complex with higher energy deposits made up of multiple incised channels showing sharp channel boundaries. Only the western edge of the eastern channel is within the oil leg of the Nelson Field; the bulk of the channel complex extends to the east below the original oil–water contact (OWC).

Sea water injection is provided by four injection wells, situated peripherally around the field and located in the channel complex areas. These provide pressure and waterflood support to the production wells. The two seawater injectors in the north of the field are now used for produced water reinjection.

The use of analogue information to help understand remaining oil configurations in the Nelson Field

The Nelson Field produces from sediments that formed in a channelized turbidite setting. A review of technical papers on analogue producing fields and outcrops of channelized turbidite systems has been made with the aim of determining whether common patterns exist that can give an idea of how the geological characteristics of channelized turbidites control production behaviour and the location of bypassed oil volumes. A number of production patterns are known or have been inferred from analogue data and these are discussed below (Fig. 8).

Production patterns in channelized turbidite reservoirs

Amalgamation of sand complexes. Reservoir connectivity is controlled by the degree of lateral and vertical amalgamation of individual channel complexes. A spectrum of connectivity relationships can be seen in analogue reservoirs varying from total isolation of individual channels to widespread amalgamation of channel complexes to form a well-connected reservoir volume (e.g. Eubanks 1987).

Mud drapes. Sand-to-sand connectivity is sensitive to the amount of shale interbeds in the channel complexes (Weimer & Slatt 2004). Mud drapes are elements which act as baffles or barriers in these systems, forming as silty intervals overlying incised channel-form erosional surfaces (Beaubouef *et al.* 1999; Larue 2004).

Shale blankets. Thin but laterally extensive shale and debris flow horizons are known to act as vertical flow barriers in turbidite systems (Lowry *et al.* 1993; Hempton *et al.* 2005). They can act as surfaces to support water over-run and can also trap oil beneath them. An example of oil trapped below extensive shales is described from the Magnus Field (Fig. 8) (MacGregor *et al.* 2005).

Bypassed oil in channel margins. The channel complex fairways act as the main conduits for waterfloods, whereas channel margins commonly contain bypassed oil volumes. These volumes may be depositionally isolated as a result of flow barriers caused by complex channel–levee–overbank stratigraphic relationships (Cronin *et al.* 2000; Beaubouef 2004). Collapse structures are common on levee margins in channel–levee complexes and this may also contribute to poor connectivity. Alternatively, bypassed oil may occur even where there is good reservoir connectivity between the channels and the channel margins. The channel axes tend to be well swept in waterflooded reservoirs and there can be a tendency for oil to be bypassed or ‘banked’ in the channel margin areas. Subsequent sweep can isolate and immobilize large individual oil pockets in these areas as has been described for the Yowlumne Field in the United States (Clark *et al.* 1997).

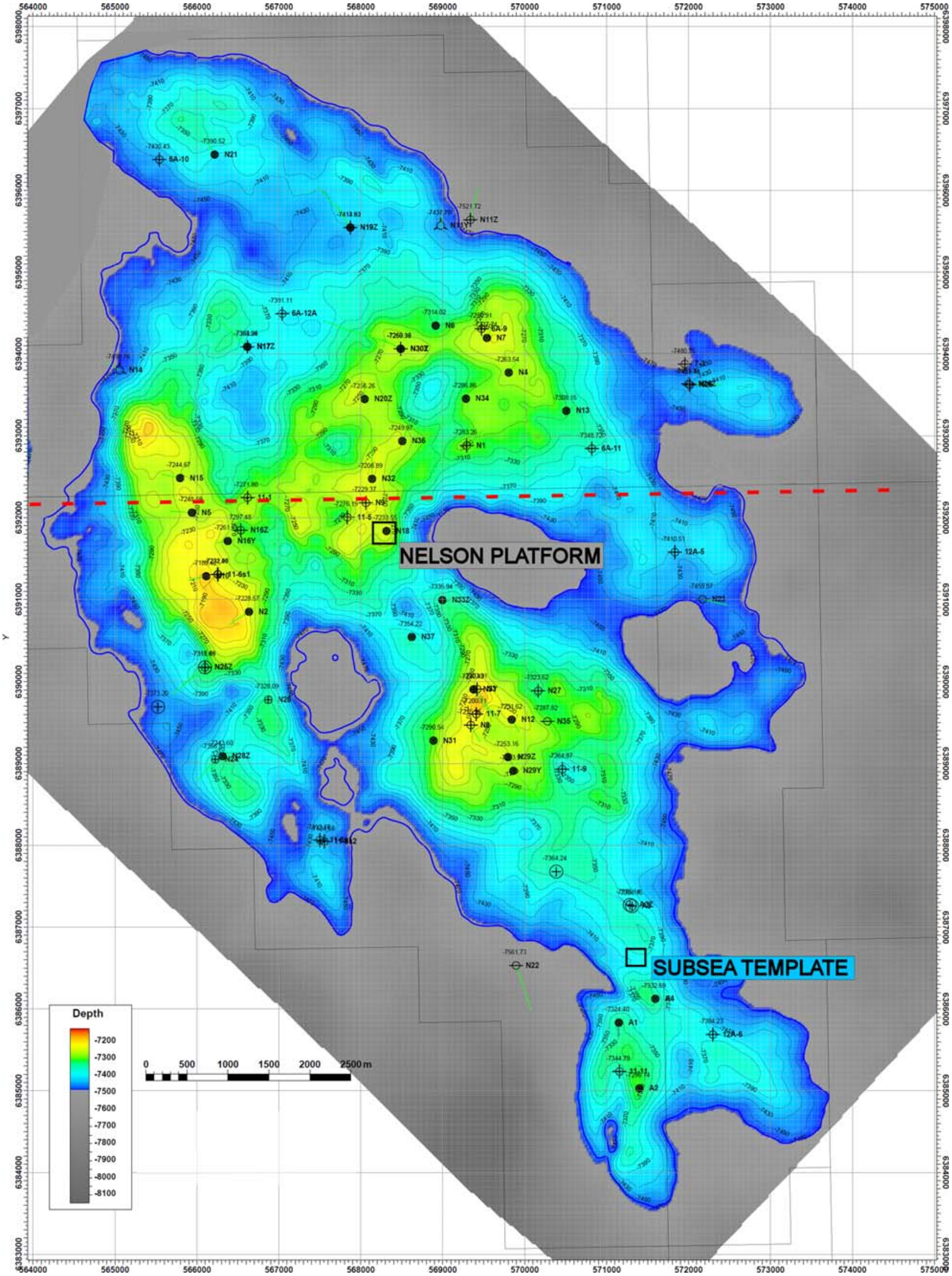

Fig. 3. Top structure map for the Nelson Field. The contour interval is 20 ft, TVDSS. The blue line indicates the original OWC. The dashed red line indicates the line of section for Figure 4.

Data integration

As a generalization, each producing field has a distinctive character in terms of its reservoir performance; certain dominant character traits tend to control the production behaviour. In order to understand the reservoir performance in this way, it is necessary to carry out a detailed analysis as to how the geological framework influences fluid flow.

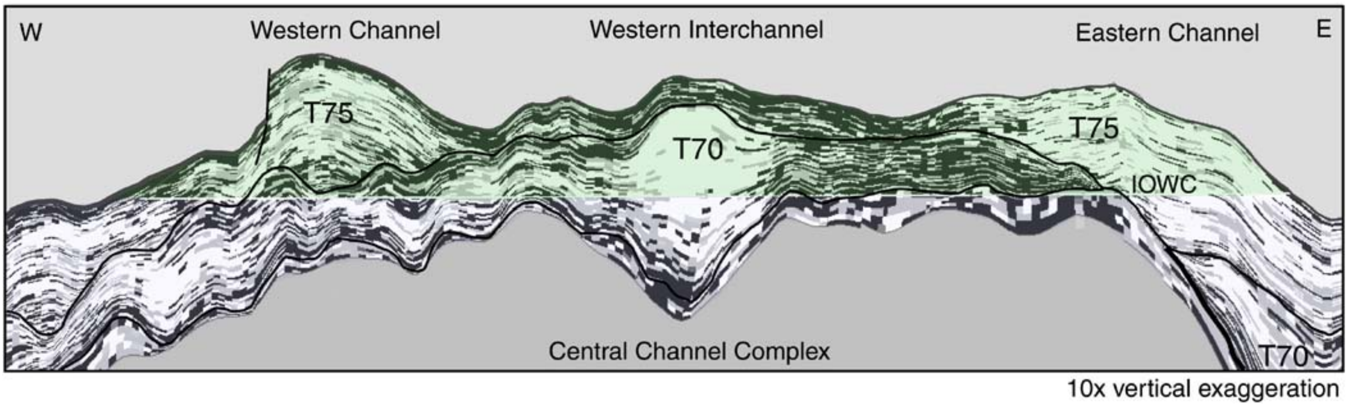

Fig. 4. Schematic net to gross cross-section west–east through Nelson Field showing the principal reservoir intervals. For the line of section see Figure 3. IOWC, initial oil–water contact.

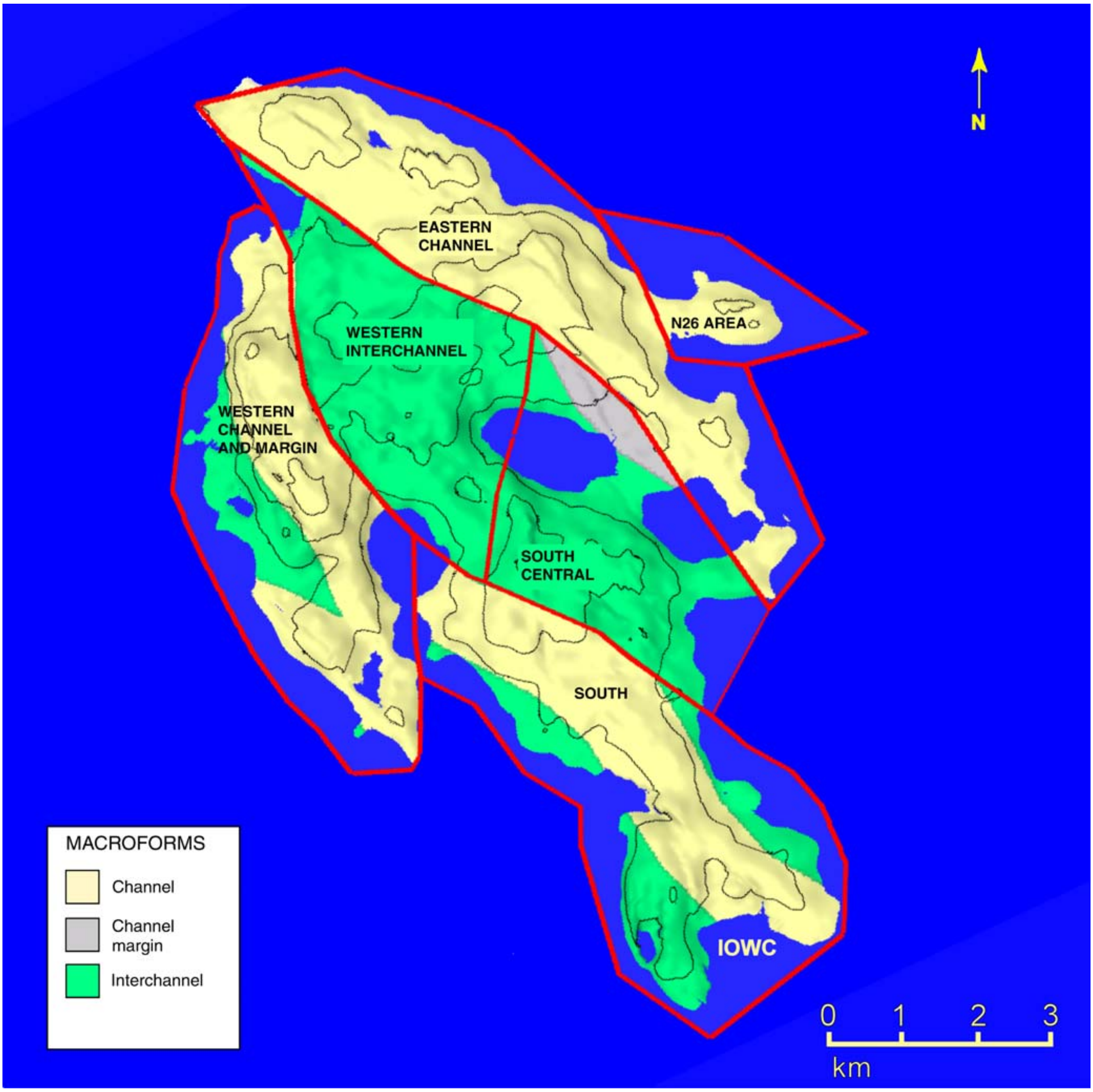

Fig. 5. Macroforms and drainage cells within the T75 reservoir unit. IOWC, initial oil–water contact.

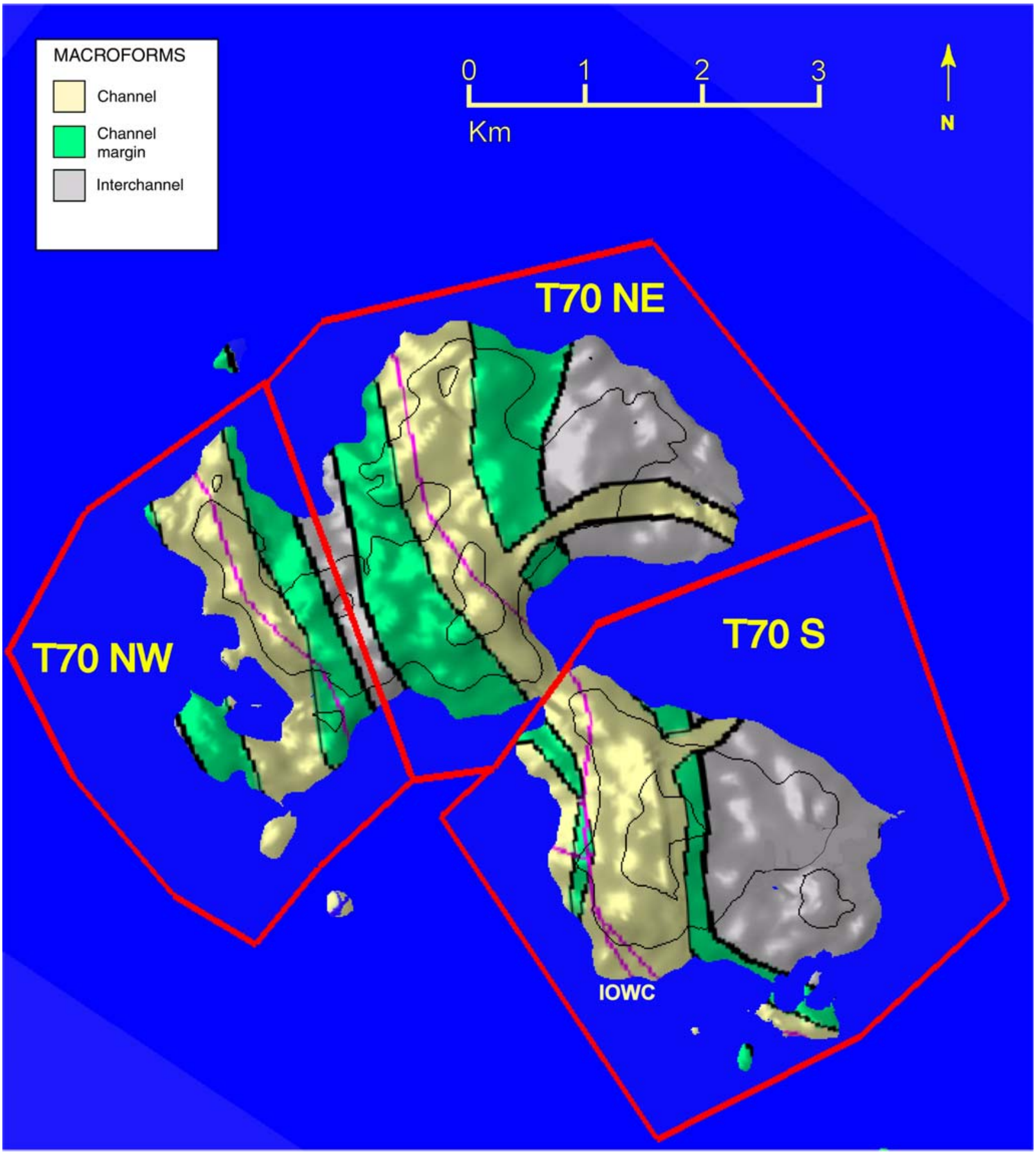

Fig. 6. Macroforms and drainage cells within the T70 reservoir unit. IOWC, initial oil–water contact.

Data integration involves compiling a dossier of individual observations relating sweep patterns to the geological framework. Over a hundred observations have been collected for the Nelson Field. Most of these have been made on a well-by-well basis. The observations are then linked together and illustrated by annotated maps and cross-sections showing both the geological framework and the sweep patterns. The aim is to produce a field-scale conceptual model to help explain the production behaviour of the reservoir. The process can be compared with using individual clues to help solve a giant 3D puzzle.

Data integration as applied to the Nelson Field

As applied to the Nelson Field, data integration methods tend to produce two types of 'clue'. Overlays of production data onto geological cross-sections provide clues on vertical flow controls; overlays of production data onto lithofacies maps give clues as to the controls on the horizontal flow component within the reservoir. To help with this analysis, the geological interpretation for Nelson was revised with the objective of providing lithofacies maps for each reservoir sequence (Figs 5 & 6).

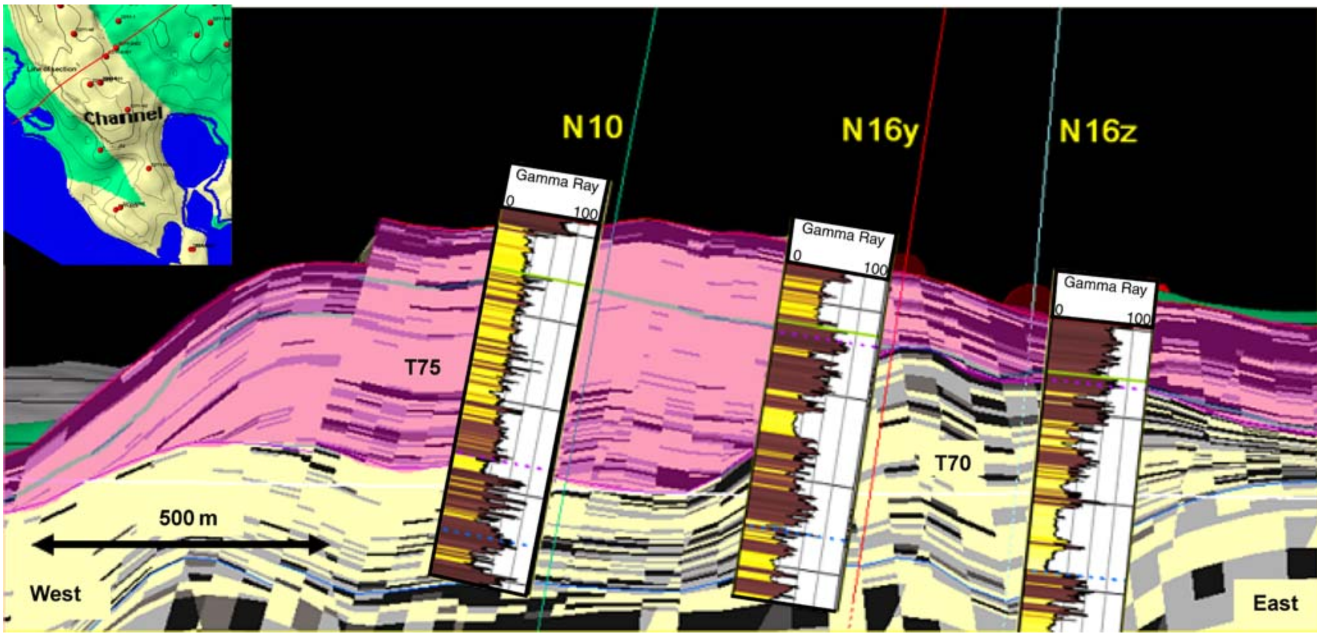

Fig. 7. West–east cross-section through the western channel showing the fill and spill geometry of the T75 unit; five times vertical exaggeration. The lower section onlaps onto the basal surface, with the sediments having ponded into a pre-existing channel feature. The upper portion is more tabular, and extends beyond the area of ponded channel fill sediments.

Methods of detecting geological influence on vertical flow

Methods used to detect geological influences on vertical flow have involved the investigation of patterns of OWC movement, water cut histories and documentation of pressure differences across shales and geochemistry. The aim is to subdivide the reservoir vertically into hydraulic units. The term hydraulic unit is used in the sense that these are reservoir intervals that show internal communication, but are bounded at the top and base by extensive permeability barriers to flow (Haldorsen & Lake 1984).

Oil–water contact movement. The OWC in a producing field will rise as a consequence of production. In the Nelson Field, the OWC rise can be measured by open hole logging in new infill wells or by production logging in existing wells. There have been several phases of infill drilling and open hole logs from these wells have provided good quality data to track OWC movement as a result of production (Fig. 9). Production logs, including pulsed neutron logs, have been run repeatedly in key oil producers in the field. Repeat production logs will give a history of how the OWC is rising over time. Various patterns may be seen such as a steady, continuous rise in the OWC, a static OWC or an OWC that rises for a few years and then becomes static, typically below a shale bed. These patterns can be used to infer the nature of aquifer influx. A continuously rising OWC indicates a bottom-water drive mechanism, whereas a static OWC is indicative of a baffled or edge-water drive operating. If a shale bed is observed to impede the rise in the OWC for a long period of time, then it is likely to be acting as a major baffle or a widespread permeability barrier to vertical flow.

The movement in the OWC is referenced to the initial oil–water contact (IOWC) as a datum level. In the Nelson Field the depth of the IOWC varies from 7449 to 7502 ft true vertical depth subsea (TVDSS) with a mean of 7470 ft TVDSS (Kunka *et al.* 2003).

Water shut-off performance. Water produced from the perforated interval of a production well can cause the fluids flowing up a well to be loaded with water, thus reducing the total flow rate. Once water cuts are in excess of 90–95%, the water-producing interval will be isolated by inserting a plug above them. The plug will be located opposite a shale interval in the wellbore. If the shale is laterally extensive then the water shut-off operation will prove successful in isolating or reducing the water production for some time. Both the plug and the shale in the reservoir behind the liner act together to isolate the open perforations in the well from a direct pathway for water influx from the swept zone. If the shale is not extensive, then water production will be unaffected in the well or will be reduced for only a short period. Water shut-off performance was used by Hamilton *et al.* (1998) to evaluate the status of permeability barriers within the Jackson Field in Australia. The result of each operation was recorded as a water shut-off table in terms of the reduction in water cut and for how long the plug was successful in doing this. This table gives a qualitative idea of the extent of individual flow barriers within the reservoir. Water shut-off events have been analysed for the Nelson Field. An example of successful water shut-off was seen in the N20z production well. A bridge plug was set opposite the T75 MFS in late 2004. This reduced the water cut from 80% to zero water production. Thus the T75 MFS appears to act as an effective barrier in this part of the field (Fig. 10).

Post-production formation tester logs. A vertical profile of formation pressures can be measured in infill wells using formation tester logs, for example, Schlumberger's RFT and MDT logs. The data are used to make a pressure–depth profile and this can show where differential depletion has resulted in a pressure difference across a barrier to vertical flow, a shale for instance. For example, the 22/11-A3 well was drilled in the south of the field in 1995. The formation tester logs run seven months after the start of field production showed a 210 psi pressure differential across the shale marking the T75 MFS (Fig. 11). This indicates that the shale is a significant permeability barrier to flow in the south of the field. In this area of the reservoir, production at the time was mainly from the T75 sand sequence, whereas the T70 sand sequence was effectively undepleted.

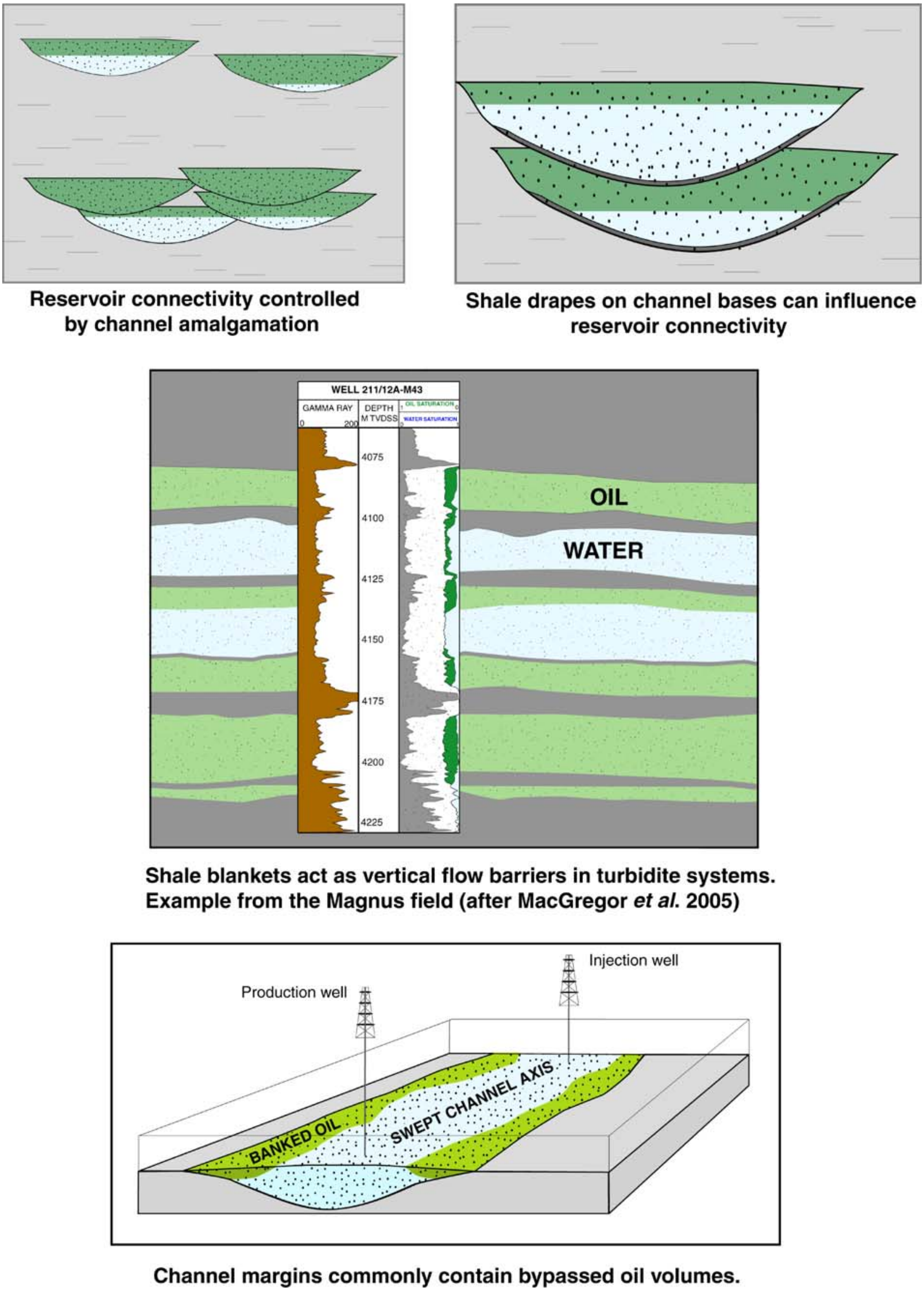

Fig. 8. Analogue information from fields with turbidite reservoirs has been used to help locate the remaining oil in the Nelson Field. Reservoir connectivity is controlled by the degree of channel amalgamation. Lateral connectivity is affected by shale drapes and shales blankets. Water over-run and bypassed oil is shown from the Magnus Field (MacGregor *et al.* 2005). Banked oil results from the preferential ingress of a waterflood along channel axes as in the Yowlumne Field, California (Clark *et al.* 1997).

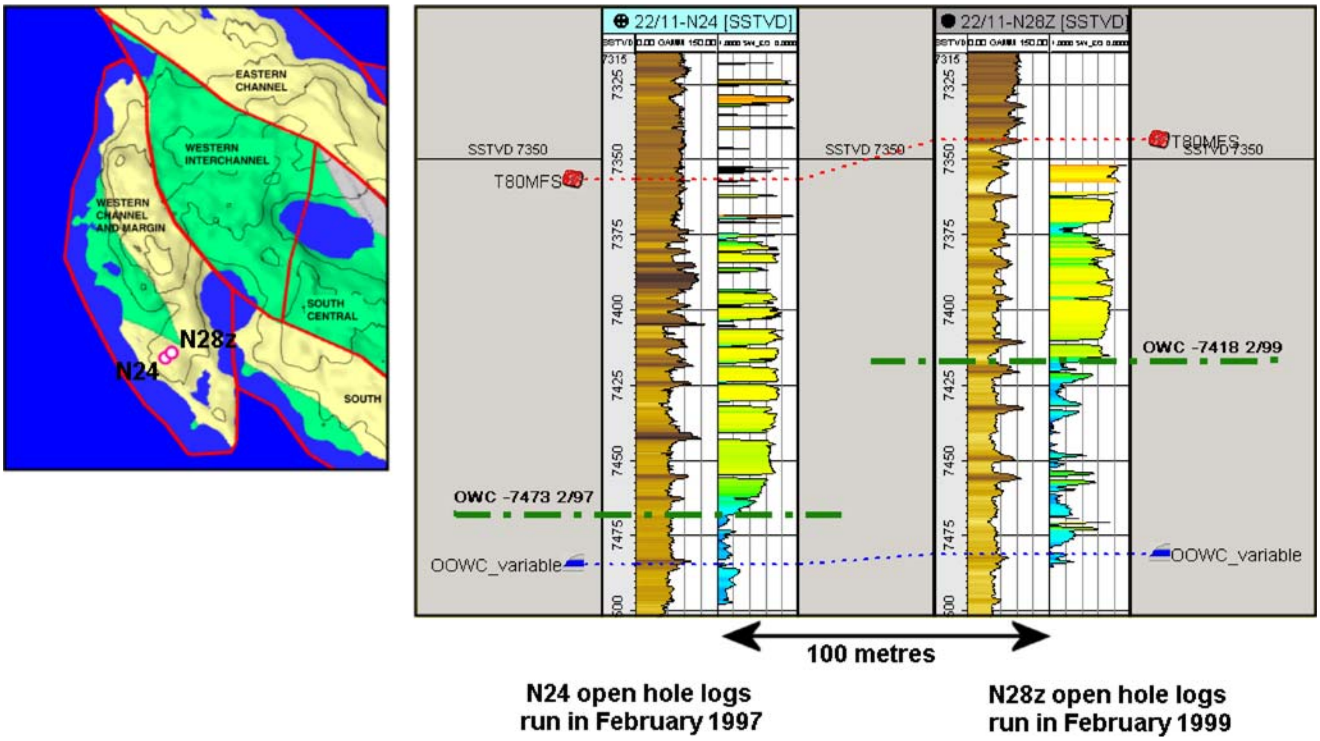

Fig. 9. Open hole gamma-ray and resistivity logs from two closely spaced (100 m apart) wells in the Western Channel (22/11-N24 and 22/11-N28Z). The OWC, shown as a green dashed line, had risen by 55 ft in two years. This is a fast-rising OWC which does not appear to have been impeded by shales. The resistivity log in 22/11-N28Z shows some thin zones, about 2–3 ft thick, showing some minor unswept oil left behind. The inset map shows the position of the wells.

Shut-in crossflow. It is common practice to record a shut-in flowmeter pass while running production logs in an oil producer. These will show where crossflow is taking place because of the presence of differentially pressured zones opposite the perforated interval of the well. The well is shut in so there is no flow to surface while logging. The log will show flow from a high pressure zone into a low pressure zone within the reservoir, if these exist. The permeability barrier separating the zones can often be picked on these logs. This marks the depth where flow out of the high-pressured interval flips over to flow entering the low-pressured interval. For example, shut-in flowmeter passes were used to establish the presence of a major shale baffle in well N15 in the western channel (Fig. 12). There is also evidence for a slow-moving OWC immediately beneath the shale.

Water geochemistry. The continuous sampling of produced water from each individual well throughout the lifetime of the Nelson Field means that it is possible to plot the variation in produced water compositions between wells across the field area and in individual wells with time. The ability to monitor variations in water major element chemistry with time can be considered as a time-lapse geochemistry method akin to similar methods that use oil geochemistry data (Milkov *et al.* 2007). In addition, the changing intervals open to production in the wells gives some sense as to the vertical variation in water composition.

For example, there is a systematic decrease in the produced water chloride ion concentration upwards through the reservoir. The uppermost unit in the reservoir produces water with the lowest chloride ion concentration. These low-salinity water samples are

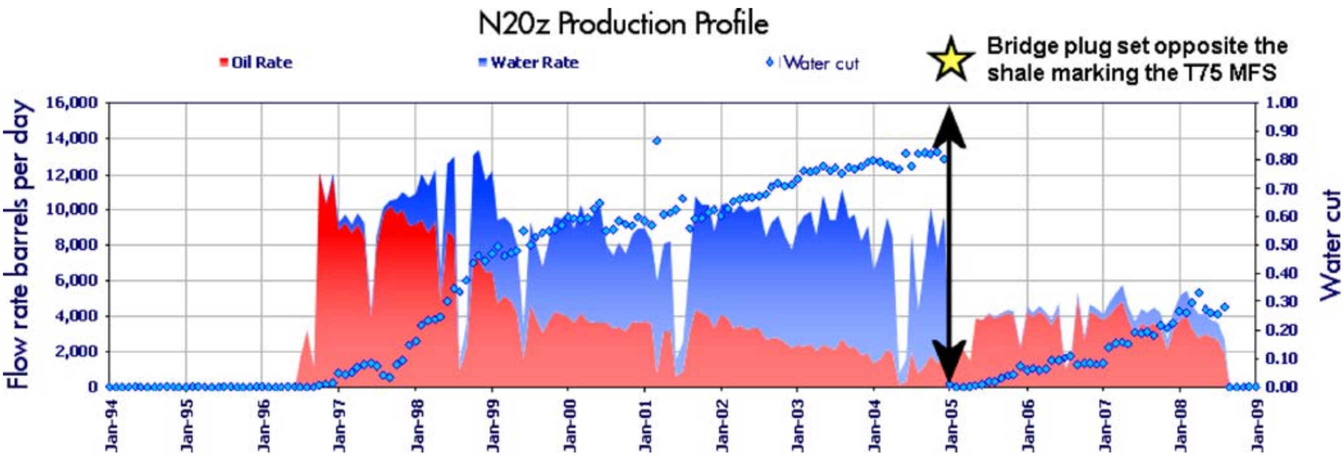

Fig. 10. A bridge plug set in late 2004 opposite the shale marking the T75 MFS was effective in reducing water production in well N20z. This indicates that the shale is laterally extensive and acts to impede the upward movement of water.

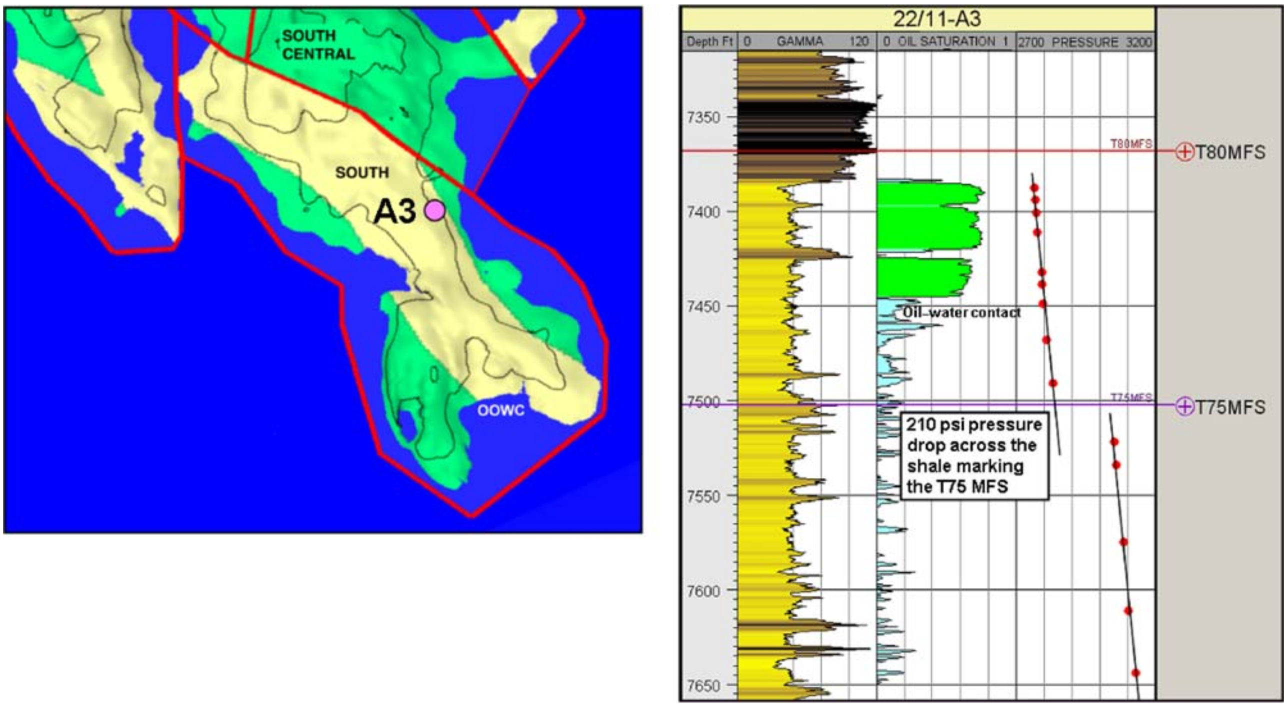

Fig. 11. Formation pressure-tester plot for well A3. The plot shows a 210 psi pressure drop across the shale marking the T75 MFS between the T75 and T70 reservoir units. The shale is extensive enough to separate reservoir zones at different pressures.

also typically sampled from producing intervals at a significant height above the initial OWC. The deepest samples (taken from the water leg in appraisal wells and from the lowermost perforated intervals in the oil leg) have the highest chloride ion concentration. For instance, the western channel shows an aquifer composition of about 60 800 mg l^{-1} chloride ion concentration, whereas produced water from the stratigraphically highest sand in the western channel area shows a mean chloride ion concentration of 57 949 mg l^{-1}.

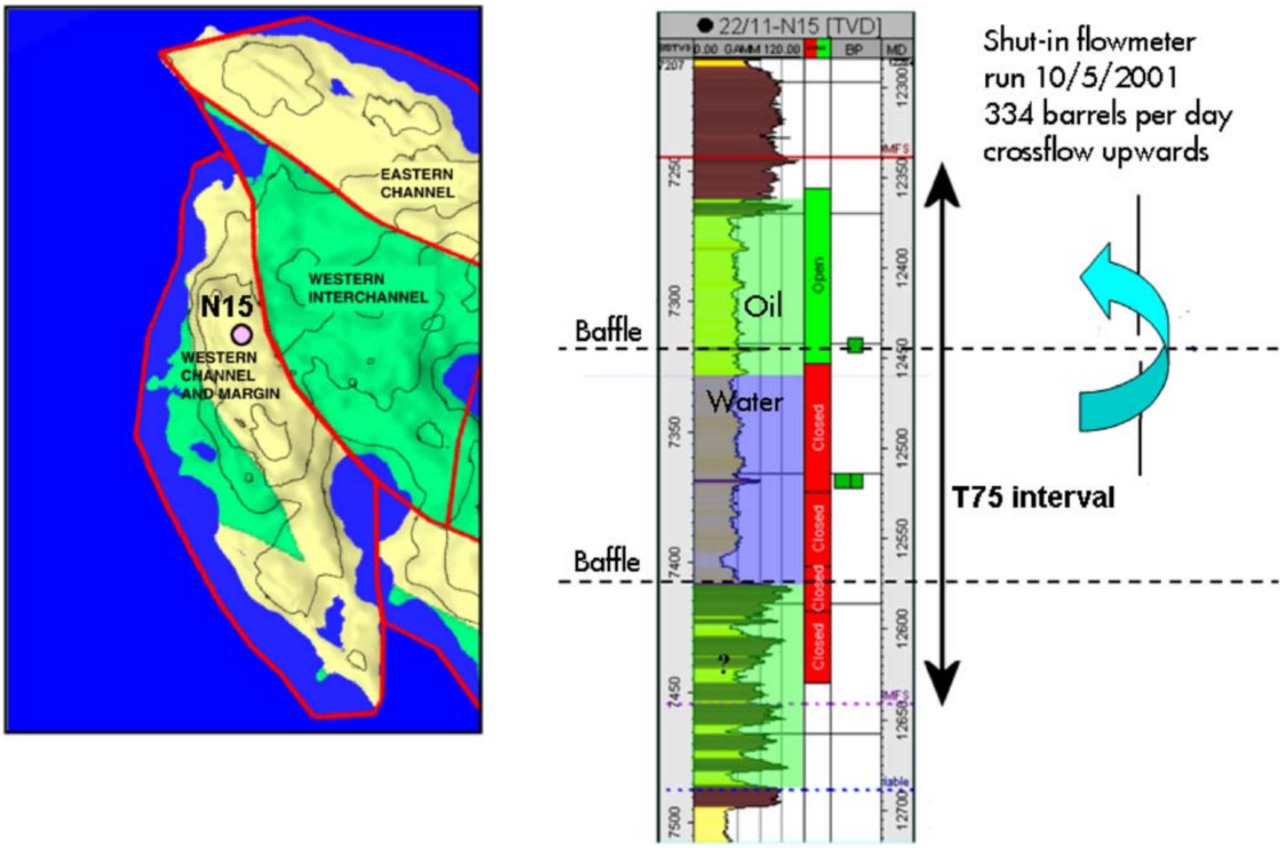

Fig. 12. A shut-in flowmeter pass shows crossflow from a high pressured reservoir unit to a low-pressure reservoir unit across the laterally extensive Last Chance Shale in the western channel well, N15. A bridge plug was set opposite the shale in order to isolate water influx from the lower perforations. SSTVD, subsea true vertical depth; BP, bridge plug setting depth; GAMM, gamma-ray log; MD, measured depth.

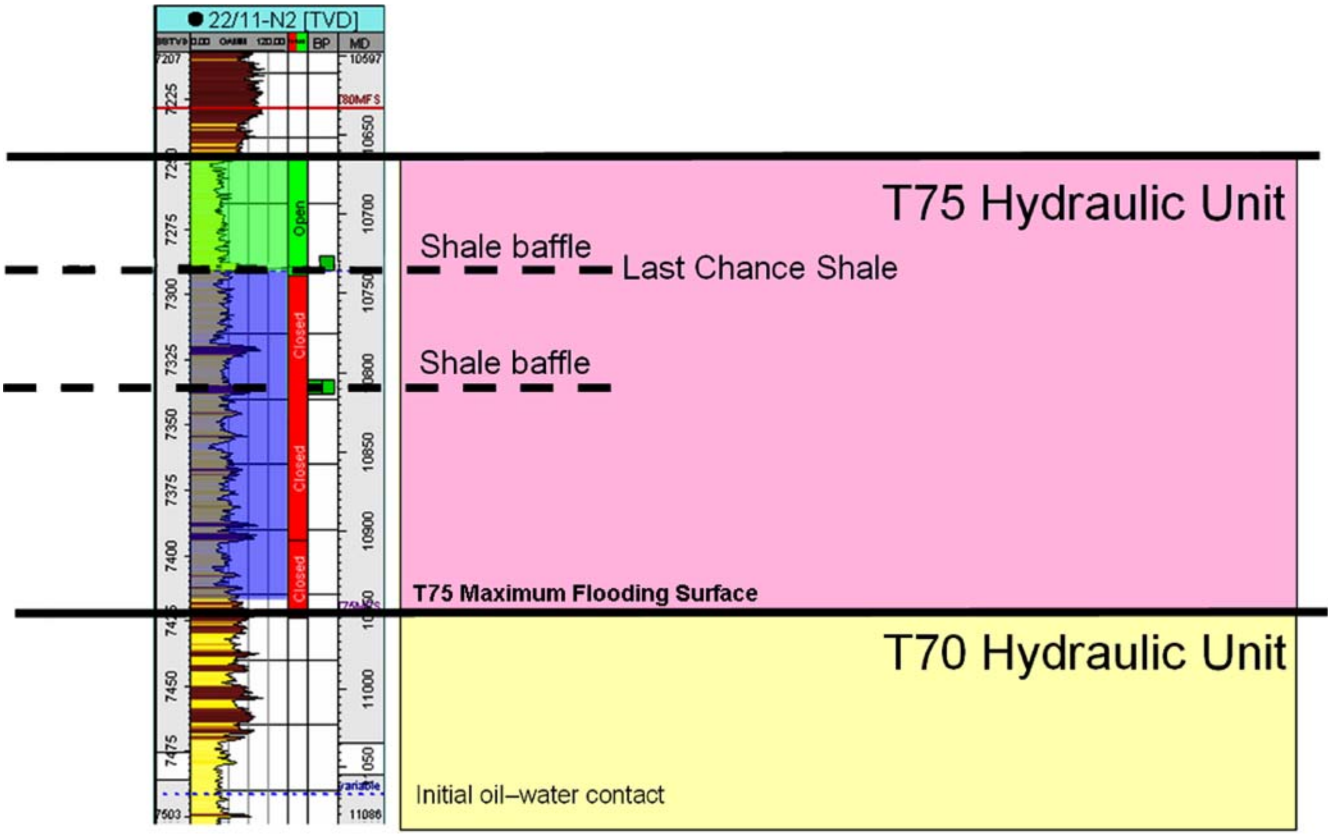

Fig. 13. The two main hydraulic units in the Nelson Field correspond to the T70 and T75 sequences, separated by the shale corresponding to the T75 maximum flooding surface. Two shale baffles are found within the T75 reservoir unit. The uppermost unit has been termed the 'Last Chance Shale'.

Lateral compartmentalization is shown by a correspondence between a specific produced water composition from wells and the macroform in which they are located. Laterally the eastern channel of the Nelson Field produces water with a lower chloride ion concentration than the western channel at all reservoir levels. The western interchannel region shows an intermediate composition to both flanking channel bodies.

Thus, the major element chemistry of produced water in individual wells is observed to change after successful water shut-off events, allowing shale barriers or major baffles to be detected (Gill *et al.* 2010).

Vertical flow barriers and baffles in the Nelson Field

The results of data integration indicate that there is one major flow barrier to vertical flow, a shale interval corresponding to the T75 MFS. This separates the Nelson reservoir into two hydraulic units corresponding to the T70 sequence (below) and the T75 sequence (above). Produced water geochemistry, water shut-off tables and formation tester log data are consistent with this interpretation (Fig. 13).

There are no obvious major baffles within the T70 central channel area, with the exception of some thin shales near the top of the interval in the south of the field. A rapid rise in the OWC was observed in the early years of production in the central channel complex.

There are two major baffles within the T75 western channel area, indicated by shut-in crossflow, punctuated OWC rises and water shut-off tables. The upper baffle is referred to informally as the 'Last Chance Shale'; so named because, in the more mature parts of the field, there are no more shales above this level where it is possible to set a bridge plug. The sandstone interval above is called the Last Chance Sand. In the eastern channel, the Last Chance Shale is the only shale interval that acts as a baffle. Pressure data suggests that it is leaky in both areas, more so in the west than the east. Nevertheless both baffles are extensive enough to separate high- and low-pressure sand intervals on the evidence of shut-in crossflow on flowmeter logs. There is evidence that the Last Chance Shale comprises a widespread series of low permeability debris flows (Fig. 14).

Geological significance of the vertical flow barriers and baffles

The main vertical flow barrier is the T75 MFS. There is a known correspondence between maximum flooding surfaces and in-field vertical flow barriers in the Jurassic deep-water sandstone reservoirs of the Northern North Sea (Partington *et al.* 1993). This is also potentially the case for the Cenozoic deep-water sandstone reservoirs.

The two major shale baffles in the T75 sequence cover large areas. Thin blanket mudstones are commonly extensive baffles and barriers in North Sea deep-water reservoirs (Hempton *et al.* 2005). For example, laterally extensive mudstones have been described as acting as permeability barriers or baffles in the Jurassic reservoirs of the Magnus Field (Shepherd *et al.* 1990) and the Miller Field (Garland *et al.* 1999); the Paleocene reservoirs of the Forties Field (Wills 1991) and the Balmoral Field (Gambaro & Currie 2003); and the Montrose and Arbroath Fields (Hogg 2003). Local erosion or minor faulting may be responsible for breaches in the shales, allowing a modicum of communication across them.

Methods of detecting controls on areal flow in the Nelson Field

The controls on areal flow are partly detected using data integration and partly inferred from the geological interpretation. For the Nelson Field, the assumption was made that compartmentalization

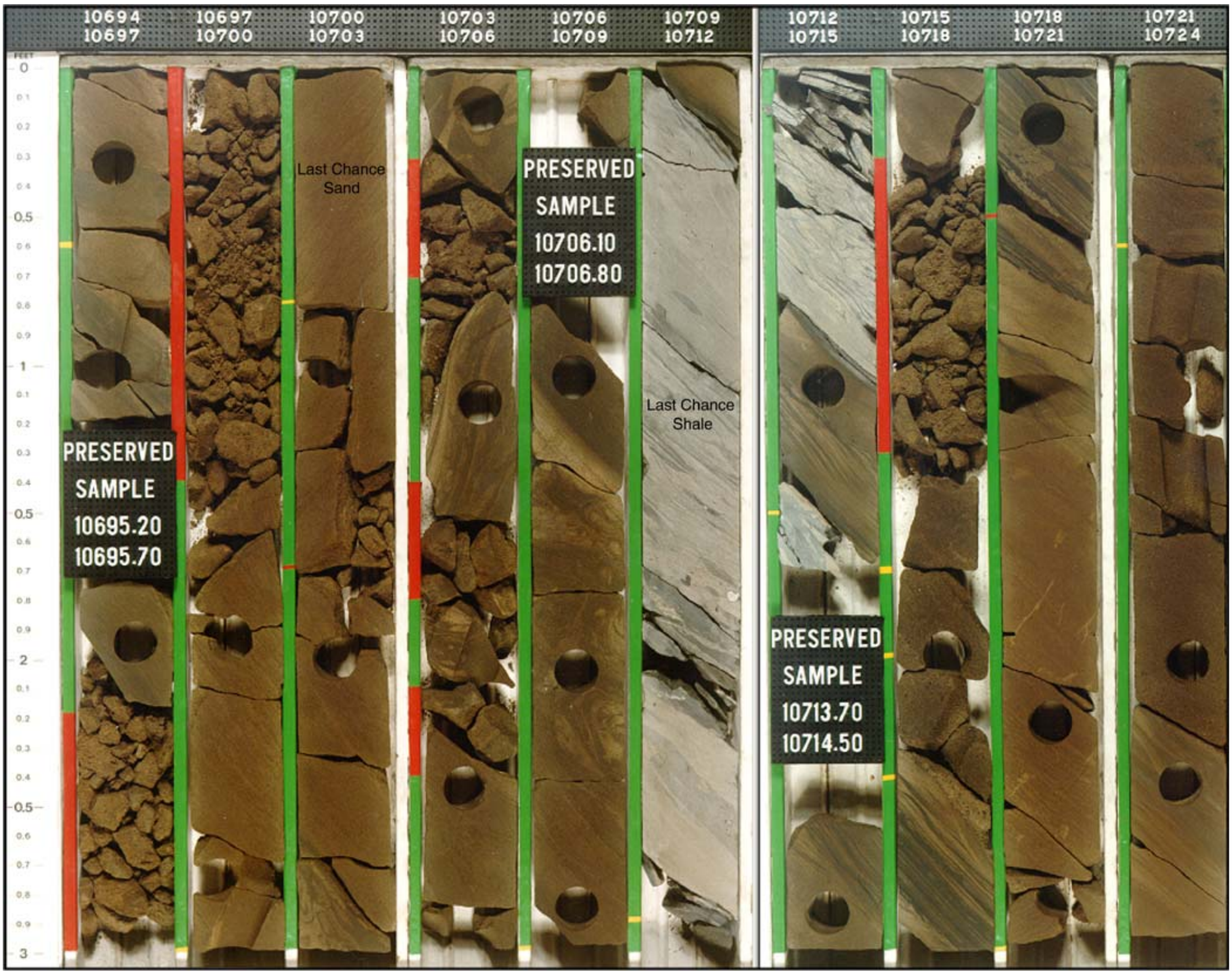

Fig. 14. Core photograph from well 22/11-N2 showing the debris flow at 10,709–10,716 ft cored depth, known to act as a baffle on a production timescale. This correlates to the unit known as the Last Chance Shale.

in the field results from poor to no connectivity through low net to gross areas defined by interchannel sediments in combination with structural cols that provide a significant degree of dip closure at or just above the level of the initial OWC. Data integration has not shown any features that would conflict with these initial assumptions.

The methods used to detect controls on areal flow include the recognition of OWC rise domains using water cut maps in conjunction with log facies maps, oil and water geochemistry and 4D seismic data.

Water cut maps used in conjunction with log facies maps

The comparison of water cut maps to log facies maps can be effective in establishing OWC rise domains, specifically areas where either bottom-water influx or edge-water influx is occurring. In the Nelson Field, areas of bottom-water influx are characterized by wells with high water cuts and log facies maps showing sand-prone reservoir intervals with only a small number of interbedded shales (Fig. 15). By contrast areas showing predominantly edge-water drive tend to show wells with low water cuts and numerous interbedded shales. Here, the lateral inflow of water has a longer path (along the shales) to reach the production wells and water cuts tend to be lower as a result. Figure 15 shows the contrast in log facies character between the western channel in the T75 interval (undergoing bottom-water drive) and the western interchannel area (undergoing edge-water drive). There is a marked dissimilarity in water cut behaviour between the two areas.

Water and oil geochemistry

Provincial variation in produced water geochemistry has been used to infer the location of compartments within the Nelson Field (Gill *et al.* 2010). Provincial variation in oil geochemistry is also seen. For example, the N26 area has markedly different oil compositions from the rest of the field.

4D seismic data

Nelson has a long history of the use of 4D seismic surveys, building on a 1990 pre-production 3D survey with one of the first dedicated marine 4D surveys in 1997 (Boyd-Gorst *et al.* 2001). Additional 4D monitor datasets were acquired in 2000 (McInally *et al.* 2003), 2003, 2006 and 2009. With each new survey, improved acquisition repeatability and combined reprocessing of vintage seismic data has led to successive improvements in time-lapse matching and differencing.

For the purposes of acquiring usable 4D seismic data, the Nelson fluid parameters can be considered to be relatively simple with a water sweep (fluid saturation) dominated signal and a strong aquifer. However, the interpretation of the 4D seismic signal is complicated by the labyrinthine reservoir geometry combined with areal and vertical variation in the net to gross. This creates

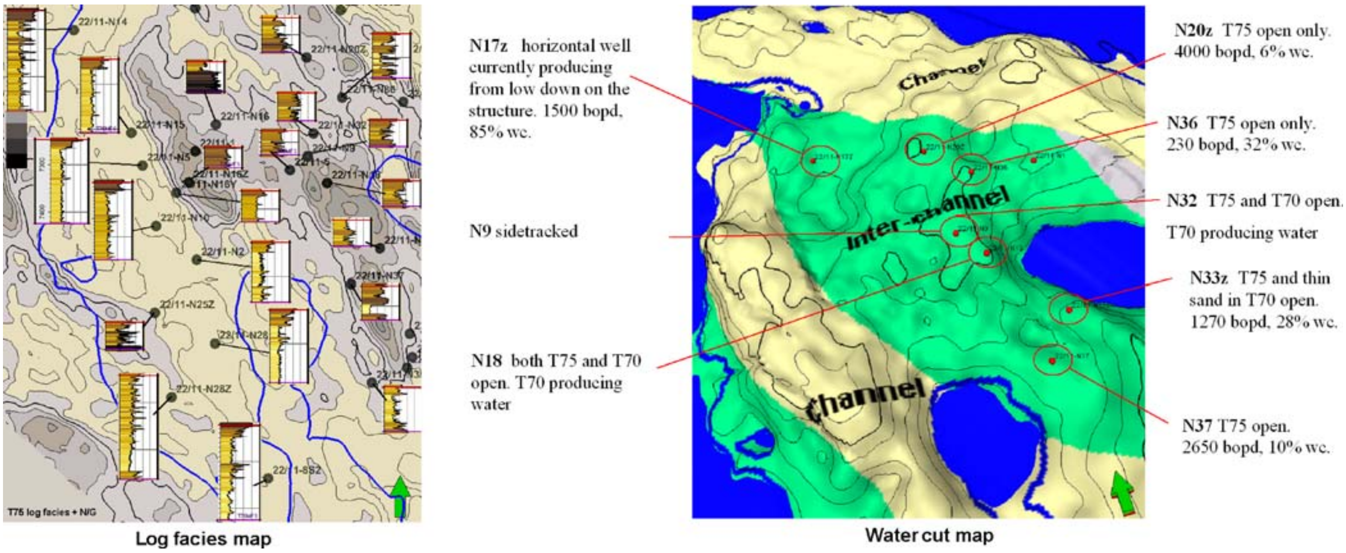

Fig. 15. Log facies map for the western channel complex and interchannel area showing the bedding style in both areas. The western channel shows few interbedded shales, bottom-water drive predominates and the water cuts are high in the wells located here. The interchannel area shows numerous interbedded shales, a predominantly edge-water drive with low water cuts. Bopd, barrels of oil per day; wc, water cut.

the situation where the existence of a 4D signal is a likely indication of sweep within a high net to gross sand body; however away from the main channel sands, the absence of a signal either could be due to an unswept sand, to poor quality reservoir within thin-bedded sands that are below seismic resolution or to the presence of non-reservoir rock.

Variable pressure-up signals (softening and slowdown causing a train of signal below top reservoir due to misalignment in the difference signal) are observed around the four water injectors; the extent of the response is an indication of each injector's connectivity to channel sands. As expected from a field with strong aquifer drive, no depletion signal has been detected in this relatively low-depletion (900 psi decrease from initial pressure) and pressure-connected reservoir.

Variability in the 4D signal is accounted for through an understanding of the stratigraphic geometry and the relative connectivity of reservoir sandstone units. Reservoir surveillance and the 4D seismic response can be considered consistent with a dominant bottom-water drive acting within the major channel complex fairways bodies. The 4D seismic response is much more ambiguous in the lower net to gross areas of the field where much of the remaining oil volumes are thought to reside (Fig. 16). Nevertheless, the main value of the information of the 4D seismic dataset in the Nelson Field is that it provides the means of screening out those areas of the reservoir that are probably swept.

Areal flow barriers and baffles in the Nelson Field

The main feature shown by data integration analysis is a distinction between the major eastern and western channel complex fairways and the central interchannel area in the T75 unit. The major channel areas show production wells with high water cuts and indications of a drive mechanism dominated by bottom-water influx. The interchannel area contains wells with low water cuts, showing interbedded sandstone–mudstone intervals with a dominant edge-water drive pattern.

Screening tools

Data integration allows the main geological controls on fluid flow to be established. The major elements are shales acting as barriers or baffles to vertical flow and combination stratigraphic/structural areal compartments. The net effect is to create drainage cells, which are self-contained volumes bounded by lateral and vertical permeability barriers (Shepherd 2009; Gill *et al.* 2010). The concept of a drainage cell is similar to what some geologists would refer to as a 'compartment'. For instance, Larue & Hovadik (2006) defined a compartment as a non-connected part of the reservoir. The phrase 'drainage cell' is used by preference to 'compartment' in the sense that it is an operational term for the purposes of screening reservoir volumes. A drainage cell may be slightly leaky, but if the rate of leakage is small compared to production rates then this will not be a matter of great importance to the reservoir management team.

Nine drainage cells have been defined in the Nelson Field as a result of data integration (Figs 5 & 6). It can be shown that the field does not drain as a single entity with a common OWC throughout. Instead, the field behaves in a multicellular manner, with each drainage cell having its own producing OWC. The drainage cells are more or less self-contained with minor to no connectivity between them on the producing time-scale of the field. In the T75 reservoir interval the drainage cells are defined by the macroforms present and are named after the location and the dominant macroform in the cell: these are the western channel and margin, western interchannel, eastern channel, south central, south and the N26 area drainage cells (Fig. 4). In the T70 reservoir interval the drainage cells are designated as the NW, NE and south drainage cells (Fig. 5).

The definition of drainage cells allows the subsurface team to localize areas of the field where there are significant remaining oil volumes. This has been done by compiling maturity tables which show for each drainage cells the total STOIIP, produced oil volume and an estimate of the remaining unrecovered mobile oil volume (Vining 1997). A maturity table can be illustrated as a fuel tank display showing the relative volumes of produced to remaining mobile oil. An example of such a display is shown for the T75 interval (Fig. 17). Maturity tables and fuel tank displays allow the remaining oil volumes to be localized and then screened for infill well potential. Drainage cells with low production rates and significant remaining mobile oil volumes are likely to be those areas of the field with large enough bypassed oil volumes to be worth targeting. Areas which are largely swept such as the main permeability fairways can also be identified. Maturity tables for the Nelson Field show that the genetically linked low-permeability macroforms may potentially contain significant volumes of remaining oil.

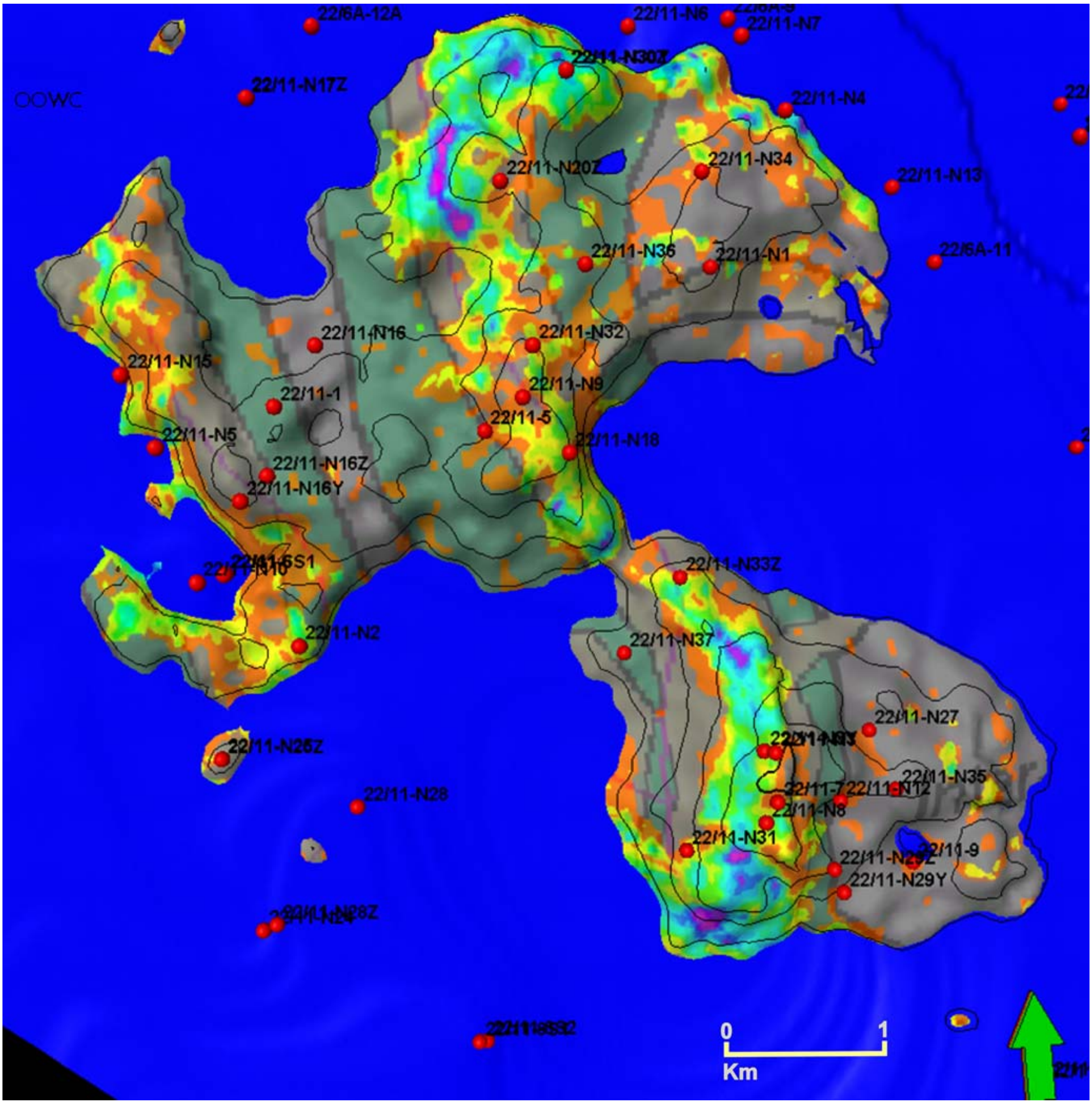

Fig. 16. Four-dimensional seismic response in the T70 sequence overlain on a map showing macroforms. A clear sweep signal is seen within the central channel complex (bright colours), whereas the channel margins show only a limited or no sweep response (grey tones). OOWC, original oil–water contact.

Four out of the nine drainage cells defined in the Nelson Field show significant remaining oil volumes; these are the western interchannel, the N26 area and the southern drainage cells in the T75 interval, together with the northeastern drainage cell in the T70 interval.

Having screened the more promising drainage cells for their remaining oil potential, the next stage is to determine the trapping style of the oil pockets within the identified drainage cells. The intent is to look for targets which may be of a large enough size to justify drilling with an infill well. In practice, these oil targets will either be found in dead-end structures with bypassed oil or will be held up in slow moving oil columns within low permeability rock. Trapped oil will also be found in smaller, uneconomic volumes.

Uneconomic oil volumes

For a typical North Sea platform well target to be economic, it should produce incremental reserves of at least $1–2 \times 10^6$ bbl. Data integration methods are able to identify bypassed oil volumes of this size, and these are discussed later. However, where sizable targets are not immediately obvious within a drainage cell that appears to have significant remaining oil volumes, there will be a concern that much of the unrecovered mobile oil is located in numerous small oil pockets which are unlikely to provide economic targets. At this stage, there is a need to judge from known observations, the use of outcrop analogues and general experience as to the likely level of the balance between the volume of uneconomic oil pockets v. the larger target volumes. Note though that there is

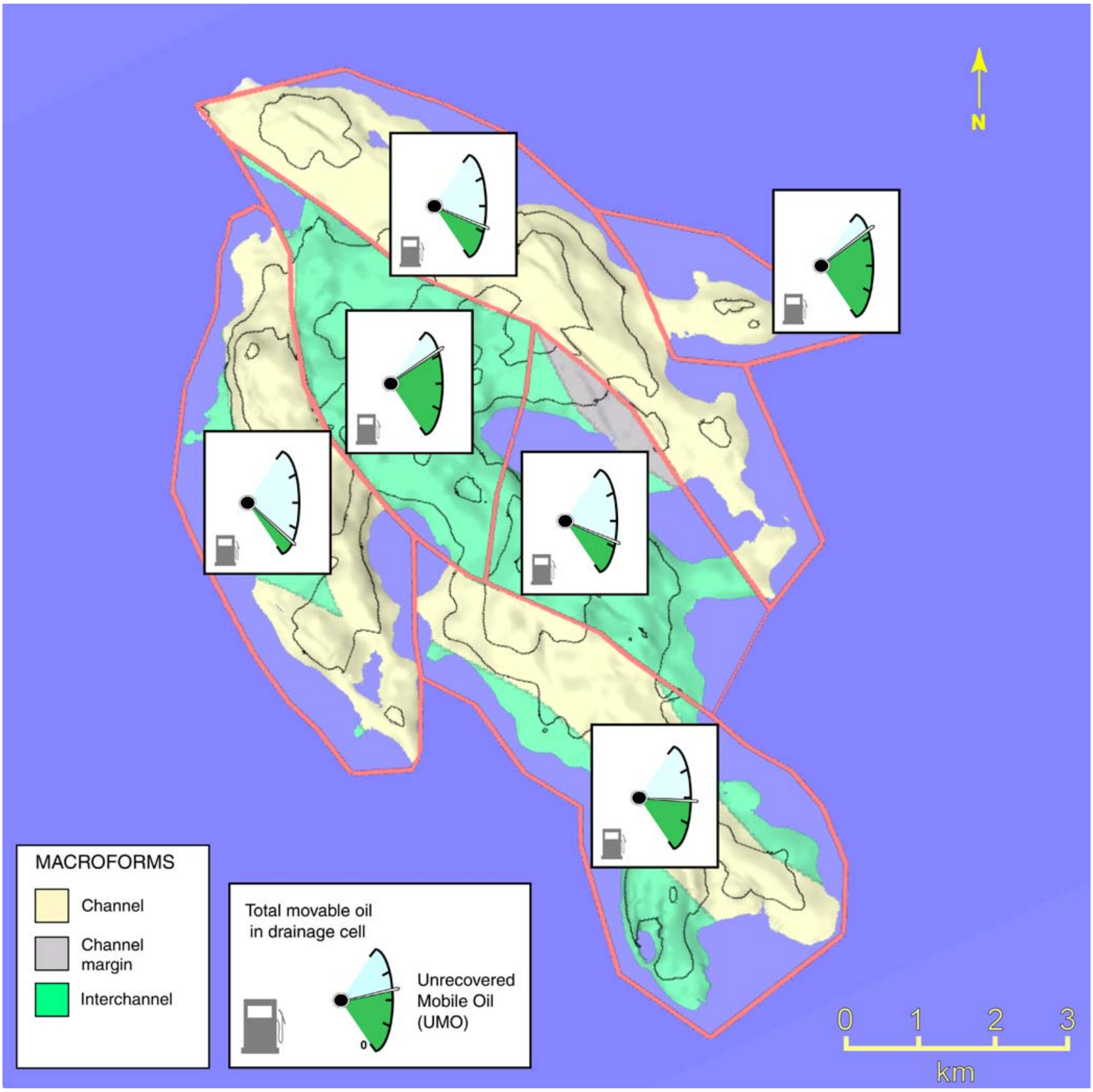

Fig. 17. Fuel tank display for the T75 unit. A full tank is equal to the total movable oil in the drainage cell. The fuel gauge shows the volume of remaining mobile oil left in each cell.

always an issue with small uneconomic volumes that they could be transformed into feasible targets under more favourable economic conditions or if the cost of infill drilling can be reduced.

The various associations for uneconomic oil volumes in the Nelson Field are thought to include thin beds, minor attic oil volumes, heterogeneous reservoir intervals, thin beds disconnected by faulting, local sand pinch-outs and volumes associated with channel margin complexities.

Thin beds

Poorly swept oil volumes occur in thin beds. It is noticeable that open hole logs in infill wells with swept oil columns show a small number of thin intervals 2–3 ft thick with oil saturations that are higher than residual saturations (i.e. greater than 20–25% oil). Some of these are capped by thin mudstone beds, although for others it is not clear from the log response as to why the oil is trapped. This observation is resonant of the comment by Wetzaeler *et al.* (1996) on remaining oil configurations in the Brent Field, that it can only take a subtle lithological change for oil to be trapped. It should be noted, however, that there is a possibility that some of these features may be artefacts of the log interpretation.

Minor attic oil volumes

An attic oil target occurs when oil is trapped in a structural culmination above the highest producing interval in an adjacent well (Shepherd 2009). Small unproducible attic oil volumes occur both at top reservoir level and underneath extensive blanket

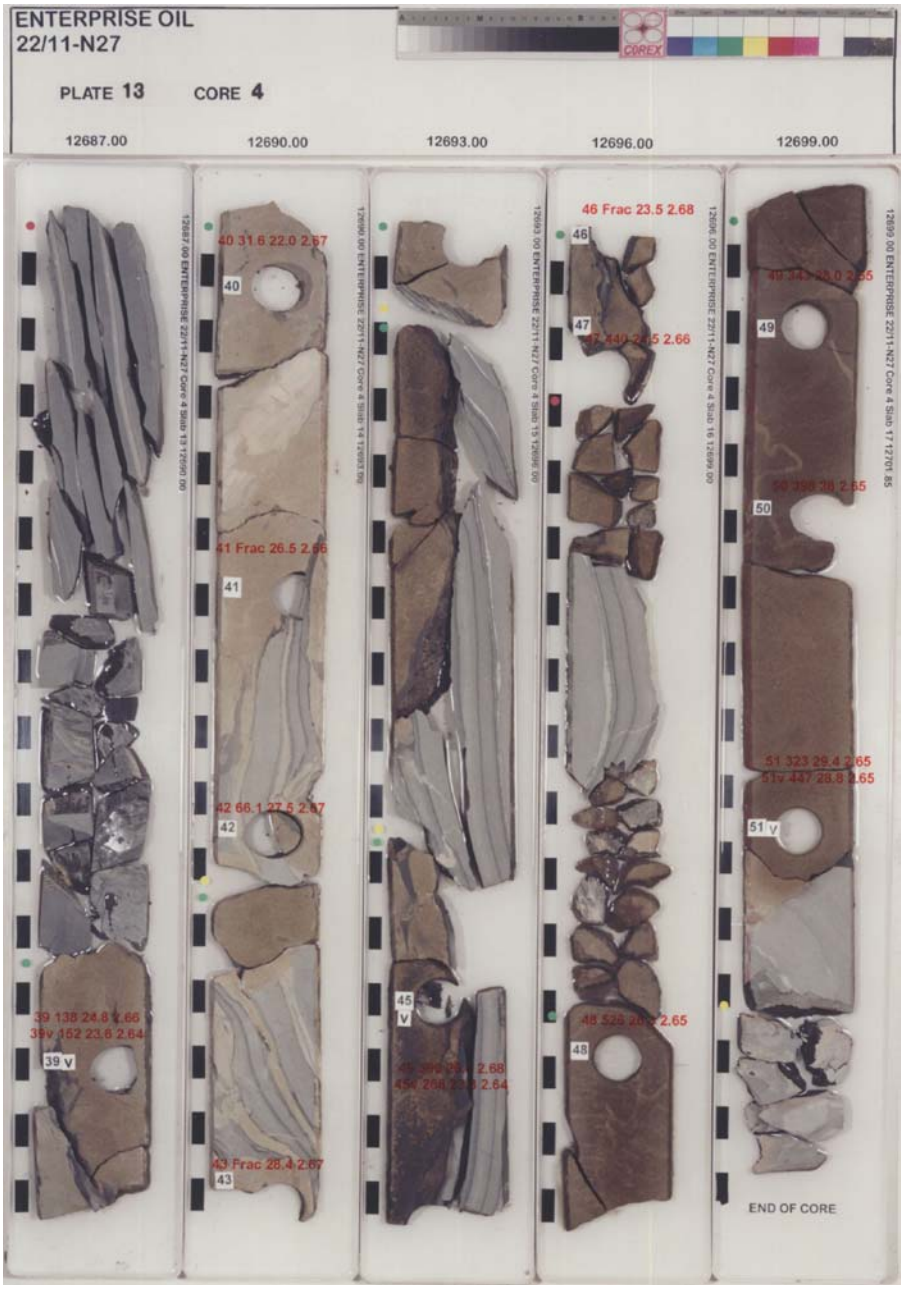

Fig. 18. Highly slumped and injected heterolithic sediments in well N27. The figures in red refer to the permeability, porosity and grain density values for each core plug. Frac, fracture.

mudstones. These are unproducible in the sense that the likely volumes will be too small to justify the expense of drilling them.

Heterogeneous reservoir intervals

Highly heterogeneous reservoir intervals may contain uneconomic oil volumes. For example, core in production well N27 shows an interval of highly slumped and injected turbidites (Fig. 18). This is the only example of extremely heterolithic sediments known to date in the Nelson Field. It is likely that the individual sandstone bodies in these features are small and tortuously connected with the potential for numerous small-scale dead ends and small isolated oil volumes.

Thin beds partially disconnected by faulting

Poor connectivity in thin-bedded intervals may be the result of minor faults. An observation has been made from modelling studies in the Westphalian succession in the Carboniferous East Pennine Coalfield that faults generally lead to a decrease in connectivity for reservoirs comprising thin, low net to gross channelized systems (Bailey *et al.* 2002). Although the observation is locality specific, the study highlights the potential effect of faults on reservoir connectivity in channelized sediments.

Local sand pinch-outs

Local sand pinch-outs may trap uneconomic oil volumes. Updip pinch-outs of thin interbedded sandstones may locally create reservoir dead-ends trapping oil.

Channel margin architecture

Complex channel margin relationships may contain small oil pockets that are uneconomic to produce. Channel margins in field exposures can show evidence for multiple incision, slumping

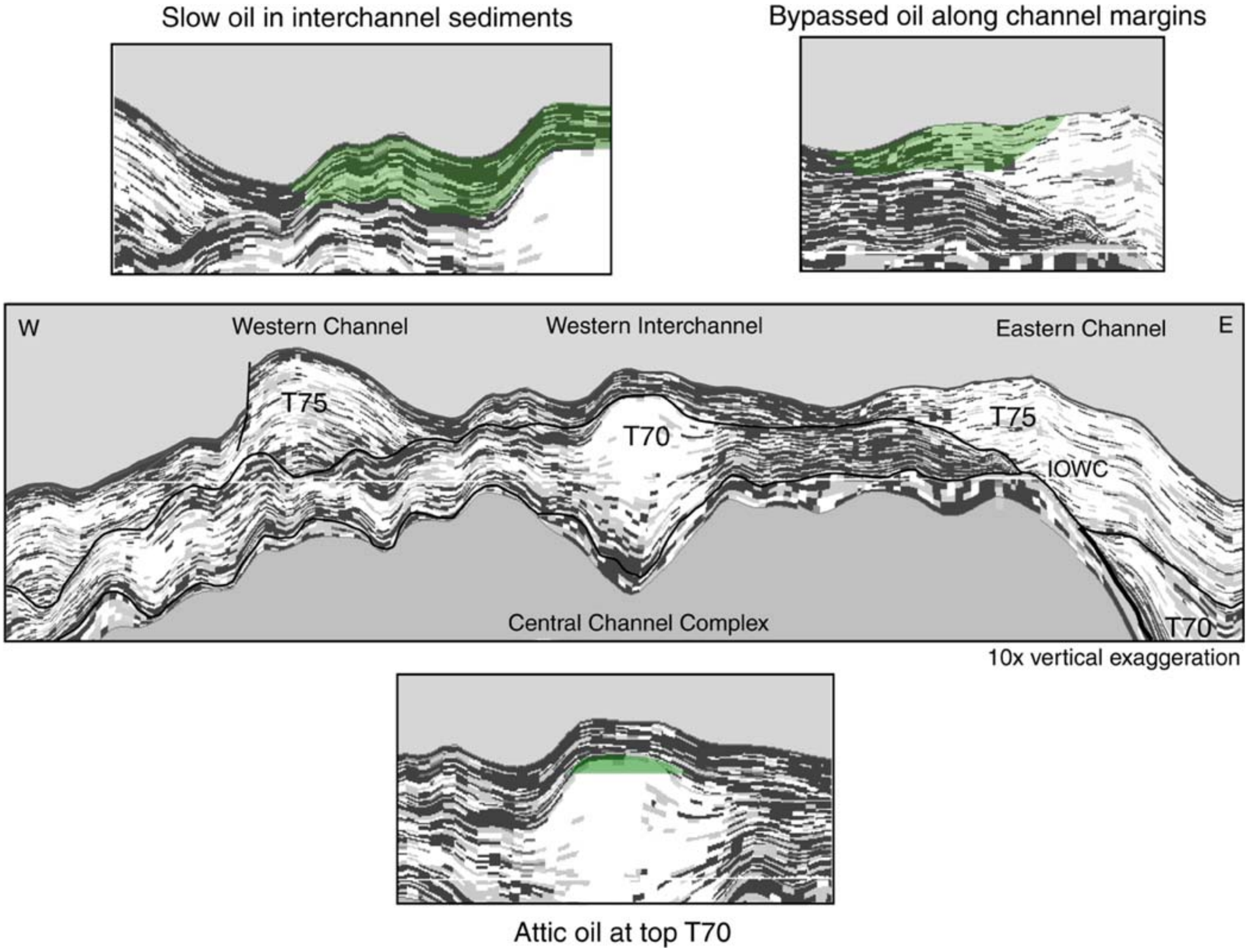

Fig. 19. Conceptual model showing different bypassed oil configurations in the Nelson Field. These include slow oil volumes in interchannel sediments, bypassed oil in the channel margins and attic oil configurations. IOWC, initial oil–water contact.

and localized shale drapes. There may be a significant volume of small dead-end volumes associated with these heterogeneities.

Target oil volumes

Target oil volumes are oil pockets that are likely to produce enough incremental oil to justify the cost of drilling the well and to provide an economic return on the money invested in the operation. Experience with producing fields suggests that it is possible to categorize specific type of target oil configurations (Wetzaeler *et al.* 1996). In the Nelson Field, there are three main types of target: These are attic oil, slow oil in the interchannel areas and channel margin oil. These are shown conceptually in Figure 19.

Significant attic oil volumes

The structural culmination defining attic oil volumes in the Nelson Field is typically a four-way dip closure beneath a permeability barrier (e.g. at the top of the reservoir), or a three-way dip closure bounded by a sealing fault. The attic oil configurations are generally low-relief dip closures updip from existing wells. Although these targets are easy to define, the volumes are generally small and are subject to depth conversion uncertainty. Attics are an important target in the Nelson Field as they are the simplest to identify.

Attic targets are not only recognized at the top of the T75 sequence (top reservoir) but are also identified at the top of the T70 sequence (with the T75 MFS as the top seal) and at top Lista level (with the T65 MFS as the top seal). In areas where there is an un-penetrated structural high at multiple reservoir levels and laterally continuous MFS shales at all levels it is also possible that stacked attic oil accumulations exist.

Fault bounded three-way dip closed attic volumes have also been recognized and can be identified on 4D seismic volumes.

Slow oil

This remaining oil type is specific to the large T75 interchannel area which lies between the two channel complexes. The area contains wells with low water cuts. In a mature field this can be a sign that there is a large volume of oil between the production wells and the source of water influx. There is a concern that there may not be enough producers to guarantee effective areal sweep and to ensure that the oil in this area will be produced by the end of field life.

Interchannel targets are defined within thinly developed overbank sands in two areas of low net to gross interbedded sandstone/shale sequences between the channel complexes. The initial Nelson exploration well 22/11-1 encountered such a low N/G shale-prone sequence in the inter-channel facies that the field was not properly evaluated as commercial until 18 years later. Currently producing sandstone intervals demonstrate the reservoir potential in these areas, but quality, rate, connectivity and volumes for infill wells are sensitive to localized variation in the interval net to gross.

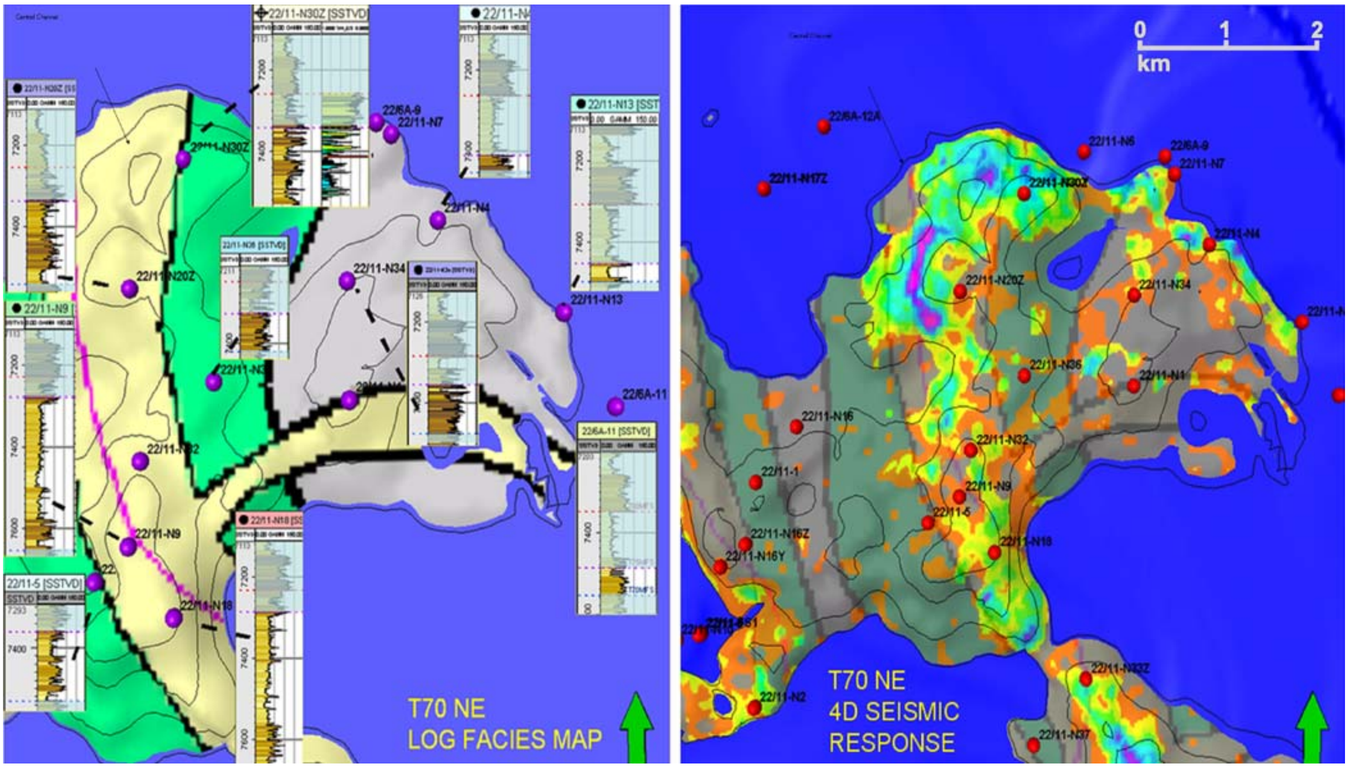

Fig. 20. Log facies map and the equivalent 4D seismic response for the NE sector of the T70 unit. The maps indicate that the channel margin areas potentially contain bypassed oil volumes.

Oil bypassed in channel margins

Maturity tables and 4D seismic data indicate that some of the channel axis drainage cells contain significant volumes of unrecovered mobile oil. Wells in the channels show indications of good sweep. The likelihood is that much of the remaining oil is located in the channel margin areas on the wings of the channels. This configuration is known to be a major bypassed oil target in the Forties Field (Vaughan *et al.* 2007). One possibility to explain bypassed oil in the channel margins is that the waterflood has occurred preferentially along the main channel axes and that oil has been banked along the channel margins. Viscous forces may be insufficient to displace oil in channel margin locations.

Channel margin opportunities represent bypassed oil in both channel margin sand pinch-outs in the main channel complexes and/or volumes trapped in thinner channel margin stacked sands (see Fig. 20). The 4D signal shows limited sweep in T75 and T70 sands along the margins of the central and western channels and this has driven the target identification process. The thin nature of channel margins (reducing sand thickness) is at the limit of seismic resolution. In order to more accurately identify the position of channel margins, inversion techniques were used.

The majority of the margin targets are located on both sides of the western channel complex in T75 sands. Reservoir surveillance suggests a relatively low offtake in this area as compared with other parts of the field and it is likely that significant remaining reserves exist here.

The southern end of the T70 central channel shows bypassed oil in the channel margins. The channel margins to the central channel complex extend eastward into a poorly understood low N/G area where a high level of heterogeneity has resulted in low recovery from the existing wells.

The western side of the eastern channel complex is predicted to show an erosive channel margin back-filled with sands and few intervening shales. The eastern margin of the eastern channel complex extends to the east beyond the field limit.

Discussion

The main theme of this paper is a discussion of the methods used to help locate the remaining oil in mature fields. The reservoir engineering-led approach commonly uses a reservoir simulation model as the main tool for reservoir management in offshore fields. These models are typically built with a coarse grid representation of the geological model as the framework for matching and predicting reservoir performance. Simulation models are ideal for solving reservoir management problems at the early stage of field development and in fields with relatively simple geology where high-confidence predictions of reservoir performance can be made throughout the field life. They may not work as well in fields with complex geology, particularly at the mature stage of development (Hansen *et al.* 2002). The reservoir simulation model is often too coarse to indicate the location of the subtler and smaller stranded oil volumes ($1-2 \times 10^6$ bbl). Paradoxically, these models can be considered to be reliable in predicting where not to drill in mature fields, that is in the largely swept, main production fairways. However, they do not have the detail to resolve the location of unswept oil volumes in the areas of more complex geology. In these areas, the simulation model will tend to show an abstract and diffuse range in oil saturations, generally above residual oil saturation; however, the more promising unswept areas will tend to be inadequately represented.

The geophysical-led approach works best in fields where there is good 4D seismic resolution and where there are no problems with survey repeatability. Although 4D seismic surveys are available for the Nelson Field, their main use to date has been less to locate the remaining oil than to provide information on where the reservoir is swept. In this way the 4D seismic method is performing a similar role to the reservoir simulation model as a screening tool to eliminate those areas of the reservoir where large remaining oil volumes are unlikely to be found.

The mature stage of field development is ideally suited to the geology-led approach, particularly if the other two approaches lack the resolution to help locate the remaining oil volumes in detail. A modified workflow for reservoir modelling is used compared with the conventional practice for fields at the appraisal or early production phase. The large amount of production data available for a mature oil field allows an evidence-based assessment of reservoir connectivity to be made in tandem with reservoir modelling studies, whereas a largely model-based approach is used to evaluate connectivity for reservoirs where there is much less production data.

The workflow given here focuses on those methods that have been used to help understand the reservoir performance in the Nelson Field. These are only part of the larger toolkit of techniques available to help determine the key geological features influencing fluid flow in reservoirs (Shepherd 2009). Whereas fluid flow in the Nelson Field is strongly controlled by stratigraphic compartmentalization and laterally extensive shales, other fields may show different features pertinent to the reservoir behaviour, for example, in a reservoir where the waterflood performance is dominated by major vertical permeability variation and where a flow unit characterization would be relevant. Nevertheless, the broad aspects of the workflow used in the Nelson Field is applicable to most producing reservoirs. These involve determining the main geological features controlling fluid flow in the field, establishing the number and location of drainage cells as a means to localizing and screening remaining oil volumes, and the analysis of trapping styles at the drainage cell level.

Conclusions

A 'Locate the Remaining Oil' analysis of the Nelson Field has resulted in the division of the Nelson Field into nine drainage cells which are defined by reservoir macroforms. Screening of these nine drainage cells has identified four cells that contain significant remaining volumes of mobile oil. These have then been investigated in order to locate any stranded oil volumes that are unlikely to be produced by the existing well stock, and to determine if these are large enough to justify infill well drilling. A number of opportunities have been identified which have led to a focussed drilling campaign in order to target these volumes.

The authors would like to thank the Nelson Field partners Shell UK Limited, Esso Exploration and Production UK Ltd, Total E & P UK plc, Petro Summit Investment UK Ltd and Premier Oil for publishing permission. The authors would like to thank all those who have worked on Nelson during the course of this study and G. Murray for assistance with drafting.

References

Bailey, W. R., Manzocchi, T. *et al*. 2002. The effect of faults on the 3D connectivity of reservoir bodies: a case study from the East Pennine Coalfield, UK. *Petroleum Geoscience*, **8**, 263–277.

Beaubouef, R. T. 2004. Deep-water leveed channel complexes of the Cerro Toro Formation, Upper Cretaceous, southern Chile. *AAPG Bulletin*, **11**, 1471–1500.

Beaubouef, R. T., Rossen, C., Zelt, F. B., Sullivan, M. D., Mohrig, D. C. & Jennette, G. D. C. 1999. *Field Guide for AAPG Hedberg Field Research Conference – April 15–20, 1999. Deep-Water Sandstones, Brushy Canyon Formation, West Texas*. AAPG, Tulsa, OK, Continuing Education Course Note Series, **40**.

Boyd-Gorst, J., Fail, P. & Pointing, L. 2001. 4D time lapse reservoir monitoring of the Nelson Field, Central North Sea: successful use of an integrated rock physics model to predict and track reservoir production. *The Leading Edge*, **20**, 1336–1350.

Bryant, I. D. & Livera, S. E. 1991. Identification of unswept oil volumes in a mature field by using integrated data analysis: Ness Formation, Brent field, UK North Sea. *In*: Spencer, A. M. (ed.) *Generation, Accumulation and Production of Europe's Hydrocarbons*. European Association of Petroleum Geoscientists, Special Publications, **1**, 75–88.

Clark, M. S., Melvin, J. D., Prather, R. K. & Marino, A. W. 1997. Characterization and exploitation of the distal margin of a layered, low-permeability turbidite reservoir, Yowlumne field, San Joaquin Basin, California. Houston Geological Society Bulletin, December 1997, 12–15.

Cronin, B. T., Hurst, A., Celik, H. & Turkmen, I. 2000. Superb exposures of a channel, levee and overbank complex in an ancient, deep-water slope environment. *Sedimentary Geology*, **132**, 205–216.

Eubanks, L. G. 1987. North Sabine Lake Field: complex deposition and reservoir morphology of lower Hackberry (Oligocene), Southwest Louisiana. *AAPG Bulletin*, **71**, 1162–1170.

Gambaro, M. & Currie, M. 2003. The Balmoral, Glamis and Stirling fields, UK Central North Sea. *In*: Gluyas, J. & Hitchen, H. (eds) *United Kingdom Oil and Gas Fields Commemorative Millennium Volume*. Geological Society, London, Memoirs, **20**, 395–413.

Garland, C. R., Haughton, P., King, R. F. & Moulds, T. P. 1999. Capturing reservoir heterogeneity in a sand-rich submarine fan, Miller Field. *In*: Fleet, A. J. & Boldy, S. A. R. (eds) *Petroleum Geology of Northwest Europe: Proceedings of the 5th Conference*. Geological Society, London, 1199–1208; doi: 10.1144/0051199.

Gill, C. E., Shepherd, M. & Millington, J. 2010. Compartmentalization of the Nelson Field, Central North Sea: evidence from produced water chemistry analysis. *In*: Jolley, S. J., Fisher, Q. J., Ainsworth, R. B., Vrolijk, P. J. & Delisle, S. D. (eds) *Reservoir Compartmentalization*. Geological Society, London, Special Publications, **347**, 71–87.

Haldorsen, H. H. & Lake, L. W. 1984. A new approach to shale management in field-scale models. Presented at the 1982 SPE Annual Technical Conference and Exhibition, New Orleans. SPE **10976**.

Hamilton, D. S., Holtz, M. H., Ryles, P., Lonergan, T. & Hillyer, M. 1998. Approaches to identifying reservoir heterogeneity and reserve growth opportunities in a continental-scale bed-load fluvial system: Hutton Sandstone, Jackson field. *AAPG Bulletin*, **82**, 2192–2219.

Hansen, A.-G., Brendsdal, A., Arnesen, D. S. & Morris, M. 2002. *Optimisation of an aggressive drilling programme at the Statfjord Field – maximising production in a mature field*. SPE **78347**.

Hempton, M., Marshall, J., Sadler, S., Hogg, N., Charles, R. & Harvey, C. 2005. Turbidite reservoirs of the Sele Formation, Central North Sea: geological challenges for improving production. *In*: Doré, A. G. & Vining, B. A. (eds) *Petroleum Geology: Northwest Europe and Global Perspectives: Proceedings of the 6th Petroleum Geology Conference*. Geological Society, London, 449–459; doi: 10.1144/0060449.

Hogg, A. J. C. 2003. The Montrose, Arbroath and Arkwright Fields, blocks 22/17, 22/18, 22/23a, UK North Sea. *In*: Gluyas, J. & Hitchen, H. (eds) *United Kingdom Oil and Gas Fields Commemorative Millennium Volume*. Geological Society, London, Memoirs, **20**, 611–616.

Holtz, M. H. & Hamilton, D. S. 1998. *Reservoir Characterization Methodology to Identify Reserve Growth Potential*. Presented at the International Petroleum Conference and Exhibition of Mexico, Society of Petroleum Engineers, 3–5 March, Villahermosa, Mexico. SPE Paper **39867**.

Kunka, J. M., Williams, G. *et al*. 2003. The Nelson Field, Blocks 22/11, 22/6a, 22/7, 22/12a, UK North Sea. *In*: Gluyas, J. G. & Hichens, M. H. (eds) *United Kingdom Oil and Gas Fields, Commemorative Millennium Volume*. Geological Society, London, Memoirs, **20**, 617–646.

Larue, D. K. 2004. Outcrop and waterflood simulation modeling of the 100-foot Channel Complex, Texas, and the Ainsa II Channel Complex, Spain: analogs to multistory and multilateral channelized slope reservoirs. *In*: Grammer, G. M., Harris, P. M. & Eberli, G. P. (eds) *Integration of Outcrop and Modern Analogs in Reservoir Modelling*. AAPG, Tulsa, OK, Memoir, **81**, 337–364.

Larue, D. K. & Hovadik, J. 2006. Connectivity of channelized reservoirs: a modelling approach. *Petroleum Geoscience*, **12**, 291–308.

Lowry, P., Jenkins, C. D. & Phelps, D. J. 1993. Reservoir scale sandbody architecture of Pliocene turbidite sequences, Long Beach Unit, Wilmington oil field, California. Presented at the SPE Annual Technical Conference and Exhibition, 3–6 October, Houston, TX. SPE Paper **26440**.

MacGregor, A. G., Trussell, P., Lauver, S., Bedrock, M., Bryce, J. & Moulds, T. 2005. The Magnus field; extending field life through good reservoir management and enhanced oil recovery. *In*: Doré, A. G. & Vining, B. A. (eds) *Petroleum Geology: Northwest Europe and Global Perspectives: Proceedings of the 6th Petroleum Geology Conference*. Geological Society, London, 469–475; doi: 10.1144/0060469.

McInally, A. T., Redondo-López, T., Garnham, J., Kunka, J., Brooks, A. D., Stenstrup-Hansen, L., Barclay, F. & Davies, D. 2003. Optimising 4D fluid imaging. *Petroleum Geoscience*, **9**, 91–101.

Milkov, A. V., Goebel, E., Dzou, L., Fisher, D. A., Kutch, A., McCaslin, N. & Bergman, D. F. 2007. Compartmentalization and time lapse geochemical reservoir surveillance of the Horn Mountain oil field, deep-water Gulf of Mexico. *AAPG Bulletin*, **91**, 847–876.

Partington, M. A., Mitchener, B. C., Milton, N. J. & Fraser, A. J. 1993. Genetic sequence stratigraphy for the North Sea Late Jurassic and early Cretaceous: distribution and prediction of Kimmeridgian–Late Ryazanian reservoirs in the North Sea and adjacent areas. *In*: Parker, J. R. (ed.) *Petroleum Geology of Northwest Europe: Proceedings of the 4th Conference*. Geological Society, London, 347–370; doi: 10.1144/0040347.

Shepherd, M. 2009. *Oil Field Production Geology*. AAPG, Tulsa, OK, Memoir **91**.

Shepherd, M., Kearney, C. J. & Milne, J. H. 1990. Magnus field. *In*: Beaumont, E. A. & Foster, N. H. (eds) *1990, Structural Traps II Traps Associated with Tectonic Faulting. Treatise of Petroleum Geology of Oil and Gas Fields*. AAPG, Tulsa, OK, 95–125.

Vaughan, O., Jones, R. & Plahn, S. 2007. Reservoir management aspects of the rejuvenation of the Forties Field, UKCS. Presented at Offshore Europe, Society of Petroleum Engineers, 4–7 September 2007, Aberdeen. SPE Paper **109012**.

Vining, M. R. 1997. Reserve growth in a mixed sequence of deltaic and barrier-island Frio Sandstones: Umbrella Point field, Chambers County, Texas. *Gulf Coast of Geological Societies Transactions*, **47**, 612–619.

Weber, K. J. 1999. The prize – what's possible? *Petroleum Geoscience*, **5**, 135–144.

Weimier, P. & Slatt, R. M. 2004. *Petroleum Systems of Deep-Water Settings*. SEG/EAGE (Society of Exploration Geophysicists/European Association of Geoscientists and Engineers) Distinguished Instructor Series, **7**. 465 pp.

Wetzaeler, A., Hildebrandt, A., Coutts, S. D. & Veeman, S. W. 1996. Locating the remaining oil in the Brent field prior to depressurisation. Presented at the European Petroleum Conference, Society of Petroleum Engineers, 22–24 October 1996, Milan. SPE Paper **36891**.

Wills, J. M. 1991. The Forties Field, Block 21/10, 22/6a, UK North Sea. *In*: Abbots, I. L. (ed.) *United Kingdom Oil and Gas Fields, 25 Years Commemorative Volume*. Geological Society, London, Memoirs, **14**, 301–308.

The Buzzard Field: anatomy of the reservoir from appraisal to production

F. M. RAY, S. J. PINNOCK, H. KATAMISH and J. B. TURNBULL

Nexen Petroleum UK Ltd., Charter Place, Vine Street, Uxbridge, Middlesex, UB8 1JG (e-mail: Francesca_Ray@nexeninc.com)

Abstract: The Buzzard oil field in the Outer Moray Firth, Central North Sea was discovered in 2001 and rapidly appraised during 2001–2002. Pre-production development drilling began in 2005 and the field was brought on stream in January 2007 by operator Nexen Petroleum UK Ltd. The Buzzard reservoir consists of Upper Jurassic deep marine turbidites within the Kimmeridge Clay Formation. Sands were derived from the shelf to the west and the resulting mass flow deposits were contained within a fault-bounded basin, whose margins were prone to mass wastage. The deposits pinchout to the west and thicken eastwards into the basin and hydrocarbon source kitchen. Following appraisal drilling, the high net-to-gross reservoir was interpreted as well connected. Interbedded shale layers were thought unlikely to control flow through the reservoir. However, a biostratigraphic review indicated that a consistent biostratigraphic event, indicative of reworking, could be identified field-wide. This shale layer is interpreted as a large-scale, muddy slump, extensive enough to form a significant vertical barrier to flow. Subsequent production data, modelling and chemostratigraphy studies suggest greater subdivision and vertical baffling within the main reservoir. Interpretation of these data has led to a move away from early models of Buzzard as a tank-like reservoir to a model dominated by compensationally stacked lobes, where hydraulic flow is influenced by sand body geometry and extensive shales. A comprehensive understanding of the Buzzard Field has only been possible through full integration of core, log and dynamic data, benefiting from a high density of well control, an extensive data acquisition programme and early reservoir monitoring. Ongoing reservoir management, involving continuous update of both the geological and dynamic models in response to new data, has enabled an evolving understanding of the Buzzard reservoirs, and placed the operator in an excellent position to proactively address future development challenges.

Keywords: turbidite, Upper Jurassic, integration, biostratigraphy, chemostratigraphy

The Buzzard Field development area is located across four blocks of the UK Central North Sea, 19/05, 19/10, 20/01 and 20/06, although the majority of the field occurs within part block 20/06a where the platform facilities are located. The field is situated approximately 50 km NE of the Scottish mainland in a water depth of 318 ft. The accumulation lies within the Outer Moray Firth region of the UK North Sea, at the western end of the Buchan Graben and at the southwestern limit of the Ettrick sub-basin (Fig. 1). To the west lies the Grampian Spur, an Upper Jurassic platform area, while the Peterhead Graben is located to the south. The Ettrick sub-basin is separated from the Peterhead Graben by a SW–NE trending Mesozoic structural high drilled by well 20/06-1 (Fig. 2). This structure constrains the southern limit of the Buzzard Field.

Structure and trap

Within the Buzzard Field development area, the main accumulation is offset by several west–east oriented normal faults (Fig. 3). These divide the field into three main regions referred to as the Southern, Central and Northern Panels, flanked by smaller structural terraces. The faults have a maximum offset of about 250 ft and are more or less continuous across the area of the accumulation. Both the Southern-Central and Central-Northern Panel bounding faults throw down to the north. The Northern Panel is limited on its northern margin by a down to the south, west–east oriented normal fault. Beyond this lies the Buzzard Northern Terrace into which the 20/01-5 appraisal well was drilled.

The trapping mechanism for the field is exclusively stratigraphic in nature as Buzzard sands are completely enclosed within sealing shales of the Kimmeridge Clay Formation. The sands were deposited by turbidite flows, from the west, into a structural low between the southerly Mesozoic high and the Buzzard Northern Terrace (Fig. 2). This gave rise to a thick sandy sequence in the centre of the low pinching-out onto the northern and southern flanks (the sands were not deposited in 20/06-1) and also westwards, towards the shelfal source area. Regional dip down to the east limits the oil accumulation with the field oil–water contact lying west and slightly updip of well 20/06-2 (Fig. 3).

Jurassic stratigraphy

Initial marine flooding of this part of the Buchan Graben can be dated to the Oxfordian and is recorded by the transgressive shallow marine Sgiath Sandstone (Fig. 4). Extension along SW–NE oriented fault systems resulted in rapid deepening of the graben in the Buzzard Field area. The Late Kimmeridgian to Early Volgian Buzzard Sandstone Member was deposited during this syn-rift phase into a relatively deep and anoxic basin. Extensional fault trends within the Late Volgian and Ryazanian were oriented west to east and lead to modification of the original SW–NE structural grain. It is this later trend that offsets the field, giving the present-day structural configuration.

The gross Jurassic interval in Buzzard wells is primarily subdivided on the basis of lithological variations and biostratigraphic markers which relate directly to the established Upper Jurassic chronostratigraphy of the North Sea (Fig. 4) (Partington *et al.* 1993). The total Jurassic package can be split into four formations (Kimmeridge Clay, Heather, Sgiath and Pentland) of which the Kimmeridge Clay is the thickest and contains the reservoir sands in the Buchan Graben area. Three major phases of turbidite sand deposition are informally recognized within the Kimmeridge Clay Formation: the Buzzard, Ettrick and Burns Sandstone Members, of which Buzzard is the oldest. In the Buzzard Field

VINING, B. A. & PICKERING, S. C. (eds) *Petroleum Geology: From Mature Basins to New Frontiers – Proceedings of the 7th Petroleum Geology Conference*, 369–386. DOI: 10.1144/0070369

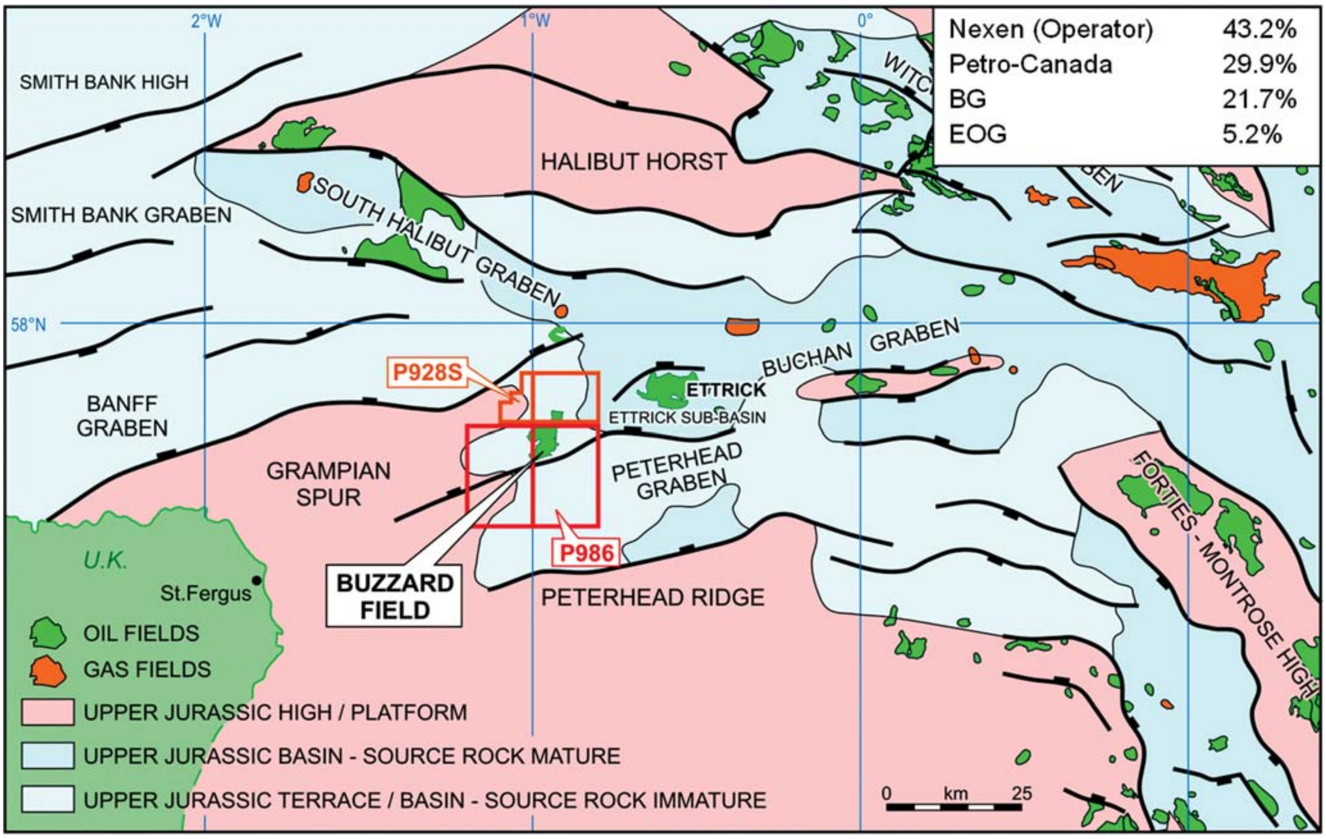

Fig. 1. Buzzard Field development area location map.

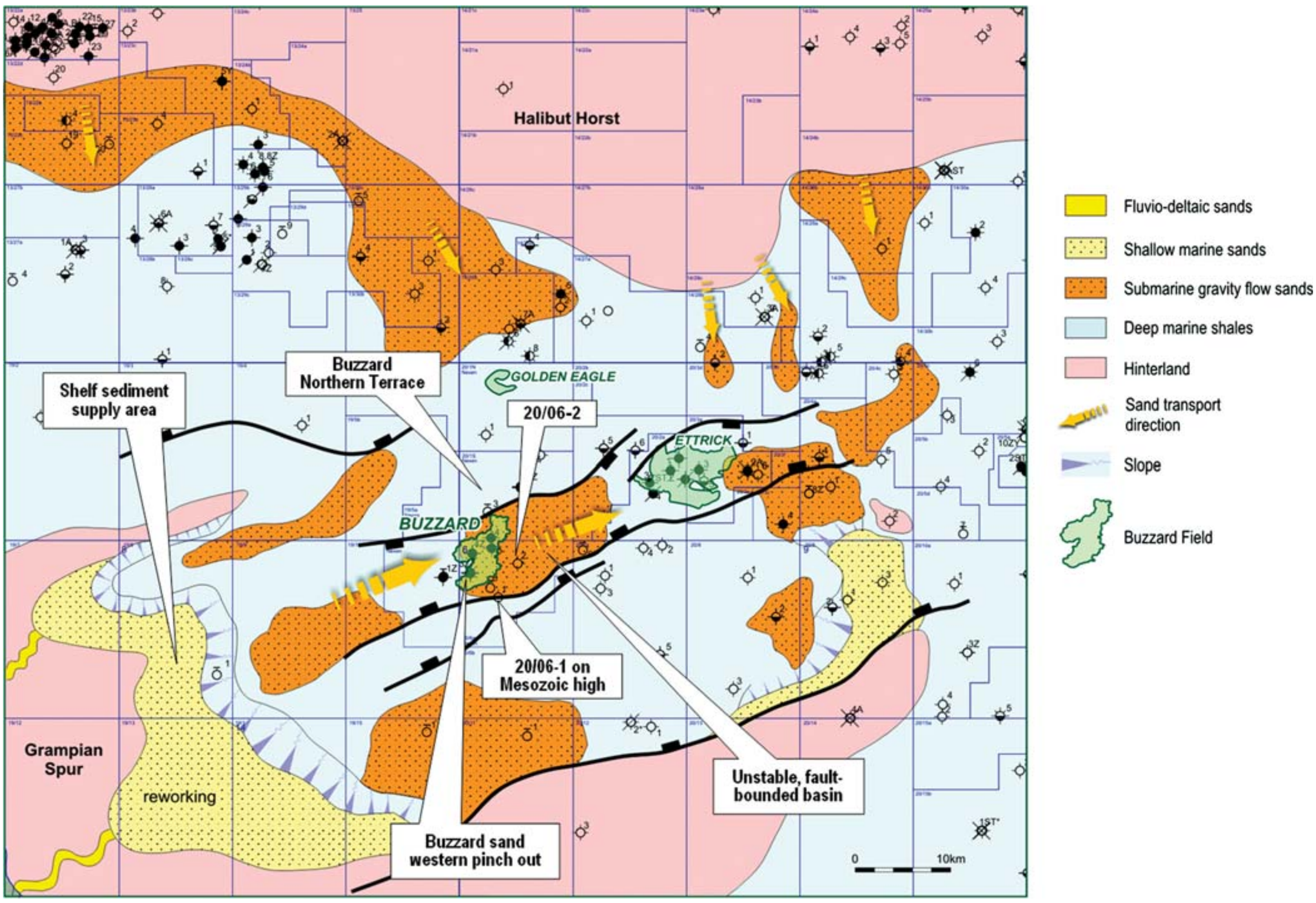

Fig. 2. Palaeogeography of the Buzzard Sandstone Member.

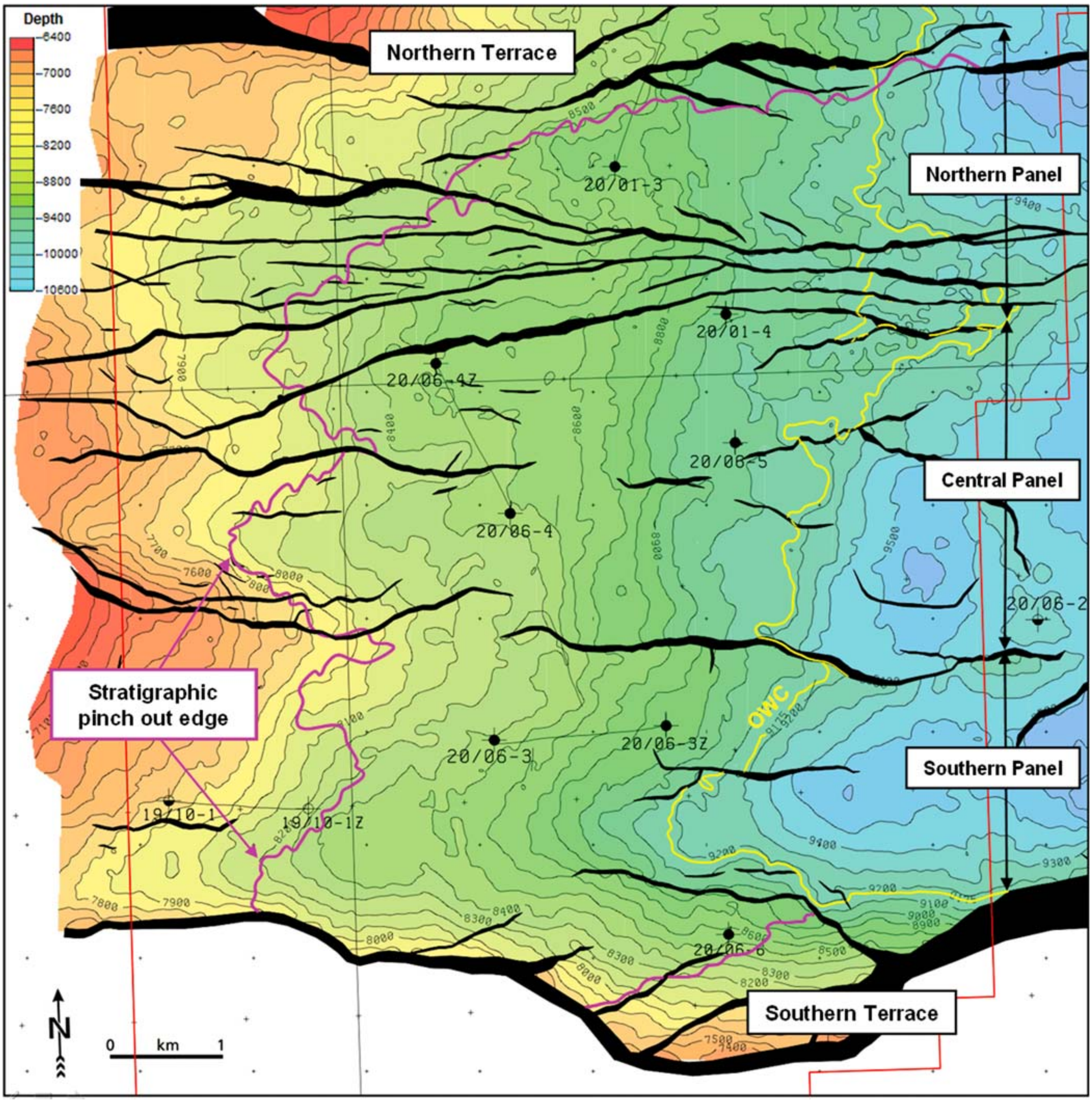

Fig. 3. Buzzard Field top reservoir depth map, structural configuration and location of exploration and appraisal wells.

area the Upper Jurassic interval is dominated by the Buzzard Sandstone Member, overlain by very thin, shale-prone Ettrick and Burns sections.

Field discovery and appraisal

Prospectivity in this part of the Buchan Graben was initiated by well 20/06-2, drilled in 1987 to test a relatively small four-way dip closure mapped within the Jurassic sequence (Fig. 3). The well is located eastward and downdip of the Buzzard Field but encountered a thick Buzzard Sandstone Member. An 11 ft oil column at the top of the Buzzard Sandstone Member in this well confirmed an active petroleum system in this part of the basin. However, the large potential prospectivity westward and updip of 20/06-2 was not tested for a further 14 years due to the perceived high-risk nature of the stratigraphic play.

The Buzzard discovery well, 20/06-3, was drilled in 2001. The well was sidetracked downdip as 20/06-3Z and together these wells proved a 753 ft oil column within the Buzzard Sandstone Member (Doré & Robbins 2005). During 2001 and 2002 six appraisal wells and two associated sidetracks were drilled (Fig. 3). Locations were based on the existing 3D seismic data, which was qualitatively interpreted to identify intra-reservoir packages defined by thickness, amplitude and morphology. These appraisal wells delineated most of the accumulation, confirming Buzzard as the biggest find in the North Sea since the discovery of the Nelson Field in 1988, and allowed an early commitment to field development. Since then, the field's structurally highest delineation well has proven an oil column height of over 1400 ft.

The Buzzard reservoir contains undersaturated 32° API oil at a reference pressure of 4628 psia and temperature of 195°F at a reservoir datum of 8735 ft TVDSS. The accumulation is some

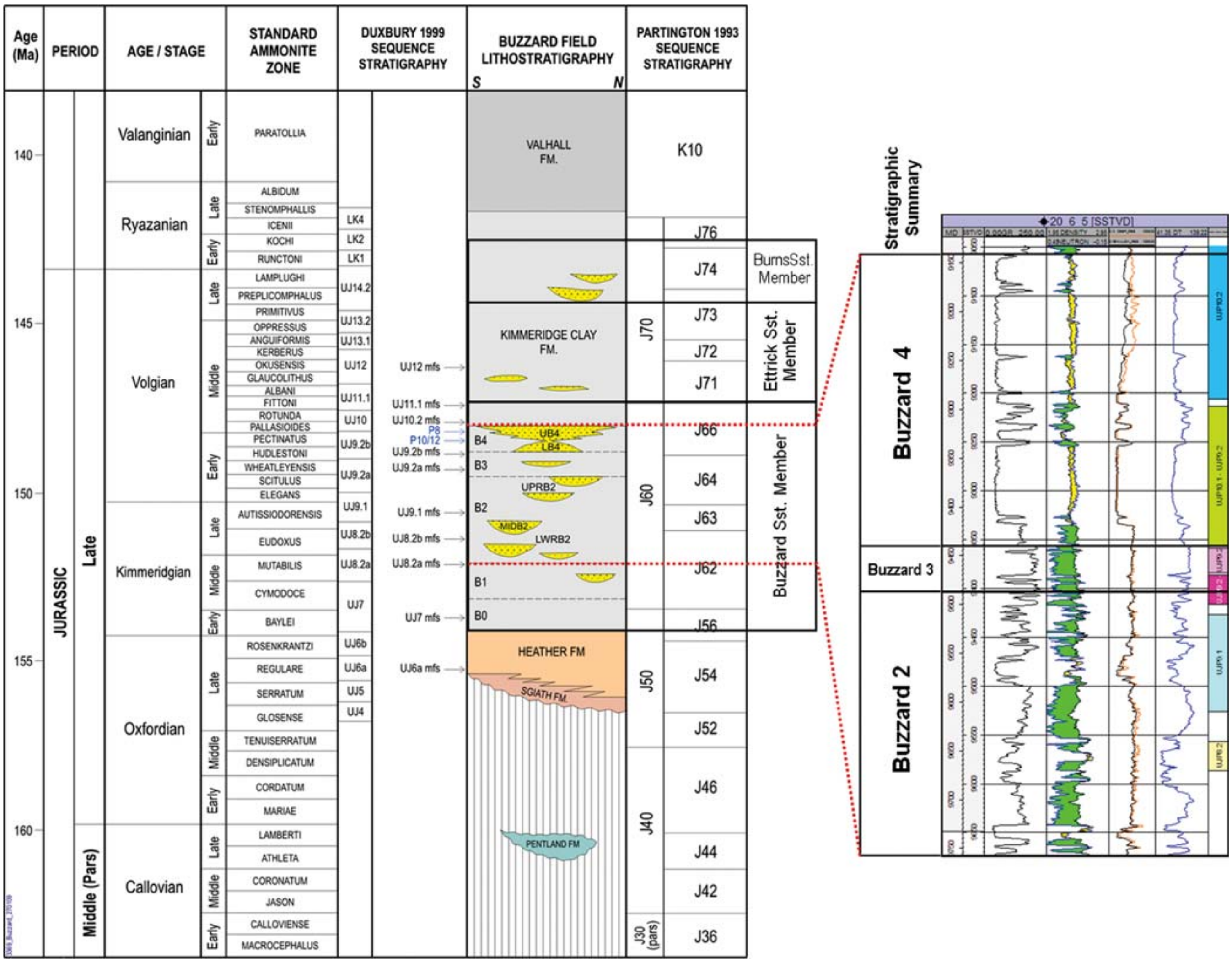

Fig. 4. Buzzard Field stratigraphy illustrated by appraisal well 20/06-5, which penetrated the OWC in the Central Panel. Tracks, from left to right, are measured depth (MD); subsea true vertical depth (SSTVD); gamma ray (GR); density-neutron; resistivity (deep and shallow); sonic (DT) and Duxbury palynological zonation (Partington *et al.* 1993; Duxbury *et al.* 1999).

600 psia over-pressured relative to a normal hydrostatic gradient, suggesting the system is pressure isolated within the surrounding Kimmeridge Clay Formation shales.

Theme of the paper

The main focus of this paper is on the uppermost Buzzard Sandstone Member, the Buzzard 4 (B4) reservoir (Fig. 4), as it holds the majority of the STOIIP and reserves (approximately 90%). The format for the rest of the paper continues the timeline onwards from field appraisal through field development planning to the present day. The text is subdivided into four sections representing points in time (Mid 2003, End 2006, End 2007 and Mid 2009). In each, the critical data acquisition and interpretations of the time are discussed, illustrating the evolution in understanding of the Buzzard Field. This paper also demonstrates how development of the field has been adapted to account for revised subsurface interpretations in order to optimize field recovery, and exemplifies the benefits of early and continuous static and dynamic data acquisition and integration.

The Buzzard Field: mid 2003

The Buzzard Field Development Plan (FDP) was submitted during 2003 on the basis of 11 exploration and appraisal wells, together with the 3D seismic survey upon which the discovery was made. This survey was acquired in 1995 and reprocessed in 2000. Dynamic and fluid data was acquired from four drill stem tests (DSTs) carried out in the exploration and appraisal wells. Three of these were performed on discrete oil intervals, whilst the fourth was a production and injectivity test below the oil–water contact. At the time of the FDP, the base case estimate of oil-in-place and reserves was around 1000 and 500×10^6 stb, respectively.

Reservoir stratigraphy

The FDP reservoir subdivision, originally defined in the discovery well 20/06-3, was both lithostratigraphically and biostratigraphically driven. The reservoir sequence was subdivided into five chronostratigraphically constrained packages referred to, from top to bottom, as the Buzzard 4 (B4), Buzzard 3 (B3), Buzzard 2 (B2), Buzzard 1 (B1) and Buzzard 0 (B0) units (Fig. 4).

At this time, the uppermost reservoir unit, B4, was described as a laterally extensive, massive sand unit, dominated by high net-to-gross, high-density turbidites in the Central and Southern Panels (Fig. 5a). The extent of subordinate thin shales was uncertain. The B3 unit, underlying the B4, was interpreted as a laterally extensive hemipelagic shale unit. The B2 unit was described as a laterally extensive unit of variable reservoir quality, with high-quality B2 sands interpreted only in the Southern Panel. The

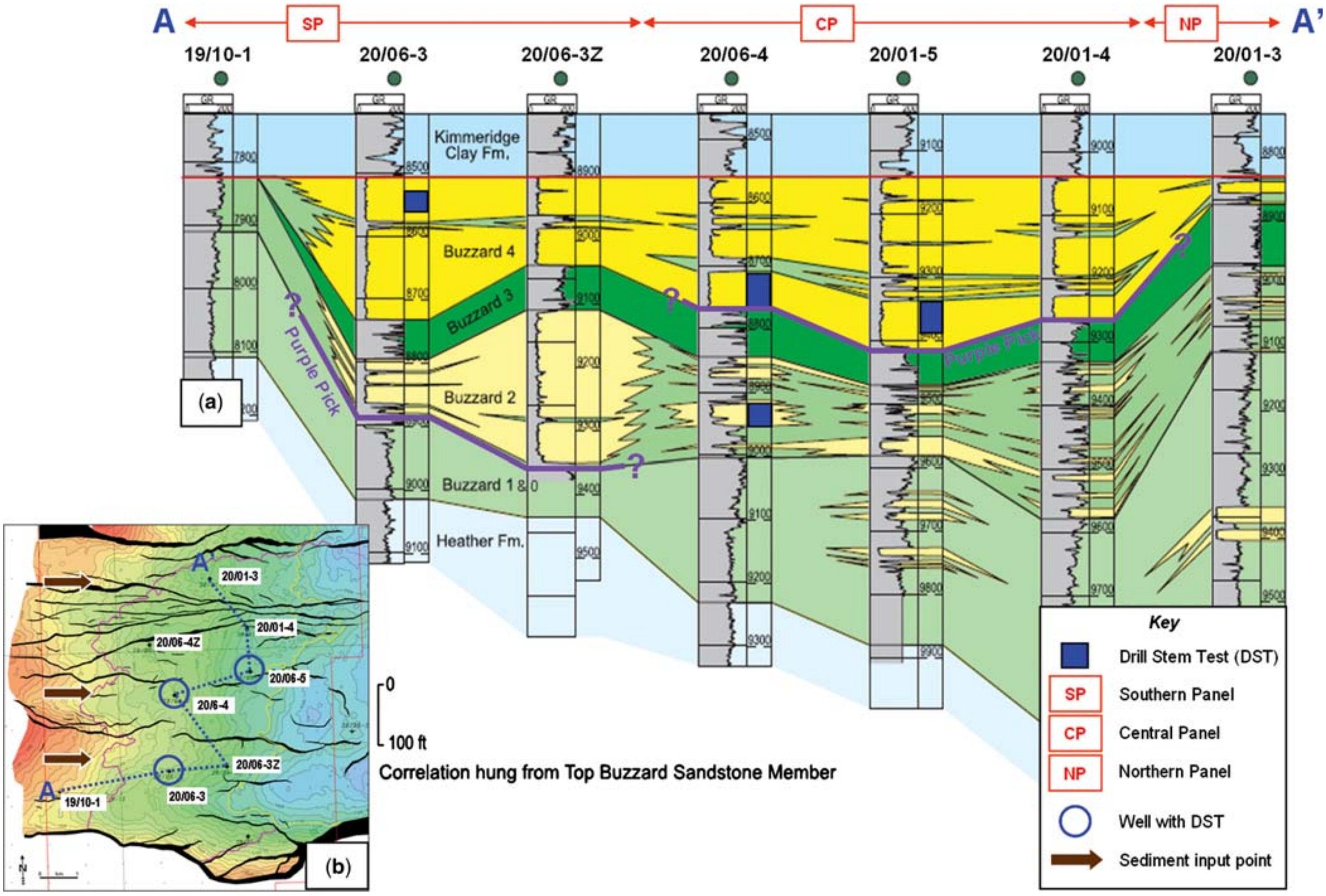

Fig. 5. (**a**) Appraisal well correlation A–A′ through the Southern, Central and Northern Panels. Note correlation into 20/06-3Z (discovery well sidetrack), where the thick, lower sand body is assigned to the B2 package. Tracks, from left to right, are GR infilled by stratigraphic unit and SSTVD. (**b**) Buzzard top structure map showing location of cross-section and postulated sediment input points.

oldest Buzzard units, B1 and B0, are laterally extensive, shale-dominated packages with very low to no reservoir potential.

Seismic interpretation

The FDP seismic interpretation characterized the Buzzard reservoir by three events: Top Buzzard, intra-Buzzard (referred to as the ‘Purple Pick’) and Base Buzzard. Top Buzzard corresponded to the top of the high net to gross, massive sand: the Buzzard 4 (B4) unit. The ‘Purple Pick’ was a conspicuous intra-reservoir event marking the base of the high net to gross package. The pick was apparently diachronous since the interpretation at that time was unable to reconcile the biostratigraphic and geophysical data. This resulted in the ‘Purple Pick’ coinciding with the base of the B4 unit in the Central Panel, but the base of the B2 in the Southern Panel (Fig. 5a). The Base Buzzard horizon was picked on an event close to the base of the B2 unit.

In general, the gross Buzzard reservoir envelope was considered to be well constrained within the core of the Southern, Central and Northern Panels. The areas with most uncertainty in reservoir pinchout definition were SE of well 19/10-1 in the Southern Panel, around 20/06-4Z in the Central Panel and west of 20/01-3 in the Northern Panel (Fig. 5b). Continuity of the Buzzard reservoir sands into the Northern Terrace was also uncertain, although there was strong evidence for thinning of the B4–B2 interval towards the north.

Geological model at field sanction

At FDP time, reservoir development and intra-reservoir stratigraphy were believed to be closely related to structural development. The depositional model was based on a concept whereby interactions between sediment supply and creation of accommodation space, through initiation and movement on half-graben faults, led to preferential deposition of sand rich flows. This seemed to explain the stratigraphic architecture of the sandy B4 unit in the Central and Southern Panels and the B2 in the Southern Panel (Fig. 5a). It was postulated that sand input kept pace with, or exceeded, the development of accommodation space via fault movement, resulting in thick sand accumulations. Other areas of the Buzzard Field, the Southern Terrace, Northern Panel and the Central Panel at the time of B2 unit deposition, were thought to have remained relatively ‘high’, with the resulting sedimentation being dominated by shale and limited sand.

It was postulated that the primary sediment supply to the area was via multiple input points, to the SW, west and NW (Fig. 5b). The major east–west faults which separated the field structural panels and terraces were mapped as having variable throw (up to a maximum of 250 ft), but were believed to be of sufficient magnitude along the majority of the fault to seal it as a result of clay smear. It was recognized that windows potentially existed along the fault plane, where throws were smaller, which might allow communication.

Using this geological model as a guide, seismic was used qualitatively to identify intra-reservoir packages defined by thickness, total absolute amplitude and morphology and correlated with well data to define areas of low, medium and high net to gross within the Buzzard Field. This approach had proved successful as a predictive model for appraisal drilling, and so formed the basis of the FDP Buzzard reservoir model used for initial development well planning. Gross reservoir packages, such as the B4, were defined deterministically as sandy units within which shales were stochastically populated, constrained by the seismically derived net to gross maps and honouring the well data. As per the conceptual model, this typically allowed full communication throughout the B4, as shales were modelled with very limited lateral extent.

A range of studies completed prior to the FDP, designed to further refine both vertical and lateral heterogeneity and compartmentalization in the field, proved difficult to integrate with the geological model at the time. These studies included chemostratigraphy, heavy mineral analysis, strontium residual salt analysis, core palaeomagnetic analysis and fault seal analysis. More recent follow-up studies, made with the benefit of twice as much well data plus dynamic data, have since proved the value of these alternative studies and contributed to the development of current geological models consistent with all the data.

Reservoir performance and fluids

The DSTs confirmed the presence and continuity of high permeability sands in the B4 and B2 units contributing to high well deliverability. Fluid analysis on bottom hole samples obtained from DSTs in 20/06-3 and 20/06-4 indicated the presence of H_2S. The highest values of H_2S in oil observed during the appraisal campaign were from a DST in 20/06-4 which tested the B4 sands in the Central Panel (Fig. 5b). This equated to well stream values of 42.1 ppm weight as H_2S. The 20/06-3 well DST tested the B4 interval in the Southern Panel and showed lower well stream values of 5 ppm weight as H_2S. The fluid composition from the 20/06-4 DST in the B4 unit was adopted for topsides design purposes, since it had showed the highest H_2S levels and was believed to represent approximately 40% of the oil in place.

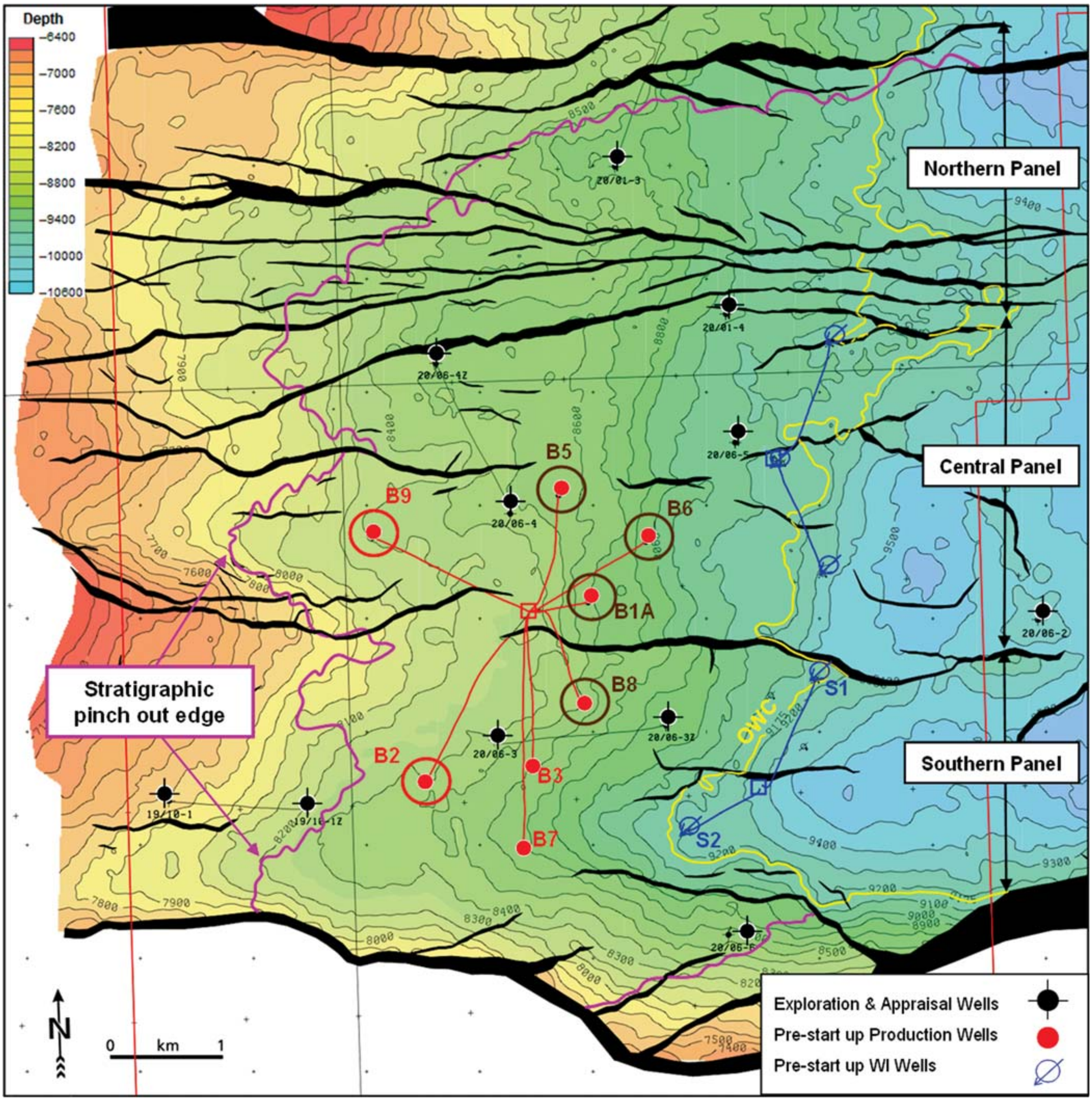

Fig. 6. Top structure map showing platform, subsea manifold locations and the 16 wells drilled prior to field start-up. Wells circled red are revised, updip production locations. Wells circled brown are perforated as pressure monitoring wells, rather than production wells as originally planned, due to higher than expected levels of H_2S.

The Buzzard Field: late 2005 to end 2006

In accordance with the FDP, a number of production and injection wells were drilled prior to the start of field production, between October 2005 and the end of 2006. Location of these pre-development wells was intended to provide a balance between the desire to produce the field at the design capacity from soon after start-up and the need to improve reservoir understanding prior to first oil. The strategy for pre-development production wells was to initially drill mid-flank wells covering a north to south span across the Southern and Central Panels. This was to mitigate against the risk of NW–SE trending compartmentalization through structural elements or stratigraphic pinchouts, which early studies had highlighted as a risk. Mid-flank producers were to be followed later in field life by updip production wells, with all wells completed progressively downwards from the B4 to the B2 unit, or converted to injectors in the B4 unit. Little scope was seen for water shut-off of individual sands within the B4 unit due to the perceived lack of laterally extensive sealing shales and the relatively high vertical permeabilities within the unit. Wells were to be drilled from a drilling platform located above the Central Panel (Fig. 6). This was installed, together with the production facility, in 2005–2006. Injection wells were to be drilled from two subsea manifolds located above the Southern and Central Panels.

Pre-development drilling results

Thirteen wells were drilled and completed between 2005 and first oil in 2007, eight producers and five injectors (Fig. 6). The strategy for the location of injection wells, which was to place them as close to the original oil–water contact (OOWC) as possible, did not change as a result of pre-development drilling. In contrast to the injection wells, production well planning changed dramatically as a consequence of pre-development drilling. The first well, 20/01-B1A, targeting the core of the field and 1–1.5 km from the nearest appraisal wells (Fig. 6), found H_2S levels three times greater than expected based on appraisal well predictions. Subsequent wells throughout the field demonstrated that the H_2S distribution varied significantly over short distances (Beilby *et al.* 2009). As a result, a solution for handling of higher H_2S levels later in field life was required and the decision to install a fourth platform to handle the fluids was made. This platform is due to be commissioned in 2010.

A more immediate consequence of the H_2S problem was a change in the pre-development drilling strategy. Mid-flank, potentially high H_2S, producer locations were revised to target updip areas believed to contain sweeter oil (Fig. 6, wells circled red). This change in strategy was successful and had the unforeseen benefit of leaving four mid-flank wells, which could not immediately come on stream due to high H_2S levels, available as pressure observation wells (Fig. 6, wells circled brown). These four wells in the Central and Southern Panels have subsequently provided invaluable information for understanding the performance of the B4 reservoir unit in the Buzzard Field.

Pre-development wells also clearly demonstrated the absence of any relationship between reservoir sand development and seismic amplitudes (or other properties), the FDP observations apparently being coincidental. While this did not significantly compromise

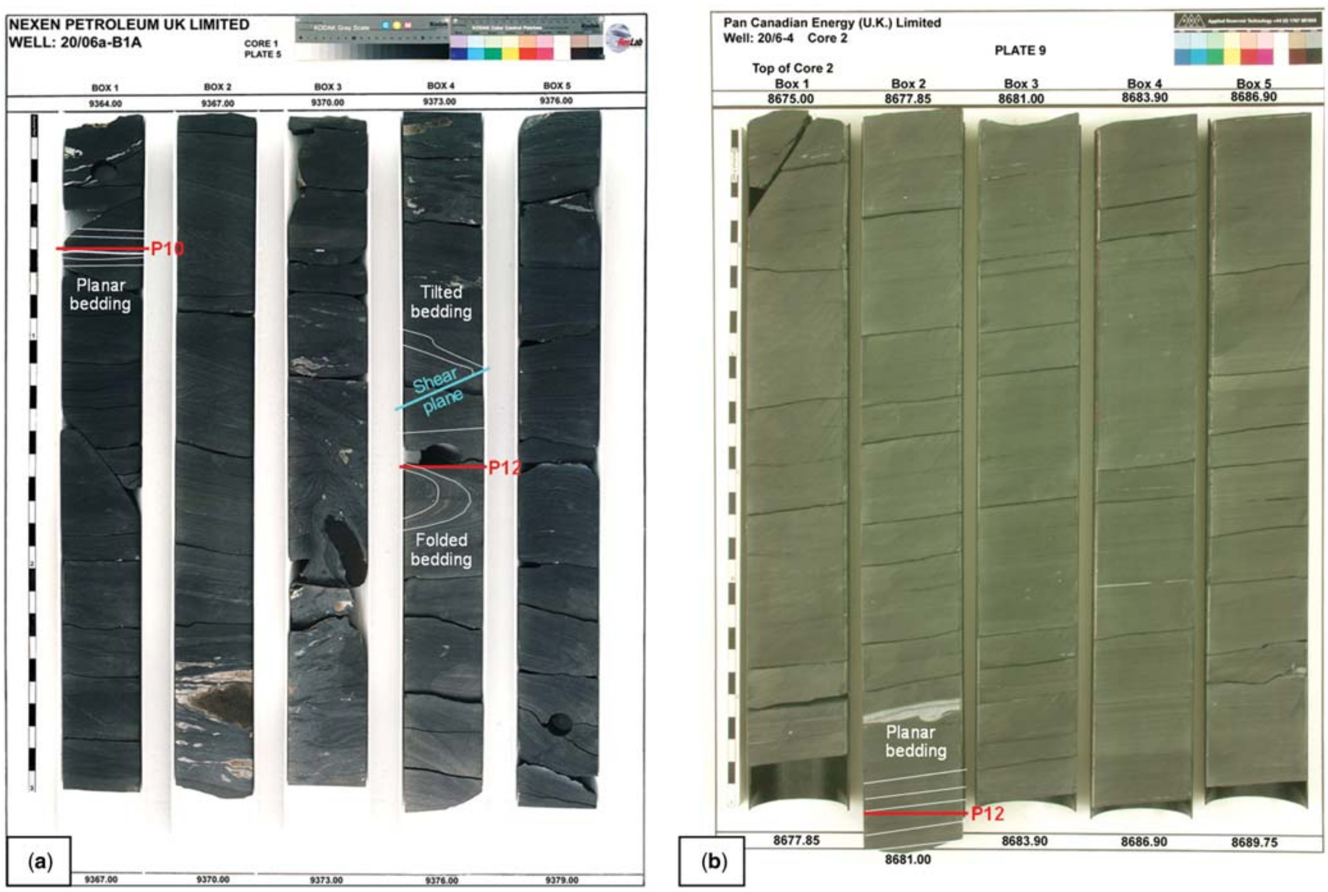

Fig. 7. Shales in core with field-wide consistent biostratigraphy markers P10 and P12. (**a**) P10 shale is planar laminated, whilst P12 shale is folded, tilted and sheared. (**b**) P12 event within a significant thickness of planar laminated shale. Assemblages of taxa in both P10 and P12 shales are consistent with an origin that includes reworked sediments, giving rise to the possibility that some of the planar laminated shales are not *in situ*, but are in fact large-scale slump blocks of partially lithified shale.

the results from these early development wells it did demonstrate both the caution that should be applied to such amplitude-based interpretations and the need for alternative methods of predicting reservoir quality and extent.

A consistent biostratigraphic interpretation

Wells drilled during the pre-development phase added to the considerable data acquisition programme begun by the appraisal wells. Full log suites were acquired in all wells, including pressure measurements, fluid samples, image logs and percussion sidewall cores. The additional conventional core taken at this stage doubled the total amount of core from the field to nearly 3000 ft.

Biostratigraphy had already been recognized as the most reliable aid to reservoir correlation, with palynological analysis providing by far the best stratigraphic resolution. Following a re-evaluation of the biostratigraphy in two appraisal wells in 2005, an intense programme of biostratigraphic analysis of conventional core, sidewall core and cuttings material was instigated covering a further five wells, with the aim of providing a robust biostratigraphic framework. This study confirmed the existence of consistent palynological events within the B4 unit, where previously the resolution had been limited to definition of only the gross B4–B0 packages.

Two particularly consistent events, recognized in all wells and referred to as the P10 and P12 events, displayed a range of palynoflora composed of B3 age markers together with younger taxa. At the time of the FDP, this assemblage was not recognized in all wells and, where it was observed, the shale containing it was assigned to the B3 unit. The constituent younger taxa were considered statistically insignificant. The new interpretation considered the younger taxa as more indicative of the age of deposition, implying that the B3 age taxa had been reworked and were incorporated as a result of slumping of older sediments. Sedimentological logging of these shales revealed a potentially confusing picture. Some of the P10 and P12 shales show clear evidence of remobilization, indicative of slump deposits (Fig. 7a), whereas others are planar laminated and appeared to be hemipelagic in origin (Fig. 7a, b). Correlation and mapping of the shale unit characterized by the P10 and P12 biostratigraphic events supported the interpretation of a laterally extensive intra-B4 shale, which was thickest in the Southern Panel and thinned towards the north (Fig. 8a). Evidence for slumping in core, in combination with reworked palynoflora, was the basis for suggesting that the Intra-B4 shale represented a kilometre-scale slump unit, probably derived through catastrophic failure of the southern basin margin. In places, the slump unit contains large-scale, partially lithified, blocks of shale.

Recognition of the Intra-B4 shale led to a redefinition of the B4 reservoir into an Upper and Lower unit and resulted in a notable revision to the correlation of the B4 and B2 units in the Southern Panel. In some wells, the shale originally picked as the B3 shale was re-defined as the Intra-B4 shale (Fig. 8b). In wells such as 20/06-3Z, sands originally designated as B2 became B4 units, giving rise to a Lower B4 unit up to 240 ft thick, but resulting in a thinner B2 package with considerably lower net to gross. This

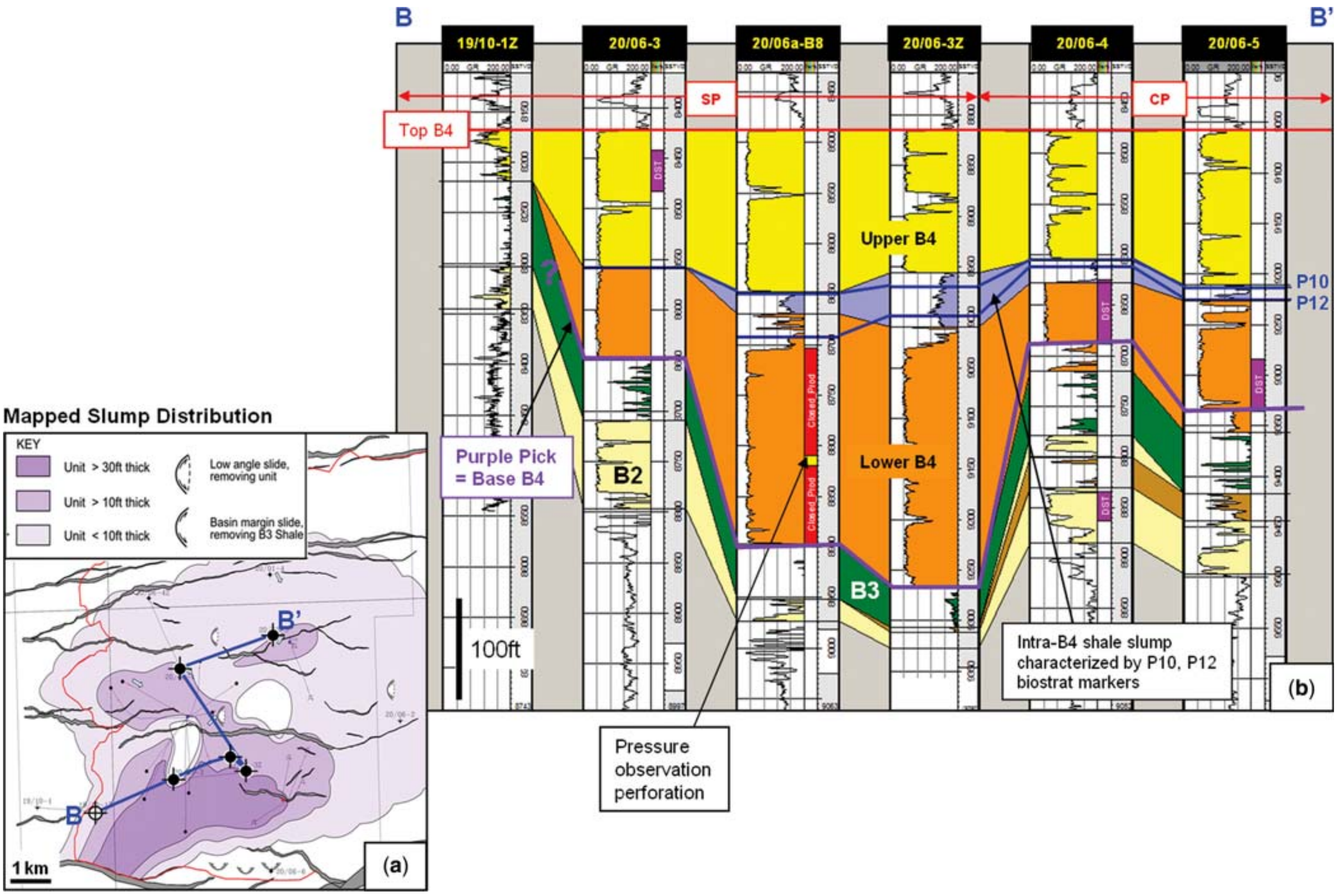

Fig. 8. Field-wide correlation and map of the Intra-B4 shale slump. Note the revised correlation in 20/06-3Z compared with Figure 5. The purple coloured shale unit has been re-interpreted from the B3 unit to the Intra-B4 shale and the underlying thick sand, coloured orange, formerly interpreted as the B2 unit, is now a Lower B4 unit. The Upper and Lower B4 are still considered to be laterally extensive sand-dominated units. Tracks, from left to right, are GR infilled by stratigraphic unit; perforation interval DST and SSTVD. SP, Southern Panel; CP, Central Panel.

alternative interpretation reconciled the seismic 'Purple Pick' with biostratigraphically driven correlations of wells field-wide and clarified the 'Purple Pick' as a base B4 marker. This allowed the gross B4 isochore package to be mapped directly on seismic.

Pre-development geological model

The revised correlation and seismic mapping no longer supported the tectonically controlled depositional model as proposed in the FDP. Thickest accumulations of sand were not confined to individual fault panels and hence there was little evidence to support the creation of accommodation space in associated half-grabens. Although it was supposed that the area remained tectonically active during deposition of the Buzzard sequence, this was confined to slight movements on the basin bounding faults, which triggered large-scale slumping as exemplified by the Intra-B4 shale unit. It became apparent that pre-existing basin topography must have played a significant role in controlling sand depositional geometries. In addition, mapping of the newly defined Upper and Lower B4 units indicated that a single source point, west of the Central Panel, rather than three separate source points, best fitted the new geometries. The modified correlation and mapping of the Upper and Lower B4 packages resulted in a radical change in the interpretation of sand connectivity and a shift in volumetric distribution within the Southern Panel, re-assigning more than 50×10^6 bbl from the B2 to the B4 unit. The development plan for the Southern Panel, which had expected to recomplete wells from the B4 to the B2 unit within the second year of field life, was revised to account for the new model, downgrading the importance of the B2 as a reservoir unit in the Buzzard Field and pushing its planned development further into the future.

Importantly, the geological model just prior to production start-up maintained the Upper and Lower B4 as discrete, field-wide hydraulic units, individually likely to behave in a tank-like manner. Shales within the body of each unit were considered to be small-scale features which would act as minor baffles only. The Upper and Lower B4 units were considered effectively isolated from each other, although it was thought that minor communication pathways could exist through fault juxtaposition. 'Holes' in the Intra-B4 shale, created by erosional downcutting of later, Upper B4-age flows, were also postulated to exist and to have the potential to provide leaky pathways between the Lower and Upper B4. This was based on evidence from the 20/06-3 well, where the Intra-B4 shale is absent, although the thick, sandy B4 unit present does contain large rip-up clasts with biomarkers commonly associated with the Intra-B4 shale (Fig. 8b).

The Buzzard Field: end 2007

Water injection began in December 2006, followed by first oil in January 2007. Prior to the field coming on stream, pressure data acquired in almost every pre-development well simply confirmed that all the wells lay on a common oil gradient, indicating that all sand units were potentially in hydraulic communication. Whether or not the Upper and Lower B4 units would communicate over a production time scale was a key question to be answered by post production start-up dynamic data.

By the end of 2007, an additional eight development wells had been drilled, bringing the total number of wells in the field to 35. Dynamic data, acquired after production start-up, provided an invaluable insight into the performance of the Buzzard Field. Key to this was downhole and tubing head pressure measurements acquired during interference testing.

Interference tests

At the time of field start-up, a set of interference tests were performed to gather information about lateral connectivity in the reservoir. Prior to production, pressure signals resulting from downdip injection were monitored in updip producers. The initial injection volume into the B4 was not large; only 300 000 barrels of water were injected into two Southern Panel injection wells, yet every single producer showed a pressure response, including wells located in the Central Panel. Even the most updip production well, 20/06a-B9, some 4 km away, saw a pressure response within 10 days (Fig. 9). These observations argued for a fairly open pressure system areally, even between the Central and Southern Panels. This was contrary to predictions based on the FDP model that the main structural panel bounding faults would be sealing.

Evidence for connectivity from pressure measurements

Prior to production start-up it was believed that the Intra-B4 shale, the biostratigraphically defined, laterally extensive shale between the Upper and Lower B4, would act as a vertical flow barrier. It was thought that only minimal connection between the two units existed, effectively resulting in segregated flow behaviour in the two B4 sands. However, post production start-up pressure profiles indicated that there was good communication across the Intra-B4 shale, indicative of highly effective Lower to Upper B4 connectivity, either through more widespread Upper to Lower B4 erosional contacts and/or fault juxtaposition of the two B4 units. The pressure profile in development well 20/06a-B14Z showed significant depletion both in the Upper and Lower B4, despite there being no off-take from the Lower B4 prior to drilling this well (Fig. 10a). The B2 unit was also depleted, to much the same level as the Lower B4. This was entirely unexpected, since the B2 unit was not under production and the field-wide B3 shale exists between the B4 and B2 packages. These data led to a review of the seismic in the area of the well and the identification of a small normal fault, south of the 20/06a-B14Z, which tips out rapidly to the east and west. At the point of maximum offset, where the throw is approximately 75 ft, the Upper and Lower B4 are juxtaposed and the Lower B4 and B2 are juxtaposed. Since the fault tips out, the pressure wave can easily travel around the ends of the fault to produce a localized system in which all the units communicate (Fig. 10b). Without the pressure data, this fault would not have been firmly identified on seismic since the amount of throw is close to seismic resolution. This example provided good evidence that faults of this magnitude exist and provide communication pathways between reservoir units in the Buzzard Field. More recent work has identified additional areas of fault juxtaposition which allow such cross-unit communication.

In contrast, pressure profiles from Southern Panel wells show a different story, in which only minor depletion in the B2 is observed, suggesting that the effects of such faulting may be localized.

Evidence for compartmentalization from pressure measurements

Whilst early monitoring of reservoir pressures has provided positive evidence of communication within the B4 and to the B2 unit, it has also, critically, enabled identification of isolated sand packages within the B4 reservoir. Mid flank, pre-production wells which could not come on stream due to H_2S levels were nevertheless perforated as pressure monitoring wells. Figure 11 shows the response of four pressure monitoring wells as a Southern Panel production well, 20/06a-B3, came on stream in January 2007.

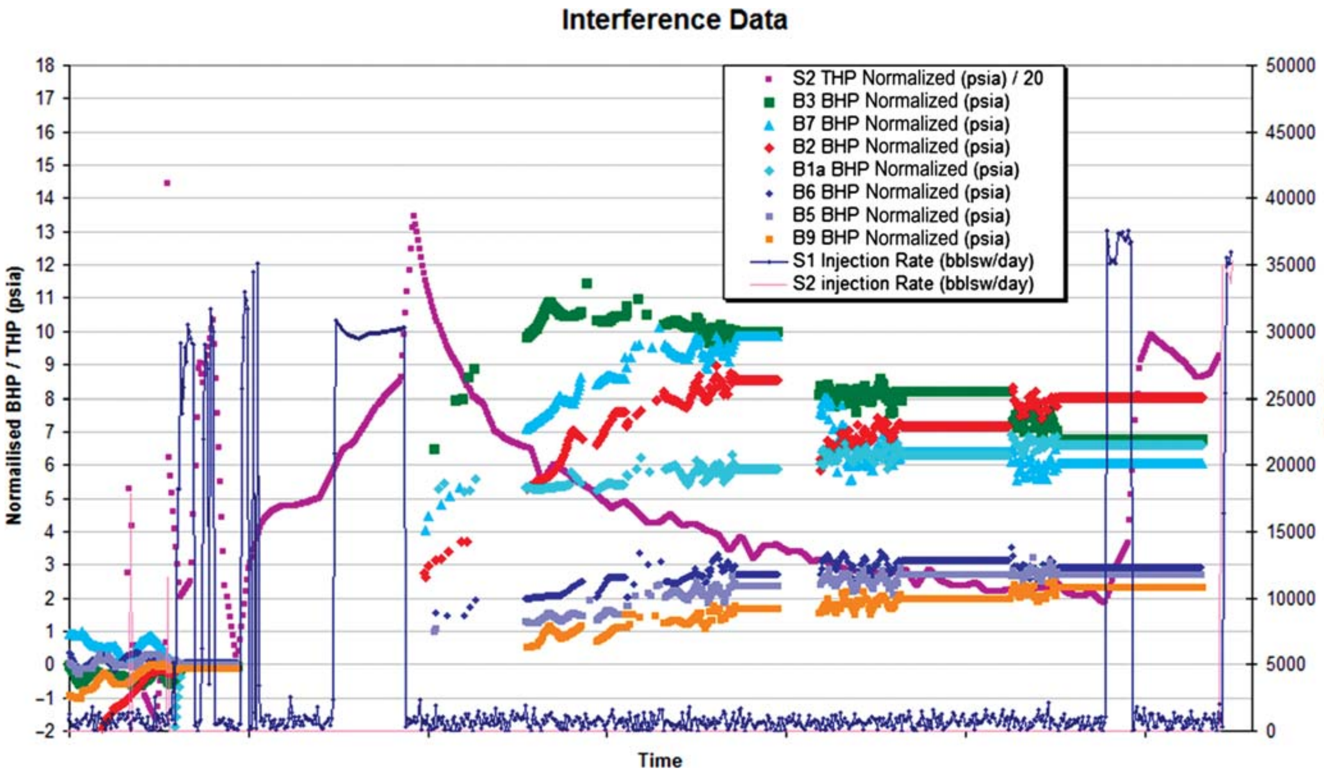

Fig. 9. Interference data plot showing production well bottom hole pressure (BHP) response in seven wells to initial water injection rate shown in barrels per day (Bbls/day) in Southern Panel injectors, 20/06a-S1 and 20/06a-S2. BHP shown as points and injection rate shown as lines. Tubing head pressure (THP) in the 20/06a-S2 injection well is also shown as points. All wells show a pressure response, including Central Panel pressure monitoring wells 20/06a-B1A, 20/06a-B6 and 20/06a-B5, and updip Central Panel producer 20/06a-B9. Refer to Figure 6 for well locations.

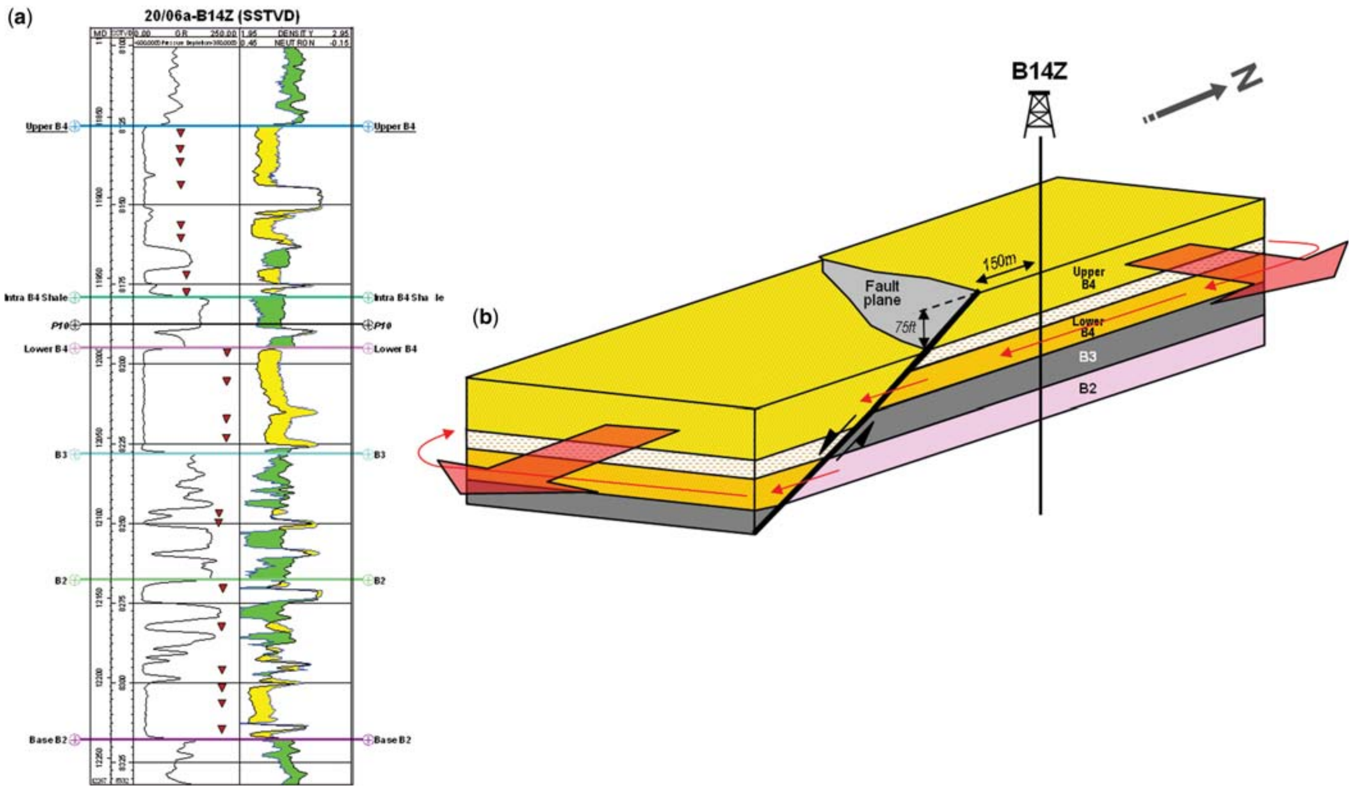

Fig. 10. (**a**) Central Panel updip production well 20/06a-B14Z drilled in 2007 showing pressure depletion as red triangles (track 3) relative to virgin reservoir conditions represented by the right hand side of the GR track. This illustrates depletion in Upper and Lower B4 units and the B2 unit, despite no offtake from the Lower B4 or B2 units. Tracks, from left to right, are MD; SSTVD; GR and density-neutron. (**b**) Cartoon block diagram showing how sand-to-sand juxtaposition across the tipping out fault near 20/06a-B14Z results in depletion of Upper and Lower B4 and B2 units. Inferred local flow pathways shown as small red arrows, with flow out of area to Upper B4 production wells as thick red arrows.

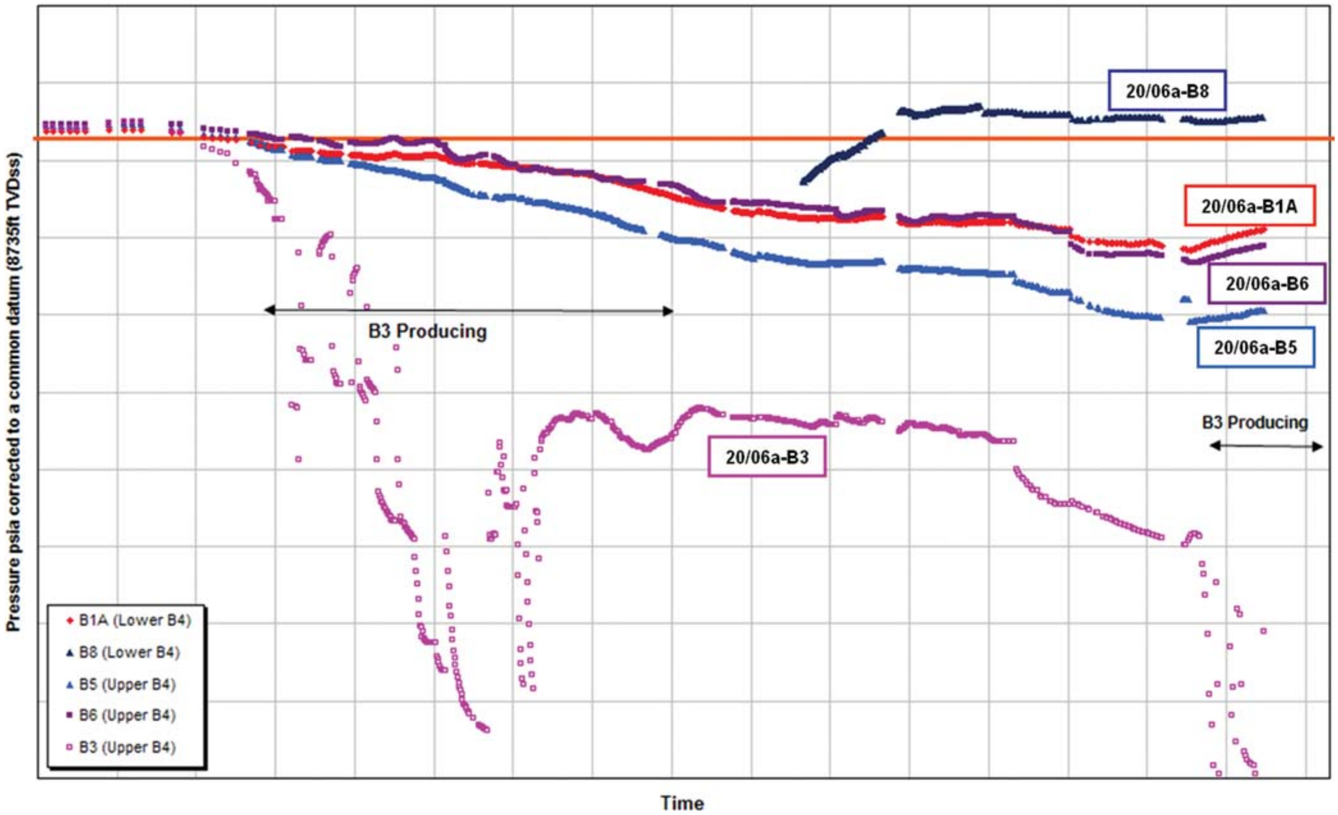

Fig. 11. Downhole gauge data (BHP) in mid flank pressure monitoring wells showing the response to Southern Panel well, 20/06a-B3, coming on stream. Orange line represents virgin reservoir pressure – all wells BHP slightly elevated initially due to injection as illustrated in Figure 9. Note pressure increase in Southern Panel well 20/06a-B8 in contrast to pressure decline seen in the Central Panel wells 20/06a-B1A, 20/06a-B5 and 20/06a-B6. Refer to Figure 6 for well locations.

Three of the wells (20/06a-B1A, -B5, -B6), located in the Central Panel, show consistent pressure decline, but the fourth well, 20/06a-B8, in the Southern Panel, continues to show pressure increase. Of these, the Southern Panel well, 20/06a-B8, and the closest Central Panel well, 20/06a-B1A, are completed in the same, Lower B4 interval. Early interference tests had indicated that all wells communicated with downdip injectors. The response in the Central Panel observation wells was interpreted as a balance between injection downdip and offtake updip. However, 20/06a-B8 in the Southern Panel, whilst responding to downdip injection, was clearly disconnected from any of the producing wells at the time, either in the Southern or Central Panel. In order to understand the dynamic information, seismic mapping and stratigraphic correlation of the B4 package in the Southern Panel were reassessed. Figure 12 shows the revised interpretation of the Lower B4 in the Southern Panel (Fig. 12a), which better honours all the data, and produces an excellent history match for the 20/06a-B8 well (Fig. 12b). Originally, the Lower B4 unit extended updip from 20/06a-B8 through the 20/06-3 well (Fig. 8). In this new model, still valid today, the thick sand package representing the Lower B4 in the Southern Panel pinches out rapidly updip of 20/06a-B8, allowing no communication with Southern Panel production wells.

History matching also indicated that the Lower B4 sand in the 20/06a-B8 does not fully communicate with the Upper B4, against which it is juxtaposed, across the Southern-Central Panel bounding fault. Optimum history matches were achieved by assigning low transmissibility to the western portion of the fault, whilst the eastern half was fully open. Whilst most of the early dynamic data were pointing towards a very open system, here was a clear indication that at least part of the Southern-Central bounding fault was not fully transmissible after all.

In this case, perhaps fortuitously, well 20/06a-B8 was in a good position to monitor reservoir pressure in this Lower B4 sand unit, without which early identification of stratigraphic compartmentalization would not have been possible. As a result, the extensive accumulation monitored by the 20/06a-B8 well, an estimated 70×10^6 bbl, can be targeted in the future to ensure fluids are efficiently recovered. The design of future infill well drilling strategies will have to take into account the possibility of similar stratigraphic compartmentalization, ensuring sufficient areal well coverage and extensive pressure sampling for all sand units. This data, and the revised geological model it led to, brought about a change in attitude to the Buzzard reservoirs, whereby the reservoir model containing simplistic, laterally extensive, 'tank-like' reservoir units was no longer considered viable.

The Buzzard Field today: mid 2009

During 2008, one appraisal, two production and two injection wells were drilled, bringing the total number of wells in the field development area to 40 (Fig. 13). As had been the strategy prior to first oil, and throughout the first year of production, the data acquisition programme continued with an emphasis on obtaining dynamic data. Cased hole production logs, saturation logs and reservoir pressures were acquired across the field to enhance understanding of production contribution from individual sand units and to determine whether there was evidence for any differential depletion between sands.

Efforts to dynamically model the field continued throughout, with model updates being made in order to capture the most recent information. One of the key results of simulation modelling was an indication that the B4 reservoir was more complex than the

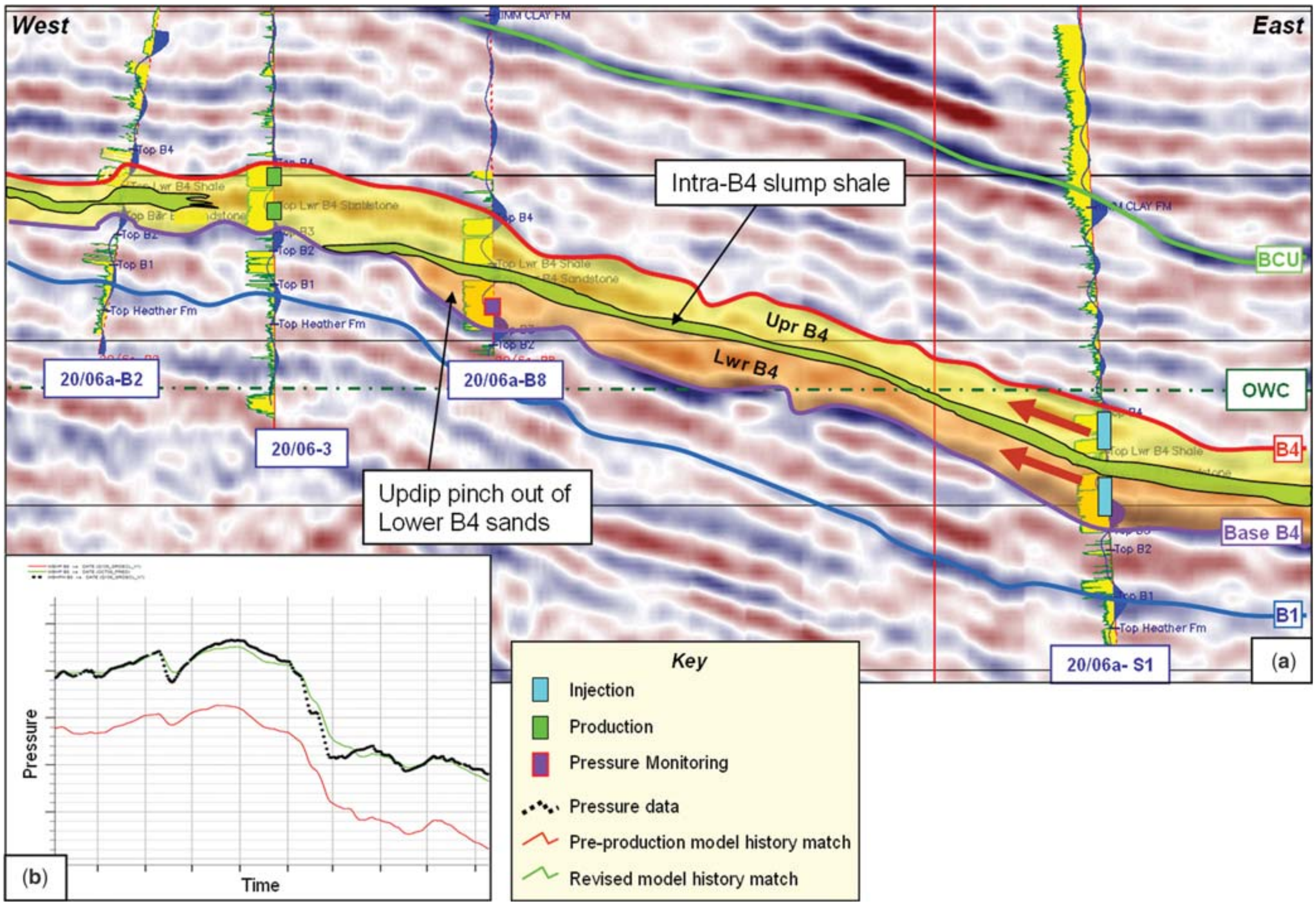

Fig. 12. (**a**) Revised interpretation of the Lower B4 unit in the Southern Panel (refer to Figure 6 for well locations). GR log displayed in wells together with perforation interval and type. (**b**) History match of the 20/06a-B8 well (actual data shown as black dots), before (red line) and after (green line) editing to capture the pinchout of the Lower B4 unit updip of the well.

simple Upper and Lower split built into the early production models of the field. Pressure surveys acquired in new wells typically indicated the presence of more than two hydraulic units (Fig. 14) and it became increasingly difficult to match field pressures in a simple two-layer model of the B4 reservoir. Matches were achieved by invoking an additional, extensive barrier to vertical flow within the Upper B4 and it became clear that a review of the field stratigraphy was required to determine whether a more complex vertical layering scheme, involving additional, laterally extensive shales, was supported by all the data.

In addition to the dynamic data incoming throughout this time, the results of a number of core-based studies also became available and, in conjunction with the continued biostratigraphic analysis of Buzzard wells, afforded a means to further subdivide the B4 reservoir. These studies were largely a continuation of work initiated at FDP time, but it was only through the addition of considerably more core material, some 2050 ft acquired in development wells, that useful patterns began to emerge, allowing improved integration of all the data towards a consistent Buzzard reservoir model. The most informative of these studies, outlined here, utilized chemostratigraphy.

Integration of Buzzard chemostratigraphy

Whilst a consistent approach to biostratigraphic analysis had provided a framework for correlation within the Buzzard Field, it is based solely on data from shale sections. The very sandy nature of the Buzzard reservoirs, together with their rapid mode of deposition as turbidites, precludes finding sufficient palynofloral material to be able to distinguish within sandy sections. Chemostratigraphy, on the other hand, characterizes sedimentary rock successions by using inorganic geochemical data and so is not limited by lithology. Rock geochemistry is sensitive to subtle changes in mineral abundance and composition. Apparently uniform sedimentary successions usually show primary differences in the geochemistry of their constituent minerals, or in the proportions of accessory minerals. The latter, which include heavy minerals and clay minerals, commonly have very distinctive trace element contents.

During 2007 and 2008, 355 sandstone and 292 claystone samples from core, cuttings and sidewall cores were analysed, providing data covering 34 different elements. This was used as the basis for defining sandstone and claystone chemostratigraphic packages within the Buzzard reservoir, with the most confident definition achieved through the B4 unit where the majority of samples came from.

Interpretation of the geochemical data allows the recognition of six sandstone and four claystone chemostratigraphic packages, although not all the packages are identified in all the wells (Fig. 15). The chemostratigraphic characterization of the sandstones (Fig. 15a) is largely based on changes related to potassium feldspar abundance and heavy mineral types, particularly zircon and rutile, which reflect variations in either provenance or the depositional pathways along which flows have travelled. The chemostratigraphic characterization of Buzzard claystones (Fig. 15b), on the other hand, may represent facies changes. Older claystones, with relatively higher calcium levels, appear to have been deposited in more oxic conditions, above the carbonate compensation depth (CCD). Younger claystones show decreased calcium levels,

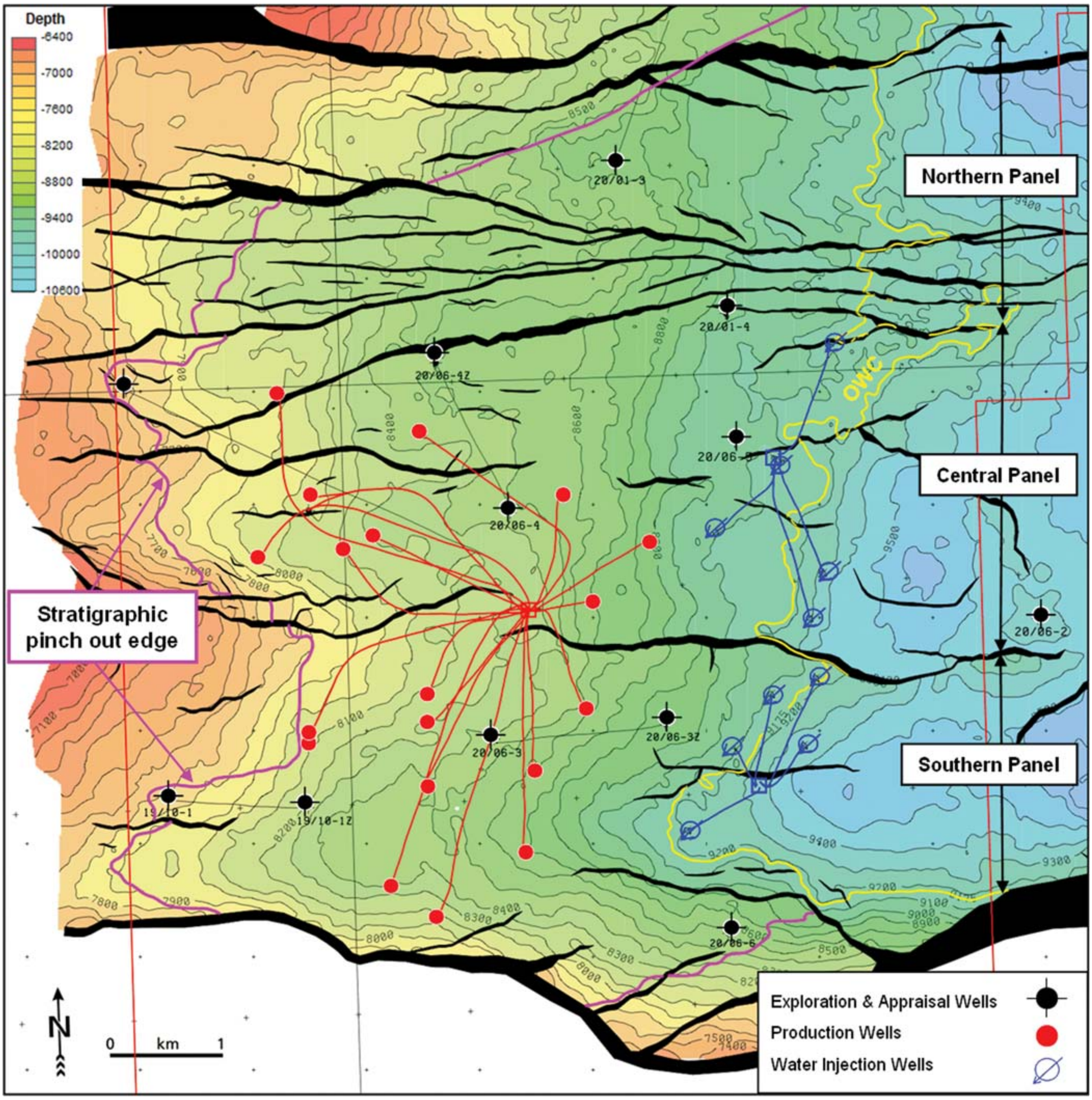

Fig. 13. Buzzard Field B4 reservoir top depth map showing present-day well coverage (as of March 2009), comprising 11 exploration and appraisal wells, 19 production wells and 10 water injection wells. Note the extension of the stratigraphic pinchout edge westwards due to new well results and revised geological interpretations.

indicating deposition below the CCD. Finer-scale geochemical variations may even help to distinguish within claystone packages, between hemipelagic and slump deposits.

When used in conjunction with the existing biostratigraphic framework, the large-scale chemostratigraphic packages help define four sandstone units in the Upper B4 and three in the Lower B4, interbedded with distinct shales (Fig. 16). The two most confidently defined claystone chemostratigraphic packages are consistent with the biostratigraphically defined Intra-B4 and B3 shales and have signatures relating to slumped or debritic, and hemipelagic type deposits, respectively. The resultant B4 reservoir zonation scheme, shown in Figure 16, has greater vertical heterogeneity than previously described but, when modelled, provides a better match to dynamic data.

Revised geological model

The integration of biostratigraphy and chemostratigraphy with feedback from dynamic data and modelling has enabled a more detailed subdivision of the Buzzard reservoir which is intrinsically linked to our understanding of how the reservoir is behaving under development conditions. Isopach mapping of individual Upper and Lower B4 units, defined by the new zonation scheme, supports the interpretation of each sandy unit as a separate turbidite lobe and demonstrates the topographic control of existing lobes and muddy slumps on subsequent depositional packages (Fig. 17). The maps illustrate how the B4 lobes were deposited through compensational stacking, whereby successive sandy flows fill the topographic lows adjacent to relative highs formed by previous deposits. These ‘highs’ may have been in the form of existing turbidite lobes or,

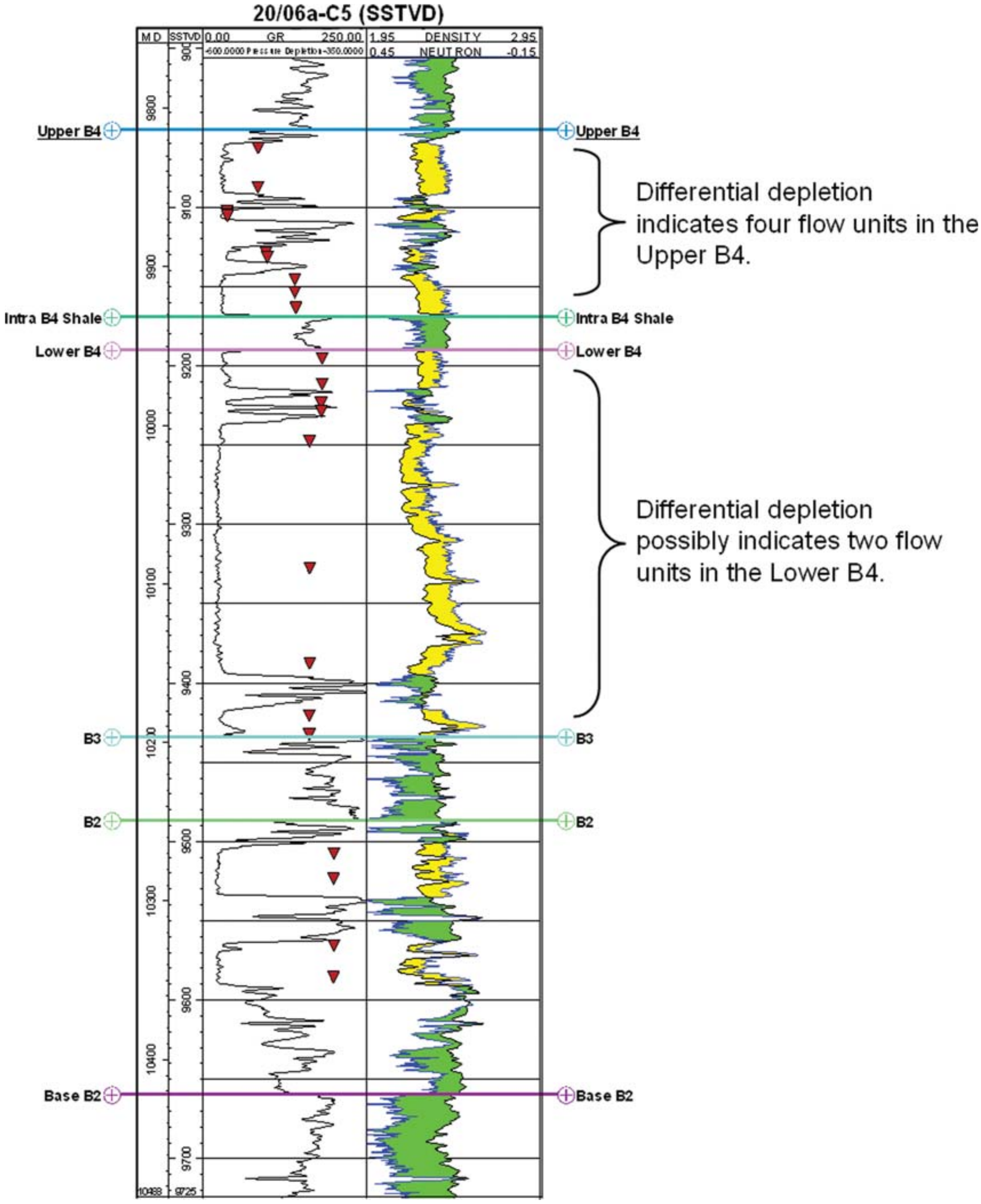

Fig. 14. Central Panel injection well drilled in 2008 showing pressure depletion as red triangles (track 3) relative to virgin reservoir conditions, represented by the right-hand side of the GR track, illustrating the potential for multiple flow units within the stratigraphic sequence already defined. Tracks, from left to right, are MD; SSTVD; GR and density-neutron.

as shown in Figure 17, the positive relief features created by periodic, catastrophic muddy slumps from the basin margins. Isopach maps of the individual reservoir units thicken eastwards, away from a westerly source point. Subtle changes in the maps over time suggest that the position of that source point may have shifted from a location in the Central Panel, during deposition of the Lower B4 units, to the Southern Panel during deposition of the Upper B4 units. Limited palaeoflow indicators from core and image log interpretations in Southern Panel wells are also supportive of a southerly source point during deposition of the Upper B4.

A similar model of deposition has been described by Gervais *et al.* (2004, 2006) for the Pleistocene age Golo turbidite system off the eastern margin of Corsica. This modern, sandy turbidite system is fed by a single river and canyon feeder and is confined by a structural ridge on one side and the continental shelf slope on the other, giving rise to a basin with similar dimensions and setting as the Buzzard Field. The processes for supplying sand into Buzzard may also have been similar to those proposed for some of these East Corsican fans, via turbidity currents generated through failure of pro-delta slopes where sediment was temporarily stored (Deptuck *et al.* 2008).

Current understanding of reservoir connectivity

The revised stratigraphy for the Buzzard Field has been used in recent modelling efforts and has proved successful in matching dynamic field data. The current model supports excellent field-wide communication despite the presence of laterally extensive shale layers within the B4 unit. The mechanism by which this communication is allowed is believed to be dominantly via sand

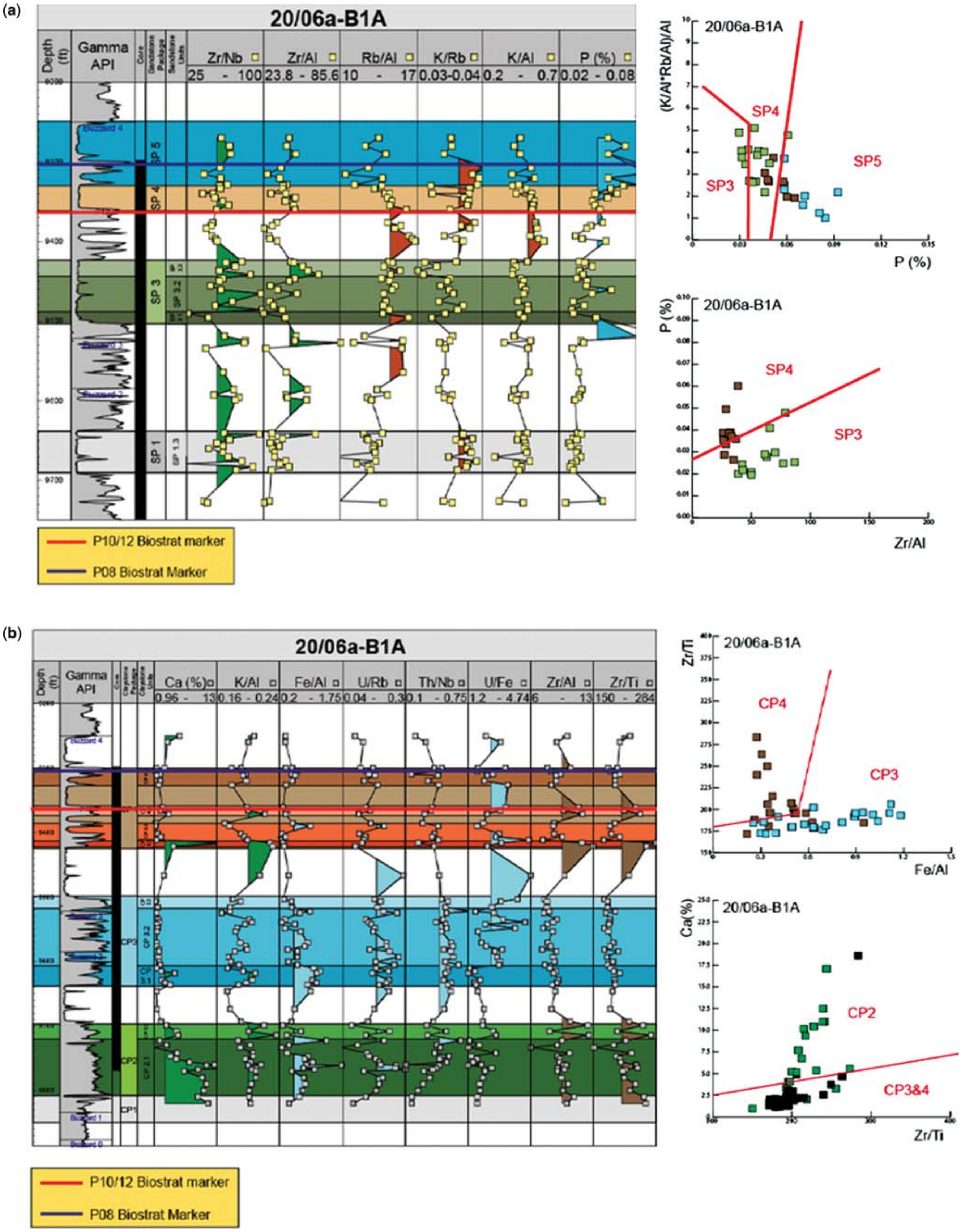

Fig. 15. Selected geochemical profiles and binary diagrams for well 20/06a-B1A, illustrating some of the (**a**) sand and (**b**) shale chemostratigraphic packages defined in the Buzzard wells. (a) Sandstone package SP5 is clearly characterized by high P levels, linked to abundance of biogenic apatite and carbonaceous debris. (b) Claystone package CP4 is characterized by high overall Zr–Al and Zr–Ti values, reflecting the abundance of silt-sized zircon grains as well as lower Fe–Al values related to lower abundance of pyrite.

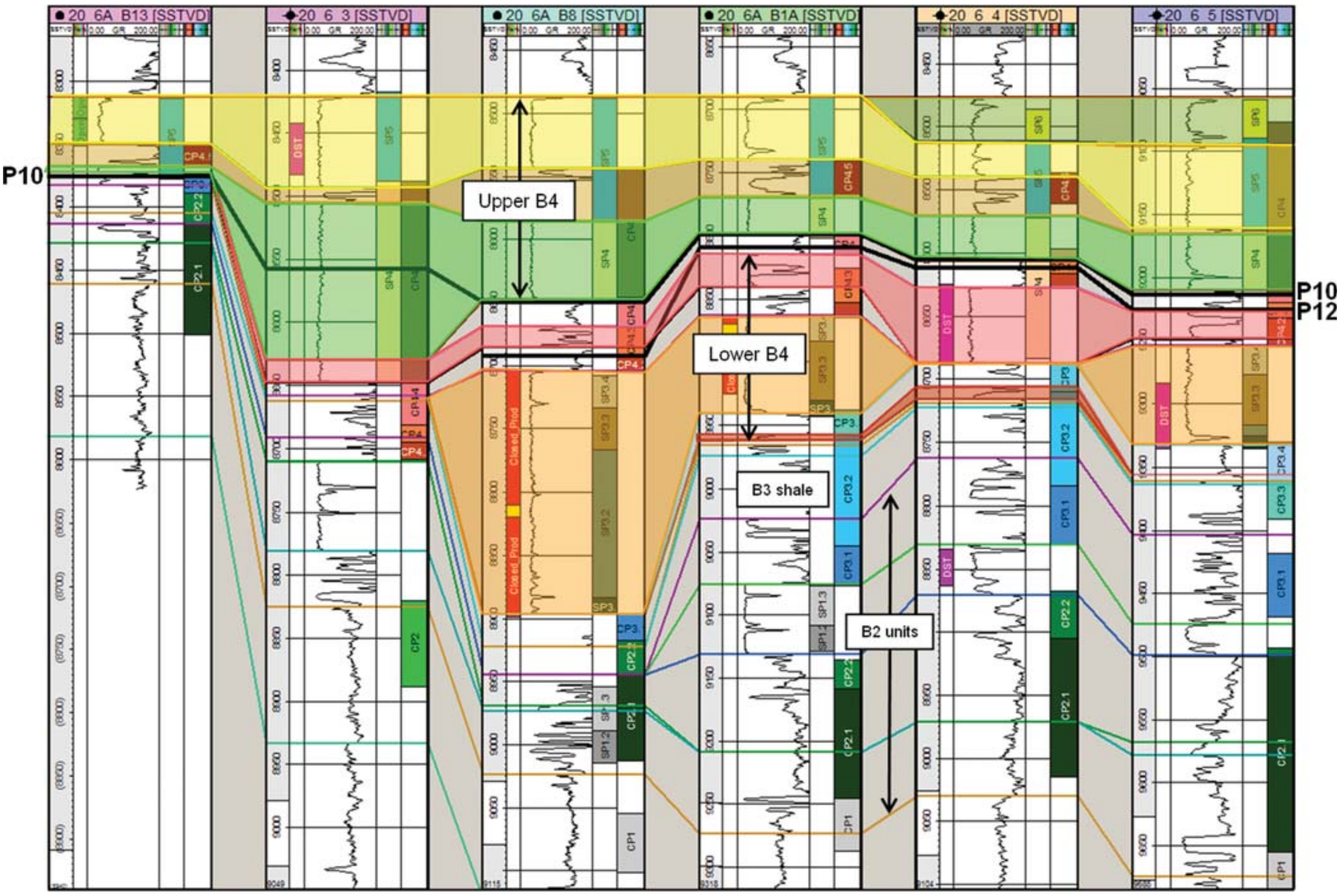

Fig. 16. South to north cross-section through Southern and Central Panel wells showing chemostratigraphic sand and claystone packages (tracks 4 and 5, respectively), relevant biostrat markers, P10 and P12 (black lines) and the current reservoir stratigraphy (coloured lines and shading). Tracks, from left to right, are subsea true vertical depth (SSTVD); perforated intervals [green, open; red, closed; yellow, pressure observation; purple, DST]; GR; chemostratigraphic sandstone packages and chemostratigraphic claystone packages.

to sand juxtaposition across non-sealing faults. There may also be a minor element of erosional sand on sand contact, but there is little evidence for significant erosion in Buzzard cores, with the exception of that observed and commented upon in well 20/06-3. The effect of the extensive shale layers is to promote strong flow layering within the B4, giving rise to the differential pressure depletion signals seen in recently drilled wells (Fig. 14).

The current model enhances understanding and prediction of production contribution, differential depletion and water breakthrough in the individual B4 reservoir sands. This will help to optimize future well planning and perforation strategy in production and injection wells to balance the water flood front advance and manage voidage within the field.

In addition, the improved reservoir zonation and sedimentological understanding provides a sound basis for more detailed investigation into variability in facies, grain size, porosity and permeability within the reservoir units. A greater appreciation of the controls on, and distribution of, these factors will further refine the reservoir model and hence its prediction capability.

Conclusions

The geological model for the Buzzard reservoir has changed over the last six years, in response to continuous data acquisition, integration and analysis through the pre- and post-startup phases of field life. The 'tank-like' reservoirs of FDP time have been superseded by a more complex model of compensationally stacked sand lobes. Shales, derived through intermittent, large-scale muddy slumps from the basin margins, are considerably more extensive than originally modelled, creating barriers to vertical flow within the gross reservoir package. These muddy slumps also create positive seafloor topography, influencing deposition of subsequent sandy flows. Conversely, sand lobes potentially have depositional limits within the main field area, such that prediction of sand presence and thickness across the field is far from straight forward. Understanding the geometry and distribution of sands and shale units is now seen as critical for successful reservoir management.

Evolution of the geological model has gone hand in hand with our understanding of connectivity within the B4 reservoir. The early FDP model of a highly connected B4 'tank' sand confined within fault panels by sealing faults was superseded by a model in which the FDP 'tank' was divided into an Upper and Lower unit. The expectation was of a high level of connectivity within each B4 unit, but a significant amount of vertical baffling between the units as faults were still considered sealing. Early development interference testing indicated faults were, on the whole, not sealing, but it also became apparent that stratigraphic compartmentalization, due to sand unit pinchout within the limits of the development area, could limit communication across the whole field. With the benefit of two and a half years of production data and continued data acquisition in newly drilled development wells, it is now evident that the B4 reservoir is divided into multiple hydraulic units, defined by individual sand lobes and laterally extensive shales acting as vertical baffles. Some of these lobes pinchout within the field development area. The effect of

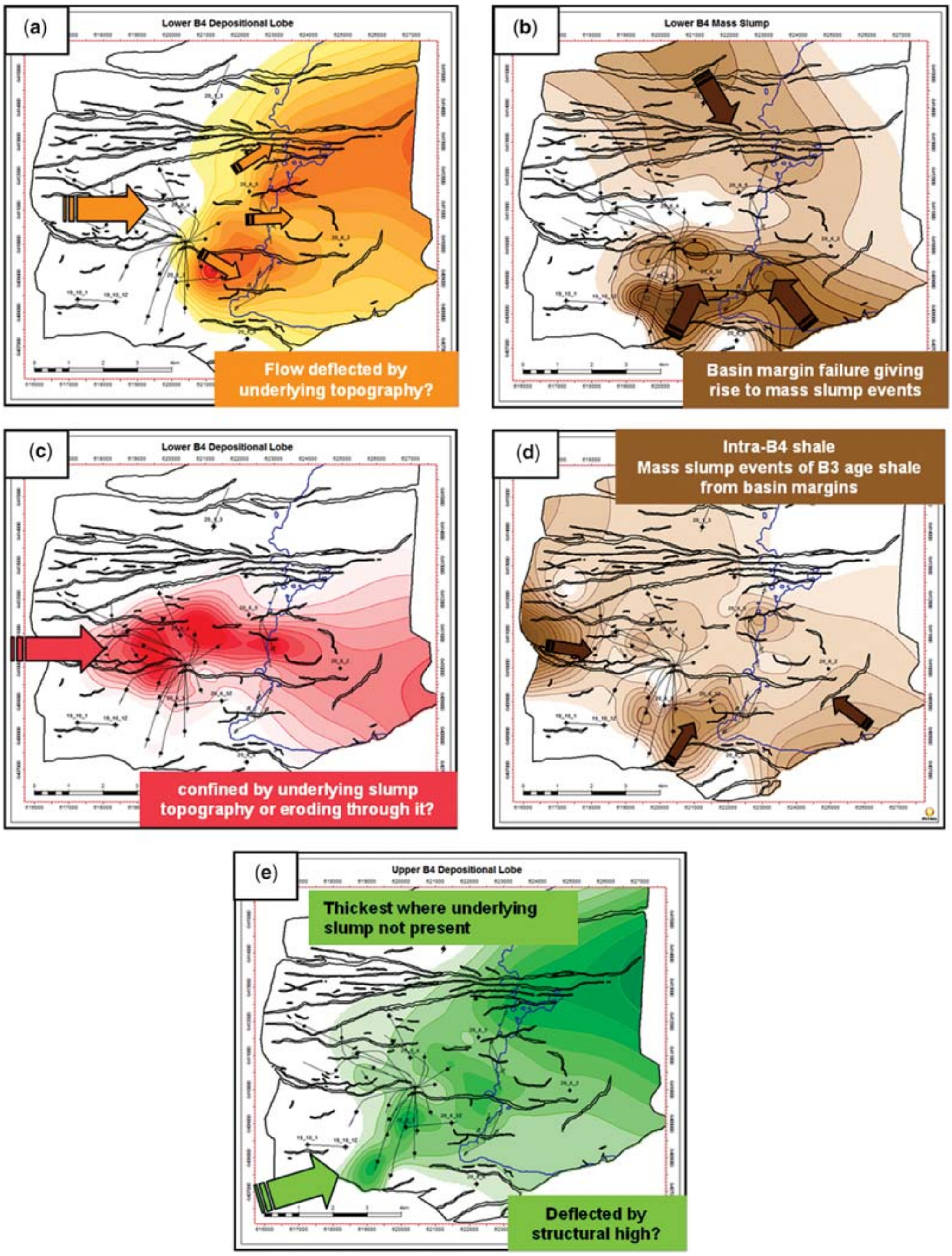

Fig. 17. Compensational stacking of the depositional sequence of some of the B4 units, from oldest, Lower B4 (**a–d**) to youngest, Upper B4 (**e**) illustrated with unit isochore maps; colours of units as per Figure 16. Lower B4 sands are derived from a westerly, Central Panel source point. Sand deposition is strongly influenced by existing topography as created by previous sands and mass slump deposits. Not all Upper B4 units are shown, but sand deposition post the Intra-B4 shale may be derived from a more southerly source point.

non-sealing faults within this vertically baffled reservoir is to maintain excellent lateral connectivity over the field as a whole.

Our present-day understanding of the Buzzard depositional system has been greatly assisted by the high density of well control, extensive data acquisition programmes, the use of wells for reservoir monitoring and full integration of static and dynamic reservoir data. This, in combination with an undeniably world class reservoir provided by mother nature, has enabled the operator to exceed FDP expectations, reaching plateau production levels of over 200 000 BOPD within six months of the field coming on stream. STOIIP and reserves expectations have increased by more than 40% since the FDP was written, which is partly attributable to improvements in the mapping of field net to gross in the geological model. Going forward, our improved understanding of the field will provide input into reservoir management and well planning strategies as well as supporting targeted data acquisition and studies programmes.

The authors would like to thank Nexen Petroleum UK Ltd, BG Group plc, Petro-Canada UK Ltd and Edinburgh Oil and Gas for their kind permission to publish this paper.

References

Beilby, P., Clayton, C. & Moffat, B. 2009. Distribution of hydrogen sulphide in the Buzzard Field. SPE 123875. *2009 SPE Annual Technical Conference and Exhibition*.

Deptuck, M. E., Piper, D. J. W., Savoye, B. & Gervais, A. 2008. Dimensions and architecture of late Pleistocene submarine lobes off the northern margin of East Corsica. *Sedimentology*, **55**, 869–898.

Doré, G. & Robbins, J. 2005. The Buzzard Field. *In*: Doré, A. G. & Vining, B. (eds) *Petroleum Geology: North-West Europe and Global Perspectives: Proceedings of the 6th Conference*. Geological Society, London, 241–252. DOI: 10.1144/0060241.

Duxbury, S., Kadolsky, D. & Johansen, S. J. 1999. Sequence stratigraphic subdivision of the Humber Group in the Outer Moray Firth area (UKCS, North Sea). *In*: Jones, R. W. & Simmons, M. D. (eds) *Biostratigraphy in Production and Development Geology*. Geological Society, London, Special Publications, **152**, 23–54.

Gervais, A., Savoye, B., Mulder, T., Piper, D., Cremer, M. & Pichevin, L. 2004. Present morphology and depositional architecture of a sandy submarine system: the Golo turbidite system (Eastern margin of Corsica). *In*: Lomas, S. & Joseph, P. (eds) *Confined Turbidite Systems*. Geological Society, London, Special Publications, **222**, 59–89.

Gervais, A., Savoye, B., Mulder, T. & Gonthier, E. 2006. Sandy modern turbidite lobes: a new insight from high resolution seismic data. *Marine and Petroleum Geology*, **23**, 485–502.

Partington, M. A., Copestake, P., Mitchener, B. C. & Underhill, J. R. 1993. Biostratigraphic calibration of genetic stratigraphic sequences in the Jurassic-lowermost Cretaceous (Hettangian to Ryazanian) of the North Sea and adjacent areas. *In*: Parker, J. R. (ed.) *Petroleum Geology of Northwest Europe: Proceedings of the 4th Conference*. Geological Society, London, 371–386; doi: 10.1144/0040371.

The Scott Field: revitalization of a mature field

G. R. BROOK, J. R. WARDELL, S. F. FLANAGAN and T. P. REGAN

Nexen Petroleum (UK) Ltd, Charter Place, Vine Street, Uxbridge, Middlesex UB8 1JG, UK (e-mail: glen_brook@nexeninc.com)

Abstract: The Scott Field, located in the UK Central North Sea, is in a mature stage of development. The Scott platform has been on production since 1993, when the Scott Field came on stream, followed in 1996 by the subsea tie-back of the Telford Field development, located to the south of Scott. By 2005 the Scott Field had produced 400×10^6 boe cumulative production. However, the field was producing at water cuts approaching 90% and the previously completed 2002–2004 infill drilling campaign had not met expectations. A change in strategy was undertaken in the subsequent 2005–2007 Scott drilling campaign, which yielded positive results, adding reserves and significantly increasing platform export rates. The focus moved from peripheral targets towards the edge of the field to lower risk targets closer to existing well control. Success was also attributed to focusing on the seismic interpretation of block bounding faults in poorly imaged areas of the field, allowing identification of small fault-bound targets. The recent drilling has demonstrated that significant value can be found in small and often complex accumulations within an extensively drilled mature field.

Keywords: mature asset, drilling, case study, North Sea, late field life development

The Scott Field lies in Blocks 15/21 and 15/22 of the UK sector of the North Sea (Fig. 1). It is operated by Nexen Petroleum (UK) Ltd. The field began production in September 1993 and reached plateau production of 200 000 bbl/day within several months, through seven pre-drilled production wells, with supporting injectors. The production potential of the field is currently around 20 000 bbl/day at a field watercut of 90%.

As the asset matures, it is getting more and more difficult to find reserve and production adding opportunities. Infill drilling targets have progressively decreased in size since the early field drilling. Additionally, the targets were of higher risk as infill opportunities at the margins of the field were being pursued.

Infill drilling on the field was paused in 2004 after a series of drilling results that were poorer than prognosed. A change in strategy was undertaken in the subsequent 2005–2007 campaign which yielded positive results, adding reserves and significantly increasing platform export rates. The focus moved from peripheral targets at the edge of the field towards lower risk targets closer to existing well control. In some instances the drilling targets were located just over 500 m from existing production wells in the same targeted reservoir interval. Success was also attributed to focusing on the seismic interpretation of block bounding faults in poorly imaged areas of the field. This increased the confidence on the interpretation of the reservoir adjacent to the bounding faults and also identified minor faulting that may have impacted on the sweep behaviour of the field, resulting in fault shadow accumulations. The recent drilling has demonstrated that significant value can be found in small and often complex accumulations within an extensively drilled mature field.

Geological description

The Scott Field is a structurally complex, Upper Jurassic sandstone reservoir located in the Outer Moray Firth, Scotland. The tectono-stratigraphic evolution of the Witch Ground Graben and the Scott and Telford fields have been documented by numerous workers (Boldy & Brealey 1990; O'Driscoll *et al.* 1990; Hibbert & Mackertich 1993; Jones *et al.* 1999; Guscott *et al.* 2003) and is only briefly summarized in this paper.

The Scott Field is highly compartmentalized with major faulting subdividing the field into a number of blocks (Fig. 2); two main fault trends are identified. The older of the fault trends forms part of the NE–SW trending Theta Graben fault system. This represents a mid Cimmerian extensional phase along a reactivated Caledonide trend. The principal expression of this fault is the Block I/Block II bounding fault and there is evidence for syn-depositional activity along this trend in the Scott Field. A later east–west orientated set of faults result from the Late Jurassic extension associated with the opening of the Witch Ground Graben. This episode of faulting postdates the deposition of the Scott and Piper reservoirs of the Scott Field and is responsible for the tilted fault block geometry of the field. Whilst the observed throw is greatest on the NE–SW trending fault separating Blocks I and II on the field, both orientations of faulting have sealing potential resulting in different fluid contacts in the main blocks of the field (Fig. 3).

Reservoir characterization has been performed from a combination of logging data, core data and production performance. There was an immense amount of core taken, particularly in the early days of Scott drilling with 62 wells wholly or partially cored, giving a total of about 19 000 feet of core (Thickpenny & Russell 2000). The abundance of data has led to the development of a robust depositional model for the Scott Field reservoirs.

The reservoir comprises four main sandstone units, the Upper and Lower Scott and the Upper and Lower Piper sandstones (Fig. 4). The reservoir sequence is defined by shales which separate the sandstones into flow units. The base of the reservoir sequence is the Skene Shale; the Upper and Lower Scott sandstones are divided by the G-Shale. The Mid-Shale, which represents a regionally correlatable flooding event, lies between the Scott and Piper and the Piper is partitioned by the Piper Shale. The entire sequence is overlain by the marine shales of the Kimmeridge Clay Formation (KCF). The KCF acts as both regional source rock and seal to the Scott Field.

Although the Scott sandstones are split into two distinct lobes, they are best considered as part of a single progradational coarsening and cleaning upwards shoreface system. The Lower Scott lobe is seen as a progradational shoreface overlain by two aggradational back barrier units which are separated by a correlatable coal.

VINING, B. A. & PICKERING, S. C. (eds) *Petroleum Geology: From Mature Basins to New Frontiers – Proceedings of the 7th Petroleum Geology Conference*, 387–403. DOI: 10.1144/0070387

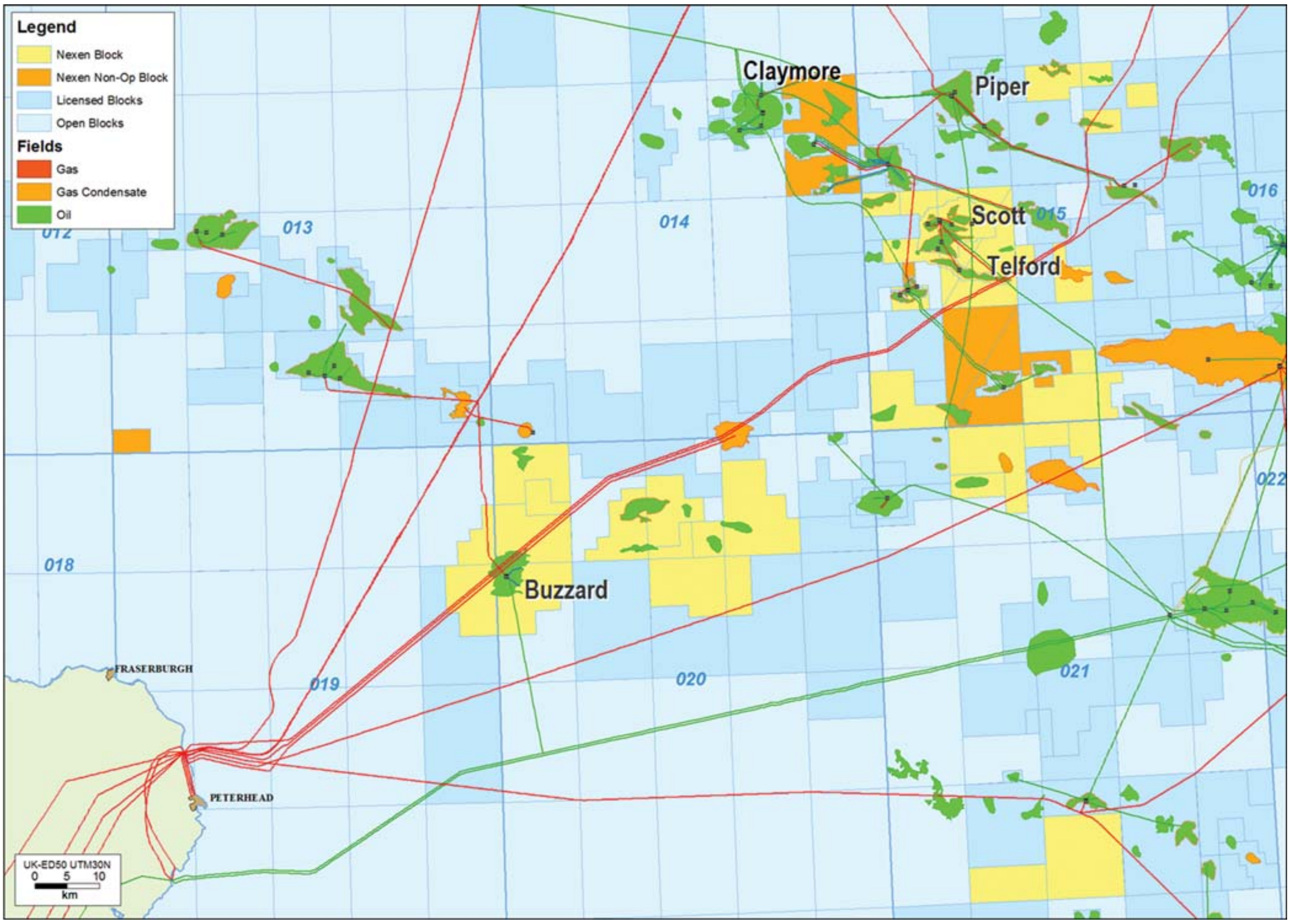

Fig. 1. Scott Field location map.

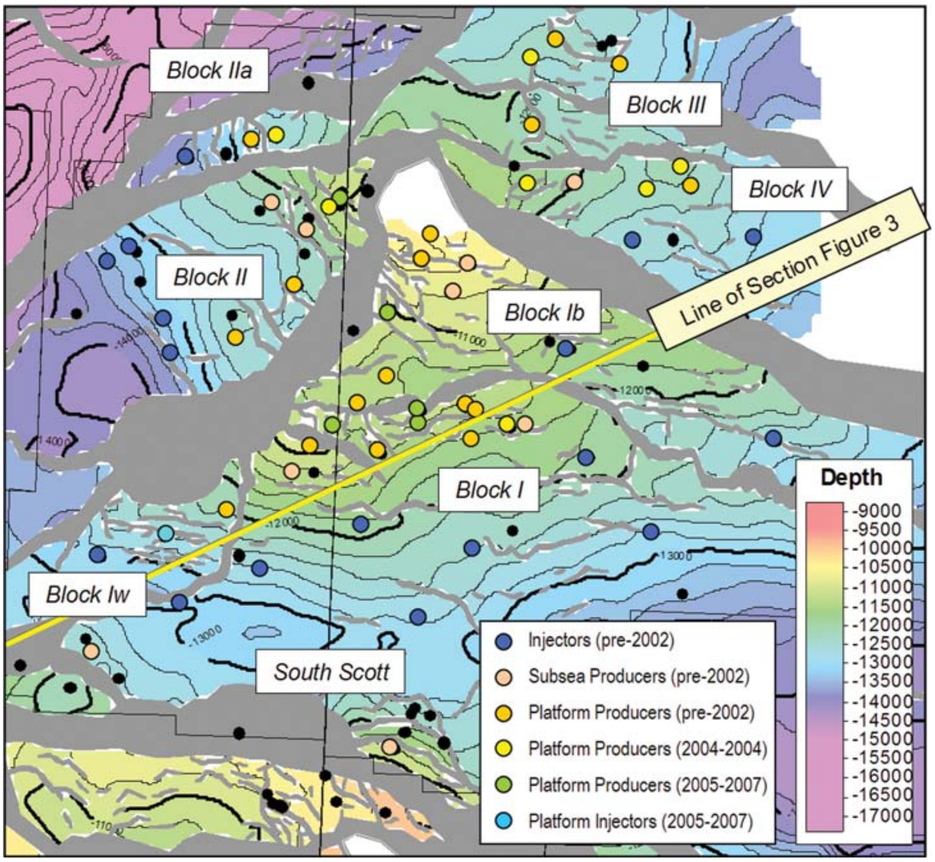

Fig. 2. Scott Field structure map.

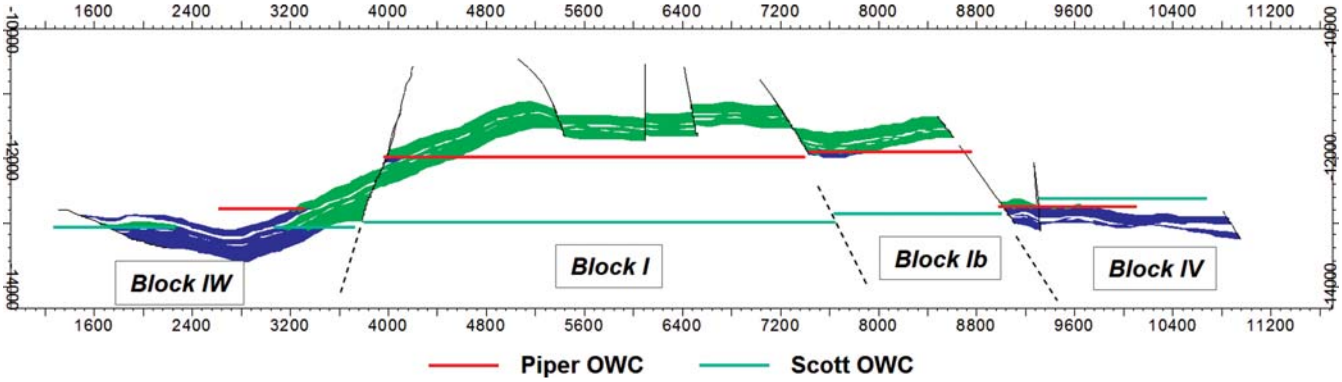

Fig. 3. Line of section shown in Figure 2, indicating structuration and variable OWC.

The shoreface sands and the lower back barrier units are of consistently good reservoir quality where found but the upper back barrier unit is of more variable quality. The Scott Formation sandstones thicken to the west in response to syn-sedimentary faulting, particularly across the Block I/Block II bounding fault and deposition towards a more basinal setting. The Scott Formation is thin to absent over much of Telford due to non-deposition.

The Piper sandstones are similarly split into two distinct units. The Lower Piper is further divided into two units, the 'ratty' Lower Piper below the 'blocky' Lower Piper. In both the 'ratty' and

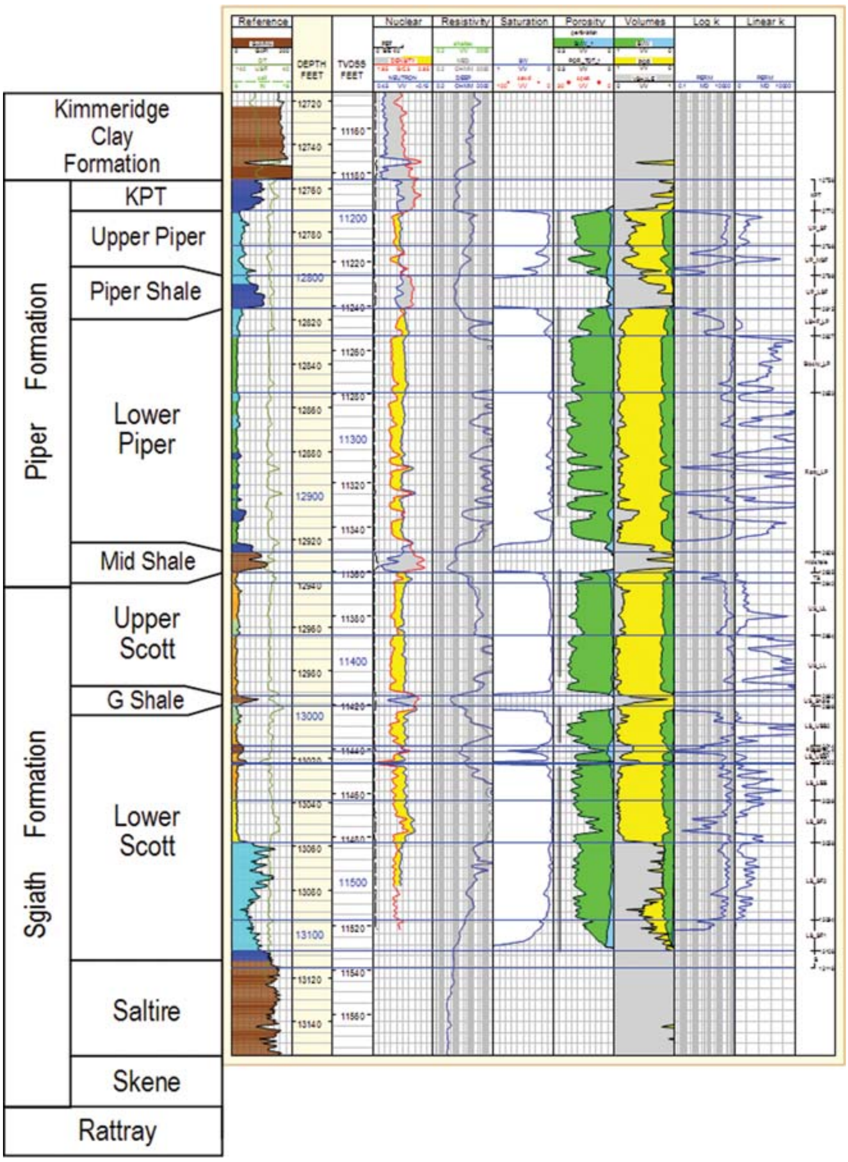

Fig. 4. Example log of a Scott well indicating zonation; track 1, GR/DT/CALI; track 2, PEF/DENS/NEUT; track 3, RES; track 4, SW; track 5, PERFS/PORO/BVW; track 6, VSH/PORO/BVW; tracks 7 and 8, PERM estimated.

'blocky' units, the better quality sands are submarine mass flow deposits. The 'ratty' and 'blocky' units are differentiated by the predominance of the background lower shoreface sediments into which the submarine mass flows were deposited; the more background lower shoreface sediments there are, the rattier the log signature. The Upper Piper sandstone is a progradational marine sequence capped by the Kimmeridge–Piper Transition unit (KPT), which comprises extensive back barrier deposits which grade upwards into the overlying KCF. The KPT unit is not of reservoir quality in the Scott Field. Both the Scott and the Piper formations display excellent reservoir quality with permeabilities in excess of 1 Da. The Piper Formation, in contrast to the Scott Formation, thickens to the east over the Scott Field toward the inferred palaeo-shoreline, and is the predominant reservoir unit in the Telford Field, with the KPT also being of reservoir quality at Telford.

The result of this tectonostratigraphic development of the field has resulted in the Scott Field comprising a number of complex tilted fault block traps (Fig. 2). Although depositional pinchouts are mapped, these are not thought to influence the trapping geometry. The structural style and the widespread Mid-Shale unit which separates the Scott and Piper formations has led to different fluid contacts within the individual blocks and between the two formations (Fig. 3).

Seismic database

The original 3D seismic survey over the Scott Field was acquired in 1992 and was used for the initial development drilling. Following several poor well results a new dataset was acquired in 1996. Ocean Bottom Cable (OBC) data were acquired in the centre of the field in order to avoid a two-boat undershoot of the Scott platform and conventional towed streamer data were acquired over the rest of the field. Although an improvement on the 1992 data, operational problems and poor weather conditions meant the data were very noisy with severe multiple problems. The dataset was reprocessed on several occasions and finally underwent Pre Stack Depth Migration (PreSDM) processing in 1999. This markedly improved the focussing of the data but did not improve the vertical resolution; nor did it remove the presence of the multiples. Reprocessing tests, primarily aimed at multiple attenuation, continued throughout 2000 without major success.

In 2001 the decision to shoot a new 3D survey over the Scott Field was made. A 4C/3D OBC survey was acquired primarily for the added advantages of the PZ multiple suppression, the improved spatial resolution and the improved coverage under the platform area. This was initially PSTM processed; however, an issue with the OBC survey was that the area covered was long and relatively narrow. As a consequence a large proportion of the data was in the migration aperture and suffered from mis-migration. It was decided therefore to merge the OBC data with the pre-existing 1996 streamer survey. In addition, the improvements seen from the 1999 PreSDM reprocessing justified a similar processing approach and PreSDM processing was also performed. This data was available in 2003 and showed significant improvements in the overall signal/noise, multiple suppression and fault definition (Fig. 5).

In 2006 post stack processing of the 2003 PreSDM data was carried. Noise cancellation and spectral whitening techniques were applied which increased the frequency content and vertical resolution at the reservoir level.

Seismic interpretation

In 2003 a seismic re-interpretation of the field was carried out using the new merged PreSDM 3D seismic data. The dramatic improvement in data quality resulting from the increase in the signal/noise ratio and the suppression of the worst of the multiples meant reflectors were more accurately positioned in the correct subsurface space. This allowed a more confident interpretation to be made over the highly faulted areas of the field where previously it was deemed impossible to site a well.

During 2003–2004 several wells were drilled in these more complex areas with varying levels of success. As a result a further seismic reinterpretation was carried out in 2005 which incorporated the results of these new wells. An extensive review of the faulting, together with a comprehensive 3D fault plane mapping exercise, was carried out. Well ties were also re-examined

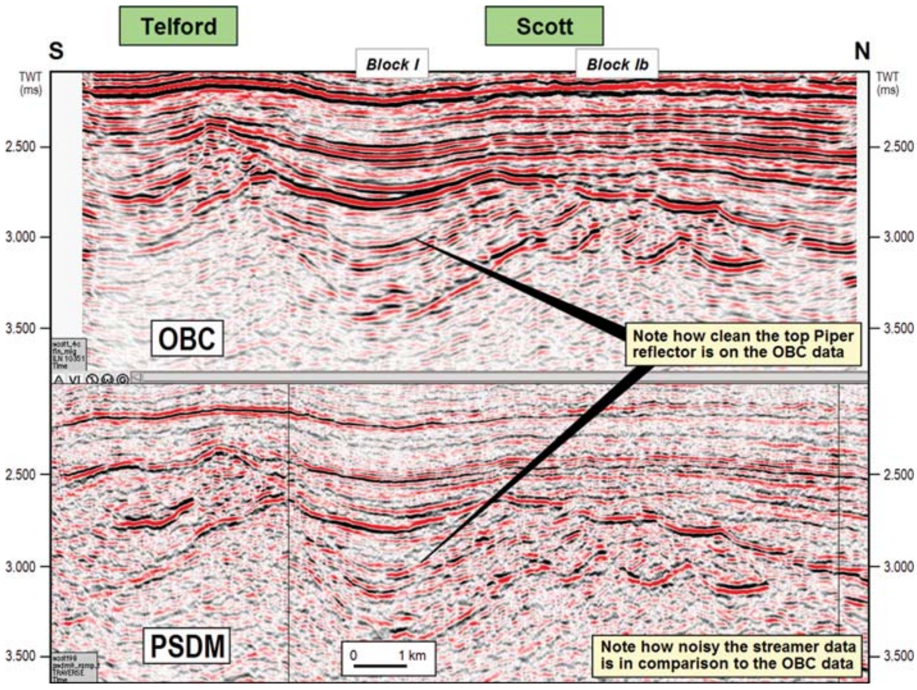

Fig. 5. Comparison of 2001 OBC data with 1999 PSDM data.

and two key markers, the BCU and a near Top Mid-Shale pick (located between the Piper and Scott reservoir units), were mapped in detail over the field. Previous mapping had attempted to pick a near Top Piper seismic event which the recent well ties suggested could not be accurately defined. Even though this seismic dataset was a marked improvement, the data quality was still of insufficient resolution to permit any further picking of intra-reservoir horizons.

The 2006 post–stack reprocessing improved the resolution at the reservoir level. Although it was still not possible to map intra-reservoir seismic events on this dataset, it did provide more reservoir detail and allowed mapping of smaller scale faults which had not been previously possible.

Production overview

From start-up to the end of 2008, the Scott Field has produced 400×10^6 bbl of oil, with peak rates in excess of 200 000 bbl/day, and cumulative gas production of 268 bcf. The current field oil production potential is around 20 000 bbl/day. Initially the field was produced through seven pre-drilled production wells, supported by water injection through seven injection wells that commenced injection a month after first oil. To date there have been a total of 34 production wells drilled of which 10 were sidetracks of previously drilled wells. There are 19 injection wells in the field providing pressure maintenance to the field continuously since start-up. The Scott platform has 350 000 bbl/day of injection capacity. The injection strategy has been to maintain voidage replacement in each of the identified fault blocks in the field. Voidage replacement has not always been maintained due to operational issues, which has resulted in fluctuations of the reservoir pressure at various times during the production life of the field. The majority of the production wells are located in the crestal regions of the major fault blocks. The injectors are located downdip, but still above the oil–water contact (OWC) due to deteriorating reservoir quality in the water leg that has been shown to severely impact injectivity. The typical spacing between the producers and the injectors is of the order of 1000 m.

Although plateau rates were achieved soon after start-up, production of water was earlier than anticipated and oil rates from several wells began to decline. The field water cut had climbed to 10% after just over one year of production. This compared unfavourably with other large developments in the area, which produced at minimal or low water cut for considerably longer. The Claymore Field did not reach a water cut of 10% until after two and a half years of production, whereas the Piper Field required four years of production to achieve a 10% water cut (DECC 2010). The overall production rate from the Scott Field was maintained by a continuous drilling programme, targeting areas of reservoir unswept by water flooding. Although generally successful, there were early indications of the difficulties in drilling at the margins of the major fault blocks. Drilling results during the producing life of the field have increased the interpreted complexity of the reservoir in terms of structure, facies and connectivity. The drilling campaign of 2003–2004 demonstrated that this complexity was still not fully understood, with wells generally underperforming prognosis.

2005–2007 infill campaign

Prior to the 2005 drilling campaign, a complete seismic re-interpretation and geological re-mapping of the field was performed. In addition, dynamic simulation models were built and history matched to aid the positioning of drilling targets.

There was a shift in strategy for the 2005 drilling campaign. Some of the well results from the previous drilling campaign had been disappointing. This was particularly the case with wells targeting the northern and southern edges of the field. There appeared to be greater than anticipated structural complexity at the tested edges of the field. As a result, these wells suffered from a number of issues including compartmentalization and lack of adequate pressure support. In addition, one of the wells encountered either a perched OWC or uncharged reservoir sands.

Owing to the lessons of the previous campaign, the 2005 drilling campaign focused on areas well within the defined area of the field and closer to well control. The targets identified included updip attic targets mainly identified from the seismic reinterpretation, areas of bypassed sweep as indicated by dynamic modelling as well as a downdip injection target identified through an extended well test. Examples of each type, comparing pre-drill expectations and post-drill results, are discussed below.

Updip attic targets

As a result of the presence of numerous independent tilted fault blocks, the potential for a number of updip attic targets was identified. Updip attic type targets formed the basis of the J33 and J35 wells in the drilling campaign.

The J35 well, drilled as the last well of the campaign in 2007, targeted the area updip of the J7 well in the NE area of Block I. Faulting out of the reservoir was viewed as the principal risk and a primary well location and a contingent fallback location were identified.

The location of the J35 target (Fig. 6) was originally mapped and identified on the 2003 PreSDM data and was chosen to access both the Piper and Scott reservoirs in Block I. The target is bounded to the north by the main Block I/Block Ib west–east striking fault and to the south and west by the NW–SE trending fault which was encountered by J4 (Fig. 7).

The interpretation of 2006 post-stack reprocessed volumes confirmed the presence of this target and identified an additional north–south trending fault to the east of the proposed J35 primary location. This fault downthrows to the east, has a maximum throw of *c.* 100 ft and appears to reduce to zero throw to the north. This created an upthrown fault terrace which formed the primary target for the well. Because of the close proximity of both the bounding faults, the area did carry a risk on reservoir presence. A downdip fall-back location (J35_FB) was therefore identified in the event that the well did not encounter any reservoir.

The size of the J35 target area fault terrace was controlled by the position and dip of the major bounding faults to the north and SW; shallow dipping faults would reduce the volume of reservoir under the fault plane, and potentially result in the reservoir being faulted out at the J35 location. Unfortunately, other than the seismic data there was little hard data, such as dipmeter logs in offset wells, to constrain the dip of these faults and as a consequence the dip of the faults remained uncertain.

A review of analogous faults in the vicinity of J35 was undertaken. Previously drilled wells in the campaign, J30 and J34, penetrated a fault which was believed to be a splay of the Block I/Block Ib boundary fault. Triangulation of the well–fault intersection points indicated that the fault plane, at this location, had a dip of approximately 60° to the north.

Seismic interpretation of the Block I/Block Ib bounding fault plane indicated that the J14 well to the NW should have intersected the Block I/Block Ib bounding fault. This well had a complete Piper and Scott section present. However, a detailed review of the underlying Skene and Rattray sections indicated that a portion of this section was missing, potentially due to faulting or non-deposition. The presence of a fault in the deeper section of the J14 well would support the interpretation of a steeply inclined

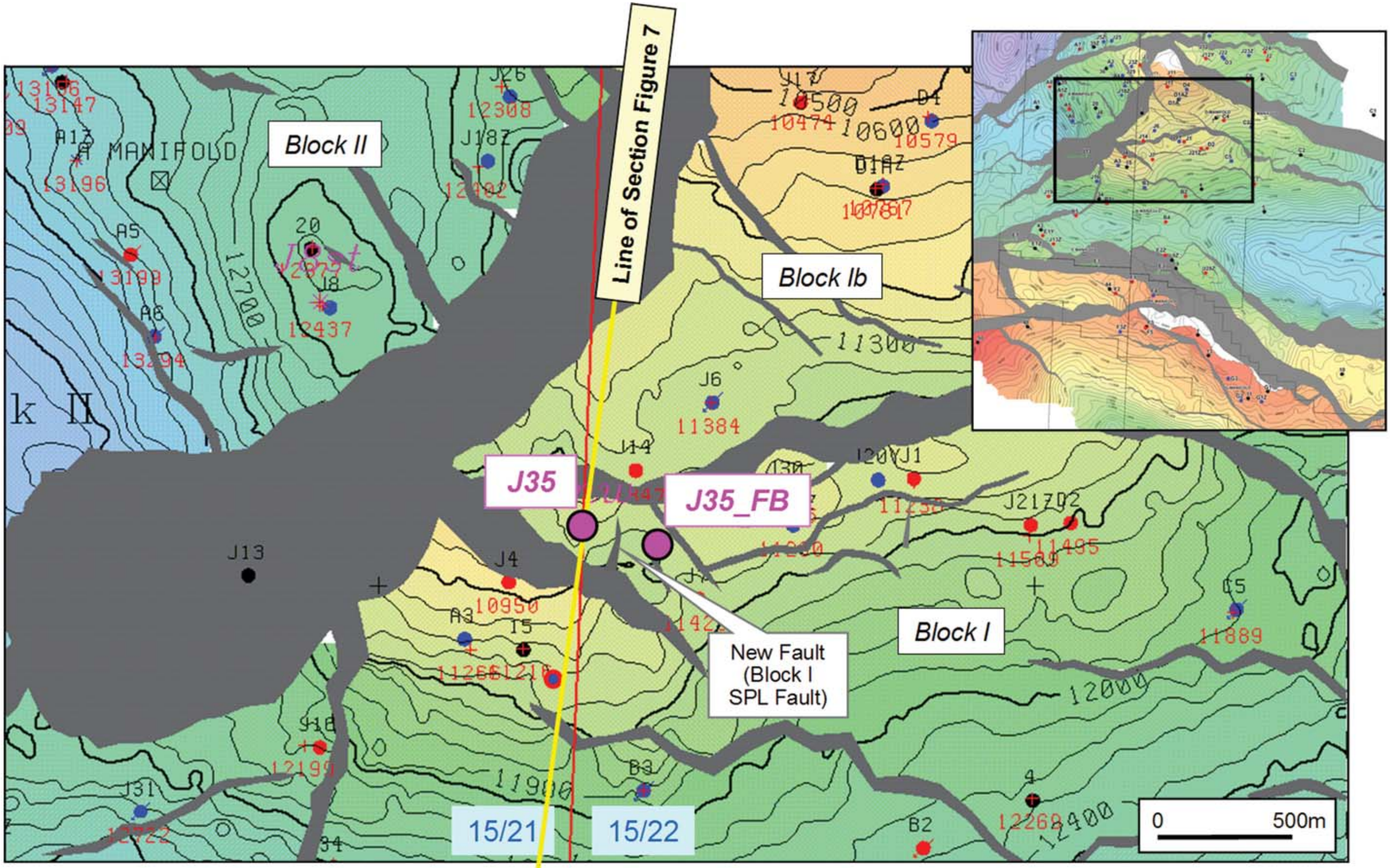

Fig. 6. Location of J35 target and J35 fall-back target on Mid Shale structure map (ft TVDSS). Red numbers indicate Mid Shale depth at well locations.

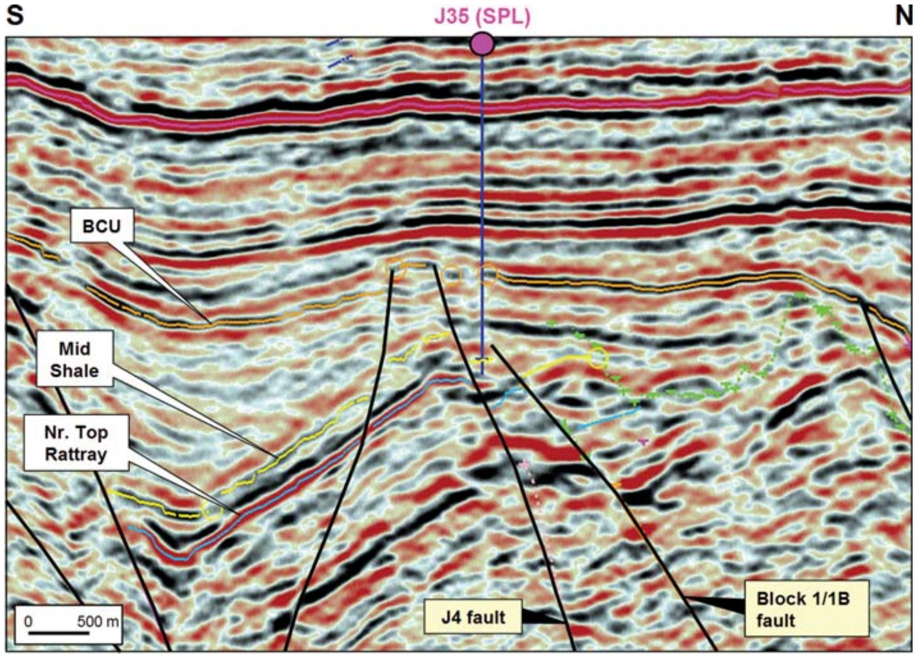

Fig. 7. Seismic line through J35 target.

Block I/Block Ib bounding fault plane, with dips similar to or greater than that seen in the J30, J34 wells.

Reservoir development from a depositional perspective was not an issue for the J35 location; offset wells clearly demonstrated that a thick sand sequence was deposited over the target location. All of the main reservoir units are present and show relatively uniform thickness and quality. There was no evidence in this region of the field that reservoir quality was reduced near faults. Wells J4, J30 and J34 all penetrate major faults, but showed no significant reservoir cementation or degradation as a result.

Dynamic modelling was used to confirm the presence of the unswept area since this target was a local fault bound high on the block. After history matching the model did indeed show the area not to have been fully swept, the principal risk being some partial oversweep updip of the J7 well. The model was also used to predict recovery of the fall-back target location. Recovery for the primary target was based on a volumetric uncertainty analysis.

The pre-drill volumetric recovery estimate for the primary target was $0.9–3.9 \times 10^6$ boe. The primary target was given a 50% chance of success, with absence of reservoir due to faulting identified as the primary risk. Compartmentalization and lack of pressure support were identified as risks, albeit minor, at the primary location due to the presence of the newly identified north–south trending fault to the east of the target. To aid any potential sidetrack decision, MDT logs were planned to identify any differences in pressure between the primary target and the rest of Block I that might indicate compartmentalization. In the event that the primary target was a failure due to the absence of reservoir sands through faulting, the recovery at the fallback target was estimated to be $0.7–1.8 \times 10^6$ boe with an 80% chance of success.

The well was drilled successfully at the primary location in the first quarter of 2007. The reservoir intervals came in between 30 and 80 feet shallow to prognosis. The well encountered full Upper and Lower Piper sections. Minor subseismic faulting, interpreted from image log interpretation, resulted in partial absence of the Lower Scott Sands (Fig. 8) leading to the shallow penetration of the base of the reservoir. Stratigraphic thinning was discounted due to the uniformity in Lower Scott thickness observed in offset wells. Some heavy minerals were believed to be present in the Lower Piper and Upper Scott sands, resulting in depressed resistivity along with elevated density, although there was no impact observed on the reservoir quality as exhibited by the gamma ray (GR) log (Fig. 9). This heavy mineral concentration is a feature commonly seen in the wells along the Block I/Block Ib fault and other block bounding faults, although the cause of this is not fully understood.

MDT logs were run prior to completing the well. The measured pressures indicated pressure depletion of at least 1000 psi from the assumed virgin reservoir pressure of *c.* 8000 psi. The Lower Piper was depleted by almost 2000 psi. The Upper and Lower Scott exhibited a common pressure gradient and were slightly less depleted than the Lower Piper. The Upper Piper was the least depleted but still had pressures 1000 psi below the estimated virgin reservoir pressure. These observations, along with some apparent partial sweep at the base of the Lower Scott, indicated that communication with the rest of Block I was very likely and that compartmentalization was not an issue.

The well was initially perforated in the Upper Scott sands which were believed to be unswept. However, the well initially produced at an oil rate of 8000 bbl/day with a water cut of 20%, potentially indicating communication with the partially swept Lower Scott sands. The water cut rose quickly to 40% before stabilizing. Despite the higher than expected early water cut, the performance of the well has been good, having produced 0.7×10^6 bbl of oil from the Upper Scott, with additional production potential remaining in the Piper sands.

The early water cut behaviour observed in well J35 is not unique. The other updip attic target, J33, had very good openhole results (Fig. 10), indicating unswept full sections of both Piper and Scott sands. Despite these results the well was producing at a water cut of 50% two weeks after initial perforation of the Lower Scott sands. The well has performed well, producing 1.8×10^6 bbl of oil with significant remaining unperforated production potential in the uphole zones.

Bypassed sweep targets

Because of the complex interplay of structure, depositional architecture and reservoir quality a number of bypassed or unswept

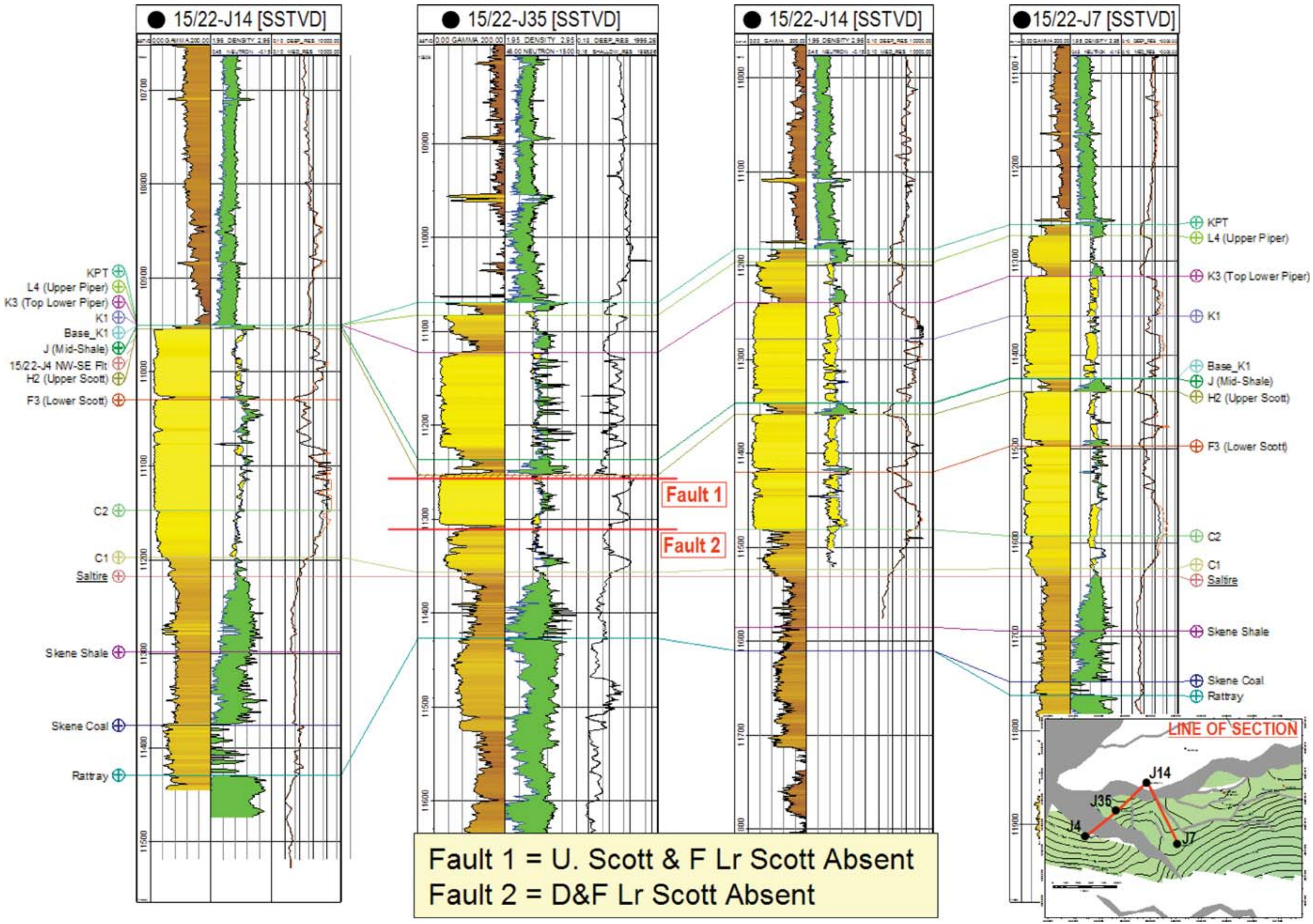

Fig. 8. J35 post-drill correlation, flattened on Saltire Fm., lLogs shown: track 1, GR; track 2, DENS/NEUT; track 3, RESISTIVITY.

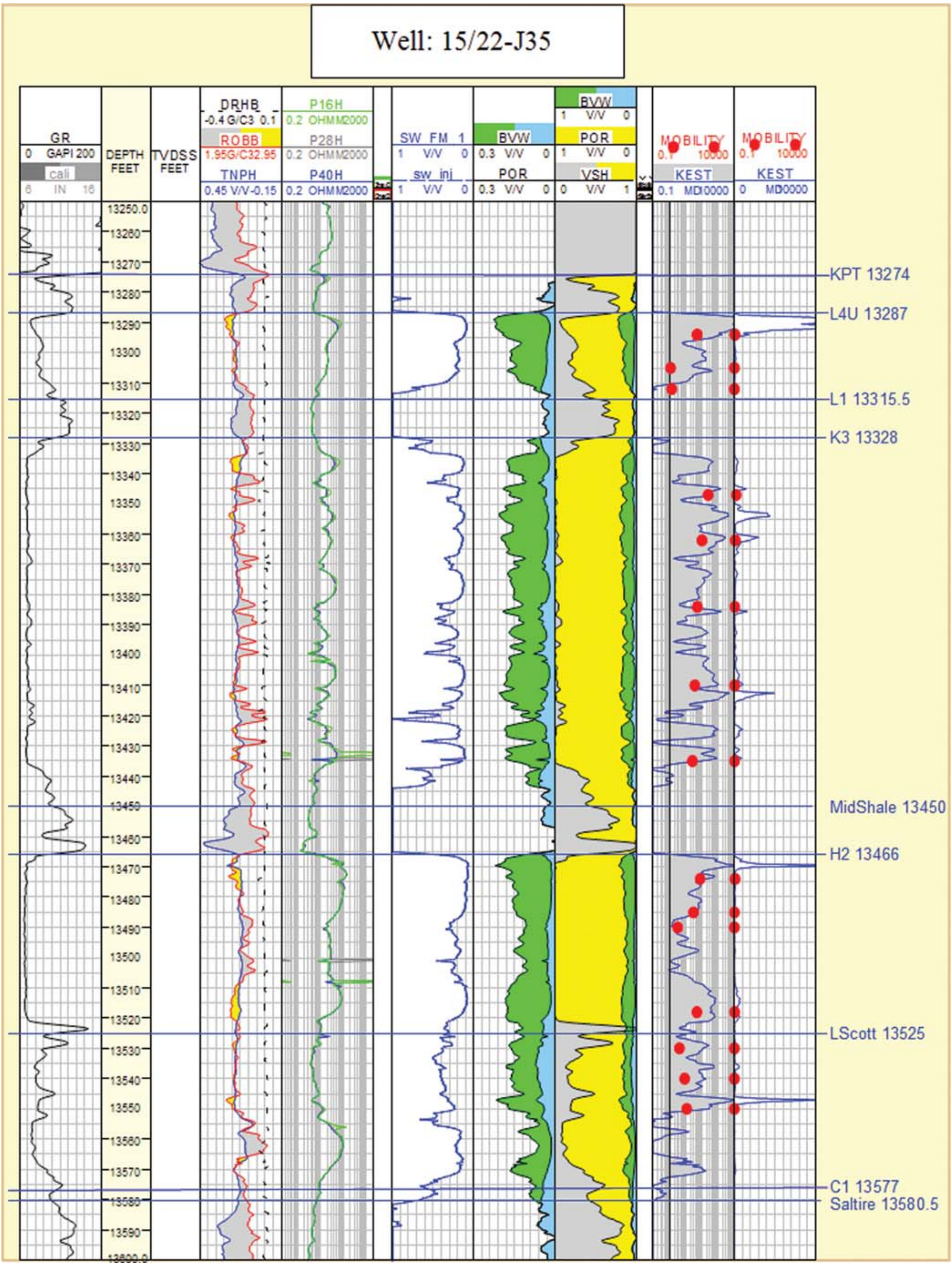

Fig. 9. J35 interpreted open hole results.

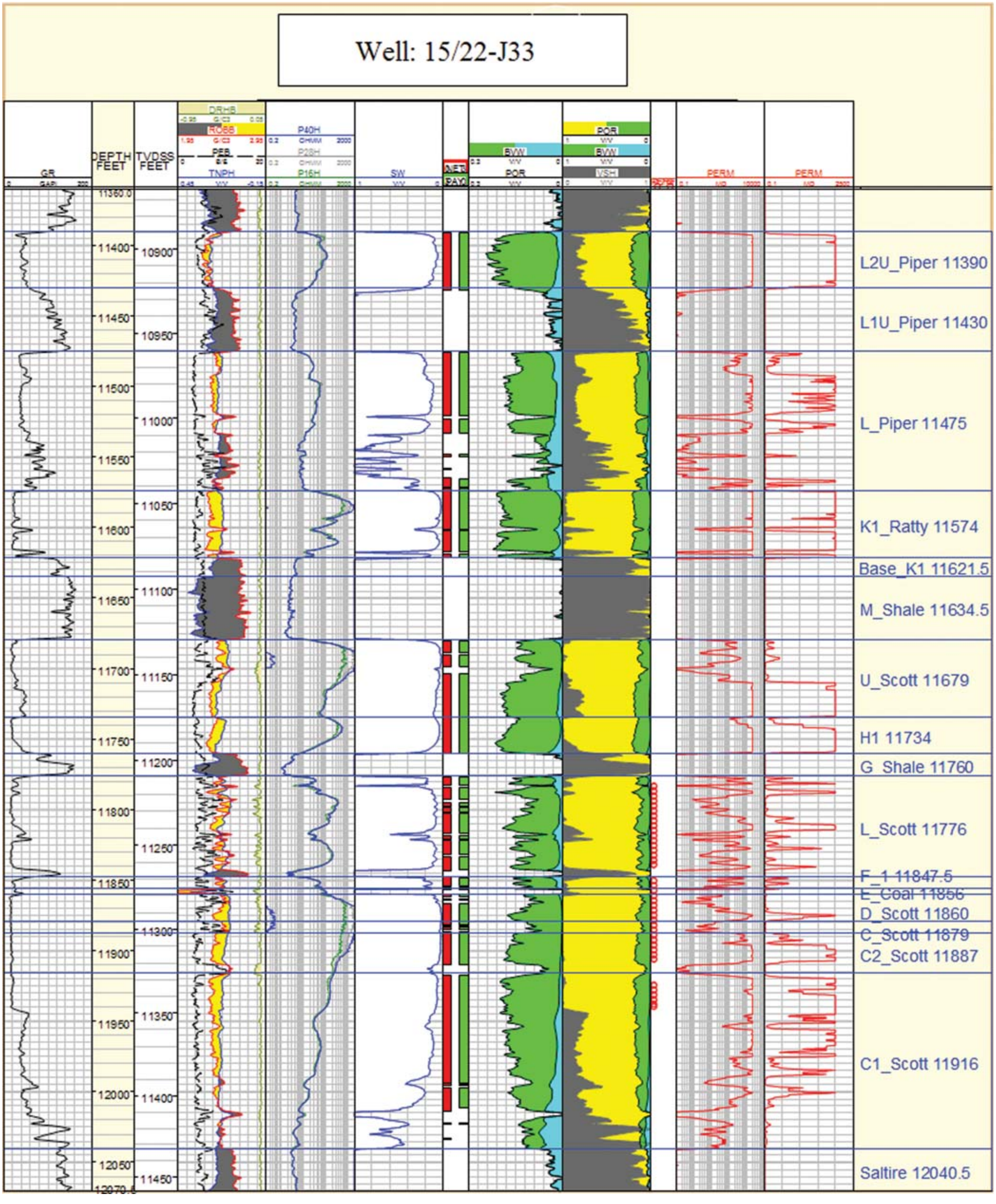

Fig. 10. J33 interpreted open hole results; tracks as in Figure 4.

targets were identified within the Scott Field. Such targets are often reliant on the sealing nature of intra-block faults with bypassed oil present in the shadow of sealing or baffling faults. Identification of such targets requires the integration of seismic interpretation, geological and simulation modelling studies to prove the validity of the target. The J32Z and J34 wells drilled in the campaign are representative of this type of target.

The J32Z location was chosen to access a mapped by-passed volume of hydrocarbon to the west of Block 1b (Fig. 11). The target is bounded to the north and south by two NW–SE striking faults which are both downthrown to the SW. The throw on the most northerly of these faults (fault '3' in Fig. 11) decreases to the SE from a maximum value of approximately 300 ft in the NW. This throw was deemed sufficient over some of its length

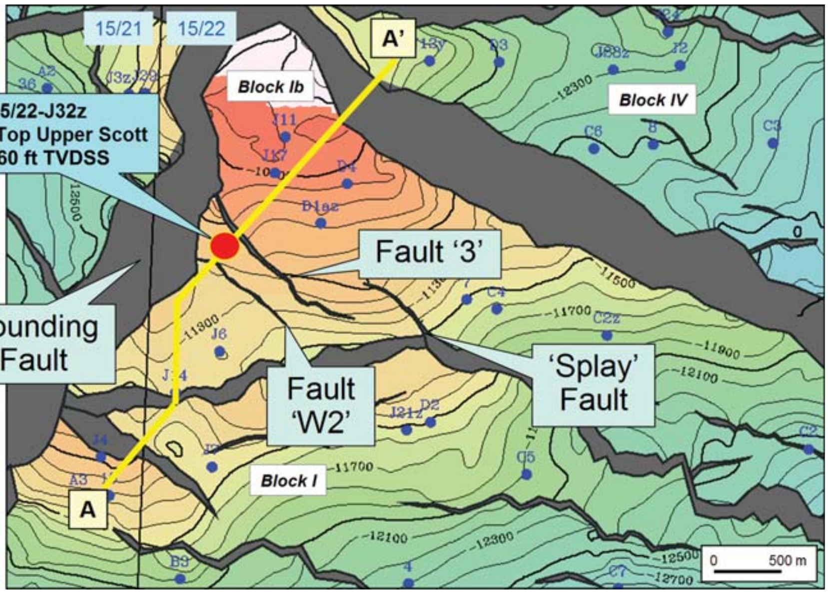

Fig. 11. Location of J32z target.

that it should offset the Scott Formation reservoir against older impermeable rocks of the Saltire Shale and Rattray Volcanics. Even where the throw was insufficient to completely offset reservoir against non-reservoir, the presence of clays and shales either side of the fault was thought to have generated sufficient shale gouge to seal the fault or at least significantly reduce permeability in the fault zone. The principal risk identified on the target was considered to be the sealing nature of the fault to the north of the proposed location with sweep likely if this fault was not sealing.

A dynamic modelling study was performed on Block Ib to assess the J32Z target area. Based on the 2004 geophysical fault interpretation, a number of modifications were made to the faulting pattern within the existing model to more accurately reflect the revised views on the faulting. The main changes were regarding the faulting between the main part of Block 1b and the J6/J14 area, namely faults '3' and 'W2', which were more pronounced than previously mapped (Figs 11 & 12). As a result of these changes, when the model was run through a history matching process, the J32Z target location became the most obvious remaining target within the block.

At the end of the history matching process, the target area was identified as having a significant volume of unswept oil associated with it, particularly in the Scott reservoir, which had been downthrown against non-reservoir at fault '3'. Given the non-unique nature of a history match solution in a large mature field, there was still an element of uncertainty associated with the model. As a result a risk factor was applied to all well production

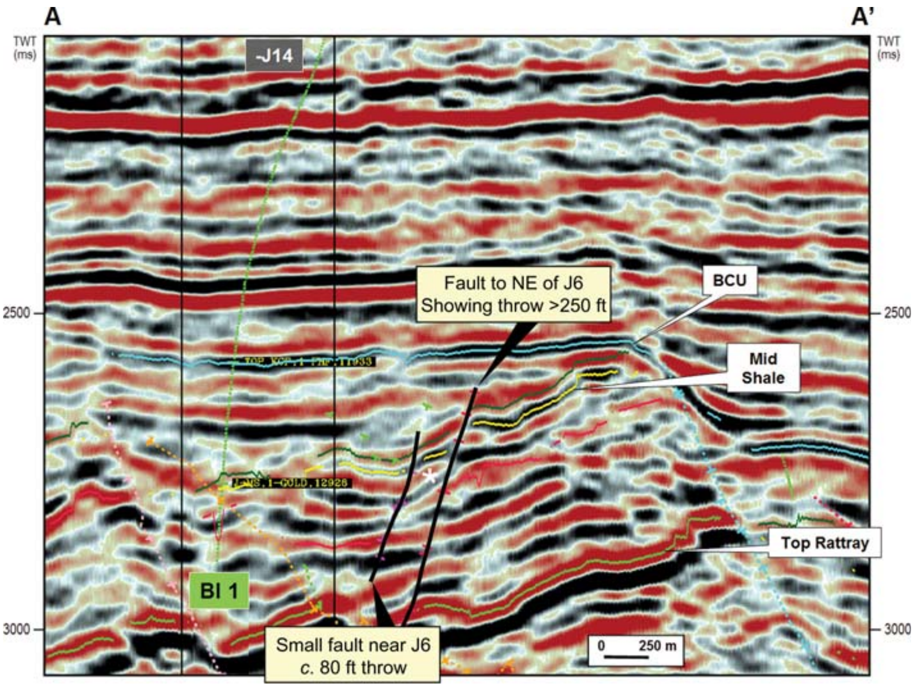

Fig. 12. Seismic line through J32z target.

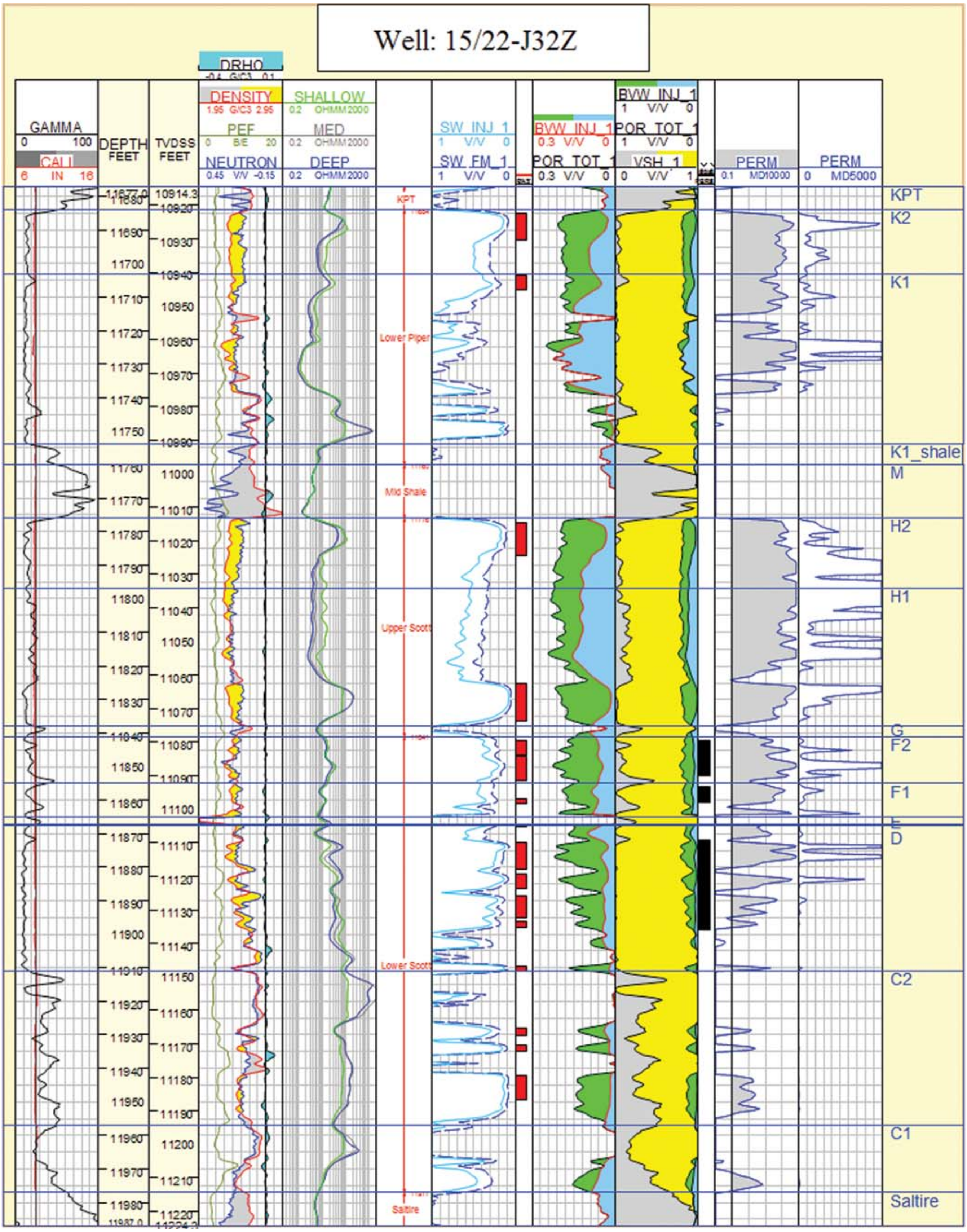

Fig. 13. J32z interpreted open hole results; tracks as in Figure 4.

rates coming from the model to give a more realistic expectation case. After running numerous prediction runs and sensitivities, J32Z had pre-drill estimated incremental recoveries of 1.1–2.7×10^6 bbl.

The well was drilled as the third well of the campaign as a sidetrack of the neighbouring J6 well. Geological results were as prognosed with thick Piper and Scott sands penetrated, although the Upper Piper sands were absent through faulting. Reservoir

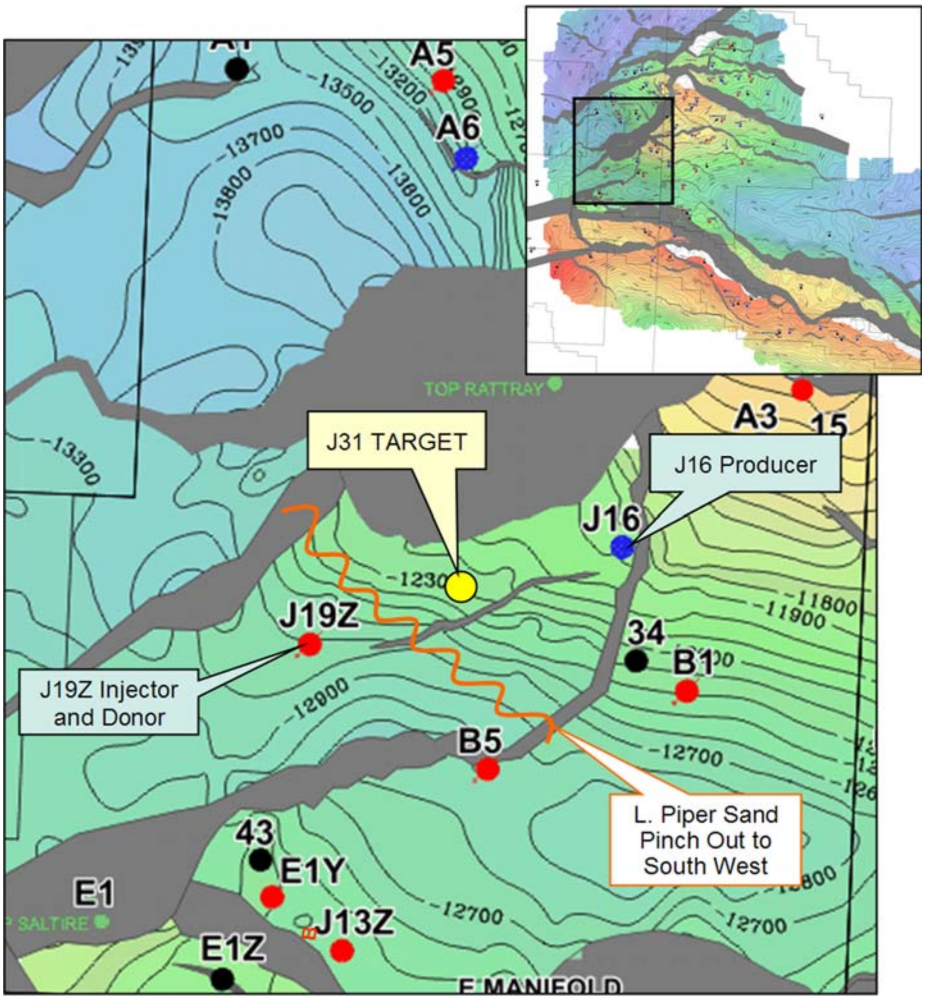

Fig. 14. Location of J31 target.

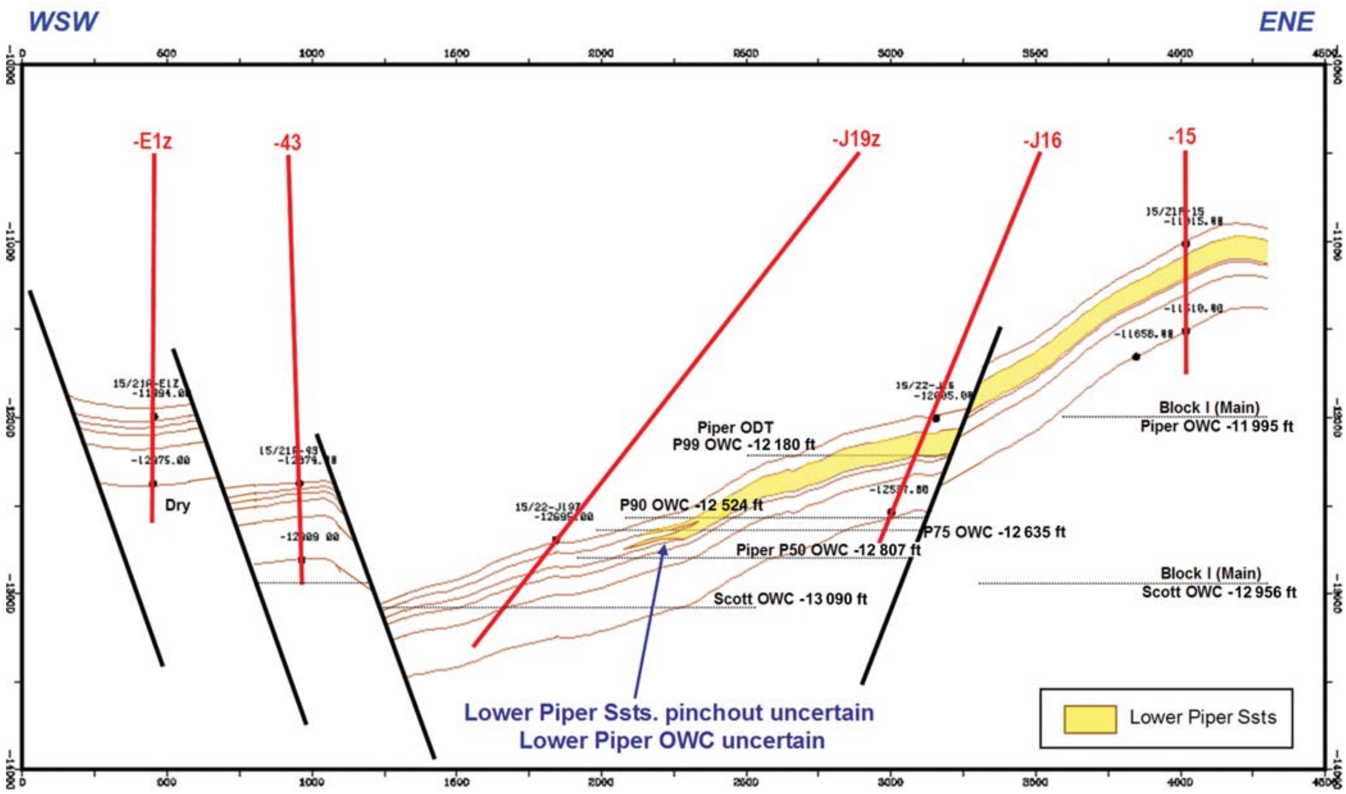

Fig. 15. Block IW, SW–NE cross section.

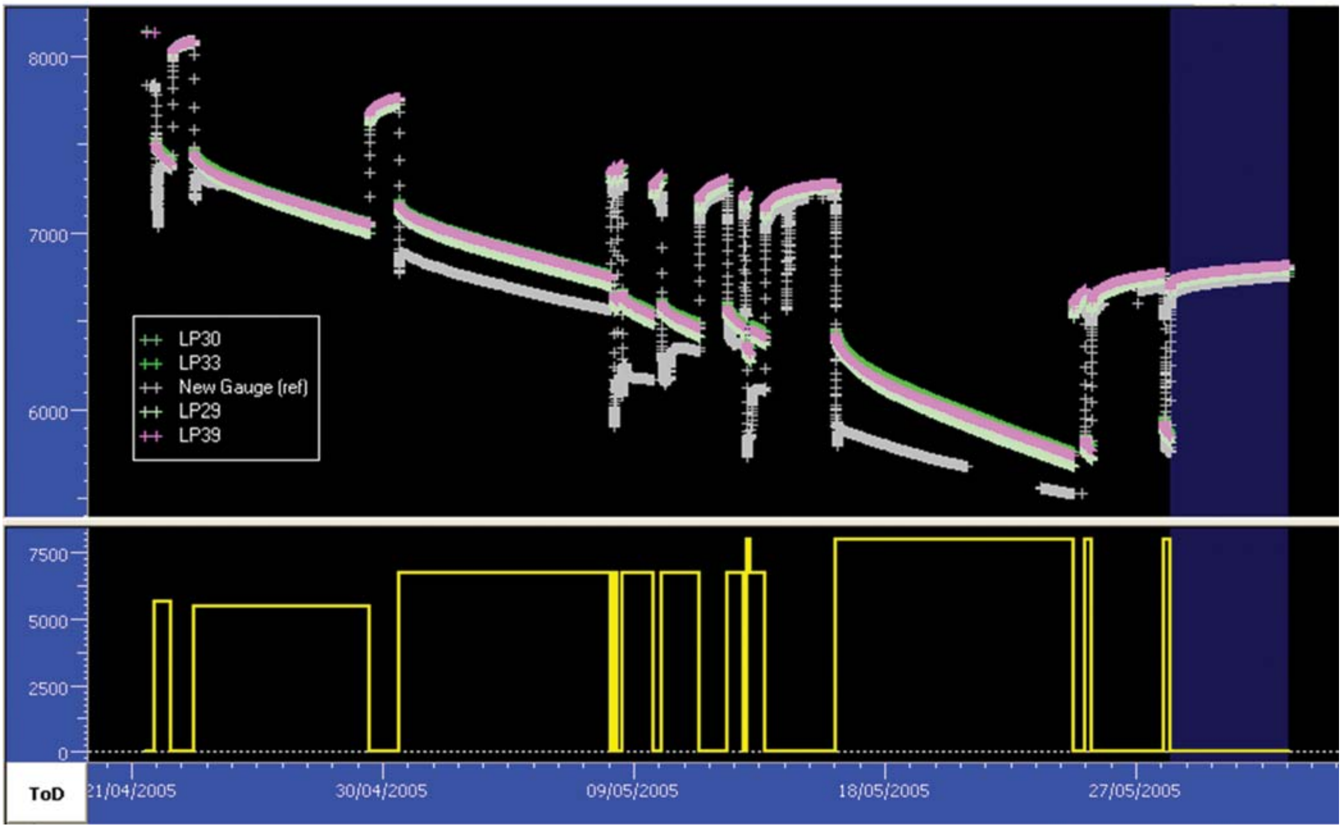

Fig. 16. Simulation match of J16 Piper depletion: four different models; upper plot, pressure (psia) v. date; lower plot, rate (stb/d) v. date.

quality was good with high NTG, porosity and permeable sands, and generally reservoir quality was higher than anticipated (Fig. 13). Saturations were somewhat disappointing with evidence of sweep in both the Scott and Piper sands. The observed water saturation in the Upper Scott appeared to be higher in the lower quality sands, which would not normally be expected in a swept environment. This could possibly be a result of recharging or due to variable wettability in the Upper Scott sands.

The J32Z well initially produced at an oil rate of approximately 5000 bbl/day and a water cut of 80%. The water cut increased to 90% in about one month before levelling off. Although the water cut performance was poorer than had been anticipated, the well still added significant production rates. The ultimate recovery from the well is estimated at 1.4×10^6 bbl. The log interpreted sweep and the high water cut on initial production can be interpreted to indicate that the fault to the north of the well does not provide an adequate seal from updip producer wells. This is despite the significant throw and assumed shale gouge mapped along its length. Further production analysis and history matching including J32Z production data indicates that bypassed oil potential remains present in the block downdip of the fault identified to the south of the well.

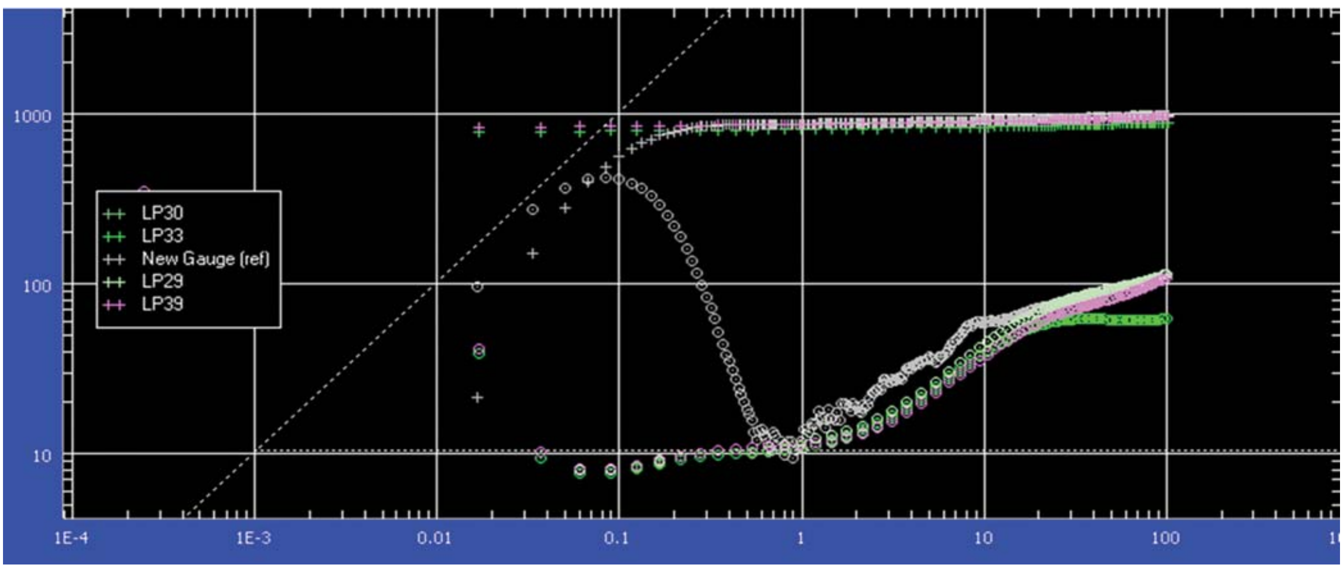

Fig. 17. Simulation match of J16 log-log PBU derivative response; ΔP (psia) and ΔP′ v. Δt (hours): four different models.

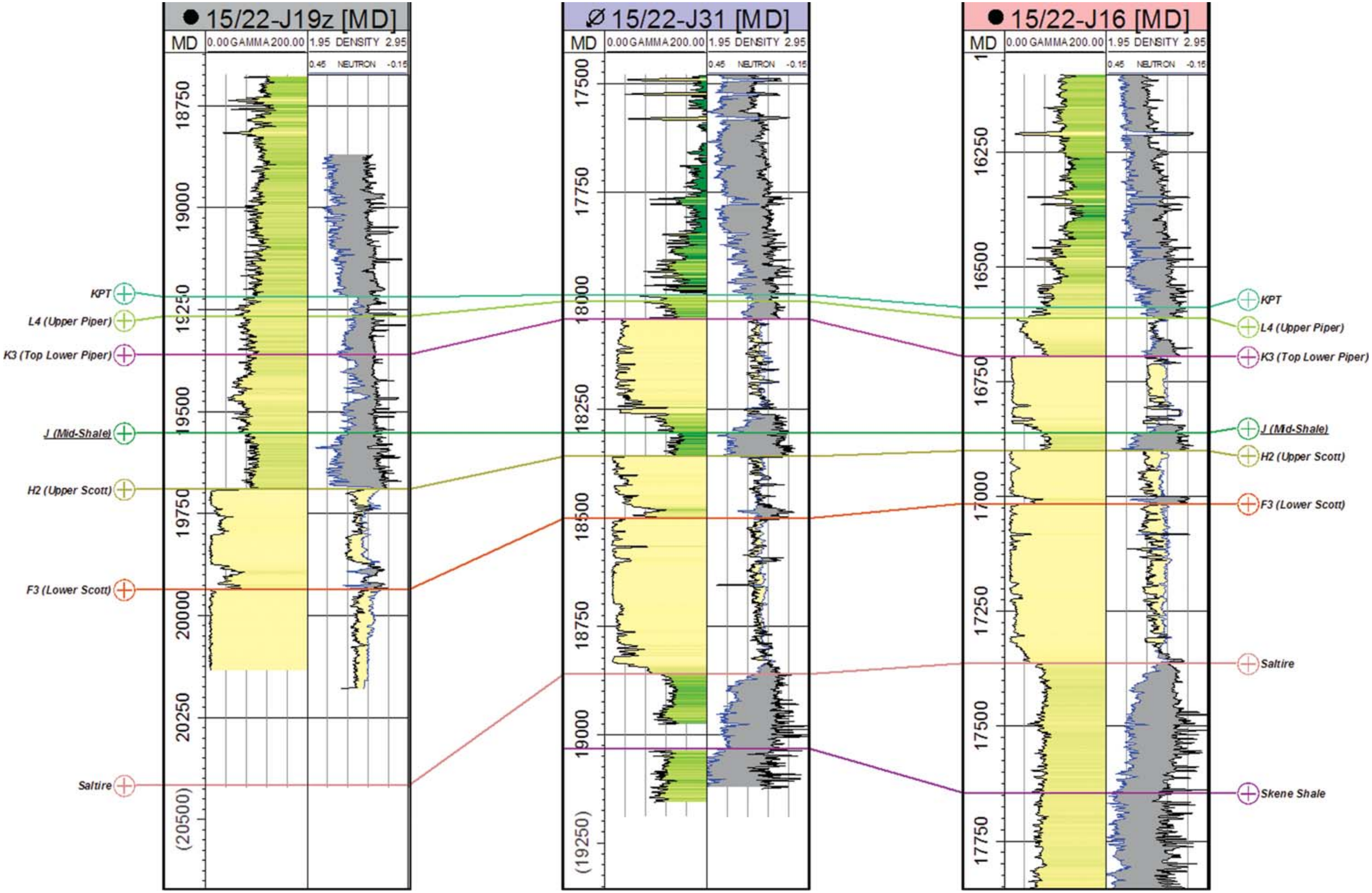

Fig. 18. J31 post-drill correlation. Logs shown: track 1, GR; track 2, DENS/NEUT.

Downdip injector

Block Iw, at the western end of Block I, had been recognized as an isolated compartment since the well J16 was put on production. The J16 well encountered both Scott and Piper reservoirs, at pressures below initial reservoir pressure. Despite this apparent depletion, initial production from the Scott Formation indicated that the interval was not receiving any significant pressure support from the injectors in the main area of Block I to the east.

As a consequence of the lack of pressure support, the J19Z injection well (the first Scott platform injection well) was drilled downdip to provide water injection to the Scott and Piper reservoirs penetrated in the updip J16 well (Fig. 14). However, the J19Z well did not encounter any Piper sands, interpreted to be due to a transition from stacked mass flow sands observed in the J16 well to shale prone lower shoreface in J19Z to the west (Fig. 15).

One of the opportunities identified for the drilling campaign was a downdip injector to intercept the Piper sands encountered in J16. The key uncertainty in the reserves potential for the well was the oil in place in the Lower Piper in Block Iw. A large range of oil in place, from 1.5 to 20×10^6 bbl, could be mapped in the Lower Piper due to the lack of well control on the pinchout edge of the sand, and the unknown OWC. Furthermore, the pinchout edge could not be readily inferred from the seismic data.

As part of the pre-drill ranking for the drilling campaign, it was critical to reduce the uncertainty on the oil in place in the Lower Piper of Block 1w. An intervention was planned and executed that isolated the producing Scott perforations in the J16 well (flowing at 90% water cut), and added a small perforation interval to the Piper sands. The well was produced on depletion for several weeks with several build-ups scheduled, all the time with pressure data recorded from the permanent downhole gauge.

Integrated analysis of the depletion trends and pressure buildup response indicated that the J16 Piper perforations were connected to $3-10 \times 10^6$ bbl of unsupported oil in place. Boundaries could be interpreted from pressure transient analysis consistent with the seismically mapped faults. Material balance analysis of the drawdown could establish only total compressibility of the connected system, but could not distinguish between aquifer and oil. The well data constrained the maximum total sand volume in Block Iw Lower Piper, thus placing a limit on the minimum oil leg/maximum aquifer scenario that would also match the calculated total compressibility of the system. Simulation models confirmed the material balance conclusions; multiple models could be constructed that matched the depletion and the pressure buildup derivative (Figs 16 & 17).

Simulation modelling indicated an incremental recovery of 10–40% from water injection (over depletion recovery) from the Piper sands. The value of a new dedicated Piper water injector, updip of the J19Z well, was compared with a sidetrack of the existing J19Z well – significant reserves remained to be recovered by the J19Z–J16 well pair from the Scott sands. Analysis indicated that the reserves potentially lost from the Scott sands were small compared with the value saving of a sidetrack over a new well.

The principal risk to the target was the presence of the Piper sands. Because of the uncertainty in the pinchout location the well was planned with contingent sidetracks. The J31 injection well was drilled as a sidetrack of the J19Z well as the second well of the campaign. The Piper sands encountered were thicker, but deeper than prognosed, and fully oil-bearing (Fig. 18). Reservoir quality was, however, lower than expected with an increased proportion of finer-grained, silty layers, probably reflecting the position of the Piper sands toward the edge of a depositional pinchout. The Scott sands were swept as prognosed. Post-drill estimates of the oil in place in the Lower Piper of Block Iw were revised towards the upper end of the pre-drill expectations.

A further complication arose during the time between execution of the J16 pressure data gathering, and the drilling of the well. The plug isolating the J16 Scott sands (overpressured due to injection) and the Piper sands (underpressured due to depletion) failed, resulting in cross-flow and causing apparent total loss of productivity from the Piper perforation. It was unclear if there would be total reservoir damage in the Piper sands in the vicinity of the J16 well bore (despite only a small interval having been perforated). In conjunction with putting the J31 well on injection, a remedial intervention was carried out in the J16 well to reinstate the bridge plug and add perforations over the whole J16 Piper interval.

Both wells were brought online. Injection rates in the J31 well were lower than pre-drill expectations, owing to the lower reservoir quality, but the damage to the J16 Piper was less than expected. The J16 well produced 3.1×10^6 bbl from the Piper interval before water breakthrough, ahead of expectations, and ultimate recovery from injection at the J31 well is expected to be 3.8×10^6 bbl.

Impact of drilling campaign on field production

The 2005–2007 drilling campaign had a significant positive impact on the production of the field. The addition of six successful wells saw Scott production increase from pre-campaign levels of 15 to greater than 35 kbbl/day at peak levels. Even though the high initial rates of Scott infill wells tend to decline quickly with

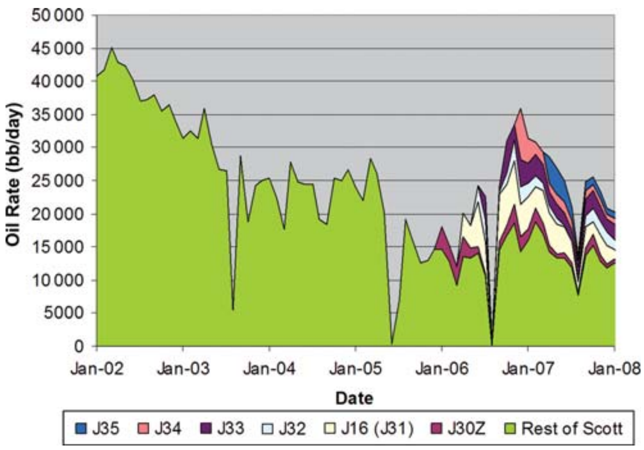

Fig. 19. Scott Field production illustrating impact of 2005–2007 drilling campaign.

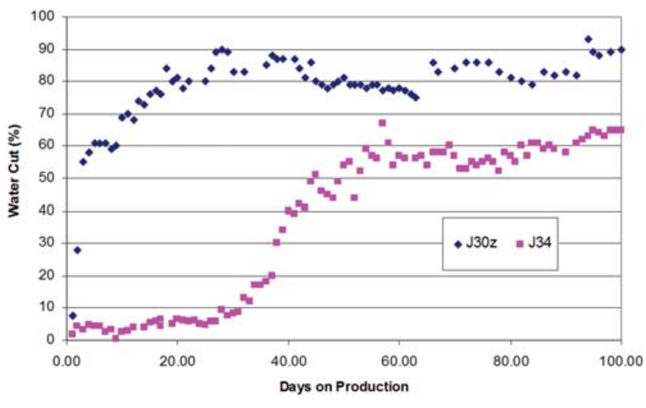

Fig. 20. Wellhead water cut measurements, wells J30Z and J34.

increasing water cut, the increase in field production rate was observed for about three years before returning to pre-campaign levels. When viewed in the context of the field historical production performance (Fig. 19), the benefit of the recent campaign is clearly demonstrated, showing a larger impact than previous infill campaigns.

Despite the considerable amount of production and drilling history on the Scott Field, the nature of the waterflood sweep is still not fully understood. The J32Z and J35 wells both encountered partially swept reservoir sections. The nature of the sweep in the J32Z well, with the higher quality sands showing sweep, cannot be fully explained. In general, the earlier wells in the campaign (J30Z, J32Z, J33), exhibited more rapid water cut evolution than had been anticipated. This led to more pessimistic pre-drill predictions of water cut for the later wells in the 2005–2007 drilling campaign (J34, J35). However, the production performance of these latter wells turned out to be much better than anticipated with more conventional and slower increases in water cut. A comparison of J30Z and J34 illustrates the variation in water cut performance of the infill targets (Fig. 20).

Conclusions

The overall impact of the 2005–2007 drilling campaign has been positive for the Scott Field, both in terms of increased production rates and reserves additions. The six successfully drilled infill wells have all contributed value to the asset.

A number of lessons have been learned from the results of the drilling campaign. Updip attic targets were very successful. The identified pre-drill risk of faulting out due to proximity of the major block bounding faults proved not to be an issue. The seismic interpretation based on the PreSDM volume has been shown to be reliable with respect to the major faults. However, minor faulting continues to be difficult to image and can result in partial absence of reservoir sands, as was experienced with the J35 well.

The downdip injector concept was successful with the J31 target and is easily justified for unsupported reservoir compartments. However, the scope for similar targets on the field is limited with most identified fault blocks currently receiving injection support.

The impact on field production of the campaign has been significant, particularly when compared with the previous drilling results. The strategy of drilling less risky targets, well within the field boundary, has been shown to be value adding even in a mature field that has already been extensively drilled.

The extensive drilling history on Scott has enabled the construction of robust depositional models for the Scott and Piper sands. However the results indicate that some uncertainty still exists in the seismic mapping (faults and horizons) and reservoir behaviour over the field. It is likely that future drilling campaigns will eventually have to target smaller higher risk areas as remaining targets closer to existing well control are drilled up. These are likely to be in areas of increased structural risk due to the poor imaging and complex nature of the faulting areas or where a detailed understanding of reservoir and fault characterization will be required to minimize risks.

The authors would like to thank Nexen Petroleum (UK) Ltd, Petro-Canada UK Ltd, Exxon Mobil Corp., Maersk Oil and Premier Oil plc for their kind permission to publish this paper.

References

Boldy, S. R. & Brealey, S. 1990. Timing, nature and sedimentary results of Jurassic tectonism in the Outer Moray Firth. *In*: Hardman, R. F. P. & Brooks, J. (eds) *Tectonic Events Responsible for Britain's Oil and Gas Reserves*. Geological Society, London, Special Publications, **55**, 254–279.

DECC 2010. Department of Energy and Climate Change, UKCS Field Information. World Wide Web address: https://www.og.decc.gov.uk/fields/fields_index.htm.

Guscott, S., Russell, K., Thickpenny, A. & Poddubiuk, R. 2003. The Scott Field, Blocks 15/21a, 15/22, UK North Sea. *In*: Gluyas, J. G. & Hichens, H. M. (eds) *United Kingdom Oil and Gas Fields Commemorative Millennium Volume*. Geological Society, London, Memoirs, **20**, 467–482. doi: 10.1144/GSL.MEM.2003.020.01.38.

Hibbert, M. J. & Mackertich, D. S. 1993. The structural evolution of the eastern end of the Halibut Horst, Block 15/21, Outer Moray Firth, UK North Sea. *In*: Parker, J. R. (ed.) *Petroleum Geology of Northwest Europe: Proceedings of the 4th Conference*. Geological Society, London, 1179–1188; doi: 10.1144/0041179.

Jones, G., Rorison, P., Frost, R., Knipe, R. & Colleran, J. 1999. Tectono-stratigraphic development of the southern part of UKCS Quadrant 15 (eastern Witch Ground Graben): implications for the Mesozoic-Tertiary evolution of the Central North Sea Basin. *In*: Fleet, A. J. & Boldy, S. A. R. (eds) *Petroleum Geology of Northwest Europe: Proceedings of the 5th Conference*. Geological Society, London, 133–152; doi: 10.1144/0050133.

O'Driscoll, D., Hindle, A. D. & Long, D. C. 1990. The structural controls on Upper Jurassic and Lower Cretaceous reservoir sandstones in the Witch Ground Graben, UK North Sea. *In*: Hardman, R. F. P. & Brooks, J. (eds) *Tectonic Events Responsible for Britain's Oil and Gas Reserves*. Geological Society, London, Special Publications, **55**, 299–323.

Thickpenny, A. & Russell, K. 2000. *A Depositional Model for Scott and Telford Fields*. Lomond Report No. **2083f**, August 2000.

Predicting production behaviour from deep HPHT Triassic reservoirs and the impact of sedimentary architecture on recovery

S. KAPE, O. DIAZ DE SOUZA, I. BUSHNAQ, M. HAYES and I. TURNER

BG Group, Thames Valley Park, Reading, Berkshire RG6 1PT, UK
(e-mail: stephanie.kape@bg-group.com)

Abstract: The Triassic Skaggerak Formation is one of the main reservoirs in the high pressure–high temperature province of the North Sea. Production to date has come from fields located on the intra-basinal highs within the Central Graben, between 10 000 and 15 000 ft TVDss. Undrilled prospectivity has been recognized in structural traps in the deeper parts of the Central Graben up to 20 000 ft TVDss, yet reservoir effectiveness remains a key risk. Therefore, in order to optimize future exploration, appraisal and development programmes, it is necessary to consider the likely reservoir performance and production behaviour of these deeper Skaggerak prospects. The Skagerrak Formation comprises two main reservoir sandstones, the Judy Member and the overlying Joanne Member, separated by a thick shale interval, the Julius Member mudstone (Goldsmith *et al.* 2003). The two reservoirs show markedly different production behaviour despite their apparently similar character on wireline logs. Integration of the production behaviour from the Jade and Judy fields with the sedimentology has enabled the causes of this different production behaviour to be better understood, allowing the controls on reservoir flow to be modelled in both a static and dynamic environment. The understanding of the reservoir behaviour in the currently producing fields has been carried through to a predictive phase of simulation and modelling to determine the range of production behaviours expected for a deeper exploration portfolio. A clear porosity–depth trend exists within the Skagerrak Formation and this has been used to translate the robust history-matched reservoir models from the producing fields to the depth of the prospects. Sensitivity to fluid, porosity–depth trend and permeability of the deep reservoirs have been tested, and a range of likely production rates and behaviours established.

Keywords: Skagerrak Formation, Judy Member, Joanne Member, reservoir architecture, production performance, depth

The Skagerrak Formation of the UK and Norwegian high pressure–high temperature (HPHT) province has been on production since the mid 1990s. Judy (1996), Heron (1998), Egret (1999), Skua (2001) and Jade (2002) are well documented examples of Skagerrak Formation reservoirs (Jones *et al.* 2005; Keller *et al.* 2005; McKie & Audretsch 2005). The J Block area alone has produced over 240 mmboe to date from the Skaggerak Formation. With over 13 years of production performance from these fields, the understanding of the reservoir behaviour of the Skagerrak Formation is improving.

Increasingly, exploration in the HPHT province is targeting deep structural traps (often over 3000 ft deeper than the existing fields on production) within the Skagerrak Formation. Understanding the likely production behaviour of these reservoirs where porosity is known to degrade with depth has been key to defining the risks for exploration in this play. To this end, a reservoir modelling and simulation study has been undertaken to look at the interaction of degrading porosity (and hence permeability) with depth and its sensitivity to increasing reservoir pressure (improving recovery), for a range of fluids, for both the Joanne and Judy members. The study has been based on the history-matched modelling and simulation studies carried out on the Jade Field and the methodology used to generate the predictive history-matched model has been applied to generic models of the Judy and Joanne Member reservoirs at greater depths.

A difference in production behaviour can be seen between the Joanne and Judy Member sandstones over both the Jade and Judy Fields. The sedimentology has been integrated with the production behaviour and well test interpretation to determine the controls of the different sedimentary architectures on production performance. The different sedimentary architectures for the Joanne and Judy members have been incorporated into the reservoir model of the Jade Field, enabling a better simulation match to be obtained to the production.

Given the lack of well data at depth, the modelling is subject to a range of uncertainties; sensitivities have been carried out to test for different porosity–depth trends, different porosity–permeability relationships and sensitivity to hydrocarbon saturation. Fluid type is a key uncertainty when dealing with exploration; however, owing to the location of the prospects in the deep Central Graben, a lean gas condensate fluid was thought to be the most likely fluid present. This was modelled along with a richer gas condensate and a light volatile oil.

Models were run as simulation grids with a range of parameters (both geological and fluid) and recovery and well flow rates were analysed. The increased depth and pressure of the prospects was expected to result in an improved recovery (due to a large pressure drop between initial reservoir pressure and abandonment pressure); however, the effect of the fluid and the degradation of the porosity–permeability with depth was expected to counteract this. The study was designed to investigate the sensitivity of both the Joanne and the Judy members to these controls on production performance. Given the high costs and technical challenges of extreme HPHT exploration and developments, this understanding is critical to the future success and design of any appraisal/development activities as well as de-risking the exploration play.

Geology of the Skaggerak Formation

The geological setting has been well described in a series of regional background papers (Bartholomew *et al.* 1993; Helgeson 1999; Errat *et al.* 2005). The Triassic Skagerrak Formation was

Vining, B. A. & Pickering, S. C. (eds) *Petroleum Geology: From Mature Basins to New Frontiers – Proceedings of the 7th Petroleum Geology Conference*, 405–417. DOI: 10.1144/0070405

deposited in a series of salt and fault controlled mini-basins or 'pods' (Smith *et al.* 1993) within an overall rift basin. The Triassic is deposited immediately overlying a thick Zechstein salt section, which began to form pods (withdrawal basins) due to a combination of sediment loading and structural extension (Smith *et al.* 1993). In the Central Graben the salt section was relatively thick and the pods in general did not become grounded at this time on the underlying Rotliegend rifted basement. This allowed thick accumulations of sediment within the pods to be deposited. The basal part of the Triassic Heron Group (Goldsmith *et al.* 1995, 2003) is the Smith Bank Formation (shales, evaporites and thin sands), which forms the bulk of the fill of the pods. The overlying Skagerrak Formation (thickly interbedded units of sandstones and shales) is found in the upper parts of the pods, often being thinned but present between pods as the basin infilled. The pods represent localized depocentres but were not thought to have formed topographic lows (as they were largely maintained by sediment loading); they are responsible for the increased preservation of the sediments relative to the inter-pod areas. The Triassic is interpreted to have been deposited on a broad plain within the pre-existing Permo-Triassic rift basin.

The Skaggerak Formation is unconformably overlain by Mid and Late Jurassic, or Cretaceous sediments, which form a regional seal. The basin has become highly overpressured in the pre-Cretaceous section (Erratt *et al.* 1999, 2005; Haszeldine *et al.* 1999).

The Skagerrak Formation comprises three thick, continental sandstone sequences (Judy, Joanne and Josephine members), interbedded with predominantly mudstone units (Julius, Jonathan and Joshua members). The upper Josephine and Joshua members are only preserved in the deepest basinal areas and are not volumetrically significant in terms of production. The stratigraphic nomenclature used in this paper was first developed by Goldsmith *et al.* (1995, 2003) (Figs 1 & 2), and is still widely used in the UKCS Quad 30 (J Block) area to date. To the north, in the Heron and Marnock and ETAP area, a different stratigraphic naming convention is used (McKie & Audretsch 2005).

A thorough description of depositional facies found in the Skagerrak Formation is given by previous authors (Goldsmith *et al.* 2003; Jones *et al.* 2005; Keller *et al.* 2005; McKie & Audretsch 2005). Description of the Judy Field (Keller *et al.* 2005) splits the Skagerrak Formation sandstones into four main facies associations: channel sandstone, sheetflood sandstone, argillaceous sandstone and lacustrine mudstone. Palaeosols are also present within the Skaggerak and are found in all facies associations. The channel sandstones provide the best reservoir quality but the sheetflood sandstones also comprise net reservoir. The depositional environment for both the Joanne and the Judy sandstones is interpreted as 'deposition on the margins of an ephemeral lake to a relatively proximal alluvial plain or fluvial braidplain environment' (Keller *et al.* 2005). This covers quite a wide range of dryland depositional environments with potentially very different sedimentary architectures. Nichols & Fisher (2007) give a useful summary of a range of sedimentary architectures seen in an endorheic dryland system (Fig. 3). The Joanne Member of the

Fig. 1. Map of the Quad 30 area of the CNS showing locations of the producing Triassic Fields.

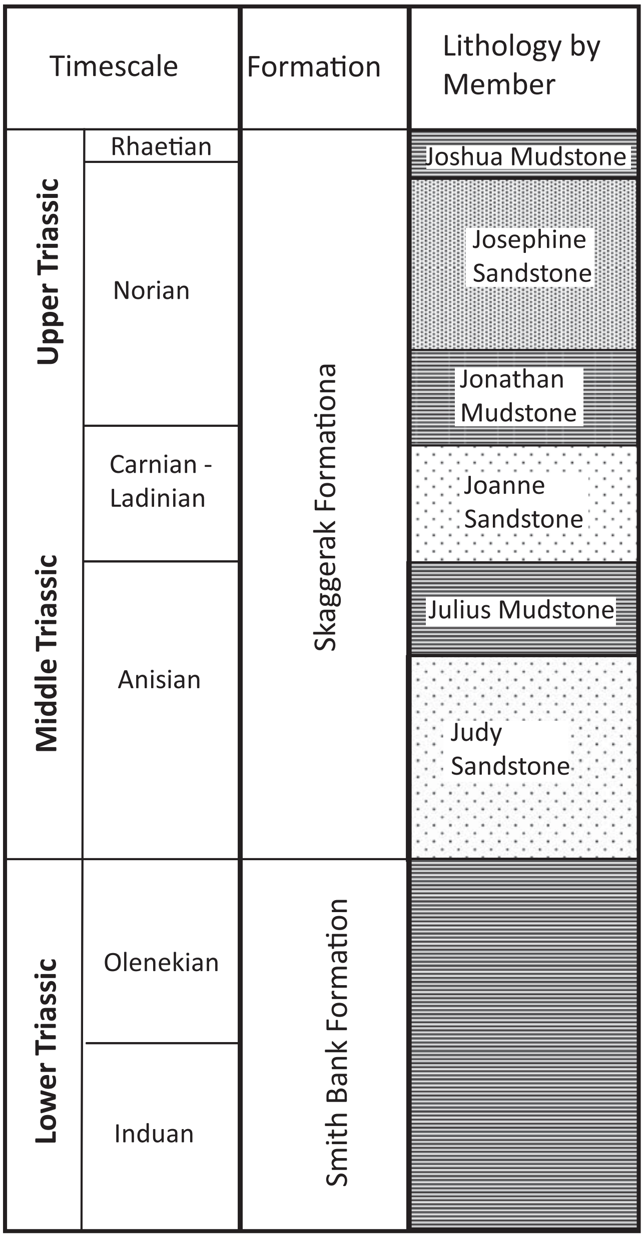

Fig. 2. Stratigraphic column of CNS Triassic (from Goldsmith *et al.* 2003) showing subdivision of the Skagerrak Formation.

Jade Field (Jones *et al.* 2005) is subdivided into an upper more channel-dominated interval and a lower more sheetflood-dominated section, based on a wireline log interpretation. The lower part of the Joanne Member and the Judy Member are not cored in Jade Field. The Judy Member is cored in offset well 30/7a-7 and is there described as finer grained with permeabilities an order of magnitude lower than those seen in the Joanne Member of the Jade Field. The depth difference between the Judy Member in these fields is *c.* 4000 ft true vertical depth subsea (TVDss) (Judy Field is the shallower).

Proprietary sedimentology and diagenesis studies carried out for the J Block partnership and BG Group by A. Melvin of PM Geos and AM Geos discriminate further between sedimentary environments in the Skagerrak (A. Melvin, pers. comm.). From the 30/7a-7 Judy Member core, the reservoir sandstones are described as being arkosic, very fine to fine grained, well sorted, laminated and of a fluvial (sheetflood) origin. These sandstones form the bulk of the reservoir facies although the core also comprises a cleaner, massive, fine grained sandstone, interpreted to be an ephemeral fluvial channel (A. Melvin, pers. comm.). The sandstones in the Judy core are interbedded with fine grained facies interpreted as flood basin and lacustrine and show a high degree of lamination. These facies are more thinly laminated and micaceous than in the core from the Joanne Member.

It is noted that the fluvial channel facies from the Joanne Member sandstones contrast with that seen in the Judy Member, in that it is commonly coarser grained with improved textural characteristics. The Joanne Member sandstones comprise fine to very fine arkosic sandstones but the sands are dominated by coarser-grained cleaner fluvial channel sandstones which show a low degree of compaction and cementation. Sheetflood facies are described as finer grained and better sorted than the channels but include micaceous laminae which serve to reduce porosity and permeability. The sheetflood facies are volumetrically less significant in the Joanne Member than the Judy Member (A. Melvin, pers. comm.). The variation in facies proportions between the Judy Member and the Joanne Member is interpreted to be the dominant control on the production behaviour as described in the following section.

Field production and well test behaviour

Over the 13 years of production from the Judy and Jade fields, the Skagerrak Formation reservoirs (Judy and Joanne members) have shown very different production and well test behaviour. The earlier fields (Judy, Heron, Egret) initially showed a disappointing production performance due to issues of fault compartmentalization and the misinterpretation of early well test data (Keller *et al.* 2005; McKie & Audretsch 2005).

The Joanne Member shows a characteristic decline on a P/Z plot (see Fig. 4) of an initial steep decline in pressure followed by a more gentle pressure decline. This behaviour is also seen in the Heron–Skua–Egret area and is interpreted by McKie & Audretsch (2005) as resulting from initial depletion from the high permeability channel systems followed by a later contribution from poorer quality splay sands (sheetfloods). This behaviour makes early analysis of connected volume (material balance) studies very misleading in the Joanne Member, as they show a far more limited connected volume than is eventually accessed by the well through time. McKie & Audretsch (2005) also note the presence from well test analysis of many localized boundaries which are not seen to affect longer term production performance. This behaviour is also seen on well tests from the Joanne Member in the J Block fields (Fig. 5a). A log–log analysis (pressure derivative) of the 30/7a-P03 well from (Joanne Member, Judy Field) is typical; all Joanne Member well tests from the J Block area show a similar pressure derivative analysis. The log–log plots show strong linear flow characteristics, indicating a linear body of width 80–200 ft. The linear bodies could also be fault constrained; however, the consistency of the well test character between Joanne Member wells indicates a sedimentological rather than a local fault control. The tests indicate initial high permeabilities (100–500 mD) followed by later background permeability of at least an order of magnitude lower (2–10 mD).

In contrast, Judy Member well tests (Fig. 5b) show a characteristic radial flow pattern and do not show barriers close to the wellbore (unless the well is located close to a known fault). The Judy Member well tests typically indicate permeabilities ranging in the tens of milliDarcy.

Both the Joanne and the Judy members show vertical pressure barriers in depleted pressure test datasets within the section. These support pressure differentials post production and are laterally persistent on a field scale. These vertical barriers are likely to correspond to very thin lacustrine and floodbasin shales seen in core. It is difficult to correlate these shales between wells; however, post-production pressure differentials supported across thin shales indicates their lateral continuity within the J Block

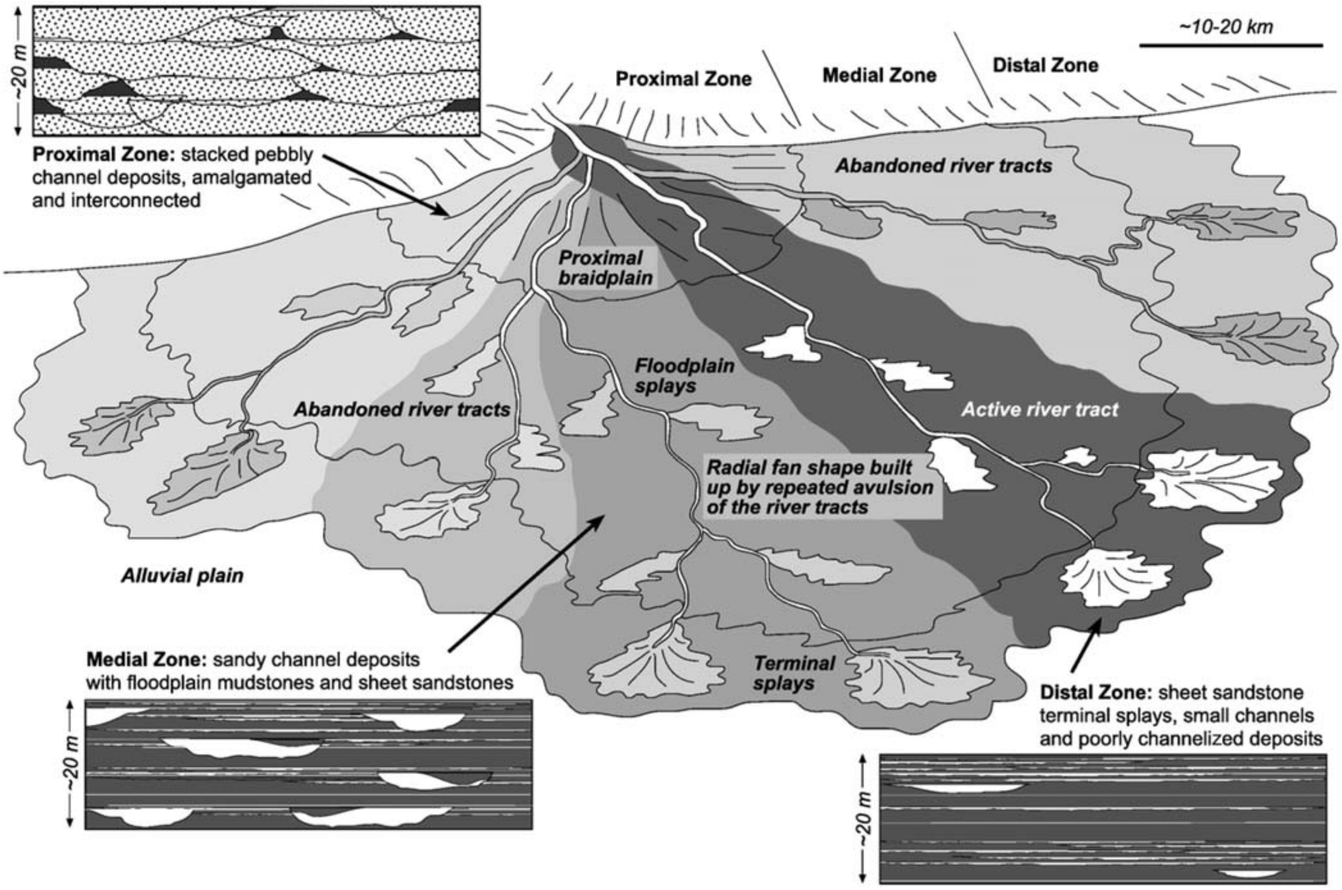

Fig. 3. Proximal to distal trends in channel and overbank processes across a fluvial distributary system. The Joanne Member is interpreted to be part of the medial zone of the system, and the Judy Member in the distal terminal splays (Nichols & Fisher 2007).

fields. Vertical barriers are also noted by McKie & Audretsch (2005) from the Heron cluster area to the north.

Implications of the reservoir behaviour for the sedimentological interpretation

This marked difference in production behaviour between the Judy Member and the Joanne Member is strongly indicative of different reservoir architecture and is seen consistently across both Jade and Judy Fields and offset satellites.

Although the dryland facies seen in the Joanne and Judy members originate in a similar environment, sedimentology studies (see above) point to differing proportions of these facies within the two reservoirs. This, coupled with the variation in production behaviour, suggests that the two reservoirs actually represent different dryland environments. The channel-dominated Joanne Member is more likely to represent a fluvial drainage system from a medial zone of a fluvial system (Nichols & Fisher 2007), where sandy, channelized, bedload-dominated and occasional meandering channels are interbedded with overbank splays and floodplain fines. The channel systems migrate through time

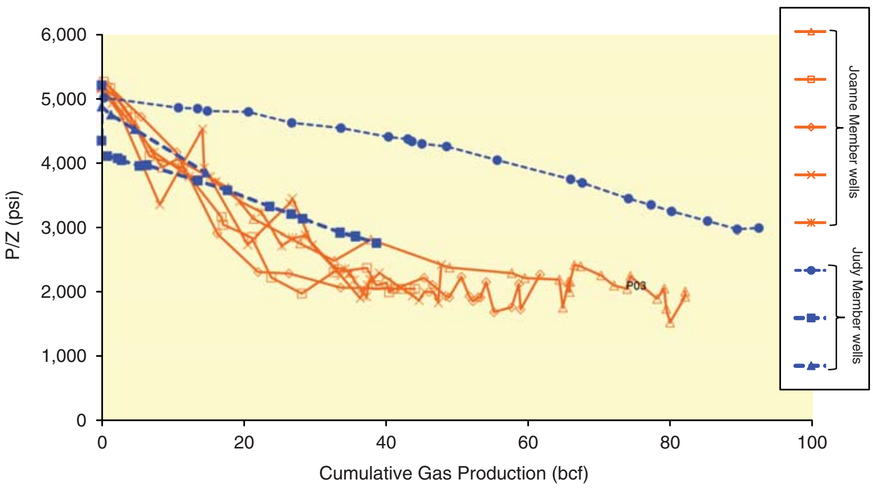

Fig. 4. Cumulative gas production plotted against pressure–time for the Judy Field. Judy Member wells show a steady decline in pressure through time, Joanne Member wells show a faster initial decline followed by a low later pressure decline.

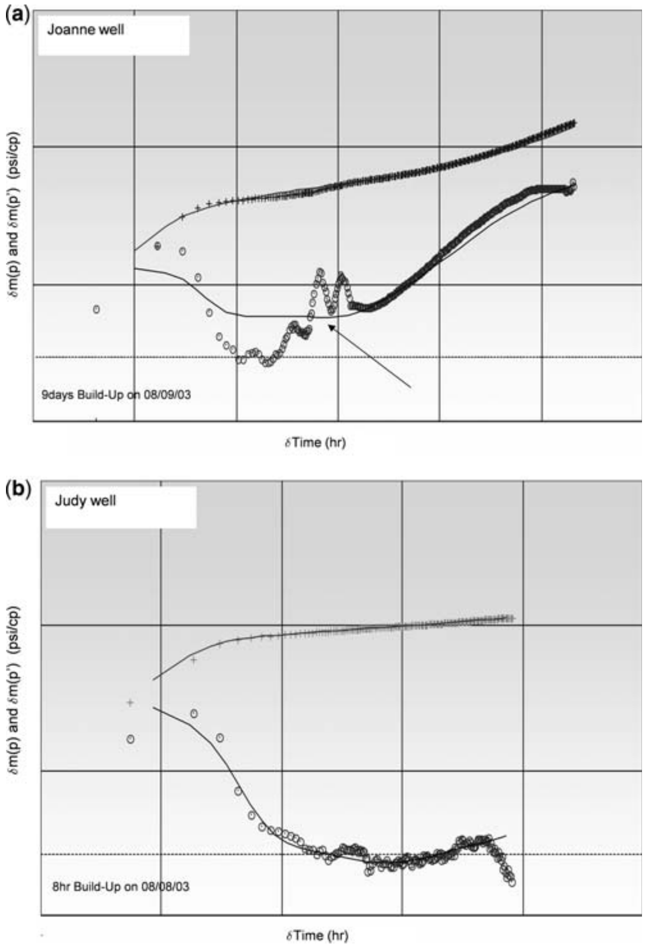

Fig. 5. (**a**) Log–log plot of 30/a-P03 well test. The plot shows the characteristic radial composite model of the Joanne Member well tests, with channels of high permeability seen initially and a lower permeability background seen later. (**b**) Log–log plot of 30/7a-P18 well test. This shows radial flow with no boundaries, indicating tank like pressure behaviour. This is characteristic of the Judy Member.

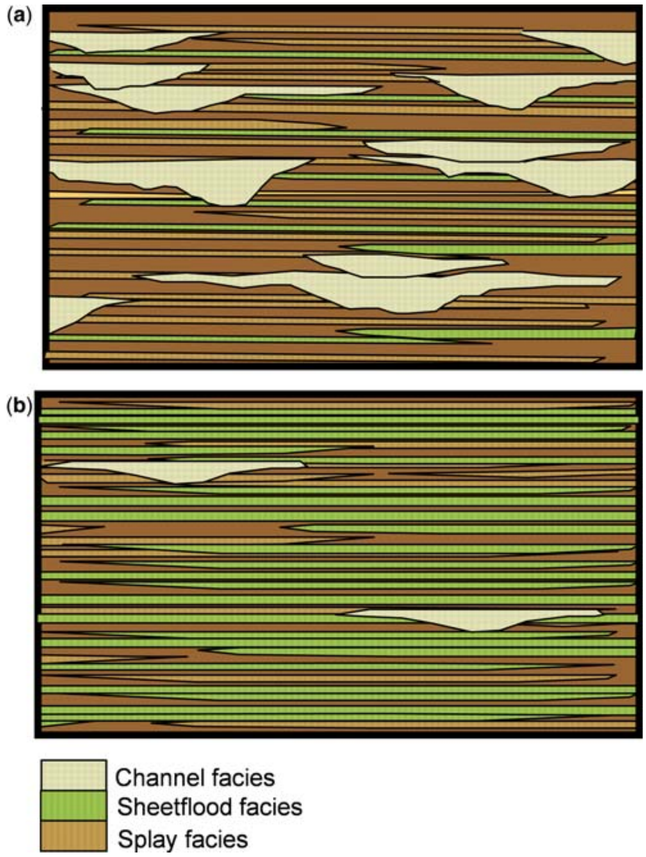

Fig. 6. (**a**) Conceptual stratigraphic architecture of the Joanne Member. (**b**) Conceptual stratigraphic architecture of the Judy Member.

across the pod area (and between pods), occasionally bypassing the pod entirely, allowing the establishment of thin lacustrine shales and palaeosols. The previous interpretation of the Joanne fluvial systems as 'unconfined' (Jones *et al.* 2005) is not compatible with the well test data where clear boundaries are seen on all tests. The fact that the channels are mostly bedload-dominated (braided) does not exclude deposition in a confined channel belt (Nichols & Fisher 2007). The linear flow behaviour seen on Joanne Member well tests is unlikely to be representing the margins of the pods, as the fields are generally located within the thickest part of the pods.

The sheetflood-dominated Judy Member may be interpreted as a sandy terminal splay system (Nichols & Fisher 2007), where sheetfloods are interbedded with thin, single-story ephemeral channels. The sheetfloods themselves are laterally more continuous and more homogenous in porosity–permeability characteristics. Vertical communication in this kind of reservoir architecture is poor, yet lateral connectivity is good, giving rise to the radial flow seen on the Judy Formation well tests and the steady homogenous depletion. The resultant architectures of these systems are likely to be very different (Fig. 6) and hence have been modelled separately in this study.

Previous studies on the J Block fields (Jones *et al.* 2005; Keller *et al.* 2005) have noted the range of sedimentary environments in the J Block Fields, but not the variation in architecture between the Joanne and Judy members, nor its control on the production behaviour.

Skagerrak diagenesis and relationship of porosity with depth

The depositional facies exerts the primary control on reservoir quality (A. Melvin, pers. comm.). The diagenetic history of the Skagerrak Formation sandstones shows episodes of both porosity loss (due to compaction and precipitation of cements), porosity gain (secondary dissolution) and porosity preservation (hydrocarbon emplacement, chlorite rims, overpressure). Much of the porosity loss is interpreted (A. Melvin, pers. comm.) as occurring from early burial to the Early Cretaceous accelerated by high heat flow, particularly in the deeper fault compartments. This resulted in silica and dolomite cementation and localized fault-related calcite cementation. Diagenesis was retarded during the Late Cretaceous–Recent burial, with the onset of overpressure and lower heat flow.

Secondary porosity preservation due to leaching from meteoric water below the Base Cretaceous Unconformity (BCU) is described as a porosity enhancing mechanism (A. Melvin, pers. comm.). Whilst this process is likely to have occurred on the very crestal parts of the upthrown fault blocks (J Block, Jade Field), it does not account for the significant preservation of porosity seen in deeper J Block wells (30/13-5, 30/8-3), where the Triassic reservoirs are overlain by a thick Jurassic section and are not directly bisected by the BCU. Likewise, retardation of quartz precipitation due to hydrocarbon charge is also not thought to be a significant factor in the preservation of porosity as good quality sandstones are seen in wells that have never been hydrocarbon charged or have only residual hydrocarbons (30/13-5, 30/13-3)

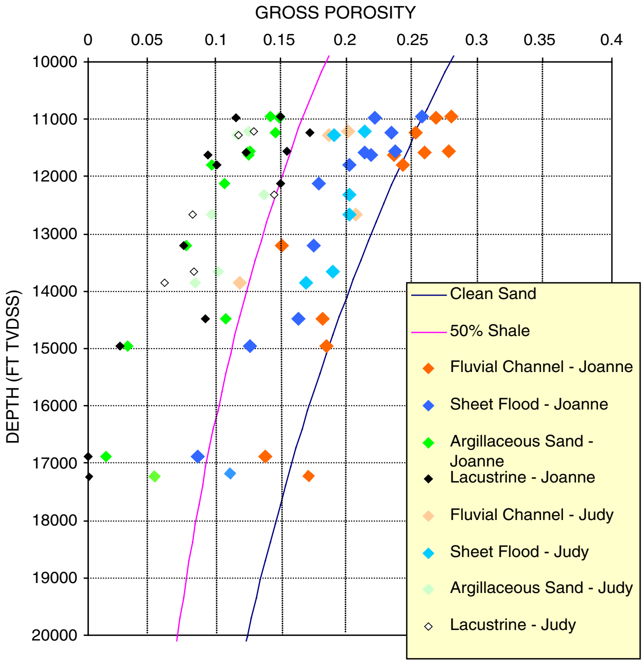

Fig. 7. Average gross porosity plotted with depth by facies for cored wells for the Joanne and Judy members. Sclater & Christie (1980) compaction curves are overlain.

(A. Melvin, pers. comm.). A strong relationship of porosity with depth can be derived from the existing well data (Fig. 7). What is not known is the impact of increasing overpressure with depth in the deep Triassic from 17 000 to 20 000 ft (TVDss) at top reservoir and its impact on retarding compaction (and cementation) related porosity loss.

Methods

The aim of the modelling was to determine the flow characteristics of deep Skaggerak Formation reservoirs from the known production behaviour from the Judy and Joanne Member reservoirs. The models were conditioned to ambient conditions at depth (pressure, temperature, etc.) with a range of fluids.

In order to model a range of possible production behaviour for deep Triassic reservoirs [17 000–20 000 ft (TVDss) at top reservoir], a range of porosity–depth relationships have been applied to the Jade well data to simulate a 'deep Joanne model' and a 'deep Judy model'. A single well (30/2c-J5) was chosen from the deepest offset producing field, Jade, with a Top reservoir depth of 14 340 ft TVDss. The well was translated to depth by applying a range of porosity–depth functions to obtain a high, mid and low case porosity log for the analogue model. A synthetic static and simulation model was built around the well to simulate reservoir behaviour at depth.

The 30/2c-J5 (Jade Field) well was chosen as an analogue for both the Joanne Member and Judy Member as it represents an 'average' Jade Field well and has a full coverage of basic log data (gamma ray, resistivity, density/neutron, sonic) to obtain the best estimation of wireline porosity. It also has a complete section of Joanne Member reservoir and is not eroded at the crest. Although the Skagerrak Formation varies in net to gross (NTG) character between Triassic pods and it is understood that a single well from a field will not accurately predict the NTG and porosity to be found in the exploration prospects, the 30/2c-J5 well was thought to represent a good 'average' well in both the Joanne and Judy members. The range in porosity–depth trends applied to the well to translate the porosity log to the synthetic model depths will go some way towards bracketing a NTG range for the Skagerrak Formation; however, a very low or very high NTG well would have a different production performance. The deep Judy and deep Joanne reservoirs were modelled separately as horizontal slabs, and translated to depth using a porosity–depth trend.

Porosity–depth trends

For the deep Judy model, a range of porosity–depth trends were chosen: 1.4 pu/1000 ft represented the regional porosity–depth trend taken from all the Judy Member well data in the area and was considered to be a good base case. By using core data taken from Judy Member sheetflood facies alone, a linear trend could be fitted through the data of 2.7 porosity units – %(pu)/1000 ft. This was considered a 'worst case' as there was little core control from deeper sections and it may reflect the effects of high porosities seen at shallow depths in the Judy Field, immediately below the BCU, thought to represent the effects of diagenetic leaching related to the unconformity. A trend of 1 pu/1000 ft enabled a match to the wireline porosities seen in the deepest Skagerrak Formation well to date (30/8-3) in the Judy Member (not cored from this well in the Judy Member) at around 18 100 ft, possibly showing some effect of porosity preservation due to overpressure (in addition to the diagenetic mechanisms mentioned previously). A 'high high' case was also run of 0.5 pu/1000 ft to capture a possible increase in the effect of increasing overpressure with depth and also to account for a higher NTG Judy Member section by proxy.

The J Block Joanne Member core data shows that different facies have different porosity decline trends with depth (fluvial channels decline at 2.2 pu/1000 ft, sheetfloods at 2.6 pu/1000 ft and the fine-grained argillaceous facies at 1.66 pu/1000 ft). Three alternative depth trends have been applied to the deep Joanne model, a high case of 1.4 pu/1000 ft, a low case of 3.0 pu/100 ft and a mid case of 2.2 pu/1000 ft. This reflects the fact that the Joanne Member channels are the main flowing zone in this unit and so the porosity–depth trend has been biased towards this. The high and low cases were designed to bracket the range of possible trends; in the high case this would account for a section with more sheetfloods or where overpressure had retarded compaction- and cementation-related porosity loss, and in the low case it would account for a lower NTG section. A sensitivity test was carried out whereby the log data were transformed by individual facies to the depths required; this was found to be very close to the base case porosity–depth trend (on account of the channels being the dominant facies in the Joanne Member).

Modelling parameters

A static geological grid was constructed for both the deep Judy and the deep Joanne reservoirs of 2 × 2 km. The workflow described in Figure 8 was used to generate the static and dynamic models. This workflow is consistent with that which had been used in the Jade Field to achieve a history-matched predictive simulation. The models were translated to a top reservoir depth to reflect possible well locations in offset deep Triassic prospects, such that the results of the simulation could be directly compared with well test esults.

Tables 1 and 2 show the parameter ranges applied to both the deep Judy and the deep Joanne models.

A facies based model was built for both the deep Joanne and deep Judy models. Table 3 details the modelling parameters applied to each grid. For the Joanne model a background facies conditioned by sequential indicator simulation (SIS) (a stochastic, variograms controlled distribution) was used to model the distribution of

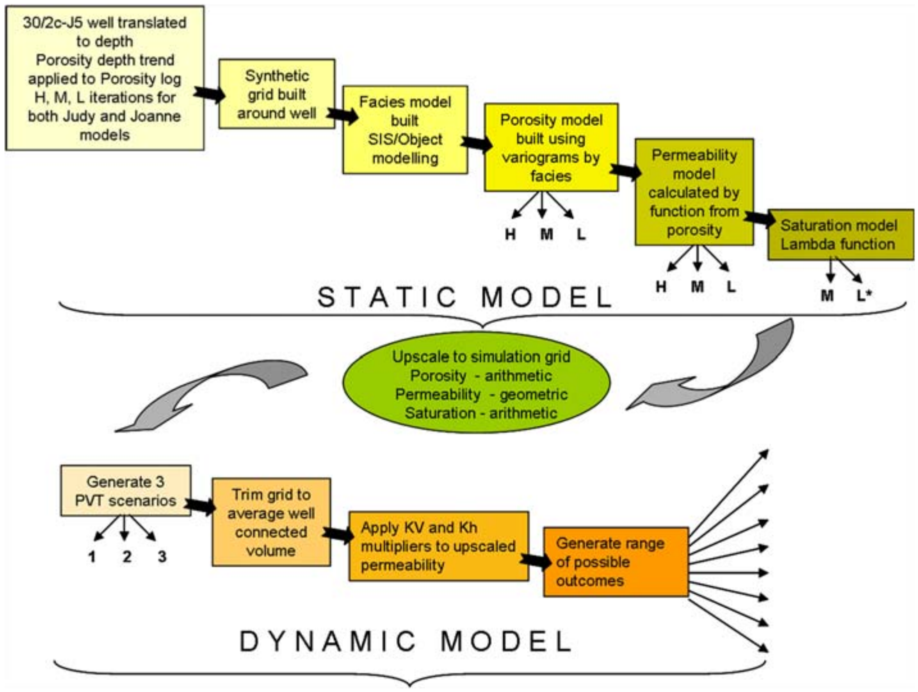

Fig. 8. Static and dynamic modelling workflow used in the construction of the deep Judy and deep Joanne models.

Table 1. Shows the range of parameter sensitivities tested for the deep Judy model

	Low	Base	High	High–high
Porosity–depth trend (pu/100 ft)	2.7	1.4	1	0.5
Porosity–permeability (applied by facies)	H, M, L	H, M, L	H, M, L	H, M, L
S_w (Lambda function)	Base, low	Base, low	Base, low	Base, low
Fluid – CGR (bbl/mmscf)	50/200/408	50/200/408	50/200/408	50/200/408

Table 2. The range of parameter sensitivities tested for the deep Joanne model

	Low	Base	High
Porosity–depth trend (pu/100 ft)	3	2.2	1.4
Porosity–permeability (applied by facies)	H, M, L	H, M, L	H, M, L
Fluid – CGR (bbl/mmscf)	50/200/408	50/200/408	50/200/408

argillaceous sandstones and sheetflood sandstones. An object-based channel distribution was then applied using the previously defined stochastic facies as a background. A ‘channel object’ was used to model the deposits of a confined braided channel and was thought to be representative as the main sand facies were likely to have been deposited in mid channel bars. The channel widths were based on the width of the boundaries determined by well test analysis and other dimensions from core data (thickness). Modern day analogues suggested a straight to sinuous form for these channels (Nichols & Fisher 2007). It should be noted that the channel bodies often represent a series of stacked amalgamated multi-storey channels. From the work of Larue & Hovadik (2006) for NTG over 35% the dimensions and shape of the bodies used becomes less important as connectivity in 3D increases. In the Skaggerak where vertical permeability is poor, the channel dimensions are important despite the relatively high NTG. Connectivity between the channels determines the initial high rate period of production in the Joanne Member. This model has been conditioned to the Jade Field production data through the production history match – and an iterative loop carried out with the facies modelling to condition the body sizes to match the production rates.

The Judy model uses a similar approach to the Joanne Member, with variogram-controlled SIS simulation. Owing to the connected nature of the sheetflood, larger variogram ranges were used of 1500 m. Smaller channel bodies were inserted into this background to represent the single-story nature of the channels seen in core and log.

Porosity distributions in the 3D grid were modelled by facies, using a sequential gaussian simulation and matched to well distributions and a 3% porosity net cutoff applied. No VClay cutoff was applied due to the difficulties of accurately determining a VClay log in the Skagerrak Formation due to the presence of heavy minerals. The 3% porosity cutoff is consistent with the offset Judy Field and Jade Field data, where production is seen from low porosity–permeability facies.

A core derived function between porosity and permeability was applied for each facies (Fig. 9) and sensitivities applied to this

Table 3. Model data for the deep Judy and the deep Joanne models

	Deep Judy model	Deep Joanne model
Top Reservoir depth (ft TVDss)	18 870	18 880
Depth translation from J5 (ΔD) (ft)	2657	4540
Reservoir thickness (ft)	1198	1436
Static grid cell size (W × L × T)	50 × 50 × 2 m	50 × 50 × 4.6 m
Upscaled grid cell size	75 × 75 × 2 m	60 × 60 × 4.6 m
OGIP final trimmed grid (variation due to PVT variation)	155–200 bcf	190–240 bcf
Initial model surface pressure (psia)	16 800	16 900
Vertical permeability (K_v) multiplier	0.01	0.01
Horizontal permeability (K_h) multiplier	1	0.1

to generate a high, low and base case permeability model for each porosity–depth realization. The same porosity–permeability functions were applied to both the deep Joanne and the deep Judy models.

Different saturation height models were applied to both models and were derived from Judy Member and Joanne Member well data. These used a lambda function (Brooks & Corey 1966). In the Judy Member much of the well data input to these models was derived from the transition zone (and the intention of the synthetic models was to generate a flow model from above the transition zone); a sensitivity was applied to this function to model the sensitivity low case saturations as the data were not thought to provide good constraint to the simulation model. The base case water saturations (S_w) ranged from 13 to 29%, for porosity values of 20–9% respectively at 1400 ft above the free water level (FWL). The sensitivity to the low side had a S_w range of 17–38% for the same porosity range, by varying the parameters *A* and *B* in the lambda function (Brooks & Corey 1966).

A FWL was set at the base of the deep Joanne model to coincide with the spill point seen on the prospect which the synthetic model was built to simulate. The Joanne Member showed a shorter transition zone than the Judy Member and the data used to derive a lambda saturation height function were primarily based on data considerably above the FWL; therefore a sensitivity to saturation function was not carried out on the deep Joanne model. The range of saturations seen at 1400 ft above the FWL was from 13 to 30% for 20–9% porosity.

Evaluation runs were generated on the upscaled grid, which had been trimmed to give an original gas in place (OGIP) comparable to that seen by wells in the offset J Block Fields. The grid was equilibrated with an initial pressure (Table 3) corresponding to the top reservoir depth. Unconstrained tubing was used and a minimum bottom-hole pressure of 5000 psi for both models. The simulation was run for a 20 year period. Both models were run with three alternate fluids, a light gas condensate of gas condensate ratio (CGR) of 50 (seen as the most likely case), a richer gas condensate (CGR = 200) and a volatile oil [gas oil ratio (GOR) = 2450]. Vertical (K_v) and horizontal (K_h) permeability multipliers were added to the deep Joanne and deep Judy models to achieve consistency with the history-matched Jade Field model. A K_v multiplier of 0.01 was applied to both models to reflect the poor vertical permeability seen in the offset fields. A K_h multiplier was applied to the deep Joanne model only of 0.1, which had been used to match the long-term production performance of the Joanne reservoir in the Jade Field. A match to the 30/2c-4 Joanne Member well test calculated permeability results in a K_h multiplier of 0.4. This decrease in effective flowing permeability through time is thought to reflect the increasing heterogeneity of the fluvial Joanne reservoir with distance from the wellbore.

Results

Deep Judy model results

The graphs in Figures 10 and 12 show the results of the low, base and high-high case porosity realizations (the high case was found to be close to the base case) for the synthetic Judy model, plotted by CGR.

Recovery Factor (RF) v. CGR/GOR (Fig. 10a, b). The RF for both gas and oil is significantly higher in the low CGR case than the volatile oil case. The gas RF shows an overlap between the porosity cases between the high and low permeability sensitivities. The oil RF plot shows less overlap between the porosity cases.

Initial gas rate v. CGR (Fig. 10c). This graph shows a decrease in initial gas production with increasing CGR/GOR (as would be expected). As with the RF, there is a good deal of overlap between the runs. The low porosity–low permeability case and the mid porosity–low permeability case both show significantly lower initial gas production rate than the other cases. All other cases produce an initial rate of around 45–57 mmscf/day in the low CGR = 50 (most likely) case. This mid porosity–permeability case with a CGR of 200 has an initial gas rate of around 30 mmscf/day, comparable with initial gas rates from Judy Fields of 50 mmscf/day for the P18 Judy Member well, around 7000 ft shallower (Jones *et al.* 2005; Keller *et al.* 2005).

Figure 10d shows gas RF plotted against mean net permeability. All three fluids follow a similar trend, showing a marked decrease in RF below 2 mD net permeability. However, for the light gas condensate case the RF remains above 50% even in the lowest porosity–permeability run. The sensitivity of the model to a low case saturation height function is shown in Figure 10e. There is relatively little sensitivity to CGR/GOR with a low case saturation model, and only in the lowest porosity–permeability case is a significant impact on gas RF seen (20–25%).

The expected ultimate recovery (EUR) recovery per model (Fig. 12a) over a 20 year time period shows little variation again between the CGR cases. The permeability sensitivities result in a few mmboe EUR difference for each porosity case. The cases plot in order of porosity–depth trend, with the lowest porosity cases producing less than 15 mmboe/well over 20 years.

Production profiles (Fig. 12b) for the mid porosity–permeability run show a steady rate decline through time with an initial rate of around 47 mmscf/day in the light gas condensate case. The volatile oil shows a drop off in gas recovery after four years, followed by a lower rate gas tail.

Deep Joanne model results

The graphs shown in Figure 11 show the results of the synthetic deep Joanne model.

The gas and oil recovery factors both show the low permeability sensitivities plotting at the low end of the range below the mid-case permeability realizations. Both the gas and oil RF are particularly poor for the high GOR (volatile oil) runs (Fig. 11a, b), with RFs at 10% or less for both gas and oil in the low permeability cases.

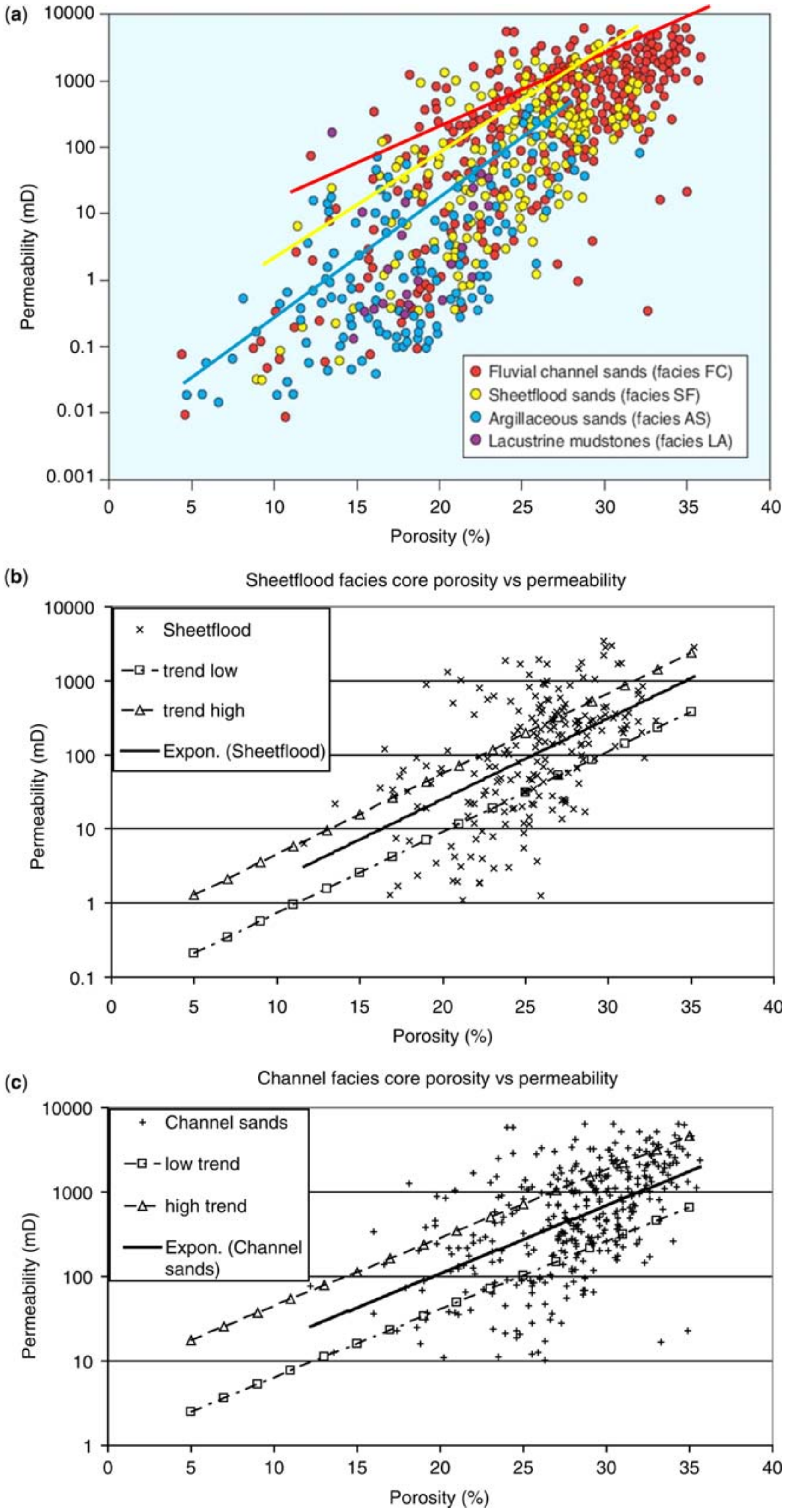

Fig. 9. Porosity v. permeability plot coloured by facies from the Joanne Formation of the UK Central North Sea (CNS) (Goldsmith *et al.* 2003). Data appear to be on one trend, yet split by facies it is composed of three trends. (**b**) Porosity v. permeability plot for the sheetflood facies only, showing the best fit exponential trend, plus a low and high case sensitivity. (**c**) Porosity v. permeability plot for the channel facies only, showing the best fit exponential trend, plus a low and high case sensitivity.

The gas RF when plotted against mean net permeability shows a significant reduction in RF below 10 mD net permeability (Fig. 11d) in all three cases of around 10–20%. For the volatile oil cases this reduction in RF seems to occur at round 20 mD.

Good RF and rates can be achieved in the low CGR case in all but the lowest permeability cases. For the richer gas condensate (CGR = 200) the RF and rates are more sensitive to permeability.

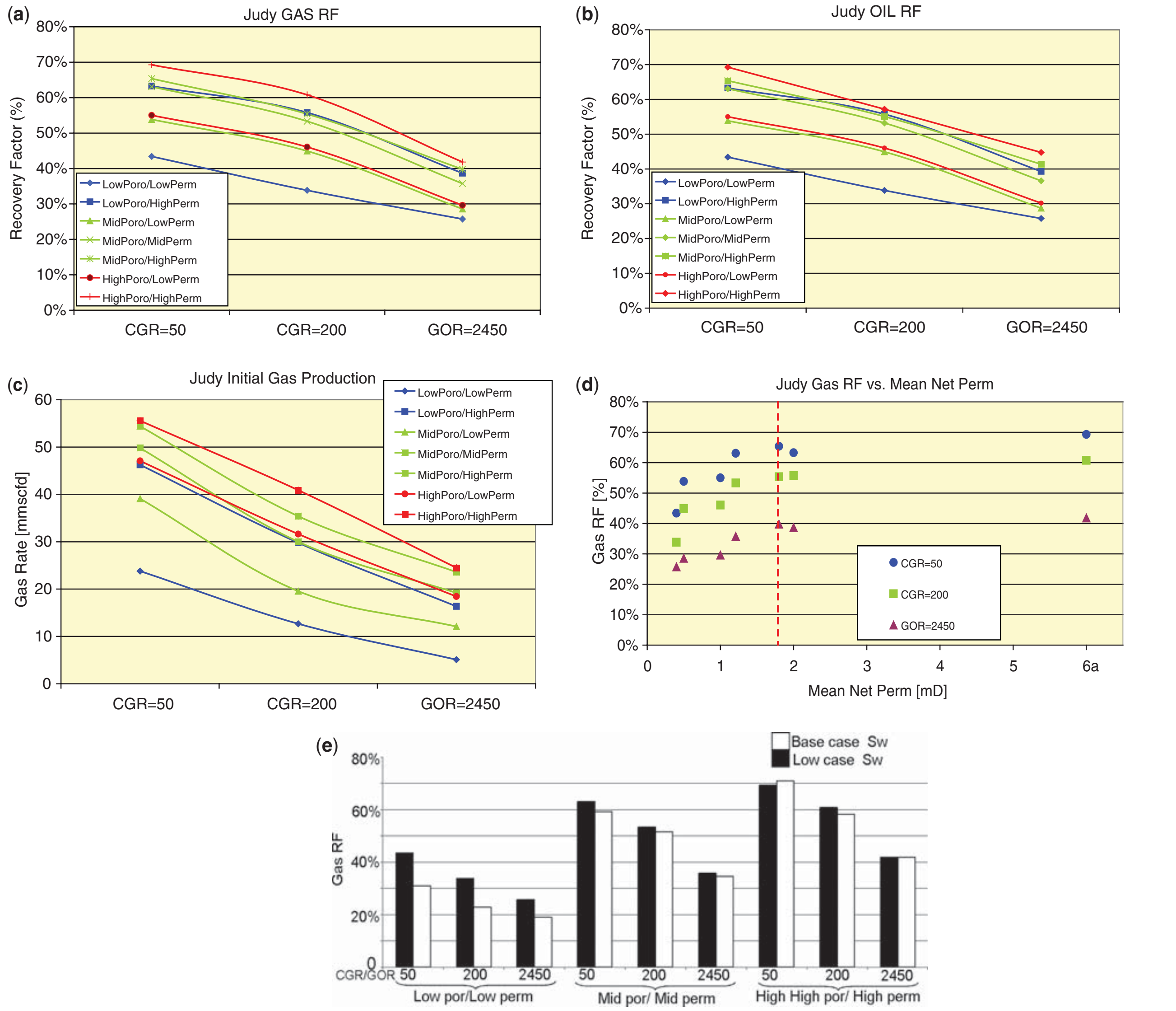

Fig. 10. (**a**) Judy Gas RF v. CGR/GOR. (**b**) Judy oil RF v. CGR/GOR. (**c**) Judy initial gas production rate v. CGR (**d**). Judy gas RF v. mean net model permeability. Red line shows permeability at which little incremental RF is achieved. (**e**) Sensitivity of deep Judy model mid case porosity run to a low case saturation height function.

The initial gas rate (Fig. 11c) is also strongly affected by CGR, with the volatile oil case producing at a rate of less than 5 mmscf/day. The low permeability cases for the lean and rich gas condensates are also less than 20 mmscf/day. The mid porosity–permeability case with a CGR of 200 has an initial gas rate of 28 mmscf/day. This is can be compared with published Jade Field rates at a similar CGR of 50–75 mmscf/day (Jones *et al.* 2006) from wells *c*. 2500 ft shallower.

The ultimate recoverable resources over the 20 year run life (Fig. 12a) show low recoveries in the high CGR case in all but the highest permeability sensitivities. For the gas condensate runs, the ultimate recoverable resources rank in order of porosity with no overlap between the permeability cases. The recovery is less than 15 mmboe in the low porosity–permeability run for all cases.

Discussion

The deep Judy model shows that gas recovery factor is controlled by both porosity and permeability, whereas oil RF is more strongly controlled by porosity. EUR resources through time are likely to be controlled by porosity rather than permeability. The model produces in a stable manner above 2 mD net permeability, with little incremental recovery above this value. Sensitivities to low case saturations also show a limited effect on recovery; the key controlling factor on recovery is porosity. The model is not sensitive to variations in CGR, suggesting that a volatile oil case would also be producible in the Judy Member reservoir under the extreme HPHT conditions expected. Initial gas rate is more sensitive to permeability and it is likely that the low permeability–low porosity cases may not prove to be effective reservoir.

The initial gas rates compare favourably with the P18 well on Judy Field (the 30/2c-J5 Judy Member producer on Jade Field is comingled with the Joanne Member), showing a third of the initial gas rate. The Judy Field is 7000 ft shallower than the deep models. In the deep models, the most likely fluid is predicted to be a light gas condensate – for which initial gas rates are comparable at 50 mmscf/day, suggesting that a lighter fluid may compensate for the decrease in reservoir properties with depth.

As the model initializes at a high pressure, it never falls below the dew point in the 20 year run time. This means that the sensitivity to the effects of condensate banking have not been studied but are likely to have an effect in the low permeability cases (due to lower flow rate) and high CGR cases. This effect would only be seen towards the end of the field life.

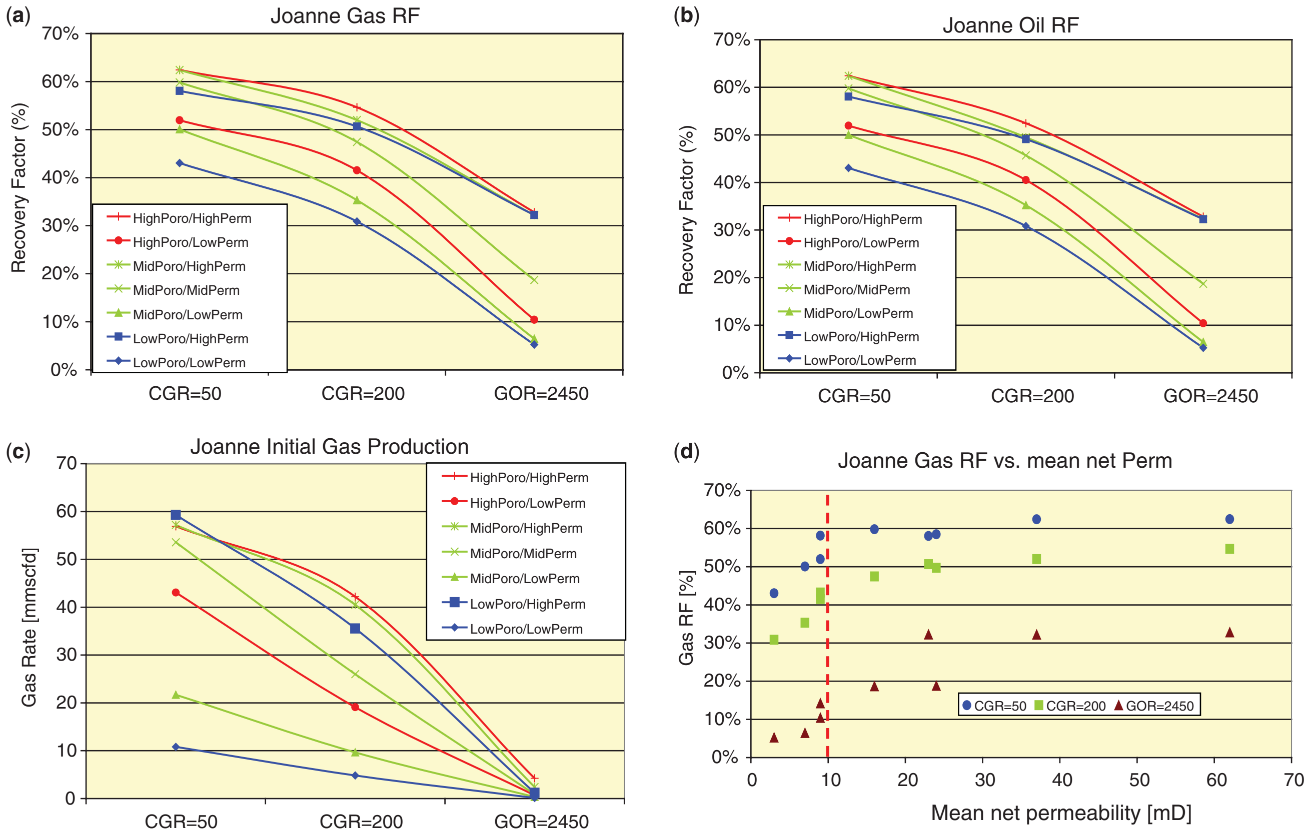

Fig. 11. (**a**) Joanne Gas RF v. CGR/GOR. (**b**) Joanne oil RF v. CGR/GOR. (**c**) Joanne initial gas production rate v. CGR (**d**) Joanne gas RF v. mean net model permeability. Red line shows permeability at which little incremental RF is achieved.

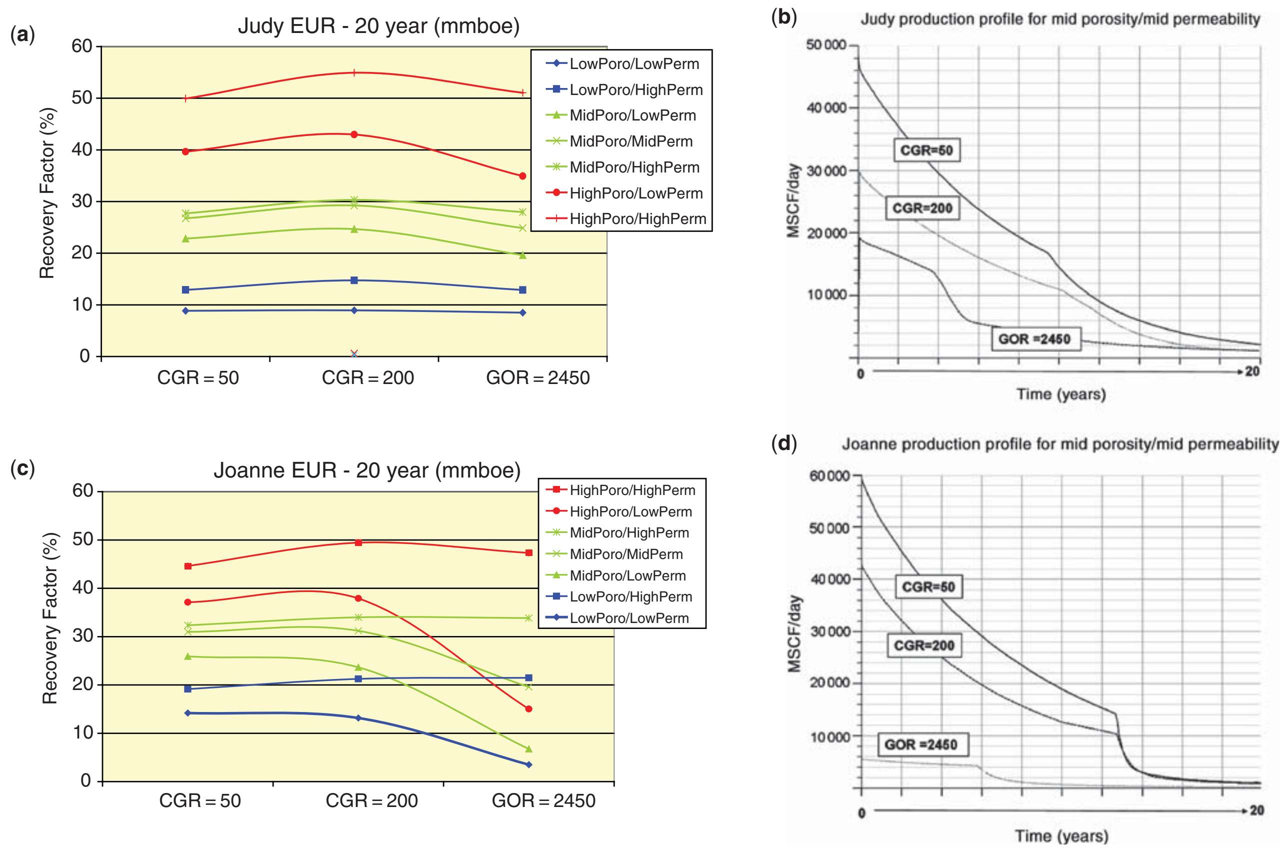

Fig. 12. (**a**) Judy EUR resources over 20 years. (**b**) Judy production profile v. CGR for mid porosity–permeability case. (**c**) Joanne EUR resources over 20 years. (**d**) Joanne production profile v. CGR for mid porosity–permeability case.

The Judy Member reservoir is interpreted as sheetflood-dominated. The production and well test behaviour show radial flow through a relatively homogenous system. Although the porosity–permeability characteristics of the Judy Member reservoir are poorer than the channel-dominated Joanne Member, this homogeneity allows a steady production decline and the good lateral connectivity results in much of the model volume being connected, increasing recovery. No K_h multiplier has been applied to the deep Judy model (consistent with the methodology used in the history-matched Jade Field model). The lack of K_h multipliers results from the laterally homogenous properties of sheetflood deposits, suggesting that the flowing permeability does not vary away from the well bore due to the lack of lateral baffles/barriers to flow.

The porosity–permeability transform used is based on core data that has not been corrected for reservoir pressure, temperature and fluids. This would imply that this dataset would be expected to be 'optimistic' in its prediction of permeability from porosity. As a best fit linear transform has been applied to this data set (by facies) and the permeability is plotted on a logarithmic scale, this will always lead to a low side estimation of the permeability in the model. It is acknowledged that the prediction of permeability from porosity remains a key uncertainty in this workflow as no core data from the depth of the prospects have yet been obtained to define this relationship at depth and that sensitivity of the Judy model to permeability may be greater than shown in this study. The behaviour of the deep Judy model contrasts with the deep Joanne model. The Joanne Member has consistently higher porosities and permeabilities in the channel sands in the Jade and Judy fields than the Judy Member, yet the deep production behaviour and RF show a much stronger control from permeability than that seen in the deep Judy model.

The deep Joanne model shows a strong control from both permeability and fluid type, both of which may significantly reduce gas rate. The deep Joanne model shows no incremental increase in gas RF above a 10 mD average net permeability cutoff (as compared with a 2 mD cutoff in the Judy model). The inherent production behaviour of the Joanne Member as a dual permeability system with the poorer quality sheetflood and overbank deposits serving to connect the higher permeability channels increases the dependency of the production on the lower permeability facies. When these are extrapolated to depth, the productivity of the entire Joanne reservoir declines. In the Joanne model, porosity controls the ultimate recoverable resources, yet permeability has a stronger control on liquid production and rate. The volatile oil cases are particularly adversely affected by the reduction in permeability and only the high porosity–permeability sensitivities recover more than 20 mmboe/well in the 20 year run time.

The gas production profiles for the mid case porosity–permeability realization for both the deep Joanne and Judy models (Fig. 11b, d) show that the deep Joanne model produces at higher rates (5000–10 000 mmscf/day more) for the gas condensate cases, but the volatile oil case is significantly poorer than for the deep Judy model.

The Joanne Member has had a K_h multiplier of 0.1 applied (consistent with that applied in the history-matched Jade Field model), which reflects the increasing sedimentological heterogeneity seen (baffles and barriers to flow) away from the well bore, consistent with its interpretation as a channel-dominated facies.

Porosity–depth trends remain a significant source of uncertainty in both the Joanne and Judy members. In both forward-modelled examples it is the low case porosity–depth trend that results in low recovery; this is 2.7 pu/1000 ft in the deep Judy model and 3 pu/1000 ft in the deep Joanne model. These results suggest that, in either reservoir, if the low case porosity–depth trend is coupled with poor permeability and/or low NTG, the reservoir is unlikely be effective. The deep Joanne model is more sensitive to permeability than the deep Judy model and there may be more reservoir risk associated with a deep Joanne prospect as a result.

As a single 'average Skagerrak Formation' well has been used as an analogue, the effect of significantly poorer or better NTG has not been explicitly modelled in this study. It is known that Skagerrak Formation stratigraphy changes between pods and that NTG varies also within pods, such that the applicability of a single 'representative well' must be questioned, and its applicability away from the Jade Field discussed. Although the stratigraphy may vary within the Judy Member, the overall homogeneous nature of the sheetflood sands means that the model will be likely to represent this type of facies within the region. The Heron–Marnock area to the north show a similar facies in the Lower Judy, with the upper Judy showing a fluvial dominated facies. In this area the deep Joanne model will better represent the production from the Upper Judy in the Heron–Marnock area. NTG variations within the Joanne and the Judy will significantly impact production and connectivity – particularly within the Joanne Member, which is very sensitive to variations in connectivity between the channels. This is seen in the offset fields and an NTG of $>25\%$ is likely to severely limit recovery. These results are consistent with plots of recovery v. NTG for heterogeneous reservoirs derived by Larue & Hovadik (2006), which show an 'S curve' decline in recovery below 35% NTG for most channelized reservoirs. The Judy Member reservoir may be less susceptible to low NTG scenarios as lateral connectivity is generally better than in the Joanne Member. However given that in a low NTG scenario the pore volume connected to the well bore will reduce and vertical permeability is poor, ultimate recovery per well may be severely reduced.

Given that the aim of this study is to study deep Skagerrak production behaviours, it can be seen that the mid and high porosity–depth trend cases all produced at viable rates. Structural complexity was not considered in this evaluation and production wells drilled into areas with significant faulting could be expected to have significantly poorer performance. Structural tilt will also impact production performance but has not been accounted for in this generic study.

Conclusions

The understanding of the Joanne and Judy reservoir production data from the currently producing J Block fields has allowed better understanding of the risks for deep Skagerrak Formation exploration targets, in that for the majority of cases the reservoir is able to flow over production timescales and at effective rates.

Recognition that the Joanne and Judy members have different characteristic reservoir production and well test behaviours has improved understanding of sedimentological architecture and connectivity. This can be related to different environments of deposition within an overall dryland setting for the Joanne and the Judy members of a medial fluvial system for the Joanne Member and a terminal splay for the Judy Member. Understanding of this fundamental difference in production style linked to sedimentary architecture has allowed facies-based models to be constructed that captured the fundamental heterogeneity of both the Joanne and the Judy reservoirs, resulting in a predictive history-matched model for the Jade Field. This tested methodology had been extrapolated to the deep Skagerrak Formation reservoirs to understand likely production behaviour with depth.

The deep Judy model flow rate and RF at depth are controlled mainly by porosity. The model is not as sensitive to CGR/GOR variations as the deep Joanne model and permeability is a secondary not a primary control on production. For net permeabilities of greater than 2 mD the recovery is stable.

The Joanne Member is more heterogeneous than the Judy Member and recovery from the deep Joanne model is more strongly controlled by permeability, particularly oil recovery. Increased CGR has a strongly detrimental effect on both recovery and rate. For net permeabilities of less than 10 mD there is a marked reduction in RF in all CGR cases. Either low permeability or a volatile oil may limit the effectiveness of a deep Joanne Member reservoir.

The behaviour of the two models has been used to understand the possible implications for production from deep Skagerrak Formation Reservoirs. In all but the lowest porosity–permeability and NTG cases the reservoir is predicted to be effective, due mainly to higher predicted overpressures and large differences between initial reservoir pressure and dew point.

The authors would like to thank BG Group for allowing publication of this material. The J Block and Jade partners are also thanked [Conoco Phillips UK Ltd, ENI (UK) Ltd, Chevron UK Ltd and OMV (UK) Ltd]. The opinions and interpretations expressed in this paper are the views of the authors and do not necessarily represent those of BG Group Ltd or its co-venturers. Proprietary sedimentology and diagenesis studies were carried out on the cored intervals in J Block and offset wells for the J Block partnership and BG Group by A. Melvin of PM Geos and AM Geos. The authors have also benefitted from discussion with other J Block workers: A. Gabb, R. Hiney, R. Charles, J. Hilton. M. Hardman and G. Cowan are also thanked for their comments and edits. Three anonymous reviewers are thanked for their time and helpful comments.

References

Bartholomew, I. D., Peters, J. M. & Powell, C. M. 1993. Regional structural evolution of the North Sea: oblique slip and the reactivation of basement lineaments. *In*: Parker, J. R. (ed.) *Petroleum Geology of North West Europe: Proceedings of the 4th Conference*, Geological Society, London, 1109–1122, doi: 10.1144/0041109.

Brooks, R. H. & Corey, A. T. 1966. Properties of porous media affecting fluid flow. *Journal of the Irrigation and Drainage Division, Proceedings, ASCE*, **92**, 61–88.

Errat, D., Nicholson, P. H., Winefield, P., Milton-Worssell, R. J., Cayley, G. T. & Arter, G. 2005. Exploration history of the high-pressure, high-temperature plays: UK Central North Sea. *In*: Doré, A. G. & Vining, B. A. (eds) *Petroleum Geology: North-West Europe and Global Perspectives: Proceedings of the 6th Petroleum Geology Conference*. Geological Society, London, 253–267, doi: 10.1144/0060253.

Erratt, D., Thomas, G. M. & Wall, G. R. T. 1999. The evolution of the Central North Sea Rift. *In*: Fleet, A. J. & Boldy, S. A. R. (eds) *Petroleum Geology of Northwest Europe: Proceedings of the 5th Conference*. Geological Society, London, 63–82, doi: 10.1144/0050063.

Goldsmith, P. J., Hudson, G. & Van Veen, P. 2003. Triassic. *In*: Evans, D., Graham, C., Armour, A. & Bathurst, P. (eds) *The Millennium Atlas: Petroleum Geology of the Central and Northern North Sea*. Geological Society, London, 105–127.

Goldsmith, P. J., Rich, B. & Standring, J. 1995. Triassic correlation and stratigraphy in the South Central Graben, UK North Sea. *In*: Boldy, S. A. R. (ed.) *Permian and Triassic Rifting in Northwest Europe*. Geological Society, London, Special Publications, **91**, 123–143.

Haszeldine, R. S., Wilkinson, M. *et al*. 1999. Diagenetic porosity creation in an overpressured graben. *In*: Fleet, A. J. & Boldy, S. A. R. (eds) *Petroleum Geology of Northwest Europe: Proceedings of the 5th Conference*. Geological Society, London, 1339–1351, doi: 10.1144/0051339.

Helgeson, D. E. 1999. Structural development and trap formation in the Central North Sea HP/HT play. *In*: Fleet, A. J. & Boldy, S. A. R. (eds) *Petroleum Geology of Northwest Europe: Proceedings of the 5th Conference*. Geological Society, London, 1029–1034, doi: 10.1144/0051029.

Jones, A. D., Auld, H. A. *et al*. 2005. Jade Field. *In*: Doré, A. G. & Vining, B. A. (eds) *Petroleum Geology: North-West Europe and Global Perspectives: Proceedings of the 6th Petroleum Geology Conference*. Geological Society, London, 269–283, doi: 10.1144/0060269.

Keller, T., Bayes, R., Auld, H. & Lines, M. 2005. Judy Field: rejuvenation through a second phase of drilling. *In*: Doré, A. G. & Vining, B. A. (eds) *Petroleum Geology: North-West Europe and Global Perspectives: Proceedings of the 6th Petroleum Geology Conference*. Geological Society, London, 651–661, doi: 10.1144/0060651.

Larue, D. J. & Hovadik, J. 2006. Connectivity of channelized reservoirs: a modelling approach. *Petroleum Geoscience*, **12**, 291–308.

McKie, T. & Audretsch, P. 2005. Depositional and structural controls on Triassic reservoir performance in the Heron Cluster, ETAP, Central North Sea. *In*: Doré, A. G. & Vining, B. A. (eds) *Petroleum Geology: North-West Europe and Global Perspectives: Proceedings of the 6th Petroleum Geology Conference*. Geological Society, London, 285–297, doi: 10.1144/0060285.

Nichols, G. J. & Fisher, J. A. 2007. Processes, facies and architecture of fluvial distributary system deposits. *Sedimentary Geology*, **195**, 75–90.

Sclater, J. G. & Christie, P. A. F. 1980. Continental stretching: an explanation of the post Mid-Cretaceous subsidence of the Central North Sea basin. *Journal of Geophysical Research*, **85**, 3711–3739.

Smith, R. I., Hodgson, N. & Fulton, M. 1993. Salt control on the Triassic reservoir distribution. UKCS Central North Sea. *In*: Parker, J. R. (ed.) *Petroleum Geology of Northwest Europe: Proceedings of the 4th Conference*. Geological Society, London, 469–483, doi: 10.1144/0040469.

Sedimentology and unexpected pressure decline: the HP/HT Kristin Field

J. G. QUIN, P. ZWEIGEL, E. ELDHOLM, O. R. HANSEN, K. R. CHRISTOFFERSEN and A. ZAOSTROVSKI

Statoil, Strandveien 4, NO-7501 Stjørdal, Norway (e-mail: jqu@statoil.com)

Abstract: Since production began in the HP/HT Kristin Field off mid-Norway, reservoir pressure in each of the three mid to late Jurassic reservoir units (the Garn, Ile and Tofte formations) has declined significantly more rapidly than was initially predicted. In the Garn Formation, the Tofte Formation and to some extent also the Ile Formation, this has occurred at least partly because an unusual distribution of reservoir properties led to bias in the four-well appraisal dataset and this in turn resulted in an overestimation of reservoir properties. Of particular importance to this bias was the fact that very good but unrepresentative reservoir properties were encountered in all three reservoir zones in the discovery well located in the centre of the field. These, it is now realized, are not even typical of most of the central part of the field but are, instead, restricted within one, small, anomalous area. Study of cores and thin sections indicates that in each reservoir unit this directly reflects a concentration of more energetic depositional facies in the area while less energetic facies are present on three sides. This pattern was not predictable from the original dataset and seems to have arisen because there was structural control upon facies positioning during accumulation of the reservoir section. This influenced the distribution of cleaner, coarser grained, more proximal depositional facies and, ultimately, reservoir quality distribution and pressure development. What is interesting about Kristin Field is that the structural influence upon sedimentation is observed within the footwall stratigraphy of a major relay structure where the primary provenance direction was on the hanging-wall side. This pattern is the reverse of what is normally reported in tectono-stratigraphic studies.

Keywords: depletion, growth strata, shallow marine sandstone, tectono-stratigraphy, HP/HT

The high-pressure, high-temperature (HP/HT) Kristin Field lies 220 km off the mid-Norwegian coast (Fig. 1) in 350 m water depth and is a conventional structural trap comprising an elongate north–south oriented horst block (25 km long and 5 km across). The structure dips gently to the east and is partly eroded along the northern part of the western margin by the Base Cretaceous Unconformity (BCU). The field contains gas condensate in three Lower to Middle Jurassic paralic sandstone units buried at between 4600 and 4850 m ss and was discovered by Saga Petroleum in 1996. Three appraisal wells were subsequently drilled and a substantial discovery was proven with estimated original in-place volumes of around 100 MSm^3 of condensate and 100 GSm^3 of gas, a dew point of *c.* 400 bar and a gas–oil ratio of *c.* 1000 Sm^3/Sm^3 (Christoffersen *et al.* 2008). Statoil became the operator of Kristin Field in January 2000 and production began in November 2005. Since then, pressure in each of the three Kristin Field reservoir units has declined significantly more rapidly than was predicted at the appraisal stage. This has occurred at least partly because reservoir properties (mainly permeability) were initially overestimated as a result of a skewed appraisal well dataset. Of particular importance to this bias was the persistent presence of unrepresentatively high reservoir quality in the discovery well (well 2-3) which is located in the volumetrically important central part of the field. This manuscript examines what geological controls led to this phenomenon, how it skewed initial impressions of Kristin Field, and what impact it has had on field development.

Tectonics and burial history

From the early Carboniferous through to the opening of the north Atlantic in the early Eocene, the Norwegian continental margin underwent a prolonged episode of tectonic extension (Glennie & Underhill 1998; Doré *et al.* 1999; Brekke *et al.* 2001). This began with widespread active rifting between the Carboniferous and Permian, was followed by a phase of thermal relaxation between the Middle Triassic and the late Early Jurassic, and continued with intermittent tectonic activity from the Middle Jurassic through to the Cenozoic (Brekke *et al.* 2001). In the Halten Terrace area in which Kristin Field is located, the Middle Jurassic to Cenozoic rifting stage has traditionally been thought to have begun between deposition of the shallow marine Fangst Group and the overlying shelf mudrocks of the Upper Jurassic Viking Group (Dalland *et al.* 1988; Ehrenberg *et al.* 1992; Koch & Heum 1995; see Fig. 1). While this would place the reservoir section in Kristin Field (mainly Fangst Group) within the pre-rift section, some syn-depositional fault movement is nevertheless reported within the interval regionally (Corfield & Sharp 2000; Corfield *et al.* 2001; Marsh 2008) and is occasionally observed from growth across faults within the Kristin Field reservoir section. Deposition of the overlying Upper Jurassic Viking Group mudrocks coincided with much more intense tectonic activity (late Oxfordian/early Kimmeridgian and the Ryazanian/Valangian, e.g. Blystad *et al.* 1995; Underhill 1998) which is observed from major growth across faults within the interval. This pulse of tectonism also led to most of the structuration that is now associated with hydrocarbon accumulation in the Halten Terrace and in the area around Kristin Field this episode was characterized by thin-skinned gravitational sliding (Marsh 2008) towards the west. The faulted Jurassic section is capped by the BCU while the overlying succession is dominated by eastward onlapping marine shales with minor sandstone units derived from the Norwegian mainland.

Both hydrocarbon generation and the development of overpressure in the western part of the Halten Terrace seem to have been associated with a pulse of subsidence in the Pliocene (Skar *et al.* 1999). The overpressure is thought to have developed either in response to local mechanical compaction of shales (Borge 2002) or through transfer of pressure from the deep and highly

VINING, B. A. & PICKERING, S. C. (eds) *Petroleum Geology: From Mature Basins to New Frontiers – Proceedings of the 7th Petroleum Geology Conference*, 419–429. DOI: 10.1144/0070419

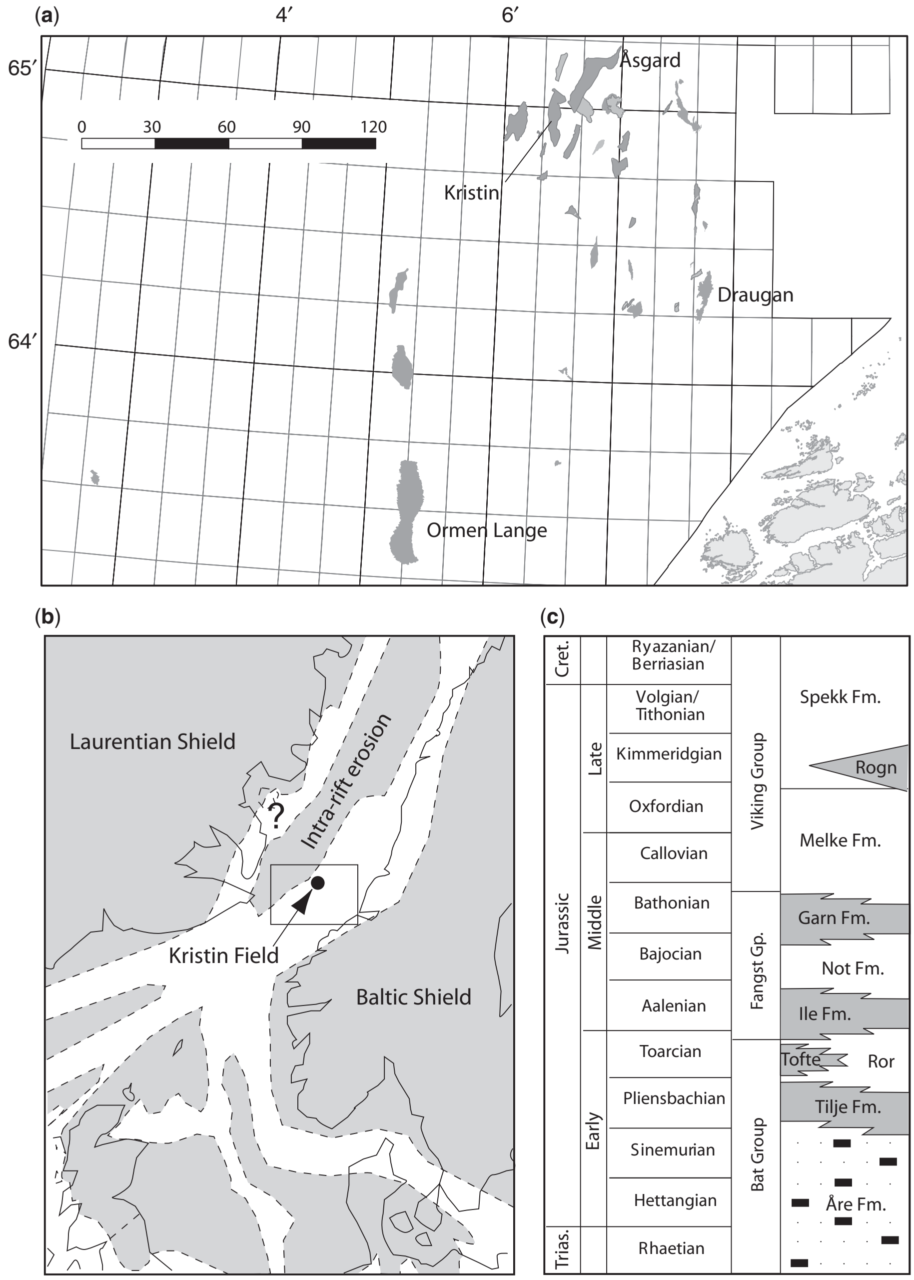

Fig. 1. (**a**) Kristin Field location map (NPD); (**b**) Middle Jurassic palaeogeography (modified from Doré 1992); and (**c**) Haltenbanken stratigraphic column (solid circles indicate producing reservoirs).

overpressured Rås Basin to the west (see Skar *et al.* 1999 for discussion). However, because overpressure developed late on in the burial history of the western Halten Terrace, it has a relatively minor impact upon both shale porosity calculated from logs (Hermanrud *et al.* 1998) and upon the reservoir quality of the sandstones.

Palaeogeography

Regional palaeogeographic reconstructions suggest that the Kristin Field reservoir section accumulated in the western part of the Halten-Trøndelag Basin – part of a long north to south oriented Jurassic seaway which is thought to have linked the Boreal and Tethys Oceans (Fig. 1). In the mid-Norway area (offshore), Gjelberg *et al.* (1987) and Jongepier *et al.* (1996) report sand influx from the west into this area, during accumulation of the Kristin Field reservoir section (i.e. Early to Middle Jurassic). This is supported both by well data and from outcrop studies (Dalland 1979) and has been taken to imply that the deep Cretaceous Møre and Vøring basins, to the west of the Halten Terrace, were areas of uplift sub-aerial exposure and sediment export (Doré 1992). In the Jameson Land area of East Greenland, Surlyk (1990) reports sediment influx from the north and east in time-equivalent strata. This implies that the proposed uplift extended to the western side of the present Norwegian Sea while the main north to south seaway lay to the east of the present day rift axis (Brekke *et al.* 2001). The palaeoaltitude of the Halten Terrace during the Jurassic was between 49 and 53° (Smith *et al.* 1994), while climatic conditions were probably warm with potential for strong seasonal differences in temperature and rainfall (Hallam *et al.* 1994).

Kristin Field

With an initial reservoir pressure of 911 bar and an initial temperature of 170°C, Kristin Field is the most extreme HP/HT field on the Norwegian shelf. The field is being produced by pure

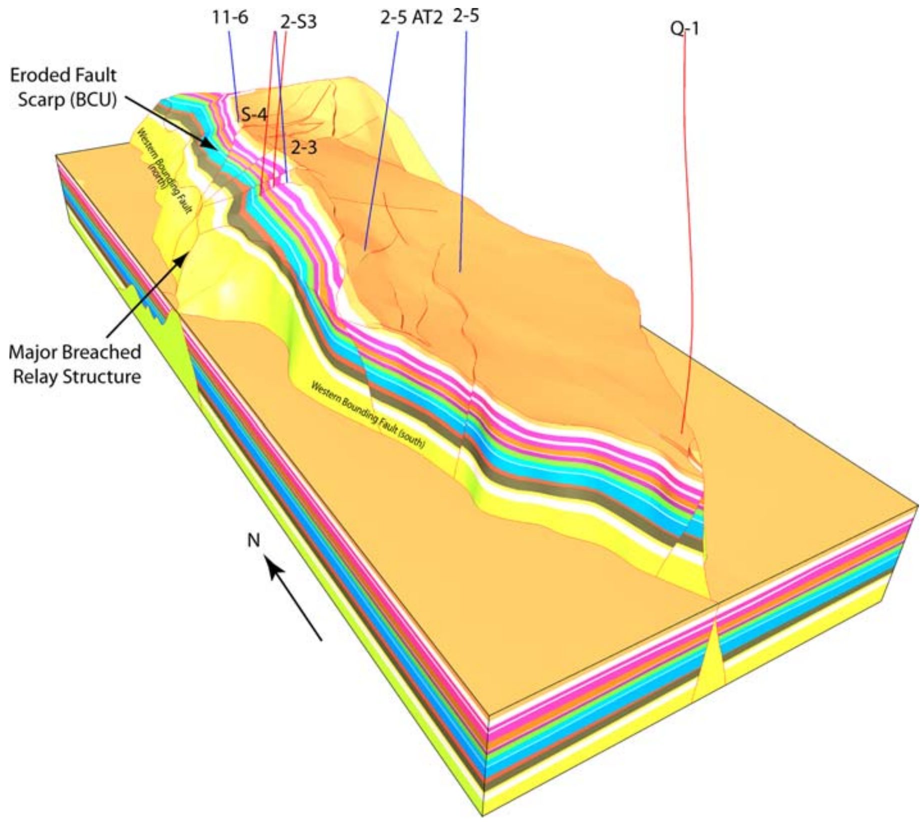

Fig. 2. Kristin Field structural model. Also shown are: the discovery well (2-3); the three appraisal wells (11-6, 2-5 and 2-5AT2) and three development wells (S-4H and S-3 HT3 adjacent to the discovery well and Q-1H in the south of the field).

depletion from 12 wells, almost all of which are located along the western structural crest (Fig. 2). The producing wells include: five dedicated Garn Formation producers; one dedicated Ile Formation producer; five co-mingled Garn and Ile formation producers; and one dedicated Tofte Formation producer. The dedicated producers are located in the central area, while comingled producers are situated towards the north and south. Although there is some uncertainty regarding the zonal production allocation in comingled wells (i.e. Garn and Ile formations), gas–oil ratios do give a reasonable indication of the relative flow contributions from the different reservoir units. There is also, in general, a good link between permeability calculated from logs (and calibrated to core) with flow tests and well productivity index (PI) and, consequently, log permeability is used directly in the simulation model without modification (see Fig. 3 for reservoir properties and porosity permeability plots). The field is covered by a variety of 3D and 4D seismic surveys which have allowed detailed mapping of the structure but have not provided robust insight into reservoir property distribution.

Diagenetic controls on reservoir quality

Despite major differences in the sedimentology of the three Kristin Field reservoir units, study of thin sections and core indicates that there is a strong link between primary depositional fabric and reservoir quality variation in all three units (i.e. depositional fabric drives diagenetic differences). The main depositional controls upon reservoir quality are: (1) the sorting and clay content of the sandstones which influences the degree of physical and chemical compaction (e.g. stylolites are abundant in mud-draped intervals but are almost absent in cleaner sandstones); (2) grain

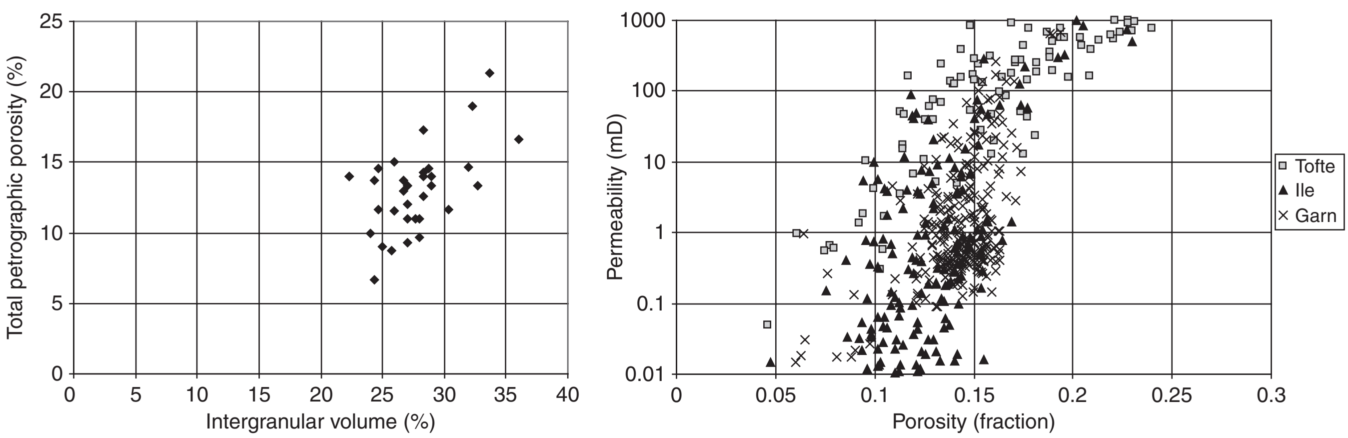

Fig. 3. Intergranular volume plotted against petrographic porosity for Garn Formation thin sections (left), and porosity to permeability plots for the discovery well (right).

size, which influences both the pore throat size and the quartz surface area available for growth of quartz cement; and (3) clay grain coats which also influence available quartz surface area. The most important grain coating mineral is chlorite, although illite and illite-chlorite mixtures are also reported in the Garn Formation (Storvoll *et al.* 2002). Grain coats typically exhibit an inner layer of concentrically laminated ooidal chlorite which probably formed by mechanical accretion of chlorite (or more probably an iron-rich precursor clay) as grains were rolled along the bottom. The actual source of iron is generally agreed to be river water, which carries a relatively rich load of colloidally suspended iron derived from weathering. Near the river mouth, increased salinity causes the iron to be flocculated and deposited in an amorphous reactive state (Ehrenberg 1993). The distribution of grain coats is poorly understood in Kristin Field, but they are more common in coarser cleaner intervals of sandstones and in facies interpreted to reflect deposition within tidal channels rather than the open shelf.

Although non-depositional controls upon reservoir quality distribution (i.e. variation) have been considered, they can be discounted as major controls upon reservoir quality distribution. For example, the structure is deep and relatively flat and depth trends are poor over the available dataset. Neither is there a good relationship between structural highs and enhanced reservoir quality, so evidence for an early hydrocarbon charge-preserving reservoir quality during burial is lacking. Nor is there a geographical association between the major bounding faults and better reservoir quality, so migration of porosity-enhancing corrosive fluids associated with the faults has not occurred. Indeed, the main bounding faults are not even in contact with the reservoir section in central and northern areas because of BCU erosion. There is also no evidence for a relationship between the distribution of enhanced reservoir quality and the proximity of the BCU, which indicates that porosity improvement due to leaching is not influential (nor is this phenomena observed in adjacent fields). Most importantly, however, there is a clear link between grain size, sorting and mud content with zones of enhanced reservoir quality.

Reservoir sedimentology

Given the strong link between reservoir quality distribution and primary depositional facies, the following section briefly describes the sedimentology of the three reservoir units and links this to Kristin Field pressure decline (e.g. Fig. 4).

Garn Formation

The *c.* 110 m thick Garn Formation is the uppermost of three formations that constitute the Fangst Group and the uppermost Kristin reservoir unit. The interval is contemporaneous with the Brent Group of the North Sea (Ehrenberg 1990) and is equivalent to the transgressive sandstones of the Pelion Formation in East Greenland (Doré 1992). The Garn Formation exhibits relatively constant thickness in both Kristin Field (where there are 18 well penetrations and 716 m of core) and where the unit is penetrated in wells further east across the Halten Terrace. However, the interval thins gradually both to the north and south along the axis of the Halten–Trøndelag Basin. The Garn Formation in Kristin Field exhibits fairly constant porosity (*c.* 13%), which compares favourably to the general depth trend for the unit. This is at least partly due to the presence of more grain coats, increased grain-size and fewer mud drapes. Permeability variation is more dramatic and strongly impacts production. Two broad permeability groups are observed from the current well dataset: (1) a low permeability background (typically <1 mD) which dominates the interval and is more common in the east of the field, and (2) higher permeability layers (typically up to tens of millidarcy) which are present (very) locally along the western flank of the field and which die out eastwards over short distances.

Description. The Garn Formation in Kristin Field is characterized by high net-to-gross ratios (>95%) and low gamma ray (GR) signatures and, in general, it is not normally possible to confidently correlate surfaces/units between wells. The base of the interval is defined by a rather abrupt upwards decrease in GR response which is the culmination of a cleaning upward succession within the upper part of the underlying Not Formation. The actual contact between the units corresponds to an upward step in grain size observed in core and an increase in reservoir properties. Nevertheless comparable facies are consistently observed either side of this surface and Si–Al ratios, measured across it, show that the clear cleaning upward profile which begins in the central part of the Not Formation continues into the basal part of the Garn Formation (Si–Al ratios from core-based chemostratigraphic analysis; Ichron). The Garn Formation itself is dominated by very fine to coarse grained subarkosic arenites (Ehrenberg 1990; Chuhan *et al.* 2001) which, while superficially homogeneous, can be divided into two main depositional facies in Kristin Field (for brevity, volumetrically minor facies are not described). Most important from a reservoir quality perspective are intervals of clean, typically cross-bedded sandstones which are usually several metres thick and which also include sections of parallel lamination or massive bedding and rare trace fossils (mainly *Trichichnus*, *Skolithos*, *Arenicolites*, *Ophiomorpha*, *Cylindrichnus*, bivalve burrows, resting traces and non-specific burrow mottles). Poorly developed coarsening and cleaning-upward trends are also occasionally observed. While permeability is not always

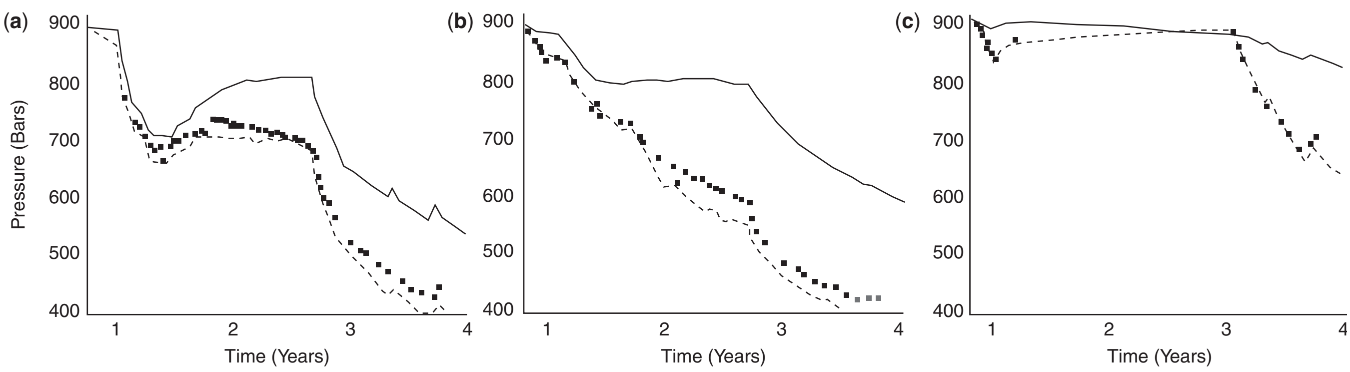

Fig. 4. Pressure profiles taken from: (**a**) a Garn Formation well; (**b**) an Ile Formation well; and (**c**) a Tofte Formation well. In each case the solid upper line refers to initial pressure prognoses, the lower solid line to the current history matched reservoir model, and the circles to calculated down-hole pressure measurements.

significantly higher in this facies, all intervals of high permeability within the Garn Formation occur within it. This facies dominates the Garn Formation in the west of the field (hence higher permeability in this area) and is also anomalously abundant in the central area where it is also notably coarser grained (mainly coarse sandstone). Intervals of this facies are normally thinner and less common in wells in the eastern part of the field (e.g. 30% in well 6406/2-5 compared with up to 80% on the western margin). The second and more volumetrically important depositional facies comprises cross-bedded very fine to medium grained sandstones with thin drapes rich in mudrock and mica which are prone to stylolite formation. Bioturbation is rare but can be prevalent and includes (*Ophiomorpha*, *Trichichnus*, *Skolithos*, bivalve burrows, resting traces, *Planolites*, *Palaeophycus* and *Chondrites*). This facies association is always associated with very poor reservoir quality and is common in the middle part of the Garn Formation and in the eastern part of the field.

Depositional synthesis. The depositional model for the Garn Formation implies accumulation within stacked, possibly tidally influenced shoreface successions. These accumulated during eastwards (and perhaps northeastwards) progradation through Kristin Field and are presumably separated by transgressive surfaces (generated during shoreface retreat) although these surfaces are seldom obvious. The general absence of either well-defined coarsening and cleaning upward trends (within shoreface packages) or well-developed shale-prone flooding intervals (between them) reflects a lack of accommodation in what was presumably a proximal part of the depositional system. In contrast, bioturbated shale-prone intervals and well-defined cleaning upward trends are present further east (e.g. Tyrihans Field). The clean cross-bedded facies is interpreted to represent upper shoreface environments while the draped cross-bedded facies is thought to reflect accumulation in lower shoreface settings. Given this depositional model, the observed reduction in the abundance of the clean cross-bedded facies over short distances from west to east across Kristin Field (over 2–3 km) is strange when one considers that coastlines almost certainly migrated some tens of kilometres to the east and NE of Kristin during regressive stages. A possible explanation for this pattern is that it results from shoreface stacking patterns (e.g. Fig. 5). One also has to question why intervals of higher permeability are encountered in some intervals of the clean cross-bedded facies but not in others. Here, it seems likely that these intervals reflect subtle intra-facies changes in mineralogy, sorting and grain size which are not readily observable in core. For example, chemostratigraphy suggests that these intervals reflect the mineralogically cleanest (most proximal?) parts of the shoreface (core-based chemostratigraphic analysis; Ichron). The fact that the coarsest grained sandstones (with better reservoir properties) are most prevalent in the central western area through several cycles of progradation and back-stepping potentially suggests that the distributary systems feeding sediment into the area and thus into the upper shoreface (or in another model perhaps ebb and flood tidal deltas) were structurally controlled.

Explanation for rapid pressure decline. The unusual distribution of reservoir facies within the Garn Formation of Kristin Field led to a highly biased appraisal well dataset which skewed initial understanding of the interval. Two unusual deposition/reservoir quality trends led to this bias. The first was the west to east decrease in the volume fraction of the clean cross-bedded facies and associated eastwards decrease in permeability. This biased (and continues to bias) the well dataset because most wells are located close to the western margin of the structure (Fig. 2). As a result, while mean (arithmetic) permeability calculated from the present total well dataset is *c*. 6 mD and was even higher in the PDO model, the mean permeability in the current reservoir model for the interval is only 0.4 mD. As the only appraisal well (well 2-5) intersecting the poorer quality reservoir (typical of the eastern part of Kristin) was located well to the south and only a little to the east of the other appraisal wells it did not, unfortunately, help define the orientation of this trend. The second misleading aspect of the appraisal well dataset was the presence of unusually coarse and clean sandstones with unrepresentatively good reservoir quality in the discovery well (well 2-3) in the centre of the field. This is still the best well drilled to date in the Garn Formation of Kristin Field with 18 other penetrations. The well particularly biased understanding of the volumetrically important central area of Kristin because, while appraisal well spacing is on an order of 5 km, the good properties encountered by the discovery well probably extend for just a few hundred metres to the east. Current reservoir models which include both a rapid west to east decrease in permeability and a concentration of better permeability in the central western area now provide a fairly accurate prediction of pressure development for the interval.

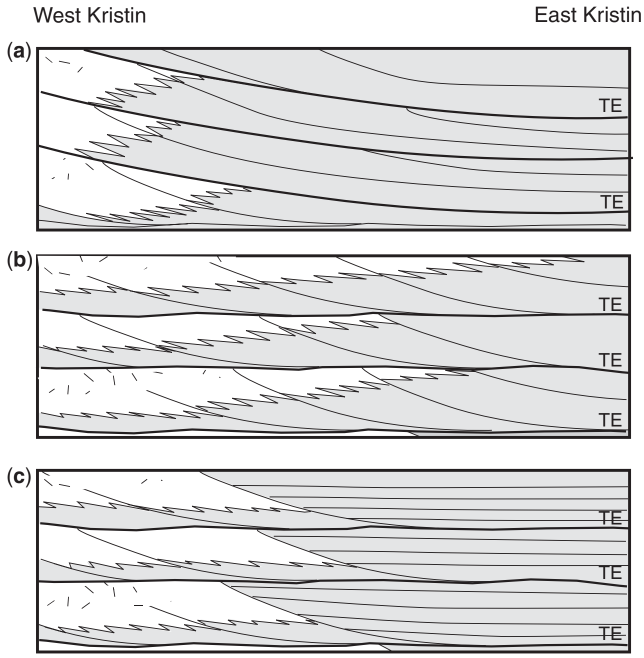

Fig. 5. Sketch models explaining why clean cross-bedded sandstones may be more common in the Garn Formation of western Kristin Field compared with the east. White shade, clean cross-bedded facies; grey shade, draped facies; stipple, high reservoir quality. (**a**) How this pattern might arise from a combination of changes in shoreface aggradation rate and later transgressive erosion; (**b**) how it might result from a progressive reduction in upper shoreface thickness due to a decrease in wave energy (as regression progressed eastwards); and (**c**) a scenario whereby there is a fundamental change in the style of the coastline and/or its orientation as regression proceeded eastwards (e.g. easterly regression from the basin margin is terminated by northerly axial regression).

Not Formation

Separating the Garn and Ile formations, the Not Formation is a regionally extensive mud-prone unit (45–55 m thick). The interval can be divided into two parts: a lower shale-prone section, which is characterized by high GR values, and an upper section which is more sand-prone and cleans upward. Core from both intervals includes a diverse trace fossil suite but traces become less common towards the top of the upper interval close to the transition with the Garn Formation. The lower shale-prone part of the Not Formation is interpreted to reflect accumulation in relatively distal shelf settings while the upper unit reflects accumulation in front of a prograding wave-dominated coast.

Ile Formation

The *c.* 85 m thick Ile Formation (penetrated by 12 wells and with 354 m of core) is the middle of the three Kristin reservoir units and is an important regional hydrocarbon-bearing interval (Koch & Heum 1995). The unit is sand-prone but is commonly heterolithic with flaser and wavy bedding present throughout and, in Kristin Field at least, the interval becomes increasingly heterolithic upwards. Accumulation of the unit (together with the Not Formation) is thought to have coincided with a significant hiatus (Aalenian–early Bajocian) in East Greenland (Doré 1992).

Description. The basal part of the unit (Ile 1: *c.* 5 m thick) comprises an upward-cleaning package of fine-grained sandstones in which the abundance of mud-drapes and bioturbation decreases up-section. The interval is intensely quartz cemented and is of minor reservoir significance. It is overlain, across an erosion surface, by a thick section (Ile 2: *c.* 20 m thick) dominated by two major facies (Fig. 6). The first and volumetrically more important comprises medium to coarse grained, predominantly trough cross-bedded sandstone with intercalated intervals containing climbing ripples, parallel lamination, intraclasts, vein quartz clasts, thin calcite cemented horizons and rare trace fossils (e.g. *Planolites*, *Palaeophycus*, *Skolithos*). Petrographic studies suggest that chlorite grain coats are common and reservoir quality is excellent (e.g. 19%, *c.* 300 mD). The second facies in this interval comprises decimetre to metre-scale intervals of flaser to wavy bedded, very-fine to medium grained heterolith which include abundant cross-bedding and asymmetric ripples, mud-drapes, fluid muds, mud clasts (some organic rich), thin calcite cemented horizons and a more diverse (although still limited) suite of trace fossils (*Planolites*, *Palaeophycus*, *Chondrites*, *Skolithos*, *Ophiomorpha*, *Asterosoma*, *Phycosiphon*). This facies is characterized by poor reservoir quality (e.g. 12%, <1 mD) due to high levels of quartz cementation and compaction which is in turn probably related to the finer grain size, higher clay content and rarity of grain-coating clay minerals. Two facies trends are observed in the interval. The first is that the heterolithic facies becomes more abundant up-section while the second is that the trough cross-bedded facies (with good properties) is more common in the central western part of the field near the discovery well. An intra-facies trend of increasing permeability towards this area is also observed. The overlying upper part of the Ile Formation (Ile 3: *c.* 53 m thick) begins with a 1–3 m thick, bioturbated, mud-prone interval which is present in all five cored Ile Formation wells and is considered a marker bed (*Planolites*, *Palaeophycus*, *Thalassinoides*, *Skolithos*, *Asterosoma*). Overlying this, the facies assemblage reverts to that observed in the lower Ile section (i.e. Ile 2) with the same two basic facies elements: (1) an excellent quality, predominantly trough cross-bedded sandstone facies; and (2) a heterolithic facies displaying very poor reservoir quality. Major facies trends also continue from the underlying, lower part of the Ile Formation with an up-section increase in the proportion of the heterolithic facies and a higher volume fraction of the trough cross-bedded sandstone facies within a small area in the central western part of the field.

Depositional synthesis. The thin, cleaning-upward, lower part of the Ile Formation (Ile 1) represents progradation (probably) from

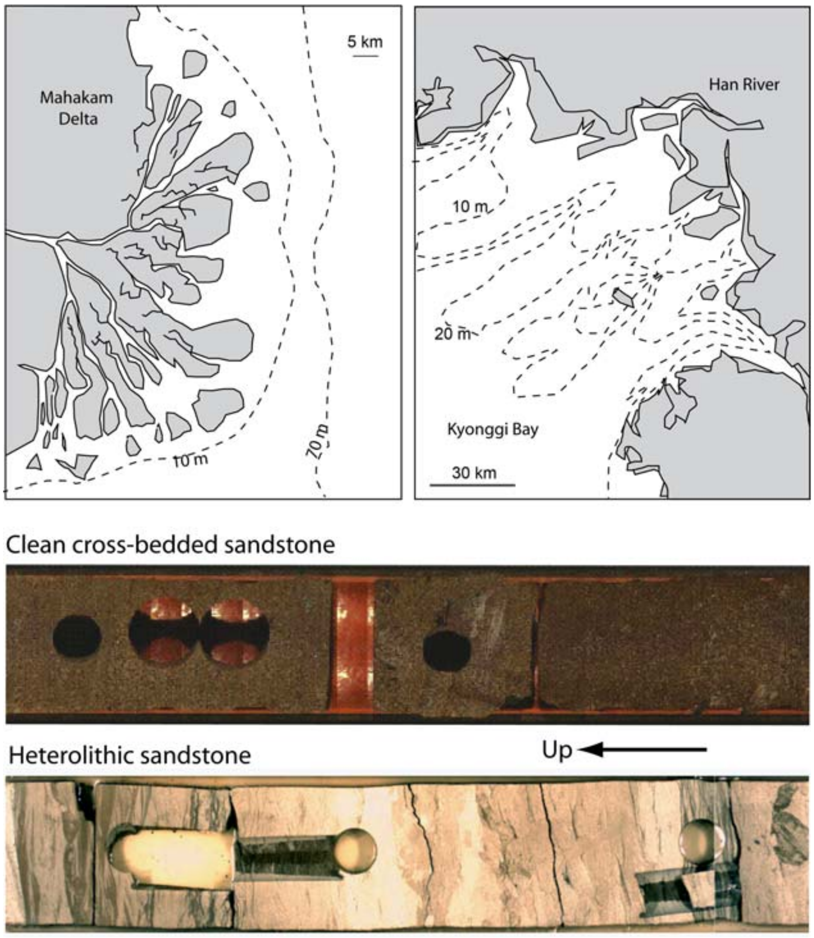

Fig. 6. Core photos illustrating the main facies components of the Ile Formation in Kristin Field. Above: possible modern analogues for the Ile Formation. (Left: Mahakem Delta, Indonesia. Right: Han River, Korea).

the west and shoaling of the succession from the shelf deposits of the Upper Ror Formation into proximal delta-front settings. Overlying this (across an erosion surface), a complicated stack of probable tide influenced bar and channel deposits (Ile 2) is generally interpreted to reflect deposition within a large tide influenced delta (McIlroy 2004) similar to that envisaged by Martinius *et al.* (2001) for the slightly older Tilje Formation. The trough cross-bedded facies is interpreted to reflect stronger fluvial influence while the heterolithic facies is thought to reflect stronger marine and tide influence. However fine-scale inter-bedding of both elements indicates that they clearly co-existed across much of the delta and, as a result, the observed facies assemblage is highly heterogeneous (Fig. 6). The bioturbated shale-prone interval at the base of Ile 3 is interpreted to represent an episode of marine transgression while the rest of Ile 3 (i.e. the upper part of the Ile Formation) reflects similar depositional environments to those interpreted for Ile 2. The fact that the heterolithic facies becomes more abundant up-section in both intervals is interpreted to reflect the predominance of transgression and back-stepping of the system westwards. The abundance of the coarser grained facies (with better reservoir properties) within a small area in the central western part of the field seems to indicate structural control on the location of the distributary system/tidal delta feeding through the area.

Explanation for rapid pressure decline. As in the Garn Formation, it is now clear that the Ile Formation properties in the central western area are unusually good with a higher volume fraction of the good-quality cross-bedded facies than elsewhere in the field. Unlike the Garn Formation, however, inclusion of this pattern in current reservoir models only improves, rather than resolves, the problem of overestimating pressure support. As a result, the current model can only be history-matched by including additional horizontal barriers and invoking considerable fault seal. Both host rock lithology (greater mud content) and faulting history (deeper deformation and thus more grain crushing and subsequent cementation) might explain why Ile Formation faults could be less permeable than those in the Garn Formation which are known to be relatively open. It remains questionable, however, whether the Ile Formation faults really can withhold the pressure differences implied by history-matched reservoir simulations (e.g. 400 bar) and it seems likely that understanding of the interval and the approach to modelling has some way to go.

Upper Ror Formation

Underlying the Ile Formation, the Upper Ror Formation is a mud-prone interval, *c.* 50–70 m thick. In Kristin Field it is less mud-prone than the Not Formation and may not form a perfect pressure seal to the Tofte Formation, an interpretation suggested by similar GWCs in the Tofte and Ile formations (fluid properties differ somewhat). The unit thickens and becomes more shale-prone eastward across the Kristin structure and is thinner to the SW in the Erlend Field (*c.* 5 km from Kristin Field). The Ror Formation contains a diverse trace fossil suite characteristic of accumulation in an open shelf setting.

Tofte Formation

The sand-prone Tofte Formation (*c.* 135 m thick) is the lowermost of the three Kristin Field reservoir units. It is only present along the western margin of the Halten Terrace because further to the east it shales out (over *c.* 15 km) as the Upper and Lower Ror Formation shales merge. As most of this eastward thinning is compensated by thickening of the Upper Ror Formation shale (rather than the Lower Ror Formation), it appears that maximum regression occurred near the base of the Tofte Formation. Following initial regression, the coastline then seems to have slowly back-stepped westwards such that the central and upper part of the Tofte Formation in the wells in the western part of Kristin Field accumulated contemporaneously with shelf mudrock in wells further east. The unit has been penetrated by six wells in Kristin Field, three of which (exploration wells) also penetrate the shaley Lower Ror Formation. Core has been taken in four wells (111 m) and comprises markedly different depositional facies both along depositional dip (east–west) and strike (north–south).

Description. In the northern part of Kristin Field in well 11–6 (Fig. 2), the cored interval (near the top of the Tofte Formation) is dominated by a thick section of lightly bioturbated, fine-grained sandstone comprising numerous draped cross-beds (trace fossils include bivalve burrows, *Rosselia* and *Siphonichnus*). Log signatures in both the cored and underlying uncored interval indicate subtle upwards cleaning patterns, 10–20 m thick, which in the cored section correspond to an upwards decrease in mud-drapes, mica content and bioturbation intensity, as well as an increase in maximum clast size. Permeability throughout the Tofte succession in this well is typically less than 1 mD. In well 2-5, located some 5 km SE of the central area, a similar succession with numerous stylolites, abundant organic rich clasts and bioturbation was encountered and, again, exhibits very poor reservoir properties.

In contrast to the successions encountered in both the northern and southern appraisal wells, three closely spaced, east–west aligned wells in the central area intersected markedly better reservoir properties (porosity of 19% compared to 9%). Core was taken from the upper part of the two easternmost of these wells. In well 2-S 3 (middle well), the lower and middle part of the cored section includes a thick interval dominated by red to brown massive sandstones which also contain rare low-angle cross-bedding. The interval displays excellent reservoir quality, lacks any bioturbation or mud-drapes and includes numerous floating sandstone intra-clasts, commonly up to pebble grade. In contrast, the cored section in the discovery well 2-3 (just 440 m to the east) is medium to coarse grained (i.e. slightly finer) and includes cross-beds throughout with some mud/mica drapes together with rare bioturbation (J-shaped burrows, *Trichichnus*, *Siphonichnus* resting traces, general burrow mottling). This change in depositional facies between the two wells seems to be associated with a rapid decrease in reservoir properties which is observed across all three wells, at least in the upper part of the Tofte Formation (e.g. 23% in S-4 to 19% in 2-S-3 to 12% well 2-3).

Depositional synthesis. The diverse trace fossil suite, abundance of mud drapes and presence of cleaning-upward cycles in the middle and upper parts of the Tofte Formation in the northern and southern parts of Kristin Field suggest a depositional environment dominated by prograding tide-influenced shelf deposits (with very poor reservoir quality). In contrast, in the central western part of the field, the unit comprises markedly coarser grained, commonly massive sandstones which display excellent reservoir properties. These are thought to reflect either rapid deposition within distributary channel bars or shallow sandy debris flows at the mouths of distributary channels which fed coarse sediment into the upper shoreface (Fig. 7). The persistent presence of coarser grained, less bioturbated facies (with better reservoir properties) in the central western area through several cycles of progradation and back-stepping (e.g. equivalent to several stacked cleaning upward cycles in northern and southern wells) seems to indicate that the distributary system feeding onto the Tofte shelf was somehow locked into this one fairly small area – at least during deposition of the middle and upper part of the unit.

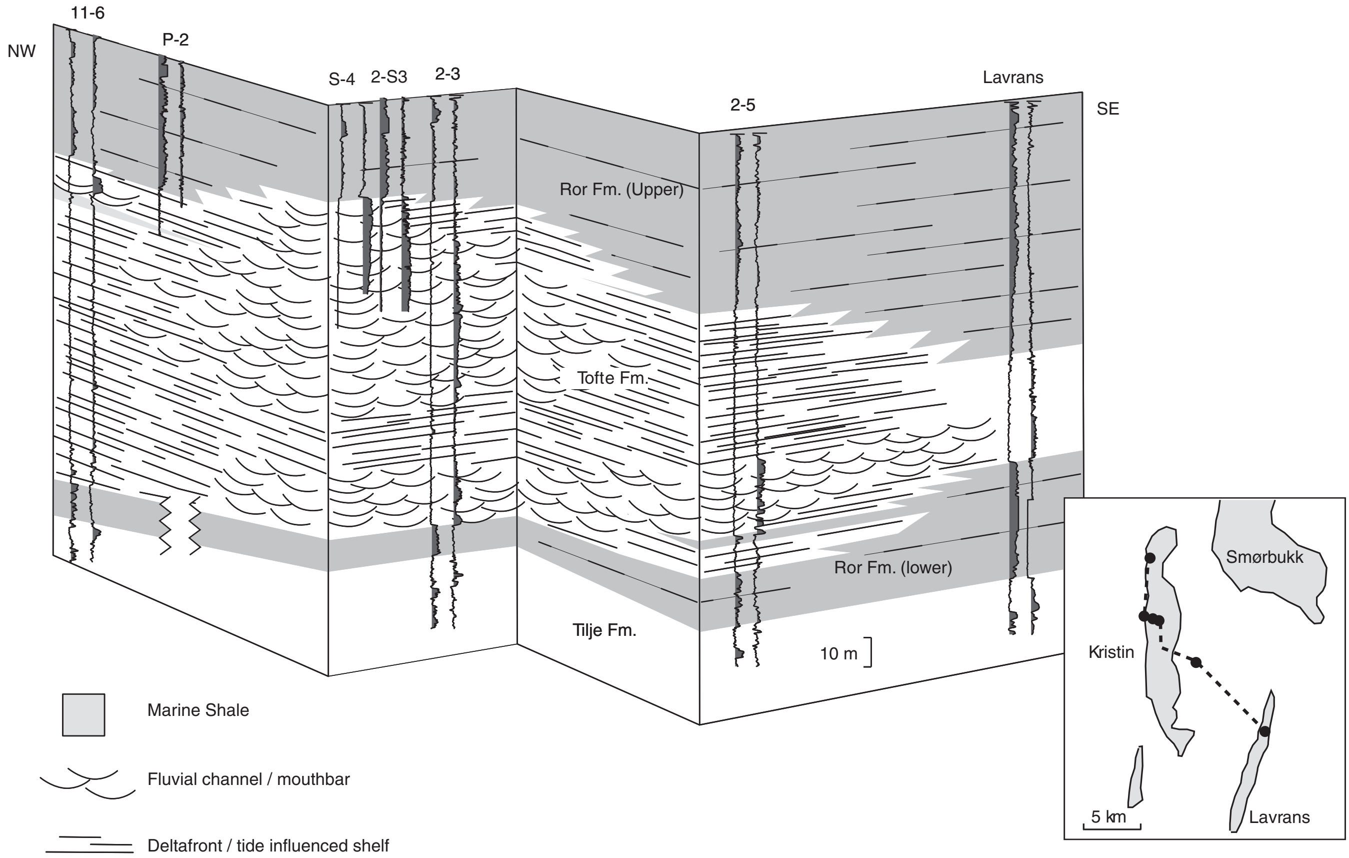

Fig. 7. Distribution of primary facies elements within the Tofte Formation of Kristin Field. Well logs, per well, are GR (left) and permeability (right).

Explanation for rapid pressure decline. The pressure observed from the one well which produces from the Tofte Formation (S-4) has declined significantly more rapidly than initially expected. This is thought to reflect a more rapid than predicted reduction in reservoir properties away from the central western area which probably occurs over just a few hundred metres to the east of the producing well. This pattern significantly reduces aquifer support but the intensity of this important trend towards poorer properties only became clear following the drilling of two closely spaced development wells immediately adjacent to the discovery well (Fig. 2).

Discussion

Since production began in 2005, reservoir pressure in each of the three Kristin Field reservoir sections has declined significantly more rapidly than was initially predicted. In the Garn Formation, the Tofte Formation and to some extent also the Ile Formation, this has occurred at least partly because the appraisal well dataset was biased and because this in turn led to an overprediction of reservoir properties. Although the appraisal well dataset was skewed in a number of ways, the most important bias resulted from the persistent presence of good but unrepresentative reservoir properties in the discovery well which is located in the volumetrically important central part of the field. It is now realized (with additional data) that these are in no way typical of the field as a whole or, indeed, even of most of the central area. This is illustrated in Figure 8, which shows that in eight of the 10 main Kristin Field reservoir sub-zones, mean (arithmetic) permeability is highest in just one of two closely spaced wells (both extensively cored) in the western central part of the field. The fact that reservoir properties seem to be repeatedly higher within this one small area suggests that the origin of the enhanced properties is the same in the different reservoir sub-zones and, based on study of thin sections and cores, is interpreted to reflect the persistent presence of more proximal depositional facies in the area (coarser grain-sizes, less bioturbation, fewer mud-drapes, better grain coats). The most likely explanation for this phenomenon is that the location of the fluvial or deltaic systems feeding sediment into the different reservoir units (or in another model perhaps, tidal inlets) was structurally influenced – presumably up-depositional-dip to the west. Further, given the smallness of the zone and the fact that reservoir properties seem to decrease rapidly as one moves eastwards across it, it seems likely that whatever exerted this control was in close geographic proximity. For this reason, the major breached relay structure located immediately west of the central part of the field is perhaps the most likely structural element to have exerted this control (Fig. 2). Although there are other possible explanations (see below), this model is interesting because it suggests that fault oversteps/relay ramps can influence the distribution of facies, not only within hanging-wall successions (e.g. Gawthorpe & Leeder 2000), but also within footwall successions in cases where the primary provenance direction is on the hanging-wall side (Fig. 9). Alternative models which could also explain the unusual facies/reservoir quality pattern observed across Kristin Field include: deflection of the fluvial system by only the northernmost of the two western bounding faults (which has larger displacement); the influence of other unidentified faults up-depositional-dip to the west; antecedent drainage; or salt movement. However regardless of what exactly caused this pattern, it is clear that it had an important and misleading influence on early understanding of the field. As a result, current reserve and pressure estimates are between base case and P90 estimates and problems related to condensate blockage will potentially be brought forward (to date, fluids seem to behave as expected). To bring the field back towards base case predictions, high-angle producers have been drilled where

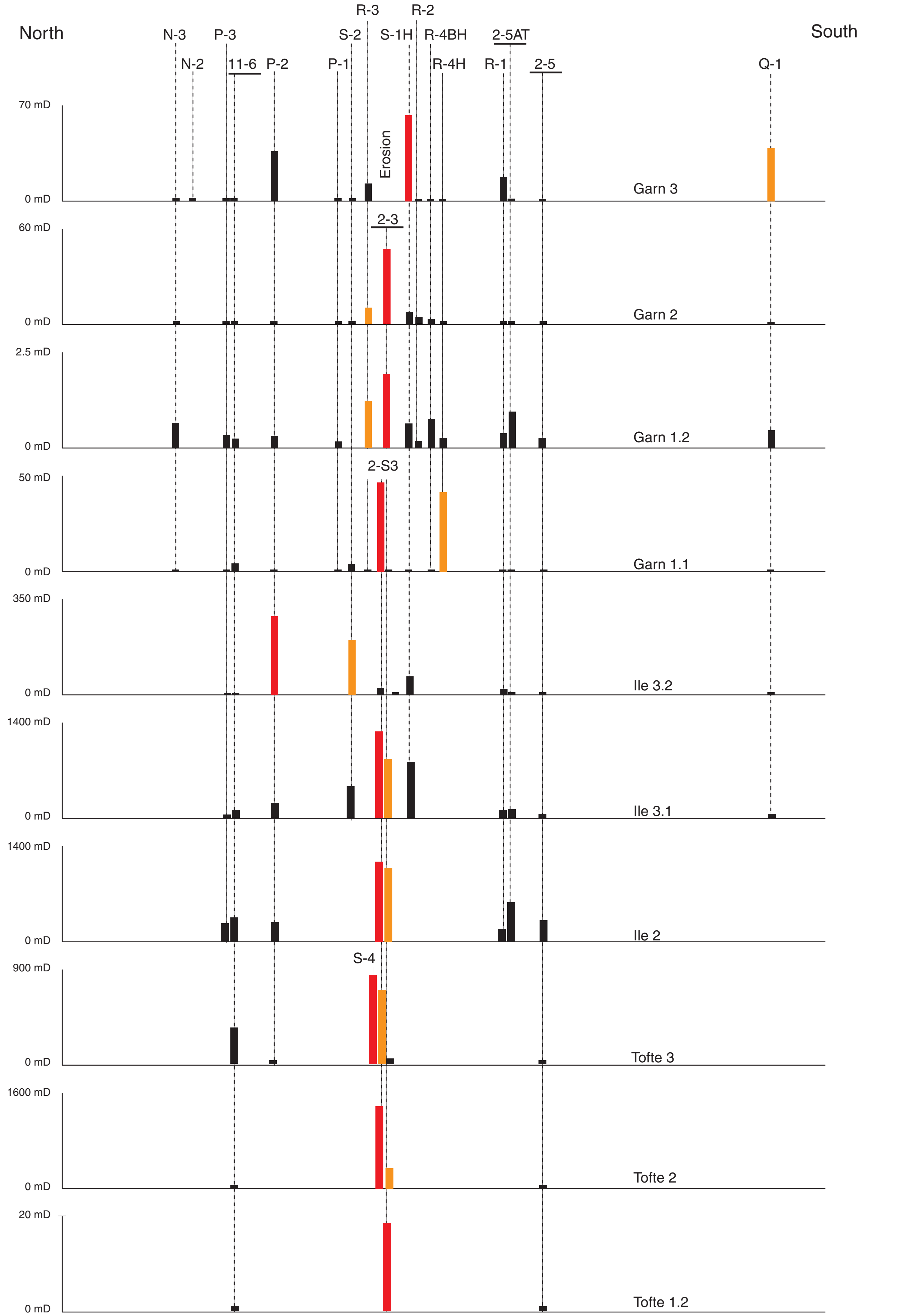

Fig. 8. North to south permeability distribution across Kristin Field with the highest and second highest permeability (per reservoir zone) highlighted (highest, red; second highest, orange). Appraisal wells are underlined. Note that in one of the two reservoir zones (Garn 3) where permeability is not highest in either of these wells the interval is not actually even present (it has been eroded out) yet production data still suggest anomalously good permeability immediately to the east.

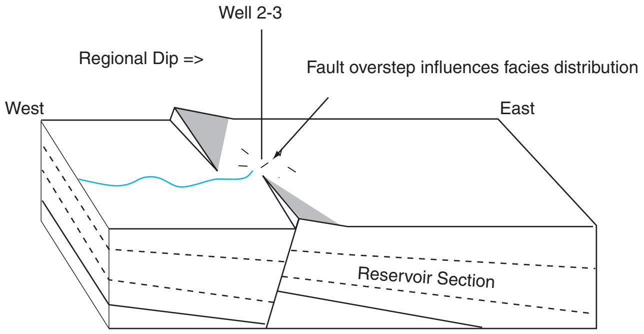

Fig. 9. The possible impact of a major fault overstep (on the western margin of Kristin Field) upon facies distribution and ultimately reservoir quality (view: looking north).

low-angle wells had originally been planned and a number of infill wells have been drilled.

Conclusions

Early impressions of the HP/HT Kristin Field were significantly skewed by the presence of very good but unrepresentative reservoir properties in the discovery well. This biased the appraisal well dataset which was itself significantly biased in some units. With the larger information dataset now available (wells, production data, etc.), it is clear that the good properties encountered by the discovery well are to a large extent limited to a very small anomalous area in the central western part of the field. This unusual pattern was not predictable from the original dataset and is thought to have arisen because of structural control upon the location of depositional facies. What is interesting about Kristin Field is that this structural influence is observed within the footwall stratigraphy of a major relay structure where the primary provenance direction was on the hanging-wall side. This pattern is the reverse of what is normally reported in tectono-stratigraphic studies.

The authors wish to thank Tony Peters and an anonymous reviewer for their comments which significantly improved the manuscript. We would also like to thank Rob Gawthorpe, Christian Brostrøm, Tanja Tora Blekastad, Peter McFadzean, Holger Rieke, Mari-Anne Hetle and Nicola Marsh. The study also draws from reports prepared by Ichron (particularly by Stuart Gowland) and from internal reports and studies including those by Olav Walderhaug, Carlo Messina and Carsten Elfenbein. The views expressed in this manuscript do not necessarily reflect those of the Kristin Unit partners and are not necessarily the only explanation for more rapid pressure decline than had been predicted. The partners, ExxonMobil, Total Norge, ENI Norge and Petoro, are thanked for granting permission to publish.

References

Blystad, P., Brekke, H., Færseth, R. B., Larsen, B. T., Skogsteid, J. & Tørrudbakken, B. 1995. Structural elements of the Norwegian continental margin. *Norwegian Petroleum Directorate Bulletin*, **8**, 1–45.

Borge, H. 2002. Modeling generation and dissipation of overpressure in sedimentary basins; an example from the Halten Terrace, offshore Norway. *In*: Al-Aasm, I. S., Scotchman, I. C. & Verweij, H. (eds) *Origin, Characterization and Significance of Fluids in Sedimentary Basins. Marine and Petroleum Geology*, **19**, 377–388.

Brekke, H., Sjulstad, H. I., Magnus, C. & Williams, R. W. 2001. Chapter 2. *In*: Martinsen, O. J. & Dreyer, T. (eds) *Sedimentary Environments Offshore Norway: Paleozoic to Recent*. Norwegian Petroleum Society, Oslo, Special Publications, **10**, 7–37.

Chuhan, F. A., Bjorlykke, K. & Lowrey, C. J. 2001. Closed-system burial diagenesis in reservoir sandstones; examples from the Garn Formation, Haltenbanken area, offshore Mid-Norway. *Journal of Sedimentary Research*, **71**, 15–26.

Christoffersen, K. R., Quin, J. G., Zweigel, P., Hansen, O. R. & Zaostrovski, A. 2008. Continuous history matching an HP/HT gas condensate field during the first two years of production. *Society of Petroleum Engineers*, **113861-MS**.

Corfield, S. & Sharp, I. R. 2000. Structural style and stratigraphic architecture of fault propagation folding in extensional settings: a seismic example from the Smørbukk area, Halten Terrace, Mid-Norway. *Basin Research*, **12**, 329–341.

Corfield, S., Sharp, I., Häger, K. O., Dreyer, T. & Underhill, J. 2001. An integrated study of the Garn and Melke Formations (Middle to Upper Jurassic) of the Smørbukk area, Halten Terrace, mid-Norway. *In*: Martinsen, O. J. & Dreyer, T. (eds) *Sedimentary Environments Offshore Norway: Palaeozoic to Recent*. Norwegian Petroleum Society, Oslo, Special Publications, **10**, 199–210.

Dalland, A. 1979. The sedimentary and sequence of Andøya, Northern Norway. *In*: *Norwegian Sea Symposium*. Norwegian Petroleum Society, Oslo, 1977, Article 9.

Dalland, A., Worsley, D. & Ofstad, K. 1988. *Lithostratigraphic Scheme for the Mesozoic and Cenozoic Succession Offshore Mid and Northern Norway*. Oljedirektoratet, Bulletin, **4**.

Doré, A. G. 1992. Synoptic palaeogeography of the Northeast Atlantic seaway; late Permian to Cretaceous. *In*: Parnell, J. (ed.) *Basins on the Atlantic Seaboard: Petroleum Geology, Sedimentology and Basin Evolution*. Geological Society, London, Special Publications, **62**, 191–202.

Doré, A. G., Lundin, E. R., Jensen, L. N., Birkeland, Ø., Eliassen, P. E. & Fichler, C. 1999. Principle tectonic events in the evolution of the northwest European Atlantic margin. *In*: Fleet, A. J. & Boldy, S. A. R. (eds) *Petroleum Geology of Northwest Europe: Proceedings of the 5th Conference*, Geological Society, London, 41–61; doi: 10.1144/0050041.

Ehrenberg, S. N. 1990. Relationship between diagenesis and reservoir quality in sandstones of the Garn Formation, Haltenbanken, mid-Norwegian continental shelf. *American Association of Petroleum Geologists Bulletin*, **74**, 1538–1558.

Ehrenberg, S. N. 1993. Preservation of anomalously high porosity in deeply buried sandstones by grain-coating chlorite: examples from the Norwegian continental shelf. *American Association of Petroleum Geologists Bulletin*, **77**, 1260–1286.

Ehrenberg, S. N., Gjerstad, H. M. & Hadler-Jacobsen, F. 1992. Smørbukk field. A gas condensate fault trap in the Haltenbanken Province, Offshore Mid-Norway. *In*: Halbouty, M. T. (ed.) *Giant Oil and Gas Fields of the Decade 1978–1988*. American Association of Petroleum Geologists, Tulsa, OK, Memoirs, **54**, 471–481.

Gawthorpe, R. L. & Leeder, M. R. 2000. Tectono-stratigraphic evolution of active extensional basins. *Basin Research*, **12**, 195–218.

Gjelberg, J., Dreyer, T., Høie, A., Tjelland, T. & Lilleng, T. 1987. Late Triassic to Mid-Jurassic sandbody development on the Barents and mid-Norwegian shelf. *In*: Brooks, J. & Glennie, K. W. (eds) *Petroleum Geology of North West Europe*. Graham & Trotman, London, 1105–1129.

Glennie, K. W. & Underhill, J. R. 1998. Origin, development and evolution of structural styles. *In*: Glennie, K. W. (ed.) *Petroleum Geology of the North Sea; Basic Concepts and Recent Advances*. 4th edn. Blackwell Science, Oxford, 42–84.

Hallam, A., Crame, J. A., Mancenido, M. O., Francis, J. & Parrish, J. T. 1994. Jurassic climates as inferred from the sedimentary and fossil record; discussion and reply. *In*: Allen, J. R. L., Hoskins, B. J., Sellwood, B. W., Spicer, R. A. & Valdes, P. J. (eds) *Palaeoclimates and their Modelling; with Special Reference to the Mesozoic Era*. Chapman & Hall, London, 79–88.

Hermanrud, C., Wensaas, L, Teige, G. M. G., Nordgard-Bolas, H. M., Hansen, S. & Vik, E. 1998. Shale porosities from well logs on Haltenbanken (offshore mid-Norway) show no influence of overpressuring. *In*: Law, B. E., Ulmishek, G. F. & Slavin, V. (eds) *Abnormal Pressures in Hydrocarbon Environments*. American Association of Petroleum Geologists, Tulsa, OK, Memoirs, **70**, 65–85.

Jongepier, K., Rui, J. C. & Grue, K. 1996. Triassic to Early Cretaceous stratigraphic and structural development of the northeastern More

Basin margin, off mid-Norway. *Norsk Geologisk Tidsskrift*, **76**, 199–214.

Koch, J. O. & Heum, O. R. 1995. Exploration trends of the Halten Terrace. *In*: Hanslien, S. (ed.) *Petroleum Exploration and Exploitation in Norway*. Norwegian Petroleum Society, Oslo, Special Publications, **4**, 235–251.

Marsh, N. A. 2008. The influences of crustal extension, salt tectonics and gravity-driven deformation on the structural evolution of the Halten Terrace, offshore mid-Norway: new insights from 3D seismic data and fault analysis. Thesis, University of Durham.

Martinius, A. W., Kaas, I., Næss, A., Helgesen, G., Kjærefjord, J. M. & Leith, D. 2001. Sedimentology of the heterolithic and tide-dominated Tilje Formation (Early Jurassic, Halten Terrace, offshore mid-Norway). *In*: Martinsen, O. J. & Dreyer, T. (eds) *Sedimentary Environments Offshore Norway – Palaeozoic to Recent*. Norwegian Petroleum Society, Oslo, Special Publications, **10**, 103–144.

McIlroy, D. 2004. Ichnofabrics and sedimentary facies of a tide-dominated delta; Jurassic Ile Formation of Kristin Field, Haltenbanken, offshore mid-Norway. *In*: McIlroy, D. (ed.) *The Application of Ichnology to Palaeoenvironmental and Stratigraphic Analysis*. Geological Society, London, Special Publications, **228**, 237–272.

Skar, T., van Balen, R. T., Arnesen, L. & Cloetingh, S. 1999. Origin of overpressures on the Halten Terrace, offshore mid-Norway; the potential role of mechanical compaction, pressure transfer and stress. *In*: Aplin, A. C., Fleet, A. J. & Macquaker, J. H. S. (eds) *Muds and Mudstone; Physical and Fluid-Flow Properties*. Geological Society, London, Special Publications, **158**, 137–156.

Smith, A. G., Smith, D. G. & Funnel, B. M. 1994. *Atlas of Mesozoic and Cenozoic Coastlines*. Cambridge University Press, Cambridge.

Storvoll, V., Bjorlykke, K., Karlsen, D. & Saigal, G. 2002. Porosity preservation in reservoir sandstones due to grain-coating illite; a study of the Jurassic Garn Formation from the Kristin and Lavrans fields, offshore mid-Norway. *Marine and Petroleum Geology*, **19**, 767–781.

Surlyk, F. 1990. A Jurassic sea-level curve for East Greenland. *Palaeogeography, Palaeoclimatology, Palaeoecology*, **7–8**, 71–85.

Underhill, J. R. 1998. Jurassic. *In*: Glennie, K. W. (ed.) *Petroleum Geology of the North Sea; Basic Concepts and Recent Advances*. Blackwell Science, Oxford, 245–292.

An old field in a new landscape: the renaissance of Donan

R. R. A. REEKIE, E. L. DAVIES, N. J. HART, A. T. MCINALLY, J. R. TODD, J. R. MCATEER, L. FRANOUX and E. L. M. FERGUSON

Maersk Oil North Sea UK Limited, Maersk House, Crawpeel Road, Altens, Aberdeen AB12 3LG, UK (e-mail: russell.reekie@maerskoil.com)

Abstract: The Donan Field was discovered in 1987 by BP well 15/20a-4. Oil is reservoired in Paleocene Lower Balmoral Sandstones of the Lista Formation. First oil was achieved from Donan on 28 April 1992 via two crestal producers to the Single Well Oil Production System (SWOPS) vessel *O.P.V. Seillean*. Peak production rates of 15 mstb/day were achieved before high well watercuts caused a significant drop in gross rates. Further attempts at development proved unsuccessful at the time. No further infill attempts were made as the field continued to be produced until it reached its economic limit in 1997. The field had produced 15.3×10^6 stb. Subsequently, block 15/20a was awarded to a partnership led by Kerr–McGee (North Sea) UK Ltd (now Maersk Oil North Sea UK Limited) in 2002 as part of the twentieth licensing round. Drilling results whilst testing the prospectivity on the block led to a focus towards Donan redevelopment. A combination of Rock Physics modelling and AVO, calibrated by appraisal drilling, and the integration of high-resolution biostratigraphy, played a significant role in the successful first phase of the 'Dumbarton Project', consisting of five horizontal producers and one produced water reinjection well. 'Second oil' from Donan was achieved on 19 January 2007 to the Global Producer III FPSO. Early production performance was in line with expectations with the field producing 20×10^6 stb within the first two years. In 2008 and 2009 further phases of development drilling took place on Donan with 2009 also expected to deliver two development wells in the Lochranza Field, a smaller, structurally distinct field to the east of Donan.

Keywords: Donan, Dumbarton, Paleocene, redevelopment, AVO, turbidite, Balmoral

The Donan Field has produced in excess of 20×10^6 bbl oil from its Paleocene reservoir since coming online in January 2007. At the time of writing, a second phase of infill development drilling is planned and due to commence in 2009. Thereafter, development drilling will commence on Lochranza, a satellite field located a short distance east of Donan. Whilst this introduction to Donan is not especially unusual, such a cursory assessment ignores the less-than-ordinary history of a field with a previous life, which was abandoned, and has subsequently been brought 'back from the dead'.

First discovered in 1987, the field was on production from 1992 to 1997 before being abandoned. This paper reviews the history of Donan. Using period reports it discusses the discovery of the field in the 1980s, first oil in 1992 and its eventual abandonment. It then documents the 2002 award of Block 15/20a in the twentieth licensing round for Jurassic prospectivity, the 're-discovery' of the Paleocene and the birth of the 'Dumbarton Project'. At a time when many are reflecting on the past four decades of North Sea Exploration and Production, the renaissance of Donan is an excellent example of how advances in technology coupled with a fresh insight can stimulate success.

A first life: Donan 1987–1997

Location and block history

The Donan field is located in blocks 15/20a and 15/20b, 27 km SW of Tiffany and 11 km NE of MacCulloch in the Central North Sea. Structurally, this places the field on the northern flank of the Witch Ground Graben to the SW of the Fladen Ground Spur (Fig. 1).

Block 15/20 was first awarded to BP in 1972 as part of the fourth licensing round. The part of the block covering Donan stayed in BP's operatorship through its various subdivisions until 1991, when block 15/20b was created for the twelfth licensing round. BP retained 100% of 15/20a with only 7.5% equity stake in 15/20b along with Conoco (60%), Croft Exploration (2.5%) and OMV (30%). In 1993 the Donan Field Area was unitized between BP (70%) and the Conoco Group (30%).

Block 15/20a was relinquished by BP in 2000 and awarded to Kerr–McGee (40%), EDC Europe [later to become Noble Energy (Europe) Ltd] (30%) and Enterprise Oil (30%) as part of the twentieth licensing round in 2002. In 2003, Enterprise Oil left the 15/20a block with their equity passing to Kerr–McGee. Meanwhile, 15/20b was acquired by Kerr–McGee (100%) for a cash consideration. In 2004 Noble Energy farmed into a 30% stake of 15/20b, unitizing the equity across the two blocks. Finally Maersk Oil bought Kerr–McGee's interest in both blocks in 2005 as part of a large Kerr–McGee UK asset sale.

Discovery and appraisal of Donan

Mapping of the 2D seismic data available at the time identified a structural closure at base Cretaceous and Paleocene levels in 15/20a. This structural closure was observed to become less pronounced between the lower Intra-Danian and the upper Early Eocene horizons that were used to define the Paleocene envelope. Towards the upper Early Eocene horizon, the structure was observed to be of lower relief (Fig. 2). Hence, the trapping mechanism was identified as the key risk associated with the Paleocene prospect. A secondary target at Jurassic level was also identified. Correlation from nearby wells suggested the presence of Upper Jurassic Piper reservoir sandstones and a closure. The key risk at this level was fault seal.

The 15/20a-3 well was drilled to test these prospects in 1986 and resulted in the discovery of a 75 ft oil column comprising light crude of 41° API in interbedded turbidites of the Andrew Formation (Deegan & Scull 1977) which were later re-classified as the Lower Balmoral Sandstone Unit (Knox & Holloway 1992). The well also

VINING, B. A. & PICKERING, S. C. (eds) *Petroleum Geology: From Mature Basins to New Frontiers – Proceedings of the 7th Petroleum Geology Conference*, 431–450. DOI: 10.1144/0070431

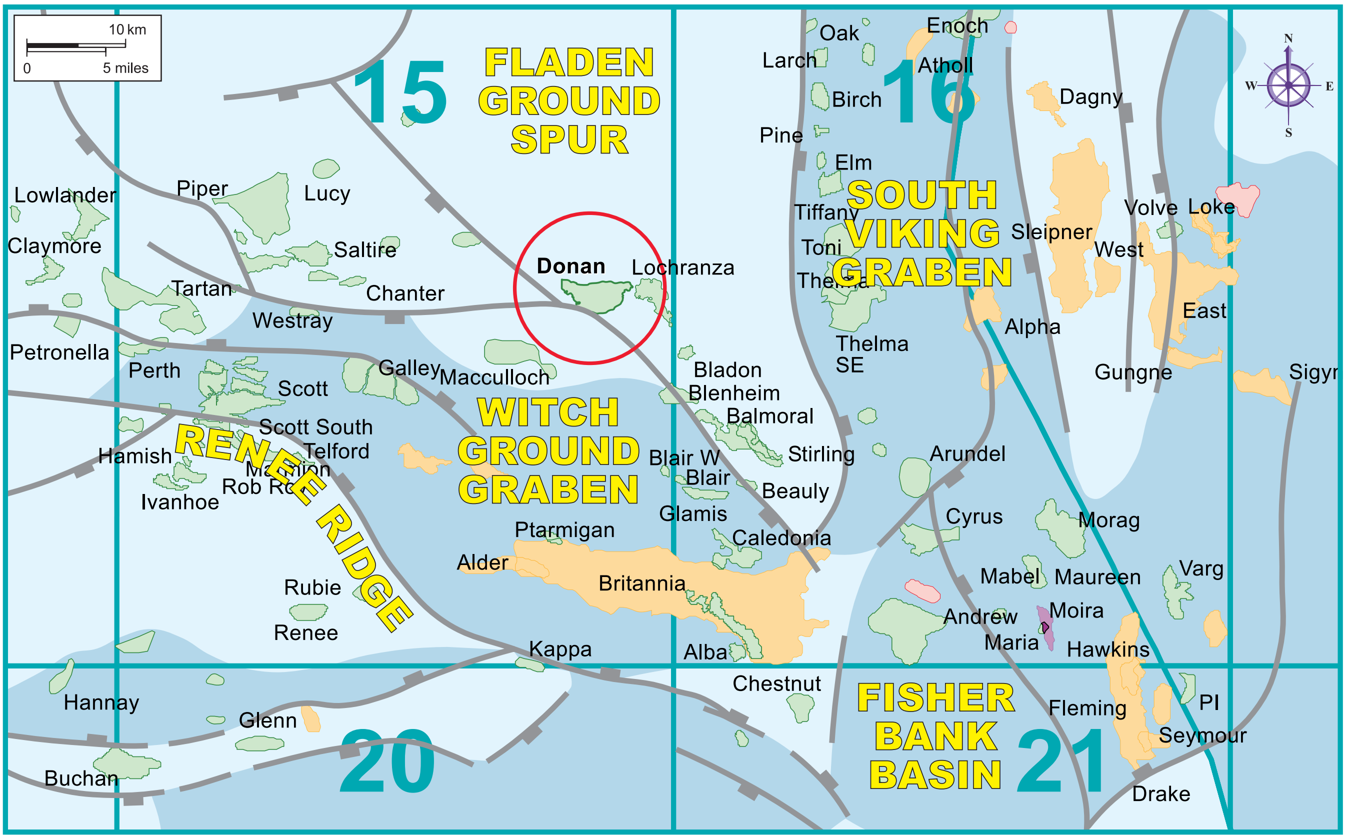

Fig. 1. Donan Field location map showing key structural elements.

successfully penetrated Jurassic Piper sandstones, although these were found to be water-wet. The well results are summarized in Table 1. Analysis of the discovery well results suggested that thicker Paleocene reservoir might be found further to the west.

This western culmination was appraised by the 15/20a-4 well in 1987 (Fig. 3). Identification of an oil column with a water-up-to (WUT) that was shallower than the contact observed in the eastern discovery well indicated that this accumulation was separate from the original discovery. The well was suspended upon completion of operations pending a development decision. A second appraisal well (15/20a-6) was drilled in 1990 from the same seabed location as 15/20a-4 to test the western part of the Donan structure and identify an original oil–water contact (OWC). This deviated well encountered thicker pay sands than the 15/20a-4 well and confirmed the contact at −6466 ft total vertical depth subsea (TVDss). This well was also suspended as a possible producer.

Further appraisal wells were drilled in the eastern accumulation, later called Pladda, in the early 1990s. Whilst these wells successfully identified hydrocarbons in the Paleocene, the volumes in place were assessed to be subeconomic for production.

At the end of the appraisal campaign, the Donan geological model was a simple layer-cake arrangement generated by the correlation of unconstrained wireline logs and the correlation of tuffs which are now believed to have been reworked and diachronous (Fig. 4). At this time, no field-specific biostratigraphy had been attempted to constrain any of the correlations and the existing biostratigraphic control was of too low resolution to be used in a meaningful way (Payne *et al.* 1999). The low net to gross reservoir sands were interpreted by BP as having been deposited during gradual and regional scale east-to-west retreat of the Andrew Fan. The layer-cake nature of the model, with laterally continuous shale layers separating the sands, led to the interpretation that production would be driven by aquifer influx along each sand layer. At this time the field had an estimated stock tank oil initially implace (STOIIP) of 82×10^6 stb with a range between 58 and 115×10^6 stb.

Donan field development

BP submitted an Annex B document for the development of the Donan Field to the Department of Energy in 1991 and first oil was achieved on 28 April 1992. The field was developed through the two existing wells via a detachable steel riser to the Single Well Oil Production System (SWOPS) vessel *O.P.V. Seillean*. The vessels name originates from the Gaelic for honey bee and had been used successfully on the Cyrus field prior to it being stationed on Donan. The SWOPS concept was part of BP's strategy for producing from its smaller fields in the North Sea with the vessel moving from field to field like a honey bee producing from the wells that would fill it to capacity in the shortest time. The *Seillean* was designed with the capability to process liquids onboard with a handling capacity of up to 15 mstb/d of oil from a maximum of two wells. However, the 300 mstb storage capacity meant that production was intermittent as the vessel had to disconnect to deliver its load to market. Using this development strategy, it was expected that the field would produce reserves of *c.* 16.5×10^6 stb of oil.

Other development schemes were considered for Donan, such as the deployment of a semi-submersible production system or tie-back to existing nearby facilities. The first year of production to the *O.P.V. Seillean* allowed well production performance to be monitored and integrated with subsurface studies before committing to a final development scheme. It was noted in the Annex B document that a further two wells may have been required to ensure effective development of reserves.

Early field performance

Upon production start-up on 28 April 1992, initial rates were good at around 13 000 bbl oil/day. The 15/20a-4 well saw early

(a)

(b)

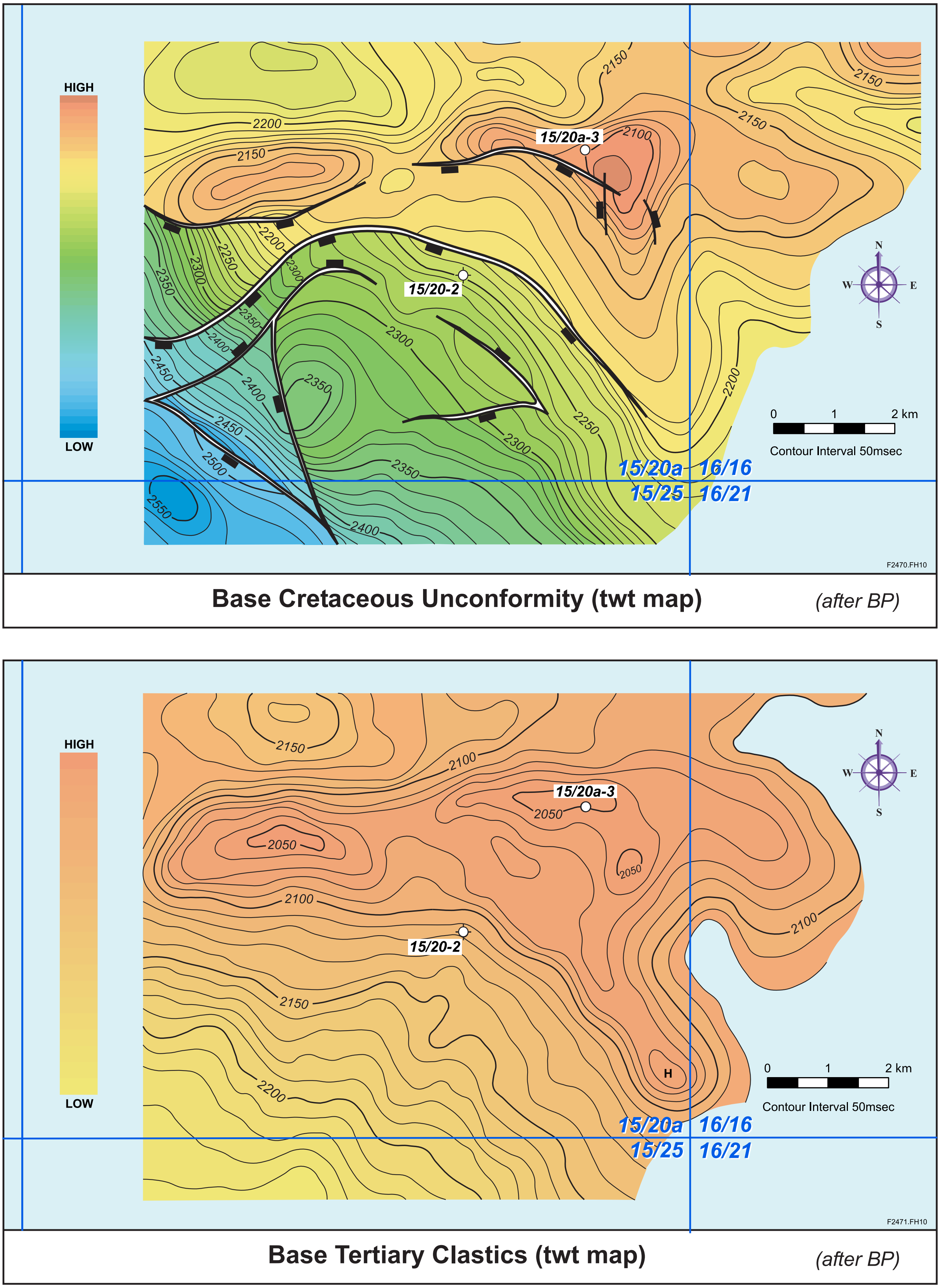

Fig. 2. Original prospect map at (**a**) Base Cretaceous and (**b**) 'Base Cenozoic clastics' levels shows structural relief, decreasing.

Table 1. Donan discovery and appraisal well results

Well	Operator	Year	Objective	Lower Balmoral net pay thickness	Contact	Flow rate
15/20a-3, 3Z	BP	1986	Paleocene Lower Balmoral and Jurassic Piper Sands	11 ft TVD	OWC – 6509 ft tvdss	Not tested
15/20a-4	BP	1987	Lower Balmoral	46 ft TVD	ODT – 6455 ft tvdss	4170
15/20a-6	BP	1990	Lower Balmoral	62 ft TVD	OWC – 6466 ft tvdss	Not tested

water-breakthrough with well watercut increasing steadily over time, whilst the 15/20a-6 well had a year of dry production owing to its location high in the structure, the proximity of a shale baffle below and its limited completion length (Fig. 5). After unitization of the field, an Annex B Addendum for continued production was submitted and approved in 1993. Between 1993 and 1994, a programme of modifications was carried out to upgrade the vessel and flowlines to enhance gross liquid throughput from 16 to 23 mbpd. Production was also interrupted regularly when the SWOPS vessel reached capacity and had to sail to market.

Studies carried out during 1994, which included interpretation of a new 3D seismic volume acquired in 1993, revised the most likely STOIIP to 77.2×10^6 stb from 82×10^6 stb and indicated that the optimum development scheme was the continued use of the SWOPS vessel. Life of Field production consent for Donan was awarded to the partnership in early 1995. At this stage, gross rate and oil rate had started to decline since there was no operational gas lift system in the two producers to maintain liquid rates as the total watercut began to exceed 50% (Fig. 4).

Infill drilling

In order to improve the understanding of the reservoir architecture during these first years of production, a high-resolution dinocyst-based biostratigraphy study was initiated using core data (Payne *et al.* 1999). This led to a revision of the geological model from a simple layer-cake model with an upper sand deposited contemporaneously across the whole field, to a more heterogeneous system with sand bodies pinching out over relatively short distances (Fig. 6). Given the high watercut in the existing wells, the partnership initiated an infill drilling campaign in February 1995 designed to replace the original two wells with two new drier horizontal wells. These were drilled to the west of 15/20a-6 where the uppermost sand layer was expected to thicken based on the new geomodel (Targets A and B; Fig. 7). Inclined pilot holes were planned to test the reservoir model and oil column height prior to drilling the horizontal wells. Wellsite biostratigraphy was also employed to aid well placement.

The first pilot well drilled was 15/20b-12. This well encountered significant borehole instability in the Eocene section. Nevertheless

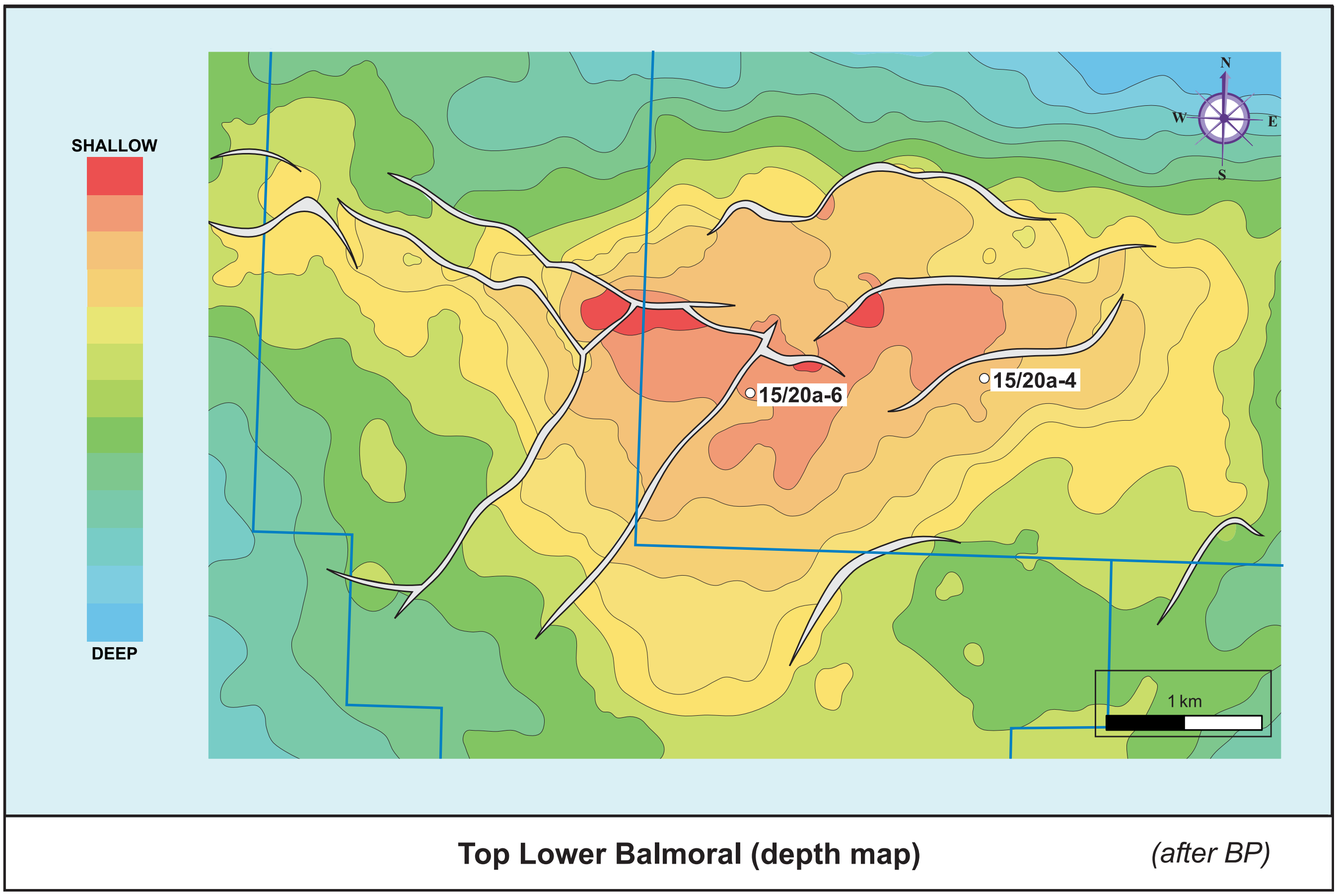

Fig. 3. Donan structure map showing appraisal well locations.

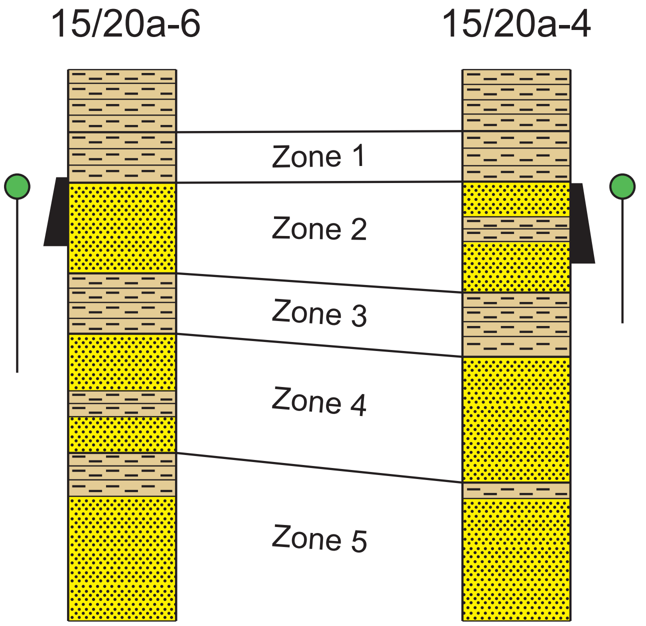

Fig. 4. Original layer-cake Donan model adapted from Payne *et al.* (1999).

the reservoir section was successfully penetrated on prognosis. On attempting to pull out of hole, the drilling assembly became stuck in the Eocene section and could not be recovered. Consequently, no wireline log data was acquired in the well. Despite the absence of log data, high gas readings in the reservoir section and high sand percentage in the drill-cuttings led to the decision to proceed with the main horizontal section (15/20b-12Z). The uppermost sand layer above the *Areoligera gippingensis* biomarker (Fig. 6) was expected to be of a similar thickness to that encountered in the pilot hole – *c*. 33 ft. The 15/20b-12Z well penetrated top reservoir and set a $9\frac{5}{8}$ ft casing only 100 m away from the original pilot wellbore. However, the upper sand layer encountered was only 7 ft thick in this location. This rapid change in layer thickness was attributed at the time to intra-reservoir faulting. Therefore a second sidetrack was planned to target the footwall of this fault where the upper sand layer was expected to be thicker. In the event, the *Areoligera gippingensis* marker came in prior to any sand being encountered, indicating that the upper sand layer was absent in this location. This led to the adoption of an alternative sedimentological model where rapid stratigraphic thinning was responsible for the variability of sand thickness, rather than faulting as previously proposed. Deepening the 15/20b-12Y well to test if the lower reservoir sands would be producible found them to be poorly developed and thin, with an apparent swept zone at the base of the reservoir section. This led to the abandonment of Target A as a viable infill option.

Despite poor results at Target A, Target B was still considered a robust option given its location between the 15/20a-6 well, where the upper sand layer above *Areoligera gippingensis* marker was of sufficient thickness, and the predicted source of the reservoir sands to the NW. Sidetrack 15/20b-12X was drilled as a pilot to test Target B (Fig. 7). Top sand was encountered 26 ft high to prognosis, was 7 ft thick and of poor quality. A 33 ft mud-prone layer was encountered before the quality of the sands began to improve. The best quality sands were identified some 82 ft below top sand but these were found to be in direct communication with the aquifer. A 16 ft swept zone was identified confirming the upward movement of the OWC caused by earlier field production from the 4 and 6 wells. The movement of the OWC indicated that the main mechanism of displacement was bottom-up drive by the aquifer, rather than lateral sweep of the individual sand layers. Analysis of this well data suggested that a reasonable producer could be drilled and completed subhorizontally (*c*. 86°) over the upper sand layers, which would be protected from the strong aquifer by the mud prone layer below. The 15/20b-12W well was drilled to the east of the pilot well as it was anticipated that the sand would thicken towards 15/20a-6. A gradational top sand was encountered high to prognosis. However, contrary to expectations, no well-developed sand was encountered in the upper section. Only thin sands were penetrated which were too close to the moved OWC identified in the 15/20b-12X well to be completed. These discouraging well results led to the abandonment of Target B as a viable infill location and to the suspension of infill drilling.

The changing geological view of Donan

The Donan geological model had changed significantly between 1992 and 1995. The validation of the high-resolution biostratigraphy study by the 15/20b-12 wells had shown that the nature of sand and shale distribution in the oil leg was far more complex than the original layer-cake model suggested. Rapid lateral facies changes of the upper reservoir observed during BP's infill campaign of 1995 was attributed to smaller, localized fans that

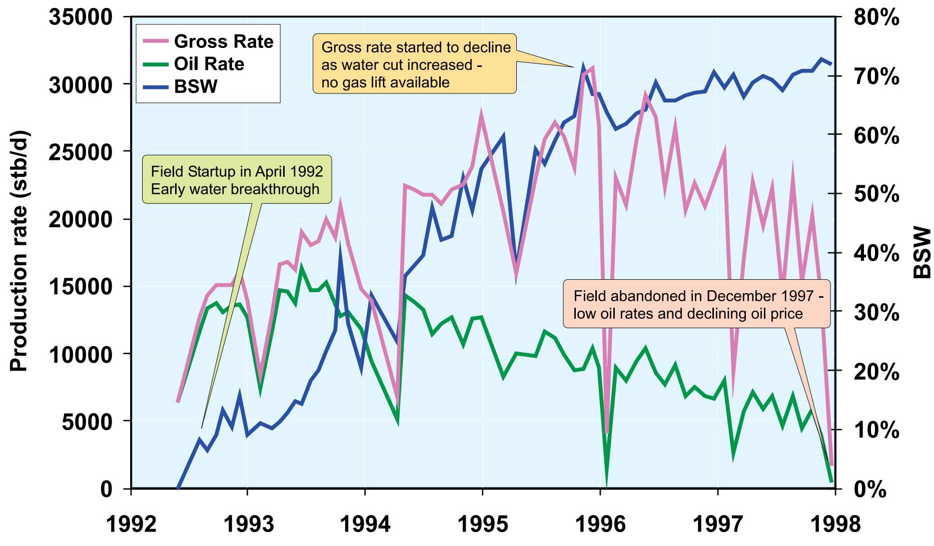

Fig. 5. Production plot showing Donan field performance between 1992 and 1997.

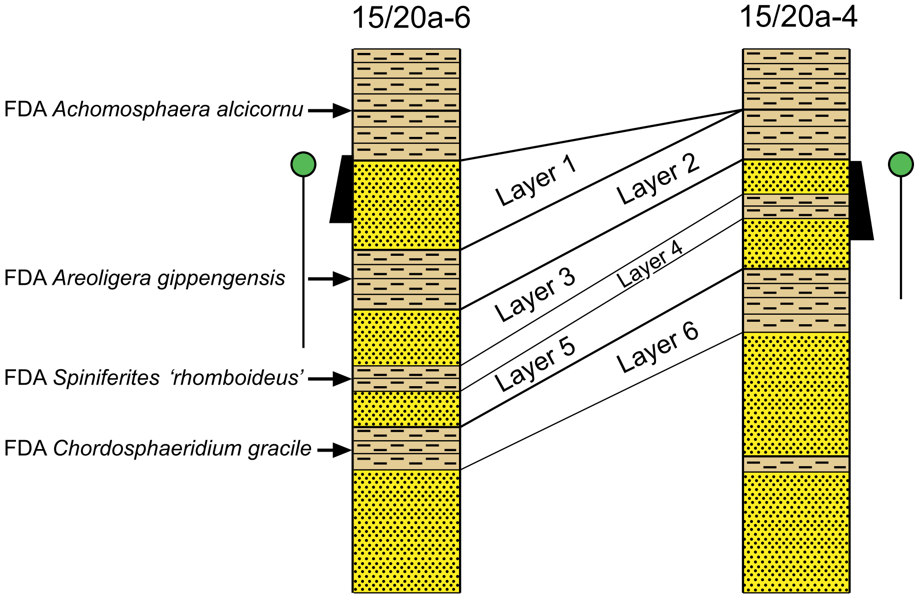

Fig. 6. Revised Donan model adapted from Payne *et al.* (1999) based on high-resolution biostratigraphy indicating a more heterogeneous system than previously modelled.

existed on the flanks of the major 'Andrew' fan axis that did not correspond to the more regional fan trends. Over Donan, a minor fan or splay may have been present with the unpredictable nature of sand distribution being related to splay or fan abandonment creating dilute sand events which were unevenly distributed around the field. Deeper, better quality reservoir sands were interpreted to reflect more stable conditions during the main phase of fan activity. However, these better quality reservoir elements were not accommodated to a great extent within the low relief Donan structure. The observation of raised OWCs in the 15/20b-12Y and -12X wells provided evidence for an aquifer-driven bottom drive mechanism indicating that whilst laterally extensive shales persisted

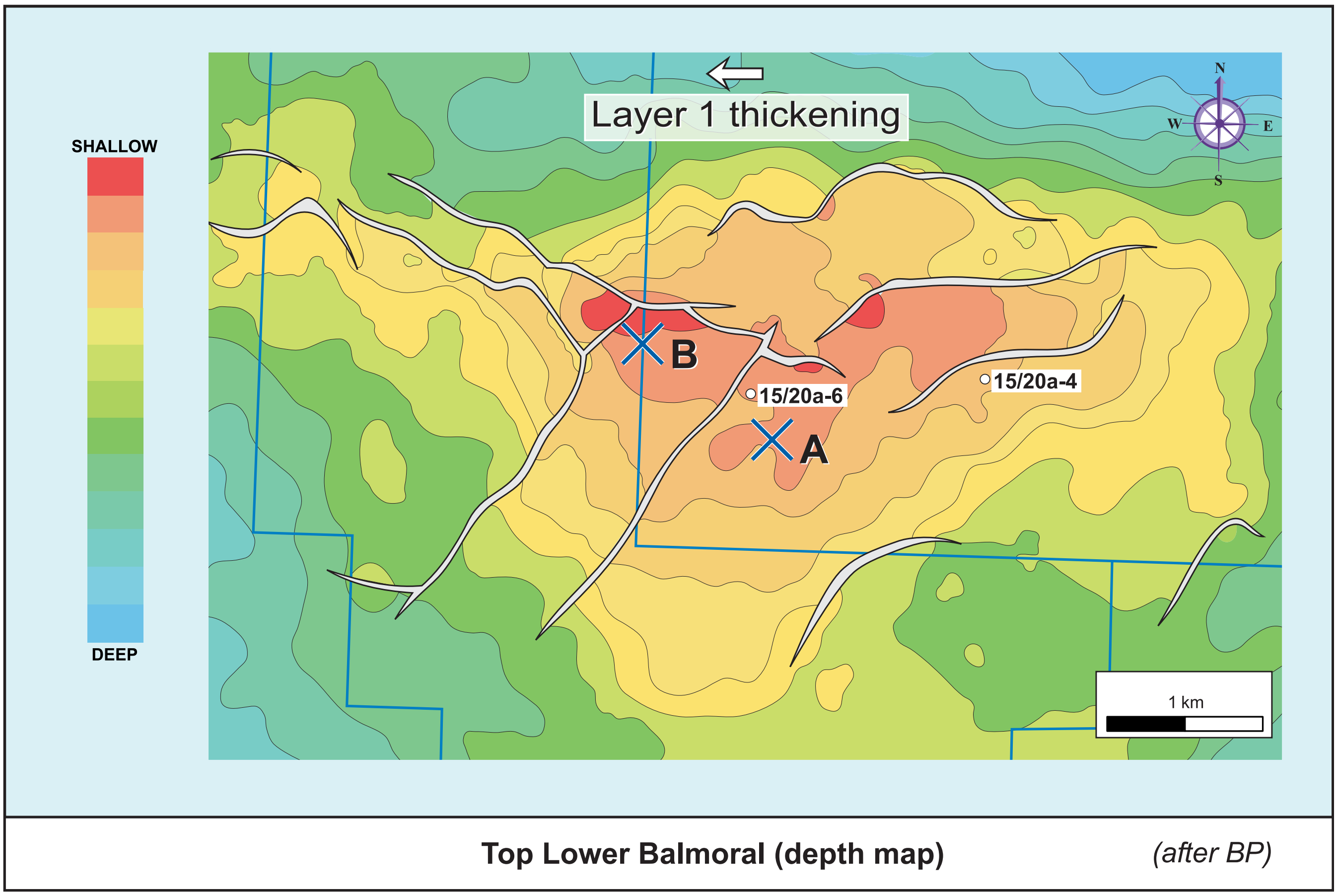

Fig. 7. Donan structure map showing infill locations (A), targeted by 15/20b-12, 12Z and 12Y, and (B), targeted by 15/20b-12X and 12W in 1995.

over much of the field, sufficient fluid pathways existed to allow vertical fluid flow.

Improved biostratigraphic data combined with modifications to the seismic pick made after infill drilling were used to create a new layering scheme for the reservoir. However, given the unpredictable nature of the sands encountered in the wells, it was deemed impossible to accurately represent the complete internal structure of the reservoir for simulation purposes.

Abandonment

In light of the disappointing infill well results and the increasingly complex picture of the reservoir, the STOIIP for the field was revised downwards from a most likely volume of 77.2 to 54×10^6 stb. The optimum development scheme for the field was to cease further development and continue production to the SWOPS vessel until this became uneconomic.

In the end, the *O.P.V Seillean* left the field on 24 December 1997 for the final time with the oil price on a downward trend that would see it reach the $10/bbl mark in 1999 (Fig. 8). The Donan field was abandoned by BP, having produced 15.3×10^6 stb.

Prospects of a new beginning: Donan 2001–2007

Following a screening study encompassing a number of blocks in the area, a partnership led by Kerr–McGee was awarded block 15/20a in 2002. The group recognized the potential of two discoveries in the block (Fig. 9). The first was the Jurassic age 'Jura' prospect that was discovered by the 15/20b-11Y well in 1992. Its closure was believed to lie somewhere to the NW beneath the abandoned Donan field. The second prospect was the Paleocene Pladda prospect penetrated by the 15/20a-3/3Z, 15/20a-9 and 15/20b-11Y wells. At the time, Pladda was considered too small to be economic unless developed after the success of Jura. In addition to the two prospects on the block, the group also saw significant potential for the redevelopment of Donan, which could, if successful, also facilitate the development of Pladda.

The twentieth licensing round award was based on a work programme that included a firm well to test the Jura prospect and a contingent well to test Pladda, the latter being dependent on the success of the firm well or success of a Donan redevelopment feasibility study. The firm well commitment was fulfilled by exploration well 15/20a-13, which was drilled in March 2003 to the east of the Donan structure. The primary objective of this well was to test the Piper Formation sandstone of the Jura prospect which had been discovered by 15/20b-11Y. This location was thought to lie *c.* 100 ft structurally updip of the 15/20b-11Y well with thicker development of the Upper Jurassic Sand. A secondary objective was to test the Paleocene sandstones of the

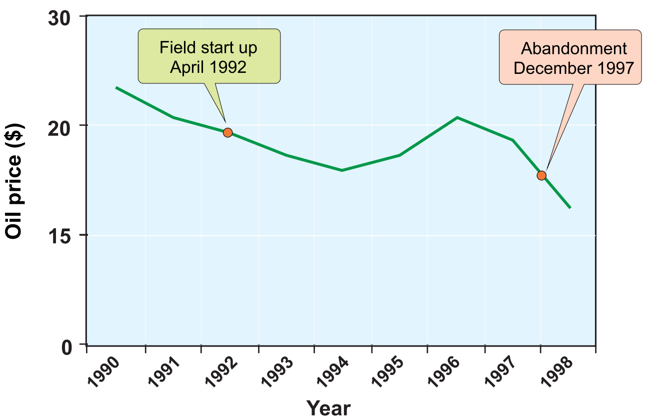

Fig. 8. Chart of oil price trends affecting the first life of Donan.

Pladda prospect. Mapping indicated that the well was targeting an area to the west of the structural closure of Pladda, therefore having a low chance of success. The well encountered a 40 ft oil column in the Paleocene Lower Balmoral sandstones whilst the Jurassic came in deeper than expected, was water-wet and well cemented. These well results, along with promising findings from initial Donan redevelopment study, prompted focus on the Paleocene and the implementation of a Donan appraisal campaign.

Key technologies influencing appraisal

Two key initiatives implemented by the partnership that had significant influence over the Donan appraisal and redevelopment were the application of detailed seismic analysis and high-resolution biostratigraphy.

Following the 15/20a-13 well results, the migrated stacks for the complete 1993 survey were purchased through standard seismic data release procedures. These post-stack migrated volumes were observed to be of poor quality so the field tapes over blocks 15/20a and 15/20b were purchased to enable reprocessing. Reprocessed pre-stack time migrated (PSTM) data was delivered and loaded in November 2003. Whilst this dataset was a significant improvement, acquisition-related artefacts such as trace-to-trace amplitude and timing jitter, poor signal-to-noise and low frequency content at the reservoir interval remained. The tuning thickness of this new data was *c.* 76 ft.

Rock physics analysis carried out in-house using the 15/20a-4 well indicated that Class II amplitude variation with offset (AVO) (Rutherford & Williams 1989) should be observed in the seismic data at this location in the presence of oil. Synthetic well ties indicated that this AVO was characterized by the presence of a weak trough ('hard' – positive impedance change) on near traces with a bright peak ('soft' – negative impedance change) on fars (Fig. 10). At first, it was difficult to quantify the reliability of this AVO. There was some degree of uncertainty over the relationship between reflection amplitude and hydrocarbon pore thickness. Furthermore, there was the possibility that the presence of hydrocarbons could also be associated with dimming effects on both near and far angles. What was clear, however, was that the reprocessed PSTM data did demonstrate a clear AVO signature when far and near stacks were subtracted (Fig. 11). It was believed that this signature could be used to optimally place appraisal wells. The appraisal wells would acquire a full suite of sonic and shear sonic logs to calibrate the rock physics model and address the remaining uncertainties. It was expected that this calibration would have a major de-risking effect on development well placement.

Whilst a useful pay indicator, the AVO response made conventional seismic interpretation on full-stack reflection data difficult. Off the main structure, brine-filled reservoir sands could be picked on a hard trough event. On the crest of the field where the net-pay thickness was sufficient to generate AVO, the top reservoir could be picked on a soft peak (Fig. 12). Near and far angle stacks had to be used together to decide which was the most appropriate pick away from well control. The pick itself was considered to represent the 'top of the reservoir envelope' due to individual reservoir sands and oil column thickness in many areas being below seismic resolution.

In parallel with seismic re-processing and AVO analysis, a high-resolution biostratigraphy/sedimentology study was undertaken building on the earlier BP work. Five cored wells were used for interpretation along with several hundred cuttings samples. This study was used to develop an understanding of apparent stratigraphic heterogeneity, characterize claystones and to define the facies distribution so that this new biostratigraphic scheme could be used in a predictive manner. All of these were crucial to building

(a)

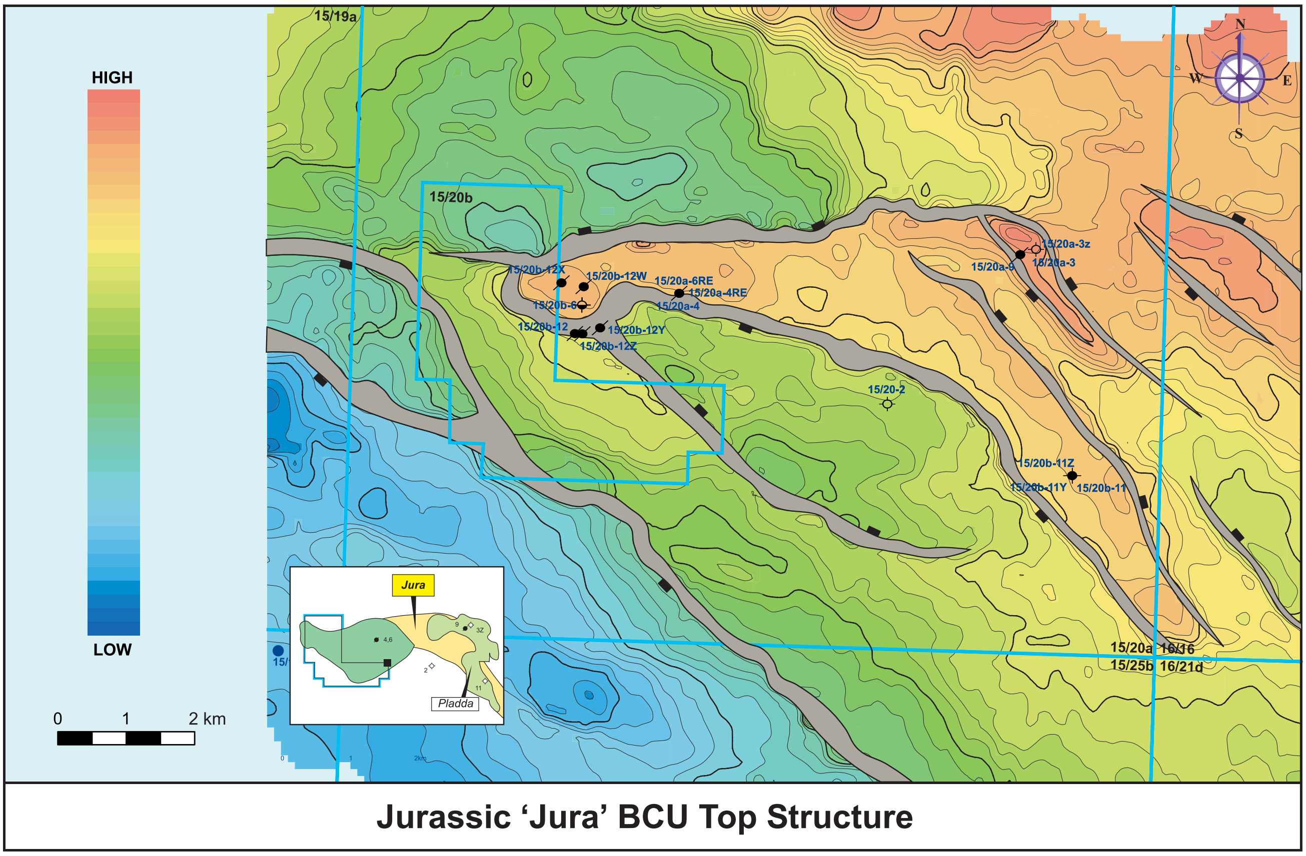

(b)

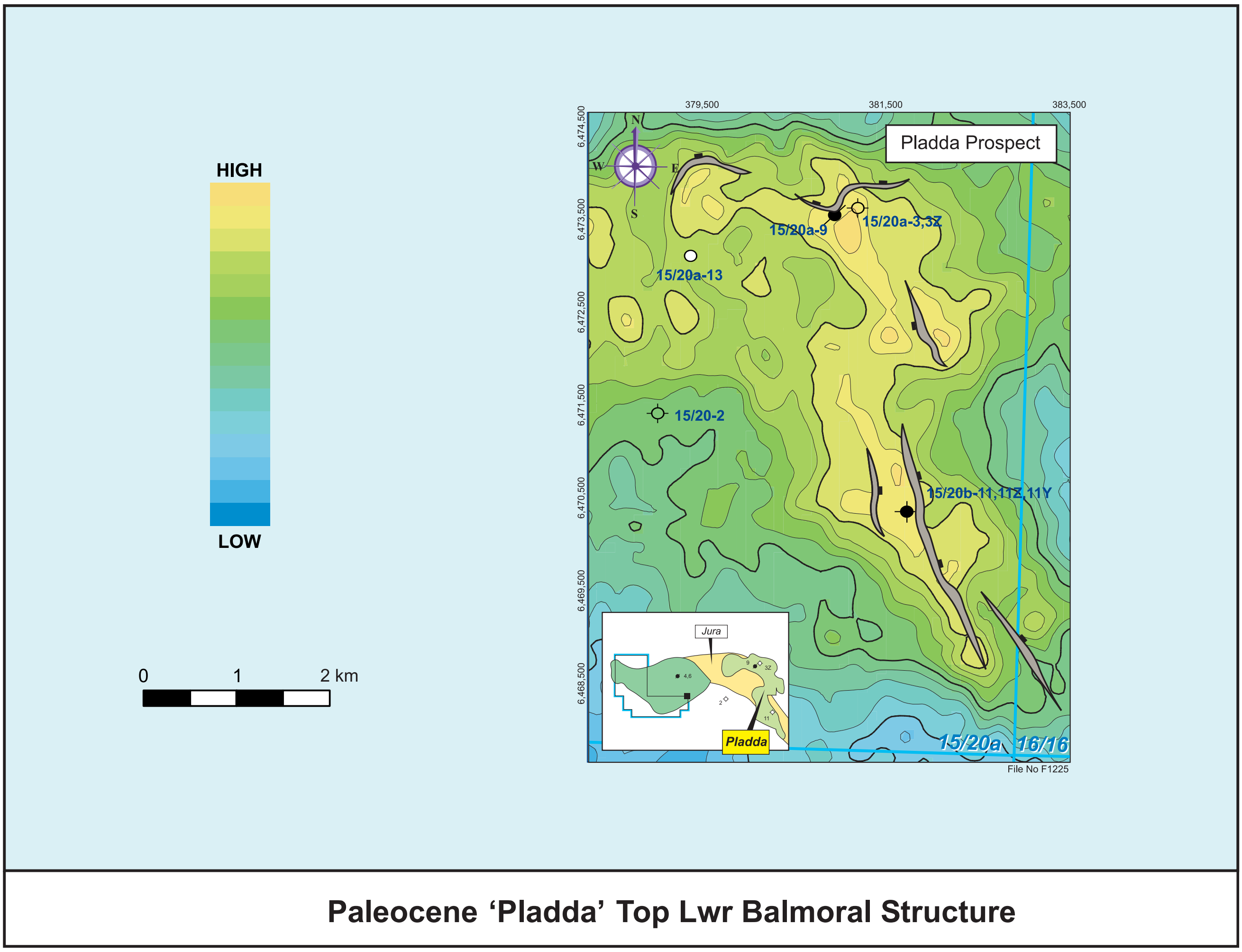

Fig. 9. (**a**) Jurassic 'Jura' and (**b**) Paleocene 'Pladda' prospects recognized by the partnership in the twentieth round in 2002.

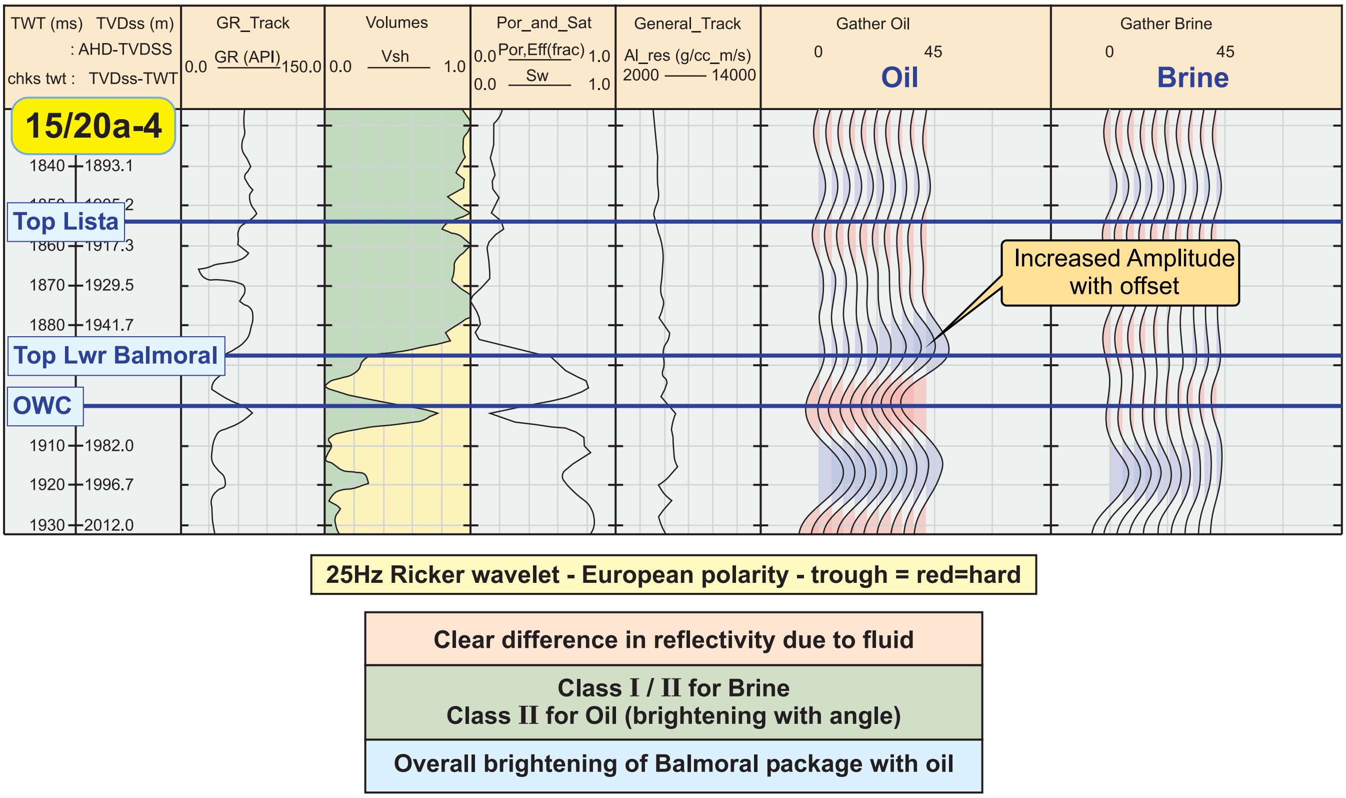

Fig. 10. Rock physics model for Donan showing AVO response in the presence of hydrocarbons in Lower Balmoral reservoir.

a working reservoir model that reflected the stratigraphic, depositional and facies relationships within and between the Donan and Pladda accumulations. Additionally, a framework of sufficient resolution was created to be used for geosteering future horizontal wells.

The new interpretation divided the reservoir into 10 units with six genetically linked sandstones deposited in a background of biostratigraphically correlated hemipelagic claystone intervals (Fig. 13). The sands themselves were interpreted as being deposited in sheet-like systems from high-density sand-rich gravity flows.

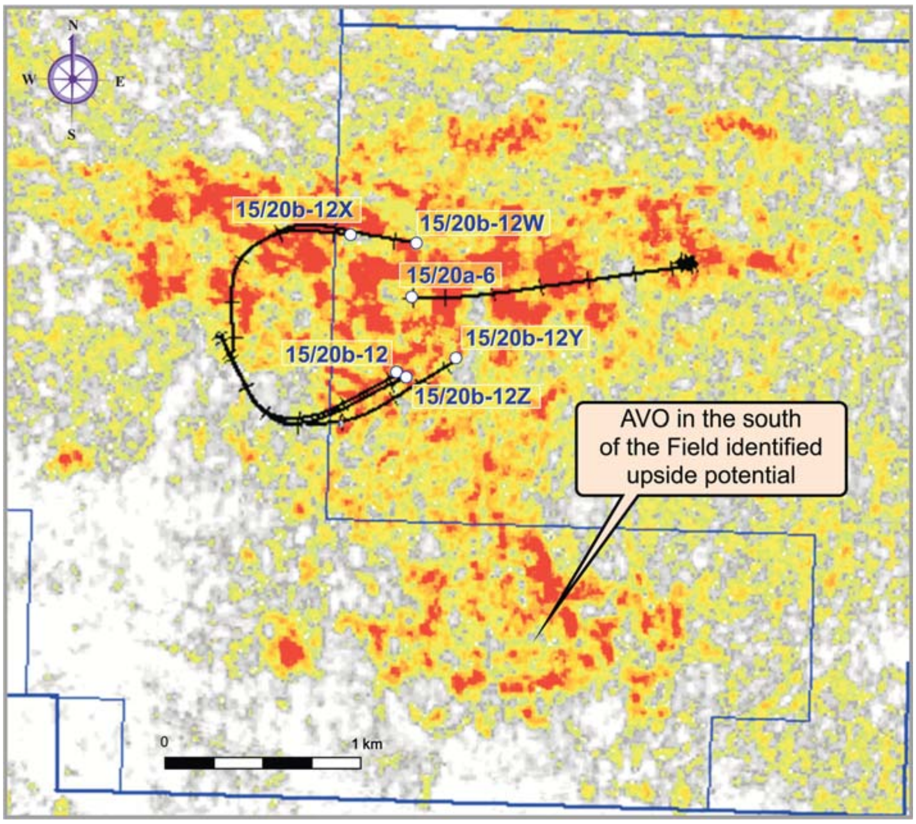

Fig. 11. Map of far minus near envelope over Donan showing clear AVO signature.

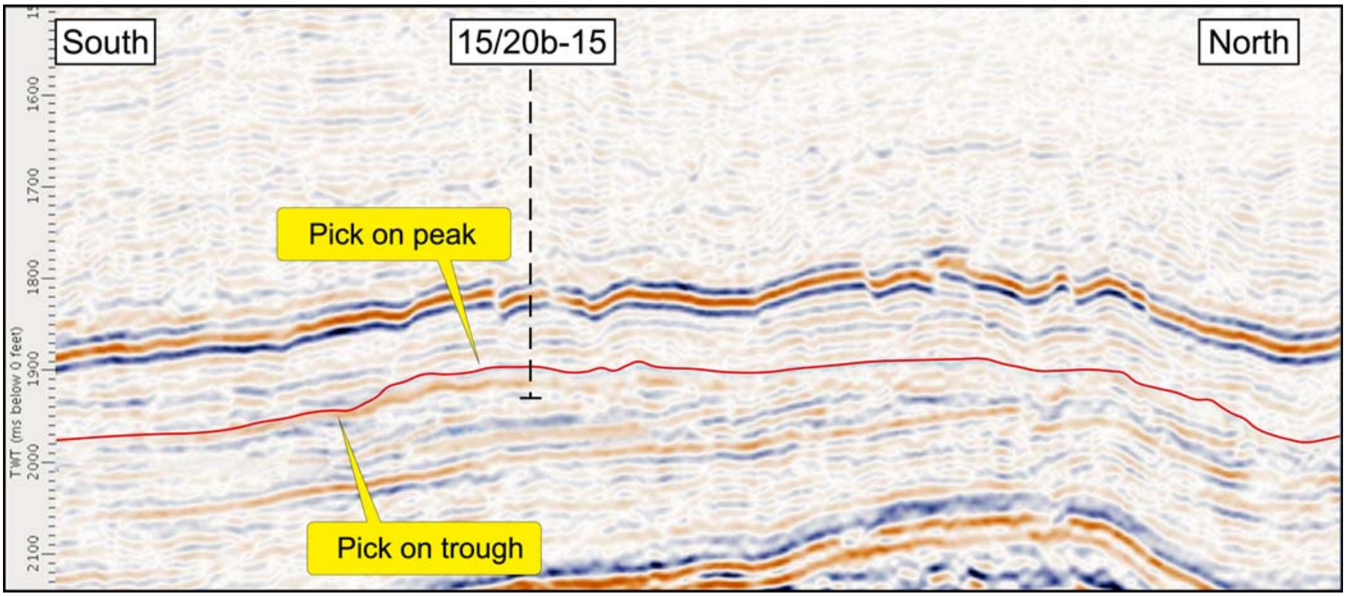

Fig. 12. Inline through full stack seismic data illustrating difficulty in picking on the flanks of the field where polarity flip occurs.

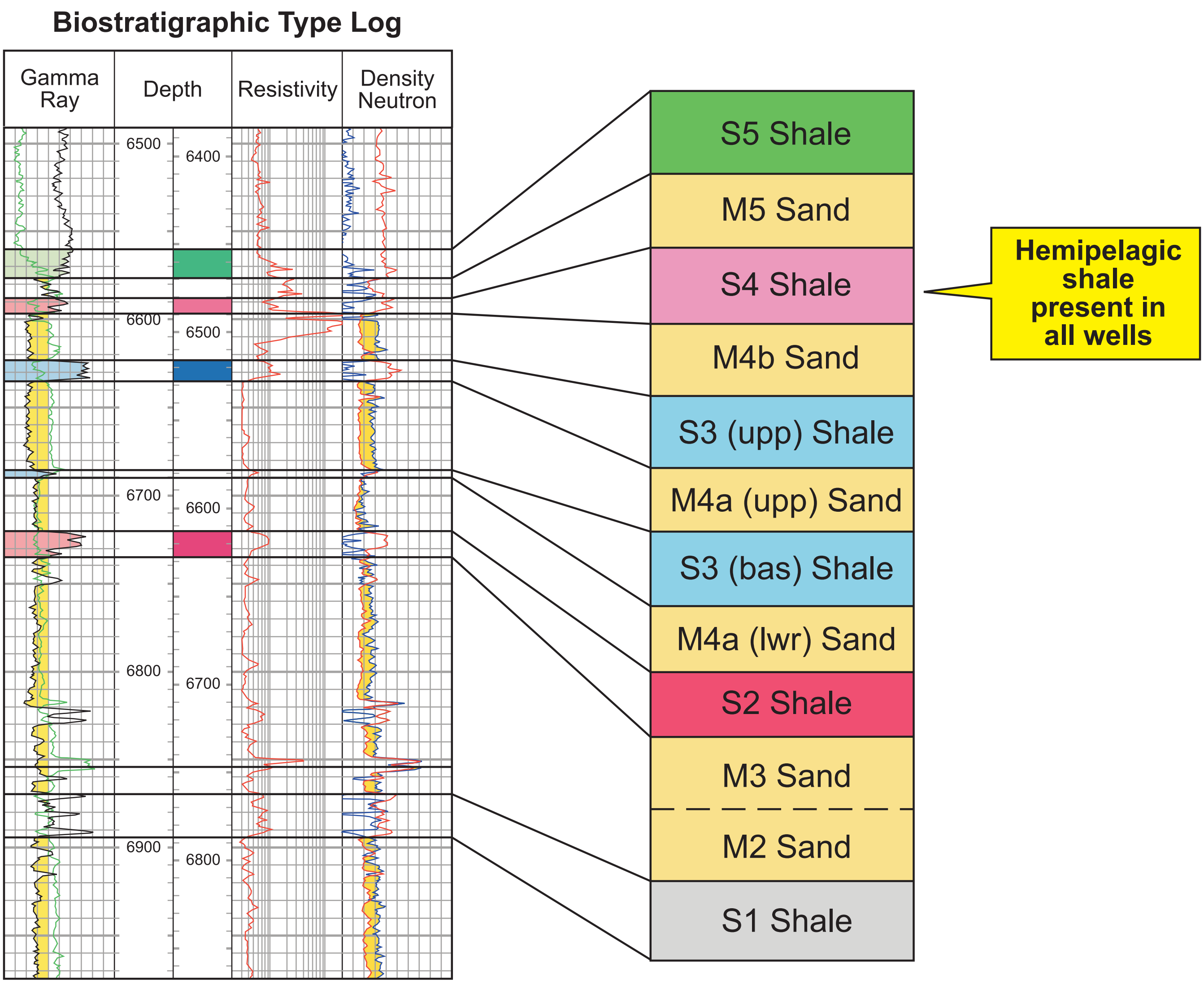

Fig. 13. Biostratigraphic subdivision Lower Balmoral sandstone reservoir units.

Only the youngest sandstone units were interpreted as showing any degree of flow-confinement, based on their lateral distribution. However, no overbank or channel margin deposits were recognized from core. A further level of complexity was added by the recognition of post-deposition remobilization and injection of sands during burial from core data. This injection is now believed to play a significant role in influencing vertical communication and water breakthrough.

Biostratigraphic data collected throughout the Donan appraisal campaign was integrated with a regional study to better understand the field's position in the larger Balmoral sandstone system.

Donan re-appraisal and the birth of the Dumbarton Project

The first appraisal well, 15/20a-14, was drilled in Q4 2003 to test a structural high that had been mapped to the east of the 15/20a-4 well (Fig. 14). The well was designed to calibrate the top reservoir pick, find sufficient net pay so that this well could act as a pilot for a future horizontal producer, confirm the field's moved OWC as predicted from dynamic modelling and verify possible remaining reserves.

The top sand was encountered some 91 ft TVD deep to prognosis at −6412 ft TVDss. However the well identified 17.5 ft net pay above a moved OWC, obtained from MDT pressures, of −6452 ft TVDss. The contact at this location had moved up 14 ft as a result of BP production.

Post-well analysis of the seismic data around the 15/20a-14 well indicated that the localized structural high may have been generated by a seismic artefact as well as the pick being made on the soft peak when the correct post-drill interpretation would have picked on the underlying hard trough below. This highlighted the difficulties in picking top reservoir. Indeed this target had primarily been driven by structure and not the AVO distribution.

Well 15/20b-15 was drilled in 2004 to test upside identified by a re-mapping of top Lower Balmoral on the re-processed seismic data and by the presence of a strong AVO anomaly at the structure's southern flank that extended outside BP's structure map (Fig. 14). The well was designed to calibrate the rock physics model, confirm reservoir presence and net pay and therefore determine likely reserves. At the time, the minimum economic field size for Donan redevelopment was assessed to be *c.* 16×10^6 stb and the field's recoverable range was believed to be around 10–53×10^6 stb (P90-P10). This wide range reflected the volumetric uncertainty associated with this untested area on the southern flank and areas to the North, away from the existing producers. Therefore, success in this upside location would justify further work and go a long way to confirming the viability of field redevelopment. The most likely redevelopment concept for Donan was considered to be a two-well scheme. However, pre-drill analysis suggested that, if a net pay thickness of 35 ft or greater were encountered in the southern area, then the likely reserves addition would justify a change of strategy to a three, or more, well development.

The 15/20b-15 well successfully encountered top sand close to prognosis and found 55 ft of net pay before identifying an OWC from well logs (Sw > 50%) of −6460 ft TVDss. This net pay thickness had considerable impact on the field development plan (FDP).

The final appraisal well drilled on Donan was 15/20b-16 which was spudded in June 2005. The success in the southern flank of the field had confirmed that the partnership would press ahead with an FDP. The objective of this final well was to characterize the likely additional reserves close to the northwestern structural closure of the field. The well was placed in an area of mapped structural elevation. However, the AVO signature was only patchy at this location (Fig. 14).

The well encountered top sand 44 ft TVD deep to prognosis and penetrated 18 ft of net pay before identifying an OWC from well logs of −6458 ft TVDss. Analysis of vertical seismic profile (VSP) data acquired during drilling indicated that once again the top Lower Balmoral had been picked on the wrong event in the seismic data and should have been tied to the trough instead of the upper peak event. This uncertainty over the seismic pick made it difficult to resolve field closure to the NW. Based on these well results, it was believed that the field closed just to the

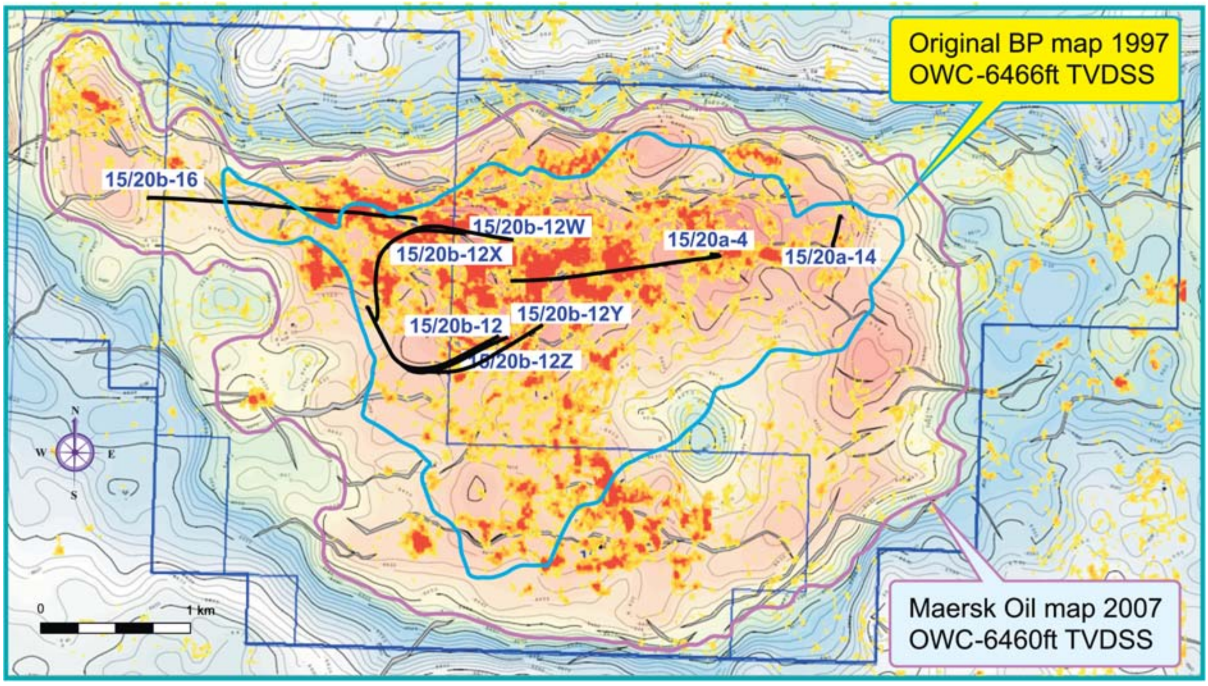

Fig. 14. Map showing appraisal well locations relative to AVO.

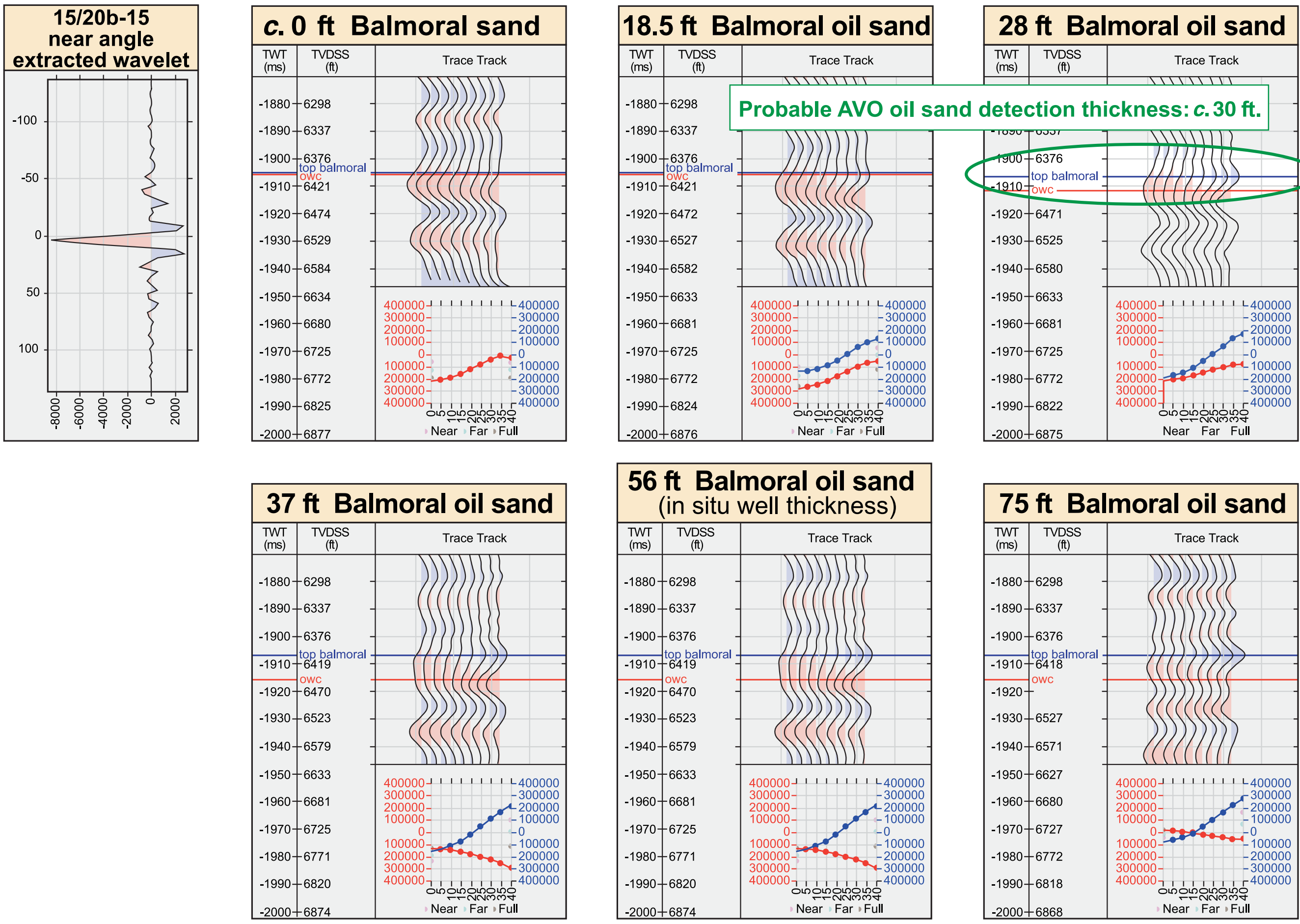

Fig. 15. Wedge modelling of reservoir sands indicating that the AVO response observed on Donan can be generated by net pay thicknesses of greater than 30 ft.

west of the well. However, this left a tempting area of AVO further to the NW, in a structurally higher position, just inside the block boundary, which would have to be further interrogated in the future.

By the end of the appraisal campaign, sufficient data had been gathered to suggest that the field would require a multi-well development plan to effectively realize reserves. The hypothesis that AVO could act as a net pay indicator had been validated and further wedge modelling using the well data indicated that areas where net pay was greater than 30 ft would exhibit Class II AVO (Fig. 15). Therefore, this could be used to aid development well placement using new seismic data which was acquired specifically for Donan by the partnership in 2005. Furthermore, the regional biostratigraphy study combined with the new appraisal data had allowed refinement of the geological model and given confidence that biosteering could be used to aid the placement of development wells in a particular sandbody.

The appraisal campaign had been a success and work began on the FDP. The partnership called the redevelopment the ‘Dumbarton Project’. Subsequent requests to change the field name to Dumbarton were turned down on the grounds that the 15/20b block had never been relinquished. However, in-house the field became known as Dumbarton.

Reservoir modelling

Following the successful appraisal campaign, a new geological model was constructed to reflect the current understanding of the field. Stratigraphic data collected from the wells was combined with the structural interpretation from seismic data to create a geocellular model which was then populated using rock property modelling. The consistency of reservoir sand properties across the field meant that constant values could be used with *J*-curves from a saturation-height model (applied to the original free water level) used to populate the variable oil saturations observed across the field. This model was input directly into simulation software for dynamic modelling.

Analysis of the historical behaviour of the field demonstrated that pressure was very well supported by the large aquifer. BP had concluded from surface pressure buildups during production shut-ins that there was no significant depletion in the field. A thorough review of regional formation pressure data, including the latest appraisal wells, suggested that *c.* 69 psi of depletion had in fact occurred since 1990 (Fig. 16). This depletion coincided with the extraction of fluids from Donan. However the trend appeared to have started two years before Donan came on stream, and continued afterwards. The effect of production from neighbouring fields (e.g. Balmoral and MacCulloch) was assessed to be the most likely explanation for this pressure depletion. In modelling the aquifer, compressibility calculations suggested an aquifer size of at least 50×10^9 bbl was present. The analysis of production and RFT data also demonstrated that depletion had occurred to the same extent across all sandstone units. This indicated that none of the hemipelagic shale units formed significant flow barriers. Flow across these hemipelagic shales could be explained by the presence of core scale sand injections and sub-seismic faulting. The main recovery mechanism was anticipated to be displacement of oil by aquifer influx from below. This was based on observation of sweep recorded in the 15/20a-12X well.

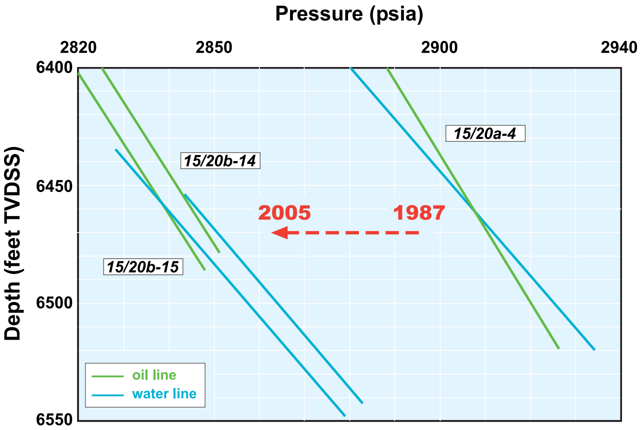

Fig. 16. Pressure plot showing depletion of Donan reservoir pre- and post-1992–1997 production.

Reservoir simulation of BP's five-year production history by Maersk demonstrated rapid local water coning at the two well locations. This left behind significant attic volumes which, at the time, were targeted by the 15/20b-12 wells. At the end of production, where field watercut was 70%, there were still significant reserves remaining. Simulation studies indicated that, in the 10 years of non-production, the water cones would have subsided somewhat (Fig. 17). Using BP's production as a constraint for history matching, further simulation was carried out to analyse the redevelopment potential. Simulation of new development wells indicated that water would rapidly encroach on horizontal producers with localized coning around the wellbore. Therefore, it was recognized that field development planning would have to optimize development well spacing to take this coning into account. With water cuts expected to be high, gas lift would be required to help lift the oil as water rates increased with production. A full suite of wellhead chokes, gauges and downhole gauges would allow the engineers to optimize gas lift distribution between the wells.

Field (re-)development plan

Reservoir modelling indicated that a phased development scheme would be optimal with five initial horizontal producers and one reinjection well for disposal of produced water (PWRI). Further phases of development drilling would depend on Phase I geological results and production performance. Data collected during development drilling would also address the remaining uncertainties of well performance (PI), the development of the water cones and the STOIIP. Given the number of development wells planned and detailed reviews of production facility options, it was decided that a stand-alone floating production storage and offloading (FPSO) facility would be used for the development. This would be owned jointly by Maersk Oil North Sea UK Limited (who had purchased Kerr–McGee's interests) and Noble Energy (Europe) Ltd. The Global Producer III (GPIII) FPSO was identified as a ready made candidate for Donan. At the time (2005) it was stationed at Maersk Oil's Leadon Field where production was close to the economic limit. The FPSO would provide processing systems for oil, gas, water production/treatment, water injection, oil and gas offload metering and have a storage capacity of 500 mbbl. Excess produced gas and condensate would be exported via pipeline. A project was initiated to carry out modifications on the FPSO's fluid handling capacities to suit the Donan fluids and handle the high volumes of produced water expected from the field.

The development wells themselves were designed to be drilled from a single drill centre cluster, batch set down to $12\frac{1}{4}$ inch hole before geosteering the horizontal sections and completing using a combination of excluder and equalizer screens.

Development drilling

Having completed the subsurface and facilities studies and with the FDP approved, detailed well planning commenced in the last quarter of 2005. This was carried out using the new 3D seismic dataset that was acquired by the partnership earlier in the year. Depth conversion was accomplished using a simple time–depth methodology utilizing the top reservoir time horizon mapped on seismic and well picks from wells in the area. The main cause of depth conversion uncertainty was interpretation uncertainty of the top reservoir horizon. This was due to changes in AVO character away from well control and at the flanks of the field where net pay thickness dropped below 25 ft. Overburden velocity anomalies created by Quaternary canyons and Eocene channels also proved problematic (Fig. 18).

The impact of overburden velocity anomalies on depth conversion has been examined by Armstrong *et al.* (2001). Their methodology of regional-residual separation was used on Donan to identify and correct time distortions of reflections at top reservoir level associated with shallow canyons and channels. This aided both well prognoses and the calculation of volumetrics in the areas where these distortions were greatest (Fig. 19). However, systematic errors in time interpretation created by picking on full-stack seismic data in the presence of AVO remained.

Development drilling commenced in January 2006 from the Noble Ton van Langeveld semisubmersible drilling rig. Each well was drilled down to $12\frac{1}{4}$ ft with the $9\frac{5}{8}$ ft casing set once reservoir sand was identified on landout by logging while drilling (LWD) gamma ray (GR), resistivity and neutron/density logs. Each $8\frac{1}{2}$ ft hole section was then drilled using an LWD logging suite of GR, resistivity and neutron/density logs as well as density and GR image logs, resistivity at bit and deep-reading azimuthal resistivity. These tools allowed the well to be geosteered as close to the roof as possible, maximizing standoff from the OWC at -6460 ft TVDss (Fig. 20). Wellsite biostratigraphy allowed both landouts and geosteered sections to be drilled within the pre-existing framework, ensuring that well positioning within the reservoir was understood. Following the drilling of each $8\frac{1}{2}$ ft section the well was completed, cleaned up and tested to the rig.

The drilling campaign lasted six months and successfully delivered five horizontal producers and one PWRI well (Fig. 21). Three sidetracks were required during drilling. Two of these sidetracks were geological, to locate/maximize reservoir, with one mechanical sidetrack required due to losses caused by drilling along a fault plane. The horizontal sections measured between 4000 and 6000 ft with pay lengths of 2000–3500 ft MD, giving an average net sand of around 65%. The wells achieved high productivities between 150 and 340 stb/d/psi.

Development drilling was followed by a further six months of subsea work and tie-in to the GPIII before production began in January of 2007.

Bringing Donan back: leveraging technology

The success of the Donan redevelopment (the Dumbarton Project) was influenced by a number of advances across the various technical disciplines:

- Rock physics modelling and seismic re-processing using pre-stack time migration allowed de-risking of wells and identification of significant upside that was previously unrecognized.

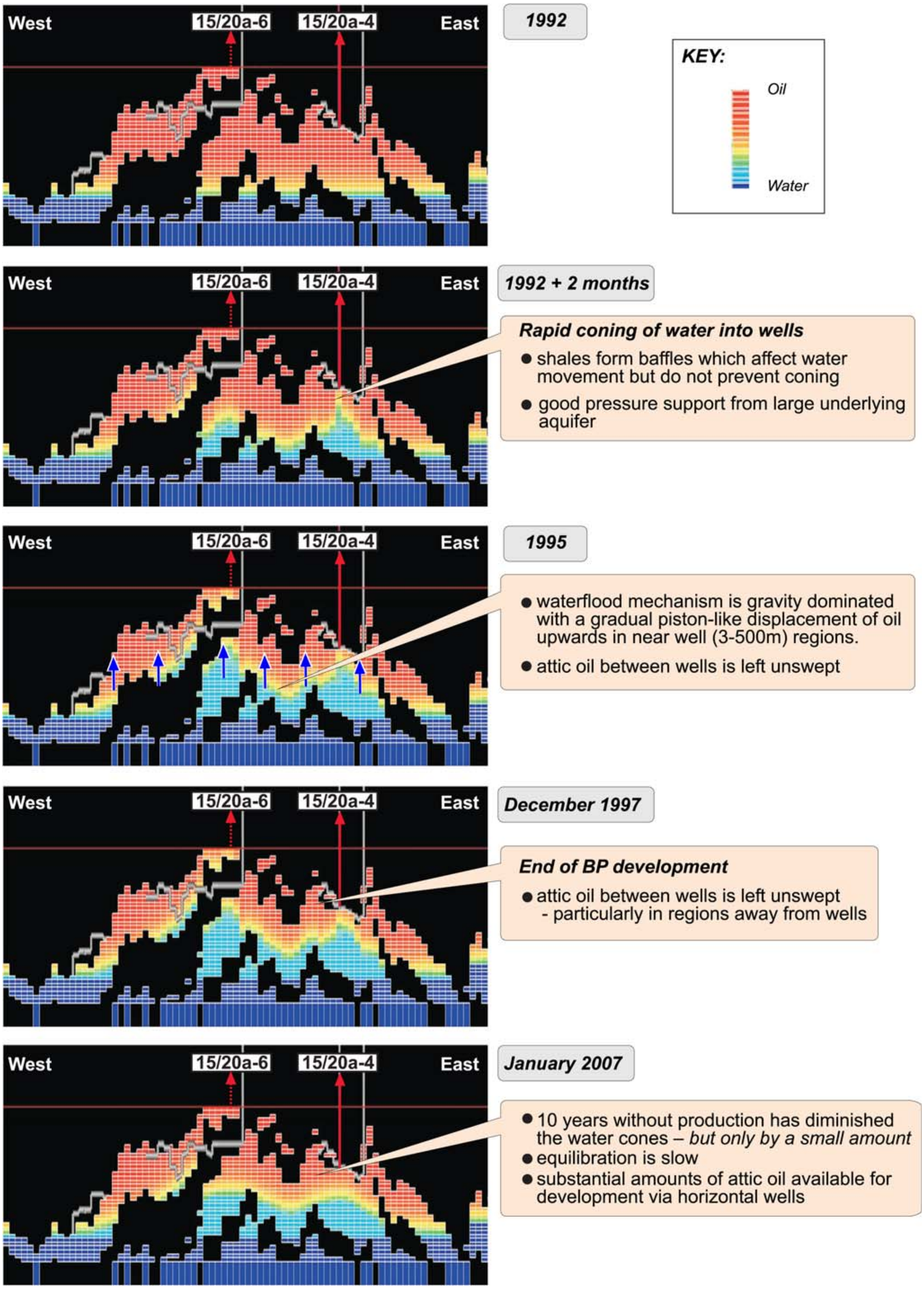

Fig. 17. Cross-sections through simulation model illustrating OWC behaviour during past production and the equilibration of cones since field abandonment.

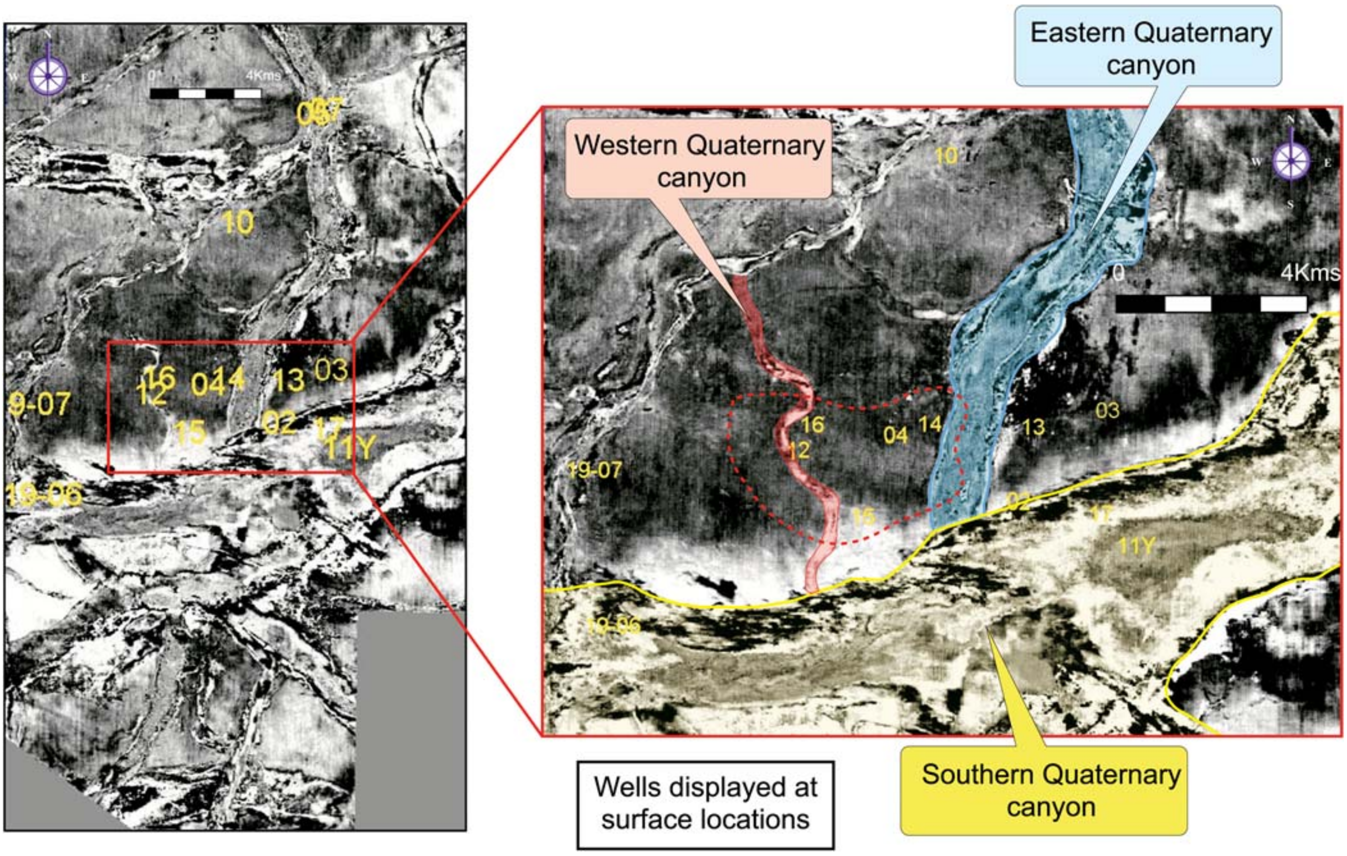

Fig. 18. Time slice showing overburden canyons that create depth uncertainties at Donan.

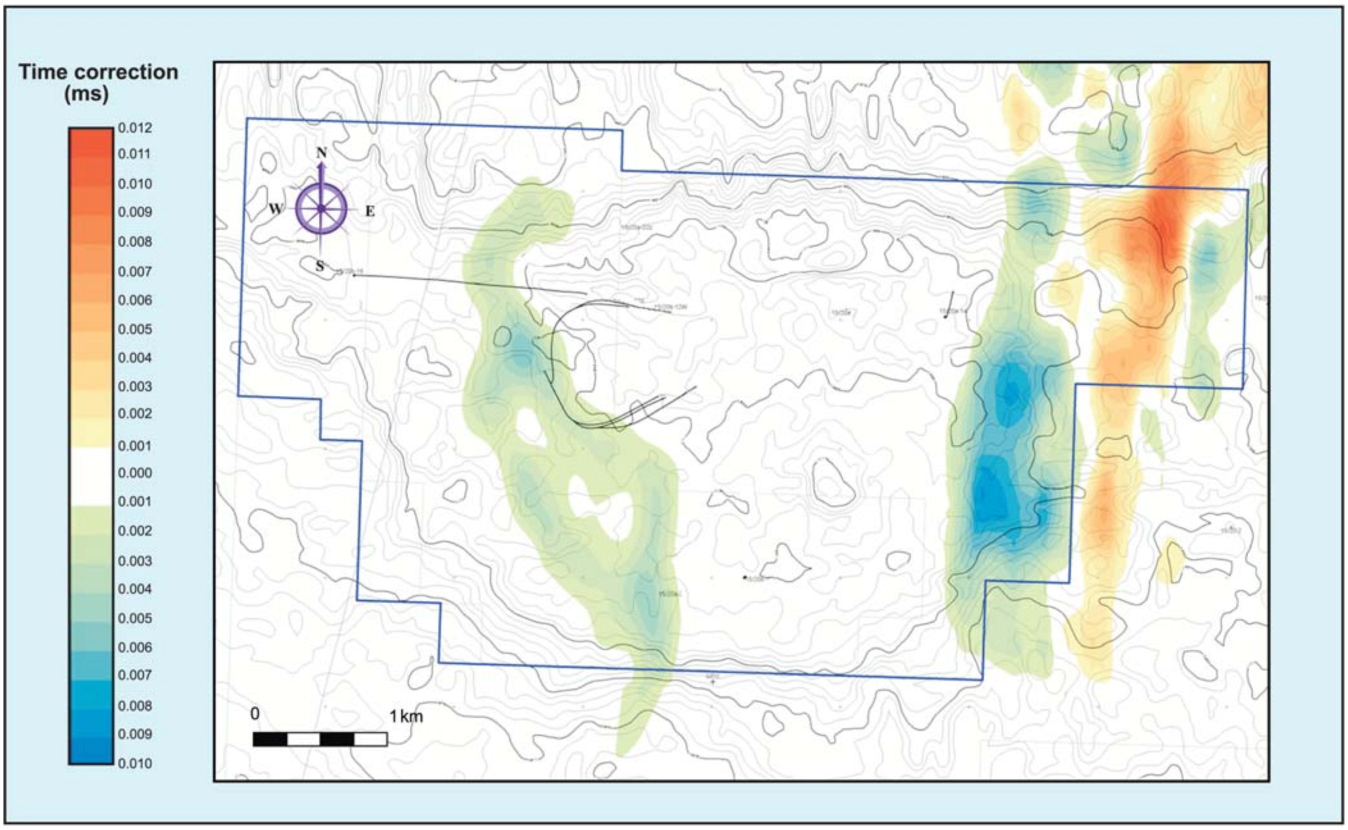

Fig. 19. Residuals map showing the time correction applied at top reservoir level to remove time distortion generated by overburden canyons.

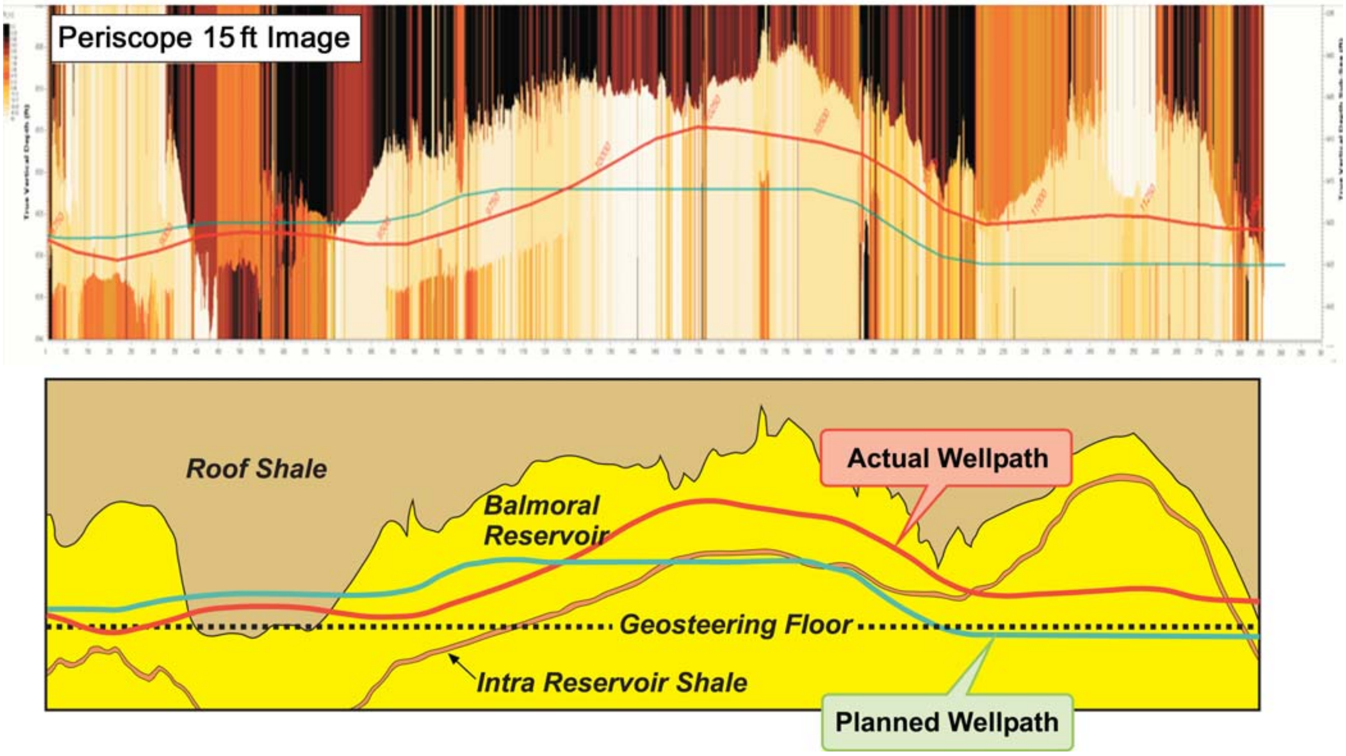

Fig. 20. Curtain plot from Periscope 15 (Schlumberger) showing planned v. actual geosteered wellpath.

- Advances in LWD technology, not least the advent of deep reading azimuthal resistivity tools, were crucial in ensuring accurate well placement and maximum standoff from the OWC. Well placement was also complemented by improvements in rotary steerable drilling assemblies with land-out accuracies significantly improved compared with what was achievable in the mid 1990s, with measurement while drilling (MWD) sensors located much closer to the drill-bit.
- The use of rotary steerable assemblies with improved hole cleaning made wellsite biostratigraphy more reliable than during the mid 1990s when inefficient hole cleaning by motor drilling meant that samples were commonly smeared. Detailed

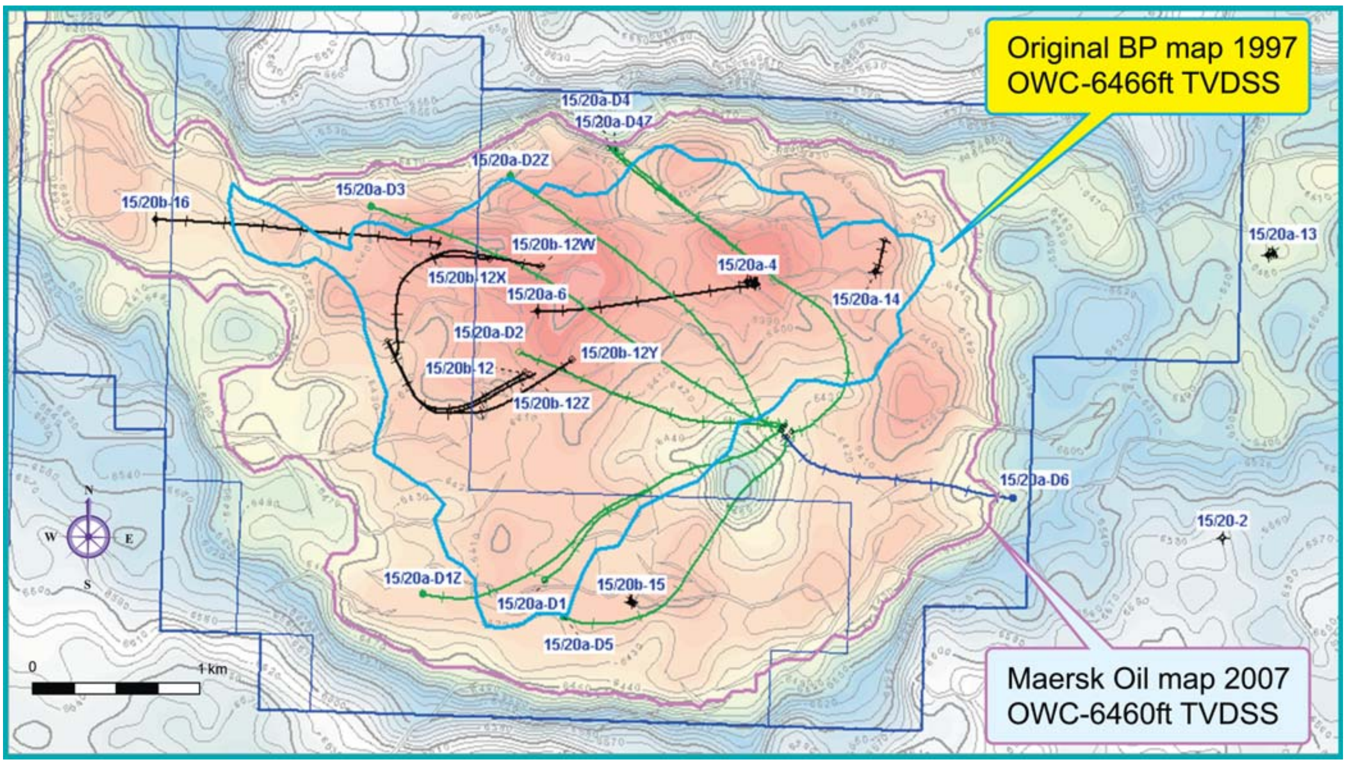

Fig. 21. Map showing development wells drilled as Phase I of the Dumbarton Project.

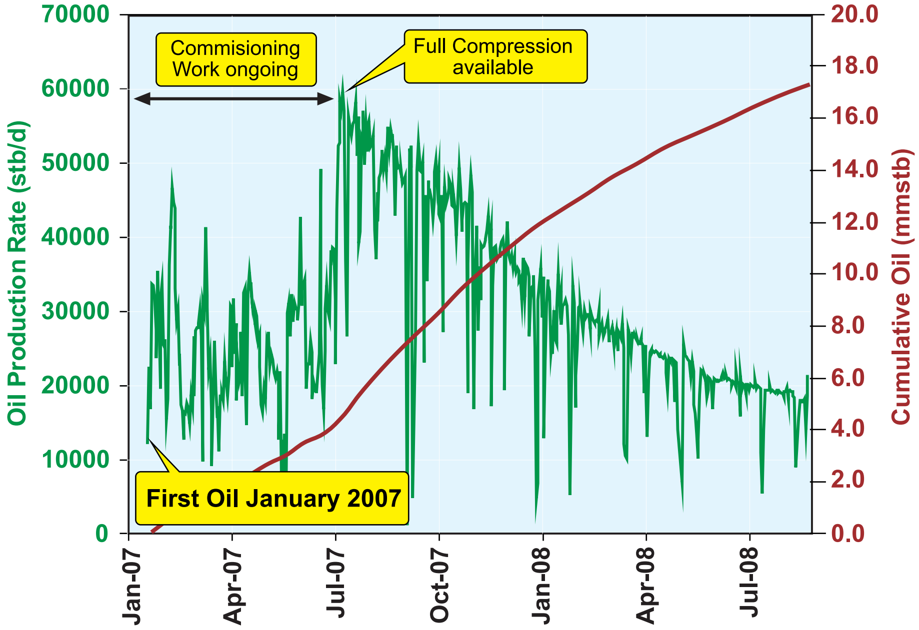

Fig. 22. Plot showing production performance from Phase I of the Dumbarton Project.

biostratigraphy and integration to a regional framework allowed correlation across the field and wells to be placed accurately.

- Improvements in wellbore stability management and drilling mud technology enabled the successful drilling of long horizontal sections.

Beyond 'second' oil: Donan 2007–?

Well performance

First oil from Phase 1 of the Dumbarton Project was produced on 19 January 2007. Early production was constrained due to commissioning activities (Fig. 22). However from mid July 2007, gross production rose and exceeded the expectation case as well rates increased to a range of 10–20 mstb/d/well. Well rates were, and are, ultimately constrained by a combination of facilities, ullage, flowline capacity and tubing performance. Water breakthrough occurred in well D2Z (Fig. 21) in April 2007 and in the other wells soon after. Gross rates fell through the latter half of 2007 as the watercut rose, and in November 2007 gas lift was employed to aid well performance. Since July 2007 excess gas has been injected back into the field using production well D2Z, due to the fact that gas export has not yet been fully commissioned. The watercut has risen in line with expectations.

The Dumbarton Project reached the milestone of 15.3×10^6 stb in May 2008, matching and then surpassing BP's five-year production total from Donan in a little over a year (Fig. 22).

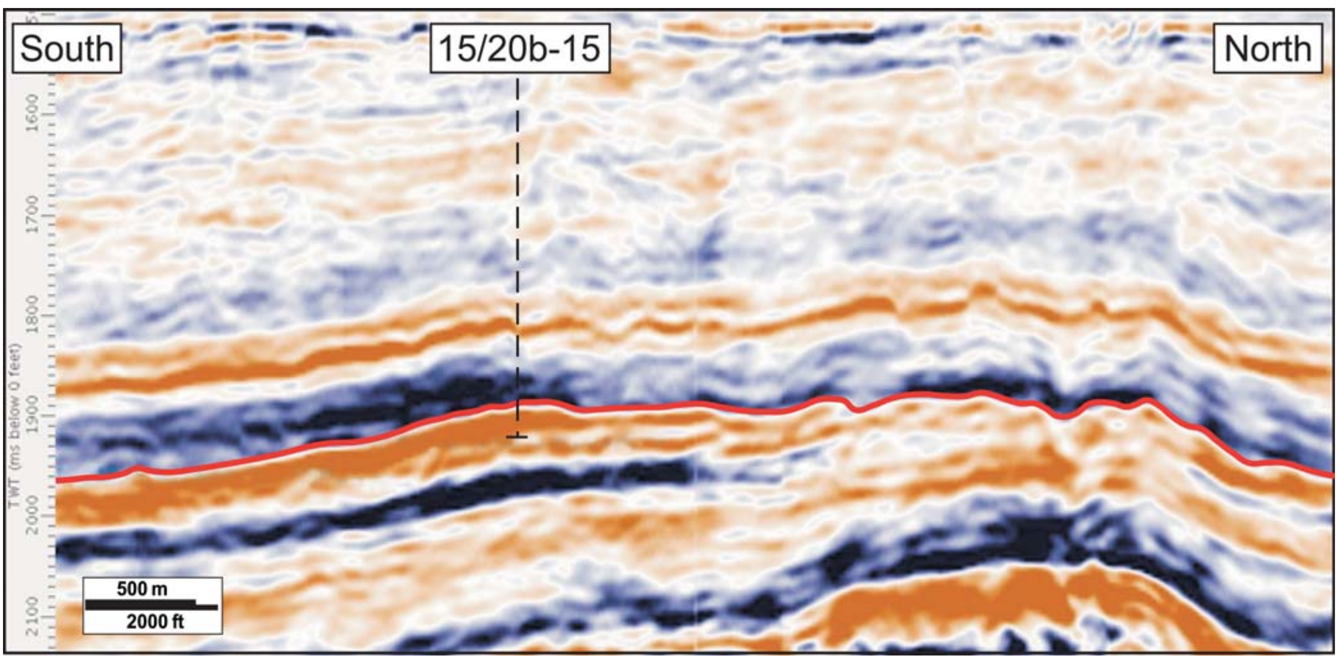

Fig. 23. Inline through lithology impedance volume showing more consistent pick on and off structure than previously achieved.

Preparing for infill drilling

In early 2008, well planning work commenced to place two additional horizontal producers and a further PWRI well on Donan. These new wells were covered by the original FDP and so became known as Phase Ib. A new top reservoir structure map was created using a reprocessed subset of the 2005 seismic data which had significantly improved signal-to-noise ratio. In order to make a consistent pick away from well control, the AI/GI cross-plot method (Whitcombe & Fletcher 2001) was used to create a lithology impedance volume. This separated the top Lower Balmoral unit from the overlying Lista roof shales and allowed a top reservoir pick to be made that was unaffected by fluid effects (Fig. 23). The geological model was then adjusted to honour this new depth structure map.

Re-mapping of the field showed a number of areas of structural relief with no associated AVO. As part of Phase Ib it was decided to test these areas for the presence of 'dim oil'. Given the success of AVO on Phase I, the D9 well was only given a 25% chance of success. Indeed, the new structure map placed top reservoir very close to the geosteering floor of −6430 ft TVDss, where 30 ft TVD was assessed to be the minimum acceptable standoff from the OWC. The well was designed such that if no reservoir was found at landout, the well would interrogate the structure before dropping inclination to find sand and log the OWC before sidetracking to a planned location that would intersect two AVO anomalies (Fig. 24). In order to further appraise the eastern side of the field, the PWRI (D8) well was designed to interrogate the highest structural point to the east of the field with no AVO to finally rule out the possibility of 'dim-oil'. The remaining infill development well in Phase Ib (D7) was planned to be the longest well to date on Donan, drilling on a north-westerly azimuth along a structural high marked by strong AVO (Fig. 24).

Since these would be the last wells covered by the original Donan FDP, an FDP addendum was submitted and approved that would allow a further phase of development to take place. Mapping had identified further potential targets that could be drilled as part of Phase II. These included a sidetrack of 15/20b-16 well to test a patchy AVO signature to the NW and apparently updip of the 15/20b-16 appraisal well and the 15/20a-D10 well which was planned to drill in a northwesterly azimuth very close to the 15/20b-12 well drilled by BP (Fig. 24).

2008 Drilling campaign

Infill drilling commenced in April 2008, once again from the Noble Ton van Langeveld drilling rig. The D7 well successfully found sand on prognosis. The D9 well, designed to appraise the area with no AVO to the SE of the field, found sand *c.* 5 ft deep to prognosis and below the geosteering floor. This confirmed the rock physics model that suggested that there was less than 25 ft net pay in this location. The well was then sidetracked to the D9Z location where it successfully entered top sand on prognosis corresponding to the observed AVO.

The D7 and D9Z (Fig. 24) wells had horizontal sections of 5899 and 1856 ft respectively and very high net to gross. Once again, the use of azimuthal resistivity and biostratigraphic control aided well

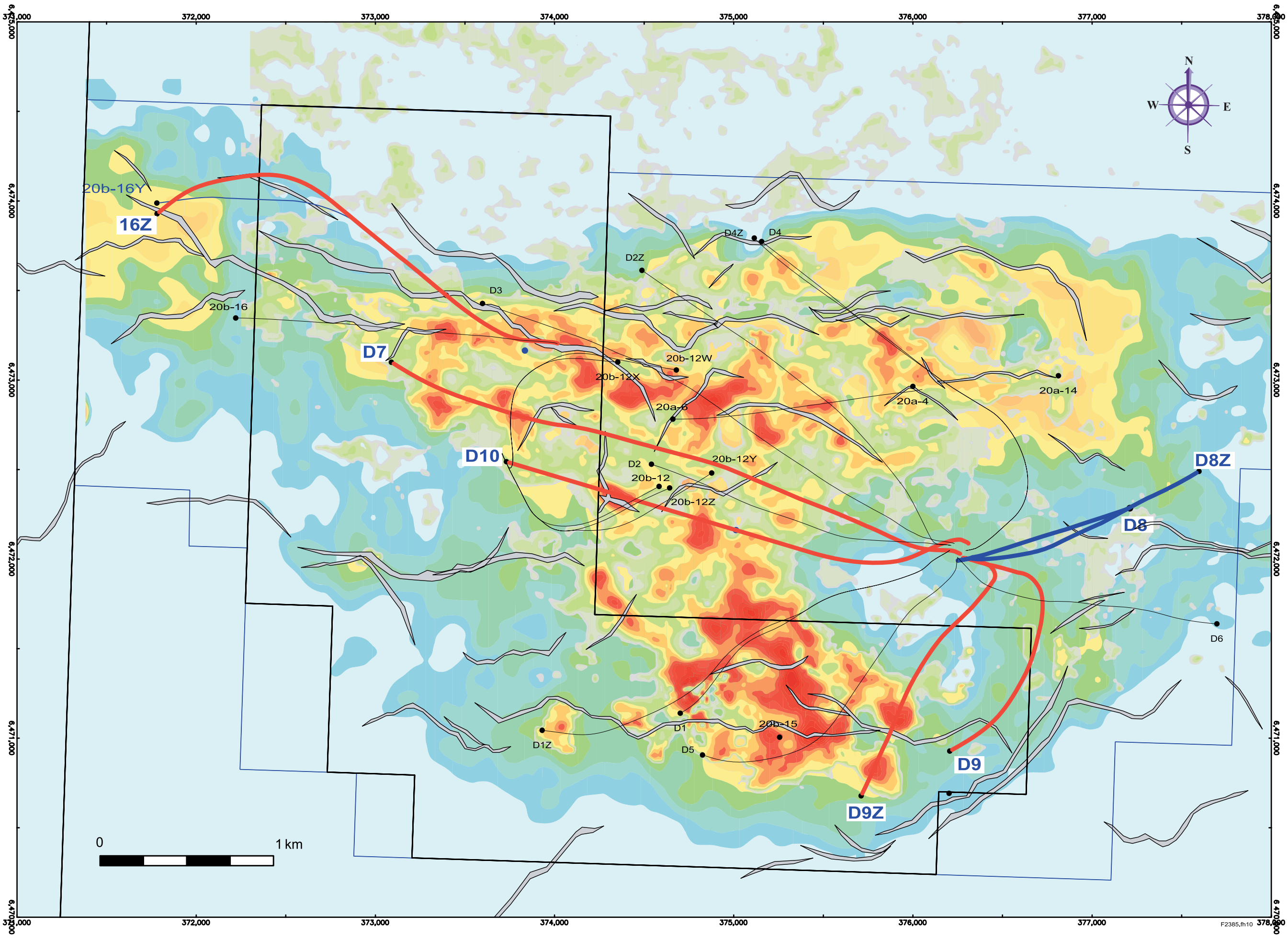

Fig. 24. Map showing Phase Ib, D7, D9 and D9Z infill well locations with AVO overlay and Phase II (D10 and 16Z) planned locations.

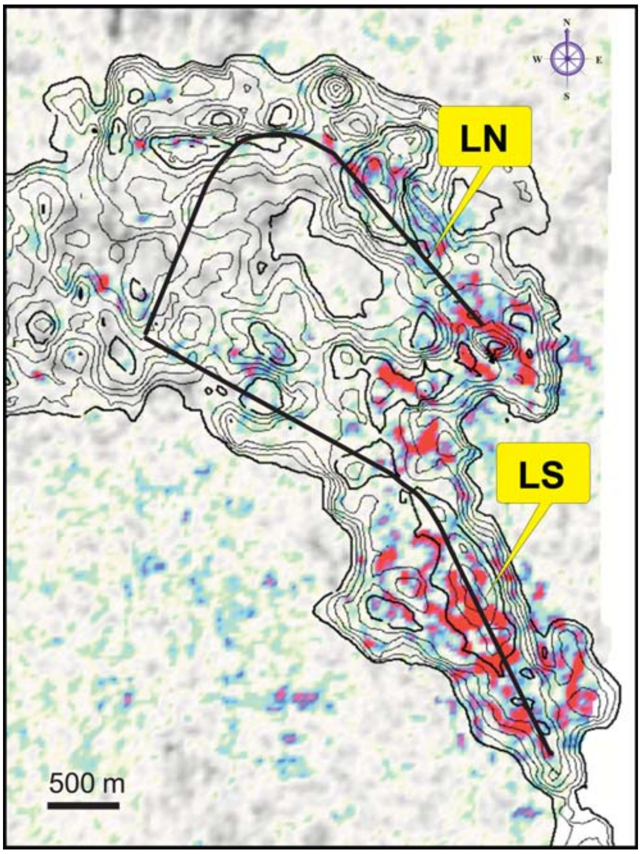

Fig. 25. Map showing AVO and structure along with planned development well locations for Lochranza field development.

placement. Both wells were completed using excluder screens and cleaned up to the rig, achieving very high productivities (PI) of 300–481 stb/d/psi. The D8 PWRI well drilled to test the structure to the east and encountered top Lower Balmoral on prognosis. However, the unit was shale prone with top sand being encountered at −6460 ft TVDss, below the OWC. This further confirmed the rock physics model and reliability of the AVO as a net pay indicator.

Exceptional drilling efficiencies meant that one of the Phase II wells could be accelerated. The suspended 15/20b-16 well was re-entered with a view to placing a development well in the AVO anomaly updip of the 18 ft oil column identified in the 15/20b-16 well. The 15/20b-16Z well encountered hydrocarbon-filled reservoir sand on prognosis. However, a WUT of −6415 ft TVDss was observed on logs, some 45 ft shallower than anticipated. The well was sidetracked and the 15/20b-16Y well was drilled to target the absolute crest of the local structure and confirmed the OWC at −6413 ft TVDss. This indicated that the Donan field must indeed close somewhere between 15/20b-16 and this location and that the original −6466 ft TVDss contact represents the structural spill to the NW. Whilst net pay thickness was sufficient to generate the AVO observed, the shallower contact and limited lateral extent of this local structure meant that the volumes were too small to be economic. The well was plugged and abandoned.

Infill well performance

In September 2008 the D7 and D9Z Phase Ib wells were brought on stream. These wells were given priority over the earlier wells for pipeline ullage, and high early gross production rates led to production being constrained by the surface equipment. These wells were brought back on stream after new subsea facilities were installed in October 2009 to accommodate further infill wells.

Future challenges

Next phase of development: the birth of Lochranza

At the time of writing, drilling of the remaining Phase II well on Donan is about to commence. This will place a further development well towards the west of the field, passing close to the 15/20b-12 well drilled by BP in 1995. Thereafter the drilling rig will move around 5 km east of Donan to commence development drilling on Lochranza, the renamed Pladda prospect.

Work to characterize Lochranza has continued in parallel to Donan development. Lochranza's small size would mean that, without the success of Donan and convenient subsea tieback, its reserves would never be realized economically. The development will comprise two horizontal producers that will be geosteered in the same manner as previous Donan wells (Fig. 25). It is expected that the field will be of lower net to gross than Donan with thinner sandstones providing a greater geosteering challenge than those drilled thus far.

Identifying remaining potential

As Donan matures, infill targets of sufficient size will become increasingly difficult to identify. The intensive well planning and operations of the last 2–3 years have limited the time available to carry out detailed subsurface studies to fully integrate the dynamic data with the reservoir model. At the end of the current drilling campaign, a full geological model re-build will take place to integrate new stratigraphic data with dynamic performance data. This study is expected to shed new light on the field, perhaps de-risking targets that currently seem marginal or identifying entirely new infill possibilities.

Conclusions

The Dumbarton Project has been a technical and commercial success for Maersk Oil North Sea Limited and partners Noble Energy (Europe) Limited. The renaissance of Donan has been achieved thanks to a number of technological advances since initial field abandonment in 1997. Advances in seismic technology and AVO processing have enabled the preservation of amplitudes in seismic data and the identification of the AVO expected from rock physics modelling. The development of more sophisticated drilling technology and LWD tools have allowed long, tortuous wellpaths to be drilled quickly and cheaply whilst optimizing well placement in the reservoir. These technological advances have been leveraged within an integrated and multidisciplinary framework by the many geoscientists and engineers who have worked on the project since its inception. Furthermore the realization at the corporate level that the abandoned Donan field represented a good opportunity worth pursuing illustrates the ambition of the partnership.

At a time when many are reflecting on the last four decades of exploration and production in the UKCS and assessing the current landscape, the renaissance of Donan and birth of Lochranza may represent the first of many opportunities to realize stranded value in this mature province.

The authors would like to thank the management of Maersk Oil North Sea UK Limited and Noble Energy (Europe) Ltd for permission to publish this paper. Thanks also to the reviewers of this paper for their constructive suggestions. Finally (and importantly) thanks are owed to all the geoscientists and engineers who have contributed to the Donan story over its 22-year history.

Appendix A: Donan Field data summary

Trap			
Type	Four-way dip closure – large basal aquifer	Gas–oil ratio (initial)	380 scf/stb
Depth to crest	−6340 ft tvss	Formation volume factor	1.21
Lowest closing contour	−6466 ft tvss	Bubble point (initial)	1408 psia
Oil–water contact	−6460 ft tvss	*Formation water*	
Oil column	Max 120 ft at crest	Salinity (average)	84550 mg l^{-1}
Pay zone			
Formation	Lower Balmoral Sandstone	Resistivity (average)	0.119 Ω m at 60 °F
Age	Thanetian (Late Paleocene)	*Reservoir conditions*	
Gross thickness	300 ft	Temperature	183°F
Lithology	Sandstone	Pressure (initial)	2830 psia (at −6460 ft TVDSS)
Porosity (average)	28%	*Production*	
Hydrocarbon saturation (average)	85%	Start-up	19 January 2007
Permeability	800 mD	Development	Five producers +1 PRWI, two infill wells drilled late 2008, one infill well drilled Q1 2009
Net to gross (average)	90%	Production rate	Gross rate 70 mbpd will increase to 150 mbpd
Hydrocarbons			
Density	38.7 API 0.83 g cm^3	Cumulative production	22 × 10^6 stb January 2007 to March 2009 plus 15.3 × 10^6 stb 1992–1997

References

Armstrong, T., McAteer, J. & Connolly, P. 2001. Removal of overburden velocity anomaly effects for depth conversion. *Geophysical Prospecting*, **49**, 79–99.

Deegan, C. E. & Scull, B. J. 1977. *A Proposed Standard Lithostratigraphic Nomenclature for the Central and Northern North Sea*. Report of the Institute of Geological Sciences, No. 77/25; Bulletin of the Norwegian Petroleum Directorate, **1**.

Knox, R. W. O'B. & Holloway, S. 1992. Paleogene of the Central and Northern North Sea. *In*: Knox, R. W. O'B. & Cordey, W. G. (eds) *Lithostratigraphic Nomenclature of the UK North Sea*, **1**. British Geological Survey, Nottingham.

Payne, S. N. J., Ewen, D. F. & Bowman, M. J. 1999. The role and value of 'high impact biostratigraphy' in reservoir appraisal and development. *In*: Jones, R. W. & Simmons, M. D. (eds) *Biostratigraphy in Production and Development Geology*. Geological Society, London, Special Publications, **152**, 5–22.

Rutherford, S. R. & Williams, R. H. 1989. Amplitude-v.-offset in gas sands. *Geophysics*, **54**, 680–688.

Whitcombe, D. N. & Fletcher, J. G. 2001. The AIGI cross plot as an aid to AVO analysis and calibration. *SEG International Exposition and Annual Meeting 2001*.

Session: Europe

Techniques in Exploration and Exploitation

A road map for the identification and recovery of by-passed pay

P. F. WORTHINGTON

Gaffney, Cline & Associates (Consultants) Pte Ltd, 80 Anson Road #31-01C, Fuji Xerox Towers, Singapore 079907 (e-mail: pworthington@gaffney-cline.com)

Abstract: By-passed pay can occur at or between wells. Either way, it constitutes a lower risk prospect than hydrocarbon accumulations in unappraised areas. Beyond this, there are three contemporary drivers for its exploitation. First, new technology in the form of sharper reservoir imaging allows insights that were not achievable previously. Second, an evolving understanding of how reservoirs work has led to improved procedures for maximizing the exploitation of even the most problematic accumulations. Third, market forces amid global post-peak production fears are giving the incremental development of by-passed pay an even greater commercial impetus today. An examination of case histories that illustrate the role of these drivers has led to a six-fold type classification of by-passed pay. Type 1 can be produced using an existing identified well. Type 2 requires a side track or a new well in order to capture the reserves. Each type is further subdivided into three classes. The classification scheme has provided the context for an emerging *modus operandi* to maximize commercially recoverable hydrocarbons in developed assets. Thus, the approach takes the form of a road map for practical application. By corollary, the type classification demonstrably accommodates a wide range of reported exploitations of by-passed pay from diverse reservoirs. Therefore, this classification constitutes a potential foundation for further systemic refinements to the identification and recovery of by-passed pay.

Keywords: net pay, by-passed pay, reserves, resources

Pay

Changing market conditions are encouraging operators to search out untapped hydrocarbon volumes within mature fields. The production of these volumes requires that they be incrementally economic. In conventional oil field parlance, this requirement becomes one of sufficient net hydrocarbon volumes to justify further development in terms of return on investment. This justification is partly based on an analysis of net pay as an input to the estimation of petroleum resources. In the following discussion, the use of terms such as 'Resources' and 'Reserves' tracks the Petroleum Resources Management System (PRMS) published by the Society of Petroleum Engineers *et al.* (2007).

Net pay

The literature contains various definitions of net pay as well as several different protocols for distinguishing net-pay from non-pay intervals. This paper adopts the scheme of Worthington & Cosentino (2005). Following this scheme, for a vertical well net pay is defined as the thickness of a reservoir or reservoir zone that contains significant quantities of movable hydrocarbons: in many cases it is the aggregated thickness of two or more subintervals. The product of reservoir area and net pay is the subsurface volume that expresses itself at a wellbore in terms of significant hydrocarbon production. This expression takes place through supracritical levels of porosity, permeability and hydrocarbon saturation, that is, those values that satisfy net-pay criteria, and how these properties vary over the net-pay interval(s).

Net pay can only be measured at a wellbore: elsewhere, it has to be interpolated or estimated. It is quantified from downhole logs using one or more petrophysical cut-offs and then propagated through a 3D reservoir model. There is no industry standard method for doing this, but one of the more common approaches is the conjunctive application of cut-offs for shale volume fraction, porosity, and water or hydrocarbon saturation (Worthington & Cosentino 2005). It is important that these cut-offs are dynamically conditioned, so that they take account of the requirement that net pay contains movable hydrocarbons (Worthington 2008).

By-passed pay

By-passed pay relates to significant movable hydrocarbons that cannot be drained by any existing well and will be left behind in the subsurface if nothing is done. In other words, by-passed pay satisfies the technical requirements for being classified as net pay but it has not been developed and might not even have been seen. This definition is set within the context of conventional reservoirs. It excludes residual hydrocarbons, which are immobile and therefore will stay in the reservoir. By-passed pay can occur at or between wells.

By-passed pay may or may not be a subset of the initial net pay. It depends on why the pay has been by-passed. There are four principal reasons.

- The accumulation was identified but was originally considered to be uneconomic.
- The pay was not seen either because downhole measurements did not identify it or because of inadequate perceptions on the part of the analyst.
- The degree of reservoir complexity was not fully evident at the time of formulating a field development plan. In other words, the field database and its interpretation were not adequate for a sufficiently detailed reservoir description, so that there was an oversimplified geoscience model at production start-up. This explanation has a widespread validity, because reservoir models tend to become more complex as more data are acquired.
- The recovery mechanism has been less efficient and effective than initial projections indicated, perhaps because of a preferential watering out or simply because discrete sand bodies were not intersected by a wellbore.

These are all common occurrences and therefore it follows that by-passed pay is potentially a common occurrence too. This is an

VINING, B. A. & PICKERING, S. C. (eds) *Petroleum Geology: From Mature Basins to New Frontiers – Proceedings of the 7th Petroleum Geology Conference*, 453–462. DOI: 10.1144/0070453

important contention because the exploitation of by-passed pay carries a lower risk and can be more cost effective than standard field operations. This paper considers different kinds of by-passed pay and identifies approaches for capturing them.

Types of by-passed pay

There are two types of by-passed pay. Type 1 is that which could be produced using an existing identified well, for example, where a hydrocarbon-bearing interval has never been perforated. Type 2 is that which requires a sidetrack or a new well in order to capture the reserves, for example, unswept hydrocarbon volumes in an inter-well region. On this basis alone, the term 'by-passed pay' is inappropriate, because pay is a thickness that can only be measured at a wellbore. The phrase 'by-passed hydrocarbons' would be more generally applicable. Types 1 and 2 can each be further subdivided in terms of three scenarios (Table 1).

Type 1: Scenario A

Hydrocarbons were seen but not developed at the time of well completion, for example, because there was no (gas) market at the time, the accumulation was not economically recoverable with the technology of the day (e.g. stimulation practices), there were safety concerns, or the recoverable volume was considered too small to be economically attractive (in terms of commodity prices, lifting costs and/or production sharing contractual terms). Once identified, the recoverable volumes should be classified as Contingent Resources until there is a plan to develop them. Another explanation is that the original net-pay cut-offs were too severe, so that the in-place volumes were considered to be unrecoverable and therefore could not be classified as Contingent Resources at the time. The ongoing requirement is to monitor continuously commodity prices vis-à-vis evolving technology, field/regional infrastructure and net storage/flow criteria, so that (incrementally economic) workover opportunities can be generated.

Type 1: Scenario B

Hydrocarbons were present but not seen at the time of well completion. At the most basic level, the hydrocarbons might simply have been outside the originally perceived evaluation interval, for example, shallow gas sands. The local perceptions of net pay might have been flawed, or the pay interval might literally have been overlooked. More profoundly, these Scenario B situations can arise because of deep invasion by drilling mud filtrate, laminated sedimentary sequences, fresh formation water or high capillarity of the reservoir rock caused by siltiness or microporosity. It is important to gather sufficient data so that departures from classical reservoir character can be identified. Fortunately, there are downhole technologies available to help deal with these situations. They include (through-casing) deep-sensing resistivity logs that see beyond the invaded zone, microresistivity imaging tools for identifying and demarcating thin beds, high-resolution multifrequency dielectric measurements to distinguish fresh water from oil, and magnetic resonance logs for identifying capillary-bound water. The deployment of these tools should be guided by special core analysis from a representative appraisal well. Such data have a potentially high value because, without them, hidden hydrocarbons can be lost forever.

A Scenario B situation might also arise because the concept of net pay evolves during the life of a field. For example, net pay is conditioned by the recovery mechanism, and that can change during field life (George & Stiles 1978). Another situation is that of late-onset gas production. This is most commonly found in an alternating sequence of tight and permeable gas-bearing sands. The permeable sands are identified as net pay: the tight sands are rightly excluded from net pay because they do not satisfy the cut-off criteria for flow. However, as pressure declines with depletion of the permeable sands, the induced pressure difference between the tight and permeable layers allows gas to flow into the permeable sands and thence be produced at the wellbore. The tight sands remain non-pay but the permeable sands can be assigned a recovery factor that is greater than 100%.

Table 1. Type classification of by-passed pay

Scenario	Description	Type 1: At wellbore	Type 2: Inter-well region
A	Recognizable at outset but not developed	1A	2A
B	Not recognized at outset but identified now	1B	2B
C	Developed at outset but unswept volumes evident	1C	2C

Type 1: Scenario C

Hydrocarbon intervals were seen and perforated at the time of well completion but post-production they have been identified as containing unswept volumes, for example, through formation damage, reservoir heterogeneity, premature well decline or early breakthrough of water fronts (either aquifer-sourced or injected). In other words, the in-place volumes might have been estimated meaningfully but there is no significant recovery along sections of the pay interval. Unswept volumes can be identified using through-casing resistivity logs, carbon–oxygen logs and/or pulsed neutron tools in time-lapse mode. Some of these situations might be obviated by utilizing more realistic models for predicting well performance. These models should be updated in response to evolving concepts of reservoir connectivity during production.

Type 2: Scenario A

Hydrocarbon occurrences were theoretically detectable through geoscience but either they were recognized but not drilled or they were recognized insufficiently. The former case might have arisen because of economic perceptions and/or drilling limitations. The latter case might be due to geoscience misinterpretation (especially in the presence of faulting), erroneous depth conversion placing the structure too low, or perhaps an uncalibrated attribute analysis. In many situations, this occurrence of by-passed pay is due to reservoir complexity or, more specifically, to the adoption of a field database that does not capture the geoscience complexity of the field. To some extent, this situation can be obviated by carrying out a commensurate reservoir appraisal, noting that a knowledge of hydrocarbon volumes on the flanks of the field does contribute to this process. There has been a tendency to short-cut appraisal by drilling only crestal or subcrestal wells: this strategy may appear financially beneficial in the short term, but over the life of a field it will almost certainly detract from the booking of Proved Reserves and in this regard alone it constitutes negligence. Further remedial action would be to integrate more effectively the benefits of enhanced workstation technology, better seismic-to-well ties, and advancing reservoir characterization concepts. In connection with this last point, note that stochastic methods of populating geoscience models may be limited in their added value. These methods generate realizations, which are intended to be analysed statistically. A realization does not constitute reality, because it is a member of a population that should be treated as a whole.

Type 2: Scenario B

Some inter-well hydrocarbon volumes were not indicated geologically or geophysically at the outset, for example, because of reservoir complexity, weak seismic imaging or inadequate (vertical) spatial resolution. Where the size of the field justifies it, the acquisition of sharper-imaging seismic data before the field has reached its mid-life stage, in conjunction with refined reservoir characterization, can help to extend plateau production considerably. The structural model and the encompassed geological architecture should be refined as more data become available. In this respect, contiguous field extensions that are identified in mid-life might also be regarded as by-passed pay. All things being equal, the potential upside associated with by-passed pay is likely to be greater for larger fields. At the same time, consider the conjunctive use of geophysical deliverables such as seismic attributes and inter-well products such as electromagnetic tomography, especially in complex reservoirs. Calibrated seismic attributes have a potential semiquantitative application to net reservoir and/or net pay mapping. Subject to the principles of geophysical equivalence and suppression, electromagnetic tomography can distinguish net pay from net reservoir.

Type 2: Scenario C

Untapped hydrocarbon accumulations are indicated during development, for example, through seismic time-lapse monitoring, early water production or exposed shortcomings in the geoscience model. The most important response is to revise one's geological concepts to conform to the realities of production data. This should lead to a refined geological architecture and most probably a more complex one, given that reservoirs become more complex as more data are acquired. It will also lead to a refined initialization of a reservoir simulator. In the light of this refined model, flood front(s) should be monitored with the object of ascertaining their effectiveness.

Application

The above classification scheme is illustrated through its application to some reported case histories from the past 15 years (Table 2).

Exploitation of by-passed pay

There are three overprints, two technical and one commercial. First, new technology in the form of sharper reservoir imaging, both downhole and in the inter-well region, allows insights that were not achievable previously. New production technologies lead to improved wellbore efficiencies. Today, the main technology drivers are the service companies, in contrast to 25 years ago when they were the (now diluted or sometimes even defunct) shared resource teams of the operators. Second, an evolving understanding of how reservoirs work has led to enhanced procedures for maximizing the exploitation of even the most problematic accumulations. These advances include better perceptions of reservoir connectivity and flow units as well as improved insights into how *in-situ* hydrocarbon volumes express themselves at the wellbore. Third, market forces amid global post-peak-production fears are imparting an even greater commercial impetus to the exploitation of by-passed pay. When commodity prices are high, the prize is greater. However, even in an economic downturn, there are opportunities in the form of acquisition targets (Sneider & Sneider 2001).

Identification

The first step is the recognition of by-passed pay. As implied above, this brings together input from sister disciplines that should be viewed conjunctively. The principal thrusts are itemized below:

- reservoir performance vis-à-vis a history-matched simulator;
- material balance studies in the light of estimated ultimate recovery;

Table 2. Type classification of some reported examples of by-passed pay

Investigator(s)	Formation/Field/Province	Type
Sibley & Mastoris (1994)	Eugene Island Block 338 Field, offshore Louisiana, USA	2C
Palar *et al.* (1999)	Sepinggan Field, East Kalimantan, Indonesia	2C
Pauzi *et al.* (1999)	West Lutong Field, Sarawak, Malaysia	2B
McConkey & Stromquist (2000)	Medicine Hat Sandstone, Alberta/Saskatchewan, Canada	1A
Bartenhagen *et al.* (2001)	Permian Basin, New Mexico/Texas, USA	1B
Gómez *et al.* (2001)	Vernet Field, Macuspana Basin, Mexico	1B
Mendoza & Duran (2002)	Tía Juana Field, Lake Maracaibo, Venezuela	1C
Thatcher *et al.* (2003)	Bowdoin Field, north-central Montana, USA	1A
Pranter *et al.* (2004)	Vacuum Field, Permian Basin, New Mexico, USA	2B
Conner & Blesener (2005)	Sante Fe Springs Field, California, USA	1C
Nikijuluw *et al.* (2005)	Semberah Field, East Kalimantan, Indonesia	2A
Xiaoguang *et al.* (2005)	Makmur Field, south Sumatra, Indonesia	2A
Youssef (2006)	Badr-1 Field, Western Desert, Egypt	2C
Fairhurst *et al.* (2007)	Olmos/Escondido Sands, LaSalle County, south Texas, USA	1B
Chu & Welch (2008)	Acacus Formation, Ghdames Basin, southern Tunisia	1B
Energy Partners Ltd (2008)	East Bay Field, Gulf of Mexico, USA	2B
Grant *et al.* (2008)	Offshore Louisiana, USA	1C
Nishikiori *et al.* (2008)	Gyda Field, southern North Sea	2C

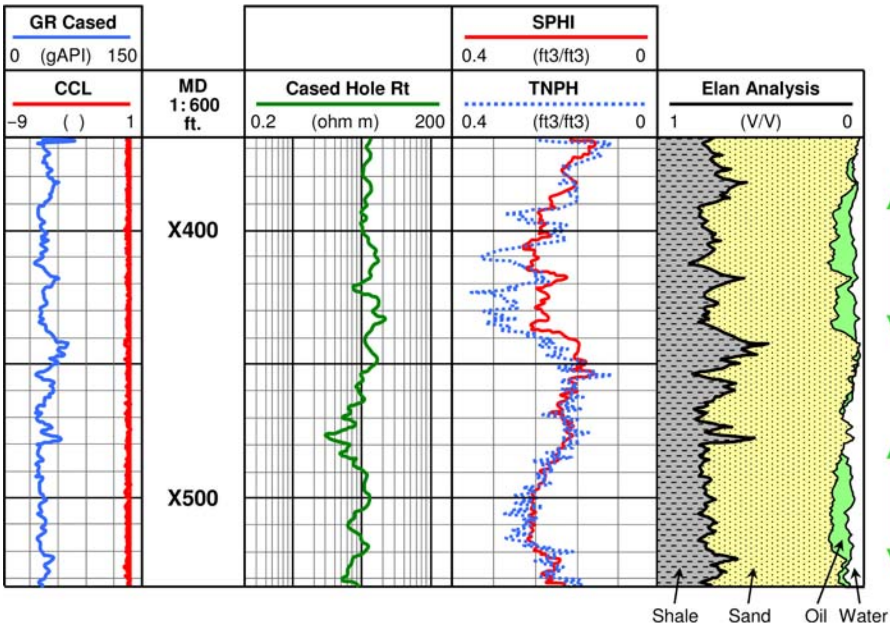

Fig. 1. Delaware Formation, west Permian Basin, USA: intervals previously missed because of large-scale invasion effects on the open-hole resistivity log now appear as by-passed pay when analysed using the deep-sensing cased-hole resistivity log. ELAN, elemental analysis (Schlumberger); GR, gamma ray log; MD, measured depth; Rt, true formation resistivity; SPHI, porosity from sonic log; TNPH, neutron porosity log response (Schlumberger); gAPI, gamma ray units as per American Petroleum Institute standard. (Redrawn from Bartenhagen *et al.* 2001.)

- (interwell) geophysics, principally 3D/4D seismic and electromagnetic imaging;
- improved structural modelling, especially faults and their transmissibilities;
- advanced reservoir characterization techniques, for example, high-resolution geological models, fracture modelling, analysis of reservoir connectivity, flow-unit identification;
- well performance relative to a 3D geoscience model;
- movement of fluid contacts – observed v. predicted;
- time-lapse well logging to expose undepleted intervals;
- re-evaluation of older wells in the light of new understanding to discover previously ‘hidden’ pay;
- retrospective identification of formation damage.

In pulling these matters together, reservoir analogues have an important reference role. Elements of the above have been used by many investigators (e.g. Montgomery 1998; Choon 2007; Von Pattay *et al.* 2007; Hustedt & Snippe 2008; Nishikiori 2008; Tioe *et al.* 2008).

Estimation of Resources

The second step is to estimate the additional Resources through the technical approaches listed above. By-passed pay will initially fall into the class of Contingent Resources (Society of Petroleum Engineers *et al.* 2007). This class refers to remaining hydrocarbon volumes that have been discovered, either directly at a wellbore or by interpolation of producing zones, so that the volumes are known to be present in significant quantities. The admitted volumes must also be recoverable in that the hydrocarbons will flow into a wellbore.

Commerciality

The third step encompasses an economic evaluation. This exercise benefits from the incremental nature of the hydrocarbon accumulations, which allows the evaluation to be more definitive. In general, larger by-passed volumes occur in larger fields: disappointments have usually related to smaller accumulations (e.g. Conner & Blesener 2005). To be classified as Reserves, the recovery must satisfy all the criteria for being classified as Contingent Resources and it must also be commercial, that is, it is not just economic, but there is also a commitment to develop the volumes and there is a plan to do so, for example, through recompletions or sidetrack drilling. Risk and uncertainty are lower, because the project is already advanced and knowledge of the reservoir is more detailed than it was at the time of production start-up.

Case histories

The above principles underpin the following case histories, which have been selected from Table 2.

Type 1: Scenario A

There are numerous cases of Type 1A by-passed pay. One example is the multilayer shallow gas sands of Western Canada, specifically the Medicine Hat Sandstone within southeast Alberta and southwest Saskatchewan, Canada (McConkey & Stromquist 2000).

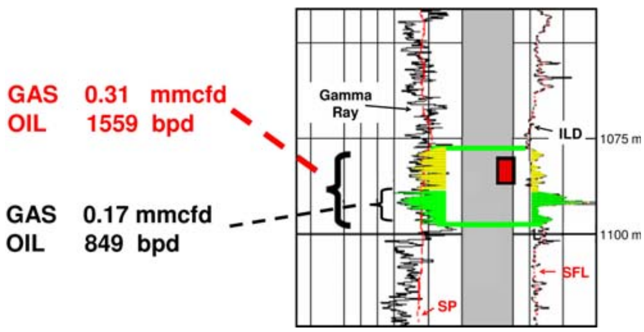

Fig. 2. Macuspana Basin, Gulf of Mexico: exploitation of by-passed hydrocarbons in a (yellow) layered sand/shale sequence leads to a doubling of production from the target zone. SP, self potential log; ILD, deep induction log; SFL, spherically focused log. (Adapted from Gómez *et al.* 2001.)

Of the 21 000 shallow gas wells that have been drilled in this region, many contain gas-bearing intervals that were never completed. The reasons lay in the earlier perceptions of uneconomic gas volumes within zones that were too thin to be completed with conventional limited-entry fracturing technology. As gas prices increased and conventional fracturing could be integrated with coiled tubing and retrievable downhole tool technology, these by-passed gas zones could be accessed economically. A similar situation has been reported in the Bowdoin Field in north-central Montana, USA (Thatcher *et al.* 2003).

Type 1: Scenario B

A Type 1B example of by-passed pay owing to deep invasion comes from the complex Delaware Formation in the western Permian Basin of Texas and New Mexico (Bartenhagen *et al.* 2001). A well drilled with a light water-base mud was completed around 1980. Resistivity logs saw aqueous filtrate and the recorded resistivity was therefore suppressed, so that the interpreted water saturations were excessively high. The original well completion was based on mud log shows and the neutron log together with resistivity logs in an offset well. The well was earmarked for abandonment in 2000. It was re-logged with cased-hole gamma ray (GR), neutron, sonic and resistivity logs. The cased-hole resistivity log is a deep-sensing measurement that sees beyond any remaining invasion: in contrast, the more traditional pulsed-neutron and carbon–oxygen tools have a shallow depth of investigation. The evaluation indicated several oil-bearing zones above the producing interval. Two of these are shown in Figure 1. Preliminary tests indicated that these additional zones would breathe new life into the well. Thus, the cased-hole survey found pay that previously had been hidden by drilling-induced formation damage.

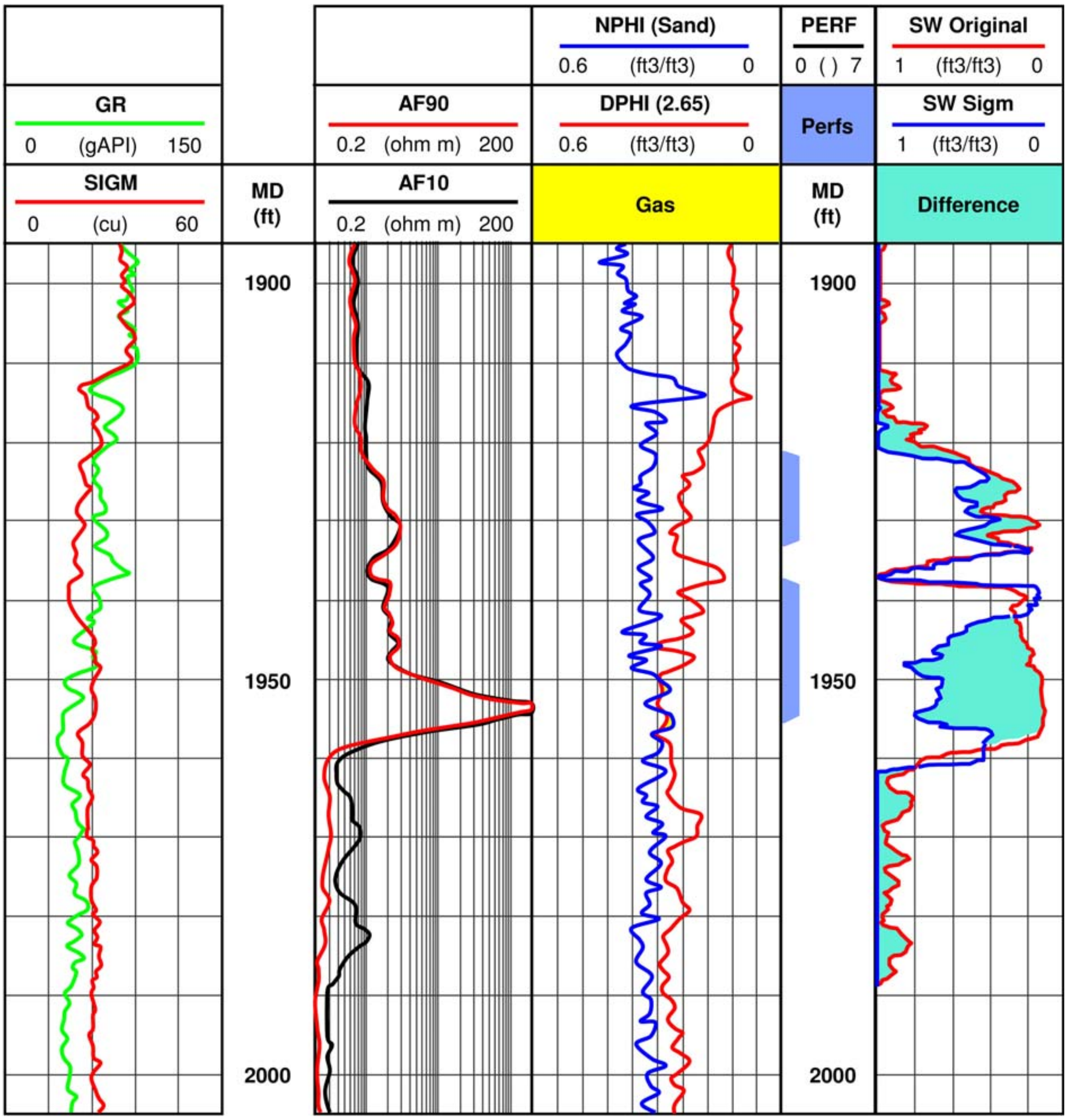

Fig. 3. Offshore Louisiana, USA: water saturation data derived from a (cased-hole) pulsed neutron log and compared with initial data (from open-hole logs) have exposed an unswept interval (around 1930 ft MD) above a swept zone. GR, gamma ray log; gAPI, gamma ray units as per American Petroleum Institute standard; SIGM, neutron capture cross-section; CU, capture units; AF90, array induction (deep) resistivity log (Schlumberger); AF10, array induction (shallow) resistivity log (Schlumberger); NPHI, porosity from neutron log; DPHI, porosity from density log; MD, measured depth; SW, water saturation. (Redrawn from Grant *et al.* 2008.)

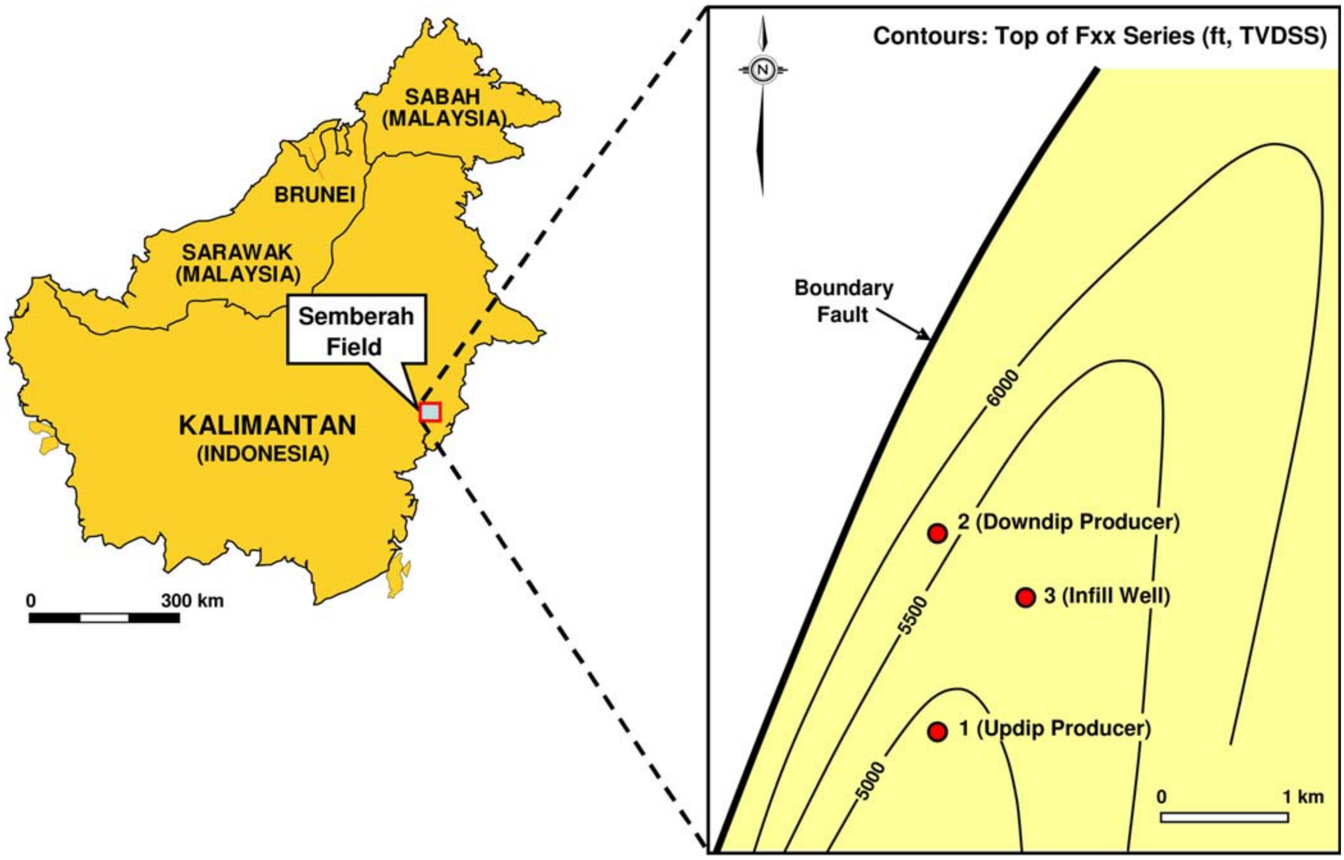

Fig. 4. Semberah Field, East Kalimantan, Indonesia: locations of updip producing Well 1, downdip producing Well 2, and infill Well 3. TVDSS, true vertical depth subsea. (Redrawn from Nikijuluw *et al.* 2005.)

A second example of hidden pay, this time owing to the nature of the rock itself, comes from the Vernet Field, Macuspana Basin, Gulf of Mexico (Gómez *et al.* 2001). The basin has been exploited since the early 1900s. The original interpretations of net pay are being re-visited in the light of contemporary understanding. The laminated sand-shale sequences (yellow in Fig. 2) were previously dismissed as water zones on the basis of a formation resistivity less than 2 Ω m. Yet, when perforated, they contributed to a doubling of production from the target interval.

Suppressed resistivity owing to laminated sand-shale sequences is the biggest cause of missed pay around the wellbore (Worthington 2000). It is a component of the low-resistivity (contrast) pay problem. It is encountered where the thicknesses of the laminations are below the spatial resolutions of conventional logging tools. The laminations act as resistors in parallel so that the average resistivity of the hydrocarbon-bearing sand (high resistivity) and the intraformational shale (low resistivity) is weighted towards the lower value. The best approach is to use key wells from the same geological province to set up an alert flag for the occurrence of laminated reservoirs. The approach draws upon core data and resistivity micro-imaging logs. Once the flag has been activated, well-log analysis should be customized.

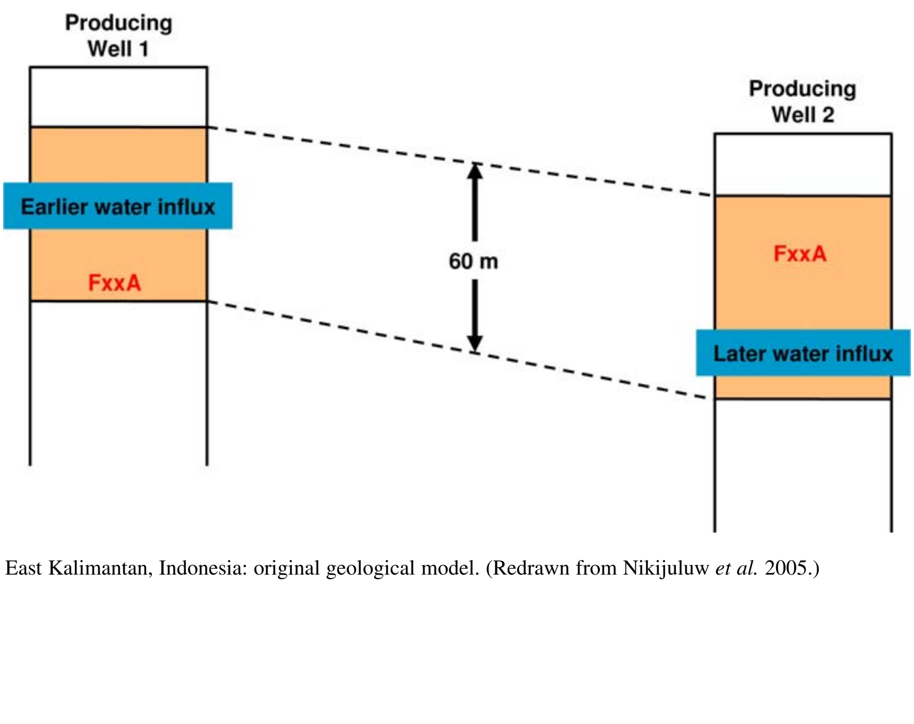

Fig. 5. Semberah Field, East Kalimantan, Indonesia: original geological model. (Redrawn from Nikijuluw *et al.* 2005.)

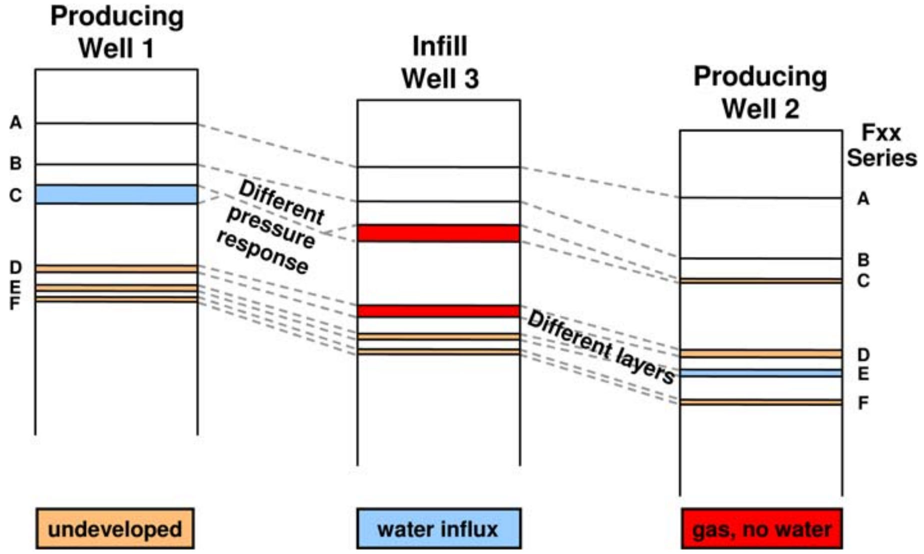

Fig. 6. Semberah Field, East Kalimantan, Indonesia: refined geological model. (Redrawn from Nikijuluw *et al.* 2005.)

These are important messages because the current drive to explore deep-water prospects on passive margins is impacted by the proliferation of turbidites, which invariably present a laminated-sand problem.

Type 1: Scenario C

Figure 3 shows a Type 1C example from an oil and gas field, offshore Louisiana (Grant *et al.* 2008). Pulsed neutron measurements were run through casing so that the neutron capture cross-section (sigma) could be used to infer water saturation (S_w), as a snapshot in time, for comparison with the S_w originally estimated from open-hole logs. Figure 3 shows two perforated intervals. The lower interval is being swept but the upper interval is not and therefore it is a candidate for recompletion to access the by-passed pay.

Type 2: Scenario A

A Type 2A example of an initially oversimplified geological model relates to the Semberah Field, East Kalimantan, Indonesia (Nikijuluw *et al.* 2005). The depositional setting is deltaic with channel/bar sands. The field contains both oil and gas. The geological model turned out to be at variance with water influx. Specifically, the updip producer (Well 1) showed earlier water influx than the downdip producer (Well 2) (Fig. 4). The model was initially that of a single reservoir unit (Fig. 5). This model was perceived to be inadequate. A campaign to locate by-passed pay in gas intervals led to a revised model based on an analysis of log and pressure data that included infill wells (e.g. Well 3, Fig. 4). The revised model comprised six reservoir zones, a distributary channel A and five delta front bars B–F (Fig. 6). It can be seen from Figure 6 that the (early) water influx in producing Well 1 occurred in a different layer from that in producing Well 2. The refined lithostratigraphy exposed undeveloped layers with potential for by-passed gas (Fig. 6).

This case history elucidates two key points. First, production data are the groundtruth for how the reservoir is working and, as such, they take precedence. All other data are spot samples or visualizations. However, note that the interpretation of production data can be ambiguous, for example, where there is comingling. Second, the greatest benefits can be secured through the integrated use of diverse data, in this case reservoir-pressure measurements and well logs within a stratigraphic framework.

Type 2: Scenario B

A Type 2B example of geological re-evaluation is taken from the West Lutong Field, offshore Sarawak (Pauzi *et al.* 1999). Most of

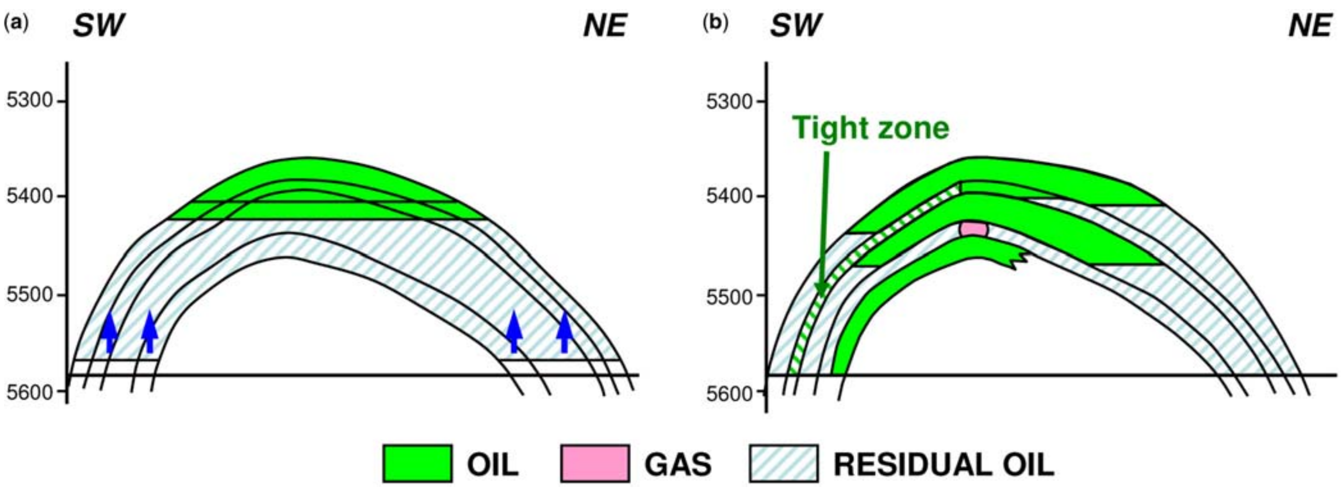

Fig. 7. West Lutong Field, offshore Sarawak, Malaysia: comparison of (**a**) initial and (**b**) reconstructed geological models. Depth units – ft. (After Pauzi *et al.* 1999.)

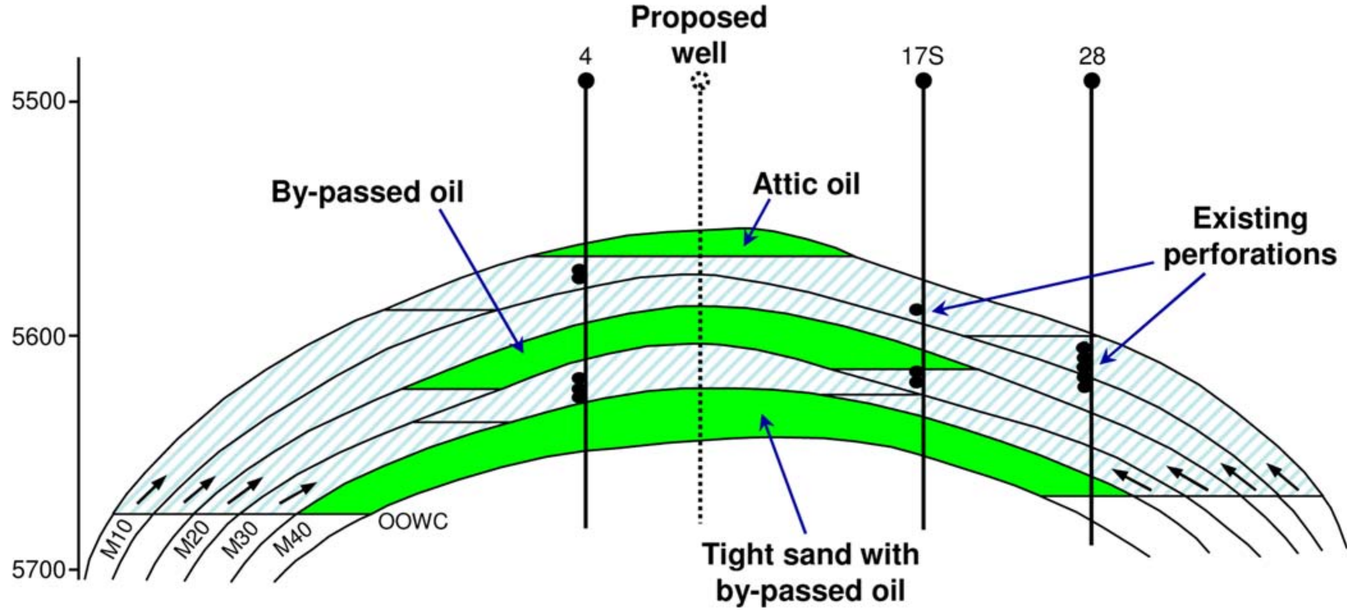

Fig. 8. West Lutong Field, offshore Sarawak, Malaysia: identification of by-passed hydrocarbons in the M-sand through the reconstruction of the field-wide geological model. Depth units – ft. (After Pauzi *et al.* 1999.)

the wells are clustered around the crest. The field was in decline despite several attempted rejuvenations. The original geological model was a homogeneous tank (Fig. 7a). A revised geological model comprised shale-separated sand layers of variable reservoir quality and possibly some inter-layer connectivity (Fig. 7b). The new model revealed opportunities for accessing by-passed pay in its various forms (Fig. 8).

Another Type 2B example with a more commercial emphasis is described in a press release put out by Energy Partners Ltd (EPL) on 31 March 2008. This announced the penetration of by-passed oil by an infill well in the heart of EPL's 100% owned East Bay Field, Gulf of Mexico, which was discovered 'nearly 60 years ago'. The press release alluded to further opportunities in undrilled fault blocks containing 'multiple oil-bearing sands'. It is typical of many others.

Type 2: Scenario C

A Type 2C example comes from the Eugene Island Block 338 oil field, offshore Louisiana (Sibley & Mastoris 1994). The field saw first production in 1972 with a water/pressure drive depletion mechanism. By 1982, production had declined to one-quarter of the peak in 1976 (Fig. 9). In 1988, the field became a candidate for sale during a time of low commodity prices because of its high operating costs. That same year 3D seismic was shot and subsequently interpreted to identify additional development potential. Data analysis revealed that high compressional wave velocity corresponded to high water saturation. This meant that a migrating water front could be resolved seismically provided that the residual oil saturation behind the front was no greater than 20% (Fig. 10). The analysis was supported by the fact that high seismic amplitudes

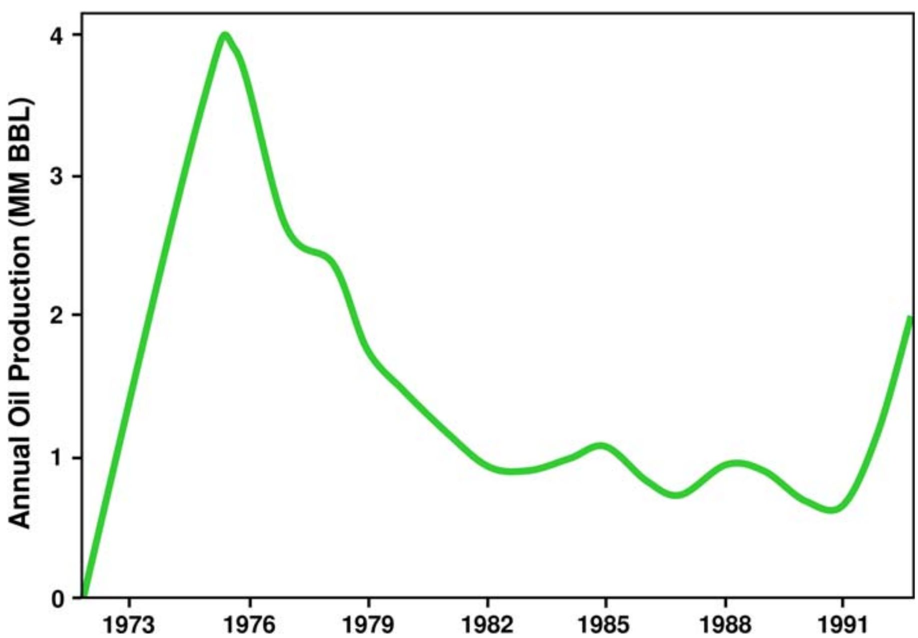

Fig. 9. Eugene Island Block 338 Field, offshore Louisiana: production profile 1972–1992. (Redrawn from Sibley & Mastoris 1994.)

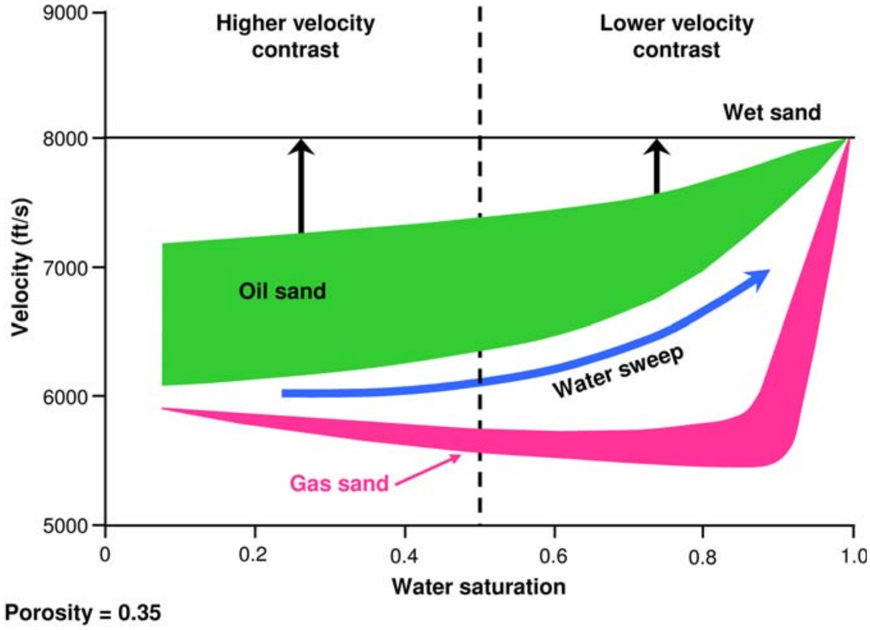

Fig. 10. Eugene Island Block 338 Field, offshore Louisiana: crossplot of seismic velocity and fluid saturation for oil and gas sands. (Redrawn from Sibley & Mastoris 1994.)

corresponded to hydrocarbon accumulations. Thus, unswept zones could be identified and targeted by drilling. The ensuing drilling campaign delivered a high success rate of commercial producers and this doubled field production after one year (Fig. 9).

Conclusions

A classification scheme has been proposed as the basis for a road map for the exploitation of by-passed pay. The recognition of Type 1 and Type 2 by-passed hydrocarbons draws strongly upon (through-casing) well logs and (3D/4D) seismic data, respectively. The exploitation of by-passed hydrocarbons is likely to be more economic for larger fields: reported disappointments usually relate to smaller accumulations. Current trends are directed towards the re-interpretation of existing field databases, cross-hole geophysics, time-lapse seismic with permanent sensors, and advancing the petrophysics of problematic reservoirs. The improvement of poorly performing waterfloods remains a highly pertinent objective. The fruits of these ongoing efforts are evident in contemporary press releases from operators who specifically report the discovery of (hitherto) by-passed hydrocarbons, with corresponding uplifts in reserves.

The author thanks the Society of Petroleum Engineers for allowing the use of certain artworks as referenced. Thanks are due to Gaffney, Cline & Associates for supporting the publication of this work and to Mr Steve Fahy for inspired draughting support.

References

Bartenhagen, K. J., Bradford, J. C. & Logan, D. 2001. *Cased Hole Formation Resistivity: Changing the Way We Find Oil and Gas*. SPE Paper **70042**. Society of Petroleum Engineers, Richardson, TX.

Choon, T. T. 2007. *Identification of Bypassed Oil for Development in Mature Water-drive Reservoirs*. SPE Paper **109077**. Society of Petroleum Engineers, Richardson, TX.

Chu, W.-C. & Welch, P. M. 2008. *Identification of By-passed Pays in Low-resistivity, Thinly-bedded, Sand–Shale Sequences in the Ghdames Basin of North Africa Through Use of the Wireline Formation Tester*. SPE Paper **114478**. Society of Petroleum Engineers, Richardson, TX.

Conner, M. G. & Blesener, J. A. 2005. Development of bypassed oil reserves using behind casing resistivity measurements: Santa Fe Springs Field, Los Angeles County, California. Semiannual Technical Progress Report, DoE Award No. DE-FG26-03NT15435, US DoE Office of Scientific and Technical Information, Washington, DC.

Energy Partners Ltd. 2008. EPL finds bypassed oil in the heart of its 100% owned East Bay Field. News Release, 31 March 2008. EPL, New Orleans, LA.

Fairhurst, D. L., Semmelbeck, M. E. *et al*. 2007. *Fracturing Previously Bypassed Highly Laminated Tight Gas Sands: a Production Optimization Case Study in South Texas*. SPE Paper **105681**. Society of Petroleum Engineers, Richardson, TX.

George, C. J. & Stiles, L. H. 1978. Improved techniques for evaluating carbonate waterfloods in west Texas. *Journal of Petroleum Technology*, **30**, 1547–1554.

Gómez, L. A., Andrade, C. B. & Sneider, J. S. 2001. *In Search of Bypassed Gas Pays in the Macuspana Basin Wells*. AMGP/AAPG Joint Conference, November.

Grant, J., May, D. & Pinto, K. 2008. *The Use of Pulsed Neutron Measurements for Determination of Bypassed Pay: a Multi-well Study*. SPE Paper **114027**. Society of Petroleum Engineers, Richardson, TX.

Hustedt, B. & Snippe, J. R. 2008. *Integrated Data Analysis and Dynamic Fracture Modelling Key to Understand Complex Waterflood: Case Study of the Pierce Field, North Sea*. IPTC Paper **12533**. Society of Petroleum Engineers, Richardson, TX.

McConkey, S. & Stromquist, M. 2000. *Integration of Conventional Fracturing, Coiled Tubing, and Retrievable Tool Technology*. SPE Paper **60709**. Society of Petroleum Engineers, Richardson, TX.

Mendoza, E. & Duran, W. 2002. *Identifying Bypassed Reserves and Monitoring Fluids using Carbon–Oxygen Logs in Tía Juana Field, Lake Maracaibo, Venezuela*. SPE Paper **77784**. Society of Petroleum Engineers, Richardson, TX.

Montgomery, S. L. 1998. Increasing reserves in a mature giant: Wilmington Field, Los Angeles Basin, Part 1: reservoir characterization to identify bypassed oil. *American Association of Petroleum Geologists Bulletin*, **82**, 367–385.

Nikijuluw, R., Suwito, Z. A. & Arianto, M. A. 2005. *Integrated Reservoir Assessment: a Way to Identify 'Overlooked' Multi-layered Reservoirs*. SPE Paper **93198**. Society of Petroleum Engineers, Richardson, TX.

Nishikiori, N., Sugai, K., Normann, C., Onstein, A., Melberg, O. & Eilertsen, T. 2008. *An Integrated Workflow for Gas Injection EOR and a Successful Application to a Heterogeneous Sandstone Reservoir in the Southern North Sea*. IPTC Paper **12025**. Society of Petroleum Engineers, Richardson, TX.

Palar, S., Bowen, J. F. *et al*. 1999. *Sepinggan Field Development: a Cross-functional Team Effort to Develop Bypassed Attic Oil*. SPE Paper **54369**. Society of Petroleum Engineers, Richardson, TX.

Pauzi, N., Low, F. N., Abas, A., Juwaini, A. R. & Maksari, H. 1999. *Revitalizing the West Lutong Field*. SPE Paper **57266**. Society of Petroleum Engineers, Richardson, TX.

Pranter, M. J., Hurley, N. F., Davis, T. L., Raines, M. A. & Wehner, S. C. 2004. Dual-lateral horizontal wells successfully target bypassed pay in the San Andres Formation, Vacuum Field, New Mexico. *American Association of Petroleum Geologists Bulletin*, **88**, 99–113.

Sibley, D. M. & Mastoris, S. S. 1994. *Rethinking Conventional Field Development: 3D Shows Direct Detection of Bypassed Oil Reserves*. SPE Paper **28719**. Society of Petroleum Engineers, Richardson, TX.

Sneider, R. M. & Sneider, J. S. 2001. New oil in old places: the value of mature field development. *In*: Downey, M. W., Threet, J. C. & Morgan, W. A. (eds) *Petroleum Provinces of the Twenty-first Century*. American Association of Petroleum Geologists, Tulsa, OK, Memoirs, **64**, 63–84.

Society of Petroleum Engineers, World Petroleum Council, American Association of Petroleum Geologists & Society of Petroleum Evaluation Engineers. 2007. *Petroleum Resources Management System*. Society of Petroleum Engineers, Richardson, TX.

Thatcher, D., Glanville, S., Zander, D., Jirges, H. & Weishoff, J. 2003. *Re-completion Techniques on Shallow Gas Wells using Coiled Tubing Conveyed Fracturing*. SPE Paper **81708**. Society of Petroleum Engineers, Richardson, TX.

Tioe, E., Sarif, M. R., Elias, M. R. & Vrolijk, P. J. 2008. *Understanding the Plumbing in your Field: Application of Reservoir Connectivity Analysis to Improve Oil and Gas Recovery*. IPTC Paper **12383**. Society of Petroleum Engineers, Richardson, TX.

Von Pattay, P. W., Hamer, F. & Strassner, R. 2007. *Unlocking the Potential of Mature Fields – an Innovative Filtering and Analysis Approach to Identify Sidetracking Candidates in Mature Water Flooded Fields*. SPE Paper **110927**. Society of Petroleum Engineers, Richardson, TX.

Worthington, P. F. 2000. Recognition and evaluation of low-resistivity pay. *Petroleum Geoscience*, **6**, 77–92.

Worthington, P. F. 2008. The application of cut-offs in integrated reservoir studies. *SPE Reservoir Evaluation & Engineering*, **11**, 968–975.

Worthington, P. F. & Cosentino, L. 2005. The role of cut-offs in integrated reservoir studies. *SPE Reservoir Evaluation & Engineering*, **8**, 276–290.

Xiaoguang, L., Xuewen, Z., Sincock, B., Handono, B. W. & Mayanullah, F. 2005. *Integrated Approach for Improving Development of a Mature Field*. SPE Paper **92895**. Society of Petroleum Engineers, Richardson, TX.

Youssef, M. I. 2006. *New Oil Recovery from an Old Field: a Unique Case Study in Badr-1 Concession, Western Desert, Egypt*. SPE Paper **99401**. Society of Petroleum Engineers, Richardson, TX.

Tilting oil–water contact in the chalk of Tyra Field as interpreted from capillary pressure data

I. L. FABRICIUS[1] and M. A. RANA[2]

[1]*DTU Environment, Miljoevej 113, DK-2800 Kgs. Lyngby, Denmark (e-mail: ilf@env.dtu.dk)*
[2]*Talisman Energy (UK) Limited, 163 Holburn Street, Aberdeen AB10 6BZ, UK*

Abstract: The Tyra Field in the central North Sea is located in Palaeogene and Upper Cretaceous chalk. It contains a natural gas zone underlain by an oil leg. Based on analysis of logs and core data from ten wells drilled prior to the field being put into production, normalized water saturation depth-trends from logs were compared with normalized water saturation depth-trends predicted from capillary pressure core data. The ten wells lie close to a SW–NE cross section of the field. For the gas–oil contact, a free contact measured in one well corresponds to a practically horizontal contact interpreted from logging data in the remaining wells. A westerly dipping oil–water contact was found from logging data. Comparison of the depth-wise trends in normalized water saturation among the different wells indicates a regional pattern: in the western side of the field, the trends correspond to a situation of imbibition, where the free water level overlies an interval of residual oil, whereas in the eastern part of the field, the depth-wise trends in normalized water saturation correspond to a situation of drainage. The free water level apparently dips to the east due either to hydrodynamic action or to pressure inequilibrium in the aquifer following tectonic tilting.

Keywords: chalk, North Sea, capillary pressure, water saturation, fluid contacts

In the central North Sea, the Palaeogene and Upper Cretaceous Chalk Formations host accumulations of natural gas and oil (Andersen 1995). Several chalk fields had already been discovered by 1980, and in many cases operators of the fields found that oil–water contact (OWC) and free water level (FWL) tilt, and in some cases also the gas–oil contact (GOC) (Jacobsen *et al.* 1999). Figure 1 shows a cross section through a field with a horizontal GOC, a tilting OWC, and a tilting FWL. The presence of tilting contacts is a challenge in field delineation and in reservoir engineering. It also causes debate about the origin of the tilt. Regional subsidence or local tectonic action may cause lateral gradients in fluid pressure, which can cause tilt of the fluid contacts. Vejbæk *et al.* (2005) list three scenarios:

- Pressure equilibrium in hydrocarbon phases causes horizontal GOC, whereas a lateral pressure gradient in the water leg causes the FWL to dip in the direction of declining lateral pressure.
- Lateral pressure gradients in the same direction in hydrocarbon zone and in the water leg cause both GOC and FWL to dip in the same direction.
- Pressure equilibrium resides in the water leg, whereas a lateral pressure gradient in the oil zone alone causes GOC and FWL to tilt in opposing directions: GOC tilts in the direction of declining oil zone pressure, while FWL tilts in the direction of increasing oil zone pressure.

The question of interpreting fluid contacts is complicated by the high capillarity of the chalk, which causes free fluid contacts to differ from fluid contacts in the rock pores so that OWC differs from FWL (Figs 1 & 2; Engstrøm 1995). In the case of hydrocarbons flowing into the rock matrix from fractures, the drainage process may require an entry pressure, so that OWC is above the FWL. In the case of hydrocarbons seeping out of the seal at a higher rate than hydrocarbons entering the structure, the water imbibition process may cause OWC to be deeper than FWL. The present paper addresses FWL and fluid contacts in the chalk of the Tyra Field.

Tyra Field

The Tyra Field is a low-relief structure in the North Sea Central Graben (Fig. 3). It is situated in the Palaeogene and Upper Cretaceous Chalk Group (Fig. 4). It contains gas underlain by a rim of oil. Chalk porosity varies stratigraphically and regionally from 20 to 45%. Gas permeability also varies and is up to 20 mD. Natural fracturing is sparse. Core and logging data indicate that the OWC is not horizontal, but rather is relatively shallow in the northeastern part of the field, while it is relatively deep in the southwestern part of the field (Doyle & Conlin 1990; Nykjaer 1994).

Chalk is primarily composed of calcitic biogenic mud representing nannofossil remains. The mud is partly recrystallized through interaction with the pore water, so that the single mud particles tend to have surfaces representing calcitic rhombohedra. It also contains sand-size microfossils, which may be filled with calcitic cement or locally with silica cement. The Palaeogene chalk constitutes the Ekofisk Formation, which in addition to calcitic fossil remains contains clay and a relatively high and variable amount of microcrystalline quartz. The latter largely represents diagenetically mobilized biogenic opal as evidenced by the presence of

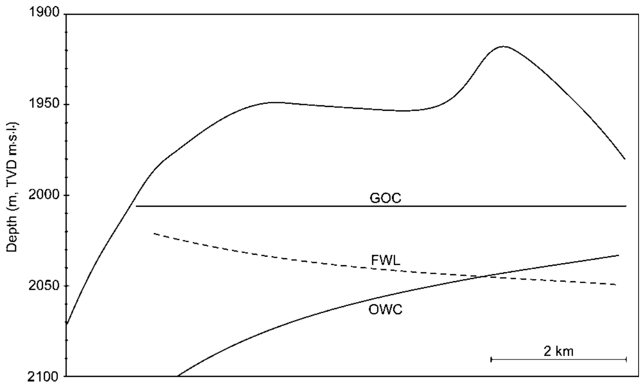

Fig. 1. Conceptual cross section through field with horizontal GOC, tilting OWC and tilting FWL.

VINING, B. A. & PICKERING, S. C. (eds) *Petroleum Geology: From Mature Basins to New Frontiers – Proceedings of the 7th Petroleum Geology Conference*, 463–472. DOI: 10.1144/0070463

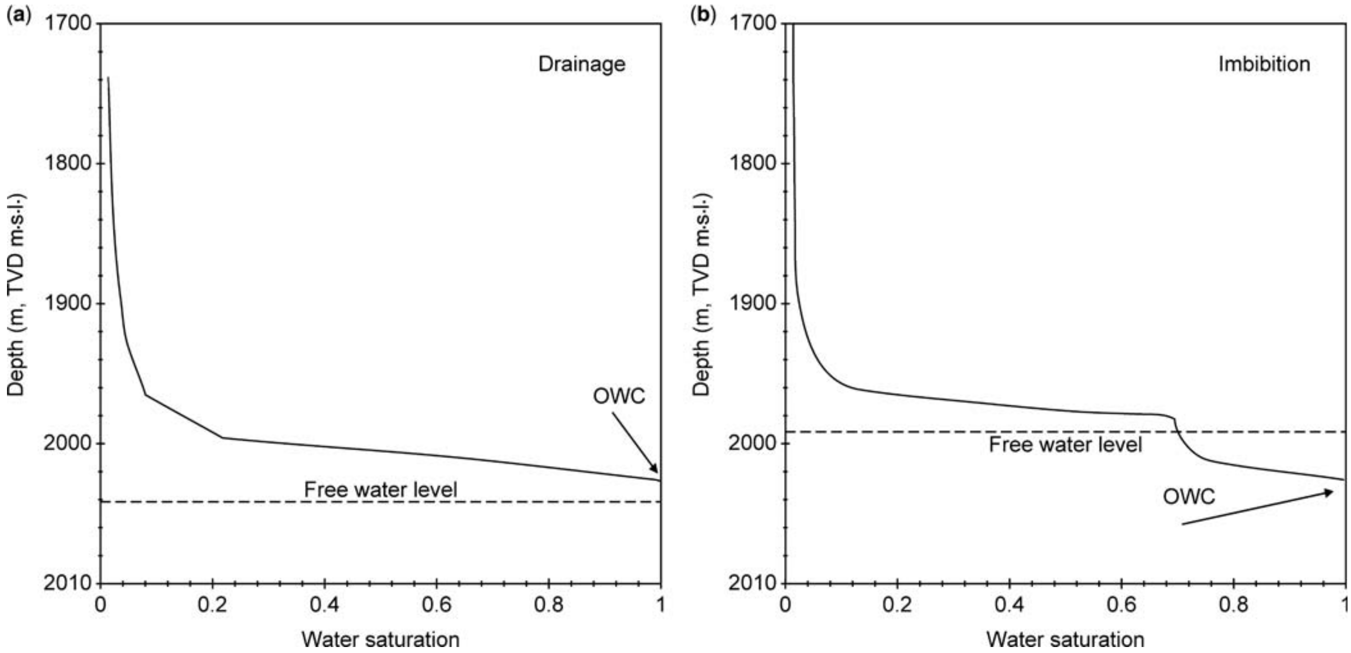

Fig. 2. Conceptual water saturation–depth trends for a water-wet, homogeneous chalk in (**a**) drainage, and (**b**) in subsequent imbibition caused by rising FWL.

moulds after opaline fossils (Fig. 5a, Røgen & Fabricius 2002). Porosity in the Ekofisk Formation varies stratigraphically as a reflection of varying content of microfossils and microcrystalline quartz (Fig. 4). The Upper Cretaceous chalk is split into several formations. The uppermost, Tor Formation, is almost purely calcitic (Fig. 5b) and the porosity varies locally as a consequence of varying content of calcite-cemented microfossils. These local porosity variations scatter an overall depth-wise porosity decrease due to pore-filling cementation (Fig. 4; Fabricius *et al.* 2007). Because of the high and variable content of microcrystalline quartz, the chalk of Ekofisk Formation has higher and more variable specific surface than the chalk of the Tor Formation, and consequently, for a given porosity, chalk from Ekofisk Formation will have lower and less predictable permeability than chalk from Tor Formation (Mortensen *et al.* 1998; Røgen & Fabricius 2002).

Analysis of log- and core data

In order to evaluate how the tilting OWC relates to the FWL, we used conventional core analysis data, logging data, as well as data from Hg capillary pressure experiments including drainage as well as imbibition curves (Fig. 6). Data from ten wells (Table 1) were used in the study, including one well (TEB-8) where wireline formation tester data are available. TEB-8 is

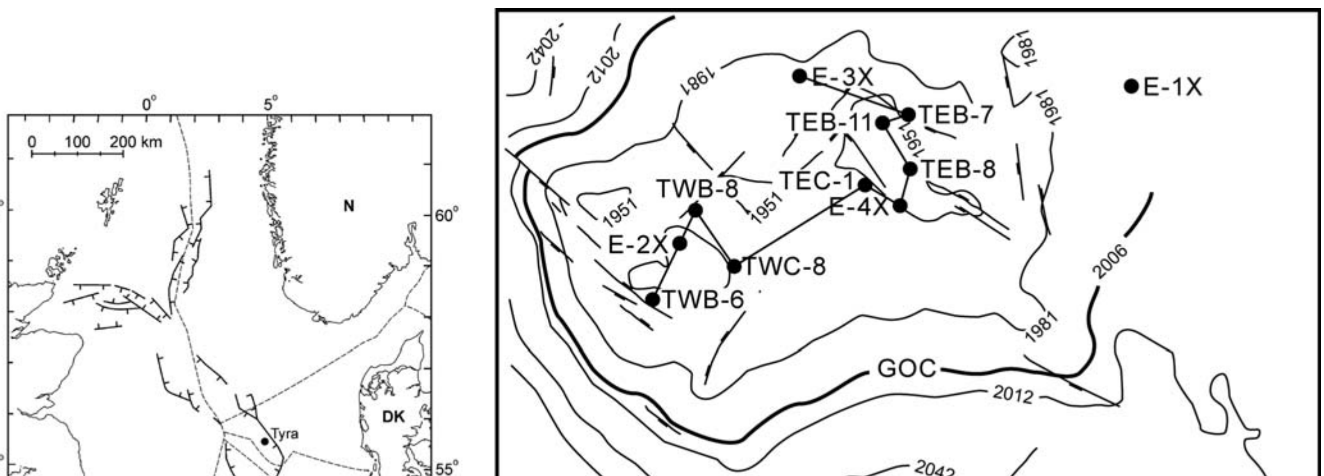

Fig. 3. Depth structure map of Tyra Field, modified after Halberg (2008). Interpreted GOC is shown. The original contour values in feet have been recalculated to metres.

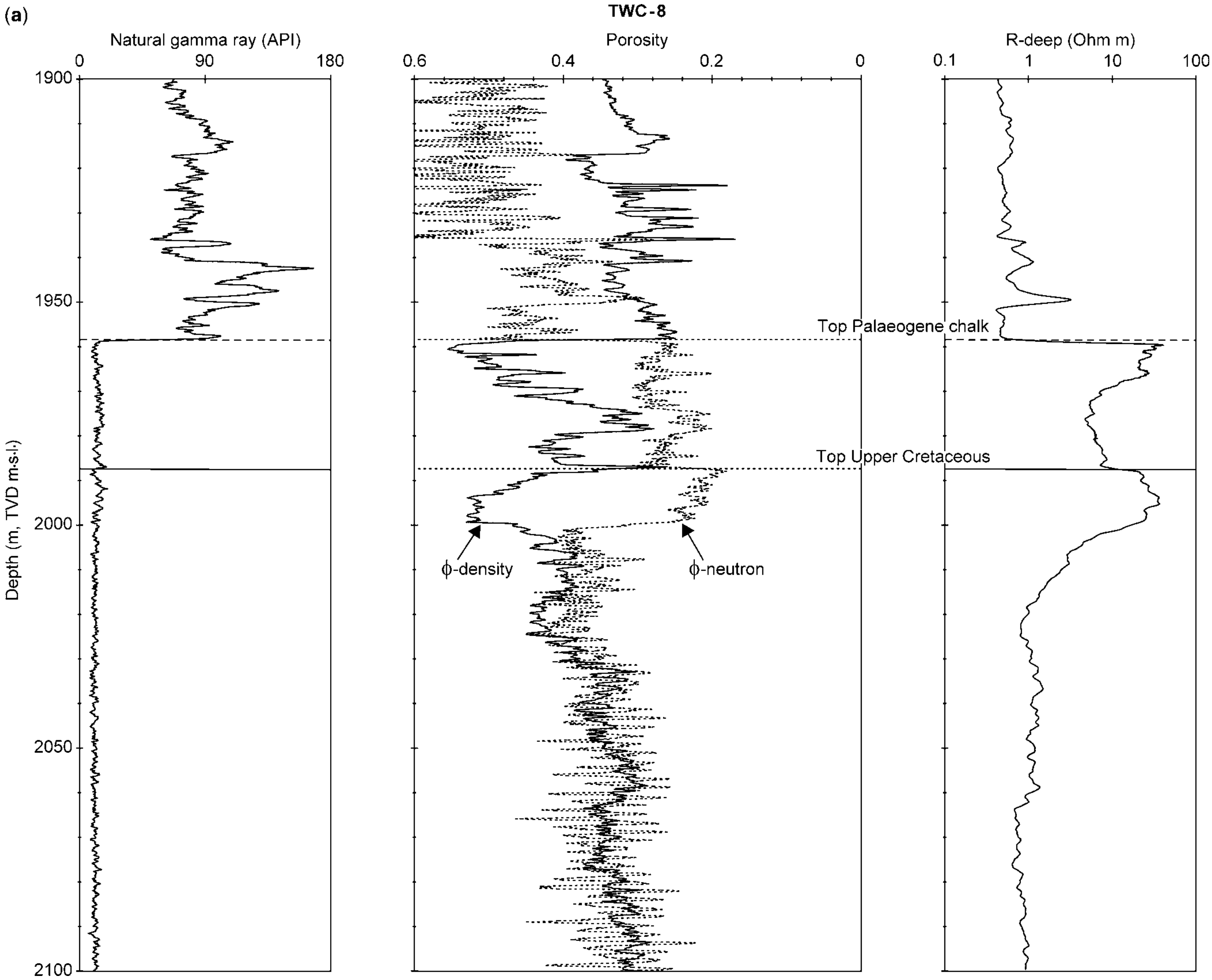

Fig. 4. Natural gamma ray log, limestone porosity from neutron and density logs, as well as deep resistivity log from wells (**a**) TWC-8 and (**b**) TEB-11. Top Palaeogene chalk is shown by a broken line, top Upper Cretaceous chalk by a solid line.

located in the eastern part of the field. The ten wells comprise all wells drilled before the field was put into production in 1984 (Tables 1 & 2). The old exploration wells (E-2X, E-3X and E-4X) were drilled with water-based mud, whereas the remaining studied wells were drilled with oil-based mud. All wells were cored and conventional core analysis data are available. Top chalk, which is also the top of the gas zone, is accompanied by a distinct drop in natural gamma radiation, but it is also easy to define from the crossover of the neutron and density logs at the transition from shale to gas-bearing chalk (Fig. 4). In an interval with relatively low porosity in the Ekofisk Formation, the gas effect is small. The resistivity in this interval is also relatively small (Fig. 4). This indicates a high water saturation, probably due to high specific surface (i.e. 'small pore size') in the presumed water-wet chalk. The GOC is not always easy to define in intervals of high water saturation where the neutron-density gas effect is low. In some wells GOC interferes with the low-porosity interval in the Ekofisk Formation. In other wells the depth-wise increase in water-saturation in the transition zone causes low gas effect. The chosen GOC of 2006 m TVD msl is the value derived from the wireline formation tester data. This value is not in contradiction with the deeper limit of the neutron-density effect in any of the studied wells, bearing in mind that the error on depth determination from wirelines is probably larger than 1 per mil. The uncertainty also implies that a minor regional tilt in GOC cannot be excluded.

The OWC in each well was preliminarily picked from the resistivity log. Data from nine of the studied wells indicate practically the same reservoir temperature, but TWB-8 data indicate an anomalously high temperature (Table 2). The density of gas at reservoir conditions was derived from the pressure–depth gradient of the wireline formation tester data (Table 2). The density of the oil is less easy to define because of sparse wireline formation tester data points, but the noticeable hydrocarbon effect below the gas zone indicates relatively light oil (Fig. 4, Table 2).

The calculated water saturation from wireline logs depends on the interpreted water resistivity. If the water resistivity is calculated by Archie's method from the water leg in each well independently, we find apparent water resistivity to be relatively high in well TWB-8 in the western part of the field, where the OWC is low and difficult to define. This is not caused by a relatively high temperature in TWB-8, as this would rather cause a relatively low water resistivity for a given salinity. In our interpretation we for simplicity assume constant low water resistivity as derived from the remaining wells (Table 2). The water resistivity corresponds to a salinity of 35 700 ppm, which was used for calculating water density at reservoir pressure and temperature using Batzle and Wangs relations as cited in Mavko *et al.* (1998). This water density, ρ_w is consistent with wire-line formation tester data. The density of water-based mud filtrate, ρ_{mf}, was calculated by the same method from mud filtrate resistivity, R_{mf}.

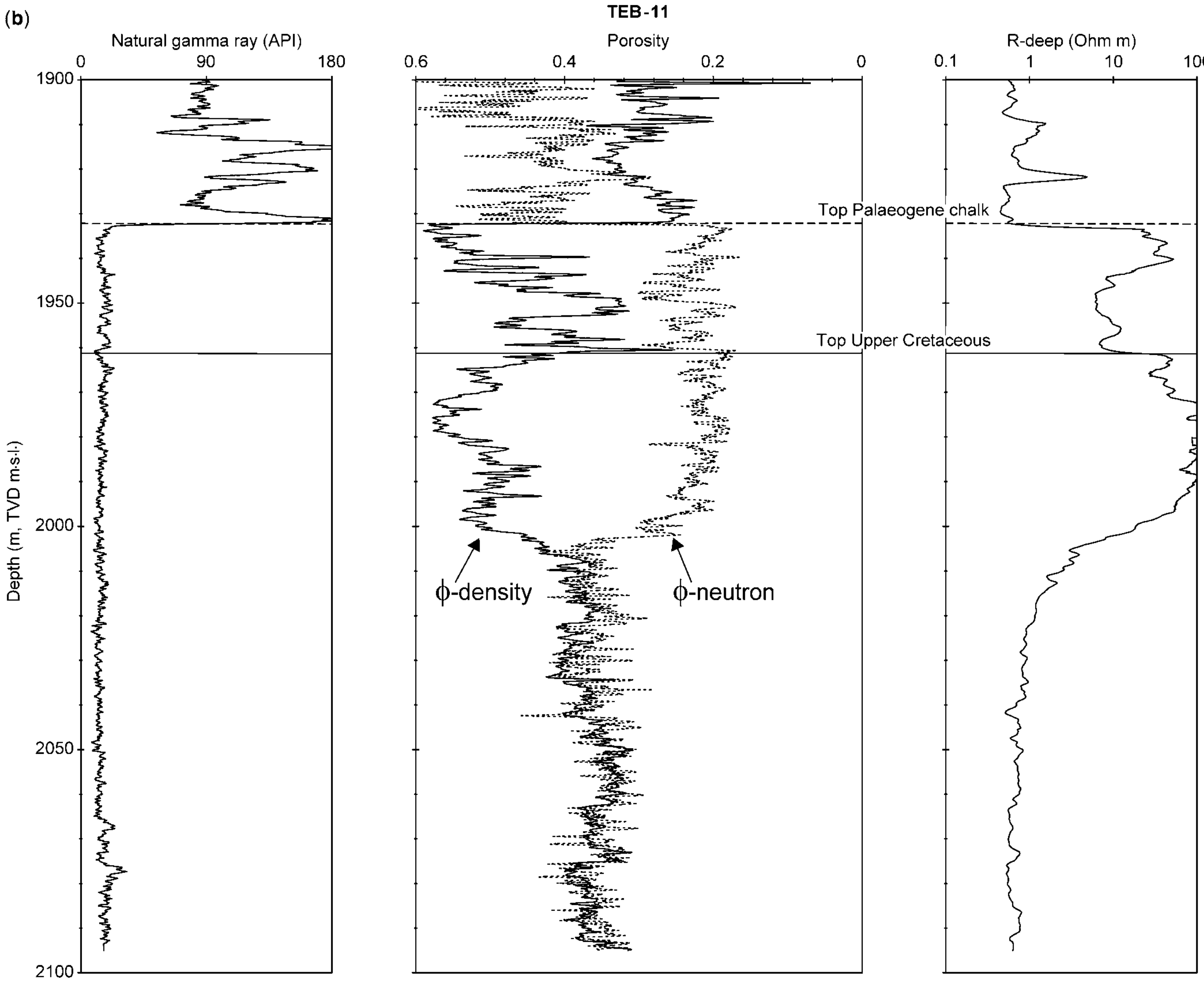

Fig. 4.

Porosity, ϕ, was calculated from bulk density, ρ_b and the shallowest resistivity log, R_{xo} in each well as checked by core porosity. In wells with water-based mud the resulting porosity log was matched to available core data by iteration, involving adjusting the resistivity R_{mfx} of mixed formation water and mud filtrate:

$$\rho_b = \rho_{calcite}(1-\phi) + \rho_{mfx}S_{xo}\phi + \rho_{hc}(1-S_{xo})\phi \tag{1}$$

$$S_{xo}^n = \frac{R_{mfx}}{(R_{xo}\phi^m)} \tag{2}$$

where $\rho_{calcite}$ is the density of calcite and ρ_{hc} is the density of either gas or oil depending on reservoir interval.

In wells drilled with oil-based mud, the resulting porosity log was fitted to available core data by iteration involving selection of a suitably high ρ_{hc} in the invaded zone, where the heavy mud filtrate is mixed with the formation hydrocarbons, and solving for bulk density and water saturation in the invaded zone, S_{xo}:

$$\rho_b = \rho_{calcite}(1-\phi) + \rho_w S_{xo}\phi + \rho_{hc}(1-S_{xo})\phi \tag{3}$$

$$S_{xo}^n = \frac{R_w}{(R_{xo}\phi^m)}. \tag{4}$$

Subsequently water saturation, S_w, was in both cases calculated from porosity and deep resistivity, R_t:

$$S_w^n = \frac{R_w}{(R_t\phi^m)}. \tag{5}$$

The cementation factor m was for simplicity assumed to be 2, although the higher specific surface of Ekofisk Formation would imply a slightly higher m (Olsen *et al.* 2008). The saturation exponent, n, was for simplicity assumed to be equal to m and thus set to 2. According to Van DeVerg *et al.* (1999), this is a sensible value for n where S_w is a result of imbibition; whereas when S_w is a result of drainage, they obtained values of n as low as 1.6. If the water saturation in a well is indeed a result of drainage rather than imbibition, the choice of $n = 2$ rather than $n = 1.6$ will cause too high water saturation, but will not influence the location of OWC. When comparing the resulting S_{xo} and S_w, in accordance with the procedure, we find that in wells drilled with water-based mud $S_w < S_{xo}$ in the upper part of the reservoir, whereas S_w and S_{xo} are similar in the transition zone. In wells drilled with oil-based mud we find S_w and S_{xo} to be similar in the upper part of the reservoir and $S_{xo} < S_w$ in the transition zone.

Direct comparison of OWC and FWL is only possible in TEB-8, where wireline formation tester data are available. In principle, in a homogeneous water-wet reservoir, the shape of

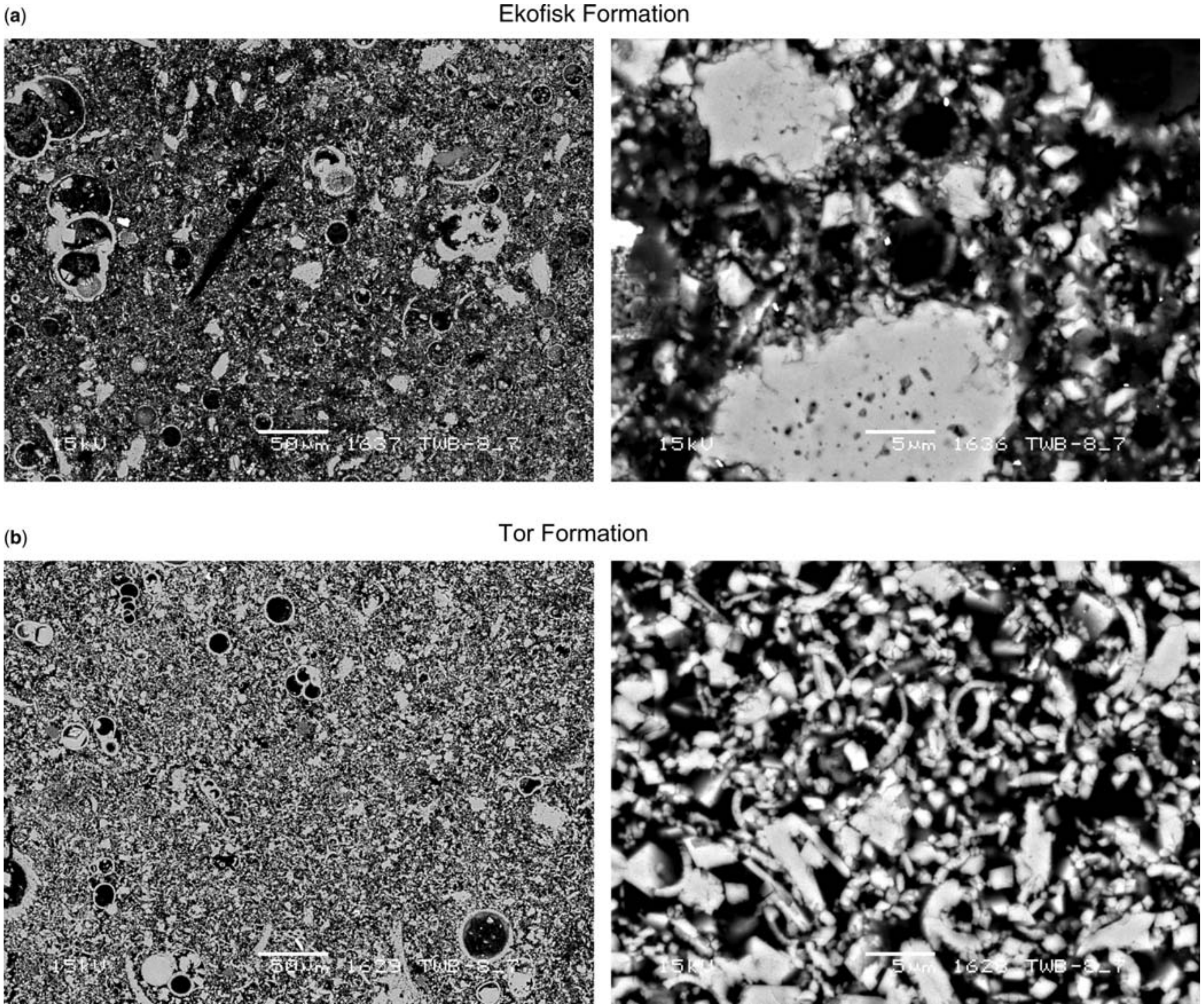

Fig. 5. Backscatter electron micrographs of chalk from well TWB-8. Images to the right represent a close-up of images to the left. (**a**) Sample from 1972 m, TVD m.s.l., Ekofisk Formation. (**b**) Sample from 1995 m, TVD m.s.l., Tor Formation.

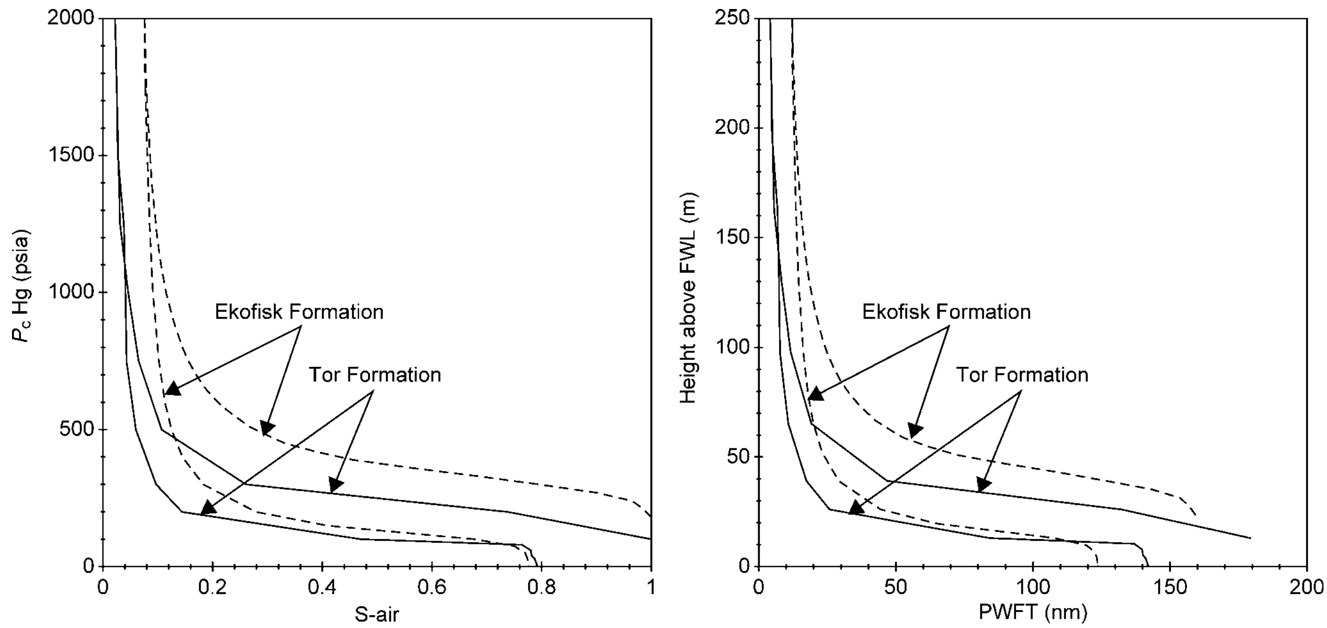

Fig. 6. Hg-capillary pressure curves recalculated to height above FWL v. pseudo water film thickness (PWFT) in a gas–water system. Data from Tor Formation follow the thick line. Data from Ekofisk Formation are shown by the broken line.

Table 1. Interpreted lithostratigraphic and fluid contacts in wells (m, TVD m.s.l.)

	TWB-6	E-2X	TWB-8	TWC-8	TEC-1	E-4X	TEB-8	TEB-11	TEB-7	E-3X
Year logged	1983	1968	1982	1984	1983	1976	1982	1982	1982	1974
Top chalk	1968	1958	1963	1958	1956	1947	1941	1932	1981	1981
Top Cretaceous	1983	1976	1991	1987	1993	1984	1975	1961	2011	2015
OWC*	2082	2073	>2117?	2063	2055	2062	2047	2047	2027	2037
FWL-i†	2031	2025	2023	2023	2021	2024	2024	2023		
FWL-d§					2041	2051	2045	2045	2051	2054

*OWC defined as level of 100% water saturation.
†FWL corresponding to a state of imbibition.
§FWL corresponding to state of drainage.

Table 2. Assumed properties and constants for analysis of well logs

Property	Value	Unit	Estimated uncertainty
Pressure at FWL in TEB-8	29	MPa	2
ρ_{gas}	290	kg m^{-3}	20
ρ_{oil}	690	kg m^{-3}	20
ρ_{water}	1013	kg m^{-3}	2
GOC*	2006	m, TVD m.s.l.	5
Temperature	72†	°C	2
Cementation factor, m	2		0.1
Saturation exponent, n	2		0.1
Water resistivity, R_w	0.087	Ω m	0.003
Sg§ Ekofisk Fm.	6.5	m^2 cm^{-3}	2
Sg§ Tor Fm.	3.5	m^2 cm^{-3}	1

*GOC apparently varies less than a few metres across the field.
†Temperature in well TWB-8 was measured to be anomalously high: 85 °C.
§Effective specific surface of solids as calculated from core-data on porosity and permeability.

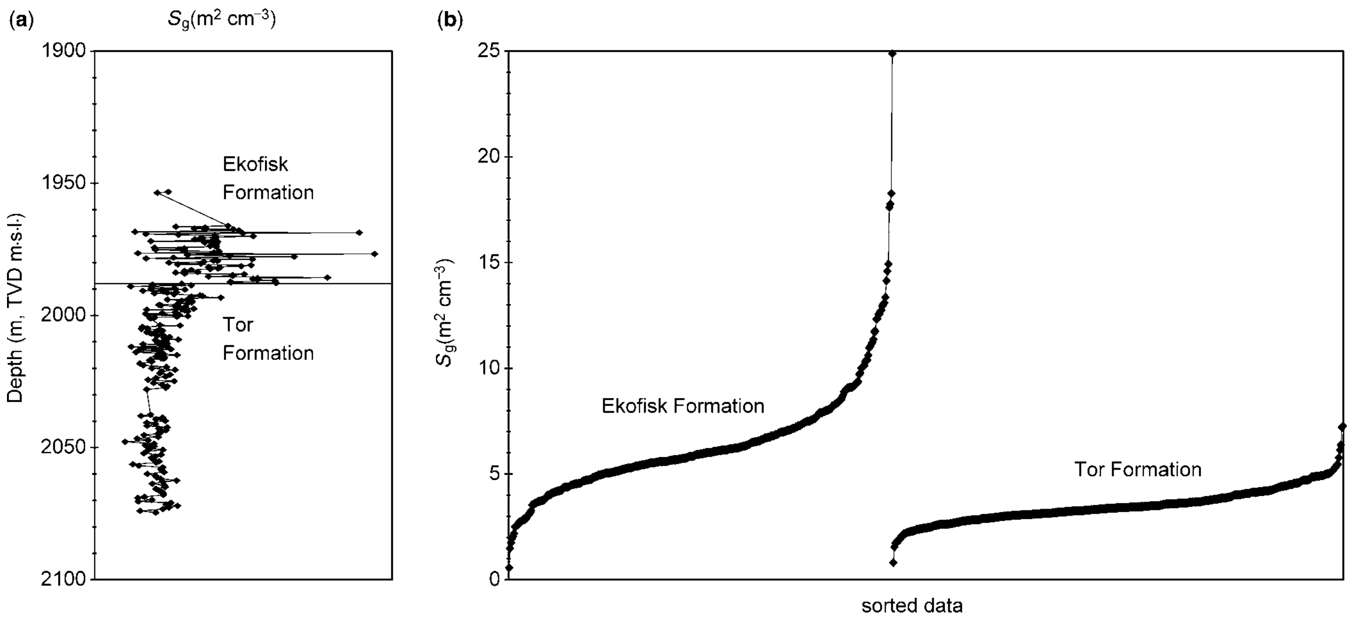

Fig. 7. Specific surface of solids as calculated from equation (6). (**a**) Depth trend for core data from Well E-4X; (**b**) core data from all wells sorted by formation and by value.

the water-saturation–depth curve should correspond directly to a capillary pressure curve. The Tyra Field is not homogeneous: porosity and specific surface vary stratigraphically. In order to overcome this problem, all water saturation data were normalized to the specific surface of pores, and expressed as pseudo water film thickness (PWFT, Larsen & Fabricius 2004). The specific surface of pores, S_p was estimated from conventional core analysis data on porosity and permeability, k, by use of Kozeny's equation:

$$k = c\frac{\phi^3}{S^2} = c\frac{\phi^3}{[(1-\phi)S_g]^2} = c\frac{\phi}{S_p^2} \tag{6}$$

where S is specific surface with respect to bulk volume, S_g is specific surface of solids and c, according to Mortensen *et al.* (1998), is a function of porosity which may be expressed by:

$$c = \left(4\cos\left(\frac{1}{3}\arccos\left(\phi\frac{8^2}{\pi^3}-1\right)+\frac{4}{3}\pi\right)+4\right)^{-1}. \tag{7}$$

Klinkenberg permeability, k, was estimated from air permeability by the empirical relation for chalk (Mortensen *et al.* 1998):

$$\begin{aligned} k &= 0.52k_a^{1.083} \quad (\text{where } k \text{ and } k_a \text{ are given in mD) or} \\ k &= 9.15k_a^{1.083} \quad (\text{where } k \text{ and } k_a \text{ are given in m}^2). \end{aligned} \tag{8}$$

From core analysis data we find a relatively constant S_g for each of the Formations, Ekofisk and Tor, although data from Ekofisk Formation scatter more than data from Tor Formation (Table 2, Fig. 7). $S_p = S_g\,(1-\phi)/\phi$ may then be calculated from the porosity log and PWFT calculated from:

$$\text{PWFT} = \frac{S_w}{S_p}. \tag{9}$$

Special core analysis data on air–mercury capillary pressure, P_c, for a number of core samples from Ekofisk and Tor formations were recalculated to PWFT v. height over FWL for the gas–water

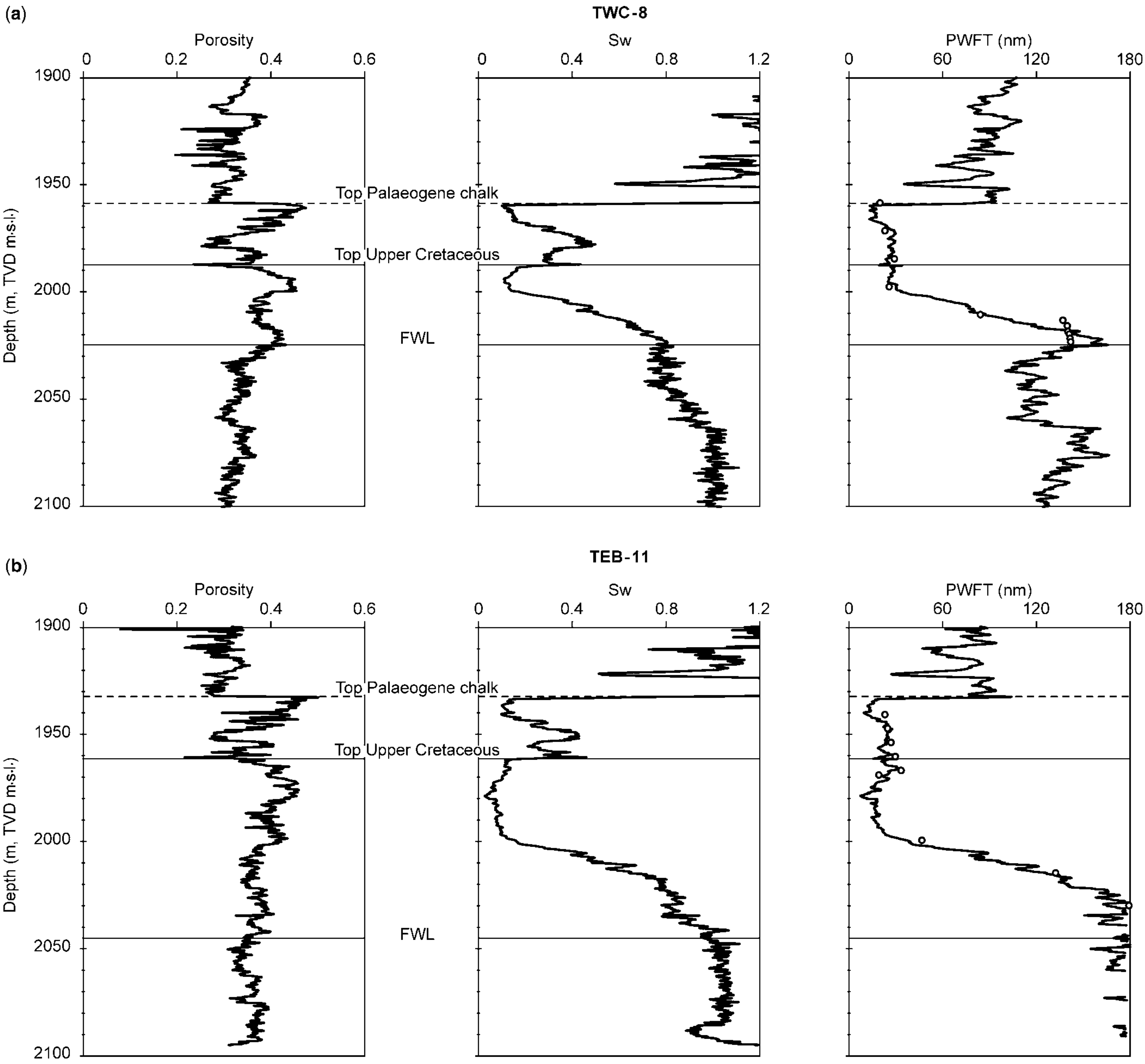

Fig. 8. Porosity, water saturation (S_w) and PWFT as calculated from logging data and core data. (**a**) Well TWC-8. On the PWFT figures open circles represent Hg-imbibition data for samples from Tor and Ekofisk Formation, recalculated to the proper pore fluids. (**b**) Well TEB-11. On the PWFT figures open circles represent Hg-drainage data for samples from Tor and Ekofisk Formation, recalculated to the proper pore fluids.

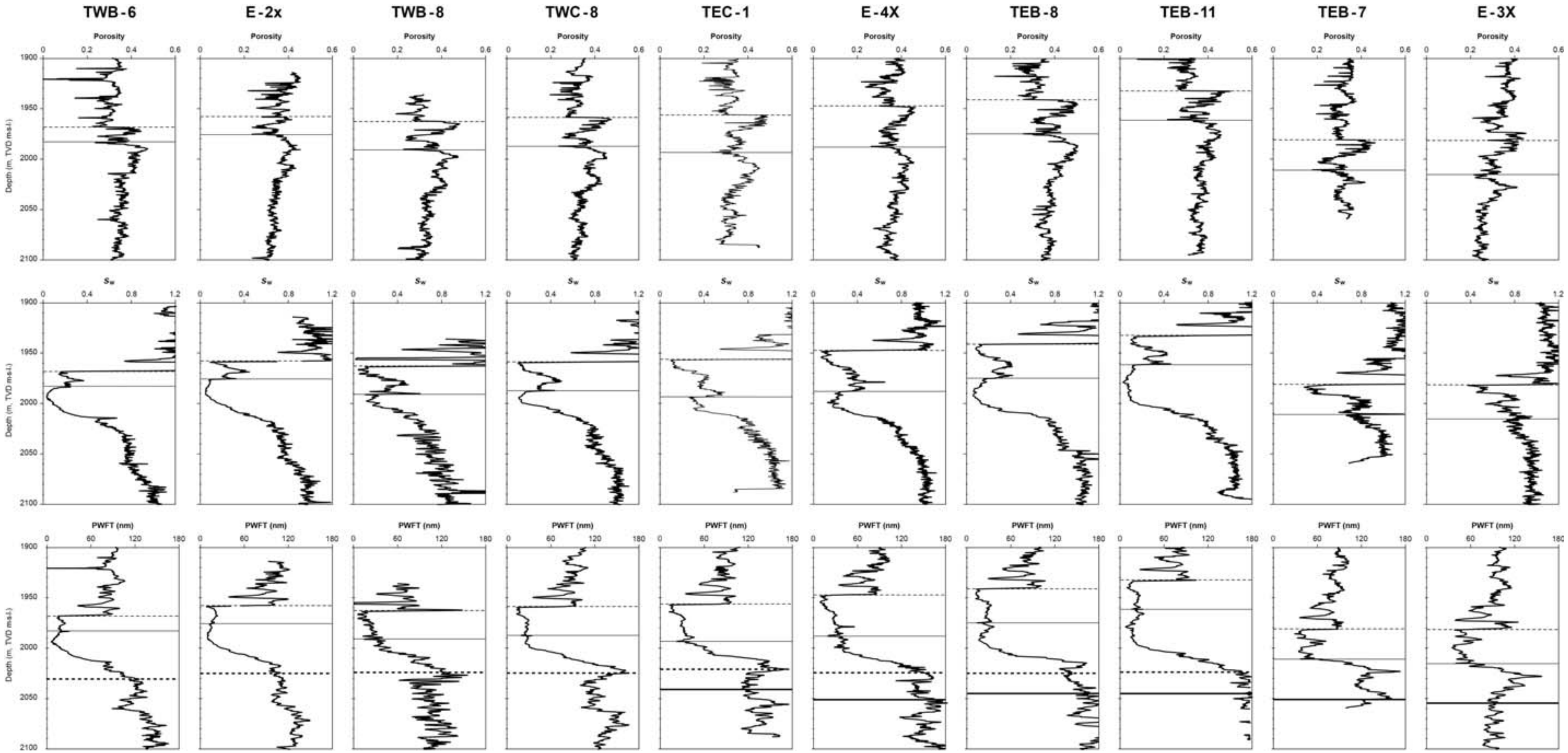

Fig. 9. Porosity, water saturation (S_w) and PWFT as calculated from logging data and core data of all wells in a SW–NE transect (refer to Fig. 3). In the PWFT figures, an FWL corresponding to imbibition is indicated by a broken line, whereas an FWL corresponding to drainage is indicated by a solid line.

system (Figs 6 & 8) and for the oil–water system using the Leverett J-function:

$$J(S_{we}) = \frac{P_c(S_{we})\sqrt{k/\phi}}{\sigma \cos\,\theta} \quad (10)$$

where S_{we} is the wetting phase saturation, σ is surface tension and θ is the contact angle. For the air–mercury system $\sigma \cos\theta = 372$ dyn/cm was chosen, for the water–oil system at reservoir conditions, $\sigma \cos\theta = 26$ dyn/cm was chosen, and for the water–gas system at reservoir conditions, $\sigma \cos\theta = 50$ dyn/cm was chosen.

Capillary pressure, P_c was recalculated to depth, D by:

$$P_c = (\mathrm{D} - \mathrm{FWL})g\rho_w - (\mathrm{D} - \mathrm{FWL})g\rho_{hc} \quad (11)$$

where g is the acceleration of gravity (in latitude of Tyra Field: 9.82 m s^{-2}) and ρ_{hc} is the density of gas in the gas zone and the density of oil in the oil zone. We thus assume the chalk to be water-wet and assume no capillary action between gas and oil. FWL for the gas and the oil zone was in the present case estimated to differ by less than a metre. From porosity and permeability, S_p was calculated from equations (6)–(8) and PWFT was calculated from equation (9).

Results

The depth trends of porosity, water saturation and PWFT vary among the studied wells along a roughly SW–NE trend (Figs 3 & 9). The two westernmost wells, TWB-6 and E-2X, are characterized by a relatively thin Ekofisk Formation, a relatively deep OWC, and shallower FWL. The PWFT-depth trends correspond to an imbibition curve with FWL at a depth of 2025 − 31 m, TVD m.s.l. (Table 1). The difference in mud type (water-based in E-2X and oil-based in TWB-6) does not seem to influence results. The next two wells, TWB-8 and TWC-8, have a thicker Ekofisk Formation and, based on the concept of imbibition, a FWL of 2023 m, TVD m.s.l. was found. OWC is deep although for TWC-8 not as deep as in the westernmost wells. For TWB-8, OWC is ambiguous. It may be below total depth or around the same level as in TWC-8 depending on the choice of pore water salinity in the water saturation calculation (Table 1). TEC-1 and E-4X are located further to the east (Figs 3 & 9). The Ekofisk Formation is relatively thick in these wells and OWC is relatively deep, so a drainage interpretation of the PWFT trend would require FWL to be slightly above OWC, and an imbibition interpretation may thus be more likely. This indicates an FWL of 2021–2024 m, TVD msl (Fig. 9, Table 1). TEB-8 and TEB-11 are located near the crest of the structure and hold thick gas columns (Figs 3 & 9). The hydrocarbon-bearing interval is relatively porous, and this may explain why FWL according to a drainage model falls close to the OWC (Fig. 9, Table 1). TEB-7 and E-3X are located where the structure is relatively deep and the hydrocarbon column relatively thin (Figs 3 & 9). The overall porosity in the hydrocarbon-bearing interval is lower than in the other wells. OWC is relatively shallow and distinctly shallower than the FWL, which according to the PWFT–depth trends represents a situation of drainage (Fig. 9, Table 1).

Discussion

The OWC of Tyra Field apparently dips to the SW whereas, from the studied wells, no significant tilt was observed on the GOC. This could be interpreted as a scenario of pressure equilibrium within and between the hydrocarbon phases, and towards the SW a declining pressure in the water phase. When taking into account the interpreted FWL, which dips to the NE, we rather expect a pressure declining towards the NE in the water phase. Apparently the OWC is then dipping in one direction and the FWL in another direction (Figs 1 & 9). At the same time hydrocarbons in the westerly wells seem to have been leaving the structure while water has been imbibed, whereas in the northeasternmost wells, hydrocarbons seem to have been entering the structure while water has drained out.

A way to account for the lateral pressure gradient in the water phase could be hydrodynamic action caused by easterly flow in the aquifer (Megson 1992). A situation of pressure compartments in the aquifer is also possible (Caillet *et al.* 1997), or rather a gradient in pore pressure caused by tilting of chalk with low lateral permeability in the aquifer. A simplified sequence of events could be: a structure at top chalk level forms; hydrocarbons are generated in a deeper source rock and migrate into the structure; in the underlying aquifer and the capillary transition zone porosity and permeability decrease due to partial cementation; the structure tilts to the SW; hydrocarbons consequently move to the NE leaving a residual oil leg in the SW; in the vertical direction pressure equilibrates between water and hydrocarbon phase; in the less permeable underlying aquifer pressure is not yet equilibrated, so that a lateral pressure gradient persists. The difference in perceived FWL in the northeastern and southwestern parts of the field corresponds to a minimum tectonic tilt corresponding to around 25 m in a vertical direction (Table 1).

Conclusions

Water saturation–depth trends through chalk of varying porosity and permeability may be related to capillary pressure curves when water saturations on log or capillary curves are normalized to PWFT on the pore walls. This procedure was applied to ten wells in the Tyra Field, and it indicates that water saturation in the easternmost part of the field matches a drainage capillary pressure curve, where the FWL corresponds to that derived from wireline formation testing. By contrast, in the western side of the field the water saturation matches an imbibition capillary pressure curve. These results would indicate that the Tyra structure has tilted to the west subsequent to the introduction of hydrocarbons, so that at the time just prior to production, hydrocarbons had been filling into the eastern part of the field, while hydrocarbons had been leaving the western side of the field.

References

Andersen, M. A. 1995. *Petroleum Research in Chalk*. Joint Chalk Research Phase IV. Rogaland Research, Stavanger.

Caillet, G., Judge, N. C., Bramwell, N. P., Meciani, L., Green, M. & Adam, P. 1997. Overpressure and hydrocarbon trapping in the chalk of the Norwegian Central Graben. *Petroleum Geoscience*, **3**, 33–42.

Doyle, M. C. & Conlin, J. M. 1990. The Tyra Field. *In*: Buller, A. T., Berg, R., Hjelmeland, O., Kleppe, J., Torsæter, O. & Aasen, J. O. (eds) *North Sea Oil and Gas Reservoirs II*. Graham & Trotman, London, 47–65.

Engstrøm, F. 1995. A new method to normalize capillary pressure curves. SCA-9535. *International Symposium of the Society of Core Analysts*, California.

Fabricius, I. L., Røgen, B. & Gommesen, L. 2007. How depositional texture and diagenesis control petrophysical and elastic properties of samples from five North Sea chalk fields. *Petroleum Geoscience*, **13**, 81–95.

Halberg, H. (ed.) 2008. *Danmarks Olie og Gasproduktion 2007*. Danish Energy Agency, Copenhagen.

Jacobsen, N. L., Engstrøm, F., Uldall, A. & Pedersen, N. W. 1999. Delineation of hydrodynamic/geodynamic trapped oil in lower permeability chalk. Society of Petroleum Engineers, SPE paper **56514**.

Larsen, J. K. & Fabricius, I. L. 2004. Interpretation of water saturation above the transitional zone in chalk reservoirs. *SPE Reservoir Evaluation and Engineering*, **7**, 155–163.

Mavko, G., Mukerji, T. & Dvorkin, J. 1998. *The Rock Physics Handbook*. Cambridge University Press, Cambridge.

Megson, J. B. 1992. The North Sea Chalk Play: examples from the Danish Central Graben. *In*: Hardman, R. F. P. (ed.) *Geological Insights for the Next Decade*. Geological Society, London, Special Publications, **67**, 247–282.

Mortensen, J., Engstrøm, F. & Lind, I. 1998. The relation among porosity, permeability, and specific surface of chalk from the Gorm field, Danish North Sea. *SPE Reservoir Evaluation & Engineering*, **1**, 245–251.

Nykjaer, O. 1994. Development of a thin oil rim with horizontal wells in a low relief chalk gas field, Tyra Field, Danish North Sea. Society of Petroleum Engineers, SPE paper **28834**.

Olsen, C., Hongdul, T. & Fabricius, I. L. 2008. Prediction of Archie's cementation factor from porosity and permeability through specific surface. *Geophysics*, **73**, E81–E87.

Røgen, B. & Fabricius, I. L. 2002. Influence of clay and silica on permeability and capillary entry pressure of chalk reservoirs in the North Sea. *Petroleum Geoscience*, **8**, 287–293.

Van DeVerg, P. E., Howard, J. J., Fidan, M. & Nesvold, R. L. 1999. Water saturation breakthrough intervals, Ekofisk Field, Norway. *Society of Professional Well Log Analysts 40th Annual Logging Symposium*, 30 May to 3 June 1999, Paper LL.

Vejbæk, O. V., Frykman, P., Bech, N. & Nielsen, C. M. 2005. The history of hydrocarbon filling of Danish chalk fields. *In*: Doré, A. G. & Vining, B. A. (eds) *Petroleum Geology: North-West Europe and Global Perspectives: Proceedings of the 6th Petroleum Geology Conference*. Geological Society, London, 1331–1345; doi: 10.1144/0061331.

A holostratigraphic approach to the chalk of the North Sea Eldfisk Field, Norway

M. J. HAMPTON,[1] H. W. BAILEY[1] and A. D. JONES[2]

[1]*Network Stratigraphic Consulting Ltd, Harvest House, Cranborne Road, Potters Bar, Herts, UK (e-mail: mj.hampton@btconnect.com)*
[2]*ConocoPhillips Norway, Postbox 3, 4064 Stavanger, Norway*

Abstract: A biostratigraphic review, conducted on 34 wells from the chalk of the Eldfisk Field, Norwegian Central Graben, has been integrated with petrophysical, geophysical and sedimentological information resulting in a revised lithostratigraphic framework for the chalk on this structure. Chalk of Danian to Turonian age is divided into five formations: the established Ekofisk Formation of Danian age and Tor Formation of Maastrichtian age, together with a new three-fold division of the Hod Formation, namely the Magne Formation of Campanian age, the Thud Formation of Santonian age and Narve Formation of Coniacian to Turonian age. This work demonstrates the application of this three-fold division of the Hod Formation. Internal field specific subdivisions of all formations are also presented for the Eldfisk Field. This lithostratigraphic framework is applied across the Eldfisk Field, together with the recognition of erosional features, unconformities, areas of non-deposition, reworking and lateral changes in biofacies. The results have also allowed recognition of the following regionally synchronous tectonic phases for the first time on a Norwegian chalk structure: Stille's Ilsede phase (Late Turonian–Coniacian) and Wernigerode phase (Late Santonian–'earliest' Campanian), Mittel–Santon phase (Middle Santonian) of Niebuhr *et al.* and Reidel's Peine phase ('latest' Early Campanian), together with un-named phases of 'latest' Campanian, intra Mid Maastrichtian and (previously unrecognized?) intra Danian age. Evidence for these tectonic phases is compared with work from Denmark, Germany and the Anglo-Paris Basin. An innovative approach to mapping lateral biofacies (principally water depth) variations has been applied using the microfaunal database. This enhances understanding of the timing of structural phases when integrated with time lines generated by nanoplankton data. Biofacies proxies for silica content in the sediment may also correlate with changes in reservoir quality. Biofacies interpretations have also facilitated the identification and mapping of allochthonous bioclastic rich debris flow deposits. The fully calibrated biostratigraphic, lithostratigraphic and tectonostratigraphic frameworks presented can be applied to chalk structures regionally.

Keywords: Eldfisk Field, chalk, North Sea, holostratigraphy, biostratigraphy

The Eldfisk Field, located in Block 2/7 in the Norwegian Sector of the North Sea (Fig. 1), has a total estimated in place volume of *c.* 3.0 BBoe (Brasher 1995). Production began in 1979 through a depletion drive mechanism and in 2001 a water injection programme was introduced to improve recovery. Compaction has led to well casing deformation problems and the need to constantly renew wells. Approximately 75 vertical wells were drilled during early field development; a subset of which provide the main stratigraphic input to this study. Since the mid 1990s over 50 geosteered horizontal wells have been drilled and it is likely that the any future drilling will be mainly horizontal in design.

The field, located on an inversion high called the Lindesnes Ridge in the Central Graben, consists of two domal structures (Alpha and Bravo) and a smaller low relief structure known as East Eldfisk. The Central Graben was tectonically active during chalk deposition, characterized by a complex and dynamic interplay between graben subsidence along major bounding faults, inversion and halokinetic tectonics. The chalk basinal areas surrounding Eldfisk exhibit chalk thicknesses of >2500 ft, whilst over the Eldfisk structure the chalk thins in places to *c.* 700 ft due to the interaction of erosion, unconformities, gravity flow deposition and structural history. This geological complexity, combined with the extremely poor seismic quality over the field due to shallow gas, means reservoir modelling is problematic. Detailed discussion on the tectonic history of Eldfisk can be found in Brewster & Dangerfield (1984), D'Heur (1984), Herrington *et al.* (1987), Michaud (1987) and Brasher (1995); a more regional summary can be found in Bramwell *et al.* (1999).

This holostratigraphic study was designed to improve the understanding of chalk deposition, stratigraphy, facies distribution and to link this to the tectonic history of the structure. All available geological data, including biostratigraphy, petrophysics, geophysics and lithofacies have been used to derive the study results.

Stratigraphic background

The lithostratigraphic nomenclature conventionally applied to Central Graben chalks, namely the Ekofisk, Tor, Hod and Hidra Formations, was initially published by Deegan & Scull (1977) and later updated by Isaksen & Tonstad (1989). A breakdown of Danish chalks has been published by Lieberkind *et al.* (1982) and in the UK by Johnson & Lott (1993). To integrate the wide variety of internal, informal chalk sub-divisions that were used by various operating companies, the Joint Chalk Research (JCR) project, Phase V, Fritsen (1999) was commissioned. This established a common stratigraphic nomenclature for the chalk in the Central Graben and divided the Hod Formation into the Magne, Thud and Narve Formations (Fig. 2). These formations are herein tied to a series of regionally synchronous tectonic phases recognized through the Late Cretaceous succession which can be geophysically mapped. Many of these events have been identified across NW Europe and the wider geographical implications of these events have been described by Mortimore & Pomerol (1997), Mortimore *et al.* (1998) and Niebuhr *et al.* (2000). These events were initially described by Stille (1924) and Reidel (1940, 1942) from the German Hartz Mountain region. Vejbaek & Andersen (2002) also recognized potentially synchronous regional phases of inversion from the Danish sector of the North Sea. Early Campanian to Maastrichtian inversion tectonics have also been described from Belgium, Netherlands and Germany by Bless *et al.* (1986).

Vining, B. A. & Pickering, S. C. (eds) *Petroleum Geology: From Mature Basins to New Frontiers – Proceedings of the 7th Petroleum Geology Conference*, 473–492. DOI: 10.1144/0070473

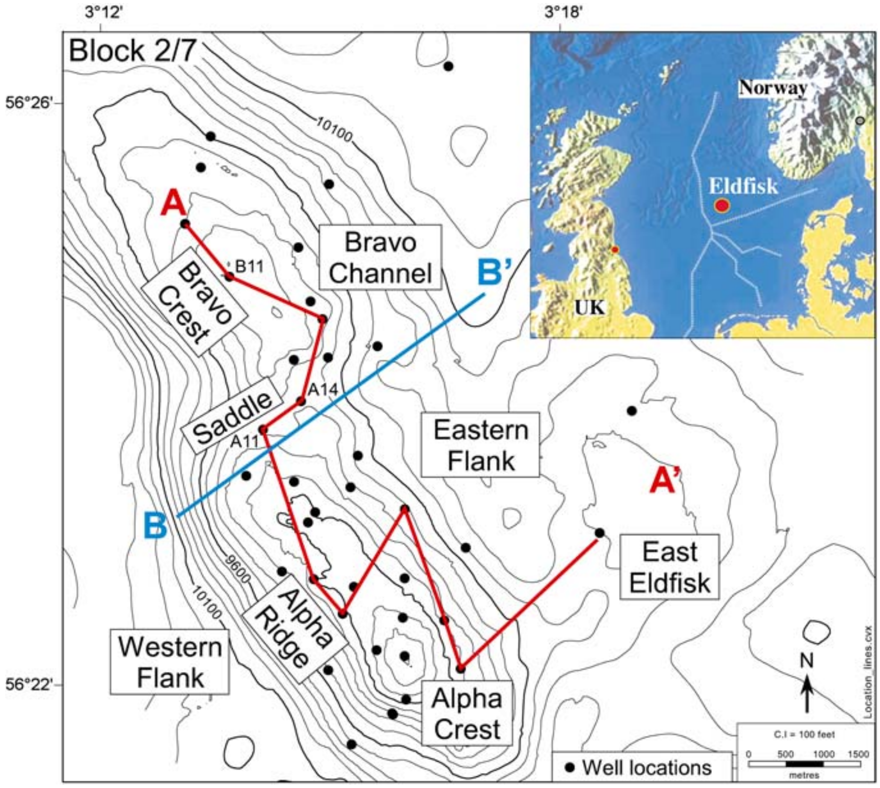

Fig. 1. Eldfisk Field location map (inset) and top Ekofisk Formation depth map (block 2/7). Map also shows wells used in the study and line of section A–A′ for Figure 4 and seismic line B–B′ in Figure 8. Informal geographical names used in the text are presented here.

Study objectives

Following a review of recent drilling activities and whilst planning for future development of the Eldfisk Field, it became apparent that the vast biostratigraphical database, gathered over 30 years of drilling, could be further integrated to improve the understanding of the field. Vertical wells hold a wealth of detailed stratigraphic information, are spread geographically across the field and are particularly well suited for the creation of 3D geological and reservoir models; however, many of these early wells were not analysed for biostratigraphy or were analysed approximately 30 years ago for microfauna only. As taxonomic concepts and biostratigraphic methods have improved significantly since these wells were first interpreted, it was decided to undertake a new, fully holostratigraphic study with the following objectives:

(1) to update the stratigraphic understanding of the chalk on Eldfisk to constrain the new 3D geological and simulation model and gain a better understanding of the growth of the structure and controls on chalk deposition;
(2) to improve understanding of stratigraphic layering, reworking events and the distribution of unconformities to aid horizontal geosteering;
(3) to enhance the geophysical interpretation, particularly in the large seismically obscured area that occurs across Eldfisk;
(4) to tie the biostratigraphy to the petrophysical interpretation and review anomalies in the database.

Methodology and integration of results

Detailed biostratigraphy was used as the foundation for the study as the chalk is well suited to biostratigraphic analysis due to the abundance of microfauna, nanoflora and macrofaunal remains that can be recovered. Results from cored wells were generated first in order to establish a correlation between biostratigraphy, lithofacies, petrophysics, lithostratigraphy and the geological model. Once calibrated, results were applied to wells containing ditch cuttings samples. Samples were analysed for microfaunal and nanofloral content and results were plotted against data from other geological disciplines. The nanofloral and microfaunal data were then used to build the stratigraphic framework; the microfaunal assemblages were also used to interpret biofacies changes along time lines generated by the nanofossil results.

Whilst the operator's 3D model is flow unit-based, it has been calibrated with the combined biostratigraphic scheme described here (Fig. 2). This scheme fully integrates all microfaunal and nanofloral events and has been developed following extensive biostratigraphic work on and around Eldfisk by Network Stratigraphic Consulting Ltd staff, building on previous published works on the region (King *et al.* 1989; Burnett *et al.* 1998; Fritsen 1999). This combined scheme has also been applied regionally to Central Graben chalks.

The complex depositional controls in the chalk have resulted in significant variations in lithofacies and a myriad unconformities that are manifested as significant vertical and lateral variations in petrophysical character. Therefore, without stratigraphic context various petrophysical correlations are possible. With time lines applied to the correlation panels it is possible to identify isochronous, widespread petrophysical features of correlative utility, punctuated by intervals of variable petrophysical character. In order to build and test the stratigraphic framework, the biostratigraphic interpretations were plotted alongside petrophysical CPI logs as stratigraphic summary logs for each well (Fig. 3). Integration of the biostratigraphy with the petrophysics (Fig. 4) allowed time lines to be drawn across correlation panels to identify:

(1) correlatable intervals with consistent and pervasive petrophysical characteristics;
(2) intervals that display variable petrophysical characteristics but are of the same age.

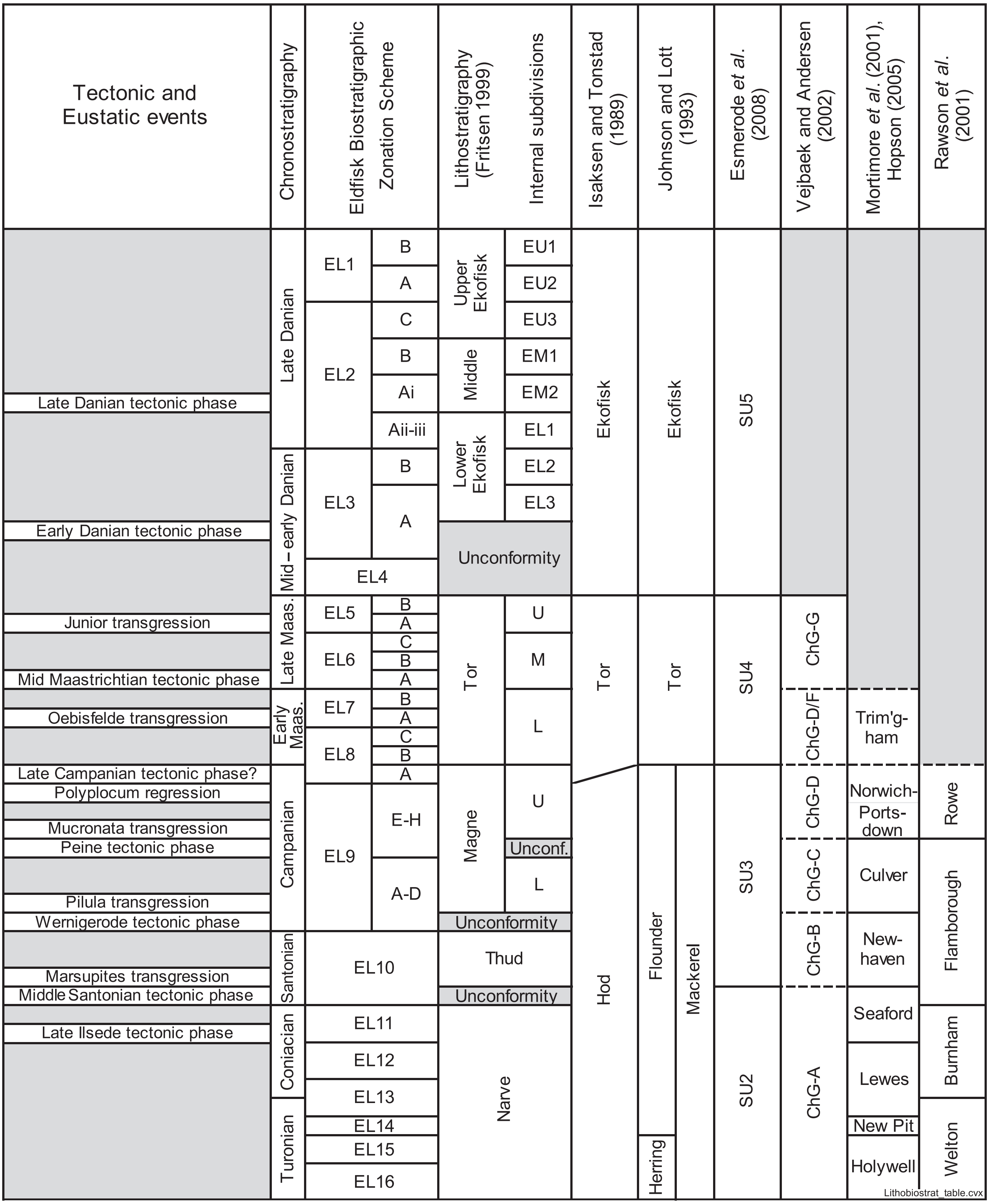

Fig. 2. Biozonation, chronostratigraphy and lithostratigraphy of the chalk on Eldfisk correlated with regional lithostratigraphic nomenclature, eustatic and tectonic events.

Examples of consistent correlative features include:

(a) Upper Ekofisk (EU) – this regionally pervasive unit is characterized at its base by high-porosity, low-density, clean hydrocarbon saturated chalks which display increasing gamma ray, decreasing porosity and increasing density trends up. Biostratigraphy dates this hemipelagic, autochthonous sequence as 'latest' Danian Subzones EL2C–EL1A. Lithofacies grade from massive, homogeneous chalks at the base to argillaceous, bioturbated periodites at the top.

(b) Lower Ekofisk (EL) – a widespread unit displaying higher gamma ray, higher density values and lower porosity characteristics than immediately adjacent sediments. The lithofacies are

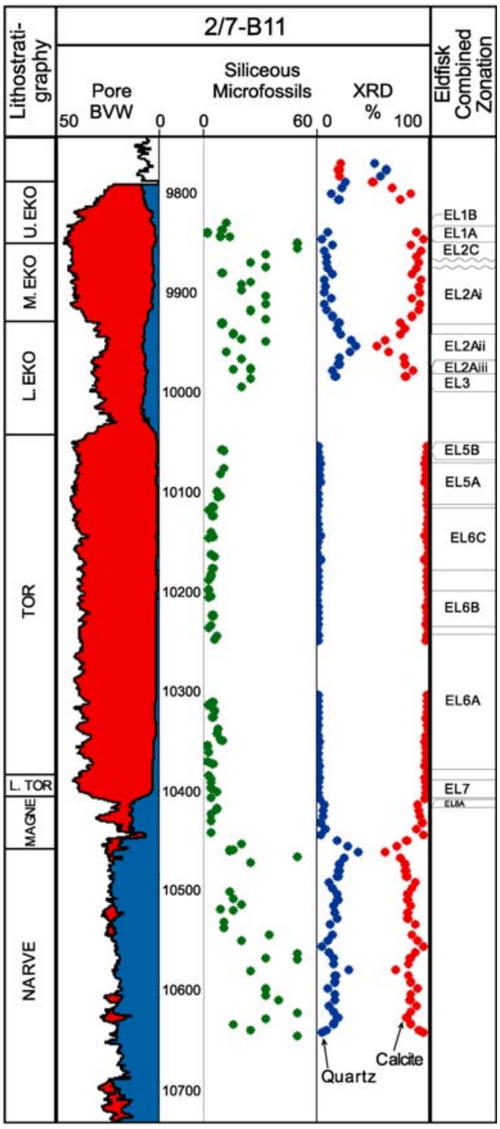

Fig. 3. Example stratigraphic summary log, from well 2/7-B-11, displaying the biostratigraphic interpretation alongside selected petrophysical data. This example also plots siliceous microfossil abundance (radiolarian) abundance against silica (quartz) content illustrating the relationship between high radiolarian abundance and high silica content in the sediment and its subsequent detrimental effect on porosity.

characterized by argillaceous hemipelagic periodites, dated as ‘early’ Danian subzones EL2Aii to Zone EL4.

Therefore, sequences displaying isochronously consistent petrophysical and lithological character were identified which in turn are punctuated by intervals of variable petrophysical and lithological character, for example:

(c) Middle Ekofisk (EM). Once the time lines are applied and the consistent character of the EU and EL is identified, it is apparent that there is considerable variation within the intervening EM unit; logs display laterally and vertically variable porosity and thickness in this unit. The biostratigraphic data reveals that these variations are influenced by differences in the geographical extent and temporal source of the reworking. The top of the Middle Ekofisk Formation is characterized by a phase of intra Ekofisk Formation (‘early’ Danian) derived reworking and is assigned to Subzone EL2B. This unit is characterized by higher gamma ray, higher density and lower porosity values than adjacent sediments (Fig. 4) and yields high proportions of chert.

The lower part of the Middle Ekofisk Formation is assigned to Subzone EL2Ai and yields dominantly *in situ*, ‘late’ Danian assemblages. This clean, low-gamma ray, high-porosity, low-density chalk is an important reservoir horizon. Within Subzone EL2Ai a phase of Late Cretaceous reworking can be recognized. This is focused in the ‘saddle area’, which acted as a depocentre for the remobilized Tor Formation derived sediments. These reworking levels clearly have a detrimental effect on the porosity which contrasts with the neighbouring Ekofisk trough where large-scale reworking equates with high-porosity reservoir horizons. However, the relationships between allochthonous and autochthonous levels within the EM are complex (Fig. 5). The Late Cretaceous reworking is concentrated in the saddle area (attaining up to 20% of assemblages) where it lies within otherwise autochthonous EM sediments which are in turn overlain by reworked intra Danian sediments. Further on to the structure these reworking events converge with little evidence for autochthonous sedimentation in between. Finally, in crestal locations the intra Danian and Late Cretaceous reworking is absent, resulting in high-porosity EU sediment lying contiguously upon high-porosity EM sediments. Therefore, these reworked horizons appear to act as permeability barriers or aquicludes in certain locations. The Middle Ekofisk Formation is characterized by a variety of lithofacies including conglomeratic and brecciated chalks, evidence for soft sediment deformation, including slump structures, convoluted bedding, overturned folds and homogenous massive chalks, together with evidence for hemipelagic rhythmic chalk and marl couplets, illustrating the mixture of autochthonous and allochthonous deposits.

(d) Tor Formation (EL6) – the integration of petrophysics and biostratigraphic results has improved the understanding of the distribution and generation of Tor Formation sediments. Late Maastrichtian Tor Formation Zone EL6 is characterized by high-porosity clean chalks which vary in thickness across the region. This interval comprises abundant, distinctive inoceramid debris in excess of 40% of the microfaunal recovery and often as high as 75–80%; the coarse bioclastic nature of these sediments may account for the high porosities. Given that inoceramid numbers were diminishing during the Maastrichtian, reaching extinction at the Cretaceous–Cenozoic boundary (inoceramids that occurred at this time were small and unlikely to be present in the numbers required to generate the high recovery of prismatic fragments recorded), the most likely explanation for deposition of this bioclast-dominated carbonate is by hydrodynamic sorting as part of an allochthonous process of sedimentation. This is a well established feature of Late Cretaceous carbonate turbidites (Neuweiler 1989) in which prismatic fragments of inoceramid shells act as coarse detrital elements in what is otherwise a normal Bouma turbidite sequence (Fig. 6). The faunal associations displayed on this figure are typical of the Tor Formation.

This zone appears to achieve maximum thickness on East Eldfisk and on the SW, southern and SE margins of the Alpha structure and in the Bravo channel on the Bravo structure. It is thin to absent on ‘crestal’ areas of Eldfisk Alpha and Bravo as defined during the Early Maastrichtian, suggesting the gravity flows were not deposited on structural highs. Overall depositional trends mirror those of the Early Maastrichtian, suggesting the palaeotopography developed at this time-controlled deposition of the Zone EL6 gravity flows. Hatton (1986) and Kennedy (1987) suggest penecontemporaneous allochthonous sediments were derived from the graben margin towards the NE. Conversely, derivation of these sediments could potentially be from a southerly source area, at least in part, as the area to the south was a more positive structure at this time and debris flows were being generated in this area during the ‘mid’ Maastrichtian (Sikora *et al.* 1999). Therefore knowledge of where these high-porosity gravity flows have been deposited helps in the selection of Tor Formation well locations. The presence of reworked nanofossil taxa and intraclasts supports the gravity flow

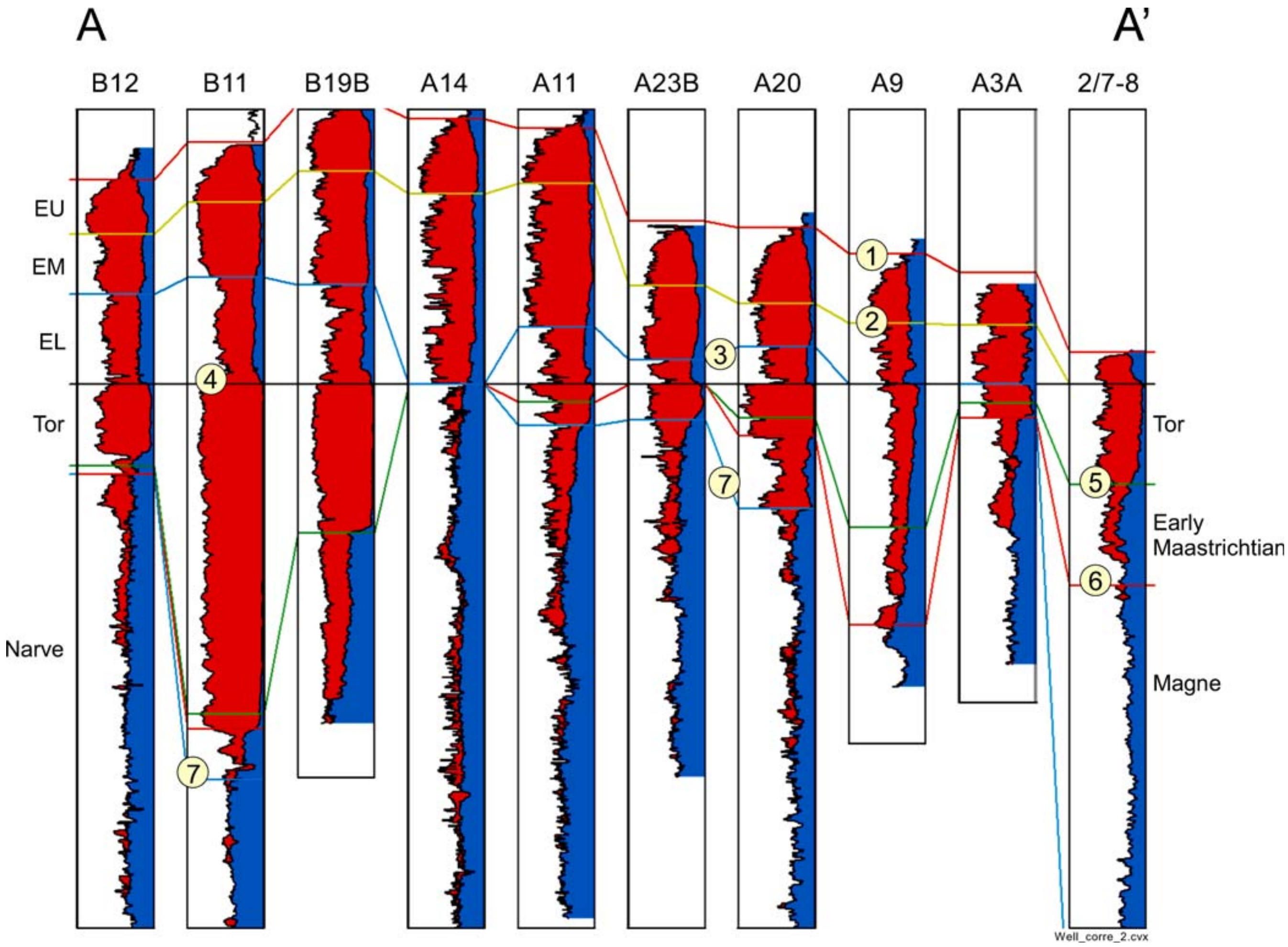

Fig. 4. Key well correlation (section A–A′ in Fig. 1) flattened on top Cretaceous. Lines represent the following horizon tops: (1) Ekofisk, (2) Middle Ekofisk, (3) Lower Ekofisk, (4) Tor, (5) Early Maastrichtian, (6) Magne, (7) Narve. Porosity (red) and Bulk Volume Water (blue) 50–0%.

origin for these sediments. The Tor Formation is also generally devoid of siliceous microfossils such as radiolaria. There appears to be a good relationship between the abundance of siliceous microfossils, the proportion of quartz determined by XRD analyses and porosity (Fig. 3); therefore the potential exists for radiolarian abundance to act as an inverse proxy for porosity.

(e) Magne Formation. Sediments that display Tor Formation petrophysical properties (high porosity with good separation between the porosity and BVW on CPI logs, e.g. Well 2/7-A-23B on Fig. 4), are present across the northern part of the Alpha ridge and NW flank of the Alpha structure. Prior to biostratigraphic analyses these sediments have previously been assigned to the Tor Formation, based principally on petrophysical character (clean, low gamma ray and high porosity). The presence of an allochthonous debris flow, including small chalk clasts, recorded in core from the western flank may well have contributed to the assignment of this unit to the Tor Formation. However, biostratigraphic results reveal these sediments to be Late Campanian Magne Formation. Porosity and permeability plots from the Magne Formation in well 2/7-A-23B (Fig. 7) illustrate that the Magne Formation follows Hod Formation poroperm trends rather than Tor Formation trends when plotted against data from across Eldfisk Alpha and is therefore genetically unrelated to the Tor Formation. Subtle poroperm differences suggest this unit may not act as a single flow unit when in contact with the Tor Formation.

When the geological data is integrated, it is apparent that there are autochthonous, hemipelagic, undisturbed, often rhythmic, isochronous intervals characterized by widespread, consistent characteristics. These intervals are punctuated by intervals of variable petrophysical character, yielding evidence for allochthonous sedimentation. Therefore, chalk deposition on Eldfisk is characterized by periods of eustatically controlled, tectonically quiescent sedimentation, interrupted by synchronous episodes of tectonically controlled sedimentation.

Improved understanding of the timing and differential growth of various parts of the structure can be determined by integration of the biostratigraphy with geophysical and biofacies data. The importance of mapping the variations in reworking and facies distribution is not only important from a reservoir modelling perspective but is also critical when geosteering horizontal wells in any particular reservoir layer.

Geophysical data

The presence of shallow gas in the overburden of Eldfisk means that approximately 60% of the wells drilled on Eldfisk are located in a seismically obscured zone. A four-component 3D Ocean Bottom Cable acquisition programme was acquired and processed in 2001, with the primary purpose of undershooting the Alpha and Bravo complexes and attempting to obtain a better image through the gas affected overburden. In 2007 a P-wave prestack depth migration project was instigated to further improve the image. The resultant PZ imaged data volume reduced this obscured area by 20% and improved the overall imaging on the flanks of the

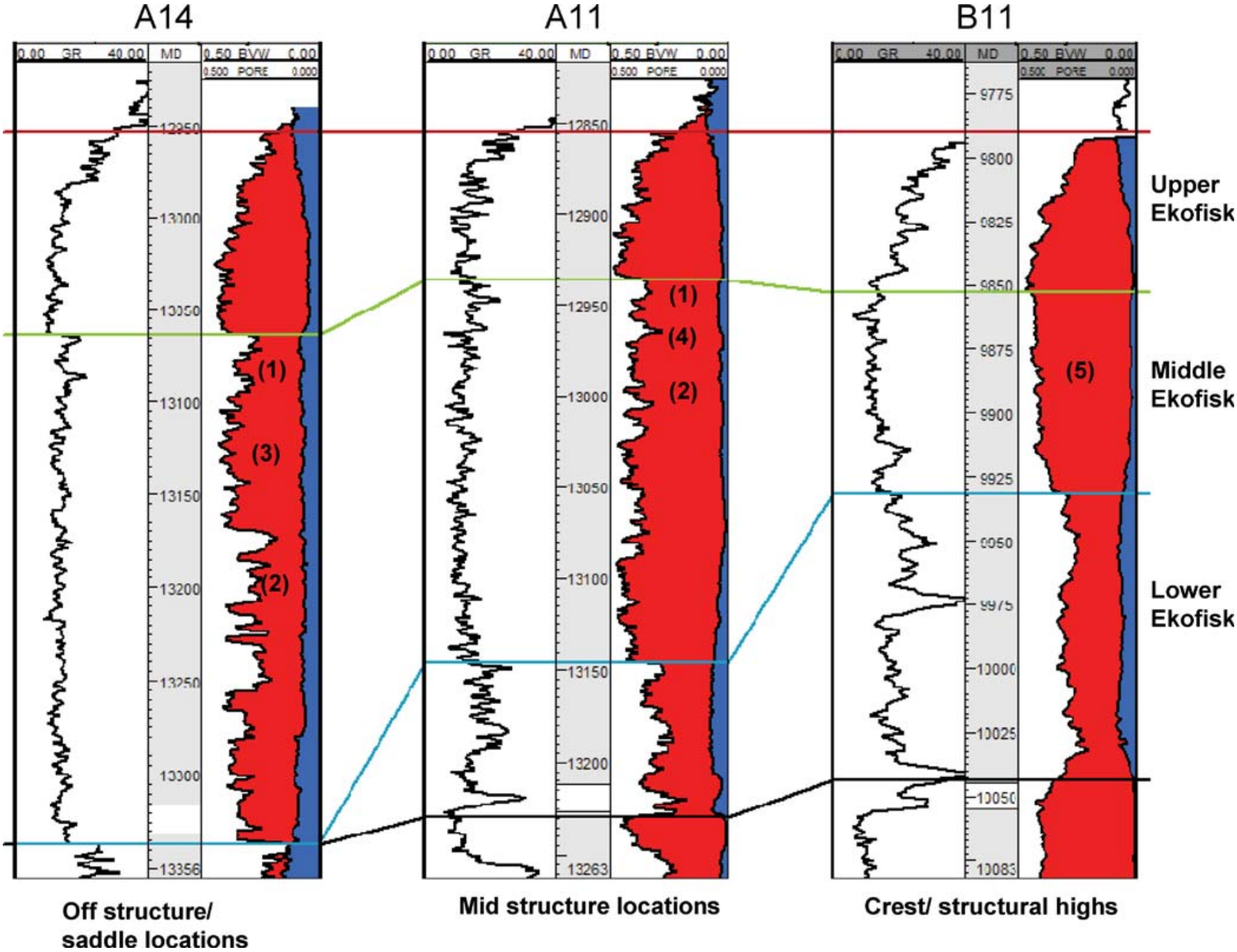

Fig. 5. Intra Danian reworking (1) and Cretaceous reworking (2) levels are characterized by reduced porosity. In the saddle area reworked horizons (3) are separated by autochthonous, high-porosity sediments. These reworked horizons converge towards structural highs and are not separated by high-porosity autochthonous beds (4). However no low-porosity reworked horizons (5) are present on the crest. Traditional log correlation could lead to ambiguous results, however, when tied to the biostratigraphy mappable patterns of reworking emerge and these maps are presented in this paper. This in turn leads to improved 3D modelling and is extremely important when geo-steering horizontal wells. Track 1, gamma ray 0–50 API; track 2, porosity (red) and bulk volume water (blue) 50–0%.

field. The new seismic volume was then integrated with the biostratigraphic analyses to produce a meaningful interpretation of the Alpha and Bravo crests (Fig. 8). The following chalk horizons were calibrated with the petrophysics and biostratigraphy in the interpretation:

(1) Narve Formation – the top of the Narve Formation is picked at a weak reflector overlying a generally ‘washed out’ seismic character that can be tracked regionally.
(2) Thud Formation – this is generally thin or absent in the study area and therefore beyond seismic resolution. The lower boundary is described geophysically in Fritsen (1999) as an onlap surface, suggesting a phase of structural growth between deposition of the Narve and Thud Formations.
(3) Magne Formation – Fritsen (1999) defines the seismic criterion for the boundary between the Magne and Thud Formation as an onlap surface, again suggesting a phase of structural growth between deposition of these formations. Regionally, the seismic criterion for picking the boundary between the Magne and Tor Formation in Fritsen (1999) is a well defined reflector separating a lower amplitude interval below from a higher amplitude interval above and is also locally an onlap surface. The presence of a stronger geophysical signature supports differentiation of this (former Hod Formation) unit from the Narve Formation
(4) Tor Formation – the top of this formation can be difficult to pick without well ties due to lack of contrast attributed to the presence of an unconformity and the absence of the basal ‘Ekofisk tight zone’ in the study area. The presence of a more continuous reflector pattern in the upper part may reflect the hemipelagic Zone EL5, while the discontinuous pattern observed within the Tor Formation may represent the remobilized deposits assigned to Zone EL6, where seismic resolution allows.
(5) Ekofisk Formation – in Fritsen (1999) the top of the Ekofisk Formation is evident as a clear seismic event, the result of an increase in acoustic impedance. Poor seismic resolution prohibits internal subdivision, although the chaotic internal seismic character may be related to allochthonous deposition.

The seismic interpretation of the flanks of the structure is reasonably straight forward as the stratigraphy is relatively thick and not restricted by the tuning thickness of the seismic (horizontal resolution limits). However, as the interpretation is pushed towards the crest the combination of thinning and the obscured seismic zones means that the picks become increasingly more driven by

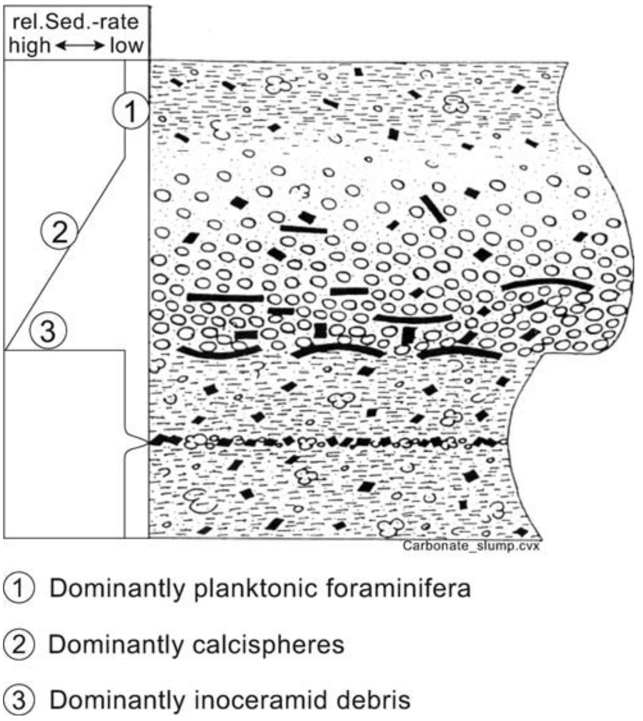

Fig. 6. Typical carbonate slump with concentrations of inoceramid debris, planktonic foraminifera and calcispheres, after Neuweiler (1989). This hydrodynamic sorting pattern is particularly common in the Tor Formation regionally.

the biostratigraphic and structural controls. The final interpretation consists of hand-contoured maps and relies on the extensive and consistent biostratigraphic input outlined in this paper. The integration of seismic and biostratigraphy on the flanks has brought more confidence in the mapping of the field and this is particularly apparent where the seismic image degrades and more reliance is placed on the integrated petrophysical and biostratigraphic

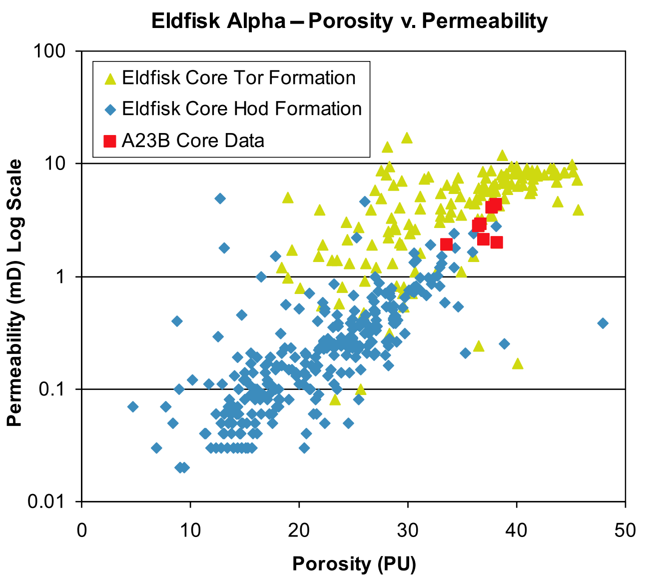

Fig. 7. Porosity v. permeability plots from the Magne Formation from well 2/7A-23B, illustrating that the Magne Formation follows Hod Formation porosity permeability trends rather than Tor Formation trends when plotted against core data from Eldfisk Alpha. These sediments, which display good reservoir characteristics, had previously been assigned to the Tor Formation.

derived tops. The flow units used in the 3D model are below seismic resolution and mapping of these is reliant on the isopachs derived from this study.

Biofacies methodology

The biofacies component of this study is targeted at determining the relative palaeobathymetry of chalk deposition over the Eldfisk region to aid facies mapping, improve understanding of the structural growth of the field and identify possible future drilling targets. To achieve this, the palaeoslope biofacies model defined by Olsson & Nyong (1984), Nyong & Olsson (1984) and Sikora & Olsson (1991) has been used. Following their defining criteria, all benthic foraminifera are ascribed to either a biofacies group or range of groups. Their model is applicable to the North Sea area as it was initially developed within the North Atlantic region and many species are common to both areas. The original statistical definition of their depth/biofacies groups has been accepted here. However, additional work has been undertaken identifying the palaeobathymetric groups to which foraminifera recorded in this study, but not utilized by Nyong & Olsson (1984) and Sikora & Olsson (1991), belong. While other environmental factors such as temperature, current circulation, nutrient and oxygen supply also have an effect, the distribution of benthic taxa is interpreted largely as a response to bathymetric controls and is consequently used to assess changing palaeobathymetric trends. Six main biofacies groups have been recognized during this study, using the Nyong & Olsson (1984) model as an initial basis. However, additional factors will have had an effect, particularly the development of dysaerobic conditions at the seafloor, resulting in apparent deeper biofacies signals. Therefore, while elements of the microfauna are consistent with lower bathyal to abyssal biofacies as defined by Nyong & Olsson (1984), it is unlikely that such depths were present in North Sea chalk seas. To reflect depth trends rather than absolute values the terms Upper Slope, Middle Slope, Lower Slope and Basinal have been applied to represent the Upper, Middle, Lower Bathyal and Abyssal biofacies of Nyong & Olsson (1984) but not necessarily the absolute palaeodepths (Fig. 9). In addition, information derived from the planktonic foraminifera, radiolaria, calcispheres, ostracods and other bioclastic debris has also been used to assess changing trends in the depositional environment.

In the present study planktonic morphotypes, as identified by Hart & Bailey (1979) have been formalized and divided into component groups according to life cycle water depth preference. This technique in establishing trends in water depth changes has never previously been applied to North Sea Late Cretaceous chalks. It is strictly an experimental approach that, when compared with the benthic foraminiferal analysis outlined above, shows a similarity of trends sufficiently strong to support the value of using this method, particularly when used in conjunction with other biofacies data. This is also summarized in Figure 9; however, this correlation remains tentative given that other environmental factors mentioned above (notably palaeotemperature) can influence the distribution of planktonic foraminifera. Planktonic/benthic (P/B) ratios have not been used to imply palaeobathymetry in the chalk in this study. There is evidence to show that planktonic recovery from onshore chalk outcrop sections is approximately 10% of that seen in adjacent flint meals (Bailey & Clayton 2010). This suggests there must be a post-diagenetic factor and questions the use of P/B ratios as a palaeobathymetric tool in the chalk.

Radiolaria exhibit levels of increased abundance and diversity during periods of chalk deposition in the North Sea basin. They are useful stratigraphically and also indicate changes in original water mass movement. Their abundance at levels in the Narve, Thud and Ekofisk Formations coincide with deeper water,

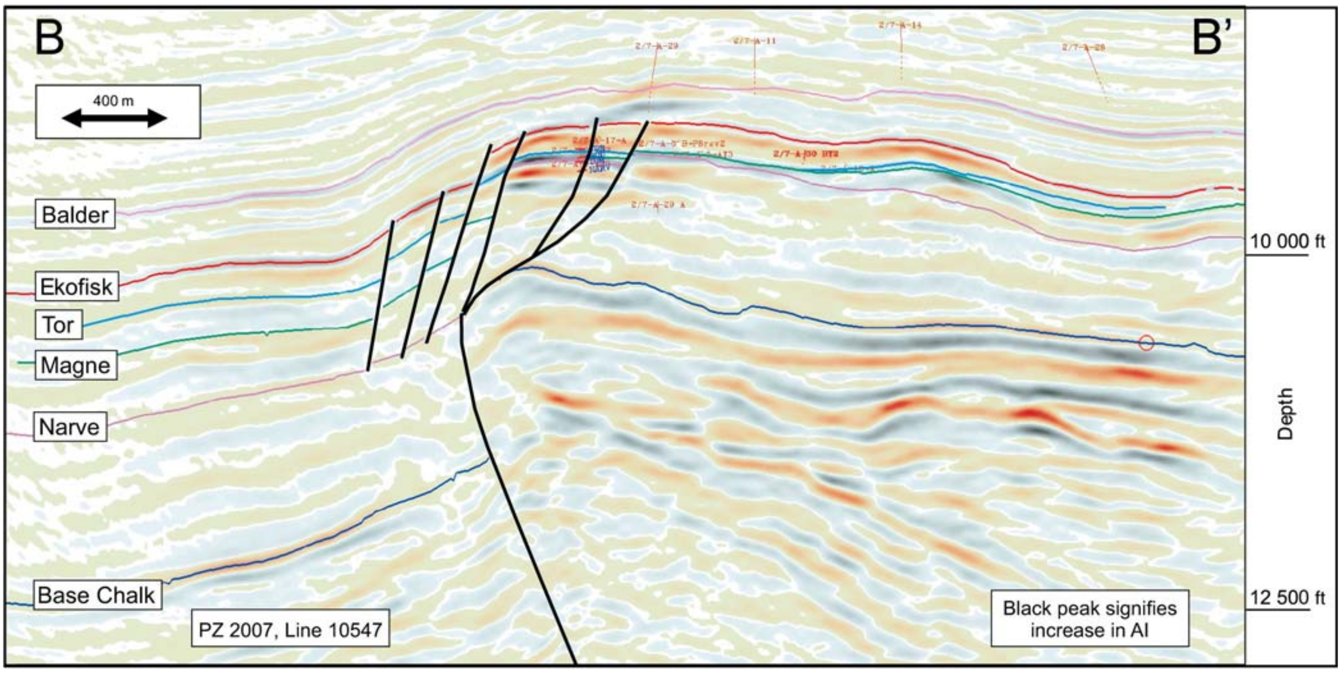

Fig. 8. The depth seismic line B–B′ across the Eldfisk Field saddle area (see Fig. 1 for location) demonstrates the array of unconformities in the chalk sequences.

hemipelagic, autochthonous depositional conditions with reduced levels of reworking. Results from this study agree with Brasher & Vagle (1996) and suggest that radiolarian abundance may act as a proxy for the silica content and therefore chalk porosity (Fig. 3).

Inoceramid bivalves occur frequently in Late Cretaceous chalks and there is evidence they were associated with dysaerobic seafloor conditions (Harries *et al.* 1996). Individual complete specimens range in size from *c.* 2 cm to 2 m and originally comprised a two-layered structure of aragonitic and prismatic calcite. The former is unstable and easily destroyed during early diagenesis, leaving a resistant prismatic layer. These shells often disaggregate and, at certain stratigraphic levels, the disaggregated prisms can form a significant constituent of the sediment. This characteristic is important during deposition of the Tor Formation, where considerable thicknesses of high-porosity chalks, associated with mass flows and comprising dominantly inoceramid debris (often 70% of microfaunal recovery), were deposited to the south and

Biofacies Groups	Sea floor environment	Planktonic Foram Groups	Descriptors	Examples
1	Inner Neritic (Shelf)	Unkeeled forms	Simple spherical - subspherical chambers, no major ext. ornam't e.g. keels	*Rugoglobigerina Whiteinella Hedbergella Heterohelix Globigerinelloides*
2	Middle Neritic (Shelf)	Keeled Group 1	Flat, biconvex morphotypes, 1 or 2 keels	*Globotruncanella, Arch. cretacea, Marg. marginata*
3	Outer Neritic (Shelf)	Keeled Group 2	Planoconvex - part trochospiral, 1 or 2 keels	*Hel'globotruncana praehelvetica, Praeglobotruncana stephani, Dicarinella primitiva, Rosita fornicata*
4	Upper Slope	Keeled Group 3		
5	Lower Slope	NB: Planktonic groups do not imply a precise depth range. Other environmental factors e.g. temperature, current circulation, oxygen supply may affect their distribution	Strongly planoconvex - high trochospiral, 1 or 2 keels	*Hel'globotruncana helvetica Praeglobotruncana gibba, Dicarinella concavata, Rosita contusa*
6	Basinal			

Fig. 9. Correlation of planktonic bathymetric foraminifera biofacies groups used in this study. Benthic biofacies groups follow Olsson & Nyong (1984) and Nyong & Olsson (1984).

east of the region (see 'Allochthonous biofacies' section below). Echinoderm debris, bryozoan debris and ostracods also form significant elements of the coarser calcitic component and concentrations may also occur at levels interpreted as being part of mass flow deposits.

Calcispheres (the encystment stage of calcareous dinoflagellate algae) are most abundantly found in shelf margin to upper slope sediments (Adams *et al.* 1967); their occurrence in deeper settings may be due to subsequent reworking downslope as part of the sediment load (Neuweiler 1989).

Allochthonous biofacies

It is important to improve understanding of the distribution of different reworking events and the variable impact of these events on porosity across the structure. Chalk reworking is well established in Norwegian Central Graben chalk fields (e.g. Perch-Nielsen *et al.* 1979), with subsequent discussion of the variable sedimentology by Hatton (1986) and Kennedy (1987). Because of the derived nature of the microfaunal components, remobilized sequences are not suited to palaeobathymetric biofacies interpretations. Late Cretaceous chalk turbidite sequences are described from onshore Germany (Neuweiler 1989), where different bioclastic elements form discrete size-sorted levels, comparable with grain size units in normal Bouma sequences (Fig. 6); comparable sequences are recorded repeatedly through the succession in Central Graben chalks. When unlithified chalk is redeposited as a gravity flow it creates turbidites/mass flows analogous with those in siliciclastic sediments. Consequently, coarser fragments (e.g. inoceramid and echinoderm debris) are deposited in more proximal, higher energy locations, whereas the finer fragmented nanoplankton-dominated fraction is deposited as distal mud cloud deposits or at lower energy levels. Other common bioclastic elements, principally foraminifera, radiolaria and calcispheres, are size sorted, with larger foraminifera in more proximal or higher energy deposits and small, lighter forms occurring with calcispheres in more intermediate locations or at intermediate energy levels within mass flows. The impact of grain size on porosity distribution in the chalk was also discussed by Brasher & Vagle (1996).

Of the fine-grained nanofossil component, robust morphotypes of calcareous nanoplankton appear to preferentially survive transportation and re-deposition within allochthonous chalks; examples include the genera *Micula*, *Lucianorhabdus*, *Prediscosphaera* and *Arkhangelskiella*. The recognition of assemblages dominated by these forms (in the absence of a diverse nanoflora also yielding delicate forms) therefore assists the identification of such sediments.

Whilst the interpretation of individual biofacies in a well can be problematic, for the reasons outlined above, the combination of petrophysics, geophysical interpretation and the collective interpretation of many wells along confirmed time lines gives confidence in a field-wide model based on many wells. The position of the changes in facies and water depth interpreted and mapped conforms to reasonable geological pattern and strengthens the confidence in the technique. The biofacies maps produced cite palaeobathymetries deeper than commonly quoted for onshore chalks. Although dysaerobic conditions at the seafloor may give an apparently deeper biofacies signal, the chalk in the Central Graben appears to have been deposited at significantly greater depths than previously appreciated. Regardless of the specific depth of deposition, the relative patterns and trends still hold.

Results (discussed in lithostratigraphic order)

The lithostratigraphic definitions of the Ekofisk and Tor formations follow Isaksen & Tonstad (1989); the definitions of the Narve, Thud and Magne formations follow Fritsen (1999), but are referred to in an informal sense pending formal validation. Regional biostratigraphic and seismic evidence suggests that the Thud Formation is best developed in basinal lows (Fritsen 1999), and this is supported by evidence for the Thud Formation off-structure on East Eldfisk. The first record of cored Thud Formation, as identified in this study (well 2/7-A-23B), allows better calibration with petrophysical and geophysical data. This also permits better definition of this formation than the original description by Fritsen (1999). The Magne Formation can be subdivided into two distinct sequences: a Late Campanian, Upper Magne Formation sequence which is relatively widespread and an Early Campanian, Lower Magne Formation sequence which is only rarely preserved and identified in the study area. The Tor Formation is restricted to the Maastrichtian on Eldfisk; the top of the Late Maastrichtian defines the upper boundary (Zone EL5), and the lower boundary equates with the base of the Early Maastrichtian (Subzone EL8B). The boundary between the Magne and Tor Formations broadly coincides with the boundary between the Campanian and Maastrichtian stages. The results of this study allow the Tor Formation to be subdivided into three distinct (allostratigraphic) sequences. Similarly, the Ekofisk Formation can be subdivided into three distinct (allostratigraphic) sequences which correlate well with the ConocoPhillips geological model subdivisions. These unit breakdowns are below seismic resolution and based on the biostratigraphic and petrophysical interpretations.

Narve Formation

Age. Turonian to Coniacian, Zones EL16–EL11. The top of the Narve Formation represents a variable unconformity surface on Eldfisk, the top of which ranges from Subzone EL11B at its youngest on Alpha; to Zone EL13 in the 'saddle', an area which also displays maximum section loss at this unconformity (overlain by 'late' Danian Ekofisk sediments, a time gap of 23 Ma).

Lithology/petrophysics. Generally deposited as 'deep' water, hemipelagic, rhythmically bedded, alternating dark grey and light grey–off-white argillaceous periodites which vary in thickness from tens of centimetres up to a metre. The relatively high argillaceous content is reflected in the relatively high gamma ray values seen in the Narve Formation on Eldfisk. Petrophysical logs typically display low-porosity, poor reservoir characteristics.

Biofacies. Described by Kennedy (1987) as a time of quiet, pelagic deposition with potentially anoxic bottom waters in bathyal settings with little evidence for strong structural relief. The poor recovery of benthic foraminifera at this time suggests probable dysaerobic conditions.

Tectonostratigraphy. The main Ilsede phase tectonics occurred in rocks older than those studied as analyses ceased on confirmation of top Narve Formation. However, inversion during this tectonic phase resulted in the early growth of the Eldfisk structure, upon which evidence for subsequent tectonic phases is expressed.

Regional correlation. Equates with the Middle Hod Member of Isaksen & Tonstad (1989), the Seaford (*pars.*), Lewes Nodular, New Pit and Holywell Formations in the UK and seismic unit SU2 of Esmerode *et al.* (2008) and seismic sequence ChG-A of Vejbaek & Andersen (2002) in Denmark.

Thud Formation

Age. Constrained to Zone EL10 of Santonian age on Eldfisk.

Lithology/petrophysics. Fritsen (1999) described alternating argillaceous and clean chalks (periodites), the higher gamma values observed therein suggest clay content higher than in the overlying Magne Formation. Cored Thud Formation sediments from this study, in which argillaceous chalk and clean chalk periodite couplets display variable but generally high gamma and low-porosity values, confirm this description.

Biofacies. Deepwater, transgressive benthic foraminifera such as *Stensioeina*, together with lithofacies data implies a deeper water (bathyal) environment and ubiquitous deposition in the area before subsequent erosion.

Tectonostratigraphy. The lower boundary of the Thud Formation on the western flank of Eldfisk Alpha is of Middle Santonian, Subzone EL10B age, and the boundary between the Thud Formation and intra Coniacian Narve Formation unconformable. These age constraints suggest the influence of 'Mittel Santon puls' tectonics. The lower boundary and therefore Thud Formation deposition on Alpha are associated with the Middle Santonian *Marsupites* transgression (as described in German outcrop sections, Niebuhr *et al.* 2000). Cored Thud Formation sediments yield a zone of irregularly shaped inoceramid bivalve shell fragments (Fig. 10a), representing soft sediment, slumped, fragmentation of a specimen of the genus *Sphenoceramus* (C. J. Wood, pers. comm. 2007). Initial pulses of the Wernigerode tectonic phase are expressed by an interval of slumping in many German and southern England outcrop sections and dated as Santonian. A phase of inversion tectonics has also been described from the Aachen–Antwerp area by Bless *et al.* (1986) close to the Santonian–Campanian boundary. The cumulative effect of these tectonic and eustatic events, together with the subsequent intra Campanian Peine tectonic event, accounts for the absence of Thud Formation sediments on structural highs. The occurrence of slumping and intraclasts within the upper part of the Thud Formation on the western margin of the Eldfisk Alpha structure appears to be an expression of the Wernigerode tectonic event. (Fig. 10b).

Correlation. Lithostratigraphic comparison of age equivalent sections in onshore northern Germany confirms the presence of argillaceous chalks in the mid Santonian to basal Early Campanian sequences and broadly equates with the marl-rich Newhaven Chalk Formation in the UK, proving the widespread geographical extent of this distinctive unit. In the Danish sector the Thud Formation equates with ChG-B of Vejbaek & Andersen (2002) and seismic unit SU3 (*pars.*) of Esmerode *et al.* (2008).

Lower Magne Formation

Sediments assigned to the Lower Magne Formation are present in flank/off structure locations on Eldfisk where they generally overlie Thud Formation sediments. However, the presence of Early Campanian age sediments resting directly on Narve Formation on the NE flank of Alpha suggests that this sequence is genetically separable from the Thud Formation.

Age. Lower Magne Formation sediments range in age from Early Campanian, Subzones EL9A–EL9E.

Lithology/petrophysics. A distinctive petrophysical log signature (characterized by 'bow-shaped' density and porosity profiles) attributable to the Early Campanian Magne Formation can be seen in off-structure locations, particularly East Eldfisk. The presence of relatively expanded sequences off structure suggests preservation of these sediments in basinal settings despite removal from structural highs.

Biofacies. Biofacies data indicates deepening from middle to lower slope/basinal water depths towards East Eldfisk and the presence of a palaeotopographic high towards Alpha.

Tectonostratigraphy. The presence of Lower Magne Formation directly overlying the Narve Formation on the NE flank suggests

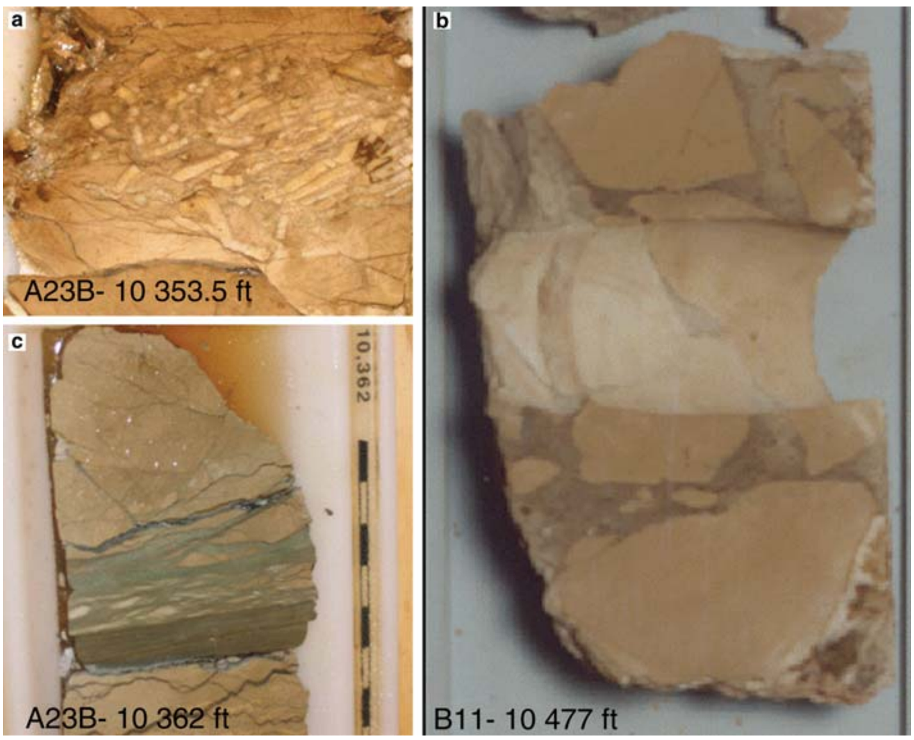

Fig. 10. (**a**) Example of Wernigerode Phase tectonics; small scale slumping recognized in the deformation of inoceramid (*Sphenoceramus*) bivalves in 2/7-A-23B. Core section represents approximately 4 inches. (**b**) Example of Wernigerode Phase tectonics; clasts in Santonian Thud Formation sediments in 2/7-A-23B. (**c**) Example of Peine Phase tectonics: clasts in Campanian age sediments in cored 2/7-B-11. Core section represents approximately 4 inches.

that the Thud Formation may have been removed during the Wernigerode tectonic event and associated eustatic lowstand, prior to the onset of Magne Formation deposition during the subsequent *pilula* and *mucronata* transgressions. Elsewhere, the scarcity of Early Campanian Lower Magne Formation relative to the Late Campanian Upper Magne Formation may suggest that its absence is a function of the 'latest' Early Campanian Peine tectonic phase, possibly combined with the effects of a coincident eustatic fall.

Correlation. The Lower Magne Formation equates with the Culver Formation, onshore UK. In the Danish sector this unit equates with seismic sequence ChG-C (Vejbaek & Andersen 2002) and seismic unit SU3 (*pars.*) (Esmerode *et al.* 2008).

Upper Magne Formation

Age. Late Campanian Subzone EL9E–EL8A.

Lithology/petrophysics. A range of lithofacies (including hemipelagic periodites, homogenous chalk and brecciated chalk) have been assigned to the Magne Formation, reflecting different depositional environments as the structure grew through the Campanian. These variations are supported herein by lateral variations in the petrophysical log curves; for example, reservoir quality Magne Formation described in well 2/7-A-23B on the Alpha structure contrasts with the low-porosity, tighter, deeper water biofacies in 'basinal' well 2/7-8 (Fig. 4). Late Campanian sediments occur in many wells across the study area, but principally across the northern part and eastern flank of the Eldfisk Alpha structure and across the East Eldfisk structure. The Magne Formation is notably absent across the highest points on the crest and southwestern parts of the Alpha structure. The distribution across the Bravo structure is less clear due to a lack of data points. The top of the Magne Formation displays higher gamma ray values than the overlying Tor Formation, which equates with red/pink chalk facies in off-structure or basinal settings.

Biofacies. Biofacies data implies a shallowing environment of deposition towards a crestal feature on the south of the Alpha structure, with a similar pattern observed on parts of the Bravo structure (Fig. 11). This indicates growth of significantly positive structures by the Late Campanian, characterized by non-deposition, condensation and hard-ground development on structural crests. This has also been reported from the adjacent Valhall structure (Sikora *et al.* 1999). The presence of reworked Narve Formation within the Magne Formation on the eastern flank of Alpha indicates that areas of Narve Formation were exposed during the Late Campanian. Surrounding areas are characterized by middle to lower slope environments giving an overall impression of a gentle dip slope to the east during the Late Campanian.

Tectonostratigraphy. Late Campanian Upper Magne Formation sediments post-date Peine phase tectonics and their deposition is associated with the subsequent *mucronata* transgression, the local European equivalent to global maximum sea levels recorded during the Late Campanian.

Correlation. In the Danish sector this unit equates with seismic sequence ChG-D (*pars.*) of Vejbaek & Andersen (2002) and seismic unit SU3 (*pars.*) of Esmerode *et al.* (2008). Sedimentological features such as intraclasts and hard-grounds in the upper part of the Magne Formation, together with an eastwards shift in the location of the structural high in the 'earliest' Maastrichtian, suggest a phase of inversion near the Campanian–Maastrichtian boundary, coincident with inversion in the Aachen–Antwerp area (Bless *et al.* 1986). Results indicate that crestal reservoir facies are genetically unrelated to the reservoir sediments within the Tor Formation. Intra Magne Formation brecciated debris flows,

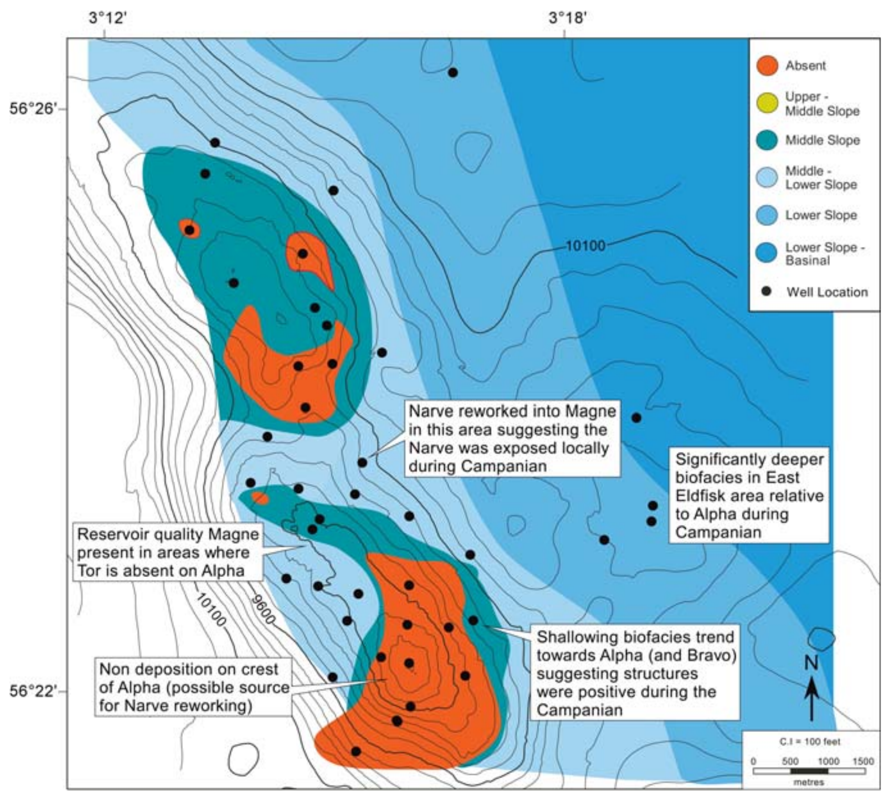

Fig. 11. Biofacies map for the Late Campanian Magne Formation showing a shallowing pattern towards, and non-deposition on structurally higher areas. P/B groups do not imply precise depth ranges but do give an impression of shallowing and deepening depth trends.

interpreted as expressions of Peine phase tectonics, can be seen in core from the Alpha and Bravo structures (Fig. 10c).

Lower Tor Formation

Age. Early Maastrichtian Subzone EL8B to Zone EL7.

Lithology/petrophysics. Petrophysical variations may be a function of biofacies and lithofacies variations reflecting the continuation of the palaeotopography established in the Late Campanian.

Biofacies. Early Maastrichtian hemipelagic sediments display onlap and infill distribution patterns, controlled by the existing palaeotopography. Distinct depocentres occur within the 'Bravo channel', along the eastern and southern flank of the Alpha structure and extending out towards the East Eldfisk structure. These depocentres exhibit middle–lower slope biofacies signatures (Fig. 12). There are areas of absence along the crest of the Alpha structure, a continuation of the pattern of non-deposition on structural highs recognized during the Campanian, combined with erosion during subsequent tectonic phases. The relatively shallower crestal 'Alpha ridge' appears to have shifted NW to encompass the whole of the present day 'saddle' area. On Bravo there is evidence of a positive crestal area NW of the 'Bravo channel' (non-deposition), surrounded by upper–middle slope deposits. To the south and east of the 'Alpha ridge', upper–middle slope depths are recorded. During this period there is biofacies evidence for progressive shallowing across the study area.

Tectonostratigraphy. Any deposition over the 'Alpha ridge' during this time was subsequently eroded. There is little evidence for tectonism during deposition of the Lower Tor Formation, although a tectonic phase is close to the Campanian–Maastrichtian (Magne–Tor Formation) boundary.

Middle Tor Formation

Age. Late Maastrichtian, Zone EL6.

Lithology/petrophysics. Sediments are rich in coarse bioclastic debris, particularly inoceramid bivalve fragments, providing high-porosity reservoir in depocentres around the Alpha structure and in the Bravo channel (Fig. 13).

Biofacies. Given the allochthonous, derived nature of sediments of this age, it is not possible to conduct palaeobathymetric biofacies interpretations.

Tectonostratigraphy. An intra Maastrichtian tectonic phase may be the mechanism for triggering this re-deposition and may correlate on a regional scale with intra Maastrichtian inversion events from the Aachen–Antwerp area onshore (Bless *et al.* 1986) and northern Europe (Ernst & Wood 2000).

Upper Tor Formation

Age. Late Maastrichtian Zone EL5.

Lithology/petrophysics. Deposition and distribution of Late Maastrichtian Zone EL5 chalks appear relatively widespread, with the exception of an area along the 'crestal ridge' area of the Alpha structure, extending into the 'saddle area' between Alpha and Bravo and locally on the northern part of East Eldfisk. Zone EL5 is characterized by clean, porous chalks at the base, becoming slightly less porous up section, reflecting the change from allochthonous to autochthonous sedimentation.

Biofacies. This zone is interpreted as a hemipelagic 'drape' across the Eldfisk structures following the cessation of the Combined Zone EL6 reworking episodes. Its absence from the areas illustrated in

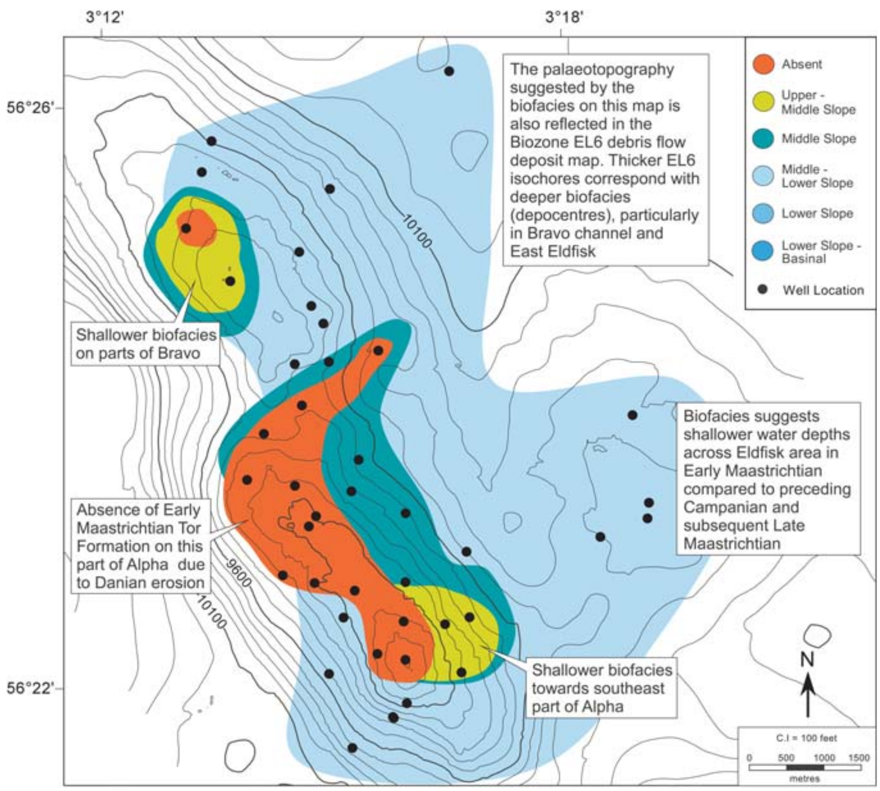

Fig. 12. Biofacies map for the Early Maastrichtian Tor Formation, showing a shallowing pattern towards, and non-deposition on structurally higher areas.

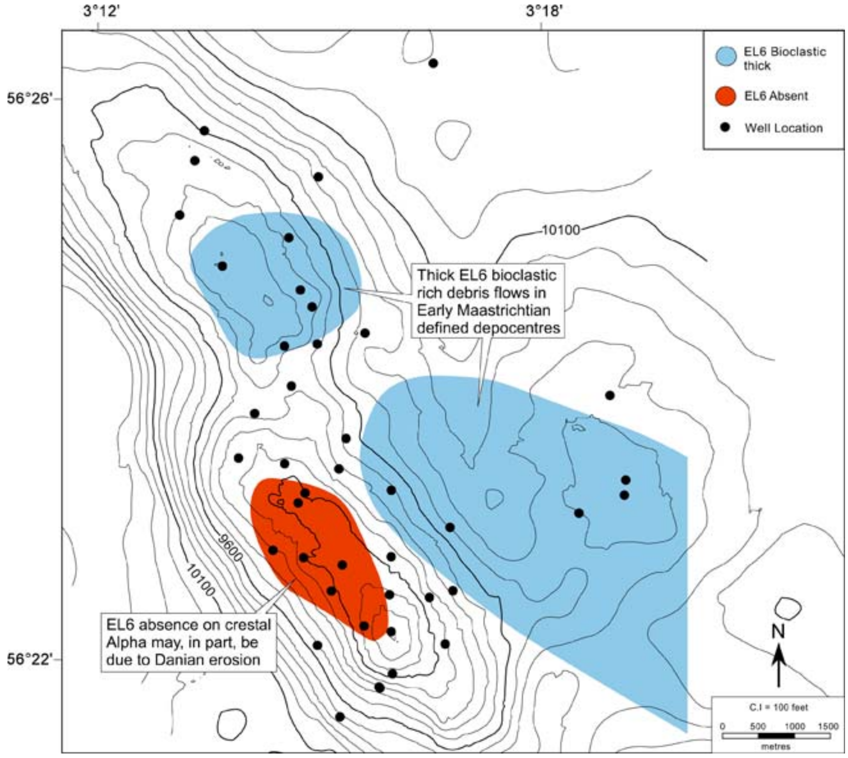

Fig. 13. Map illustrating main depocentres and areas of absence for bioclastic-rich debris flows (possibly eroded) assigned to Zone EL6.

Figures 14 and 15 is attributed to subsequent erosion during the 'early' Danian.

Late Maastrichtian Subzone EL5A represents the initial phase of a period of pervasive hemipelagic sedimentation, relatively rich in planktonic foraminifera. Subzone EL5A was deposited in middle–lower slope water depths over Alpha, increasing to lower slope towards the SW of Alpha. Structural relief is less pronounced due to backfilling of depocentres during the 'mid' Maastrichtian. An absence of Late Maastrichtian Subzone EL5A chalks on a well-defined 'ridge' along the length of the Alpha structure is attributed to subsequent erosion during the Danian. This is indicated by the absence of a pronounced biofacies shallowing trend towards this 'ridge' and by the fact that the area of absence also cuts across biofacies contours.

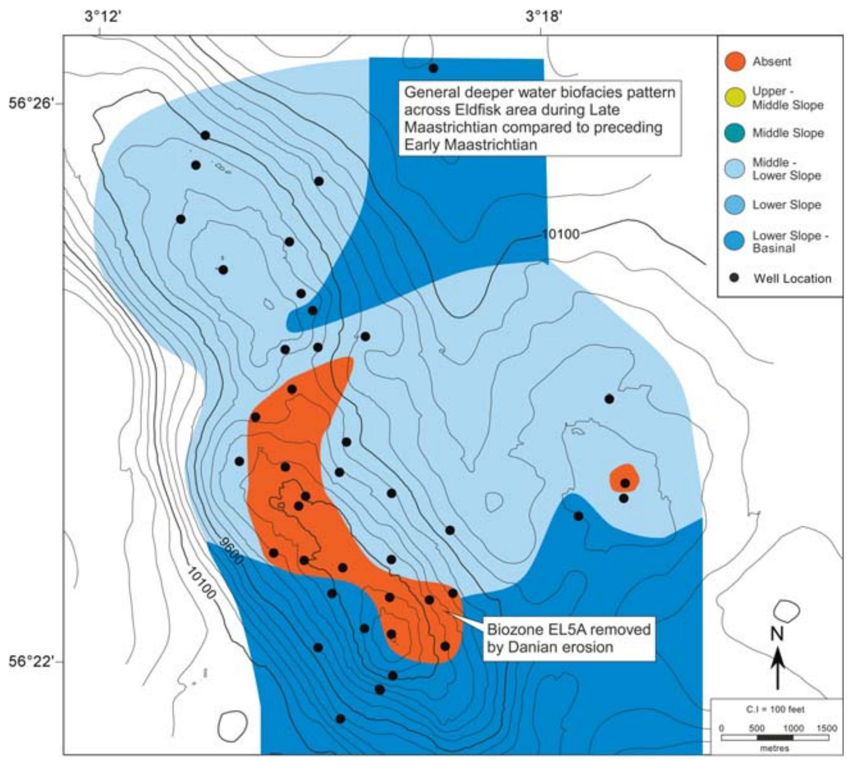

Fig. 14. Biofacies map for Late Maastrichtian Tor Formation Subzone EL5A, representing a hemipelagic drape across the structures.

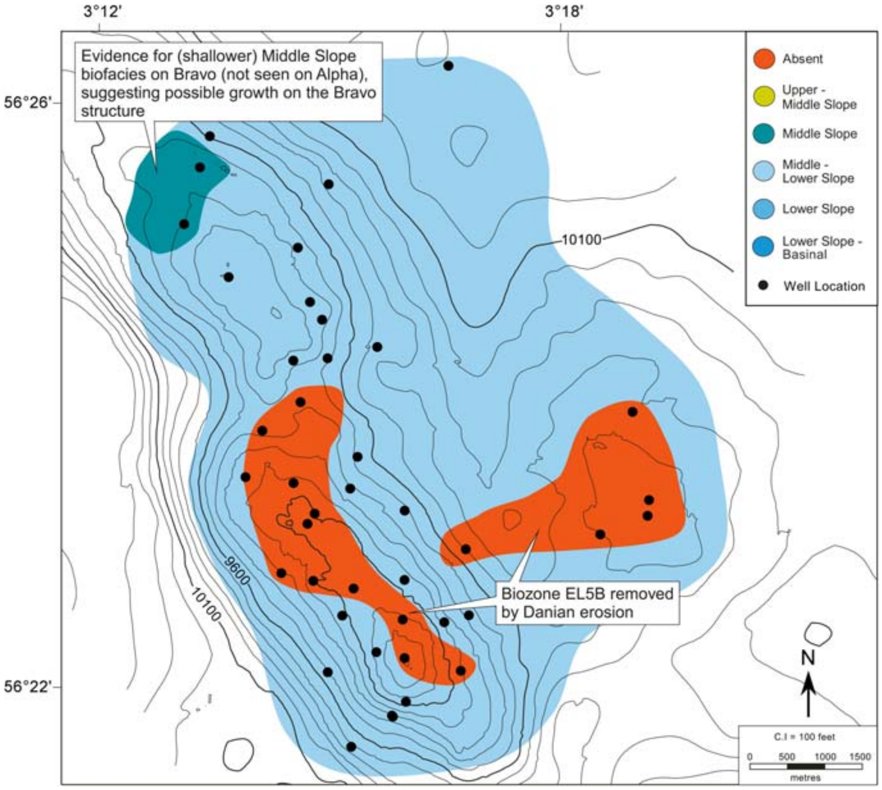

Fig. 15. Biofacies map for Late Maastrichtian Tor Formation Subzone EL5B. The areas of absence are attributable to a subsequent erosion event.

Top Tor Formation, Late Maastrichtian Subzone EL5B also represents a hemipelagic, plankton-rich drape over the Eldfisk structure deposited in middle to lower slope water depths. A shallower (middle slope) biofacies is also recorded at this time over the northern part of Eldfisk Bravo, indicating some structural relief in this area. The planktonic foraminifera which characterize this interval are generally regarded as being of relatively warm water (Tethyan) origin. There is evidence suggesting their ubiquitous record throughout the North Sea and northern Europe is due to the establishment of an Atlantic proto-Gulf Stream during the Late Cretaceous which swept southwards through the North Sea Basin towards the end Cretaceous carrying this distinctive planktonic association through the region and onto the European continental shelf (Hart 2007), where it is recorded in onshore Denmark (Troelsen 1955) and northern Germany (Koch 1977; Schulz & Schmid 1983). The hemipelagic origins of this unit imply deposition across the Eldfisk structure. Where absent, it is probably due to (uplift and) erosion at the end Cretaceous or during the earliest Danian.

Tectonostratigraphy. Time equivalent sediments from the adjacent Ekofisk trough continue to yield evidence for intra Tor Formation reworking, suggesting tectonically induced gravity flow deposition continued in that area, possibly correlatable with Late Maastrichtian inversion episodes described by Bless *et al.* (1986) from the Aachen–Antwerp area, while largely hemipelagic deposition occurred on Eldfisk.

Lower Ekofisk Formation

Age. 'Early' Danian Zone EL4 to 'late' Danian Subzone EL2Aii. Sediments of 'earliest' Danian, Zone EL4 are not routinely observed on the Eldfisk structures. It is difficult to definitively determine whether this is due to erosion or non-deposition. The occurrence of a thin Zone EL4 in core high on the western flank confirms that sediments of this age may have been deposited on (at least part of) the structure, with subsequent erosion downcutting into the Tor. Nevertheless, the thin occurrence of this zone renders it difficult to identify in ditch cuttings sample material. In contrast, Zone EL4 is well developed as the 'Ekofisk tight zone' in the adjacent Ekofisk trough. Zones EL3–EL2Aii are present on Eldfisk.

Lithology/petrophysics. Core facies interpretations reveal these sediments are characterized by argillaceous periodites, suggesting *in situ*, deep water, hemipelagic deposition. The argillaceous periodites are reflected in the petrophysical logs, displaying higher gamma ray and density values than adjacent sediments.

Biofacies. Lower Ekofisk Formation sediments assigned to Zone EL3 are more widespread in their distribution and were deposited at middle–lower slope depths (Fig. 16), with a lower slope signal along the western flank of Alpha, implying the presence of a steeper scarp structure. In contrast to Alpha, much of Bravo is characterized by a deeper lower slope microfaunal biofacies, although lower–middle slope biofacies depths interpreted towards the north suggest some structural relief.

Tectonostratigraphy. Thick sequences of Lower Ekofisk Formation (essentially Zone EL3) are developed on the Bravo structure where this unit generally caps the Tor Formation. This implies that this area acted as a depocentre at this time. The pervasive occurrence of Zone EL3 suggests any removal of Zone EL4 occurred prior to EL3 deposition, possibly associated with an unnamed 'early' Danian tectonic event. Thinner sequences of Lower Ekofisk Formation sediments are developed along the western margin of the Alpha structure; they are largely absent on the eastern margin of the Alpha structure and on the East Eldfisk structure. Subsequent erosion or non-deposition from these areas suggests they may have been structurally higher than the Bravo structure during or just after deposition of the EL. When compared with the Tor Formation (Subzone EL5B), these areas of absence

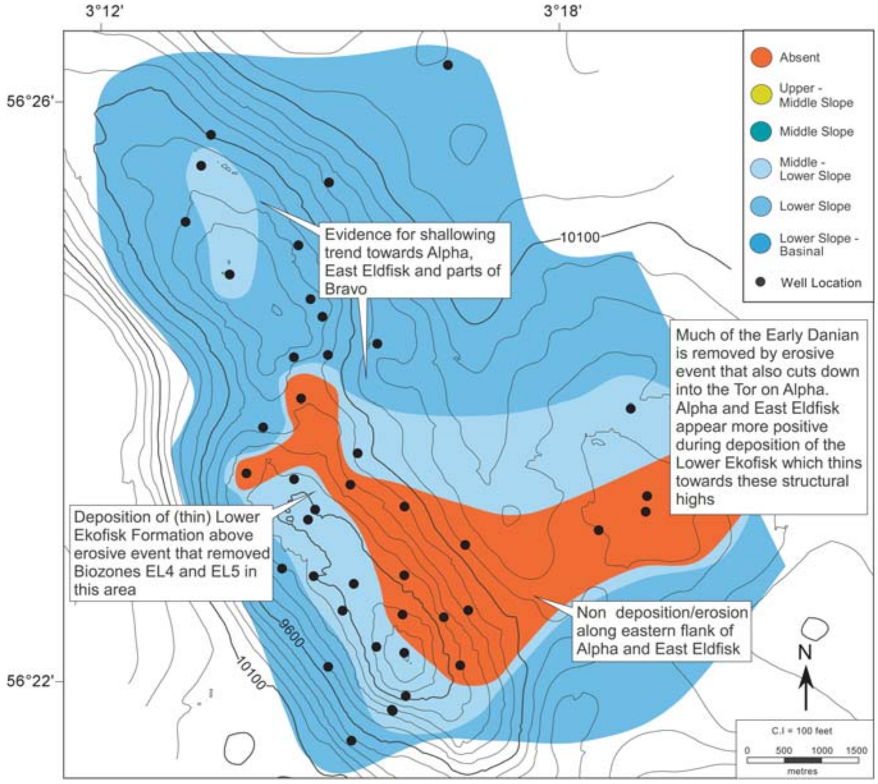

Fig. 16. Biofacies map for the 'mid-early' Danian Lower Ekofisk Formation. The areas of absence have shifted relative to the Late Maastrichtian, suggesting different erosional phases from the Late Maastrichtian.

suggest eastward migration of the crestal line of the 'Alpha ridge' due to movement on the underlying Skrubbe fault. The absence of these sediments on East Eldfisk, following backfilling and structural growth of East Eldfisk during the Maastrichtian, resulted in the presence of an eastern structurally positive area during the 'early' Danian.

Middle Ekofisk Formation

Age. 'Late' Danian, comprising Subzones EL2Ai–EL2B.

Lithology/petrophysics. Middle Ekofisk Formation sediments are the primary hydrocarbon-producing sediments in the Ekofisk Formation on Eldfisk. This ubiquitous unit across Alpha and Bravo displays considerable thickness variations. Thicker sequences are developed in the 'saddle area' between the Alpha and Bravo structure, whilst EM sediments are absent on the East Eldfisk structure. Lateral variations in thickness are attributed to variations in the proportion of *in situ* 'late' Danian material, reworked Late Cretaceous derived sediments and reworked intra Danian sediments. The reworking has a detrimental effect on the porosity in this unit.

Biofacies. The structural relief is supported by biofacies data which implies a shallower middle slope environment of deposition along the 'Alpha ridge', the southern part of crestal Alpha representing the shallowest environment (and structurally higher). No biofacies data exist for the East Eldfisk structure as no sediments of this age are preserved over this area and extending onto the SE flank of Alpha, suggesting that this area was also a structural high at this time. Around the 'Alpha ridge', middle–lower slope water depths are recognized in virtually every well; deeper water lower slope facies existed towards the SW flank (Fig. 17).

Tectonostratigraphy. An undescribed intra Danian tectonic phase may provide a mechanism for the reworking observed; such a phase has been intimated by Mackertich & Goulding (1999) on the South Arne Field. Presumably, comparable local tectonism can be invoked to account for the active reworking of both Late Cretaceous and Danian sediments during the deposition of the Middle Ekofisk Formation described here. Certainly inversion pulses along the Lindesnes Ridge, most active during the Late Cretaceous, are considered to continue through the Cenozoic by Wride (1995), who also recognizes continued reversal movements along the Skrubbe Fault during this time.

Upper Ekofisk Formation

Age. 'Late' Danian Subzones EL2C–EL1B.

Lithology/petrophysics. This unit is pervasive across Eldfisk and grades from clean, porous hydrocarbon saturated chalks in Subzone EL2C to marls transitional with the overlying Våle Formation in Subzone EL1B. This reflects progressive submergence of the region during the transitional phase from chalk deposition during the Danian to dominantly argillaceous deposits in the Selandian Våle Formation. *Zoophycos* trace fossils become conspicuous and increase in abundance in the EU, perhaps suggesting decreasing oxygen levels in the bottom waters as water depth increases. The Upper Ekofisk Formation is relatively uniformly developed across the Bravo and Alpha structures and interpreted as a largely autochthonous, hemipelagic drape which can be recognized regionally. Some variation in thickness is seen towards East Eldfisk, where this unit appears to thin, inferring the continued presence of the structural high towards East Eldfisk as recognized during deposition of the Middle Ekofisk Formation.

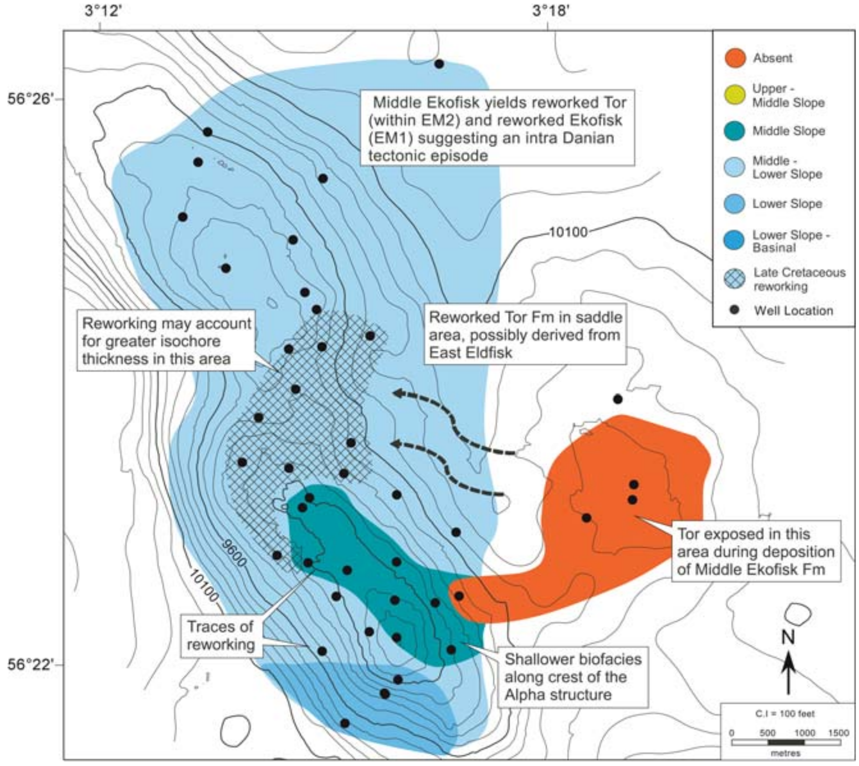

Fig. 17. Biofacies map for the 'late' Danian Middle Ekofisk Formation suggesting structural relief and growth of East Eldfisk. An area of Late Cretaceous reworking, concentrated in the saddle area, was mapped and this proved to be an important marker for geo-steering a horizontal well in the area.

Biofacies. Results imply a gradual increase in water depth from the crestal area northeastwards into East Eldfisk. Structural relief is still evident with lower slope to basinal water depths interpreted around the margins of the Eldfisk structures, shallowing slightly through lower slope on the flanks to middle-lower slope depths across crestal Alpha (Fig. 18).

Conclusions

The tectonic and eustatic events that have controlled chalk deposition on the Eldfisk structure as recognized in this study are summarized in Figures 19 and 20. They have been used in interpreting the structural history of Eldfisk, their impact on the deposition and

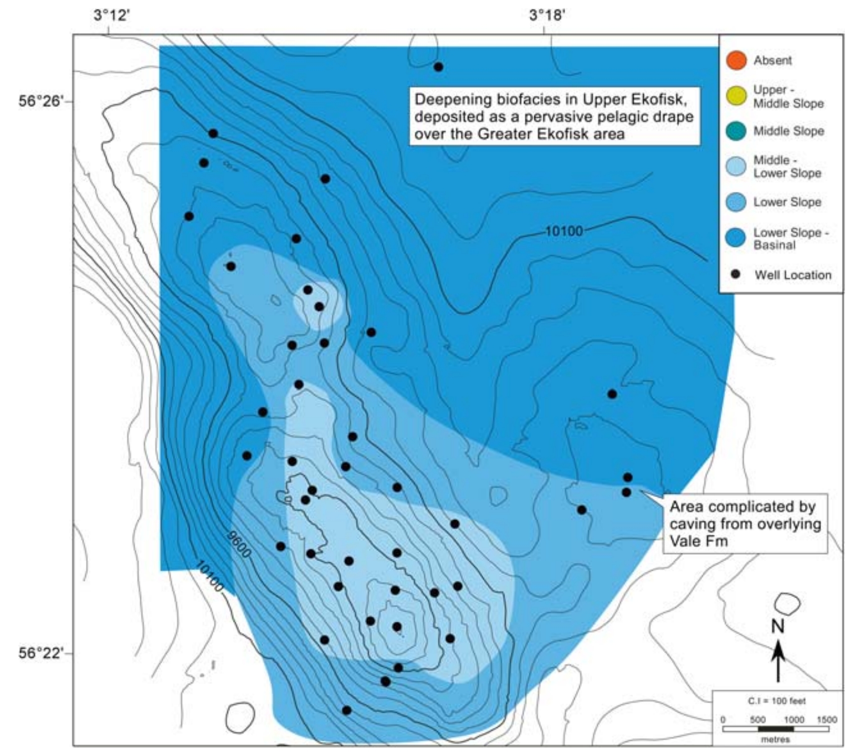

Fig. 18. Biofacies map for the 'late' Danian Upper Ekofisk Formation, suggesting deepening water trend throughout the 'latest' Danian. The deepening trend continues into the marls of the Våle Formation.

Event	Age	Formation	Comments	Reference
Unnamed mid–late (EM) Danian event	Mid–Late Danian	Mid Ekofisk	Erosion on East Eldfisk, reworking of Late Cretaceous sediments into local depocentres on Eldfisk, large scale re-deposition in the Ekofisk trough. Regionally pervasive re-deposition of 'early' Danian sediments. Growth faulting on Eldfisk? Penecontemporaneous re-mobilization of Zone EL2Ai (soft sediment overfolds seen in Ekofisk trough).	Mudge and Jones 2004
'Laramide' Tectonic event	End Cretaceous–earliest Danian structural phase	Tor	Early Danian erosive event removing Zone EL4 over Eldfisk. Erosion of Tor Formation Zone EL5 from the 'Alpha ridge'.	Hart 2007
Junior transgression	Late Maastrichtian	Tor	Brings warm water planktonics into N. Sea and deposits Zone EL5 as hemipelagic drape.	
'Mid' Maastrichtian Tectonic event	'Mid' Maastrichtian, Zone EL6	Tor	A series of minor structural events recognized across Northern Germany which may equate to generation of bioclastic rich debris flows on Eldfisk. Growth faulting resulting in eastwards shift of 'Alpha ridge'. Growth of East Eldfisk structure.	Bless *et al.* 1986; Niebuhr *et al.* 2000
Oebisfelde transgression	Early Maastrichtian	Tor	Responsible for deposition of 'lower' Tor Formation, nondeposition on structural highs.	Niebuhr *et al.* 2000
Polyplocum Regression/Late Campanian tectonic phase	Latest Campanian	Magne	Onset of sealevel fall and the onset of hardground formation on structural highs, possibly coincident with a Late Campanian tectonic phase; possibly responsible for formation of Bravo channel (crestal collapse or slope failure feature?), intraclasts in upper Magne Formation.	Bless *et al.* 1996; Niebuhr *et al.* 2000
Mucronata Transgression	Late Campanian	Magne	Widespread flooding phase - initiates high sealevels recognized globally. Magne deposited in variety of lithofacies due to presence of structure formed during earlier Peine phase. Nondeposition on crestal areas where Narve is exposed and reworked into surrounding Magne.	Niebuhr *et al.* 2000
Peine Tectonic event	Lower/Upper Campanian boundary	Magne	Major, widely recognized, structural event over Northern Europe which resulted in significant unconformities and removed the Early Campanian (and older) sediments from Eldfisk.	Riedel 1940,1942; Bless *et al.* 1986; Mortimore & Pomerol 1991, 1997, 1998
Pilula Transgression	Early Campanian transgressive phase	Magne	Recognized across northern Germany and the UK. Sediments probably deposited over the structure but only preserved in East Eldfisk and flanks of the Eldfisk structure. Base Magne shows onlap relationship (on Thud) and overstep (on Narve) reflecting previous structural growth phases.	Niebuhr *et al.* 2000
Wernigerode Tectonic event	End Santonian event	Thud	Recognized across much of Europe and into North & West Africa. Major inter-regional structural re-alignment, structural growth and erosion possibly responsible for removal of Thud over much of Eldfisk.	Stille 1924; Guiraud & Bosworth 1997; Mortimore & Pomerol 1991,1997; Mortimore *et al.* 1998;
Marsupites Transgression:	Late Santonian flooding event	Thud	Probably deposits Thud over entire area (deep water biofacies when preserved). Base Thud displays onlap relationship due to presence of structurally created topography. Thud preserved in off structure settings.	
Mittel Santon Pulse	Middle Santonian	Narve	Minor tectonic event recognized in northern Germany, London Basin and probably in the Central Graben area. Erodes Early Santonian sediments and erodes down into the Narve Formation.	Niebuhr *et al.* 2000
Undulatoplicatus Transgression	Base Santonian flooding event	Narve	Recognized across Northern Europe but evidence on Eldfisk has currently not been recognized due to subsequent erosional events.	Niebuhr *et al.* 2000
Ilsede	Early (mid Turonian) and late (Late Turonian–Early Coniacian) phases	Narve	Major phase of structural movements recognized across Europe. Initial stages of inversion during 'mid' Turonian led to growth of the Eldfisk structure upon which subsequent tectonic phases are expressed.	Stille 1924; Mortimore & Pomelro 1991, 1997; Mortimore *et al.* 1998

Fig. 19. Summary of the tectonic and eustatic events discussed in this study.

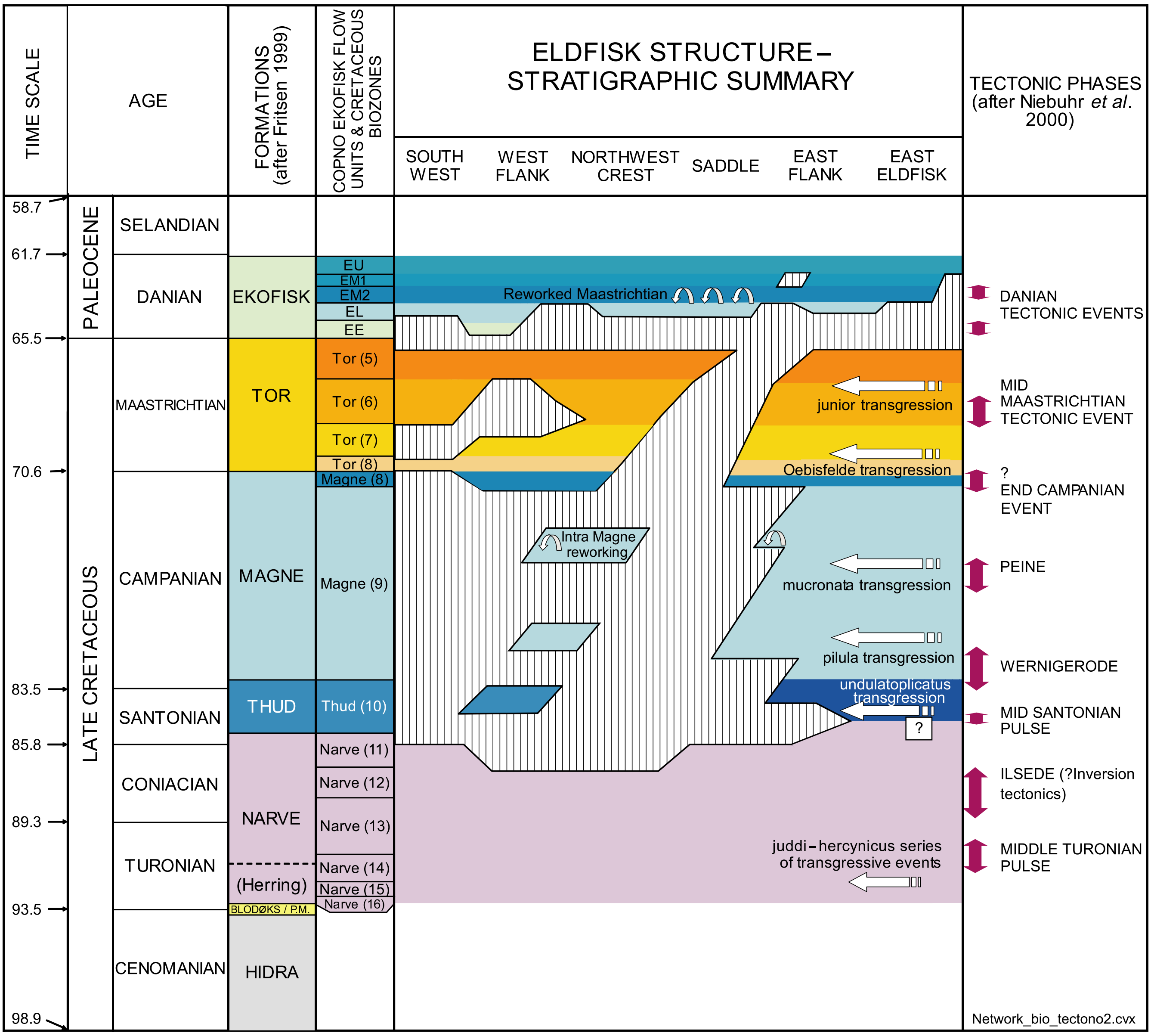

Fig. 20. Eldfisk Field biostratigraphic and tectonostratigraphic summary showing depositional variations across the structure, including a near-complete sequence on the gentle sloping eastern flank of Alpha (dominantly eustatic control) v. the punctuated (tectonic/fault control) pattern on the steeper, western flank and crestal areas.

preservation of discrete sediment packages and the various hiatuses and unconformities that bound them. Having defined this sequence of events it proved possible to create a geological model based on a tightly constrained stratigraphy, which has been shown to hold in all the wells in the study area. Tectonically controlled sedimentation in the Central Graben is well known; however, this study confirms the pulsed, punctuated nature of the tectonics. This study implies that the timing of these phases correlates with tectonic phases described from Germany, the Low Countries and the Anglo-Paris basin, thus extending the area influenced by Sub-Hercynian tectonics. Previously undescribed tectonic phases are also described from the Danian. The subdivision of the reservoir has also proven useful in the following ways:

(1) predicting where and why reservoir facies are developed on the structures;
(2) greater appreciation of the geographical and temporal extent of reworking in the EM and its effect on porosity on this structure;
(3) a new three-fold division of the Tor Formation with recognition and appreciation of the distribution of an allochthonous, bioclastic debris rich, porous Middle Tor Formation unit;
(4) recognition of variable lithofacies and petrofacies in the Magne Formation, including a crestal high-porosity reservoir facies comparable to the Tor Formation but with subtle poroperm differences.

Despite the complex inter-relationships between eustatic sea level changes, tectonic events and halokinetic movements which are acknowledged to exist, stratigraphical studies on numerous wells in this region have given rise to a stratigraphic framework in which the same sequence of events can be recognized over a large area with remarkable regularity, punctuated by unconformities and hiatuses at predictable stratigraphic levels. The holostratigraphic approach outlined here has greatly enhanced the geological appreciation of the Eldfisk Field by creating a unified geological model that ties with current regional understanding. This in turn has impacted on the geophysical interpretation and will guide the new 3D geological and simulation models that are currently under construction. The study had an immediate impact on the ongoing drilling programme, where the improved understanding has helped geo-steer horizontal wells. The biostratigraphic and lithostratigraphic framework has since been successfully applied to other chalk fields across the North Sea Basin for geosteering, geostopping and multiwell correlation studies; however, no wide-scale regional study has yet been undertaken to understand the utility of the technique on the basin scale.

Often the biggest hurdle to studies such as these is the gathering and compilation of a vast array of data that has been archived over a long period of time. However, the effort is rewarded as these types of studies become increasingly important in attempts to exploit the remaining resources on a field and prove that, even after 30 years of production and drilling, there is still a lot to be learnt on these old production assets.

The authors would like to thank the Eldfisk Group for permission to publish this paper: ConocoPhillips Skandinavia AS (Operator), Total E&P Norge AS, ENI Norge AS, StatoilHydro Petroleum AS and Petoro AS. Thanks to P. McQuillan for providing geophysical background and interpretations and L. Gallagher, R. Mortimore and F. Gradstein are thanked for advice and constructive comments throughout this project and for reading early drafts of this text. S. Balke is thanked for his continued support and enthusiasm throughout this project. The many reviewers of this paper are also thanked for their time and helpful comments. The interpretations expressed in this paper are the opinions and responsibilities of the authors and do not necessarily reflect those of ConocoPhillips or its co-venturers.

References

Adams, T. D., Khalili, M. & Said, A. K. 1967. Stratigraphic significance of some oligostegenid assemblages from Lurestan Province, northwest Iran. *Micropaleontology*, **13**, 55–67.

Bailey, H. W. & Clayton, C. J. 2010. Foraminifera from flint meals and 'rotten' flints: the choice of an eclectic. *In*: Whittaker, J. E. & Hart, M. B. (eds) *Micropalaeontology, Sedimentary Environments and Stratigraphy: A Tribute to Dennis Curry (1912–2001)*. Geological Society, London, Micropalaeontological Society Special Publications, 235–246.

Bless, M. J., Felder, P. J. & Meesen, J. P. M. T. 1986. Late Cretaceous sea level rise and inversion: their influence on the depositional environment between Aachen and Antwerp. *Annales de la Societe geologique de Belgique*, **109**, 333–355.

Bramwell, N. P., Meciani, L., Judge, N., Green, M. & Adam, P. 1999. Chalk exploration, the search for the subtle stratigraphic trap. *In*: Fleet, A. J. & Boldy, S. A. R. (eds) *Petroleum Geology of Northwest Europe: Proceedings of the 5th Conference*. Geological Society, London. 911–937; doi: 10.1144/0050911.

Brasher, J. E. 1995. Local tectonics and effects of sedimentation distribution within the Eldfisk Field. *In*: Hanslien, S. (ed.) *Petroleum Exploration and Exploitation in Norway*. NPF, Trondheim, Special Publications, **4**, 67–84.

Brasher, J. E. & Vagle, K. R. 1996. Influence of lithofacies and diagenesis on Norwegian North Sea chalk reservoirs. *AAPG Bulletin*, **80**, 746–769.

Brewster, J. & Dangerfield, J. A. 1984. Chalk fields along the Lindesnes Ridge, Eldfisk. *Marine and Petroleum Geology*, **1**, 239–278.

Burnett, J. A., Gallagher, L. T. & Hampton, M. J. 1998. Upper Cretaceous. *In*: Bown, P. R. (ed.) *Calcareous Nannofossil Biostratigraphy*. Chapman & Hall, London, 132–199.

Deegan, C. E. & Scull, B. J. 1977. *A Standard Lithostratigraphic Nomenclature for the Central and Northern North Sea*. Institute of Geological Sciences Report 77/25.

D'heur, M. 1984. Porosity and hydrocarbon distribution in the North Sea chalk reservoirs. *Marine and Petroleum Geology*, **1**, 211–238.

Ernst, G. & Wood, C. J. 2000. 3.2.10 Santon. *In*: Stratigraphische Kommission Deutschlands (Hrsg.) Stratigraphie von Deutschland III. *Die Kreide der Bunderepublik Deutschland*. Courier Forschungsinstitut Senckenberg **226**, 34–42.

Esmerode, E. V., Lykke-Andersen, H. & Surlyk, F. 2008. Interaction between bottom currents and slope failure in the Late Cretaceous of the southern Danish Central Graben, North Sea. *Journal of Geological Society, London*, **165**, 55–72.

Fritsen, A. (ed.) 1999. *A Joint Chalk Stratigraphic Framework. Volume 1. Joint Chalk Research (JCR) Program Phase V*. NPD Publication Y558. Norwegian Petroleum Directorate, Norway.

Guiraud, R. & Bosworth, W. 1997. Senonian basin inversion and rejuvenation of rifting in Africa and Arabia: synthesis and implications to plate-scale tectonics. *Tectonophysics*, **282**, 39–82.

Harries, P. J., Kauffman, E. G. & Crampton, J. S. 1996. Lower Turonian Euramerican Inoceramidae: a morphologic, taxonomic and biostratigraphic overview. *Mitteilungen aus dem Geologisch Paläonologischen Institut Der Universitat Hamburg*, **77**, 641–671.

Hart, M. B. 2007. Late Cretaceous climates and foraminiferid distributions. *In*: Williams, M., Haywood, A. M., Gregory, F. J. & Schmidt, D. N. (eds) *Deep-time Perspectives on Climate Change: Marrying the Signal from Computer Model and Biological Proxies*. The Geological Society, London, The Micropalaeontological Society Special Publications, 235–250.

Hart, M. B. & Bailey, H. W. 1979. The distribution of planktonic foraminiferida in the mid-Cretaceous of NW Europe. *Aspekte der Kreide Europas*. IUGS Series A, **6**, 527–542.

Hatton, I. R. 1986. Geometry of allochthonous Chalk Group members, Central Trough, North Sea. *Marine and Petroleum Geology*, **3**, 79–98.

Herrington, P. M., Pederstad, K. & Dickson, J. A. D. 1987. Sedimentology and diagenesis of resedimented and rhythmically bedded chalks from the Eldfisk Field, North Sea Central Graben. *AAPG Bulletin*, **75**, 1661–1674.

Hopson, P. M. 2005. *A Stratigraphical Framework for the Upper Cretaceous Chalk of England, Scotland, with Statements of the Chalk of Northern Ireland and the UK Offshore Sector*. British Geological Society Research Report, RR/05/01. HMSO, London.

Isaksen, D. & Tonstad, K. 1989. *A Revised Cretaceous and Tertiary Lithostratigraphic Nomenclature for the Norwegian North Sea*. Norwegian Petroleum Directorate (NPD), Bulletin 5.

Johnson, H. & Lott, G. K. 1993. Cretaceous of the Central and Northern North Sea. *In*: Knox, R. W. O. B. & Cordey, W. G. (eds) *Lithostratigraphic Nomenclature of the UK North Sea*. British Geological Survey, Nottingham.

Kennedy, W. J. 1987. Late Cretaceous and Early Palaeocene Chalk Group sedimentation in the Greater Ekofisk area, North Sea Central Graben. *Bulletin des Centres de Recherches Exploration-Production Elf-Aquitaine*, **11**, 91–126.

King, C., Bailey, H. W., Burton, C. & King, A. D. 1989. Cretaceous of the North Sea. *In*: Jenkins, D. G. & Murray, J. W. (eds) *Stratigraphic Atlas of Fossil Foraminifera*, 2nd edn. Ellis Horwood, Chichester, 372–417.

Koch, W. 1977. Biostratigraphie in der Oberkreide und Taxonomie von Foraminiferen. *Geologisches Jahrbuch, Reihe A*, **38**, 11–123.

Lieberkind, K., Bang, I., Mikkelsen, N. & Nygaard, E. 1982. Late Cretaceous and Danian limestone. *In*: Michelsen, O. (ed.) *Geology of the Danish Central Graben. Geological Survey of Denmark, Series B*, **8**, 49–60.

Mackertich, D. S. & Goulding, D. R. G. 1999. Exploration and appraisal of the South Arne Field, Danish North Sea. *In*: Fleet, A. J. & Boldy, S. A. R. (eds) *Petroleum Geology of Northwest Europe: Proceedings of the 5th Conference*. Geological Society, London, 959–974; doi: 10.1144/0050959.

Michaud, F. 1987. Eldfisk. *In*: Spencer, A. H. *et al.* (eds) *Geology of the Norwegian Oil and Gas Fields*. Graham & Trotman, London, 89–105.

Mortimore, R. N. & Pomerol, B. 1991. Upper Cretaceous tectonic disruptions in a placid Chalk sequence in the Anglo-Paris Basin. *Journal of the Geological Society, London*, **148**, 391–404.

Mortimore, R. N. & Pomerol, B. 1997. Upper Cretaceous tectonic phases and end Cretaceous inversion in the Chalk of the Anglo-Paris Basin. *Proceedings of the Geological Association*, **108**, 231–255.

Mortimore, R. N., Wood, C. J., Pomerol, B. & Ernst, G. 1998. Dating the phases of the Subhercynian tectonic epoch: Late Cretaceous tectonics and eustatics in the Cretaceous basins of northern Germany compared with the Anglo-Paris Basin. *Zentralblatt für Geologie und Pälaontologie, Teil I.*, **11/12**, 1349–1401.

Mortimore, R. N., Wood, C. J. & Gallois, R. W. 2001. *British Upper Cretaceous Stratigraphy. Geological Conservation Review Series, No. 23*. Joint Nature Conservation Committee, Peterborough.

Mudge, D. C. & Jones, S. M. 2004. Palaeocene uplift and subsidence events in the Scotland-Shetland and North Sea region and their relationship to the Iceland Plume. *Journal of Geological Society of London*, **161**, 381–386.

Neuweiler, F. 1989. *Facies analysis of pelagic limestones of the early Upper Cretaceous of Hilter/Haltenberge a.t.w. Part 1: Upper Cenomanian to Middle Turonian*. Diplom. Thesis, Freie Universität Berlin.

Niebuhr, B., Wood, C. J. & Ernst, G. 2000. Isolierte Oberkreide-Vorkommen zwischen Wiehengebirge und Harz. Stratigraphie von Deutschland III, Die Kreide der Bundesrepublik Deutschland. *Courier Forschungsinstitut Senckenberg*, **226**, 101–109.

Nyong, E. E. & Olsson, R. K. 1984. A paleoslope model of Campanian to Lower Maestrichtian foraminifera in the North American Basin and adjacent continental margin. *Marine Micropaleontology*, **8**, 437–477.

Olsson, R. K. & Nyong, E. E. 1984. A paleoslope model for Campanian–Lower Maestrichtian foraminifera of New Jersey and Delaware. *Journal of Foraminiferal Research*, **14**, 50–68.

Perch-Nielsen, K., Ulleberg, K. & Evensen, J. E. 1979. Comments on 'The Terminal Cretaceous event: a geologic problem with an oceanographic solution' (Gartner & Keany 1978). *Proceedings of the Cretaceous–Tertiary Boundary Events Symposium*, University of Copenhagen, **2**, 106–111.

Rawson, P. F., Allen, P. M. & Gale, A. S. 2001. The Chalk Group – a revised lithostratigraphy. *Geoscientist*, **11**, 21.

Riedel, L. 1940. Uber eine tektonische Phase an der Wende Quadraten-Mucronaten–Senon (Peine Phase) in Nordwestdeutschland. *Zeitschrift der deutschen geologischen Gesellschaft*, **92**, 253–258.

Reidel, L. 1942. Das Mesozoikum in Niedersachsen-Obere Kreide. *Schriften der Wirtschaftswissenschaftlichen Gesellschaft zum Studium Niedersachsens E. V. Neue Folge*, **2**, 1–52.

Schulz, M. G. & Schmid, F. 1983. Das Ober-Maastricht von Hemmoor (N-Deutschland): Faunenzonen-Gliederung und Korrelation mit dem Ober-Maastricht von Dänemark und Limburg. *Newsletters in Stratigraphy*, **13**, 21–39.

Sikora, P. J. & Olsson, R. K. 1991. A paleoslope model of late Albian to early Turonian foraminifera of the western Atlantic Margin and North Atlantic Basin. *Marine Micropaleontology*, **18**, 25–72.

Sikora, P. J., Bergen, J. A. & Farmer, C. L. 1999. Chalk palaeoenvironments and depositional model: Valhall & Hod fields, southern Norwegian North Sea. *In*: Jones, R. W. & Simmons, M. D. (eds) *Biostratigraphy in Production and Development Geology*. Geological Society, London, Special Publications, **152**, 113–138.

Stille, H. 1924. *Grundfragen der vergleichenden Tektonik*. Borntraeger, Berlin.

Troelsen, J. C. 1955. *Globotruncana contusa* in the White Chalk of Denmark. *Micropaleontology*, **1**, 76–82.

Vejbaek, O. V. & Andersen, C. 2002. Post mid-Cretaceous inversion tectonics in the Danish Central Graben – regionally synchronous tectonic events? *Bulletin of the Geological Society of Denmark*, **49**, 139–144.

Wride, V. C. 1995. Structural features and structural styles from the five countries area of the North Sea Central Graben. *First Break*, **13**, 395–407.

Role of the Chalk in development of deep overpressure in the Central North Sea

R. E. SWARBRICK,[1] R. W. LAHANN,[1,2] S. A. O'CONNOR[1] and A. J. MALLON[3]

[1]*GeoPressure Technology, Mountjoy Research Centre, Stockton Road, Durham DH1 3UZ, UK (e-mail: r.e.swarbrick@geopressure.co.uk)*

[2]*Indiana University, Bloomington, Indiana, USA*

[3]*Department of Earth Sciences, Durham University, South Road, Durham DH1 3LE, UK*

Abstract: A high magnitude of overpressure is a characteristic of the deep, sub-Chalk reservoirs of the Central North Sea. The Upper Cretaceous chalk there comprises both reservoir and non-reservoir intervals, the former volumetrically minor but most commonly identified near the top of the Tor Formation. The majority of non-reservoir chalk has been extensively cemented with average fractional gross porosity of 0.08, and permeability in the nano- to microDarcy range (10^{-18}–10^{-21} m^2), and sealing properties comparable to shale. Hence deeply buried chalk is comparable to shale in preventing dewatering and allowing overpressure to develop. Direct pressure measurements in the Chalk are restricted to the reservoir intervals, plus in rare fractured chalk, but reveal that Chalk pressures lie on a pressure gradient which links to the Lower Cenozoic reservoir above the Chalk and the Jurassic/Triassic reservoir pressures below. Hence a pore pressure profile of constantly increasing overpressure with increasing depth is indicated. Mud weight profiles through the Chalk, by contrast, show many borehole pressures lower than those indicated by these direct measurements, implying wells are routinely drilled underbalanced. The Chalk is therefore considered the main pressure transition zone to high pressures in sub-Chalk reservoirs. In addition to its role as a regional seal for overpressure, the Base Chalk can be shown to be highly significant to trap integrity. Analysis of dry holes and hydrocarbon discoveries relative to their aquifer seal capacity (the difference between water pressure and minimum stress) shows that the best empirical relationship exists at Base Chalk, rather than Base Seal/Top Reservoir, where the relationship is traditionally examined. Using a database of 65 wells from the HP/HT area of the Central North Sea, and extending the known aquifer gradients from the Fulmar reservoirs via Base Cretaceous to Base Chalk, leads to a risking threshold at 5.2 MPa (750 psi) aquifer seal capacity. Discoveries constitute 88% of the wells above the threshold and 36% below, with 100% dry holes where the aquifer seal capacity is zero (i.e. predicted breached trap). This relationship at Base Chalk can be used to identify leak points which control vertical hydrocarbon migration as well as assessing the risk associated with drilling high-pressure prospects in the Central North Sea.

Keywords: overpressure, Central North Sea, seal breach

A high magnitude of overpressure is a characteristic of the deep, sub-Chalk reservoirs of the Central North Sea (Gaarenstroom *et al.* 1993). The excess pressure is distributed mainly in Jurassic and Triassic pressure cells with overpressure increasing with depth. The origin of the overpressure is considered to be a function of rapid loading during late Cenozoic burial as well as contributions from thermal processes (e.g. gas generation) during deep, high-temperature burial (Swarbrick *et al.* 2002, 2005*a*, *b*). Some valid high-pressure trap structures have been drilled and have found hydrocarbons; others have been found to be water-wet (dry holes), and some of these show evidence of leakage of earlier trapped hydrocarbons.

Hydrocarbon leakage occurs either when the hydrocarbon buoyancy pressures exceed the capillary entry pressure (membrane failure) or when pore pressures exceed the fracture strength of the seal (hydraulic failure). Jurassic and Cretaceous sealing units in the Central North Sea have high capillary entry pressures which favour hydraulic failure as the main leakage process (Ingram & Urai 1999). Data in the Central North Sea show that many deep reservoirs have pore pressure close to the estimated fracture strength of the seal. The seal above these high-pressure reservoirs consists of variable thicknesses of Jurassic and Lower Cretaceous shales (with minor sandstone and limestone units in some locations) and the Upper Cretaceous Chalk. There are few direct pore pressure measurements to validate pressure profiles in these dominantly fine-grained sediments within the seal. Many published pressure profiles are based on drilling data, especially mud pressures coupled with the presence of gas. These interpretations feature a rapid increase of overpressure at the base of the Chalk and through the Lower Cretaceous and Upper Jurassic shales, where present (Holm 1998*a*, *b*). We re-assess the data in light of new permeability for the Chalk (Mallon *et al.* 2005; Mallon & Swarbrick 2008) from rare direct pressure measurements plus gas data. A high-quality database of 1248 wells was made available by IHS. The study location area is displayed in Figure 1. These data included direct pressure measurements such as Repeat Formation Tester (RFT), Drill Stem Tests (DST) and Kicks, as well as ancillary data such as stratigraphic tops and mud weights. Drilling reports were utilized where possible to provide evidence of pressures encountered during drilling such as connection gas build-ups and other drilling data.

Pressure transition zone through the Chalk

The Upper Cretaceous Chalk of the Central North Sea varies in thickness between 850 and 1500 m (2800 and 5000 ft) at burial depths of 2000–4000 m (6600–13 100 ft). The chalk comprises both reservoir and non-reservoir intervals, the former most commonly identified near the top of the Tor Formation (although porous units are present also in the Herring Formation). Reservoir chalk is interpreted as a re-deposited chalk, rapidly buried and removed from the sediment–water interface, thereby reducing cementation (Brasher & Vagle 1996).

VINING, B. A. & PICKERING, S. C. (eds) *Petroleum Geology: From Mature Basins to New Frontiers – Proceedings of the 7th Petroleum Geology Conference*, 493–507. DOI: 10.1144/0070493 © Petroleum Geology Conferences Ltd. Published by the Geological Society, London.

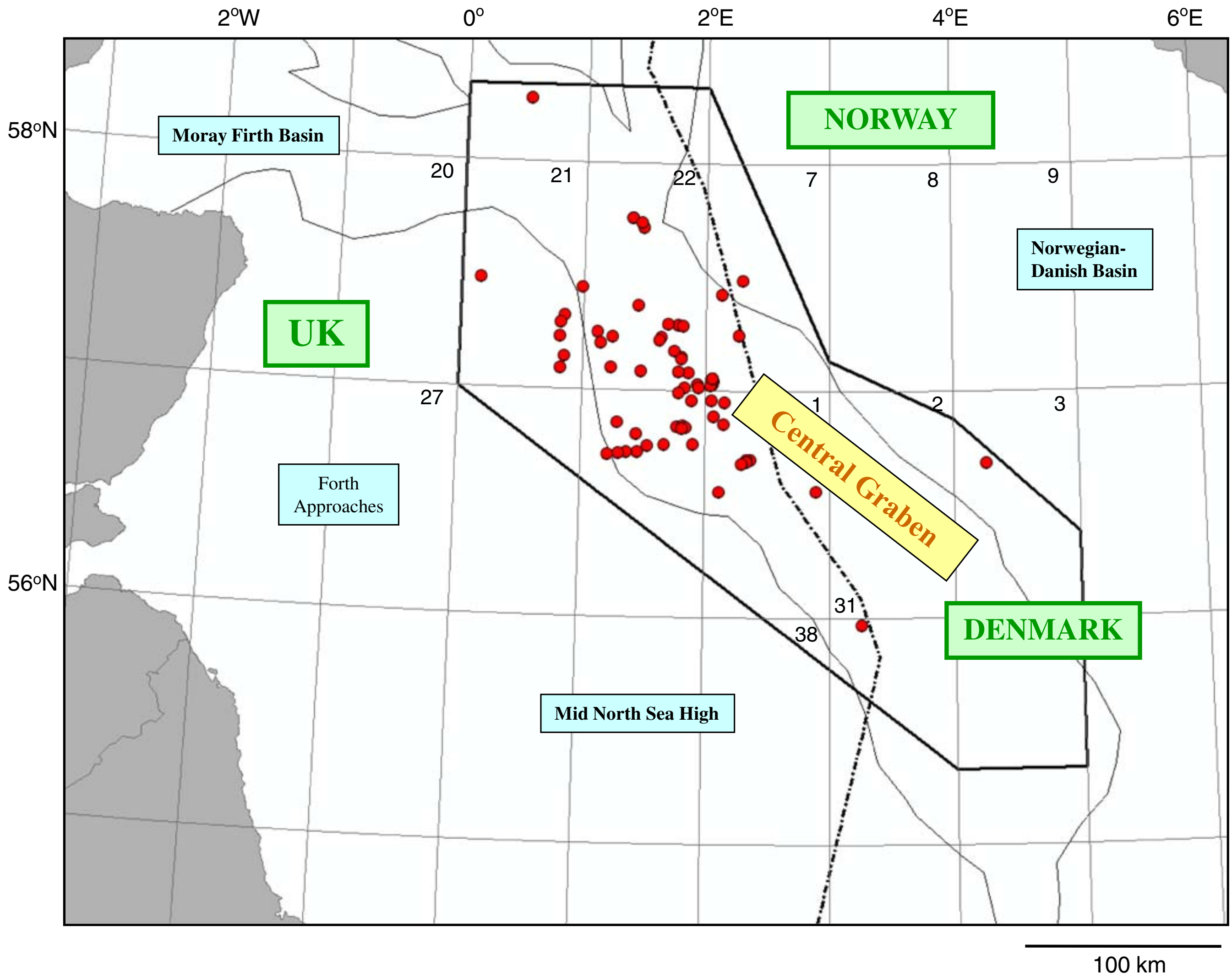

Fig. 1. Location of the North Sea Central Graben. Red dots represent the location of the 65 wells used in the analysis of hydraulic top-seal failure (see text).

Characteristics of non-reservoir chalk

The non-reservoir chalk is dominantly pelagic with varied lithofacies: (a) massive, clean chalk comprising coccolith fragments with early contact cements; (b) massive, clean chalk with localized stylolites; and (c) burrowed, laminated argillaceous chalk containing dissolution seams (Fig. 2). Mallon *et al.* (2005, 2008) describe the deeply buried non-reservoir chalk as extensively cemented with fractional gross porosity from 0.04 to 0.18 (average 0.08), compared with 0.20–0.40 in the reservoir intervals at similar depths. The permeability of the reservoir chalk is in the milliDarcy to microDarcy range (10^{-15}–10^{-18} m^2), compared with non-reservoir chalk permeability in the nano- to microDarcy range (10^{-18}–10^{-21} m^2) depending on depth of burial. Low values in non-reservoir chalk are comparable to shale permeability (Mallon *et al.* 2005). Hence deeply buried chalk has equal ability as shale to seal overpressure in underlying highly pressured reservoirs. Moreover, core reveals the chalk to be predominantly massive and cemented and unlike the highly layered fabric of the underlying Cretaceous (Cromer Knoll) and Upper Jurassic (Kimmeridge and Heather) shales.

Pressures in the Upper Cretaceous Chalk

Direct pressure measurements in the chalk are restricted to the reservoir intervals, plus rare measurements in fractured chalk. It is not possible to independently assess the pore fluid pressures in non-reservoir chalk due to a lack of relationship between porosity and effective stress (Lubanzadio *et al.* 2002). When plotted on a pressure–depth plot, Chalk fluid pressures recorded in reservoir units such as the Tor and Herring Formations normally lie on a pressure gradient linking pressures found in Lower Cenozoic reservoir above the Chalk with Jurassic/Triassic reservoir pressures below (Fig. 3). The resulting profiles show pressure transition zones of constantly increasing overpressure with increasing depth.

Mud pressure profiles through Chalk succession

Mud pressures represent an upper limit to pore pressures where the rocks are sufficiently permeable to allow fluid flow into the borehole during drilling operations. In the non-reservoir chalk we believe the permeability is low enough for mud weights to be below the actual pore fluid pressures. Sediments can only be drilled underbalanced (pore pressures are higher than mud weight) when they have extremely low permeability. This situation applies to non-reservoir chalk. We calculate that for a 1000 m (3300 ft), non-reservoir chalk section of $12\frac{1}{4}$ in diameter borehole with formation water 6.9 MPa (1000 psi) higher pressure than the borehole pressure, and assuming 50 nD permeability Chalk, the fluid influx approximates only 0.5 barrels per day, that is, below influx detection levels.

The low permeability and potential to drill underbalanced helps explain the mud weight profiles observed through the Chalk. In UK well 22/30a-2 (Heron Discovery) (Fig. 4), the mud weight was

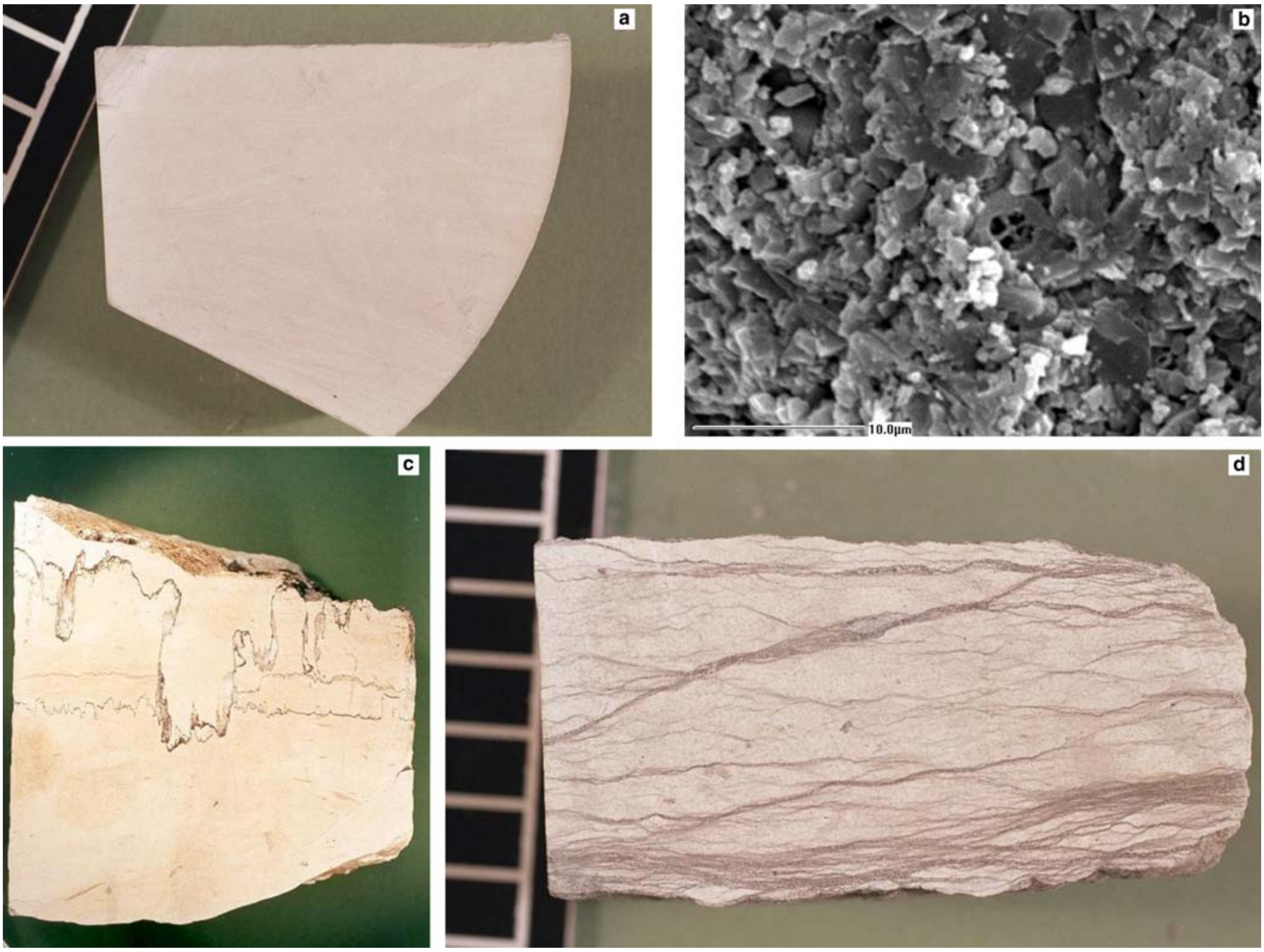

Fig. 2. Reservoir and non-reservoir chalk facies: (**a**) massive, clean chalk comprising coccolith fragments with early contact cements; (**b**) SEM view of the same; (**c**) massive, clean chalk with localized stylolites; and (**d**) burrowed, laminated, argillaceous chalk containing dissolution seams.

maintained at 12.3 ppg through the Cromer Knoll to a deep casing point. After setting casing, the mud weight was increased to 17.5 ppg, prior to drilling into the Fulmar reservoir with 47.7 MPa (6920 psi) overpressure. In our model for Chalk pressures the pore pressure was much higher through the Chalk than represented by the mud weight profile, but no measureable influx occurred because of the low permeability. Other wells, such as UK well 22/30c-10 (Elgin Appraisal; Fig. 4), show mud weight increased several times through the Hod and Hidra Formations to control increases in gas. Influx of gas is consistent with higher formation pressures than balanced by the mud weight (Holm *et al.* 2008).

Furthermore, the relevance of thick sub-Chalk shales above the high-pressure Fulmar reservoir for sealing of high pressure reservoirs is also challenged. In Figure 5, four UK wells situated in the deeper parts of the Central North Sea have variable thicknesses of sub-Chalk mudrocks above highly overpressured Fulmar reservoir beneath. The mud weight profiles in UK wells 22/29-2 and 22/30b-4 are lower than the corresponding pressure transition zones associated with these wells. In well 22/29-2, the thickness of the Base Chalk to Top Fulmar reservoir is only 34 m (109 ft), yet there is 39 MPa (5700 psi) overpressure in the Fulmar. Since the Chalk and sub-Chalk mudrocks/shales have similar permeability the Chalk is acting as part of the pressure seal in this example.

The role of the Chalk as a regional seal

The Chalk is considered the main pressure transition zone to high pressures in sub-chalk reservoirs, rather than the sharp transition zone starting near Base Chalk and continuing through the Cromer Knoll/Kimmeridge Clay favoured by other authors (e.g. Holm 1998*a*, *b*; Daniel 2001; Winefield *et al.* 2005). We believe the evidence for the actual pore pressure profile, based on available but rare pressure measurements in the more permeable units, points to a steady-state pressure profile controlled by low overpressure, Cenozoic reservoirs above, and reservoir and sub-Chalk mudrock pressures below the Chalk.

The evidence presented above implies that the North Sea Chalk must play a significant role in the development of the high overpressures found in deeper reservoirs, especially in the Central North Sea area. Earlier emphasis on the rock properties of the volumetrically minor reservoir chalk may have led to the belief that the chalk did not contribute to trapping of overpressure beneath. The results revealed in this paper, coupled with permeability data from non-reservoir chalk, dispel that assessment. We now explore the evidence for the Base Chalk as a significant barrier to upwards hydrocarbon migration and hence a major influence on the preservation of hydrocarbons in Jurassic/Triassic traps, located deeper in the section.

Seal breach analysis

Seals leak, or breach, and hydrocarbons are re-migrated to younger reservoirs by either hydraulic failure (either by shear, i.e. faulting or reactivation of an existing fault, or by opening of tensile fractures) or membrane leakage (when the hydrocarbon buoyancy pressure

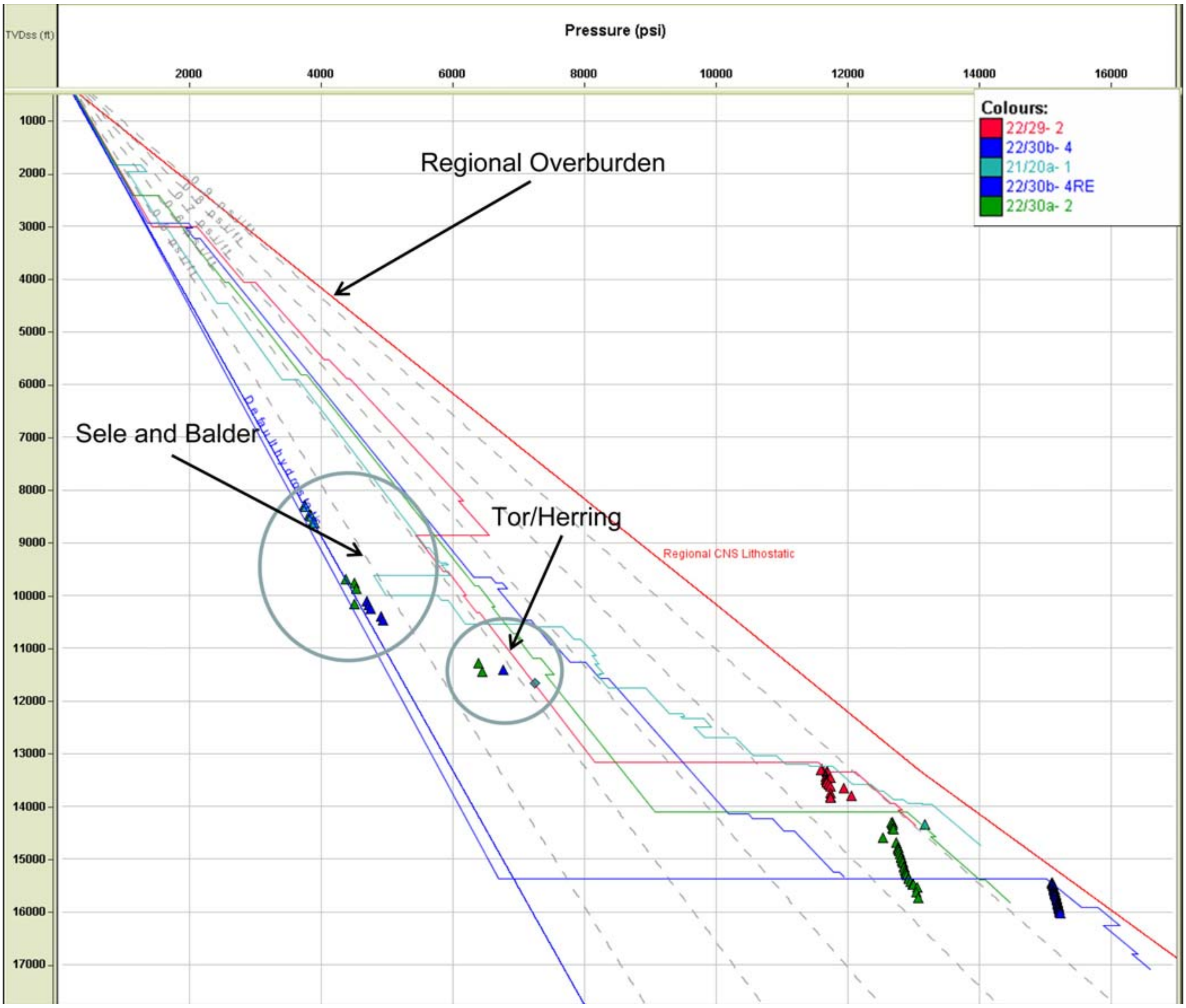

Fig. 3. Pressure–depth plot showing data from UK wells 22/29-2 (Seagull discovery), 22/30b-4 (Shearwater discovery) and RE, 21/20a-1 and 22/30a-2 (Heron Discovery) displaying profiles of increasing overpressures with increasing depth of burial. Coloured lines represent mud weights used to drill these wells.

exceeds the capillary entry pressures of the seal). As Jurassic and Cretaceous sealing units in the Central North Sea have high capillary entry pressures (due to their fine-grained lithology), hydraulic failure is the main leakage process. Gaarenstroom *et al.* (1993) assessed the risk of seal breach in the Central North Sea by calculating the 'retention capacity' (their term) of the top seal in relation to hydraulic failure and concluded that when the difference between pore fluid pressures and minimum horizontal stress at Top Reservoir is less than approximately 7.0 MPa (1000 psi) there is a high risk of seal breach into the overlying seal. Similar conclusions were reached by Holm (1998*a*, *b*) and Winefield *et al.* (2005), who also emphasized the role of the overlying shales (i.e. Jurassic Kimmeridge/Heather Formations and the Lower Cretaceous Cromer Knoll Group) in sealing the deep high-pressure reservoirs beneath.

Aquifer seal capacity

We have re-examined the analysis of Gaarenstroom *et al.* (1993), using a larger database of high pressure wells over a wider geographical region of the Central North Sea (Fig. 1). For each well the **aquifer seal capacity**, here defined as the difference between water pressure, extrapolated from the reservoir pressure data, and minimum compressive stress at the reservoir/field crest, have been estimated (Fig. 6) using all available data. The influence of hydrocarbon buoyancy has been examined later in relation to the data using hydrocarbon seal capacity in discovery wells. Measured pore fluid pressure can be used to determine both aquifer and hydrocarbon gradients. Fracture strength was estimated using a relationship built from rock stress relationships coupled with borehole Leak Off Test and incorporating a fluid pressure–stress coupling terms to capture the poroelastic fluid–stress interaction (see Engelder & Fischer 1994). Lithostatic stress was determined from five wells with almost complete density log coverage, to depths of nearly 5500 m (18 000 ft). Analysis of top seal failure (seal breach) ideally compares aquifer pressure with minimum stress at the crestal location of a structure (Fig. 6), and we have assumed that each well penetrated the reservoir within 150 m (492 ft) of the crest.

Assuming a water-wet reservoir, the buoyancy pressure in the hydrocarbon phase is considered to have a minor influence on rock behaviour, and hydraulic failure is most closely linked to aquifer pressure. Given that in a petroleum accumulation, the pores in the trap are filled with a two-phase fluid system, and the

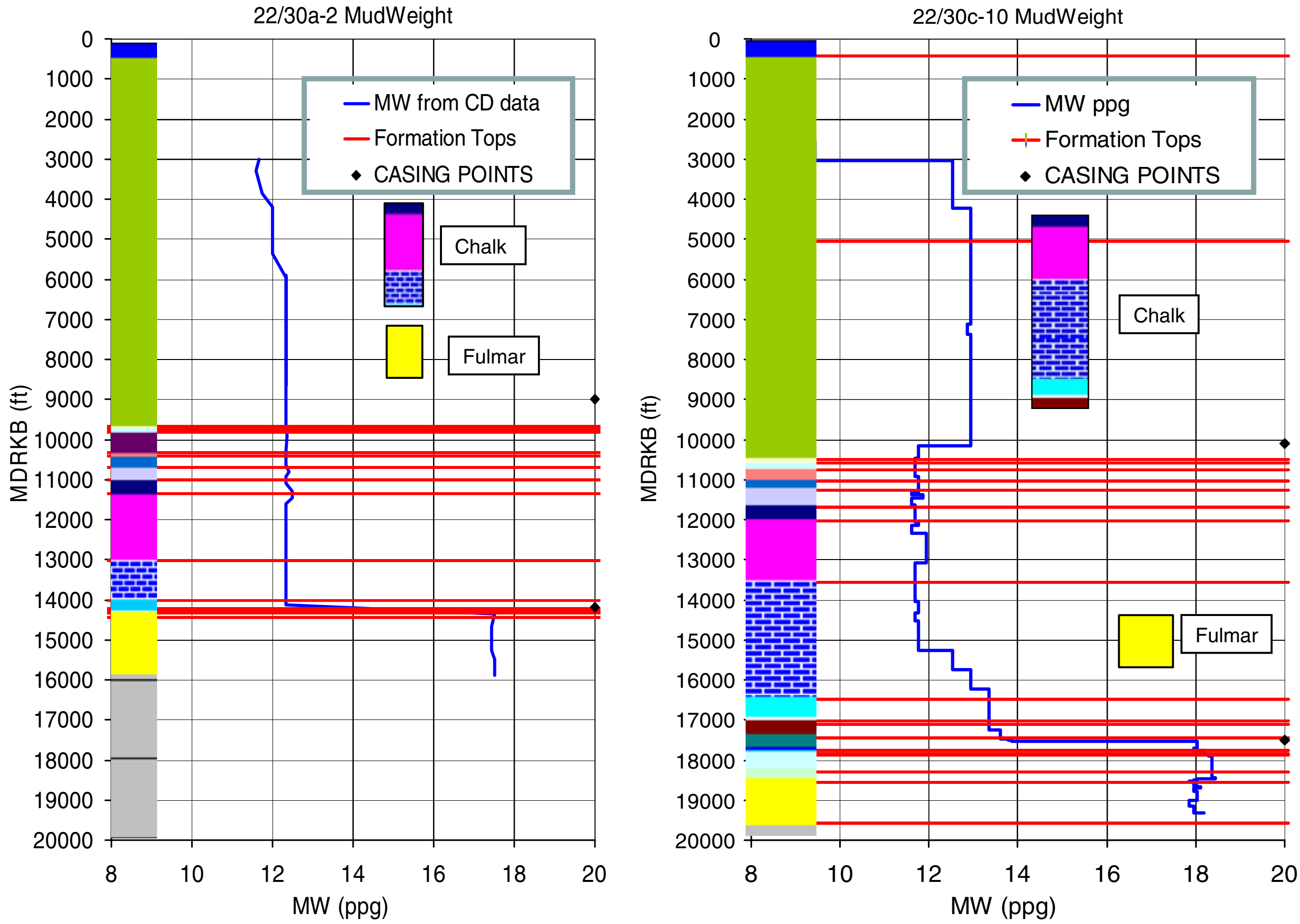

Fig. 4. A typical UK well 22/30a-2 has been drilled with a low mud weight to near Base Chalk. In contrast, in some wells, such as 22/30c-10, mud weight increases several times over the same stratigraphic intervals, to subdue high gas readings interpreted as high pressure. The absence of indications of high fluid pressures in the chalk in many wells is on account of the low porosity and low permeability of deeply buried Central North Sea chalk.

petroleum and water are immiscible, then in such a water-wet reservoir (i.e. one in which water coats the rock grains in a continuous phase or film, as it does in the overlying seal lithology), the overpressure in the hydrocarbon phase relative to the water phase does not increase the risk of hydrofracturing the reservoir's seal. Bjørkum *et al.* (1998) reason that the interfacial tension (elastic forces at the fluid interface and an influence on capillary entry pressure of the seal) balances the hydrocarbon buoyancy. This assumption appears to be reasonable for the typical hydrocarbon column heights found in the Central North Sea, that is, 160 m (500 ft), and is supported by data in Hermanrud *et al.* (2005) where pressure differences between the oil and water phases in a water-wet, oil-saturated core were equivalent to these column lengths. Gaarenstroom *et al.* (1993), along with a list of others referred to by Bjørkum *et al.* (1998), consider that buoyancy pressure in the hydrocarbon column contributes to hydrofracturing of the reservoir cap rock seal.

Comparison of methods

Differences between the results for sealing at Top Reservoir presented here and other studies in the same area arise from two main factors: (a) our reliance on aquifer seal capacity (this study) v. hydrocarbon pressure in hydrocarbon discoveries and aquifer pressure for dry holes (e.g. Gaarenstroom *et al.* 1993) and (b) our use of the lower of either (i) fracture gradient based on an algorithm incorporating a fluid pressure–horizontal stress term or (ii) lithostatic stress v. use of a minimum bound for Leak Off Test (Gaarenstroom *et al.* 1993; Winefield *et al.* 2005).

Using all available aquifer pressures, a lithostatic stress relationship was generated from density data in selected wells (rather than utilizing a default 1.0 psi/ft). A fracture strength model, based on a regional dataset of Leak Off Tests incorporating a fluid pressure–horizontal stress coupling term, was also generated. The minimum stress in the North Sea Central Graben is then assumed to be the smaller of the fracture strength or the lithostatic stress. We observe that at depths of >4300 m (approximately 14 000 ft) the Leak Off Tests can exceed the lithostatic stress. This apparent stress reversal most likely results from the high pore pressures at depth, as well as the reliance on data from vertical or near-vertical boreholes. Leak Off Tests in vertical boreholes, conducted where the vertical stress is the minimum stress, create vertical fractures initially near the borehole wall, due to the reordering of the stress magnitudes by the Hoop stresses. As these fractures controlled by the horizontal stress magnitude lengthen outside the region of Hoop stresses, they rotate to horizontal in the far field area, responding to the vertical stress field. In these circumstances leak-off pressures are higher than lithostatic result. Other explanations for leak-off pressures higher than the vertical stress are (1) high tensile strength of the rock and (2) increase in lateral compressive stress in the basin (as suggested for many deep basins by Grauls 1998).

Comparison of dry holes and discoveries

Dry hole v. hydrocarbon discovery assignment of well-bores in this study of 65 wells (Fig. 1) are based on (a) published data sources such as Gaarenstroom *et al.* (1993) and Winefield *et al.* (2005) and (b) examination of well logs in other wells. Dry holes were

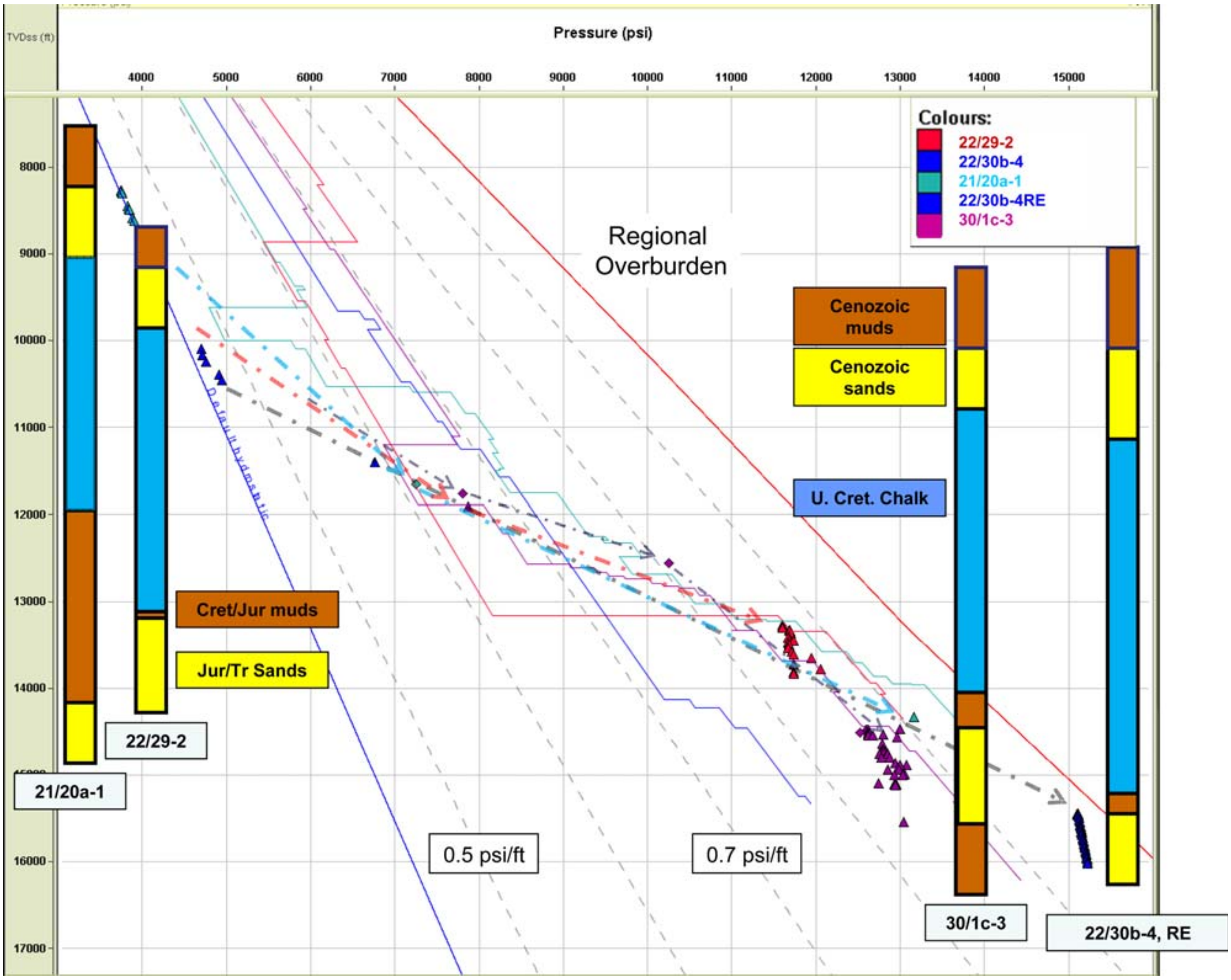

Fig. 5. Direct pressures in the chalk are relatively rare. Several UK wells with these pressure tests are shown, and each indicates increasing overpressure through the chalk, supporting a pressure transition zone of steady increase in overpressure into the underlying Cretaceous/Jurassic shale and reservoir beneath. Mud weights in UK wells 22/29-2 and 22/30b-4 are lower than the corresponding pressure transition zones inferred for these wells. In UK well 22/29-2, the shale thickness between chalk and Fulmar Reservoir is only 109 ft, with a measured overpressure of 39.3 MPa (5700 psi).

assumed to have leaked due to seal failure. Those dry wells where published sources showed the well was drilled off-structure were eliminated from the analysis (e.g. 21/16-3). Only one well per structure was included, so as to remove field-bias. Only wells with an aquifer seal capacity <17.2 MPa (2500 psi) at Top Reservoir are included, leaving a total of 65 wells in the final study set. All data used in the analysis are displayed in Table 1.

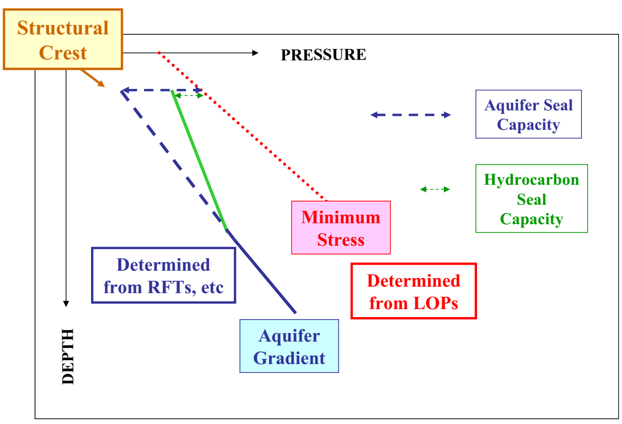

Fig. 6. Aquifer seal capacity is determined where the aquifer overpressure is established and compared with the minimum stress at the structural crest. In a discovery hydrocarbon seal capacity is the difference between hydrocarbon-phase pressure and minimum stress. Minimum stress refers to either fracture or lithostatic pressure.

Top reservoir/base seal

The initial evaluation of aquifer seal capacity relative to distribution of dry holes and hydrocarbon discoveries was completed at Top Fulmar reservoir (the traditional stratigraphic level for analysis of top-seal failure; Fig. 7). There is a marked difference in statistics for discoveries above and below a threshold of 9.7 MPa (1400 psi): 83% discoveries when aquifer seal capacity is above and only 43% discoveries when it is below the threshold. The results compare with a threshold at 7.0 MPa (1000 psi) in Gaarenstroom *et al.* (1993). We note, however, that some dry holes known (from analysis of core) to be ‘leaking’ (hydrocarbon-stained vertical fractures), such as UK wells 21/20a-1 and 22/8a-3, have a higher aquifer seal capacity than UK well 22/30a-4, which has one of the smallest aquifer seal capacities, yet with a 460 m (1510 ft) hydrocarbon column. Whilst we believe the analysis of aquifer seal capacity is appropriate for assessing seal risk, for comparison we have also completed the analysis using hydrocarbon seal capacity at Top Reservoir for discoveries (Fig. 8). Since the hydrocarbon column heights are generally less than 150 m (480 ft) in the Central

Table 1. Data utilized in the calculations of aquifer and hydrocarbon seal capacity at Top Reservoir, Base Cretaceous and Base Chalk horizons

Well number	HC column height (ft)	Aquifer O/P (psi)	Base Chalk (TVDSS feet)	BCU (TVDSS feet)	Top Reservoir (TVDSS feet)	Fracture pressure at Top Reservoir (psi)	Vertical stress at Top Reservoir (psi)	HC sealing capacity at Top Reservoir (psi)	Aquifer sealing capacity at Top Reservoir (psi)	Fracture pressure at BCU (psi)	Vertical stress at BCU (psi)	Aquifer sealing capacity (psi) at BCU	Fracture pressure at Base Chalk (psi)	Vertical stress at Base Chalk (psi)	Aquifer sealing capacity at Base Chalk (psi)
22/27a-1	0	6707	13 746	14 123	14 648	14 696	14 298		1073	14 195	13 721	729	13 835	13 306	482
NO1/6-7	0	7363	13 971	14 326	15 758	15 904	15 422		1047	14 539	13 847	109	14 200	13 456	−124
NO3/4-1	0	1746	8607	8832	8841	7806	8305		2126	7798	8295	2122	7583	8048	2007
NO7/7-2	0	4307	10 115	10 554	10 863	10 427	10 295		1154	10 133	9955	952	9714	9472	664
22/28a-1	0	7510	14 614	15 520	15 815	16 005	15 489		941	15 723	15 164	748	14 859	14 168	154
22/29-6s2	0	7837	15 150	15 280	15 450	15 687	14 990		278	15 525	14 803	167	15 401	14 660	81
30/1c-2A	0	6302	13 391	13 391	13 445	13 284	12 810		525	13 233	12 751	490	13 233	12 751	490
22/21-7	0	6670	12 354	12 850	13 900	14 012	13 502		647	13 011	12 347	−41	12 538	11 801	−366
22/30a-1	0	7789	14 542	14 757	15 118	15 431	14 712		195	15 087	14 315	−41	14 882	14 079	−182
23/16d-6	24	5859	12 016	12 884	13 242	13 043	12 697	940	946	12 702	12 304	711	11 874	11 349	143
21/30-3	58	2182	7163	7453	8381	7650	7933	1721	1738	6765	6912	1266	6488	6593	1119
21/30-19	143	2166	7358	8018	8707	7984	8333	1908	1944	7327	7576	1593	6698	6850	1257
23/26-7	150	7076	14 830	15 056	15 358	15 311	14 855	907	945	15 023	14 523	747	14 808	14 274	599
39/02-2Z	162	1850	8652	8652	8657	7619	8040	1904	1917	7614	8034	1914	7614	8034	1914
22/18-6	181	2312	10 161	10 169	10 172	9024	9475	2143	2185	9021	9472	2184	9013	9463	2179
23/26b-8	475	7062	14 806	14 806	15 009	14 984	14 483	631	742	14 790	14 260	610	14 790	14 260	610
15/23a-12	578	4991	11 061	12 602	12 628	12 329	12 223	1506	1613	12 304	12 195	1596	10 834	10 499	586
22/30c-10	437	8076	16 512	16 942	17 644	17 858	17 425	1401	1498	17 189	16 652	1038	16 778	16 179	756
22/24b-8	50	6109	12 620	12 873	12 928	12 778	12 295	425	433	12 726	12 235	397	12 484	11 957	232
22/30a-2	1066	6077	13 930	14 190	14 294	13 999	13 733	1094	1296	13 900	13 619	1228	13 652	13 333	1057
29/4d-4	502	8117	16 838	17 691	18 209	18 419	18 063	1700	1843	17 925	17 493	1504	17 112	16 555	945
22/30b-4	1510	7861	15 316	15 467	15 667	15 905	15 236	46	402	15 714	15 016	271	15 570	14 850	173
29/10a-2	0	5849	11 179	13 292	13 590	13 517	13 250		1353	13 233	12 922	1158	11 218	10 598	−226
22/07a-2	0	6563	12 956	13 616	14 261	14 255	13 829		920	13 640	13 120	498	13 011	12 394	65
22/08a-3	0	6518	13 045	13 468	14 311	14 302	13 904		1018	13 498	12 977	466	13 094	12 512	189
22/8a-4	0	5047	12 919	13 356	13 502	13 011	13 006		1951	12 871	12 845	1855	12 455	12 365	1569
22/21-4	0	6636	12 053	12 399	13 753	13 893	13 377		622	12 602	11 888	−265	12 272	11 507	−492

(*Continued*)

Table 1. *Continued*

Well number	HC column height (ft)	Aquifer O/P (psi)	Base Chalk (TVDSS feet)	BCU (TVDSS feet)	Top Reservoir (TVDSS feet)	Fracture pressure at Top Reservoir (psi)	Vertical stress at Top Reservoir (psi)	HC sealing capacity at Top Reservoir (psi)	Aquifer sealing capacity at Top Reservoir (psi)	Fracture pressure at BCU (psi)	Vertical stress at BCU (psi)	Aquifer sealing capacity (psi) at BCU	Fracture pressure at Base Chalk (psi)	Vertical stress at Base Chalk (psi)	Aquifer sealing capacity at Base Chalk (psi)
21/20a-1	0	6778	12 047	13 010	14 315	14 544	14 078		929	13 299	12 642	75	12 381	11 583	−556
30/1c-4	424	5934	13 601	13 632	13 812	13 467	13 169	1004	1088	13 296	12 971	970	13 266	12 937	950
30/11b-3	240	5877	13 554	14 228	14 788	14 349	14 204	1682	1746	13 815	13 588	1380	13 172	12 847	938
23/22b-4	120	5225	13 046	13 652	13 730	13 222	13 171	1806	1836	13 147	13 086	1785	12 569	12 419	1388
23/26b-15	149	7177	15 206	15 266	15 332	15 332	14 847	810	848	15 269	14 775	805	15 212	14 709	765
29/2a-2	270	5182	11 235	11 730	12 620	12 354	12 177	1308	1379	11 505	11 198	796	11 033	10 654	472
29/5a-3	367	6274	13 433	13 917	13 956	13 846	13 481	900	996	13 809	13 438	971	13 347	12 905	654
29/10-3 sti	521	6129	13 540	14 380	14 384	14 235	13 994	1408	1465	14 231	13 990	1462	13 430	13 066	912
21/25-12	0	3865	9448	10 125	10 373	9866	9820		1339	9629	9547	1176	8984	8802	733
22/22b-4	0	6461	13 404	13 564	14 720	14 660	14 347		1335	13 558	13 075	578	13 405	12 899	473
22/24d-10	671	5890	13 614	13 916	14 103	13 766	13 535	1270	1369	13 587	13 330	1247	13 299	12 997	1049
22/25b-2	0	6282	13 328	13 835	14 245	14 066	13 722		1101	13 675	13 271	832	13 192	12 713	500
22/30a-6	444	6135	14 377	14 813	15 001	14 672	14 492	1621	1682	14 493	14 286	1559	14 077	13 806	1273
22/30b-11	520	7776	15 594	15 755	16 359	16 528	15 993	799	937	15 952	15 329	542	15 798	15 151	436
23/26-3	0	7121	14 881	15 232	15 273	15 241	14 757		839	15 202	14 712	812	14 868	14 326	583
23/26b-14	173	7067	14 663	14 909	15 273	15 233	14 765	864	902	14 886	14 365	663	14 651	14 094	502
29/05b-4Z	646	7995	16 095	16 275	16 993	17 216	16 709	1011	1152	16 531	15 919	682	16 359	15 721	564
29/07a-5	164	2429	9130	10 020	10 220	9230	9662	2250	2253	9040	9442	2152	8191	8463	1699
29/07a-7	512	2556	9755	9856	10 088	9081	9442	1920	2036	8860	9187	1918	8763	9076	1867

(*Continued*)

Table 1. *Continued*

Well number	HC column height (ft)	Aquifer O/P (psi)	Base Chalk (TVDSS feet)	BCU (TVDSS feet)	Top Reservoir (TVDSS feet)	Fracture pressure at Top Reservoir (psi)	Vertical stress at Top Reservoir (psi)	HC sealing capacity at Top Reservoir (psi)	Aquifer sealing capacity at Top Reservoir (psi)	Fracture pressure at BCU (psi)	Vertical stress at BCU (psi)	Aquifer sealing capacity (psi) at BCU	Fracture pressure at Base Chalk (psi)	Vertical stress at Base Chalk (psi)	Aquifer sealing capacity at Base Chalk (psi)
29/08a-3	349	5093	11 384	12 491	12 852	12 499	12 378	1507	1565	12 154	11 981	1329	11 099	10 763	604
29/08a-4	0	5019	11 613	12 687	13 492	13 097	13 105		2074	12 330	12 219	1554	11 305	11 038	851
29/08b-5	0	4803	10 904	11 403	11 910	11 524	11 365		1262	11 041	10 807	930	10 565	10 258	603
29/09c-4	0	6124	12 508	14 378	14 405	14 290	14 044		1510	14 264	14 014	1492	12 481	11 957	267
30/07a-6	23	3828	11 966	12 041	12 115	11 286	11 494	2065	2067	11 215	11 412	2029	11 144	11 330	1991
30/07a-8	198	3738	11 265	11 404	11 555	10 746	10 897	1819	1866	10 602	10 731	1789	10 469	10 578	1718
30/07a-P1	134	3758	11 076	11 464	11 542	10 756	10 899	1834	1862	10 682	10 813	1822	10 311	10 386	1625
29/07a-4	95	2496	10 050	10 570	10 688	9482	9915	2218	2230	9370	9785	2170	8874	9213	1906
21/25-8	157	2772	9700	10 255	10 665	9809	10 206	2268	2291	9418	9755	2082	8888	9145	1800
29/4a-2	0	6416	13 411	14 012	14 255	14 219	13 858		1098	13 987	13 590	939	13 414	12 929	545
23/27-6	0	3647	11 987	11 987	12 472	11 495	11 800		2298	11 033	11 266	2052	11 033	11 266	2052
29/5a-5	117	6256	13 639	14 245	14 277	14 155	13 849	1217	1240	14 124	13 814	1219	13 546	13 148	822
30/01c-3	556	6172	13 826	13 826	14 544	14 259	13 992	1269	1348	13 574	13 202	877	13 574	13 202	877
30/01f-8	0	7486	15 307	15 320	15 665	15 730	15 179		722	15 401	14 800	496	15 388	14 785	488
22/24-7	399	3985	11 614	11 665	11 665	10 881	10 951	1628	1705	10 881	10 951	1705	10 832	10 895	1679
22/24b-9	494	3990	11 710	11 790	11 790	10 988	11 072	1713	1751	10 988	11 072	1751	10 912	10 984	1711
22/24a-2	671	3915	11 412	11 412	11 412	10 638	10 698	1494	1705	10 638	10 698	1705	10 638	10 698	1705
30/7a-7	80	3749	11 050	11 050	11 240	10 463	10 564	1692	1712	10 282	10 355	1616	10 282	10 355	1616
21/25-10	323	2453	8300	9100	9450	8624	8952	1909	1965	8290	8567	1787	7527	7687	1380

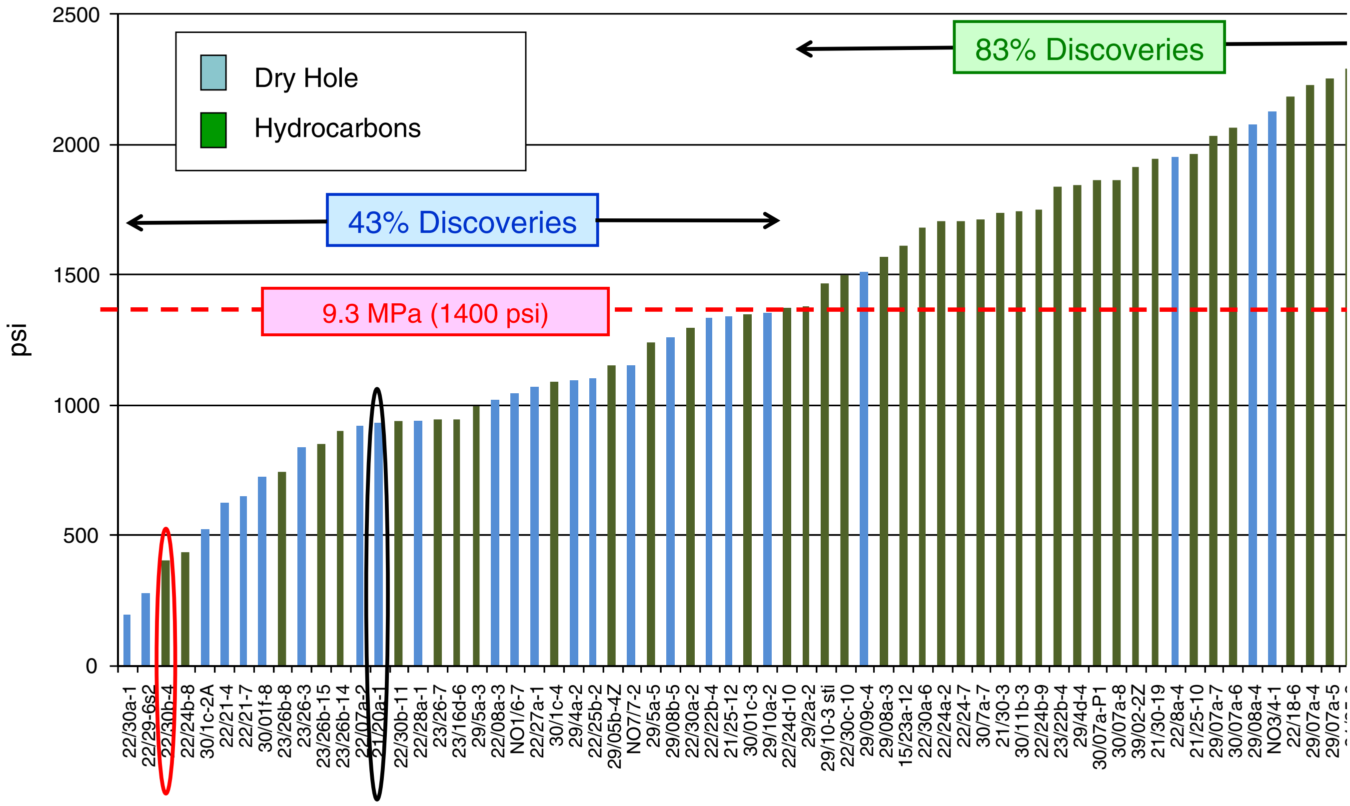

Fig. 7. Histogram of dry hole and hydrocarbon discoveries v. aquifer seal capacity at Top Reservoir. Out of 65 wells 83% are discoveries and 43% are dry holes when an aquifer seal capacity of 9.3 MPa (1400 psi) is used as threshold. However the analysis does not adequately explain UK well 21/20a-1 (black oval), a dry hole with 929 psi aquifer seal capacity but hydrocarbon shows in vertical fractures through the chalk, and UK well 22/30b-4 (red oval), with its long gas column but only 402 psi aquifer seal capacity.

North Sea there is little change in overall results, with the same threshold of 9.7 MPa (1400 psi) between discovery statistics of 82% above and 46% below the threshold. Plotting hydrocarbon or aquifer seal capacity v. hydrocarbon column height shows no relationship since all wells, except UK well 22/30a-4, have an aquifer seal capacity which exceeds the hydrocarbon buoyancy created by the hydrocarbon column height in the Fulmar reservoir.

Base Cretaceous Unconformity

Analysis of direct pressure measurements from turbidite sandstone within both the Heather and Kimmeridge Clay Formations shows that these thin reservoirs generally share the same aquifer gradient as the underlying Fulmar reservoir within any one pressure compartment (Fig. 9). We have therefore re-examined the relationship between aquifer seal capacity and dry hole/discovery at Base Cretaceous Unconformity. To calculate aquifer seal capacity the aquifer gradient in each of the wells was projected to the Base Cretaceous Unconformity, a stratigraphic marker identified in all study wells. Extrapolating the aquifer gradient to Base Cretaceous Unconformity results in smaller aquifer seal capacity estimates in all wells, the reduction dependent on the stratigraphic thickness of the Jurassic section above Top Reservoir (Fig. 10). For example in UK well 22/30a-4 the Top Fulmar to Base Cretaceous Unconformity interval is 61 m (200 ft) leading to a reduction of aquifer seal capacity of just 0.9 MPa (131 psi), whereas the same interval in UK well 21/20a-1 is 398 m (1305 ft) with reduction of aquifer seal capacity of 5.9 MPa (854 psi).

The relative position of the study wells is changed at Base Cretaceous Unconformity (Fig. 11). The threshold based on high frequency of hydrocarbon discoveries has now moved to 8.3 MPa (1200 psi) with 84% discoveries above and 41% discoveries beneath this threshold. There are three wells with ‘negative’ aquifer seal capacity, each therefore predicted to be breached, and each is a dry hole.

Base Chalk

There are no direct indications of fluid pressures in the Cromer Knoll except in the Greater Britannia area in the north of the study area. Hence over much of the study area the fluid pressures between Base Cretaceous Unconformity and Base Chalk are unknown. In order to examine the potential of the Chalk as a key horizon controlling hydrocarbon retention we have extended the aquifer gradients for each pressure cell to Base Chalk in each of the wells. The analysis at Base Chalk (Fig. 12) reveals a threshold aquifer seal capacity of 5.2 MPa (750 psi), with 88% discoveries above and 36% discoveries below. Further there are six wells with zero or negative seal capacity, all of them dry holes. We note that UK well 22/30a-4, with its long hydrocarbon column, remains with a positive aquifer seal capacity of 1.2 MPa (173 psi) at Base Chalk, reflecting the thin stratigraphic thickness between Top Fulmar and Base Chalk. Care was taken to avoid the Britannia Field area that has been affected by lateral drainage of pressures in Lower Cretaceous Britannia Sandstone since these reservoir pressures are not representative of the Cromer Knoll shales (O’Connor & Swarbrick 2008).

Discussion

Analysis of dry holes and hydrocarbon discoveries relative to their aquifer seal capacity shows the best empirical relationship at Base Chalk, as opposed to Top Reservoir, where the relationship is traditionally examined. At both Base Cretaceous Unconformity and Base Chalk, 100% dry holes are observed where the aquifer seal

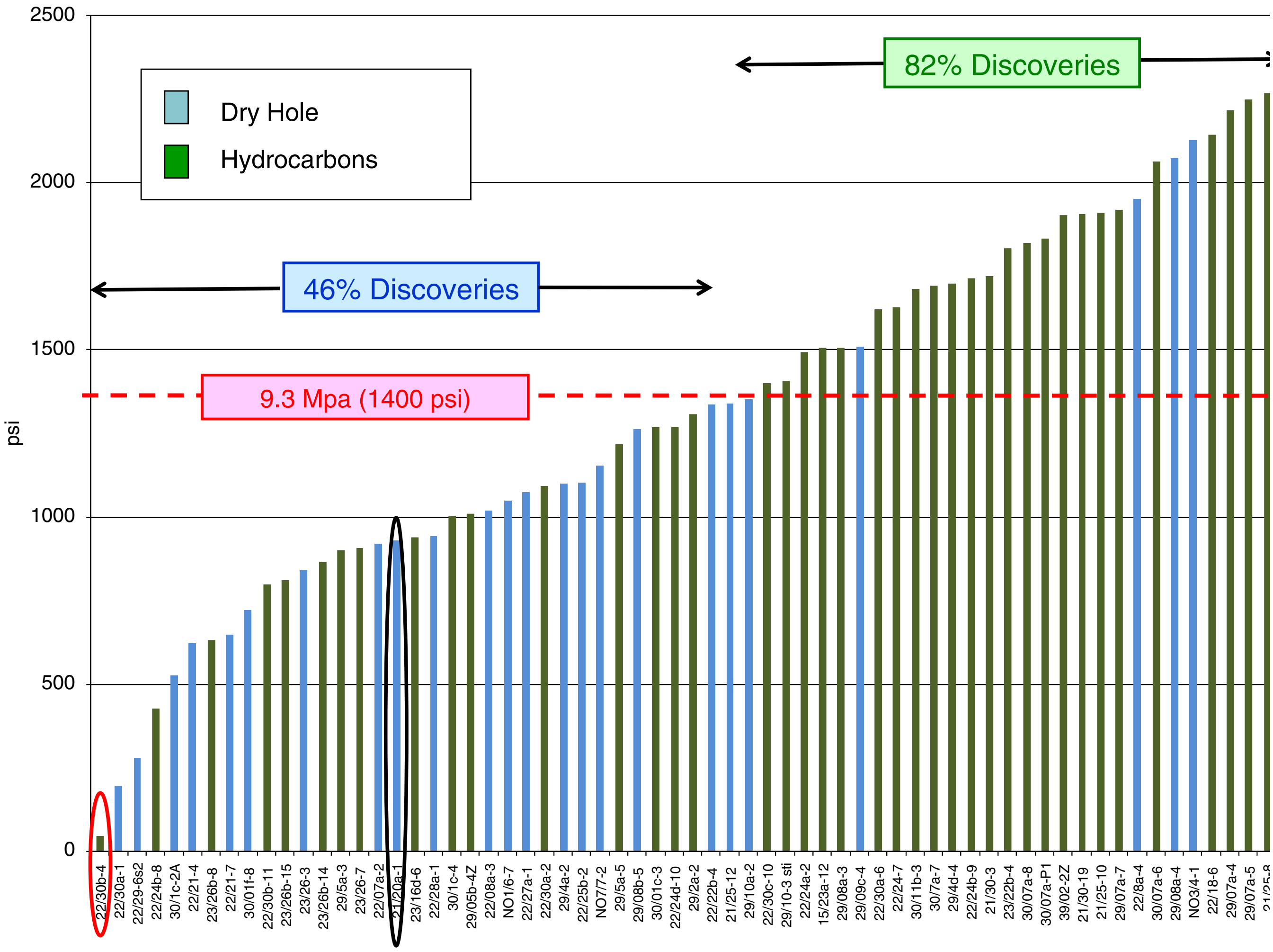

Fig. 8. Analysis of dry holes and discoveries at Top Reservoir using hydrocarbon seal capacity (in psi) for discoveries and the same values of aquifer seal capacity as shown in Figure 7 for dry holes.

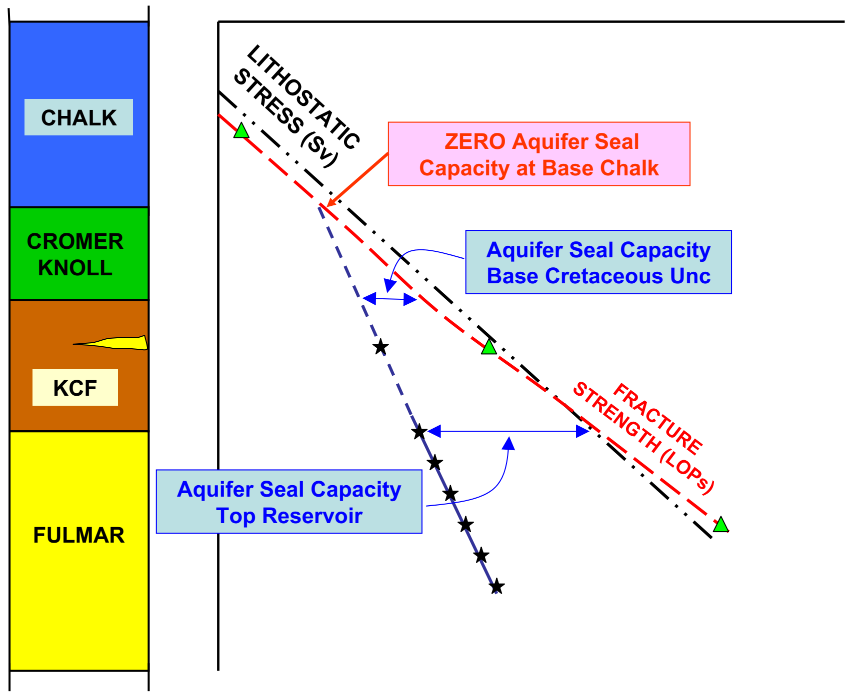

Fig. 9. Evidence from pressures in turbidite sands in the Kimmeridge Clay Formation (KCF) indicates pressure continuity between Fulmar and KCF sandstone reservoirs. The same aquifer gradient can be projected to shallower stratigraphic levels (e.g. Base Cretaceous Unconformity, Base Chalk), reducing the aquifer seal capacity reduces. Pressures in the Cromer Knoll Group are not known but have been extended to Base Chalk in order to examine the sealing/trapping relationship there.

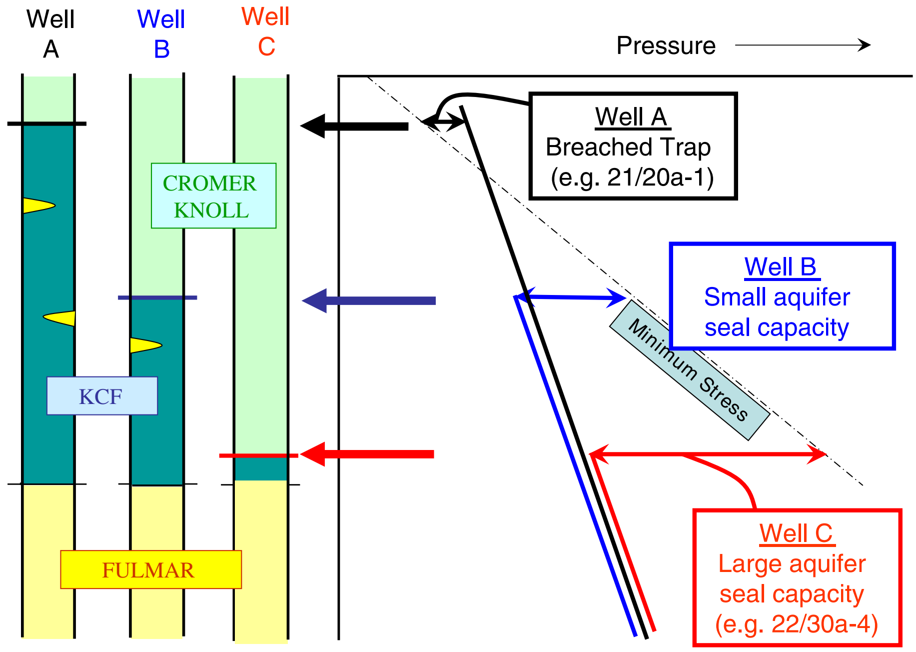

Fig. 10. Schematic diagram to illustrate how stratigraphic thicknesses control changes in aquifer seal capacity when an aquifer gradient is extended up-section. As an illustration well 22/30a-4 has very thin KCF and hence a similar aquifer seal capacity as at Top Fulmar. Where the stratigraphic thickness of KCF is large the aquifer pressure can reach the pressure of the minimum stress, implying seal breach conditions.

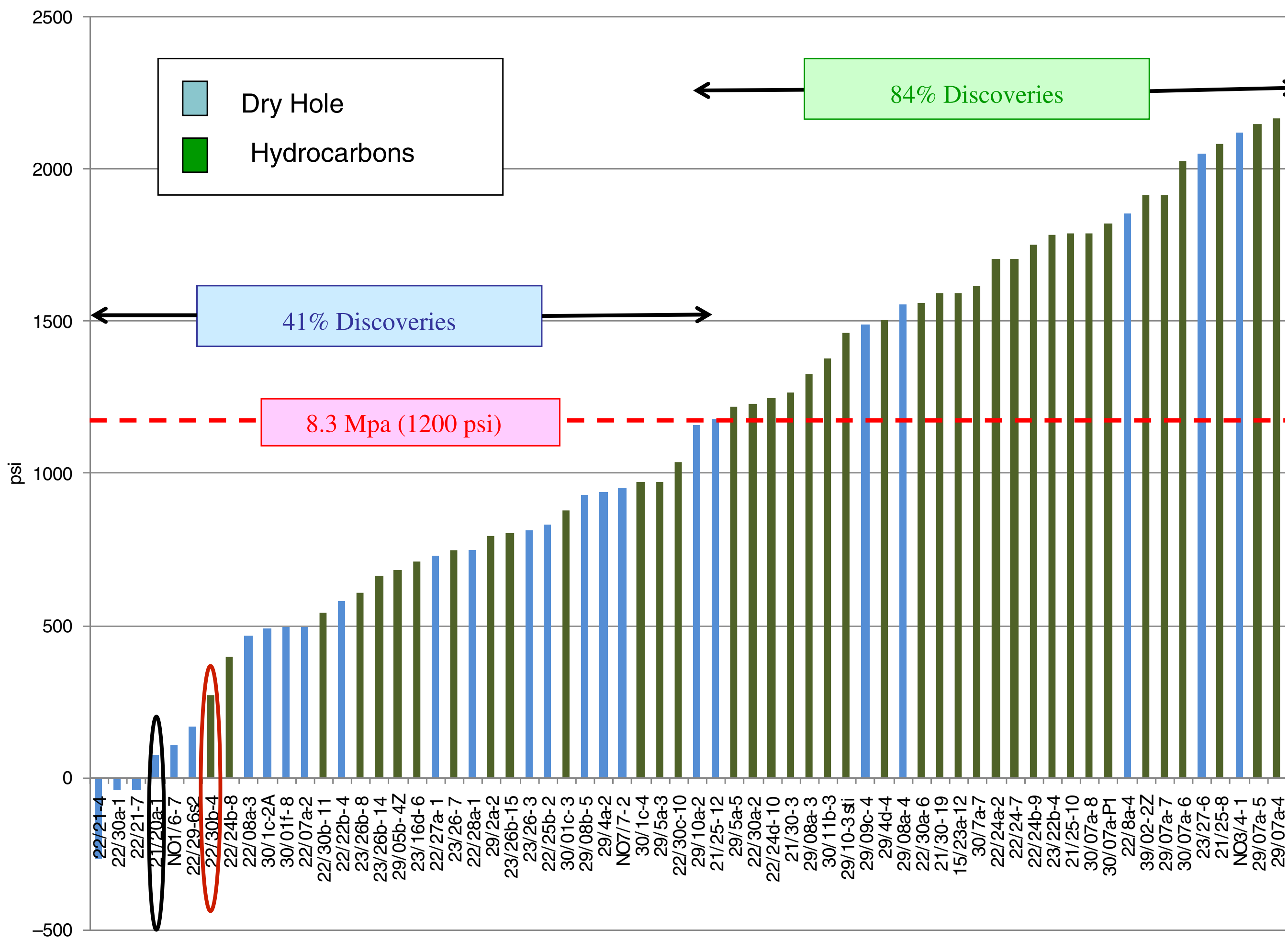

Fig. 11. Histogram of dry hole and hydrocarbon discoveries v. aquifer seal capacity at Base Cretaceous Unconformity. Out of 65 wells 84% are discoveries and 41% are dry holes when an aquifer seal capacity of 8.3 MPa (1200 psi) is used as threshold.

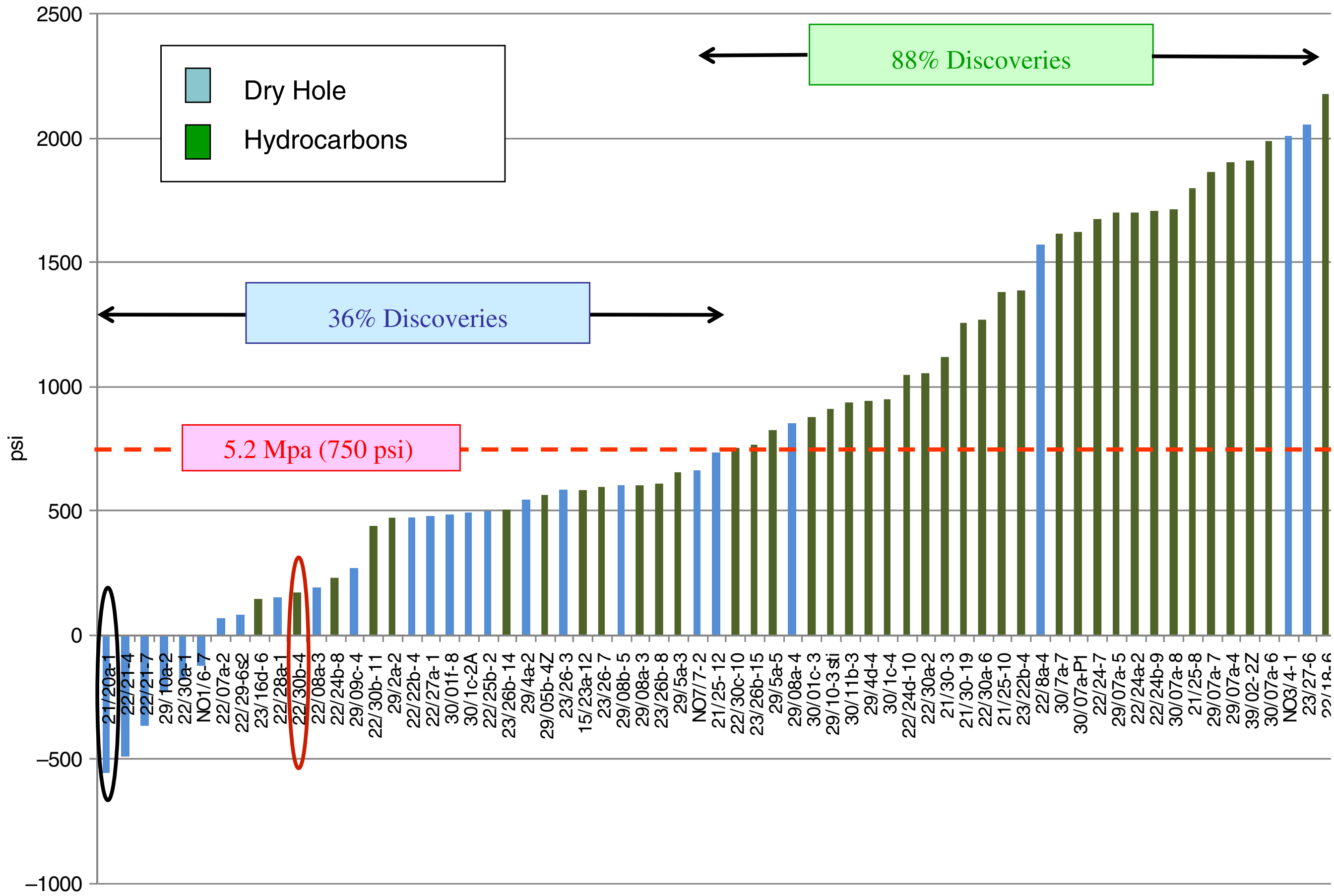

Fig. 12. Histogram of dry hole and hydrocarbon discoveries v. aquifer seal capacity at Base Chalk. Out of 65 wells 88% are discoveries and 36% are dry holes when an aquifer seal capacity of 5.2 MPa (750 psi) is used as threshold. Of those wells with negative aquifer seal capacity values, and hence predicted to be breached traps, all are dry holes.

capacity is zero or negative (i.e. predicted breached trap). At aquifer seal capacity magnitudes of >5.2 MPa (750 psi), 88% of wells drilled in the HP/HT area of the Central Graben are discoveries. We suggest, therefore, that Base Chalk may exert a controlling influence on hydrocarbon retention in this area.

There are leaking/leaked traps with positive values of aquifer seal capacity up to 750 psi (Fig. 12), such as UK well 22/8a-3 with core-based evidence for active petroleum leakage along vertical fractures in the Chalk. There are also wells with negative aquifer seal capacity values down to approximately −3.8 MPa (−556 psi), such as UK well 21/20a-1, with the same core-based evidence for active leakage. Whilst accepting the challenge of what the negative values of aquifer seal capacity may mean in terms of hydraulic failure and pressure retention, we believe that the data are not so precise that we can expect zero to be the breach value for all wells in that condition. We are therefore suggesting that the technique has an uncertainty of ±3.4 MPa (500 psi) around the zero value. It would be an over-interpretation of the data and processes to try to explain how a value of –3.4 MPa (−500 psi) for well 21/20a-1 might be created.

A field analogue from the Catskill Mountains, Upstate New York (Fig. 13) shows gas-generated hydraulic fractures extending only as far as the cemented sandstone, beyond which these fractures are unable to propagate. We suggest that the same concept may apply in the Central North Sea, that is, the cemented, and often massive, Chalk has higher fracture strength than the underlying stratified shales, which are more susceptible to hydraulic failure. The photograph also shows a later fracture set with different orientation (marked by arrow), which extends upwards through the entire section, but dated as much later, during uplift.

The Chalk is the hydrocarbon seal in several fields in the Central North Sea where chalk immediately overlies the Fulmar (e.g. 30/16-6) or Triassic reservoirs, for example, 22/24-2 Marnoch. We have demonstrated above that the pressure transition zones through the chalk indicated by rare direct pressure measurements also demonstrate that the Chalk is a pressure seal. Analysis of aquifer seal capacity in relation to hydrocarbon trapping also points to the Chalk as a potential control on hydrocarbon retention in these high-pressure areas, where hydraulic failure can lead to breached traps. The continuity of an aquifer gradient from Top Fulmar reservoir at least to Base Cretaceous Unconformity helps to explain the improved relationship between trapping and aquifer seal capacity estimates for our current dataset. However, the mechanism by which the pressures in thin multiple turbidites approximately equilibrate with the underlying Fulmar reservoir remains uncertain. Since the area where most of these wells are located coincides with areas where the Kimmeridge Clay Formation source rock is gas-generative (Cayley 1987), it is tempting to suggest that excess pressure due to gas generation has generated hydraulic fractures which have propagated downwards, thereby linking the reservoirs. Simultaneous upwards propagation may also help explain how aquifer gradients may also extend to Base Chalk, although this remains unproven. The common occurrence of gas influxes and reported issues relating to borehole instability when drilling the sub-Chalk section in many wells we examined suggests not only high pore pressure in the late Jurassic and Cromer Knoll mudrocks but also a high concentration of fractures.

We have highlighted that there is a major lithological distinction between the late Jurassic and Cromer Knoll Group mudrocks, and the fine-grained carbonates of the Chalk. The massive nature of the

Fig. 13. Field analogue from the Catskill Mountains, Upstate New York. Fractures believed to be created by gas at depth, which are arrested by a thin cemented clastic unit. We suggest comparison to the chalk arresting hydraulic fractures extending from Top Reservoir to Base Chalk. The photograph also shows a late fracture set (marked by an arrow), which extends upwards through the entire section, but related to stress release during uplift.

Chalk carbonates, compared with the more lithologically varied shales, may be significant in terms of how stresses are accommodated in the basin-fill, that is, brittle or ductile failure. Alternatively the fracture strength of the Chalk may be superior to the deeper strata.

In terms of implications for the risking of deep, high pressure traps in the Central North Sea, the above analysis allows for a pre-drill risk strategy. Specifically where the fluid pressure prediction has been predicted for the Top Fulmar reservoir, an aquifer gradient can be projected to Base Cretaceous Unconformity and Base Chalk. Using the predictions of fracture gradient and lithostatic at these depths, if the aquifer seal capacity is less than 5.2 MPa at Base Chalk or 8.3 MPa at Base Cretaceous Unconformity, there is a higher probability of dry hole than discovery. If a negative or zero value is predicted at either stratigraphic level a dry hole is predicted.

Conclusions

(1) Deeply buried Upper Cretaceous Chalk in the North Sea Central Graben is as effective as shale at creating a pressure seal.
(2) The pressure transition zone through the chalk in this area can be best described by a steady-state pressure profile.
(3) The chalk appears to have been drilled underbalanced in most wells in the study area.
(4) The low permeability of the non-reservoir chalks precludes influx during drilling, except where locally higher permeability (by several orders of magnitude) or fractures/faults exist.
(5) Analysis of aquifer seal capacity based on aquifer gradients extended from Fulmar Reservoir through Base Cretaceous Unconformity to Base Chalk indicates the most robust relationship between dry holes and discoveries is at Base Chalk.
(6) Further research is needed to understand more fully how fluid pressures equilibrate between Top Reservoir and Base Chalk through the Heather, Kimmeridge Clay and Cromer Knoll mudrock units, and why the Base Chalk may be a preferred stratigraphic unit relative to hydrocarbon entrapment.

The authors would like to thank IHS for provision of data and permission to use the data as part of the study. Thanks also to Patricia Kelly for generation of the well location map. An earlier version of the manuscript was helpfully improved by comments from John Smallwood and an anonymous referee.

References

Bjørkum, P. A., Walderhaug, O. & Nadeau, P. H. 1998. Physical constraints on hydrocarbon leakage and trapping revisited. *Petroleum Geoscience*, **4**, 237–239.

Brasher, J. E. & Vagle, K. R. 1996. Influence of lithofacies and diagenesis on Norwegian North Sea chalk reservoirs. *AAPG Bulletin*, **80**, 746–769.

Cayley, G. T. 1987. Hydrocarbon migration in the Central North Sea. *In*: Brooks, J. & Glennie, K. (eds) *Petroleum Geology of North West Europe*. Graham & Trotman, London, 549–555.

Daniel, R. B. 2001. Pressure prediction for a Central Graben wildcat well, UK North Sea. *Marine & Petroleum Geology*, **18**, 235–250.

Engelder, T. & Fischer, M. P. 1994. Influence of poroelastic behaviour on the magnitude of minimum horizontal stress, S_h, in overpressured parts of sedimentary basins. *Geology*, **22**, 949–952.

Gaarenstroom, L., Tromp, R. A. J., de Jong, M. C. & Bradenburg, A. M. 1993. Overpressures in the Central North Sea: implications for trap integrity and drilling safety. *In*: Parker, J. R. (ed.) *Petroleum Geology of NW Europe. Proceedings of the 4th Petroleum Conference*. Geological Society, London, 1305–1313; doi: 10.1144/0041305.

Grauls, D. 1998. Overpressure assessment using a minimum principal stress approach. *Overpressures in Petroleum Exploration. Proceedings of Workshop*, Pau, 1999. Bull. Centre Research. Elf Explor. Prod., Memoirs, **22**, 137–147.

Hermanrud, C., Norgard Bolas, H. M. & Tiege, G. M. G. 2005. Seal failure related to Basin-scale processes. *In*: Boult, P. & Kaldi, J. (eds) *Evaluating Fault and Cap Rock Seals*. AAPG Hedberg Series, **2**. American Association of Petroleum Geologists, Tulsa, OK, 13–22.

Holm, G. M. 1998*a*. Distribution and origin of overpressure in the Central Graben of the North Sea. *In*: Law, B. E., Ulmishek, G. F. & Slavin, V. I. (eds) *Abnormal Pressures in Hydrocarbon Environments*. American Association of Petroleum Geologists, Memoir, **70**, 123–144.

Holm, G. M. 1998*b*. Gas chromatography monitoring: an empirical method to detect the onset and magnitude of overpressure while drilling. With particular reference to Elgin Well 22/30c-G4. Overpressures in Petroleum Exploration Proceedings Workshop, Pau, 1999. Bulletin of the Centre for Research. Elf Exploration Production, Memoirs, **22**, 233–241.

Holm, G., Onu, C., Gray, R., Neillo, V., Tindle, C. & Joffroy, G. 2008. Observed indications of changes in pore pressure, fracture gradient following depletion of an HPHT reservoir – a case history from Franklin Well 29/5b-F8Z. Overpressure 2008 Present and Future Challenges, Durham University/CeREES conference abstracts.

Ingram, G. M. & Urai, J. L. 1999. *Top-Seal Leakage Through Faults and Fractures: The Role of Mudrock Properties*. Geological Society, London, Special Publications, **158**, 125–135.

Lubanzadio, M., Goulty, N. R. & Swarbrick, R. E. 2002. Variation of velocity with effective stress in chalk: null result from North Sea well data. *Marine and Petroleum Geology*, **19**, 921–927.

Mallon, A. J. & Swarbrick, R. E. 2008. Diagenetic characteristics of low permeability, non-reservoir chalks from the Central North Sea. *Marine and Petroleum Geology*, **25**, 1097–1108.

Mallon, A. J., Swarbrick, R. E. & Katsube, J. 2005. Permeability of fine-grained rocks: new evidence from chalks. *Geology*, **33**, 21–24.

O'Connor, S. A. & Swarbrick, R. E. 2008. Pressure regression, fluid drainage and a hydrodynamically-controlled fluid contact in the North Sea, Lower Cretaceous, Britannia Sandstone Formation. *Petroleum Geoscience*, **14**, 1–14.

Swarbrick, R. E., Osborne, M. J. & Yardley, G. S. 2002. Comparison of overpressure magnitude resulting from the main generating mechanisms. *American Association of Petroleum Geologists, Memoir*, **76**, 1–12.

Swarbrick, R. E., O'Connor, S. A. & Lahann, R. 2005*a*. Maximizing geological information from pressure tests and depth plots. *Oil & Gas Journal*, 26 September.

Swarbrick, R. E., Seldon, B. & Mallon, A. J. 2005*b*. Modelling the Central North Sea pressure history. *In*: Doré, A. G. & Vining, B. A. (eds) *Petroleum Geology: North-West Europe and Global Perspectives: Proceedings of the 6th Petroleum Geology Conference*. Geological Society, London, 1237–1245; doi: 10.1144/0060001.

Winefield, R., Gilham, R. & Elsinger, B. 2005. Plumbing the depths of the Central Graben: towards an integrated pressure, fluid and charge model for the Central North Sea HPHT Play. *In*: Doré, A. G. & Vining, B. A. (eds) *Petroleum Geology: North-West Europe and Global Perspectives: Proceedings of the 6th Petroleum Geology Conference*. Geological Society, London, 1301; doi: 10.1144/0061301.

Investigating fault-sealing potential through fault relative seismic volume analysis

J.-F. DUTZER,[1] H. BASFORD[2] and S. PURVES[2]

[1]*GDFSUEZ, Direction Exploration-Production, 361 Avenue du President Wilson 93211 Saint-Denis, La Plaine Cedex, France*

[2]*ffA, Newcastle Technopole, Kings Manor, Newcastle upon Tyne NE1 6PA, UK*

(e-mail: spurves@ffa.co.uk)

Abstract: Accurate fault interpretation is key to building a robust and reliable reservoir model, and is essential for further study of fault-seal behaviour and reservoir compartmentalization. Conventional fault interpretation defines faults as planar features. Although the concept of fault damage zones (FDZ) is well established, manual delineation of FDZ from subsurface imaging data is difficult and rarely attempted. In this work we are using the concept of a seismic fault distortion zone (SFDZ). The SFDZ differs from the geological FDZ and is the 3D extent of the regions where the presence of a fault has perturbed the seismic image. The SFDZ represents an area of significant uncertainty within the seismic volume where the signal is distorted either by changes in geology associated with faulting or by imaging problems due to the presence of the fault. Delineation of the SFDZ is a key step in further analysing 3D seismic data to provide information regarding variations in seismic attributes across a fault that can be used to indicate how juxtaposition of strata influences a potential sealing fault. The SFDZ is delineated using an adaptive region growing algorithm and produces a set of detailed 3D SFDZ geobodies. The delineated SFDZ is then used as the input to a set of analysis techniques that examine 3D volumetric juxtaposition of seismic attributes, and properties relative to the fault. The techniques involve automated statistical measurement along seismic structure relative to the fault itself. The workflow has been applied and its utility assessed on an underground gas storage dataset. Initial results suggest that by taking account of the 3D geometry of the SFDZ and subsequently analysing 3D frequency and acoustic impedance volumes relative to these structures, an improved understanding of the juxtaposition of layers across the fault and the lateral variability, juxtaposition can be determined at seismic resolution, and subsequently used to assess the potential for fault seal and fluid migration.

Keywords: fault network, juxtaposition, inner distortion zones, outer distortion zone

When faults are picked during interpretation of seismic data, they are commonly picked as a single plane running through the centre of a faulted zone. A fault's expression in seismic data is rarely a sharp discontinuity and both manual and automated methods for picking faults must address the problem of precise placement of the fault surface. There is uncertainty in the fault's 'true' position at seismic scale, whichever method is used.

However, both outcrop and well data studies show that complex and often asymmetric zones of disturbance, such as fracturing, grain crushing and bending of rock layers, exist around fault surfaces that can typically range from several centimetres up to 200 m on a single side. The reader is directed to Berg & Skar (2005) for an illustration of the disturbance surrounding the Moab Fault, Utah. Although the character of these zones varies to a great degree, they can generally be classified into a fault core and more extensive fault damage zones (FDZ). Typically, the fault core is characterized by fault gouge, internal fault rock, slip surfaces, clay smear and alteration, and will have accommodated the majority of displacement. The FDZ is characterized by subsidiary faults, folds, deformation bands, veins and joints, which reduce in frequency away from the fault core. Subsidiary faulting is dominantly parallel to the main fault, but can also occur in vertical or antithetic planes to the main fault (Kim *et al.* 2004; Berg & Skar 2005). Towards the extent of the FDZ there are often significant regions of drag in the surrounding strata, which may or may not be characterized as damage.

On a seismic scale, the fault core is not resolvable. In standard seismic acquisition, the typical bin spacing of 12.5–25 m is well above the width of the fault core for the majority of faults on a reservoir scale. Therefore the focus of this research is solely on a wider seismic fault distortion zone (SFDZ) that is generally resolvable on high-quality 3D PSTM or PSDM seismic data. We further classify this into an inner seismic distortion zone and an outer seismic distortion zone where these are defined through appropriate use of seismic attributes.

- **The inner zone** is generally expressed by a disruption to the reflectors and reduction in seismic amplitudes (shown schematically in Fig. 1). The inner zone represents the limits to the zone of uncertainty associated with the positioning of the fault core within the seismic volume. The seismic response here is likely to be unreliable, as the fault itself will have introduced distortion during the imaging process. Traditional fault attributes such as semblance-based measurements are used in characterizing the inner zone.
- **The outer zone** is a wider zone within which reflector drag, folding and distortion related to faulting is present and resolvable (shown schematically in Fig. 1). This type of expression can be defined through the use of curvature- and flexure-type seismic attributes.

Note, this classification is similar to that adopted by Jones & Knipe (1996) in their interpretation of 'fault damage zones' across a range of scales using seismic attribute maps, although here we work consistently with 3D seismic data-based measurements.

Defining the fault network

Prior to analysing the fault network, structurally oriented, adaptive and edge-preserving noise cancellation algorithms are applied.

VINING, B. A. & PICKERING, S. C. (eds) *Petroleum Geology: From Mature Basins to New Frontiers – Proceedings of the 7th Petroleum Geology Conference*, 509–515. DOI: 10.1144/0070509

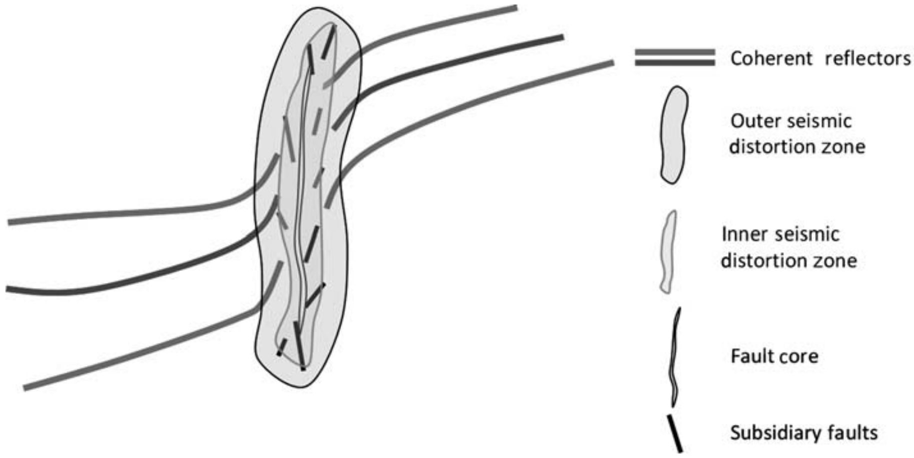

Fig. 1. Schematic demonstrating the inner and outer seismic distortion zones associated with faulting.

By increasing the signal-to-noise ratio whilst preserving edges, a clearer definition of fault v. non-fault can be obtained.

A 3D seismic processing workflow has been defined and implemented in order to allow fault systems to be analysed by drawing on the information available within noise-cancelled 3D seismic reflectivity, derived seismic attribute and inverted seismic property volumes. This workflow builds on existing post-stack fault imaging and fault network skeleton extraction methods (Fig. 2a, b) to provide a starting point for the fault relative seismic analysis workflow that we discuss here. The process of fault imaging provides us with a number of fault attributes, typically computed through trace-to-trace correlation and/or discontinuity detection algorithms, which are used to extract a skeleton of single-voxel-thick surfaces across the whole dataset.

This fault skeleton represents potential faults as exhibited in the chosen seismic fault attribute response and is a data-driven approach to positioning a 3D fault surface within the zones of uncertainty around faults in the seismic.

Defining the damage zone

In order to define the limits of the SFDZ across the volume of interest, an automatic region-growing algorithm is utilized. The fault skeleton is used as a starting seed for a region-growing process. Used in combination with a selected seismic attribute which highlights the extent of SFDZ in the data, fault structures within the fault skeleton are extended in three dimensions so that they cover the corresponding SFDZ regions. The algorithm analyses all adjoining voxels to the seed and those that meet interpreter-defined growth criteria are accepted as part of the SFDZ geobody (Fig. 2c).

The nature and thickness of the SFDZ geobodies that are extracted vary according to the attribute used in the calculation. This in turn responds to different SFDZ expressions within the seismic data (i.e. flexures in reflectors, dimming of amplitude, phase change, apparent reflector termination). Seismic expression of the faults can vary significantly within a single seismic dataset. As a result, faults are rarely completely captured by individual attributes across a dataset and optimum results often come from using a number of attributes in combination.

Figure 3 shows a selection of attributes and how they image the SFDZs of two faults. The inner zone is well defined by attributes such as deformation distance (a vector-based measurement of disruption), semblance, dip and tensor (a measurement of disruption based on eigenvalues of the gradient structural tensor). The outer zone is well defined by measurements of curvature, including the measure of structurally oriented curvature shown here.

Fault relative analysis associated with damage zones

Once an SFDZ has been defined (either the inner or outer zone depending on user focus), both its lateral thickness and changes in a selected seismic attribute response across the SFDZ can be evaluated. The thickness of the damage zone is mapped directly onto the fault network and enables the user to rapidly see variations in the extent of fault-related distortion. The outer surface of the SFDZ geobody is also extracted (Fig. 2d) and this ‘skin’ is used to constrain statistical analysis of seismic attributes. By studying the juxtaposition across the damage zones of the defined SFDZ and calculating the difference in these attribute values on either side of the SFDZ, areas of significant contrast and areas of no contrast are readily highlighted. This is achieved via the application of structurally oriented filters that initially sample then juxtapose data from either side of the damage zone onto the central fault plane. Steering volumes are used to align the structurally oriented filter footprints along dominant reflectors and thus maintain structural variations. By taking the local mean of an attribute, a noise-free representation of it is provided, whilst the variance gives a measure of its distribution. Results are initially stored on the skin of the damage zone (Fig. 2f), then horizontally juxtaposed from both sides onto the central plane in a direction perpendicular to the trend of the central fault. With the variance and mean attribute value on either side of the fault now stored co-incident to the fault plane, a difference volume can be generated and the contrast in properties across the fault visualized in a single volume, which is named the juxtaposition difference (Fig. 2g). The result of this process is a data-derived juxtaposition map being produced, at seismic resolution, on the 3D fault surface representation itself.

Attributes proposed for this workflow include acoustic impedance (AI), porosity or frequency. However juxtaposition difference maps for any seismic attribute or inverted volume could be applied during this process. Through the use of appropriate seismic attributes and inversion data, the juxtaposition difference can aid in the overall process of assessing fault seal by allowing detailed examination of subsurface properties around faults via seismic resolution attribute maps as opposed to interpretation-based juxtaposition diagrams.

In the case of AI, we see the following behaviour: where there is shale-to-sandstone contact at the SFDZ, the juxtaposition difference will yield high values and where there is either a sandstone-to-sandstone or shale-to-shale contact at the damage zone, the FSC index will yield low values. By restricting the evaluation zone of interest to centre on the reservoir interval and calibrating with known lithologies at well locations, low juxtaposition difference regions corresponding to sandstone-to-sandstone

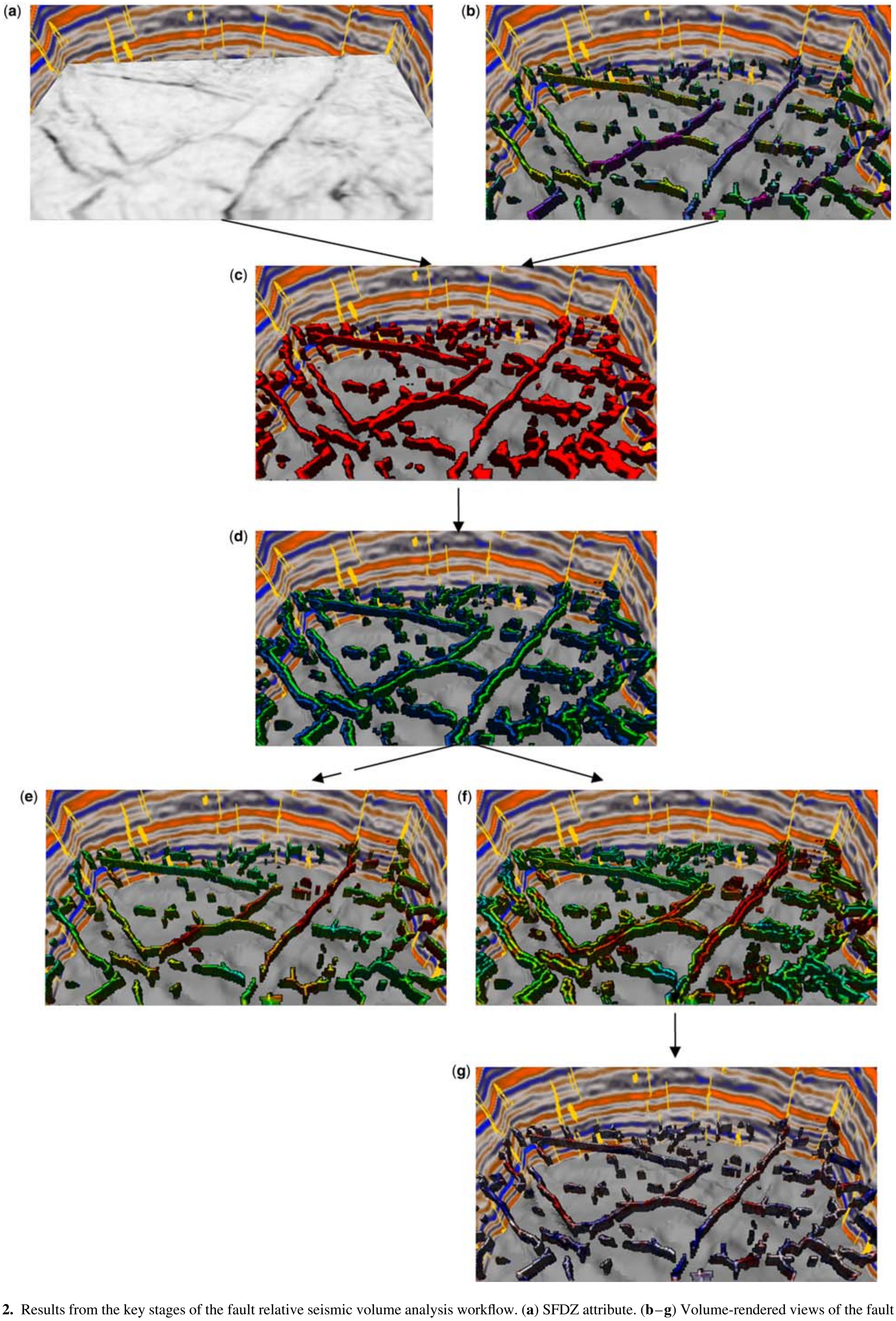

Fig. 2. Results from the key stages of the fault relative seismic volume analysis workflow. (**a**) SFDZ attribute. (**b**–**g**) Volume-rendered views of the fault and SFDZ-based measurements: (b) fault network skeleton mapped with fault trend; (c) SFDZ geobody; (d) SFDZ skin geometries; (e) mean AI from within the SFDZ; (f) structurally oriented average of AI outside of the SFDZ; (g) AI juxtaposition difference.

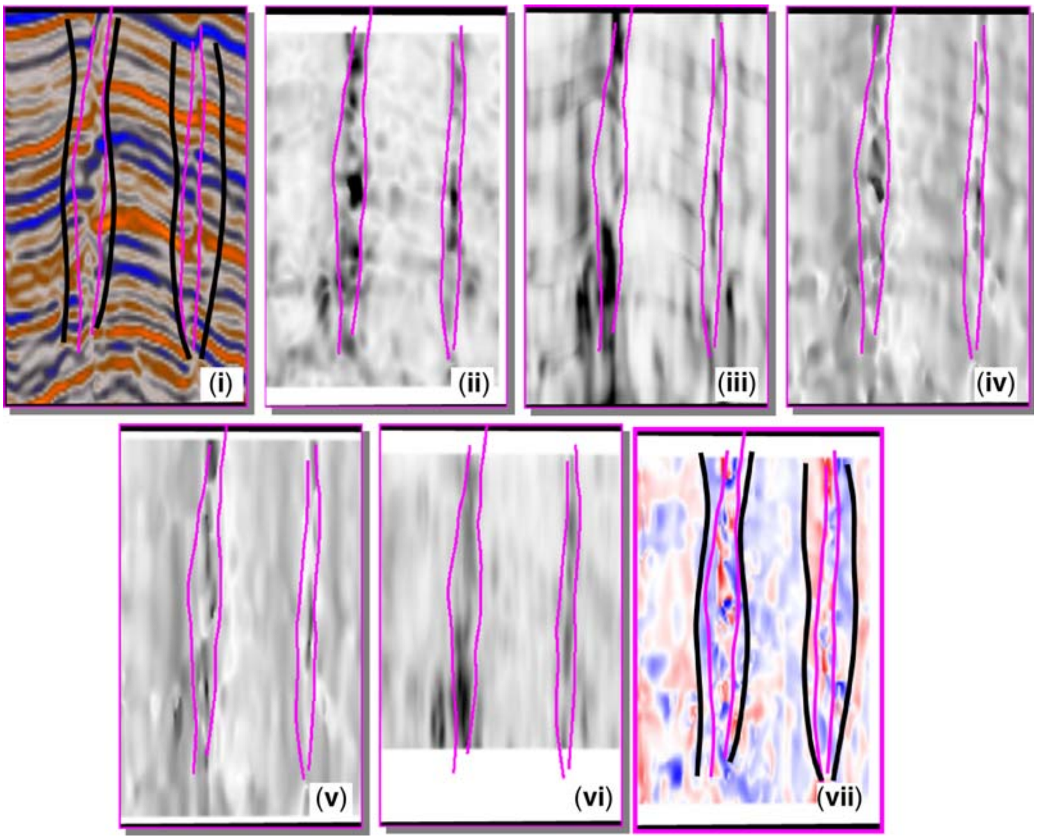

Fig. 3. Expressions of the SFDZ. (**i**) Reflectivity; (**ii–vi**) volumetric fault attributes; (ii) deformation; (iii) semblance; (iv) dip A; (v) dip B; (vi) gradient structure tensor; (**vii**) volumetric local curvature. Pink represents a manual interpretation of the inner seismic distortion zone and black a manual interpretation of the outer seismic distortion zone.

contacts can be identified, and thus potential non-sealing regions are highlighted and spatially defined for further analysis within an overall fault seal analysis workflow.

In the case of a sandstone-to-sandstone contact, a juxtaposition difference value of zero implies that the AI on either side of the fault is identical and a small value implies that there are differences in AI of the sandstone on either side of the fault. The 3D nature of the analysis enables the lateral and vertical variation of these contrasts to be viewed along the length of a single fault or across a fault network.

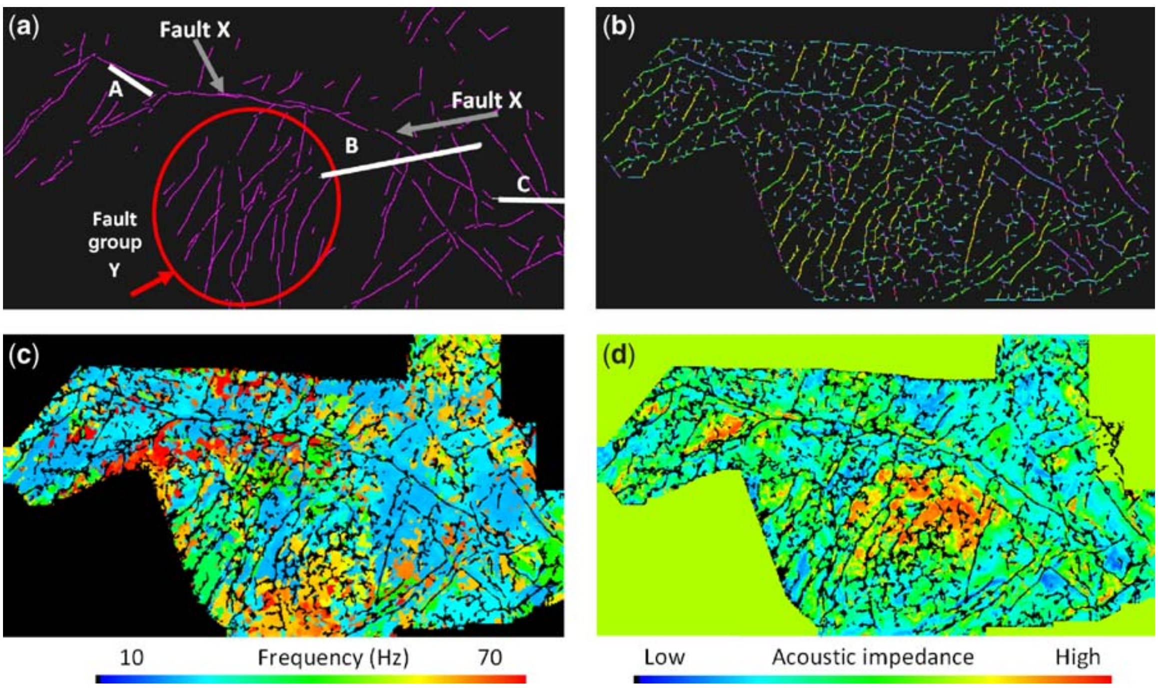

Fig. 4. Fault imaging: (**a**) manual interpretation of fault network with key wells marked A–C; (**b**) automatically detected fault network mapped with 2D trend; (**c**) SFDZ (black) mapped on to frequency; and (**d**) SFDZ (black) mapped on to AI. This analysis can be seen in time-slices or in a horizon-consistent manner.

In the juxtaposition analysis described above, the data-derived SFDZ is used to ensure that only data samples outside of the SFDZ are included in the measurement. In an additional step within the workflow, the statistics of the selected seismic property volume can also be assessed within the SFDZ. Within the SFDZ the analysis is performed relative to the seismic sampling grid, as (by definition) there are no conformable reflectors present here, and larger sample neighbourhoods are typically adopted. The calculation of the bulk mean and variance within the SFDZ is used to produce a further attribute map of the fault surface (Fig. 2e). This can be used to examine the apparent continuity of seismic properties within the SFDZ.

Case study

The workflow described above has been applied to approximately 100 km^2 of 3D seismic data acquired over an onshore underground gas storage area (UGS). The data is a merge of three different vintages that have been processed to produce a single seismic reflectivity volume. The seismic data is of fair to very good quality with bin spacing of 20×20 m and elevated noise in some areas as a result of varying fold due to the presence of surface facilities.

The target level contains three reservoir intervals, with an approximate total thickness of 70–160 m. This interval is contaminated by noise, remaining internal multiples and intrinsic complexity (three reservoir levels, themselves divided into four levels). However, the current interpretation of the entire sequence has good well control, with more than 100 wells present in the area.

Within this data, several fault studies have been performed, focusing at different levels: above the top reservoir, adjacent to top reservoir, and inside the reservoir itself. The decoupling of fault studies into depth ranges is a direct consequence of tectonic decoupling that can be observed on seismic reflectivity.

Initial mapping and manual interpretation of faults provides a good but simple understanding of the faulting present in each of

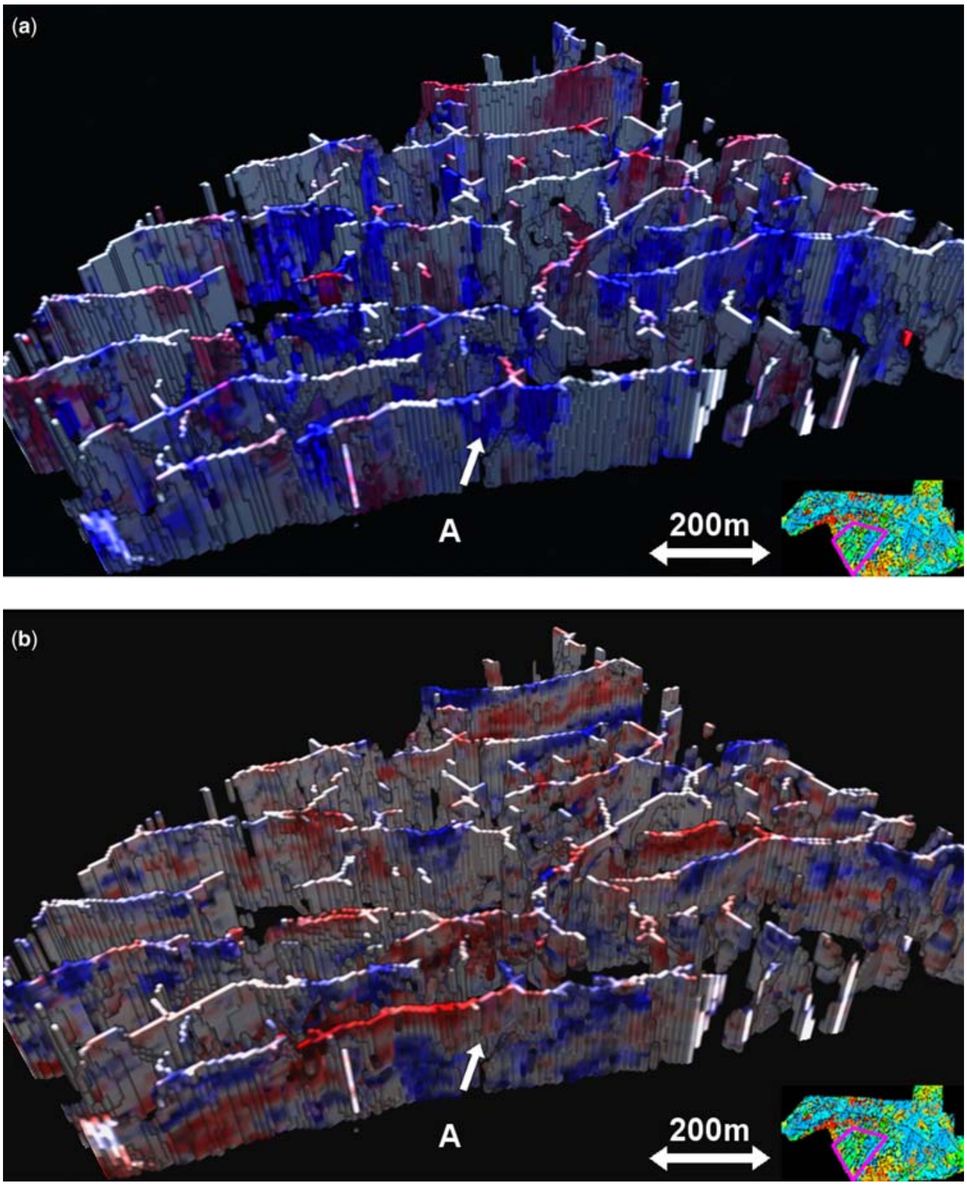

Fig. 5. (**a**) Frequency and (**b**) AI volume-rendered view of the fault network skeleton mapped with the juxtaposition difference values. (a) FDZ index volumes for frequency. Blue shows an increase in frequency to the top of the 3D image, red shows a decrease in frequency to the top of the 3D image and white shows no contrast in frequency. The small base map in the right-hand corner shows the position of the sub volume on the images seen in Figure 4. (b) FDZ index volumes for AI. Blue shows an increase in A1 to the top of the 3D image, red shows a decrease in A1 to the top of the 3D image and white shows no contrast in A1. The small base map in the right-hand corner shows the position of the sub-volume on the images seen in Figure 4.

the levels (Fig. 4a), but does not provide information about the interplay between faults and fluid movement, although different pressure regimes have been discovered between some specific pairs of wells (well pairs A–B and B–C in Fig. 4a).

In order to optimize results, structurally oriented edge-preserving and adaptive noise-cancellation filters were applied to remove the coherent and random noise within the seismic reflectivity data whilst maintaining the structure of subtle faults and discontinuities. By utilizing automated fault detection and extraction workflows, a more detailed map of faulting than previously interpreted has been defined (Fig. 4b), enabling interpreters to distinguish and study internal fractured zones in addition to major and en-echelon faults seen in the area. By mapping the volumetrically calculated SFDZ onto a horizon of interest or viewing simply along a time slice, we can see the variation in thickness between and along faults (Fig. 4c, d). Varying damage zone thickness can relate to different fault mechanisms as well as the lithology in which faulting has occurred and is of interest as it can influence fluid flow across a fault. Damage zones along both fault X and fault group Y have similar widths, which range from 80 to 120 m.

SFDZ analysis has been applied to both frequency and AI volumes. Seismic frequency can be affected and attenuated by depth, lithology, bed thickness, porosity and fluid fill. In particular, the presence of gas is often seen to reduce frequency. It can be clearly seen in Figure 4c that dominant faults (such as those in fault group Y) and their associated damage zones are often sharply bounding areas of high and low frequency.

The juxtaposition difference (Fig. 5a) for this volume provides increased detail of how the contrast in frequency changes spatially along the length of faults within fault group Y. Reds and blues both indicate zones of high frequency contrast (up to 60 Hz). Blue shows an increase in frequency across the fault towards the top of the 3D image, red shows a decrease in frequency across the fault towards the top of the 3D image and white shows no contrast in frequency. The juxtaposition difference volume implies that the sealing potential based on frequency juxtaposition alone is much more variable

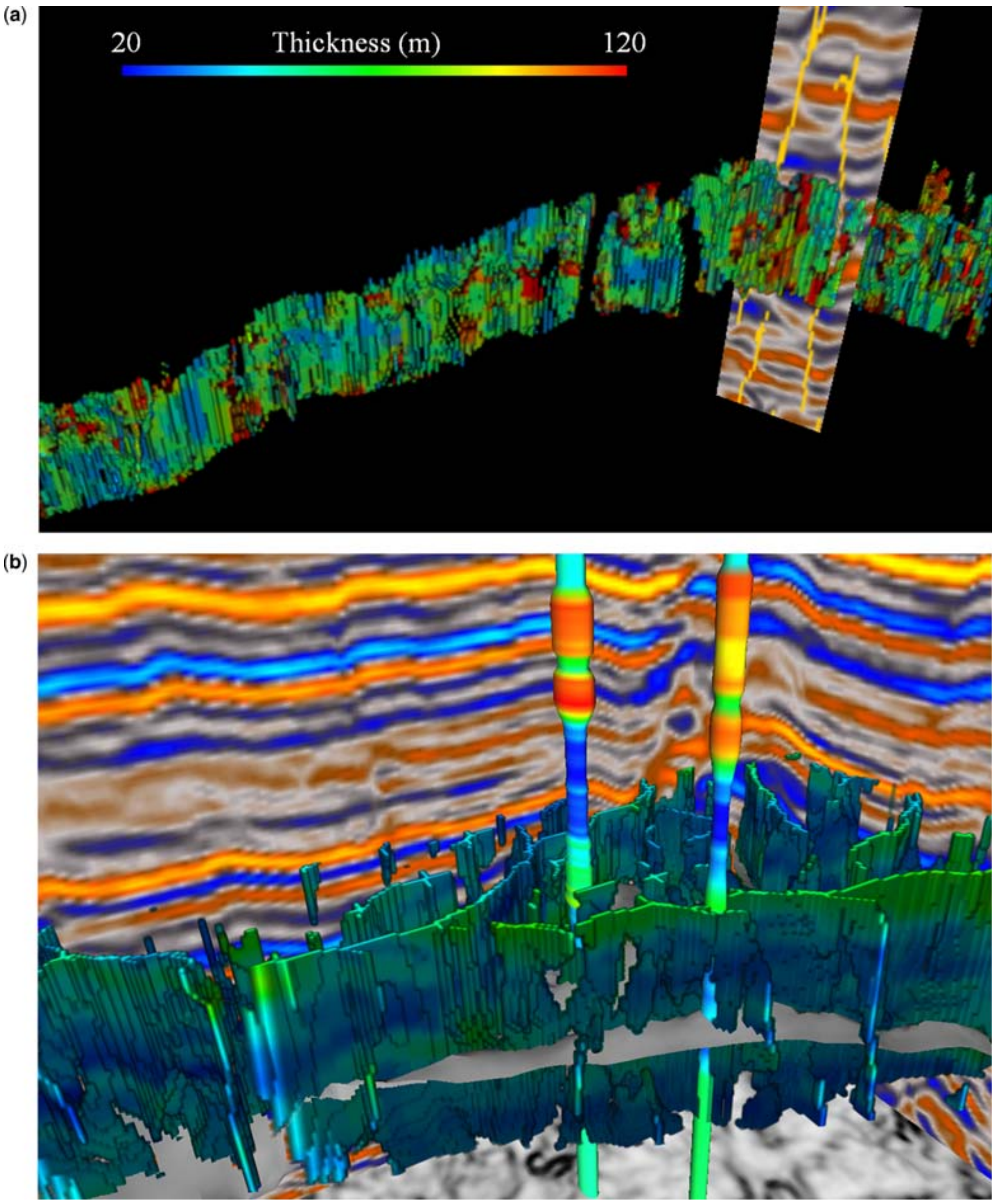

Fig. 6. (**a**) Volume render of a single fault cropped to the reservoir level alone and mapped with SFDZ thickness. Variations from low (blue) to high (red) thickness can be observed. Rapid lateral and vertical changes suggest possible areas of fluid transmissibility are localized. (**b**) Well information. The AI within the inner damage zone (mapped onto fault network) is seen to correlate with *P* wave velocity (Vp) logs, bringing thus the first step in the well calibration procedure (using the porosity logs and pressure measurements).

along the length of these faults than the horizon slice initially suggests. Analysing the AI yields similar results. By embedding the SFDZ into the AI volume, zones where faults are bounding large contrasts in AI can easily be seen (Fig. 4d). FSC index volumes for both frequency and AI reveal high contrasts and thus high potential for juxtaposition-based sealing at many locations, such as that marked A on Figure 5a, b. However, it is apparent that these regions of potential sealing are all localized and there are many (white) regions of no contrast that have the potential to provide pathways for fluid migration.

Focusing on a particular fault at the reservoir zone enables detailed juxtaposition difference and thickness variations (Fig. 6a) to be mapped. Rapid lateral and vertical changes in thickness as well as juxtaposition difference suggest possible areas of fluid transmissibility are localized.

Visualization and correlation of well logs as displayed in Figure 6b demonstrates that the information borne by fault analysis (local sample mean of inverted AI within the damage zone) is supported by existing well data. The incorporation of additional and more advanced well information could thus be used for further extrapolation and calibration.

Caveats and discussion

- The analysis of seismic-scale FDZ and contrast in attributes/properties across them can provide additional information and a greater degree of detail regarding the juxtaposition-based sealing potential of a fault, or fault network. It must be noted that this is just one of several mechanisms for sealing as a result of faulting.
- The technique relies on seismic reflectivity data and seismic attributes with a high lateral resolution and yields more accurate results when data has been acquired with a small bin spacing (i.e. 12.5 m).
- The fault imaging and fault network skeleton can be used to highlight significantly more detail at and around existing fault interpretations as well as highlighting new unconsidered candidate faults that may positively impact on the overall understanding of reservoir sealing behaviour.
- Although the seismic data under observation is highly perturbed (faulted and even acting as wave propagation barriers), much information can be directly inferred from fault and SFDZ studies. Nevertheless, it is believed that seismic data is statistically sufficient to derive accurate information on sealing/non-sealing capacities (varying within one fault), provided some calibrating additional data (pressure from wells) is given.
- Future work includes applying this new workflow to other datasets, particularly those with interpreted fault, FDZ geometries and including parallel fault sealing studies.
- As a data-driven workflow to examine subsurface properties around faults, it is highly dependent upon the use of robust attributes and inverted data, and upon the availability of well data in order to calibrate the results.
- As far as UGS projects are concerned, a dynamic/historic view of the fault-sealing behaviour should also be sought, as there are likely to be significant variations in seismic response with time.

Conclusions

We have an established workflow that has been applied to a number of case studies. The techniques for extracting a damage zone around the fault are well defined. More work is required in order to understand the best combination of information, from both seismic and wells, needed to demonstrate the behaviour of fluid across an identified damage zone.

For the UGS study presented here, damage zone thickness and symmetry measures, contrast in AI response across the damaged zone, AI variability and spectral decomposition techniques have been used in combination to produce indicators of potential fault-sealing behaviour.

Prior to this study, the structural system was simplified in order to fit with current models, but the detailed interpretation of the complete fault network, including small faults subsets, and the behaviour provided by FDZ analysis, is delivering a better understanding of the fault network and will have an impact on the forecast of production profiles.

One may highlight that the varying behaviour vertically and horizontally of what were previously considered to be simple single faults brings a clear call for more integration between reservoir models and detailed geological (horizons and faults behaviour included) models derived from seismic data.

The authors are grateful for Storengy (formerly GdF/DGI) for making this data available. The seismic acquisition was partly funded by TEN-E Network from the European Community. Elements of the workflow presented have been developed as part of the following R&D Collaborations: FSC (Fault Seal Capacity) Workflow Stage I – ffA, GDFSUEZ; FSC Workflow Stage II Joint Industry Project – ffA, GDFSUEZ, StatoilHydro.

References

Berg, S. S. & Skar, T. 2005. Controls on damage zone asymmetry of a normal fault zone: outcrop analyses of a segment of the Moab fault, SE Utah. *Journal of Structural Geology*, **27**, 1803–1822.

Jones, G. & Knipe, R. J. 1996. Seismic attribute maps; application to structural interpretation and fault seal analysis in the North Sea Basin. *First Break*, **14**.

Kim, Y.-S., Peacock, D. C. P. & Sanderson, D. J. 2004. Fault damage zones. *Journal of Structural Geology*, **26**, 503–517.

4D acquisition and processing: a North Sea case study on the relative contributions to improved 4D repeatability

E. C. RUSHMERE, M. DYCE, S. CAMPBELL and A. J. HILL

BP, Dyce Complex, 1–4 Wellheads Avenue, Stoneywood Park, Dyce, Aberdeen AB21 7DF, UK (e-mail: ed.rushmere@uk.bp.com)

Abstract: Using a case study from the Mungo Field in the Central North Sea, we investigate the relative impact of acquisition and processing improvements on 4D seismic repeatability. The results show that, while advancements in both have helped to reduce 4D noise, significant noise reduction can be attributed to processing alone. 4D noise can be thought of as any non-production-related amplitudes that are observable on a 4D difference section, and has both random and coherent components. Both are undesirable as they can mask any real 4D signal. A great deal of effort is employed to reduce noise levels by optimizing acquisition and processing between the 3D surveys, which are differenced to highlight the 4D signal. This paper studies the changes introduced by acquisition and processing improvements using the calibrated difference in reflectivity measure.

Keywords: 4D, repeatability, North Sea, acquisition, processing

4D noise levels were calculated between three acquisition vintages, upon which two processing flows were applied. An additional application of 'STAR', a 4D post-stack noise reduction process was tested (Zamorouev *et al.* 2006). Comparisons of repeatability were made using calibrated difference reflectivity (CDR) to highlight improvements through processing, acquisition and combinations of both. For each result a CDR value, map and amplitude spectrum were calculated to represent the 4D noise in that 4D difference volume.

For the Mungo 4D Noise Case Study, the total contribution of all improvement is to drive down the 4D noise level by a factor of 3. Acquisition efforts to better match source and receiver locations between baseline and monitor surveys account for approximately one-third of this uplift. The application of STAR accounts for approximately one-third of the total noise reduction, while improvements to the 4D processing flow provide the remaining uplift.

A typical method for the analysis of 4D anomalies is the study of 3D seismic difference volumes. The energy in a difference volume is a sum of the 4D signal, random noise which does not match between datasets, and coherent noise caused by the imperfect matching of events. Both forms of noise are undesirable as they can mask any 4D signal that would otherwise be interpretable, as shown in Figure 1. A great deal of effort is employed to reduce 4D noise levels and improve repeatability by optimizing acquisition and processing parameters between 3D surveys, the final objective being to remove both coherent and random noise from the difference volume and improve our ability to interpret the 4D signal. This paper studies the changes introduced by each acquisition and processing step of a typical flow, and attempts to identify where the greatest reduction in 4D noise is achieved.

Repeatability measurements

It is common to use an attribute to measure the level of noise in a 4D difference volume. This can be recalculated as new processing or acquisition is introduced to determine the improvement in the seismic difference, or reduction in the noise level. One measure is the CDR (Dyce *et al.* 2004).

This attribute computes the RMS amplitudes in a 4D difference volume between two 3D seismic surveys. However, CDR is different from many industry standard repeatability measures, for example normalized root mean square (NRMS), in that it also calibrates the seismic amplitudes to the well reflectivity by matching the spectra of the data and the well over the seismic bandwidth through an application of blueing. Blueing the seismic difference volume ensures the CDR measure can be directly compared with predictions of 4D signal from rock properties modelling, both in terms of reflectivity and predicted change of acoustic impedance. The definition of CDR, the windowed RMS amplitude from the difference of two blued seismic volumes A and B, is shown in equation (1):

$$\mathrm{CDR} = \mathrm{RMS}(A - B). \tag{1}$$

The definition of NRMS is given in equation (2):

$$\mathrm{NRMS} = \frac{\mathrm{RMS}(A - B)}{\left(\frac{\mathrm{RMS}(A) + \mathrm{RMS}(B)}{2}\right)}. \tag{2}$$

The simple relationship between the two attributes can be seen as the reciprocal of the average of the RMS amplitude of the two seismic volumes.

Improvements in acquisition or processing should reduce random noise and better align primaries between surveys, lowering the amplitudes in the difference and reducing the CDR. From this we can determine which aspect of the flow provides the most improvement, and whether poor acquisition repeatability can be compensated for in later processing.

The intention of CDR is to measure 4D noise; therefore the repeatability analysis should take place over a window of seismic difference data in the region of the reservoir, but not in an area where a 4D signal is expected. This could be just above the top reservoir (assuming there are no 4D geo-mechanical changes in the overburden), or at the reservoir level but away from any production/injection effects.

Case study details

In many 4D projects, a CDR value is only calculated on the baseline and monitor surveys following the final processing. This only

VINING, B. A. & PICKERING, S. C. (eds) *Petroleum Geology: From Mature Basins to New Frontiers – Proceedings of the 7th Petroleum Geology Conference*, 517–522. DOI: 10.1144/0070517

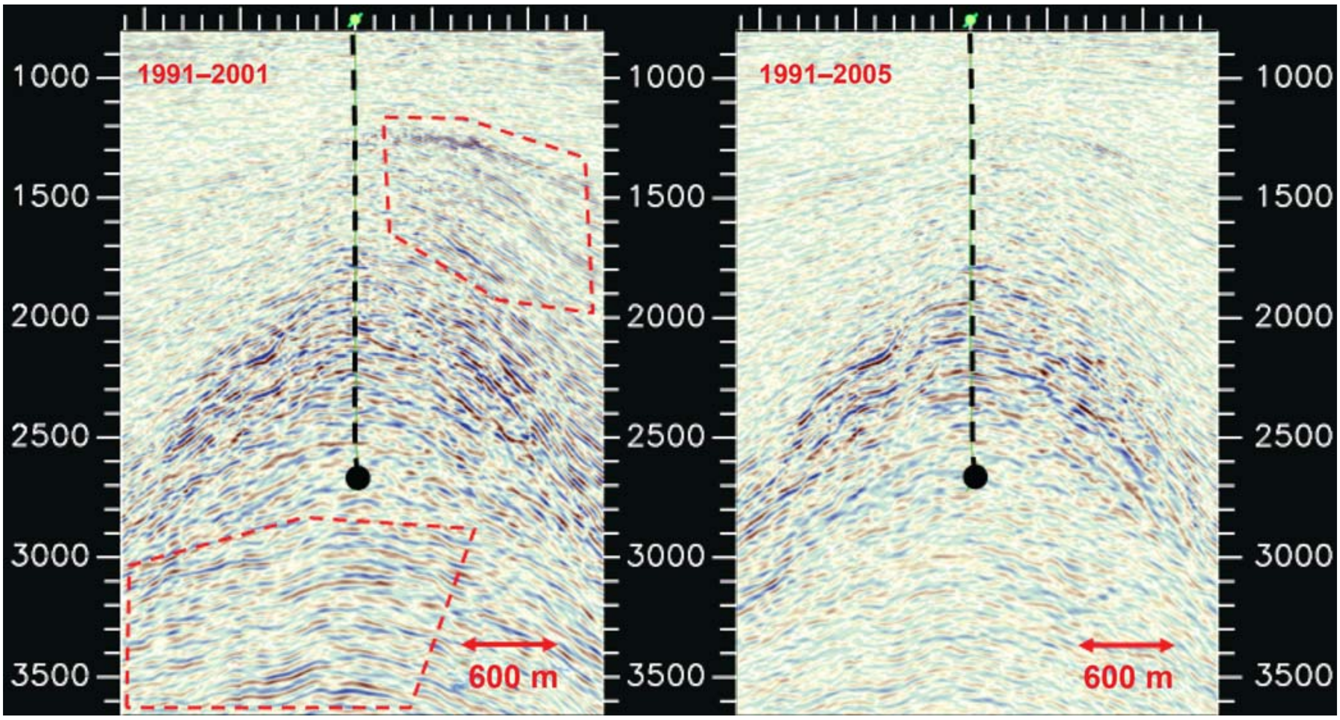

Fig. 1. Seismic time difference volumes over the Mungo Central North Sea (CNS) field comparing 1991, 2001 and 2005 vintages. Areas of 4D noise reduction are highlighted in the dashed boxes. Vertical magnification is *c.* 1.5×.

provides information on the combined result of all acquisition and processing improvements. In this study, I intend to show the improvements from each aspect of an acquisition and processing flow, including which steps are most important for improving 4D repeatability. The study area is the Mungo field as shown in Figure 2. It is a diapir flank structure in the Eastern Trough of the Central North Sea (CNS), located mainly in Paleocene turbidite sandstones (Sele formation) sealed beneath Eocene mudstones with an updip termination against Zechstein salt. The flanks dip at up to 50° with 1500 m of vertical relief. These steep dips introduce significant challenges when trying to image the 4D response within the 100–400 m thick reservoir oil leg (Pooler & Amory 1999).

In addition, the updip event terminations reduce the interpretable area of many of the horizons of interest. The CDR calculations are taken from a 300 ms window extracted over the flanks of the structure, ending 100 ms above the section predicted to show 4D signal.

CDR calculation

The CDR attribute can be presented in three ways: a single value representative of the entire analysis area, a map of local variability, or an amplitude spectrum showing the CDR relationship with frequency. Figure 3 shows two of these methods, a map of local

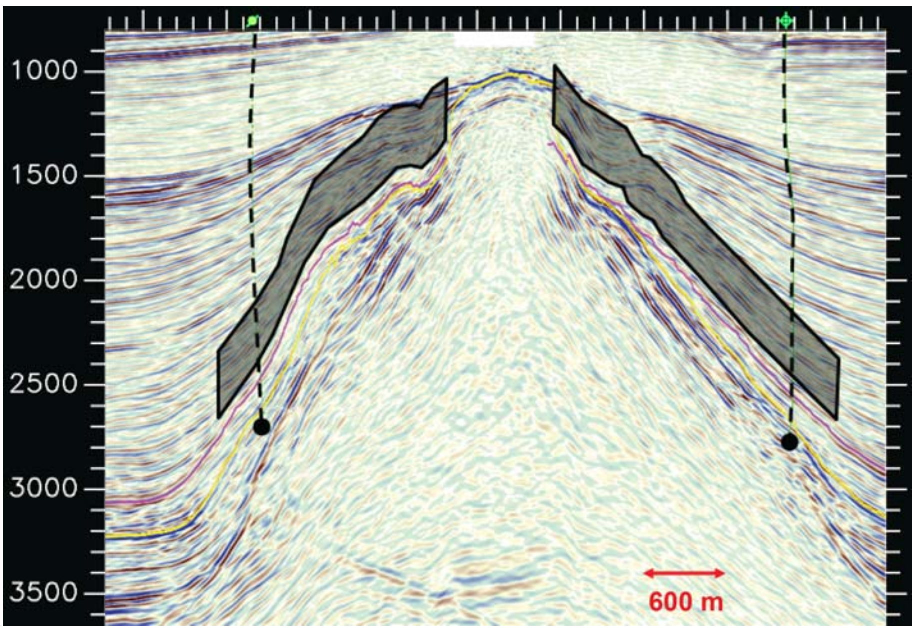

Fig. 2. Seismic time section through the Mungo diapir showing two projected well paths and two key horizons (top chalk (lower) and top Sele formation (upper)). Highlighted in dashed boxes are the windows of interest used to calculate 4D repeatability. Vertical magnification is *c.* 1.5×.

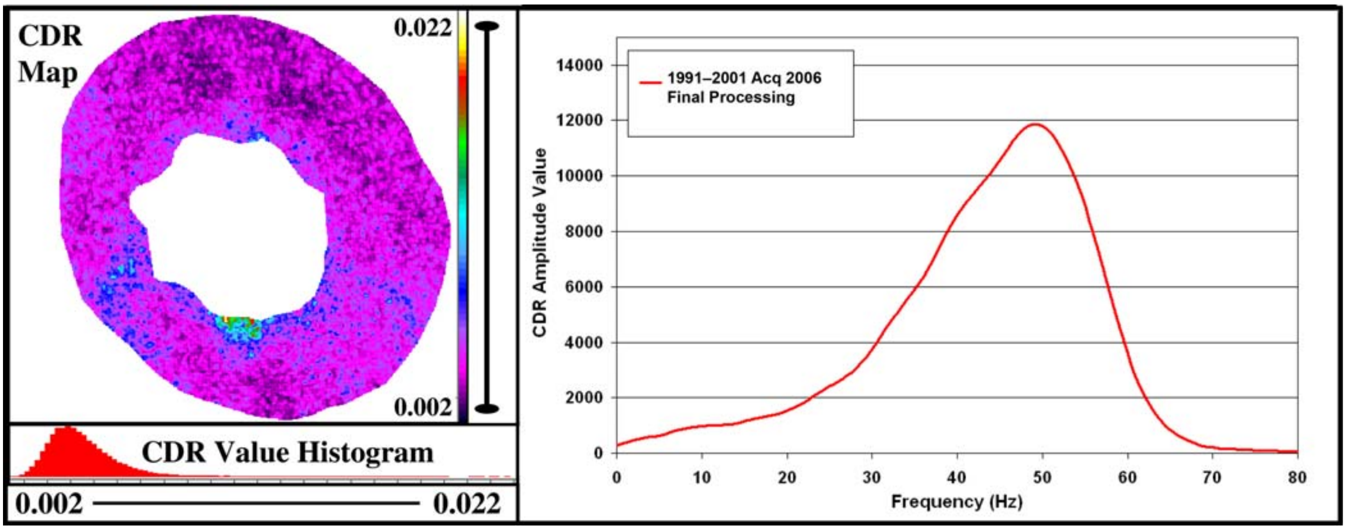

Fig. 3. Map of local CDR variations (left) and CDR frequency spectrum (right) for Mungo CNS field, 2001 monitor v. 1991 baseline acquisition and 2006 full processing flow. The CDR drops above 50 Hz due to the limit in the frequency content of the data.

variations of CDR and an amplitude variation with frequency. The light grey areas on the map indicate high CDR values relating to a platform undershoot where the acquisition repeatability deteriorates. The spectrum shows an average frequency content of the difference volume for the seismic area covered by the map. The difficulty in interpreting regions of interest based on incomplete horizons can be observed here, with the updip terminations leading to a ‘donut’-shaped horizon.

The CDR calculations were taken from surveys acquired in 1991, 2001 and 2005. The acquisition parameters for the three surveys are presented in Table 1, showing the similarities and differences in the acquisition methods which may result in variability in the final seismic volumes. 4D processing was carried out in 2001 and 2006, and included a series of fast-track products where a subset of the final processing steps were applied. An additional application of STAR (Zamorouev *et al.* 2006), a 4D post-stack noise reduction process, was also tested. This utilizes the higher signal-to-noise properties of a sum of multiple seismic vintages to help clean up each individual vintage through the application of a local scalar to each sample. This scalar is defined as the value that will move the sample amplitude onto a best fit linear trend calculated from a cross plot of the average amplitudes of the two vintages against the individual vintage, extracted over a window centred on the sample, as shown in Figure 4. It is a process that reduces noise in

Table 1. Acquisition parameters for the three seismic survey vintages

	Survey vintage 1991	Survey vintage 2001	Survey vintage 2005
Total volume of source	2 × 5012 cubic inches	2 × 3397 cubic inches (source x) 2 × 3000 cubic inches (source y)	2 × 3490 cubic inches
Type of energy source	Bolt Airguns	Bolt LongLife Airguns (source x) Sleeve guns (source y)	Airgun − G-gun + sleeve
Source depth	5 m	5 m	5 m
Shot point interval	50 m (25 m flip-flop)	50 m (25 m flip-flop)	50 m (25 m flip-flop)
Sail line direction	0°/180°	0°/180°	Repeat 1991 source positioning
Number of cables	3	6	7
Nominal xline streamer separation	100 m	100 m	75 m
Cable length	3.0 km	4.0 km	4.0 km
Cable depth	8 m	8 m	8 m
Number of channels	240	320	324
Group interval	12.5 m	12.5 m	12.5 m
Total no. of channels	720	1920	2268
Cable direction	0°/180°	0°/180°	Repeat 1991 receiver positioning
Inline near offset (centre source a near receiver)	136 m	189 m	130 m
Nominal stacking fold	30	40	40

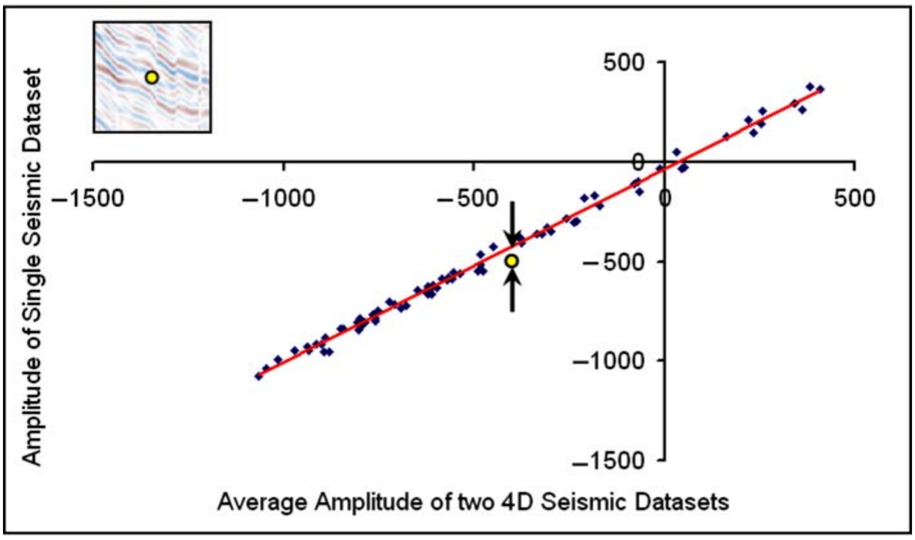

Fig. 4. The STAR methodology, where the highlighted sample is scaled to lie on the trend line calculated from all the amplitudes in the window of seismic data shown in the top left. The size of the window can vary.

the 4D difference volume, but if applied carelessly can deteriorate time shifts which could be due to real 4D changes.

For each combination of acquisition and processing a CDR value, map and spectrum were calculated. The individual CDR value was recorded for each acquisition and processing combination, whilst the frequency spectrum and map were only used in the study of regional and frequency variability. The full suite of individual CDR measures is presented in Figure 5, indicating the CDR drops from 0.0105 to 0.0038 following the implementation of all processing and acquisition improvements. This is interpreted as an approximate three-fold reduction in 4D noise. The CDR measure was recorded over a 10–45 Hz bandwidth for all cases to ensure consistency, and the parameterization and velocity models used in a given processing flows were not varied between the three seismic volumes.

The three most significant comparisons are:

(1) *Processing flow improvements* – the 2006 processing flow included improved regularization and enhanced pre-stack noise attenuation compared with the 2001 flow. By calculating the repeatability following each flow for the 1991 and 2001 acquisition vintage difference, we can assess the impact of processing improvements.
(2) *Improved acquisition repeatability* – in both the 2001 and 2005 monitor surveys the seismic acquisition was designed to repeat the line orientation of the 1991 baseline survey. However, in

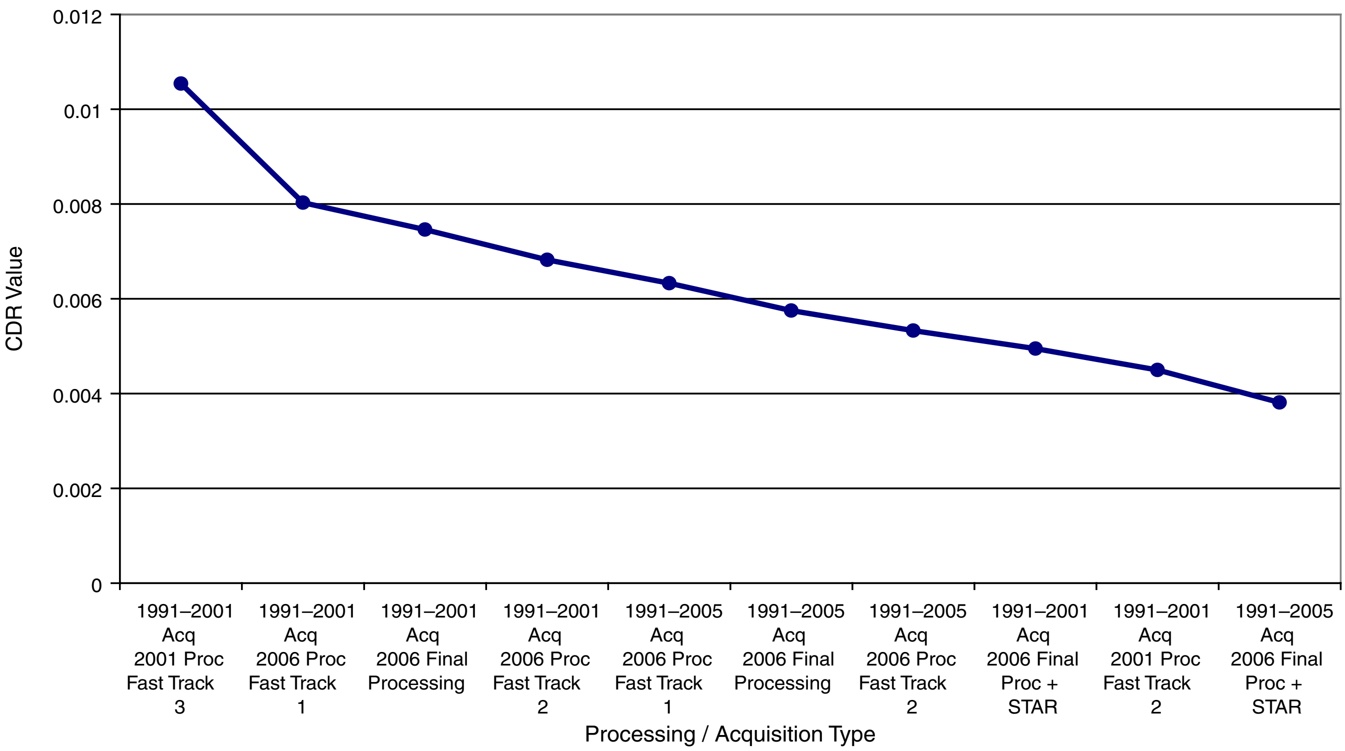

Fig. 5. The reductions in CDR from improved repeatability for different acquisition vintages and processing runs.

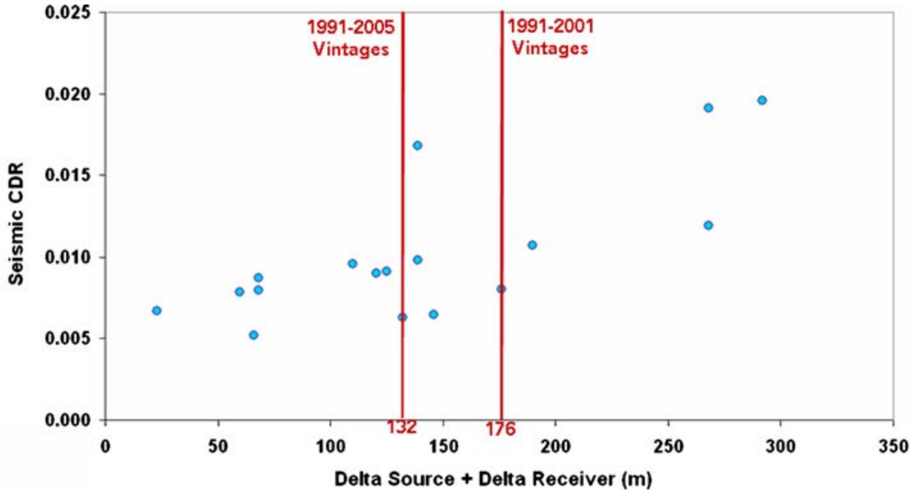

Fig. 6. Relationship between acquisition repeatability (delta source + delta receiver) and seismic CDR for a series of 4D surveys. The vertical lines show the DS + DR for the Mungo monitor surveys, annotated with the relevant vintages.

2005 particular care was taken to match the original source and receiver locations as far as surface currents and the positioning systems of the acquisition would allow. A simple measure used to assess the acquisition repeatability is the average of the variation in source and receiver locations between each monitor and the baseline survey at a reference offset, in this case 1000 m. This measure is referred to as delta source plus delta receiver, or DS + DR. By comparing the 1991–2001 and 1991–2005 acquisition repeatability for the 2006 processing flow, we can assess the impact of the increased effort to improve acquisition repeatability. We can observe the relationship between acquisition and seismic repeatability for a series of field examples in Figure 6, all taken for a 1000 m offset but with different acquisition parameters and conditions. The 2005 monitor survey shows a lower values of DS + DR when compared with the 2001 acquisition, and assuming the 1000 m offset positioning is indicative of the full offset range, it more closely matched the original acquisition repeatability. The CDR value decreases as the DS + DR is minimized, indicating the enhanced repeatability of the 2005 monitor due to the acquisition improvements.

(3) *Additional 4D noise reduction* – the repeatability calculation pre and post the application of STAR provides an assessment of the improvement in repeatability achieved by including specific 4D noise reduction techniques. We can observe these significant comparisons in Figure 7.

The relative percentage improvements are detailed in Table 2. The results show a decrease in CDR, and hence a reduction in the 4D noise, for both processing and acquisition enhancement. For this case study the largest relative improvement comes from the application of STAR compared with both 2001 and 2005 monitor surveys with final 2006 processing. This is a simple post-stack specific 4D noise reduction processing step. The acquisition changes in this study offer the lowest overall relative repeatability improvement. However, all results are comparable, including what can be achieved from additional steps during the processing flow to better reduce 3D noise and align data.

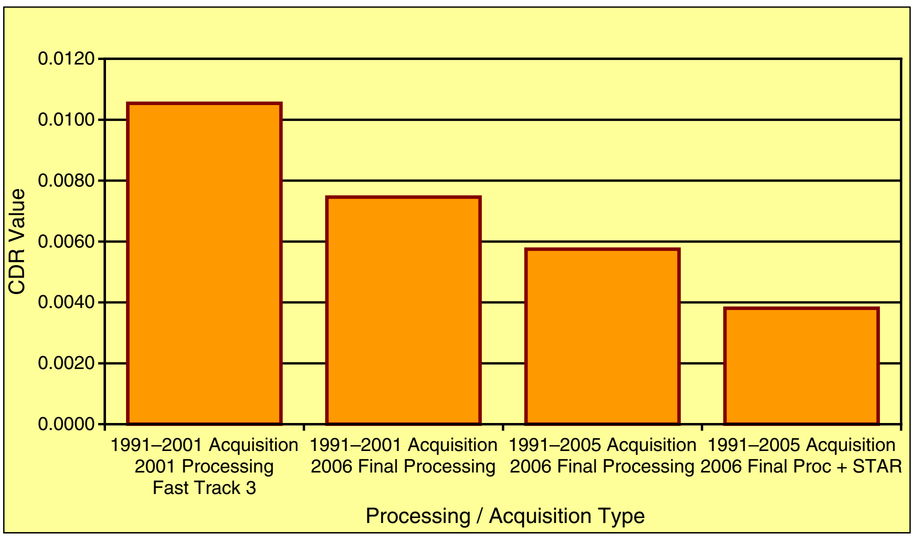

Fig. 7. CDR variations with improving processing and acquisition. Processing improvements are highlighted in columns 1 and 2, acquisition improvement in columns 2 and 3 and STAR improvements in column 3 and 4.

Table 2. CDR improvements. The last column shows percentage improvements in repeatability for different processing and acquisition. The fifth row is an additional test on the percentage improvement from the STAR process compared with row 2

	Processing and acquisition	CDR value	CDR incremental improvement
1	1991–2001 acquisition 2001 processing Fast_Track_3	0.0105	
2	1991–2001 acquisition 2006 final processing	0.0075	29% (v. row 1)
3	1991–2005 acquisition 2006 final processing	0.0058	23% (v. row 2)
4	1991–2005 acquisition 2006 Final Proc + STAR	0.0038	34% (v. row 3)
5	1991–2001 acquisition 2006 final proc + STAR	0.0050	34% (v. row 2)

Conclusions

This case study indicates that repeatability can be improved using the following methods in the order of significance:

(1) specific post-stack 4D noise attenuation;
(2) more extensive and tailored 4D processing flows;
(3) higher acquisition repeatability.

The results suggest that, in terms of the level of 4D noise, the most significant improvements can be achieved by the application of STAR. However, it is evident that no single aspect of the flow enhances the data dramatically enough to be considered in isolation; it is the combination of all efforts which leads to the three-fold improvement. Furthermore, it should be noted that, although it appears that the acquisition refinements produce the least significant reduction in 4D noise, this is likely to be due to the high level of acquisition repeatability achieved in the original monitor survey in 2001. Further improvements would be difficult to achieve, as opposed to a base case of two 3D surveys acquired and processed individually with no attempt made to match source–receiver locations or processing flow.

Whilst good acquisition repeatability helps align primary energy between acquisition vintages and therefore low 4D noise levels, it is clear that substantial reductions in 4D noise can also be achieved through 4D processing improvements. Finally, it should be highlighted that the value gained by investing in the methods described in this study is that 4D noise can be significantly reduced, leading to an improvement in the interpretability of the 4D signal, and thus a greater understanding of the dynamics of a reservoir during its development.

The authors would like to thank BP management and the Mungo field partners, Murphy Petroleum, Total E&P UK and NOEX Co. for providing feedback and allowing permission to publish information on the study area.

References

Dyce, M., Whitcombe, D., McKenzie, C. & Hodgson, L. 2004. The quantification of 4D noise. *66th EAGE Conference Workshop: Can Time Lapse Seismic be more Quantitative*, Paris.

Pooler, J. & Amory, M. 1999. A subsurface perspective on ETAP – an integrated development of seven Central North Sea fields. *Proceedings of the 5th Geological Society Conference: Petroleum Geology of Northwest Europe*, London, 993–1006; doi: 10.1144/0050993.

Zamorouev, A., Whitcombe, D., Dyce, M. & Hodgson, L. 2006. A simple methodology for 4D noise reduction and repeatability improvement. SEG Expanded Abstracts, **25**, 3155–3159.

Applying time-lapse seismic methods to reservoir management and field development planning at South Arne, Danish North Sea

J. V. HERWANGER,[1] C. R. SCHIØTT,[2] R. FREDERIKSEN,[2] F. IF,[2] O. V. VEJBÆK,[2] R. WOLD,[3] H. J. HANSEN,[4] E. PALMER[5] and N. KOUTSABELOULIS[6]

[1]*WesternGeco, 10001 Richmond Avenue, Houston, TX 77042, USA (e-mail: jherwanger@houston.westerngeco.slb.com)*
[2]*Hess, Østergade 26B, 1100 Copenhagen, Denmark*
[3]*Schlumberger Information Solutions, 1325 South Dairy Ashford, Houston, TX 77077, USA*
[4]*Schlumberger Reservoir Seismic Services, Titangade 15, 2200 Copenhagen, Denmark*
[5]*WesternGeco, Schlumberger House, Buckingham Gate, Gatwick Airport, Gatwick RH6 0NZ, UK*
[6]*Schlumberger Reservoir Geomechanics Centre of Excellence, 10 The Courtyard, Eastern Road, Bracknell RG12 2XB, UK*

Abstract: At South Arne a highly repeatable time-lapse seismic survey (normalized root-mean-square error or NRMS of less than 0.1) allowed us to reliably monitor reservoir production processes during five years of reservoir depletion. Time-lapse AVO (amplitude v. offset) inversion and rock-physics analysis enables accurate monitoring of fluid pathways. On the crest of the field, water injection results in a heterogeneous sweep of the reservoir, whereby the majority of the injected water intrudes into a highly porous body. This is in contrast to a pre-existing reservoir simulation model predicting a homogeneous sweep. On the SW flank, time-lapse AVO inversion to changes in water saturation ΔS_w reveals that the drainage pattern is fault controlled. Time-lapse seismic data furthermore explain the lack of production from the far end of a horizontal producer (as observed by production logging), by showing that the injected water does not result in the expected pressure support. On the highly porous crest of the reservoir compaction occurs. Time-lapse time shifts in the overburden are used as a measure for compaction and are compared with predictions of reservoir compaction from reservoir geomechanical modelling. In areas where compaction observations and predictions disagree, time-lapse seismic data give the necessary insight to validate, calibrate and update the reservoir geomechanical model. The information contained in time-lapse seismic data can only be fully extracted and used when the reservoir simulation model, the reservoir geomechanical model and the time-lapse seismic inversion models are co-visualized and available in the same software application with one set of coordinates. This allows for easy and reliable investigation of reservoir depletion and gives deeper insight than using reservoir simulation or time-lapse seismic individually.

Keywords: time-lapse seismic, rock physics, AVO inversion, reservoir geomechanics, compaction

Petroleum geology and reservoir production of South Arne

The South Arne field is situated in the Danish sector of the North Sea. It is a chalk field extending 12.5 by 4 km with the long axis of the double-dipping anticline trending in a NNW–SSE direction. Production started in July 1999 predominantly from horizontal wells oriented along the axis of the reservoir in a NNW–SSE direction (Fig. 1). Cumulative production to date (March 2008) is 116 MMstb of 34.2 API oil and 166 Bscf of gas. For comparison, at Valhall a total of 500 MMstb of oil have been produced in the first 20 years (Barkved *et al.* 2003). On the north shoulder of the anticline, post-depositional faults create a graben-like structure at the crest of the reservoir (Mackertich & Goulding 1999). The graben strikes in a NNW–SSE direction, the same direction as the anticline. A second set of WNW–ESE trending faults can be interpreted from 3D seismic data over the entire field, except in an area obscured by a gas cloud. The second set of faults contributes significantly to reservoir depletion. The oil-bearing intervals are the Late Cretaceous Tor (referred to as lower reservoir in this paper) and overlying early Cretaceous Ekofisk (upper reservoir) formations. Reservoir quality is variable and the best reservoir quality is found on the crest of the north flank with a total reservoir thickness up to 65 m, split between Tor (approximately 40 m) and the overlying Ekofisk (approximately 25 m) formations (Fig. 2). The Ekofisk and Tor formations are separated by the Ekofisk tight zone. Porosity values on the north flank in the Tor range from 25 to 46%, with an average porosity of 37%. Matrix permeability in the Tor ranges of 1–10 mD, with fractures and faults adding significantly to permeability. On the western and eastern flank of the reservoir the chalk sequence thickens with distance from the axis of the anticline (Fig. 2), increasing the thickness of the reservoir interval. At the same time porosity and permeability drop significantly (Mackertich & Goulding 1999; Megson & Hardman 2001). Because of the low permeability in the distal part of the chalk sequence, pressure support by the water table is minimal and water injection is necessary to provide the necessary drive energy for hydrocarbon production. In the high-porosity region on the crest of the reservoir, compaction adds additional drive energy, estimated at 20% of total drive energy. Source rock is provided by the underlying Late Jurassic shale sequences.

The reservoir produces from horizontal wells, interleaved with horizontal water injection wells (Figs 1 & 2). Production is enhanced by induced vertical fractures and further supported by water injection. Both producers and injectors are stimulated by acid frac or hydro-facing using a proppant. The induced fractures are vertical and aligned with the direction of the horizontal wells, drilled in the direction of minimal horizontal stress, to enable a

VINING, B. A. & PICKERING, S. C. (eds) *Petroleum Geology: From Mature Basins to New Frontiers – Proceedings of the 7th Petroleum Geology Conference*, 523–535. DOI: 10.1144/0070523

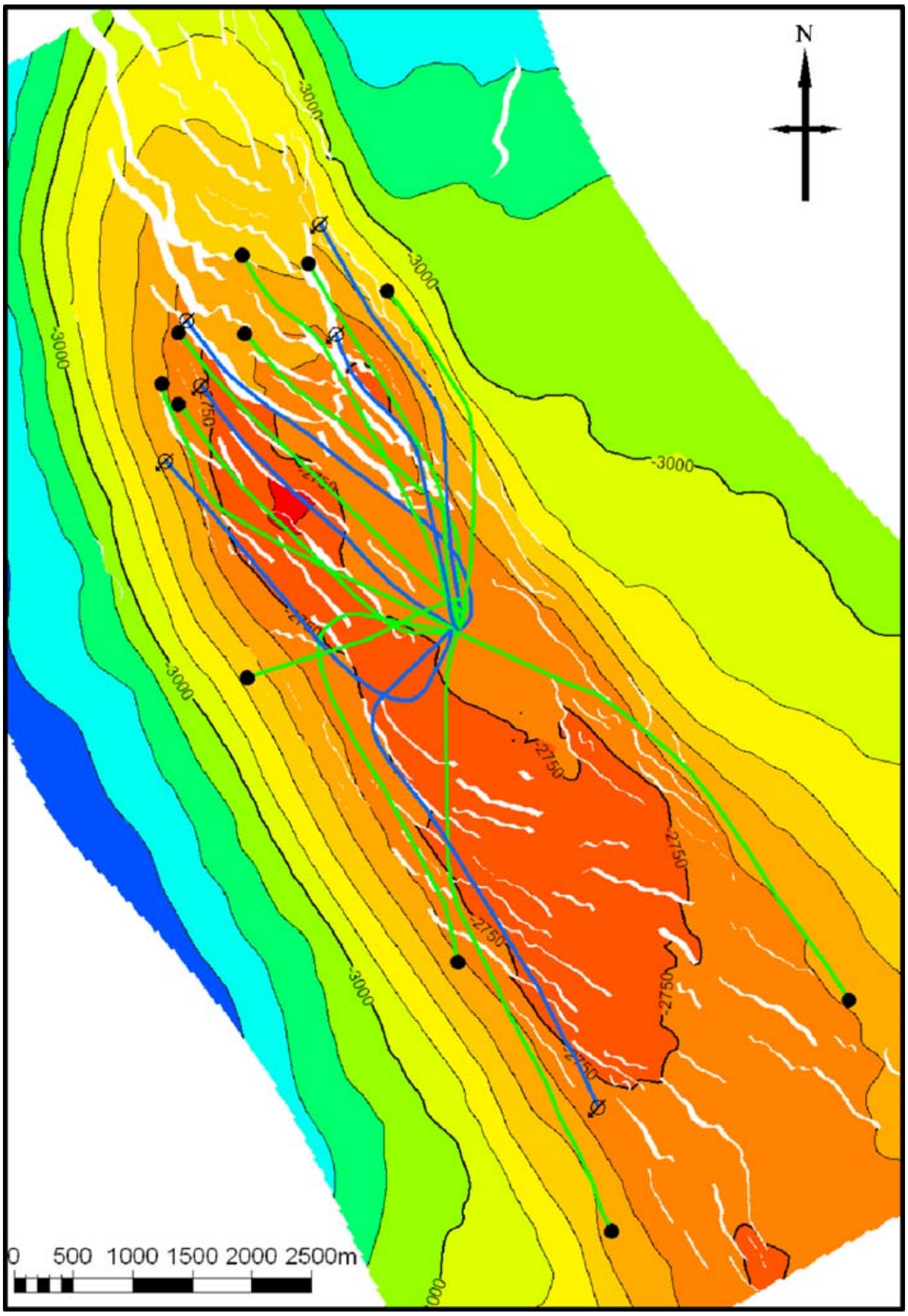

Fig. 1. Top-reservoir structure shows an elongated anticline. The northern crest exhibits a graben structure on the crest of the reservoir. The reservoir is produced by interleaved horizontal producers (in green, with solid black dot at toe of well) and water injectors (in blue, with black circle and arrow).

homogenous sweep across the reservoir interval. For an in-depth discussion of the petroleum geology of South Arne and field history, the reader is referred to the excellent paper of Mackertich & Goulding (1999).

Time-lapse seismic data: acquisition, processing and inversion

In recent years, time-lapse seismic data are increasingly used as a reservoir management tool and to assist in field development planning. The use of time-lapse seismic data in conjunction with reservoir simulation models and production data allows the creation of an internally consistent subsurface model. Published field examples of such integrated case studies include Lena, Gulf of Mexico (Johnston *et al.* 2000), Gullfaks, North Sea (Najjar *et al.* 2003), Jotun, North Sea (Gouveia *et al.* 2004), Girassol and Jasmin, West Africa (Gonzalez-Carballo *et al.* 2006), Gannet C (Staples *et al.* 2006) and Marlim (Thedy *et al.* 2007). More recently, the impact of reservoir compaction on time-lapse seismic data has been studied in more detail (Guilbot & Smith 2002; Hatchell *et al.* 2003) and reservoir geomechanical models are included into workflows that integrate time-lapse seismic data with subsurface flow and geomechanical models (Barkved & Kristiansen 2005; Staples *et al.* 2006; De Gennaro *et al.* 2008). In this paper we demonstrate that high quality time-lapse seismic data, in conjunction with careful time-lapse seismic processing and application of advanced reservoir seismic inversion methods, yields detailed insight into reservoir fluid flow and geomechanical processes. By co-visualizing the subsurface models derived from time-lapse seismic data, the reservoir simulation model and the reservoir geomechanical model, we generate an understanding of reservoir production processes that could not be achieved when using each model individually.

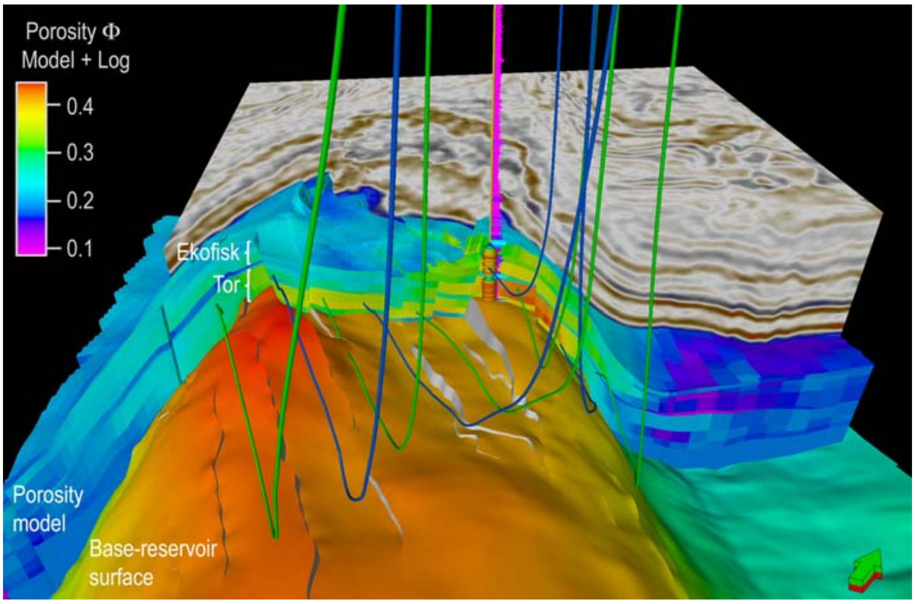

Fig. 2. Three-dimensional view of northern crest. The base reservoir surface clearly shows the graben structure. The simulator porosity model shows the highest porosities (in excess of 40%) on the crest of the reservoir, with a clear division between the upper (Ekofisk) and lower (Tor) reservoir. The porosity log at the appraisal well also clearly shows the low porosity tight zone separating the two reservoirs. Also note the excellent anti-correlation between the porosity log (displayed as barrel) and the velocity log (displayed as a vane). Finally note the strong top-reservoir reflector visible in the seismic data, facilitating the interpretation of reservoir geometry.

Acquisition and processing

Two 3D seismic surveys are available for a time-lapse seismic study. A pre-production baseline survey was acquired in 1995, using 4×4600 m streamers at 100 m streamer separation and a 50 m source interval. The monitor survey was shot during five weeks in September and October 2005 after five years of reservoir production. This acquisition time includes downtime due to bad weather (about one-third of the time) at the end of the North Sea seismic season. The monitor survey was shot using 8×4600 m streamers at 50 m separation and a source interval of 25 m. The survey design for the monitor survey aimed to repeat the acquisition geometry of the base survey as closely as possible, and using steerable streamers helped to closely match the baseline geometry during acquisition. This resulted in a good repeatability of seismic data in areas where no time-lapse changes occur and consequently provided good visibility and high signal-to-noise ratio of the time-lapse seismic signal. At South Arne, the repeatability (Kragh & Christie 2002), using normalized root-mean-square error (NRMS) between traces of base and monitor survey as a metric, was 0.15 at reservoir level after fast-track processing, which was available three weeks after the end of data acquisition (Schiøtt & King 2006). After careful time-lapse processing and 4D matching, an NRMS value of less than 0.10 was measured across the reservoir interval. In comparison with other time-lapse surveys (e.g. Smit *et al.* 2005 report values between 7 and 37%) the NRMS value of the South Arne survey is low, showing that a high repeatability was achieved. The final processing sequence included the application of tidal static corrections, swell noise attenuation, tau-p deconvolution and Kirchoff pre-stack time-migration. Both base and monitor surveys were co-processed using a deterministic processing sequence, carefully maintaining amplitude preserved time-lapse signal.

Time-lapse time shifts and amplitude changes

Seismic data observations include the amplitude and the arrival time of a wavelet reflected from an interface in the subsurface. At South Arne the interfaces between the reservoir and the overburden, as well as the reservoir and the underburden, are strong reflectors (Figs 2 & 3). Figure 3a, b displays vertical sections of the baseline survey and the monitor survey, respectively. The top- and base-reservoir reflector interpretations are indicated by black lines. Additionally, the interface between the upper (Ekofisk) reservoir and the lower (Tor) reservoir is marked. The displayed section contains the vertical well displayed in Figure 2 and the well location is indicated by a vertical line. For further analysis, traces from the 1995 baseline survey and the 2005 monitor survey are extracted and displayed in Figure 3c, d. The trace from the baseline survey is displayed in green and the monitor survey trace is displayed in blue. Amplitude changes ΔA and time-lapse time shifts Δt are readily visible. At reservoir level, the arrival times of the baseline survey t_1 (in green) are consistently earlier than the corresponding arrival times of the equivalent reflections in the monitor survey t_2 (in blue). The observed time-lapse time shifts $\Delta t = t_1 - t_2$ are negative, with a maximum observed value of approximately -7 ms. The measurement of time-lapse time shifts can be automated (Nickel *et al.* 2003) and the results can be used to time-align corresponding traces of base and monitor survey (Fig. 4a, b). The time-aligned traces can then be subtracted and the amplitude differences plotted (Fig. 4c), giving a first qualitative indication of reservoir production processes. The amplitude changes ΔA show a clear fault control of the time-lapse seismic response and therefore fault control of the reservoir depletion process. The location of the largest amplitude change furthermore corresponds with the location of an injector well.

Time-lapse time shifts can be used to time-align different vintages of time-lapse seismic surveys. On the other hand, time-lapse time shifts also have a diagnostic value in monitoring reservoir compaction (Guilbot & Smith 2002; Hatchell *et al.* 2003; Nickel *et al.* 2003). The time shifts in the overburden can be explained by a combination of geomechanical modelling (predicting reservoir compaction as pore-pressure in the reservoir is reduced) and associated overburden stretching. Overburden stretching affects seismic time-lapse data in two ways. Firstly, the path length of the monitor survey increases as the overburden elongates and secondly, the vertical velocity decreases as the overburden stretches and

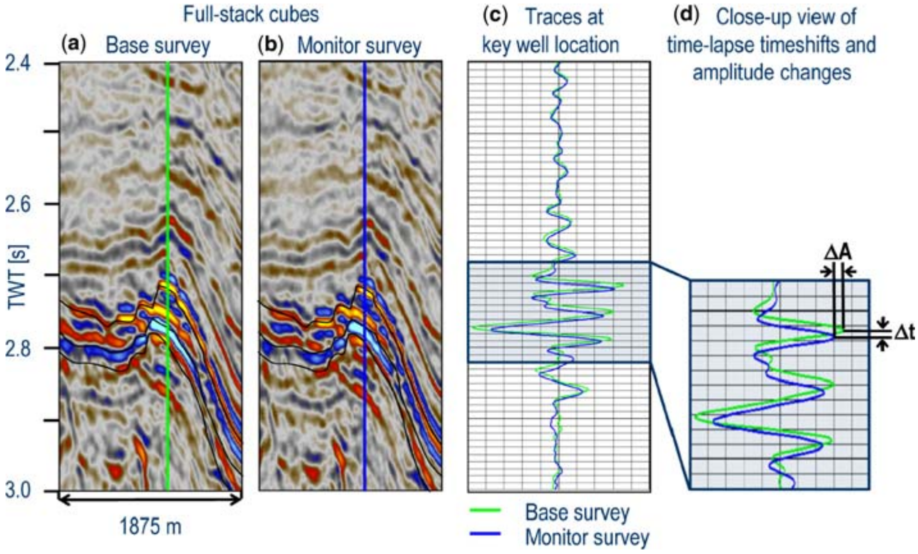

Fig. 3. Vertical sections of full-stack seismic cubes after pre-stack Kirchhoff time migration for (**a**) base survey and (**b**) monitor survey. The location of the appraisal well (see Fig. 2) is indicated by the vertical lines. (**c**) Extracting a single trace at the location of the appraisal well allows investigation of time-lapse signal changes at this location. (**d**) A close-up look shows an increase in travel-time Δt (time-lapse time shift caused by reservoir compaction) and a dimming in amplitude ΔA between the base and monitor surveys.

vertical effective stress decreases (Hatchell & Bourne 2005; Herwanger & Horne 2005). Both effects cause an increase in travel time for the monitor survey compared with the base survey in compacting reservoirs. In Figure 4d we plot the measured time shifts in a vertical section along a profile containing the appraisal well (for well location see Fig. 2). Note that the time shifts are clearly fault-bounded. This will become even more apparent when we investigate the time shifts extracted along the top-reservoir horizon later in this paper.

Time-lapse AVO inversion

In time-lapse AVO inversion, we use the fact that the amplitude of a reflected wave depends on the change of elastic properties across the interface. The reflection coefficients as a function of the incidence angle are given by the Zoeppritz equations (e.g. Mavko *et al.* 1998). A variety of approximations exist that allow for a deeper insight which parameters govern the AVO response. For vertical incidence, the reflection amplitude of a reflected P-wave is determined by the contrast in acoustic impedance (AI) above and below the interface:

$$R(0^\circ) = \frac{(AI_2 - AI_1)}{(AI_2 + AI_1)}$$

where AI_2 and AI_1 are the acoustic impedances (i.e. the product of seismic P-wave velocity V_p and bulk density ρ) in the lower and upper layer, respectively. At intermediate angles of incidence Θ

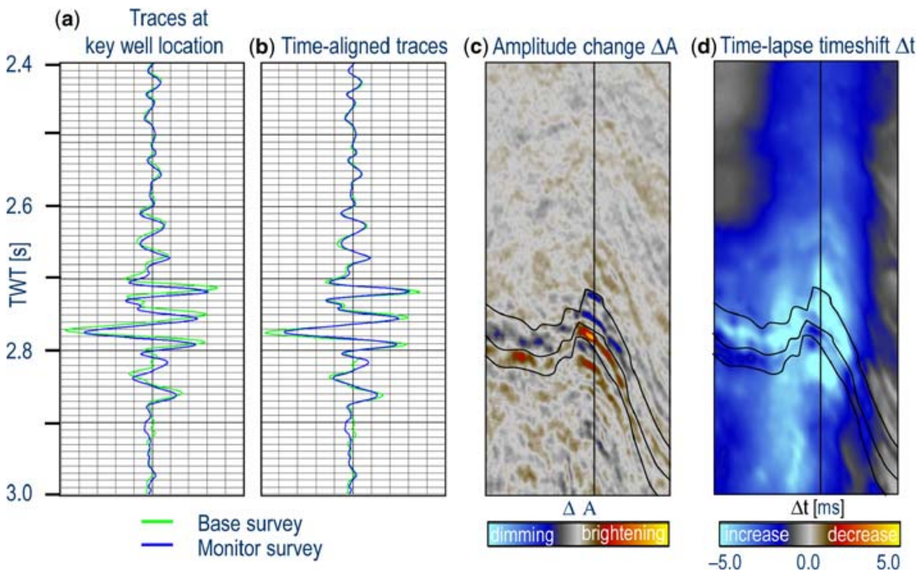

Fig. 4. (**a**) Single trace of the base and monitor surveys at the location of the appraisal well. (**b**) Same traces as (a) with time-lapse time shift removed. (**c**) After removing time-lapse time shifts, a difference cube can be generated. Note the fault control of the amplitude changes, giving a first indication of fault control of depletion processes. (**d**) Time-lapse time shifts at each sample location can be plotted and used as a diagnostic tool. Note that the time shifts are fault controlled and that the largest shifts occur above the region of the reservoir that shows the largest amplitude changes. This region, not surprisingly, also correlates with the location of the best producer.

of the seismic wave on an interface, the contrast in shear-wave velocities or Poisson's ratio v becomes influential (Shuey 1985):

$$R(\Theta) = R(0^\circ) + \left(A_0 R(0^\circ) + \frac{\Delta v}{(1-v)^2}\right) \sin^2 \Theta.$$

Here $R(0^\circ)$ is the normal incidence reflection coefficient, governed by the acoustic impedance contrast, A_0 specifies a normal, gradual decrease of amplitude with offset (full expression given in Shuey 1985), and finally Δv and v specify the Poisson's ratio difference $\Delta v = v_2 - v_1$ across the interface and the average $v = 0.5(v_2 + v_1)$ of Poisson's ratio below and above the interface.

The variation of reflection coefficient with incidence angle, recorded in seismic data, can be used to estimate 3D volumes of acoustic impedance and Poisson's ratio using 3D AVO inversions. Here we use seven cubes of seismic angle-band stacks as input, with incidence angles ranging from 0 to 35°. The seven angle-band stacks are inverted simultaneously using an angle-band stack specific wavelet (Rasmussen *et al.* 2004). The outputs of the 3D AVO inversions are 3D models of acoustic impedance and Poisson's ratio at each sample of a seismic cube, in this case a regularly sampled grid of 12.5 × 25 m in horizontal directions and 2 ms in the vertical direction. In Figure 5a, b, we display cross-sections through the acoustic impedance and Poisson's ratio model, respectively. The location of the appraisal well is indicated by the black line. Note that the low acoustic impedance in the AVO inversion model corresponds with the high porosity observed in the log (Fig. 2).

For time-lapse AVO inversion, we use angle-band stacks for both base and monitor surveys as input and simultaneously invert for acoustic impedance (AI_{Baseline}), Poisson's ratio (v_{Baseline}) and additionally for the ratio changes $AI_{\text{Monitor}}/AI_{\text{Baseline}}$ and $v_{\text{Monitor}}/v_{\text{Baseline}}$ of these parameters (see Fig. 5c, d). The time-lapse AVO inversion is described in more detail in Schiøtt *et al.* (2008). For reservoir management purposes, it is desirable to understand the change in reservoir properties, such as changes in water saturation ΔS_w, reservoir pressure ΔP and porosity $\Delta\Phi$. The inverted changes in acoustic impedance AI or Poisson's ratio ν are an intermediate step to seismically monitor changes in reservoir engineering parameters. To determine reservoir engineering parameters, it is necessary to first derive a calibrated rock physics model that allows translation of the observed changes in AI and v to changes in reservoir properties. At South Arne, acoustic impedance AI is closely correlated with porosity Φ in the chalk sequences and Poisson's ratio v is a sensitive fluid indicator. Note that other factors, such as depositional environment and compaction history, will also influence the seismic behaviour of the chalks comprising the reservoir (Vejbæk *et al.* 2005). Therefore, the rock physics model needs to be calibrated for each reservoir unit. The calibration is done using log data and, where available, laboratory measurements. In Gommesen *et al.* (2004), three different rock physics models are each fitted to observations of acoustic impedance and Poisson's ratio as functions of porosity and water saturation. All models agree that, for the South Arne chalks, acoustic impedance is a good porosity indicator, whereas Poisson's ratio is a good fluid indicator.

The rock physics model employed for the lower reservoir (Tor) in this study is displayed in Figure 6. Each dot in the figure represents a prediction of Poisson's ratio (on the abscissa) and acoustic impedance (on the ordinate) for a given porosity Φ (colour coded) and water saturation S_w using a rock physics model at virgin reservoir pressure. Note again the predominant dependence of acoustic impedance on porosity and of Poisson's ratio on water saturation. Application of the rock physics model allows the effective translation of changes in acoustic impedance ΔAI and Poisson's ratio $\Delta\nu$ to changes in water saturation ΔS_w and porosity $\Delta\Phi$, and vice versa. The resulting rock physics time-lapse AVO inversion images of porosity change $\Delta\Phi$, water saturation change ΔS_w and gas saturation change ΔS_g are displayed in Figure 7a–c, respectively. The estimation of three quantities ($\Delta\Phi$, ΔS_w, ΔS_g) from two independent quantities (ΔAI, Δv) is essentially underdetermined. However it is made possible by the fact that an extreme decrease in Poisson's ratio cannot be explained by water saturation changes alone, whereas an increase in gas saturation can explain this effect. Note also that for the shale sequences outside the reservoir, no calibrated rock physics model is available. Therefore the overburden and underburden are masked out for the rock physics inversion. It would be of interest, however, to relate inverted changes in elastic properties in the overburden and underburden to changes in strain or porosity for geomechanical applications such as seal-integrity studies.

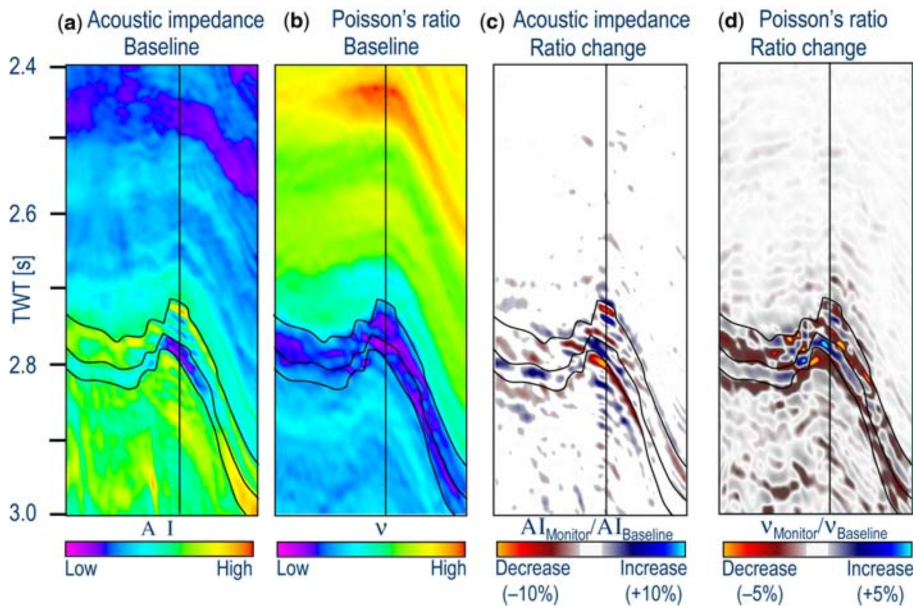

Fig. 5. (**a**) Acoustic impedance and (**b**) Poisson's ratio can be derived from 3D AVO inversion. Time-lapse AVO inversion additionally allows computation of (**c**) change in acoustic impedance and (**d**) change in Poisson's ratio. See text for detail.

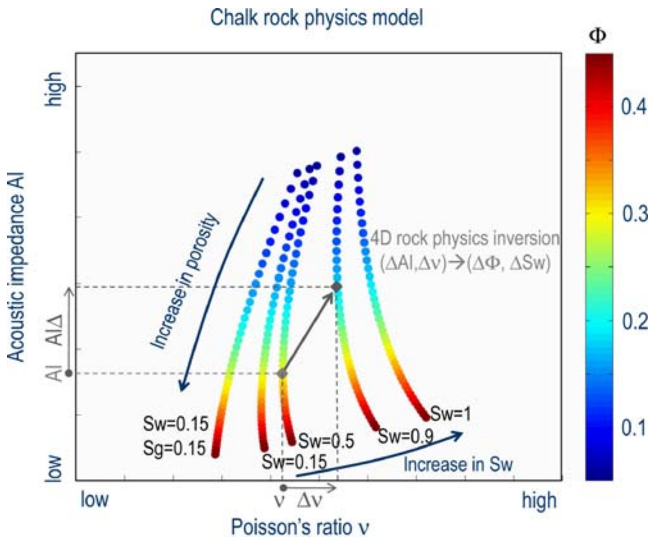

Fig. 6. Acoustic impedance and Poisson's ratio are closely related to porosity and water saturation in South Arne chalks. An increase in porosity causes a decrease in acoustic impedance, with hardly any influence on Poisson's ratio. Increasing water saturation (at constant porosity) causes a strong increase in Poisson's ratio, with hardly any imprint on acoustic impedance. A rock physics model allows translation of elastic properties observed from AVO inversion to reservoir properties.

Application of time-lapse rock physics AVO inversion and time-lapse time shift observations

Applied time-lapse seismic interpretation helps to address questions about reservoir production dynamics. The challenge for the reservoir engineers and the asset team is to determine an interpretative mental image of the production process and create a subsurface model that can be reconciled with all available information. In this section, we co-visualize the production-induced time-lapse seismic results with corresponding properties from reservoir simulation models. This allows a direct comparison of reservoir depletion as seen by time-lapse seismic and as predicted from either a reservoir simulation model or a reservoir geomechanical model.

Reservoir depletion of the northern crest

In a first example, we study the depletion pattern on the northern crest of the reservoir. To this end, we compare water saturation changes derived by time-lapse seismic rock physics AVO inversion (seismic ΔS_w) and water saturation changes predicted from the reservoir simulation model (simulation ΔS_w). The key findings are that (i) water pathways are more heterogeneous than the simulation model predicts, (ii) the reservoir drains mainly from a high porosity body and (iii) the injected water spreads predominantly in the lateral updip direction, whereas the simulation model had predicted more of a vertical movement.

In Figure 8 the seismic ΔS_w (Fig. 8a) and simulation ΔS_w (Fig. 8b) are displayed along a vertical profile. The location of the profile is indicated on the map inset in Figure 8a. Both figures use the same colour scale: areas with the strongest increase in water saturation are displayed by the deep shades of blue and areas with marginal or no change of water saturation are displayed by light hues and in white. The intersections of the horizontal wells with the displayed vertical section through the reservoir are indicated by solid black dots for oil producers and circles with tilted arrows for water injectors. The seismic ΔS_w shows strong lateral continuity and is concentrated in the lower (Tor) reservoir. The only change in seismic ΔS_w in the upper reservoir occurs around the injection well I2. The water injected at I1 appears to be moving updip and remains in the lower reservoir. This observation is in contrast to the simulation model prediction that the injected water would spread vertically into the upper reservoir.

To investigate the lateral spread of the injected water, we compute a map of average change in water saturation for the

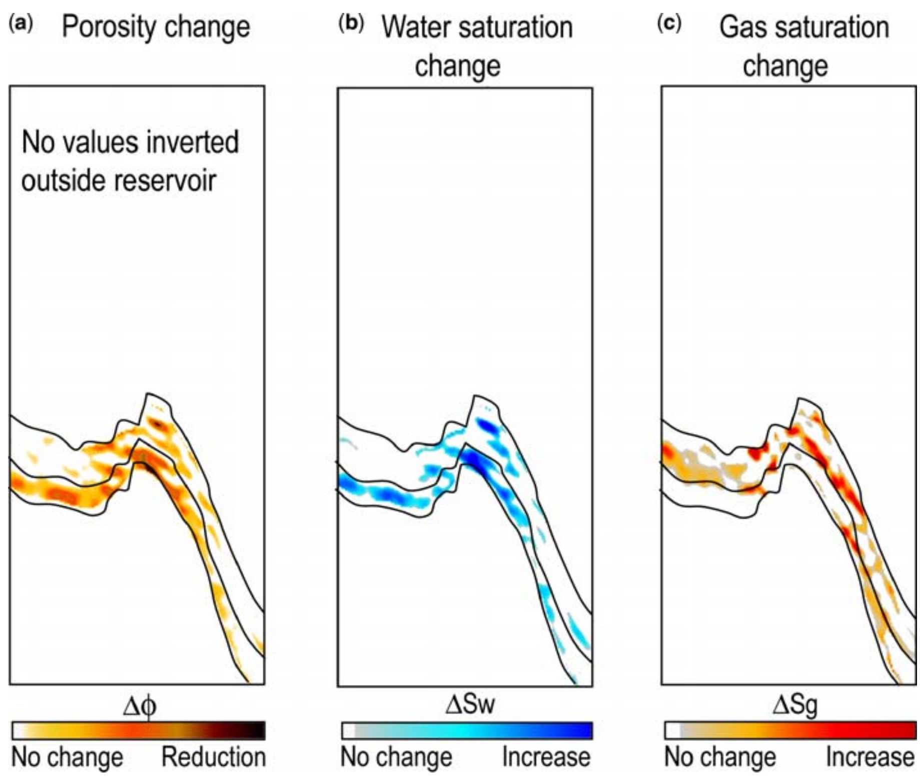

Fig. 7. Application of the South Arne rock physics model allows estimates of (**a**) change in porosity Φ, (**b**) change in water saturation ΔS_w and (**c**) change in gas saturation ΔS_g. No calibrated rock physics model existed for the over- and underburden and therefore these zones are masked for the inversion procedure.

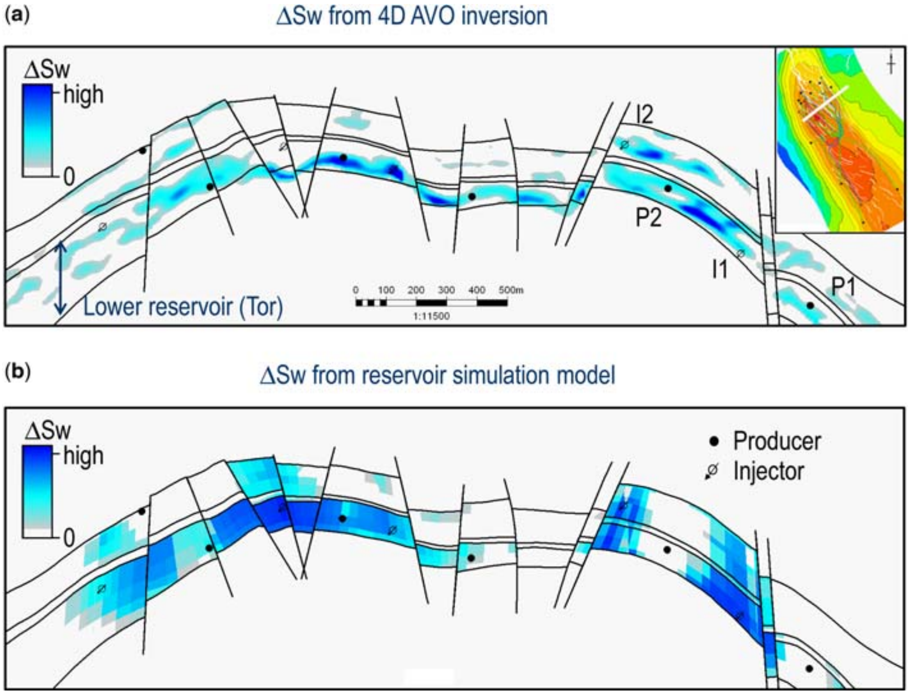

Fig. 8. (**a**) ΔS_w derived from time-lapse rock physics inversion and (**b**) ΔS_w predicted by the reservoir simulation model. Profile length is approximately 3 km and vertical exaggeration is by a factor of 3. Change in water saturation is colour coded with large increases in water saturation indicated by dark blue colours. The locations of producing wells are indicated by the solid black dots and the locations of injector wells are indicated by circles with arrows. Producer and injector wells discussed in the text are labelled P1, P2, I1 and I2.

lower reservoir by vertically averaging ΔS_w in the lower (Tor) reservoir for both seismic ΔS_w and simulator ΔS_w. The average Tor ΔS_w is then plotted on the bottom reservoir surface (Fig. 9a, b). Simulation ΔS_w shows three fingers of increased water saturation. The two left fingers are centred on injector wells I1 and I2, and the third finger originates from an abandoned injector well (not displayed in this map). Seismic ΔS_w, on the other hand, shows a heterogeneous water front moving updip from injector I1 along most of the well, with a strong change in water saturation at the centre of the well. Based on the seismic ΔS_w map the water injected into the I2 injector well seems to gather in an elongated zigzag shaped feature of about 700 m length and a width varying between 200 and 300 m, whereas the simulation ΔS_w predicts a uniform injection pattern centred along the I2 injector.

To investigate the observed heterogeneous nature of change in ΔS_w further, we display the seismic and simulator ΔS_w in a 3D plot together with the porosity from the reservoir simulation model (Fig. 10a, b). The simulation model shows a homogeneous

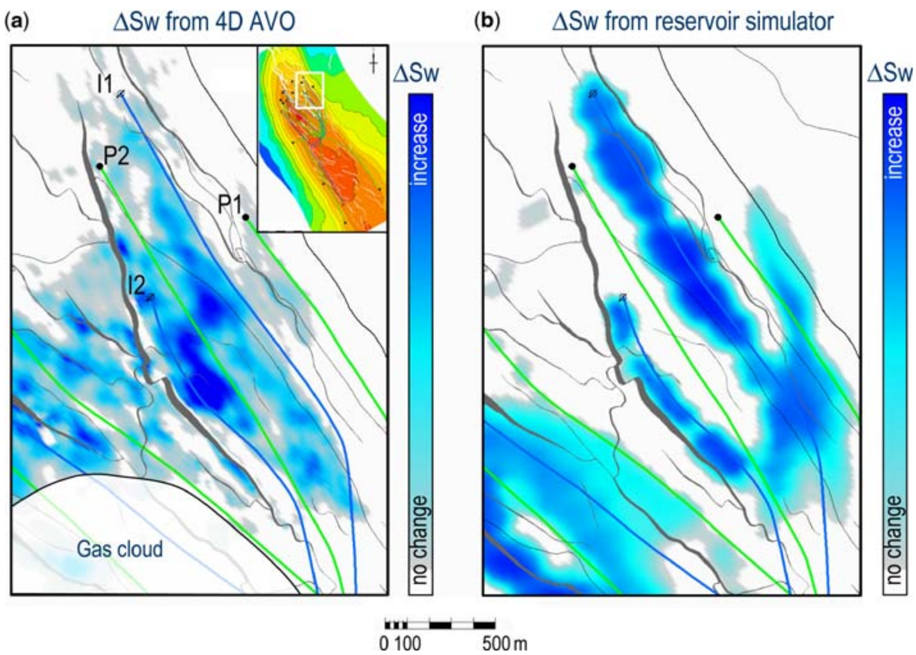

Fig. 9. (**a**) Map of ΔS_w derived from time-lapse rock physics inversion and (**b**) map of ΔS_w predicted by the reservoir simulation model. The average water saturation in the lower reservoir (Tor) is vertically averaged and the average ΔS_w is displayed on the base reservoir surface. Note the zigzag shaped pattern for increased seismic ΔS_w and the three-fingered pattern in simulator ΔS_w. See text for a detailed discussion.

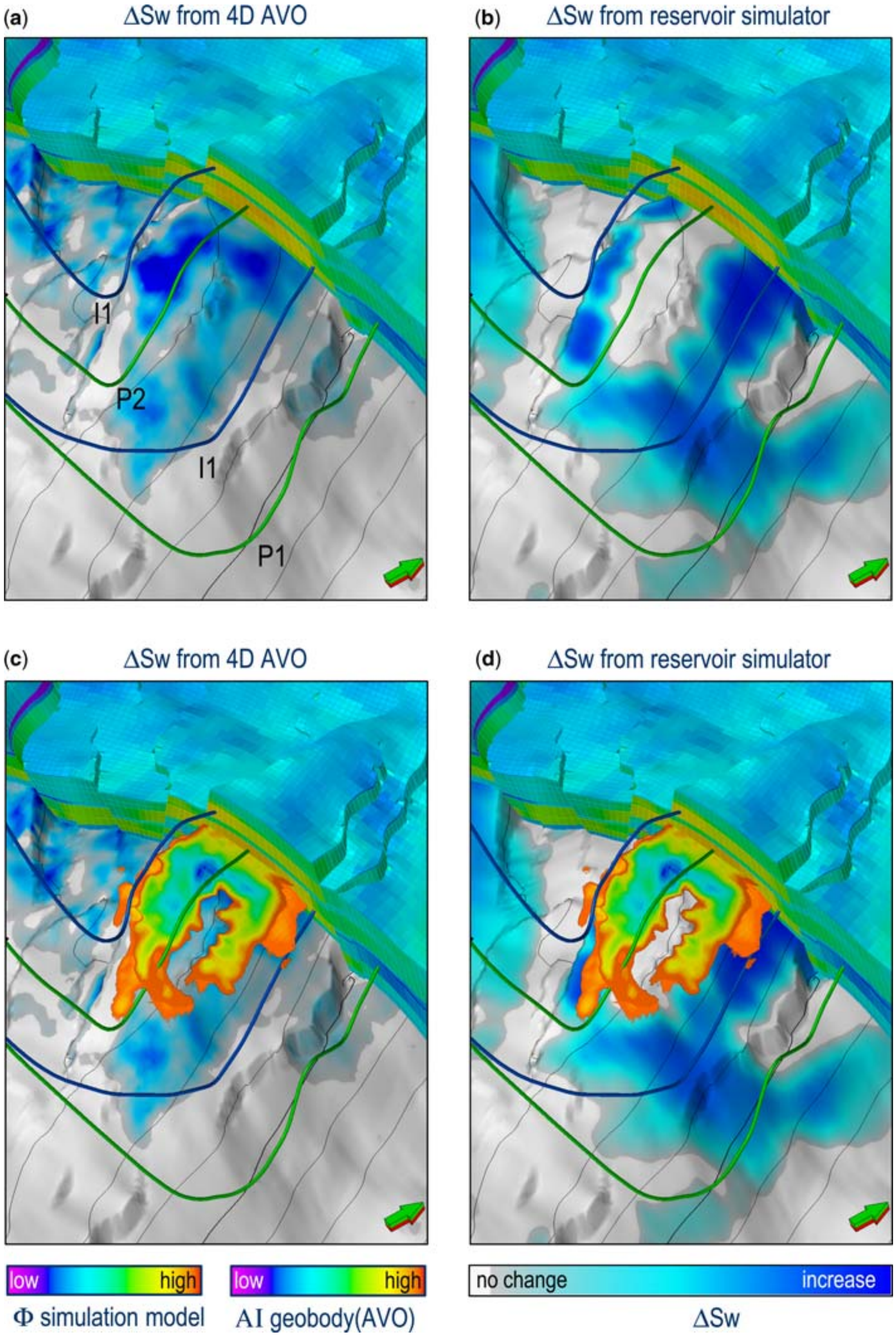

Fig. 10. Three-dimensional view of (**a**) seismic ΔS_w and (**b**) simulator ΔS_w co-visualized with the simulator porosity and the producer (green) and injector (blue) well locations on the northern crest. The ΔS_w maps are the same as in Figure 9. When adding a seismically derived geobody of acoustic impedance (**c** and **d**), it becomes apparent that the water saturation changes in (a) follow the high porosity/high permeability zone outlined by the geobody, whereas the water saturation changes in (b) follow a simplistic porosity/permeability model. See text for discussion.

porosity (and thus homogeneous permeability) distribution in the lower (Tor) reservoir. This explains the symmetric spread of the injected water around the injector wells. New insight is gained when additionally displaying a geobody of seismic-derived acoustic impedance (Fig. 10c, d) in the 3D image. The geobody is extracted in such a way that it represents a volume of low acoustic impedance; that is, a volume of high porosity (Fig. 6). The top of the geobody is sliced off such that the distribution of values inside the geobody can also be seen. In Figure 10c it becomes immediately clear that the changes in regions of high water saturation mirror the regions of high porosity and permeability. The injected water is simply intruding a permeable zone, creating a heterogeneous water saturation pattern.

The information gained from seismic ΔS_w gives a clear picture of a heterogeneous reservoir sweep within a body of high porosity and permeability. This additional knowledge can potentially be used to selectively sweep the lesser drained areas by fracturing these areas to increase permeability.

Fault control of injected water on the SW flank

Faults can act as flow barriers or fluid conduits. For accurate production forecasts from reservoir simulation models, faults and fractures need to be included in the reservoir model. However, including faults in a reservoir model adds additional complexity, since their location and physical properties need to be determined – information that is not always readily available. On the other hand, a huge number of minor faults can often be extracted from 3D seismic data – the question of which of these faults contribute to fluid flow (and therefore need to be included into a flow model) still needs to be addressed. In this section, we show that time-lapse seismic observations can assist in finding the locations of transmissive faults. We can clearly demonstrate that fluid flow on the SW flank is fault dominated. The joint use of time-lapse seismic observations and production logging data creates a clearer and consistent picture of drainage of the SW flank.

In Figure 11, we compare changes in water saturation ΔS_w observed from time-lapse seismic AVO inversion (Fig. 11a), and predicted from the reservoir simulation model (Fig. 11b). The location of the displayed area and the view direction for the 3D plot are indicated in the inset in Figure 11a. Again, we compute the vertically averaged ΔS_w and display the averaged ΔS_w as a map attached to the bottom reservoir surface. Additionally, we display the injector well I3 and two producers P4 and P5, and a vertical seismic section. The seismic ΔS_w shows several streaks of increased water saturation emanating downdip from injector well I3, whereas the simulation ΔS_w shows a homogeneous spread of injected water around well I3. The locations of the streaks of increased water saturation coincide with the locations of minor faults (marked by red arrows) that are visible in the seismic data. The seismic data suggest that the injected water has found a conductive pathway from injector I3 to producer P4 along three conductive zones and the majority of the water seems to be injected into the first half of I3. In a similar manner, production logging data has shown that the P5 well produces predominantly from the first half of the well, indicating a lack of pressure support in the toe-half of P5. The time-lapse seismic data show only minor changes in ΔS_w towards the toe of producer P5, indicating that only a negligible amount of water is injected into this region. This is consistent with the lack of production towards the toe of the well, indicating a lack of pressure support and is consistent with the production logging data. This additional insight may be used for a workover campaign to re-fracture the toe end of injector I3 and producer P5, in order to increase production from this low permeability zone.

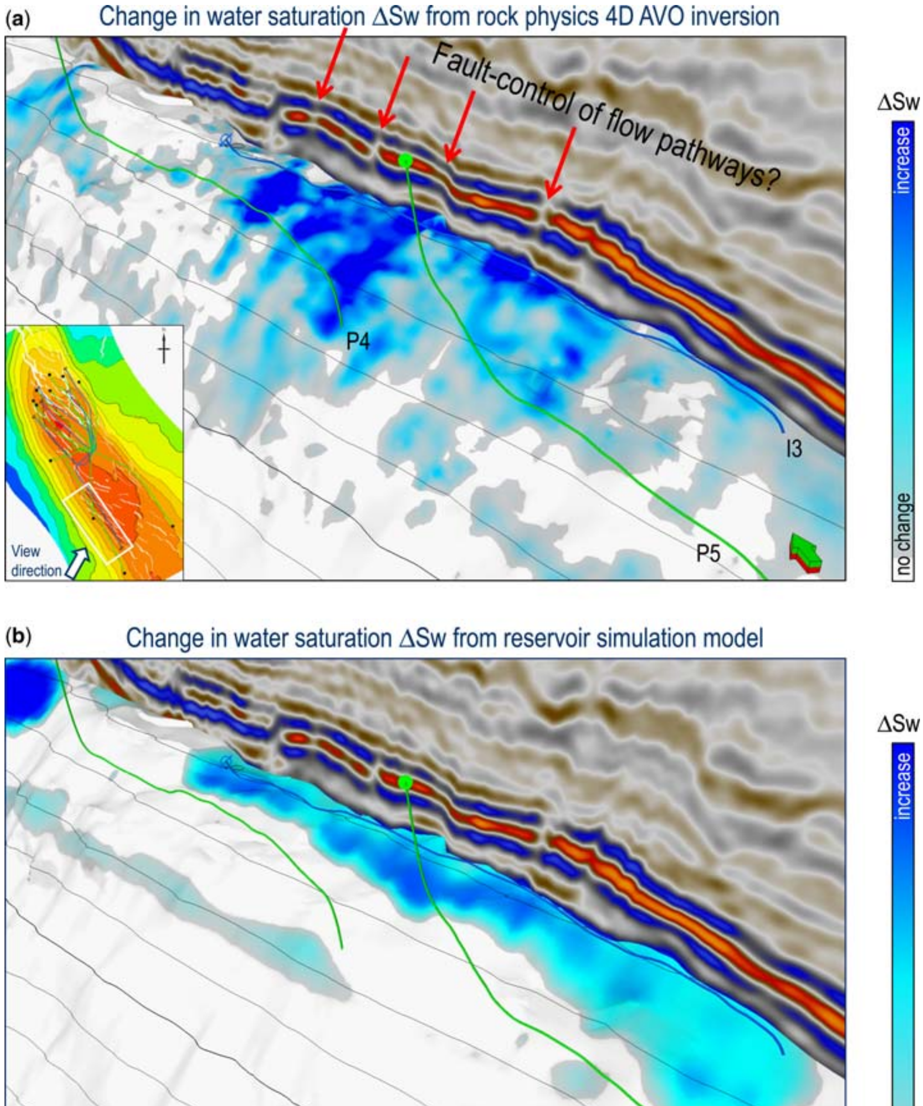

Fig. 11. Changes in water saturation ΔS_w (**a**) observed from time-lapse rock physics inversion and (**b**) predicted from reservoir simulation. Injector well I3 is marked in blue and two producers P4 and P5 are marked in green. The seismic derived ΔS_w shows a series of blue streaks indicating conductive pathways. Their locations coincide with minor faults (marked by red arrows) observed in seismic data.

The observations of fault control on reservoir depletion have also had implications for the field development of an extension of South Arne to the north of the currently producing region. Three new appraisal wells were drilled – an appraisal well to the north and NE tested the reservoir at virgin pressure, whereas an appraisal well to the NW tested at substantially lower pressure. Fault control along radial faults offers a suitable explanation as to why the well towards the NW is already partially pressure depleted. The faults are observed in seismic data (Mackertich & Goulding 1999) and the time-lapse seismic data have given a strong indication of the faults acting as fluid conduits. Hess has therefore built several reservoir models of the northern extension, simulating different depletion scenarios, including fault-controlled reservoir depletion, causing a skewed map of pressure depletion.

Compaction monitoring on the northern crest

The high porosity chalk comprising the reservoir on the northern crest makes production-induced reservoir compaction a distinct possibility, and reservoir compaction at the nearby Ekofisk (e.g. Boade *et al.* 1989; Chin & Nagel 2004) and Valhall (Cook & Jewell 1996; Barkved *et al.* 2003) chalk fields is well published. Laboratory experiments from the upper (Ekofisk) and lower (Tor) reservoir show the typical chalk compaction behaviour (Fig. 12a, b): as pore-pressure is reduced and mean effective stress increases, the chalk initially shows a slow (but reversible) decline in porosity. At a critical effective stress, irreversible compaction occurs as the weakly cemented grain-to-grain bonds fail and porosity drops sharply. High porosity in chalks causes a lower critical stress at which porosity collapse starts to occur. In the lower reservoir, the critical stress can be as low as 12 MPa at an initial porosity of 45%. Replacing oil by water in the pore space additionally lowers the critical stress, as water weakens the grain contacts.

In order to predict reservoir compaction and associated porosity and permeability changes, a full-field reservoir geomechanical model was built and coupled to the reservoir simulation model. A calibrated reservoir geomechanical model will assist in reliably assessing the amount of compaction drive energy. This allows for a better production forecast by including stress-dependent permeability and allows the operator to assess the risk of well failure by differential compaction. Geomechanical simulations also need to be calibrated (i.e. matched) with data observations in the same way that reservoir simulation models can be history matched using produced water and hydrocarbon volume and observed reservoir pressure. For compaction simulations, time-lapse seismic can produce the necessary calibration tool. In Figure 13, we compare time-lapse time shifts Δt on the top-reservoir horizon with displacement Δz of the same horizon predicted from reservoir geomechanical modelling. The time-lapse time shifts are taken as a proxy for the predicted vertical displacement. This seems a reasonable assumption, since the time shifts are caused by the compaction-induced stretching of the overburden and an associated velocity slowdown. However, the exact nature and means of calibrating the relationship between overburden stretching, velocity slowdown and observed time shifts is still a field of active research and debate (Hatchell & Bourne 2005; Staples *et al.* 2007; De Gennaro *et al.* 2008).

The observed time-lapse time shift Δt map (Fig. 13a) and computed vertical displacement Δz map (Fig. 13b) broadly agree. Maximum Δt is 6 ms and the maximum Δz is 1.5 m. This relationship between time-lapse time shifts and vertical displacement is in broad agreement with observations at Valhall (Hatchell & Bourne 2005) and Ekofisk (Janssen *et al.* 2006). Both maps show fault control of reservoir compaction, where faults clearly act as flow barriers. However, more interesting than the similarities are the subtle differences between the two maps. Areas where the observed compaction is stronger than predicted are indicated by yellow ellipses, and vice versa, areas where observed compaction is less than predicted are marked by red ellipses in Figure 13a, b. This can be seen especially clearly for the area drained by producer P1, where compaction of up to 75cm is predicted, but no time-lapse time shifts are observed.

These observations can be used to adjust the material properties of the reservoir geomechanical model. In areas that are seen to be compacting from seismic, but where the simulation model does not predict compaction, either the porosity may be increased or the critical stress at which irreversible deformation occurs can be lowered. For producer P3 it would be reasonable to increase porosity in the central area marked by the yellow ellipse and decrease porosity in the area marked by the red ellipse. The net result on production for the entire producer P3 may then be left unchanged and the history matching of production for the entire well would not be affected. The inversion results for acoustic impedance *AI* or rock physics inversion to porosity Φ can additionally assist in determining whether the simulator porosity model should be updated.

A quantitative comparison between compaction estimates from time-lapse seismic AVO inversions and reservoir geomechanical modelling gives a similar picture of compaction as given by time-lapse time shifts and vertical strain images. In

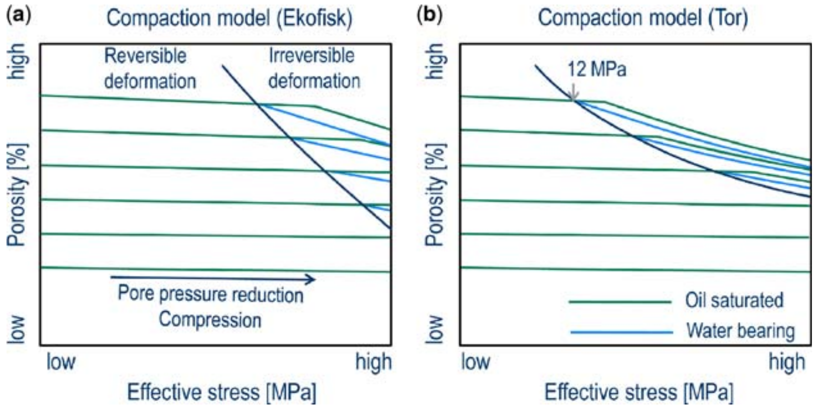

Fig. 12. Porosity as a function of effective stress for the (**a**) Ekofisk formation and (**b**) Tor formation. Each curve shows the porosity–effective stress relationship for a different initial porosity. Blue curves show the behaviour for water-bearing chalk and green curves show the behaviour for hydrocarbon-bearing chalk. For small effective stress, the porosity reduction is reversible (elastic deformation). At a critical stress, irreversible deformation occurs. Water in the pore space reduces the critical stress to as low as 12 MPa for chalk with 45% porosity in the Tor interval.

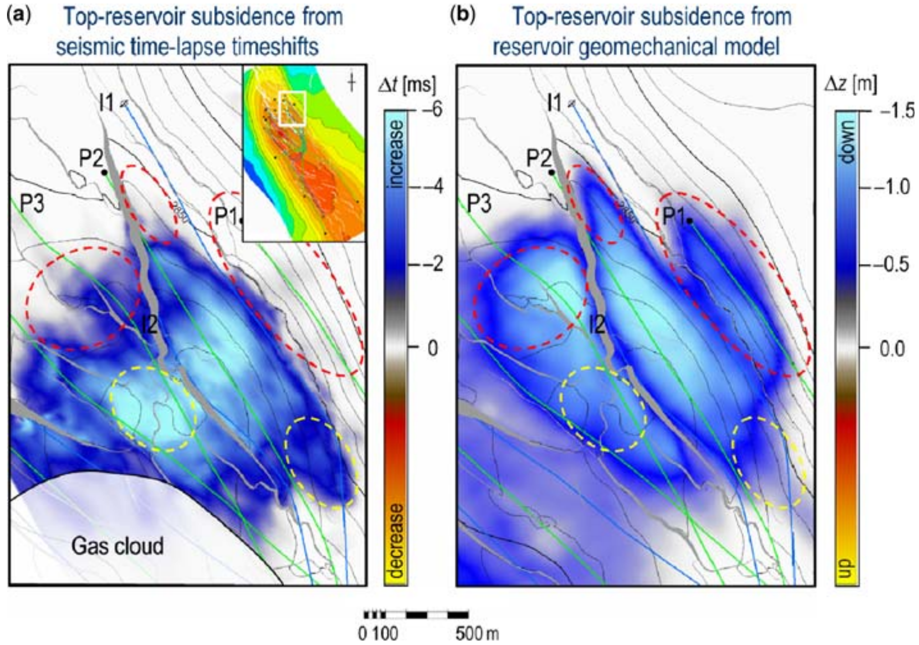

Fig. 13. Observed and predicted reservoir compaction. (**a**) Compaction-induced travel time changes to the top-reservoir reflector (time-lapse time shifts Δt) as a measure for top-reservoir subsidence. (**b**) Predicted vertical displacement Δz of the top-reservoir surface. A 6 ms increase in travel time corresponds roughly to 1.5 m top-reservoir subsidence. Areas where observed subsidence is larger than predicted subsidence are marked by yellow ellipses, and vice versa, areas where observed subsidence is less than predicted subsidence are marked by red ellipses. Note the clear fault control in both observed and predicted subsidence.

Figure 14, we compare porosity changes $\Delta\Phi$, inferred from time-lapse AVO inversion and volumetric strain ε_V from the reservoir geomechanical model. Assuming that a negative volumetric strain (i.e. a decrease in volume) is caused by reduction in porosity, the two quantities describe the same process. Porosity reduction of approximately -2.5% is measured by time-lapse seismic data across the lower (Tor) reservoir across most of the crestal area, with predicted volumetric strain of *c.* -3%. Discrepancies are again observed around producer P1, where time-lapse seismic observations detect only negligible porosity reduction and the reservoir geomechanical model predicts volumetric strains of -1.5%.

Discussion

The aim of time-lapse seismic interpretation should be to identify differences between a current understanding of reservoir dynamics and the reservoir dynamics inferred from time-lapse seismic data. Only then does time-lapse seismic add value by creating a new

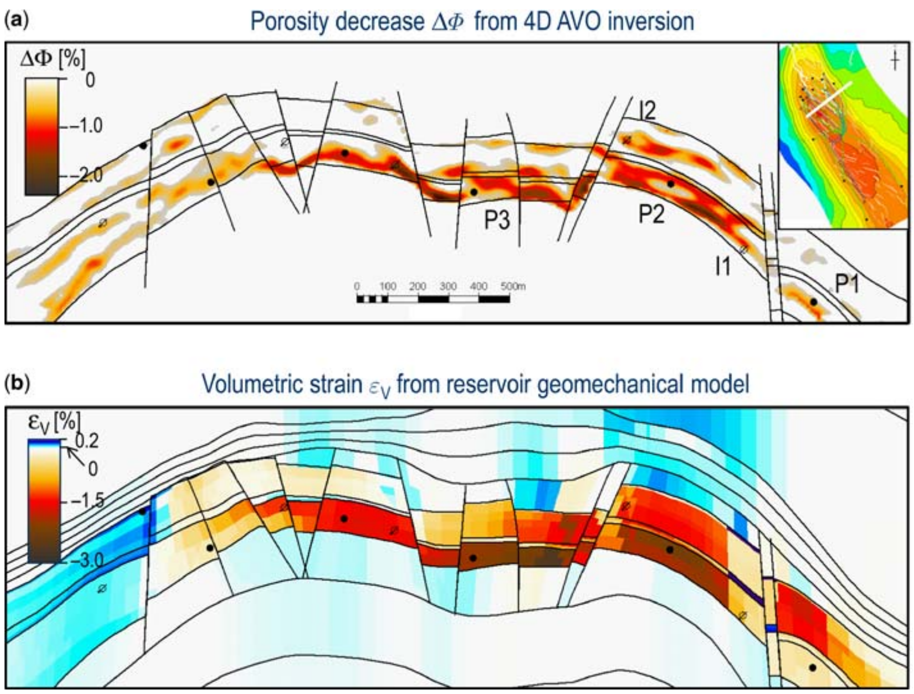

Fig. 14. (**a**) Porosity reduction $\Delta\Phi$ derived from time-lapse rock physics AVO inversion. (**b**) Volumetric strain change ε_V predicted from reservoir geomechanical modelling. Under the assumption that porosity decrease is the primary reason for volumetric strain change, the two images are directly comparable. See text for discussion.

understanding of the field. If time-lapse seismic confirms what we already know, its application simply adds peace of mind.

At South Arne, we have identified a high-porosity, high-permeability zone on the northern crest of the reservoir that may be responsible for a heterogeneous sweep, whereas the simulation model predicts a homogeneous sweep. Nevertheless, the seismically derived ΔS_w and $\Delta\Phi$ needs to be investigated with a critical eye: the employed rock physics model accurately describes the effect of changes in water saturation in intact rock. However, we also know that the rock on the crest of the reservoir experiences approximately -3% of volumetric strain and undergoes irreversible compaction with grain-to-grain bonds failing and a possible occurrence of grain-crushing. We are currently striving for a deeper understanding how irreversible compaction influences the acoustic impedance and Poisson's ratio as determined by seismic observations. This lack of understanding adds some uncertainty to our interpretations.

Time-lapse seismic has given a clear indication of faults adding additional hydraulic permeability at South Arne, and we have shown a particularly clear example from the SW flank of the field. It must be noted that, in this part of the field, the strike-direction of the faults and the sail direction during seismic acquisition are aligned, and some of the fault-related time-lapse changes may be related to acquisition artefacts. We do not believe that this is the case. Firstly the fault-related time-lapse differences do not extend into the overburden above the reservoir whereas an acquisition footprint on the time-lapse differences would. Secondly, there is no correlation between any 'striping' in repeatability plots and the location of the interpreted conductive pathways. If the interpreted conductive pathways were spurious, other minor faults would also show up with time-lapse differences. Thirdly, the time-lapse observations confirm and explain reservoir dynamics from production logging adding to a consistent picture of reservoir drainage.

Besides adding hydraulic permeability along fault strike direction, faults clearly cause compartmentalization of the field. We gave an example of fault-controlled reservoir compartmentalization on the north flank, where time shift maps clearly show an imprint from fault locations. Faults therefore clearly cause macroscopic permeability anisotropy, with flow enabled along the strike direction and impaired across the fault. This behaviour has been included in a reservoir simulation model for a planned field extension to the north of the currently productive area. Including permeability anisotropy by introducing hydraulically conductive faults causes skewed maps of pressure depletion, which are in accordance to the reservoir pressure encountered when drilling appraisal wells for the extension.

In order to extract the full information contained in time-lapse seismic data, it is necessary to use time-lapse seismic data and inversion models in conjunction with all other data available on the dynamic behaviour of the field. In this paper we showed that co-visualization and joint interpretation of reservoir dynamics from time-lapse seismic data and reservoir simulation models creates deeper insight than could be gained from either tool individually.

Conclusion

We have presented a case study applying time-lapse seismic to obtain a clearer understanding of reservoir depletion patterns, production dynamics, the influence of faults on fluid flow and reservoir compaction. Using time-lapse seismic data in conjunction with a reservoir simulation model in the same software environment, using common colour tables and common scales for maps and cross-sections, allows for rapid scanning of differences and similarities between the depletion patterns derived from time-lapse seismic and reservoir simulation. Reconciliation of the reservoir simulation model and the reservoir geomechanical model with time-lapse seismic data and inversion models results in a well calibrated simulation model. The calibrated models, in turn, have a higher probability of accurately predicting future reservoir production and therefore allow for more efficient day-to-day reservoir management and for optimization of future field development.

The authors wish to thank the South Arne partnership Hess, DONG Energy, Noreco and Danoil for permission to publish this paper. We also would like to acknowledge the work of Frédéric Bourgeois and James Minton in building and running the South Arne reservoir geomechanical model; the work of Valerie Biran and Kjetil Westeng on rock physics modelling and low frequency model building for rock physics AVO inversion; and the work of Paul Groombridge and Paul Ramsden on time-lapse data processing of the South Arne dataset.

References

Barkved, O. I. & Kristiansen, T. 2005. Seismic time-lapse effects and stress changes: examples from a compacting reservoir. *The Leading Edge*, **24**, 1244–1248.

Barkved, O., Heavey, P., Kjelstadli, R., Kleppan, T. & Kristiansen, T. G. 2003. Valhall field – still on plateau after 20 years of production. *Proceedings of Offshore Europe*, SPE 83957; doi: 10.2118/83957-MS.

Boade, R. R., Chin, L. Y. & Siemers, W. T. 1989. Forecasting of Ekofisk reservoir compaction and subsidence by numerical simulation. SPE 17855. *Journal of Petroleum Technology*, **41**, 723–728.

Chin, L. Y. & Nagel, N. B. 2004. Modeling of subsidence and reservoir compaction under waterflood operations. *International Journal of Geomechanics*, **4**, 28–34.

Cook, C. C. & Jewell, S. 1996. Simulation of a North Sea Field experiencing significant compaction drive. *In*: *SPE Reservoir Engineering*, **SPE 29132**, 48–53.

De Gennaro, S., Onaisi, A., Grandi, A., Ben-Brahim, L. & Neillo, V. 2008. 4D reservoir geomechanics: a case study from the HP/HT reservoirs of the Elgin and Franklin fields. *First Break*, **26**, 53–59.

Gommesen, L., Hansen, H. P., Pedersen, J. M., Marsden, G. & Schiøtt, C. R. 2004. Rock-physics templates and seismic modelling of chalk reservoirs in the South Arne field of the Danish North Sea. *EAGE 66th Conference and Exhibition*, Paris, France, 7–10 June, G019.

Gonzalez-Carballo, A., Guyonnet, P.-Y., Levallois, B., Veillerette, A. & Deboiasne, R. 2006. 4D monitoring in Angola and its impact on reservoir understanding and economics. *The Leading Edge*, **25**, 1150–1159.

Gouveia, W. P., Johnston, D. H., Solberg, A. & Lauritzen, M. 2004. Jotun 4D: characterization of fluid contact movement from time-lapse seismic and production logging data. *The Leading Edge*, 1187–1194.

Guilbot, J. & Smith, B. 2002. 4-D constrained depth conversion for reservoir compaction estimation: application to Ekofisk Field. *The Leading Edge*, **21**, 302–308.

Hatchell, P. & Bourne, S. 2005. Rocks under strain: strain-induced time-lapse time-shifts are observed for depleting reservoirs. *The Leading Edge*, **24**, 1222–1225.

Hatchell, P. J., van den Beukel, A., Molenaar, M. M., Maron, K. P., Kenter, C. J., Stammeijer, J. G. F., van der Velde, J. J. & Sayers, C. M. 2003. Whole earth 4D: reservoir monitoring geomechanics. *SEG International Exposition and 74th Annual Meeting*, Dallas, TX, 26–31 October.

Herwanger, J. & Horne, S. 2005. Predicting time-lapse stress effects in seismic data. *The Leading Edge*, **24**, 1234–1242.

Janssen, A. L., Smith, B. A. & Byerley, G. W. 2006. Measuring velocity sensitivity to production-induced strain at the Ekofisk Field using time-lapse time-shifts and compaction logs. *SEG International Exposition and 76th Annual Meeting*, New Orleans, LA, 1–6 October.

Johnston, D. H., Eastwood, J. E., Shyeh, J. J., Vauthrin, R., Khan, M. & Stanley, L. R. 2000. Using legacy seismic data in an integrated time-lapse study: Lena Field, Gulf of Mexico. *The Leading Edge*, **19**, 294–302.

Kragh, E. & Christie, P. 2002. Seismic repeatability, normalized rms, and predictability. *The Leading Edge*, **21**, 640–647.

Mackertich, D. S. & Goulding, D. R. G. 1999. Exploration and appraisal of the South Arne Field, Danish North Sea. *In*: Fleet, A. J. & Boldy, S. A. R. (eds) *Petroleum Geology of Northwest Europe: Proceedings of the 5th Conference*, 959–974; doi: 10.1144/0050959.

Mavko, G., Mukerji, T. & Dvorkin, J. 1998. *The Rock Physics Handbook: Tools for Seismic Analysis in Porous Media*. Cambridge University Press, Cambridge.

Megson, J. & Hardman, R. 2001. Exploration for and development of hydrocarbon in the Chalk of the North Sea: a low permeability system. *Petroleum Geoscience*, **7**, 3–12.

Najjar, N. F., Stronen, L. K. & Alsos, T. 2003. Time-lapse seismic programme at Gullfaks: value and the road ahead. *Petroleum Geoscience*, **9**, 35–41.

Nickel, M., Schlaf, J. & Sønneland, L. 2003. New tools for 4D seismic analysis in compacting reservoirs. *Petroleum Geoscience*, **9**, 53–59.

Rasmussen, K. B., Bruun, A. & Pedersen, J. M. 2004. Simultaneous seismic inversion. *EAGE 66th Conference & Exhibition*, Paris, 7–10 June 2004.

Schiøtt, C. R. & King, A. 2006. Plan, acquire, process and interpret – how to turn around a time lapse survey in three weeks. *EAGE 68th Conference and Exhibition*, Vienna, 12–15 June, E033.

Schiøtt, C. R., Bertrand-Biran, V., Hansen, H. J., Koutsabeloulis, N. & Westeng, K. 2008. Time-lapse inversion and geomechanical modelling of the South Arne field. *First Break*, **26**, 85–91.

Shuey, R. T. 1985. A simplification of the Zoeppritz equations. *Geophysics*, **50**, 609–614.

Smit, F., Brain, J. & Watt, K. 2005. Repeatability monitoring during marine 4D acquisition. *EAGE 67th Conference and Exhibition*, 13–16 June, C015.

Staples, R., Cook, A., Braisby, J., Hodgson, B. & Mabillard, A. 2006. Integration of 4D seismic data and the dynamic reservoir model reveal new targets in Gannet C. *The Leading Edge*, **25**, 1126–1133.

Staples, R., Ita, J., Burrell, R. & Nash, R. 2007. Monitoring pressure depletion and improving geomechanical models of the Shearwater field using 4D seismic. *The Leading Edge*, **26**, 636–642.

Thedy, E. A., Salomão, M. C., Corá, C. A. G., Santos, M. S., Pumputis, A., Gomes, R. M. & Caletti, L. 2007. Understanding flow paths – new opportunities from time-lapse seismic data. *69th EAGE Conference and Exhibition*, London, 11–14 June, D001.

Vejbæk, O. V., Rasmussen, R., Japsen, P., Bruun, A., Pedersen, J. M., Marsden, G. & Fabricius, I. L. 2005. Seismic response from North Sea chalk. *In*: Doré, A. G. & Vining, B. A. (eds) *Petroleum Geology: North-West Europe and Global Perspectives – Proceedings of the 6th Petroleum Geology Conference*, 1401–1413; doi: 10.1144/0061401.

3D seismic mapping and porosity variation of intra-chalk units in the southern Danish North Sea

T. ABRAMOVITZ, C. ANDERSEN, F. C. JAKOBSEN, L. KRISTENSEN and E. SHELDON

Geological Survey of Denmark and Greenland (GEUS), Øster Voldgade 10, DK-1350 Copenhagen K, Denmark (e-mail: tab@geus.dk)

Abstract: Deposition of the Upper Cretaceous–Danian Chalk Group in the Salt Dome Province of the southern Danish Central Graben took place during a tectonic period dominated by post-rift subsidence, halokinesis and structural inversion. This resulted in highly variable chalk distribution with >1300 m of chalk located in synclines and <200 m preserved on inversion highs and salt structures. The area is mature with respect to exploration with most of the chalk fields located in structural traps discovered in the 1970s. However, the Halfdan discovery in 1999 illustrates the existence of off-structural traps, leading to renewed exploration interest. To locate additional off-structural traps, a detailed geological model is necessary for prediction of chalk intervals with reservoir potential. To unravel basin development, we combine 3D seismic interpretation, well log correlation and 2D seismic inversion to estimate acoustic impedance along selected profiles. The 2D acoustic impedance profiles are converted to total porosity and used to identify areas with potential untargeted reservoirs. A prominent high-amplitude reflection is interpreted as a regional unconformity separating two distinctly different chalk deposition patterns. Nannofossil biostratigraphy suggests a latest Campanian to early Maastrichtian age for the unconformity. It corresponds to an increase in acoustic impedance and decrease in porosity in wells. The Tor Formation contains porous intervals while the underlying Hod Formation contains less porous chalk. The Hod Formation has a maximum porosity of <20% based on well log and inversion data. In contrast, inversion data indicate that the Tor Formation comprises reservoir-grade porosity at several locations on downflank structures. In several areas, the inversion-based maximum porosity is predicted to be higher than expected, compared with porosity/depth trends derived from well data. Therefore, the spatial porosity variation in chalk is complex and controlled by factors other than burial depth.

Keywords: Chalk Group, Danish North Sea, GR/DT well log correlation, 3D seismic interpretation, seismic inversion, porosity anomalies, chalk reservoir potential

The majority of present-day oil and gas production in the Danish part of the North Sea is from fields with chalk reservoirs of Late Cretaceous (Maastrichtian) and Early Paleocene (Danian) ages (Fig. 1). The application of seismic data inverted for acoustic impedance (AI) has been a rewarding technology for porosity prediction in chalk exploration (Mackertich & Goulding 1999; Albrechtsen *et al.* 2001; Megson & Tygesen 2005). The predominantly mono-mineralic nature of chalk enables a robust empirical correlation between AI derived from the inversion of seismic data and total porosity (PHIT) (Anderson 1999; Jacobsen *et al.* 1999). The Halfdan discovery in 1999 was largely due to seismic inversion results that revealed low AI corresponding to high porosity values in the Maastrichtian chalk. This was later proven to contain non-structurally trapped oil.

In this paper, we use 3D seismic interpretation, well log correlation and 2D seismic inversion to estimate AI, and thus porosity, along key profiles in the Southern Salt Dome Province of the Danish Central Graben. The 2D AI profiles are converted to total porosity using an AI-PHIT transform for the entire Chalk Group based on 14 wells located in the study area. Our aim is to unravel the basin development and to distinguish between areas with potential untargeted reservoirs and areas acting as baffles to flow. We argue that the Maastrichtian Tor Formation has reservoir-grade porosity at several locations on downflank structures. These locations are situated where the inversion-based porosity is higher than expected when compared with porosity/depth trends derived from well data.

Database

The study area comprises parts of the Southern Salt Dome Province in the Danish Central Graben. It is covered by a 3D seismic data set, the Kraka Extension survey, which was acquired by Mærsk Olie and Gas AS in 2000. The survey has inline and crossline intervals of 12.5 m and covers an area of 1150 km^2. The data were time-migrated and converted to zero phase. Post-stack seismic processing included spectral balancing with a subsequent scaling to improve the resolution of the original seismic data. The main frequency content is 10–60 Hz after reprocessing and the vertical seismic resolution is 12–15 m for the upper part of the Chalk Group.

The survey covers the basin extending from the Coffee Soil Fault in the east to the Rolf Field near the Danish/German border in the west. The northwestern limit of the seismic survey reaches the flank of the Tyra Gas Field. Most of the Danish hydrocarbon reserves are located in chalk fields in the study area. These reserves include the large Dan, Halfdan, Gorm and Skjold Fields and the small Kraka, Rolf, Dagmar and Regnar Fields (Fig. 2). The latter three plus Skjold are located on shallow salt-piercement structures with a thin chalk section, typically less than 200 m thick. The combined ultimate recoverable reserves in the eight fields are estimated to be 370×10^6 m^3 of oil and 80×10^9 Nm^3 of gas (Danish Energy Agency 2008).

Six key wells, all of which penetrate the entire chalk section, have been selected for detailed seismic well ties and as input for

VINING, B. A. & PICKERING, S. C. (eds) *Petroleum Geology: From Mature Basins to New Frontiers – Proceedings of the 7th Petroleum Geology Conference*, 537–548. DOI: 10.1144/0070537

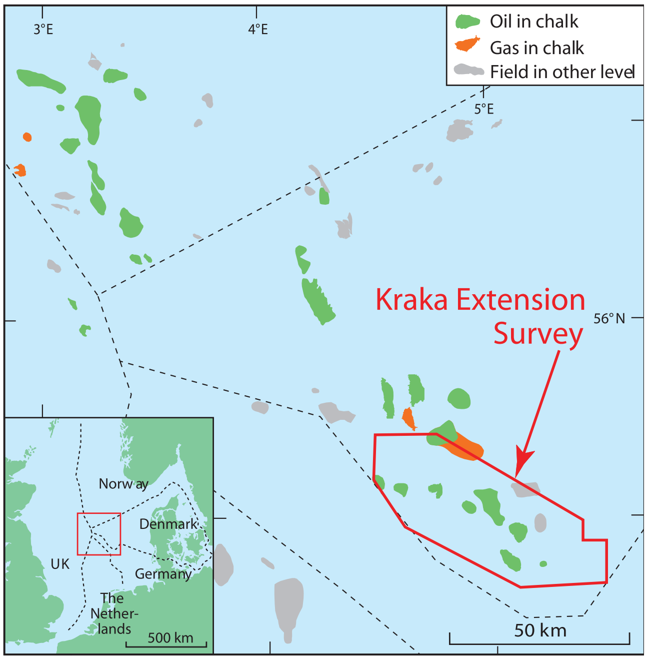

Fig. 1. Location map of the study area in the Danish North Sea.

wavelet extraction for seismic inversion. These wells are Olga-1X and Anne-3 on the Kraka structure, M-8X on the Dan structure, Nana-1XP, which is the vertical discovery well on the non-structural Halfdan accumulation, and finally U-1X and Skjold Flank-1, the latter situated in a basinal setting. Four 2D profiles crossing the well locations have been extracted from the 3D volume and inverted for AI. The profiles have been selected in such a way that they represent a range of structural settings and chalk burial depths (Fig. 2).

Geological setting

Deposition of the Late Cretaceous–Danian Chalk Group in the southern part of the Danish Central Graben took place during a phase of regional subsidence following Late Jurassic rifting. This period was marked by high sea-level, high sea-surface temperature and a peak in production of organic matter. The Late Cretaceous regional subsidence pattern was modified by halokinesis of the Zechstein salt and was punctuated by widespread structural inversion in the form of compression along old extensional fault trends, flexuring and folding of basin infill (e.g. Cartwright 1989; Vejbæk & Andersen 2002). This resulted in the development of areas with bathymetric elevations and the formation of local depocentres in the intervening lows. The structural movements gave rise to a

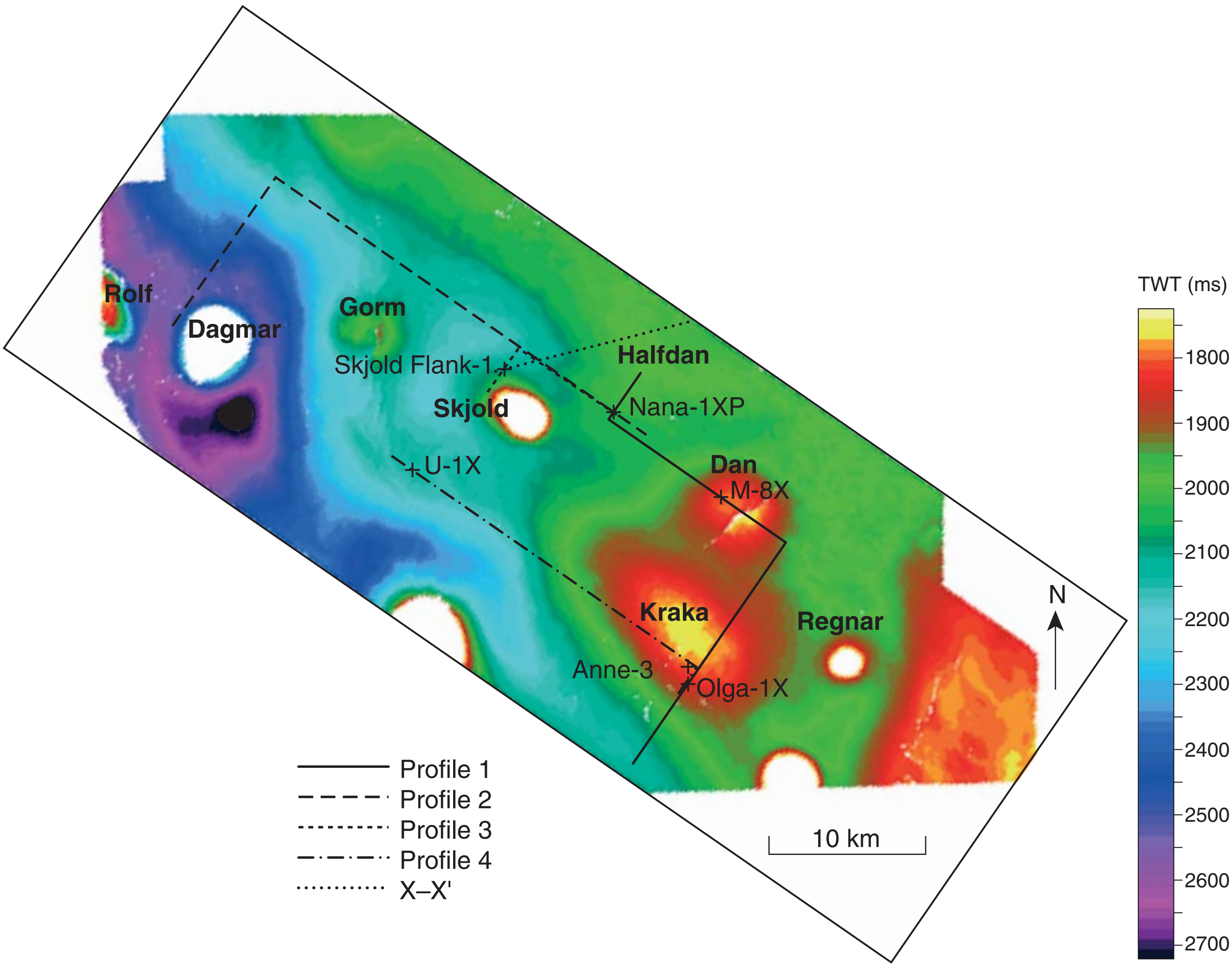

Fig. 2. Top Chalk Group time–structure map with location of 2D profiles, key wells and producing fields. Note: contours on the shallow salt diapirs with thin Chalk not shown.

number of unconformities that are easily recognized as truncation and onlap surfaces on seismic profiles and to stratigraphic hiatuses recorded in wells.

Chalk represents a unique, very fine-grained reservoir rock, characterized by high porosity and low matrix permeability. It is a pelagic carbonate sediment formed by settling of calcareous nannoplankton remains (i.e. coccoliths) from suspension in the water column (Hancock 1975). The North Sea chalk is a mono-mineralic carbonate rock that consists of 96–99% calcite ($CaCO_3$), non-carbonate biogenic particles (radiolarian, diatoms and sponge spicules) and small amounts of clay minerals due to influx of erosional detritus (Håkansson *et al.* 1974; Kennedy 1987). After pelagic deposition, the chalk deposits were subjected to redistribution by various processes. These include downslope mass flow movements from slope instability caused by syn-depositional tectonics as well as alongslope bottom currents that caused seafloor geometry modifications in the form of incised valleys, channels, drifts, ridges and mounds (Evans *et al.* 2003; Lykke-Andersen & Surlyk 2004; Surlyk *et al.* 2008). In the lower part of the chalk section, the interaction of downslope and alongslope processes has been demonstrated by Esmerode *et al.* (2008) in an area immediately north of the present study area.

The structural style in the Kraka Extension survey area is illustrated by the time isochore of the Chalk Group (Fig. 3). This shows very large thickness variations from less than 100 ms on top of the salt diapirs and up to 650 ms (*c*. 1300 m; Britze *et al.* 1995) in the rim-syncline east of the Dagmar Field. The chalk is reduced in thickness over the Dan and Kraka structures, which are caused by growth of underlying salt pillows. Similarly, the chalk time isochores are less than 200 ms on the flanks of a NW–SE trending inversion ridge east of the Nana-1XP location ('Igor-Tyra Ridge' by Britze *et al.* 1995) and on a north–south oriented ridge extending from the U-1X well northwards to the Gorm Field. The latter, termed the 'Gorm-Lola Ridge', is caused by a combination of structural inversion and halokinesis.

Stratigraphic subdivision of the chalk and reservoir properties

The lithology and stratigraphic subdivision of the chalk section in five of the key study wells are illustrated in the well correlation diagram (Fig. 4) together with seismic ties of the mapped horizons. In addition, the log-derived hydrocarbon saturation profiles in the field wells are shown.

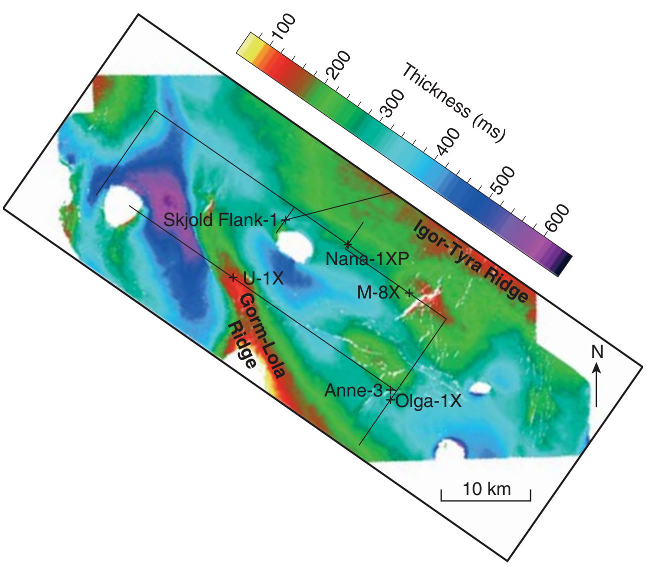

Fig. 3. Time isochore map of the total Chalk Group with location of key wells and major inversion ridges. Note: isochores on the salt diapirs not shown.

The lithology is illustrated by the gamma ray (GR) and sonic (DT) log curves. A distinction is made between 'high' GR argillaceous chalk and 'low' GR clean chalk. The DT log response serves as a porosity indicator in the clean chalk, which has been divided into four porosity classes to highlight the porosity variations.

We have used the standard lithostratigraphic nomenclature for the Central North Sea (Surlyk *et al.* 2003) and subdivided the chalk section into the Hod, Tor and Ekofisk Formations. The Cenomanian and lowermost Turonian Hidra and Blodøks Formations are thin in the area and are usually below seismic resolution.

The boundary in the wells between the Tor and Hod Formations is generally marked by a sharp decrease in porosity and can be traced seismically as an unconformity (prominent high amplitude reflection) over most of the study area. New biostratigraphic studies carried out on cuttings samples from the Olga-1X well suggest that the unconformity is Late Campanian to Early Maastrichtian in age. Using the 'UC^{BP}' (Late Cretaceous boreal province) nannofossil biozonation scheme of Burnett (1998), the unconformity separates chalk dated as $UC16^{BP}$ (Campanian/Maastrichtian boundary interval) from the overlying chalk unit dated as $UC19^{BP}$ ('Middle' Maastrichtian). A distinct intra-Hod unconformity is picked as a continuous peak and is identified by a relatively strong negative reflection coefficient. It is locally truncated and merges with the overlying near-top Hod unconformity. In most well sections, it corresponds to the top of an argillaceous interval. The age is biostratigraphically unconstrained, but a Santonian age has been suggested by Vejbæk & Andersen (2002).

The Maastrichtian Tor Formation is divided into an upper and lower unit separated by an intra-Tor seismic marker. In the Anne-3 well on the Kraka structure, the lower unit is missing and the upper part of the Tor Formation directly overlies the near-top Hod unconformity. The top of the Tor Formation is marked by a ubiquitous hardground, separating it from the overlying Ekofisk Formation of Danian age. The uppermost part of the Tor Formation is the main reservoir in the Dan and Halfdan Fields. It is a pelagic chalk that exhibits a characteristic cyclic pattern of high and low porosity over a 1–3 m scale that is regionally correlatable (Scholle *et al.* 1998). In the high-porosity intervals, the porosity may reach 35–37%. On a reservoir scale, the average porosity is 25–30%.

The Danian Ekofisk Formation is the main reservoir in the underfilled Kraka Field (Klinkby *et al.* 2005). The formation is divided into an upper unit characterized by relatively clean chalk and a lower unit characterized by impure argillaceous and siliceous chalk, which may form a barrier to vertical flow during production.

The effective porosity (PHIE) v. depth trends for each of the mapped chalk units in 14 vertical exploration wells have been analysed and compared with the classical model of Scholle (1977) (Fig. 5). This model predicts porosity as a function of burial depth and is based on empirical data of normally compacted chalk without overpressure and hydrocarbons. The recorded trends deviate considerably from the Scholle curve with more than 20% excess porosity in the shallow parts and rapid porosity deterioration with depth in the basal part, where the porosity trend approaches the model. The excess porosity in the uppermost chalk units is mostly caused by the porosity preserving effects related to overpressure, early hydrocarbon emplacement and possibly also reworking. In the southern part of Danish Central Graben, the chalk reservoirs are overpressured 6–10 MPa, which reduces the effective stress (Brasher & Vagle 1996; Japsen *et al.* 2005) – the magnitude of the overpressure is, however, only half the overpressure observed in the Norwegian chalk fields like Valhall and Ekofisk. Despite the modest overpressure in the study area, the abnormal pressure conditions restrict fluid removal, resulting in undercompacted

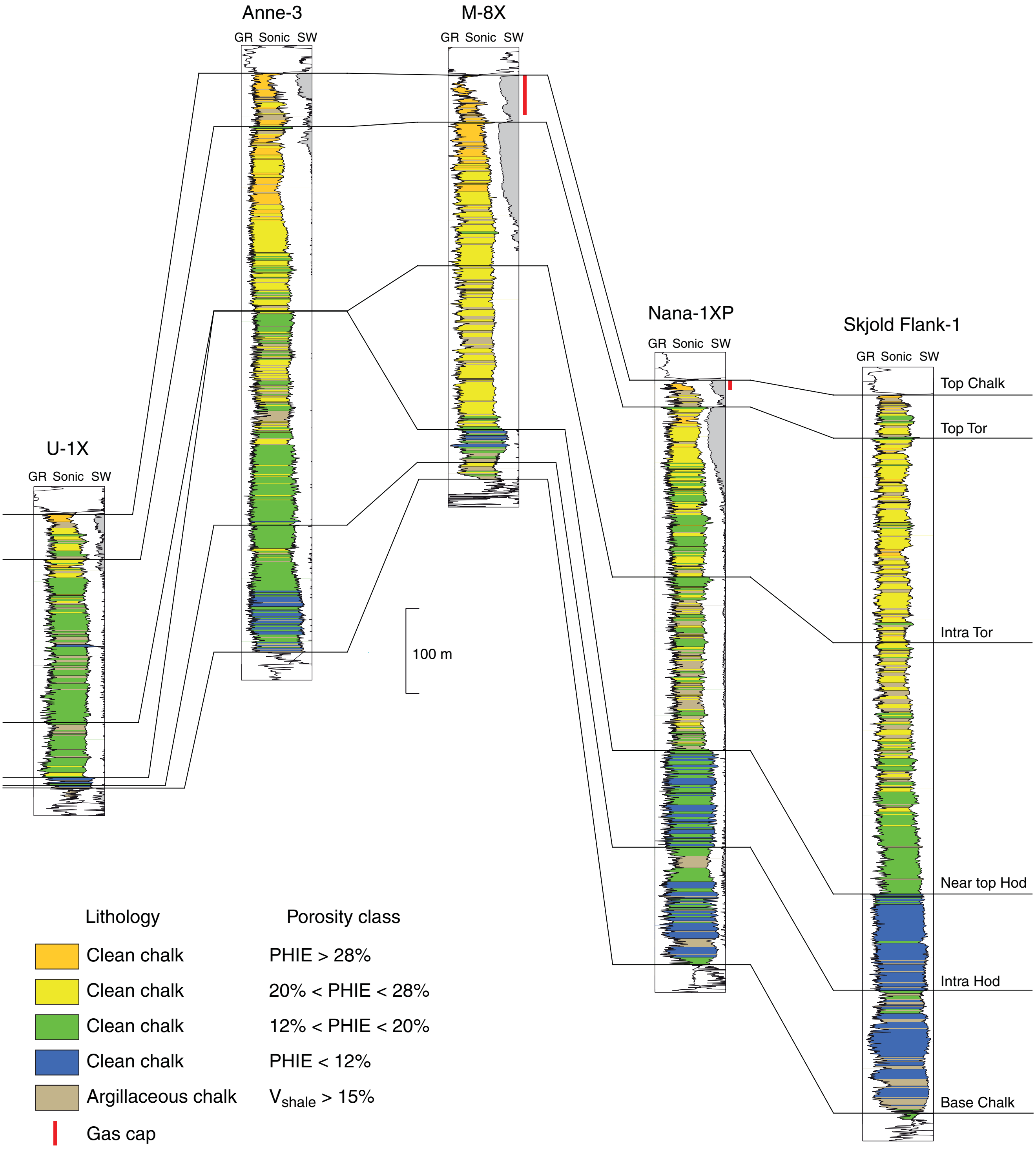

Fig. 4. Well correlation diagram through five key wells showing the lithology, hydrocarbon saturation and seismic tie of mapped horizons. The DT-log response is used as porosity indicator in clean chalk, which has been subdivided into four porosity classes.

chalk sections and higher than normal porosities. In many Danish chalk fields the porosity deterioration gradient is steeper than expected in the light of a normal porosity/depth trend, suggesting that hydrocarbon migration into the formation is a secondary source of porosity preservation. Furthermore, porosity above 40% is recorded in wells with high hydrocarbon saturations, illustrating that the presence of oil and gas also influences porosity preservation by impeding chemical compaction. Moreover, it is commonly accepted that re-sedimented chalk may *in general* exhibit a higher porosity level than pelagic chalk at the same depth known from the Norwegian greater Ekofisk area (Hatton 1986) and the northern part of the Danish Central Graben area (Nygaard *et al.* 1983).

The marked drop in porosity in the deep well sections shows that the effectiveness of overpressure in preserving high porosity is lost. Hence, the drilled pre-Tor Formation chalks in the Southern Salt Dome Province are generally tight (<20% PHIE) and without reservoir properties unless heavily fractured.

Basin development

The Late Cretaceous–Danian basin development in the survey area is illustrated in a series of time-isochore maps (Fig. 6a–f). The pre-Maastrichtian interval, which includes the Hod Formation and the thin Blodøks and Hidra Formations, shows large thickness

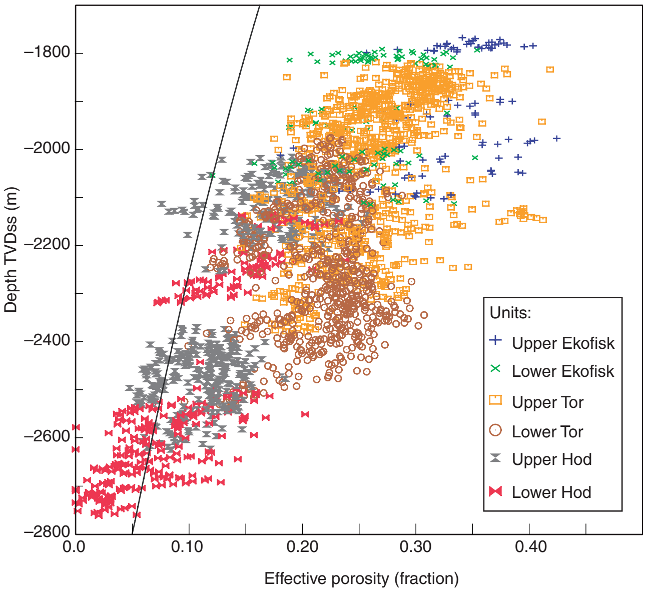

Fig. 5. Effective porosity (PHIE) v. true vertical depth colour coded with respect to stratigraphic unit. The plot is based on interpreted well log data from 14 selected wells located in the study area. The black solid line represents the model by Scholle (1977), which predicts the porosity as function of burial depth for normally compacted chalks.

variations (Fig. 6a). The main depocentre, which is up to 300 ms thick, is found in the rim-syncline north and east of the Dagmar salt diapir. The Gorm–Lola Ridge separates it from a NW–SE oriented depocentre that covers the southern flank of the Kraka structure. The Hod interval is also thin over the Dan Field area, indicating structural growth caused by underlying salt. The marked unconformity at near-top Hod level is clearly imaged on a composite seismic section through three key wells (Fig. 7). Clear truncations of underlying reflections are observed in the synclinal area between the present day Kraka and Dan structures.

The early basin development can be further illustrated by the time isochore of the lower Hod interval, which lies between the intra-Hod unconformity and the Base Chalk reflector (Fig. 6b). The interval shows basal onlap and is absent on the Gorm–Lola Ridge and the Dan and Kraka structures. A conspicuous NW–SE trending ridge system is mapped north of the Nana-1XP location parallel to the Tyra–Igor inversion ridge. The ridge system is a result of the effects of low-angle listric faults caused by slides and channel cuts developed on the flank of a rising inversion structure (Fig. 8). We suggest that these features are derived from an interaction of downslope mass movements and alongslope currents as described by Esmerode *et al.* (2008) in the adjacent area to the north.

The time isochore of the Maastrichtian Tor Formation (Fig. 6c) shows a shift in depocentre locations compared with Hod Formation depocentres. Most notable is a northeastward shift of the NW–SE oriented depocentre mapped in the central part of the area that contains up to 200 ms of Tor Formation chalk. The basin development during the Maastrichtian can be differentiated further when considering the time-isochores of the lower and upper part of the interval (Fig. 6d, e). The lower part of the Tor Formation, between the near-top Hod and the intra-Tor seismic markers, onlaps the near-top Hod unconformity towards the SW in the Kraka area (Fig. 7) and towards the NE in the direction of the Tyra–Igor inversion ridge. This is in contrast to the upper part of the Tor Formation, which has a more uniform thickness distribution across the area. Only minor thickness variations are observed in the central Kraka and Dan areas, suggesting quiet depositional conditions with little or no structural growth during the Late Maastrichtian (Kristensen *et al.* 1995; Klinkby *et al.* 2005).

The Danian Ekofisk Formation is generally thin, with time isochores greater than 50 ms mapped only in the areas on the northeastern flank of the Dan structure and the southern flank of Kraka (Fig. 6f). Here, local thickness minima and maxima are attributed to early post-Danian sliding of poorly consolidated chalk sediments (Surlyk *et al.* 2003; Klinkby *et al.* 2005).

Seismic inversion

Application of seismic inversion techniques for predicting porosity in North Sea chalk is a standard geophysical tool as there is a robust relationship between AI and porosity in clean chalk without gas-bearing zones. Excluding gas-zones and using a V_{shale} cut-off of 2%, a cross-plot of log-derived AI and PHIT of 14 wells in the study area shows a well-defined correlation with only minor scatter around a second-order polynomial regression line. This is expressed as: PHIT $= 0.729 - 7.08 \times 10^{-5}\text{AI} + 1.55 \times 10^{-9}\ \text{AI}^2$, where porosity is given as a fraction and AI is in $\text{g cm}^{-3} \times \text{m s}^{-1}$ (Fig. 9). The total (or apparent) porosity was calculated using the density log only, which may introduce a minor error in the estimate since no correction is made for hydrocarbon and shale content. The use of PHIT instead of PHIE for correlation with seismically derived porosity estimates is considered the most applicable, since porosity derived from the seismic data is 'bulk' porosity that includes any porosity bound in clay (e.g. clay-bound water) and other minerals. Furthermore, our analysis has shown that use of the above equation will locally overestimate total porosity by up to 5 p.u. in chalk with shale content above 10%. A similar overestimate of porosity is demonstrated in gas-bearing intervals.

In the present study, seismic inversion along four selected 2D key profiles was performed using the commercial ISIS software package developed for the petroleum industry. The inversion algorithm is a deterministic approach based on a simulated annealing algorithm (Maver & Rasmussen 1995; Rasmussen & Maver 1996).

The 2D seismic inversion work flow

The general 2D workflow is an iterative process carried out in loops as illustrated in Figure 10. It involves loading and conditioning the input data, performing a log to seismic calibration, wavelet estimation, low-frequency (i.e. background impedance) model generation and seismic inversion defined by four inversion parameters: signal-to-noise ratio, horizontal continuity, relative deviation of the low-frequency model and a threshold for reflection coefficients (Maver & Rasmussen 1995; Rasmussen & Maver 1996). The input data consists of 2D seismic profiles extracted from the 3D Kraka extension survey and the well log data (sonic, density and time-depth data) from the relevant wells.

The well-to-seismic tie is the most crucial step in the inversion procedure. The available check-shots (time–depth data) are used to create a reflectivity series with the same sampling rate (4 ms) as the input seismic data and to convert the log data from the depth domain into the two-way travel time (TWT) domain. The AI is calculated by multiplying the calibrated density log and the velocity log derived from the calibrated sonic log. The reflectivity series is computed by differentiating the AI series. After the initial log calibration, a preliminary wavelet is estimated by deriving the convolution operator between the reflectivity log and the seismic trace at the well location using a least squares wavelet estimation method. If necessary, visual ties are added to shift, stretch or squeeze the logs. The best-fit wavelet models as much of the coherent seismic data as possible and as little of the noise as possible, and is derived using the Akaike's final prediction error (FPE) criterion

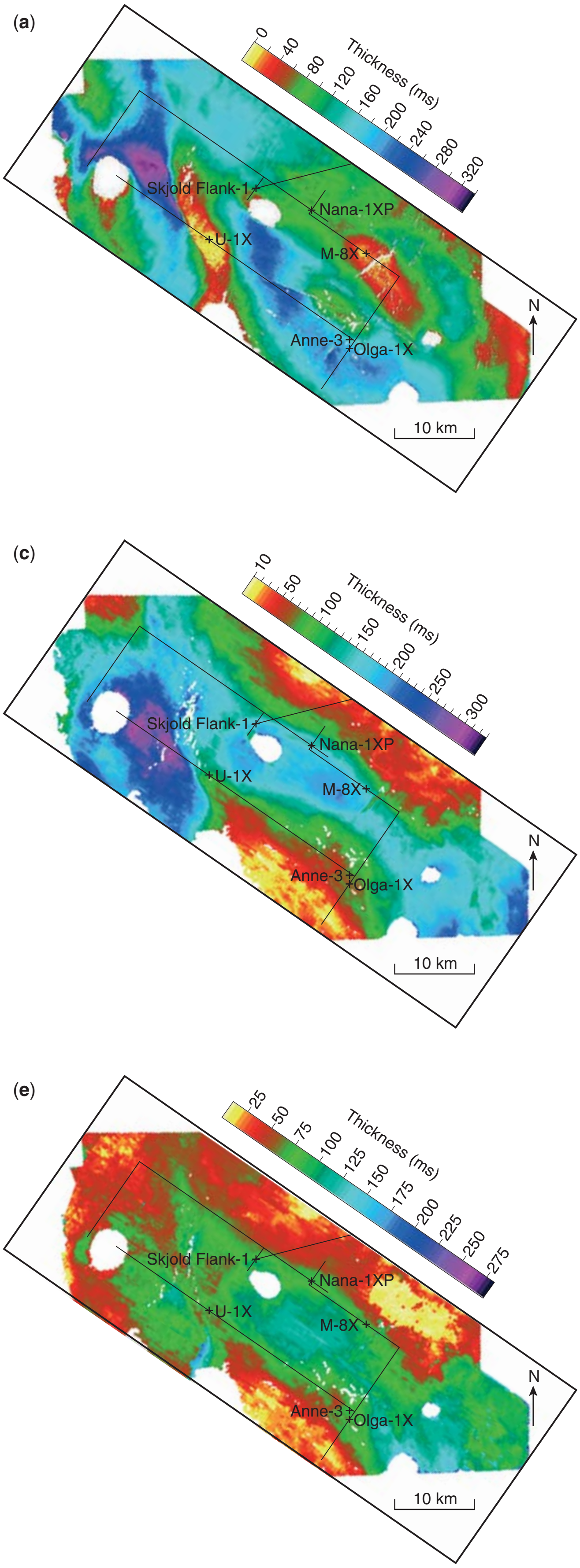

Fig. 6. Time isochore maps of individual seismic units: (**a**) time isochore of the total Hod Formation; (**b**) time isochore of the Lower Hod Formation; (**c**) time isochore of the total Tor Formation; (**d**) time isochore of the Lower Tor Formation; (**e**) time isochore of the Upper Tor Formation; (**f**) time isochore of the Ekofisk Formation.

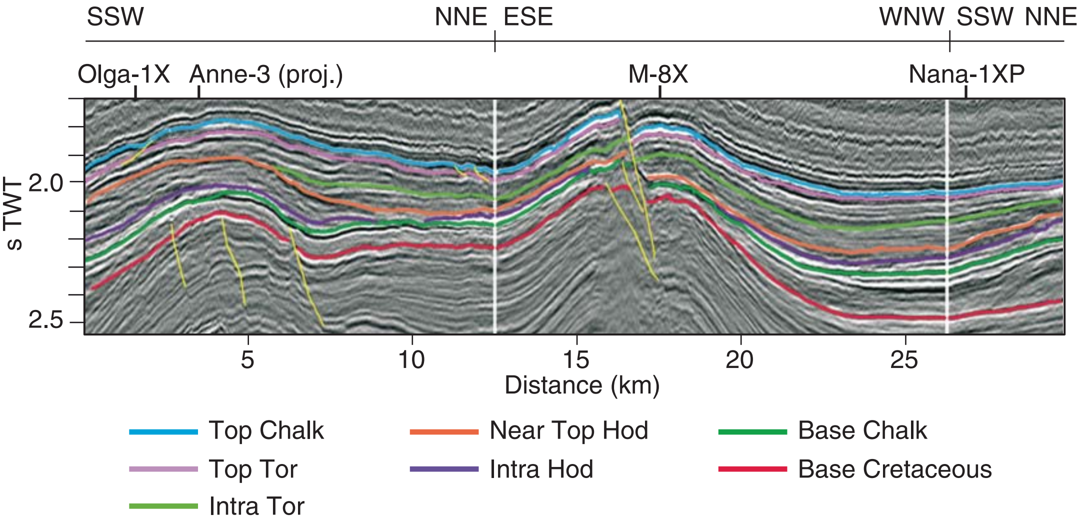

Fig. 7. Composite seismic section through Olga-1X, M-8X and Nana-1XP with the mapped horizons. Location is shown as profile 1 on Figure 2.

in combination with visual inspection of the wavelet and synthetic seismic trace (Maver & Rasmussen 1995). For each well location, the log calibration and wavelet estimation experiments are repeated until no further improvements are needed. The optimum wavelet used for the inversion is the one with the smallest relative misfit and the highest cross-correlation factor at the different well locations.

The low-frequency components of the AI variations are not present in the seismic data and have to be taken into account in the seismic inversion process. A low-frequency model (*a priori* model) introduces the sub-seismic frequencies into the seismic inversion result. The 2D low-frequency model is constructed by laterally extrapolating the final calibrated impedance logs from the wells along interpreted seismic horizons extracted from the 3D seismic data to guide and yield the absolute level of AIs along the seismic profile.

The four 2D profiles selected for this study (for location see Fig. 2) all have well ties to at least one of the five wells displayed in the well correlation profile (Fig. 4). The Nana-1XP well serves as a type well used for wavelet estimation for three of the 2D key profiles (Fig. 10). The absolute acoustic impedance (AAI) inversion results that include the low frequency model are based on the final calibrated impedance logs from the wells along each profile. Hence, no blind tests are used. The 2D AI inversion results are converted to total porosity using the AI–PHIT transform obtained from the second-order polynomial regression line shown in Figure 9 and are imaged as 2D PHIT profiles (s TWT) (Figs 12 & 13).

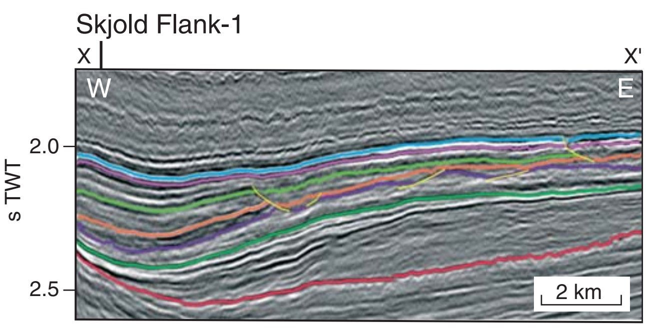

Fig. 8. Low-angle, listric faults and channel cuts in Hod Formation on the flank of the Tyra–Igor inversion ridge. Location is shown as profile X–X′ on Figure 2.

Inversion results along key profiles

Key profile 1. This profile is a composite, 30 km-long cross-section that strikes SSW–NNE across the Kraka Field (Olga-1X and Anne-3) and the Dan Field (M-8X) and then strikes ESE–WNW through the Nana-1XP well (Figs 2, 7 & 12). The Olga-1X, M-8X and Nana-1XP are all vertical wells and have suitable sonic, density and time–depth log curves covering the entire Chalk Group. The deviated Anne-3 well is located 1 km NE of profile 1 and was not used for wavelet estimation. The optimum wavelet is a least squares wavelet estimation obtained from Nana-1XP (Fig. 11).

A 2D low-frequency model was constructed by laterally guiding and extrapolating the calibrated impedance log from the four wells along the top Chalk, top Tor, near-top Hod and base Chalk reflectors, and then low-pass filtering the model (Fig. 12a). Between the Kraka and Dan Fields, the absolute level of AI reveals intermediate values (7–8.1 $\times$ 10^6 kg ms^{-2}) in the Tor interval and high values (>8.5 $\times$ 10^6 10^6 kg ms^{-2}) below the near-top Hod reflector as defined by the impedance logs from the Olga-1X and M-8X

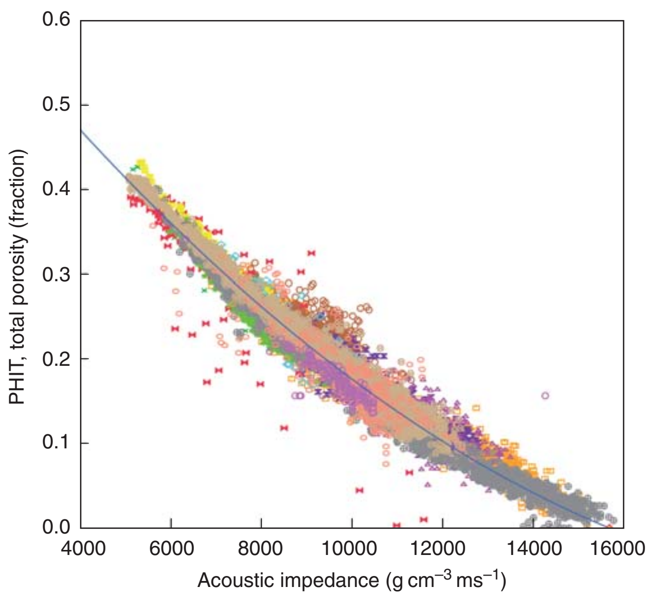

Fig. 9. Acoustic impedance v. total porosity (PHIT) in clean chalk from 14 chalk wells in the study area. A V-shale cut-off of 2% is applied. Gas-bearing zones are omitted.

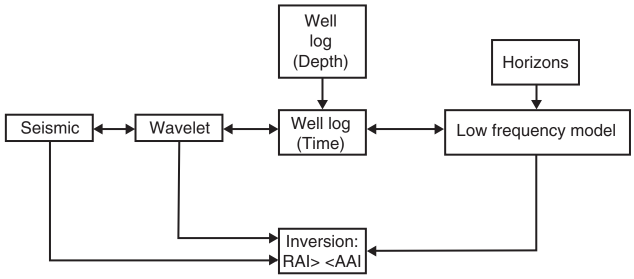

Fig. 10. Diagram for the ISIS 2D inversion workflow.

wells. Further to the NE near the Nana-1XP well, the Tor interval is dominated by a higher AI level and significantly higher values ($>10 \times 10^6$ kg ms^{-2}) below the near-top Hod reflector.

The inversion result as seen in the 2D AAI profile (Fig. 12b) clearly illustrates the fine-scale impedance variations within the Chalk Group. This implies the presence of alternating high and low AI layers onlapping onto the near-top Hod reflector in the deeper part of the Tor interval in the syncline between the Kraka and Dan Fields. These alternating high and low AI layers have a total porosity in the range of 20–25 and 29–32%, respectively (Fig. 12c). A maximum total porosity (above 30%) is found in the upper Ekofisk Formation and the topmost part of the Tor Formation. In the pre-Tor interval, the calculated PHIT values are mostly below 20%.

Key profile 2. Profile 2 is an arbitrary, 40 km long cross-section that extends from the NE flank of the Dagmar Field, covers the basin north of the Gorm and Skjold Fields, and continues past the Nana-1XP to the SE (Figs 2 & 13*a*). For the 2D low-frequency model, the calibrated impedance log from the Nana-1XP well and three interpreted horizons (top chalk, near-top Hod and the base Chalk) were used. A least squares wavelet estimated in the Nana-1XP well was used for the inversion.

The thickness of the Tor interval is fairly constant, but increases slightly in the rim-syncline north of the Dagmar Field. The uppermost part of this unit is characterized by a high porosity (>28%)

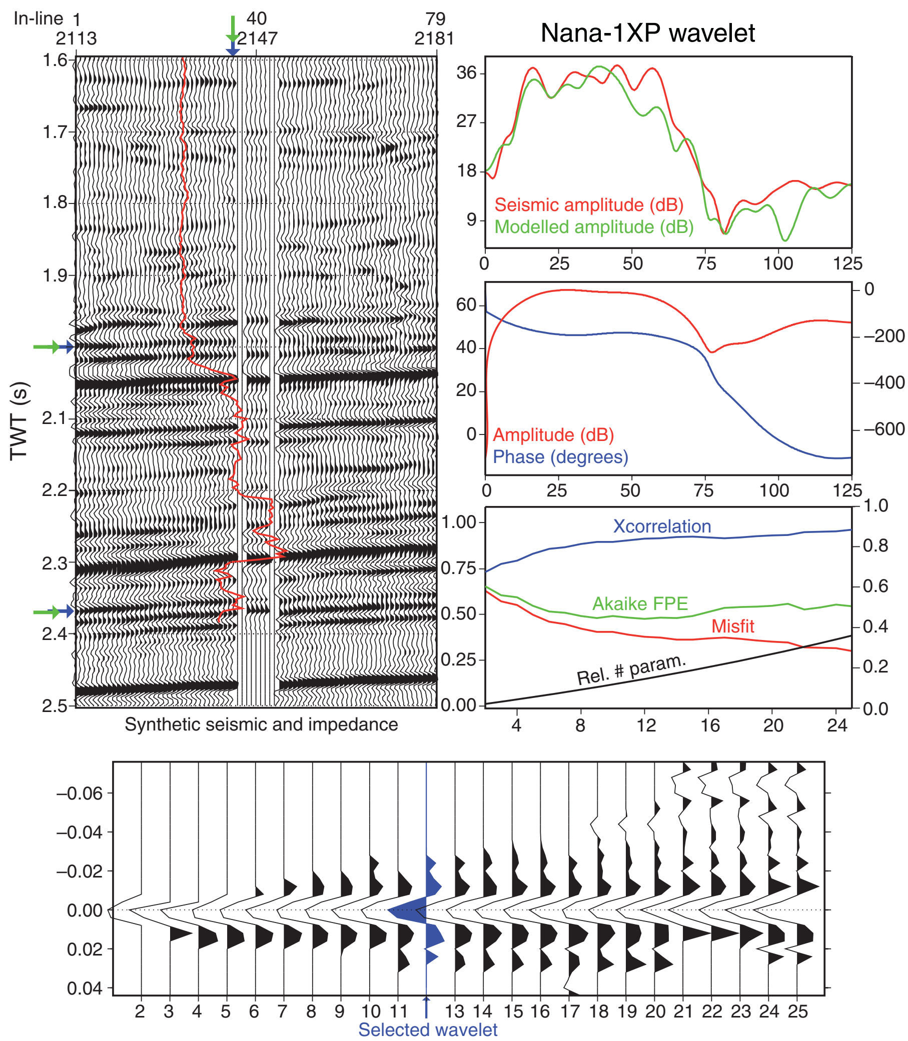

Fig. 11. Quality-control plot of the least squares wavelet estimation in the Nana-1XP well. *Bottom panel*: the stable wavelet suite with wavelet lengths ranging between 2 and 25 samples (8–100 ms) on the horizontal axis. *Left panel*: the synthetic trace derived by convolution of the optimum wavelet with the reflectivity log from the well is inserted into the seismic data. The AI log is shown in red. *Top right panel*: amplitude spectra of the seismic trace at the well location and the modelled synthetic trace in the wavelet estimation window by blue arrows on the left panel. *Middle right panel*: phase and amplitude spectra of the optimum wavelet (estimated between the green arrows on left panel). *Bottom right panel*: the relative misfit energy, Akaike's FPE cross-correlation and relative number of parameters. Akaike's FPE is a function of the misfit, which decreases as a function of the wavelet length, and the relative number of parameters, which increases as a function of the wavelet length. The relative number of parameters is equal to the length of the estimation window within which the misfit between the synthetic trace and the seismic data is calculated. The wavelet with the minimum value of Akaike's FPE, that is, the optimum wavelet, models as much of the coherent seismic signal as possible without modelling a significant amount of local noise.

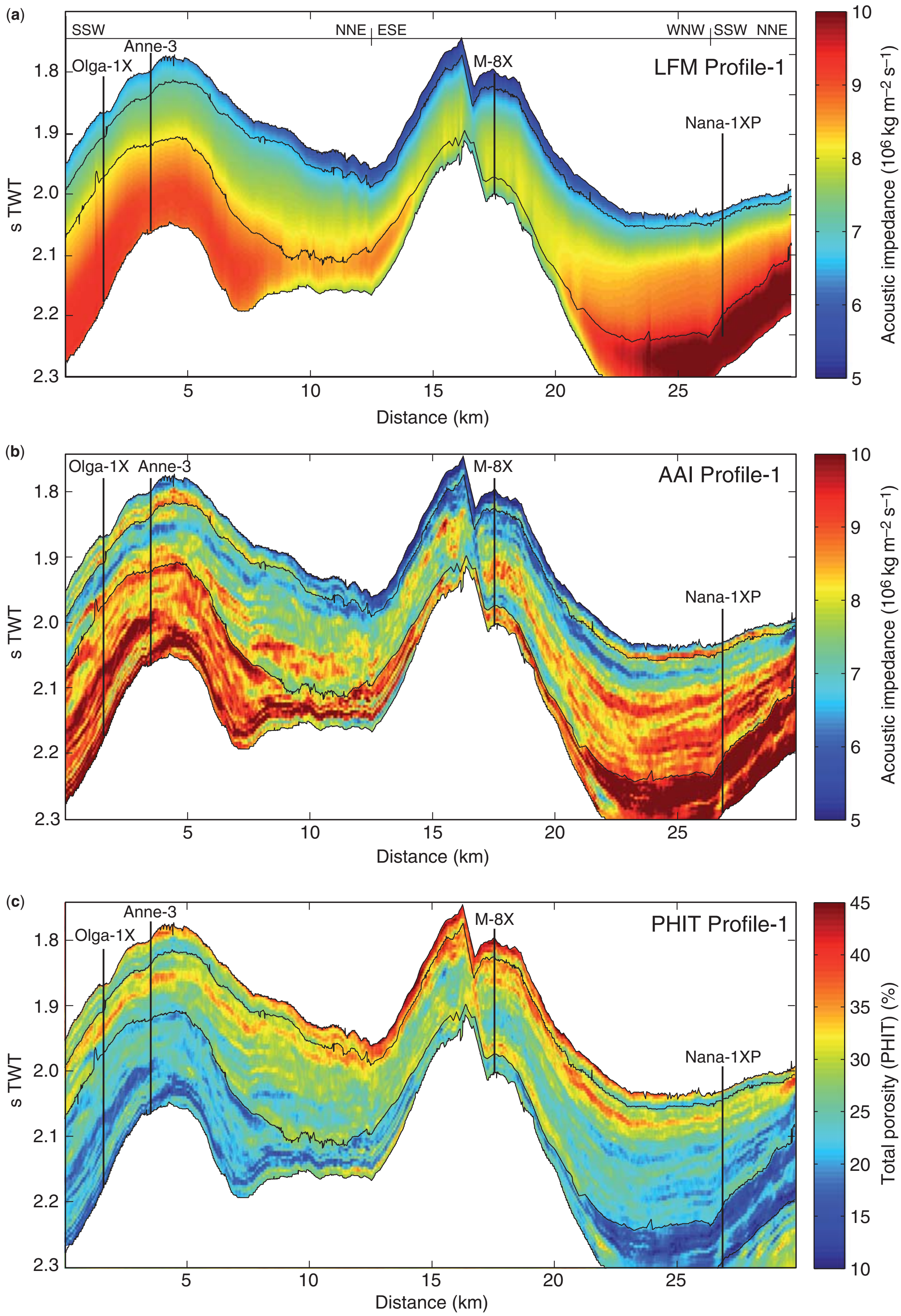

Fig. 12. Inversion results of key profile 1 corresponding to the seismic section shown in Figure 7. The profile location is indicated in Figure 2. (**a**) The 2D low-frequency model; (**b**) the 2D AAI section; (**c**) the calculated total porosity (PHIT) as a percentage.

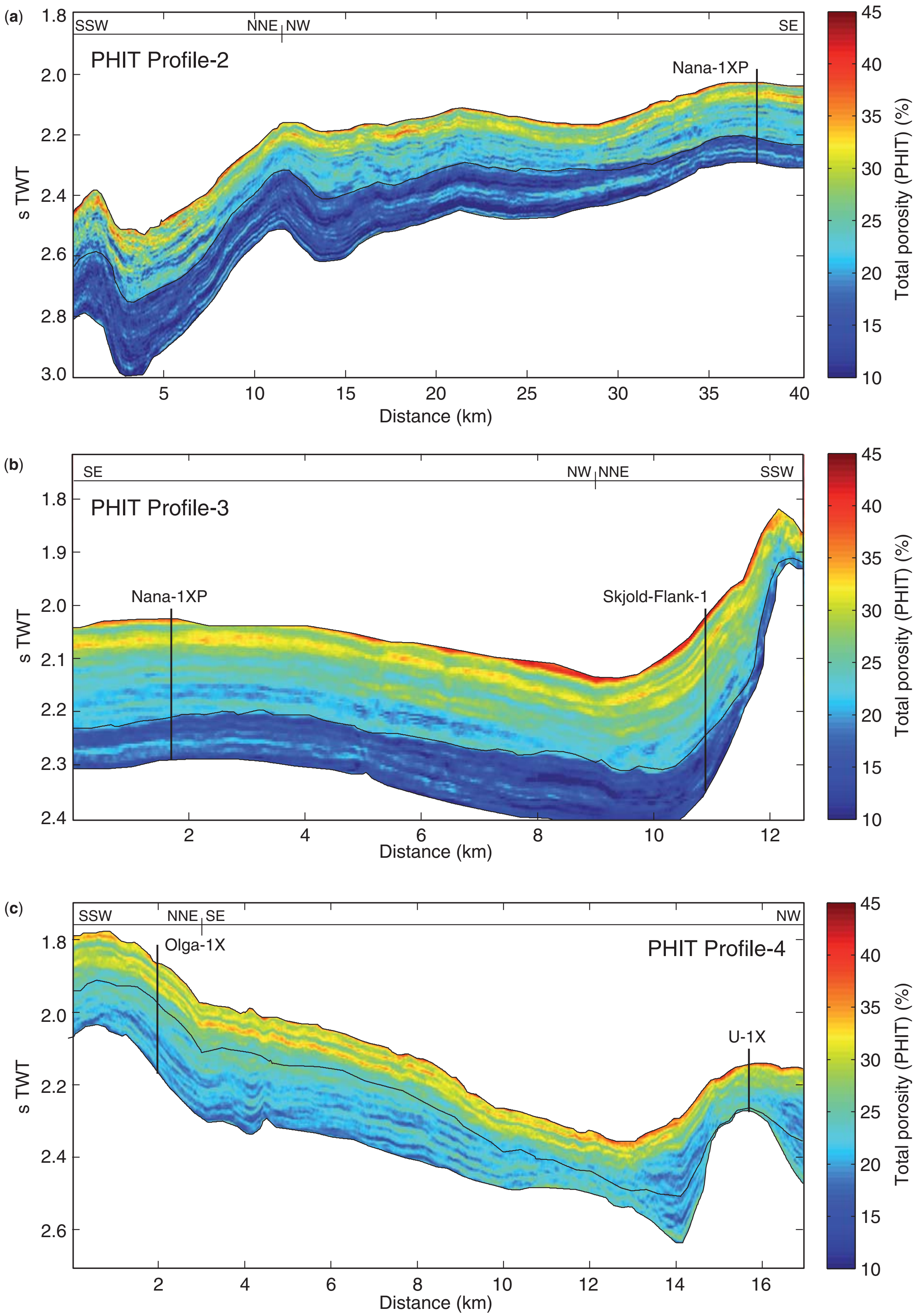

Fig. 13. Selected total porosity (PHIT) 2D sections discussed in the text: (**a**) profile 2; (**b**) profile 3; (**c**) profile 4.

along the profile. In some parts, the PHIT values are as high as 30–40%, mainly concentrated in the Dagmar rim-syncline. Similar high values are found in a zone in the central part of the profile (at distance 20 km) and close to the Nana-1XP well. The deeper part of the Tor Formation is characterized by alternating high- and low-porosity layers in the rim syncline of the Dagmar high. The thin, high-porosity layers have PHIT values in the range of 30–40% and are found in a deeper time window between 2.5 and 2.8 s TWT. In general, the Hod Formation is rather tight, with PHIT values of less than 20%. However, the impedance-derived porosity indicates the existence of a thin layer with a total porosity of approximately 25% extending from the Nana-1XP well and further to the NW. This may partly be an artefact, since this layer ties to the section immediately below the intra-Hod unconformity and is characterized by argillaceous chalk that gives rise to a slight overestimation of the effective porosity.

Key profile 3. Profile 3 is a 12 km long composite cross-section extending from the Nana-1XP well in the Haldan Field area to the Skjold Flank-1 well that was drilled on the flank of the Skjold diapir (Figs 2 & 13b). The 2D low-frequency model was constructed using the calibrated impedance logs from the Nana-1XP and Skjold Flank-1 wells and three interpreted horizons (top Chalk, near top Hod and the base Chalk). The least squares wavelet estimated in the Nana-1XP well was used for the inversion.

A continuous high-porosity (PHIT $>$ 30%) layer is observed in the upper part of the Tor Formation along the entire profile. The lower part of the Tor Formation is characterized by lower porosity (generally PHIT $<$ 25%), apart from a region in the central part of the profile north of the Skjold Field, where PHIT values are as high as 30–32%. The pre-Tor interval is tight with a total porosity below 20%.

Key profile 4. Profile 4 is a 16 km long cross-section extending from the Olga-1X well on the SE flank of the Kraka structure to the U-1X well on the Gorm-Lola Ridge (Figs 2 & 13c). The 2D low-frequency model was constructed using the calibrated impedance logs from the Olga-1X and U-1X wells and three interpreted horizons (top Chalk, near-top Hod and the base Chalk). For this profile, a least squares wavelet estimated in the Olga-1X well was used for the inversion. The profile covers the basin south of the Kraka Field, where the Chalk Group is as thick as 400 ms (Fig. 3). Two separate high-porosity layers with a total porosity in the range of 32–37% are found in the upper part of the chalk section along the entire length of the profile and are independent of the present day burial depth.

Fine-scaled impedance variations are observed in the pre-Tor section. Here, the maximum total porosity appears slightly higher (20–25%) compared with the other key profiles. This difference is caused by inverting with the Olga-1X wavelet compared with the other profiles where Nana-1XP was used. The Olga-1X well log has lower AI values in the Hod Formation than Nana-1XP.

Discussion and conclusion

A multi-disciplinary approach consisting of detailed 3D seismic mapping, well log correlation, petrophysical log analysis and seismic inversion enables a consistent division and mapping of individual depositional units within the Chalk Group. The 2D seismic inversion data allow estimation of the distribution of porosity variations in each unit and are used to distinguish between areas with potential untargeted reservoirs and areas acting as baffles to flow.

An AI-PHIT relationship is established for the entire Chalk Group in the study area and 2D AI profiles are converted to total porosity. The 2D profiles from the seismic inversion (Figs 12 & 13) clearly illustrate highly porous units in the uppermost Ekofisk Formation and the uppermost Tor Formation. The porosity bodies in the upper Tor appear as continuous layers and are found throughout the entire study area, including both structural highs and basinal settings. The study also demonstrates the existence of high-porosity layers at deeper levels in the Maastrichtian Tor Formation, where discrete high-porosity layers onlap the near-top Hod unconformity. Below the unconformity, the Hod Formation appears as a generally tight unit with porosity $<$20%.

Significant tectonic inversion transformed former basin areas into morphological highs. Isochore maps of the various chalk units (Fig. 6) illustrate the basin development in the study area. The Chalk Group is thickest in the western basin between the Dagmar and Gorm Fields; the latter are located at the northern end of a NNW–SSE striking ridge with a reduced thickness. The isochore maps for the Hod Formation (Fig. 6a) and the Tor Formation (Fig. 6c) indicate a change in the tectonic regime and the location of depocentres. In fact, the formations are an inverse of each other like a mould and a cast: the Hod Formation is thick where Tor Formation is thin and vice versa. The deposition of the Hod Formation is assumed to take place in a basinal setting with relatively high clay content.

The Maastrichtian Tor Formation is divided into an upper and lower unit separated by an intra-Tor seismic marker. The lower Tor Formation is found in local basins associated with syn-depositional uplift and the generation of rim synclines. The syn-depositional uplift and the associated development of a pronounced high relief morphology triggered slope instability that resulted in intra-Chalk sediment mass-movement. Alternating high and low AI layers that onlap the near–top Hod unconformity have a total porosity of between 20–25 and 29–32% and thus demonstrate the presence of high-porosity units in the deeper part of the Maastrichtian interval (Fig. 12c). The porosity distribution in the lower Tor Formation determined from the inversion is most likely related to the reworked chalk units as identified in the section. A highly discontinuous reflection pattern in the lower Tor Formation may be interpreted to be related to strong bottom currents that lead to the development of intra-Chalk channels, drifts and mounds (e.g. Lykke-Andersen & Surlyk 2004; Esmerode *et al.* 2008; Surlyk *et al.* 2008). An alternative explanation for the formation of many of the significant deep intra-Chalk seismic and stratal discontinuities is suggested by interpreting these as being caused by gravity-driven erosion and sedimentary processes that developed in response to the intense syn-depositional tectonics.

The uppermost part of the Tor Formation is the main reservoir in the Dan, Halfdan and Gorm Fields. It is a pelagic chalk that exhibits a characteristic cyclic pattern of high and low porosity over a 1–3 m scale that is regionally correlatable (Scholle *et al.* 1998). In the high-porosity intervals, the porosity may reach 35–37% and on a reservoir scale the average porosity is 25–30%.

The excess porosity in the uppermost part of the Chalk Group is mostly caused by porosity preserving effects related to overpressure (6–10 MPa in the study area), which reduces the effective stress (Brasher & Vagle 1996; Japsen *et al.* 2005). However, porosity above 40% is locally recorded in wells with high hydrocarbon saturations, illustrating that the presence of oil and gas also influences porosity preservation by impeding chemical compaction. The drop in porosity in the Hod Formation shows that the effectiveness of overpressure in preserving high porosity appears to decrease with depth.

The inverted AI data and derived total porosity values along selected 2D key profiles show good agreement with the values observed in wells. The uppermost part of the Tor Formation has the highest porosity ($>$28%). In some parts, PHIT values are as high as 30–40%. In the rim syncline of the Dagmar salt diapir, the lower part of the Tor Formation is characterized by alternating high- and low-porosity layers. The thin, high-porosity layers have PHIT values of 30–40% in a time window between 2.5 and 2.8 s TWT.

The inversion-based maximum porosity is predicted to be higher than expected based on the porosity/depth trends from well data only. This indicates that the spatial porosity variation of the chalk is complex and is controlled by more than burial depth. The inversion results show that porous chalk is not restricted to shallow features only, but reservoir-grade chalk of the Tor Formation is regionally widespread and may be found at exceptional depths.

We would like to thank J. A. Cartwright for the very constructive review of the paper. Jette Halskov (GEUS) is acknowledged for preparing the figures, and John Hopper (GEUS) is thanked for critical reading of the first draft.

References

Albrechtsen, T., Andersen, S. J., Dons, T., Engstrøm, F., Jørgensen, O. & Sørensen, F. W. 2001. Halfdan: developing non-structurally trapped oil in North Sea Chalk. Paper SPE 71322.

Anderson, J. K. 1999. The capabilities and challenges of the seismic method in chalk exploration. *In*: Fleet, A. J. & Boldy, S. A. R. (eds) *Petroleum Geology of Northwest Europe: Proceedings of the 5th Conference*. Geological Society, London, 939–947; doi: 10.1144/0050939.

Brasher, J. E. & Vagle, K. R. 1996. Influence of lithofacies and diagenesis on Norwegian North Sea Chalk reservoirs. *AAPG Bulletin*, **80**, 746–769.

Britze, P., Japsen, P. & Andersen, C. 1995. Geological map of Denmark, 1:200 000. The Danish Central Graben. 'Top Chalk' and the Post Chalk Group (two-way travel time, depth and interval velocity). *Danmarks Geologiske Undersøgelse Kortserie* **47**, 7, 3 maps.

Burnett, J. A. with contributions from Gallagher, L. T. & Hampton, M. J. 1998. Upper Cretaceous. *In*: Bown, P. R. (ed.) *Calcareous Nannofossil Biostratigraphy*. British Micropalaeontological Society Series. Chapman & Hall/Kluwer Academic, London, 132–199.

Cartwright, J. A. 1989. The kinematics of inversion in the Danish Central Graben. *In*: Cooper, M. A. & Williams, G. D. (eds) *Inversion Tectonics*. Geological Society, London, Special Publications, **44**, 153–175.

Danish Energy Agency (DEA) 2008. *Oil and Gas Production in Denmark, 2007.*

Esmerode, E. V., Lykke-Andersen, H. & Surlyk, F. 2008. Interaction between bottom currents and slope failure in the Late Cretaceous of the southern Danish Central Graben, North Sea. *Journal of the Geological Society, London*, **165**, 55–72.

Evans, D. J., Hopson, P. M., Kirky, G. A. & Bristow, C. R. 2003. The development and seismic expression of syn-sedimentary features within the Chalk of southern England. *Journal of the Geological Society, London*, **160**, 797–813.

Håkansson, E., Bromley, E. G. & Perch-Nielsen, K. 1974. Maastrichtian chalk from North West Europe – a pelagic shelf sediment. *Special Publication, International Association of Sedimentologists*, **1**, 211–233.

Hancock, J. M. 1975. The petrology of the chalk. *Proceedings of the Geologists' Association*, **86**, 499–535.

Hatton, I. R. 1986. Geometry of allochthonous Chalk Group members, Central Trough, North Sea. *Marine Petroleum Geology*, **3**, 79–98.

Jacobsen, F. L., Engstrøm, F., Uldall, A. & Petersen, N. W. 1999. Delineation of hydrodynamic/geodynamic trapped oil in low permeability Chalk. Paper SPE 56514.

Japsen, P., Mavko, G. ET AL. 2005. Chalk background velocity: influence of effective stress and texture. *EAGE 67th Conference and Exhibition, Madrid, Spain, 13–16 June 2005.*

Kennedy, W. J. 1987. Sedimentology of Late Cretaceous/Paleocene chalk reservoirs, North Sea Central Graben. *In*: Brooks, J. & Glennie, K. (eds) *Petroleum Geology of North West Europe*. Graham & Trotman, London, 469–481.

Klinkby, L., Kristensen, L., Nielsen, E. B., Zinck-Jørgensen, K. & Stemmerik, L. 2005. Mapping and characterisation of thin chalk reservoirs using data integration: the Kraka Field, Danish North Sea. *Petroleum Geoscience*, **11**, 113–124.

Kristensen, L., Dons, T., Maver, K. G. & Schiøler, P. 1995. A multidisciplinary approach to reservoir subdivision of the Maastrichtian Chalk in the Dan Field, Danish North Sea. *AAPG Bulletin*, **79**, 1650–1660.

Lykke-Andersen, H. & Surlyk, F. 2004. The Cretaceous–Palaeogene boundary at Stevns Klint, Denmark: inversion tectonics or seafloor topography? *Journal of the Geological Society, London*, **161**, 343–352.

Mackertich, D. S. & Goulding, D. R. G. 1999. Exploration and appraisal of the South Arne Field, Danish North Sea. *In*: Fleet, A. J. & Boldy, S. A. R. (eds) *Petroleum Geology of Northwest Europe: Proceedings of the 5th Conference*. Geological Society, London, 959–974; doi: 10.1144/0050959.

Maver, K. G. & Rasmussen, K. B. 1995. Seismic inversion for reservoir delineation and description. Paper SPE 29798.

Megson, J. & Tygesen, T. 2005. The North Sea Chalk: an underexplored and underdeveloped play. *In*: Doré, A. G. & Vining, B. A. (eds) *Petroleum Geology: North-West Europe and Global Perspectives. Proceedings of the 6th Petroleum Geology Conference*, Geological Society, London, 159–168; doi: 10.1144/0060159.

Nygaard, E., Lieberkind, K. & Frykman, P. 1983. Sedimentology and reservoir parameters of the Chalk Group in the Danish Central Graben. *Geologie en Mijnbouw*, **62**, 177–190.

Rasmussen, K. B. & Maver, K. G. 1996. Direct inversion for porosity of post stack seismic data. Paper SPE 35509.

Scholle, P. A. 1977. Chalk diagenesis and its relation to petroleum exploration: oil from chalk, a modern miracle? *AAPG Bulletin*, **61**, 982–1009.

Scholle, P. A., Albrechtsen, T. & Tirsgaard, H. 1998. Formation and diagenesis of bedding cycles in uppermost Cretaceous chalk of the Dan Field, Danish North Sea. *Sedimentology*, **45**, 223–245.

Surlyk, F., Dons, T., Clausen, C. K. & Higham, J. 2003. Upper Cretaceous. *In*: Evans, D., Graham, C., Armour, A. & Bathurst, P. (eds) *Millennium Atlas: Petroleum Geology of the Central and Northern North Sea*. Geological Society, London, 213–233.

Surlyk, F., Jensen, S. K. & Engkilde, M. 2008. Deep channels in the Cenomanian–Danian Chalk Group of the German North Sea sector: evidence of strong constructional and erosional bottom currents and effect on reservoir quality distribution. *AAPG Bulletin*, **92**, 1565–1586.

Vejbæk, O. V. & Andersen, C. 2002. Post mid-Cretaceous inversion tectonics in the Danish Central Graben – regionally synchronous tectonic events? *Bulletin of the Geological Society of Denmark*, **49**, 129–144.

Seismic imaging of variable water layer sound speed in Rockall Trough, NE Atlantic and implications for seismic surveying in deep water

S. M. JONES,[1,2] C. SUTTON,[2] R. J. J. HARDY[2] and D. HARDY[2]

[1]*Present Address: University of Birmingham, School of Geography, Earth and Environmental Sciences, Edgbaston, Birmingham B15 2TT, UK (e-mail: s.jones.4@bham.ac.uk)*
[2]*Trinity College Dublin, School of Natural Sciences, Department of Geology, Dublin 2, Ireland*

Abstract: Natural variation in sound speed within ocean water can degrade sub-seabed images from 2D, 3D and 4D seismic reflection datasets. Degrading effects include vertical offset of reflections between adjacent or intersecting sail lines and difficulties in suppressing multiples from water layer reverberations. Here we investigate water layer variability in Rockall Trough, offshore Ireland, in water depths ranging from 200 m to 3.5 km. A compilation of vertical sound speed profiles, calculated from temperature and salinity profiles obtained by probes lowered from ships, shows that the mean sound speed in the water layer mostly varies between 1490 and 1500 m s^{-1}. Vertical offsets of up to about 15 ms two-way travel time are predicted at seismic line intersections. A significant amount of the total observed sound speed variability can occur along a single seismic sail line. These effects result mainly from spatial and temporal fluctuations in the thicknesses of, and vertical sound speed gradients within, an upper layer of North Atlantic Central Water and a mid-depth layer of Mediterranean Outflow Water. Seismic sections across Rockall Trough commonly show lateral variability in reflectivity within these same two water layers. Some reflective packages contain lens-shaped structures consisting of reflective rims and transparent cores and with diameters between 10 and 50 km. Other reflective packages have abrupt, almost vertical boundaries and no distinct transparent core. We infer that the lateral boundaries of the reflective packages are likely to be associated with significant variations in average water layer sound speed. When processing 2D, 3D and 4D seismic surveys of regions of high oceanic variability, such as Rockall Trough, it is necessary to employ techniques that can solve for and then remove the effect of significant fluctuations in water layer sound speed over time periods as short as a few hours and distances as short as a kilometre.

Keywords: seismic reflection imaging, seismic oceanography, seismic data processing, oceanic circulation, mixing, Rockall Trough

Variation in sound speed within ocean water can cause problems in sub-seabed seismic reflection imaging (Wombell 1997; Barley 1999; Bertrand & Macbeth 2003; Mackay *et al.* 2003; Xu & Pham 2003; Lacombe *et al.* 2006, 2009). Water layer sound speed variations arise from natural variations in temperature and salinity associated with oceanic currents. In 2D and 3D seismic surveying, water layer sound speed variations cause travel time offsets and amplitude variations between adjacent and intersecting sail lines. Water layer variability also complicates the suppression of multiples from water layer reverberations (Jakubowicz 2006; Hatchell *et al.* 2008; Hardy & Jones 2009). Four-dimensional seismic surveying compounds these problems (Bertrand & Macbeth 2003; Lacombe *et al.* 2009). Other risks related to oceanic variability affect prospect evaluation and production (Vogel & Symonds 2002). Riser design must account for shear from the water currents that are associated with sound speed variability. Water temperature variability over time affects oil viscosity within the riser. All of these risks are expected to increase as hydrocarbon exploration steps out into deeper water, partly because a thicker water layer accentuates mistakes in assigning water layer sound speeds during processing, and also because oceanic mixing, and consequent high sound speed variability, is often concentrated at steep seabed slopes along continental edges (Barley 1999; Egbert & Ray 2001).

Several important questions arise when planning acquisition and processing of seismic reflection datasets for hydrocarbon exploration or field management. How might water layer sound speed vary during acquisition of a single sail line? How might sound speed vary between acquisitions of adjacent or crossing sail lines? How might sound speed vary between repeated 3D survey acquisitions in a 4D programme? What acquisition and processing strategies are required to cope with the expected water layer variability, in order to minimize subsurface image degradation and hence reduce risk in exploration or production?

The recent realization that oceanic sound speed variations can be directly imaged using standard seismic reflection data and processing techniques provides a new method to investigate these questions (Holbrook *et al.* 2003; Jones *et al.* 2008). The deepwater basins offshore west of the UK and Ireland are good locations to study the effect of water layer variability in water depths between 200 m and 3.5 km (Fig. 1). Sound speed variation within the water column can be imaged directly using seismic reflection data (Figs 2–4). Long seismic profiles show considerable variation in water column sound speed structure from place to place within Rockall Trough (Fig. 2). Lines adjacent to the Rockall Trough margin suggest that sound speed structure is influenced by interaction between oceanic currents with the steep seabed topography (Fig. 3). Short overlapping sections of 2D lines, collected following air-gun failure and repair, show that the water layer sound structure can vary significantly over only a few hours (Fig. 4).

In this paper, we first examine legacy oceanographic observations in order to illustrate the cause of the sound speed fluctuations, and to define the scale of the problem facing sub-seabed seismic imaging. We then interpret the seismic images in order to

VINING, B. A. & PICKERING, S. C. (eds) *Petroleum Geology: From Mature Basins to New Frontiers – Proceedings of the 7th Petroleum Geology Conference*, 549–558. DOI: 10.1144/0070549

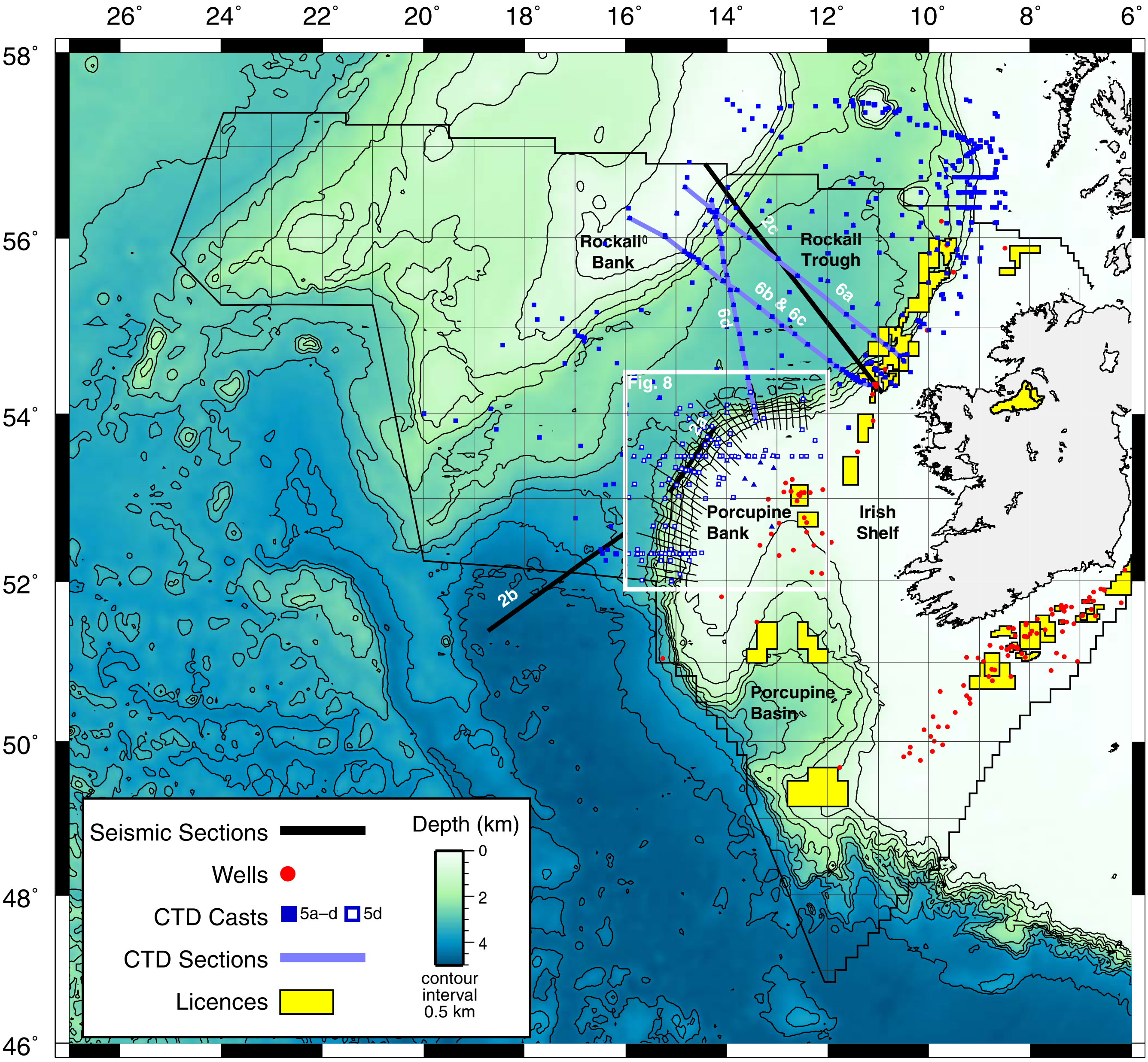

Fig. 1. Location of Rockall Trough in the North Atlantic, and locations of oceanographic and seismic data discussed in the text.

begin to address some of the questions raised above. Finally, we discuss the implications for the planning, acquisition and processing of seismic surveys in deep water regions.

Oceanic variability from legacy oceanographic data

The North Atlantic is an important hub in the global oceanic thermohaline circulation. Irish offshore territory is situated just south of the sea between Norway and Greenland where warm surface water arrives from the south, sinks to form cold deep water and returns southward along the Atlantic seabed (Sherwin & Turrell 2005). In Rockall Trough, this oceanic stratification is easily visible in vertical temperature and salinity profiles obtained by lowering conductivity–temperature–depth (CTD) probes from research vessels, and in sound speed profiles calculated from these (Fig. 5). Four water layers can be distinguished and each layer has a distinctive pattern of sound speed variability (New & Smythe-Wright 2001). In the surface layer, down to a depth of about 100 m, sound speed varies by >20 m s^{-1} and can either increase or decrease with depth. The next layer down, termed North Atlantic Central Water by oceanographers, has increasing sound speed with depth. In the third layer, composed of a mixture of Mediterranean Outflow Water and Labrador Sea Water, sound speed decreases with depth. The deepest layer, cold North Atlantic Deep Water, has increasing sound speed with depth.

Several different modes of variability can be seen in this compilation of oceanographic data (Fig. 5). At a given depth, sound speed can vary by more than 20 m s^{-1} in layer 1 and by 10 m s^{-1} in layers 2 and 3. The vertical sound speed gradient across the layer can vary significantly in layers 1–3 and can even change sign in layer 1. These variations in sound speed magnitude and gradient mean that the depth to the boundary between layers 2 and 3 can vary by more than a kilometre. Smaller scale variability with a vertical wavelength of 100 to <10 m often occurs within layers 2 and 3. This type of variation, termed fine structure by oceanographers, is important because its wavelength is similar to the seismic wavelength. Fine structure is responsible for the reflective packages observed within the water layer of seismic sections (Figs 2–4). The amplitude and vertical wavelength of fine structure in layers 2 and 3 is very variable. The sound speed compilation in

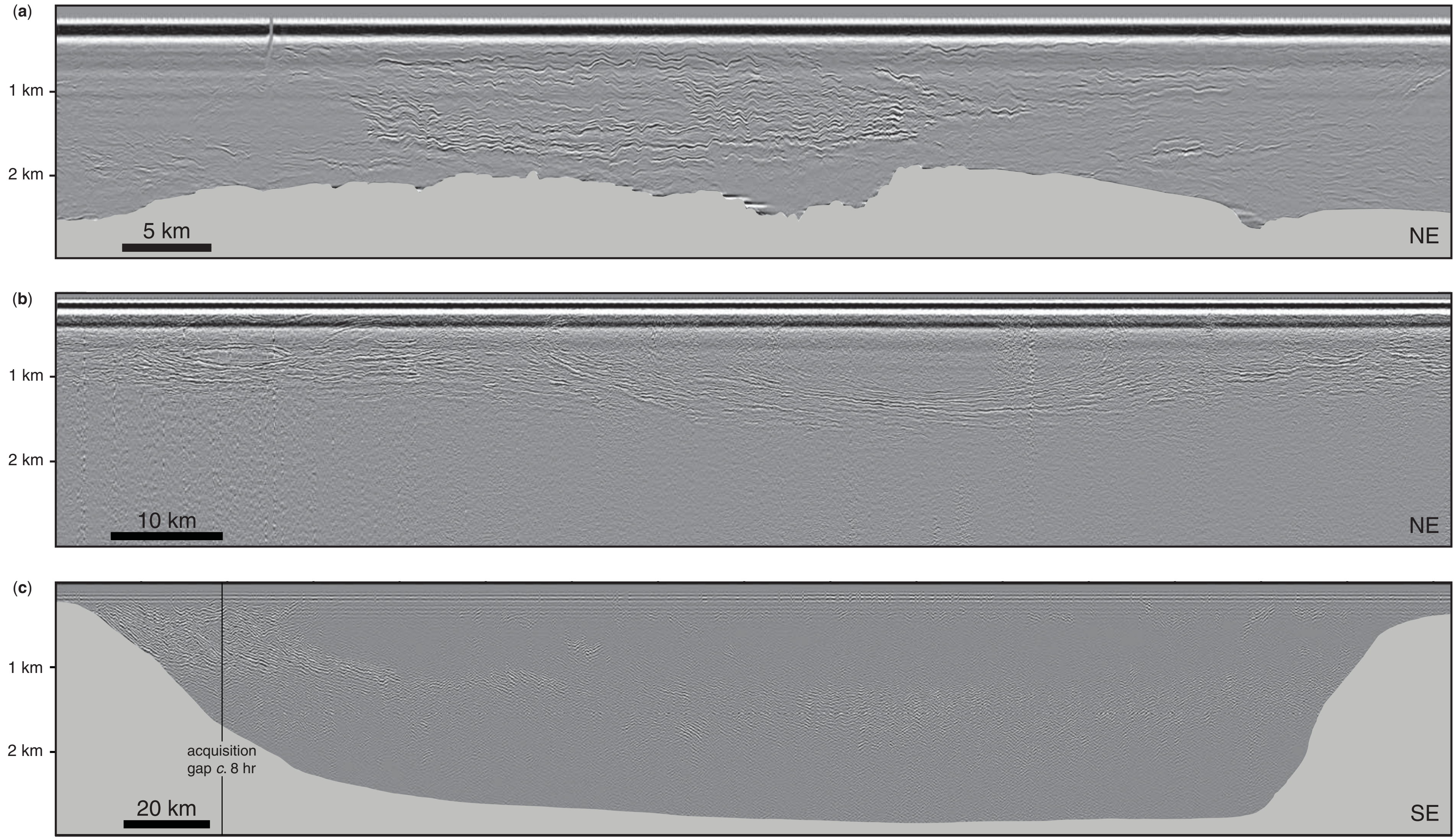

Fig. 2. Regional seismic profiles showing water layer reflectivity: (**a**) ISROCK-96-09; (**b**) PAD-95-11; (**c**) WESTLINE. Line locations marked on Figure 1. Processing sequence given in Jones *et al.* (2008), where a typical shot gather is illustrated. Normal move-out (NMO) correction was done at a constant velocity of 1500 m s^{-1} to produce the stacked sections in Figures 2–4. Move-out on water layer reflections contains both a normal hyperbolic component and a component related to water motion, so applying standard velocity analysis does not necessarily provide a physically meaningful velocity field (Jones *et al.* 2008). There is no difference in gross reflectivity structure, which is the main focus of this paper, between sections stacked after constant-velocity NMO and variable-velocity NMO, although the curvature of individual reflections on scales of a few hundred metres can vary. Figures 2–4 have not been migrated because of these difficulties arising from water motion.

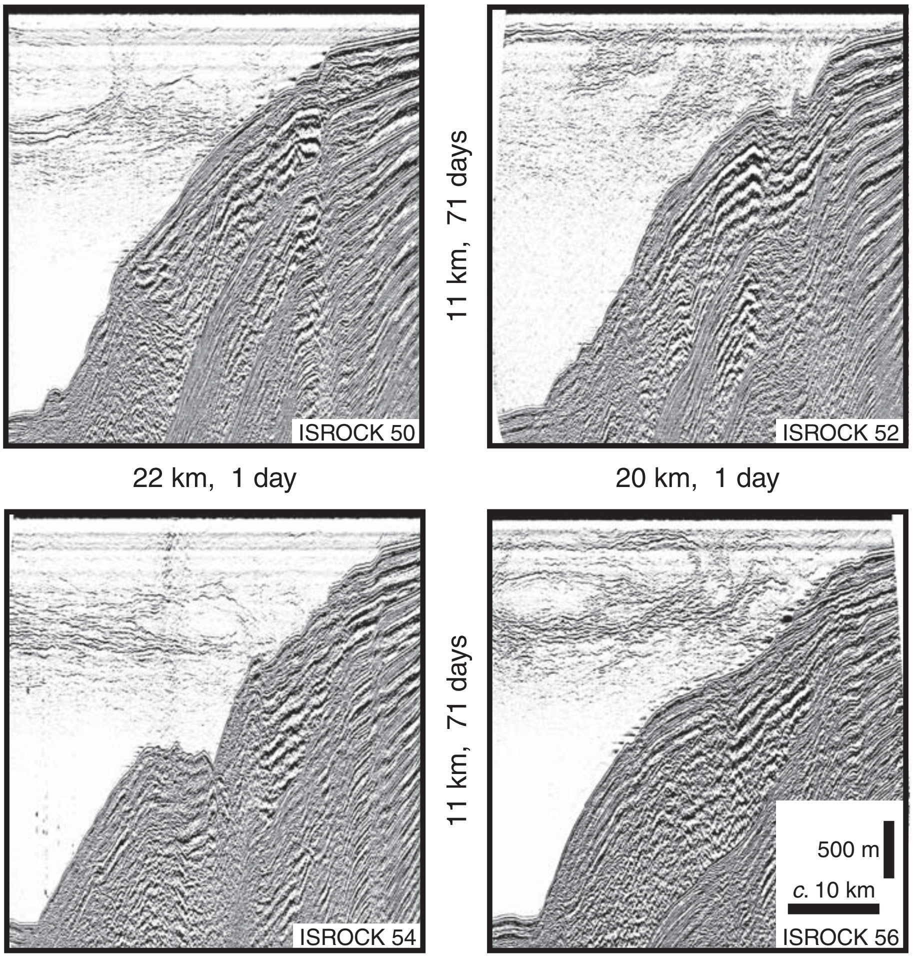

Fig. 3. Four adjacent lines perpendicular to the seabed slope on the western margin of Porcupine Bank (line locations on Fig. 8). Lines 50 and 54 were shot 22 km apart on consecutive days in late June 1996; lines 52 and 56 were shot 20 km apart on consecutive days in early September, 71 days later. The scale on bottom right panel applies to all panels; the vertical scale applies to the water layer only. See caption to Figure 1 for processing sequence.

Figure 5c covers the whole of Rockall Trough but significant variability can still occur within limited geographical regions (Fig. 5d).

Several water layer sound speed sections across Rockall Trough are plotted in Figure 6. Each sound speed section is reconstructed from a series of CTD probe casts along a straight transect obtained over a period of several days, similar to the time periods taken to acquire the regional seismic sections in Figure 2. An important observation is that layers 2 and 3 are each composed of strings of lens-shaped features. The lateral positions and the differences in sound speed from edge to centre of each lens vary from section to section. Annual variation along a single transect is demonstrated by comparing the November 1996 and 1997 sections. Seasonal variation between nearby transects is demonstrated by comparing the May and November 1997 sections. Satellite monitoring of sea-surface height anomalies shows that the Rockall Trough is covered by a set of swells and depressions that have similar diameters to the sound speed lenses within the water column, and which change significantly on a time-scale of weeks. It is tempting to link these sea-surface height anomalies with the sound speed lenses observed on the sound speed sections, thereby indicating a time-scale of weeks for variation of the sound speed lenses, but the detailed work required to test this hypothesis has not yet been carried out.

The implications of all this variability for seismic imaging are summarized in Figure 7. The risk of vertical two-way travel time offsets is mainly controlled by uncertainty over the average sound speed of the water column. Mean water layer sound speed in Rockall Trough mostly varies between 1490 and 1500 m s^{-1} (Fig. 7a). Variability is greater in winter and less, though still significant, during the summer seismic acquisition season. Large uncertainty in mean sound speed occurs above 2 km and uncertainty decreases somewhat in deeper water (Fig. 7b). The decrease in uncertainty in the deepest water occurs because the strong sound speed variability in layers 2 and 3 is progressively offset by the uniform gradient of layer 4 (Fig. 5). The right-hand column of Figure 7 estimates the vertical offset in two-way travel time at the seabed that is expected to result if the water layer is assigned a constant sound speed. Vertical offsets of over 15 ms are expected when the water layer is assigned the modal mean sound speed of 1496.5 m s^{-1} (Fig. 7c, d). Worse choices for mean water layer sound speed will lead to larger offsets. Large offsets are more likely in deeper water if the modal value is chosen to represent the water layer sound speed.

Oceanic variability from seismic data

The sound speed cross-sections in Figure 6 suggest that a significant component of the total oceanic variability summarized in Figure 7 can occur on the space–time scale of a single seismic line. However, horizontal resolution of the sound speed sections is limited by the sparse cast spacing. The ability to image sound speed variability on seismic data itself offers the opportunity to resolve the true spatial and temporal scales over which variability occurs.

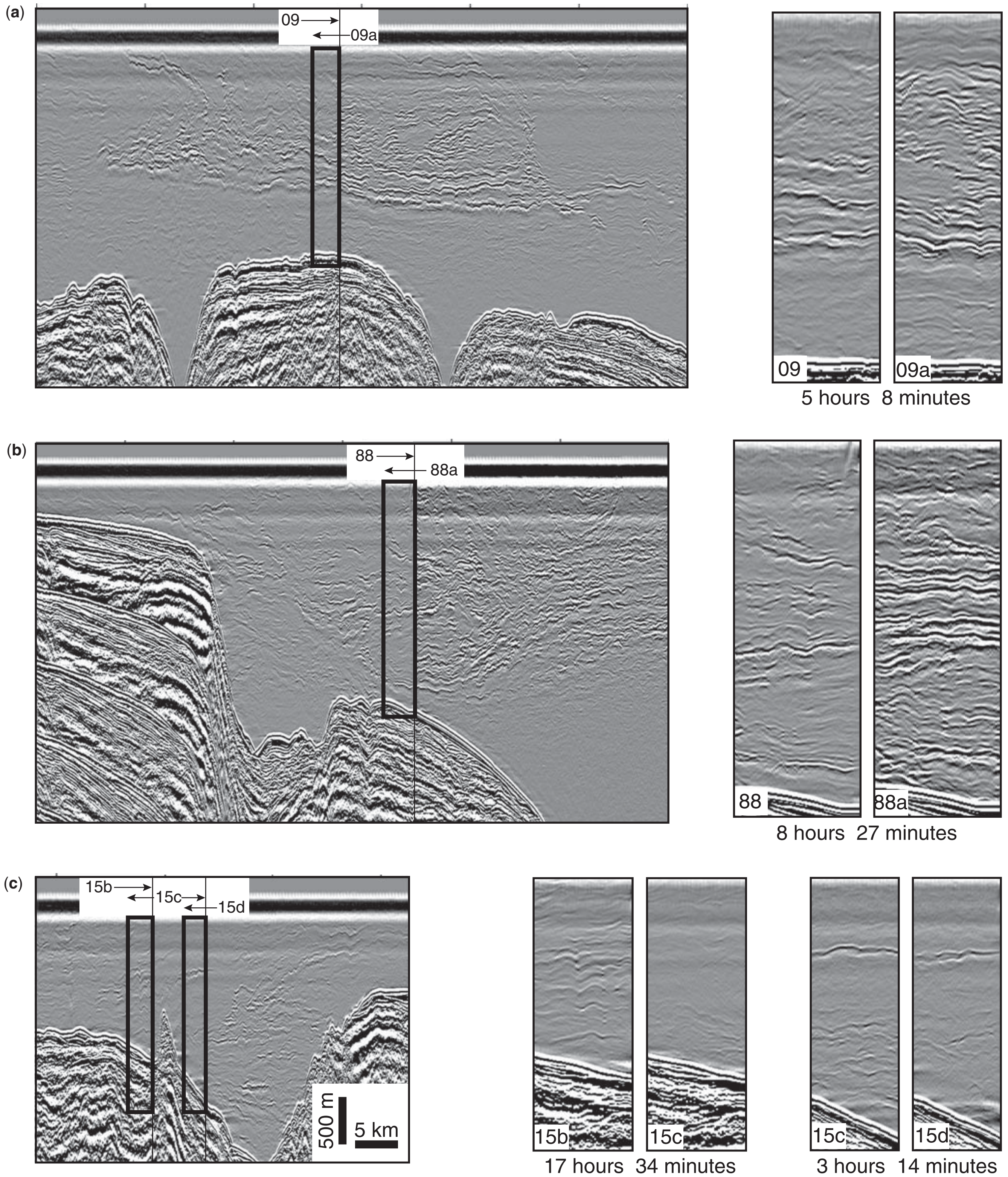

Fig. 4. Overlapping seismic sections to illustrate variability in water layer structure over a few hours: (**a**) ISROCK line 09; (**b**) line 88; (**c**) line 15. Line locations marked on Figure 8. Locations of overlapping sections are marked with bold boxes on the left-hand panels; re-started lines are named by adding a, b etc. to the line number. Both overlapping sections in each pair are expanded to the right and the separation in time is indicated beneath. The scale on left-hand panel (c) applies to all three left-hand panels; the vertical scale applies to the water layer only. See caption to Figure 1 for processing sequence.

Spatial variation

In Rockall Trough, oceanic sound speed structure commonly appears on seismic sections as a strongly reflective layer at depths above 1.5 km (Figs 2–4). Comparison with sound speed profiles from CTD probe data (Fig. 5) suggests that the seismic energy is reflected by the fine-structure (that is the variations with a vertical wavelength of 100 to <10 m, similar to the seismic wavelength) observed over the same depth range. We cannot test this idea directly in Rockall Trough since we do not have direct measurements of water layer sound speed coincident with the seismic sections. However, the relationship between

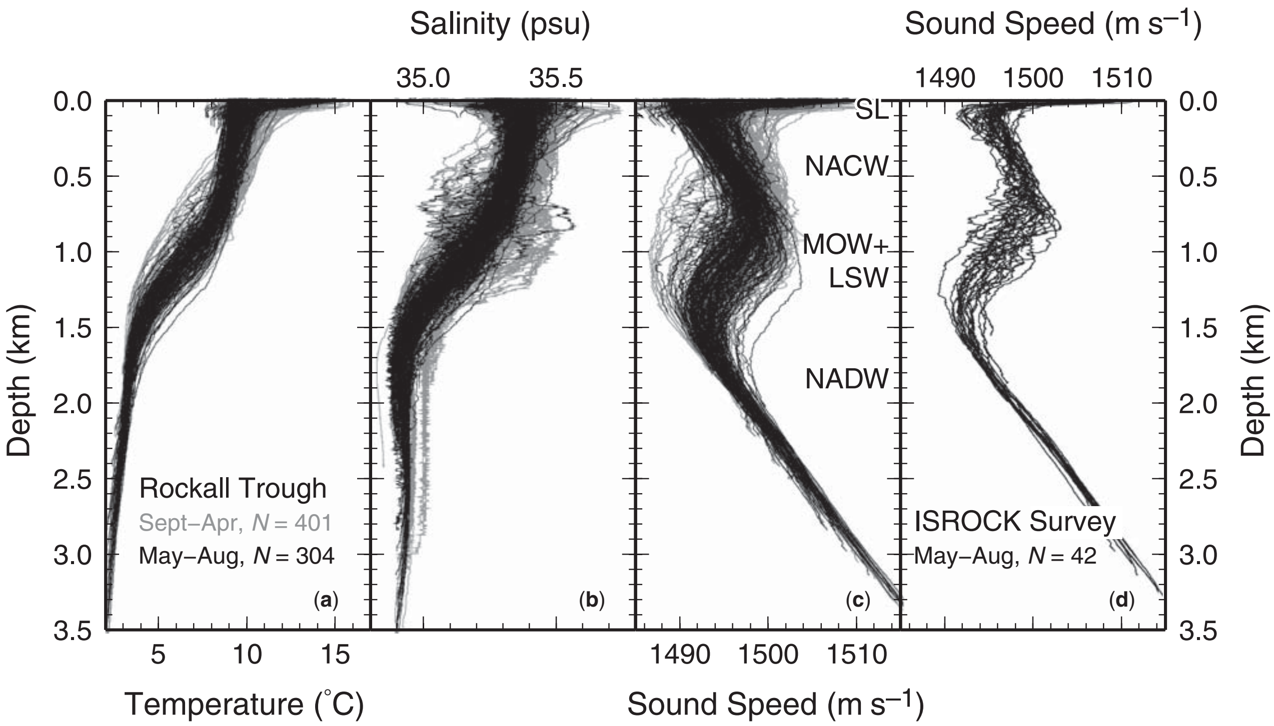

Fig. 5. Water layer stratigraphy in Rockall Trough. (**a**) Temperature, (**b**) salinity and (**c**) sound speed calculated from the temperatures and salinities using the 1980 Equation of State of Seawater (EOS-80; Fofonoff & Millard 1983). Profiles on panels (a–c) cover the entire area of Rockall Trough (all blue squares on Fig. 1). (**d**) Sound speed profiles in the region of the ISROCK seismic survey (white-filled blue squares on Fig. 1). Abbreviations: SL, surface layer; NACW, North Atlantic Central Water; MOW + LSW, Mediterranean Outflow Water and Labrador Sea Water; NADW, North Atlantic Deep Water.

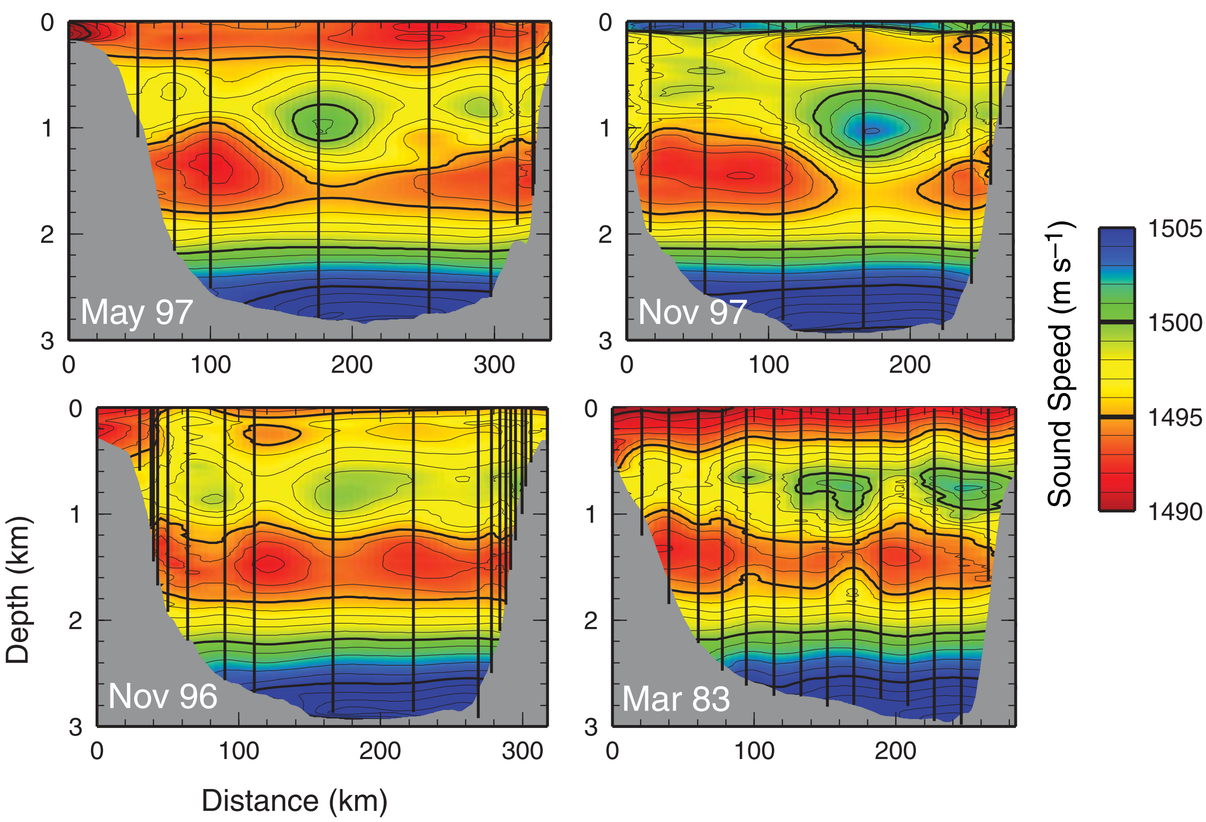

Fig. 6. Regional cross-sections of sound speed from CTD probe casts (locations on Fig. 1). The temperature and salinity profiles were converted to sound speed using the 1980 Equation of State of Seawater (EOS-80; Fofonoff & Millard 1983). Cast locations were projected onto straight lines; locations of measured profiles on each projected section are denoted by vertical black lines. Where unconstrained by data, the edges of each sound speed section were set to the average sound speed profile for Rockall Trough, obtained by averaging the dataset in Figure 5c. The sections were gridded using a using the minimum curvature scheme from the Generic Mapping Tools (GMT) with a mesh size of 5 km by 20 m. Finally, the seabed along each section was interpolated from the GEBCO database.

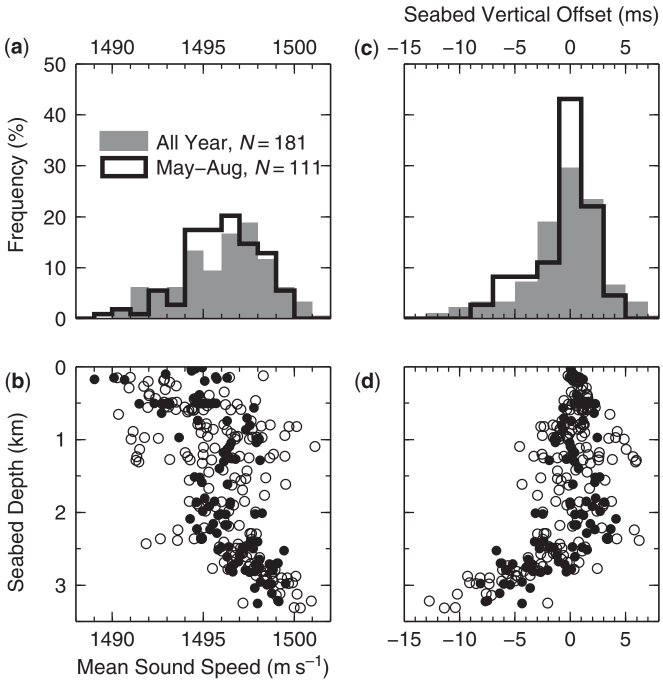

Fig. 7. Statistical variation in mean water layer sound speed and resulting vertical offset in two-way travel time at the seabed, calculated using the Rockall Trough sound speed profiles in Figure 5a–c.

individual seismic reflections and vertical sound speed gradients has been confirmed in joint seismic/oceanographic experiments offshore Norway and in the Gulf of Cadiz (Nandi *et al.* 2004; Biescas *et al.* 2008).

There is strong lateral variation in the reflection strength and internal structure of the reflective regions in Rockall Trough. Figure 2a shows an example of a discrete package of reflective water about 30 km wide and surrounded by seismically transparent water. This seismic section lies adjacent to the Porcupine Bank, parallel to the margin of Rockall Trough. The base of the reflective package is defined by a series of high-amplitude, fairly continuous reflections. The reflection strength is more variable within the upper part of the package. The southern boundary is defined by abrupt terminations of reflections over a horizontal distance of <1 km. The northern boundary is shaped more like the edge of a lens and covers a lateral distance of about 5 km. Another type of lateral variation is illustrated in Figure 2b, which crosses deep water where the Rockall Trough opens southward into the Atlantic oceanic basin. Undulations in the reflections define two lens-shaped features, the smaller with a diameter of 10 km and the larger with a diameter of 40 km. Each lens consists of a marginal zone of continuous high-amplitude reflections enclosing a seismically transparent interior. Such lenticular features are common within our Rockall Trough seismic database.

Seismic reflectivity is generated by vertical sound speed gradients on the scale of the seismic wavelength (<100 m; Ruddick *et al.* 2009), whereas the variability in water layer travel time summarized in Figure 7 is mainly controlled by the larger scale (100 m to 1 km) structure of the water layers. Do the packages of reflective and transparent water visible on seismic sections correspond to spatial changes in sound speed? It is hard to answer this question in the absence of oceanic probe measurements coincident with the seismic sections. However, two pieces of evidence suggest that packages of different reflectivity structure do have significantly different average sound speed. First, the reflective packages commonly have similar dimensions and occur at the same levels in the water column as the sound speed variations in Figure 6. Secondly, the lens-shaped reflective features resemble eddies recognized on a coincident seismic and oceanographic dataset in the Gulf of Cadiz (Biescas *et al.* 2008). Following this interpretation, the Rockall lenticular features might consist of a core of relatively warm, salty Mediterranean Outflow Water, probably mixed to some degree with Labrador Sea Water (New & Smythe-Wright 2001), and surrounded by fresher, cooler water. These variations in temperature and salinity are expected to be associated with sound speed variations. Furthermore, the sharp edges of some of the reflective packages imply that significant sound speed variations can occur over horizontal distances of a kilometre.

Temporal variation

Sea water is in constant motion, and all seismic reflection surveys contain information on how the water layer changes through time. Individual shots records effectively provide snapshots of oceanic reflectivity structure because the distances that water can move over the few seconds of the record are too small to be resolved by industry seismic data. Common Mid Point gathers typically contain traces collected over more than 15 min and it appears possible to detect movement in the reflectivity structure over such periods (Jones *et al.* 2008). Seismic sail lines take many hours or even a few days to acquire, during which time significant amounts of water motion can occur. In this section we provide a few examples of evidence for hourly to monthly variability in reflectivity structure that can be obtained from the typical 2D speculative survey ISROCK, acquired over the western margin of Porcupine Bank, adjacent to Rockall Trough, in 1996 (Fig. 8).

Short-term (hourly) variability. Changes in the water layer over a few hours to a day can be demonstrated by comparing overlapping line segments. There are 22 overlapping sections in the ISROCK survey and four are shown in Figure 4. In each case acquisition was suspended following an air-gun fault, repairs were made (always well within a day), and the line was resumed with an overlapping segment in order to build up a full fold of coverage. Figure 4a shows an overlapping pair that image the package of highly reflective water in Figure 2a. Although, the bottom of the reflective package remained at roughly the same

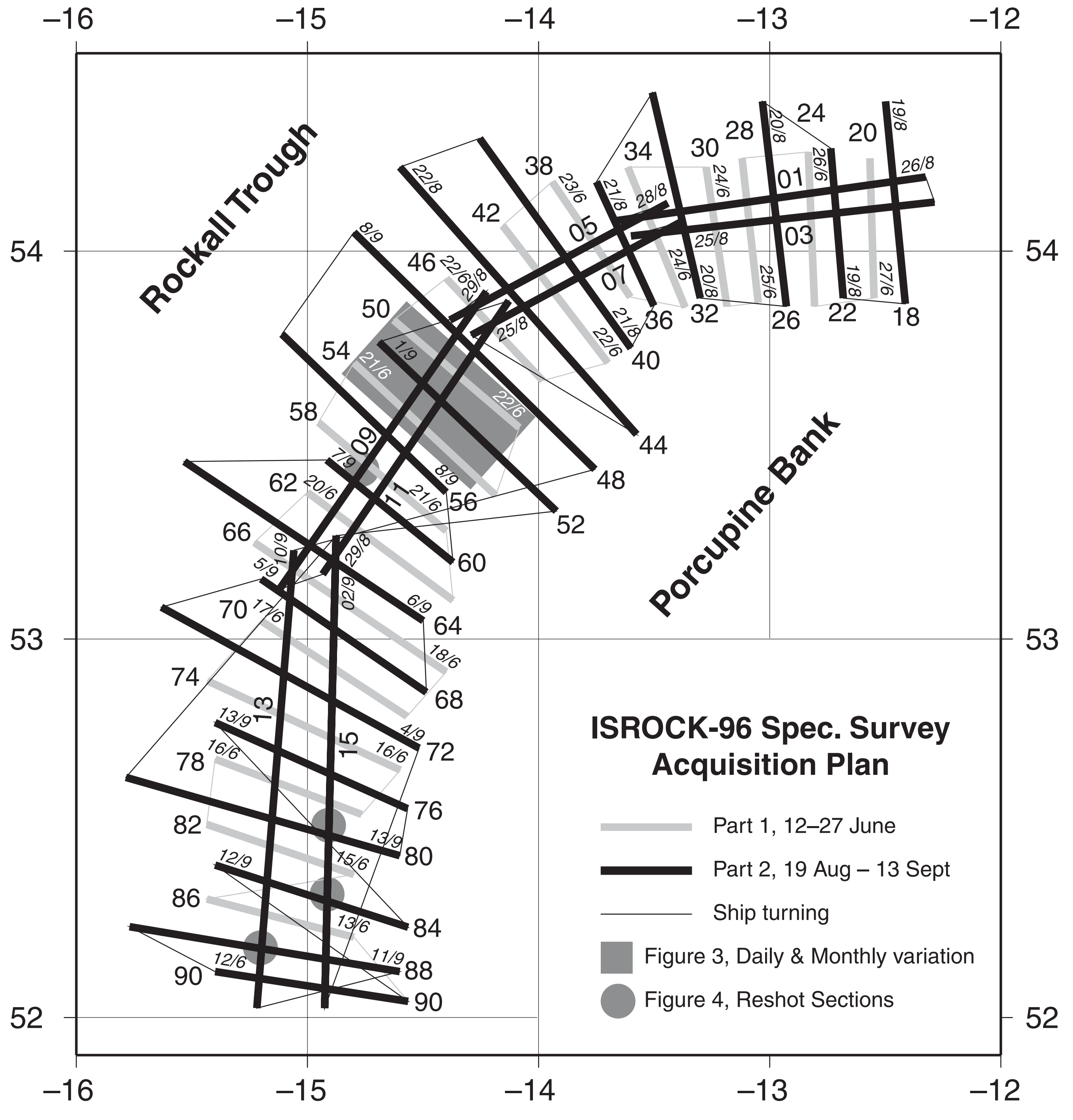

Fig. 8. Acquisition plan for the ISROCK-96 seismic survey. Roman numbers next to each line are line numbers and italicized numbers show day and month of acquisition.

depth, the internal reflectivity structure near the base of the package changed somewhat and the internal structure near the top of the package altered significantly over a period of just over 5 h. Figure 4c shows two pairs of overlapping sections: in the first (15b/c) the water changes from moderately reflective to almost transparent over a period of 17.5 h; in the second (15c/d) a single prominent reflection is visible in the middle of the water column for more than 3 h.

These examples clearly show that the reflectivity structure of the water column overlying a particular point on the seabed can either remain similar or change radically over a period of a few hours. From the industrial point of view, it would be useful to know the changes in average sound speed that accompany these changes in reflectivity structure. The arguments in the previous sections suggest that changes in the order of several metres per second might occur. This question might be answered in future by careful velocity analysis of the water layer. From the point of view of oceanographic research, this observation method gives the rate of change of reflectivity in a reference frame fixed to the seabed; that is, the Eulerian derivative of the reflectivity structure. It would be interesting to separate the effects of fluid motion over the observation point and change within a particular parcel of water; that is, to measure both components of the Lagrangian derivative. This question cannot be easily answered using overlapping sections of 2D seismic data, although it could be addressed in future using 3D data.

Longer term (daily to monthly) variability. ISROCK consists of 45 lines, with 68 ties between two lines and six ties between three lines. The line ties range in time gap from several days to several months (Fig. 8). This survey was shot in two halves, with a set of lines at about 20 km spacing shot in late June (coloured grey in Fig. 8) and an interleaving set shot in late August to early September (coloured black). Figure 3 exploits this acquisition pattern to illustrate water layer variability. Lines 50 and 54 (shot 1 day and 20 km apart) both show a reflective package at moderate depth that impinges on the continental slope and relatively transparent shallow water. Lines 52 and 56 show the same area more than 2 months later, when reflectivity at shallower levels is observed. There are distinct changes in water structure over months to years, and these are the variations that cause difficulty in 4D seismic surveying.

Implications for seismic surveying

When planning a seismic survey in deep water, we have shown above that freely available legacy oceanographic data can be used to assess the likely extent of oceanic variability. Legacy seismic data can also be used to estimate how rapidly and by how much the water layer sound speed is likely to vary at a given location. Significant variability in water layer sound speed is to be expected in areas where water masses that differ in temperature and salinity come into contact and also near to steep seabed topography (Egbert & Ray 2001; Biescas *et al.* 2008).

When processing 2D, 3D and 4D seismic surveys of regions of high oceanic variability, such as Rockall Trough, it may be necessary to employ techniques that can solve for and then remove the effect of significant fluctuations in water layer sound speed over time periods as short as a few hours and distances as short as a kilometre. The current industry standard solution is known as 'cold-water statics' (Wombell 1997; Xu & Pham 2003). This approach corrects for variation in the average sound speed in the water layer using a layer replacement method borrowed from land-based seismic processing. However, the standard implementations do not account for the sort of rapid lateral and temporal variability in water layer sound speed observed in Rockall Trough. Processing schemes that account for strong spatial and temporal water layer variations do exist; for example, Mackay *et al.* (2003) discussed the possibility of measuring seismic water layer sound speeds directly using semblance analysis and inversion of direct arrivals.

During seismic acquisition, it may be helpful to measure oceanic sound speed directly using CTD or sound speed probes if legacy seismic and oceanographic data indicate that strong variability might occur. Expendable probes are designed to be deployed from an underway vessel and need not interfere with seismic acquisition, especially if deployed from a chase boat. Two useful types are the expendable sound speed probe (XSP) and the expendable conductivity–temperature–depth (XCTD) probe. Portable, re-usable probes are available that can be deployed from a chase boat using nothing more than a small winch and a suitable length of line. We have successfully operated both expendable and re-usable oceanic probes to augment industrial and academic 2D and 3D seismic surveys. It is neither practical nor necessary to make closely spaced probe casts and produce sound speed sections comparable to those in Figure 6. Instead the aim should be to analyse probe data collected across the entire footprint and time-span of the survey, as in Figure 7, to ascertain whether the survey was affected by significant water layer sound speed variation. This analysis should be completed by the end of seismic acquisition and used to decide whether to invest in processing steps that can account for strong spatial and temporal water layer sound speed variations.

Implications for oceanography

Seismic reflection surveying provides a remote sensing tool that can rapidly image large volumes of the oceanic interior at a lateral resolution of tens of metres. For comparison, the spacing between the traditional oceanographic probe casts used to build the sound speed cross-sections in Figure 7 ranges from a few kilometres to tens of kilometres. Seismic reflection data is therefore providing new opportunities to investigate the detailed structure of oceanic features, such as fronts between water masses and eddies, and to observe how these features evolve and how they interact with seabed topography. The seismic data presented here show strong spatial and temporal variability. Whilst this variability represents a risk to the hydrocarbon industry, it represents an opportunity to oceanographers. The variations in sound speed that generate seismic reflectivity arise from mixing between water masses of distinctive physical properties, so that measurements of the variability can potentially constrain oceanic mixing rates. An accurate description of oceanic mixing is an integral part of ocean circulation models, which are an in turn part of global climate models. We therefore recommend that the hydrocarbon industry makes the water layer part of seismic reflection data available for academic research.

Conclusions

(1) Natural variation in sound speed occurs within the water layer of some deepwater oceanic regions such as Rockall Trough, offshore west of Ireland. This variation is likely to degrade sub-seabed reflection images. Degrading effects include vertical offset of reflections between adjacent sail lines and line intersections, and difficulties in suppressing multiples from water layer reverberations.

(2) Risk assessment for water layer sound speed variation is an essential part of planning 2D, 3D and 4D seismic surveying in deep water. An initial assessment of water layer risk can be made from legacy oceanographic probe data. Legacy seismic data can be used to refine the risk assessment by showing how rapidly and by how much the water layer sound speed is likely to vary at a given location.

(3) In areas of vigorous oceanic mixing, such as offshore west of the UK and Ireland, expect strong water layer variability along individual sail lines. In Rockall Trough, the mean water layer sound speed mostly varies between 1490 and 1500 m s^{-1}, and vertical offsets of up to about 15 ms travel time at line intersections are predicted.

(4) Currently standard processing techniques for removing the effect of water layer variability are not designed to cope with the variability observed in Rockall Trough. Instead, it is necessary to employ techniques that can solve for and then remove the effect of fluctuations in water layer sound speed over time periods as short as a few hours and distances as short as a kilometre.

We are grateful to the Irish Petroleum Affairs Division (in particular to Peter Croker) and to Spectrum Geo Ltd for providing the seismic data illustrated here. We also acknowledge the support of the Irish Marine Institute, both by providing access to oceanographic datasets and by granting use of the R/V *Celtic Explorer* to SMJ under the SSTI (Strategy for Science, Technology and Innovation) Ship-Time Programme 2007, funded under the Irish Government's National Development Plan (Marine Research Sub-Programme). We thank the Irish Petroleum Infrastructure Project for supporting the seismic processing facility at Trinity College Dublin. Other supporters of our oceanography work are Providence Resources, Statoil Ireland, ExxonMobil and BG Group. C. Sutton is supported by a studentship from Trinity College Dublin. All seismic processing was performed using the Seismic Unix system. We thank Richard Hobbs, John Smallwood and an anonymous reviewer for their comments on the original version of this manuscript.

References

Barley, B. 1999. Deep-water problems around the world. *The Leading Edge*, **18**, 488–494.

Bertrand, A. & MacBeth, C. 2003. Seawater velocity variations and real time reservoir monitoring. *The Leading Edge*, **22**, 351–355.

Biescas, B., Sallarès, V. *et al*. 2008. Imaging meddy finestructure using multichannel seismic reflection data. *Geophysical Research Letters*, **35**, L11609; doi: 10.1029/2008GL033971.

Egbert, G. D. & Ray, R. D. 2001. Estimates of M2 tidal energy dissipation from TOPEX/Poseidon altimeter data. *Journal of Geophysical Research*, **106**, 22475–22502.

Fofonoff, N. P. & Millard, Jr, R. C. 1983. Algorithms for computation of fundamental properties of seawater. *Unesco Technical Papers in Marine Science*, 44.

Hardy, R. J. J. & Jones, S. M. 2009. Identifying and quantifying the effects of water column velocity variation on surface related multiple elimination. *European Association of Geoscientists & Engineers, 71st Conference*. Expanded Abstract V027.

Hatchell, P., Wills, P. & Didraga, C. 2008. Identifying and removing effects of multiples on time-lapse interpretation at Valhall. *First Break*, **26**, 69–76.

Holbrook, W. S., Páramo, P., Pearse, S. & Schmitt, R. W. 2003. Thermohaline fine structure in an oceanographic front from seismic reflection profiling. *Science*, **301**, 821–824.

Jakubowicz, H. 2006. *Multiple Suppression Workshop*. EAGE European Association of Geoscientists and Engineers, London.

Jones, S. M., Hardy, R. J. J., Hardy, D. & Hobbs, R. W. 2008. The new synergy between seismic reflection imaging and oceanography. *First Break*, **26**, 51–57.

Lacombe, C., Schultzen, J., Butt, S. & Lecerf, S. 2006. Correction for water velocity variations and tidal statics. *Society of Exploration Geophysicists, Expanded Abstracts* **25**, 2881.

Lacombe, C., Butt, S., MacKenzie, G., Schons, M. & Bornard, R. 2009. Correcting for water column variations. *The Leading Edge*, **28**, 198–201.

Mackay, S., Fried, J. & Carvill, C. 2003. The impact of water-velocity variations on deepwater seismic data. *The Leading Edge*, **22**, 344–350.

Nandi, P., Holbrook, W. S., Pearse, S., Páramo, P. & Schmitt, R. W. 2004. Seismic reflection imaging of water mass boundary in the Norwegian Sea. *Geophysical Research Letters*, **31**, L23311.

New, A. L. & Smythe-Wright, D. 2001. Aspects of circulation in the Rockall Trough. *Continental Shelf Research*, **21**, 777–810.

Ruddick, B., Song, H., Dong, C. & Pinheiro, L. 2009. Water column seismic images as maps of temperature gradient. *Oceanography* **22**, 192–205.

Sherwin, T. J. & Turrell, W. R. 2005. Mixing and advection of a cold water cascade across the Wyville Thompson Ridge. *Deep Sea Research I*, **52**, 1392–1413.

Vogel, M. & Symonds, D. 2002. Real-time ocean current data from 3000 m and beyond. *Offshore Engineer*, April, 57–60.

Wombell, R. 1997. Water velocity variations and static corrections in 3D data processing. *European Association of Geoscientists & Engineers, 59th Conference*, Expanded Abstract A029.

Xu, S. & Pham, D. 2003. Global solution to water column statics: a new approach to an old problem. *Society of Exploration Geophysicists, Expanded Abstracts*, **22**, 1885.

New aeromagnetic and gravity compilations from Norway and adjacent areas: methods and applications

O. OLESEN,[1] M. BRÖNNER,[1] J. EBBING,[1] J. GELLEIN,[1] L. GERNIGON,[1] J. KOZIEL,[1] T. LAURITSEN,[1] R. MYKLEBUST,[2] C. PASCAL,[1] M. SAND,[3] D. SOLHEIM[4] and S. USOV[2]

[1]*Geological Survey of Norway (NGU), Leiv Eirikssons vei 39, NO 7491 Trondheim, Norway (e-mail: odleiv.olesen@ngu.no)*
[2]*TGS-NOPEC Geophysical Company ASA (TGS), Hagaløkkveien 13, NO 1383 Asker, Norway*
[3]*Norwegian Petroleum Directorate (NPD), Professor Olav Hanssens vei 10, NO 4021 Stavanger, Norway*
[4]*Norwegian Mapping Authority (SK), Kartverksveien 21, NO 3507 Hønefoss, Norway*

Abstract: The Geological Survey of Norway (NGU) has produced new aeromagnetic and gravity maps from Norway and adjacent areas, compiled from ground, airborne and satellite data. Petrophysical measurements on core samples, hand specimens and on *in situ* bedrock exposures are essential for the interpretation of these maps. Onshore, the most prominent gravity and magnetic anomalies are attributed to lower crustal rocks that have been brought closer to the surface. The asymmetry of the gravity anomalies along the Lapland Granulite Belt and Kongsberg–Bamble Complex, combined with the steep gradient, points to the overthrusted high-density granulites as being the main source of the observed anomalies. The Kongsberg–Bamble anomaly can be traced southwards through the Kattegat to southern Sweden. This concept of gravity field modelling can also be applied to the Mid-Norwegian continental shelf and could partially explain the observed high-density rocks occurring below the Møre and Vøring basins and in the Lofoten area. Extrapolations of Late-Caledonian detachment structures occurring on the mainland can be traced on aeromagnetic and gravimetric images towards the NW across the continental margin. Subcropping Late Palaeozoic to Cenozoic sedimentary units along the mid-Norwegian coast produce a conspicuous magnetic anomaly pattern. The asymmetry of the low-amplitude anomalies, with a steep gradient and a negative anomaly to the east and a gentler gradient to the west, relates the anomalies to gently westward dipping strata. Recent aeromagnetic surveys in the Barents Sea have revealed negative magnetic anomalies associated with shallow salt diapirs. Buried Quaternary channels partly filled with gravel and boulders of crystalline rocks generate magnetic anomalies in the North Sea. The new maps also show that the opening of the Norwegian–Greenland Sea occurred along stable continental margins without offsets across minor fracture zones, or involving jumps in the spreading axis. A triple junction formed at 48 Ma between the Lofoten and Norway Basins.

Keywords: aeromagnetic data, gravity data, petrophysical data, Norway, North Sea, Norwegian Sea, Barents Sea

The Geological Survey of Norway (NGU) has acquired aeromagnetic and gravity data over the last 50 and 40 years, respectively, and has recently decided to release new aeromagnetic and gravity maps of Norway and adjacent areas. In addition to managing the datasets, we actively utilize the data to improve our understanding of the structure and evolution of the Norwegian mainland and adjacent continental margin and oceanic domains.

NGU has national responsibility for operating and maintaining the potential field databases in Norway. The survey acquired aeromagnetic data from the Norwegian mainland and continental shelf during the period 1959–1976. A second programme of high-resolution aeromagnetic mapping was initiated in offshore areas in 1993.

Gravity data have been systematically measured on mainland Norway by NGU over the last 40 years. In conjunction with marine data, which are often obtained in connection with seismic data acquisition, the gravity coverage is extensive enough to study both local and regional features.

Over the last 30 years, NGU has also carried out a petrophysical sampling programme on hand specimens from the Norwegian mainland, as well as on offshore drillcores. The petrophysical data on hand specimens can be utilized to estimate the magnetic properties of basement rocks in the offshore areas.

The new aeromagnetic and gravity maps contain many features ascribed to major tectonic elements, and portray their regional distribution. Aeromagnetic data reflect rock distributions at any depths from the surface to depths where the magnetic rocks reach the Curie temperature. The first-generation, offshore gravity and magnetic datasets were used mainly for interpretation of basement topography and detection of intra-sedimentary volcanic units and intrusions. The high quality of the data acquired in recent years provides the possibility of mapping high-frequency anomalies caused by sources located within the sedimentary successions. The improved quality is due to the use of (1) state-of-the-art instrumentation, (2) real-time, differential GPS navigation equipment, (3) a denser line spacing and (4) advanced micro-levelling software. Magnetic data are also utilized to reduce the well-bore positional uncertainty in offshore wells (Russell *et al.* 1995).

This review paper summarizes the results of recent studies carried out by NGU and collaborators and is intended to illustrate various scientific and petroleum implications of our recent high-quality aeromagnetic and gravity surveys.

Datasets

Bathymetric and topographic data

A combined bathymetry–topography compilation is particularly useful for (1) terrain corrections of the mainland gravity data, (2) Bouguer corrections of the offshore data and (3) Airy isostatic

VINING, B. A. & PICKERING, S. C. (eds) *Petroleum Geology: From Mature Basins to New Frontiers – Proceedings of the 7th Petroleum Geology Conference*, 559–586. DOI: 10.1144/0070559

correction of the final Bouguer grid. Bathymetric data includes (1) modern multi-beam echo sounder data, (2) digitized naval maps in areas adjacent to the coast and (3) depth data collected during seismic surveys. Dataset 1 has the highest quality whilst dataset 3 is the poorest. Norwegian Hydrographic Service supplied data in shallow Norwegian waters. A revised version of the International Bathymetric Chart of the Arctic Ocean, IBCAO v. 2.23 (Jakobsson *et al.* 2008), was included for the remaining area of the Norwegian–Greenland Sea and the eastern Barents Sea. This DEM is available in polar stereographic projection, with 2 km cell size. We further inserted data from the arc-minute grid of the General Bathymetric Chart of the Oceans (GEBCO) in the North Sea area (http://www.gebco.net/data_and_products/gridded_bathymetry_data/).

High-resolution topography grids for mainland Norway (100×100 m) and Svalbard (1×1 km) were supplied by the Norwegian Mapping Authority. Topography for Fennoscandia, Iceland, Faroe Islands, Scotland and eastern Greenland was downloaded from the GTOPO30 dataset (http://edcwww.cr.usgs.gov/landdaac/gtopo30/gtopo30.html). The final grid shown in Figure 1 was displayed using the shaded-relief technique with illumination from the NE. The cell size of the combined grid is 250×250 m.

Aeromagnetic data

As noted above, the whole of Norway (including the largest continental shelf in western Europe) was covered with aeromagnetic surveys from 1959 to 1975. In 1957, NGU acquired the first fluxgate magnetometer from the US Geological Survey in exchange for an electromagnetic Turam system. The first onshore survey was flown in 1959 in the Løkken and Kautokeino regions, and the first offshore survey was completed in 1962 in the Skagerrak region.

Aeromagnetic data collected on the Norwegian mainland prior to 1976 are provided in the form of a matrix digitized from manually drawn contour maps (Norges geologiske undersøkelse 1992; Smethurst *et al.* 1994). Flight altitudes and directions, and line-spacings of the aeromagnetic surveys, varied widely. The areas of low flight altitude of mainland Norway (150–300 m) were covered between 1959 and 1968 using a stinger-mounted fluxgate magnetometer. From 1969 to 1976, a stinger-mounted proton magnetometer was used, covering western Norway and most of northern Norway with measurements made at flight altitudes ranging from 800 to 1500 m a.s.l. (Table 1). The cell size of the grid is 500×500 m. The magnetic total field is reduced to anomaly values using the Definite Geomagnetic Reference Field 1965.0 (DGRF 1965.0). NGU and Amarok (now TGS-NOPEC Geophysical Company) launched a programme for remapping the Norwegian continental shelf in 1993, applying a line spacing of 2 km.

Both vintage and new surveys were levelled applying the standard Geosoft (2006) statistical method to the tie-lines, followed by a statistical levelling of the profiles utilizing the levelled tie-lines. The IGRF field was calculated and subtracted from the levelled survey lines to produce the magnetic anomalies of the survey areas. We applied the more sophisticated, moving median filtering method (Mauring & Kihle 2006) in areas where levelling errors still existed subsequent to the standard statistical levelling. This was often the case for the vintage surveys where the number of tie-lines was inadequate for a thorough levelling (Fig. 2a). The median method can also be applied to profiles with varying orientation, such as the 1970–1975 surveys that were acquired along parabolic Decca lanes. The median method was also successfully applied in areas with subtle low-frequency anomalies in reflown areas on the shallow continental shelf. The moving median levelling technique showed its advantages, and errors down to less than one nanoTesla (nT) have been removed. Specifications for the different subareas are given in Table 1. The individual datasets have been interpolated to square grids of 500×500 m using the minimum curvature method (Briggs 1974; Geosoft 2005). The grids were trimmed to a *c.* 10 km overlap and merged using a minimum curvature algorithm, GridKnit, developed by Geosoft (2008).

The coverage has been extended into the oceanic domain outside the continental margin with the line/tie-line spacing of 5/20 km. A total of 240 000 km was acquired by NGU covering an area of *c.* 500 000 km^2. NGU and TGS have both acquired their surveys with cesium vapour magnetometers installed in a towed bird located 70 m below the aeroplane and in a tail stinger, respectively. During the last 15 years, the two systems have been flown with Piper PA-31 aeroplanes. They were tested in a joint flight in 1996 and the performances of the two systems were almost identical. The noise envelope of the magnetometers is usually less than 0.2 nT and most of the data are within limits of ± 0.04 nT. Real-time differential GPS navigation with a minimum of four satellites was used throughout the surveys, resulting in a navigation accuracy better than ± 3 m.

The final aeromagnetic map (Fig. 3) also includes aeromagnetic data from Great Britain and mainland Greenland from the 5×5 km GAMMAA5 grid (Verhoef *et al.* 1996). This grid was regridded to 500×500 m cells before being merged into the final compilation.

The southwestern part of the Barents Sea was remapped in 1997–2009. The more recent NGU datasets (SNAS-06, BAS-06, BASAR-08, BARSAR-09; Løvaas *et al.* 2006; Gernigon *et al.* 2007; Brönner *et al.* 2009) are not included in the present compilation since they are not yet released. The resolution of these modern aeromagnetic data is 0.1–0.2 nT.

Long-wavelength magnetic anomalies are not reliably represented in regional aeromagnetic compilations. We have therefore applied a high-pass filter on the compiled grid using a 330 km Gaussian filter, and added the spherical harmonic degrees ≤ 120 (i.e. ≥ 330 km wavelength) of the CHAMP satellite magnetic anomaly model MF6 (Maus *et al.* 2008). The removed 330 km low-pass filtered component of the aeromagnetic compilation is shown in Figure 2c, while Figure 2d shows the substituted 330 km low-pass version of the MF6 model. The final corrected map is presented in Figure 3.

Gravity data

The gravity compilation represents an update of the 1:3 million scale gravity map published by Skilbrei *et al.* (2000). We have added substantially more data on the Mid-Norwegian continental shelf and on the mainland of southern Norway. We have also carried out a more detailed terrain correction and removed the bathymetric effects of the fjords in the mainland gravity data. The terrain correction of the up to 1400 m-deep fjords amounts to 15×10^{-5} m s^{-2} (mGal). The marine gravity database consists of 554 000 km of ship profiles collected by the Norwegian Petroleum Directorate (NPD), TGS-NOPEC Geophysical Company (TGS), the Norwegian Mapping Authority (SK) and various commercial companies. We have included *c.* 68 000 land gravity stations measured by NGU, SK and several Norwegian and foreign universities from mainland Norway and *c.* 1000 stations measured by SK on Svalbard. The mainland data are stored in the national gravity database at NGU (Gellein *et al.* 1993). Bouguer gravity data from mainland Greenland (Strykowski & Forsberg 1998), Iceland (Thorbergsson *et al.* 1990) and Scotland (British Geological Survey 1997) are also included in the compilation.

The profile data offshore Norway have been levelled using the median levelling technique (Mauring & Kihle 2006). The compiled free-air dataset has been interpolated to a square grid of 2×2 km

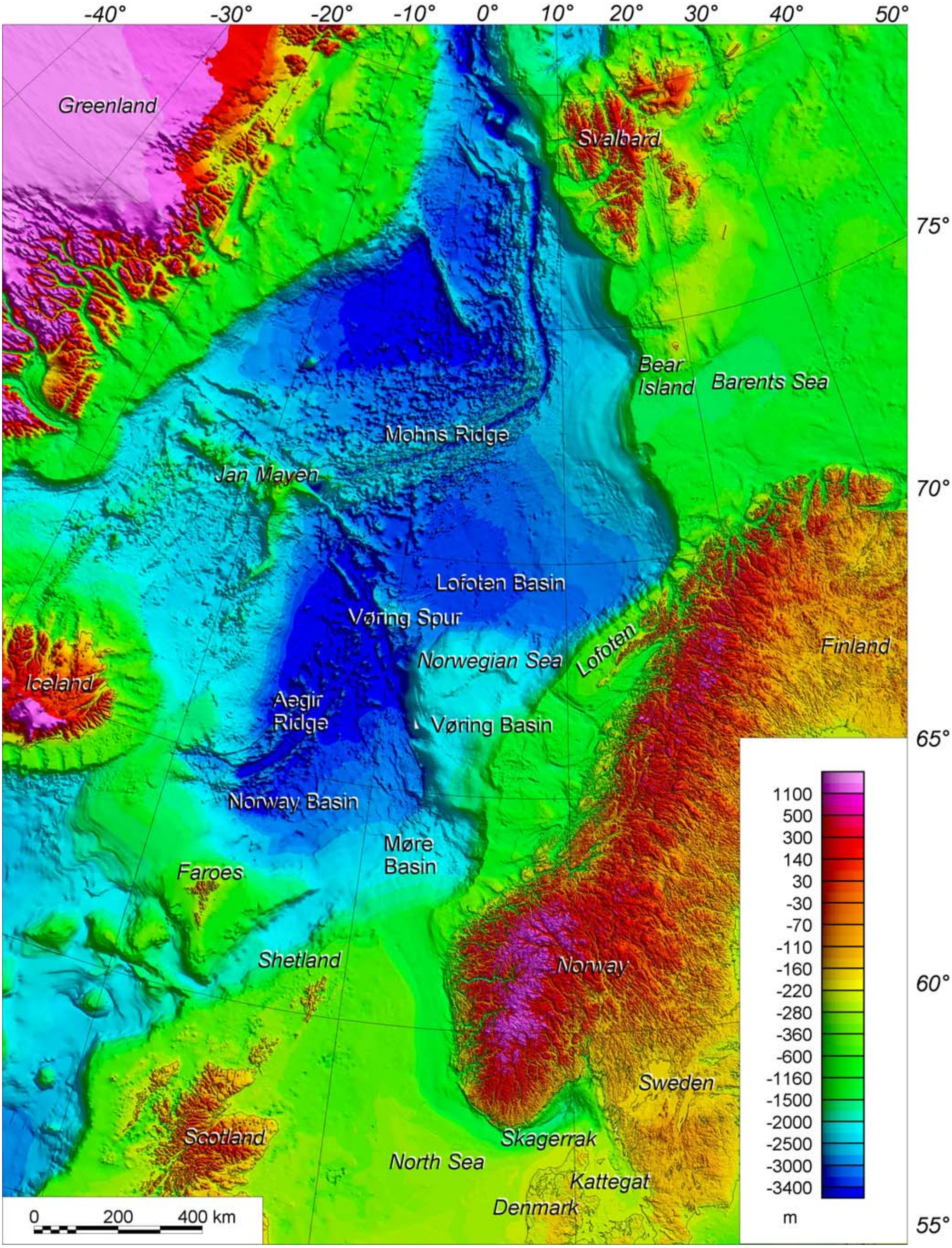

Fig. 1. Bathymetry and topography map of the NE Atlantic. The 250 × 250 m grid represents an updated version of the Dehls *et al.* (2000) compilation using new releases of bathymetric data from the Arctic Ocean, IBCAO v. 2.23 (Jakobsson *et al.* 2008) and the world oceans (GEBCO). High-resolution topography data (100 × 100 m) for Norway and the adjacent land areas were supplied by the Norwegian Mapping Authority and the US Geological Survey, respectively.

Table 1. Offshore aeromagnetic surveys compiled for the present study (Figs 2, 3 & 6a)

Year	Area	Operator, reference	Survey name	Sensor elevation (m)	Line spacing (km)	Length (km)
1968–1992	Iceland	University of Iceland 1, 2	UoI-68/92	900–1200	3–6	56 900
1969	SW Barents Sea	NGU, 3	NGU-69	200	4	26 200
1970	SE Barents Sea	NGU, 3	NGU-70	200	4–8	22 800
1971	Viking Graben	Fairey, 4	Fairey-71a	300	2	11 100
1971	Shetland Basin	Fairey, 5	Fairey-71b	500	7.5	13 500
1972	Shetland Basin	Fairey, 5	Fairey-72	500	5	20 100
1973	Shetland Basin	Fairey, 5	Fairey-73	500	15	32 600
1973	Vøring Basin	NGU, 3	NGU-73	500	5	35 000
1972	North Norwegian–Greenland Sea	NRL, 6	NRL-72	300	7.5	38 500
1973	South Norwegian–Greenland Sea	NRL, 6	NRL-73	300	10 (20)	50 600
1973	Denmark Strait	NOO, 7	NOO-73	160	5.5	60 400
1974	Norwegian Sea, east of Iceland	NOO, 8	NOO-74a	160	10	5500
1974	Norwegian Sea, SE of Iceland	NOO, 8	NOO-74b	160	10	2000
1974	NE Atlantic, south of Iceland	NOO, 8	NOO-74c	160	5	22 200
1974	Norwegian North Sea	NGU, 9	NGU-74	300	2–7	23 000
1974	East Greenland mainland	GEUS, 10	GEUS-74	1820	8	15 200
1975	Norwegian North Sea	NGU, 9	NGU-75	300	1–6	19 000
1976	Jan Mayen Ridge	CGG/NPD, 11	CGG-76	700	5	11 600
1979	East Greenland shelf	GEUS, 12	GEUS-79	600	8	48 300
1983	Greenland Sea	NRL, 5	NRL-83	300	20	13 000
1985	SW Barents Sea	CGG, 13	BAMS-85	200	4	16 900
1985	S of Faroe Islands	NOO, 5	NOO-85	230	3	18 100
1986	Trøndelag Platform	Hunting, 14	Hunting-86	200	2	57 000
1987	Vøring Plateau	NOO, 5	NOO-87	230	5	16 900
1987	NW Barents Sea	NGU, 15	BSA-87	250	4–8	34 000
1988	Spitsbergen	NGU, 16	SPA-88	1550	5.5	13 300
1989	Lofoten	NGU, 17	LAS-89	250	2	30 000
1990	Ægir Ridge	NRL, 18	NRL-90	0 ship	6	11 000
1991	Svalbard	Amarok/TGS, 19	SVA-91	900	7.5	27 800
1993	N. Viking Graben	NGU, 20	Viking-93	150	0.5–2	28 000
1993	Hel Graben–Nyk High	World Geoscience, 21	SPT-93	80	0.75	19 000
1994	Vøring Basin	Amarok/TGS, 22	VGVB-94	140	1–3	31 800
1994	Nordland Ridge–Helgeland Basin	NGU, 23	NAS-94	150	2	36 000
1994	S. Viking Graben	Amarok/TGS, 24	VGVG-94	160	0.2	44 800
1996	Skagerrak	NGU, 25	SAS-96	150	2	42 000
1997	Møre Basin	Amarok/TGS, 26	MBAM-97	220	1–2	46 600
1998	Vestfjorden	NGU, 27	VAS-98	150	2	6000
2000	Vøring Basin	TGS, 28	VBE-AM-00	130	1–4	17 300
2003	Røst Basin	NGU, 29	RAS-03	230	2	30 000
2005	Jan Mayen FZ	NGU, 30	JAS-05	230	5	32 600
2007	Norway Basin	NGU, 31	NB-07	230	5	38 500
	Norway Basin	NGDC, 32	NGDC	0 ship		15 200
Total						1 173 500

CGG, Compagnie Générale de Géophysique; GEUS, Geological Survey of Denmark and Greenland; NOO, Naval Oceanographic Office; NGU, Geological Survey of Norway; NPD, Norwegian Petroleum Directorate; NRL, Naval Research Laboratory.
References: (1) Kristjánsson *et al.* 1989, (2) Jónsson *et al.* 1991, (3) Åm 1975, (4) Åm 1973*a*, (5) Verhoef *et al.* 1996, (6) Vogt *et al.* 1979, (7) Vogt *et al.* 1980, (8) US Naval Oceanographic Office 1982, Vogt *et al.* 1981, (9) Olesen *et al.* 1997*a*, (10) Larsen 1974, (11) Compagnie Générale de Géophysique 1977, Navrestad & Jørgensen 1979, (12) Larsen & Thorning 1979, (14) Skilbrei & Kihle 1995, (15) Skilbrei 1991, (16) Skilbrei 1992, (17) Olesen *et al.* 2002, (18) Jung & Vogt 1997, (19) Breivik & Faleide 2004, (20) Smethurst 2000, (23) Olesen *et al.* 2002, (25) Olesen *et al.* 2004, (27) Olesen *et al.* 2002, (29) Olesen *et al.* 2007, (30) Olesen *et al.* 2006, (31) Gernigon *et al.* 2008, (32) Maus *et al.* 2009. The individual datasets are stored in NGUs Dragon database (DiRect Access to Geophysics On the Net, Smethurst & Lauritsen 2003).

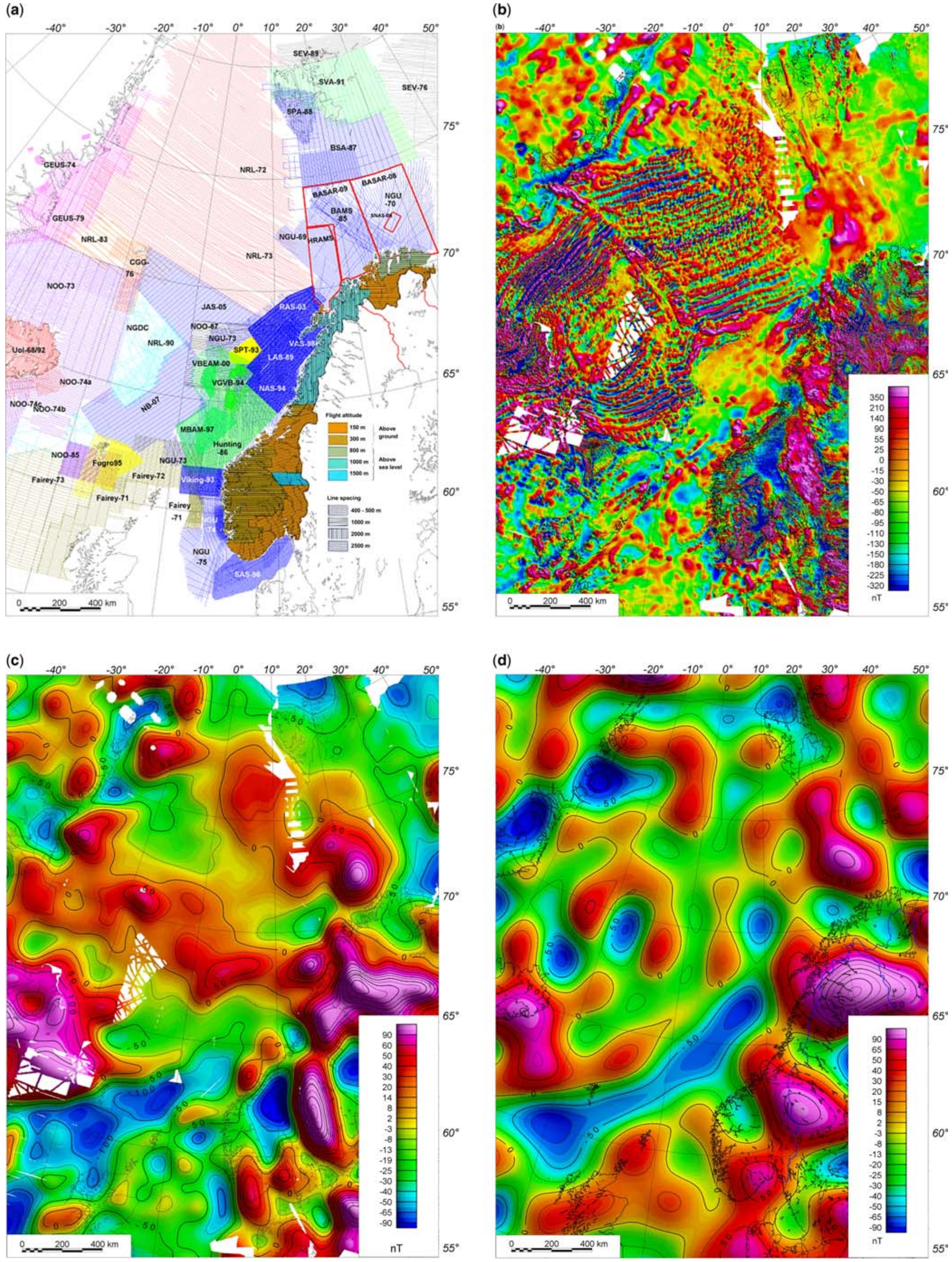

Fig. 2. (**a**) Compilation of magnetic surveys in the NE Atlantic area. The subgrids from the 40 aeromagnetic surveys and two marine magnetic datasets listed in Table 1 are produced from original profile data and added to the mainland Norway compilation. The red frames in the Barents Sea show three high-resolution surveys that are not included in the compilation for confidentiality reasons. (**b**) Grid compilation of the surveys. The total magnetic field is referred to the IGRF. We have filled in data from Scotland and East Greenland from the North Atlantic aeromagnetic compilation by Verhoef *et al.* (1996) and in Denmark, Sweden and Finland from the Fennoscandia aeromagnetic compilation by Korhonen *et al.* (2002*a*). (**c**) A 330 km long-wavelength component has been removed from the magnetic dataset and replaced by (**d**) the 330 km long-wavelength component of the MF6 magnetic model by Maus *et al.* (2008) based on the CHAMP satellite data. The final magnetic grid is shown in Figure 3.

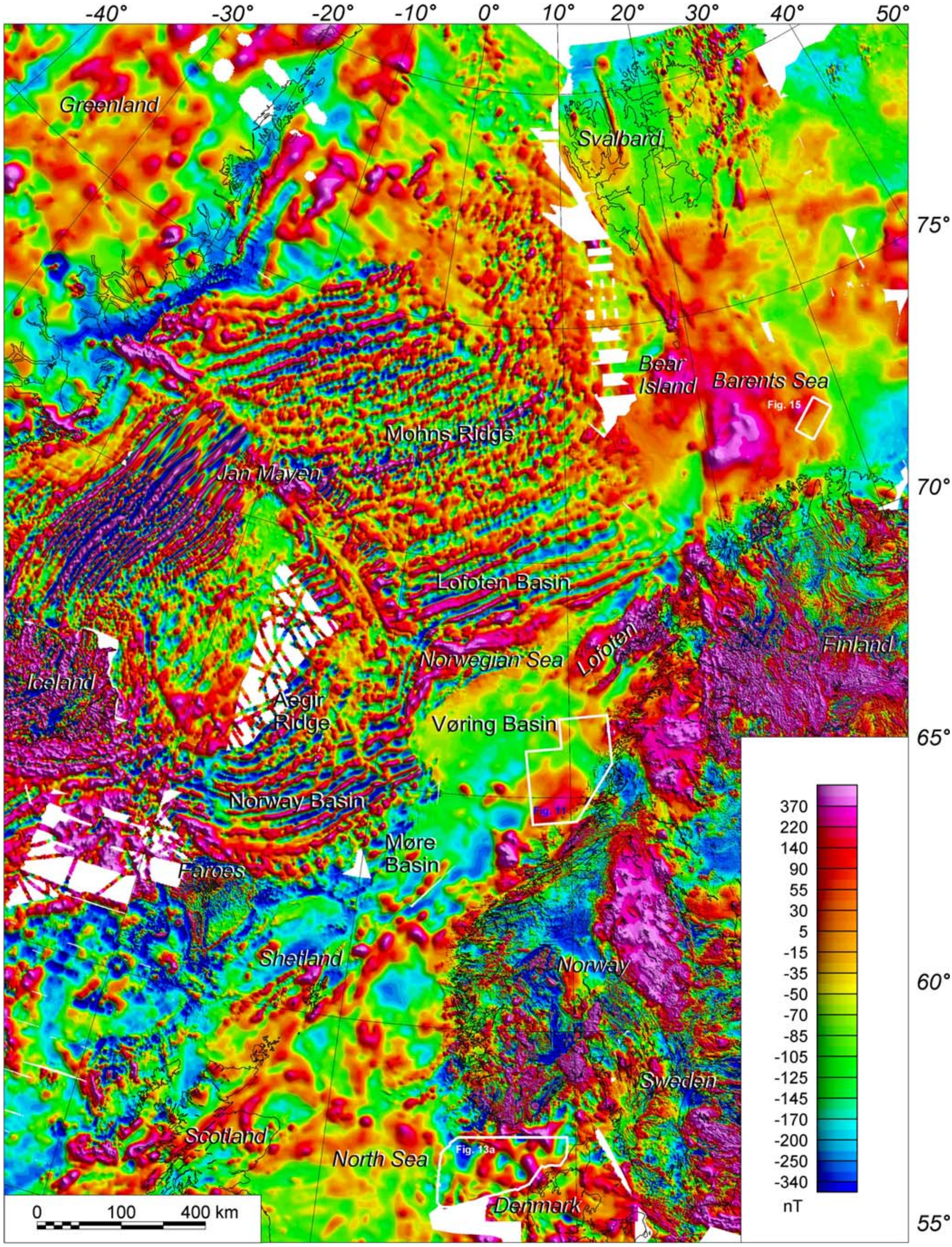

Fig. 3. Magnetic compilation of the NE Atlantic. Total magnetic field referred to IGRF. The map is displayed using the shaded-relief technique with illumination from the SE. The long-wavelength component ($\geq$330 km) of the grid was replaced with the spherical harmonic degrees $\leq$120 (i.e. $\geq$330 km wavelength) of the CHAMP satellite magnetic anomaly model MF6 (Maus *et al.* 2008). The white frames in the Norwegian Sea and the North Sea show the location maps of the analytic signal of the total magnetic field shown in Figures 11 & 13a, respectively. The white frame in the Barents Sea shows the outline of the southern Nordkapp Basin Aeromagnetic Survey 2006 (SNAS-06) where the salt diapir in Figure 15 is located. A 1 : 3 million scale version of the map can be downloaded from http://www.ngu.no/upload/Kart%20og%20data/Geofysikkart%20stort%20format/Mag_3_mill.pdf.

using the minimum curvature method (Briggs 1974; Geosoft 2005). The simple Bouguer correction at sea (Mathisen 1976) was carried out using a density of 2200 kg m^{-3}. The International Standardization Net 1971 (IGSN 71) and the Gravity Formula 1980 for normal gravity have been used to level the surveys. The compiled dataset was merged with the gravity data from the 2.5×2.5 km Fennoscandian grid to the east and south (Denmark, Finland and Sweden; Korhonen *et al.* 2002*b*), and the DNSC08 satellite altimetry gravity data from the National Space Institute, Technical University of Denmark, in the deepwater areas of the Norwegian Sea and the eastern Barents Sea (Andersen *et al.* 2008). The Fennoscandian grid had to be shifted by a constant of -16.3×10^{-5} m s^{-2} to make it fit to our IGSN 71 data. Figure 4a shows the locations of the individual datasets. Figure 4b shows the free-air gravity field at sea and Bouguer gravity on the mainland while Figure 4c displays the Bouguer gravity on the mainland as well as in the offshore areas.

The Airy–Heiskanen 'root' (Heiskanen & Moritz 1967) was calculated from a smoothed version of the compiled topographic and bathymetric dataset in Figure 1. The gravitational attraction (Fig. 4d) from the 'root' was calculated using the AIRYROOT algorithm (Simpson *et al.* 1983). The isostatic residual (Fig. 5) was achieved by subtracting the gravity response of the Airy–Heiskanen 'root' from the calculated Bouguer gravity data in Figure 4c. The Airy isostatic residual map enhances crustal anomalies better than traditional free-air and Bouguer gravity maps.

Petrophysical data

Some of the pronounced magnetic and gravity anomalies present along the coast of Norway are continuous from the mainland onto the continental shelf. Consequently, it is important to know the magnetic properties of the rocks on land when assessing the 3D structure of the basement. NGU has therefore carried out petrophysical sampling programmes (including susceptibility and remanence measurements) to assist the bedrock mapping and mineral exploration programmes on mainland Norway (Åm & Oftedahl 1977; Sindre 1977; Olesen *et al.* 1990, 1991, 1997*b*, 2002; Skilbrei *et al.* 1991; McEnroe *et al.* 2001). In addition, density measurements have been carried out on bedrock samples in conjunction with gravity campaigns (Svela 1971; Chroston 1974; Lønne & Sellevoll 1975; Ramberg 1976).

Approximately 28 000 rock samples (Fig. 6), collected during geological mapping and geophysical studies, have been measured with respect to density, susceptibility and remanence (Torsvik & Olesen 1988). The data are stored in NGUs petrophysical database (Olesen *et al.* 1993).

We have produced maps of susceptibility and density by calculating the average values within each geological unit represented on the Norwegian part of the northern Europe bedrock map (Sigmond 2002) (Fig. 7). Non-representative samples (e.g. sulphide mineralizations, hydrothermal alterations, mylonites, diabase and eclogite) were removed from the dataset before map production. The applied colour scale for the susceptibility map is logarithmic in order to depict the several magnitude-wide distributions within each rock unit.

The susceptibility can locally be high within the crystalline bedrock of Norway (Fig. 7a, Tables 2 & 3). The directions of the natural remanent magnetization (NRM) are mostly dominated by a viscous component (close to the present Earth field direction), especially in felsic and intermediate igneous rocks such as granites and orthogneisses. The high-amplitude magnetic anomalies in the Kongsberg–Bamble area, on the Fosen Peninsula (Roan) in mid Norway, Lofoten–Vesterålen and the northwestern part of Senja in northern Norway are caused by granulite-facies gneisses and intrusions (mangerites) (Schlinger 1985; Olesen *et al.* 1991; Skilbrei *et al.* 1991; Fabian *et al.* 2008). The orthopyroxene isograd in the Vesterålen area coincides with the boundary between the high-magnetic and low-magnetic gneisses. The migmatites to the west of this line are in granulite facies whereas to the east they are in amphibolite facies. In this particular area, the magnetic basement surface reflects the depth to the granulite-facies gneisses. The *Q*-values (ratio of remanent to induced magnetization) are generally low, in the order of 0.5 or lower, but mafic and ultramafic rocks frequently show high *Q*-values (Tables 2 & 3). These particular rocks often have a more stable remanence, such as, for example, the norites from the Sveconorwegian Rogaland Igneous Province, which show negative inclination (McEnroe *et al.* 2001).

The intermediate-amplitude magnetic anomalies on the mainland are mostly caused by granitic and quartz–dioritic rocks and migmatitic gneisses. The susceptibilities of the Caledonian rocks are mostly low, with the exception of some banded iron formations and mafic to ultramafic intrusions that frequently show high values. These units appear as high-frequency magnetic anomalies on the mainland (Fig. 3). The magnetically transparent Caledonian nappes in southern Nordland extend to the NW below the Helgeland Basin and the Nordland Ridge, causing the large depths to magnetic sources in this area (Fig. 10).

We have also considered information from petroleum exploration wells as constraints for the potential field modelling. Densities of sedimentary successions have been calculated from well logs and refraction seismic profiles.

Hauger & van Veen (1995) and Løvlie & van Veen (1995) have reported magnetic studies of the Brent Formation sandstones in the North Sea. This formation, however, is dominated by pure, quartz-bearing, high-quality reservoir sandstone with low susceptibility. The OSRAM Project (Origin of Sediment-Related AeroMagnetics) documented, however, that parts of the offshore sedimentary succession are magnetic (Mørk *et al.* 1996, 2002) as in other basin areas of similar age. Reynolds *et al.* (1994) documented, for example, magnetic Fe–Ti oxide- and siderite-bearing, Cretaceous sediments from the North Slope Basin in Alaska (Table 4).

A total of *c.* 11 000 susceptibility measurements were carried out on *c.* 10 km of cores from the IKU shallow drilling programme and exploration wells along the coast of Norway (Fig. 6). These petrophysical studies have been reported by Mørk & Olesen (1995), Mørk *et al.* (1996, 2002) and Lauritsen *et al.* (2007). The distributions are generally wide, covering two orders of magnitude. Sandstone has generally a lower susceptibility than mudstone, siltstone and claystone, $5–30 \times 10^{-5}$ v. $15–60 \times 10^{-5}$ SI (Table 4). This is comparable to the susceptibility of the metamorphosed paramagnetic equivalents in mainland Norway [e.g. histograms from the Klubben and Storelv formations within the Kalak Nappe Complex in Finnmark (Olesen *et al.* 1990)]. Ferro-magnetic metasedimentary rocks in the crystalline basement on the mainland, however, may have a susceptibility more than two orders of magnitude higher than the paramagnetic equivalents. Red-coloured sandstones in the offshore wells may contain Fe–Ti oxides and hydroxides and commonly have higher susceptibilities (up to 100×10^{-5} SI) than other sedimentary rocks. The highest susceptibility recorded in bedrock lithologies was encountered in siderite-cemented claystones and siltstones of Cretaceous age; up to 400×10^{-5} SI. These cemented zones occur in 5–20 cm-wide sections of the SINTEF-IKU cores and are the most common source of magnetization within the offshore sedimentary column (Mørk *et al.* 2002). They seem to be associated with locally small-scale faulting. Caliche, which is a lithified desert soil formed by the near-surface crystallization of calcite and/or other soluble minerals by upward-moving solutions, has intermediate susceptibilities reaching up to 100×10^{-5} SI. Anhydrite, gypsum and coal have the lowest susceptibilities; anhydrite has susceptibilities in the range -2 to $+1 \times 10^{-5}$ SI, and gypsum can be diamagnetic – a finding consistent with published data (e.g. Clark 1997). The thickness of the

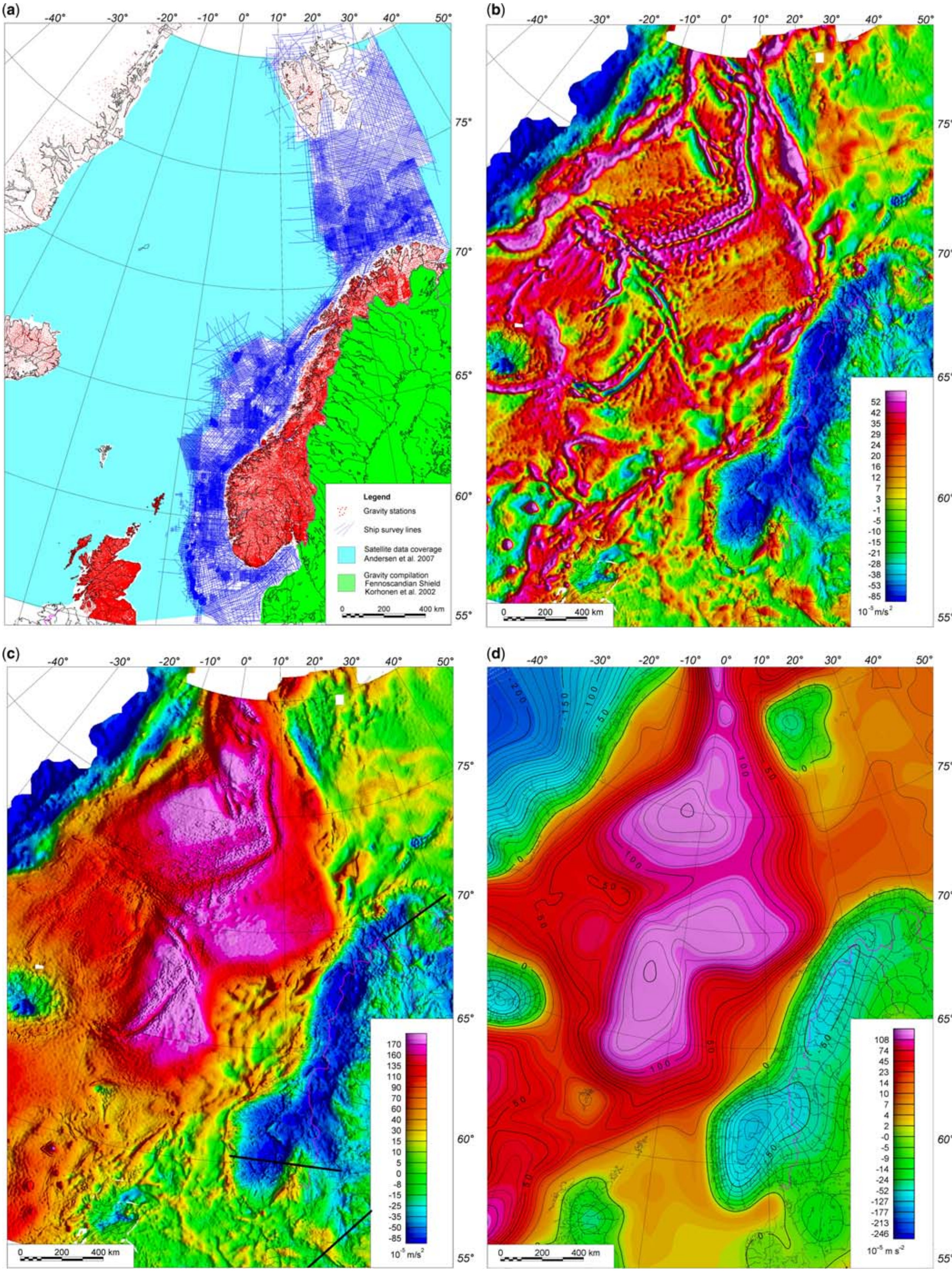

Fig. 4. (**a**) Compilation of gravity surveys in the NE Atlantic. Data from the Fennoscandian gravity compilation (Korhonen *et al.* 2002*b*) and the DNSC08 ocean-wide altimetry derived gravity field (Andersen *et al.* 2008) have been added to the new Norwegian compilation, which represents an update of the 1:3 million gravity map by Skilbrei *et al.* (2000). (**b**) Bouguer gravity on mainland Scandinavia and free-air anomalies from the adjacent sea areas. (**c**) Bouguer gravity of the NE Atlantic area. We have for the Bouguer correction applied a density of 2670 kg m^{-3} on the mainland and 2200 kg m^{-3} in the offshore regions. (**d**) The gravitational attraction from the 'root' is calculated using the AIRYROOT algorithm (Simpson *et al.* 1983) and the bathymetry and topography in Figure 1. The depth of the root at the coast is chosen at 30 km and the density contrast at the mantle-crust interface is 300 kg m^{-3}.

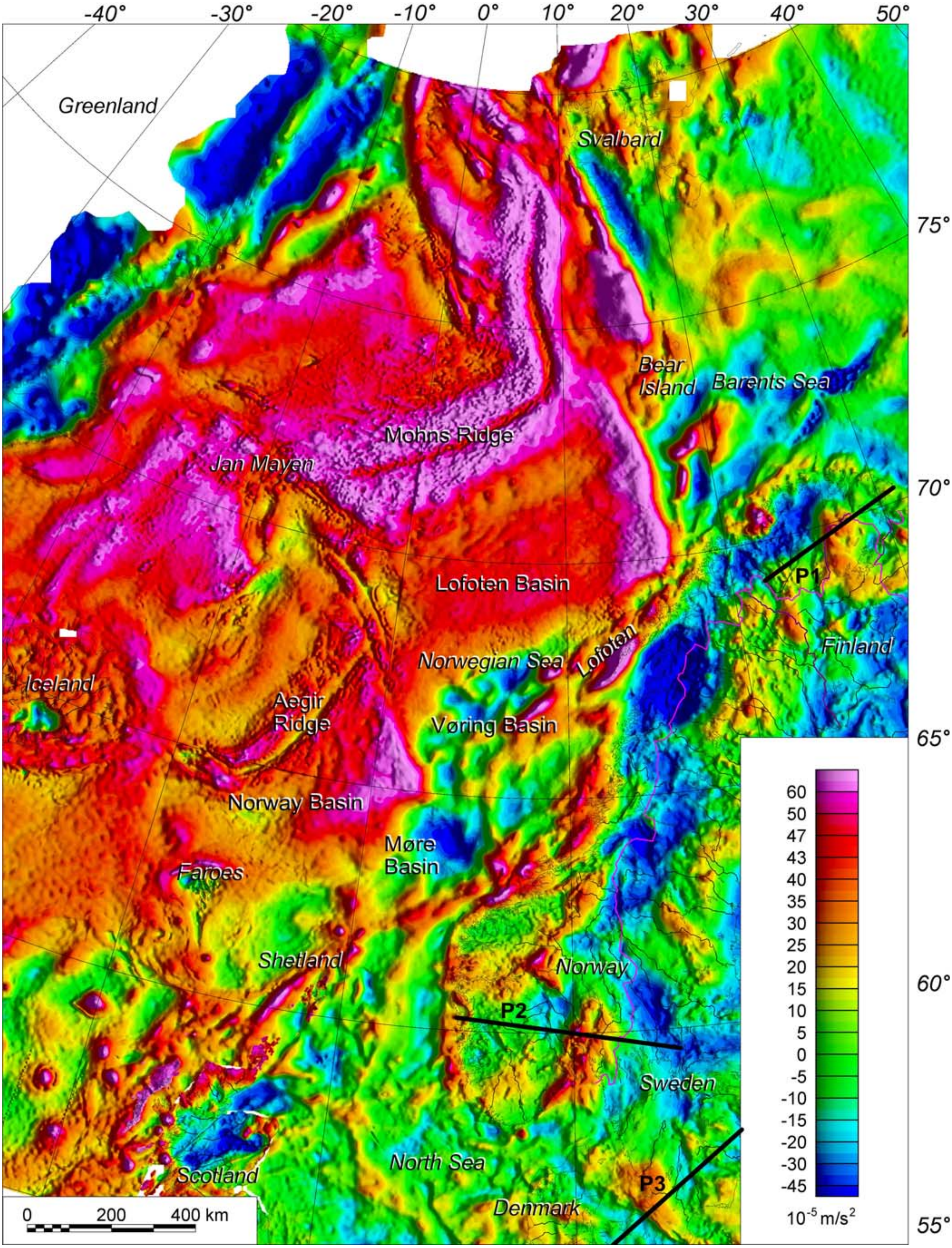

Fig. 5. Residual gravity after isostatic correction of Bouguer gravity data. The isostatic correction has been calculated applying the AIRYROOT algorithm (Simpson *et al.* 1983) to the topography/bathymetry dataset in Figure 1 as shown in Figure 4. The Bouguer gravity along profiles P1, P2 and P3 is shown in Fig. 9. A 1 : 3 million scale version of the map can be downloaded from http://www.ngu.no/upload/Kart%20og%20data/Geofysikkart%20stort%20format/Grav_3_mill.pdf.

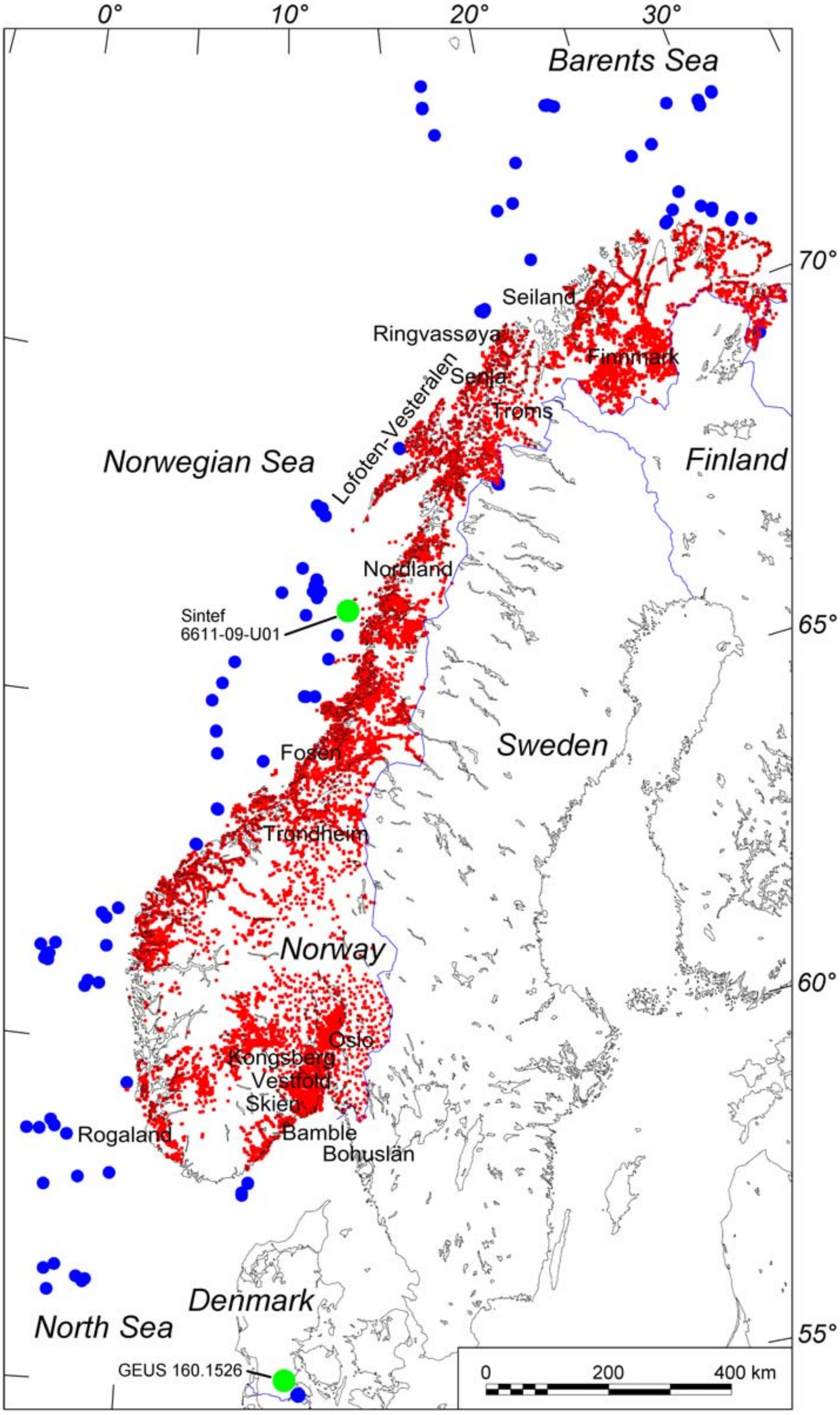

Fig. 6. Locations of petrophysical samples on the Norwegian mainland (red dots) and continental shelf (blue circles). The green circles show the locations of two drillholes offshore Nordland and in southern Denmark. The susceptibility logs of these two wells are shown in Figures 12 and 14, respectively.

magnetic layers generally varies from decimetres to a few tens of metres. We think that these rocks are representative of magnetic units within the stratigraphical column of the Norwegian continental shelf.

The Pleistocene overburden, especially glaciomarine clay, has even higher susceptibilities than the underlying sedimentary rocks (Table 4). The source of the Quaternary sediments is partly the very magnetic crystalline basement rocks in Scandinavia. The susceptibility values vary between 6 and 600×10^{-5} SI.

Susceptibility measurements on the Eocene volcanic rocks from the Vøring Basin were reported by Eldholm *et al.* (1987) and Kent & Opdyke (1978) and are listed in Table 3. These rocks are the most magnetic within the sedimentary basins on the Norwegian continental shelf and continental margin. They reveal high remanence intensities with alternating positive and negative directions (field reversals). Field reversals recorded in remanent magnetizations also cause the characteristic stripes over the oceanic crust in the Norwegian–Greenland Sea to the west (Fig. 3). The

NRM-directions carried by Permian volcanic rocks, as measured in the Oslo Rift by Thorning & Abrahamsen (1980) and Torsvik & Rehnström (2003), are characterized by a viscous component (close to the present-day Earth field direction) and by a flat-lying, slightly upward, Permian direction (Table 3).

Results

Basement structures

The aeromagnetic data show that the Precambrian igneous rocks of the Baltic Shield can be followed below the Caledonian nappes to the tectonic windows and to the western gneiss region in both southern and northern Norway (Figs 3 & 7a). They constitute parts of the Svecokarelian greenstone belts (Gaal & Gorbatschev 1987) in northern Norway and the continuous Transscandinavian Igneous Belt (TIB), and a north–south trending chain of Sveconorwegian post-collision granites in southern Norway (Smethurst *et al.* 1994). The two last-mentioned rock units are shown on the interpretation map in Figure 8. The TIB granitoids extend to great depths (*c.* 20 km, Olesen *et al.* 2002; Skilbrei *et al.* 2002). Analogous deep granitoids related to Mesozoic plate subduction occur within the Sierra Nevada Batholith in California (Ducea 2001). Consequently, the negative gravity field in the northern and central Scandinavian mountains seems to originate from intra-crustal, low-density rocks in addition to variations in the Moho depth (Olesen *et al.* 2002; Skilbrei *et al.* 2002; Ebbing & Olesen 2006). These results are in contrast to southern Norway where the mountains, to some extent, are supported by low-density rocks within the mantle (Olesen *et al.* 2002; Ebbing & Olesen 2006). The intrusive rocks in the Lofoten–Senja–Ringvassøya basement complex are interpreted to represent, in part, a deep level of the TIB (Griffin *et al.* 1978; Olesen *et al.* 1997*b*).

Distinctive, paired, negative–positive gravity anomalies can be observed along the Lapland Granulite Belt in northern Fennoscandia, and along the Kongsberg–Bamble Complex in southern Norway (Figs 5, 8 & 9a). These anomalies have been attributed to lower crustal rocks occurring at a shallower level in the crust. The emplacement of high-grade and high-density lower crustal rocks on top of upper crustal rocks produces the distinct paired gravity anomaly with a steep gradient along the suture zone and a much gentler gradient on the hinterland side. The asymmetry of the gravity anomalies along the Lapland Granulite Belt and Kongsberg–Bamble Complex, combined with the steep gradient, points to the overthrusted high-grade and high-density granulites as the main source of the observed positive gravity anomaly (Midtun 1988; Ebbing *et al.* 2007). Similar paired anomalies have been observed along other Palaeo- to Meso-Proterozoic suture zones in Canada (Gibb *et al.* 1983), India (Narain & Subrahmanyam 1986; Mishra *et al.* 2006) and South Africa (Emenike 1986), and along Neoproterozoic and Early Phanerozoic mobile belts in western Africa and Brazil (Lesquer *et al.* 1984) and in Australia (Forman & Shaw 1973). The northwestward thrusting of the Kongsberg–Bamble Complex is supported by reflection seismic data in the Skagerrak area (Lie & Husebye 1994; Balling 2000). The Bouguer gravity anomaly associated with the Kongsberg–Bamble Complex can be traced southwards through the Kattegat to the Scania region in southern Sweden. This anomaly has previously been related to deep-seated mafic intrusions of Permian age (Thybo 2000), but this model could not explain the asymmetry of the anomaly. We present an alternative model in Figure 9b where lower crustal rocks are thrust on top of upper crustal rocks along a Sveconorwegian suture zone. The regional suture zones were later reactivated as continental rifts, that is the Oslo Rift to the north and the Norwegian–Danish Basin to the south. This concept of gravity field modelling can also be applied to the Mid-Norwegian continental shelf and partially explains the observed high-density rocks occurring below the Møre and Vøring basins and in the Lofoten area (Olesen *et al.* 2002; Osmundsen & Ebbing 2008).

Coinciding positive gravity anomalies and negative magnetic anomalies offshore Kristiansand and in central Jutland can also be related to Neoproterozoic intrusions. Gravity and magnetic anomalies have previously been interpreted to indicate strongly magnetic Permian or even Cenozoic intrusive bodies beneath the Skagerrak, such as the 'Skagerrak volcano' (Sharma 1970; Åm 1973*b*), and beneath Silkeborg in Denmark (Thybo & Schönharting 1991). Combined modelling of the magnetic and gravity anomalies over these rock bodies has, however, indicated that a steep upward magnetization is required to explain the magnetic anomalies at the surface (Olesen *et al.* 2004), reminiscent of the magnetic direction in the Sveconorwegian rocks of the Rogaland Igneous Province in southern Norway (McEnroe *et al.* 1996, 2001). The younger rocks of the Permian Oslo Rift region have an intermediate and flat magnetization (Torsvik *et al.* 1998; Torsvik & Rehnström 2003) that is inadequate to explain the observed magnetic field. The positive part of the Skagerrak magnetic anomaly is continuous with the induced anomalies associated with the eastward extension of the Rogaland Igneous Province (shown as anorthosite complex, RIP, in Fig. 8). This relationship also suggests that rocks of the Rogaland Igneous Province and its offshore extension are responsible for the Skagerrak anomalies. Both the negative, remanence-dominated, magnetic anomaly and the positive gravity anomaly can be modelled using constraints from seismic reflection lines, the available density data and rock-magnetic properties (Olesen *et al.* 2004). A 7 km-thick complex of ultramafic/mafic intrusions is located below a southward-dipping, 1–4 km-thick section of Mesozoic sediments and 1–2 km of Palaeozoic sedimentary rocks. The application of similar petrophysical properties in the forward modelling of the Silkeborg magmatic body (SMB in Fig. 8) provides a more likely explanation of the observed gravity and magnetic anomalies as compared with earlier studies. Integrated modelling shows that a model with a reverse magnetic body (anorthosite?) situated above a dense, mafic/ultramafic body may account for the Silkeborg anomalies.

Figure 8 shows the spatial relationship between core complexes, low-angle detachments and the TIB. In our interpretation, the TIB can tentatively be followed all the way into the Barents Sea (Fig. 8). The lower crustal rocks were exhumed along the low-angle detachments during a late phase of the Scandian orogeny (Osmundsen *et al.* 2002, 2003, 2006). Of particular interest is the recognition of the structurally denuded basement culminations in mainland Norway, and their bounding detachments. These major detachments formed mainly during a phase of orogen-parallel extension (Figs 8 & 10) (Braathen *et al.* 2000, 2002).

Detachments of similar age and style have been mapped in East Greenland: the Fjord Region and Ardencaple Detachments (Hartz *et al.* 2002). Mapping in Norway and East Greenland has revealed the presence of NE–SW-trending (orogen-parallel), Late-Scandian gravity collapse structures. The Kollstraumen Detachment and the Nesna and Sagfjord shear zones extend northwestwards below the Helgeland, Vestfjorden and Ribban basins. Down-faulted, low-magnetic, Caledonian nappes are interpreted to constitute the 'basement' SW of the Bivrost Lineament. Such an interpretation is supported by the correspondence between the depth extent of the low-magnetic nappes on land and the thickness of the offshore low-magnetic basement (calculated as the difference between the offshore magnetic depth estimates and the depths obtained from gravity and seismic interpretations). Some of the offshore, low-magnetic basement may also comprise Devonian sandstones deposited above the offshore extensions of the Nesna and Kollstraumen detachments, that is similar to the tectonic situation farther south along the Nordfjord–Sogn and

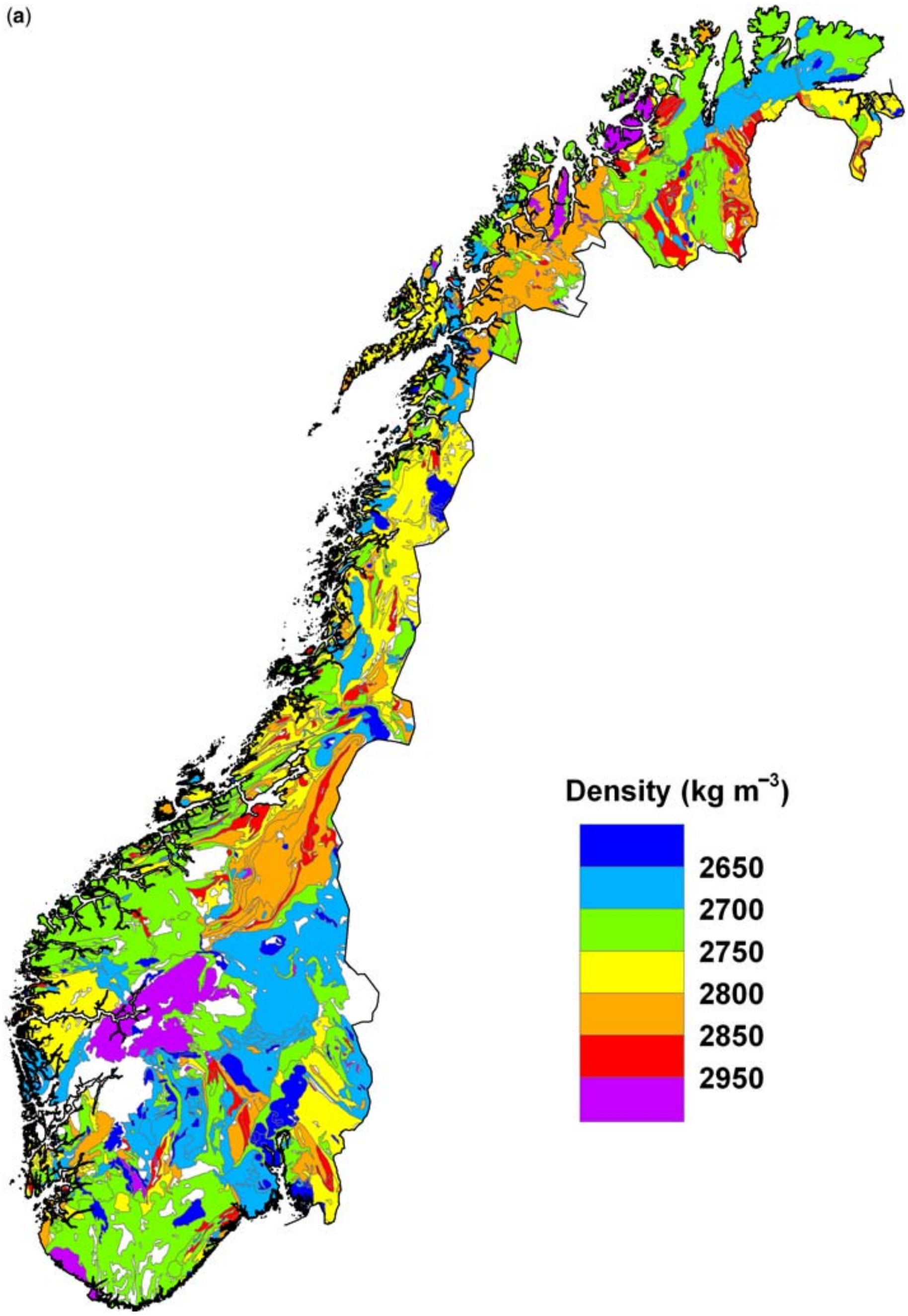

Fig. 7. (**a**) Average density in kg m^{-3}.

Table 2. Magnetic properties of basement rocks from the coastal part of mainland Norway

Rock type	Location	No.	Susceptibility	Q-value	NRM Dec./Inc.	Reference
Greenstone	Alta-Kautokeino, Finnmark	698	0.003	0.21		Olesen *et al.* (1990)
Gabbro	Seiland, Finnmark	78	0.019	0.71		Olesen *et al.* (1990)
Gneiss	Senja and Kvaløya, Troms	500	0.005	0.59		Olesen *et al.* (1997*b*)
Gneiss	Vesterålen, granulite facies	153	0.021	0.27	$2/81$ ($n = 11$)	Olesen *et al.* (1991)
Gneiss	Vesterålen, amphibolite facies	98	0.001	2.0		Olesen *et al.* (1991)
Gneiss	Roan, Fosen Peninsula	66	0.023	0.25	$348/74$ ($n = 10$)	Skilbrei *et al.* (1991)
Gabbro	Smøla	11	0.020			Sindre (1977)
Norite	Tellnes, Rogaland	191	0.037	7.3	$293/-64$ ($n = 32$)	McEnroe *et al.* (1996)

Declination (Dec.) and inclination (Inc.) of the NRM are reported from some of the locations. No., number of samples.

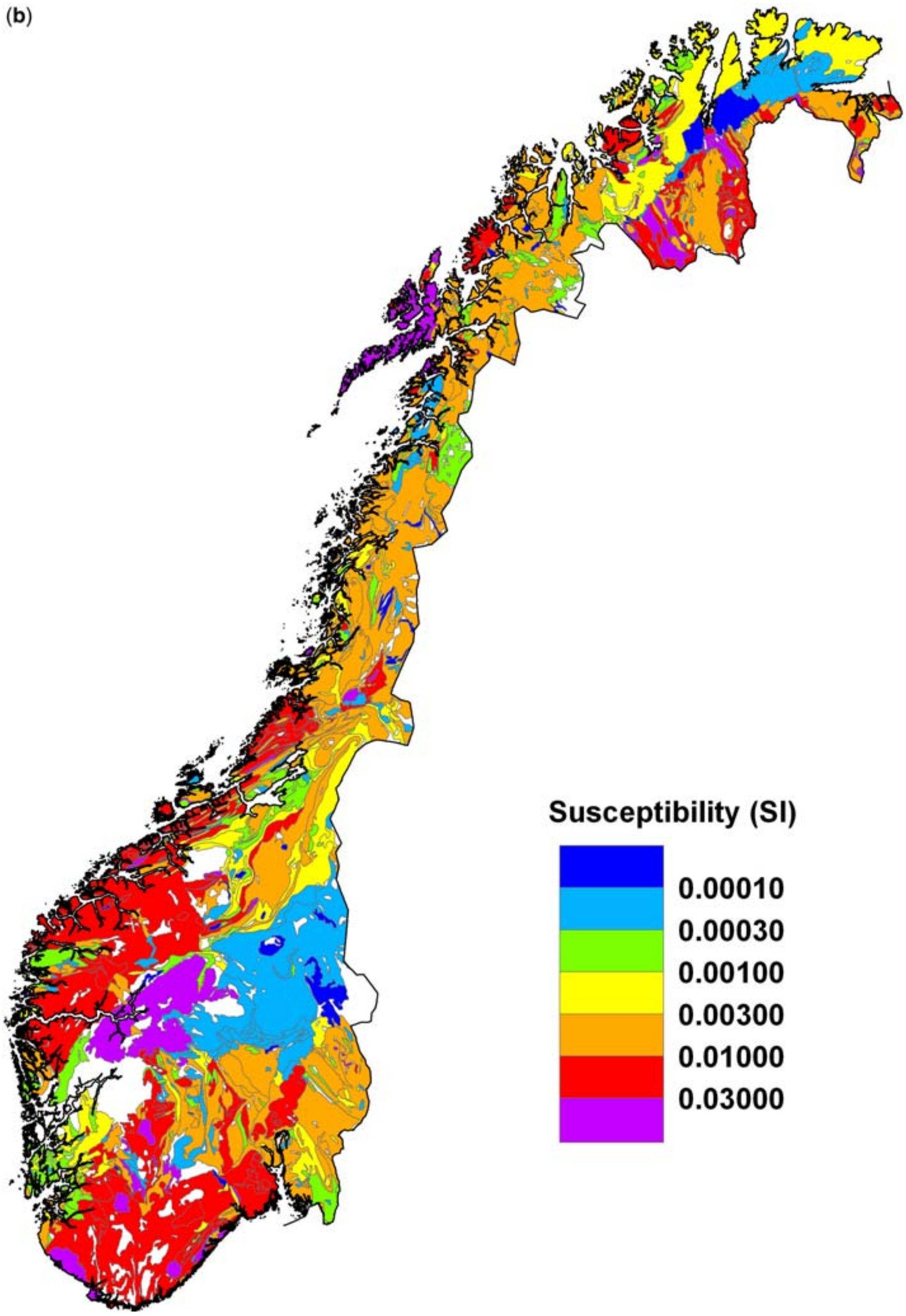

Fig. 7. (*Continued*) (**b**) Average susceptibility in SI units of bedrock samples within each geological unit on the Norwegian part of the northern Europe bedrock map (Sigmond 2002). The applied colour scale for the susceptibility data is logarithmic to depict the wide distributions of mean values.

Høybakken detachments. The major basement detachment structures coincide with major discontinuities in the NE–SW trending basement blocks within the offshore Late Palaeozoic and Mesozoic rifts (Olesen *et al.* 2002; Osmundsen *et al.* 2002). The detachments controlled the location of the younger transfer zones. The major Bivrost transfer zone also coincides with regional changes in Moho depth (Olesen *et al.* 2002) and is consequently a deep-seated crustal feature, characteristic of segmentation of the margin.

Modelling of the aeromagnetic data suggests that the Bivrost Lineament is a detachment dipping 5–15° to the SW (Olesen *et al.* 2002). Undulations of the offshore extension of the Sagfjord shear zone (SSZ) may have governed the location of the large-scale, Mesozoic, normal fault zones that bound the sides of the Lofoten and Utrøst Ridges (Olesen *et al.* 2002). The Nesna Shear Zone (Fig. 8) can be extended in more detail along the Bivrost Lineament to the continent–ocean boundary and may possibly be represented on the East Greenland margin as the northern Ardencaple Fjord detachment (NAD; Fig. 8). In a similar way, the Kollstraumen and Høybakken detachments can be traced across the Trøndelag Platform and may appear again on the East Greenland Margin as the southern Ardencaple Fjord detachment and northern segment of the Fjord Region Detachment system.

A section of the offshore extension of the Kollstraumen detachment trends ENE–WSW and coincides partly with the Ylvingen Fault (Fig. 11), indicating that Late Mesozoic structures are governed by deep-seated structures. Negative and positive gravity anomalies on the continental shelf reflect, to a large extent, sedimentary basins and structural highs, respectively, and can also be utilized to interpret the depth to crystalline basement as shown by Ebbing & Olesen (2010). Recent thermo-kinematical modelling (Gernigon *et al.* 2006; Wangen *et al.* 2008) has shown that the magnetization of the offshore basement can decrease at the COT

Table 3. Magnetic properties of Permian volcanic rocks on the mainland of southern Scandinavia (Åm & Oftedahl 1977; Thorning & Abrahamsen 1980; Torsvik & Rehnström 2003) and drillcore samples of Cenozoic igneous rocks from the Vøring area sampled in the Deep Sea Drilling Project (DSDP) and Ocean Drilling Program (ODP) in 1974 and 1985, respectively (Kent & Opdyke 1978; Eldholm *et al.* 1987). The ODP susceptibility data are claimed to be in cgs units, but they are most likely in SI units because a corresponding magnetite content of 30–40% in the volcanic rocks is highly unlikely

Rock type	Location	No.	Mean susceptibility	Q-value	NRM Dec./Inc.	Reference
Basalt	Bærum & Oslo	20	0.072	0.3		Åm & Oftedahl (1977)
Basalt	Vestfold	42	0.067	0.8		Åm & Oftedahl (1977)
Basalt	Skien	60	0.109	1.3		Åm & Oftedahl (1977)
Diabase	Bohuslän	6	0.068	0.66	$181/-6$ ($n = 5$)	Thorning & Abrahamsen (1980)
					$264/81$ ($n = 1$)	
Diabase	Tvedestrand, Vestfold	15	0.015	2.7	$216/-27$ ($n = 15$)	Torsvik & Rehnström (2003)
Basalt	Vøring Basin (site 338)	7	0.016	4.8	?/70.4	Kent & Opdyke (1978)
Basalt	Vøring Basin (site 342)	3	0.015	2.3	$?/-81.0$	Kent & Opdyke (1978)
Basalt	Vøring Basin (site 642)	221	0.030	4.1	$?/-63.0$	Eldholm *et al.* (1987)

(continent–ocean transition) to zero at a minimum depth of 20–25 km where the basement rocks locally reach the Curie temperature for magnetite (580 °C). In general, the magnetic pattern of the Mid-Norwegian margin reflects the depth to the high-magnetic basement below the Caledonian type basement, and not a change in the depth of the Curie temperature (Ebbing *et al.* 2009).

It is important to realize that structures of Palaeoproterozoic age similar to the Late-Caledonian core-complexes of Proterozoic rocks exist in northern Fennoscandia (Fig. 8). There, they have usually been referred to as gneiss domes (e.g. Lindroos & Henkel 1978; Midtun 1988; Henkel 1991; Olesen & Sandstad 1993) and are characterized by positive gravity and magnetic anomalies similar to the younger core complexes in Mid-Norway. The gneiss domes in northern Fennoscandia were most likely formed during a gravity collapse of the Svecofennian orogen that formed subsequent to continent–continent collision along the Lapland Granulite Belt (Fig. 8) (Marker 1985; Daly *et al.* 2006).

Further to the north in the Barents Sea, the isostatic gravity anomaly (Fig. 5) reveals the deep and narrow rift basins (e.g. Nordkapp basin), reflecting large changes in the geometry of the top basement. Even more spectacular is the magnetic signatures of the Loppa and Stappen highs (Fig. 3). Barrère *et al.* (2009) presented a division of basement types for the southwestern Barents Sea. In their interpretation, the Loppa High is caused by a core-complex upthrusting similar to core complexes on the

Table 4. Magnetic properties of sedimentary rocks from mainland Denmark and the continental shelf offshore Norway and Alaska

Rock type	Location	No.	Susceptibility	Q-value/NRM-intensity	Reference
Quaternary sand channel	Southern Jutland	257	0.00040		Merechi (2006)
Pleistocene sediments	Offshore Nordland, northern Norway, Triassic	55	0.00107		Mørk & Olesen (1995)
Miocene clay and sand	Southern Jutland	78	0.00004		Merechi (2006)
Sandstone	Brent Formation, Viking Graben	162	0.00013	0.20 0.001 A m^{-1}	Løvlie & van Veen (1995), Hauger & van Veen (1995)
Sandstone	Norwegian continental shelf, Triassic–Neogene	2912	0.00013		Mørk *et al.* (1996, 2002)
Claystone	Norwegian continental shelf, Triassic–Neogene	1685	0.00024		Mørk *et al.* (1996, 2002)
Coal	Norwegian continental shelf, Triassic–Jurassic	21	0.00007		Mørk *et al.* (1996, 2002)
Fe–Ti oxide-bearing sandstone	Offshore Nordland, northern Norway, Triassic	2	0.00133		Mørk & Olesen (1995)
Siderite-bearing sedimentary rocks	Norwegian continental shelf, Triassic–Palaeogene	520	0.00135		Mørk *et al.* (1996, 2002)
Fe–Ti oxide-bearing sandstone	Simpson Peninsula, Alaska, Cretaceous units	4	0.00140	0.07 0.004 A m^{-1}	Reynolds *et al.* (1994)
Siderite-bearing mudstone	Simpson Peninsula, Alaska, Cretaceous units	4	0.00240	0.02 0.002 A m^{-1}	Reynolds *et al.* (1994)
Caliche	Offshore Nordland, northern Norway	11	0.00057		Mørk & Olesen (1995)

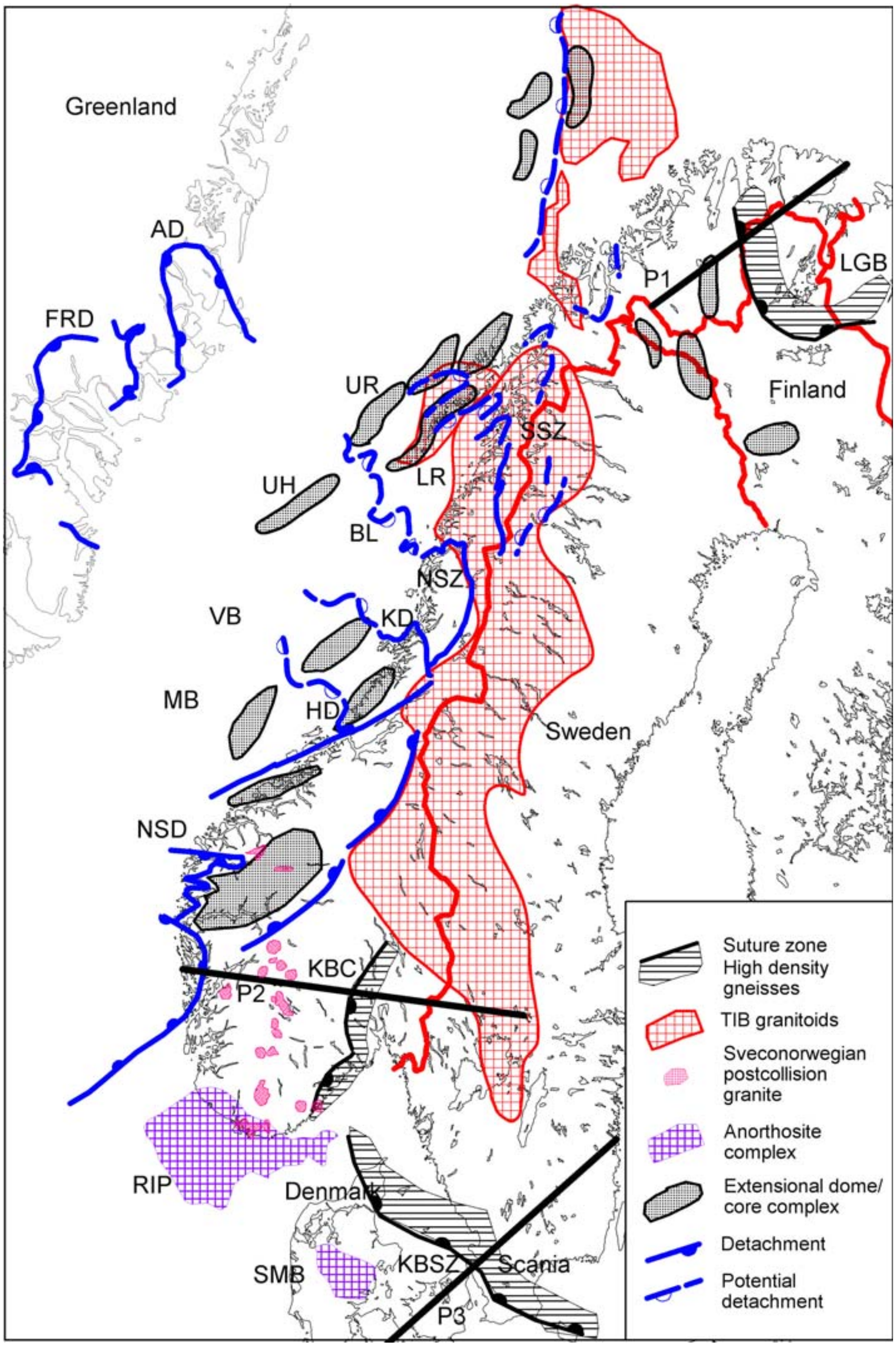

Fig. 8. Regional structures compiled from interpretations of potential field data and bedrock mapping (Lindroos & Henkel 1978; Midtun 1988; Henkel 1991; Olesen & Sandstad 1993; Braathen *et al.* 2002; Hartz *et al.* 2002; Olesen *et al.* 2002, 2004; Skilbrei *et al.* 2002; Ebbing *et al.* 2007; Barrère *et al.* 2009). Greenland is rotated back to pre-opening of the Atlantic in the Eocene. The Bouguer gravity along profiles P1, P2 and P3 is shown in Fig. 9. AD, Ardencaple Fjord Detachment; BL, Bivrost Lineament; FRD, Fjord Region Detachment system; HD, Høybakken Detachment; KBSZ, Kongsberg–Bornholm Suture Zone; KBC, Kongsberg–Bamble Complex; KD, Kollstraumen Detachment; LGB, Lapland Granulite Belt; LR, Lofoten Ridge; MB, Møre Basin; NSZ, Nesna Shear Zone; NSD, Nordfjord–Sogn Detachment; RIP, Rogaland Igneous Province; SSZ, Sagfjord Shear Zone; SMB, Silkeborg Magmatic Body; UH, Utgard High; UR, Utrøst Ridge; VB, Vøring Basin.

Mid-Norwegian margin (Osmundsen *et al.* 2002). Both highs, however, belong to an elbow-shaped feature that may conceivably be interpreted as the northward continuation of the TIB (Fig. 8). The detachment to the west of the inferred extension of the TIB is believed to mark the boundary between Baltica and Laurentia and can be traced southwards off Lofoten (Fig. 8). Although still tentative, the structural interpretation in Figure 8 provides a complete link between onshore and offshore structures for the entire Norwegian continental shelf and points to similarities of the structural style between the Mid-Norwegian margin and the southwestern Barents Sea.

Sedimentary subcrop pattern

The modern aeromagnetic surveys on the Mid-Norwegian shelf (Hunting-86, LAS-89, NAS-94 and VAS-98) have revealed several sets of high-frequency anomalies caused by magnetic sources within the sedimentary successions (Olesen & Smethurst 1995; Skilbrei & Kihle 1999; Olesen *et al.* 2002). When compared with susceptibility measurements on cores from the shallow drilling programme of SINTEF Petroleum Research (previously IKU; Mørk *et al.* 2002), the bulk of the anomaly pattern is caused by subcropping sedimentary rock units (Fig. 11). The asymmetry of

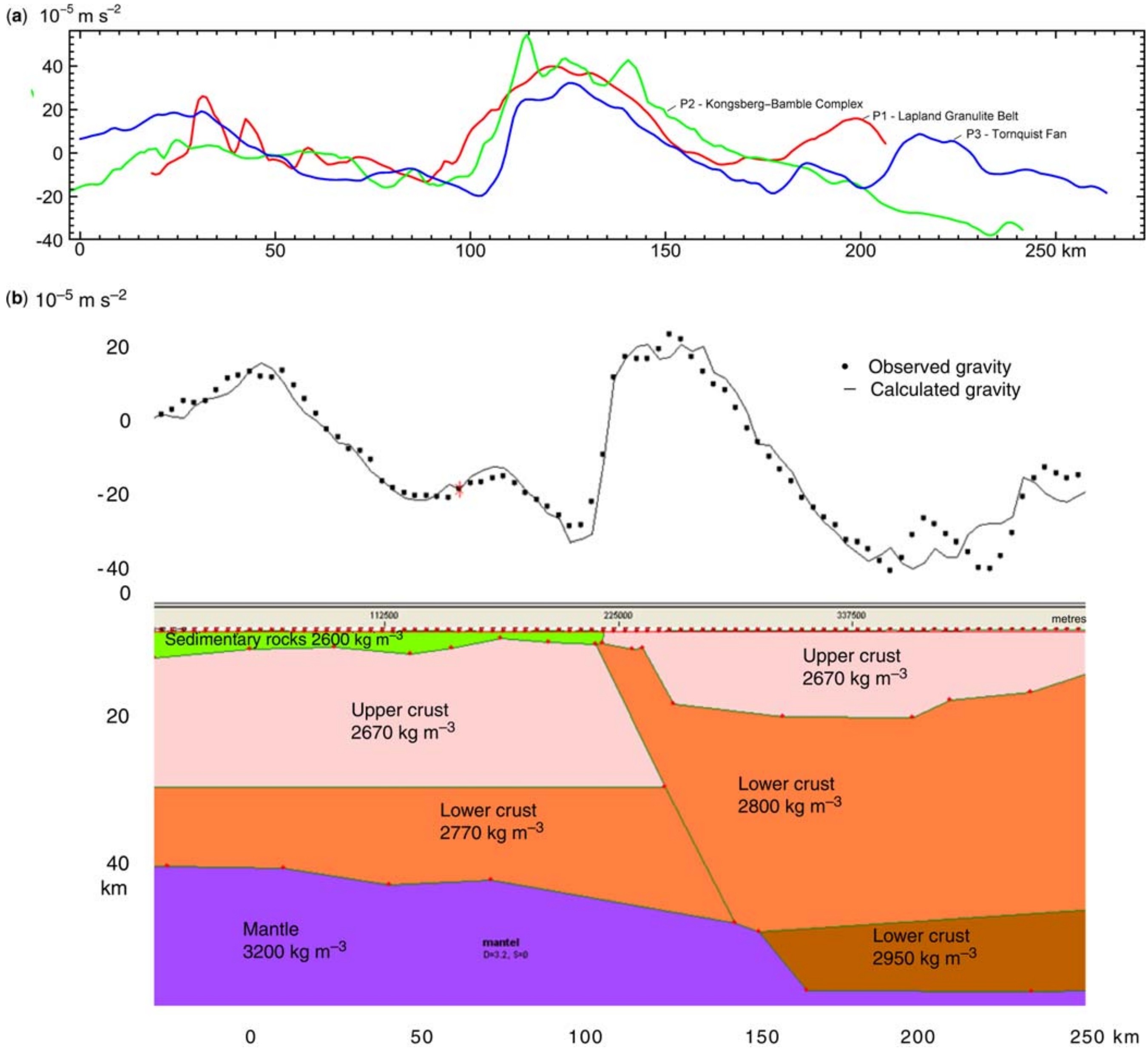

Fig. 9. (**a**) Bouguer gravity profiles across the Lapland Granulite Belt (red line), Kongsberg–Bamble Complex (green line) and Tornquist Fan (blue line). All three profiles have the same characteristics with a steep gradient to the west and a much gentler gradient to the east. This asymmetry is most likely caused by over-thrusted high-grade and high-density rocks. (**b**) Alternative interpretation of the Tornquist Fan (Profile P3). Previous interpretations have suggested that the gravity anomaly is caused by a more than 10 km-thick complex of Permian mafic intrusions (Thybo 2000). The location of profiles P1, P2 and P3 is shown in Figs 5 and 8.

the anomalies, with a steep gradient and a negative anomaly to the east and a more gentle gradient to the west (Olesen & Smethurst 1995), shows that the sources of the anomalies dip gently towards the west, consistent with interpretations of seismic data (Rokoengen *et al.* 1988). The susceptibility measurements on SINTEF Petroleum's cores (Table 4; Fig. 12) indicate that the positive, coast-parallel anomalies are caused by (1) alternating beds of sandstone and claystone/siltstone/mudstone, (2) siderite-cemented sedimentary rocks or (3) sedimentary units containing detrital Fe–Ti oxides (magnetite, ilmenite or hematite) or pyrrhotite. Negative anomalies are most likely caused by low-magnetic sandstones, gypsum or coal.

Another set of anomalies trends WSW–ENE (Fig. 11) and coincides with the graben segments of the Ylvingen Fault Zone bounding the Vega High. Susceptibility measurements on cores from the IKU shallow drilling programme (Table 4 and Mørk *et al.* 2002) show that Lower Cretaceous claystones and siltstones have higher susceptibilities than Jurassic sandstones. A susceptibility contrast between the Cretaceous sedimentary infill in the grabens along the Ylvingen Fault Zone and the juxtaposed Jurassic sandstones on both sides may explain the magnetic anomalies.

The lowest amplitude magnetic anomalies (commonly less than 1 nT) trend WNW–ESE and occur on the Trøndelag Platform between the Træna Basin in the west and the Nordland coast in the east (Olesen & Smethurst 1995). The only sedimentary unit on the shelf with such a wide geographical distribution is the Quaternary overburden. These anomalies are best seen on the north–south, horizontal, magnetic gradient maps. Comparisons with the Quaternary deposits map of Rise *et al.* (1988) show that some magnetic anomalies coincide with thick sequences of overburden. Some of the magnetic anomalies also coincide with other bathymetric features, such as in the Trændjupet area in the north. Susceptibility measurements (Table 4; Mørk & Olesen 1995) show that the overburden (especially glaciomarine clay) is frequently

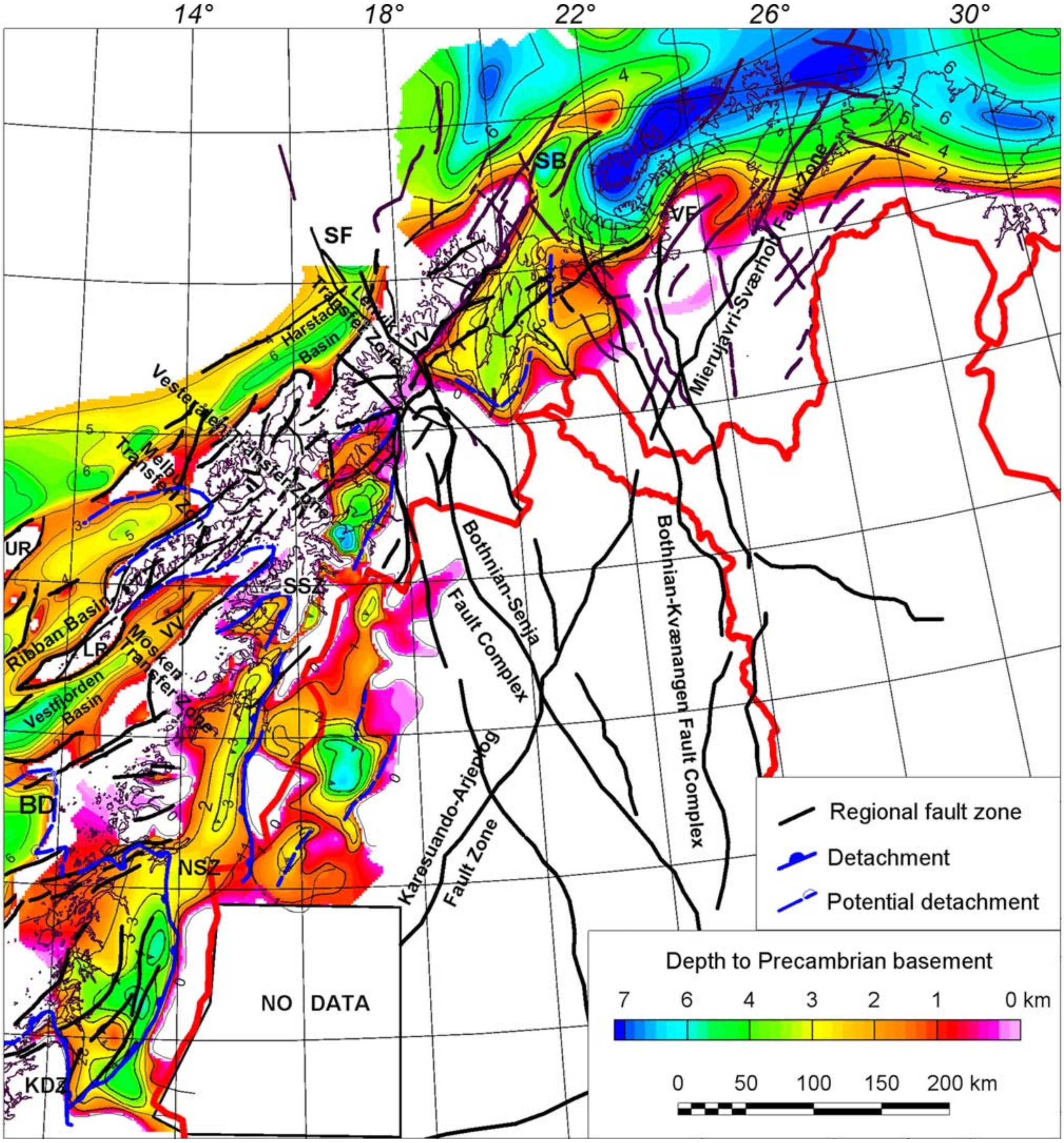

Fig. 10. Basement structure map from northern Norway compiled from Olesen *et al.* (1990, 1997*b*, 2002), Henkel (1991) and Braathen *et al.* (2002). BD, Bivrost Detachment; KDZ, Kollstraumen Detachment; LR, Lofoten Ridge; NSZ, Nesna Shear Zone; SB, Sørvær Basin; SF, Senja Fracture Zone; SSZ, Sagfjord Shear Zone; UR, Utrøst Ridge; VF, Vargsund Fault; VV, Vestfjorden–Vanna Fault Complex. Different methods, both automatic inversion methods and manual graphical methods, were utilized in the different studies and are described in the respective papers. The base of the Caledonian nappes extends to depths of more than 8 km.

more magnetic than the underlying sediments. The magnetic carriers were identified as magnetite and/or hematite.

Quaternary sand channels

A very distinct set of high-frequency, NE–SW to ENE–WSW-trending, aeromagnetic anomalies (Fig. 13a) occurs regionally in the Norwegian and Danish parts of the southern North Sea and is oriented perpendicular to the general trend of the subcropping Cenozoic and Mesozoic units (Sigmond 2002). The 5–50 km long curvilinear anomalies terminate towards the Norwegian Channel to the NE at a water depth between 100 and 150 m. The symmetry of the anomaly curves and the general NE–SW trend indicate that deep incisions are cutting into Middle and Upper Miocene successions. Studies of 3D seismic data (e.g. Fig. 13b) from the area indeed show that the anomalies are caused by shallow sand channels (Olesen *et al.* 1997*c*; Gausland 1998; Fichler *et al.* 2005; Merechi 2006). Magnetic modelling (Olesen *et al.* 1997*c*; Merechi 2006) of one of these sand channels (250 m thickness and 2000 m width buried below 100 m of younger sediments) showed that a susceptibility of 500×10^{-6} SI was needed to generate a 2 nT amplitude anomaly. Susceptibility measurements on sand and gravel samples from a groundwater well *c*. 400 km to the SE on the mainland of Jutland show an

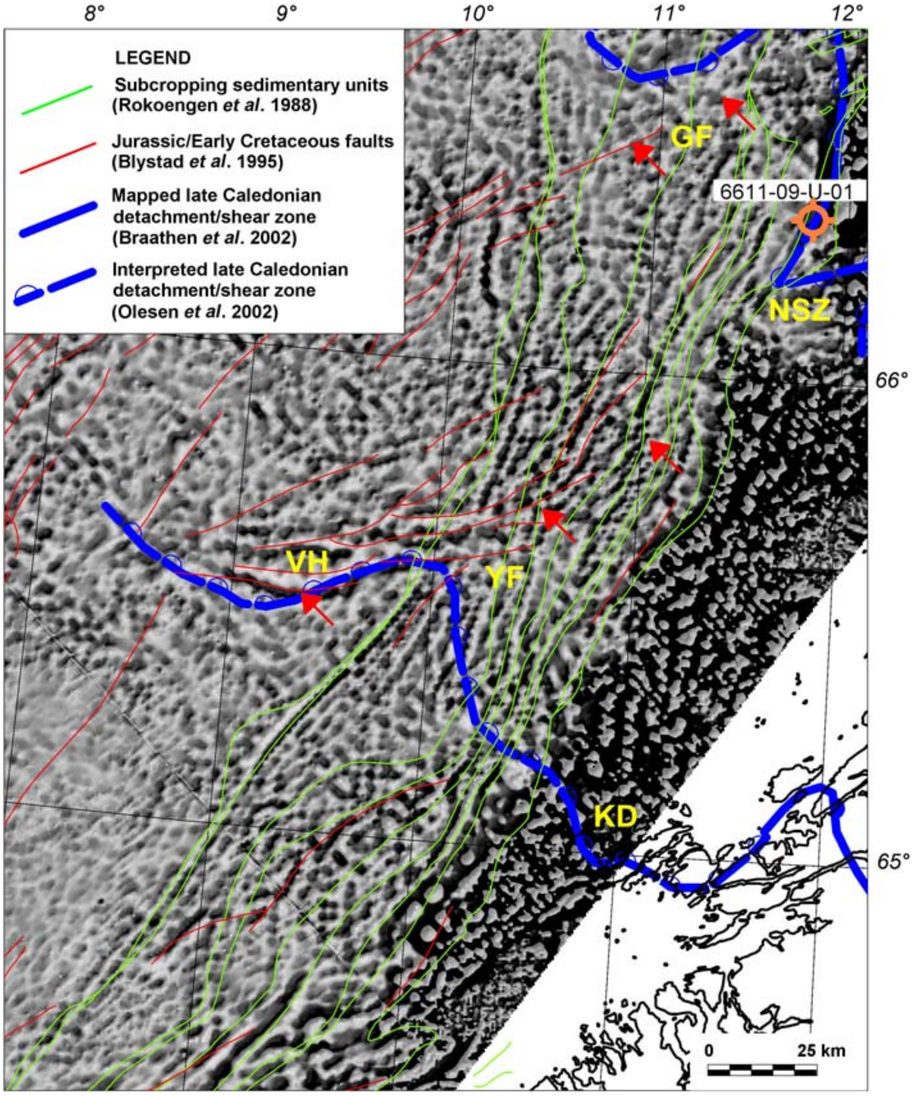

Fig. 11. Shaded relief map of analytic signal (total gradient amplitude) from high-resolution aeromagnetic surveys with superimposed subcrop pattern and Jurassic/Early Cretaceous faults (modified from Olesen *et al.* 2002). GF, Grønna Fault; KD, Kollstraumen Detachment; NSZ, Nesna Shear Zone; VH, Vega High; YF, Ylvingen Fault Zone. The map offers a plane view of the subcrop and fault pattern in the Nordland area. The red arrows show the offshore ENE–WSW-oriented Ylvingen and Grønna faults cutting through Late Palaeozoic and Mesozoic sedimentary rocks. The location of the map area is shown with a white frame in Figure 3.

average susceptibility of *c*. 360×10^{-6} SI from a Quaternary sand channel (Table 4 and Fig. 14). Magnetization along the present-day Earth field is assumed. These channels partly coincide with fault segments.

The varying orientation of the channels as they appear in the aeromagnetic dataset (Fig. 13a) may indicate that they represent channels of different age within the sedimentary column. A 3D seismic study has also revealed that at least two different generations of channels exist, since one set of channels is cutting another. These sand channels seem to occur widely beneath the northern continental shelf and lowlands of Europe. The origin of the channels, however, is contentious. Ehlers & Linke (1989) argued that the channels were eroded by end-glacial and subglacial meltwater and are consequently the erosive analogues of eskers in areas of soft, deformable bedrock. The channels were filled in by meltwater deposits when the ice sheet melted, and by Early Saalian time (before 130 000 years) the channels were completely filled. Wingfield (1990) considered that the major incisions are the product of a singular mechanism: the outburst of intra-ice-sheet lakes forming jøkulhlaup plunge pools (catastrophic meltwater release) in the marginal parts of the ice sheets. Kristensen *et al.* (2007) argues on the other hand that the valleys formed time-transgressively during ice retreat, whereby sediments eroded further up-ice were re-reposited along adverse subglacial slopes of the valleys close to the ice margin. The aeromagnetic method has proved to be an adequate tool for the mapping of sand channels in the North Sea, as has also been reported offshore Australia (Gunn 1997).

Salt-related magnetic anomalies

Three high-resolution, aeromagnetic surveys in the Barents Sea during the time period 2006–2008 have revealed negative magnetic anomalies partly caused by the magnetic properties of the exposed salt diapirs in the Nordkapp Basin (Løvaas *et al.* 2006; Fichler *et al.* 2007; Gernigon *et al.* 2007). Similar negative aeromagnetic anomalies have been observed in the Norwegian–Danish Basin (Olesen *et al.* 1997*c*). This phenomenon is only observable in the magnetic quiet zones, that is in the deep sedimentary basins. The negative anomalies are caused by the negative susceptibility of salt and anhydrite, that is diamagnetic behaviour. The salt-related magnetic anomalies are more pronounced in the

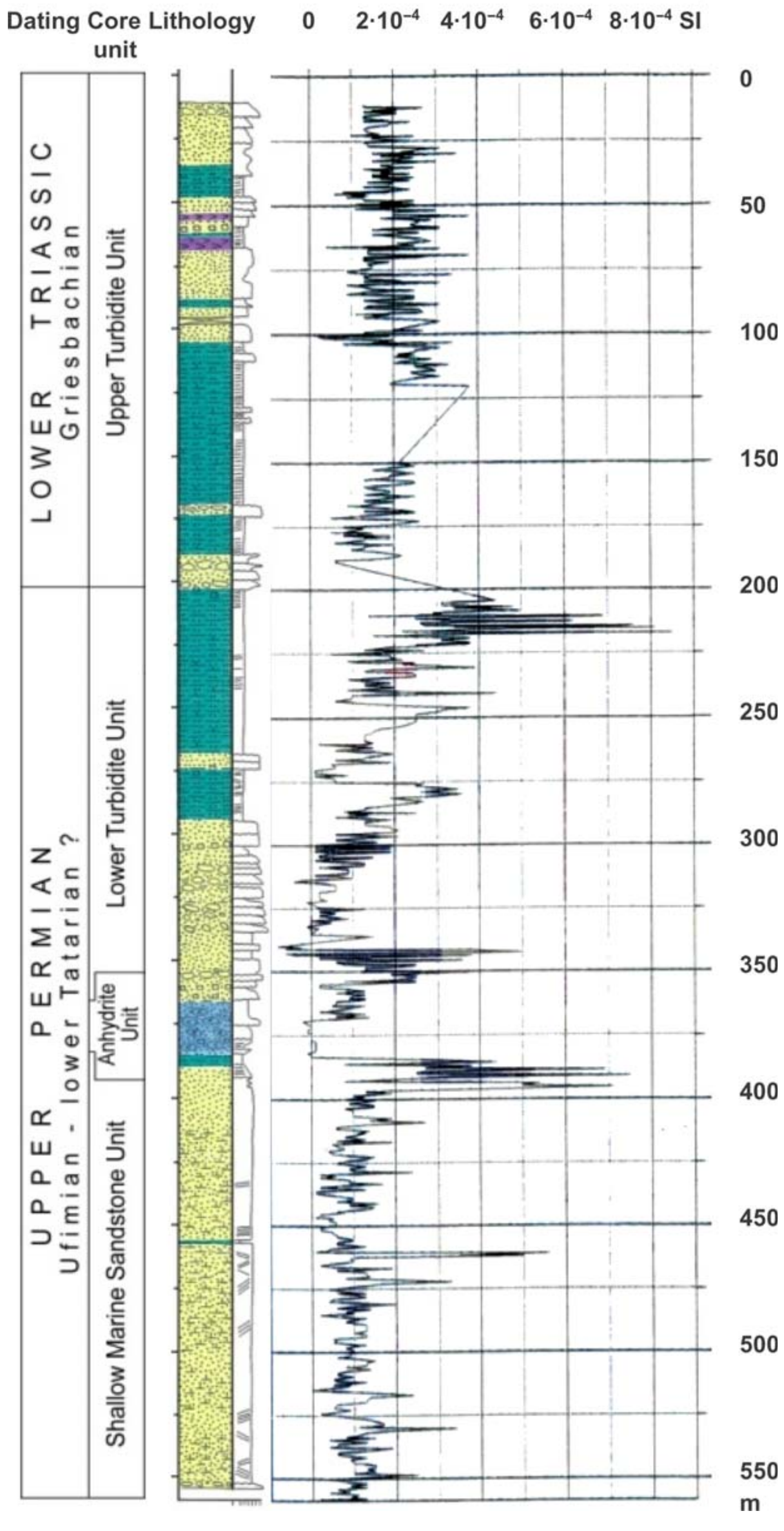

Fig. 12. Susceptibility log from the Nordland area, northern Norway (SINTEF Petroleum borehole no. 6611-09-U01) reveals that magnetic anomalies are caused by subcropping Palaeozoic and Mesozoic sedimentary rocks with varying contents of magnetic minerals such as siderite and detrital Fe–Ti oxides. The lithology and stratigraphy log is adapted from Bugge *et al.* (2002). The location of the bore hole is shown in Figure 6.

Barents Sea where significant Plio-Pleistocene glacial erosion and passive diapirism have allowed the salt diapirs to reach shallower levels.

Reflection-seismic investigation of salt diapirs commonly has problems in defining the base of the salt. To overcome this problem, gravity data are often used to distinguish between different models, particularly those defined from the seismic and salt-tectonic models. Gravity gradiometry has further improved the method by its higher accuracy, as well as by setting geometric constraints (Fichler *et al.* 2007). Inherent limitations, as density contrasts are the only rock parameters defining the gravity anomaly and its derivatives, lead to a number of limitations (Fichler *et al.* 2007):

(1) Sediment compaction leads to increased densities with depth, which causes a non-contrast zone (‘nil zone’; Bain *et al.*

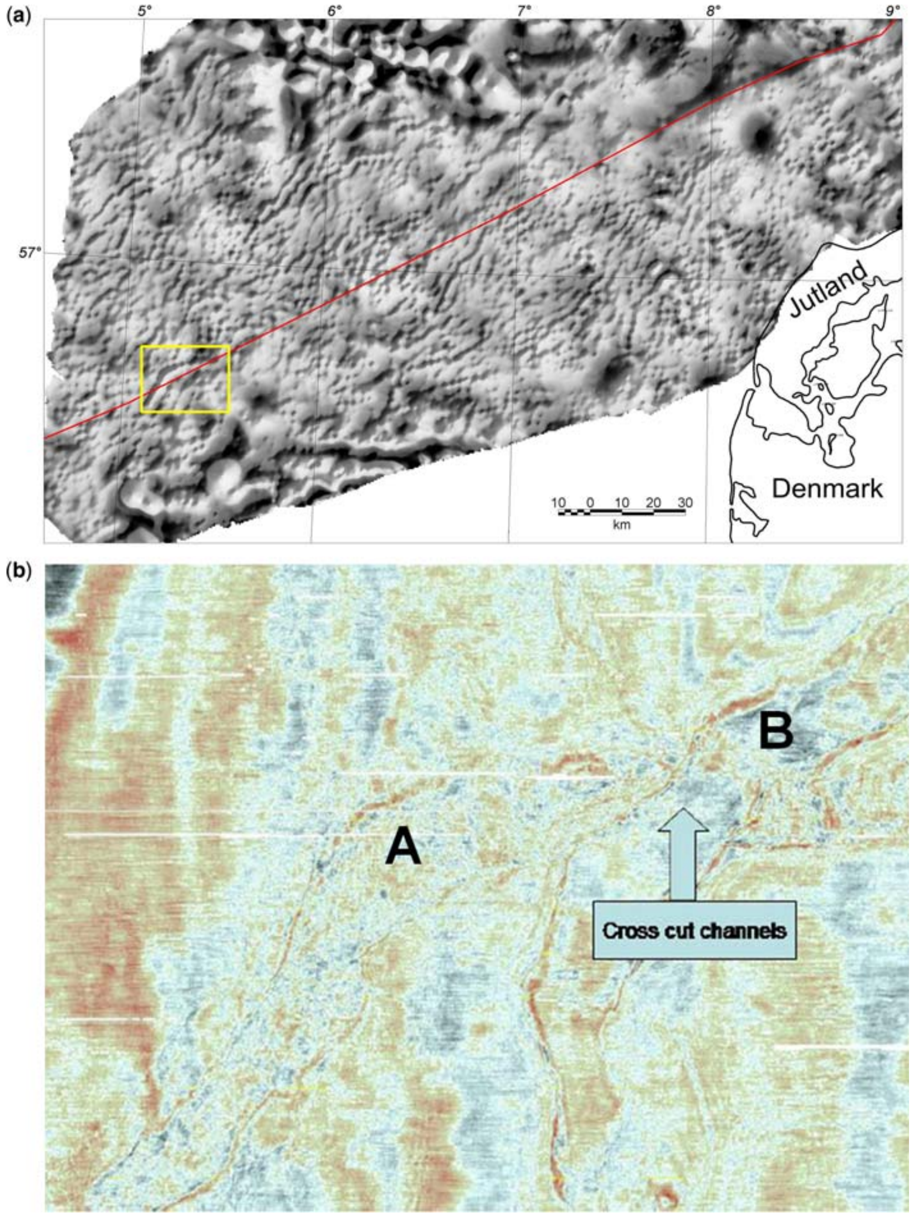

Fig. 13. (**a**) Analytical signal (total gradient amplitude) anomalies reflect Quaternary sand channels. The location of the map area is shown with a white frame in Figure 3. The WesternGeco NCS QUAD4 3D is located within the yellow frame. (**b**) Time slice at 320 ms (TWT) of the 3D seismic survey shows in detail that the pronounced aeromagnetic anomaly within the yellow frame on the map above coincides with a Quaternary sand channel (A) incised into the underlying Miocene sediments during subglacial drainage (Merechi 2006; Kristensen *et al.* 2007). The sand channel is cut by another channel (B) to the east which is less pronounced on the aeromagnetic map.

1993) where salt and sediment densities are similar. Salt occurring above and below the nil zone produces gravity anomalies of the opposite direction, which result in destructive interference.

(2) The mineral composition of a salt diapir is rarely pure halite and a whole suite of evaporite minerals may be present. Anhydrites with densities up to 2.9 g cm^{-3} have the most marked deviation from 'normal' salt density.

(3) Negative gravity anomalies from depths below the salt diapirs can be caused by deep salt, that is a salt pillow, feeder or mother salt, but also by fault throws in basins below the salt diapirs. By conventional gravity alone, we cannot distinguish between these sources.

Magnetic data have none of these problems. Induced magnetic susceptibilities of sediments are generally positive, whereas the susceptibilities of evaporite rocks, including both halite and anhydrite, are usually weakly negative. This will effectively overcome the limitations for the densities described in (1) and (2). Problem (3) can also be solved by magnetics, as a basement fault will normally generate a much stronger magnetic anomaly than any salt feature, due to a much higher susceptibility contrast.

Fichler *et al.* (2007) produced an integrated 3D interpretation of a salt diapir from seismic, magnetic and gravity gradiometry data (Fig. 15). The salt diapir is located within the SNAS-06 survey (Løvaas *et al.* 2006) shown in Figure 3. The petrophysical database (Fig. 6) was used to constrain the susceptibility and remanence of the different rock bodies in the 3D model.

North Atlantic oceanic spreading

Remapping of the oceanic crust with improved magnetometers and navigation has also improved our understanding of the early spreading history and structure of the Norwegian–Greenland Sea.

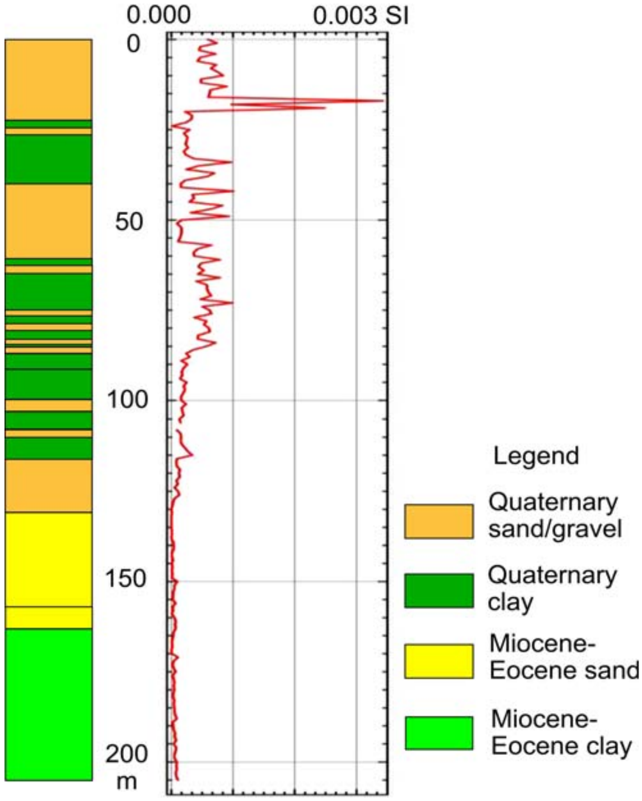

Fig. 14. Lithological and susceptibility log from southern Jutland (GEUS borehole no. 160.1526) reveals that magnetic anomalies are caused by Quaternary channels containing sand and gravel derived from the Fennoscandian Shield. Low-magnetic Miocene sediments were encountered at a depth of *c*. 129 m. The location of the borehole is shown in Figure 6.

Transfer zones have previously been associated with oceanic fracture zones along the Mid-Norwegian and East-Greenland margins (Tsikalas *et al.* 2002). Transfer zones are important entry points for sedimentary drainage systems, a relationship that has also been suggested for the transport of Cretaceous sands to the Mid-Norwegian margin. Tectonic reconstruction using the new aeromagnetic datasets has shown that the Cenozoic opening of the Norwegian–Greenland Sea between the Jan Mayen and Senja fracture zones occurred along a stable axis without offsets of the oceanic spreading anomalies and without jumps in the spreading axis (Fig. 16; Olesen *et al.* 2007). Consequently, our new interpretations have implications for evaluating the petroleum potential in the Vøring Basin.

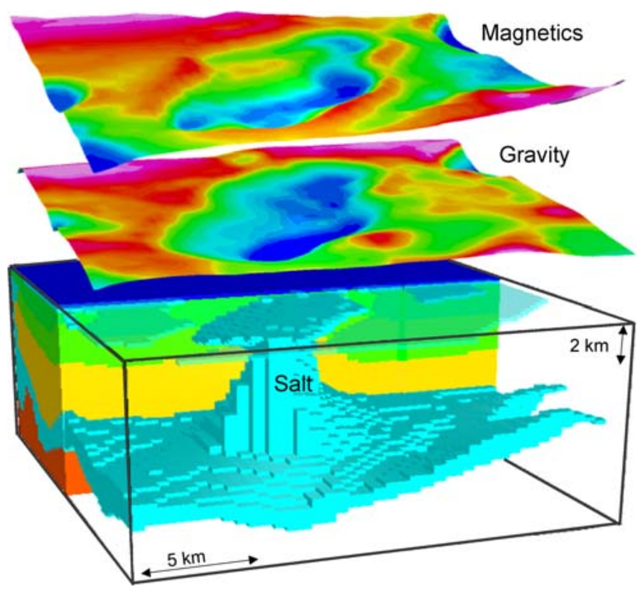

Fig. 15. Magnetic data (vertical derivative of TMI), gravity gradiometry data (gzz) and a possible model for the salt diapir displayed as a 3D grid in a simplified sedimentary strata (Fichler *et al.* 2007).

Palaeogeographic reconstruction of the aeromagnetic map to Anomaly 22 (Fig. 16) has revealed a major discordance on the East Greenland and Mid-Norway margins, between the NAD and the SSZ, marking the boundary between clearly differentiated anomalies 23 and 24, to the NE, from a much more diffuse pattern to the west. The irregular magnetic pattern is most likely due to more igneous activity to the west during the early stage of oceanic spreading. The palaeogeographic reconstruction shows also a *c*. 50 km-wide magnetic anomaly cutting across spreading anomalies 24A, 24B and 23 from the Vøring Marginal High on the Norwegian margin to Traill Ø on the East Greenland coast (Fig. 16). The anomaly is interpreted to represent an igneous complex referred to as the Traill–Vøring igneous complex (TVIC). The complex cuts across anomaly 22 on the Greenland margin, suggesting that this atypical and oblique igneous activity was active until *c*. 50 Ma. This magmatism may be associated with a previously proposed, NNE–SSW-trending, initial magmatic lineament (IML) extending between Traill Ø and Kangerlussuaq (Larsen 1988). The IML has been suggested to relate to a failed attempt of direct linkage between the Reykjanes and Mohns Ridges. The magnetic response of the TVIC along the Vøring margin has previously been interpreted as representing anomaly 24A and 24B (Hagevang *et al.* 1983). Interpretation of a more recent aeromagnetic survey along the Jan Mayen Fracture Zone (JMFZ) has revealed that the TVIC may represent the leaky transform of a pseudo triple junction resembling the present-day tectonic situation observed on the Azores Plateau in the Central Atlantic (Fig. 17; Gernigon *et al.* 2009).

The new aeromagnetic surveys in the Norwegian–Greenland Sea have allowed us to significantly refine our knowledge of the structure of the JMFZ (Gernigon *et al.* 2009). The JMFZ is a complex oceanic corridor affected by episodic phases of anomalous accretion, observed and modelled along the Vøring Spur (VS) (Fig. 1). The VS represents an atypical bathymetric high, west of the Vøring Marginal High. The origin of the VS is tectonic and partly related to deep magmatic processes. Anomalous melt production and crustal thickening observed along the VS is due to Eocene overcrusting formed during the spreading between the Lofoten Basin and the VS (Gernigon *et al.* 2009). The thickening of the oceanic crust is syn-accretion and is not necessarily related to Late Miocene underplating (post-accretion), as previously assumed by Breivik *et al.* (2008). In the model of Gernigon *et al.* (2009), anomalous melt production started near the Vøring Basin during breakup and continued episodically to the west along the trend of the Jan Mayen leaky transform.

Spreading rates between the Ægir and Mohns ridges have also been refined, thanks to the new magnetic compilation, and differ by *c*. 2 mm a^{-1} for much of the period ranging from continental breakup to extinction of the Ægir Ridge. The contrasting spreading rates on either side of the Jan Mayen Fracture Zone should have resulted in dextral strike-slip along the EJMFZ and perhaps along the palaeo-JMFZ on the continental side, in turn resulting in inversion of the Vøring Basin, as was also suggested by for example, Mosar *et al.* (2002). According to seismic interpretations of inversion structures in the Vøring Margin, inversion has been going on from continental breakup until present-day either by discrete pulses (Lundin & Doré 2002; Gómez & Vergés 2005) or more or less continuously (Vågnes *et al.* 1998). There is an apparent lack

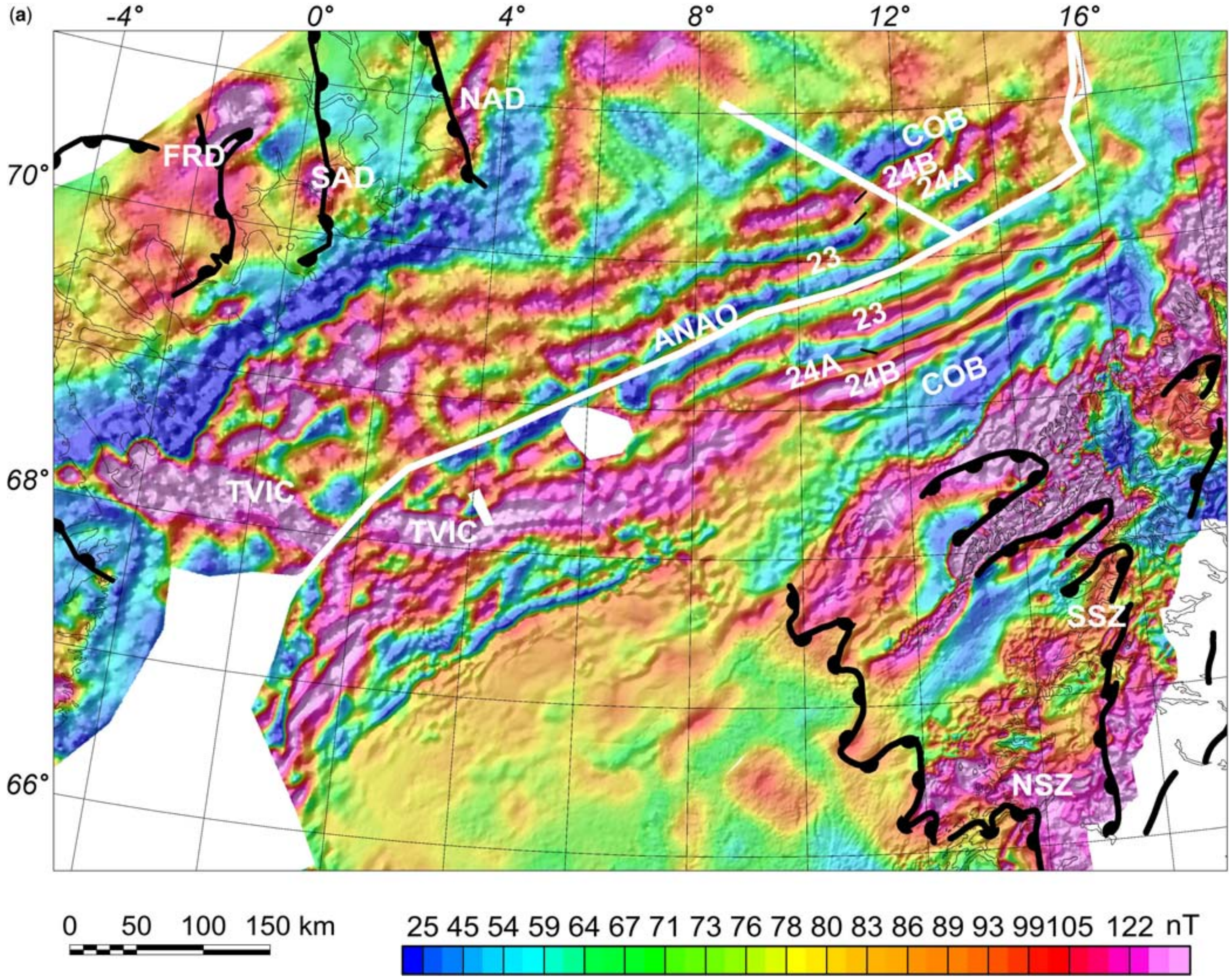

Fig. 16. (**a**) Reconstruction of the Greenland margin aeromagnetic data to Chron 22 (*c*. 49.7 Ma). Note that the *c*. 50 km-wide, diffuse, high-amplitude aeromagnetic anomaly to the NW of the Vøring Marginal High appears to be continuous across the oceanic spreading anomalies 23, 24A and 24B as far as Traill Ø (on the East Greenland coast) where Cenozoic igneous complexes occur at the surface. This anomaly has earlier been interpreted as anomalies 24A and 24B in the Norwegian Sea. The width of the anomaly, however, is considerably wider than the corresponding anomalies offshore Lofoten farther to the north. The anomaly is most likely caused by an igneous complex (referred to as the Traill–Vøring igneous complex). The introduction of this inferred igneous complex simplifies the initial opening history and excludes the need to invoke the abandoned spreading ridge and the Gleipne and Bivrost fracture zones along the Vøring margin (e.g. as in Hagevang *et al.* 1983; Blystad *et al.* 1995). The bold black lines show the Late-Caledonian detachment zones of Braathen *et al.* (2000, 2002), Hartz *et al.* (2002) and Olesen *et al.* (2002). ANAO, axis of North Atlantic opening. White holes represent gaps in the data coverage. (**b**) Reconstruction of tectonic interpretations to Chron 22 (49.7 Ma). Regional basement faults and sill intrusions on the Vøring Lofoten continental margin. Note that the TVIC intrudes continental crust on either side of the early Norwegian-Greenland Sea. COB, continent–ocean boundary; EJMFZ, Eastern Jan Mayen Fracture Zone; WJMFZ, future location of Western Jan Mayen Fracture Zone; IML, northern termination of the initial magmatic lineament; TVIC, Traill–Vøring igneous complex; SSZ, Sagfjord Shear Zone; NSZ, Nesna Shear Zone; NAD, Northern Ardencaple Fjord Detachment; SAD, Southern Ardencaple Fjord Detachment; FRD, Fjord Region Detachment system; SGFZ, Senja–Greenland Fracture Zone. Modified from Larsen (1988), Brekke (2000), Braathen *et al.* (2002), Hartz *et al.* (2002), Olesen *et al.* (2002, 2007), Osmundsen *et al.* (2003, 2006), Ebbing *et al.* (2006) and Gernigon *et al.* (2009).

of consensus on the precise timing but most authors agree on a marked inversion phase from Early Eocene until Early Oligocene. This has been tested using 2D finite-element techniques involving elasto-plastic rheologies and contact elements (Olesen *et al.* 2006). Three main domains were defined according to their rheological parameters (Fig. 18): (1) the oceanic domain assumed to be relatively rigid, (2) the continental domain (i.e. margin) where plastic parameters were selected in order to simulate yielding of weakened crust, and (3) the JMFZ, a 50 km wide zone in the model, also assumed to be relatively weak. In this preliminary modelling attempt, the boundary conditions depicted in Figure 18a were applied for a time period of 5 Ma. Our modelling suggests that shortening of the Vøring Margin occurred between continental breakup and extinction of the Aegir Ridge and could have reached up to *c*. 10% in the first 5 Ma. However, the shortening is far from being uniform and is predicted to have mainly affected the COB and the eastern end of the palaeo-JMFZ (Fig. 18b). We speculate that inversion also occurred later than Oligocene due to a different mechanism than the one represented in this model (see Olesen *et al.* 2006).

Conclusions

(1) Modern high-resolution aeromagnetic and gravity data along the Norwegian shelf and continental margin have revealed previously unknown geological structures, and led to refinements in our knowledge of existing ones. This is partly due to the use of more sensitive magnetometers, closer line

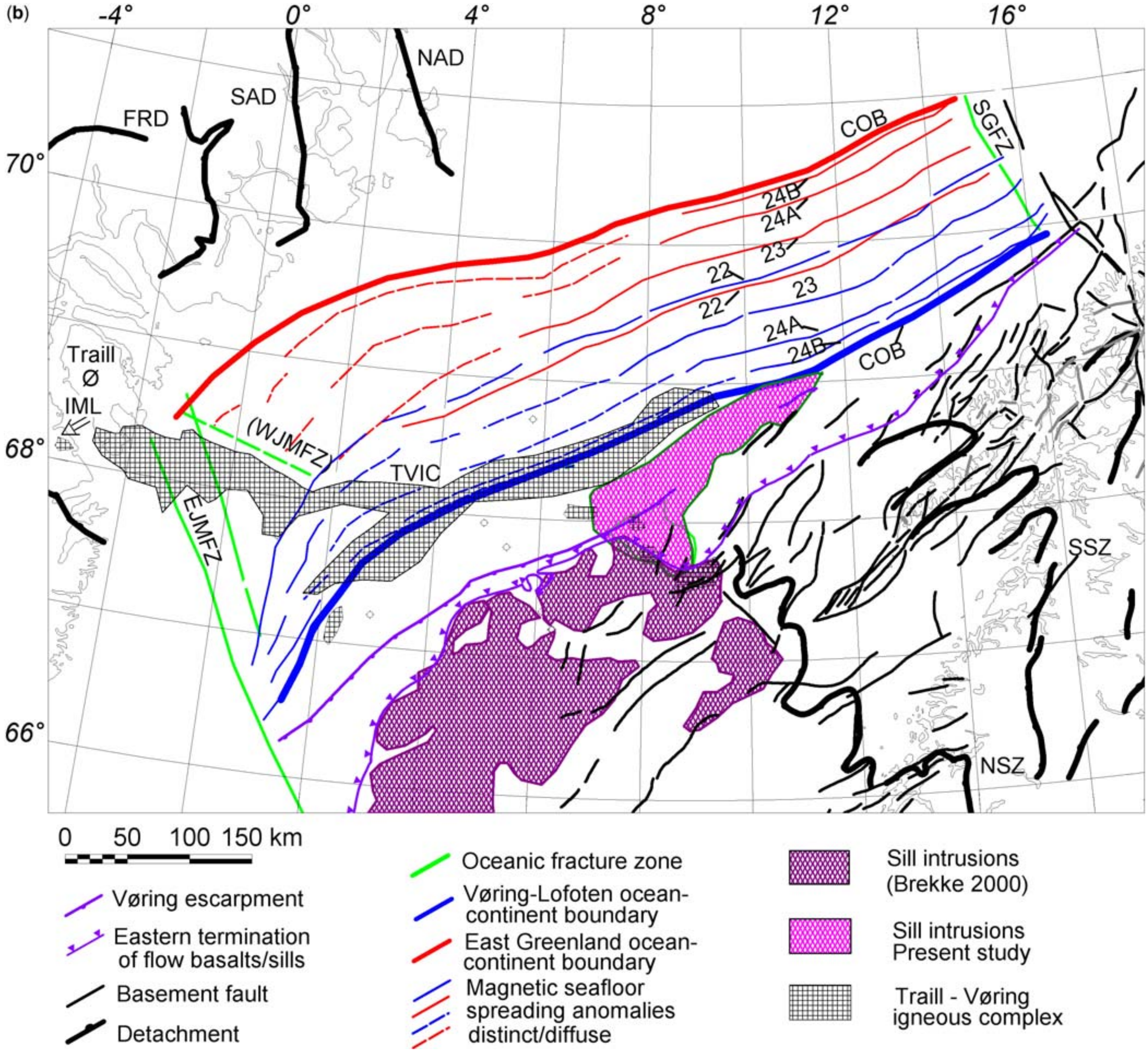

Fig. 16. (*Continued*).

spacing, more accurate navigation, and improved processing and data presentation during the last two decades.

(2) The compilation of petrophysical data (density magnetic susceptibility and remanence) from *c*. 28 000 rock samples from the Norwegian mainland and offshore wells, and susceptibility measurements on 10 km of offshore drillcores, have constrained the interpretation of the potential field data. The interpretation of high-sensitivity aeromagnetic data has been elaborated by studying naturally occurring intra-formational anomalies and linking them as closely as possible with petrophysical measurements on actual sedimentary material of appropriate formations.

(3) Potential field data in Norway provide a continuous coverage of areas onshore the mainland and Svalbard and the areas offshore. The data thus act as a bridge between areas traditionally mapped by two different methods, bedrock mapping and seismic interpretation, respectively. These data compilations have allowed tracing and correlating basement structures across the transition zone between the mainland and the offshore areas.

(4) The magnetic anomaly pattern in Norway and adjacent areas is interpreted to reflect different types of magnetic sources: (a) a magnetic basement of Precambrian or Cambro-Silurian age that continues from mainland Norway below the continental shelf, (b) Permian to Cenozoic igneous rocks, (c) subcropping sedimentary rocks of Late Palaeozoic, Mesozoic and Cenozoic age along the coast, (d) salt diapirs, (e) Quaternary till and sand channels of varying thickness on the continental shelf and (f) topographic and bathymetric features. The last four sources are generally producing low-amplitude, high-frequency anomalies. These are mostly seen in modern, high-sensitivity data, but are generally not discernible in the vintage (pre-1976) datasets.

(5) Coinciding magnetic and gravity anomalies along the Norwegian coast and continental margin represent to a large extent gneissic domes formed during exhumation of lower crustal rocks along Late-Caledonian, low-angle detachment zones. Similar core complexes of Proterozoic age in northern Fennoscandia are usually referred to as gneiss domes. They were most likely formed during a gravity collapse of the

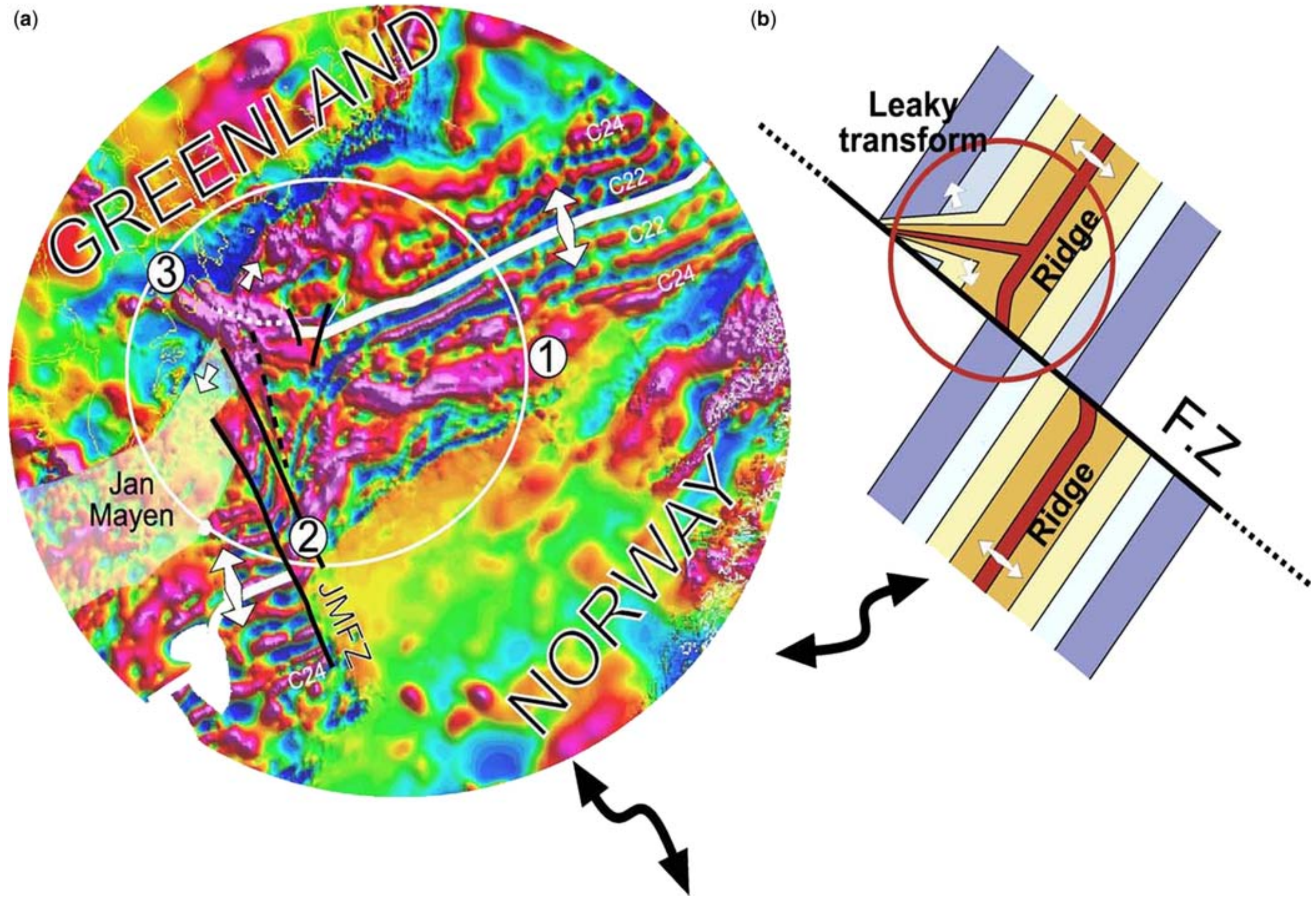

Fig. 17. (**a**) Plate reconstruction of the Norwegian margin, Greenland and the Jan Mayen microcontinent, at C21 (*c*. 47 Ma ago), after Gernigon *et al.* (2009). This picture illustrates a triple junction between two magnetic (magmatic) branches (1) and (2) which represent the basaltic SDRs along the Vøring Marginal High and the Greenland part of the TVIC branch (3). In this kinematic reconstruction, the VS lies in the central part of the complex. (**b**) A leaky transform model can be proposed for both, and the TVIC lying in the trend of the VS could have formed obliquely along the trend of the pre-existing EJMFZ.

Palaeoproterozoic Svecofennian orogen subsequent to continent–continent collision along the Lapland Granulite Belt.

(6) The depth to magnetic basement estimates indicate a general depth of 4–15 km beneath the basins on the Norwegian continental shelf. The basement on the inner Mid-Norwegian shelf consists partly of Caledonian nappes. Estimates of depths to magnetic sources are therefore larger than estimates of depths to gravity contrasts in the same area.

(7) A correlation between magnetic anomalies caused by Mesozoic faulting on the continental shelf and anomalies due to underlying basement topography indicates that the deep structural setting may have guided the location of the later faulting.

(8) Opening of the Norwegian–Greenland Sea (between the Jan Mayen and Senja fracture zones) occurred along stable continental margins without offsets across minor fracture zones, or involving jumps in spreading axis. The previously proposed offset zones were merely artefacts of wide profile spacing, poor navigation and poor profile levelling of the vintage aeromagnetic profiles.

(9) The 50 km wide and 500 km long, TVIC cuts across spreading anomalies 24A, 24B and 23 from the Vøring Marginal High on the Norwegian margin to Traill Ø on the Greenland coast. Hence, the igneous activity must have lasted until *c*. 50 Ma and was most likely part of a triple junction formed between the Lofoten and Norway Basins.

(10) The aeromagnetic anomalies related to the subcropping sedimentary units along the coast of Trøndelag and Nordland are caused by (i) alternating beds of sandstone and claystone/siltstone/mudstone (mean susceptibility 0.00013 and 0.00025 SI), (ii) siderite-cemented sedimentary rocks (mean susceptibility 0.00135 SI) and (iii) sedimentary units containing detrital Fe–Ti oxides (susceptibility 0.00100–0.01000 SI). Negative anomalies are caused by low-magnetic gypsum, anhydrite, salt or coal (mean susceptibility 0.00007 SI). The measured *Q*-values (ratio of remanent to induced magnetization) are usually low for these sedimentary units (0.04–0.21).

(11) The distinct positive magnetic anomalies related to buried Quaternary sand channels in the North Sea and Denmark are caused by gravel and boulders consisting of typical basement rocks from the Fennoscandian Shield (e.g. granite, gneiss and amphibolite). The average susceptibility of the infill is 0.00043 SI whereas the underlying Miocene shales have 0.00007 SI. The small contrast of 0.00036 SI is sufficient to produce magnetic anomalies in the order of 1–2 nT.

The acquisition of recent aeromagnetic, gravity and petrophysical measurements along the Norwegian continental margin has been financed by a large number of institutes and companies: the Geological Survey of Denmark and Greenland (GEUS), BP Norge, Chevron Norge, ConocoPhillips Norge, Det norske oljeselskap, Eni Norge, ExxonMobil Exploration and Production Norway, Faroese Earth and Energy Directorate (Jarðfeingi), GDF SUEZ Norge, Norwegian Petroleum Directorate (NPD), RWE-Dea Norge, Statoil, Total Norge and the Geological Survey of Norway (NGU). Oddvar Blokkum, Kolbjørn Brandhaug, Einar Dalsegg, Harald Elvebakk, Henrik Håbrekke, Rolf Lynum, John Olav Mogaard, Stig Rønning, Atle

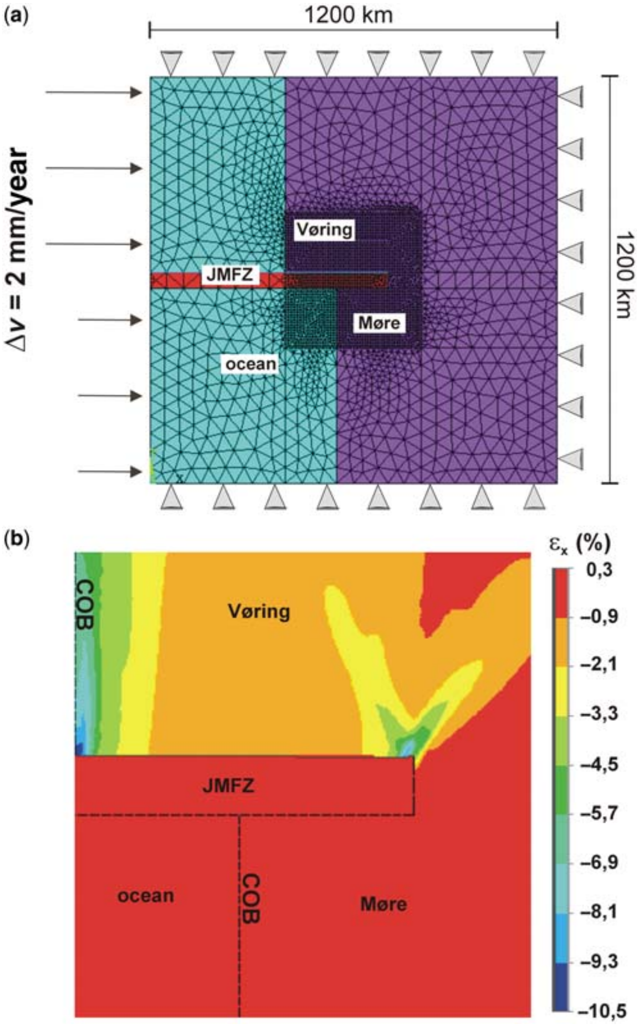

Fig. 18. Modelled strains after 5 Ma. Negative values are associated with shortening. Note significant strain concentrations at the COB and at the termination of the JMFZ in the Vøring Basin.

Sindre and Jan Fredrik Tønnesen carried out aeromagnetic and gravity data acquisition. NPD and TGS provided the offshore gravity datasets. Torben Bidstrup and Torkild Rasmussen, GEUS, Juha Korhonen, GTK, Martin Heinesen and Thomas Varming, Jarđfeingi, Kajsa Hult and Sven Aaro, SGU, Leó Kristjánsson and Geirfinnur Jónsson, Institute of Earth Sciences, University of Iceland, Geoffrey S. Kimbell and Christopher P. Royles, BGS supplied aeromagnetic and gravity data from Denmark, Finland, Faroe Islands, Sweden, Iceland and Scotland, respectively. Gordon Oakey, Atlantic Geoscience Center, Canadian Geological Survey, provided all the processed NOO, NRL and the Fairey surveys from the NE Atlantic region. Numerous geologists at NGU, in addition to Charles Schlinger and Gunnar Raade, provided bedrock samples for petrophysical measurements. Henry Kalvøy carried out a large number of the petrophysical laboratory measurements. Hermann Weiss and Atle Mørk, SINTEF Petroleum Research, provided core samples from their shallow drilling programme and provided the lithological log from the Nordland area. Tibor Czaka, GEUS, provided sample material from borehole no. 160.1526 through a Quaternary sand channel in southern Jutland. The compilation of the datasets was carried out during the first author's 2.5-month sabbatical stay at the US Geological Survey. Discussions with Rick Saltus and Bob Kucks were very useful. David Roberts improved the English of the paper. We express our sincere thanks to all these persons, companies and institutes.

References

Åm, K. 1973*a*. *Tolkning av magnetiske og gravimetriske data, Kontinentalsokkelen Stavanger/Stad (59–62°N)*. Norges geologiske undersøkelse Report **1175**.

Åm, K. 1973*b*. Geophysical indications of Permian and Tertiary igneous activity in the Skagerrak. *Norges Geologiske Undersøkelse*, **287**, 1–25.

Åm, K. 1975. Aeromagnetic basement complex mapping north of latitude 62°N, Norway. *Norges Geologiske Undersøkelse*, **316**, 351–374.

Åm, K. & Oftedahl, C. 1977. Brief comments on some aeromagnetic anomalies in the Oslo Region. *In*: Heier, K. S. (ed.) *The Norwegian Geotraverse Project. A Norwegian Contribution to the International Upper Mantle Project and The International Geodynamics Project*. Norwegian Research Council for Science and the Humanities, Oslo, 209–222.

Andersen, O. B., Knudsen, P., Berry, P., Kenyon, S. & Trimmer, R. 2008. The DNSC08 ocean wide altimetry derived gravity field. Abstract. European Geosciences Union *General Assembly* 2008, Vienna, 14–18 April, 2008.

Bain, J. E., Weyand, J., Horscroft, T. R., Saad, A. H. & Bulling, D. N. 1993. Complex salt features resolved by integrating seismics, gravity, and magnetics. *EAEG/EAPG 1993 Annual Conference and Exhibition*, Extended Abstract.

Balling, N. 2000. Deep seismic reflection evidence for ancient subduction and collision zones within the continental lithosphere of northwestern Europe. *Tectonophysics*, **329**, 269–300.

Barrère, C., Ebbing, J. & Gernigon, L. 2009. Offshore prolongation of Caledonian structures and basement characterisation in the western Barents Sea from geophysical modelling. *Tectonophysics*, **470**, 71–88.

Blystad, P., Brekke, H., Færseth, R. B., Larsen, B. T., Skogseid, J. & Tørudbakken, B. 1995. *Structural Elements of the Norwegian Continental Shelf, Part II. The Norwegian Sea Region*. Norwegian Petroleum Directorate Bulletin, **8**.

Braathen, A., Nordgulen, Ø., Osmundsen, P. T., Andersen, T. B., Solli, A. & Roberts, D. 2000. Devonian, orogen-parallel, opposed extension in the Central Norwegian Caledonides. *Geology*, **28**, 615–618.

Braathen, A., Osmundsen, P. T., Nordgulen, Ø., Roberts, D. & Meyer, G. B. 2002. Orogen-parallel extension of the Caledonides in northern Central Norway: an overview. *Norwegian Journal of Geology*, **82**, 225–241.

Breivik, A. & Faleide, J. I. 2004. *Geophysical Atlas of the Barents Sea, Integrated Seismic, Gravity and Magnetic Interpretation*. Confidential VBPR and TGS-NOPEC Report, Oslo.

Breivik, A., Faleide, J. I. & Mjelde, R. 2008. Neogene magmatism northeast of the Aegir and Kolbeinsey ridges, NE Atlantic: Spreading ridge mantle plume interaction?: G-Cube. *Geochemistry, Geophysics, Geosystems: an Electronic Journal of the Earth Sciences*, **9**, Q02004; doi: 10.1029/2007GC001750.

Brekke, H. 2000. The tectonic evolution of the Norwegian Sea continental margin with emphasis on the Vøring and Møre basins. *In*: Nøttvedt, A. *et al*. (eds) *Dynamics of the Norwegian Margin*. Geological Society, London, Special Publications, **167**, 327–378.

Briggs, I. C. 1974. Machine contouring using minimum curvature. *Geophysics*, **39**, 39–48.

British Geological Survey. 1997. *Colour Shaded Relief Gravity Anomaly Map of Britain, Ireland and Adjacent Areas*. Smith, I. F. & Edwards, J. W. F. (compilers) 1 : 500 000 scale. British Geological Survey, Keyworth, UK.

Brönner, M., Gernigon, L., Ebbing, J., Olesen, O., Roberts, D., Barrère, C. & Koziel, J. 2009. *Barents Sea Aeromagnetic Remapping 2008 – BASAR-08 Acquisition, Processing and Interpretation*. Norges geologiske undersøkelse Report **2009.020** (confidential).

Bugge, T., Ringås, J. E., Leith, D. A., Mangerud, G., Weiss, H. M. & Leith, T. L. 2002. Upper Permian as a new play model on the Mid-Norwegian continental shelf: investigated by shallow stratigraphic drilling. *AAPG Bulletin*, **86**, 107–127.

Chroston, P. N. 1974. Geological interpretation of gravity data between Tromsø and Øksfjord (Finnmark). *Norges geologiske undersøkelse Bulletin*, **312**, 59–90.

Clark, D. A. 1997. Magnetic petrophysics and magnetic petrology: aids to geological interpretation of magnetic surveys. *AGSO Journal of Geology & Geophysics*, **17**, 83–103.

Compagnie Générale de Géophysique. 1977. Norwegian Petroleum Directorate, Aeromagnetic Survey Jan Mayen Area, Interpretation Report.

Daly, J. S., Balagansky, V. V., Timmerman, M. J. & Whitehouse, M. J. 2006. The Lapland-Kola Orogen: Palaeoproterozoic collision and accretion of the northern Fennoscandian lithosphere. *In*: Gee, D. G. & Stephenson, R. (eds) *European Lithosphere Dynamics*. Geological Society, London, Memoirs, **32**, 579–597.

Dehls, J. F., Olesen, O., Bungum, H., Hicks, E., Lindholm, C. D. & Riis, F. 2000. *Neotectonic Map, Norway and Adjacent Areas, 1:3 Mill*. Geological Survey of Norway, Trondheim.

Ducea, M. 2001. The California Arc: thick granitic batholiths, eclogitic residues, lithospheric-scale thrusting, and magmatic flare-ups. *GSA Today*, **11**, 5–10.

Ebbing, J. & Olesen, O. 2006. The Northern and Southern Scandes – structural differences revealed by an analysis of gravity anomalies, the geoid and regional isostasy. *Tectonophysics*, **411**, 73–87.

Ebbing, J. & Olesen, O. 2010. New compilation of top basement and basement thickness for the Norwegian continental shelf reveals the segmentation of the passive margin system. *In*: *Petroleum Geology: From Mature Basins to New Frontiers. Proceedings of the 7th Petroleum Geology Conference*. Geological Society, London, 885–897.

Ebbing, J., Lundin, E., Olesen, O. & Hansen, E. K. 2006. The Mid-Norwegian margin: a discussion of crustal lineaments, mafic intrusions, and remnants of the Caledonian root by 3D density modelling and structural interpretation. *Journal of the Geological Society, London*, **163**, 47–60.

Ebbing, J., Skilbrei, J. R. & Olesen, O. 2007. Insights into the magmatic architecture of the Oslo Graben by petrophysically constrained analysis of the gravity and magnetic field. *Journal of Geophysical Research*, **112**, B4404; doi: 10.1029/2006JB004694.

Ebbing, J., Gernigon, L., Pascal, C., Olesen, O. & Osmundsen, P. T. 2009. A discussion of structural and thermal control of magnetic anomalies on the Mid-Norwegian margin. *Geophysical Prospecting*, **57**, 665–681; doi: 10.1111/j.1365–2478.2009.00800.x.

Ehlers, J. & Linke, G. 1989. The origin of deep buried channels of Elsterian age in Northwest Germany. *Journal of Quaternary Sciences*, **4**, 255–265.

Eldholm, O., Thiede, J. *et al*. (eds) 1987. *Proceedings of the ODP, Initial Reports 104*. Ocean Drilling Programme, College Station, TX.

Emenike, E. A. 1986. Gravity signature of the Limpopo–Kaapvaal fossil plate boundary in southern Africa. *Tectonophysics*, **128**, 127–137.

Fabian, K., McEnroe, S. A., Robinson, P. & Shcherbakov, V. P. 2008. Exchange bias identifies lamellar magnetism as the origin of the natural remanent magnetisation in ilmenohematite from Modum, Norway. *Earth Planetary Science Letters*, **268**; doi: 10.1016/j.epsl.2008.01.034.

Fichler, C., Henriksen, S., Rueslåtten, H. & Hovland, M. 2005. North Sea Quaternary morphology from seismic and magnetic data: indications for gas hydrates during glaciation? *Petroleum Geoscience*, **11**, 331–337.

Fichler, C., Rueslåtten, H., Gram, C., Ingebrigtsen, A. & Olesen, O. 2007. Salt interpretation with special focus on magnetic data, Nordkapp Basin, Barents Sea 2007. *EGM 2007 International Workshop Innovation in EM, Grav and Mag Methods: a New Perspective for Exploration*, Capri, 16–18 April 2007, Extended Abstract.

Forman, D. J. & Shaw, R. D. 1973. Deformation of the crust and mantle in central Australia. *Bureau of Mineral Resources Australia Bulletin*, **144**.

Gaal, G. & Gorbatschev, R. 1987. An outline of the Precambrian evolution of the Baltic Shield. *Precambrian Research*, **35**, 15–52.

Gausland, A. K. 1998. *Distribution and Genesis of Late Pleistocene Buried Channels in the Central North Sea*. Unpublished Cand. Scient. Thesis, University of Oslo.

Gellein, J., Olesen, O., Reitan, M. & Sæther, P. O. 1993. *Brukerbeskrivelse – database og prosessering av gravimetriske data*. Norges geologiske undersøkelse Internal Report **93.019**.

Geosoft. 2005. *Montaj GridKnit, Grid Extension for OASIS Montaj 6.1, Tutorial and User Guide*. Geosoft Incorporated.

Geosoft. 2006. *Montaj Geophysics Levelling System, Processing and Enhancing Geophysical Data Extension for Oasis Montaj 6.3. Tutorial and User Guide*. Geosoft Incorporated.

Geosoft. 2008. *OASIS Montaj 7.0 Mapping and Processing System. The Core Software Platform for Working with Large Volume Spatial Data. Quick Start Tutorials*. Geosoft Incorporated.

Gernigon, L., Lucazeau, F., Brigaud, F., Ringenbach, J. C., Planke, S. & Le Gall, B. 2006. A moderate melting model for the Voring margin (Norway) based on structural observations and a thermo-kinematical modelling: implication for the meaning of the lower crustal bodies. *Tectonophysics*, **412**, 255–278.

Gernigon, L., Marello, L., Mogaard, J. O., Werner, S. C. & Skilbrei, J. R. 2007. *Barents Sea Aeromagnetic Survey BAS-06: Acquisition-processing Report and Preliminary Interpretation: Geological Survey of Norway*. Norges geologiske undersøkelse Report **2007.035**.

Gernigon, L., Olesen, O., Koziel, J. & Lynum, R. 2008. *Norway Basin Aeromagnetic Survey NB-07 – Acquisition, Processing and Interpretation*. Norges geologiske undersøkelse Report **2008.052**.

Gernigon, L., Olesen, O. *et al*. 2009. Geophysical insights and early spreading history in the vicinity of the Jan Mayen Fracture Zone, Norwegian-Greenland Sea. *Tectonophysics*, **468**, 185–205.

Gibb, R. A., Thomas, M. D., Lapointe, P. L. & Mukhopadhay, M. 1983. Geophysics of proposed Proterozoic sutures in Canada. *Precambrian Research*, **19**, 349–384.

Gómez, M. & Vergés, J. 2005. Quantifying the contribution of tectonics vs. Differential compaction in the development of domes along the Mid-Norwegian Atlantic margin. *Basin Research*, **17**, 289–310.

Griffin, W. L., Taylor, P. N. *et al*. 1978. Archaean and Proterozoic crustal evolution in Lofoten-Vesterålen, North Norway. *Journal of the Geological Society London*, **135**, 629–647.

Gunn, P. J. 1997. Application of aeromagnetic surveys to sedimentary basin studies. *AGSO Journal Australian Geology & Geophysics*, **17**, 133–144.

Hagevang, T., Eldholm, O. & Aalstad, I. 1983. Pre-23 magnetic anomalies between Jan Mayen and Greenland-Senja Fracture Zones in the Norwegian Sea. *Marine Geophysical Researches*, **5**, 345–363.

Hartz, E. H., Eide, E. A., Andresen, A., Midbøe, P., Hodges, K. V. & Kristiansen, S. N. 2002. $^{40}Ar/^{39}Ar$ geochronology and structural analysis: basin evolution and detrital feedback mechanisms, Hold With Hope region, East Greenland. *Norsk Geologisk Tidsskrift*, **82**, 341–358.

Hauger, E. & van Veen, P. 1995. Application of magnetostratigraphy to Brent Group reservoir zonation in the Visund Basin. *In*: Turner, P. & Turner, A. (eds) *Palaeomagnetic Applications in Hydrocarbon Exploration and Production*. Geological Society, London, Special Publications, **98**, 187–204.

Heiskanen, W. A. & Moritz, H. 1967. *Physical Geodesy*. W.H. Freeman, San Francisco, CA.

Henkel, H. 1991. Magnetic crustal structures in Northern Fennoscandia. *In*: Wasilewski, P. & Hood, P. (eds) Magnetic Anomalies – Land and Sea. *Tectonophysics*, **192**, 57–79.

Jakobsson, M., Macnab, R. *et al*. 2008. An improved bathymetric portrayal of the Arctic Ocean: implications for ocean modeling and geological, geophysical and oceanographic analyses. *Geophysical Research Letters*, **35**, L07602; doi: 10.1029/2008GL033520.

Jónsson, G., Kristjánsson, L. & Sverrisson, M. 1991. Magnetic surveys of Iceland. *Tectonophysics*, **189**, 229–247.

Jung, W. Y. & Vogt, P. R. 1997. A gravity and magnetic anomaly study of the extinct Aegir Ridge, Norwegian Sea. *Journal of Geophysical Research*, **12**, 5065–5089.

Kent, D. V. & Opdyke, N. D. 1978. Paleomagnetism and magnetic properties of igneous rock samples – Leg 38. *In*: Talvani, Udintsev *et al*. (eds) *Initial Reports of the Deep Sea Drilling Project, Supplements to Vol. 38, 39, 40 & 41*. Government Printing Office, Washington, DC, 3–8.

Korhonen, J. V., Aaro, S. *et al*. 2002*a*. *Magnetic Anomaly Map of the Fennoscandian Shield 1:2,000,000*. The Geological Surveys of Finland, Norway and Sweden and Ministry of Natural Resources of the Russian Federation.

Korhonen, J. V., Aaro, S. *et al*. 2002*b*. *Bouguer Anomaly Map of the Fennoscandian Shield 1:2,000,000*. Geological Surveys of Finland, Norway and Sweden and Ministry of Natural Resources of the Russian Federation.

Kristensen, T. B., Huuse, M., Piotrowski, J. A. & Clausen, O. R. 2007. A morphometric analysis of tunnel valleys in the eastern North Sea based on 3D seismic data. *Journal of Quaternary Science*, **22**, 801–815.

Kristjánsson, L., Jónsson, G. & Sverrisson, M. 1989. *Magnetic Surveys at the Science Institute. Documentation to Accompany a Colored Map of Total-field Anomalies in Scale 1:1 000 000, and Computer Diskettes* *of Survey Data*. Science Institute, University of Iceland Report **RH01.89**.

Larsen, H. C. 1974. *Airborne Geophysical Survey in the Central East Greenland.* Grønlands Geologiske Undersøkelse Report **75**.

Larsen, H. C. 1988. A multiple and propagating rift model for the NE Atlantic. *In*: Morton, A.C. & Parson, L.M. (eds) *Early Tertiary Volcanism and the Opening of the NE Atlantic*. Geological Society, London, Special Publications, **39**, 157–158.

Larsen, H. C. & Thorning, L. 1979. *Project Eastmar: Acquisition of High Sensitivity Aeromagnetic Data off East*. Greenland, Grønlands Geologiske Undersøkelse Report **100**.

Lauritsen, T., Blomstrand, L. B., Olesen, O. & Mørk, A. 2007. *OSRAM II – Origin of Sediment-Related AeroMagnetics II, Magnetic Susceptibility Measurements on Shallow Stratigraphic Cores from the Finnmark Platform, Nordkapp Basin and Svalis Dome*. Norges geologiske undersøkelse Report **2007.028**.

Lesquer, A., Beltrao, J. F. & De Abreu, F. A. M. 1984. Proterozoic links between northeastern Brazil and West Africa: a plate tectonic model based on gravity data. *Tectonophysics*, **110**, 9–26.

Lie, J. E. & Husebye, E. S. 1994. Simple-shear deformation of the Skagerrak lithosphere during the formation of the Oslo Rift. *Tectonophysics*, **232**, 133–141.

Lindroos, H. & Henkel, H. 1978. *Regional Geological and Geophysical Interpretation of Precambrian Structures in Northeastern Sweden*. Sveriges geologiska undersökning, **C751**.

Lønne, W. & Sellevoll, M. A. 1975. A reconnaissance gravity study of Magerøy, Finnmark, northern Norway. *Norges Geologiske Undersøkelse*, **319**, 1–15.

Løvaas, L., Mogaard, J. O., Olesen, O., Koziel, J. & Lynum, R. 2006. *Southern Nordkapp Basin Aeromagnetic Survey 2006 (SNS-06). Data Acquisition and Processing Report*. Norges geologiske undersøkelse Report **2006.089**.

Løvlie, R. & van Veen, P. 1995. Magnetic susceptibility of a 180 m sediment core: reliability of incremental sampling and evidence for a relationship between susceptibility and gamma activity. *In*: Turner, P. & Turner, A. (eds) *Palaeomagnetic Applications in Hydrocarbon Exploration and Production*. Geological Society, London, Special Publications, **98**, 259–266.

Lundin, E. R. & Doré, A. G. 2002. Mid-Cenozoic post-breakup deformation in the 'passive' margins bordering the Norwegian–Greenland Sea. *Marine & Petroleum Geology*, **19**, 79–93.

Marker, M. 1985. Early Proterozoic (ca. 2000–1950 Ma) crustal structure of the northeastern Baltic Shield: tectonic division and tectogenesis. *Norges geologiske undersøkelse Bulletin*, **403**, 55–74.

Mathisen, O. 1976. A method for Bouger reduction with rapid calculation of terrain corrections. *Geographic Survey of Norway Geodetic Publications*, **18**.

Mauring, E. & Kihle, O. 2006. Leveling aerogeophysical data using moving differential median filter. *Geophysics*, **71**, L5–L11.

Maus, S., Yin, F. *et al*. 2008. Resolution of direction of oceanic magnetic lineations by the sixth generation lithospheric magnetic field model from CHAMP satellite magnetic measurements. *Geochemistry, Geophysics, Geosystems*, **9**, 7021; doi: 10.1029/2008GC001949.

Maus, S., Barckhausen, U. *et al*. 2009. EMAG2: A 2-arc-minute resolution Earth Magnetic Anomaly Grid compiled from satellite, airborne and marine magnetic measurements. *Geochemistry, Geophysics, Geosystems*, **10**, Q08005; doi: 10.1029/2009GC002471.

McEnroe, S. A., Robinson, P. & Panish, P. 1996. *Rock-magnetic Properties, Oxide Mineralogy and Mineral Chemistry in Relation to Aeromagnetic Interpretation and Search for Ilmenite Reserves*. Norges geologiske undersøkelse Report **96.060**.

McEnroe, S. A., Robinson, P. & Panish, P. 2001. Aeromagnetic anomalies, magnetic petrology, and rock magnetism of hemo-ilmenite- and magnetite-rich cumulate rocks from the Sokndal Region, South Rogaland, Norway. *American Mineralogist*, **86**, 1447–1468.

Merechi, Z. T. 2006. *Aeromagnetic mapping of Quaternary buried sand-channels in southern North Sea basin.* Unpublished Masters thesis, Norwegian University of Science and Technology.

Midtun, R. D. 1988. *Karasjok-grønnsteinsbeltet, Regional geofysisk og geologisk tolkning*. Norges geologiske undersøkelse Skrifter, **88**.

Mishra, D. C., Vijaya Kumar, V. & Rajasekhar, R. P. 2006. Crustal structure and tectonic evolution of the southern Granulite Terrain, India. *Gondwana Research*, **10**, 6–17.

Mørk, M. B. E. & Olesen, O. 1995. *Magnetic Susceptibility of Sedimentary Rocks from Shallow Cores off Mid-Norway and Crystalline Rocks from the Adjacent Onland Areas. NAS-94 Interpretation Report, Part II: Petrophysical data*. Norges geologiske undersøkelse Report **95.039**.

Mørk, M. B. E., McEnroe, S. & Olesen, O. 1996. *OSRAM – Origin of Sediment-related Aeromagnetics, Magnetic Properties of Mesozoic and Cenozoic sediments from the Northern North Sea and the Norwegian Sea: Measurements and Interpretation*. Continental Shelf and Petroleum Technology Research Institute (IKU) Report **23.2570.00/01/96**.

Mørk, M. B. E., McEnroe, S. A. & Olesen, O. 2002. Magnetic susceptibility of Mesozoic and Cenozoic sediments off Mid Norway and the role of siderite: implications for interpretation of high-resolution aeromagnetic anomalies. *Marine and Petroleum Geology*, **19**, 1115–1126.

Mosar, J., Lewis, G. & Torsvik, T. H. 2002. North Atlantic sea-floor spreading rates: implications for the Tertiary Development of inversion structures of the Norwegian–Greenland Sea. *Journal of the Geological Society, London*, **159**, 503–515.

Narain, H. & Subrahmanyam, C. 1986. Precambrian tectonics of the south Indian shield inferred from geophysical data. *Journal of Geology*, **94**, 187–198.

Navrestad, T. & Jørgensen, F. 1979. *Aeromagnetic investigation on the Jan Mayen Ridge*. Norwegian Petroleum Society, NSS/9.

Norges geologiske undersøkelse. 1992. *Aeromagnetisk anomalikart, Norge M 1:1 mill.* Norges geologiske undersøkelse.

Olesen, O. & Sandstad, J. S. 1993. Interpretation of the Proterozoic Kautokeino Greenstone Belt, Finnmark, Norway from combined geophysical and geological data. *Norges geologiske undersøkelse Bulletin*, **425**, 41–62.

Olesen, O. & Smethurst, M. A. 1995. *NAS-94 Interpretation Report, Part III: Combined Interpretation of Aeromagnetic and Gravity Data*. Norges geologiske undersøkelse Report **95.040**.

Olesen, O., Roberts, D., Henkel, H., Lile, O. B. & Torsvik, T. H. 1990. Aeromagnetic and gravimetric interpretation of regional structural features in the Caledonides of West Finnmark and North Troms, northern Norway. *Norges geologiske undersøkelse Bulletin*, **419**, 1–24.

Olesen, O., Henkel, H., Kaada, K. & Tveten, E. 1991. Petrophysical properties of a prograde amphibolite – granulite facies transition zone at Sigerfjord, Vesterålen, northern Norway. *In*: Wasilewski, P. & Hood, P. (eds) Magnetic Anomalies – Land and Sea. *Tectonophysics*, **192**, 33–39.

Olesen, O., Reitan, M. & Sæther, P. O. 1993. *Petrofysisk database PETBASE 3.0, Brukerbeskrivelse*. Norges geologiske undersøkelse Internal Report **93.023**.

Olesen, O., Gellein, J., Håbrekke, H., Kihle, O., Skilbrei, J. R. & Smethurst, M. 1997*a*. *Magnetic Anomaly Map of Norway and Adjacent Ocean Areas, scale 1:3 million*. Geological Survey of Norway, Trondheim.

Olesen, O., Torsvik, T. H., Tveten, E., Zwaan, K. B., Løseth, H. & Henningsen, T. 1997*b*. Basement structure of the continental margin in the Lofoten–Lopphavet area, northern Norway: constraints from potential field data, on-land structural mapping and palaeomagnetic data. *Norsk Geologisk Tidsskrift*, **77**, 15–33.

Olesen, O., Smethurst, M. A., Beard, L., Torsvik, T. H., Bidstrup, T. & Egeland, B. 1997*c*. *SAS-96 Part II, Skagerrak Aeromagnetic Survey 1996, Interpretation Report*. Norges geologiske undersøkelse Report **97.022**.

Olesen, O., Lundin, E. *et al*. 2002. Bridging the gap between the Nordland onshore and offshore geology. *Norwegian Journal of Geology*, **82**, 243–262.

Olesen, O., Smethurst, M. A., Torsvik, T. H. & Bidstrup, T. 2004. Sveconorwegian igneous complexes beneath the Norwegian–Danish Basin. *Tectonophysics*, **387**, 105–130.

Olesen, O., Gernigon, L., Ebbing, J., Mogaard, J. O., Pascal, C. & Wienecke, S. 2006. *Interpretation of Aeromagnetic Data along the Jan Mayen Fracture Zone, JAS-05*. Norges geologiske undersøkelse Report **2006.018**.

Olesen, O., Ebbing, J. *et al*. 2007. An improved tectonic model for the Eocene opening of the Norwegian-Greenland Sea: use of modern magnetic data. *Marine and Petroleum Geology*, **24**, 53–66.

Osmundsen, P. T. & Ebbing, J. 2008. Styles of extension offshore Mid Norway and implications for mechanisms of Late Jurassic–Early Cretaceous rifting. Basement configuration of the Mid-Norwegian margin. *Tectonics*, **27**, TC6016; doi: 10.1029/2007TC002242.

Osmundsen, P. T., Sommaruga, A., Skilbrei, J. R. & Olesen, O. 2002. Deep structure of the Norwegian Sea area, NE Atlantic margin. *Norwegian Journal of Geology*, **82**, 205–224.

Osmundsen, P. T., Braathen, A., Nordgulen, Ø., Roberts, D., Meyer, G. B. & Eide, E. 2003. The Devonian Nesna shear zone and adjacent gneiss-cored culminations, North–Central Norwegian Caledonides. *Journal of the Geological Society, London*, **160**, 137–150.

Osmundsen, P. T., Eide, E. A. *et al*. 2006. Kinematics of the Høybakken detachment zone and the Møre–Trøndelag Fault Complex, central Norway. *Journal of the Geological Society, London*, **163**, 303–318.

Ramberg, I. B. 1976. *Gravity Interpretation of the Oslo Graben and Associated Igneous Rocks*. Norges geologiske undersøkelse Bulletin, **325**.

Reynolds, R. L., Tuttle, M. L., Rice, C. A., Fishman, N. S., Karachewski, J. A. & Sherman, D. 1994. Magnetization and geochemistry of greigite-bearing Cretaceous strata, North Slope Basin, Alaska. *American Journal of Sciences*, **294**, 485–528.

Rise, L., Rokoengen, K., Sættem, J. & Bugge, T. 1988. *Thickness of Quaternary Deposits on the Mid Norwegian Continental Shelf. Scale 1:1 000 000*. Continental Shelf and Petroleum Technology Research Institute (IKU), **119**.

Rokoengen, K., Rise, L., Bugge, T. & Sættem, J. 1988. *Bedrock Geology of the Mid Norwegian Continental Shelf. Scale 1:1 000 000*. Continental Shelf and Petroleum Technology Research Institute (IKU), **118**.

Russell, J. P., Shiells, G. & Kerridge, D. J. 1995. Reduction of well-bore positional uncertainty through application of a new geomagnetic in-field referencing technique. Paper SPE 30452, *Society of Petroleum Engineers Annual Technical Conference & Exhibition, Dallas*, 22–25 October 1995.

Schlinger, C. M. 1985. Magnetization of lower crust and interpretation of regional magnetic anomalies: example from Lofoten and Vesterålen, Norway. *Journal of Geophysical Research*, **90**, 11 484–11 504.

Sharma, P. V. 1970. Geophysical evidence for a buried volcanic mount in the Skagerrak. *Bulletin of the Geological Society of Denmark*, **19**, 368–377.

Sigmond, E. M. O. 2002. *Geological Map, Land and Sea Areas of Northern Europe. Scale 1:4 million*. Geological Survey of Norway, Trondheim.

Simpson, R. W., Jachens, R. C. & Blakely, R. J. 1983. *AIRYROOT: A Fortran Program for Calculating the Gravitational Attraction of an Airy Isostatic Root out to 166.7 km*. United States Department of the Interior, Geological Survey, Open-File Report **83–883**.

Sindre, A. 1977. Geofysiske undersøkelser innen kartbladet Smøla. (Med geofysisk kart M 1:50 000). *Norges geologiske undersøkelse Skrifter*, **330**, 25–32.

Skilbrei, J. R. 1991. Interpretation of depth to the magnetic basement in the northern Barents Sea (south of Svalbard). *Tectonophysics*, **200**, 127–141.

Skilbrei, J. R. 1992. Preliminary interpretation of aeromagnetic data from Spitsbergen, Svalbard Archipelago (78°–79°n): implications for structure of the basement. *Marine Geology*, **106**, 53–68.

Skilbrei, J. R. & Kihle, O. 1995. *Reprocessing and Interpretation of the Hunting 1986 Aeromagnetic Data*. Norges geologiske undersøkelse Report **95.026**.

Skilbrei, J. R. & Kihle, O. 1999. Display of residual profiles v. Gridded image data in aeromagnetic study of sedimentary basins: a case history. *Geophysics*, **64**, 1740–1748.

Skilbrei, J. R., Skyseth, T. & Olesen, O. 1991. Petrophysical data and opaque mineralogy of high grade and retrogressed lithologies: implications for the interpretations of aeromagnetic anomalies in northern Vestranden, Western Gneiss Region, central Norway. *In*: Wasilewski, P. & Hood, P. (eds) Magnetic Anomalies – Land and Sea. *Tectonophysics*, **192**, 21–31.

Skilbrei, J. R., Kihle, O., Olesen, O., Gellein, J., Sindre, A., Solheim, D. & Nyland, B. 2000. *Gravity Anomaly Map, Norway and Adjacent Ocean Areas. Scale 1:3 million*. Geological Survey of Norway, Trondheim.

Skilbrei, J. R., Olesen, O., Osmundsen, P. T., Kihle, O., Aaro, S. & Fjellanger, E. 2002. A study of basement structures and some onshore–offshore correlations in Central Norway. *Norwegian Journal of Geology*, **82**, 263–279.

Smethurst, M. A. 2000. Land-offshore tectonic links in western Norway and the northern North Sea. *Journal of the Geological Society, London*, **157**, 769–781.

Smethurst, M. A. & Lauritsen, T. 2003. *Norwegian National Archive for Geophysical Potential Field Survey Data*. Norges geologiske undersøkelse Internal Report **2003.010**.

Smethurst, M. A., Olesen, O. & Håbrekke, H. 1994. An aeromagnetic compilation over mainland Norway. *First Break*, **12**, 203–210.

Strykowski, G. & Forsberg, R. 1998. Operational merging of satellite, airborne and surface gravity data by draping techniques. *In*: Forsberg, R., Feissel, M. & Dietrich, R. (eds) *Geodesy on the Move: Gravity, Geoid, Geodynamics and Antarctica*, IAG Symposia **119**, IAG Scientific Assembly, Rio de Janeiro, 3–9 September 1997, Springer, Berlin, 243–248.

Svela, P. T. 1971. *Gravimetriske undersøkelser av Lofoten-Vesterålen området*. Unpublished Cand. real. thesis, University of Bergen.

Thorbergsson, G., Magnusson, I. T. & Palmason, G. 1990. *Thyngdarmæligogn og þyngdarkort af Íslandi (Gravity data and gravity map of Iceland)*. National Energy Authority Report **OS-90001/JHD-01**, and color map at scale 1:1 000 000 (in Icelandic).

Thorning, L. & Abrahamsen, N. 1980. Palaeomagnetism of Permian multiple intrusion dykes in Bohuslän, SW Sweden. *Geophysical Journal of the Royal Astronomical Society*, **60**, 163–185.

Thybo, H. 2000. Crustal structure and tectonic evolution of the Tornquist Fan region as revealed by geophysical methods. *Bulletin of the Geological Society of Denmark*, **46**, 145–160.

Thybo, H. & Schönharting, G. 1991. Geophysical evidence for Early Permian igneous activity in a transtensional environment, Denmark. *Tectonophysics*, **189**, 193–208.

Torsvik, T. H. & Olesen, O. 1988. *Petrophysics and Palaeomagnetism: Initial Report of the Norwegian Geological Survey Laboratory*. Norges geologiske undersøkelse Report **88.171**.

Torsvik, T. H. & Rehnström, E. F. 2003. The Tornquist Sea and Baltica–Avalonia docking. *Tectonophysics*, **362**, 67–82.

Torsvik, T. H., Smethurst, M. A. *et al*. 1996. Continental break-up and collision in the Neoproterozoic and Palaeozoic: a tale of Baltica and Laurentia. *Earth Science Reviews*, **40**, 229–258.

Torsvik, T. H., Eide, E. A., Meert, J. G., Smethurst, M. A. & Walderhaug, H. J. 1998. The Oslo Rift: new palaeomagnetic and ^{40}Ar/^{39}Ar age constraints. *Geophysical Journal International*, **135**, 1045–1059.

Tsikalas, F., Eldholm, O. & Faleide, J. I. 2002. Early Eocene sea floor spreading and continent-ocean boundary between Gleipne and Senja fracture zones in Norwegian–Greenland Sea. *Marine Geophysical Researches*, **23**, 247–270.

US Naval Oceanographic Office. 1982. *Geomagnetic Surveys*. US Naval Oceanographic Office, **RP-23**.

Vågnes, E., Gabrielsen, R. H. & Haremo, P. 1998. Late Cretaceous–Cenozoic intraplate contractional deformation at the Norwegian continental shelf: timing, magnitude and regional publications. *Tectonophysics*, **300**, 29–46.

Verhoef, J., Roest, W. R., Macnab, R., Arkani-Hamed, J. & members of the Project Team. 1996. *Magnetic Anomalies of the Arctic and North Atlantic Oceans and Adjacent Land Areas*. Geological Survey of Canada Open File Report **3125**, Parts a and b (CD-ROM and project report).

Vogt, P. R., Taylor, P., Kovacs, L. C. & Johnson, G. L. 1979. Detailed aeromagnetic investigation of the Arctic Basin. *Journal of Geophysical Research*, **84**, 1071–1089.

Vogt, P. R., Johnson, G. L. & Kristjansson, L. 1980. Morphology and magnetic anomalies north of Iceland. *Journal of Geophysics*, **47**, 67–80.

Vogt, P. R., Bernero, C., Kovacs, L. C. & Taylor, P. 1981. Structure and plate tectonic evolution of the marine Arctic as revealed by aeromagnetics. *Oceanologica Acta*, **SP**, 25–40.

Wangen, M., Fjeldskaar, W., Faleide, J. I., Wilson, J., Zweigel, J. & Austegard, A. 2008. Forward modeling of stretching episodes and paleo heat flow of the Voring margin, NE Atlantic. *Journal of Geodynamics*, **45**, 83–98.

Wingfield, R. 1990. The origin of major incisions within the Pleistocene deposits of the North Sea. *Marine Geology*, **91**, 31–52.

Session: Russia, Former Soviet Union and the Circum-Arctic

Russia, FSU and the Circum-Arctic: 'the final frontier'

J. R. MAYNARD,[1] A. J. FRASER,[2] M. B. ALLEN,[3] R. A. SCOTT[4] and S. DRACHEV[1]

[1]*ExxonMobil, ExxonMobil House, Ermyn Way, Leatherhead, Surrey KT22 8UX, UK*
[2]*BP Exploration, Chertsey Road, Middlesex TW166 7LN, UK (e-mail: alastair.fraser@imperial.com)*
[3]*Department of Earth Sciences, University of Durham, Durham DH1 3LE, UK*
[4]*CASP, University of Cambridge, 181A Huntingdon Road, Cambridge CB3 0DH, UK*

Sixteen papers representing the petroleum geology of the Arctic, Russia and former Soviet Union were presented over the first day and a half of PGC VII. The region is huge, diverse and has generated a great deal of excitement and outside investment in the industry over the 20 years since the collapse of the Soviet Union. The Arctic region in particular has significance as perhaps the last great frontier hydrocarbon province on Earth. The region is large, approximately 5000 km across a polar view north of the Arctic Circle (Fig. 1). Importantly, from an oil and gas exploration perspective, the Arctic Ocean has the most extensive continental shelf area of any ocean basin (*c*. 50% of offshore area). Much of this sits in the broad Russian offshore Arctic in water depths of less than 50 m. There are numerous sedimentary basins in the Arctic, some well known, but most poorly understood. Art Grantz (United States Geological Survey) and colleagues estimated resources at 114×10^9 barrels of undiscovered oil and 2000×10^{12} standard cubic feet (SCF) of natural gas. If the estimates are correct, these hydrocarbons would account for more than a fifth of the world's undiscovered resources. This great prize, in a world of diminishing reserves, has recently brought territorial issues into focus between the five countries with claims in the Arctic Ocean (Russia, Norway, Denmark, Canada and the USA). All of this is taking place against a backdrop of increasing concern for the fragile Arctic environment.

Day one was dominated by the Arctic, the first half of which focused on the various models that are considered responsible for the tectonic origin of the Arctic and its basins. That such a wide variety of models is possible emphasized how much we still need to learn about the region. The discussions prompted by this session spilled over into lively debate in the poster session. The keynote by Al Fraser (BP) on the regional context of the Arctic Frontier Basins of Canada, Russia, Norway and the USA was given by John Berry and Edith Fugelli, who had stepped in to present at short notice. They described the Arctic as comprising two major deepwater basins floored by oceanic crust. These are the Eurasia Basin and the Amerasia Basin (Fig. 1). The Eurasia Basin as the extension of the North Atlantic rift system is relatively well constrained. However, the spreading history of the Amerasia Basin is less certain and is still the subject of some debate.

This was followed by Steve Bergman (Shell) who outlined the model for the development of the Arctic Ocean. Art Grantz (USGS) spoke about the recent work undertaken by the US Survey and collaborators to assess the petroleum potential of the region. Paul Green (Geotrack International) presented the results of numerous fission track studies that show synchronous widespread Cenozoic exhumation in the region and discussed its potential impact on hydrocarbon migration and trap integrity. Sergey Drachev (ExxonMobil) discussed the tectonic and petroleum geology of the Russian Arctic sector, outlining evidence for the various theories on the opening of the Arctic Ocean and the creation of the basins in this region.

Papers in the second half of the day discussed individual Arctic basins of the Russian and Norwegian Arctic sectors. Vladimir Verzhbitsky (TGS-NOPEC) showed the results of recently acquired seismic data in the North Chukchi Basin in the Russian Arctic, which have been used to construct an interpretation of the region's geological history and contain evidence for an active petroleum system. Jan Inge Faleide (University of Oslo) presented a paper on the sedimentary basins of the Barents Sea, comparing and contrasting the Western and Eastern basins. Jorg Ebbing (Geological Survey of Norway) described a joint project with the Russian VSEGEI institute on the palaeogeographic and tectonic evolution and present-day structure of the Barents and Kara Seas. Timothy Klett (USGS) expanded on the recent Arctic assessment by highlighting the potential of the Siberian shelf and craton, which has an estimated 28 MMBOE to be discovered.

Day two was the turn of Russia's petroleum geology to be examined and the keynote delivered by Steve Creaney (ExxonMobil) gave an overview of the numerous prospective basins in this vast country, using a genetic approach. The tectonic development of the region was used as a framework to address the diverse complexity of these different basins and their hydrocarbon systems. The tectonic evolution of the prolific West Siberian Basin from the Palaeozoic to the present was described by Mark Allen (Durham University), adding to the debate on the tectonic evolution of the Arctic started on the previous day. Robert Scott (CASP) presented an explanation of the curvature of the Novaya Zemlya fold-and-thrust belt and its offset from the remainder of the Uralian Orogen, based on recently collected field observations and regional tectonic synthesis. The significance of this interpretation for adjacent hydrocarbon basins was discussed. Erik Fjellanger (ExxonMobil) described 3D modelling of the hydrocarbon system of the northern West Siberian Basin, where he characterized the plays and source rocks and calibrated the model with some of the world's giant gas fields.

The neotectonics and effects of the Fennoscandian de-glaciation on Siberia were discussed by Mark Allen (Durham University). Finally the discussion moved to the Caspian, where two Kazakh field developments were explained. Firstly the exploration and appraisal of the technically and environmentally challenging, super giant Kashagan Field was presented by Didier Terroir (ENI), and lastly Simon Beavington-Penny (BG) presented work on integrating carbonate sedimentology and cross-well seismic to optimize the phased gas injection at Karachaganak.

The discussion continued into the poster sessions which, in a change from past conferences, allocated the authors a chance to present their posters. A steady number of 15–20 people contributed to these discussions with a free flow of debate amongst the audience and presenters. Robert Scott (CASP) continued the discussion on the opening of the Arctic Ocean by considering the

VINING, B. A. & PICKERING, S. C. (eds) *Petroleum Geology: From Mature Basins to New Frontiers – Proceedings of the 7th Petroleum Geology Conference*, 589–590. DOI: 10.1144/0070589

Fig. 1. Sedimentary basins of the Arctic. The Arctic region is large, approximately 5000 km across this polar view north of the Arctic Circle. There are two deepwater basins floored by oceanic crust and separated by the Lomonosov Ridge. These are the Eurasia Basin and the Amerasia Basin.

various models and their significance for how sediment was dispersed in the Arctic. New seismic from offshore Sakhalin was used to explore the petroleum potential of the Deriugin Basin by Alice Little (TGS-NOPEC), an area of recent developments by western companies. A collaboration to map the basins of the Arctic was presented by two of the joint authors (Sergey Drachev, ExxonMobil and Robert Scott, CASP). This map categorizes the sedimentary accumulations of the Arctic according to their tectonic affinity. Henrik Stendal (Bureau of Minerals and Petroleum) presented his poster on the hydrocarbon potential of the East Greenland Margin. Finally, the prospectivity of the eastern Black Sea was discussed by Li Guo (CASP), who presented work on the analogue late Jurassic reefs of the western Caucasus and Crimea.

Tectonic history and petroleum geology of the Russian Arctic Shelves: an overview

S. S. DRACHEV,[1] N. A. MALYSHEV[2] and A. M. NIKISHIN[3]

[1]*ExxonMobil International Ltd, ExxonMobil House, MP44, Ermyn Way, Leatherhead, Surrey KT22 8UX, UK (e-mail: sergey.s.drachev@exxonmobil.com)*

[2]*Russian State Oil Company 'OAO NK Rosneft', 26/1 Sofiiskaya Embankment, Moscow 115035, Russia*

[3]*Geological Department of Moscow State University, 1 Vorob'evy Gory, Moscow 119899, Russia*

Abstract: The Eastern Barents, Kara, Laptev, East Siberian seas and the western Chukchi Sea occupy a large part of the Eurasian Arctic epicontinental shelf in the Russian Arctic. Recent studies have shown that this huge region consists of over 40 sedimentary basins of variable age and genesis which are thought to bear significant undiscovered hydrocarbon resources. Important tectonic events controlling the structure and petroleum geology of the basins are the Caledonian collision and orogeny followed by Late Devonian to Early Carboniferous rifting, Late Palaeozoic Baltica–Siberia collision and Uralian orogeny, Triassic and Early Jurassic rifting, Late Jurassic to Early Cretaceous Canada Basin opening accompanied by closure of the South Anyui Ocean, the Late Mesozoic Verkhoyansk–Brookian orogeny and Cenozoic opening of the Eurasia Oceanic Basin. The majority of the sedimentary basins were formed and developed in a rift and post-rift setting and later modified through a series of structural inversions. Using available regional seismic lines correlated with borehole data, onshore geology in areas with no exploration drilling, and recent Arctic-wide magnetic, bathymetry and gravity grids, we provide more confident characterization of the regional structural elements of the Russian Arctic shelf, and constrain the timing of basin formation, structural styles, lithostratigraphy and possible hydrocarbon systems and petroleum play elements in frontier areas.

Keywords: Eurasian Arctic, Barents Sea, Kara Sea, Laptev Sea, East Siberian Sea, Chukchi Sea, sedimentary basin, rift, petroleum potential, hydrocarbon system

A significant part of the Arctic is represented by the Eurasian epicontinental shelf which is the largest shelf on Earth. Its major portion (about 3.5 million km^2) is located in the Russian Arctic and is occupied by the eastern part of the Barents, Kara, Laptev, East Siberian and a western part of the Chukchi seas (Fig. 1). A systematic geological study and airborne gravity and magnetic measurements of the vast Russian Arctic shelves (RAS) was commenced soon after the end of the World War II, by the Research Institute of Arctic Geology (NIIGA, former Leningrad) and later by State Research Enterprise 'SevMorGeo' (see references below). The general results were summarized by Vol'nov *et al.* (1970), Vinogradov *et al.* (1974, 1977), Gramberg & Pogrebitskiy (1984), and recently by Suprunenko & Kos'ko (2005), Petrov *et al.* (2008), and Burlin & Stoupakova (2008).

The main exploration effort over the entire RAS was undertaken during the latest period of the Soviet era, when extensive coverage of refraction and 2D reflection seismic lines was acquired over the eastern Barents and southern Kara seas by Polar Marine Geological Expedition (PMGRE, St Petersburg), Marine Arctic Geological Expedition (MAGE, Murmansk), SevMorGeologiya (SMG, St Petersburg) and SevMorNefteGeofizika (SMNG, Murmansk) (Fig. 2). Some of the large prospects were successfully tested during the 1980s and several large discoveries were made, including the gigantic Shtokman, Rusanovskoe and Leningradskoe gas and gas condensate fields. Today the Russian Barents and southern Kara shelves represent the most explored petroleum provinces of the RAS, bearing *c.* 130×10^9 barrels of oil equivalent (BBOE) of proven resources.

The Siberian shelves, which are the most remote from the present-day markets, remain poorly explored. They represent one of the most promising petroleum frontiers worldwide. They have been explored by an irregular grid of wide-angle refraction and 2D regional multichannel seismic reflection (MCS) lines acquired mostly between 1975 and 1997 by PMGRE, MAGE, Laboratory of Regional Geodynamics (LARGE, Moscow) and SMNG in cooperation with German Federal Institute for Geosciences and Natural Resources (BGR, Hannover) in the Laptev Sea; and by LARGE and DalMorNefteGeofizika (DMNG, Sakhalin) in cooperation with Halliburton Geophysical Services, in the East Siberian and Chukchi seas. A recent seismic survey by the TGS-Nopec Geophysical Company AS provided modern high-quality data acquired with a 6 km long streamer in the Russian Chukchi Sea (Verzhbitsky *et al.* 2008).

Although the post-Soviet period did not bring new offshore discoveries due to suspended exploration activity, it was generally a time of broad regional compilation of the Soviet-era data. These became publicly available, and were incorporated into Arctic-wide digital bathymetric, gravity and magnetic grids through implementation of several international projects: International Bathymetric Chart of the Arctic Ocean (IBCAO, http://www.ibcao.org), Arctic Gravity Project (AGP, http://earth-info.nga.mil/GandG/wgs84/agp/index.html) and several compilations of the Arctic magnetic and gravity fields (Verhoef *et al.* 1996; Glebovsky *et al.* 2000; Maschenkov *et al.* 2001). Interpretation of these digital gravity and magnetic grids in combination with MCS lines allowed much more confident and accurate mapping and characterization of the Arctic regional structural elements and sedimentary basins (Ivanova *et al.* 1990; Warren *et al.* 1995; Drachev *et al.* 1998, 1999, 2001; Franke *et al.* 2000, 2001, 2004; Glebovsky *et al.* 2000; Sekretov 2000, 2001; Sherwood *et al.* 2002; Franke & Hinz 2005; Sharov *et al.* 2005; Grantz *et al.* 2009).

Sedimentary basins of the RAS are thought to bear significant volumes of undiscovered hydrocarbon (HC) resources which are still difficult to estimate due to limited geological and geophysical data. According to a recent assessment by the Russian Ministry of Natural resources, the RAS could contain as much as 700 BBOE of

VINING, B. A. & PICKERING, S. C. (eds) *Petroleum Geology: From Mature Basins to New Frontiers – Proceedings of the 7th Petroleum Geology Conference*, 591–619. DOI: 10.1144/0070591

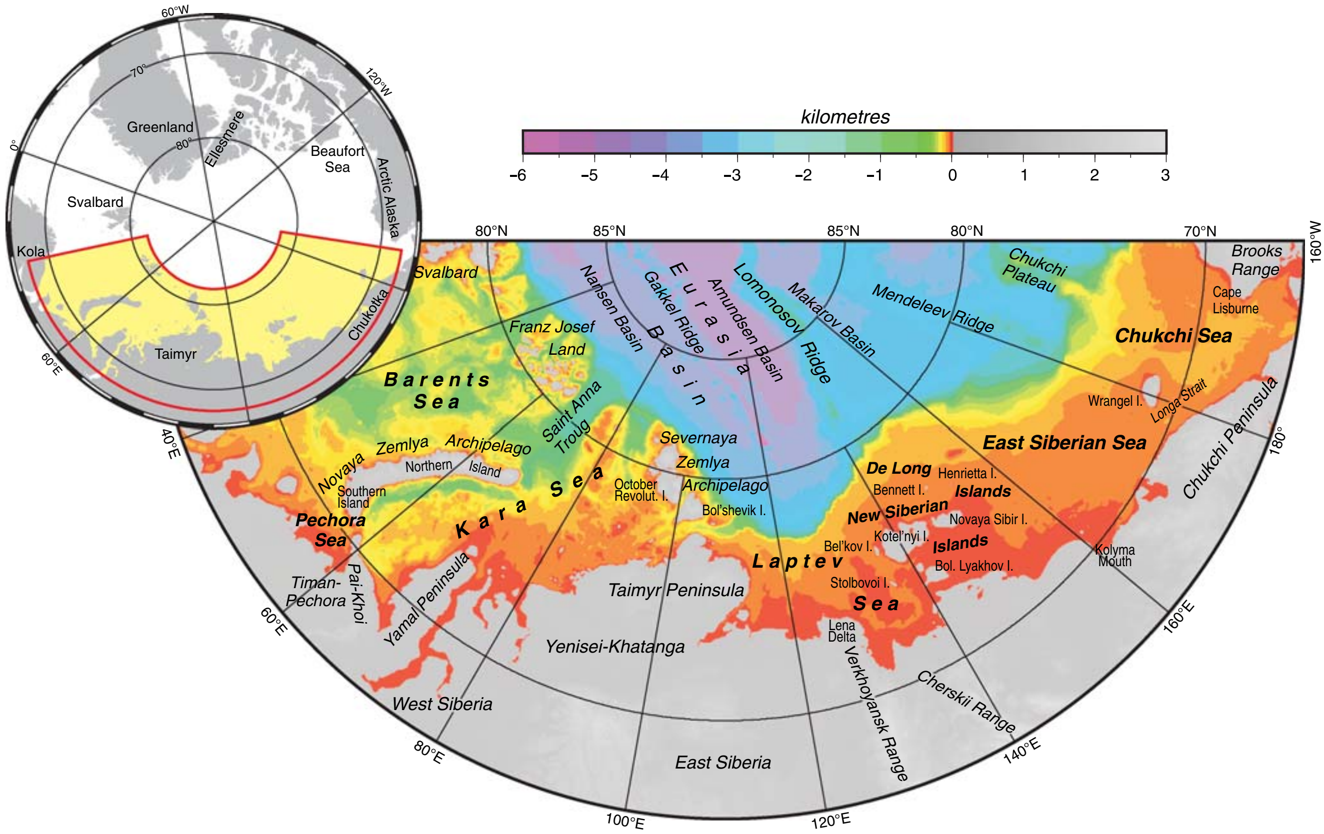

Fig. 1. Physiography of the Russian Arctic shelf. Topography is given after International Bathymetric Chart of the Arctic Ocean (IBCAO; http://www.ibcao.org). The inserted map in the upper left corner shows the location of the study area (red outline) in the Circum-Arctic.

total (discovered and undiscovered) resources. Data describing the age, composition and structural styles of the rocks composing the Arctic continental masses and islands remain a principal source of information about undrilled pre-Jurassic HC plays of the Barents–Kara region and the entire section of the Siberian Arctic shelves. This paper presents a brief overview of the RAS regional and petroleum geology. Based on available seismic, gravity/magnetic and geological data, we describe the main structural features of the East Barents, North and South Kara, Laptev, East Siberian Sea and western Chukchi provinces. The paper also summarizes the most important data on the evolution of these basins, and their known petroleum systems, and tries to apply general tectonic

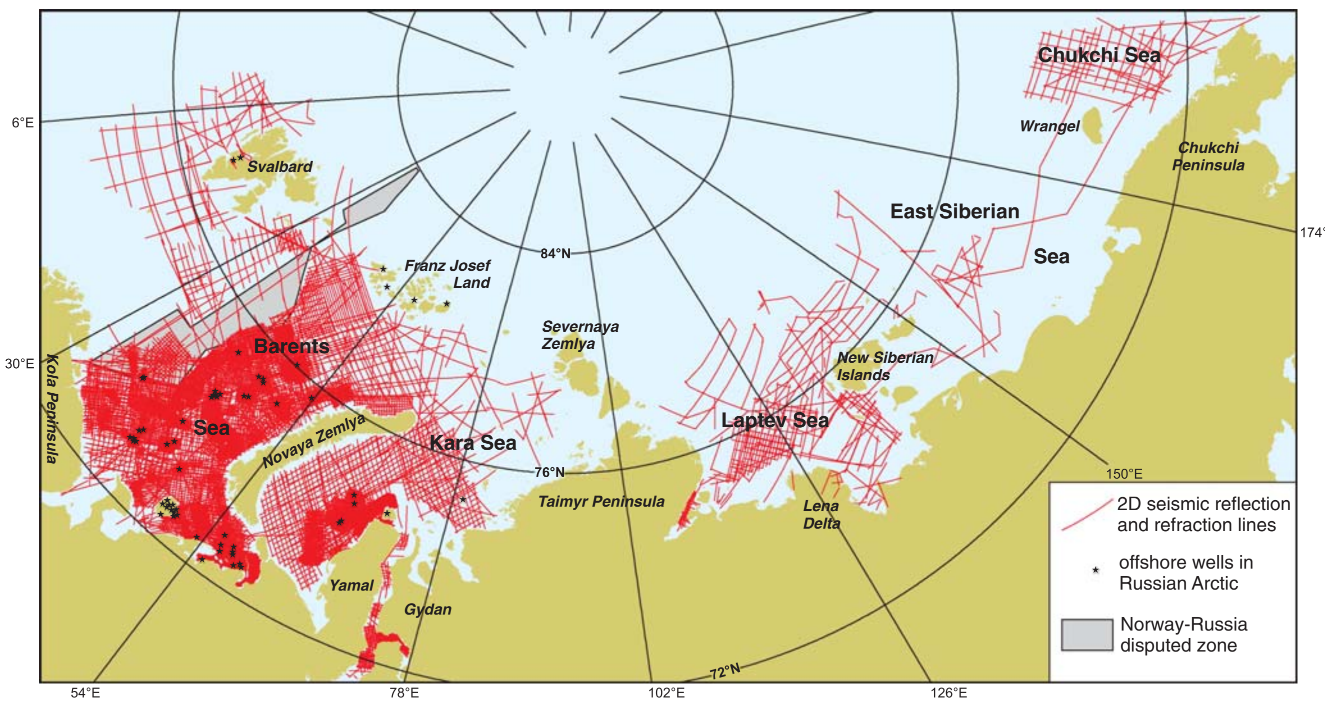

Fig. 2. Location of the 2D seismic reflection and refraction surveys and offshore wells in the Russian Arctic.

models and trans-regional correlations to draw some conclusions for those parts of the shelves where no direct observations exist to infer their geology.

Tectonic setting

As is consistent with modern plate-tectonic ideas of Arctic evolution, the structure of the consolidated continental crust underlying the Eurasian continental margin was formed during much of the Phanerozoic as a result of a series of collisions between the Laurentia, Baltica and Siberia continents and with a number of smaller microcontinents. Sedimentary basins post-dating the main Phanerozoic collisions mainly formed in response to initial rifting related to post-orogenic collapse and/or to the formation of Arctic spreading basins, for example, Eurasia and Amerasia basins. Many of these sedimentary basins were later modified through a series of intraplate structural inversions.

The formation of the RAS basins has generally been migrating over time east- and northeastward (present-day coordinates), thus basin complexity and age decrease in the same direction. The oldest Early Palaeozoic basins formed in the western sector of the RAS, and then the basin formation progressed through the Palaeozoic in the east Barents and north Kara shelves, and throughout the Early–Mid Mesozoic in the South Kara Sea and the Yenisei–Khatanga region.

The latest phase of basin formation in the RAS took place in the Laptev Sea region, where a series of rift-related basins have been evolving due to the opening of the Eurasia oceanic basin and the development of the present-day boundary between the Eurasian (EUR) and North American (NA) lithospheric plates. The Cenozoic plate-tectonic history of the Arctic is well constrained due to the decipherable set of seafloor spreading magnetic anomalies in the North Atlantic and Eurasia basins (Karasik 1968, 1974; Pitman & Talwani 1972; Vogt *et al.* 1979; Savostin & Karasik 1981; Karasik *et al.* 1983; Savostin *et al.* 1984*a*; Srivastava 1985; Cook *et al.* 1986; Harbert *et al.* 1990; Kristoffersen 1990; Glebovsky *et al.* 2006), and we refer to these publications when more details are required with regard to the Cenozoic plate-tectonic framework of the Arctic.

Therefore the basins of the Barents–Kara region, which rest on continental crust of the Palaeoproterozoic craton and Palaeozoic accreted crust, are mostly composed of Neoproterozoic, Palaeozoic and Mesozoic–Cenozoic carbonate and siliciclastic sequences, whereas most of the Siberian Arctic basins (the Laptev, East Siberian and Chukchi shelves) are underlain by the younger crust of the Late Mesozoic fold belts, and are filled with the Cretaceous (Aptian–Albian and younger) and Cenozoic siliciclastic sediments.

The most important tectonic events controlling the structure and petroleum geology of the entire Eurasian Arctic shelf are:

(1) Neoproterozoic to Early Cambrian Timanian orogeny;
(2) Caledonian orogeny followed by a phase of orogen collapse and crustal extension in Late Devonian–Early Carboniferous;
(3) Late Palaeozoic (Uralian) collision of the Baltica and Siberian continents;
(4) Permo-Triassic plume-related volcanic event and associated crustal extension;
(5) Jurassic rifting and subsequent opening of the Canada oceanic basin, accommodated by separation of the Arctic Alaska–Chukchi Microplate (AACM) from the Canadian margin of North America and its movement towards Siberia;
(6) Early Cretaceous closure of the Anyui Ocean due to convergence of the AACM with the Verkhoyansk-Omolon Siberian margin along the South Anyui Suture;
(7) Late Cretaceous to Paleocene opening of the Labrador Sea and Baffin Bay basins, which may also have affected the Central Arctic region between the Lomonosov and the Alpha-Mendeleev ridges;
(8) Greenland–Ellesmere and Greenland–West Barents margin convergence at 55–33 Ma and related crustal microplate re-adjustment in the Barents–Kara region;
(9) opening of the Eurasia oceanic basin at 55–0 Ma and related rifting and crustal microplate re-adjustment in the Laptev–East Siberian seas sector;
(10) the India–Eurasia collision at 40–10 Ma, causing large-scale crustal re-adjustment throughout Asia and NE Asia, which may also have reached the Eurasian Arctic continental margins.

The Cenozoic development of the RAS was controlled by continuous interaction of the NA and EUR lithospheric plates, which caused a drastic impact on the Siberian Arctic shelves. Since this region has always been in an intra-plate setting near the pole of plate rotation, even small changes in the plates' rotation have resulted in drastic changes in the basins' tectonic development and depositional environments.

Main characteristics of the RAS consolidated basement

Structurally the RAS is bordered on the south by the Baltica (also called East European, or Russian) and Siberian (also called East Siberian) cratons and adjoining Neoproterozoic, Palaeozoic and Mesozoic fold-and-thrust belts (hereinafter called fold belts). All of these first-order structures approach the Eurasian Arctic coast, and apparently extend farther offshore, where they form a tectonic basement (hereinafter also called basement) underlying sedimentary basins (Fig. 3). (By a tectonic basement we mean strongly deformed and/or metamorphosed units of rocks and their associations, compared with generally undeformed/weakly deformed and unmetamorphosed sedimentary successions existing within a sedimentary basin.)

The fact that the Eurasian Arctic onshore fold belt domains extend offshore is also supported by a number of MCS lines located close to the shoreline, as well as by gravity and magnetic maps. However, due to the lack of reliable data, there are as many points of view on possible offshore basement tectonics as there are researchers. However, many agree that a fundamental difference in tectonics and geological history exists between the western and eastern sectors of the RAS, as was earlier recognized by Vinogradov *et al.* (1974, 1977), Gramberg & Pogrebitskiy (1984), Savostin *et al.* (1984*b*), Zonenshain *et al.* (1990) and others.

Figure 3 illustrates our understanding of large-scale crustal structural pattern of the RAS based on geological data from coastal areas, published and unpublished MSC lines and publicly available gravity and magnetic grids.

Western sector of the RAS (eastern Barents and Kara shelves)

The western RAS is dominated by pre-Cambrian, Palaeozoic and Early Mesozoic crustal domains: the Neoproterozoic Timan–Varanger Fold Belt (Timanides by Gee & Pease 2005), Scandinavian Caledonides, a hypothetical Mesoproterozoic Svalbard Massif, Late Palaeozoic Uralian and Taimyr fold belts (Uralides and Taimyrides, respectively), the Early Mesozoic Novaya Zemlya and, to a small extent, South Taimyr fold belts (Fig. 3). There are still many highly disputed issues concerning possible outlines and relationships of these first-order structural domains beneath thick sedimentary cover of the Arctic seas (for the latest review see Pease 2011). Below we provide a short description of the main structural domains of the offshore basement relevant to understanding the formation and evolution of the RAS sedimentary basins.

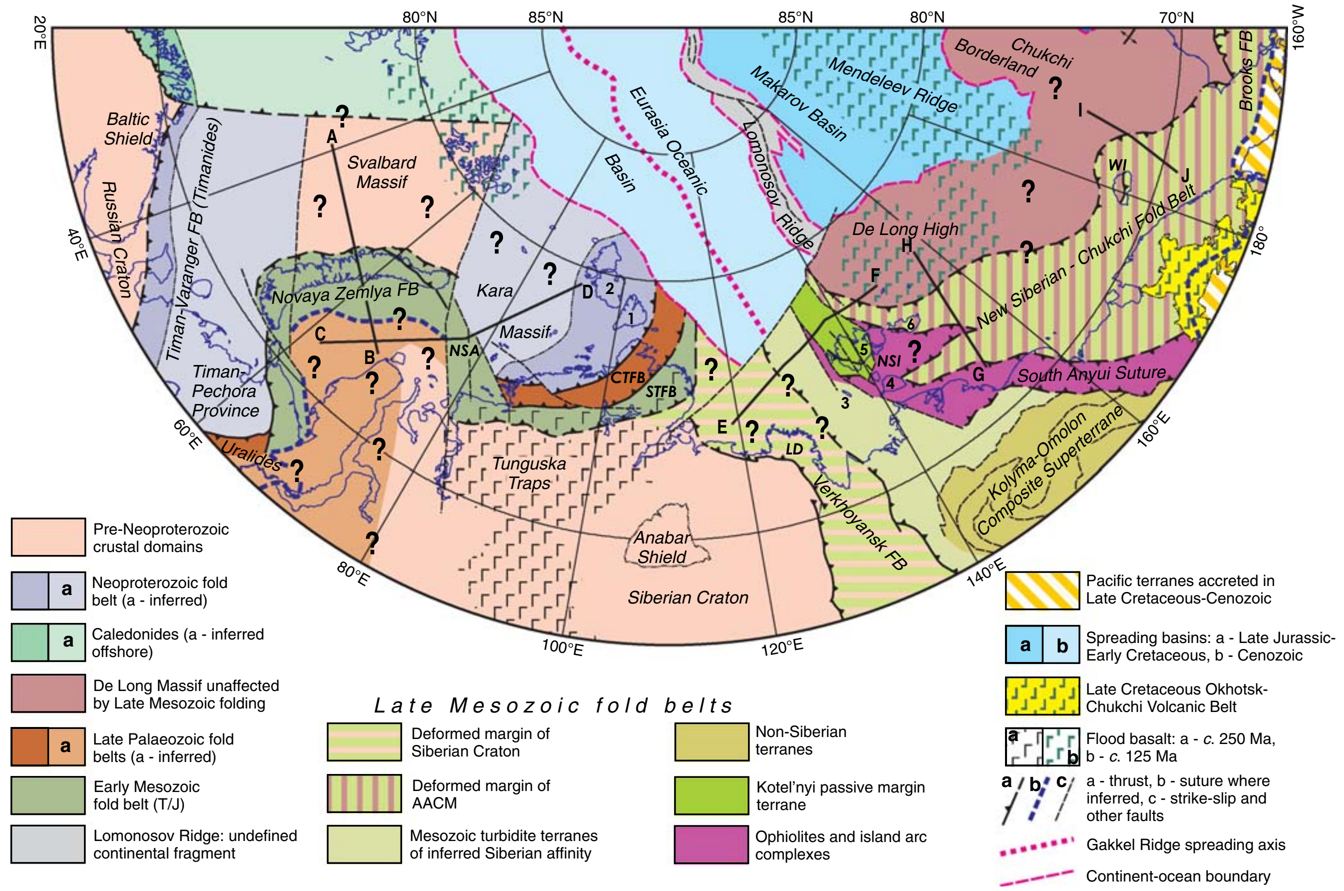

Fig. 3. Crustal tectonics of the Russian Arctic shelf and adjacent onshore and offshore regions. Bold solid lines labelled A–B, C–D, E–F, G–H and I–J show the location of crustal cross-sections given in Figures 6a, b, 11b, 14 & 16, respectively. The bold italic letters denote: NSA, North Siberian Arch; CTFB, Central Taimyr Fold Belt; STFB, South Taimyr Fold Belt; LD, Lena Delta; NSI, New Siberian Islands; WI, Wrangel Island. The bold numbers denote the following islands: 1, Bol'shevik; 2, October Revolution; 3, Stolbovoi; 4, Bol'shoi Lyakhov; 5, Kotel'nyi; 6, Novaya Sibir'. For other geographic names see Figure 1. Bold question marks denote the areas with least constrained interpretation of the basement type and age. FB denotes fold belt.

The Novaya Zemlya Fold Belt (NZFB) has a critical significance for understanding the tectonic history of the western RAS. It was formed at a very complex junction of the Baltica and Siberian cratons with the northern part of the Late Palaeozoic Uralides. It also divides two major HC provinces – East Barents and Northwest Siberian – and thus is the only area where the Palaeozoic HC systems of both provinces are exposed and thus available for direct studies.

As shown by Bondarev (1982), Lopatin *et al.* (2001), Pogrebitskiy (2004), Korago *et al.* (2004, 2009) and Vinokurov *et al.* (2009), the NZFB is mostly composed of Palaeozoic to Early Triassic successions deposited in a shelf to basin transition setting with shallow shelf facies developed along the western flank of the fold belt. The total thickness of the known section exceeds 13 km. The entire section was severely deformed at the end of the Triassic–earliest Jurassic to form a west-verging arcuate fold belt (Scott *et al.* 2010).

The basement of the NZFB is exposed locally and consists of Meso- and Neoproterozoic metaclastic and metacarbonate rocks, compressionally (east–west trending) deformed and metamorphosed in epidote–amphibolite and greenschist facies, and intruded by Neoproterozoic granite and granodiorite rocks (Korago *et al.* 2004). The recent study of metaclastic turbidites, which underlie a sharp angular unconformity at the base of unmetamorphosed variegated clastic sediments of Early Ordovician at Southern Novaya Zemlya Island, revealed the presence of Cambrian ages of detrital zircons (Pease & Scott 2009). This implies that at least some of the previously inferred Neoproterozoic rock complexes have, in fact, Cambrian age, and that the age of 'Timanian' unconformity is not older than Late Cambrian to Early Ordovician. Therefore, according to Pease (2011), the Timanian orogeny on southern Novaya Zemlya lasted until the end of Cambrian time, and the regional limit of the Timanian deformation probably extends beyond the Novaya Zemlya Archipelago into the Northern Kara region, where a contemporaneous unconformity between Cambrian and Ordovician is present on October Revolution Island (see below). A similar point of view about possible Cambrian extent of the Timanian orogeny was proposed by Bogolepova & Gee (2004).

The east–west compressed and unmetamorphosed Palaeozoic to Lower Triassic strata were deposited along the eastern margin of the Baltica (present-day orientation). The southern and central parts of the NZFB are composed of the following tectonostratigraphic rock assemblages, or complexes (Lopatin *et al.* 2001):

(1) Cambrian to Middle Devonian shallow water sandstones, dolomites, limestones, shales, siltstones, gravelites and conglomerates.
(2) Late Devonian to Early Carboniferous shallow water limestones, calcarenites, bioherms and calcareous sandstones.
(3) Middle to Late Devonian assemblage of clastic, volcanic and volcaniclastic rocks – claystones, siltstones, shales, polymictic sandstones, gravelites, conglomerates, tholeiitic basalts and tuffs. The intrusive analogues are represented by sills and dykes of gabbro-dolerites. The rock geochemistry suggest their intracontinental rift affinity.
(4) Late Devonian to Permian open marine and deepwater claystones, siltstones, rhodochrosite-bearing siliceous rocks, turbidites, olistostromes.

(5) Late Permian siliciclastic deepwater turbidites with horizons of olistostromes and calcareous sandstones.
(6) Later Permian to Lower Triassic shallow water and continental coarse-grained clastic rocks.

These rock complexes are intruded by a few small bodies of granitic rocks with Late Triassic to Early Jurassic isotopic ages (Pogrebitskiy 2004).

Baltica Timanide sources for the Palaeozoic clastic rocks are determined by detrital zircon ages (Pease & Scott 2009). Korago *et al.* (2009) suggested that the Upper Silurian clastic sediments, in contrast to the underlying beds, were derived predominantly from a northwesterly located Caledonian orogen. However, the Caledonian source is still highly debated (Pease 2011).

The northern part of the NZFB reveals a different type of stratigraphy. According to Lopatin *et al.* (2001), Pogrebitskiy (2004) and Korago *et al.* (2004), it is composed of a continuous *c.* 10–13 km thick Neoproterozoic to Lower Devonian section, which lacks any significant unconformities. The deepwater fine-grained siliciclastic metaturbidites are predominant within the Neoproterozoic to Lower Silurian successions. The overlying Upper Silurian to Lower Devonian strata are composed of shallow marine clastic and coarse clastic sediments, and the uppermost part of the section consists of Lower to Middle Devonian shallow water carbonate succession. Thin Upper Devonian and Carboniferous shallow water clastic and carbonate sediments occur sporadically and reveal a number of stratigraphic gaps. This interval could be related to the Late Palaeozoic orogenic event, which strongly affected the Taimyr Peninsula, and apparently the adjacent Kara Massif. Upper Carboniferous to Permian shallow-marine and continental coarse-grained clastic sediments coeval to main phase of the orogeny cap the section of the northern part of the fold belt.

The absence of unconformities within the Neoproterozoic to Lower Palaeozoic section of the northern block of the NZFB, which could be expected in proximity to the Timanian and possibly Caledonian (see Gee *et al.* 2006) deformation fronts, is one of the enigmas of the Arctic geology. One possible explanation given by Korago *et al.* (2004) is that this block had an independent Neoproterozoic and Palaeozoic history and became a part of the fold belt during its formation in Permian–Triassic.

The age of compressional deformations associated with the NZFB was for a long time one of the most disputed issues of the Arctic geology (see Pease 2011). The youngest strata recognized to be involved into the deformations are the Lower Triassic, which could assume a younger age of the deformations. Modern MCS data acquired in the vicinity of the western coast of Novaya Zemlya show a sharp angular unconformity at about the Triassic–Jurassic boundary, which probably corresponds to the main deformation phase (Pavlov *et al.* 2008).

The Kara Massif, or Microcontinent (KM) is traditionally outlined in the northern part of the Kara Sea. Structurally it is separated from the Late Palaeozoic to Early Mesozoic structural assemblage at the basement of the South Kara Basin (SKB) by a prominent linear North Siberian basement arch (or Step in the Russian literature). As depicted by the gravity field (Fig. 4, number 11), the arch strikes from the northern tip of the Novaya Zemlya Archipelago to the northwestern coast of the Taimyr Peninsula, indicating a structural relationship between the Novaya Zemlya and Taimyr fold belts. Its origin may be related to the Early Mesozoic compressional event and, given almost orthogonal orientation of the arch

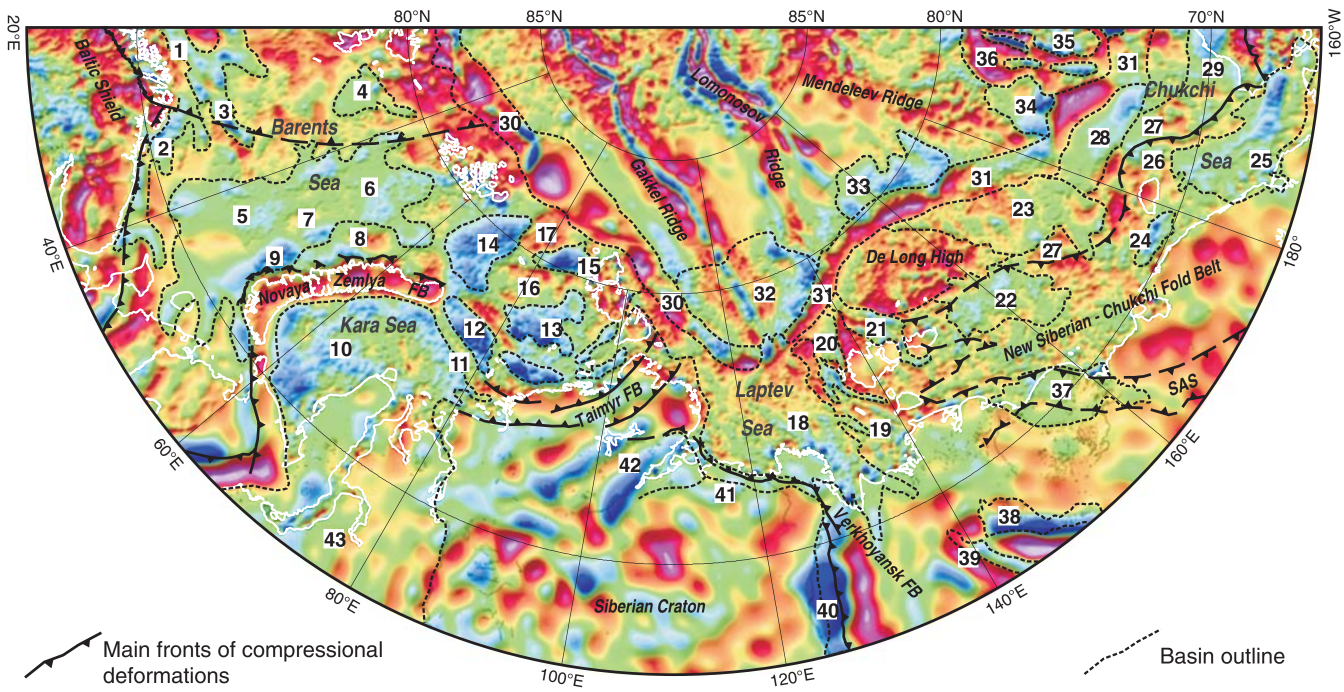

Fig. 4. Free-air gravity field over the Russian Arctic shelf and adjacent areas with outlines of the main sedimentary basins and basement highs (gravity data source is Arctic Gravity Project, http://earth-info.nga.mil/GandG/wgs84/agp). Numbers denote the following structural elements: *Barents Sea* – 1, Hammerfest Basin; 2, Varanger Trough; 3, Nordkapp Rift; 4, Olga Basin; 5–7, East Barents Megatrough (5, South Barents Basin; 6, North Barents Basin; 7, Ludlov Saddle); 8, Admiralty High; 9, Pri-Novaya Zemlya Basin. *Kara Sea:* 10, South Kara Basin; 11, North Siberian Arch; 12, Litke Trough; 13, North Kara Basin; 14, St Anna Trough; 15, Schmidt Trough; 16, Central Kara High; 17, Ushakov High. *Laptev Sea:* 18, Ust' Lena Rift; 19, Stolbovoi Horst; 20, Anisin Rift; 21, New Siberian Rift. *East Siberian Sea:* 22, East Siberian Sea Basin (East Siberian Depocentre); 23, Vil'kitskii Basin; 24, Longa Basin. *Chukchi Sea:* 25, South Chukchi (Hope) Basin; 26, Wrangel-Herald Structural Arch; 27, New Siberian-Wrangel Basin; 28, North Chukchi Basin; 29, Colville Basin. *Eurasian Continental Margin:* 30, Barents–Kara–West Laptev marginal basin; 31, East Laptev–East Siberian–Chukchi marginal basin. *Oceanic deepwater basins:* 32, South Eurasia Basin; 33, Podvodnikov Basin; 34, Chukchi Abyssal Plane Basin; 35, Northwind Basin; 36, Chukchi Plateau. *Continental realm:* 37, Lower Kolyma Basin; 38, Zyryanka Basin; 39, Moma Rift; 40, Priverkhoyansk Basin; 41, Lena-Anabar Basin; 42, Yenisei–Khatanga Basin; 43, West Siberian Basin. SAS is South Anyui Suture.

with regard to the NZFB, a considerable dextral strike-slip deformation may be expected.

The KM remains poorly studied and its geology is mainly projected from the Severnaya Zemlya Archipelago and northern Taimyr Peninsula. The first reliable isotopic data constraining the ages of magmatic, metamorphic and, therefore, tectonic events were obtained by Vernikovsky (1995, 1996). Recently new data on geology of Severnaya Zemlya were published by Metelkin *et al.* (2005), Lorenz *et al.* (2006, 2007, 2008), and Männik *et al.* (2009). Lorenz *et al.* describe the KM as the North Kara Terrane.

Tectonic basement of the KM is exposed in the northern part of the Taimyr Peninsula, and on northerly located Bol'shevik Island (Fig. 3). It is represented by a succession of Neoproterozoic siliciclastic turbidites that are commonly attributed to a passive margin of the KM (Vernikovsky 1996; Lorenz *et al.* 2006–2008). The detrital zircon ages provide solid argument for a Timanian Baltica source of the clastic sediments and therefore constrain Neoproterozoic setting of the KM as a part of the Baltica Continent (Lorenz *et al.* 2008; Pease & Scott 2009). The rocks are intensively deformed and regionally metamorphosed to lower greenschist (Bol'shevik Island) and amphibolite (Northern Taimyr) facies and intruded by Late Palaeozoic syn- and post-collisional granites (300–265 Ma, Vernikovsky 1995; Vernikovsky & Vernikovskaya 2001). While the Northern Taimyr metamorphism is related to the Late Palaeozoic Uralian orogeny (Vernikovsky 1995; Pease & Scott 2009), the data on the Neoproterozoic metaturbidites of Bol'shevik Island may suggest a Neoproterozoic (Vendian, according to Proskurnin (1999), or Riphean, according to Lorenz *et al.* (2008)) phase of compressional deformation and metamorphism, which may be related to a 740–600 Ma collision of the KM with an island arc terrane (currently the Central Taimyr Fold Belt; Vernikovsky & Vernikovskaya 2001).

Cambrian marine siliciclastic sediments occur on eastern October Revolution Island. The lower part of the section is represented by unfossiliferous turbidites which, according to Proskurnin (1999), reveal some similarities with the Neoproterozoic turbidites of Bolshevik Island, and therefore may have Neoproterozoic age. The fossiliferous Cambrian strata are composed of shallow marine and basinal clastic sediments with some limestone beds in the Upper Cambrian. The section is compressed in north–south trending tight folds, but the rocks are unmetamorphosed as compared with the Neoproterozoic rocks of the Bol'shevik Island (Lorenz *et al.* 2007, 2008).

The Ordovician shallow water clastic sediments overlie Cambrian strata with a prominent angular unconformity on eastern October Revolution Island (the Kan'on River Unconformity). Lorenz *et al.* (2006) consider the deformations of the Neoproterozoic turbidites and Cambrian clastics as manifestations of a Caledonian compressional phase. The Kan'on River Unconformity is a coeval analogue to the Cambrian–Ordovician unconformity on Northern Novaya Zemlya Island, and therefore may be attributed to the latest stage of the Timanian orogeny, as suggested by Pease & Scott (2009) and Pease (2011).

Multi-coloured poly-facial Early Ordovician to Late Devonian calcareous, evaporite and clastic successions form an unmetamorphosed *c.* 3.5–5 km thick cover of the KM. Accumulation of the Ordovician to Silurian strata was taking place in shallow-water semi-restricted basins (Männik *et al.* 2009). In the Early Ordovician time a magmatic event took place with emplacement of intrusive and extrusive rocks: alkaline gabbro, syenite, granite, andesite, rhyolite and trachytes. The rock geochemistry is consistent with their origin in an intracontinental rift setting (Proskurnin 1995; Gramberg & Ushakov 2000). The Mid-Ordovician section is dominated by dark shales and gypsiferous limestones. The Late Ordovician quartz-sandstones probably related to a local uplift of the KM, which was followed by deposition of carbonate rocks through most of the Silurian. Lorenz *et al.* (2008) correlate the Devonian shallow water and fluvial sandstone dominated clastic strata to the Old Red Sandstone Formation.

In the earliest Carboniferous, the whole Early to Middle Palaeozoic KM cover within present-day limits of the Severnaya Zemlya was affected by slight to moderate compressional or transpressional deformation, and intruded by post-orogenic granites with U–Pb zircon ages 342 ± 3.6 and 343.5 ± 4.1 Ma. This Severnaya Zemlya folding is regarded by Lorenz *et al.* (2007, 2008) as Caledonian related. Another coeval compressional tectonic event, which could be a potential cause of the Severnaya Zemlya deformations, is Ellesmerian, or Innuitian, folding in the Canadian Arctic (Trettin 1991).

The Carboniferous and Permian shallow marine and continental clastic sediments, post-dating compression, occur locally on the Severnaya Zemlya. These strata do not reveal any deformation, assuming this part of the KM was not affected by a compression during its collision with the Siberian continent in Late Palaeozoic, which formed a south verging Central Taimyr Fold Belt.

An Early Mesozoic phase of compression has also been reported for the South Taimyr Fold Belt (Inger *et al.* 1999). In the Southern Taimyr Peninsula, the Tunguska-like flood basalts with $^{40}Ar/^{39}Ar$ ages *c.* 229–227 Ma are folded together with Carboniferous to Lower Triassic continental clastic rocks, and are unconformably overlain by Early Jurassic strata that constrain the age of the compressional event to the Late Triassic time (Walderhaug *et al.* 2005). Therefore, the Early Mesozoic compression occurred across a large domain of the RAS, which is almost 2000 km in the east–west direction, from the Novaya Zemlya Archipelago to the eastern coast of the Taimyr Peninsula. The regional extent and the magnitude of the folding are comparable to other first-order tectonic events which occurred in the Arctic, like the Caledonian, Late Palaeozoic and Late Mesozoic events.

Eastern sector of the RAS (east of Taimyr Peninsula)

The eastern Siberian shelves of the RAS are considered to be mostly underlain by Late Mesozoic fold belts (Vinogradov *et al.* 1974; Drachev *et al.* 1999; Drachev 2002), which occupy a huge onshore region between the Lena River in the west and the Mackenzie River in Alaska in the east. These fold belts originated in Late Jurassic to Early Cretaceous in the course of several collisional episodes of large terranes (AACM, Omolon) with Siberian margin, and were finally consolidated in Aptian during so-called Verkhoyansk–Brookian (or Chukotka–Brookian) orogeny. The fold belts are inferred to continue offshore where the Late Mesozoic folded structural domains are exposed on New Siberian and Wrangel islands (Fig. 3).

The Verkhoyansk Fold Belt and its western branch, the Olenek fold zone, surround the Siberian Craton in the east and NE. Their sections consist of over 10 km of Upper Palaeozoic to Lower Cretaceous (Hauterivian) siliciclastic sediments, known also as a Verkhoyansk Complex, which vary from fluvial to shallow marine sediments in the proximity to the craton to deepwater turbidites in the distal zones of the fold belts. The Verkhoyansk Complex is underlain by Riphean to Middle Palaeozoic carbonate and clastic–carbonate formations, belonging to the marginal parts of the Siberian Craton. This Palaeo-Siberian passive continental margin was compressionally deformed in the Early Cretaceous (*c.* 130–125 Ma) in the course of collisions with Kolyma–Omolon Composite Superterrane (Kolyma Structural Loop) and the AACM. Based on available MCS and gravity data, Vinogradov & Drachev (2000) and Drachev (2002) outlined the possible offshore extent of the Verkhoyansk and Olenek fold belts beneath the Laptev Sea rifted basins post-dating the Late Mesozoic compressional deformation (Figs 3 & 10).

The Kotel'nyi Terrane is defined in the western part of the New Siberian Archipelago *c.* 350–500 km north from onshore Late Mesozoic fold belts (Fig. 3). It provides solid evidence of a major Late Mesozoic compression event affected eastern portion of the RAS. The terrane is prevailed by Middle Ordovician to Upper Devonian and Mesozoic sedimentary rocks deposited in a passive margin setting. Three main tectonostratigraphic rock assemblages were defined (Kos'ko & Nepomiluev 1975; Kos'ko *et al.* 1990; Kos'ko 1994):

(1) A 3–5 km thick Middle Ordovician to Middle Devonian succession of carbonate rocks, mainly represented by lagoonal and shallow water marine fossiliferous limestones; basinal facies of black limestones and shales are known within Lower Silurian and Lower Devonian.
(2) A 7–9 km thick Upper Devonian to lowermost Carboniferous succession of grey mudstones and siltstones with minor carbonates and sandstones occurring within a prominent NW elongated synform-like structure (the Bel'kov-Nerpalakh Trough by Kos'ko *et al.* 1990), which may represent an infill of a structurally inverted Late Devonian rift. The share of carbonates and sandstones increases in the uppermost Devonian to Carboniferous interval, where the variegated rocks appear.
(3) A 1200–1300 m thick Triassic to Jurassic succession of claystone, clayey siltstone, siltstone and sandstone. The fine-grained clastic rocks occur predominantly within the Jurassic part of the section while the Triassic interval reveals an almost total absence of clastic material and is abundant in calcite and phosphorite nodules, which may be an evidence of deepwater sedimentation (Egorov *et al.* 1987).

The Carboniferous to Permian rocks occur sporadically, and are absent over most of the terrane. Their known sections are represented by very thin (30–130 m) beds of Serpukhovian and Bashkitian shallow water fossiliferous limestones, and by *c.* 200 m thick Lower Permian black shales with siltstone and limestone interbeds. Both the Carboniferous and Permian strata overlie, with a prominent unconformity at their base, the Ordovician to Devonian strata. In several localities the unconformity is characterized as an angular unconformity (Kos'ko & Nepomiluev 1975). Therefore, these facts may suggest an occurrence of a compressional phase at earliest Carboniferous time, which may be related to Ellesmerian orogeny in the Canadian Arctic. Another possible cause for the deformation may be the tilting of blocks of lower Palaeozoic rocks during the formation of the Bel'kov–Nerpalakh Trough. At present, the lack of structural data does not allow any further conclusions to be drawn on the possible nature of the Mid Palaeozoic deformation.

The whole section of the terrane is intruded by numerous sills and dykes of gabbro-diabases that closely resemble in age and composition the Permian–Triassic Tunguska flood basalts (Kuzmichev & Pease 2007). The whole rock package of the terrane was intensively compressed in the Early Cretaceous, prior to Aptian, with clear dextral transpression component.

A narrow and highly deformed *South Anyui ophiolitic suture (SAS)* separates the New Siberian–Chukchi and Verkhoyansk–Kolyma fold belts. As shown by aeromagnetic data (Rusakov & Vinogradov 1969; Vinogradov *et al.* 1974; Spektor *et al.* 1981), it extends from the Kolyma River mouth onto the shelf where dismembered ophiolites and island-arc volcanic complexes are exposed on Bol'shoi Lyakhov Island (Drachev & Savostin 1993; Kuzmichev 2009). The further offshore continuation of the suture, though obscured by younger extensional structures, is still definable by magnetic data, which show two branches of positive anomalies: between Stolbovoi and Kotel'nyi islands and ENE of the latter (Fig. 3).

The suture formed as a result of the closure of the Anyui Ocean – a large embayment of the Late Palaeozoic–Mesozoic Pantallassa to the Pangaea II – in the course of collision between the AACM and the Siberian margin in the Late Jurassic–Early Cretaceous (prior to Aptian) time (Savostin *et al.* 1984*b*; Parfenov & Natal'in 1986; Zonenshain *et al.* 1990; Sokolov *et al.* 2002).

The Siberian portion of the *Arctic Alaska–Chukchi Microplate*, or microcontinent, is inferred to consist of two parts (Fig. 3):

(1) the New Siberian–Chukchi Fold Belt, which constitutes the southern, adjacent to the South Anyui Suture, deformed margin of the microcontinent;
(2) the De Long Massif located north of the Late Mesozoic deformation front and composed of Lower and Middle Palaeozoic complexes.

The New Siberian–Chukchi Fold Belt occupies the Chukchi Peninsula and provisionally extends offshore to include the Late Mesozoic folded complexes of Wrangel Island, and a broad area of the East Siberian Sea north of the proposed limits of the South Anyui Suture. The northern offshore limit of the fold belt has been identified on several MCS lines south of the De Long Islands and north and east of Wrangel Island, where it follows the northern flank of the Wrangel–Herald Arch (Drachev *et al.* 1999, 2001; Verzhbitsky *et al.* 2008).

Stratigraphic and structural relationships between various lithostratigraphic units of Wrangel Island remain poorly understood, although ongoing studies may illuminate its tectonic evolution. The oldest Neoproterozoic Wrangel Complex is composed of metavolcanic, metavolcanoclastic and metaclastic rocks, intruded by basic dykes and sills and small granitic bodies with isotopic ages 600–700 Ma (Kos'ko *et al.* 1993). The rocks were intensively deformed prior to deposition of thick sedimentary successions of Upper Silurian–Devonian and Carboniferous to Permian shallow marine siliciclastic rocks and shales, with some carbonate units deposited in a continental shelf setting. The uppermost part of the section is represented by an over 1–1.5 km thick unit of Triassic siliciclastic turbidites (medium to fine-grained sandstone alternating with shale and siltstone), which contrast with the older Palaeozoic shelfal strata (Kos'ko *et al.* 1993; Miller *et al.* 2010). Data on the U–Pb age of detrital zircons from Wrangel sections reveal similarities between the Upper Palaeozoic rocks of the island and the Lisburne Hills area (Western Alaska). Zircon populations from the Triassic turbidites differ significantly from both older Palaeozoic rocks of the island and from coeval rocks of the Lisburne area, although they are similar to the Triassic turbidites of the Chukchi Peninsula (Miller *et al.* 2010). All sedimentary successions were deformed in the latest Jurassic to Early Cretaceous, probably simultaneously with deformations in the Lisburne Hills area (132–115 Ma, according to Moore *et al.* 2002). On the Chukchi Peninsula and probably Wrangel Island the orogenic event was followed by an uplift and profound erosion between *c.* 117 and 95 Ma (Miller & Verzhbitsky 2009).

The De Long Massif has a very contrasting expression in gravity and magnetic fields, due to the occurrence of highly uplifted and eroded basement, and the presence of the Early Cretaceous flood basalts. The massif has repeatedly been attributed by Soviet geologists to a pre-Cambrian craton, often named the Hyperborean, or East Arctic Platform (Obruchev 1934; Shatskii 1935; Pushcharovskii 1963; Atlasov *et al.* 1970 and many others). However, today we have more evidence in favour of either Caledonian or Ellesmerian (Late Devonian) age for this feature (see below).

On Bennett Island, a 1.5 km thick succession of Middle Cambrian to Middle Ordovician fossiliferous shales and distal siliciclastic and clastic carbonate turbidites reveals rather weak deformation and a lack of metamorphism (Vol'nov *et al.* 1970; Drachev 1989). This section is quite unique since no similar rocks are known from the nearest Siberian Arctic. The closest occurrences of the Cambrian to Ordovician rocks to which the Bennett succession could be correlated are deepwater turbidites exposed in the Northern Greenland and the Northern Ellesmerian Island (Trettin 1991).

Henrietta Island is composed of moderately deformed clastic and volcano-clastic complexes and a unit of calc-alkaline basalts of unclear stratigraphic setting (Vinogradov *et al.* 1975). The section is intruded by diabase and diorite sills and dykes whose unpublished $^{40}Ar/^{39}Ar$ dates could possibly reveal a Caledonian age for the magmatism (Kaplan *et al.* 2001), while rock chemistry points to their island-arc affinity. The other two occurrences of the Caledonian-age structural domains in the High Arctic are at Spitsbergen and northern Ellesmere Island (Peary Terrane and adjacent area of the island). Therefore, based on the possible Caledonian age of the Henrietta magmatic rocks, we infer that a location of the De Long Massif was close to Northern Ellesmere Island prior to the Late Jurassic to Early Cretaceous opening of the Canada Basin.

On Bennett Island, Aptian coal-bearing muddy sediments, and a 200–300 m thick unit of plume-like flood basalts are separated from the underlying Lower Palaeozoic section by a sharp basal unconformity. A few K–Ar radiometric dates in the range of $119–112 \pm 5$ Ma constrain the age of the basalts to the Aptian to Albian (Drachev 1989; Drachev & Saunders 2006).

The above characterization of the RAS's heterogeneous folded tectonic basement points to some major uncertainties regarding the areal extent and structural relationships of the basement domains. These are:

(1) existence and extent of the Svalbard Massif (Microcontinent) and adjoining Scandinavian Caledonides and Timanides;
(2) relationships between the Kara and Svalbard massifs, and their relationship with the Baltica Continent;
(3) relationships between Late Palaeozoic Uralides and Taimyrides; extent of the Early Mesozoic Novaya Zemlya Fold Belt, and the mechanism of its formation;
(4) offshore extent of the Late Mesozoic fold belts, structural factors controlling their formation;
(5) palaeorelationships of the Kotel'nyi Terrane and the De Long Massif with Siberia, Arctic Canada, and Arctic Alaska;
(6) occurrence of Caledonian and/or Ellesmerian deformations on Kotel'nyi and Wrangel islands;
(7) offshore extent and magnitude of Permian–Triassic and Aptian–Albian flood basalt magmatic.

Presently no reliable data exist to constrain these uncertainties. However the fact that the western sector of the RAS is generally dominated by Neoproterozoic crustal domains, and the eastern sector by Late Mesozoic and, to a smaller extent, by Palaeozoic fold belts, is well supported by the modern geological and geophysical data. This has fundamental implications for characterizing the RAS sedimentary basins, history of their formations and their established and inferred HC systems.

RAS sedimentary basins and their petroleum geology

According to Grantz *et al.* (2009), as many as 37 large sedimentary basins of variable age and genesis exist over the entire RAS and adjoining deepwater areas. Figure 4 shows their outlines derived from MCS and gravity data. Based on the age of the basins, inferred mechanisms of their formation, composition of sedimentary infill, and known and inferred HC systems, we describe six groups of basins, or provinces, which generally fit into geographically isolated shelves: the East Barents (including offshore continuation of Timan–Pechora Basin), South Kara, North Kara, Laptev, East Siberian and Chukchi Sea (Russian sector).

East Barents Province

The structure, lithostratigraphy and petroleum geology of the East Barents and Pechora shelves are known due to the relatively dense grid of 2D seismic surveys, and a number of offshore wells (Gramberg & Pogrebitskiy 1984; Gramberg 1988; Verba *et al.* 1992; Bogdanov & Khain 1996; Shipilov & Tarasov 1998; Kogan *et al.* 2004). Shtokman, Ludlov, Ledovoe, Murmanskoe, Severo–Kildinskoe gas and gas condensate fields, Prirazlomnoe, Severo–Gulyaevskoe, Varandey–More and other oil fields are the biggest among those discovered so far.

The East Barents Province is dominated by the gigantic East Barents Megabasin (EBMB) which, due to its elongated shape, is often called a megatrough. It is bounded by the Central and North Barents platforms in the west and NW, respectively, and by the Novaya Zemlya Fold Belt in the east (Fig. 5). The southern rim of the EBMB is formed by a steep slope of the Fennoscandian Shield (Kola Monocline) and a series of NW-elongated horsts of the Timanian basement. In the north, it is limited by a high-standing block of basement of the Franz Josef Land Archipelago (Fig. 5). Some researchers also include the St Anna Trough in the EBMB. However, this basin is located in the North Kara Shelf, and is isolated from the East Barents Province by a zone of high-standing basement (the Al'banov-Gorbov Arch), and thus may have a different geological history.

The *East Barents Megabasin* extends south–north for over 1000 km, while its west–east width reaches 400–450 km. Despite a large amount of 2D MCS and refraction data and drilled wells, the EBMB is still poorly imaged beneath Jurassic strata due to the great thickness of Triassic and Upper Permian successions. Its internal structure and lithostratigraphic architecture are therefore disputable.

The EBMB is composed of two smaller depocentres: the South Barents and the North Barents basins divided by a basement high named the Ludlov Saddle (Fig. 5). Crustal velocity data show that in the central parts of the depocentres, where the total thickness of presumed post-Middle Devonian sediments reaches over 22 km, the underlying consolidated continental crust is highly attenuated or even could be completely absent (Kogan *et al.* 2004; Kaminsky *et al.* 2009). This fact is used by several researchers to propose that the EBMB is underlain by an oceanic lithosphere formed due to a failed spreading episode (Aplonov *et al.* 1996), or trapped during the Uralian collision event (Ustritsky 1989). As imaged by the deep seismic refraction data (Kogan *et al.* 2004; Ivanova *et al.* 2006), the EBMB generally resembles rift/post-rift basins with significant post-rift cover exceeding 20 km, for example the Pricaspian Basin.

MCS data supported by well ties both within the basin and along its southern margin in the Pechora Sea provide a good basis for understanding of the basin tectonostratigraphy. Six main seismic stratigraphic units have been identified so far (Fig. 6a). These are correlated to the siliciclastic sequences of Cretaceous (1), Jurassic (2), Triassic (3) and Late Permian (4) age, to the Late Carboniferous–Early Permian carbonate rocks (5), and to the Late Devonian to Early Carboniferous syn- and pre-rift clastic and carbonate rocks (6). The first three are well documented by numerous offshore wells that penetrated these stratigraphic intervals. Beneath the unit (6), on the flanks of the megabasin, an older pre-rift seismic stratigraphic unit is visible in seismic data (number 7 in Fig. 6a), which we correlate to Lower Palaeozoic strata known in the Timan–Pechora Basin.

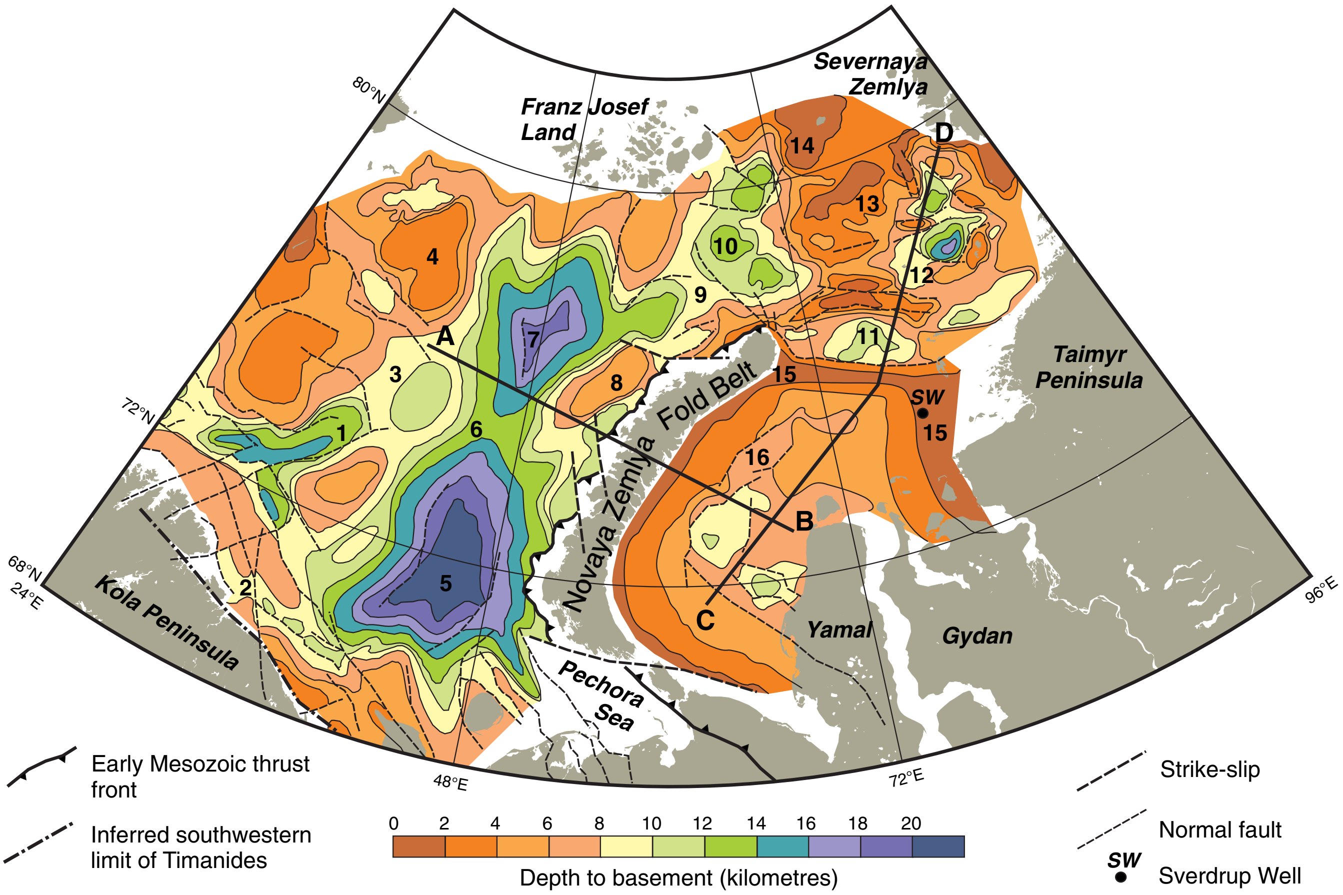

Fig. 5. Simplified depth-to-basement map of the Barents–Kara shelf based on seismic reflection and refraction data and ERS-2 gravity field (see text for the references). Numbered structures are: 1, Nordkapp Basin; 2, Varanger Basin; 3, Central Barents Platform; 4, North Barents Platform; 5, South Barents Basin; 6, Ludlov Saddle; 7, North Barents Basin; 8, Admiralty High; 9, Al'banov-Gorbov Arch. 10, St Anna Trough; 11, Litke Trough; 12, North Kara Basin; 13, Central Kara High; 14, Ushakov High; 15, North Siberian Arch; 16, South Kara Basin. Bold solid lines labelled A–B and C–D show location of cross-sections given in Figure 6.

Because of uncertainties with the stratigraphic correlation of the lower seismic horizons, the timing of basin formation is highly disputed. Proposed models differ significantly with regard to the age of the main rift event, which varies from Mezo-Neoproterozoic to Permo-Triassic (Gramberg & Pogrebitskiy 1984; Gramberg 1988; Nikishin *et al.* 1996; Shipilov & Tarasov 1998; Malyshev 2002; Sharov *et al.* 2005 and references contained therein). We support the point of view proposed in Lopatin (2000), and infer the main rifting phase to occur at Frasnian–Early Carboniferous time based on the following facts: (1) Late Devonian and Early to Mid Carboniferous rift episodes are well documented in the Norwegian Barents Shelf (Gudlaugsson *et al.* 1998); (2) Caledonian compressional deformation affecting the western Barents Shelf in Ordovician–Silurian terminated by Frasnian (Gee & Stephenson 2006).

The tectonic history of the EBMB can be described as a succession of the following events (Fig. 7):

(1) In Cambrian to Silurian, the basin may have been developing mainly in a shelf setting adjacent to the Uralian palaeocean. Its western (present-day) margin may have been subjected to compression and developing of a foreland basin in front of the Caledonides. Depositional environments may have varied though the EBMB from continental and fluvial–deltaic systems in the west, to carbonate platforms and deepwater conditions along its eastern flank. In the Late Silurian, clastic sediments derived from Caledonian orogen may have dominated the entire basin (Korago *et al.* 2009).

(2) In the latest Silurian to beginning of Devonian, large-scale strike-slip deformation and the formation of small pull-apart basins may have occurred in the southern part of the EBMB (by analogy with the Timan–Pechora Basin), followed by regional uplift and erosion during Middle to Late Devonian, prior to Frasnian. The latter could be correlated to a Svalbard Late Caledonian compressional phase, and therefore a compressional setting and basin inversion could be inferred for EBMB at the Middle to Late Devonian.

(3) Frasnian to Early Carboniferous was a time of a main rift phase accompanied by syn-rift basaltic volcanism. Continental crust was severely attenuated and formation of initial oceanic lithosphere could have taken place in the deepest parts of the mega-basin. Geodynamic factors controlling the rifting are unknown. A possible association with a mantle plume event could be inferred as proposed earlier for the Russian Craton (Nikishin *et al.* 1996; Wilson & Lyashkevich 1996; Wilson *et al.* 1999). The collapse of the Caledonian orogen could also provide a possible mechanism for crustal extension. Some analogues could be drawn to the Sverdrup Basin in Canadian Arctic to explain crustal attenuation within the EBMB.

(4) The Late Carboniferous to Early Permian was a period of thermal subsidence. Carbonate platforms and buildups formed along the basin flanks while its central parts were dominated by deposition of basinal carbonates and shales.

(5) In Late Permian to Triassic, a rapid subsidence of the entire EBMB took place, accompanied by accumulation of large volume of siliciclastic sediments. Permian clinoforms show

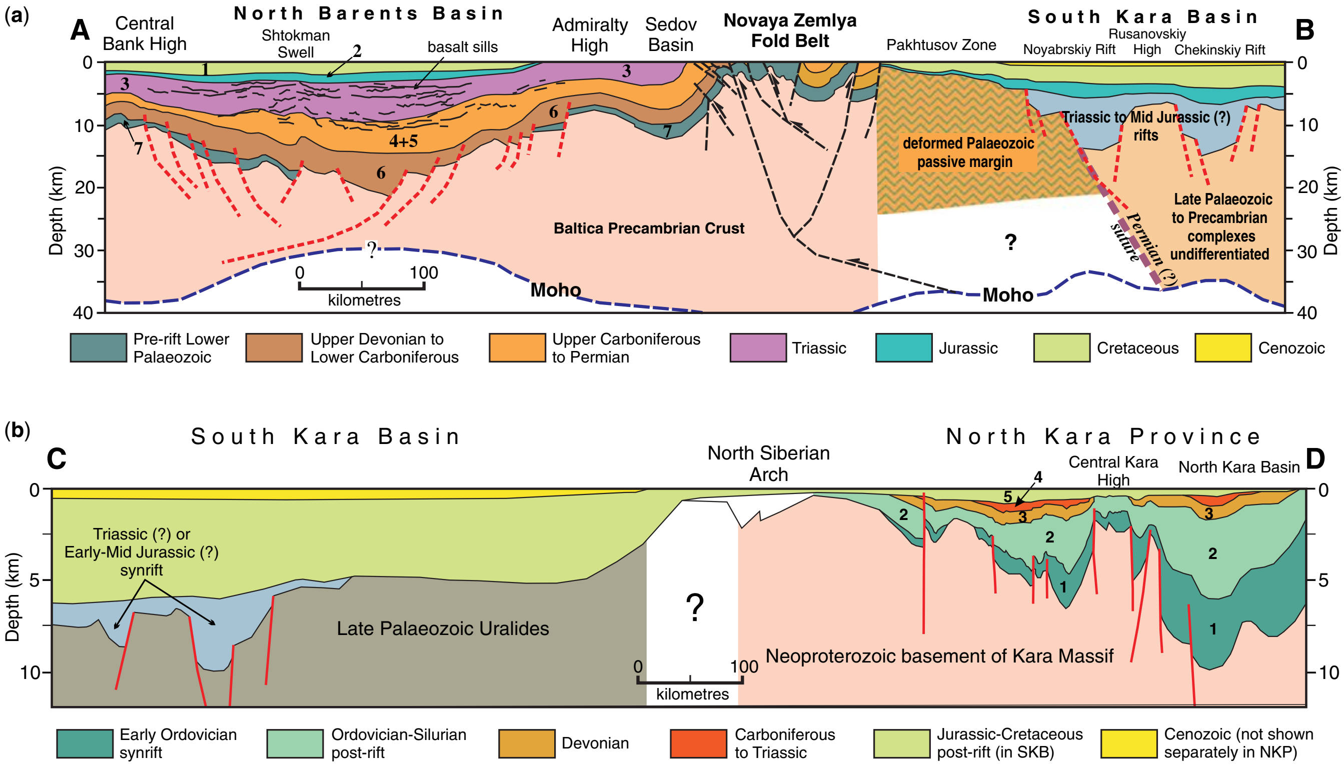

Fig. 6. Schematic geological cross-sections based on re-interpretation of deep seismic reflection and refraction data acquired and published by SMG (Sharov *et al.* 2005; Ivanova *et al.* 2006): (**a**) through the Eastern Barents and South Kara basins based on seismic transect 2-AP, (**b**) though the North Kara Province based on seismic transect 3-AP. Location is shown in Figures 3 and 5. Bold numbers from 1 to 6 in (a) and from 1 to 5 in (b) denote seismic stratigraphic units (see the text for the details).

that the main provenance areas were in the Russian Craton–Timan Pechora–Urals to the SSE of the EBMB, and to the NE within the present North Kara Shelf. Both of these regions were affected by the Late Palaeozoic Uralian orogenesis. Central and eastern parts of the EBMB remained uncompensated through the Late Permian to Early Triassic, and were probably part of a deepwater depression extending and deepening toward the present SKB. Many MCS lines approaching the Novaya Zemlya Fold Belt from the west show thickening of the Upper Permian and Lower Triassic intervals eastward, that is basinward. At the Permian–Triassic boundary, a plume-related basaltic volcanism affected some parts of the EBMB as indicated by basalts of the Pai–Khoi and Timan–Pechora (Nikishin *et al.* 2002). By the end of the Triassic the basin was probably completely filled with clastic sediments.

(6) At the Triassic–Jurassic boundary, the main Novaya Zemlya orogenic phase occurred, accompanied by inversion of the EBMB eastern flank in a foreland setting. Jurassic strata are eroded in the vicinity of the Novaya Zemlya, suggesting that the EBMB eastern flank was uplifted and subjected to erosion during most of Jurassic time.

(7) In Jurassic to Cretaceous, the central part of the EBMB continued to subside and received clastic sediments. During the latest Jurassic, the subsidence became undercompensated by sediment supply, and the EBMB became a starved basin accumulating marine organic rich sediments. By this time, the Novaya Zemlya orogen was probably completely eroded and had subsided below sea-level, uniting the EBMB with the SKB. Both of these became a part of the huge West Siberian depression and were gradually filled up in Early Cretaceous by easterly and northerly derived clastic sediments, as shown by the orientation of the Early Cretaceous clinoforms.

(8) In Aptian to Albian, there was a plume-related magmatic event that caused broad eruption of flood basalts known on Franz Josef Land and Eastern Svalbard (Amundsen *et al.* 1998).

Post-Cretaceous sediments are generally absent over most of the EBMB, which may be related to: (1) tectonic uplift during the Eocene-Oligocene and probably Early Miocene; and/or (2) recent glacial erosion. Cenozoic erosional phases were probably triggered by plate interactions in the North Atlantic and High Arctic, and by hard collision between India and Eurasia beginning around Eocene and continuing through Oligocene and Miocene. These global plate-tectonic factors caused the growth of a series of inversional swells and anticlinal structures (Fig. 8). Some of these inverted features (e.g. the Admiralty High) were formed at the Triassic–Jurassic boundary, and then re-activated in the Cenozoic time. Simultaneously, the Novaya Zemlya orogen was uplifted and became again the major divide between the Barents and Kara provinces.

The formation of the EBMB, as a whole, and especially the mechanisms of its rapid subsidence in the Triassic, remains highly debatable. Several models have been published by Nikishin *et al.* (1996), Artyushkov (2005), Levshin *et al.* (2007), Ritzmann & Faleide (2009) and others (for more comprehensive review see Gee & Stephenson 2006), and we refer readers to these publications and references contained therein for further details on the subject. In this paper we support a concept proposed by Sullivan *et al.* (2007) and by Scott *et al.* (2010), which involves the trapping of Uralian oceanic lithosphere in a pre-existing embayment of Baltica margin (present-day South Kara) during the main Late Palaeozoic collision, and following westward roll-back and pulldown of the trapped lithospheric slab, accompanied by slab to cause rapid subsidence of the adjacent Barents margin (Fig. 9).

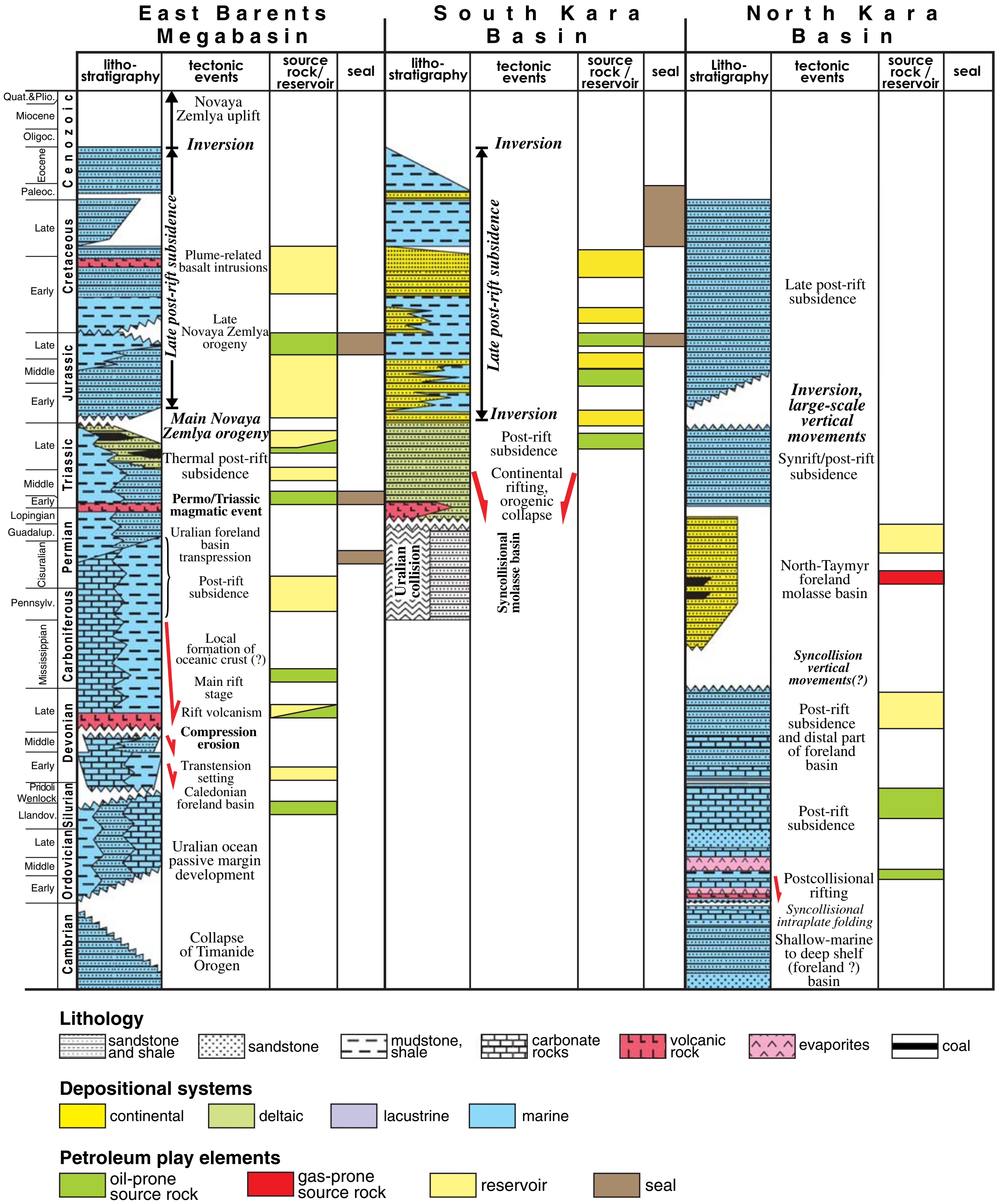

Fig. 7. Summary chart of tectonostratigraphy and petroleum play elements for the Barents–Kara Region.

Petroleum geology. HC systems and petroleum plays of the East Barents Province are known from numerous offshore wells (Fig. 2). The Palaeozoic and Lower Mesozoic plays, which occurred at greater depths throughout the basin and are currently undrilled, were tested in the Pechora Sea, and have been used to decipher the petroleum geology of the lower part of the EBMB infill. The younger Jurassic and Cretaceous plays are well studied in the EBMB where they have accumulated significant gas resources. Many data on the petroleum geology of the Barents–Pechora Shelf were summarized by Ulmishek (1982), Johansen *et al.* (1993), Ostisty & Fedorovsky (1993) and Doré (1995), and we refer readers to these publications for more detailed information. A summary of the petroleum systems and play elements of the East Barents province is given in Figure 7.

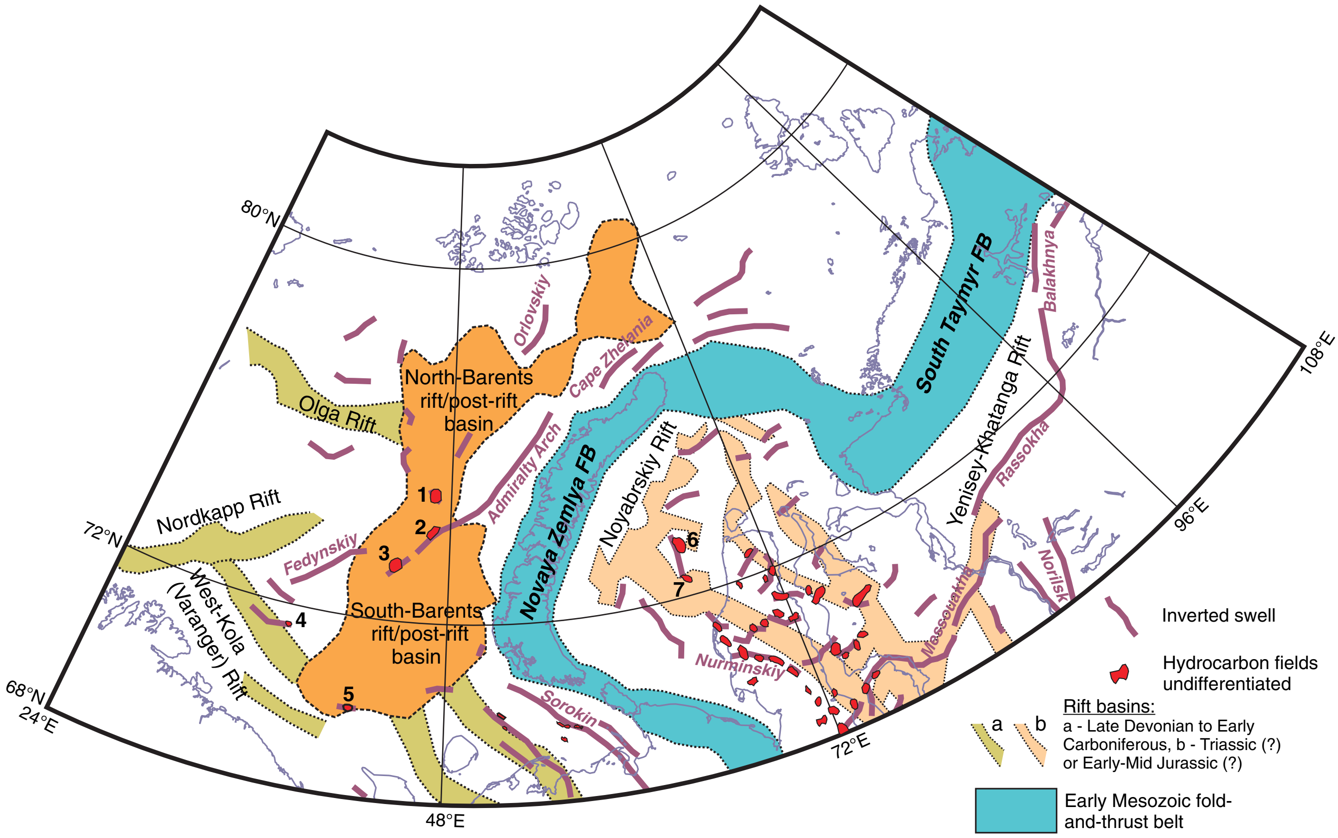

Fig. 8. Areal occurrence of main Mesozoic and Cenozoic intraplate inversional swells in the Barents–Kara Region. Bold numbers denote main gas and gas condensate fields: 1, Ludlov; 2, Ledovoe; 3, Shtokman; 4, Severo-Kil'dinskoe; 5, Murmarskoe; 6, Rusanovskoe; 7, Leningradskoe.

In the Timan–Pechora Basin, the Palaeozoic oil-prone source rocks are represented by:

(1) Upper Silurian shales;
(2) Devonian (lower Frasnian) carbonates and shales (Domanic Formation);
(3) Lower to Middle Carboniferous coaly-argillaceous sediments with mixed kerogen types.

The Lower Permian shaly sediments reveal high content of total organic carbon (TOC) in some sections, and thus could also be a local oil source.

The main reservoirs include:

(1) the Lower Devonian limestones and dolomitized limestones (encountered by a few wells at the lower levels of the Medyn–More and Prirazlomnoe fields);
(2) the Upper Carboniferous and Lower Permian carbonate rocks, especially carbonate buildups and organo-clastic limestones (the Prirazlomnoe Field);
(3) The Upper Permian to Triassic sandstones.

The properties of the Lower Devonian carbonate reservoirs are mainly controlled by highly irregular secondary porosity (7–8%) and low permeability. The Upper Carboniferous to Lower Permian carbonate rocks are the main reservoir for oil accumulations over the entire Timan–Pechora Basin. They also host the Medyn–More and Prirazlomnoe oil fields offshore. These rocks have good properties due to higher porosity, which reaches 25% in fossiliferous layers.

The main seals within the Palaeozoic and Lower Mesozoic plays of Timan–Pechora Basin are represented by:

(1) the Upper Devonian (Kynovsk–Sargaev) argillaceous succession;
(2) the Lower Carboniferous (Visean–Serpukhovian) evaporate succession;
(3) the Lower Permian (Kungurian–Upper Artinskian) carbonate–shale succession;
(4) the Lower Triassic shaly–argillaceous succession.

The Kynovsk–Sargaev and Kungurian–Upper Artinskian are the regional seals which developed throughout most of the Timan–Pechora Basin, while the others have a more limited occurrence.

The main phase of HC generation in the Timan–Pechora Basin occurred in the Permo-Triassic when about 70% of total source rocks entered the oil maturation window (Malyshev 2002).

In the EBMB, the main HC source rocks, which are inferred to charge the gigantic gas accumulations, are the Triassic organic-rich (up to 4.7–6.5% TOC) gas-prone coal-bearing shaly sediments of continental, lagoonal and shallow-marine origin. Their potential for oil generation is unknown, but cannot be ruled out, since marine facies with type II kerogen could have been deposited in the central parts of the EBMB. Marine Upper Jurassic organic rich shales (an analogue of the Bazhenov Suite of the West Siberian Basin) with TOC reaching 16% are widespread within the basin but are generally thermally immature.

The main Mesozoic petroleum plays in the EBMB are related to the Middle–Upper Jurassic (Shtokman, Ledovoe) and Lower–Middle Triassic (Severo-Kil'dinskoe and Murmansk fields) fluvial–deltaic and shallow-marine sandstones. The main pay

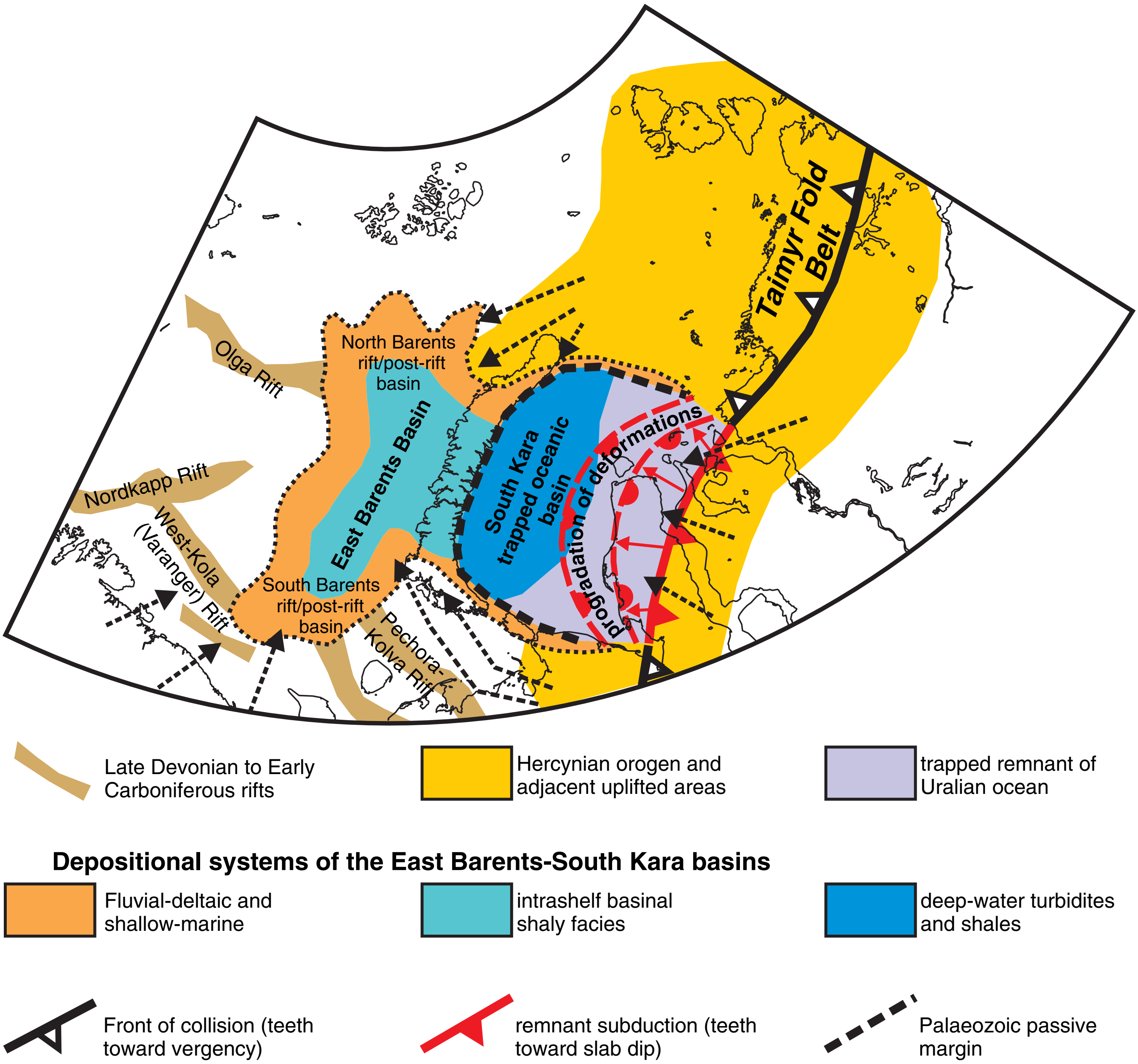

Fig. 9. Schematic chart illustrating the plate-tectonic setting and depositional environments of the East Barents and South Kara basins in Permian–Triassic and possible structural mechanism of the Novaya Zemlya Fold Belt formation. Black dashed arrows show main directions of sedimentary supply into the basins. Red arrows indicate direction of the subducted lithospheric slab roll-back.

interval of the Severo-Kil'dinskoe gas field occurs at 2440 m depth, and is hosted by Lower Triassic sandstones with porosity of *c.* 20%. Potential reservoirs can also be inferred within the Upper Permian siliciclastic successions forming clinoforms along the southern and northern margins of the EBMB, as well as within the Palaeozoic carbonate rocks, where these occur at drillable depths.

The only regional seal occurring throughout the EBMB is composed of the Upper Jurassic immature organic rich shales. In some parts of the basin the seal extends down-section to include the Callovian shales.

Oil and gas trap formation in the East Barents region is generally related to two inversion events:

(1) the Triassic–Jurassic orogeny;
(2) the Early Cenozoic (Eocene to Oligocene) crustal adjustment triggered by the Greenland–EUR–NA plate interactions in the North Atlantic and the Arctic.

The former has a greater impact on the eastern margin of the EBMB affected by a Novaya Zemlya foreland deformation, while the latter resulted in formation of large anticlinal quasi-isometric or elongated arches throughout the basin (Fig. 8).

The main phase of the HC generation in the EBMB started around 55–50 Ma, when the Triassic coaly source rocks became mature. Charge timing was favourable for both the traps formed in Early Cenozoic and for any older traps.

South Kara Province

The SKB is the second most petroliferous province in the RAS with established HC resources. Two large HC accumulations were discovered there at the end of the 1980s: the Leningranskoe gas and the Rusanovskoe gas condensate fields (Fig. 8). Generally the basin is fairly well explored, and many leads and prospects are known (Gramberg 1988; Shipilov

& Tarasov 1998; Kontorovich *et al.* 2001; Sharov *et al.* 2005; Vinokurov *et al.* 2009).

The SKB is located at a junction of the Baltica and East Siberian cratons and the intervening northern termination of the Late Palaeozoic Uralides and western flank of Taimyrides (Figs 3 & 5). It is also located at the hinterland of the Early Mesozoic Novaya Zemlya Fold Belt separating it from the EBMB (Fig. 6). Although it is generally accepted that the SKB is underlain by a basement consisting of these structural domains, the structural pattern of this tectonically complex region is not properly understood. The precise timing of the basin origin, as well as a tectonic regime causing its initiation, also remain unclear. There have been four structural mechanisms proposed so far:

(1) trapped lithosphere of Palaeozoic Uralian Ocean (Ustritsky, 1985);
(2) Late Permian to Early Triassic (Post-Uralian) abandoned small oceanic basin (Aplonov *et al.* 1996);
(3) Late Permian to Early/Mid Triassic intracontinental rifting (Surkov *et al.* 1997, and many others);
(4) Late Permian/Early Triassic subduction rollback and simultaneous crustal extension (see references below).

MCS data reveal extensional structures, dominated by half-grabens, beneath thick sedimentary cover post-dating the extension (Shipilov & Tarasov 1998; Sharov *et al.* 2005; Vyssotski *et al.* 2006). Because of the great thickness of the post-rift sediments, their lower stratigraphic intervals have not been penetrated by drilling, which results in a lack of clarity with regard to the age of the crustal extension affecting the basement beneath the basin. By analogy with the far better studied West Siberian Basin, where the age of crustal extension is considered to be Late Permian to Early Triassic (Kontorovich *et al.* 1975; Surkov & Zhero 1981; Nikishin *et al.* 2002), many researchers attribute the SKB rifts to the same Permo-Triassic extensional event. However, bearing in mind the magnitude of the Triassic–Jurassic compression, which resulted in the formation of the Novaya Zemlya and South Taimyr fold belts, we do not exclude a younger age for the South Kara rifting. Although this does not preclude the existence of the older Permo-Triassic rifts, the latter might have been affected by the Early Mesozoic compression and become a part of a folded basement underlying the SKB. The SKB grabens and half-grabens could be attributed to a crustal extension post-dating the main Triassic–Jurassic orogeny, and could therefore have originated in Early to Middle Jurassic, since the Upper Jurassic Bazhenov horizon is a well-defined seismic marker in the lower part of the post-rift cover. Indirect evidence in favour of this model is derived from the SE–NW strike of the Noyabrskiy Rift in the SKB – almost orthogonal to the dominant direction of the West Siberian rifts (Fig. 8), which suggests that these rifts could have originated independently.

The following events are considered to contribute to the origin of the SKB and its petroleum potential:

(1) the Permian Baltica–Siberia collision and possible trapping of oceanic lithosphere in the future SKB;
(2) the Permian–Triassic plume-related magmatic event;
(3) the Triassic–Jurassic compression and orogeny;
(4) the Early to Middle Jurassic rifting probably related to a collapse of the Early Mesozoic orogen.

Since the Middle Jurassic the SKB became an area of a post-rift thermal subsidence, providing room for accumulation of more than 6 km of fluvial–deltaic, shallow-marine and deepwater siliciclastic sediments. The main sedimentary supply into the basin was from the east (through the Yenisei–Khatanga Depression) and from the north.

Possible models for the SKB formation have to deal with explanation of the rapid subsidence of the EBMB in the Late Permian–Triassic, and remarkable curvature of the Novaya Zemlya Fold Belt. We believe that all these events could be integrated in the model shown in Figure 9. According to this, the slab rollback would be continuously accommodated by the westward expansion of the Uralian orogenic front into the remnant oceanic basin, which could have been completely consumed by the end of the Triassic. Modern seismic tomography data seem to support the existence of an oceanic lithospheric slab beneath the Eastern Barents and Southern Kara shelves (Levshin *et al.* 2007).

Petroleum geology. HC systems of the SKB are projected from the onshore West Siberian Basin. The main source rocks are the bituminous shales of the Bazhenov Formation. In addition, based on well data from the Yamal Peninsula, organic-rich beds are also present in older Early–Mid Jurassic marine shaly succession, and especially in the Tyumen Formation. Aptian–Albian deltaic coals of the Tanopchin Formation are one of the major gas sources (see Fjellanger *et al.* 2010). If the Triassic sediments survived the post-Triassic orogeny, they, by analogy with the East Barents Province, can also be considered as a potential source of HC.

The main gas and gas condensate accumulations of the SKB occur in the Cretaceous Tanopchin and Pokur fluvio-deltaic sandstones and pelitic sandstones. In the Rusanovskoe Field, 12 pay zones with average effective porosity *c.* 20% were established in Cenomanian (one zone), Albian (three zones) and Aptian (eight zones) strata. In the Leningradskoe Field, pay zones with average effective porosities of 26% were tested in Cenomanian (one zone), Albian (three zones) and Aptian (three zones) sediments. Potential clastic reservoirs may occur within the Lower Cretaceous (Neocomian) clinoforms and within the Jurassic Vasyugan Formation.

Regional seals within the SKB are represented by Turonian–Paleocene and Albian marine shaly successions. The former is a seal over 50 m thick for the Leningradskoe Field, while the latter is a 100 m thick seal in the Rusanovskoe Field. Upper Jurassic–Neocomian shales and shaly sediments form another basin-wide seal for the deeper undrilled prospects.

Numerous anticlinal structures, identified by the MCS data in the SKB, affect the Cenozoic sediments. This suggests inversion at the latest stages of the basin's formation. As shown by Vyssotski *et al.* (2006), the inversion in the West Siberian basin could have started as early as Campanian–Maastrichtian and culminated in the Oligocene. The existence of two systems of inverted anticlines striking to the eastnortheastern and northwestern directions, almost orthogonal one to another (Fig. 8) suggests at least two main directions of tectonic stress. Many researches refer to the far-field stresses sourced by the India–Eurasia collision to explain the West Siberia Basin inversion (e.g. Allen & Davies 2007). We believe that there could also be a more proximal source for inversion caused by convergence of the EUR–Greenland and EUR–NA plates in Early Cenozoic time.

HC generation in the SKB could have started as early as Barremian, when Tyumen Formation first entered the oil window, and persisted through the Late Cretaceous with the main HC generation from the Bazhenov Formation. One important difference between the West Siberian Basin and its offshore continuation is that all the pre-Bazhenov sources and most of the Bazhenov Formation are deeply buried within the SKB, and thus are located in the gas maturation window. Therefore, the potential for oil generation is limited to the marginal parts of the basin. According to Fjellanger *et al.* (2010), gas accumulations in the gigantic fields of the Yamal–Tazov Region and SKB can only be explained by the combined charge from all possible sources, including biogenic gas.

North Kara Province

North Kara Province (NKP) is the least explored part of the western RAS (Fig. 2). Current understanding of its geology is mostly based on a few published MCS lines (Shipilov & Tarasov 1998; Sharov *et al.* 2005; Ivanova *et al.* 2006), potential field data and geological observations from the Severnaya Zemlya Archipelago (Kaban'kov & Lazarenko 1982; Bogolepova *et al.* 2001; Metelkin *et al.* 2005; Lorenz *et al.* 2006–2008).

Tectonically the NKP is separated from the South Kara Basin by the North Siberian Arch (see above). As shown by the seismic reflection and refraction data along the 3-AP line (Sharov *et al.* 2005; Ivanova *et al.* 2006), the post-rift, especially Jurassic, sediments filling the SKB thin dramatically towards the arch. Sverdrup Well, drilled on a small same-named island in the eastern Kara Sea (Fig. 5), located just on the North Siberian Arch, penetrated about 1350 m of the Lower Cretaceous sediments and only 170 m of the Upper Jurassic sediments, which rest unconformably on metamorphic rocks of inferred pre-Cambrian age. This implies that the basement arch existed during most of the post-rift history of South Kara Province. MCS data do not show any significant faulting associated with the arch.

There are four contrasting gravity lows in the Northern Kara Sea corresponding to the main depocentres: St Anna Trough (Fig. 4, number 14; & Fig. 5, number 10), Litke Trough (Fig. 4, number 12; & Fig. 5, number 11), Schmidt Trough (Fig. 4, number 15) and North Kara Basin (Fig. 4, number 13; & Fig. 5, number 12). As shown by the MCS data, they have an extensional origin and contain *c.* 10 km of syn-rift and post-rift sediments (Shipilov & Vernikovsky 2010). Age calibration of the MCS data is highly controversial and can only be based on lithostratigraphic correlations with the sections described from northern part of the Novaya Zemlya and Severnaya Zemlya archipelagos.

Based on MCS data interpretation correlated with the above-described stratigraphy of the Severnaya Zemlya, we infer the following seismic stratigraphic units within the NKP offshore basins (Fig. 6b):

(1) Early Ordovician syn-rift unit consisting of shallow-marine clastic rocks and volcanic rocks;
(2) Ordovician–Silurian post-rift unit dominated by clastic rocks and shales (Ordovician), carbonate and evaporate rocks;
(3) Devonian unit dominated by syn-orogenic continental clastic molasses;
(4) Carboniferous to Triassic unit dominated by continental clastic sediments synchronous with the Taimyr orogeny;
(5) Mesozoic to Cenozoic unit composed of continental and shallow-marine sediments overlying older units with a sharp basal unconformity.

Whether the Neoproterozoic to Cambrian strata are present within the NKP sedimentary basins remains unclear. Considering data on the Northern Block of the NZFB, the pre-Cambrian siliciclastic rocks may, together with the Lower to Middle Palaeozoic strata, participate in the sedimentary cover of the KM, while the data on Severnaya Zemlya Archipelago evidences their involvement into folded Neoproterozoic basement.

Geological and MCS data suggests that the main structural inversion of the NKP basins took place in post-Triassic time, perhaps at the Triassic–Jurassic boundary, synchronous with the formation of the Novaya Zemlya Fold Belt. The inversion was accompanied by large-scale vertical movements of basement blocks, and may have generally had a transpressional character.

Petroleum geology. HC systems of the North Kara Sea and adjacent islands are not studied, and thus can only be inferred based on lithological composition and depositional environment observed in the Severnaya Zemlya sections. However, natural bitumen is reported from Silurian, Devonian and Triassic–Jurassic sediments, which may indicate the presence of source rocks generating these HCs. Oil-prone source rocks are inferred in the Middle Ordovician dark shales and Silurian carbonates, while clastic reservoirs could be expected within Devonian and Late Palaeozoic strata. The main trap formation phase may have occurred at the Triassic–Jurassic boundary, and the related structures could have been charged from Palaeozoic sources. The main exploration risks are related to seal presence, as perhaps Upper Jurassic–Lower Cretaceous (Neocomian) regional seals might not have been formed due to post-orogenic uplift of the entire NKP in Mesozoic time.

Laptev Sea Province

The Laptev Shelf is the most studied of the Siberian shelves (Fig. 2). Tectonically it represents a large, about 500 km wide and 700 km long, rift system that has been developing since Late Cretaceous time in response to the Eurasia oceanic basin breakup and consequent spreading along the Gakkel Ridge (Figs 4 & 10). Its geology has been described in detail by Drachev *et al.* (1998, 1999), Drachev (2000), Franke *et al.* (2000, 2001, 2004), Sekretov (2000) and Franke & Hinz (2005), and therefore we refer the reader to these publications for more comprehensive insight into structure and seismic stratigraphy of the Laptev shelf.

The Laptev Rift System (LRS) consists of a series of wide extensional basins and relatively narrow grabens, as shown in Figures 4, 10 and 11. These are (from west to east): the SW Laptev (Fig. 11a, number 1), Ust' Lena (Fig. 4, number 18; & Fig. 11a, number 2), Anisin (Fig. 4, number 20; & Fig. 11a, number 6), Bel'kov (Fig. 10, number 5; & Fig. 11a, number 7) and Svyatoi Nos (Fig. 11a, number 8), separated by high-standing blocks of underlying Late Mesozoic basement (East Laptev, Stolbovoi, Shiroston, and Kotel'nyi horsts, or highs; see Fig. 11a). The New Siberian Rift (Fig. 4, number 21; & Fig. 11a, number 10) occurring NE of Kotel'nyi Island is structurally isolated from the LRS, and thus is considered as a structural element of the East Siberian Shelf.

The internal structure of the LRS is controlled by a series of large-offset listric normal faults, with the main extensional detachments generally located at the eastern shoulders of the rifts (Fig. 11b). Inverted structures are widespread and occur along the listric faults; they are considered the result of compression, due to slight convergence between the EUR and NA plates in the Oligocene to Early Miocene (Savostin & Drachev 1988).

Stratigraphic correlation of the rift infill is disputable. Ivanova *et al.* (1990) and Sekretov (2000), based on the earlier idea of extension of the Siberian Craton far offshore (Vinogradov 1984), speculated that the rifts contain Neoproterozoic, Palaeozoic and Lower Mesozoic rocks, which represent a lithostratigraphic analogue of the craton's sedimentary cover. This concept suffers from lack of geological evidence supporting the offshore continuation of the Siberian Craton. An opposing point of view, supported in this paper, is based on a fact that the Laptev Shelf is surrounded by the Late Palaeozoic and Late Mesozoic fold belts, which apparently continue offshore and form a pre-rift basement of the rift system (Vinogradov & Drachev 2000; Drachev 2002). Therefore this concept limits the total stratigraphic range of the Laptev rift basins infill to the Upper Cretaceous and Cenozoic, and is in agreement with onshore stratigraphy of the Laptev region (Grinenko 1989; Alekseev *et al.* 1992).

The rift infill is composed of mainly siliciclastic non-marine, deltaic and shallow marine sediments whose total thicknesses vary from 1.5–3 to 8–10 km, and reach 13–14 km in the deepest parts of the Ust' Lena Rift (Fig. 11a, b). A clear eastward decrease of thickness and stratigraphic completeness of the syn-rift

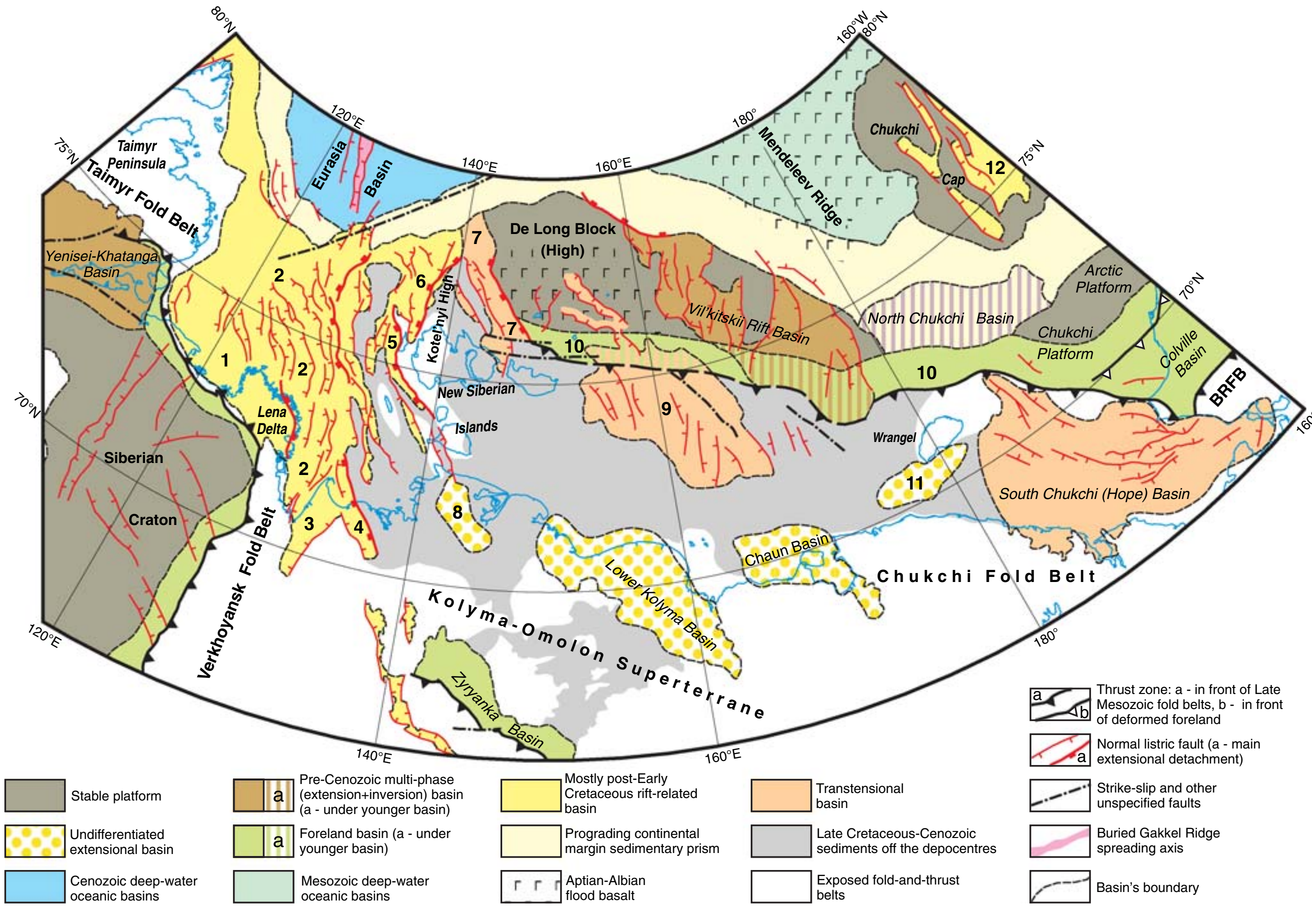

Fig. 10. Main sedimentary basins of the Siberian Arctic Shelf (modified from Grantz *et al.* 2009). Bold numbers denote the following basins: 1, Southwest Laptev Basin; 2, Ust' Lena Rift; 3, Omoloy Graben; 4, Ust' Yana Graben; 5, Bel'kov Rift; 6, Anisin Rift; 7, New Siberian Rift; 8, Tas–Takh Depression; 9, East Siberian Sea Basin; 10, New Siberian–Wrangel Basin; 11, Longa Basin; 12, Northwind Basin. BRFB, Brooks Range Fold Belt.

sequences, as well as a decrease in structural complexity of the rifts, may indicate an eastward rejuvenation of the rifts.

Based on the known history of the NA–EUR plate interaction in the Arctic, the following scenario for the evolution of the LRS is proposed (Fig. 12):

(1) In the Late Cretaceous to Paleocene, an initial rifting culminated in a breakup event and the onset of seafloor spreading in the Eurasia Basin at *c.* 55 Ma.
(2) In the Eocene, a non-rift setting existed as a result of the accommodation of the Eurasia Basin opening by the Khatanga–Lomonosov shear zone, which then became a segment of the plate boundary, and thus prevented the penetration of extensional strain onto the Laptev Shelf.
(3) During the Oligocene to Early Miocene, a non-rift or compressional setting existed, caused by global plate re-arrangement at 33 Ma.
(4) During the Late Miocene to Pleistocene, a re-activation of crustal extension occurred, representing the Second Rift Stage.

Interpreted MCS data correlated with onshore lithostratigraphy support this model and show the presence of successions deposited in a non-rift setting. These units truncate many of the earlier normal faults, and a sharp seismic stratigraphic unconformity at their base is regarded as a break-up unconformity at 55 Ma. The high reflectivity pattern on MCS data may be related to a high coaly material content. This is supported by a widespread occurrence onshore of Eocene and Oligocene strata abundant in brown coals and lignites deposited in low coastal plains during warm climatic conditions (Grinenko 1989; Stein 2008).

Petroleum geology. Data on HC systems of the Laptev Sea Province are generally absent. However, based on the lithostratigraphy of the onshore Cenozoic sections, and the inferred tectonic history of the LRS, we can speculate on possible source/reservoir/seal rock occurrences within the offshore rift basins (Fig. 12).

The main potential sources of HCs in the LRS can be attributed to:

(1) Paleocene to Eocene and, to some extent, Oligocene sediments with abundant terrestrial organic matter are potential gas-prone sources. However, Paleocene and Mid-Eocene marine organic-rich beds should not be excluded within the rift depocentres. They could be analogues of organic-rich marine shales recently encountered on the Lomonosov Ridge (Moran *et al.* 2006). Despite the uncertainty as to whether these beds could produce oil or not, their great contribution into the total HC potential of the Arctic deepwater basins and adjacent shelves cannot be ignored in future assessments.
(2) The Late Cretaceous and Paleocene syn-rift successions may contain both terrestrial and lacustrine organic-rich beds. These potential sources are presently buried at depths generally greater than 4–5 km in the main rift depocentres, and hence are likely to be mainly gas-prone.

Oligocene and particularly Lower Miocene sediments in many onshore localities are dominated by coarse-grained clastic sediments and thus can be considered as reservoir-prone successions. Little is known about the mineral composition of the sands, but considering the Palaeo-Lena River as a major supplier of the clastic sediments into the rift depocentres, especially into the Ust' Lena

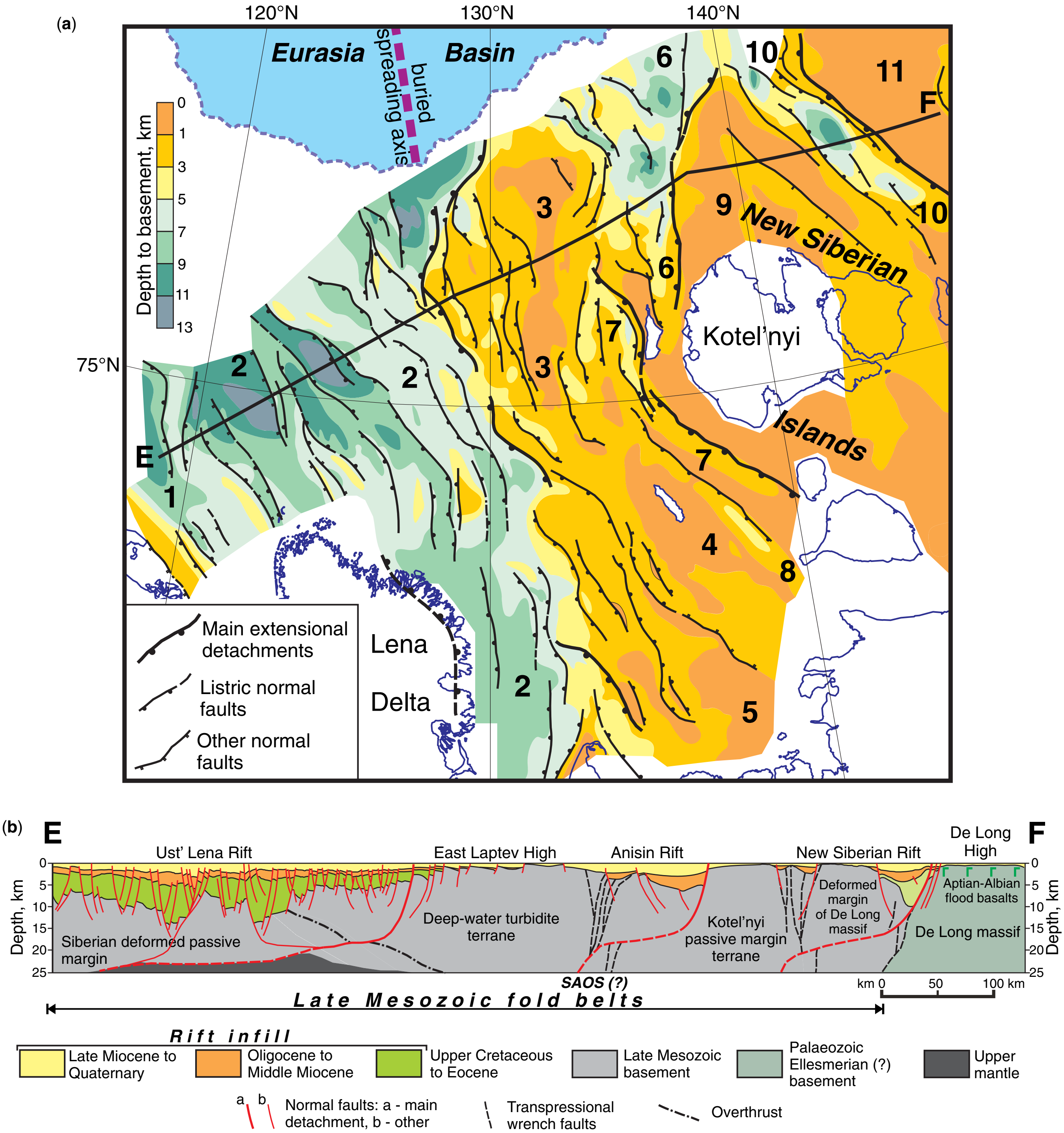

Fig. 11. Structure of the Laptev Rift System: (**a**) simplified depth-to-basement map of the Laptev Shelf based on 2D seismic and ERS-2 gravity data; (**b**) cross-section based on geological data and published BGR regional seismic lines (Franke *et al.* 2000, 2001). Location of the cross-section is shown in (a). Bold numbers in (a) denote following elements of the rift system: 1, Southwest Laptev Rift Basin; 2, Ust' Lena Rift; 3, East Laptev Horst; 4, Stolbovoi Horst; 5, Shiroston Horst; 6, Anisin Rift; 7, Bel'kov Rift; 8, Svyatoi Nos Graben; 9, Kotel'nyi High; 10, New Siberian Rift; 11, De Long High. *SAS (?)* in (b) denotes possible offshore projection of the South Anyui Suture.

Rift, we conclude that the reservoirs may potentially be of good or very good quality. Based on the broad areal extent of the Oligocene to Lower Miocene fluvial clastic sediments around the Laptev Shelf, we can predict their widespread occurrence offshore. That, in turn, makes this interval a main future HC exploration play.

In the onshore sections the Upper Miocene to Quaternary strata are dominated by clastic material against the suppressed accumulation of terrestrial organic matter. However, offshore sections are generally dominated by marine fine-grained muddy sediments, allowing the Upper Miocene and especially Pliocene to Quaternary sediments to be considered as a main regional seal.

Earliest oil generation could have started *c.* 13 Ma ago in the main rift depocentres of the western Laptev Shelf, and progressed until the end of Miocene time when the source rock is estimated to leave the oil maturation window, and the whole petroleum system became gas generating. The second phase of oil generation could have begun along the rift flanks during Late Miocene time, and has progressed up to the present.

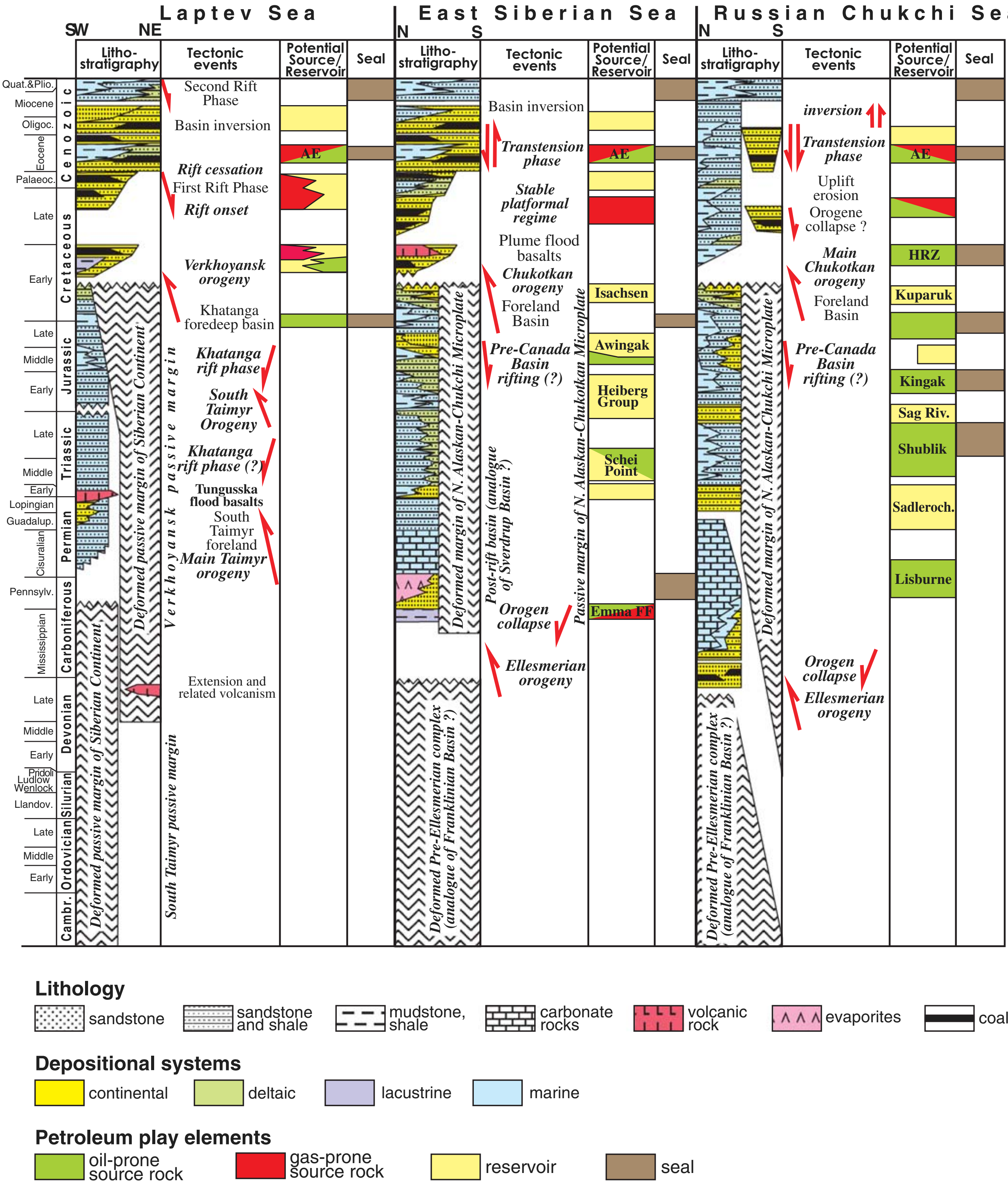

Fig. 12. Summary chart of tectonostratigraphy and petroleum play elements of the Siberian Arctic Shelf. AE denotes Azolla Event. Other bold italic words in Potential source/Reservoir columns denote names of analogue formations in the Sverdrup Basin (East Siberian Sea column) and the Alaskan Northern Slope (Chukchi Sea column). Emma FF denotes Emma Fiord Formation, and HRZ denotes Highly Radioactive Zone.

The estimated time of primary oil generation phases is quite favourable in terms of the capturing of migrating HCs in pre-existing structural traps, formed during the Oligocene to Early Miocene basin inversion, and the onset of the Second Rift Phase (Fig. 12). In most cases the traps are represented by tilted blocks and faulted rollover anticlines, as well as inverted anticlines and drapes over basement highs. The width of the structural traps is controlled by the distance between normal faults, which commonly varies around 5–7 km, while the length of the traps could be in the range of 10–20 km.

Older pre-rift HC plays may have a lesser contribution to the overall HC potential of the Laptev Shelf, as compared with the syn-rift plays. One of the pre-rift plays could be inferred in the southwestern part of the shelf, where marine organic-rich beds of latest Jurassic to earliest Cretaceous age are known to crop out along the shore in a foreland setting (Kaplan *et al.* 1973). There, a younger Neocomian succession is formed by reservoir-prone fluvial and deltaic/shallow marine facies, correlative to a set of Neocomian clinoforms that are well developed throughout the entire Yenisei–Khatanga Basin (Baldin 2001). If this basin extends offshore beneath syn-rift sedimentary cover, then the shelf area between the Lena Delta and Khatanga Bay could be favourable for both oil and gas pre-rift HC plays.

East Siberian Sea Province (ESSP)

The ESSP is the largest part of the Siberian Arctic shelf extending for over 1000 km from New Siberian Islands to Wrangel Island (Fig. 1). It is also the least studied part of the RAS (Fig. 2), and thus only general conclusions on its geology and possible HC systems can be drawn based on limited MCS, gravity and magnetic data, supported by the offshore projection of onshore geology. Earlier tectonic concepts published by Vinogradov *et al.* (1974, 1977), Kos'ko (1984) and Kos'ko *et al.* (1990) were recently reviewed with the use of regional MCS data (Roeser *et al.* 1995; Drachev *et al.* 1999, 2001; Franke *et al.* 2004; Franke & Hinz 2005). The following description summarizes the tectonic concepts of the ESSP history drawn from our interpretation of the available MCS data.

Two main crustal domains are recognized within the ESSP (Figs 10 & 13):

(1) the De Long Massif representing a northern (present-day) part of the AACM unaffected by the Late Mesozoic Verkhoyansk–Brookian orogeny;
(2) the New-Siberian–Chukchi Fold Belt – a southern part of the AACM involved in the Late Mesozoic compression deformation and orogeny.

Consequently, we outline two main generations of the basins whose occurrence is controlled by the above basement domains:

(1) Palaeozoic (post-Devonian?) to Mesozoic basins preserved north of the Late Mesozoic frontal thrusts (stratigraphic analogue of the US Chukchi Ellesmerian Sequence);
(2) Early Cretaceous (Aptian–Albian) to Quaternary basins, post-dating the Verkhoyansk–Brookian orogeny, and evolving mainly over the New-Siberian–Chukchi Fold Belt (stratigraphic analogue of the US Chukchi Brookian Sequence).

The 70–100 km wide New Siberian Rift is clearly expressed in the gravity field (Fig. 4, number 21). It occurs between two high-standing blocks of tectonic basement – Kotel'nyi High on the west and De Long High on the east (Fig. 10). The rift sedimentary infill thickens from 5 km in the southern part of the rift, where it onlaps onto the Late Mesozoic folded basement of the Kotel'nyi High (Fig. 11b), to 10 km in the northern part of the rift, and is composed of several seismic units forming two main sets of strata:

(1) a syn-rift sequence correlates with Upper Cretaceous and Paleocene–Eocene siliciclastic terrestrial and shallow-marine sediments containing abundant coaly material;
(2) a set of post-rift seismic sequences interpreted as Oligocene to Lower Miocene, Middle to Upper Miocene and Pliocene to Quaternary sequences, deposited mainly in shallow-marine conditions.

Drachev *et al.* (1998, 1999) proposed that the New Siberian Rift was formed in response to a postulated divergent plate-tectonic boundary linked to the Late Cretaceous–Paleocene Labrador Sea–Baffin Bay spreading axis. Generally the rhomboid-like shape of the rift, its rather limited extent and evidence of strike-slip dislocations within its interior, are interpreted as evidence of a pull-apart origin.

The East Siberian Sea Basin (ESSB) is a NW–SE elongated 450 km long by 350 km wide depocentre, occurring in the central part of the ESSP (Fig. 4, number 22; Fig. 10, number 6; & Fig. 13). Its structural style differs significantly from the severely rifted Laptev Shelf, and is interpreted as being transtensional in origin (Franke *et al.* 2004; Franke & Hinz 2005). A possible cause for the transtensional regime can be inferred from the tectonic setting of the ESSP within a broad region of Early Cenozoic crustal re-adjustment between the NA and EUR lithospheric plates.

The basin is filled with siliciclastic sediments exceeding 8 km in the deepest depocentres. Their stratigraphic range is inferred to be Late Cretaceous to Quaternary in age. Based on reflection MCS data, the basin infill is subdivided into three main units (Fig. 14):

(1) a Lower Unit correlated to Upper Cretaceous (Cenomanian to Turonian), and Paleocene successions of coal-rich continental and deltaic clastic sediments exposed on Novaya Sibir' Island;
(2) a Middle Unit inferred to consist of Eocene to Middle Miocene fluvial–deltaic and shallow-marine successions, accumulated during the main stage of basin subsidence;
(3) an Upper Unit post-dating the main subsidence stage, and truncating the majority of faults identified within the Middle Unit. We correlate the Upper Unit to a set of Late Miocene to Pleistocene sequences dominated by shallow-marine shaly clastic sediments, which occur widely throughout northeastern Asia.

Considering the tectonic history of the ESSB, we can distinguish the following stages:

(1) Late Cretaceous and Paleocene – a tectonically 'quiet' platformal regime existed with accumulations of the Lower Unit, which is abundant in terrestrial organic matter.
(2) Eocene to Middle Miocene – rapid subsidence of the basin occurred in a transtensional setting controlled by dextral divergence of the NA and EUR plates. By the end of Oligocene to Early Miocene a change in the interaction of the plates caused the compression and structural inversion of some parts of the basin.
(3) Late Miocene to Pleistocene – the active tectonic movements ceased across the entire East Siberian Sea as the main zone of interaction between the EUR and NA plates moved over to the Laptev Sea region. During this sag phase the entire ESS shelf experienced thermal subsidence, and experienced broad marine transgressions.

The *New Siberian–Wrangel Foreland Basin* is recognized below the northern limb of the ESSB (Fig. 10, number 10). This narrow west–east trending basin is traced by a few lines across the ESS and north of Wrangel Island (see below) into the US Chukchi shelf, where it possibly merges into offshore prolongation of the Colville Foreland Basin (Grantz *et al.* 2009).

The MCS data along seismic line LARGE-8901 show the presence of two wedge-shaped packages of seismic reflectors beneath the Lower Unit north of the Late Mesozoic frontal thrust (Fig. 14). The reflectors of the upper package progressively onlap northward onto the lower wedge-shaped package, and both packages are involved into compressional deformations in the vicinity of the frontal thrust. We interpret the upper package as a siliciclastic coal-bearing infill of the foreland basin formed at terminal stages of the Verkhoyansk–Brookian orogeny (Drachev *et al.* 2001). The lower package may represent the Lower Mesozoic and/or Late Palaeozoic strata of the De Long Massif – analogues of the Ellesmerian Sequence of the Arctic Alaska. Alternatively, it could consist of the Lower Cretaceous flood basalts cropped

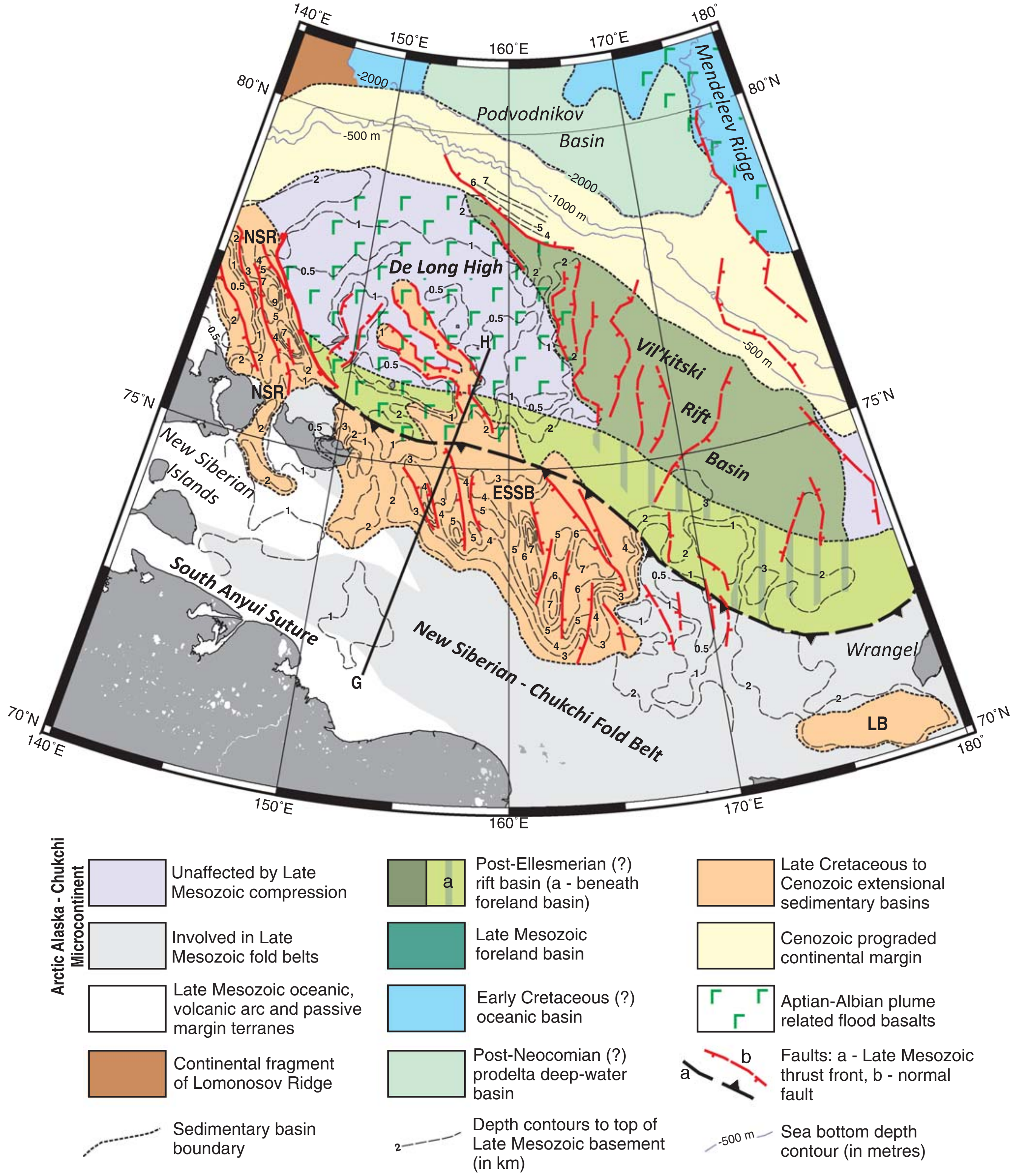

Fig. 13. Main structural features of the East Siberian Sea Shelf. NSR, ESSB and LB denote New Siberian Rift, East Siberian Sea Basin and Longa Basin accordingly. Bold line indexed G–H shows location of a cross-section given in Figure 14. The italic capital letters index the following islands: KT, Kotel'nyi; NS, Novaya Sibir'; BL, Bol'shoi Lyakhov. The accuracy of the scale bar increases towards 75°N.

out on Bennett Island. Presently we do not have data to constrain these possible interpretations.

The northeastern ESSP remains virtually unexplored, since no seismic data exist east of the De Long Archipelago (Fig. 2). The tectonic pattern of this vast area can only be inferred from the study of geophysical fields. The gravity field reveals a series of closely spaced SSE trending linear and rhomboid-shaped lows (Fig. 4, number 23) interpreted as an expression of extensional crustal features called the Vil'kitskii Trough by Kos'ko (1984), Fujita & Cook (1990) and Kos'ko *et al.* (1990) or the Vil'kitskii Rift System by Drachev *et al.* (1999). There are no data to infer the sediment age and composition in the Vil'kitskii Rift System, or to infer the scale and timing of possible crustal extension. Based on the suggested proximity of the northern ESS shelf to the Canadian Arctic prior to opening of the Canada Basin, we can only speculate as to the possible structural and stratigraphic relationships between the Vil'kitski Rift Basin and the Sverdrup Basin. If these basins are tectonically related, then

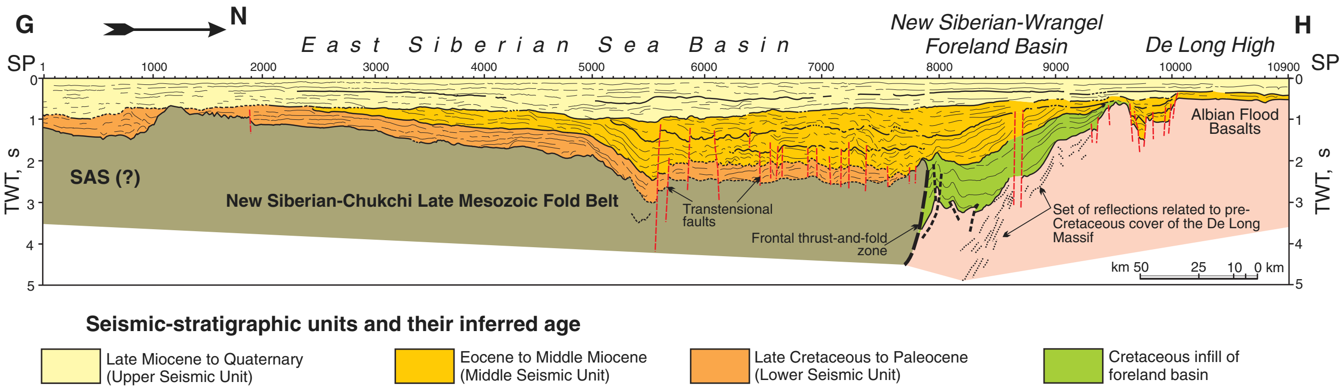

Fig. 14. Geological cross-section along seismic reflection line LARGE-89001 showing structural style and inferred seismic stratigraphy of the East Siberian Sea Basin (modified from S. Drachev *et al.* 1999). For location see Figures 3 and 13. SAS(?) denotes an offshore extent of the South-Anyui Suture.

the following tectonostratigraphic history can be proposed for the former:

(1) Early Carboniferous – the collapse of the Ellesmerian orogen, and formation of the rift system;
(2) Carboniferous to Mid Jurassic – post-rift thermal sagging and deposition of shelf carbonates, evaporates and clastic sediments, an analogue of Sverdrup Basin infill;
(3) Mid-Late Jurassic – a phase of crustal extension and initial rifting culminated probably during latest Jurassic to earliest Cretaceous, with continental breakup and spreading in the Amerasia Basin;
(4) Early Cretaceous (Neocomian) – the southern part of the basin became involved in Late Mesozoic compressional deformation and structural inversion occurred in its northern part;
(5) End Early Cretaceous – a plume-related magmatism influenced the northern part of the basin;
(6) Late Cretaceous to Early Cenozoic – followed the same development stages as the ESS Basin.

Petroleum geology. Two distinct differences exist between lithostratigraphy and, therefore, depositional environments of the Laptev and East Siberian Sea provinces:

(1) Cenomanian–Turonian terrestrial coal-bearing sediments deposited in a fluvial coastal plain setting are present on Novaya Sibir' Island, suggesting marine conditions existed northward in early Late Cretaceous time.
(2) In the Oligocene to Early Miocene, in contrast to the Laptev Province that experienced tectonic uplift and long-term regression with a prevalence of continental fluvial depositional systems, the ESSP, in turn, experienced a long period of subsidence and a dominance of marine and coastal plain environment with accumulation of mainly fine-grained sediments with abundant terrestrial organic matter and coaly material as far south as the present-day coastline (Patyk-Kara & Laukhin 1986).

This suggests that marine depositional environments were widespread through the entire Late Cretaceous and Cenozoic history of the ESSP, and therefore the corresponding sequences could be more favourable for the occurrence of marine organic rich beds – potential oil sources.

Based on this, the main potential HC sources could be expected in (Fig. 12):

(1) Upper Cretaceous to Paleocene sediments with abundant terrestrial organic matter (Lower Seismic Unit) – most probably a gas-prone source;
(2) Eocene and possibly Oligocene to Early Miocene sections.

Based on simple analysis of basin subsidence, initiation of HC generation could have started as early as 54 Ma when potential Lower Cretaceous source rocks entered the oil maturation window and may have continued until 23 Ma. Given the mainly terrestrial composition of organic matter, most of the generated HCs are probably in the gassy fraction, although the possibility of oil generation cannot be excluded. At approximately 23 Ma, possible Oligocene source rocks may have entered the oil maturation window and the period between 23 Ma and present time could represent the main phase of HC generation.

Presently, we do not have data to constrain possible HC systems and petroleum plays of the completely unexplored Vil'kitskii Rift Basin. Speculating on possible pre-Jurassic relationships between the Canadian Arctic and ESSP, we may infer an analogue to the Sverdrup HC systems to be present in the Vil'kitskii Basin north of the Late Mesozoic deformation front (Fig. 12). However, considering the magnitude of the Cenozoic tectonically driven subsidence in better known depocentres, preservation of the oil-prone Late Palaeozoic and Early Mesozoic source rocks at the depths not exceeding the oil window becomes very questionable.

Russian sector of Chukchi Sea Province (CSP)

The Russian sector of the Chukchi Shelf has much better seismic coverage compared with the East Siberian Sea (Fig. 2), and hence its geology is better constrained. The geology and tectonic history of this region were considered by Vinogradov *et al.* (1974, 1977), Pol'kin (1984), Grantz *et al.* (1986, 1990) and recently by Verzhbitsky *et al.* (2008) and Petrovskaya *et al.* (2008), and some data on petroleum geology were summarized by Haimila *et al.* (1990) and by Warren *et al.* (1995).

Tectonically the Russian CSP is similar to the East Siberian Sea shelf (Fig. 13). Two main tectonic domains divided by a zone of frontal thrusts of the Wrangel–Herald Arch are outlined (Fig. 15):

(1) the northern part of the AACM with preserved pre-Late Cretaceous (pre-Barremian?) basins mostly filled with stratigraphic analogues of the Ellesmerian Sequence of the US Chukchi Shelf;
(2) the southern part of the AACM affected by the Late Mesozoic Chukotka–Brookian compressional event and orogeny. It comprises basins post-dating the orogeny and filled with stratigraphic analogues of the Brookian Sequence of the US Chukchi Shelf.

Three first-order basins are outlined in the Russian CSP with use of the MCS and gravity data. Two of them, the New Siberian–Wrangel and the North Chukchi basins (Fig. 4, numbers 27 and 28), occur within the older crustal domain north of the

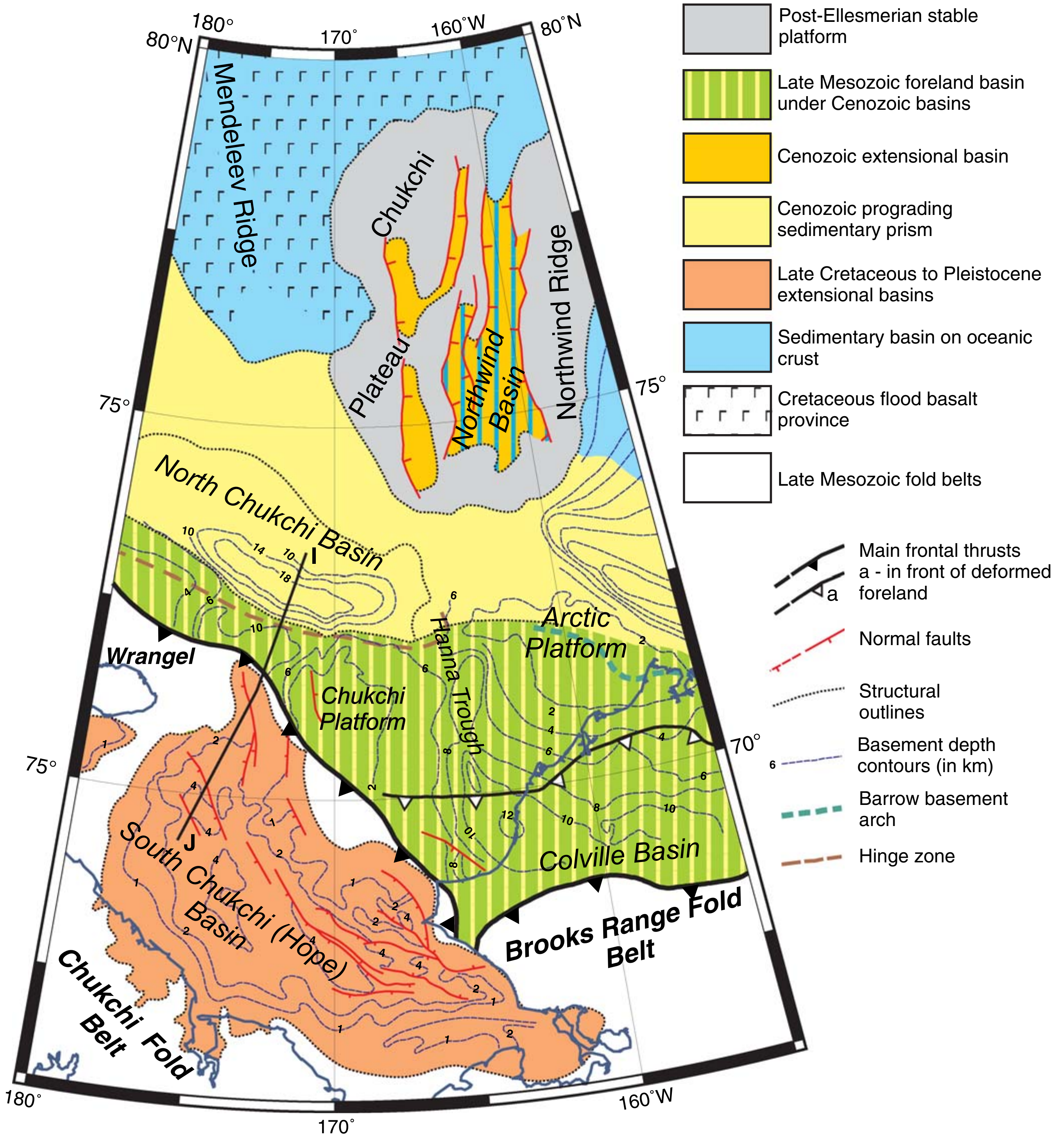

Fig. 15. Main structural elements of the Chukchi Shelf (modified from Grantz *et al.* 2009). Bold solid line labelled 'J–I' shows location of cross-section given in Figure 16. Capital italic letters denote: HT, Hanna Trough; SCB, South Chukchi Basin; KSB, Kotzebue Sound Bay. The accuracy of the scale bar increases towards 75°N.

deformational front, and the South Chukchi (Hope) Basin exists south of the Wrangel–Herald Arch (Fig. 15). A similar view on the Russian CSP tectonics was presented earlier by Grantz *et al.* (1990) and Warren *et al.* (1995).

The eastern part of the New Siberian–Wrangel Foreland Basin is well mapped by the numerous DNMG (Petrovskaya *et al.* 2008) and TGS–Nopec (Verzhbitsky *et al.* 2008) MCS lines north of Wrangel Island between the late Mesozoic deformational front and the North Chukchi Basin. From the latter it is divided by a sharp basement surface break which is assumed to be an analogue of the Hinge line by Grantz *et al.* (1990). Existence of a basin in this location was first proposed by Pol'kin (1984), who named it the North Wrangel Trough. Most of the basin infill is represented by the seismic stratigraphic units CS-2 and CS-3, which are inferred to be composed of Upper Jurassic to Lower Cretaceous clastic rocks (Fig. 16). These units are underlain by the CS-1 unit interpreted to represent Upper Palaeozoic to Lower Mesozoic sedimentary rocks, which may be analogues of the Ellesmerian Sequence of Arctic Alaska. The CS-3 forms the upper part of the basin infill and continues over the hinge line into the North Chukchi Basin. All these units are affected by moderate fold-and-thrust deformations in the vicinity of the Late Mesozoic compressional front.

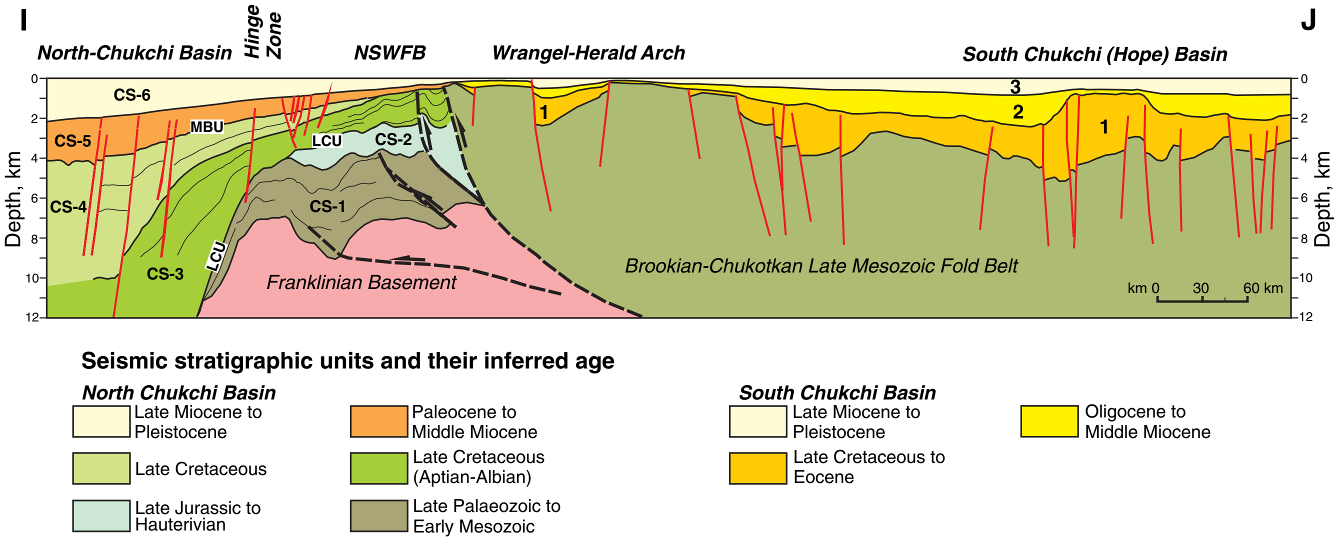

Fig. 16. Simplified cross-section illustrating internal structure and inferred stratigraphy of the South Chukchi and North Chukchi basins. Based on seismic data acquired and published by DMNG and TGS-Nopec (Petrovskaya *et al.* 2008; Verzhbitsky *et al.* 2008) and ERS-2 gravity data. Location is given in Figures 3 and 15. The bold numbers are indexes of the seismic sequences in the South Chukchi Basin after Tolson (1987). The alpha-numeric indexes CS-1 through CS-6 denote seismic sequences identified in the North Chukchi and the New Siberian–Wrangel basins (see text for further details). LCU, Lower Cretaceous Unconformity; MBU, Mid Brookian Unconformity. NSWFB denotes the New Siberian–Wrangel Foreland Basin.

The *North Chukchi Basin* extends east for more than 500 km from the 180° meridian towards the North Slope of Alaska (Figs 10 & 15). Its full extent is depicted by a prominent gravity low of −40 to −60 mGal (Fig. 4, number 28). According to interpretations of the MCS data, the basin can contain over 12 km thick sedimentary fill, which can locally reach 18 or even 20 km. Most of the basin fill is inferred to be composed of Cretaceous to Cenozoic clastic strata (Thurston & Theiss 1987; Grantz *et al.* 1990), although the presence of older sediments in the most subsided parts of the basin is highly likely.

Several seismic units have been identified within the basin and interpreted to reflect the main development stages (Fig. 16). A sharp unconformity is observed at the bottom of the seismic unit CS-3 along the steep southern slope of the basin. It deepens sharply from *c.* 3 to 12 km and more to the north, towards the basin interior. To the south, the unconformity extends into the New Siberian–Wrangel Foreland Basin, where it forms the top of seismic unit CS-2 corresponding to an early stage of the foreland deformations (Fig. 16). Therefore, we interpret this prominent seismic stratigraphic unconformity to be related to onset of the main orogenic phase which, based on geological data from the Chukchi Peninsula (Sokolov *et al.* 2002), occurred around Hauterivian to Barremian time (130–125 Ma). We further correlate this unconformity with the Lower Cretaceous Unconformity (LCU), which is one of the most distinct regional unconformities in the US Chukchi–Beaufort shelf (Craig *et al.* 1985; Thurston & Theiss 1987). A similar interpretation has been proposed by Grantz *et al.* (1990), and more recently by Verzhbitsky *et al.* (2008). The seismic stratigraphic units above the LCU form the main infill of the North Chukchi Basin, which is thus interpreted to be mostly a post-Barremian basin.

Another sharp seismic stratigraphic unconformity at the top of the seismic unit CS-4 truncates folds in the foreland basin, and extends into the central part of the North Chukchi Basin (Fig. 16). The closest analogue in the US Chukchi Sea is the well established regional Mid Brookian Unconformity (MBU) at the Cretaceous–Cenozoic boundary (Thurston & Theiss 1987). The well-laminated seismic pattern of the CS-4 unit between the LCU and MBU allows for conclusion that the post-Barremian Cretaceous infill can be dominated by marine facies, reflecting the main phase of the subsidence within the North Chukchi Basin.

The *South Chukchi (Hope) Basin* extends for over 1000 km from the Longa Strait up to the Western Alaska coast, and is limited by the transpressional Wrangel–Herald Arch in the north, and by the Chukchi Peninsula in the south (Fig. 4, number 25; Fig. 10, number 8 & Fig. 15). The basin is underlain by folded complexes of the Chukotka–Brooks Fold Belt exposed on Wrangel Island, Chukchi Peninsula and along the Alaskan rim of the basin. Two onshore exploration wells near Kotzebue in the southern US Hope Basin encountered basement of Palaeozoic schists and marbles (Thurston & Theiss 1987). In the US Chukchi Sea this basin is known as the Hope Basin, whose geology and petroleum systems were characterized by Tolson (1987) and Haimila *et al.* (1990).

MCS data reveal an asymmetric geometry of the basin. Its southern limb is formed by a gradual southward basement rise while the northern fractured limit, at the junction with the Wrangel–Herald Arch, is rather steep (Fig. 16). The internal structure of the basin is formed by a series of NW–SE trending grabens, half-grabens and dividing horsts, whose assemblage was described by Tolson (1987) as transtensional. Sediment thickness in the basin does not exceed 5–6 km in its deepest parts. Three main seismic stratigraphic units are interpreted (Fig. 16):

(1) A Lower Unit is inferred to be represented by Paleocene (perhaps, Upper Cretaceous) to Eocene continental coal-bearing and fluvial, lacustrine and shallow marine clastic sediments. In the Alaskan onshore extent of the basin, a lower stratigraphic interval penetrated by two exploration wells is known to consist of volcanic and non-marine volcaniclastic rocks, possibly of Eocene age. However, there is no direct tie of the seismic horizons with these wells, and therefore the well data may not be indicative for the offshore lithostratigraphy of the basin (Thurston & Theiss 1987).
(2) A Middle Unit is inferred to be represented by Oligocene–Middle Miocene predominantly continental clastic sediments.
(3) An Upper Unit is represented by Miocene to Quaternary mainly shallow-marine clastic and shaly sediments.

Based on the above characteristics of the Russian CSP geology, we draw the following conclusions about the tectonic history of its sedimentary basins:

(1) The North Chukchi Basin was probably initiated as a rift basin in the Early to Middle Jurassic during an extensional stage precursor to the Canada Basin opening (Grantz *et al.* 1998). However this remains a speculative assumption since the rocks coeval with the early stage of the North Chukchi Basin formation are buried below the depths imaged by MCS data.
(2) In latest Jurassic to Barremian, a major collision occurred between the AACM and the Siberian margin, followed by orogeny and formation of a foreland basin north of the deformation front.
(3) In Aptian to Albian, the North Chukchi Basin was affected by a drastic subsidence resulting in accumulation of a *c.* 10 km thick succession of clastic sediments. This event is coeval to a severe erosion which occurred at Western Alaska around 115 Ma (Moore *et al.* 2002).
(4) In the Late Cretaceous, formation of the South Chukchi Basin began in response to a post-orogenic collapse. The end of the stage was marked by an uplift and erosion caused by convergence of the NA and EUR plates.
(5) Paleocene to latest Eocene/earliest Oligocene – the basins evolved in an intraplate setting controlled by dextral motion between the NA and EUR plates. This is also the main phase of subsidence in the South Chukchi Basin.
(6) Oligocene to Miocene – the South Chukchi Basin was affected by NE–SW plate convergence compression causing transpressional growth of the Wrangel–Herald Arch.

Petroleum geology. Petroleum systems and HC play elements of the South Chukchi Basin can be projected from the drilled and thus to some extent better known Hope Basin. According to Haimila *et al.* (1990) the petroleum potential of the latter is considered to be rather limited with no identified oil-prone source and only thermally immature terrestrial organic rich beds identified in nearby onshore wells. However, offshore depocentres that subsided to significant depths may still be more prospective for generation and accumulation of HCs. During the main Eocene to Oligocene phase of tectonic subsidence, the basin remained structurally isolated from marine environment existing to the north by the Wrangel–Herald basement arch, and therefore the presence of the marine source beds in this inland basin is highly unlikely.

The older North Chukchi Basin is much more prospective for oil generation. The structural setting of the basin is quite similar to the Alaska North Slope and therefore a number of HC plays prospective for both gas and oil can be expected in this part of the Chukchi Shelf (Fig. 12).

As described above, the entire seismically imaged section of the North Chukchi Basin down to the depths of 12 km, and possibly greater, is apparently composed of Cretaceous and Cenozoic strata only. Depth to the Cenozoic base increases rapidly from a few hundred metres along the southern flank of the basin, up to 4–5 km at the basin's axial depocentre (Fig. 16). This suggests that any possible oil source rocks beneath the MBU in the central North Chukchi Basin would have already passed way below the conventional oil maturity window.

The section above the MBU has a much greater chance for the presence of lower Cenozoic marine organic rich beds – analogues of the Middle to Upper Eocene oil-prone Richards sequence in the Beaufort-Mackenzie region. However, an almost complete absence of tectonic structures within this part of the aggraded section significantly limits future exploration potential over the main part of the North Chukchi Basin axial depocentre to the stratigraphic traps.

Greater chances of finding large oil accumulations are more likely along the southern margin of the basin at the hinge zone, and to the south of the hinge zone, where pre-LCU strata occur at drillable depths for exploration wells – around 4–5 km. As illustrated in Figure 16, a basement high dividing the North Chukchi depocentre from the New Siberian–Wrangel Foreland Basin resembles the Barrow Arch. Therefore, mature HC plays existing along the Arctic coast of Alaska could be considered as the closest analogues of the potential untested petroleum plays of the southern flank of the North Chukchi Basin in the Russian CSP.

Summary and conclusions

The vast Russian Arctic Shelf is, to a large extent, sparsely explored due to its harsh environment, high cost of operations and remoteness from modern markets, and its undiscovered HC potential is still highly unconstrained. We have summarized the results of many regional geological and geophysical studies accomplished over the past few decades. Based on 2D regional seismic surveys correlated with borehole data and with onshore geological data in the areas where no exploration wells have yet been drilled, as well as on low-resolution gravity and magnetic data, we have outlined the main sedimentary basins and constrained their structural styles, lithostratigraphy and possible HC systems. Concluding this review of the RAS, we would like to highlight the following major points:

- The Barents and South Kara seas have the largest discovered gas resources in the Russian Arctic, and thus are commonly considered as gas-prone provinces. However, the chances for finding oil plays in the marginal zones of these basins are relatively high, and thus these could be of future exploration interest.
- The NKP is virtually unexplored, and its tectonostratigraphy is mainly constrained by available geological data from adjacent land areas. Several mid-sized depocentres inferred from gravity data are considered to be of mostly Early to Middle Palaeozoic age, and probably experienced inversion related to the Late Palaeozoic and Early Mesozoic orogenic events. Petroleum systems of the North Kara Shelf are unconstrained.
- The Siberian Arctic shelves were severely affected by the Late Mesozoic (Neocomian) orogeny, which largely shaped their tectonic basement and also had a dramatic impact on their potential petroleum systems.
- The Laptev rift province provides solid evidence of high HC potential. The basins are filled with thick Late Cretaceous to Cenozoic terrestrially sourced clastic sediments with abundant coaly matter, and thus are inferred to be mainly gas prone. However, if the pre-rift Bazhenov-type source rocks were not destroyed by the Late Mesozoic orogeny in the southwestern part of the Laptev shelf, or if the Early Cenozoic marine oil-prone source rocks accumulated within the rift depocentres, the Laptev shelf could also be prospective for the presence of oil plays. As the Laptev Shelf was the site of active rifting in Late Cretaceous to Paleocene and Recent times, and many normal faults reach the sea bottom, significant exploration risks may be related to the seal integrity.
- The East Siberian and Chukchi shelves are dominated by two generations of basins: (1) the Late Cretaceous to Cenozoic basins occurring south of the offshore extent of the Late Mesozoic deformational front; and (2) older (Late Palaeozoic(?) to Early Cretaceous) basins occurring north of the Late Mesozoic deformation front.
- The Late Cretaceous to Cenozoic basins are interpreted to have originated in a transtensional setting caused by dextral relative

motions of the NA and EUR lithospheric plates. Lithostratigraphy and possible HC systems of these basins are inferred from the better studied Hope Basin in the US Chukchi Sea, and are also constrained by onshore sedimentary sections. Their potential is considered to be mainly related to gas-prone terrestrial sources, although the presence of Early Cenozoic thermally mature lacustrine or shallow marine oil-prone sources cannot be disregarded.

- The inferred Late Palaeozoic to Early Mesozoic basins may be similar tectonostratigraphically to the Sverdrup Basin in the Canadian Arctic. The petroleum geology of the latter has been used to constrain possible HC systems of the Vil'kitsky Basin, which is identified on the basis of gravity and magnetic data only.
- The New Siberian–Wrangel Foreland Basin occurs in front of the Late Mesozoic compressional deformations. Its tectonostratigraphy is inferred to resemble the basins of the Alaska's North Slope and thus the petroleum geology of the latter with its rich oil potential has been projected north of Wrangel Island to highlight possible oil potential of this foreland basin.
- North Chukchi Basin dominates the Russian Chukchi Sea and is mainly filled with post-Neocomian siliciclastic sediments with a total thickness exceeding 18 km. Its petroleum plays may be similar to the known Late Cretaceous and Cenozoic plays of the Beaufort Sea.

The authors during their research career have collaborated with many geoscientists from Russia (G. E. Bondarenko, L. I. Lobkovskiy, V. E. Khain, A. V. Savitskiy, L. A. Savostin, K. O. Sobornov, S. D. Sokolov) and from Western countries (S. Creaney, A. Grantz, K. Hinz, L. Johnson, W. Jokat, N. Kaul, R. Scott, J. Thiede, G. Ulmishek, P. Ziegler). We extend our gratitude to all of them for contributing to our understanding of the Arctic geology. We are thankful to the management of ExxonMobil and Rosneft for providing the opportunity to publish this article. The whole paper was considerably improved after it had been thoroughly reviewed by N. McAllister, V. Pease and D. Thurston. E. A. Miloradovskaya (Karasik) helped with the editing of the text.

References

Alekseev, M. N., Arkhangelov, A. A. *et al*. 1992. Laptev and East Siberian Seas. Cenozoic. *In*: *Palaeogeographic Atlas of the Shelf Regions of Eurasia for the Mesozoic and Cenozoic*, **1**. Robertson Group plc, UK, and Geological Institute, Academy of the Sciences, USSR, 1-14–1-33.

Allen, M. B. & Davies, C. E. 2007. Unstable Asia: active deformation of Siberia revealed by drainage shifts. *Basin Research*, **19**, 379–392.

Amundsen, H., Evdokimov, A., Dibner, V. & Andresen, A. 1998. Petrogenetic significance and evolution of Mesozoic magmatism, Franz Josef Land and the Barents Sea. *In*: Solheim, A., Musatov, E. & Heintz, N. (eds) *Geological Aspects of Franz Josef Land and the Northernmost Barents Sea (the Northern Barents Sea Geotraverse).* Norsk Polarinstitutt, Meddelelser, **151**.

Aplonov, S. V., Shmelev, G. B. & Krasnov, D. K. 1996. Geodynamics of the Barents–Kara Shelf: geophysical evidence. *Geotectonics*, **30**, 309–326.

Artyushkov, E. V. 2005. The formation mechanism of the Barents basin. *Russian Geology and Geophysics*, **46**, 700–713.

Atlasov, I. P., Dibner, V. D. *et al*. 1970. *Explanatory Notes to Tectonic Map of the Arctic and Sub-Arctic*. Scale 1:5,000,000. Nedra, Leningrad (in Russian).

Baldin, V. A. 2001. *Geology and petroleum potential of Upper Jurassic to Neocomian successions of the western Yenisei–Khatanga Depression.* Candidate of Sciences Thesis, Moscow (in Russian).

Bogdanov, N. A. & Khain, V. E. (eds) 1996. *Explanatory Notes to the Tectonic Map of the Barents Sea and the Northern Part of European Russia*. Scale 1:2,500,000. ILRAN, Moscow (in Russian).

Bogolepova, O. K. & Gee, D. 2004. Early Paleozoic unconformity across the Timanides, NW Russia. *In*: Gee, D. & Pease, V. (eds) *The Neoproterozoic Timanide Orogen of Eastern Baltica*. Geological Society, London, Memoirs, **30**, 145–158.

Bogolepova, O. K., Gubanov, A. P. & Raevskaya, E. G. 2001. The Cambrian of the Severnaya Zemlya Archipelago, Russia. *Newsletter Stratigraphy*, **39**, 73–91.

Bondarev, V. I. (ed.) 1982. *Geology of the South Island of Novaya Zemlya*. PGO 'Sevmorgeologiya', Leningrad.

Burlin, Yu. K. & Stoupakova, A. V. 2008. Geological conditions of petroleum potential of the Russian Arctic. *Oil and Gas Geology*, **4**, 13–23 (in Russian).

Cook, D. B., Fujita, K. & McMullen, C. A. 1986. Present-day plate interactions in Northeast Asia: North American, Eurasian, and Okhotsk plates. *Journal of Geodynamics*, **6**, 33–51.

Craig, J. D., Sherwood, K. W. & Johnson, P. P. 1985. *Geologic Report for the Beaufort Sea Planning Area, Alaska*. US Minerals Management Service OCS Report 85-0111.

Doré, A. G. 1995. Barents Sea geology, petroleum resources and commercial potential. *Arctic*, **48**, 207–221.

Drachev, S. S. 1989. *Tectonics and Mesozoic to Cenozoic geodynamics of the New Siberian Islands*. PhD (Candidate of Geological and Mineralogical Sciences) thesis. Geological Department of Moscow State University.

Drachev, S. S. 2000. Tectonics of the Laptev Sea rift system. *Geotectonics*, **34**, 467–482.

Drachev, S. S. 2002. On the basement tectonics of the Laptev Sea Shelf. *Geotectonics*, **36**, 483–498.

Drachev, S. S. & Saunders, A. 2006. The Early Cretaceous Arctic LIP: its geodynamic setting and implications for Canada Basin opening. *In*: Scott, R. A. & Thurston, D. K. (eds) *Proceedings of the Fourth International Conference on Arctic Margins*, Dartmouth, Nova Scotia, 30 September to 3 October. U. Department of the Interior, Anchorage, Alaska, 216–223.

Drachev, S. S. & Savostin, L. A. 1993. Ophiolites of Bol'shoi Lyakhov Island (New Siberian Islands). *Geotektonika*, **6**, 33–51 (in Russian).

Drachev, S. S., Savostin, L. A., Groshev, V. G. & Bruni, I. E. 1998. Structure and geology of the continental shelf of the Laptev Sea, Eastern Russian Arctic. *Tectonophysics*, **298**, 357–393.

Drachev, S. S., Johnson, G. L., Laxon, S., McAdoo, D. & Kassens, H. 1999. Main structural elements of the Eastern Russian Arctic Continental Margin derived from satellite gravity and multichannel seismic reflection data. *In*: Kassens, H., Bauch, H. A. *et al*. (eds) *Land–Ocean Systems in the Siberian Arctic: Dynamics and History*. Springer, Berlin, 667–682.

Drachev, S. S., Elistratov, A. V. & Savostin, L. A. 2001. Structure and seismostratigraphy of the East Siberian Sea Shelf along the Indigirka Bay–Jeannette Island seismic profile. *Doklady Earth Sciences*, **377A**, 293–297.

Egorov, A. Y., Bogomolov, Y. A., Konstantinov, A. G. & Kurushin, N. I. 1987. Stratigraphy of Triassic rocks of Kotel'nyi Island (New Siberian Islands). *In*: Dagys, A. S. (ed.) *Boreal Triassic*. Nauka, Moscow, 66–80 (in Russian).

Fjellanger, E., Kontorovich, A. E., Barboza, S. A., Burshtein, L. M., Hardy, M. J. & Livshits, V. R. 2010. Charging the giant gas fields of the NW Siberia Basin. *In*: Vining, B. A. & Pickering, S. C. (eds) *Petroleum Geology: From Mature Basins to New Frontiers – Proceedings of the 7th Petroleum Geology Conference*. Geological Society, London, 659–668; doi: 10.1144/0070659.

Franke, D. & Hinz, K. 2005. The structural style of sedimentary basins on the shelves of the Laptev Sea and western East Siberian Sea, Siberian Arctic. *Journal of Petroleum Geology*, **28**, 269–286.

Franke, D., Hinz, K. *et al*. 2000. Tectonics of the Laptev Sea Region in North-Eastern Siberia. *In*: Roland, N. W. & Tessensohn, F. (eds) *III International Conference on Arctic Margins. Polarforschung*, **68**, 51–58.

Franke, D., Hinz, K. & Oncken, O. 2001. The Laptev Sea rift. *Marine and Petroleum Geology*, **18**, 1083–1127.

Franke, D., Hinz, K. & Reichert, Ch. 2004. Geology of the East Siberian Sea, Russian Arctic, from seismic images: structures, evolution, and implications for the evolution of the Arctic Ocean Basin. *Journal of Geophysical Research*, **109**, 1–19.

Fujita, K. & Cook, D. B. 1990. The Arctic continental margin of eastern Siberia. *In*: Grantz, A., Johnson, G. L. & Sweeney, J. F. (eds) *The Arctic Ocean Region*. The Geology of North America, L. Geological Society of America, Boulder, CO, 257–288.

Gee, D. G. & Pease, V. (eds) 2005. *The Neoproterozoic Timanide Orogen of Eastern Baltica*. Geological Society, London, Memoirs, **32**.

Gee, D. G. & Stephenson, R. A. (eds) 2006. *European Lithosphere Dynamics*. Geological Society, London, Memoirs, **30**.

Gee, D. G., Bogolepova, O. K. & Lorenz, H. 2006. The Timanide, Caledonide and Uralian orogens in the Eurasian high Arctic, and relationships to the palaeo-continents Laurentia, Baltica and Siberia. *In*: Gee, D. G. & Stephenson, R. A. (eds) *European Lithosphere Dynamics*. Geological Society, London, Memoirs, **32**, 507–520.

Glebovsky, V., Kovacs, L. C., Maschenkov, S. P. & Brozena, J. M. 2000. Joint compilation of Russian and US Navy Aeromagnetic data in the Central Arctic Seas. *Polarforschung*, **68**, 35–40.

Glebovsky, V. Yu., Kaminsky, V. D., Minakov, A. N., Merkur'ev, S. A., Childers, V. A. & Brozena, J. M. 2006. Formation of the Eurasia Basin in the Arctic Ocean as inferred from geohistorical analysis of the anomalous magnetic field. *Geotectonics*, **40**, 263–281.

Gramberg, I. S. (ed.) 1988. *Barents Shelf Plate*. Nedra, Leningrad.

Gramberg, I. S. & Pogrebitskiy, Yu. E. (eds) 1984. *Geological Structure of the USSR and Trends in Distribution of Mineral Resources, 9, Soviet Arctic Seas*. Nedra, Leningrad (in Russian).

Gramberg, I. S. & Ushakov, V. I. 2000. *Severnaya Zemlya – Geology and Mineral Resources*. VNIIOkeangeologia, St Petersburg (in Russian).

Grantz, A., Mann, D. M. & May, S. D. 1986. *Multichannel Seismic-reflection Data Collected in 1978 in the Eastern Chukchi Sea*. US Geological Survey Open-File Report, **86-206**.

Grantz, A., May, S. D. & Hart, P. E. 1990. Geology of the Arctic continental margin of Alaska. *In*: Grantz, A., Johnson, G. L. & Sweeney, J. F. (eds) *The Arctic Ocean Region*. The Geology of North America, L. Geological Society of America, Boulder, CO, 257–288.

Grantz, A., Clark, D. L., Phillips, R. L. & Srivastava, S. P. 1998. Phanerozoic stratigraphy of Northwind Ridge, magnetic anomalies in the Canada basin, and the geometry and timing of rifting in the Amerasia basin, Arctic Ocean. *Geological Society of America Bulletin*, **110**, 801–820.

Grantz, A., Scott, R. A., Drachev, S. S. & Moore, T. E. 2009. *Map Showing the Sedimentary Successions of the Arctic Region (58°–64° to 90°N) that May be Prospective for HCs.* Open-File Spatial Library, World Wide Web Address: http://gisudril.aapg.org/gisdemo/.

Grinenko, O. V. (ed.) 1989. *Palaeogene and Neogene of North-East of the USSR*. Scientific Center of Siberian Department of Academy of Sciences of USSR, Yakutsk (in Russian).

Gudlaugsson, S. T., Faleide, J. I., Johansen, S. E. & Breivik, A. 1998. Late Palaeozoic structural development of the south-western Barents Sea. *Marine and Petroleum Geology*, **15**, 73–102.

Haimila, N. E., Kirschner, C. E., Nassichuk, W. W., Ulmichek, G. & Procter, R. M. 1990. Sedimentary basins and petroleum resource potential of the Arctic Ocean region. *In*: Grantz, A., Johnson, G. L. & Sweeney, J. F. (eds) *The Arctic Ocean Region*. The Geology of North America, L. Geological Society of America, Boulder, CO, 503–538.

Harbert, W., Frei, L., Jarrard, R., Halgedahl, S. & Engebretson, D. 1990. Palaeomagnetic and plate-tectonic constraints on the evolution of the Alaskan-eastern Siberian Arctic. *In*: Grantz, A., Johnson, G. L. & Sweeney, J. F. (eds) *The Arctic Ocean Region*. The Geology of North America, L. Geological Society of America, Boulder, CO, 567–592.

Inger, S., Scott, R. A. & Golionko, B. G. 1999. Tectonic evolution of the Taimyr Peninsula, northern Russia: implications for Arctic continental assembly. *Journal of the Geological Society, London*, **156**, 1069–1072.

Ivanova, N. M., Sekretov, S. B. & Shkarubo, S. I. 1990. Geological structure of the Laptev Sea shelf according to seismic studies. *Oceanology*, **29**, 600–604.

Ivanova, N. M., Sakoulina, T. S. & Roslov, Yu. V. 2006. Deep seismic investigation across the Barents–Kara region and Novozemelskiy Fold Belt (Arctic Shelf). *Tectonophysics*, **420**, 123–140.

Johansen, S. E., Ostisty, B. K. *et al*. 1993. Hydrocarbon potential in the Barents Sea region: play distribution and potential. *In*: Vorren, T. O., Bergsaker, E., Dahl-Stamnes, Ø. A., Holter, E., Johansen, B., Lie, E. & Lund, T. N. (eds) *Arctic Geology and Petroleum Potential*, Norwegian Petroleum Society Special Publication 2. Elsevier, Amsterdam, 273–320.

Kaban'kov, V. Ya. & Lazarenko, N. P. (eds) 1982. *Geology of Severnaya Zemlya Archipelago*. Sevmorgeo, Leningrad (in Russian).

Kaminsky, V. D., Glebovsky, V. Yu., Leychenkov, G. L., Golynsky, A. V., Masolov, V. N. & Gandyukhin, V. V. 2009. Role of geophysical methods in geological study of mineral resources of Arctic and Antarctic and some results. *In*: *Geology of Polar Regions of the Earth. Materials of XLII Tectonic Conference, I*. GEOS, Moscow, 253–257 (in Russian).

Kaplan, A. A., Copeland, P. *et al*. 2001. New radiometric ages of igneous and metamorphic rocks from the Russian Arctic. *In*: *Abstracts of AAPG Regional Conference 2001*. VNIGRI and AAPG, St Petersburg, 2001.

Kaplan, M. E., Yudovnyi, E. G. & Zakharov, V. A. 1973. Depositional environment of marine sediments of Paksa Peninsula transitional between Jurassic and Cretaceous (Anabar Bay). *Doklady Academii Nauk SSSR*, **209**, 691–694 (in Russian).

Karasik, A. M. 1968. Magnetic anomalies of the Gakkel Ridge and the origin of the Eurasian Subbasin of the Arctic Ocean. *In*: *Geophysical Survey Methods in the Arctic*. NIIGA, Leningrad, **5**, 8–19 (in Russian).

Karasik, A. M. 1974. The Eurasia Basin of the Arctic Ocean from the point of view of plate tectonic. *In*: *Problems in Geology of Polar Areas of the Earth*. Nauchno-Issledovatel'skii Institut Geologii Arktiki, Leningrad, 23–31 (in Russian).

Karasik, A. M., Savostin, L. A. & Zonenshain, L. P. 1983. Parameters of the lithospheric plate movements within Eurasia Basin of North Polar Ocean. *Doklady Academii Nauk SSSR, Earth Sciences Section*, **273**, 1191–1196 (in Russian).

Kogan, L. I., Malovitski, Ya. P. & Murzin, R. R. 2004. Deep structure of the East Barents Megabasin: evidence from wide-angle deep seismic profiling. *Geotectonics*, **38**, 224–238.

Kontorovich, A. E., Nesterov, I. I., Salmanov, F. K., Surkov, V. S., Trofimuk, A. A. & Ervye, Yu. G. 1975. *Geology of Oil and Gas of West Siberia*. Nedra, Moscow (in Russian).

Kontorovich, V. A., Belyaev, S. Yu., Kontorovich, A. E., Krasavchikov, V. A., Kontorovich, A. A. & Suprunenko, O. I. 2001. Tectonic structure and history of development of the East-Siberian geosineclise. *Russian Geology and Geophysics*, **42**, 1832–1845.

Korago, E. A., Kovaleva, G. N., Lopatin, B. G. & Orgo, V. V. 2004. The Precambrian rocks of Novaya Zemlya. *In*: Gee, D. G. & Pease, V. L. (eds) *The Neoproterozoic Timanide Orogen of Eastern Baltica*. Geological Society, London, Memoirs, **30**, 135–143.

Korago, E. A., Kovaleva, G. N. *et al*. 2009. To a problem of continental crust age on west of Eurasian Arctic (based on data from zircon geochronology from Ordovician and Silurian of north-western Novaya Zemlya). *In*: *Geology of Polar Regions of the Earth. Materials of XLII Tectonic Conference, I*. GEOS, Moscow, 285–289 (in Russian).

Kos'ko, M. K. 1984. East Siberian Sea. *In*: Gramberg, I. S. & Pogrebitskii, Yu. E. (eds) *Geological Structure of the USSR and Trends in Distribution of Mineral Resources, 9, Seas of the Soviet Arctic*. Nedra, Leningrad, 60–67 (in Russian).

Kos'ko, M. K. & Nepomiluev, V. F. 1975. Reconstructing Palaeozoic litho-structural zonation of Anzhu Islands. *In*: *Tectonics of the Arctic*. NIIGA, Leningrad, **1**, 26–30 (in Russian).

Kos'ko, M. K., Lopatin, B. G. & Ganelin, V. G. 1990. Major geological features of the islands of the East Siberian and Chukchi Seas and the northern coast of Chukotka. *Marine Geology*, **93**, 349–367.

Kos'ko, M. K., Cecile, M. P., Harrison, J. C., Ganelin, V. G., Khandoshko, N. V. & Lopatin, B. G. 1993. Geology of Wrangel Island, between Chukchi and East Siberian Seas, Northeastern Russia. *Geological Survey of Canada Bulletin*, **461**.

Kos'ko, M. K. 1994. Major tectonic interpretations and constraints for the new Siberian Islands region, Russian Arctic. *In*: *Proceedings International Conference on Arctic Margins*, Anchorage, AK, September 1992. US Department of the Interior, Minerals Management, 195–200.

Kristoffersen, Y. 1990. Eurasia Basin. *In*: Grantz, A., Johnson, G. L. & Sweeney, J. F. (eds) *The Arctic Ocean Region*. The Geology of

North America, L. Geological Society of America, Boulder, CO, 365–378.

Kuzmichev, A. B. 2009. Where does the South Anyui suture go in the New Siberian Islands and Laptev Sea? Implications for the Amerasia basin origin. *Tectonophysics*, **463**, 86–108.

Kuzmichev, A. B. & Pease, V. 2007. Siberian trap magmatism on the New Siberian Islands: constraints for east Arctic Mesozoic plate tectonic reconstructions. *Journal of the Geological Society, London*, **164**, 959–968.

Levshin, A. L., Schweitzer, J., Weidle, C., Shapiro, N. M. & Ritzwoller, M. H. 2007. Surface wave tomography of the Barents Sea and surrounding region. *Geophysical Journal International*, **170**, 441–459.

Lopatin, B. G. (ed.) 2000. *State Geological Map of Russian Federation*. Scale 1,000,000 (New Series). Sheet S-36, 37 – Barents Sea. Explanatory Notes. St Petersburg, P. P. Karpinsky Russian Geological Research Institute.

Lopatin, B. G., Pavlov, L. G., Orgo, V. V. & Shkarubo, S. I. 2001. Tectonic structure of Novaya Zemlya. *Polarforschung*, **69**, 131–135.

Lorenz, H., Gee, D. G. & Bogolepova, O. K. 2006. Early Palaeozoic unconformity on Severnaya Zemlya and Relationships to the Timanian margin of Baltica. *In*: Scott, R. A. & Thurston, D. K. (eds) *Proceedings of the Fourth International Conference on Arctic Margins*, Dartmouth, Nova Scotia, 30 September to 3 October 2003. US Department of the Interior, Anchorage, AK, 14–30.

Lorenz, H., Gee, D. G. & Whitehouse, M. J. 2007. New geochronological data on Palaeozoic igneous activity and deformation in the Severnaya Zemlya Archipelago, Russia, and implications for the development of the Eurasian Arctic margin. *Geological Magazine*, **144**, 105–125; doi: 10.1017/S001675680600272X.

Lorenz, H., Männik, P., Gee, D. G. & Proskurnin, V. 2008. Geology of the Severnaya Zemlya Archipelago and the North Kara Terrane in the Russian high Arctic. *International Journal of Earth Sciences (Geol. Rundsch.)*, **97**, 519–547; doi: 10.1007/s00531-007-0182-2.

Malyshev, N. A. 2002. *Tectonics, Evolution and Petroleum Potential of Sedimentary Basins of the Russian European North*. Uralian Branch of Russian Academy of Sciences, Ekaterinburg (in Russian).

Männik, P., Bogolepova, O. G., Poldvere, A. & Gubanov, A. P. 2009. New data on Ordovician–Silurian conodonts and stratigraphy from the Severnay Zemlya Archipelago, Russian Arctic. *Geological Magazine*, 497–516; doi: 10.1017/S0016756809006372.

Maschenkov, S. P., Glebovsky, V. Yu. & Zayonchek, A. V. 2001. New digital compilation of Russian aeromagnetic and gravity data over the North Eurasian Shelf. *Polarforschung*, **69**, 35–39.

Metelkin, D. V., Vernikovsky, V. A., Kazansky, A. Yu., Bogolepova, O. K. & Gubanov, A. P. 2005. Palaeozoic history of the Kara microcontinent and its relation to Siberia and Baltica: paleomagnetism, paleogeography and tectonics. *Tectonophysics*, **398**, 225–243.

Miller, E. L. & Verzhbitsky, V. 2009. Structural studies in the Pevek region, Russia: implications for the evolution of the East Siberian Shelf and Makarov Basin of the Arctic Ocean. *In*: Stone, D. B., Fujita, K., Layer, P. W., Miller, E. L., Prokopiev, A. V. & Toro, J. (eds) *Geology, Geophysics and Tectonics of Northeastern Russia: A Tribute to Leonid Parfenov*. Stephan Mueller, Special Publications Series, **4**, 223–241.

Miller, E. L., Gehrels, G. E., Pease, V. & Sokolov, S. 2010. Stratigraphy and U-Pb detrital zircon geochronology of Wrangel Island, Russia: implications for Arctic paleogeography. *AAPG Bulletin*, **94**, 665–692.

Moore, T. E., Dumitru, T. A., Adams, K. E., Witebsky, S. N. & Harris, A. G. 2002. Origin of the Lisburne Hills–Herald Arch–Wrangel Arch structural belt: stratigraphic, structural, and fission-track evidence from the Cape Lisburne area, northwestern Alaska. *In*: Miller, E. L., Grantz, A. & Klemperer, S. L. (eds) *Tectonic Evolution of the Bering Shelf–Chukchi Sea–Arctic Margin and Adjacent Landmasses*. Geological Society of America, Boulder, CO, Special Papers, **360**, 77–109.

Moran, K., Backman, J. *et al*. 2006. The Cenozoic palaeoenvironment of the Arctic Ocean. *Nature*, **441**; doi: 10.1038/nature04800.

Nikishin, A. M., Ziegler, P. A. *et al*. 1996. Late Precambrian to Triassic history of the East-European Craton: dynamics of sedimentary basin evolution. *Tectonophysics*, **268**, 23–63.

Nikishin, A. M., Ziegler, P. A., Abbott, D., Brunet, M.-F. & Cloetingh, S. 2002. Permo-Triassic intraplate magmatism and rifting in Eurasia: implications for mantle dynamics. *Tectonophysics*, **351**, 3–39.

Obruchev, S. V. 1934. Materials on tectonics of Northeastern Asia. *Aspects of Soviet Geology*, **6**, 182–200, 77–78 (in Russian).

Ostisty, B. K. & Fedorovsky, Y. F. 1993. Main results of oil and gas prospecting in the Barents and Kara Seas inspire optimism. *In*: Vorren, T. O., Bergsaker, E. *et al*. (eds) *Arctic Geology and Petroleum Potential*, Norwegian Petroleum Society Special Publication 2. Elsevier, Amsterdam, 243–252.

Parfenov, L. M. & Natal'in, B. A. 1986. Mesozoic tectonic evolution of northeastern Asia. *Tectonophysics*, **127**, 291–304.

Patyk-Kara, N. G. & Laukhin, S. A. 1986. Cenozoic evolution of the Arctic coastal relief of North-Eastern Asia. *Sovetskaya Geologiya*, **1**, 75–84 (in Russian).

Pavlov, S. P., Shlykova, V. V. & Grigoryeva, B. M. 2008. HC potential of Palaeozoic deposits of eastern flank of North Barents depression. *In*: *Proceedings of the International Conference 'Oil and Gas of the Arctic Shelf'*, Murmansk, 12–14 November (CDROM).

Pease, V. 2011. Eurasian orogens and Arctic tectonics: an overview. *In*: Spencer, A. M., Gautier, D., Stoupakova, A., Embry, A. & Sørensen, K. (eds) *Arctic Petroleum Geology*. Geological Society, London, Memoirs (in press).

Pease, V. & Scott, R. A. 2009. Crustal affinities in the Arctic Uralides, northern Russia: significance of detrital zircon ages from Neoproterozoic and Paleozoic sediments in Novaya Zemlya and Taimyr. *Journal of the Geological Society, London*, **166**, 517–527; doi: 10.1144/0016-76492008-093.

Petrov, O. V., Morozov, A. F., Strelnikov, S. I., Ivanov, V. L., Kaminsky, V. D. & Pogrebitskiy, Yu. E. (eds) 2008. *Geological Map of Russian Federation and Adjoining Seas*. Scale 1:2,500,000. Ministry of Natural Resources of the Russian Federation, Federal Agency for Mineral Resources, All-Russia Geological Research Institute, All-Russia Research Institute of Geology and Mineral Resources of World Ocean. 12 sheets.

Petrovskaya, N. A., Trishkina, C. V. & Savishkina, M. A. 2008. Main geological features of the Russian Chukchi Sea. *Oil and Gas Geology*, **6**, 20–28 (in Russian).

Pitman, W. C. III & Talwani, M. 1972. Sea-floor spreading in the North Atlantic. *Geological Society of America Bulletin*, **83**, 619–649.

Pogrebitskiy, Yu. E. (ed.) 2004. *Novaya Zemlya and Vaigach Island. Geological Structure and Miragenia*. NIIGA-VNIIOkeangeologiya, St Petersburg, **205** (in Russian).

Pol'kin, Ya. I. 1984. Chukchi Sea. *In*: Gramberg, I. S. & Pogrebitskiy, Yu. E. (eds) *Geological Structure of the USSR and Trends in Distribution of Mineral Resources, 9, Seas of the Soviet Arctic*. Nedra, Leningrad, 67–77 (in Russian).

Proskurnin, V. F. 1995. New volcano-plutonic association of Severnaya Zemlya and the features of its metallogeny. *In*: Samojlov, A. G. (ed.) *Taimyr's Subsoil. Collection of the Papers*. VSEGEI, Taimyrkomprirodresursy, Norilsk, 93–100 (in Russian).

Proskurnin, V. F. 1999. On angle unconformities in upper Pre-Cambrian and lower Palaeozoic of the Severnaya Zemlya Archipelago. *In*: Simonov, O. N. (ed.) *Taimyr's Subsoil. Collection of the Papers*. VSEGEI, Taimyrkomprirodresursy, Norilsk, 68–76 (in Russian).

Pushcharovskii, Yu. M. (ed.) 1963. *Tectonic Map of the Arctic*. Scale 1:10 000 000. Geological Institute of USSR Academy of Sciences, Moscow (in Russian).

Ritzmann, O. & Faleide, J. I. 2009. The crust and mantle lithosphere in the Barents Sea/Kara Sea region. *Tectonophysics*, **470**, 89–104.

Roeser, H. A., Block, M., Hinz, K. & Reichert, C. 1995. *Marine Geophysical Investigations in the Laptev Sea and the Western Part of the East Siberian Sea.* Alfred Wegener Institute for Polar and Marine Research, Reports on Polar Research, **176**, 367–377.

Rusakov, I. M. & Vinogradov, V. A. 1969. Eugeosynclinal and miogeosynclinal areas of North-East of USSR. *In*: *Proceedings of NIIGA, Regional Geology*, **15**, 5–27 (in Russian).

Savostin, L. A. & Drachev, S. S. 1988. The Cenozoic compression in New Siberian Islands region and its relationship with Eurasia basin opening. *Okeanologiya*, **28**, 775–782 (in Russian).

Savostin, L. A. & Karasik, A. M. 1981. Recent plate tectonics of the Arctic basin and of northeastern Asia. *Tectonophysics*, **74**, 111–145.

Savostin, L. A., Karasik, A. M. & Zonenshain, L. P. 1984*a*. The history of the opening of the Eurasia basin in the Arctic. *Doklady Earth Sciences*, **275**, 79–83.

Savostin, L. A., Natapov, L. M. & Stavsky, A. P. 1984*b*. Mesozoic palaeogeodynamics and palaeogeography of the Arctic region. *In*: *27th International Geological Congress (Moscow), Arctic Geology. Reports*, **4**. Nauka, Moscow, 217–237.

Scott, R. A., Howard, J. P., Guo, L., Schekoldin, R. & Pease, V. 2010. Offset and curvature of the Novaya Zemla fold-and-thrust belt, Arctic Russia. *In*: Vining, B. A. & Pickering, S. C. (eds) *Petroleum Geology: From Mature Basins to New Frontiers – Proceedings of the 7th Petroleum Geology Conference*. Geological Society, London, 645–657; doi: 10.1144/0070645.

Sekretov, S. B. 2000. Petroleum potential of the Laptev Sea basins: geological, tectonic and geodynamic factors. *In*: Roland, N. W. & Tessensohn, F. (eds) *III International Conference on Arctic Margins. Polarforschung*, **68**, 179–186.

Sekretov, S. B. 2001. Northwestern margin of the East Siberian Sea, Russian Arctic: seismic stratigraphy, structure of the sedimentary cover and some remarks on the tectonic history. *Tectonophysics*, **339**, 353–371.

Sharov, N. V., Mitrofanov, F. P., Verba, M. L. & Gillen, K. (eds) 2005. *Lithospheric Structure of the Russian Barents Sea Region*. Karelian Research Centre of Russian Academy of Sciences, Petrozavodsk (in Russian).

Shatskii, N. S. 1935. On tectonics of the Arctic. *Geology and Mineral Resources of the USSR's North*. Glavsevmorput', Leningrad, 149–165 (in Russian).

Sherwood, K. W., Johnson, P. P. *et al*. 2002. Structure and stratigraphy of the Hanna Trough, U.S. Chukchi Shelf, Alaska. *In*: Miller, E. L., Grantz, A. & Klemperer, S. L. (eds) *Tectonic Evolution of the Bering Shelf–Chukchi Sea-Arctic Margin and Adjacent Landmasses*. Geological Society of America, Boulder, CO, Special Papers, **360**, 39–66.

Shipilov, E. V. & Tarasov, G. A. 1998. *Regional Geology of Oil and Gas Bearing Sedimentary Basins of the Russian West-Arctic Shelf*. Kola Science Centre of Russian Academy of Sciences, Apatity (in Russian).

Shipilov, E. V. & Vernikovsky, V. A. 2010. The Svalbard–Kara plates junction: structure and geodynamic history. *Russian Geology and Geophysics*, **51**, 58–71.

Sokolov, S. D., Bondarenko, G. Y., Morozov, O. L., Shekhovtsov, V. A., Glotov, S. P., Ganelin, A. V. & Kravchenko-Berezhnoy, I. R. 2002. South Anyui suture, northeast Arctic Russia: facts and problems. *In*: Miller, E. L., Grantz, A. & Klemperer, S. L. (eds) *Tectonic Evolution of the Bering Shelf–Chukchi Sea-Arctic Margin and Adjacent Landmasses*. Geological Society of America, Boulder, CO, Special Papers, **360**, 209–224.

Spektor, V. B., Andrusenko, A. M., Dunko, E. A. & Kareva, N. F. 1981. Continuation of the South Anyui suture in the Primorya lowlands. *Doklady Academii Nauk SSSR, Earth Science Section*, **260**, 1447–1450 (in Russian).

Srivastava, S. P. 1985. Evolution of the Eurasian Basin and its implications to the motion of Greenland along Nares Strait. *Tectonophysics*, **113**, 29–53.

Stein, R. 2008. *Arctic Ocean Sediments: Processes, Proxies, and Palaeoenvironment. Developments in Marine Geology, 2*. Elsevier, Amsterdam.

Sullivan, M. A., Creaney, S. *et al*. 2007. Hydrocarbon system framework of Russia: Pre-Cambrian to present-day. *In*: *International AAPG Conference Athens Greece*, 19–27 November. Abstracts.

Suprunenko, O. I. & Kos'ko, M. K. 2005. Russian Arctic shelf sedimentary basins. *Developments in Sedimentology*, **57**, 237–271.

Surkov, V. S. & Zhero, O. G. 1981. *Basement and Development of the Platform Cover of the West Siberian Platform*. Nedra, Moscow (in Russian).

Surkov, V. S., Kazakov, A. M., Devyatkov, V. P. & Smirnov, V. L. 1997. Lower-Middle Triassic rift sequence of the West Siberian basin. *Otechestvennaya Geologiya*, **3**, 31–37 (in Russian).

Thurston, D. K. & Theiss, L. A. 1987. *Geologic Report for the Chukchi Sea Planning Area, Alaska*. Minerals Management Service Outer Continental Shelf Report 87-0046.

Tolson, R. B. 1987. Structure and stratigraphy of the Hope Basin, Southern Chukchi Sea, Alaska. *In*: Scholl, D. W., Grantz, A. & Vedder, J. G. (eds) *Geology and Resource Potential of the Continental Margin of Western North America and Adjacent Ocean Basins; Beaufort Sea to Baja California*. Earth Sciences Series. Circum-Pacific Council for Energy and Mineral Resources, Houston, TX, **6**, 59–72.

Trettin, H. P. (ed.) 1991. *Geology of the Innuitian Orogen and Arctic Platform of Canada and Greenland*. The Geology of North America, E. Geological Society of America, Boulder, CO.

Ulmishek, G. 1982. *Petroleum Geology and Resource Assessment of the Timan–Pechora Basin, USSR, and the Adjacent Barents–Northern Kara Shelf*. Argonne National Laboratory, Report EES-TM-199.

Ustritsky, V. I. 1985. On the relationship between the Urals, Pay–Khoy, Novaya Zemlya and Taymyr. *Geotectonics*, **538**, 51–61.

Ustritsky, V. I. 1989. On the tectonic origin of the Barents–North Kara Megabasin. *In*: *Problems of Petroleum Geology of the World Ocean. Moscow*. Nedra, Leningrad, 182–191.

Verba, M. L., Daragan-Sushchova, L. A. & Pavlenkin, A. D. 1992. Riftogenic structures of the western Arctic shelf investigated by refraction studies. *International Geology Review*, **34**, 753–764.

Verhoef, J., Walter, R. R., Macnab, R. & Arkani-Hamed, J. Members of the Project Team 1996. *Magnetic Anomalies of the Arctic and North Atlantic Oceans and Adjacent Land Areas*. Geological Survey of Canada. Open File 3125a.

Vernikovsky, V. 1995. Riphean and Paleozoic metamorphic complexes of the Taimyr foldbelt: condition of formation. *Petrol*, **3**, 55–72.

Vernikovsky, V. A. 1996. The geodynamic evolution of the Taimyr folded area. *Geology of the Pacific Ocean*, **12**, 691–704.

Vernikovsky, V. & Vernikovskaya, A. 2001. Central Taimyr accretionary belt (Arctic Asia): Meso-Neoproterozoic tectonic evolution and Rodinia breakup. *Precambrian Research*, **110**, 127–141.

Verzhbitsky, V., Frantzen, E. *et al*. 2008. New seismic data on the South and North Chukchi sedimentary basins and the Wrangel Arch and their significance for the geology of Chukchi Sea shelf (Russian Arctic). *In*: *Proceedings of the EAGE 3rd St. Petersburg International Conference & Exhibition*, Saint Petersburg.

Vinogradov, V. A. 1984. Laptev Sea. *In*: Gramberg, I. S. & Pogrebitskiy, Yu. E. (eds) *Geological Structure of the USSR and Trends in Distribution of Mineral Resources, 9, Seas of the Soviet Arctic*. Nedra, Leningrad, 51–60 (in Russian).

Vinogradov, V. A. & Drachev, S. S. 2000. Southwestern shelf of the Laptev Sea and tectonic nature of its basement. *Doklady Earth Sciences*, **372**, 601–603.

Vinogradov, V. A., Gaponenko, G. I., Rusakov, I. M. & Shimaraev, V. N. 1974. *Tectonics of the Eastern Arctic Shelves of the USSR*. Nedra, Leningrad (in Russian).

Vinogradov, V. A., Kameneva, G. I. & Yavshits, G. P. 1975. On Hyperborean Platform in light of new data on geology of the Henrietta Island. *In*: *Tectonics of Arctic*, **1**. NIIGA, Leningrad, 21–25 (in Russian).

Vinogradov, V. A., Gaponenko, G. I., Gramberg, I. S. & Shimaraev, V. N. 1977. Structural-associational complexes of the Arctic shelf of eastern Siberia. *International Geology Review*, **19**, 1331–1343.

Vinokurov, I. Yu., Belyaev, V. I., Egorov, A. S., Kalenich, A. P., Matveev, Yu. I., Prudnikov, A. N. & Roslov, Yu. V. 2009. Deep-crustal model and evolution of Barents-Kara region. *In*: *Geology of Polar Regions of the Earth. Materials of XLII Tectonic Conference*, **I**. GEOS, Moscow, 102–106 (in Russian).

Vogt, P. R., Kovacs, L. C., Johnson, G. L. & Feden, R. H. 1979. The evolution of the Arctic Ocean with emphasis on the Eurasia Basin. *In*: *Proceedings of Norwegian Sea Symposium*. Norwegian Petroleum Society, Oslo, 1–29.

Vol'nov, D. A., Voitsekhovsky, V. N., Ivanov, O. A., Sorokov, D. S. & Yashin, D. S. 1970. New Siberian Islands. *In*: Tkachenko, B. V. & Egiazarov, B. K. (eds) *Geology of USSR*, **26**. Nedra, Moscow, 224–274 (in Russian).

Vyssotski, A. V., Vyssotski, V. N. & Nezhdanov, A. A. 2006. Evolution of the West Siberian Basin. *Marine and Petroleum Geology*, **23**, 93–126.

Walderhaug, H. J., Eide, E. A., Scott, R. A., Inger, S. & Golionko, E. G. 2005. Palaeomagnetism and $^{40}Ar/^{39}Ar$ geochronology from the South Taimyr igneous complex, Arctic Russia: a Middle–Late Triassic magmatic pulse after Siberian flood-basalt volcanism. *Geophysical Journal International*, **163**, 501–517; doi: 10.1111/j.1365–246X.2005.02741.x.

Warren, T., Sherwood, K. W. *et al*. 1995. Petroleum exploration opportunities on the US-Russia Chukchi Sea continental shelf. *In*: *Proceedings of the Fifth International Offshore and Polar Engineering Conference*, The Hague, June 11–16, 493–500.

Wilson, B. M. & Lyashkevich, Z. M. 1996. Magmatism and the geodynamics of rifting of the Pripyat-Dnieper-Donets Rift, East European Platform. *Tectonophysics*, **268**, 65–81.

Wilson, M., Wijbrans, J., Fokin, P. A., Nikishin, A. M., Gorbachev, V. I. & Nazarevich, B. P. 1999. $^{40}Ar/^{39}Ar$ dating, geochemistry and tectonic setting of Early Carboniferous dolerite sills in the Pechora basin, foreland of the Polar Urals. *Tectonophysics*, **313**, 107–118.

Zonenshain, L. P., Kuz'min, M. I. & Natapov, L. M. 1990. *Geology of the USSR: A Plate-Tectonic Synthesis*. Page, B. M. (ed.) Geodynamics Series, **21**. American Geophysical Union, Washington, DC.

Assessment of undiscovered petroleum resources of the north and east margins of the Siberian craton north of the Arctic Circle

T. R. KLETT, C. J. WANDREY and J. K. PITMAN

US Geological Survey, Denver Federal Center, MS 939, Box 25046, Denver, CO 80225 USA (e-mail: tklett@usgs.gov)

Abstract: The Siberian craton consists of crystalline rocks and superimposed Precambrian sedimentary rocks deposited in rift basins. Palaeozoic rocks, mainly carbonates, were deposited along the margins of the craton to form an outwardly younger concentric pattern that underlies an outward-thickening Mesozoic sedimentary section. The north and east margins of the Siberian craton subsequently became foreland basins created by compressional deformation during collision with other tectonic plates. The Tunguska Basin developed as a Palaeozoic rift/sag basin over Proterozoic rifts.

The geological provinces along the north and east margins of the Siberian craton are immature with respect to exploration, so exploration-history analysis alone cannot be used for assessing undiscovered petroleum resources. Therefore, other areas from around the world having greater petroleum exploration maturity and similar geological characteristics, and which have been previously assessed, were used as analogues to aid in this assessment. The analogues included those of foreland basins and rift/sag basins that were later subjected to compression. The US Geological Survey estimated the mean undiscovered, technically recoverable conventional petroleum resources to be *c.* 28 billion barrels of oil equivalent, including *c.* 8 billion barrels of crude oil, 103 trillion cubic feet of natural gas, and 3 billion barrels of natural gas liquids.

Keywords: Siberian craton, undiscovered petroleum resources, geological analogues, assessment methodology

This study describes the method used by the US Geological Survey (USGS) to assess undiscovered, technically recoverable conventional petroleum resources of the Siberian craton. The assessed areas are north of the Arctic Circle. Areas south of the Arctic Circle were previously assessed by the USGS (Ulmishek 2001*a*, *b*) and will not be addressed in this paper. Petroleum occurrences in the Siberian craton have been studied for many years, and numerous papers have been written on the subject. This study synthesizes results of previous studies of the Siberian craton and recasts the geological models on the basis of petroleum system elements.

The Siberian craton is located in the Russian Federation between longitude 86° and 138°E and between latitude 52° and 73°N. The craton, surrounded by fold and thrust belts (Fig. 1), covers *c.* 4 500 000 km^2, extending north and south of the Arctic Circle. Most of the craton is located south of the Arctic Circle.

Geological provinces

The Siberian craton consists of continental blocks that were originally separated by ocean basins but had accreted during early Proterozoic time (Rosen *et al.* 1994; Smelov & Timofeev 2007). Various tectonic structures that developed within and among the accreted blocks and along the margins of the Siberian craton separate the area into individual geological provinces (Fig. 1). Geological provinces are defined by the USGS as spatial entities with common geological attributes. Attributes might include a single dominant structural element such as a basin or a fold belt, or a number of contiguous related elements (Klett *et al.* 1997). The geological provinces along the north and east margins of the Siberian craton and north of the Arctic Circle that were delineated for this study are (from west to east): (1) Tunguska Basin (includes Turukhansk–Norilsk Folded Zone and part of the Turukhansk–Igarka Uplift); (2) Yenisey–Khatanga Basin (includes Khatanga Saddle); (3) Lena–Anabar Basin; and (4) Lena–Vilyui Basin (northern part only) (Fig. 1). Some of these provinces extend south of the Arctic Circle.

The Siberian craton consists of crystalline rocks and superimposed Proterozoic sedimentary rocks deposited in intracratonic rifts (Ulmishek 2001*a*). Palaeozoic rocks, mainly carbonates, were deposited along the margins of the craton and are overlain by a progressively outward-thickening Mesozoic section (Persits *et al.* 1998). The north and east margins subsequently became foreland basins created by compressional deformation during collision with other tectonic plates during the Mesozoic (Zonenshain *et al.* 1990). The Tunguska Basin developed as a Palaeozoic rift/sag basin over Proterozoic rifts. The main styles of the basins are primarily Proterozoic to Palaeozoic extensional rift/sag, rifted passive margin and foreland basins that were later deformed by compression, uplift and tilting (Clarke 1991).

Geological models of petroleum occurrence

The sedimentary successions of the geological provinces along the north and east margins of the Siberian craton are similar because of their proximity and similar depositional histories (compare cross-sections in Fig. 3). Known and inferred petroleum sources include organic-rich mudstone in the Proterozoic, Cambrian, Permian, Triassic and Jurassic stratigraphic sections (Bakhturov 1985; Bakhturov *et al.* 1990; Kontorovich *et al.* 1991; Shenfil' 1991; Kuznetsov 1997; Shishkin & Isaev 1999). Reservoirs include Proterozoic, Permian, Triassic, Jurassic and Lower Cretaceous sandstones and seals are intraformational mudstones (Kontorovich *et al.* 1991; Kuznetsov 1997). Traps include compressional structures, updip stratigraphic pinchouts, progradational systems, and karsted platform and reef-related carbonates (Kontorovich *et al.* 1991). Based on petroleum-generation modelling, major petroleum generation and migration probably occurred during the Mesozoic.

Numerous discoveries of crude oil and natural gas were made along the margins of the craton (Fig. 1; IHS Energy 2007). In the Tunguska Basin Province, seven gas and condensate fields have

VINING, B. A. & PICKERING, S. C. (eds) *Petroleum Geology: From Mature Basins to New Frontiers – Proceedings of the 7th Petroleum Geology Conference*, 621–631. DOI: 10.1144/0070621

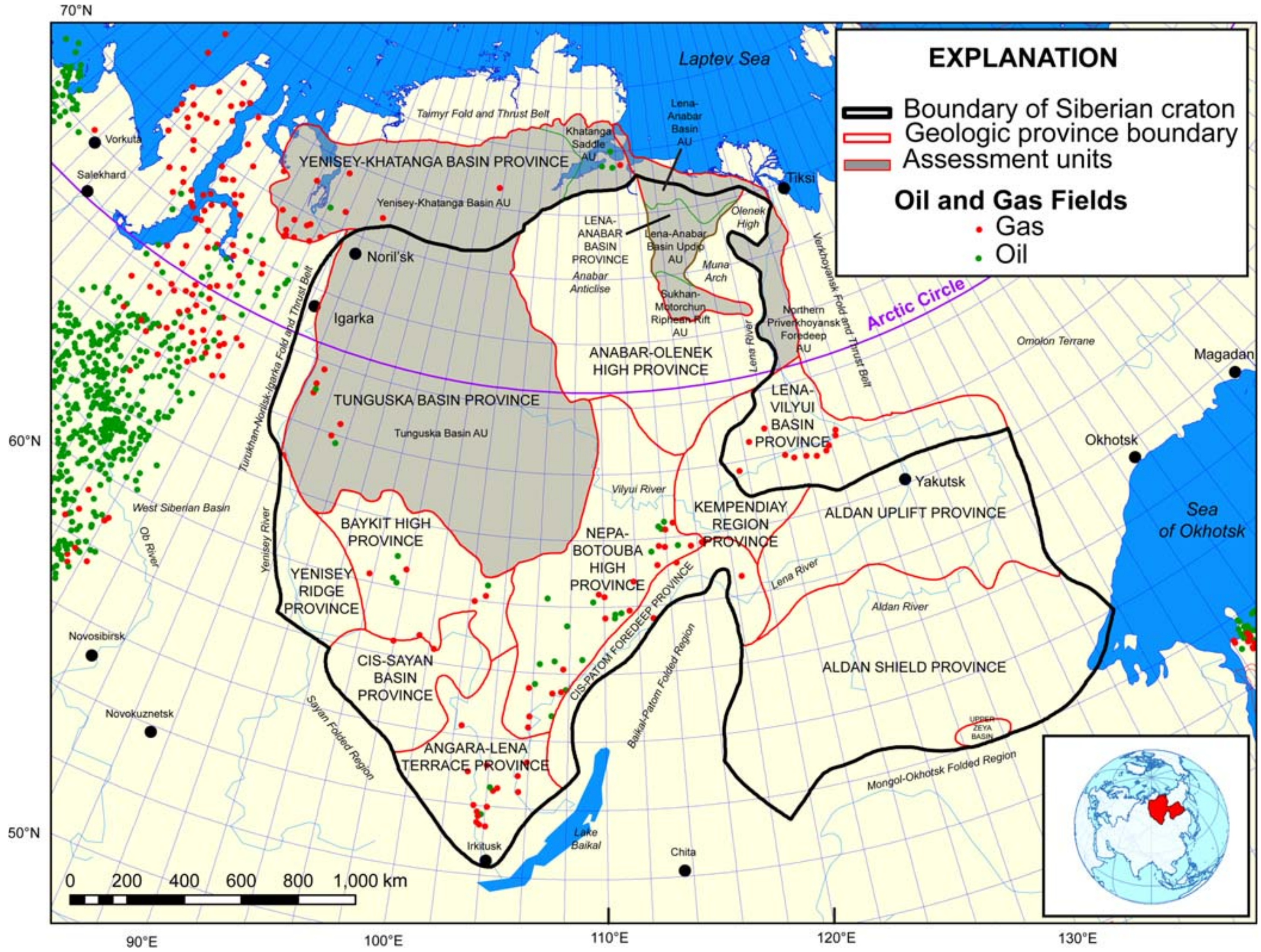

Fig. 1. Map showing locations of geological provinces and assessment units. Data from Persits & Ulmishek (2003); Persits *et al.* (1998); Environmental Systems Research Institute Inc. (1999); and IHS Energy (2007).

been discovered in Proterozoic rocks, but these fields are south of the Arctic Circle. Several gas and condensate fields were discovered north of the craton in the Yenisey–Khatanga Basin Province. Petroleum in these fields is in upper Palaeozoic and Mesozoic clastic rocks (Grebenyuk *et al.* 1988; Kontorovich *et al.* 1991). No fields have been discovered in the Lena–Anabar Basin Province, but some wells indicate the presence of petroleum (Grausman 1996; Sekretov 2003). In the Lena–Vilyui Basin Province south of the Arctic Circle, fields contain mostly natural gas and condensates in upper Palaeozoic and Mesozoic clastic rocks (Vagin *et al.* 1987; Sokolov 1989). Extensive degraded petroleum (bitumen, not assessed in this study) deposits crop out along the margins of the Anabar–Olenek High (Ivanov 1979), but no fields have been discovered on the high.

Assessment units

Assessment units (AUs), which are mappable volumes of rock that are sufficiently homogeneous so that the methodology of resource assessment is applicable (Klett *et al.* 1997), were delineated in each of the geological provinces of the northern and eastern Siberian craton (Fig. 1). One AU, Tunguska Basin, was delineated in the Tunguska Basin Province, but it was not quantitatively assessed. Two AUs, Yenisey–Khatanga Basin and Khatanga Saddle, were delineated in the Yenisey–Khatanga Basin Province. Three AUs, Lena–Anabar Basin, Lena–Anabar Basin Updip and Sukhan–Motorchun Riphean Rift, were delineated in the Lena–Anabar Basin Province; however, the Lena–Anabar Basin Updip and Sukhan–Motorchun Riphean Rift AUs were not quantitatively assessed. One AU, Northern Priverkhoyansk Foredeep, was delineated in the Lena–Vilyui Basin Province north of the Arctic Circle.

Geological analogues for assessment

The required input for the assessment of undiscovered petroleum resources is primarily estimates of the number and sizes of undiscovered fields. In areas that are mature with respect to exploration, the input can be estimated from exploration-history analysis. However, the geological provinces along the north and east margins of the Siberian craton are immature with respect to exploration. Therefore, other areas from around the world having greater petroleum exploration maturity and similar geological characteristics, and that have been previously assessed, were used as analogues to aid in this assessment.

Estimates of undiscovered petroleum resources were calculated by statistically combining the number, sizes in terms of recoverable quantities including reserve growth, and geological risk (as AU probability) of undiscovered oil and gas fields. The statistical combination uses Monte Carlo simulation with 50 000 iterations. Calculated resource quantities and the largest field size selected during each iteration are recorded. The results are given as probability distributions. The calculated largest field size distribution is used to calibrate estimates of the practical largest undiscovered field size.

Table 1. Field densities, median oil and gas field sizes, and exploration maturities of geological analogues used for the assessment of the Khatanga Saddle, Lena–Anabar Basin, and Northern Priverkhoyansk Foredeep AUs

Province name (AU number)	Area (km^2)	Field density (no. discovered per 1000 km^2)	Field density (no. discovered + undiscovered per 1000 km^2)	Median field size, fields ≥50 MMBOE	Largest discovered field size (binned MMBOE)	Exploration maturity (percentage petroleum discovered per total assessed)
Provinces with foreland basin AUs						
Middle Caspian Basin (11090101)	36 452	0.38	1.15	116	2826	61
Amu–Darya Basin (11540101)	156 543	0.12	0.13	111	2826	94
Amu–Darya Basin (11540102)	58 199	0.17	0.29	110	11 305	97
Amu–Darya Basin (11540103)	180 786	0.08	0.09	149	2826	96
Rub Al Khali Basin (20190101)	172 931	0.09	0.18	204	22 610	90
Rub Al Khali Basin (20190102)	57 336	0.54	0.80	175	22 610	95
Rub Al Khali Basin (20190103)	40 737	0.27	0.55	109	707	54
Zagros Fold Belt (20300101)	655 783	0.20	0.57	162	45 220	79
Zagros Fold Belt (20300102)	350 545	0.19	0.59	126	22 610	83
Zagros Fold Belt (20300201)	30 409	0.30	1.55	213	5652	57
Junggar Basin (31150101)	66 347	0.11	0.17	121	5652	98
Sichuan Basin (31420101)	99 141	0.07	0.12	98	353	89
Tarim Basin (31540101)	453 119	0.02	0.13	112	353	14
North Carpathian Basin (40470101)	40 958	0.22	0.27	119	353	99
North Carpathian Basin (40470201)	57 909	0.09	0.10	77	707	98
San Jorge Basin (60580102)	14 185	0.07	0.29	124	177	99
Middle Magdalena Basin (60900101)	6178	1.13	1.25	177	707	99
Middle Magdalena Basin (60900102)	5504	0.73	0.92	115	177	91
Llanos Basin (60960101)	24 630	0.24	0.44	123	707	58
Llanos Basin (60960102)	92 074	0.09	0.22	147	1413	66
East Venezuela Basin (60980101)	35 724	0.64	1.38	187	2826	73
East Venezuela Basin (60980102)	40 319	0.07	0.46	90	353	16
Maracaibo Basin (60990102)	13 549	0.44	0.60	112	353	90
Greater Antilles Deformed Belt (61170101)	138 853	0.02	0.03	102	177	67
Median		0.18	0.37	120	874	89
Mean		0.26	0.51	132	9626	78
Provinces with AUs having rifted passive margins and foreland basin components						
Timan–Pechora Basin (11090102)	203 079	0.26	0.44	115	1413	74
Timan–Pechora Basin (11090103)	86 305	0.01	0.23	103	2826	53
Volga–Ural Basin (10150101)	471 793	0.25	0.29	114	11 305	100
Volga–Ural Basin (10150102)	95 001	0.14	0.14	116	353	100
Middle Caspian Basin (11090101)	36 452	0.38	1.15	116	2826	61
Amu–Darya Basin (11540101)	156 543	0.12	0.13	111	2826	94
Nepa–Botuba Arch (12100101)	40 737	0.02	0.07	117	11 305	76
Ma'Rib–Al Jawf/Masila Basin (20040101)	90 789	0.20	0.41	100	707	66
Fahud Salt Basin (20160201)	17 281	0.23	0.28	223	1413	92
Zagros Fold Belt (20300101)	655 783	0.20	0.57	162	45 220	79
Zagros Fold Belt (20300102)	350 545	0.19	0.59	126	22 610	83

(*Continued*)

Table 1. *Continued*

Province name (AU number)	Area (km^2)	Field density (no. discovered per 1000 km^2)	Field density (no. discovered + undiscovered per 1000 km^2)	Median field size, fields $\geq$50 MMBOE	Largest discovered field size (binned MMBOE)	Exploration maturity (percentage petroleum discovered per total assessed)
Pelagian Basin (20480101)	93 016	0.12	0.19	157	707	94
Pelagian Basin (20480201)	180 311	0.01	0.02	63	177	66
Tarim Basin (31540101)	453 119	0.02	0.13	112	353	14
Bombay (80430101)	180 720	0.06	0.11	106	2826	82
Median		0.14	0.23	115	1666	79
Mean		0.15	0.32	123	8007	76
Combined analogues (duplicates removed)						
Median		0.15	0.29	116	1025	86
Mean		0.22	0.43	129	5810	78
Maximum		1.13	1.55	223	45 220	100

Three elements of geological risk are incorporated in the AU probability: charge, adequate reservoir and seal rocks, and timing of maturation and trap formation. The AU probability is the probability of the existence of one field anywhere in the AU exceeding a minimum size of 50 million barrels of oil equivalent (MMBOE). AUs having a probability of 0.10 or less were not quantitatively assessed.

The numbers of undiscovered fields in an AU were estimated by comparing field densities (estimated number of undiscovered fields plus number of discovered fields, exceeding 50 MMBOE per 1000 km^2) of the analogue datasets. The density of discovered fields, which is less than the density of both discovered and undiscovered fields, was used to calibrate the densities of the undiscovered fields.

Sizes of undiscovered fields were estimated by comparing the median and maximum sizes of the analogue datasets (discovered and undiscovered fields exceeding 50 MMBOE). Minimum sizes are always 50 MMBOE, which is 50 million barrels (MMB) of crude oil or 300 billion cubic feet (BCF) of natural gas (6 BCF equals 1 MMBOE). Petroleum composition and properties of undiscovered fields estimated for an AU are based on fields both discovered in the AUs and in the analogue datasets and on global statistics.

For the assessment of the Khatanga Saddle, Lena–Anabar Basin and Northern Priverkhoyansk Foredeep AUs, two analogue datasets (Table 1) were chosen from the USGS Analogue Database (Charpentier *et al.* 2007): (1) foreland basins (24 analogues) and (2) rifted passive margins and foreland basins with mixed clastic and carbonate depositional systems (15 analogues). The analogues were used to estimate the numbers and sizes of undiscovered fields (Fig. 2). Both analogue sets have discovered fields greater than the minimum size defined for this assessment (50 MMBOE). The analogue categories include extensional and compressional structures and traps having carbonate and clastic depositional systems. Four AUs are common to both analogue sets.

Two different analogue datasets (Table 2) were used to estimate the number of undiscovered fields for the Yenisey–Khatanga Basin AU: (1) rift/sag basins that were subsequently compressed (seven analogues); and (2) basins with slope, clinoforms and turbidites depositional systems (20 analogues) (Fig. 3). The analogue sets contain primarily clastic reservoir rocks and have discovered fields of 50 MMBOE or greater.

Khatanga Saddle, Lena–Anabar Basin, and Northern Priverkhoyansk Foredeep Assessment Units

The median and maximum densities of discovered fields in the combined analogue datasets are 0.2 and 1.1 fields per 1000 km^2, respectively, whereas the median and maximum densities of discovered plus undiscovered fields are 0.3 and 1.6 fields per 1000 km^2, respectively. The median undiscovered oil field size of the combined analogue datasets is 116 MMBOE (Fig. 2) and the median of maximum undiscovered field size is 1000 MMBOE.

Khatanga Saddle Assessment Unit

The area of the Khatanga Saddle AU is *c.* 45 000 km^2 and is located entirely north of the Arctic Circle (Fig. 1). The likelihood that the Khatanga Saddle AU contains at least one field equal to or greater than the minimum size of 50 MMBOE is estimated at 50% (0.50). Input distributions and AU probabilities for this AU are shown in Figure 4.

Densities of 0.02, 0.22 and 1.1 (minimum, median and maximum, respectively) were estimated for numbers of fields per 1000 km^2 in the assessment of the Khatanga Saddle AU. The total minimum, median and maximum numbers of undiscovered fields are estimated at 1, 10 and 50, respectively (Fig. 4). The estimated number of undiscovered oil fields is 0 (minimum), 4 (median) and 40 (maximum), and the estimated numbers of undiscovered gas fields are 1 (minimum), 6 (median) and 45 (maximum), assuming oil–gas mixtures of 0.1 (minimum), 0.4 (mode) and 0.8 (maximum).

The median undiscovered field sizes in the AU are 100 MMB of crude oil and 400 BCF of natural gas. The median undiscovered oil field size (100 MMBOE) is slightly less than the median field size of the analogue dataset (116 MMBOE; Fig. 2). The low-probability maximum field size of 1000 MMBOE equals the median size of the maximum values of the combined analogue datasets (1000 MMBOE). On an oil-equivalent basis, the median and maximum (4000 BCF) sizes of undiscovered gas fields are smaller than undiscovered oil fields because of a greater risk for preservation. The mean of the largest undiscovered field sizes (called the 'expected maximum size') is chosen based on the analogue dataset and matches those provided by the Monte Carlo simulation to calculate resource quantities, *c.* 200 million barrels (MMB) for undiscovered oil fields and *c.* 900 BCF, or 150 MMBOE, for

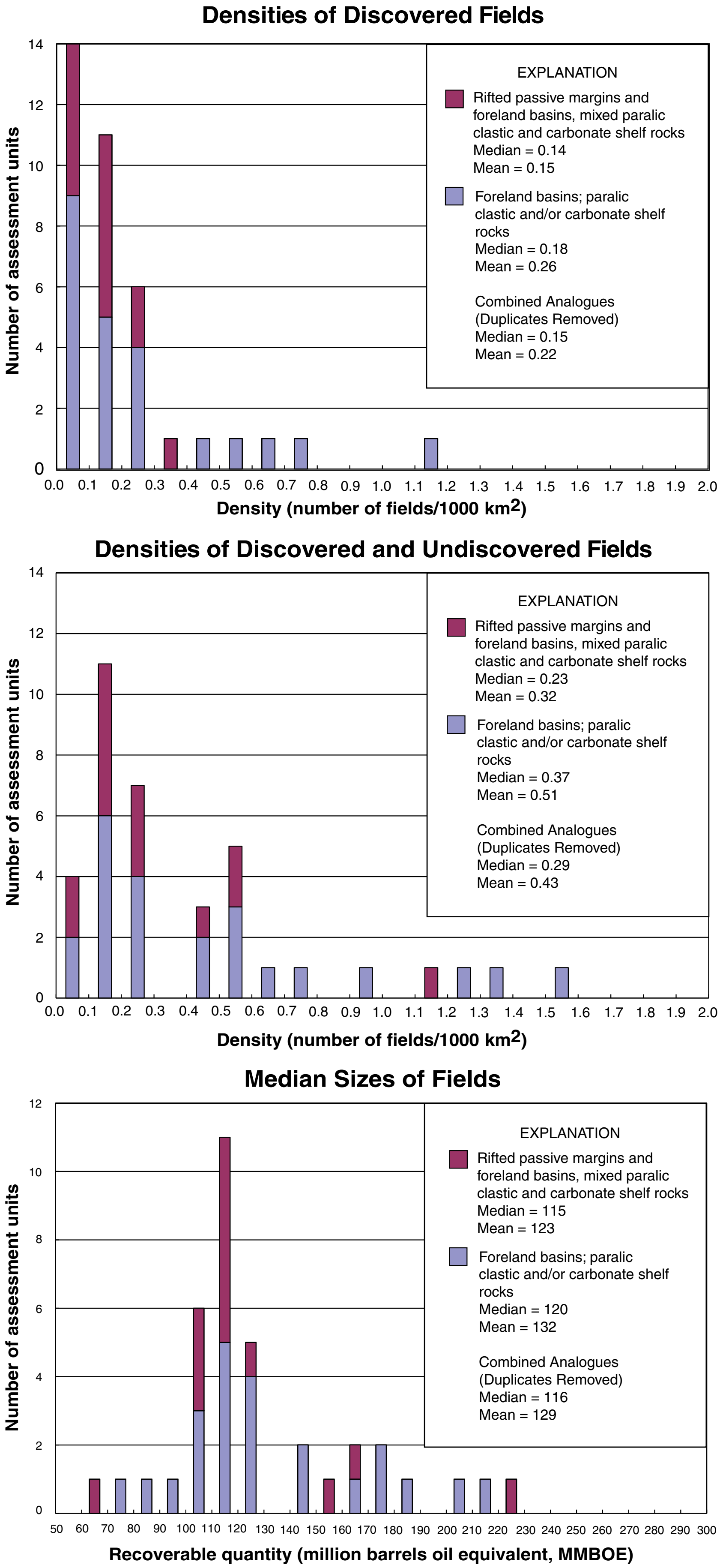

Fig. 2. Densities and median sizes of fields in the geological analogues used for the assessment of the Khatanga Saddle, Lena–Anabar Basin and Northern Priverkhoyansk Foredeep AUs. Four AUs are common to both analogue sets. Data from Charpentier *et al.* (2007).

Table 2. Field densities, median oil and gas field sizes, and exploration maturities of geological analogues used for the assessment of the Yenisey–Khatanga Basin AUs

Province name (AU number)	Area (km^2)	Field density (no. discovered per 1000 km^2)	Field density (no. discovered + undiscovered per 1000 km^2)	Median field size, fields ≥50 MMBOE	Largest discovered field size (binned MMBOE)	Exploration maturity (percentage petroleum discovered per total assessed)
Provinces with rift/sag basin AUs that were later compressed						
Middle Caspian Basin (11090201)	80 295	0.09	0.15	142	2826	95
North Ustyurt Basin (11500101)	24 898	0.16	0.29	251	1413	82
North Ustyurt Basin (11500201)	141 758	0.01	0.04	105	177	84
West Siberia Basin (11740101)	999 936	0.15	0.32	132	22 610	79
West Siberia Basin (11740301)	423 539	0.15	0.35	224	45 220	92
Malay Basin (37030101)	72 558	0.39	0.64	108	707	69
Malay Basin (37030201)	32 955	0.36	0.51	186	707	94
Median		0.15	0.32	142	1268	84
Mean		0.19	0.33	164	13 749	85
Provinces with AUs having slope, clinoforms, and turbidites depositional systems						
Baram Delta/Brunei–Sabah (37010102)	54 084	0.09	0.28	100	353	39
Bonaparte Gulf Basin (39100201)	72 634	0.03	0.14	95	353	8
Bonaparte Gulf Basin (39100201)	146 975	0.03	0.14	112	1413	68
Browse Basin (39130101)	133 150	0.02	0.14	125	1413	48
Northwest Shelf (39480101)	50 436	0.40	1.53	108	2826	56
Northwest Shelf (39480201)	309 715	0.00	0.02	111	707	41
Pannonian Basin (40480101)	99 022	0.11	0.09	102	353	98
Pannonian Basin (40480201)	54 076	0.15	0.13	95	177	99
Po Basin (40600101)	75 427	0.21	0.35	110	707	76
Sergipe–Alagoas Basin (60290102)	23 320	0.09	0.51	105	353	5
Campos Basin (60350101)	40 408	0.74	1.74	178	2826	55
Santa Cruz–Tarija Basin (60450101)	98 239	0.19	0.38	115	1413	68
Neuquen Basin (60550103)	7734	0.65	0.76	130	177	98
Tobago Trough (61030101)	23 864	0.38	0.94	128	707	42
West-Central Coastal (72030201)	258 108	0.05	0.14	114	1413	24

(*Continued*)

Table 2. *Continued*

Province name (AU number)	Area (km^2)	Field density (no. discovered per 1000 km^2)	Field density (no. discovered + undiscovered per 1000 km^2)	Median field size, fields ≥50 MMBOE	Largest discovered field size (binned MMBOE)	Exploration maturity (percentage petroleum discovered per total assessed)
West-Central Coastal (72030302)	199 541	0.01	0.49	140	2826	23
Orange River Coastal (73030101)	394 664	0.00	0.01	110	353	50
Bombay (80430102)	65 776	0.20	0.24	114	707	88
Ganges–Brahmaputra Delta (80470301)	176 260	0.05	0.18	116	353	41
Irrawaddy (80480102)	466 281	0.01	0.04	107	707	37
Median		0.09	0.21	112	575	49
Mean		0.17	0.41	116	1075	53
Combined analogues (duplicates removed)						
Median		0.11	0.28	114	850	68
Mean		0.17	0.39	128	4361	62
Maximum		0.74	1.74	251	45 220	99

undiscovered gas fields (Fig. 4). The sizes are reduced in this AU from the median of the largest discovered field size in the analogue dataset because of the complex tectonic history and uplift since petroleum generation.

Lena–Anabar Basin Assessment Unit

The area of the Lena–Anabar Basin AU is *c.* 55 000 km^2 and is located entirely north of the Arctic Circle. Input distributions and AU probabilities for the Lena–Anabar Basin AU are shown in Figure 4.

Assessment of the Lena–Anabar Basin AU was based on two scenarios because a single timing probability was not sufficient to characterize the age of petroleum generation in Proterozoic and Palaeozoic source rocks with respect to trap development. Permian and Mesozoic rocks directly overlie Cambrian rocks over much of the AU, but whether or not a complete Palaeozoic section was deposited and subsequently eroded is unknown. The scenarios are: (1) base case (having a 90% probability) – non-deposition of a middle and late Palaeozoic section followed by deposition, petroleum generation and accumulation during the Permian and Mesozoic; and (2) worst case (having a 10% probability) – deposition of a middle and upper Palaeozoic section with petroleum generation and accumulation followed by middle to late Palaeozoic erosion. The likelihood that the Lena–Anabar Basin AU contains at least one field equal to or greater than the minimum field size of 50 MMBOE is estimated to be *c.* 48% (0.48) for the base case scenario and 32% (0.32) for the worse case scenario.

Densities of 0.02, 0.4 and 1.8 (minimum, median, and maximum, respectively) were estimated for scenario 1 in the assessment of the Lena Anabar Basin AU because accumulations sourced by Proterozoic and Palaeozoic source rocks could exist in the Mesozoic section. For scenario 2, the median and maximum densities were estimated to be approximately half of those of scenario 1 (0.02, 0.2 and 0.9) because accumulations sourced by Proterozoic and Palaeozoic source rocks would exist only in the Palaeozoic section. For scenario 1, the total minimum, median and maximum numbers of undiscovered fields are 1, 20 and 100, respectively (Fig. 4). The estimated numbers of undiscovered oil fields are 1 (minimum), 20 (median) and 100 (maximum) and the estimated numbers of undiscovered gas fields are 0 (minimum), 2 (median) and 20 (maximum), assuming oil–gas mixtures of 0.8 (minimum), 0.9 (mode) and 1.0 (maximum). The densities and estimated numbers of undiscovered fields for scenario 2 are half of those for scenario 1 (Fig. 4). The total minimum, median and maximum numbers of undiscovered fields are 1, 10 and 50, respectively. The estimated numbers of undiscovered oil fields are 1 (minimum), 9 (median) and 50 (maximum) and the estimated numbers of undiscovered gas fields are 0 (minimum), 1 (median) and 10 (maximum).

The median sizes of undiscovered oil fields (125 and 100 MMBOE, scenarios 1 and 2, respectively) in the AU were estimated to approximate the median size of the analogue datasets (Fig. 2). The low-probability maximum oil field size, 2500 MMBOE (Fig. 4), is larger than the median of the largest discovered field size in the rifted passive margin and foreland basin analogue dataset (1700 MMBOE), whereas sizes of gas fields are lower (median sizes of 83 and 75 MMBOE and maximum sizes of 167 MMBOE) because gas-prone Mesozoic source rocks may not be fully mature with respect to generation, resulting in incomplete trap fill. The expected maximum crude oil size (*c.* 750 MMBOE; Fig. 4) is based on the distribution of sizes of discovered fields in the analogue dataset, particularly the median of the maximum discovered field sizes. The expected maximum gas field size (*c.* 600 BCF or 100 MMBOE; Fig. 4) is less because gas-prone Mesozoic source rocks may not be fully mature with respect to generation.

Northern Priverkhoyansk Foredeep Assessment Unit

The area of the Northern Priverkhoyansk Foredeep AU is *c.* 56 000 km^2 and 99% of the area is located north of the Arctic Circle. The likelihood that the AU contains at least one field equal to or greater than the minimum field size (50 MMBOE) is 40% (0.40). Input distributions and AU probabilities for the Northern Priverkhoyansk Foredeep AU are shown in Figure 5.

Densities of 0.02, 0.1 and 0.9 (minimum, median and maximum, respectively) were used in the assessment of the Northern Priverkhoyansk Foredeep AU. These densities are slightly less

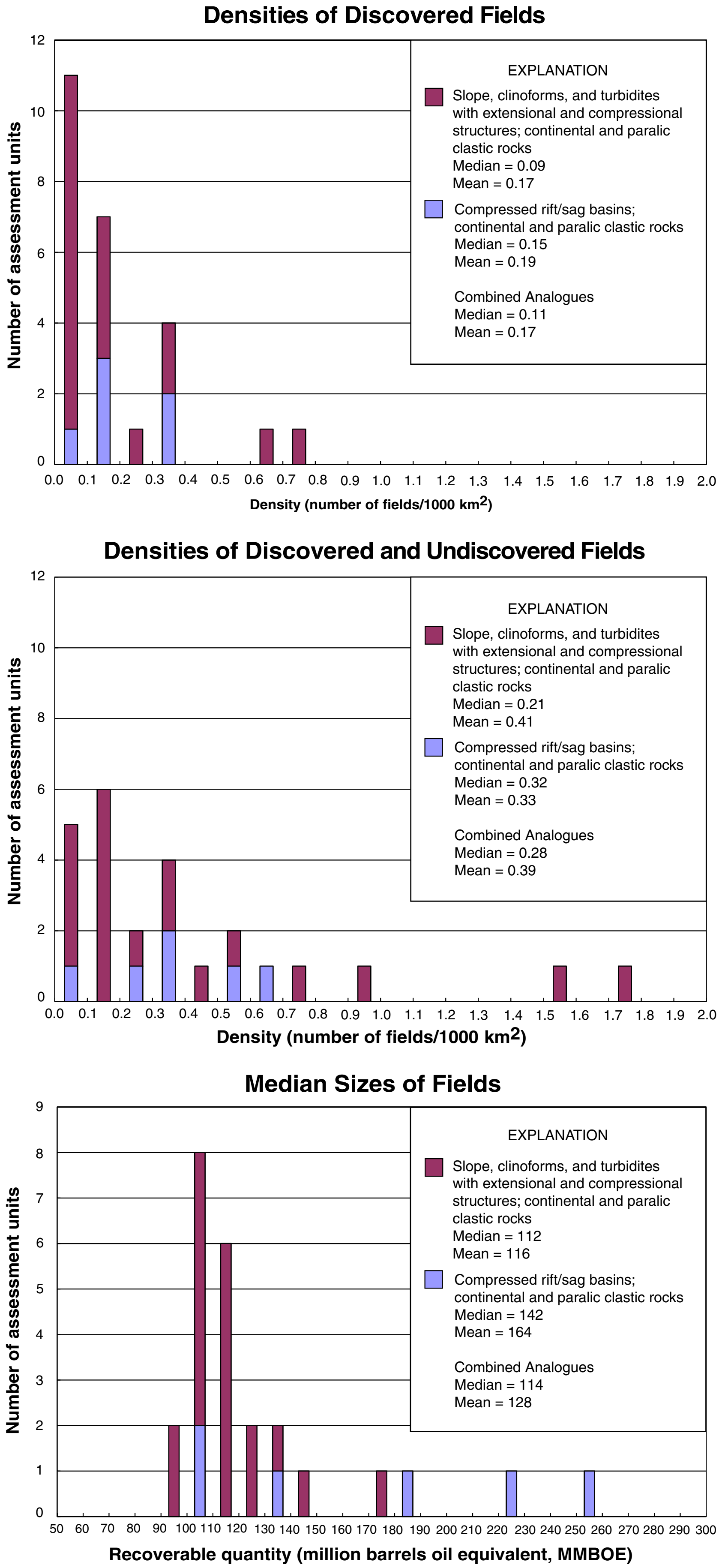

Fig. 3. Densities and median sizes of fields in the geological analogues used for the assessment of the Yenisey–Khatanga Basin Assessment Unit. Data from Charpentier *et al.* (2007).

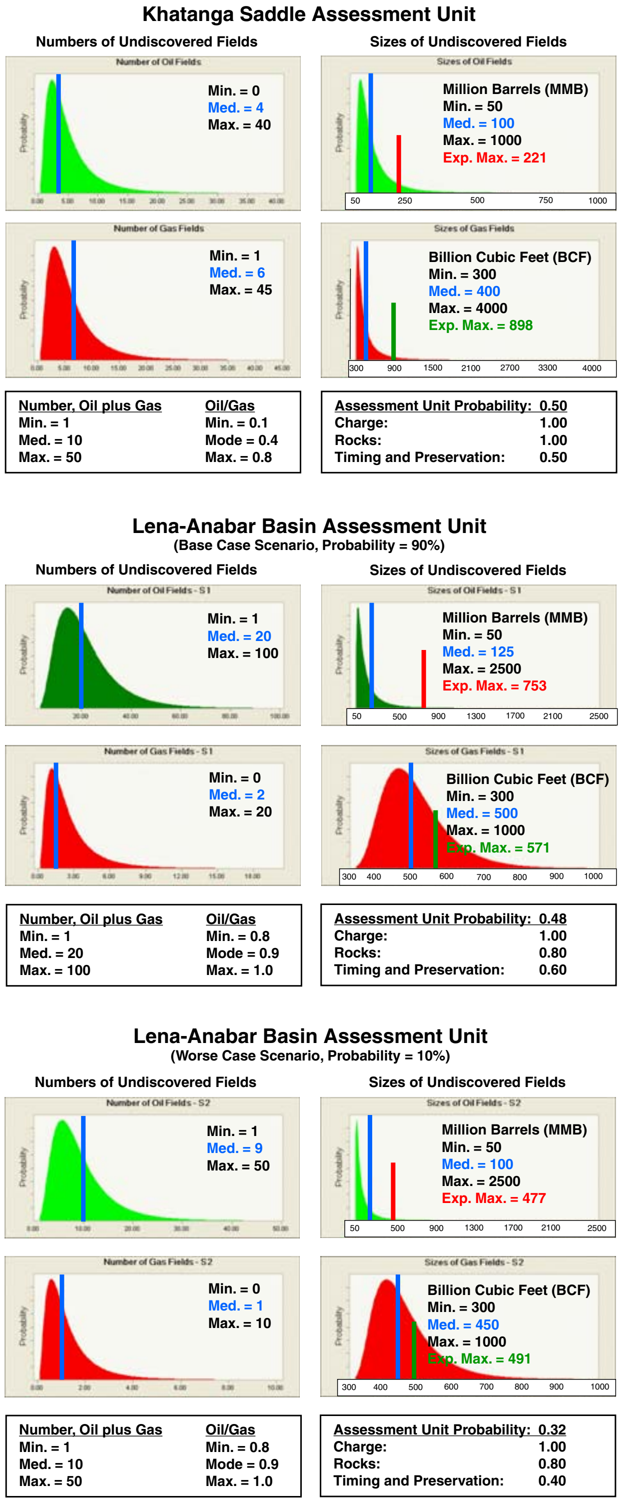

Fig. 4. Input distributions and AUs probabilities for the Khatanga Saddle and Lena–Anabar Assessment Units. Min., minimum; Med., median; Max., maximum; Exp. Max., calculated expected maximum.

than those of the analogue dataset (Fig. 2) because: (1) outlying values in the analogue set that do not represent this AU were excluded; (2) no economic discoveries were made in the AU despite exploration; and (3) a carbonate shelf might not have existed over the entire area. The total minimum, median and maximum numbers of undiscovered fields are 1, 7 and 50, respectively (Fig. 5). The estimated numbers of undiscovered oil fields are 1 (minimum), 4 (median) and 35 (maximum), and the estimated numbers of undiscovered gas fields are 1 (minimum), 4 (median)

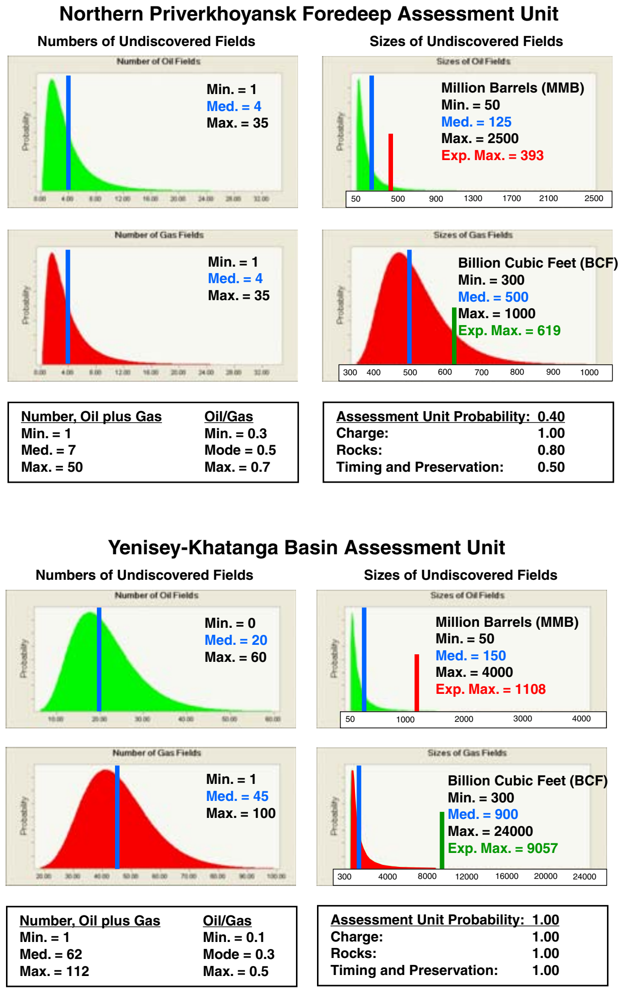

Fig. 5. Input distributions and assessment unit probabilities for the Northern Priverkhoyansk Foredeep and Yenisey–Khatanga Basin AUs. Min., minimum; Med., median; Max., maximum; Exp. Max., calculated expected maximum.

and 35 (maximum), assuming an oil–gas mixture of 0.3 (minimum), 0.5 (mode) and 0.7 (maximum).

The median undiscovered field sizes in the AU are 125 MMB of crude oil and 500 BCF of natural gas (Fig. 5). The median undiscovered oil field size is approximately equal to the mean size of the analogue dataset (*c.* 130 MMBOE; Fig. 2), but the median undiscovered gas field size is considerably less because traps for natural gas in this AU might not be efficient. Low-probability maximum undiscovered oil and gas field sizes in the AU are 2500 MMB and 1000 BCF, allowing for the probability of a large oil field within the Proterozoic and Palaeozoic section. The expected maximum oil and gas field sizes (*c.* 400 and 100 MMBOE, respectively; Fig. 5) are based on the distribution of sizes of discovered fields in the analogue dataset, particularly the median of the maximum discovered field sizes, but excluding values that do not represent this AU.

Yenisey–Khatanga Basin Assessment Unit

The area of the Yenisey–Khatanga Basin AU is *c.* 345 000 km^2 and is located entirely north of the Arctic Circle. The likelihood that the AU contains at least one field equal to or greater than the minimum field size of 50 MMBOE is estimated at 100% (1.00). Input distributions and AU probabilities for the Yenisey–Khatanga Basin Assessment Unit are shown in Figure 5.

The median and maximum densities of discovered fields in the combined analogue datasets are 0.1 and 0.7 fields per 1000 km^2, respectively, whereas the median and maximum densities of discovered plus undiscovered fields are 0.3 and 1.7 fields per 1000 km^2, respectively (Fig. 3). Minimum sizes of undiscovered fields defined for the AU are 50 MMB of crude oil and 300 BCF of natural gas. The median undiscovered oil field size of the combined analogue datasets is 114 MMBOE (Fig. 3), and the median of maximum undiscovered field sizes is 850 MMBOE.

Densities of <0.01, 0.2 and 0.3 (minimum, median and maximum, respectively) were estimated for numbers of fields per 1000 km^2 in this AU. The median density of 0.2 is between the median densities of the analogue datasets, and the maximum density of 0.3 approximates the density of the neighbouring West Siberian Basin AUs (0.35, included in the analogue set). The total minimum, median and maximum numbers of undiscovered fields are 1, 62 and 112, respectively (Fig. 5). The estimated numbers of undiscovered oil fields are 0 (minimum), 20 (median) and 60 (maximum), and the estimated numbers of undiscovered gas fields are 1 (minimum), 45 (median) and 100 (maximum), assuming oil–gas mixtures of 0.1 (minimum), 0.3 (mode) and 0.5 (maximum).

The median field size, 150 MMBOE, approximates the median size of the rift/sag basin analogue set (142 MMBOE), but is greater than the median field size of the combined analogue dataset (114 MMBOE; Fig. 3). This median field size is consistent with the average size of discovered fields in this AU and the neighbouring Northern West Siberian Onshore Gas AU (with a median size of *c*. 200–300 MMBOE, included in the analogue set). The low-probability maximum field sizes of 4000 MMB for undiscovered oil accumulations and 24 000 BCF for undiscovered gas accumulations (Fig. 5) approximates the means of the maximum field sizes in the combined analogue database. The expected maximum size of undiscovered fields is based on the analogue dataset with a smaller oil field size than gas to be consistent with the sizes of discovered fields in this AU: *c*. 1000 MMB for undiscovered oil fields and 1500 MMBOE for undiscovered gas fields (9000 BCF; Fig. 5). These sizes are based on a distribution of

Table 3. Assessment results of geological provinces along the north and east margins of the Siberian craton (technically recoverable, conventional, undiscovered resources)

Assessment unit	Khatanga Saddle	Yenisey–Khatanga Basin	Lena–Anabar Basin (aggregated)	Northern Priverkhoyansk Foredeep	Total (means only)
Assessment unit code	11750101	11750102	12000101	12140101	
Oil in oil fields (MMB)					
F95	0	2201	0	0	
F50	0	4847	0	0	
F05	1376	9716	7207	1732	
Mean	327	5257	1913	377	7874
Gas in oil fields (associated and dissolved gas) (BCF)					
F95	0	11 604	0	0	
F50	0	26 571	0	0	
F05	932	55 375	6022	1448	
Mean	206	29 078	1502	296	31 082
Natural gas liquids in oil fields (MMB)					
F95	0	305	0	0	
F50	0	710	0	0	
F05	25	1529	163	39	
Mean	6	786	40	8	840
Gas in gas fields (non-associated gas) (BCF)					
F95	0	38 629	0	0	
F50	0	66 089	0	0	
F05	6764	108 413	2538	4319	
Mean	1797	68 884	605	1039	72 325
Natural gas liquids in gas fields (MMB)					
F95	0	1009	0	0	
F50	0	1754	0	0	
F05	182	2929	69	116	
Mean	48	1835	16	28	1927

MMB, million barrels; BCF, billion cubic feet. Results shown are fully risked estimates. For gas fields, all liquids are included under the natural gas liquids category. F95 denotes a 95% of at least the amount tabulated; other fractiles are defined similarly. Fractiles are additive under the assumption of perfect positive correlation.

sizes of fields in this AU and neighbouring AUs, and are constrained by the discovery history.

Tunguska Basin Assessment Unit

The Tunguska Basin AU is *c.* 854 000 km^2 and 39% of the area is located north of the Arctic Circle. It was not quantitatively assessed and no analogues were selected. The likelihood that the AU contains at least one field equal to or greater than 50 MMBOE is *c.* 6% (0.06). AUs with probabilities less than 1% were not quantitatively assessed.

Assessment results

The USGS estimated the mean undiscovered, technically recoverable, conventional petroleum resources in the seven AUs in the Arctic portion of the Siberian craton (Fig. 1) to be *c.* 28 billion barrels of oil equivalent, including *c.* 8 billion barrels of crude oil, 103 trillion cubic feet of natural gas and 3 billion barrels of natural gas liquids (Table 3).

Conclusions

The assessment of undiscovered petroleum resources along the north and east margins of the Siberian craton was accomplished using geological analogues. Individual analogues, sets of analogues with similar geological characteristics, and combinations of analogue sets (as used in this study) facilitate the assessment of geological provinces that are immature with respect to exploration such that exploration-history analysis alone cannot be used. Number and sizes of undiscovered oil and gas fields can be obtained from analogues and, when statistically combined with AU probability, provide estimates of undiscovered petroleum resources.

The authors would like to acknowledge F. M. Persits for GIS support, and D. L. Gautier and G. F. Ulmishek for their valuable reviews and comments. The manuscript was greatly improved by the reviews and comments of A. Khudoley, A. Stoupakova, S. Drachev and S. Pickering. The authors are grateful to the USGS Library staff for their help in obtaining hard-to-find and rare geological articles from the Russian scientific literature.

References

Bakhturov, S. F. 1985. *Bituminoznye karbonatno-slantsevye formatsii Vostochnoy Sibiri (Bituminous carbonate-shale formations of eastern Siberia).* Trudy Instituta Geologii i Geofiziki, **617**. Sibirskoye Otdelenie, Akademiya Nauk SSSR (in Russian).

Bakhturov, S. F., Yevtushenko, V. M. & Pereladov, V. S. 1990. Kuonam bituminous carbonate shale complex. *Petroleum Geology*, **24**, 124–133; translated from Trudy Instituta Geologii i Geofiziki, **671**, Sibirskoye Otdelenie, Akademiya Nauk SSSR (1988).

Charpentier, R. R., Klett, T. R. & Attanasi, E. D. 2007. *Database for Assessment Unit-scale Analogs (Exclusive of the United States).* United States Geological Survey Open-File Report 2007-1404.

Clarke, J. W. 1991. Petroleum geology of East Siberia (abstract). American Association of Petroleum Geologists Bulletin, **75**, 554 (presented at the *1991 American Association of Petroleum Geologists Annual Convention*, Dallas, TX, 7–10 April 1991).

Environmental Systems Research Institute Inc. 1999. *ESRI Data and Maps.* Environmental Systems Research Institute Inc., Redlands, CA.

Grausman, V. V. 1996. Upper Precambrian deposits of the Olenek Uplift from deep drilling data. *Tikhookeanskaya Geologiya*, **12**, 775–781.

Grebenyuk, V. V., Gurari, F. G., Lugovtsov, A. D. & Moskvin, V. I. 1988. Specifics of oil–gas formation in the Mesozoic depressions of the Siberian Platform. *Petroleum Geology*, **19**, 602–605; translated from *Geologiya i neftegasonosnost' mesozoiskikh sedimentatsionnnikh basseinov Sibiri*. Akademiia Nauk SSSR, Sibirskoe Otdelenie, Trudy Institut Geologii i Geofiziki, **532**, 132–139 (1983).

IHS Energy. 2007 [includes data current through October 2007]. *International Exploration and Production Database*. IHS Energy Group, Englewood, CO.

Ivanov, V. L. 1979. *Olenekskoe mestorozhdenie bitumov (Geologicheskoe stroenie i usloviia formirovaniia)* (Olenek bitumen field, geologic layer and conditions of formation). Nauchno-issledovatel'skii institut geologii Arktiki, Trudy (Leningrad, 'Nedra', Leningrad Branch), **182**.

Klett, T. R., Ahlbrandt, T. S., Schmoker, J. W. & Dolton, G. L. 1997. *Ranking of the World's Oil and Gas Provinces by Known Petroleum Volumes*. United States Geological Survey Open-File Report 97-463.

Kontorovich, A. Eh., Bakin, V. E., Grebenyuk, V. V., Kuznetsov, L. L. & Nakaryakov, V. D. 1991. Khatanga-Vilyui Upper Paleozoic–Mesozoic petroleum province (abstract). American Association of Petroleum Geologists Bulletin, **75**, 1414 (presented at the *American Association of Petroleum Geologists International Conference*, London, 29 September to 2 October, 1991).

Kuznetsov, V. G. 1997. Riphean hydrocarbon reservoirs of the Yurubchen–Tokhom zone, Lena–Tunguska province, NE Russia. *Journal of Petroleum Geology*, **20**, 459–474.

Persits, F. M. & Ulmishek, G. F. 2003. *Maps Showing Geology, Oil and Gas Fields, and Geologic Provinces of the Arctic*. United States Geological Survey Open-File Report 97-470-J.

Persits, F. M., Ulmishek, G. F. & Steinshouer, D. W. 1998. *Map Showing Geology, Oil and Gas Fields, and Geologic Provinces of the Former Soviet Union*. United States Geological Survey Open-File Report 97-470E.

Rosen, O. M., Condie, K. C., Natapov, L. M. & Nozhkin, A. D. 1994. Archean and early Proterozoic evolution of the Siberian Craton: a preliminary assessment. *In*: Condie, K. C. (ed.) *Archean Crustal Evolution, Developments in Precambrian Geology*, **11**. Elsevier, Amsterdam, 411–459.

Sekretov, S. B. 2003. Hydrocarbon potential of the Yenisei–Lena region of the Arctic Siberia and adjacent southwestern Laptev Sea (abstract). Abstracts of the *Fourth International Conference on Arctic Margins (ICAM IV)*, Dartmouth, Nova Scotia, 30 September–3 October, 2003).

Shenfil', V. Yu. 1991. *The Late Precambrian of the Siberian Platform.* Nauka Sibirskoye Otdelenie, Novosibirsk.

Shishkin, B. B. & Isaev, A. V. 1999. Structure of the Precambrian and Cambrian deposits in the northeast of the Siberian platform. *Russian Geology and Geophysics*, **40**, 1763–1775.

Smelov, A. P. & Timofeev, V. F. 2007. The age of the North Asian Cratonic basement: an overview. *Gondwana Research*, **12**, 279–288.

Sokolov, B. A. (ed.) 1989. History of oil–gas formation and accumulation in the east of the Siberian Craton. *Petroleum Geology*, **23**, 12–45; translated from Akademiya Nauk SSSR, Sibirskovo Otdeleniya, Yakutskii Filial, Institut Geologii, Moscow, Izdatelctvo Nauka, (1986).

Ulmishek, G. F. 2001*a*. *Petroleum Geology and Resources of the Nepa–Botuoba High, Angara–Lena Terrace, and Cis–Patom Foredeep, southeastern Siberian Craton, Russia.* United States Geological Survey Bulletin 2201-C.

Ulmishek, G. F. 2001*b*. *Petroleum Geology and Resources of the Baykit High Province, East Siberia, Russia.* United States Geological Survey Bulletin 2201-F.

Vagin, S. B., Samsonov, Yu. V., Shashin, A. V. & Dongaryan, L. Sh. 1987. Paleo-geologic and paleo-hydrogeologic bases for assessing the oil–gas prospects of the Vilyuy Basin. *Petroleum Geology*, **22**, 458–460; translated from *Neftegazovaya Geologiya i Geofizika*, **1986**, 2–4.

Zonenshain, L. P., Kuzmin, M. I. & Natapov, L. M. 1990. Geology of the USSR; a plate-tectonic synthesis. *In*: Page, B. M. (ed.) *Geodynamics Series*. American Geophysical Union, Washington, DC, **21**.

Synchronous exhumation events around the Arctic including examples from Barents Sea and Alaska North Slope

P. F. GREEN and I. R. DUDDY

Geotrack International Pty Ltd, 37 Melville Road, West Brunswick, Victoria 3055, Australia (e-mail: mail@geotrack.com.au)

Abstract: In many areas of the Arctic, sedimentary sequences have been exhumed from significantly greater depths during the Cenozoic, with 2 km of section or more removed in some areas. Implications for exploration include enhanced maturity levels, possible loss of reservoired hydrocarbons as a result of seal breach, and phase changes due to pressure reduction. While the importance of Cenozoic exhumation to hydrocarbon prospectivity in individual basins is widely recognized, less well recognized is the regional synchroneity in the main phases of Cenozoic exhumation over wide areas of the Arctic and North Atlantic. Thermal history reconstruction studies in the Barents Sea and the Alaskan North Slope, based on application of apatite fission track analysis and vitrinite reflectance, reveal three main episodes of exhumation, in Paleocene, Eocene–Oligocene and Miocene times, and correlative exhumation episodes have been identified in a number of published studies in these and other areas. Previous attempts to explain these episodes of exhumation have been focussed on local mechanisms. However, our results reveal a pattern of regionally synchronous exhumation over a wide region, not only of the Arctic but also in many areas around the European North Atlantic margin, suggesting that events in each area are a regional response to events at plate boundaries, perhaps coupled to imbalances of crustal forces at continental boundaries. To date, no convincing mechanism has been put forward for producing such regional exhumation episodes, despite the fact that in many areas they exert critical control on regional hydrocarbon prospectivity. We suggest that serious attention should be directed to investigating the underlying mechanisms.

Keywords: AFTA, exhumation, Barents Sea, Alaskan North Slope, thermal history, burial history reconstruction

In many areas of the Arctic, sedimentary sequences have been exhumed from significantly greater depths during the Cenozoic, with up to 2 km of section or more removed in some areas. Examples include Barents Sea (Cavanagh *et al.* 2006), Svalbard (Blythe & Kleinspehn 1998), North Slope Alaska (O'Sullivan *et al.* 1993; O'Sullivan 1996, 1999), Sverdrup Basin (Arne *et al.* 2002), West Greenland (Japsen *et al.* 2005) and East Greenland (Thomson *et al.* 1999; Hansen *et al.* 2001). Implications for exploration include enhanced maturity levels (compared with assessments that underestimate former burial depths), possible loss of reservoired hydrocarbons as a result of seal breach and spillage, and phase changes due to pressure reduction (see Doré *et al.* 2002, for an extensive review of the influence of exhumation on hydrocarbon systems). In addition, the timing of generation becomes a key issue in such areas, particularly for plays involving structures formed in the initial stages of exhumation, as these structures were not available for charging during the main phase of generation, which occurred during burial prior to the onset of exhumation.

Exhumation is often considered as a negative factor for prospectivity, but exhumed basins in many parts of the world contain significant quantities of hydrocarbons, such as the East Irish Sea Basin (e.g. Jackson *et al.* 1995) and southern North Sea (Cameron *et al.* 1992) of the UK, the Reconcavo Basin of Brazil (Magnavita *et al.* 1994) and much of North Africa (e.g. Logan & Duddy 1998). In these basins, discovering hydrocarbons requires detailed knowledge of magnitude and timing of exhumation and associated effects.

As evidence accumulates regarding the relatively common occurrence of exhumed basins, it is becoming increasingly clear that episodes of exhumation display a broad regional synchroneity across wide areas. A recent synthesis of stratigraphic information from the European North Atlantic margin (Praeg *et al.* 2005; Stoker *et al.* 2005) highlighted the presence of synchronous unconformities at Paleocene, Eocene–Oligocene, Base Miocene, Middle Miocene and Early Pliocene levels from offshore Ireland (Porcupine) to offshore Norway (Lofoten). As discussed below, each of these unconformities was interpreted as representing a plate-wide response to a major tectonic episode. Holford *et al.* (2009) showed that these unconformities correlate with episodes of kilometre-scale exhumation affecting wide areas of the East Irish Sea Basin and adjacent regions of the UK, in an intra-plate setting well inboard of the continental margin. In these regions, the magnitude of these events was such that up to a kilometre or more of section has been removed and all stratigraphic evidence for these events has been erased, whereas lower amounts of erosion along the margin have resulted in the preservation of evidence as hiatuses in the incomplete stratigraphic record.

Here we show that episodes of exhumation in many areas of the Arctic, including the Barents Sea, Alaskan North Slope, Arctic Canada, West and East Greenland, also correlate with these key episodes of tectonism originally defined along the European North Atlantic Margin. While the importance of Cenozoic exhumation to hydrocarbon prospectivity is now widely recognized in many areas of the Arctic, the nature of the underlying processes is poorly understood. Previous attempts to explain exhumation in these regions have been focussed purely on local mechanisms (e.g. Cavanagh *et al.* 2006 in the Barents Sea). However the results discussed here reveal a pattern of broadly synchronous exhumation over wide regions, suggesting that events in these areas represent manifestations of a regional response to events at plate boundaries.

The work reported here is based on application of apatite fission track analysis (AFTA®) and vitrinite reflectance (VR) to provide rigorous constraints not only on the magnitude but also on the timing of exhumation. We present case studies based on individual

VINING, B. A. & PICKERING, S. C. (eds) *Petroleum Geology: From Mature Basins to New Frontiers – Proceedings of the 7th Petroleum Geology Conference*, 633–644. DOI: 10.1144/0070633 © Petroleum Geology Conferences Ltd. Published by the Geological Society, London.

wells from two key areas to illustrate how AFTA provides independent timing constraints on the onset of exhumation, followed by a brief review of results from other areas. We then synthesize this information to show that major phases of exhumation show a broad synchroneity across wide areas of the Arctic in three key time intervals, viz. Paleocene, Latest Eocene and Miocene–Pliocene. We then briefly discuss possible underlying mechanisms, and the resulting implications for hydrocarbon exploration. However, first we present a brief outline of the methods employed.

Thermal history reconstruction using AFTA and VR

Constraints on the magnitude and timing of exhumation episodes have been defined using thermal history reconstruction based on integrated application of AFTA and VR data (e.g. Green *et al.* 2004; Japsen *et al.* 2007). Application of AFTA in sedimentary basins allows determination of the maximum palaeotemperature attained by an individual rock sample from a sedimentary unit, and the time at which the sample cooled from that palaeotemperature. Multiple cooling episodes can often be resolved from data in individual samples. VR data allow complementary determinations of the maximum post-depositional palaeotemperatures of individual sedimentary units.

Extraction of thermal history information from AFTA and VR data begins by construction of a Default Thermal History, which is the history that can be reconstructed based on the preserved stratigraphic section and present-day thermal regime. Because the responses of both the AFTA and VR systems are dominated by maximum temperature, if the measured parameters can be explained purely by the Default Thermal History (possibly combined with the presence of shorter tracks inherited from sediment provenance regions), then no further information on the post-depositional thermal history can be extracted from the data. However, if the AFTA data show a greater degree of fission track annealing, and/or if VR values are higher than predicted from the Default Thermal History, then the sampled unit has been hotter in the past. In this case, information on the timing and magnitude of the palaeothermal maximum can be extracted from the data, by forward modelling of AFTA parameters through a range of likely thermal history scenarios, to define the range of conditions that match the measured values within 95% confidence limits. More details of factors which determine precision and accuracy of the resulting estimates are provided by Green *et al.* (2002).

Combination of the two methods, with AFTA data from sandstones and VR data from fine-grained units, allows data to be gathered over as wide a range of section as possible, allowing definition of the variation of palaeotemperatures with depth in key palaeothermal episodes. The slope of these palaeotemperature profiles then provides quantitative estimates of the range of allowed palaeogeothermal gradients, and extrapolation of the fitted linear profiles to an appropriate palaeosurface temperature provides definition of the corresponding amounts of additional section required to produce the observed palaeotemperatures in each episode. For further examples of this approach and practical details, see for example Green *et al.* (2004), Japsen *et al.* (2005) and Turner *et al.* (2008). It is emphasized that this approach is totally data-driven, and is independent of any assumptions or theoretical considerations regarding basin formation and tectonic processes.

Wherever possible, additional constraints on the magnitude of removed section are sought from methods based on sediment compaction, such as sonic velocities or porosity (e.g. Holford *et al.* 2005; Japsen *et al.* 2007). Consistency between amounts of removed section determined from palaeothermal (i.e. AFTA and VR) and palaeoburial methods (sonic velocities) provides evidence of exhumation that can be regarded as highly reliable.

Exhumation histories in the Barents Sea

The Barents Sea forms a broad offshore shelf to the north of the Norwegian mainland, containing significant thicknesses of dominantly Late Palaeozoic and Mesozoic sedimentary units in a mosaic of basins and platforms (Doré 1995). Further details of the regional geology and stratigraphy are provided by, for example, Faleide *et al.* (1993) and Gabrielsen *et al.* (1997). Cenozoic exhumation across the Barents Sea is widely recognized. Cavanagh *et al.* (2006) provided an extensive review of published studies, illustrating the wide diversity of opinions as to both the timing and magnitude of exhumation.

The main reason for the wide disparity of views regarding the timing of exhumation is that few studies actually employ methods which constrain the timing directly. Instead, most studies have been based on assumed timings derived from ideas regarding the nature of the underlying processes. Many studies favour a dominant phase of Late Pliocene to Pleistocene exhumation, based on the presence of marginal sedimentary wedges and perceived mechanisms of erosion related to glaciation (e.g. Nyland *et al.* 1992; Riis & Fjeldskaar 1992; Cavanagh *et al.* 2006).

Here we review AFTA and VR data from the 7120/9-2 well, located in the Hammerfest Basin (Fig. 1). The well encountered *c*. 60 m of Pliocene to Quaternary section, separated by an unconformity from *c*. 700 m of Paleocene to Eocene section, which in turn unconformably overlies *c*. 840 m of Hauterivian to Santonian section. Further unconformities separate *c*. 50 m of Kimmeridgian section, *c*. 130 m of Pliensbachian to Bajocian section, and *c*. 2970 m of Upper Permian to Hettangian section, and the well reached total depth (TD) in Upper Permian section at a depth of 5072 m (rkb). A present-day geothermal gradient of 30.1°C/km was derived from corrected BHT data, using a sea-bed temperature of 5°C.

Results from this well form part of a larger (unpublished) study, and are typical of those from other wells in the Hammerfest Basin. AFTA parameters from the 7120/9-2 well are plotted against depth in Figure 2a, where they are compared with trends predicted from the default burial history (derived from the preserved section in this well and the present-day thermal regime described above). These trends define the patterns of fission track age and mean track length that would be expected if units throughout this well are currently at their maximum post-depositional palaeotemperatures.

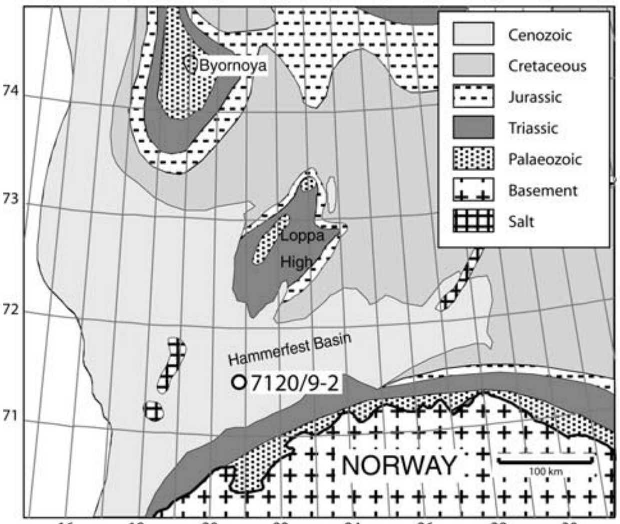

Fig. 1. Simplified geology of the Barents Sea, showing the location of the 7120/9-2 well. Generalized pre-Quaternary subcrop geology after Nøttvedt *et al.* (1993).

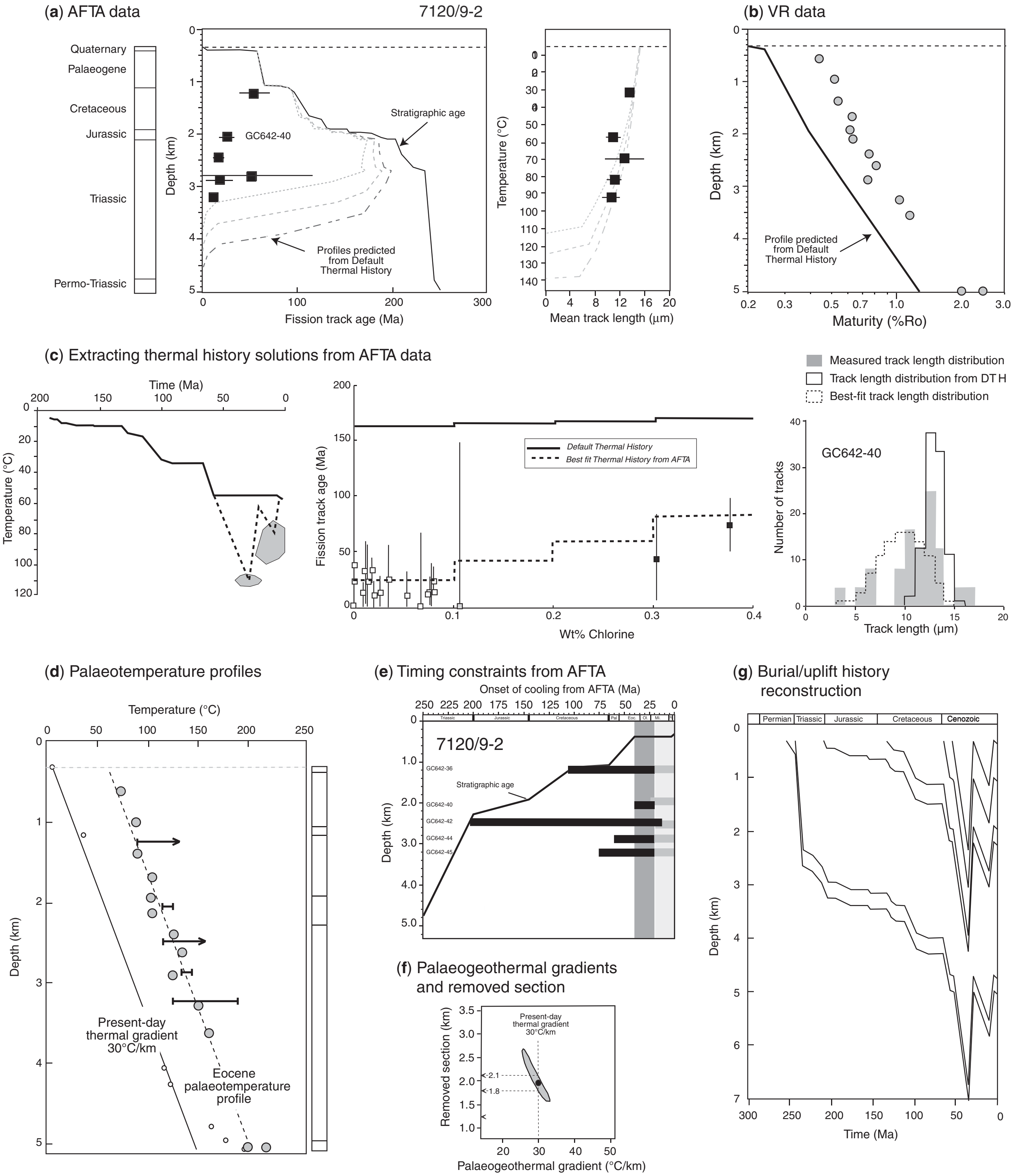

Fig. 2. AFTA and VR data in 7120/9-2, illustrating the process of burial history reconstruction. (**a**) AFTA parameters plotted against depth and compared with predictions of the Default Thermal History. A stratigraphic column is shown on the left, and the variation of stratigraphic age through the section is shown in the central panel. (**b**) VR data, also plotted against depth and compared with the profile predicted from the Default Thermal History. (**c**) Quantitative assessment of the AFTA data in sample GC642-40 shows that two episodes of heating and cooling in addition to the Default Thermal History are required to explain all aspects of the data. (**d**) Maximum post-depositional palaeotemperatures derived from AFTA and VR data in this well define a linear profile, sub-parallel to the present-day temperature profile and offset to higher temperatures by *c*. 60 °C. This is diagnostic of heating due to deeper burial, with little or no change in heat flow. Results from a later episode as shown in (e) have been omitted for clarity. (**e**) AFTA data in all samples define two major episodes of cooling, which began in the intervals 40–20 Ma and 20–0 Ma. (**f**) Variation of palaeotemperatures with depth as shown in (d) allow definition of the range of allowed values (within 95% confidence limits) of palaeogeothermal gradient and removed section, as shown by the hyperbolic elliptical shaded region. Constraints on the later episode are much broader and are not shown. (**g**) Integration of the palaeothermal episodes with the preserved stratigraphic section results in reconstruction of the history of post-Early Eocene burial and subsequent exhumation. The option illustrated here, with all Eocene section removed and a further 1 km or so of Oligocene to Early Miocene section deposited prior to the final phase of exhumation, represents one end-member of a range of viable solutions.

The measured fission track ages are all much younger than predicted from the Default Thermal History scenario, showing that the sampled units have been hotter than the present-day temperatures at some time since deposition.

The measured fission track ages show the characteristic pattern of a section that has been significantly hotter in the past (Green *et al.* 2002), with a rapid decrease at shallow depths and a break in slope (at around 2 km) denoting the transition from partial to total annealing of tracks formed prior to the onset of cooling. Fission track ages around 20 Ma below the break in slope show that these samples have only retained tracks since cooling to sufficiently low temperatures in the mid-Cenozoic. However, these ages do not directly date the onset of cooling, because tracks formed after cooling have been reduced in length (mean lengths are *c.* 12 μm in these samples, Fig. 2a) due to the prevailing temperatures. Nevertheless, this initial, qualitative assessment of the AFTA data from the 7120/9-2 well shows quite clearly that the section in this well began to cool from palaeotemperatures considerably higher than present-day temperatures at some time in the mid-Cenozoic.

Quantitative assessment of the data, including the fission track age and track length data and their variation with chlorine content in each sample (following principles outlined by Green *et al.* 2002), allows extraction of thermal history solutions from the AFTA data. This process is illustrated in Figure 2c, based on AFTA data in sample GC642-40, collected from depths between 1980 and 2130 m (rkb) in Early Jurassic section. Two episodes of heating and cooling in addition to the Default Thermal History are required to explain the AFTA data in this sample. Synthesis of AFTA data in all samples from this well (Fig. 2e) results in definition of two dominant episodes of cooling, beginning in the intervals 40–20 Ma (Eocene to Early Miocene) and 20–0 Ma (Early Miocene to Recent). Note that such estimates of the onset of cooling from AFTA refer to the 95% confidence interval within which cooling *began*, and we do not imply that cooling was restricted to this interval.

VR data are plotted against depth in Figure 2b, where they are compared with the profile predicted from the Default Thermal History. Measured VR values are consistently higher than predicted from the Default Thermal History, confirming that the sampled units have been hotter at some time after deposition. Note particularly that this well contains a significant thickness of Paleocene to Early Eocene section (see stratigraphic column and variation of stratigraphic age with depth in Fig. 2), and VR values from this sequence plot well above the profile predicted from the Default Thermal History and define a consistent trend with deeper values, showing that cooling from the palaeothermal maximum post-dates deposition of the Early Eocene section.

Palaeotemperatures characterizing the earlier of the two episodes identified from AFTA, and the independent estimates of maximum post-depositional palaeotemperature derived from the VR data, are highly consistent (Fig. 2e) and define a linear depth profile, subparallel to the present-day temperature profile and offset to higher temperatures by *c.* 60 °C. This is a clear signature of heating due dominantly to deeper burial by additional section (Bray *et al.* 1992) with cooling due mainly to subsequent removal of this additional section by uplift and erosion (exhumation). Palaeotemperatures characterizing the Early Miocene to Recent episode are less clearly defined in this well, but a similar interpretation is inferred on the basis of results in other wells (Geotrack, unpublished results). The onset of cooling in both episodes identified from AFTA, between 40 and 20 Ma and between 20 and 0 Ma, falls within the time interval represented by the unconformity in this well between Early Eocene and Quaternary sedimentary units (Fig. 2), which is also consistent with this style of interpretation.

Figure 2f shows the range of values of palaeogeothermal gradient and additional burial ('removed section') consistent with the Eocene–Early Miocene palaeotemperatures in this well within 95% confidence limits (using methods outlined e.g. by Bray *et al.* 1992; Green *et al.* 2002). The present-day thermal gradient of *c.* 30°C/km falls towards the centre of the allowed range of palaeogradients, and corresponds to between 1.8 and 2.1 km of additional section, assuming a constant surface temperature of 5°C. Importantly, the constraints in Figure 2f show that palaeogeothermal gradients higher than *c.* 33°C/km are not compatible with the results from this well, and scenarios involving significantly elevated basal heat flow can therefore be ruled out. Constraints on the more recent episode are less well defined, but for a constant palaeogeothermal gradient are consistent with between 0.25 and 1.35 km of additional burial at the palaeothermal peak between 20 and 0 Ma. Thus, the AFTA data in this well suggest a history involving little or no significant change in heat flow with time, with around 2 km of additional section deposited on top of the youngest preserved Early Eocene section, and subsequently removed in two episodes of exhumation.

Note that the constant surface temperature adopted for this study represents a convenient simplification, and it is possible that higher or lower values may be more appropriate for each episode. The magnitude of removed section required to explain the observed palaeotemperatures can be easily adjusted by subtracting or adding the difference in depth equivalent to the change in palaeosurface temperature, for the appropriate palaeogeothermal gradient. Increasing the palaeosurface temperature by 10°C, for a palaeogeothermal gradient of 30°C/km, would require a reduction of 333 m in the amount of removed section needed to explain the observed palaeotemperatures.

As already noted, both episodes of cooling identified in this well began during the interval represented by the unconformity between Earliest Eocene and Quaternary units (Fig. 2). Because AFTA and VR define only the maximum palaeotemperatures in the Eocene to Early Miocene episode and the peak palaeotemperatures in the Early Miocene to Recent episode, and not the

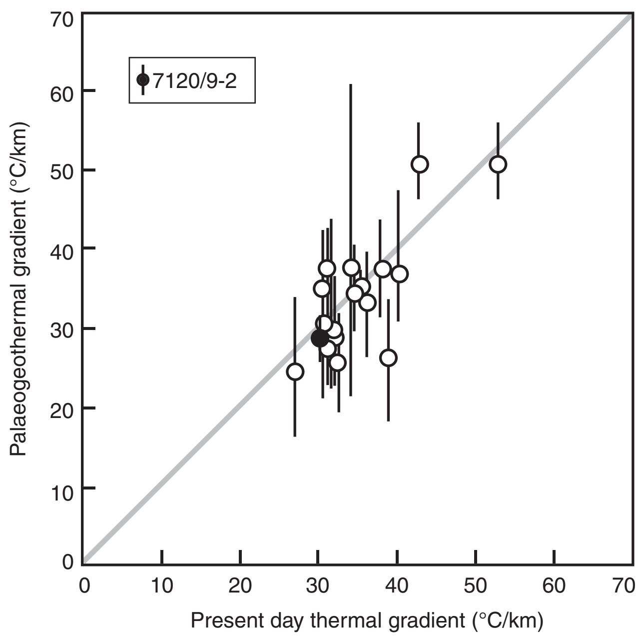

Fig. 3. Paleocene and Eocene palaeogeothermal gradients derived from AFTA and VR data in a number of Barents Sea wells, plotted against present-day thermal gradient. These results provide strong evidence for an explanation of the observed heating expressed in the AFTA and VR data in terms of deeper burial, with little or no change in heat flow.

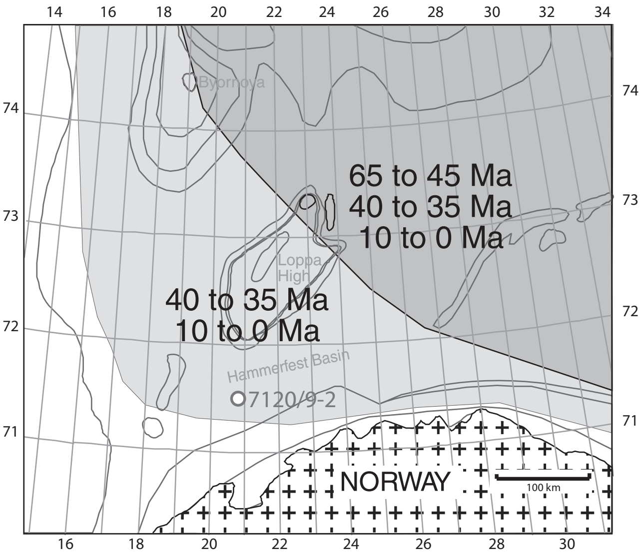

Fig. 4. Summary of areas of the Barents Sea dominated by different Cenozoic exhumation episodes.

intervening history, it is not possible to delineate the total amount of section removed in the Eocene–Early Miocene episode, because of the lack of constraint on the degree of reburial before the re-commencement of cooling (exhumation) from the Miocene to Recent palaeothermal peak. In this context, the estimates of 'removed section' shown in Figure 2 are better considered as estimates of 'additional burial' at the time that cooling in each episode began. That is, the quoted values refer to the amount by which the present unconformity horizon was more deeply buried at the onset of each cooling episode.

The final burial/uplift history reconstruction for the 7120/9-2 well is shown in Figure 2g. In this reconstruction, all of the additional section deposited prior to Latest Eocene cooling is removed and a further 1 km of Oligocene–Miocene section is deposited prior to the onset of Late Miocene exhumation. On the basis of the above discussion, this represents one end-member of a range of viable styles of Late Cenozoic uplift and erosion, with the other end-member being removal of around half of the additional Eocene section in the Latest Eocene episode, with the remainder removed in the Late Miocene episode.

Similar burial/uplift histories to that shown for the 7120/9-2 well in Figure 2g have been identified in a number of wells from the region, while other wells also show evidence of an earlier episode of Paleocene cooling (Geotrack, unpublished results). Combining evidence from all wells in the Barents Sea in which data are available shows that all results can be described in terms of three dominant episodes of Cenozoic cooling, beginning in the intervals 65–55 Ma (Paleocene), 40–30 Ma (Eocene–Oligocene) and 10–5 Ma (Late Miocene). As shown in Figure 3, palaeogeothermal gradients in each of these episodes are very close to present-day gradients, showing no evidence to suggest any significant variation of basal heat flow throughout the Cenozoic.

Figure 4 summarizes unpublished results from a number of wells across the Barents Sea region, distinguishing between those regions where Cenozoic exhumation began in the Paleocene and those characterized by an onset of exhumation in Eocene–Oligocene times. Paleocene exhumation dominates the NE of the region, where Palaeogene sediments are not present, while in the SE, Cenozoic exhumation began in the Eocene–Oligocene, following deposition of the Palaeogene sedimentary units in that region. However, Eocene–Oligocene exhumation is also recognized in the NE, and this episode together with Late Miocene exhumation are recognized across the entire region. It seems likely that the Palaeogene sediments present in the SW of the region represent the erosional products of the Paleocene erosion recognized in the AFTA data from the NE.

With data from all Barents Sea wells pointing to a most recent phase of major cooling/exhumation beginning in the interval 10–5 Ma (above), no results from the Barents Sea region show any evidence for significant amounts of cooling beginning within the last few million years that could be attributed to glacial action, as suggested in many earlier studies as discussed earlier. This is not to say that there has been no significant exhumation in this region in Late Pliocene to Recent times, and significant uplift and erosion at this time is indicated by Pliocene to Pleistocene sediment fans to the west of the shelf break (e.g. Cavanagh *et al.* 2006). However, any exhumation/cooling over this period is clearly negligible compared with that achieved in earlier events, and is not recorded in the AFTA data.

Exhumation histories from the North Slope Alaska

While the mountains of the Brooks Range, Alaska, display obvious contractional deformation and present-day high relief, indicating major Cenozoic denudation (e.g. O'Sullivan *et al.* 1997), the adjacent North Slope region is characterized by low relief at the present day. Nevertheless, numerous studies of the North Slope have provided abundant evidence of widespread Cenozoic exhumation across the region (e.g. Johnsson *et al.* 1993; Burns *et al.* 2005),

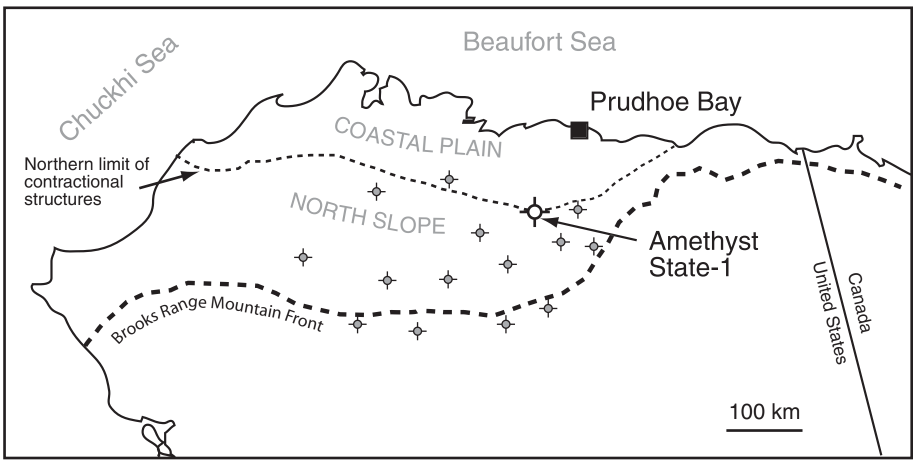

Fig. 5. Location map of the North Slope of Alaska, showing the Amethyst State-1 well, together with other wells from which results are synthesized here. Structural features are taken from figure 1 of Houseknecht & Bird (2005).

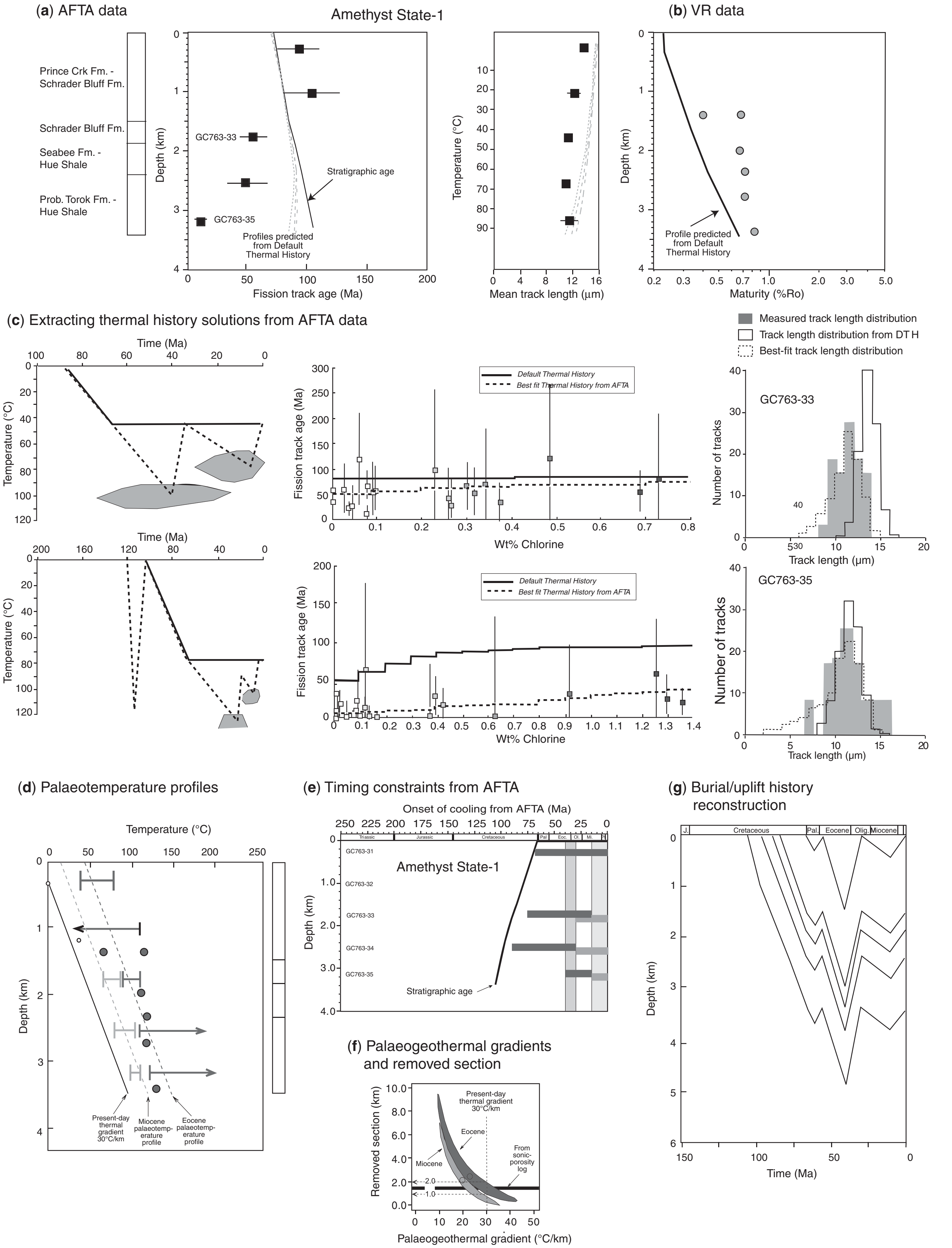

Fig. 6. AFTA and VR data in the Amethyst State-1 well, Alaska. All details are as in Figure 2. The Default Thermal History employed in construction of this figure is based on a thermal gradient below base permafrost of 30°C/km, as indicated by the AFTA data.

with amounts of section removed increasing from north to south across the region towards the Brooks Range fold-and-thrust belt. Bird & Molenaar (1992) provide a detailed review of the regional geological framework. Previous apatite fission track studies in the region (O'Sullivan *et al.* 1993; O'Sullivan 1996, 1999) have shown that exhumation began in Paleocene times, between 64 and 56 Ma, while also suggesting at least three later episodes of exhumation beginning at *c.* 45, 40–30 and 28–22 Ma (again quoting the *onset* of exhumation in each episode).

Here we discuss AFTA and VR data from the Amethyst State-1 well (Fig. 5). Again, results from this well form part of a wider (unpublished) study, and are typical of results from other wells in the immediate vicinity. The Amethyst State-1 well intersected Colville Group sediments of Cretaceous (Campanian to Albian) age, containing no recognized unconformities, and reached a total depth of 3394.5 m. A present-day geothermal gradient of 38°C/km from base permafrost at a depth of 304.8 m was estimated from corrected BHT values, but this was revised to 30°C/km on the basis of the AFTA data. Summary AFTA parameters in samples from this well are plotted against depth in Figure 6a (all details being similar to those for well 7120/9-2 in Fig. 2). Fission track ages in two shallower samples are greater than the respective depositional ages, suggesting only relatively mild post-depositional heating in these samples, but mean track lengths are significantly less than predicted from the Default Thermal History. Measured fission track ages in the three deepest samples are significantly less than predicted from the Default Thermal History. Thus, initial qualitative assessment of these data shows that all five have been hotter than present-day temperatures at some time since deposition.

Detailed analysis of the AFTA data in the five samples from this well results in definition of two major cooling episodes (Fig. 6c, e). Synthesis of data from all samples analysed from this well shows that cooling from maximum post-depositional palaeotemperatures began at some time between 40 and 30 Ma (Eocene–Oligocene), while cooling from a later palaeothermal peak began between 15 and 0 Ma (Miocene–Recent). VR data from this well, plotted against depth in Figure 6b, all plot above the profile predicted from the Default Thermal History, again confirming that the sampled units have been hotter in the past. Maximum palaeotemperatures derived from these VR data are highly consistent with the Eocene–Oligocene palaeotemperatures derived from AFTA data (Fig. 6e) and the combined constraints define a linear profile, sub-parallel to the present-day temperature profile and offset to higher temperatures by *c.* 40°C. Again, this is a clear signature of heating due dominantly to deeper burial by additional section (Bray *et al.* 1992) with cooling due mainly to subsequent removal of this additional section by uplift and erosion (exhumation).

While these palaeotemperatures allow quite a range of palaeogeothermal gradients (Fig. 6f), due largely to the relatively small number of VR values in this well, the present-day thermal gradient of 30°C/km falls well within the range of allowed palaeogradients, and corresponds to between 1000 and 2000 m of additional section, removed since the onset of cooling between 40 and 30 Ma. Miocene to Recent palaeotemperatures result in much broader constraints on the amount of additional section present at the Miocene to Recent palaeothermal peak, but again assuming a constant thermal gradient, the results suggest a value between 250 and 650 m. The resulting burial/uplift history reconstruction for the well is shown in Figure 6g.

Whereas results from the Amethyst State-1 well show that exhumation at the location of this well began between 40 and 30 Ma, results from our wider (unpublished) study in other wells across the region show that, to the west, exhumation began earlier, at around 60 Ma (consistent with earlier studies, as reviewed above), while the two episodes identified in the Amethyst State-1 well are recognized in wells across the region. Synthesis of all data defines three major episodes of exhumation which began in the intervals 60–50, 40–35 and 15–10 Ma. The magnitude of

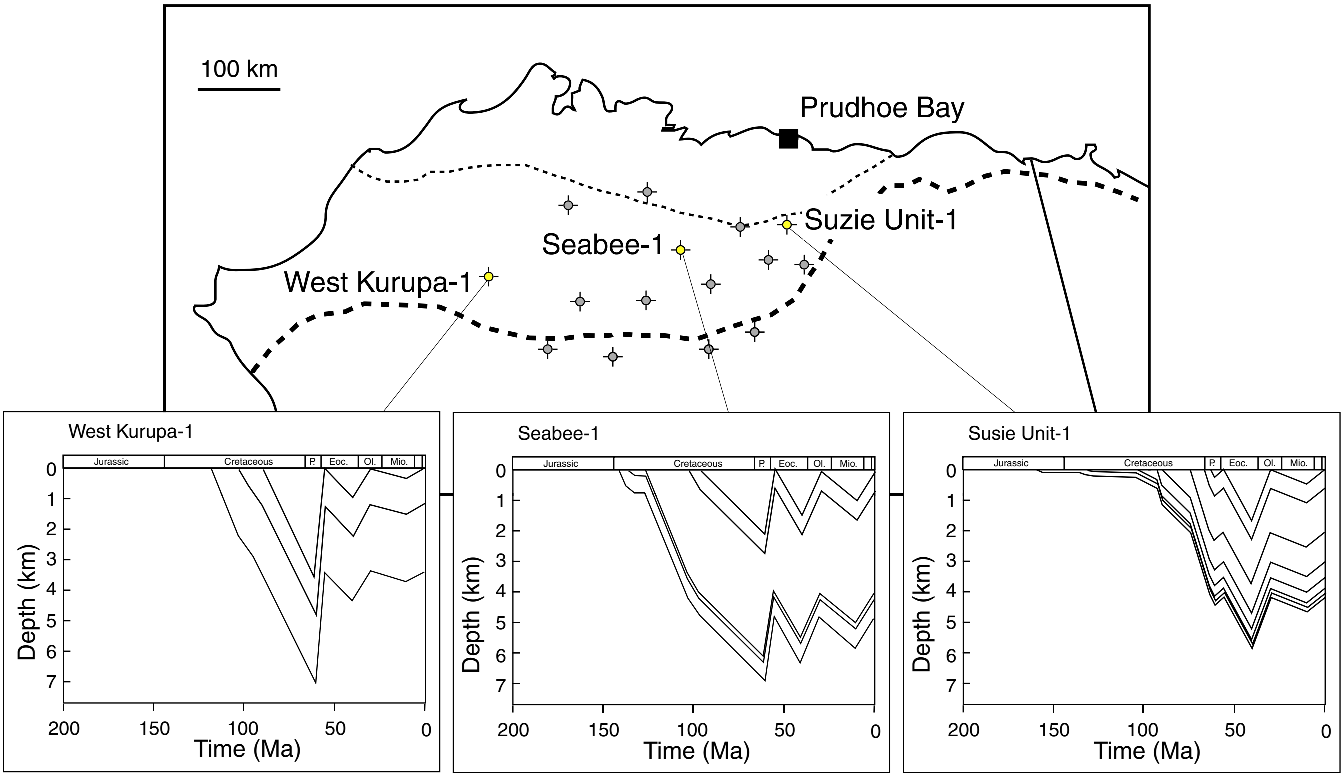

Fig. 7. Variation in burial/uplift history styles across the Alaskan North Slope. From west to east, the magnitude of Paleocene exhumation decreases, such that in wells located to the east, the onset of exhumation from maximum burial depths began in the Eocene episode. Structural elements as in Figure 5.

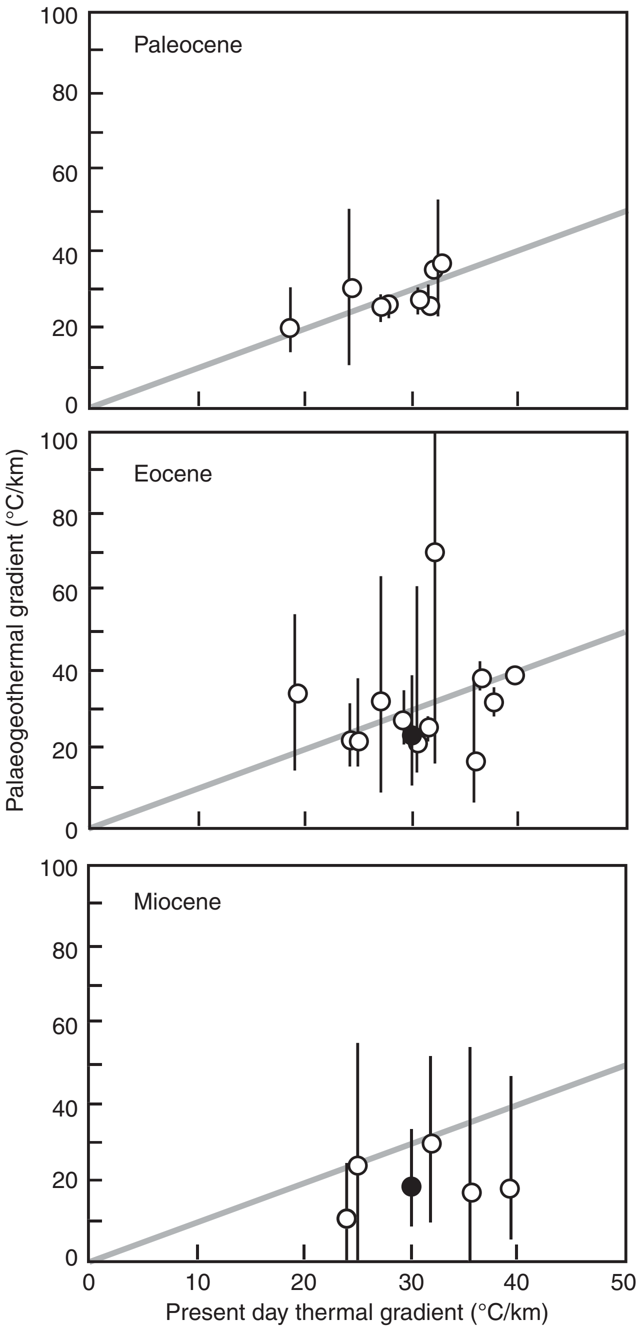

Fig. 8. Paleocene, Eocene and Miocene palaeogeothermal gradients derived from AFTA and VR data in a number of North Slope Alaska wells (locations shown in Fig. 6), plotted against present-day thermal gradient. Values for the Amethyst State-1 well are shown with black symbols. These results provide strong evidence for an explanation of the observed heating expressed in the AFTA and VR data in terms of deeper burial, with little or no change in heat flow.

the Paleocene event shows a general increase to the west, as illustrated in Figure 7, towards the northward extension of the Brooks Range deformation front.

While the constant thermal gradient option adopted here for the Amethyst State-1 well is only one of a range of scenarios that would be allowed by the AFTA and VR data, results from other wells in the vicinity of the Amethyst State-1 well show a high degree of consistency between palaeogeothermal gradients and present-day thermal gradients in all three episodes (Fig. 8), and show no suggestion of elevated heat flow at any time. We therefore regard this scenario as the most realistic style of reconstruction for wells of the Alaskan North Slope.

Note that the estimated amount of additional section derived from AFTA and VR data in this well (between 1000 and 2000 m) is highly consistent with the value of 1486 m (4875 ft) estimated from porosity–depth relationships in this well by Burns *et al.* (2005), as illustrated in Figure 6f. This consistency suggests that the reconstruction provided for this well can be regarded with some confidence. Burns *et al.* (2005) suggested that VR data are ‘demonstrably unreliable predictors of amounts of exhumation’, compared with sonic-porosity methods and AFTA. We suggest that this perceived problem with VR data is related mainly to problems with data quality and analytical approach, rather than representing an inherent shortcoming of the technique. As discussed in detail elsewhere (Green *et al.* 2002, 2004), analysis of VR using the methods recommended by the International Committee on Coal and Organic Petrography (www.iccop.org), based on identification of indigenous vitrinite in polished thick rock sections, invariably provides results which are consistent with AFTA data from adjacent samples, and generates reliable indications of amounts of additional burial.

Other areas

A number of published studies have reported evidence of Cenozoic exhumation in Arctic regions. Arne *et al.* (2002) reported evidence based on apatite fission track data for Paleocene exhumation across the Sverdrup Basin of Arctic Canada, with an onset of exhumation in the range 65–60 Ma or perhaps earlier in some places.

Blythe & Kleinspehn (1998) reported evidence from apatite fission track data in Svalbard for three discrete phases of cooling, with the earliest beginning in the interval 70–50 Ma with further phases at *c.* 35 and 5 Ma. While their data provided no direct constraints on palaeogeothermal gradients and the mechanisms of heating and cooling, Blythe & Kleinspehn (1998) interpreted their three cooling episodes as all representing periods of exhumation, with the two earliest linked to tectonic influences – the most recent episode resulting from climate deterioration. The timing of these events is consistent with our own (unpublished) results from outcrops on Svalbard. AFTA data in samples of Mesozoic and Palaeozoic sedimentary units define cooling in the intervals 65–45 and 10–0 Ma, while samples of Paleocene sandstones began to cool from their maximum post-depositional palaeotemperatures in the 50–35 Ma interval and also show evidence of later cooling in the 10–0 Ma interval.

Green *et al.* (2005) reported evidence from AFTA for exhumation beginning in the interval 60–40 Ma in the Mackenzie Valley of the Northwest Territory of Canada, as well as a later phase in the last 15 Ma. Because data across much of this region are dominated by initial exhumation in the Jurassic (190–170 Ma) during a period of elevated heat flow, resolution of the detail of the Cenozoic exhumation history is less well defined than in other areas. Based on data from Alaska and the other areas discussed here, it seems likely that three Cenozoic episodes also affected this region.

AFTA and VR data from the Gro-3 well in the Nuussuaq Basin, West Greenland (Japsen *et al.* 2005), reveal a major phase of exhumation in this region which began in the interval 40–30 Ma, with subsequent episodes which began between 11 and 10 Ma and between 7 and 2 Ma. It is notable that this region shows no evidence of a Paleocene phase of exhumation, although there is evidence of latest Cretaceous to earliest Cenozoic uplift in the region from incised valleys that were filled by latest Maastrichtian sediments which later underwent sub-aerial erosion, prior to burial beneath overlying Palaeogene flood basalts. Japsen *et al.* (2009) subsequently showed using AFTA that Eocene–Oligocene exhumation also affected the basement region adjacent to the Nuussuaq basin, with the onset of exhumation refined to the interval 36–30 Ma. Again, dominance of earlier episodes in the AFTA

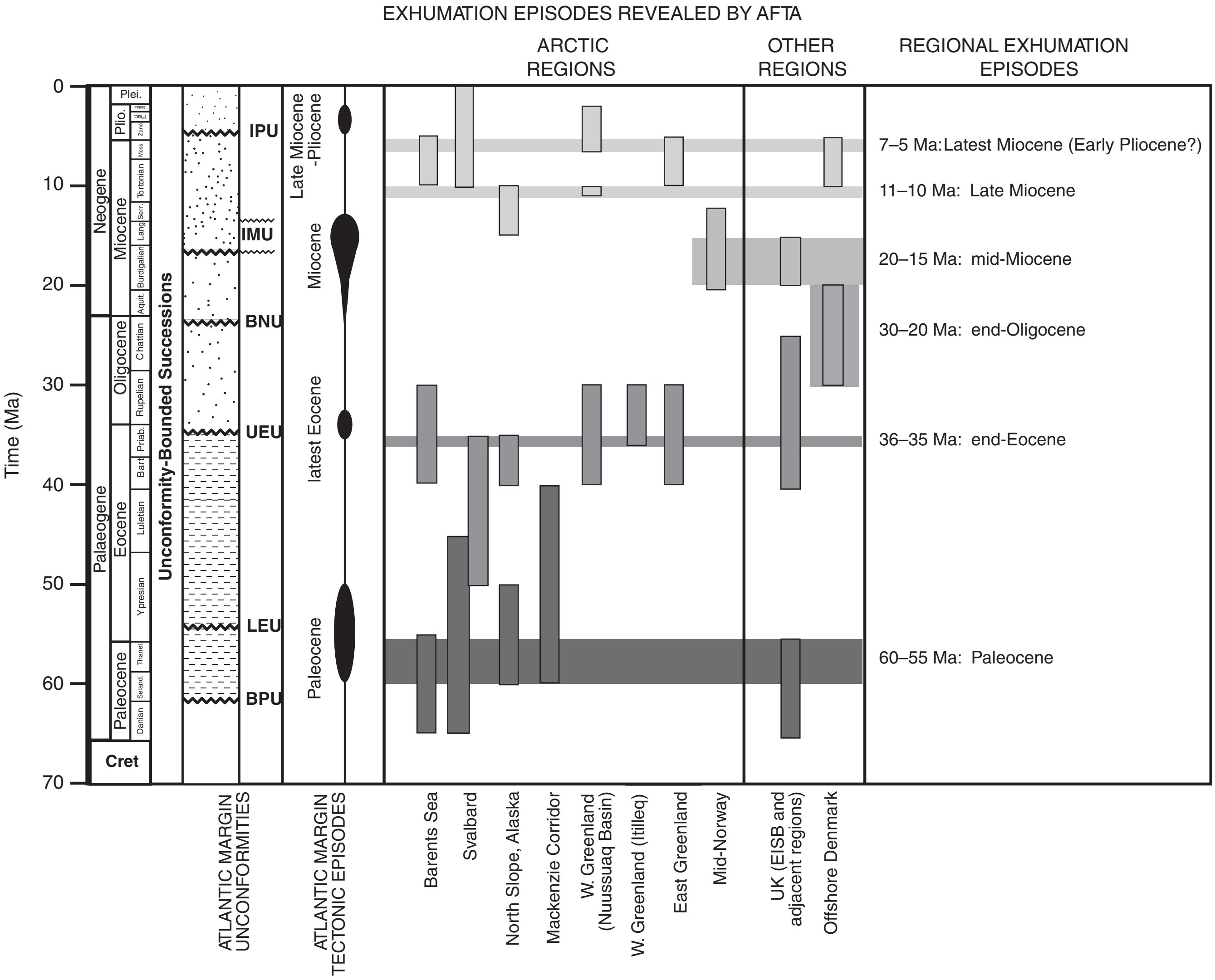

Fig. 9. Timing constraints on Cenozoic episodes of exhumation identified from AFTA and VR data in a number of regions across the Arctic and North Atlantic region, as discussed here, not only show a regional consistency between themselves (horizontal bars) but also correlate with regional unconformities defined along the Atlantic margin and to major episodes of tectonism (Praeg *et al.* 2005; Stoker *et al.* 2005). This emphasizes that these episodes of exhumation are controlled by regional processes acting on the scale of tectonic plates, rather than being due to local processes. References to results from individual areas are provided in the text. Note only results from our own studies are shown here, to ensure consistency of approach.

data from this region precludes resolution of any later cooling episodes.

A number of thermal history studies in East Greenland have provided important insights into the exhumation history of Mesozoic and Palaeozoic sediments of the Jamesonland Basin and NE Greenland, as well as adjacent basement terrains. Thomson *et al.* (1999) reported two episodes of Cenozoic cooling, based on AFTA data in a series of outcrop samples from Traill Island, which began between 40 and 30 Ma (Eocene–Oligocene) and between 10 and 5 Ma (Late Miocene). While this later episode was interpreted as due to uplift and erosion related to a change in the North Atlantic spreading vector, the origin of the Eocene–Oligocene cooling was not immediately clear, because the timing for the onset of cooling closely matches the timing of syenite intrusions at Kap Parry and Kap Simpson (*c.* 35 Ma). Thomson *et al.* (1999) suggested that hydrothermal circulation, deeper burial prior to exhumation (uplift and erosion) or elevated basal heat flow (or some combination of the three) provided viable alternative mechanisms for the Eocene–Oligocene palaeotemperatures.

Johnson & Gallagher (2000) reported apatite fission track data in a series of samples of Carboniferous sandstone from a vertical section on Clavering Island and found that the section began to cool from maximum post-depositional palaeotemperatures at *c.* 274 Ma (Early Permian), with subsequent cooling episodes at *c.* 206, 140 and 23 Ma. Johnson & Gallagher (2000) interpreted these cooling episodes largely in terms of denudation involving removal of several kilometres of section, but suggested that Cenozoic palaeothermal effects could be related, at least in part, to Palaeogene volcanic activity. Although the section sampled by Johnson & Gallagher (2000) is overlain by Palaeogene sediments and basalts, their analysis failed to take full account of this basic constraint on the thermal history of the sequence and this may explain the mismatch between their preferred onset of Cenozoic cooling and the other studies described above.

Hansen *et al.* (2001) reported results of an extensive regional apatite fission track study of the Jamesonland Basin and adjacent regions, and interpreted their results to reflect a complex interplay between deeper burial prior to Cenozoic exhumation, circulation of hot fluids associated with Mid-Cenozoic intrusive activity, and locally elevated heat flow associated with the intrusive activity. Hansen *et al.* (2001) favoured an onset of exhumation at *c.* 55 Ma in the south of the basin, and 'before 25 Ma' in the north. However, preservation of fission track ages in excess of

200 Ma in relatively close proximity to much younger ages, together with significant variations in VR levels over short distances, suggest that regional Cenozoic heating is relatively minor in this region, and that local heating effects dominate the data. We believe that all evidence suggests that any Palaeogene palaeothermal effects in this area are due either to contact heating from the widespread minor intrusions of this age or associated hydrothermal effects (or both). Based on a compilation of all available data, we conclude that the main phase of Cenozoic exhumation in East Greenland began in the interval 40–30 Ma, and continued through possibly several later episodes, some of which appear to vary in magnitude across the region.

Regional synchroneity of exhumation episodes, and underlying mechanisms

Figure 9 illustrates the timing of the exhumation episodes discussed in preceding sections (showing results from our own studies only, for consistency), within the context of the synthesis of key tectonic events along the North Atlantic margin and regional unconformities from Stoker *et al.* (2005) and Praeg *et al.* (2005), together with the timing of major episodes of intra-plate exhumation recognized in the UK by Holford *et al.* (2009). It is clear from Figure 9 that many of these exhumation episodes display a broad regional synchroneity (within the limits of uncertainty on the timing from AFTA across a wide region), while other events appear to be more restricted in extent.

Results from Alaska, Arctic Canada and the Barents Sea all show consistent evidence for major cooling which began in the Paleocene, with all results consistent with an onset of cooling due to exhumation in the interval 60–55 Ma (Late Paleocene). Results from a large area of the UK presented by Holford *et al.* (2009) also define a major period of exhumation at this time. As illustrated in Figure 9, this timing correlates with a period of pronounced tectonic activity affecting the North Atlantic region (Praeg *et al.* 2005), as well as the Arctic, as expressed for example by the Eurekan Orogeny (De Paor *et al.* 1989; Harland 1997).

Results from all the areas showing Paleocene cooling (above), as well as West and East Greenland, also show evidence for cooling which began at around 36–35 Ma (Latest Eocene). Again, the timing of this episode shows a close correlation with Latest Eocene tectonism in the North Atlantic, as expressed by the Upper Eocene Unconformity recognized by Stoker *et al.* (2005). Cooling at a similar time was again recognized in the UK region by Holford *et al.* (2009).

In contrast, the timing of the most recent exhumation episodes in Alaska, the Barents Sea and Greenland does not show the degree of consistency shown by the two earlier episodes. However, results from most areas are consistent with exhumation beginning in the 7–5 Ma interval (Fig. 9), which is very close to the timing of the 'Intra-Pliocene Unconformity' ('IPU' in Fig. 9) defined by Stoker *et al.* (2005). Results from a number of wells onshore and offshore Denmark (Japsen *et al.* 2007) also record this Late Miocene episode (Fig. 9). Japsen *et al.* (2007) suggested that the slight mismatch between the onset of exhumation from AFTA and the stratigraphically defined timing may be due to an anomalous result in one sample in their study, but the results shown in Figure 9 confirm the slight mismatch, which remains unresolved. Results from West Greenland and Alaska define an additional, slightly earlier episode, which is particularly well defined in the Gro-3 well from West Greenland (Japsen *et al.* 2005). These results appear to indicate further episodes of Miocene cooling, which either have not as yet been recognized in the stratigraphic record or else are of only local extent. Further work is required in order to resolve this uncertainty.

AFTA data from the Felicia-1 and Hans-1 wells, Offshore Denmark (Japsen *et al.* 2007), also define a period of Late Oligocene to Early Miocene (30–20 Ma) exhumation. Japsen *et al.* (2007) correlated this episode with the 'base-Neogene Unconformity' defined by Stoker *et al.* (2005), indicated by 'BNU' in Figure 9. Similarly, results from the UK (Holford *et al.*

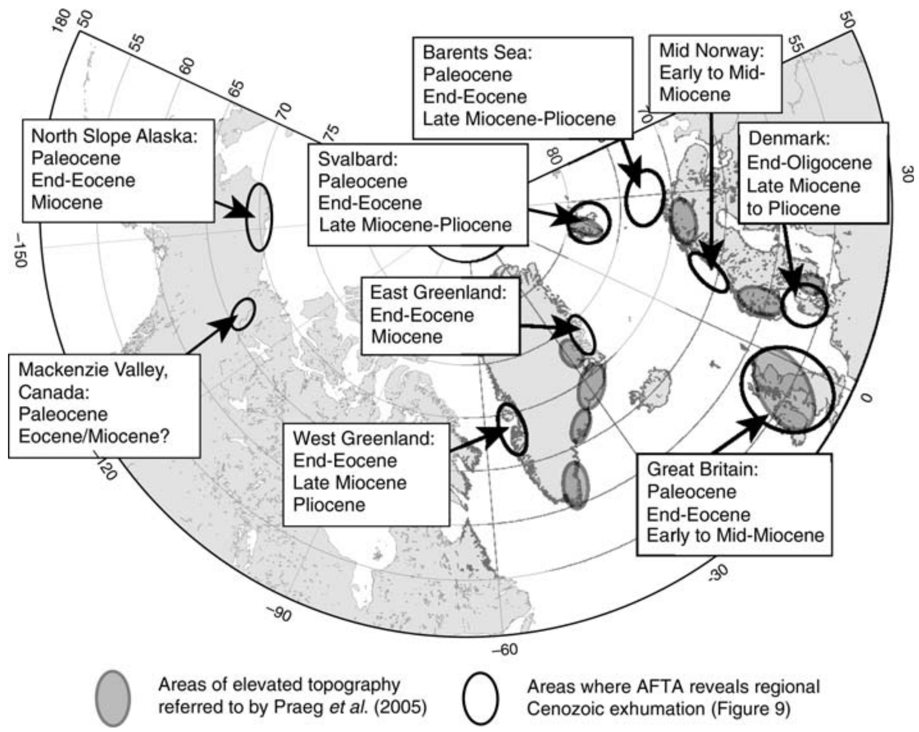

Fig. 10. Areas displaying Cenozoic exhumation with timing displayed in Figure 9 are highlighted, emphasizing the regional nature of these events. Also shown are regions of present-day elevated topography around the North Atlantic region discussed by Praeg *et al.* (2005). The mismatch between areas of exhumation and the modern topography emphasizes that the latter provides only limited insight into the extent of Cenozoic exhumation.

2009) define a Mid-Miocene onset of cooling (20–15 Ma) which correlates with the Intra-Miocene unconformity (IMU in Fig. 9). Cooling at this time is also identified in AFTA data from wells along the Mid-Norway margin (Green *et al.* 2007).

While it is beyond the scope of the present paper to provide a detailed synthesis of regional tectonic events across the Arctic, Figure 9 emphasizes that the timing of exhumation episodes identified across a wide area of the Arctic and North Atlantic not only shows a close correlation from region to region but also correlates with regional unconformities identified by Praeg *et al.* (2005) and Stoker *et al.* (2005) as reflecting major tectonic events affecting adjacent plate boundaries. While the true nature of the underlying processes remains as yet unknown, Figure 9 provides strong evidence that each of these exhumation episodes represents part of a regional response to plate boundary events, possibly as a result of compressive intra-plate stresses transmitted from plate boundaries. Similar observations have been made in other parts of the world, for example by Cobbold *et al.* (2001), who pointed out that episodes of Cretaceous to Cenozoic exhumation affecting the Atlantic margin of Brazil correlate closely in time with three prominent phases of Andean orogeny, representing periods of rapid convergence at the Andean margin of South America.

Regional extent of Cenozoic exhumation episodes

Figure 10 illustrates those areas where the effects of Paleocene, Eocene and Miocene exhumation have been identified to date. While data coverage is relatively sparse on the scale of Figure 10, these apparently synchronous episodes have clearly been recognized over a wide region, and it is likely that as further results become available these episodes will become increasingly familiar. The regional extent of these Cenozoic exhumation episodes suggests that the controlling processes act on a plate scale.

Note that the areas affected by these episodes show little correspondence with regions of high modern-day topography. Praeg *et al.* (2005) presented a description of the European North Atlantic margin characterized by a series of topographic highs resulting from two main episodes of Cenozoic uplift, accompanied by subsidence of offshore basins. The results of this study show that this picture is over-simplistic, and that many areas that now form offshore basins, as well as the onshore highs, have undergone multiple episodes of Cenozoic uplift and erosion, as reflected in the exhumation histories described here. Thus, the differentiation between topographic highs and basins of deposition depicted by figure 2 of Praeg *et al.* (2005) simply reflects the present-day setting, and holds only limited clues to earlier episodes of uplift and erosion that have affected wide areas through the Cenozoic (further discussion on the relationship between Cenozoic exhumation and modern topography is provided by Japsen *et al.* 2010). Again, the nature of the underlying processes remains uncertain, due in large part to the fact that in previous studies the effects of multiple episodes of uplift and erosion have not been recognized. The timing constraints on exhumation episodes established by AFTA and complementary methods, as summarized here, provide a rigorous framework within which a more complete understanding of the processes affecting these regions can be achieved.

Implications for hydrocarbon prospectivity

The exhumation episodes identified in this study, together with the corresponding prior burial, exert critical control on regional hydrocarbon prospectivity in many areas, including the Barents Sea, the Sverdrup Basin and both west and east Greenland. A fundamental issue in these and other exhumed basins is that maturity levels are considerably higher than expected on the basis of current burial depths. In these areas, the main phase of hydrocarbon generation took place during deeper burial prior to the onset of exhumation, and generation effectively ceased when exhumation began. One important outcome in relation to prospectivity is that traps formed as a result of the uplift which initiated exhumation were not present during generation and only earlier structures will have been available for charging. Subsequent episodes of uplift and erosion may have led to redistribution of any hydrocarbons trapped in those early structures, while phase changes as a result of the reduction in pressure during exhumation will favour preservation of gas and condensate over oil at the present day. Possible breaching of seals during exhumation is another key factor that must be taken into account.

The relative magnitude of the individual episodes clearly varies across the Barents Sea and the Alaskan North Slope, and in some parts of each region the Paleocene palaeothermal episode is of lesser magnitude than that of the Eocene–Oligocene episode, which represents the palaeothermal maximum (and hence the termination of hydrocarbon generation) in these areas. This implies that the later maturation in areas dominated by Eocene–Oligocene effects can produce hydrocarbons to charge structures formed during the Paleocene episode. With factors such as this crucial in the preservation of hydrocarbons to the present day, a detailed understanding of the magnitude and timing of exhumation is essential in order to ensure further discoveries in these exhumed basins.

References

Arne, D. C., Grist, A. M., Zentilli, M., Collins, M., Embry, A. & Gentzis, T. 2002. Cooling of the Sverdrup Basin during Tertiary basin inversion: implications for hydrocarbon exploration. *Basin Research*, **14**, 183–205.

Bird, K. J. & Molenaar, C. M. 1992. The North Slope foreland basin, Alaska. *In*: Macqueen, R. W. & Leckie, D. A. (eds) *Foreland Basins and Fold Belts*. American Association of Petroleum Geologists, Tulsa, OK, Memoirs, **55**, 363–393.

Blythe, A. & Kleinspehn, K. L. 1998. Tectonically versus climatically driven Cenozoic exhumation of the Eurasian plate margin, Svalbard: fission track analyses. *Tectonics*, **17**, 621–639.

Bray, R. J., Green, P. F. & Duddy, I. R. 1992. Thermal history reconstruction using apatite fission track analysis and vitrinite reflectance: a case study from the UK East Midlands and the Southern North Sea. *In*: Hardman, R. F. P. (ed.) *Exploration Britain: Into the Next Decade*. Geological Society, London, Special Publications, **67**, 3–25.

Burns, M., Hayba, D. O., Rowan, E. L. & Houseknecht, D. W. 2005. Estimating the amount of eroded section in a partially exhumed basin from geophysical well logs: an example from the North Slope. USGS Geological Survey Profession Paper **1732-D**.

Cameron, T. D. J., Crosby, A., Balson, P. S., Jeffrey, D. H., Lott, G. K., Bulat, J. & Harrison, D. J. 1992. *United Kingdom Offshore Regional Report: The Geology of the Southern North Sea*. British Geological Survey, London.

Cavanagh, A. J., Di Primio, R., Scheck-Wenderoth, M. & Horsfield, B. 2006. Severity and timing of Cenozoic exhumation in the southwestern Barents Sea. *Journal of the Geological Society, London*, **163**, 761–774.

Cobbold, P. R., Meisling, K. & Mount, V. S. 2001. Reactivation of an obliquely rifted margin, Campos and Santos basins, southeastern Brazil. *American Association of Petroleum Geologists Bulletin*, **85**, 1925–1944.

De Paor, D. G., Bradley, D. C., Eisenstadt, G. & Phillips, S. M. 1989. The Arctic Eurekan Orogeny: a most unusual fold-and-thrust belt. *Bulletin of the Geological Society of America*, **101**, 952–967.

Doré, A. G. 1995. Barents Sea geology, petroleum resources and commercial potential. *Arctic*, **48**, 207–221.

Doré, A. G., Corcoran, D. V. & Scotchman, I. C. 2002. Prediction of the hydrocarbon system in exhumed basins, and application to the NW European margin. *In*: Doré, A. G., Cartwright, J., Stoker, M. S., Turner, J. P. & White, N. (eds) *Exhumation of the North Atlantic Margin: Timing, Mechanisms and Implications for Petroleum Exploration*. Geological Society, London, Special Publications, **196**, 331–354.

Faleide, J. I., Vagnes, E. & Gudlaugsson, S. T. 1993. Late Mesozoic–Cenozoic evolution of the southwestern Barents Sea. *In*: Parker, J. R. (ed.) *Petroleum Geology of Northwest Europe: Proceedings of the 4th Conference*. Geological Society, London, 993–950; doi: 10.1144/0040993.

Gabrielsen, R. H., Grunnaleite, I. & Rasmussen, E. 1997. Cretaceous and tertiary inversion in the Bjørnøyrenna fault complex, southwestern Barents Sea. *Marine and Petroleum Geology*, **14**, 165–178.

Green, P. F., Crowhurst, P. V. & Duddy, I. R. 2004. Integration of AFTA and (U-Th)/He thermochronology to enhance the resolution and precision of thermal history reconstruction in the Anglesea-1 well, Otway Basin, SE Australia. *In*: Boult, P. J., Johns, D. R. & Lang, S. C. (eds) *Eastern Australian Basins Symposium II*. Petroleum Exploration Society of Australia, Special Publications, 117–131.

Green, P. F., Duddy, I. R. & Hegarty, K. A. 2002. Quantifying exhumation from apatite fission-track analysis and vitrinite reflectance data: precision, accuracy and latest results from the Atlantic margin of NW Europe. *In*: Doré, A. G., Cartwright, J., Stoker, M. S., Turner, J. P. & White, N. (eds) *Exhumation of the North Atlantic Margin: Timing, Mechanisms and Implications for Petroleum Exploration*. Geological Society, London, Special Publications, **196**, 331–354.

Green, P. F., Duddy, I. R., Japsen, P. & Holford, S. P. 2007. Synchronous regional kilometre-scale Late Cenozoic exhumation events around the North Atlantic region (extended abstract). *ICAM V Conference*, Tromso.

Green, P. F., Duddy, I. R., Slind, L., Calverley, F. & Rayer, F. 2005. Multiple paleo-thermal episodes in Mackenzie Corridor, NWT, Canada revealed by THR: implications for hydrocarbon prospectivity (extended abstract). *AAPG Meeting*, Calgary.

Hansen, K., Bergman, S. C. & Henk, B. 2001. The Jameson Land basin (East Greenland): a fission track study of the tectonic and thermal evolution in the Cenozoic North Atlantic spreading regime. *Tectonophysics*, **331**, 307–339.

Harland, W. B. 1997. *The Geology of Svalbard*. Geological Society, London, Memoirs, **17**.

Holford, S. P., Green, P. F., Duddy, I. R., Turner, J. P., Hillis, R. R. & Stoker, M. S. 2009. Regional intraplate exhumation episodes related to plate boundary deformation. *Bulletin of the Geological Society of America*, **121**, 1611–1628.

Holford, S. P., Green, P. F. & Turner, J. P. 2005. Palaeothermal and compaction studies in the Mochras borehole (NW Wales) reveal early Cretaceous and Neogene exhumation and argue against regional Paleogene uplift in the southern Irish Sea. *Journal of the Geological Society, London*, **162**, 829–840.

Houseknecht, D. W. & Bird, K. J. 2005. *Oil and gas resources of the Arctic Alaska petroleum province*. Geological Society of America, Boulder, CO, Professional Papers, **1732-A**.

Jackson, D. I., Jackson, A. A., Evans, D., Wingfield, R. T. R., Barnes, R. P. & Arthur, M. J. 1995. *United Kingdom Offshore Regional Report: The Geology of the Irish Sea*. British Geological Survey, London.

Japsen, P., Bonow, J. M., Green, P. F., Chalmers, J. A. & Lidmar-Bergström, K. 2009. Formation, uplift and dissection of planation surfaces at passive continental margins – a new approach. *Earth Surface Processes and Landforms*, **34**, 683–699.

Japsen, P. J., Green, P. F., Bonow, J. M., Rasmussen, E. S., Chalmers, J. A. & Kjennerud, T. 2010. Episodic uplift and exhumation along North Atlantic passive margins: implications for hydrocarbon prospectivity. *In*: Vining, B. A. & Pickering, S. C. (eds) *Petroleum Geology: From Mature Basins to New Frontiers – Proceedings of the 7th Petroleum Geology Conference*. Geological Society, London, 979–1004; doi: 10.1144/0070979.

Japsen, P., Green, P. F. & Chalmers, J. A. 2005. Separation of Palaeogene and Neogene uplift on Nuussuaq, West Greenland. *Journal of the Geological Society, London*, **162**, 299–314.

Japsen, P., Green, P. F., Nielsen, L. H., Rasmussen, E. S. & Bidstrup, T. 2007. Mesozoic-Cenozoic exhumation in the eastern North Sea Basin: a multi-disciplinary study based on palaeo-thermal, palaeoburial, stratigraphic and seismic data. *Basin Research*, **19**, 451–490.

Johnson, K. & Gallagher, K. 2000. A preliminary Mesozoic and Cenozoic denudation history of the North East Greenland onshore margin. *Global and Planetary Change*, **24**, 303–309.

Johnsson, M. J., Howell, D. G. & Bird, K. J. 1993. Thermal maturity patterns in Alaska: implications for tectonic evolution and hydrocarbon potential. *AAPG Bulletin*, **77**, 1874–1903.

Logan, P. & Duddy, I. R. 1998. An investigation of the thermal history of the Ahnet and Reggane Basins, Central Algeria, and the consequences for hydrocarbon generation and accumulation. *In*: MacGregor, D. S., Moody, R. T. & Clark-Lowes, D. D. (eds) *Petroleum Geology of North Africa*. Geological Society, London, Special Publications, **132**, 131–155.

Magnavita, L. P., Davison, I. & Kusznir, N. J. 1994. Rifting, erosion, and uplift history of the Reconcavo-Tucano-Jatoba Rift, northeast Brazil. *Tectonics*, **13**, 367–388.

Nøttvedt, A., Cecchi, M. *et al*. 1993. Svalbard-Barents Sea correlation: a short review. *In*: Vorren, T. O., Bergsager, E., Dahl-Stammes, Ø. A., Holter, E., Johansen, B., Lie, E. & Lund, T. B. (eds) *Arctic Geology and Petroleum Potential*. Norwegian Petroleum Society, Trondheim, Special Publications, **2**, 363–375.

Nyland, B., Jensen, L. N., Skagen, J., Skarpnes, O. & Vorren, T. 1992. Tertiary uplift and erosion in the Barents Sea: magnitude, timing and consequences. *In*: Larsen, R. M., Brekke, H., Larsen, B. T. & Talleraas, E. (eds) *Structural and Tectonic Modelling and its Application to Petroleum Geology*. Norwegian Petroleum Society, Trondheim, Special Publications, **1**, 153–162.

O'Sullivan, P. B. 1996. Late Mesozoic and Cenozoic thermotectonic evolution of the Colville Basin, North Slope, Alaska. *In*: Johnsson, M. J. & Howell, D. G. (eds) *Thermal Evolution of Sedimentary Basins in Alaska*. US Geological Survey, Reston, VA, Bulletins, **2142**, 45–79.

O'Sullivan, P. B. 1999. Thermochronology, denudation and variations in paleo-surface temperature: a case study from the North Slope foreland basin, Alaska. *Basin Research*, **11**, 191–204.

O'Sullivan, P. B., Green, P. F., Bergman, S. C., Decker, J. U., Duddy, I. R., Gleadow, A. J. W. & Turner, D. L. 1993. Multiple phases of Tertiary uplift and erosion in the Arctic National Wildlife Refuge, Alaska, revealed by apatite fission track analysis. *AAPG Bulletin*, **77**, 359–385.

O'Sullivan, P. B., Murphy, J. M. & Blythe, A. E. 1997. Late Mesozoic and Cenozoic thermotectonic evolution of the central Brooks Range and adjacent North Slope foreland basin, Alaska: including fission track results from the Trans-Alaska Crustal Transect (TACT). *Journal of Geophysics Research*, **102**, 20 821–20 845.

Praeg, D., Stoker, M. S., Shannon, P. M., Ceramicola, S., Hjelstuen, B. O., Laberg, J. S. & Mathiesen, A. 2005. Episodic Cenozoic tectonism and the development of the NW European 'passive' continental margin. *Marine and Petroleum Geology*, **22**, 977–1005.

Riis, F. & Fjeldskaar, W. 1992. On the magnitude of the late Tertiary and Quaternary erosion and its significance for the uplift of Scandinavia and the Barents Sea. *In*: Larsen, R. M., Brekke, H., Larsen, B. T. & Talleraas, E. (eds) *Structural and Tectonic Modelling and its Application to Petroleum Geology*. Norwegian Petroleum Society, Trondheim, Special Publications, **1**, 163–185.

Stoker, M. S., Praeg, D., Hjelstuen, B. O., Laberg, J. S., Nielsen, T. & Shannon, P. M. 2005. Neogene stratigraphy and the sedimentary and oceanographic development of the NW European Atlantic margin. *Marine and Petroleum Geology*, **22**, 977–1005.

Thomson, K., Green, P. F., Whitham, A. G., Price, S. P. & Underhill, J. R. 1999. New constraints on the thermal history of North-East Greenland from apatite fission-track analysis. *Geological Society of America Bulletin*, **111**, 1054–1068.

Turner, J. P., Green, P. F., Holford, S. P. & Lawrence, S. R. 2008. Thermal history of the Rio-Muni (West Africa)–NE Brazil margins during continental breakup. *Earth and Planetary Science Letters*, **270**, 354–367.

Offset and curvature of the Novaya Zemlya fold-and-thrust belt, Arctic Russia

R. A. SCOTT,[1] J. P. HOWARD,[1] L. GUO,[1] R. SCHEKOLDIN[2] and V. PEASE[3]

[1]*CASP, Department of Earth Sciences, University of Cambridge, West Building, 181A Huntingdon Road, Cambridge CB3 0DH, UK (e-mail: robert.scott@casp.cam.ac.uk)*

[2]*Department of Historical and Dynamic Geology, St Petersburg State Mining Institute, House 2, 21 Line, 199106 St Petersburg, Russia*

[3]*Department of Geology & Geochemistry, Stockholm University, 104 05 Stockholm, Sweden*

Abstract: The Novaya Zemlya archipelago contains a predominantly west-vergent fold-and-thrust belt that separates two contrasting hydrocarbon basins with enigmatic subsidence histories. On the foreland side is the deep depression of the eastern Barents Shelf that hosts the Shtokman gas condensate discovery; on the hinterland side is the South Kara Basin, an offshore continuation of the gas-dominated northern West Siberian Basin. Much of the compressional deformation recorded in Novaya Zemlya appears to have been later than the onset of subsidence in adjacent basins, and may therefore be expected to have had a potentially significant influence on hydrocarbon systems within them. Two characteristics of Novaya Zemlya immediately stand out on any topographic map: the *c*. 600 km westward offset compared with the remainder of the Uralian Orogen and the plan-view curvature (convex towards the Barents Shelf). Any regional tectonic model developed for the Novaya Zemlya fold-and-thrust belt must be able to explain these first-order features, and a wide range of mechanisms, geometries and timings has been proposed in the literature. However, as far as we are aware, there has been no previous attempt to link the geometry of structures on the archipelago with a potential mechanism that explains their curvature in plan view. Using field observations, information on geological maps and interpretation of satellite imagery, we demonstrate the link between structural geometries in Novaya Zemlya and the basins of the adjacent eastern Barents Shelf. We find no evidence to support previous interpretations of the fold-and-thrust belt as an orocline (bending of an originally straight deformation belt) or a far-travelled thin-skinned allochthon, and conclude that the offset from the remainder of the Uralian Orogen is a primary feature that results from an original embayment on the margin of Baltica.

Keywords: tectonics, Novaya Zemlya, Barents Shelf, Russia, Arctic, fold-and-thrust belt, orogeny

A continuous belt of compressional deformation can be traced from the Aral Sea in Kazakhstan, northwards along the linear Ural mountain chain and then curving eastward through the Russian Arctic toward the edge of the Arctic Ocean in eastern Taimyr (Fig. 1). The overall cause of this deformation was the collision of the Siberia and Kazakhstan palaeocontinents with the Baltica margin of Euramerica (Laurussia) (e.g. Hamilton 1970; Zonenshain *et al.* 1984; Ziegler 1988, 1989), one of the final stages in the construction of Pangea. Most of the deformation took place in Late Palaeozoic time and is attributed to the Uralian Orogeny (Puchkov 1997), with contemporaneous granitic magmatism present in the Ural mountains (Montero *et al.* 2000) and in Taimyr (Vernikovsky *et al.* 1995). For the most part, this deformation belt does not display any abrupt changes in plan-view orientation. However, the Novaya Zemlya archipelago is the exception to this rule. When viewed on a large-scale map, two first-order characteristics of Novaya Zemlya immediately stand out: its westward offset of *c*. 600 km from the general trend of the orogen and its curvature (convex towards the Barents Shelf) (Fig. 1). An explanation for these features is the principal concern of this contribution.

Previous studies have adopted two contrasting hypotheses.

(1) Novaya Zemlya was originally aligned with the remainder of the Uralian orogen, such that the offset and curvature of Novaya Zemlya must result from late-stage displacement events during orogeny (i.e. Novaya Zemlya was transported *c*. 600 km westward during deformation). This mechanism implies significant relative movement between Novaya Zemlya and adjacent crustal blocks to the north and south.

(2) Novaya Zemlya was always offset relative to the remainder of the Uralian orogen owing to a specific characteristic of the pre-collisional continental margin, such as the presence of an embayment. This mechanism requires no relative movement between Novaya Zemlya and adjacent crustal blocks during deformation.

In the first category of model (i.e. those that explain offset and curvature to be a consequence of displacement events during orogeny), the orocline hypothesis is one of the earliest; Carey (1955) used Novaya Zemlya as an example in his development of the orocline concept, in which an initially straight orogen is subsequently bent around a vertical axis to create curvature, implying a two-stage deformation process. Hamilton (1970) proposed a variant of the orocline concept in which the *c*. 90° bend between Novaya Zemlya and Pai Khoi was an oroclinal fold, but the connection between northern Novaya Zemlya and Taimyr was a strike-slip fault. Mezhvilk (1995) suggested that both margins of the Novaya Zemlya block were strike-slip faults and that Novaya Zemlya had been emplaced NW relative to the remainder of the Uralides. In the same year, Otto & Bailey (1995) published an interpretation in which Novaya Zemlya was originally part of a continuous linear Uralian Orogen that was transported NW during Triassic time as a gravity-driven, thin-skinned allochthon bounded by strike-slip faults. The mechanism proposed by Otto & Bailey has remained influential in subsequent tectonic interpretations (e.g. O'Leary *et al.* 2004; Torsvik & Cocks 2004; Gee *et al.* 2006). Some authors (e.g. Zonenshain *et al.* 1990; Metelkin *et al.* 2005 and references therein) have suggested that the North Kara

VINING, B. A. & PICKERING, S. C. (eds) *Petroleum Geology: From Mature Basins to New Frontiers – Proceedings of the 7th Petroleum Geology Conference*, 645–657. DOI: 10.1144/0070645

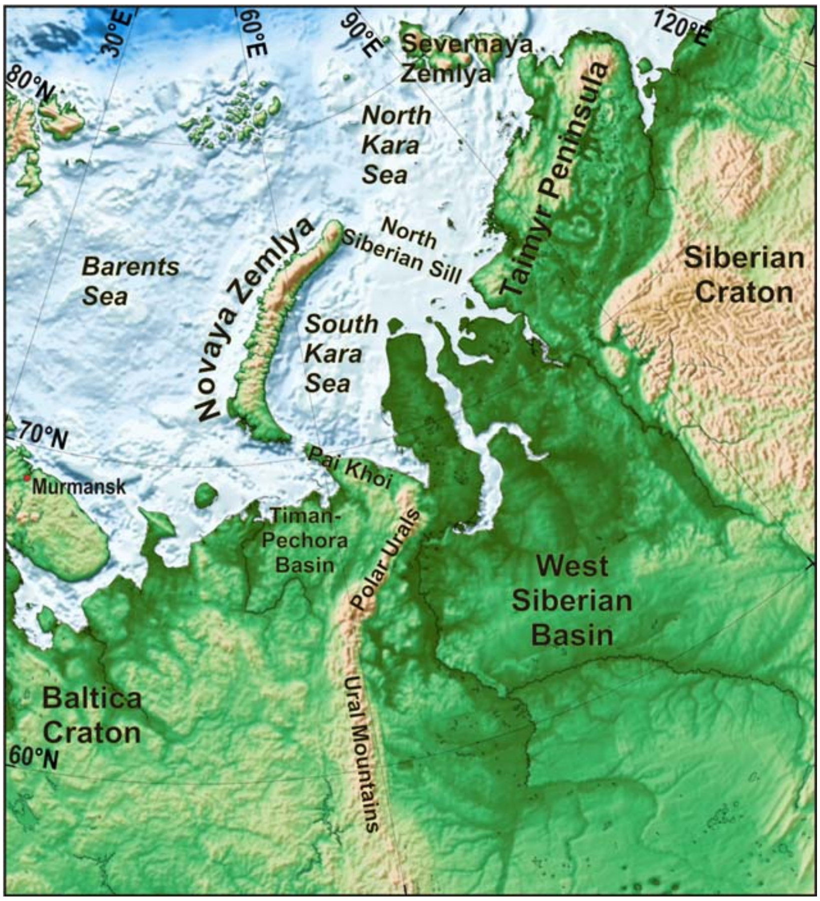

Fig. 1. Topography of northern Russia showing the curvature of the Novaya Zemlya archipelago (convex towards the Barents Shelf) and its offset with respect to the Urals and Taimyr.

region (comprising northern Taimyr, Severnaya Zemlya and the northern Kara Sea) was an independent crustal block, named the North Kara Terrane or Kara Massif, thus complicating the collisional history between Baltica and Siberia in the Arctic.

In the second category of model (i.e. those in which a pre-collisional embayment on the continental margin of Baltica predetermines offset and curvature), the interpretations of Ustritsky (1985) and Ziegler (1988, 1989) are the principal examples. Ustritsky (1985) proposed that a segment of oceanic crust became trapped in the South Kara Basin region, although the absence of specific tectonic information on his diagrams makes objective discussion of the subsequent deformation mechanism impossible. Ziegler (1988, 1989) depicted a pre-collisional embayment on the margin of Baltica, into which a promontory on the margin of Siberia (located in the Yamal Peninsula region) then entered during Uralian collision. This implies that a hinterland indenter was also involved in the creation of curvature. No strike-slip displacement along the margins of the embayment was depicted on Ziegler's palaeogeographic reconstructions during or after collision, although the Novaya Zemlya segment of the fold belt was depicted to propagate westward relative to the remainder of the Uralian Orogen during Permian to Early Triassic time.

In addition to identifying the mechanism(s) by which offset and curvature of Novaya Zemlya developed, we are also concerned with how the development of these features is related to the subsidence histories of adjacent basins. The fold-and-thrust belt in Novaya Zemlya is surrounded and, in part, overlain by some of the most important hydrocarbon basins in Russia (Barents Sea, Timan–Pechora, West Siberia, South Kara Sea). For the offshore basins in particular, many questions remain about the timing, magnitude and mechanism of subsidence. Furthermore, the relationship between extension and subsidence in these basins and the Novaya Zemlya compressional deformation zone that separates them is a significant issue.

In contrast to the predominantly Late Palaeozoic age of Uralian deformation elsewhere, the principal phase of compression in Novaya Zemlya is considered by the majority of authors to be Early Mesozoic (e.g. Korago *et al.* 1992). Stratigraphic relationships in adjacent basins and the preliminary results of our own fission track studies are consistent with this interpretation. An unresolved question in the literature, however, is whether the Early Mesozoic deformation is superimposed on earlier deformation of typical Late Palaeozoic Uralian age. Although we focus here specifically on the development of the fold-and-thrust belt, this research is part of a larger study seeking to develop a coherent tectonic model that links the Barents Shelf to the Kara Sea through Novaya Zemlya.

The South Kara Basin is generally considered to be a northward continuation of the West Siberian Basin, and began rifting in latest Permian to Early Triassic time, with a temporal, and potentially genetic, link to the eruption of the Siberian traps and/or cessation of Late Palaeozoic Uralian deformation (e.g. Hamilton 1970; Ziegler 1988, 1989; Şengör & Natal'in 1996; Allen *et al.* 2006; Vyssotski *et al.* 2006). However, this potential link with Late Palaeozoic orogenic collapse is more difficult to explain in the South Kara Basin if the main compressional deformation in Novaya Zemlya occurred in Late Triassic time (i.e. *c.* 50 Ma after the onset of subsidence).

The North and South Barents basins are characterized by successions approaching 20 km thick (see Fig. 6), of which around half are interpreted to be of Permo-Triassic age (e.g. Johansen *et al.* 1993). It is theoretically possible to model subsidence in these depocentres as the product of Permo-Triassic lithospheric extension alone (e.g. Corfield *et al.* 2006); however, this mechanism in isolation is considered to be an unlikely explanation of total subsidence because insufficient normal faults are visible on seismic reflection profiles to accommodate Permo-Triassic extension of the magnitude required. Additional subsidence is therefore required from pre-Permian rift events, and/or from some alternative subsidence mechanism. However, identifying any pre-Permian subsidence events on the eastern Barents Shelf, let alone constraining their timing and magnitude, is extremely difficult because the thick package of Permo-Triassic sediment masks underlying successions. It is logical to extrapolate information on pre-Permian Palaeozoic rift events from Timan–Pechora (e.g. O'Leary *et al.* 2004), but this inevitably relies on assumptions that are impossible to validate with current datasets. There are very few papers in which the relationship between Novaya Zemlya and the eastern Barents Shelf is directly addressed. Otto & Bailey (1995) concluded that Late Permian extension-driven subsidence in the eastern Barents Shelf produced the necessary gradient and gravitational instability to promote Late Triassic allochthonous emplacement of the Novaya Zemlya fold-and-thrust belt from an original position approximately 600 km further east. During this emplacement, the allochthonous thin-skinned thrust sheets overrode any foreland basin deposits, an argument used by O'Leary *et al.* (2004) to explain their modelled 1D subsidence data from the South Barents Basin.

No detailed database of structural measurements exists for Novaya Zemlya, nor is the collection of such a comprehensive dataset ever likely to be possible, considering the access restrictions to substantial portions of the archipelago, the permanent ice cap in the north and the deleterious effects of frost-shattering on many inland exposures in subdued terrain. However, using data collected during CASP expeditions to the south (2004) and north (2005) of the archipelago, interpretation of satellite images and published maps, and regional considerations, it is possible to draw some new conclusions concerning the origin of curvature and offset, and its significance for adjacent basins. As far as we aware there has been no previous attempt to link the geometry of structures on the archipelago with a potential mechanism that explains their curvature in plan view.

Curvature in fold-and-thrust belts: causes and classification schemes

Many fold-and-thrust belts have an element of curvature in plan view, and contain a distinctive pattern of structural trend lines (fault traces, fold axial plane traces and cleavage) within them – Novaya Zemlya represents a typical example. However, relatively few, if any, fold-and-thrust belts have been studied in sufficient detail for the processes involved in generating curvature to be unequivocally identified (Wezel 1986; Hindle & Burkhard 1999). It is clear that no single mechanism can explain all cases, and a number of genetic classification schemes for arcuate fold-and-thrust belts have been proposed (e.g. Marshak 1988, 2004; Ferrill & Groshong 1993; Hindle & Burkhard 1999; Macedo & Marshak 1999). Even in the most thoroughly studied examples (e.g. the Jura arc; Hindle & Burkhard 1999) where there is a comprehensive understanding of structural geometries and a substantial database of strain measurements with which to predict the precise trajectory of material during deformation, the mechanism by which the curvature developed is still controversial.

Hindle & Burkhard (1999) suggested a genetic classification scheme with three end-members identified on the basis of total strain patterns and displacement vector fields (Fig. 2). The end-members were: (1) oroclines (pure bending of an initially straight orogen, implying a two-stage process); (2) Piedmont glacier (divergent transport directions); (3) primary arcs (uniform transport direction). Identification of end-member categories based on displacement directions requires knowledge of the total strain distribution in a fold-and-thrust belt (or at least gradients in strain along- and across-strike) and such data are not available for Novaya Zemlya. However, our principal reason for citing Hindle & Burkhard (1999) is that they depicted Novaya Zemlya as an example of the 'orocline' end-member, reproducing illustrations from Carey (1955), that is, two-stage formation with bending of an originally straight Uralian Orogen about a vertical axis. This starting geometry was also proposed by Otto & Bailey (1995), although their model then invokes a different mechanism to generate offset and curvature. We therefore approach the problem of explaining the curvature of Novaya Zemlya, and its offset with respect to the remainder of the Uralian Orogen, with these previous hypotheses in mind.

The classification scheme employed by Macedo & Marshak (1999) and Marshak (2004) is similar to that proposed by Hindle & Burkhard (1999) and identifies two end-members: (1) rotational curves (equivalent to the orocline of Hindle & Burkhard 1999); and (2) non-rotational curves (equivalent to the primary arc of Hindle & Burkhard 1999) (Fig. 2). The Macedo & Marshak (1999) and Marshak (2004) classification is, however, more readily applied to Novaya Zemlya because it draws additionally on the information that can be obtained from plan-view patterns of structural trend lines (Fig. 3), without the need for detailed strain data.

The most common control on plan-view curvature in fold-and-thrust belts identified by Macedo & Marshak (1999) and Marshak (2004) was some geometric and/or mechanical property inherited from pre-existing sedimentary basins within the foreland of a fold-and-thrust belt, either acting alone or in combination. They referred to this type of curvature as 'basin controlled'. Properties of precursor sedimentary depocentres such as along-strike variations in the thickness of the deformed succession, critical-taper angle and angle of basal detachment determine the width of a fold-and-thrust belt for a given quantity of upper-crustal shortening (Fig. 3). The wider segments of the fold-and-thrust belt develop into salients (plan-view curves that are convex in the direction of tectonic transport; e.g. Aitken & Long 1978; Marshak & Wilkerson 1992; Marshak *et al.* 1992; Calassou *et al.* 1993; Boyer 1995; Mitra 1997; Macedo & Marshak 1999; Marshak 2004). Basin-controlled salients are characterized by structural trend lines that are more widely spaced at the apex than at the endpoints (Fig. 3). Thrusts are also commonly blind near the apex and emergent closer towards the endpoints, where deeper levels of the geology may be exposed. A further important characteristic of basin-controlled curves noted by Marshak (2004) is that structures are generally initiated as curves and do not involve oroclinal bending.

Of all these properties inherited from pre-existing sedimentary basins, the most significant appears to be along-strike change in the depth to detachment. In a study of fold-and-thrust belts worldwide, Macedo & Marshak (1999) noted a significant coincidence between salient apex location and pre-deformational depocentre position, implying that salients form where sediment thickness is greatest. The greater the sediment thickness, the greater the depth to detachment, and thus, for a given critical taper angle, the greater the width of the resulting fold-and-thrust belt, given the need to maintain volume balance (Fig. 3). The position of a depocentre may also coincide with a weaker basal detachment horizon compared with adjacent fold belt segments (e.g. because the lithology forming the detachment is thicker and/or more continuous in the basin). Where an underlying detachment is relatively weak, the critical taper angle decreases (Boyer 1995; Mitra 1997), forming wedges that can be transported further into the foreland than adjacent stronger rock masses for a given amount of

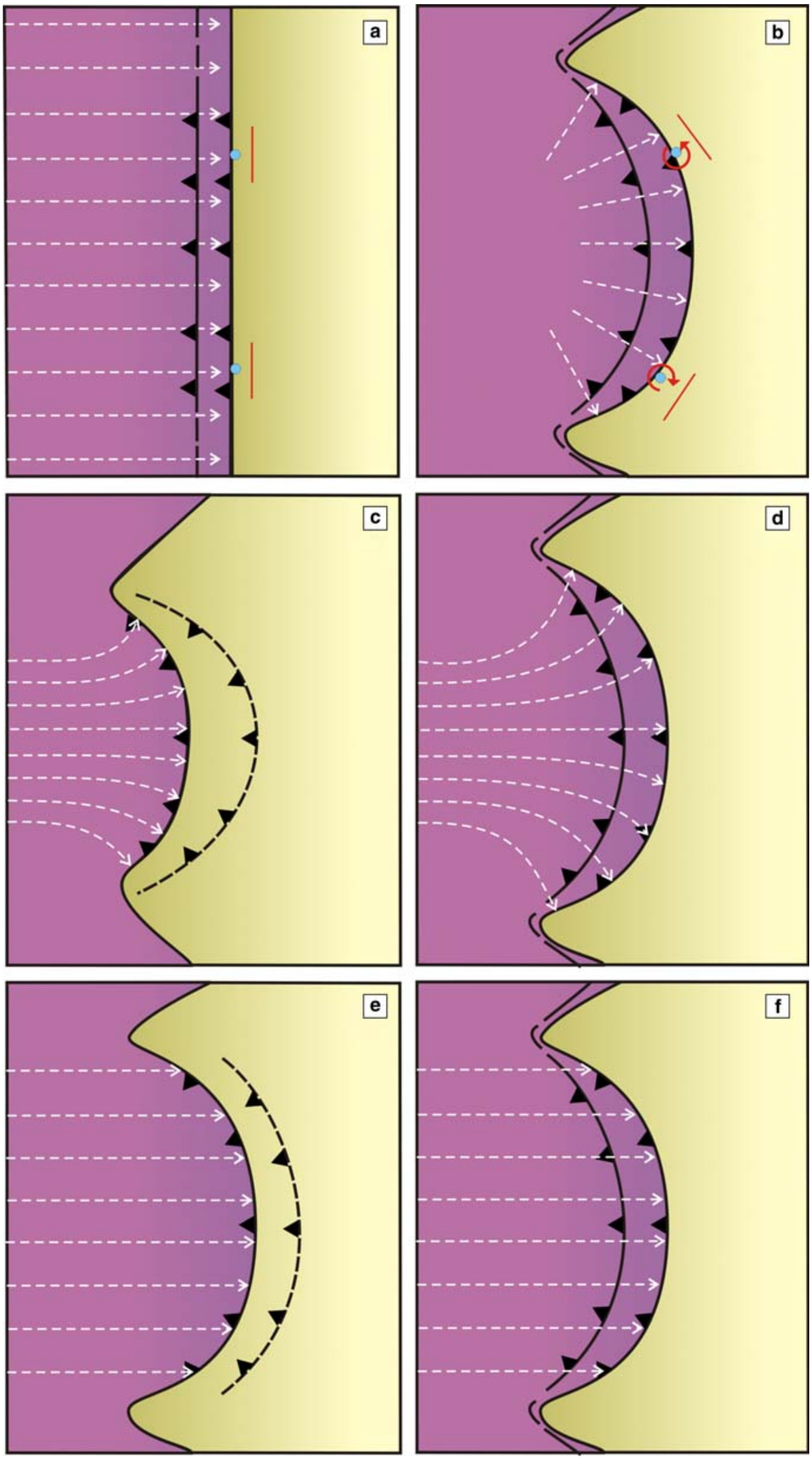

Fig. 2. The three end-member classification of arcuate fold-and-thrust belts proposed by Hindle & Burkhard (1999). In each case, the right-hand side diagram represents a later stage in development compared with left-hand side. (**a**, **b**) 'Orocline' (bending of an initially straight belt); (**c**, **d**) 'Piedmont glacier' (divergent transport directions); (**e**, **f**) 'primary arc' (uniform transport direction). White arrows represent displacement vectors. Red arrows in (b) denote the sense of rotation on the fold belt flanks as curvature develops. Thrusts indicated in (c) and (e) with a dashed line represent their incipient position in the foreland as the fold-and-thrust belt propagates. In the Marshak (2004) classification, (a) and (b) represent development of a rotational curve and (e) and (f) illustrate the development of a non-rotational curve. Marshak (2004) did not include the intermediate 'Piedmont glacier' curve in his classification scheme.

regional shortening (Davis & Engelder 1985; Jaumé & Lillie 1988; Marshak 2004).

Less common stimuli to the development of curvature identified by Macedo & Marshak (1999) and Marshak (2004) include irregularities on colliding margins (e.g. hinterland indenters or foreland promontories), interaction with later strike-slip faults, and distortion of the underthrust slab. The collision of a hinterland indenter into a sedimentary basin will generate a salient in the

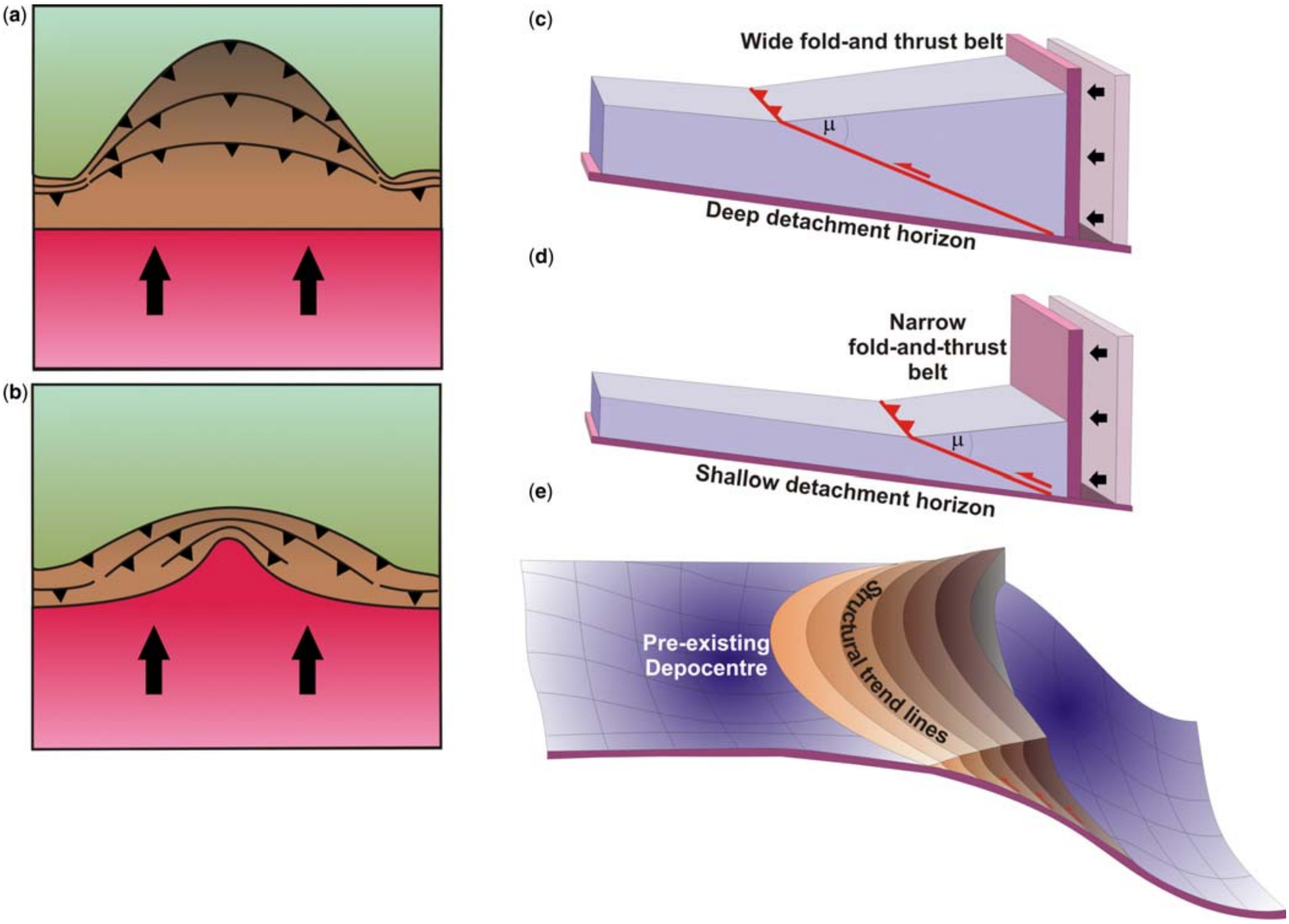

Fig. 3. Comparison of typical structural trend-line patterns in (**a**) a basin-controlled salient v. (**b**) a salient formed by collision of a hinterland indenter. (**c**, **d**) Schematic illustrations demonstrating how depth to detachment influences the width of a fold-and-thrust belt for a given amount of displacement. (**e**) Schematic illustration of the frontal part of a salient demonstrating how a pre-existing depocentre with gradually sloping margins produces smooth curvature. If the pre-existing depocentre has abrupt, steeply dipping margins, the salient margins are more likely to be affected by strike-slip faults. μ, critical taper angle. All diagrams adapted from illustrations in Marshak (2004).

foreland, but with precisely the opposite pattern of structural trend lines compared with a basin-controlled salient (Macedo & Marshak 1999) (Fig. 3). If the foreland to an advancing fold-and-thrust belt is irregular (i.e. it has promontories and/or embayments), a margin-controlled curve may develop as the deformation belt adapts to the shape of the margin. As Marshak (2004) pointed out, the effect of pre-deformational shape of a continental margin may be intimately linked with the effect of basin geometry on curve formation, because recesses in a continental margin may correspond to the location of wider and deeper basins. Rotation of segments of a fold-and-thrust belt around a vertical axis (i.e. oroclinal bending *sensu stricto*) is most likely to occur if curvature is induced by strike-slip faulting and/or foreland obstacles.

Structural patterns in Novaya Zemlya

The Novaya Zemlya archipelago separates the eastern Barents Shelf from the southern Kara Sea and contains a fold-and-thrust belt that exposes a Precambrian through Early Triassic succession. The fold-and-thrust belt is structurally connected to the Polar Urals through the Pai Khoi fold belt in the south, and to the Taimyr fold belt through the submerged Siberian Sill in the north (Fig. 1). The depositional setting and fauna of the Palaeozoic succession exposed on the Novaya Zemlya archipelago implies that it was located along the eastern margin of Baltica (present-day orientation) prior to deformation, with platform sediments predominant on the western side of the archipelago and slope deposits on the eastern side (e.g. Bondarev 1982) adjacent to the Uralian Ocean. The affinity with Baltica has been confirmed using detrital zircon ages from Early Palaeozoic sediments (Pease & Scott 2009). The west-to-east transition from platform to slope deposits on the margin of Baltica is also characteristic of the external parts of the main Uralian deformation belt further south (e.g. Puchkov 1997).

The Novaya Zemlya archipelago comprises two main islands separated by a narrow channel located around 73°20′ N, and forms a sweeping arc more than 900 km long that separates the Barents Sea from the Kara Sea (Figs 1 & 4). The pattern of major structures exposed on Novaya Zemlya broadly follows the trend of the archipelago. In detail, however, the plan-view shape of the archipelago is more complex, and is not a simple curve of constant curvature. The southern part of the archipelago is characterized by a relatively tight curve coincident with a broadening of the south island to *c*. 140 km wide (Fig. 4). The central part of the archipelago has virtually no curvature, with the width decreasing to <90 km in the vicinity of the channel between the north and south islands. In the northern part of the archipelago the width of the north island increases to *c*. 110 km as the curvature also increases, and towards the northernmost part of the island curvature decreases again as the width is reduced to around 60 km.

The main structural trend lines in Novaya Zemlya are summarized on Figure 5, which is based on more detailed compilations

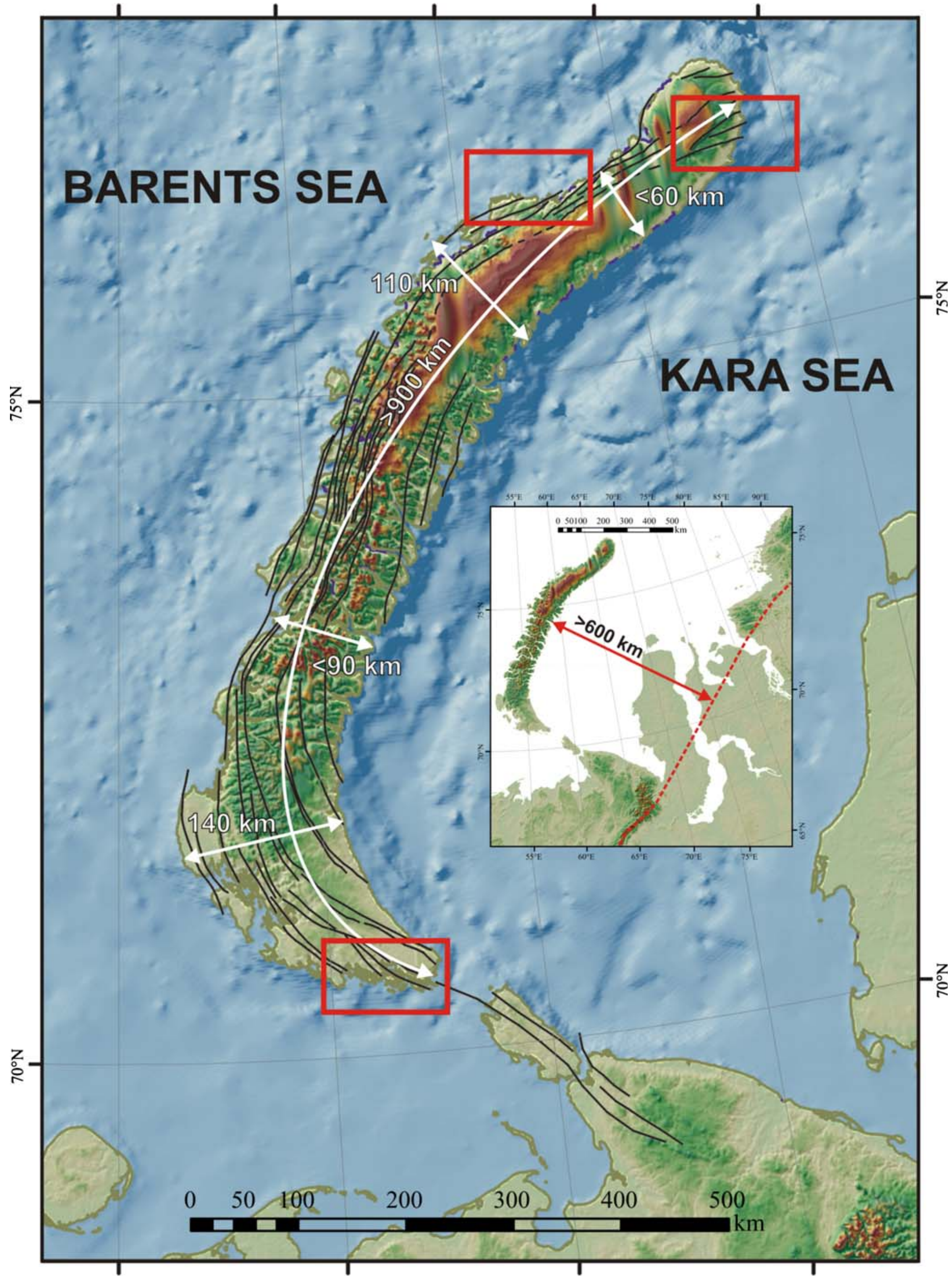

Fig. 4. Principal dimensions of the Novaya Zemlya archipelago. Structural trend lines (major faults and fold axes) are shown in black. Field work localities are indicated by the red boxes.

from geological maps and public-domain Landsat and Corona satellite imagery. Also shown is the assumed structural zonation of the fold-and-thrust belt, extrapolated from information presented in Korago *et al.* (1992). Korago *et al.* identified four north–south trending structural domains in the central portion of the archipelago (outlined by the white dashed box in Fig. 5). From west to east, these structural domains were described by Korago *et al.* (1992) as follows:

- Western Structural Domain – contains the most intense deformation and is characterized by an imbricate, west-directed thrust belt.
- Central Structural Domain – described as a negative structure, with less intense deformation than adjacent zones and with more continuity and better preservation of folds.
- Axial Structural Domain – structural intensity approaches that in the Western Structural Domain, but is characterized by eastward vergence.
- Eastern Structural Domain – low-lying region with limited exposure, but is characterized by less intense deformation and generally upright symmetrical or slightly east-verging folds.

The structural domains, as defined by Korago *et al.* (1992), occur in an area of Novaya Zemlya that is inaccessible to western geologists and therefore cannot be corroborated with our own observations. We have extrapolated these four domains along the length of the entire archipelago using the pattern of structural trend lines on the basis that our own observations in southern and northern Novaya Zemlya are broadly consistent with the Korago *et al.* (1992) descriptions. The overall structural style that we observed in the field, which is reported by Korago *et al.* (1992) and can be discerned on published geological maps and sections, is consistent with a predominantly thick-skinned style of deformation characterized by limited horizontal transport (a few tens of kilometres maximum). Only on the western side of the fold-and-thrust belt do structures exhibit a trend towards more thin-skinned geometries. For the arguments presented here, however, the trend of the domains is more important than the internal detail of their structural architecture.

Using the terminology of Marshak (2004), the entire fold-and-thrust belt exposed on Novaya Zemlya constitutes a large salient. However, it is apparent from the pattern of structural trend lines and structural domains depicted in Figure 5 that the large salient is a compound feature comprising two smaller salients: a gentle curve in the north which is convex towards the NW, and a tighter curve in the south which is convex towards the SW. Although the current geographic width of the archipelago is not completely equivalent to the width of the known fold-and-thrust belt (see Fig. 5), there is a clear systematic relationship between the pattern of structural trend lines and the width of the archipelago: (1) the northern salient coincides with the broadening of the archipelago to *c*. 110 km, and the southern salient coincides with the broadening of the archipelago to *c*. 140 km (Fig. 4); (2) trend lines are further apart near the apexes of each of these salients than at the endpoints, and trend lines are most closely spaced in the central part of the archipelago between the two salients – this is the part of the archipelago which thins to <90 km and has no significant curvature (Fig. 4).

It is also apparent that the northern and southern salients expose different elements of the structural domains. In the northern salient all four of the domains defined by Korago *et al.* (1992) are exposed, and this is the only part of the archipelago where the Eastern Structural Domain is exposed. Structural trend lines have to be projected beneath the permanent ice sheet in northern Novaya Zemlya, adding an element of uncertainty. Further south, structures consistently trend offshore on the eastern (Kara Sea) side of the archipelago so that the southern salient is dominated only by exposures of the Western and Central Structural Domains. We assume that the Axial and Eastern Structural Domains are present beneath the SW part of the Kara Sea shelf (Fig. 5).

The extrapolated trend lines suggest that the Central Structural Domain has a much greater outcrop width in the southern salient than in the northern salient. This may be an artefact of the inherent uncertainties involved in extrapolation, but arguments could equally be made that the change of width is real. For example, the northern salient is characterized by much higher topographic relief than the southern salient (Fig. 4), which may indicate some basement impediment to horizontal propagation of the fold-and-thrust belt in the north compared with the south. This impediment may have been the Admiralty Arch, located in the Barents Sea close to the apex of the northern salient (Fig. 5). This structural high is commonly depicted as a long-lived positive feature on palaeogeographic maps (e.g. Smelror *et al.* 2009).

The outcrops of Precambrian–Cambrian 'basement' rocks are also shown on Figure 5. Precambrian–Cambrian rocks crop out in only a few locations in Novaya Zemlya and are unconformably overlain by Palaeozoic strata (Korago *et al.* 2004; Pease & Scott 2009). Although the outcrops are relatively small, they are highly significant for understanding the evolution of the fold-and-thrust belt because they represent the areas in which the deepest geological levels are exposed. The 'basement' outcrops have a clearly defined relationship with the structural pattern: (1) they are consistently located close to the boundary between the Western Structural Domain and the Central Structural Domain; (2) they occur only at the margins of the salients and are symmetrically disposed with respect to the apex of each salient (Fig. 5).

Interpretation of structural patterns in Novaya Zemlya

Cause of curvature

The plan-view geometry of structures in Novaya Zemlya is consistent with an overall westward emplacement of thrust sheets, and the structural pattern clearly implies that the basinal geometry of the eastern Barents Shelf had a significant influence on development of the Novaya Zemlya fold-and-thrust belt. The two salients that we have identified on Novaya Zemlya were emplaced towards the two main depocentres on the eastern Barents Shelf, whereas the intervening recess lies adjacent to the Ludlov Saddle, the structural high that separates the North Barents Basin from the South Barents Basin (Fig. 6). This implies that the two salients are basin-controlled curves in the terminology of Marshak (2004), and demonstrates that the North and South Barents basins were distinct entities separated by an intervening high at the onset of deformation.

The distribution of Precambrian–Cambrian outcrops (Fig. 5) is consistent with the observation that deeper structural levels are exposed at the margins of salients (Macedo & Marshak 1999; Marshak 2004). This adds further weight to the argument that increased depth to detachment in the pre-existing eastern Barents depocentres was an important element that controlled curvature. With estimated sediment thicknesses up to 20 km in the South and North Barents basins, the detachment horizon(s) would be expected to be significantly deeper in the basin centres than the basin margins, although this pattern may have been disrupted in the north by the presence of the Admiralty Arch (this potential disruption to palaeogeographic connectivity may explain why the northern salient is less well developed than the southern salient). The expanding pattern of structural trend lines towards the apex of the salients is also consistent with basin-controlled curves, and there is no evidence from the pattern of trend lines that hinterland indenters were significant (cf. Ziegler 1988, 1989).

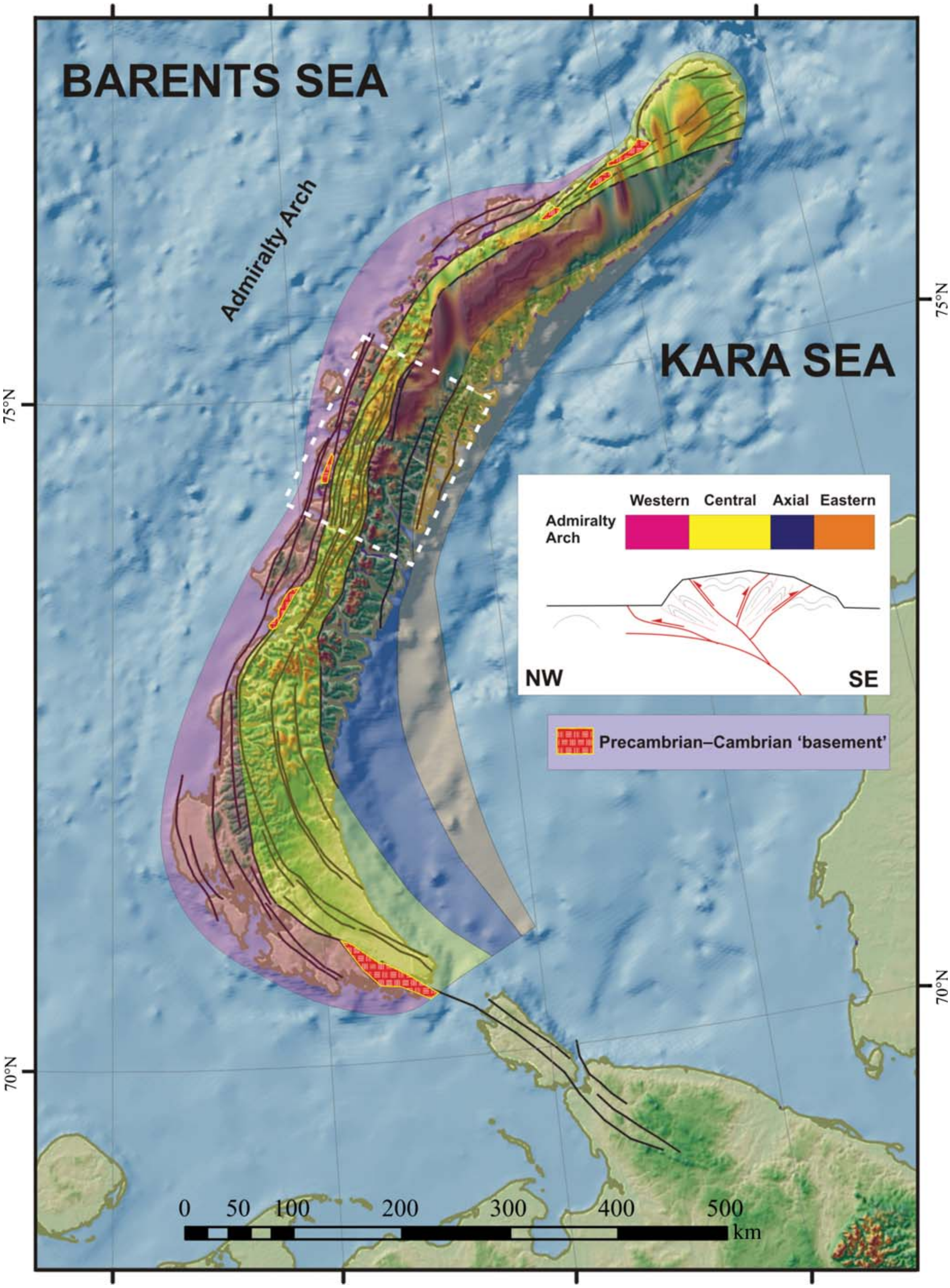

Fig. 5. Topography and structural trend lines of Novaya Zemlya from Figure 4, overlain by structural domains extrapolated from those defined by Korago *et al.* (1992) in central Novaya Zemlya (in the area outlined by the white dashed box). Inset figure shows a schematic cross-section across the northern half of Novaya Zemlya illustrating the assumed relationships between the four structural domains. Structural trend lines (major faults and fold axes) are shown in black. Precambrian–Cambrian exposures are also shown.

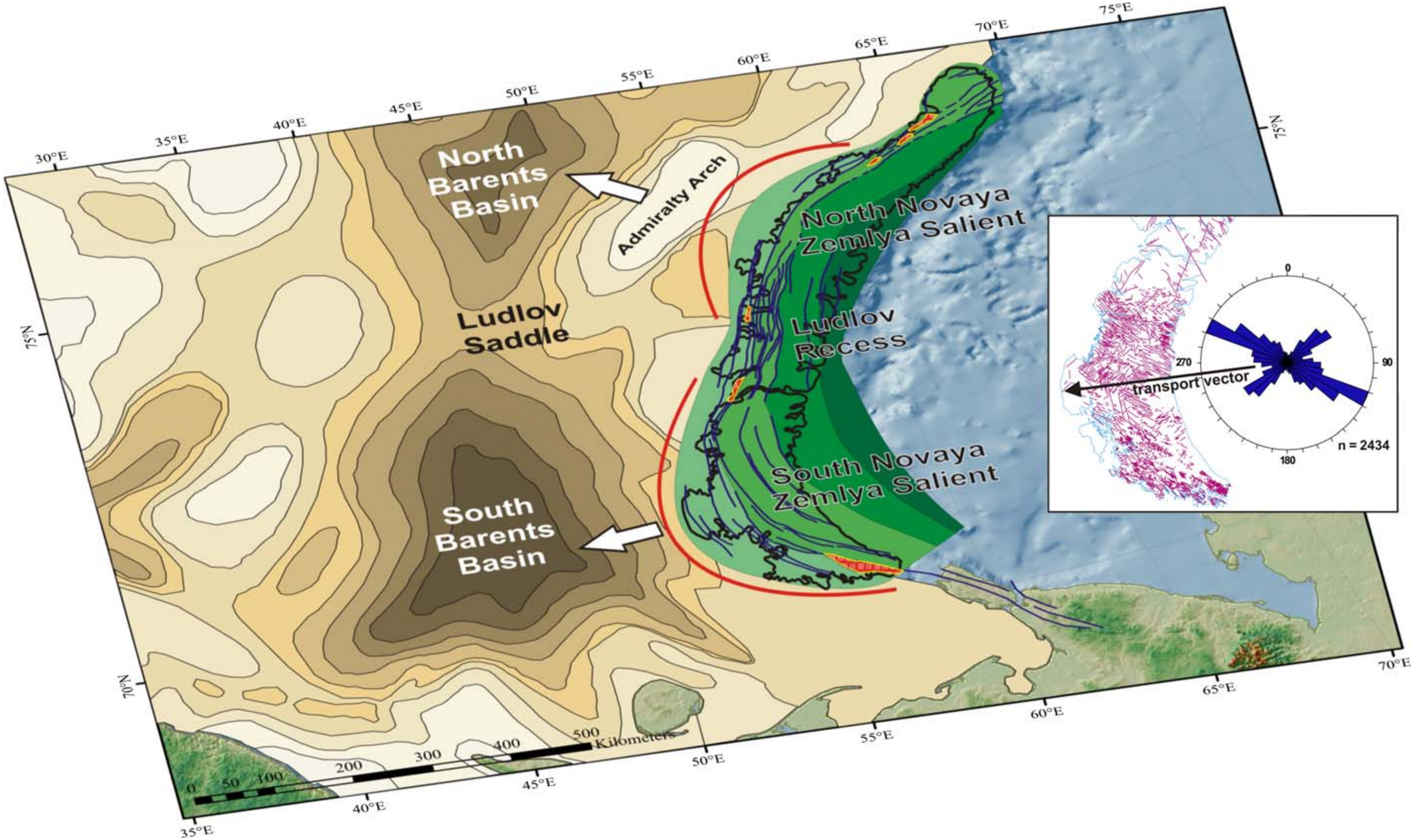

Fig. 6. Oblique view illustrating the relationship between the geometry of the Novaya Zemlya fold-and-thrust belt and structure features on the eastern Barents Shelf. Contouring on Barents Shelf represents depth to basement, with sediment thicknesses of *c.* 20 km in the South Barents Basin. The North Novaya Zemlya Salient and South Novaya Zemlya Salient have developed by enhanced propagation induced by a deepening of basal detachment levels in the pre-existing North Barents Basin and South Barents Basin, respectively (cf. Fig. 3e). Note that the presence of the Admiralty Arch may have inhibited the development of the northern salient compared with the southern salient. The Ludlov Recess has formed in response to the presence of a pre-existing high in the vicinity of the Ludlov Saddle. Novaya Zemlya structural domains (green shading) are named on Figure 5. Precambrian/Cambrian exposures are also shown (see also Fig. 5). The inset shows the relationship between lineament orientation taken from satellite images and the South Novaya Zemlya salient.

It is not clear from field observations at what stratigraphic level the main detachment occurs on the foreland side of the Novaya Zemlya fold-and-thrust belt, and in this respect it is difficult to predict whether the weakness of any particular detachment is enhanced in the basinal areas. In the southern and middle Urals, Brown *et al.* (2006) recognized foreland detachments in units of Late Riphean, Late Vendian and Ordovician age. In Timan–Pechora, Sobornov (1994) illustrated Early Palaeozoic and Artinskian (mid-Permian) detachments. Fine-grained clastic units occur at many levels in the Late Precambrian and Palaeozoic succession exposed on Novaya Zemlya, offering numerous potential décollement levels.

When seeking to explain the formation of an arcuate fold-and-thrust belt, the instinctive interpretation implied by the geometry is that thrust sheets are transported perpendicular to the thrust front at all localities, and thus there must have been radially divergent spreading of material toward the foreland. In the case of Novaya Zemlya, this line of reasoning could be used to explain significant extensional collapse in the hinterland (i.e. formation of the South Kara Basin). However, structural lineaments visible in satellite imagery of southern Novaya Zemlya are arranged in a simple conjugate pattern that is symmetrically distributed about the salient apex (Fig. 6). This symmetry with the presumed transport vector towards the South Barents Basin implies that formation of these lineaments was intimately linked with emplacement of the fold-and-thrust belt. Furthermore, the simple symmetrical pattern is consistent with a single emplacement event and would argue against significant divergent transport or oroclinal bending. We therefore conclude the southern salient in Novaya Zemlya is more likely to be closer to the ‘non-rotational curve’ end-member in the classification of Marshak (2004) (equivalent to the ‘primary arc’ end-member of Hindle & Burkhard 1999). Owing to the permanent ice sheet in northern Novaya Zemlya, insufficient lineaments can be identified to draw inferences for the northern salient with the same certainty; however, there is no evidence to suggest that it is any different to the southern salient.

We note also that Hindle & Burkhard (1999) considered their ‘primary arc’ end-member to be the most appropriate interpretation for the Jura arc based on extensive analysis of 2D balanced sections and other strain data. As they pointed out, severe space problems would be encountered in the hinterland after even limited radial divergence of material because so much rock mass is required to be derived from the same area in the centre of the arc.

Cause of offset

Structural patterns in Novaya Zemlya argue against significant oroclinal bending. It follows, therefore, that the only way that the fold-and-thrust belt could have been offset from a position originally in straight-line continuity with the remainder of the Uralian Orogen is by long-distance (*c*. 600 km) emplacement of a crustal block bounded by strike-slip faults. The model of Otto & Bailey (1995) invokes such a mechanism, with a thin-skinned allochthon bounded by major strike-slip fault systems in the Pai Khoi region and between northern Novaya Zemlya and Taimyr.

A number of observations lead us to question a long-distance, thin-skinned emplacement mechanism involving substantial horizontal thrust transport:

(1) the overall structural style of Novaya Zemlya is thick-skinned and implies limited horizontal translation.
(2) if Novaya Zemlya had originally been aligned with the remainder of the Late Palaeozoic Uralian Orogen and then emplaced westward at a later stage, the fold-and-thrust belt would be expected to preserve a complex, multi-stage deformation history, although, as we describe above, only a simple structural pattern is apparent, consistent with a single, uncomplicated emplacement event.
(3) no structural evidence was observed for significant strike-slip displacement, discontinuity of major structures or rotation of rock masses during CASP field work, even though this field work includes some of the most likely localities in which evidence would be expected according to the Otto & Bailey hypothesis (e.g. southernmost and northernmost Novaya Zemlya; Fig. 4). Significant strike-slip displacement or structural discontinuity is also not obvious on satellite images, nor can it be observed on geological maps. (We accept, however, that on its own this lack of evidence is not proof, because the main bounding fault systems may be offshore.)
(4) Even with a basal décollement that has a dip of $<1^{\circ}$, the gravity-induced lateral translation of 600 km proposed by Otto & Bailey (1995) would require an elevation difference between each end of the décollement of >10 km. The cross-section through Novaya Zemlya and the eastern Barents Sea depicted by Otto & Bailey (their fig. 4) shows a decollement beneath Novaya Zemlya at a depth of 2–2.5 km below sea level. On this basis, the hinterland end of the décollement should have been at an elevation of *c*. 8 km, which is clearly unfeasible, particularly considering the fact that subsidence in the South Kara Basin may well have begun prior to emplacement of the fold-and-thrust belt.

Given these reservations about the scale of thrust-sheet transport, we consider that the offset of Novaya Zemlya with respect to the remainder of the Uralian Orogen most probably reflects the presence of an original embayment along the margin of Baltica. Such embayments are not unusual, and may reflect segments of oceanic crust that have a different spreading history to adjacent segments along a continental margin. For example, the embayment in the Norwegian–Greenland Sea adjacent to the Møre Basin coincides with a segment of oceanic crust that has a different spreading history to areas north and south (e.g. Scott *et al.* 2005).

Assuming that the presence of an original embayment along the margin of Baltica controlled the offset of Novaya Zemlya, this would make Novaya Zemlya a margin-controlled salient in the terminology of Marshak (2004). However, as we have demonstrated in the current study, superimposed on the broad curve of Novaya Zemlya are two smaller salients, the plan-view morphology of which must at least in part be generated in response to the presence of pre-existing depocentres on the former margin of Baltica. In this respect, therefore, Novaya Zemlya is probably best considered to represent a combination of margin- and basin-controlled salients.

Relationship between structural curvature in Novaya Zemlya and the subsidence history of the eastern Barents Shelf

The double salient structure of the Novaya Zemlya fold-and-thrust belt provides independent evidence that the North and South Barents basins were discrete depocentres, separated by an intervening high, prior to the inception of fold-and-thrust belt development. This raises the question of precisely when and how they achieved this bipartite morphology. According to Otto & Bailey (1995), separation of the North and South Barents basins into discrete depocentres occurred in mid Triassic time due to uplift of the Ludlov Saddle during sinistral transpression along a reactivated Timanide fault trend. This is only shortly before, or penecontemporaneous with, development of the fold-and-thrust belt. The timing of depocentre development on the eastern Barents Shelf is important to our understanding of the later subsidence history, the thermal history of

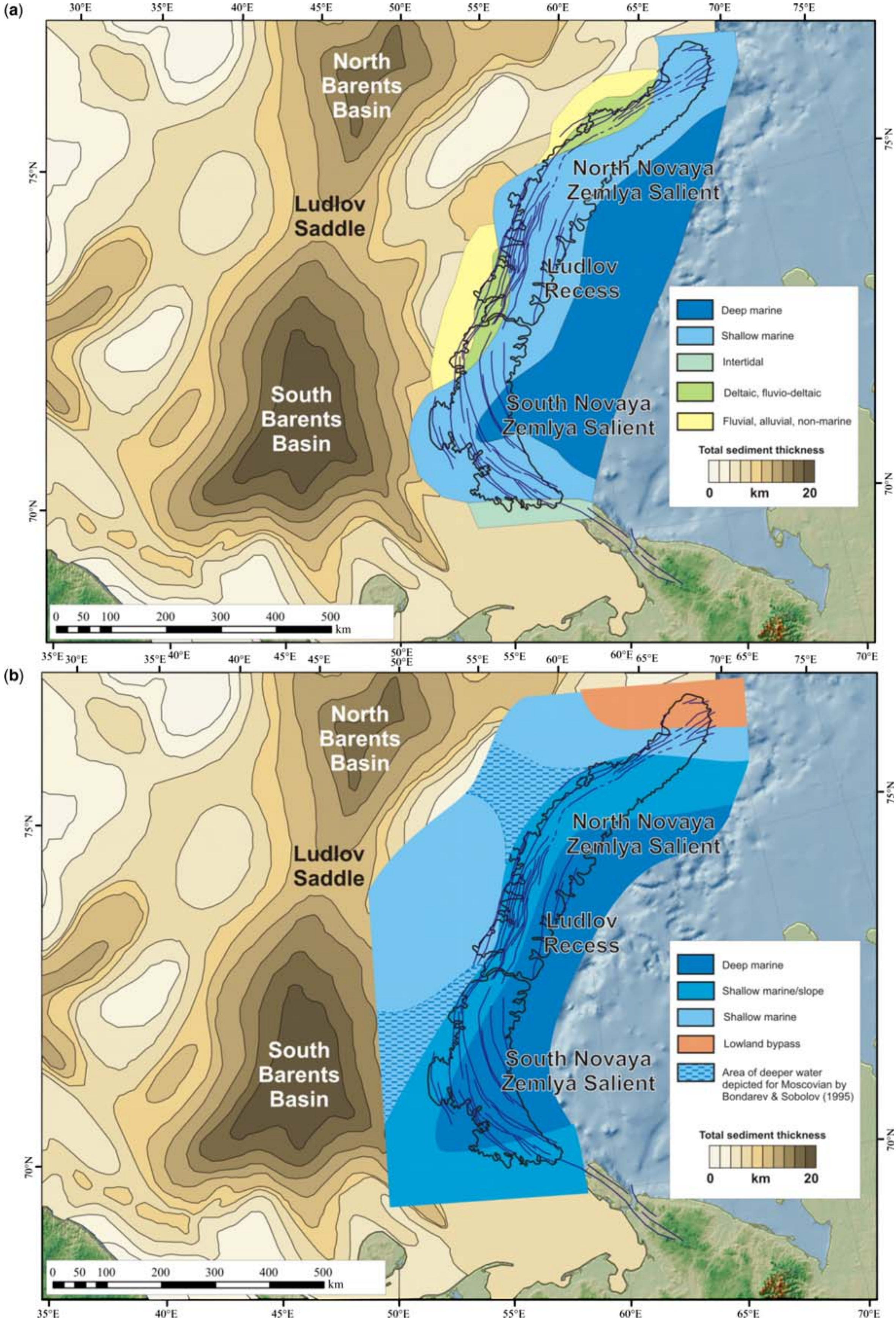

Fig. 7. (**a**) Lochkovian (Early Devonian) and (**b**) Kasimovian (Late Carboniferous) palaeogeography maps of Novaya Zemlya superimposed on a map showing total sediment thickness of the Barents Shelf and structural trend lines on Novaya Zemlya. There is a clear relationship between salient location, structural trend lines and palaeogeographic environment boundaries which implies that the North and South Barents basins, or their precursors, existed as distinct entities at these times.

the basin and the palaeogeographic evolution, which, for example, may have implications for the distribution of potential source rocks.

Palaeogeographic maps of Novaya Zemlya for the Palaeozoic consistently show deeper water to the east, reflecting a location at the margin of Baltica adjacent to the Uralian Ocean. These map sequences also show periodic deeper-water connections from the Uralian margin across Novaya Zemlya, which have been extrapolated through to the eastern Barents Shelf (e.g. Smelror *et al.* 2009; Guo *et al.* 2010; Fig. 7). Recognition of the two basin-controlled salients in Novaya Zemlya allows us to consider the significance of these possible basinal connections with new understanding.

As all the exposures in Novaya Zemlya used to constrain our palaeogeographic maps (Fig. 7) are now within an early Mesozoic fold-and-thrust belt, it can be assumed that the current distribution of palaeogeographic environments has been modified by deformation to some degree. For example, many of the maps also show a distribution of palaeo-environment boundaries that at least in part reflects the curvature of the fold-and-thrust belt, including the double salient structure (Fig. 7). However, we argue that, if any of the palaeogeographic environment boundaries can be demonstrated to cross-cut structural trend lines within the fold-and-thrust belt in a systematic fashion, it implies that the current distribution of palaeogeographic environments is not solely a function of tectonic transport but also reflects some pre-existing palaeobathymetric control. In the case of a basin-controlled salient, if palaeogeographic environment boundaries for any particular age have a more acute curvature than structural trend lines (i.e. are more acutely convex toward the foreland), it implies that the basin already existed at that age. Two pre-Permian palaeogeographic maps for Novaya Zemlya are presented as examples in Figure 7, with the structural trend lines superimposed. Inevitably, there are limitations imposed by the accuracy of palaeogeographic maps and only tentative conclusions can be drawn. However, many of the maps that we have prepared (spanning Late Ordovician to Late Carboniferous time) show palaeogeographic boundaries systematically cross-cutting structural trend lines, a phenomenon particularly apparent in the South Barents Basin. This would imply a prolonged pre-Permian history of differential subsidence on the eastern Barents Shelf, consistent with the rifting history of Timan–Pechora.

Conclusions

Novaya Zemlya contains an early Mesozoic fold-and-thrust belt characterized by an overall thick-skinned structural style and relatively low levels of exhumation compared with the Polar Urals and Taimyr, implying a 'soft' collision with limited horizontal transport of thrust sheets. Curvature of the fold-and-thrust belt was controlled by west-directed transport as a non-rotational primary arc, modified by the geometry of pre-existing sedimentary basins on the eastern Barents Shelf. The substantial offset of the Novaya Zemlya fold-and-thrust belt from the remainder of the Uralian orogen was determined largely by the presence of an original embayment on the margin of Baltica, and there is little evidence to support either development as an orocline (bending of an originally straight deformation belt) or emplacement of a thin-skinned allochthonous segment on bounding strike-slip faults. Furthermore, the pattern of structural trend lines does not support the influence of a hinterland indenter.

Compressional deformation in Novaya Zemlya occurred significantly after the onset of subsidence in adjacent basins. Palaeogeographic maps for the Palaeozoic, drawn with no attempt to compensate for later compressional deformation in the Novaya Zemlya fold-and-thrust belt, show periodic connections between the Uralian Ocean margin and depocentres on the eastern Barents Shelf, crossing Novaya Zemlya. Recognition of the two basin-controlled salients in the Novaya Zemlya fold-and-thrust belt, and of the significance of cross-cutting relationships between palaeo-environment boundaries and structural trend lines within the salients, provides tangible evidence in support of these interpretations and affords an understanding of why these connections have the form that they do. The relationship between structural trend-lines and palaeogeographic environment boundaries indicates that discrete depocentres may have been present on the eastern Barents Shelf through a significant portion of Palaeozoic time.

We thank the captains and crews of the research vessels *Gorizont* and *Gydrolog*, both operated by the Russian Hydrographic Office in Murmansk, for their logistic support during expeditions to Novaya Zemlya in 2004 and 2005, respectively. We also thank VNIIOkeangeologiya in St Petersburg and David Gee (Uppsala) for their organizational role in the Novaya Zemlya expeditions, and Henning Lorenz (Uppsala) for assistance with the satellite imagery. CASP acknowledges the industrial sponsors of its Arctic research with gratitude. Tim Kinnaird provided helpful comments on an earlier version of this manuscript. Sergey Drachev and Anatoly Nikishin provided constructive criticism which improved the quality of the manuscript.

References

Aitken, J. D. & Long, D. G. F. 1978. Mackenzie tectonic arc – reflection of early basin configuration? *Geology*, **6**, 626–629.

Allen, M. B., Anderson, L., Searle, R. C. & Buslov, M. M. 2006. Oblique rift geometry of the West Siberian Basin: tectonic setting for the Siberian flood basalts. *Journal of the Geological Society, London*, **163**, 901–904.

Bondarev, V. I. (ed.) 1982. *Geologiya Yuzhnogo ostrova Novoy Zemli (Geology of the South Island of Novaya Zemlya)*. PGO 'Sevmorgeologiya', Leningrad.

Bondarev, V. I. & Sobolev, N. N. 1995. The Paleozoic of Novaya Zemla. Arctic and Russian Report 609. Unpublished report. CASP, Cambridge.

Boyer, S. E. 1995. Sedimentary basin taper as a factor controlling the geometry and advance of thrust belts. *American Journal of Science*, **295**, 1220–1254.

Brown, D., Juhlin, C., Tryggvason, A., Friberg, M., Rybalka, A., Puchkov, V. & Petrov, G. 2006. Structural architecture of the southern and middle Urals foreland from reflection seismic profiles. *Tectonics*, **25**, TC1002.

Calassou, S., Larroque, C. & Malavieille, J. 1993. Transfer zones of deformation in thrust wedges: an experimental study. *Tectonophysics*, **221**, 325–344.

Carey, S. W. 1955. The orocline concept in geotectonics. *Proceedings of the Royal Society of Tasmania*, **89**, 255–288.

Corfield, R. I., Hansen, E.-K., Fugelli, E., Milner, P., Kittilsen, J.-E., Roberts, A. & Matthews, S. 2006. Structural evolution of the Russian Barents Sea. *In*: Fraser, A., Allen, M., O'Callaghan, M. & Hamilton, R. (eds) *Oil and Gas Habitats of Russia and Surrounding Regions*. Geological Society, London, **9**. (abstract volume).

Davis, D. M. & Engelder, T. 1985. The role of salt in fold-and-thrust belts. *Tectonophysics*, **119**, 67–88.

Ferrill, D. A. & Groshong, R. H. J. 1993. Kinematic model for the curvature of the northern Subalpine Chain, France. *Journal of Structural Geology*, **15**, 523–541.

Gee, D. G., Bogolepova, O. K. & Lorenz, H. O. 2006. *The Timanide, Caledonide and Uralide Orogens in the Eurasian High Arctic, and Relationships to the Palaeo-continents Laurentia, Baltica and Siberia*. Geological Society, London, Memoirs, **32**, 507–520.

Guo, L., Schekoldin, R. & Scott, R. A. 2010. Sedimentology, palaeogeography and hydrocarbon significance of the Devonian succession in northern Novaya Zemlya, Arctic Russia. *Journal of Petroleum Geology*, **33**, 105–122.

Hamilton, W. 1970. The Uralides and the motion of the Siberian and Russian platforms. *Bulletin of the Geological Society of America*, **81**, 2553–2576.

Hindle, D. & Burkhard, M. 1999. Strain, displacement and rotation associated with the formation of curvature in fold belts; the example of the Jura arc. *Journal of Structural Geology*, **21**, 1089–1101.

Jaumé, S. C. & Lillie, R. J. 1988. Mechanics of the Salt Range–Potwar Plateau, Pakistan: a fold-and-thrust belt underlain by evaporites. *Tectonics*, **7**, 57–71.

Johansen, S. E., Ostisty, B. K. *et al*. 1993. Hydrocarbon potential in the Barents Sea region: play distribution and potential. *In*: Vorren, T. O., Bergsager, E., Dahl-Stamnes, Ø. A., Holter, E., Johansen, B., Lie, E. & Lund, T. B. (eds) *Arctic Geology and Petroleum Potential*. NPF Special Publication 2. Elsevier, Amsterdam, 273–320.

Korago, E. A., Kovaleva, G. N., Il'in, V. F. & Pavlov, L. G. 1992. *The Tectonics and Metallogeny of the Early Kimmerides of Novaya Zemlya*. Nedra, Leningrad.

Korago, E. A., Kovaleva, G. N., Lopatin, B. G. & Orgo, V. V. 2004. *The Precambrian Rocks of Novaya Zemlya*. Geological Society, London, Memoirs, **30**, 135–143.

Macedo, J. & Marshak, S. 1999. Controls on the geometry of fold-thrust belt salients. *Bulletin of the Geological Society of America*, **111**, 1808–1822.

Marshak, S. 1988. Kinematics of arc and orocline formation in thin-skinned orogens. *Tectonics*, **7**, 73–86.

Marshak, S. 2004. *Salients, Recesses, Arcs, Oroclines, and Syntaxes – a Review of Ideas Concerning the Formation of Map-view Curves in Fold-thrust Belts*. American Association of Petroleum Geologists, Tulsa, OK, Memoirs, **82**, 131–156.

Marshak, S. & Wilkerson, M. S. 1992. Effects of overburden thickness on thrust belt geometry and development. *Tectonics*, **11**, 560–566.

Marshak, S., Wilkerson, M. S. & Hsui, A. 1992. Generation of curved fold-thrust belts: insights from simple physical and analytical models. *In*: McClay, K. R. (ed.) *Thrust Tectonics*. Chapman & Hall, London, 83–92.

Metelkin, D. V., Vernikovsky, V. A., Kazansky, A. Y., Bogolepova, O. K. & Gubanov, A. P. 2005. Paleozoic history of the Kara microcontinent and its relation to Siberia and Baltica: paleomagnetism, paleogeography and tectonics. *Tectonophysics*, **398**, 225–243.

Mezhvilk, A. A. 1995. Thrust and strike-slip zones in northern Russia. *Geotectonics*, **28**, 298–305.

Mitra, G. 1997. Evolution of salients in a fold-and-thrust belt: the effects of sedimentary basin geometry, strain distribution and critical taper. *In*: Sengupta, S. (ed.) *Evolution of Geological Structures in Micro- and Macro-scales*. Chapman & Hall, London, 59–90.

Montero, P., Bea, F. *et al*. 2000. Single-zircon evaporation ages and Rb–Sr dating of four major Variscan batholiths of the Urals: a perspective on the timing of deformation and granite generation. *Tectonophysics*, **317**, 93–108.

O'Leary, N., White, N. J., Tull, S., Bashilov, V., Kuprin, V., Natapov, L. M. & Macdonald, D. 2004. Evolution of the Timan–Pechora and South Barents Sea basins. *Geological Magazine*, **141**, 141–160.

Otto, S. C. & Bailey, R. J. 1995. Tectonic evolution of the northern Ural Orogen. *Journal of the Geological Society, London*, **152**, 903–906.

Pease, V. & Scott, R. A. 2009. Crustal affinities in the Arctic Uralides, northern Russia: significance of detrital zircon ages from Neoproterozoic and Paleozoic sediments in Novaya Zemlya and Taimyr. *Journal of the Geological Society, London*, **166**, 517–527.

Puchkov, V. N. 1997. *Structure and Geodynamics of the Uralian Orogen*. Geological Society, London, Special Publications, **121**, 201–236.

Scott, R. A., Ramsey, L. A., Jones, S. M., Sinclair, S. & Pickles, C. S. 2005. *Development of the Jan Mayen Microcontinent by Linked Propagation and Retreat of Spreading Ridges*. Norsk Petroleumsforening, Trondheim, Special Publications, **12**, 69–82.

Şengör, A. M. C. & Natal'in, B. A. 1996. Paleotectonics of Asia: fragments of a synthesis. *In*: Yin, A. & Harrison, T. M. (eds) *The Tectonic Evolution of Asia*. Cambridge University Press, Cambridge, 486–640.

Smelror, M., Petrov, O. V., Larssen, G. B. & Werner, S. C. (eds) 2009. *Geological History of the Barents Sea*. Geological Survey of Norway, Trondheim.

Sobornov, K. O. 1994. *Structural Relationship of the Northern Urals and Adjacent Basins*. Canadian Society of Petroleum Geologists, Alberta, Memoirs, **17**, 145–154.

Torsvik, T. H. & Cocks, L. R. M. 2004. Earth geography from 400 to 250 Ma: a palaeomagnetic, faunal and facies review. *Journal of the Geological Society*, **161**, 555–572.

Ustritsky, V. I. 1985. On the relationship between the Urals, Pay-Khoy, Novaya Zemlya and Taymyr. *Geotectonics*, **1**, 51–61.

Vernikovsky, V. A., Neimark, L. A., Ponomarchuk, V. A., Vernikovskaya, A. E., Kireev, A. D. & Kuz'min, D. S. 1995. Geochemistry and age of collision granitoids and metamorphites of the Kara microcontinent (Northern Taimyr). *Geologiya i Geofizika*, **36**, 46–60.

Vyssotski, A. V., Vyssotski, V. N. & Nezhdanov, A. A. 2006. Evolution of the West Siberian Basin. *Marine and Petroleum Geology*, **23**, 93–126.

Wezel, F. C. (ed.) 1986. *The Origin of Arcs*. Elsevier, Amsterdam.

Ziegler, P. A. 1988. *Evolution of the Arctic–North Atlantic and the Western Tethys*. American Association of Petroleum Geologists, Tulsa, OK, Memoirs, **43**, 1–198 + 30 plates.

Ziegler, P. A. 1989. *Evolution of Laurussia: a Study in Late Palaeozoic Plate Tectonics*. Kluwer, Dordrecht.

Zonenshain, L. P., Korinevsky, V. G., Kazmin, V. G., Matveenkov, V. V. & Khain, V. V. 1984. Plate tectonic model for the development of the south Urals. *Tectonophysics*, **109**, 95–135.

Zonenshain, L. P., Kuzmin, M. I. & Natapov, L. M. 1990. *Geology of the USSR: a Plate Tectonic Synthesis*. American Geophysical Union, Washington, DC.

Charging the giant gas fields of the NW Siberia basin

E. FJELLANGER,[1] A. E. KONTOROVICH,[2] S. A. BARBOZA,[3] L. M. BURSHTEIN,[2] M. J. HARDY[4] and V. R. LIVSHITS[2]

[1]*Esso Norge AS, PO Box 60, 4064 Stavanger, Norway (e-mail: erik.fjellanger@exxonmobil.com)*
[2]*Institute of Petroleum Geology and Geophysics, Russian Academy of Sciences Siberian Branch, Koptuga 3, Novosibirsk, 630090, Russia*
[3]*ExxonMobil Upstream Research Company, PO Box 2189, Houston, TX 77008, USA*
[4]*ExxonMobil International Ltd., Ermyn Way, Leatherhead, Surrey KT22 8UX, UK*

Abstract: The West Siberia basin is the largest petroleum province in Russia, with 80% of the country's gas resources in the Cenomanian Pokur Formation. Significant undiscovered gas resources have been assessed as on trend with the giant gas fields. However, the origin of the large amounts of dry, isotopically light gas is still an enigma, albeit extensively addressed in the literature. This study aims at quantifying the gas contribution from all relevant thermal sources. The West Siberia Basin is the world's largest intracratonic basin, comprising up to 12 km of Mesozoic and Cenozoic clastic rocks. The Basement is composed of Palaeozoic accretionary crust. Northward-trending Permian–Triassic rifts were filled by fluvial–deltaic sediments from the south and east, punctuated by marine transgressions from the north. Cenozoic basin inversion formed traps for petroleum. A regional high-resolution 3D basin simulation was used to model the thermal evolution of the northern West Siberia basin. Geostatistical modelling was applied to assess source rock richness and quality. Basal heat flow was modelled by calibration to bottom-hole temperature and vitrinite measurements. Hydrocarbon generation kinetic parameters were derived from measurements performed on West Siberia rock samples. Thermal gas charge expelled from the hydrocarbon kitchen drainage areas of key fields were compared with the gas volumes accumulated in these fields. The study found that Cretaceous terrestrial sources can generate sufficient early thermal gas to charge accumulations in the South Kara Sea area, and additional Jurassic sources can charge the remaining accumulations of the study area if favourable conditions apply. Biogenic gas is likely to have contributed to the gas accumulations. Mixing of thermal and biogenic gas could explain the observed isotopic composition. Sensitivity analyses show that the timing of structuring and uplift is the most critical factor of the assessment. Variations in glaciation, heat flow and source kinetics show less effect on the hydrocarbon accumulation.

Keywords: basin modelling, source rock, gas charge, Cenomanian, Pokur Formation (Fm.), West Siberia

The West Siberia Basin is one of the world's largest petroleum provinces, estimated to contain 356 billion barrels of oil equivalent (BBOE) of petroleum resources, of which 40% is oil and 60% is gas (Ulmishek 2003). The West Siberia basin is estimated to contain more than 70% of Russia's remaining undiscovered petroleum resources (USGS 2000), and the northern West Siberia basin is assessed to hold the largest undiscovered gas potential of any Arctic basin (Bird *et al.* 2008).

While the dominant oil play is the Neocomian clastics in the central parts of the basin, the dominant gas play is the Cenomanian Pokur Fm. in the northern West Siberia basin (Figs 1–3; Kontorovich *et al.* 1975; Surkov & Zhero 1981; Peterson & Clarke 1991). The Cenomanian gas play is moderately explored onshore in the Yamal and Gydan peninsulas, and poorly explored offshore in South Kara Sea.

Several giant gas fields have been discovered in the Cenomanian play (Grace & Hart 1986; Ulmishek 2003). The gas is characterized by being very dry and isotopically light. Methane content is normally up to 99%, and the average isotope ratio is in the range −45 to −65‰ δ^{13}C (Grace & Hart 1986; Littke *et al.* 1999). The largest gas field in West Siberia is the Urengoy Field with 330×10^{12} SCF in place, the second largest gas field in the world. In this study, Urengoy, together with Bovanenkovskoye (170×10^{12} SCF) and Leningradskoye (40×10^{12} SCF), will be used as reference fields to estimate gas expelled from different sources and drainage areas to charge these fields (gas-in-place estimates are approximate numbers from the ExxonMobil internal database).

The Cenomanian reservoir section consists of fluvial–deltaic sandstone, grading to shallow marine sandstone northward into the South Kara Sea (Fig. 2b). Maastrichtian marine, transgressive mudstones form an excellent seal rock in addition to intraformational sealing mudstones causing multi-reservoir levels in many of the fields. Cenozoic compression formed valid traps as four-way dip closures or fault-bounded inverted structures. Stratigraphic traps by facies pinchout add to the petroleum potential.

Several potential source rocks are present in the northern West Siberia basin to charge the Cenomanian fields. However, the single source or combination of sources to provide the large amounts of dry and isotopically light gas is still an enigma in spite of being actively studied by many authors for years (Kortsenshteyn 1977; Vasilyev *et al.* 1979; Rice & Claypool 1981; Kontorovich 1984; Grace & Hart 1986; Galimov 1988; Prasolov 1990; Stroganov 1990; Rovenskaya & Nemchenko 1992; Surkov & Smirnov 1994; Schoell *et al.* 1997; Cramer *et al.* 1999; Kontorovich *et al.* 1999; Littke *et al.* 1999; Nemchenko *et al.* 1999; Ulmishek 2003).

The main proposed models are (Ulmishek 2003):

(1) Early thermal gas from Cretaceous terrestrial organic matter (Vasilyev *et al.* 1979; Galimov 1988; Stroganov 1990; Rovenskaya & Nemchenko 1992; Nemchenko *et al.* 1999). Coals and disseminated organic matter in the Pokur Fm. and Tanopcha Fm. can produce isotopically light gas to match the gas in Cenomanian fields. However, the formations are early to immature

VINING, B. A. & PICKERING, S. C. (eds) *Petroleum Geology: From Mature Basins to New Frontiers – Proceedings of the 7th Petroleum Geology Conference*, 659–668. DOI: 10.1144/0070659

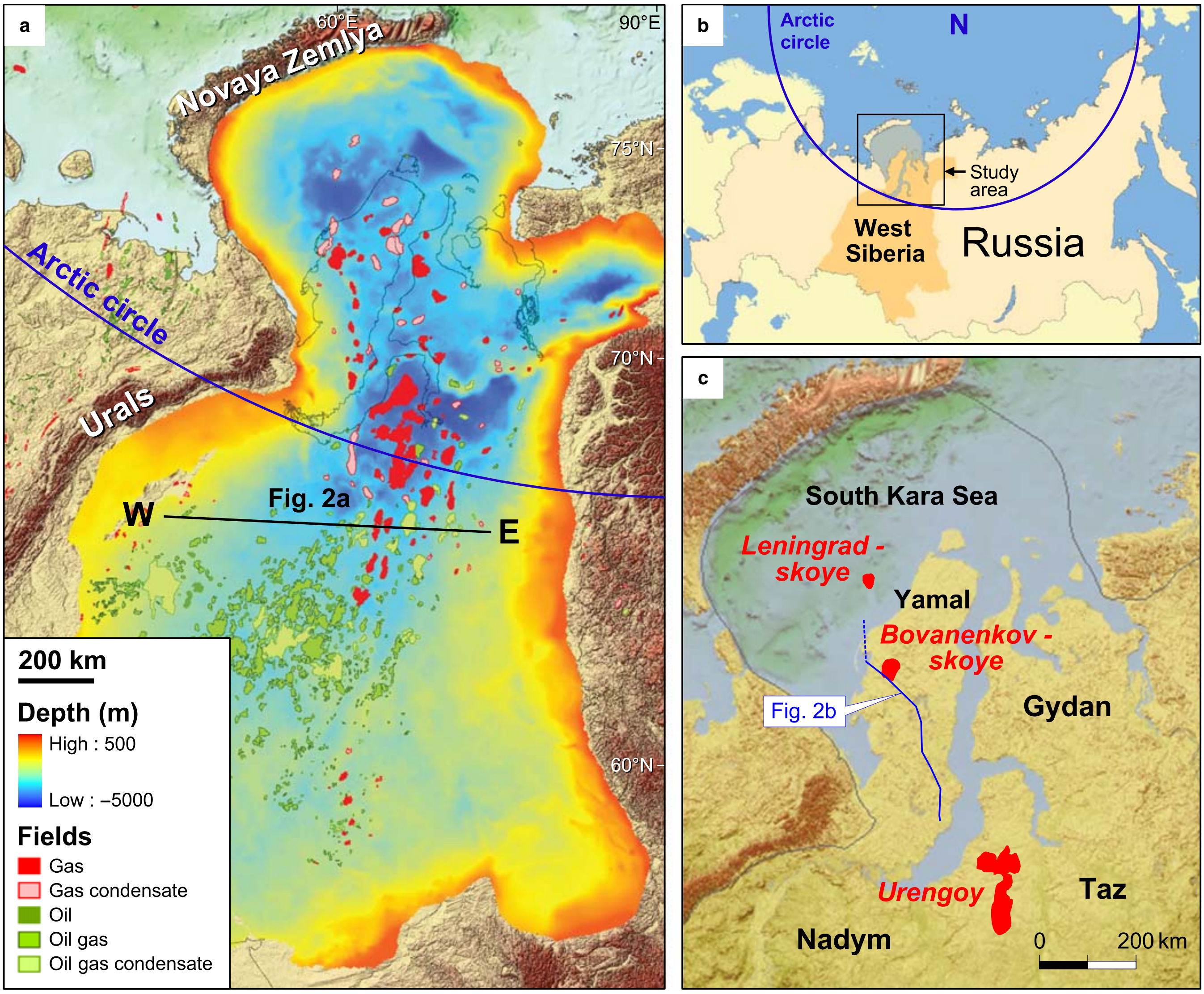

Fig. 1. (**a**) West Siberia basin Top Jurassic depth map including hydrocarbon fields superimposed on present-day topography. (**b**) Russia index map including West Siberia basin and study outline. (**c**) Northern West Siberia study area of 3D basin modelling project including reference fields.

for gas generation, and sufficient expulsion to charge the giant fields may not be achieved.

(2) Late thermal gas from Jurassic marine organic matter (Prasolov 1990). The prolific Jurassic Bazhenov Fm. and Tyumen Fm. oil-prone mudstones are currently in the gas window in most of the study area (Fig. 4), and gas produced from kerogen or cracked from oil may charge the Cenomanian fields. Migration pathways from the Jurassic sources to the Cenomanian fields are known to exist from source to oil correlation of remnant oil along the rims of Cenomanian fields (Kontorovich *et al.* 1999). However, the isotopic composition and dryness of the Cenomanian gas is not in agreement with a heavy and wet gas charge expected from late thermal gas sources.

(3) Biogenic gas is dry and isotopically light, but the volume generated is difficult to estimate. Cretaceous coals and mudstones may be in a favourable position for biogenic gas production, and methane may have been produced by biodegradation from previous hydrocarbon accumulations (Larter *et al.* 2005).

(4) Storage of thermal gas in Cretaceous water coupled with degassing after uplift and trap formation. This method was first discussed by Kortsenshteyn (1977) and later by Littke *et al.* (1999).

(5) Diffusion is discussed as a potential method by Ulmishek (2003).

The aim of this study was to apply a high-resolution 3D basin model to quantitatively assess contribution from Cretaceous and Jurassic sources to charge the Cenomanian gas fields (models 1 and 2 above) and to qualitatively assess the conditions for biogenic gas contribution from Cretaceous organic matter (model 3 above). The study was performed as a joint research project between the Institute of Petroleum Geology and Geophysics – Russian Academy of Sciences Siberian Branch (IPGG – RAS SB) and ExxonMobil.

Geology

Structure

The West Siberia basin is the world's largest intracratonic basin covering more than 3×10^6 km^2 (Fig. 1). It extends under the South Kara Sea, and is delineated by Novaya Zemlya in the north, the Ural mountains in the west, the East Siberia craton in the east and the Altay mountains in the south (Kontorovich *et al.* 1975; Surkov & Zhero 1981; Peterson & Clarke 1991). The basement was formed during the Carboniferous–Earliest Permian as accretionary crust between the colliding Baltic and Siberian cratons, forming a significant part of the Pangea supercontinent (Ziegler 1989; Sengor & Natal'in 1996). The collision formed the

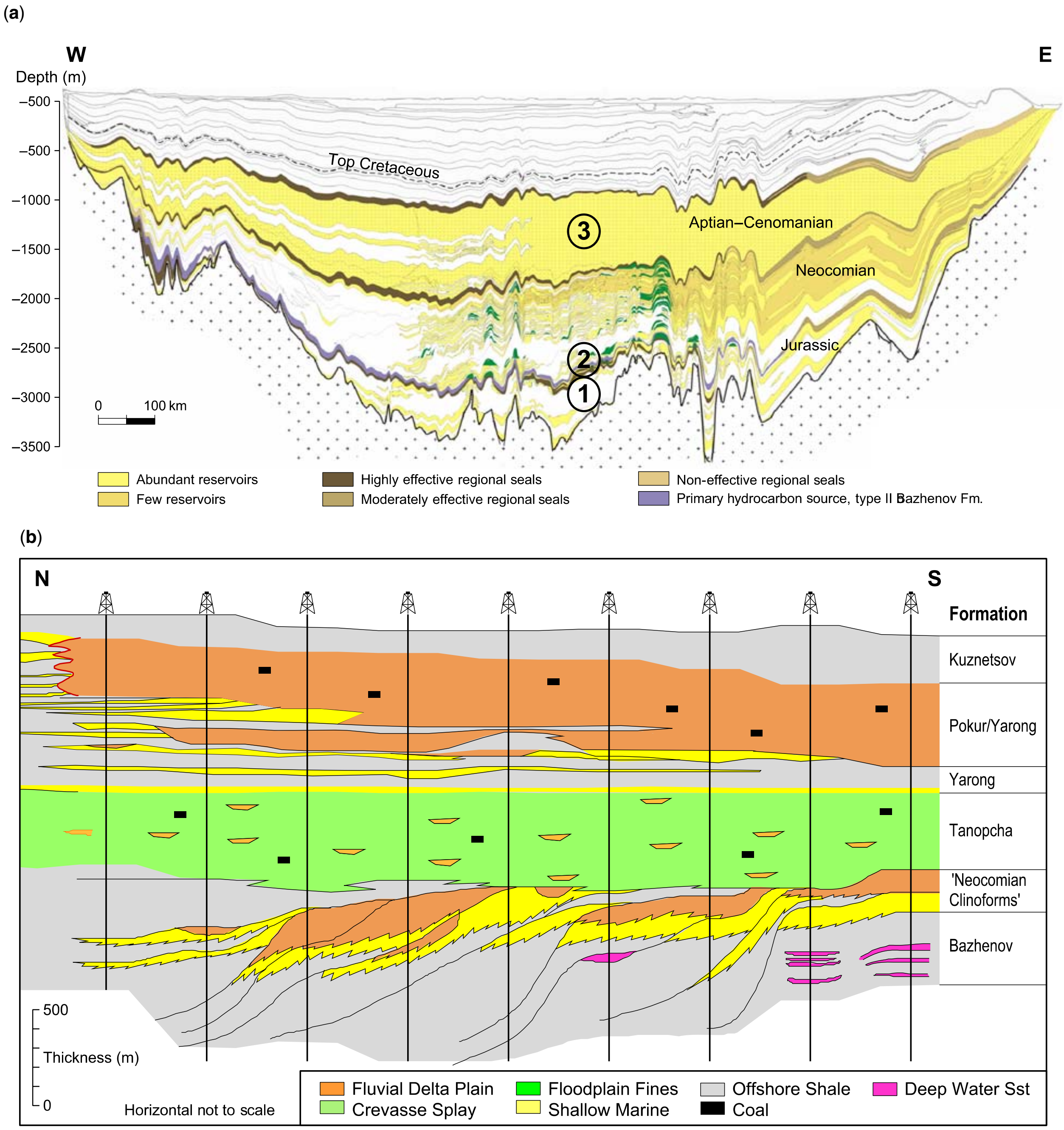

Fig. 2. (**a**) Schematic cross-section of the petroleum systems of West Siberia basin. For location see Figure 1. Key source intervals are (1) Mid Jurassic Tyumen Fm. coal and shale, (2) Late Jurassic Bazhenov Fm. marine shale and (3) Aptian–Cenomanian Pokur Fm. terrestrial coal and shale. (**b**) Schematic correlation through fields in the Kara Sea and Northern Yamal Peninsula (J. Maynard, pers. comm.).

Urals in the west by structural compression migrating from the south to the north (Nikishin *et al.* 1996; Fokin *et al.* 2001).

During the Early Permian, Pangea started breaking up, and a compressional phase formed the Novaya Zemlya Island in the north (Nikishin *et al.* 1996; Fokin *et al.* 2001). A dominantly north–south trending rift developed in northern West Siberia. Thick and extensive basalts were extruded to fill the rifts and surrounding areas, known as the East Siberian traps (Shipilov & Tarasov 1998; Vyssotski *et al.* 2006).

Clastics contributed to fill the Permian rifts, and during the subsequent thermal sag, the basin was filled with up to 12 km of Mesozoic sediments. In the Cenozoic the basin was uplifted and eroded as a result of India's collision and the opening of the arctic Eurasia basin (Vyssotski *et al.* 2006). Faults were inverted, forming traps for hydrocarbon fields.

Stratigraphy

The northern and central West Siberia basin stratigraphy is summarized in Figure 3. During the Permian continental deposits and volcanics filled the rift graben, and up to 7 km of Triassic clastics were deposited in the northern West Siberia basin.

In the Jurassic, fluvial and deltaic deposits were sourced from the Altay mountains in the south. However, marine transgressions periodically flooded the rifted basin from the north, gradually covering large parts of the basin with marine sediments. Organic-rich mudstones of Tyumen Fm. and Bazhenov Fm. were deposited and became excellent source rocks, with shallow marine sandstones of the Tyumen Fm. and Vasyugan Fm. forming good reservoirs.

During the Early Cretaceous (Neocomian) fluvial–deltaic deposits of the Megion Fm. prograded from east to west as a series of

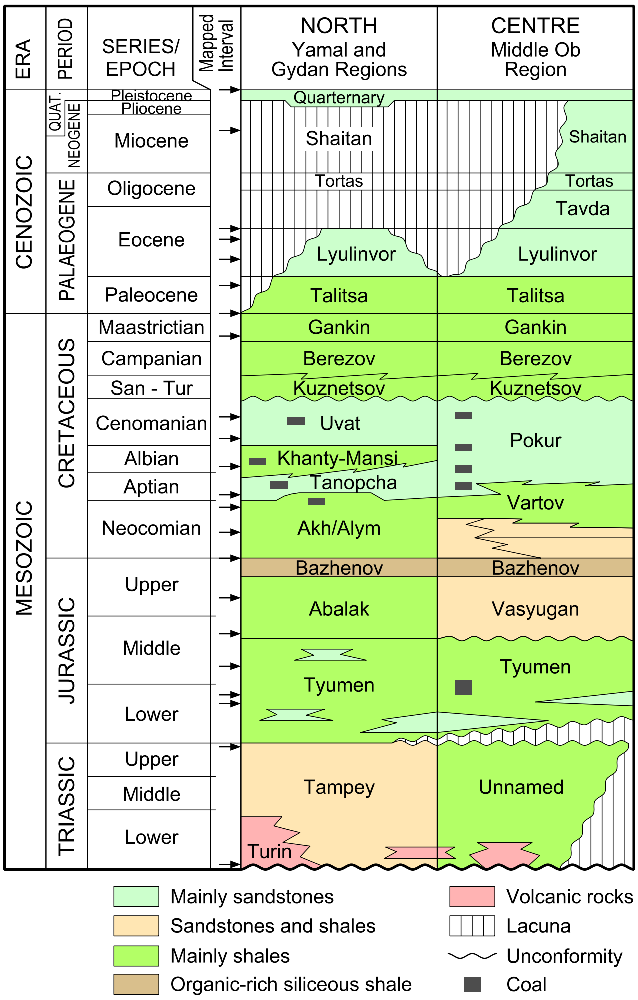

Fig. 3. Mesozoic chronostratigraphy of the northern and central West Siberia basin (modified from Ulmishek 2003). Stratigraphic levels of structure maps used for the study are marked by arrows.

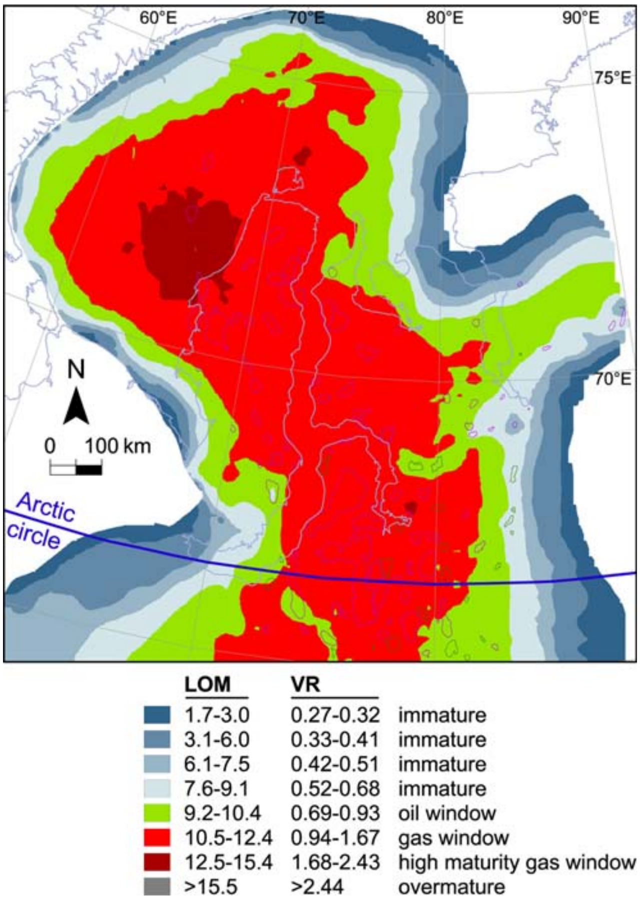

Fig. 4. Bazhenov Fm. present-day maturity map. Coastline and field outlines are annotated.

clinoforms (Fig. 2a). Deep-marine sands of the Achimov Fm. were deposited at the toe slope of the clinoforms. The Neocomian fluvial–deltaic deposits constitute the main oil play in the central West Siberia basin. An Aptian marine flooding event caused deposition of continuous mudstone (Alym Fm.) that acted as a regional seal to the Neocomian deposits.

Two renewed phases of fluvial–deltaic sediments filled the basin, firstly in Aptian (Tanopcha Fm./Pokur Fm.) and then, following an Albian marine flooding event (Yarong Fm.), Cenomanian fluvial–deltaic deposits (Pokur Fm.). These deposits grade to shallow marine sandstones in the northern part of the West Siberia basin, and deep marine mudstones in central parts of the South Kara Sea (Fig. 2b). The Pokur Fm. is interpreted as dominantly fluvial–deltaic along the South Kara Sea basin margins. These deposits form the Cenomanian gas play discussed in this paper. A Turonian flooding event (Kuznetsov Fm.) formed marine mudstone acting as a seal to the Pokur Fm. play.

In central parts of the West Siberia basin the Pokur Fm. includes the Aptian to Cenomanian fluvial–deltaic sediments. In the northern West Siberia basin, the Albian Yarong Fm. marine mudstone separates the Aptian from the Cenomanian fluvial–deltaic sediments, and the Aptian section is named Tanopcha Fm. (Fig. 3). For simplicity, in this paper the Aptian fluvial–deltaic sediments are referred to as the Tanopcha Fm. and the Albian to Cenomanian fluvial–deltaic sediments are referred to as the Pokur Fm. within the entire study area.

Cenozoic uplift brought continental conditions to the West Siberia basin, with erosion, sediment by-pass or fluvial deposits at various times (Fig. 3; Surkov & Smirnov 1994; Ulmishek 2003). During Pleistocene several glacial events caused ice cover and tills to be deposited in NW Siberia.

Today the West Siberia basin is a flat-lying, swampy basin with permafrost in the upper 300–500 m and a shallow sea (South Kara Sea) in the northernmost part of the basin.

Analyses

A high-resolution 3D basin model was constructed for the northern West Siberia basin (Fig. 1), using ExxonMobil's proprietary Stellar^{TM} 3D basin modelling software. The model had many purposes, one of which was to assess the gas charge to the Cenomanian play. Questions raised were: how much gas is generated from thermal sources within the drainage areas of selected fields after trap formation? To what extent can this help in understanding the gas charge to the Cenomanian fields?

The high-resolution 3D basin model was constructed by establishing a stratigraphic section, boundary conditions and a source model. The stratigraphic section was built from isopach maps of 22 structural horizons covering the entire Triassic to present-day sedimentary interval (Fig. 3). The structure maps were dominantly derived from well information onshore and seismic interpretation offshore. Missing section maps were produced from estimated erosion during Cenozoic uplift. Lithology composition was entered for each isopach, split into percentage sandstone, mudstone and coal. The lithology composition was calibrated against well logs from a large number of onshore wells, and then extrapolated to the offshore and undrilled areas based on depositional environment maps.

Thermal boundary conditions were defined to enable source maturity calculations to be performed. The thermal model is bounded by the surface temperature at the top of the sedimentary section and the basal heat flow from below the sediments through time.

The palaeosurface temperatures were entered using ExxonMobil's global climate model through geological history. Palaeowater depth maps at 16 key intervals were entered to provide correct subsea temperature, palaeotopography and decompaction of the sedimentary section. Surface temperature estimates during the Quaternary glaciation required special consideration. Mapped permafrost thickness was used to calibrate the effect of glaciation on present-day subsurface temperature.

The basal heat flow was modelled as the sum of the Triassic (240 Ma) rifting heat flow anomaly and the background heat flow. The background heat flow represents the heat loss from the earth's interior together with radiogenic heat production, and is modelled as constant through time. The heat flow associated with the Triassic rifting is represented by a gamma map, which represents the thinning of the crust during rifting. The present-day regional basal heat flow map was calibrated against more than 2000 temperature and vitrinite measurements from 72 wells across the study area.

A source model was built to perform yield (expulsion) calculations. Maps of source richness (total organic carbon, TOC) and quality (hydrogen index, HI) are required as input parameters for yield analyses. An extensive rock-eval database was established and geostatistical analyses performed to determine the optimal mapped representation of the source richness and quality.

Four sources for thermogenic hydrocarbons were considered for the basin model: (1) Cenomanian deltaic coals and mudstones (Pokur Fm.); (2) Aptian deltaic coals and mudstones (Tanopcha Fm.); (3) Upper Jurassic marine mudstones (Bazhenov Fm.); and (4) Middle Jurassic marine mudstones and coals (Tyumen Fm.).

Stellar^{TM} default kinetic parameters for kerogen transformation were applied. However, with respect to the sensitivity analyses of early gas generation from Cretaceous mudstones and coals, the parameters were derived from relevant Cretaceous coals in West Siberia.

Results

The gas charge to the Cenomanian play was tested by running the Stellar 3D basin model over the entire study area, and then calculating the amounts of gas expelled within the drainage areas of three representative fields. The gas yield was then compared with the original gas-in-place volumes accumulated in the Cenomanian reservoirs of these fields. The three fields were Urengoy, Bovanenkovskoye and Leningradskoye, comprising 330, 130 and 40×10^{12} SCF gas, respectively.

First the thermal yields from the Cretaceous sources Pokur Fm. and Tanopcha Fm. were calculated within the drainage areas, applying best estimate parameters ('base case Cretaceous sources'). Secondly, key parameters were optimized to evaluate a scenario of early gas generation from the Cretaceous sources ('high case Cretaceous sources'). The parameters were also each varied to test their relative contribution to the increased volumes obtained by the early gas case scenario. Thirdly, the cumulative thermal yields from both the Cretaceous and the Jurassic sources were calculated for the same drainage areas ('base case all sources'). Finally, an early gas scenario was run to optimize the expelled amounts of gas including both Cretaceous and Jurassic sources ('high case all sources').

The yield from the Cretaceous sources applying base case parameters is represented on Figure 5. The graph on Figure 5a

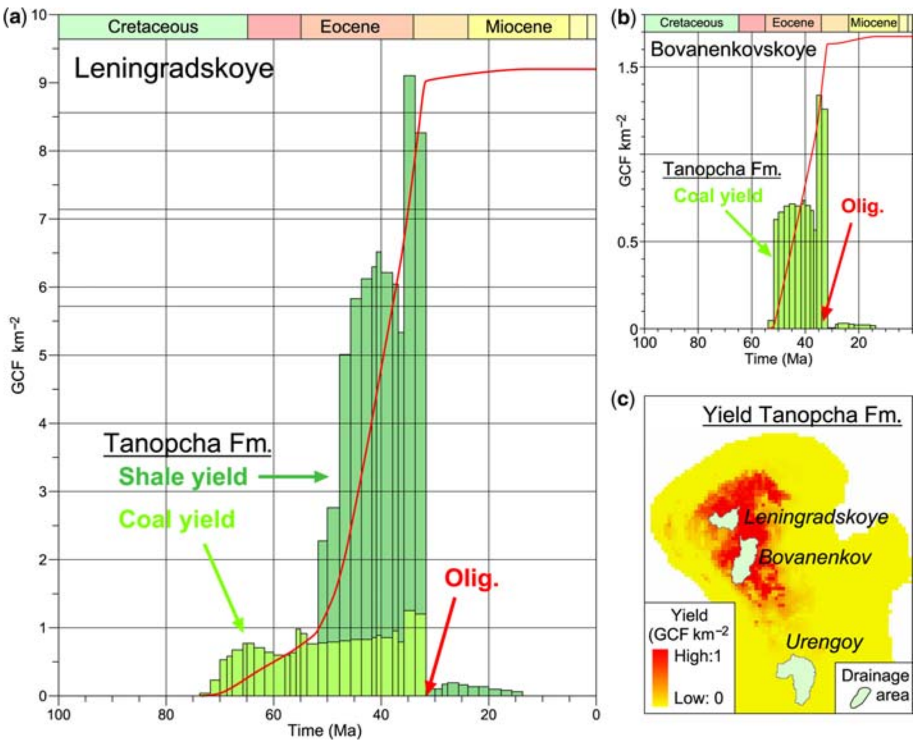

Fig. 5. Base case Cretaceous sources: (**a**) gas yield (in GCF km^{-2}) through time for the Leningradskoye field drainage area for the Tanopcha Fm. source applying base case parameters (Table 2). The Pokur Fm. was immature for gas generation. Shale yield is plotted in dark green and coal yield in bright green. Note the large volumes expelled post-Paleocene compared with post-Oligocene, and thus the importance of trap timing. (**b**) Gas yield through time for the Bovanenkovskoye field drainage area for the Tanopcha Fm. source applying base case parameters (Table 2). The Pokur Fm. was immature for gas generation. (**c**) Map of gas yield for Cretaceous sources applying base case sensitivity. Drainage areas of the selected fields are shown. All yield is from the Tanopcha Fm. The Pokur Fm. was immature for gas generation in the entire study area.

Table 1. Gas volumes accumulated in Cenomanian reservoirs and expelled from sources in the drainage areas of the Leningradskoye, Bovanenkovskoye and Urengoy fields (approximate numbers)

Field/drainage gas volumes	Leningradskoye ($\times 10^{12}$ SCF)	Bovanenkovskoye ($\times 10^{12}$ SCF)	Urengoy ($\times 10^{12}$ SCF)
Cenomanian field in-place gas volume (approximate)	40	170	330
Gas available from drainage area			
Base case Cretaceous source	2	3	0
Base case Jurassic + Cretaceous sources	8	8	7
High-case Cretaceous source	333	81	0
High-case Jurassic + Cretaceous sources	504	618	411

shows gas yield per km^2 within the drainage area of the Leningradskoye field plotted against time. Gas yield occurs from the Tanopcha Fm. only as the younger Pokur Fm. is not buried sufficiently deep for gas generation to be initiated. The Tanopcha Fm. yield started in late Cretaceous and peaked in late Eocene. A subsequent marked drop in yield is modelled due to basin uplift and folding. This folding event corresponds to the time of trap formation in the base case scenario, which implies that only a minor amount of gas expelled after the start of the Oligocene at 32 Ma is available for entrapment. In the Leningradskoye drainage area, 2×10^{12} SCF only were generated post-Eocene in our base case, which is far from sufficient to charge the 40×10^{12} SCF gas-in-place in Leningradskoye (Table 1).

A similar situation applies for Bovanenkovskoye, where 1×10^{12} SCF gas only is expelled from the drainage area (Fig. 5b), and gas from coals only are generated here. In the Urengoy drainage area there is no gas yield from Cretaceous sources in the base case.

The regional distribution of gas yield from the Cretaceous sources is displayed on Figure 5c. The drainage areas of the study fields Leningradskoye, Bovanenkovskoye and Urengoy are also annotated on the map. Gas expulsion from Cretaceous sources is limited to the deepest parts of the basin in South Kara Sea, and from the Tanopcha Fm. only when base case parameters apply.

Table 2. Sensitivity parameters applied to base case and high case scenarios listed in order of impact on results

Sensitivity factor	Base case	High case
Trap timing	Early Oligocene	Early Palaeocene
Eocene erosion (m)	300	0
Source thickness	Best estimate map	Best estimate +20% map
Kinetic parameters	Best estimate	Early generation
Basal heat flow	Best estimate map	Best estimate map +5 mW m^{-2}

Eocene erosion adds to the missing section maps prepared for post-Eocene isopach maps, which was applied to all sensitivity cases.

A high case scenario was defined by applying a sensitivity range on key parameters to realistically improve the yield from the Cretaceous sources. In the base case, trap timing was defined to occur in Early Oligocene at 32 Ma, representing a major tectonic folding phase in West Siberia related to the collision of India with the Asian plate. All Cenomanian traps were in place after this event. In the high case, trap timing was set to the Early

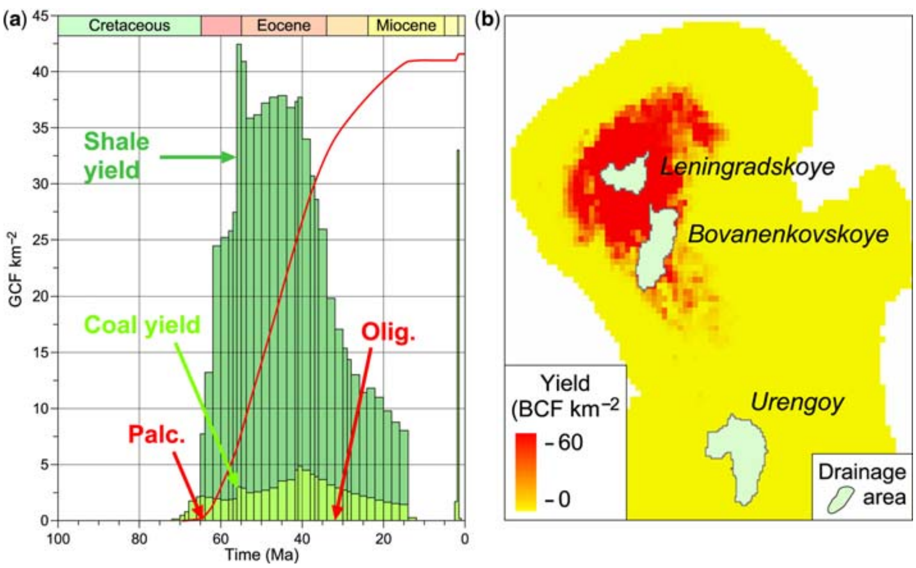

Fig. 6. High case Cretaceous sources: (**a**) Gas yield through time for the Leningradskoye field drainage area for the Tanopcha Fm. source applying high case sensitivity (Table 2). The Pokur Fm. was immature for gas generation. Note the large volumes expelled post-Paleocene compared with post-Oligocene, and thus the importance of trap timing. (**b**) Map of gas yield for Cretaceous sources applying high case sensitivity. Drainage areas of the selected fields are shown. All yield is from the Tanopcha Fm. The Pokur Fm. was immature for gas generation in the entire study area. Note the scale difference between Figures 5b and 6c.

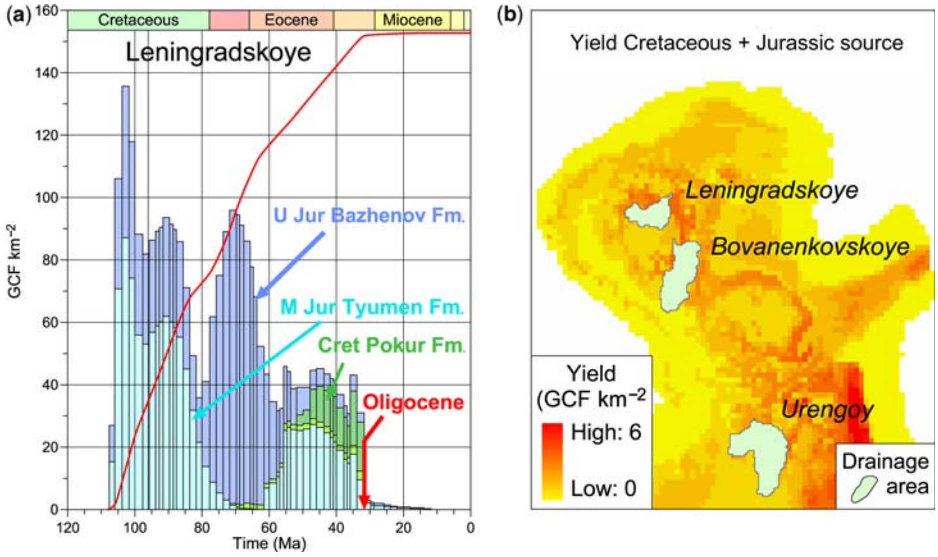

Fig. 7. Base case all sources: (**a**) gas yield through time for the Leningradskoye field drainage area for Cretaceous and Jurassic sources (Table 2 base case). Bazhenov Fm. source yield is in dark blue, Tyumen Fm. yield in light blue and Tanopcha Fm. yield in green. (**b**) Map of gas yield for Cretaceous and Jurassic sources using base case parameters.

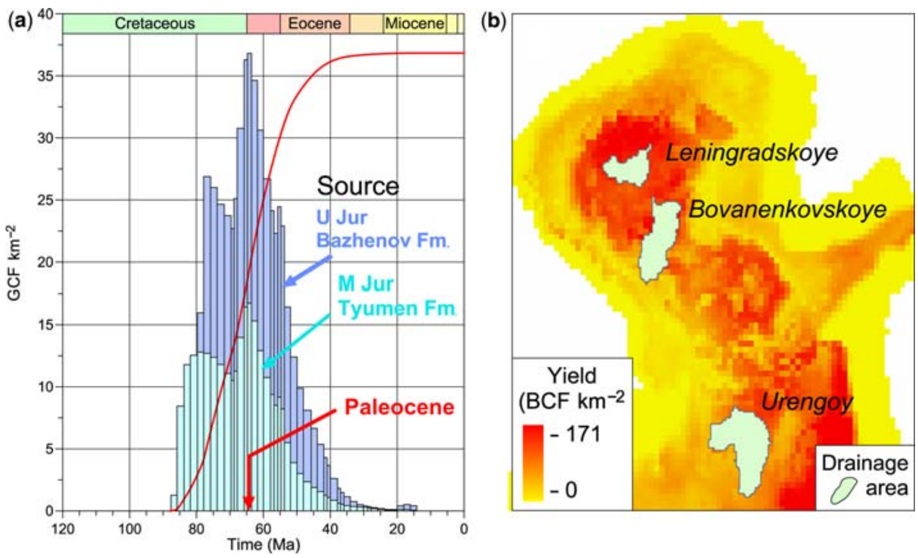

Fig. 8. High case all sources: (**a**) gas yield through time for the Urengoy field drainage area for Cretaceous and Jurassic sources (Table 2 high case). The contribution is from Jurassic sources only as the Cretaceous sources are immature at this location. (**b**) Map of gas yield for Cretaceous and Jurassic sources (high case sensitivity).

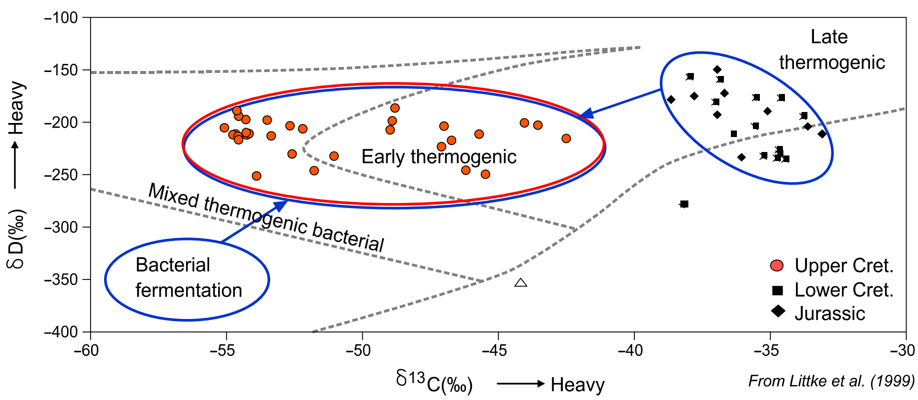

Fig. 9. Isotopic composition of methane from fields in northern West Siberia. Modified from Littke *et al.* (1999). Genetic classification after Schoell (1980) and Whiticar (1990).

Paleocene at 65 Ma. Uplift and basin inversion are described in the literature (Vyssotski *et al.* 2006) and interpreted on seismic lines to be as early as Maastrichtian in age, which means that Cenomanian traps may have started forming already in the Paleocene. The exact trap timing varies across the basin, and thus trap timing is used as a sensitivity factor. Uplift and erosion were also important factors that affected the gas yield. Cenozoic erosion was estimated based on missing section maps of Cenozoic intervals, and for simplicity interpreted to take place at Base Quaternary. However, additional erosion was set to occur in the Eocene, being varied between 0 and 500 m as a sensitivity factor. Source thickness was varied by $\pm 20\%$, a range of kinetic parameters were applied, and heat flow was varied by $\pm 5\%$ (Table 2).

The gas yield from the Cretaceous sources, including all high case parameters within the Leningradskoye drainage area, is displayed in Figure 6a. The cumulative gas yield has increased significantly, from 9 to 42 GCF km^{-2} (red curves on Figs 5a & 6a). Generation started in the Maastrichtian (70 Ma), but significant generation did not start until the Early Paleocene (65 Ma). The yield peaked in the Eocene and then gradually decreased during the Oligocene–Miocene due to restricted burial.

Simulations were also run varying one parameter at the time. The relative contribution from each parameter in the high case is listed in Table 2. Trap timing stands out as the dominant factor. Large additional volumes are included by changing trap timing from 32 Ma in Early Oligocene to 65 Ma in Early Paleocene (Fig. 6a). The effect of reducing uplift and erosion is expressed by additional late gas yield compared with the base case (post 30 Ma). Source thickness, kinetics and heat flow as defined in the model had a minor impact on the results.

The high case parameters for charge from Cretaceous sources were also applied to the Bovanenkovskoye and Urengoy drainage areas (Fig. 6b). When applying high case yield parameters, the Bovanenkovskoye gas charge is about half that required to fill the trap, and there is still no expulsion in the Urengoy drainage area. This shows that the Cretaceous sources alone cannot charge all the Cretaceous fields.

Two Jurassic sources, the Upper Jurassic Bazhenov Fm. and the Middle Jurassic Tyumen Fm., were introduced to the 3D basin simulation, and base case sensitivity parameters were applied. Figure 7 shows the gas yield for the base case scenario from the Leningradskoye field drainage area through time for all thermal sources. In dark blue is the Bazhenov Fm. source yield and in light blue the Tyumen Fm. yield. Jurassic gas yield starts in Early Cretaceous. Gas co-generated with oil is expelled until Campanian (80 Ma). After Campanian the Bazhenov Fm. passed through the late gas generation stage with expulsion of significant amounts of cracked gas. The Tyumen Fm. expelled cracked gas during the Cenozoic, in parallel with early mature gas from the Tanopcha Fm. A marked drop in gas expulsion occurred during uplift and erosion post-Eocene.

The total volume expelled in the drainage area is 8×10^{12} SCF, which is not enough to charge the Leningradskoye field. Similar situations apply for Bovanenkovskoye and for Urengoy drainage areas, charging 8 and 7×10^{12} SCF, respectively (Table 1).

As a final test, the high case parameters were applied to all thermal sources. Significant gas volumes are expelled in all drainage areas, including the Urengoy drainage area (Fig. 8). Table 1 shows that when all high case parameters are applied, the Urengoy drainage area yields more than 400×10^{12} SCF gas. This is 25% more than the 300×10^{12} SCF gas stored in the Urengoy Cenomanian reservoir, that is, a charge multiplier of 1.25. Table 1 shows that the charge multiplier is 4 for Bovanenkovskoye and 10 for Leningradskoye. By varying the sensitivity parameters one by one, trap timing became the dominant factor and erosion was of second most importance.

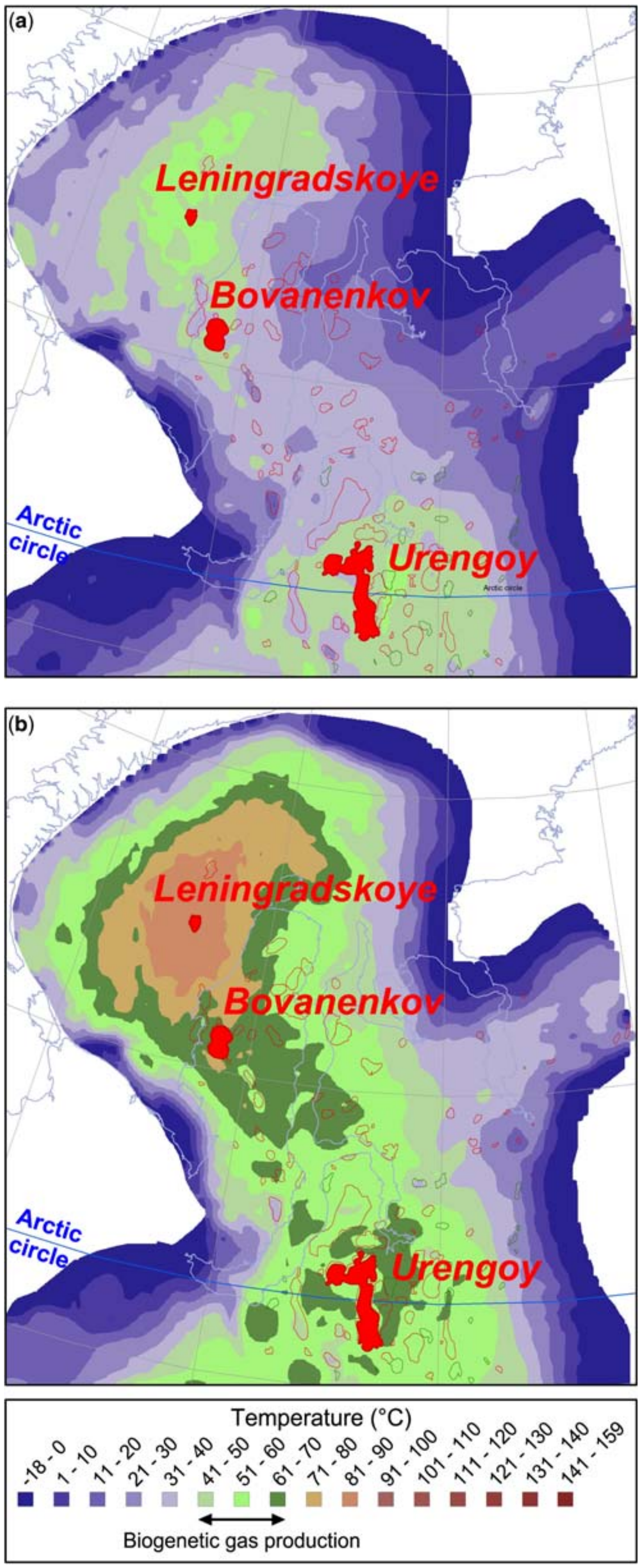

Fig. 10. (**a**) Pokur Fm. temperature map in Miocene (10 Ma). (**b**) Tanopcha Fm. temperature map in Miocene (10 Ma).

In summary, more thermal gas has been generated in the drainage areas of the Cenomanian fields in northern West Siberia than accumulated in the traps if all thermal sources are taken into account and if very favourable geological conditions apply.

Discussion

The simulation results show that, when applying high case parameters for all sources, the amounts of thermal gas expelled in the drainage areas of the selected fields exceeds the original in-place volumes in the fields. However, migration loss has not been taken into account. The Urengoy field has a charge multiplier of 1.25 and it is unlikely that sufficient gas has reached the structure from its immediate kitchen. However, fill–spill mechanisms have not been considered, and this may expand the drainage area for Urengoy substantially.

Even if additional volumes of late thermal gas from Jurassic sources are made available by expanding the drainage area to the Urengoy field, its gas charge cannot be explained by Jurassic charge alone since the isotopic composition of the gas stored in the field does not correspond to a late thermal source. This is documented by Littke *et al.* (1999), who plotted isotopic values of $\delta^{13}C$ against deuterium of methane from fields in northern West Siberia (Fig. 9). The graph shows the zones where early and late thermogenic methane and biogenic methane generally plots. Gases from the West Siberia Cenomanian reservoirs plot in the early thermogenic range, marked in red. This is consistent with the maturity of the Cretaceous sources.

West Siberia gases from Jurassic sources plot in the late thermogenic area, marked in black. Hence Jurassic sources cannot be the only source charging Urengoy since the isotopic ratios do not match. However, if the Jurassic gases are mixed with bacteria-produced gas, the mixture may plot in the zone of the Cenomanian fields, and thus be the origin of the gas, or at least make a contribution together with gas from the Cretaceous sources.

Hence a unique source to gas correlation is hard to establish. Furthermore, the extreme dryness of the gas (98–99%) implies that biomarkers and wet gas parameters cannot be used to discriminate the origin of the gas.

Biogenic gas is formed at shallow depths and low temperatures, between 40°C (or even lower) and 70–80°C, by anaerobic bacterial decomposition (biodegradation) of sedimentary organic matter and accumulated oil (e.g. Winters & Williams 1969). The Tanopcha Fm. and Pokur Fm. contain significant amounts of coals and disseminated organic matter. Figure 10 shows the temperature map of the Tanopcha Fm. and Pokur Fm. 10 Ma ago. The Stellar model shows that for the last 10 million years, the Tanopcha Fm. in the Urengoy area was between 40 and 70°C, marked by green colours on the map. The Leningradskoye and Bovanenkovskoye drainage areas are buried deeper and have temperatures above 70°C. In the last 10 Ma the Pokur Fm. has been exposed to temperatures in the range 40°C–70°C in the entire study area. It is therefore likely that biogenic gas is produced from the Pokur Fm.

Biodegraded oils from Jurassic sources are present in Cenomanian gas fields (e.g. Kontorovich 1984; Peters *et al.* 1994), and residual oil is normally found along the rim of the gas accumulations (Grace & Hart 1986). In biodegraded oil fields, isotopically lighter methane is commonly found mixed with thermogenic methane (Larter *et al.* 2005). The carbon isotopic composition of methane associated with subsurface oil biodegradation conditions in marine petroleum systems is frequently in the range of -45 to -55‰ $\delta^{13}C$, which is in agreement with the observations made by Littke *et al.* (1999) for the West Siberia Cenomanian gas fields (Fig. 9). Therefore, isotopically light methane in the Cenomanian fields may have been generated from biodegradation of oil charged from Jurassic sources.

In summary, there are favourable conditions for biogenic gas to supplement the gas volumes stored in the Cenomanian gas fields, as biogenic gas generated both from disseminated organic matter and from biodegraded oil pools.

Conclusions

The Cenomanian gas fields in northern West Siberia comprise the world's largest gas province. However, the gas charge to the fields is poorly understood in spite of being extensively studied by many authors.

In this study, gas yield from established Cretaceous and Jurassic sources was calculated using ExxonMobil's Stellar™ 3D basin modelling software to quantitatively estimate charge to selected Cenomanian fields. This quantitative approach eluded the most likely source intervals to charge the fields in different parts of the basin.

The study showed that Cretaceous terrestrial sources generate sufficient early thermal gas to charge fields in the deepest areas of South Kara Sea (e.g. Leningradskoye), and may contribute to the gas charge in the Yamal area (e.g. Bovanenkovskoye). No gas is generated from Cretaceous sources in the Nadym–Taz regions (e.g. Urengoy) due to shallow burial. Hence Cretaceous sources can fully or partly charge the Cenomanian gas fields in the deepest parts of South Kara Sea, and may contribute to charging gas fields on the Yamal peninsula.

Additional Jurassic sources may generate sufficient thermal gas to charge the fields in the entire study area, but only if favourable geological conditions apply. Sensitivity analyses showed that trap timing and amount of erosion were the most sensitive geological factors for thermal gas charge. Kinetics, heat flow and source thickness were of less importance in this study.

The isotopic composition of methane from Cenomanian fields shows an early gas generation signature, which is consistent with early thermal gas from the shallow Cretaceous sources, but not with the late thermal gas generated from the deeply buried Jurassic sources in the study area (Fig. 9). However, biogenic gas admixing with late thermal gas from Jurassic sources may balance the isotopic composition observed for the Cenomanian gas accumulations and plot as a gas with an early thermal generation signature. There are favourable temperature conditions for biogenic gas production from organic-rich intervals in the basin. Hence biogenic gas is likely to have contributed to the gas fields and admixed with gas from Jurassic sources.

The authors would like to thank ExxonMobil and IPGG–RAS SB for permission to publish this paper. Many thanks to the numerous geoscientists in IPGG and ExxonMobil who provided technical input during the course of the study. Special thanks to Michael Brown and James Maynard for their thorough review of the paper.

References

Bird, K. J., Charpentier, R. R. *et al.* 2008. Circum-Arctic Resource Appraisal: Estimates of Undiscovered Oil and Gas North of the Arctic Circle. US Geological Survey Fact Sheet 2008-3049.

Cramer, B., Poelchau, H. S., Gerling, P., Lopatin, N. V. & Littke, R. 1999. Methane released from groundwater – the source of natural gas accumulations in northern West Siberia. *Marine and Petroleum Geology*, **16**, 225–244.

Fokin, P. A., Nikishin, A. & Ziegler, P. A. 2001. Pre-Uralian and Peri-Palaeo-Tethyan Rift systems of the East European Craton. *In*: Ziegler, P. A., Cavazza, W., Robertson, A. H. F. & Crasquin-Soleau, S. (eds) *Peri-Tethys Memoir 6: Peri-Tethyan Rift/Wrench Basins and Passive Margins.* Muséum National d'Histoire Naturelle, Mémoires, **186**, 347–368.

Galimov, E. M. 1988. Sources and mechanisms of formation of gaseous hydrocarbons in sedimentary rocks. *Chemical Geology*, **71**, 77–95.

Grace, J. D. & Hart, G. F. 1986. Giant gas fields of northern West Siberia. *American Association of Petroleum Geologists Bulletin*, **70**, 830–852.

Kontorovich, A. E. 1984. Geochemical methods for the quantitative evaluation of the petroleum potential of sedimentary basins. *In*: Demaison, G. J. & Murris, R. J. (eds) *Petroleum Geochemistry and Basin Evaluation*. American Association of Petroleum Geologists, Tulsa, OK, Memoirs, **35**, 79–109.

Kontorovich, A. E., Danilova, V. P. *et al.* 1999. Oil-source formations of West Siberia – old and new looks at the problem. *In*: Kontorovich, A. E. &

Vyshemirsky, V. S. (eds) *Organic Geochemistry of Oil-source Rocks of West Siberia (Organicheskaya geokhimiya nefteproizvodyashchikh porod Zapadnoy Sibiri)*. NITS OIGGM, Novosibirsk, 10–12.

Kontorovich, A. E., Nesterov, I. I., Salmanov, F. K., Surkov, V. S., Trofimuk, A. A. & Ervye, Yu. G. 1975. *Geology of Oil and Gas of West Siberia (Geologiya nefti i gaza Zapadnoy Sibiri)*. Nedra, Moscow.

Kortsenshteyn, V. N. 1977. *Aquifer Systems of the Largest Gas and Gas Condensate Fields of the USSR (Vodonapornye sistemy krupneyshikh gazovykh i gazikondensatnykh mestorozhdeniy SSSR)*. Nedra, Moscow.

Larter, S. R., Head, I. M. *et al*. 2005. Biodegradation, gas destruction and methane generation in deep subsurface petroleum reservoirs: an overview. *In*: Doré, A. G. & Vining, B. A. (eds) *Petroleum Geology: North-West Europe and Global Perspectives: Proceedings of the 6th Petroleum Geology Conference*. Geological Society, London, 633–640, doi: 10.1144/0060633.

Littke, R., Cramer, B. *et al*. 1999. Gas generation and accumulation in the West Siberian basin. *AAPG Bulletin*, **83**, 1642–1665.

Nemchenko, N. N., Rovenskaya, A. S. & Schoell, M. 1999. Origin of natural gases in giant gas fields of northern West Siberia. *Geologiya Nefti i Gaza*, **1–2**, 45–56.

Nikishin, A. M., Ziegler, P. A. *et al*. 1996. Late Precambrian to Triassic history of the East European Craton: dynamics of sedimentary basin evolution. *Tectonophysics*, **268**, 23–63.

Peters, K. E., Kontorovich, A. E., Huizinga, B. J., Moldowan, J. M. & Lee, C. Y. 1994. Multiple oil families in the West Siberian Basin. *AAPG Bulletin*, **78**, 893–909.

Peterson, J. A. & Clarke, J. W. 1991. *Geology and Hydrocarbon Habitat of the West Siberian Basin*. AAPG Studies in Geology #32. American Association of Petroleum Geologists, Tulsa, OK.

Prasolov, E. M. 1990. *Isotopic Geochemistry and Origin of Natural Gases (Izotopnaya geokhimiya i proiskhozhdeniye prirodnykh gazov)*. Nedra, Leningrad.

Rice, D. D. & Claypool, G. E. 1981. Generation, accumulation, and resource potential of biogenic gas. *AAPG Bulletin*, **65**, 5–25.

Rovenskaya, A. S. & Nemchenko, N. N. 1992. Prediction of hydrocarbons in the West Siberian basin. *Bulletin Centre de Recherche Exploration – Production Elf Aquitaine*, **16**, 285–318.

Schoell, M. 1980. The hydrogen and carbon isotopic composition of methane from natural gases of various origins. *Geochimica et Cosmochimica Acta*, **44**, 649–661.

Schoell, M., Picha, F., Rovenskaya, A. & Nemchenko, N. 1997. Genetic characterization of natural gases in NW Siberia [abstract]. *American Association of Petroleum Geologists International Conference*, Vienna, Abstract Volume, 46–47.

Sengor, A. M. C. & Natal'in, B. A. 1996. Paleotectonics of Asia: fragments of a synthesis. *In*: Yin, A. & Harrison, T. M. (eds) *The Tectonic Evolution of Asia*. Cambridge University Press, New York, 486–641.

Shipilov, V. & Tarasov, G. A. 1998. *Regional Geology of Oil and Gas Bearing Sedimentary Basins of the Russian West-Arctic Shelf*. Apatity, Russia, 306.

Stroganov, L. V. 1990. Genetic criteria and prognosis of zones of oil accumulation on Yamal Peninsula. *Geologiya Nefti i Gaza*, **10**, 2–5.

Surkov, V. S. & Smirnov, L. V. 1994. Cenozoic tectonic events and phase differentiation of hydrocarbons in the Hauterivian–Cenomanian complex of the West Siberian basin. *Geologiya Nefti i Gaza*, **11**, 3–6.

Surkov, V. S. & Zhero, O. G. 1981. *Basement and Development of the Platform Cover of the West Siberian Platform*. Nedra, Moscow, 142.

Ulmishek, G. F. 2003. Petroleum Geology and Resources of the West Siberia Basin, Russia. *USGS Bulletin*, **2201-G**, 1–49.

USGS World Energy Assessment Team. 2000. *US Geological Survey World Petroleum Assessment 2000 – Description and Results*. US Geological Survey Digital data Series – DDS60. World Wide Web Address. http://pubs.usgs.gov/dds/dds-060.

Vasilyev, V. N., Yermakov, V. I. & Nemchenko, N. N. 1979. Origin of natural gas in fields of the northern West Siberian plain. *Geologiya Nefti i Gaza*, **4**, 7–10.

Vyssotski, A. V., Vyssotski, V. N. & Nezhdanov, A. A. 2006. Evolution of the West Siberia Basin. *Marine and Petroleum Geology*, **23**, 93–126.

Winters, J. C. & Williams, J. A. 1969. *Microbiological Alteration of Crude Oil in the Reservoir*. American Chemical Society, Division of Petroleum Chemistry, New York, Meeting Preprints, **14**, E22–E31.

Whiticar, M. J. 1990. A geochemical perspective of natural gas and atmospheric methane. *Organic Geochemistry*, **16**, 531–547.

Ziegler, P. A. 1989. *Evolution of Laurussia*. Kluwer Academic, London, **102**, 14 plts.

Session: North Africa and Middle East

Middle East and North Africa: overview

J. REDFERN[1] and J. CRAIG[2]

[1]*University of Manchester, School of Earth, Atmospheric and Environmental Sciences, Basin Analysis and Petroleum Geoscience Group, Williamson Building, Oxford Road, Manchester M13 9PL, UK*
[2]*Eni Exploration & Production Division, Via Emilia 1, 20097 San Donato Milanese, Milan, Italy (e-mail: jonathan.craig@eni.com)*

North Africa and the Middle East hold huge reserves and resources of oil and gas and are some of the most important regions for future hydrocarbon production. Recent drilling successes onshore Algeria and offshore Egypt, and renewed industry interest in Libya have re-invigorated exploration in North Africa. The Middle East holds the majority of the world's remaining oil and gas and offers a showcase for new research into the major plays and recent exploration/production advances. The North Africa and Middle East session at the 7th Petroleum Geology Conference brought together 12 papers ranging from keynotes on regional play evaluation to detailed field studies. Ten of those papers are published in this volume.

Craig *et al.* provide a regional perspective that spans North Africa and the Middle East. The paper examines the entire stratigraphic interval and highlights the more challenging, older and deeper plays and higher risk, but more conventional, plays in under-explored frontier areas. It offers some thoughts on the potential to develop new play concepts and to extend known producing plays into new areas. Focusing on North Africa, Eschard *et al.* discuss the timing of uplift of palaeohighs and how they have influenced the Palaeozoic petroleum systems in terms of reservoir and source rock development and trapping configuration. They document how the interplay of tectonics, eustacy and subsidence rate produce complex stratigraphic wedge geometries which have important exploration significance. The paper by Lubeseder *et al.* concentrates on the early Carboniferous (Tournaisian to Visean) interval in North Africa, an alternating series of widespread shallow marine and more discrete fluvial reservoirs with interbedded offshore mudstone seals. It examines the glacio-eustatic controls of facies patterns along the stable continental margin, and identifies four potential stratigraphic trap types, using selected outcrop examples placed into a regional sequence stratigraphic context. Dixon *et al.* provide a case study of an integrated petroleum systems and play fairway analysis of the Ghadames Basin. Pulling together a large regional dataset and linking this to published work, the results offer insight into the timing of hydrocarbon charge and prospectivity of the basin. Luening *et al.* examine the frontier Kufra Basin in SE Libya. This basin is the subject of a current exploration campaign by several companies, hoping to unlock its as yet unproven potential. This paper provides information on the recent well, A1-NC198, drilled by RWE. Despite being dry and lacking hydrocarbon shows, the well still provides important data to improve the understanding of the regional petroleum play.

Moving east, two papers cover important petroleum plays in Egypt. Dancer *et al.* review the Gulf of Suez Basin, a classic extensional rift basin of Miocene age, with both syn-rift and pre-rift hydrocarbon plays. Exploration has been carried out here since the late 1800s, with over 10 billion barrels discovered to date, but poor seismic quality has hindered the identification of deep targets, such as the key pre-rift Nubia Sandstone reservoir. The paper highlights improvements in seismic data acquisition, using 3D ocean bottom cable (OBC) to enhance imaging. The authors present models of the tectonically controlled sedimentation that characterizes the syn-rift section, and show how this approach can re-invigorate exploration. Gordon *et al.* present recent work by a multi-disciplinary team evaluating the prospectivity of the North Red Sea. A new regional biostratigraphic and environmental analysis is presented from North to South through the Gulf of Suez and into the Red Sea, placing the Nubian sequences into a regional chronostratigraphic framework. Again, recent reprocessing and newly acquired seismic data has produced a step change improvement in imaging of the prospective pre-rift section. The authors suggest that all the key elements of the Gulf of Suez petroleum system exist in the North Red Sea, thereby high grading the prospectivity of the area.

Finally, three papers on the Middle East, the first by Fraser, uses an analysis of the prolific Upper Jurassic 'Arab' play fairway of the Middle East, and the application of play fairway risk mapping techniques, to demonstrate the play systems and assess remaining prospectivity. Ismail *et al.* present a short paper on analysis of the Late Cretaceous Shiranish Fm, in the Central Euphrates Graben of Syria. Detailed analyses characterize this potentially important source rock that is within the oil window in many areas. Finally, Garland *et al.* describe a detailed study of the appraisal of the Taq Taq Field, located within an anticline in the gently folded zone of the Zagros mountains, northeastern Iraq. This paper reviews the main reservoirs and the importance of characterizing the pervasive fracture system, which provides the reservoir connectivity and deliverability. The authors describe modelling of the fractures using data from core and image logs, and their critical role in a dual-media dynamic model used for field development planning.

VINING, B. A. & PICKERING, S. C. (eds) *Petroleum Geology: From Mature Basins to New Frontiers – Proceedings of the 7th Petroleum Geology Conference*, 671. DOI: 10.1144/0070671

From Neoproterozoic to Early Cenozoic: exploring the potential of older and deeper hydrocarbon plays across North Africa and the Middle East

J. CRAIG, D. GRIGO, A. REBORA, G. SERAFINI and E. TEBALDI

Eni Exploration & Production Division, Via Emilia 1, 20097 San Donato Milanese, Milan, Italy (e-mail: jonathan.craig@eni.com)

Abstract: As the traditional exploration plays in the main productive basins of North Africa and the Middle East become more 'mature', attention is increasingly focusing on more challenging, older and deeper plays in the main producing basins and on high-risk, but more conventional, plays in under-explored frontier areas. This shift brings with it a range of technical and commercial challenges that must be addressed, if exploration in the region is to remain an attractive proposition. Exploration in North Africa and the Middle East has traditionally focused on the prolific Mesozoic- and Cenozoic-sourced petroleum systems of the Nile Delta, the Sirte Basin, the Pelagian Shelf, and the Arabian Plate and on the Palaeozoic-sourced petroleum systems of the Berkine, Ghadames, Illizi, Ahnet and Murzuq basins, the Central Arabian Basin, the Qatar Arch and the Rub Al Khali Basin. Together these form one of the most prolific petroleum provinces in the world and, as a consequence, there has been little commercial incentive to invest in exploring more challenging and riskier plays in these areas. However, as the need to find new reserves becomes imperative, attempts are increasingly being made to test new play concepts and to extend already proven plays into new areas. Key recent developments in this regard include the recognition of the hydrocarbon potential of the Neoproterozoic to Early Cambrian ('Infracambrian') sedimentary section lying below the traditionally explored Palaeozoic succession in many basins in North Africa. In some areas, particularly the Berkine Basin in Algeria, the Nile Delta in Egypt and the Rub Al Khali Basin in Saudi Arabia, attention is also increasingly being focused on developing deeper gas plays, both in new areas and beneath existing producing fields. The technical challenges associated with these deeper gas plays are immense and include difficult seismic imaging of deep prospects, low porosity and permeability, high temperature and pressure and a critical need to identify 'sweet spots' where either locally preserved primary reservoir characteristics or secondary enhancement of reservoir quality through palaeo-weathering and/or fracturing allow commercial rates of gas production to be achieved. Despite these challenges, it is clear that the future for exploration in many of the more mature basins of North Africa and the Middle East will increasingly lie in evaluating such older and more deeply-buried plays.

Keywords: North Africa, West Africa, petroleum systems, Neoproterozoic, Palaeozoic, Oligocene, Taoudenni Basin, Berkine Basin, Nile Delta

Older and deeply buried petroleum systems are usually characterized by complex geological histories, and this is certainly the case for the Neoproterozoic and Palaeozoic petroleum systems of North Africa and the Middle East. In these systems, the efficiency of the source rocks and the potential to generate, migrate and trap hydrocarbons in a time-frame that allows hydrocarbons to be retained are often the most critical risks. Hydrocarbons can usually only be trapped for a few tens of millions of years (Berg 1975; Watts 1987; Sylta 1991, 1993) because even the most perfect seals are permeable over longer periods of time. One of the most critical issues determining the efficiency of older and/or deeply buried petroleum systems is, therefore, their burial history, and specifically the existence of a 'late' burial phase that can allow hydrocarbons to be generated, expelled, migrated and trapped in a suitably recent timeframe. Exceptions, such as the Neoproterozoic petroleum system of the Amadeus and Officer basins of Australia (Ghori *et al.* 2009) or the Late Neoproterozoic–Early Cambrian petroleum systems of Oman (Blood 2001; Al-Siyabi 2005) and the Indian Sub-continent (Peters *et al.* 1995) generally occur where evaporate super-seals are present (Schoenherr *et al.* 2007) and/or where the post-trapping history is dominated by extreme tectonic stability.

Burial history, thermal history and the presence, quality and reactivity of source rocks are key factors in determining the efficiency of the older and deeper petroleum systems in basins across North Africa and the Middle East (Fig. 1). Thermal events are particularly important in North Africa where rift-related volcanic activity in the Early Jurassic, related to incipient Atlantic rifting (Weis *et al.* 1987; Liegeois *et al.* 1991; Logan & Duddy 1998), and the passage of a mantle plume beneath the region during the Cenozoic (Busrewil & Wadsworth 1980*a*, *b*; Woller & Fediuk 1980; Loper 1991; Nataf 1991) are locally as important, or even more important, in controlling hydrocarbon maturation than the history of burial and uplift.

The presence of Cenozoic volcanic centres in North Africa that decrease in age from the Mediterranean coast to the Hoggar and Tibesti massifs records the progressive movement of the African Plate eastwards above a mantle plume or plumes (Busrewil & Wadsworth 1980*a*, *b*; Woller & Fediuk 1980). The increased heat flow produced by the passage over this plume system seems to be an important factor in rejuvenating the Palaeozoic-sourced petroleum systems in several North African basins, particularly where the overlying Mesozoic succession is thin or absent and the Palaeozoic source rocks are primarily affected only by older, pre-Hercynian, phases of burial.

The burial history, thermal evolution and hydrocarbon prospectivity of the even older and more deeply buried Proterozoic petroleum systems in North Africa and the Middle East are even more uncertain, partly because of the long period of geological time involved and the difficulty of dating the sequences, but also because their pre-Palaeozoic tectonic evolution and their geometry and facies architecture are poorly known. For these systems to be prospective, it is seems to be essential that there is residual hydrocarbon potential remaining after the long Neoproterozoic

VINING, B. A. & PICKERING, S. C. (eds) *Petroleum Geology: From Mature Basins to New Frontiers – Proceedings of the 7th Petroleum Geology Conference*, 673–705. DOI: 10.1144/0070673

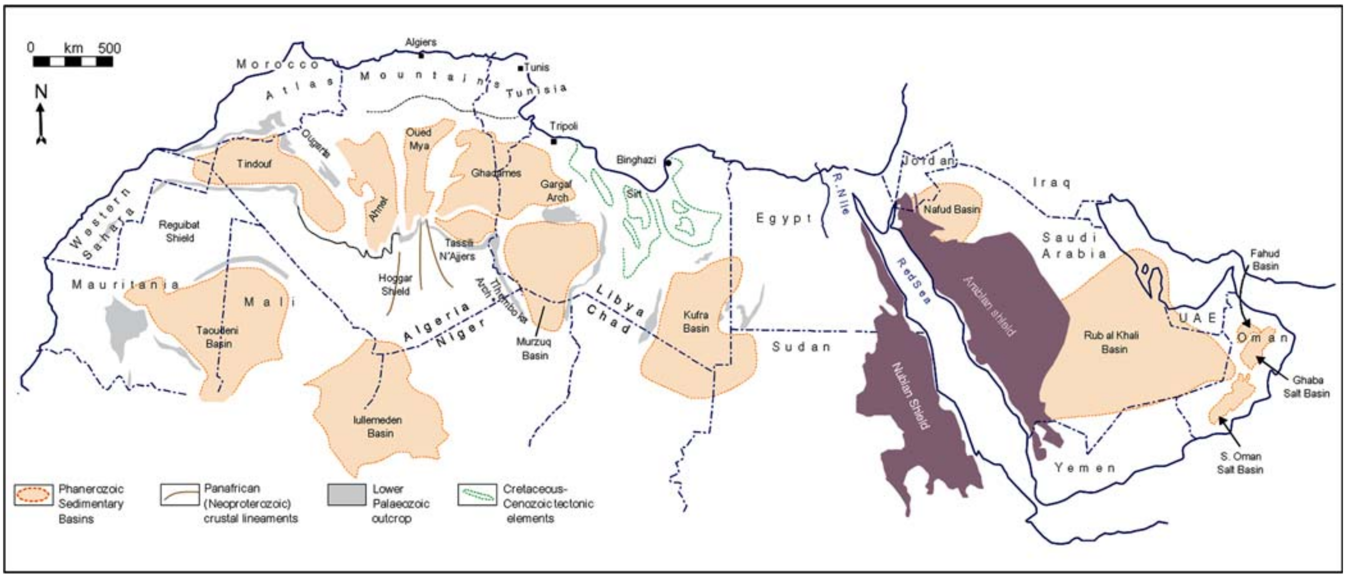

Fig. 1. Major Palaeozoic Basins of North Africa and the Middle East (after Le Heron *et al.* 2009).

and Palaeozoic history and that this residual potential is then activated during the subsequent Mesozoic and Cenozoic evolution, due either to volcanic activity and/or a phase of 'late' burial.

Neoproterozoic plays: the new frontier for exploration in North Africa and the Middle East

The Neoproterozoic Eon, which extends from 1000 Ma to the base of the Cambrian at 542 Ma, is relatively poorly known from a petroleum perspective, despite the existence of potential, proven or producing plays in many parts of the world, including Oman, Mauritania, Siberia, China, India, Pakistan, Australia and both North and South America (Bhat *et al*. 2009; Craig *et al.* 2009; Ghori *et al.* 2009).

The Neoproterozoic was a period of massive atmospheric, climatic and tectonic change. It was dominated by the 'freeze-fry' cycles of the Cryogenian (850–650 Ma) 'Snowball Earth' glaciations, when global mean surface temperature may have oscillated between -50 and $+50$ °C over periods of ± 5–10 Ma (Hoffman *et al.* 1998; Hoffman & Schrag 2000; Halverson *et al.* 2005; Smith 2009). Evolution studies suggest that these extreme climatic variations were ultimately responsible for the emergence of the first animal life around 600 Ma during the Ediacaran (630 Ma–542 Ma) and, in turn, for the eventual explosion of life forms in the latest Neoproterozoic and Early Cambrian. In climatic, tectonic and petroleum systems terms, the Neoproterozoic to Early Cambrian period can be divided into three distinct phases: a Tonian to Early Cryogenian phase, prior to about 750 Ma, dominated by the formation, stabilization and initial breakup of the supercontinent of Rodinia; a Mid Cryogenian to Early Ediacaran phase (*c.* 750–600 Ma) including the major global-scale 'Sturtian' and 'Marinoan' glaciations and a Mid Ediacaran to Early Cambrian (*c.* post 600 Ma) phase corresponding to the formation and stabilization of the Gondwana Supercontinent (Trompette 1997; Collins & Pisarevsky 2005; Zhu *et al.* 2008; Craig *et al.* 2009; Scotese 2009; Fig. 2).

Many of the proven 'Infracambrian' (Neoproterozoic to Early Cambrian) hydrocarbon plays around the world depend on the presence of prolific 'Infracambrian' source rocks. There is increasing evidence that the deposition of many of these organic-rich units was triggered by strong post-glacial sea-level rise, on a global scale, following the major Neoproterozoic glaciations, coupled, in some areas at least, with basin development and rifting on a more local scale (e.g. Le Heron *et al.* 2009).

Interest in exploring for stratigraphically older and deeper 'Infracambrian' plays along the margin of the Gondwana supercontinent, from northern South America, across North Africa and the Middle East, into Pakistan and India (Fig. 3), is growing. This interest is rooted in the greatly improved understanding of the prolific Neoproterozoic to Early Cambrian (Huqf Supergroup), intra-salt Ara 'Stringer' carbonate and Athel silicilyte plays, and the increasingly important older 'pre-salt' plays, in the South Oman Salt Basin, and of the prolific Neoproterozoic and 'Infracambrian' plays in Siberia and southern China.

Oman and the Middle East

The Late Neoproterozoic–Early Cambrian Ara Group portion of the Huqf Supergroup in Oman (Sharland *et al.* 2001; Allen 2007) contains one of the oldest proven hydrocarbon systems in the world (Fig. 2). The reservoirs are dolomitic carbonates and silicilytes encased in salt, with complex trapping geometries, usually strongly affected by salt movements (Amthor *et al.* 2005). Predicting the nature and spatial distribution of these reservoirs in the subsurface is extremely challenging due to their complex geometry and tectonic history (e.g. Droste 1997; Blood 2001). Oil was initially, and rather unexpectedly, discovered in the 'intrasalt Ara carbonate stringers' in 1976 and the play was then explored for the next two decades with indifferent results. Commerciality was achieved in 1997 with the Harweel Deep-1 well and through this and subsequent discoveries the play now accounts for some 70% of the oil production in Oman (Al-Siyabi 2005).

The older Neoproterozoic pre-salt section, underlying the Ara Group, is called the Nafun Group. This consists of five formations, containing both siliciclastic and carbonate lithologies. Pre-salt exploration in Oman started in the 1950s, but renewed interest was triggered in the late 1990s by the discoveries in the Ara Group. The Buah Formation is the youngest and most prospective of the pre-salt formations. It consists of carbonates deposited in a ramp environment with high-quality reservoirs in shallow water peloidal-ooidal and/or stromatolitic facies. These can be laterally extensive over distances of tens of kilometres. Reservoir quality and deliverability are enhanced locally by fractures and karst phenomena. The Buah Formation petroleum system is 'self-sourced' by off-ramp basinal facies shales with total organic content (TOC) values in the range of 2.5–3.5% (Cozzi & Al Siyabi 2004; Cozzi *et al.* 2004).

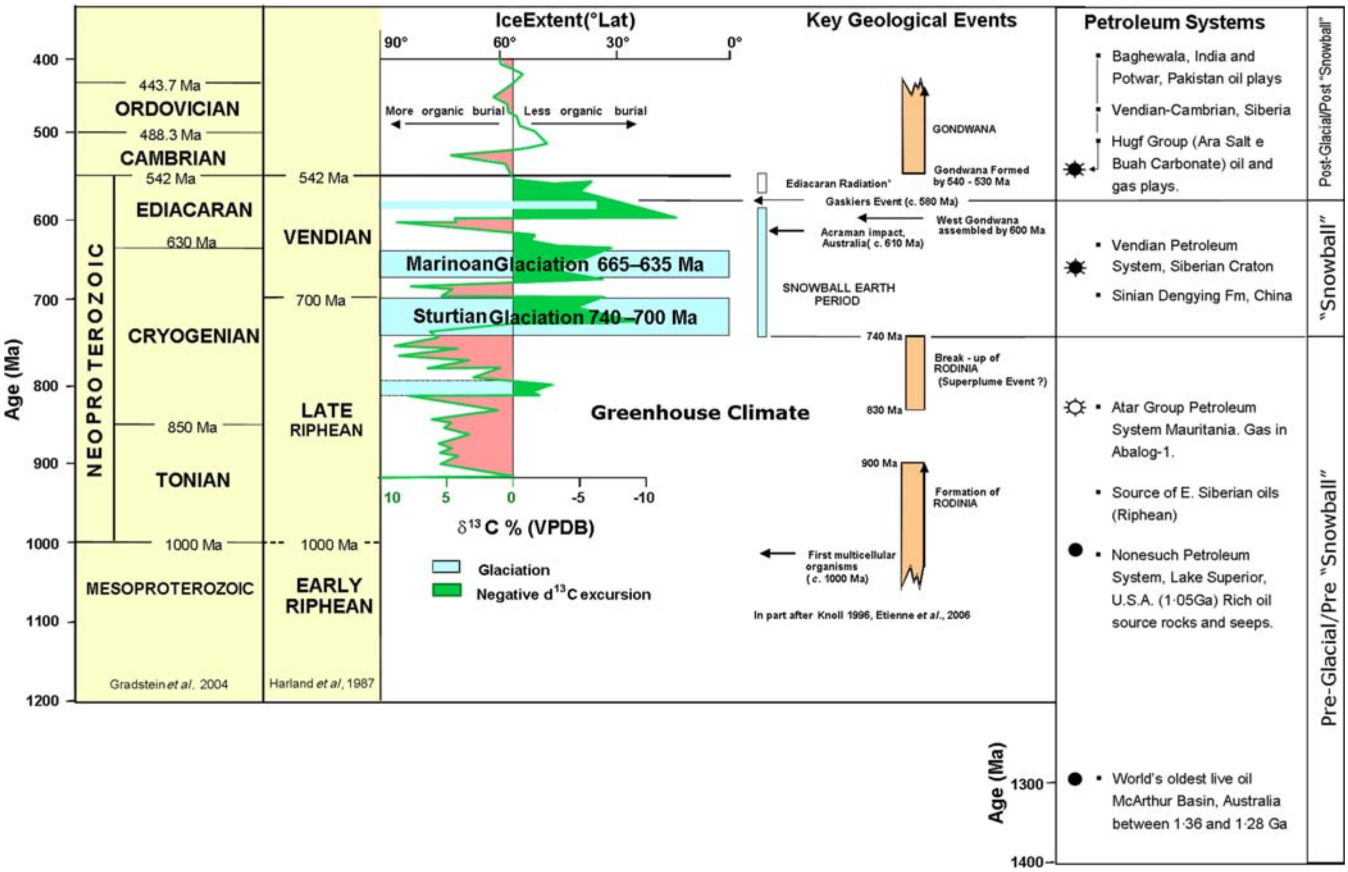

Fig. 2. Summary of Neoproterozoic timescale, carbon isotope record, ice extent, key geological events and petroleum systems (after Craig *et al.* 2009).

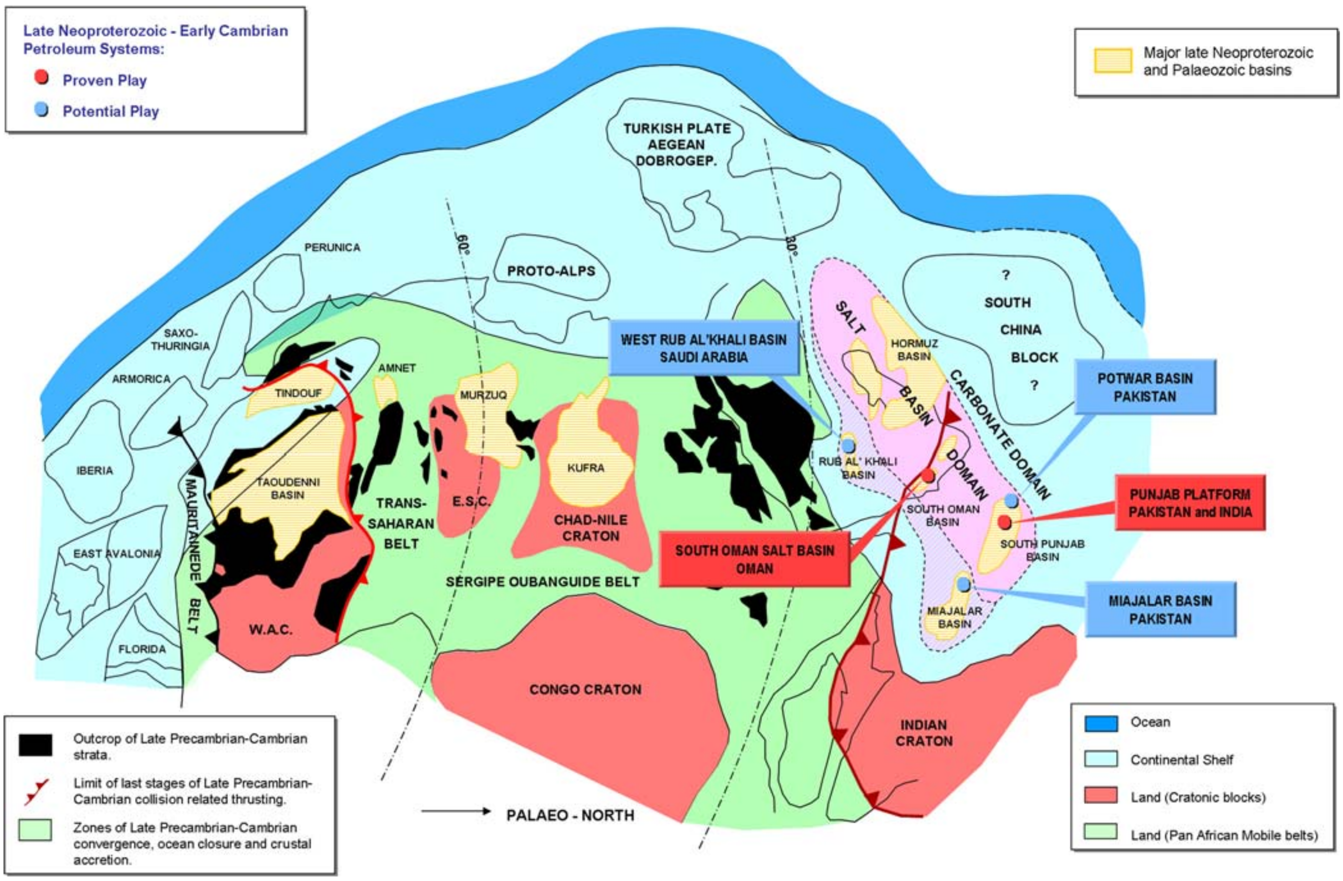

Fig. 3. Generalized Late Neoproterozoic (Ediacaran) to Early Cambrian palaeogeography of the 'Peri-Gondwana Margin' (*c.* 610–520 Ma) with associated petroleum systems (after Craig *et al.* 2009).

It is possible that Neoproterozoic plays, similar to those in Oman, exist within and beneath the Hormoz salt in neighbouring Saudi Arabia and Yemen, and perhaps also in Iran (Waltham 2009) and Iraq, but relevant data are currently very limited, with few well penetrations. Similar plays are, however, already being explored actively within the age-equivalent Marwar and Machh supergroups in the Sindh and Punjab regions of Pakistan and in Rajasthan State in western India (e.g. Sati *et al.* 1997; Riaz *et al.* 2003), and attention is increasingly turning to the potential for age-equivalent, and possibly older, Neoproterozoic plays across the rest of the Middle East. Neoproterozoic to Early Cambrian sediments occur at outcrop in Saudi Arabia (e.g. Delfour 1970), southern Jordan, Yemen and Oman (e.g. Beydoun 1991) and seismic evidence suggests the presence of Neoproterozoic–Early Cambrian Hormoz/Ara-equivalent salt within 'Infracambrian' graben beneath the Rub Al Khali Basin along the NW–SE trending Najd fault system extending from Saudi Arabia into northern Yemen. The outcropping Neoproterozoic to Early Cambrian sediments are predominantly conglomerates, sandstones and shales, locally with andesite and basalt and often with carbonates and evaporates in the upper parts, deposited under shallow marine to tidal flat conditions along the Gondwana margin. They rest unconformably on Precambrian basement rocks and are commonly overlain unconformably by Cambro–Ordovician sandstones. Interestingly, oil recovered from the Tarfyat-1 well on the North Hadramaut Arch in Yemen is geochemically similar to oil derived from Neoproterozoic to Early Cambrian Huqf Supergroup source rocks in the South Oman Salt Basin (Grosjean *et al.* 2008). Most of the Persian Gulf region is underlain by the Hormoz salt at depths of 4–10 km, which has been mobilized to form diapirs that reach the surface in more than 200 salt domes, mainly in the coastal region and the Zagros Mountains of Iran. The Hormoz salt was originally more than a kilometre thick in this region. It was deposited in two major units separated by a suite of volcanic rocks and shales which occur as rafts, some more than 1 km across, within the salt domes. The shales contain Cambrian trilobites which date the sequence. Rafts of granitic and gabbroic basement rocks (probably detached from basement faults and then entrained in the flowing salt), together with beds of anhydrite and sylvite, are also preserved in some of the salt domes. The depositional red banding of the salt, produced by the inclusion of some 2–10% of insoluble material (including 'earthy' hematite of syngenetic origin) in thin beds within the pure white halite, defines spectacular flow folds in many of the diapirs in Iran (Waltham 2009). In the Zagros region, salt movement largely began during the Jurassic, with the development of salt pillows, and the diapirism driven by the subsequent increase in overpressure during the Cretaceous and Cenozoic.

North and west Africa

The Neoproterozoic to Early Cambrian ('Infracambrian') successions in northern and western Africa are also emerging as hydrocarbon exploration targets with proven petroleum systems in several areas, including the Taoudenni Basin in Mauritania, Mali and southern Algeria, the Tindouf Basin in southern Morocco and NW Algeria and the Sirte–Cyrenaica rift margin in NE Libya. Large basins with excellent surface outcrops and thick sedimentary fills of Neoproterozoic and Early Palaeozoic age are widespread throughout north and west Africa (Fig. 1). Away from the outcrops, relatively little is known about these successions because they have only rarely been penetrated by wells. However, in the Taoudenni Basin, the Tindouf Basin and the Sirte–Cyrenaica rift margin, the few wells that have been drilled suggest that these successions contain tantalizing evidence of active petroleum systems with clear analogies to major producing Neoproterozoic petroleum systems in other parts of the world.

New biostratigraphic analysis has recently provided the first definitive Tonian–Cryogenian (Late Riphean) age dates for reservoir sequences containing gas in the Taoudenni Basin in Mauritania (Lottaroli *et al.* 2009). Similar dates were obtained for subsurface sequences in the Cyrenaica Platform bordering the eastern Sirte Basin of Libya in the 1970s (described in Arnauti & Shelmani 1988). Recent fieldwork in the Taoudenni Basin (Deynoux *et al.* 2006; Shields *et al.* 2007), in the Anti-Atlas region of Morocco (e.g. Geyer & Landing 2006), and in Al Kufrah Basin in Libya (Le Heron & Howard 2008) has also added to our understanding of reservoir, source and seal relationships in the Neoproterozoic to Early Cambrian successions in these basins and has confirmed the widespread presence of stromatolitic carbonate units of potential reservoir facies (Trompette 1969, 1973; Bertrand-Sarfati & Trompette 1976; Bertrand-Sarfati & Moussine-Pouchkine 1985).

Neoproterozoic to Early Cambrian organic-rich strata were deposited in both high latitudes (e.g. Mauritania) and low latitudes (e.g. Oman) on the 'Peri–Gondwana Margin'. Some of the black shales deposited on the West African Craton may be as old as 1000 Ma and clearly predate the Pan-African orogenic event (e.g. the Bleida–Tachdamt Group, in Morocco; Leblanc & Moussine-Pouchkine 1994). These are substantially older than the majority of the Neoproterozoic ('Infracambrian') organic-rich units that occur across much of North Africa and the Middle East (including those in Oman), which typically range from *c.* 850 to *c.* 540 Ma in age. 'Infracambrian' black 'oil shales' and laminated organic-rich dolomites, that are broadly equivalent in age to the prolific Late Neoproterozoic–Early Cambrian source rocks in Oman, are also known to generate, respectively, mature, low-sulphur, light oil (42–50° API) capable of relatively long distance migration and low-maturity, high-sulphur, heavy oil capable of only short distance migration, in northern and eastern Pakistan and in western India. The giant Baghewala Oil Field in Rajasthan, India contains an estimated 628 MBBL in place of heavy oil in four separate reservoirs of Neoproterozoic, Neoproterozoic to Early Cambrian and Late Cambrian age. Biomarkers in the oil recovered in the Baghewala-1 well suggest that it is derived from a Late Neoproterozoic–Early Cambrian ('Infracambrian') source rock (Peters *et al.* 1995).

Neoproterozoic petroleum system in the Taoudenni Basin, West Africa

The most prospective Neoproterozoic plays in northern and western Africa appear to be in the Taoudenni Basin in Mali, Mauritania and southern Algeria, and in the Kufra Basin (Al Kufrah) in southeastern Libya. These basins have broadly similar stratigraphy and tectonic evolution, despite being more 2500 km apart.

The Taoudenni Basin lies on the West African Craton, one of the pre-Pan-African cratonic blocks that formed the core of the Gondwana Supercontinent during the Late Neoproterozoic and the Early Palaeozoic (Trompette 1973). Palaeomagnetic constraints on the position of West African Craton during the earlier Neoproterozoic, before the amalgamation of West Gondwana, are rather poor, but most modern palaeogeographic reconstructions place it as a separate continental fragment located close to the palaeo-south pole (e.g. Collins & Pisarevsky 2005; Pisarevsky *et al.* 2008; Scotese 2009). Today, the West African Craton and the overlying Taoudenni Basin occupy most of NW Africa and are flanked to the west and east by north–south trending Pan-African 'mobile belts', formed during the accretion of the Gondwana Supercontinent and reactivated, at least partly, during the Late Carboniferous–Early Permian Hercynian orogeny (Fig. 4).

Stratigraphy and tectonic evolution

Outcrops around the margins of the Taoudenni Basin allow a robust stratigraphic and facies framework to be developed for the

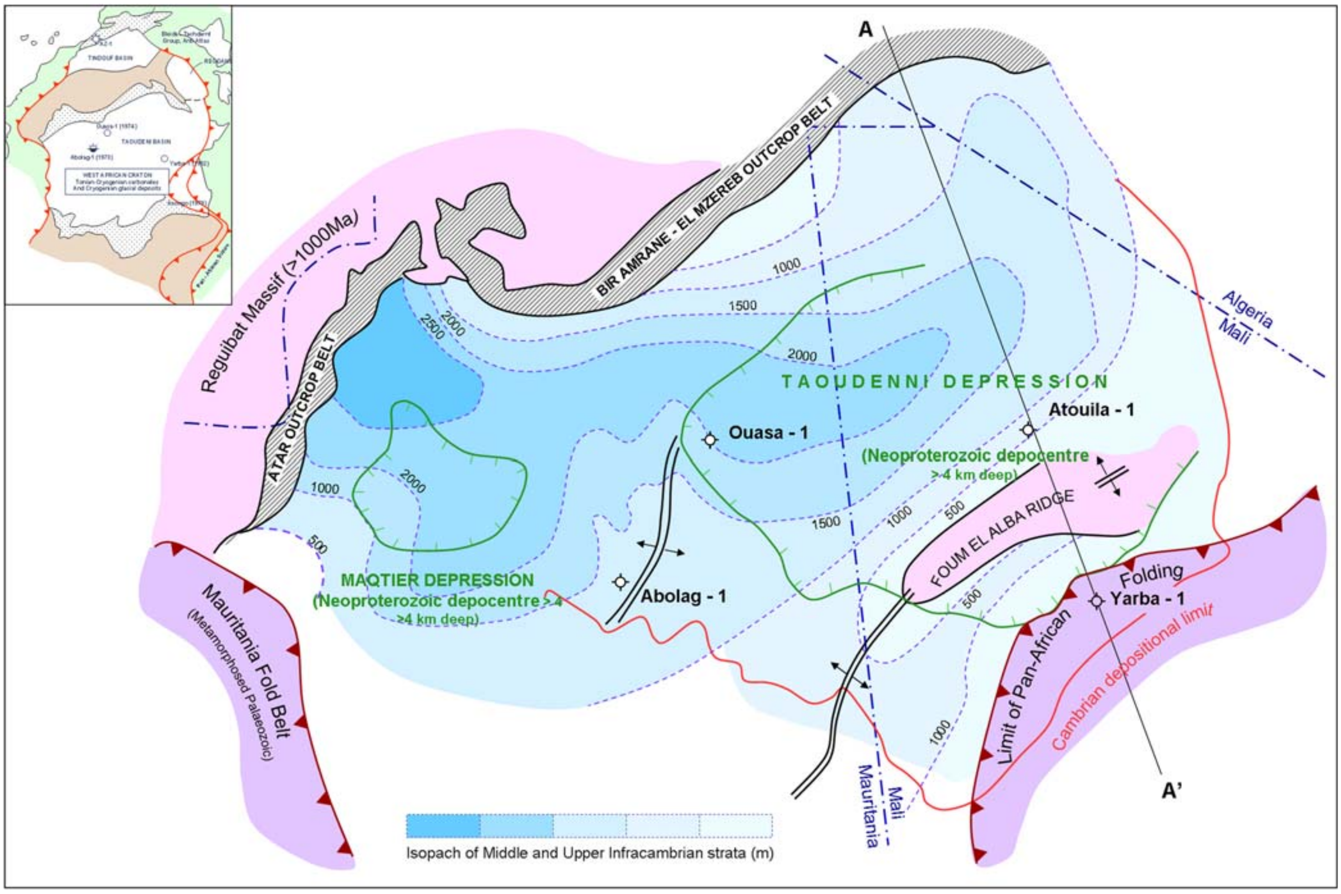

Fig. 4. Neoproterozoic geology of the Taoudenni Basin, Mauritania, Mali and southern Algeria (in part after Moussine-Pouchkine & Bertrand-Sarfati 1997, Baraka Petroleum, Mali Petroleum SA and Societé Mauritanienne des Hydrocarbures 2007).

Meso- and Neoproterozoic succession (Fig. 5). The main tectonic events are recorded by major unconformities within the 1000 m thick succession exposed along the 1100 km long outcrop belt on the northern flank of the basin through Mauritania, northern Mali and into southernmost Algeria. The outcrops in the Atar Region of Mauritania, at the SW end of this belt, are relatively well known and are documented in a series of comprehensive and accurate geological maps and sections (e.g. Moussine-Pouchkine & Bertrand-Sarfati 1997; Deynoux *et al.* 2006 and references therein; Alvaro *et al.* 2007). The Neoproterozoic succession here is well defined and radiometrically dated (e.g. Clauer 1981, 1982). An unconformity at the base of the succession marks the Eburnean Orogeny and defines the boundary between the igneous basement and the oldest sediments derived from the weathering and erosion of the Rodinia Supercontinent. The overlying Mesoproterozoic (Early Riphean) Char Group was deposited during a phase of intra-cratonic extension and consists of clastic sediments deposited in fluvial to shallow marine environments. These are overlain by a uniformly east-dipping succession of interbedded stromatolitic carbonates and black shales belonging to the Tonian to Mid-Cryogenian Atar Group that range in age from *c.* 1000 Ma to somewhat younger than 775 Ma. The top of the Atar Group marks the final breakup of Rodinia supercontinent and is overlain unconformably by a sub-horizontal succession of younger Neoproterozoic sediments with, at the base, a series of glacial/interglacial cycles represented by the alternating clastic and calcareous deposits of the Late Cryogenian Dar Cheikh Group. These glaciogenic sediments are radiometrically dated as younger than 630 Ma which, if correct, would suggest that they are broadly 'Marinoan' or younger in age (Fig. 2). Rapid lateral changes in thickness of the glacial units reflect inherited relief resulting from a long period of erosion and uplift associated with the initial stages of the Pan-African orogeny, combined with palaeo-relief associated with the Cryogenian glaciation. A thin glacial diamictite marks the unconformity associated with the glaciation and is overlain by the sandstones, siltstones and shales of the Late Neoproterozoic (Ediacaran) Assabet Group. A marked unconformity at the base of the Assabet Group is related to the Pan-African compression (Phase 1). Another unconformity associated with a second phase of Pan-African compression (Phase 2) seals the Assabet Group and marks the onset of the Eocambrian glaciation.

All the major unconformities observed in the outcrops surrounding the Taoudenni Basin can be identified on seismic data in the subsurface in areas of the basin where intra-cratonic sub-basins are well developed and the sedimentary successions exhibit clear geometries and internal architectures. Recently acquired seismic data suggest that much of the uplift along the southeastern flank of the Taoudenni Basin is younger than Lower Palaeozoic in age and most probably occurred during the Hercynian Orogeny (Fig. 6).

Hydrocarbon plays

The main Neoproterozoic hydrocarbon play in the Taoudenni Basin comprises Atar Group stromatolitic limestone reservoirs, with hydrocarbons sourced laterally and vertically from organic-rich shales deposited in restricted sub-basins between the stromatolic carbonate complexes, sealed by interbedded shales. The subsurface portion of the Taoudenni Basin remains extremely under-explored. There are only four exploration wells in the basin and only two of these, Abolag-1 drilled in 1973 in Mauritania and Yarba-1 drilled in 1982 in Mali, have tested the Neoproterozoic play. Abolag-1 penetrated more than 600 m of succession which, although undated at

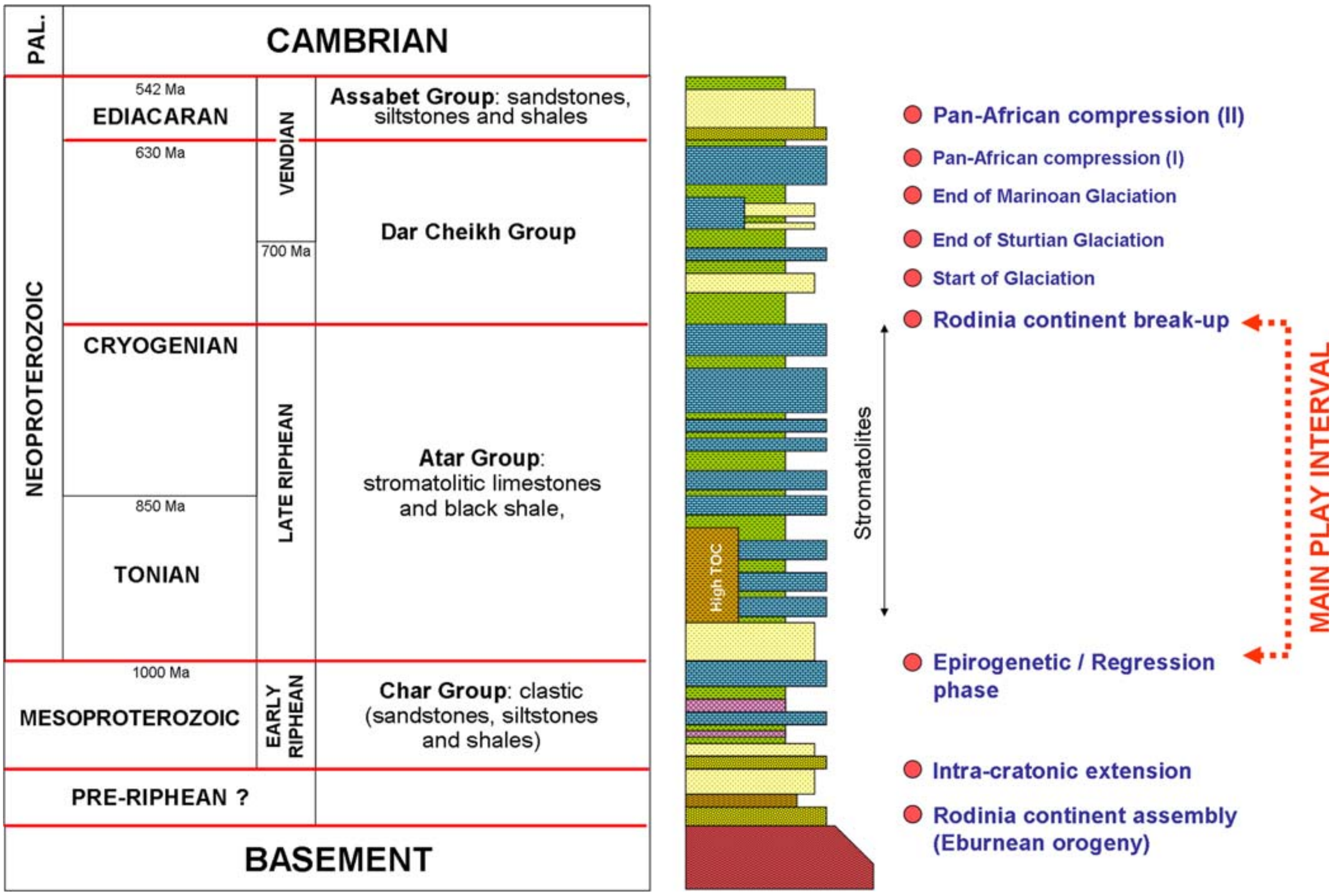

Fig. 5. Summary of the Precambrian stratigraphy, lithologies, main tectonic events and hydrocarbon play in the Taoudenni Basin.

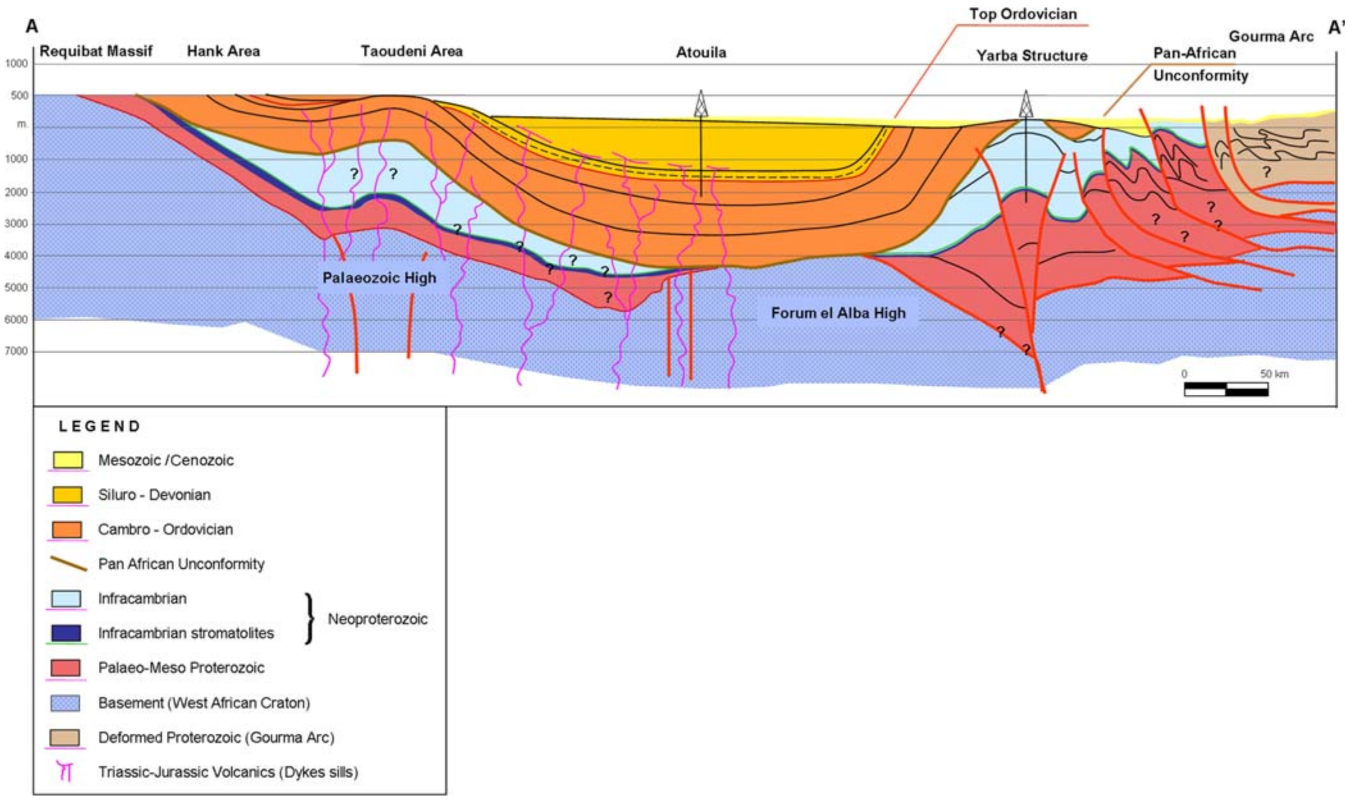

Fig. 6. Schematic geological cross-section through the Taoudenni Basin in western Mali (see Fig. 4 for location) based on seismic and well data.

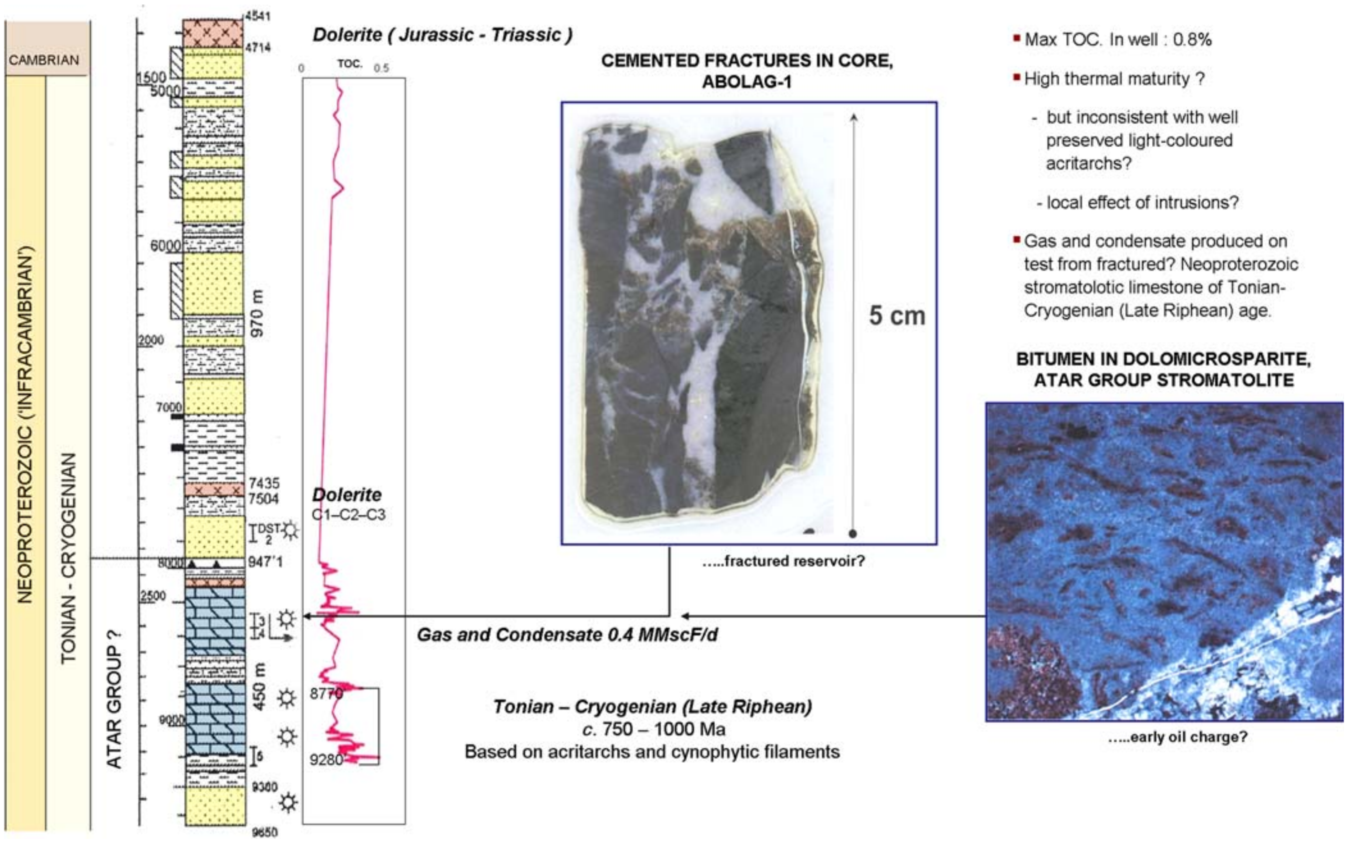

Fig. 7. Summary of the Neoproterozoic succession and the associated petroleum system encountered in the Abolag-1 well in the Taoudenni Basin, Mali.

the time, was assigned to the 'Infracambrian' (Fig. 7). The succession consists of an upper clastic sequence and a lower carbonate sequence, both of which contain hydrocarbons. Gas (and condensate?) was recovered from the carbonate sequence on test at a rate of 13 600 m^3 per day. The carbonate succession in the Abolag-1 well has subsequently been dated biostratigraphically to *c.* 1000–800 Ma on the basis of an assemblage of acritarchs similar to those recovered from Tonian to Early Cryogenian successions in Siberia, Australia and southern Poland (Lottaroli *et al.* 2009). There is, therefore, little doubt that the lower, predominantly stromatolitic carbonate succession in Abolag-1 is of Tonian to Early Cryogenian age and that the gas bearing section is the lateral equivalent of the Atar Group at outcrop. The succession in the well has a low TOC and appears to be of high thermal maturity, although this is somewhat inconsistent with the well preserved state of the acritarchs and could be partially a local thermal effect associated with the abundant dolerite intrusions. At outcrop, the equivalent black shales within the Atar Group are of low thermal maturity. The carbonates in the well are tight, heavily fractured and contain bitumen (Fig. 7; Lottaroli *et al.* 2009), which might suggest that there was an earlier phase of oil generation and migration in this part of the basin.

The distribution and geometry of the stromatolitic carbonates in the Taoudenni Basin can be interpreted using the depositional model of a distally steepened ramp developed by Cozzi & Al Siyabi (2004) for the probably somewhat younger Neoproterozoic stromatolitic carbonate reservoir of the Buah Formation in Oman. In this model, the inner ramp is characterized by the deposition of columnar stromatolites, with oolitic, cross-stratified, grainstones occurring in more distal locations. The latter facies, which in Oman have the best reservoir quality, appears not to have been penetrated by the wells drilled so far in the Taoudenni Basin. Recent interpretations of the depositional setting suggest that the wells are in a mid-outer ramp setting where limited, metre-scale stromatolites with an overall orientation perpendicular to the palaeocoastline are characteristic (Fig. 8). This suggests that there may be areas of the Taoudenni Basin where the reservoir quality of the Neoproterozoic carbonates may be significantly better. Predicting the location of these more prospective areas remains one of the key challenges for future exploration in the Taoudenni Basin and for the Neoproterozoic stromatolitic carbonate play elsewhere in North Africa.

Thermal evolution and hydrocarbon generation

The thermal evolution of the Neoproterozoic petroleum system in the Taoudenni Basin is dominated by two major phases of burial, the first during the Neoproterozoic and terminated by the Pan-African orogeny, and the second during the Palaeozoic and terminated by the Hercynian orogeny (Fig. 9), which was responsible for the emplacement of the internal nappes in the Mauritanide fold belt (Alvaro *et al.* 2007). The magnitude of the uplift and erosion associated with these two orogenic events varies across the basin. The Pan-African erosion is greatest in the eastern sub-basin, while the Hercynian erosion is more significant in the western sub-basin. Maximum burial was reached just prior to the Hercynian uplift and erosion (at *c.* 250 Ma) in both sub-basins, and there is little or no significant re-burial after the Hercynian orogeny. This burial history implies that there were two main phases of hydrocarbon generation and migration from any potential Early Neoproterozoic source rocks in the Taoudenni Basin, the first at *c.* 550 Ma during the latest Neoproterozoic and the Early Cambrian, and the second at *c.* 250 Ma during the Late Permian and the Early Triassic. Significant volumes of hydrocarbons were probably generated, expelled, migrated and, potentially, trapped during the earlier phase but then leaked away or were re-migrated when traps were tilted or breached during subsequent tectonic events. The lack of significant Mesozoic or Cenozoic burial

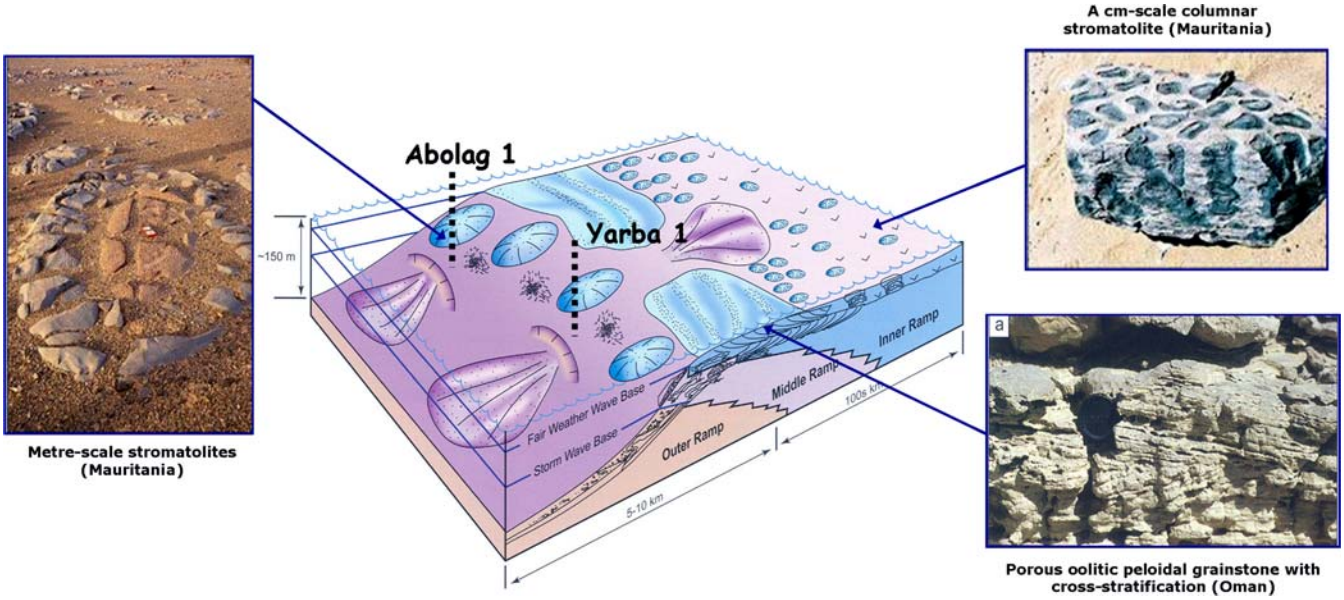

Fig. 8. Depositional model for stromatolitic carbonates in a distally-steepened ramp setting (after Cozzi & Al-Siyabi 2004) and the inferred location of the Neoproterozoic stromatolitic carbonates penetrated by the Abolag-1 and Yarba-1 wells in the Taoudenni Basin in Mauritania and Mali, respectively.

precludes more recent hydrocarbon generation. This is particularly the case around the flanks of the basin where there is remaining residual hydrocarbon potential.

The existence of a viable Neoproterozoic petroleum system in the Taoudenni Basin has yet to be proven and remains the subject of considerable debate. A new phase of exploration is currently underway in the basin and there are both negative and positive indications from the data now available. The negative factors include the low porosity (*c.* 2–5%) of the main stromatolitic carbonate reservoir and the low flow rate achieved in the Abolag-1 well, the general absence of thick shale seals in the wells, the complex tectonic evolution of the basin, the presence of extensive Triassic–Early Jurassic intrusions and the probability that any Neoproterozoic source rocks have reached high thermal maturities, at least in the central parts of the basin, and that 'early' generation of hydrocarbons (from Ordovician times onwards) resulted in any

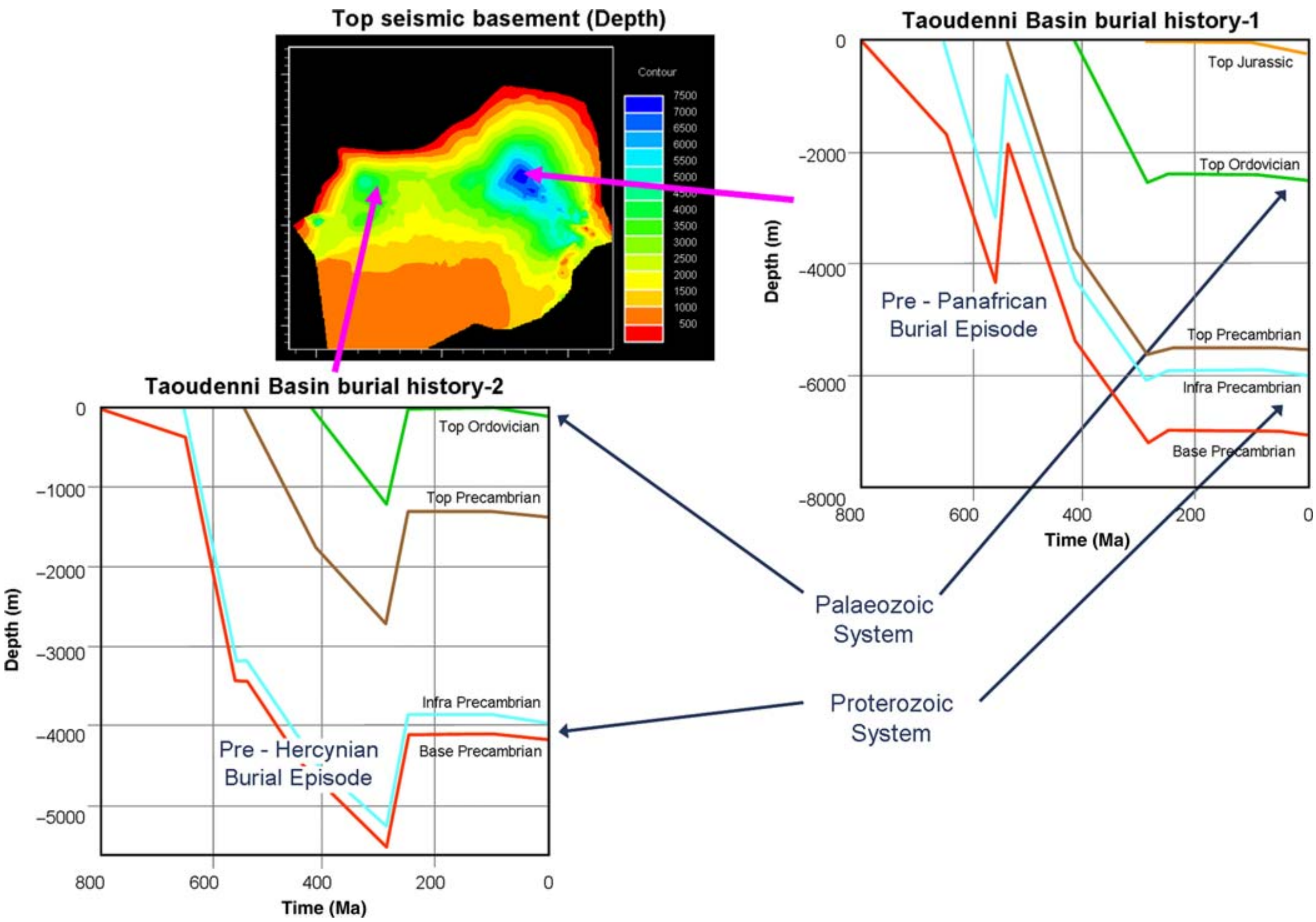

Fig. 9. Burial histories and regional tectonic events for the western and eastern sub-basins of the Taoudenni Basin, Mali and Mauritania.

liquid hydrocarbons being cracked to gas during the Triassic–Early Jurassic thermal event. These are balanced by several positive indications, including the presence of gas (and, possibly, condensate) in Abolag-1, the reported occurrence of gas shows in either Neoproterozoic or Lower Palaeozoic formations in the Ouasa, Asongo, Yarba and Atouilla wells, the existence of oil-prone black shales with a TOC of 10–20% (the so-called 'burning shales') within the Atar Group which are 'early mature' at outcrop, the presence of saline formation water, the low present-day thermal gradients (15–18°C/km), the uncertain thermal history of the basin with conflicting 'high' and 'lower' maturity indicators and, finally, the presence of numerous untested four-way dip and fault-related closures, mainly of 'Hercynian' age.

Neoproterozoic plays in other parts of North and West Africa

Exploration for Neoproterozoic or 'Infracambrian' (Late Neoproterozoic–Early Cambrian) plays in other parts of northern and western Africa is rather less well advanced. The presence of gas shows in the post-Pan-African, mixed clastic and carbonate, Neoproterozoic and Early Cambrian succession (including the Late Neoproterozoic Adoudou, Lie de Vin and Igoudine/Tislit formations) in the AZ-1 well in the Anti-Atlas of Morocco suggests that there may also be some potential both here and in the Tindouf Basin to the south. In addition, oil is produced from fractured granitic basement and overlying 'basal sandstones' on the Augila–Nafoora High along the Sirte–Cyrenaica rift margin in NE Libya. The basement in this area has been radiometrically dated and is Late Precambrian (Neoproterozoic) in age, but the 'Basal sandstones', which are preserved in downfaulted blocks along the flanks of the high, are largely undated and could be, at least in part, 'Infracambrian' in age. However, the source of the oil in this region is clearly not the 'Infracambrian' (which appears to lack any source potential in this area), but is probably the onlapping Cretaceous succession (including the Rachmat Shale), so this is not a true Neoproterozoic petroleum system. Interest has also been sparked by what is assumed to be a remnant Neoproterozoic or 'Infracambrian' basin, containing more than 1500 m of strata, observed on seismic data in the Kufra Basin (Al Kufrah) in SE Libya (Fig. 10) lying, with marked unconformity, below the relatively uniform and flat-lying Palaeozoic succession (e.g. Craig *et al.* 2008). This has been variously interpreted as an erosional remnant of a once much more extensive 'Infracambrian' succession, possibly preserved in a graben or even, perhaps, given the broadly rhombohedral shape and relationship with potential bounding faults, in a 'pull-apart' basin. The succession remains undrilled and, therefore, undated but, from a seismic facies perspective, it appears to consist of three distinct stratigraphic units, truncated by two well defined unconformities in the upper part. These unconformities have been interpreted as representing the two main phases of Pan-African compression that are observed in the Taoudenni Basin and elsewhere.

The very limited and fragmented nature of both the outcrops and the subsurface penetrations of the Neoproterozoic to Early Cambrian succession in North Africa make it extremely difficult to develop general models of prospectivity or to define prospective play fairways. Further investigations of the Neoproterozoic and Neoproterozoic–Early Cambrian ('Infracambrian') black shales in northern Africa are required in order to better understand their source potential and their relationship with the Cryogenian glaciations. High-resolution biostratigraphic, isotope and other palaeotemperature proxy records need to be documented for suitable type sections and constrained, where possible, with absolute radiometric dates, so that the timing of black shale deposition

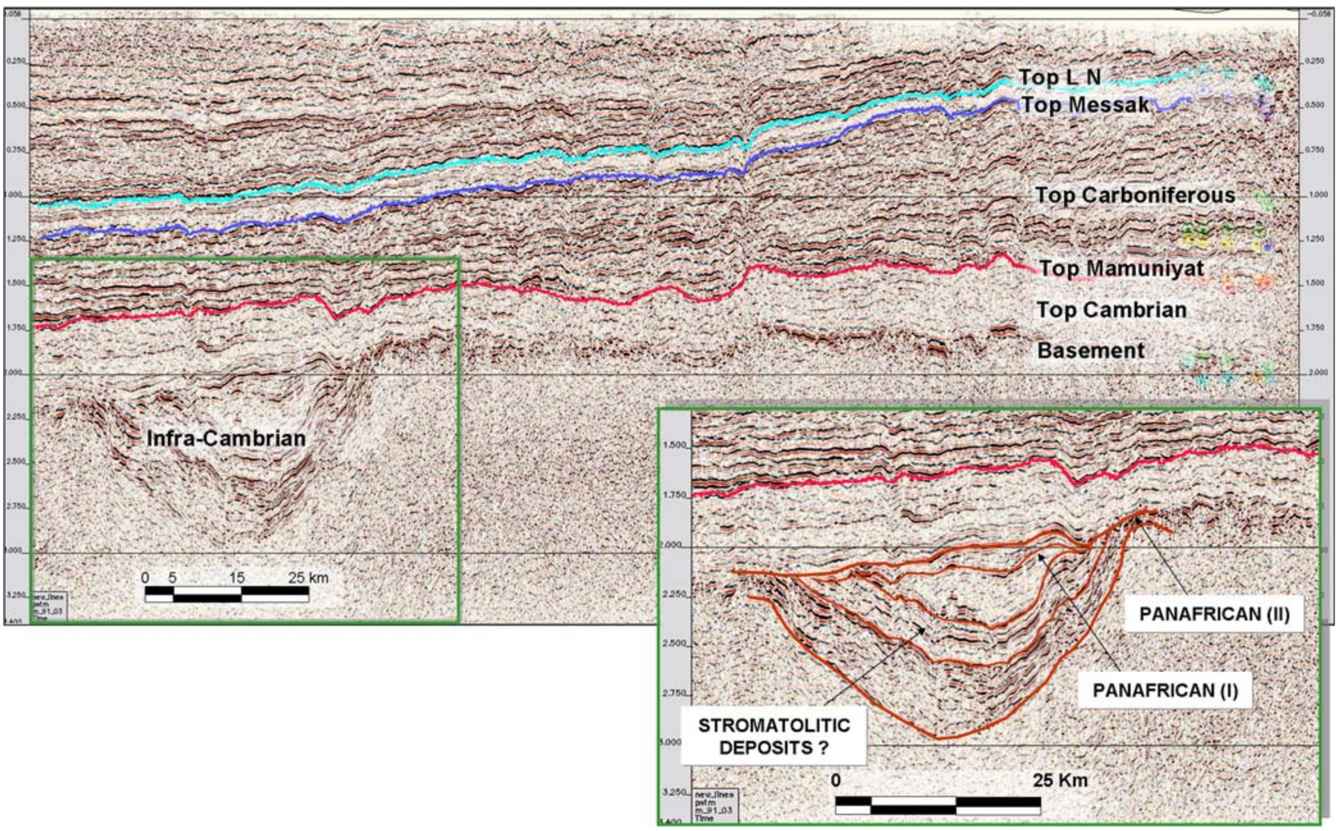

Fig. 10. Seismic section through the central Kufra Basin, SE Libya showing a potential remnant Neoproterozoic–Early Cambrian basin below relatively flat-lying Palaeozoic strata.

can be determined and placed within the Neoproterozoic to Early Cambrian climatic context. Initial observations suggest that there is a higher chance of encountering viable Neoproterozoic petroleum systems in areas underlain by the stable Precambrian cratons than in those underlain by the Pan-African mobile belts (Fig. 11). Areas such as the Taoudenni Basin on the West African craton contain, at least locally, relatively undeformed Neoproterozoic–Early Cambrian successions with Pre-Cryogenian, Cryogenian and Post-Cryogenian plays and rich Neoproterozoic source rocks (see Craig *et al.* 2009 for discussion). In contrast, the pre-Pan-African Neoproterozoic successions within the Pan-African mobile belts are typically heavily deformed and any 'Infracambrian' plays in theses areas are probably restricted to post-Pan-African inter-montane basins or graben which are typically filled with molasse sediments that have little or no source potential. Overall, our knowledge of the Neoproterozoic Eon and its global petroleum systems is growing rapidly and there is a widespread perception that Neoproterozoic and Late Neoproterozoic–Early Cambrian ('Infracambrian') plays will continue to be an important target for exploration in North Africa and the Middle East in the future.

Palaeozoic plays: expanding the play – the future for frontier oil and deep gas exploration in North Africa and the Middle East

The Palaeozoic hydrocarbon plays of the North African Saharan Platform and the Middle East are far better known and generally more widely explored than their Neoproterozoic counterparts. However, over large parts of the region the Palaeozoic succession is deeply buried beneath Mesozoic and Cenozoic successions (Fig. 12) that themselves contain prolific petroleum systems and, as a result, in the past there has been relatively little commercial incentive to address these more challenging, deeper and therefore, riskier, plays, particularly in the central parts of the main basins which still remain relatively under-explored (Rusk 2001). As the traditional Mesozoic and Cenozoic plays in these areas have become more mature and as the need to find new reserves has become imperative, attention has increasingly turned towards extending the Palaeozoic plays into new areas, including both 'frontier' areas on the periphery of the proven play fairway and the more deeply buried parts of the main proven fairway.

The collisional amalgamation of the African, South American, Indian, Australian and Antarctic basement terrains during the Late Precambrian, and the subsequent delamination of the underlying mantle, resulted in the uplift and subsequent peneplanation of basement rocks across the new Gondwana Supercontinent and the development of a wide, relatively stable shelf around its margins. The assembly of the Gondwana Supercontinent occurred in two main phases, *c.* 640–600 and *c.* 570–510 Ma, and was largely complete by the Mid Cambrian (e.g. Collins & Pisarevsky 2005; Pisarevsky *et al.* 2008; Craig *et al.* 2009). The peneplanation resulted in the development of an extensive and very gently inclined surface across much of the Gondwana margin encompassing North Africa, the Middle East and the Indian subcontinent. This surface was gradually buried under sediment eroded and transported broadly northwards from the remains of the Pan-African mountains to the south and was periodically flooded by marine transgressions from the north to form a broad shallow marine continental shelf throughout much of the Palaeozoic (Casati & Craig 2003). Reactivation of Pan-African structures during the Early Palaeozoic triggered the development of broad intra-cratonic sag basins that remained active depocentres throughout the Palaeozoic. Thick successions of Palaeozoic strata accumulated

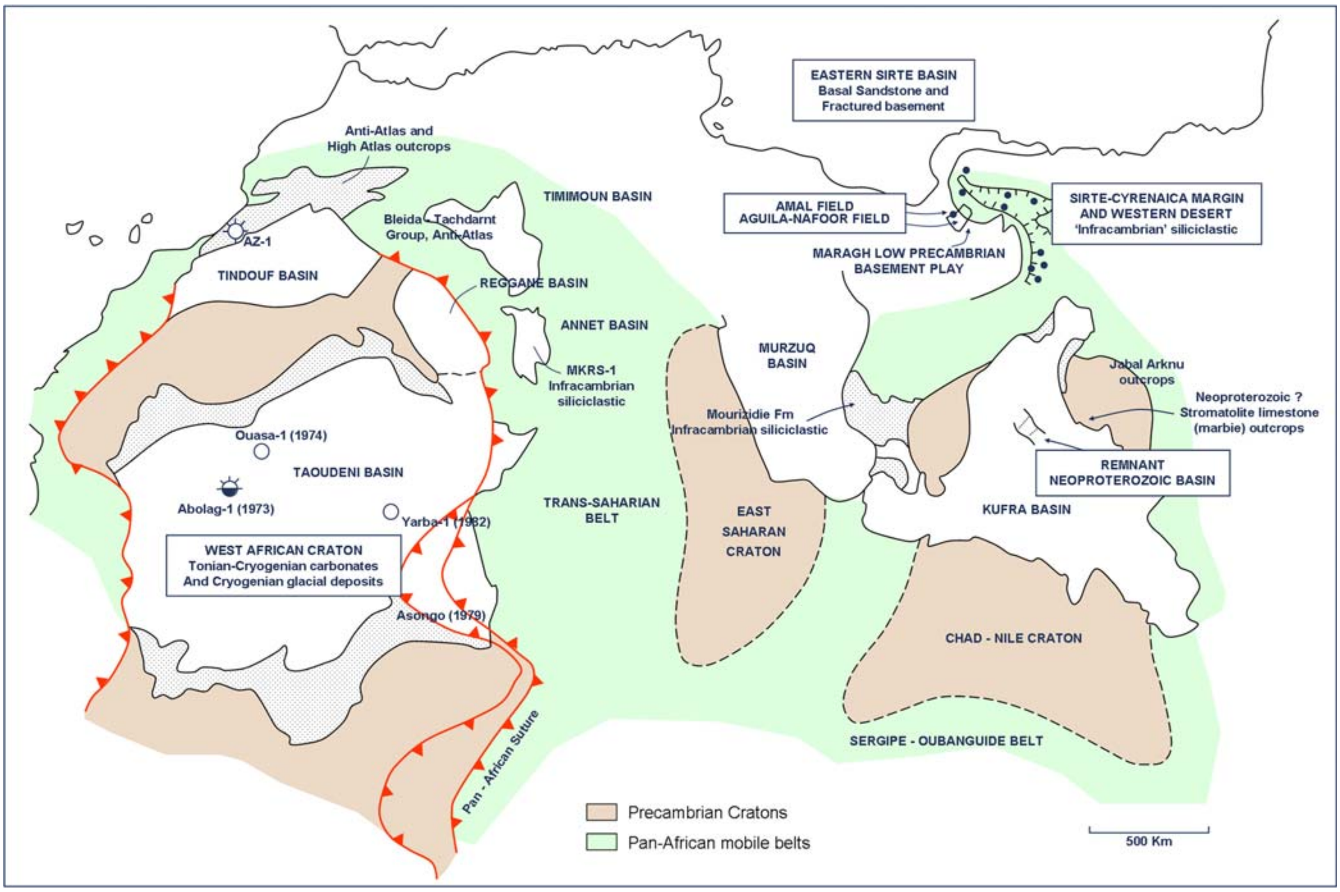

Fig. 11. Summary of Neoproterozoic and Neoproterozoic–Early Cambrian plays in North Africa.

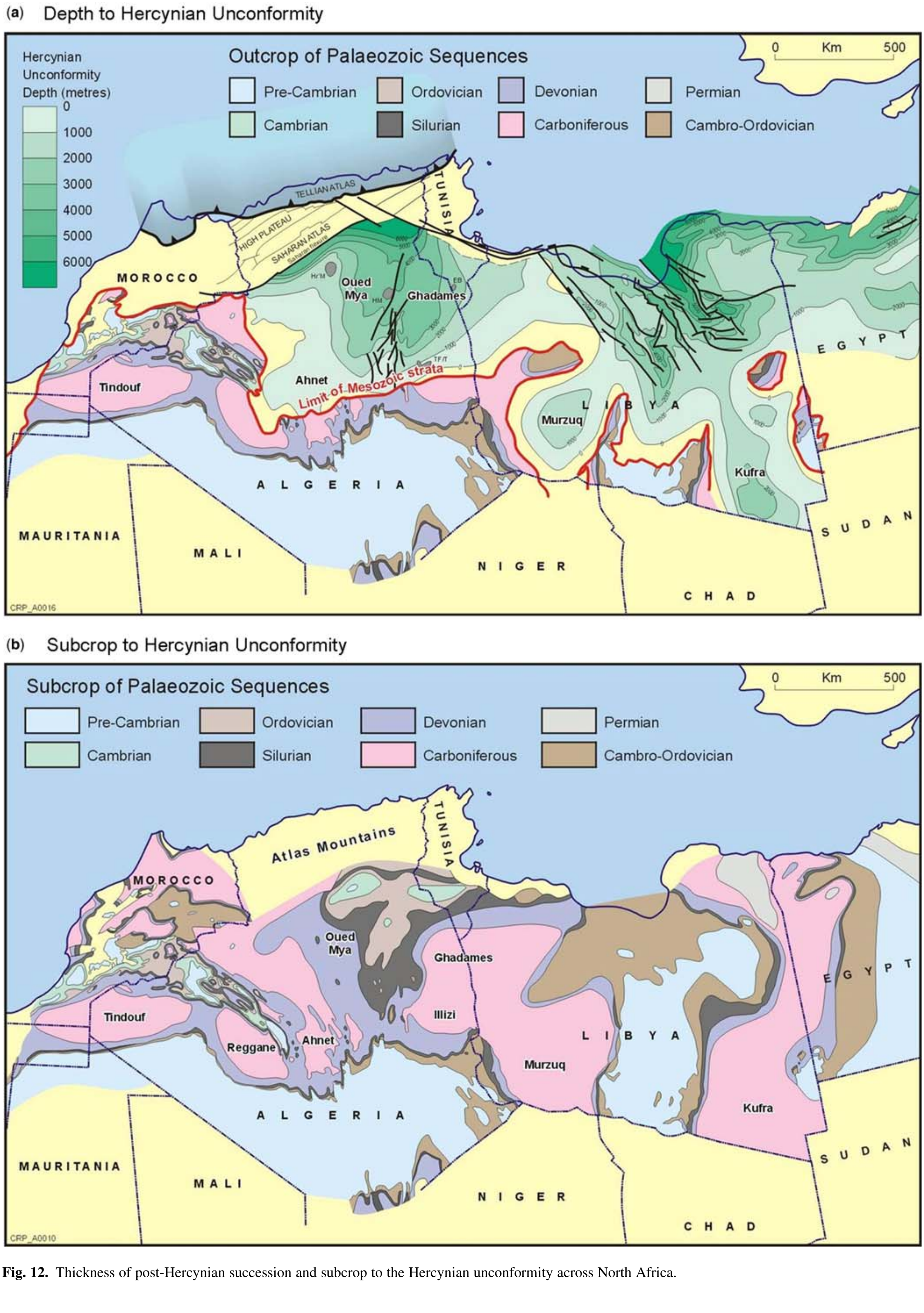

Fig. 12. Thickness of post-Hercynian succession and subcrop to the Hercynian unconformity across North Africa.

in many of these basins, but the shelf was sufficiently stable that similar and broadly correlatable sequences were deposited along the entire margin.

The Cambrian succession in both North Africa and across the Arabian plate typically rests unconformably on Precambrian crystalline or meta-sedimentary rocks or on Neoproterozoic or Neoproterozoic–Early Cambrian ('Infracambrian') sediments. It consists predominantly of fine- to coarse-grained sandstones with occasional pebble beds and conglomerates, deposited in a fluvial to marginal marine environment with primary sediment provenance from the south. The Silurian, Devonian and Early Carboniferous sequence are dominated by belts of marginal to shallow marine sandstones that migrated laterally with changing sea level and pass into deeper marine shales further offshore. The Cambro-Ordovician and Siluro-Devonian sequences are predominantly lowstand systems consisting of coarse clastic sediments deposited in a variety of continental fluvial and shallow marine environments. Major transgressions during the Rhuddanian (earliest Silurian) and the Frasnian (Late Devonian) flooded large parts of the shelf with variably anoxic waters. The associated transgressive and highstand systems contain organic-rich, radioactive ('hot') shales which form primary hydrocarbon source rocks and leaner shales which together act as regionally extensive seals.

North Africa

Cambro-Ordovician stratigraphy, tectonic evolution and hydrocarbon prospectivity

The Cambro-Ordovician succession in North Africa (Fig. 13) was deposited during a period of rifting associated with the opening of the Rheic Ocean (Stampfli & Borel 2002). The main Cambrian reservoirs are separated from the overlying Ordovician Quartzite de Hamra ('Hamra Quartzites') by a *c.* 200 m thick sequence of Argiles D'El Gassi (El Gassi Shale). This vertical barrier has probably isolated the Cambrian succession from overlying younger reservoir units and from the key Early Silurian and Devonian (Frasnian) source rocks in most areas. The charge risk that this creates is substantially reduced where there is lateral fault contact between the Silurian source rocks and Cambrian reservoirs or between Cambrian reservoirs and Ordovician reservoirs, but such occurrences appear to be relatively rare because vertical fault displacements rarely achieve the 500 m required to juxtapose the Cambrian and Silurian successions. The petrophysical properties of the Cambrian reservoirs are generally poor due to extensive quartz cementation, although some porosity is retained locally in facies where kaolinite has been transformed into dickite during burial. The porosity and permeability of the Cambrian sandstones is higher over the Hassi Messaoud High where there was less re-burial after the Hercynian uplift and fracturing is more intense.

The black and dark grey, indurated, silty and locally pyritic El Gassi Shale is sometimes considered to be a viable source rock, but the limited data available suggest that the organic content varies considerably, is usually low (less than 1.5%), although locally as high as 8.6%, and it is almost invariably overmature, although this still requires further study. There have been suggestions that the oil in the super-giant Hassi Messaoud Field (9–11 BBOE recoverable) is derived from both Silurian and Ordovician sources (Balducchi & Pommier 1970; Bacheller & Peterson 1991). Other Ordovician shale units (e.g. The Azzel Shales and the 'Microconglomeratique' Shales) appear to have rather limited source rock potential with TOC values typically less than 1%.

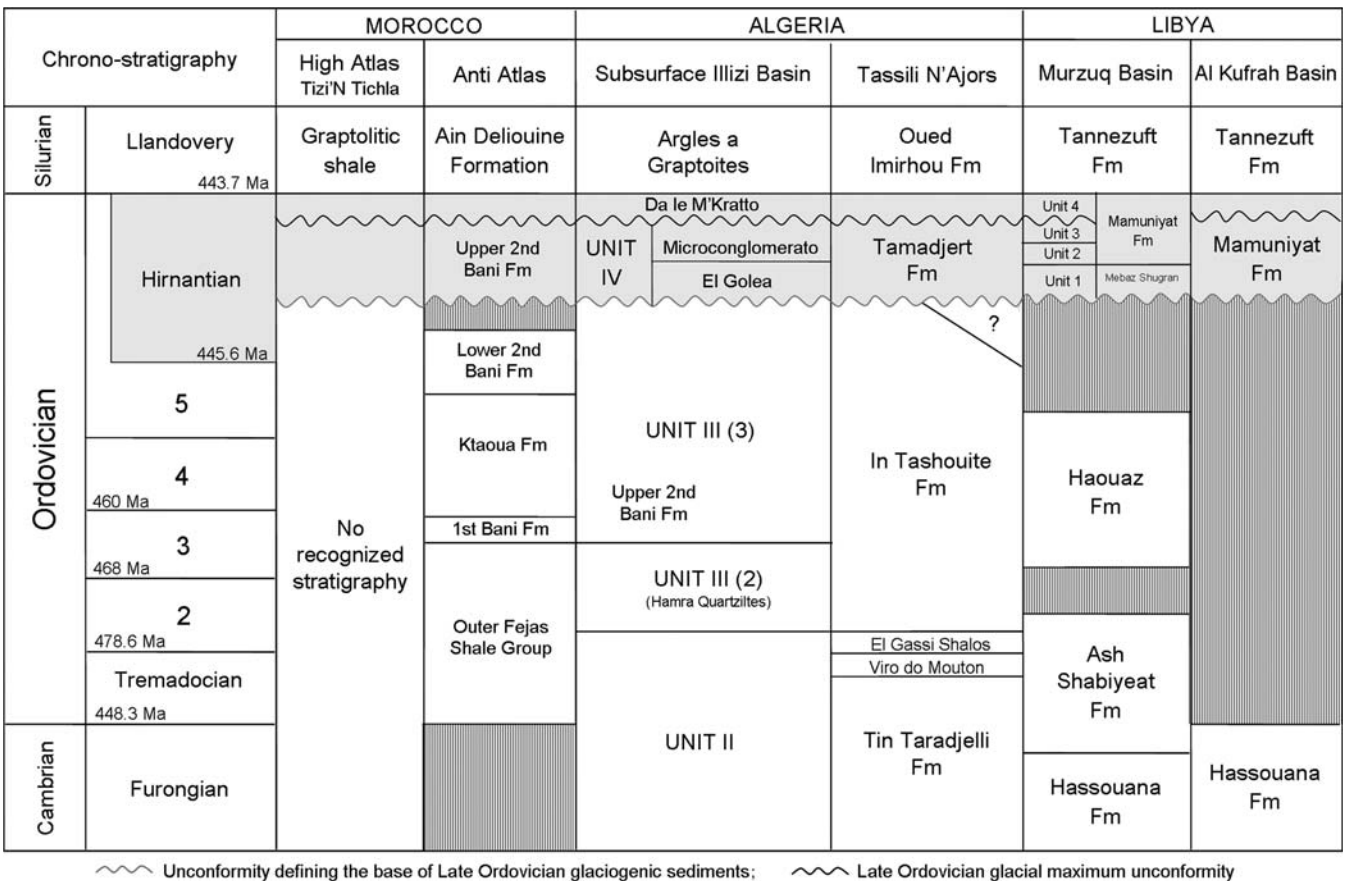

Fig. 13. Cambro-Ordovician stratigraphy of North Africa (after Le Heron *et al.* 2009).

The reservoir potential of the Ordovician Hamra Quartzites is typically relatively low as a result of extensive quartz cementation during pre- and post-Hercynian burial. The highest remaining porosity is confined to areas where bitumen coating developed during the pre-Hercynian phase of hydrocarbon generation and migration. Fracture development is also important in enhancing the reservoir potential of the Hamra Quartzites, as even in areas where the matrix porosity is very low (typically less than 1%), the presence of fractures increases the overall reservoir permeability substantially. The search for highly fractured 'sweet-spots' in the Hamra Quartzite and equivalent reservoirs is one of the key technical challenges facing future exploration across much of northern Africa.

The equivalent Cambrian to Lower Ordovician succession (the Hassauna and Haouaz formations; Fig. 13) in the Libyan portion of the Ghadames Basin consists of a thick sequence of continental to shallow marine sands and is overlain by a sequence of transgressive marine shales, assigned to the Melez Chograne Formation (Bertello *et al.* 2003; Craig *et al.* 2008; Galeazzi *et al.* 2010).

The Upper Ordovician reservoirs in North Africa (Unit IV, Mamouniat Formation and equivalents) contain at least 5 BBOE of reserves in more than 50 fields scattered across a broad area from the Murzuq Basin in SW Libya to the Ahnet Basin in central Algeria (Fig. 14), including the giant El Feel (more than 500 MMBBL), Tiguentourine (1.2×10^{12} SCF and 40 MMBBL) and Tin Fouye (8×10^{12} SCF and 710 MMBBL) fields (Davidson *et al.* 2000; Echikh & Sola 2000; Hirst *et al.* 2002; Ghienne 2003; Le Heron *et al.* 2004). Most of these reservoirs were deposited in glacially influenced, generally shallow marine settings, on the continental shelf at, or beyond, the margins of a continental ice sheet (Craig *et al.* 2009; Le Heron & Craig 2008; Le Heron & Dowdeswell 2009; Le Heron *et al.* 2009). In keeping with their ice-proximal to distal setting, they exhibit complex and rapid changes in facies and reservoir quality, and contain a wide range of glacially induced, syn-sedimentary structures. Deposition was controlled at the basin-scale by the location of fast-flowing ice streams active during glacial maxima, and by meltwater release during glacial recession. Much of the succession consists of fluvioglacial and glaciomarine sediments deposited in a series of deep subglacial incisions into the underlying pre-glacial strata at or near the ice margin (Le Heron & Craig 2009). These tunnel valleys were filled in two main phases. The initial phase was characterized by debris flow release, while during later phases of glacial retreat, glaciofluvial, shallow glaciomarine to shelf sediments were deposited dependent on the water depth at the ice front. The reservoir sand bodies deposited in these tunnel valleys have a complex and irregular distribution that is directly related to the topography created by the erosive action of the ice sheets. The reservoir distribution is closely associated with the position of 'grounding lines' where the glacial topography was enhanced and sediment accumulated in thick glacial outwash ice-contact fans (Le Heron & Craig 2009). Unequivocal evidence of the presence of ice on the continental shelf of North Africa is sparse, but includes isolated occurrences of outsized, exotic, faceted and striated (ice-rafted?) clasts in shales and the presence of locally extensive soft sediment striated 'ice-pavements' (Sutcliffe *et al.* 2005). The Upper Ordovician glaciogenic rocks characteristically exhibit very rapid lateral and vertical changes in facies (e.g. Sutcliffe *et al.* 2000; Ghienne 2003). These make it notoriously difficult to establish a sound stratigraphic framework for the sediments, or to correlate them from one area to another, even within a single oil field. However, new work has enabled the Upper Ordovician glaciogenic sediments of North Africa to be subdivided into ice-contact, glacimarine shelf,

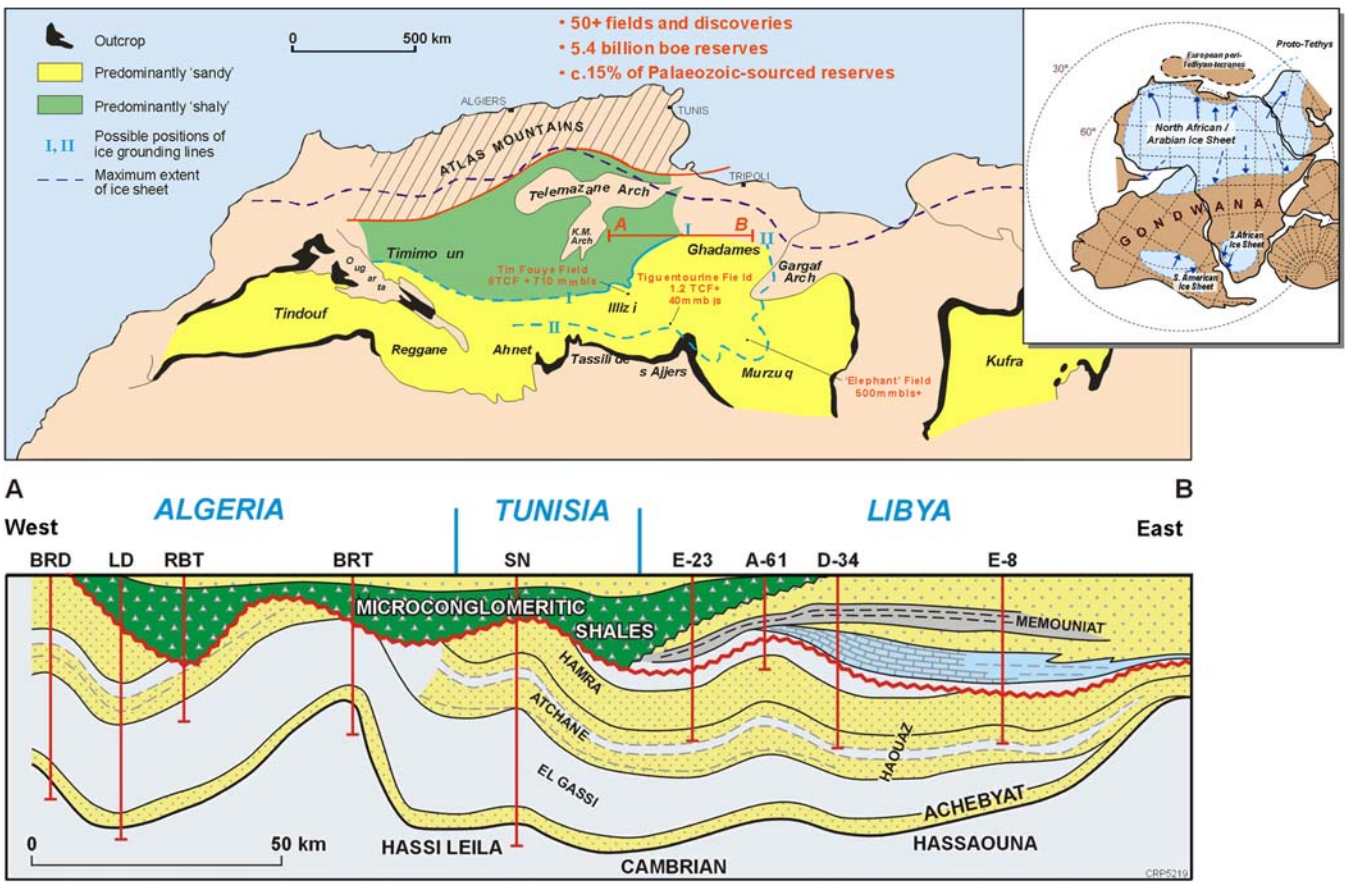

Fig. 14. Distribution and facies of the Late Ordovician glaciogenic Mamouniyat Formation and equivalents in North Africa (after Craig *et al.* 2008). Inset: distribution of the Late Ordovician ice sheets (after Le Heron & Dowdeswell 2009).

and rebound units, based on an analysis of the facies preserved within the Upper Second Bani Formation in Morocco, the Hassi el Hadjar Formation in Algeria, and the Melez Chograne and Memouniat Formations in Libya. Together these indicate ice-contact to distal glacimarine shelf settings on a high-latitude shelf influenced by an extensive grounded ice sheet (Le Heron & Craig 2009; Le Heron *et al.* 2010; Craig *et al.* in preparation). The different facies of the Upper Ordovician glaciogenic succession have widely differing reservoir properties. Successful exploration for, and development of these reservoirs requires a detailed understanding of sand body distribution, geometry and vertical and lateral continuity. Ice-proximal fluvioglacial deposits and high-density turbidites typically form the best-quality reservoirs, but punctuated coarsening-up shoreface deposits in the post-glacial isostatic rebound succession also have considerable potential. Appraisal and development of these glaciogenic reservoirs is further complicated by the presence of a wide range of syn-depositional, glacially induced heterogeneities, including subglacial and ice marginal fold-thrust belts, tunnel valleys, soft-sediment load structures, intra-formational shear surfaces, dewatering structures and micro-faults, all of which have the potential to act variously as barriers, baffles or conduits for fluid flow on both geological and production time-scales.

The Late Ordovician glaciation was short lived (<0.5 Ma) and glacial conditions ended abruptly near the base of the Late Hirnantian *persculptus* Zone (Vecoli 2000; Vecoli *et al.* 2009). The glacio-eustatic sea level rise associated with the collapse of the ice sheets produced a return to normal oceanic stratification and flooded the previously exposed continental shelf with anoxic waters, pushing the contemporary shoreline southwards by many hundreds of kilometres. Organic-rich, graptolitic pyritic, radioactive ('hot') shales were deposited in isolated topographic depressions in the former glacial landscapes in the Rhuddanian (earliest Llandovery), during the initial stages of the transgression. The organic-rich 'hot' shale intervals are typically 10–60 m thick with TOC contents ranging from 3 to 17%. A younger, less well developed and more areally restricted organic-rich 'hot' shale horizon occurs higher in the Silurian succession, within the Telychian, in some parts of the Ghadames Basin (Luning *et al.* 2000). The organic-rich horizons produce very distinctive high amplitude events on seismic data which, when combined with information from well penetrations, allows the distribution of the 'hot' shale source rocks to be mapped in detail (Fig. 15, Luning *et al.* 2000; Craig *et al.* 2009). The basal Silurian 'hot' shale interval appears to be thicker and more laterally continuous in the more distal or 'out-board' areas of central and western Algeria and Tunisia than in the proximal or 'in-board' areas such as the Murzuq Basin of SE Libya, where it is thinner, discontinuous and its deposition was strongly controlled by the relict topography of the Late Ordovician glacial landscape (Luning *et al.* 2000; Le Heron *et al.* 2009). The complex post-glacial topography in these areas reflects a combination of palaeo-ice stream pathways, 'underfilled' tunnel valley incisions, glaciotectonic deformation structures and re-activation of older crustal structures during post-glacial isostatic rebound. Competing hypotheses link the formation of these organic-rich source rocks to either coastal upwelling or freshening of marine water due to the influx of meltwater as the ice sheets collapse (Luning *et al.* 2000; Armstrong *et al.* 2005, 2009). These locally discontinuous basal Silurian black shales are the source of at least 80% of the Palaeozoic-derived hydrocarbons discovered in North Africa to date.

Estimates of the potential volumes of gas that remain to be found in the deep Cambrian and Ordovician reservoirs underlying the more conventional Silurian–Devonian Acacus plays in the Ghadames Basin of eastern Algeria and western Libya and the Triassic plays in the Berkine Basin in central Algeria, vary widely. Detailed 3D petroleum systems models suggest that P50 volumes in the range of $70–100 \times 10^{12}$ SCF would not be unreasonable for the Berkine Basin. About half of this volume is likely to be trapped in the Hamra Quartzite and deeper Cambrian reservoirs because the size of the structures generally increases with depth. Our models also suggest that most of this gas will be trapped in a limited number of very large structures, most of which underlie existing producing Triassic fields. The petrophysical characteristics of these deeply buried reservoirs are very uncertain, largely due to the very limited number of well penetrations at these depths, but it would be reasonable to assume that low porosities and permeabilities will be the norm and that tight gas production technologies will need to be utilized, with the consequent impact on the commercial viability. However locally, sandstones in the Late Ordovician Memouniat Formation can have porosities in the range of 8–12% with fair permeabilities (Bertello *et al.* 2003).

Silurian and Devonian stratigraphy, tectonic evolution and hydrocarbon prospectivity

Sea level continued to rise through the Early Silurian, flooding most of the remaining topography by the Aeronian (mid-Llandovery), before a major north to northeastward-prograding delta system deposited the sandy sediments of the Acacus Formation across much of the North African margin. The basal members of this formation are one of the primary Palaeozoic reservoir targets in the southern and eastern portions of the Ghadames Basin, particularly in northwestern Libyan and southern Tunisia, where they have porosities ranging from 10 to 20% and permeabilities that are often in excess of 100 mD (Bertello *et al.* 2003). Inversion-related uplift and erosion during the Early Devonian (the so-called 'Caledonian event'), associated with the separation of the 'Hun Superterrane' from African Gondwana (Stampfli & Borel 2002), resulted in variable erosion of the Acacus Formation and was followed by the deposition of fluvio-deltaic and shallow marine sandstones of the Tadrat Formation on the resulting unconformity surface. Stratigraphic traps are developed locally where the Acacus sands are truncated by the Hercynian unconformity (e.g. the Tigi Field, Ghadames Basin). The succeeding Devonian succession in the Ghadames Basin includes transgressive shallow marine sandstones of the Ouan Kasa Formation, the Emgyet Shale (representing a maximum flooding surface), the shelf sandstones and overlying shallow marine shales of the Aouinet–Ouenine Formation and, finally, the shelf sandstones of the Tahara Formation. Stratigraphic trapping as a result of pinchout of the Aouinet–Ouenine sands against the Tihemboka High is responsible for the giant El Wafa Field in the Ghadames Basin of western Libya, while the nearby El Hamra Fields are the result of structural trapping of oil in updip closures against faults within the Tadrart Formation.

The Upper Devonian (Frasnian) sequence (the upper shaly part of the Aouinet–Ouenine Formation) contains the second major 'hot' shale source rock interval n the Palaeozoic succession and is estimated to be the origin of some of 10% of the Palaeozoic-sourced hydrocarbons in North Africa. Its distribution is more restricted than that of the deeper Silurian 'hot' shales, due in part to the fact that it was deposited in an active foredeep (Dixon *et al.* 2010) so it is best developed in the basin centre and thin to absent on the regional arches and local inversion structures, and partly due to the later effects of erosion at the Hercynian Unconformity. It is a key source interval in the Berkine and Illizi basins and also has an important role in the Palaeozoic petroleum system in the Ahnet and Reggane basins. The organic-rich shale was deposited in a restricted, poorly oxygenated environment during regional transgression of an unconformity surface (the 'Frasnian Unconformity') with palaeo-relief of at least 200 m in the northern Berkine Basin. The 'Frasnian shale' (Frasnian–Famennian?) varies in

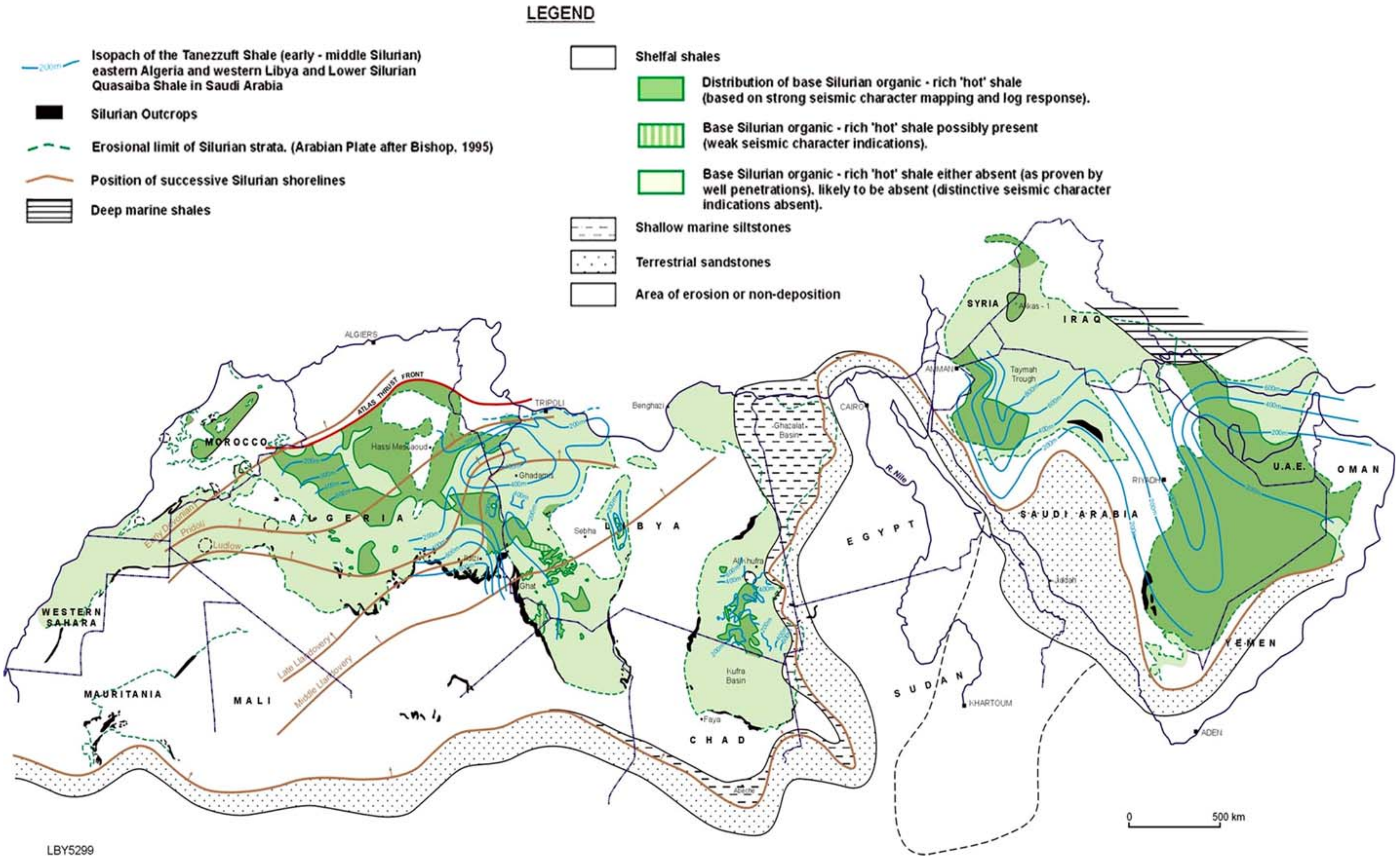

Fig. 15. Distribution of the Silurian Tannezuft Formation and equivalents across North Africa and the Middle East.

thickness from 0 to 150 m across this topography and consists of a series of high-frequency, high-amplitude, metre-scale, gamma ray cycles with TOC typically in the range of 3–5%, but locally up to 14%. As in the Silurian succession, there is a second organic-rich interval present locally, particularly in the northern parts of the Berkine Basin. Hydrocarbons expelled from the Frasnian source rock are sometimes encountered in younger Devonian and Lower Triassic reservoirs (Bertello *et al.* 2003).

The lateral continuity of the major stratigraphic sequences was a key characteristic of Palaeozoic deposition on the North African continental margin until Late Carboniferous times when more isolated and restricted continental basins developed as a result of tectonic movements marking the initial pulses of the Hercynian orogeny. During the Carboniferous, several mostly shaly units of shelfal and shallow marine facies (the M'rar, Assedjefar and Tiguentourine formations) were deposited before sedimentation was terminated abruptly by uplift, erosion and regional northward tilting as a result of the Hercynian orogeny, during the Late Carboniferous and Early Permian.

The Hercynian orogeny produced widespread compressional deformation in northern and western Morocco and in northern Algeria and uplift and, locally, profound erosion in intra-plate areas such as Algeria and western Libya. Petroleum systems established as a result of burial and maturation of Palaeozoic source rocks prior to the Hercynian orogeny were largely 'frozen' or destroyed by the deformation, uplift and erosion that accompanied the development of the Hercynian unconformity (Casati & Craig 2003; Craig *et al.* 2008). The subcrop pattern and the topography of the Hercynian unconformity surface (Fig. 12) are key elements in the present-day petroleum systems of North Africa. They control the gross distribution of Palaeozoic reservoirs, the communication pathways between the Palaeozoic source rocks and reservoirs and the pattern of long distance migration into post-Hercynian reservoirs.

Sedimentation resumed in the Early Permian with carbonate deposition in parts of southern Tunisia, but was delayed until the Early to Mid Triassic over much of North Africa with the deposition of clastic, carbonate and evaporitic sediments, that wedge strongly towards the north (Fig. 12). These include, at the base, the important Lower Triassic fluvio-deltaic reservoir sandstones of the TAGI/TAGS in the Algerian portion and the broadly equivalent Ouled Cheb and Ras Hamia formations in the Libyan and Tunisian portions of the Ghadames Basin. The early post-Hercynian sedimentation in the Oued Maya, Berkine and Ghadames basins of eastern Algeria and western Libya was characterized by the deposition of a complex system of Triassic fluvial, aeolian and sabkha sediments across the subtle erosional topography of the Hercynian unconformity surface with regional drainage towards the NNE into the developing Neo-Tethys rift (Turner *et al.* 2001; Turner & Sherif 2007). Sedimentation and associated volcanism during the Late Triassic and Early Jurassic was increasingly influenced by NE–SW trending extensional faults. The Triassic fluvial and aeolian sandstones are the traditional primary exploration target in these areas. They host some 50% of the Palaeozoic-sourced reserves in structural, stratigraphic and combination traps that are ultimately sealed by thick Early Jurassic (Liassic) evaporates and, locally, by laterally equivalent volcanic lavas.

It is notable that some of the younger Palaeozoic reservoirs in these areas locally retain very high porosities (up to 25%) due to the preservation of porosity by chlorite grain coatings formed during early diagenesis in the presence of mixed marine and fresh water in estuarine depositional environments. These reservoirs constitute more attractive and less risky exploration targets. Most of the Lower–Middle Devonian (Eifelian and Emsian) successions in this area were deposited in offshore or shoreface environments and typically have low reservoir porosities and permeabilities. However, Emsian and Eifelian (F4/F5) sandstones form thin, laterally discontinuous, but relatively porous reservoirs where they are embedded in offshore shales, with the preservation of reservoir quality being, at least in part, due to early overpressure development.

Thermal evolution and hydrocarbon generation

The thermal evolution of the Palaeozoic petroleum systems in North Africa and the Middle East is generally well constrained by the large well database. This is particularly the case for the maturity data necessary to reconstruct the burial history of the basins, although the maturity measurements for pre-Carboniferous sequences are not usually based on vitrinite data, but use other methods to estimate equivalent values, which are inherently less reliable.

The Taoudenni Basin was contiguous with the Tindouf and Reggane basins to the north during the Early Palaeozoic and this connection was only broken as a result of regional inversion and uplift of the Regubiat Rise during the Late Silurian and Early Devonian (Guerrak 1989). The Taoudenni Basin was uplifted and eroded at this time and the resulting unconformity completely removes the Silurian succession in some areas of the basin (Dixon *et al.* 2010). The thermal evolution of any potential Early Silurian Tannezuft Formation source rocks in the Taoudenni Basin is influenced strongly by burial prior to the Hercynian orogeny (Fig. 9). Uplift and erosion associated with the Hercynian events was quite significant in the western Taoudenni sub-basin, but comparatively minor in the eastern sub-basin. Basin modelling suggests that the maximum burial, reached at 250 Ma, was not sufficient to cause generation, expulsion and migration of significant amounts of hydrocarbons from any potential basal Silurian source rocks in either sub-basin, but particularly in the west, although this is highly dependent on the assumed thermal regime. There was also insufficient re-burial during the Mesozoic and Cenozoic to increase the maturity and reactivate the residual hydrocarbon potential.

The evolution of the Palaeozoic petroleum systems in the Berkine Basin is very different (Fig. 16). Here, the amount of burial during the Palaeozoic, prior to Hercynian orogeny, was comparatively minor in the present-day basin centre, but much greater on the flanks. The key difference in the evolution compared with the Taoudenni Basin is the occurrence of a second important burial phase during the Mesozoic, prior to a minor episode of uplift and erosion related to the Alpine deformation. The lack of substantial Hercynian erosion in the basin centre combined with the pre-Alpine re-burial is sufficient to produce late hydrocarbon generation and an efficient petroleum system in areas of the basin where the source rock potential was not exhausted during the pre-Hercynian burial phase. A similar evolution is observed in many other Palaeozoic basins in North Africa, including the Oued Mya Basin, the Reggane and Ahnet basins (Fig. 1), although the evolution appears to complicated locally by a pronounced heating event at around 200 Ma, recorded through apatite and zircon fission track analysis and the presence of both intrusive and extrusive volcanic rocks. This heating event is related to Late Triassic to Early Jurassic volcanic activity associated with the onset of Atlantic rifting and it overprints the effects of heating caused by simple burial before the Hercynian uplift. In the Reggane and Ahnet basins, this seems to have produced a two-stage maturation history, with an early phase of generation and expulsion of mainly liquid hydrocarbons and a later phase, associated with the *c.* 200 Ma 'heat spike', during which significant quantities of dry gas were generated and expelled (Logan & Duddy 1998).

In many of the Palaeozoic basins of North Africa, additional burial during Jurassic and Early Cretaceous times seems to have been sufficient to at least partially reactivate the hydrocarbon generation of the main Palaeozoic source rocks and result in further

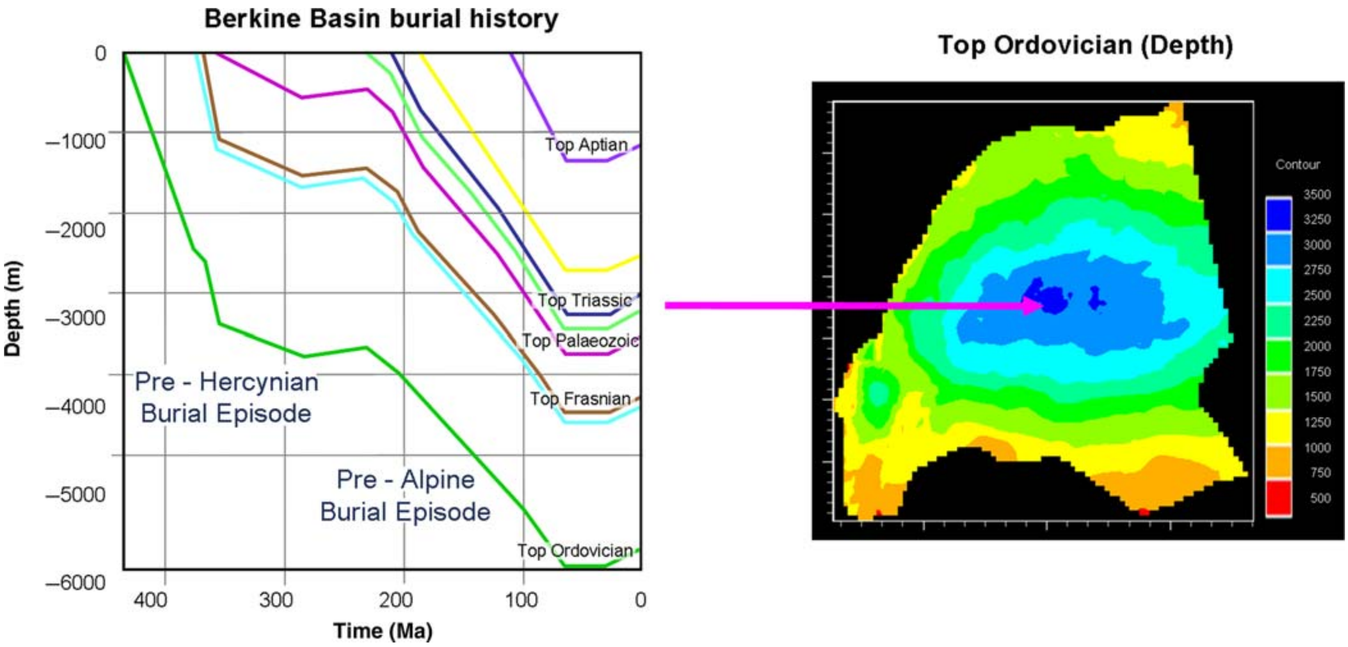

Fig. 16. Burial history and regional tectonic events in the Berkine Basin, central Algeria.

expulsion and migration of both oil and gas into Palaeozoic and basal Triassic reservoirs between the Late Cretaceous and the present day. Deformation and uplift during the Early Cretaceous 'Austrian' and Mid Cenozoic 'Alpine' events modified existing traps, and created new traps in many areas. Locally, a final phase of tilting, re-migration of hydrocarbons and freshwater flushing of reservoirs occurred with the massive Mid to Late Cenozoic uplift of the Hoggar Massif.

The presence or absence of significant Hercynian erosion is often considered to be a critical element in the maturation history of the key Silurian and Devonian source rocks in North Africa. However, detailed 3D Petroleum Systems Modelling of the Tunisian portion of the Ghadames Basin (Tonetti & Grigo 2007) suggests that this may be less important than generally envisaged. In this area, the Silurian source rocks reach approximately the same level of present-day maturity irrespective of whether the Hercynian subcrop is considered to represent palaeotopographic relief with thicker Palaeozoic sequences deposited in topographic lows and thinner sequences or depositional hiatus over the topographic highs, or the result of variously eroded thicknesses of more uniformly distributed Palaeozoic strata. The main difference between these two scenarios is in the timing of generation and expulsion, with the Silurian source rock entering the oil window earlier, just prior to the onset of Hercynian erosion, in the basin depocentre in the latter case. However, the overall quantity, and the phases, of the trapped hydrocarbons are similar in both cases, with the maximum expulsion of both oil and gas during the Middle Oligocene as a result of the combination of burial and of a peak in heat flux related to the passage of a Cenozoic hot spot beneath North Africa.

There is a strong correlation between the fluid phase trapped in the overlying Triassic reservoirs in the Berkine Basin and the maturity and lateral extent of the main basal Silurian and Frasnian source rocks. Gas fields predominate in the SW and east of the Berkine Basin, where the Frasnian source rock is eroded and the charge is probably directly from the highly mature Silurian source rock. Oil fields predominate in the north of the basin where the Frasnian source rock is early mature or in the peak oil generation window and condensates or mixed oil and gas fields characterize the central part of the basin where the Frasnian source rock is highly mature. A similar relationship is observed in the northern Oued Mya Basin (Fig. 17) where the Frasnian source has a more restricted distribution but there is a strong correlation between the phase of hydrocarbons in the fields and the maturity of the Silurian source rock within the corresponding 'fetch areas'. There is a strong differentiation between the SW portion of the Oued Mya Basin and the Mouydir Basin, where generation and migration occurred before the Hercynian orogeny and where there are no significant remaining accumulations, and the northern Oued Mya Basin where maximum maturity was achieved mainly in Albian–Aptian times and where all the major present-day oil and gas fields are located. The Hassi Messaoud, El Gassi and Rhourde El Baguel fields can all be charged from areas subject to post-Hercynian oil and wet gas generation with the southwestward increasing gas–oil ratio (GOR) of the fields along the Hassi Messaoud Arch corresponding with increasing maturity of the Silurian source rock. It is notable that in this scenario the giant Hassi R'Mel Gas Field cannot be charged from the Oued Mya Basin, but must be charged from a deep gas kitchen further to the north. This is consistent with the concept that the Hassi R'Mel Field is stratigraphically trapped along its southern edge.

There was also significant pre-Hercynian generation of oil and gas from the Silurian Tannezuft 'hot' shale source in the Ghadames and Illizi basins and probably also more minor generation of oil and gas from the Frasnian source in the deepest part of the Ghadames Basin (e.g. Dixon *et al.* 2010). Present day, the Silurian source rock is overmature and the Frasnian source rock is in the gas window in the central part of the Ghadames Basin (Craig *et al.* 2008).

The basal Silurian 'hot' shale source rock in the Murzuq Basin in SW Libya has a similar two-phase burial history (Fig. 18), with an initial pre-Hercynian burial phase and a subsequent Mesozoic phase, during which the source rock reached its maximum burial in most parts of the basin. The depth of burial in the Murzuq Basin is generally less than in the Oued Mya and Berkine basins and significant volumes of hydrocarbons were only generated and expelled during the later Mesozoic, pre-Alpine burial. Pre-Hercynian and pre-Alpine burial phases also occur in the Kufra Basin (Al Kufrah) in SE Libya, but here the pre-Hercynian phase is relatively weak and there appears to be a significant amount of Alpine uplift

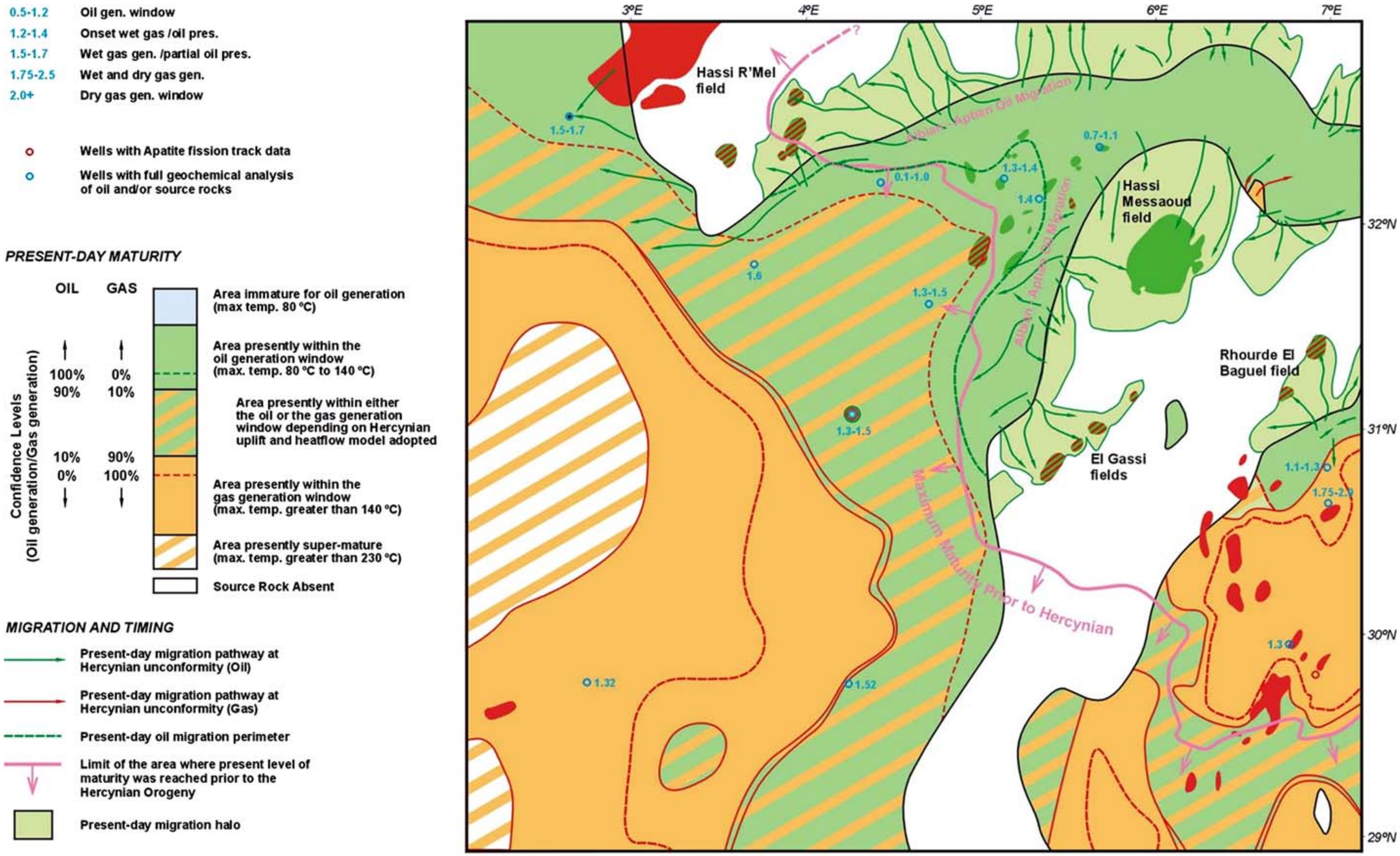

Fig. 17. Thermal maturity of the Early Silurian Tannezuft 'Hot' shale and relationship to the distribution of oil, gas and gas condensate fields in the northern Oued Mya Basin, central Algeria.

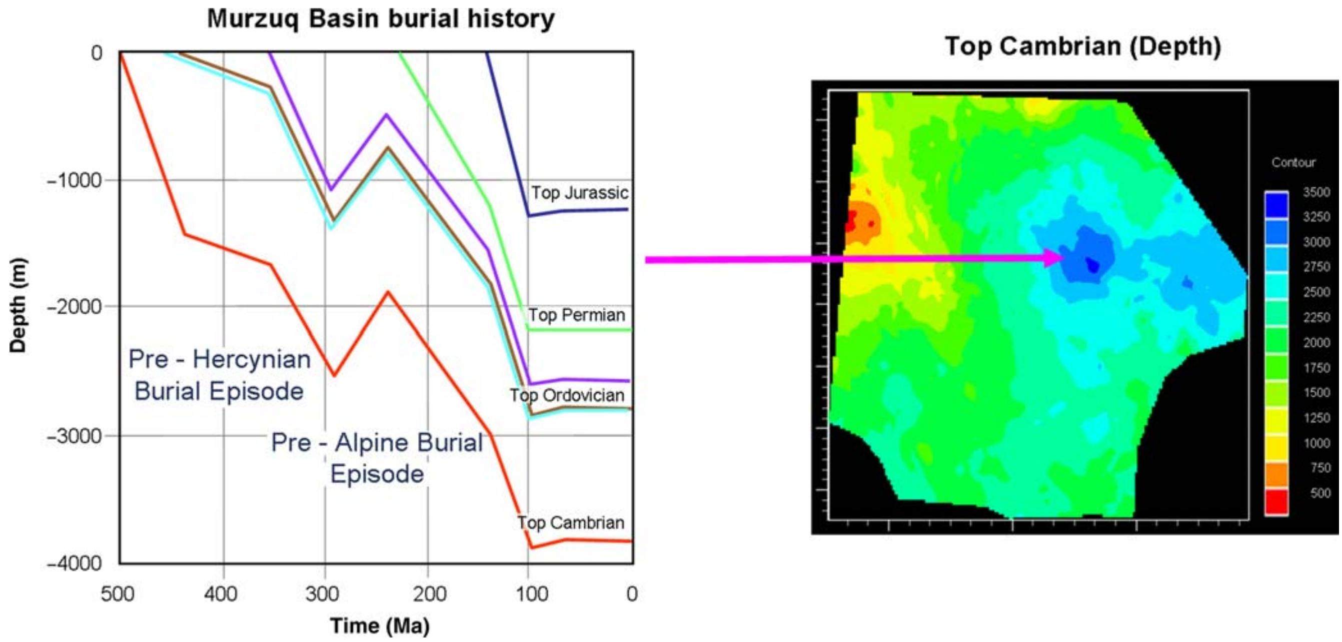

Fig. 18. Burial history and regional tectonic events in the Murzuq Basin, SW Libya.

(Fig. 19). This is likely to have resulted in a rather inefficient Palaeozoic petroleum system in this basin because any potential mature Silurian source rocks are likely to have been lifted out of the 'oil window' rather rapidly during the Alpine uplift.

The ultimate intensity of deformation and the degree of thermal maturity of the main Palaeozoic hydrocarbon source rocks in North Africa decreases broadly eastwards away from the Hercynian and Alpine collision zones (Craig *et al.* 2008). The present-day concentration of large oil and gas fields in eastern Algeria and southwestern Libya is a direct result of the favourable timing of hydrocarbon generation and expulsion, trap formation and, crucially, hydrocarbon preservation in these areas on the margins of the main orogenic belts. It is in these same areas that the best remaining potential for deeper accumulations below the traditional Triassic and/or Devonian objectives in North Africa is likely to be found (Fig. 20).

Saudi Arabia and the Middle East

The sedimentary basins of the Arabian Plate are universally recognized as one of the richest petroleum provinces in the world. The remaining reserves in the Kingdom of Saudi Arabia alone are estimated to be some 300×10^9 BOE, with the majority being light oil in the 'traditional' reservoirs of Jurassic and Cretaceous age (Pollastro 2003). Exploration of the deeper Palaeozoic sequences in Saudi Arabia only began in the 1980s. The first success came in 1989, with the discovery of oil in the Permian Unayzah Formation in what subsequently became the Hawtah field. Many new Palaeozoic oil and gas fields have been discovered in Saudi Arabia over the past 30 years and a significant proportion of the Saudi Arabia production now comes from Palaeozoic reservoirs. The Palaeozoic succession is well exposed in the central western

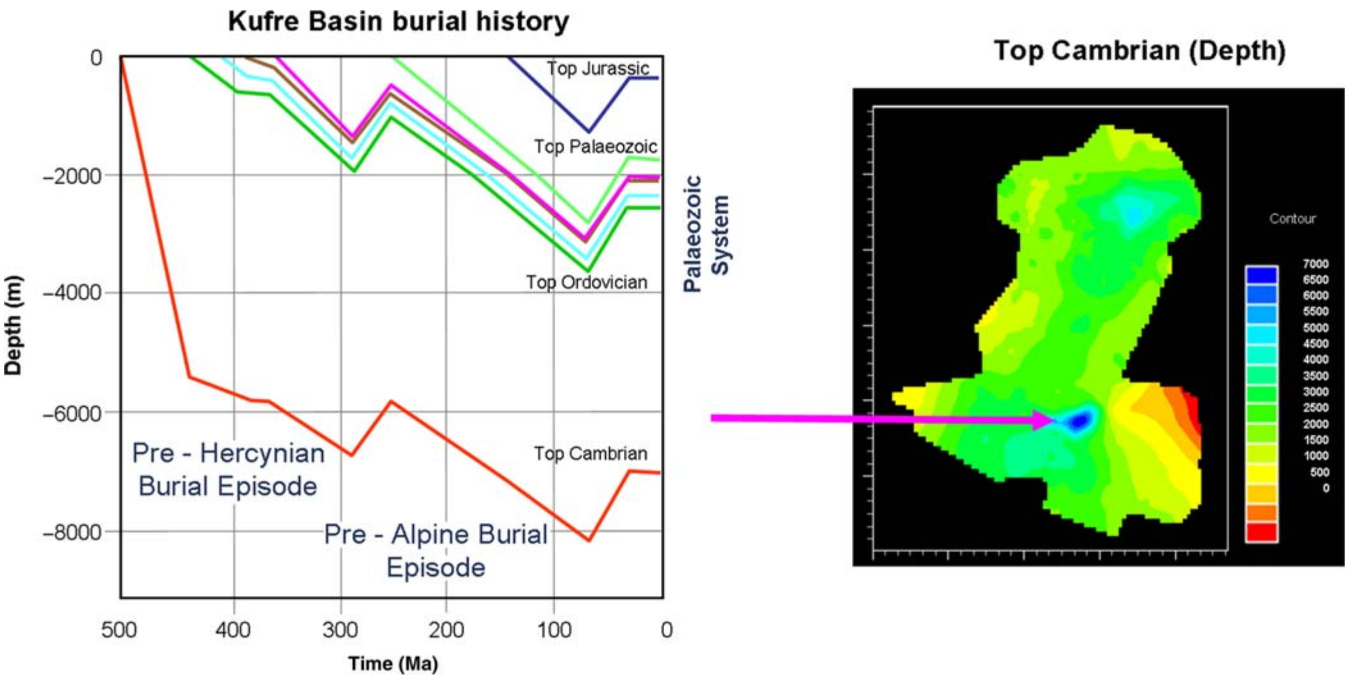

Fig. 19. Burial history and regional tectonic events in the Kufra Basin, SE Libya.

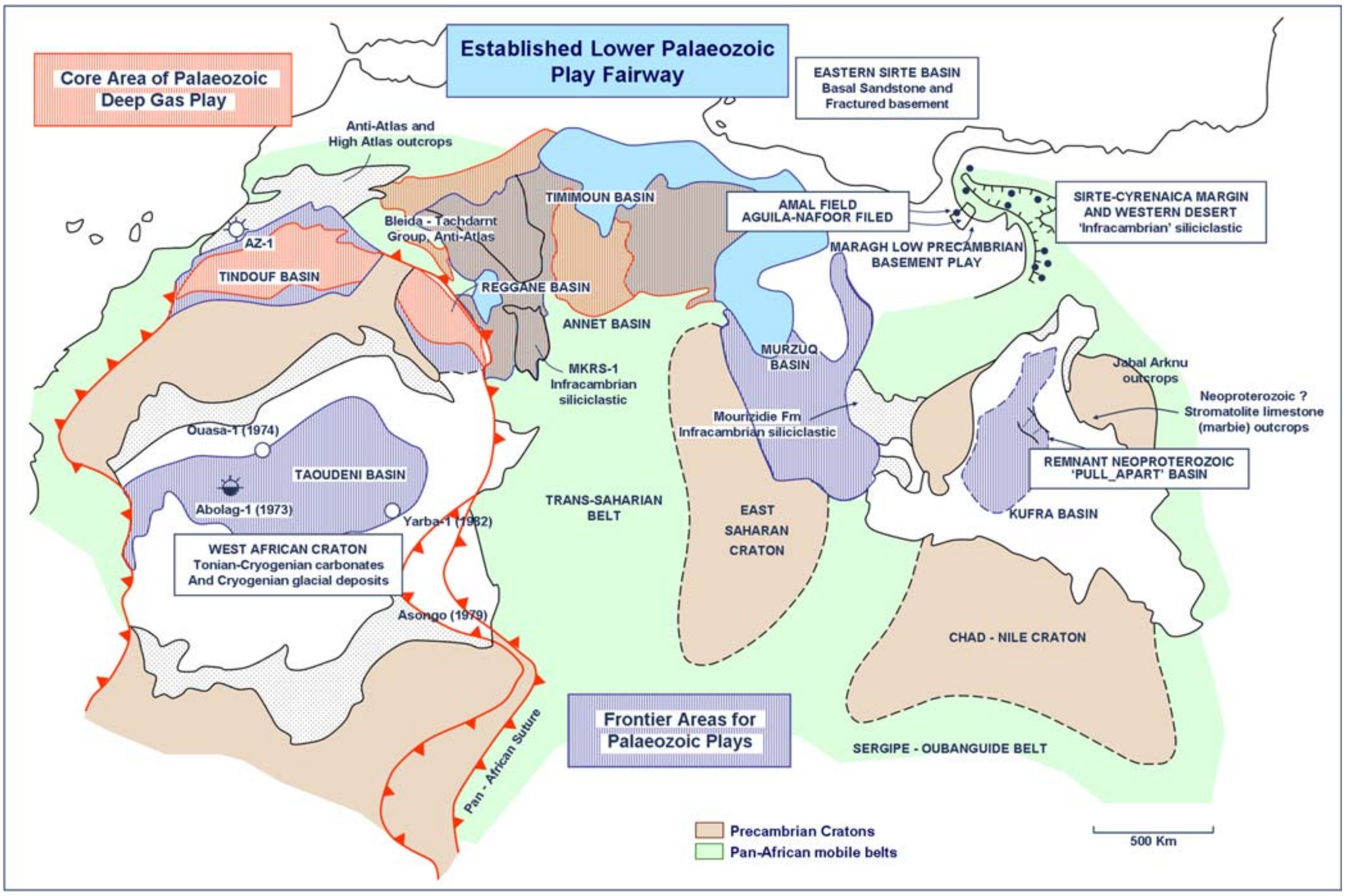

Fig. 20. Summary of Precambrian and Palaeozoic plays in North Africa.

part of the Arabian Peninsula, where it forms extensive outcrops along the eastern flank of the Arabian Shield (Fig. 21). The Palaeozoic succession in these outcrops dips gently eastwards and is soon buried under a thick sequence of mostly Mesozoic sediments which are more than 6000 m thick in the centre of the main Rub Al Khali Basin (Fig. 21).

Stratigraphy and tectonic evolution

The Late Permian Khuff Formation is the best explored and most prolific Palaeozoic reservoir in the Arabian Gulf region. It is the main reservoir in the super-giant North Field in Qatar, which was discovered in 1971, but was not brought on production until 1989. The Khuff Formation is also a reservoir for gas and condensate in Saudi Arabia (e.g. in the Ghawar, Abqaiq and Abu Safah fields) and for gas in Bahrain (Awali Field). It consists mainly of limestone and dolomite, deposited in shallow to open marine environments, with interbedded evaporites that form local intra-formational seals (Ziegler 2001).

The Palaeozoic units below the Khuff Formation in Saudi Arabia are traditionally referred to as the 'pre-Khuff section' and this is indicative of the more limited exploration for, and more limited knowledge of, these older units. The most important and best explored 'pre-Khuff' reservoir is the Late Carboniferous to Mid Permian Unayzah 'Group', a highly variable complex of clastic units of continental to shallow marine facies, with frequent fluvioglacial, fluvial and aeolian intervals (Fig. 22; Senalp & Al-Duaiji 1995). There are several major gas condensate fields in the Unayzah Group in Saudi Arabia, mainly in the so-called 'Central Area' to the south and west of the Ghawar Field. The aeolian facies sandstones typically have the best reservoir characteristics in these fields with good porosity, but locally with reduced permeability. In the tightest sandstones, effective permeability is only present where the formations are heavily fractured.

The base of the Unayzah complex in Saudi Arabia is represented by the regionally extensive Hercynian unconformity surface which cuts across the underlying Early–Middle Carboniferous to Cambrian succession. The main prospective reservoir unit in this pre-Hercynian succession is the Devonian Jauf Formation which comprises a sequence of interbedded shales and sandstones deposited in shallow marine to fluvio-deltaic environments. Trapping in the Jauf Formation is often stratigraphic and related either to the pinchout of the individual sandstone reservoirs or to their truncation by the Hercynian unconformity. Gas condensate is produced from the Jauf Formation in the Hawiyah field, NE of Ghawar (Wender *et al.* 1998). The Hawiyah Field is one of the largest gas projects in the Kingdom of Saudi Arabia and the first to be dedicated solely to the production of non-associated gas.

The underlying Silurian succession is characterized by shallow to deep marine deposition with, at its base, organic-rich radioactive ('hot') shales (Qalibah Formation, Qusaiba Member) that are age-equivalent to the basal Silurian Tannezuft 'hot' shales in North Africa. These organic-rich shales are considered to be the main hydrocarbon source rock for the entire Arabian Palaeozoic petroleum system (Abu-Ali *et al.* 1999; Konert *et al.* 2001; Abu-Ali & Littke 2005; Fig. 22). Some sandy facies within the Qalibah Formation, including the so-called 'Mid Qusaiba Sandstones' and the 'Rhuddanian Sandstones' at the base of Qusaiba Member have also recently become targets for exploration. These units usually have poor to fair reservoir properties, but their distribution and geometry are still very poorly known. Under

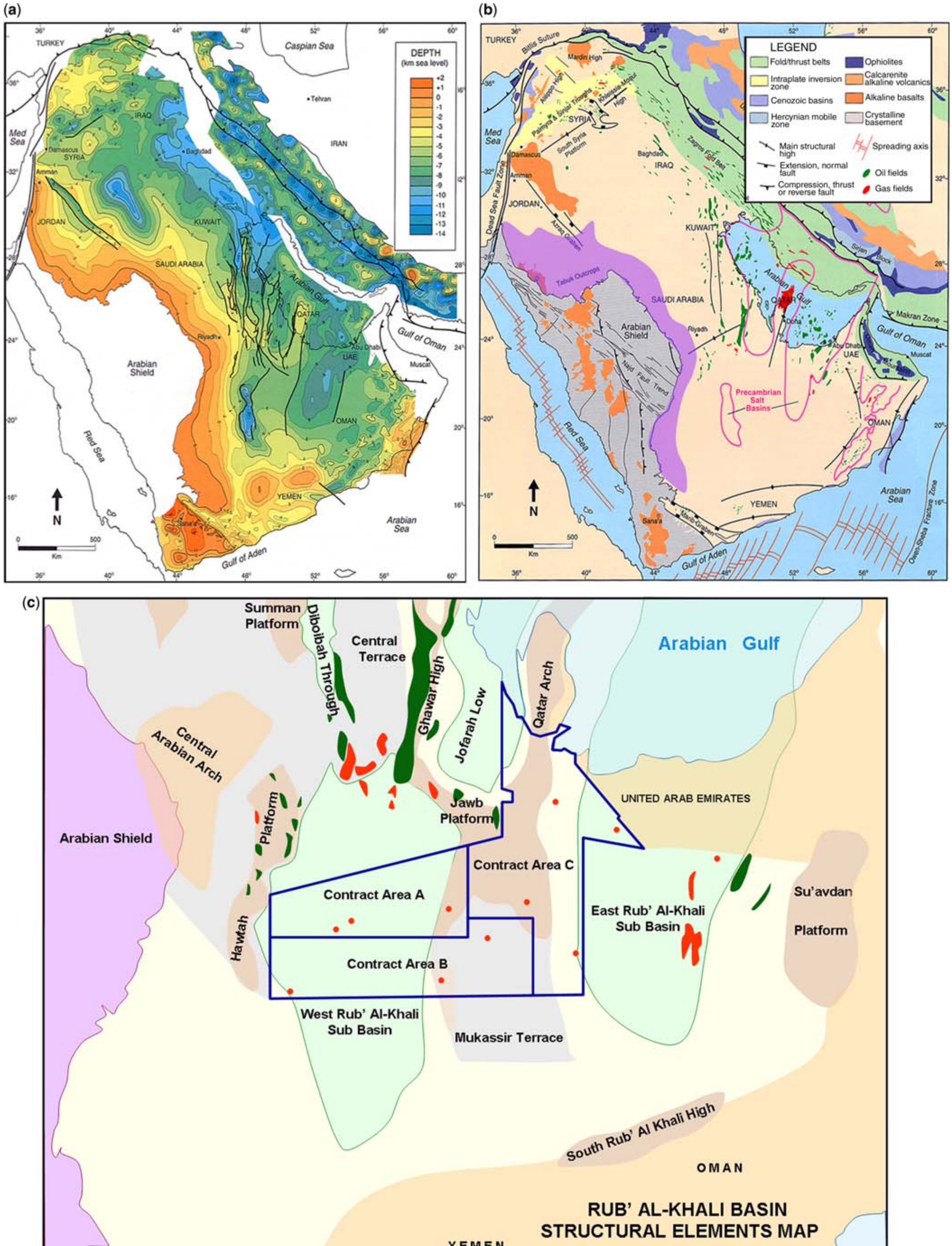

Fig. 21. Regional geology of the Middle East. (**a**) Depth to basement. (**b**) Major tectonic elements. (**c**) Structural elements of the Rub Al Khali Basin and the location of contract areas A, B and C.

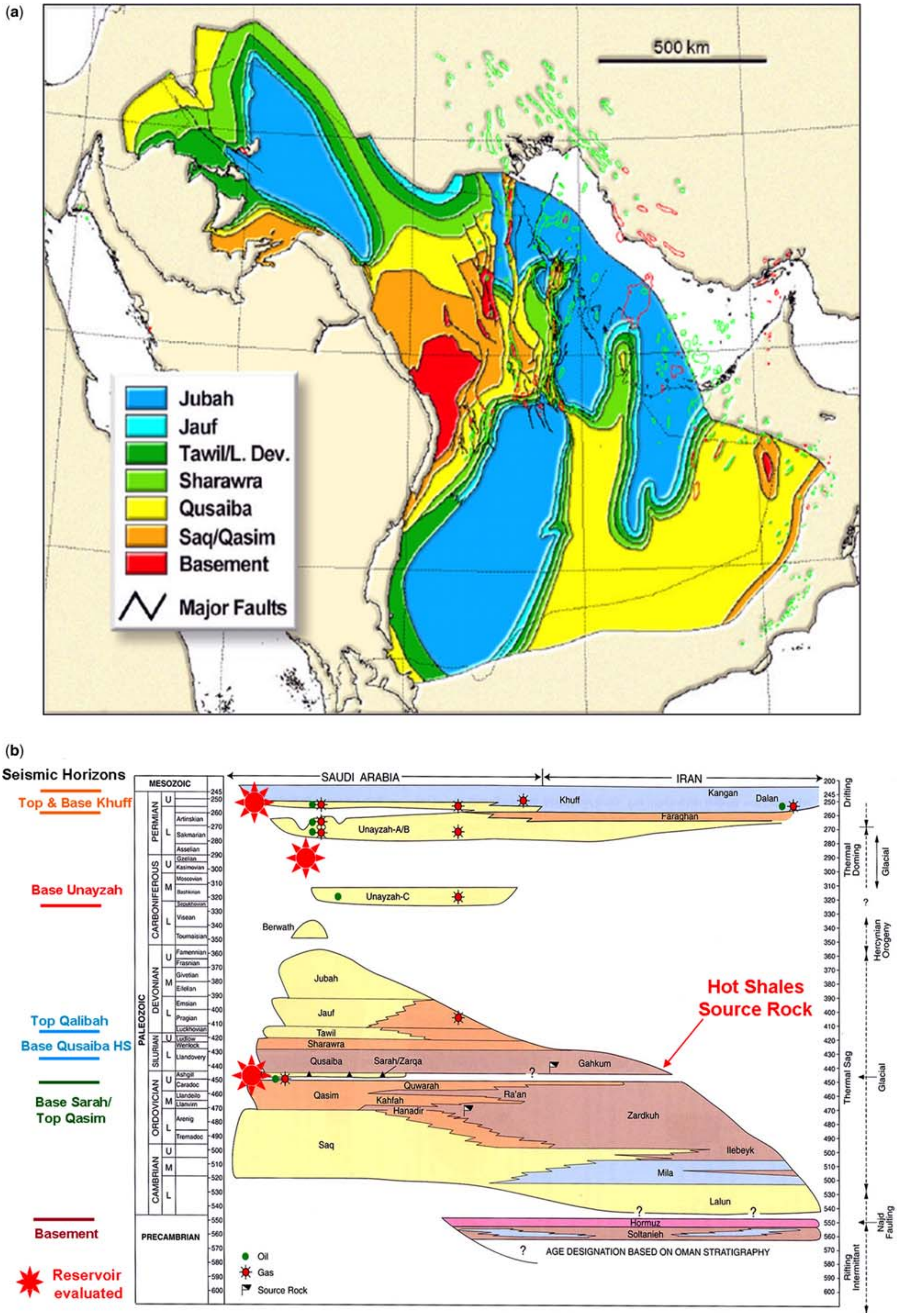

Fig. 22. Palaeozoic geology of the Middle East. (**a**) Subcrop to the Hercynian unconformity. (**b**) Chronostratigraphy, seismic horizons and distribution of source rocks, reservoirs and hydrocarbons.

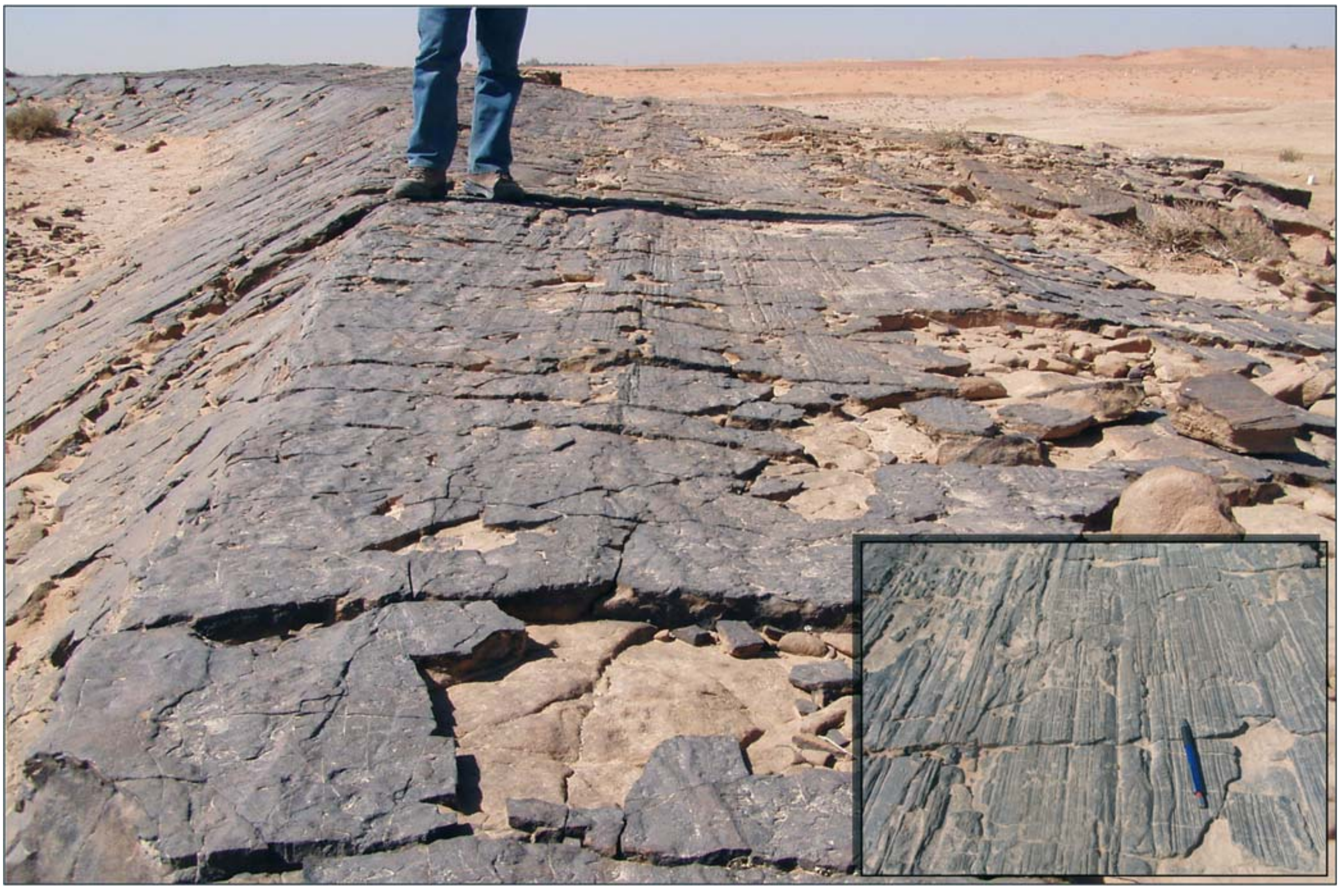

Fig. 23. Outcrop of a striated glacial surface within the Late Ordovician Sarah Formation, western Saudi Arabia.

favourable conditions, the basal Silurian Qusaiba Member source rock can also charge the underlying Ordovician sandstones of the Sarah and Qasim formations, either by downward migration or through fault juxtaposition.

The latest Ordovician (Ashgillian) Sarah Formation in the Rub Al Khali Basin consists of sandstones and conglomerates deposited in braided-fluvial and fluvioglacial environments, while the underlying Caradocian Qasim Formation consists of shallow marine sandstones and open marine shales. Deposition of the Sarah Formation is strongly controlled by a well developed system of glacial valleys, and sedimentary structures of probably glacial origin are well exposed and documented at outcrop along the western flank of the basin (Fig. 23).

There are relatively few subsurface penetrations of these Ordovician reservoir targets, so information about their reservoir quality at depth is still very limited. The Palaeozoic petroleum system in the Rub Al Khali Basin is largely unaffected by major erosion episodes, with almost continuous burial until the end of the Mesozoic and only relatively minor Alpine uplift and erosion thereafter (Fig. 24). This burial history produces the optimum conditions for generation and expulsion of significant volumes of hydrocarbons (Fig. 25). The main risk seems to be the possible local absence of the basal Silurian 'hot' shale source, particularly in the eastern sub-basin.

The only commercial development of hydrocarbons in the Ordovician succession in Saudi Arabia to date has been in the Khurais region, but most penetrations of the Palaeozoic succession have been the result of deepening of wells targeted at reservoirs in the shallower Mesozoic sequences, with the Palaeozoic succession representing a relatively low-cost 'near-field' upside potential. As a consequence, most of these penetrations are concentrated in the Saudi Aramco core development areas and the Palaeozoic potential in many other areas of the Arabian plate, including the vast Rub Al Khali Basin, remains largely unexplored. It is only recently that exploration for non-associated gas in deep Palaeozoic targets has become a priority in Saudi Arabia, with the award of exploration acreage in the Rub Al Khali Basin to international companies in 2003. Four joint operating companies, Luksar (Lukoil), SRAK (Shell), SSGL (Sinopec) and EniRepSa (Eni and Repsol), each in partnership with Saudi Aramco, are now actively exploring for Palaeozoic gas plays in the Rub Al Khali Basin.

Exploration challenges

The challenges in exploring for Palaeozoic plays as 'stand alone' targets in this region are considerable. The Rub Al Khali desert is an extremely remote area, and considerable time and investment is required for the construction of skid roads and the preparation of well sites under very hostile climatic conditions. In addition, the Palaeozoic targets are extremely deep, typically in the range of 5000–6000 m, and are associated with high-pressure/high-temperature regimes that are close to, and sometimes exceed, the normal operational limits for drilling and logging tools and materials. Rates of penetration are generally extremely low because of the hard and abrasive nature of the Palaeozoic sandstones and the drilling and testing of a single well commonly takes more than one year to complete.

In total, some 22 exploration wells have been drilled (or are currently under operation) in the Rub Al Khali Basin in the past five years by the four operating companies as part of their contractual work commitments. Most of these have been drilled to the Ordovician Sarah and Qasim formations, at depths often exceeding 6000 m. Few results have been released, but several wells are reported to have been tested and flowed unspecified quantities

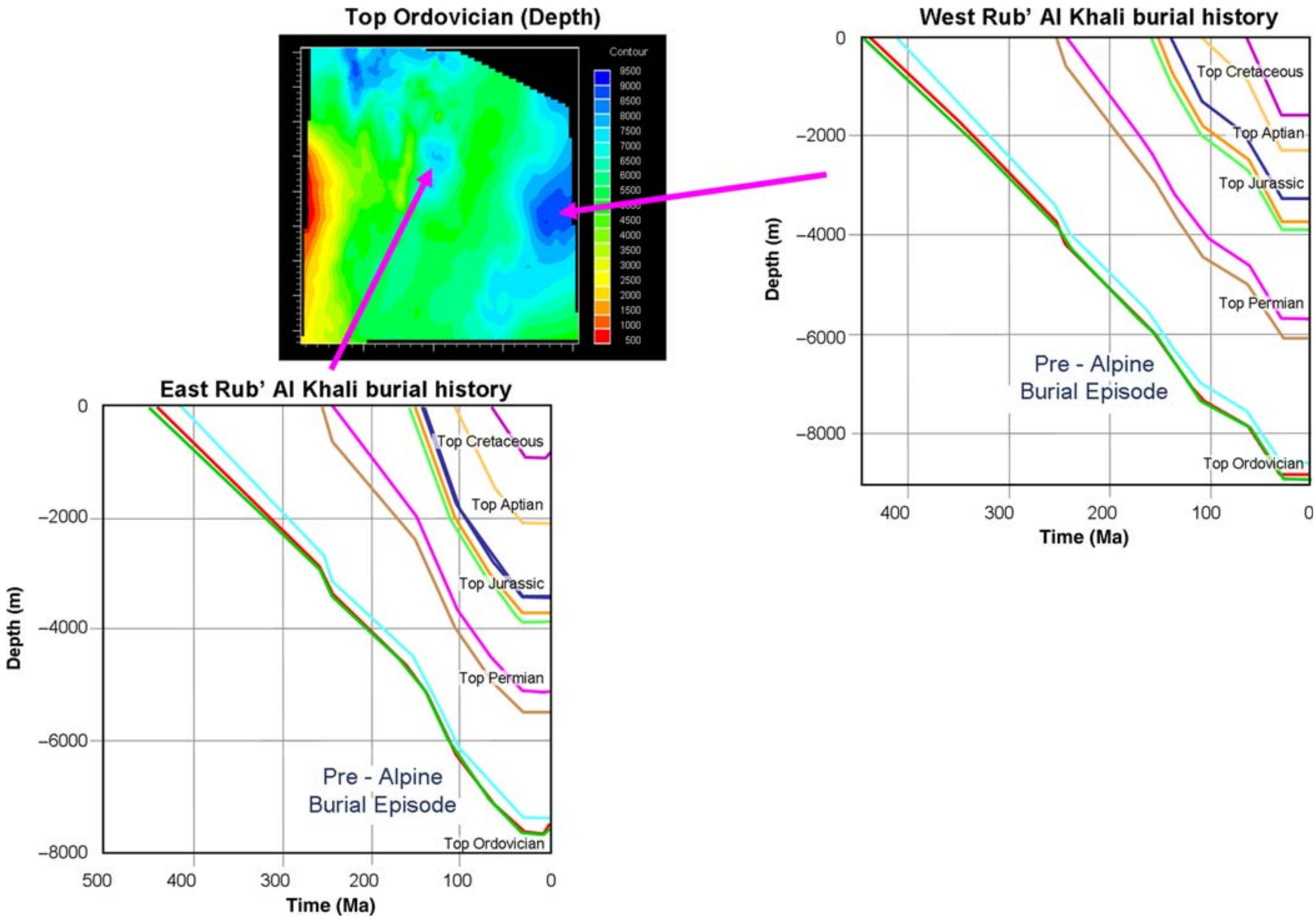

Fig. 24. Burial history and associated regional tectonic events in the Rub Al Khali Basin, Saudi Arabia.

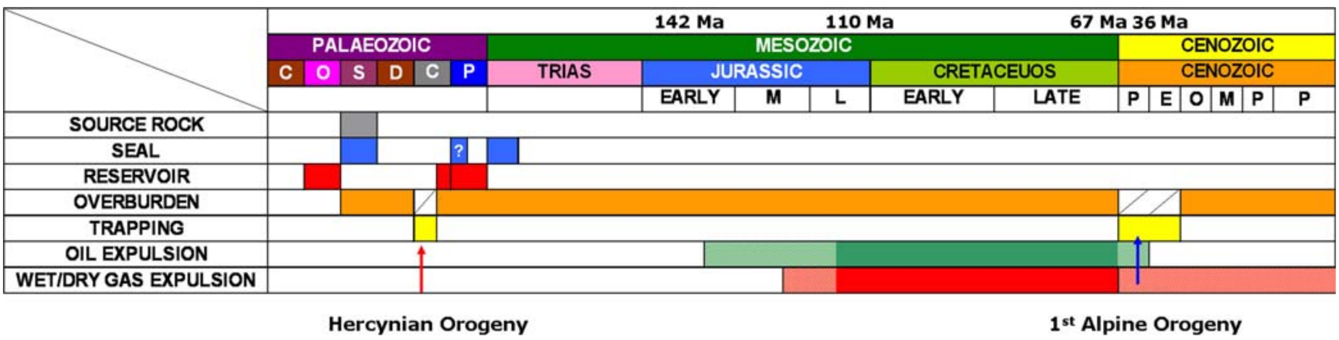

Reservoirs

- Sarah Fm. (Ordovician) sandstones
- Lower Unayzah (Permo-Caroniferous) sandstones
- Upper Unayzah (Permo-Caroniferous) sandstones

Source Rock

- Silurian Hot Shales (Qusaiba Fm.) (Kerogene type II, T.O.C. 4%, H.I. 400)

Seals

- *Qusaiba Shales (Silurian)*
- Lower Unayzah Shales
- Khuff basal clastic shales and Khuff tight limestones and anydrite

Wet/Dry Gas Expulsion Time

- End of Jurassic to recent (142-0 Ma)

Traps

- Four ways dip closure

Time of Trap Development

- Carboniferous (Sarah Fm.)
- Upper Cretaceous – Base Cenozoic

Oil Expulsion Time

- End of Jurassic to Eocene (142-52 Ma)

Fig. 25. Petroleum systems summary chart for the Rub Al Khali Basin, Saudi Arabia.

of gas and/or condensate, confirming that there is an effective Palaeozoic petroleum system in the basin, although no 'commercial' discoveries have yet been announced. Most of the exploration effort has been targeted at the Ordovician Sarah and the Permo-Carboniferous Unayzah formations. These typically exhibit fair to poor reservoir quality, particularly in terms of permeability, and constitute a 'tight gas' play, with significant technical and commercial challenges. The likely low ultimate recovery per well, coupled with the very high costs due to the difficult surface and subsurface environments, makes the economic development of any discoveries in this play extremely challenging. The current price scenario for domestic gas in Saudi Arabia also has a significant impact on project economics and the present scenario makes wet gas discoveries, with high condensate yields, far more attractive than dry gas discoveries. However, condensate production can represent an additional challenge in such low-permeability reservoirs due to 'condensate banking'. In the light of these challenges, significant effort has been devoted to locating reservoir 'sweet spots' where deliverability may be enhanced, either as a result of better primary reservoir characteristics (such as in the aeolian facies of the Unayzah Formation) or by the presence of connected fracture networks. Experience from Palaeozoic discoveries and fields elsewhere in Saudi Arabia suggests that there is likely to be a significant stratigraphic component to any hydrocarbon traps in the Rub Al Khali Basin. An overall improvement in the seismic imaging of these deep and tight formations is critical for further de-risking of prospects, with the application of appropriate surface static corrections and suppression of multiples being key steps towards achieving reliable seismic attribute analysis for reservoir quality prediction.

Palaeozoic plays in other parts of the Middle East

Palaeozoic plays remain relatively unexplored elsewhere in the Middle East with, to date, one significant discovery in western Iraq, five Palaeozoic discoveries in Syria, two Ordovician gas discoveries in Jordan, a single important Ordovician gas and condensate discovery in northern Saudi Arabia (Whaley 2004) and three producing gas fields (Barik, Saih Rawl and Saih Nihayda) and one recent giant gas discovery (Khazzan) in the Upper Cambrian to Lower Ordovician low porosity–very low permeability Barik Sandstone Member in Oman (Millson *et al.* 2008). There is also further deep potential in the Cambrian clastic reservoirs (Barik, Miqrat and Amin formations, Droste 1997) in Oman (e.g. Millson *et al.* 2008) and for Cambro-Ordovician, Devonian and Lower Permian clastic reservoirs in adjacent parts of Yemen. Reservoir quality appears to be a key issue for the Palaeozoic reservoirs in many of theses areas. In the Akkas Field in western Iraq, the Ordovician and Silurian sandstone reservoirs have porosities of 6.5–7.6% and permeabilities of 0.13–0.2 mD (Al-Hadidy 2007), but there is clearly considerable potential for further tight gas exploration in deep Palaeozoic plays throughout NW Arabia (Ramseyer *et al.* 2004). The reservoir quality of the Cambro-Ordovician sandstones encountered in Yemen seems to be rather better with porosities of up to 20% and permeabilities of several hundred milliDarcies recorded in some wells. Although the gas sector is relatively underdeveloped in much of the Middle East, the demand for gas is increasing steadily. For example, in Oman, the supply–demand balance suggests that without further significant gas discoveries Oman may need to import gas by 2012 and the government is actively encouraging gas exploration with an objective of discovering an additional 1×10^{12} SCF of gas per year. Such requirements should make deep gas exploration an increasingly attractive commercial proposition in many parts of the Middle East.

Mesozoic plays: the Sirte Basin, Western Desert and Levantine Basin

The Mesozoic plays in North Africa and the Middle East are, without doubt, the most studied and best explored in the region and are becoming increasingly mature from an exploration perspective, with the possible exception of the deep graben systems within the Sirte Basin of Libya, parts of the western desert of Egypt and the Levantine Basin, the easternmost portion of the Mediterranean basin. This latter, largely under-explored area has yet to be evaluated fully, but several wells in the offshore Sinai Peninsula and offshore Israel have highlighted the existence of active Mesozoic petroleum systems, below more traditional Cenozoic objectives. The major structural elements of the eastern Mediterranean offshore (Garfunkel 1998, 2004; Robertson 1998; Robertson & Comas 1998; Walley 1998; Ziegler 2001; Ben-Avraham *et al.* 2002; Longacre *et al.* 2007; Roberts & Peace 2007; Peck 2008)

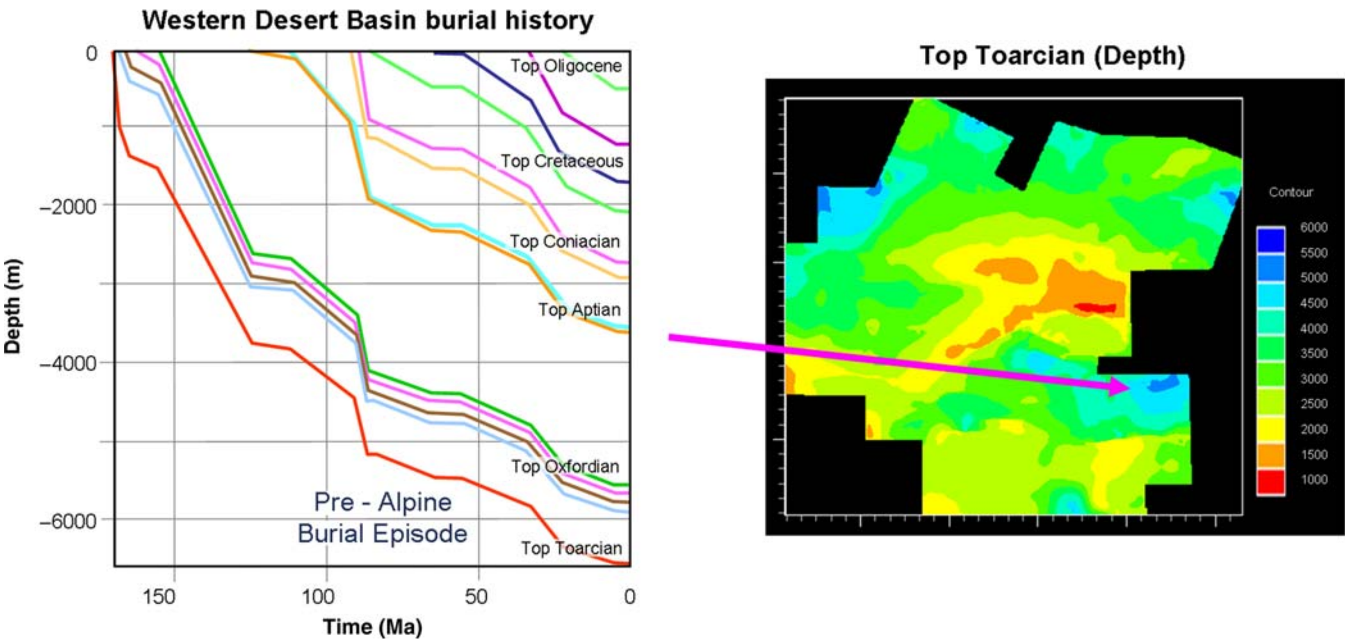

Fig. 26. Burial history and regional tectonic events in the Western Desert, Egypt.

show a marked similarity to the main Syrian Arc folds in the Egyptian Western Desert, where the availability of well data allows the main factors controlling the effectiveness of different Mesozoic petroleum systems to be better constrained. The burial history of the deep Mesozoic petroleum system in the Western Desert (cf. also Metwalli & Piggot 2005) is characterized by almost continuous burial, with some local variation in the rate of subsidence, but no major periods of uplift and erosion through the Cenozoic (Fig. 26). Critical factors controlling the effectiveness of the Mesozoic petroleum system in the Western Desert seem to include the rather indifferent quality of the Mesozoic source rock and the general lack of regional seals. In the Sirte Basin of Libya, the Upper Jurassic–Lower Cretaceous Nubian sandstone members seem to offer significant potential for future exploration below the more traditional and better explored Upper Cretaceous and Cenozoic reservoirs (e.g. Rusk 2001).

Cenozoic plays: deep Oligocene play in the offshore Nile Delta

The offshore Nile Delta of Egypt is a mature gas province with several well explored and proven plays and more than 60×10^{12} SCF of proven reserves. Most of the fields discovered to date are in the shallow portion of the delta (Fig. 27), in reservoirs ranging from Upper Miocene to Plio-Pleistocene in age (Bertello *et al.* 1996; Hart *et al.* 2002; Marten *et al.* 2004; Samuel *et al.* 2005). This Late Cenozoic interval is the most significant and well known portion of the delta sediment cone and has been the subject of numerous studies over the past 20 years (e.g. Dolson *et al.* 2000*a*, *b*; Aal *et al.* 2001; El Barkooky & Helal 2002), Recent detailed mapping of fluid released structures (pockmarks, mud volcanoes associated with gas chimney, etc.) on the seafloor across the Nile Delta cone has revealed significant new information about these shallow petroleum systems (Loncke & Mascle 2004; Loncke *et al.* 2006).

The deeper, Upper Oligocene and older portion of the Nile Delta cone (Fig. 28) is much less well known and remains largely unexplored. However, it forms a significant, if challenging, new frontier for exploration in the region. Recent high-pressure/high-temperature discoveries such as Satis and Port Foaud Marine Deep, at depths in excess of 5000 m, have confirmed the potential of these deep plays to deliver significant new gas and condensate reserves.

Stratigraphy, tectonic evolution and hydrocarbon generation

The main stratigraphic and tectonic events of the Nile Delta region are illustrated in Figure 29 (modified from Meciani *et al.* 2002). The deltaic system initially developed during the late Early Oligocene and subsequent deposition has been characterized by a general increase in terrigenous input, punctuated by several progradational and retrogradational cycles. The most dramatic event to disrupt this long-term depositional trend occurred in Messinian time, when isolation and subsequent desiccation of the Mediterranean resulted in the deposition of a laterally extensive evaporite succession that reaches a maximum thickness of 2000 m in the eastern part of the delta.

The relationship between the younger Late Cenozoic and the older and deeper Early Cenozoic portions of the Nile Delta sedimentary cone is shown in Figure 29. This regional dip geological section shows two different tectonostratigraphic regimes:

(1) a thick sedimentary succession ranging from Late Miocene to Recent in age and 0 to *c*. 5000 m in depth with a well defined delta progradational geometry and prominent growth faulting in the upper part;
(2) a deeper sedimentary succession of Mesozoic and Early Cenozoic age cut by transpressional features that reactivate older (Mesozoic) tectonic lineaments.

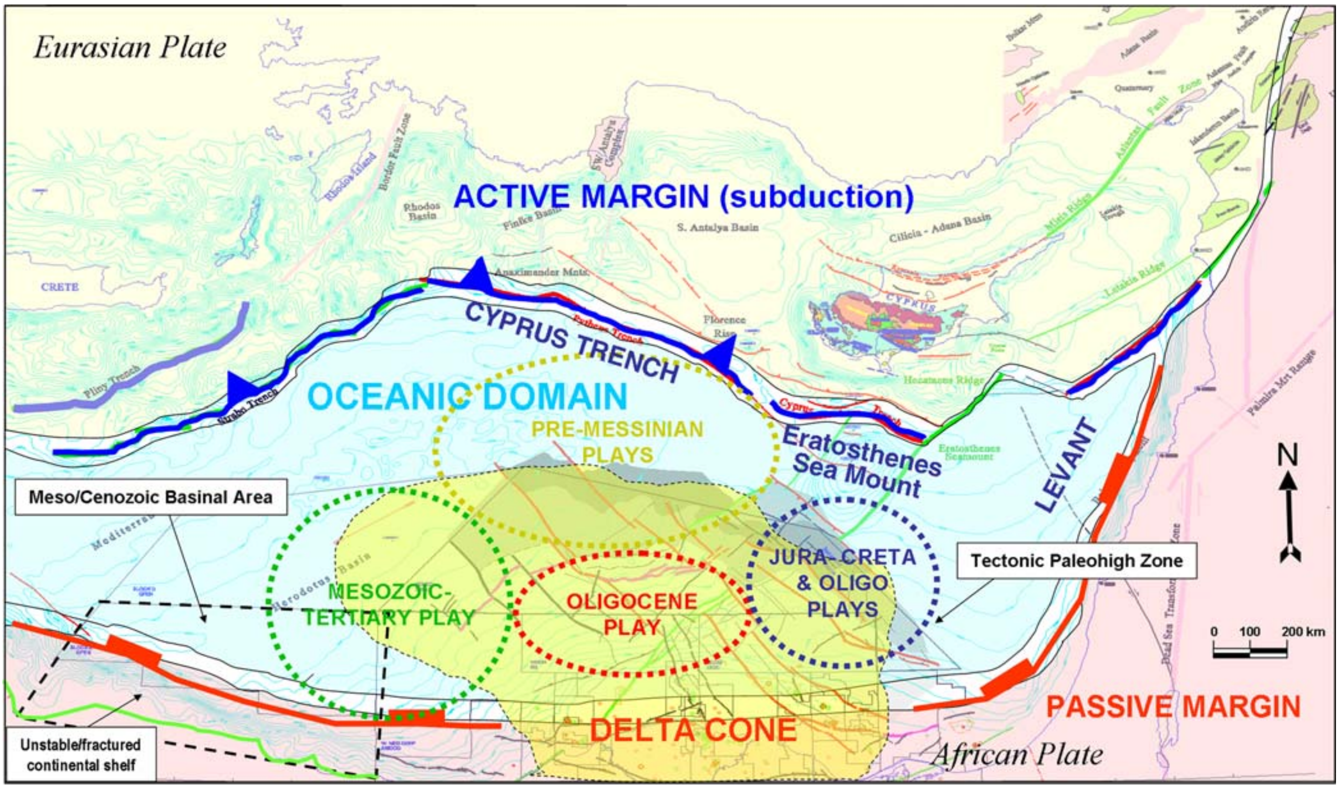

Fig. 27. Major tectonic elements of the eastern Mediterranean Basin.

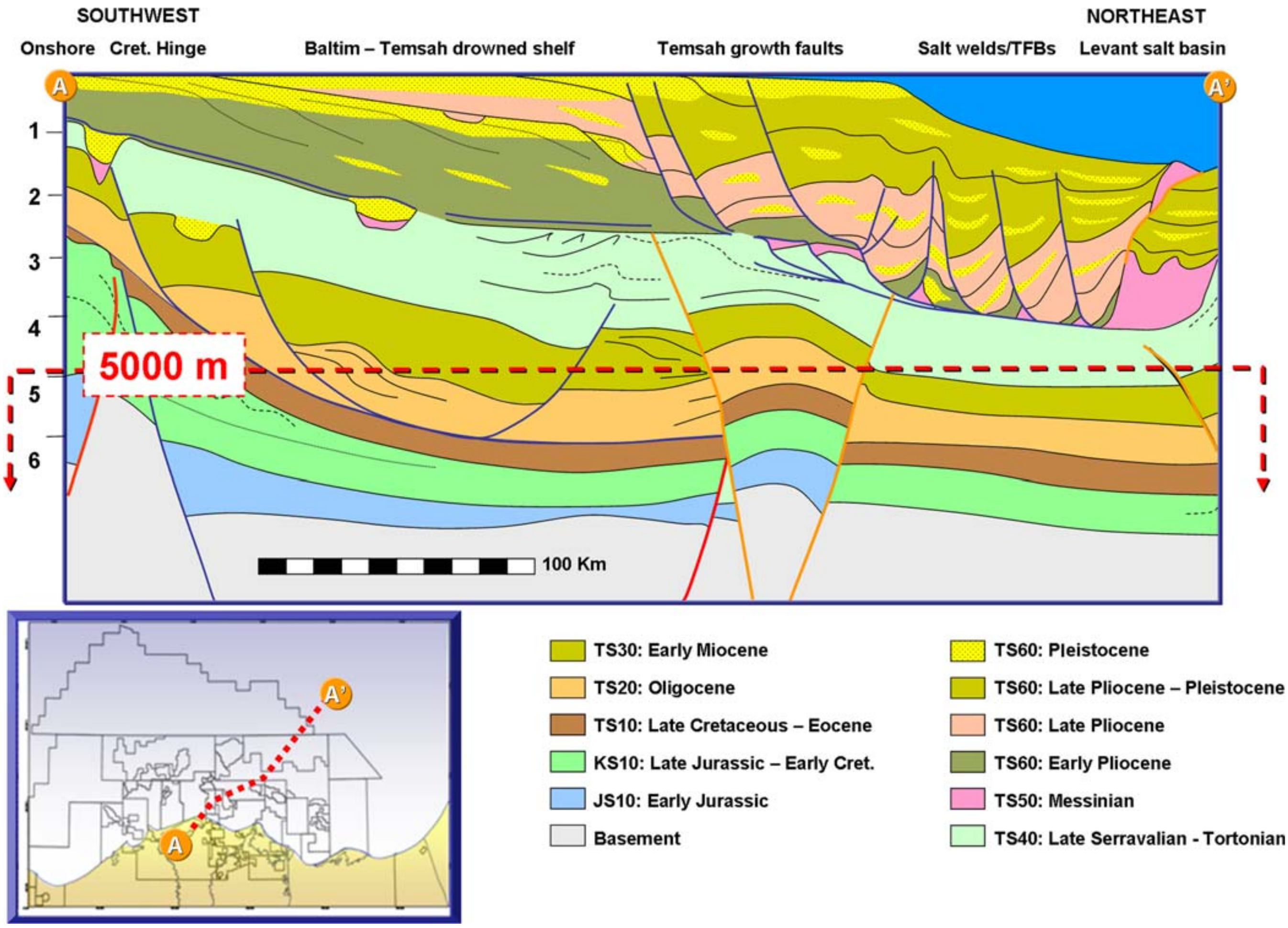

Fig. 28. Regional geological section across the Nile Delta cone, offshore Egypt (modified from Dolson 2001).

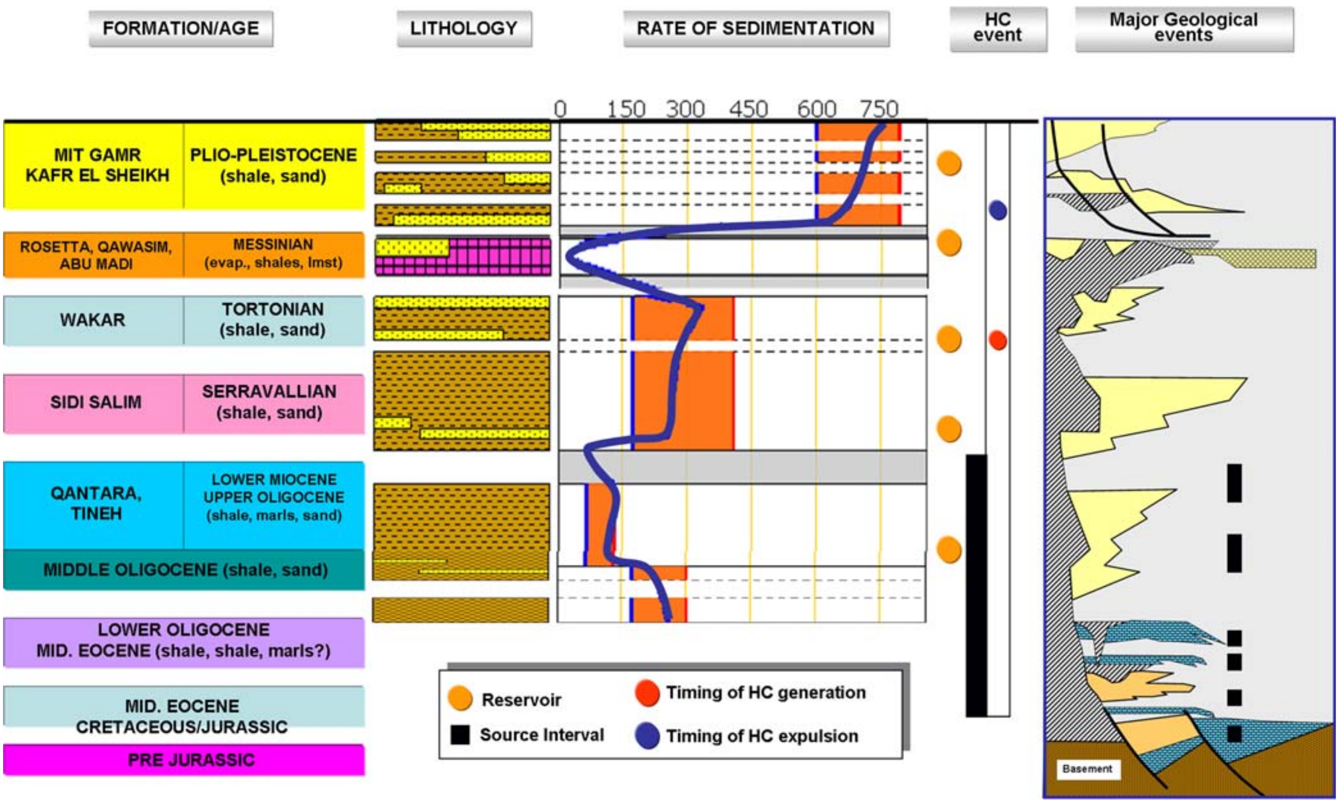

Fig. 29. Lithology, sedimentary stacking patterns, major tectonic events and effective petroleum systems of the offshore Nile Delta, Egypt.

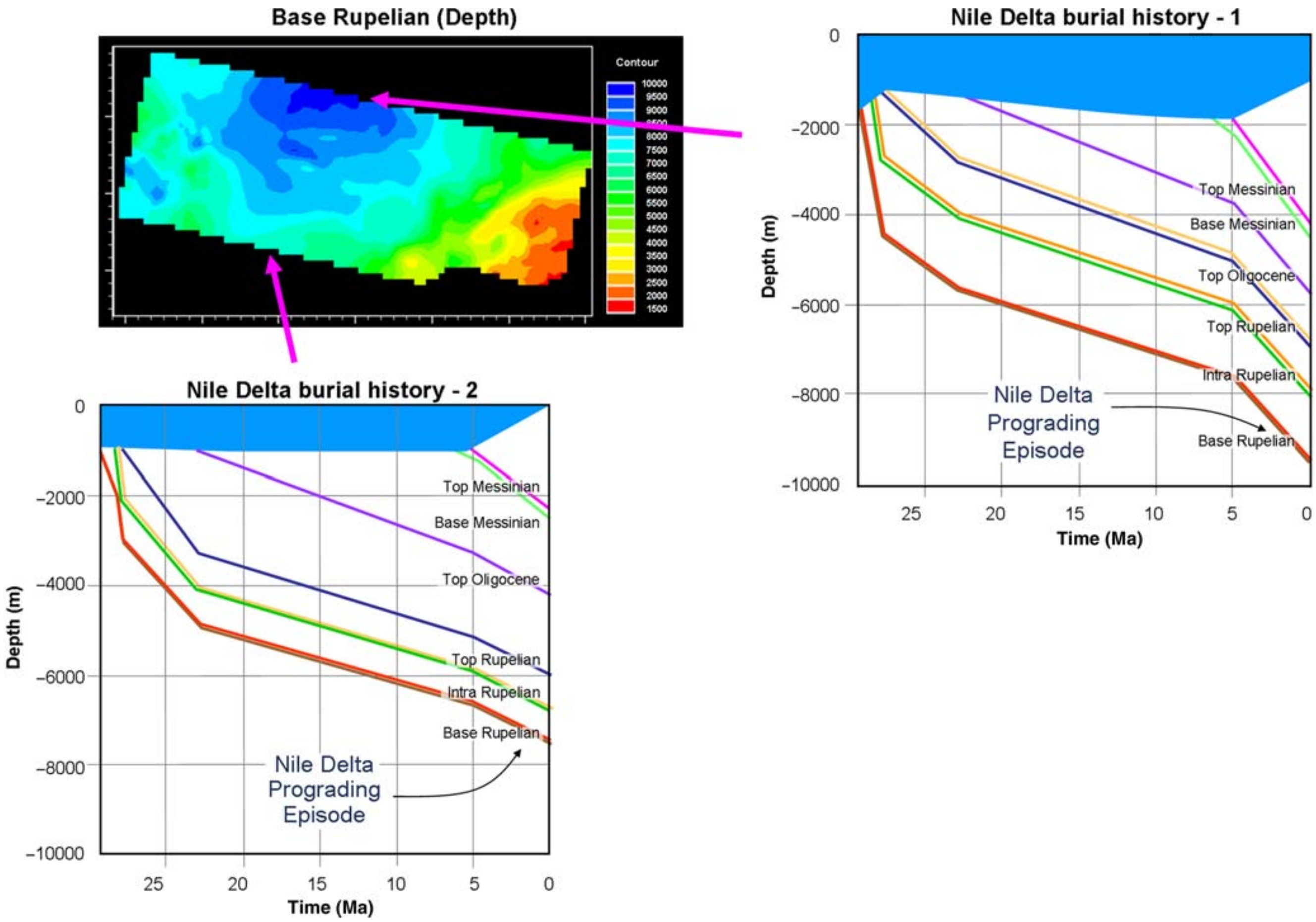

Fig. 30. Stratigraphy and sedimentary characteristics of the Oligocene sequence in the Nile Delta, offshore Egypt.

Early Cenozoic regional tectonic events were responsible for the initiation of the Nile Delta and the first pulses of clastic deposition are well dated biostratigraphically as Middle to Late Oligocene in age (Fig. 30). Detailed palaeogeographic reconstructions indicate that there were two distinct phases of deposition during the early stages of development of the Nile Delta. Initially, the lack of a significant terrigenous platform allowed a channelized turbidite system to develop through which sediment was carried northwards directly into the Mediterranean basin. Later, during a second phase, an increase in accommodation space at the basin margin triggered the development of marginal marine environments and the onset of delta progradation. The loading effect of the delta sediment cone during the past 5 million years (Fig. 31) is directly responsible for the relatively recent maturation of the Early Cenozoic source rock and the localized preservation of reservoir quality in the sandstones as a result of overpressuring of the interbedded shales. The pressuring of the system is also responsible for the re-migration of hydrocarbons through the different petroleum systems through repeated hydraulic fracturing of the intervening seals.

The acquisition of high-quality 3D seismic data across most of the offshore Nile Delta area in recent years (e.g. Wescott & Boucher 2000; Galbiati *et al.* 2009) has allowed new play concepts to be developed and applied to the deep petroleum systems. Mapping of the distribution of potential reservoirs has, in particular, benefited from the rigorous application of seismic amplitude extraction techniques and has led to the identification of well defined reservoir fairways characterized by sand-prone turbidites and individual meandering deepwater channel systems (Fig. 32).

Exploration challenges

The exploration of these deep targets in the offshore Nile Delta region carries significant risks from both a technical and an operational perspective. The considerable depth of the reservoirs, coupled with the high-temperature/high-pressure environment, means that reservoir quality, seal integrity, the high cost of drilling and the optimization of high-pressure/high-temperature well design are all critical issues. Understanding the reasons for the success of wells that have targeted the play, and of the failures in terms of lack of charge, top seal breach, dis-migration through faults or other reasons, will be critical to continued exploration success as will the application of 'state of the art' techniques of seal efficiency analysis (combing mechanical, geological and geochemical data), elastic inversion of 3D seismic data for overpressure and the integration of reservoir quality prediction for the main reservoir units in the petroleum systems models. Despite the technical challenges and uncertainties, the recent discoveries made in both the eastern and western portions of the delta have already proven more than 3×10^{12} SCF of reserves and indicate that the Oligocene play represents a very promising challenge for the future of exploration in the region.

Conclusions

As the traditional exploration plays in the main productive basins of North Africa and the Middle East become more 'mature', attention is increasingly focusing on more challenging, older and deeper plays in the main producing basins and on high-risk, but more conventional, plays in underexplored frontier areas. This shift brings with it a wide range of technical, operational and commercial challenges that must be addressed if exploration in the region is to remain an attractive proposition. Although these older and deeper plays have widely differing ages, from Neoproterozoic to Early Cenozoic, they share many characteristics. The technical challenges involved in their exploration include difficult seismic

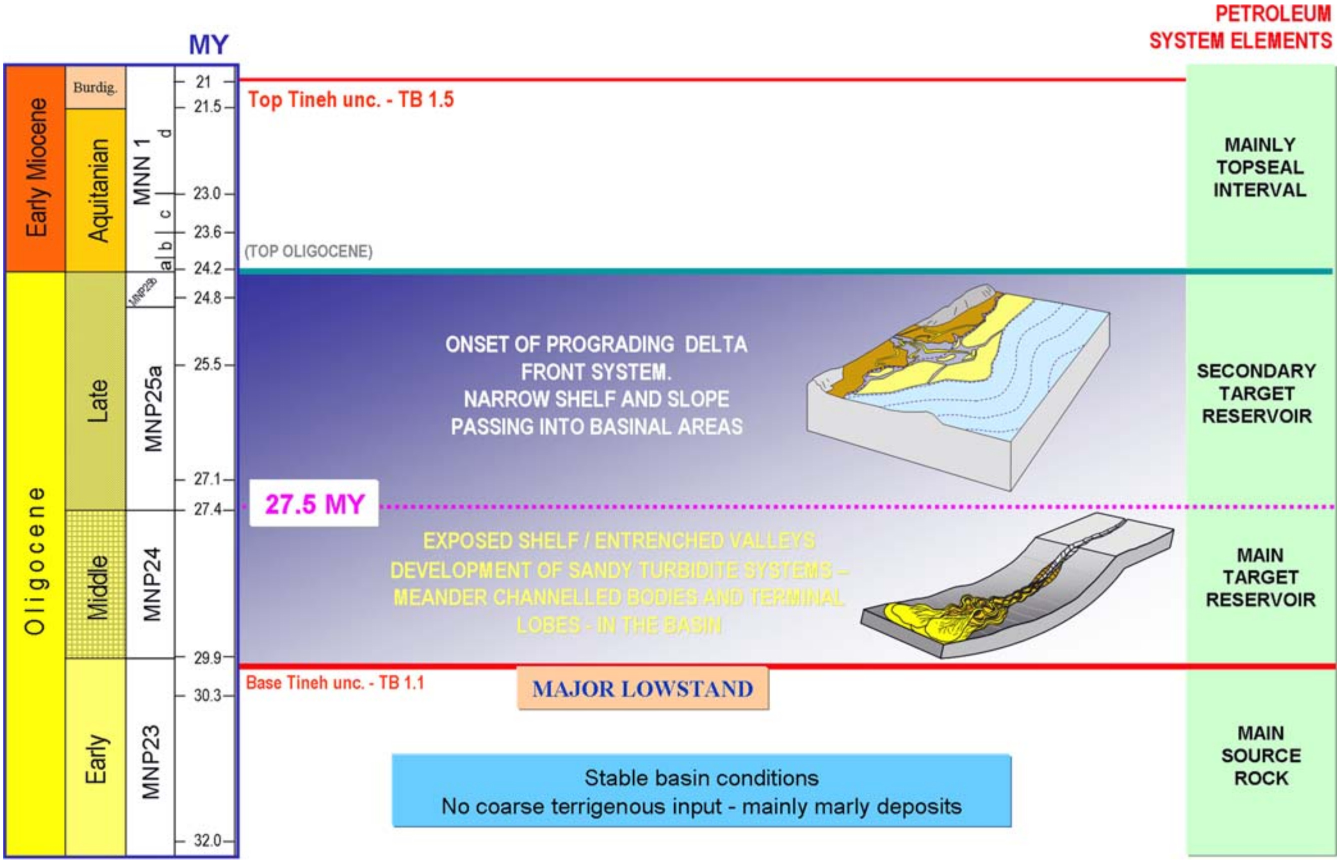

Fig. 31. Burial history and regional tectonic events of the Nile Delta depositional system, offshore Egypt.

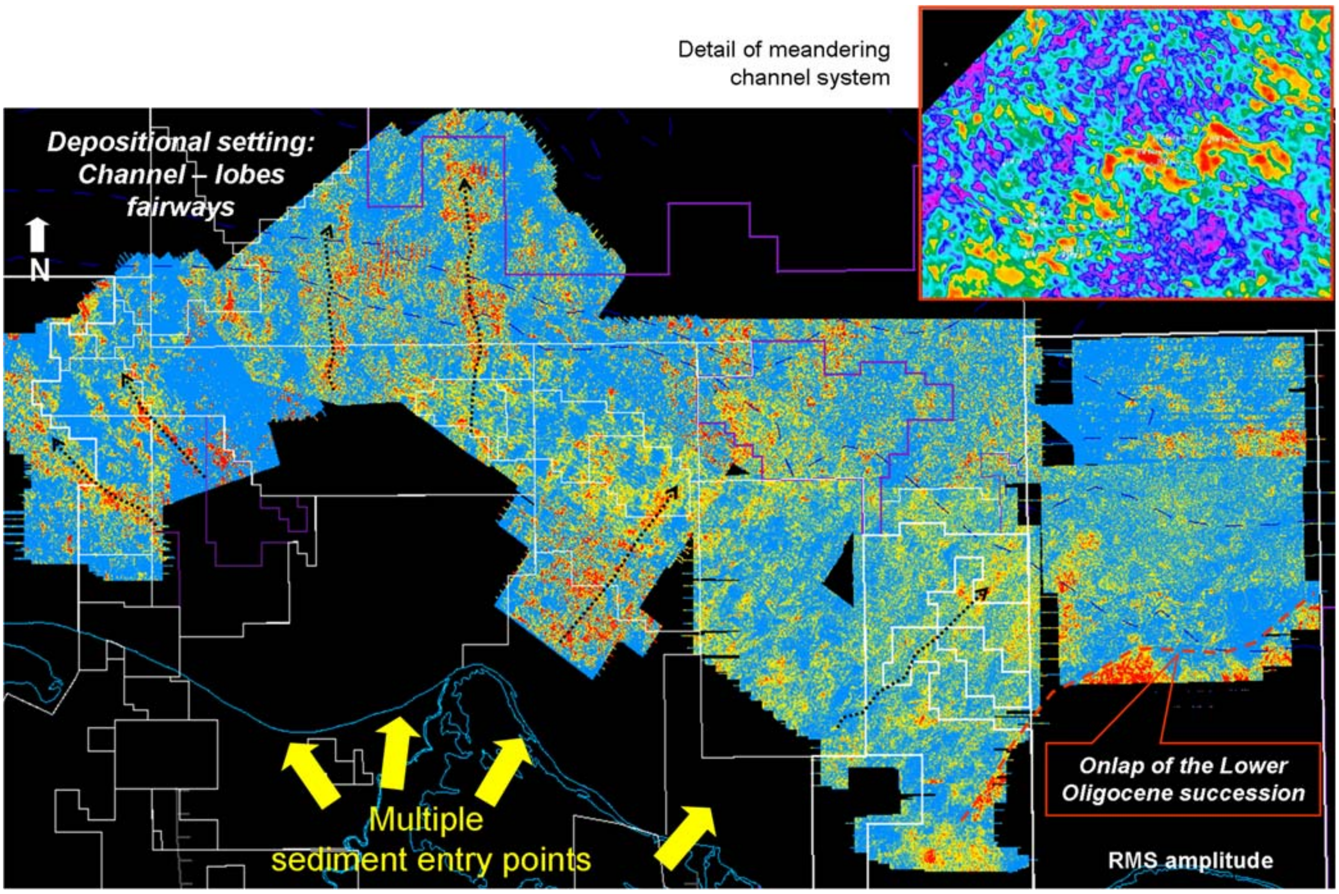

Fig. 32. Regional seismic amplitude anomaly display showing depositional features of the Oligocene succession, offshore Nile Delta, Egypt.

imaging, low porosity and permeability, high temperature and pressure and a critical need to identify reservoir 'sweet spots' where deliverability may be enhanced either through the preservation of primary reservoir quality or secondary enhancement through fracturing. In the case of the Neoproterozoic and Palaeozoic plays, the distribution and continuity of source rocks and the risk of early generation of hydrocarbons due to the deep burial are additional risks. From an operational perspective, many of these deep plays are located in areas with hostile surface and subsurface environments, in remote locations, where the extreme temperatures and pressures at objective depths that commonly exceed 5000 m place drilling and logging tools at, or sometimes beyond, their operational tolerances. The associated high drilling costs and the need for 'tight gas' development technologies renders it extremely challenging to make these projects commerciality attractive, but it is becoming increasingly clear that the potential rewards from doing so could be immense.

References

Aal, A., El Barkooky, A., Gerrits, M., Meyer, H., Schwander, M. & Zaki, H. 2001. Tectonic evolution of the eastern Mediterranean basin and its significance for hydrocarbon prospectivity in the ultradeepwater of the Nile delta. *GeoArabia*, **6**, 363–384.

Abu-Ali, M. A. & Littke, R. 2005. Paleozoic petroleum systems of Saudi Arabia: a basin modeling approach. *GeoArabia*, **10**, 131–168.

Abu-Ali, M. A., Behar, F., McGillivray, J. G. & Rudkiewicz, J. L. 1999. Paleozoic petroleum system of Central Saudi Arabia. *GeoArabia*, **4**, Gulf PetroLink, Bahrain.

Al-Hadidy, A. B. 2007. Palaeozoic stratigraphic lexicon and hydrocarbon habitat of Iraq. *GeoArabia*, **12**, 63–130.

Allen, P. A. 2007. The Huqf Supergroup of Oman: basin development and context for Neoproterozoic glaciation. *Earth Science Reviews*, **84**, 139–185.

Al-Siyabi, H. A. 2005. Exploration history of the Ara intrasalt carbonate stringers in the South Oman Salt Basin. *GeoArabia*, **10**, 39–72.

Alvaro, J. J. *et al*. 2007. The Ediacaran sedimentary architecture and carbonate productivity in the Atar cliffs, Adrar, Mauritania: palaeoenvironments, chemostratigraphy and diagenesis. *Precambrian Research*, **153**, 236–261.

Amthor, J. E., Ramseyer, K., Faulkner, T. & Lucas, P. 2005. Stratigraphy and sedimentology of a chert reservoir at the Precambrian–Cambrian Boundary: the Al Shomou Silicilyte, South Oman Salt Basin. *GeoArabia*, **10**, 89–122.

Armstrong, H. A., Turner, B. R., Makhlouf, I. M., Weedon, G. P., Williams, M., Alsmadi, A. & Abu Salah, A. 2005. Origin, sequence stratigraphy and depositional environment of an upper Ordovician (Hirnantian) deglacial black shale, Jordan. *Palaeogeography, Palaeoclimatology, Palaeoecology*, **220**, 356–360.

Armstrong, H. A., Abbott, G. D., Turner, B. R., Makhlouf, I. M., Muhammad, A. B., Pedentchouk, N. & Peters, H. 2009. Black shale deposition in an Upper Ordovician–Silurian permanently stratified, peri-glacial basin, southern Jordan. *Palaeogeography, Palaeoclimatology, Palaeoecology*, **273**, 368–377.

Arnauti, A. & Shelmani, M. 1988. A contribution to the northeast Libyan stratigraphy with emphasis on the Pre-Mesozoic. *In*: Arnauti, A., Owens, B. & Thusu, B. (eds) *Subsurface Palynostratigraphy of Northeast Libya*. Garyounis University Publications, Benghazi.

Bacheller, W. D. & Peterson, R. M. 1991. Hassi Messaoud Field; Algeria, Trias Basin, Eastern Sahara Desert. *In*: Foster, N. H. & Beaumont, E. A. (comps) *AAPG Treatise of Petroleum Geology: Atlas of Oil and Gas Fields*. American Association of Petroleum Geologists, Tulsa, OK, 211–225.

Balducchi, A. & Pommier, G. 1970. Cambrian Oil Field of Hassi Messaoud, Algeria. *In*: Halbouty, M. T. (ed.) *Geology of Giant Petroleum Fields*. American Association of Petroleum Geologists, Tulsa, OK, Memoirs, **14**, 477–488.

Ben-Avraham, Z., Ginzburg, A., Makris, J. & Eppelbaum, L. 2002. Crustal structure of the Levant Basin, eastern Mediterranean. *Tectonophysics* **346**, 23–43.

Berg, R. R. 1975. Capillary pressure in stratigraphic traps. *American Association of Petroleum Geologist Bulletin*, **59**, 939–956.

Bertello, F., Barsoum, K., Dalla, S. & Guessarian, S. 1996. Temsah discovery: a giant gas field in a deep sea turbidite environment. *In*: Youssef, M. (ed.) *Proceedings of the 13th Petroleum Conference*, Cairo, Egypt. Egyptian General Petroleum Corporation, 165–180.

Bertello, F., Visentin, C. & Ziza, W. 2003. An overview of the evolution and the petroleum systems of the Eastern Ghadames (Hamra) Basin, Libya. *AAPG Hedburg Conference 'Palaeozoic and Triassic Petroleum Systems in North Africa'*, February 2003, Algiers, Algeria, 18–20.

Bertrand-Sarfati, J. & Moussine-Pouchkine, A. 1985. Evolution and environmental conditions of the Conophyton associations in the Atar Dolomite (Upper Proterozoic, Mauritania). *Precambrian Research*, **29**, 207–234.

Bertrand-Sarfati, J. & Trompette, R. 1976. Use of stromatolites for intrabasinal correlation: example from the Late Proterozoic of the north western margin of the Taoudenni Basin. *In*: Walter, M. R. (ed.) *Stromatolites*. Elsevier, Oxford, 517–522.

Beydoun, Z. R. 1991. *Arabian Plate Hydrocarbon Geology and Potential – a Plate Tectonic Approach*. American Association of Petroleum and Geological Studies, Tulsa, OK, **33**.

Bhat, G. M., Ram, G. & Koul, S. 2009. Potential for oil and gas in the Proterozoic Carbonates (Sirban limestone) of Jammu, North India. *In*: Craig, J. *et al*. (eds) *Global Neoproterozoic Petroleum Systems and the Emerging Potential in North Africa*. Geological Society, London, Special Publications.

Blood, M. F. 2001. Exploration for a Frontier Salt Basin in Southwest Oman. *GeoArabia*, **6**, 159–176.

Busrewil, M. T. & Wadsworth, W. J. 1980*a*. *Preliminary Chemical Data on the Volcanic Rocks of Al Haruj Area, Central Libya*. Geology of Libya. Academic Press, London, **3**, 1077–1080.

Busrewil, M. T. & Wadsworth, W. J. 1980*b*. *The Basanitic Volcanoes of Gharyan Area, NW Libya*. Geology of Libya. Academic Press, London, **3**, 1095–1105.

Casati, L. & Craig, J. 2003. Petroleum Geology Overview of the North Africa Saharan Platform. AAPG Hedburg Conference '*Palaeozoic and Triassic Petroleum Systems in North Africa*', Algiers, Algeria February 2003, 18–20.

Clauer, N. 1981. Rb–Sr and K–Ar dating of Precambrian clays and glauconites. *Precambrian Research*, **15**, 331–352.

Clauer, N. 1982. Geochronology of sedimentary and metasedimentary Precambrian rocks of the West African Craton. *Precambrian Research*, **18**, 53–71.

Collins, A. S. & Pisarevsky, S. A. 2005. Amalgamating eastern Gondwana: the evolution of the Circum-Indian Orogens. *Earth Science Reviews*, **71**, 229–270.

Cozzi, A. & Al-Siyabi, H. A. 2004. Sedimentology and play potential of the late Neoproterozoic Buah Carbonates of Oman. *GeoArabia*, **9**, 11–36.

Cozzi, A., Grotzinger, J. P. & Allen, P. A. 2004. Evolution of a terminal Neoproterozoic carbonate ramp system (Buah formation, Sultanate of Oman): effects of basement paleotopography. *GSA Bullettin*, **116**, 1367–1384.

Craig, J., Rizzi, C. *et al*. 2008. Structural styles and prospectivity in the Precambrian and Palaeozoic hydrocarbon systems of North Africa. *Geology of East Libya*, **4**, 51–122.

Craig, J., Thurow, J., Thusu, B., Whitham, A. & Abutarruma, Y. 2009. *Global Neoproterozoic Petroleum Systems and the Emerging Potential in North Africa*. Geological Society, London, Special Publications, **326**.

Davidson, L., Beswetherick, S. *et al*. 2000. The structure, stratigraphy and petroleum geology of the Murzuq Basin, southwest Libya. *In*: Sola, M. A. & Worsley, D. (eds) *Geological Exploration of the Murzuq Basin*. Elsevier, Amsterdam, 295–320.

Delfour, J. 1970. Le groupe de J'Balah – une nouvelle unite du bouclier arabe. *Bullétin de BRGM (deuxieme series), Section IV*, **4**, 19–32.

Deynoux, M., Affaton, P., Trompette, R. & Villeneuve, M. 2006. Pan-African tectonic evolution and glacial events registered in Neoproterozoic to Cambrian cratonic and foreland basins of West Africa. *Journal of African Earth Sciences*, **46**, 397–426.

Dixon, R. J., Moore, J. K. S. *et al*. 2010. Integrated petroleum systems and play fairway analysis in a complex Palaeozoic basin: Ghadames/Illizi Basin, North Africa. *In*: Vining, B. A. & Pickering, S. C. (eds)

Petroleum Geology: From Mature Basins to New Frontiers – Proceedings of the 7th Petroleum Geology Conference. Geological Society, London, 735–760; doi: 10.1144/0070735.

Dolson, J. C. 2001. *The Petroleum Potential of Egypt*. American Association of Petroleum Geologists, Tulsa, OK, Memoirs, **74**.

Dolson, J. C., Boucher, P. J. & Shann, M. V. 2000*a*. Exploration potential in the offshore Mediterranean, Egypt: perspectives from the context of Egypt's future resources and business challenges. *EAGE Conference on Geology and Petroleum Geology, Malta*.

Dolson, J. C., Shann, M., Matbouly, S. I., Hammouda, H. & Rashed, R. M. 2000*b*. Egypt in the twenty-first century: petroleum potential in offshore trends. *GeoArabia*, **6**.

Droste, H. J. 1997. Stratigraphy of the lower Paleozoic Haima supergroup of Oman. *GeoArabia*, **2**, 419–472.

Echikh, K. & Sola, M. 2000. Geology and hydrocarbon occurrences in the Murzuq Basin, S.W. Libya. *In*: Sola, M. A. & Worsley, D. (eds) *Geological Exploration in the Murzuq Basin*. Elsevier, Amsterdam, 175–222.

El-Barkooky, A. N. & Helal, M. A. 2002. Some Neogene stratigraphic aspects of the Nile Delta. *Mediterranean Offshore Conference, Alexandria*.

Galbiati, M., Fervari, M. & Cavanna, G. 2009. Seismic evaluation of reservoir quality and gas reserves of DHI supported deep water systems in the offshore Nile Delta. *First Break*, **27**, 95–102.

Galeazzi, S., Point, O. N., Haddadi, N., Mather, J. & Druesne, D. 2010. Regional geology and petroleum systems of the Illizi–Berkine area of the Algerian Saharan Platform: an overview. *Marine and Petroleum Geology*, **27**, 143–178.

Garfunkel, Z. 1998. Constraints on the origin and history of the Eastern mediterranean Basin. *Tectonophysics*, **298**, 5–35.

Garfunkel, Z. 2004. Origin of the Eastern Mediterranean basin: a reevaluation. *Tectonophysics*, **391**, 11–34.

Geyer, G. & Landing, E. 2006. Ediacaran–Cambrian depositional environments and stratigraphy of the western Atlas Regions, Morocco. UCL Maghreb Petroleum Research Group (MPRG) Infracambrian/ Early Palaeozoic Field Guide Series No. 1. *Beringeria*, Special Issue **6**.

Ghienne, J. F. 2003. Late Ordovician sedimentary environments, glacial cycles, and post-glacial transgression in the Taoudeni Basin, West Africa. *Palaeogeography, Palaeoclimatology, Palaeoecology*, **189**, 117–145.

Ghori, K. A. R., Craig, J., Thusu, B., Luning, S. & Geiger, M. 2009. Global Infracambrian petroleum systems. *In*: Craig, J., Thurow, J., Thusu, B., Whitham, A. & Abutarruma, Y. (eds) *Global Neoproterozoic Petroleum Systems and the Emerging Potential in North Africa*. Geological Society, London, Special Publications, **326**, 109–136.

Grosjean, E., Love, G. D., Stalvies, C., Fike, D. A. & Summons, R. E. 2008. Origin of petroleum in the Neoproterozoic-Cambrian South Oman Salt Basin. *Organic Geochemistry*, **40**, 87–110.

Guerrak, S. 1989. Time & Space distribution of Palaeozoic oolitic ironstones in the Tindouf Basin, Algerian Sahara. *Journal of the Geological Society, London*, **46**, 197–212.

Halverson, G. P., Hoffman, P. F., Schrag, D. P., Maloof, A. C. & Rice, A. H. 2005. Towards a Neoproterozoic composite carbon-isotope record. *Geological Society of America Bulletin*, **117**, 1181–1207.

Hart, S., Gerrits, M. *et al*. 2002. The Northeast Mediterranean deep water area – results of first drilling campaign & Regional Framework Study or ... Finding the Sweet Spots in a large under-explored block. *Mediterranean Offshore Conference*, *Alexandria*.

Hirst, J. P. P., Benbakir, A., Payne, D. F. & Westlake, I. R. 2002. Tunnel valleys and density flow processes in the upper Ordovician glacial succession, Illizi Basin, Algeria: influence on reservoir quality. *Journal of Petroleum Geology*, **25**, 297–324.

Hoffman, P. F. & Schrag, D. P. 2000. Snowball earth. *Scientific American*, **285**, 50–57.

Hoffman, P. F., Kaufman, A. J., Halverson, G. P. & Schrag, D. P. 1998. A Neoproterozoic snowball Earth. *Science*, **281**, 1342–1346.

Konert, G., Afifi, A. M., Al Hajri, S. A. & Droste, H. J. 2001. Paleozoic stratigraphy and hydrocarbon habitat of the Arabian Plate. *GeoArabia*, **6**, 407–442.

LeBlanc, M. & Moussine-Pouchkine, A. 1994. Sedimentary and volcanic evolution of a Neoproterozoic continental margin (Bleida, Anti-Atlas, Morocco). *Precambrian Research*, **70**, 25–44.

Le Heron, D. P. & Craig, J. 2008. First-order reconstructions of the Late Ordovician Saharan Ice Sheet. *Journal of the Geological Society*, **165**, 19–29.

Le Heron, D. P. & Dowdeswell, J. A. 2009. Calculating ice volumes and ice flux to constrain the dimensions of a 440 Ma North African ice sheet. *Journal of the Geological Society, London*, **166**, 277–281.

Le Heron, D. P. & Howard, J. 2008. Short notes and guidebook on the geology of the Jabal az-Zalmah region, Northern Al Kufrah Basin. *Geology of Southern Libya*, *Field trip*, 21–25 November 2008, 60.

Le Heron, D., Sutcliffe, O., Bourgig, K., Craig, J., Visentin, C. & Whittington, R. 2004. Sedimentary architecture of Upper Ordovician tunnel valleys, Gargaf Arch, Libya: implications for the genesis of a hydrocarbon reservoir. *GeoArabia*, **9**, 137–159.

Le Heron, D. P., Craig, J. & Etienne, J. L. 2009. Ancient glaciations and hydrocarbon accumulations in North Africa and the Middle East. *Earth Science Reviews*, **93**, 47–76.

Le Heron, D. P., Armstrong, H. A., Wilson, C., Howard, J. P. & Gindre, L. 2010. Glaciation and deglaciation of the Libyan Desert: the Late Ordovician record. *Sedimentary Geology*, **223**, 100–125.

Liegeois, J. P., Sauvage, J. F. & Black, R. 1991. The Permo-Jurassic alkaline province of Tadhak, Mali: geology, geochronology and tectonic significance. *Lithos*, **27**, 95–105.

Logan, P. & Duddy, I. 1998. An investigation of the thermal history of the Ahnet and Reggane Basins, Central Algeria, and the consequences for hydrocarbon generation and accumulation. *In*: MacGregor, D. S., Moody, R. T. J. & Clark-Lowes, D. D. (eds) *Petroleum Geology of North Africa*. Geological Society, London, Special Publications, **132**, 131–155.

Loncke, L. & Mascle, J. F. 2004. Mud volcanoes, gas chimneys, pockmarks and mounds in the Nile deep sea fan (eastern Mediterranean): geophysical evidences. *Marine and Petroleum Geology*, **21**, 669–689.

Loncke, L., Gaullier, V., Mascle, J., Vendeville, B. & Camera, L. 2006. The Nile deep-sea fan: an example of interacting sedimentation, salt tectonics, and inherited subsalt paleotopographic features. *Marine and Petroleum Geology*, **23**, 297–315.

Longacre, M., Bentham, P., Hanbal, I., Cotton, J. & Edwards, R. 2007. New crustal structure of the Eastern Mediterranean basin: detailed integration and modeling of gravity, magnetic, seismic refraction, and seismic reflection data. *EGM International Workshop on Innovation in EM, Grav and Mag Methods: a new Perspective for Exploration*, Capri.

Loper, D. E. 1991. Mantle plumes. *Tectonophysics*, **187**, 372–384.

Lottaroli, F., Craig, J. & Thusu, B. 2009. Neoproterozoic–Early Cambrian (Infracambrian) hydrocarbon prospectivity of North Africa: a synthesis. *In*: Craig, J., Thurow, J., Thusu, B., Whitham, A. & Abutarruma, Y. (eds) *Global Neoproterozoic Petroleum Systems and the Emerging Potential in North Africa*. Geological Society, London, Special Publications, **326**, 137–156.

Luning, S., Craig, J., Loydell, D. K., Storch, P. & Fitches, B. 2000. Lower Silurian 'hot shales' in North Africa and Arabia: regional distribution and depositional model. *Earth Science Reviews*, **49**, 121–200.

Marten, R., Shann, M., Mika, J., Rothe, S. & Quist, Y. 2004. Seismic challenges of developing the pre-Pliocene Akhen Field offshore Nile Delta. *The Leading Edge*, April, **23**, 314–320.

Meciani, L., Laura, S. A. & Khalil, M. 2002. Tectono-sedimentary provinces of the Oligo-Quaternary in the Offshore Nile Delta: relevance to hydrocarbon trapping and reservoirs distribution. *AAPG Conference*, Cairo, October 2002.

Metwalli, F. I. & Piggot, J. D. 2005. Analysis of petroleum system criticals of the Matruh-Shushan Basin, Western Desert, Egypt. *Petroleum Geoscience*, **11**, 157–178.

Millson, J. A., Quin, J. G., Idiz, E., Turner, P. & Al-Harthy, A. 2008. The Khazzan gas accumulation, a giant combination trap in the Cambrian Barik Sandstone Member, Sultanate of Oman: implications for Cambrian petroleum systems and reservoirs. *AAPG Bulletin*, **92**, 885–917.

Moussine-Pouchkine, A. & Bertrand-Sarfati, J. 1997. Tectonosedimentary subdivisions in the Neoproterozoic to Early Cambrian over of the Taoudenni Basin (Algeria, Mauritania, Mali). *Journal African Earth Sciences*, **24**, 425–443.

Nataf, H. C. 1991. Mantle convection, plates and hotspots. *Tectonophysics*, **187**, 361–371.

Pankhurst, R. J., Trouw, R. A. J., de Brito Neves, B. B. & de Wit, M. J. (eds) *West Gondwana: Pre-Cenozoic Correlation Across the South Atlantic Region*. Geological Society, London, Special Publications, **294**, 9–31.

Peck, J. 2008. Giant oil prospects lie in distal portion of offshore East Mediterranean Basin. *Oil & Gas Journal/Oct 6*.

Peters, K. E., Clark, M. E., Das Gupta, U., McCaffrey, A. M. & Lee, C. Y. 1995. Recognition of an Infracambrian source rock based on biomarkers in the Baghewala-1 Oil, India. *AAPG Bulletin*, **79**, 1481–1494.

Pisarevsky, S. A., Murphy, J. B., Cawood, P. A. & Collins, A. S. 2008. Late Neoproterozoic and Early Cambrian palaeogeography; models and problems. *In*: Pollastro, R. M. 2003. *Total Petroleum Systems of the Paleozoic and Jurassic, Greater Ghawar Uplift and Adjoining Provinces of Central Saudi Arabia and Northern Arabian–Persian Gulf*. US Geological Survey Bulletins, **2202-H**.

Ramseyer, K., Amthor, J. E., Spotl, C., Terken, J. M. J., Matter, A., Vroonten Hove, M. & Borgomano, J. R. F. 2004. Impact of basin evolution, depositional environment, pore water evolution and diagenesis on reservoir-quality of Lower Paleozoic Haima Supergroup sandstones, Sultanate of Oman. *GeoArabia*, **9**, 107–138.

Riaz, A. S., Jamil, A. M., McCann, J. & Saqi, M. I. 2003. Distribution of infracambrian reservoirs on Punjab Platform in Central Indus Basin of Pakistan. *ATC 2003 Conference & Oil Show*, Islamabad, 1–17.

Roberts, G. & Peace, D. 2007. Hydrocarbon plays and prospectivity of the Levantine Basin, offshore Lebanon and Syria from modern seismic data. *GeoArabia*, **12**, 3.

Robertson, A. F. H. 1998. Mesozoic–Tertiary tectonic evolution of the easternmost Mediterranean area: integration of marine and land evidence. *In*: Robertson, A. H. F., Emeis, K.-C., Richter, C. & Camerlenghi, A. (eds) *Proceedings of the Ocean Drilling Program, Scientific Results*, **160**.

Robertson, A. & Comas, M. 1998. Collision-related processes in the Mediterranean region – introduction. *Tectonophysics*, **298**, 1–4.

Rusk, D. 2001. Libya: petroleum potential of the underexplored basin centers – a twenty-first century challenge. *In*: Downey, M. W., Threet, J. C. & Morgan, W. A. (eds) *Petroleum Provinces of the Twenty-First Century*. American Association of Petroleum Geologists, Tulsa, OK, Memoirs, **74**, 429–452.

Samuel, A., Kneller, B., Raslan, S., Sharp, A. & Parsons, C. 2005. Prolific deep-marine slope channels of the Nile Delta, Egypt. *AAPG Bulletin*, **87**, 541–560.

Sati, G. C., Zutshi, P. B., Pati, P. B. & Lal, N. K. 1997. Late Proterozoic–Early Palaeozoic sequence in Southeastern Jaisalmer Basin: a new play for hydrocarbon exploration. *Indian Journal of Petroleum Geology*, **6**, 43–54.

Schoenherr, J., Ural, J. L., Kukla, P. A., Littkre, R., Schleder, Z., Larroque, J. M. & Newall, M. 2007. Salt: a case study of the Infra-cambrian Ara Salt from the South Oman Salt Basin. *AAPG Bulletin*, **91**, 1541–1557.

Scotese, C. R. 2009. Late Proterozoic plate tectonics and palaeogeography: a tale of two supercontinents, Rodinia and Pannotia. *In*: Craig, J., Thurow, J., Thusu, B., Whitham, A. & Abutarruma, Y. (eds) *Global Neoproterozoic Petroleum Systems and the Emerging Potential in North Africa*. Geological Society, London, Special Publications, **326**, 67–83.

Senalp, M. & Al-Duaiji, A. 1995. Stratigraphy and sedimentation of the Unayzah reservoir, central Saudi Arabia. *In*: Al-Husseini, M. I. (ed.) *Middle East Petroleum Geosciences, GEO'94*. *GeoArabia*, **2**, 837–847.

Sharland, P. R., Archer, R., Casey, D. M., Davies, R. B., Hall, S. H., Heward, A. P., Horbury, A. D. & Simmons, M. D. 2001. *Arabian Plate Sequence Stratigraphy*. *GeoArabia*, Special Publications, **2**.

Shields, G. A., Deynoux, M., Culver, S. J., Brasier, M. D., Affaton, P. & Vandamme, D. 2007. *Neoproterozoic Glaciomarine and Cap Dolostone Facies of the Southwestern Taoudeni Basin (Walidiala Valley, Senegal/Guinea, NW Africa)*. Comptes Rendus Geoscience, Paris, **339**, 3–4, 186–199.

Smith, A. G. 2009. Neoproterozoic timescales and stratigraphy. *In*: Craig, J., Thurow, J., Thusu, B., Whitham, A. & Abutarruma, Y. (eds) *Global Neoproterozoic Petroleum Systems and the Emerging Potential in North Africa*. Geological Society, London, Special Publications, **326**, 27–54.

Societé Mauritanienne de Hydrocarbures. 2007. *Hydrocarbon Potential of Taoudeni Basin*. Promotional Brochure, December 2007.

Stampfli, G. M. & Borel, G. D. 2002. A plate tectonic model for the Palaeozoic and Mesozoic constrained by dynamic plate boundaries and restored synthetic oceanic isochrones. *Earth and Planetary Science Letters*, **196**, 17–33.

Sutcliffe, O. E., Dowdeswell, J. A., Whittington, R. J., Theron, J. N. & Craig, J. 2000. Calibrating the late Ordovician glaciation and mass extinction by the eccentricity cycles of the Earth's orbit. *Geology*, **23**, 967–970.

Sutcliffe, O. E., Craig, J. & Whittington, R. 2005. Late ordovician glacial pavements revisited: a reappraisal of the origin of striated surfaces. *Terra Nova*, **17**, 486–487.

Sylta, O. 1991. Modelling of secondary migration and entrapment of multicomponent hydrocarbon mixtures using equation of state and raytracing modeling techniques. *In*: England, W. A. & Fleet, A. J. (eds) *Petroleum Migration*. Geological Society, London, Special Publications, **59**, 111–122.

Sylta, O. 1993. New techniques and their application in the analysis of secondary migration. *In*: Doré, A. G. *et al*. (eds) *Basin Modelling: Advances and Applications*. Elsevier, Amsterdam/Norwegian Petroleum Society, Oslo, Special Publications, **3**, 385–398.

Tonetti, M. & Grigo, D. 2007. The role of Hercynian event in Tunisian Ghadames Basin: an innovative comparison between two petroleum systems modelling studies. *Epitome*, **2**, 406–407.

Trompette, R. 1969. Les stromatolites du Précambrien supérieur de l'Adrar de Mauritanie (sahara occidental). *Sedimentology*, **13**, 123–154.

Trompette, R. 1973. *Le Precambrien superieur et le Paleozoique inferieur de l'Adrar de Mauritanie (bordure occidentale du bassin de Taoudeni, Afrique de l'Ouest). Un exemple de sedimentation de craton*. Etude stratigraphique et sedimentologique. Travaux des Laboratoires des Sciences de la Terre St-Jerome, Marseille, **B-7**.

Trompette, R. 1997. Neoproterozoic (600 Ma) aggregation of Western Gondwana: a tentative scenario. *Precambrian Research*, **82**, 101–112.

Turner, P. & Sherif, H. 2007. A giant Late Triassic–Early Jurassic evaporitic basin on the Saharan Platform, North Africa. *In*: Schreiber, B. C., Lugli, S. & Babel, M. (eds) *Evaporites through Space and Time*. Geological Society, London, Special Publications, **285**, 87–105.

Turner, P., Pilling, D., Walker, D., Exton, J., Binnie, J. & Sabaou, N. 2001. Sequence stratigraphy and sedimentology of the late Triassic TAG-I (Blocks 401/402, Berkine Basin, Algeria). *Marine & Petroleum Geology*, **18**, 959–981.

Vecoli, M. 2000. Palaeoenvironmental interpretation of microphytoplankton diversity trends in the Cambrian–Ordovician of the northern Sahara Platform. *Palaeogeography, Palaeoclimatology, Palaeoecology*, **160**, 329–346.

Vecoli, M., Riboulleau, A. & Versteegh, G. J. M. 2009. Palynology, organic geochemistry and carbon isotope analysis of a latest Ordovician through Silurian clastic succession from borehole Tt1, Ghadamis Basin, southern Tunisia, North Africa: palaeoenvironmental interpretation. *Palaeogeography, Palaeoclimatology, Palaeoecology*, **273**, 378–394.

Walley, C. D. 1998. Some outstanding issues in the geology of Lebanon and their importance in the tectonic evolution of the Levantine region. *Tectonophysics*, **298**, 36–62.

Waltham, A. 2009. Salt terrains of Iran. *Geology Today*, **24**, 188–194.

Watts, N. L. 1987. Theoretical aspects of cap-rock and fault seals for single and two-phase hydrocarbon columns. *Marine and Petroleum Geology*, **4**, 274–307.

Whaley, J. 2004. The hydrocarbon potential of the underexplored Palaeozoic and Triassic petroleum systems of Northwest Arabia. *Abstract in 6th Middle East Geosciences Conference, GEO 2004*. GeoArabia, **9**, 143.

Weis, D., Liegeois, J. P. & Black, R. 1987. Tadhak alkaline ring-complex (Mali): existence of U–Pb isochrones and 'Dupal' signature 270 Ma ago. *Earth and Planetary Science Letters*, **82**, 316–322.

Wender, L. E., Bryant, J. W., Dickens, M. F., Neville, A. S. & Al Moqbel, A. M. 1998. Paleozoic (Pre-Khuff) hydrocarbon geology of the Ghawar area, Eastern Saudi Arabia. *GeoArabia*, **3**, Gulf PetroLink, Bahrain, 273–302.

Wescott, W. A. & Boucher, P. J. 2000. Imaging submarine channels in the western Nile Delta and interpreting their paleohydraulic characteristics from 3-D seismic. *The Leading Edge*, June, **19**, 580–591.

Woller, F. & Fediuk, F. 1980. *Volcanic Rocks of Jabal as Sawda; Geology of Libya*. Academic Press, London, **3**, 1081–1093.

Zhu, W., Zhang, Z., Shu, L., Lu, H., Su, J. & Yang, W. 2008. SHRIMP U–Pb zircon geochronology of Neoproterozoic Korla mafic dykes in the northern Tarim Block, NW China: implications for the long-lasting break-up process of Rodinia. *Journal of the Geological Society*, **165**, 887–890.

Ziegler, M. A. 2001. Late Permian to Holocene paleofacies evolution of the Arabian Plate and its hydrocarbon occurrences. *GeoArabia*, **6**, Gulf PetroLink, Bahrain, 445–504.

Palaeohighs: their influence on the North African Palaeozoic petroleum systems

R. ESCHARD,[1] F. BRAIK,[2] D. BEKKOUCHE,[2] M. BEN RAHUMA,[3] G. DESAUBLIAUX,[4] R. DESCHAMPS[1] and J. N. PROUST[5]

[1]*IFP, 1, 4 Avenue de Bois Préau, 92 506 Rueil-Malmaison, France (e-mail: remi.eschard@ifp.fr)*
[2]*Sonatrach Activité Amont, Avenue du 1^er^ Novembre, Boumerdes, 35 000, Algeria*
[3]*Libyan Petroleum Institute, Tripoli, Libya*
[4]*IFP, 1, 4 Avenue de Bois Préau, 92 506, Rueil-Malmaison, France; Present address: GDF-Suez, 93 210 Saint-Denis, France*
[5]*Rennes I University, Campus de Beaulieu, 35042 Rennes, France*

Abstract: We present new insights for the characterization of the petroleum system evolution in North Africa based on a review of the stratigraphic architecture description of some selected North African Palaeozoic basins. During Palaeozoic time, the Gondwana platform was divided into sub-basins bounded by structural highs. Most of the highs were inherited from north–south and SW–NE Pan-African crustal faults which were reactivated during the Palaeozoic and later, in the Austrian and Alpine tectonic phases. We studied the stratigraphic architecture of the Palaeozoic succession around four main highs showing a clear tectonic activity during the Palaeozoic sedimentation. The Gargaff Arch, in Libya, is a major SW–NE broad anticline which slowly grew up during the Cambrian and Ordovician and stopped rising during the Silurian. The activity resumed during Late Silurian and early Devonian and during the Late Devonian. The Tihemboka High is a north–south anticline in between Libya and Algeria. The uplift started during the Cambro-Ordovician then stopped during most of the Silurian. The activity resumed during the Late Silurian and continued until the Lower Carboniferous. The Ahara High, separating the Illizi and Berkine basins in Algeria, has continuously grown during the Cambro-Ordovician, stopped rising during the Silurian, and grew again continuously during the Devonian. The Bled El-Mass High is a part of the Azzel-Matti Ridge separating the Ahnet and Reggane basins in Algeria. The high mostly rose during the Cambro-Ordovician then subsided relatively less quickly than the surrounding basins during the Silurian and Devonian. The uplift timing and chronology of each palaeohigh partly controlled the petroleum systems of the surrounding basins. Topographic lows favoured the occurrence of anoxic conditions and the preservation of Lower Silurian and Frasnian source rocks. Complex progressive unconformities developed around the palaeohighs form potential complex tectonostratigraphic traps. Finally, hydrocarbons could have been trapped around the highs during pre-Hercynian times, preserving reservoir porosity from early silicification. Mixed stratigraphic–structural plays could then be present today around the highs.

Keywords: palaeohighs, Palaeozoic, Algeria, petroleum system, stratigraphic architecture, stratigraphic trap

The Palaeozoic basins in North Africa represent one of the most prolific petroleum systems of the world. Two major source rocks, several stacked potential reservoir levels and a succession of tectonic phases favoured the accumulation of hydrocarbons in a large variety of traps and reservoirs. Hydrocarbons were first discovered and produced in the early 1960s from giant fields, such as the Hassi Messaoud or the Hassi R'Mel fields in Algeria. Since that time, tens of fields have been discovered and produced in Algeria and Libya, the exploration strategy being still mostly driven by the identification of structural traps from seismic data. Today, exploration is facing new challenges, the new targets being the deep tight reservoir gas prospects of the Lower Palaeozoic, and Palaeozoic reservoir subtle traps. Consequently, a good understanding of the reservoir and seal distribution together with the timing of the fluid migration is key for successful exploration. The objective of this paper is to describe the stratigraphic architecture of the Palaeozoic succession around four palaeohighs in Libya and Algeria from outcrop and subsurface data: the Gargaff Arch in Libya, the Ahara and Tihemboka arches in eastern Algeria, and the Bled el Mass Arch in western Algeria. We compare the timing of the uplifts and their petroleum implications.

Geological setting of the Palaeozoic platform in North Africa

Sub-basins and arches across the Algerian and Libyan platform

During Palaeozoic times, the Saharan platform was a part of the northern passive margin of the Gondwana supercontinent. The tectonic setting of this rigid craton was remarkably calm from Cambrian to Devonian times, while deformation progressively increased during Upper Devonian and Carboniferous times, announcing the late Carboniferous Hercynian compression. Major phases of deformation nevertheless episodically affected the craton, inducing low-angle regional unconformity associated with significant erosion during the Upper Ordovician (Taconic unconformity) and the Upper Silurian–Lower Devonian (Caledonian unconformity). On the Saharan platform, fluvial sedimentation episodes alternated with shallow marine ones, depending on the competition between the relative sea-level changes and subsidence. The epicontinental seas opened to the Rheic ocean located to the NW (Scotese *et al.* 1999).

VINING, B. A. & PICKERING, S. C. (eds) *Petroleum Geology: From Mature Basins to New Frontiers – Proceedings of the 7th Petroleum Geology Conference*, 707–724. DOI: 10.1144/0070707

The Gondwana craton itself consisted of several terranes accreted during the Pan-African orogen (Bertrand & Caby 1978; Fabre 1988; Caby 2003; Coward & Ries 2003). The main suture zone was located between the West African craton and the Touareg shield, and is marked today by a north–south fault zone in SW Algeria turning NW in the Ougarta range and in the Anti-Atlas in Morocco (Fabre 1988). Other major north–south Pan-African faults also cut the Touareg shield into narrow strips and were reactivated several times during the geological history. Away from these mobile areas, the craton was remarkably stable and rigid. As a result, the platform showed a succession of sub-basins separated by structural highs (Fig. 1) located above the Pan-African main faults. From east to west, we can recognize the Brak bin Ghanimah uplift marking the eastern termination of the Murzuk and Ghadames basins in Libya (Massa 1988); the Tihemboka High separating the Illizi from the Murzuk basins; the Amguid–El Biod, making a major north–south ridge separating the Illizi–Berkine basins from the Mouydir/Oued-Mya basins to the west; the Arak/Foum–Belrem ridge forming the eastern flank of the Ahnet Basin; and the Bled-el-Mass/Azzel–Matti Ridge limiting the Ahnet Basin from the Reggane Basin and connected northwards to the Ougarta chain. The Reggane Basin was itself limited from the Tindouf Basin by the Bou-Bernous High. Some highs also have an east–west or NE–SW orientation, such as the Gargaff High separating the Ghadames Basin from the Murzuk Basin in Libya. Similarly, the Ahara Arch separated the Illizi and Berkine basins, this basin being itself bounded northwards by the Talemzane–Dahar High.

The cited structures influenced the Palaeozoic sedimentation. However, many other highs were formed latterly during the Hercynian orogeny or during the Austrian Mid-Cretaceous or Cenozoic Alpine compressive phases.

Summary of the stratigraphic architecture of the Cambrian to Devonian succession

The different second-order cycles of the sedimentation have been already described by Boote *et al.* (1998) and Eschard *et al.* (2005). An overall transgressive trend from Cambrian to Middle Ordovician was followed by a regressive trend during Upper Ordovician. Erosion occurred in many places during an intra-Arenig unconformity. The Upper Ordovician successions were preserved in the Ougarta trough (Ghienne *et al*. 2007*a*, *b*), in the Anti-Atlas succession in Morocco (Destombes *et al.* 1985) and Libya (Echikh 1998), but was eroded in most of the Algerian sector by the Taconic unconformity, a low-angle and low-relief tectonic unconformity associated with a large flexure of the Saharan craton that occurred during the Upper Ordovician. A major glacial event then occurred during Late Ordovician (Hirnantian times), inducing a network of glacial pathways and glacial valleys (Ghienne *et al.* 2007*a*, *b*; Le Heron & Craig 2007). The Taconic unconformity locally merged with the Ashgill glacial erosion surface, making the interpretation rather complex.

Silurian times were marked by a major transgression depositing a thick succession of offshore shale. It includes basal hot shale layers corresponding to the main source rock that has generated hydrocarbons in almost every basin across North Africa (Legrand 2003). The Upper Silurian was deposited during a regressive event, ended by the Caledonian unconformity, another low-angle tectonic unconformity at the Siluro-Devonian boundary. The Devonian

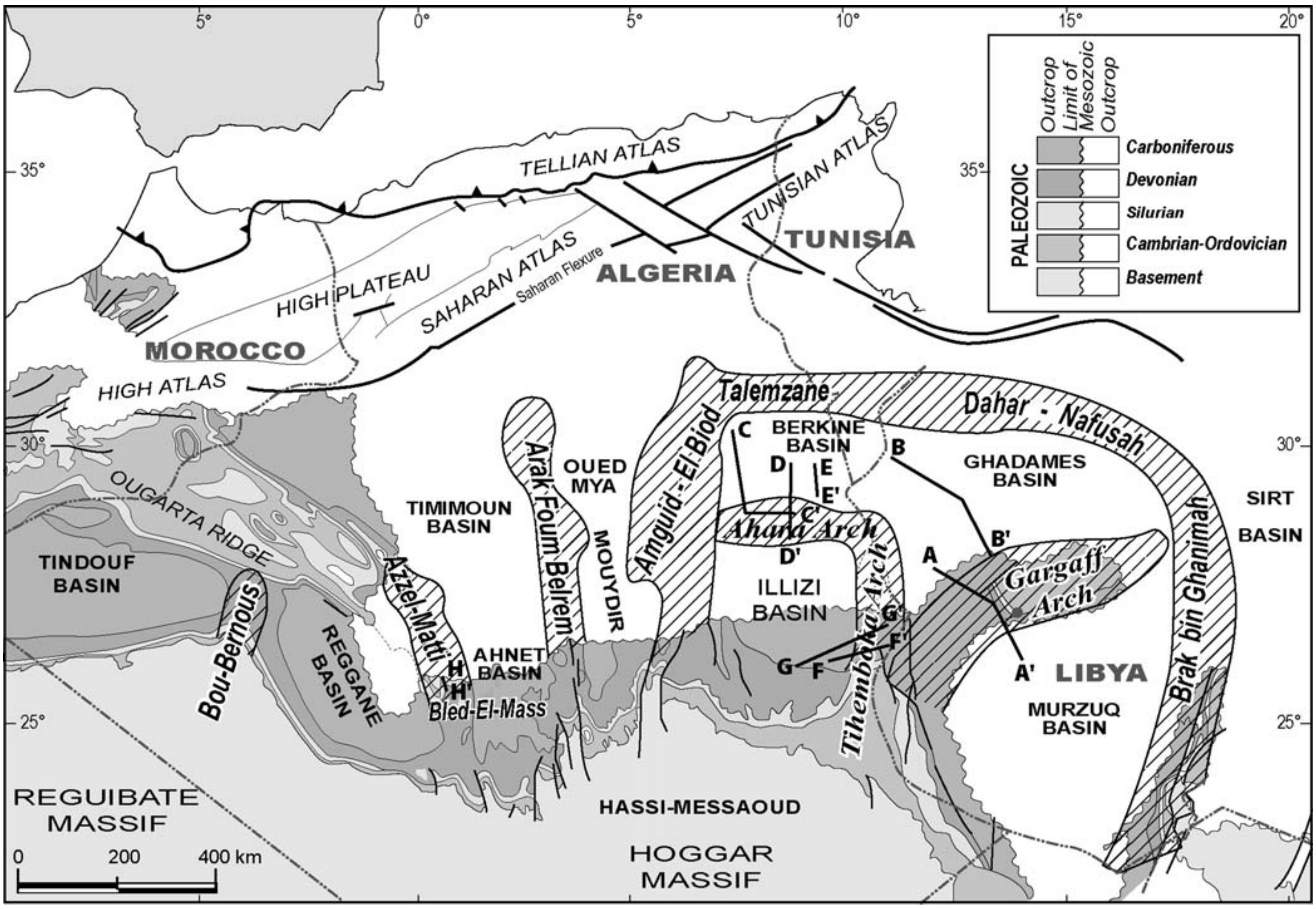

Fig. 1. Structural map showing the distribution of the main highs and basins across the Saharan Platform (partially redrawn from Boote *et al.* 1998). The hatched areas correspond to the main highs described in the text.

cycle initiated with low-stand deposits above the Caledonian unconformity, followed by a major transgression culminating with the deposition of the Frasnian hot-shale, forming another prolific source rock. Deformation of the craton then progressively increased during the Upper Devonian and Carboniferous, announcing the Hercynian compression.

The main characteristics of the Lower Palaeozoic sedimentation were already described by Beuf *et al.* (1971), summarized by Eschard *et al.* (2005). Figure 2 shows a summary of the stratigraphic sections observed in the Berkine, Ahnet, Ghadames and Illizi basins, and in the Tassili outcrops in Algeria. Within sub-basins, the Lower Palaeozoic stratigraphic architecture was

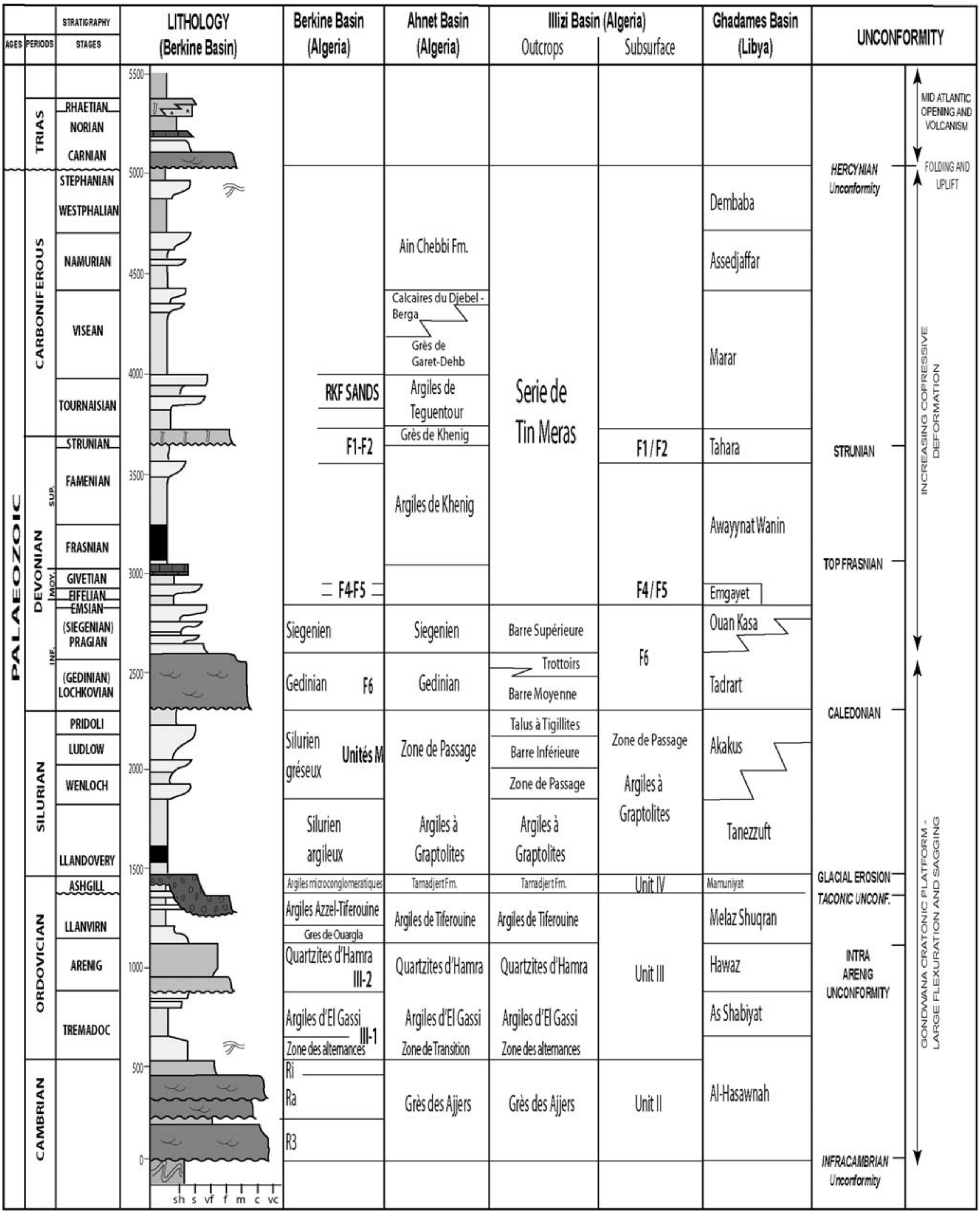

Fig. 2. Stratigraphic column of the Palaeozoic succession in the Berkine Basin, with the lithostratigraphic nomenclature of the Ahnet, Illizi, Ghadames basins and of the Ajjer Tassil outcrops.

remarkably organized in third-order sequences showing a well defined and laterally constant stacking pattern at the basin-scale. The lateral facies variations were very progressive, depositional environments being more and more distal in a NW direction. However, the stratigraphic architecture of the Palaeozoic succession abruptly changes within a few kilometres distance of the palaeohighs. The series rapidly thins out, making complex wedges with an amalgamation of several unconformities.

Stratigraphic architecture of the Palaeozoic succession around syn-tectonic highs

Gargaff Arch, Ghadames and Murzuq basins, Libya

Stratigraphic architecture. The Gargaff Arch (Fig. 3a) is a conspicuous WSW–ENE structural feature separating the Murzuq Basin from the Ghadames Basin in Libya. The arch plunges in the subsurface to the SW and probably connects to the north–south Tihemboka Arch. The Gargaff Arch continues to the NE and connects to the Tripoli–Assawada Arch. The arch forms a broad asymmetric anticline, with a relatively steep southern flank compared with the northern one (Fig. 3b).

Proterozoic granites and low-grade meta-sediments that crop out in Jabal Hasawnah were covered by Cambrian (Al-Hasawnah Formation) and Ordovician sediments (As Shabiyat, Hawaz, Melaz Shuqran and Mamuniyat formations). Lower Devonian sediments only crop out in the NW part of the high while, in the southern flank, Upper Devonian sediments directly onlap a reduced section of Silurian (Rubino & Blanpied 2000). The Hercynian unconformity then eroded the Palaeozoic sediments below, and the unconformity was itself onlapped by Cretaceous and Cenozoic sediments.

While in the subsurface to the SW of the Gargaff Arch, the Cambro-Ordovician succession thins out (Hallett 2002), in outcrops, the Cambrian sandstones remain thick (600 m, according to Massa 1988). Palaeocurrents measured in outcrops in the Cambrian and Ordovician sediments show north–NW flow directions (Vos 1981; Massa 1988; Ramos *et al.* 2006), which are the ones observed regionally by Beuf *et al.* (1971). The Ordovician succession presents a rather complex geometry in outcrops. In the western termination of the high, Lower–Middle Ordovician units (Ash Shabiyat, Hawaz and Melaz Shuqran formations) pinch out below the Late Ordovician glacial valleys (Mamouniyat Formation) from north to south.

A regional cross-section between the Ghadames Basin and the Gargaff Arch illustrates the overall geometry of the Silurian and Devonian succession (Fig. 4). In the outcrops of the northern flank of the high, only a few metres of the lower part of the Llandovery Tanezzouft shales are left above the Upper Ordovician sediments (Fig. 5), and further westwards, the Silurian is completely eroded, with Lower Devonian Tadrart Formation directly overlying the Cambro-Ordovician (Massa 1988; Dardour *et al.* 2004). Correlations in the Figure 4 show evidence for a discrete onlap of the lower hot-shale levels on the relief made by the Gargaff Arch; the hot shales pinch out southward. In contrast, the upper part of the Silurian succession (Akakus Formation) was progressively eroded below the base of the Lower Devonian Tadrart sandstones (Fig. 5) when approaching the palaeohigh, and is not present any more in outcrops.

The Devonian stratigraphic succession progressively thins out when approaching the high, in the southern flank of the Ghadames Basin (Fig. 4) and northern flank of Murzuk Basin (Hallett 2002). The Tadrart fluvio-estuarine sandstones are 30 m thick in outcrops,

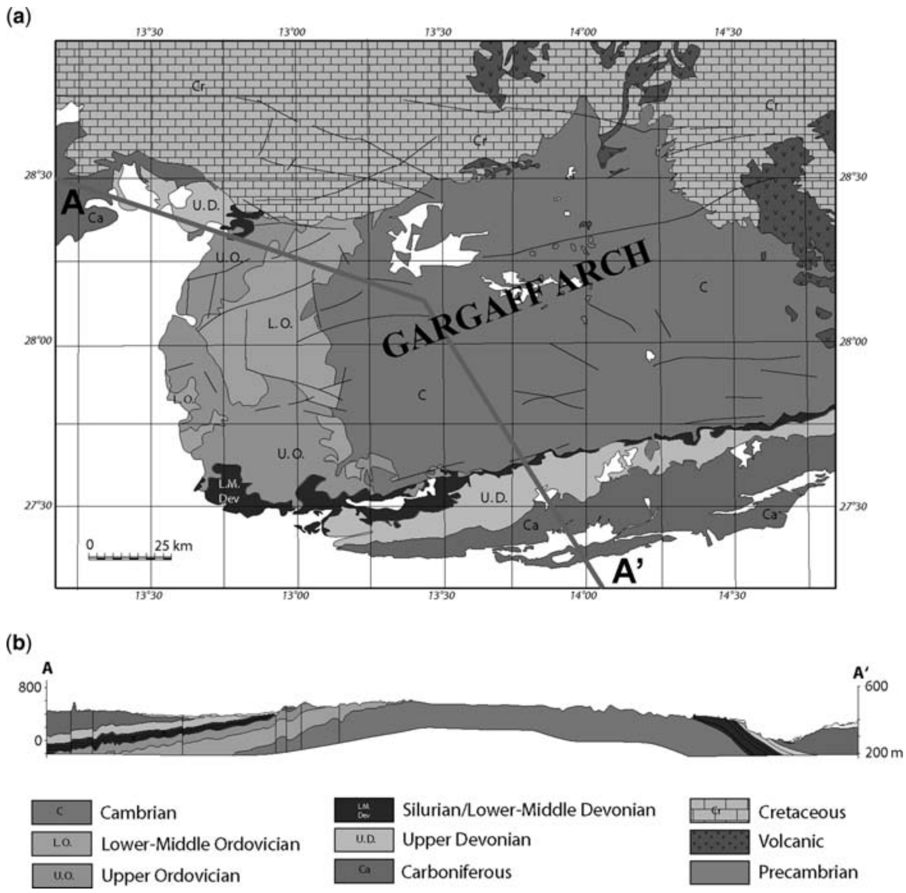

Fig. 3. (**a**) Simplified geological map of the Gargaf Arch. (**b**) Cross-section across the arch redrawn from the geological maps. Observe the asymmetry of the high and the difference in the wedge architecture between the North and South flanks.

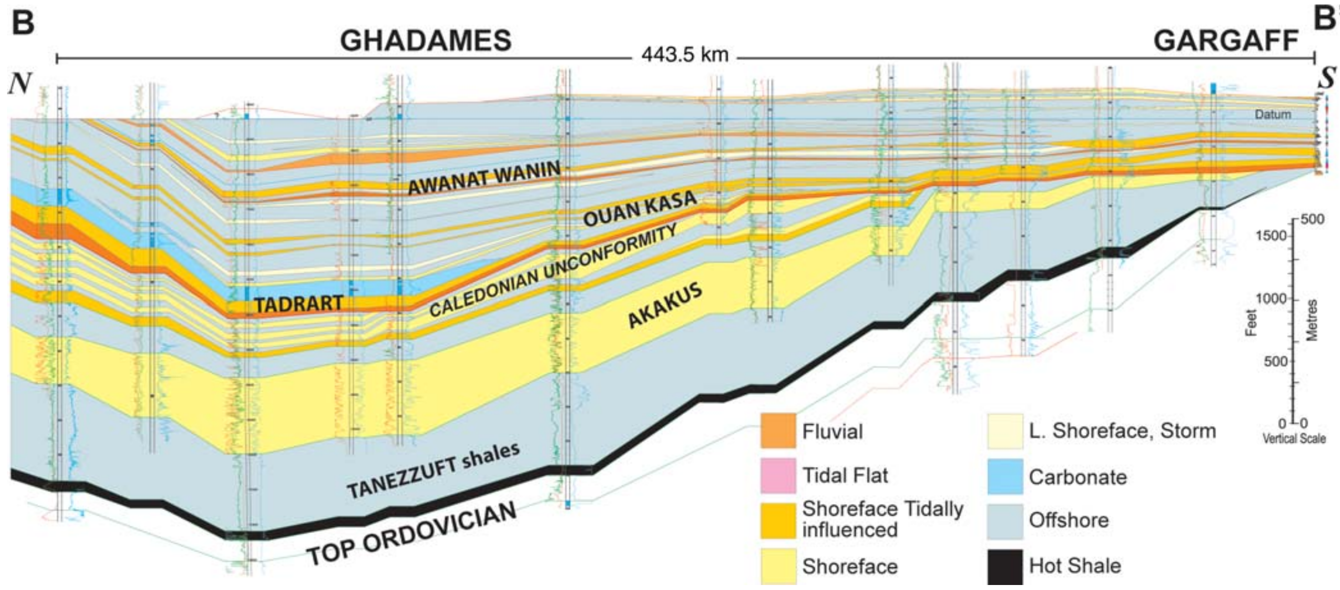

Fig. 4. Cross-section showing the stratigraphic architecture of the Siluro-Devonian succession between the Ghadames Basin and the Gargaff Arch.

thicken to 100 m in the centre of the Ghadames Basin and reach 300 m in thickness in the Berkine Basin. On the southern flank of the palaeohigh, the Lower Devonian succession is missing (Rubino & Blanpied 2000). According to Massa (1988), the Lower Devonian succession is completely pinching out over the Gargaff Arch westward in the subsurface between the Murzuk and Ghadames basins.

The Middle to Upper Devonian succession consists of fluvial, deltaic and marine sediments organized in third-order sequences which have already been described by Sutcliffe *et al.* (2000) for the northern flank of the Gargaff High, and by Rubino & Blanpied (2000) for its southern flank. We observed current directions and progradation northwestwards on the northern flank, and southwards on the southern flank, suggesting that the palaeohigh was expressed at that time.

In outcrops, the Devonian unconformities are of two types. First, fluvial incised valleys formed a network of narrow and deep channels filled by either fluvial or tidal sediments. An example of intra-Givetian incised valleys (Awanat Wanin Formation), formerly interpreted by Vos (1981) as a distributary channel, can be seen in Figure 6. Incised valleys, 300 m wide and 25 m thick, were incised into shelfal silty mudstones during a relative sea-level fall and filled during the subsequent relative sea-level rise by tidal deposits. Other examples of fluvial incisions can be also observed in the Eifelian sediments (Awanat Wanin/Emgayet). Second, forced regression wedges, bounded by sharp and flat erosional surfaces at their base and flooding surfaces on top, consist of laterally continuous fluvio-estuarine wedges (base of the Emsian Ouan Kasa sandstone and at the base of the Strunian Tahara sandstone) passing distally to tidal deposits. The units considerably thicken in the subsurface of the Ghadames Basin, forming lowstand prograding wedges during periods of relative sea-level fall.

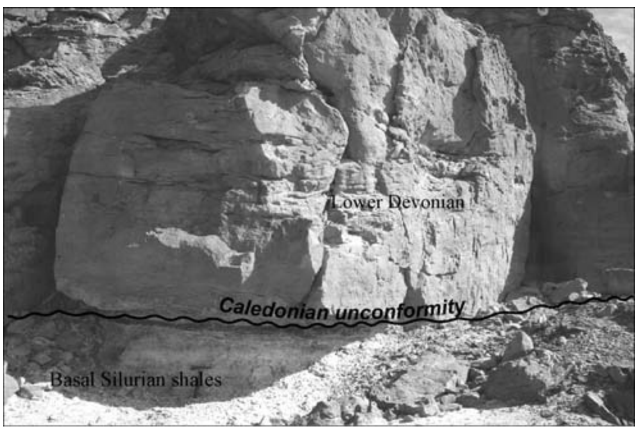

Fig. 5. Outcrop photo showing the Lower Devonian Tadrart formation unconformably overlying the Lower Silurian Tanezzouft Shales, Wadi Shati area, Gargaff region. Only a few metres of basal Silurian shales were preserved below the Caledonian unconformity.

Interpretation. The uplift of the Gargaff Arch started during the Cambrian, as shown by the thinning of the succession when approaching the palaeohigh. However, the palaeohigh was itself subsiding and the Cambrian fluvial system was not affected by the uplift, as proved by the constant palaeocurrent directions measured in the Cambrian fluvial channels. The Ordovician succession progressively pinched out from north to south on the western region of the high, below Upper Devonian sediments, but it is still difficult to differentiate the effects of the Taconic unconformity from Late Ordovician glacial incision and from the ones due to the local uplift.

During Lower Silurian times, the palaeohigh formed a discrete positive relief on the seafloor, which was onlapped by the basal hot shale layers. Afterwards, the palaeohigh probably remained inactive during most of the Silurian times and was covered by the Silurian succession (Fig. 4).

The major phase of uplift occurred during the Upper Silurian and Lower Devonian associated with the Caledonian unconformity. Above the high, the Upper Silurian succession was completely eroded. The thinning of the Tadrart Formation from the Ghadames Basin to the Gargaff Arch suggests a fluvial onlap configuration, and the lower part of the Devonian is probably missing in the outcrops. The Gargaff palaeohigh was emergent, and was the site of a fluvial by-pass during the Lower Devonian (Lochkovian). During the Middle and Upper Devonian, the high continually grew. Palaeocurrent orientations measured on both flanks of the high show a divergence of the palaeocurrent orientations (Rubino & Blanpied 2000), suggesting that the palaeohigh was eroded and supplied sediments both northwards and southwards.

The Hercynian orogen probably modified the shape of the arch, and the present-day Gargaff Arch was also exhumed during the Alpine compression (Underdown & Redfern 2008). The western

Fig. 6. Incised valleys observed in the Upper Devonian, Awanat Wanin I formation, Wadi Shati area, Gargaff region. Car for scale.

part of the arch is now outcropping in the Gargaff area, while the eastern part is still buried in the subsurface separating the Murzuq and Ghadames basins. According to Hallett (2002), the highest part of the arch during the Cambro-Ordovician is now located in the subsurface between the Murzuk and the Ghadames basins. The arch has continued to influence sedimentation until the present day.

Ahara High, Illizi and Berkine basins, Algeria

Stratigraphic architecture. The Ahara High is a broad east–west anticline separating the Illizi Basin from the Berkine Basin during the Cambrian up to the Upper Devonian (Figs 7–9). The palaeohigh can be seen in the subsurface only, as it is buried under a thick series of Carboniferous and Mesozoic sediments. The structure plunges westwards and is offset by the major north–south Ramade fault complex bounding the El-Biod High. Above the El Biod High, strong uplift occurred during the Hercynian event, Cretaceous Austrian compression and Cenozoic Alpine compression, resulting in the partial erosion of the Palaeozoic succession. Eastwards, the high merges in a complex manner with the Tihemboka north–south structure. During the Mesozoic, subsidence increased in the Berkine Basin, inducing a general tilting of the Ahara High northwards (Chaouche 1992).

The pinchout of the Cambro-Ordovician succession across the palaeohigh can be seen in seismic section (Fig. 10) and in the stratigraphic correlation (Fig. 7). The thickness of the Cambro-Ordovician is still unknown in the centre of the Berkine Basin, where the succession is deeply buried. The Cambro-Ordovician sandstones onlapped a high located further eastwards than its present day position; a broad north–south trough (the Marfag trough) connected the Illizi and Berkine basins westwards at that time (Fig. 11a). The Ordovician succession in the Berkine Basin shows a series of progressive unconformities which were better expressed when approaching the palaeohigh. Hence, the 'Quartzite de Hamra' Formation successively overlies the units below (El Atchane Sandstones and El Gassi Shales), and was in turn eroded and overlain by the Ouargla Sandstones. Finally, above the palaeohigh, only a thin section of Upper Ordovician sediment, including glacial deposits (Unit IV in Algeria), was preserved below the Silurian shales. Cambrian and Lower Ordovician sediments thickened again southwards into the Illizi Basin. These successive erosions suggest that the palaeohigh was progressively growing during most of the Lower Ordovician times.

The basal Silurian succession (Argiles à Graptolithes) was deposited across the palaeohigh. However, detailed stratigraphic correlation provides evidence for an onlap of the basal Llandovery hot shales over the palaeohigh, arguing for palaeorelief at the time of the Silurian transgression. Above, the successive shoreface and tidal sequences of the Silurian prograded from south to north across the high without showing any facies or thickness change. The upper parts of the Silurian (Pridoli stage) are missing above the Ahara High, eroded below the Caledonian unconformity. The fluvial units of the lower Devonian also completely pinched out on both sides of the palaeohigh (Fig. 9). The Gedinnian unit, which is 300 m thick in the Berkine Basin first thins then pinches out both in relation with a basal fluvial onlap and with the subsequent erosion of the overlying units.

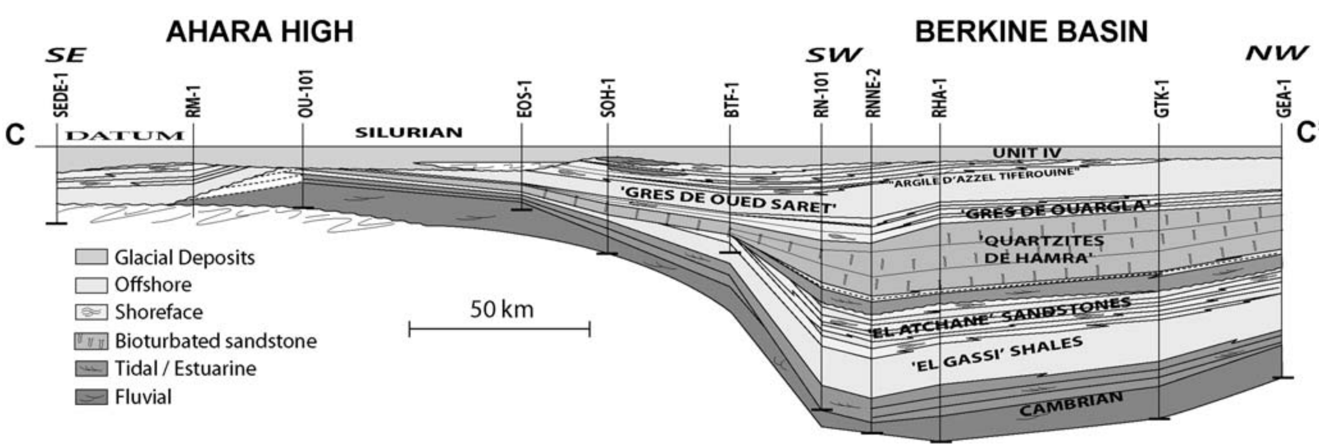

Fig. 7. Cross-section between in the Berkine Basin and the Ahara High, showing the stratigraphic pinchout of the Cambro-Ordovician succession on the northern flank of the Ahara High. The section is flattened on the Silurian flooding. Location map on Figure 1.

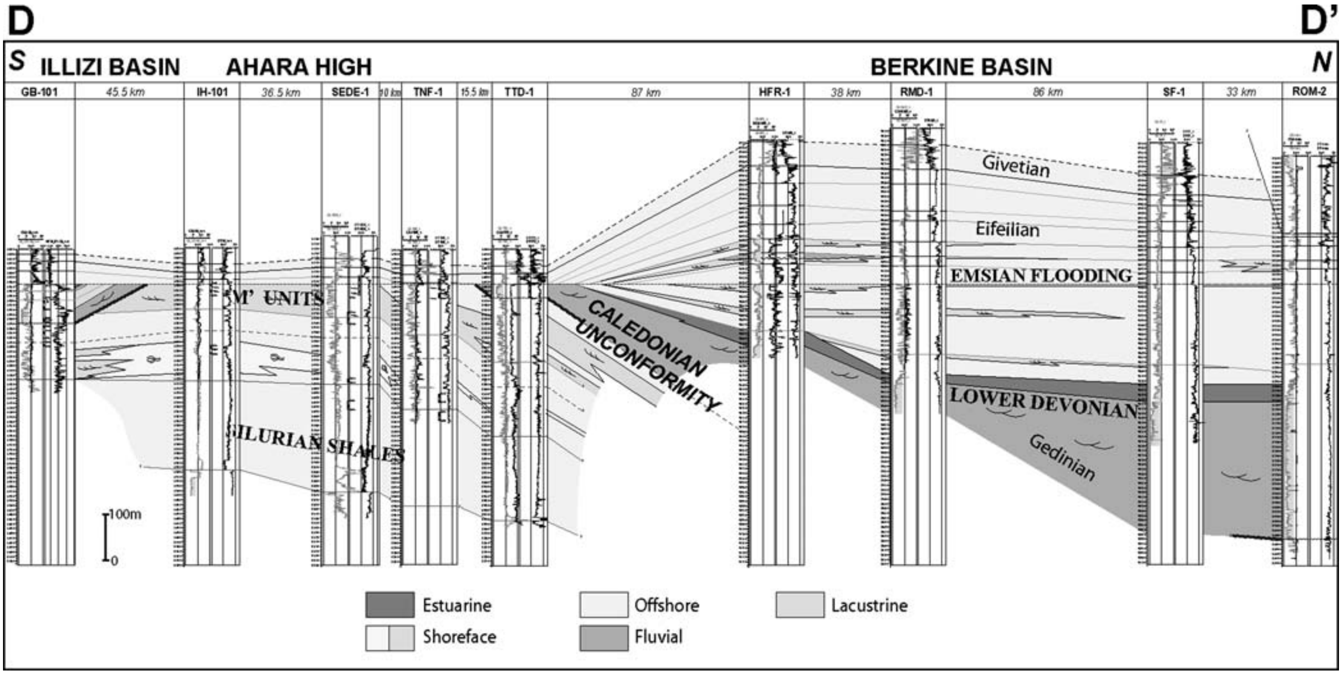

Fig. 8. Correlation of the Devonian succession on the northern flank of the Ahara High. The section is flattened on the Emsian flooding surface. Location map on Figure 1. Observe the complete pinchout of the Gedinnian fluvial unit on the flank of the high.

During Middle and Upper Devonian times, major facies and thickness variations occurred around the Ahara High. Emsian, Eifelian and Givetian sediments were onlapping on both eastern and western flanks of the palaeohigh, and sandy facies belts of shoreface and deltaic sediments extend in the southern part of the Berkine Basin (Fig. 8). In this area, the units successively pinched out southwards when onlapping the high, and passed to distal shaly facies towards the centre of the Berkine Basin. The sandstone units often show incised valleys and sharp-based shoreface sequences on logs. Finally, Upper Frasnian shales sealed the palaeohigh directly overlying the Upper Silurian sediments above the axis of the Ahara High.

Interpretation. The shape of the Ahara High has changed during the Lower Palaeozoic and the uplift rate was not constant. From Cambrian to Middle Ordovician, the uplift of the high was limited to its eastern end, and at that time (Fig. 11a), a south–north trough connected the Illizi Basin with the Berkine Basin between the El Biod and the Ahara Highs. The sediments onlapped the margin of the palaeohigh, forming wedges with a complex architecture as the constant uplift modified the available accommodation space.

The Silurian was a period during which the growth of the Ahara uplift almost completely stopped. The Silurian transgression occurred over a smoothed positive residual relief, influencing the deposition of the Lower Silurian hot shales in the lows while condensation occurred above the highs. The progradation of the Upper Silurian shorefaces and deltas was not affected at all by the high and, at that time, the Illizi Basin opened to the Berkine Basin. The uplift was reactivated during the Caledonian event, with the formation of an angular unconformity between the Upper Silurian and the Lower Devonian. The palaeohigh formed a positive relief separating the Illizi Basin from the Berkine Basin. In the Berkine Basin, an east–west trough was formed and rapidly subsided (Fig. 11b) in which a thick sedimentary succession accumulated. In contrast, the Illizi Basin formed a slowly subsiding sag. In

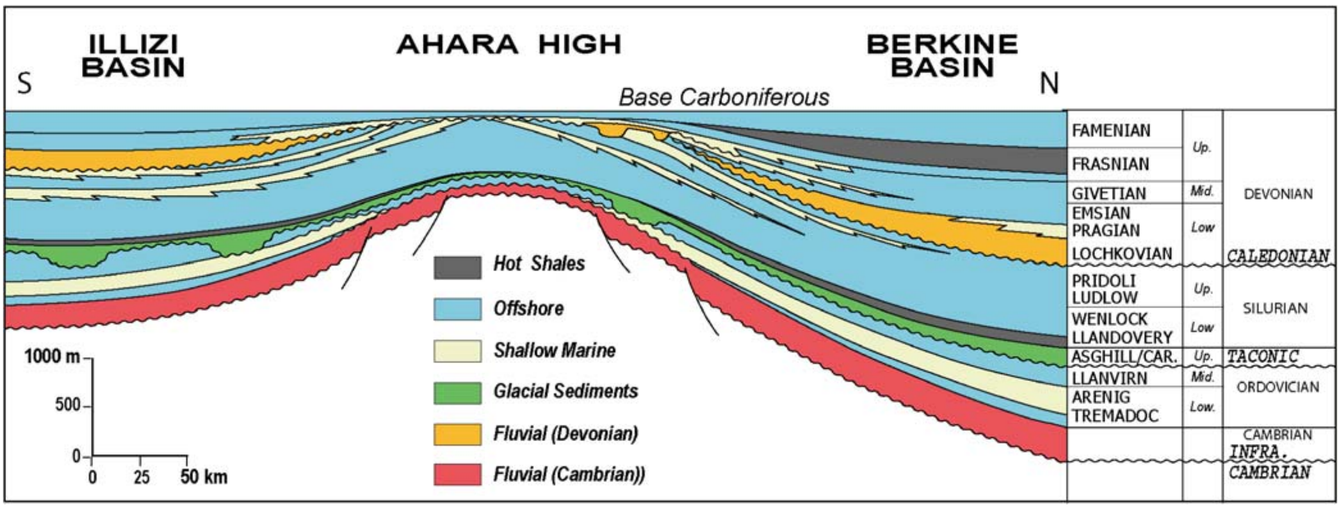

Fig. 9. Synthetic cross-section between the Illizi and Berkine basins, showing the complex stratigraphic architecture of the series around the Ahara High.

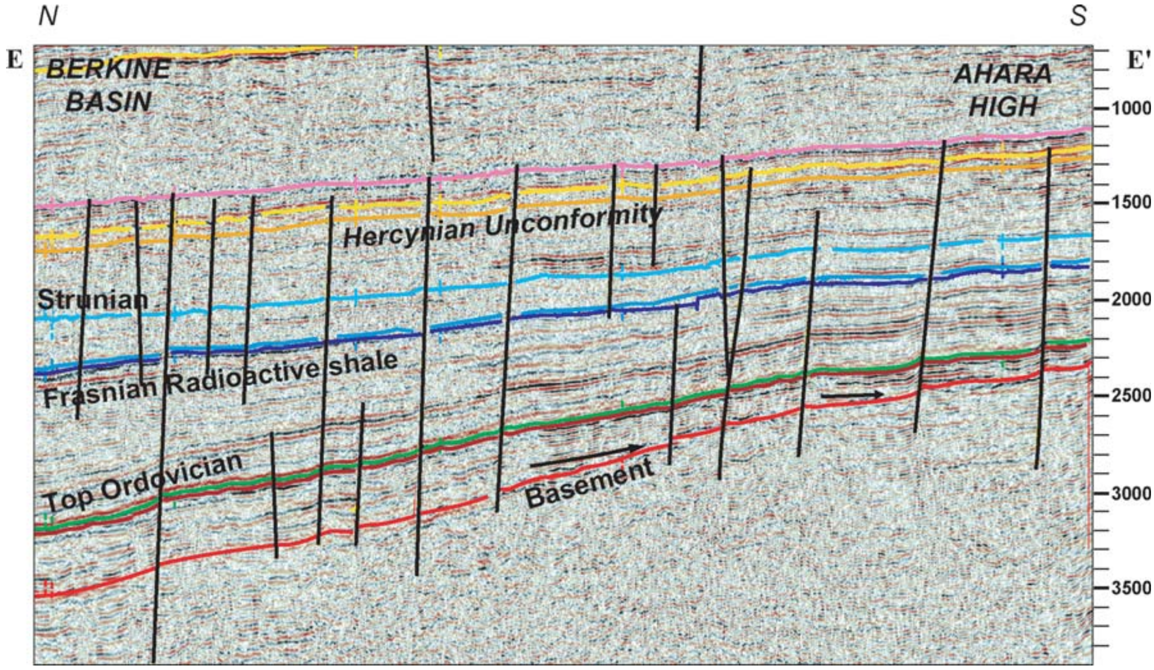

Fig. 10. Seismic section on the southern flank of the Berkine Basin illustrating the onlap configuration of the Cambro-Ordovician, and the thickness reduction of the Silurian and Devonian succession.

between, the Ahara High was the site of uplift and erosion and intermittently supplied the two basins with sediments.

The fluvial sediments of the Lower Devonian (Lochkovian and Lower Pragian) completely pinched out on the flanks of the Ahara High and the Illizi and Berkine basins were probably not connected at that time, except through narrow troughs on the eastern and western sides of the high. During Pragian, a transgression started in the Berkine Basin, and the shallow marine sediments of the Siegenien succession were deposited, while lacustrine and fluvial sediments still aggraded in the Illizi Basin during the same period. The transgression continued with the Emsian flooding, and offshore sediments were deposited all over the area, forming a major reference horizon. A regression then followed and, at that time, the Ahara High was eroded, supplying sediments towards the Berkine Basin while the high continued to rise. Periods of erosion and marine transgression then alternated during Middle and Upper Devonian times: the palaeohigh was periodically eroded during relative sea-level falls, while coastal onlaps occurred during relative sea-level rises. Forced regression wedges developed around the palaeohigh, especially in the southern part of the Berkine Basin, while less sediment arrived in the Illizi Basin, suggesting an asymmetry in the high topography (Fig. 9). Finally, the Frasnian offshore shales transgressed the palaeohigh when the uplift stopped. Frasnian shales then unconformably onlapped over the different terms of the eroded Devonian units.

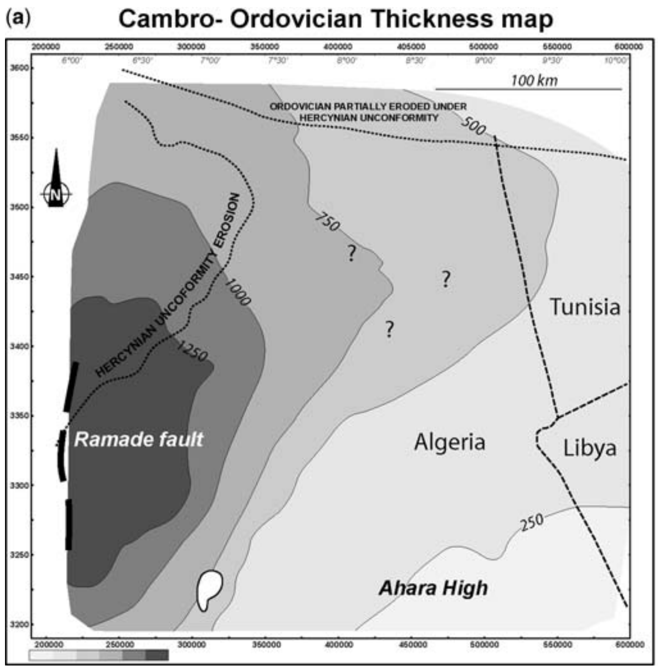

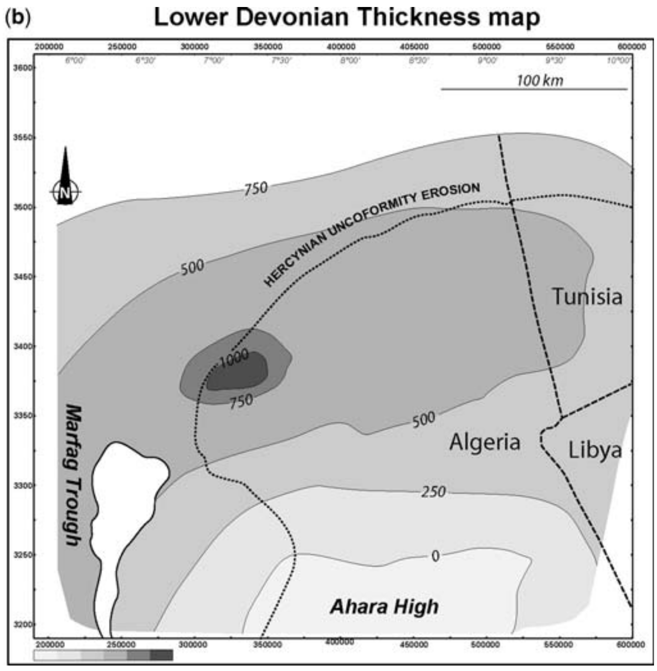

Fig. 11. (**a**) Isopach map of the Hamra Quartzite in the Bekine Basin; (**b**) Isopach map of the Lower Devonian in the Berkine Basin.

Tihemboka High, Illizi and Murzuq basins, Algeria and Libya

Stratigraphic architecture. The Tihemboka High is a major north–south structure straddling the Algerian–Libyan border. The structure extends southwards as a series of flexures and faults. Northwards, the axis of the high plunges in the subsurface of the Berkine and Ghadames basins. The Tihemboka structure may turn eastwards and possibly connect to the Gargaff Arch in Libya. The Tihemboka Arch also merges to the Ahara Arch in a complex manner.

The geometry of the Devonian stratigraphic wedges around the high was first described by Beuf *et al.* (1971) and we detail here its stratigraphic architecture by new field data and subsurface correlations in the Illizi Basin. According to the surface geology (Beuf *et al.* 1971), the Cambrian succession does not show any significant thickness variation nor palaeocurrent variation across the high in the Djanet/Ghat area. However, a stratigraphic wedge of the Cambrian and Lower Ordovician units can be observed in the subsurface in the Illizi Basin when approaching the palaeohigh from the west (Fig. 13a). The unit III-3 (Middle Ordovician) directly overlies the Precambrian in the vicinity of the Algerian–Libyan border. The Upper Ordovician glacial related valleys (Unit IV) then eroded the units below, almost reaching the Precambrian basement. Normal faults sealed by the glacial valleys may also contribute to the thickness variations of the Cambro-Ordovician units. A similar truncation of the Upper Ordovician can also be observed in the outcrops of the Djanet area in Algeria, where the Unit IV directly eroded the Cambrian sandstone (Beuf *et al.* 1971).

The Siluro-Devonian stratigraphic architecture of the Tihemboka western flank was studied in detail from outcrop and subsurface data, whereas the interpretation of the eastern flank is based on published data and map observations (Fig. 13). The high formed a broad and smooth anticline; no syn-sedimentary faults are observed in the western flank outcrops. The Lower Silurian shales (Llandovery) can be observed in outcrops and correlate on the flanks of the high without showing any significant variations (Fig. 13b). In the subsurface, the basal radioactive hot shale layers are continuous in the wells and do not onlap the palaeohigh. In contrast, the upper part of the Silurian succession was severely eroded above the palaeohigh. According to Massa (1988), the erosion reached the Middle Llandovery level (Lower Silurian) in the high Libyan flank. The upper units of the Silurian succession were progressively eroded below the Caledonian unconformity when approaching the palaeohigh, forming a low-angle regional unconformity.

The Lower Devonian succession partly pinches out over the high axis, as shown in the geological maps (Fig. 12) and well cross-sections (Fig. 13b). In the Tassili outcrops and in the Illizi Basin, the Lower Devonian succession consists of two sand-rich fluvial units separated by a fluvio-lacustrine one (see reference section in Eschard *et al.* 2005). The units progressively merged when approaching the palaeohigh, the upper one progressively truncating the lower ones, forming a progressive unconformity. In outcrops, the fluvial systems do not show any major lateral facies changes nor significant palaeocurrent rotations, even close to the high axis.

Middle and Upper Devonian units also progressively onlapped the palaeohigh. In the Emsian and Givetian sandy units, lateral facies variations can be observed, with coarser and more proximal facies towards the axis of the palaeohigh while the units thin and fine towards the Illizi Basin. The Frasnian shales onlapped the structure. The Upper Devonian units were finally eroded beneath the Carboniferous ones along the axis of the palaeohigh. In the eastern flank of the Tihemboka High in Libya, Massa (1988) observed the Frasnian shales directly overlying the Lower Silurian (Llandovery).

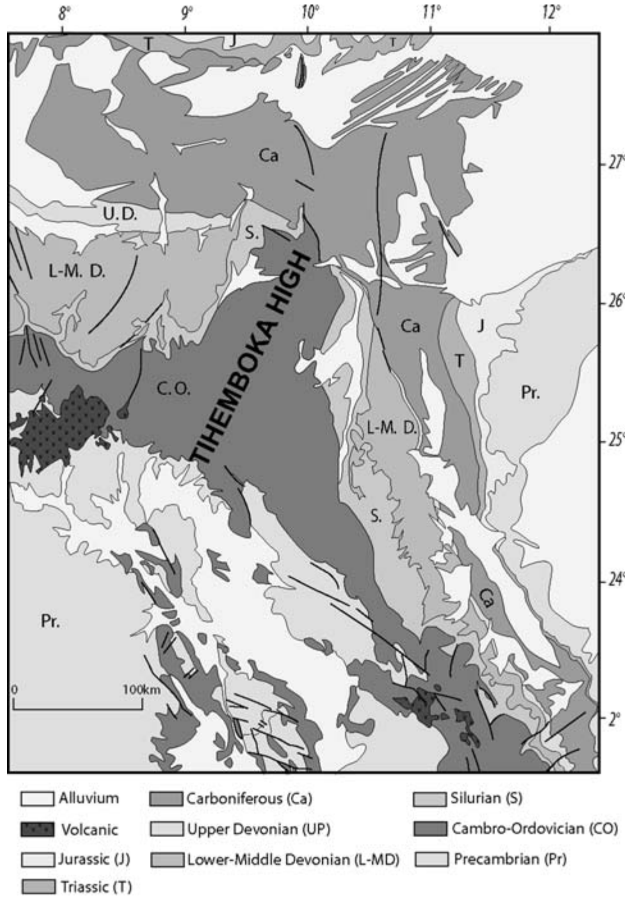

Fig. 12. Simplified geological map of the Tihemboka area.

Interpretation. The Tihemboka structure was inherited from a major north–south Pan-African fault system. The large flexure probably accommodated the motion of a deep crustal fault, forming the present-day broad anticline.

The Tihemboka area was uplifted during Cambro-Ordovician times. In the subsurface, the uplift was associated with a complex fault pattern probably forming a kind of horst which is still difficult to map precisely, as the faults were later reactivated during late compressive events. The structure continuously grew during Cambrian and Lower Ordovician times; the Cambrian units (unit II) and the lower Ordovician units (units III-3 and III-2) were progressively eroded below the Middle Ordovician units (unit III-3). The Upper Ordovician is missing because of the combined effects of the regional Taconic unconformity and of the erosion of the glacial valleys (unit IV).

The Silurian marked a period of quiescence of the palaeohigh; the Lower Silurian shales were deposited across the Upper Ordovician surface without any facies or thickness changes. Similarly, the palaeohigh did not affect the Upper Silurian shoreface progradation. Erosion resumed during Caledonian unconformity. The entire Upper Silurian shoreface succession was eroded above the high, which continued to grow almost continuously during the Devonian, forming a complex progressive unconformity. Lower Devonian fluvial units show erosive unconformities at their base while they progressively pinch out towards the axis of the palaeohigh. Each fluvial unit was first deposited on the Tihemboka High, before being eroded beneath the one above. This geometry suggests that the relative rise (i.e. the result of the tectonic uplift and of the eustasy) was not constant at that time, with base-levels falls interfering with the uplift, causing the fluvial re-incision.

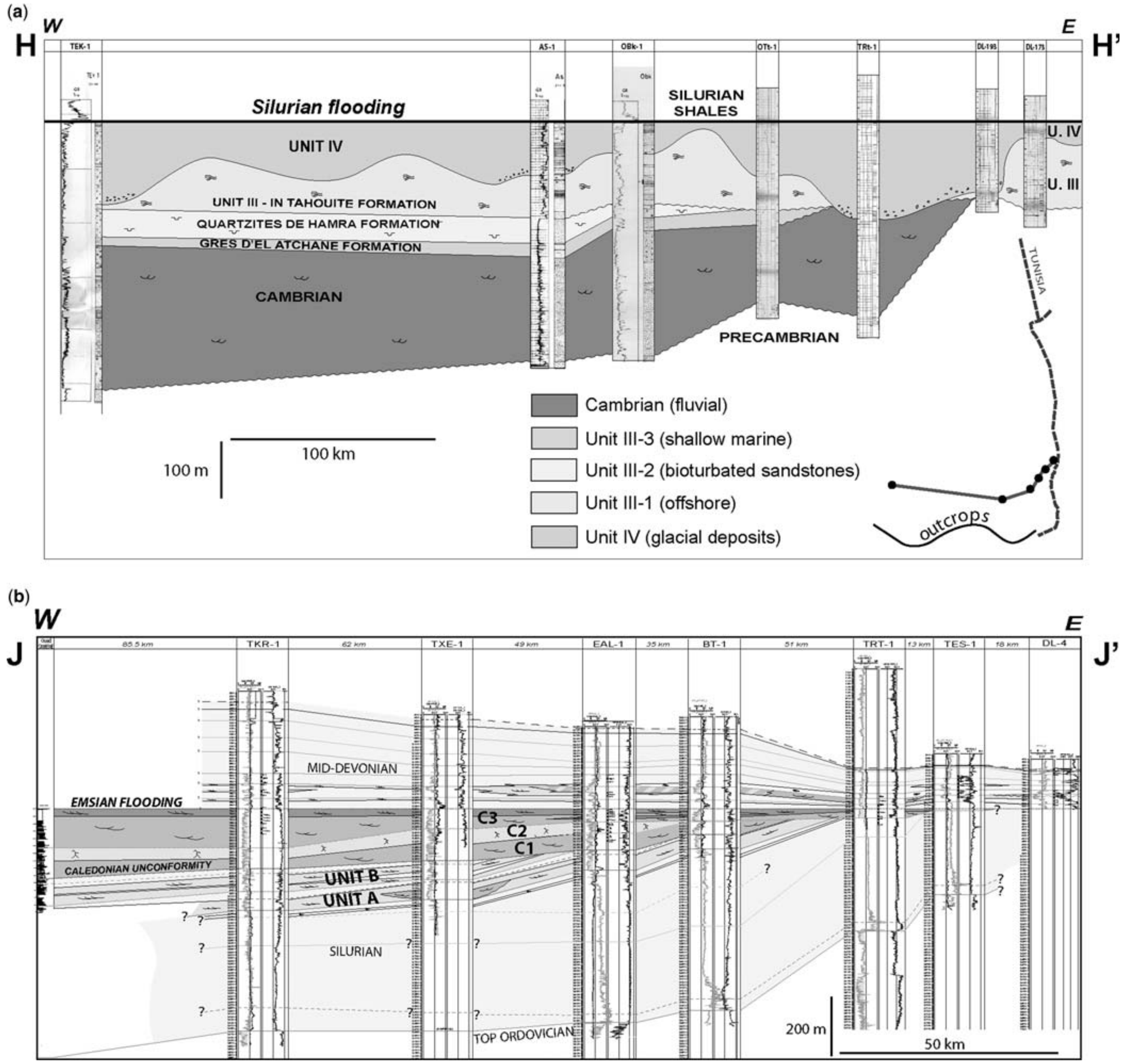

Fig. 13. East–west cross-section in the subsurface of the Illizi Basin, showing (**a**) the stratigraphic pinchout of the Cambrian and Lower Ordovician units. The section is flattened on the Silurian flooding. (**b**) The complex geometry of the Devonian stratigraphic wedge. The section was flattened on the Emsian flooding surface. Location map in Figure 1 and legend in Figure 8.

During the Upper Devonian, Emsian, Eifelian, Givetian and Frasnian shorefaces and tidal units successively onlapped the palaeohigh during transgressive events before being eroded during the following sea-level falls. At that time, the palaeohigh was eroded and supplied a clastic sediment belt around an emerged highland. Carboniferous sediments then definitively sealed the palaeohigh.

Djebel Tamamat in the Bled el Mass area

Stratigraphic architecture. The Bled el Mass area is a structurally complex zone within the Azzel Matti Ridge, a north–south high between the Ahnet and Reggane basins (Fig. 14). The Azzel Matti Ridge continues in the subsurface northwards and turns westward to connect to the Ougarta chain, finally continuing towards the Anti-Atlas area in Morocco. Southwards, the Azzel Matti Ridge can be mapped in the southern part of the Ahnet Basin. This complex structure was inherited from collision between the Reguibat and Hoggar shields during the Pan-African orogeny (Bertrand & Caby 1978). The collision implied north–south crustal transpressional faults with hundreds of kilometre offsets. From Cambrian to Devonian, a trough formed the Ougarta and Anti-Atlas areas in which accumulated a very thick stratigraphic succession (Ghienne *et al.* 2007*a*, *b*). In the Bled el Mass outcrops, the north–south folds (Fig. 14) at present day were formed during the Hercynian orogen, and reactivated latterly, probably during the Mid-Cretaceous Austrian event as interpreted from palaeomagnetic measurements (Haddoum *et al.* 2001; Zazoun 2001; Smith *et al.* 2006).

The studied outcrops are just a small part of the Azzel Matti and Bled El Mass ridge, as seen in the structural section in Figure 14. The outcrops of the Djebel Tamamat (Fig. 14) were recently studied, an area where Beuf *et al.* (1968) first identified a stratigraphic pinchout of the Cambro-Ordovician succession over a basement high. The north–south section shown in Figure 15 was

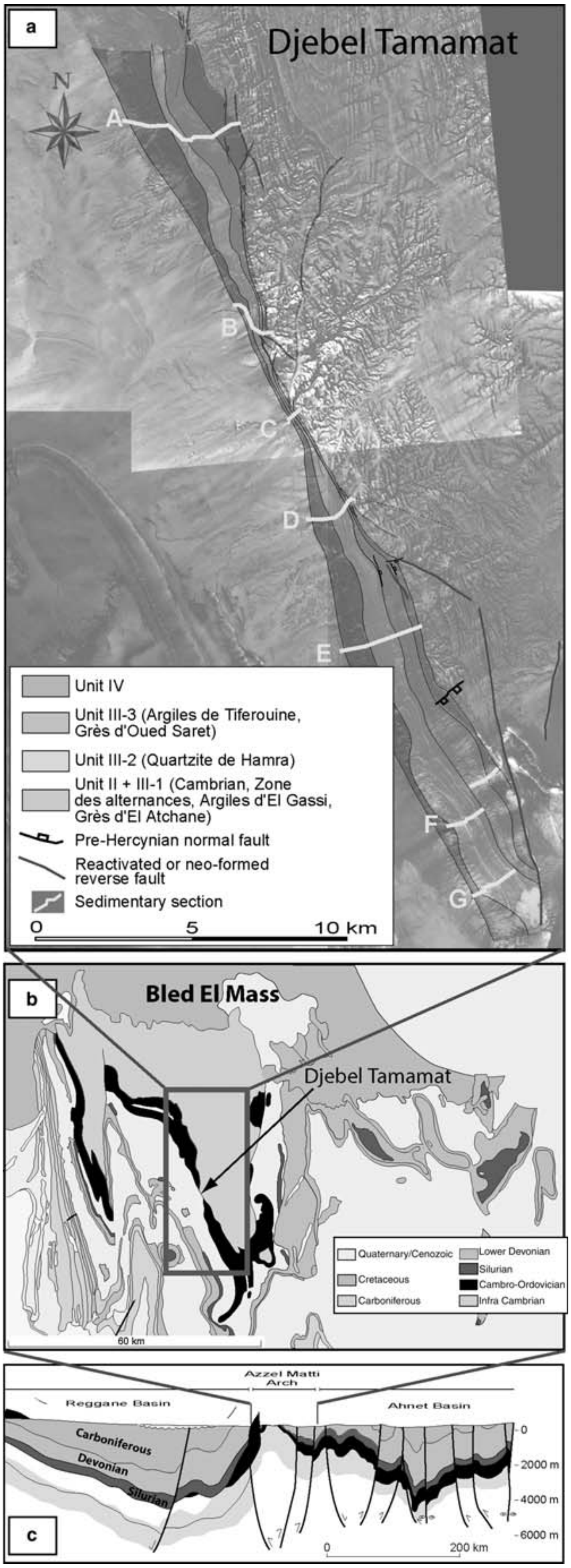

Fig. 14. (**a**) Photo-interpretation of the Djebel Tamamat area showing the wedge geometry. (**b**) Simplified geological map of the Djebal Tamamat area, showing the onlaps of the Lower Palaeozoic succession over the 'serie Pourprée'. (**c**) Section across the Reggane Basin, Azzel Matti Ridge and the Ahnet Basin (modified from Craig *et al.* 2006).

made along the western flank of a north–south fold. The contact between the Infra-Cambrian meta-sediments of the 'Serie Pourprée' and the Cambrian sandstones was also locally offset by a reverse fault. The wedge geometry observed in the map (Fig. 14a) then results from both stratigraphic pinchout and reverse faults effect.

The Cambrian succession consists of coarse-grained fluvial sandstones which onlap a basement palaeohigh on both flanks and completely pinch out over the high. The palaeohigh formed a horst, with normal syn-sedimentary faults and tilted blocks on both sides (Fig. 15). Normal syn-sedimentary faults were sealed by the Lower Ordovician marine siltstones and shales (El Gassi Formation), which in turn onlap then pinch out over the high. Above, Lower and Middle Ordovician sediments consist of bioturbated sandstone units alternating with marine shales and siltstones (Grès d'El Atchane, Quartzites de Hamra, Argiles de Tiferouine and Grès de Oued Saret Formations). The succession significantly thins when approaching the palaeohigh, where progressive angular unconformities can be observed. Facies changes occur across the high (Fig. 15). The Quartzites de Hamra unit, which usually consists of fine-grained bioturbated sandstones, shows a transition to coarse-grained levels and gravel lags with quartzite pebbles and fragments of Precambrian schist when approaching the basement high. The material was obviously eroded from the Infra-Cambrian 'Série Pourprée', testifying that the palaeohigh was exposed during the Hamra time. Another angular unconformity overlain by conglomerates was observed at the base of the 'Argiles de Tiferouine' unit.

Ashgill aged glacial valleys can be observed flanking the palaeohigh, suggesting that the topography also influenced the glacial valley location. However, these glacial sediments sealed the palaeohigh and, just above, the Silurian shales were also deposited across the palaeohigh. The Devonian succession also regionally thins out above the high, at the scale of the Azzel Matti Ridge.

Interpretation. The 3D geometry of the palaeohigh is difficult to reconstruct only from the 2D outcrop section and map, the eastern flank of the present-day fold being also affected by a major fault. The palaeohigh probably had a NNE–SSW axis and a width of around 10 km. However, the entire Bled el Mass area was above a major mobile zone, and we observe in the outcrops only a small portion of a much larger high, the Azzel Matti Ridge.

During Cambrian times, the palaeohigh formed a horst bounded by normal faults, Cambrian fluvial sandstones being progressively eroded during the uplift as they were deposited. The palaeohigh was then flooded by a shallow sea during the Lower Ordovician. During most of the Ordovician, the palaeohigh continuously grew, as documented by progressive unconformities and the facies changes. The palaeohigh was alternatively drowned and exposed according to the sea-level variations. During the deposition of the Quartzite de Hamra Formation, the palaeohigh was sub-aerially exposed, and the products of the erosion were reworked downflank in the shoreface and tidal deposits. Then, the high was flooded while it continued to rise, marine sediments of the Argiles de Tiferouine thinning over the relief.

The activity of the high ceased before the deposition of the Late Ashgill glacial sediments. However, the Upper Ordovician sediments are missing in the area, probably due to the erosion of the Upper Ordovician Taconic unconformity, as suggested by the complex thickness variations observed at a regional scale at this level in the subsurface of the Ahnet Basin.

Silurian sediments finally sealed the high, which was inactive at that time. At the scale of the Azzel Matti Ridge, thickness variations can be observed in the Lower Devonian sections when comparing the Reggane, Bled el Mass and Ahnet areas, suggesting that the entire Bled El mass area was a still a mobile zone during the

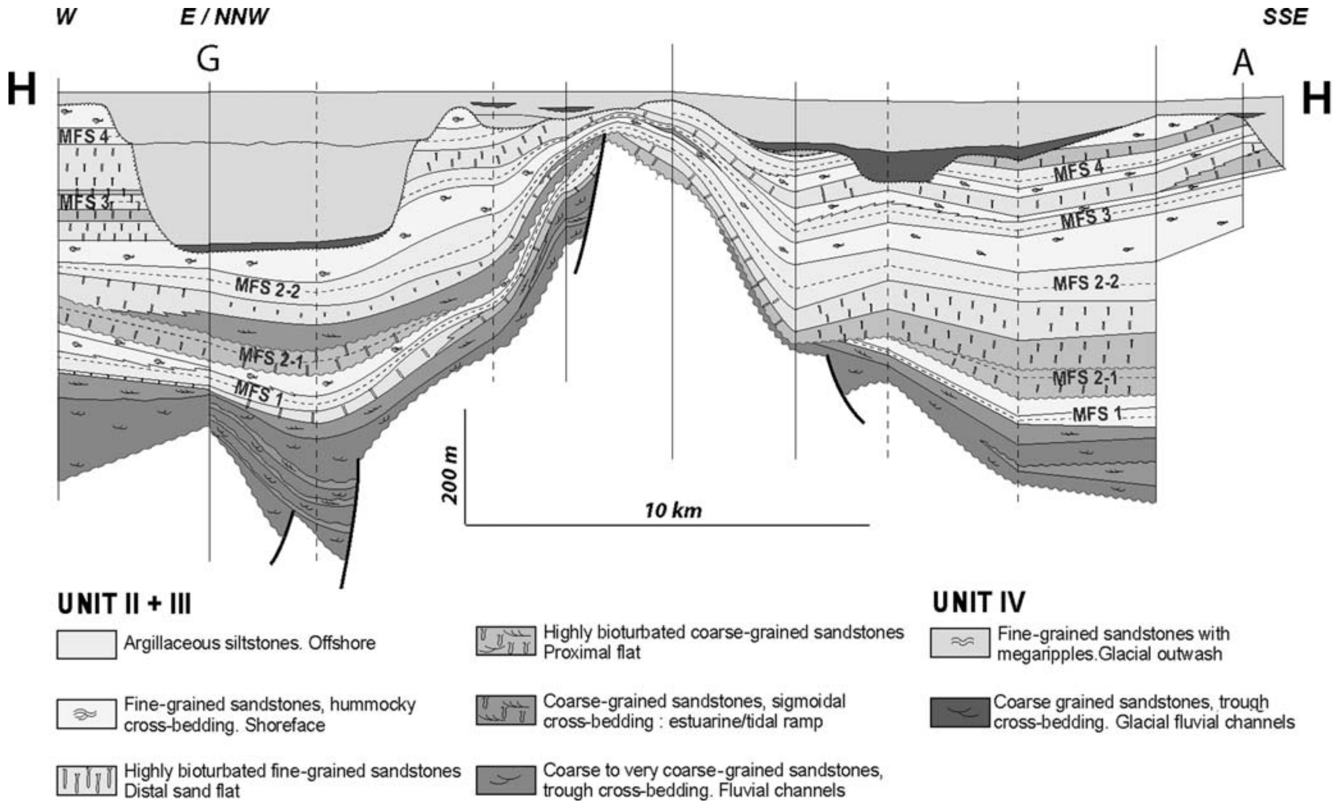

Fig. 15. Outcrop north–south cross-section illustrating the stratigraphic architecture of the Lower Palaeozoic succession apart from the high.

Devonian. The movements significantly increased during the Upper Devonian times, as proved by the major thickness variations of these series in the Ahnet Basin (Wendt *et al.* 2005).

Synthesis: tectonostratigraphic evolution

Structural style: the Pan-African heritage

The palaeohighs studied here were linked to the reactivation of major crustal structures. They are located at the boundary between different terranes and rigid shields accreted during the Pan-African orogeny to form the Gondwana supercontinent (Bertrand & Caby 1978). The north–south lineaments were formed during the oblique collision between the West African shield and the Hoggar shield, and were associated with major strike-slip movements (Black *et al.* 1979; Craig *et al.* 2006). The Bled el Mass/Azzel Matti Ridge was located close to the suture zone, between the Reguibat and the Hoggar shields. The Tihemboka High, the Idjerane/Arak/Foum–Belrem Ridge, the Amguid/El Biod/Hassi-Messaoud High and the Bin Ghanimah Highs (Fig. 1) are also linked to a north–south crustal fault. The crustal lineaments were then occasionally reactivated depending on the stress regime orientation and the geodynamic events which succeeded through time such as the Hercynian compression, and the Mid-Cretaceous Austrian and Cenozoic Alpine compressions. Other highs present a global east–west orientation, such as the Ahara High, the Gargaff Arch and the Talemzane–Dahar High. These structural features are more difficult to understand in the context of the Gondwana accretion.

The studied palaeohighs always present the same overall geometry: they form broad anticlines, tens of kilometres wide, with a maximum of 15° of structural dip on their flanks. The Tamamat High is apparently smaller, but outcrops are only a part of the much wider Azzel Matti Ridge.

The structural style of the palaeohighs also evolved through time (Fig. 16). During Cambro-Ordovician times, the deformation had a brittle behaviour. Several normal faults with a limited vertical throw, tilted block and half-grabens were observed along the flank of the Tamamat (Bled El Mass). In contrast, during Silurian and Devonian times, the palaeohigh formed large anticlines without any faults on their flanks. The thick Silurian shales layer then probably decoupled the deformation. The palaeohighs also recorded the change from an extensional structural style during Cambro-Ordovician to a compressive style during the Devonian. The shapes of the palaeohigh themselves changed through time, as illustrated by the geometry evolution of the Ahara High and of the surrounding basins between Cambrian and Devonian (Fig. 11).

Timing of the uplifts

The stratigraphic architecture of the series around the palaeohigh registered the different uplift phases, making possible a comparison of the uplift timing (Fig. 17). During Cambrian and Lower Ordovician times, the uplift activity of the palaeohighs varied depending on their location. The Tamamat High in the Bled el Mass area (part of the Azzel Matti Ridge), the Ahara High and the Tihemboka High grew almost continuously at that time, such as other ridges like the Foum Belrem–Arak Ridge (Fig. 1; Beuf *et al.* 1971). In contrast, the uplift activity of the Gargaff Arch was more limited; Cambrian and Ordovician sediments could have covered the palaeohigh before being eroded. Other prominent structures, such as the Amguid-El Biod High (Fig. 1), were not active at that time as proved by the development of the Cambro-Ordovician succession in the Hassi–Messaoud field (Boudjema 1987). The structure formed later during the Hercynian and Alpine compressions (Boudjema 1987). It is worth noting that an erosive event, the Intra-Arenig unconformity (Fig. 17), is also well registered in most of the highs.

Upper Ordovician times are complex to understand because the effects of the local uplift interfered with the Taconic unconformity, a major low-angle unconformity which occurred before the late Asghill glacial event. In many places around Algeria, the Upper Ordovician succession was not preserved and the exact nature of

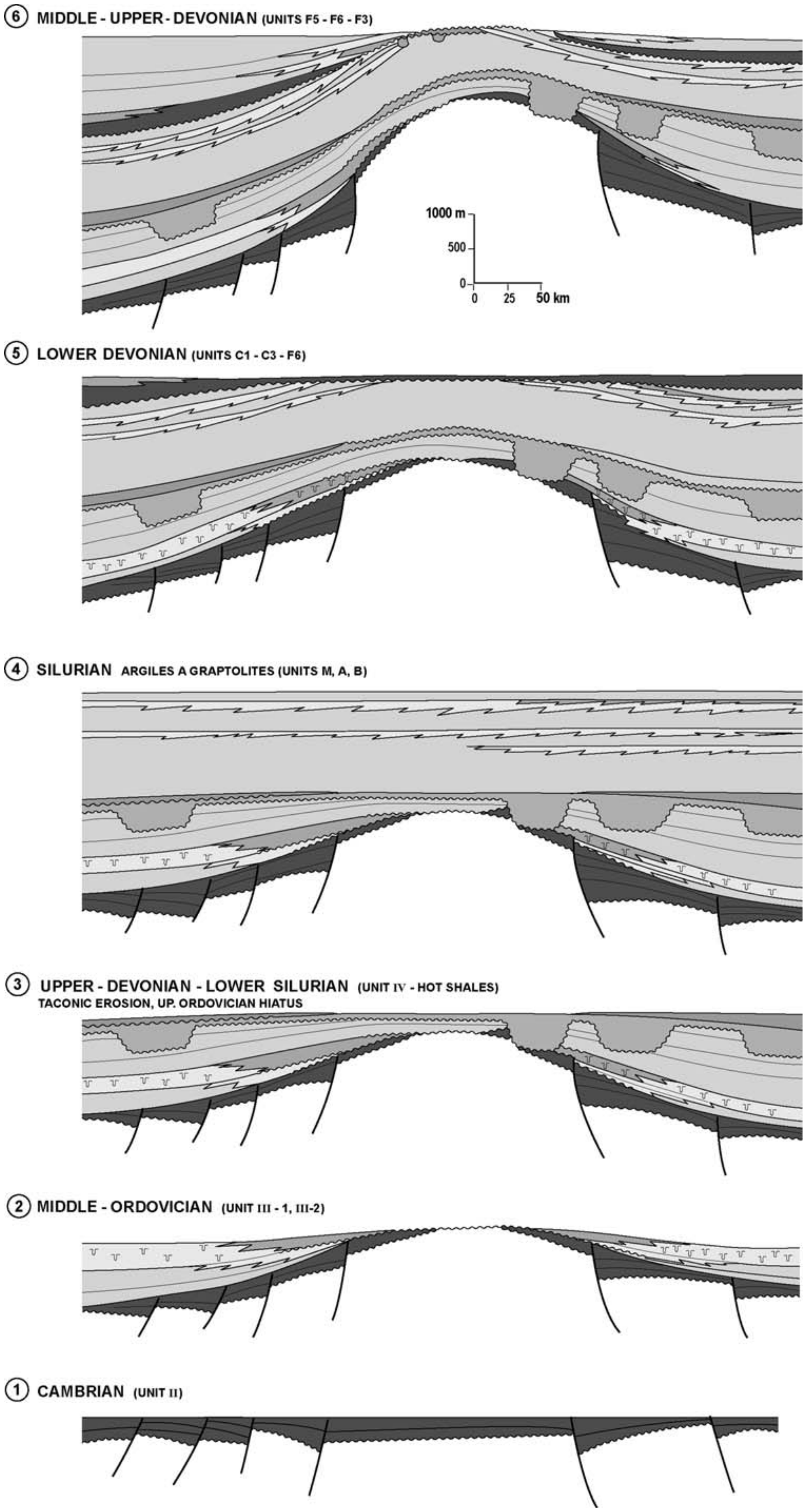

Fig. 16. Synthetic scheme showing the sedimentation associated with the deformation due to uprising palaeohigh during Palaeozoic times. Explanation in text.

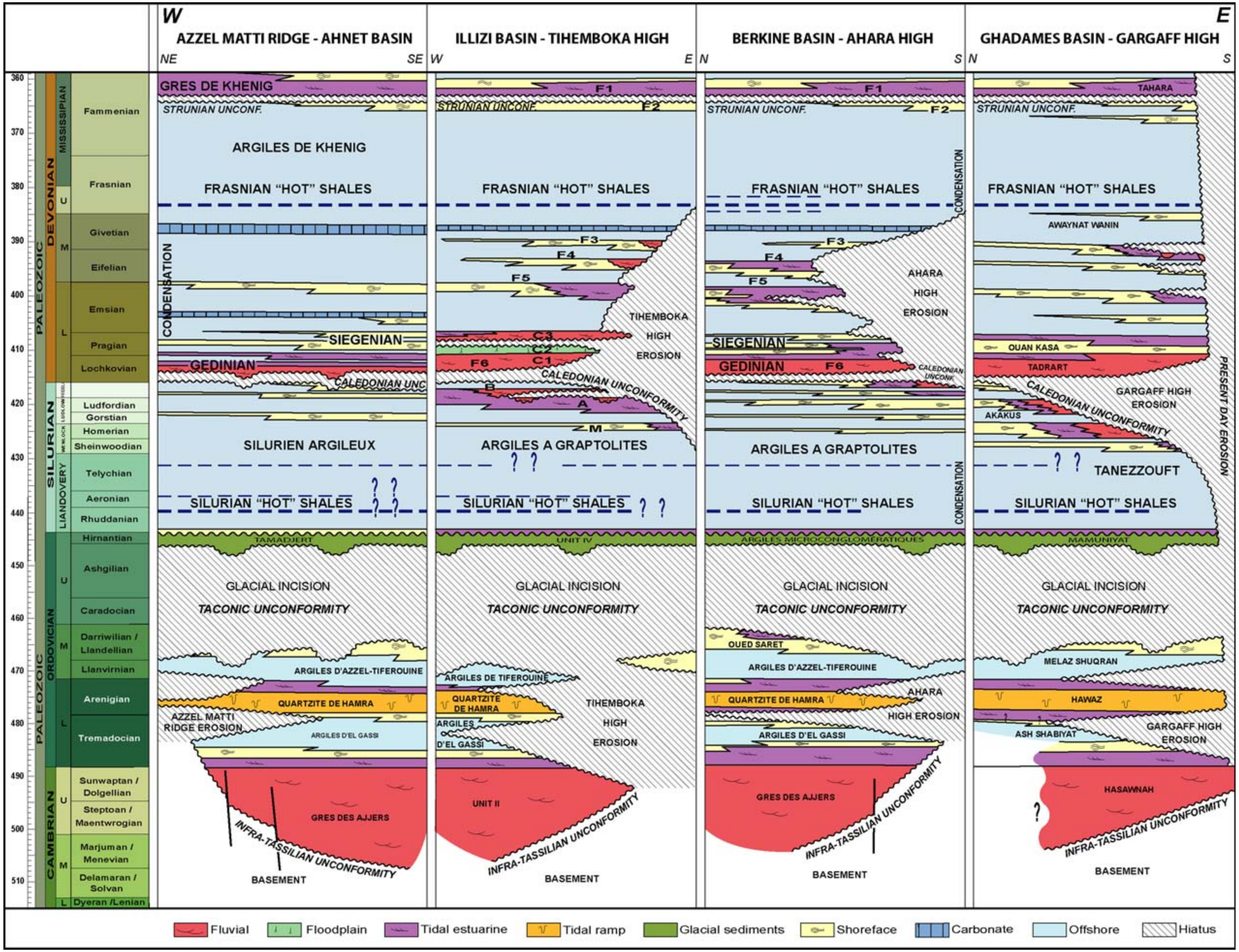

Fig. 17. Synthetic chronostratigraphic chart of the Azzel Matti Ridge–Ahnet Basin, Illzi Basin and Tihemboka Arch, Berkine Basin and Ahara High, and Ghadames Basin and Gargaff Arch. Note the very good correlation of most of the unconformities above the highs, suggesting that global eustatic variations interfered with the uplift.

the palaeohighs is poorly known for this period of time. During the Late Ordovician, the glacial pathway network itself was possibly controlled by the topography (Ghienne *et al*. 2007*a*, *b*; Le Heron & Craig 2007), but there is no direct evidence of tectonic activity during sedimentation except the glacio-tectonics effects. The glaciation period was probably too short (between 0.2 and 0.5 years; Brenchley *et al.* 1994; Sutcliffe *et al.* 2000) to register the effects of the long-term tectonic subsidence.

Silurian times were characterized by the stability of all palaeohighs, which were passively flooded during the Lower Silurian transgression. At that time, a residual topography remained, and was onlapped by the basal part of the transgressive Silurian shales. The Middle and Upper Silurian progradational sequences were deposited without being influenced by the palaeohigh topography.

Lower Devonian times were marked by a rejuvenation of most of the palaeohighs during the Caledonian event. As a result, the Upper Silurian succession was dramatically eroded over the Gargaff and Tihemboka arches and to a lesser extent, over the Ahara Arch. During Devonian times, significant structural growth occurred in most of the palaeohighs, with the noticeable exception of the Gargaff Arch that only slowly grew. Upper Frasnian shales generally sealed the palaeohighs, as seen over the Ahara, Gargaff and Tihemboka Highs. Frasnian shales can be then seen directly onlapping different elements of the Palaeozoic succession below. The deformation also increased significantly during Upper Devonian, especially in the western part of Algeria (Wendt *et al.* 2005). Compressive deformation increased again during the Carboniferous, inducing a migration of the depocentres: the Ahara High started to subside and the Tihemboka High was sealed by the Carboniferous sediments.

Controlling factors of the stratigraphic architecture around the palaeohighs

The palaeohighs were alternatively flooded or emerged depending on the eustatic sea-level variations, the uplift rates and the global deformation affecting the craton. The wedge geometry can then be rather complex when local progressive unconformities interfered with more global regional unconformities. This is especially the case for the Upper Ordovician Taconic unconformity or the Caledonian unconformity at the Silurian–Devonian boundary. These events were manifest as large flexures at the scale of the craton, inducing regional tilts and large amplitude folding. They were subjected to erosion or non-deposition of the Upper Ordovician and Upper Silurian successions, respectively. The resulting regional low-angle unconformities were then superimposed on local ones around the palaeohighs. Interpretation of the Taconic unconformity is further complicated by the Ashgill glacial valleys.

The third-order sequence architecture was controlled by the interaction between the uplift rate and the eustatic sea-level variations (Fig. 18). During transgression (or base level rise for the fluvial units), sediments were deposited above the highs, which continued slowly to rise. They were then eroded during the subsequent relative sea-level fall, inducing the creation of a network of incised valleys and forced regression wedges of shoreface and tidal sediments around the palaeohighs. The alternation of relative sea-level rise and falls explains the peculiar shape of the unconformities above the palaeohighs, which were continuously rising during some periods.

The sequence organization between the different highs is remarkably similar. This suggests that the main controlling factor of third-order sequences was related to the eustatic variations, the

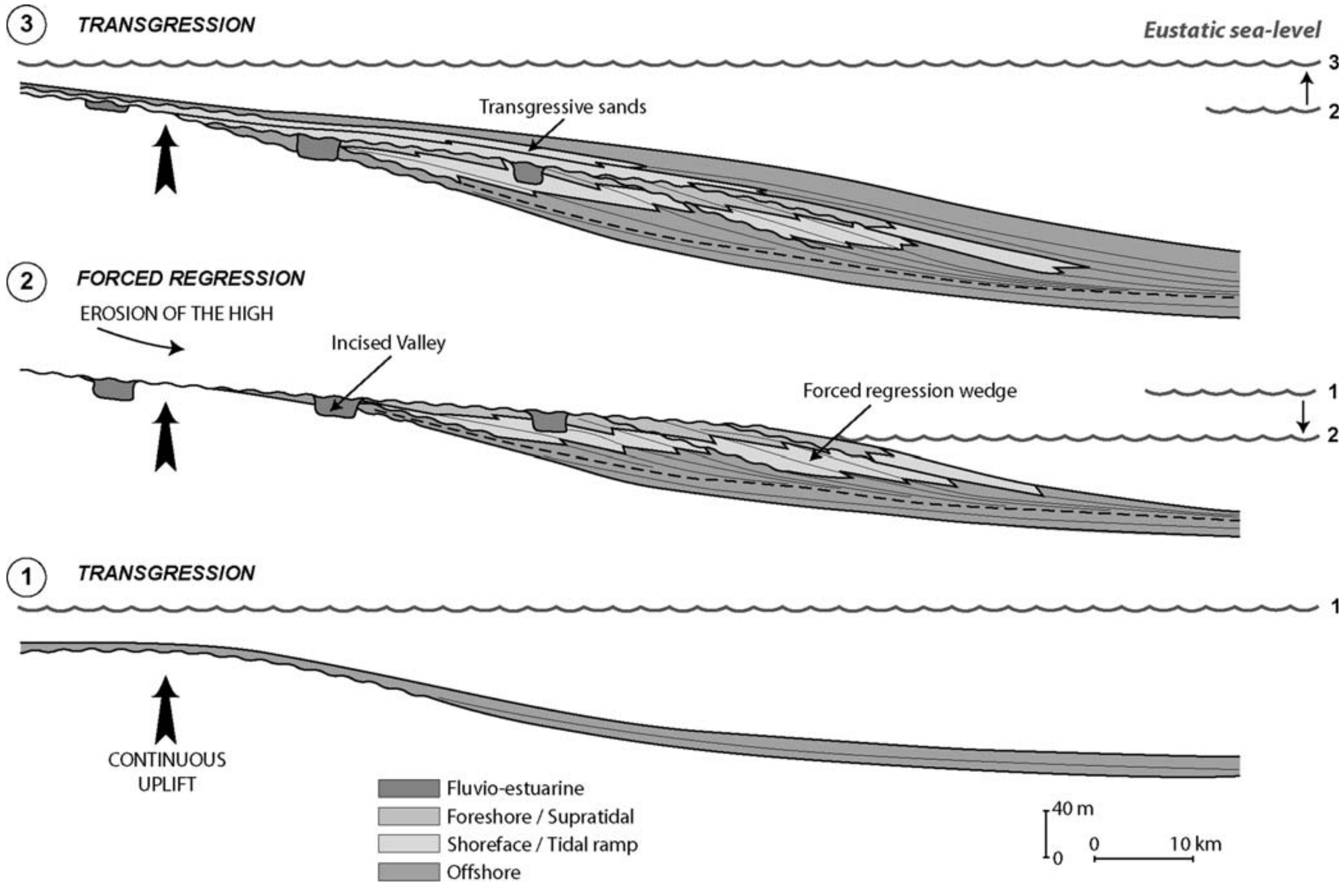

Fig. 18. Model of Devonian stratigraphic wedge developed around a high continuously rising while eustatic sea-level varied. 1, Transgression and coastal onlap during relative sea-level rise. 2, Erosion above the high during relative sea-level drop, creation of incised valley network and deposition of a forced regression wedge in the basin. 3, New transgression. Such cycles repeated several times during the Devonian.

relative sea-level changes being amplified above the highs which slowly rose during the Devonian. In such a cratonic context, the uplift rate of the highs is expected to be slow and constant. The Palaeozoic eustatic charts (Haq & Schutter 2008) show that the eustatic variations during the Devonian were relatively limited in amplitude, but sufficient to create the emersion of the palaeohighs during the eustatic sea-level falls.

Petroleum system implications

Source rock deposition

The growth of the palaeohighs had some major implications for the petroleum systems evolution. The Lower Silurian 'hot' shale layers, which constitute the oldest significant source-rock, were influenced by the topography of the Silurian flooding surface (Lüning *et al.* 2000, 2003*a*). The basal hot shale layers often onlap the residual topography above the highs. Furthermore, facies changes are also observed laterally when approaching a high within the source rock levels. Lüning *et al.* (2000) proposed that anoxic conditions prevailed in the topographic lows during the Silurian transgression. Above the palaeohighs, the organic-rich shales were not deposited or not preserved because of the hydrodynamics in the shallower setting (Figs 4 & 9), favouring organic matter oxidation or its erosion by marine currents (Lüning *et al.* 2000).

Similarly, the Frasnian source rocks deposition was controlled by the differential subsidence in the sub-basins, with anoxic conditions being created in the lows where the source rock with the best quality was preserved (Lüning *et al.* 2003*b*). In the centre of the Berkine Basin, for example, 250 m of radioactive organic-hot, Frasnian shales were deposited, sourcing the Triassic reservoirs. On the flank of the Ahara High, the source-rock layer progressively thinned out southwards and less than 5 m of organic Frasnian shales were left above the Ahara High.

Stratigraphic architecture and potential tectonostratigraphic traps

The stratigraphic relationship developed on the flanks of the palaeohighs set up potential stratigraphic trapping configurations around the palaeohighs. Toplaps of Upper Silurian shallow marine sequences can be particularly found below the Caledonian unconformity close to the palaeohighs. The Upper Silurian shoreface and tidal units were tilted and eroded during this event, especially above the palaeohighs, which were reactivated at that time. The transect between the Ghadames Basin and the Gargaff Arch (Fig. 4) illustrates this truncation. Such a geometry potentially favoured hydrocarbon migration through the Silurian drainage system to source the Devonian reservoirs.

Erosional onlaps are a common geometry observed around the palaeohighs. They formed during transgression above the rising highs, each unit onlapping the one below, which was eroded as the palaeohigh grew. These types of truncations were very frequently observed around the palaeohighs. In the Djebel Tamamat in the Bled el Mass area, the Lower Ordovician units were successively eroded onto the high as it was rising during the Ordovician transgression (Fig. 15). Above the Tihemboka, Ahara and Gargaff highs, the Lower Devonian fluvial units were also progressively eroded while onlapping the palaeohighs (Fig. 13). A major stratigraphic wedge of the Gedinnian fluvial sandstone unit can then be observed along the northern flank of the Ahara High. In this example, 250 m of fluvio-estuarine sandstones are present in the centre of the Berkine Basin, which completely pinches out on the northern flank of the Ahara High (Fig. 8). The pinchout is due to the basal fluvial onlap and erosion as the palaeohigh grew.

Lowstand wedges and incised valleys developed around the palaeohighs during the Middle and Upper Devonian times, a period during which the palaeohighs were alternatively flooded during the transgressive events and subaerially exposed during the relative sea-levels falls. At that time, the surface exposed to erosion was large enough to supply a significant amount of sediments in the adjacent basins around. A network of fluvio-estuarine incised valleys developed during the sea-level falls in Emsian, Eifelian and Givetian times around the main highs. Such valleys can be observed in the outcrops of the Gargaff Arch, and also in the subsurface of the Berkine, Illizi and Reggane basins. As in the classical models (Posamentier *et al.* 1992), during the incision phase, sediments transited through the valleys to accumulate in forced regression wedges during the lowstand periods (Fig. 18). Sharp-based shoreface and tidal units can be frequently observed in the clastic belts around the highs, thinning and pinching out basinwards in the offshore setting.

The geometry of the shale layers sealing the palaeohigh during the transgression is also critical to ensure the seals of the stratigraphic wedge. As the palaeohighs were uplifted, these shales were also eroded, reducing their sealing capacities, and their continuity must be carefully evaluated when chasing stratigraphic traps to ensure their closure.

Pre-Hercynian migration process and implications on reservoir quality

The petroleum systems of the North African Palaeozoic basins suffered a very long and complex geological history. The Hercynian event especially affected the geometry of the basins together with the Jurassic extensional phase, and the Austrian and Alpine compressional phases. Basin modelling approaches suggest that, in many basins, a significant amount of hydrocarbons was generated during the Palaeozoic times, from both the Silurian and the Frasnian source rocks. Understanding the Palaeozoic migration pathways and trapping is very important to predict the most porous reservoirs, as early charge inhibited porosity and permeability reduction. Different silicification phases affected the reservoir during the burial history, often significantly reducing the porosity. In the Palaeozoic traps, the oil coatings in the reservoir may have preserved porosity during cementation during later phases of diagenesis, even if most of these traps were inverted during Austrian and Alpine compressional phases. Early oil migration probably occurred in the stratigraphic wedges around the palaeohighs, explaining the unusually high porosity ranges observed in some of these reservoirs. In the Berkine Basin, after the Hercynian compression, a second phase of subsidence generated most of the hydrocarbons, charging the present-day in structures, which mostly formed during the Austrian and Cenozoic compressive phases (Underdown & Redfern 2008).

Another issue is the hydrocarbon charging of the stratigraphic wedges around the highs. As mentioned previously, the Silurian and the Frasnian source rocks are thinning out over the high. This implies a long-distance lateral migration between the oil kitchen and the stratigraphic traps to fill the stratigraphic wedges.

Conclusions

Knowledge of the timing of the uplift of the tectonic palaeohighs separating the Saharan craton into sub-basins is critical to our understanding the petroleum system evolution. The cited palaeohighs influenced sedimentation during most of the Palaeozoic times, but others may have formed during the Hercynian deformation, later during Mid-Cretaceous or Alpine deformation. In some cases (e.g. the Bled el Mass area), the same structure was reactivated during each of these major tectonic phases. Every palaeohigh formed above crustal mobile zones resulting from the terrane accretion during the Pan-African collision. Most of the crustal faults had a north–south orientation and may have branched to other NE–SW faults, and were then reactivated through geological times.

The Cambrian and Lower Ordovician was a period of active uplift, with palaeohighs forming slowly rising broad horsts. The palaeohighs were covered by the Cambro-Ordovician sediments before being eroded during the uplift phase. Although Cambrian sediments were deposited across the craton, thickness variations occurred across these palaeohighs but without major facies variations. The effect of the uplift was more pronounced during Ordovician times, during which significant erosion occurred above the palaeohighs, controlling the sequence architecture and facies distribution. Silurian times marked a period of general quiescence with limited uplift of the highs. Lower Silurian successions, including the main source rock levels, onlapped a residual topography. The subsequent progradation of the Upper Silurian from south to north across the craton was not affected by palaeorelief on the highs. The uplift resumed during latest Silurian and Lower Devonian times. Upper Silurian sediments were eroded below the Caledonian unconformity, especially at the margins of the palaeohighs. The palaeohighs then continuously grew during the Devonian, separating distinct palaeogeographic domains and controlling the local facies distribution. During Middle and Upper Devonian times, the palaeohighs were alternatively flooded and emergent depending on the relative sea-level variations. The activity of the palaeohighs almost ceased during the Frasnian times, with marine shales onlapping and sealing most of the palaeohighs. Late Devonian and Carboniferous were marked by a complete reorganization of the depocentres on the craton (Wendt *et al.* 2005), in relation to the beginning of the Hercynian compression, except for the Gargaff High, which continuously grew to the present day.

The depositional sequence architecture in such a context was controlled by the eustatic variations interfering with the palaeohigh uplift and subsidence rates, which were extremely low (a few metres per million years). In such a low accommodation context, eustatic sea-level falls were better registered above the rising palaeohighs. Progressive unconformities around the palaeohighs were superimposed onto the global tectonic unconformities, making complex stratigraphic wedge geometries. These result from the successive erosion of the reservoir levels associated with the progressive unconformities, and with the occurrence of incised valleys and forced regression wedges which developed during the relative sea-level falls.

The uplift of the palaeohigh controlled both the source rocks and reservoir rock distributions. The Lower Silurian and Frasnian source rocks were preferentially preserved in the lows where anoxic conditions prevailed, while they were less developed or absent above the palaeohighs.

The hydrocarbon prospects associated with these stratigraphic wedges must be carefully evaluated with 3D seismic surveys. If the presence of such stratigraphic wedges has been already proved and produces hydrocarbon around the palaeohighs, the lateral closure of the reservoir and the continuity of the seal above have to be investigated in detail in the prospects. The sealing offshore shales layers deposited above the palaeohighs during transgression may have been themselves eroded during the uplift, reducing their sealing capacities.

Finally, the sourcing of the wedges implies lateral hydrocarbon migration from both Silurian and Frasnian source rocks. The reconstruction of the geometry of the drainage system and its evolution during the deformation of the basin have to be taken into account to restore the migration history through time. An early pre-Hercynian migration in such traps may have prevented silicification of the reservoir, favouring relatively high-porosity ranges which make very good reservoirs during the post-Hercynian migration.

This manuscript is based on 15 years of work in Algeria performed during Triassic, Devonian, Illizi-Berkine and BerkineGas joint Sonatrach-IFP projects. Many geologists from Sonatrach and from the IFP Group were involved and they are too numerous to be individually cited, together with those in the companies who sponsored the studies (Anadarko, BP, Cepsa, ENI, GDF-Suez, Talisman Energy, Total, Repsol, Statoil). Special thanks go to D. Takherist (Alnaft), H. Chebourou, M. Malla, C. Hellal and N. Mokhtari (Sonatrach), to T. Euzen and C. Ravenne (IFP) and to T. Lorin and G. Philippe (Beicip-Franlab). Discussions with J. L. Rubino and C. Blanpied (Total) were very fruitful for improving the description of the Libyan outcrops. Special thanks are extended to the LPI management in Tripoli for their support of M. Ben Rahuma's PhD study. The contribution of F. Paris (Rennes University) and K. Boumendjel (Sonatrach) for dating the series is also invaluable. The comments from T. Patton (BP) and an anonymous reviewer improved the manuscript quality greatly.

References

Bertrand, J. & Caby, R. 1978. Geodynamic evolution of the Pan-African orogenic belt: a new interpretation of the Hoggar shield. *Geologisches Rundschau*, **67**, 357–388.

Beuf, S., Biju-Duval, B., Mauvier, A. & Legrand, Ph. 1968. Nouvelles observations sur le 'Cambro-Ordovicien' du Bled El Mass (Sahara central). *Publication du Service Géologique Algérie, Bulletin*, **38**, 39–51.

Beuf, S., Biju-duval, B., De Charpal, O., Rognon, P., Gariel, O. & Bennacef, A. 1971. *Les grès du Paléozoïque inférieur du Sahara. Sédimentologie et discontinuités. Evolution d'un craton*. Publication Institut Francais du Pétrole, Collection Science et Techniques Pétrolières, **18**. Editions Technip, Paris.

Black, R., Caby, R. *et al.* 1979. Evidence for Late Precambrian plate tectonics in West Africa. *Nature*, **278**, 223–227.

Boote, D. R., Clark-Lowes, D. D. & Traut, M. W. 1998. Paleozoic Petroleum systems of North Africa. *In*: Macgregor, D. S., Moody, R. T. J. & Clark-Lowes, D. D. (eds) *Petroleum Geology of North Africa*. Geological Society, London, Special Publications, **132**, 7–69.

Boudjema, A. 1987. Evolution Structurale Du Bassin Pétrolier (Triassique) du Sahara Nord Orientale (Algerie), Unpublished PhD thesis, Université de Paris Sud, Orsay.

Brenchley, P. J., Marshall, J. D. *et al.* 1994. Bathymetric and isotopic evidence for a short-lived late Ordovician glaciation in a greenhouse period. *Geology*, **22**, 295–298.

Caby, R. 2003. Terranes assembly and geodynamic evolution of central-western Hoggar: a synthesis. *Journal of African Earth Sciences*, **37**, 133–159.

Chaouche, A. 1992. *Genèse et mise en place des hydrocarbures dans les basins de l'Erg Oriental (Sahara Algérien)*. Thesis, Université de Bordeaux III.

Coward, M. P. & Ries, A. C. 2003. Tectonic development of North African basins. *In*: Arthur, T. J., Macgregor, D. S. & Cameron, N. R. (eds) *Petroleum Geology of Africa*. Geological Society, London, Special Publications, **207**, 61–83.

Craig, J., Rizzi, C. *et al.* 2006. Structural Styles and Prospectivity in the Precambrian and Palaeozoic Hydrocarbon Systems of North Africa. *III Symposium Geology of East Libya Binghazi*, GSPLAJ.

Dardour, A. A., Boote, D. R. D. & Baird, A. W. 2004. Stratigraphic controls on Palaeozoic petroleum systems, Ghadames Basin, Libya. *Journal of Petroleum Geology*, **27**, 141–162.

Destombes, J., Holland, H. & Willefert, S. 1985. Lower Paleozoic rocks of Morocco. *In*: Holland, C. (ed.) *Lower Paleozoic Rocks of North-western and Western Africa*. Wiley, New York, 91–336.

Echikh, K. 1998. Geology and hydrocarbon occurrences in the Ghadamis Basin, Algeria, Tunisia, Libya. *In*: Macgregor, D. S., Moody, R. T. J. & Clark-Lowes, D. D. (eds) *Petroleum Geology of North Africa*. Geological Society, London, Special Publications, **132**, 109–129.

Eschard, R., Abdhallah, H., Braïk, F. H. & Desaubliaux, G. 2005. The Lower Paleozoic succession in the Tasilli outcrops, Algeria: sedimentology and sequence stratigraphy. *First Break*, **23**, 27–36.

Fabre, J. 1988. Les séries du paléozoïque d'Afrique: une approche. *Journal of African Earth Sciences*, **7**, 1–40.

Ghienne, J. F., Boumendjel, K., Paris, F., Videt, B., Racheboeuf, P. & Salem, H. A. 2007*a*. The Cambrian-Ordovician succession in the Ougarta Range (western Algeria, North Africa) and interference of the Late Ordovician glaciation on the development of the Lower Palaeozoic transgression on northern Gondwana. *Bulletin of Geosciences*, **82**, 183–214.

Ghienne, J. F., Le Heron, D. P., Moreau, J., Denis, M. & Deynoux, M. 2007*b*. The Late Ordovician glacial sedimentary system of the North Gondwana platform. *In*: Hambrey, M., Christoffersen, P., Glasser, N., Janssen, P., Hubbard, B. & Siegert, M. (eds) *Glacial Sedimentary Processes and Products*. International Association of Sedimentologists, Special Publications, **39**. Blackwells, Oxford, 239.

Haddoum, H., Guiraud, R. & Moussine-Pouchkine, A. 2001. Hercynian compressional deformations of the Ahnet-Mouydir Basin, Algerian Saharan Platform: far-field stress effects of the Late Palaeozoic orogeny. *Terra Nova*, **13**, 220–226.

Hallett, D. 2002. *Petroleum Geology of Libya*. Elsevier Science, Amsterdam, 503.

Haq, B. U. & Schutter, S. R. 2008. A chronology of Paleozoic sea-level changes. *Science*, **322**, 64–68.

Legrand, P. 2003. Paléogéographie du Sahara algérien à l'Ordovicien terminal et au Silurien inférieur. *Bulletin de la Société Géologique de France*, **174**, 19–32.

Le Heron, D. P. & Craig, J. 2007. First order reconstruction of a Late Ordovician Ice sheet. *Journal of the Geological Society, London*, **93**, 47–76.

Lüning, S., Craig, J., Loydell, D. K., Storch, P. & Fitches, L. 2000. Lower Silurian 'hot shales' in North Africa: regional distribution and depositional model. *Earth Science Review*, **49**, 121–200.

Lüning, S., Archer, R., Craig, J. & Loydell, D. K. 2003*a*. The Lower Silurian 'Hot Shales' and 'Double Hot Shales' in North Africa and Arabia. *In*: Salem, M. J., Oun, K. M. & Seddiq, H. M. (eds) *The Geology of Northwest Libya (Ghadamis, Jifarah, Tarabulus and Sabratah Basins)*. Earth Science Society of Libya, Tripoli, **3**, 91–105.

Lüning, S., Adamson, K. & Craig, J. 2003*b*. Frasnian organic-rich shales in North Africa: regional distribution and depositional model. *In*: Arthur, T. J., MacGregor, D. S. & Cameron, N. R. (eds) *Petroleum Geology of North Africa: New Themes and Developing Technologies*. Geological Society, London, Special Publications, **207**, 165–184.

Massa, D. 1988. Paléozoique de Libye occidentale – Stratigraphie et Paleogéographie. Doctoral thesis, Université Nice.

Posamentier, H. W., Allen, G. P., James, D. P. & Tesson, M. 1992. Forced regressions in a sequence stratigraphic framework: concepts, examples and exploration significance. *AAPG Bulletin*, **76**, 1687–1709.

Ramos, E., Marzo, J. M., de Gibert, K. S., Tawengi, A. A., Khoja, & Bollati, N. D. 2006. Stratigraphy and sedimentology of the Middle Ordovician Hawaz Formation (Murzuq basin, Libya). *AAPG Bulletin*, **90**, 1309–1136.

Rubino, J. L. & Blanpied, C. 2000. Sedimentology and sequence stratigraphy of the Devonian to lowermost Carboniferous succession on the Gargaf Uplift (Murzuq Basin, Libya). *In*: Sola, M. & Worsley, D. (eds) *Geological Exploration in Murzuq Basin*. Elsevier Science, Amsterdam, 321–348.

Scotese, C. R., Boucot, A. J. & Mckerrow, W. S. 1999. Gondwanan palaeogeography and palaeoclimatology. *Journal of African Earth Sciences*, **28**, 99–114.

Smith, B., Derder, M. E. M. *et al*. 2006. Relative importance of the Hercynian and post-Jurassic tectonic phases in the Saharan platform: a palaeomagnetic study of Jurassic sills in the Reggane Basin (Algeria). *Geophysics Journal International*, **167**, 380–396.

Sutcliffe, O. E., Adamson, K. & Ben Rahuma, M. M. 2000. The geological evolution of the Palaeozoic rocks of western Libya: a review and field guide. Second Symposium on the Sedimentary Basins of Libya. Geology of northwestern Libya. Field Guide. *Earth Sciences Society of Libya*, **93**.

Underdown, R. & Redfern, J. 2008. Petroleum generation and migration in the Ghadames Basin, north Africa: a two-dimensional basin-modeling study. *AAPG Bulletin*, **92**, 53–76.

Vos, R. G. 1981. Deltaic sedimentation in the Devonian of Western Libya. *Sediment Geology*, **29**, 67–88.

Wendt, J., Kaufmann, B., Belka, Z., Klug, C. & Lubeseder, S. 2005. Sedimentary evolution of a Palaeozoic basin and ridge system: the Middle and Upper Devonian of the Ahnet and Mouydir (Algerian Sahara). *Geological Magazine*, **143**, 269–299.

Zazoun, R. S. 2001. La tectogenèse hercynienne dans la partie occidentale du bassin de l'Ahnet et la région de Bled El-Mass, Sahara algérien: un continuum de deformation. *Journal of African Earth Sciences*, **32**, 869–887.

Stratigraphic trapping potential in the Carboniferous of North Africa: developing new play concepts based on integrated outcrop sedimentology and regional sequence stratigraphy (Morocco, Algeria, Libya)

S. LUBESEDER, J. REDFERN, L. PETITPIERRE and S. FRÖHLICH

School of Earth, Atmospheric and Environmental Sciences, University of Manchester, Oxford Rd, Manchester M13 9PL, UK (e-mail: jonathan.redfern@manchester.ac.uk)

Abstract: The lower Carboniferous (Tournaisian to Visean) of North Africa is characterized by cycle-stacks of predominantly shelfal to marginal marine sandstones and limestones, thick shelfal mudstones and less common but important interbedded fluvio-deltaic sandstones. The cyclic sedimentation pattern continues into the Mid Carboniferous (Serpukhovian to Bashkirian), when mixed siliciclastic–carbonate sequences give way to tropical carbonates, before an abrupt return to continental deposits in the upper Carboniferous (Bashkirian to Gzhelian). The alternation of widespread shallow marine and more discrete fluvial reservoirs with interbedded offshore mudstone seals is interpreted to result from high-frequency, high-amplitude Carboniferous glacio-eustatic sea-level changes. The large base-level changes during that time, combined with climatic conditions that produced high amounts of terrigenous mud, provided favourable conditions for the development of stratigraphic traps in the clastic-prone lower Carboniferous, while the advent of tropical carbonates produced reefal buildups in the Mid Carboniferous. Four stratigraphic trapping types are recognized: (1) truncation traps in which reservoir units were eroded on subaerially exposed proximal palaeohighs and thick underlying transgressive and highstand systems tract (TST and HST) mudstones form the bottom-seal and the rapid transgression of the offshore facies forms the top-seal; (2) pinchout traps of lowstand wedges on the flanks of distal palaeohighs, which were only affected by subaqueous reworking of previous TST–HST mudstones and were buried during the subsequent transgression; (3) incised valleys of the lowstand systems tract (LST), filled with thick fluvial and tidal sandstones, cutting either into TST–HST mudstones in the lower Carboniferous, or into exposed carbonate platforms in the Mid Carboniferous; (4) Waulsortian-type reefal buildups of the Mid Carboniferous. The four trapping types are discussed using selected outcrop examples, and are placed into regional sequence stratigraphic context of the Carboniferous depositional systems and sequence development of North Africa. These concepts can be readily applied to the subsurface and offer significant potential for new plays across North Africa.

Keywords: stratigraphic traps, sequence stratigraphy, Carboniferous, Morocco, Algeria, Libya

A tentative sequence stratigraphic scheme for the Carboniferous of North Africa has been developed to guide reservoir prediction in poorly explored areas and to provide a framework for further analysis of potential stratigraphic traps. Seven important outcrop sections across North Africa were reviewed and correlated. Of these, five sections have been interpreted based on published sources and two sections (SW Anti-Atlas, Morocco; NW Murzuk Basin, Libya) were logged for this study (Figs 1 & 2). All sections are located along the southern Palaeozoic outcrop belt, comprising exposures in the Anti-Atlas, the Bechar Basin, the Reggane, Ahnet and Mouydir Basins, the southern Illizi Basin, and the northern Murzuk to southern Ghadames Basins. The presented chronostratigraphic chart has been compiled based on a comprehensive review of a large amount of published literature, of which only selected key publications are referred to in this summary paper.

North African Carboniferous sequence framework

Over many decades of studies in North Africa there have been a number of publications on the stratigraphy and sedimentology of the Carboniferous; an excellent regional summary is provided by Diaz *et al.* (1985). However, of these studies, only a few attempt any sequence-type interpretation. In this paper we present the first regional sequence stratigraphic scheme, based on a large amount of available published biostratigraphic and sedimentological data, integrated with new field work.

Good quality sedimentological and biostratigraphic published work on a regional scale is very limited, despite the vast outcrops of fossiliferous Carboniferous sediments. The sequence stratigraphic scheme and correlation presented here must be considered a preliminary working document due to the vast area covered and the relatively widely spaced dataset currently available. In certain data-poor areas the scheme remains very conjectural at present. In addition to the limited dataset, different fossil groups used for biostratigraphic dating sometimes suggest very different ages (Wendt *et al.* 2009), exemplifying the need to continue and update the research on the extensive outcrops.

The regional correlation shows the general facies patterns and palaeogeography of the Carboniferous from Morocco to western Libya. This correlation allows assessment of the broad trends, although it should be emphasized that in detail, on a basin scale, the stratigraphy and sedimentology are undoubtedly more complicated than can be shown on the generalized correlation panel.

The following sections describe each phase of Late Devonian to Late Carboniferous deposition, ending with a comparison of these phases with global sea-level cycles.

Late Devonian ('Strunian') regression

A latest Devonian ('Strunian') regression is recognized across all of NW Africa, with the deposition of shelf sandstones in the Anti-Atlas (e.g. Kaiser *et al.* 2004), Bechar Basin, Ougarta Arch, northern Hoggar region and the Illizi and Ghadames Basins (Conrad *et al.* 1986; Lubeseder 2005; Fig. 3). A regionally extensive unconformity developed in the Murzuq Basin of Libya and across surrounding palaeohighs (the Gargaf Arch and Tihemboka Arch) and presumably reached far into the Ghadames Basin. The

VINING, B. A. & PICKERING, S. C. (eds) *Petroleum Geology: From Mature Basins to New Frontiers – Proceedings of the 7th Petroleum Geology Conference*, 725–734. DOI: 10.1144/0070725

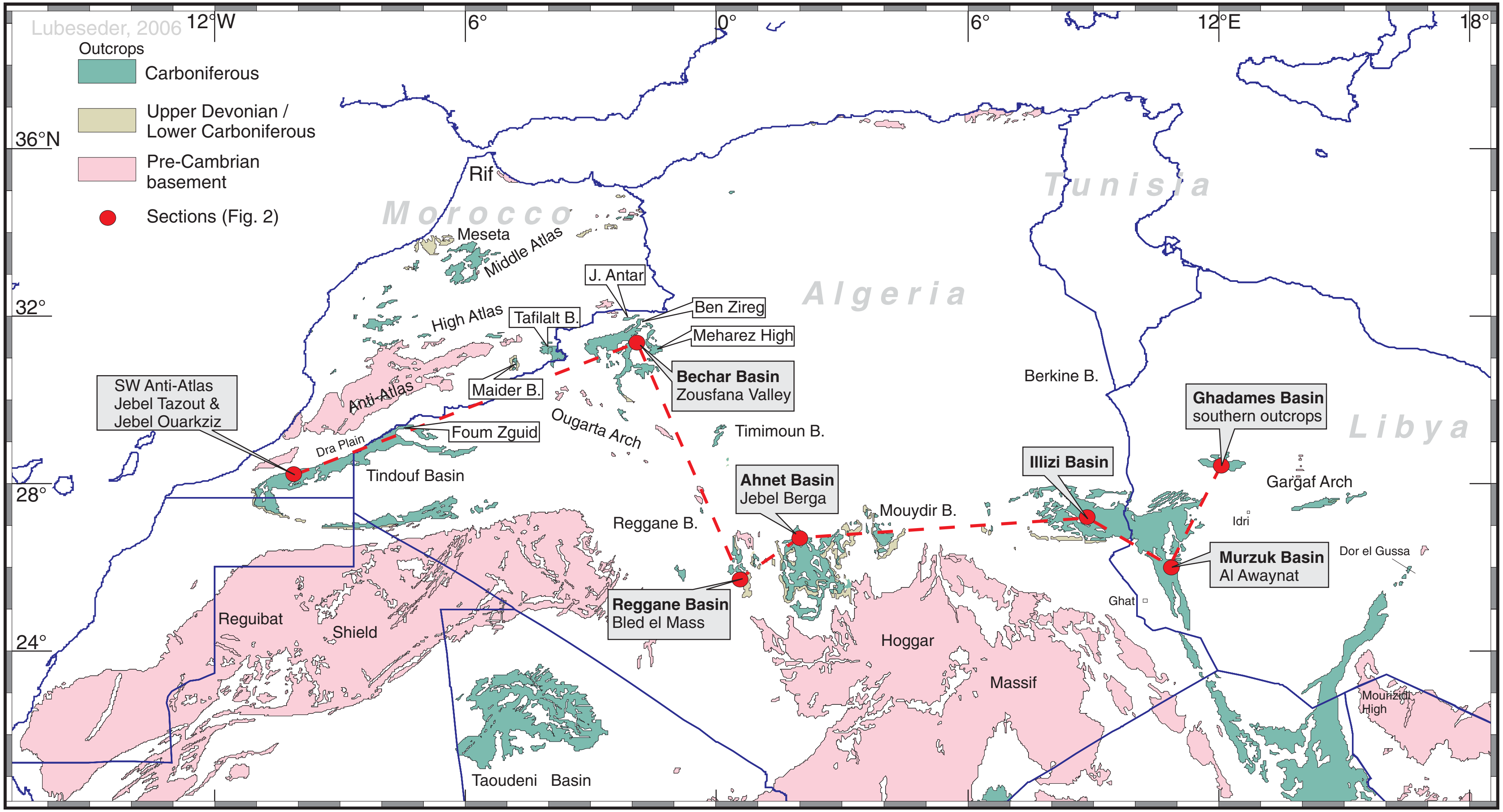

Fig. 1. Map of North Africa showing Carboniferous outcrops, location of sections (red dots), and line of correlation (shown in Fig. 2). Geological basemap after Persits *et al.* (1997).

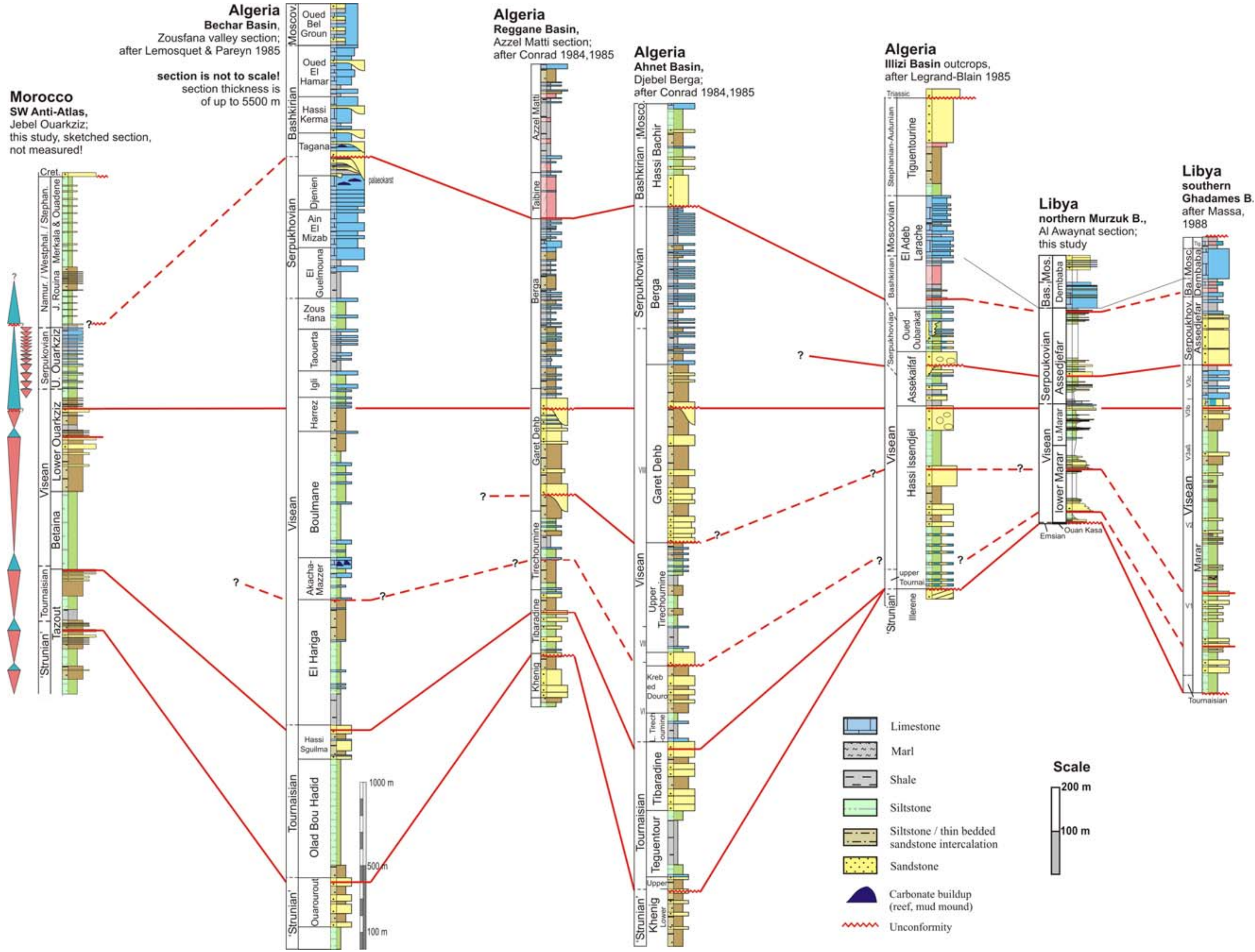

Fig. 2. Correlation of selected North African Carboniferous outcrop sections.

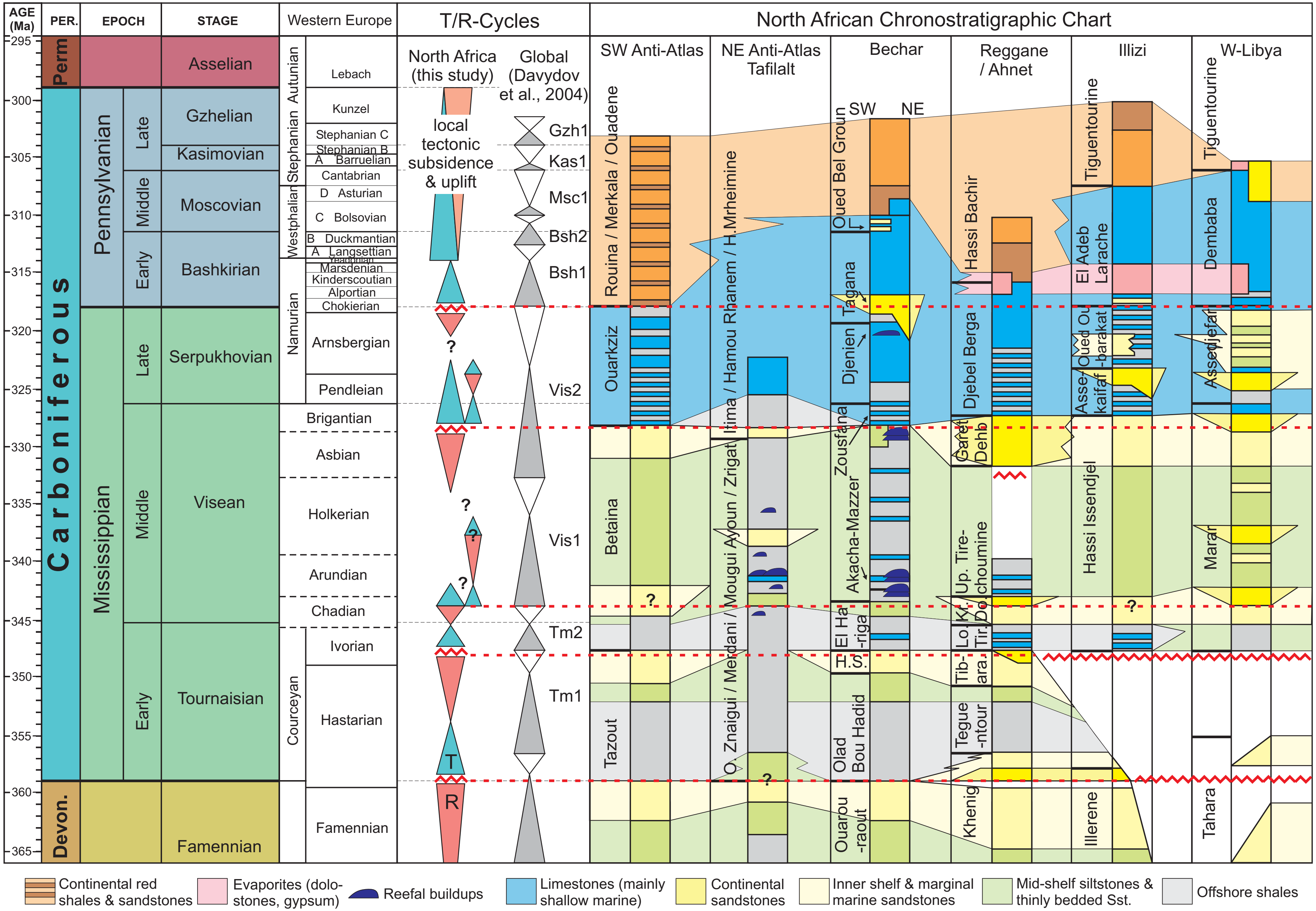

Fig. 3. Tentative chronostratigraphic correlation and transgressive-regressive (T/R) sequence framework of the Carboniferous of North Africa. Note that much more integrated biostratigraphic and sedimentological work on the Carboniferous sections of North Africa will have to be carried out before a satisfactory regional sequence framework can be achieved, and that the proposed scheme presented here is only a starting-point.

unconformity is also developed in the Reggane and Ahnet Basins of Algeria (Conrad 1984, 1985).

Early to Middle Tournaisian transgression

In the northwestern regions (the Anti-Atlas, Bechar Basin and Ougarta Arch), the subsequent transgression led to the deposition of marine shales with an Early Tournaisian fauna (the ammonoid *Gattendorfia* sp.). These shales are correlated to the shales of the Teguentour Formation in the Ahnet Basin, dated to the Mid to Late Tournaisian (Wendt *et al.* 2009). The emergence interpreted by these authors in the Ahnet Basin is interpreted here as a hiatus caused by non-deposition during maximum flooding. In the more proximal near-shore to continental dominated southwestern areas, transgressive sandstones were deposited bearing Early Tournaisian brachiopods (e.g. the upper Tahara and Ashkidah Formations of the Gargaf Arch; Mergl & Massa 2000).

Late Tournaisian regression

In the Anti-Atlas and the Bechar, Reggane and Ahnet Basins, a Late Tournaisian regression formed a shale-to-sandstone coarsening-upward hemi-cycle comparable to those of the latest Devonian. It is likely that this hemi-cycle also developed in the subsurface of several other basins (e.g. the Timimoun, Ghadames and Berkine Basins) and may have been incorporated into the 'Strunian' reservoir interval by some workers. In the southern Ahnet Basin, fluvial sandstones occur locally within the Late Tournaisian Tibaradine Formation (Conrad 1985). In the Murzuq Basin and in the southern Illizi Basin outcrops, Late Tournaisian strata were eroded or sediments bypassed these basins during this regressive phase.

Latest Tournaisian to earliest Visean transgression

The Late Tournaisian shelf sandstones are succeeded by a thick interval of outer-shelf shales in the Anti-Atlas and the Bechar Basin (Betaina Formation; El Hariga Formation), which contain latest Tournaisian faunas at their bases. In the Ahnet Basin, the shales and limestones of the Lower Tirechoumine Formation (Iridet Formation *sensu* Wendt *et al.* 2009) are dated by conodonts, ammonoids and foraminifera to the Late Tournaisian to Early Visean (Conrad 1985; Wendt *et al.* 2009). This latest Tournaisian transgression also led to the deposition of marine sediments directly above the basal Hassi Issendjel Formation unconformity (Legrand-Blain 1985) and above the basal Marar Formation unconformity in the southern Illizi and Murzuq Basins. The very bases of these two formations have been assigned to the latest Tournaisian.

Visean transgressive–regressive cycles

Most of the Visean essentially forms one large-scale regressive phase (seen in the SW Anti-Atlas Betaina Formation, more poorly developed in the Ahnet and Illizi Basins, and well developed in the Marar Formation of Libya), which ended with the onset of widespread carbonate deposition during the latest Visean. Correlation of several intra-Visean cycles across the Saharan Platform, however, is uncertain (Fig. 2). It is proposed that the Visean large-scale regression is subdivided into two, or possibly three, higher-order cycles (Fig. 3).

Two well developed Visean cycles are evident in the Betaina Formation of the Anti-Atlas and are possibly represented by the El Hariga Formation, and (partially) by the Akacha–Mazzer Formation (lower cycle), and by the Boulmane and the Harrez Formations (upper cycle), in the Bechar Basin.

In the Ahnet Basin, the regressive deltaic-marine to fluvial sandstones of the Kreb ed Douro Formation are well dated to the Early Visean by the under- and overlying marine shales and limestones with ammonoids, conodonts and foraminifera (Conrad 1985; Wendt *et al.* 2009). We suggest a different interpretation from that of Wendt *et al.* (2009), placing the subsequent fluvially dominated and undated Garet Dheb Formation into the Late Visean, not the Early Visean. Fluvial channels that are reported to have incised several tens of metres within this formation (Conrad 1985) correlate better with the Late Visean major regressive phase than with the relatively minor regression in the Early Visean. The long-lasting Visean hiatus proposed by Wendt *et al.* (2009) would, in this re-interpretation, underlie a Late Visean unconformity.

At least two higher-order cycles also occur in the Hassi Issendjel Formation of the southern Illizi Basin (Legrand-Blain 1985), but there is little detailed information available on this section. In the western Libyan outcrops, the Marar Formation shows three well developed Visean sequences, the upper two starting with incised fluvial channels at the base that grade upwards into shelf sandstones and shale (sequences LC1, LC2 and LC3 of Fröhlich *et al.* in press; biostratigraphic data mainly based on Massa & Vachard 1979 and Massa 1988).

Latest Visean to Serpukhovian transgression

In all of the reviewed sections the start of the regionally widespread carbonate deposition above the Late Visean clastics was proposed to occur in the latest Visean. In the west (the Anti-Atlas and the Bechar, Reggane and Ahnet Basins), deposition of the carbonate-rich interval continued throughout the Serpukhovian, while siliciclastics remained important in the SE (the Murzuk, Ghadames and southern Illizi Basins).

In the Anti-Atlas (Jebel Ouarkziz section) the uppermost Visean to Serpukhovian forms a well-expressed cyclic succession of shallow marine limestones, siltstones and sandstones with an overall long-term transgressive trend from lagoonal to open-shelf carbonates and a gradual disappearance of intercalated siliciclastics (Fig. 4). Similar cyclic Serpukhovian strata are recorded from the Bechar, Reggane and Ahnet Basin sections (Fig. 2). In the Libyan outcrops, oolitic and stromatolitic limestones (Collenia Beds) are part of these Serpukhovian mixed depositional systems. It appears that relative sea-level during the latest Visean and Serpukhovian rose gently, punctuated by many high-order fluctuations.

It must be noted that biostratigraphic dating in this interval is very controversial. In the Ahnet Basin, Wendt *et al.* (2009) proposed that the carbonates of the Jebel Berga Formation date entirely to the Bashkirian based on conodont data, yet foraminifera suggest a Late Visean to Serpukhovian age (Conrad 1985; Wendt *et al.* 2009). We follow the foraminifera dating since most of the other Algerian and Libyan sections were also dated using foraminifera.

Early Bashkirian regression

It appears that the gently rising Serpukhovian sea-level fell abruptly around the Serpukhovian–Bashkirian boundary, around which time a marked regression is observed that terminated the shelf carbonate deposition in the Anti-Atlas, the Reggane Basin and the Ahnet Basin. In these areas, the Bashkirian commenced with deposition of continental sandstones, marginal-marine gypsum deposits and dolomites as well as lacustrine carbonates. In the Bechar Basin, sea-level fall exposed the carbonate platform and a palaeokarst surface developed, into which sandstone-filled channels up to 150 m deep were cut (Lemosquet & Pareyn 1985). This major regression is less evident in the Libyan sections, where shelf carbonate deposition continued into the Bashkirian. Clearly, the palaeogeography and facies patterns across North Africa became more complicated across the Saharan Platform during the Bashkirian, suggesting that Variscan tectonics began

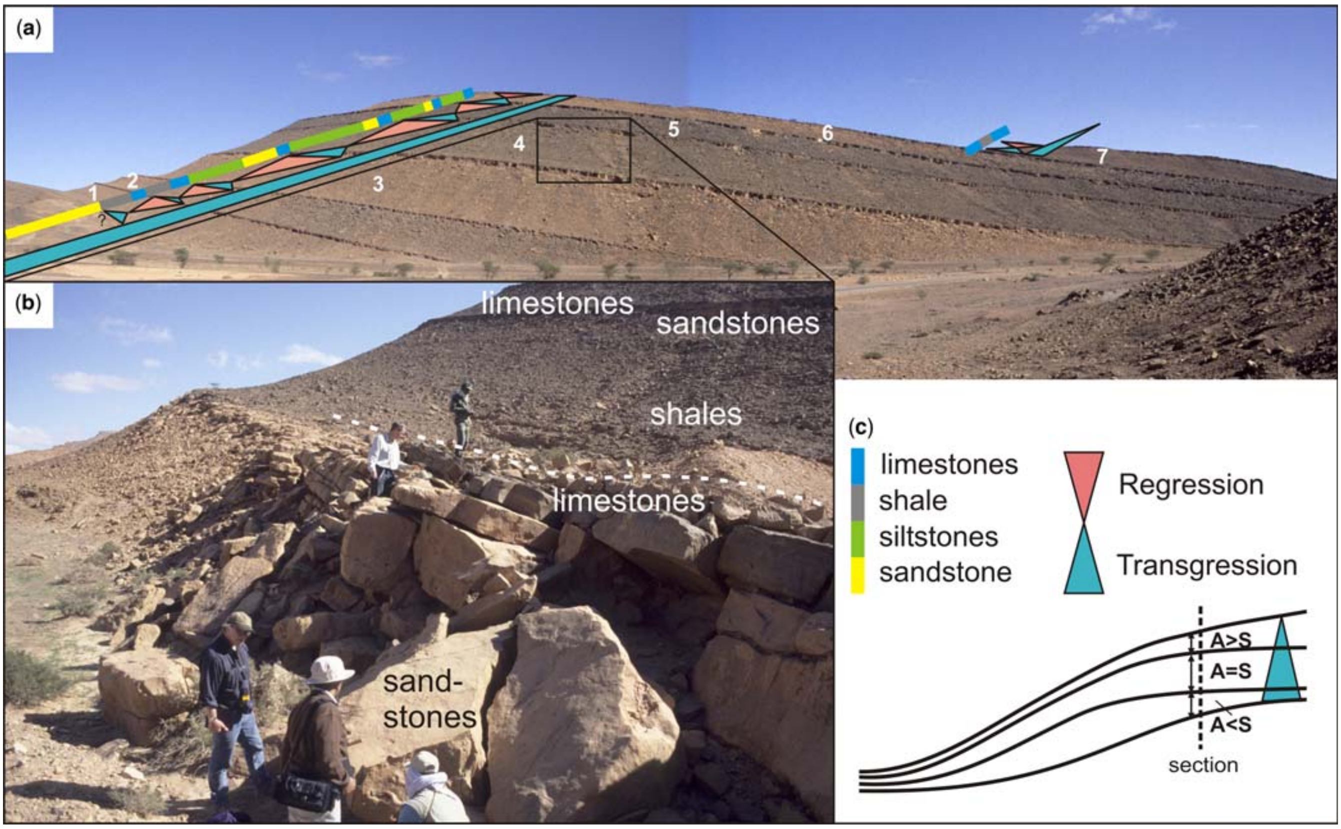

Fig. 4. (**a**) Serpukhovian transgressive succession of the SW Anti-Atlas (Ouarkziz Formation south of Assa) consisting of several higher-order transgressive limestone–regressive shale, siltstone, sandstone cycles (numbered 1–7). Note the overall transgressive sequence that is expressed in the upward decrease of terrigenous supply and increase of carbonate deposition as well as in the cyclical thin (cycles 1 and 2) to thick (cycles 2 and 3) to thin (cycles 4–7) stacking pattern. The section continues above the last crest with at least the same thickness of carbonate-dominated cycles. (**b**) Close-up view of cycle 4. (**c**) Legend and sketch to illustrate the interpretation of the stacking pattern as an upward passage through changing accommodation to sediment supply ratios (A/S) due to transgression (cycles 1 and 2, near-shore A < S; cycles 2 and 3, mid-shelf A = S; cycles 4–7, offshore A > S).

to destabilize the platform more effectively than the subtle tectonic movements that had prevailed since the Middle Devonian.

Late Carboniferous

Following the major end-Early Carboniferous regression, the Late Carboniferous sections vary across the region. Whilst in the Anti-Atlas (Tindouf Basin) and the Reggane and the Ahnet Basins, continental sandstones, mudstones and gypsum were deposited during the Late Carboniferous, carbonate deposition continued in the Bechar Basin, the southern Illizi Basin, and the Libyan basins during the early Late Carboniferous (Bashkirian to Moscovian). In the latter regions, continental red beds were deposited during the late Late Carboniferous (middle Moscovian to Gzhelian; middle Westphalian to Stephanian), although the full extent of their deposition is unclear, since the Hercynian Unconformity cuts down through the area. Upper Carboniferous cycles are difficult to constrain in terms of their sedimentology and biostratigraphy from the literature descriptions and are likely only to be valid locally.

Comparison of North African and global transgressive–regressive cycles

Four Early Carboniferous second-order transgressive–regressive (T/R) cycles are recognized in North Africa, which is the same as the number of cycles shown on the global scheme (Davydov *et al.* 2004; Fig. 3). Three out of nine North African hemi-cycle boundaries (maximum regressions and maximum transgressions) differ in age from the global scheme. Of the remaining six boundaries, four show a good correlation with the global scheme, but two are biostratigraphically too poorly constrained to allow a comparison. An additional Mid Visean cycle in North Africa is at present speculative.

The first Early Carboniferous cycle of North Africa, comprising the Devonian–Carboniferous boundary maximum regression, the Early Tournaisian transgression and the Late Tournaisian regression, compares well with the global T/R cycle Tm1 of Davydov *et al.* (2004) (Fig. 3). A fundamental difference between the schemes, however, exists in the preceding latest Devonian cycle. On global T/R schemes, the latest Devonian is considered to be transgressive (Johnson *et al.* 1985) and the following regressive phase is thought to fall entirely into the earliest Tournaisian. Yet, in North Africa, a wealth of biostratigraphic data suggest a latest Devonian ('Strunian') regression, succeeded by an Early Tournaisian transgression.

The interpreted second and third Early Carboniferous T/R cycles fit well with those of the global scheme (Tm2, Vis1; Fig. 3), although the Late Visean maximum regression appears to be younger in North Africa, constrained mainly by the age of the overlying transgressive limestones.

The fourth identified cycle, comprising the latest Visean and Serpukhovian transgression and the regression at the Serpukhovian–Bashkirian boundary, corresponds approximately to the global T/R cycle Vis2.

Although Early Hercynian tectonic activity is known to have started during the Middle Devonian and continued throughout the Late Devonian and Carboniferous in North Africa, the close match of North African and global T/R cycles suggests that Early Carboniferous sedimentary sequences were mainly controlled by eustatic sea-level fluctuations rather than tectonics. In contrast, the Late Carboniferous sequence ages, architectures and depositional systems are likely to have been controlled predominantly by regional to local tectonics and climate changes; however, the increasingly continental nature of the depositional environment means that research to date has struggled to constrain these sequences, making any conclusion regarding controls somewhat tentative.

Potential stratigraphic trapping types

Four potential stratigraphic trapping mechanisms are recognized within the Carboniferous interval. Two of the four stratigraphic trap types (truncation traps and depositional pinchout traps, Fig. 5) are controlled by the topography of palaeohighs and basins during the Carboniferous. Many of these highs are old structures that already influenced sediment distribution during the Early Palaeozoic. The structures were re-activated during the Middle to Late Devonian, and subsequently the syn-depositional relief became more and more pronounced until Hercynian uplift and peneplanation, especially in the northern basins (e.g. Bechar Basin; Malti *et al.* 2008). The other two potential trapping types are more related to depositional architecture (incised valleys, carbonate buildups, Fig. 5).

Truncation traps

Truncation, and subsequent onlap by a sealing lithology, is a proven trapping mechanism in Algeria. In several places the 'Strunian'–Tournaisian sandstones have been eroded on palaeohighs (e.g. the western Meharez High flanking the Bechar Basin, the Timimoun Basin margins and the Tihemboka Arch separating the Illizi Basin from the Ghadames Basin) either shortly after deposition (within-sequence) or later by the Hercynian Unconformity. Top-seals are either Visean shales or Triassic–Liassic shales and evaporites. The bottom-seal is provided by the Frasnian–Famennian shales. Risk of top-seal failure occurs in the case of within-sequence truncation, since laterally continuous sandstones of the following transgression may overlie the unconformity and trapping may therefore rely on sealing faults. However, the fault offsets required to give seals may only be small, since the thicknesses of the stacked transgressive sandstones are expected to be limited due to high-amplitude Carboniferous sea-level fluctuations.

Depositional pinchout of lowstand wedges on palaeohigh flanks

This stratigraphic trapping concept is probably the least-known and least-documented type in North Africa. It is similar to the truncation trap and may have been misinterpreted as such in some cases, but differs in the genetic sense and the predicted reservoir facies.

Topographic relief on the Saharan Platform influenced the facies patterns in all depositional environments, including outer shelf settings. This is well documented in the Middle to Upper Devonian carbonate facies (e.g. Wendt *et al.* 2006). In distal mid-shelf to outer-shelf dominated settings, siliciclastic supply into the basin either directly bypassed the highs or was subsequently removed by bottom-currents or storm reworking. This led to the deposition of only thinly bedded, rippled sandstones and siltstones on the highs and thickly bedded storm-induced siliciclastic turbidites and distal storm beds in the adjacent basin.

An example of this sediment partitioning is found in the 'Strunian'–Tournaisian of the Maider and Tafilalt Basins (Morocco), which are separated by a regional palaeohigh. In the centre of the Maider Basin, sandstones with large flute-marks

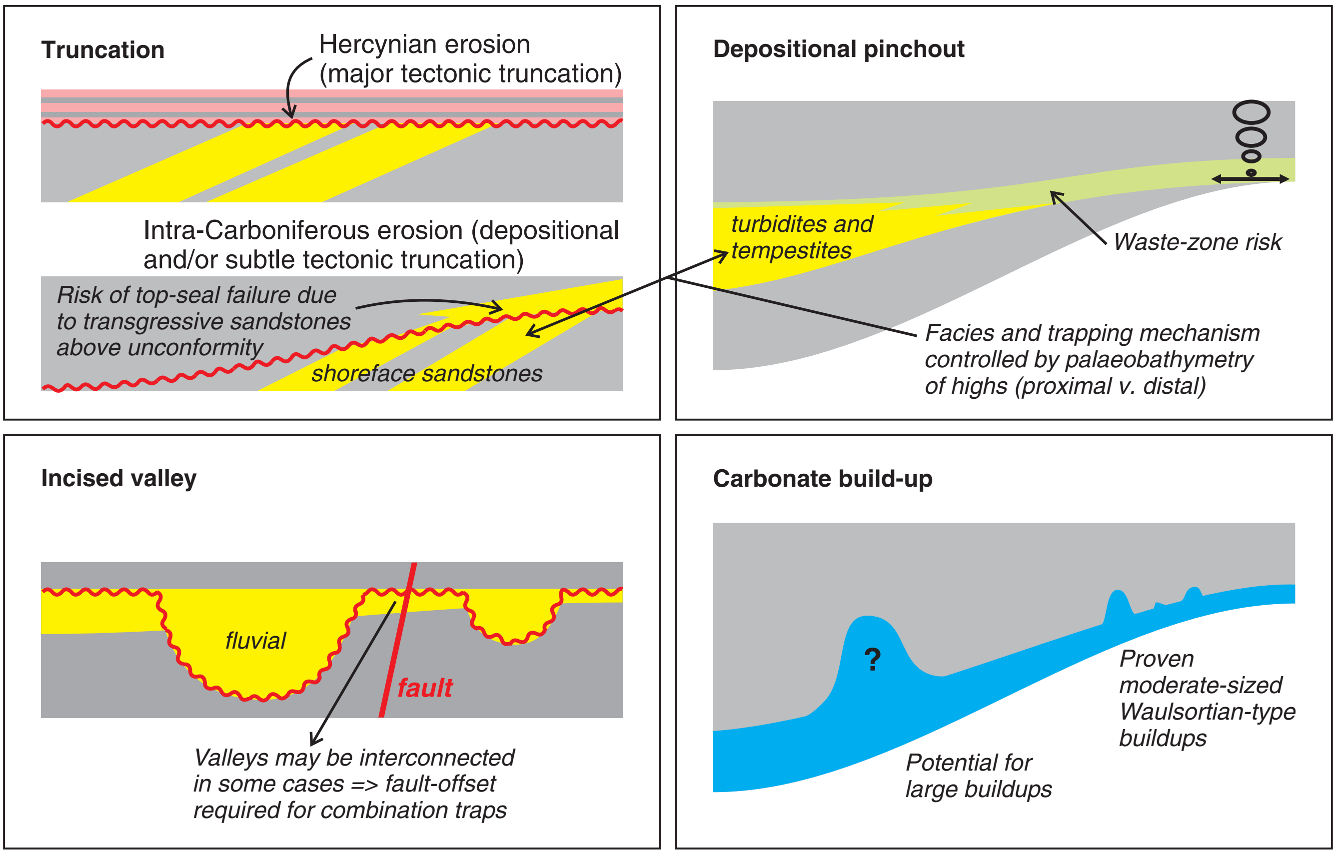

Fig. 5. The four main stratigraphic trapping types recognized in Carboniferous plays in North Africa. See text for explanations.

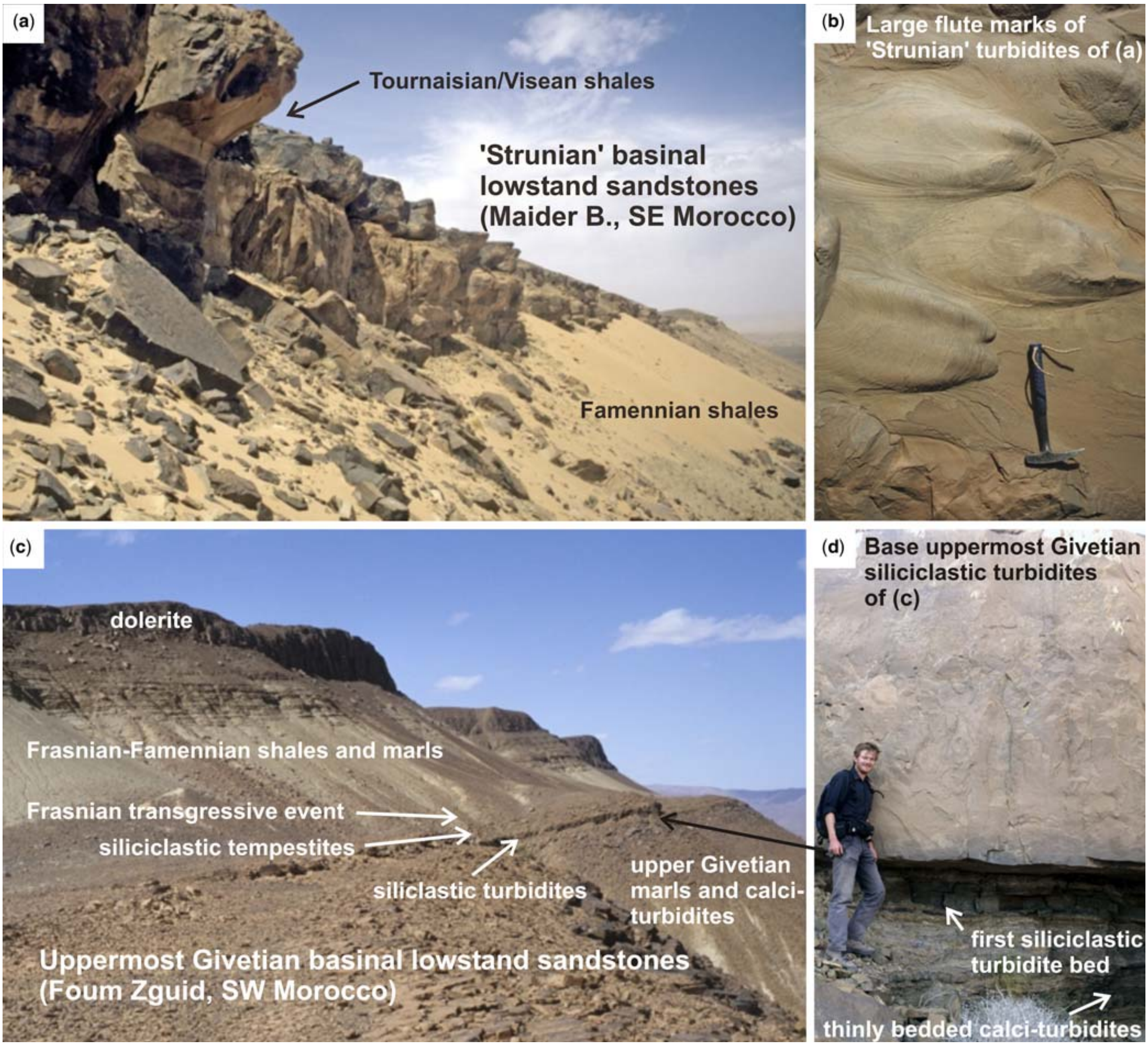

Fig. 6. Examples of basin-centred, distal lowstand sandstones that pinch out towards adjacent palaeo-structures thus forming potential pinchout traps on their flanks. The sandstones form 5–8 m thick bodies consisting of massive siliciclastic turbidites that pass upwards into storm deposits. The first example is the uppermost Devonian ('Strunian') sandstone exposed in the Maider Basin of Morocco (**a**) exhibiting large flute marks (**b**); note that the flute marks are filled by cross-beds and that the turbidites start at the base with the Bouma–Tc sequence. The second example is from the uppermost Givetian of the NE Dra Plain (Morocco) (**c**, **d**), where the sandstone is sandwiched between upper Givetian marls to thinly bedded calci-turbidites and Frasnian 'black' shales. Both examples are from the Middle and Upper Devonian, but very similar basin-centred lowstand sandstones are expected to occur in the NW African Carboniferous basins.

(Fig. 6) sharply overlie upper Devonian (Famennian) dark-coloured shales and are interpreted as turbiditic lowstand wedges. The sandstones pinch out onto the Tafilalt ridge and re-appear in the Tafilalt Basin. Another example of these lowstand basin-centred sandstones is the uppermost Givetian Megsem–Medersam Sandstone at Foum Zguid (SW Morocco) (Fig. 6). This sandstone sharply overlies upper Givetian thinly bedded calciturbidites, and its lower 4 m are entirely structureless. In its upper part there is a transition to hummocky cross-stratification. The transitional contact with the overlying Frasnian dark shales (related to a base Frasnian transgressive event, and elsewhere a proven source rock interval) is characterized by levels enriched in large corals and wood fragments (Meyer-Berthaud *et al.* 2004).

For a pinchout trap to be effective, it requires rapid pinchout of reservoir facies against the high; change from reservoir to non-reservoir facies must ideally happen over a short distance to minimize the potential for a mixed-facies 'waste-zone'. Such clear separation of reservoir-quality lowstand wedge deposits from non-reservoir deposits on the palaeohigh may require reasonable palaeo-relief, and may therefore limit this trapping style to the northwestern and northern Saharan Platform basins with, for example, known elevated subsidence rates during the Famennian.

Incised valley-fills

Fluvial channels interpreted to occur within incised valleys have been reported from several outcrop localities and stratigraphic levels of the uppermost Devonian and lower Carboniferous; and occasionally also from subsurface data. Because of the predominantly mud-rich lithologies of under- and overlying strata, these incised valley-fills may have good trapping potential, unless they pass laterally into extensive shoreline successions.

'Strunian' to Tournaisian incised valleys

Fluvial sandstones of the 'Strunian' and Tournaisian have been described (e.g. the Khenig Formation of the Ahnet and Reggane Basins, Conrad 1985; the Tazout Formation of the SW Anti-Atlas, Vos 1977), but no examples of isolated incised systems have been found in the literature. In the SW Anti-Atlas, on the northern flank of the Tindouf Basin, coarse-grained delta plain deposits occurring in up to 55 m thick and 60 km wide belts, pass laterally into extensive shoreface deposits (Vos 1977). These belts may significantly increase net reservoir thickness in structural traps, but because of the juxtaposition to the extensive shoreface deposits, they have low stratigraphic trapping potential.

Visean incised valleys

Fluvial sandstones of Visean age are widespread in the Ahnet and Reggane Basins (Garet Dehb Formation) and channels cut down several tens of metres into the underlying strata. Two main channel systems have been logged, one in the lower and one in the upper part of the formation (Azzel Matti section, Fig. 2).

Similar delta distributary channels cutting into underlying strata also occur in the southern Illizi Basin outcrops ('Gres de Champinngons Superieur'). In the northern Murzuk Basin, the Marar Formation contains recently recognized incised valleys about 0.5–3 km wide and 15–50 m thick (this study).

Serpukhovian–Bashkirian incised valleys

A different stratigraphic trapping potential may exist in the Bechar Basin. A sea-level drop towards the end of the Serpukhovian exposed the carbonate platform of the Bechar Basin, and a palaeokarst surface developed, into which cut sandstone-filled channels up to 150 m deep (Lemosquet & Pareyn 1985).

According to these authors, the fluvial sandstones were derived from the SW (Arlal Land) from the area of the future Kenadza and Abadla 'coal basins' (Colombo & Bensalah 1991).

The channels are filled with coarse, plant-bearing sandstones and occasional conglomerates. Each channel-filling episode was followed by deposition of well stratified shales and limestones containing marine faunas. The cycle of incision, fluvial sandstone deposition and open marine carbonate sedimentation suggests high-amplitude sea-level fluctuations at this time.

Carbonate buildups (Waulsortian reefs)

Visean Waulsortian-type carbonate buildups are exposed along the margins of the larger Bechar Basin (the Meharez High to the east, the Ben Zireg and Jebel Antar outcrops to the north and the Tafilalt Basin to the west). On the Meharez High, the sponge-bryozoan mounds grew vertically during times of high relative sea-level. Growth terminated when the buildups were covered by crinoidal and oolitic limestones during falling sea-level and lowstand stages (Bourque *et al.* 1995).

In the Tafilalt, approximately 100 Visean carbonate mud mounds are exposed (Wendt *et al.* 2001). However, several of these have also been interpreted as channels, filled with calcarenitic and finer-grained material, and not representing true mud mounds (Klug *et al.* 2006).

On the Meharez High, the exposed buildups are 50 m (locally up to 120 m) high and 2–3 km broad (Bourque *et al.* 1995). It may well be that even larger buildups exist in the subsurface. The size distribution of the Devonian mud mounds shows that it is inadvisable only to consider the well known examples as analogues. Most of the famous Devonian mounds in Morocco and Algeria (Brachert *et al.* 1992; Kaufmann 1998; Wendt & Kaufmann 1998) are rather small (few metres to tens of metres high and wide), economically unattractive buildups, but the less well-known Middle Devonian reefal mounds of the Zemour in the SW Tindouf Basin (Dumestre & Illing 1967) show that buildups at this time were also capable of accumulating 80 m thick coral-stromatoporoid-rich limestones with good reservoir potential, with aerial extents of up to 2 km.

Conclusions

A preliminary sequence stratigraphic framework is presented for the Early Carboniferous of North Africa that shows a good correlation with published global sequences and eustatic sea-level curves. However, the relatively sparse sedimentological database available regionally, and the limited biostratigraphic control, further hampered by contradictory published biostratigraphic interpretations, emphasize the need for further work in the region to develop a more robust regional synthesis of the Carboniferous sequence development in North Africa.

Four types of potential stratigraphic traps are recognized (truncation traps, depositional pinchout traps, incised valley-fills and carbonate buildups). Of these, truncation plays have the highest potential as exploration targets. Depositional pinchout traps of basin-centred sands may have been overlooked in the past and offer a higher risk but potentially volumetrically significant target. These may be imaged on future high-quality 3D seismic. Such reservoirs are believed to be a particular feature of the middle to upper Palaeozoic succession, as the basins changed from low-relief intra-cratonic sag basins (Late Cambrian to Early Devonian) to ramps with locally steepened profiles (Middle Devonian to Carboniferous). High-amplitude sea-level falls in the Carboniferous provided a mechanism to deliver clastics into the distal parts of the basins and may even have led to detached lowstand accumulations (the latter being a hypothesis that is not yet confirmed). Incised valley-fills also provide opportunities for thickened and stratigraphically discrete reservoir sections, and require a detailed knowledge of the sequence stratigraphic framework for prediction.

This study was funded by the North Africa Research Group (University of Manchester) sponsored by Anadarko, BG Group, ConocoPhillips, Hess, Maersk, Oxy, Petro-Canada, PlusPetrol, RepsolYPF, RWE, Wintershall and Woodside.

References

Bourque, P. A., Madi, A. & Mamet, B. L. 1995. Waulsortian-type bioherm development and response to sea-level fluctuations: upper Visean of Béchar Basin, western Algeria. *Journal of Sedimentary Research*, **B65**, 80–95.

Brachert, T. C., Buggisch, W., Flügel, E., Hüssner, H. M., Joachimski, M. M., Tourneur, F. & Walliser, O. H. 1992. Controls of mud mound formation: the Early Devonian Kess–Kess carbonates of the Hamar Laghdad, Antiatlas, Morocco. *Geologische Rundschau*, **81**, 15–44.

Colombo, F. & Bensalah, M. 1991. Le Westphalien continental de la région de Bechar (Algérie) Considérations sédimetologiques. *Bulletin d'Office Nationale Géologique Algérie*, **2**, 49–52.

Conrad, J. 1984. *Les séries carbonifères du Sahara central algérien. Stratigraphie, sédimentation, évolution structurale*. PhD thesis, Université d'Aix-Marseille, France.

Conrad, J. 1985. Northwestern and central Saharan areas – Ahnet–Mouydir area. *In*: Diaz, C. M., Wagner, R. H., Winkler-Prins, C. F. & Granados, L. F. (eds) *The Carboniferous of the World II: Australia, Indian Subcontinent, South Africa, South America, & North Africa*. IUGS Publication Instituto Geologico y Minero de España & Empresa Naçional Adaro de Investigaçiones Mineras, Spain, **20**, 317–322.

Conrad, J., Massa, D. & Weynant, M. 1986. Late Devonian regression and early Carboniferous transgression of the North African Platform. *Annales Société Géologique Belgique*, **109**, 113–122.

Davydov, V., Wardlaw, B. R. & Gradstein, F. M. 2004. The Carboniferous period. *In*: Gradstein, F. M., Ogg, J. O. & Smith, A. G. (eds) *A Geological Time Scale 2004*. Cambridge University Press, Cambridge, 222–248.

Diaz, C. M., Wagner, R. H., Winkler-Prins, C. F. & Granados, L. F. 1985. *The Carboniferous of the World II: Australia, Indian Subcontinent, South Africa, South America, & North Africa*. IUGS Publication Instituto Geologico y Minero de España & Empresa Naçional Adaro de Investigaçiones Mineras, Spain, **20**, 298–477.

Dumestre, A. & Illing, L. V. 1967. Middle Devonian reefs in Spanish Sahara. *In*: Oswald, D. H. (ed.) *International Symposium on the Devonian System*. Alberta Society of Petroleum Geology, Calgary, **II**, 333–350.

Fröhlich, S., Petitpierre, L., Redfern, J., Grech, P., Bodin, S. & Lang, S. in press. Sedimentological and sequence stratigraphic analysis of Carboniferous deposits in western Libya: recording the sedimentary response of the northern Gondwana margin to climate and sea-level changes. *Journal of African Earth Sciences*; doi: 10.1016/j.jafrearsci.2009.09.007.

Johnson, J. G., Klapper, G. & Sandberg, C. A. 1985. Devonian eustatic fluctuations in Euramerica. *Geological Society of America Bulletin*, **96**, 567–587.

Kaiser, S., Becker, T. R. *et al*. 2004. Sedimentary succession and neritic faunas around the Devonian-Carboniferous boundary at Kheneg Lakahal south of Assa (Dra Valley, SW Morocco). *In*: El Hassani, A. (ed.) *Devonian of the Western Anti Atlas: Correlations and Events*. Documents de l'Institut Scientifique, Université Mohammed V Agdal, Rabat, **19**, 69–74.

Kaufmann, B. 1998. Middle Devonian reef and mud mounds on a carbonate ramp: Mader Basin (eastern Anti-Atlas, Morocco). *In*: Wright, V. P. & Burchette, T. P. (eds) *Carbonate Ramps*. Geological Society, London, Special Publications, **149**, 417–435.

Klug, C., Döring, S., Korn, D. & Ebbighausen, V. 2006. The Viséan sedimentary succession at the Gara el Itima (Anti-Atlas, Morocco) and its ammonoid faunas. *Fossil Record*, **9**, 3–60.

Legrand-Blain, M. 1985. Northwestern and central Saharan areas – Illizi Basin. *In*: Diaz, C. M., Wagner, R. H., Winkler-Prins, C. F. & Granados, L. F. (eds) *The Carboniferous of the World II: Australia, Indian Subcontinent, South Africa, South America, & North Africa*. IUGS Publication Instituto Geologico y Minero de España & Empresa Naçional Adaro de Investigaçiones Mineras, Spain, **20**, 329–333.

Lemosquet, Y. & Pareyn, C. 1985. Northwestern and central Saharan areas – Bechar Basin. *In*: Diaz, C. M., Wagner, R. H., Winkler-Prins, C. F. & Granados, L. F. (eds) *The Carboniferous of the World II: Australia, Indian Subcontinent, South Africa, South America, & North Africa*. IUGS Publication Instituto Geologico y Minero de España & Empresa Naçional Adaro de Investigaçiones Mineras, Spain, **20**, 306–315.

Lubeseder, S. 2005. *Silurian and Devonian sequence stratigraphy of North Africa: regional correlation and sedimentology (Morocco, Algeria, Libya)*. PhD thesis, University of Manchester.

Malti, F. Z., Benhamou, M., Mekahli, L. & Benyoucef, M. 2008. The development of the Carboniferous Ben-Zireg-Zousfana Trough in the northern part of the Bechar Basin, Western Algeria: implications for its structural evolution, sequence stratigraphy and palaeogeography. *Geological Journal*, **43**, 337–360.

Massa, D. 1988. *Paleozoique de Libye occidentale – stratigraphie et paleogeographie*. PhD thesis, Université de Nice, France.

Massa, D. & Vachard, D. 1979. Le Carbonifère de Libye occidentale. Biostratigraphie et Micropaléontologie. Position dans le domaine téthysien d'Afrique du Nord. *Revue Institute Français du Pétrole*, **34**, 1–65.

Mergl, M. & Massa, D. 2000. A palaeontological review of the Devonian and the Carboniferous succession of the Murzuq Basin and the Djado Sub-Basin. *In*: Sola, M. A. & Worsley, D. (eds) *Geological Exploration in Murzuq Basin*. Elsevier, Amsterdam, 41–88.

Meyer-Berthaud, B., Rücklin, M., Soria, A., Belka, Z. & Lardeux, H. 2004. Fransian plants from the Dra Valley, southern Anti-Atlas, Morocco. *Geological Magazine*, **141**, 675–686.

Persits, F., Ahlbrandt, T., Tuttle, M., Charpentier, R., Brownfield, M. & Takahashi, K. 1997. Maps showing geology, oil and gas fields and geological provinces of Africa. United States Geological Survey, Open-File Report **97-470A**, 1–10.

Vos, R. G. 1977. Sedimentology of an Upper Paleozoic river, wave and tide influenced delta system in southern Morocco. *Journal of Sedimentary Petrology*, **47**, 1242–1260.

Wendt, J. & Kaufmann, B. 1998. Mud buildups on a Middle Devonian carbonate ramp (Algerian Sahara). *In*: Wright, V. P. & Burchette, T. P. (eds) *Carbonate Ramps*. Geological Society, London, Special Publications, **149**, 397–415.

Wendt, J., Kaufmann, B. & Belka, Z. 2001. An exhumed Palaeozoic underwater scenery; the Visean mud mounds of the eastern Anti-Atlas (Morocco). *Sedimentary Geology*, **145**, 215–233.

Wendt, J., Kaufmann, B., Belka, Z., Klug, C. & Lubeseder, S. 2006. Sedimentary evolution of a Palaeozoic basin and ridge system: the Middle and Upper Devonian of the Ahnet and Mouydir (Algerian Sahara). *Geological Magazine*, **143**, 269–299.

Wendt, J., Kaufmann, B., Belka, Z. & Korn, D. 2009. Carboniferous stratigraphy and depositional environments in the Ahnet Mouydir area (Algerian Sahara). *Facies*, **55**, 443–472.

Integrated petroleum systems and play fairway analysis in a complex Palaeozoic basin: Ghadames–Illizi Basin, North Africa

R. J. DIXON, J. K. S. MOORE, M. BOURNE, E. DUNN, D. B. HAIG, J. HOSSACK, N. ROBERTS, T. PARSONS and C. J. SIMMONS

BP Exploration, Chertsey Road, Sunbury-on-Thames, Middlesex TW16 7LN, UK
(e-mail: dixonr2@bp.com)

Abstract: The Ghadames–Illizi Basin system is a highly productive petroleum province with a long exploration history in Algeria, Libya and Tunisia (from the late 1950s to present day). Ongoing exploration success in all three countries suggests that it will continue to provide attractive exploration targets in the future. The basin has a long (Cambrian to Plio-Pleistocene) and complex geological evolution characterized by multiple phases of subsidence punctuated by significant regional uplift events. Two 'world-class' petroleum source rocks of different geological age are present (Lower Silurian and Upper Devonian) with similar depositional environments and geochemical characters. Both source horizons have generated significant volumes of oil and gas. Migration is strongly influenced by the stratigraphic architecture of the basin fill, notably distribution of regional seals and the complex patterns of subcrop and onlap across regional unconformities. Multiple reservoir–seal combinations are presented by Late Ordovician glaciogenic sediments and younger Silurian through to Carboniferous paralic sequences. Integrating the stratigraphic relationships with the complex burial history of the basin (timing of uplift, degree of tilting, amount of section removed by erosion) is not a trivial task, but is key to exploration success in such a complex basin. With the aid of 3D basin reconstruction and fluid flow modelling software, we can attempt to capture the stratigraphic and structural complexity and make exploration predictions. If basin modelling techniques are to be optimally applied in such settings, a fully integrated and geologically realistic approach involving sedimentologists, structural geologists, geophysicists and geochemists is required. A modelling approach, workflow and some results are presented.

Keywords: Ghadames–Illizi basin, petroleum systems, play fairway analysis

The location of the major Palaeozoic basins in North Africa and the major tectonic elements of the North African Margin are shown in Figure 1. At a crustal scale African Gondwana is dominated by two major cratonic blocks, the West African Craton in the west and the Saharan Metacraton in the east (Fig. 1). A strong, Late Proterozoic tectonic grain inherited from the Pan-African Orogeny runs between these two cratonic masses and has been reactivated many times, most notably and severely during the Hercynian collision of Gondwana and Laurussia. Great escarpments of tilted, resistant, Palaeozoic strata (Fig. 1) date from this time (LeFranc & Guiraud 1990) and define the remnant Palaeozoic basins as well as strongly influencing subsequent Mesozoic–Cenozoic deposition (LeFranc & Guiraud 1990; Schroter 1996). In the offshore Pelagian Basin, the Sirt Basin and the offshore areas of Egypt and the Levant Palaeozoic sequences are probably present at depth beneath thick sequences of Mesozoic and Cenozoic strata. The most likely position of the Tauride Block (most of southern Turkey) during the Palaeozoic was adjacent to African Gondwana (Fig. 1). The great similarities in Palaeozoic stratigraphy and lithology between the Tauride Block and African Gondwana have led to this hypothesis (Demirtash 1984; Monod *et al.* 2003; Smith 2006). The Tauride Block and other previously conjugate terrains (e.g. Apulia and the Hellenides; Smith 2006) are now separated from African Gondwana by Neotethyan oceanic crust (of probable Cretaceous age).

Ghadames–Illizi Basin

Figure 1 shows the location of the Ghadames–Illizi Basin. The basin is large, covering an area of some 400 000 km^2 and reaches a maximum depth in its northwestern part, where the top of crystalline basement is found at depths approaching 8000 m. In a regional sense the basin has a relatively simple 'saucer-like' structure. The basin was first explored by the oil industry in the 1950s and in total 32 BBOE of petroleum (oil and gas) have been discovered to date. Despite its relatively simple regional structure, the Ghadames–Illizi Basin has a long and complex history. For example, although now separated from the Ahnet Basin to the west and the Murzuq Basin to the SE by regional highs or arches (Fig. 1), it is considered likely that all of these basins were connected during the early part of the Palaeozoic (Beuf *et al.* 1971), only becoming separate depositional entities from the Middle Devonian onwards as the effects of 'Hercynian' compression became increasingly pronounced. The interaction of tectonics with sedimentation has exerted a very strong influence on the distribution of both reservoir and source facies as well as on later source rock maturation and migration. Our evaluation of the Ghadames–Illizi Basin has involved a combination of geological fieldwork on the surrounding outcrops in Algeria, Tunisia and Libya and subsurface studies of a large well and seismic database (*c.* 200 wells and *c.* 125 000 km of 2D seismic).

Megasequence framework

For the basin model to be geologically realistic the basin's burial history must be reconstructed using all available data (cores, wells, seismic and outcrops). The purpose of this section is to review the structural and stratigraphic framework of the basin. The key basin forming and uplift episodes represented in the Ghadames–Illizi Basin (and in the other North African basins illustrated in Fig. 1) are shown in Figure 2. Several megasequences are recognized.

VINING, B. A. & PICKERING, S. C. (eds) *Petroleum Geology: From Mature Basins to New Frontiers – Proceedings of the 7th Petroleum Geology Conference*, 735–760. DOI: 10.1144/0070735

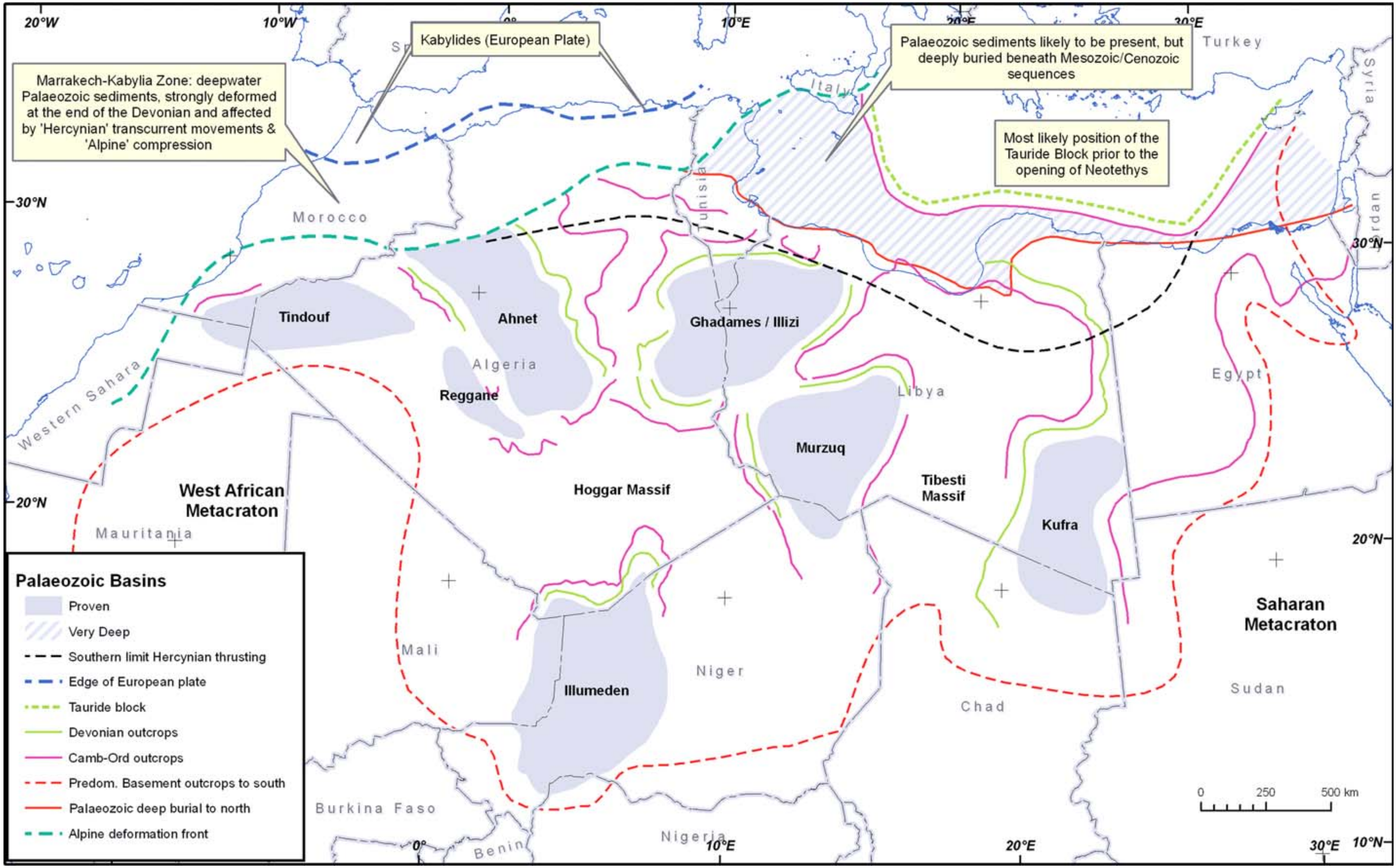

Fig. 1. Major tectonic elements and Palaeozoic basins of North Africa.

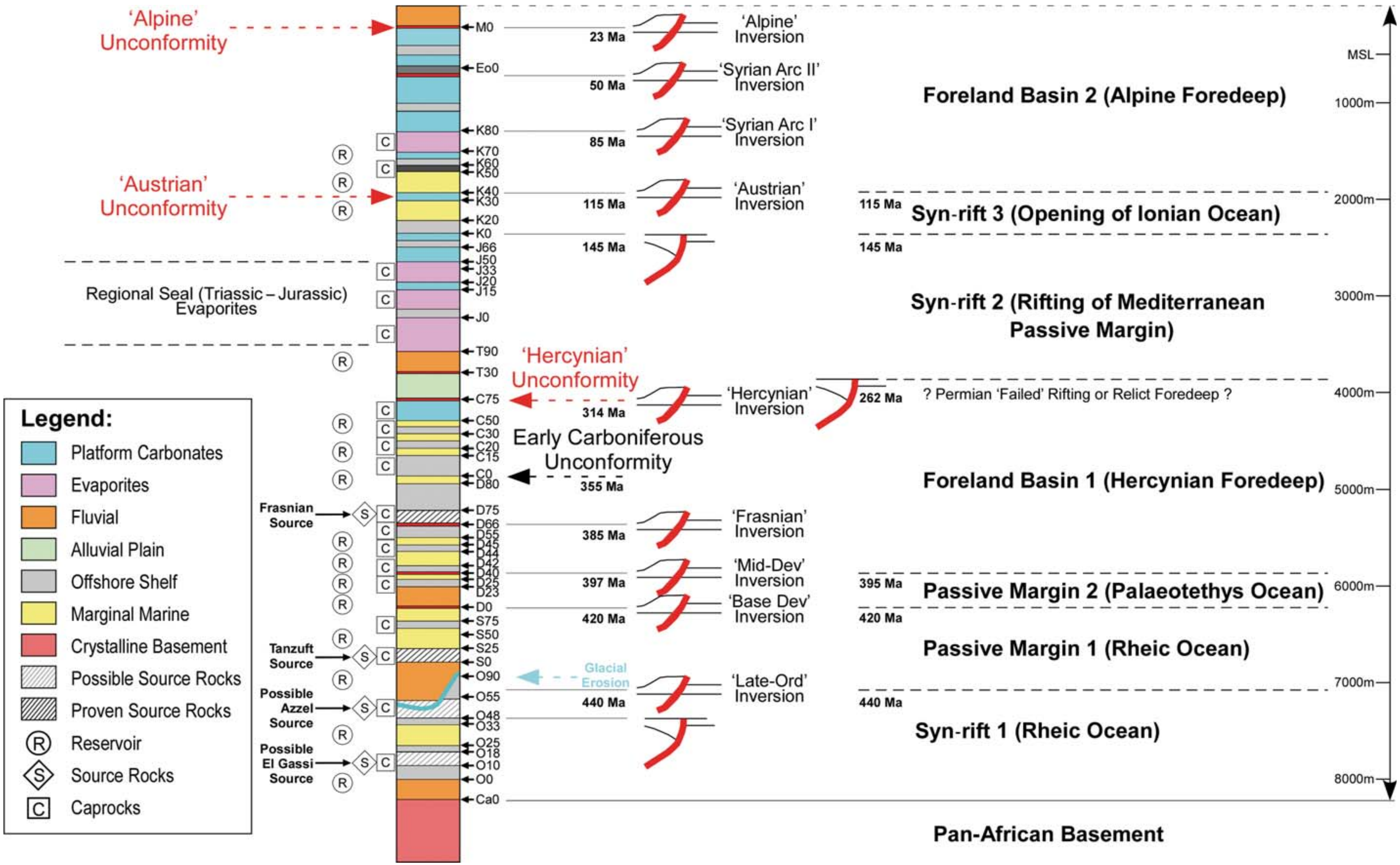

Fig. 2. Stratigraphic framework of the Ghadames–Illizi Basin. Section is schematic, but is based on the central part of the basin where up to 8000 m of sediment is preserved (arrows denote structural surfaces incorporated in the 3D basin model).

Syn-rift 1 Megasequence (Rheic Ocean rifting)

After a poorly defined Cambro-Ordovician Syn-Rift phase (opening of the Rheic Ocean; Stampfli & Borel 2002), two passive margin 'drift' megasequences were deposited, related to the Rheic Ocean and Palaeotethys Ocean, respectively, before the onset of the 'Hercynian Foredeep' (Foreland Basin 1 in Fig. 2).

Passive Margin 1 Megasequence (Rheic Ocean drift)

The first passive margin megasequence is the Rheic Ocean Drift succession, including the O90–S75 sequences of the Mamuniyat (O90–S0), Tanzuft (S0–S25) and Akakus (S25–S75). This megasequence is separated from the later Palaeotethys Ocean Drift succession by the Base Devonian Unconformity ('Caledonian'). According to Stampfli & Borel (2002), this unconformity records uplift associated with the separation of the 'Hun Superterrane' from African Gondwana ('Ridge–Push' mechanism of Stampfli & Borel 2002). The Tanzuft is a major petroleum source rock.

Passive Margin 2 Megasequence (Palaeotethys Ocean drift)

The Palaeotethys Ocean Drift succession ranges in age from D0 to D40 including the Tadrart (D0–D23), Emsian Shale (D23–D25) and Wan Kasa (D25–D40). Stampfli & Borel's (2002) 380 Ma plate reconstruction shows a wide Palaeotethys Ocean during the Late Devonian, although there are other authors who disagree with this interpretation and place Laurussia and Gondwana much closer together at this time (McKerrow *et al.* 2000). Both authors agree that continental collision began in the west and progressed eastwards with time, but we would agree with the McKerrow *et al.* interpretation and would argue that the continents started to collide in the Mid Devonian (Emsian–Eifelian). This is consistent with regional evidence of important uplift and erosion during the Middle Devonian (Emsian and Frasnian events, discussed below; Fig. 8) The Frasnian shale is a major petroleum source rock (Lüning *et al.* 2004*b*).

Foreland Basin 1 Megasequence ('Hercynian' Foredeep)

In order to reconstruct the early history of the 'Hercynian Foredeep' it is important to understand the evolution of the western Palaeozoic basins and the role of the West African Craton. The West African Craton is characterized by extremely thick crust [up to 250 km (Liegeois *et al.* 2005)]. Throughout the Neoproterozoic and Palaeozoic the craton remained at or close to sea-level. In the intracratonic Taoudenni Basin *c.* 5 km of paralic–shelfal sediment is preserved in the Gourma Trough (Villeneuve 2005). During the Lower Palaeozoic the Taoudenni Basin was connected to the Tindouf and Reggane basins (Fig. 1) and it shares a similar Cambro-Ordovician and Silurian stratigraphy. This connection was broken by regional uplift of the Regubiat Rise in the Late Silurian–Early Devonian (Guerrak 1989). The Taoudenni Basin was also uplifted and eroded at this time and a strong Base Devonian Unconformity locally completely removes the Silurian section. Deposition did not recommence in the Taoudenni area until the Emsian (Guerrak 1989; Herrera & Racheboeuf 2001).

The depositional history of the western Palaeozoic basins (Taoudenni, Tindouf, Reggane and Ahnet) starts to diverge from that of the more easterly basins (Ghadames–Illizi and Murzuq) during the Eifelian (D40–D42). Up until this time the pattern of regressions and transgressions seen in the Ghadames–Illizi Basin can be matched in the Ahnet, Reggane and Tindouf basins, suggesting that sediment supply and subsidence were balanced across the margin. During the Eifelian (D40–D42) the West African Craton appears to have stopped supplying clastic detritus into the westerly basins and they become carbonate dominated. We interpret the regional change from clastics to carbonates as the result of tectonic loading associated with the onset of the Laurussia–Gondwana collision. The West African Craton is depressed and clastic sediment supply can no longer keep pace with subsidence. The resulting clear waters allow carbonates to thrive and aggrade (e.g. Wendt *et al.* 1997). Accelerating tectonic subsidence also led to the establishment of deepwater conditions in the Ahnet Basin by Frasnian times (Dixon 1997*c*). The emergence of the deforming Marrakech–Kabylia Zone to the north is indicated by the development of a marginal offshore carbonate belt in the northernmost Ahnet Basin and in the Tindouf Basin (Fig. 5). This northern uplift (and related regional uplifts within the basins, e.g. Mole D'Ahara) generated a number of silled, anoxic depocentres where the organically rich, Frasnian source facies accumulated (Lüning *et al.* 2004*a*, *b*).

Up to 800 m of Fammenian sediments (D75–D80) overlie the Frasnian in the southern part of the Ahnet Basin and clinoform heights from regional 2D seismic (Barr *et al.* 1994) confirm progradation into deepwater (300–400 m). The clinoforms record the northward progradation of a large but 'muddy' delta, the topsets of which are the so-called 'Strunian Sands' (D80–C0), the equivalent of the 'F2' or 'Tahara' sandstones of the Ghadames–Illizi Basin. In the Tindouf Basin the Late Devonian section is even thicker (up to 1.8 km thick; Guerrak 1989), suggesting that it was also subsiding rapidly. Latest Fammenian sandy deltas fringe its northern margin (Cavaroc *et al.* 1976; Vos 1977; Graham 1982; Brice *et al.* 2007). These deltas are derived from the actively uplifting Marrakech–Kabylia Zone and imply that continental collision was well advanced by the end of the Devonian (cf. McKerrow *et al.* 2000).

'Pre-Hercynian' burial. Estimates of Pre-Hercynian burial are always fraught with uncertainty, because significant Post-Hercynian erosion has removed large amounts of this stratigraphy. Recent regional work on the Carboniferous has helped to constrain erosion estimates for the Ghadames–Illizi Basin. A maximum Carboniferous thickness of 1.4 km seems reasonable based on well data and biostratigraphic data (which proves a virtually complete section). In the Ghadames–Illizi Basin the transition from the Devonian to the Carboniferous is essentially conformable from a regional perspective (there is a stratigraphic hiatus – the Early Tournaisian is apparently missing or extremely condensed; Jones 1997). The depositional facies on either side of this hiatus are similar, although there is a marked shallowing of water depth into the Carboniferous. In the Ahnet Basin further west, the Early Tournaisian is also missing and Middle Tournaisian fluvial sediments rest unconformably on 'Strunian' shoreface sequences (Dixon 1997*a, b, c*). Visean marine sediments (clastics and carbonates) are also present in the Bechar area further north, unconformably overlying Frasnian shales (Madi *et al.* 2000), but no younger Carboniferous sediments are preserved. Barr *et al.* (1994) estimate that up to 2.0 km of Carboniferous was originally present in the Ahnet Basin. The Tindouf Basin is similar to the Ahnet in that nothing younger than Visean is preserved. Boote *et al.* (1988) estimate that at least 2.5 km of Carboniferous was originally present. The large thicknesses of Mid–Late Devonian and Carboniferous sediments in the western basins (over 4 km in the Tindouf Basin) led to significant maturation of both Early Silurian and Late Devonian source rocks during the Carboniferous and it seems likely that they passed through the gas window at this time (Boote *et al.* 1988).

'Pre-Hercynian' structures. In some cases it is possible to demonstrate that the regional arches also had a Pre-Hercynian expression. This can be shown for the Mole D'Ahara in the

Ghadames–Illizi Basin where subsurface mapping (2D seismic and wells) has illustrated that the structure was uplifted several times, in the Late Silurian–Early Devonian (Base Devonian or 'Caledonian' Unconformity), in the Mid Devonian and in the Late Devonian (Base Frasnian Unconformity). Further east, Devonian outcrops on the flanks of the Tibesti–Sirt Arch reveal a similar phase of Late Silurian–Early Devonian uplift. The cross-bedded fluvial sandstones in Dor el Gussa (western flank of the arch) show palaeocurrents toward the west, whereas those at Jebel Eighi (eastern flank) show palaeocurrents toward the NE (Clark-Lowes & Ward 1991). In the Ahnet Basin similar trends are seen at the southern end of the Ougarta Foldbelt, where the Bled el Mass basement high was exposed during the Middle Devonian and actively shedding sediment westward into the basin (Dixon 1997*b*). The Devonian and Early Carboniferous sequences accumulated on a very broad (hundreds of kilometres) fairly shallow shelf with a gentle ramp into the deeper waters of the Tindouf Basin toward the NW. Sand supply was from a poorly vegetated land area south of the Hoggar Massif (Fig. 1). Although this is regionally the case, it is clear that in a number of areas subtle, but, large -scale, regional uplift events punctuate the stratigraphy (Fig. 2). Each uplift event probably led to the emergence of new land areas and the erosion of earlier shelfal sequences, thus providing new sediment source areas for the syn-uplift sequences. A good example of this is the Mid Devonian 'F3' sand that fringes the northern and eastern flank of the Mole D'Ahara (Chaouchi *et al.* 1998). A wide range of shelfal sandstone architectures is possible in this environment (sheets, bars, spits, incised valleys, tidal estuaries, etc.). All of these locally offer excellent stratigraphic trapping potential (e.g. the giant Alrar and Al Wafa Fields; Chaouchi *et al.* 1998).

'Hercynian' Orogeny. The climax of the Hercynian orogenic phase in North Africa took place in the Late Carboniferous, although it is clear that significant pulses of deformation had been propagating through African Gondwana since the Mid Devonian (onset of Laurussia–Gondwana collision), including a major Early Carboniferous Unconformity at the northern margin of the basin (Fig. 2; Dixon *et al.* 2009). The southern limit of Hercynian thrusting (determined by seismic mapping; Dixon *et al.* 2009) is shown in Figure 1. For most of the Lower Palaeozoic regional drainage is from south to north (Beuf *et al.* 1971). The first evidence of a change in regional drainage comes from the Tindouf Basin in the Late Devonian where southerly directed drainage suggests that the Marrakech–Kabylia zone was a land area at this time (Cavaroc *et al.* 1976; Vos 1977). Early Carboniferous regional uplift is marked at the northwestern margin of the Ghadames–Illizi Basin by a pulse of Visean clastic sediments that prograde from the NW towards the basin centre (IFP/Sonatrach/Beicip-Franlab 2006) and by northward-prograding, marine clastic systems in Tunisia, Cyrenaica and Crete. Later in the Carboniferous there is a widespread change from marine to non-marine sedimentation across African Gondwana (C75–P5 sequence). These non-marine conditions prevail in all of the internal basins (probably represented by the basal sequences of the 'Continental Intercalaire'; Lefranc & Guiraud 1990), whereas limited data from outcrops in Tunisia (Busson & Burrollet 1973) and Crete (Robertson 2007) and subsurface data in Cyrenaica (El-Arnauti & Shelmani 1988) confirm the continuation of marine conditions into the Early Permian north of the Hercynian Deformation Front.

Following the deposition of these Early Permian sediments there was a prolonged hiatus (*c*. 60 Ma), before deposition resumed in Gondwana with the accumulation of Late Permian carbonates in Tunisia, the Levant and on the Tauride Block (Demirtash 1984). A marked angular unconformity records this event and can be seen both in the field and on regional seismic data (Fig. 4). This unconformity is most often called the 'Hercynian' Unconformity but in fact it formed some 60 Ma later than the 'Hercynian' event and is probably more related to the opening of the Neotethys Ocean (Dixon *et al.* 2009). Palaeozoic sediments were removed over large areas of the North African margin at this time leaving the current basins as erosional remnants (Fig. 1). The regional 'Hercynian Unconformity' map (Fig. 3) nicely illustrates the 'saucer-like' geometry of the Ghadames–Illizi Basin.

In the Ghadames–Illizi Basin the 'Hercynian' Unconformity is progressively onlapped from north to south by Mesozoic sediments. In southern Tunisia Late Permian carbonates rest unconformably on Late Carboniferous–Early Permian carbonates (Wahlman 1991). In the Djebel Tebaga outcrops Middle to Late Permian carbonate facies are exposed including reefal buildups (Archaeolithoporella–Tubiphytes boundstones). A NW–SE trending reef belt is developed (Toomey 1991) bounded to the north by a 'shale' basin and to the south by mixed carbonate and clastic shoreline fringing the northern flank of the emergent Talemzane Arch (Fig. 4). In the 'shale basin' over 4000 m of Late Permian 'shelf' facies were deposited (Wahlman 1991). The existence of very thick, Middle to Late Permian sequences to the north of Djebel Tebaga has led some authors to suggest that this may be evidence of rifting (Dridi 2000) and other authors (e.g. Stampfli *et al.* 2001) to suggest that Permian oceanic crust might be present in the Eastern Mediterranean. This is a controversial topic as evidence from the Eastern Mediterranean ophiolites suggests that the most likely age of/oldest oceanic crust is Jurassic or Early Cretaceous (Robertson & Dixon 1984). An alternative model is that the Tunisian, Late Permian basin represents a small transtensional basin underlain by attenuated continental crust.

Syn-rift 2 Megasequence (rifting of Mediterranean passive margin)

Evidence for Triassic rifting in the Eastern Mediterranean is strong (Druckman 1984; Garfunkel & Derin 1984). Similar strong evidence for Triassic rifting is found in Morocco (e.g. The Argana Basin; Beauchamp 1988) and its counterpart in North America (Benson & Doyle 1988). Analysis of regional seismic data from the Ghadames–Illizi Basin reveals little evidence of Triassic rifting, although it has been described locally from the northwestern part of the basin in the Berkine area (Turner *et al.* 2001). In this area NNE to SSW trending 'Pan-African' lineaments have been reactivated as extensional faults. These faults controlled the thickness and facies of Triassic sediments and probably also localized extrusive volcanic activity (fissure fed eruptions) that in turn led to the development of extensive fields of basaltic lava of Carnian age [up to 68 000 km^2 in the northwestern part of the basin (IFP 1998)]. Regional drainage at this time was toward the NNE (Acheche *et al.* 2001; Turner *et al.* 2001) into the developing 'Neotethyan' rift and it seems likely that most, if not all, of the sediment was derived from uplifted Lower Palaeozoic sandstones and basement in the Hoggar region to the south (Fig. 1). The northern margin of the Ghadames–Illizi Basin at this time was formed by the Medenine High (Benton *et al.* 2000) a subtle NW–SE-trending feature broadly coincident with the old Permian reef trend and located on the northern flank of the Talemzane Arch. Triassic fluvial sediments thin over this high and have locally been removed completely by later erosion (Aptian), although it seems likely that they were originally deposited across the high, as palaeocurrents at Djebel Rehach (on the immediate southwestern flank of the structure) are uniformly toward the north (suggesting that the high was not there at the time). A similar relationship can be observed on the eastern flank of the Ghadames–Illizi Basin at Djebel Gharian in Libya. Here palaeocurrents suggest flow from east to west, suggesting the existence of a high on the eastern margin of the basin (Assereto & Benelli 1971). Further north in

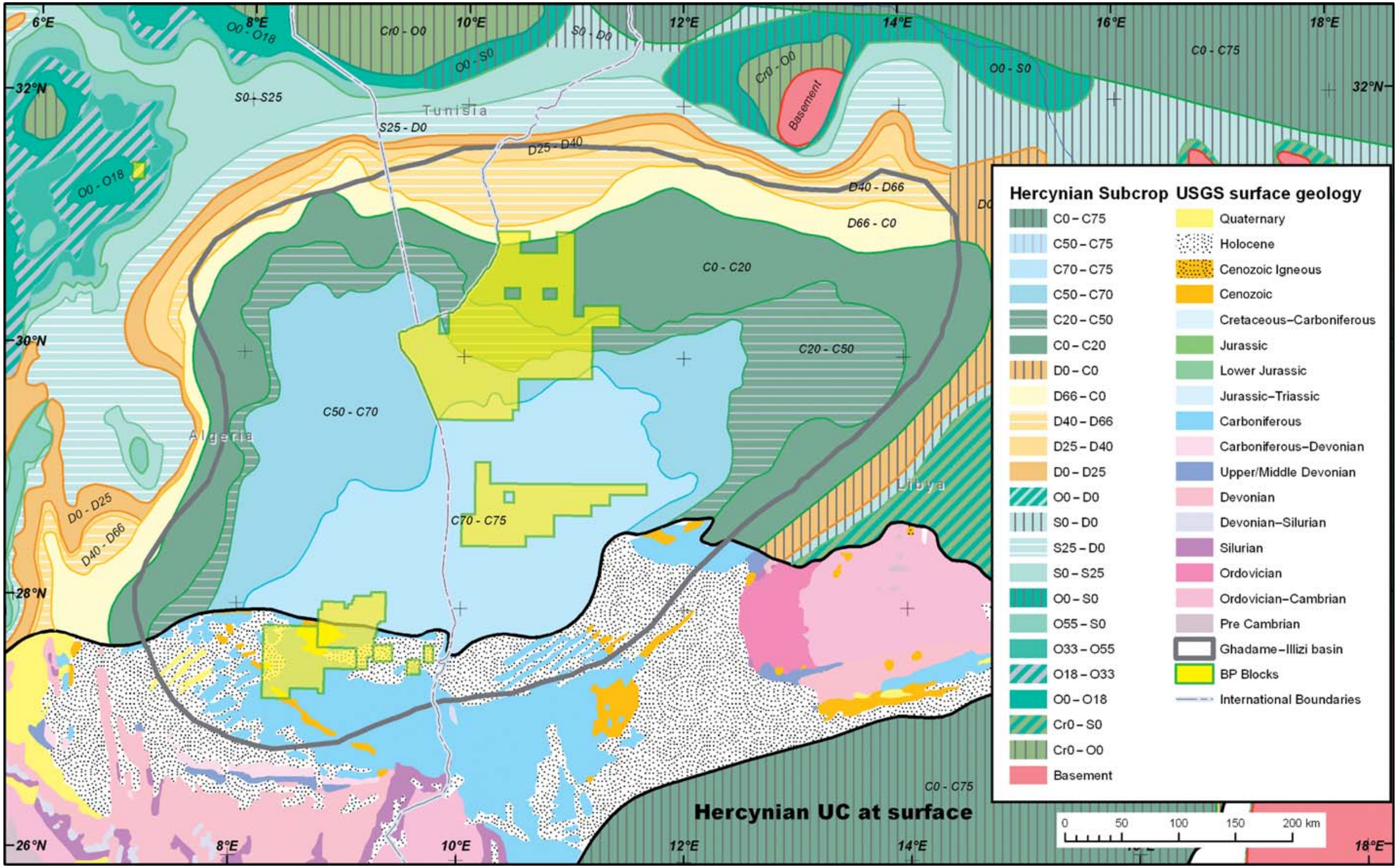

Fig. 3. Outline of the Ghadames–Illizi Basin (solid grey line) and subcrop map to the 'Hercynian' Unconformity (based on BP data).

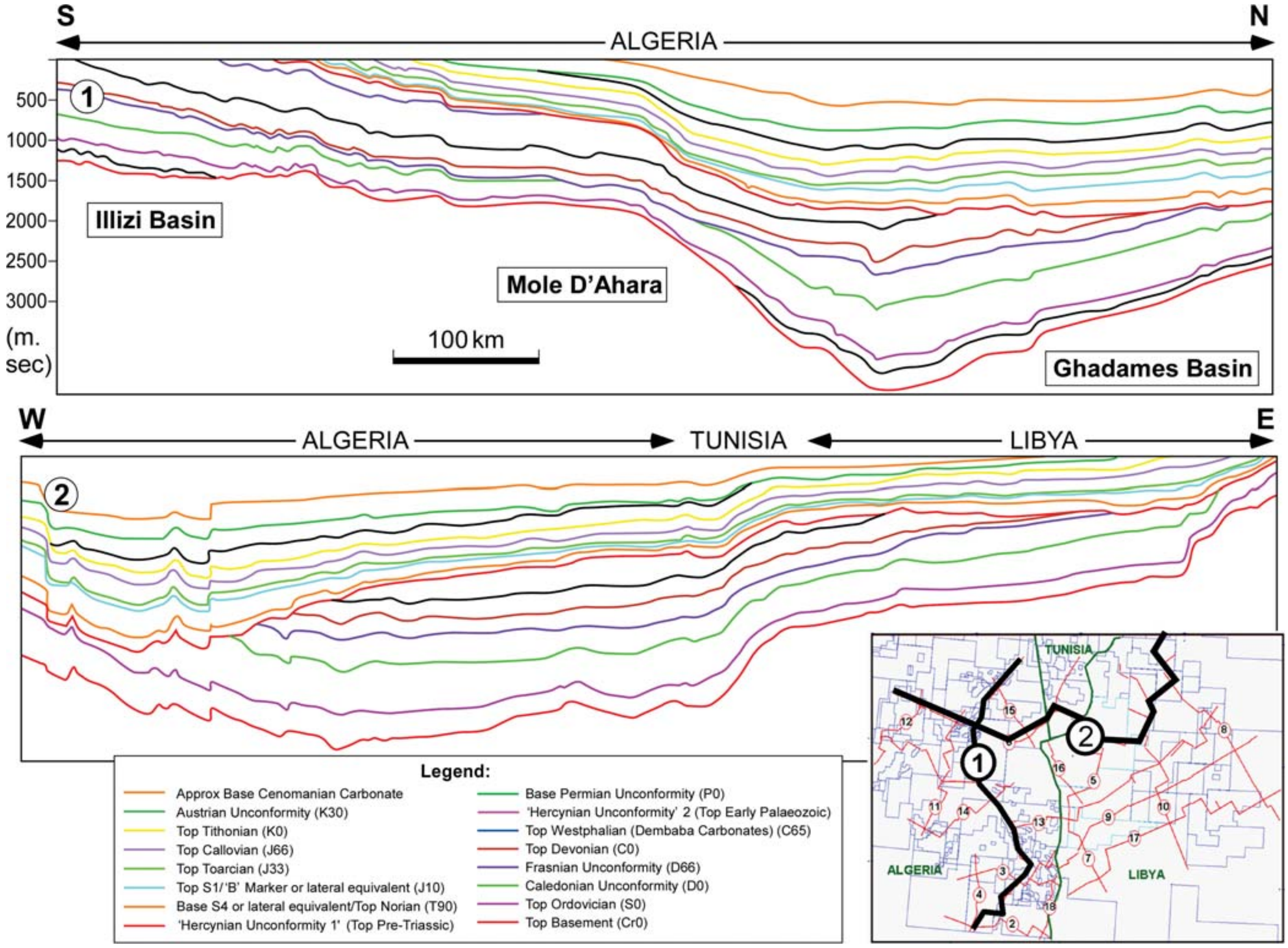

Fig. 4. Line drawings of two mega-regional seismic profiles that cross the Ghadames–Illizi Basin.

the Pelagian Basin and in Malta and Sicily, the Triassic is represented by a thick succession of platform carbonates. The Djebel Tebaga–Medenine High continued to be an important structure throughout the Jurassic, although it is unlikely ever to have been elevated above sea-level. The Jurassic sequences thin over it (Benton *et al.* 2000; Turner & Sherif 2007) and there are some important facies changes from south to north across it, but it seems likely that the Jurassic was only removed by later (Cretaceous–Aptian) erosion.

Post-rift 2 Megasequence (carbonates and evaporites)

Post-rift thermal subsidence after Early Triassic rifting created a broad area of Late Triassic and Jurassic evaporitic deposition in a basin that also extended northwestwards into the Moroccan Atlas (Turner & Sherif 2007). Up to 1250 m of evaporitic facies accumulated in the basin, typically with halite in the centre of the basin grading outward through anhydrites to interbedded dolomites and shales toward the edges of the basin (Turner & Sherif 2007). To the north of the Medenine High Mid Triassic evaporites are also present (Acheche *et al.* 2001) and are widespread across the Mediterranean, but the Jurassic is dominated by platform carbonates (Soussi & Ben Ismail 2000). The Djebel Tebaga–Medenine High seems to have acted as a 'sill' separating this marine area to the north from the evaporitic system to the south. Thinning and facies changes in wells are illustrated by Turner & Sherif (2007) and can also be observed on regional seismic lines (Fig. 4). The evaporitic sequence forms a very effective regional caprock to the underlying Triassic fluvial sandstones. These sandstones are locally juxtaposed against the Lower Palaeozoic source rocks (Early Silurian Tanzuft and the Frasnian shale) across the 'Hercynian' Unconformity (Figs 2 & 3), allowing them to be charged with petroleum. The unconformity therefore sets up a very prolific petroleum system containing the super-giant Hassi R'Mel gasfield and a number of giant oilfields in the Berkine area. As shown in Figure 4 (profile 2), the Mesozoic depocentre is offset from the Palaeozoic depocentre; this is also shown in Figure 5, a 3D representation of the main structural surfaces we mapped using our regional 2D seismic database.

Syn-rift 3 Megasequence (formation of the Ionian Ocean)

The Ghadames–Illizi Basin was on the periphery of the Early Cretaceous rifting episode so evident in the Sirt Basin (Gras & Thusu 1998), Gabes Basin (Ben Ferjani *et al.* 1990) and in other similar basins in Central Africa (e.g. Genik 1993) and the Sudan (e.g. Mohamed *et al.* 2001). No evidence of Early Cretaceous rifting has been observed on regional seismic lines from the Ghadames–Illizi Basin (Fig. 4), but Figure 2 clearly shows that the Early Cretaceous was a time of pronounced clastic input into the basin, suggesting that clastic source areas to the south of the basin (the Ougarta Chain and Hoggar Massif) were being rejuvenated at this time (Lefranc & Guiraud 1990; Benton *et al.* 2000). The gently tilted, Palaeozoic sandstones that form the great escarpments of the Tassili N'Ager on the northern flank of the Hoggar Massif were clearly elevated above sea-level at this time as they are onlapped by Early Cretaceous fluvio-lacustrine sediments in the Serouenout area of Hoggar in Algeria (Lefranc & Guiraud

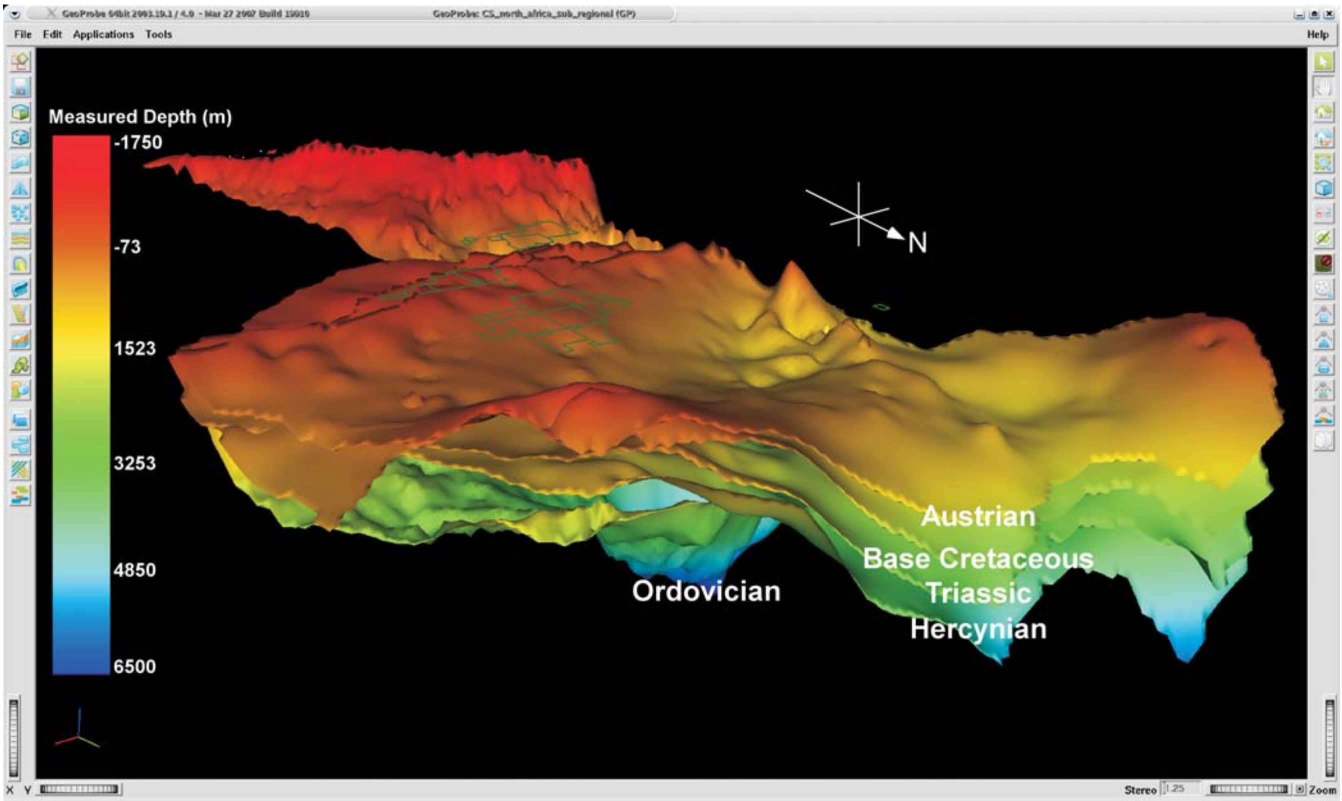

Fig. 5. Three-dimensional 'Geoprobe' image showing the offset Palaeozoic and Mesozoic depocentres and the 'Hercynian' Unconformity (Late Permian Unconformity of Dixon *et al.* 2009).

1990) and in Libya [Djebel Nafusa (Hammuda 1971) and the Sirt Basin (Schroter 1996)]. In the Ghadames–Illizi Basin the Early–Mid Cretaceous sandstones are dominated by fluvial facies (Lefranc & Guiraud 1990) and contain a rich reptilian fauna [including dinosaurs (Benton *et al.* 2000)] together with abundant flora [including ferns and very large tree trunks and stumps (Benton *et al.* 2000; Bamford *et al.* 2002)] suggestive of a stable, humid, non-seasonal, tropical environment (Lefranc & Guiraud 1990).

Slight thickening of the Early Cretaceous into the Ghadames–Illizi Basin suggests that the basin was still subsiding at this time, but the greatest variations in Early Cretaceous thickness are north of the Djebel Tebega–Medenine High, where up to 2000 m of Early Cretaceous deltaic facies are seen (Bishop 1975), and within the grabens of the Sirt Basin, where over 500 m of clastic sediment is preserved (El-Hawat *et al.* 1996; Gras & Thusu 1998). The rift shoulder of the Early Cretaceous rift was located along the northern and eastern margins of the Ghadames–Illizi Basin. The 'Neocomian' through Barremian time interval is dominated by coarse-grained, clastic sediments, but the Aptian is marked by a dramatic return to carbonate facies (in Algeria, Tunisia and Egypt), signifying a major marine transgression southward into North Africa (reaching as far south as the Sudan; Klitzch 1990). The limestone unit forms a good regional seismic horizon (Fig. 4) and is also an excellent reference point in wireline logs from the region. Detailed sedimentological and biostratigraphic work on outcrops of this stratigraphic sequence in Central Tunisia has revealed that an important stratigraphic hiatus, the 'Austrian' Unconformity, also occurs within the Aptian (Chaabani & Razgallah 2006).

The unconformity can be mapped on regional seismic and is locally a strong angular unconformity (Figs 4 & 5). Uplift, tilting and erosion are noticeable on regional seismic profiles from the southern and eastern flanks of the basin and are locally significant (Fig. 4). In the field the 'Austrian' Unconformity is locally spectacular, for example at Djebel Tebaga in southern Tunisia (Fig. 5), where gently dipping Albian sandy limestones rest with marked angular unconformity on more steeply dipping (*c.* 20°) Late Permian carbonates. Similar relationships are also observed further to the east in Jebel Gharian (Assereto & Benelli 1971) and much further to the east in the subsurface of the Western Desert of Egypt, where the karstified Early Aptian, 'Alamein' Dolomite is overlain by the Late Aptian, Dahab Shale. The origin of the 'Austrian' Unconformity in North Africa is uncertain, but it is clearly a major 'plate-scale' event generally characterized by uplift, tilting and erosion at a regional scale, that is, over major regional arches with structural wave lengths of hundreds of kilometres (see Fig. 4).The timing of this event is roughly synchronous with the maturation of and migration from the Palaeozoic source rocks in the Ghadames–Illizi Basin.

Post-rift 3 Megasequence (Neotethys and the Trans-Saharan Seaway)

To the north of the Cretaceous rift shoulder, thick sections of fine-grained limestone and chalk interbedded with shales accumulated at this time. Rich petroleum source rocks of Cenomanian–Turonian and Campanian age are commonly present (Lüning *et al.* 2004*a*). Further south, the Ghadames–Illizi Basin was part of the Trans-Saharan seaway with marine connections to the South Atlantic around both sides of the Hoggar Massif. By latest Campanian the eastern seaway was apparently disconnected and only the western seaway was active, persisting until the Late Paleocene (Zaborski & Morris 1999), when the Trans-Saharan Seaway finally disappeared. The rift shoulder formed an effective 'sill' between Neotethys and the Ghadames–Illizi Basin and the Late Cretaceous sequences in the northern part of the basin are commonly evaporitic (Bracene *et al.* 2003). At the eastern end of

Djebel Nafusa the Albian Kiklah Sandstone onlaps the 'Austrian' Unconformity and the overlying Cenomanian–Turonian, Ain Tobi carbonates thin dramatically (Hammuda 1971), suggesting that this area was topographically high during the Late Cretaceous. The early phases of compression between North Africa and Europe are recorded by the Syrian Arc events (Fig. 2). Although classically expressed in Egypt and the Levant, similar aged structures may also be observed at outcrops in Libya [Jebel Akhdar (Bosworth *et al.* 2008)] and further west in Central Tunisia (e.g. the Kesra Plateau; Zaier *et al.* 1998). Typically the 'Syrian Arc' events inverted pre-existing faults. Syrian Arc 1 is a Late Cretaceous event (Santonian) whereas Syrian Arc 2 is an Eocene event.

Foreland Basin 2 Megasequence (Alpine Foredeep)

We have taken the Syrian Arc 2 event (Fig. 2) as the base of our Foreland Basin 2 Megasequence (Alpine Foredeep), although in truth this is probably a great oversimplification and the actual transition is probably more gradational and complex. To the north of the old Cretaceous rift shoulder the Cenozoic section is thick (over 3000 m) and predominantly carbonate (Swezey 2008), but to the south the Cenozoic section is thin (*c.* 300 m maximum, Swezey 2008). Analysis of well data and regional seismic profiles confirms that the Palaeogene is relatively thin (typically less than 100 m) in the Ghadames–Illizi Basin and that the Paleocene is mostly absent. The Eocene sequence is thin (rarely more than 50 m) and predominantly evaporitic, passing northwards into fully marine carbonates. It seems likely that during the Early Cenozoic the basin had a very similar geometry to that seen in the present day, but with a limited, 'silled' marine connection to the north somewhere between the Tunisian Dorsale range and the 'Djebel Tebaga–Djebel Nafusa Uplift'. In the latter area the Cenozoic was probably not deposited.

To the south of the 'sill' evaporitic facies were extensively developed whereas to the north the fully marine carbonates described by Zaier *et al.* (1998) were flourishing. The Eocene sediments are overlain unconformably by coarse-grained sandstones that are usually ascribed to the Mio-Pliocene on most oil company composite logs, although this section is very poorly dated. The main 'Alpine' Unconformity is probably of 'Miocene' age (Fig. 2) and is locally a strong angular unconformity on regional seismic profiles with locally, well defined 'channels' or canyons. The Late Cretaceous and Cenozoic sequences are also locally strongly folded (Fig. 4) and sometimes these folds may be mapped at the surface. The structural wavelength of these late folds is typically short (Fig. 4) and suggestive of reactivation of basement faults in the final phases of Alpine compression.

Petroleum source rocks

The Early Silurian and Late Devonian source rocks are very similar from a geochemical point of view, but were deposited in slightly different settings. The Early Silurian, Tanzuft source was deposited in a passive margin setting (Passive Margin 1 Megasequence) and associated with a major transgression caused by the demise of the Late Ordovician Ice Cap. The Late Devonian, Frasnian source was deposited in a Foreland Basin setting associated with widespread regional inversion (Foreland Basin 1 Megasequence). The salient points relating to the distribution of these two world-class source rocks are discussed below. Figure 2 shows the stratigraphic position of the basin's two major source rock horizons.

Early Silurian: 'Tanzuft'

In general terms the major regional control on the distribution of the Tanzuft source rock is the Saharan Metacraton. Throughout the Palaeozoic this cratonic block has been a major supplier of sandy sediment and this is particularly marked during the Silurian, Devonian and Early Carboniferous. Well data from Cyrenaica and the Western Desert of Egypt show that the Early Silurian shales are organically lean and outcrops around Djebel Uweinat show that the same stratigraphic section is dominated by sandstones (Fig. 7). To the west the source rock is generally present, although there are areas where it is not (as shown in Fig. 7). Established

Fig. 6. 'Austrian' Unconformity at Djebel Tebaga (Tunisia). Gently dipping, Albian sandy limestones overlie more steeply dipping (to the south) Late Permian carbonates. Cenomanian–Turonian carbonates cap the high escarpment in the background. Halk el Menzel locality, view to west.

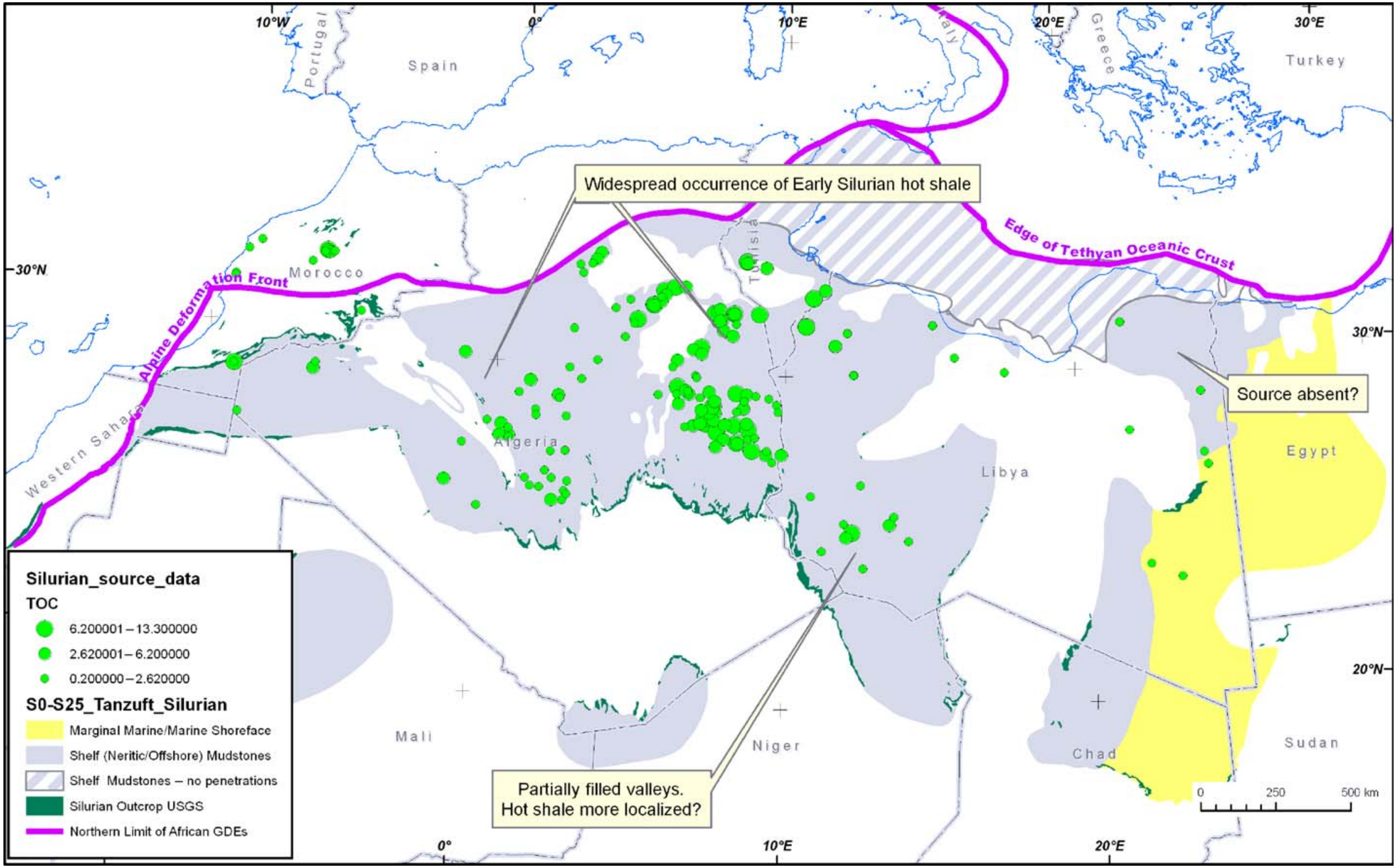

Fig. 7. Early Silurian, Tanzuft Source Rock gross depositional environment (GDE) map (green circles represent calibration points; the bigger the circles the higher the TOC content).

models for the distribution of the Tanzuft source facies (Lüning *et al.* 2000) invoke remnant glacial topography to provide 'silled', anoxic basins.

Late Devonian: 'Frasnian'

The distribution of the Frasnian source rock is principally controlled by the overall geometry of the evolving Hercynian Foredeep and the locally developed inversion structures that developed along its southern and eastern margins (Fig. 8). In general terms the Frasnian source facies is best developed in the basin centres and is thin to absent on the regional arches. In Cyrenaica shallow marine sandstones fringing the emergent Tibesti–Sirte Arch dilute the source facies (El-Arnauti & Shelmani 1988). In the Western Desert of Egypt the Frasnian is dominated by sandstones derived from the Saharan Metacraton (Paleoservices Report 1986). The areas covered by our gross depositional environment (GDE) maps are essentially restricted to African Gondwana. We have not attempted to extend our GDE maps into the highly deformed Marrakech–Kabylia zone, although we have extrapolated our facies belts into the deeply buried offshore zone (Fig. 1).

Reservoir–seal combinations

Figure 2 shows the main reservoir–seal combinations in the Ghadames–Illizi Basin. In our regional play fairway and 3D basin modelling we have considered 13 reservoir–seal combinations. With the exception of the glaciogenic Mamuniyat sequence, all of the other potential reservoir sequences are of a paralic character, that is, they were deposited at or close to sea-level. A wide variety of facies are represented in this category, such as fluvial, tidally influenced fluvial, shoreface. The Palaeozoic outcrops of the Tassili N'Ager and Djebel Akakus on the southern flank of the Ghadames–Illizi Basin convincingly demonstrate that a great many of these paralic sandstone units are sheet-like, regionally extensive bodies (Beuf *et al.* 1971) and this is confirmed in the subsurface by regional seismic mapping (Fig. 4) and evaluation/correlation of well sections.

Palaeocurrents collected from the Tassili N'Ager outcrops (Cambrian–Devonian) record gross sediment transport from south to north (Beuf *et al.* 1971). A similar sense of sediment transport is recorded by Dardour *et al.* (2004) from large-scale clinoform geometries seen the Silurian Akakus sequence. In very broad terms the Silurian and Devonian of North Africa record a second-order regressive–transgressive cycle (Fig. 8). The Lower Devonian, 'Tadrart' reservoir sequence represents the maximum northward regressive extent of paralic sandstones across the platform (Fig. 8) and the overlying Frasnian, Awaynat Wanin C shales the subsequent maximum transgression southwards across the craton. For each reservoir sequence and each seal sequence we have compiled GDE maps, examples of which are shown below (Figs 8 & 9). Each reservoir GDE shows the maximum regressive extent of the reservoir and the reservoir facies. Sand–shale ratio from wireline log data is also posted on the maps to highlight regional trends (e.g. increasing shale content northwards in Fig. 11). Each seal GDE shows the maximum transgressive extent of the seal and seal facies. Sand–shale ratios are also added to these maps to show regional trends (e.g. increasing sand content southwards in the Middle Akakus Shale; Fig. 11).

Integrated basin modelling approach and workflow

The philosophy of this work prioritizes integration across geological disciplines. A particular emphasis was placed on creating burial and uplift models that are consistent with the structural and tectonic interpretation for the basin(s) in question; it is all too easy for geochemists to settle on a model that seemingly calibrates their data with limited regard to its geological veracity. Figure 12 illustrates the multi-disciplinary approach that we have applied to Ghadames–Illizi Basin modelling. Team members collaborated and integrated their work from the start, considering palaeoclimatic change, plate reconstruction, GDE/facies mapping (including well correlation, outcrop data and field studies), structural restoration, seismic mapping (including subcrop mapping) and crustal modelling/thermal history. We used this integrated approach to utilize increasingly complex basin modelling approaches as our understanding matured, for example, 1D 'Genesis' → 2D map based 'Trinity' → 3D 'Temis' full physics.

Missing section map and erosion maps

Velocity analysis when applied to uplift requires thick shale sections, reliable logs and appropriate depth–velocity relationships. Departures from a virgin-compaction velocity–depth relationship can be used to quantify the degree of uplift (within a range of error). As such the thick, argillaceous sections recorded within the Devonian and Silurian sections of the Ghadames and Illizi basins are good candidates for this type of investigation. An example of the velocity analysis is shown in Figures 13 and 14 for the Devonian argillaceous and Silurian argillaceous shales. Organic-rich 'hot' shales were not included due to the complexity that high organic contents cause in simple stress–velocity relationships. The depth–velocity relationships used here have been derived from an extension of the work by Yang & Aplin (1999) on the practical definition of practical mudstone porosity–effective stress relationships.

The quantitative estimates of uplift obtained from shale velocity and analysis and calibration to geochemical data such as vitrinite reflectance provide insight into maximum burial depth and maximum palaeotemperature reached. However, they do not necessarily provide insight into the timing of these events, particularly in areas of long and complex geological history with multiple candidate unconformities. In order to address this issue we both tested multiple models and incorporated insights and interpretations from the structural geologists and sedimentologists. Focusing upon the Illizi Basin it was clear that significant uplift had occurred from the velocity analysis work (Figs 13 & 14), but a variety of models could account for the timing of this uplift. Three models with differing burial and uplift histories were tested and are illustrated in Figure 15. Whilst all three models can calibrate the available geochemical data and uplift estimates, not all were consistent with the observations made from the regional geology.

Observations made around the Hoggar area were particularly important. Cretaceous strata are seen to lie directly upon basement in the Amguid area and near Serouenout (Lefranc & Guiraud 1990). Reports of shoreline features suggest that this area was at or at least close to sea-level during the Early Cretaceous (Lefranc & Guiraud 1990). Given that seismic interpretation shows no evidence of thinning as the Palaeozoic approaches the surface outcrops, we conclude that over 4 km of Palaeozoic sediment which originally lay above the basement have been eroded prior to deposition of the Cretaceous sediments. The Cretaceous sediments contain vertebrate and plant fossils that indicate that they lay close to sea-level at the time of deposition (Lefranc & Guiraud 1990) but are now at 1000–1700 m a.s.l. and have been gently tilted to the north. Clearly the uplift of Hoggar was pulsed and consisted of pre- and post-Cretaceous events. In our preferred model the pre-Cretaceous uplift involved up to 4 km of exhumation (*sensu* England & Molnar 1990) whereas the post-Cretaceous comprised rock uplift (*sensu* England & Molnar 1990). The evidence that led to us to prefer this model is outlined below.

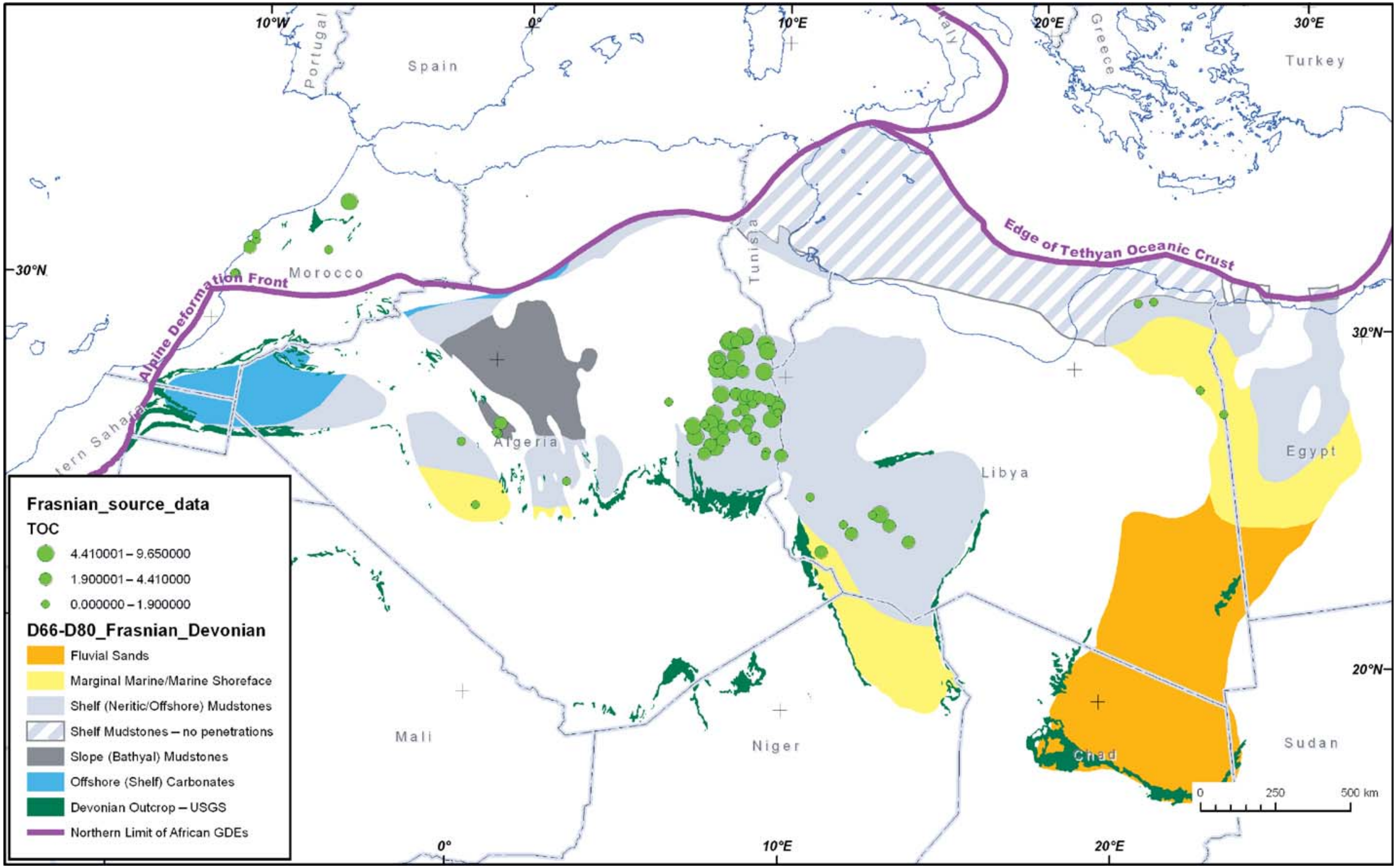

Fig. 8. Late Devonian, Frasnian GDE map (green circles are well calibration points; the bigger the circle the higher the TOC).

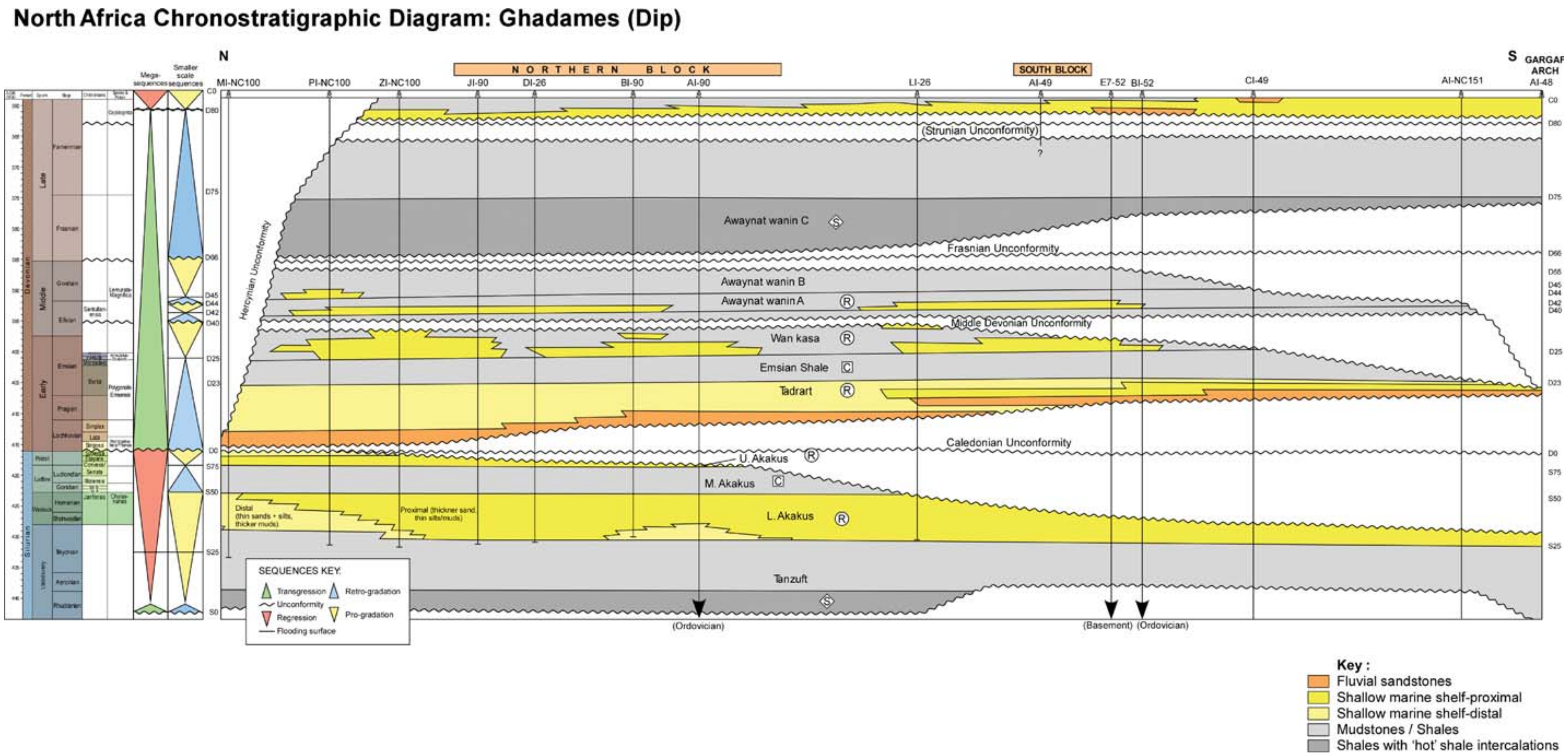

Fig. 9. North–south chronostratigraphic diagram through the Silurian and Devonian of the Ghadames–Illizi Basin.

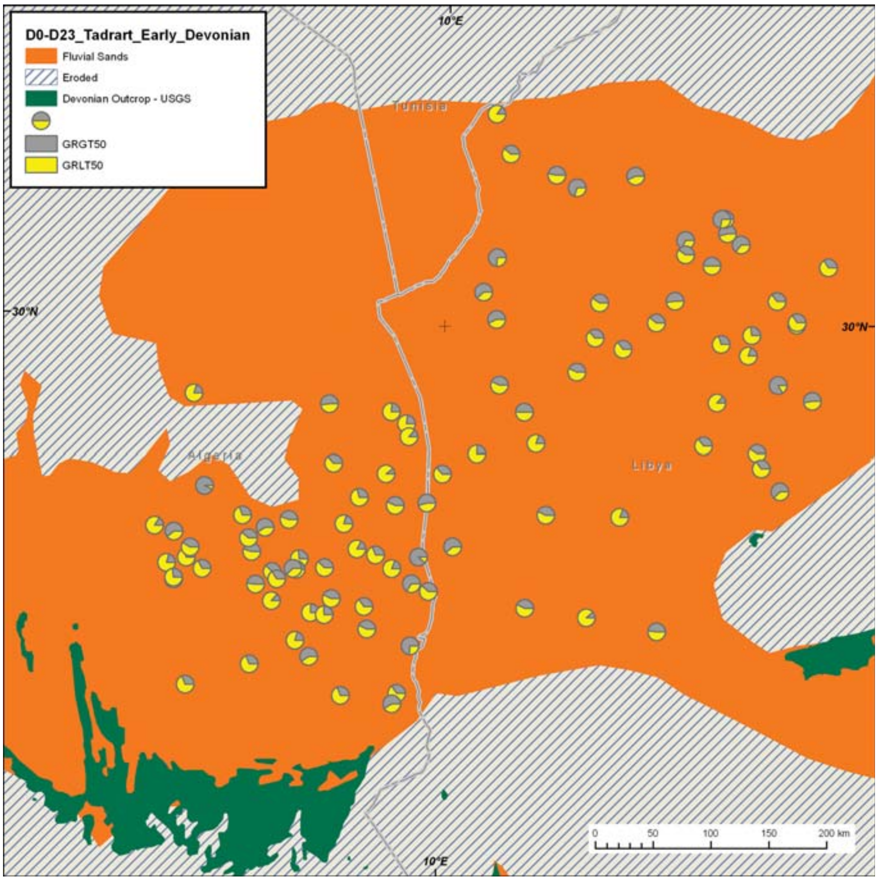

Fig. 10. GDE map for the Lower Devonian, 'Tadrart' reservoir sequence.

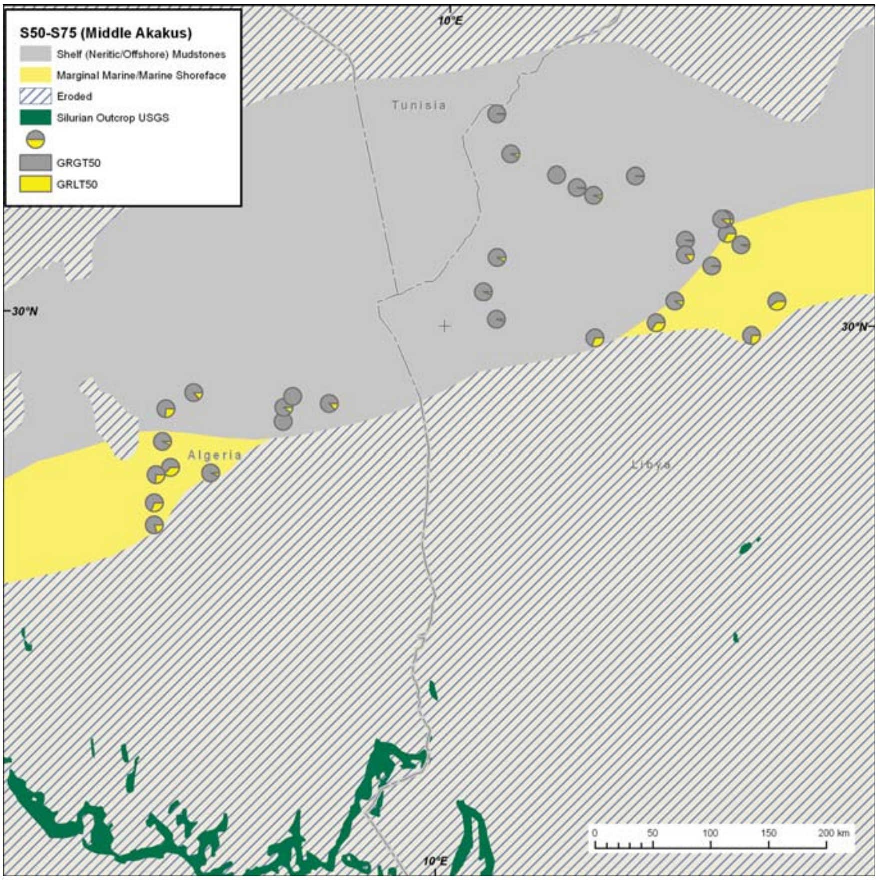

Fig. 11. GDE map for the Silurian, Middle Akakus Shale sequence.

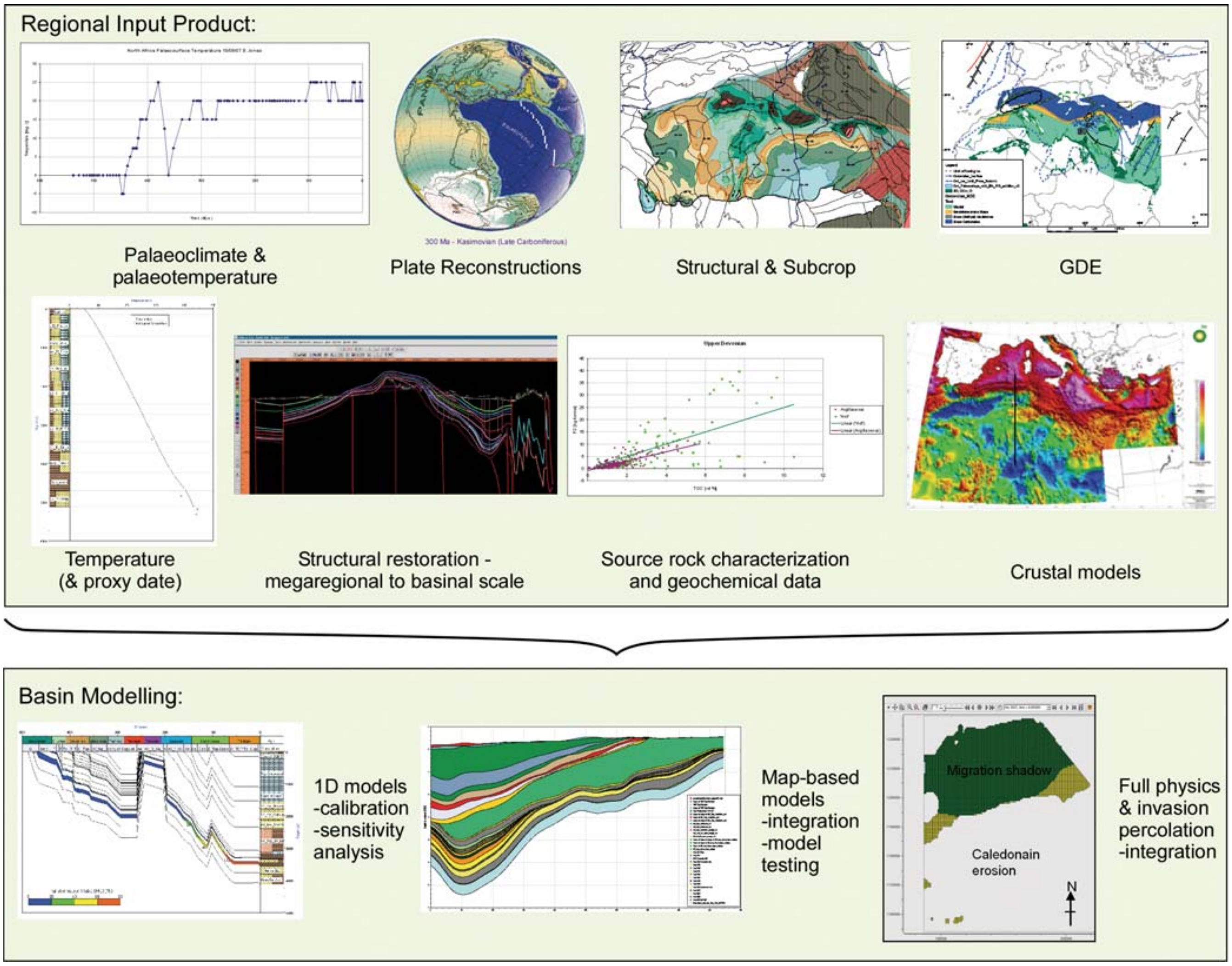

Fig. 12. Integrated basin modelling approach and workflow.

The simplest interpretation of model A would suggest that, during the Cretaceous, Hoggar (to the South of Illizi) would have been buried by a significant thickness of Palaeozoic stratigraphy, which is not consistent with the observations of Lefranc & Guiraud (1990). Similarly the observation of Early Cretaceous sediments sitting directly upon basement is also not consistent with model B. The model that most closely matches structural restorations at the mega-regional and regional scale and the apatite fission-track data is model C. This model invokes removal of most of the Palaeozoic section during the Hercynian, consistent with observation from Hoggar and the Tassili escarpment being in place at this time (cf. Lefranc & Guiraud 1990). Permian apatite fission track cooling ages (Carpena *et al.* 1988) from basement rocks suggest initiation of uplift post-dating the Hercynian unconformity. Outcrop observations from the In Amenas area suggest that Mesozoic sediments onlap onto the Hercynian erosion surface, potentially suggesting a gentle tilting of this surface (from south to north). There is no tectonic evidence for significant Cenozoic accommodation space being generated in the Illizi Basin; however, the observations of Cretaceous freshwater fauna around Hoggar relevant to its current elevation suggest that significant rock uplift (*sensu* England & Molnar 1990; whereby rock is displaced with respect to the geoid) has occurred. Assuming that much of the Cretaceous was deposited at or close to sea-level, back-interpolating the topography onto the base Cretaceous contacts and then contouring, allows estimation of the amount of post-Cretaceous uplift on the Hoggar (Fig. 15). In doing so this suggests a post-Mesozoic rock uplift of 300–700 m across the Illizi Basin.

Our model has largely viewed the basin along an effective dip-line orientated north–south from the Hoggar area to the Berkine fields of the central Ghadames Basin. This view contrasts with the approach taken by Underdown *et al.* (Underdown & Redfern 2007, 2008; Underdown *et al.* 2007), who described the basin and its evolution from a strike-line. A variety of techniques were used to estimate both gross missing section and to partition this to three main erosion events: 'Hercynian', 'Austrian' and 'Alpine' (Fig. 16). These include structural restoration, shale velocity analysis, fluid inclusions, temperature data and source maturity data. The maps at the bottom show the amount of missing section we calculated at each unconformity. Blue shows the greatest amount of erosion, whereas red indicates no erosion. From our analysis we predict that the major loss of section was during the 'Hercynian' when up to *c.* 2000 m was eroded. Up to *c.* 600 m was lost during the 'Austrian' and a further *c.* 200 m at the 'Alpine' event (Fig. 17).

The recognition of the 'Austrian Unconformity' and the potentially significant erosion at this time is the major difference between this study and previous Ghadames–Illizi Basin models (e.g. Underdown & Redfern 2008 and references therein). Underdown & Redfern (2008) partition the uplift at the southern and eastern margins of the basin between the 'Hercynian' and 'Alpine'; we achieve it by having a similar loss of section between the 'Hercynian' and 'Austrian' so that maximum burial

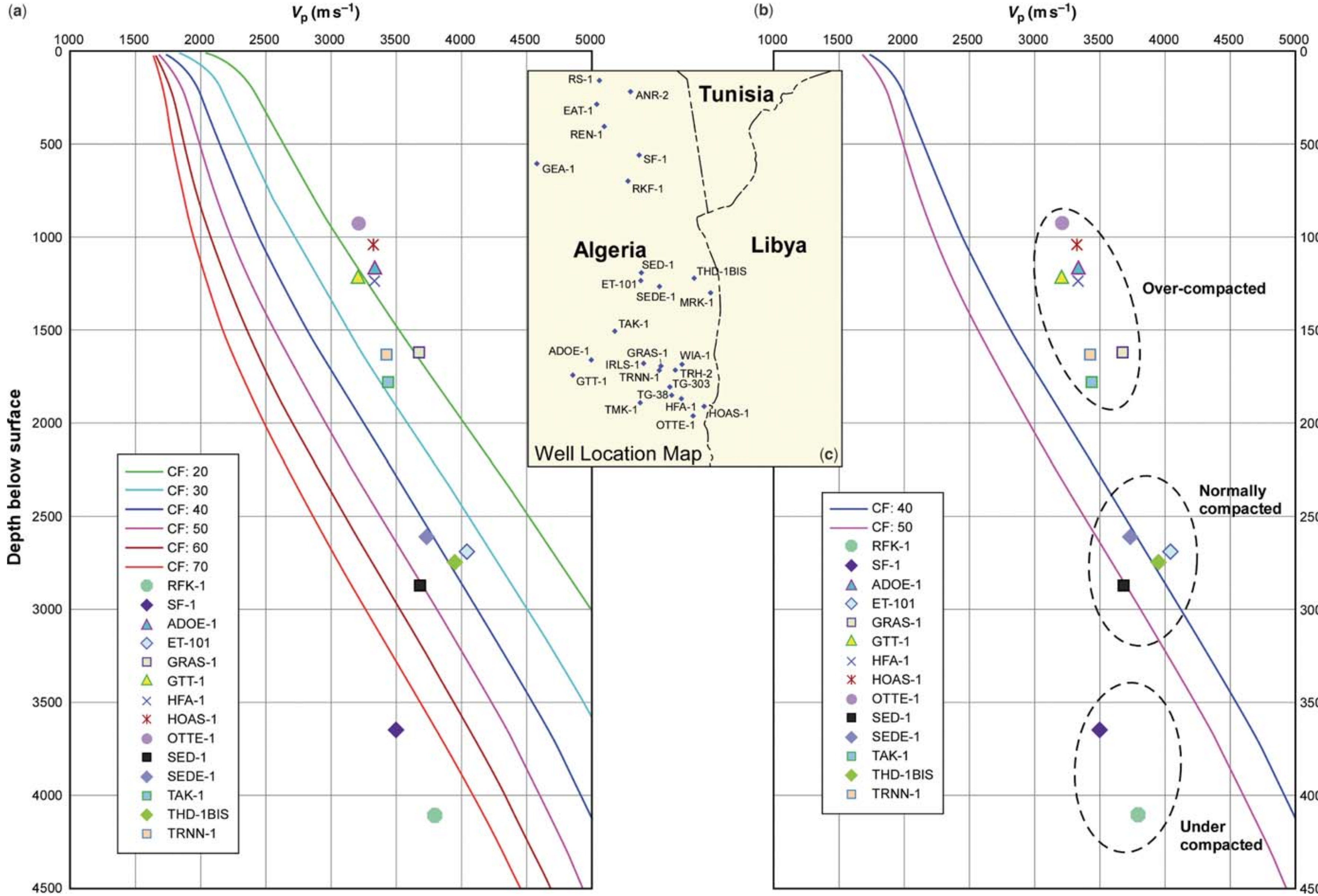

Fig. 13. (**a**) Depth velocity plots for Devonian argillaceous shales from the Ghadames and Illizi basins with a variety of depth–velocity curves based upon BP's proprietary mudrock physical properties database. (**b**) Preferred virgin compaction depth–velocity relationships and compaction state interpretation of the 14 wells analysed. (**c**) Location map.

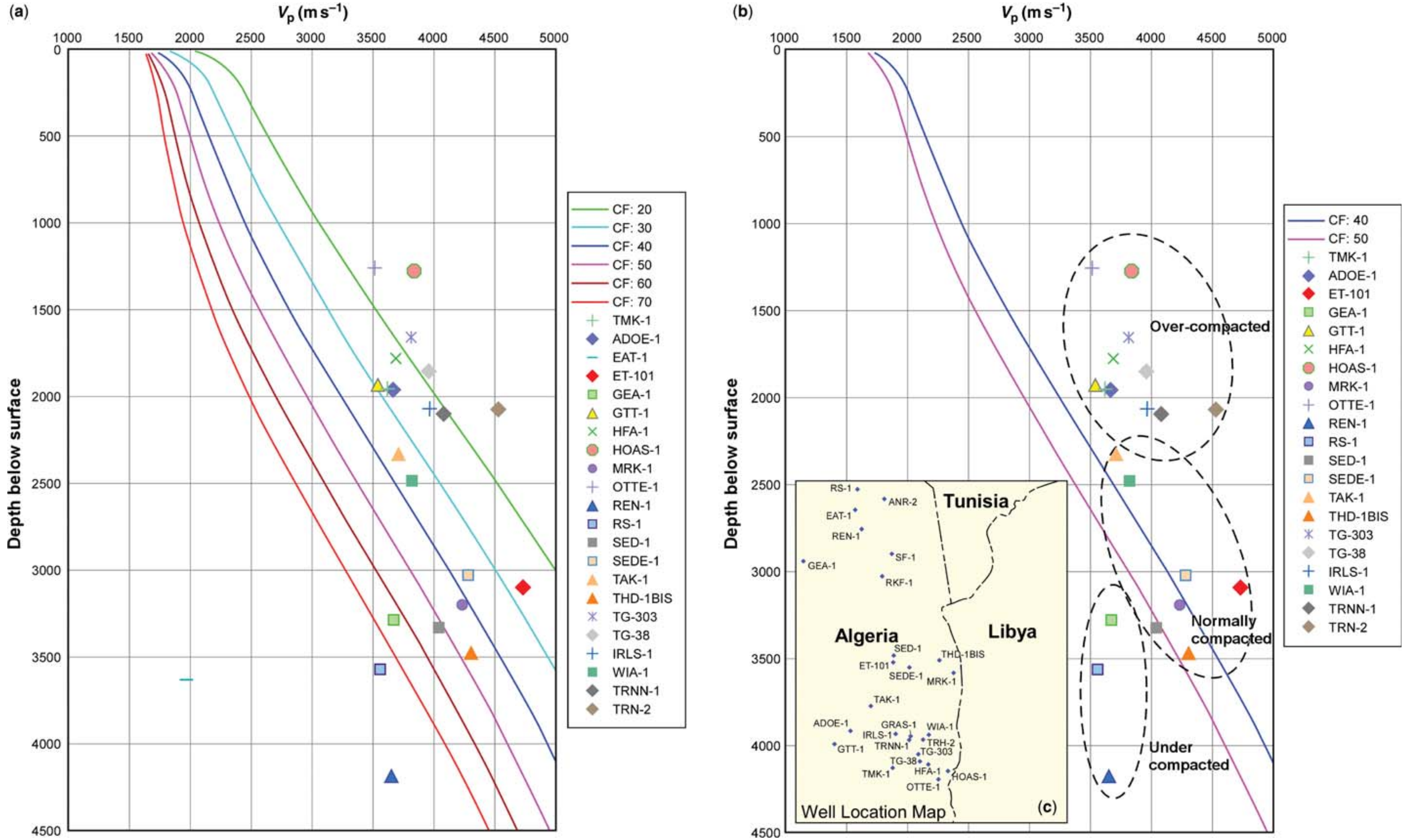

Fig. 14. (**a**) Depth velocity plots for Silurian argillaceous shales from the Ghadames and Illizi basins with a variety of depth–velocity curves based upon BP's proprietary mudrock physical properties database. (**b**) Preferred virgin compaction depth–velocity relationships and compaction state interpretation of the 22 wells analysed. (**c**) Location map.

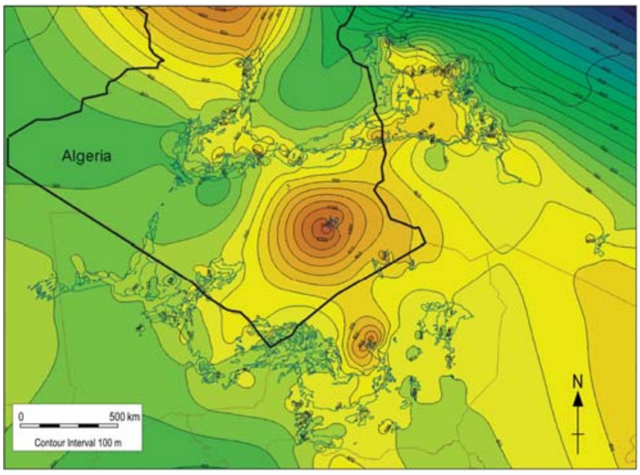

Fig. 15. Map of the base of the Cretaceous outcrops across the Hoggar; back-interpolating the topography onto the base Cretaceous contacts and then contouring allows estimation of the amount of post Cretaceous uplift on the Hoggar (courtesy of Tom Patton, BP Exploration).

is achieved in the Cretaceous rather than Miocene as in the Underdown & Redfern (2008) model in the east, but agree that maximum burial is reached in the Cenozoic in the central and western portions of the basin. Field observations (e.g. Fig. 6), well data and regional 2D seismic profiles (e.g. Fig. 4) clearly demonstrate the importance of the 'Austrian Unconformity' and also the generally thin nature of the Cenozoic section in the Ghadames–Illizi Basin. There is no geological evidence for the deposition of a thick (*c*. 1700 m) Cenozoic section at the eastern margin of the Ghadames–Illizi Basin and its subsequent removal during the 'Alpine' phase, rather the evidence is that this margin of the basin has been a high since the Cretaceous with little or no Cenozoic deposition (Hammuda 1971; Drake *et al.* 2008).

Hydrocarbon distribution

There are significant (32 BBOE) discovered resources of oil and gas in the Ghadames–Illizi Basin with the phase split of oil to gas and condensate of *c*. 50:50. The bulk of these resources are in Algeria in comparison to Libya and Tunisia (Fig. 18). In

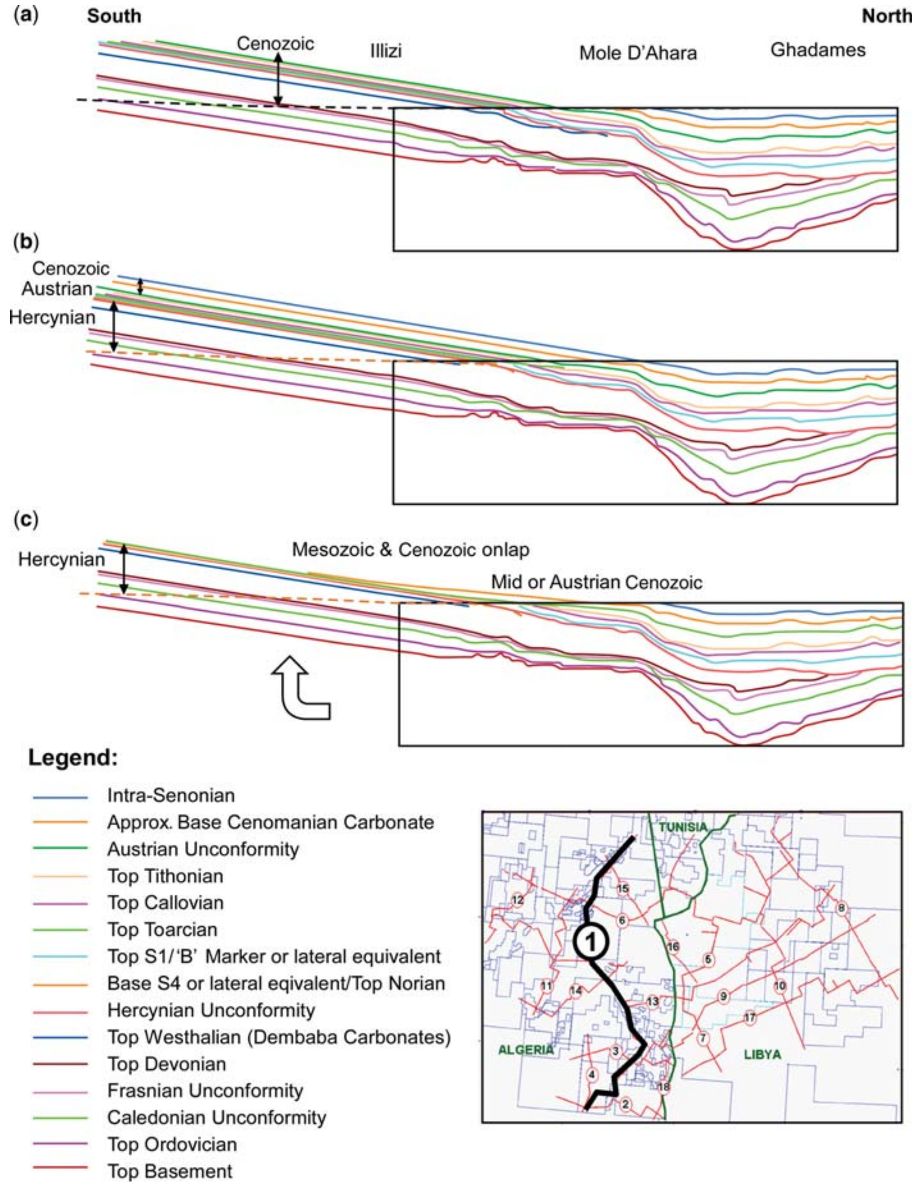

Fig. 16. Cartoon regional sections illustrating the differing burial and uplift models tested for the Illizi Basin. (**a**) Cenozoic to Hercynian section removed by the Alpine unconformity; (**b**) Cenozoic to Hercynian section removed incrementally by the Hercynian, Austrian and Alpine unconformities; (**c**) Palaeozoic section removed by the Hercynian unconformity; onlap of Mesozoic section onto this surface and erosion at the Austrian unconformity and minor Cenozoic deposition followed by uplift of rock (*sensu* England & Molnar 1990).

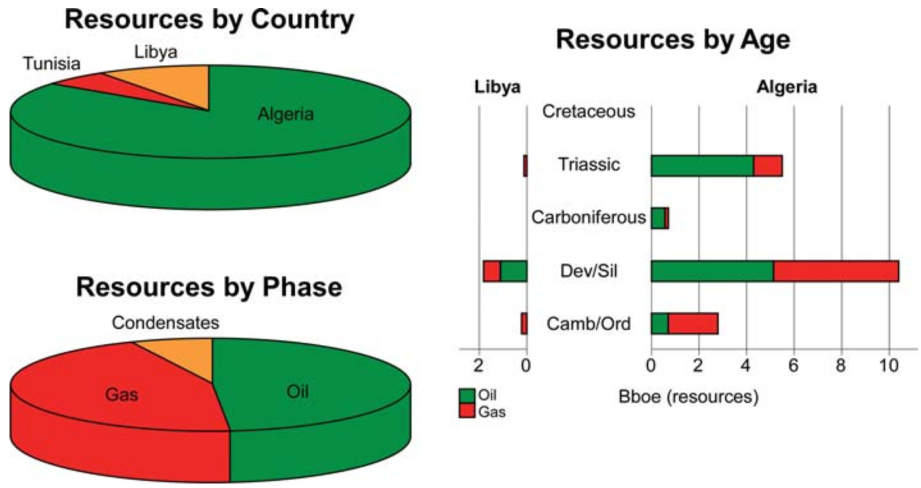

Fig. 17. Ghadames–Illizi Basin petroleum resources by country, phase and age (data from IHS and BP).

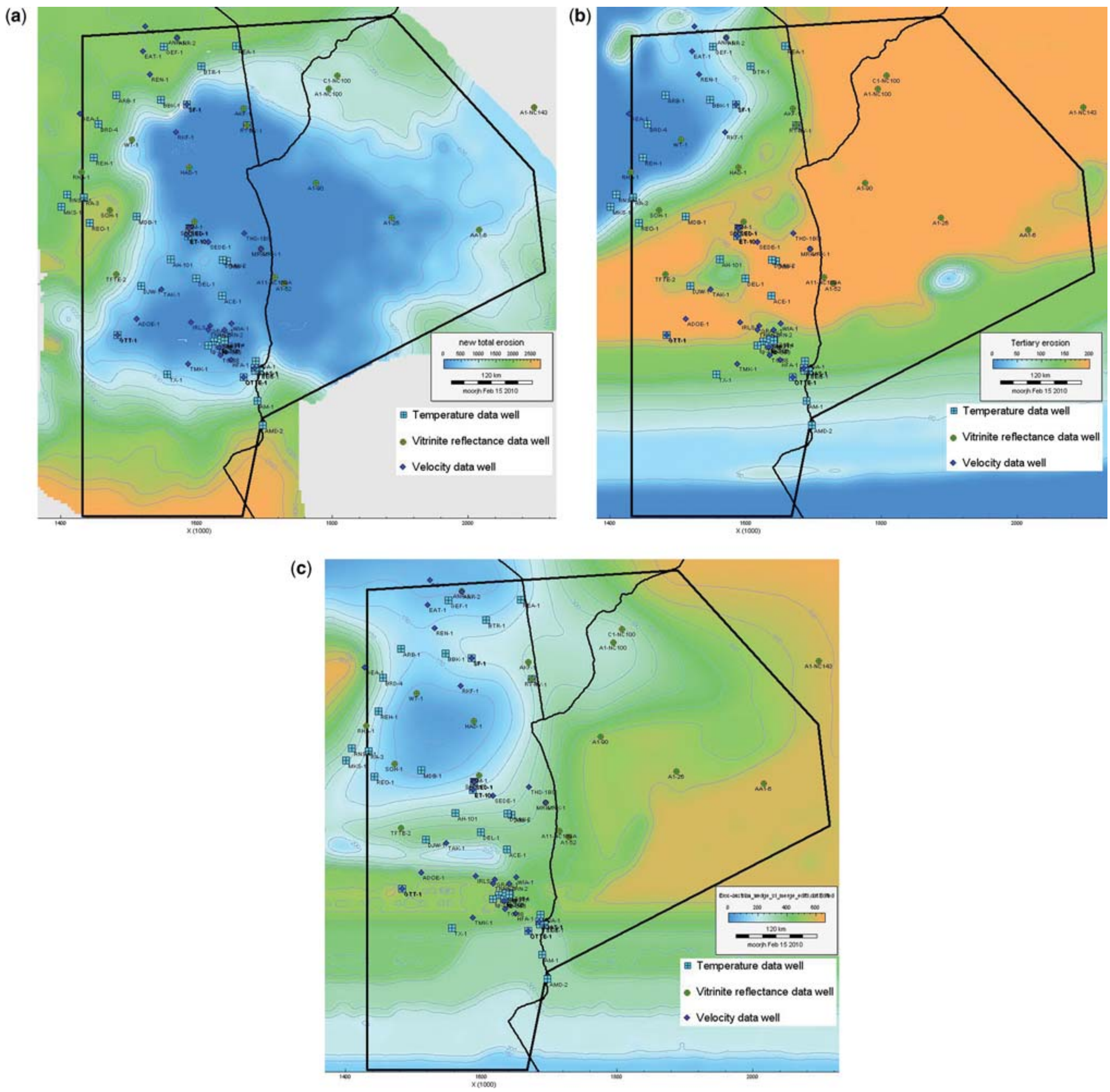

Fig. 18. Ghadames–Illizi Basin erosion estimates.

Algeria, these hydrocarbons are predominantly reservoired in the Cambro–Ordovician, Silurian–Devonian and Triassic clastic reservoirs with only moderate resources in the Carboniferous. Gas is the dominant phase in the Cambro–Ordovician, oil is the dominant phase in the Triassic and there is an *c.* 50:50 split of oil and gas in the Silurian–Devonian reservoirs (Fig. 18). In Libya the bulk of the resources are in the Silurian–Devonian clastic reservoirs and the phase split is slightly biased to oil. Only minor resources are present in the Cambro–Ordovician and Triassic clastic reservoirs (Fig. 18).

Source rock presence

All of the available source screening data were plotted on the GDE maps for the Frasnian (Fig. 8) and the Tanzuft 'hot' shales (Fig. 7) intervals. These data indicate that both these intervals are excellent oil-prone source rock intervals. These source intervals have TOC values up to 20 wt% and P2 values up to 100 kg/tonne.

Source access

A 'Trinity' 3D basin model was built using 35 structural surfaces and thus 34 layers. These surfaces were either derived directly by seismic mapping or by using seismic and well data. GDE maps were input for these 34 layers as were palaeo-bathymetry and surface temperature through time. In addition to the 35 structural surfaces, three major unconformities are also represented in the model (as above). Temperature data (DST and PLT data) used to calibrate the Trinity model came from three principle sources (BP, IFP (2003) and Libyan NOC). When these temperatures are plotted against depth (Fig. 19), it can be observed that the Ghadames–Illizi Basin is a moderately warm basin and that there is reasonable variation in temperature at any given depth. The warm nature of the basin is consistent with gravity and magnetics studies which indicate that the continental crust is fairly thick. Prior to running the 'Temis 3D' basin model, a limited 1D basin modelling exercise was carried out using 'Genesis'. The four 'shotpoints' modelled include the central part of the Ghadames Basin, the southern flank of the Ghadames Basin, the crest of the Mole D'Ahara and the Illizi Basin depocentre.

Representative Genesis burial plots for the Ghadames and Illizi Basin depocentres are shown in Figure 20. The deeper Ghadames Basin was separated from the shallower Illizi Basin by the long-lived Mole D'Ahara structural arch (Fig. 4). There is minimal loss of section for the Ghadames and Illizi Basin depocentre at each of the three main unconformities, with the exception of the Illizi Basin depocentre, where *c.* 500 m were lost at the 'Austrian' Unconformity. The timings of oil and gas expulsion relative to the 'Hercynian' Unconformity are shown for the Tanzuft and Frasnian 'hot' shales at the four modelled shot point locations in Figure 21. For the Tanzuft 'hot' shale most of the oil expulsion took place prior to the 'Hercynian' Unconformity with the exception of the crest of the Mole D'Ahara. In the present day the Mole D'Ahara and Illizi depocentres are within the gas window, whereas the central part of the Ghadames Basin is overmature for gas. For the Frasnian 'hot' shale there was some oil expulsion Pre-Hercynian, but only from the deepest part of the Ghadames Basin. Present day, the central part of the Ghadames Basin is into the gas window whereas the Mole D'hara and Illizi depocentres are within the oil window (Fig. 21).

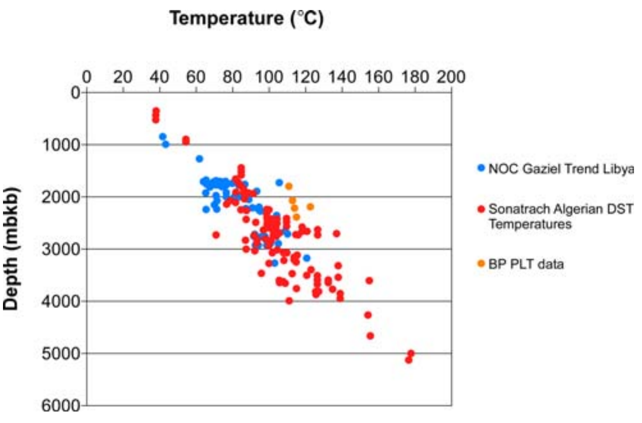

Fig. 19. Ghadames–Illizi Basin temperatures v. depth.

Kitchen maps were then produced within 'Trinity' but these were then superseded by the kitchen maps produced within 'Temis 3D'. Three thermal models were run initially which varied the upper crustal ratio (UC/UC + LC) and the total basement thickness to ensure a good calibration for all wells with DST temperature data. The three models were a cooler model (crust ratio 0.4 and total basement thickness 110 km), an initial model (crust ratio 0.5 and total basement thickness 90 km) and a warmer model (crust ratio 0.6 and total basement thickness 70 km).

All of the calibration wells were then used to produce gridded crustal ratio and total basement thickness maps which were used to run the most likely model. Present day transformation ratio kitchen maps for this most likely model were produced for the Tanzuft 'hot' shale and the Frasnian 'hot' shale. Present day the Tanzuft 'hot' shale is overmature (even for gas) in the Ghadames depocentre. This kitchen map would indicate that gas would be the most likely phase in the central parts of the basin and oil would be the most likely phase in the basin margins (Fig. 22). In the present day the Frasnian 'hot' shale is in the gas window in the Ghadames depocentre where the source rock is at its richest and thickest. There was also significant 'Pre-Hercynian' generation of oil and gas throughout the Ghadames–Illizi Basin from the Tanzuft 'hot' shale. Prior to the 'Hercynian', oil and minor gas generation did take place from the Frasnian source rock, but only in the very deepest part of the Ghadames Basin.

Migration modelling

Representative cross-sections and lithology distributions within the 'Temis 3D' model are illustrated in Figure 23. The cross-sections clearly resemble the seismic lines (Fig. 4) and also illustrate the multiple reservoir–seal combinations shown in Figure 2. The Tanzuft 'hot' shale generally overlies the Cambro–Ordovician reservoir interval. Downward migration of petroleum into this interval is low risk and the phase is predominantly gas towards the basin centre and oil on the basin flanks (Fig. 22). Petroleum also migrates vertically out of the Tanzuft and into the Akakus (Fig. 24). In the northern part of the basin most of this charge will be trapped in the Lower Akakus reservoir because of the overlying Middle Akakus Shale (Fig. 11). The Lower Akakus contains a number of intra-formational seals (Dardour *et al.* 2004), giving potential 'stacked pay' with varying column heights. In the south the Middle Akakus Shale is absent, because it has been removed by 'Caledonian' erosion (Fig. 23). Petroleum therefore migrates through the Lower Akakus into the Lower Devonian Tadrart reservoir (Fig. 10). Initial 'Mpath' modelling predicts the presence of a migration shadow for the Tadrart reservoir in the north due to the presence of the Middle Akakus seal beneath it and low-risk access of charge to the Tadrart reservoir in the south due to the absence of the Middle Akakus seal (Fig. 25). These modelling conclusions are consistent with the field observations, which indicate that the Akakus fields are in the north and the Tadrart fields are in the southern part of the basin. The Frasnian charge will

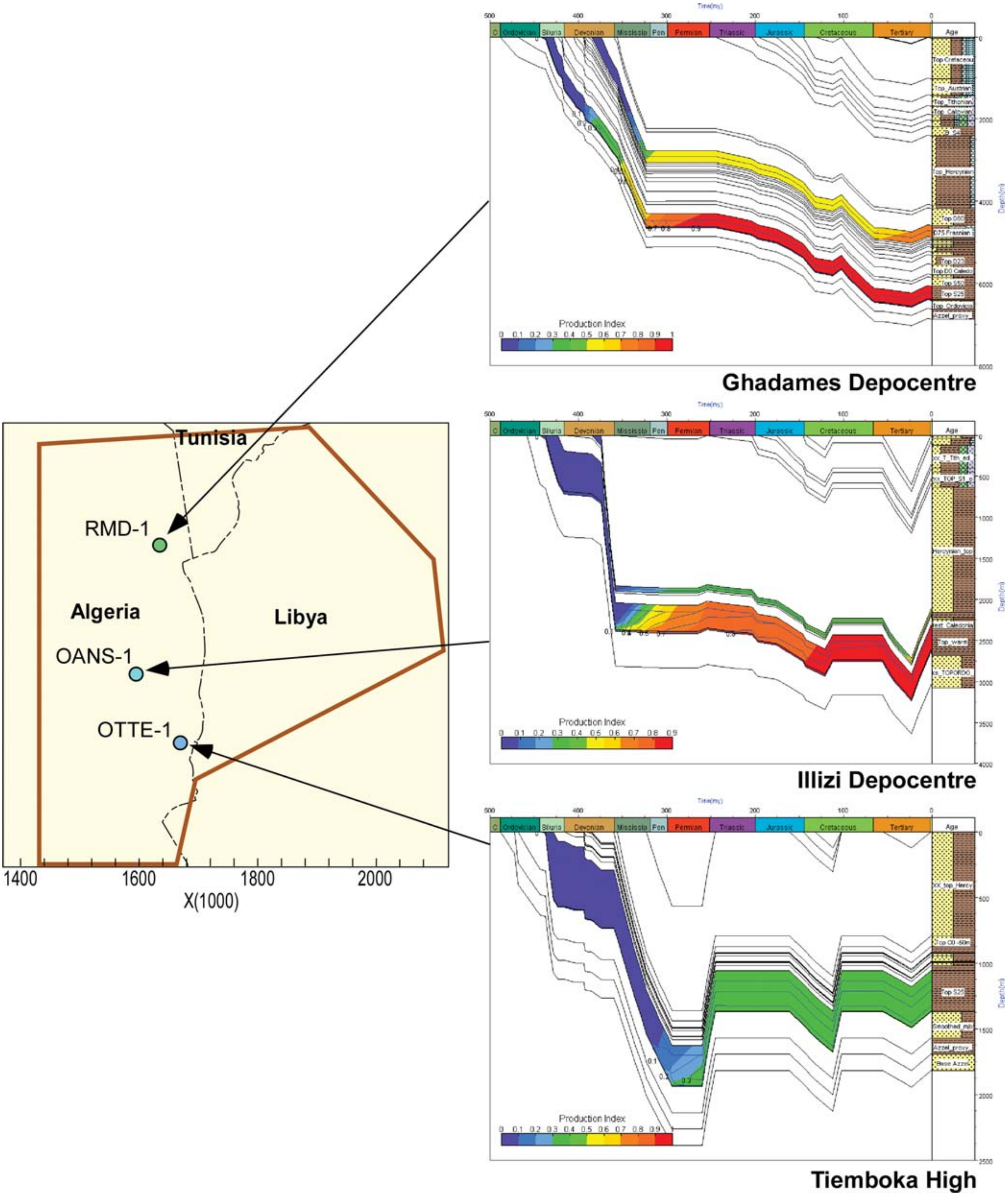

Fig. 20. Representative 'Genesis' burial plots for the Ghadames and Illizi depocentres.

migrate primarily into the Late Devonian 'F2' sand. Lateral migration will carry the charge to the 'Hercynian' subcrop where the charge will then migrate updip within the Triassic reservoir by fill and spill. Thus charge risk is low for the Triassic reservoirs close to the 'Hercynian' subcrop to the NW of the basin and this is where all the giant Triassic fields have been found. The charge risk will increase away from the Hercynian subcrop for these Triassic reservoirs as longer fill and spill chains are required. In the basin centre it is unclear what the main migration mechanism is.

Summary

The Ghadames–Illizi Basin has a long (Cambrian to Plio-Pleistocene) and complex geological evolution characterized by

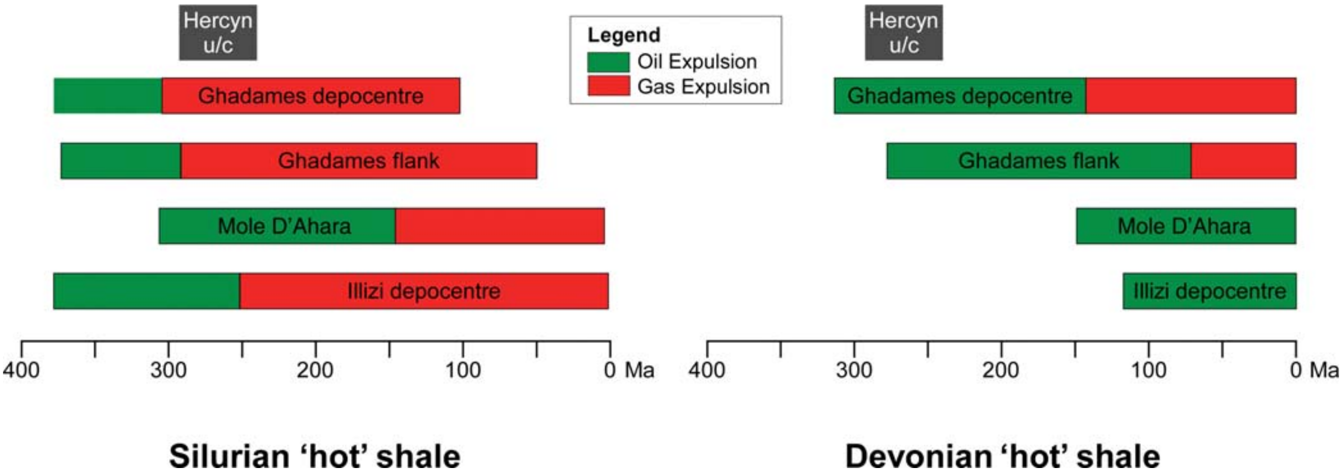

Fig. 21. Timing of oil and gas expulsion for the four modelled 'shotpoint' locations. Oil expulsion, green; gas expulsion, red.

multiple phases of subsidence punctuated by significant regional uplift events. Two major petroleum source rocks of different geological age are present (Lower Silurian and Upper Devonian) with similar depositional environment and geochemical character. Multiple reservoir–seal combinations are presented by Late Ordovician glaciogenic sediments and younger Silurian through to Carboniferous paralic sequences. The sedimentary architecture of the basin fill has been captured in a 'Temis 3D' basin model with 35 structural surfaces and thus 34 layers. Lithology calibration came from GDE maps and palaeo-bathymetry and surface temperature through time (for each layer) was also included. Three regional unconformities have had a major impact on the Ghadames–Illizi Basin petroleum system, the 'Hercynian', 'Austrian' and 'Alpine'. These events are significant, because they were characterized by uplift, tilting and erosion and their timing overlapped with petroleum maturation and migration. The 'Hercynian' event probably had the greatest impact, stopping the active 'Pre-Hercynian' petroleum system and leading to wholesale remigration of its trapped petroleum (oil and gas). Erosion is greatest in the northwestern and southern flanks of the basin. The uplift and tilting associated with the 'Austrian' event is regional in extent, but probably an order of magnitude less than the 'Hercynian'. Erosion is greatest on the eastern flank of the basin and in the south. There is little evidence of erosion associated with the 'Alpine' event in the Ghadames–Illizi Basin. The Paleocene and Eocene sequences are thin and it is likely that the basin was an area of non-deposition for most of the Oligocene. Alpine compression led to the reactivation of a number of basement faults and the propagation of folds through to the surface. At the play fairway level the Ghadames–Illizi Basin is considered low risk for source presence and reservoir presence, although charge access for some sequences is high risk. For example, initial 'Mpath' modelling predicts the presence of a migration shadow for the Tadrart reservoir in the northern part of the basin (due to the presence of the Middle Akakus Shale seal between it and the Tanzuft source). In the southern part of the basin, however, the Tadrart has a low charge access risk, because the Middle Akakus Shale seal is absent (removed by erosion) and Tanzuft charge can access the Tadrart directly from the Lower Akakus sandstones across the 'Caledonian' Unconformity. These modelling

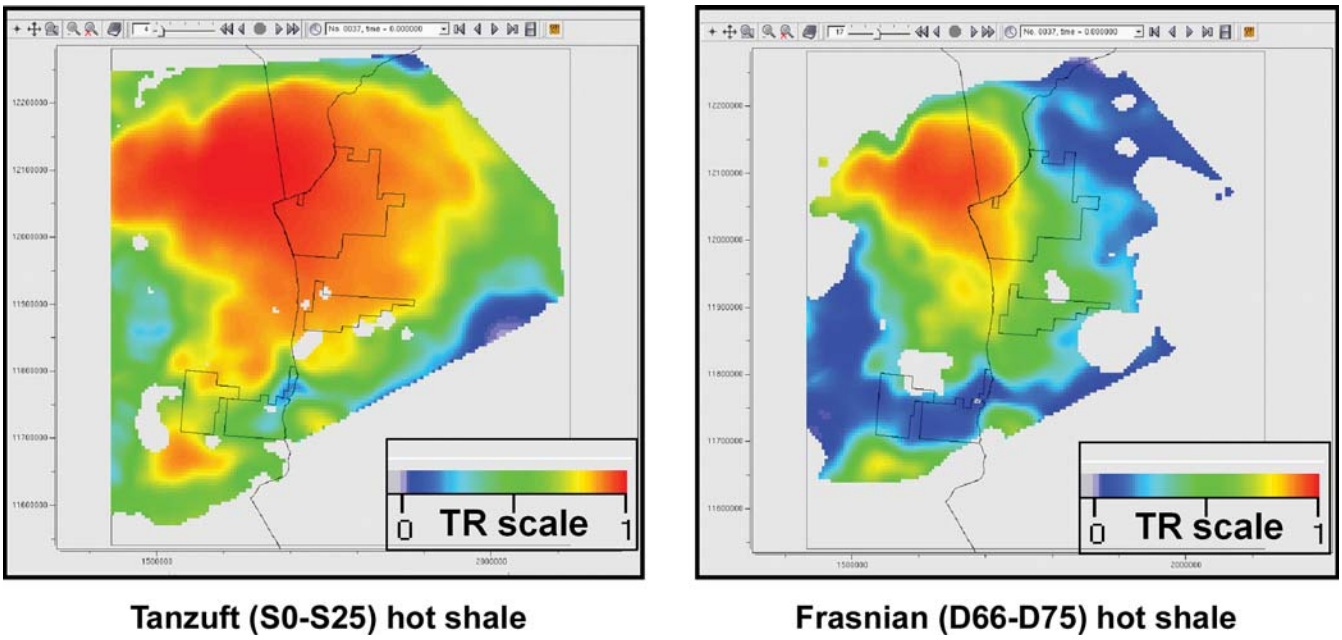

Fig. 22. Kitchen maps: present day transformation ratio for the Tanzuft and Frasnian source rocks.

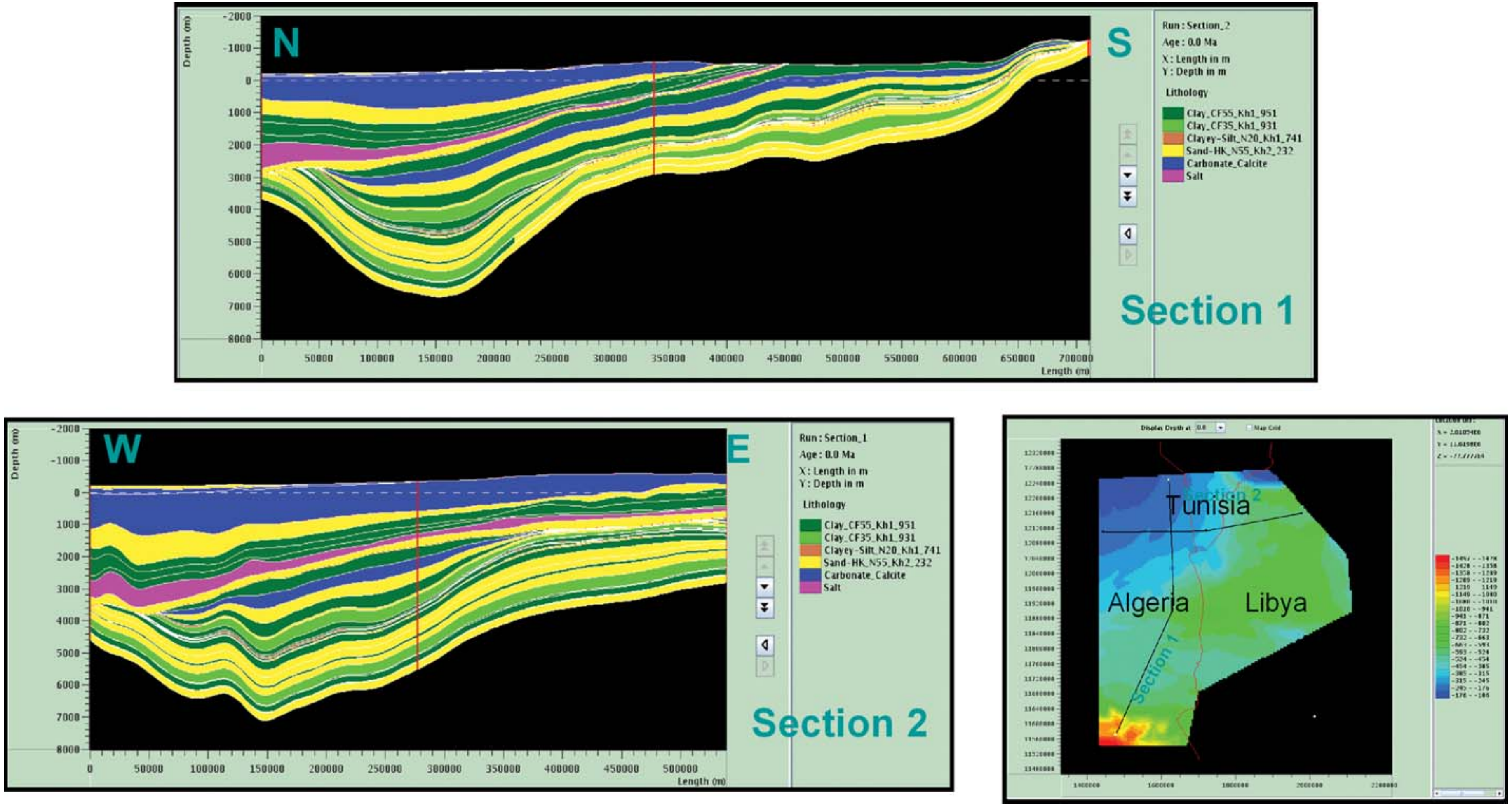

Fig. 23. 'Temis 3D' model: representative cross-sections and lithology distributions.

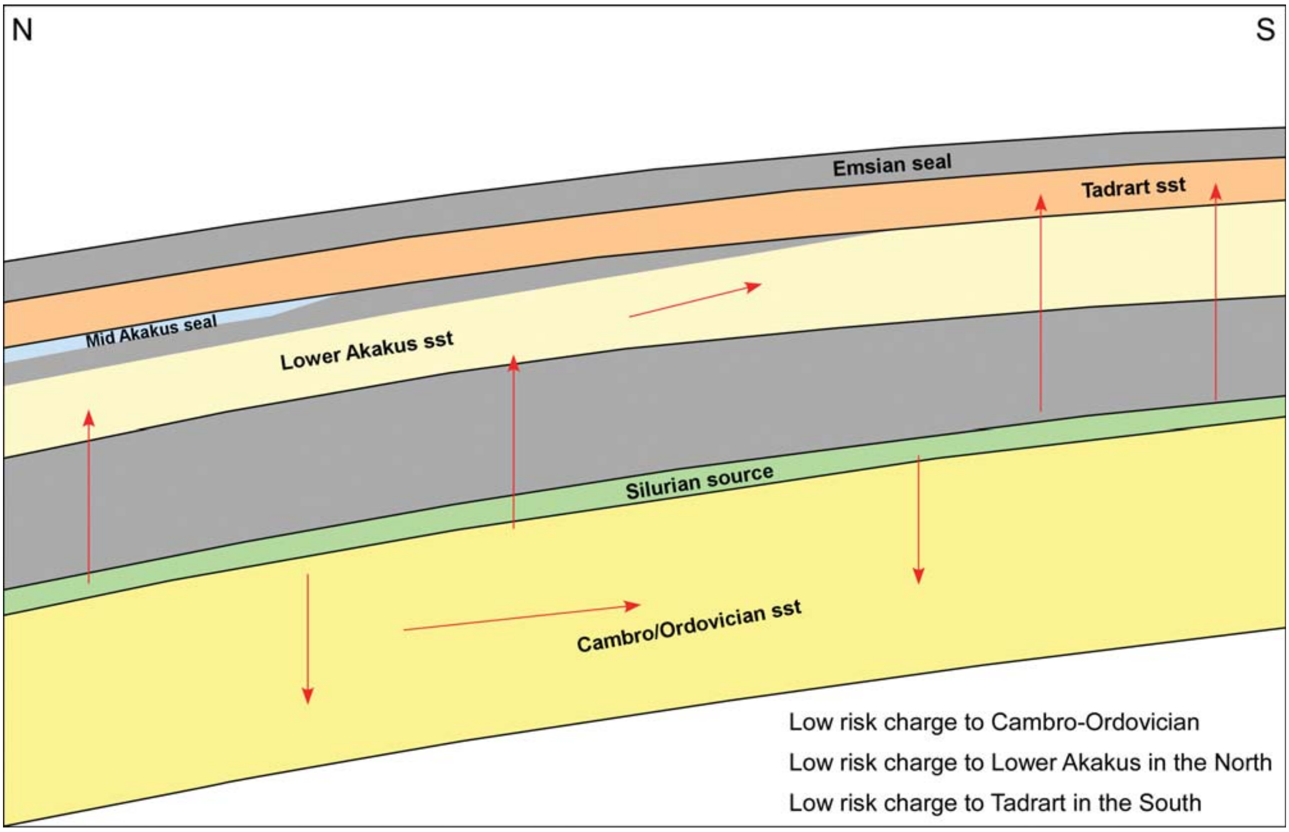

Fig. 24. Ghadames–Illizi Basin charge access cartoon for the Tanzuft source rock.

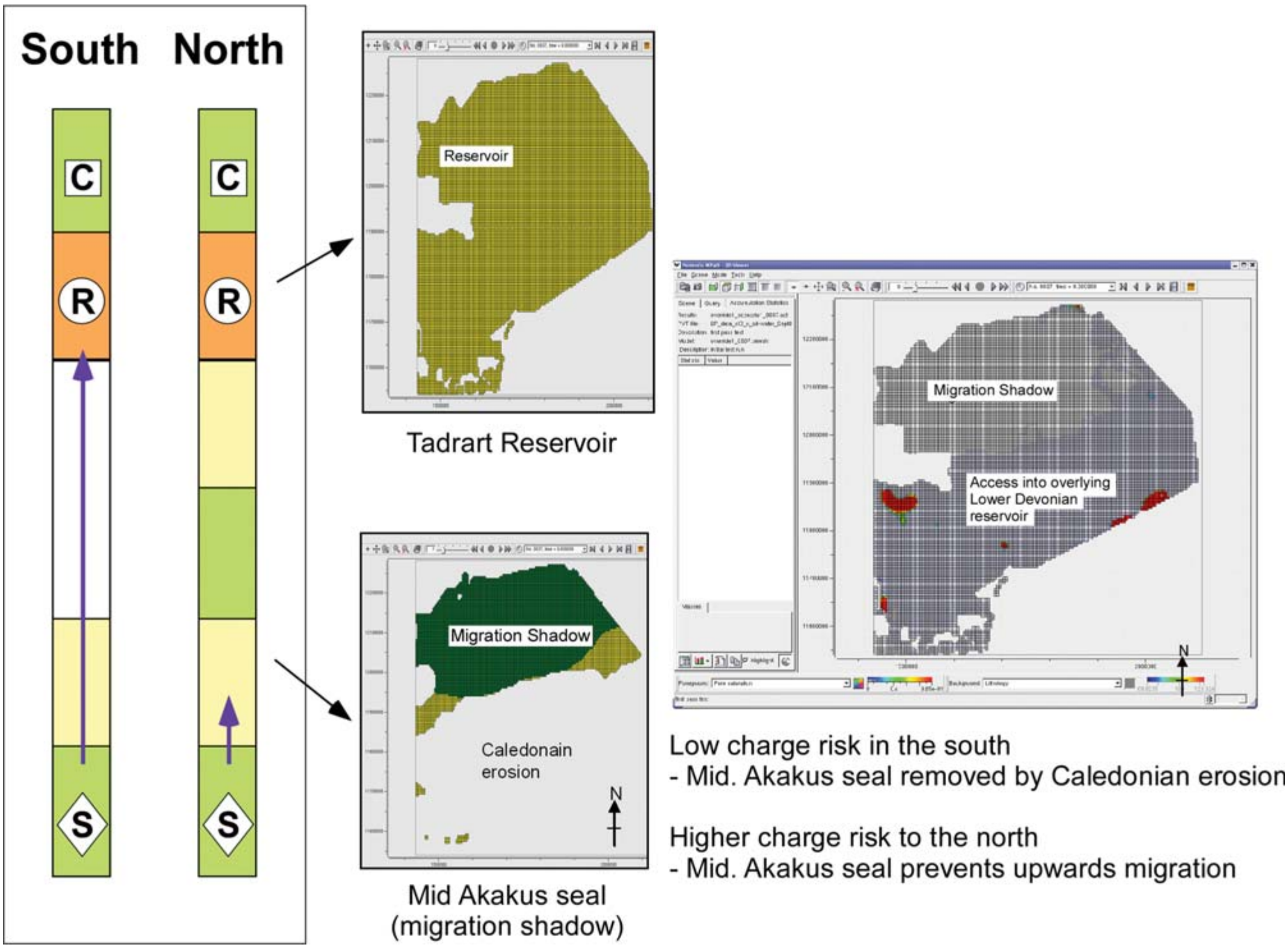

Fig. 25. ‘MPath’ modelling highlighting the Lower Devonian ‘Tadrart play’.

conclusions are consistent with the field observations which indicate that the Akakus fields are in the north and the Tadrart fields are in the southern part of the basin.

We acknowledge BP Exploration for permission to publish. The comments of two reviewers improved the content and presentation of the manuscript.

References

Acheche, M. H., M'Rabet, A., Ghariani, H., Ouahchi, A. & Montgomery, S. L. 2001. Ghadames Basin, Southern Tunisia: a reappraisal of Triassic reservoirs and future prospectivity. *American Association of Petroleum Geologists Bulletin*, **85**, 765–780.

Assereto, R. & Benelli, F. 1971. Sedimentology of the Pre-Cenomanian Formations of the Jebel Gharian, Libya. *In*: Grey, C. (ed.) *Symposium on the Geology of Libya*. Faculty of Science, University of Libya, Tripoli, 37–87.

Bamford, M. K., Roberts, E. M., Famory, S., Mamadou, L. B. & O'Leary, M. A. 2002. An extensive deposit of fossil conifer wood from the Mesozoic of Mali, Southern Sahara. *Palaeogeography, Palaeoclimatology. Palaeoecology*, **186**, 115–126.

Barr, D., Benkali, M., Riviere, M. & Wilson, N. 1994. Algeria District 3 Convention BP/Sonatrach Joint Study. Module 2: Tectonics and Basin Evolution. BP Report EXT67024/2.

Beauchamp, J. 1988. Triassic sedimentation and rifting in the High Atlas (Morocco). *In*: Manspeizer, W. (ed.) *Triassic–Jurassic Rifting. Part A*. Elsevier, Amsterdam, 477–497.

Ben Ferjani, A., Burollet, P. F. & Mejri, F. 1990. *Petroleum Geology of Tunisia*. Entreprise Tunisienne d'Activities Petrolieres.

Benson, R. N. & Doyle, R. G. 1988. Early Mesozoic rift basins and the development of the United States middle Atlantic continental margin. *In*: Manspeizer, W. (ed.) *Triassic–Jurassic Rifting. Part A*. Elsevier, Amsterdam, 41–79.

Benton, M. J., Bouaziz, S., Buffetaut, E., Martill, M., Ouaja, M., Soussi, M. & Trueman, C. 2000. Dinosaurs and other fossil vertebrates from fluvial deposits in the Lower Cretaceous of Southern Tunisia. *Palaeogeography, Palaeoclimatology, Palaeontology*, **157**, 227–246.

Beuf, S., Biju-Duval, B., De Charpal, O., Rognon, P., Gariel, A. & Bennacef, A. 1971. *Les Gres Du Palaeozoique Inferieur Au Sahara*. L'Institut Francais Du Petrole, **18**.

Bishop, W. F. 1975. Geology of Tunisia and adjacent parts of Algeria & Libya. *American Association of Petroleum Geologists Bulletin*, **59**, 413–450.

Boote, D. R. D., Clark-Lowes, D. D. & Traut, M. W. 1988. Palaeozoic petroleum systems of North Africa. *In*: Macgregor, D. S., Moody, R. T. J. & Clark-Lowes, D. D. (eds) *Petroleum Geology of North Africa*. Geological Society, London, Special Publications, **132**, 7–68.

Bosworth, W., El-Hawat, A. S., Helgeson, D. E. & Burke, K. 2008. Cyrenaican 'shock absorber' and associated inversion strain shadow in the collision zone of north–east Africa. *Geological Society of America Bulletin*, **36**, 695–698.

Bracene, R., Patriat, M., Ellouz, N. & Gaulier, J. M. 2003. Subsidence history of basins in Northern Algeria. *Sedimentary Geology*, **156**, 213–239.

Brice, D., Legrand Blain, M. & Nicollin, J. P. 2007. *Brachiopod Faunal Changes Across the Devonian/Carboniferous Boundary in North West Sahara (Morocco & Algeria)*. Geological Society, London, Special Publications, **278**, 261–271.

Busson, G. & Burollet, P. F. 1973. *La limite Permien-Trias sur la plateforme saharienne (Algérie, Tunisie, Libye)*. Canadian Society of Petroleum Geologists, Memoirs, **2**, 74–88.

Carpena, J., Kienast, J. R., Ouzegone, K. & Tehamo, C. 1988. Evidence of contrasted fission-track clock behaviour of the apatite from In Ouzzal Carbonates (north west Hoggar): the low-temperature thermal history of Archean basement. *Bulletin of the Geological Society of America*, **100**, 1237–1243.

Cavaroc, V. V., Padgett, G., Stephens, D. G., Kanes, W. E., Boudda, A. & Woolen, I. D. 1976. Late Palaeozoic of the Tindouf Basin – North Africa. *Journal of Sedimentary Petrology*, **46**, 77–88.

Chaabani, F. & Razgallah, S. 2006. Aptian sedimentation: an example of the interaction of tectonics and eustatics in Central Tunisia. *In*: Moratti, G. & Chalouan, A. (eds) *Tectonics of the Western Mediterranean and North Africa*. Geological Society, London, Special Publications, **262**, 55–74.

Chaouchi, R., Malla, M. S. & Kechou, F. 1998. Sedimentological evolution of the Givetian–Eifelian (F3) sandbar of West Alrar Field, Illizi Basin, Algeria. *In*: Macgregor, D. S., Moody, R. T. J. & Clark-Lowes, D. D. (eds) *Petroleum Geology of North Africa*. Geological Society, London, Special Publications, **132**, 187–200.

Clark-Lowes, D. D. & Ward, J. 1991. Palaeoenvironmental evidence from the Palaeozoic 'Nubian sandstones' of the Sahara. *In*: Salem, M. J., Sbeta, A. M. & Bakbak, M. R. (eds) *The Geology of Libya*. Elsevier, Amsterdam, **VI**, 2099–2153.

Dardour, A. M., Boote, D. R. D. & Baird, A. W. 2004. Stratigraphic controls on Palaeozoic petroleum systems, Ghadames Basin, Libya. *Journal of Petroleum Geology*, **27**, 141–162.

Demirtash, E. 1984. Stratigraphic evidence of Variscan and early Alpine tectonics in Southern Turkey. *In*: Dixon, J. E. & Robertson, A. H. F. (eds) *The Geological Evolution of the Eastern Mediterranean*. Geological Society, London, Special Publications, **17**, 129–145.

Dixon, R. J. 1997*a*. Depositional Facies and Key Stratal Surfaces of the Late Devonian (D70) and Early Carboniferous (C10), Ahnet Basin, District 3, Algeria. Part II – Field Geology Report: Timimoun Anticline. BP Report SDT/001/97.

Dixon, R. J. 1997*b*. Depositional Facies and Key Stratal Surfaces of the Lower Devonian (D51) and Middle Devonian (D65), Ahnet Basin, District 3, Algeria. BP Report SDT/005/97.

Dixon, R. J. 1997*c*. Depositional Facies and Key Stratal Surfaces of the Late Devonian (D70) and Early Carboniferous (C10), Ahnet Basin, District 3, Algeria. Part III – Gross Depositional Environments. BP Report SDT/013/97.

Dixon, R. J., Moore, J. K. S. *et al*. 2009. The 'Hercynian' Unconformity in North Africa: Its nature & significance; a case study from Southern Tunisia & North West Libya. Extended Abstract PESGB/HGS Africa Conference, September 2009.

Drake, N. A., El-Hawat, A. S., Turner, P., Armitage, S. J., Salem, M. J., White, K. J. & McLaren, S. 2008. Palaeohydrology of the Fazzan Basin: the last 7 million years. *Palaeogeography, Palaeoclimatology, Palaeoecology*, **263**, 131–145.

Dridi, M. 2000. *Overview on the Stratigraphy, Palaeogeography and Structural Evolution in Southern Tunisia during the Mesozoic as Part of the African Margin*. CIESM Workshop Series, **13**, 57–59.

Druckman, Y. 1984. Evidence for early–middle Triassic faulting and possible rifting from the Helez Deep Borehole in the coastal plain of Israel. *In*: Dixon, J. E. & Robertson, A. H. F. (eds) *The Geological Evolution of the Eastern Mediterranean*. Geological Society, London, Special Publications, **17**, 203–212.

El-Arnauti, A. & Shelmani, M. 1988. A contribution to the North East Libyan subsurface stratigraphy with emphasis on pre-mesozoic. *In*: El-Arnauti, A., Owens, B. & Thusu, B. (eds) *Subsurface Palynostratigraphy of North East Libya*. Garyounis University, Benghazi.

El-Hawat, A. S., Missallati, A. A., Bezan, A. & Taleb, T. N. 1996. The Nubian Sandstone in the Sirt Basin and its correlatives. *In*: Salem, M. J., El-Hawat, A. S. & Sbeta, A. M. (eds) *The Geology of Sirt Basin*. Elsevier, Amsterdam, 3–29.

England, P. & Molnar, P. 1990. Surface uplift, uplift of rocks and exhumation of rocks. *Geology*, **18**, 1173–1177.

Garfunkel, Z. & Derin, B. 1984. Permian–early Mesozoic tectonism and continental margin formation in Israel and its implications for the history of the Eastern Mediterranean. *In*: Dixon, J. E. & Robertson, A. H. F. (eds) *The Geological Evolution of the Eastern Mediterranean*. Geological Society, London, Special Publications, **17**, 187–201.

Genik, G. J. 1993. Petroleum geology of Cretaceous–Tertiary rift basins in Niger, Chad and Central African Republic. *American Association of Petroleum Geologists Bulletin*, **77**, 1405–1434.

Graham, J. R. 1982. Wave-dominated shallow marine sediments in the Lower Carboniferous of Morocco. *Journal of Sedimentary Petrology*, **52**, 1271–1276.

Gras, R. & Thusu, B. 1998. Trap architecture of early Cretaceous Sarir Sandstone in the Eastern Sirte Basin, Libya. *In*: Macgregor, D. S., Moody, R. T. J. & Clark-Lowes, D. D. (eds) *Petroleum Geology of*

North Africa. Geological Society, London, Special Publications, **132**, 317–334.

Guerrak, S. 1989. *Time and Space Distribution of Palaeozoic Oolitic Ironstones in the Tindouf Basin, Algerian Sahara*. Geological Society, London, **46**, 197–212.

Hammuda, O. S. 1971. Nature and significance of the lower Cretaceous Unconformity in Jebel Nafusa, North West Libya. *In*: Gray, C. (ed.) *Symposium on the Geology of Libya*. Faculty of Science, University of Libya, Tripoli, 87–99.

Herrera, Z. A. & Racheboeuf, P. R. 2001. Les Eodevonariides (*Chonetoidea, Brachiopoda*) Du Devonien des Bassins de Taoudeni et du Sud du Hoggar, Sahara. *Geobios*, **34**, 493–503.

IFP. 1998. Regional Synthesis of the Triassic Reservoir in Algeria. Oil Industry Consortium Report (4 Volumes).

IFP. 2003. Regional Basin Modelling Study of the Berkine/Illizi Basin (Algeria). Oil Industry Consortium Report (1 Volume).

IFP/Sonatrach/Beicip-Franlab. 2006. Berkine Gas Project: Evaluation of the Gas Potential of the Berkine Basin (Algeria). Oil Industry Consortium Project (3 Volumes).

Jones, R. W. 1997. Devonian–Carboniferous Stratigraphy of District 3, Algeria: Results of the 1996 Biostratigraphic Work Programme (Phase 1), March 1997. BP Report EXT 72613.

Klitzch, E. 1990. Palaeogeographical development and correlation of continental Strata (former Nubian Sandstone) in North East Africa. *Journal of African Earth Sciences*, **10**, 199–213.

Lefranc, J. P. & Guiraud, R. 1990. The continental intercalaire of North Western Sahara and its equivalents in the neighbouring regions. *Journal of African Earth Sciences*, **10**, 27–77.

Liegeois, J. P., Benhallou, A., Azzouni-Sekkal, A., Yahyao, R. & Bonnin, B. 2005. The Hoggar swell and volcanism: reactivation of the Precambrian Taureg Shield during Alpine Convergence and West African Cenozoic Volcanism. *In*: Foulger, G. R., Natland, J. H., Presnall, D. C. & Anderson, D. C. (eds) *Plates, Plumes & Paradigms*. Geological Society of America, Boulder, CO, Special Papers, **388**, 379–400.

Lüning, S., Craig, J., Loydell, D. K., Storch, P. & Fitches, B. 2000. Lower Silurian 'Hot Shales' in North Africa and Arabia: regional distribution and depositional model. *Earth Science Reviews*, **49**, 121–200.

Lüning, S., Kolonic, S., Belhadj, E. M., Cota, L., Baric, G. & Wagner, T. 2004*a*. Integrated depositional model for the Cenomanian–Turonian organic-rich strata in North Africa. *Earth Science Reviews*, **64**, 51–117.

Lüning, S., Wendt, J., Belka, Z. & Kaufmann, B. 2004*b*. Temporal/spatial reconstruction of the early Frasnian (Late Devonian) anoxia in NW Africa: new field data from the Ahnet Basin (Algeria). *Sedimentary Geology*, **163**, 237–264.

Madi, A., Savard, M. M., Bourque, P. A. & Chi, G. 2000. Hydrocarbon potential of the Mississippian Carbonate Platform, Bechar Basin, Algerian Sahara. *American Association of Petroleum Geologists Bulletin*, **84**, 256–287.

McKerrow, W. S., Mac Niocaill, C., Ahlberg, P. E., Clayton, G., Cleal, C. J. & Eager, R. M. C. 2000. The late Palaeozoic relations between Gondwana & Laurussia. *In*: Franke, W., Haak, V., Oncken, O. & Tanner, D. (eds) *Orogenic Processes: Quantification and Modelling in the Variscan Belt*. Geological Society, London, Special Publications, **179**, 9–20.

Mohamed, A. Y., Pearson, M. J., Ashcroft, W. A. & Whiteman, A. J. 2001. Structural development and crustal stretching in the Muglad Basin, Sudan. *Journal of African Earth Sciences*, **32**, 179–191.

Monod, O., Kozlu, H. *et al*. 2003. Late Ordovician glaciation in Southern Turkey. *Terra Nova*, **15**, 249–257.

Paleoservices Report. 1986. The Hydrocarbon Potential of the Palaeozoic Rocks of the Western Desert of Egypt. BP Report EXT 52158/1.

Robertson, A. H. F. 2007. Sedimentary evidence from the south Mediterranean region (Sicily, Crete, Peloponnese, Evia) used to test alternative models for the regional tectonic setting of Tethys during Late Palaeozoic–Early Mesozoic time. *In*: Robertson, A. H. F. & Mountrakis, D. (eds) *Tectonic Development of the Eastern Mediterranean Region*. Geological Society, London, Special Publications, **260**, 91–154.

Robertson, A. H. F. & Dixon, J. E. 1984. Aspects of the geological evolution of the Eastern Mediterranean. *In*: Dixon, J. E. & Robertson, A. H. F. (eds) *The Geological Evolution of the Eastern Mediterranean*. Geological Society, London, Special Publications, **17**, 1–74.

Schroter, T. 1996. Tectonic and sedimentary development of the Central Zallah Trough. *In*: Salem, M. J., Busrewil, M. T., Misallati, A. A. & Sola, M. A. (eds) *The Geology of the Sirt Basin*. Elsevier, Amsterdam, 123–137.

Smith, A. G. 2006. Tethyan ophiolite emplacement, Africa to Europe motions and Atlantic spreading. *In*: Robertson, A. H. F. & Mountrakis, D. (eds) *Tectonic Development of the Eastern Mediterranean Region*. Geological Society, London, Special Publications, **260**, 11–34.

Soussi, M. & Ben Ismail, M. H. 2000. Platform collapse and pelagic seamount facies, Jurassic development of Central Tunisia. *Sedimentary Geology*, **133**, 93–113.

Stampfli, G. M. & Borel, G. D. 2002. A plate tectonic model for the Palaeozoic and Mesozoic constrained by dynamic plate boundaries and restored synthetic oceanic isochrones. *Earth and Planetary Science Letters*, **196**, 17–33.

Stampfli, G. M., Borel, G. D., Cavazza, W., Mosar, J. & Zeigler, P. A. 2001. Palaeotectonic and palaeogeographic evolution of western Tethys and Peritethyan domain. *Episodes*, **24**, 222–228.

Swezey, C. S. 2008. Cenozoic stratigraphy of the Sahara. *Journal of African Earth Sciences*, **53**, 89–121.

Toomey, D. F. 1991. Late Permian reefs of Southern Tunisia: facies patterns and comparison with Capitan Reef, South Western United States. *Facies*, **25**, 119–146.

Turner, P. & Sherif, H. 2007. A giant late Triassic–early Jurassic evaporitic basin on the Saharan Platform, North Africa. *In*: Schreiber, B. C., Lugli, S. & Babel, M. (eds) *Evaporites through Space and Time*. Geological Society, London, Special Publications, **285**, 87–105.

Turner, P., Pilling, D., Walker, D., Exton, J., Binnie, J. & Sabaou, N. 2001. Sequence stratigraphy and sedimentology of the late Triassic TAG-I (Blocks 401/402, Berkine Basin, Algeria). *Marine & Petroleum Geology*, **18**, 959–981.

Underdown, R. & Redfern, J. 2007. The importance of constraining regional exhumation in basin modelling: a hydrocarbon maturation history of the Ghadames Basin, North Africa. *Petroleum Geoscience*, **13**, 253–270.

Underdown, R. & Redfern, J. 2008. Petroleum generation and migration in the Ghadames Basin, North Africa: a two-dimensional basin modelling study. *American Association of Petroleum Geologists Bulletin*, **92**, 53–76.

Underdown, R., Redfern, J. & Lisker, F. 2007. Constraining the burial history of the Ghadames Basin, North Africa: an integrated analysis using sonic velocities, vitrinite reflectance data and apatite fission track ages. *Basin Research*, **19**, 557–578.

Villeneuve, M. 2005. Paleozoic basins in West Africa and the Mauritanide Thrust Belt. *Journal of African Earth Sciences*, **43**, 166–195.

Vos, R. G. 1977. Sedimentology of an Upper Palaeozoic river, wave and tide influenced delta system in Southern Morocco. *Journal of Sedimentary Petrology*, **47**, 1242–1260.

Wahlman, G. P. 1991. Permian and Late Carboniferous Carbonates of South Central Tunisia: Biostratigraphy, Reefs and Associated Carbonate Facies. Amoco Internal Report.

Wendt, J., Belka, B., Kaufman, B., Kostrewa, R. & Hayer, J. 1997. The world's most spectacular carbonate mud mounds (Middle Devonian, Algerian Sahara). *Journal of Sedimentary Research*, **67**, 424–436.

Yang, Y. & Aplin, A. C. 1999. Definition and practical application of mudstone porosity–effective stress relationships. *Petroleum Geoscience*, April 2004, **10**, 153–162.

Zaborski, P. M. & Morris, N. J. 1999. The late cretaceous ammonite genus *Libyoceras* in the Lullemeden Basin (West Africa) and its palaeogeographical significance. *Cretaceous Research*, **20**, 63–79.

Zaier, A., Beji-Sassi, A., Sassi, S. & Moody, R. T. J. 1998. Basin evolution and deposition during the Early Palaeogene in Tunisia. *In*: Macgregor, D. S., Moody, R. T. J. & Clark-Lowes, D. D. (eds) *Petroleum Geology of North Africa*. Geological Society, London.

Biostratigraphy, chemostratigraphy and thermal maturity of the A1-NC198 exploration well in the Kufra Basin, SE Libya

S. LÜNING,[1] N. MILES,[2] T. PEARCE,[3] E. BROOKER,[3] P. BARNARD,[4] G. JOHANNSON[5] and S. SCHÄFER[1,5]

[1]*RWE Dea, Überseering 40, 22297 Hamburg, Germany (e-mail: Sebastian.Luening@rwe.com)*
[2]*Petrostrat Ltd, Tan-y-Graig, Parc Caer Seion, Conwy LL32 8FA, UK*
[3]*Chemostrat Ltd, Unit 1, Ravenscroft Court, Buttington Enterprise Park, Welshpool, Powys SY21 8SL, UK*
[4]*Applied Petroleum Technology (UK) Ltd, Second Floor, 14 Wynnstay Road, Colwyn Bay LL29 8NB, UK*
[5]*RWE Dea Libya, Barcelona Street, 15A Hai Andalus, Tripoli, Libya*

Abstract: The A1-NC198 exploration well was drilled in the Kufra Basin in 2007 by RWE Dea and represented only the third well in a large, 400 000 km^2 frontier basin. Despite being dry and lacking any hydrocarbon shows, the well provides important data to improve the understanding of the regional petroleum play. In the 1980s and 1990s the basin's prospectivity was questioned largely because of supposed (1) lack of structuration, (2) lack of source rock and (3) thermal immaturity at Silurian level. Following a series of academic and industry studies over the past 10 years, these assertions can no longer be upheld. The analysis of available seismic has proven the existence of Murzuq-style fault blocks as well as late Ordovician glacial erosional relict buried hills, potentially forming suitable structural and stratigraphic traps. The presence of hot shale in the Kufra Basin is evidenced by typical seismic onlaps of strong amplitude reflectors at base Silurian levels, shallow drilling results and outcrop spectral gamma-ray evidence. A spore colouration study of A1-NC198 cuttings indicates a deep oil window maturity for the Silurian, implying potential oil generation in the basin if suitable Silurian source rocks exist. The stratigraphy of the A1-NC198 succession was analysed by means of biostratigraphy and chemostratigraphy, which form the basis for improved well correlations within the basin.

Keywords: Kufra Basin, Libya, chemostratigraphy, petroleum geology

The Kufra Basin is a large, underexplored Palaeozoic frontier basin covering 400 000 km^2 in SE Libya and NE Chad, and extending into NW Sudan and SW Egypt (Fig. 1). Only four petroleum wildcat wells have been drilled in the basin to date, A1-NC43 and B1-NC43 in 1978 and 1981 by AGIP (Bellini *et al.* 1991), A1-NC198 by RWE Dea in 2007 and A1-171/4 by Statoil in 2008. All of these were dry (Fig. 2). Another four dry wells were drilled just outside the basin, two by Oasis in the 1960s (A1-71 and D1-71) and two by Repsol in 2009 (A1-NC203 and B1-NC203) (Fig. 2). Because of its large size, the basin remains significantly underexplored.

The petroleum play pursued by explorers in the Kufra Basin is similar to the neighbouring Murzuq Basin in SW Libya, which hosts a series of medium to large oil fields in a similar geological setting (Fig. 3) (Davidson *et al.* 2000; Lüning *et al.* 2000; Herzog *et al.* 2008). Most of the hydrocarbon play elements known from the Murzuq Basin also occur in the Kufra Basin. As in the Murzuq Basin, the Ordovician sedimentary package contains thick porous sandstones with potential reservoir quality (Turner 1980). Late Ordovician deposition was strongly influenced by glacial processes as evidenced by buried hill morphologies on seismic and glacial striations at outcrop (Le Heron *et al.* 2010).

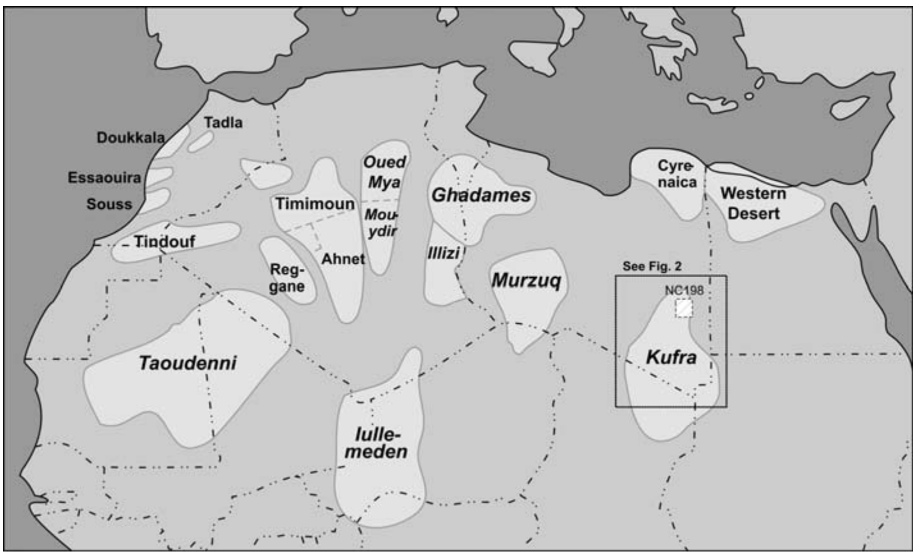

Fig. 1. Palaeozoic basins of North Africa and location of Kufra Basin and Block NC198.

VINING, B. A. & PICKERING, S. C. (eds) *Petroleum Geology: From Mature Basins to New Frontiers – Proceedings of the 7th Petroleum Geology Conference*, 761–770. DOI: 10.1144/0070761

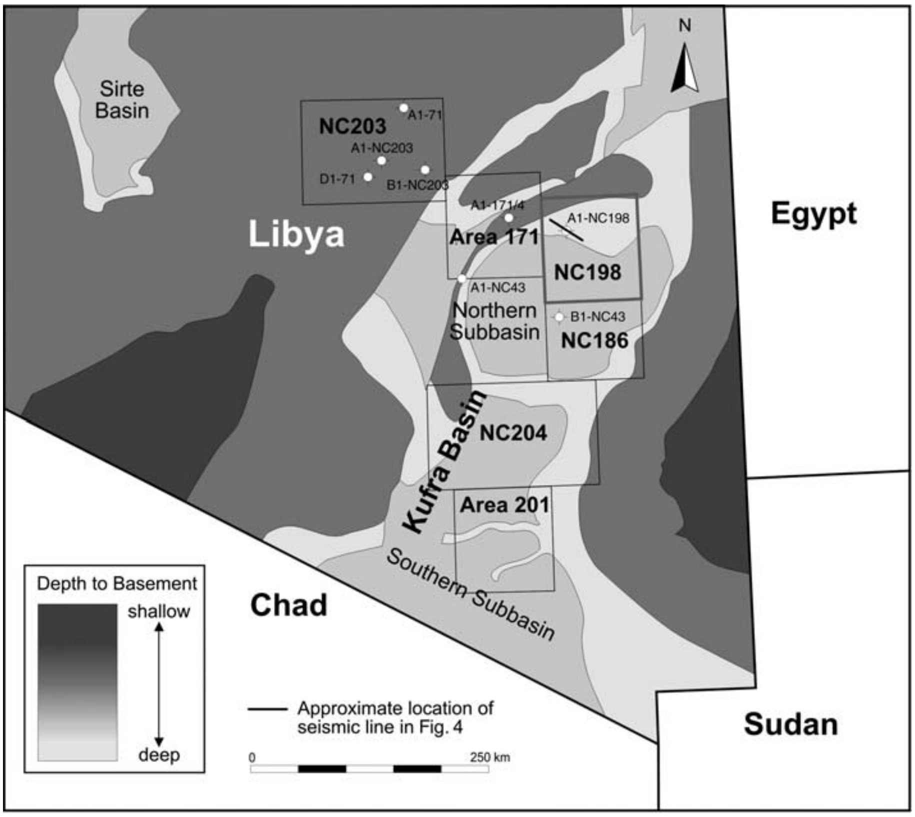

Fig. 2. Depth-to-basement map (modified after FrOGTech 2008, published with permission) and locations of wells drilled in and nearby the Kufra Basin.

In addition to buried hill palaeotopographic stratigraphic traps, a series of structural traps defined by fault blocks have also been mapped on seismic in the Kufra Basin.

The Silurian Tanezzuft Shale represents both seal and source rock for the petroleum play and is the most critical element of the play (Lüning *et al.* 1999). The basal Tanezzuft 'lower hot shale' has a patchy distribution and was deposited in palaeodepressions. It is the only source rock in the Murzuq Basin (Lüning *et al.* 2000). The hot shale also occurs in the Kufra Basin and has been identified in several outcrop sections by means of gamma-ray (GR)

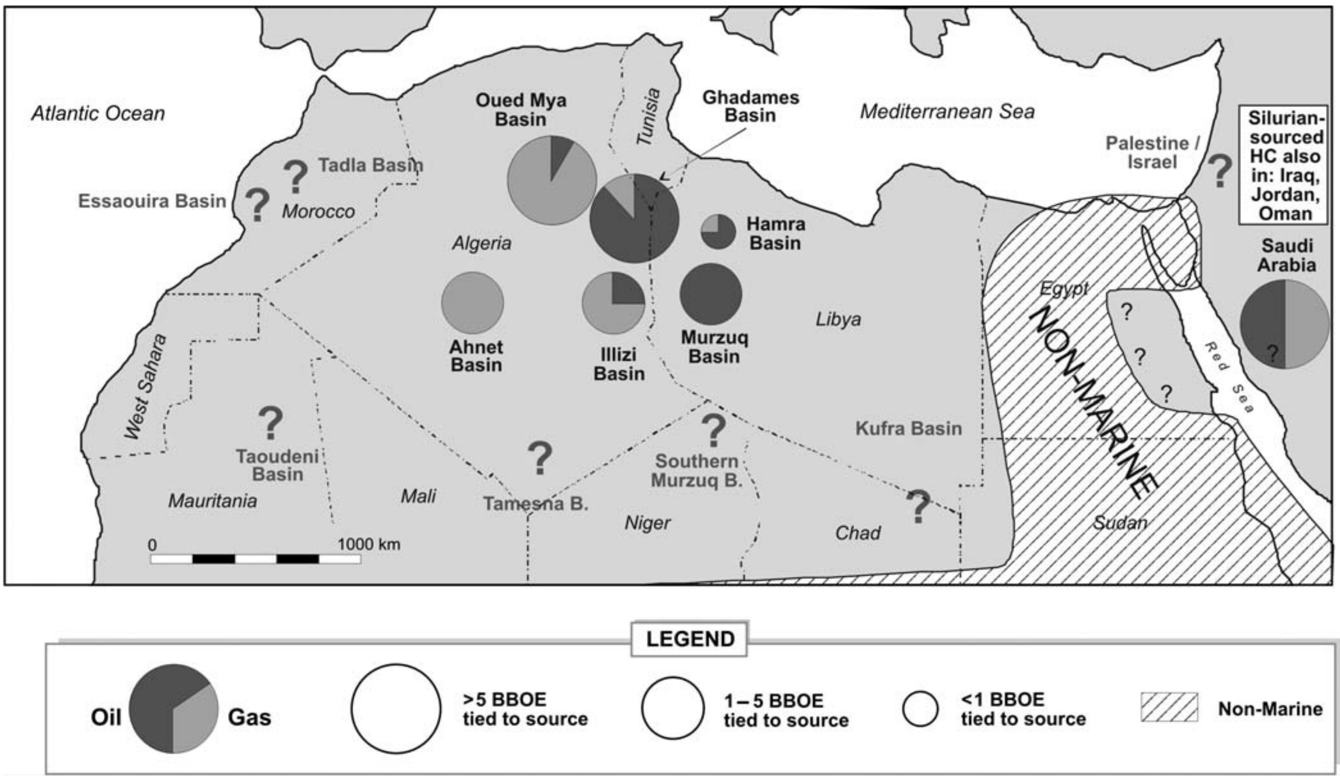

Fig. 3. Proven oil and gas occurrences in North Africa sourced by the Silurian black shales. Modified after Macgregor (1996).

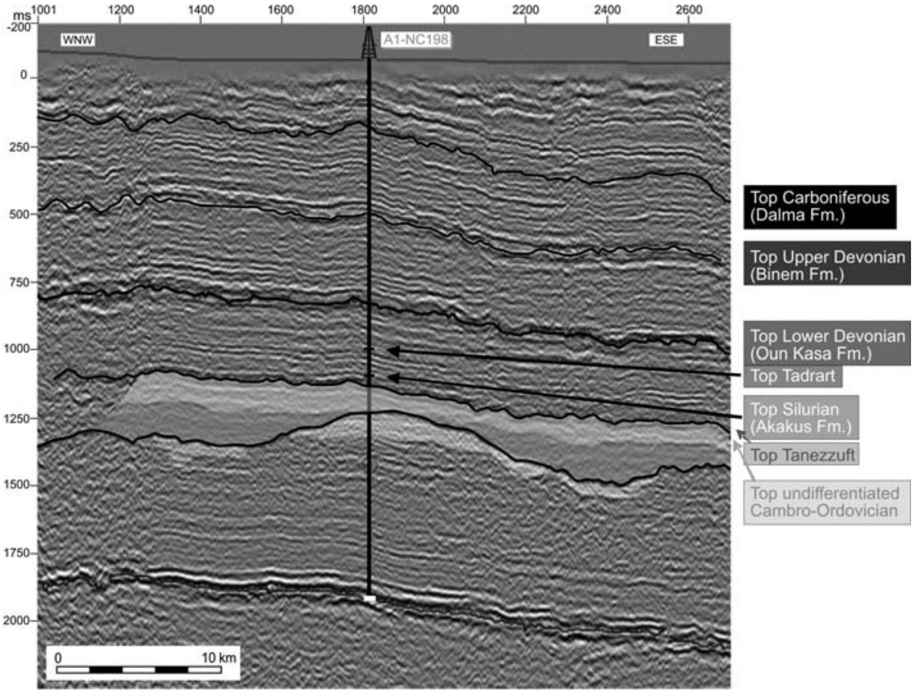

Fig. 4. Seismic cross-section through the A1-NC198 buried hill structure. Vertical scale in two-way time.

spectrometry based on its characteristic enrichment in uranium (Lüning *et al.* 2003; Fello *et al.* 2006). The source rock was also penetrated by AGIP's shallow borehole KW2 and is interpreted in the subsurface based on strong seismic amplitudes and onlap geometries. The thickness of the total Tanezzuft shale package varies greatly across the Kufra Basin (Lüning *et al.* 1999). In surface outcrops the Tanezzuft may be a few metres to more than 100 m thick and shale-dominated. In wells A1-NC43 and A1-NC198 the Tanezzuft is about 60 m thick; in B1-NC43 it is only 20 m (Fig. 6). The Tanezzuft shales also provide the main seal for the underlying Ordovician reservoirs. Compared with the Murzuq Basin, where Tanezzuft thicknesses of up to 500 m have been recorded, providing an excellent regional seal, the seal risk in the Kufra Basin may be higher because in some areas there is increased risk that fault offsets are greater than seal thickness. In cases where the Tanezzuft seal is breached by faults, hydrocarbons may have migrated into the Devonian–Carboniferous section, which also has reservoir potential and is characterized by a thick series of interbedded sandstones and sealing shales.

Exploration well A1-NC198 was drilled in block NC198, in the northern sub-basin (Fig. 2), between 13 April and 26 May 2007. The well targeted an upper Ordovician 'buried hill' prospect (Fig. 4), and reached basement at TD (12 193 ft, 3716 m). The well proved to be dry and did not encounter any visible hydrocarbon shows. A series of studies was carried out, including palynology, chemostratigraphy, fluid inclusions, organic geochemistry and thermal maturity, in order to better understand the petroleum play elements and implications for regional hydrocarbon prospectivity of the Kufra Basin.

Palynology

Study objective

Establishing a palyno-biostratigraphical subdivision of the section drilled by well A1-NC198 was important because the typical monotonous interbedded sandstones and shales are easily mis-correlated, especially due to the limited number of offset wells available to provide control in this frontier basin. A secondary objective was the study of depositional environments. The comprehensive biostratigraphic dataset acquired in the A1-NC198 well has enabled a more reliable correlation with AGIP's A1-NC43 and B1-NC43 wells (Fig. 5), which were palynologically studied in detail by Grigagni *et al.* (1991).

Material and methods

The study was based on 71 cuttings samples, mostly claystones, sampled throughout the entire well section. The analysis is based on counts of 200 palyno-specimens per sample, using 10 μm sieved preparations. The rest of the slide was then scanned for rarer taxa. In addition a 53 μm sieved preparation was analysed for most samples in order to concentrate chitinozoans, with counts of up to 100 made where possible (Fig. 6).

Results

Based on palynology, a robust biostratigraphic framework was erected for the uppermost Ordovician to Early Carboniferous encountered by well A1-NC198 (Fig. 7). Spores, chitinozoans, acritarchs and algae all proved useful in the biostratigraphic interpretation of this well section. The bulk of the Cambro-Ordovician as well as the strata overlying the Lower Carboniferous siliciclastics could not be age-dated by palynomorphs due to poor palynomorph recovery or barren samples. The majority of analysed Palaeozoic samples indicated marginal marine to inner shelf depositional environments. Only a few samples yielded evidence for non-marine settings, a scarcity which however may be related to the paucity of palynomorphs in continental sedimentary successions.

Chemostratigraphy

Chemostratigraphy involves the characterization and correlation of sedimentary strata using stratigraphic variations in inorganic geochemistry (e.g. Pearce *et al.* 2005; Ratcliffe *et al.* 2006). The technique is particularly sensitive to these variations and in many instances has proved successful in detecting and correlating them when dealing with apparently uniform lithological successions. Consequently, reservoir correlations and stratigraphic picks may

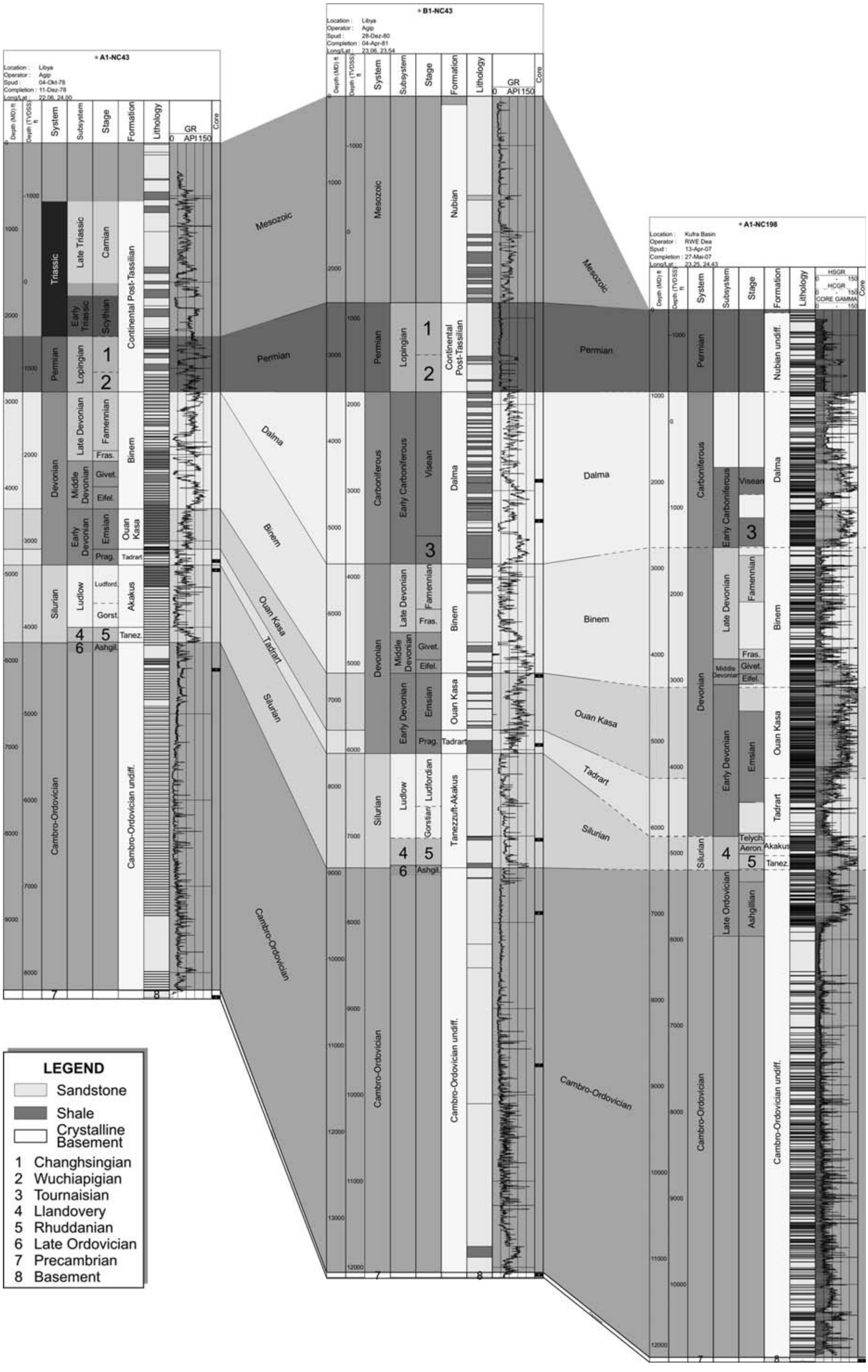

Fig. 5. Correlation of wells A1-NC43, B1-NC43 and A1-NC198 (flattened on base Permian).

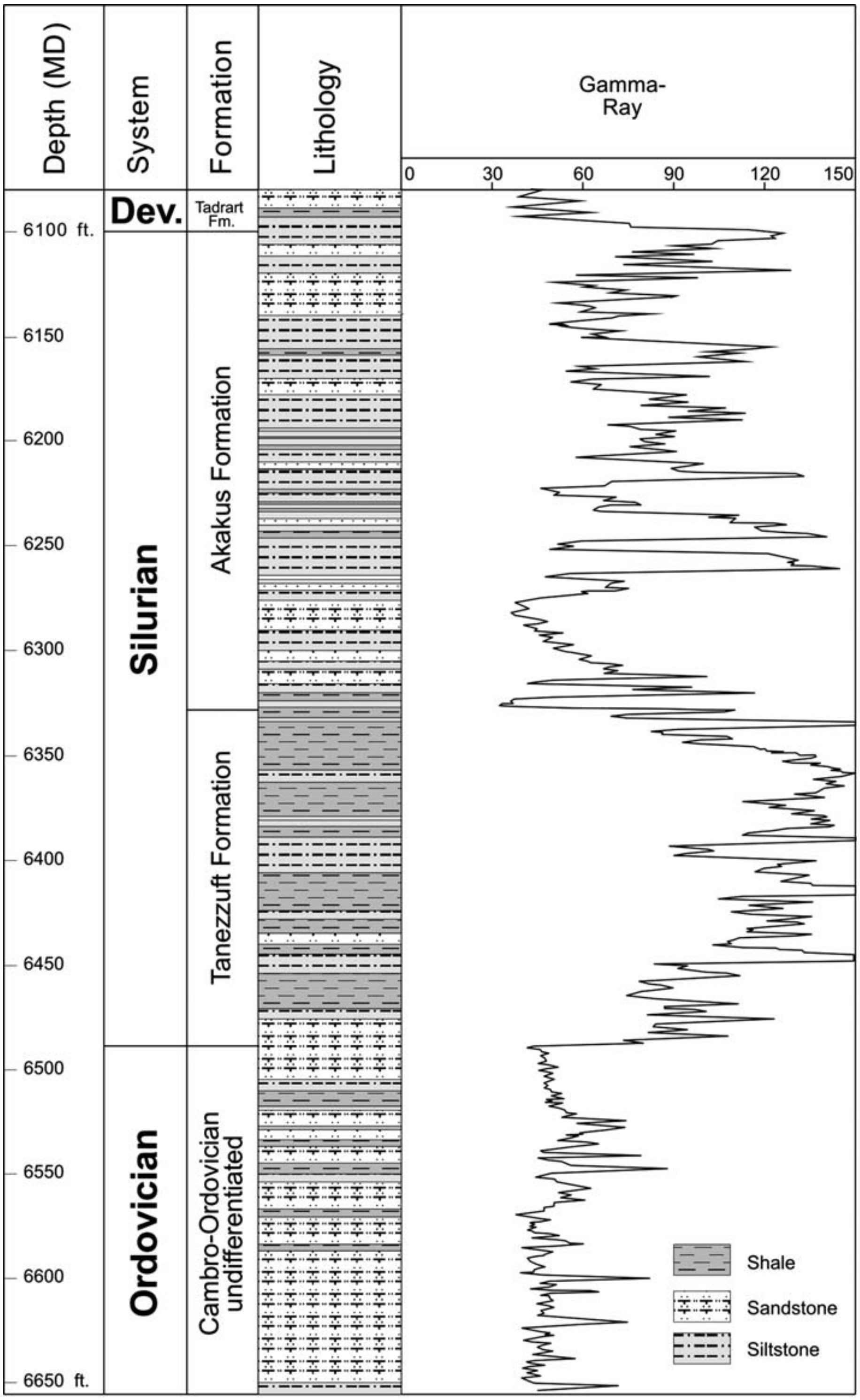

Fig. 6. Lithology and GR characteristics of the Silurian Tanezzuft Formation in well A1-NC198. GR in API units.

now be established with confidence, even for those sequences over which the E-log traces show little significant change.

Study objective

Chemostratigraphy was carried out, targeting specifically the gaps in the Cambrian to mid Ordovician and post-lower Carboniferous succession that were not resolved by palynostratigraphy.

Material and methods

A total of 69 cuttings samples were selected, distributed over the entire well, and comprised mostly sandstones but also some claystones. All samples were analysed by inductively coupled plasma–optical emission spectrometry (ICP-OES) and inductively coupled plasma–mass spectrometry (ICP-MS), with data being acquired for 50 elements.

Results

Based on the chemostratigraphic analysis, the section drilled by well A1-NC198 was subdivided into 15 discrete sedimentary packages, named P1–P15 (Fig. 8). Each package possesses a distinct set of geochemical characteristics. Because of the limited number of samples and the great thickness of the interval analysed,

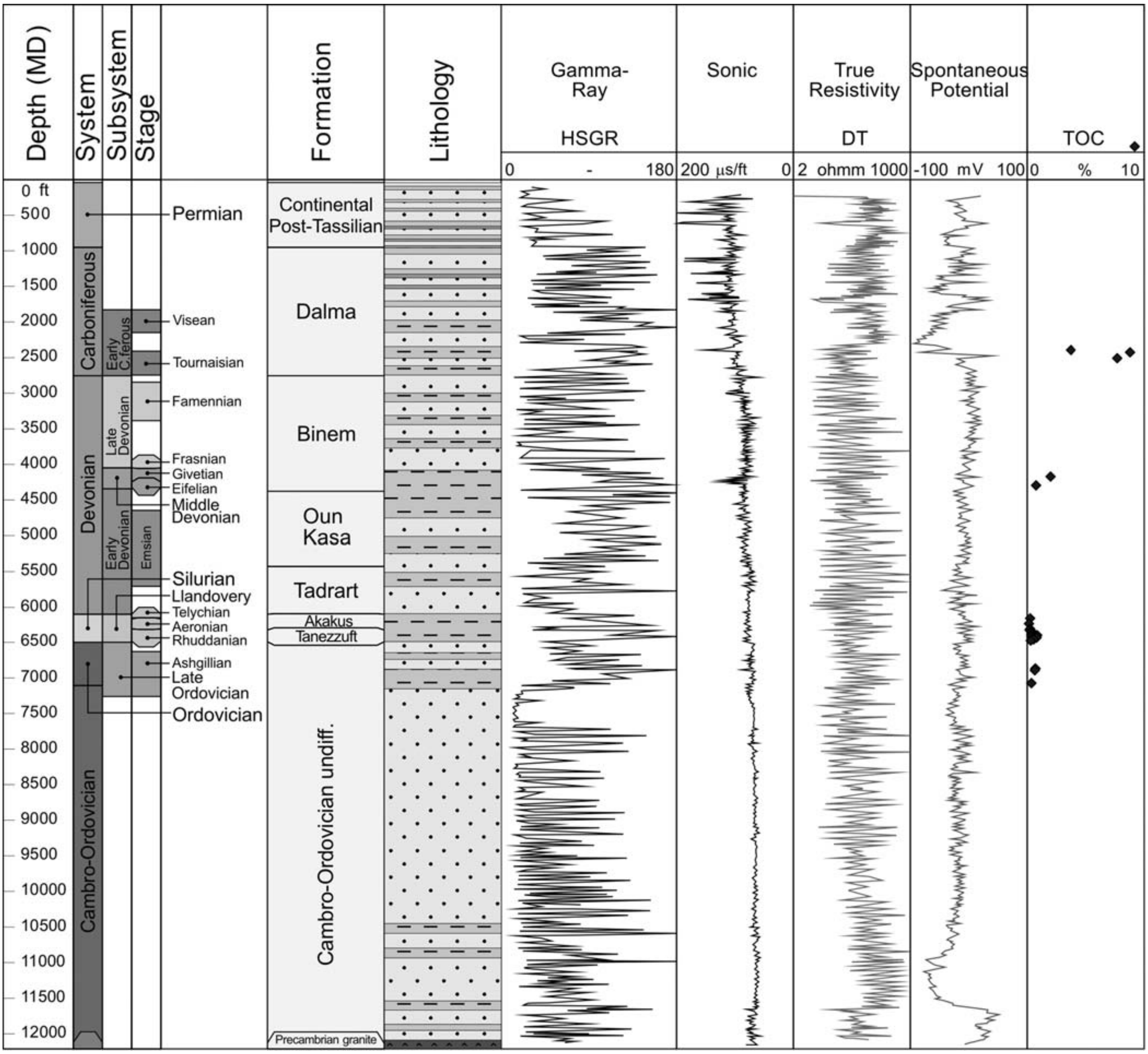

Fig. 7. Simplified well log from the A1-NC198 wildcat well and plot of measured TOC data.

chemostratigraphic distribution curves remain rather coarse for this well. However, typical trends exist both in the Cambro-Ordovician and post-lower Carboniferous that might allow chemostratigraphic correlation with neighbouring wells. In the Murzuq Basin (Kaaber *et al.* 2007) chemostratigraphy has been used successfully to subdivide and correlate the Cambro-Ordovician succession. Overall, the geochemical signature of the Achebayat, Hawaz and Bir Tlascin intervals identified in the Murzuq Basin are comparable to those recognized in well A1-NC198 with, for example, high Ga/Rb (attributed to high kaolinite/illite ratios) characterizing the Achebayat and moderately high K–Al (K-feldspar) occurring in the Bir Tlascin Formations. Notably, the sandstones of the Mamuniyat Formation are not identified geochemically in well A1-NC198. The Silurian/Devonian sandstones and shales of the Akakus, Tadrart and Binem Formations can each be differentiated geochemically based on variations in, amongst others, K–Al, Fe–Mn and Ti–Mg, attributed to fluctuations in feldspar, siderite and Ti-rich heavy minerals respectively. Carboniferous deposits exhibit high Na–Al associated with the occurrence of plagioclase feldspar reworked from basic volcanic provenance. Notably, the Permian section is marked by high K–Al attributed to major influx of arkosic sandstones derived from a granitic provenance (Fig. 8).

Fluid inclusions

Fluid inclusions are representative microscopic samples of past or present-day subsurface fluids that become entrapped in rocks during the formation of diagenetic cements or healed microfractures. They are not subject to fractionation during sampling or evaporative loss during sample storage for any length of time. Fluid inclusions persist in the geological record long after the parent fluids have moved on, but are continuously formed even up to the very recent past (Hall *et al.* 2002).

Study objective

The study objective was the identification and quantitative analysis of volatile hydrocarbon traces within micron-sized cavities in cuttings rock samples.

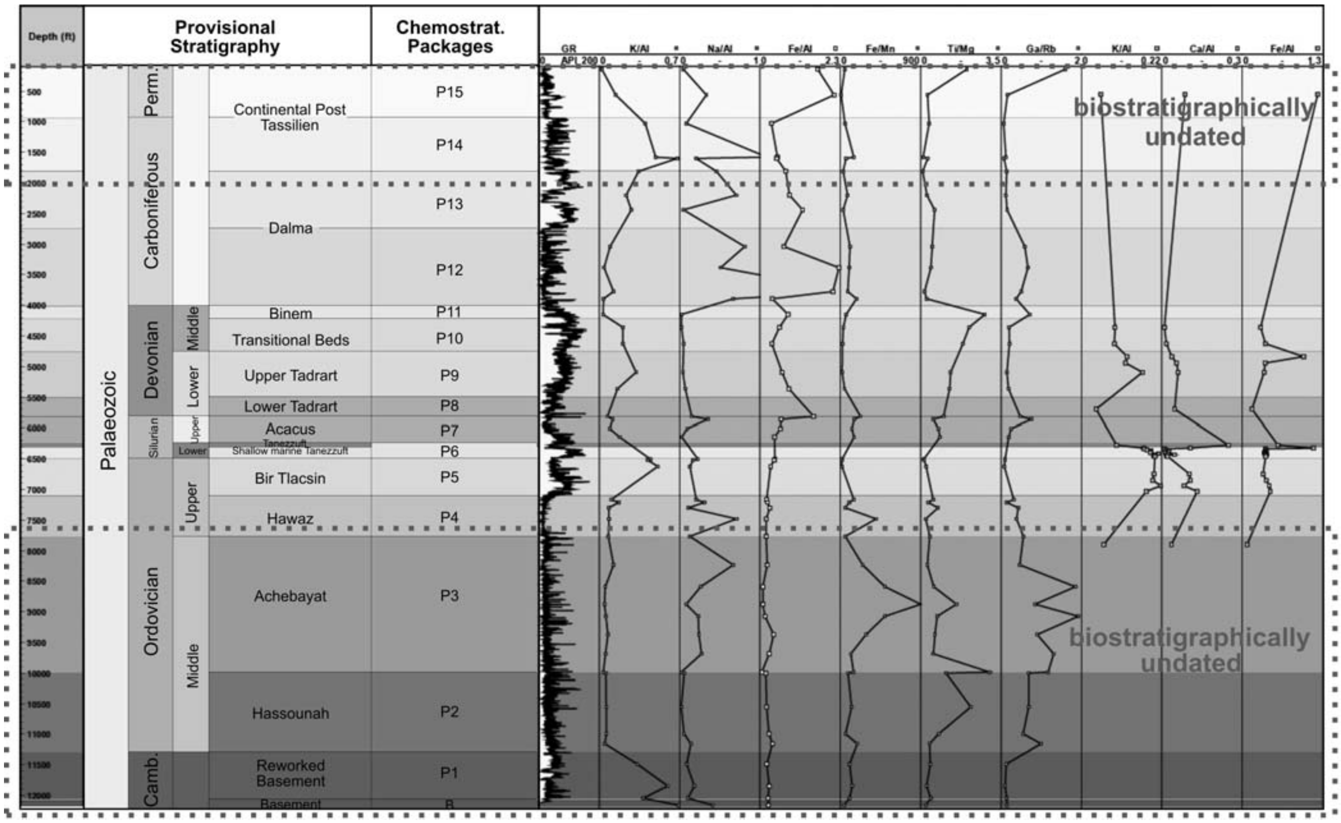

Fig. 8. Chemostratigraphy of well A1-NC198. Zones boxed with dashed lines mark intervals that could not be dated by palynology due to poor palynomorph recovery. Silurian to Carboniferous stratigraphy is based on palynomorphs.

Material and methods

The study was carried out by fluid inclusion technologies (FIT) using the fluid inclusion stratigraphy (FIS) method, a patented Amoco technology, licensed to FIT Inc. The study in well A1-NC198 was based on 78 cuttings samples, mostly sandstones. The samples were mechanically crushed and the volatile substances released instantaneously. The fluids were then pumped through mass analysers where they were ionized, separated according to their mass/charge and recorded.

Results

No liquid petroleum fluids were recorded by FIS throughout the well, indicating sub-anomalous hydrocarbon concentrations. Nevertheless, visual inspection of thin sections of Devonian and Ordovician samples resulted in the identification of rare oil inclusions (Fig. 9). In addition, a few thin zones with weak dry gas responses were recorded by FIS.

Additional evidence for the presence of liquid hydrocarbons and hence a working petroleum system in the NC198 area of the Kufra Basin also comes from a Gore™ surface geochemistry micro-seepage survey that yielded a series of positive seepage anomalies.

Petroleum source rock evaluation

Study objective

Despite the positive evidence from high seismic amplitudes, seismically defined onlaps and radioactive Silurian shales at outcrop, an organic-rich Silurian source rock has not yet been penetrated by any of the existing exploration wells in the Kufra Basin (Lüning *et al.* 1999). As most wells are drilled on positive structures

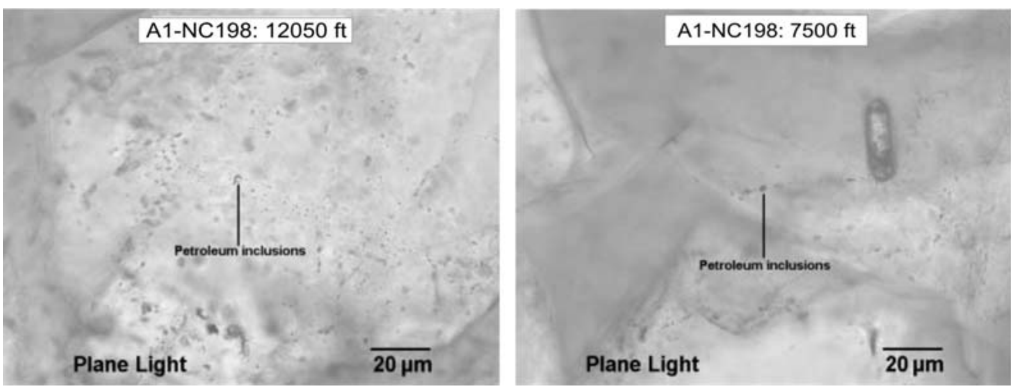

Fig. 9. Fluid inclusions containing hydrocarbon fluids in Cambro-Ordovician sandstone.

that might also have been palaeohighs during the early Silurian, the absence of organic-rich shales in these locations is not unexpected. The study objective was to evaluate whether the Lower Silurian source rock is present in well A1-NC198 and to determine the organic richness of the interval.

Material and methods

The study is based on 11 Silurian Tanezzuft samples and five Devonian-Carboniferous samples. Total organic carbon content (TOC) was analysed using a Leco system.

Results

All of the Tanezzuft samples recorded low organic richness with TOCs ranging between 0.21 and 0.84%. This is consistent with the rather low GR values of only up to 180 API, indicating the absence of the typical radioactive Silurian 'hot shale' at this location. Slightly elevated TOCs of around 2% were recorded in the Middle Devonian within the Binem Formation (Fig. 7). In contrast, high TOCs of up to 9% occur in the Carboniferous Dalma Formation (Fig. 7).

Spore colouration and vitrinite reflectivity

Study objective

The thermal maturity history of the Kufra Basin to date has been largely unknown. Therefore, a detailed thermal maturity study on the basis of spore colouration and vitrinite reflectance has been carried out on samples from the A1-NC198 well.

Material and methods

The study is based on 28 cuttings samples, mostly shales, originating from the depth range of 1995 to 7740 ft. The vitrinite reflectivity studies were carried out on isolated 10 μm sieved kerogen concentrates which were mounted in resin and polished ready for reflectivity studies.

Results

Both spore colour indices and vitrinite reflectivity data indicate that the Lower Carboniferous and the upper part of the Devonian sediments have been within the main oil window (Figs 10 & 11). Spore colour indices indicate that the Silurian and Ordovician interval is late mature for oil generation. No vitrinite-like material was observed in the Lower Palaeozoic section. Extrapolation of maturity gradients to surface intercepts indicate significant missing section, with erosion of post-Lower Carboniferous section due to uplift. Apatite fission track analyses suggest that this uplift occurred sometime during the Late Cretaceous to Cenozoic period (Lisker, pers. comm. 2009).

Implications for regional hydrocarbon prospectivity

Contrary to previous interpretations, the new results show that the potential Silurian hot shale source rock was previously deeply buried, into the oil window, as evidenced by high spore colouration indices. Unpublished apatite fission track data indicate that this oil generation phase must have terminated due to significant uplift sometime around Late Cretaceous to Early Cenozoic time.

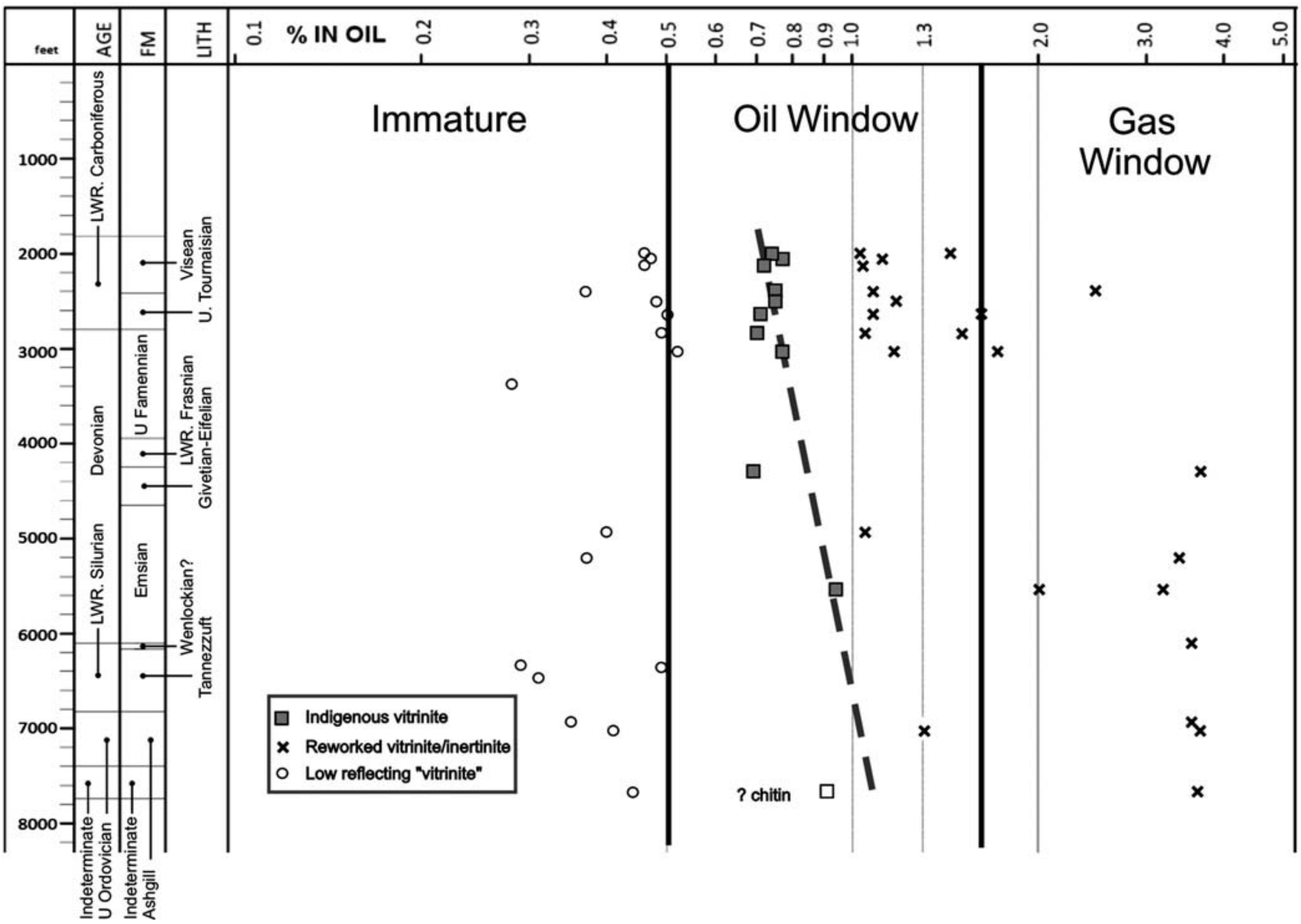

Fig. 10. Vitrinite reflectance against depth, well A1-NC198.

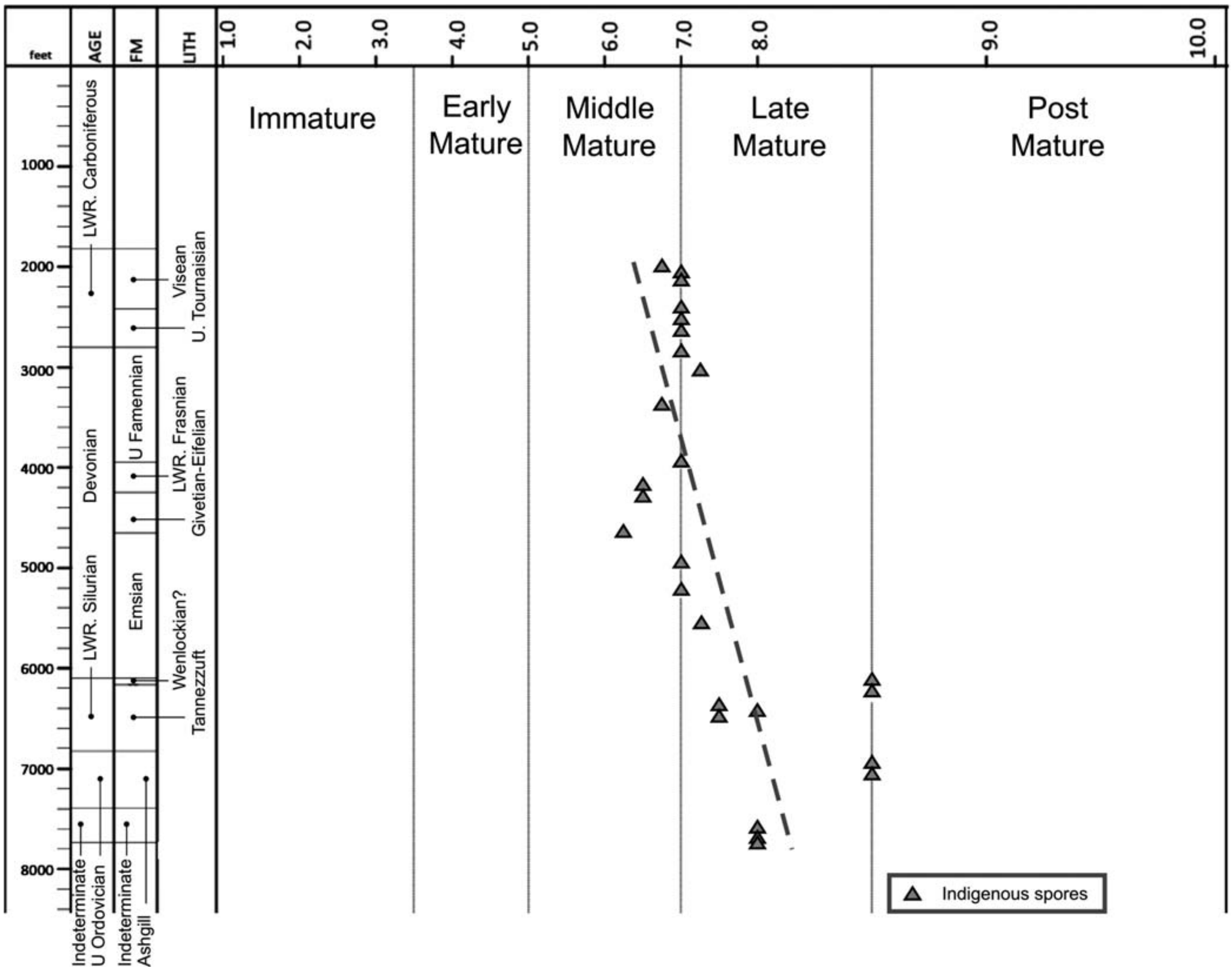

Fig. 11. Spore Colour Index against depth, well A1-NC198.

A similar structural history is known from the Murzuq and Ghadames basins (e.g. Dardour 2004; Underdown & Redfern 2008).

Based on seismic data, both glacial buried hills and tilted fault block structural traps can be identified in the Kufra Basin. However, the Tanezzuft shales which onlap these palaeohighs may not be thick enough to serve as an effective seal for the underlying Ordovician reservoirs, especially in areas where large faults exist. Over some buried hills the Tanezzuft shales may be extremely thin or even pinch out. Possible 'leakage' might have opened up migration pathways into Devonian–Carboniferous sandstones. Thick Devonian–Carboniferous shale units exist that may act as more effective seals in such cases. At the Ordovician reservoir level it may be more promising to concentrate on structural traps that developed later, such as tilted fault blocks, which may be better sealed by Tanezzuft shales than the buried hills.

In terms of source rock development, the absence of the Silurian hot shale in A1-NC198 does not challenge the current model of patchy distribution of the lower Silurian hot shale areally restricted to palaeodepressions. Evidence for the presence of the hot shale in the Kufra Basin is provided by typical seismic onlaps and strong amplitudes at base Silurian levels, and has been confirmed by shallow stratigraphic drilling results and outcrop spectral GR evidence.

Despite the two new recent dry wells in the Kufra Basin, the basin is still largely underexplored and a final determination of its hydrocarbon prospectivity is some way off. In the light of the petroliferous Murzuq Basin to the west, where a similar play exists, and which also initially had a number of negative well results before large accumulations were discovered, exploration of the Kufra basin remains a challenge well worth pursuing.

We thank RWE Dea and NOC for permission to publish this paper. The manuscript benefited greatly from helpful reviews by Professor Jonathan Redfern (University of Manchester) and an anonymous colleague.

References

Bellini, E., Giori, I., Ashuri, O. & Benelli, F. 1991. Geology of Al Kufrah Basin, Libya. *In*: Salem, M. J., Sbeta, A. M. & Bakbak, M. R. (eds) *The Geology of Libya*. Vol. 6. Elsevier, Amsterdam, 2155–2184.

Dardour, A. M. 2004. Stratigraphic controls on Palaeozoic petroleum systems, Ghadames Basin, Libya. *Journal of Petroleum Geology*, **27**, 141–162.

Davidson, L. *et al*. 2000. The structure, stratigraphy and petroleum geology of the Murzuq Basin, Southwest Libya. *In*: Sola, M. A. & Worsley, D. (eds) *Geological Exploration in the Murzuq Basin*. Elsevier, Amsterdam, 295–320.

Fello, N., Lüning, S., Štorch, P. & Redfern, J. 2006. Identification of early Llandovery (Silurian) anoxic palaeo-depressions at the western margin of the Murzuq Basin (southwest-Libya) based on gamma-ray spectrometry in surface exposures. *GeoArabia*, **11**, 101–118.

FrOGTech. 2008. *Kufra Basin SE Libya Zoom Study* (unpublished proprietary multiclient report).

Grigagni, D., Lanzoni, E. & Elatrash, H. 1991. Palaeozoic and mesozoic subsurface palynostratigraphy in the Al Kufrah Basin, Libya. *In*: Salem, M. J., Hammuda, O. S. & Eliagoubi, B. A. (eds) *The Geology of Libya*, Vol. IV. Elsevier, Amsterdam, 1160–1227.

Hall, D. L., Sterner, S. M., Shentwu, W. & Bigge, M. A. 2002. Applying fluid inclusions to petroleum exploration and production. AAPG Search and Discovery, www.searchanddiscovery.com, **40042**, 1–62.

Herzog, U., El-Ila, A. & Saad, S. O. 2008. Al Kufrah Basin, Libya – geological history review and refinement. *In*: Salem, A. E.-A. M. J. & El Sogher Saleh, A. (eds) *The Geology of East Libya*, Vol. 3. Earth Science Society of Libya, Tripoli, 3–18.

Kaabar, O., Algibez, J. L., Pearce, T. & Khoja, A. 2007. Chemostratigraphy of Cambro-Ordivician to Silurian sequences from Block NC186 in the Murzuq Basin, Western Libya. *Extended abstract*, 3rd North African/ Mediterranean Petroleum & Geosciences Conference & Exhibition, Tripoli, Libya, 26–28 February 2007.

Le Heron, D. P., Armstrong, H. A., Wilson, C., Howard, J. P. & Gindre, L. 2010. Glaciation and deglaciation of the Libyan Desert: the Late Ordovician record. *Sedimentary Geology*, **223**, 100–125.

Lüning, S. *et al*. 1999. Re-evaluation of the petroleum potential of the Kufra Basin (SE Libya, NE Chad): does the source rock barrier fall? *Marine and Petroleum Geology*, **16**, 693–718.

Lüning, S., Craig, J., Loydell, D. K., Štorch, P. & Fitches, W. R. 2000. Lowermost Silurian 'hot shales' in North Africa and Arabia: regional distribution and depositional model. *Earth Science Reviews*, **49**, 121–200.

Lüning, S., Kolonic, S., Loydell, D. & Craig, J. 2003. Reconstruction of the original organic richness in weathered Silurian shale outcrops (Murzuq and Kufra basins, southern Libya). *GeoArabia*, **8**, 299–308.

Macgregor, D. S. 1996. The hydrocarbon systems of North Africa. *Marine and Petroleum Geology*, **13**, 329–340.

Pearce, T. J., Wray, D., Ratcliffe, K. & Wright, D. K. 2005. Chemostratigraphy of the Schooner Formation, Southern North Sea. *Proceedings of Yorkshire Geological Society, Occasional Publications*, **7**, 147–164.

Ratcliffe, K. T. *et al*. 2006. A regional chemostratigraphically-defined correlation framework for the late Triassic TAG-I Formation in Blocks 402 and 405a, Algeria. *Petroleum Geoscience*, **12**, 3–12.

Turner, B. R. 1980. Palaeozoic sedimentology of the southeastern part of Al Kufrah Basin, Libya: a model for oil exploration. *In*: Salem, M. J. & Busrewil, M. T. (eds) *The Geology of Libya*, Vol. 2. Academic Press, London, 351–374.

Underdown, R. & Redfern, J. 2008. Petroleum generation and migration in the Ghadames basin, North Africa: a two-dimensional modeling study. *AAPG Bulletin*, **92**, 53–76.

Exploring subtle exploration plays in the Gulf of Suez

P. N. DANCER,[1] J. COLLINS,[2] A. BECKLY,[2] K. JOHNSON,[3] G. CAMPBELL,[3] G. MUMAW[2] and B. HEPWORTH[3]

[1]*Dana Petroleum, Zahret El Maadi Tower (Secon Building), Corniche El Nile, Maadi, Cairo, Egypt (e-mail: nick.dancer@dana-petroleum.com)*
[2]*Senergy, 15 Bon Accord Crescent, Aberdeen AB11 6DE, UK*
[3]*Helix RDS (a Baker Hughes Incorporated Company), Peregrine Road, Westhill Business Park, Westhill, Aberdeen AB32 6JL, UK*

Abstract: The Gulf of Suez Basin is a classic extensional rift basin of Miocene age, with a number of syn- and pre-rift hydrocarbon plays. Exploration started in 1886, targeting areas around documented oil seeps, and was highly successful. During the boom in offshore exploration in the 1950s and 1960s, a combination of diligent geology and serendipity resulted in the discovery of a number of giant fields whose reserves form a major part of some 10 billion barrels discovered to date. However, the pursuit of smaller fields, both structural and stratigraphic, has been hampered by the poor quality seismic data characteristic of the basin. The poor quality of the seismic data is due to the interbedded shales and evaporites of shallow post-rift Zeit and South Gharib formations that create massive reverberation and severe attenuation of the seismic signal. Incremental progress in imaging the deeper horizons, including the key pre-rift Nubia Sandstone reservoir, has been achieved through low frequency enhancement and 3D seismic data acquisition. However it is still common for exploration and development wells to miss the Nubia objective due to the poor imaging and consequent misinterpretation of the seismic data. Exploration is now directed towards the smaller targets and subtle plays of the Gulf of Suez. To improve seismic imaging the focus has been on improved acquisition, with 3D ocean-bottom cable seismic data. This has the advantages of reduced multiple energy, higher fold and a broader bandwidth over streamer 3D data. Combined with detailed models of the tectonically controlled sedimentation that characterizes the syn-rift section, this has allowed the development of a re-invigorated exploration programme.

Keywords: Gulf of Suez, rifts, syn-rift sedimentation, petroleum systems

The Gulf of Suez has been an active exploration area since the first well (Gemsa D-1) was drilled in 1886. Oil seeps along the basin margin, especially in the Gebel Zeit area, have been historically reported, with evidence that these oils had been used during Pharonic times in the preservation of mummies (Harrell & Lewan 2002). Since the initial discovery of the Gemsa Oil Field, some 10×10^9 barrels of oil have been discovered, in approximately 132 oil fields.

The majority of the large oil fields lie offshore in the present-day Gulf, but two-thirds of the rift basin is onshore. The outcrops produced by variable erosion of the onshore areas have been the focus of much research. As a result the Gulf of Suez is often used as an analogue for other ‘failed’ extensional basins, including the UK and Norwegian North Sea and adjacent areas.

Gulf of Suez structural setting

The Gulf of Suez formed in Late Oligocene/Early Miocene times as the northern extension of the Red Sea Rift (Bosworth 1995; Bosworth & McClay 2001). The Red Sea Rift is the northeastern arm of the Neogene separation of the Nubia, Arabian and Somalian plates. In Mid–Late Miocene times the continued extension in the Red Sea was accommodated by sinistral strike-slip displacement along the NE–SW Gulf of Aqaba–Dead Sea transform fault system, resulting in the Gulf of Suez becoming a failed rift system. Extension within the Gulf ranges from *c.* 16 km in the northern part of the rift (extension factor $\beta = 1.33$) to *c.* 30 km in the southern part ($\beta = 1.51$) (Moustafa 2002). The primary extensional faults are commonly referred to as the clysmic faults or trend, and the movement on these faults as clysmic events (Hume 1916; Robson 1971).

The Suez Rift divides into three segments with opposite sense of fault throw and half graben dip, separated by NE–SW trending transform/accommodation zones (Fig. 1; Colletta *et al.* 1988). The segments are, from north to south, the Darag Basin (SW-dipping half graben), the Belayim Province (NE-dipping half graben) and Amal–Zeit Province (SW-dipping half graben), separated by the Galala–Abu Zenima Accommodation Zone and Morgan Accommodation Zone, respectively. The southern Amal–Zeit Province, as formed during rifting, continues south into the Red Sea to the city of Quseir, with the Quseir–Brothers–Aslam Accommodation Zone marking the southern boundary, but this is now dissected by the Late Miocene Gulf of Aqaba strike-slip system. Orthogonally to the rift access, the Suez Rift also divides into three large half graben, parallel to the clysmic trend with the central portion defining the contemporary Gulf of Suez, flanked on either side by the uplifted rotated fault blocks that form part of the rift system.

Pre-rift and syn-rift beds dip at an average of 10–15°, but due to the increased extension in the southern part of the rift, pre-rift strata locally dip up to 45–50°. Although the Gulf of Suez is considered a failed rift system, minor structural movement/uplift continues today. This is demonstrated along the coast at Gebel Zeit, where successions of Quaternary reef terraces have been uplifted on the eroded footwall. This contributes to the uplift of the rift shoulders, locally by as much as 2 km, since the cessation of extensional rifting in the Late Miocene.

Regional stratigraphy

The Gulf of Suez stratigraphy is divided into three tectonostratigraphic intervals, (1) basement and pre-rift, (2) syn-rift and (3) post-rift (Fig. 2). The basement is part of the Precambrian Pan-African craton, created by the amalgamation of several

VINING, B. A. & PICKERING, S. C. (eds) *Petroleum Geology: From Mature Basins to New Frontiers – Proceedings of the 7th Petroleum Geology Conference*, 771–781. DOI: 10.1144/0070771

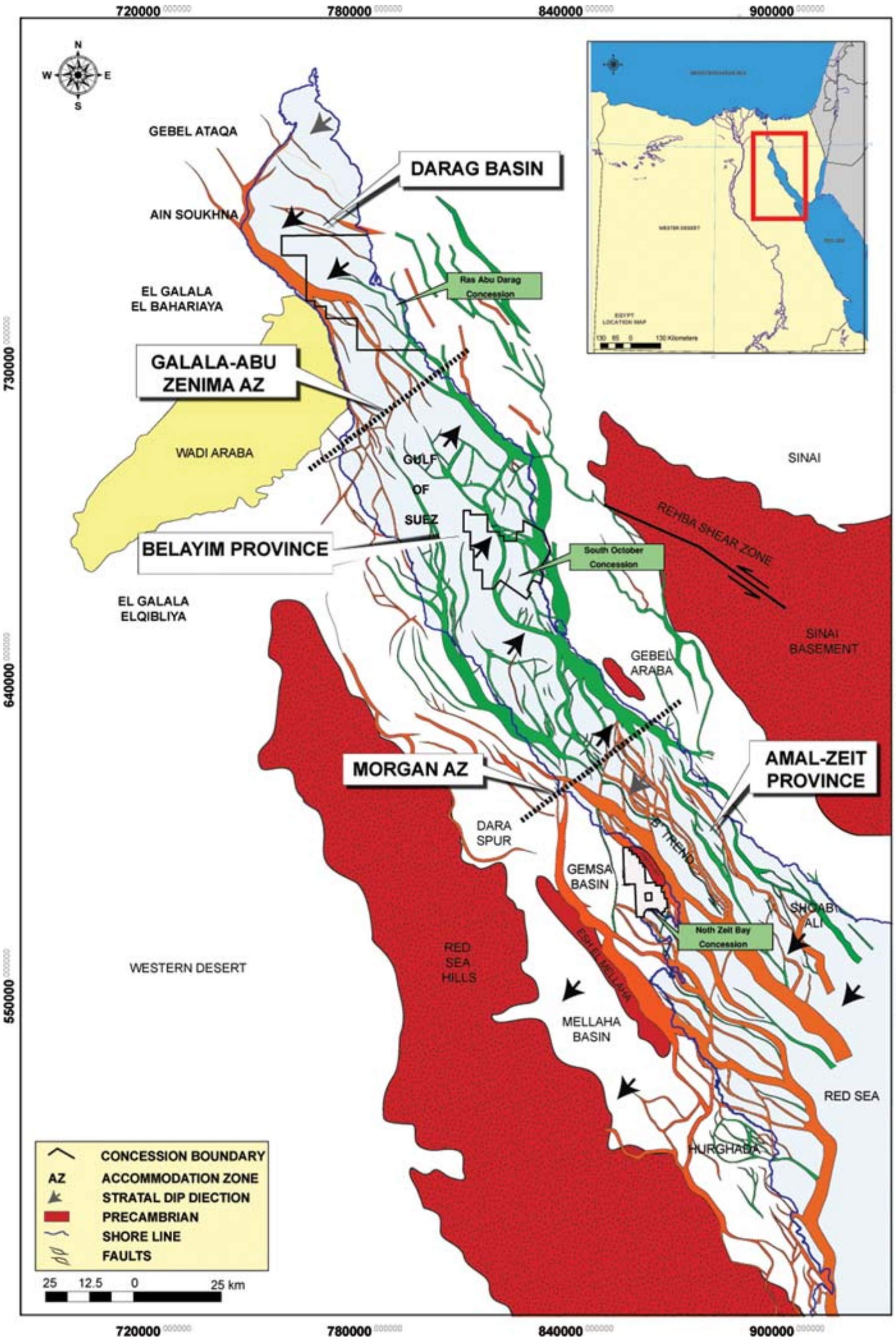

Fig. 1. Gulf of Suez – location map and structural elements.

island arcs (630–715 Ma) and modified by later transcurrent tectonics and widespread granitic intrusions. The basement is overlain by the Nubia Sandstone which comprises a number of units, predominantly of fluvial sandstones, ranging in age from Cambrian to Early Cretaceous. Overlying the Nubia are Late Cretaceous formations comprising an interbedded mixture of carbonate and clastic dominated intervals, reflecting the regional marine transgression over the continental Nubia deposits. The overlying Eocene sequence is predominantly carbonate and shale rich. The entire pre-rift stratigraphy thins dramatically southward from >2000 m at the northern tip of the Gulf to <400 m at its junction with the Red Sea. This is due to a combination of increased depositional thickness in the north due to greater subsidence, and increased erosion in the south at the onset of rifting.

The syn-rift stratigraphy encompasses the Abu Zenima and/or Nukhul Formations, overlain by the Rudeis and Kareem Formations. The Abu Zenima Formation, where present, represents the onset of the Gulf of Suez rifting and consists of continental red beds and volcanics. In southern parts of the Gulf, the formation is missing and the first representation of syn-rift sedimentation is the Nukhul basal conglomerates, resting directly on the pre-rift units. This, however, may reflect differences in the onshore exposures with the basal rift unit of the immediate hanging wall areas exposed in the north, but only footwall crests in the south.

This represents the breakup of the pre-rift structure (pre-Early Miocene) along clysmic faults, with half graben development, transgression and establishment of generally shallow marine, mixed clastic and carbonate environments. Extensive carbonate reef build-ups developed on the footwall crest palaeo-highs at this time, especially on the fault margins of the rift.

The overlying Rudeis Formation represents the regional highstand reflecting both the rift maximum and eustatic sea-level

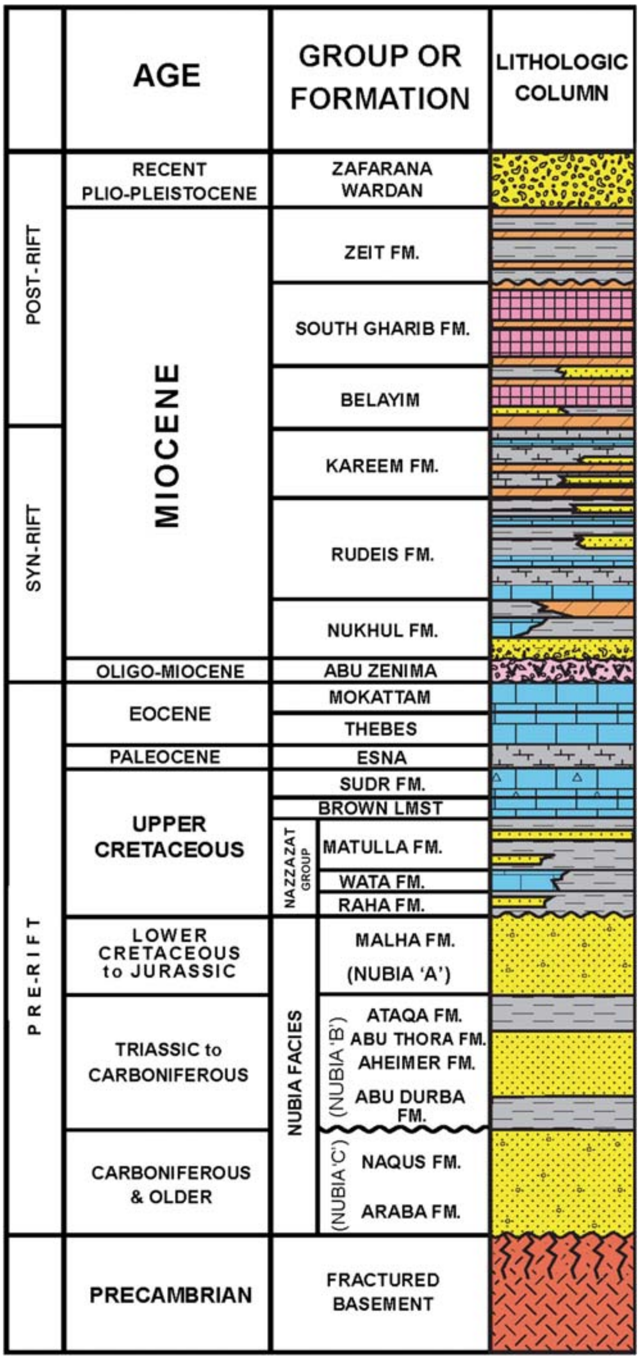

Fig. 2. Generalized stratigraphic column for the Gulf of Suez.

high. Carbonaceous and marl lithologies predominate, with clastic deposits being common at the base of the formation. Carbonate reefs continued to develop on palaeo-highs throughout Rudeis times on the rift margin.

The Kareem Formation comprises similar lithologies to the Rudeis Formation with local development of evaporite units. Clastic deposits are variably developed during lowstands, in particular at the mid-Rudeis unconformity and in the lower part of the Kareem Formation. These clastic intervals reflect the exposure and erosion of footwall crests from earlier, marginal rift basins. Sediment input is both into the hanging wall of the fault scarp and down the dip-slope from the footwall crest, although the most significant sedimentation is focused through offsets in the clysmic faults, particularly at transfer zones. The direction of sediment dispersal is critical to reservoir development and is dependent on the interaction of the contemporary drainage system with cross-faults. This is discussed further in the sections on specific sub-basins. The basin axes, independent of sediment input direction, are characterized by axial turbidite systems.

The overlying post-rift units are dominated by evaporites. The South Gharib and Belayim Formations consist of massive halite and anhydrite units, with interbedded carbonate, shale and clastic units. The evaporites form the regional top seal for many Gulf of Suez fields. They also pose a major challenge in acquisition and processing of seismic.

Source rocks

The primary source rocks in the basin are considered to occur in the pre-rift interval, but the sourcing of oil in the reservoirs of the Gulf of Suez is still subject to debate (Wever 2000). The major source rock is the Type II/I oil prone Brown Limestone (Duwi) Member of the Upper Cretaceous Sudr Formation. Secondary source rock intervals occur locally in the pre-rift Eocene Thebes Limestone (type II/I oil prone), and in the Miocene syn- and post-rift Rudeis, Kareem and Belayim Formations (type II oil and gas prone rocks). Oil generation began during the Late Miocene or Pliocene times, and is considered to be present day mature.

Reservoirs

Reservoir intervals in the Gulf are found throughout the entire stratigraphy.

Pre-rift reservoirs

The Nubia Formation Sandstone is the primary reservoir in the Gulf (Ras el Ush, October and East Zeit Fields), varying from 200 to 600 m in thickness and is known to be present across the whole of the Gulf of Suez. In some areas it has been subdivided into three members, A, B and C, where B is largely shale prone, but this stratification is not present across the whole of the Suez rift basin. The Nubia was deposited in a range of environments from continental to shallow marine. It is a high quality reservoir, but burial reduces the effective porosity such that, at 4000 m burial, porosities are in the range of 9–13%. In general, the other pre-rift reservoirs which have significantly less net reservoir, become economic when associated with Nubia accumulations, and include fractured Precambrian basement (Zeit Bay Field) as well as the overlying Nezzazat Group.

The overlying Nezzazat Group consists of clastic and carbonate sediments interpreted to have been deposited in a range of shelf environments. The group contains three formations with reservoir potential: Matulla, Wata and Raha Formations. The Matulla Formation is present across the Gulf, usually between 100–150 m thick, with high reservoir quality sandstones (B Trend Fields). The Wata and Raha Formations have minor sandstones with limestones, and are not generally effective reservoirs (indeed the Raha Formation is a potential source rock in the northern part of the Gulf).

The Lower to Middle Eocene Thebes Formation is a massive limestone with thin chert bands. Although generally a tight limestone (and potentially a seal), variable facies and secondary porosity development have allowed this locally to become an effective reservoir (Ras Bakr Field, Ras Sudr Field).

Syn-rift reservoirs

The Nukhul Formation covers most of the central Gulf of Suez. Areas with no Nukhul Formation present relate to erosion of fault block crests or non-deposition. Facies range from non-marine sandstones to marine sandstones, shales and carbonates. The distribution of facies varies dramatically, reflecting multiple sediment input points and different hinterland lithology. Deposition is locally accompanied by syn-rift volcanism (Abu Rudeis–Sidri Field).

The Rudeis Formation is a deeper, more open marine, shale-dominated section containing significant syn-rift sandstones. The sands were deposited as a system of major basin margin alluvial outwash fans feeding deepwater submarine fans in active hanging wall depocentres. Sediment input is structurally controlled at transfer faults which breach the clysmic trend. This means that the sandstones can reach over 350 m thick (well South July-1X) and yet pinchout rapidly away from the clastic source and entry point. Distinctive productive reservoirs are the Ysur Sandstone in the Lower Rudeis (e.g. July Field) and the Asl Sandstone in the Upper Rudeis (e.g. Belayim Marine Field).

Post-rift reservoirs

Reservoir sandstones are present within the post-rift section (Zeit, South Gharib and Belayim Formations; Gemsa Field and Belayim Land Field), but they are not volumetrically significant in terms of discovered hydrocarbons. The key risk with these reservoirs is the unlikelihood of hydrocarbon charge, as they lie within the halite top seal.

Play types

The primary hydrocarbon play in the Gulf of Suez is the crest of rotated fault blocks, both as primary footwall crests (B Trend Fields, Zeit Bay Field and July Field) and downthrown terraces from these (e.g. Ras el Ush Field). The primary seal in all cases is provided by drape of post-rift evaporites. The large angle of rotation of the fault blocks allows the high-quality Nubia Sandstones to be within closure, with secondary reservoir intervals in the overlying Nezzazat Group.

Generally there is no effective seal between the Nubia Sandstones and the overlying Nezzazat Group. This results in a single oil–water contact (OWC) for multi-reservoir pre-rift fields and, to have a successful Nubia accumulation, fault throw needs to be sufficient to juxtapose the Nubia against syn- and post-rift marls and evaporites. Significant intrafield faults do not appear to form barriers and may in fact contribute to vertical connectivity through juxtaposition or open fractures. A consequence of this is that, when the Nezzazat Group has no well developed sandstone members, it can be regarded as a waste zone for exploration, occupying pre-rift closure at the expense of the Nubia Sandstone.

A secondary issue for the pre-rift play is charge, as the source rock stratigraphically overlies the main reservoirs. Effective charge is therefore generally achieved by juxtaposition.

In the syn-rift interval, there are three-way faulted dip closures (e.g. Belayim Marine Field) as well as occasional four-way dip closed anticlines (e.g. Belayim Land Field), both of which are again sealed by the overlying post-rift evaporates.

Combination structural–stratigraphic traps are also common, but contain smaller accumulations than the pure structural traps. These occur due to the rapid thickness variations associated with the syn-rift sedimentation; the thinner reservoir intervals allow stratigraphic plays and subtle hanging wall structural closures to be developed against faults. These include unconformity-related truncations, onlap pinchouts (e.g. Nukhul and Rudeis Formation sandstones) and reefal carbonates. In all cases the seal to the clastic reservoirs is provided by the overlying shales, and in contrast to the pre-rift plays, sands within the same stratigraphic unit can have different fluids and contacts.

Seismic data quality

The seismic data quality in the area ranges from poor to fair, depending on the local overburden geology and the depth or stratigraphic level of the target. The prime causes of poor seismic data are the lack of energy propagation to the target reflectors and the significant reverberation caused to the seismic signal. The water depth and seabed characteristics are benign to seismic acquisition, and the data is not heavily contaminated with seabed multiples. However, the mid-range section, from typically 300–500 ms until 1500 ms, is dominated by the Zeit and South Gharib Formations, which contain interbedded halites, anhydrites, shales and sands. This is compounded in areas by thick halite salt swells, which add seismic distortion to the already degraded signal. Traditional 2D data have limited penetration beneath the syn-rift section, and even relatively modern 3D seismic datasets struggle to image the pre-rift reservoirs. In addition to not successfully imaging structural configurations, the poor data quality precludes any amplitude analysis to relate to fluid types within the reservoir intervals.

Various attempts to improve the imaging by pre-stack depth migration have not significantly improved data quality, as the lack of signal propagation, and deep stratigraphic illumination, cannot be resolved with depth imaging. More recently, 3D ocean-bottom cable (OBC) surveys have been acquired, which show significant improvement in data quality. Initially these surveys were acquired due to shallow-water constraints at the margins of the Gulf, but the improved data quality is promoting their use in areas that were previously covered by streamer surveys. The reason why OBC data offers improved resolution is three-fold. Firstly, OBC surveys tend to be acquired with higher fold, enhancing the signal-to-noise ratio and hence the suppression of noise. Secondly, the OBC data have greater bandwidth (due to the receiver ghost effect, and also the use of geophones), especially at the lower end of the frequency spectrum, which is less prone to attenuation from thin interbedded stratigraphy. Finally the OBC acquisition layout allows for a more uniform azimuthal illumination.

Exploration targets

The dearth of high-quality seismic datasets has hampered recent exploration in the Gulf of Suez and continues to prove problematic as the remaining trap size diminishes. Initial exploration in the Gulf focused on the extrapolation of surface geological features and limited gravity data. With the advent of reflection seismology, the identification of the Upper Miocene evaporite became relatively straightforward. Significant four-way dip closures were identified at this level and most of the major fields were discovered underlying these highs. However, a number of dry holes were drilled based on the premise of a hard linkage between pre- and post-evaporite structure. The gradual understanding that there is an offset structural relationship has led to improvement in well prognosis in targeting the syn- and pre-rift fault blocks.

With the extensive drilling in the Gulf of Suez, most (if not all) of the simple fault blocks and anticlinal features have been drilled, leaving little potential for pre-rift plays requiring large fault offsets. Thus current exploration focus is on smaller structures. This is challenging even with 3D seismic data due to the limitations of imaging in this area: even over producing fields it is still possible to drill wells that do not encounter the reservoir horizons, due to the poor structural control provided by seismic data. Therefore the potential for significant discoveries is in the underexplored but riskier stratigraphic and downthrown fault block of the syn-rift suite.

These play types in the syn-rift are discussed in more detail below, with reference to selected sub-basins, which encompass the three main structural provinces of the Gulf of Suez. Firstly, in the southern Gulf, the syn-rift plays of the Amal–Zeit Province are discussed with reference to the Gemsa Basin. Secondly, the syn-rift plays of the central and northern Gulf (the Belayim and Darag Basin Provinces) are jointly discussed by reference to two concessions: the South October Concession in the Belayim Province and the Ras Abu Darag Concession in the Darag Province (Fig. 1).

Gemsa Basin footwall prospectivity

The Gemsa Basin is located onshore in the southern Gulf of Suez, Amal–Zeit Province. Immediately north of the basin lies the Morgan Accommodation Zone, while the basin is bordered to the SW by Esh el Mellaha (Fig. 1). Both areas are major hinterland sources for clastic deposition in the northwest and SW of the basin. The basin is a highly rotated half graben block, with the entire stratigraphy exposed, but thinned, in the footwall crest to the NE at Gebel Zeit. The pre-rift stratigraphy dips by as much as 45–50°SW, while the top syn-rift succession dips 15°SW (Fig. 3).

The basement exposures at the footwall crest are separated into North and South Gebel Zeit by a saddle draped by post-rift evaporites. In the larger exposure of North Gebel Zeit the erosion of the softer Nubia Formation creates a fault parallel valley, Wadi Kabrit, between the Precambrian basement and the harder Miocene deposits (Fig. 4). At South Gebel Zeit the basement complex also forms a prominent ridge, but the area is structurally complex and the majority of the pre-rift stratigraphy is absent, resulting in a more random topography.

With the exposure of the footwall, the footwall crest play is precluded in this area. The exposures at Gebel Zeit, however, have provided an excellent opportunity to examine the stratigraphy and structure of a footwall crest, which is the main play of the Gulf of Suez and as such the area has been intensely studied (Evans & Moxon 1988; Helmy 1990; Bosworth 1995; Winn *et al.* 2001; Aboud *et al.* 2003). Poor seismic imaging has also resulted in the pre-rift being considered an unattractive target in the Gemsa Basin.

The syn-rift Rudeis and Kareem Formations progressively onlap and pinchout onto the footwall crest (Fig. 3). The only tested discoveries in the updip area are in the Kareem Formation of Abydos and Gazwarina 1 wells. Each contains two vertically isolated thin (less than 6 m) sandstones and their relationship to a pair of anhydrite marker beds indicates that sandstones are developed at a minimum of three stratigraphic levels, indicating that they are not laterally continuous. The same marker beds are used to subdivide the Kareem Formation lithostratigraphically into the Shagar and Rahmi Members; an anhydrite is taken as the base of each. The lower anhydrite therefore marks the boundary between the Kareem and Rudeis Formations, although biostratigraphy suggests the formation boundary is slightly deeper. This is consistent with a repeated upward succession of lithofacies for each of the anhydrites from laminated shale, through birdcage anhydrite into banded anhydrite. The sand at the base of the Shagar Member clearly erodes into and locally removes the upper anhydrite. The development of the anhydrite indicates the isolation of the Gemsa Basin from the rest of the Gulf and therefore the emergence of the footwall area. However, whether the renewed clastic input reflects further lowering of sea-level, tectonic footwall uplift or climatic shift to wetter conditions is less clear.

The drainage system associated with such run-off is critical to the distribution of coarse clastics in the basin. The structural position, high on the dip-slope of the footwall, clearly indicates that any clastic sediments in this area will have been derived from the emergence of the footwall crest. Today, Wadi Kabrit and the comparable system of Wadi Araba to the north are characterized by axial drainage (Fig. 4) with entry onto the adjacent dip and scarp slopes controlled by cross-faults. Although it is difficult to demonstrate whether an equivalent drainage system existed during the Kareem Formation, the presence of a large incised feeder system towards the southern end of the present day Wadi Kabrit is certainly compatible with this. The incision cuts down into the pre-rift, and limited biostratigraphic evidence suggests it may be of Kareem age (Evans & Moxon 1988), a view supported by the absence of sandstones in the Rudeis Formation.

The Kareem depositional environment has been a subject of much conjecture and the sands have been regarded as turbidite deposits, largely on the evidence of deepwater bio-facies above and below. However, this view can be questioned based on a number of observations:

(1) The feeder system, previously described as a turbidite channel, is in a very proximal position with respect to the footwall crest, which has adequate hinterland to allow the erosion.
(2) The fill of the feeder contains abundant bioturbation indicative of *Thalassinoides/Ophiomorpha* ichnofacies, suggesting shallow marine conditions.
(3) The anhydrite units commonly display chicken-wire fabric, which in isolation is a poor environmental indicator, but when supported by the other observations is consistent with a shallow-water/sabkha environment (Machel & Burton 1991). The foraminifer genus *Amphistegina* has been reported from the anhydrite in one well. This shallow-marine genus has been particularly successful in invading the eastern Mediterranean through the Suez Canal (Gruber *et al.* 2007). The occurrence of *Amphistegina* would therefore be consistent with sporadic flooding of a restricted basin.

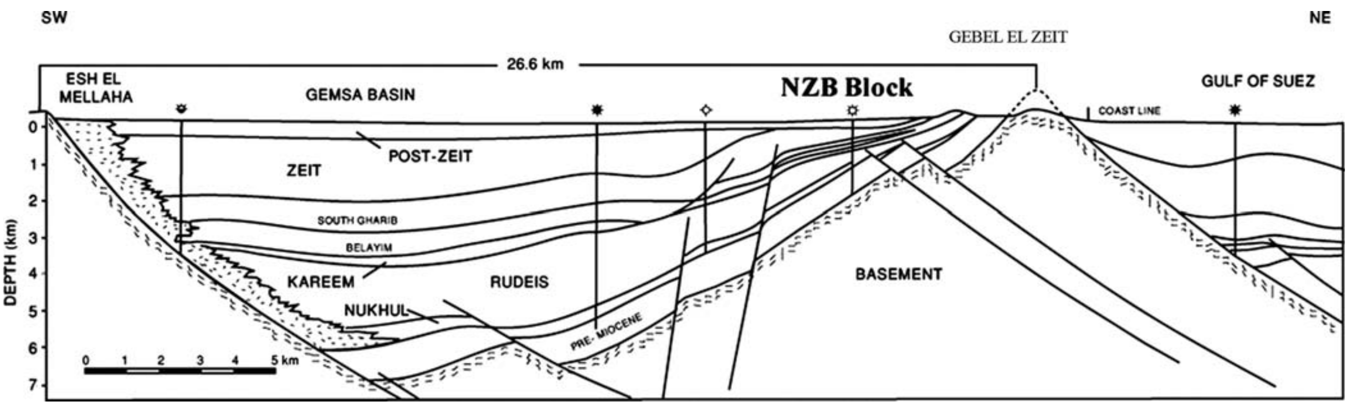

Fig. 3. Gemsa Basin half graben cross-section (after Bosworth 1995).

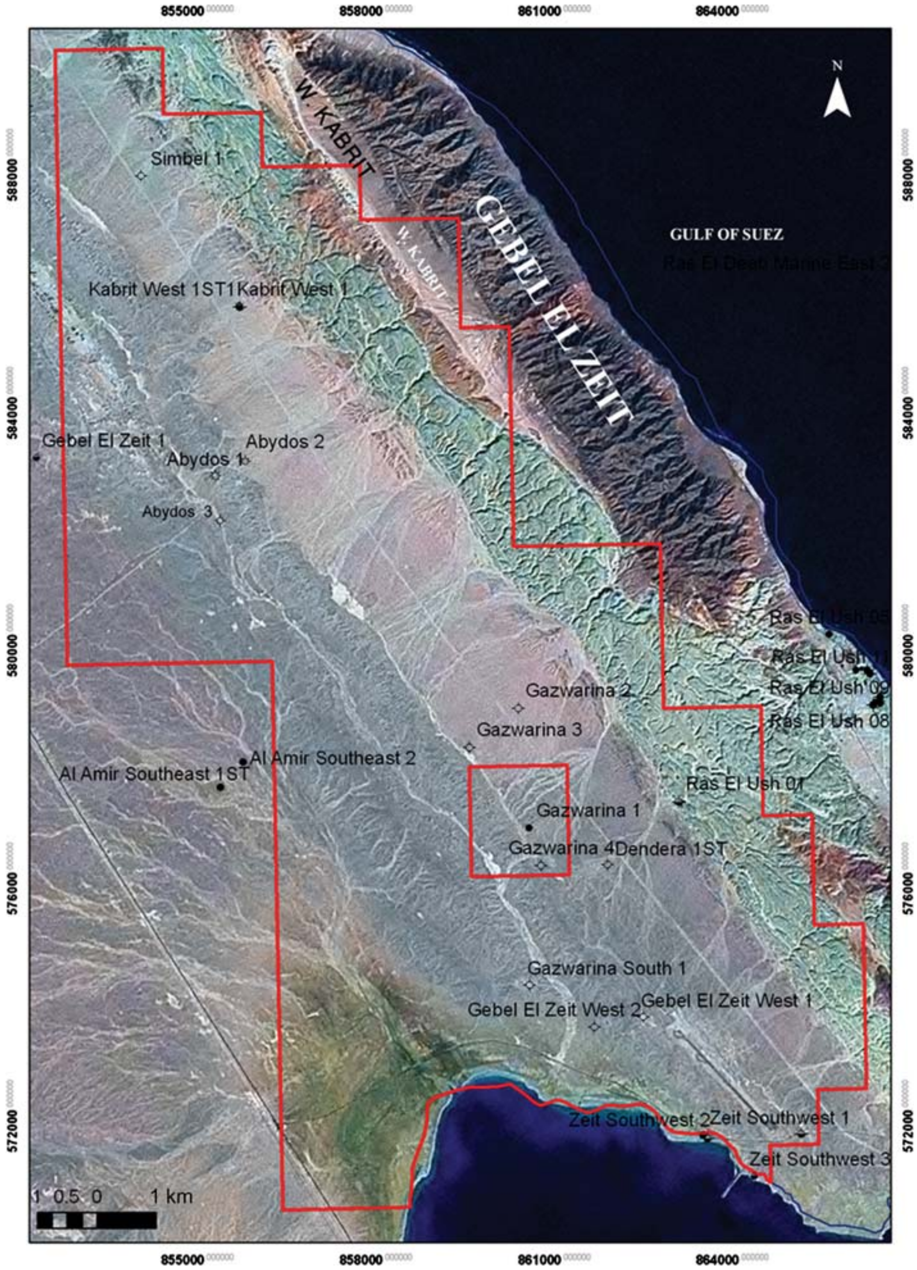

Fig. 4. Gemsa Basin, landsat 7742: geological image.

The channelized turbidite model has been used to propose sediment by-pass of the slope area, with deposition limited to isolated channels. However, an alternative interpretation of the outcrop channel is a shallow marine fill of a sub-aerially eroded incised valley. This allows potential for shallow water re-working and lateral distribution across the dip-slope.

Although it has to be tempered with the uncertainty in the quality of the seismic data, the seismic character of the Kareem interval appears to support this. On seismic data, the Kareem interval can be divided into an upper, relatively continuous unit, and a much more variable lower unit, which appears to onlap an incised surface (a possible palaeo-shoreline and cliff) on the dip-slope. This is broadly compatible with the character of the Shagar and Rahmi Formations seen on log correlation, although it has to be emphasized that the thickened interval has been very poorly constrained by well data. The alternative model suggested here is that the incised surface represents a lowstand erosive down-cut and this may have provided accommodation space for additional sands. The recent drilling of the Abydos-2X well supports this model, encountering Base Shagar sands in an erosive down-cut of the Rahmi Formation, which were not present in the Abydos-1X well some 500 m away.

The trapping mechanism remains conjectural because the individual sandstones are below seismic resolution, but is suspected to be a combination of stratigraphic pinchout and small fault offsets, given the individual units are thin. However, the recovery of 2.3×10^6 stock tank barrels (MMSTB) on depletion drive from Gazwarina 1 does suggest reasonable connectivity. In conjunction with this updip trapping there is clear evidence from the seismic of low amplitude folding of the Kareem Formation. These fold axes appear to be oblique to the cross-faults, which may indicate an element of strike-slip movement in their genesis.

Evidence of continued tectonic activity into the 'post-rift' phase in the area of Gebel Zeit is demonstrated by the majority of movement on an antithetic fault, 9 km downdip of the footwall crest, occurring during the post-rift Zeit Formation. This fault movement may also contribute to the continued uplift of Gebel Zeit. The area of Gebel Zeit therefore offers a very different perspective on the depositional processes to those derived from the exposures in the north-eastern Gulf (Young *et al.* 2000, 2003; Jackson *et al.* 2005). There the studies have focused on the deeply dissected deposits of the immediate hanging wall in areas of only moderate rotation, close to transfer zones. In Gebel Zeit, outcrop shows the deposition environment on the proximal dip-slope of the footwall crest, in an area of much greater rotation, and the position in the southern Gulf seems to have allowed continued tectonic activity into the period of Red Sea rifting, questioning the designation of the Kareem as post-rift, and the rigid syn-rift/post-rift division of the Gulf of Suez.

Upper Rudeis prospectivity of the offshore Ras Abu Darag and South October Concessions

The Ras Abu Darag and South October Concessions lie either side of Galala–Abu Zenima Accommodation Zone in the Darag Basin and Belayim Province, respectively (Fig. 1). This results in a shift from SW-dipping half graben in the Darag Basin to NE-dipping half graben in the Belayim Province. Geologically both concessions are representative of their respective sub-basin and share a common depositional history as axial basins within the Gulf of Suez rift.

Pre-rift reservoirs have been drilled in both concessions. However, deep burial and poor seismic imaging with the currently available 2D and 3D datasets make the pre-rift targets less attractive than those in the syn-rift sequence.

The syn-rift stratigraphy is dominated by the Nukhul and Rudeis Formations and, in contrast to the Gemsa Basin further south, sandstones are developed in the Rudeis Formation and not in the Kareem Formation. The major clysmic faults control the thickness of the Upper Rudeis Formation, with the maximum thickness of the Rudeis Formation within the two concessions occurring in well GS 56-1A in the Ras Abu Darag Concession, where it attains 2125 m. Active rifting appears to have ended before the deposition of the Kareem Formation evaporates, and hence the syn-rift hydrocarbon prospectivity focuses on the Upper Rudeis Formation, in which the main reservoir sandstone is informally called Asl Sandstone. The Lower and Middle Rudeis Formation are also described, as this sets the prospective interval in its depositional, sequence stratigraphical and structural context.

In contrast to the generally shallow marine to brackish depositional conditions of the underlying Nukhul Formation, planktonic foraminifera assemblages at the base of the Rudeis Formation show a sharp increase in water depth to upper bathyal conditions. The Rudeis Formation is generally conformable on the Nukhul Formation. However, the Nukhul Formation and the basal part of the Rudeis Formation are absent in wells in the southwestern part of the Ras Abu Darag Concession associated with footwall crests. This may reflect onlap of the Early Miocene clastic systems onto the evolving, rotated fault blocks, particularly on the flanks of the graben. In the east of the South October concession, structural terraces flanking the main basin margin fault show the Rudeis Formation directly overlying basement. It is unclear whether this is a fault contact or a major unconformity, possibly recording transpressional uplift along fault-bounded structural terraces before the onset of rift subsidence and onlap by the deepwater Rudeis system.

The three-fold subdivision of the Rudeis Formation is based on the ‘N’ zonation of planktonic foraminifer (Blow 1969), derived from 1980s vintage reports from wells in both the South October and the Ras Abu Darag Concessions:

- Upper Rudeis: *Globigerinoides sicanus – Praeorbulina transitoria* zone (lower part of N8), described in (Schütz 1994).
- Middle Rudeis: *Globigerina ciperoensis – Globigerinoides trilobus* zone (N7).
- Lower Rudeis: *Globigerinoides primordius – Globigerina ciperoensis* zone (?N6).

Well picks of the three units were adjusted to maximum flooding surfaces where possible (Fig. 5). The regional, *c.* 18.25 Ma T_{20} Mid-Clysmic Unconformity, as described in proprietary well and outcrop studies, could not be identified biostratigraphically in the Ras Abu Darag and South October Concessions, probably reflecting the basinal position of the wells during Rudeis times. However, it is possible that this regional structural event may be an important control on the distribution of Rudeis Formation Asl Sandstone reservoirs on the correlative unconformity (Fig. 5).

- *Lower–Middle Rudeis Formation.* In the hanging wall of the major clysmic faults, the Lower–Middle Rudeis Formation is interpreted as a rift climax, deep marine sedimentary system. The lower part of the Rudeis contains (?benthonic) foraminifera indicative of upper bathyal conditions, which pass upwards into outer shelf assemblages and finally into sub-littoral conditions at the upper part of the formation. This overall shallowing-upward profile probably reflects the progressive development of the T_{20} Mid-Clysmic Unconformity. Rapid facies changes into shallower water, more calcareous or sandy sediments occur towards the basin margins and around palaeo-highs (Schütz 1994).
- *Upper Rudeis Formation.* This unit is characterized by rift margin fan deltas feeding deep marine clastic systems in hanging-wall depocentres. The thick development of potential reservoir quality sandstones (Asl Sandstone) is limited to the Upper Rudeis Formation. These occur mainly as sharp-based sand bodies, possibly as lowstand fans associated with the T_{20} Mid-Clysmic Unconformity (Fig. 5). Deposition is either in incised channels/valleys which are back-filled during transgression, or on slope apron systems deposited in front of clysmic faults. Other Asl sands occur as progradational, submarine fan, lobe and channel complexes.

A map of Upper Rudeis sandstone distribution from well data shows the inferred lateral input and axial transport dispersal patterns controlled by the clysmic faults in the northern Gulf of Suez (Fig. 6). Three main types of Upper Rudeis sediment supply have been identified:

(1) Point sources of sediment input structurally controlled by transfer zones which offset the major clysmic faults, for example, the Belayim Transfer and the Ekma Transfer faults.
(2) Axial transport southward of coarse-grained clastics input from the Wadi Araba High. These sands were focused along the rift axis in the immediate hanging wall of normal faults.
(3) Hanging-wall sands locally derived from the erosion of intra-rift footwall highs, for example, erosion of the Belayim Marine Field crest resulted in deposition of submarine fan systems in the immediate hanging wall. Notably this contrasts with the Gemsa Basin where the focus is on sands derived from the footwall crest onto the dip-slope.

The Rudeis Formation in the South October Concession

Reservoir development is clearly controlled by the nature of the eroded hinterland. The onshore area south of the Nezzazat Fault (Fig. 6) has undergone extensive uplift with erosion down to basement in many places. This has resulted in erosion of the Nubia

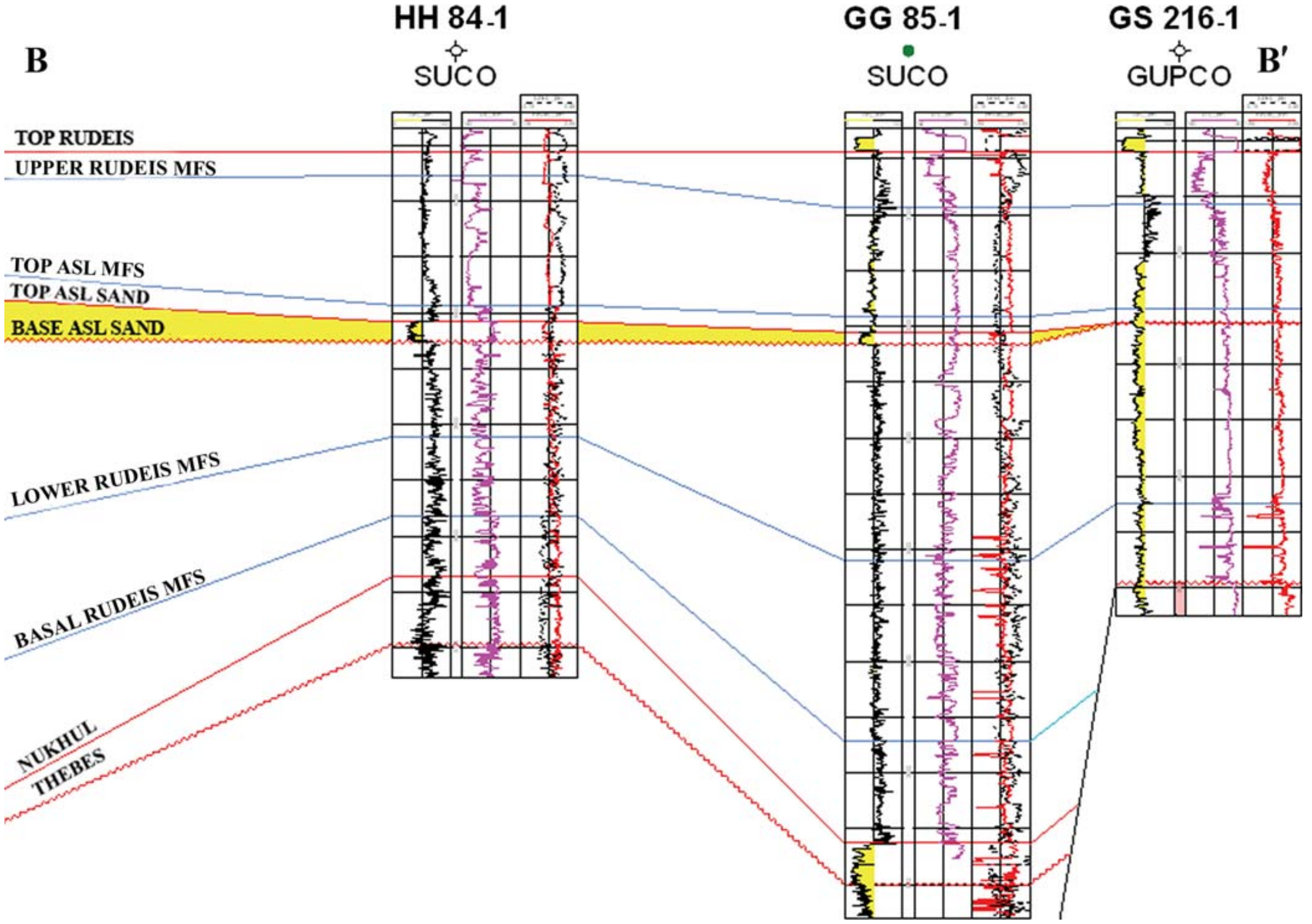

Fig. 5. Correlation of Asl Sandstone between wells HH84-1, GG85-1 and GS216-1, showing thickness variation. Log curves are gamma ray (black), resistivity (pink) and density/neutron (red/dashed black). Location of correlation shown in Figure 6. Vertical scale: 50 m per division.

Sandstone which has been reworked and deposited as syn-rift sandstones. In contrast, within the Belayim province (Fig. 6) there has been less uplift with erosion of predominantly pre-rift carbonates. This has resulted in the local development of calcarenitic syn-rift sediments along the eastern basin margins. However within the rift axis, quartzose sands are present, having been transported south from the Wadi Araba High.

In the South October Concession the thickness of the Rudeis Formation is greatest in the immediate hanging wall of clysmic faults. However the Rudeis Formation shows an overall thinning to the SE in accordance with regional sediment distribution patterns. Thickness ranges from 700 m in the hanging wall to 300 m on the dipslope. Rudeis Formation depocentres do not necessarily contain a significant thickness of sandstone, the input of which is controlled by the composition of the hinterland and location of transfer zones (Fig. 6). However the overall Rudeis Formation thickness is significantly less than that seen in the Ras Abu Darag Concession.

The Asl Sandstone is a proven reservoir in the GG85-1 discovery, which is located in the southeastern part of the South October Concession, on terraces flanking the main basin-bounding fault (Fig. 6). The Belayim Land Field lies directly south of the discovery and is separated from it by a structural low. GG85-1 occurs in the hanging wall of the major fault and is a possible transpressional feature associated with a transfer zone. It is a combined structural–stratigraphic trap, consisting of a SW-plunging anticline. From well data it is known to have lateral stratigraphic pinch-out of the reservoir sandstones to the north. This is demonstrated by the gradual thinning and absence of the sands in wells GS216-1 (Fig. 5). Trapping to the east is provided by hanging wall fault closure, possibly against basement. Top seal is provided by Upper Rudeis Formation shales. Well GG 85-1 was drilled in 1983 and tested 27° API oil from an 11 m thick Asl sandstone reservoir. Understanding of the precise depositional nature (i.e. deep v. shallow marine to continental) and the distribution of the Asl sands in the discovery is uncertain. The discovery lies along-strike from thick (>300 m of net reservoir) Asl sands of probable alluvial fan origin in the Belayim Land Field located to the south, adjacent to a major transfer zone that acts as a point source for significant sediment input. To the west of the Belayim field lies the deepwater, turbidite-prone basin of the central Gulf. One possibility, given the sharp base to the reservoir sand interval, is that the sands occur above an unconformity as a transgressive package within an erosional valley, but other interpretations (e.g. deepwater slope apron sands) are possible.

The Rudeis Formation in the Ras Abu Darag Concession

North of the Galala–Abu Zenima Accommodation Zone there is good evidence showing thickening of the Rudeis Formation in the northwestern part of the Ras Abu Darag Concession. This suggests a sediment entry point in this part of the northern Gulf of Suez, probably feeding from the west (Fig. 6). This requires connection to a large antecedent drainage network in the hinterland (possibly the Wadi El-Abyad drainage system). Widespread reservoir sands in the NE part of the Ras Abu Darag Concession suggest another structurally controlled point source fed by the Wadi Sudr drainage system.

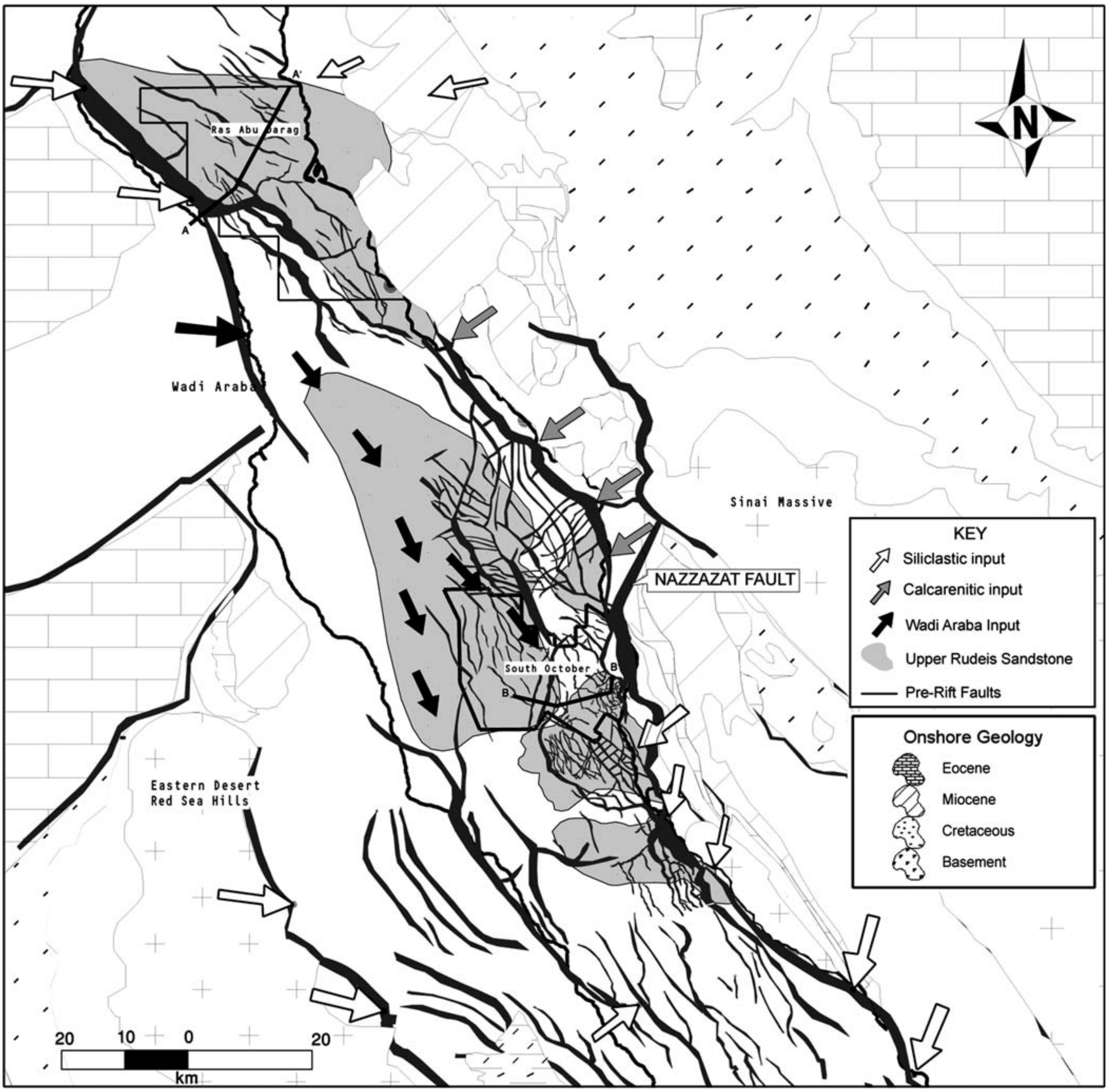

Fig. 6. Upper Rudeis sandstone distribution in the central and northern Gulf of Suez. A–A′ is the location of the discussed seismic section (Fig. 7). B–B′ is the location of the discussed well correlation (Fig. 5).

Increased distance from the clastic source leads to sand-poor distal portions of fan lobes near the base of the Upper Rudeis. Coarsening-upwards packages with carbonate-rich tops may reflect shallowing to shelfal conditions. Geological interpretation suggests that the Darag and Belayim Provinces behaved as separate en-echelon structurally controlled basins, each with its own sediment entry and dispersal patterns, but sharing synchronous rifting and sea-level variation.

Although the basinal Ras Abu Darag wells have encountered significant sections of Upper Rudeis formation, where thicknesses range between 460 and 1035 m, on the footwall crest of the main basin-bounding fault in the southwestern part of Ras Abu Darag, the Upper Rudeis is absent to thin (23–140 m). Possible causes of the thinning may be due to a combination of reduction in accommodation space on structural highs, onlap, faulting at footwall crests and erosion of footwall crests. The evidence from the Gemsa Basin is that all of these may occur. Any footwall-sourced sediment is likely to be more variable in character and quality and volumetrically less important. The scale of the sand distribution in the Gemsa Basin in this structural setting confirms that economic accumulations in an offshore setting are unlikely.

Given the narrowness of the deepwater Darag Basin during Upper Rudeis times, it is probable that large areas of the basin floor are sand-prone, given that the likely sediment transport processes are gravity-driven mass flows, allowing for distal sand deposition. Contemporary shelf deposits are known on the regional dip-slope offshore and onshore east of the Gulf within the Darag Basin.

Ras Abu Darag well Nebwi 81-1 encountered a 73 m thick sandstone interval which contains high proportions of net reservoir within the Upper Rudeis Formation. Non-net intervals within these gross sand intervals are either calcite-cemented sandstones or primary carbonates. Average PHIE of the Asl sands is 16%. Petrophysical work identified a unit called the Asl Sandy Limestone with thick (up to 30 m), high net-to-gross units with average

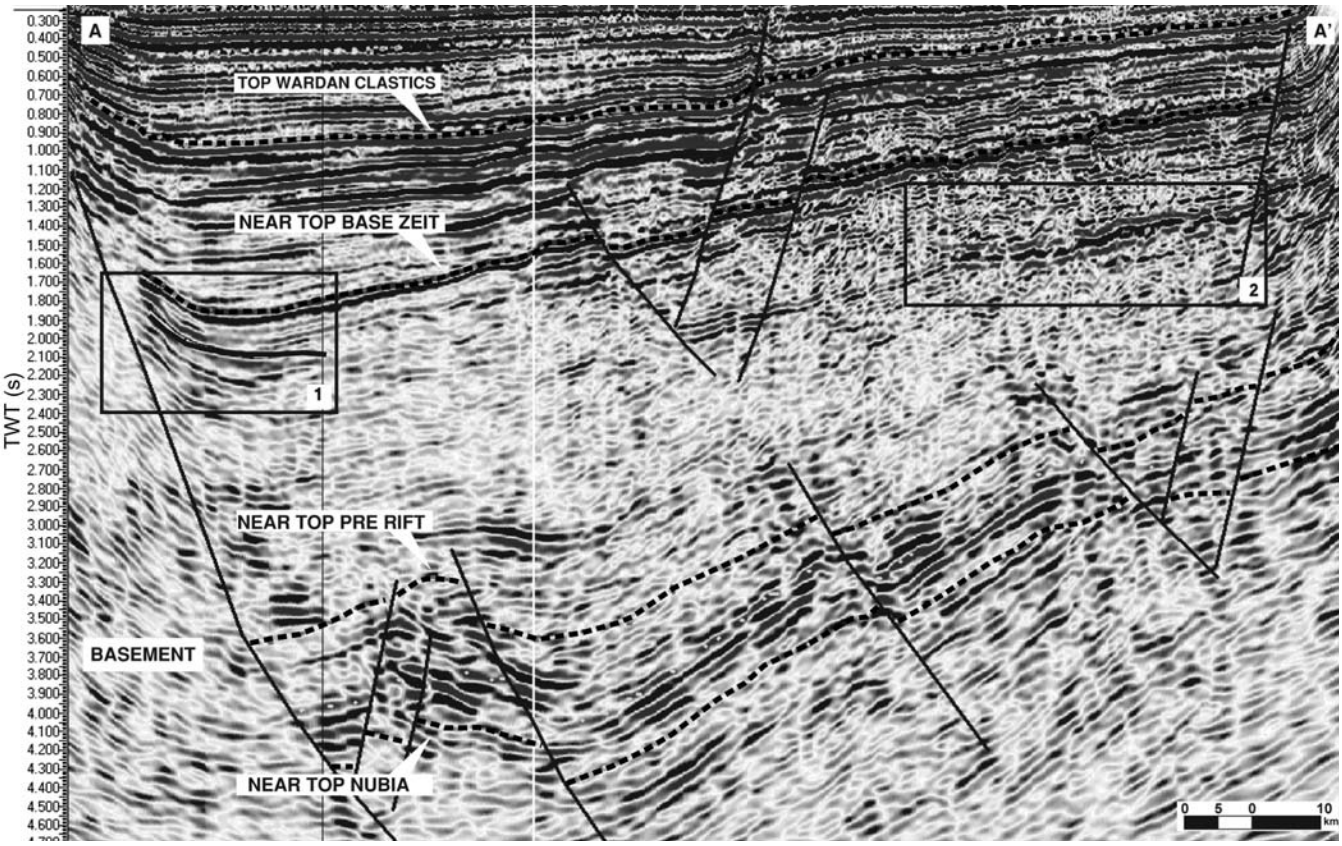

Fig. 7. Seismic profile through the Darag sub-basin. Box 1 shows a Rudeis proximal sandstone fan. Box 2 shows a shallow water carbonate. Profile location shown in Figure 6.

porosities of 15%. The top of the Upper Rudeis Formation in the Fina Z 80-1/1A well contains a 24 m thick, stacked sand body, which consists almost entirely of net reservoir and has an average porosity of 19%.

Away from the well control in Ras Abu Darag, seismic amplitude anomalies (Fig. 7) are identified as likely sandstones or calarenites, both in hanging wall and dip-slope settings, which offer potential targets in the Upper Rudeis. Hanging-wall traps offer the additional advantage of updip seal against major faults. Submarine slope apron deposits may be associated with the active major fault scarps. Dip-slope sands rely more heavily on updip stratigraphic termination of the reservoirs, as demonstrated in the Kareem Formation in the Gema Basin. This may result from either depositional pinchout of the reservoir or erosional truncation during relative sea-level fall acting on the generally uniformly dipping, ramped margin. As suggested for Gebel Zeit, such ramps in shallow marine settings could act as sites of sand deposition associated with forced regressions during the falling stage of the relative sea-level cycle. Carbonate build-ups and shoals may also be developed along the ramp margin. In deeper marine settings, lowstand submarine fans represent another possible play. However, most of these stratigraphic configurations require the addition of structural closure to form effective traps so that the acquisition of high-quality seismic data remains paramount.

Conclusion

With mean expected field sizes getting smaller, it is increasingly difficult to detect reliable traps with conventional 3D streamer seismic data. Even with good definition from the use of high-fold 3D OBC seismic data, these targets are without Direct Hydrocarbon Indicators, and therefore are significantly riskier than comparable targets in other basins. However the Gulf benefits from excellent outcrop exposure that directly relates to onshore/offshore prospectivity, and combined with geological control from adjacent wells, the structural and sedimentological risk can be managed.

Unless widespread 3D OBC seismic data is acquired to offer a step chance in deep pre-rift imaging, the lack of clearly defined pre-rift fault blocks will cause exploration to focus on more subtle plays within the syn-rift section. Outcrop geology shows clearly the rapid variation in syn-rift sedimentation and the occurrence of sand pinchouts. This play also benefits by being above the regional source rocks and closer to the regional seal. The Gemsa Basin is a clear example where significant exploration effort focused on the pre-rift has failed, but the syn-rift Kareem Formation reservoirs demonstrate successful stratigraphic trapping and downthrow fault plays. These plays are difficult to define seismically, but the combination of excellent outcrop and well control allow for moderately risked exploration targets to be created and drilled successfully. However, this is in an onshore setting and the very different economics of offshore drilling increase the challenge in the offshore areas.

Remaining potential exists for further hydrocarbon discoveries with a significant stratigraphic component in the syn-rift systems of the Gulf of Suez. Current understanding of the syn-rift systems in terms of their stratigraphy, provenance, sedimentary architecture and sequence stratigraphic and structural context should form the basis for increased recognition of these potential reservoirs.

Further application of this type of play, and the conventional fault block play within the Rudeis and the Kareem Formations, will allow additional targets in the offshore Gulf to be defined. If combination structural stratigraphic targets can be developed these should provide attractive volumes to pursue.

This paper is published with the permission of Dana Petroleum, and the authors would like to thank Dana Petroleum and EGPC for their support. The authors are grateful for the constructive discussion from various co-workers within their respective companies and would like to thank Paul Wilson and Paul Woodman for introducing the complexities of the Gulf of Suez to the authors as field trip leaders in 2008. The authors also thank Hassan Aboudy for drafting the figures. Stefan Lubesedar is gratefully thanked for his review and constructive remarks for improving the clarity of this paper. Since completion of this paper we regret to announce the death of our respected colleague Barry Hepworth who made an invaluable contribution to this paper.

References

Aboud, E., Salem, A. & Ushijima, K. 2003. Interpretation of aeromagnetic data of Gebel El-Zeit area, Gulf of Suez, Egypt using magnetic gradient techniques. *Memoirs of the Faculty of Engineering, Kyushu University*, **63**, 139–149.

Blow, W. H. 1969. Late Middle Eocene to Recent planktonic foraminiferal biostratigraphy. *In*: Bronnimann, R. & Renz, H. H. (eds) *Proceedings of the First International Conference on Planktonic Microfossils*, Geneva, 1967, **1**, 199–421.

Bosworth, W. 1995. A high-strain rift model for the southern Gulf of Suez (Egypt). *In*: Lambiase, J. J. (ed.) *Hydrocarbon Habitat in Rift Basins*. Geological Society, London, Special Publications, **80**, 72–102.

Bosworth, W. & McClay, K. R. 2001. Structural and stratigraphic evolution of the Gulf of Suez rift: a synthesis. *In*: Zeigler, P. A., Cavazza, W., Robertson, A. H. F. R. & Crasquin Soleau, S. (eds) *Peritethyian Rift/Wrench Basins and Passive Margins*. Museum National d'Historie Naturelle de Paris, Memoirs, **186**, 567–606.

Colletta, B., Le Quellec, P., Letouzy, J. & Moretti, I. 1988. Longitudinal evolution of the Suez rift structure (Egypt). *Tectonophysics*, **153**, 221–233.

Evans, A. L. & Moxon, W. 1988. Gebel Zeit chronostratigraphy: Neogene syn-rift sedimentation atop a long-lived palaeohigh. *In*: Hantar, G. (ed.) *Proceedings of the 8th Egyptian General Petroleum Corporation Exploration Seminar*, Cairo, **1**, 251–265.

Gruber, L., Lazar, S., Hyams, O., Sivan, D., Herut, B. & Almogi-Labin, A. 2007. *Amphistegina lobifera*, a larger symbiont-bearing foraminiferal migrant from the Red Sea, now dominates rocky coasts of the Israeli Mediterranean. *Geophysical Research Abstracts*, **9**, 01407.

Harrell, J. A. & Lewan, M. D. 2002. Sources of mummy bitumen in Ancient Egypt and Palestine. *Archaeometry*, **44**, 285–293.

Helmy, H. M. 1990. Southern Gulf of Suez, Egypt: structural geology of the B-Trend oil fields. *In*: Brooks, J. (ed.) *Classic Petroleum Provinces*. Geological Society, London, Special Publications, **50**, 353–363.

Hume, W. F. 1916. *Report on the Oilfield Region of Egypt, with a Geological Report on the Abu Shaar El Quibli (Black Hill) District*. Petroleum Reservoir Bulletin, **6**. Government Press, Cairo.

Jackson, C. A. L., Gawthorpe, R. L., Carr, I. D. & Sharp, I. R. 2005. Normal faulting as a control on the stratigraphic development of the shallow marine syn-rift sequences: the Nukhul and Lower Rudeis Formations, Hammam Faraun fault block, Suez rift, Egypt. *Sedimentology*, **52**, 313–338.

Machel, H. G. & Burton, E. A. 1991. Burial-diagenetic sabkha-like gypsum and anhydrite nodules. *Sedimentary Petrology*, **61**, 394–405.

Moustafa, A. R. 2002. Controls on the geometry of transfer zones in the Suez rift and northwest Red Sea: implications for the structural geometry of rift systems. *AAPG Bulletin*, **86**, 979–1002.

Robson, D. A. 1971. The structure of the Gulf of Suez (clysmic) rift, with special reference to the eastern side. *Journal of the Geological Society, London*, **127**, 247–276.

Schütz, K. K. 1994. Structure and stratigraphy of the Gulf of Suez, Egypt. *In*: Landon, S. M. (ed.) *Interior Rift Basins*. American Association of Petroleum Geologists, Tulsa, OK, Memoirs, **59**, 57–96.

Wever, H. E. 2000. Petroleum and source rock characterization based on C7 star plot results: examples from Egypt. *AAPG Bulletin*, **84**, 1041–1054.

Winn, R. D., Crevello, W. D. & Bosworth, W. 2001. Lower Miocene Nukhul Formation, Gebel el Zeit, Egypt: model for structural control on early synrift strata and reservoirs, Gulf of Suez. *AAPG Bulletin*, **85**, 1871–1890.

Young, M. J., Gawthorpe, R. L. & Sharp, I. R. 2000. Sedimentology and sequence stratigraphy of a transfer zone coarse-grained delta, Miocene Suez rift, Egypt. *Sedimentology*, **47**, 1081–1104.

Young, M. J., Gawthorpe, R. L. & Sharp, I. R. 2003. Normal fault growth and early syn-rift sedimentology and sequence stratigraphy: Thal Fault, Suez rift, Egypt. *Basin Research*, **15**, 479–502.

The hydrocarbon prospectivity of the Egyptian North Red Sea basin

G. GORDON, B. HANSEN, J. SCOTT, C. HIRST, R. GRAHAM, T. GROW, A. SPEDDING, S. FAIRHEAD, L. FULLARTON and D. GRIFFIN

Hess, Level 9, The Adelphi Building, 1–11 John Adam Street, London WC2N 6AG, UK (e-mail: graeme.gordon@hess.com)

Abstract: Recent work by a multi-disciplinary team has led to a significantly better understanding of the prospectivity of the North Red Sea. New regional biostratigraphic and environmental analysis from north to south through the Gulf of Suez and into the Red Sea have placed the Nubian sequences into a regional chronostratigraphic framework. The Nubian Upper Cretaceous pre-rift sandstones are observed in the field on both the Egyptian and Saudi Arabian side of the North Red Sea. This regionally extensive sequence was deposited in a continental to shallow marine setting fringing the Mesozoic Tethys Ocean, which lay further north. Extensive onshore fieldwork and mapping of sediment input points, fault orientations and fault linkages have helped to develop an understanding of the expected controls on syn-rift sandstone and carbonate deposition offshore. Thick halite with interbedded evaporite and clastics in the Late Miocene sequences of the Red Sea pose seismic imaging challenges. Recent reprocessing and newly acquired seismic data have produced a step change improvement in imaging of the prospective pre-rift section. Petroleum systems modelling incorporating new information on rift timing and crustal thinning as well as onshore core analysis for source rock properties and temperature variation through time indicates that oil expulsion occurs in the inboard section of North Red Sea – Block 1. This is supported by hydrocarbon shows in the drilled offshore wells which can be typed to pre-rift source rocks from stable isotope and biomarker data. All the key elements of the Gulf of Suez petroleum system exist in the North Red Sea. An integrated exploration approach has enabled prospective areas in the North Red Sea – Block 1 to be high-graded for drilling in early 2011.

Keywords: Red Sea, Gulf of Suez, Dakhla, Duwa, Nubia, seismic imaging, subsalt, Gebel Duwi, gravity magnetics

The North Red Sea – Block 1 concession is located in the NW of the Red Sea, near the mouth of the Gulf of Suez and covers *c.* 9445 km^2 (Fig. 1). Esso held the block from the mid 1970s through to 1984. They acquired 2D seismic and drilled five unsuccessful wells between 1976 and 1981. Phillips drilled two dry wells to the south of the block in 1977. Failure of these wells was largely attributed to the difficulties in drilling valid structures due to the poor quality seismic, which suffered from serious multiple contamination and limited sub-salt illumination. BG was awarded the block in 1995 and acquired 1600 km^2 of 3D seismic in 1999, then relinquished it in 2000. BP took the block in 2004, then farmed it out to Hess in 2006, who acquired 2008 km^2 3D seismic in 2006 and a further 753 km^2 in 2008 (Fig. 2).

Stratigraphy and tectonic framework

Prior to the development of the Red Sea rift system, this part of North Africa was located on the southern margin of the Tethys Ocean (Stampfli & Borel 2002). An extensive passive margin succession developed showing an overall transgressive character, culminating with extensive carbonate deposition in the Late Cretaceous and Eocene, resulting in the passive margin megasequence stratigraphy of the Red Sea and Gulf of Suez (Guiraud & Bosworth 1999; Bosworth & McClay 2001; Ziegler 2001; Khalil & McClay 2009). This pre-rift sequence contains the primary reservoir target of the Upper Cretaceous Nubian sandstone and the prolific Maastrichtian age Dakhla source (equivalent to the Gulf of Suez Brown Limestone) (Fig. 3) (Robison & Engel 1993). Onshore exposure of the pre-rift shows depositional thickness variations along old structural trends, as well as some erosion from footwall highs exposed in the Miocene. South of Quseir the pre-rift section is not exposed onshore and is postulated to be absent offshore due to non-deposition and/or erosion. These onshore observations significantly upgrade the exploration potential of the pre-rift in the Northern Red Sea relative to the central area south of Quseir.

A variety of fault orientations are mapped onshore and can be interpreted on seismic. These fall into three main categories:

- Precambrian – ESE–WNW Najd shear zone features (Fig. 4);
- rift parallel SE–NW clysmic trend faults from Gulf of Suez rift extension – 25–15 Ma;
- Gulf of Aqaba parallel NNE–SSW structures due to the oblique spreading – 15–0 Ma (Lelek *et al.* 1992; Patton *et al.* 1994; Seber 2000; Ziegler 2001; Bosworth *et al.* 2005; Polis *et al.* 2005).

Source

The Cretaceous Maastrichtian age Dakhla formation, a carbonate-rich shale, overlies the leaner Campanian Duwi regionally. Dakhla data from surface samples and cores analysed from the Red Sea Hills in 2005–2008, as well as regional studies, indicate a world class source rock. From onshore unweathered cores, total organic content (TOC) values for the Dakhla range from 2 to >8%, hydrogen index (HI) from 400 to 600 mg g^{-1} and the source rock thickness is >50 m, similar to that of the Brown Limestone in the Gulf of Suez (Robison & Engel 1993). The age equivalent of the Brown Limestone is the Duwi in the Red Sea. This is a leaner shallow marine source rock with lower TOCs and HIs. From petroleum systems modelling, oil generation began at 20 Ma with peak generation at 17–15 Ma. This correlates with oil show extracts from on-block wells contain geochemical biomarkers correlating to pre-rift source rocks (Fig. 5).

From: VINING, B. A. & PICKERING, S. C. (eds) *Petroleum Geology: From Mature Basins to New Frontiers – Proceedings of the 7th Petroleum Geology Conference*, 783–789. DOI: 10.1144/0070783

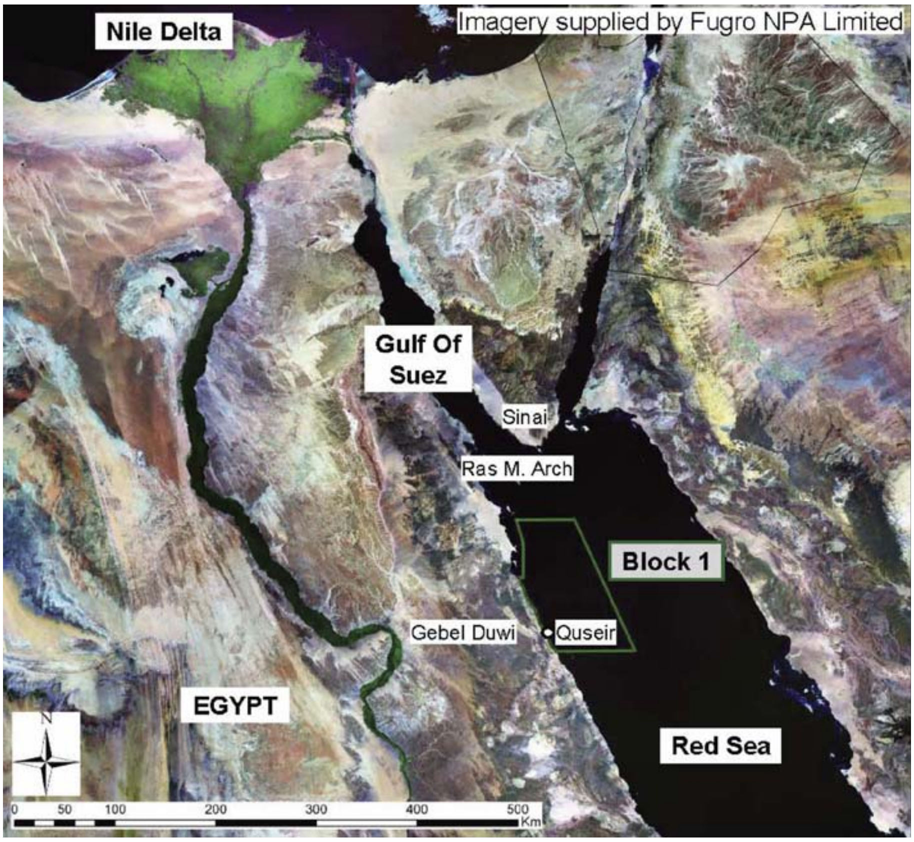

Fig. 1. Location map of Block 1, North Red Sea, Egypt.

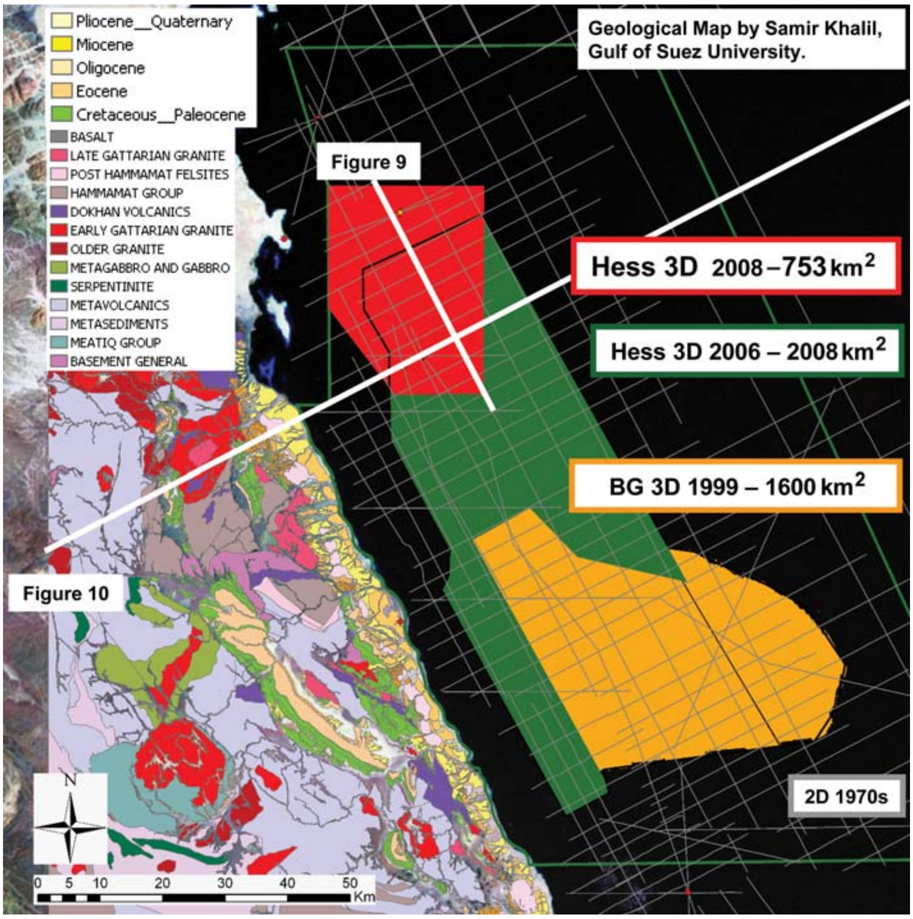

Fig. 2. Block outline showing seismic data coverage and onshore field mapping. Locations of seismic line and aeromagnetic modelling section are labelled, see Figs 9 and 10.

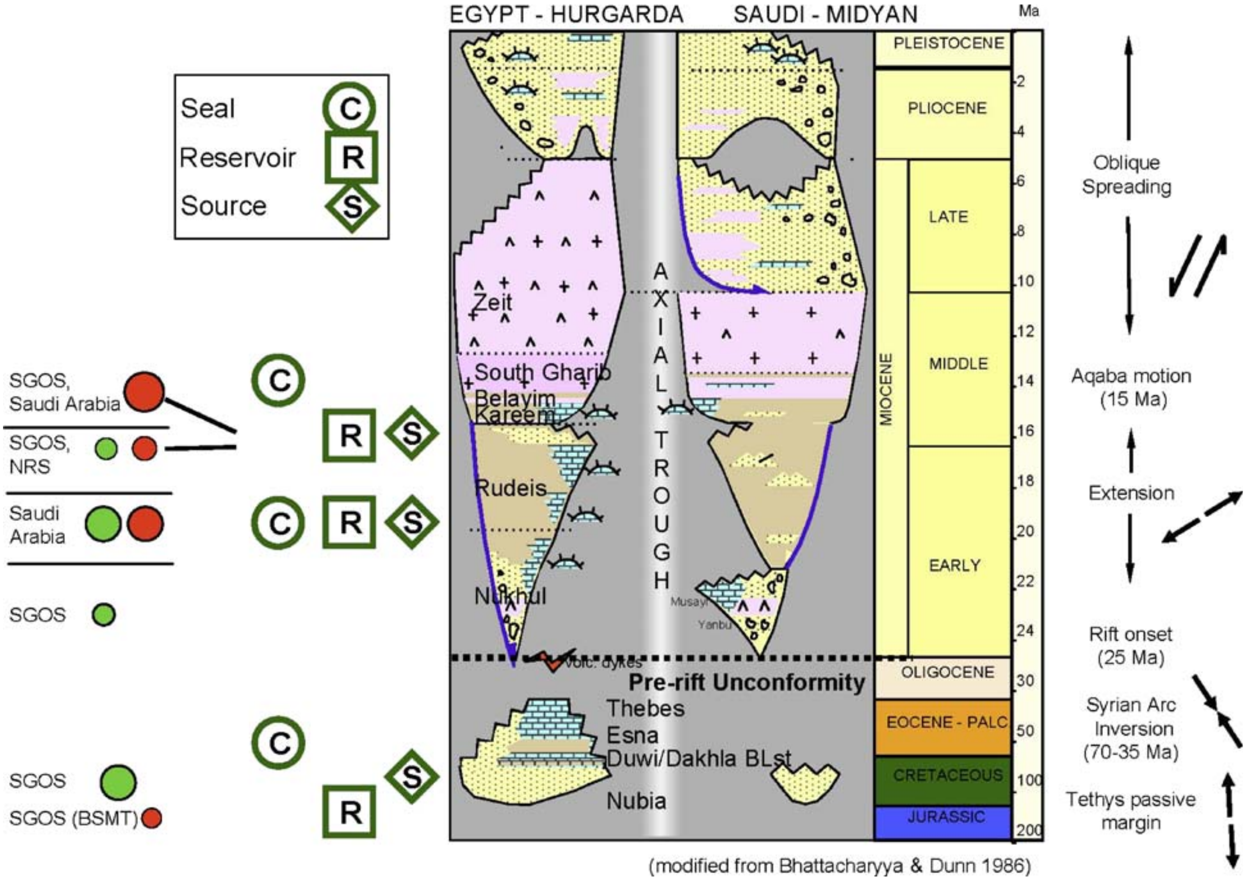

Fig. 3. Stratigraphy and tectonic framework of the North Red Sea showing ages of important tectonic events and petroleum system elements.

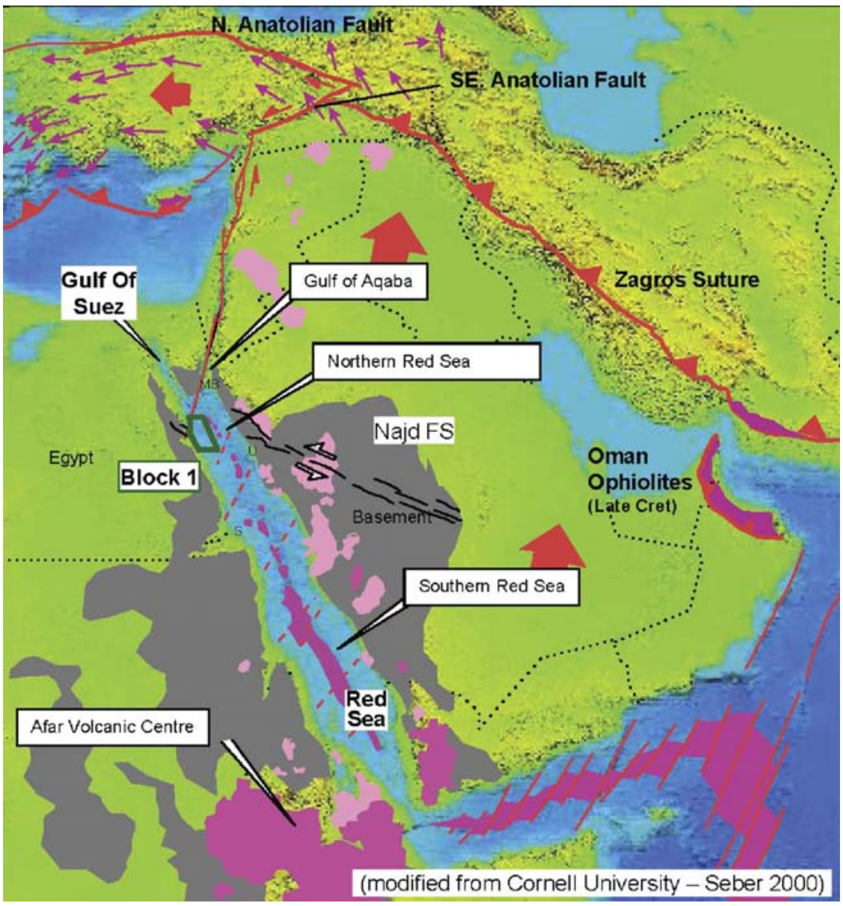

Fig. 4. Regional tectonic setting of North Red Sea, Block 1, showing major tectonic elements.

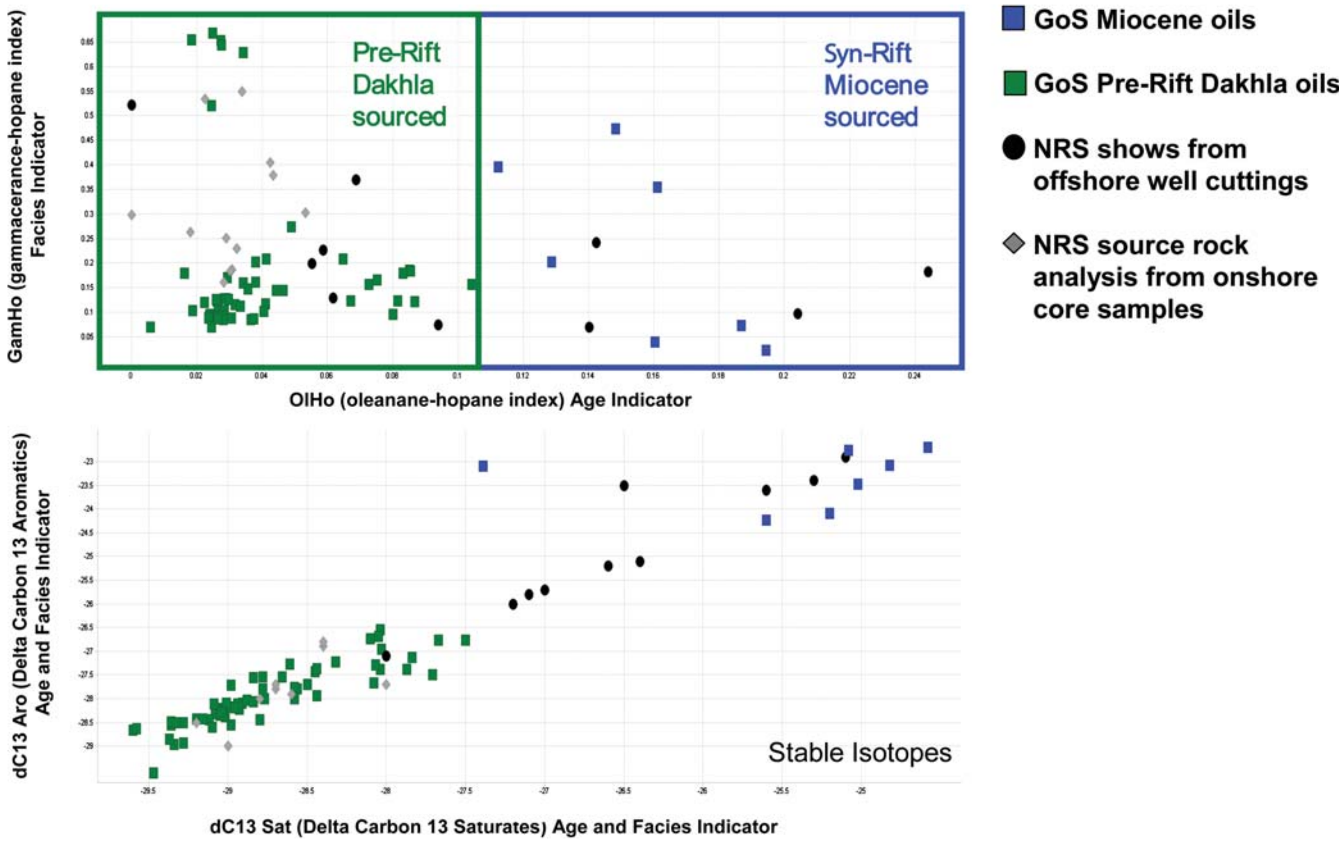

Fig. 5. Comparison of Gulf of Suez (GoS) v. North Red Sea (NRS) source rock biomarker and isotope analysis. NRS offshore shows from well cuttings and onshore core samples type to Cretaceous age GoS brown limestone.

Reservoir and seal

The principal reservoir interval within the pre-rift is the Cretaceous and older Nubian sands. The Nubia represents the initial clastic dominated continental to shallow marine fringe with the Tethyan passive margin and was deposited directly upon basement (McDonald 1979; Ward & McDonald 1979). The Nubian section thins southwards through the Gulf of Suez and is locally absent across the Kharga Arch at the southern tip of the Sinai Peninsula (Klitzch & Squyres 1990; Patton *et al.* 1994; Guiraud & Bosworth 1999). South of this feature, the Nubia thickens dramatically as seen in outcrop at Gebel Duwi, located onshore of the North Red Sea Block 1, where in excess of 300 m of Nubia is present (Fig. 6) (Bhattacharyya & Dunn 1986; Mitchell *et al.* 1992). The Nubia age-equivalent Adaffa sands are also present on the Saudi Arabian side of the North Red Sea (Hughes & Johnson 2005). As the rift evolved, sediment entry points became fixed at major fault transfer points. In the Gulf of Suez the Holocene drainage pattern is indicative of key sediment entry points into the rift basin. Likewise, in the Red Sea the main onshore wadis and drainage basin fall lines interpreted from topographic maps are considered keys to the past when evaluating point sources for Miocene sands (Fig. 7; Richardson & Arthur 1988; Gawthorpe *et al.* 1990; Heath *et al.* 1998; Younes & McClay 2002; Polis *et al.* 2005; Khalil & McClay 2009). In the pre-rift section, the main sela is the Maastrichtian age Dakhla and in the syn-rift. Lower Miocene intraformational shales are penetrated in the offshore wells, as well as an ultimate seal at the evaporite layers of the South Gharib, and Zeit.

Seismic acquisition and processing

Thick halite with interbedded evaporites and clastics, as well as diapiric salt, pose severe challenges to the seismic imaging of sub-salt targets. A 753 km^2 3D seismic survey was acquired in 2008 at 30° azimuth to the vintage data to provide improved subsalt illumination and a lower signal to noise multiazimuth dataset in the overlap area. Deeper streamers and sources were used than in the 2006 acquisition and the source configuration was optimized to help maximize low frequency signal penetration of the thick evaporite section. Hess has then carefully merged and reprocessed the full 3D vintage seismic datasets on-block during 2008–2009. 3D surface related multiple elimination (SRME) processing was used to reduce the impact of multiples from the rugose seabed and Top Zeit. Previous depth migrations used a flood velocity beneath the Top Zeit, but the cleaner reprocessed data allowed a laterally varying velocity field within the evaporite sequence to be generated using tomography. This replaced the flood velocity model with a more geologically consistent velocity variation (Fig. 8). Reverse-time depth migration (RTM) processing also provided a cleaner, more coherent image sub-salt where low frequencies dominate. Overall, optimized acquisition parameters and the application of the latest geophysical processing techniques have resulted in a significant uplift in the quality of subsalt imaging as compared with the 1999 BG and original 2006 3D seismic volumes. The 2D data shot in 1975 and 1988 which formed the basis for the earlier drilled wells was unable to image below the salt.

Seismic mapping

The imaging of the pre- and syn-rift sequences has markedly improved from the original time-migrated data (Fig. 9). Each of the acquisition and processing steps has provided an incremental improvement which when added together help to de-risk the sub-salt prospectivity of this new frontier basin. The latest seismic data quality at the target level has a wider frequency bandwidth, a reduction in migration noise and reduced multiple contamination. This has led to better fault definition and allows

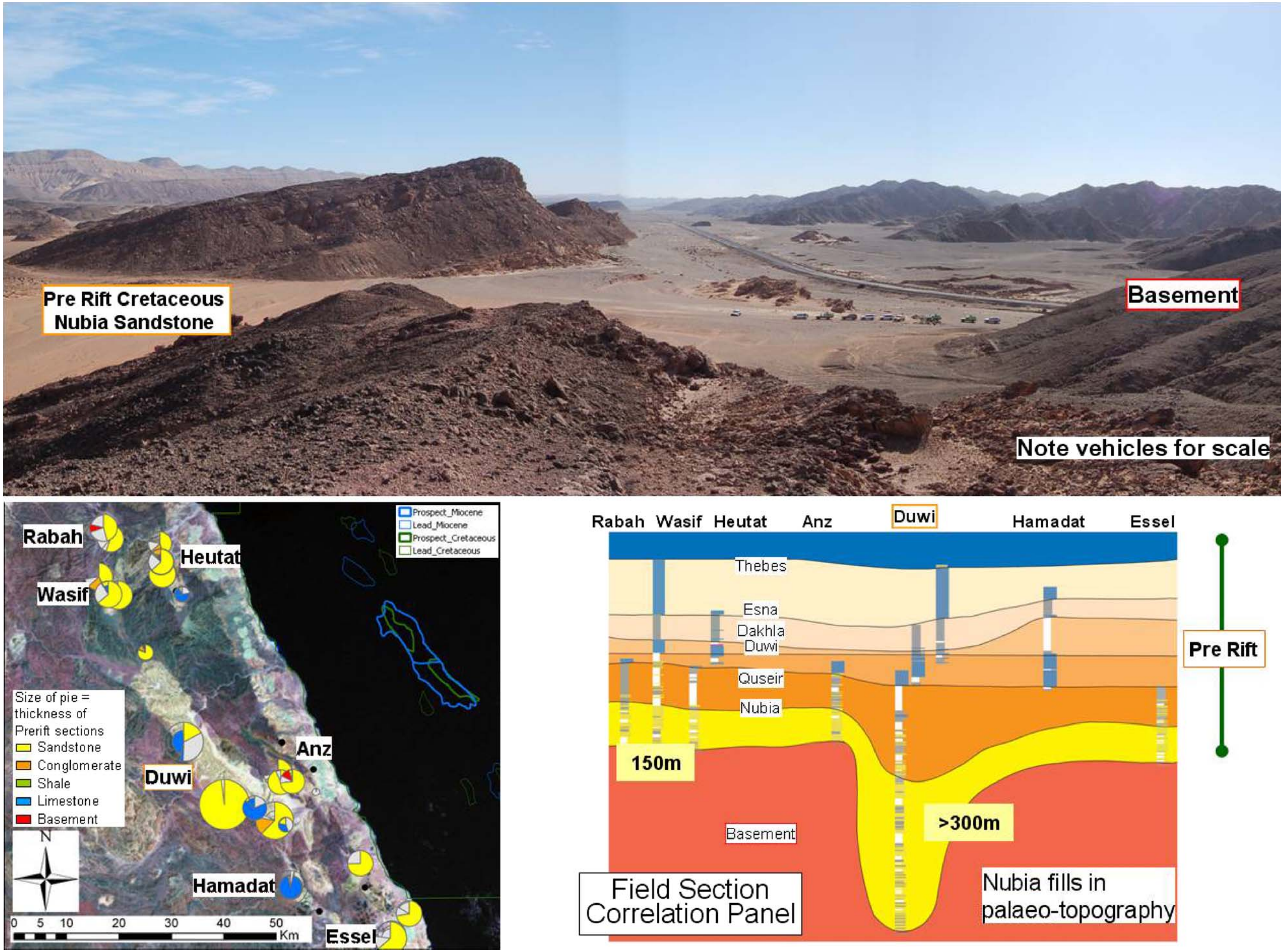

Fig. 6. Field photograph of Gebel Duwi North Red Sea Hills. Showing the geometry of a tilted pre-rift Cretaceous Nubia sandstone on basement. Map and cross section show consistent regional thickness of Nubia sandstone of 150 m with thickening at Gebel Duwi due to infilling of palaeotopography of palaeostructuring

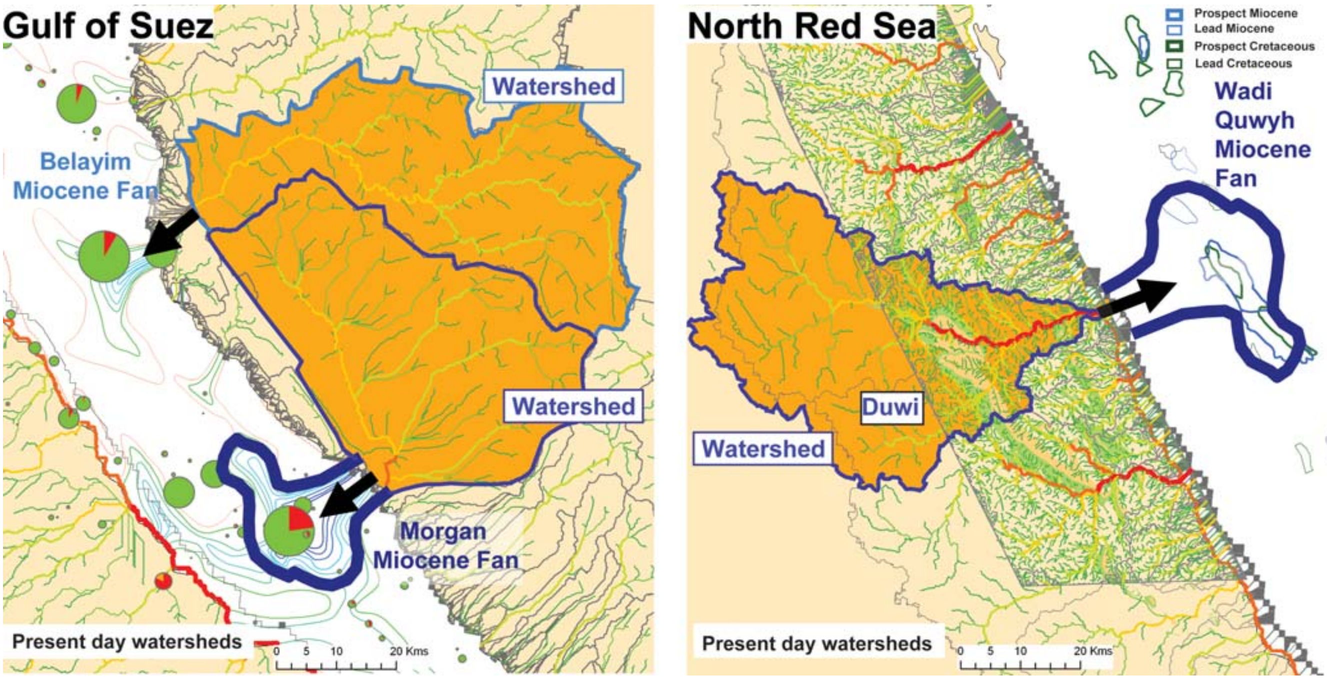

Fig. 7. Present day watersheds from digital elevation data. In the Gulf of Suez, the present day drainage system outputs correlate with Miocene syn-rift depositional thicks. This Miocene fan delta analogue was used to compare between Gulf of Suez discovered fields and North Red Sea prospects and leads.

increased confidence in the mapping of subsalt events. However, the current 3D data quality still does not lend itself to an intricate sequence-stratigraphic or AVO/amplitude mapping approach. Rather, the top and base of gross tectonic sequences have been mapped, such as the top evaporites (Top Zeit), the base evaporites (base Belayim), the rift-onset unconformity and the top of igneous basement (Fig. 9). Mapping at these levels allows detailed structural interpretation and geological models based on onshore mapping and regional understanding has identified prospectivity at both syn-rift and pre-rift levels.

Gravity/magnetics

The aeromagnetic survey coverage acquired in 2006 provides a link between the outcrops on the Red Sea margin, offshore well penetrations and seismic data. Integration with the 2008 ship-borne

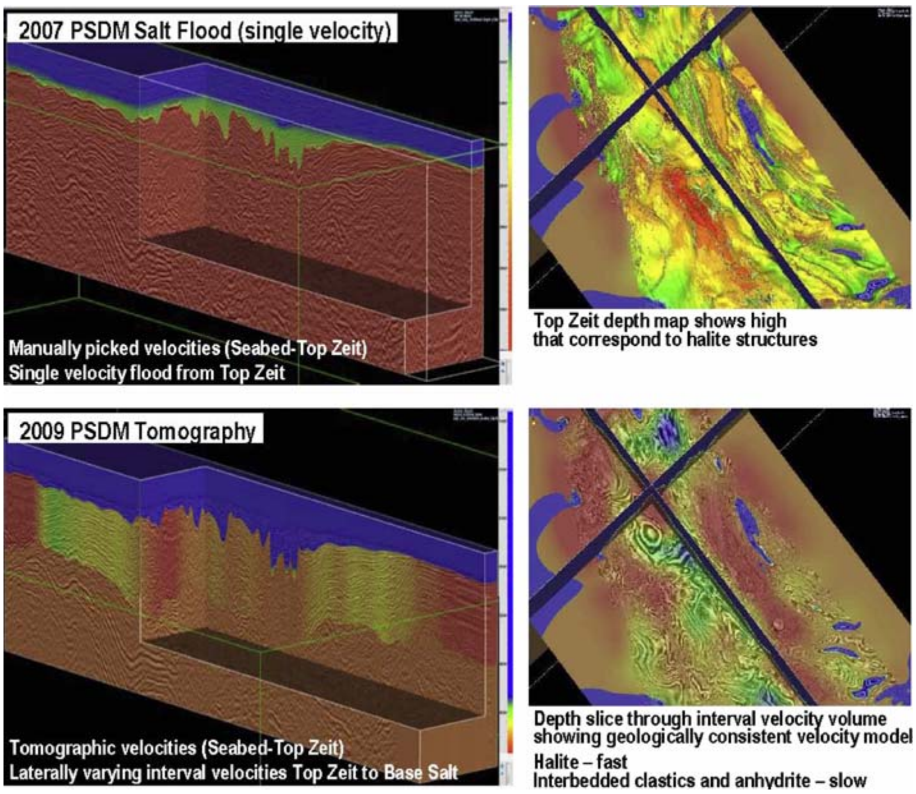

Fig. 8. 3D views of 2007 and 2009 pre-stack depth migration (PSDM) velocity models. The 2009 result shows improved imaging due to a more geologically consistent velocity model, incorporating Top Zeit rugosity and laterally varying velocities within the South Gharib and Zeit evaporite section.

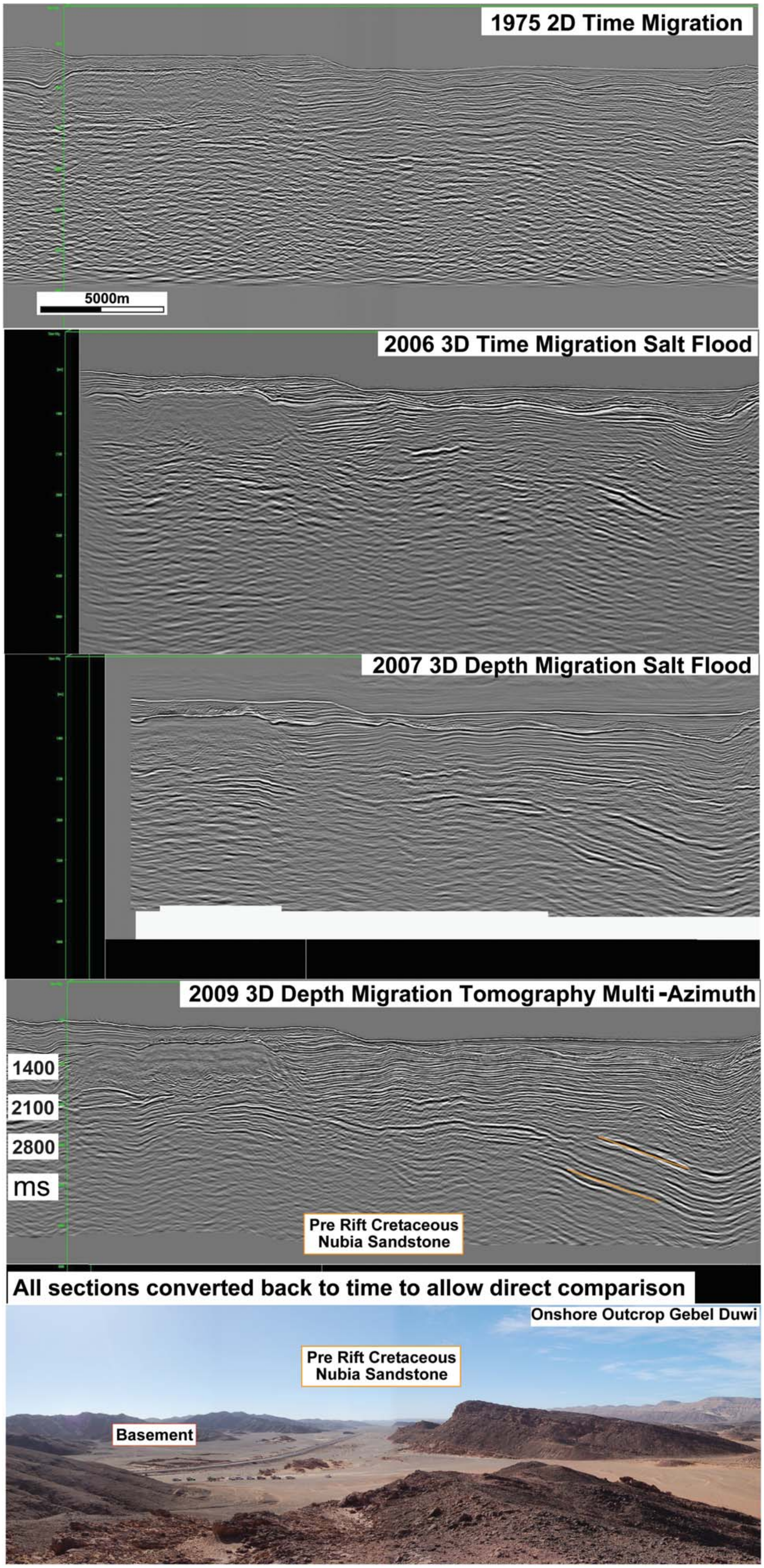

Fig. 9. Comparison of seismic datasets covering northern area of Block 1. Data quality steadily improves moving from 2D seismic to 3D seismic, from pre-stack time migration (PSTM) to pre-stack depth migration (PSDM), and form a salt flood velocity model to a laterally varying velocity model derived from tomography. With improved data quality faults are more easily delineated and the pre-rift section is imaged.

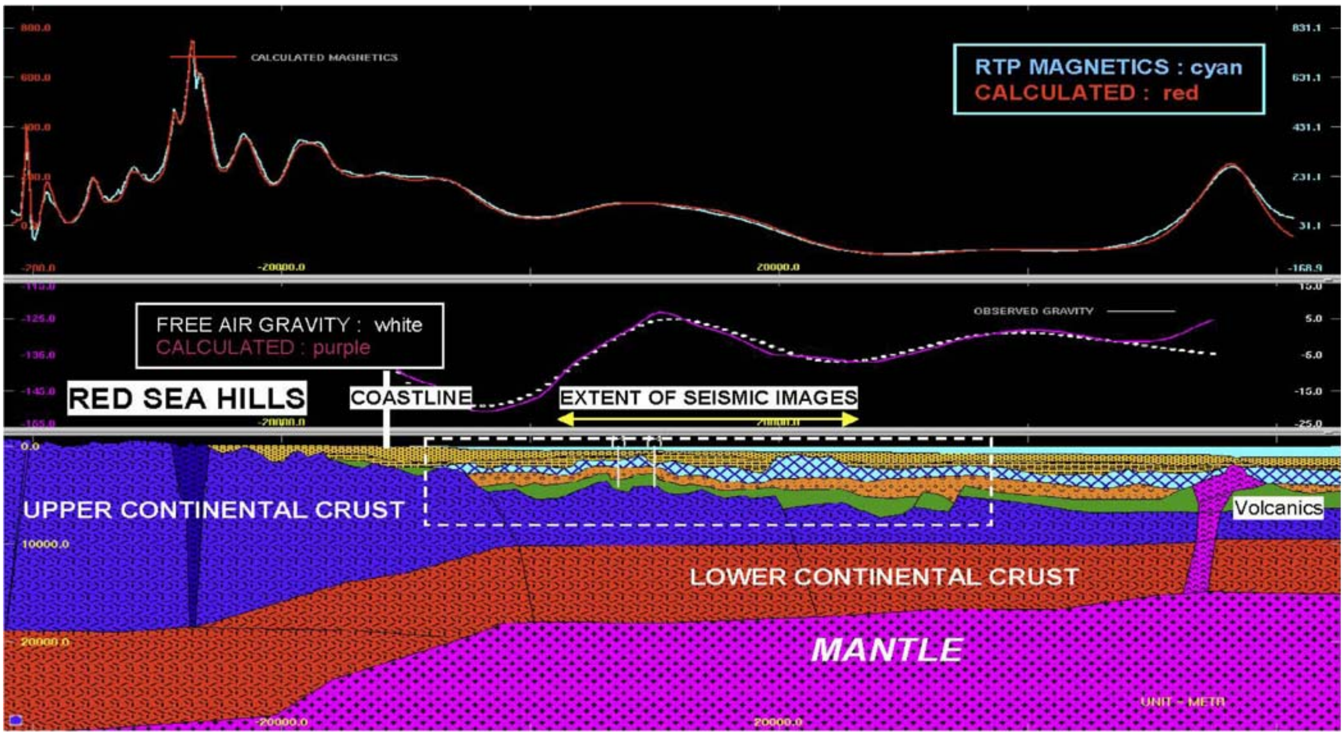

Fig. 10. Joint modelling of high frequency aeromagnetic data and regional gravity data allows salt thickness and depth to basement to be modelled for comparison with seismic interpretation.

gravity and magnetics data helps to constrain the offshore seismic interpretation (Fig. 10). In areas of imaging uncertainty, this has been particularly beneficial for placement of sub-salt faults, and to determine the thickness of salt and depth to basement where the seismic is poorly imaged.

Summary

From the extensive regional work, the northwestern margin of the North Red Sea is interpreted to be a continuation of the Gulf of Suez petroleum system. The primary play is the pre-rift Dakhla source rock charging pre-rift Nubian sands in structural traps set up by extensional tilted fault blocks. Onshore the basis for a working petroleum system can be demonstrated in the source rock exposure at outcrop and oil shows in the wells offshore have been typed to pre-rift Dakhla source rock. This confirms that the pre-rift play extends into the offshore region albeit that the wells only saw syn-rift on basement. A secondary play also exisits with syn- and/or pre-rift source rocks charging both clastic and carbonate potential reservoirs in the syn-rift Miocene. Improved seismic imaging has de-risked these plays and an integrated exploration approach summarized in this paper has enabled prospective areas to be high-graded.

The authors would like to thank EGPC for their permission to present this paper and Dr Samir Khalil, Suez Canal University, Egypt, for inclusion of his geological map. Special thanks for the contributions made by Dave Peel, Laura Lawton, Dr Paul Whitehouse, Andy Pepper, Hans Ladegaard, Dr Niall McCormack and Dr Stuart Lake from Hess, Dr Ahmed Barkooky from Cairo University, Jonathan Redfern from the University of Manchester, and Dr Nicky White from the University of Cambridge.

References

Bhattacharyya, D. P. & Dunn, L. G. 1986. Sedimentologic evidence for repeated pre-Cenozoic vertical movements along the North-East margin of the Nubian Craton. *Journal of African Earth Sciences*, **5**, 147–153.

Bosworth, W. & McClay, K. 2001. Structural and stratigraphic evolution of the Gulf of Suez Rift, Egypt, a synthesis (in Peri-Tethys memoir 6, Peri-Tethyan Rift/Wrench basins and passive margins). *Memoires du Museum National d'Histoire Naturelle*, **186**, 567–606.

Bosworth, W., Huchon, P. & McClay, K. 2005. The Red Sea and Gulf of Aden basins. *Journal of African Earth Sciences*, **43**, 334–378.

Gawthorpe, R. L., Hurst, J. M. & Sladen, C. P. 1990. Evolution of Miocene footwall-derived coarse-grained deltas, Gulf of Suez, Egypt, implications for exploration. *AAPG Bulletin*, **74**, 1077–1086.

Guiraud, R. & Bosworth, W. 1999. Phanerozoic geodynamic evolution of North-Eastern Africa and the northwestern Arabian Platform (in basin dynamics and basin fill, models and constraints; Part I). *Tectonophysics*, **315**, 73–108.

Heath, R., Vanstone, S. *et al*. 1998. Renewed exploration in the offshore North Red Sea region–Egypt. *In*: Eloui, M. (ed.) *Proceedings of the 14th Petroleum Conference*. Egyptian General Petroleum Corporation, Cairo, 16–34.

Hughes, G. & Johnson, R. S. 2005. Lithostratigraphy of the Saudi Arabian Red Sea. *GeoArabia*, **10**, 49–126.

Khalil, S. M. & McClay, K. R. 2009. Structural control on syn-rift sedimentation, northwestern Red Sea Margin, Egypt. *Marine and Petroleum Geology*, **26**, 1018–1034.

Klitzch, E. H. & Squyres, C. H. 1990. Paleozoic and mesozoic geological history of Northeastern Africa based upon new interpretation of Nubian Strata. *AAPG Bulletin*, **74**, 1203–1211.

Lelek, J. J., Shepherd, D. B., Stone, D. M. & Abdine, A. S. 1992. October Field: The Latest Giant under Development in Egypt's Gulf of Suez. *In*: *Giant Oil and Gas Fields of the Decade 1978–1988*. American Association of Petroleum Geologists, Tulsa, OK, Special Volumes, **M54**, 231–249.

McDonald, K. C. 1979. *The Nubia Formation, Quseir – Safaga Area, Eastern Desert*. University of Kansas, Egypt.

Mitchell, D. J. W., Allen, R. B., Salama, W. & Abouzakm, A. 1992. Tectonostratigraphic framework and hydrocarbon potential of the Red Sea (in The Red Sea–Gulf of Aden, II, Beydoun). *Journal of Petroleum Geology*, **15**, 187–209.

Patton, T. L., Moustafa, A. R., Nelson, R. A. & Abdine, A. S. 1994. *Tectonic Evolution and Structural Setting of the Suez Rift (in Interior Rift*

Basins, Landon). American Association of Petroleum Geologists, Tulsa, OK, Memoirs, **59**, 9–55.

Polis, S. R., Angelich, M. T. *et al*. 2005. Preferential deposition and preservation of structurally-controlled synrift reservoirs. *Northeast Red Sea and Gulf of Suez*, **10**, 97–124.

Richardson, M. & Arthur, M. A. 1988. The Gulf of Suez-Northern Red Sea Neogene Rift, a quantitive basin analysis. *Marine and Petroleum Geology*, **5**, 247–270.

Robison, V. D. & Engel, M. H. 1993. Characterization of the source horizons within the Late Cretaceous transgressive sequence of Egypt. *In*: Katz, B. J. & Pratt, L. M. (eds) *Source Rocks in a Sequence Stratigraphic Framework*. AAPG Studies in Geology, **37**, 101–117.

Seber, D., Steer, D., Sandvol, E., Sandvol, C., Brindisi, C. & Barazangi, M. 2000. Design and development of information systems for the geosciences; an application to the Middle East. *GeoArabia (Manama)*, **5**, 269–296.

Stampfli, G. M. & Borel, G. D. 2002. A plate tectonic model for the paleozoic and mesozoic constrained by dynamic plate boundaries and restored synthetic oceanic isochron. *Earth and Planetary Science Letters*, **196**, 17–33.

Ward, W. C. & McDonald, K. C. 1979. Nubia formation of central Eastern Desert, Egypt, major subdivisions and depositional setting. *AAPG Bulletin*, **63**, 975–983.

Younes, A. I. & McClay, K. 2002. Development of accommodation zones in the Gulf of Suez-Red Sea Rift, Egypt. *AAPG Bulletin*, **86**, 1003–1026.

Ziegler, M. A. 2001. Late Permian to holocene paleofacies evolution of the Arabian plate and its hydrocarbon occurrences. *GeoArabia (Manama)*, **6**, 445–504.

A regional overview of the exploration potential of the Middle East: a case study in the application of play fairway risk mapping techniques

A. J. FRASER

BP Exploration, Chertsey Road, Sunbury-on-Thames, Middlesex TW16 7LN, UK
(e-mail: alastair.fraser@imperial.ac.uk)

Abstract: The Middle East is the world's most prolific petroleum province, containing the world's top five countries in terms of oil reserves and four of the top 10 oil producers. This success is largely due to the stacked nature of what are essentially very simple play systems with multiple carbonate platform and deltaic clastic reservoirs, widespread evaporitic seals, world class source rocks and the overprint of very large compressional anticlines in both fold belt and foreland settings. As with most working petroleum systems, all areas of the Middle East are not equally endowed with petroleum resources and future potential. Using an analysis of the prolific Upper Jurassic 'Arab' play fairway of the Middle East, the application of play fairway risk mapping techniques is demonstrated.

Keywords: Middle East play fairway analysis, common risk segments, exploration triangle

In terms of future global oil and gas resources, the Middle East is of immense importance. Much has already been written about its scale and the fundamental geological reasons underlying this (Murris 1980; Beydoun 1986, 1998; Stoneley 1990; Konert *et al.* 2001; Sharland *et al.* 2001; Alsharhan & Nairn 2003; Sorkhabi 2010). This assessment suggests that the Middle East contains a significant volume of undiscovered oil and gas: that yet to be found is almost certainly well in excess of 100 BBOE (billion barrels of oil equivalent). Applying existing best in class technology to the more difficult or currently inaccessible parts of the play system suggests it is very likely that world class, super-giant fields, containing more than 1 BBOE remain to be found.

The constraints on delivering this resource are two-fold. Firstly, there is a general lack of competitive fiscal terms. These are needed if companies are to earn returns that are accretive to their financial performance. Secondly, there are very serious non-technical barriers and obstacles to foreign participation.

In this short paper, frequent reference will be made to an extensive regional study undertaken to assess the existing and future resource potential of the Arabian plate. The paper will address the principles and benefits of constructing a series of plate-scale, gross depositional environment (GDE) maps to describe basin evolution and as the fundamental building blocks of the common risk segment (CRS) mapping process. The prolific Upper Jurassic 'Arab' fairway which has estimated resources of around 300×10^9 barrels in the region will be used as an example of how these GDE maps are turned into a series of plate-wide CRS maps and subsequently used to focus exploration effort.

History

Exploration in the Middle East effectively commenced on 26 May 1908 when William Knox D'Arcy made the discovery at Masjid-i-Sulaiman in Cenozoic Asmari limestones in the Persian Zagros Mountains in what is now Iran. The photograph (Fig. 1) taken in 1911 shows one of the early wells on the field. Reserves are estimated at 1.3×10^9 barrels. The first discoveries were made on the basis of field mapping which identified surface anticlines and associated seeps. Today, we have access to modern 3D seismic data, sophisticated petroleum systems models and play fairway analysis tools to locate new oil and gas resources.

The Middle East contains estimated proven reserves of some 750×10^9 barrels of oil and 2680×10^{12} SCF of gas, representing *c.* 65 and 35% of global oil and gas reserves, respectively, making it, by some margin, the world's richest petroleum province (BP Statistical Review of World Energy 2009). These reserves are encountered in reservoirs of Late Palaeozoic to Cenozoic age in a NW–SE trending zone that runs from Oman to Turkey. The world's largest oil field (Ghawar) and gas field (South Pars/North Dome) are located in the region (Fig. 2). Masjid-i-Sulaiman (discovered by D'Arcy, later to form BP) is also highlighted on this map.

Saudi Arabia contains by far the majority of the oil resources of the region but this analysis is not just about Saudi Arabia (although this is the focus of the play fairway risk mapping), but also Iran, Iraq, Kuwait and Abu Dhabi, five of the top six in terms of proven oil reserves at the present day (BP Statistical Review 2009). This study utilizes a unique database of surface and subsurface information covering the region, sourced from the archives of the three heritage companies BP, Amoco and ARCO.

Fig. 1. Photograph taken in 1911 showing one of the very early BP wells drilled on Masjid-i-Sulaiman after penetrating the Cenozoic Asmari carbonate reservoir. Reserves are estimated at 1.3×10^9 barrels of oil. Photo BP archives.

VINING, B. A. & PICKERING, S. C. (eds) *Petroleum Geology: From Mature Basins to New Frontiers – Proceedings of the 7th Petroleum Geology Conference*, 791–800. DOI: 10.1144/0070791

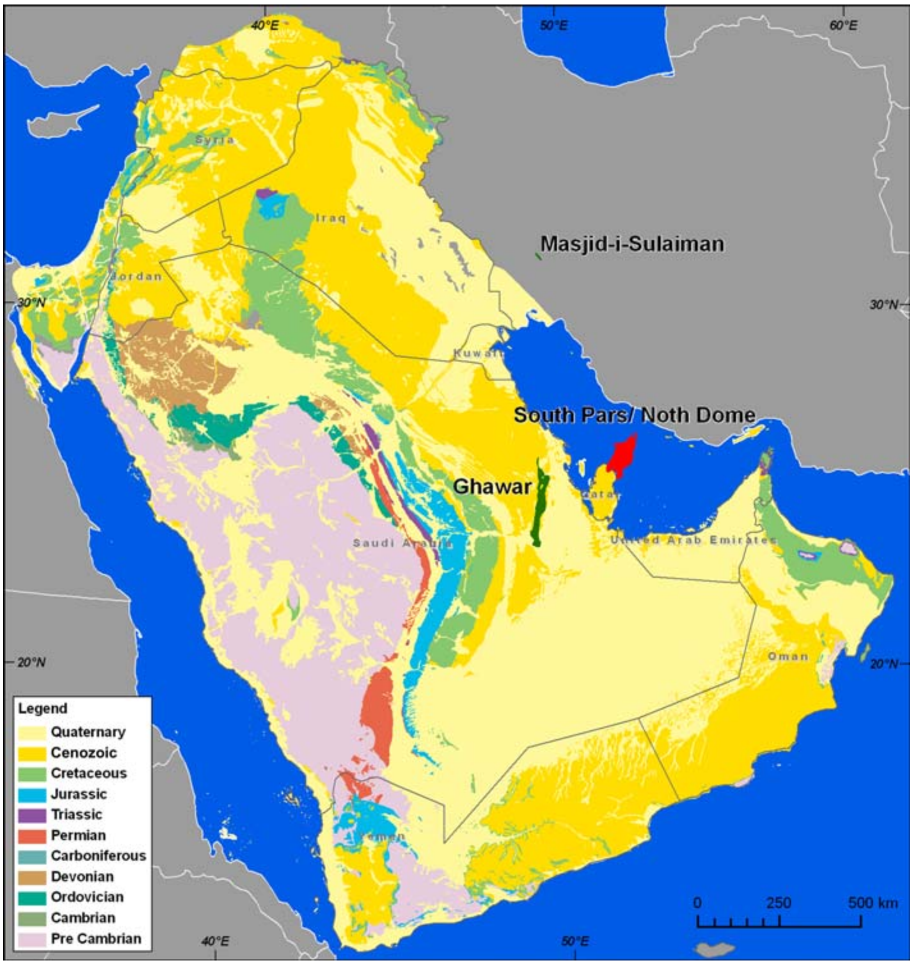

Fig. 2. Geology of the Arabian Plate.

Middle East plays

Figure 3 illustrates a tectonostratigraphic diagram to summarize the tectonic history and stratigraphic fill of the Arabian plate. It is best thought of as a horizontally compressed chronostratigraphic diagram. In essence both charts fulfil a similar function. The chronostratigraphic section is consistent along the line of section with the GDE maps, and complements them by providing a temporal interpretation of the facies associations. Additionally, the chronostratigraphic diagram illustrates the missing sections and time, something a suite of GDE maps are unable to achieve on their own. The chronostratigraphic chart also shows the spatial relationship of plays through time, such as the multiple stacked shale, carbonate and evaporite cycles observed in the Permian to Cenozoic section of the Middle East. It is used to highlight the key tectonic events recorded in the region and link these to broader plate margin processes. The stratigraphy is divided into megasequences and their constituent sequences, to identify the spatial and temporal distribution of the key reservoir, source and seal facies. A link between trap and charge timing can be observed. Ultimately, the chronostratigraphic chart highlights the major play fairways, typically based on the presence of major reservoir intervals having both a regional seal and charge system.

The most notable aspects of Middle East geology that are illustrated on this chart are as follows:

- Early north–south oriented Infra-Cambrian rifts that developed on the northern margin of Gondwanaland and contain in some places fairly thick salt – the Hormuz salt (Edgell 1996; Sharland *et al.* 2001).
- A long-lived post-rift phase through much of the Palaeozoic which ended with the onset of NW–SE trending Neo-Tethyan rifting from the early Permian (Konert *et al.* 2001; Sharland *et al.* 2001).
- A repeated set of shale (source rocks), carbonate (reservoirs) and evaporite (seal) cycles throughout the Mesozoic forming a series of stacked, essentially self-contained play fairways. For the purposes of this short paper we will concentrate on the most prolific of these, the late Jurassic 'Arab' play fairway, when discussing the principles of GDE and CRS mapping (Murris 1980; Ellis *et al.* 1996; Loosveld *et al.* 1996; Youssif & Nouman 1997; Sharland *et al.* 2001).
- Closure of Neo-Tethys and formation of the Zagros Mountains in late Cretaceous and Cenozoic times, the major trap-forming event on the Arabian plate (Sharland *et al.* 2001).

A play cartoon generated to describe the play systems of the Middle East is shown in Figure 4. The cartoon illustrates a section running roughly west–east through southern Iraq, northern Kuwait and across the Persian Gulf into Iran and is loosely based on a regional 2D seismic line from the region.

The Middle East can, in simple terms, be described as a series of inverted north–south trending Infra-Cambrian and NW–SE trending Early Permian (Neo-Tethyan) rifts. The Zagros Mountains are interpreted as a largely thick skinned fold belt with the foreland dominated by a series of associated inversion anticlines. Ghawar, the largest oilfield in the world, is effectively a large inversion anticline underpinned by an inverted north–south trending Infra-Cambrian rift.

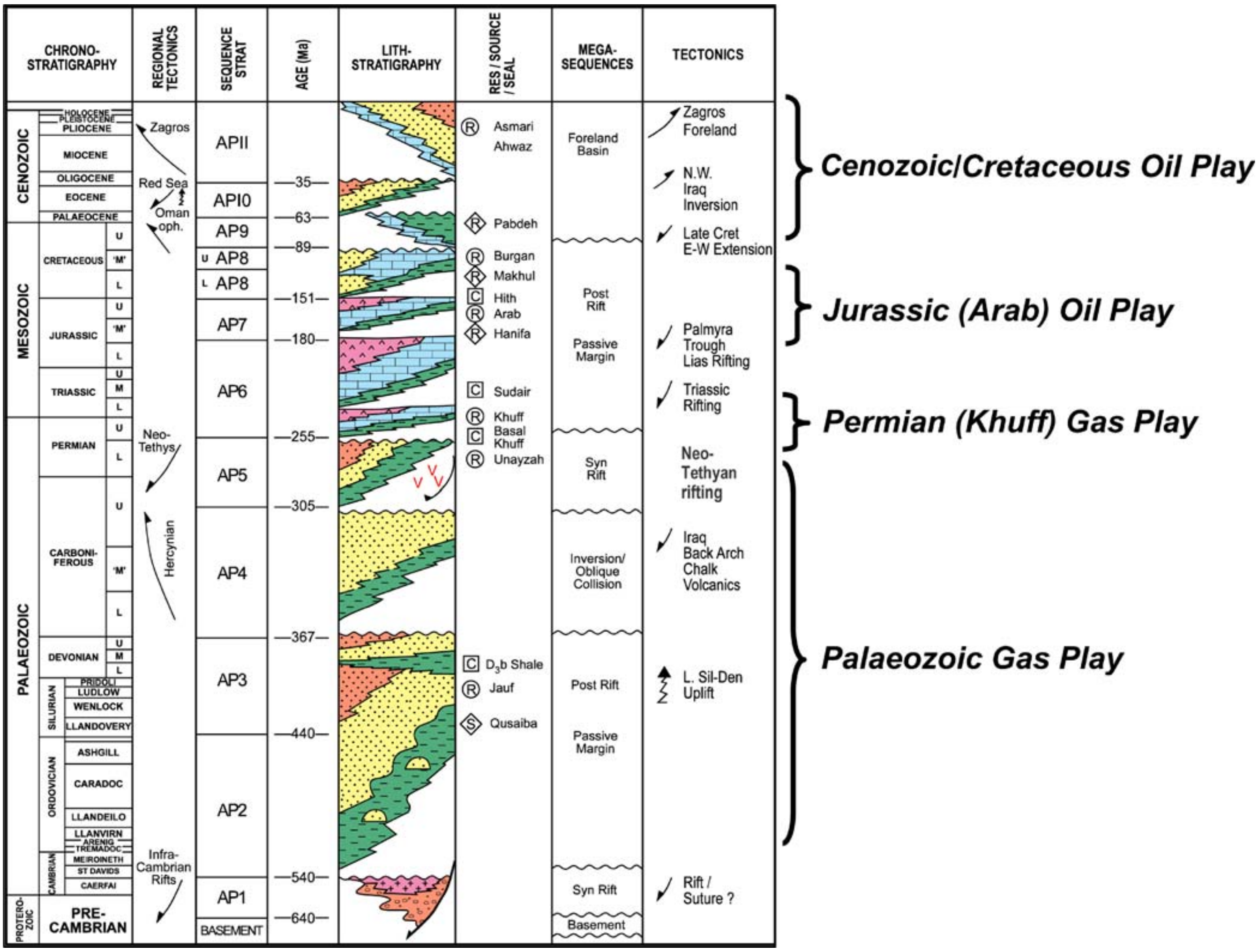

Fig. 3. Tectonostratigraphic chart for the Middle East showing key stratigraphic, tectonic and play elements. R, reservoir; S, source; C, seal. Sequence stratigraphy after Sharland *et al.* (2001).

The play cartoon also highlights the five world-class source rocks in the region. These are the Qasaiba in the Silurian, the Hanifa in the Jurassic, the Khaz Dumi and Garau in the Cretaceous and the Pabdeh in the Cenozoic. All are associated with multiple reservoir-seal pairs. In fields such as Rumaila, West Qurna and Burgan, there are up to 12 individual reservoir-seal pairs resulting in super-giant fields with reserves in excess of 40×10^9 barrels (Jassim & Al-Gailani 2006).

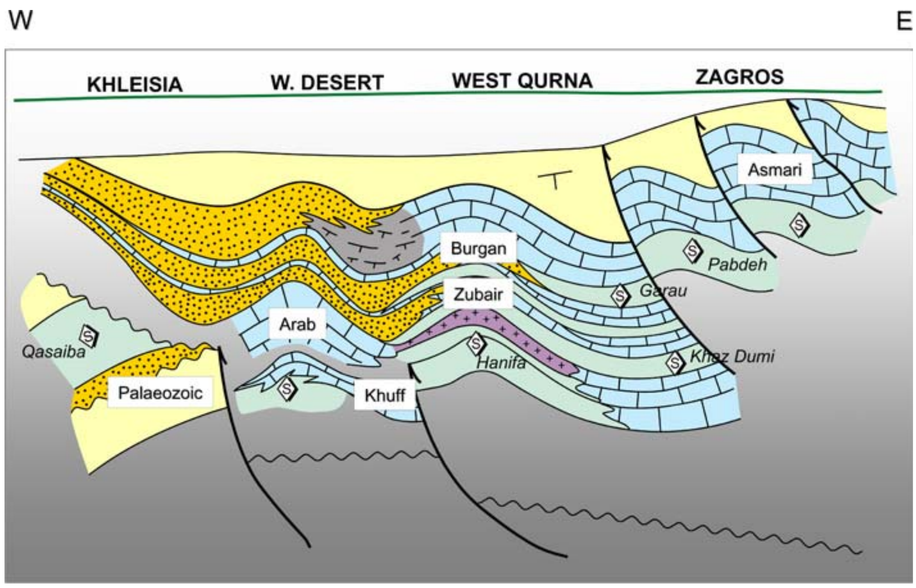

Fig. 4. Play cartoon describing the major play systems of the Middle East. Of note are the five world-class source rocks present in the region. These are the Qasaiba in the Silurian, the Hanifa in the Jurassic, the Khaz Dumi and Garau in the Cretaceous and the Pabdeh in the Cenozoic.

Exploration process

The fundamental understanding of what makes basins work has evolved over the past 15 years into a systematic approach which focuses thinking at the regional or basin scale before considering individual prospects and leads. The strength of the methodology presented in this paper, which we refer to as 'geology from the bottom up', is that it allows the early high-grading of basins and plays for further study/investment, thus negating much wasted time, effort and money in areas with little potential. The process can be elegantly summarized in the form of the 'exploration triangle' (Fig. 5). The bottom part of the triangle is about focusing on the basins/plays which are likely to work at a scale that fits with our exploration strategy of targeting basins with billion barrel potential, that is, being in the right basins and the right parts of these basins. The top part of the triangle is about shotpoint risk – locating wells and drilling 'no dry holes' using techniques such as surgical mapping, detailed charge modelling, AI/AVO analysis, etc. and ultimately building a quality prospect inventory that allows us to make better exploration investment decisions through a process of 'quality through choice'.

Jurassic of the Arabian plate

GDE maps form an essential tool in the exploration process. They fulfil two important roles. Firstly, they provide an easily comprehensible view of the depositional fill of the basin through time. Secondly, they constrain the areal distribution of source, seal and reservoir facies and thus provide the basis for defining and risking play fairways. They are used at all scales of exploration work from the regional basin scale to prospect scale analysis.

For this Middle East study, a suite of 14 individual GDE maps were generated which describe the stratigraphic evolution of the Arabian Plate from the Infra-Cambrian to the present. For the purposes of this short paper we will concentrate on the two GDE maps used to constrain the areal distribution of reservoir, source and seal for the late Jurassic (Arab) play fairway, one of the most prolific play systems in the world with over 300×10^9 barrels of oil reserves. The maps for the Upper Jurassic describe a broad carbonate shelf located on the southeastern margin of Neo-Tethys. Two isolated, intra-shelf basins that were subsiding at a faster rate than the surrounding areas are highlighted in shaded green/blue – perhaps related to underlying Infra-Cambrian salt (Fig. 6). Widespread anoxia developed in these areas, resulting in the widespread deposition of the Hanifa and equivalent type IIs source rocks. These outlines can be transferred directly to a source presence CRS map and combined with source rock maturity to produce a map combining charge presence and effectiveness for oil (Fig. 7).

A CRS is defined as an area of a play fairway which has common critical risk factors. The risk factors include charge, reservoir and seal, although the latter in some settings (e.g. conformable sequences) may be a prospect specific issue. CRS maps are typically constructed at the basin scale for each of the key risk factors. The detail of these depends entirely on the density of available data. The individual components are convolved together to produce a composite CRS description of the fairway. These maps provide the focus on the lowest risk segments of the play fairway.

The real value of CRS mapping is its simplicity. Having refined the technique over the past 15 years, we have seen it evolve to fulfil several important functions.

- Firstly, it provides a process whereby each explorer is forced to work through a systematic assessment which addresses all (stratigraphic) elements in a play fairway analysis.
- Secondly, once individual maps are combined into a composite CRS map we have a very effective means of focusing on the key 'low-risk' part of a basin or play fairway and by implication defocusing on the higher-risk 'red' areas of the map.
- Thirdly, by the use of only three 'traffic light' colours to describe relative play risk (green for low-risk, yellow for moderate-risk and red for high-risk), we as geoscientists are able to share often complex geological analyses in an easily comprehensible fashion.

As mentioned above, hydrocarbons in the Upper Jurassic 'Arab' reservoir are sourced directly from the underlying Upper Jurassic (Oxfordian), Lower Hanifa Formation. The classic oil-producing region of central Saudi Arabia is situated in an area of thick

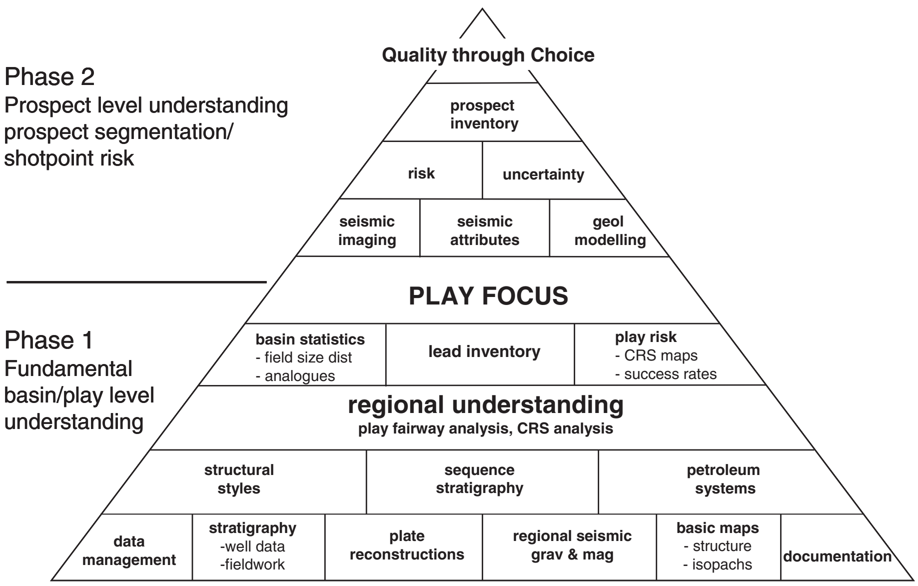

Fig. 5. The exploration process triangle. The base of the triangle focuses on gaining a fundamental basin and play level understanding using subsurface integration tools such as GDE and CRS mapping. The top part of the triangle is about shot-point risk, that is, locating wells, drilling no dry holes, using techniques such as surgical mapping, detailed charge modelling and AI/AVO analysis, and ultimately building a quality prospect inventory.

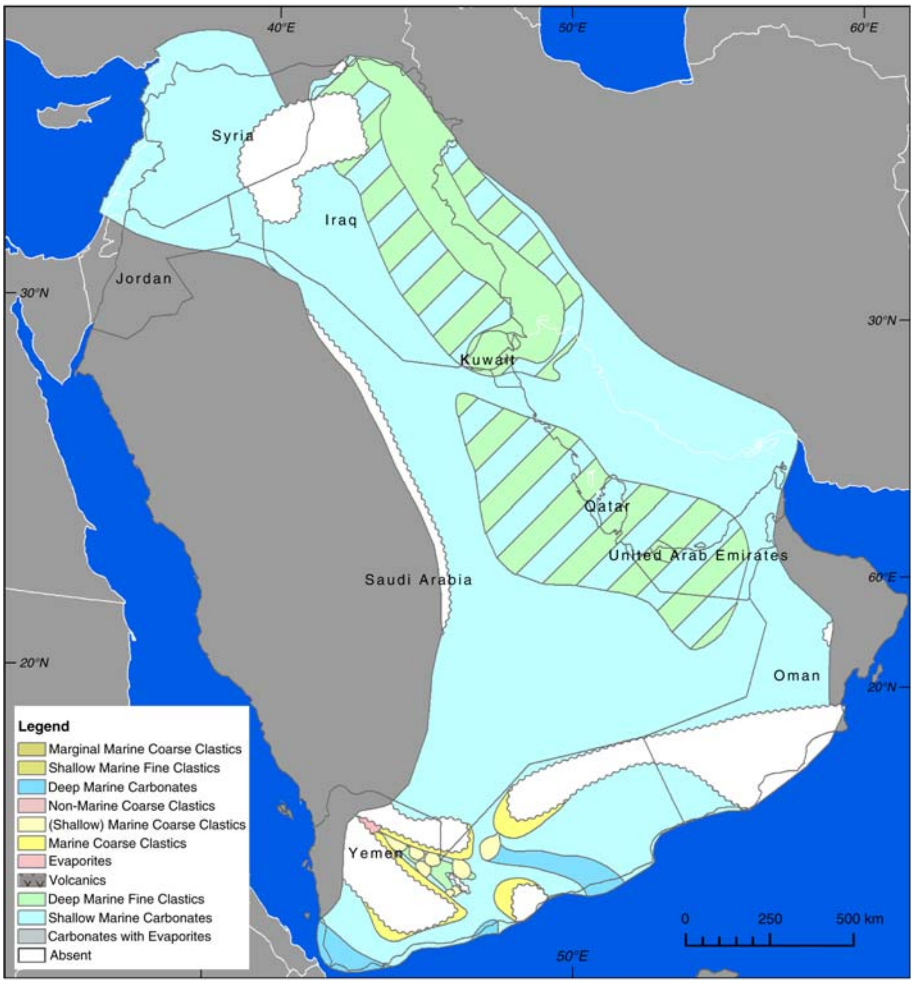

Fig. 6. Upper Jurassic GDE map for the Hanifa (source rock) and Arab (reservoir) formations. This map illustrates a broad carbonate shelf located on the southern margin of Neo-Tethys. Shaded green/blue are two intra-shelf basins that were subsiding faster than the surrounding areas. Widespread anoxia developed in these areas, resulting in the accumulation of the world-class Hanifa and equivalent class IIs source rocks. Compiled from extensive BP in-house database and reference to Murris (1980), Edgell (1996), Ellis *et al.* (1996), Loosveld *et al.* (1996), Youssif & Nouman (1997) and Sharland *et al.* (2001).

Hanifa source rock development that lies in the present-day oil window. The more deeply buried source rocks to the east in the Rub Al Khali basin are currently in the gas window. Note that on the resulting CRS oil charge map (Fig. 7), this area is coloured yellow for moderate-risk on the premise that the Hanifa oil-prone source rocks were in the oil window in the past and it is only recent gas flushing that makes gas the most likely, but not the sole, petroleum phase.

The Arab Formation carbonate grainstones are widespread across the Arabian Plate around the margins of the two intra-shelf basins, as illustrated on the Upper Jurassic (Hanifa/Arab) GDE map (Fig. 6). In the southern basin the carbonates were able to prograde out over the basin and importantly were deposited upon the Hanifa source rocks during periods of sea-level highstand. In the northern Gotnia basin continued subsidence confined the carbonates to rimmed shelves on the margins of the basin. Clearly this has important implications for reservoir prediction in the northern Gotnia depocentre situated in Kuwait, southern Iraq and Iran. This analysis from the GDE map is transferred directly to the reservoir presence and effectiveness CRS map (Fig. 8).

The GDE map for the upper part of the Upper Jurassic (Hith Formation) highlights the presence of widespread evaporite seals over the Arabian Plate overlying the Arab reservoirs particularly in the area of the southern basin in Saudi Arabia (Fig. 9). Note the presence of halites in the northern area which rest directly on Hanifa equivalent source rocks with Arab equivalent reservoir only present around the margins of the basin. There is an important facies change to the east where the Hith anhydrite pinches out into eastern Saudi Arabia and Abu Dhabi. This facies change effectively defines the eastern limit of the working Upper Jurassic 'Arab' play fairway and is represented by a rapid transition from low-risk (green) to high-risk (red) on the Seal Presence and Effectiveness CRS map (Fig. 10).

The Hith evaporites have been very effective in providing a classic regional seal for the giant Arab oil fields of the Arabian Peninsula. Additionally, intra-formational evaporitic seals exist within the Arab at the top of each of the A, B, C and D members. Beyond the eastern limit of the Hith seal, oil sourced in the Jurassic migrates vertically to charge Cretaceous reservoirs, as illustrated in Figure 11.

The stratigraphic elements of the Upper Jurassic 'Arab' play described in the GDE and CRS maps above can be summarized on a simplified play cartoon (Fig. 11). This elegantly makes the point that big oil really is simple. The more complicated the play system is required to be, the less likely it is to work. The diagram is a representation of the southern passive margin of Neo-Tethys as it existed during the Late Jurassic. The outer part of the platform is formed by a rimmed carbonate shelf. In the intra-shelf basin, silled behind this barrier, the type IIs, Hanifa source rocks were deposited. As relative sea-level fell in the intra-shelf basin, the

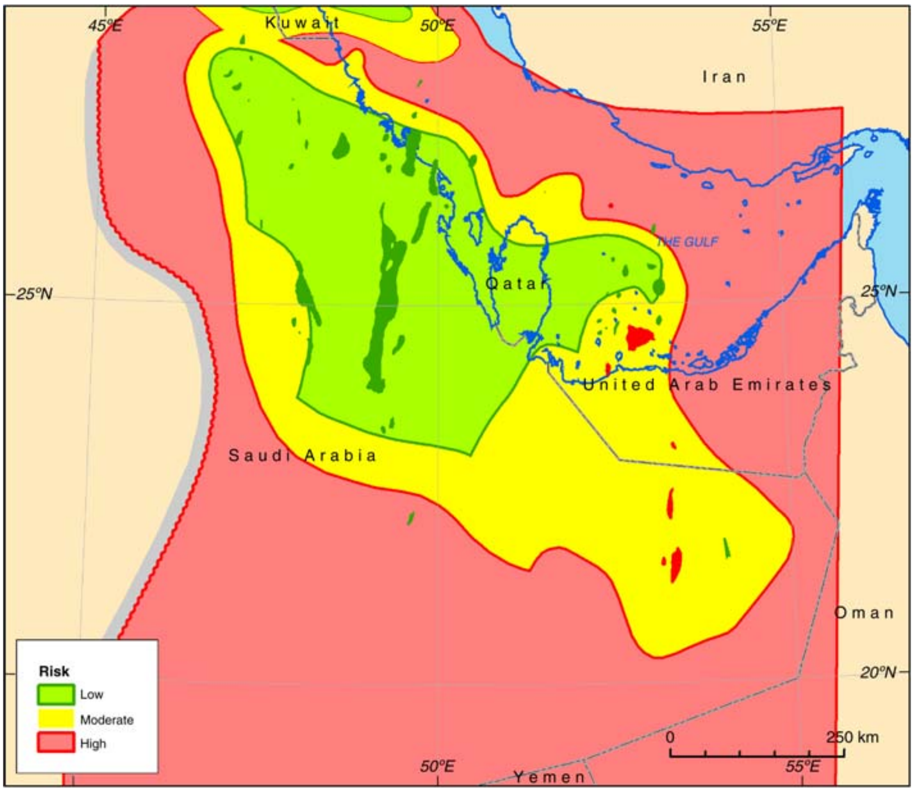

Fig. 7. Upper Jurassic 'Arab' play fairway. CRS map for oil charge presence and effectiveness. Existing oil and gas fields are shown in dark green and red, respectively.

Arab Formation grainstones were able to prograde from both the eastern and western margins to fill the intra-shelf basin. As sea-level fell further below the level of the outer margin, the basin was capped by Hith evaporites comprising mainly anhydrites with halites towards the central part of the basin. This vertical facies association repeated itself several times through the Late Jurassic and into the Cretaceous, forming multiple stacked world class source, reservoir and seal combinations.

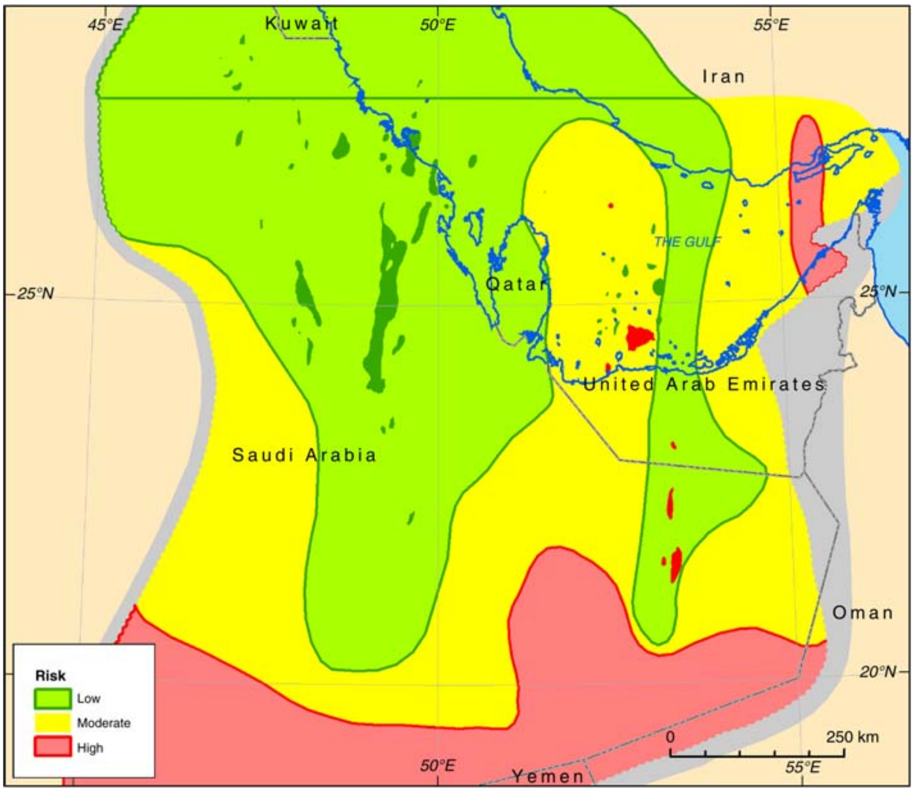

Fig. 8. Upper Jurassic 'Arab' play fairway. CRS map for reservoir presence and effectiveness. Existing oil and gas fields are shown in dark green and red, respectively.

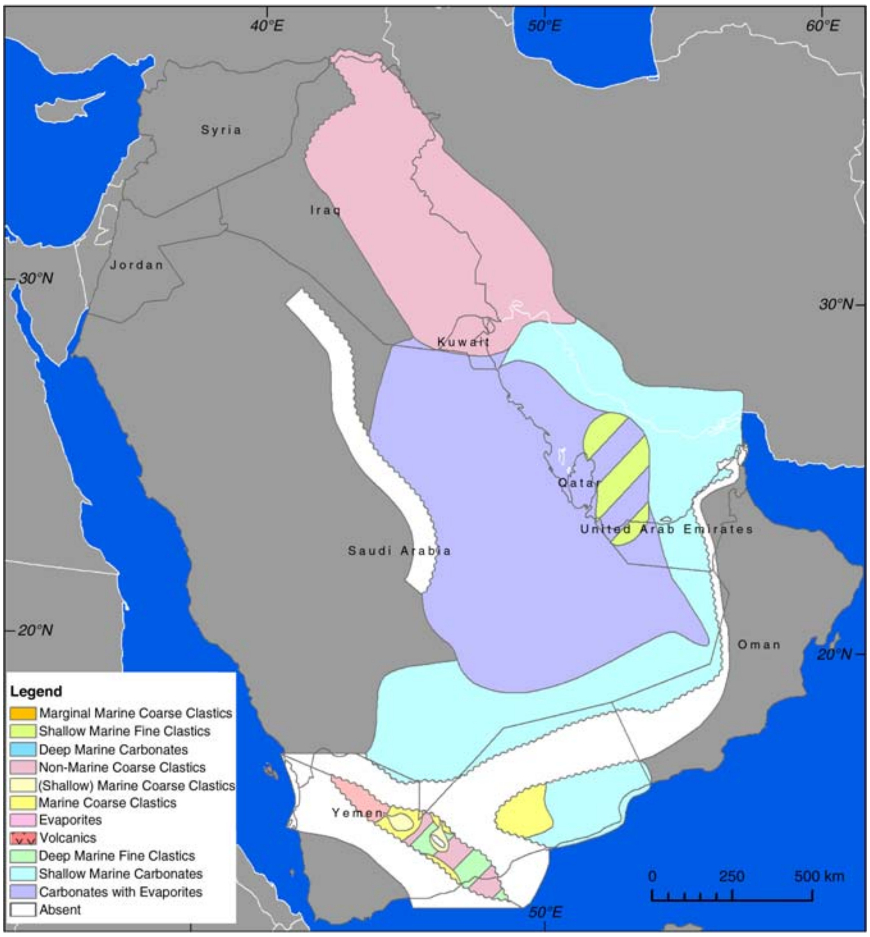

Fig. 9. Upper Jurassic GDE map for the Hith (seal) Formation. The map highlights the presence of widespread halite and anhydrite seals over the Arabian plate. Compiled from extensive BP in-house database and reference to Murris (1980), Edgell (1996), Ellis *et al.* (1996), Loosveld *et al.* (1996), Youssif & Nouman (1997) and Sharland *et al.* (2001).

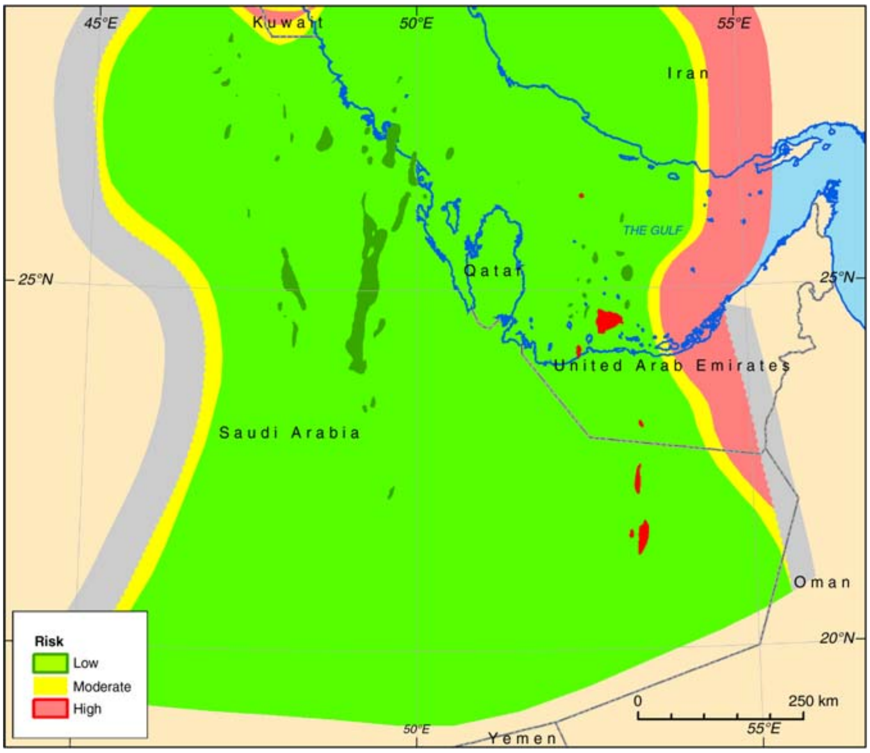

Fig. 10. Upper Jurassic 'Arab' play fairway. CRS map for seal presence and effectiveness. Existing oil and gas fields are shown in dark green and red, respectively.

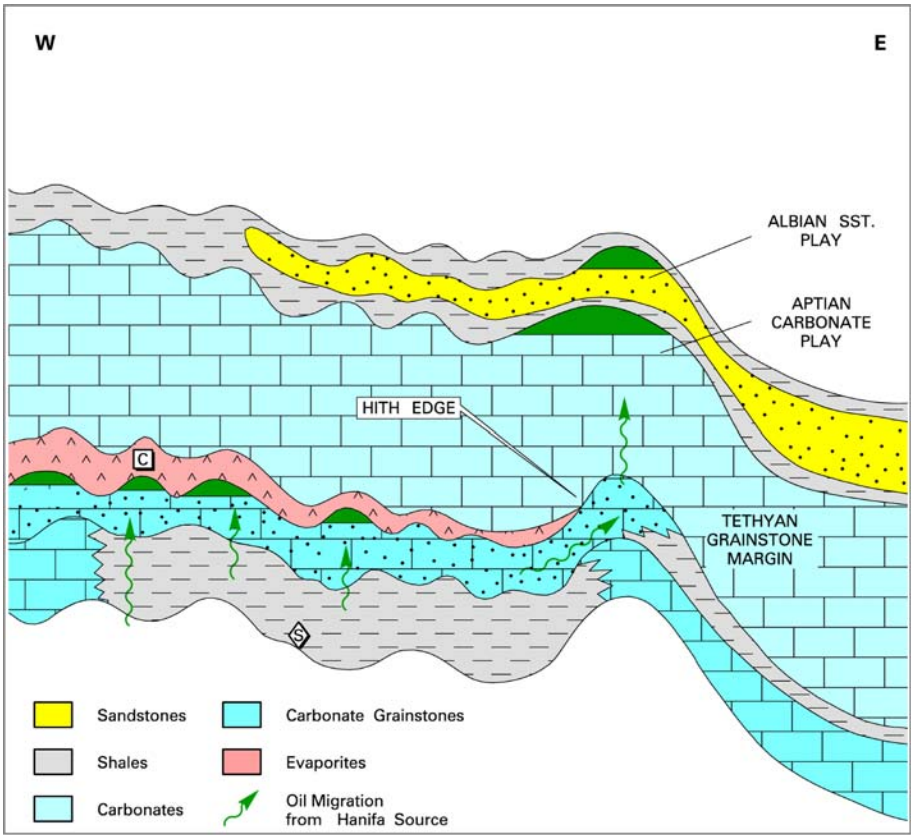

Fig. 11. Play cartoon illustrating the Upper Jurassic 'Arab' play fairway. Inherently a very simple petroleum system with the seal sitting directly above the reservoir and source. All elements of 'world class' quality. These are gently folded into large simple traps. Beyond the Hith edge, Upper Jurassic sourced hydrocarbons are free to migrate vertically into Cretaceous reservoirs.

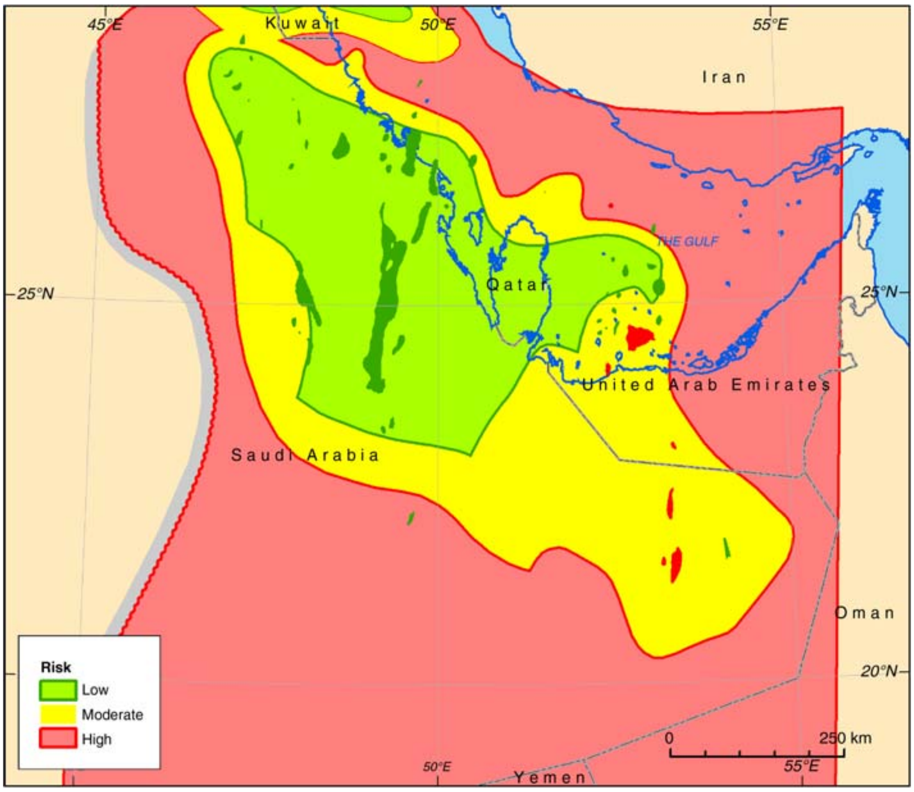

Fig. 12. Upper Jurassic 'Arab' play fairway. Composite CRS map for oil. Existing oil and gas fields are shown in dark green and red, respectively. The map presents no surprises as all the large Arab Formation oilfields such as Ghawar are located within the low-risk (green) segment.

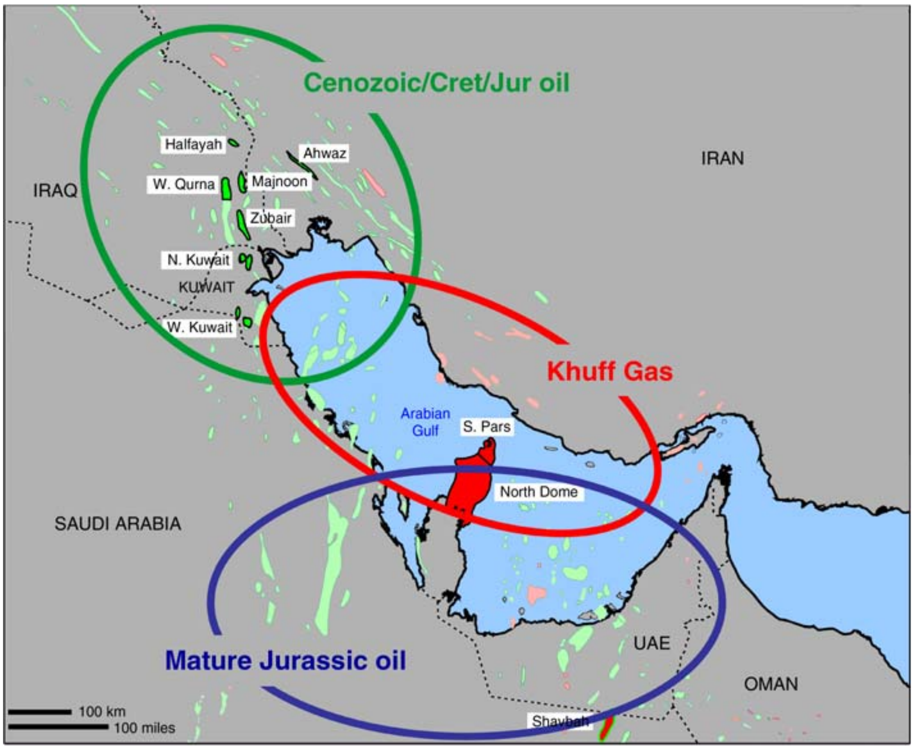

Fig. 13. Composite play fairway map of Middle East summarizing future resource potential. The map is based on a synthesis of all play fairways reviewed in this study.

To summarize, world-class Hanifa Formation source rocks are overlain by a world-class reservoir in the Arab Formation grainstones, which are in turn overlain by the Hith Formation evaporite seals. To be an effective petroleum system, it only needed sufficient late Mesozoic and Cenozoic burial to mature the source rocks and some gentle Zagros compression to form the simple, broad inversion structures which contain the oil fields.

The composite CRS map for oil for the Upper Jurassic 'Arab' play fairway is shown in Figure 12. Before discussing the results it is important to recap the process for compiling a composite CRS map. The composite CRS is assigned the risk of the most risky component CRS. Thus when the component maps are convolved, only three combined low-risk (green) segments (for reservoir, charge and seal) will generate an overall low-risk (green) composite CRS. The presence of one high-risk (red) component is sufficient to turn the composite CRS high-risk (red). Likewise, one moderate-risk (yellow) will turn an otherwise low-risk (green) segment moderate-risk (yellow).

The composite CRS map for the Upper Jurassic 'Arab' play fairway presents somewhat of a self-fulfilling prophesy with all the large Arab Formation oilfields firmly located within the low-risk (green) segment. The gas fields of the central Rub Al Khali are contained within a moderate-risk (yellow) segment as this is a map for oil. However, one oil accumulation, the North Dome field in the Persian Gulf, sits in the high-risk (red) segment. This is a classic case of long-distance lateral migration to the NE along the major Qatar Arch, revealing the only real flaw in the CRS methodology. In an essentially vertically stacked evaluation process it is has proven difficult to adequately address the impact of lateral migration of petroleum through regional carrier beds.

Summary of Middle East future potential

The future exploration potential of the Middle East is summarized in a composite play fairway map which combines the results of play fairway analyses for all the major plays in the region (Fig. 13). The already discovered and developed giant and super-giant fields of the region provide the basis for the majority of the long term reserves and are located in the Upper Jurassic of eastern Saudi Arabia and the UAE. Further significant reserves are expected to be delivered from these fields by continuing investment in improved oil recovery. The bulk of the undiscovered gas resources are expected to lie in deep Upper Palaeozoic reservoirs in an area centred on the Persian Gulf. However, the majority of the remaining undiscovered oil potential is likely to lie further north in the Cenozoic and Mesozoic trends of the Zagros fold belt and related foreland areas. However, having a technical view on the scale and location of additional hydrocarbon resources in a region the size of the Middle East is only part of the story. There are very serious non-technical barriers and obstacles to foreign participation in the region such as regional politics and the lack of competitive fiscal terms. Overcoming these and other constraints will be a major test of industry leadership in the next decade.

As with any significant piece of regional work there are many colleagues involved in locating, compiling and interpreting the large dataset required to provide a synthesis of the Arabian plate on this scale. In particular, I would like to acknowledge the work of Jeremy Goff, Bob Jones, Christoph Lehman, Steve Matthews and Ivor Simpson. For the graphics I am indebted to the efforts of Pat Randell and Dave Johnson. I also thank Jonathan Redfern of Manchester University for his comments on an earlier draft which significantly improved the text.

References

Alsharhan, A. S. & Nairn, A. E. M. 2003. *Sedimentary Basins and Petroleum Geology of the Middle East*. Elsevier, Amsterdam.

Beydoun, Z. R. 1986. The petroleum resources of the Middle East: a review. *Journal of Petroleum Geology*, **9**, 5–28.

Beydoun, Z. R. 1998. Arabian plate oil and gas: why so rich and prolific? *Episodes*, **21**, 74–81.

BP Statistical Review of World Energy 2009. BP plc, London.

Edgell, H. S. 1996. Salt tectonism in the Persian Gulf Basin. *In*: Alsop, G. I., Blundell, G. J. & Davidson, I. (eds) *Salt Tectonics*. Geological Society, London, Special Publications, **100**, 129–151.

Ellis, A. C., Kerr, H. M., Cornwell, C. P. & Williams, D. O. 1996. A tectono-stratigraphic framework for yemen and its implications for hydrocarbon potential. *Petroleum Geoscience*, **2**, 29–42.

Jassim, S. Z. & Al-Gailani, M. 2006. Hydrocarbons. *In*: Jassim, S. Z. & Goff, J. C. (eds) *Geology of Iraq*. Dolin, Prague, 232–250.

Konert, G., Afifi, A. M., Al-Hajri, S. A., de Groos, K., Al Naim, A. A. & Droste, H. J. 2001. Paleozoic stratigraphy and hydrocarbon habitat of the Arabian Plate. *In*: Downey, M. W., Threet, J. C. & Morgan, W. A. (eds) *Petroleum Provinces of the Twenty-First Century*. American Association of Petroleum Geologists, Tulsa, OK, Memoirs, **74**, 483–515.

Loosveld, R. J. H., Bell, A. & Terken, J. J. M. 1996. The tectonic evolution of interior Oman. *GeoArabia*, **1**, 28–51.

Murris, R. J. 1980. The Middle East: stratigraphic evolution and oil habitat. *American Association of Petroleum Geologists Bulletin*, **64**, 597–618.

Sharland, P. R., Archer, R. *et al*. 2001. Arabian plate sequence stratigraphy. *GeoArabia Special Publications*, **2**, 1–371.

Sorkhabi, R. 2010. Why so much oil in the Middle East? *GeoExpro*, **7**, 21–26.

Stoneley, R. 1990. The Middle East basin: a summary overview. *In*: Brooks, J. (ed.) *Classic Petroleum Provinces*. Geological Society, London, Special Publications, **50**, 293–298.

Youssif, S. & Nouman, G. 1997. Jurassic geology of Kuwait. *GeoArabia*, **2**, 91–110.

Appraisal and development of the Taq Taq field, Kurdistan region, Iraq

C. R. GARLAND,[1] I. ABALIOGLU,[2] L. AKCA,[3] A. CASSIDY,[1] Y. CHIFFOLEAU,[1] L. GODAIL,[1] M. A. S. GRACE,[1] H. J. KADER,[2] F. KHALEK,[1] H. LEGARRE,[1] H. B. NAZHAT[4] and B. SALLIER[1]

[1]*Addax Petroleum Services and Sinopec, 16 Avenue Eugène-Pittard, CH1211, Geneva, Switzerland (e-mail: chris.garland@addaxpetroleum.com)*

[2]*Taq Taq Operating Company Limited, Via Tower Bestepeler Mahallesi, Nergiz Sokak No 7/52, Sogutozu Ankara, Turkey*

[3]*Genel Enerji AS, Via Tower Bestepeler Mahallesi, Nergiz Sokak No 7/8, Sogutozu Ankara, Turkey*

[4]*Kurdistan Regional Government-IRAQ, Council of Ministers, Ministry of Natural Resources*

Abstract: The Taq Taq Field is located within an anticline in the gently folded zone of the Zagros mountains, northeastern Iraq, approximately 50 km ESE of Erbil. The main reservoirs are fractured limestones and dolomites of Late Cretaceous age, with an oil column exceeding 500 m in thickness. Eocene limestones and dolomites at shallow depth form a subsidiary reservoir. The structure is a gentle thrust-related fold which has also been affected by dextral transpression. A pervasive fracture system is present within the reservoirs, giving good connectivity and deliverability. Initial discovery and appraisal was made in 1978 when three wells were drilled. The recent appraisal programme started in 2005 and by the end of 2008 two seismic surveys had been acquired and eight additional wells had been drilled. Mapping has incorporated a seismic principal component analysis for horizon and lithology identification. Modelling of the fractures has utilized a comprehensive data set derived from core and image logs. Special core analysis has been directed towards the understanding of the pore system and its interaction with the fractures. Synthesis of all these elements is performed in a dual-media dynamic model which is currently in use for development planning.

Keywords: fracture model, Iraq, Middle East Cretaceous reservoirs, seismic facies analysis, thrust-related fold

Taq Taq was one of the first new oil accumulations to be put on production in northern Iraq for 40 years. It had been discovered in 1978 by the Northern Oil Company of Iraq, who drilled a well on the crest of a four-way dip-closed anticline 60 km NE of Kirkuk in the Zagros gently folded zone (Fig. 1). Two other wells, TT-02 and TT-03, were also drilled in this period. Production commenced in 1994 under the auspices of the Kurdistan Regional Government (KRG): the project consisted of the building of a workover rig, the testing and completion of wells TT-02 (2150 bopd from the Cenozoic Pilaspi Fm.) and TT-01 (5000 bopd from the Cretaceous Shiranish Fm.) and the construction of a refinery in Suleimaniya (Kader 2002). Delivery was by tanker from the site to the refinery and over 4×10^6 barrels of crude oil have been produced from the Cretaceous and 1×10^6 barrels from the Cenozoic up until October 2008.

Genel Enerji AS signed the first PSA in July 2002 and operation of the Taq Taq field was assigned to Genel in February 2003. In 2006 operatorship of the field was transferred to the Taq Taq Operating Company (TTOPCO), a joint venture between Genel Enerji AS and Addax Petroleum Corporation. Appraisal commenced with the acquisition of a 170 km 2D seismic survey and by the end of 2008 eight new wells had been drilled and 166 km^2 of new 3D seismic had been acquired. In 2009 a production facility was installed and connected to seven wells. At the time of proof-reading (March 2010), production of up to 55 000 bo had been achieved totalling 8×10^6 bo.

The anticline is clearly visible at the surface, where Miocene sandstones crop out forming ridges in an elliptical shape approximately 13 km long and 7 km wide. The stratigraphy comprises (from the top, Fig. 2): red beds, fluviatile clastics and conglomerates of the Fars Formations of Miocene–Pliocene age; limestones and dolomites of the Pila Spi Formation of Eocene age, which form a minor reservoir at the crest of the structure; shelf and shoal limestones overlying marine clastics of the Kolosh Formation of Paleocene–Eocene age, which form the main seal to the Cretaceous fractured reservoirs at a depth of approximately 1000 m below

Fig. 1. Iraq location map showing main outcrop, Taq Taq and other fields noted in the text. BH, Bai Hassan.

VINING, B. A. & PICKERING, S. C. (eds) *Petroleum Geology: From Mature Basins to New Frontiers – Proceedings of the 7th Petroleum Geology Conference*, 801–810. DOI: 10.1144/0070801

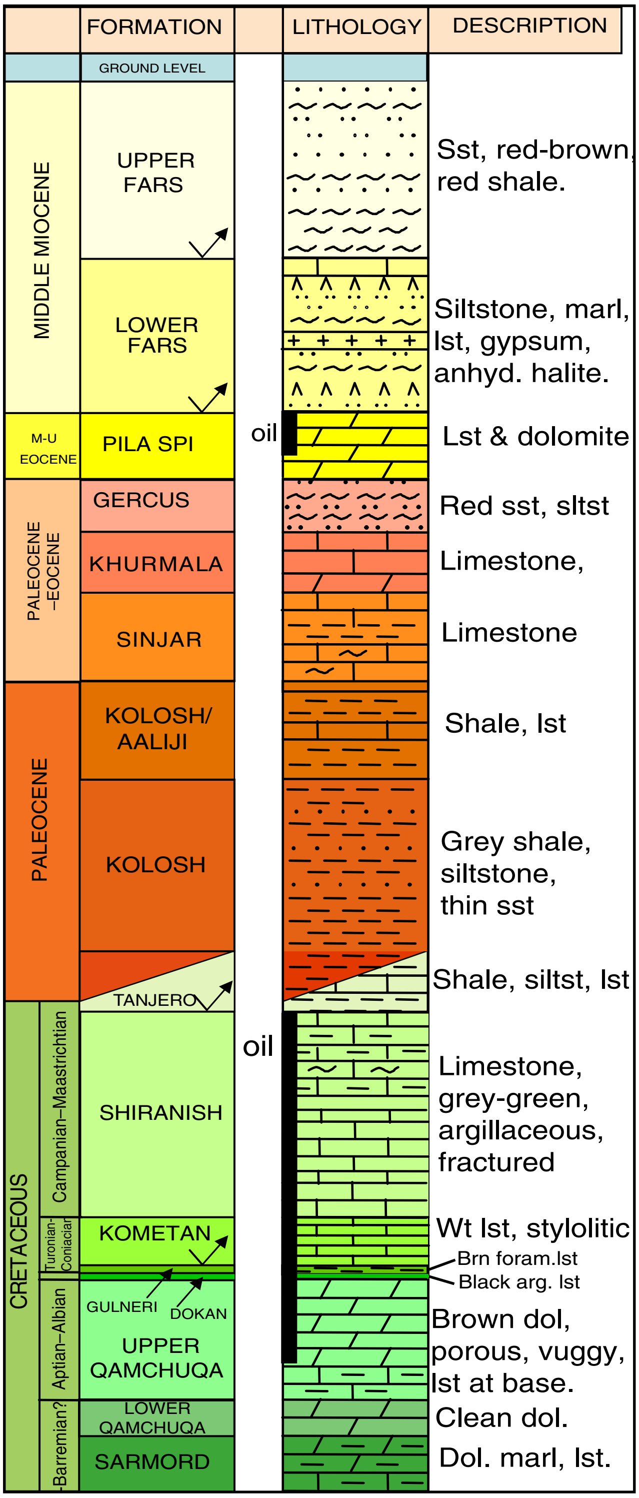

Fig. 2. General stratigraphy at Taq Taq showing reservoirs, lithology, formation names and approximate ages. Colours selected for contrast only.

mean sea level (bmsl). This paper is concerned with these main Cretaceous reservoirs. Beneath these, TT-01 penetrated the entire Cretaceous and Jurassic sections, terminating in the Triassic at approximately 3300 m bmsl.

Source rocks for Taq Taq oil have been shown to be Jurassic in age: this is consistent with regional studies (Pitman *et al.* 2003) which show the Naokelekan and Sargelu Formations (which are present in Taq Taq) to be the main source rocks in northern Iraq. These began generating hydrocarbons in the Miocene prior to the main compressional phase of Zagros folding (Ameen 1991).

Reservoirs

The main productive stratigraphic formations are described in detail in van Bellen *et al.* (1959) and Jassim & Goff (2008) and include three main reservoirs:

(1) The *Shiranish Formation* (Campanian–Maastrichtian) comprises up to 350 m of greenish-grey to dark brown foraminiferal

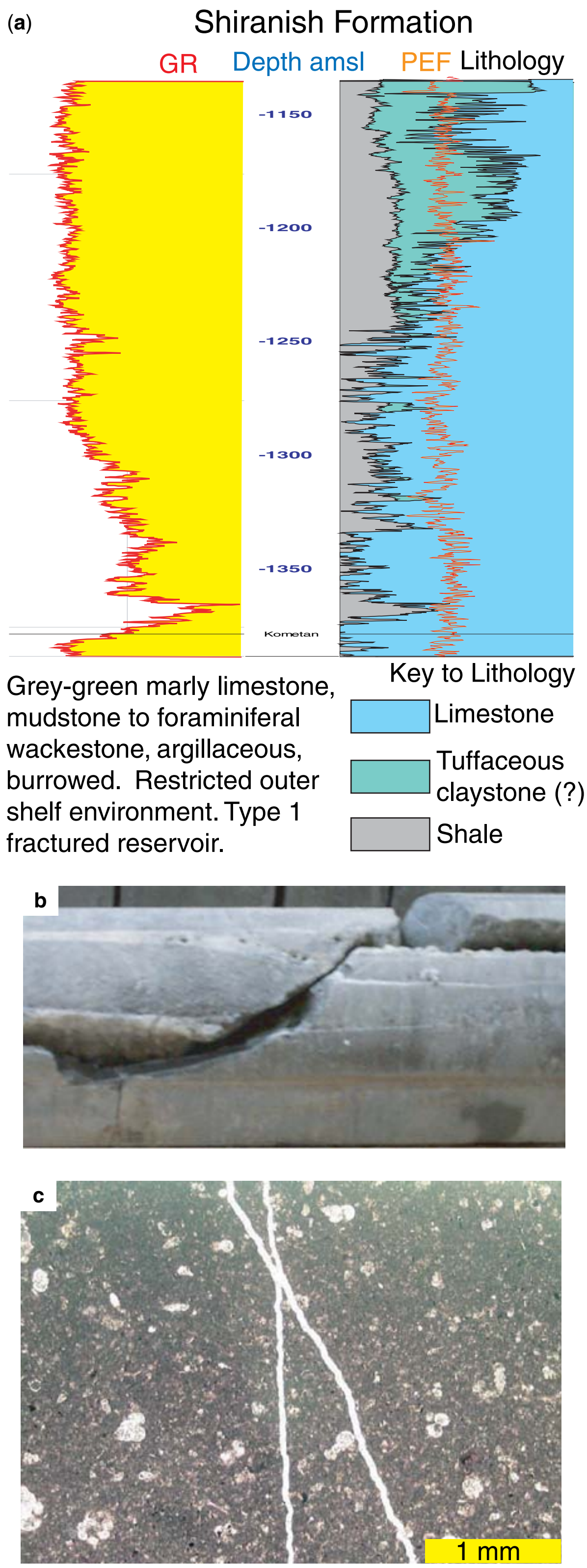

Fig. 3. Shiranish Formation. Brief description and (**a**) typical well logs; (**b**) partially cemented en-echelon open fractures in core; (**c**) thin section (plane polarized light) showing foraminifera and cemented fractures.

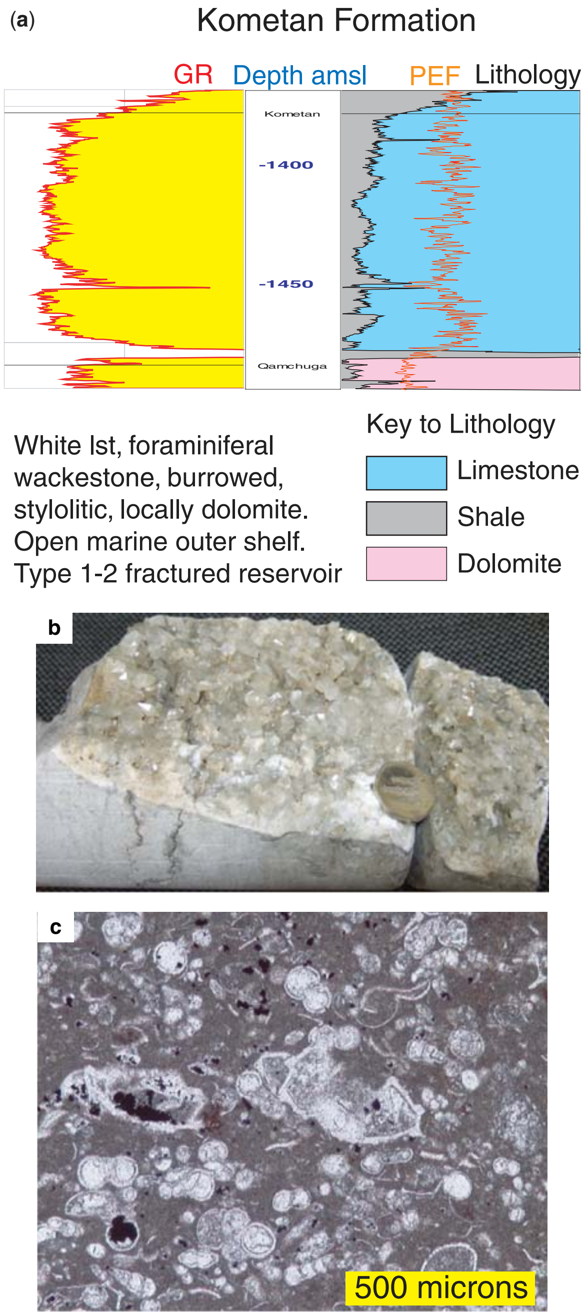

Fig. 4. Kometan Formation. Brief description and (**a**) typical well logs; (**b**) core of white limestone displaying stylolites and partially cemented open fracture; (**c**) thin section (plane polarized light) showing foraminifera.

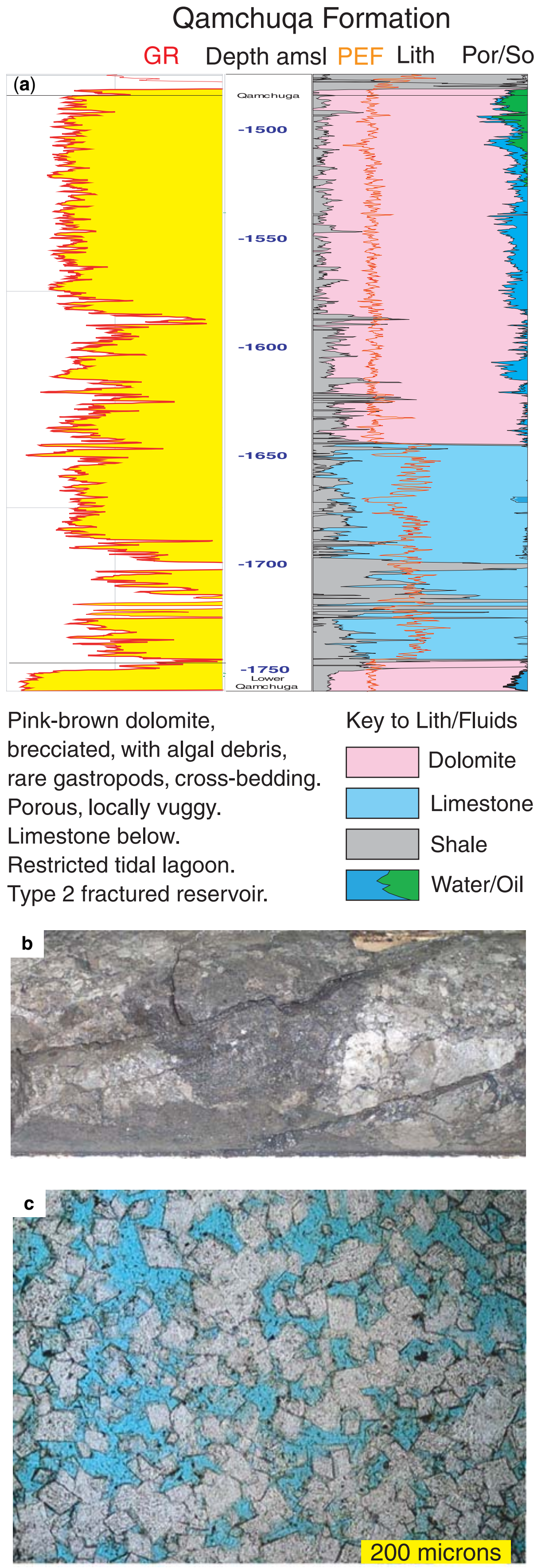

Fig. 5. Qamchuqa Formation. Brief description of upper part of reservoir and (**a**) typical well logs with porosity and oil-saturation evaluation; (**b**) core showing brecciated lithology and steeply-dipping sub-parallel open fractures; (**c**) thin section showing dolomite crystals and blue stain in pore space.

wackestone and packstone in an argillaceous matrix, interbedded with marly argillaceous limestone, deposited in a restricted marine outer shelf environment (Fig. 3). It displays a shallowing-up profile and an upward increase in low-density clays and lithic fragments (showing green on the log) which have been attributed to wind-transported dust or volcanic material. Its thickness is reduced over the crests of the fault blocks. Despite its low matrix porosity, the Shiranish is pervasively fractured, especially in the lower part, which makes it a significant hydrocarbon reservoir with high deliverability exceeding 19 000 bopd.

(2) The *Kometan Formation* (Turonian–Santonian) comprises up to 120 m of white to light-grey, compact, burrowed, well-bedded, stylolitic, foraminiferal wackestone, similar to the Shiranish but without the major argillaceous component (Fig. 4). It was deposited in a pelagic marine environment. A disconformity is

developed at the top of the Kometan: this is interpreted from variations in thickness of the overlying Shiranish Formation and from seismic evidence that shows many faults terminating upwards at this level. There is, however, no evidence of subaerial exposure or karstification and matrix porosity is generally low. This confirms the results of regional outcrop studies (Karim *et al.* 2008). Locally, especially where fracturing is intense, the Kometan is dolomitized and displays a higher matrix porosity. Studies of this dolomite indicate that it has a post-depositional, hydrothermal origin (Davies & Smith 2006). The Kometan is generally more fractured than the Shiranish and flowed over 16 000 bopd on test. A thin interval (6–10 m) below the Kometan is occupied by the Gulneri and Dokan Formations.

(3) The *Qamchuqa Formation* (Aptian–Albian) comprises over 300 m of light brown microcrystalline dolomite, originally wackestones to grainstones whose original fabrics are locally preserved, including: mouldic pores after gastropods, bivalves, ostracods and gypsum crystals; laminated algal fabrics and crusts cut by burrows of various sizes; and brecciated intervals comprising angular lithified carbonate fragments, suggesting clastic gully fill or debris flow (Fig. 5). The upper part of the Qamchuqa displays a karst fabric of interconnected vugs and fracture fill, indicating subaerial exposure of the original sediment, which would have been deposited with a very high primary porosity (>50%). This indicates a lagoonal and tidal flat setting with erosion during periods of lowered sea-level. With depth, its composition becomes increasingly dominated by limestone and marl (blue on the log) down to an unconformity at its base. The connected matrix porosity of the Qamchuqa Formation makes this the main hydrocarbon reservoir. The Qamchuqa is pervasively fractured and produced over 17 000 bopd on test: the fractures are an important feature of the recovery mechanism and give access to hydrocarbon resources in the low-permeability matrix. The Qamchuqa is also a matrix reservoir in the Kirkuk area some 80 km to the SW (Al Shdidi *et al.* 1995). The cleaner water-bearing dolomite at the base of the log, currently termed 'Lower Qamchuqa', is probably the equivalent of the Shuaiba Formation further south.

Structure

A key seismic section from the 2D survey (Fig. 6a) shows the structure as a simple anticline with increasing complexity at depth. The interpretation (Fig. 6b) includes structural as well as stratigraphic elements. At the western end of the section the synclinal part of the fold indicates maximum depths of burial; at the base of the section the Jurassic shows reverse faulting and other complexities indicative of compressional stress; two major reversed faults emerge upward from the Jurassic on the southwestern and northeastern limbs of the fold; between them the Cretaceous reservoir shows a block-faulted style within the anticline and, in the shallow part, the Cenozoic is gently curved into a smooth parallel fold with outer-arc extension. The Cretaceous reservoirs between the two reverse faults occupy an intermediate structural position, isolated from the outer arc above by décollement within the shales and siltstones of the Kolosh Formation and separated from the deeper compressive regime by another discontinuity in the shales and limestones of the Sarmord formation.

The latest folding and faulting is related to the compressive phase of Zagros mountain-building which reached its climax in Late Miocene to Pliocene time (Ameen 1991). This late history of the structure is written in the deposition and parallel folding of the fluviatile sands and conglomerates of the Bakhtiari and Upper Fars Formations, which together attain 1500 m in thickness west of Taq Taq. The main anticline was formed as a result of compression above a thrust plane which probably lies several kilometres below the recorded seismic data. The present-day maximum horizontal stress in this area has been calculated, both from induced fractures in the Taq Taq wells and from regional earthquake studies (Reinecker *et al.* 2004), to be approximately NNE–SSW. This is consistent with the major orientation of the open fractures in the reservoir. Uplift of the anticline was enhanced by unloading of the crest of the structure by the erosion of at least 1500 m of clastic deposits. This unloading may also have enhanced some of the open fracturing in the Cenozoic and Cretaceous: it is only one of many factors that have been found to determine the final style of fracturing and faulting in a folded zone (Bazalgette & Petit 2007). Since the formation of the structure began subsequently to the commencement of oil generation, the open state of the fracture system may be partly due to inhibition of cementation by the presence of oil.

When the anticline is restored to its Late Cretaceous position (Fig. 7), the faults cutting it delineate a tilted block arrangement. This appears to have many similarities with that previously described for Northern Iraq in which the ramp-and-flat block-faulted style of the Cretaceous is due to one or more episodes of extension and faulting in Late Cretaceous time (Haddad & Ameen 2007). The depositional effect of this configuration in wells on the Bai Hassan and Qara Chauq structures to the SW of Taq Taq (Fig. 1) was described in terms of the sequence stratigraphy of the Gulneri and Kometan Formations and their position on the fault blocks. A similar structural control on deposition is confirmed by well data also to have taken place in the Taq Taq reservoirs, where the more shaly lower part of the Shiranish is only present in the deeper fault blocks. This phase of faulting clearly occurred following deposition of the Kometan because, whilst Top Kometan is displaced by several faults, it is not possible to trace their displacement upwards through the Shiranish. The minor variations in Kometan thickness may be related to an earlier phase of movement on these faults. Even though the two major faults have been reactivated as reverse faults during the formation of the anticline, it appears that the other faults have not been reactivated with any vertical displacement.

The depth map of Top Shiranish (Fig. 8) is derived from a principal component interpretation of the 3D seismic survey and shows details in the anticline which point to the presence of a strike-slip element in the generation of the fold. The double-plunging anticline is traversed by a set of subsidiary short folds crossing the axis, which are interpreted to be parasitic to the main anticline. These anticlines are predicted to occur in an oblique orientation to a right-lateral wrench fault (Harding 1974): in this case its orientation is NW–SE parallel to the main faults giving parasitic folds in a northeasterly to easterly direction. It has been shown from core and image-log analysis that the dominant open fracture direction is usually close to that of the nearest one of these folds and it is concluded that they are the loci of fracture corridors. Having made this connection, curvature processing has enabled them to be delineated with greater accuracy and adopted in the fracture model.

Evidence for this strike-slip element has also been found during mapping of the surface outcrop of sandstones and red shales of the Upper Fars Formation. These are extensively fractured and faulted into tilted blocks with a dominantly north–south azimuth. Detailed study of these fractures at several different localities revealed strike-slip displacements that point to dextral transpression along a NW–SE orientation. In this scenario the dominantly north–south fractures seen at the surface are synthetic Riedel shears. Strike-slip movement is also suggested by oblique-slip slickensides on cored faults. It is interpreted that, in the reservoir, the stress regime naturally exploited existing faults and fractures rather than creating new ones, and retained the Cretaceous dominant NE–SW open fracture direction during the uplift of the anticline

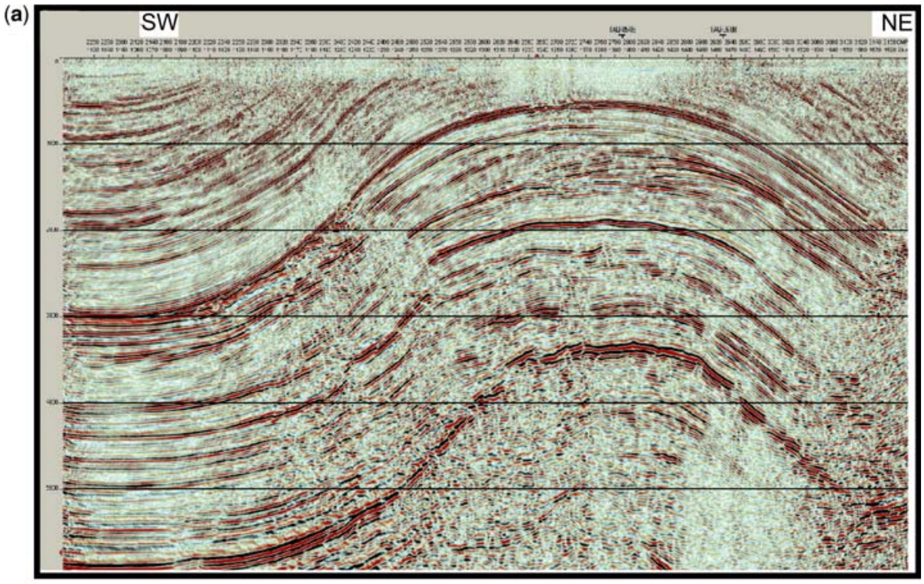

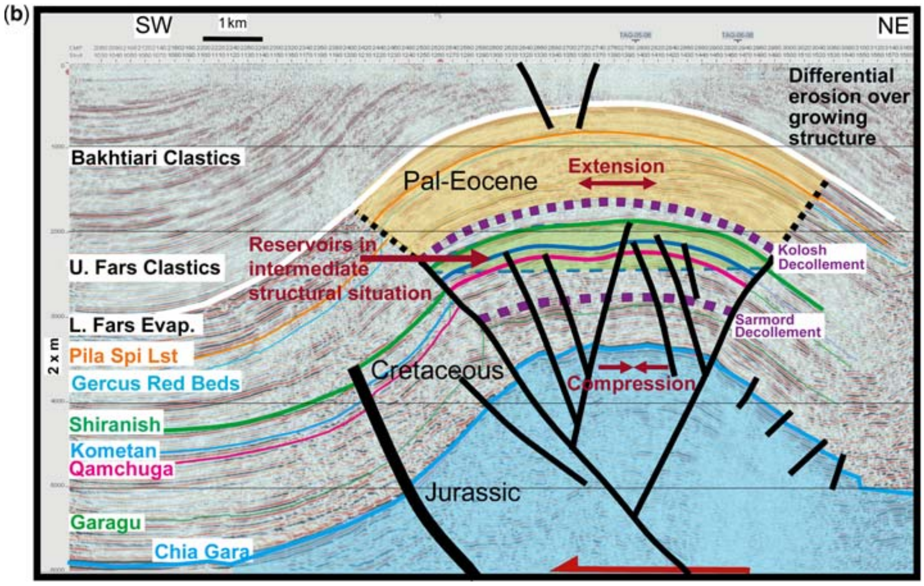

Fig. 6. (**a**) 2D seismic dip line across Taq Taq field. (**b**) The same line showing stratigraphic units and structural interpretation. The Taq Taq anticline is a response to shortening along a deep thrust plane lying below the base of the seismic section. Reverse faulting within the Jurassic indicates compression and normal faulting in the Cenozoic section indicates extension. The Cretaceous lies in an intermediate to extensional position between two neutral surfaces and is also affected by strike-slip movement.

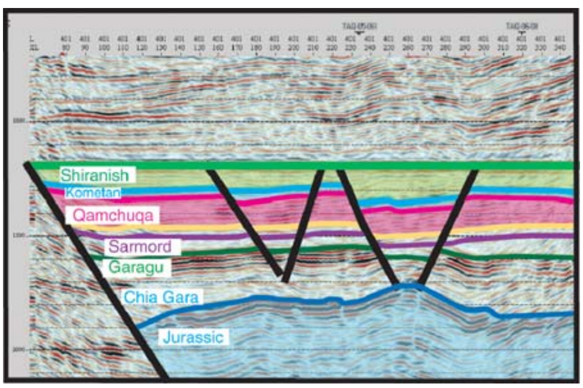

Fig. 7. 3D seismic line flattened on top Shiranish. This emphasizes fault movement prior to Late Cretaceous deposition of the Shiranish Formation.

and during filling of the growing structure with oil. Reactivation of the normal faults as strike-slip faults may also have occurred, but without any vertical movement.

Thus the Cretaceous reservoirs are in the favourable position of retaining original extensional structures as well as undergoing subsequent shear, which explains the dominant NE–SW fracture direction in the reservoir, in contrast to the north–south fractures in the Cenozoic sandstones at the surface, which formed for the first time within the later dextral shear regime. The low compressional stress within the reservoir is interpreted to partly explain the relatively open state of the fracture system.

Seismic facies analysis

Core obtained from the reservoirs and special analysis of many core plugs were a basis for the identification from logs of facies groups to be used for each well in the matrix model of the Qamchuqa and the Kometan Formations. Following a conventional system, the spectral gamma-ray log was used to differentiate clay from

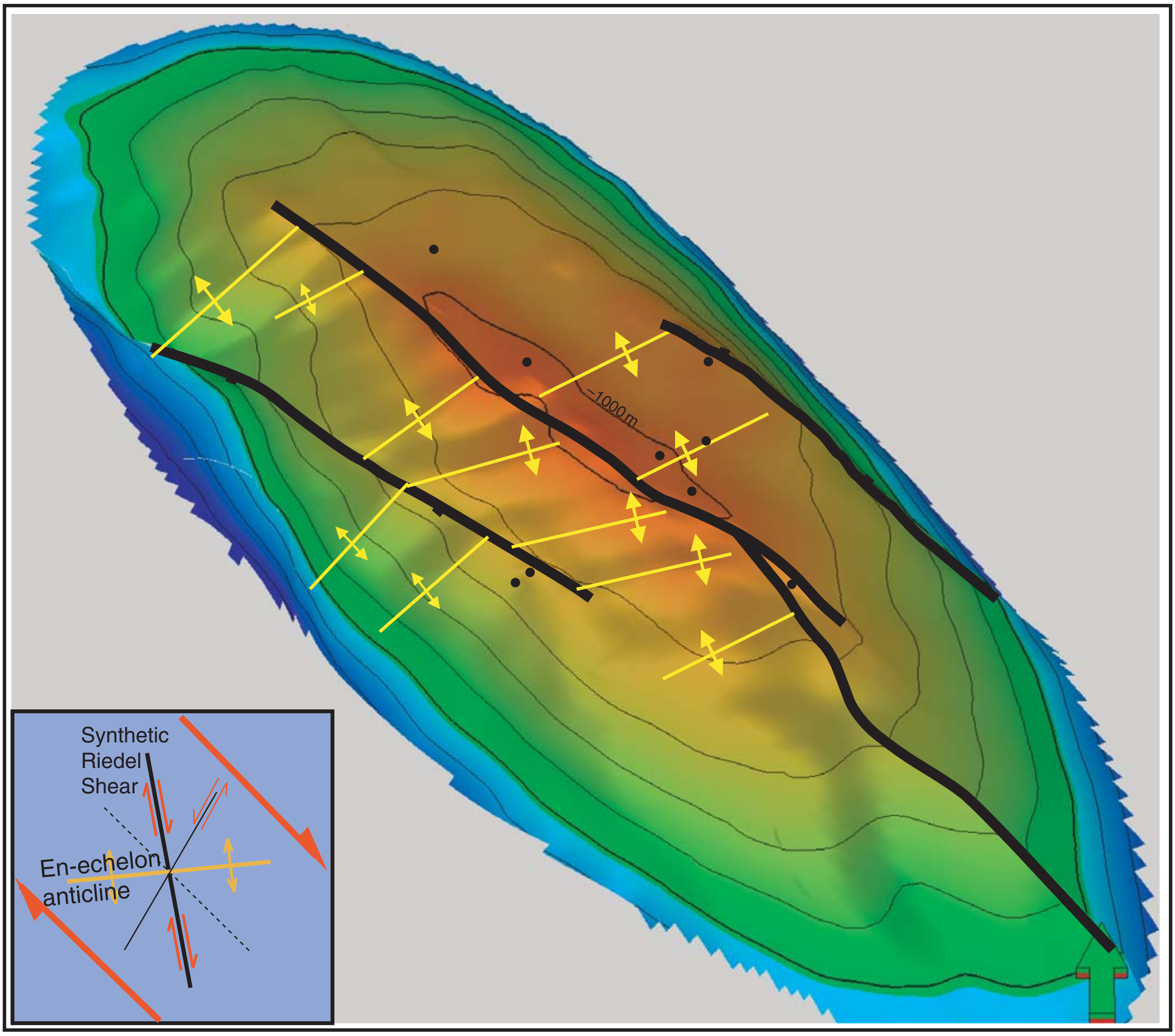

Fig. 8. Top Shiranish model depth surface, colour interval (c.i.) 100 m. Main fault displacement is strike-slip at this level. Parasitic folds, marked in yellow, perturb the smooth surface of the main anticline and are the major control on fracture corridors. Inset shows orientation of strike-slip features (after Harding 1974).

carbonate, the PEF log was used to differentiate dolomite from calcite and sonic v. density porosity was used to identify vuggy porosity from disseminated matrix porosity (Dehghani *et al.* 1997). These were used to define facies groups with different porosity statistics, different porosity–permeability characteristics and different water saturation response under the varying capillary pressure regime within a long transition zone. These groups were shale, limestone, low-porous dolomite, medium-porous dolomite, high-porous dolomite, medium-porous vuggy dolomite and high-porous vuggy dolomite. A study of seismic attributes was carried out to assist the mapping of these facies classes and their porosity.

Prediction of lithofacies from seismic amplitudes is difficult in carbonates where reflectivity variations are typically subtle. A statistically based modelling method was developed, consisting of sampling seismic amplitudes using a narrow sliding time window and analysing a large number of windowed samples using principal component analysis (Scheevel & Payrazyan 1999). The method made a selection of principal components to capture variance and other information within the seismic signal. These attributes of seismic samples projected into a multi-attribute space enabled a classification to be made according to the lithofacies distribution at the wells. Prediction of lithofacies was then carried out probabilistically throughout the seismic volume using a geostatistical approach via sequential gaussian simulation. This yielded the most probable facies at any location, giving a statistical, but geologically constrained, lithofacies model, as shown on the section (Fig. 9). The resultant facies volume confirmed some of the suspected trends in the data and revealed others that had not been interpreted from the limited well data alone.

Pore system

Estimation of matrix porosity in the Qamchuqa Formation has been a major target of the coring programme, partly because its character is, to some extent, masked by the exceptionally high well deliverability due to the fractures. Detailed study of the cores has confirmed the importance of the karstic episode in late Albian time. Porosity in the karstified upper zones of the Qamchuqa locally exceeds 20% with average in the order 4–12% and low permeability in the range 0.1–10 mD. In addition, late hydrothermal

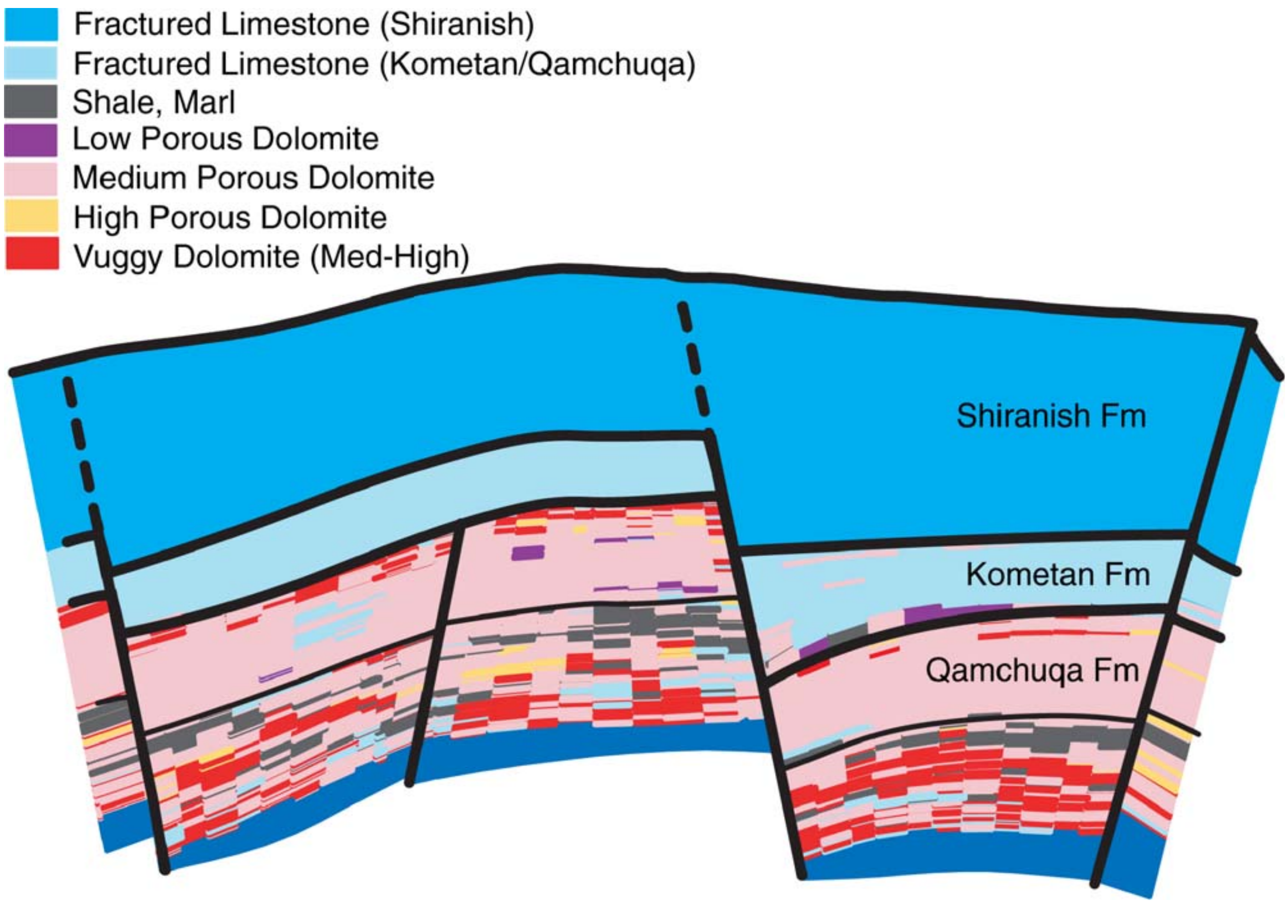

Fig. 9. Lithological model derived from seismic facies analysis (not to scale). The model shows development of vuggy porosity in the Qamchuqa formation on the crestal part of the anticline and lower porosity in the graben. The Kometan includes local dolomitization with low matrix porosity. The lithology is one of the controlling factors in the generation of fractures in each formation.

dolomitization has led to local development of matrix porosity in the Shiranish and Kometan formations, as identified by the seismic analysis. The porosity has been mapped together with facies using the seismic amplitude method described above.

A pervasive and well connected fracture system is seen as a benefit in this low-permeability matrix, which under natural or assisted water flood enables imbibition and effective oil displacement during production. The process is illustrated in Figure 10. Overall recovery will be dependent on the extent and characteristics of the fracture system, including spacing, connectivity and permeability.

A dual-media model is in use with the whole system being treated as a type 2 fractured reservoir in which connectivity within the matrix is largely provided by the fractures. To optimize recovery, the production strategy will be directed towards achieving a steady rise in water level in the fracture system so that imbibition has time to act in the matrix before the producing wells are overwhelmed by the water flood. It is believed that, with this treatment, the matrix, which contains up to 50% of the total STOIIP, will yield a high percentage of its movable oil to production. A wide range in probable volumes is carried for the porous matrix.

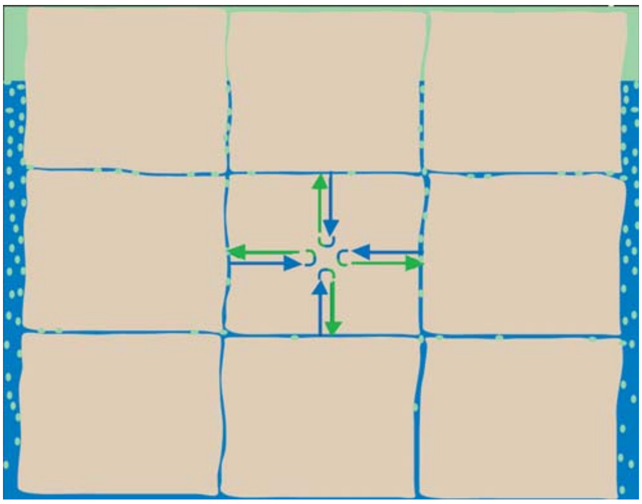

Fig. 10. Cartoon of matrix–fracture interaction under water flood. Rock matrix blocks (tan) are initially oil-bearing. Water introduced into the fractures is imbibed (blue arrows) into the matrix and oil is displaced into the fractures (green arrows). Oil droplets (green) form in the fractures, rise through the water column and merge into the oil column in the fracture network.

Fractures

Drill stem tests performed on well Taq Taq-1 in 1978 showed high productivity from the Shiranish formation, which has very low porosity and permeability. This paradox was interpreted to indicate the presence of a major fracture system in the well.

During the recent appraisal programme, high productivity has also been achieved from both the Kometan and the Qamchuqa formations, and it was interpreted at an early stage that the Shiranish and Kometan formations could be considered to be type 1 fractured reservoirs, in which both storage and deliverability are provided only by the fractures. The Qamchuqa, however, would have to be treated as a type 2 fractured reservoir, in which storage is provided by the matrix and deliverability is provided by the fractures (Hubbert & Willis 1955). The appraisal programme was directed towards understanding both the matrix and the fractures. XRMI borehole image logs, WSTT dipole sonic logs and oriented cores were obtained from the initial appraisal wells. At the same time, surface mapping was carried out with emphasis on the fractures in the Upper Fars sandstones to gain an understanding of the stress fields related to the formation of the anticline. The cores have been studied intensively and every one of more than 1100 individual cored fractures has been described with respect to orientation, aperture, fill, hydrocarbons and kinematic indicators. The image logs across the cored intervals have been set up as standards for the whole reservoir section and a complete suite of fracture descriptions has been established for a total of over 6000 open conductive fractures (Fig. 11). The powerful statistical analysis tools available in FRACA software have been used to group fractures into families within the 'diffuse fracture system' and the 'fracture corridors'. A lithological and stratigraphic control has emerged from these analyses. Mud loss and inflow data have enabled the most significant open fractures to be identified in the wells from the appropriate image log trace. Finally, well tests, including interference and monitoring data, have verified the interpretation of a system so well connected that, for example, a pressure pulse due to testing of the flank well TT-08 could be detected almost immediately both in TT-07, 3 km to the south and in TT-06 2 km to the NW.

The trends of the axis-parallel faults interpreted from the 3D survey are also seen in those of one of the fracture families but, as noted above, the numerous small-scale anticlines with broadly ENE–WSW orientation, transverse to the main fold axis but parallel to the dominant fracture directions, are taken to be the loci of major fracture zones. This relationship has been described in many tectonic settings (e.g. Keating & Fischer 2008) and seismic curvature processing, which has improved the definition of these features, has been a major element in the interpretation. The current fracture model (Fig. 12) incorporates the interpreted clusters of fracture corridors and swarms with the statistical frequency and orientations of the two conjugate families in the diffuse system. The model has been the framework for uncertainty studies investigating likely scenarios within the assessed variability of the data. In terms of reservoir volume, a wide uncertainty remains regarding the overall fracture porosity. Fracture modelling will guide the development of the field and the location and orientation of the remaining development wells.

Fluids

Analysis of the Cretaceous oil indicates a 48° API gravity combined with a low viscosity and a low GOR of approximately 25 scf/bbl which is unusual and has facilitated the safe drilling and completion of all seven of the development wells. The source rock has been identified geochemically to be the Jurassic Sargelu and Naokelekan Formations, which have been penetrated within the field area. Another feature of the Taq Taq oil is its lower sulphur content (300 ppm) compared with the older producing

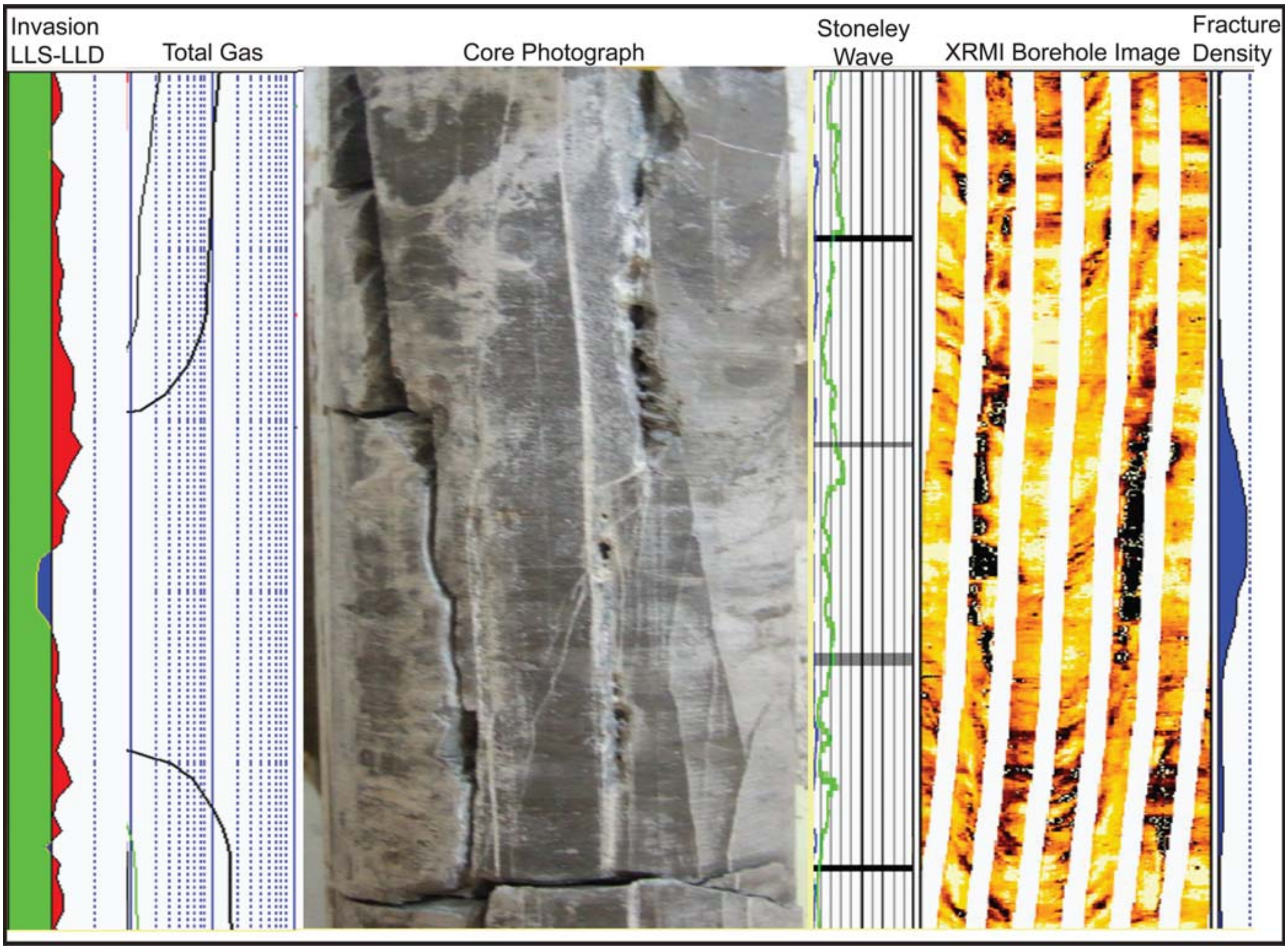

Fig. 11. Log, core, mud gas and image interpretation over fractured reservoir (not to scale). Total gas drops with severe mud loss during drilling. Core photograph of oriented whole core prior to slabbing. Stoneley wave from dipole sonic indicates zone of fractures. XRMI image detects fracture on both sides of the borehole. Fracture density calculated from core and/or from image calibrated to mean aperture.

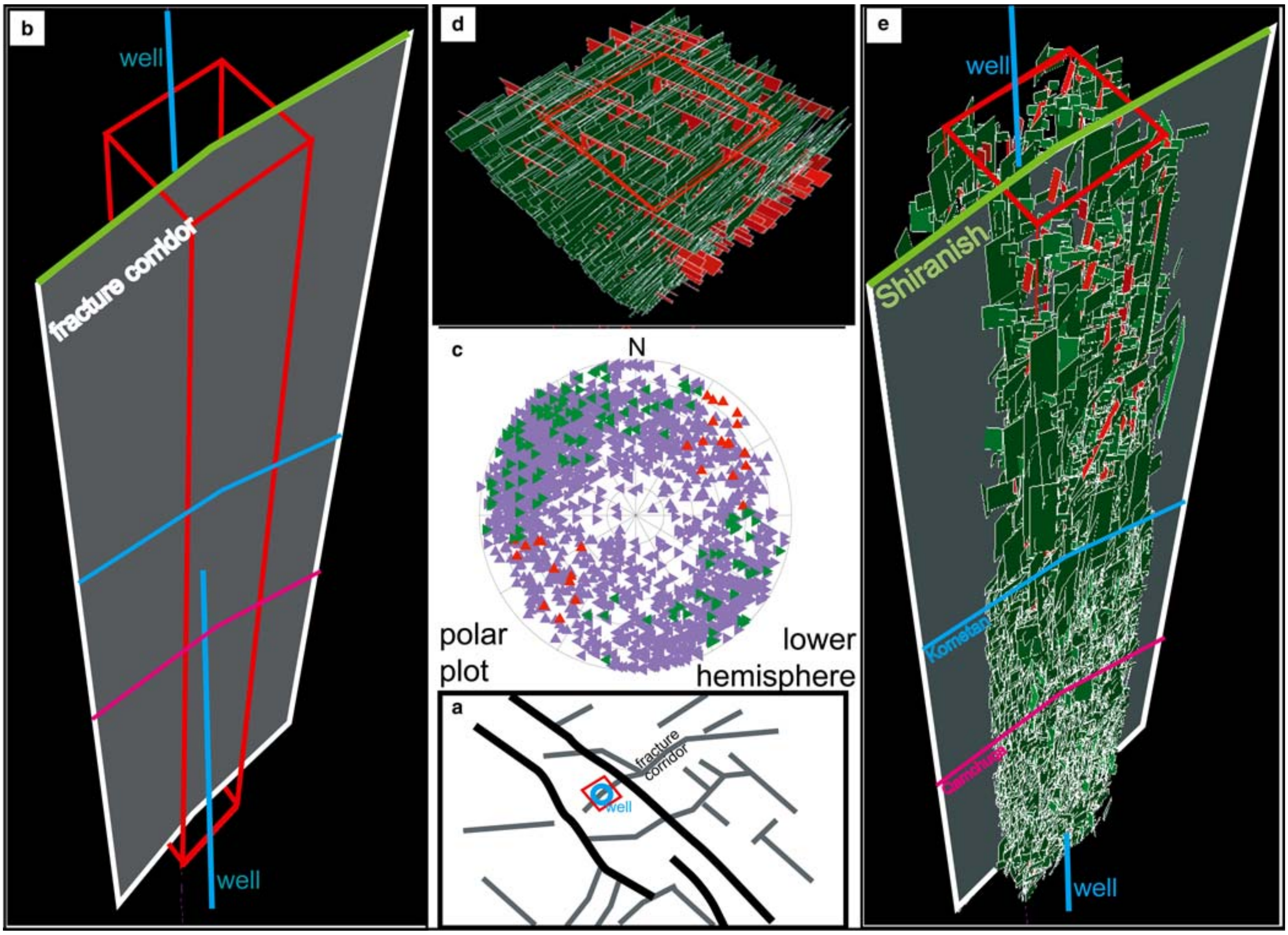

Fig. 12. Fracture model. Well located on fracture corridor (**a**) is explicitly incorporated into model (**b**). Statistics of all the fractures identified as open are analysed and split into red and green families of the diffuse fracture system (**c**). Fractures are propagated into the model for each zone based on the statistics (**d**). Zones are combined with the corridor (**e**) and the other wells in the final model.

fields in Iraq, and handling of the hydrogen sulphide has been relatively simple to incorporate into the design of the treatment facilities. Special core analysis has indicated an intermediate wettability for the Qamchuqa matrix with effective imbibition under water flood, which implies the potential for a favourable recovery factor, especially where the fracture density is high (Warren & Root 1963; Kazemi 1969). As has been found in many carbonate reservoirs, it has not been possible to define a single OWC from log interpretation. Part of the problem is due to varying water salinity where the formation water was originally saline but the active aquifer has been flushed with meteoric water since the emergence of the Zagros in Oligocene time and may still be in the process of displacing the original fluids. Also, as in many carbonate reservoirs, it has not everywhere been possible to obtain good RFT pressure data due to the difficulty of obtaining a good seal with the probe in hard and fractured dolomite. So far, the pressure gradients derived from static pressure data in both the oil column and the aquifer following production tests (of which there have been over 20) indicate a free water level implying a total potential oil column of some 525 m. It is planned to measure the true free water level in an open hole static test in a future well.

Current plans

Dynamic simulation of this hydrocarbon system, incorporating both the matrix and the fracture models, is being carried out with a dual media simulator which will enable optimization of well locations, orientations and production strategy under several possible scenarios within the uncertainty range. A production facility is being built close to the field with initial plans for tanker loading. At the time of writing (December 2008), various plans were being considered including a pipeline and possibilities for ramping up production. These facilities have been in production (March 2010) at rates up to 55 000 bopd with export by tanker. For the present, our models carry a wide uncertainty in many parameters: with production these uncertainties will narrow as the Taq Taq reservoirs progressively reveal their petrophysical secrets.

The support and cooperation of the Ministry of Natural Resources of the Kurdistan Regional Government of Iraq is acknowledged both for the writing of this paper and for the development of the Taq Taq field. Significant assistance is also acknowledged from the staff and students of the Department of Geology, University of Sulaimani, for helping to put Taq Taq subsurface geology into the context of local outcrops. Core and XRMI fracture analysis and sedimentological studies have been carried out by P. Lucas and A. Mann of Fugro-Robertson Ltd. Principal-component seismic facies analysis was carried out by J. Scheevel, of Scheevel Geotechnologies. The initial structural interpretation was carried out by B. Meier of Proseis AG, Zurich. Thanks are also due to the management of Genel Enerji (SA) and of Addax Petroleum Corporation.

References

Al Shdidi, S., Thomas, G. & Delfaud, J. 1995. Sedimentology, diagenesis and oil habitat of the qamchuqa group, N Iraq. *AAPG Bulletin*, **79**, 763–779.

Ameen, M. S. 1991. Alpine geowarpings in the Zagros-taurus range: influence on hydrocarbon generation, migration and accumulation. *Journal of Petroleum Geology*, **14**, 417–428.

Bazalgette, L. & Petit, J.-P. 2007. Fold amplification and style transition involving fractured dip-domain boundaries. *In*: Lonergan, L., Jolly, R. J. H., Rawnsley, K. & Sanderson, D. J. (eds) *Fractured Reservoirs*. Geological Society, London, Special Publications, **270**, 157–169.

Davies, G. R. & Smith, L. B. 2006. Structurally controlled hydrothermal dolomite reservoir facies: an overview. *AAPG Bulletin*, **90**, 1641–1690.

Dehghani, K., Edwards, K. A. & Harris, P. M. 1997. *Modeling of Waterflood in a Vuggy Carbonate Reservoir*. SPE Annual Technical Conference and Exhibition, San Antonio, Texas, SPE 38910.

Haddad, S. N. S. & Ameen, M. A. 2007. Mid-Turonian–Early Campanian sequence stratigraphy of northeast Iraq. *GeoArabia*, **12**, 135–176.

Harding, T. P. 1974. Petroleum traps associated with wrench faults. *Journal of Structural Geology*, **19**, 59–75.

Hubbert, M. K. & Willis, D. G. 1955. Important fractured reservoirs in the United States. *Proceedings of the 4th World Petroleum Congress*, 57–81.

Jassim, Z. J. & Goff, J. C. 2008. *The Geology of Iraq*. Dolin, Prague.

Kader, H. J. 2002. *Taqtaq Oil Field developed by Kurdistan Regional Government*. Babagurgur Centre for Kurdistan Resources Studies.

Karim, K. H., Ismail, K. M. & Ameen, B. M. 2008. Lithostratigraphic study of the contact between Kometan and Shiranish Formations (Cretaceous) from Suleimaniya Governorate, Kurdistan Region, NE Iraq. *Iraqi Bulletin of Geology and Mining*, **4**, 16–27.

Kazemi, H. 1969. Pressure transient analysis of naturally fractured reservoirs with uniform fracture distribution. *SPE Journal*, **9**, 451–462.

Keating, D. P. & Fischer, M. P. 2008. An experimental evaluation of the curvature-strain relation in fault-related folds. *AAPG Bulletin*, **92**, 869–884.

Pitman, J. K., Steinshouer, D. W. & Lewan, M. D. 2003. *Generation and Migration of Petroleum in Iraq: Modeling Study of Jurassic Source Rocks*. US Geological Survey Open-File Report.

Reinecker, J., Heidbach, O., Tingay, M., Connolly, P. & Muller, B. 2004. *World Stress Map*. Heidelberg Academy of Sciences and Humanities.

Scheevel, J. R. & Payrazyan, K. 1999. Principal component analysis applied to 3D seismic data for reservoir property estimation. *SPE Annual Technical Conference and Exhibition*, Houston, TX, SPE 56734.

van Bellen, R. C., Dunnington, H. V., Wetzel, R. & Morton, V. 1959. *Lexique Stratigraphique International Asie Iraq Vol 3c (Stratigraphic Lexicon of Iraq)*. CNRS Editions, France, reprinted by Gulf PetroLink 2005.

Warren, J. & Root, P. 1963. The behavior of naturally fractured reservoirs. *SPE Journal*, **3**, 245–255, SPE 426.

Sedimentology, geochemistry and hydrocarbon potential of the Late Cretaceous Shiranish Formation in the Euphrates Graben (Syria)

S. ISMAIL,[1] H.-M. SCHULZ,[1] H. WILKES,[1] B. HORSFIELD,[1] R. DI PRIMO,[1] M. DRANSFIELD,[2] P. NEDERLOF[3] and R. TOMEH[2]

[1]*Helmholtz Centre Potsdam-GFZ German Research Centre for Geosciences, Sect. 4.3 Organic Geochemistry, Telegrafenberg, D-14473 Potsdam, Germany (e-mail: shirin78@gfz-potsdam.de)*
[2]*Al-Furat AFPC, Damascus, Syria*
[3]*Shell International E&P, Rijswijk, the Netherlands*

Abstract: The Shiranish Formation consists of mudstones and wackestones in the central Euphrates Graben which are rich in organic carbon. Here the Shiranish Formation is more than 700 m thick with a minor increase in organic maturity with depth. The Shiranish Formation sediments are characterized by a continuously increasing hydrogen index to the top whereas the oxygen index is markedly lower in the Upper Shiranish Formation (USF). The Lower Shiranish Formation (LSF) is characterized by lower hydrogen indices and higher oxygen indices relative to the USF. These organic geochemical characteristics enable a rough subdivision into a lower and an upper part of the Shiranish Formation. Furthermore, mineralogical results enable a subdivision of the USF into two parts (USF-1, lower part; USF-2, upper part) each with individual mineralogical signatures due to a modified depositional environment and differing diagenetic history. The LSF resembles mineralogically the USF-2. Ankerite, together with higher pyrite contents in the LSF and USF-2, reflect similar diagenetic pathways which were controlled by higher clay contents. During early diagenesis, a traceable conversion of metabolizable organic matter led to mineral assemblages due to significant methanogenesis. Intervals in the USF with total organic carbon (TOC) contents up to around 4% and hydrogen indexes up to 500 mg HC/g TOC indicate the presence of very good potential source rock intervals for oil generation. Additionally, intervals of the LSF also contain gas-prone organic material. Bulk kinetic investigations show a broad activation energy of the LSF and a narrow activation energy pattern for the USF for hydrocarbon generation. Furthermore, the predicted petroleum formation temperatures are 136°C for the USF and 144°C for the LSF, respectively. This corresponds to *c.* 630 m difference in burial depth for petroleum formation. These differences in activation energies and corresponding depth to reach oil window maturity are controlled by facies, and less by maturity.

Keywords: organic carbon, hydrocarbon source rock, Cretaceous, graben, petroleum

Organic matter-rich sediments in modern and ancient depositional environments are the result of a complex interaction between several factors, such as primary productivity in the water column, supply of nutrients, redox–oxidation processes and sediment accumulation rates (Demaison & Moore 1980; Pedersen & Calvert 1990; Tyson 1995). An extraordinary geological test site to unravel the significance of these single factors which may have controlled organic matter richness is the marine Shiranish Formation in the Euphrates Graben (Figs 1 & 2). Sediments of the Shiranish Formation can locally reach more than 1000 m thickness in the central Graben and were deposited during the late Campanian and Maastrichtian. The thickness of the Shiranish Formation predominantly is a result of syn- and post-rift controlled subsidence which changed regionally and temporally. The Lower Shiranish Formation (LSF) was deposited during the syn-rift development of the graben, whereas the Upper Shiranish Formation (USF) is a part of the post-rift sequence (De Ruiter *et al.* 1995; Litak *et al.* 1998). The Tayarat Limestone intercalated between the Lower and Upper Shiranish Formation marks this change. The Shiranish Formation exhibits strong variations in thickness along the graben axis (e.g. up to 1800 m in the SE; De Ruiter *et al.* 1995). The remarkable thickness of the Shiranish Formation deposited within a relatively short time is the result of high sedimentation rates both of the clayey and carbonate mineral matrix, coupled with a strong subsidence, predominantly in the graben area. In terms of petroleum geology, these sediments are considered as seal and source rock having total organic carbon (TOC) contents of up to 1.7% (De Ruiter *et al.* 1995; Brew *et al.* 2001). On the other hand, the Shiranish Formation has reservoir properties outside the Euphrates Graben where shallow marine depositional environments prevailed (e.g. Oudeh Field in northern Syria and Kirkuk and Mosul area in Iraq, after Ziegler 2001).

In this manuscript we present detailed investigations of the source rock potential of the Shiranish Formation in the Euphrates Graben at a high resolution. Our investigations focus on two wells (well A and well B both drilled in 1987; Fig. 2), which are located in the central part of the Euphrates Graben. Well A was drilled with water-based mud and well B was drilled with oil-based mud. Well A recovered cuttings material from the Shiranish Formation between 2840 and 3550 m depth (well B: 2760–3525 m depth). In both wells the Shiranish Formation exhibits all features of continuous sedimentation and has a thickness of about 800 m.

The organic matter-rich sediments of the Shiranish Formation are an attractive research topic due to the high TOC contents in a thick sedimentary column deposited within a relatively short time interval during the latest Cretaceous. It is the aim of this contribution to couple data from geochemical, mineralogical and sedimentological investigations in order to evaluate the source rock properties as a consequence of depositional environment and diagenesis.

Regional and petroleum geology of Syria

Four major tectonic zones occur in Syria: the Palmyride foldbelt, the Euphrates Graben system, the Abd El Aziz/Sinjar uplifts and

VINING, B. A. & PICKERING, S. C. (eds) *Petroleum Geology: From Mature Basins to New Frontiers – Proceedings of the 7th Petroleum Geology Conference*, 811–819. DOI: 10.1144/0070811

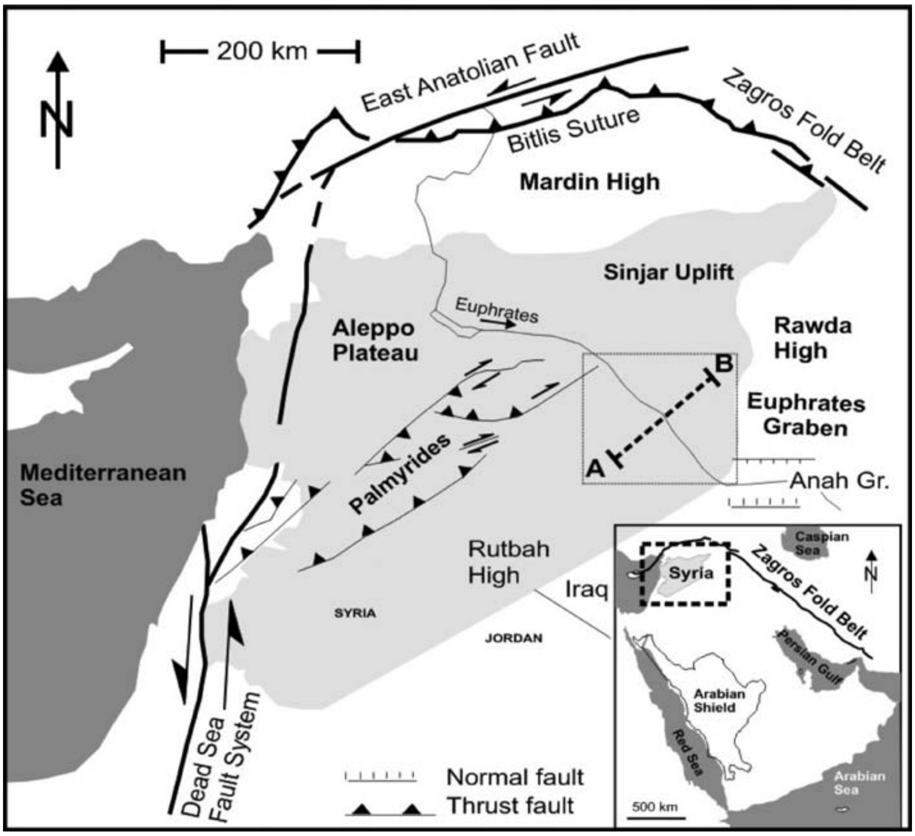

Fig. 1. Tectonic map of Syria. Geological cross-section A–B in Fig. 2.

the Dead Sea fault system (Barazangi *et al.* 1993; Brew *et al.* 2001; Fig. 1). The 160 km long Euphrates Graben system is interpreted as an aborted NW-trending intercontinental rift of Late Cretaceous age that has subsequently been hidden by sediments due to Cenozoic burial (Litak *et al.* 1998). It consists of a system of normal and strike-slip faults and is a result of a transtensive regime during the Late Cretaceous. The tectonic processes formed a complex of many smaller grabens and half-grabens which are less expressed in the northwestern part. The underplating of the Arabian plate in the Neo-Tethys subduction zone ended the rifting in the Late Cretaceous. It is related to convergence associated with the emplacement of amphibolites along the Arabian Plate (Litak *et al.* 1998). On a wider regional scale, the depositional environment during the uppermost Cretaceous in the Middle East is controlled by the northeastwards dipping Arabian Plate. This stable tectonic element enabled the deposition of carbonates with minor variation of facies (shallow and open-marine) which graded into deep marine clastics in the Levantine Basin and the Mesopotamian foreland basin (Brew *et al.* 2001; Ziegler 2001).

Oil and gas fields occur throughout the tectonic zones with the exception of the Dead Sea fault system. However, the majority of the oil fields are located in the Euphrates Graben system. This graben system is a relatively small but highly prolific oil province with more than 38 oil fields discovered since the mid-1980s. Reservoirs are predominantly siliciclastic and of Triassic and Early Cretaceous age (De Ruiter *et al.* 1995).

Potential source rock units in Syria can be subdivided into two groups on the basis of their lithofacies characteristics: (1) relatively deep and open-marine lithofacies, which include the Palaeozoic

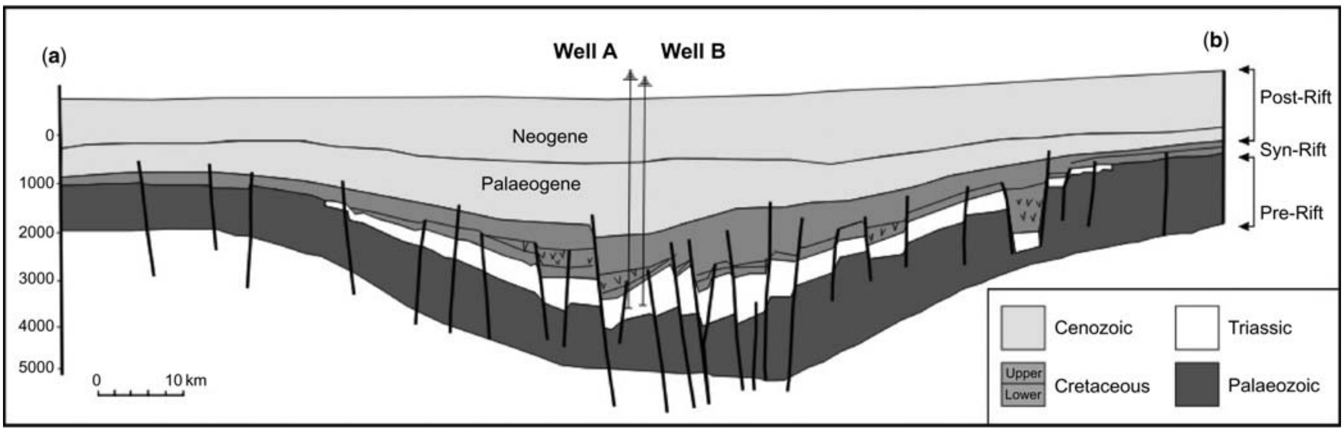

Fig. 2. Geological cross-section across the Euphrates Graben (modified after De Ruiter *et al.* 1995).

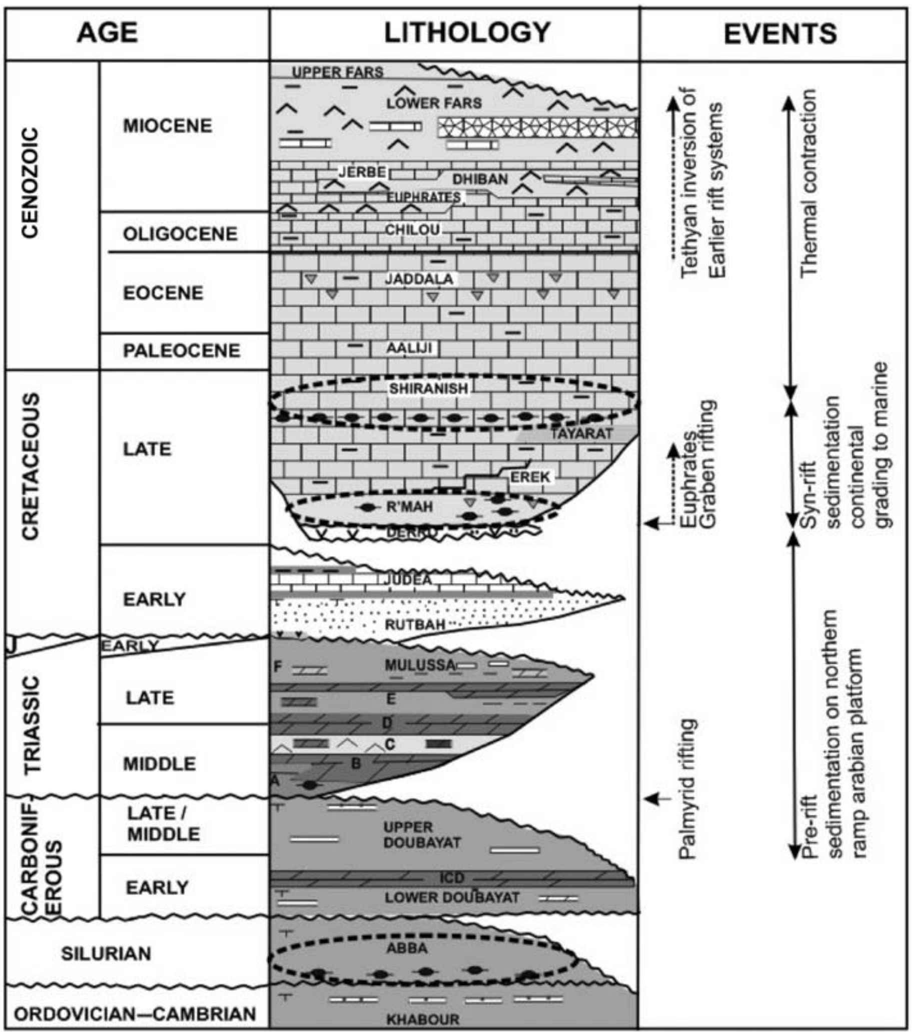

Fig. 3. General stratigraphy of the Euphrates Graben (modified after De Ruiter *et al*. 1995). Potential source rocks are presented in dotted circles.

Swab–Tanf Formation, the Late Cretaceous Shiranish Formation and the Paleocene Kermav Formation; and (2) shallow-marine and lagoonal lithofacies, including the Amanus Shale Kurra Chine Formation (Lower–Middle Triassic) and the Upper Cretaceous Soukhne Formation (Abboud *et al.* 2005).

Besides supposed Palaeozoic source rocks (e.g. the Silurian Tanf/Abba Formation) sediments predominantly of Cretaceous age are regarded as source rocks in the Euphrates Graben (De Ruiter *et al.* 1995, Fig. 3). A proven source rock is the R'mah Formation (alternatively Soukhne Formation) which is considered to be deposited as a first central grabenfill during the Early Upper Cretaceous (De Ruiter *et al.* 1995).

Samples and methods

The sample set was provided by Al-Furat (Damascus, Syria) and Shell (Rijswijk, The Netherlands). Additionally, data from Rock-Eval Pyrolysis and TOC contents of 28 samples from well A were kindly provided. Because of the limited amount of cuttings material from well A, inorganic geochemical and mineralogical analyses were carried out on cuttings material from well B. A direct comparison of data is possible, as both wells are close to each other and are similar in thickness and sedimentology.

The mineralogical and inorganic chemical composition of 30 cuttings samples from well B was investigated by XRD and XRF analysis respectively. Bulk pyrolysis was performed using 11 cuttings samples from well A. Kinetic parameters of hydrocarbon generation were determined using the experiential setup described by Schaefer *et al.* (1990).

Results and interpretation

The Shiranish Formation in well A is *c*. 700 m thick (Fig. 4). Lithologically, it consists of alternating mudstones and wackestones (terminology according Dunham 1962). A subdivision into a Lower and Upper Shiranish Formation with the Tayarat Limestone at their boundary follows internal considerations by Shell and Al-Furat, and is supported by the analysis of petrophysical properties (Ismail *et al.* 2008). This subdivision into a lower and an upper unit of the Shiranish Formation is kept in this contribution (Fig. 4) and extended to a further subdivision of the USF (Fig. 7).

Maturity and hydrocarbon source rock potential

A potential hydrocarbon source rock is characterized by its organic carbon content, the type and quality of the organic matter, and organic maturity. A compilation of different data log motifs from RockEval pyrolysis for the Shiranish Formation in well A (Fig. 4) together with a compilation of selected data in interpretive x–y plots (Fig. 5) shows the subdivision of a Lower and an Upper Shiranish Formation, the latter of marginally lower organic maturity (T_{max} averages slightly lower than 440 °C). In general, The LSF is characterized by TOC contents between 1.37 and

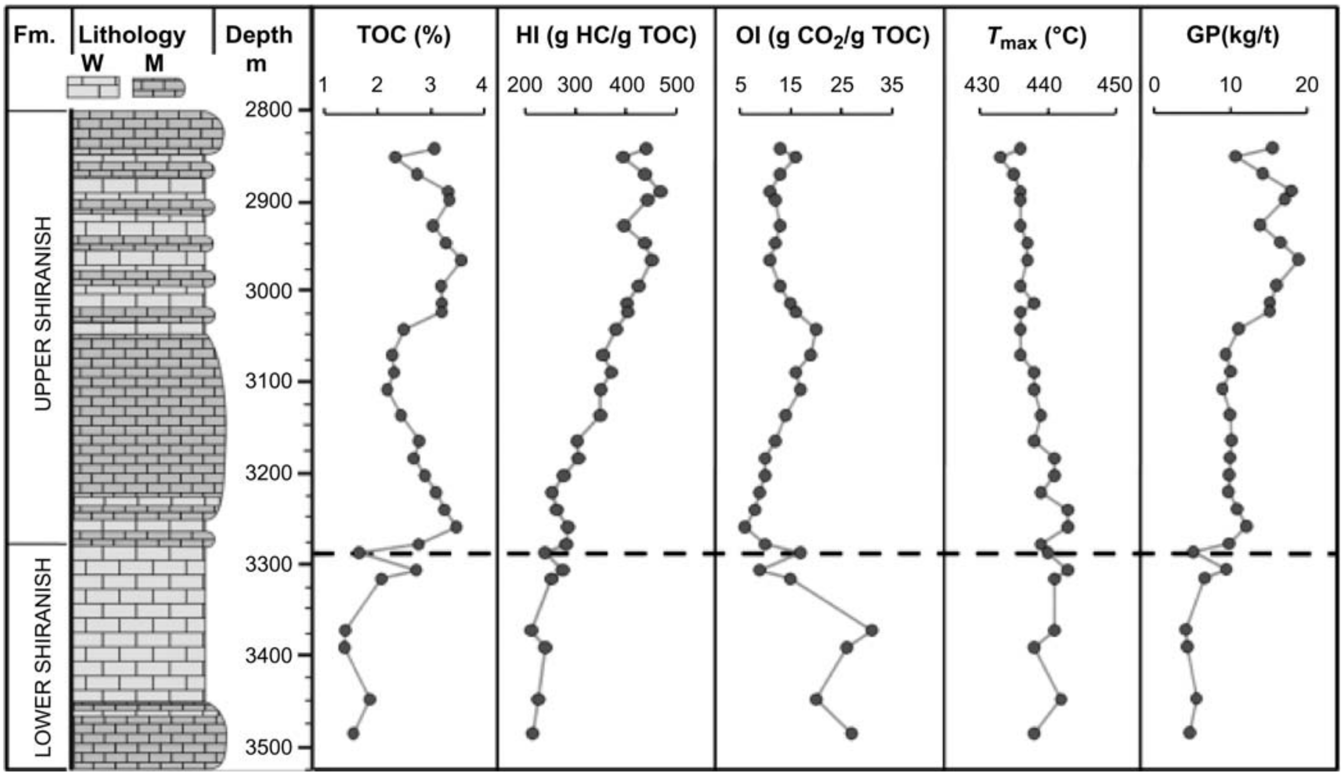

Fig. 4. Lithology and organic geochemical proxies for well A. Fm., Formation; W, wackestone; M, mudstone.

2.73%, hydrogen indices ranging from 212 to 275 mg HC/g TOC, and oxygen indices with values between 9–31 mg CO_2/g TOC. Moreover, a maximum temperature T_{max} of around 440°C is needed for the total thermal conversion into hydrocarbons. These characteristics of the LSF enable the calculation of the genetic potential (GP) of around 5 kg/t, and a production index PI of more than 0.2 (equilibrium at 0.5). In contrast, higher organic carbon contents (2.27–3.58%) occur in the USF, which has relatively higher hydrogen indices with values from 263 to 469 mg HC/g TOC, but lower oxygen indices (8–20 mg CO_2/g TOC). This organic material requires a temperature (T_{max}) slightly lower than 440°C to start releasing thermogenic hydrocarbons. As a

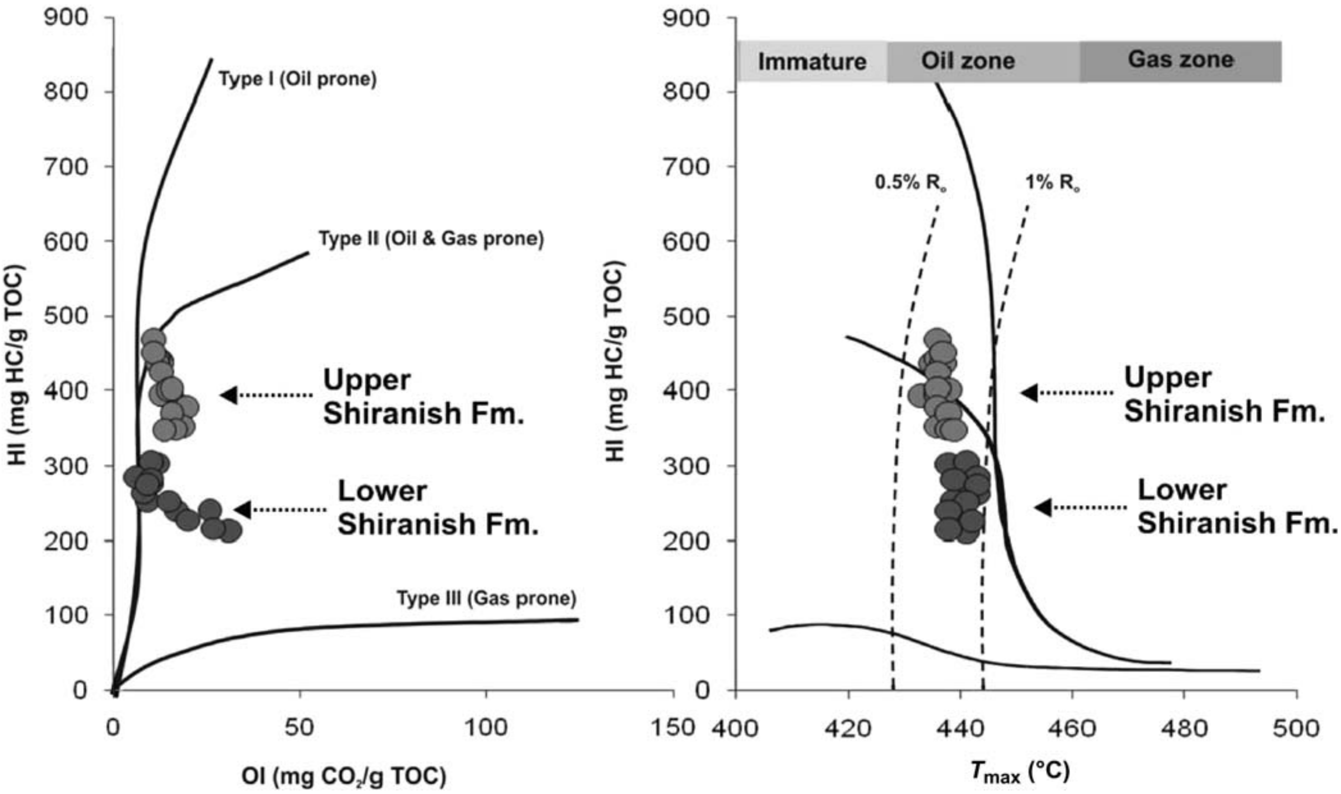

Fig. 5. Organic geochemical characterization of cutting samples from well A. Fm., Formation.

consequence, the organic material of the USF has a higher GP, due to a lower content of terrigenous organic matter, but a lower PI.

Organic facies

The organic matter of the Shiranish Formation can be classified into two groups, similar to the subdivision into the Lower and Upper Shiranish Formation. According to the van-Krevelen definition (Espitalié *et al.* 1980; Fig. 5), the USF contains a type II kerogen, whereas a type II–III kerogen mixture occurs in the LSF. However, TOC contents and Rock-Eval data have to be critically evaluated regarding their significance for a useful interpretation (Dembicki 2009). For example, the mineral matrix of a source rock with TOC contents less than 2.0% (as for intervals in the LSF excluding an interval at depth 3330 m) can also influence Rock-Eval kerogen typing. This phenomenon can be the result of retention on mineral grains, which cause a significant reduction in the hydrogen index (HI; Espitalié *et al.* 1980; Katz 1983). As the Shiranish Formation is calcareous in lithology, thermal decomposition of small amounts of carbonate minerals during the Rock-Eval analysis can contribute carbon dioxide and increase the oxygen index (OI) in low TOC sediments (Katz 1983). However, there are alternative ways to correct the interpretation of Rock-Eval data in terms of organic matter typing and to define organic matter sources. The first one is to simply deconvolve the HI into its two components, S2 and TOC (Katz & Elrod 1983; Langford & Blanc-Valleron 1990; Fig. 7). Second, higher C_1–C_5 contents generated by pyrolysis-gas chromatography from the LSF relative to the USF (Ismail *et al.* 2008, Fig. 6) are evidence for a correct interpretation of Rock-Eval data in terms of organic matter type. The S2:TOC ratio calculated for the corresponding material thus implies well characterized organic material with good source rock properties for the LSF and excellent source rock properties for the USF (Fig. 7). What are the factors causing variations of TOC content and the Rock-Eval parameters in the Shiranish Formation? The observed trend in the hydrogen index appears to be related to the nature of the organic matter in the Shiranish Formation. Increasing HI values can reflect either differences in the degree of organic preservation of marine organic matter or higher changes in the relative abundance of marine and terrestrial organic matter (Katz *et al.* 1993). According to this, higher HI values in the USF would be indicative of better preservation and/or higher relative abundance of marine organic matter. In contrast, the lower HI values in the LSF reflect terrestrial input. Moreover, a wide range of HI values indicates variations of the organic facies. In summary, a higher palaeoproductivity led to an

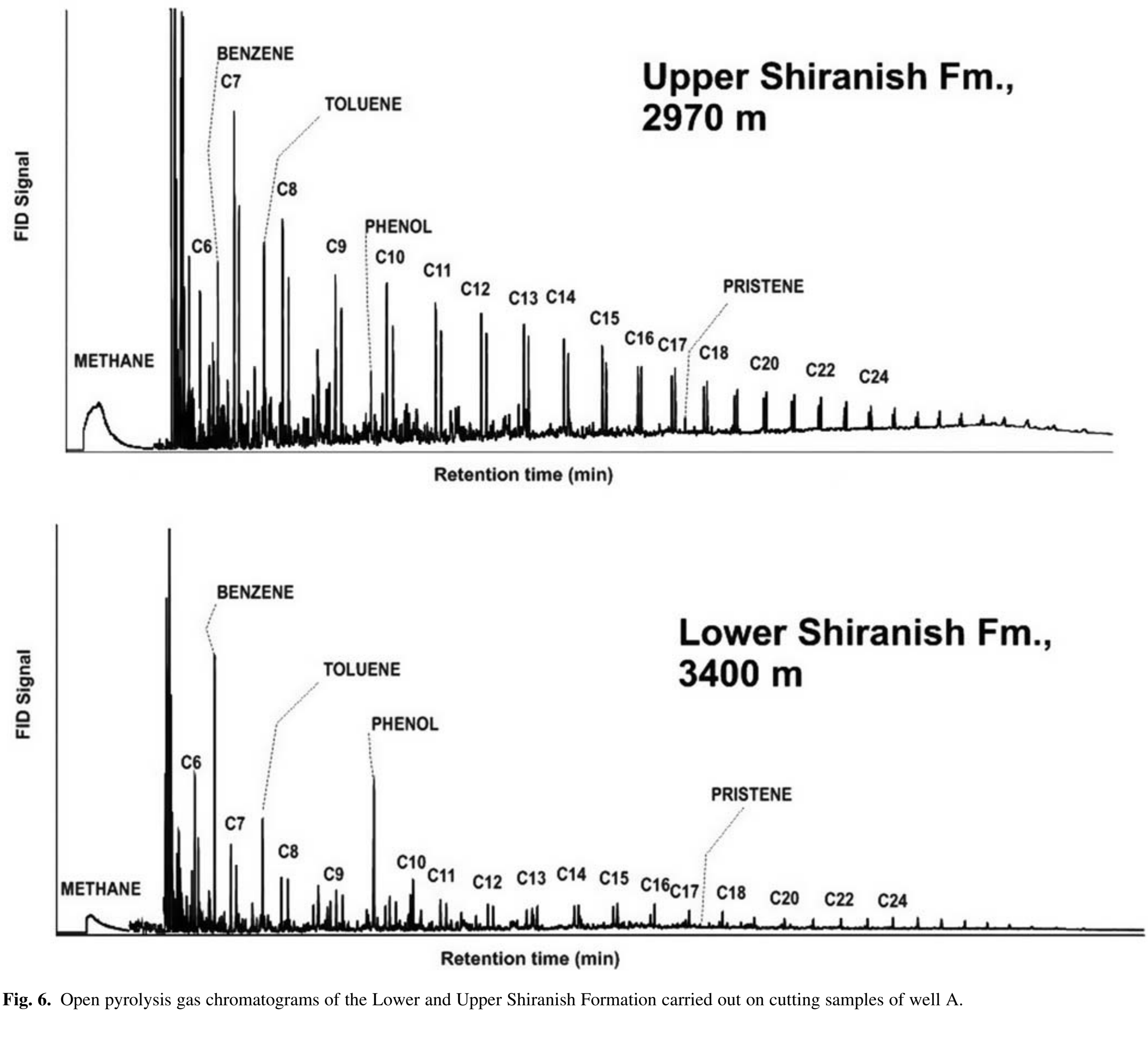

Fig. 6. Open pyrolysis gas chromatograms of the Lower and Upper Shiranish Formation carried out on cutting samples of well A.

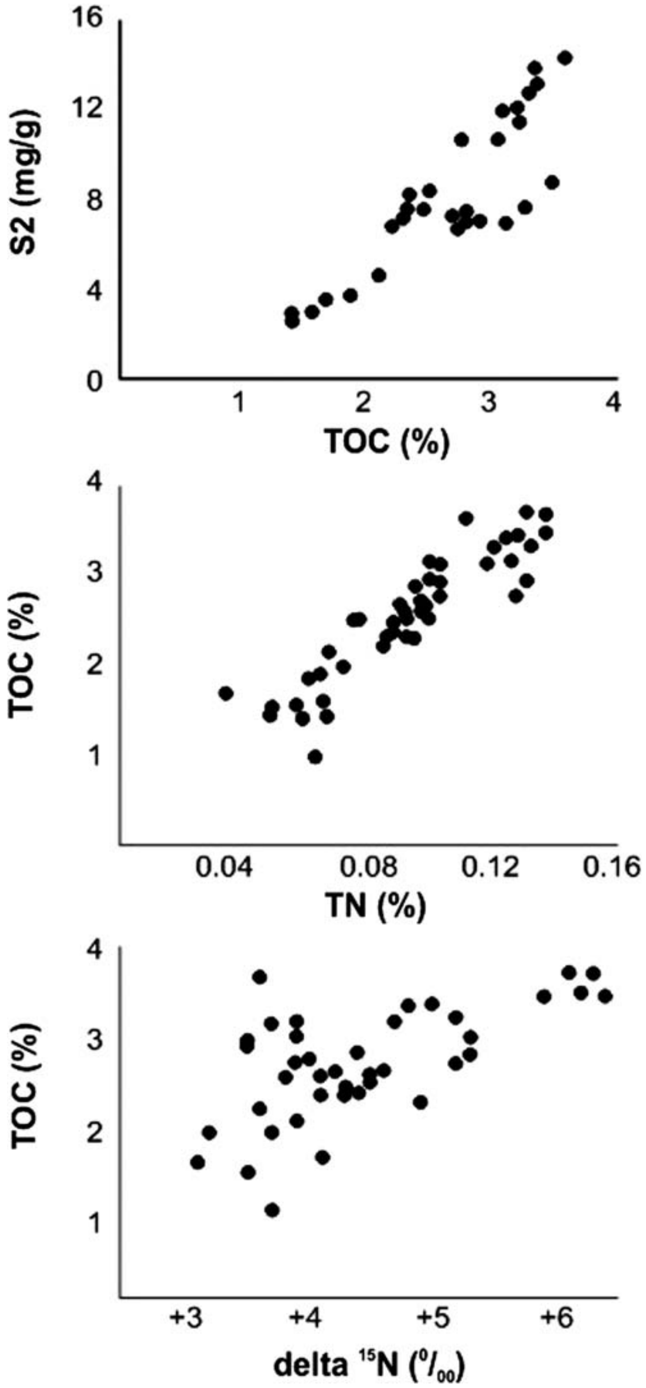

Fig. 7. TOC v. S2, total nitrogen content and $\delta^{15}N$ of cutting material from well A.

enhanced preservation potential of marine organic material due to clayey sedimentation during deposition of the USF in open marine conditions. In contrast, input of terrestrial organic material occurred during deposition of the LSF in shallow marine conditions.

TOC:N_{total} ratios remain fairly constant throughout the whole Shiranish Formation and suggest similar organic material (Fig. 7). Moreover, hydrogen indices positively correlate with $\delta^{15}N$ (Fig. 7). $\delta^{15}N$ can be used to distinguish between organic matter derived from algae and land plants (Meyers 1997). Atmospheric N_2 ($\delta^{15}N \approx 0‰$) is the nitrogen source for terrestrial plants, whereas dissolved nitrate with higher $\delta^{15}N$ values is the nitrogen source for plankton. $\delta^{15}N‰$ increases from 3 to 7‰ towards the top of the Shiranish Formation. Two scenarios can be considered as factors controlling $\delta^{15}N‰$ variability throughout the Shiranish Formation. The first one is water-column denitrification caused by relatively lower $\delta^{15}N‰$ values in the LSF due to nitrogen utilization by N-fixers. Progressive water-column denitrification may have led to relatively heavier $\delta^{15}N‰$ values in the USF due to increased productivity. Second, variations of $\delta^{15}N‰$ can be the result of mixing of isotopically light terrestrial organic matter with marine organic matter. The controversy of this interpretive approach and relevant references are presented in Calvert (2004).

Mineralogy of the Shiranish Formation and early diagenesis

The inorganic matrix of the cuttings material from well B is predominantly composed of calcite (up to *c*. 90%). Quartz, kaolinite and ankerite occur as well as calcite, and traces of pyrite have been found (Fig. 8). Besides the general subdivision into a Lower and Upper Shiranish Formation, the distribution patterns of the single mineral phases allow a further subdivision of the USF into a lower and upper unit, both with different mineralogical compositions. Consequently, a new classification of the Shiranish Formation into three sub-units is proposed into units A (the LSF), B (lower part of the USF) and C (upper part of the USF). In terms of mineralogical composition, unit C resembles unit A (Fig. 8). The carbonate contents are similar in both units A and C, ranging from 51 to 80%, while higher carbonate contents (72–91%) occur in unit B. High concentrations of siliciclastic minerals such as quartz and kaolinite are observed in units A and C. Tracer minerals to unravel the diagenetic pathways of the Shiranish Formation are ankerite and pyrite. The contents of both are lower in unit B.

Several mineral phases occur in the Shiranish Formation, either deposited primarily or the result of early diagenesis of organic matter-rich matrix. Calcite, quartz and kaolinite are regarded as primary minerals whereas pyrite and ankerite are interpreted as characteristic diagenetic products in organic-rich sediments (for an overview see Einsele 2000).

In general, relative sea-level changes can greatly affect carbonate sedimentation as widespread carbonate accumulations are often associated with global sea-level highstands (Tucker & Wright 1990). Thick carbonate sequences are thus deposited as transgressive systems tracts, and relative sea-level change may affect carbonate sediments by a diagenetic process (Tucker & Wright 1990). The variation in relative calcite content throughout the Shiranish Formation can therefore be considered as a general proxy for sea-level variations. As a consequence, high calcite contents in unit B could point to a highstand. Moreover, high calcite contents may reflect high palaeoproductivities due to positive correlations with relatively higher TOC contents. Periods with less carbonate flux and deposition were coupled to increased terrigenous input (high oxygen indices together with higher quartz and clay contents, here kaolinite). In general, kaolinite is associated with very low energy depositional environments (Chamley 1989; Hallam *et al.* 1991), but can also be formed diagenetically (Ghandour *et al.* 2003). Kaolinite is the predominant clay mineral in the Shiranish Formation and is at its lowest concentration in unit B (Fig. 8). This variation may be related to relative sea-level changes, which affect the distribution of clay minerals such as kaolinite and smectite (Steinke *et al.* 2008). As kaolinite is of sedimentary origin in the Shiranish Formation, increased contents can be related to a relative sea-level lowstand during sedimentation of unit B.

High clay mineral content decreases sediment permeability. Thus, the positive correlation between the kaolinite content and the pyrite and ankerite content indicates less permeable sediment properties which enhance sulphate reduction and minor pyrite precipitation followed by intense ankerite crystallization (Berner

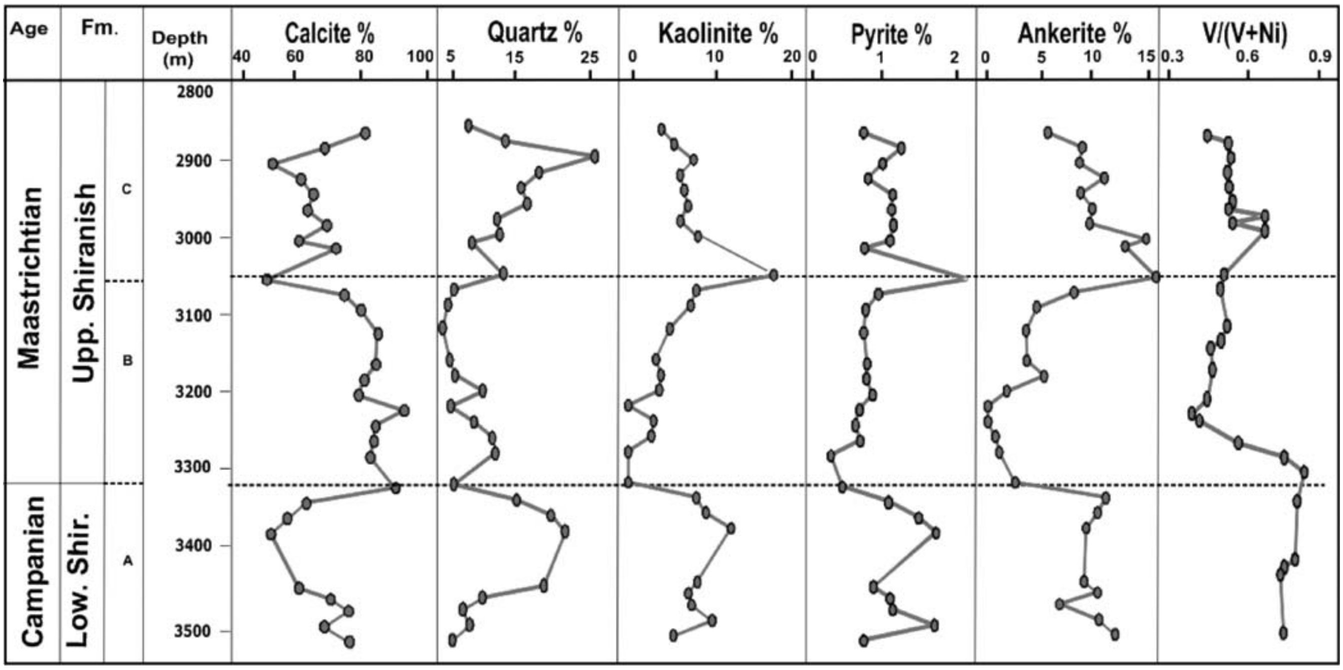

Fig. 8. Mineralogical composition of the Shiranish Formation in well B.

1982). Ankerite may indicate that intervals with relatively high kaolinite contents had methanogenic pore water conditions during early diagenesis, during which organic matter was intensively converted. Thus, intervals with significant ankerite contents originally had relatively higher TOC contents than those with low ankerite contents.

Trace element palaeoredox proxies

Trace element concentrations and ratios of significant elements have successfully been applied to evaluate the palaeo-O_2/H_2S boundary in ancient, stratified water columns (e.g. Cr/V, V/(V + Ni) etc.; Hatch & Leventhal 1992).

For example, vanadium is more effectively fixed than nickel in sediments under anoxic water conditions and in the presence of hydrogen sulphide (Lewan & Maynard 1982; Breit & Wanty 1991). The application of the ratio V/(V + Ni) suggests relative changes in oxygenation in the water column throughout deposition of the Shiranish Formation (according to Lewan & Maynard 1982; Breit & Wanty 1991). Hatch & Leventhal (1992) suggested V/(V + Ni) ratios >0.84 to indicate euxinic conditions, and lower values indicate higher oxygen contents in the bottom-water column. According to this classification, V/(V + Ni) ratios around 0.8 in the LSF could be linked to oxygen-depleted depositional conditions.

Bulk petroleum generation kinetics

The transformation of sedimentary organic matter, mainly kerogen, to petroleum during burial in a sedimentary basin can be calculated as a function of time and temperature. It is controlled by parallel and successive chemical reactions (Tissot & Welte 1984). This basic approach was applied to 11 samples from the Lower and Upper Shiranish Formation, each with a characteristic, but different organic material. The approach includes the calculation of the bulk parameters activation energy E_a and per-exponential factor A. Both will be used to determine the timing of hydrocarbon generation at a linear geological heating rate of 3.3 K/Ma. This heating rate corresponds to an average geological heating rate in sedimentary basins (Schenk *et al.* 1997), and is applied as a rough working hypothesis for the Euphrates Graben. Under consideration of this generalized heating rate, the Lower and Upper Shiranish Formations differ significantly in their diagnostic activation energy distributions and petroleum yields (Fig. 9). The USF is characterized by high petroleum yields at low activation energy (maximum at 54 kcal/mol) and frequency factors ranging between 1.52×10^{14} and

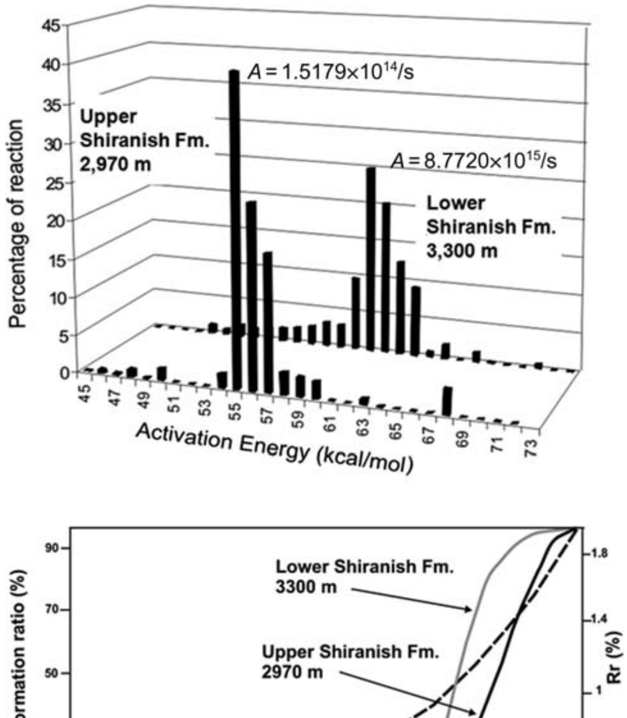

Fig. 9. Distribution of activation energy, computed transformation ratio and vitrinite reflectance in the USF and LSF.

6.3×10^{14}/s. A relatively narrow activation energy distribution indicates a kerogen type II organic matter in the USF. On the other hand, calculations for the LSF show lower petroleum yields. For the sediments of the LSF a broader activation energy distribution has been determined (54–67 kcal/mol) with frequency factors between 1.04×10^{15} and 8.77×10^{15}/s. Calculations to predict the timing of petroleum generation result in different onset and peak generation temperatures for the Lower and Upper Shiranish Formations. The generation of petroleum from the USF is predicted to start at 136°C (lowest geol. $T_{max} = 151$°C) and at 144°C (lowest geol. $T_{max} = 170$°C) in the LSF. These different temperatures would correspond to *c*. 630 m difference in burial depth for petroleum formation assuming a mean geothermal gradient of 33°C/km. This difference is due to the different organic facies within the Shiranish Formation, with higher contents of terrigenous organic material in the lower unit.

Summary and conclusions

Clear source rock facies variations, with significant impact of the timing of petroleum formation, have been identified for the Shiranish Formation in the central Euphrates Graben. Source rock screening of the Shiranish Formation reflects a subdivision into a Lower and an Upper Shiranish Formation. An organic matter type II to type II–III is preserved within the USF, while a kerogen type II–III is incorporated in the LSF.

The major controls on the heterogeneities of organofacies are changes in the depositional environment, and changes in the redox environment due to the deposition during a time of a sea-level change coupled with an input of terrestrial organic matter to the LSF. This terrestrial organic matter input delivered gas-prone material in contrast to the predominance of oil-prone organic matter in the USF.

A new classification of the Shiranish Formation into three subunits is proposed according to mineralogical composition: unit A (the LSF), unit B (lower part of the USF), and C (upper part of the USF). The units A and C resemble depositional conditions. Both are characterized by more clayey sediments and ankerite as a signal for palaeomethanogenesis.

The different organic matter types of the USF and LSF cause differences in the petroleum formation kinetics. The USF characterized by HI values >350 mg HC/g TOC requires lower activation energy (53–59 kcal/mol) and frequency factors (1.52×10^{14} to 6.3×10^{14}/s). A uniform heating rate of 3.3°C/Ma can cause an onset of petroleum formation (10% TR) at *c*. 136°C. In contrast, the LSF has HI values <350 mg HC/g TOC and shows a higher activation energy (54–67 kcal/mol) associated with frequency factors between 1.04×10^{15} to 8.77×10^{15}/s. The onset of petroleum formation (10% transformation ratio (TR)) is predicted to be at *c*. 144 °C.

In summary, the more than 700 m thick Shiranish Formation in the central Euphrates Graben is a unique example of a potential hydrocarbon source rock which has efficiently stored organic carbon during the uppermost Cretaceous. The large thickness in relation to the relatively short period of deposition requires both strong subsidence and high sedimentation rates. Further investigations will show how the huge amounts of organic material could have been produced and which factors led to an efficient storage, but also how these processes affect the today's hydrocarbon potential. A complex interaction of factors like productivity, favourable incorporation in the mineral matrix and less effective diagenetic overprint offer potential for a high resolution of depositional features.

This study is part of the Ph.D. studies of S. Ismail. The authors thank Shell International E&P and Al-Furat AFPC for providing cutting material and data. We are grateful to Dr R. Naumann for his mineralogical and inorganic analyses, Dr B. Plessen for the analysis of stable nitrogen isotopes, and F. Perssen for pyrolysis experiments.

References

Abboud, M., Philp, R. P. & Allen, J. 2005. Geochemical correlation of oils and source rocks from central and NE Syria. *Petroleum Geology*, **28**, 203–218.

Barazangi, M., Serber, D., Chaimov, T., Best, J., Litak, R., Al-Saad, D. & Sawaf, T. 1993. Tectonic evolution of the northern Arabian plate in western Syria. *In*: Boschi, E., Mantonani, E. & Morelli, A. (eds) *Recent Evolution and Seismicity of the Mediterranean Region*. Kluwer Academic, Dordrecht, 117–140.

Berner, R. A. 1982. Burial of organic carbon and pyrite sulfur in the modern ocean: its geochemical and environmental significance. *American Journal of Science*, **282**, 451–473.

Breit, G. N. & Wanty, R. B. 1991. Vanadium accumulation in carbonaceous rocks: a review of geochemical controls during deposition and diagenesis. *Chemical Geology*, **91**, 83–97.

Brew, G., Barazangi, M., Al-Maleh, A. K. & Sawaf, T. 2001. Tectonic and geologic evolution of Syria. *Gulf PetroLink, Bahrain. GeoArabia*, **6**, 573–616.

Calvert, S. E. 2004. Beware intercepts: interpreting compositional ratios in multi-component sediments and sedimentary rocks. *Organic Geochemistry*, **35**, 981–987.

Chamley, H. 1989. *Clay Sedimentology*. Springer, Heidelberg, 623.

De Ruiter, R. S. C., Lovelock, P. E. R. & Nabulsi, N. 1995. The Euphrates Graben of eastern Syria: a new petroleum province in the northern Middle East. *In*: Al-Husseini, M. I. (ed.) *GEO 94: The Middle East Petroleum Geosciences*, **1**. Gulf PetroLink, Manama, Bahrain, 357–368.

Demaison, G. J. & Moore, G. T. 1980. Anoxic environments and oil source bed genesis. *American Association of Petroleum Geologists Bulletin*, **64**, 1179–1209.

Dembicki, Jr, H. 2009. Three common source rock evaluation errors made by geologists during prospect or play appraisals. *American Association of Petroleum Geologists Bulletin*, **93**, 341–356.

Dunham, R. J. 1962. Classification of carbonate rocks according to depositional texture. *In*: Ham, W. E. (ed.) *Classification of Carbonate Rocks – A Symposium*. AAPG, Tulsa, OK, Memoirs, **1**, 108–121.

Einsele, G. 2000. *Sedimentary Basins. Evolution, Facies and Sediment Budget*. Springer, Berlin, **685**.

Espitalié, J., Madec, M. & Tissot, B. 1980. Role of mineral matrix in kerogen pyrolysis: influence on petroleum generation and migration. *American Association of Petroleum Geologists Bulletin*, **64**, 59–66.

Ghandour, I. M., Harue, M. & Wataru, M. 2003. Mineralogical and chemical characteristics of Bajocian-Bathonian shales, G. Al-Maghara, North Sinai, Egypt: climatic and environmental significance. *Geochemical Journal*, **37**, 87–108.

Hallam, A., Grose, J. A. & Ruffell, A. H. 1991. Paleoclimatic significance of changes in clay mineralogy across the Jurassic–Cretaceous boundary in England and France. *Palaeogeography, Palaeoclimatology, Palaeoecology*, **81**, 173–187.

Hatch, J. R. & Leventhal, J. S. 1992. Relationship between inferred redox potential of the depositional environment and geochemistry of the Upper Pennsylvanian (Missourian) Stark Shale Member of the Dennis Limestone, Wabaunsee County, Kansas, USA. *Chemical Geology*, **99**, 65–82.

Ismail, S., Schulz, H. M., Wilkes, H., Horsfield, B., Dominik, W. & Nederlof, P. 2008. Petroleum source rock characteristics of the Shiranish Formation in the Euphrates Graben, Syria. *GEO 2008 – 8th Middle East Geoscience Conference and Exhibition*. Manama, Bahrain.

Katz, B. J. 1983. Limitations of Rock-Eval pyrolysis for typing organic matter. *Organic Geochemistry*, **4**, 195–199.

Katz, B. J. & Elrod, L. W. 1983. Organic geochemistry of DSDP Site 467, offshore California, Middle Miocene to Lower Pliocene strata. *Geochimica et Cosmochimica Acta*, **47**, 389–396.

Katz, B. J., Breaux, T. M. *et al*. 1993. Implications of stratigraphic variability of source rocks. *AAPG Studies in Geology*, **37**, 5–16.

Langford, F. F. & Blanc-Valleron, M. M. 1990. Interpreting Rock-Eval Pyrolysis data using graphs of pyrolizable hydrocarbons vs. total organic carbon. *American Association of Petroleum Geologists Bulletin*, **74**, 799–804.

Lewan, M. D. & Maynard, J. B. 1982. Factors controlling enrichment of Vanadium and nickel in the bitumen of organic sedimentary rocks. *Geochimica et Cosmochimica Acta*, **46**, 2547–2560.

Litak, R. K., Barazangi, M., Brew, G., Sawaf, T., Al-Imam, A. & Al-Youssef, W. 1998. Structure and evolution of the petroliferous Euphrates graben system, southeast Syria. *American Association of Petroleum Geologists Bulletin*, **82**, 1173–1190.

Meyers, P. A. 1997. Organic geochemical proxies of paleoceanographic, paleolimnologic, and paleoclimatic processes. *Organic Geochemistry*, **27**, 213–250.

Pedersen, T. F. & Calvert, S. E. 1990. Anoxic vs. productivity: what controls the formation of organic carbon-rich sediments and sedimentary rocks? *American Association of Petroleum Geologists Bulletin*, **74**, 454–466.

Schaefer, R. G., Schenk, H. J., Hardelauf, H. & Harms, R. 1990. Determination of gross kinetic parameters for petroleum formation from Jurassic source rocks of different maturity levels by means of laboratory experiments. *Organic Geochemistry*, **16**, 115–120.

Schenk, H. J., Horsfield, B., Kroos, B., Schaefer, R. G. & Schwochau, K. 1997. Kinetics of petroleum generation and cracking. *In*: Welte, D. H., Horsfield, B. & Baker, D. R. (eds) *Petroleum and Basin Evolution*. Springer, Berlin, 231–270.

Steinke, S., Hanebuth, T. J. J., Vogt, C. & Stattegger, K. 2008. Sea level induced variations in clay mineral composition in the southwestern South China sea over the past 17 000 yr. *Marine Geology*, **250**, 199–210.

Tissot, B. P. & Welte, D. H. 1984. *Petroleum Formation and Occurrence*. Springer, Berlin, **699**.

Tucker, M. & Wright, V. 1990. *Carbonate Sedimentology*. Blackwell Science, Oxford, 28–308.

Tyson, R. V. 1995. *Sedimentary Organic Matter*. Chapman and Hall, London, **615**.

Ziegler, M. A. 2001. Late Permian to Holocene paleofacies evolution of the Arabian Plate and its hydrocarbon occurrences. Gulf PetroLink, Bahrain. *GeoArabia*, **6**, 445–504.

Session: Passive Margins

Passive margins: overview

B. LEVELL,[1] J. ARGENT,[2] A. G. DORÉ[3] and S. FRASER[4]

[1]*Shell International E and P bv., Kessler Park 1, Rijswijk, 2280AB, The Netherlands (e-mail: bruce.levell@Shell.com)*
[2]*BG Group plc, Thames Valley Park, Reading, Berkshire RG6 1PT, UK*
[3]*Statoil USA E&P, 2103 CityWest Boulevard, Suite 800, Houston, TX 77042, USA*
[4]*BHP Billiton Petroleum Inc, 1360 Post Oak Boulevard, Suite 150, Houston, TX 77056, USA*

Abstract: Passive margins have been the reliable, accessible mainstay of exploration success worldwide for the last 25 years, and have hosted the spectacularly fast exploitation of deepwater resources (Angola, Nigeria, Brazil, Trinidad, USA Gulf of Mexico, Egypt, Australia and India). Despite, or perhaps because of this, there is still much to learn about the variety of hydrocarbon habitats they present.

For example: (1) deep seismic observations and deep sea drilling have revealed more of the diversity of passive margins geodynamics. This liberates explorationists from simple geodynamic models, with consequences not only for new views of thermal history but also for the whole tectonic and stratigraphic evolution. For example, the time significance assigned to the geometries traditionally labelled 'pre-rift, syn-rift and sag' may be misleading. This has implications for correlations, the significance assigned to unconformities and sequence boundaries, heat flow and structural history. (2) New deep imaging of the sedimentary sections has revealed mistaken assumptions about the importance of 'mobile substrate' in major deltas and allowed the detailed unravelling of salt and shale movement and its implications for reservoir and trap. (3) Depositional models for deepwater reservoirs have increased in predictive capability and modern seismic imaging supports new models for shallow water sequences. (4) Discoveries of very large amounts of dry bacterial methane in stratigraphic traps have challenged old assumptions about prospectivity based on thermally matured source rocks. (5) New engineering and development technologies are opening up the commercialization of remote frontiers. As a consequence there is legitimate scope to re-visit old 'dogmas' and to propose that each passive margin segment is best regarded as unique, with analysis and interpretation rooted in observation rather than models (at least while the newly proposed models evolve to stability). Many of these themes were visited in the Passive Margins session of the Seventh Petroleum Geology Conference, held in London in 2009. This paper outlines some of these ideas, and considers how exploration along passive margins in the next decade can use new geoscience thinking.

Keywords: passive margins, exploration technology, petroleum systems, rifting, continental breakup, deepwater plays

Despite more than 70 years of active exploration, modern passive continental margins still remain an exploration frontier. With a current aggregate length of 105 000 km (for a recent review see Bradley 2008), they represent a substantial exploration domain, and also a long-lived one: mean Phanerozoic passive margin preservational lifetime, including the modern passive margins, is about 135 Ma (Bradley 2008). Present day passive margins have a mean (incomplete) life span of 104 Ma. The passive margin sequences (post rift) are estimated to host approximately 35% of all giant field discoveries (Mann *et al.* 2003), which in turn represent 67% of discovered conventional hydrocarbons.

Deep sea drilling, a wide variety of geophysical methods (e.g. SCREECH, Funck *et al.* 2003; Van Avendonk *et al.* 2008; ISIMM, White *et al.* 2008, 2010) and geological studies have demonstrated that there is substantial variety in the history of passive margins. In this paper we set out to identify some new thoughts which can trigger critical re-examination of already partly explored areas, and add to the effectiveness of exploration in new frontiers in this basin type.

A snapshot of industry activity shows the diversity of plays currently being pursued including:

(1) major deltaic depocentres (e.g. Cenozoic of US Gulf of Mexico; Venezuela, Orinoco; Brazil Campos, Santos; Niger, Congo and Baram Deltas);
(2) smaller deltaic depocentres (e.g. Alaska, Beaufort Sea; Cameroon, Isongo; Equatorial Guinea; India, Mahanadi, Cauvery; Guyana, Essequibo; South Africa, Orange; Mozambique, Rovuma; Tanzania, Rufiji; Kenya, Lomu);
(3) slope by-pass systems (Ghana; Equatorial Guinea; India, Krishna-Godavari);
(4) carbonate platforms and their margins (Pakistan, Indus; Senegal; Mauritania; Morocco);
(5) deepwater fold belts (Mozambique, Rovuma; Nigeria, São Tomé and Príncipe);
(6) lightly explored frontier Arctic margins (USA Beaufort Sea; Canada, deepwater Mackenzie Delta);
(7) deepwater far-outboard areas with a wide variety of reservoirs and tectonic settings (Norway Outboard Voring; Brazil Santos; Australia, Outer Exmouth);
(8) syn-rift sections (Gabon sub-salt; India Krishna-Godavari; Norway, Voring Nordland);
(9) pre-rift sections on many margins.

Passive margin evolution and its implications

Better understanding of passive margins is demonstrated by the observation that it is now surprisingly hard to find an example of a 'classical' model of margin evolution (e.g. Allen & Allen 2005). Perhaps the best is the Labrador margin (Chalmers &

VINING, B. A. & PICKERING, S. C. (eds) *Petroleum Geology: From Mature Basins to New Frontiers – Proceedings of the 7th Petroleum Geology Conference*, 823–830. DOI: 10.1144/0070823

Pulvertaft 2001). The exciting new information on deeper structure of continental margins generated by large-scale refraction and reflection experiments as well as direct drilling supports a wide spectrum of plausible passive margin evolutionary mechanisms. This variety has triggered a wave of model-based inferences, in particular on post-rift evolution of continental margins. These insights have, to some extent at least, liberated the exploration geologist, struggling to interpret the deeper data on industry reflection seismic lines from simple models of the rift, thermal sag, rift/drift unconformity and drift phases. They include:

(1) The common occurrence of multiple rifting events with an irregular relationship to the line of final breakup (Doré *et al.* 1999; Ren *et al.* 2003). A recently identified potential example is described by Scotchman *et al.* (2010), who postulate a pre-breakup rift, oblique to the continental margin, in the Santos Basin, offshore Brazil, thought to have proceeded almost to oceanic status.
(2) The possibility of polyphase faulting in any given rift event. Redfern *et al.* (2010) suggest multiple rift events in the Permo-Triassic sequences of the North Atlantic margins, more varied than the overlying Jurassic and younger basins.
(3) A better understanding of magmatic addition to passive margins. Reynisson *et al.* (2010) systematically describe high-velocity, high-density lower crustal bodies on the mid-Norwegian margin and infer that, contrary to the common view that these bodies constitute magmatic additions to the base of the crust, many such features may be better explained as high-grade metamorphics remaining from the Caledonian orogeny, or as serpentinized mantle. In a similar vein, White *et al.* (2010) show from deep penetration and wide-angle seismic data on the Faroes–Hatton margin the probable existence of massive lower crustal intrusion, confined to the margin and with a sharp landward boundary. This again calls into question the concept of a widespread underplate, and the many phenomena assumed to result from it.
(4) The occurrence of very wide sag-type basins, relative to the syn-rift phase, possibly related to differential lower to mid-crustal stretching rather than a thermal sag related to pure shear rifting. The importance of this structural regime is attested to by recent discoveries on São Paulo Plateau of the Santos Basin (Machado *et al.* 2009).
(5) The possibilities of either hot/wet spot rifting with intra-crustal and supra-crustal magmatic addition or cold/dry-spot or otherwise amagmatic rifting margin. For a summary of magma-poor margins see Reston (2008). Hyperextension and mantle exhumation are currently the source of prolific literature and more examples of hyperextension are regularly being proposed. Blaich *et al.* (2010) discuss the nature of the conjugate magma-poor Camamu–Almada (Brazil) and Gabon margins, and in particular the nature of a prominent deep detachment surface, the M-Reflector. It is uncertain whether the reflector is underlain by exhumed mantle, but it appears to be an intraplate decoupling surface that accommodated significant pre-breakup extension.

As well as the obvious and ubiquitous thermal maturation implications, these insights also potentially impact other issues important to explorers, for example:

(1) the 3D isostatic behaviour of margins, and their consequent palaeobathymetric evolution;
(2) the correlation of poorly dated 'syn-rift units', possibly representing multiple rift phases, and the interpretation of basement penetrations or reflections as non-conformities v. rotated fault planes (and hence the significance to be attached to 'basement' penetrations in terms of completely testing a play);
(3) the nature and significance of unconformities, in particular the presence, significance and age of the 'rift-drift' unconformity (Tucholke *et al.* 2007) – other considerations include local footwall uplifts v. regional changes in crustal stretching and thinning and, again, unconformities due to poly-phase rifting rather than the single rift event of classic passive margin evolution.

Two-dimensional views of margin evolution are clearly only partial. Segmentation of margins can relate to pre-existing geomechanical interfaces in the basement. Many margin geometries are typically attributed to the breaking of continental crust along old lines of structural weakness. Ebbing & Olesen (2010) follow this line in documenting basement thickness variations and structural segmentation along the mid-Norwegian margin. These variations are correlated with Caledonian and Precambrian basement domains, and also with later basement detachments and normal faults mapped close to shore or onshore, and prolongated oceanwards. This paper also provides a valuable compilation of Moho depth and basement thickness for the entire mid-Norwegian shelf and western Barents Sea. It is worth noting, however, that only about 50% of the entire Gondwana supercontinent's rifted margins are even sub-parallel to pre-existing structure, based at least on the structural level of the current Gondwana surface geological map. Hence old structures are not necessarily parallel to either rift/drift tectonic strike or depositional strike. Together with intracontinental deformation, these factors can cause significant trend complexity and segmentation along margins. This can be obscured, particularly in restoring early rift units by generalized continental fits, especially those that do not accommodate intracontinental deformation (De Wit *et al.* 2008).

Hydrocarbon charge and maturation

Major marine source rocks and oceanic anoxic events

The explored passive margin source rocks have typically been the few, major, regionally extensive source rock-bearing intervals characteristic of whole sets of basins and seemingly preponderant in the Atlantic Oceans (e.g. Toarcian, Aptian Turonian and Lower Eocene).

In this respect passive margins are of course no different from other hydrocarbon provinces. For the world as a whole, almost 60% of discovered conventional hydrocarbons were sourced from the major source rocks of the Jurassic and Cretaceous and 75% if the Cenozoic is included (Klemme & Ulmishek 1991). Plays associated with these source rocks have largely been proven, or at least defined. Future potential in these known petroleum systems will arise from changing political/environmental or commercial circumstances. Examples of such 'political' openings include: Guyana (Upper Cretaceous petroleum system); potentially Mexico (Jurassic and Cretaceous); the Eastern seaboard of the USA; Georges Bank off Canada; east Greenland; and Nordland, off northern Norway (Upper Jurassic/Lower Cretaceous).

Local source rocks

Excitingly, much future passive margin exploration may rely on currently unknown, missed or more local or marginal source rocks. For example, driving the Niger Delta play into still deeper water will require an Oligocene or older charge system. In margins where the Middle or Upper Jurassic source is absent or too deep, and the Upper Cretaceous is immature due to lack of a depositional overburden, the Lower Cretaceous is often in the present-day maturity window. The often-marginal source rocks of the Lower Cretaceous will, however, need to deliver! Future large passive margin plays which would benefit from a prolific Lower Cretaceous source rock facies include: west Greenland; much of Africa – NW Africa from Morocco and the Canaries to Liberia, southern Africa, and east Africa; the Great Australian Bight; the South Atlantic, Uruguay and Argentina; and the Lord Howe Rise. Interestingly the geochemistry of the early Aptian oceanic anoxic event suggests that it is a deeper water anoxic event than, for example, the Toarcian, which was characterized by photic zone euxinia (Jenkyns 2003). The specific organic and inorganic geochemistry of source rock pods, reflecting their palaeo-ecology, may enable extrapolation from known occurrences into shallower sections and predict onlap or dilution.

Important clues to missed source rocks are provided by modern geochemical methods. Examples include diamondoid and C isotope analysis (Sassen & Post 2008), which when carried out on minor condensate in the Baltimore Canyon Trough on the eastern North American passive margin (Prather 1991) possibly point to extreme thermal cracking of oils from a Lower–Middle Jurassic source rock. Elsewhere dilution of a minor but effective charge system by a prolific one may obscure a secondary play. Detailed biomarker geochemistry can tease out the secondary charge system.

Hydrates and biogenic gas

In addition to conventional source rocks, biogenic gas has proven in the Nile, Krishna Godavari and Mahanadi deltas to be able to source major fields. A better understanding of biogenic gas, even a predictive understanding, may unlock many new plays.

In the Krishna Godavari (K-G) Basin a detailed model of gas generation, charge focusing and migration has been developed by workers from Reliance, following the discovery of the multi Tcf-Dhirubbai Field and its satellites (Bastia 2006; Kundu *et al.* 2008). The K-G play is believed to be biogenic based on uniformly high negative $\delta^{13}C > 90$ per mil in the gas. The impingement of an oxygen minimum zone on the slope has resulted in preservation of a steady 1–2% total organic carbon (TOC) through the Mio-Pleistocene section. In areas with too rapid accumulation (perhaps >1200 m/Ma) the source rock is too dispersed. In areas with too slow deposition (perhaps <500 m/Ma) there is insufficient organic preservation, or sulphate is not dispersed, or the methane itself can be oxidized. However, in zones with the right sedimentation rate, bacteria generate methane from the organic matter in the shallow subsurface. As the sedimentary section accumulates, this methanogenic zone rises, gas migrates upwards until it reaches the hydrate stability zone where it first forms hydrate, then pools beneath the impermeable layer. This layer itself rises through the sediment column as fresh insulating sediments are deposited and deeper layers dissociate releasing biogenic gas.

The hydrate layer, following the conical sea bottom of the delta, has focused migration updip and broadly towards the delta axis into the ponded slope turbidites of a terrace formed by a linked extensional/compressional fault system.

Biogenic gas systems can be driven not only by organic material in the sediment hosting the methanogenic bacteria, but also by supply of other substrates from thermally maturing source rocks. Known biogenic gas systems also provide a basis for chasing new plays.

Heat flow models

For conventional charge systems thermal maturation is clearly important. In the case of the K-G Basin biogenic system the cooling of the seafloor along the continental slope due to changes in oceanic circulation driven ultimately by glaciations, critically extended the hydrate stability field updip. More usually, heating from below and insulation by sediment are regarded as the major issues. Classical basin models rely on a relationship between observable, if local, sedimentation histories, through regional unloaded crustal subsidence, to a model of isostatically balanced crustal thinning which has heat flow consequences. The 'McKenzie' pure shear stretching model for rifts (McKenzie 1978) has stood the test of time as a robust basis for modelling in various different software suites. It provides, for example, a simple explanation of the occurrence of oil and gas in the passive margin off Congo and Angola related to the Cenomanian–Turonian Iabe Formation, as well as rift basins such as the Kimmeridge Clay of the North Sea. This may in part be due to its general nature which, despite the rigour of back-stripping, still allows matching of temperature histories with loosely constrained crustal and conductivity parameters. Recent observations however challenge the validity of classical pure shear rift models for the later stages of passive margin geodynamics (e.g. Kusznir & Karner 2007). It is plausible that thermal basin models have in some cases been right for the wrong reasons, or alternatively that thermal histories (when calibrated for example to recent temperature data) can be somewhat insensitive to the precise mechanisms of lithospheric deformation.

In addition there has been re-assessment of some of the 'constants', for example the heat-generating capacity and thermal structure of the continental crust itself (Jackson *et al.* 2008) and kinetic parameters used in hydrocarbon modelling (Stainforth 2009).

Seismic observations of shallow or even exposed mantle in the outer parts of passive margins, and direct drilling evidence, cannot be reconciled with pure shear extension, and imply depth-variable extension (so called 'depth-dependent'), which can be logically related to lithospheric mechanics (Reston & Perez-Gussinye 2007).

For hydrocarbon prospectivity in passive margins this has the following implications:

(1) Accommodation space creation, both in the early rift and in the late rift to drift phases, may not follow models based on pure shear. Specifically, the empirical observations are that accommodation space is lower than predicted in the early rifting phase, leading to sustained shallow water depositional environments. This is typically followed by subsidence so rapid that it may not be balanced by sediment supply leading to rapid deepening.
(2) In inboard areas, the brittle extension of the rift phase ends well prior to the onset of drifting, or may even relate to a previous phase of rifting, leading to a rift-drift transition which is younger than the level of 'top extensional faulting', sometimes picked as the rift-drift unconformity. This can lead in frontier settings to erroneous jump correlations, with implications for reservoir and source rock prediction. It may also lead to an erroneous understanding of the regional context of the older rift faulting.
(3) Conversely in outboard areas, rifting, even to an extreme degree, can continue well after true seafloor spreading has commenced (Tucholke *et al.* 2007).
(4) The heat flow models related to pure shear, and the attendant mantle upwelling, may not be relevant to mantle which although uplifted is apparently not uplifted on a 'normal' mantle adiabat, and moreover undergoes extensive serpentinization (Blaich *et al.* 2010; Reynisson *et al.* 2010).

These effects are currently being assessed. The ability to confidently model temperature history based on geodynamics awaits clarity on the physical mechanisms for lithospheric mantle and lower crustal extension.

New thermal history algorithms will probably fall into two domains:

(1) 'pick-and-mix' forward models which can deal with varying margin evolution scenarios and are used to classify margins into genetic types (e.g. magma-rich v. magma-poor, depth-dependent stretching or pure shear);
(2) use of observed geometric attributes (sedimentary backstripping, whatever crustal profiling data are available) and boundary temperature assumptions without explicit choice of a geodynamic model to invert to a crustal profile, followed by a forward temperature model.

An interesting approach to the latter is the 2D inversion of strain rate as defined by stratigraphic geometries (e.g. Bellingham & White 2002; White *et al.* 2004; Crosby *et al.* 2008). In its first exposition this approach was simplified, but it illustrates well the potential of inversion based on observation, rather than forward models based on a sometimes arbitrary choice of geodynamic model.

Exploration on oceanic crust

Exploration is already being pursued onto oceanic crust in areas where sedimentary overburden is thick enough for thermal blanketing to compensate for lower crustal heat production. Typically such plays are sourced by rocks related to major oceanic anoxic events. Examples include the Gulf of Mexico, the outer Niger Delta, the outer Congo Delta and the Ganges–Brahmaputra deep sea fan off Eastern India. There are suggestions that some thick passive margin sequences, such as the anomalously unstructured simple prograding wedges offshore Mozambique, may also be underlain by transitional oceanic crust (Watts 2001).

Reservoirs

Clearly a wide range of reservoir types have proven productive on passive margins: aeolian sandstones (Kudu, Namibia); hydrothermal dolomites (Deep Panuke; Wierzbicki *et al.* 2006); the full range of carbonate facies (Campos and Santos Basin lacustrine coquinas and microbial carbonates, reef and fore-reef limestones in Mexico–Campeche, platform sequences such as the India–Bombay High and salt-rafted limestones in Angola and Congo); shallow marine clastics (NW Australia, Gabon); deltaics (Niger, Cameroon, the Canadian Mackenzie, Nile); and last but not least slope and basin-floor turbidites (all the above deltas, Gulf of Mexico, Norway and UK Atlantic Margin, Angola, Congo, Equatorial Guinea, NW Australia).

It is probably fair to say, however, that turbidite reservoirs have stolen the show as exploration has moved into ever-deeper water. Approximately 125×10^9 BOE have been discovered in water depths of more than 400 m in the last 30 years, and with 30 plus BBOE in the last 4 years, this global play is not yet creamed. The great majority of these volumes have been from passive margins (the major exceptions being the south Caspian and NW Borneo). Reasonable estimates, based on play analysis, creamed field size distribution curves for each province or simply basin creaming curve analysis, are for a further 150–200 BBOE from passive margin deepwater plays via new discoveries and reserve growth.

Notably, recent major exploration discoveries in the deepwater Brazilian Santos Basin have taken the spotlight from turbidite reservoirs (Scotchman *et al.* 2010). These resources are hosted in Late Barremian and Aptian non-marine microbial carbonates in the late syn-rift and sag sequences prior to deposition of the South Atlantic salt basin (Machado *et al.* 2009; Wright & Racey 2009). Reservoir quality is strongly facies-controlled overprinted by a multiphase diagenetic history, culminating in late-stage corrosion enhancing the remnant primary porosity and sequent reservoir deliverability. Predicting reservoir distribution across these giant fields poses an unique challenge for development. However, these discoveries raise the question of whether similar pre-salt petroleum systems are yet to be discovered along the conjugate margins in the South Atlantic (Jones *et al.* 2009).

Reservoirs on outer margins

Outboard portions of passive margins have typically been dominated by exploration for deepwater reservoirs. A number of processes can result in shallow water deposits being drowned in the deep waters of the outer margins and yet still be at economically drillable depths:

(1) sediment starvation, outboard due for example to an active inboard rift-related basin, perhaps in its thermal sag phase;
(2) depth-dependent mid-crustal stretching (Kusznir & Karner 2007), for example on the outboard Exmouth Plateau;
(3) severe crustal thinning and mantle exhumation (e.g. review in Reston 2009);
(4) micro-continent isolation by rift jumping (e.g. São Paulo High, Scotchman *et al.* 2010).

Reservoirs and 'basement' in multi-phase rifts

Much older industry seismic data shot with 4 km streamers warrants re-analysis in the light of the realization that a classical rift then drift model of passive margin evolution is probably too simple. Apart from simply correct imaging of basement, the picking of top basement reflections and an understanding of possibly rotated early fault planes which appear to be top basement is one point to check. A second is the significance and age of 'syn-rift' or 'pre-rift' sequences. Syn- which rift? Pre- which rift? Proximal alluvial sequences may well have been dated by inference from an assumed tectonostratigraphic scheme rather than by biostratigraphic data.

Large drainage basin systems

Some 50 major river drainage systems drain most of the land surface of the present-day continents and of these about half drain to modern passive margins, giving the thermal blanketing, reservoir and seal for recent hydrocarbon generation and preservation. As exploration shifts away from the current major river deltas/or into deeper sections, it is worth questioning past palaeogeographies to see if drainage basins differed. The widespread development, for example, of Upper and 'Middle' Cretaceous inland (epeiric) seas on all continents suggests that major drainages were busy infilling these essentially foreland basin domains, with relatively minor drainages feeding the then young (Atlantic) passive margins. Earth systems, thinking about interactions between erosion, sedimentation, palaeoclimate and palaeo-oceanography, may also be a stimulating source of new ideas about reservoirs in older sequences (e.g. for the Cretaceous; Skelton *et al.* 2003). Notable Upper Cretaceous discoveries along the equatorial African margin in the Rio Muni Basin, Equatorial Guinea and the West Tano Basin, Ghana have shown that these earlier drainage systems can provide high-quality turbidite reservoirs.

Shelf edge deltas and plays

The compelling outcrop evidence that sediment supply drives deltas to the shelf edge during high stands (e.g. Uroza & Steel 2008), demonstrates that rigorous application of 'standard' sequence stratigraphic models (which for didactic purposes have underplayed the role of variable sediment supply) may have left the possibilities of these depositional systems unexplored. High stand shelf edge deltas can be expected to be characterized by thicker progradational parasequences, in general more linear and wave-dominated shorefaces, and more hyperpycnal flow direct from river mouths. The realization that interactions between palaeoclimate and changing atmospheric conditions may have caused peaks of sediment input allows explorers to investigate these controls for specific time intervals of higher weathering.

The importance of small, localized but high volume, sediment inputs controlled by drainage systems was highlighted by Martinsen *et al.* (2010). They describe a holistic 'source-to-sink' approach relating onshore drainage and geomorphology to subsurface clastic reservoirs, using the Norwegian Sea Paleocene play as an example. New geomorphological insights and data highlighting old river capture patterns are another source of inspiration for undiscovered reservoir sequences. Studies of mantle-related dynamic topography imply a variability in sediment supply due to erosion of regional uplifts, which is in contrast with the often implicit assumption of uniform sediment supply rates in some sequence stratigraphic models.

Improved techniques for establishing provenance enhance precision in this regard. For example, Redfern *et al.* (2010) and Tyrrell *et al.* (2010) describe an approach based on Pb isotope analysis of detrital feldspars that has helped to identify quite surprising and diverse basement origins for the sediments in the Rockall Basin and its margins.

Remaining deepwater plays

It can be expected that deep-marine turbidite plays will continue to be important in passive margins – not only sub-salt as in Angola and the Gulf of Mexico but also in unexplored frontier deepwater areas (e.g. the outboard Mackenzie Delta). Smaller river systems, some driven to the shelf edge as described above, and older drainage systems such as those in Cretaceous depocentres are all currently being pursued (e.g. east Greenland draining to the Norwegian outer Vøring Basin, Morocco–Canaries, Casamance Delta off Senegal). Based on improved seismic imaging, Larsen *et al.* (2010) also proposes that the Cretaceous syn-rift play of the Faroe–Shetland Basin is worth revisiting. Their interpretation revisits the source-to-sink theme, and the concept of rift segmentation, alluded to in this paper and elsewhere in this volume.

It is also possible that, in the thickest deepwater fans with massive slope by-pass of sand such as the Congo and the Ganges–Brahmaputra, largely unstructured compactional fan lobe and channel plays may be possible even on oceanic crust (Anka *et al.* 2009), given of course source rocks and a thick enough thermal blanket of sediment.

Retention

Subtle migration paths

Offshore Equatorial Guinea discoveries in Miocene slope channels spectacularly demonstrate the ability of thin (10–20 m) slope and basin floor sands to form stratigraphic traps in largely unstructured sections (Stephens *et al.* 1996), as well as the ability of oil and gas condensate to migrate vertically through thick mudstone packages from relatively deep Upper Cretaceous source rocks. This impressive feat of migration is mediated by compactional faults related to the seafloor rugosity along transform faults at the top of the oceanic crust, but which have very limited offsets. Much remains unknown about the fault-related focusing of migration flux in such systems.

Late structural evolution

Anderson (2007) argues on the basis of the lack of strength of rocks in tension that a tectonic plate can be seen as a unit of lithosphere in a state of compressive stress: part of a self-organized system essentially held in that state by plate boundary forces. It is therefore not surprising that passive margins that are born and die at plate margins but spend their middle years in plate interiors record mid-life crises, expressed as a fair amount of compressive tectonic structuring. As is well known, the World Stress Map (Heidbach *et al.* 2008) shows that the current orientation of principal horizontal stress is less related to the direction of rifting than to the current direction of plate motion, giving present-day and presumably therefore palaeocompressive stresses at oblique angles to the margins. The relationship of such plate motion-induced stresses, or body-force stresses associated with plate boundaries, to observed strain phenomena is discussed in the paper by Doré *et al.* (2008). Broad compression-related folds in the Cretaceous–Cenozoic cover successions are observed over a wide area between the Mid-Norwegian shelf and the Rockall–Faroes area. The folds appear to be episodic and to have multiple origins, and are interesting as potential late-formed hydrocarbon traps.

Late uplift, unrelated or connected only indirectly to the actual formation of a passive margin, is now well documented from many margins (e.g. Nielsen *et al.* 2008). In west Greenland, Japsen *et al.* (2006) describe three separate phases of uplift: broadly Oligocene (36–30 Ma), Miocene (11 Ma) and Pliocene (7–2 Ma), all clearly post-dating the classical rift shoulder-related uplift in the Eocene. Such events/features may have local or regional causes (Doré *et al.* 2008; Cloetingh *et al.* 2008; Holford *et al.* 2008). There is also clear evidence for substantial transient rapid uplift (Rudge *et al.* 2008; Shaw-Champion *et al.* 2008). Dynamic topography related to mantle phenomena appears to be implicated. The impacts on exploration are potentially profound, with the cessation of active maturation and possibly expulsion of hydrocarbons, embrittlement of seals, creation or destruction of overpressures, and expansion of gas caps being among the more obvious on older uplifted sequences. Furthermore the new input of sediment from erosional products may trigger very recent maturation and expulsion and far-field compressive stresses and fault reactivation may trigger new trapping possibilities. Japsen *et al.* (2010) provide comprehensive documentation of Cenozoic uplift around the North Atlantic, including timing and implications for sedimentation and petroleum systems. They suggest that uplift may be an implicit tendency of passive margin borderlands, speculatively a function of changes in crust and lithosphere thickness over short distances.

Around Africa late continental uplift, associated by many with dynamic topography, has generated seaward dips which bedevil exploration by tilting out the traps. This late uplift is sometimes obscured by salt movement or other forms of gravitational collapse, and is often multi-phase. For example in the apparently simple and 'classical' Orange River Basin margin of NW South Africa, two phases of later-than-rift uplift (Upper Cretaceous and Mid Cenozoic), are revealed (Paton *et al.* 2008).

Technology

New development concepts

The full globalization of LNG is opening up gas exploration in what were previously oil basins (e.g. Vining *et al.* 2010), or in countries or areas without developed gas markets. Furthermore, the ability to process LNG and load tankers offshore will enable development of remote fields, or fields off difficult coastlines, with the benefit also of spreading the burden of LNG plant construction around the world. Floating LNG production is currently considered likely to first be used for developments off NW Australia, but remote passive margins worldwide could follow.

New engineering technologies are also enabling smaller oil accumulations and more difficult fluids to be developed further offshore and in yet deeper water. Recent examples include very deepwater spar developments such as that in the Perdido Fold Belt, Gulf of Mexico, where the Shell group's Great White production well in 2934 m of water holds the current record. This trend too can be expected to continue.

Exploration technology refinement, leading to new exploration models

Improvements to seismic data quality are still occurring at a rapid pace. For example, Hardy *et al.* (2010) describe potential strategies and processing flows for deepwater seismic resolution, with applications for exploration off western Ireland. Wider use of multi-azimuth seismic and pre-stack depth imaging not only for seeing below salt (Ekstrand *et al.* 2010), but also simply for higher-fidelity imaging, has helped in the development of new plays such as the highly successful Gulf of Mexico and South Atlantic sub-salt, and is likely to continue to open up new plays. As costs come down (as, e.g. shooting geometries are optimized), these techniques will become even more widespread. The vastly increased visibility of sub-salt sequences in recent years has been accompanied by significant refinement of salt models, and an increased understanding of how salt and sediment behaves in areas of high sedimentation and multiphase halokinesis. Such models are important offshore Brazil and west Africa, although the key testing ground has been the US Gulf of Mexico. Jackson *et al.* (2010) describe some of these emerging concepts, such as the movement of salt canopies in the subsurface and the transport of exotic sediment rafts over tens of kilometres seaward by migrating canopies. This paper also addresses some of the current enigmas regarding minibasin formation.

Imaging beneath a thick basalt cover is a significant concern and the key to further exploration success in the North Atlantic Faroe–Shetland and Møre Basins. In the few wells that have attempted to test sub-basalt traps, the depth to base basalt has been underestimated and the wells abandoned without reaching their objective. Two studies in this volume address this theme. Davison (2010) describes imaging using deep towed seismic and its results for Cenozoic and Cretaceous trap models, while Ellefsen *et al.* (2010) stress the need for understanding internal volcanic facies at the base of the basalt succession to better resolve the key base basalt reflector.

Use of controlled source electro-magnetic surveying is increasingly becoming routine, and can, for example, usefully distinguish low saturation gas which seismic methods may not be able to separate from higher gas saturation reservoirs. Better basin models based simply on more calibration data as well as new geodynamic insights, more refined geochemical extrapolation of source rock facies based on palaeo-ecological and palaeoclimatic insights, and a clearer understanding of late uplift through fission track geothermometry and satellite-based palaeogeomorphological studies, can all be expected.

Frontiers

In addition to new ideas for already part-explored areas, there are of course still margins which have yet to be explored. Prospective margins which have suffered commercial challenges include the difficult climatic conditions of the Arctic margins and areas subject to border disputes or moratoria, such as much of the western North Atlantic margin.

Arctic

Positions are being taken along the lightly explored margins of the greater Arctic, for example, in the Beaufort Sea–Mackenzie Delta margin, with proven plays in the Paleocene to Miocene, and in west Greenland and Labrador margins. Exploratory survey work is being conducted off east Greenland. Acreage has also been offered recently in the Laptev Sea.

Palaeo-passive margins

Although not the subject of this meeting, it has to be remembered that ancient passive margins also contain oil and gas, the Brookian sequence of Alaska being a major example. In general the conversion of the passive continental margin to an active plate margin, as is currently happening between Timor and Australia, either destroys or overwrites the petroleum system. The significance of palaeo-passive margins as petroleum systems really depends on where the cratonward, updip limit of a passive margin system is placed. Examples where this might be important include the Palaeozoic of the Western Canadian Sedimentary Basin and the Mesozoic of the northeastern (Tethyan) rim of Arabia. In general these sequences are traditionally treated as belonging to continental epeiric sea basins rather than being inboard passive margins. Perhaps new insights into passive margin geodynamics will change this too.

References

Allen, P. A. & Allen, J. R. 2005. *Basin Analysis: Principles and Applications* (2nd edn). Wiley Blackwell, Chichester.

Anderson, D. L. 2007. *New Theory of the Earth*. Cambridge University Press, Cambridge.

Anka, Z., Séranne, M., Lopez, M., Scheck-Wenderoth, M. & Savoye, B. 2009. The long-term evolution of the Congo deep-sea fan: a basin-wide view of the interaction between a giant submarine fan and a mature passive margin (ZaiAngo project). *Tectonophysics*, **470**, 42–56.

Bastia, R. 2006. An overview of Indian sedimentary basins with special focus on emerging East Coast deepwater frontiers. *The Leading Edge*, July, 818–829.

Bellingham, P. & White, N. 2002. A two-dimensional inverse model for extensional sedimentary basins. 2. Applications. *Journal of Geophysical Research*, **107**, 2260; doi: 10.1029/2001JB000174.

Blaich, O. A., Faleide, J. I., Tsikalas, F., Lilletveit, R., Chiossi, D., Brockbank, P. & Cobbold, P. 2010. Structural architecture and nature of the continent–ocean transitional domain at the Camamu and Almada Basins (NE Brazil) within a conjugate margin setting. *In*: Vining, B. A. & Pickering, S. C. (eds) *Petroleum Geology: From Mature Basins to New Frontiers – Proceedings of the 7th Petroleum Geology Conference*. Geological Society, London, 867–883; doi: 10.1144/070867.

Bradley, D. C. 2008. Passive margins through earth history. *Earth Science Reviews*, **91**, 1–26; doi: 10.1016/j.earscirev.2008.08.001.

Chalmers, J. A. & Pulvertaft, T. C. R. 2001. Development of continental margins of the Labrador Sea: a review. *In*: Wilson, R. C. L., Whitmarsh, R. B., Taylor, B. & Froitzhelm, N. (eds) *Non-volcanic Rifling of Continental Margins: A Comparison of Evidence from Land and Sea*. Geological Society, London, Special Publications, **187**, 77–105.

Cloetingh, S., Beekman, F., Ziegler, P., Van Wees, J.-D. & Sokoutis, D. 2008. Post-rift compressional reactivation of passive margins and extensional basins. *In*: Johnson, H., Doré, A. G., Gatliff, R. W., Holdsworth, R., Lundin, E. R. & Ritchie, J. D. (eds) *The Nature* *and Origin of Compression in Passive Margins*. Geological Society, London, Special Publications, **306**, 27–70; doi: 10.1144/SP306.2.

Crosby, A., White, N., Edwards, G. & Shillington, D. J. 2008. Evolution of the Newfoundland–Iberia conjugate rifted margin. *Earth and Planetary Science Letters*, **273**, 214–226.

Davison, I., Stasiuk, S., Nuttall, P. & Keane, P. 2010. Sub-basalt hydrocarbon prospectivity in the Rockall, Faroe–Shetland and Møre basins, NE Atlantic. *In*: Vining, B. A. & Pickering, S. C. (eds) *Petroleum Geology: From Mature Basins to New Frontiers – Proceedings of the 7th Petroleum Geology Conference*. Geological Society, London, 1025–1032; doi: 10.1144/0071025.

De Wit, M. J., Stanciewicz, J. & Reeves, C. 2008. Restoring pan African–Brasiliano connections: more Gondwana control, less trans-Atlantic corruption. *In*: Pankhurst, R. J., Trouw, R. A. J., Brito Neves, B. B. & de Wit, M. J. (eds) *West Gondwana Pre-Cenozoic Correlations Across the South Atlantic Region*. Geological Society, London, Special Publications, **294**, 399–412.

Doré, A. G., Lundin, E. R., Jensen, L. N., Birkeland, Ø., Eliassen, P. E. & Fichler, C. 1999. Principal tectonic events in the evolution of the northwest European Atlantic margin. *In*: Fleet, A. J. & Boldy, S. A. R. (eds) *Petroleum Geology of Northwest Europe: Proceedings of the 5th Conference*. Geological Society, London, 41–61; doi: 10.1144/0050041.

Doré, A. G., Lundin, E. R., Kusznir, N. J. & Pascal, C. 2008. Potential mechanisms for the genesis of Cenozoic domal structures on the NE Atlantic margin: pros, cons and some new ideas. *In*: Johnson, H., Doré, A. G., Gatliff, R. W., Holdsworth, R., Lundin, E. R. & Ritchie, J. D. (eds) *The Nature and Origin of Compression in Passive Margins*. Geological Society, London, Special Publications, **306**, 1–26; doi: 10.1144/SP306.1.

Ebbing, J. & Olesen, O. 2010. New compilation of top basement and basement thickness for the Norwegian continental shelf reveals the segmentation of the passive margin system. *In*: Vining, B. A. & Pickering, S. C. (eds) *Petroleum Geology: From Mature Basins to New Frontiers – Proceedings of the 7th Petroleum Geology Conference*. Geological Society, London, 885–897; doi: 10.1144/0070885.

Ekstrand, E., Hickman, G., Thomas, R., Threadgold, I., Harrison, D., Los, A., Summers, T., Regone, C. & O'Brien, M. 2010. WATS it take to image an oil field subsalt offshore Angola? *In*: Vining, B. A. & Pickering, S. C. (eds) *Petroleum Geology: From Mature Basins to New Frontiers – Proceedings of the 7th Petroleum Geology Conference*. Geological Society, London, 1013–1024; doi: 10.1144/0071013.

Ellefsen, M., Boldreel, L. O. & Larsen, M. 2010. Intra-basalt units and base of the volcanic succession east of the Faroe Islands exemplified by interpretation of offshore 3D seismic data. *In*: Vining, B. A. & Pickering, S. C. (eds) *Petroleum Geology: From Mature Basins to New Frontiers – Proceedings of the 7th Petroleum Geology Conference*. Geological Society, London, 1033–1041; doi: 10.1144/0071033.

Funck, T., Hopper, J. R., Larsen, H. C., Louden, K. E., Tucholke, B. E. & Holbrook, W. S. 2003. Crustal structure of the ocean continent transition at Flemish Cap: seismic refraction results. *Journal of Geophysical Research*, **108**, 2531; doi: 10.1029/2003JB002434.

Hardy, R. J. J., Querendez, E., Biancotto, F., Jones, S. M., O'sullivan, J. & White, N. 2010. New methods of improving seismic data to aid understanding of passive margin evolution: a series of case histories from offshore west of Ireland. *In*: Vining, B. A. & Pickering, S. C. (eds) *Petroleum Geology: From Mature Basins to New Frontiers – Proceedings of the 7th Petroleum Geology Conference*. Geological Society, London, 1005–1012; doi: 10.1144/0071005.

Heidbach, O., Tingay, M., Barth, A., Reinecker, J., Kurfeß, D. & Müller, B. 2008. The 2008 release of the World Stress Map. World Wide Web Address: www.world-stress-map.org.

Holford, S. P., Green, P. F. *et al*. 2008. Evidence for kilometer-scale exhumation driven by compressional deformation in the Irish Sea basin system. *In*: Johnson, H., Doré, A. G., Gatliff, R. W., Holdsworth, R., Lundin, E. R. & Ritchie, J. D. (eds) *The Nature and Origin of Compression in Passive Margins*. Geological Society, London, Special Publications, **306**, 91–119; doi: 10.1144/SP306.4.

Jackson, M. P. A., Hudec, M. R. & Dooley, T. P. 2010. Some emerging concepts in salt tectonics in the deepwater Gulf of Mexico: intrusive plumes, canopy-margin thrusts, minibasin triggers and allochthonous fragments. *In*: Vining, B. A. & Pickering, S. C. (eds) *Petroleum Geology: From Mature Basins to New Frontiers – Proceedings of the 7th Petroleum Geology Conference*. Geological Society, London, 899–912; doi: 10.1144/0070899.

Jackson, J., McKenzie, D., Priestley, K. & Emmerson, B. 2008. New views on the structure and rheology of the lithosphere. *Journal of the Geological Society, London*, **165**, 453–465.

Japsen, P., Bonow, J. M., Green, P. F., Chalmers, J. A. & Lidmar-Bergstrom, K. 2006. Elevated passive continental margins: long term highs or Neogene uplifts? New evidence from West Greenland. *Earth and Planetary Science Letters*, **248**, 330–339; doi: 10.1016/j.epsl.2006.05.036.

Japsen, P., Green, P. F., Bonow, J. M., Rasmussen, E. S., Chalmers, J. A. & Kjennerud, T. 2010. Episodic uplift and exhumation along North Atlantic passive margins: implications for hydrocarbon prospectivity. *In*: Vining, B. A. & Pickering, S. C. (eds) *Petroleum Geology: From Mature Basins to New Frontiers – Proceedings of the 7th Petroleum Geology Conference*. Geological Society, London, 979–1004; doi: 10.1144/0070979.

Jenkyns, H. C. 2003. Evidence for rapid climate change in the Mesozoic-Palaeogene greenhouse world. *Philosophical Transactions of the Royal Society, London A*, **361**, 1885–1916.

Jones, W., Guevara, M. *et al*. 2009. The subsalt play in the lower Congo and Kwanza Basins, Angola: a seismic study. Abstract from the *American Association of Petroleum Geologists Annual Convention and Exhibition*, Denver, CO, 7–10 June.

Klemme, H. D. & Ulmishek, G. F. 1991. Effective petroleum source rocks of the world: stratigraphic distribution and controlling depositional factors. *Bulletin of the American Association of Petroleum Geologists*, **75**, 1809–1851.

Kundu, N., Pal, N., Sinha, N. & Budhiraja, I. L. 2008. Do paleo-hydrates play a major role in deepwater biogenic gas reservoirs in Krishna–Godavari Basin? *Methane Hydrate Newsletter, National Energy Technology Laboratory*, Fall 13–15.

Kusznir, N. J. & Karner, G. D. 2007. Continental lithospheric thinning and breakup in response to upwelling divergent mantle flow: application to the Woodlark, Newfoundland and Iberia margins. *In*: Karner, G. D., Manatschal, G. & Pinhero, L. M (eds) *Imaging, Mapping and Modelling Continental Lithosphere Extension and Breakup*. Geological Society, London, Special Publications, **282**, 389–419; doi: 10.1144/SP282.16.

Larsen, M., Rasmussen, T. & Hjelm, L. 2010. Cretaceous revisited: exploring the syn-rift play of the Faroe–Shetland Basin. *In*: Vining, B. A. & Pickering, S. C. (eds) *Petroleum Geology: From Mature Basins to New Frontiers – Proceedings of the 7th Petroleum Geology Conference*. Geological Society, London, 953–962; doi: 10.1144/0070953.

Machado, M. A. P., Moraes, M. F. B. *et al*. 2009. The pre-salt sequence of ultra-deep water Santos basin: geological aspects and key factors controlling the major oil accumulations. Abstract, *American Association of Petroleum Geologists International Conference and Exhibition*, Rio de Janeiro, 15–18 November.

Mann, P., Gahagan, L. & Gordon, M. B. 2003. *Tectonic Setting of the World's Giant Oil and Gas Fields*. American Association of Petroleum Geologists, Tulsa, OK, Memoirs, **78**, 15–105.

Martinsen, O. J., Sømme, T. O., Thurmond, J. B., Helland-Hansen, W. & Lunt, I. 2010. Source-to-sink systems on passive margins: theory and practice with an example from the Norwegian continental margin. *In*: Vining, B. A. & Pickering, S. C. (eds) *Petroleum Geology: From Mature Basins to New Frontiers – Proceedings of the 7th Petroleum Geology Conference*. Geological Society, London, 913–920; doi: 10.1144/0070913.

McKenzie, D. P. 1978. Some remarks on the development of sedimentary basins. *Earth and Planetary Science Letters*, **40**, 25–32.

Nielsen, S. B. *et al*. 2008. The evolution of western Scandinavian topography: a review of Neogene uplift versus the ICE (isostasy–climate–erosion) hypothesis. *Journal of Geodynamics*, **47**, 72–95; doi: 10.1016/j.jog.2008.09.001.

Paton, D. A., van der Spuy, D., di Primio, R. & Horsfield, B. 2008. Tectonically induced adjustment of passive-margin accommodation space; influence on the hydrocarbon potential of the Orange Basin, South Africa. *Bulletin of the American Association of Petroleum Geologists*, **92**, 589–609.

Prather, B. E. 1991. Petroleum geology of the Upper Jurassic and Lower Cretaceous, Baltimore Canyon Trough, Western North Atlantic Ocean. *Bulletin of the American Association of Petroleum Geologists*, **75**, 258–277.

Redfern, J. & Shannon, P. M. *et al*. 2010. An integrated study of Permo-Triassic basins along the North Atlantic passive margin: implication for future exploration. *In*: Vining, B. A. & Pickering, S. C. (eds) *Petroleum Geology: From Mature Basins to New Frontiers – Proceedings of the 7th Petroleum Geology Conference*. Geological Society, London, 921–936; doi: 10.1144/0070921.

Ren, S., Faleide, J. I., Eldholm, O., Skogseid, J. & Gradsetin, F. 2003. Late Cretaceous to Paleocene development of the NW Voring Basin. *Marine and Petroleum Geology*, **20**, 177–206.

Reston, T. J. 2009. The structure, evolution and symmetry of the magma-poor rifted margins of the North and Central Atlantic: a synthesis. *Tectonophysics*, **468**, 6–27.

Reston, T. J. & Perez-Gussinye, M. 2008. Lithospheric extension from rifting to continental breakup at magma-poor margins: rheology, serpentinization and symmetry. *In*: Bernouilli, D., Brun, J.-P. & Burg, J.-P. (eds) Special issue, Continental Extension. *International Journal of Earth Sciences*, **96**, 1033–1046.

Reynisson, R. F., Ebbing, J., Lundin, E. & Osmundsen, P. T. 2010. Properties and distribution of lower crustal bodies on the mid-Norwegian margin. *In*: Vining, B. A. & Pickering, S. C. (eds) *Petroleum Geology: From Mature Basins to New Frontiers – Proceedings of the 7th Petroleum Geology Conference*. Geological Society, London, 843–854; doi: 10.1144/0070843.

Rudge, J. F., Shaw-Champion, M. E., White, N., McKenzie, D. & Lovell, B. 2008. A plume model of transient diachronous uplift at the Earth's surface. *Earth and Planetary Science Letters*, **267**, 146–160.

Sassen, R. & Post, P. 2008. Enrichment of diamondoids and ^{13}C in condensate from Hudson Canyon, US Atlantic. *Organic Geochemistry*, **39**, 147–151; doi: 10.1016/j.orggeochem.2007.10.004.

Scotchman, I. C., Gilchrist, G., Kusznir, N. J., Roberts, A. M. & Fletcher, R. 2010. The breakup of the South Atlantic Ocean: formation of failed spreading axes and blocks of thinned continental crust in the Santos Basin, Brazil and its consequences for petroleum system development. *In*: Vining, B. A. & Pickering, S. C. (eds) *Petroleum Geology: From Mature Basins to New Frontiers – Proceedings of the 7th Petroleum Geology Conference*. Geological Society, London, 855–866; doi: 10.1144/0070855.

Shaw-Champion, M. E., White, N. J., Jones, S. M. & Lovell, J. P. B. 2008. Quantifying transient mantle convective uplift: an example from the Faroe Shetland Basin. *Tectonics*, **27**; doi: 10.1029/2007TC002106.

Skelton, P. W., Spicer, R. A., Kelley, S. P. & Gilmour, I. 2003. *In*: Skelton, P. W. (ed.) *The Cretaceous World*. The Open University/Cambridge University Press, Buckingham/Cambridge.

Stainforth, J. G. 2009. Practical kinetic modeling of petroleum generation and expulsion. *Marine and Petroleum Geology*, **26**, 552–572.

Stephens, A. R., Monson, G. D. & Reilly, J. M. 1996. *Seismic Amplitudes: Their Relevance for Hydrocarbon Exploration in the Late Miocene/Early Pliocene Sediments of the Distal Niger Delta: Examples from the Zafiro Field.* Equatorial Guinea: Offshore West Africa Conference, Libreville.

Tucholke, B. E., Sawyer, D. S. & Sibuet, J.-C. 2007. *The Iberia Newfoundland Continental Extension System (Geological and Geophysical Constraints)*. Geological Society, London, Special Publications, **282**, 9–46.

Tyrrell, S., Souders, A. K., Haughton, P. D. W., Daly, J. S. & Shannon, P. M. 2010. Sedimentology, sandstone provenance and palaeodrainage on the eastern Rockall Basin margin: evidence from the Pb isotopic composition of detrital K-feldspar. *In*: Vining, B. A. & Pickering, S. C. (eds) *Petroleum Geology: From Mature Basins to New Frontiers – Proceedings of the 7th Petroleum Geology Conference*. Geological Society, London, 937–952; doi: 10.1144/0070937.

Uroza, C. A. & Steel, R. J. 2008. A highstand shelf margin delta system from the Eocene of West Spitsbergen, Norway. *Sedimentary Geology*, **203**, 229–245.

van Avendonk, H. J. A., Lavier, L. L., Shillington, D. J. & Manatschal, G. 2008. Extension of continental crust at the margin of the eastern Grand Banks Newfoundland. *Tectonophysics*, **468**, 131–148; doi: 10.1016/j.tecto.2008.05.030.

Watts, A. B. 2001. Gravity anomalies, flexure and crustal structure at the Mozambique rifted margin. *Marine and Petroleum Geology*, **18**, 445–455.

White, R. S., Eccles, J. D. & Roberts, A. W. 2010. Constraints on volcanism, igneous intrusion and stretching on the Rockall–Faroe continental margin. *In*: Vining, B. A. & Pickering, S. C. (eds) *Petroleum Geology: From Mature Basins to New Frontiers – Proceedings of the 7th Petroleum Geology Conference*. Geological Society, London, 831–842; doi: 10.1144/0070831.

White, N., Haines, J. & Hanne, D. 2004. Towards an automated strategy for modelling extensional basins and margins in four dimensions. *In*: Davies, R. J., Cartwright, J. A., Stewart, S. A., Lappin, M. & Underhill, J. R. (eds) *3D Seismic Technology: Applications to the Exploration of Sedimentary Basins*. Geological Society, London, Memoirs, **29**, 321–331.

White, R. S., Smith, L. K., Roberts, A. W., Christie, P. A. F., Kusznir, N. J. & the rest of the ISIMM team. 2008. Lower-crustal intrusion on the North Atlantic continental margin. *Nature*, **452**, 460–464.

Wierzbicki, R., Dravis, J. J., Al-Aasm, I. & Harland, N. 2006. Burial dolomitization and dissolution of Upper Jurassic Abenaki platform carbonates, Deep Panuke reservoir, Nova Scotia, Canada. *Bulletin of the American Association of Petroleum Geologists*, **90**, 1843–1861; doi: 10.1306/03200605074.

Wright, P. V. & Racey, A. 2009. Pre-salt microbial carbonate reservoirs of the Santos Basin, offshore Brazil. Abstract from the *American Association of Petroleum Geologists Annual Convention and Exhibition*, Denver, CO, 7–10 June 2009.

Constraints on volcanism, igneous intrusion and stretching on the Rockall–Faroe continental margin

R. S. WHITE,[1] J. D. ECCLES[2] and A. W. ROBERTS[3]

[1]*Bullard Laboratories, University of Cambridge, Madingley Road, Cambridge CB3 0EZ, UK (e-mail: rsw1@cam.ac.uk)*
[2]*The Institute of Earth Science and Engineering, University of Auckland, New Zealand (present address)*
[3]*Department of Earth Sciences, Durham University, UK (present address)*

Abstract: The northern North Atlantic margins are classic examples of 'volcanic' rifted continental margins, where breakup was accompanied by massive volcanism. We discuss strategies used to obtain good intra- and sub-basalt seismic penetration so as to map the structure and the extruded and intruded igneous volume. We recorded deep penetration reflection data using a 12 000 m long single sensor (Q-)streamer and wide-angle seismic profiles with 85 4-component ocean bottom seismometers, along two transects across the Faroe and Hatton Bank continental margins in the NE Atlantic. Tomographic inversion of both compressional (P) and shear (S) wave crustal velocities are crucial in improving the reflection image and in constraining the nature of the sub-basalt lithology and the volume of extruded and intruded melt. Beneath the basalts, which reach 5 km thickness, is a low-velocity zone with P- and S-wave velocities characteristic of sedimentary rocks intruded by basalt sills. The underlying stretched continental basement contains abundant intrusive igneous sills on the rifted margin. Near the Faroe Islands, for every 1 km along-strike, 340–420 km^3 of basalt was extruded, while 560–780 km^3 was intruded into the continent–ocean transition (COT). Lower-crustal intrusions are focussed mainly into a narrow zone less than 50 km wide on the COT, whereas extruded basalts flow >100 km from the rift. Melt on the COT is intruded into the lower crust as sills which cross-cut the stretched and tilted continental fabric, rather than as 'underplate' of 100% melt, as has often been assumed previously. Our igneous thickness and velocity observations are consistent with the dominant control on the melt production being rifting above mantle with a temperature elevated above normal. The mantle temperature anomaly was up to 150°C above normal at the time of continental breakup, decreasing by *c*. 70–80°C over the first 10 Ma of seafloor spreading.

Keywords: North Atlantic, rifted continental margin, volcanism, igneous intrusion, subsidence, crustal structure

Continental breakup of the northern North Atlantic at *c*. 55 Ma was accompanied by the eruption of huge volumes of basaltic lavas. The basalts flowed across the continental hinterlands on both sides of the new ocean basin. In the North Atlantic region, the volume of extrusive lavas reached more than 1×10^6 km^3 (White & McKenzie 1989; Coffin & Eldholm 1994; Eldholm & Grue 1994). The evolved composition of the extruded basalts (typically 6–8% MgO, compared with 16–18% MgO for the primitive melts from which they were derived) means that considerable volumes of residual igneous rocks must remain either in the crust or in the upper mantle. For flood basalts, Cox (1980) estimated on petrological grounds that the intrusive volume must be 'at least as large as the amount of erupted surface lava'. Just how much of the total igneous budget remains below surface is much debated, with literature estimates of the ratio of intruded to extruded igneous rock ranging from 0.25:1 to 4:1 (Coffin & Eldholm 1994). It is important to constrain the total volume of igneous rocks not just for understanding the geological history of the new ocean basin, but also for calculating the subsidence history, its heat flow and maturation history, and the temperature and properties of the underlying mantle from which the melt was generated. This is crucial both in understanding the geological history of the continental margins and adjacent shelves and for assessing their hydrocarbon potential.

In this paper we summarize the geophysical techniques used to image the igneous rocks and to constrain their volumes. A major focus of the iSIMM (integrated Seismic Imaging and Modelling of Margins) project from which seismic work is reported here was on quantifying the total amount and distribution of igneous rocks produced during the breakup of the Rockall and Faroe continental margins. Many of the detailed results are discussed in fuller publications to which we refer at the relevant points.

When volcanic continental margins were first studied in detail, it became apparent that the widespread extrusive volcanics were invariably accompanied by high-velocity lower-crust (HVLC, P-wave velocities higher than 7.0 km s^{-1}) beneath the continent–ocean transition (COT). This was generally interpreted as due to 'underplated' igneous crust (e.g. Mutter *et al.* 1984; LASE 1986; Vogt *et al.* 1998; Klingelhöfer *et al.* 2005; Voss & Jokat 2007). Our high-quality iSIMM seismic reflection profiles across the Faroes continental margin show the presence of numerous lower-crustal reflections beneath the COT in the region displaying HVLC. We interpret these reflections as caused by igneous sills intruding the country rock. Therefore the HVLC on the Faroes margin is better interpreted as 'intruded lower-crust' than as 'underplated' igneous crust (White *et al.* 2008; White & Smith 2009). It is likely that, where similar HVLC wedges are observed elsewhere on the COT, they are also caused by sill intrusions. The widespread use of the terminology of 'underplated' igneous crust rather than 'intruded lower-crust' makes a significant and, we argue, sometimes erroneous, difference to the way the cause of the widespread magmatism at the time of continental breakup is interpreted.

The locations of the two main iSIMM profiles that cross the Faroes and Hatton continental margins of NW Europe on which we report in this paper are shown in Figure 1. Both profiles had dense deployments of 85 ocean bottom seismometers (OBS) along them. These OBS provide control on the structure from wide-angle seismic data with an unprecedented density and

Vining, B. A. & Pickering, S. C. (eds) *Petroleum Geology: From Mature Basins to New Frontiers – Proceedings of the 7th Petroleum Geology Conference*, 831–842. DOI: 10.1144/0070831

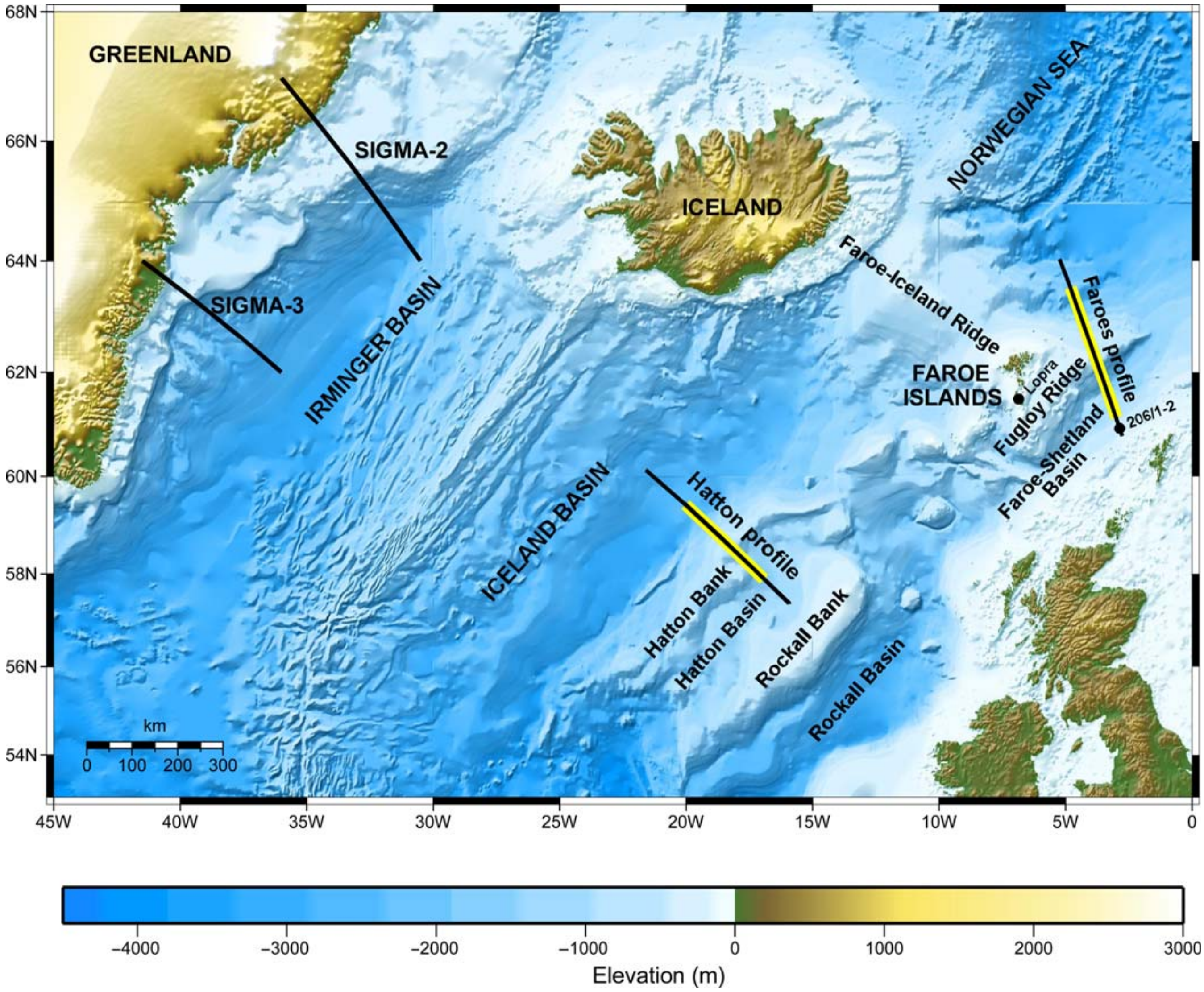

Fig. 1. Location of seismic profiles across the North Atlantic rifted continental margins. Portions of Faroes and Hatton profiles highlighted in yellow are shown in Figure 4, and results from the SIGMA profiles (Korenaga *et al.* 2000; Hopper *et al.* 2003), on the conjugate east Greenland margin, are shown in Figure 5. Lopra and 206/1-2 refer to location of wells from which data are shown on Figure 7.

number of arrivals. Only the Faroes profile had a coincident deep penetration reflection profile, although the reflection data recorded while shooting into the OBS on the Hatton profile was sufficient to constrain the sediment thickness, which was used in the analysis of the wide-angle data.

Source and receiver design

In order to achieve penetration of seismic energy through thick (*c.* 1 km or more) layered basalts, it is necessary to tune the seismic source to produce low frequencies. This is because the basalts strongly attenuate higher frequency energy (Ziolkowski *et al.* 2001; Maresh & White 2005). If the attenuation is expressed as an effective quality factor, Q_{eff}, then values of typically 25–45, but sometimes as low as 15, are measured from vertical seismic profiles in boreholes through basalts on the North Atlantic margin (Maresh *et al.* 2006; Shaw *et al.* 2008). These values of Q_{eff} are as low as those of near-surface unconsolidated sediments. The reason for the high attenuation is not the intrinsic absorption of basalts, for which Q is in the region of 200–600 (i.e. low intrinsic attenuation; Gordon & Davis 1968; Brennan & Stacey 1977; Maresh *et al.* 2006), but is probably due to scattering and/or, if the crack configurations and interconnectedness are right, to energy loss by water squirt between cracks as the seismic wave propagates (Shaw *et al.* 2008). The high-frequency scattering may arise from the fine velocity layering created by the alternation of the interiors of basalt flows with relatively high velocities, alternating with weathered and altered flow tops with much lower seismic velocities. The presence of inter-flow sediments may produce even lower velocity layers. These alternating high and low velocity layers can cause high frequency loss even if the media are flat-lying and laterally homogenous (Christie *et al.* 2006*a*; Maresh *et al.* 2006). Scattering of the high frequencies may also be caused by the 3D irregular undulating nature of the interfaces between individual flows within the basalt units (Maresh *et al.* 2006).

The iSIMM airgun source was tuned to produce peak output at 9–10 Hz. Low frequencies were generated in both the wide-angle and conventional seismic reflection sources using large airgun chambers and large total capacities (the source array for the Faroes reflection profile totalled 167 litre (10 170 cubic in.) from 48 guns). Towing the guns deeper than usual at 18 m below the sea surface also provided low-frequency enhancement due to the sea-surface ghost reflection. The choice of the source tow depth is a trade-off between enhancing the low frequencies with the reflection off the sea surface, which is better the deeper the guns, and the increase in frequency produced by an airgun of given chamber size which results from the increased ambient pressure as it is towed deeper. We also implemented an experimental configuration of shooting so as to align the bubble pulses from the individual guns rather than the conventional method of aligning the first peaks. Bubble tuning produces a lower frequency waveform than does conventional peak tuning, and also produces a more compact waveform at low frequencies (Lunnon *et al.* 2003; Christie *et al.* 2006*b*): a similar method termed 'single-bubble' tuning was implemented by Avedik *et al.* (1993, 1995). The final effect of all these factors was to produce a source for the reflection profile with a peak output of 228 dB re 1 μPa Hz^{-1} at 1 m, and a peak frequency of 9 Hz (Christie *et al.* 2006*b*). Although the bubble tuning did enhance the low-frequency output, our conclusion from comparison between the bubble-tuned and a conventional peak-tuned source with the same chamber sizes and distribution is that for most purposes the peak-tuned source is preferable because it has a smaller dependence of the waveform on the take-off angle than does the bubble-tuned source. The greatest improvement in producing low frequencies comes from the simple expedient of towing the airguns deep.

At the receiver end it is beneficial to tow the streamer at a similar depth to the source so as to also benefit from the enhancement of low frequencies by the sea surface ghost reflection. The OBS on the seafloor in deep water are far removed from the surface ghost, so the low frequencies are not enhanced in the same way, but have the additional benefit that the downward travelling water multiples can be attenuated by stacking the hydrophone and vertical geophone data because these arrivals have opposite polarities. The seabed receivers are also far removed from the acoustic noise generated by rough weather and remained quiet even when there was a Force 7 storm at the surface in the data we recorded on the iSIMM project. However, an additional source of noise to which seabed receivers may be exposed arises from strong bottom currents, which in our study were most apparent in degrading the signal-to-noise ratio of OBS at the foot of the continental slope.

Wide-angle seismic data

By deploying fixed OBS, it is possible to record out to any desired offset, limited only by the power of the source and the noise levels on the OBS. In practice we routinely recorded wide-angle arrivals to offsets of 150 km on the iSIMM profiles reported here. The importance of this is that we were able to record turning waves from throughout the lower crust, as well as wide-angle reflections from the Moho. These phases arrive outside the water wave and are normally muted when building velocity models from conventional seismic reflection data. However, they carry information on the velocity structure which can be used through tomographic inversion to create a well constrained model of the velocity variations throughout the entire crust. Furthermore, the diving waves from the deep crust appear as first arrivals for much of their trajectory, so are not contaminated by the intra-bed multiples which are such a problem in analysing conventional reflection data from shorter offset streamers. Typically the resolution of the velocities available from semblance analysis or from velocity focusing in prestack depth migration decreases with depth and, even with streamers as long as 12 000 m, provides only poor discrimination on velocities in the lower crust. This is in marked contrast to diving waves, which have maximum velocity resolution at the depths in the crust at which they are turned back towards the surface.

Two further advantages of wide-angle arrivals have been utilized in basalt covered areas. The first is the characteristic 'step-back' in the diving waves caused by a low velocity zone (LVZ), such as may occur when basalts flow across a pre-existing sedimentary system (Richardson *et al.* 1999; White *et al.* 1999). An example of such step-backs is shown in Figure 2a, from an OBS positioned on the crest of the Fugloy Ridge on the Faroes shelf, where 3.6 km thick basalt flows overlie a 1.2 km thick LVZ (Fig. 2c). The accompanying ray-trace diagram (Fig. 2b) shows rays traced through the final velocity model for the Fugloy Ridge (from Roberts *et al.* 2009), which produce travel times that match the observed data. The red rays are returned by the velocity gradient in the basalt layer. The maximum range to which the rays within the basalt layer propagate is governed by the thickness of the layer and the velocity gradient within it (Fliedner & White 2001): at maximum range the turning rays just graze the base of the basalt layer.

As we discuss later, the sub-basalt LVZ is probably caused by sedimentary rock intruded by igneous sills. The magnitude of the travel time step-back depends on the velocity and thickness of the LVZ and is an easily identifiable indicator of the presence of low-velocity material beneath the basalts. However, for basalt thicknesses typical of the Faroes shelf, this step-back in the diving waves usually occurs at ranges in excess of 15 km, which means that it is beyond the maximum offset of conventional streamers. Hence the need either to synthesize super-long streamers using two-ship methods, or to shoot into fixed seabed receivers. Using the presence and magnitude of the step-backs recorded by two-ship profiles in conjunction with conventional 4000 and 6000 m profiles enabled White *et al.* (2003) to map the regional variations in thickness of both the basalt flows and the sub-basalt LVZ from a 2D grid of profiles across the Faroes shelf.

A further advantage of using wide-angle reflections is that their amplitudes increase markedly towards the critical distance at which refractions from the underlying layer emerge (Fliedner & White 2001). This means that the wide-angle reflections produce arrivals with excellent signal-to-noise ratios, and they can be migrated to produce normal incidence reflection profiles with high amplitudes, largely free of multiples. By this means the base-basalt reflection has been identified and imaged on profiles across the Faroes shelf (Fliedner & White 2003). Conventional seismic reflection profiles still provide better images of the subsurface than do the wide-angle images, because the conventional shorter offsets exhibit less distortion from the stretching of the signal in the normal moveout correction stretch than do the far-offset arrivals, but the migrated wide-angle reflections can be used to identify which of the much weaker reflections on the conventional reflection profile are primary rather than multiple, and then the interpretation made from the conventional profile.

The use of three-component geophones in the seabed seismometers also allows the direct detection of S-waves. Airguns in water only produce acoustic waves, but significant S-wave energy may be generated by mode conversion at suitable boundaries as the energy propagates through the crust. The most efficient mode conversion occurs when the P-wave velocity on one side of an interface is similar to the S-wave velocity on the other side, provided the interface is sharp with respect to the wavelength (White & Stephen 1980). On the North Atlantic margins, such an interface is found at the top of the basalt flows where unconsolidated sediments overlie basalts, and there is indeed strong mode conversion at this interface (Eccles *et al.* 2007, 2009). The arrivals can be verified as S-waves from their travel times, their moveout and their particle motions.

An example of strong converted S-wave arrivals on wide-angle data is shown in Figure 3, using data recorded by OBS79, which lies near the oceanward end of the Faroes profile. The vertical component geophone of the OBS (Fig. 3a) records strong P-waves from the crustal diving wave (Pg) and from the Moho reflection off the base of the crust (PmP). A linear reduction

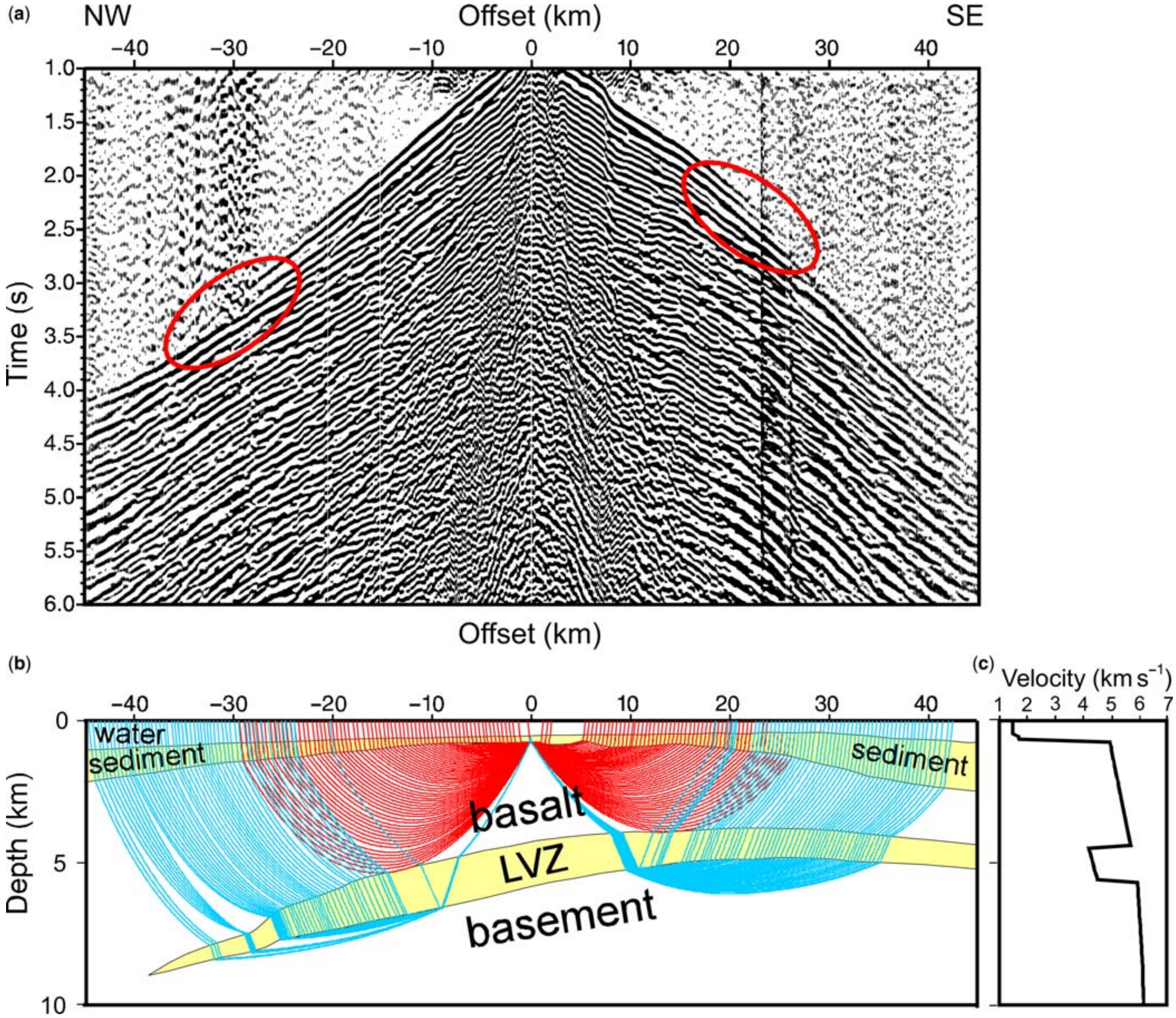

Fig. 2. (**a**) Example of seismic data from the vertical component of OBS53 on the Fugloy Ridge, Faroes profile to illustrate the effect of the LVZ on the travel times of diving waves. The location of 'step-backs' in the first arrival diving waves, which are characteristic of the presence of LVZs, are marked by red ovals. Note that the step-back occurs later in travel time and at a greater offset on the northwestern, seaward side (negative offsets) than on the southeastern, landward side (positive offsets) of OBS53 due to the deeper location of the LVZ on the seaward side. (**b**) Raytracing for first arrivals recorded at OBS53 through the final velocity model including the LVZ. Only one-third of the rays are shown for clarity. Red rays are from diving waves returned from within the extrusive basalt layer, and blue rays are from rays which have penetrated through the LVZ to the crust of the basement beneath. Note the termination of basalt diving waves (red) at the offset where they penetrate to the base of the basalt layer. (**c**) P-wave velocity-depth profile from Roberts *et al.* (2009) at the location of OBS53 (0 km offset on this figure).

velocity of 7.0 km s^{-1} has been applied to the travel times, which causes phases turning at 7.0 km s^{-1} to appear as horizontal arrivals on the time–offset plot.

The radial component of the OBS (Fig. 3b) shows the converted arrivals which are recorded as S-waves at the seafloor. The travel times have a linear velocity moveout of 3.9 km s^{-1} applied, so arrivals with a phase velocity of 3.9 km s^{-1} appear as horizontal on this plot. The ratio of the reduction velocities between Figure 3a, b is *c*. 1.8, which approximates the V_p/V_s ratio of the lower oceanic crust. Thus the Pg and PmP arrivals on the vertical component are sub-horizontal on Figure 3a, while the equivalent Sg and SmS arrivals on the radial component are sub-horizontal on Figure 3b. Sg and SmS are phases which were converted to S-waves at the interface between the sediment and the top of the basalt on the path down from the shot, and then travelled through the remainder of their paths as S-waves. Note too that the Pg phases are much weaker on the radial than on the vertical component, as is to be expected since they produce particle motions parallel to the ray path, which is sub-vertical at the seafloor. A clear example of this is shown by the PPS phase, which is converted on the way up at the sediment-basalt interface, and the P-wave water multiple generated near the OBS receiver (Fig. 3a, b). Both repeat the travel time v. offset behaviour of the primary crustal diving wave Pg and the Moho reflection PmP, but the PPS phase is delayed an additional 2.5 s by the path through the sediments as a S-wave and the water multiple phase is delayed 3.6 s by the additional two paths through the water layer. On the vertical component (Fig. 3a) the PPS phase is weak but the water multiple Pg phase is strong. On the radial component (Fig. 3b) the relative amplitudes of the PPS and water multiple arrivals are reversed: the PPS phase is strong because it arrives as a S-wave while the water multiple P-phase is weak. The delay between the

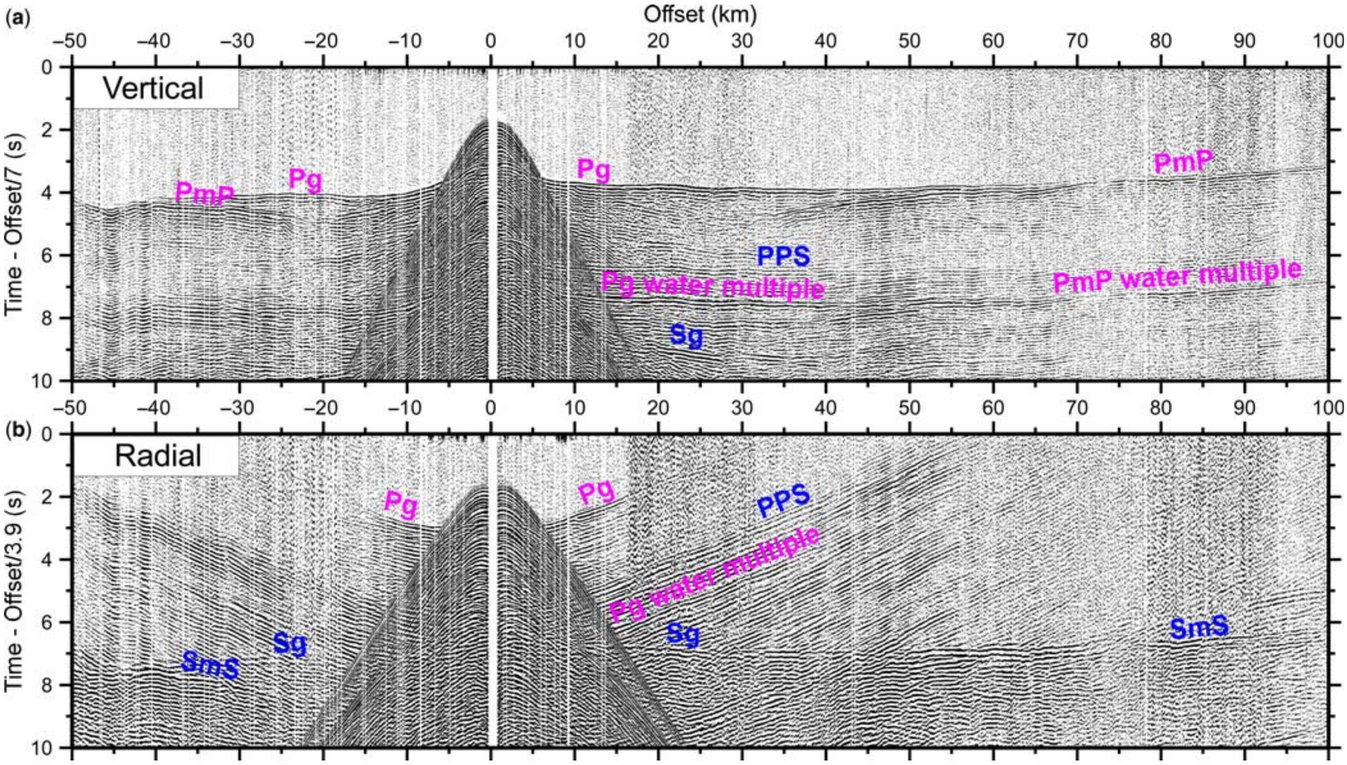

Fig. 3. Example of wide-angle data from OBS79 at the oceanic end of the Faroes profile (location shown in Fig. 1). Arrival phases labelled in red are direct P-wave arrivals: Pg are diving waves returned from the crust; PmP are reflections off the Moho and the Pg and PmP water multiples are delayed by a water multiple bounce in the water at the OBS end of the path. Arrivals labelled in blue are recorded as S-waves at the OBS: Sg and SmS are diving waves returned from the crust and reflections off the Moho, respectively, with conversion from P- to S-wave at the top basalt interface on the down-going path. The PPS phase has travelled as a P-wave through the crust and converted to S-wave at the top-basalt interface beneath the OBS on the upward travelling path. The labels of all the phases on this figure sit immediately above the phase to which they refer. (**a**) Vertical geophone component receiver gather displayed with a linear reduction velocity of 7.0 km s^{-1}. (**b**) Rotated radial geophone component displayed with a linear reduction velocity of 3.9 km s^{-1} to emphasize the converted shear wave arrivals. Figure modified from Eccles *et al.* (2009).

primary P-wave arrival and the corresponding PPS arrival allows the V_p/V_s ratio in the sediments beneath the OBS to be constrained and thus these strong converted S-waves recorded on the horizontal components of the OBS allow us to model the S-wave structure of the entire crust, which adds considerable value to the conventional P-wave velocity structure. As we discuss later, the additional information from S-wave velocities can be of crucial importance in discriminating between possible lithologies.

Crustal velocity models

The crustal velocity structure was modelled by picking the travel times of individual wide-angle arrivals recorded by each OBS from each shot and then performing a tomographic velocity analysis using the arrival times. Over 103 000 wide-angle P-wave arrivals and more than 60 000 converted S-wave arrivals were picked from the two wide-angle profiles discussed here (see Table 1). Sediment velocities were calculated from semblance analysis of wide-angle reflections on the 12 000 m long streamer data. For the sediments, this gave better velocity control than the sediment diving waves, which were largely obscured beneath the water wave and its coda. Furthermore, the diving waves are only available beyond the critical distance, whereas the reflections can be traced back to zero-offset arrivals.

The crustal velocity structure was derived first by a raytracing inversion, which used a layered model to match the modelled travel times to the observed arrival times, with the model iterated one layer at a time until the observed and modelled travel times matched to within their estimated uncertainties (Zelt & Smith 1992). This was followed by a grid-based joint reflection and refraction tomographic inversion (Korenaga *et al.* 2000). The grid-based inversion is more objective because it does not assume any initial layered boundaries, but it is poor at handling LVZs because it attempts to fit a smooth velocity field through them, whereas in reality they may have sharp interfaces with discontinuous velocities. In the extracts of P-wave velocity models shown here in Figure 4, we therefore used the grid-based result for the Hatton profile (Fig. 4a), and the raytraced model for the Faroes profile with its prominent LVZ (Fig. 4b). Uncertainties in the velocities were estimated by making multiple inversions with

Table 1. Number of wide-angle arrival times used in tomographic inversions

Phase	No. of arrival picks
Faroes Profile	
Pg	52 050
PmP	25 800
Sg	26 900
SmS	14 900
Hatton Profile	
Pg	17 650
PmP	7850
Sg	9500
SmS	9000

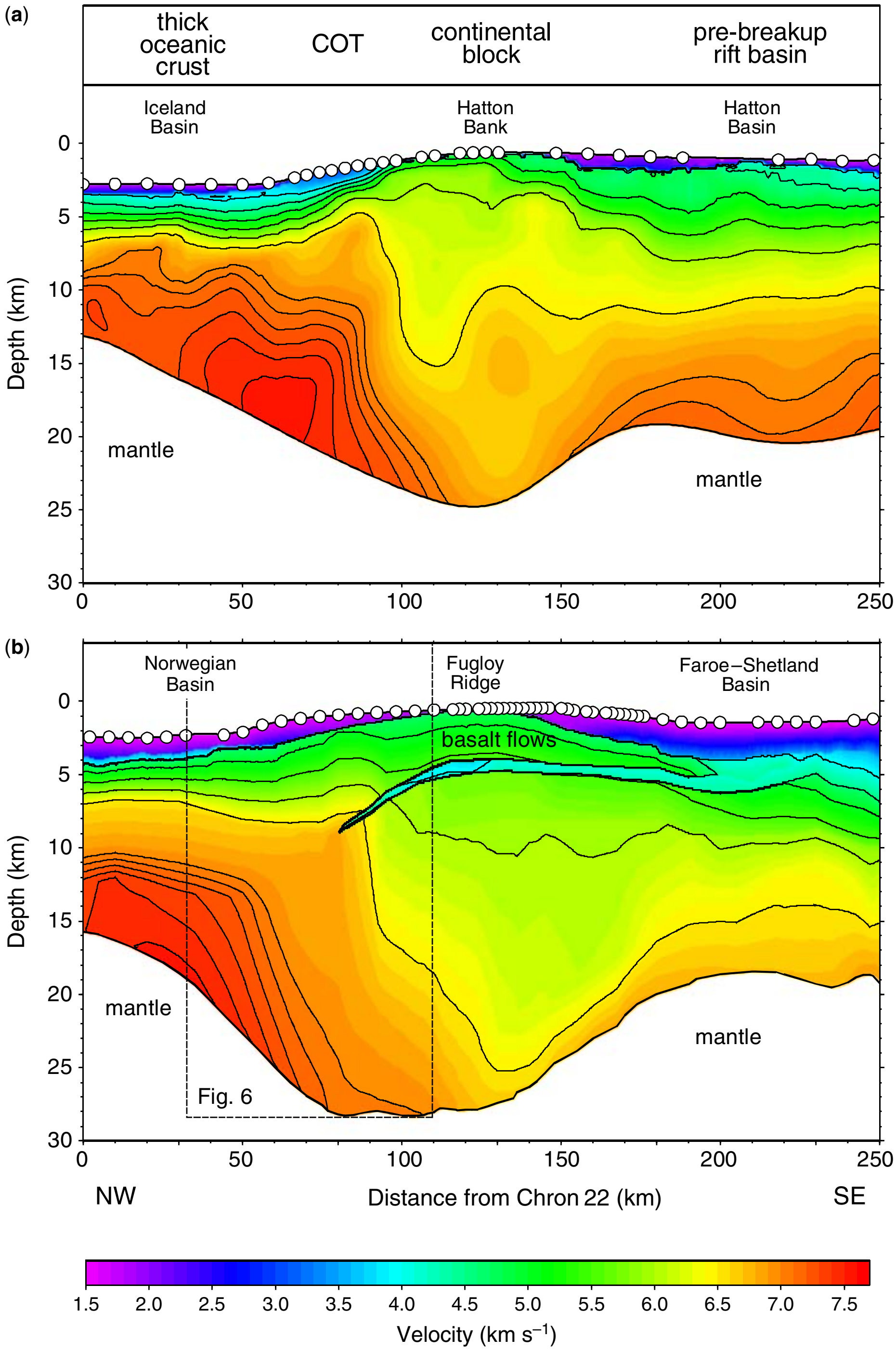

Fig. 4. Seismic velocity structure of crust across the COT near (**a**) Hatton Bank and (**b**) the Faroe Islands. For line locations see Figure 1. Profiles are aligned with 0 km distance at seafloor spreading magnetic anomaly chron 22. The main structural regions, which are found consistently on both profiles, are labelled along the top of the figure. Velocities of post-rift Cenozoic sediments (purple) are constrained by semblance moveout analysis of reflections recorded on the 12 km long hydrophone streamer and sub-sediment crustal velocities are constrained by tomography using wide-angle reflections and diving waves from OBS data (OBS locations shown by circles at seafloor). Colour bands are at 0.1 km s^{-1} intervals, with contours above 7.0 km s^{-1} spaced every 0.1 km s^{-1} to highlight the lower-crustal velocity. Diagram modified from White *et al.* (2008).

100 randomized starting velocity models: velocities are generally constrained to better than 0.1 km s^{-1} and Moho depths to within 1 km. The P-wave structure of the oceanic sections of both profiles was modelled by Craig Parkin (Parkin & White 2008), the Hatton P-wave profile by Lindsey Smith (White & Smith 2009), the Faroes P-wave profile by Alan Roberts (Roberts *et al.* 2009) and the S-wave structure across both profiles by Jennifer Eccles (Eccles *et al.* 2009): the reader is referred to these papers for full details of the modelling, the resolution testing and the uncertainty tests.

The P-wave velocity structure across both the Hatton and the Faroes rifted continental margins shows striking similarities, as marked by the summary of crustal type along the top of Figure 4, though the two profiles are some 800 km apart along strike and are at different distances from the centre of the thermal anomaly in the mantle at the time of continental breakup. Both profiles are aligned with 0 km distance at the prominent seafloor spreading magnetic anomaly 22, which is visible on the oceanic sections. Both profiles are bounded on the landward side by older Mesozoic failed rifts with thinned crust, the Hatton–Rockall Basin in

Figure 4a and the Faroe–Shetland Basin in Figure 4b. Immediately adjacent to the COT on the landward side are blocks of continental crust some 24–27 km thick, called the Hatton Bank on the southern profile and the Fugloy Ridge on the northern profile near the Faroe Islands. These continental blocks are covered in both cases by basalts which flowed landward from the continental breakup rift. The continental blocks are thinned a little from the presumed original continental crustal thickness of 30–32 km found beneath nearby Ireland and northern Britain (e.g. Barton 1992; Landes *et al.* 2005; Tomlinson *et al.* 2006). The seismic velocity of the Hatton Bank and Fugloy Ridge continental blocks averages 6.7 km s^{-1} in the lower crust, which is typical of the velocity of continental crust beneath the UK well away from the oceanic rift. This suggests that there has been only limited lateral intrusion of igneous rocks away from the COT during the breakup phase, because otherwise the igneous intrusions would have caused the seismic velocity of the lower crust beneath Hatton Bank and the Fugloy Ridge to be increased.

The transition from this continental crust to fully igneous oceanic crust is surprisingly narrow, with the COT being less than 50 km wide. Over this interval the seismic velocity of the lower crust increases by approximately 0.6 km s^{-1}, from an average of 6.7 km s^{-1} beneath the Hatton Bank to 7.3 km s^{-1} beneath the first-formed oceanic crust (White & Smith 2009), and with a similar increase across the Faroes margin. As we show later, the increase in seismic velocity of the lower crust is due to an increasing percentage of igneous sill intrusion as the oceanic rift is approached.

The first formed (i.e. the oldest) oceanic crust which, apart from the subsequently deposited sediments, is 100% igneous, exhibits the highest seismic velocities on the profiles, with the average lower-crustal (oceanic layer 3) velocity reaching 7.3 km s^{-1}: this velocity is markedly higher than the average layer 3 velocity for normal oceanic crust of 6.95 km s^{-1} (White *et al.* 1992). The oceanic crustal thickness of 8–17 km is also considerably greater than the normal oceanic thickness of 6.5 km (White *et al.* 1992). Both observations, of increased seismic velocity and increased thickness, can be explained by the generation of the melt which forms the oceanic igneous crust from mantle with its temperature elevated as much as 150 °C above normal (White & Smith 2009). Over the subsequent 10 million years following the onset of seafloor spreading in the North Atlantic both the average lower-crustal velocity and the crustal thickness of the oceanic crust measured along our profiles decreased (Fig. 5), suggesting that the mantle plume temperature decreased by about 70–80 °C from its peak at the time of continental breakup (Parkin & White 2008; White & Smith 2009). Besides controlling the formation of melt, this change in mantle temperature would have exerted a strong regional control on the subsidence history. The rifted margin and its hinterland was elevated above, or near, sea-level during breakup in the Paleocene and then subsided as the mantle thermal anomaly decreased (Barton & White 1997; White & Lovell 1997). It is important to include such changes in the regional base-level in studies of subsidence relevant to hydrocarbon exploration.

In modelling subsidence, changes in crustal thickness are the dominant control on the uplift or subsidence history. Stretching and crustal thinning causes subsidence. The addition of mass to the crust causes uplift. On the continent–ocean boundaries the thinning caused by stretching at the rift is counteracted by the thickening caused by igneous intrusion and extrusion. This often results in the surface remaining at about the same elevation. Thus the extrusive volcanics on the COT were erupted close to sea-level throughout the rifting history, despite the original crust having been thinned by more than a factor of five. Landward of the COT, there is much less stretching, but still some crustal thickening by the injection of igneous rocks and the flow of basalts across the surface. The thickening of the crust by magmatism causes permanent uplift,

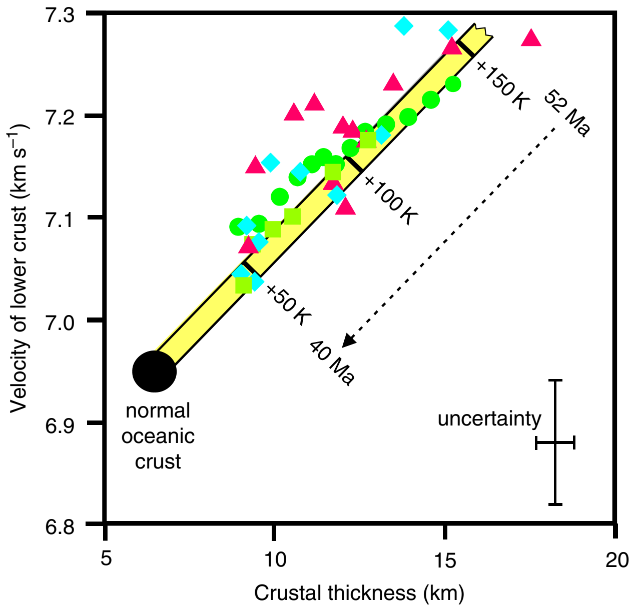

Fig. 5. Average crustal thickness and lower-crustal (oceanic seismic layer 3) P-wave velocity after correction to a standard reference pressure of 230 MPa and a reference temperature of 150 °C, calculated every 10 km along the oceanic portions of the Faroes profile (red triangles, data from Roberts *et al.* 2009), the Hatton profile (blue diamonds, data from White & Smith 2009), and the east Greenland SIGMA-3 profile approximately conjugate to the Hatton profile (green circles, data from Hopper *et al.* 2003), and the east Greenland SIGMA-2 profile (green squares, data from Korenaga *et al.* 2000), which is a similar distance from the centre of the mantle thermal anomaly as is the Faroes profile. Locations of profiles are shown in Figure 1. Uncertainty ranges typical of the data points are shown in the bottom right corner. Yellow arrow shows representative trend of changes in total igneous thickness and lower-crustal P-wave velocity for passive decompression beneath an oceanic spreading centre of mantle of increasing temperature, with tick marks approximately every 50 K above the normal mantle temperature (White & Smith 2008).

whilst temperature increases in the underlying mantle cause transient uplift which decreases as the mantle cools back to its normal temperature. So again there can be a delicate balance between subsidence and uplift that is governed largely by the magmatism and changes in underlying mantle temperature. These factors are frequently ignored in modelling the subsidence history, but are clearly of prime importance.

In the Rockall–Faroes region, local compressional structures that post-date the tectonics associated with the continental breakup are often superimposed on them (Tuitt *et al.* 2010). Thus there is evidence that Hatton Bank, which was already a structurally relatively high region at the end of continental breakup, was subsequently further uplifted during the Mid to Late Eocene by compressional forces unrelated to the breakup and that the Fugloy Ridge on the Faroes shelf was formed by inversion after the rift-related basalts had flowed across the shelf.

Geological interpretation from combined seismic reflection and wide-angle data

The combination of good velocity control from wide-angle seismic data with a deep penetration seismic reflection profile not only enables improvements to be made to the processing of the seismic reflection data in order to enhance the image, but also allows better interpretation to be made of the crustal structure. This is shown well by the section of the reflection profile across the Faroes COT and first-formed oceanic crust shown in Figure 6 (for the location see the box on Fig. 4b). The seismic P-wave velocity structure from Roberts *et al.* (2009) has been superimposed in colour on the reflection profile, using the same colour scale as in Figure 4. One of the most striking results on Figure 6 is that the region of high-velocity (6.7–7.3 km s^{-1}) lower crust under the COT between 55 and 90 km distance exhibits marked sub-horizontal reflectivity. This is interpreted as caused by lower-crustal igneous intrusions. They underlie the thickest section of extrusive basalts, which on the COT produce striking upward-convex seaward-dipping reflectors. Both the intrusions and the seaward dipping reflectors were produced in the continental rift zone at the time of continental breakup. The intrusions cross-cut the local dipping fabric of the continental basement visible between 75–110 km distance on Figure 6.

The region of HVLC containing the intrusions has velocities intermediate between that of the continental crust on the landward side and the fully oceanic crust on the seaward side. If we take the velocities of the continental and oceanic crust as the two end-members, then the percentage of intrusion at any position across the COT can be estimated by a simple mixing law. By summing the percentage of intrusion at all positions and depths across the COT, it is then possible to estimate the total area on the 2D profile of intruded igneous rock emplaced during continental breakup. For a 1 km deep slice centred on the Faroes profile this yields a total intruded igneous volume of 560–780 km^3 (Roberts *et al.* 2009). The total area in cross-section of extruded basalt which accompanied this intrusion can be measured directly off the seismic reflection profile, remembering that it flowed more than 100 km landward (Fig. 4b), so has to be summed across that region. On the Faroes profile, the area can be measured easily because the base of the basalt is defined well by the underlying LVZ (Figs 2, 4b & 6). On the Hatton profile the basalts lie directly over higher velocity crust, and their base cannot be so easily delineated. For a 1 km deep slice centred on the Faroes profile the total volume of extruded basalts is 340–420 km^3 (Roberts *et al.* 2009).

Although we do not know the age of the lower-crustal intruded rocks, because they have never been sampled directly, it is known in the North Atlantic flood basalt province, as is true of others around the world, that the main phase of the extrusive igneous activity was very short-lived, lasting typically less than 1 million years (White & McKenzie 1989, 1995; Eldhom & Grue 1994). Therefore it is likely that the entire volume of igneous melt including the intrusions, totalling 900–1200 km^3 for every 1 km alongstrike in the Faroes region, was produced in a geologically short time beneath the continental rift as it opened to form the new ocean basin. A similar volume was emplaced at the same time on the conjugate margin (White & Smith 2009). This is an astonishingly large volume of melt, which is most plausibly explained by decompression melting of abnormally hot mantle some 150 °C hotter than normal as the rift opened. As we have seen from Figure 5, the mantle temperature subsequently decreased by 79–80 °C over the next 10 Ma as the ocean opened. It is a feature of thermal boundary layer instabilities such as those

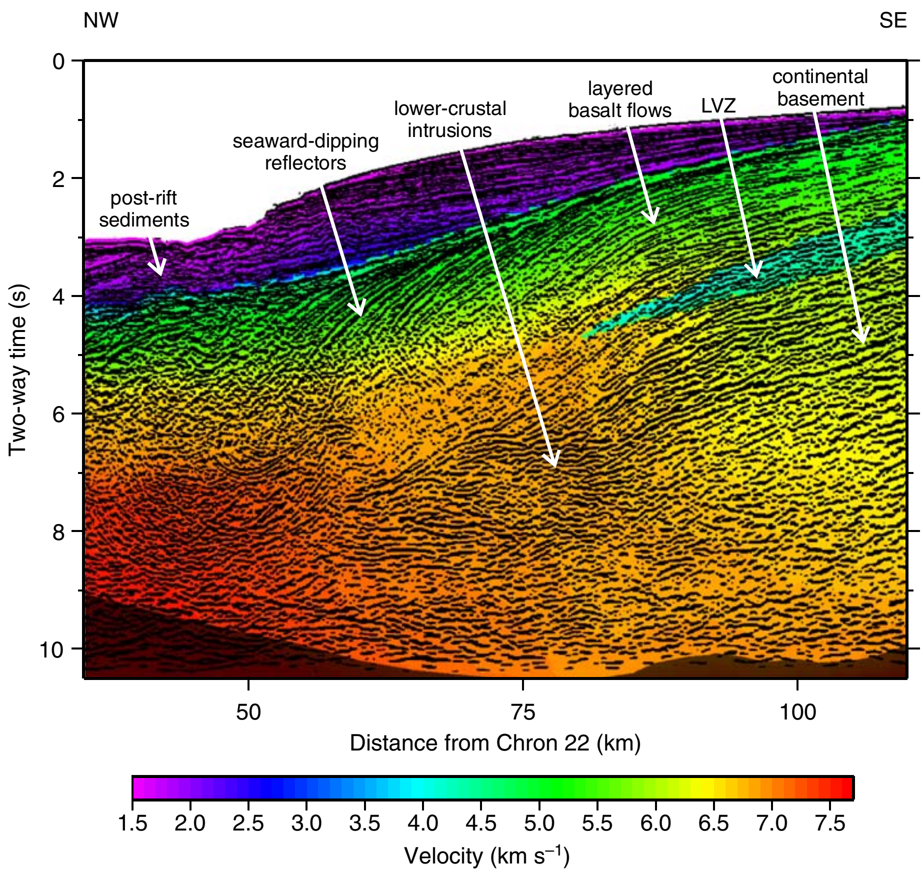

Fig. 6. Section of iSIMM seismic profile crossing the COT north of the Faroe Islands (see Fig. 1 for location) with superimposed P-wave velocity field from tomographic inversion of wide-angle arrivals on OBS (from White *et al.* 2008 and Roberts *et al.* 2009). Purple section beneath seafloor is post-rift Cenozoic sediments. Underlying extrusive lava flows are imaged as seaward-dipping reflectors between 50 and 90 km along profile and as sub-horizontal layered basalts at distances >90 km. LVZ marks the low-velocity zone immediately beneath the basalt flows. Lower-crustal layering coincident with high (>7.0 km s^{-1}) velocities, caused by igneous intrusions, lies beneath the basalts on the COT, with a termination at *c*. 90 km against continental crust with lower velocities. Moho reflection at base of crust shallows markedly from continental (SE) to oceanic (NW). Processing of the reflection profile included source designature, multiple suppression and post-stack time migration.

postulated to form mantle plumes that they are hotter at the time of initiation and then cool as convection continues, so this behaviour fits well the observations in the North Atlantic, with the anomalously hot mantle of the Iceland plume arriving shortly before rifting. The oldest volcanic rocks in the North Atlantic province date from 62 Ma, so this age probably marks the arrival of the mantle plume.

Lithological constraints from P- and S-wave velocities

Measurements of the *in-situ* S-wave velocity (V_s) in addition to the P-wave velocity (V_p) provide useful constraints on the composition of subsurface rocks that are not available from V_p measurements alone. We demonstrate this by considering two crucial regions that have been the subject of differing interpretations in the past: the LVZ that immediately underlies the basalts on the Faroes shelf, and the region of HVLC that is found beneath the COT.

The presence of a LVZ under the basalt flows on the Faroes shelf has been well established by wide-angle seismic constraints from first-arriving P-waves (Figs 2 & 4b), as discussed above, and is visible by a change of reflection character on the seismic reflection profile (Fig. 6). The main question concerning the LVZ under the basalt flows is whether it comprises sedimentary rock or igneous hyaloclastite material. This makes a large difference to its hydrocarbon prospectivity. One of the deepest penetrating wells through the basalts in the Faroes region is the Lopra 1/1A borehole (Fig. 1). The original 2178 m deep well was deepened to 3565 m on the basis of strong sub-bottom reflectors that were interpreted to be sedimentary. However, drilling showed that the deepest section was hyaloclastites (with lower P-wave velocity than the overlying basalt flows) and that the strong reflectors previously interpreted as sedimentary in origin were caused by basalt sills (Christie *et al.* 2006*a*). Sedimentary units were not reached before the Lopra well was abandoned. Elsewhere, on the eastern flank of the Fugloy Ridge, Spitzer *et al.* (2005) inferred on the basis of P-wave velocities derived from the 12 km offset seismic reflection data that there was a layer of hyaloclastite immediately beneath the base of the basalts, but that this was underlain by lower velocity material that was interpreted as sedimentary in origin.

Wide-angle seismic constraints from the Faroes profile constrain the average P-wave velocity in the LVZ as 4.5 km s^{-1}, with a possible range from 4.0–4.8 km s^{-1} and an average V_p/V_s ratio of 1.81 $\pm$ 0.1. Plotted on a graph of V_p v. V_p/V_s ratio (Fig. 7), it is clear that these velocities fall outside the main region of hyaloclastite properties measured from the nearby Faroes Lopra 1/1A well. The P-wave velocity of the material in the LVZ is lower than most hyaloclastites and the V_p/V_s ratio is also towards the lower limit of the bulk of hyaloclastite values. However, the P-wave velocity is somewhat higher than expected for the sedimentary rocks that are likely to lie under the basalts. On Figure 7 we show the average velocities of Paleocene sedimentary rocks recovered from well 206/1-2 located towards the southeastern end of our Faroes profile (see Fig. 1 for location), beyond the feather edge of the basalts. These sedimentary units may be similar to those found under the basalts. The deeper section of the Paleocene sediments, which lie at the same depth as the LVZ, has an average P-wave velocity of 3.8 km s^{-1}, with an inferred V_p/V_s ratio similar to that of the LVZ (Fig. 7). For comparison, we show on Figure 7 the equivalent values for Brent sandstone, which have similar seismic properties to the well 206/1-2 sediments. The P- and S-wave velocities of the material in the LVZ therefore indicate the presence of neither pure sedimentary rock nor hyaloclastites. The most likely explanation is that the LVZ primarily comprises sedimentary units intruded by basaltic sills, since the LVZ V_p and V_p/V_s values lie on a mixing line intermediate between these two end-members

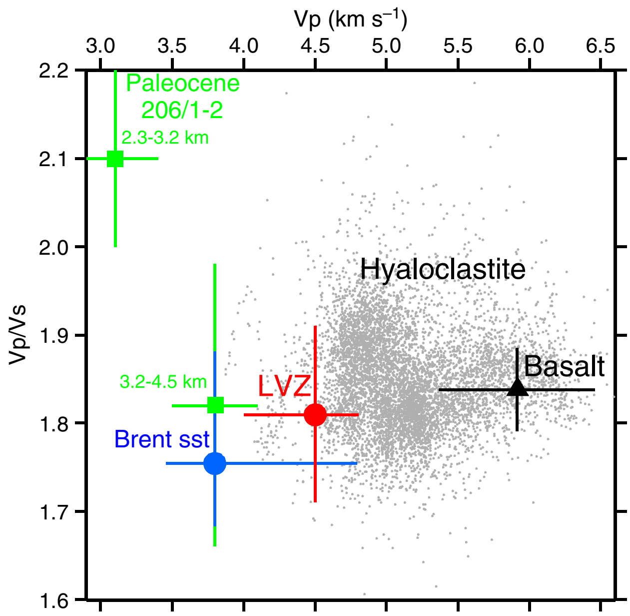

Fig. 7. V_p v. V_p/V_s ratio for the sub-basalt LVZ on the Faroes shelf and literature comparisons. The average result determined for the LVZ from analysis of the wide-angle seismic data is shown by the red circle. Grey dots represent well log measurements of hyaloclastites from the Faroes Islands Lopra-1/1A well (see Fig. 1 for location); the black triangle is an average literature value for basalt at 200 MPa (Christensen 1996). The properties of the Paleocene sedimentary section from the 206/1-2 well (see Fig. 1 for location), subdivided into two sections based on a major change in geophysical character, are shown in green, with V_s calculated using the mudrock relation of Castagna *et al.* (1985). The properties of Jurassic sandstone from the Brent field (Strandenes 1991) are shown by the blue circle for comparison. Data from Eccles *et al.* (2009).

(Fig. 7). There are sills throughout the sedimentary section in the Faroe–Shetland Trough, as well as in the hyaloclastites penetrated by the Lopra well (Christie *et al.* 2006*a*), and it would be surprising if sills were not also present in the sedimentary section beneath the basalt flows on the Faroes Shelf.

The S-wave measurements also assist the interpretation of the material which forms the HVLC under the continent–ocean boundary. We have already noted the lateral change in the average P-wave velocity of the lower crust from the continental end-member to the fully igneous oceanic end-member across the COT: the average P-wave lower crustal velocity increases from *c.* 6.7 to *c.* 7.3 km s^{-1} (Figs 4 & 6). Incorporation of S-wave measurements shows that there is also a linked change in the V_p/V_s ratio across the same COT region, with an increase from *c.* 1.75 at the continental end to *c.* 1.80 at the oceanic end (Fig. 8). The same trend is visible on both the Hatton profile data (blue diamonds) and the Faroes profile data (red triangles). We have already suggested that the gradient in P-wave velocity across the COT is caused by an increasingly dense intrusion of high-velocity igneous sills into the lower-velocity continental crust, an interpretation supported by the imaging of sub-horizontal reflectors in this part of the crust, inferred to be sills (Fig. 6). The trend of the V_p/V_s ratio confirms this interpretation. The continental lower crust in the region is likely to comprise Lewisian Gneiss, and *in-situ* seismic measurements from beneath northern Britain show that the lower crust exhibits not only relatively low P-wave velocities, but also a low V_p/V_s ratio (black square on Fig. 8, from Assumpção & Bamford 1978). The mafic intrusions by contrast have high P-wave velocities and higher V_p/V_s ratios. The systematic trends of increasing V_p and increasing V_p/V_s ratio across the COT are thus entirely compatible with a linear mixing trend between the

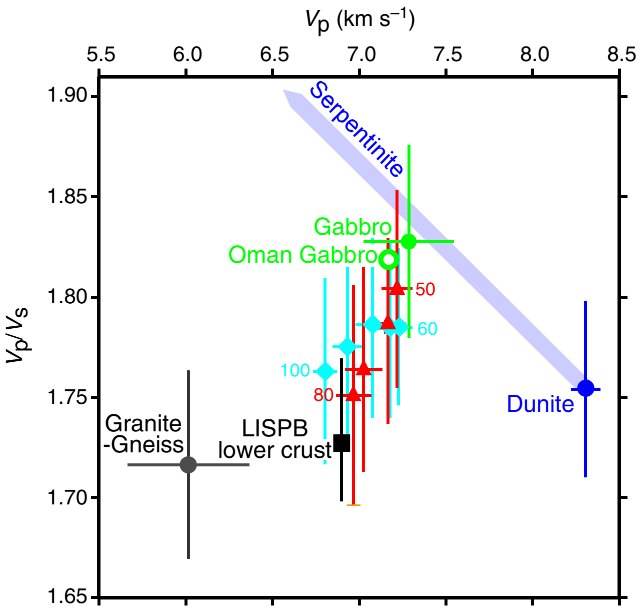

Fig. 8. V_p v. V_p/V_s ratio of the lower crust across the Faroes (red triangles) and Hatton (blue diamonds) COTs, corrected to a standard pressure of 230 MPa and a temperature of 200 °C. Values are averaged over a 10 km distance window. Small numbers show distance in km from chron 22 along the Faroes (red numbers) and the Hatton (blue numbers) profiles, matching the distance scales on Figures 4 and 6. The *in-situ* value for the lower crust under Scotland from the LISPB seismic experiment (black square) is from Assumpção & Bamford (1978). The properties of dunite, gabbro and granite-gneiss from laboratory experiments, corrected to 230 MPa, are from Christensen (1996). The properties of an Oman olivine gabbro with 10% olivine (Browning 1984) are shown by an open green circle. The properties of serpentinite with variable degrees of serpentinization (purple band) are from Horen *et al.* (1996) and Carlson & Miller (1997). The trend of increasing V_p/V_s ratio with decreasing V_p as the degree of serpentinization increases is orthogonal to the trend of increasing V_p/V_s ratio with increasing V_p measured for the HVLC on the continental margins, ruling out serpentinization as the cause of the HVLC. The trend of values observed for the HVLC on the Faroes and Hatton profiles is consistent with increasing intrusion of mafic material as sills into the continental lower crust, since they lie on a mixing line between the end-points for the lower crust (from LISPB) and high magnesium gabbro.

end members of Lewisian gneiss at the continental end and high magnesium gabbros at the oceanic end (Fig. 8). An interpretation which is ruled out by the V_p/V_s constraints is that the wedge of HVLC on the COT might be serpentinite, as has been postulated for parts of the Møre continental margin off Norway by Reynisson *et al.* (2010). Although serpentinite can certainly exhibit the range of P-wave velocities of 6.7–7.3 km s^{-1} that we observe, the accompanying V_p/V_s ratios of *c.* 1.89–1.84 for these degrees of serpentinization are much higher than are observed on the North Atlantic margins. Furthermore, the trend of increasing V_p/V_s ratio with decreasing V_p as the degree of serpentinization increases (purple shading on Fig. 8) is orthogonal to the trend of increasing V_p/V_s ratio with increasing V_p measured for the HVLC on the continental margins.

Conclusions

Layered basalts pose problems for deep sub-basalt imaging for two main reasons: high-frequency seismic energy is scattered and the high impedance contrasts at the margins of basalt sequences produce strong interbed multiples which make the interpretation of sub-basalt structure difficult. The iSIMM project has shown that sub-basalt imaging can be improved greatly by careful attention to the source and receiver design, to ensure that the source spectrum contains sufficient energy at low frequencies to make it capable of penetrating through layered basalt sequences. In order to address the problem of interbed multiples, the use of long streamers helps discriminate between primary and multiple arrivals during processing.

In addition to improvements to the conventional seismic reflection imaging mentioned above, the deployment of OBS along a profile adds another dimension by making it possible to construct a well constrained P-wave velocity model of the crust. This is useful in the mechanics of improving the reflection image through pre-stack depth migration and other processing, but it is also useful in a further way because by combining the velocity information with the reflection image it allows greatly improved geological interpretations to be made, as we have discussed with specific reference to the layered intrusions in the HVLC on the COT. Further constraints on the S-wave velocities obtained from mode-converted waves recorded directly at the OBS have the potential to add even more value to the interpretation by allowing lithological discrimination in a way which may remain ambiguous if only P-wave velocities are available. Both these improvements are of importance in hydrocarbon exploration.

Combination of tomographic velocity results with reflection imaging allows us to constrain quantitatively the total volume of melt produced during continental breakup at the rift underlying the COT. The profile across the Faroes margin, which is close to the centre of the mantle thermal anomaly, shows that a total of approximately 1000 km^3 of melt is generated from the mantle for every kilometre along strike. This is a huge volume, but of course is only half of the total produced at the continental rift near the Faroe Islands, because there is a similar volume on the east Greenland conjugate margin. Furthermore we have shown that more than half the melt is intruded in the lower crust on the COT, and never reaches the surface. This is consistent with earlier suggestions by Cox (1980, 1993) based on petrological arguments. We are able to show, at least near the Faroe Islands, that the ratio of intruded to extruded melt is about 1.5:1, thus considerably tightening the possible range of 0.25–4:1 reported by Coffin & Eldholm (1994). This is of crucial importance in modelling the subsidence and heat flow history of the continental margin and adjacent shelf.

Furthermore our conclusion that large quantities of melt are intruded in the lower crust at the rift zone is consistent with recent results from the northern volcanic rift in Iceland reported by Maclennan *et al.* (2003). They show that melt inclusions carried in extruded basalts had stalled in magma chambers near the base of the crust or in the uppermost mantle, and that some fractionation occurred before they were subsequently carried to shallow magma chambers near the surface and eventually erupted. The current northern volcanic rift of Iceland has many similarities to the Faroes margin at the time of early Cenozoic breakup, because it is a place where rifting is presently occurring through older crust between 20–30 km thick, above a thermal anomaly in the mantle caused by a mantle plume (Darbyshire *et al.* 2000*a*, *b*). Studies of the seismicity currently occurring under the Icelandic rift show considerable numbers of small earthquakes at depths of 15–30 km beneath the active Askja volcano, which are interpreted as caused by melt intrusion happening now in the lower crust (Soosalu *et al.* 2010). So it seems that we have consistent information from the seismic profiles across the Cenozoic rifted continental margin, from petrological and geochemical arguments and from seismic activity currently occurring beneath an active volcanic rift zone, that large quantities of melt are intruded in the lower crust before fractionating, moving upward towards the surface and finally erupting.

The presence of these enormous quantities of igneous rock intruded and extruded at volcanic rifts are important not only for understanding the geological history of such rifts, but also for modelling the thermal and subsidence history. Most subsidence modelling programmes assume that mass is conserved in the crust: if in fact large volumes of melt are added as the results presented here make clear, this makes an enormous difference to the subsidence pattern and the thermal history of the rifts (Barton & White 1997). Coupled to this are large base-level changes caused by changes in the temperature of the underlying mantle. Unless the mass and crustal thickness changes caused by magmatism and the elevation changes caused by the thermal history of the mantle are included in the subsidence analysis, the predicted subsidence history may be greatly in error.

We are grateful for support of the iSIMM project by Liverpool and Cambridge Universities, Schlumberger Cambridge Research Ltd, Badley Geoscience Ltd, WesternGeco, Amerada Hess, Anadarko, BP, ConocoPhillips, ENI UK, Statoil, Shell, the NERC and the DTI. The Q-streamer acquisition was undertaken by WesternGeco. The full iSIMM team comprises A. Chappell, P. A. F. Christie, J. D. Eccles, R. Fletcher, D. Healy, N. Hurst, N. J. Kusznir, H. Lau, Z. Lunnon, C. J. Parkin, A. M. Roberts, A. W. Roberts, L. K. Smith, R. Spitzer, V. J. Tymms and R. S. White. Department of Earth Sciences, Cambridge contribution number ESC1284.

References

Assumpção, M. & Bamford, D. 1978. LISPB – V. Studies of crustal shear waves. *Geophysical Journal of the Royal Astronomical Society*, **54**, 61–73.

Avedik, F., Renard, V., Allenou, J. P. & Morvan, B. 1993. 'Single-bubble' air-gun array for deep exploration. *Geophysics*, **58**, 366–382.

Avedik, F., Nicolich, R., Hirn, A., Maltezou, F., McBride, J., Cernobori, L. & the Streamers/Profiles Group. 1995. Appraisal of a new, high-energy low-frequency seismic pulse generating method on a deep seismic reflection profile in the Central Mediterranean Sea. *First Break*, **13** (July), 277–290.

Barton, P. J. 1992. LISPB revisited: a new look under the Caledonides of northern Britain. *Geophysical Journal International*, **110**, 371–391.

Barton, A. J. & White, R. S. 1997. Crustal structure of the Edoras Bank continental margin and mantle thermal anomalies beneath the North Atlantic. *Journal of Geophysical Research*, **102**, 3109–3129.

Brennan, B. J. & Stacey, F. D. 1977. Frequency dependence of elasticity of rock – tests of seismic velocity dispersion. *Nature*, **268**, 220–222.

Browning, P. 1984. Cryptic variation within the cumulate sequence of the Oman ophiolite: magma chamber depth and petrological implications. *In*: Gass, I. G., Lippard, S. J. & Shelton, A. W. (eds) *Ophiolites and Oceanic Lithosphere*. Geological Society, London, Special Publications, **13**, 71–82.

Carlson, R. L. & Miller, D. J. 1997. A new assessment of the abundance of serpentinite in the oceanic crust. *Geophysical Research Letters*, **24**, 457–460.

Castagna, J. P., Batzle, M. L. & Eastwood, R. L. 1985. Relationships between compressional-wave and shear-wave velocities in clastic silicate rocks. *Geophysics*, **50**, 571–581.

Christensen, N. I. 1996. Poisson's ratio and crustal seismology. *Journal of Geophysical Research*, **101**, 3129–3156.

Christie, P., Gollifer, I. & Cowper, D. 2006*a*. Borehole seismic studies of a volcanic succession from the Lopra-1/1A borehole in the Faroe Islands, NE Atlantic. *Geology of Denmark Survey*, **9**, 23–40.

Christie, P. A. F., Lunnon, Z. C., White, R. S. & iSIMM Team. 2006*b*. iSIMM experience with peak- and bubble-tuned sources for generating low frequencies. *68th Meeting of the European Association of Geoscientists and Engineers, Vienna, expanded abstract* A034.

Coffin, M. F. & Eldholm, O. 1994. Large igneous provinces: crustal structure, dimensions, and external consequences. *Reviews of Geophysics*, **32**, 1–36.

Cox, K. G. 1980. A model for flood basalt vulcanism. *Journal of Petrology*, **21**, 629–650.

Cox, K. G. 1993. Continental magmatic underplating. *Philosophical Transactions of the Royal Society, London, A*, **342**, 155–166.

Darbyshire, F. A., White, R. S. & Priestley, K. P. 2000*a*. Structure of the crust and uppermost mantle of Iceland from a combined seismic and gravity study. *Earth and Planetary Science Letters*, **181**, 409–428.

Darbyshire, F. A., Priestley, K. P., White, R. S., Stefánsson, R., Gudmundsson, G. B. & Jakobsdóttir, S. S. 2000*b*. Crustal structure of central and northern Iceland from analysis of teleseismic receiver functions. *Geophysical Journal International*, **143**, 163–184.

Eccles, J. D., White, R. S., Roberts, A. W., Christie, P. A. F. & iSIMM Team. 2007. Wide angle converted shear wave analysis of a North Atlantic volcanic rifted continental margin: constraint on sub-basalt lithology. *First Break*, **25** (October 2007), 63–70.

Eccles, J. D., White, R. S. & Christie, P. A. F. 2009. Identification and inversion of converted shear waves: case studies from the European North Atlantic continental margins. *Geophysical Journal International*, **179**, 381–400; doi: 10.1111/j.1365-246X.2009.04290.x.

Eldholm, O. & Grue, K. 1994. North Atlantic volcanic margins: dimensions and production rates. *Journal of Geophysical Research*, **99**, 2955–2988.

Fliedner, M. M. & White, R. S. 2001. Seismic structure of basalt flows from surface seismic data, borehole measurements and synthetic seismogram modeling. *Geophysics*, **66**, 1925–1936.

Fliedner, M. M. & White, R. S. 2003. Depth imaging basalt flows in the Faeroe-Shetland Basin. *Geophysical Journal International*, **152**, 353–371.

Gordon, R. B. & Davis, L. A. 1968. Velocity and attenuation of seismic waves in imperfectly elastic rock. *Journal of Geophysical Research*, **73**, 3917–3935.

Hopper, J. R., Dahl-Jensen, T. *et al*. 2003. Structure of the SE Greenland margin from seismic reflection and refraction data: implications for nascent spreading center subsidence and asymmetric crustal accretion during North Atlantic opening. *Journal of Geophysical Research*, **108**, 2261–2291; doi: 10.1029/2002JB001996.

Horen, H., Zamora, M. & Dubuisson, G. 1996. Seismic wave velocities and anisotropy in serpentinized peridotites from Xigase ophiolite: abundance of serpentinite in slow spreading ridges. *Geophysical Research Letters*, **23**, 9–12.

Klingelhöfer, F., Edwards, R. A., Hobbs, R. W. & England, R. W. 2005. Crustal structure of the NE Rockall Trough from wide-angle seismic data modelling. *Journal of Geophysical Research*, **110**, B11105; doi: 10.1029/2005JB003763.

Korenaga, J., Holbrook, W. S., Kent, G. M., Kelemen, P. B., Detrick, R. S., Hopper, J. R. & Dahl-Jensen, T. 2000. Crustal structure of the southeast Greenland margin from joint refraction and reflection seismic tomography. *Journal of Geophysical Research*, **105**, 21591–21614.

Landes, M., Ritter, J. R. R., Readman, P. W. & O'Reilly, B. 2005. A review of the Irish crustal structure and signatures from the Caledonian and Variscan orogenies. *Terra Nova*, **17**, 111–120.

LASE Study Group. 1986. Deep structure of the US East Coast passive margin from large aperture seismic experiments (LASE). *Marine Geophysical Research*, **3**, 234–242.

Lunnon, Z. C., Christie, P. A. F. & White, R. S. 2003. An evaluation of peak and bubble tuning in sub-basalt seismology: modelling and results from OBS data. *First Break*, **21** (December), 51–56.

Maclennan, J., McKenzie, D., Grönvold, K., Shimizu, N., Eiler, J. M. & Kitchen, N. 2003. Melt mixing and crystallization under Theistareykir, northeast Iceland. *G3 Geochemistry Geophysics Geosystems*, **4**, 8624; doi: 10.1029/2003GC000558.

Maresh, J. & White, R. S. 2005. Seeing through a glass, darkly: strategies for imaging through basalt. *First Break*, **23** (May), 27–32.

Maresh, J., White, R. S., Hobbs, R. W. & Smallwood, J. R. 2006. Seismic attenuation of Atlantic margin basalts: observations and modeling. *Geophysics*, **71**, B211–B221; doi: 10.1190/1.2335875.

Mutter, J. C., Talwani, M. & Stoffa, P. L. 1984. Evidence for a thick oceanic crust adjacent to the Norwegian Margin. *Journal of Geophysical Research*, **89**, 483–502.

Parkin, C. J. & White, R. S. 2008. Influence of the Iceland mantle plume on oceanic crust generation in the North Atlantic. *Geophysical Journal International*, **173**, 168–188; doi: 10.1111/j.1365-246X.2007.03689.x.

Reynisson, R. F., Ebbing, J., Lundin, E. & Osmundsen, P. T. 2010. Properties and distribution of lower crustal bodies on the mid-Norwegian margin. *In*: Vining, B. A. & Pickering, S. C. (eds) *Petroleum Geology: From Mature Basins to New Frontiers – Proceedings of the 7th Petroleum Geology Conference*, Geological Society, London, 843–854; doi: 10.1144/0070843.

Richardson, K. R., White, R. S., England, R. W. & Fruehn, J. 1999. Crustal structure east of the Faroe Islands. *Petroleum Geoscience*, **5**, 161–172.

Roberts, A. W., White, R. S. & Christie, P. A. F. 2009. Imaging igneous rocks on the North Atlantic rifted continental margin. *Geophysical Journal International*, **179**, 1024–1038; doi: 10.1111/j.1365-246X.2009.04306.x.

Shaw, F., Worthington, M. H., White, R. S., Andersen, M. S., Petersen, U. K. & the SeiFaba Group. 2008. Seismic attenuation in Faroe Islands basalts. *Geophysical Prospecting*, **56**, 5–20; doi: 10.1111/j.1365-2478.2007.00665.x.

Soosalu, H., Key, J., White, R. S., Knox, C., Einarsson, P. & Jakobsdóttir, S. S. 2010. Lower-crustal earthquakes caused by magma movement beneath Askja volcano on the north Iceland rift. *Bulletin of Volcanology*, **72**, 55–62; doi: 10.1007/s00445-009-0297-3.

Spitzer, R., White, R. S. & iSIMM Team. 2005. Advances in seismic imaging through basalts: a case study from the Faroe-Shetland Basin. *Petroleum Geoscience*, **11**, 147–156.

Strandenes, S. 1991. Rock physics analysis of the Brent Group reservoir in the Oseberg Field. *In*: *Stanford Rockphysics and Borehole Geophysics Project*, Special Volumes. Stanford University, Stanford, CA.

Tomlinson, J. P., Denton, P., Maguire, P. K. H. & Booth, D. C. 2006. Analysis of the crustal velocity structure of the British Isles using teleseismic receiver functions. *Geophysical Journal International*, **167**, 223–237.

Tuitt, A., Underhill, J. R., Ritchie, J. D., Johnson, H. & Hitchen, K. 2010. Timing, controls and consequences of compression in the Rockall–Faroe area of the NE Atlantic margin. *In*: Vining, B. A. & Pickering, S. C. (eds) *Petroleum Geology: From Mature Basins to New Frontiers – Proceedings of the 7th Petroleum Geology Conference*. Geological Society, London. 963–977; doi: 10.1144/0070963.

Vogt, U., Makris, J., O'Reilly, B. M., Hauser, F., Readman, P. W., Jacob, A. W. B. & Shannon, P. M. 1998. The Hatton Basin and continental margin: crustal structure from wide-angle seismic and gravity data. *Journal of Geophysical Research*, **103**, 12545–12566.

Voss, M. & Jokat, W. 2007. Continent–ocean transition and voluminous magmatic underplating derived from P-wave velocity modelling of the East Greenland continental margin. *Geophysical Journal International*, **170**, 580–604.

White, N. & Lovell, B. 1997. Measuring the pulse of a plume with the sedimentary record. *Nature*, **387**, 888–891.

White, R. & McKenzie, D. 1989. Magmatism at rift zones: the generation of volcanic continental margins and flood basalts. *Journal of Geophysical Research*, **94**, 7685–7729.

White, R. S. & McKenzie, D. 1995. Mantle plumes and flood basalts. *Journal of Geophysical Research*, **100**, 17543–17585.

White, R. S. & Smith, L. K. 2009. Crustal structure of the Hatton and the conjugate east Greenland rifted volcanic continental margins, NE Atlantic. *Journal of Geophysical Research*, **114**, B02305; doi: 10.1029/2008JB005856.

White, R. S. & Stephen, R. A. 1980. Compressional to shear wave conversion in oceanic crust. *Geophysical Journal of the Royal Astronomical Society*, **63**, 547–566.

White, R. S., McKenzie, D. & O'Nions, R. K. 1992. Oceanic crustal thickness from seismic measurements and rare earth element inversions. *Journal of Geophysical Research*, **97**, 19683–19715.

White, R. S., Fruehn, J., Richardson, K. R., Cullen, E., Kirk, W., Smallwood, J. R. & Latkiewicz, C. 1999. Faroes Large Aperture Research Experiment (FLARE): imaging through basalts. *In*: Fleet, A. J. & Boldy, S. A. R. (eds) *Petroleum Geology of Northwest Europe: Proceedings of the 5th Conference*. Geological Society, London, 1243–1252; doi: 10.1144/0051243.

White, R. S., Smallwood, J. R., Fliedner, M. M., Boslaugh, B., Maresh, J. & Fruehn, J. 2003. Imaging and regional distribution of basalt flows in the Faroe-Shetland Basin. *Geophysical Prospecting*, **51**, 215–231.

White, R. S., Smith, L. K., Roberts, A. W., Christie, P. A. F., Kusznir, N. J. & iSIMM Team. 2008. Lower-crustal intrusion on the North Atlantic continental margin. *Nature*, **452**, 460–464.

Zelt, C. A. & Smith, R. B. 1992. Seismic travel time inversion for 2-D crustal velocity structure. *Geophysical Journal International*, **108**, 16–24.

Ziolkowski, A., Hanssen, P., Gatliff, R., Li, X. & Jakubowicz, H. 2001. The use of low frequencies for sub–basalt imaging. *In*: *71st Annual International Meeting of the Society of Exploration Geophysicists*, 74–77.

Properties and distribution of lower crustal bodies on the mid-Norwegian margin

R. F. REYNISSON,[1,2,3] J. EBBING,[1,2] E. LUNDIN[3] and P. T. OSMUNDSEN[2]

[1]*Norwegian University of Science and Technology, Department of Petroleum Engineering and Applied Geophysics, S.P. Andersens vei 15A, 7491 Trondheim, Norway (e-mail: rrey@statoil.com)*

[2]*Geological Survey of Norway, Leiv Eirikssons vei 39, 7040 Trondheim, Norway*

[3]*Statoil, Rotvoll, Arkitekt Ebbels veg 10, 7005 Trondheim, Norway*

Abstract: Anomalously high velocity and high density bodies have been detected in the lower crust on the mid-Norwegian margin. The lower crustal bodies (LCB) are pronounced on the Møre and Vøring margins segments and have mainly been interpreted as either magmatic or high-grade metamorphic in origin. Evolutionary models of the whole margin are heavily affected by the interpretation of the LCB and so are estimates of vertical movements and thermal structure in the area. A 3D gravity and magnetic model of the mid-Norwegian margin was constructed to map the main geological features of the margin and acquire the distribution of the LCB. The model utilizes the most recent potential field compilations on the margin and is constrained by extensive reflection seismic data and published refraction profiles. Further constraints on the model were attained from studying the isostatic state of the lithosphere. We present a map showing the distribution of the different LCB and discuss the implications for the structural and thermal evolution of the margin. The properties of the LCB vary across the margin and at least three different processes may be responsible for their existence. The LCB is commonly interpreted as igneous rock either intruded into the lower crust or underplated beneath it. The distribution of the LCB along the Vøring margin has an apparent correlation with the offshore prolongations of major onshore detachments stemming from Late Caledonian orogenic collapse. This may point towards some relation between the LCB and these old zones of weakness and that the LCB represents high-grade metamorphic rocks. Detailed modelling on the Møre margin shows a spatial link between parts of the LCB and extremely thin crustal thickness, suggesting a serpentinized exhumed mantle origin.

Keywords: Norwegian continental shelf, lower crustal body, magmatic underplating, exhumed mantle, passive continental margins, flexure and isostasy, potential fields

This study focuses on the mid-Norwegian continental margin (Fig. 1), a part of the NE Atlantic margin, and addresses the origin of a high-velocity, high-density layer at the base of the crust, which is detected by ocean bottom seismometer (OBS) seismic experiments with a seismic P-wave velocity of 7.0–7.9 km s^{-1} (e.g. Skogseid *et al.* 1992; Raum *et al.* 2002; Mjelde *et al.* 2005, 2009*a*, *b*; Tsikalas *et al.* 2008). We refer to this layer as a lower crustal body (LCB) to follow convention, but suggest that it can be part of the mantle as well as the crust. The LCB is often referred to as magmatic underplating (e.g. Skogseid *et al.* 1992; van Wijk *et al.* 2004; Mjelde *et al.* 2005). However, while the high velocity/high density of the LCB may be considered as an objective observation, its origin as a layer of igneous rock either intruded into the lower crust or underplated beneath it is an interpretation that dates back to work by, for example, White *et al.* (1987). To our knowledge, underplated material has never been observed in outcrop nor sampled by drilling and the usage as a descriptive term should be abandoned; it is clearly an interpretation. In recent years, there has been a renewed discussion about the interpretation of the LCB (e.g. Gernigon *et al.* 2004; Mjelde *et al.* 2005, 2009*a*; Ebbing *et al.* 2006), and of the distinction between igneous underplating below stretched continental crust and igneous intrusion into the lower crust (White *et al.* 2008; White & Smith 2009).

The mid-Norwegian margin was formed by episodic extensional events during Late Palaeozoic–Triassic, Late Jurassic–Early Cretaceous and Late Cretaceous–Paleocene times (Ziegler 1988; Blystad *et al.* 1995; Doré *et al.* 1999; Brekke 2000). Early Cenozoic continental breakup and initial seafloor spreading between Eurasia and Greenland was characterized by emplacement of significant volumes of magmatic rocks (e.g. Eldholm & Grue 1994). The magmatic rocks were partially extruded on the surface as flood basalts and tuffs and partially intruded as central complexes, sills and dykes into the sedimentary rocks and the crystalline crust. In addition, a lower crustal high-velocity body has been recognized along many parts of the margin, and is commonly interpreted to represent magmatic material added beneath the crust (Eldholm & Grue 1994; Mjelde *et al.* 2001), or intruded in the lower crust (e.g. White *et al.* 1987, 2008; White & Smith 2009). Notably, the interpreted magmatic body has been proposed to constitute between 60 and 80% of the total magmatic rock volume in the NAIP (White *et al.* 1987, 2008; Eldholm & Grue 1994). In the southernmost Vøring basin, however, the lower crustal layer shows anomalously high P-wave velocities (8.4 km s^{-1}) and has been interpreted as eclogite by Raum *et al.* (2006) and Mjelde *et al.* (2009*b*). In the remainder of the basin the layer is interpreted as mafic intrusions emplaced during the last phase of rifting, but it cannot be excluded that the body consists of older (Caledonian?) mafic rocks (Ebbing *et al* 2006; Mjelde *et al.* 2009*a*). Determining the nature of the LCB clearly is relevant for the thermal history of volcanic margins, and arguably also for the entire concept of the development of such margins.

We present a deep crustal configuration based on the results of a 3D model of the Møre margin compiled with studies by Ebbing *et al.* (2006), Osmundsen & Ebbing (2008), Tsikalas *et al.* (2008) and Mjelde *et al.* (2009*a*). These studies provide means to address the properties of the LCB on the mid-Norwegian margin by incorporating flexural isostasy considerations.

VINING, B. A. & PICKERING, S. C. (eds) *Petroleum Geology: From Mature Basins to New Frontiers – Proceedings of the 7th Petroleum Geology Conference*, 843–854. DOI: 10.1144/0070843 © Petroleum Geology Conferences Ltd. Published by the Geological Society, London.

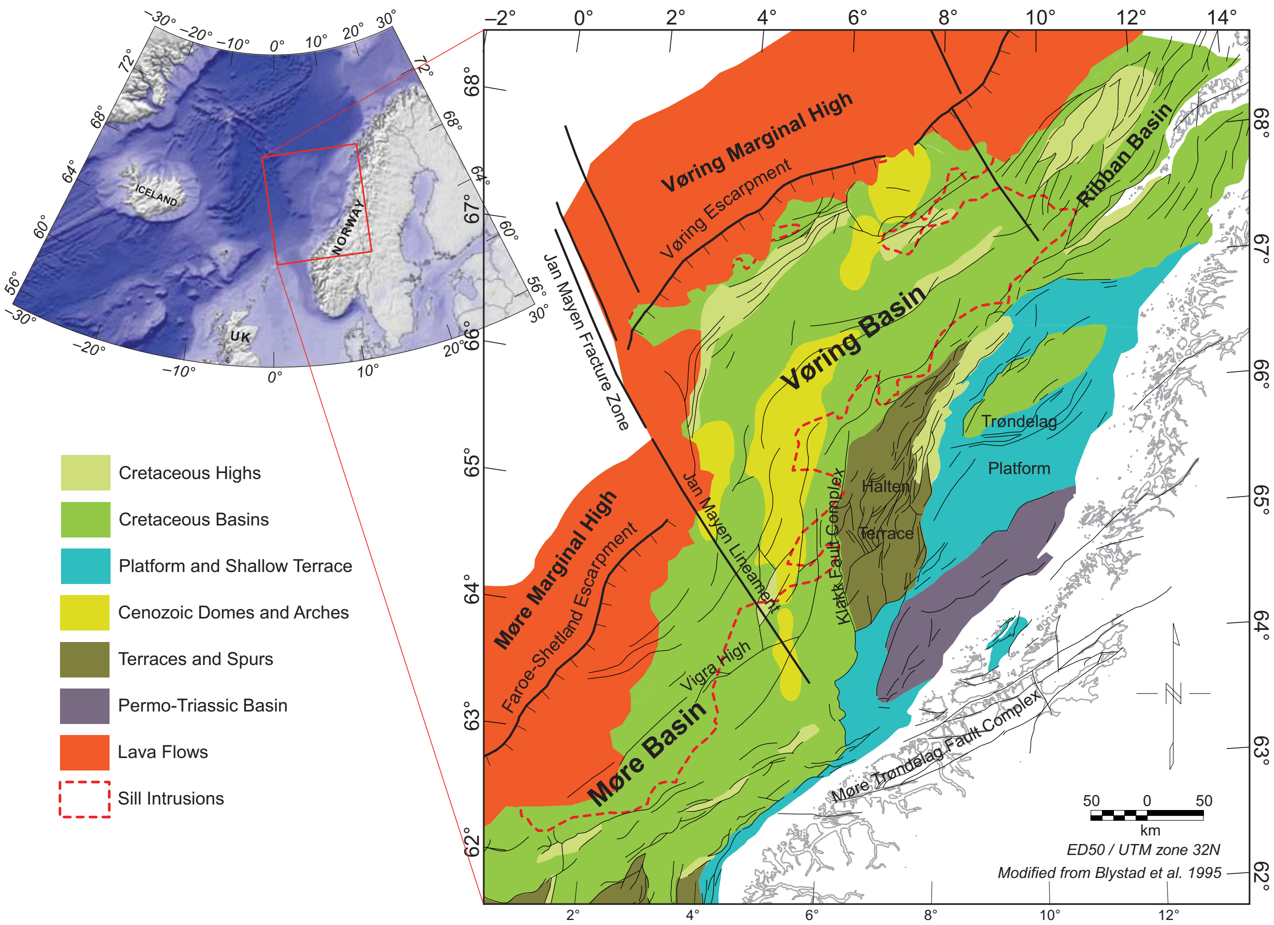

Fig. 1. Study area. The study area is the mid-Norwegian margin, a part of the NE Atlantic margin, and comprises the Møre, Vøring and Lofoten-Vesterålen margin segments. The figure shows the main geological and structural features of the margin based on Blystad *et al.* (1995).

Compilation of 3D models

The geometries of the deeper crust and the upper mantle on the mid-Norwegian margin are reasonably well defined in two dimensions by OBS data. From 3D potential field models, which have been integrated in the current study, different horizons can be mapped, which allows discussing regional changes in the geometry of the study area. The spatial extension of the horizons, with the exception of the Moho, is limited to the NW by the main escarpments and to the SE by the coast of Norway. Here, we utilize top crystalline basement, top LCB and Moho horizons in alliance with seismic interpretation and isostatic considerations to shed light on the properties of the LCB. See Ebbing *et al.* (2006) and Omsundsen & Ebbing (2008) for more details on the integration of potential field data, well information and seismic data in the construction of 3D models of the mid-Norwegian margin.

Figure 2 shows the thickness of the high-density LCB as defined by the integrated 3D models and seismic data. The LCB is primarily modelled on the Møre and Vøring margins and extends from the escarpments well into the basins. The overall structural trend of the LCB follows the general strike of the margin as indicated by seismically mapped faults. Two distinct LCB ridges that are up to 10 km thick exist on the Møre margin. The Vøring margin contains a LCB that is somewhat more evenly distributed, varying between 3 and 8 km thickness. The Lofoten margin has only a veneer of LCB that is little more than 1 km thick and is not present north of the Jennega Transfer Zone (Tsikalas *et al.* 2008).

By subtracting the Moho from the top basement horizon a crustal thickness map was acquired (Fig. 3). The map shows a very thin crystalline crust (less than 5 km) below the centre of the Møre Basin. Thin crust (less than 10 km) is noted along the whole mid-Norwegian margin and coincides with the extent of the Cretaceous depocentres, suggested to relate to Early Cretaceous rifting (Lundin & Doré 1997). Comparison of the crustal thickness with the LCB distribution reveals a strong first-order correlation along the entire mid-Norwegian margin. Locally, there is not always a one-to-one correlation between thickest modelled LCB and thinnest modelled crust. There are several possible explanations for this, such as different origin of the LCB (magmatic, metamorphic, serpentinized). In particular, densities of serpentinized mantle rocks may overlap with densities of crustal rocks and may therefore not be recognized by gravity modelling.

The distribution of volcanics in the study area was compiled from a seismic study and from previously published maps (Blystad *et al.* 1995; Olesen *et al.* 2002; Planke *et al.* 2005). Comparison of distributions of the LCB and the limit of lavas and sills (Fig. 4) reveals that all the LCB on the Vøring margin is overlain by volcanics and so is a considerable part of the Lofoten margin. On the Møre margin the LCB is overlain by volcanics, apart from the landward LCB ridge that coincides with the very thin crust.

Isostatic considerations

The Moho boundary is assumed to reflect the isostatic equilibrium surface at the base of the lithosphere (Braitenberg *et al.* 2002; Wienecke *et al.* 2007). Because the Moho is shallower than the base lithosphere and has a high density contrast, it is the main contributor of isostatic compensation to the gravity field. Comparison

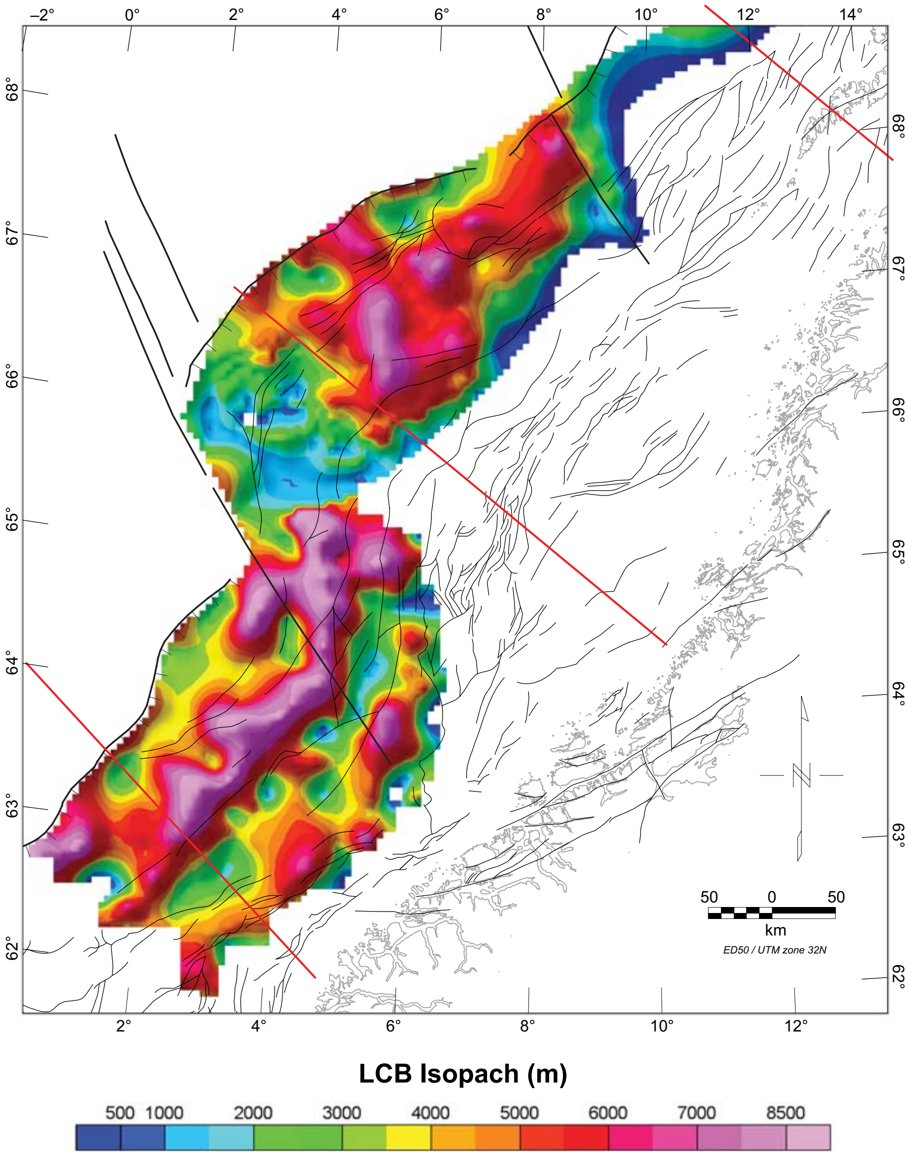

Fig. 2. LCB on the mid-Norwegian margin. LCB isopach resulting from integrated 3D models of the mid-Norwegian margin. The structural features are the same as in Figure 1. The red lines indicate the location of profiles in Figure 8.

of the Moho from the integrated models with an isostatic compensation surface provides insight into the whole crust characteristics of the study area. By comparing the two differently acquired Mohos, it is proposed that a distinction can be made between whether the LCB should be assigned to the crust or the mantle. This distinction has a profound influence on the genetic origin of the LCB. Crust-originated LCB indicates underplated or intruded igneous material in the lower crust and mantle-originated LCB reflects a low-density mantle. It is feasible to interpret the LCB associated with the mantle as serpentinized mantle and further that this body spatially coincides with very thin crust.

Assuming that the mid-Norwegian margin is in isostatic equilibrium, we calculated the isostatic compensation for the de-loading of the margin by the relatively low-density sedimentary infill and water. For the isostatic calculation, we used the LithoFlex software (Braitenberg *et al.* 2006; Wienecke *et al.* 2007). The loading of the sediments was calculated by applying a linear depth-dependent density function from 2200 kg m^{-3} at sea surface to 2700 kg m^{-3} at 10 km depth and constant below this level. The surrounding basement had density of 2750 kg m^{-3}. The simplified density distribution leads to de-loading of the lithosphere, which in an isostatic concept requires crustal thinning to balance the load. A relatively low value for the strength of the lithosphere ($T_e = 10$ km) was applied. The reference depth was 30 km and the density contrast at the isostatic flexural base was 400 kg m^{-3}, which corresponds to a lower crust density of 2900 kg m^{-3} and a mantle density of 3300 kg m^{-3}.

The resulting isostatic Moho (Fig. 5) shows a similar regional trend to the model Moho (Fig. 6) with depth decreasing from the coast to the axial part of the basins and increasing again towards the marginal high. The difference map (Fig. 7) highlights substantial differences between the isostatic and modelled Moho and gives valuable insight into the margin. A positive difference reflects that the model Moho is shallower than the isostatic Moho and negative difference indicates locations where the model Moho is deeper. In the southern Vøring, the isostatic and model Moho are at similar depths, while in the central and northern Vøring margin the isostatic Moho is more than 4 km shallower than the model Moho, corresponding to the thickness of the LCB. The same observation is made for the outer Møre margin. In the inner Møre margin and the Lofoten margin, the isostatic Moho is deeper than the model Moho. Three profiles representative for each margin segment further illustrate the difference between the isostatic and model Moho (Fig. 8).

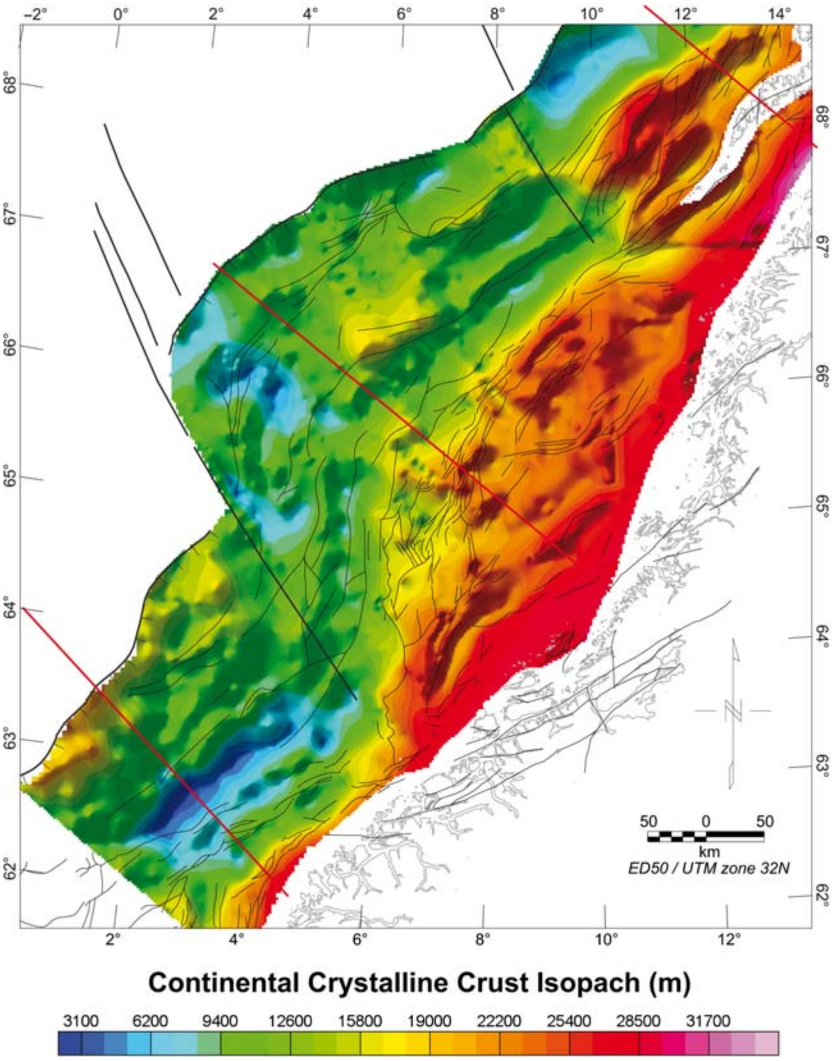

Fig. 3. Thickness of continental crystalline crust. The map shows that a very thin crystalline crust (less than 5 km) exists below the centre of the Møre Basin. Thin crust (less than 10 km) is noted locally on the whole mid-Norwegian margin and coincides with the extent of the Cretaceous depocentres, suggested to relate to Cretaceous rifting (Lundin & Doré 1997). The structural features are the same as in Figure 1. The red lines indicate the location of profiles in Figure 8.

The lateral volcanic distribution coincides mainly with negative Moho difference but the location of thin crust is most often associated with positive difference or a modelled Moho shallower than isostatic Moho (compare Figs 4 & 7). Most of the LCB has a distribution that follows the trend of the negative Moho difference, although the most inboard part of the LCB on the Møre and Vøring margins and the whole LCB on the Lofoten margin are spatially associated with positive Moho difference and thin crust. The positive difference coinciding with LCB introduces a problem to a static crustal model if the LCB is assumed part of the crust. This is because the high density body is included in the model but not in the isostatic calculations. From isostatic considerations a high-density body of LCB in the crust should suppress the Moho. It is therefore more feasible to assign the LCB in these scenarios to the mantle than the crust. Kimbell *et al.* (2004) compared Moho depth based on isostatic consideration with Moho depth observed in seismic data and noted discrepancies where estimated Moho was both shallower and deeper than observed Moho. Amongst several possibilities to explain the isostatic Moho being deeper than the seismic Moho, Kimbell *et al.* (2004) favoured a negative upper mantle density anomaly. This means that the modelled high-density LCB is not a part of the crust but a low-density mantle and the model Moho is defined at the top of the LCB, which results in an even larger positive Moho difference.

Process orientated approach

A profile from the Møre margin demonstrates the Moho configuration and the discrepancy between model Moho and isostatic Moho (Fig. 8). Accepting that LCB coinciding with a positive Moho difference represents a low-density mantle, the Moho is defined at the top of the LCB in the centre of the basin but at the base of the LCB at the flanks of the basin. In order to reconstruct this Moho configuration with isostatic and flexural considerations a process orientated approach (Watts 2001) is needed. This approach allows us to take into account different crustal strength regimes during rifting and subsequent sedimentation. We used elastic thickness values $T_e = 5$ km during rifting and $T_e = 25$ km during sedimentation to reconstruct the Moho geometry below the basin. The high Moho relief is preserved from the rifting period when the crust was weak. During sedimentation the crust is more rigid and therefore distributes the load caused by the sedimentary fill over larger areas of the crust. The resulting Moho configuration resembles the model Moho configuration in a very shallow Moho in the centre of the basin. This approach demonstrates how the positive difference between the model Moho and the isostatic Moho can exist and still be isostatically reasonable.

From the above, it possible to exclude that the LCB coinciding with positive Moho difference is magmatic underplate or highly

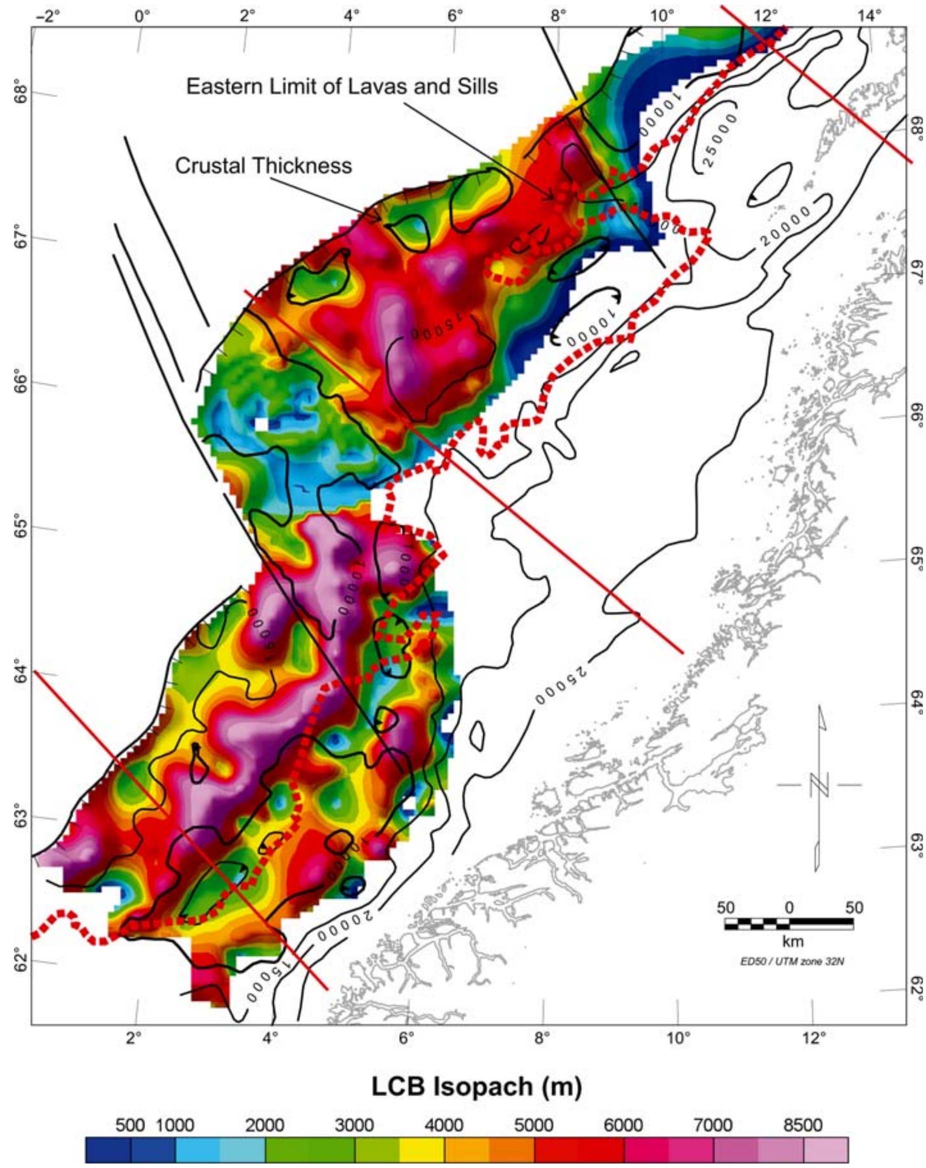

Fig. 4. LCB distribution compared to magmatic rocks and crustal thickness. The black lines are contours of the crust thickness in Figure 3 and are drawn with 5000 m interval. The red dotted line presents the eastern limit of lavas and sills on the margin. Comparison of LCB distribution and volcanic distribution reveals that all the LCB on the Vøring margin is overlain by volcanics and considerable part on the Lofoten margin. On the Møre margin the LCB is overlain by volcanics apart from the landward ridge that coincides with the very thin crust. Comparing the crustal thickness to the LCB distribution shows that in the Møre Basin the thinnest crust spatially coincides with the most landward ridge of the LCB. The landward edge of the LCB in the Vøring Basin coincides with underlying thin crust. On the Lofoten margin the whole LCB coincides with thin crust. Main lineaments are the same as in Figure 1. The red lines indicate the location of profiles in Figure 8.

intruded lower crust. An underplated or intruded lower crust would be related to the Early Cenozoic continental breakup (e.g. White *et al.* 1987; Eldholm & Grue 1994), which is much later (in the order of 80 Ma) than the main rifting period on the margin in the Late Jurassic–Early Cretaceous (Lundin & Doré 1997) and likewise after most of the sediment infill had taken place. If the lower crust is underplated or greatly intruded below the axial part of the basins the crust would reflect a more local isostatic architecture because high heat flows and consequently weak crust are the effects of magmatic underplating, which would be in disagreement with a strong crust ($T_e = 25$) during the whole sedimentation period. The spatial coincidence of very thin crust, positive Moho difference and LCB further point towards a mantle origin of the LCB. From this it is more feasible to assign the origin of the LCB to unroofed mantle rocks that have undergone serpentinization. Such settings are prone to develop décollements at the crust–serpentinized mantle interface (e.g. Reston 2009), which in turn can lead to core complex-like structural geometries. A modelled Moho deeper than isostatic Moho can on the other hand be explained by isostatic readjustments of weak crust caused by igneous underplate or intrusions in the lower crust.

Regional considerations

Geological history predating separation of the mid-Norwegian margin from that of east Greenland included two events that are particularly important with respect to the discussion of LCB origin. The first event was the Late Silurian–Early Devonian Caledonian Orogeny, which was succeeded by Devonian–Early Carboniferous extension and unroofing (e.g. Osmundsen *et al.* 2006). High-grade metamorphic rocks formed during this orogeny are well preserved in outcrop on both conjugate margins and it can readily be concluded that the deeper crust of the original

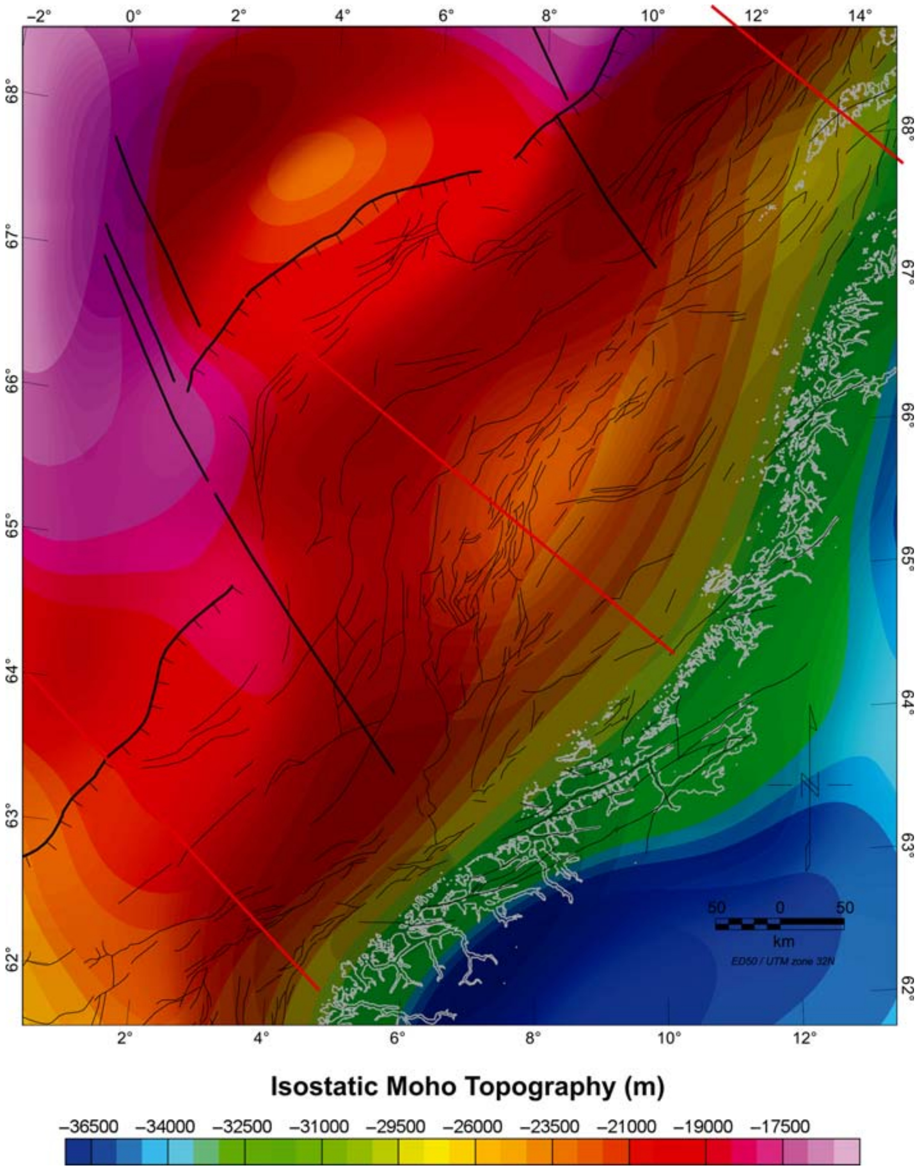

Fig. 5. Isostatic flexural Moho. Relatively low value for the strength of the lithosphere ($T_e = 10$ km) was applied to calculate the isostatic flexural Moho. The reference depth was chosen as 30 km and the density contrast at the isostatic flexural base with 400 kg m^{-3}, which correlates to a lower crust density of 2900 kg m^{-3} and a mantle density of 3300 kg m^{-3}. The structural features are the same as in Figure 1. The red lines indicate the location of profiles in Figure 8.

Caledonian root also consisted of high-grade rocks. The protoliths of this orogenic root probably varied considerably. Even so, it appears very likely that remnants from the orogenic root likely would have achieved P-wave velocities in the 7–8 km s^{-1} range (cf. Hürich *et al.* 2001).

The second important tectonic event was the Late Jurassic–Early Cretaceous rifting, which established the precursor to our current NE Atlantic margins (Doré *et al.* 1999). Following the Mid Jurassic opening of the Central Atlantic, Early Cretaceous rifting followed by plate separation that propagated northward from Iberia–Newfoundland into the Bay of Biscay, Rockall Trough and Labrador Sea (e.g. Johnston *et al.* 2001). Severe Early Cretaceous rifting also extended from the Rockall Trough via the Faroe–Shetland Basin, Møre Basin, Vøring Basin, Lofoten–NE Greenland margins into the Tromsø and Bjørnøya Basins of the SW Barents margin (e.g. Shannon 1991; Faleide *et al.* 1993; Lundin & Doré 1997). Of the mentioned areas the Iberia and Newfoundland margins have been sampled via several academic drilling campaigns, proving the presence of exhumed and serpentinized mantle (e.g. Tucholke *et al.* 2007 and references therein). For quite some time it has been clear that the Labrador Sea conjugate margins are characterized by belts of exhumed mantle (Louden & Chian 1999; Srivastava & Roest 1999). The Rockall Trough has also been interpreted to be underlain by exhumed and serpentinized mantle (O'Reilly *et al.* 1996; Morewood *et al.* 2005). The highly stretched southern axial part of the Porcupine Basin, where the so-called Median Volcanic Ridge is located, is now considered to be highly thinned continental crust underlain by serpentinized mantle (Reston 2009). A review of the mentioned magma-poor margins is provided by Reston (2009). Our contribution in this paper illustrates that also the Møre Basin is probably underlain by serpentinized mantle, and we argue that the Vøring basin is probably also underlain by serpentinized mantle, at least in part. Like the Møre Basin, the Vøring Basin is characterized by a thick Cretaceous sedimentary fill, and the basin lacks significant Cenozoic extension except in the outermost part (e.g. Lundin & Doré 1997; Roberts *et al.* 1997).

While mantle exhumation in the Porcupine Basin probably relates to Late Jurassic rifting, the other mentioned areas were thinned during Cretaceous time. Notably, the plate separation rates were slow during the Cretaceous, consistent with the development of the mentioned magma-poor margins (Bown & White

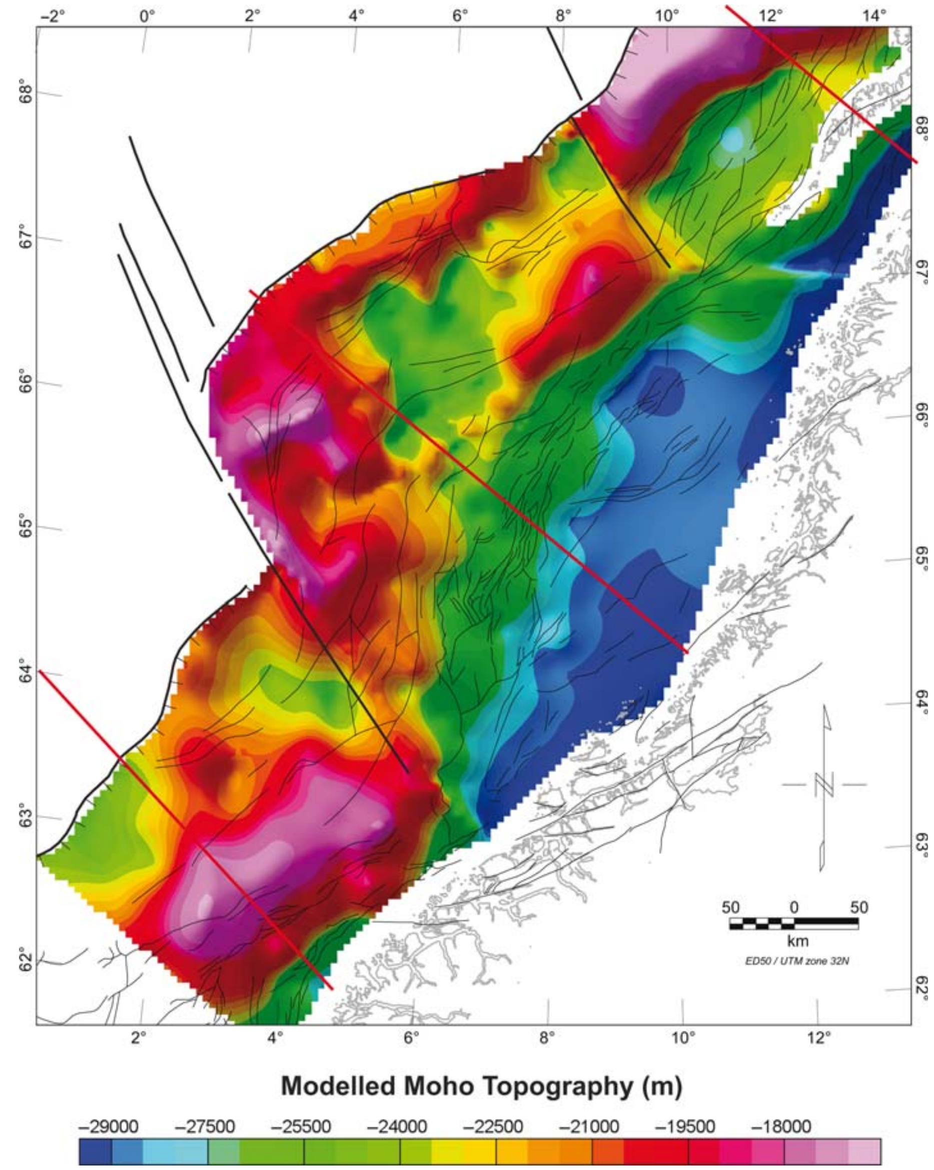

Fig. 6. Moho configuration resulting from the compiled 3D models. The structural features are the same as in Figure 1. The red lines indicate the location of profiles in Figure 8.

1995). During the Early Eocene opening of the magma-rich NE Atlantic, however, the plate separation rates increased dramatically for a short period. Commonly, this increase in plate separation rate and the magma-rich opening of the NE Atlantic is associated with the arrival of a mantle plume (e.g. White *et al.* 1987). High P-wave velocities of a LCB along the continent–ocean transition has been interpreted to represent magmatic intrusion in the lower crust or underplating, stemming from rapid decompressional melting of anomalously hot mantle related to the mantle plume (e.g. White & McKenzie 1989; Eldholm & Grue 1994). Numerous OBS studies by Mjelde and co-workers along the mid-Norwegian margin (see Mjelde *et al.* 2009*a* and references therein) have outlined an extensive LCB under the mid-Norwegian margin, and this LCB has generally been interpreted to represent Early Cenozoic magmatic underplating.

Ascribing the LCB along the Edoras–Hatton margin and the conjugate SE Greenland margin to Early Cenozoic magmatic intrusion or underplating (White *et al.* 1987; White & Smith 1989) appears reasonable. In this area breakup of Pangaea occurred within the Laurentian plate and the presence of Caledonian high-grade metamorphic rocks is unlikely. As mentioned, the path of Early Cretaceous rifting and related mantle serpentinization went via the Rockall Trough into the mid-Norwegian margin. Lack of evidence for major Cretaceous extension along the SE Greenland/Edoras–Hatton Bank part of the NE Atlantic also makes mantle serpentinization an unlikely explanation for the LCB here. However, the situation is quite different along the mid-Norwegian/East Greenland margins. Breakup of this part of the NE Atlantic certainly reopened the Caledonian Orogen, and both the mid-Norwegian Basins and Thetis Basin off NE Greenland were severely thinned during the Early Cretaceous rift event. Thus, the LCB beneath the mid-Norwegian margins in all likelihood relates to at least three different processes: (1) magmatic underplating or lower-crustal intrusion during Early Eocene breakup; (2) high-grade metamorphism during the Caledonian orogeny; and (3) mantle serpentinization during Late Jurassic–Early Cretaceous rifting. Of these processes, it appears that Early Cretaceous mantle serpentinization may be the dominant process. Recent work along the Hatton–Edoras margin reveal that the LCB there is confined to a relatively narrow body, *c*. 40 km in width (White *et al.* 2008; White & Smith 2009). We have no problem accepting that this LCB relates to Early Cenozoic intrusions of the lower crust

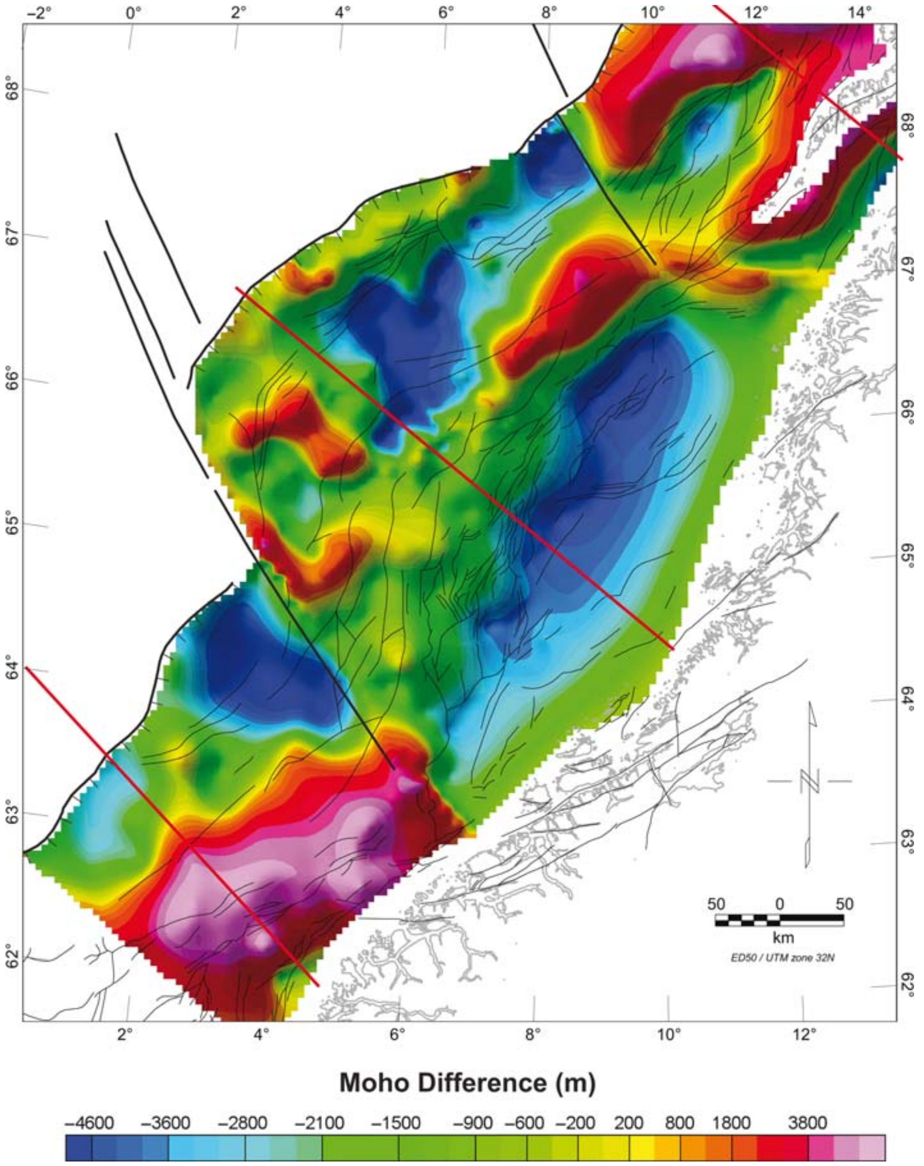

Fig. 7. Moho difference. Positive difference reflects scenarios where the model Moho is shallower than the isostatic Moho and negative difference indicates locations where the model Moho is deeper. The difference map highlights substantial differences between the isostatic and model Moho. In the southern Vøring, the isostatic and model Moho are at similar depths, while on the central and northern Vøring margin the isostatic Moho is more than 4 km shallower than the model Moho. The same observation can be made on the outer Møre margin. On the inner Møre margin and the Lofoten margin, the isostatic Moho is deeper than the model Moho. The structural features are the same as in Figure 1. The red lines indicate the location of profiles in Figure 8.

as proposed. However, the much wider LCB, observed on the mid-Norwegian margin coincides closely with the deep Cretaceous basins and we propose a genetic relationship between the severe Cretaceous extension and the LCB. Notably, V_p/V_s ratios along regional transects across the mid-Norwegian margin reveal ratios in the 1.8–1.9 range for large areas. Such V_p/V_s ratios are consistent with serpentinized mantle, but also with gabbro (Miller & Christensen 1997; Escartin *et al.* 2001). The weakness in interpreting this part of the mid-Norwegian LCB as underplated material (Mjelde *et al.* 2009*a*) lies foremost in the absence of Cenozoic extension.

Discussion and conclusions

The origin of the LCB is still under discussion and different interpretations exist for the body and the strong deep crustal reflectors, which are often associated with it (e.g. Gernigon *et al.* 2003). The early proposal that the anomalously high velocity may reflect the concentration of MgO within magmatically underplated or intruded material, which in turn was suggested to reflect mantle temperature (White & McKenzie 1989), has subsequently been challenged (Eldholm *et al.* 1995; Gernigon *et al.* 2004). Nevertheless, it is still common for workers (e.g. Mjelde *et al.* 2005) to propose that the LCB represents magmatically underplated material, and that the density and velocity distribution may signify differences in the magma composition, in turn possibly reflecting asthenospheric temperatures or compositional inhomogeneities in the asthenospheric source. OBS studies indicate large variations in the thickness and velocity within the LCB, and these have been proposed to relate to the distribution of mantle melts via feeder dykes (Mjelde *et al.* 2002). The velocities of this layer vary between 7.0 and 7.7 km s^{-1}, and have been reinterpreted as functions of differences in the magma composition due to inhomogeneities in the asthenospheric source (Mjelde *et al.* 2005) or as a function of mafic differentiation inside the LCB (Gernigon *et al.* 2005). White *et al.* (2008) suggest that variations in seismic velocity in the LCB may reflect variable percentages of intruded igneous rock into pre-existing continental crust.

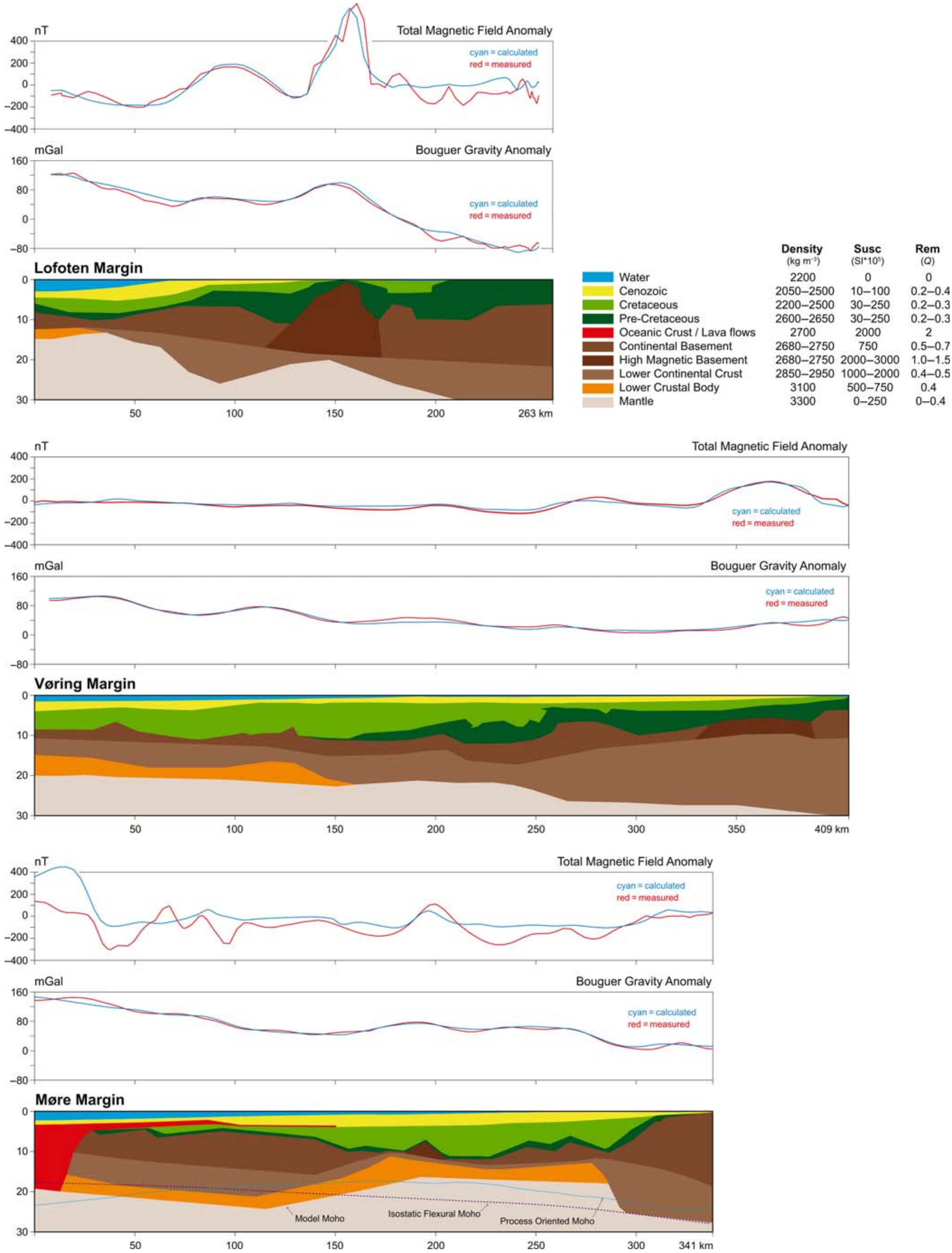

Fig. 8. Representative profiles of the mid-Norwegian margin segments. Three profiles representative for each margin segment illustrate the main geological bodies of the mid-Norwegian margin. The properties used in the potential field models are listed in the legend. See the Møre profile for comparison of different Moho types. The location of the profiles is shown with thick red lines in Figures 2–7.

Gernigon *et al.* (2003, 2004) discussed a range of possible origins for the LCB, where ultra high-pressure metamorphic rocks were the preferred alternative. Upper amphibolite to eclogite facies metamorphic rocks of a mafic composition have the same velocity range as those of the LCB (Hürich *et al.* 2001). The crust of the Horda Platform (Christiansson *et al.* 2000) and the Møre coastal area (Ólafsson *et al.* 1992) are interpreted to be underlain by eclogite. Raum *et al.* (2006) and Mjelde *et al.* (2009*b*) interpreted the lower crust in the southwestern corner of the Vøring Basin as *in situ* eclogite based on anomalously high P-wave velocities (8.4 km s^{-1}). The apparent correlation between the boundaries of the LCB and the interpreted offshore extensions of the post-Caledonian detachments support this interpretation (Ebbing *et al.* 2006), but it is unlikely that the entire region has the composition of eclogite. After all, only parts of the western gneiss region, onshore Norway, consist of these rocks and the bulk composition is a granitic or granodioritic gneiss. Depending on the protolith, metamorphism to upper amphibolite–eclogite facies can result in the same velocity range (*c.* 7–8 km s^{-1}) as the rocks that traditionally are interpreted as magmatically underplated material (Hürich *et al.* 2001). Thus, based on P-wave velocity alone it is not possible to distinguish between these alternatives and magmatic underplating. The V_p/V_s ratio should be distinctive (Eccles *et al.*, 2009; White *et al.* 2010) but V_p/V_s ratios of LCB on the mid-Norwegian margin have been reported between 1.8 and 1.9 (Mjelde *et al.* 2009*a*, *b*). These V_p/V_s ratios are compatible with mafic rocks of both igneous and metamorphic origin. Such V_p/V_s ratios are also consistent with serpentinized mantle (Miller & Christensen 1997; Escartin *et al.* 2001).

In order to address the possible genetic relationship between the LCB and interpretations of magmatic underplating, it is important to consider the tectonic setting of the layer. For instance, the LCB extends far inboard of the eastern limit of significant Cenozoic extension, while it apparently stops abruptly against the Bivrost Lineament. The abrupt termination of the LCB against the Bivrost Lineament is difficult to explain since it is clear that the passive margin continues north to the Senja Fracture Zone. Seen from a regional perspective, Cenozoic extension does not terminate

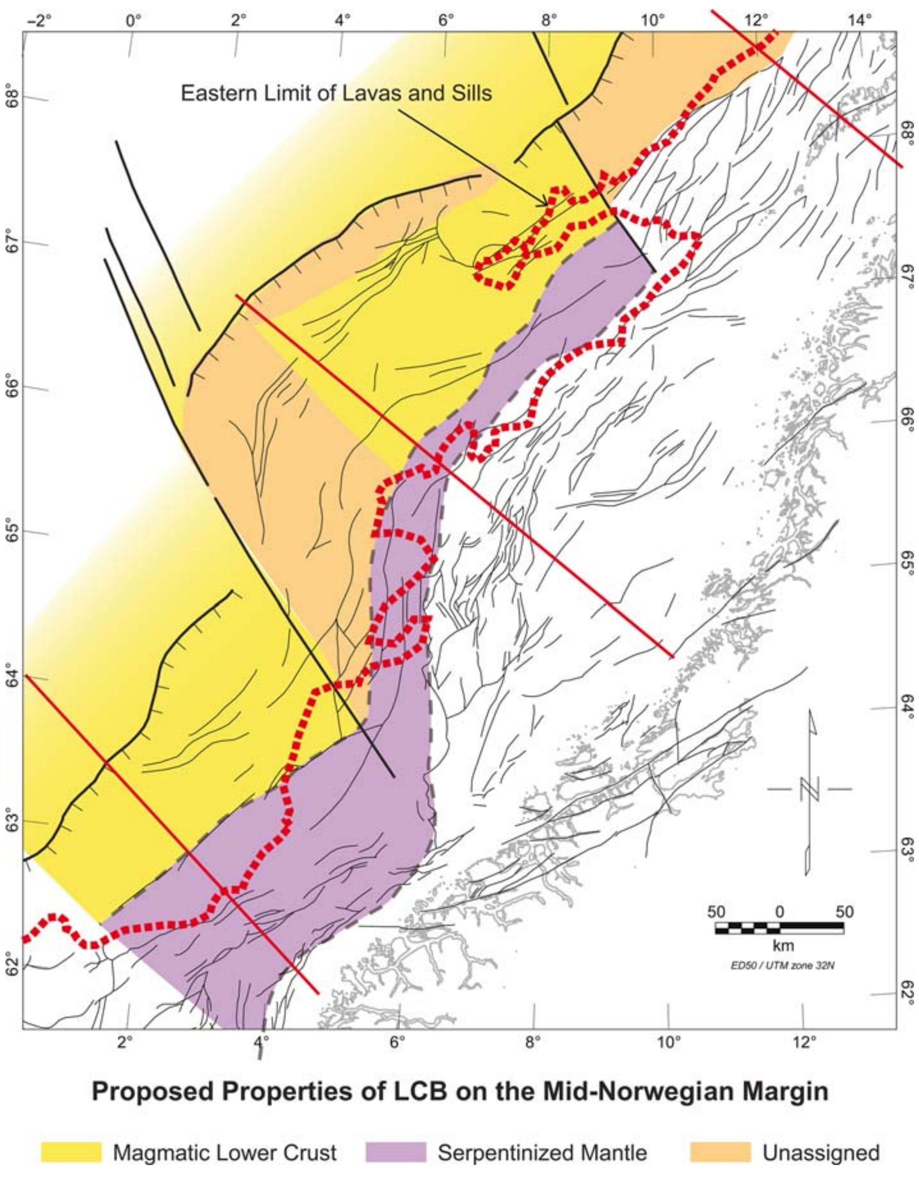

Fig. 9. Proposed properties of LCB on the mid-Norwegian margin. The main conclusions are summarized in this figure which shows the distribution of LCB on the margin and its varying properties. The yellow colour indicates LCB most likely of magmatic intrusive or underplate origin. The violet colour defines the distribution of LCB that is presumably serpentinized mantle. LCB that has indecisive origin is shown in orange. Here, the origin could be any of the proposed origins: (1) high-grade metamorphic, (2) mantle serpentinization or (3) magmatic underplating. The red dotted line presents the eastern limit of lavas and sills on the margin. The structural features are the same as in Figure 1. The red lines indicate the location of profiles in Figure 8.

against the Bivrost Lineament. Thus, it is difficult to attribute the lack of a LCB body north of the Bivrost Lineament to the lack of Cenozoic extension since it is obvious that the Lofoten margin segment also went to breakup.

Some authors (Eldholm & Grue 1994) have proposed that magmatic underplating will preferentially be located at pre-existing Moho relief locations. This concept could possibly explain how Early Cenozoic underplated material could be preferentially located under the Mesozoic Møre and Vøring basins. However, the explanation appears unlikely; the Rockall Trough is an example of a highly thinned basin that ought to have been ideally situated to preferentially receive Early Cenozoic magmatic underplating – yet it did not. It appears far easier to propose a mechanism that links the LCB in the central Møre and Vøring basins in time to the Mesozoic crustal thinning, that is, suggesting a serpentinized mantle origin. From isostatic considerations it is also unlikely, as it is not reasonable to sustain a Moho relief with material added to the base of a rifted crust without assuming unrealistically rigid crust.

On the mid-Norwegian margin, the presence of the LCB is linked to the differences between the isostatic and seismic Moho. The occurrence of LCB is either a response of the subsidence and rift history of the margin or the LCB has influenced the rift and subsidence history of the margin. Our proposal that the mid-Norwegian margin LCB can be related to at least three different geological events (Fig. 9) and processes influences several issues. The magmatic rock volume of the North Atlantic large igneous province may be significantly less than previously thought, considering that 60–80% of the volume of this LIP has been estimated to reside in the LCB (White *et al.* 1987; Eldholm & Grue 1994; White *et al.* 2008). An origin other than magmatic underplating for the LCB will change the heat flow history of the margin significantly (to a cooler scenario). The concept of ponding of magmatic underplate beneath pre-existing Moho relief is questioned.

In order to further enhance our understanding of the LCB observed on passive margins worldwide, it is important not only to integrate different geophysical methods but also to integrate different geological scale studies. The regional Moho configuration acquired by isostatic and modelling studies compared with seismically obtained Moho can shed light on the properties of LCB on all passive margins and improve understanding of the evolution of the margins.

The Geological Survey of Norway and TGS-NOPEC provided the gravity, magnetic and bathymetry data. The 3D modelling was performed using the software package IGMAS. This study is part of a PhD project titled 'Sub-basalt exploration using integrated gravimetric-, magnetometric- and seismic- (velocity) models, with isostatic considerations' financed by Shell. Odleiv Olesen is thanked for constructive feedback that led to modifications of the manuscript. We are also grateful to Robert S. White and Tony Doré, who provided helpful reviews that improved the manuscript considerably.

References

Blystad, P., Brekke, H., Færseth, R. B., Larsen, B. T., Skogseid, J. & Tørudbakken, B. 1995. *Structural Elements of the Norwegian Continental Shelf. Part II: The Norwegian Sea Region*. Norwegian Petroleum Directorate, Bulletins, **8**.

Bown, J. W. & White, R. S. 1995. Effect of finite extension rate on melt generation at rifted continental margins. *Journal of Geophysical Research*, **100**, 18011–18029.

Braitenberg, C., Ebbing, J. & Götze, H.-J. 2002. Inverse modelling of elastic thickness by convolution method – the eastern Alps as a case example. *Earth and Planetary Science Letters*, **202**, 387–404.

Braitenberg, C., Wienecke, S. & Wang, Y. 2006. Basement structures from satellite-derived gravity field: South China Sea ridge. *Journal of Geophysical Research*, **111**, B05407; doi: 10.1029/2005JB003938.

Brekke, H. 2000. The tectonic evolution of the Norwegian Sea Continental Margin with emphasis on the Vøring and Møre Basin. *In*: Nøttvedt, A. (ed.) *Dynamics of the Norwegian Margin*. Geological Society, London, Special Publications, **167**, 327–378.

Christiansson, P., Faleide, J. I. & Berge, A. M. 2000. Crustal structure in the northern North Sea; an integrated geophysical study. *In*: Nøttvedt, A. (ed.) *Dynamics of the Norwegian Margin*. Geological Society, London, Special Publications, **167**, 15–40.

Doré, A. G., Lundin, E. R., Jensen, L. N., Birkeland, Ø., Eliassen, P. E. & Fichler, C. 1999. Principal tectonic events in the evolution of the northwest European Atlantic margin. *In*: Fleet, A. J. & Boldy, S. A. R. (eds) *Petroleum Geology of Northwest Europe: Proceedings of the 5th Conference*. Geological Society, London, 41–61; doi: 10.1144/0050041.

Ebbing, J., Braitenberg, C., Bjørnseth, H. M., Fichler, C. & Skilbrei, J. R. 2006. *Basement Characterisation by Regional Isostatic Methods in the Barents Sea*. Extended Abstracts for EAGE Meeting, St Petersburg.

Eccles, J. D., White, R. S. & Christie, P. A. F. 2009. Identification and inversion of converted shear waves: case studies from the European North Atlantic continental margins. *Geophysical Journal International*, **179**, 381–400.

Eldholm, O. & Grue, K. 1994. North-Atlantic volcanic margins: dimensions and production-rates. *Journal of Geophysical Research – Solid Earth*, **99**, 2955–2968.

Eldholm, O., Skogseid, J., Planke, S. & Gladczenko, T. P. 1995. Volcanic margin concepts. *In*: Banda, E. (ed.) *Rifted Ocean–Continent Boundaries.* NATO ASI, **5**. Kluwer Academic, Norwell, MA, 1–16.

Escartín, J., Hirth, G. & Evans, B. 2001. Strength of slightly serpentinized peridotites: implications for the tectonics of oceanic lithosphere. *Geology*, **29**, 1023–1026.

Faleide, J. I., Vågnes, E. & Gudlaugsen, S. T. 1993. Late Mesozoic-Cenozoic evolution of the south-western Barents Sea in a regional rift-shear setting. *Marine and Petroleum Geology*, **10**, 186–214.

Gernigon, L., Ringenbach, J. C., Planke, S., Le Gall, B. & Jonquet-Kolstø, H. 2003. Extension, crustal structure and magmatism at the outer Voring Basin, Norwegian margin. *Journal of the Geological Society*, **160**, 197–208.

Gernigon, L., Ringenbach, J. C., Planke, S. & Le Gall, B. 2004. Deep structures and breakup along volcanic rifted margins: insights from integrated studies along the outer Voring Basin (Norway). *Marine and Petroleum Geology*, **21**, 363–372.

Gernigon, L., Ringenbach, J.-C., Planke, S. & Le Gall, B. 2005. *Tectonic and Deep Crustal Structures along the Norwegian Volcanic Margin: Implications for the 'Mantle Plume or Not?' Debate*. World Wide Web Address: http://www.mantleplumes.org/VM_Norway.html.

Hürich, C. A., Deemer, S. J., Indares, A. & Salisbury, M. 2001. Compositional and metamorphic controls on velocity and reflectivity in the continental crust: an example from the Grenville Province of eastern Quebec. *Journal of Geophysical Research*, **106**, 665–682.

Johnston, S., Doré, A. G. & Spencer, A. M. 2001. The Mesozoic evolution of the southern North Atlantic region and its relationship to basin development in the south Porcupine Basin, offshore Ireland. *In*: Shannon, P. M., Haughton, P. D. W. & Corcoran, F. V. (eds) *The Petroleum Exploration of Ireland's Offshore Basins*. Geological Society, London, Special Publications, **188**, 237–263.

Kimbell, G. S., Gatliff, R. W., Ritchie, J. D., Walker, A. S. D. & Williamson, J. P. 2004. Regional three-dimensional gravity modelling of the NE Atlantic margin. *Basin Research*, **16**, 259–278.

Louden, K. E. & Chian, D. 1999. The deep structure of non-volcanic rifted continental margin. *Philosophical Transactions of the Royal Society, London*, **357**, 767–804.

Lundin, E. & Doré, A. G. 1997. A tectonic model for the Norwegian passive margin with implications for the NE Atlantic: Early Cretaceous to breakup. *Journal of the Geological Society*, **154**, 545–550.

Miller, D. J. & Christensen, N. I. 1997. Seismic velocities of lower crustal and upper mantle rocks from the slow-spreading Mid-Atlantic Ridge, south of the Kane Fracture Transform Zone (MARK). *In*: Karson, J. A., Cannat, M., Miller, D. J. & Elthon, D. (eds) *Proceedings of ODP, Sciences Results*, **153**. Ocean Drilling Program, College Station, TX, 437–454.

Mjelde, R., Digranes, P., van Schaack, M., Shimamura, H., Shiobara, H., Kodaira, S. & Næss, O. 2001. Crustal structure of the outer Vøring Plateau, offshore Norway, from ocean bottom seismic and gravity data. *Journal of Geophysical Research*, **106**, 6769–6791.

Mjelde, R., Kasahara, J. *et al*. 2002. Lower crustal seismic velocity-anomalies; magmatic underplating or serpentinized peridotite? Evidence from the Vøring Margin, NE Atlantic. *Marine Geophysical Research*, **23**, 169–183.

Mjelde, R., Raum, T., Digranes, P., Shimamura, H. & Kodaira, S. 2003. Vp/Vs-ratio along the Vøring Margin, NE Atlantic, derived from OBS-data; implications on lithology and stress-field. *Tectonophysics*, **369**, 175–197.

Mjelde, R., Raum, T., Breivik, A., Shimamura, H., Murai, Y., Takanami, T. & Faleide, J. I. 2005. Crustal structure of the Vøring Margin, NE Atlantic: a review of geological implications based on recent OBS data. *In*: Doré, A. G. & Vining, B. A. (eds) *Petroleum Geology: North-West Europe and Global Perspectives: Proceedings of the 6th Petroleum Geology Conference*. Geological Society, London, 804–813; doi: 10.1144/0060804.

Mjelde, R., Faleide, J. I., Breivik, A. J. & Raum, T. 2009*a*. Lower crustal composition and crustal lineaments on the Vøring Margin, NE Atlantic: a review. *Tectonophysics*, **472**, 183–193.

Mjelde, R., Raum, T., Kandilarov, A., Murai, Y. & Takanami, T. 2009*b*. Crustal structure and evolution of the outer Møre Margin, NE Atlantic. *Tectonophysics*, **468**, 224–243.

Morewood, N. C., Mackenzie, G. D., Shannon, P. M., O'Reilly, B. M., Readman, P. W. & Makris, J. 2005. The crustal structure and regional development of the Irish Atlantic margin region. *In*: Doré, A. G. & Vining, B. A. (eds) *Petroleum Geology: North-West Europe and Global Perspectives: Proceedings of the 6th Petroleum Geology Conference*. Geological Society, London, 1023–1033; doi: 10.1144/0061023.

Ólafsson, I., Sundvor, E., Eldholm, O. & Grue, K. 1992. Møre margin – crustal structure from analysis of expanded spread profiles. *Marine Geophysical Researches*, **14**, 137–162.

Olesen, O., Lundin, E. *et al*. 2002. Bridging the gap between the onshore and offshore geology in Nordland, northern Norway. *Norwegian Journal of Geology*, **82**, 243–262.

O'Reilly, B. M., Hauser, F., Jacob, A. W. B. & Shannon, P. M. 1996. The lithosphere below the Rockall Trough: wide-angle seismic evidence for extensive serpentinisation. *Tectonophysics*, **255**, 1–23.

Osmundsen, P. T. & Ebbing, J. 2008. Styles of extension offshore mid-Norway and implications for mechanisms of crustal thinning at passive margins. *Tectonics*, **27**, TC6016; doi: 10.1029/2007TC002242.

Osmundsen, P. T., Eide, E. *et al*. 2006. Kinematics of the Høybakken detachment zone and the Møre-Trøndelag Fault Complex, central Norway. *Journal of the Geological Society, London*, **163**, 303–318.

Planke, S., Rasmussen, T. E., Rey, S. S. & Myklebust, R. 2005. Seismic characteristics and distribution of volcanic intrusions and hydrothermal vent complexes in the Vøring and Møre basins. *In*: Doré, A. G. & Vining, B. A. (eds) *Petroleum Geology: North-West Europe and Global Perspectives: Proceedings of the 6th Petroleum Geology Conference*. Geological Society, London, 1–12; doi: 10.1144/0060001.

Raum, T., Mjelde, R. *et al*. 2002. Crustal structure of the southern part of the Voring Basin, mid-Norway margin, from wide-angle seismic and gravity data. *Tectonophysics*, **355**, 99–126.

Raum, T., Mjelde, R. *et al*. 2006. Crustal structure and evolution of the southern Vøring Basin and Vøring Transform Margin, NE Atlantic. *Tectonophysics*, **415**, 167–202.

Reston, T. J. 2009. The structure, evolution and symmetry of the magma-poor rifted margins of the North and Central Atlantic: a synthesis. *Tectonophysics*, **468**, 6–27.

Roberts, A. M., Lundin, E. R. & Kusznir, N. J. 1997. Subsidence of the Vøring Basin and influence of the Atlantic continental margin. *Journal of the Geological Society, London*, **154**, 551–557.

Shannon, P. M. 1991. The development of Irish offshore sedimentary basins. *Journal of the Geological Society, London*, **148**, 181–189.

Skogseid, J., Pedersen, T., Eldholm, O. & Larsen, B. T. 1992. Tectonism and magmatism during NE Atlantic continental break-up: the Vøring Margin. *In*: Storey, B. C., Alabaster, T. & Pankhurst, R. J. (eds) *Magmatism and the Causes of Continental Break-up*. Geological Society, London, Special Publications, **68**, 305–320.

Srivastava, S. P. & Roest, W. R. 1999. Extent of oceanic crust in the Labrador Sea. *Marine and Petroleum Geology*, **16**, 65–84.

Tsikalas, F., Faleide, J. I. & Kusznir, N. J. 2008. Along-strike variations in rifted margin crustal architecture and lithosphere thinning between northern Vøring and Lofoten margin segments off mid-Norway. *Tectonophysics*, **458**, 68–81.

Tucholke, B. E., Sawyer, D. S. & Sibuet, J.-C. 2007. Breakup of the Newfoundland–Iberia rift. *In*: Karner, G. D., Manatchal, G. & Pinheiro, L. M. (eds) *Imaging, Mapping and Modelling Continental Lithosphere Extension and Breakup*. Geological Society, London, Special Publications, **282**, 9–46.

van Wijk, J. W., van der Meer, R. & Cloetingh, S. A. P. L. 2004. Crustal thickening in an extensional regime: application to the mid-Norwegian Vøring margin. *Tectonophysics*, **387**, 217–228.

Watts, A. B. 2001. *Isostasy and Flexure of the Lithosphere*. Cambridge University Press, Cambridge.

White, R. S. & McKenzie, D. 1989. Magmatism at rift zones: the generation of volcanic continental margins and flood basalts. *Journal of Geophysical Research – Solid Earth and Planets*, **94**, 7685–7729.

White, R. S. & Smith, L. K. 2009. Crustal structure of the Hatton and the conjugate east Greenland rifted volcanic continental margins, NE Atlantic. *Journal of Geophysical Research*, **114**, B02305; doi: 10.1029/2008JB005856.

White, R. S., Spence, G. D., Fowler, S. R., McKenzie, D. P., Westbrook, G. K. & Bowen, N. 1987. Magmatism at rifted continental margins. *Nature*, **330**, 439–444.

White, R. S., Smith, L. K., Roberts, A. W., Christie, P. A. F., Kusznir, N. J. & iSIMM Team. 2008. Lower-crustal intrusion on the North Atlantic continental margin. *Nature*, **452**, 460–464; plus supplementary information at www.nature.com,doi:10.1038/nature06687.

White, R. S., Eccles, J. D. & Roberts, A. W. 2010. Constraints on volcanism, igneous intrusion and stretching on the Rockall–Faroe continental margin. *In*: Vining, B. A. & Pickering, S. C. (eds) *Petroleum Geology: From Mature Basins to New Frontiers – Proceedings of the 7th Petroleum Geology Conference*, Geological Society, London, 831–842; doi: 10.1144/0070831.

Wienecke, S., Braitenberg, C. & Götze, H. J. 2007. A new analytical solution estimating the flexural rigidity in the Central Andes. *Geophysical Journal International*, **169**, 789–794.

Ziegler, P. A. 1988. *Evolution of the Arctic–North Atlantic and the Western Tethys*. American Association of Petroleum Geologists, Tulsa, OK, Memoirs, **43**.

The breakup of the South Atlantic Ocean: formation of failed spreading axes and blocks of thinned continental crust in the Santos Basin, Brazil and its consequences for petroleum system development

I. C. SCOTCHMAN,[1] G. GILCHRIST,[2] N. J. KUSZNIR,[3] A. M. ROBERTS[4] and R. FLETCHER[1,3]

[1]*Statoil (UK) Ltd, 1 Kingdom Street, London W2 6BD, UK (e-mail: isco@statoil.com)*
[2]*Consultant, Statoil do Brasil, Rio de Janeiro, Brazil*
[3]*Department of Earth and Ocean Sciences, University of Liverpool, Liverpool L69 3BX, UK*
[4]*Badley Geoscience Ltd, North Beck House, North Beck Lane, Spilsby, Lincolnshire PE23 5NB, UK*

Abstract: The occurrence of failed breakup basins and deepwater blocks of thinned continental crust is commonplace in the rifting and breakup of continents, as part of passive margin development. This paper examines the rifting of Pangaea–Gondwanaland and subsequent breakup to form the South Atlantic Ocean, with development of a failed breakup basin and seafloor spreading axis (the deepwater Santos Basin) and an adjacent deepwater block of thinned continental crust (the Sao Paulo Plateau) using a combination of 2D flexural backstripping and gravity inversion modelling. The effects of the varying amounts of continental crustal thinning on the contrasting depositional and petroleum systems in the Santos Basin and on the São Paulo Plateau are discussed, the former having a predominant post-breakup petroleum system compared with a pre-breakup system in the latter. An analogy is also made to a potentially similar failed breakup basin/thinned continental crustal block pairing in the Faroes region in the NE Atlantic Ocean.

Keywords: Brazilian rifted margin, continental breakup, Santos Basin, Sao Paulo Plateau, Faroes, Atlantic margin, subsidence, gravity inversion

Continental lithospheric thinning and rifted margin formation is a poorly understood process, the kinematics of which can be affected by many factors, including pre-existing lithospheric heterogeneities, variations in plate kinematics and the presence of mantle features such as plumes (e.g. Dunbar & Sawyer 1989; Corti *et al.* 2003; Ziegler & Cloetingh 2004). Evidence of complex kinematics of rifted margins is seen at many margins, such as the South Atlantic Ocean off Brazil and the NE Atlantic Ocean margin close to the Faroe Islands, both being discussed in this paper.

The Santos Basin

The Santos Basin is the southernmost of the petroliferous chain of basins along the western margin of the South Atlantic Ocean in Brazil (Fig. 1). These basins, the Santos, Campos and Espirito Santo Basins, resulted from rifting of the Gondwanaland 'supercontinent' in the earliest Cretaceous with breakup and subsequent seafloor spreading. The Santos Basin is a NE–SW-trending basin that covers about 200 000 km^2 of the Brazilian continental margin, bounded by the Cabo Frio Arch to the north and by the Florianopolis Platform to the south, both features being related to magmatic activity associated with the westward prolongation of the ocean fracture zones (Cainelli & Mohriak 1998). The western limit of the basin is defined by the uplifted Precambrian rocks of the Serra do Mar, a coastal range reaching up to 2000 m high, while to the east the basin is flanked by the Sao Paulo Plateau (SPP). The Florianopolis Fracture Zone (FFZ) is a major transform feature which defines the southern limit of the Santos Basin and marks a major break in South Atlantic Ocean breakup history. To the south, seafloor spreading is constrained by the M4 and M0 magnetic anomalies (Mueller *et al.* 1997), dated at 125.7 and 120.6 Ma, respectively. To the north of the FFZ, the age of breakup is poorly constrained as it took place during the Cretaceous normal polarity superchron between the M0 and C34 (83.5 Ma) magnetic anomalies.

The Santos Basin and the Sao Paulo Plateau

Regional geology

Rifting and breakup of the Santos Basin and SPP areas appear to have been very complex with several apparent attempts to extend seafloor spreading north of the FFZ. This resulted in various intrusive and volcanic features located in the southwestern Santos Basin and to the east of the SPP, where the Avedis volcanic chain was interpreted by several authors as a failed spreading centre (Cobbold *et al.* 2001; Meisling *et al.* 2001; Gomes *et al.* 2002). However, recent exploration and drilling indicate these features to be probably of pre-rift origin and not the result of failed Early Cretaceous-aged breakup. They form large regional structural highs (the Tupi and Sugar Loaf structures of Gomes *et al.* 2009) which drilling indicates to have trapped extremely large volumes of hydrocarbons in overlying syn-rift and sag phase reservoirs. However, data presented in this paper suggest that an earlier attempt at breakup took place in the centre of Santos Basin, extending northeastwards into the basin centre from the area of likely oceanic crust emplaced in the southwestern Santos Basin (Meisling *et al.* 2001; Gomes *et al.* 2002). The formation of the SPP and the resultant development of the prolific pre-salt hydrocarbon province recently discovered in the area appear intimately related to this failed breakup event.

Rifting in the Santos Basin began around 140 Ma in the Neocomian (Karner & Driscoll 1999), contemporaneous with eruption of the Parana volcanics (Renne *et al.* 1996; Fig. 2). Syn-rift deposition, overlying and interfingering with late stage basalts

VINING, B. A. & PICKERING, S. C. (eds) *Petroleum Geology: From Mature Basins to New Frontiers – Proceedings of the 7th Petroleum Geology Conference*, 855–866. DOI: 10.1144/0070855

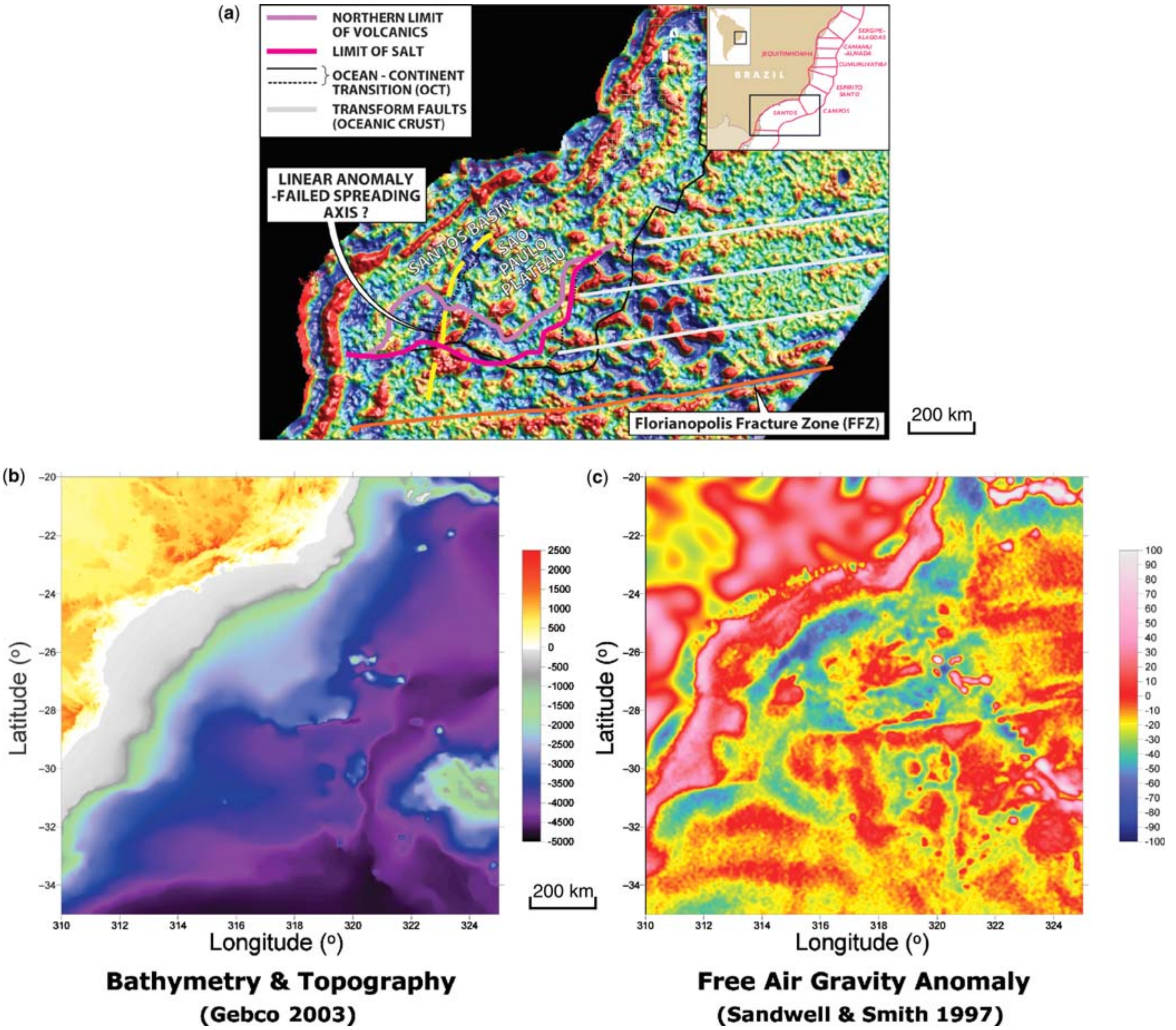

Fig. 1. (**a**) Bouguer gravity anomaly map (200 km high-pass filter) over the central area of Santos Basin showing the linear feature with strong negative gravity anomaly adjacent to the SPP. (**b**) Bathymetry (metres) and (**c**) free air gravity (mgal) data for the Santos and Campos and adjacent segments of the Brazilian rifted margin.

(Chang *et al.* 1992), comprises fluvial–lacustrine siliciclastics which infilled much of the early rift topography. Subsequent deposition, during the late rift sag phase, comprised basinal lacustrine, organic-rich shales lapping onto coquinas of the Lagoa Feia Formation, which were deposited on structural highs and the basin flanks (Pereira & Feijo 1994). The sag phase is overlain, generally unconformably (Karner & Gamboa 2007), by evaporites comprising intercalations of anhydrite and halite, reflecting development of the post-rift South Atlantic Salt Basin (Fig. 3). These evaporites were deposited in the remnant sag basin system at or at most several hundred metres below ambient sea-level (Karner & Gamboa 2007) by marine incursions from the north (Davison & Bate 2004). While Davison (2007) favours formation in a deep rift basin, evaporite formation close to ambient sea-level is indicated by several lines of evidence: the microbilitic limestones immediately underlying the salt, forming the reservoir in hydrocarbon discoveries such as Tupi, probably accumulated in less than 3 m of water (J. Lukasik, pers. comm.), the layered evaporite sequence overlying the basal halite section on the SPP was probably formed under shallow water sabkha-type conditions with periodic emergence and, finally, the large rift block bounding faults have a substantial post-salt displacement (e.g. Fig. 3, Section 2 inset). Thick evaporitic sections up to 2 km thick developed in the adjacent Santos Basin where there was more accommodation space, greatly influencing basin fill during the later evolution of the basin with extensive halokinesis producing large salt diapirs and walls within the deepwater basin.

In contrast, recent drilling on the SPP has found the structure to have thicker, well developed syn-rift and sag phase sections (Fig. 4; e.g. Gomes *et al.* 2009) which are capped by porous lacustrine limestones of algal, stromatolitic or thrombolitic origin which form the reservoir rocks in the recent large hydrocarbon discoveries in the area, such as Tupi (Mello *et al.* 2009). In contrast to the great thicknesses of evaporites seen in the Santos Basin to the west and Campos Basin to the north (Davison 2007), on the SPP a generally thinner layer of mobile salt overlies the syn-rift section; the rest of the evaporitic section of up to 2 km in thickness appears from seismic to be well bedded but is also tightly folded with diapiric structures (Fig. 3). This well bedded section above the mobile salt, previously identified as an extension of the Late Cretaceous

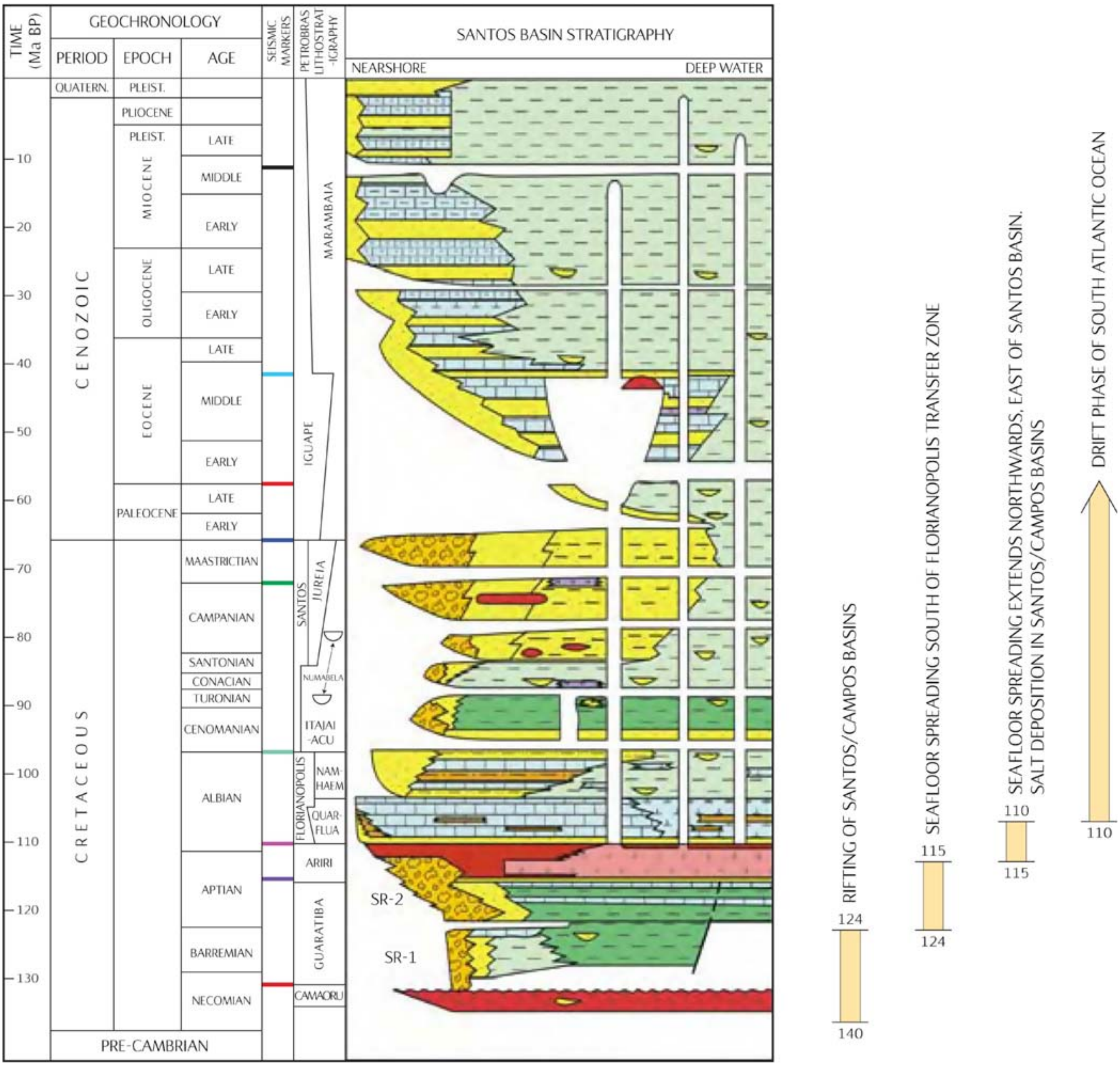

Fig. 2. Santos Basin stratigraphy and breakup history.

turbidite play north of the Santos Fault, has been found by recent drilling to consist of bedded evaporites, comprising halite and anhydrite as well as complex evaporites such as carnallite, bischofite, sylvite and tachyhydrite (Poiate *et al.* 2006). These complex minerals are 'end members' of the evaporitic system, indicating development of extreme conditions.

Karner & Gamboa (2007) suggest a date for evaporite deposition in the Santos Basin as 110–113 Ma, after which period major marine flooding of the basin took place, probably linked to breakup of the margin to the north adjacent to the Campos Basin. This was marked in the Santos Basin by deposition of Albian-age shallow marine carbonates, grey shales and sandstones which were followed by coarse turbiditic sandstones and shales deposited during progressive deepening of the basin, with the maximum flooding conditions being marked by dark grey-black shales of Cenomanian–Turonian age Itajai–Acu Formation. In the proximal areas, a thick conglomerate package and shallow marine sandstones were deposited during the Santonian to Maastrichtian in response to the first phase of Serra do Mar uplift (dated at 100–80 Ma by Lelarge 1993).

The age of the bedded evaporite deposition on the SPP is equivocal as no biostratigraphic data from recent wells has been published. Because of its extreme distal location, effectively isolated between the African and Brazilian margins, evaporite deposition under sabkha-type conditions may have continued up into the Albian as no equivalent shallow marine carbonate platform development is present, the evaporites being overlain by possibly Cenomanian or younger Late Cretaceous turbidites and shales. However, the age-equivalent section to the Albian carbonate platform may instead be present as shales at the base of the marine section overlying the evaporites.

By the Late Cretaceous and through the Cenozoic, deepwater turbidite and shale deposition was predominant across both the Santos Basin and the SPP, characterized by a basinward progradation of siliciclastics over platform/slope shales and marls. However, the SPP remained relatively sediment-poor with only

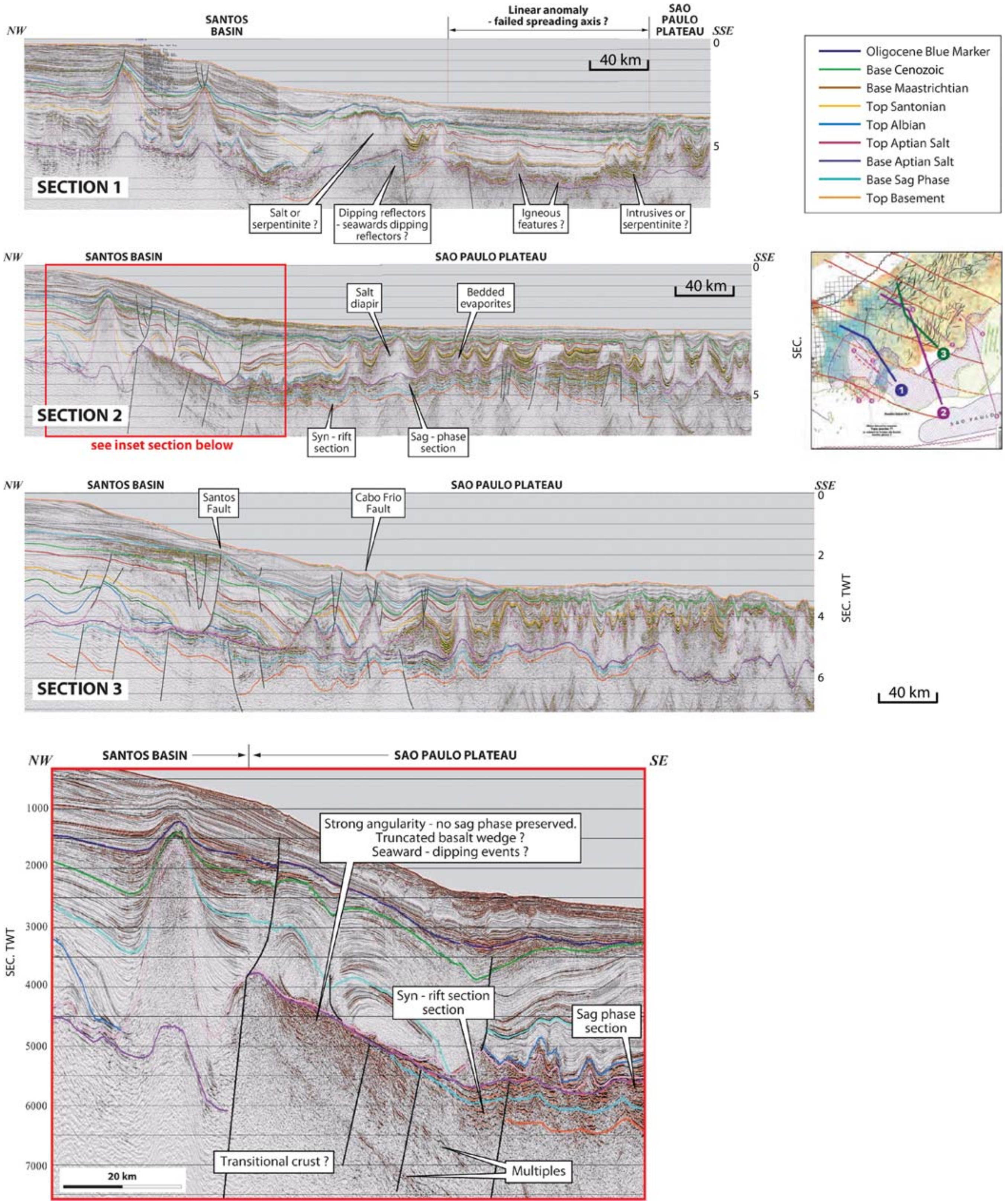

Fig. 3. Seismic cross-sections across the deepwater Santos Basin and SPP.

around 2 km drift section compared with 4–5 km or more equivalent thickness inboard in the Santos Basin.

Regional structure

Regional evaluation of the Santos Basin and SPP, using an approximate 4 × 4 km grid of 2D seismic data combined with both satellite and ship-borne gravity and magnetic data, has shown that the structure of the basin is complex with a linear negative gravity anomaly stretching from the outer southwestern part of the basin north-northeastwards into the basin centre, with a large area to the ESE comprising the SPP (Fig. 1). Regional seismic across the linear gravity anomaly in the southwestern–central Santos Basin (Fig. 3) shows a linear anomaly with volcanic features of oceanic

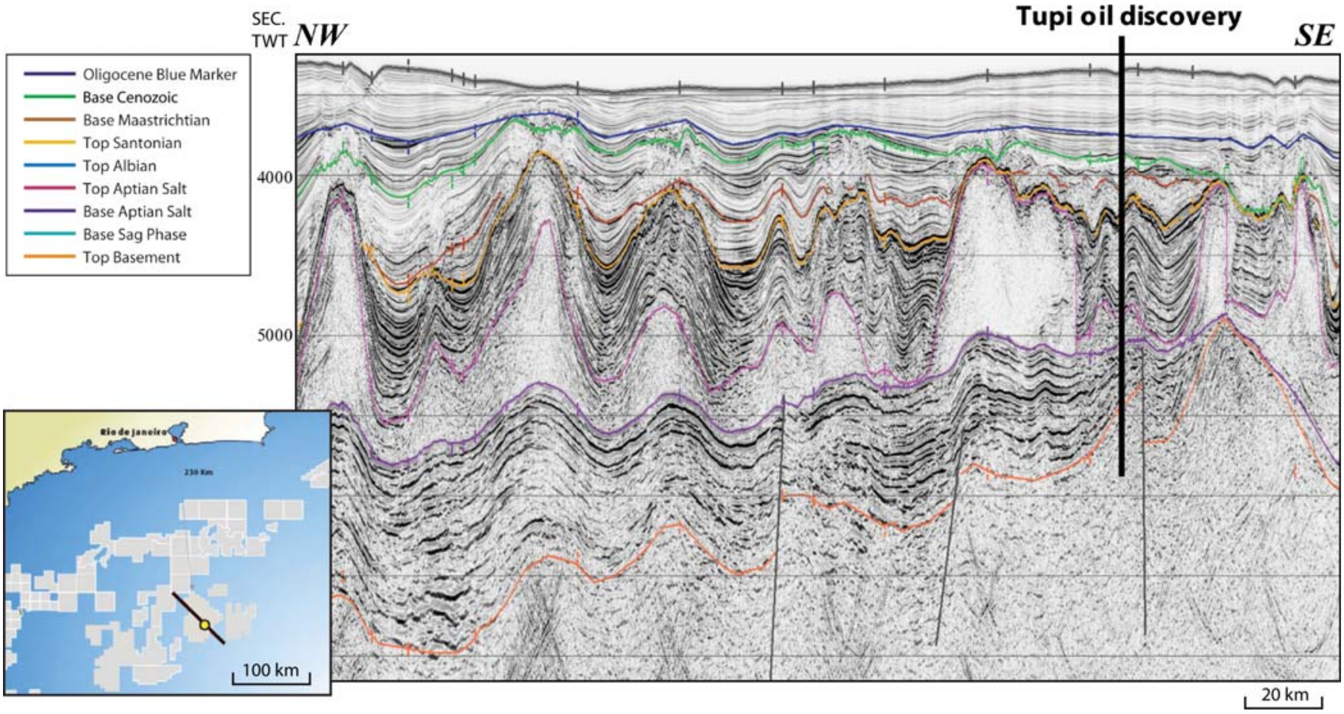

Fig. 4. SPP seismic section illustrating the Tupi oil discovery.

affinity extending from a crustal igneous feature in the southwestern part of the basin northeastwards into the basin centre where it terminates in a major fault, the Santos Fault. The feature forms the northwestern margin of the SPP, giving rise to the observation that these two features are connected. The contrasting structural and stratigraphic characteristics of the SPP and the Santos Basin to the north are illustrated by seismic line 3 of Figure 3, showing the thick, well developed syn-rift section capped by over 2 km of largely bedded evaporites in the former, while the latter shows a thin syn-rift section capped by diapiric salt buried by thick Cretaceous–Cenozoic turbidites. In contrast, the equivalent turbidite section on the SPP is only thinly developed, unlike either the Santos Basin or the other basins to the north (Campos and Espirito Santo Basins).

In order to investigate the linear anomaly within Santos Basin and its relationship to the SPP, along with the anomalous structural and sedimentary development of the latter, crustal modelling was undertaken. This used subsidence analysis from 2D backstripping, based on a regional grid of eight seismic lines, in conjunction with determination of crustal thickness from gravity inversion based on the bathymetry and free air gravity anomaly (Fig. 1) as detailed below.

Continental lithosphere thinning and crustal thickness of the Santos Basin and Sao Paulo plateau

Crustal thickness, continental lithosphere thinning and Moho depth for the Santos Basin and SPP areas of the Brazilian rifted margin were studied by subsidence analysis using flexural backstripping (Kusznir *et al.* 1995; Roberts *et al.* 1998) and gravity inversion performed in the 3D spectral domain (Parker 1972), the latter using a new method incorporating a lithosphere thermal gravity anomaly correction (Greenhalgh & Kusznir 2007; Chappell & Kusznir 2008).

Subsidence analysis

Subsidence analysis using flexural backstripping to produce water-loaded subsidence, and gravity inversion using a new method incorporating a lithosphere thermal gravity anomaly correction, were used to determine continental lithosphere thinning, Moho depth and continental crustal thickness for the Santos Basin and SPP areas of the Brazilian rifted margin. The results of the subsidence analysis using flexural backstripping are described in Scotchman *et al.* (2006) and only a brief summary is given below.

Water-loaded subsidence was determined using the 2D flexural backstripping (Roberts *et al.* 1998) of profiles across the Santos Basin and SPP. The assumption was made of the palaeobathymetric constraint of ambient sea-level for the base Aptian salt at the time of deposition, as discussed above. The water-loaded subsidence was then processed using the extensional basin formation model of McKenzie (1978) to determine continental lithosphere stretching and thinning for (i) the assumption that base salt subsidence from Aptian to present is due to both syn-rift and post-rift subsidence, and (ii) alternatively that base salt subsidence from Aptian to present is due to post-rift thermal subsidence only. An 'average' age of 120 Ma for rift development across the basin was used in the modelling, an age older than the 110–113 Ma estimates for that of the Aptian salt (Karner & Gamboa 2007), to acknowledge the existence of syn-rift deposition beneath the salt.

It is very likely that the base salt horizon within the Santos Basin experienced syn-rift tectonic subsidence, followed by continued thermal subsidence to the present day. In this likely scenario, treating the base-case salt water-loaded subsidence as only post-rift leads to an overestimate of the β stretching factors required to model the subsidence and the prediction of oceanic crust (with infinite thinning) over much of the Santos Basin (Fig. 5a). This is clearly in conflict with the seismic and gravity data as any ocean–continent transition derived from this model is too far inboard.

Conversely, the salt does not represent the whole of the syn-rift sequence and, as a consequence, treating the base salt water-loaded subsidence as representing the whole of the syn-rift and post-rift thermal subsidence underestimates continental lithosphere stretching and thinning (Fig. 5b). This assumption predicts finite (non-infinite) thinning factors for the SPP, implying that this region is underlain by thinned continental crust. A region of highly stretched and thinned continental crust is predicted in the deepwater Santos Basin to the NW, separating the SPP from the Brazilian margin.

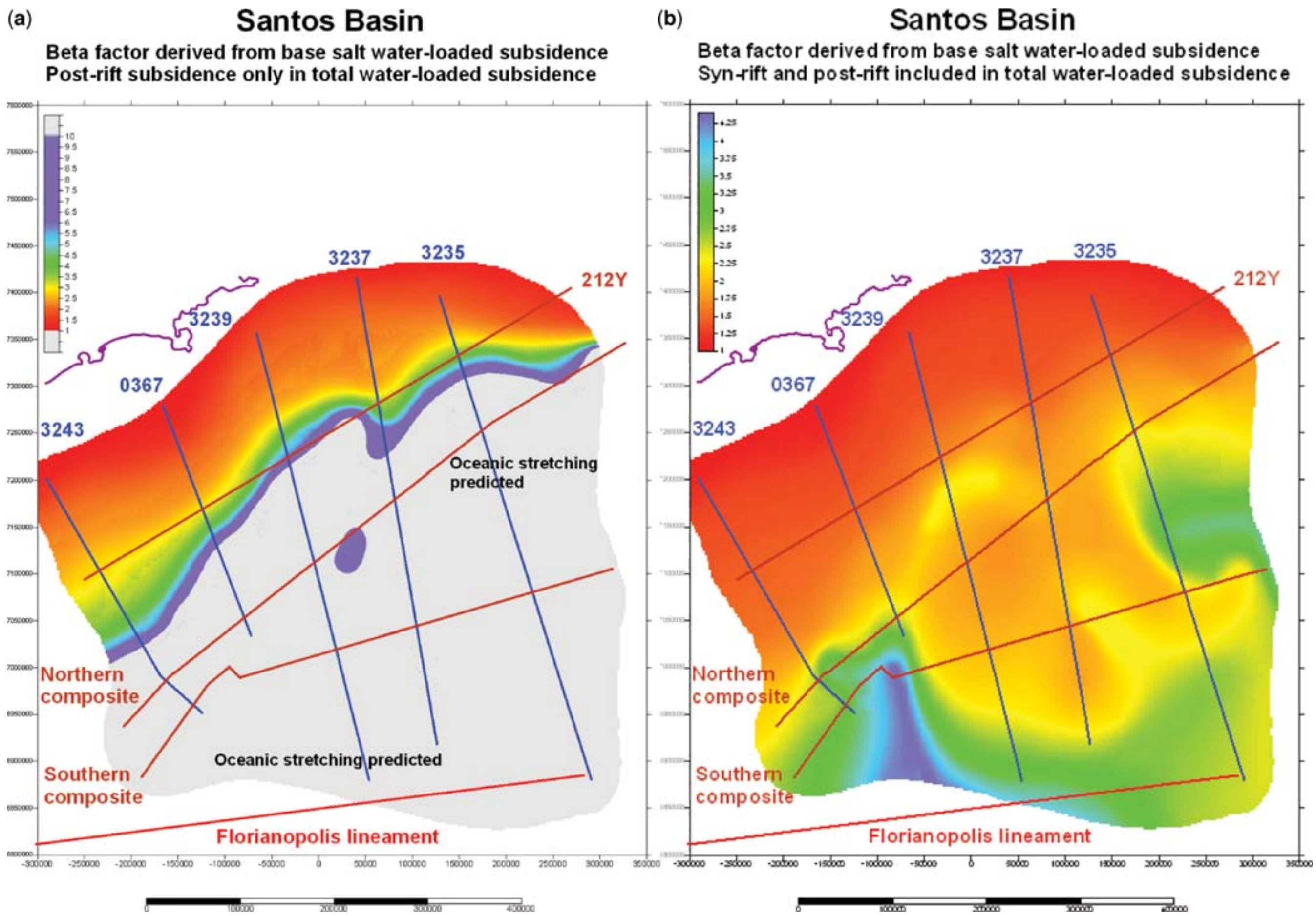

Fig. 5. Beta factor maps for the Santos Basin and SPP from 2D backstripping from Scotchman *et al.* (2006): (**a**) assuming subsidence of base salt is post-breakup only; (**b**) assuming subsidence of base salt is both syn-rift and post-breakup.

Crustal thickness determination

The input data used in the Santos Basin and SPP gravity inversion study were satellite free air gravity (Sandwell & Smith 1997), digital bathymetry (Gebco 2003), sediment thickness to base salt derived from 2D/3D seismic reflection mapping and ocean age isochrons to define unequivocal oceanic crust (Mueller *et al.* 1997). Crustal thicknesses produced by the gravity inversion applied to the Santos Basin and SPP are shown in Figure 6. Gravity inversion results are shown both omitting sediment thickness information (Fig. 6a) and including sediment thickness (Fig. 6b) to give a more accurate depth to Moho where such data exists. Crustal cross-sections with Moho depth determined using the gravity inversion method are shown in Figure 7 and indicate that crustal basement thickness in the Santos Basin decreases southwards. The low crustal thicknesses in the south of the deepwater Santos Basin, shown on cross-section 3 of Figure 7, and located to the north of the FFZ, suggest that the SW Santos Basin is underlain by oceanic crust. In contrast the SPP is underlain by crust between 12 and 16 km thick which is interpreted as thinned continental crust (Figs 6 & 7).

Both the gravity inversion results and the flexural backstripping subsidence analysis indicate that (i) the SPP is underlain by thinned continental crust and (ii) that a 'tongue' of oceanic crust extends north of the FFZ into the deepwater Santos Basin.

Discussion and conclusions

The failed breakup model for the Santos Basin

The results of the subsidence modelling from flexural backstripping indicate a zone of high subsidence in the southwestern Santos Basin, extending northeastwards into the central part of the basin, albeit with decreasing subsidence. Estimates of crustal thinning based on McKenzie (1978), backed by the regional geological reasoning, indicates that this represents both syn- and post-rift subsidence of the base salt layer, suggesting the outer part of the southwestern Santos Basin is underlain by either oceanic crust or by extremely thinned continental crust, which forms a tongue extending northeastwards into the basin centre. Seismic sections across this area confirm this finding (Fig. 3), with associated igneous features interpreted as seawards dipping reflectors observed within the basin. The results also indicate thinned continental crust to the SE of the feature beneath the SPP. The results of the gravity inversion work (Fig. 6) lead to similar conclusions with thin potentially oceanic crust in the outer part of the Santos Basin with decreasingly thinned crust northeastwards along the feature and less thinned crust beneath the SPP.

These results indicate that the feature is likely to be a failed seafloor spreading centre, representing an early attempt at breakup and initiation of seafloor spreading through the centre of the Santos Basin north of the FFZ in the early Aptian. The results suggest that extreme thinning occurred in the southern part of the feature, which probably represents incipient oceanic crust. However, the breakup and seafloor spreading event appears to have been short lived, probably due to an adjustment of plate kinematics.

Rifting and breakup history of the Santos Basin/Sao Paulo Plateau

By 140 Ma in the Neocomian, rifting followed by breakup of the southernmost South Atlantic Ocean took place south of the crustal

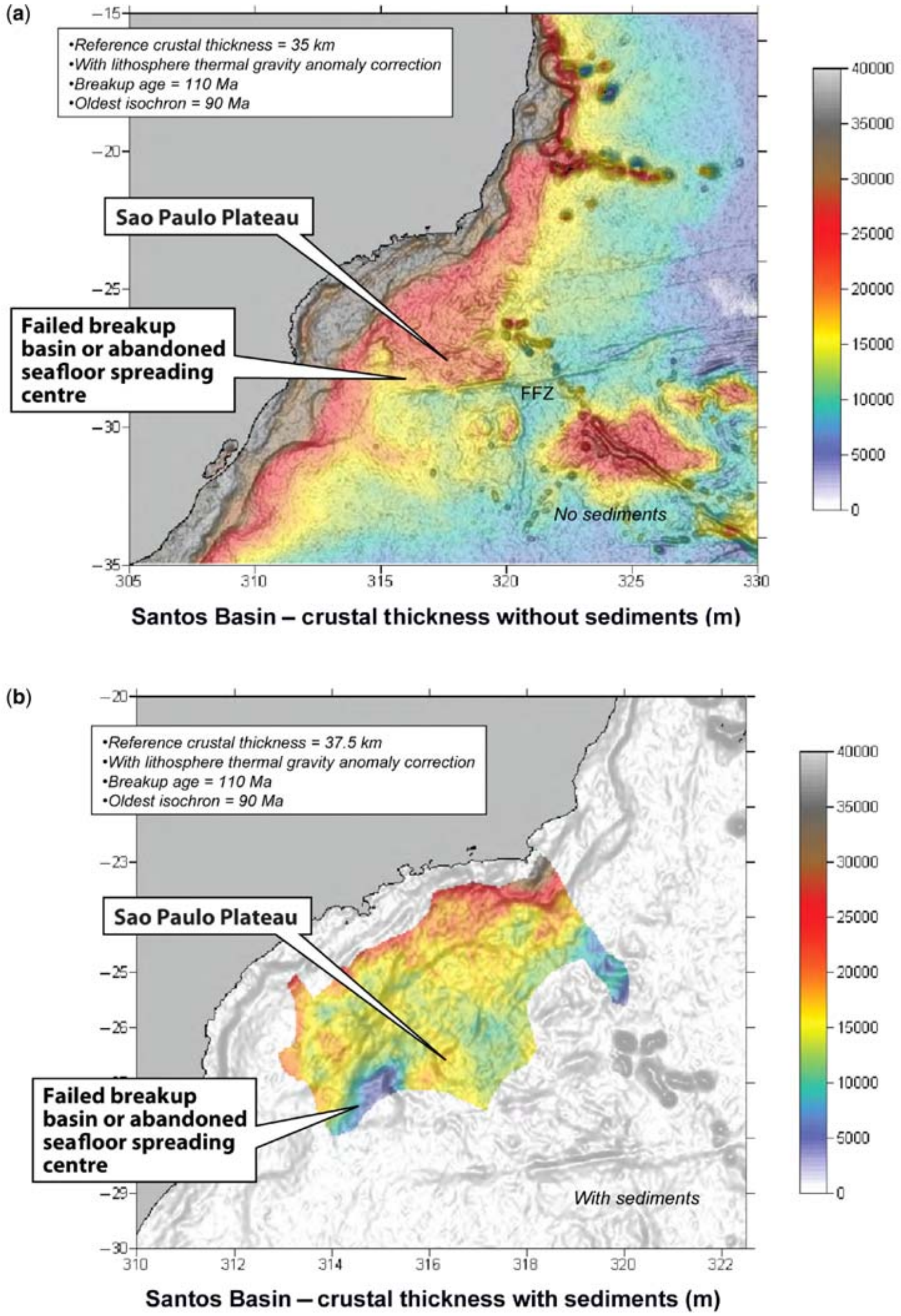

Fig. 6. (**a**) Crustal thickness map of the Santos Basin derived from gravity inversion assuming zero sediment thickness showing thick continental crust underlying the SPP and thinned crust beneath the linear anomaly in the SW Santos Basin. (**b**) Crustal basement thickness map derived from gravity inversion incorporating sediment thickness data from seismic reflection grid showing thinned continental crust underlying the SPP and oceanic crust beneath the SW Santos Basin.

lineament subsequently re-activated as the Albian-aged FFZ. North of this lineament, rifting began around 140 Ma (Fig. 8a), probably contemporaneous with the intrusion of the Ponta Grossa dyke swarm and extrusion of the Parana volcanics, associated with the Tristao da Cunha hotspot. Initiation of seafloor spreading occurred south of the FFZ by 126 Ma, while to the north sag-sequence deposition took place in the rift basin system with deposition of the lacustrine source rocks and sandstones. During this time the Tristao da Cunha hotspot appears to have moved into the rift area north of the FFZ with intrusion of igneous bodies. Associated with the hotspot, the spreading centre south of the FFZ may have ‘tipped-out’ into the rift basin on the northern side where it developed into incipient breakup and seafloor spreading on an ENE–SSW trend towards the Brazilian coastline around 120 Ma. Crustal thinning appears to have affected the area with associated thick development of sag-phase sedimentation, particularly over what is now the SPP. Extreme crustal thinning took place along the line of the incipient breakup north of the FFZ, with likely emplacement of oceanic crust in its southern part, north of the FFZ, in what is now the southwestern part of the Santos Basin. However, this phase of incipient breakup and seafloor spreading appears to have failed in the early Aptian and resulted in the formation of a failed breakup basin/seafloor spreading axis in what is now the central part of the Santos Basin with an adjacent area of thinned continental crust which became the present-day SPP.

During the late Aptian, deposition of thick halite took place in the subsiding sag basins along the whole rifted margin, which had been flooded intermittently by marine water, most likely from the

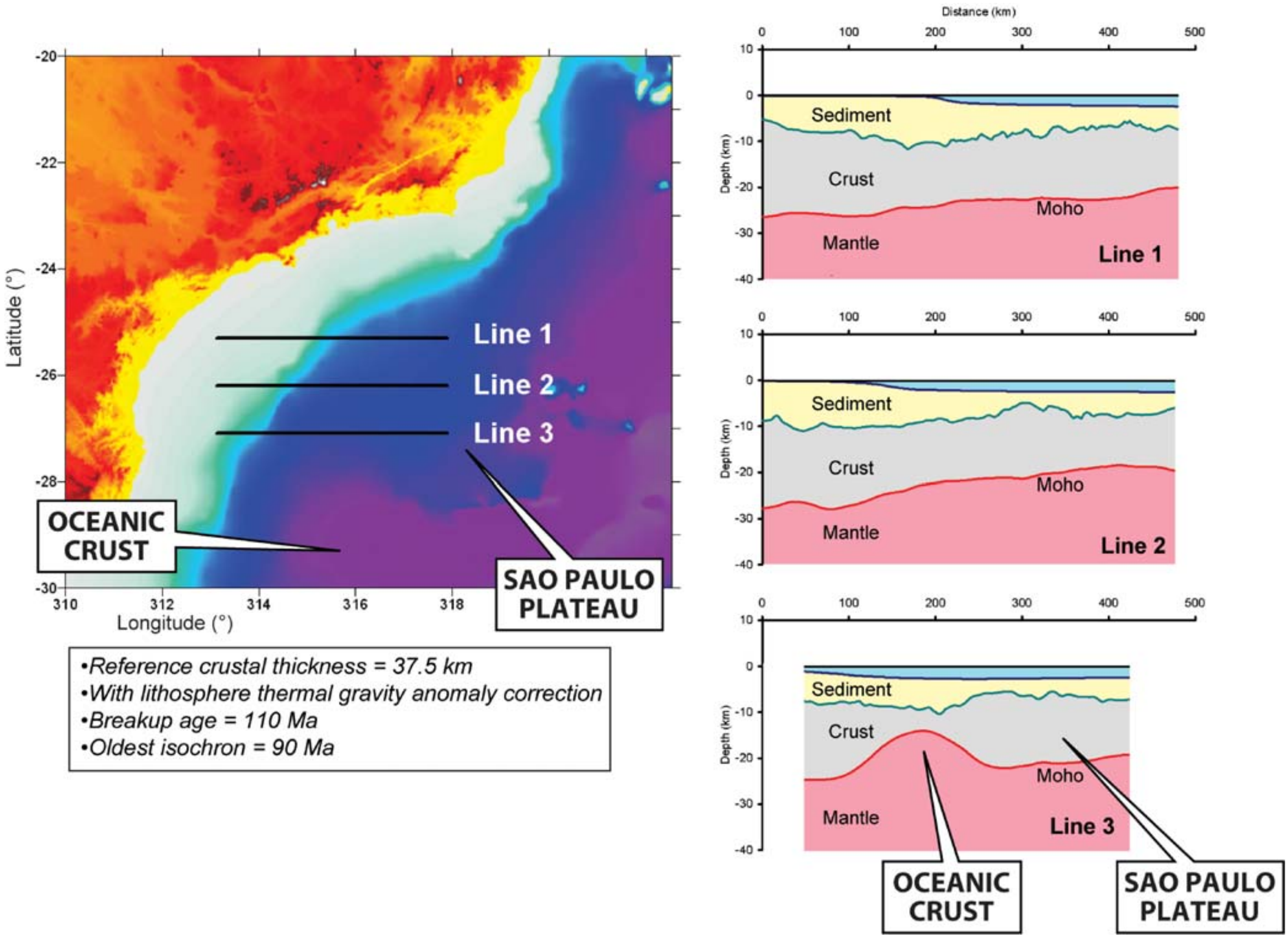

Fig. 7. Crustal cross-sections showing crustal basement thickness and Moho depth determined from gravity inversion across the Santos Basin and SPP.

north via the early rifts in the central part of the Atlantic Ocean, as the Rio Grande High appears to have prevented access by marine waters to the basin system from the south (Scotchman *et al.* 2008). The SPP area was at this time still on the African side of the rift system and remained relatively high, forming the eastern flank of the Santos failed breakup basin. Here the lack of large-scale regional subsidence appears to have resulted in the deposition of very shallow water algal/thrombolitic/stromatolitic lacustrine/brackish water limestones capping the syn-rift shales, forming the reservoir in recent discoveries such as Tupi. The area remained a positive feature during the subsequent deposition of evaporites with shallow, sabkha-like deposition of bedded evaporites. These largely comprise halite and anhydrite, but occasionally with complete evaporation leading to Mg- and K-salt precipitation.

Breakup finally appears to have taken place to the east of the SPP in the late Aptian–Albian, with evidence that this took place from the north (Scotchman *et al.* 2008), with formation of the oceanic fracture zones such as the FFZ, which as noted above appears to have re-activated an older crustal lineament. The Santos Basin to the west was flooded by shallow seas with deposition of carbonate platforms along the Brazilian flank and development of early turbiditic sandstones and shales in the deepest parts of the basin. The Albian carbonates appear to be not present or below seismic resolution on the adjacent SPP, although a lateral facies change to deep marine shales is also possible, making it difficult, without biostratigraphic data, to resolve if deposition of the marginal bedded evaporite sequence ended in the Aptian or continued into the Albian. Regional evidence perhaps favours the latter hypothesis as the Albian section in the deepwater Santos Basin flanking the northern side of the SPP comprises anoxic organic-rich black shales which form the main post-salt hydrocarbon source in the basin (Katz & Mello 2000). Marine organic shale deposition generally requires a restricted basinal setting, for example, Demaison & Moore (1980), and a narrow seaway between the coastal carbonate platform and the SPP located over the thermally subsiding failed spreading centre could easily fulfil such a role, providing additional excellent hydrocarbon source potential.

When seafloor spreading finally occurred in the area, perhaps as late as the end Albian–Cenomanian, the split between Africa and South America was completed and the Rio Grande High breached. The whole area then underwent rapid subsidence with the spread of deepwater turbidite deposition which had flooded both the Santos Basin and the SPP. Figure 8 illustrates the simplified kinematic model for the breakup of the Brazilian–African margin, showing development of the failed breakup basin (the Santos Basin) and the SPP.

Petroleum systems

The syn-rift Lagoa Feia lacustrine facies shales are the main hydrocarbon source rock in the basin system along the Brazilian Atlantic Ocean margin (Katz & Mello 2000), where they have charged post-salt turbidite reservoirs of Late Cretaceous to Cenozoic age to form a very prolific petroleum system with giant oil fields in basins such as the Campos, Espirito Santo and Santos (Guardado *et al.* 2000). Post-salt source rocks, particularly of Albian and Cenomanian–

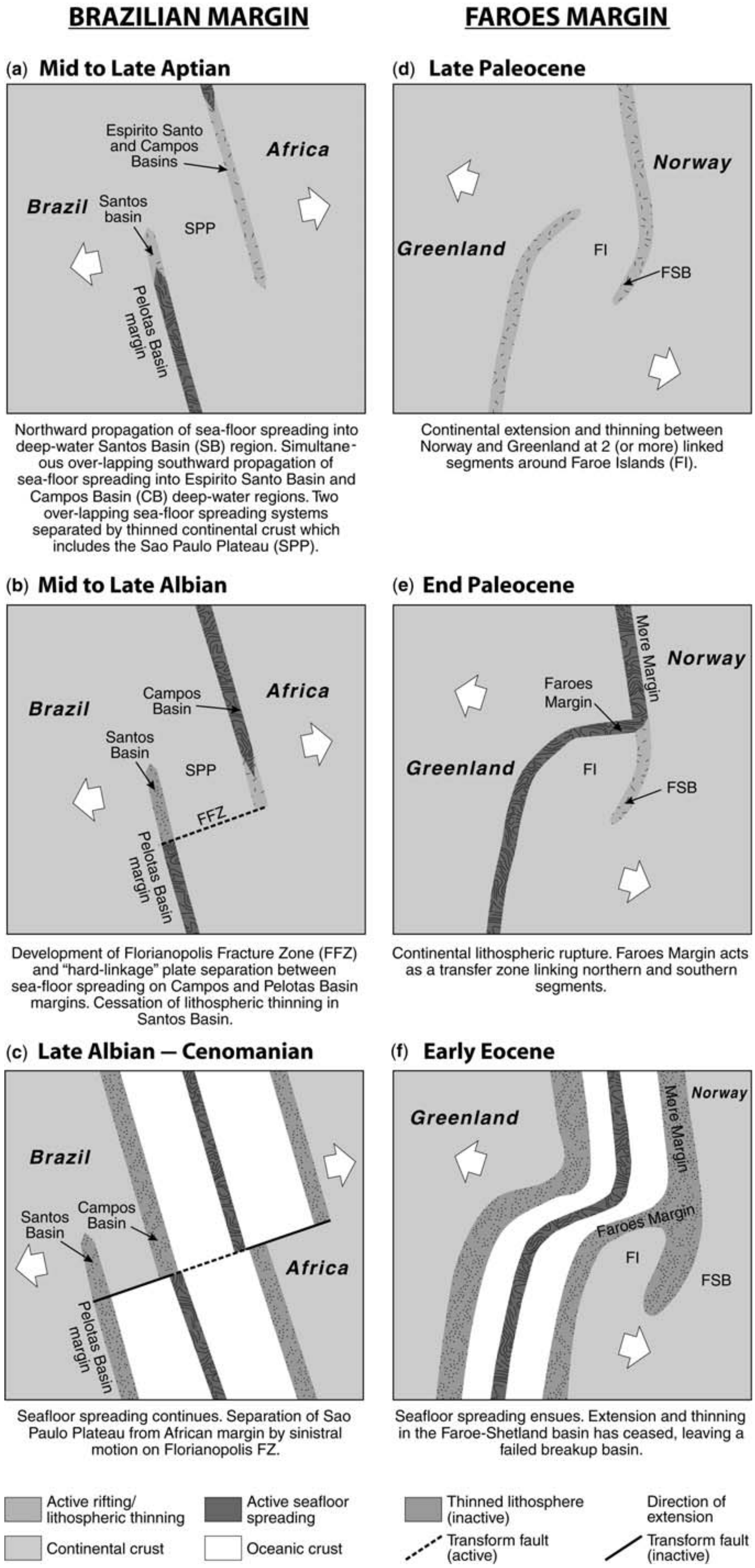

Fig. 8. Conceptual breakup models for (**a**–**c**) the South Atlantic in the Santos Basin and SPP and (**d**–**f**) the North Atlantic in the Faroes/Faroe–Shetland Basin (modified from Fletcher 2009).

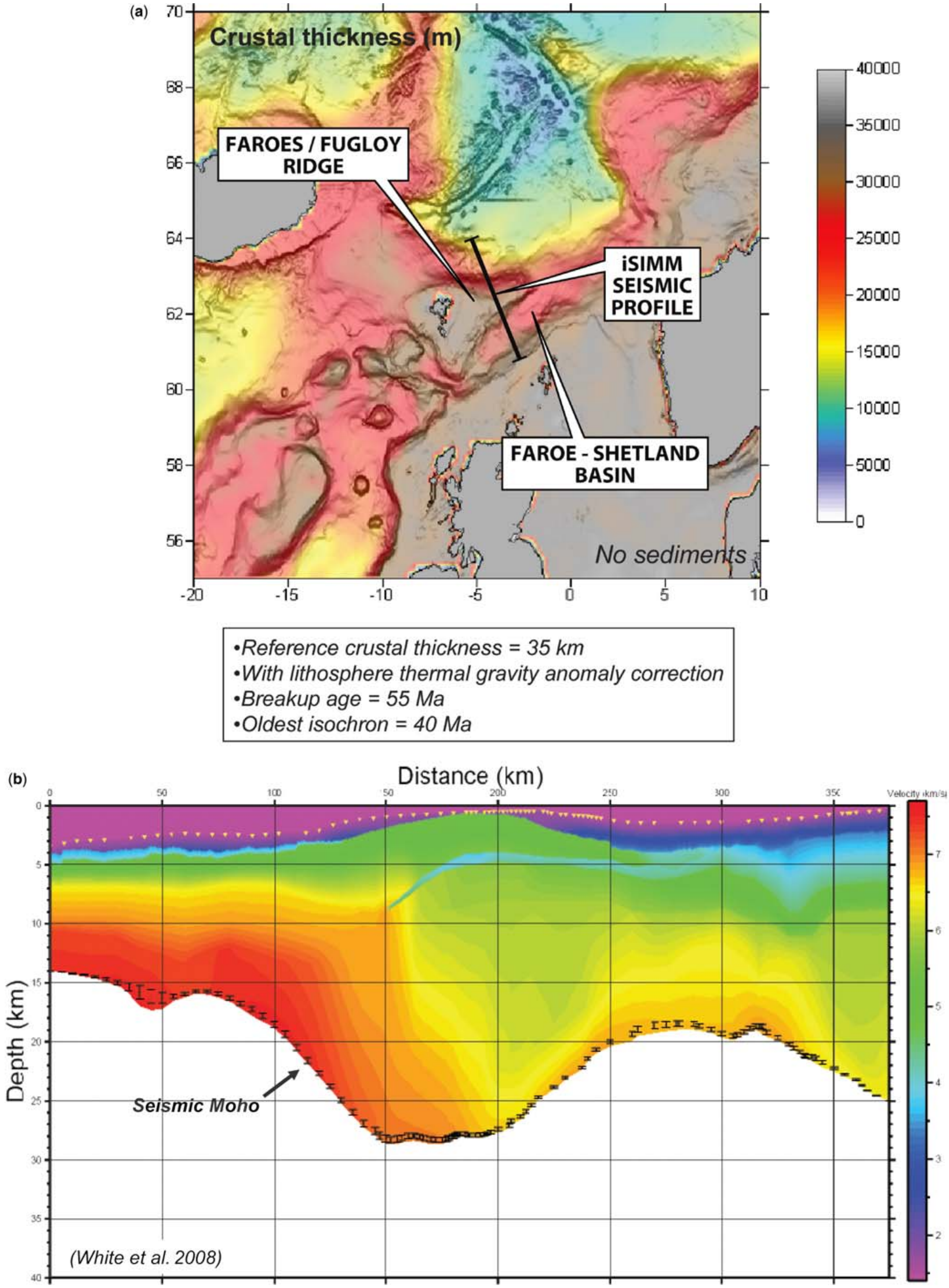

Fig. 9. (**a**) Crustal thickness map for the NE Atlantic Ocean showing thinned continental crust beneath the Faroe–Shetland Basin while the Faroes continental block comprises relatively un-thinned continental crust. (**b**) The iSIMM Deep Seismic line illustrating the deep structure of the Faroes/Faroe–Shetland Basin (from White *et al.* 2008).

Turonian, also provide important charging to these drift-phase deepwater reservoirs in the Santos and Espirito Santo Basins.

The syn-rift sourced petroleum system occurs in both the Santos Basin and the SPP; in the former the main reservoirs are in the post-salt turbidites while in the SPP the main reservoir is the pre-salt carbonate section capping the thick syn-rift/sag phase section. Importantly, due to the greatly different heatflow and burial depth between the Santos Basin and the SPP, the hydrocarbon phase is different. Within the Santos Basin, the subsidence associated with the failed seafloor spreading ridge resulted in the deep burial of the syn-rift source rock beneath a thick Late Cretaceous–Cenozoic turbidite section of 4–5 km (e.g. Fig. 3 seismic line 3), up to twice that of the equivalent section on the SPP, which remained a relatively positive feature. It is therefore not surprising that light hydrocarbons and gas, such as the giant Merluza gas field, predominate in this part of the Santos Basin. On the SPP, the large volumes of oil (28–32°API) have been discovered, reportedly in the syn-rift carbonate reservoir with estimated resources of $20–50 \times 10^9$ barrels, and a large gas discovery, Jupiter, discovered on the flank of the SPP. As well as greatly increased burial depths, the thermal regime in the Santos Basin differs from that on the SPP: at a depth of 3 km below mud-line, the typical temperature in the former is around 100 °C compared with 60 °C on the SPP (Poiate *et al.* 2006). The temperature differences appear to reflect both a lower heatflow on the SPP and the effects of the thick evaporites blanketing the structure.

Therefore the development of the prolific pre-salt oil province on the SPP appears related to its unique structural development compared to the other basins along the Brazil Atlantic Margin: the thinned crust allowed development of a thick, well developed syn-rift/sag phase section with resultant excellent source and reservoir rocks, relatively low subsidence compared with the adjacent Santos Basin and relatively low temperatures due to lower heatflows and the thick evaporites, allowing the source rocks to remain in the oil window compared with the Santos Basin, where the equivalent source rock kitchens are in the gas-window or are burnt out.

Comparison of continental lithospheric thinning and rifted margin formation in the Santos Basin/Sao Paulo Plateau with the Faroe–Shetland Basin and Faroes margin, NE Atlantic

The kinematics of continental lithosphere thinning and breakup at the Brazilian margin can be compared with those at the NE Atlantic Ocean in the Faroe–Shetland area (Fig. 9). The Faroe–Shetland Basin (FSB) and Fugloy Ridge appear to be analogous features to the Santos Basin and the SPP, respectively. The FSB, a major Cretaceous–Cenozoic depocentre, is located between the West Shetland Platform north of Scotland and the Faroes (Doré *et al.* 1999) and contains a series of NE–SW trending sub-basins formed by a complex tectonic history involving multiple phases of extension and volcanism (Carr & Scotchman 2003). The FSB underwent several periods of rifting, accommodated by extensional faulting from Devonian to Cretaceous times (e.g. Doré *et al.* 1999; Roberts *et al.* 1999). The basin also experienced lithospheric thinning in the Late Paleocene synchronously with crustal rupture and the onset of Atlantic Ocean seafloor spreading to the west of the Faroe Islands, at the Faroes margin (Fletcher 2009). This was accompanied by a massive outpouring of basalt which covers part of the FSB. The crustal thickness map of the Faroese region (Fig. 9a), derived using the method of Greenhalgh & Kusznir (2007) and the iSIMM refraction line (Fig. 9b) shows that the FSB is underlain by very thinned crust. Thin crust beneath the FSB is coaxial with thin crust at the Møre margin, and the FSB is postulated to be a failed breakup basin at the palaeopropagating tip of the Atlantic. A schematic diagram of the kinematics of breakup at the Faroes margin is shown in Figure 8b.

Both the Santos Basin and the FSB appear to be failed breakup basins associated with attempted propagation of seafloor spreading and consequent thinning of continental crust, while the adjacent structural highs, the SPP and Fugloy Ridge respectively, represent areas of relatively thick continental crust, albeit with greatly differing amounts of thinning. The SPP underwent considerable thinning and subsidence which accommodated a thick syn-rift section containing both source and reservoir rocks capped by a thick post-rift evaporitic section, resulting in a prolific petroleum province. The Fugloy Ridge also experienced considerable crustal thinning but comparison with the SPP is difficult as the crust has probably been re-thickened by the addition of both igneous intrusions and extrusive volcanics after it was thinned. Thick volcanics on the Fugloy Ridge mean that the syn-rift section is hard to image, although recent seismic data indicate the development of a sedimentary sequence beneath the post-rift sequence (Roberts 2007), indicating the potential for the development of a petroleum province.

Conclusions

The modelling suggests that the linear gravity and magnetic feature identified in the Santos Basin represent abandoned seafloor spreading propagation with the formation of oceanic or proto-oceanic crust at its southwestern end. This represents an early attempt at seafloor spreading initiation north of the FFZ during the early Aptian. The breakup process also resulted in the formation of an adjacent area of thinned continental crust, the SPP, with subsequent deposition of a thick syn-rift/sag phase section containing both hydrocarbon source and reservoir rocks capped by a thick post-rift bedded evaporitic section. A prolific pre-salt petroleum province developed on this feature due to preservation of the syn-rift/sag source rocks and reservoirs by the relatively low heatflows and subsidence compared with the adjacent Santos Basin. Breakup and seafloor spreading to the east of the SPP, marking the final breakup of the South Atlantic Ocean, appear to have been initiated from the north (Scotchman *et al.* 2008) and occurred in the late Albian–Cenomanian.

Similar analysis of the FSB area of the northeast Atlantic Ocean suggests development of a similar failed breakup/seafloor spreading basin. Both the Brazilian and Faroes margins exhibit evidence for complex breakup kinematics, where lithospheric thinning originally occurred at two or more overlapping segments before becoming linked when the lithosphere ruptured. Sedimentary basins on the regions of thinned crust on rifted continental margins have potential to be hydrocarbon provinces.

The authors would like to thank Statoil for permission to publish this work and John Kipps and Michael McCambridge for their draughting of the figures and the many revisions.

References

Cainelli, C. & Mohriak, W. U. 1998. Brazilian geology part II: geology of Atlantic Eastern Brazilian Basins. *Rio '98 AAPG International Conference and Exhibition, American Association of Petroleum Geologists/Associação Brasileira dos Geólogos de Petróleo, Short Courses*, Rio de Janeiro.

Carr, A. D. & Scotchman, I. C. 2003. Thermal history modelling in the southern Faroe–Shetland Basin. *Petroleum Geoscience*, **9**, 333–345.

Chang, K. H., Kowsmann, R. O., Figueiredo, A. M. F. & Bender, A. 1992. Tectonics and stratigraphy of the east Brazil rift system: an overview. *Tectonophysics*, **213**, 97–138.

Chappell, A. R. & Kusznir, N. J. 2008. Three-dimensional gravity inversion for Moho depth at rifted continental margins incorporating a lithosphere thermal gravity anomaly correction. *Geophysics Journal International*, **246**, 1–17; doi: 10.1111/j.1365–246X.2008.03803.x.

Cobbold, P. R., Meisling, K. & Mount, V. S. 2001. Reactivation of an obliquely rifted margin, Campos and Santos Basins, southeastern Brazil. *American Association of Petroleum Geologists Bulletin*, **85**, 1925–1944.

Corti, G., Van Wijk, J. *et al*. 2003. Transition from continental break-up to punctiform seafloor spreading: how fast, symmetric and magmatic. *Geophysical Research Letters*, **30**,1604; doi: 10.1029/2003GL017374.

Davison, I. 2007. Geology and tectonics of the south Atlantic Brazilian salt basins. *In*: Ries, A. C., Butler, R. W. H. & Graham, R. H. (eds) *Deformation of the Continental Crust: The Legacy of Mike Coward*. Geological Society, London, Special Publications, **272**, 345–359.

Davison, I. & Bate, R. 2004. Early opening of the South Atlantic: Berriasian rifting to Aptian salt deposition. *PESGB/HGS 3rd International Joint Meeting Africa: The Continent of Challenge and Opportunity*, 7–8 September.

Demaison, G. J. & Moore, G. T. 1980. Anoxic environments and oil source bed genesis. *Organic Geochemistry*, **2**, 9–31.

Doré, A. G., Lundin, E. R., Birkeland, Ø., Eliassen, P. E. & Jensen, L. N. 1999. The NE Atlantic Margin: implications for late Mesozoic and Cenozoic events for hydrocarbon prospectivity. *Petroleum Geoscience*, **3**, 117–131.

Dunbar, J. A. & Sawyer, D. S. 1989. How pre-existing weaknesses control the style of continental breakup. *Journal of Geophysical Research – Solid Earth and Planets*, **94**, 7278–7292.

Fletcher, R. J. 2009. *Mechanisms of continental lithosphere thinning and rifted margin formation*. PhD thesis, University of Liverpool.

GEBCO (IOC, IHO, and BODC). 2003. *Centenary Edition of the GEBCO Digital Atlas.* Published on CD-ROM on behalf of the Intergovernmental Oceanographic Commission and the International Hydrographic Organization as part of the General Bathymetric Chart of the Oceans. British Oceanographic Data Centre, Liverpool.

Gomes, P. O., Parry, J. & Martins, W. 2002. The outer high of the Santos Basin, southern Sao Paulo Plateau, Brazil: tectonic setting, relation to volcanic events and some comments on hydrocarbon potential. Extended Abstract. *American Association of Petroleum Geologists Hedberg Conference 'Hydrocarbon Habitat of Volcanic Rifted Passive Margins'*, 8–11 September, Stavanger. *Search and Discovery* Article **90022**.

Gomes, P. O., Kilsdonk, B., Minken, J., Grow, T. & Barragan, R. 2009. The outer high of the Santos Basin, southern Sao Paulo Plateau, Brazil: pre-salt exploration outbreak, paleogeographic setting and evolution of the syn-rift structures. *Search and Discovery* Article **10193**.

Greenhalgh, E. E. & Kusznir, N. J. 2007. Evidence for thin oceanic crust on the extinct Aegir Ridge, Norwegian Basin, NE Atlantic derived from satellite gravity inversion. *Geophysical Research Letters*, **34**, L06305, 1–5; doi: 10.1029/2007GL029440.

Guardado, L. R., Spadini, A. R., Brandao, J. S. L. & Mello, M. R. 2000. Petroleum system of the Campos Basin, Brazil. *In*: Mello, M. R. & Katz, B. J. (eds) *Petroleum Systems of South Atlantic Margins*. American Association of Petroleum Geologists, Tulsa, OK, Memoirs, **73**, 317–324.

Karner, G. D. & Driscoll, N. W. 1999. Tectonic and stratigraphic development of the West African and eastern Brazilian Margins: insights from quantitative basin modelling. *In*: Cameron, N. R., Bate, R. H. & Clure, V. S. (eds) *The Oil and Gas Habitats of the South Atlantic*. Geological Society, London, Special Publications, **153**, 11–40.

Karner, G. D. & Gamboa, L. A. P. 2007. Timing and origin of the South Atlantic pre-salt sag basins and their capping evaporites. *In*: Schreiber, B. C., Lugli, S. & Babel, M. (eds) *Evaporites Through Space and Time*. Geological Society, London, Special Publications, **285**, 15–35.

Katz, B. J. & Mello, M. R. 2000. Petroleum systems of South Atlantic marginal basins – an overview. *In*: Mello, M. R. & Katz, B. J. (eds) *Petroleum Systems of South Atlantic Margins*. American Association of Petroleum Geologists, Tulsa, OK, Memoirs, **73**, 1–13.

Kusznir, N. J., Roberts, A. M. & Morley, C. 1995. Forward and reverse modelling of rift basin formation. *In*: Lambiase, J. (ed.) *Hydrocarbon Habitat in Rift Basins*. Geological Society, London, Special Publications, **80**, 33–56.

Lelarge, M. L. M. V. 1993. *Thermochronologie par la methode des traces de fission d'une marge passive (dome de Ponta Grossa, SE Brásil) et au sein d'une chaine de collision (zone externe de lárc Alpin, France)*. PhD thesis, Université Joseph Fourier, Grenoble.

McKenzie, D. 1978. Some remarks on the development of sedimentary basins. *Earth and Planetary Science Letters*, **40**, 25–32.

Meisling, K., Cobbold, P. R. & Mount, V. S. 2001. Segmentation of an obliquely rifted margin, Campos and Santos Basins, southeastern Brazil. *American Association of Petroleum Geologists Bulletin*, **85**, 1903–1924.

Mello, M. R., Azambula Filho, N. C., de Mio, E., Bender, A. A., de Jesus, C. L. C. & Schmitt, P. 2009. 3D modelling illuminates Brazil's presalt geology. *Offshore Magazine*, **69**, PennEnergy.

Mueller, R. D., Roest, W. R., Royer, J.-Y., Gahagan, L. M. & Sclater, J. G. 1997. Digital isochrons of the world's ocean floor. *Journal of Geophysical Research*, **102**, 3211–3214.

Parker, R. L. 1972. The rapid calculation of potential anomalies. *Geophysics Journal of the Royal Astronomy Society*, **31**, 447–455.

Pereira, J. L. & Feijo, F. J. 1994. Bacia de Santos. *Boletim de Geociências da Petrobrás*, **8**, 219–234.

Poiate, E., Maia da Costa, A. & Falcão, J. L. 2006. Drilling Brazilian salt: Petrobras studies salt creep and well closure. *Oil & Gas Journal*, **104**, 88–96. World Wide Web Address: http://www.ogj.com/articles/article_display.cfm?ARTICLE_ID=256731&p=7.

Renne, P., Deckart, K., Ernesto, M., Feraud, G. & Piccirillo, E. 1996. Age of the Ponta Grossa Dyke swarm (Brazil) and implications to the Parana flood volcanism. *Earth and Planetary Science Letters*, **144**, 199–211.

Roberts, A. 2007. *Crustal structure of the Faroes North Atlantic margin from wide-angle seismic data*. PhD thesis, University of Cambridge.

Roberts, A. M., Kusznir, N. J., Yielding, G. & Styles, P. 1998. 2D flexural backstripping of extensional basins; the need for a sideways glance. *Petroleum Geoscience*, **4**, 327–338.

Roberts, D. G., Thompson, M., Mitchener, B., Hossack, J., Carmichael, S. & Bjornset, H.-M. 1999. Palaeozoic to Tertiary rift and basin dynamics: mid-Norway to the bay of Biscay – a new context for hydrocarbon prospectivity in the deep water frontier. *In*: Fleet, A. J. & Boldy, S. A. R. (eds) *Petroleum Geology of Northwest Europe: Proceedings of the 5th Conference*. Geological Society, London, 7–40; doi: 10.1144/0050007.

Sandwell, D. T. & Smith, W. H. F. 1997. Marine gravity anomaly from Geosat and ERS1 satellite altimetry. *Journal of Geophysical Research*, **102**, 10039–10054.

Scotchman, I. C., Marais-Gilchrist, G. *et al*. 2006. A failed sea-floor spreading centre, Santos Basin, Brasil. *Rio Oil and Gas Conference, IBP*, Rio de Janeiro.

Scotchman, I. C., Brockbank, P., Gilchrist, G., Hunsdale, R., Roberts, A. & Kusznir, N. 2008. The formation of the South Atlantic between Brazil and West Africa: did it un-zip South to North or North to South? Abstract, *American Association of Petroleum Geologists International Conference and Exhibition*, 26–29 October, Cape Town.

White, R. S., Smith, L. K., Roberts, A. W., Christie, P. A. F. & Kusznir, N. J. 2008. Lower-crustal intrusion on the North Atlantic continental margin. *Nature*, **452**, 460–464.

Ziegler, P. A. & Cloetingh, S. 2004. Dynamic processes controlling evolution of rifted basins. *Earth-Science Reviews*, **64**, 1–50.

Structural architecture and nature of the continent–ocean transitional domain at the Camamu and Almada Basins (NE Brazil) within a conjugate margin setting

O. A. BLAICH,[1] J. I. FALEIDE,[1] F. TSIKALAS,[1,2] R. LILLETVEIT,[3] D. CHIOSSI,[3] P. BROCKBANK[3] and P. COBBOLD[4]

[1]*Department of Geosciences, University of Oslo, PO Box 1047 Blindern, NO-0316 Oslo, Norway (e-mail: o.a.blaich@geo.uio.no)*

[2]*Eni E&P, EASS, Via Emilia 1, I-20097 San Donato Milanese, Italy (present address)*

[3]*Global Exploration, Statoil, Forusbeen 50, N-4035 Stavanger, Norway*

[4]*Géosciences-Rennes, 35042 Rennes Cedex, France*

Abstract: Regional seismic reflection profiles and potential field data across the conjugate magma-poor Camamu/Almada–Gabon margins, complemented by crustal-scale gravity modelling and plate reconstructions, are used to reveal and illustrate the relationship of crustal structure to along-margin variation of potential field anomalies, to refine and constrain the continent–ocean boundary, as well as to study the structural architecture and nature of the continent–ocean transitional domain. The analysis reveals that the prominent conjugate Salvador–N'Komi transfer system appears to be a first-order structural element, governing the margin segmentation and evolution, and may have acted as an intraplate decoupling zone. The continent–ocean transitional domain, offshore northeastern Brazil, is characterized by rotated fault-blocks and wedge-shaped syn-rift sedimentary sequences overlying a prominent and undulated reflector ('M-reflector'), which in turn characterizes the boundary between an extremely thinned, possibly magmatically intruded, continental crust and normal lithospheric mantle. The 'M-reflector' in the northeastern Brazilian margin shows remarkable similarities to the S-reflector at the West Iberia margin. In the same way, the 'M-reflector' is interpreted as a detachment surface that was active during rifting. Unlike the well studied central and northern segments of the West Iberia margin, however, the present study of the northeastern Brazilian margin does not clearly reveal evidence of an exhumation phase. The latter predicts exhumation of middle and lower crust followed by mantle exhumation. Increase in volcanic activity during the late stages of rifting may have 'interrupted' the extensional system, implying a failed exhumation phase. In this setting, the break-up and drift phase may have replaced the exhumation phase. Nevertheless, the available observations cannot discount the possibility that the 'M-reflector' is underlain by partially serpentinized mantle. Our study further leads to the development of a detailed conceptual model, accounting for the complex tectonomagmatic evolution of the conjugate northeastern Brazilian–Gabon margins. This model substantiates a polyphase rifting evolution mode, which is associated with a complex time-dependent thermal structure of the lithosphere. In the conjugate margin setting, asymmetrical lithospheric extension resulted in the formation of the thinned continental crust domain prior to the formation of the approximately symmetrical transitional domain.

Keywords: northeastern Brazilian margin, gravity modelling, continent–ocean transition, crustal extension, South Atlantic conjugate margins

The extensional margin evolution from rift through break-up rupture of the continental lithosphere to progressive oceanic crust formation remains controversial (e.g. Rosendahl *et al.* 2005; Reston & Pérez-Gussinyé 2007; Sawyer *et al.* 2007). This is due to the fact that deep crustal structures along several margins are partially or totally masked by evaporite deposits and/or by magmatic materials. There are only limited amounts of high-quality geophysical data acquired at deep and ultra-deep waters. As petroleum exploration advances towards new frontiers, there is an economic need to better define the architecture and nature of the continent–ocean boundary/transition. This also has obvious implications for the reconstruction of rifted continental margins as this boundary represents the line of final continental separation.

Drilling results combined with recent studies at the Iberia and Newfoundland margins (e.g. Sawyer *et al.* 1994; Whitmarsh *et al.* 1998; Lavier & Manatschal 2006; Péron-Pinvidic *et al.* 2007; Reston 2009) and the acquisition of high-quality geophysical data at several margins have recently cast doubt on classical models of rifted margins. The latter viewed both the concurrence of continental and oceanic crust through a well-defined sharp boundary, and the thinning of the continental crust by simple or pure shear mechanisms, or a combination of the two (McKenzie 1978; Wernicke 1985; Lister *et al.* 1986; Buck *et al.* 1988). For instance, observations from the central South Atlantic margins are not consistent with classical rifted margin model predictions (Karner *et al.* 2003; Contrucci *et al.* 2004; Moulin *et al.* 2005; Karner & Gambôa 2007). For these distinctive margins, a wide region of extremely thin continental crust is observed, overlain by relatively thin and undeformed late syn-rift sediments, deposited under shallow water conditions in 'sag' basins, and being more compatible with depth-dependent extension models (e.g. Driscoll & Karner 1998; Davis & Kusznir 2004; Karner & Gambôa 2007; Kusznir & Karner 2007). Deeply subsided and possibly anomalous crust has been recognized along several margin segments in South Atlantic and described variously as 'proto-oceanic crust,' 'attenuated continental crust' and 'transitional crust' (e.g. Meyers *et al.* 1996*a*, *b*; Rosendahl & Groschel-Becker 1999; Wilson *et al.* 2003; Contrucci *et al.* 2004; Moulin *et al.* 2005; Rosendahl *et al.* 2005). The term continent–ocean 'transitional domain' is adopted in the current study and defined as the part of the lithosphere which is located

VINING, B. A. & PICKERING, S. C. (eds) *Petroleum Geology: From Mature Basins to New Frontiers – Proceedings of the 7th Petroleum Geology Conference*, 867–883. DOI: 10.1144/070867

between the thinned crystalline crust domain and the first appearance of oceanic crust formed by seafloor spreading (e.g. Whitmarsh & Miles 1995; Dean *et al.* 2000; Srivastava *et al.* 2000; Afilhado *et al.* 2008).

In this study of the Camamu and Almada basins in the northeastern Brazilian margin (Figs 1 & 2), we analyse an available grid of regional multichannel seismic (MCS) reflection profiles. We also analyse an available grid of regional MCS profiles together with published seismic reflection/refraction profiles along the conjugate Gabon margin. In this conjugate margin context, the integration of seismic, potential field data and conducted 2D gravity modelling, together with potential field plate reconstructions, provide adequate means to study the magma-poor Camamu/Almada–Gabon margins, to elucidate structural elements and features that reflect the processes that rupture the continental crust, as well as to refine and constrain the structural architecture and nature of the continent–ocean transitional (COT) domain.

Data and methodology

Data

Together with the gridded bathymetry and potential field data along the northeastern Brazilian margin and its conjugate off Gabon, a set of deep seismic reflection profiles was at our disposal (Fig. 2). The dataset was provided courtesy of Statoil and comprises several surveys acquired between 1999 and 2001. The dataset comprises 9500 km^2 of 2D high-resolution MCS reflection profiles, acquired by TGS-NOPEC with 37.5 m shotpoint interval and 2 ms sampling interval. Published seismic reflection profiles (Meyers *et al.* 1996*a*, *b*; Rosendahl *et al.* 2005) together with industrial seismic reflection and wide-angle refraction profiles (Wannesson *et al.* 1991) on the conjugate Gabon margin have been analysed, revised and incorporated into our interpretations.

Potential field data used in this study consist of a 1 × 1 min. elevation grid (GEBCO, General Bathymetric Chart of the Oceans 2003), a 1 × 1 min. satellite radar-altimeter gravity grid (version 16.1; Sandwell & Smith 1997; Fig. 3*a*), a 3 × 3 min. gridded aeromagnetic anomaly field map (WDMAM, World Digital Magnetic Anomaly Map 2007; Fig. 3c), as well as publicly available ship-borne bathymetry and potential field anomaly data (LDEO, Lamont–Doherty Earth Observatory; Wessel & Watts 1988; Smith 1993). A comparison between the satellite and ship-borne gravity anomalies shows that there is reasonably good agreement in wavelength and amplitude of the two datasets (Marks 1996; Sandwell & Smith 1997, 2009). These results support crustal-scale modelling with the use of satellite free-air gravity. Using the broad-coverage satellite gravity data also allowed us greater flexibility in the selection of the constructed transects, being able to project the gridded data along the selected MCS profiles. Finally, a Bouguer-corrected gravity anomaly field map was constructed by utilizing the detailed bathymetry and free-air gravity anomalies and a density of 2670 kg m^{-3} as infill to the bathymetric relief (Fig. 3b).

Transect construction

The MCS profiles within the study area were compiled and extended to the ultra-deep water oceanic province, in order to construct representative regional transects used in crustal-scale gravity modelling. The regional transects are based on the seismic reflection profiles, extracted bathymetry and gravity anomaly data along the extended parts, and on initial estimates of

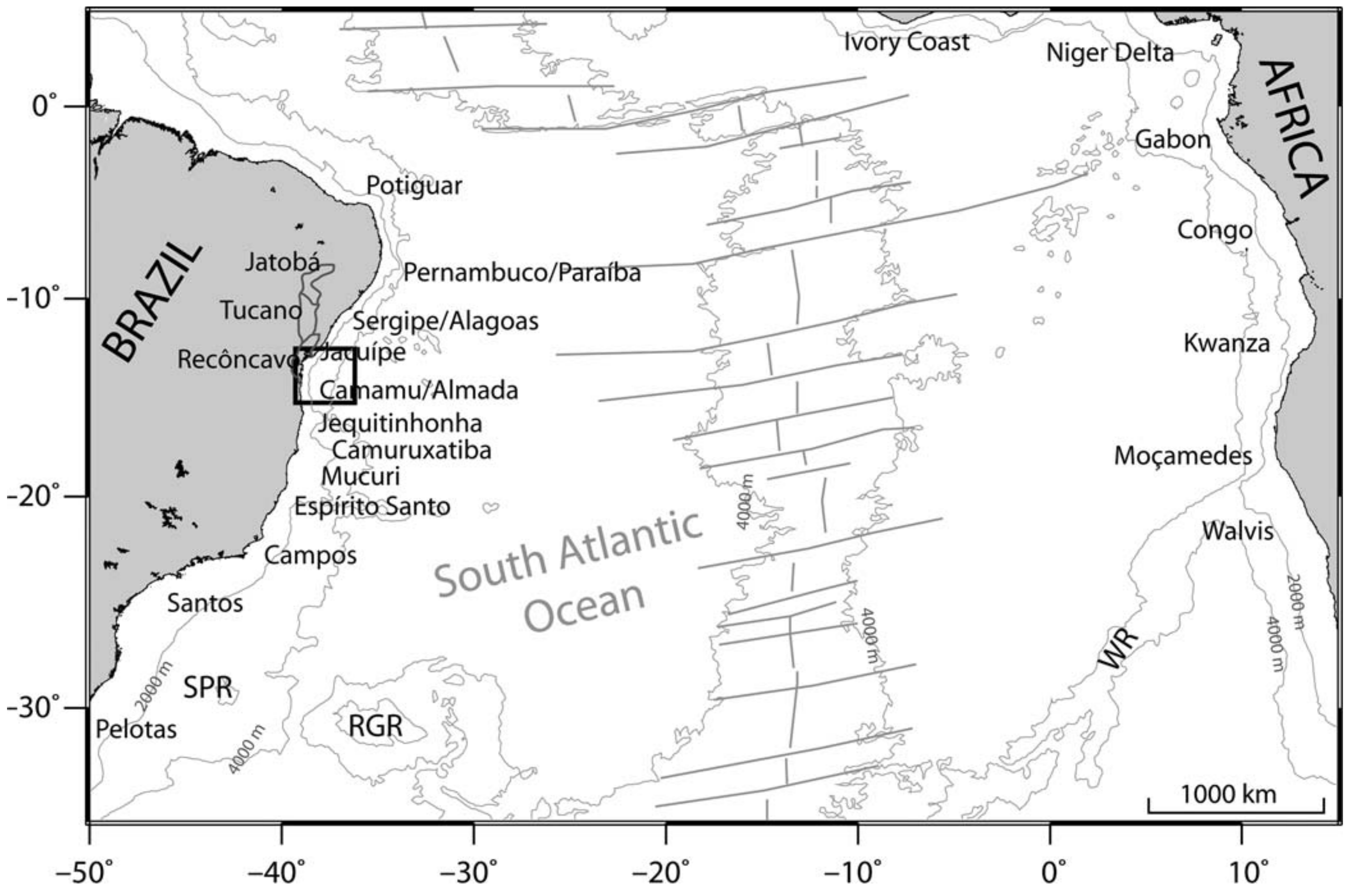

Fig. 1. South Atlantic Ocean and conjugate continental margins, outlined by the 2000 and 4000 m bathymetry contours. Rectangle outlines the study area. The location of major sedimentary basins along the East Brazilian and West Africa margins and major fracture zones are also indicated. WR, Walvis Ridge; RGR, Rio Grande Rise; SPR, São Paulo Ridge.

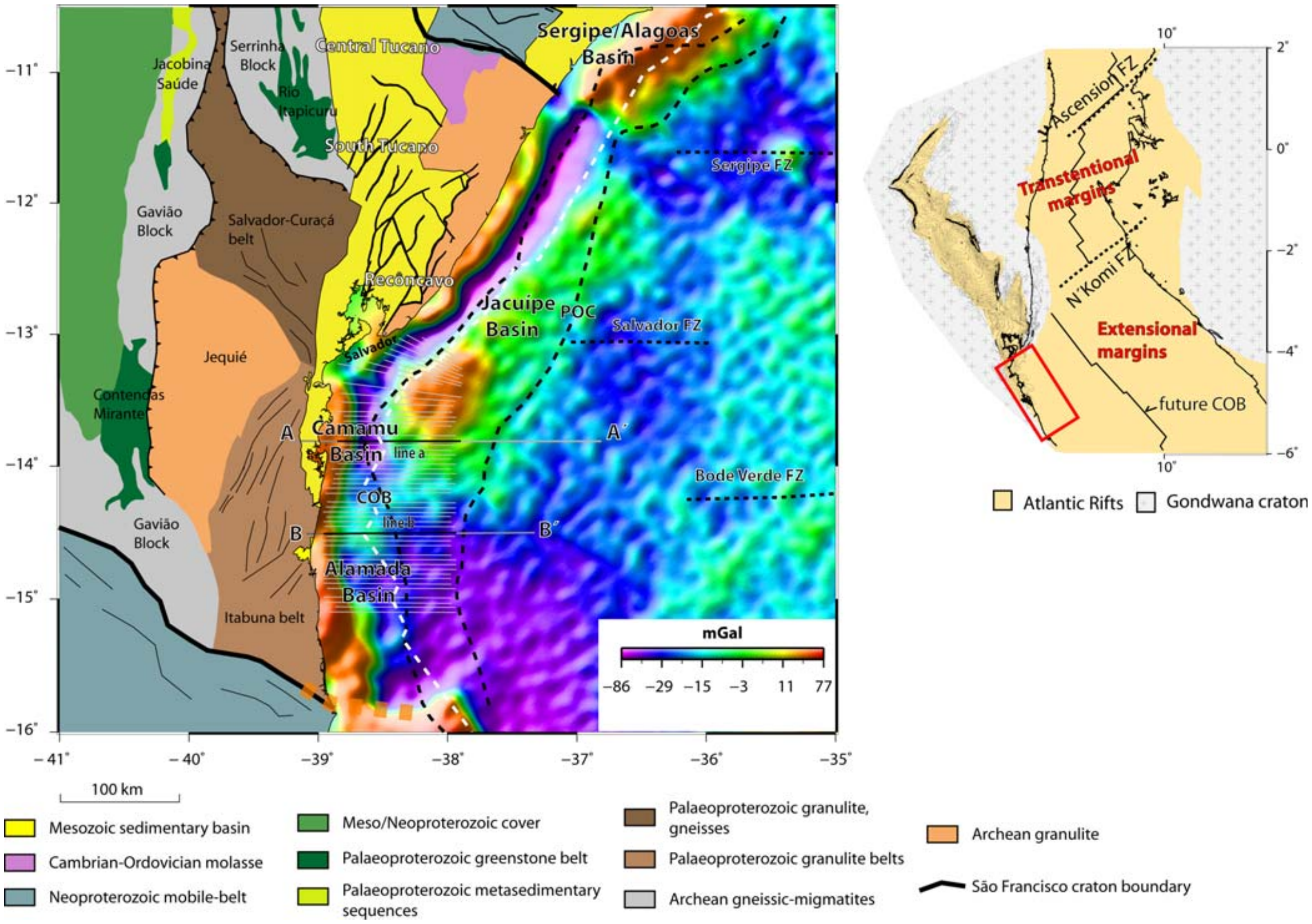

Fig. 2. Offshore: 1 × 1 min. gridded satellite radar-altimeter free-air gravity anomaly field (Sandwell & Smith 1997; version 16.1). Onshore: simplified geological and structural map of the northeastern Brazilian margin generalized from Barbosa & Sabaté (2003), Destro *et al.* (2003), Alkmim *et al.* (2006) and Leite *et al.* (2009). The constructed regional transects (A–A′ and B–B′) are also indicated together with the selected MCS profiles and the denser grid of MCS that was at our disposal. Interpreted oceanic fracture zones are based on observations made on the potential field data and on Gomes *et al.* (2000), Davison (1999) and Mohriak *et al.* (2000). COB, continent–ocean boundary (Karner & Driscoll 1999, white dashed line; Rosendahl *et al.* 2005, black dashed line); POC, proto-oceanic crust (Rosendahl *et al.* 2005). Inset: reconstruction of the rift system between northeastern Brazil and western Africa at the time of oceanic crust inception, showing major depocentres and bifurcation of the spreading axis in two branches (modified from Mohriak *et al.* 2000).

the Moho relief using both isostatic balancing and inverse gravity modelling. The latter method used in this study is described in detail by Blaich *et al.* (2008, 2009). The potential field plate reconstructions (Fig. 3) were performed using the PLATES software (Institute for Geophysics, University of Texas at Austin) and rotation poles of Torsvik *et al.* (2009). Plate reconstructions were used in this study in order to select conjugate profiles and to evaluate the tectonic evolution of the northeastern Brazilian/Gabon margins expressed on potential field data.

Margin setting

The opening of the South Atlantic Ocean and the subsequent passive margin formation resulted from lithospheric extension followed by break-up of the Palaeozoic Gondwana supercontinent and seafloor spreading during Mesozoic times (e.g. Rabinowitz & LaBrecque 1979; Chang *et al.* 1992). The opening of the South Atlantic, which probably started in the southern portion and propagated towards the north, resulted in considerable diachronic deformation in the Equatorial and eastern Brazilian margins (Matos 2000). The Equatorial margin evolved in response to transform motion between Brazil and Africa, resulting in complex shear-dominated basins. In contrast, the Eastern Brazilian margin is characterized by development of extensional basins due to divergent and semi-orthogonal crustal extension (Chang *et al.* 1992). A triple-junction is proposed near Salvador city, where the rift axis in the offshore domain changes to a more northerly direction. In this setting, the western branch of the rift forms the aborted onshore Recôncavo–Tucano–Jatobá Basins, whereas the eastern branch evolved to form the northeastern Brazilian–Gabon/Equatorial Guinea passive margin (Fig. 2; Mohriak *et al.* 2000).

Structural inheritance

Several studies of the northeastern Brazilian basin system postulate a pattern of structural inheritance, indicating that pre-existing continental lineaments, transfer zones and various basement terranes exerted important influence and rheological control on the structural development of the Mesozoic rifting and break-up (Fig. 2) (e.g. Milani & Davison 1988; Matos 1992, 1999; Szatmari & Milani 1999; Jacques 2003; Blaich *et al.* 2008). These zones of weakness played an important role in continental break-up from the earliest stage of rifting and have been correlated with failed arms of triple-junction rifts (Jacques 2003). In this setting, the pattern of extension (symmetrical v. asymmetrical), the sequence of rift phases and rift pattern leading to break-up, and the physiography of the resulting passive margin segments are all to a large extent controlled by the inherited fabric of continental lithosphere (Dunbar & Sawyer 1988, 1989).

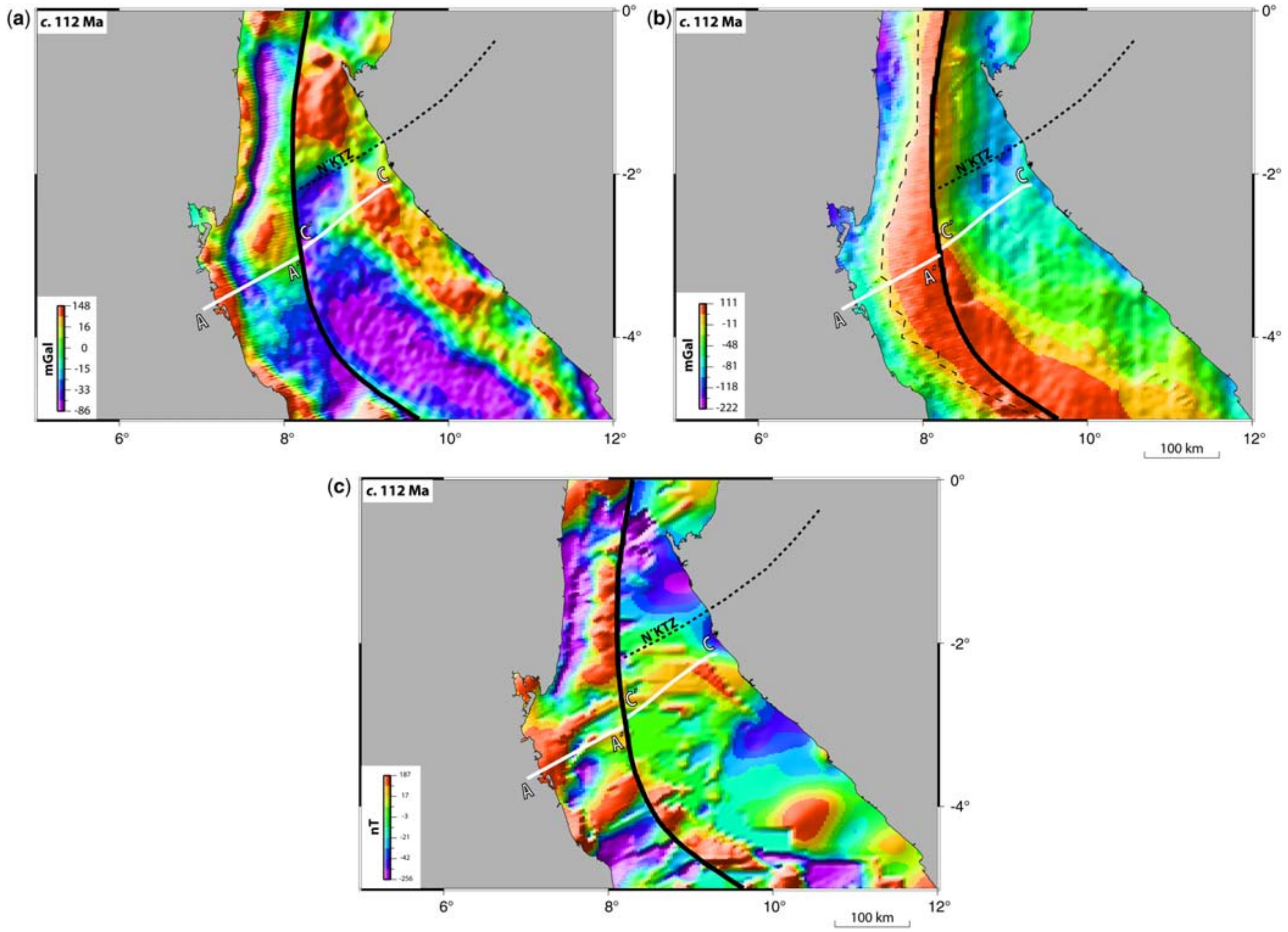

Fig. 3. Plate reconstructions at forced break-up (*c*. 112 Ma) utilizing the rotation poles of Torsvik *et al.* (2009); COB revised from Torsvik *et al.* (2009) and Karner & Driscoll (1999) fitting observations made in this study. (**a**) 1 × 1 min. satellite radar-altimeter free-air gravity anomaly field (Sandwell & Smith 1997; version 16.1). (**b**) Low-pass filtered (>200 km) Bouguer-corrected gravity anomaly field (utilizing a density of 2670 kg m^{-3} as infill to the bathymetric relief). (**c**) 3 × 3 min. gridded aeromagnetic anomaly field (WDMAM, World Digital Magnetic Anomaly Map 2007). The locations of conjugate transects A–A′ and C–C′ are indicated. Black dashed line indicates the COB as proposed by Karner & Driscoll (1999). N'KT, N'Komi Transfer Zone.

In the offshore domain, structural inheritance is reflected by the trend of the gravity anomalies. The gravity anomaly map (Fig. 2) shows that the anomaly low that flanks the 'edge-effect' anomaly high extends for 350–380 km parallel to the coastline. This anomaly low is abruptly terminated by a belt of positive anomalies to the NE, at latitude *c*. 11.2°S, along the equivalent offshore extent of the northern boundary of the São Francisco craton. The landward continuation of the Sergipe oceanic fracture zone, as proposed by Mohriak *et al.* (1995), is also closely related to this abrupt change on the gravity anomaly trend (Fig. 2). In this setting, inherited transfer zones appear to determine the location of recent oceanic fracture zones. Oceanwards, the prominent gravity anomaly high located at *c*. 13.5°S/−38°W and referred to as the Jacuípe Volcanic Complex (Davison 1999) terminates at the equivalent offshore extent of the boundary between the Salvador–Curaçá and the Itabuna Palaeoproterozoic belts (Fig. 2). Structural inheritance is also indicated by the trend of the magnetic anomalies (Fig. 3c).

Similarly, along the conjugate margin off Gabon, a prominent gravity anomaly low that flanks the 'edge-effect' gravity anomaly high abruptly terminates to the north at the N'Komi Transfer Zone (Fig. 3a). In the immediate vicinity of the prominent N'Komi Transfer Zone, abrupt changes in the deep crustal structure have been observed and the transfer zone appears to be a first-order structural element, governing the segmentation and evolution of the Gabon margin (Wannesson *et al.* 1991; Blaich *et al.* 2008). These observations suggest a distinct and probably inherited segmentation of the South Atlantic margins, where major changes in lithospheric strength may have occurred (e.g. Watts & Stewart 1998).

Crustal architecture

Northeast Brazil. The representative crustal transects obtained from the 2D gravity modelling outline the crustal structure of the individual segments along the Camamu and Almada basins. The distinct along-margin structural changes are highlighted by the modelled transects A–A′ and B–B′, which illustrate the structural complexity of the study area. Transects A–A′ and B–B′ are oriented in a west–east direction and extend *c*. 258 and *c*. 190 km eastwards along the Camamu and Almada basins, respectively (Figs 4 & 5). As the aim of this study is to illustrate the structural architecture at the transitional domain along the Camamu and Almada basins, seismic interpretation of the sedimentary units only accounts for pre-rift/syn-rift and post-rift sequences.

Interpretation of all available MCS profiles along the study area (Fig. 2) does not suggest a typical rifted continental crust, with progressive crustal thinning over an extensive distance towards oceanic crust formed due to break-up and seafloor spreading. On the contrary, although seismic interpretation combined with gravity modelling suggest extreme crustal thinning, the thick syn-rift sedimentary basins overlying the thinned crystalline

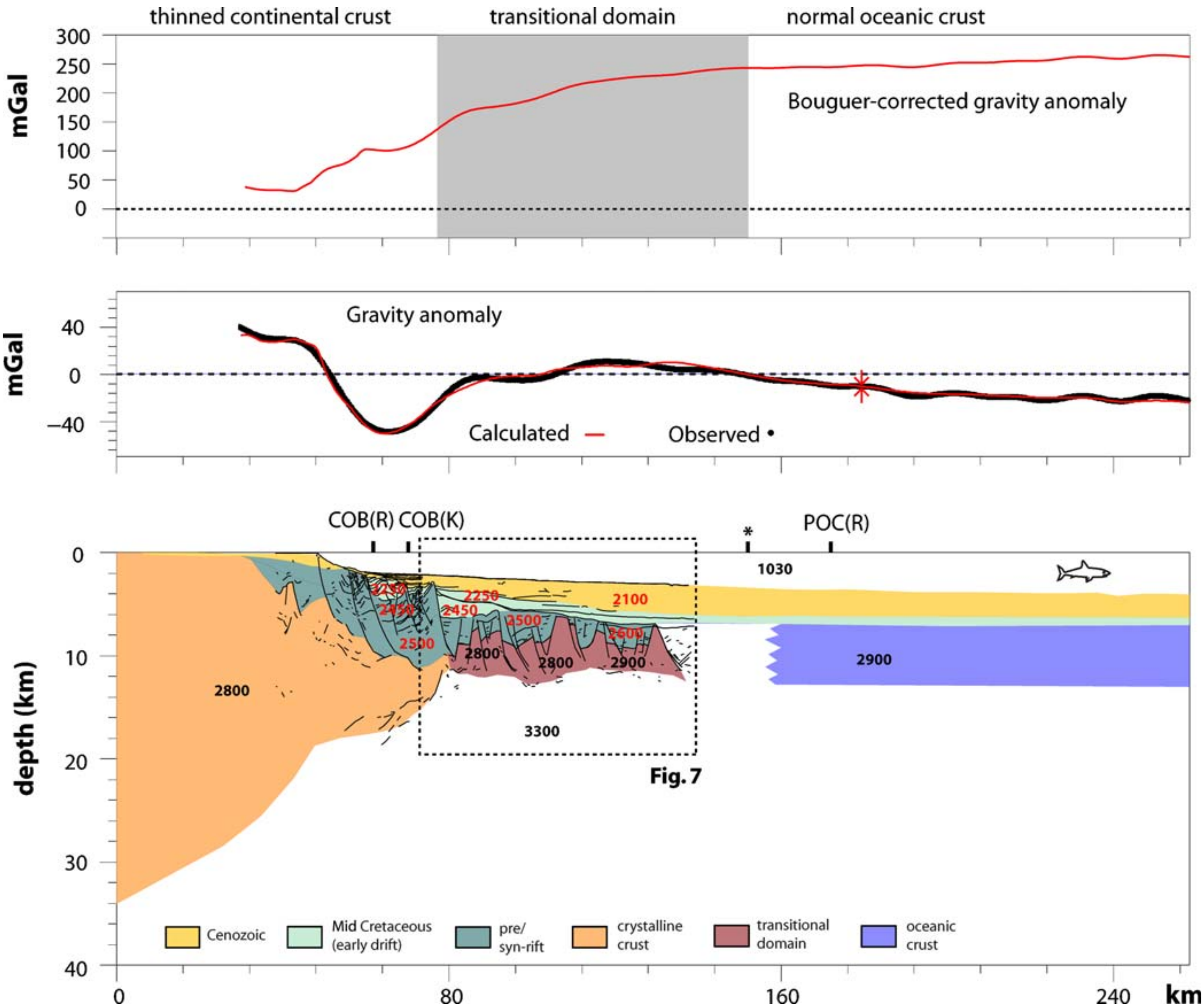

Fig. 4. Gravity modelled transect A–A′ (location in Fig. 2) utilizing the satellite radar-altimeter free-air gravity anomaly field (Sandwell & Smith 1997; version 16.1). Bouguer-corrected gravity anomaly is also shown. COB(K), continent–ocean boundary (Karner & Driscoll 1999); COB(R), continent–ocean boundary (Rosendahl *et al.* 2005); the asterisk indicates 'line of fit' used for plate reconstructions; POC(R), proto-oceanic crust (Rosendahl *et al.* 2005).

continental crust domain appear not to be the result of intense upper crust brittle deformation (Fig. 4). For instance, the data show that the continental crust along the Camamu Basin thins abruptly, from *c.* 30 to *c.* 4 km over a distance of only *c.* 80 km without prominent brittle deformation of the upper crust (Fig. 4).

Along-margin variation on the thickness of the pre/syn-rift sedimentary package is observed on the MCS profiles, and corresponds to prominent along-margin changes in the potential field data. In particular, a thick pre/syn-rift sedimentary package is characterized by a prominent and elongated gravity anomaly low along transect A–A′ (Figs 2 & 4). Further southwards, the thickness of the pre/syn-rift sedimentary package decreases considerably at places where the prominent and elongated gravity low is replaced by higher values (transect B–B′; Figs 2 & 5). A band of high-amplitude seismic reflections is observed along the thinned continental crust domain of transect B–B′ and at a depth of *c.* 14 km (Fig. 5). Such reflections are not present along transect A–A′. These reflections may represent the top of a lower crust or indicate a detachment surface; however, gravity modelling alone cannot unambiguously resolve this issue.

Although the northeastern Brazilian margin (Fig. 1) is proposed to be associated with well defined seaward-dipping reflections (Mohriak *et al.* 1995, 1998; Jackson *et al.* 2000), seismic images from this margin segment are very different from the images obtained on the well studied volcanic margins worldwide (e.g. Eldholm & Grue 1994; Gladczenko *et al.* 1998; Hinz *et al.* 1999; Franke *et al.* 2007; Tsikalas *et al.* 2008), implying that magmatic products along the northeastern Brazilian margin were not sufficiently voluminous to form seaward-dipping reflections (Sawyer *et al.* 2007). Seaward-dipping reflections were not recognized in the Camamu and Almada basins within the extensive seismic reflection dataset at our disposal (Fig. 2). Higher densities are required for the sedimentary package located adjacent to the normal oceanic crust (*c.* 110–140 km; Fig. 4), where an increase in seismic amplitude reflectivity is observed, indicating a possible increase in magmatic products characterized by volcanic flows and interbedded sediments with volcanic material.

Salt diapirs are clearly depicted along the Almada Basin, where a typical halokinetic structure is observed at the top of a well defined fault (Fig. 5). Although interpretation of the MCS profiles along the Camamu Basin indicates that prominent salt tectonism is not present (Fig. 4), previous studies have identified salt deposits along the Camamu (Karner & Gambôa 2007; Menezes & Milhomem 2009), Jacuípe (Davison 2007) and Sergipe–Alagoas basins (Castro 1988; Mohriak *et al.* 1995, 2000; Davison 2007; Souza-Lima 2009).

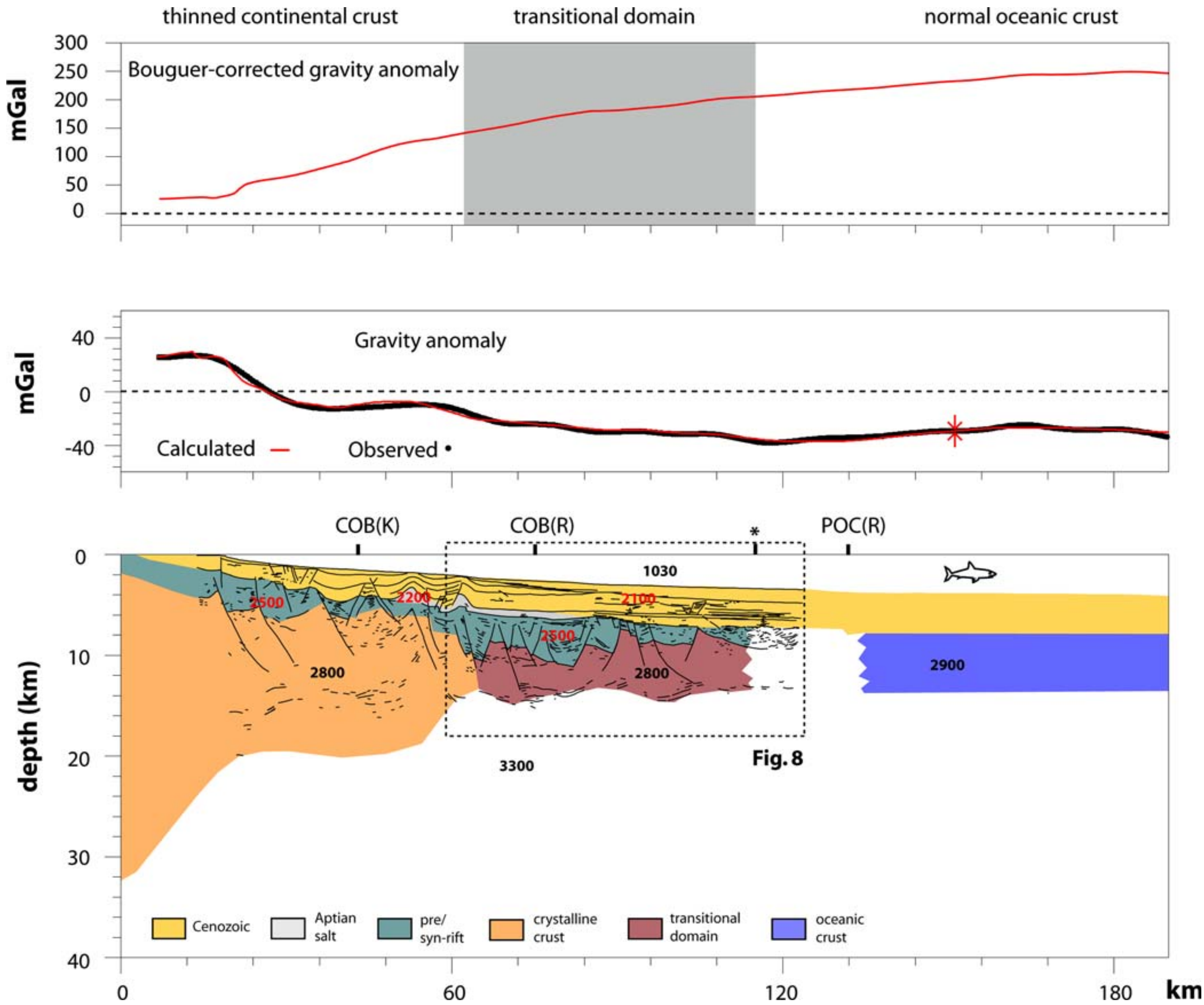

Fig. 5. Gravity modelled transect B–B′ (location in Fig. 2) utilizing the satellite radar-altimeter free-air gravity anomaly field (Sandwell & Smith 1997; version 16.1). Bouguer-corrected gravity anomaly is also shown. COB(K), continent–ocean boundary (Karner & Driscoll 1999); COB(R), continent–ocean boundary (Rosendahl *et al.* 2005); the asterisk indicates 'line of fit' used for plate reconstructions; POC(R), proto-oceanic crust (Rosendahl *et al.* 2005).

Gabon. In order to understand the total rift evolution, the conjugate margin transect C–C′ was constructed, located in the Gabon margin segment and extending for *c*. 204 km (Figs 3 & 6). The MCS profile is characterized by a wide salt basin that considerably masks the seismic reflection energy, implying that interpretation of the top basement reflection and rift structures are disputed and not easily recognized. A sub-horizontal, high-amplitude band of seismic reflections, located at a depth of *c*. 16–18 km and a distance of *c*. 0–80 km from the eastern end of transect C–C′, appears to be a good Moho candidate (Fig. 6). Several remarkable landward-dipping reflections located beneath the band of high-amplitude reflectivity are observed, indicating a different dip-pattern than the seaward-dipping structures related to the Mesozoic rifting. The Moho relief obtained by gravity modelling does not coincide with the high-amplitude band of seismic reflections discussed above (Fig. 6).

Based on seismic refraction and reflection analyses along the Gabon margin, a high-amplitude band of seismic reflections located at a depth of *c*. 16 km (depth-converted SPOG-2 profile from Wannesson *et al.* 1991) that exhibits a velocity increase from 6.1 to 6.9 km s^{-1} was earlier revealed. In addition, the gravity modelled SPOG-2 profile using densities derived from the wide-angle data of Wannesson *et al.* (1991) required a lower crustal body in order to accomplish a reliable fit in the gravity modelling. Similarly, an enigmatic high-velocity lower crustal body has also been suggested further south (Contrucci *et al.* 2004; Moulin *et al.* 2005). The analysis performed in this study indicates that the high-amplitude and sub-horizontal band of seismic reflections located at a depth of *c*. 16–18 km (Fig. 6) corresponds to the top of a lower crustal body rather than Moho. Such a lower crustal body is not necessarily magmatic in nature, but may be related to older tectonic episodes and, possibly, orogenies; for example, inheritance from Transamazonian and Pan-African collision belts (e.g. Meyers *et al.* 1996*b*).

Continent–ocean boundary

The location of the continent–ocean boundary (COB) along the northeastern Brazilian margin has been outlined in several studies based mostly on observations made on potential field anomalies and plate reconstructions (e.g. Karner & Driscoll 1999; Rosendahl *et al.* 2005). In this setting, the COB location was placed at a prominent negative–positive gradient on the Bouguer-corrected gravity field (Fig. 3b; Karner & Driscoll 1999). This location is

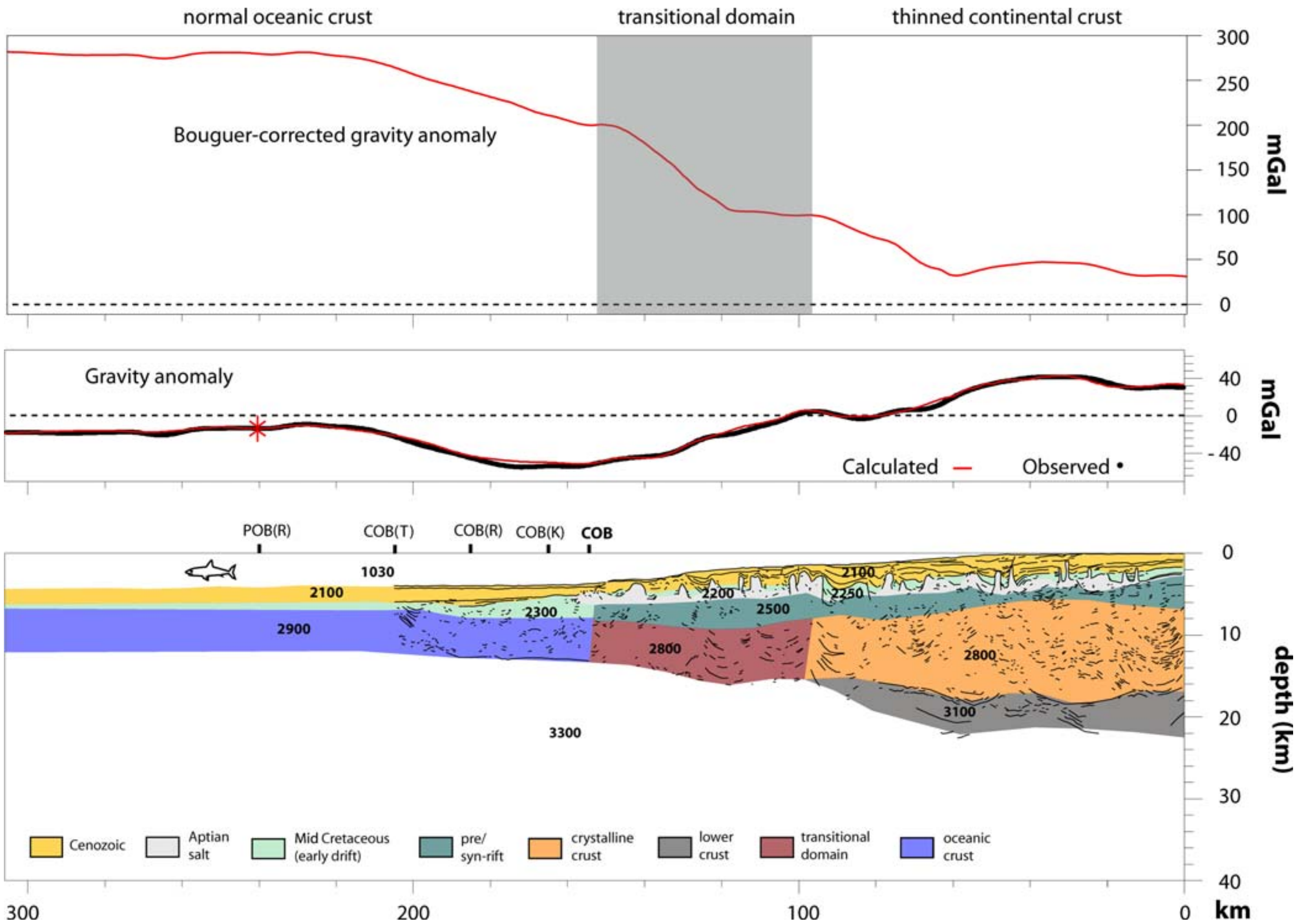

Fig. 6. Gravity modelled transect C–C′ (location in Fig. 3) utilizing the satellite radar-altimeter free-air gravity anomaly field (Sandwell & Smith 1997; version 16.1). Bouguer-corrected gravity anomaly is also shown. COB(K), continent–ocean boundary (Karner & Driscoll 1999); COB(R), continent–ocean boundary (Rosendahl *et al.* 2005); COB(T), continent–ocean boundary (Torsvik *et al.* 2009); COB, this study; POC(R), proto-oceanic crust (Rosendahl *et al.* 2005).

not consistent with current observations made on the MCS profiles, where the presence of thinned continental crust is inferred and modelled oceanwards of this boundary (e.g. along transect A–A′, Fig. 4). The COB location, as proposed earlier, seems to represent a crustal boundary; however, seismic observations and gravity modelling in the current study indicate that the crust oceanwards of the earlier proposed COB does not represent normal oceanic crust (Figs 4 & 5).

We suggest that the COB as defined by Karner & Driscoll (1999) and Blaich *et al.* (2008) is closely related to the transition from the thinned continental domain to the transitional domain. A prominent and steep fault appears to be associated with this boundary (Figs 4 & 5). The oceanwards limit of the transitional domain is, however, poorly known as the seismic reflection profiles acquired along the northeastern Brazilian margin do not extend into the normal oceanic crust domain. High-amplitude reflections within the wedge-shaped syn-rift sedimentary sequences are observed at the oceanward edge of the MCS profiles (Figs 7 & 8) and are interpreted as igneous material interbedded with sediments. The observed increased portion of volcanic features may indicate proximity to normal oceanic crust.

Along the conjugate margin off Gabon, on the other hand, a set of industrial and published deep seismic reflection profiles extends into the presumed normal oceanic crust. In this setting, the boundary between thinned continental crust and transitional domain is defined by the oceanwards edge of the anomalous lower crust, indicated by landward-dipping reflections and is characterized by shallowing of the Moho discontinuity (Fig. 6). The COB along this margin is placed approximately at the seaward limit of the salt basin, where the crust is clearly oceanic in seismic reflection character (e.g. Mohriak *et al.* 1995; Torsvik *et al.* 2009). The oceanic crust observed along the Gabon margin is highly reflective, rough and characterized by relatively flat Moho. The oceanic crust is *c.* 6 km thick and its base is imaged reasonably clear (Fig. 6). The interpreted COB along the Gabon margin is mirrored along the Camamu/Almada Basin and is defined as the 'line of fit' used for potential field plate reconstructions (Fig. 3). The 'line of fit' along the Camamu/Almada Basin is located within the portion of the transitional domain associated with increased observations of volcanic features (Figs 4 & 5).

The transitional domain along the northeastern Brazilian margin is characterized by rotated fault-blocks and wedge-shaped syn-rift sedimentary sequences (Figs 4 & 5). Below the syn-rift sediments a top basement reflector is poorly imaged; however, the transition from an area with well defined and stratified seismic reflection character to an area with more transparent character is interpreted as the top basement level. Gravity modelling of transects A–A′ and B–B′ indicates densities of 2800 kg m^{-3} for the rotated fault-blocks along the transitional domain. Somewhat higher densities (2900 kg m^{-3}) are required for the rotated fault-block located closer to the 'line of fit' along transect A–A′ (Figs 4 & 5). A high-amplitude and undulated reflector ('M-reflector') is observed and underlies the rotated fault-blocks at the transitional domain (Figs 4 & 5). These observed undulations are mainly due to a pullup effect below the tilted blocks, similar to that observed in the West Iberia margin (e.g. Reston *et al.* 2007). The performed

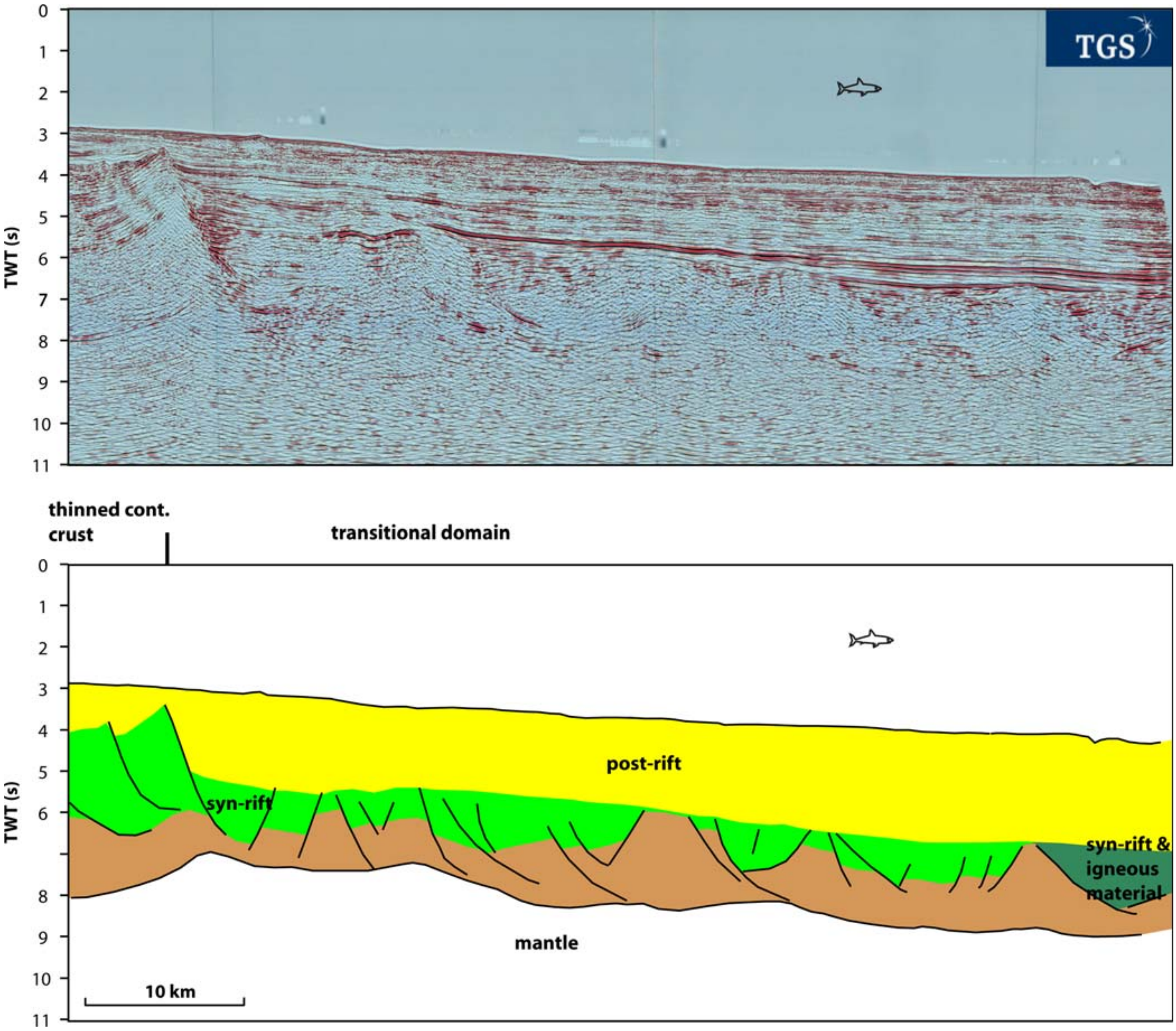

Fig. 7. Seismic example and interpretation of the transitional domain along MCS profile C-4201 (location in Fig. 2).

gravity modelling indicates that this prominent reflector probably corresponds to the Moho discontinuity that appears to be extremely shallow along transects A–A′ and B–B′ (Figs 4 & 5).

Along the Gabon conjugate margin, the evaporitic deposits considerably mask the seismic signal at the transitional domain, obscuring the potential identification of possible similar structures as in the Camamu/Almada margin, that is, rotated fault-blocks and wedge-shape syn-rift sedimentary sequences (Fig. 6). Due to the non-unique interpretation of gravity anomalies, it is difficult or even impossible to exclude such a possibility. Gravity modelling of transect C–C′ also indicates densities of 2800 kg m^{-3} for the crust at the transitional domain (Fig. 6).

Nature of the crust at the transitional domain

Our analysis indicates the existence of a transitional domain between the thinned continental crust and the oceanic crust along the northeastern Brazilian margin and its conjugate off Gabon (Figs 4–6). In most of the passive margins worldwide the nature and the precise evolution of the transitional domain from early rifting to break-up of the continental lithosphere is still unclear and subject to intense debate (Whitmarsh *et al.* 1996; Wilson *et al.* 2003; Rosendahl *et al.* 2005; Afilhado *et al.* 2008; Reston 2009). In an equivalent setting to both margins off northeastern Brazil and Gabon, the well studied magma-poor West Iberia passive continental margin also shows evidence of a transitional domain, where the crust is regarded as: (1) highly extended and intruded continental crust (Whitmarsh & Miles 1995; Whitmarsh *et al.* 1996); (2) oceanic crust derived by ultra-slow or slow seafloor spreading (Whitmarsh & Sawyer 1996; Srivastava *et al.* 2000); and (3) mantle exhumed during continental rifting by shear tectonics (Lavier & Manatschal 2006; Péron-Pinvidic *et al.* 2007; Reston *et al.* 2007; Sibuet *et al.* 2007; Reston 2009). Recent studies along this margin have indicated along-margin structural changes. While there is strong evidence of mantle exhumation along the central and northern segment of the West Iberia margin (Lavier & Manatschal 2006; Péron-Pinvidic *et al.* 2007), there is no clear evidence of an exhumation phase in the southern segment of the same margin (Afilhado *et al.* 2008).

The term ‘proto-oceanic crust’ (POC) was adopted in previous studies of the conjugate West Africa and Brazilian margins and defined as a possible anomalous crust emplaced prior to normal oceanic crust formation (Mohriak & Rosendahl 2003; Rosendahl *et al.* 2005). These studies assumed the ‘proto-oceanic crust’ to be fundamentally oceanic in nature, where POC is coupled to and subsides with the oceanic crust, exhibiting similar thermal

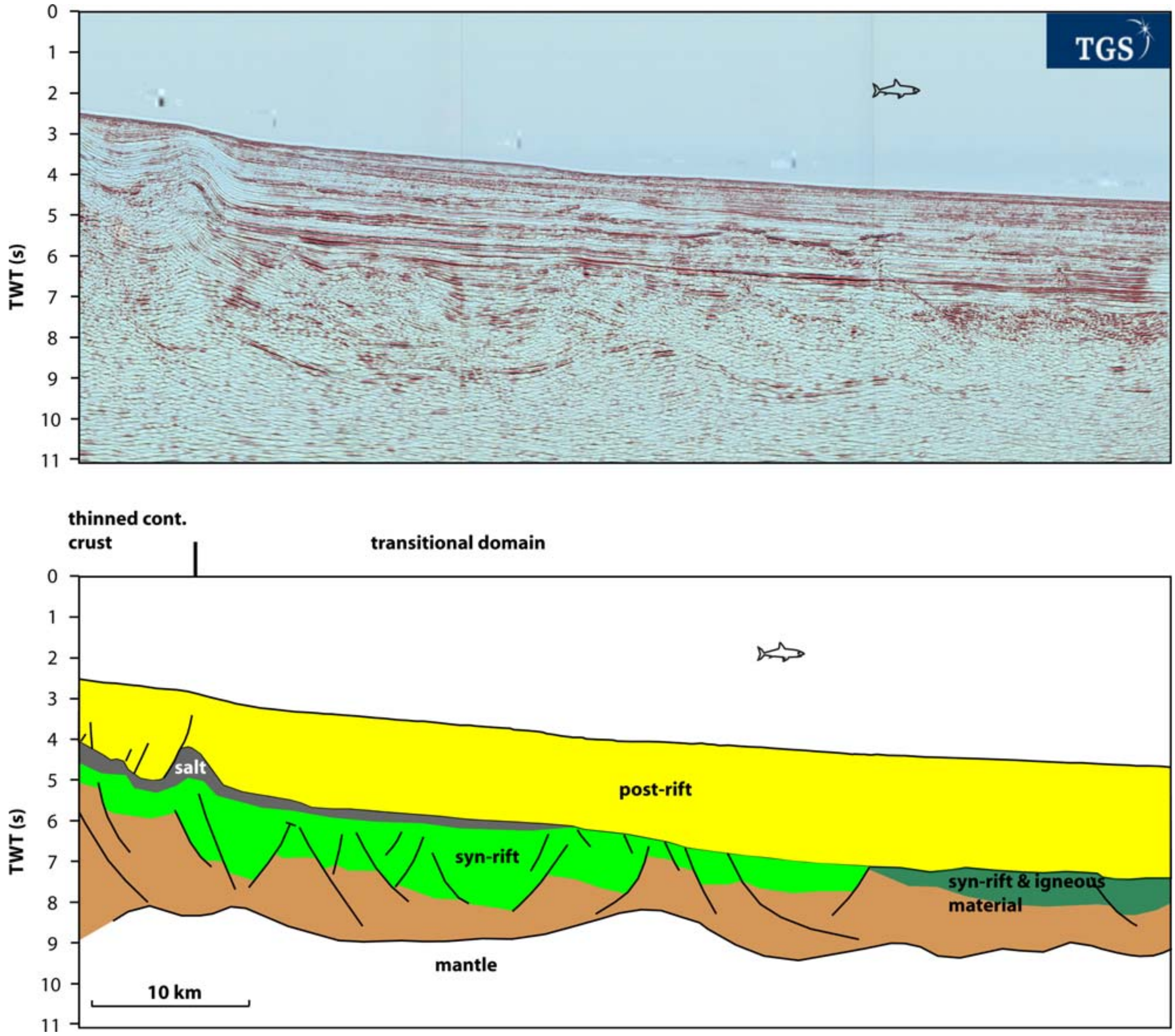

Fig. 8. Seismic example and interpretation of the transitional domain along MCS profile C-4125 (location in Fig. 2).

subsidence histories. Our analysis of seismic reflection data integrated with gravity modelling, however, casts doubt on the previous interpretation as we believe that the transitional domain observed along the conjugate northeastern Brazilian and Gabon margins is not necessarily oceanic in nature.

At several magma-dominated margins the tectonic structures at the COT zone cannot be properly resolved as they are buried beneath thick piles of lava. The deep crustal structures along the Camamu/Almada basins are not being masked by salt and/or by magmatic materials, providing a unique setting for the transitional domain to be imaged and for resolving structures related to the progressive development of a rift system through continental break-up to seafloor spreading. In this way, our analysis provides adequate means to study and refine the structural architecture and nature of the COT domain.

Exhumed mantle?

The transitional domain along the offshore northeastern Brazilian margin is characterized by rotated fault-blocks and wedge-shaped syn-rift sedimentary sequences, and occupies a zone of approximately 60 km in width. Within the transitional domain, the high-amplitude and undulated 'M-reflector' observed, at a depth of 7–9 s (TWT) shows along-margin amplitude variations. In particular, the 'M-reflector' along the Camamu Basin (Fig. 7) exhibits lower reflection coefficient than the corresponding reflector along the Almada Basin (Fig. 8). This observation has obvious implications for the composition of the crust at the transitional domain, although due to the non-unique interpretation of gravity anomalies it is not possible to account for detailed crustal heterogeneities. Along-margin variations are also observed on the gravity anomaly map (Figs 2 & 3), where a discernible gravity high characterizes the transitional domain along transect A–A′. This gravity high is related to the geometry of the Moho discontinuity and does not appear to be associated with magmatism, as earlier proposed by Davison *et al.* (1999).

The outcome of the seismic interpretation and gravity modelling of transects A–A′ and B–B′ (Figs 4 & 5) shows similarities to the results proposed in a similar study along the Rio Muni transform margin (Equatorial Guinea), West Africa, by Wilson *et al.* (2003). Similar to previous studies, however, this study also preferred the term 'proto-oceanic crust', which in this case is believed to comprise serpentinized peridotite ridges confined to discrete segments by several fracture zones. At the Rio Muni margin, serpentinized mantle was proposed to be able to move into the space generated by the oblique opening (Wilson *et al.* 2003). In contrast, the constructed transects A–A′, B–B′ and C–C′ in this study are oriented parallel to the proposed fracture zones and thus are not segmented in the same way.

In accordance with the relationship between density and serpentinized mantle fraction (Miller & Christensen 1997), the 2800 and 2900 kg m^{-3} density values required by gravity modelling for the rotated fault-blocks at the transitional domain (Figs 4–6) correspond to a serpentinization fraction of *c.* 0.64 and 0.52, respectively. With such extreme crustal thinning as observed along the study area (Figs 4 & 5), local outcrop of serpentinized peridotite ridges across the remaining thin veil of crust may not be unusual (Sibuet 1987). If this is the case, serpentinized upper lithospheric mantle has become unroofed and emplaced at the basement surface (e.g. Whitmarsh *et al.* 2001; Wilson *et al.* 2003; Lavier & Manatschal 2006; Reston & Pérez-Gussinyé 2007; Reston 2009). In this setting, the variable reflection coefficient observed on the seismic data (Figs 7 & 8) and the variable densities required for the rotated fault-blocks for transects A–A′ (Fig. 4) may be explained by diverse fractions of serpentinization and magmatic modification of the continental mantle.

Unlike the central and northern segment of the West Iberia margin, however, the present study of the Camamu/Almada Basin does not clearly reveal evidence of an exhumation phase (Figs 7 & 8). The Moho discontinuity shallows considerably at the thinned-transitional domain boundary, yet it does not cut through the crystalline crust at the transitional domain. On the contrary, the Moho discontinuity flattens out and continues beneath the rotated fault-blocks at the transitional domain (Figs 4 & 5). Finally, the rifting model for the West Iberia margin as proposed by Lavier & Manatschal (2006) predicts both an exhumation phase and a considerably large transitional domain (>100 km), as observed in the Iberia Abyssal Plain. In contrast, the transitional domain along the study area occupies only a zone of approximately 60 km in width (Figs 4 & 5).

'S-reflector' resemblance?

The high-amplitude and undulated 'M-reflector' observed at a depth of 7–9 s (TWT) along the northeastern Brazilian margin (Figs 7 & 8) shows remarkable resemblances to the prominent and undulated 'S-reflector' observed along the Galicia Bank continental margin (e.g. De Charpal *et al.* 1978; Sibuet 1987; Hoffmann & Reston 1992; Whitmarsh *et al.* 1996; Reston & Pérez-Gussinyé 2007; Reston 2009). At this margin, seismic velocities indicate that parts of the 'S-reflector' correspond to the boundary between highly thinned, fractured continental crust and the underlying zone of partially serpentinized mantle (De Charpal *et al.* 1978; Hoffmann & Reston 1992). The 'S-reflector' is therefore interpreted as the crust–mantle boundary at the time of margin formation (Boillot *et al.* 1987), characterizing a major detachment fault that was active during rifting and on which the overlying fault-blocks ride (Hoffmann & Reston 1992; Sibuet 1992; Reston *et al.* 2007). Only at its eastern end does the 'S-reflector' cut through the crust and is interpreted as a mid-crustal reflector (Whitmarsh *et al.* 1996). Similarly, the analyses performed in this study suggest that the observed undulated 'M-reflector' characterizes a major detachment surface that cuts through the crust at its western end and on which the overlying fault-blocks ride (Fig. 5).

Unlike the 'S-reflector', the 'M-reflector' described in this study does not appear to characterize a continental crust/serpentinized mantle boundary, but rather the boundary between an extremely thinned crust and normal lithospheric mantle. The undulation and discontinuity of this reflector may be distortions and imaging problems due to the passage of the seismic energy through fault-blocks characterized by a laterally varying velocity structure; equivalent observations are present in the West Iberia margin (Reston *et al.* 2007). A gravity model that accounts for serpentinized mantle beneath the 'M-reflector' is also feasible as serpentinized mantle may have a wide range of density values; however, gravity modelling alone cannot resolve this issue. Other possible explanations for the crust at the transitional domain that are applicable for the investigated conjugate margins in this study can be summarized as: slow spreading (atypic) oceanic crust (e.g. Srivastava & Keen 1995; Srivastava & Roest 1999); thinned and magmatically intruded continental crust (e.g. Whitmarsh & Miles 1995; Russell & Whitmarsh 2003); and/or exhumed lower continental crust material (e.g. Rosenbaum *et al.* 2005).

Crustal extension mode and rate

Typical rotated fault-blocks capped by sedimentary layers which parallel the sloping surfaces of the blocks are usually seen across passive continental margins that were subjected to large extension and rifting. Several studies have shown that oceanic crust formed at the early stages of break-up opening may apparently exhibit evidence of brittle deformation. In particular, excessively slow seafloor spreading (3–10 mm/year) and ridge axis propagation play an important role in thinning the oceanic crust, thereby faulting and rotating the oceanic crust (Srivastava & Keen 1995; Srivastava & Roest 1999). In the absence of identifiable magnetic anomalies, best estimates of initial half-spreading rate of *c.* 20 mm/year have been proposed for the plate separation at the northeastern Brazilian margin (Greenroyd *et al.* 2008; Müller *et al.* 2008; Torsvik *et al.* 2009), suggesting that the thin crust at the transitional domain is unlikely to be the result of ultra-slow spreading. Finally, we believe we have identified syn-rift deposits at the transitional domain along the northeastern Brazilian margin, implying that the crust there is fundamentally continental in nature (Figs 7 & 8).

Reconstructions of West Gondwana suggest that the São Francisco and Congo cratons were connected into a single continental block prior to the opening of the South Atlantic (Daziel 1997; Alkmim & Marshak 1998; Alkmim *et al.* 2006; De Wit *et al.* 2008). The Palaeoproterozoic orogeny resulted in crustal thickening within the São Francisco Craton, leading to high-grade metamorphism of the different terranes (Leite *et al.* 2008). Extension of overthickened continental crust is commonly characterized by an early core complex stage of extension, by movement along low-angle normal detachment faults, which exhume high-grade metamorphic lower crustal rocks (Lister & Davis 1989; Buck 1991; Hopper & Buck 1996; Rosenbaum *et al.* 2005). The core complex stage of extension is followed by a later stage of crustal-scale rigid block faulting (Rosenbaum *et al.* 2005). The model of core complex extension can explain the nature and character of the crust at the transitional domain, where the difference in densities for this domain required by gravity modelling for transects A–A′ may be attributed to a variable grade of metamorphism and/or a variable amount of mafic intrusives in the exhumed lower crust. In this way, the weak and intruded crust at the transitional domain may deform differently from the unintruded crust (Fig. 4). It can be definitely postulated that there is no evidence of an exhumation phase along the study area. As 'M-reflector' characterizes a major detachment surface, the eventually exhumed lower crust or exhumed mantle cannot be situated above this detachment. This implies that the rotated fault-blocks at the transitional domain cannot be composed of exhumed material. In this setting, the rotated fault-blocks observed at the transitional domain probably characterize thinned and magmatically intruded continental crust. In the initial stage of the propagating rift model (Martin 1984; Whitmarsh & Miles 1995), rifting of the continental crust leading to extension is characterized by the formation of tilted fault-blocks and half-grabens. The rising asthenosphere enables magma generated by decompression melting to begin penetrating the thinnest continental crust (transitional domain) in a diffuse manner (Whitmarsh & Miles 1995). The diffuse magmatic intrusion stage affects mainly the continent transition zone, increasing its proper densities. Consequently, the weak and magmatically intruded crust may isostatically subside relative to the unintruded crust as a consequence of the increased mean density.

Apparently, the observed seismic reflection signature and the gravity modelling results indicate that the crust at the transitional domain can be neither interpreted as normal oceanic crust, nor as exhumed lower crust/mantle. The observed 'M-reflector' is interpreted as a major detachment surface active during rifting that defines the Moho discontinuity at the transitional domain. The absence of clearly defined magnetic anomalies, as this margin was formed during the Cretaceous magnetically quite superchron, and the lack of wide-angle seismic velocity data pose an additional difficulty for the evaluation of the alternative hypotheses mentioned above. Nevertheless, the results obtained in this study favour a model in which the rotated fault-blocks located at the transitional domain are continental in nature, overlying a high-amplitude and undulated 'M-reflector'. As serpentinized mantle may have a wide range of density values, the hypothesis that the 'M-reflector' overlies a serpentinized mantle is also viable.

Total rift setting

The process of lithospheric extension that rifts and thins continental margins, resulting in symmetrical or asymmetrical lithospheric crustal structure, is much debated and focuses on the pure shear and simple shear end-member models (McKenzie 1978; Wernicke 1981; Buck *et al.* 1988). For instance, upper crust decoupling from the lower crust and mantle by strain localization into detachment zones allows the dislocation of deformation (Lavier & Manatschal 2006; Regenauer-Lieb *et al.* 2006; Weinberg *et al.* 2007). In such a setting, and when extension is slow, the lithosphere cools as it extends, thereby continuously renewing its frictional plastic layer and promoting asymmetrical behaviour and widening of the rift zone (Kusznir & Park 1987; Bassi *et al.* 1993; Huismans & Beaumont 2002).

Asymmetrical behaviour is evident on the gravity model of the conjugate pairing transect A–A′ (northeastern Brazilian margin) and transect C–C′ (Gabon margin) (Fig. 9), where a wide salt basin along the Gabon margin is conjugate to minor salt deposits along the northeastern Brazilian margin. Rifting and crustal thinning across the conjugate margins also indicate striking asymmetry. The Gabon margin is characterized by a wide area where major crustal thinning occurs, by a corresponding gradual Moho shallowing, and by relatively thin syn-rift sediments overlying the attenuated crust (Figs 9 & 10). On the other hand, the northeastern Brazilian margin is characterized by abrupt Moho shallowing and by a narrow zone of crustal thinning, where the extremely attenuated crust is overlain by relatively thick syn-rift sediments (Figs 9 & 10). This striking asymmetry is also evident on the Bouguer-corrected gravity anomaly field, where a wider area of negative–positive gradients on the Bouguer-corrected gravity anomaly map is observed along the Gabon margin, indicating a wider area of crustal thinning (Fig. 3b). The study indicates a narrow and sharp crustal tapper along the northeastern Brazilian margin that is conjugate to a wide and gentle crustal tapper along the Gabon margin.

The asymmetry observed on the conjugate northeastern Brazilian–Gabon margins may reflect an asymmetry in the process of extension (Reston & Pérez-Gussinyé 2007) and/or it may be related to the tectonic heritage of this segment (e.g. Lavier & Manatschal 2006; Aslanian *et al.* 2009). In this way, asymmetrical behaviour may be controlled by the existence of an inherited strong lower crust along the Gabon margin (Fig. 6), as well as by detachment faulting (e.g. Lavier & Manatschal 2006). Plate reconstructions indicate that the margin segment located south of the Salvador–N'Komi transfer zones has a narrow–wide conjugate margin configuration (Figs 9 & 10). In

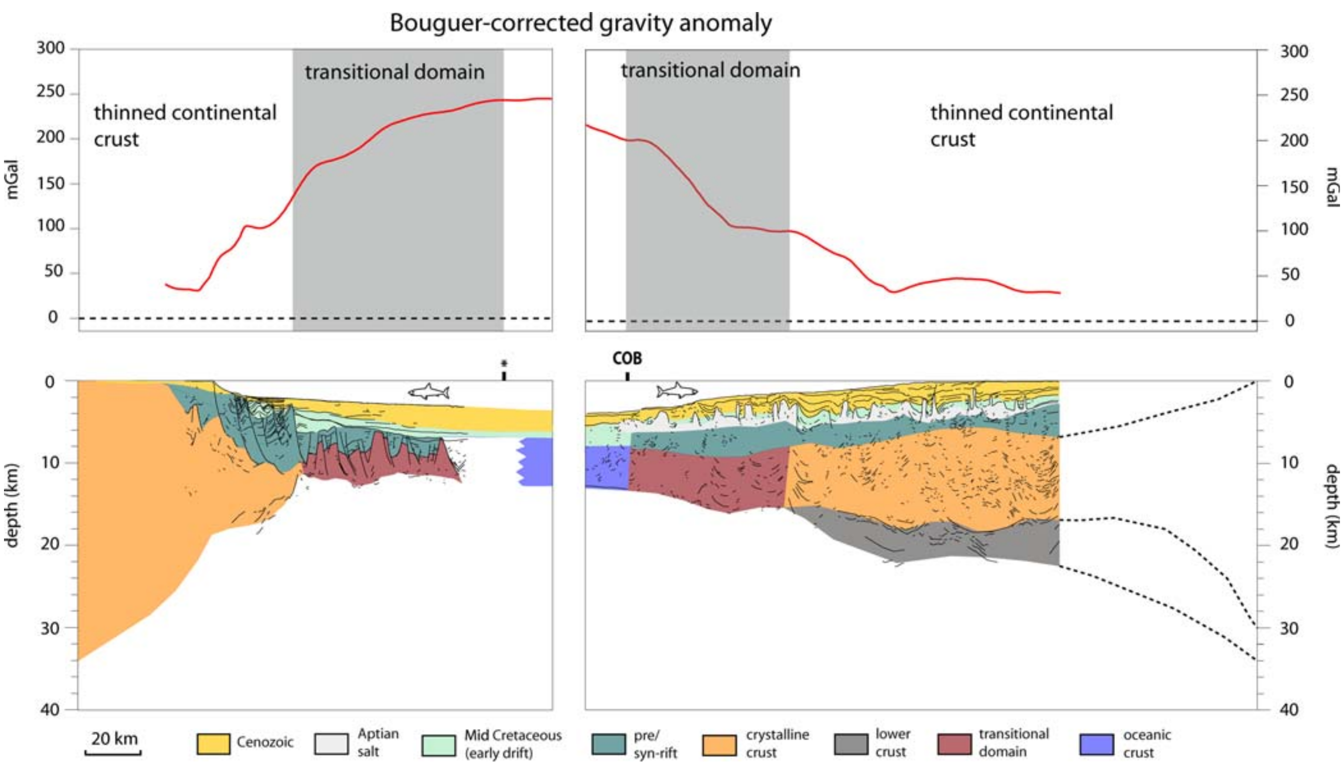

Fig. 9. (**a**) Conjugate transects A–A′ and extended transect C–C′. COB(K), continent–ocean boundary (Karner & Driscoll 1999); COB(R), continent–ocean boundary (Rosendahl *et al.* 2005); COB(T), continent–ocean boundary (Torsvik *et al.* 2009); COB, this study; the asterisk indicates 'line of fit' used for plate reconstructions; POC(R), proto-oceanic crust (Rosendahl *et al.* 2005).

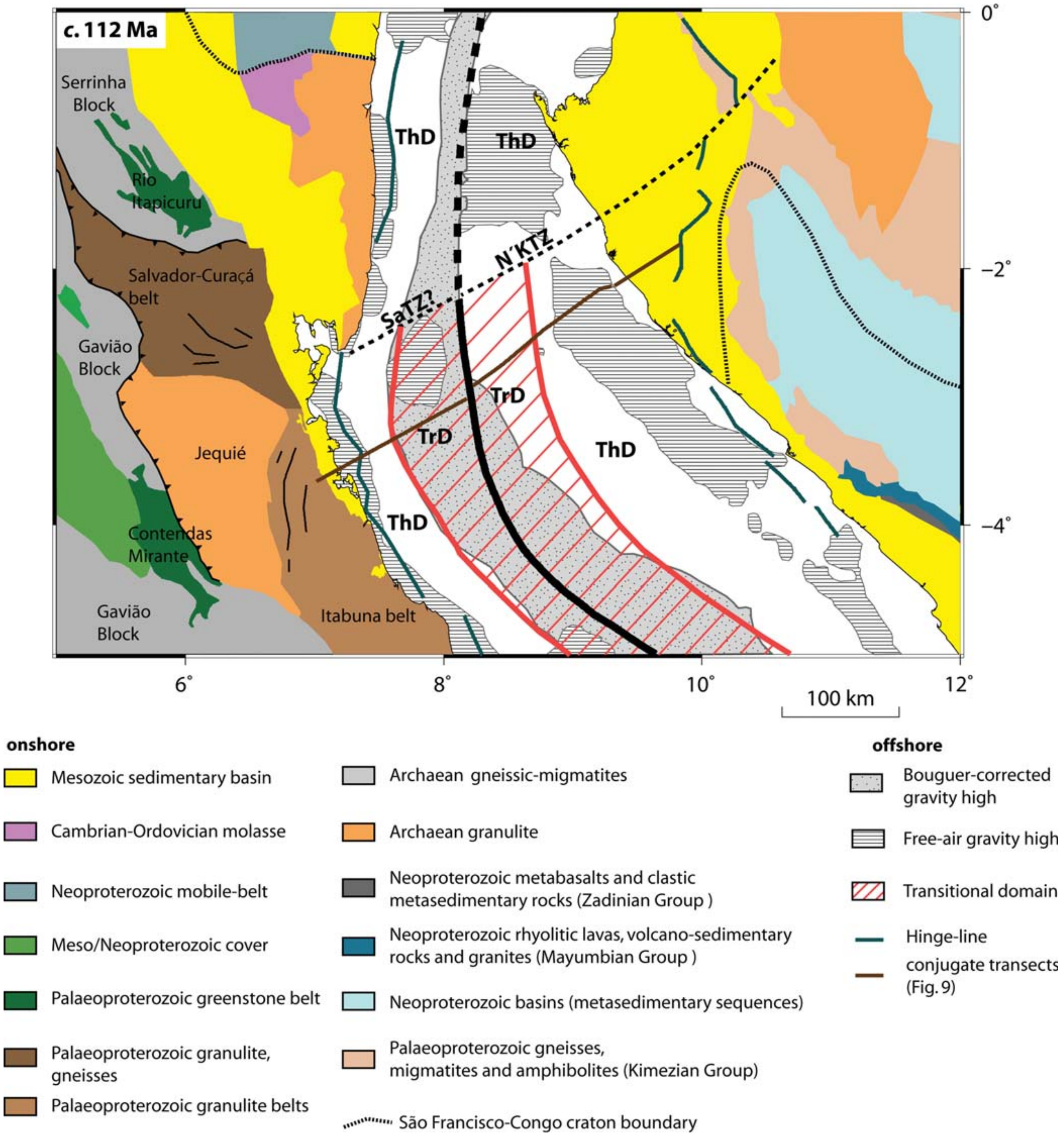

Fig. 10. Offshore: summary of prominent features observed on plate reconstructions (Fig. 3a, b); COB revised from Torsvik *et al.* (2009) and Karner & Driscoll (1999) fitting observations made in this study. Hinge-lines are derived from Karner & Driscoll (1999) for the northeastern Brazilian margin and Mounguengui & Guiraud (2009) for the Gabon margin. Onshore northeastern Brazilian margin: simplified geological and structural map generalized from Barbosa & Sabaté (2003), Destro *et al.* (2003), Alkmim *et al.* (2006) and Leite *et al.* (2009). Onshore Gabon margin: simplified geological and structural map generalized from Tack *et al.* (2001) and Alkmim *et al.* (2006). ThD, thinned crystalline crust domain; TrD, transitional domain; SaT, Salvador Transfer Zone; N'KT, N'Komi Transfer Zone.

this setting, asymmetrical lithospheric extension resulted in the formation of the thinned continental crust domain prior to the formation of the approximately symmetrical transitional domain (Fig. 10). This is further accounted for in the next section, where the analysis performed in this study suggests that the tectonic evolution of the central segment of the South Atlantic margin reflects a polyphase rifting evolution mode.

The tectono-sedimentary evolution along the central segment of the South Atlantic sedimentary basins can be summarized as indicating: (1) early Neocomian to early Barremian brittle deformation that resulted in block rotation and the deposition of characteristic syn-rift sediment wedges (early syn-rift) (Karner *et al.* 2003; Karner & Gambôa 2007); (2) early Barremian to late Aptian deposition of thick and tectonically undeformed 'sag' basins, including the evaporites, deposited under shallow water conditions (late syn-rift) (Moulin *et al.* 2005; Karner & Gambôa 2007); and (3) Albian seafloor spreading followed by significant post-rift accommodation in shallow water conditions (Karner &

Gambôa 2007). Our analysis also indicates that vertical motion prevailed in comparison to horizontal motion along the thinned continental crust domain in the northeastern Brazilian margin. In particular, the creation of syn-rift accommodation space along this domain is not characterized by horst and graben morphologies as expected for uniform extension. The observed reflections within the syn-rift basins are mostly parallel to the basement and are thus not affected by deformation that would imply significant horizontal motions (Fig. 9). On the other hand, the transitional domain suggests block rotation and the deposition of characteristic syn-rift sediment wedges (Figs 7 & 8).

The above observations are generally incompatible with uniform extension and are in better agreement with depth-dependent extension, in which stretching of the lower crust and lithospheric mantle greatly exceeds that of the upper crust (Driscoll & Karner 1998; Davis & Kusznir 2004; Karner & Gambôa 2007; Kusznir & Karner 2007). In this setting, depth-dependent thinning results in the development of relatively non-deformed upper crust (i.e. the upper plate) and a ductile-deformed lower crust and lithospheric mantle (i.e. lower plate) (Driscoll & Karner 1998).

Conjugate margin evolution

The boundary between the thinned continental crust domain and the transitional domain along the northeastern Brazilian margin coincides with a prominent Bouguer-corrected gravity high, implying abrupt crustal thinning. In contrast, the same boundary along the Gabon margin deviates gradually northwards from the prominent Bouguer-corrected gravity high (Fig. 10). This observation indicates that the Moho discontinuity along the Gabon margin shallows in a more abrupt manner in the south and progressively more gradual towards the north (Figs 9 & 10).

A similar transitional domain is also observed northwards of the prominent conjugate Salvador–N'Komi transfer zone (e.g. Rosendahl & Groschel-Becker 1999). However, the analyses performed in this study suggest that the transitional domain terminates at the conjugate Salvador–N'Komi transfer zone at break-up time (*c*. 112 Ma; Torsvik *et al.* 2009). Therefore, the conjugate Salvador–N'Komi transfer zone may have acted as an intraplate decoupling zone where a different tectono-sedimentary evolution is observed and may be associated with differential extension between the northern and the southern segments of the Gabon margin (Figs 3, 9 & 10). A similar character for the conjugate Salvador–N'Komi transfer system has also been indicated by previous studies (e.g. Teisserence & Villemin 1989; Wannesson *et al.* 1991).

The tectonomagmatic evolution of the northeastern Brazilian margin and its conjugate off Gabon is complex and may reflect a polyphase rifting evolution mode, which is associated with a complex time-dependent thermal structure of the lithosphere (e.g. Lavier & Manatschal 2006; Péron-Pinvidic *et al.* 2007; Huismans & Beaumont 2008; Aslanian *et al.* 2009). We have developed a conceptual model for the tectono-sedimentary evolution of the conjugate northeastern Brazilian–Gabon (Fig. 11). According to Lavier & Manatschal (2006), the initial extension phase is characterized by distributed listric-normal faults and symmetrical extension, resulting in block rotation and the deposition of characteristic syn-rift sedimentary wedges along the conjugate margins. The analysis performed in this study does not recognize an initial symmetrical extension phase.

The transition from a broadly distributed and symmetrical extension to asymmetrical and localized rifting is directly controlled by the existence of a strong gabbroic lower crust. In this setting, the listric-normal faulting is overprinted by localized detachment faulting (Lavier & Manatschal 2006). The thinned continental crust domain suggested in this study (Figs 9 & 10) would document the onset of the thinning phase as proposed by Lavier & Manatschal (2006), where the asymmetry between the conjugate margins is evident and probably controlled by a strong lower crust (Figs 9–11a). Since the distribution and style of subsidence

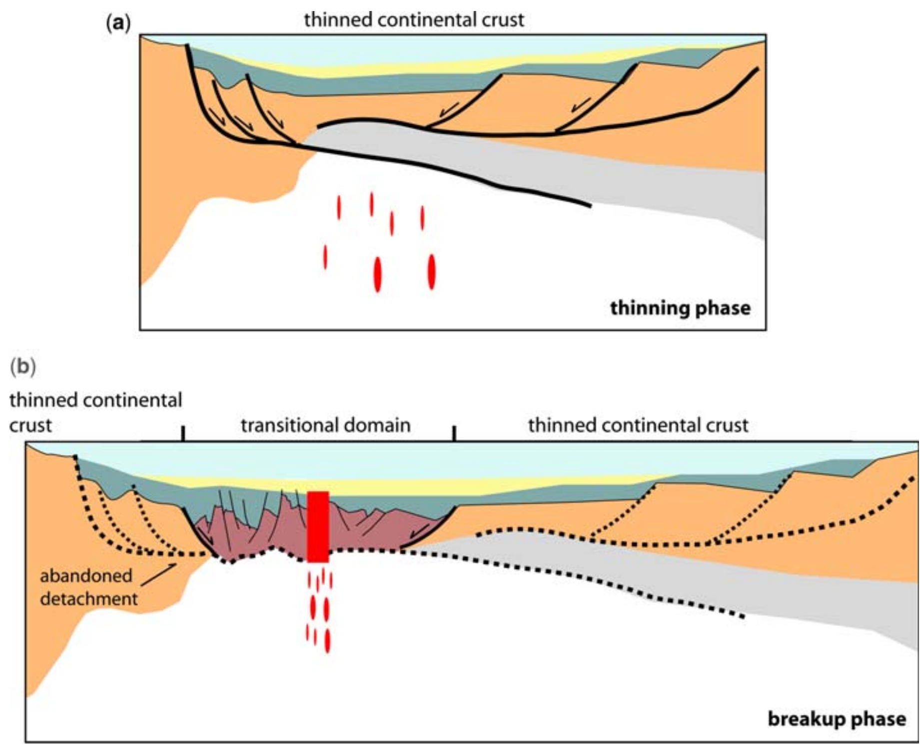

Fig. 11. Conceptual model showing the tectono-sedimentary and magmatic polyphase evolution of the conjugate northeastern Brazilian and Gabon margins. (**a**) Thinning phase, characterized by detachment faulting and depth-dependent stretching, which resulted in the deposition of thick and tectonically undeformed 'sag' basins. (**b**) Break-up phase, the increase in volcanic activity followed by the abandonment of the detachment fault may have 'interrupted' the extensional system, implying a failed exhumation phase that is replaced instead by continental break-up.

observed on both conjugate margins suggest depth-dependent stretching and upper plate subsidence patterns, detachments that separate the brittle and ductile deformation in the crust are proposed for both conjugate margins (Fig. 11a). During the thinning phase, the thick and tectonically undeformed 'sag' basin may develop under shallow water conditions (Moulin *et al.* 2005; Karner & Gambôa 2007). The subsequent exhumation phase, which predicts exhumation of middle and lower crust followed by mantle exhumation (Lavier & Manatschal 2006), is not evident along the conjugate margins off northeastern Brazil/Gabon. Even though the margins in the central segment of the South Atlantic show magma-poor affinity (Contrucci *et al.* 2004; Moulin *et al.* 2005; Sawyer *et al.* 2007), these margins also experienced magmatism during the formation of the transitional domain and break-up (Figs 7 & 8). In this setting, at the final stage of extension, magmatism increases oceanward, affecting mainly the crust at the transitional domain. The magma supply allows the release of stress by dyking, which in turn may effectively cut off the detachment fault (Ebinger & Casey 2001). The increase of volcanic activity followed by the abandoning of the detachment fault may have 'interrupted' the extensional system, implying a failed exhumation phase that is replaced instead by continental break-up.

Conclusions

An integrated analysis of regional seismic reflection profiles and potential field data across the magma-poor Camamu/Almada margin and its conjugate off Gabon, complemented by crustal-scale gravity modelling and plate reconstructions has been conducted. The analyses were used to reveal and illustrate the relationship of crustal structure to regional variation of potential field anomalies, to refine and constrain the COB, as well as to study the structural architecture and nature of the COT domain; the latter is defined as the part of the lithosphere which is located between the thinned crystalline crust domain and the first appearance of oceanic crust formed by seafloor spreading.

The study indicates the presence of along-margin tectono-sedimentary changes along the northeastern Brazilian margin and its conjugate off Gabon, and that pre-existing continental lineaments, transfer zones and various basement terranes exerted important influence and rheologic control on the structural development of the Mesozoic rifting and break-up. In particular, the prominent conjugate Salvador–N'Komi transfer zones appear to be first-order structural elements, governing the margin segmentation and evolution and may have acted as an intraplate decoupling zone.

Our analysis indicates the existence of a transitional domain between the thinned continental crust and the oceanic crust along the northeastern Brazilian margin and its conjugate off Gabon. Offshore northeastern Brazil, the transitional domain is characterized by rotated fault-blocks and wedge-shaped syn-rift sedimentary sequences overlying a high-amplitude and undulated reflector ('M-reflector') which, in turn, shows remarkable resemblances to the prominent and undulated 'S-reflector' observed along the Galicia Bank continental margin. However, unlike the 'S-reflector', the undulated reflector described in this study does not appear to characterize a continental crust/serpentinized mantle boundary, but rather the boundary between an extremely thinned, continental crust and normal lithospheric mantle. The 'M-reflector' is interpreted as a major detachment surface active during rifting that defines the Moho discontinuity at the transitional domain. Our study favours a model in which the rotated fault-blocks located at the transitional domain are continental in nature, overlying the high-amplitude and undulated 'M-reflector'. However, as serpentinized mantle may have a wide range of density values, a model that accounts for serpentinized mantle beneath the 'M-reflector' is also feasible.

Striking asymmetry is observed south of the Salvador–N'Komi transfer zones, characterized by narrow–wide thinned continental crust conjugate pair configurations. The conjugate transitional domain is approximately symmetrical. In this setting, asymmetrical lithospheric extension resulted in the formation of the thinned continental crust domain prior to the formation of the approximately symmetrical transitional domain. Vertical motion prevailed in comparison to horizontal motion along the thinned continental crust domain across the northeastern Brazilian margin reflecting depth-dependent extension. On the other hand, the transitional domain suggests block rotation and the deposition of characteristic syn-rift sedimentary wedges. A conceptual model is developed based on all our results and integrates, in a pragmatic way, several tectonic models at similar settings and regional-scale observations, providing a highly constrained polyphase model for the tectono-magmatic evolution of the conjugate Camamu/Almada–Gabon margins. This study indicates that an exhumation phase, which predicts exhumation of middle and lower crust followed by mantle exhumation, is not evident along the conjugate margins off northeastern Brazil/Gabon. The increase of volcanic activity followed by the abandoning of the detachment fault may have 'interrupted' the extensional system, implying a failed exhumation phase that is replaced instead by continental break-up. The polyphase rifting evolution mode is associated with a complex time-dependent thermal structure of the lithosphere.

We thank Statoil, TGS-NOPEC and ION for providing the MCS profiles used in this study. Eni E&P is acknowledged for providing the time and resources (to Filippos Tsikalas) to fulfil the study. We also thank the two reviewers Erik Lundin and John Argent for their constructive comments and improvements to the manuscript. The study is part of the University of Oslo Conjugate South Atlantic Margin Studies project funded by Statoil.

References

Afilhado, A., Matias, L., Shiobara, H., Hirn, A., Mendes-Victor, L. & Shimamura, H. 2008. From unthinned continent to ocean: the deep structure of the West Iberia passive continental margin at 38°N. *Tectonophysics*, **458**, 9–50.

Alkmim, F. F. & Marshak, S. 1998. Transamazonian Orogeny in the Southern São Francisco Craton Region, Minas Gerais, Brazil: evidence for Paleoproterozoic collision and collapse in the Quadrilátero Ferriféro. *Precambrian Research*, **90**, 29–58.

Alkmim, F. F., Marshak, S., Pedrosa-Soares, C., Peres, G. G., Cruz, S. C. P. & Whittington, A. 2006. Kinematic evolution of the Aracuaí–West Congo orogen in Brazil and Africa: nutcracker tectonics during the Neoproterozoic assembly of Gondwana. *Precambrian Research*, **149**, 43–64.

Aslanian, D., Moulin, M. *et al*. 2009. Brazilian and African passive margins of the Central Segment of the South Atlantic Ocean: kinematic constraints. *Tectonophysics*, **468**, 98–112.

Barbosa, J. S. F. & Sabaté, P. 2003. Colagem Paleoproterozóica de places Arqueanas do Cráton do São Francisco na Bahia. *Revista Brasileira de Geociências*, **33**, 7–14.

Bassi, G., Keen, C. E. & Potter, P. 1993. Contrasting styles of rifting; models and examples from the eastern Canadian margin. *Tectonics*, **12**, 639–655.

Blaich, O. A., Tsikalas, F. & Faleide, J. I. 2008. Northeastern Brazilian margin: regional tectonic evolution based on integrated analysis of seismic reflection and potential field data and modeling. *Tectonophysics*, **458**, 51–67.

Blaich, O. A., Faleide, J. I., Tsikalas, F., Franke, D. & León, E. 2009. Crustal-scale architecture and segmentation of the Argentine margin and its conjugate off South Africa. *Geophysical Journal International*, **178**, 85–105.

Boillot, G., Winterer, E. L. *et al.* 1987. *Proceedings of the Ocean Drilling Program, Initial Reports*, **103**. Ocean Drilling Program, College Station, TX.

Buck, W. R. 1991. Models of continental lithospheric extension. *Journal of Geophysical Research*, **96**, 20161–10178.

Buck, W. R., Martinez, F., Steckler, M. & Cochran, J. 1988. Thermal consequences of lithospheric extension: pure and simple. *Tectonics*, **7**, 213–234.

Castro, A. C. M. 1988. *Structural evolution of the Sergipe-Alagoas Basin, Brazil*. Doctorate Thesis, Rice University, TX.

Chang, H. K., Kowsmann, R. O., Figueiredo, A. M. F. & Bender, A. A. 1992. Tectonics and stratigraphy of the East Brazil Rift System; an overview. *Tectonophysics*, **213**, 97–138.

Contrucci, I., Matias, L. *et al*. 1988. Thermal consequences of lithospheric extension: pure and simple. *Tectonics*, **7**, 213–234.

Contrucci, I., Matias, L. *et al*. 2004. Deep structure of the West African continental margin (Congo, Zaire, Angola), between 5 degrees S and 8 degrees S, from reflection/refraction seismic and gravity data. *Geophysical Journal International*, **158**, 529–553.

Davis, M. & Kusznir, N. J. 2004. Depth-dependent lithospheric stretching at rifted continental margins. *In*: Karner, G. D. (ed.) *Proceedings of NSF Rifted Margins Theoretical Institute*. Columbia University Press, New York, 92–136.

Davison, I. 1999. Tectonics and hydrocarbon distribution along the Brazilian South Atlantic margin. *In*: Cameron, N. R., Bate, R. H. & Clure, V. S. (eds) *The Oil and Gas Habitats of the South Atlantic*. Geological Society, London, Special Publications, **153**, 133–151.

Davison, I. 2007. Geology and tectonics of the South Atlantic Brazilian salt basins. *In*: Ries, A. C., Butler, R. W. H. & Graham, R. H. (eds) *Deformation of the Continental Crust: The Legacy of Mike Coward*. Geological Society, London, Special Publications, **272**, 345–359.

Daziel, I. W. D. 1997. Neoproterozoic–Paleozoic geography and tectonics: review, hypothesis, environmental speculation. *Geological Society of America Bulletin*, **109**, 16–42.

Dean, S. M., Minshull, T. A., Whitmarsh, R. B. & Louden, K. E. 2000. Deep structure of the ocean–continent transition in the Southern Iberia Abyssal Plain from seismic refraction profiles. The IAM-9 transect at 40°20′N. *Journal of Geophysical Research*, **105**, 5859–5885.

De Charpal, O., Guennoc, P., Montadert, L. & Roberts, D. G. 1978. Rifting and subsidence of the northern continental margin of the Bay of Biscay. *Nature*, **275**, 706–711.

De Wit, M. J., Brito Neves, B. B., Trouw, R. A. J. & Pankhurst, R. J. 2008. Pre-Cenozoic correlations across the South Atlantic region: the ties that bind. *In*: Pankhurst, R. J., Trouw, R. A. J., Brito Neves, B. B. & De Wit, M. J. (eds) *West Gondwana: Pre-Cenozoic Correlations Across the South Atlantic Region*. Geological Society, London, Special Publications, **294**, 1–8.

Destro, N., Alkmim, F. F., Magnavita, L. P. & Szatmari, P. 2003. The Jeremoabo transpressional transfer fault, Recôncavo-Tucano Rift, NE Brazil. *Journal of Structural Geology*, **25**, 1263–1279.

Driscoll, N. W. & Karner, G. D. 1998. Lower crustal extension across the northern Carnarvon basin, Australia: evidence for an eastward dipping detachment. *Journal of Geophysical Research*, **103**, 4975–4992.

Dunbar, J. A. & Sawyer, D. S. 1988. Continental rifting at pre-existing lithospheric weaknesses. *Nature*, **242**, 565–571.

Dunbar, J. A. & Sawyer, D. S. 1989. How pre-existing weaknesses control the style of continental break-up. *Journal of Geophysical Research*, **94**, 7278–7292.

Ebinger, C. J. & Casey, M. 2001. Continental breakup in magmatic provinces: an Ethiopian example. *Geology*, **29**, 527–530.

Eldholm, O. & Grue, K. 1994. North Atlantic volcanic margins: dimensions and production rates. *Journal of Geophysical Research*, **99**, 2955–2968.

Franke, D., Neben, S., Ladage, S., Schreckenberger, B. & Hinz, K. 2007. Margin segmentation and volcano-tectonic architecture along the volcanic margin off Argentina/Uruguay, South Atlantic. *Marine Geology*, **244**, 46–67.

Gladczenko, T. P., Skogseid, J. & Eldholm, O. 1998. Namibia volcanic margin. *Marine Geophysical Researches*, **20**, 313–341.

Gomes, P. O., Gomes, B. S., Palma, J. J. C., Jinno, K. & de Souza, J. M. 2000. Ocean–continental transition and tectonic framework of the oceanic crust at the continental margin off NE Brazil: results of LEPLAC project. *In*: Mohriak, W. & Talwani, M. (eds) *Atlantic Rifts and Continental Margins*. American Geophysical Union, Washington, Geophysical Monographs **115**, 261–288.

Greenroyd, C. J., Peirce, C., Rodger, M., Watts, A. B. & Hobbs, R. W. 2008. Demerara Plateau – the structure and evolution of a transform passive margin. *Geophysical Journal International*, **172**, 549–564.

Hinz, K., Neben, S., Schreckenberger, B., Roeser, H. A., Block, M., de Souza, G. K. & Meyer, H. 1999. The Argentine continental margin north of 48°S: sedimentary successions, volcanic activity during breakup. *Marine and Petroleum Geology*, **16**, 1–25.

Hoffmann, H. J. & Reston, T. J. 1992. The nature of the S reflector beneath the Galicia Bank rifted margin: preliminary results from pre-stack depth migration. *Geology*, **20**, 1091–1094.

Hopper, J. R. & Buck, W. R. 1996. The effect of lower crustal flow on continental extension and passive margin formation. *Journal of Geophysical Research*, **101**, 20175–20194.

Huismans, R. S. & Beaumont, C. 2002. Asymmetric lithospheric extension; the role of frictional plastic strain softening inferred from numerical experiments. *Geology*, **30**, 211–214.

Huismans, R. S. & Beaumont, C. 2008. Complex rifted continental margins explained by dynamical models of depth-dependent lithospheric extension. *Geology*, **36**, 163–166.

Jackson, M. P. A., Cramez, C. & Fonck, J. M. 2000. Role of subaerial volcanic rocks and mantle plumes in creation of South Atlantic margins: implications for salt tectonics and source rocks. *Marine and Petroleum Geology*, **17**, 477–498.

Jacques, J. M. 2003. A tectonostratigraphic synthesis of the sub-Andean basins; inferences on the position of South American intraplate accommodation zones and their control on South Atlantic opening. *Journal of the Geological Society, London*, **160**, 703–717.

Karner, G. D. & Driscoll, N. W. 1999. Tectonic and stratigraphic development of the West African and eastern Brazilian margins; insights from quantitative basin modeling. *In*: Cameron, N. R., Bate, R. H. & Clure, V. S. (eds) *The Oil and Gas Habitats of the South Atlantic*. Geological Society, London, Special Publications, **153**, 11–40.

Karner, G. D. & Gambôa, L. A. P. 2007. Timing and origin of the South Atlantic pre-salt sag basins and their capping evaporites. *In*: Schreiber, B. C., Lugli, S. & Babel, M. (eds) *Evaporites Through Space and Time*. Geological Society, London, Special Publications, **285**, 15–35.

Karner, G. D., Driscoll, N. W. & Barker, D. H. N. 2003. Syn-rift regional subsidence across the West African continental margin: the role of lower plate ductile extension. *In*: Arthur, T. J., MacGregor, D. S. & Cameron, N. R. (eds) *Petroleum Geology of Africa: New Themes and Developing Technologies*. Geological Society, London, Special Publications, **207**, 105–129.

Kusznir, N. J. & Karner, G. D. 2007. Continental lithospheric thinning and breakup in response to upwelling divergent mantle flow: application to the Woodlark, Newfoundland and Iberia margins. *In*: Karner, G. D., Manatschal, G. & Pinheiro, L. M. (eds) *Imaging, Mapping and Modelling Continental Lithosphere Extension and Breakup*. Geological Society, London, Special Publications, **282**, 389–419.

Kusznir, N. J. & Park, R. G. 1987. The extensional strength of the continental lithosphere: its dependence on geothermal gradient, crustal composition and thickness. *In*: Coward, M. P., Dewey, J. F. & Hancock, P. L. (eds) *Continental Extensional Tectonics*. Geological Society, London, Special Publications, **28**, 35–42.

Lavier, L. L. & Manatschal, G. 2006. A mechanism to thin the continental lithosphere at magma-poor margins. *Nature*, **440**, 324–328.

Leite, C. De M. M., Barbosa, J. S. F., Goncalves, P., Nicollet, C. & Sabaté, P. 2009. Petrological evolution of silica-undersaturated sapphirine-bearing granulite in the Paleoproterozoic Salvador–Curacá Belt, Bahia, Brazil. *Gondwana Research*, **15**, 49–70.

Lister, G. S. & Davis, G. A. 1989. The origin of methamorphic core complexes and detachment faults formed during Tertiary continental extension in the northern Colorado River region, U.S. *Journal of Structural Geology*, **11**, 65–94.

Lister, G. S., Etheridge, M. A. & Symonds, P. A. 1986. Detachment faulting and the evolution of passive continental margins. *Geology*, **14**, 246–250.

Marks, K. M. 1996. Resolution of the Scripps/NOAA marine gravity field from satellite altimetry. *Geophysical Research Letters*, **23**, 2069–2072.

Martin, A. K. 1984. Propagating rifts: crustal extension during continental rifting. *Tectonics*, **3**, 611–617.

Matos, R. M. D. 1992. The northeast Brazilian rift system. *Tectonics*, **11**, 766–791.

Matos, R. M. D. 1999. History of the northeast Brazilian rift system; kinematic implications for the break-up between Brazil and West Africa. *In*: Cameron, N. R., Bate, R. H. & Clure, V. S. (eds) *The Oil and Gas Habitats of the South Atlantic*. Geological Society, London, Special Publications, **153**, 55–73.

Matos, R. M. D. 2000. Tectonic evolution of the Equatorial South Atlantic. *In*: Mohriak, W. & Talwani, M. (eds) *Atlantic Rifts and Continental Margins*. American Geophysical Union, Washington, Geophysical Monographs, **115**, 331–354.

McKenzie, D. P. 1978. Some remarks on the development of sedimentary basins. *Earth and Planetary Science Letters*, **40**, 25–32.

Menezes, P. E de L. & Milhomem, P da S. 2009. Tectônica de sal nas bacias de Cumuruxatiba, do Almada e de Camamu. *In*: Mohriak, W., Szatmari, P. & Couto Anjos, S. M. (eds) *Sal: Geologia e Tectônica*. São Paulo, Brasil, 232–251.

Meyers, J. B., Rosendahl, B. R., Groschel-Becker, H., Austin, J. A., Jr. & Rona, P. A. 1996*a*. Deep penetrating MCS imaging of the rift-to-drift transition, offshore Douala and North Gabon basins, West Africa. *Marine and Petroleum Geology*, **13**, 791–835.

Meyers, J. B., Rosendahl, B. R. & Austin, J. A., Jr. 1996*b*. Deep-penetrating MCS images of the South Gabon Basin: implications for rift tectonics and post-breakup salt remobilization. *Basin Research*, **8**, 65–84.

Milani, E. J. & Davison, I. 1988. Basement control and transfer tectonics in the Reconcavo-Tucano-Jatoba Rift, Northeast Brazil. *Tectonophysics*, **154**, 41–70.

Miller, D. J. & Christensen, N. I. 1997. Seismic velocities of lower and upper mantle rocks from slow-spreading Mid-Atlantic Ridge, South of the Kane Transform (MARK). *Proceedings of the Ocean Drilling Program, Scientific Results*, **153**, 437–454.

Mohriak, W. U. & Rosendahl, B. R. 2003. Transform zones in the South Atlantic rifted continental margins. *In*: Storti, F., Holdsworth, R. E. & Salvini, F. (eds) *Intraplate Strike-Slip Deformation Belts*. Geological Society, London, Special Publications, **210**, 211–228.

Mohriak, W. U., Rabelo, J. H. L., Matos, R. D. & Barros, M. C. 1995. Deep seismic reflection profiling of sedimentary basins offshore Brazil; geological objectives and preliminary results in the Sergipe Basin. *Journal of Geodynamics*, **20**, 515–539.

Mohriak, W. U., Bassetto, M. & Vieira, I. S. 1998. Crustal architecture and tectonic evolution of the Sergipe-Alagoas and Jacuípe basins, offshore northeastern Brazil. *Tectonophysics*, **288**, 199–220.

Mohriak, W. U., Bassetto, M. & Vieira, I. S. 2000. Tectonic evolution of the rift basins in the northeastern Brazilian region. *In*: Mohriak, W. & Talwani, M. (eds) *Atlantic Rifts and Continental Margins*. American Geophysical Union, Washington, Geophysical Monographs, **115**, 293–315.

Moulin, M. B., Aslanian, D. *et al*. 2005. Geological constraints on the evolution of the Angolan margin based on reflection and refraction seismic data (Zaïango Project). *Geophysical Journal International*, **162**, 793–810.

Mounguengui, M. M. & Guiraud, M. 2009. Neocomian to early Aptian syn-rift evolution of the normal to oblique-rifted North Gabon Margin (Interior and ŃKomi Basins). *Marine and Petroleum Geology*, **26**, 1000–1017.

Müller, R. D., Sdrolias, M., Gaina, C. & Roest, W. R. 2008. Age, spreading rates, and spreading asymmetry of the world's ocean crust. *Geochemistry Geophysics Geosystems*, **9**, Q04006; doi: 10.1029/2007GC001743.

Péron-Pinvidic, G., Manatschal, G., Minshull, T. A. & Sawyer, D. S. 2007. Tectonosedimentary evolution of the deep Iberia-Newfoundland margins: evidence for a complex breakup history. *Tectonics*, **26**, TC2011; doi: 10.1029/2006TC001970.

Rabinowitz, P. D. & LaBrecque, J. L. 1979. The Mesozoic South Atlantic Ocean and evolution of its continental margins. *Journal of Geophysical Research*, **84**, 5973–6002.

Regenauer-Lieb, K., Weinberg, R. F. & Rosenbaum, G. 2006. The effect of energy feedbacks on continental strength. *Nature*, **442**, 67–70.

Reston, T. J. 2009. The structure, evolution and symmetry of the magma-poor rifted margins of the North and Central Atlantic: a synthesis. *Tectonophysics*, **468**, 6–27.

Reston, T. J. & Pérez-Gussinyé, M. 2007. Lithospheric extension from rifting to continental breakup at magma-poor margins: rheology, serpentinisation and symmetry. *International Journal of Earth Sciences*, **96**, 1033–1046.

Reston, T. J., Leythaeuser, T., Booth-Rea, G., Sawyer, D., Klaeschen, D. & Long, C. 2007. Movement along a low-angle normal fault: the S reflector west of Spain. *Geochemistry Geophysics Geosystems*, **8**, Q06002; doi: 10.1029/2006GC001437.

Rosenbaum, G., Regenauer-Lieb, K. & Weinberg, R. F. 2005. Continental extension: from core complexes to rigid block faulting. *Geology*, **33**, 609–612.

Rosendahl, B. R. & Groschel-Becker, H. 1999. Deep seismic structure of the continental margin in the Gulf of Guinea: a summary report. *In*: Cameron, N. R., Bate, R. H. & Clure, V. S. (eds) *The Oil and Gas Habitats of the South Atlantic*. Geological Society, London, Special Publications, **153**, 75–83.

Rosendahl, B. R., Mohriak, W. U., Odegard, M. E., Turner, J. P. & Dickson, W. G. 2005. West Africa and Brazilian conjugate margins: crustal types, architecture, and plate configurations. *In*: Post, P. *et al*. (eds) *Petroleum Systems of Divergent Continental Margin Basins: Bob F. Perkins Research Conference*. 25th Gulf Coast Section, Society of Sedimentary Geology, Houston, TX, 4–7 December, CD-ROM.

Russell, S. M. & Whitmarsh, R. B. 2003. Magmatism at the west Iberia non-volcanic rifted continental margin: evidence from analyses of magnetic anomalies. *Geophysical Journal International*, **154**, 706–730.

Sandwell, D. T. & Smith, W. H. F. 1997. Marine gravity anomaly from Geosat and ERS 1 satellite altimetry. *Journal of Geophysical Research*, **102**, 10039–10054.

Sandwell, D. T. & Smith, W. H. F. 2009. Global marine gravity from retracked Geosat and ERS-1 altimetry: ridge segmentation versus spreading rate. *Journal of Geophysical Research*, **114**, BO1411.

Sawyer, D. S., Whitmarsh, R. B. & Shipboard Scientific Party. 1994. *Proceedings of the Ocean Drilling Program, Initial Reports*, **149**. Ocean Drilling Program, College Station, TX.

Sawyer, D. S., Coffin, M. F., Reston, T. J., Stock, J. M. & Hopper, J. R. 2007. COBBOOM: The Continental Breakup and Birth of Oceans Mission. *Scientific Drilling*, **5**, September.

Sibuet, J. C. 1987. *Contribution à l'étude des mécanismes de formation des marges continentals passives*. Doctorat d'Etat thesis. Université de Bretagne Occidentale, Brest.

Sibuet, J. C. 1992. New constraints on the formation of the nonvolcanic continental Galicia-Flemish Cap conjugate margins. *Journal of Geological Society, London*, **149**, 829–840.

Sibuet, J. C., Srivastava, S. & Manatschal, G. 2007. Exhumed mantle-forming transitional crust in the Newfoundland-Iberia rift and associated magnetic anomalies. *Journal of Geophysical Research*, **112**, B06105; doi: 10.1029/2005JB003856.

Smith, W. H. F. 1993. On the accuracy of digital bathymetric data. *Journal of Geophysical Research*, **98**, 9591–9603.

Souza-Lima, W. 2009. Seqüencias evaporíticas da bacia de Sergipe-Alagoas. *In*: Mohriak, W., Szatmari, P. & Couto Anjos, S. M. (eds) *Sal: Geologia e Tectônica*. Beca, São Paulo, 232–251.

Srivastava, S. & Keen, C. E. 1995. A deep seismic reflection profile across the extinct Mid-Labrador Sea spreading center. *Tectonics*, **14**, 372–389.

Srivastava, S. & Roest, W. R. 1999. Extent of oceanic crust in the Labrador Sea. *Marine and Petroleum Geology*, **16**, 65–84.

Srivastava, S., Sibuet, J. C., Cande, S., Roest, W. R. & Reid, I. R. 2000. Magnetic evidence for slow seafloor spreading during the formation of the Newfoundland and Iberia margins. *Earth and Planetary Science Letters*, **182**, 61–76.

Szatmari, P. & Milani, E. J. 1999. Microplate rotation in Northeast Brazil during South Atlantic rifting; analogies with the Sinai Microplate. *Geology*, **27**, 1115–1118.

Tack, L., Wingate, M. T. D., Liégeois, J. P., Fernandez-Alonso, M. & Deblond, A. 2001. Early Neoproterozoic magmatism (1000–910 Ma) of the Zadinian and Mayumbian Groups (Bas–Congo): onset of Rodinia rifting at the western edge of the Congo craton. *Precambrian Research*, **110**, 277–306.

Teisserence, P. & Villemin, J. 1989. Sedimentary basin of Gabon – geology and oil systems. *In*: Edwards, J. D. & Santogrossi, P. A. (eds) *Divergent Passive Margin Basins*. American Association of Petroleum Geologists, Memoirs, **48**, 117–199.

Torsvik, T. H., Rousse, S., Labails, C. & Smethurst, M. A. 2009. A new scheme for the opening of the South Atlantic Ocean and the dissection of an Aptian salt basin. *Geophysical Journal International*, **177**, 817–833.

Tsikalas, F., Faleide, J. I. & Kusznir, N. J. 2008. Along-strike variations in rifted margin crustal architecture and lithosphere thinning between northern Vøring and Lofoten margin segments off mid-Norway. *Tectonophysics*, **458**, 68–81.

Wannesson, J., Icart, J. C. & Ravat, J. 1991. Structure and evolution of adjoining segments of the west African margin determined from deep seismic profiling. *Geodynamics*, **22**, 275–289.

Watts, A. B. & Stewart, J. 1998. Gravity anomalies and segmentation of the continental margin offshore West Africa. *Earth and Planetary Sciences Letters*, **56**, 239–252.

Weinberg, R. F., Regenauer-Lieb, K. & Rosenbaum, G. 2007. Mantle detachments and the break-up of cold continental crust. *Geology*, **35**, 1035–1038.

Wernicke, B. 1981. Low-angle normal faults in the Basin and Range province: nappe tectonics in an extending orogen. *Nature*, **291**, 645–648.

Wernicke, B. 1985. Uniform-sense normal simple shear of the continental lithosphere. *Canadian Journal of Earth Sciences*, **22**, 331–339.

Wessel, P. & Watts, A. B. 1988. On the accuracy of marine gravity measurements. *Journal of Geophysical Research*, **93**, 393–413.

Whitmarsh, R. B. & Miles, P. R. 1995. Models of the development of the west Iberia rifted continental margin at 40°30′N deduced from surface and deep-tow magnetic anomalies. *Journal of Geophysical Research*, **100**, 3789–3806.

Whitmarsh, R. B. & Sawyer, D. S. 1996. The ocean/continent transition beneath the Iberia Abyssal Plain and continental-rifting to seafloor-spreading processes. *Proceedings of the Ocean Drilling Program, Scientific Results*, **149**. Ocean Drilling Program, College Station, TX, 713–736.

Whitmarsh, R. B., White, R. S., Horsefield, S. J., Sibuet, J. C., Recq, M. & Louvel, V. 1996. The ocean–continent boundary off the western continental margin of Iberia: crustal structure west of Galicia Bank. *Journal of Geophysical Research*, **101**, 28291–28314.

Whitmarsh, R. B., Beslier, M. O., Wallace, P. J. & Shipboard Scientific Party. 1998. *Proceedings of the Ocean Drilling Program, Initial Results*, **173**. Ocean Drilling Program, College Station, TX, 1–294.

Whitmarsh, R. B., Manatschal, G. & Minshull, T. A. 2001. Evolution of magma-poor continental margins from rifting to seafloor spreading. *Nature*, **413**, 150–154.

Wilson, P. G., Turner, J. P. & Westbrook, G. K. 2003. Structural architecture of the ocean–continent boundary at an oblique transform margin through deep-imaging seismic interpretation and gravity modelling; Equatorial Guinea, West Africa. *Tectonophysics*, **374**, 19–40.

New compilation of top basement and basement thickness for the Norwegian continental shelf reveals the segmentation of the passive margin system

J. EBBING[1,2] and O. OLESEN[1]

[1]*Geological Survey of Norway, 7491 Trondheim, Norway (e-mail: Joerg.Ebbing@ngu.no)*
[2]*Department for Petroleum Engineering and Applied Geophysics, NTNU Trondheim, 7491 Trondheim, Norway*

Abstract: We present the first complete top basement map for the passive margin system of the Norwegian continental shelf, which covers the Northern North Sea, the mid-Norwegian margin system, and the western Barents Sea. This compilation is based largely on a review and synthesis of previously published portions on detailed depth to basement and 3D modelling studies, which in turn are based on a wealth of seismic profiles, commercial and scientific drilling on the shelf and mainland Norway, petrophysical sampling and a dense coverage of gravity and aeromagnetic data. The top basement defines the base of the sedimentary strata. Sedimentary thickness is larger than 14 km on the mid-Norwegian margin and the Barents Sea, but varies strongly along the different segments of the margin. In the northeastern North Sea, the Danish–Norwegian Basin, and over the Trøndelag Platform the top basement does not exceed 8 km in depth. The top basement map highlights the transition between the different segments of the Norwegian margin, between different basement domains (e.g. Caledonian and Precambrian basement), and shows a clear correlation with the normal faults mapped on the margin and prolongated from onshore Norway into the offshore realm. The distribution of basement domains provides a new regional understanding of the evolution of the entire passive margin system. We also present an updated Moho depth compilation, which allows calculation of a thickness of crystalline basement map for the entire margin. The basement thickness map enhances differences in crustal architecture for the different margin segments and shows extremely thin crust (less than 12.5 km) for large areas on the mid-Norwegian margin and westernmost Barents Sea, intermediate thin crust (15–20 km) below the Viking Graben, but moderately thin crust (20–30 km) below the Norwegian–Danish Basin and the remaining part of the Barents Sea.

Keywords: basement, continental shelf, potential fields, onshore–offshore, Caledonian, Precambrian

The Norwegian continental shelf is of major interest for the petroleum industry. Since the first realization of the economic potential of the oil and gas prospects in the North Sea in the 1960s, a vast amount of geophysical data at all scales has been collected to enhance our understanding of the passive margin system (e.g. Blystad *et al.* 1995; Fleet & Boldy 1999; Nøttvedt 2000, and references therein). Large parts of the Norwegian shelf are covered by 2D and 3D seismic reflection surveys, which allow detailed mapping of key horizons within the sedimentary section. The base of the sedimentary strata, the top basement and the configuration of the crust below are less clearly imaged due to the large sedimentary thickness. Acquisition of OBS profiles has helped to enhance the imaging of the deep crustal configuration, as well as the top basement below the sedimentary basins, but has a less dense aerial coverage of the margin (e.g. Mjelde *et al.* 2005). The top basement is, however, of major interest for understanding the evolution of the sedimentary basins and possible migration of hydrocarbon (e.g. Doré & Vining 2005, and references therein), and in basin modelling detailed knowledge of the basin geometry is an essential input parameter (e.g. Nøttvedt 2000). Normal faults observed in seismic lines often leave their imprint in the top basement configuration, and open pathways for fluid migration, which affects potential sources and even the thermal state of the sedimentary basin. Basement structures offshore have been indirectly investigated through the combination of potential field data with seismic reflection and refraction data, as wells penetrating the top basement are only sparsely available.

In this paper, we will provide a review of the different basement studies carried out in the past and present as a synthesis of the first complete top basement map of the Norwegian continental shelf and adjacent regions. Our definition of the basement thickness regards the entire basement as a metamorphic complex. We will briefly present the individual contributions to the compilation and discuss the main structural domains as expressed in the geometry and structure of the basement. A crustal thickness map illustrates further the structure of the Norwegian margin. In the final step, we will bring our maps into the context of the evolution of the Norwegian continental shelf and its link to the onshore geology.

Geological setting

The Norwegian continental shelf is subject to the same geological processes observed onshore. Figure 1 illustrates the onshore–offshore structural links by the distribution of normal faults, which can be traced from land into the offshore basins. On land in Norway and Sweden the remnants of the Caledonides dominate the surface geology; this mountain belt formed as a result of the convergence of the North American plate with the westward subducting margin of the Baltica plate that culminated in continent–continent collision. The stacked nappes comprise allochthonous continental and oceanic crust. They were the result of thrusting and tectonic underplating of the exotic terranes from Laurentia/Iapetus (microcontinents and island arcs) and imbrications of the Palaeozoic passive margin of Baltica (e.g. Roberts 2003 and references therein). The collisional climax was followed by a general collapse of the mountain belt (e.g. Fossen 1992; Andersen 1998) and the development of Devonian basins (e.g. Osmundsen *et al.* 1998). The processes causing the mountain chain collapse and the transition in the late Devonian to Carboniferous to the purely rift-related mechanisms are still debated.

VINING, B. A. & PICKERING, S. C. (eds) *Petroleum Geology: From Mature Basins to New Frontiers – Proceedings of the 7th Petroleum Geology Conference*, 885–897. DOI: 10.1144/0070885

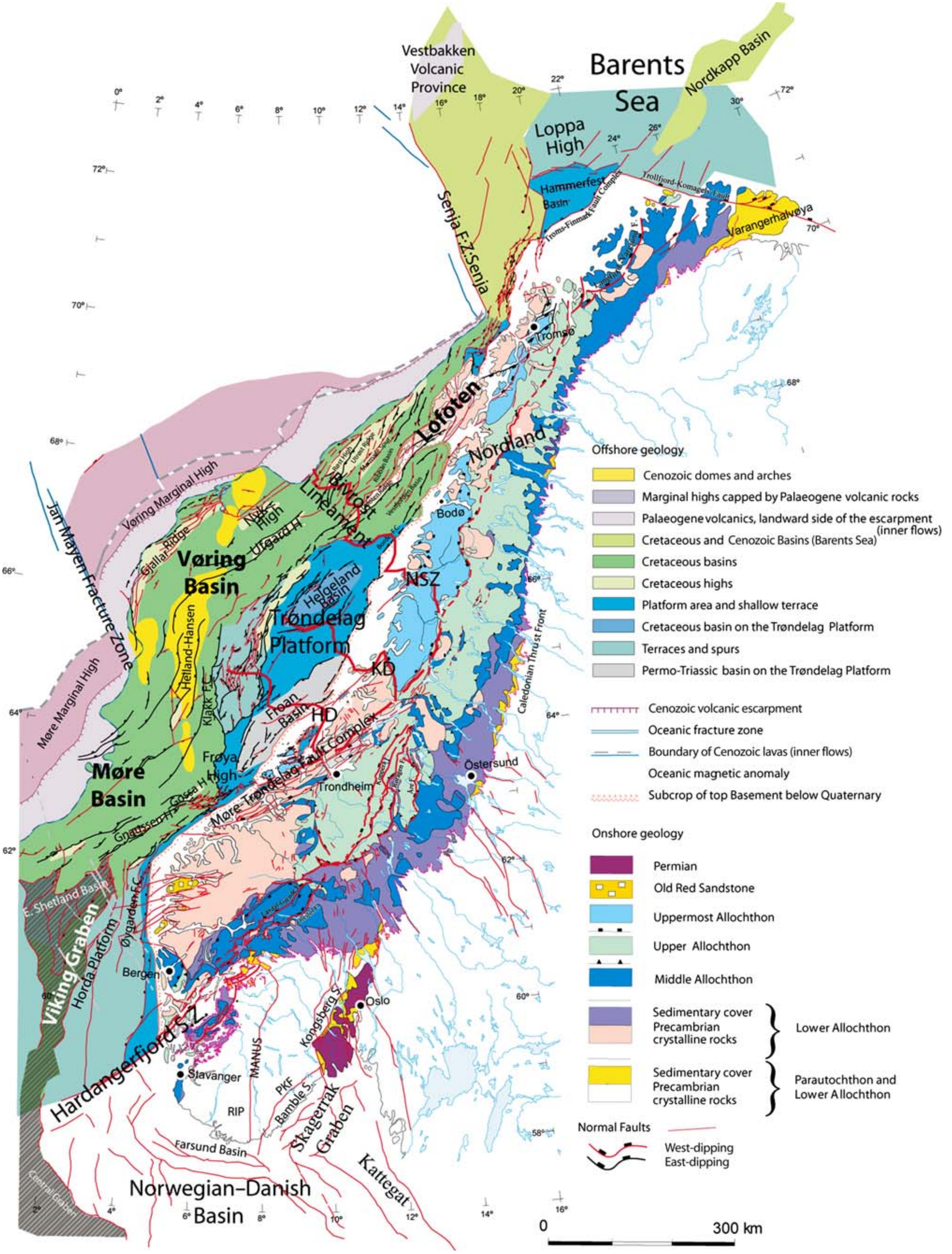

Fig. 1. Simplified onshore–offshore geological map of the Scandinavian North Atlantic passive margin (modified from Mosar 2003). In the offshore domain the different major tectono-sedimentary events are indicated (adapted and modified from Blystad *et al.* 1995; Brekke *et al.* 1999; Gabrielsen *et al.* 1999; Mosar 2000; Smethurst 2000). The dip directions of some of the major normal faults in the offshore, such as in the Nyk High, the Utgard High and the Gjallar Ridge, are shown according to interpretation of deep seismic surveys (Osmundsen *et al.* 2002). The faults have been colour-coded according to dip direction: red for west-dipping and black for east-dipping. The onshore tectonostratigraphic map is a simplified and modified version of the map by Gee *et al.* (1985). MANUS, Mandal–Ustaoset Fault; RIP, Rogaland Igneous Province; PKF, Porsgrunn–Kristiansand Fault; HD, Høybakken detachment; KD, Kollstraumen detachment; NSZ, Nesna Shear Zone.

Physiographically, the mid-Norwegian margin consists of a continental shelf and slope that vary considerably in width and steepness. The two adjacent shallow seas, the North Sea and the Barents Sea were, prior to the formation of the deep NE Atlantic ocean in early Cenozoic time, part of a much larger epicontinental sea between the continental masses of Fennoscandia, Svalbard and Greenland (Faleide *et al.* 2008).

The mid-Norwegian margin was formed by episodic extensional events during Late Palaeozoic–Triassic, Late Jurassic–Early Cretaceous and Late Cretaceous–Paleocene times (Ziegler 1988; Blystad *et al.* 1995; Doré *et al.* 1997; Brekke 2000). The Norwegian Atlantic margin is a classic passive margin that finally went from rifting to drifting in the early Cenozoic. Prior to, and during, the rift–drift transition, the margin witnessed extensive volcanic activity, which changed to normal accretionary magma volumes with subsequent continental margin subsidence and maturation from the middle Eocene to the present (Faleide *et al.* 2008).

Models for the development of the Norwegian Atlantic passive margin have in the past often focused on the sedimentary cover sequence (e.g. Doré 1992; Doré *et al.* 1997; Brekke 2000; Brekke *et al.* 2001), but in recent years the importance of the underlying basement and crustal structure on the development of the margin has been more and more recognized (e.g. Olesen *et al.* 2002; Osmundsen *et al.* 2002; Breivik *et al.* 2005).

The present structure of the passive margin reflects the cumulative effect of several consecutive rifting events that controlled basin development, and climaxed in continental breakup, the opening of the North Atlantic and formation of new oceanic crust (Mosar 2003). These rifting events were interspersed with Mesozoic uplift periods and preceded the proposed Neogene uplift that produced a significant contribution to the present-day mountain topography (e.g. Gabrielsen *et al.* 2005).

All these processes left an imprint on the structure of the basement offshore and on the topography observed onshore Norway. On the Norwegian passive margin different domains can be identified. In the north of Norway, we find the stable continental shelf of the Barents Sea, which is divided by the transform margin of the Barents Sea to the mid-Norwegian margin. On the mid-Norwegian margin three domains can be identified: (1) the Lofoten margin; (2) the Vøring Basin-Trøndelag Platform; and (3) the Møre Basin (Fig. 1). Further to the south we find the Viking and Central Graben system. The Norwegian–Danish Basin continues around the southern tip of Norway into the Skagerrak, Jutland and Kattegat.

Presentation of database

For the Norwegian continental margin and onshore Norway and Sweden a large amount of geophysical data is available. Figure 2 shows the gravity and magnetic field data and the regional seismic profiles available for the study area. Aeromagnetic and gravity data provide an important tool for mapping crustal structures both on mainland Norway and in the adjacent offshore regions.

Magnetic anomaly map

The magnetic anomaly map (Fig. 2a) is based on integration of multiple surveys at different scales and heights (Olesen *et al.* 2007, 2010). Over the last 50 years a vast number of offshore aeromagnetic surveys have been acquired with typical flight heights of 200–300 m and line spacing of 2–5 km over the continental

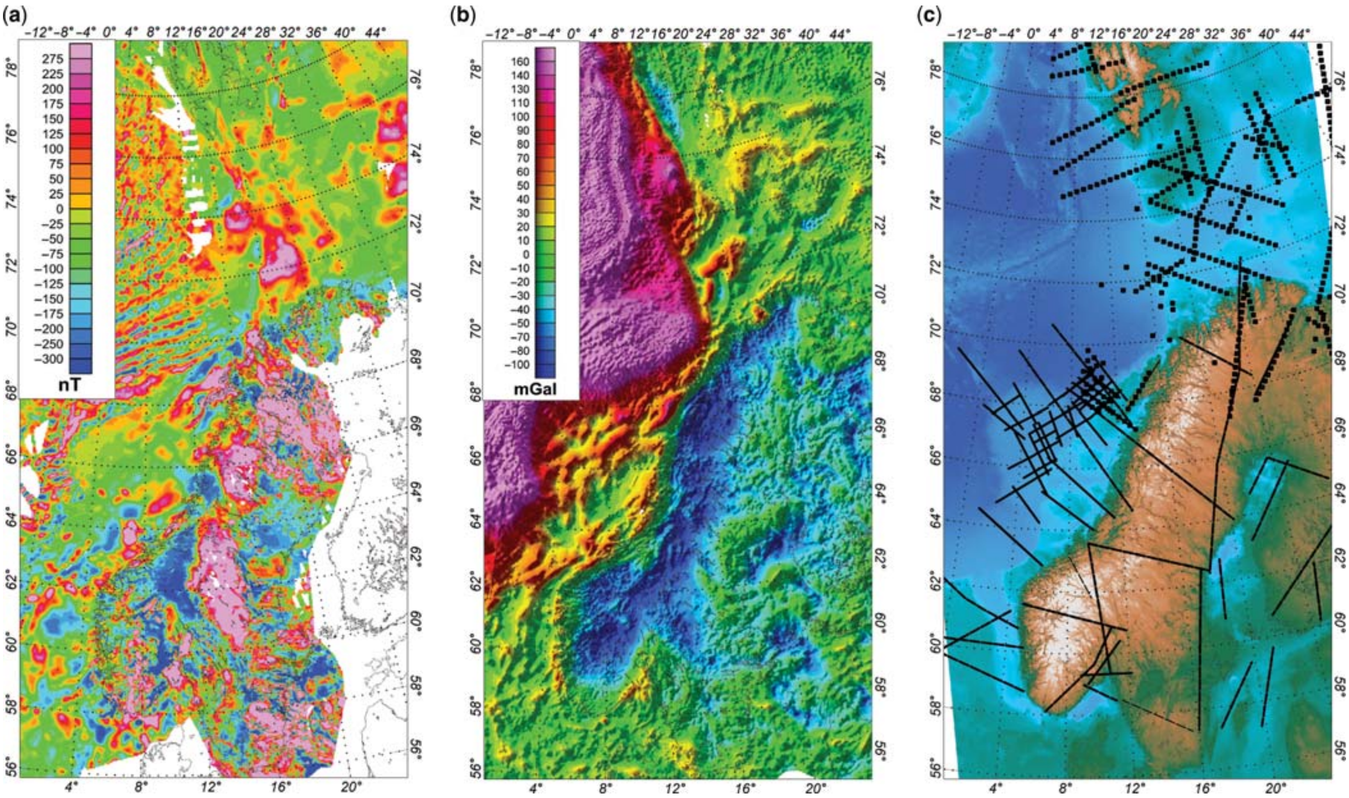

Fig. 2. Regional data for top basement studies. (**a**) Total magnetic field anomaly. The anomaly map is referred to DGRF-1965. Multiple offshore aeromagnetic surveys have been processed and merged to produce the displayed map (Olesen *et al.* 2010). (**b**) Bouguer anomaly. The map is calculated with a reduction density of 2670 kg m^{-3} onshore, and 2200 kg m^{-3} offshore (Olesen *et al.* 2010). Offshore measurements of approximately 59 000 km of marine gravity profiles have been acquired by the Norwegian Petroleum Directorate, oil companies, TGS NOPEC Geophysical Company and the Norwegian Mapping Authorities. (**c**) Regional wide-angle seismic profiles as presented in Kinck *et al.* (1993) for the onshore part, Christiansson *et al.* (2000) for the northeastern North Sea, Mjelde *et al.* (2005, 2009) for the mid-Norwegian margin, and Ritzmann *et al.* (2007) for the Barents Sea.

margin (Olesen *et al.* 2010). Outstanding features in the magnetic anomaly map are the anomalies associated with seafloor spreading, the Loppa High in the southwestern Barents Sea, the prominent high along the Lofoten islands, the Frøya High at the southern edge of the Trøndelag Platform, but also onshore structures like the magnetic high of the Oslo Graben or the north–south trending band of the Transscandinavian Igneous Belt. The anomalies are partly continuous from the Baltic Shield under the Scandinavian mountains into the continental shelf, which indicate continuous bedrock structures (e.g. Åm 1975; Olesen *et al.* 2002). The magnetic data provide important constraints on the interpretation of the regional basement configuration and distribution of volcanic rocks on the shelf (e.g. Olesen *et al.* 2002; Skilbrei *et al.* 2002).

Gravity anomaly map

The Bouguer anomaly map (Fig. 2b) is based on the integration of land measurements, ship-borne gravity surveys and satellite data (Olesen *et al.* 2010). The Bouguer anomaly is calculated with a rock density of 2670 kg m^{-3} onshore and 2200 kg m^{-3} offshore. The Bouguer anomaly map is dominated by the low along the Scandes mountain chain, and the high anomalies crossing from the continental shelf into the oceanic plate. The gravity low of the Scandes mountain belt indicates isostatic compensation, and the transition from the continental to oceanic plate reflects the crustal thinning and increase of crustal densities. On the continental shelf, anomalies are less pronounced than in the magnetic anomaly map. On the mid-Norwegian margin especially, the Trøndelag Platform stands out as a relative gravity low surrounded by higher gravity anomalies.

Regional seismic data

Seismic data are always important to constrain interpretations of potential field data. Figure 2c shows the distribution of regional seismic profiles for onshore Norway and the continental shelf. The figure does not show all available seismic lines on the shelf as many commercial 2D and 3D surveys have been and continue to be acquired. The figure features academic OBS profiles (Mjelde *et al.* 2005, 2009), the dataset available in a recent compilation for the Barents Sea (Ritzmann *et al.* 2007) and from a compilation of Moho depths for the Fennoscandian Shield (Kinck *et al.* 1993). All these published profiles have been used to image the base of the crust, and provide an indication of the offshore top basement, but with variable accuracy and resolution.

Importance of potential field data and data integration

Mapping of the top basement is based on different methods for combining the available geophysical data. The basement configuration is particularly visible in the potential fields, where it lies close to the surface, and the interpretation of potential field data helps to trace structures from the onshore to offshore realms, which can then be observed from the surface to depth. For example, the mid-Norwegian margin was studied by 3D modelling integrating a wealth of geophysical data: seismic profiles, commercial and scientific drilling on the shelf and mainland Norway, petrophysical sampling and a dense coverage of gravity and aeromagnetic data (e.g. Olesen *et al.* 2002; Skilbrei & Olesen 2005; Ebbing *et al.* 2006, 2009).

Magnetic data are extremely useful for mapping the top basement. Olesen *et al.* (1990), Skilbrei *et al.* (1991) and Mørk *et al.* (2002) show that the susceptibilities of the basement can range between 0.0005 and 0.3 SI while the susceptibilities of the overlying sediments are only in the order of 0.0003 SI, up to three orders of magnitude lower. The range of susceptibilities for the basement depends on composition and varies typically from 0.005–0.01 SI for Caledonian basement, 0.01–0.035 for Precambrian basement, to even higher values for mafic intruded basement (e.g. Barrère *et al.* 2009). Because of the large contrast between sedimentary rocks and underlying basement, magnetic depth estimates provide a good starting point for a genuine structural interpretation. Magnetic depth estimates calculated by applying, for example, Euler Deconvolution or Peter's Slope Method have been used effectively on the mid-Norwegian margin (e.g. Åm 1975; Skilbrei & Olesen 2005) and Barents Sea shelf (e.g. Skilbrei 1991, 1995), as well as in the Viking Graben and Norwegian Danish Basin (e.g. Hospers & Ediriweera 1991; Smethurst 2000; Olesen *et al.* 2004).

Skilbrei & Olesen (2005) studied the accuracy and the geological meaning of the 'magnetic basement' on the mid-Norwegian margin. They found generally good agreement between estimates made from magnetic anomalies and the depth to the Precambrian basement. In some areas non-magnetic Devonian basins may exist, and non-magnetic Caledonian nappes can overly the Precambrian basement. In the latter case, the true crystalline basement would lie above the 'magnetic basement'. Comparison of magnetic depth estimates and seismic, borehole and petrophysical data yields errors that generally vary between 5 and 15% (Skilbrei *et al.* 2002).

Gravity data are useful to a limited extent in top basement mapping as, owing to sedimentary compaction, the density contrast between sedimentary rocks and top basement becomes relatively small at depths greater than 5 km (e.g. Ramberg & Smithson 1975). The crystalline basement is also often difficult to recognize on seismic sections (e.g. Hospers & Ediriweera 1991). This is largely a result of a decrease in the contrast in acoustic impedance between sedimentary rocks and basement at greater depths. Another well known problem in the areas affected by volcanic activity is sub-basalt imaging, which makes an estimate of the top basement from seismic data very difficult (e.g. Reynisson *et al.* 2009; Reynisson 2010).

Using 3D modelling decreases the uncertainty as seismic, borehole and petrophysical data can be used directly to constrain the top basement structures, and to distinguish between different basement units. For the 3D modelling we used in most instances the Interactive Gravity and Magnetic Application System (IGMAS), which calculates the potential field effect of the model by triangulating between parallel, vertical planes (Götze & Lahmeyer 1988). The vertical planes defining the 3D geometry have typically a distance of 10–15 km depending on the geological structures and available constraining data (Ebbing *et al.* 2006, 2009; Reynisson 2010).

In the integration of datasets from the different parts of the margin we put emphasis on the consistency between the models, which was assured by careful integration of the different datasets. For example, the model of the mid-Norwegian margin after Ebbing *et al.* (2006, 2009) is an extension of the 3D model on the Nordland–Lofoten margin by Olesen *et al.* (2002) and therefore a continuous transition between the two areas on the margin is provided.

The individual 3D models also provide information about the base of the crust, which allows the calculation of total basement thickness maps, and linking of basement geometry with the overall crustal configuration. This minimizes the trade-off between sources at different crustal levels on the observed anomalies, and the effect of 3D geometries, which can heavily distort 2D models. In the areas where 3D models are absent, we use regional Moho compilations for the crustal thickness estimates.

In the following we will present the top basement compilation by giving an overview of the individual regional contributions to the top basement map of the Norwegian continental shelf and adjacent regions. Afterwards we will present the Moho depth for the same area and a basement thickness map.

Individual contributions to the basement depth map

The top basement map of the Norwegian shelf was compiled by integrating individual regional studies, shown in Figure 3 and summarized in Table 1. For the onshore part, our compilation basically corresponds to the topography. The Caledonian basement dominates the surface (Fig. 1) and is divided by thrusts, normal faults and detachments. Almost no sedimentary cover is observed. For some areas the thickness of these nappe units has been mapped, as well as the base of the Precambrian units in northern Norway (Olesen *et al.* 1990, 2002). Here we concentrate, however, on the depth to the top of the crystalline basement.

The character of the top basement surface is clearly related to different segments of the margin. For example, between the Møre margin and northeastern North Sea the grain of the top basement topography changes from SW–NE on the Møre margin to a north–south orientation, paralleling the coastline of Norway. At the same time the maximum depth of the top basement is typically less than 8 km south of the Møre margin, while on the mid-Norwegian margin the top basement is typically located at a depth of less than 10 km. Other prominent changes occur between the Vøring and Lofoten margins and in the North Sea at the offshore extension of the Hardangerfjord Shear Zone.

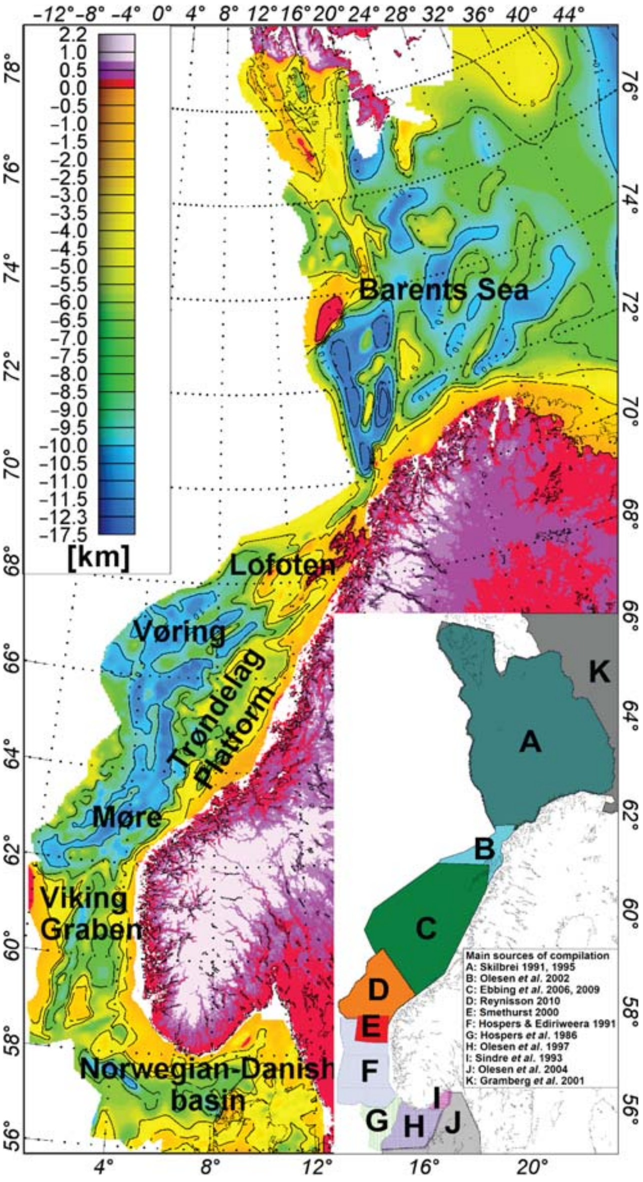

Fig. 3. Top basement map of the Norwegian continental shelf and surrounding areas. The inset map shows the distribution of the individual regional contributions. See Table 1 and text description of methodology and accuracy. Onshore top basement is represented by the topography after Dehls *et al.* (2000).

Barents Sea

The northernmost part of the compilation is the area of the Barents Sea. For the western Barents Sea, top basement maps have been presented by Johansen *et al.* (1992) and Skilbrei (1991, 1995). Johansen *et al.* (1992) used magnetic depth estimates integrated with seismic profiles and integrated further data from the eastern Barents Sea. The compilation by Skilbrei (1991, 1995) is more enhanced as new methods for the magnetic depth estimates have been used systematically (Skilbrei 1995). He integrated seismic profiles and well data to verify his top basement estimates. The resulting map was defined by hand contouring between the magnetic depth estimates.

The western limit of the top basement map is defined by the transition to North Atlantic oceanic crust, as indicated by the Senja Fracture Zone and Vestbakken Volcanic Province. The top basement depth reflects the deep Cenozoic basins of the Western Barents Sea with up to 14 km thickness (e.g. Nordkapp Basin). In the Loppa High, the basement rises to depths of less than 3 km and is associated with a Bouguer anomaly high. A magnetic high extends eastwards from this basement feature; this is due in part to the basement geometry, but also reflects compositional changes between different basement units. Barrère *et al.* (2009) showed in a recent study the influence of the different basement domains on magnetic anomalies, and provided a tentative map of their distribution. The basement is very inhomogeneous in the Barents Sea, reflecting rocks of both Caledonian and Precambrian age, as well as of younger volcanic affinity.

We also provide a top basement for the transition zone towards the eastern Barents Sea. The transition zone is associated with a basement depth of around 6–8 km before the top basement deepens rapidly below the Eastern Barents megabasins, where the top basement exceeds a depth of 20 km, just outside the map area. The data for the eastern Barents Sea are based on a study of Gramberg *et al.* (2001). According to these authors the interpretation is based on a few thousand kilometres of reflection and refraction lines, together with aeromagnetic surveys and gravity data. Even if the study by Gramberg *et al.* (2001) relies on an extended database, an unambiguous evaluation of the accuracy of their interpretation is not possible, as detailed description of the methodology is not available.

Mid-Norwegian margin

The top basement and the basement structure of the mid-Norwegian margin have been extensively studied. The first complete maps were constructed by combining regional seismic profiles and aeromagnetic depth estimates as well as onshore petrophysical studies (e.g. Olesen *et al.* 2002; Skilbrei *et al.* 2002; Skilbrei & Olesen 2005). These studies also addressed the basement type, as shown by petrophysical studies of rocks exposed in onshore areas that flank the margin. Two types of basement can be distinguished: a highly magnetic part corresponding to granulite facies Precambrian gneisses and igneous rocks and a less magnetic part corresponding to Caledonian nappes and amphibolite facies Precambrian basement (Olesen *et al.* 1991; Skilbrei *et al.* 1991).

Lofoten margin. On the Lofoten margin, the data used are from Olesen *et al.* (2002) with modifications in the transition to the Vøring margin by Ebbing *et al.* (2006). The offshore top basement estimates have been compiled from studies based on magnetic

Table 1. Overview of individual contributions to the top basement compilation

	Area	Source	Compilation type
A	Western Barents Sea	Skilbrei (1991, 1995)	Magnetic depth
B	Nordland, Lofoten margin	Olesen *et al.* (2002)	3D model
C	Vøring–Lofoten	Ebbing *et al.* (2006, 2009)	3D model
D	Møre	Reynisson (2010)	3D model
E	Northern Viking Graben	Smethurst (2000)	Magnetic depth
F	Northern North Sea	Hospers & Ediriweera (1991)	Magnetic depth
G	Central-eastern North Sea	Hospers *et al.* (1986)	Magnetic depth
H	Norwegian–Danish Basin	Olesen *et al.* (1997)	Magnetic depth, 2D modelling
I	Skagerrak	Sindre *et al.* (1993)	Magnetic depth
J	Jutland/Kattegat	Olesen *et al.* (2004)	Magnetic depth
K	Barents Sea	Gramberg *et al.* (2001)	Magnetic depth

depth estimates, and validated by forward modelling using seismic information on the sedimentary succession and petrophysical data (Olesen *et al.* 2002). Also, the thickness of the mainland Caledonian nappes has been included in the model. The top basement on this narrow portion of the margin does not exceed 10 km in depth and locally reaches the surface, for example at the Lofoten Ridge, where the Precambrian basement crops out. The Bivrost Lineament which represents the offshore extension of the Devonian Nesna Shear Zone constitutes the border with the Vøring margin to the south.

Vøring margin. Top basement on the Vøring margin has been mapped by Skilbrei & Olesen (2005), and integrated and updated with a complete model of the crust by Ebbing *et al.* (2006). The latter was well constrained on this margin, but did not address the magnetic field variations. Most recently Osmundsen & Ebbing (2008) and Ebbing *et al.* (2009) presented an updated model of the basement, where they differentiate the distribution of different basement types on the margin. Basically, a less magnetic 'Caledonian' basement overlies the highly-magnetic 'Precambrian' part.

The resulting top basement model is based on a wealth of seismic, borehole and petrophysical information (Ebbing *et al.* 2006, 2009), and the top basement coincides over the major part of the margin with the top Caledonian basement. In general, as for the entire mid-Norwegian margin, the top basement deepens from the coastal area towards the continental edge. Below the Trøndelag Platform the top basement is located at depths between 3 and 10 km, while in the Vøring Basin, top basement is generally encountered between 11 and 15 km. The top basement shows a variety of local features, for example basement highs at the Nyk and Utgard highs.

The Precambrian basement below the Caledonian cover is generally located at depths of more than 12 km, but it forms extended structural highs below the Trøndelag Platform where Precambrian rocks lie at depths of less than 3 km and the Caledonian basement is absent (Ebbing *et al.* 2009). These highs are aligned and can appear to be a continuous high from the Frøya High along the western border of the Froan Basin. However the Frøya High is very broad and is terminated in the north by the offshore prolongation of the late-Caledonian Høybakken detachment (Osmundsen & Ebbing 2008). Below the Vøring Basin the boundary between the low- and high-magnetic basement is almost horizontal and located 2–4 km below the top basement (Ebbing *et al.* 2009). This geometry explains the transition from pronounced magnetic anomalies on the mid-Norwegian margin to low-amplitude magnetic anomalies over the Vøring Basin.

Below the Helgeland Basin, the top basement in our compilation is at a depth of 3–8 km. Ebbing *et al.* (2009) suggest a deeper top basement below the Helgeland Basin with depths up to 12 km. The latter interpretation, which was based on industrial seismic data, however, differentiated between the non-magnetic Devonian and the underlying Caledonian basement. A significant portion of the basement below the Helgeland Basin is non-magnetic, most likely caused by downfaulting of the Helgeland Nappe Complex along the offshore extensions of the Devonian Nesna shear zone and the Kollstraumen detachment (Olesen *et al.* 2002). The presence of Devonian sandstones is an alternative interpretation (Olesen *et al.* 2002). The main large-scale structural changes in this map, compared with pre-existing maps, occur in the southern Vøring area, where the structural grain of the top basement bends from around the Trøndelag Platform and continues into the Møre margin. The strike direction on the southern Vøring area is north–south, which differs from the NE–SW direction dominant on the Lofoten, central Vøring and Møre margins to the south. Although, the crustal structure indicates no compositional variation along the transition between the Møre and Vøring margin, the extension of the Jan Mayen Fracture Zone on the margin appears to have controlled the changes in strike direction (e.g. Ebbing *et al.* 2006).

Møre margin. The top basement has been mapped on the Møre margin by Skilbrei *et al.* (2002), and was updated first by Osmundsen & Ebbing (2008), and more recently by Reynisson (2010). The model by Reynisson *et al.* (2010) is based on a 3D gravity and magnetic model incorporating industrial seismic horizons for the sedimentary succession, regional seismic profiles and magnetic depth estimates. Scheck-Wenderoth *et al.* (2007) presented a similar top basement map for the Møre margin as part of a 3D model, but the crustal model did not address the magnetic anomalies over the Møre margin, which are quite prominent, for example the magnetic high along the Gossa and Gnaussen highs, which is related to some extent to the crustal geometry and in some part to the compositional variation between different basement units (Reynisson 2010).

Below the central Møre Basin, the top basement is at a depth of more than 12 km and links up to the strike of the deep basins on the Vøring margin. Clearly, the basin geometry continues from the Vøring into the Møre Basin. Towards the ocean–continent transition the top basement depth increases to more than 8 km, while on the Vøring margin the top basement is located at a depth of greater than 10 km close to the continent–ocean transition. The outer margin is highly volcanic and large volumes of sills impede imaging the sedimentary successions (e.g. Planke *et al.* 2005). Only the combined interpretation of gravity and magnetic data allows a reasonable estimate of the sub-basalt sedimentary thickness for the outer part of the margin (Reynisson *et al.* 2009).

Towards the land the Møre margin is limited against the Møre–Trøndelag Fault Complex, which extends over a distance of more than 300 km from its inferred northeastwards termination in central mid-Norway to its poorly mapped offshore extension in the Norwegian Sea. Here, the Møre–Trøndelag Fault Complex separates the deep, northern Cretaceous Møre and Vøring basins from the shallower Jurassic–Cretaceous–Cenozoic basin systems to the south in the northern North Sea (Gabrielsen *et al.* 1999).

Northeastern North Sea, Skagerrak and Kattegat

Many attempts have been made to constrain the depth to top crystalline basement in the northern North Sea, but comparatively few maps have been published. Åm (1973) reported a first interpretation based on both magnetic and gravity data. Hospers & Ediriweera (1991) published a refined depth to basement map, which significantly differed from Åm's (1973) earlier work, presumably due to the greater availability of geological information. The depth to crystalline basement of the southernmost part of the maps has been compiled from six different sources: (1) Smethurst (2000), (2) Hospers & Ediriweera (1991), (3) Hospers *et al.* (1986), (4) Olesen *et al.* (1997), (5) Sindre (1993), and (6) Olesen *et al.* (2004).

Viking Graben. Our compilation for this area is based on Hospers & Ediriweera (1991) and Smethurst (2000). The Viking Graben and the Norwegian–Danish Basin constitute the main structural elements within the study area of the 'North Sea Rift Zone'. The basement depth ranges from 1–6 km on platforms and structural highs, to 7–9 km on terraces and basins and more than 10 km below the grabens. Conventionally, the Viking and Sogn Graben are regarded as first-order features, but our basement map indicates that the dominant structural feature is a north–south trending zone, approximately 150 km wide, containing a variety of structures (graben, basins and structural highs), some of which are oblique to the zone boundaries. To the west this zone is limited by the eastern boundary faults of the East Shetland Platform. To the east the zone is limited by the Øygarden Fault Zone. The Horda Platform is not a major shallow basement platform, like the Trøndelag Platform.

The study by Hospers & Ediriweera (1991) covers the entire Viking Graben and Horda Platform. The top basement estimates are based on aeromagnetic and marine magnetic data (Hospers & Ediriweera 1988), conventional seismic reflection profiles and exploration wells. Magnetic depth estimates at the flank of the anomalies were used to construct the initial top basement map. Gravity data did not contribute independent, non-redundant information on the depth and configuration of the crystalline basement, but helped to link the overall crustal structure to the sedimentary succession. The crystalline basement is often also difficult to recognize on seismic data (cf. Hospers & Ediriweera 1991). In such instances, basement depths have been extrapolated from or interpolated between basin flanks, using whatever seismic reflection evidence is available. On the flanks of the basins, where the basement lies at relatively shallow depths, the basement reflection is usually strong and can be identified by the use of well data, by seismic correlations along or between seismic sections, or by means of the earlier map based on magnetic and well data (Hospers & Ediriweera 1991).

For the northeasternmost part of the North Sea, following the acquisition of a new aeromagnetic dataset, Smethurst (1994) produced a depth to basement map based solely on the new magnetic data. The uncertainty of this map was quite high, and the map was later refined by the integration of gravity and magnetic data (Smethurst 2000). The compilation by Smethurst (2000) is based on clusters of consistent magnetic and gravity depth estimates, which were identified on the flanks of anomalies. These were then contoured by hand with a 1 km depth interval and interpolated onto a regular grid using the minimum curvature method. Incorporation of wide-angle lines (Fig. 2c; Christiansson *et al.* 2000) further constrained the top basement interpretation. The uncertainty of this top basement depth is estimated to be relatively high away from the seismic profiles.

Norwegian–Danish Basin. Further to the south the compilation is based on the interpretations by Hospers *et al.* (1986), Sindre (1993) and Olesen *et al.* (1997, 2004). They used magnetic depth estimates for an initial top basement interpretation. Two-dimensional gravity and magnetic modelling along regional seismic profiles constrained the compilation further. The top Zechstein faults interpretation of Vejbæk & Britze (1994) and exploration wells further constrain the map. Five of the wells penetrate the Precambrian basement and the other well data represent minimum depths to crystalline basement (Olesen *et al.* 2004). The top basement estimates would be more precise if derived from a complete 3D model based on the available seismic and borehole data, and potential field anomalies, and addressing the complete crustal structure. Yegorova *et al.* (2007) present a comprehensive study for the Danish–German basin and the Norwegian–Danish basin. They present a top Zechstein map, which can be used in the future to extend the model towards the south. However, they do not provide a new top basement map and do not address the magnetic anomalies of the area (Yegorova *et al.* 2007).

In our compilation the top basement below the Norwegian–Danish Basin constitutes a saucer-shaped surface with no major faulting along the basin margins. The maximum depth is more than 10 km and the shallower estimates are in general consistent with what is known from exploration drilling (Hospers *et al.* 1986; Olesen *et al.* 2004). Most of the regional aeromagnetic anomalies in the Norwegian–Danish Basin are continuous with aeromagnetic anomalies on mainland Norway and Sweden, suggesting that the offshore anomalies to a large extent are caused by the Sveconorwegian intra-basement rocks observed at the surface on land. Lyngsie *et al.* (2005) show that these anomalies in southwestern Norway coincide with the onshore Rogaland Igneous Province (RIP), Mandal–Ustaoset Fault Zone (MAGNUS) and Porsgrunn–Kristiansand Shear Zone (PKSZ), and extend for at least 200 km into the Norwegian–Danish Basin and across the Cretaceous–Cenozoic Sorgenfrei–Tornquist zone. Here, the continental scale fault zones dominate the magnetic and gravity pattern in the northern part of the Norwegian–Danish Basin.

The geometry of the top basement in the Skagerrak is influenced by the processes forming the Oslo Graben (Lyngsie *et al.* 2005), which is bound by dense Sveconorwegian complexes (Bamble and Kongsberg) to the west (Ebbing *et al.* 2007). An extension of the high-grade gneisses within the Bamble Complex also produces magnetic anomalies in the northern Skagerrak (Sindre 1993). The Kattegat–Skagerrak Platform is generally characterized by a shallow gently dipping crystalline basement surface, which is covered by an eastward thinning Meso-Cenozoic sedimentary sequence, unconformably underlain by downfaulted Palaeozoic sediments (Lassen & Thybo 2004).

Some uncertainties are also present with respect to the Moho depth in this area. The Moho depth (see below) is shallowest below the central part of the Norwegian–Danish Basin (29 km) and the Skagerrak Graben (26–28 km), and successively deepens towards the Farsund Basin and the mainland of Norway to the north (31–32 km) and towards the south (32 km). The positive gravity effect from the shallow Moho below the Norwegian–Danish Basin is, however, not sufficient to compensate for the low-gravity effect from the low-density sediments within the basin. Olesen *et al.* (2004) added a body of mafic rocks immediately above the Moho. The thickness varied between 3 and 9 km and the width between 80 and 100 km. A similar deep-seated dense mafic rock unit and shallow Moho are included in the gravity model of the Skagerrak Graben by Ramberg & Smithson (1975). A similar coinciding shallow Moho and dense mafic body in the upper part of the deep crust were also applied to model the Silkeborg gravity high in Denmark by Thybo & Schönharting (1991). However, a complete 3D model incorporating the available seismic and borehole data, in addition to the potential field anomalies, would significantly enhance the accuracy of both the top basement estimates and the base of the crust.

Moho depth and basement thickness maps

The top basement map is often associated with the top of the crystalline crust. To understand the evolution of the passive margin systems, it is of interest also to look at the base of the crust as defined by the Moho interface. Figure 4a shows the Moho depths for the Norwegian shelf, mainland Norway and surrounding areas. This Moho map has a similar database to the recent compilation for the European Moho depth by Grad *et al.* (2009), but includes more local studies on the mid-Norwegian margin.

In the depth to the Moho map the different characteristic of the Barents Sea and the southern part of the Norwegian continental margin stand out. On the mid-Norwegian margin the Moho generally deepens from the centre of the Fennoscandian Shield towards the continent–ocean transition. Typical values at the coastline are 30–35 km and the depth decreases to values around 10–15 km at the continental edge. Over the stable shelf of the Barents Sea the crustal base is for most of the area located at a depth larger than 30 km. While on the mid-Norwegian margin and the North Sea thick sedimentary sequences correlate with a shallow Moho as expected for classical extensional, pure shear, rift basins; the deep basins of the Barents Sea do not reveal a similar expression in the Moho geometry.

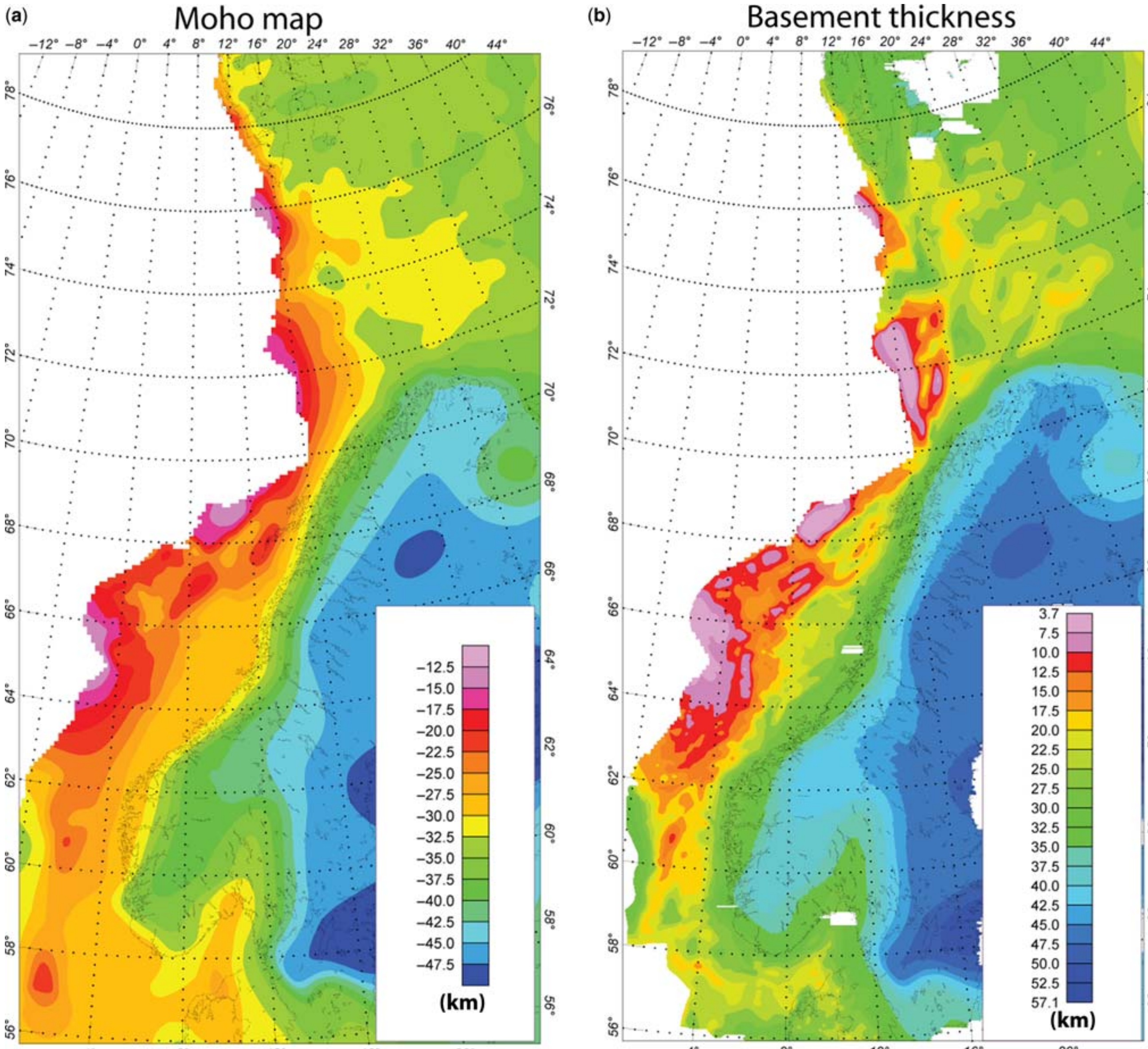

Fig. 4. (**a**) Moho map and (**b**) basement thickness. The basement thickness map corresponds to the thickness from the top basement to the Moho. The depth to Moho map is based on the regional profiles and compilations presented in Figure 2c, with modifications by Osmundsen & Ebbing (2008) for the Møre and Vøring margins, and Tsikalas *et al.* (2008) and Olesen *et al.* (2002) for the Lofoten margin.

The basement thickness map enhances this observation even more (Fig. 4b). This map is defined as the thickness of the crust between the top basement and the base of the crust (Moho). In the Barents Sea the basement thickness is typically larger than 20 km with local exceptions (e.g. the Nordkapp Basin), and despite the large sedimentary overburden, the crustal thinning is moderate. Over the Viking Graben, Møre and Vøring margins, the basement thickness is however less than 20 km, and for most areas even less than 12.5 km. Compared with the continental crustal thickness at the Norwegian coast (*c*. 32 km), this shows an enormous thinning of the crust, which reflects the influence of multiple rift episodes before the final opening of the Atlantic. An exception on the mid-Norwegian margin is the Trøndelag Platform, which is underlain by more than 20 km of crystalline crust. Similar basement thicknesses can be observed south of the Hardangerfjord Shear Zone. Clearly, the crustal thickness map reflects the distance to the continental edge, and indicates a direct link between the location of the margin segments and the opening history of the North Atlantic.

Discussion

Our definition of the basement thickness regards the entire basement as a metamorphic complex. Both low-magnetic Devonian basins and lower crustal bodies have been observed on the margin, which strictly are not part of the crystalline basement. Because of the age and often large depth, the density of the Devonian basement is likely to be similar to that of the underlying basement, and the base is often difficult to image seismically. Therefore, these Devonian basins are here regarded as part of the basement.

In our crustal thickness map, we include the entire thickness from the top basement to the crust–mantle transition (Moho). However, in the areas with extremely thin crust on the Vøring and Møre margins, a high-velocity, high-density body at the base of the crust has been mapped (e.g. Mjelde *et al.* 2005, 2009). This lower crustal body (LCB) has been mapped to have a thickness of more than 6 km, and to consist of a combination of magmatic underplated material and partially eclogitized rocks (e.g. Mjelde *et al.* 2005, 2009). This interpretation would imply that the LCB does not entirely correspond to crystalline crust and below parts of the Vøring Basin almost no crystalline crust might exist. Similar observations have been made on the southern Vøring margin and the Møre margin, where crustal-scale detachments can be observed culminating in the lower crust and the crustal thickness tapers out to less than 4 km (Osmundsen & Ebbing 2008). Below the Horda Platform a similar high-velocity body of eclogitic origin has been imaged on the landward side of the graben (Christiansson *et al.* 2000). Also below the Trøndelag Platform, increased seismic velocities and densities can be observed for the lower crust, but more in agreement with a gradual increasing velocity in normal continental crust. Hence, here the lower crust can be related to the crystalline crust.

In general, rifting that led to the formation of the Norwegian North Atlantic passive margin is associated with important detachments at depth and high-angle extensional faults near the surface (Smethurst 2000; Olesen *et al.* 2002; Osmundsen *et al.* 2002). The main structural domains of the passive margin are separated by several major normal fault systems (Fig. 1). While discussion concerning the dip directions of some major faults is ongoing, these fault systems and related structural highs and half-graben features are also reflected in the top basement map. Figure 5 shows the extension of the normal faults on the margin and their correlation with the top basement structure. The entire margin segmentation is controlled by an offshore extension of these low-angle faults and shear zones. The Hardangerfjord Shear Zone is a key example for the division of the Viking Graben to the north and the Norwegian–Danish Basin to the south. Other examples are the offshore extension of the Møre–Trøndelag Fault Complex, which divides the mid-Norwegian margin and northern North Sea, and the Nesna Shear Zone, which culminates into the Bivrost Lineament that separates the Lofoten from the Vøring margin (Blystad *et al.* 1995). The Kollstraumen and Høybakken detachments furthermore control the structural style of the Trøndelag Platform, and the latter bounds the Trøndelag Platform to the south (Osmundsen & Ebbing 2008). These major detachments formed during orogen-parallel extension, that is at a high angle to the orogenic front (Braathen *et al.* 2000, 2002; Mosar 2003).

Extrapolating the onshore structures to the offshore realm, it can be deduced that NE–SW trending (i.e. orogen-parallel) late Caledonian gravity collapse affected the entire mid-Norwegian margin, which led to the intimate link between the crust below the Trøndelag Platform and the onshore domain (Osmundsen & Ebbing 2008). Interpretation of magnetic anomalies helps to link onshore and offshore structures and correlation between detachment zones onshore and structural highs offshore can be made (e.g. Olesen *et al.* 2002; Osmundsen *et al.* 2002; Skilbrei *et al.* 2002). Of particular interest is the recognition of the structurally denuded basement culminations onshore Norway, which are bound by the detachments. These structural highs contain high-density and highly magnetized rocks of assumed lower crustal origin, which can be interpreted to represent reactivated core complexes (Osmundsen & Ebbing 2008; Ebbing *et al.* 2009).

Osmundsen & Ebbing (2008) advocate a structural model for the Jurassic–Early Cretaceous thinning of crust under the southeastern mid-Norway rifted margin, which gives an important role to the detachments. Following widespread Late Palaeozoic–Early Mesozoic half-graben formation, basin flank detachment faults developed. These faults cut the previous configuration of Palaeozoic faults and basins, and may have reactivated deep-seated older structures. At an early stage the middle and/or lower crust were still able to deform in a ductile manner, and provided a level of delamination for the early detachments, which could explain thinning of crust over the >100 km wide area that would later become the Møre and southern Vøring basins. Redistribution of ductile material led to depletion of such material (north)west of the basin flank detachments and to preferential storage of middle/lower crust under the platform and sub-basins. Isostatic denudation of the footwall and/or rotation on the Møre-Trøndelag Fault Complex led to the warping and deactivation of the Jurassic detachment, and to incision by the more planar, basin-bounding detachment fault. The main Møre fault evolved into the top basement detachment fault that, in combination with the rotated fault block arrays, controlled the basinward taper of the crystalline crust (Osmundsen & Ebbing 2008).

Basin floor detachment faults did become localized in the area of highly thinned crust 50–100 km NW of the basin flanks and the crustal thinning accommodated by the basin floor detachments resulted in extensional basins that juxtaposed rotated pre-rift and syn-rift sediments with rocks exhumed from the middle/deep crust or upper mantle (Osmundsen & Ebbing 2008).

A valuable application of our compilation will be for studies of the thermal state of the margin. Basement highs often are associated with pathways for upward fluid migration, which can lead to an anomalously high heat flow (Ritter *et al.* 2004), while the presence of granitoidal rocks can lead to a significantly increased heat-flow, as shown for the Transscandinavian Igneous Belt in the Central Scandes (Pascal *et al.* 2007). The top basement and crustal thickness map allow the influence of the crustal structure on the heat flow into the base of the sedimentary basins to be estimated.

Another step towards a better understanding of the different basement units is mapping of the base of the dominantly Caledonian or Precambrian basement. Ebbing *et al.* (2009) mapped the

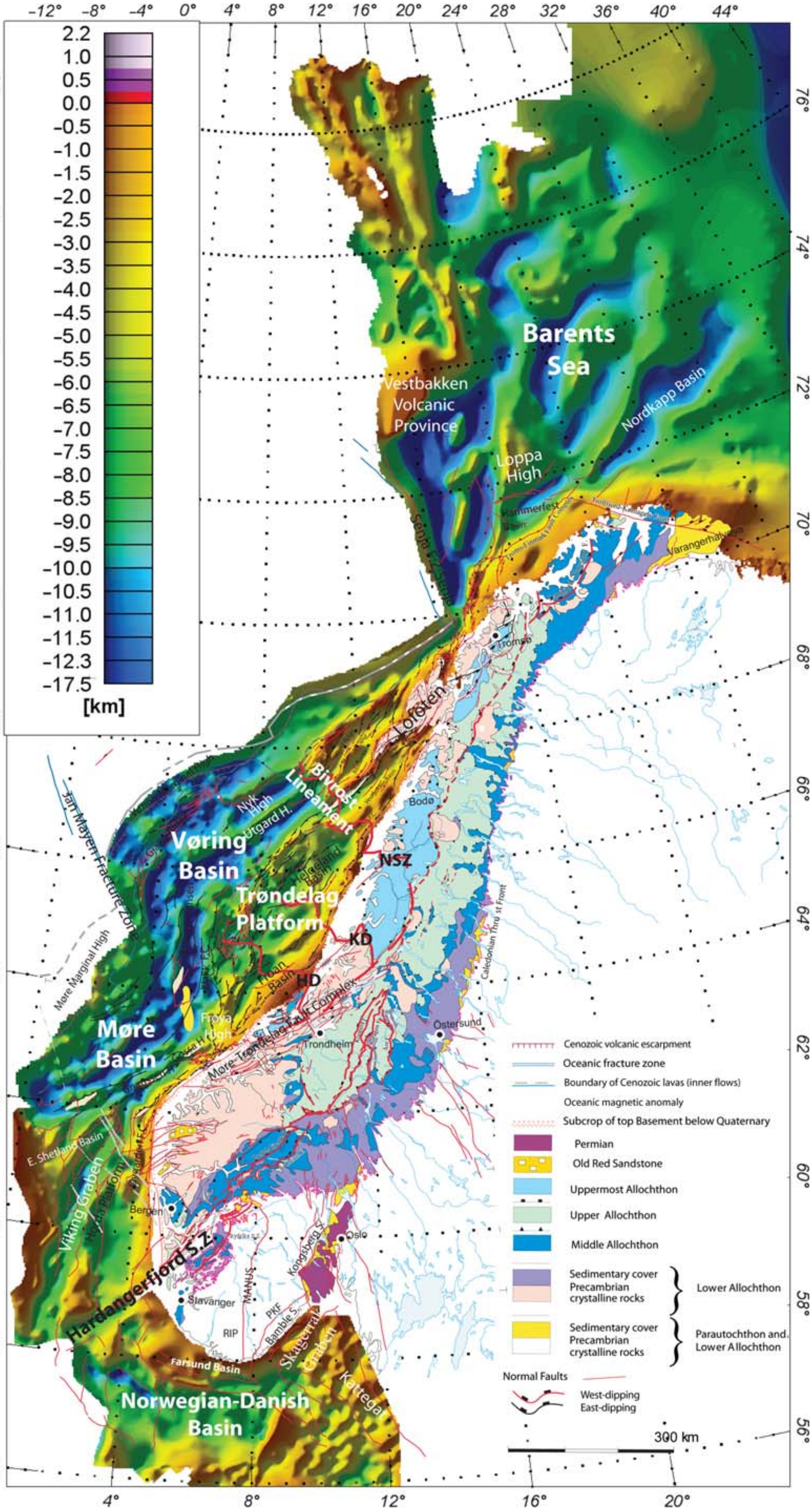

Fig. 5. Offshore top basement map and onshore tectonostratigraphic map. The map illustrates the continuation of faults from the onshore to offshore realm and illustrates the link between margin segmentation and onshore geology. Thick black lines over the Trøndelag Platform show offshore continuation of Late Caledonian detachments mapped onshore Norway.

base of the upper part of the basement on the mid-Norwegian margin, which corresponds mainly to the Caledonian basement, but also provided a tentative interpretation of the top Precambrian basement. Such studies are not yet available for the entire margin, but hopefully they will be available in the future, when the Norwegian–Danish Basin and North Sea are revisited.

Conclusions

We present for the first time a top basement map for the entire Norwegian shelf. The top basement map is based for a large part on integration of magnetic, gravity, seismic and borehole data. The quality of the compilation varies along the margin depending on the methodology used for compiling the individual contributions. The mid-Norwegian margin is the area with the largest amount of data used for the top basement mapping, partly because here the most recent studies exist. We also present a Moho compilation, which combines onshore data with the high-resolution crustal models of the margin, and which allows us to calculate the crustal thickness for the entire margin and onshore Norway. Both the top basement map and the crustal thickness map highlight the different margin segments. Comparison with the geological structure mapped onshore Norway shows the influence of normal faults on the segmentation of the margin. Previous studies mostly concentrated on different individual segments of the margin, but the compiled data will in the future allow refined studies of the evolution of the Norwegian continental shelf as a whole, and to study in more depth the influence of onshore–offshore structures on the structural style of the entire Norwegian continental shelf.

The main part of the study was done as part of the project KONTIKI (Continental Crust and Heat Generation in 3D) supported by StatoilHydro. Individual projects have been funded by different industry partners and the Research Council of Norway. We thank all authors of the individual studies for providing their results and cooperation in the individual studies, and especially appreciate the input from R. F. Reynisson, J. R. Skilbrei and M. Smethurst. We also thank the editor S. C. Pickering, an anonymous reviewer and G. S. Kimbell for their valuable comments and suggestions.

References

Åm, K. 1973. *Tolkning av magnetiske og gravimetriske data: Kontinentalsokkelen. Stavanger/Stad (59°–62°N)*. Geological Survey of Norway Report, **1175**.

Åm, K. 1975. Aeromagnetic basement complex mapping north of latitude 62 N, Norway. *Norges geologiske undersøkelse*, **316**, 351–374.

Andersen, T. B. 1998. Extensional tectonics in the Caledonides of southern Norway, an overview. *Tectonophysics*, **285**, 333–351.

Barrère, C., Ebbing, J. & Gernigon, L. 2009. Offshore prolongation of Caledonian structures and basement characterisation in the western Barents Sea from geophysical modeling. *Tectonophysics*, **470**, 71–88; doi: 10.1016/j.tecto.2008.07.012.

Blystad, P., Brekke, H., Færseth, R. B., Larsen, B. T., Skogseid, J. & Tørudbakken, B. 1995. *Structural Elements of the Norwegian Continental Shelf, Part II. The Norwegian Sea Region*. Norwegian Petroleum Directorate Bulletins, **8**.

Braathen, A., Nordgulen, Ø., Osmundsen, P. T., Andersen, T. B., Solli, A. & Roberts, D. 2000. Orogen-parallel, opposed extension in the Central Norwegian Caledonides. *Geology*, **28**, 615–618.

Braathen, A., Osmundsen, P. T., Nordgulen, Ø., Roberts, D. & Meyer, G. B. 2002. Orogen-parallel extension of the Caledonides in northern Central Norway: an overview. *Norwegian Journal of Geology*, **82**, 225–241.

Breivik, A. J., Mjelde, R., Grogan, P., Shimamura, H., Murai, Y. & Nishimura, Y. 2005. Caledonide development offshore-onshore Svalbard based on ocean bottom seismometer, conventional seismic, and potential field data. *Tectonophysics*, **401**, 79–117.

Brekke, H. 2000. The tectonic evolution of the Norwegian Sea continental margin with emphasis on the Vøring and Møre Basins. *In*: Nottvedt, A. (ed.) *Dynamics of the Norwegian Margin*. Geological Society, London, Special Publications, **167**, 327–378.

Brekke, H., Dahlgren, S., Nyland, B. & Magnus, C. 1999. The prospectivity of the Vøring and Møre basins on the Norwegian Sea continental margin. *In*: Fleet, A. J. & Boldy, S. A. R. (eds) *Petroleum Geology of Northwest Europe: Proceedings of the 5th Conference*, London, 26–29 October 1997. Geological Society, London, 261–274; doi: 10.1144/0050261.

Brekke, H., Sjulstad, H. I., Magnus, C. & Williams, R. W. 2001. Sedimentary environments offshore Norway – an overview. *In*: Martinsen, O. J. & Dreyer, T. (eds) *Sedimentary Environments Offshore Norway: Palaeozoic to Recent*. Elsevier Science, New York, 7–37.

Christiansson, P., Faleide, J. I. & Berge, A. M. 2000. Crustal structure in the northern North Sea from deep seismic reflection and refraction data. *In*: Nøttvedt, A. *et al.* (eds) *Dynamics of the Norwegian Margin*. Geological Society, London, Special Publications, **167**, 15–40.

Dehls, J. F., Olesen, O., Bungum, H., Hicks, E., Lindholm, C. & Riis, F. 2000. *Neotectonic Map: Norway and Surrounding Areas*. Geological Survey of Norway, Trondheim.

Doré, A. G. 1992. Synoptic paleogeography of the Northeast Atlantic Seaway: Late Permian to Cretaceous. *In*: Parnell, J. (ed.) *Basins on the Atlantic Seaboard: Petroleum Geology, Sedimentology and Basin Evolution*. Geological Society, London, Special Publications, **62**, 421–446.

Doré, A. G. & Vining, B. A. (eds) 2005. *Petroleum Geology: North-West Europe and Global Perspectives – Proceedings of the 6th Petroleum Geology Conference*. Geological Society, London; doi: 10.1144/0060803.

Doré, A. G., Lundin, E. R., Birkeland, Ø., Eliassen, P. E. & Jensen, L. N. 1997. The NE Atlantic Margin: implications of late Mesozoic and Cenozoic events for hydrocarbon prospectivity. *Petroleum Geosciences*, **3**, 117–131.

Ebbing, J., Lundin, E., Olesen, O. & Hansen, E. K. 2006. The mid-Norwegian margin: a discussion of crustal lineaments, mafic intrusions, and remnants of the Caledonian root by 3D density modelling and structural interpretation. *Journal of the Geological Society, London*, **163**, 47–60.

Ebbing, J., Skilbrei, J. R. & Olesen, O. 2007. Insights into the magmatic architecture of the Oslo Graben by petrophysically constrained analysis of the gravity and magnetic field. *Journal of Geophysical Research*, **112**, B4404.

Ebbing, J., Gernigon, L., Pascal, C., Olesen, O. & Osmundsen, P. T. 2009. A discussion of structural and thermal control of magnetic anomalies on the mid-Norwegian margin. *Geophysical Prospecting*, **57**, 665–681.

Faleide, J. I., Tsikalas, F. *et al.* 2008. Structure and evolution of the continental margin off Norway and the Barents Sea. *Episodes*, **31**(1), 1–10.

Fleet, A. J. & Boldy, S. A. R. (eds) 1999. *Petroleum Geology of Northwest Europe: Proceedings of the 5th Conference*, London, 26–29 October 1997. Geological Society, London.

Fossen, H. 1992. The role of extensional tectonics in the Caledonides of south Norway. *Journal of Structural Geology*, **14**, 1033–1046.

Gabrielsen, R. H., Odinsen, T. & Grunnaleite, I. 1999. Structuring of the northern Viking Graben and the Møre Basin: the influence of basement structural grain, and the particular role of the Møre–Trøndelag Fault Complex. *Marine and Petroleum Geology*, **16**, 443–465.

Gabrielsen, R. H., Braathen, A., Olesen, O., Faleide, J. I., Kyrkjebø, R. & Redfield, T. F. 2005. Vertical movements in south-western Fennoscandia: a discussion of regions and processes from the present to the Devonian. *In*: Wandås, B. T. G., Eide, E. A., Gradstein, F. & Nystuen, J. P. (eds) *Onshore–Offshore Relationships on the North Atlantic Margin*. Norwegian Petroleum Society, Oslo, Special Publications, **12**, 1–28.

Gee, D. G., Guezou, J.-C., Roberts, D. & Wolff, F. C. 1985. The central-southern part of the Scandinavian Caledonides. *In*: Gee, D. G. & Sturt, B. A. (eds) *The Caledonide Orogen – Scandinavia and Related Areas*. Wiley, New York, 109–133.

Götze, H.-J. & Lahmeyer, B. 1988. Application of three-dimensional interactive modeling in gravity and magnetic. *Geophysics*, **53**, 1096–1108.

Grad, M., Tiira, T. & ESC Working Group 2009. The Moho depth map of the European Plate. *Geophysical Journal International*, **176**, 279–292.

Gramberg, I. S. *et al*. 2001. Eurasian Arctic Margin: earth science problems and research challenges. *Polarforschung*, **69**, 3–15.

Hospers, J. & Ediriweera, K. K. 1988. *Mapping the Top of the Crystalline Continental Crust in the Viking Graben Area, North Sea*. Norwegian Geological Survey, Trondheim, Special Publications, **3**, 21–28.

Hospers, J. & Ediriweera, K. K. 1991. Depth and configuration of the crystalline basement in the Viking Graben area, Northern North Sea. *Journal of the Geological Society, London*, **148**, 261–265.

Hospers, J., Rathore, J. S., Jianhua, F. & Finnstrøm, E. G. 1986. Thickness of pre-Zechstein-salt Palaeozoic sediments in the southern part of the Norwegian sector of the North Sea. *Norsk Geologisk Tidsskrift*, **66**, 295–304.

Johansen, S. E., Ostisty, B. K. *et al*. 1992. Hydrocarbon potential in the Barents Sea region: play distribution and potential. *In*: Vorren, T. O., Bergsager, E. *et al*. (eds) *Arctic Geology and Petroleum Potential*. Elsevier, Amsterdam, NPF Special Publications, **2**, 273–320.

Kinck, J. J., Husebye, E. S. & Larsson, F. R. 1993. The Moho depth distribution in Fennoscandia and the regional tectonic evolution from Archean to Permian times. *Precambrian Research*, **64**, 23–51.

Lassen, A. & Thybo, H. 2004. Seismic evidence for Late Proterozoic orogenic structures below the Phanerozoic sedimentary cover in the Kattegat area, SW Scandinavia. *Tectonics*, **23**, TC2017; doi: 10.1029/2003TC001499.

Lyngsie, S. B., Thybo, H. & Rasmussen, T. M. 2005. Regional geological and tectonic structures of the North Sea area from potential field modeling. *Tectonophysics*, **413**, 147–170.

Mjelde, R., Raum, T. *et al*. 2005. Crustal structure of the Vøring Margin, NE Atlantic: a review of geological implications based on recent OBS data. *In*: Doré, A. G. & Vining, B. A. (eds) *Petroleum Geology: North–West Europe and Global Perspectives: Proceedings of the 6th Petroleum Geology Conference*. Geological Society, London, 803–813; doi: 10.1144/0060803.

Mjelde, R., Faleide, J. I., Breivik, A. J. & Raum, T. 2009. Lower crustal composition and crustal lineaments on the Vøring Margin, NE Atlantic: a review. *Tectonophysics*, **472**, 183–193.

Mørk, M. B. E., McEnroe, S. A. & Olesen, O. 2002. Magnetic susceptibility of Mesozoic and Cenozoic sediments off Mid Norway and the role of siderite: implications for interpretation of high-resolution aeromagnetic anomalies. *Marine and Petroleum Geology*, **19**, 1115–1126.

Mosar, J. 2000. Depth of the extensional faulting on the mid-Norway Atlantic passive margin. *Norges Geologiske Undersokelse Bulletin*, **437**, 33–41.

Mosar, J. 2003. Scandinavia's North Atlantic passive margin. *Journal of Geophysical Research*, **108**, 2360.

Nøttvedt, A. (ed.) 2000. *Dynamics of the Norwegian Margin*. Geological Society, London, Special Publications, **167**.

Olesen, O., Roberts, D., Henkel, H., Lile, O. B. & Torsvik, T. H. 1990. Aeromagnetic and gravimetric interpretation of regional structural features in the Caledonides of West Finnmark and North Troms, northern Norway. *Bulletin of the Geological Survey of Norway*, **419**, 1–24.

Olesen, O., Henkel, H., Kaada, K. & Tveten, E. 1991. Petrophysical properties of a prograde amphibolite granulite facies transition zone at Sigerfjord, Vesterålen, Northern Norway. *Tectonophysics*, **192**, 33–39.

Olesen, O., Smethurst, M., Beard, L., Torsvik, T., Bidstrup, T. & Egeland, B. 1997. *SAS-96 Part II, Skagerrak Aeromagnetic Survey 1996, Interpretation Report*. NGU Report **97.022**.

Olesen, O., Lundin, E. *et al*. 2002. Bridging the gap between the onshore and offshore geology in Nordland, northern Norway. *Norwegian Journal of Geology*, **82**, 243–262.

Olesen, O., Smethurst, M. A., Torsvik, T. H. & Bidstrup, T. 2004. Sveconorwegian igneous complexes beneath the Norwegian–Danish Basin. *Tectonophysics*, **387**, 105–130.

Olesen, O., Ebbing, J. *et al*. 2007. An improved tectonic model for the Eocene opening of the Norwegian–Greenland Sea: use of modern magnetic data. *Marine and Petroleum Geology*, **24**, 53–66.

Olesen, O., Brönner, M. *et al*. 2010. New aeromagnetic and gravity compilations from Norway and adjacent areas: methods and applications. *In*: Vining, B. A. & Pickering, S. C. (eds) *Petroleum Geology: From Mature Basins to New Frontiers – Proceedings of 7th Petroleum Geology Conference*. Geological Society, London, 559–586; doi: 10.1144/0070559.

Osmundsen, P. T. & Ebbing, J. 2008. Styles of extension offshore mid Norway and implications for mechanisms of Late Jurassic–Early Cretaceous rifting. Basement configuration of the mid-Norwegian margin. *Tectonics*, **27**, TC6016; doi: 10.1029/2007TC002242.

Osmundsen, P. T., Andersen, T. B., Markussen, S. & Svendby, A. K. 1998. Tectonics and sedimentation in the hanging wall of a major extensional detachment: the Devonian Kvamshesten Basin, western Norway. *Basin Research*, **10**, 213–224.

Osmundsen, P. T., Sommaruga, A., Skilbrei, J. R. & Olesen, O. 2002. Deep structure of the Mid Norway rifted margin. *Norwegian Journal of Geology*, **82**, 205–224.

Pascal, C., Ebbing, J. & Skilbrei, J. R. 2007. Interplay between the Scandes and the Transscandinavian Igneous Belt: integrated thermal and potential field modelling of the Central Scandes profile. *Norwegian Journal of Geology*, **87**, 3–12.

Planke, S., Rasmussen, R., Rey, S. S. & Myklebust, R. 2005. Seismic characteristics and distribution of volcanic intrusions and hydrothermal vent complexes in the Vøring and Møre basins. *In*: Doré, A. G. & Vining, B. A. (eds) *Petroleum Geology: North-West Europe and Global Perspectives: Proceedings of the 6th Petroleum Geology Conference*. Geological Society, London, 833–844; doi: 10.1144/0060833.

Ramberg, I. B. & Smithson, S. B. 1975. Geophysical interpretation of crustal structure along the southeastern coast of Norway and Skagerrak. *GSA Bulletin*, **86**, 769–774.

Reynisson, R. F. 2010. *Deep structure of the mid-Norwegian margin with emphasis on the Møre margin and sub-basalt exploration using integrated gravimetric-, and magnetometric models, with isostatic considerations*. PhD thesis, Norwegian University of Science and Technology, Trondheim.

Reynisson, R. F., Ebbing, J. & Skilbrei, J. R. 2009. The use of potential field data in revealing the basement structure in sub-basaltic settings: an example from the Møre margin, offshore Norway. *Geophysical Prospecting*, **57**, 753–771.

Ritter, U., Zielinski, G. W., Weiss, H. M., Zielinski, R. L. B. & Sættem, J. 2004. Heat flow in the Vøring Basin, Mid-Norwegian shelf. *Petroleum Geoscience*, **10**, 353–365.

Ritzmann, O., Maercklin, N., Faleide, J. I., Bungum, H., Mooney, W. D. & Detweiler, S. T. 2007. A three-dimensional geophysical model of the crust in the Barents Sea region: model construction and basement characterization. *Geophysical Journal International*, **170**, 417–435.

Roberts, D. 2003. The Scandinavian Caledonides: event chronology, palaeogeographic settings and likely modern analogues. *Tectonophysics*, **365**, 283–299.

Scheck-Wenderoth, M., Faleide, J. I., Raum, T., Mjelde, T. & Horsfield, B. 2007. The transition from the continent to the ocean: a deeper view on the Norwegian margin. *Journal of the Geological Society, London*, **164**, 855–868.

Sindre, A. 1993. *Regional tolkning av geofysiske data, kartblad Arendal*. NGU Report **92.213**.

Skilbrei, J. R. 1991. Interpretation of depth to the magnetic basement in the Northern Barents Sea (South of Svalbard). *Tectonophysics*, **200**, 127–141.

Skilbrei, J. R. 1995. Aspects of the geology of the southwestern Barents Sea from aeromagnetic data. *NGU Bulletin*, **427**, 64–67.

Skilbrei, J. R. & Olesen, O. 2005. Deep structure of the Mid-Norwegian shelf and onshore–offshore correlations: insight from potential field data. *In*: Wandås, B. T. G., Eide, E. A., Gradstein, F. & Nystuen, J. P. (eds) *Onshore–Offshore Relationships on the North Atlantic Margin*. Norwegian Petroleum Society, Oslo, Special Publications, **12**, 43–68.

Skilbrei, J. R., Skyseth, T. & Olesen, O. 1991. Petrophysical data and opaque mineralogy of high-grade and retrogressed lithologies – implications for the interpretation of aeromagnetic anomalies in Northern Vestranden, Central Norway. *Tectonophysics*, **192**, 21–31.

Skilbrei, J. R., Olesen, O., Osmundsen, P. T., Kihle, O., Aaro, S. & Fjellanger, E. 2002. A study of basement structures and onshore–offshore correlations in Central Norway. *Norwegian Journal of Geology*, **82**, 263–279.

Smethurst, M. A. 1994. *Viking-93 Aeromagnetic Survey: Interpretation Report*. NGU Report **94.011**.

Smethurst, M. A. 2000. Land–offshore tectonic links in western Norway and the northern North Sea. *Journal of the Geological Society, London*, **157**, 769–781.

Thybo, H. & Schönharting, G. 1991. Geophysical evidence for Early Permian igneous activity in a transtensional environment, Denmark. *Tectonophysics*, **189**, 193–208.

Tsikalas, F., Faleide, J. I. & Kusznir, N. J. 2008. Along-strike variations in rifted margin crustal architecture and lithosphere thinning between northern Vøring and Lofoten margin segments off mid-Norway. *Tectonophysics*, **458**, 68–81.

Vejbæk, O. V. & Britze, P. 1994. *Geological Map of Denmark 1:750 000*. Danmarks Geologiske Undersøgelse **45**.

Yegorova, T., Bayer, U., Thybo, H., Maystrenko, Y., Scheck-Wenderoth, M. & Lyngsie, S. B. 2007. Gravity signal from the lithosphere in the Central European Basin System. *Tectonophysics*, **429**, 133–163.

Some emerging concepts in salt tectonics in the deepwater Gulf of Mexico: intrusive plumes, canopy-margin thrusts, minibasin triggers and allochthonous fragments

M. P. A. JACKSON, M. R. HUDEC and T. P. DOOLEY

Bureau of Economic Geology, Jackson School of Geosciences, The University of Texas at Austin, University Station Box X, Austin, Texas 78713, USA (e-mail: martin.jackson@beg.utexas.edu)

Abstract: We summarize four emerging concepts in salt tectonics in the deepwater Gulf of Mexico, selected from a longer list of concepts that have advanced significantly in the last decade. Squeezed salt stocks are common in orogenic forelands, in inverted basins and at the toe of salt-bearing passive margins. Modelling suggests that during early shortening, an inward salt plume from the source layer inflates the diapir and arches its roof. After further shortening, diapiric salt is expelled as an outward plume back into the source layer. Salt canopies are conventionally thought to advance by glacial extrusion. However, almost all modern salt canopies are now buried and can only advance by frontal thrusting. Thrusting allows the salt canopy and its protective roof to advance together, minimizing salt dissolution. Advance is by a roof-edge thrust rooted in the leading tip of salt or by thrust imbricates forming accretionary wedges. Minibasins can sink into salt if the average density of the overburden exceeds that of salt. This requires 2–3 km of burial of siliciclastic fill, yet most minibasins first sink when much thinner. Three alternative mechanisms to negative buoyancy in the deepwater Gulf of Mexico address this paradox of initiation. First, squeezed diapirs inflate, leaving the intervening minibasins as depressions. Second, when a diapir's salt supply wanes, the overlying dynamic salt bulge subsides, allowing a minibasin to form. Third, differential loading causes the thick end of a sedimentary wedge to sink faster into the salt, creating a sag. Spreading salt canopies can transport their dismembered roof fragments tens of kilometres basinward. These exotic fragments are up to 25 km in breadth and comprise anomalously old Mesozoic through Miocene sequences. Strata of the same age underlie the salt canopy or its welded equivalent, signalling lateral transport by thick salt.

Keywords: salt tectonics, diapir, thrust, allochthonous salt, Gulf of Mexico, Louann, structural geology

Knowledge of salt tectonics has expanded rapidly on three main fronts. Petroleum exploration of passive continental margins has yielded new 3D seismic datasets, improved seismic imaging and well control, all of which reveal the large-scale geometry of salt structures. Mapping in orogenically unroofed salt basins clarifies smaller-scale field relations. Increasingly sophisticated structural modelling elucidates the kinematics and dynamics of salt tectonics.

These advances in knowledge bring new ideas and new terminology. The last attempt to summarize the conceptual growth of salt tectonics was in 1993 at the Hedberg International Research Conference on Salt Tectonics, held in Bath (UK) (Jackson 1995). That review summarized progress in understanding since 1856, when the first salt diapir was described in the geological literature.

The present paper is more restricted in scope than the Bath review. Major advances in understanding salt tectonics at seismic scale during the last decade include, for example (Fig. 1): (a) halokinetic sequences around passive diapirs (Giles & Lawton 2002; Rowan *et al.* 2003); (b) inflation and deflation of autochthonous salt layers (Hall 2002); (c) multiwavelength compressional folding in thickening strata (Peel 2003); (d) epeirogenic crustal uplift rejuvenating salt tectonics on passive margins (Hudec & Jackson 2004; Jackson *et al.* 2005); (e) emplacement of deep, old allochthonous fringes (Peel 2001); (f) directly measured rates of subaerial salt extrusion (Talbot 1998; Talbot *et al.* 2000; Talbot & Aftabi 2004); (g) salt sutures (Kadri *et al.* 2000; Liro *et al.* 2004); (h) surging salt canopies overriding small stocks (Hall 2002; Liro *et al.* 2004; Mount *et al.* 2006); and (i) strike-slip enhancing or retarding salt diapirism (Talbot & Alavi 1996; Letouzey & Sherkati 2004; Dooley *et al.* 2007). Some of these ideas have been published only as abstracts and have not been thoroughly explored.

Space allows only a brief summary of all these processes, so instead we focus on the deepwater Gulf of Mexico to highlight four advances of which we have first-hand knowledge. Despite this parochial approach, these advances could apply beyond the Gulf of Mexico, especially to equivalent deepwater settings on the West African and Brazilian continental margins or other basins where thick salt is mobilized. None of these new ideas is yet in wide currency. Some are controversial. Some may not last. However, they all seem novel and interesting. The four ideas showcased are intrusive plumes, salt-sheet thrusts, minibasin triggers and allochthonous fragments. A cross-sectional sketch shows where these processes might occur in a deepwater passive margin (Fig. 2).

Intrusive salt plumes

Within every growing diapir, salt flows upwards from its source layer. This is a classic and deeply entrenched idea (Escher & Kuenen 1929) for salt diapirs growing halokinetically and for diapirs squeezed by lateral compression. When diapirs are squeezed, salt is forced upwards, like an uncapped toothpaste tube squeezed by hand pressure. The rising salt either arches its sedimentary roof or escapes from the ruptured roof as extrusive salt.

Salt sags within model diapirs that are laterally stretched faster than they can be supplied by salt (Vendeville & Jackson 1992), and entrained dense layers partly sink inside rising model diapirs (Chemia & Koyi 2008). However, in these examples, the salt flows downward only within the diapir and does not challenge the dogma that diapiric salt does not intrude the source layer. Yet downward flow back into the source layer is indicated by modelling squeezed diapirs. Figure 3 shows this process in vertical

VINING, B. A. & PICKERING, S. C. (eds) *Petroleum Geology: From Mature Basins to New Frontiers – Proceedings of the 7th Petroleum Geology Conference*, 899–912. DOI: 10.1144/0070899

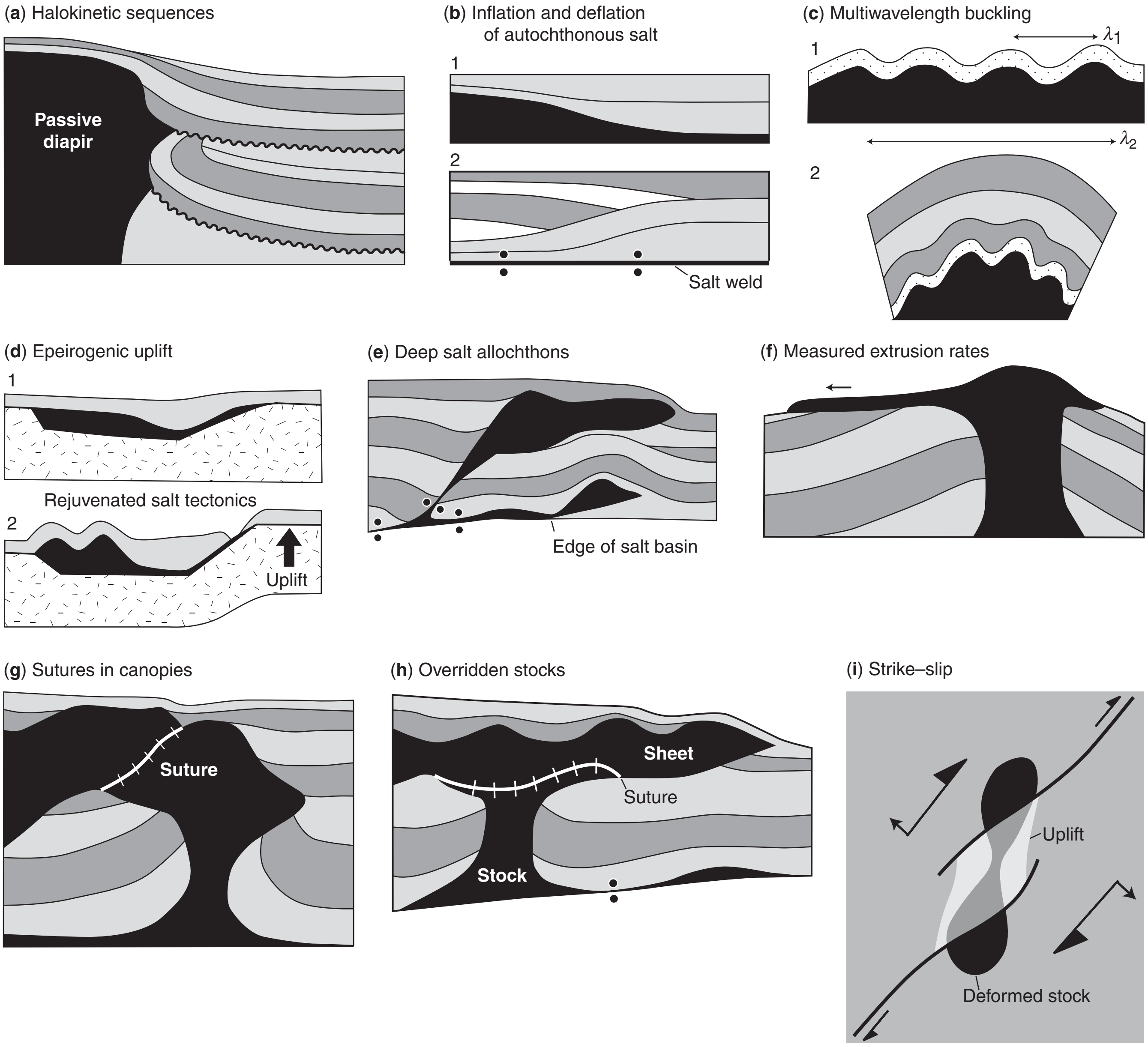

Fig. 1. Some concepts in salt tectonics recently discovered or improved: (**a**) halokinetic sequences around passive diapirs; (**b**) inflation and deflation of autochthonous salt layers; (**c**) multiwavelength (λ_1 and λ_2) compressional folding in thickening strata; (**d**) epeirogenic crustal uplift rejuvenating salt tectonics on passive margins; (**e**) emplacement of deep, old, allochthonous fringes; (**f**) directly measured rates of subaerial salt extrusion; (**g**) salt sutures; (**h**) surging salt canopies overriding small stocks; and (**i**) strike-slip (here transtensional) enhancing or retarding salt diapirism.

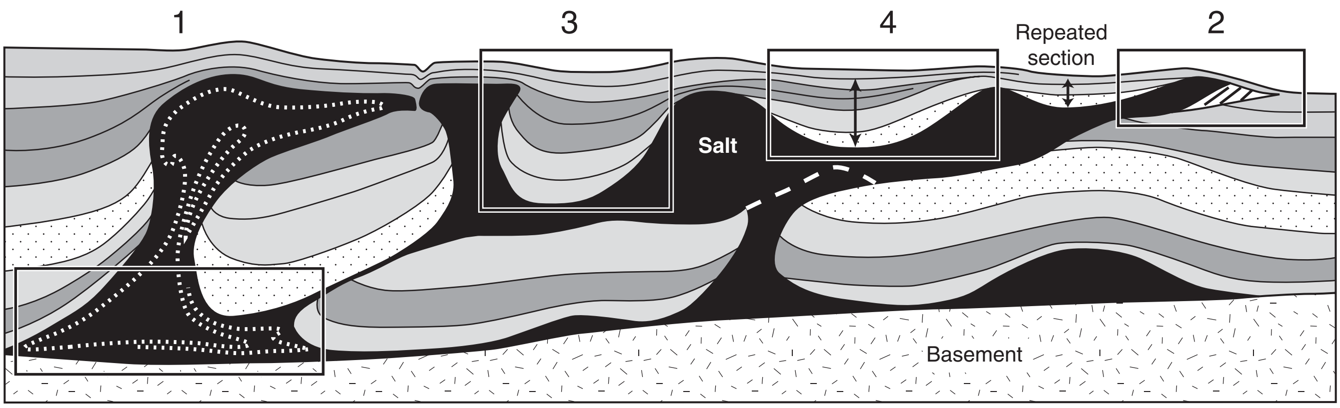

Fig. 2. Schematic cross-section of the Gulf of Mexico lower continental slope, showing the setting of the four conceptual processes highlighted in this paper. (1) Squeezed diapirs intrude plumes of salt into the source layer. (2) Buried salt canopies advance by overthrusting of allochthonous salt and its roof. (3) Three mechanisms explain why even low-density, uncompacted sediments sink into salt and start minibasins. (4) Spreading salt canopies can carry exotic fragments of the canopy roof great distances and duplicate stratigraphy above and below the canopy.

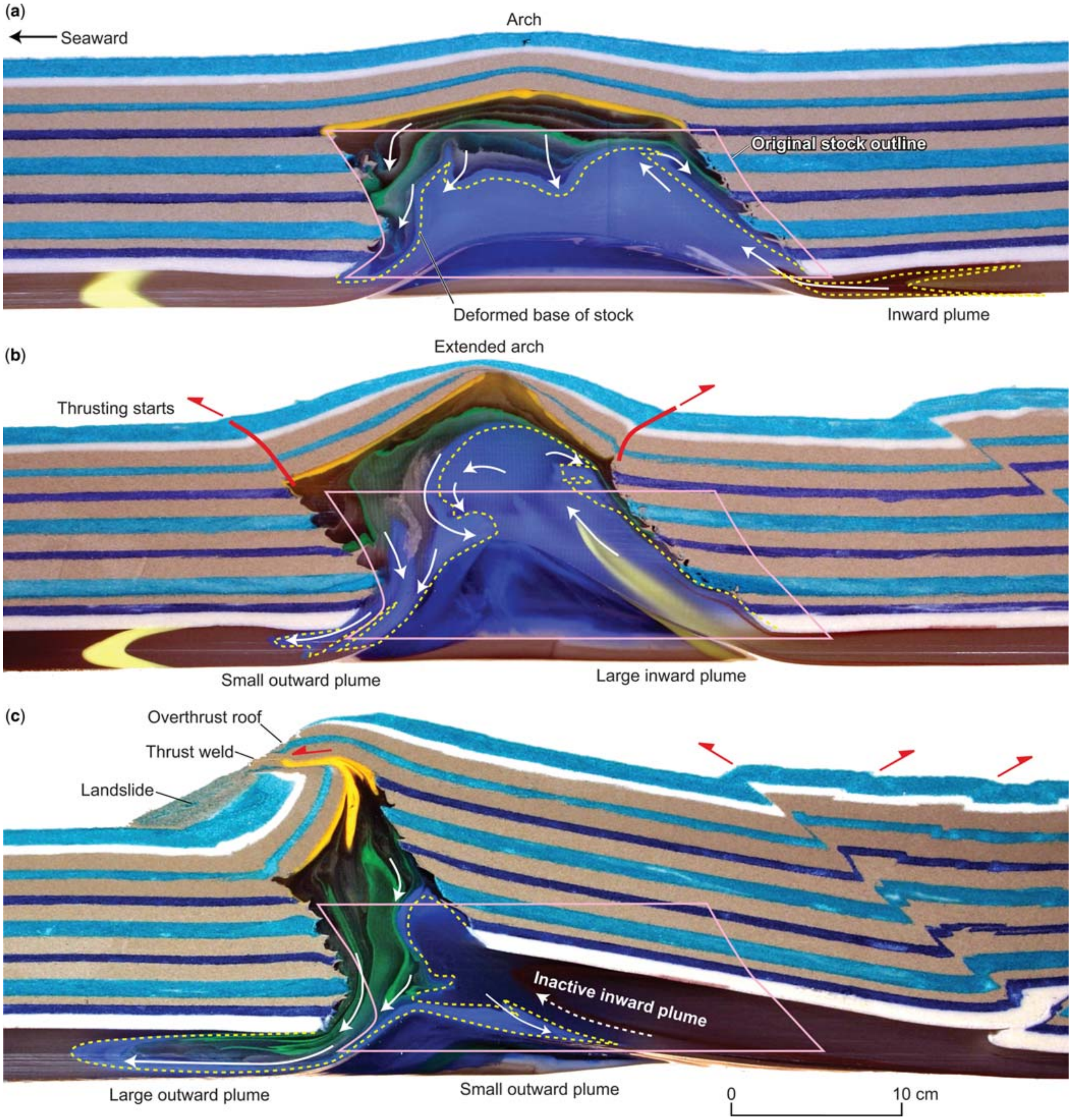

Fig. 3. Cross-sections from three physical models showing stages of squeezing of inclined stocks, whose original shapes are outlined by a polygon. (**a**) Mild shortening (7 cm) drives salt seawards. An inward-intrusive plume inflates the stock's cross-sectional area to 111% and gently arches its roof. (**b**) After moderate shortening (15 cm), the inward plume enlarges and inflates the stock area to 117%; the stock also expels a small outward plume seawards into the source layer. (**c**) After strong shortening (30 cm), two outward plumes shrink the diapir area to 42% of original area and inflate the source layer.

sections through three dynamically scaled physical models (Dooley *et al.* 2009). The models were sliced at different stages to yield snapshots of how they evolved. Apart from different durations of deformation, the three models were identical. Each model simulated the effects of shortening on seaward-inclined, cylindrical salt stocks having flat crests buried by thick roofs. The models show the effects of shortening on passive stocks that have evolved through a specific kinematic history. The resulting pre-shortening geometry modelled here is common in the Gulf of Mexico but not universal. As a moving endwall shortened the stocks at a constant rate, the squeezed diapir evolved through three stages.

In Stage 1, shortening thickened the source layer of salt and drove it seawards on both sides of the diapir (Fig. 3). Static pressures in the source layer were higher than those in the stock because salt was displaced from the thrust belt growing in the hinterland (to the right of the frame in Fig. 3a). Pressures in the source layer were also high because the overburden was 10% denser than the salt. The difference in hydraulic head injected a salt plume into the diapir from its landward side. The squeezed diapir expanded in vertical section to 111% of its original area, even though its width decreased by 2% because of shortening. The diapir dilated rather than shrank. The inward plume of salt arched the diapir roof ahead of the advancing thrust front (out of the frame in Fig. 3a).

In Stage 2, the thrust front jumped seawards of the salt stock (Fig. 3b), and the arched stock roof began to shorten. The inward plume continued to inflate the diapir to 117% of its original area in vertical section. Salt was pumped above regional because the diapir walls converged and because salt was imported from the source layer. The salt volume displaced above regional in the diapir was *c.* 1.8 times greater than the volume displaced by 11% convergence of the diapir walls. Thus salt import still dominated. However, salt export began as an outward plume of diapiric salt and began to intrude the source layer on the seaward side of the diapir.

In Stage 3, the compressed stock shrank to 42% of its original area in vertical cross-section as the inward plume of salt died and outward plumes were expelled (Fig. 3c). Serial sections show that no salt escaped along-strike. Overthrusting thickened the arched roof, which prevented salt from escaping as an extrusion. Salt flowed downwards because its roof was too thick for salt to escape upwards. The diapir grew taller because of salt inflation and lateral squeezing. Increased height of the diapir reversed the earlier hydraulic-head gradient and forced diapiric salt into the source layer, thickening it 4-fold on the landward side of the diapir. Salt intruded the source layer in outward plumes both seawards and landwards.

The three stages of shortening are shown in underside views up through the colourless, transparent silicone simulating salt (Fig. 4). Shearing of coloured marker plugs into streaked-out ribbons tracked salt flow. After minor shortening (stage 1), the blue base of the stock remained elliptical. During stage 2, salt converged seaward into the stock and rose as an inward plume. By stage 3, outward plumes of salt expelled and crumpled the blue base of the diapir and a green marker layer from half-way up the stock. Together the blue and green markers merged into the two outward plumes seawards and landwards.

The models shed light on the dynamics of squeezing of salt stocks. Gravity provides a load, as in all salt tectonics. In addition, regional compression forces together the sides of the stock. Initially the pressurized source layer intruded and inflated the stock. Then as shortening intensified, more diapiric salt was expelled as plumes. Shortening structures in the overburden rose and made space for the salt plumes.

Four other factors promote outward plumes intruding the source layer but are not essential (Dooley *et al.* 2009). First, a thick diapiric roof is strong enough to resist arching, so diapiric salt is forced to flow downwards into the source layer. Passive diapirs are interpreted to have emplaced wings of salt into thin post-Zechstein salt beds delaminated in compressional detachment folds in Germany and the North Sea (Baldschuhn *et al.* 2001; Hudec 2004; Stewart 2007). A small minority of these diapirs (e.g. Wolthausen diapir and Niendorf II diapir; Baldschuhn *et al.* 2001; Hudec 2004) appear to have been emergent during wing intrusion, suggesting that a thick roof is not necessary for outward plumes. Second, a wide diapir provides a large volume and broad conduit for salt to intrude the source layer. Third, an initially thick source layer provides a wide channel for salt flow in which boundary drag is proportionally low. Fourth, a seaward dip of the base of salt helps salt to flow seaward and entrains exported diapiric salt. The thick-roofed models in Figure 3 did not require a seaward-dipping source layer to form outward plumes, but our models of thin-roofed diapirs required a dipping source layer to expel plumes (Dooley *et al.* 2006). All four factors are more effective when combined. In contrast, although a dense overburden encourages inward salt plumes, the effect of density contrast seems small for outward plumes.

Outward plumes should be considered in restorations of cross-sections of squeezed diapirs. In a closed system the source layer thickens as salt laterally shortens. Downward expulsion of salt plumes from squeezed diapirs further thickens the source layer. Neglecting downward expulsion causes an interpreter to overestimate the original thickness of the source layer. For example, diapirs such as Hildesheimer Wald and Niendorf II (Germany)

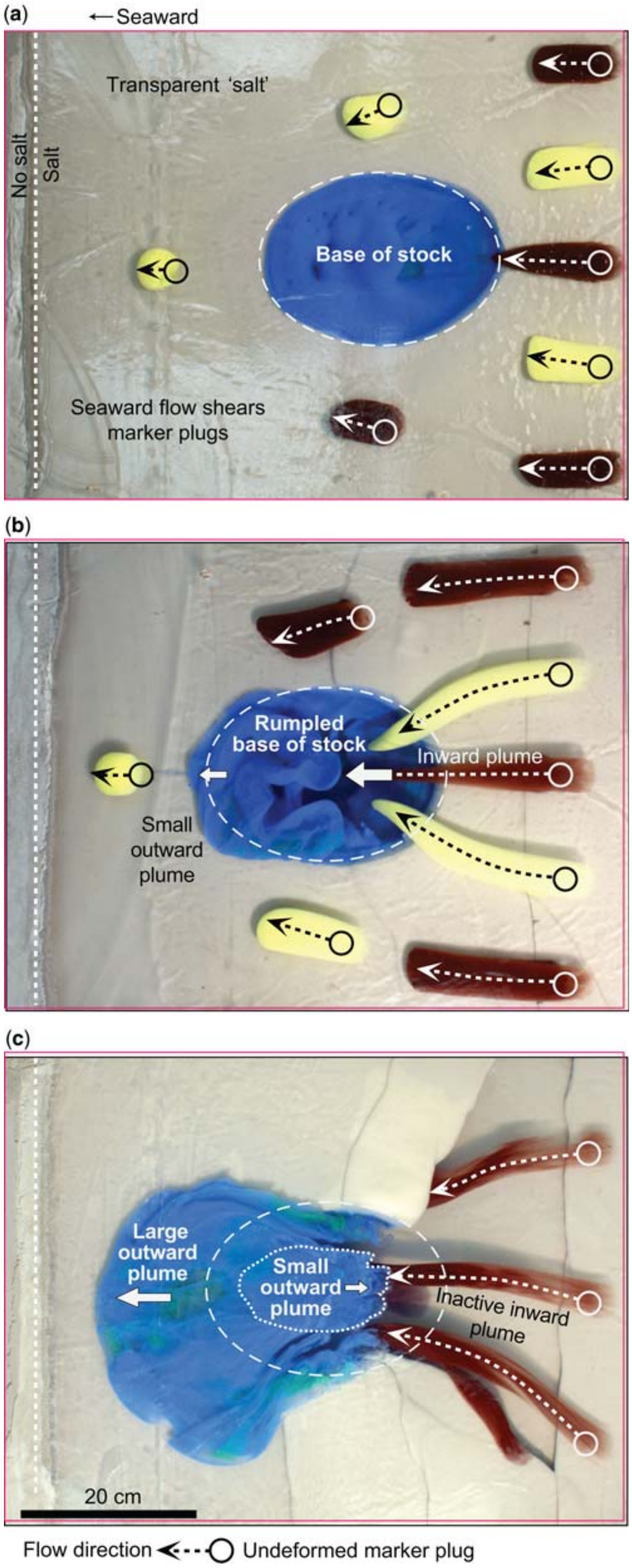

Fig. 4. Underside view upwards through the base of the physical models showing the same three stages of shortening (**a**–**c**) as in Figure 3. The salt source layer is transparent and colourless, except for the brown and yellow marker plugs embedded within it. The pale background colour is the base of the overburden. The dashed ellipse marks the shape and position of the stock before shortening.

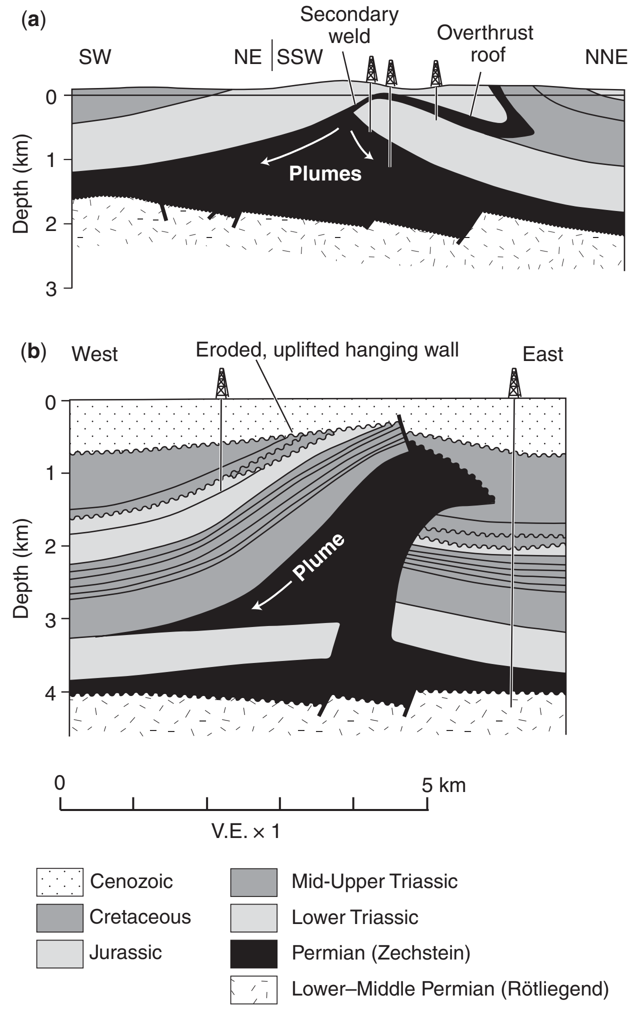

Fig. 5. Two German squeezed diapirs, showing thick adjoining salt. We attribute the thickness to plumes expelled from the diapirs by regional shortening. (**a**) Intense squeezing of Hildesheimer Wald diapir expelled an extrusive salt sheet upwards and probable plumes of diapiric salt downwards, which thickened the Permian Zechstein source layer to nearly 2 km. (**b**) Niendorf II diapir expelled Zechstein-derived diapiric salt outwards into the buckling, delaminating layer of Triassic Röt halite. Cross-sections after Baldschuhn *et al.* (2001).

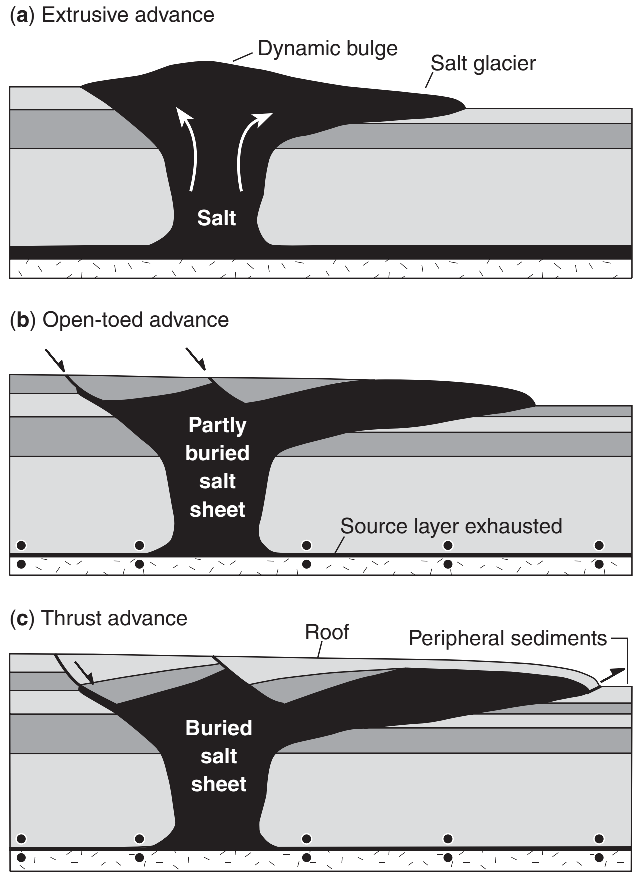

Fig. 6. Schematic cross-sections showing three ways in which salt sheets can advance, depending on their state of burial. After Hudec & Jackson (2009).

are locally flanked by an unusually thick salt next to the diapir, which could have been thickened by salt expelled from the squeezed diapirs or inherited from a structurally thickened core of an anticline (Fig. 5). In addition the geometry of Niendorf II suggests that salt plumes may intrude even thin evaporite layers such as the Röt halite. Regional shortening peeled the overburden upwards, providing space for salt to escape from the squeezed diapir. Incorrectly estimating the original thickness of a salt layer also affects estimates of palaeo-heat flow and timing of welding.

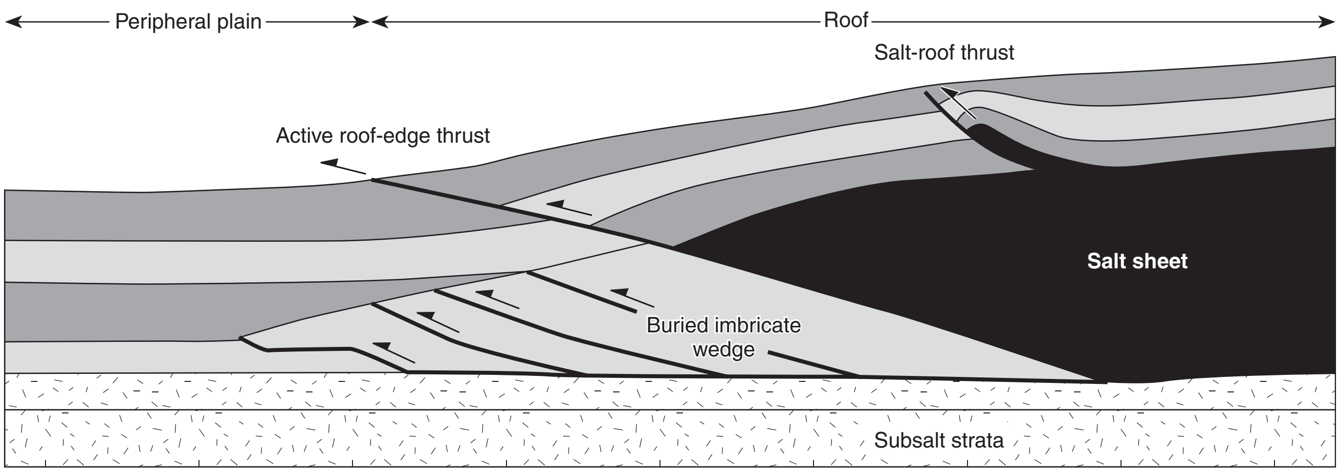

Fig. 7. Schematic cross-section of three types of thrusts in front of advancing salt canopies. (1) Roof-edge thrusts cut upsection from the salt tip and separate the condensed roof of the salt from the adjoining peripheral plain. (2) Imbricate wedges of thrusted peripheral-plain strata detach on a sole thrust rooted in the tip or base of the salt canopy. (3) Salt-roof thrusts, which shorten the roof of the canopy, are much rarer than the other two types of thrusts so are not discussed here. After Hudec & Jackson (2009).

The internal structures of most diapirs are complex (e.g. Balk 1949; Dixon 1975; Talbot & Jackson 1987; Jackson & Talbot 1989; Talbot & Aftabi 2004; Talbot *et al.* 2009). Outward intrusive plumes may further complicate the internal structure of a diapir. The models in Figure 3 show intricately refolded folds as the source layer mingled with salt originally in the diapir. Both deformed further as they intruded as an outward plume. This complexity makes it difficult to predict where even closely spaced drilling might intersect repeated anomalous layers in, for example, a potash mine. Such layers could be highly ductile potash beds (commonly sylvite and carnallite), which increase the risk of a borehole closing, or they could be shale inclusions, as in Belle Isle and Weeks Island salt mines (Gulf of Mexico; Kupfer 1974, 1980). Inclusions might increase the risk of abrupt changes in pore pressures, especially where the inclusions are continuous.

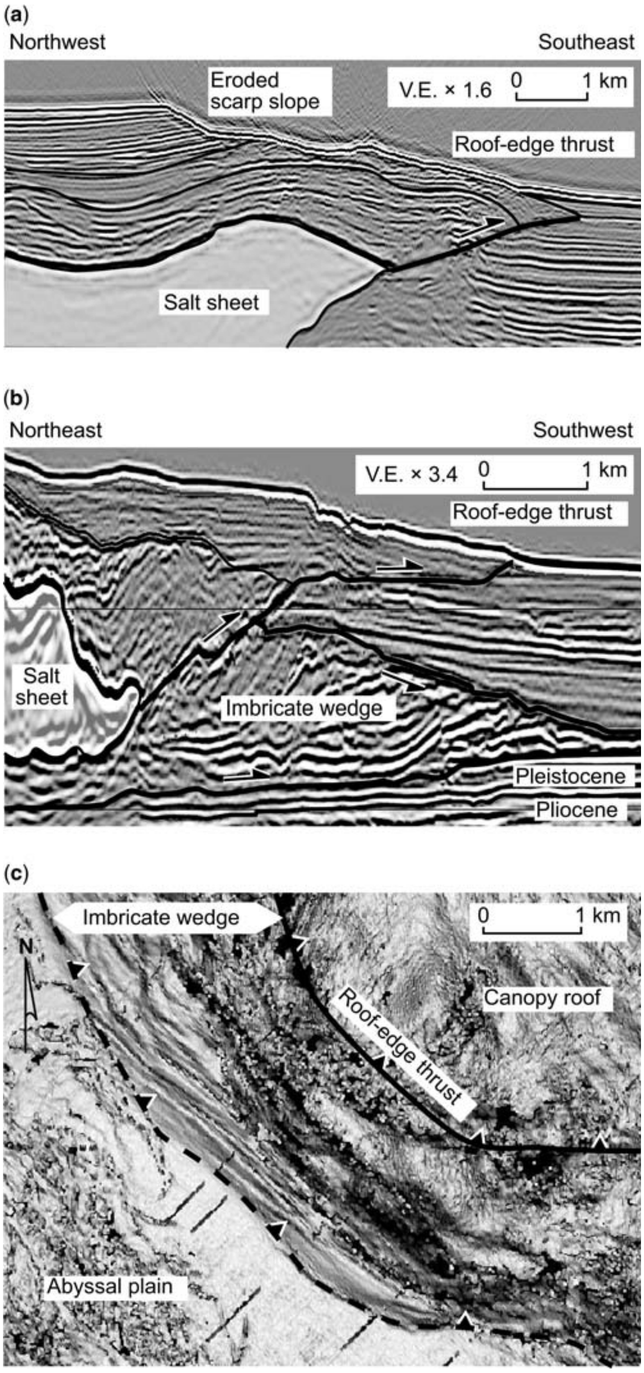

Fig. 8. Thrusts in front of advancing salt canopies in three different areas in the northern Gulf of Mexico. (**a**) A roof-edge thrust, Green Canyon area. (**b**) An imbricate wedge offset by a roof-edge thrust, Alaminos Canyon area. Horizontal lines are depth contours. (**c**) Dip map of a Pleistocene surface mapping the top of a buried imbricate wedge; backthrusts, which are rare in this setting, corrugate the top of the wedge into parallel ridges trending NW. Pre-stack depth-migrated seismic images (a) courtesy of BP, Unocal, and BHP Billiton; (b) and (c) courtesy of CGGVeritas. After Heyn *et al.* (2008).

Canopy-margin thrust systems

Since the early 1990s, geoscientists have inferred that salt canopies advance extrusively as submarine salt glaciers (McGuinness & Hossack 1993; Fletcher *et al.* 1995). Extrusive advance applies to unburied and partly buried salt sheets. However, almost all salt canopies in modern marine settings are almost completely buried by sedimentary roofs (Fig. 2). A completely buried canopy can advance only if its roof overthrusts sediments in front (Fig. 6). The canopy and its roof advance together, which minimizes dissolution (Jackson & Hudec 2004; Hudec & Jackson 2009) as exemplified by the Sigsbee Escarpment in the northern Gulf of Mexico. The escarpment has a great-circle length of 560 km and a buried, sinuous length of *c.* 1100 km, making it the longest near-surface salt structure in the world. The escarpment follows the inflated leading edge of salt canopies. Roughly 60% of the escarpment is advancing, almost entirely by thrusting. Salt is exposed along less than 1% of the escarpment length, so extrusive advance is minor today.

Along the Sigsbee Escarpment, frontal thrusts can be divided into three parts (Fig. 7). A single roof-edge thrust commonly links the tip of the salt canopy to the seafloor (Fig. 8a). The hanging wall of the roof-edge thrust comprises the canopy and its sedimentary roof, which is a stratigraphically condensed carapace. The overridden footwall comprises a peripheral plain of uncondensed strata. An imbricate wedge of subsidiary thrusts can shorten the peripheral strata. Onlapping peripheral strata bury the imbricate wedge once the wedge is no longer active (Fig. 8b, c). If so, the canopy continues to advance on a large roof-edge thrust, which overrides any imbricate wedge. Frontal thrusts also sporadically fringe salt canopies landwards of the Sigsbee Escarpment.

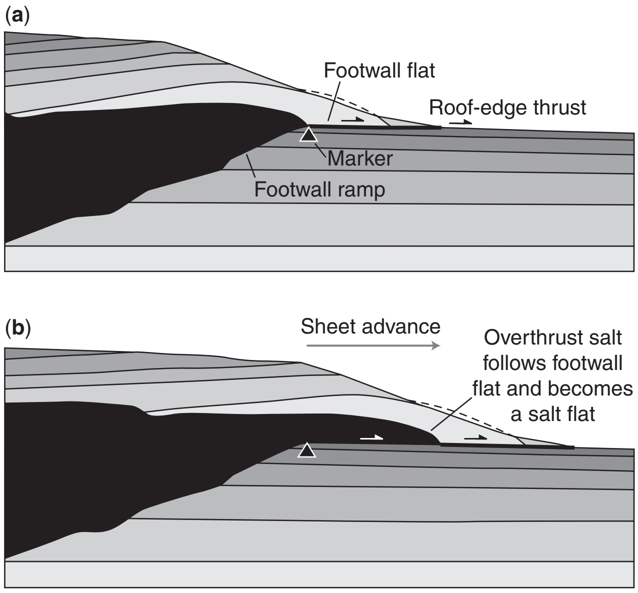

Fig. 9. Schematic cross-sections showing how a thrust flat (**a**) can later become a salt flat (**b**) as a salt canopy advances along the thrust. This change creates ambiguities in interpreting a stepped base of salt.

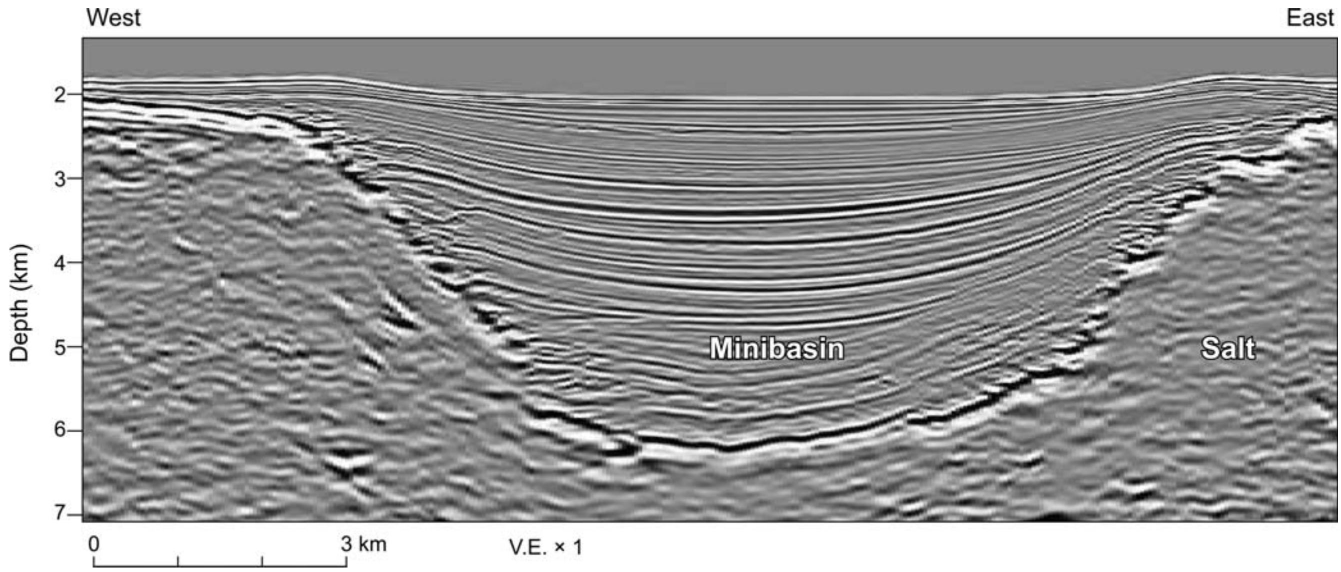

Fig. 10. A simple U-shaped minibasin sunk 4 km into a shallow salt canopy in Walker Ridge area, northern Gulf of Mexico. Pre-stack depth-migrated seismic image from Hudec *et al.* (2009), courtesy of CGGVeritas.

Evidence suggests that roof-edge thrusts continue along the base of the salt sheet for at least a few kilometres landwards (Hudec *et al.* 2009). A top-salt detachment would require a hanging-wall flat above the roof-edge thrust, which is rare. A short hanging-wall flat may be present in Figure 8a, so detachment along the top of salt might have contributed slip to the roof-edge thrust. However, Figure 8b lacks a hanging-wall flat and is far more typical. More fundamentally, the condensed hanging wall has age-equivalent cutoffs against the base of the salt sheet. Thus both the salt and its roof are in the hanging wall, and the detachment must follow the base of salt.

The preponderance of thrusting along the Sigsbee Escarpment affects how we interpret the origin of the stepped base of salt canopies. Segments of the stepped base of salt concordant with underlying strata are known as ‘salt flats’. Conversely, markedly discordant segments are called ‘salt ramps’. Since the early 1990s, salt ramps and flats have been attributed to variable rates of aggradation. A salt flat is inferred to mark a hiatus when salt extrusion was unhindered by sedimentation. Conversely, a salt ramp records when sedimentation accelerated, forcing extrusive salt to climb seawards over accumulating sediments.

This conventional interpretation of salt ramps and flats is invalid when a salt canopy is completely buried. Thrusting can create ramps and flats independent of aggradation rate during thrusting. As the thrust cuts through strata, variations in sediment strength create ramps and flats in the footwall (Fig. 9). As the canopy advances along the thrust, the base of the advancing canopy conforms to the stepped shape of the thrust footwall. As salt advances, footwall flats become salt flats; footwall ramps become salt ramps. Thus, both extrusion and thrusting form steps in the base of canopies. The geometry of the base is ambiguous and does not reveal the mechanism.

The ambiguity grows because most buried salt canopies advance first by extrusion and then by thrusting if they advance after burial. How can we infer when thrust advance began? The key is the age of the oldest roof strata. This age is rarely known in thin roofs because most subsalt wells in the deepwater Gulf of Mexico are drilled riserless for the first 600–900 m depth through suprasalt strata (R. Pilcher, pers. comm. 2009). However, where known, the age of the oldest roof strata records when a salt canopy was finally buried and extrusion changed to thrusting. At that stage, ramps and flats take on a different significance.

Minibasin triggers

Dish-shaped minibasins sinking into a broad salt canopy are deceptively simple (Figs 2 & 10), but within their synclinal form lies the puzzle of how they are initiated. Weakly compacted siliciclastic sediments are less dense than salt, so a sedimentary lens floats like an iceberg in a sea of salt (Fig. 11). Added sediments tend to be diverted off the structural high and pile up elsewhere – an unpromising start for a minibasin. How then do minibasins start to form and how do they deepen enough for sediments to compact and sink into the salt by negative buoyancy? This problem has been known for decades but has been largely ignored as just another mystery of salt tectonics, although some authors have invoked lateral variations in thickness and density to explain why buoyant sediments can sink into salt (e.g. Jackson & Talbot 1986; Kehle 1988; Cohen & Hardy 1996; Ge *et al.* 1997; Waltham 1997; Stewart & Clark 1999).

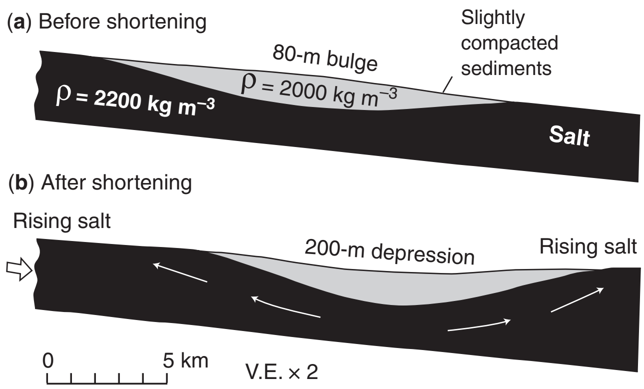

Fig. 11. Finite-element model showing the effects of gravity and regional shortening on a 1 km-thick lens of slightly compacted sediment floating on a salt canopy. (**a**) Because of its low density, the sedimentary lens floats 80 m above the surrounding salt. Extra sediments would be deflected off the bathymetric bulge and stacked on each side, so the lens does not become a minibasin. (**b**) After regional shortening, a similar lens of sediment becomes a local depression because passive diapirs rise on each side. Diapiric rise creates space for more sediments to form a minibasin. The minibasin was part of a 50 km-long model tilted 3° to the right. After Hudec *et al.* (2009).

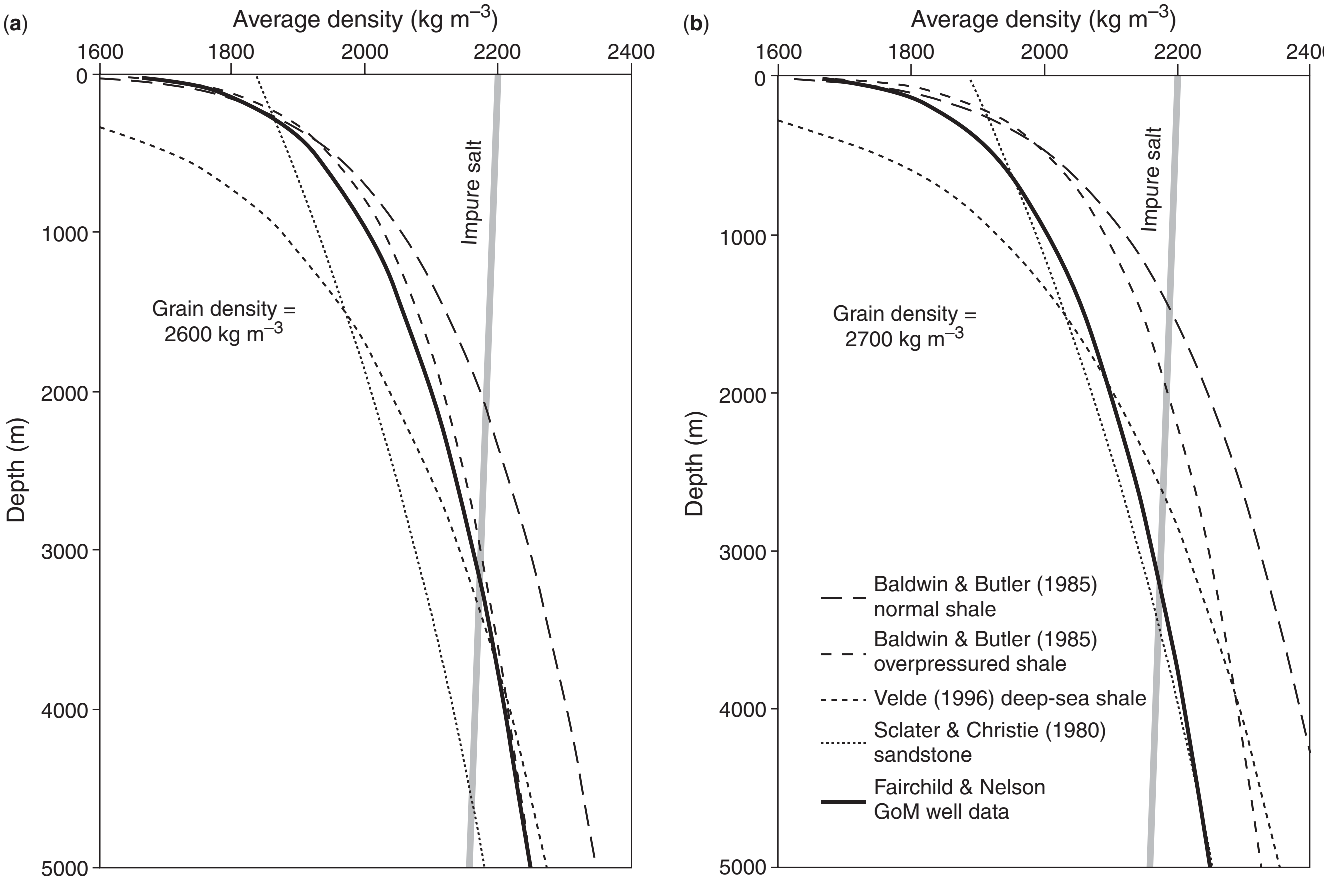

Fig. 12. Best-fit curves of depth v. average density for the entire sedimentary column in siliciclastic rocks. Compacting siliciclastic sediments must be at least 2–3 km thick before they become denser than salt. The thick black line is based on density measurements from sidewall cores and density logs (L. Fairchild & T. Nelson, pers. comm. 1989). The other curves are based on solidity measurements, assuming two different average densities of grains; an assumed grain density of 2600 kg m^{-3} (**a**) fits the measured bulk densities better than does a grain density of 2700 kg m^{-3} (**b**). The density of halite (thick grey line) at room temperature is *c*. 2160 kg m^{-3}. Typical rock salt containing anhydrite impurities has a density rounded off to 2200 kg m^{-3}, which decreases slightly on burial because of the high thermal expansion coefficient of halite. Curves compiled by Hudec *et al.* (2009), except that of salt, which is from Jackson & Talbot (1986).

Density profiles suggest that the problem is extreme. Impure rock salt is slightly denser than halite, *c.* 2200 km m^{-3}. During burial, salt is virtually incompressible (Heard *et al.* 1975) and its density decreases slightly as the crystalline rock salt warms and expands (Fig. 12). Siliciclastic sediments compact to densities equal to salt at burial depths of 1000–2000 m. However, only the deepest sediments are this dense. For the average density of the entire overburden to equal the density of salt, siliciclastic sediments must be 2000–4000 m thick, especially in overpressured basins (Fig. 12) (Hudec *et al.* 2009). Only at depths of several kilometres will

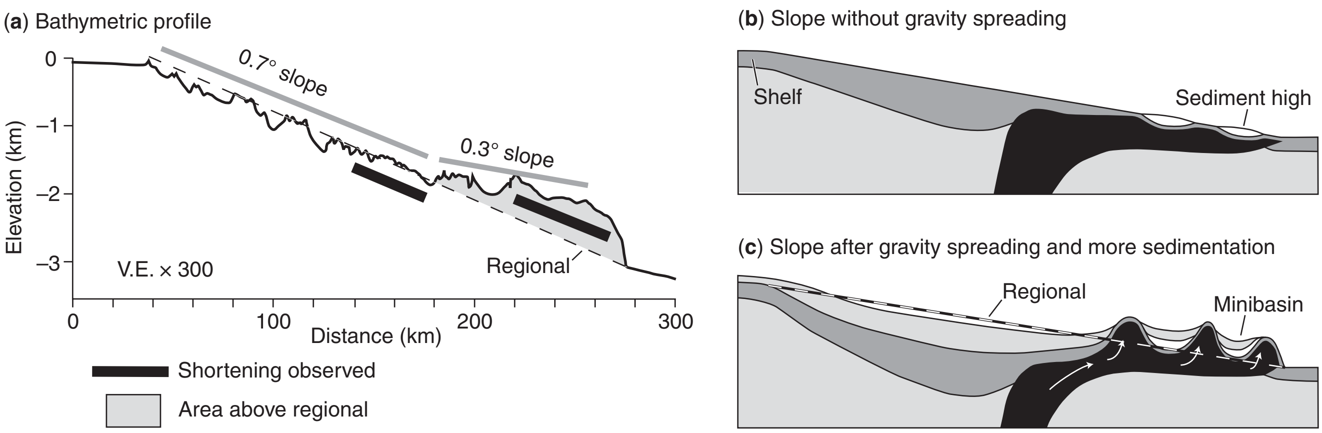

Fig. 13. Regional bathymetry can control where shortening initiates minibasins. (**a**) Bathymetric profile of the continental slope along longitude 92°35′W in the northern Gulf of Mexico; bathymetric data from Divins & Metzger (2007). The concept of an elevated lower slope trapping minibasins is from Rowan (2002). (**b**) and (**c**) Schematic cross-sections showing that in the compressed, uplifted area of the lower slope, both salt and sediment rise, but the more mobile salt diapirs rise above the adjoining minibasins.

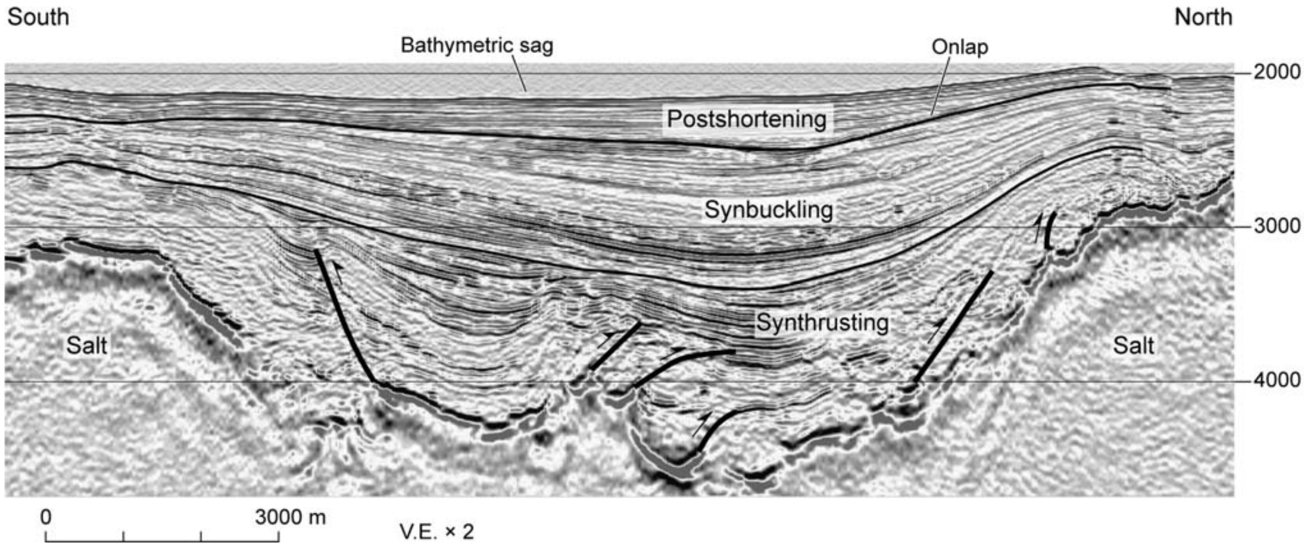

Fig. 14. Thrust faults offset the top of a salt canopy in a minibasin, Walker Ridge area, northern Gulf of Mexico. Thrusting occurred during stage 1, as shortening depressed the low-density sedimentary roof into the salt. After stage 1 thrusting ended, continued mild shortening depressed the minibasin further during stage 2. After shortening ended and stage 3 began, the minibasin compacted enough to sink by negative buoyancy. Pre-stack depth-migrated seismic data courtesy of CGGVeritas, after Hudec *et al.* (2009).

density inversion allow negative buoyancy to drive minibasin subsidence. If thick, dense carbonate or anhydrite layers overlie the salt, the density inversion will be shallower.

If buoyancy cannot initiate siliciclastic minibasins, what does? Five other mechanisms may explain minibasin subsidence when basin fill is less dense than salt (Hudec *et al.* 2009). Three of these appear common in the deepwater Gulf of Mexico: downdip shortening, decay of dynamic bulges and topographic loading. The north-central Gulf of Mexico has two zones of Pleistocene shortening above salt canopies. A landward zone of shortening in the midslope area (Fig. 13a) coincides with its probable cause: a regional break in slope from 0.7° dip to 0.3° dip. A

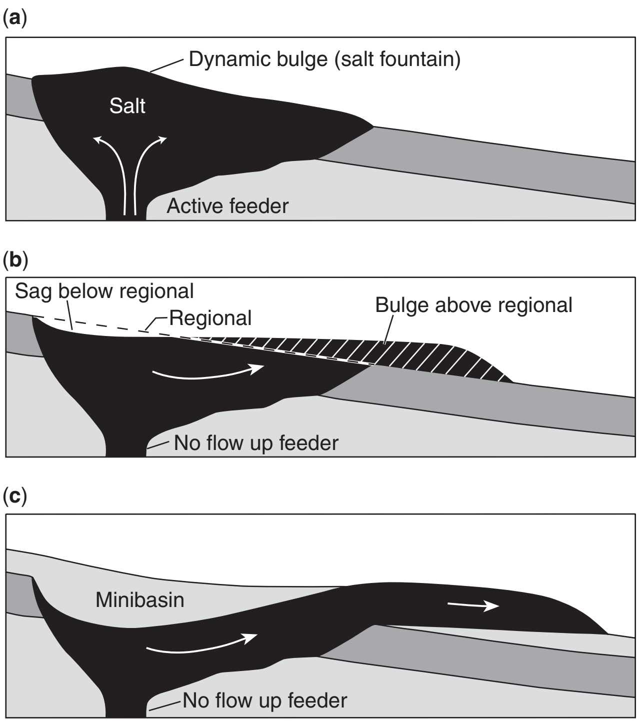

Fig. 15. Schematic cross-sections showing how decay of a dynamic bulge of salt can create a minibasin. (**a**) Above an active feeder, the dynamic pressure of rising salt supports a salt fountain. (**b**) After salt supply wanes, the unsupported salt bulge sags by gravity spreading to form a flat-topped droplet of salt. The updip part of the salt surface sags below regional, creating space for a local depocentre. (**c**) Sediments can gather in the depocentre and further deepen it to form a minibasin. After Hudec *et al.* (2009).

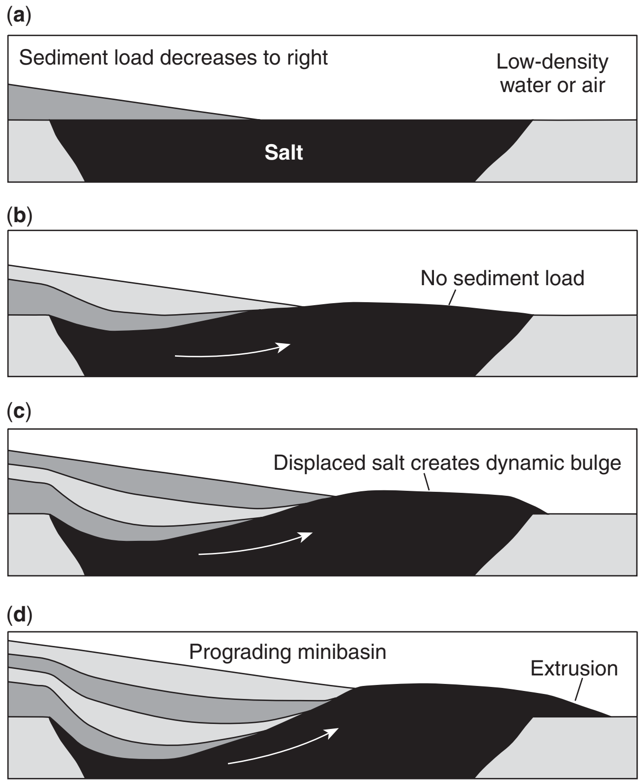

Fig. 16. Schematic cross-sections showing how the differential load of a prograding sedimentary wedge can initiate a minibasin. (**a**) A wedge of uncompacted sediments imposes a differential load because it is much denser than adjoining air or water. (**b**) The differential load causes the thick end of the sedimentary wedge to sink into salt, displacing salt seawards (**c**) and (**d**). After Hudec *et al.* (2009).

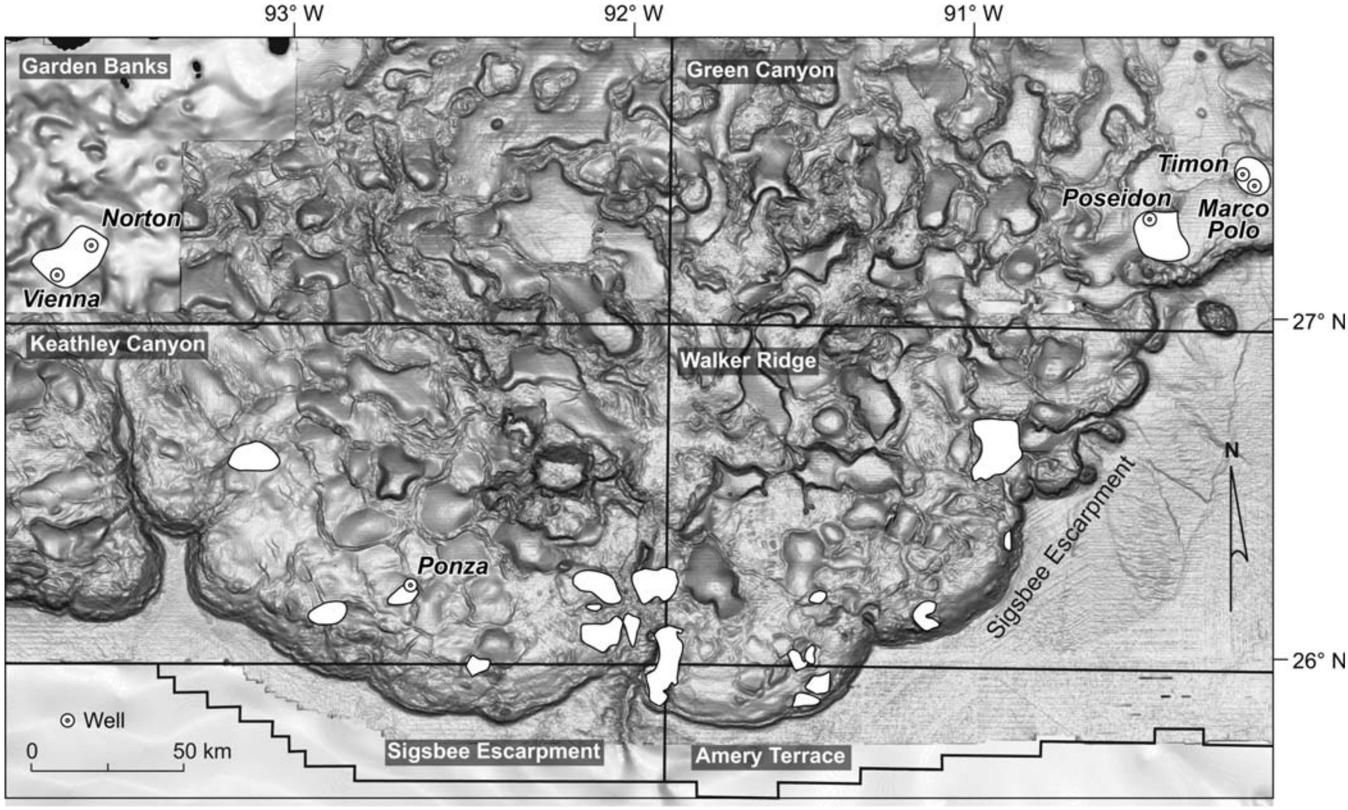

Fig. 17. Allochthonous fragments (white) interpreted to contain Mesozoic to Miocene strata at anomalously shallow burial depths in the northern Gulf of Mexico. Fragments are recognized by combinations of well penetrations from six wells, seismic character and high seismic velocities. Salt carried the exotic fragments seawards to collect near the front of the spreading Sigsbee salt canopy, which is marked by the Sigsbee Escarpment. Fragment map courtesy of Shell E&P Company, after Kilby *et al.* (2008), except for addition of Marco Polo (Mount *et al.* 2006) and Poseidon minibasins. Base map shows first derivative of bathymetric data from Bryant & Liu (2000).

seaward zone of shortening in the toe of the gravity-spreading system is raised above regional (Fig. 13a). As the canopy shortens and thickens, both salt and the floating lenses of overburden rise above regional. However, the laterally squeezed diapirs rise more than the intervening sediment lenses, leaving the minibasins as synclinal depressions perched on the inflated canopy (Fig. 13c). A compressional origin of minibasins was proposed on the basis of geometric reasoning by Rowan (2002) and later simulated by numerical modelling (Fig. 11). As further evidence, the deepest sediments in some minibasins near the Sigsbee Escarpment have been thrust (Fig. 14). Thrusting was the first of three evolutionary stages of minibasin subsidence, so a compressional trigger is plausible.

Many minibasins lack evidence of early thrusting. This lack of evidence does not preclude mild shortening that affected only intervening salt diapirs but may indicate that other mechanisms initiated minibasins. One mechanism could be the decay of salt topography above an ebbing salt feeder (Fig. 15). An emergent diapir fed by strong salt flow has a smoothly rounded summit, like a slow-moving fountain (Bailey 1931; Talbot & Jarvis 1984). The dynamic pressure of rising salt supports the bulging summit. Once upward flow ebbs, the dynamic bulge decays as the salt settles under gravity towards a flat-topped profile (Talbot 1998). The updip part of the flattening salt may sag below the sediment surface, accommodating sediments in a deepening minibasin.

Another way to trigger a minibasin without a density inversion is by the well recognized mechanism of topographic loading (Fig. 16). A wedge of sediment prograding across a flat-topped, emergent stock applies a differential load that increases toward the thick end of the wedge, which sinks fastest, regardless of density. The thick end sags as long as topography exists. Each

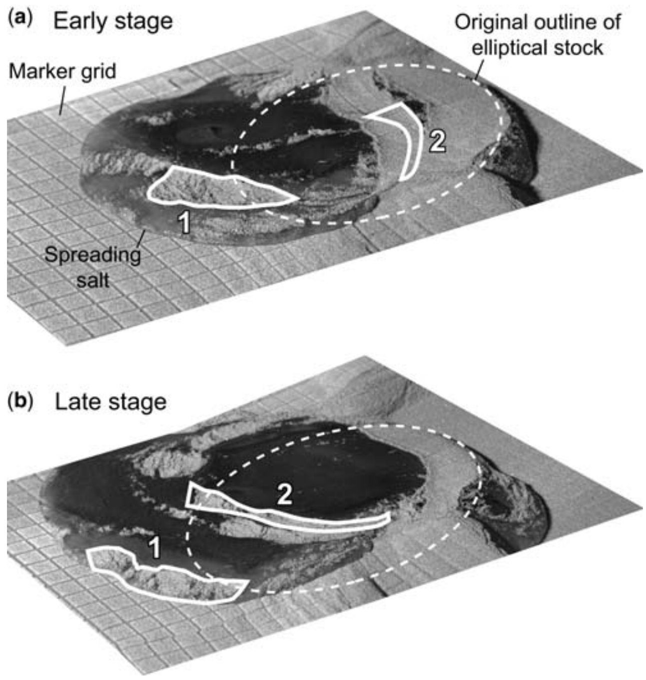

Fig. 18. Disruption of a thin roof above an extruding salt stock, shown in oblique views of a physical model. Lateral shortening forced salt to pierce and disperse a once-continuous sedimentary roof. (**a**) Extrusive salt carried roof fragment 1 almost to the salt front; fragment 2 had only begun to fracture. (**b**) Fragment 1 became stranded at the salt front, like a terminal moraine; fragment 2, now separated, was still being carried by spreading salt.

increment of sagging creates space for more sediment in the deepening minibasin.

Eroding a canyon into salt and filling it with sediments could initiate a minibasin, but only if the canyon was several kilometres deep and filled in a geological instant before the salt could respond to unroofing. More realistically, salt in the floor of an eroded canyon would well up faster than sediments could fill it, thereby inverting and destroying the canyon, as along most of Bryant Canyon where it crossed the Sigsbee salt canopy (Lee *et al.* 1996).

The mechanisms of compression, decay of salt topography and topographic loading are independent of density, thereby explaining a long-standing puzzle of how minibasins first form when loaded by siliciclastic sediments. The problem disappears in compacted minibasins more than 2–3 km thick, where negative buoyancy becomes the main force for subsidence.

Allochthonous fragments

Marine salt canopies are eventually dissolved or buried by a sedimentary carapace. Subparallel carapace strata tend to be stratigraphically condensed because they collect hemipelagically over a salt-induced bulge in the seafloor (Hart *et al.* 2004). As the canopy spreads further it may dismember a carapace into pieces that can be carried by flowing salt. The pieces are likely to be carried most effectively by freely extruding salt. A carapace fragment can be tilted or folded or come to rest subconformably on a salt weld. However, because of its distinctive character, a carapace fragment may still be recognizable as a piece of disrupted roof even when deformed or buried.

Salt flow may carry pieces of its roof basinward like glacial erratics for up to tens of kilometres, although the distance of transport is still speculative (Fig. 2). Many Mesozoic to Miocene fragments have been interpreted as salt-borne exotic pieces (Fig. 17) (Hart *et al.* 2004; Kilby *et al.* 2008). The fragmented slabs are up to 25 km in breadth and are a few kilometres thick. Two stages of a physical model (Fig. 18) show how diapiric salt can break a thin roof and widely disperse the pieces. The spreading salt strands the carapace pieces near the front of a waning flow or overrides them in a vigorous flow.

Exotic pieces are typically perched anomalously high above salt rather than buried many kilometres deeper with coeval strata. A notable example of a perched fragment was in the Norton discovery well in GB-754 (Hart *et al.* 2004; Fig. 17). The well intersected a moderately condensed Jurassic-to-Palaeogene interval overlain by condensed Neogene strata. The Mesozoic kerogen is thermally immature, so the strata were never deeply buried. The lack of

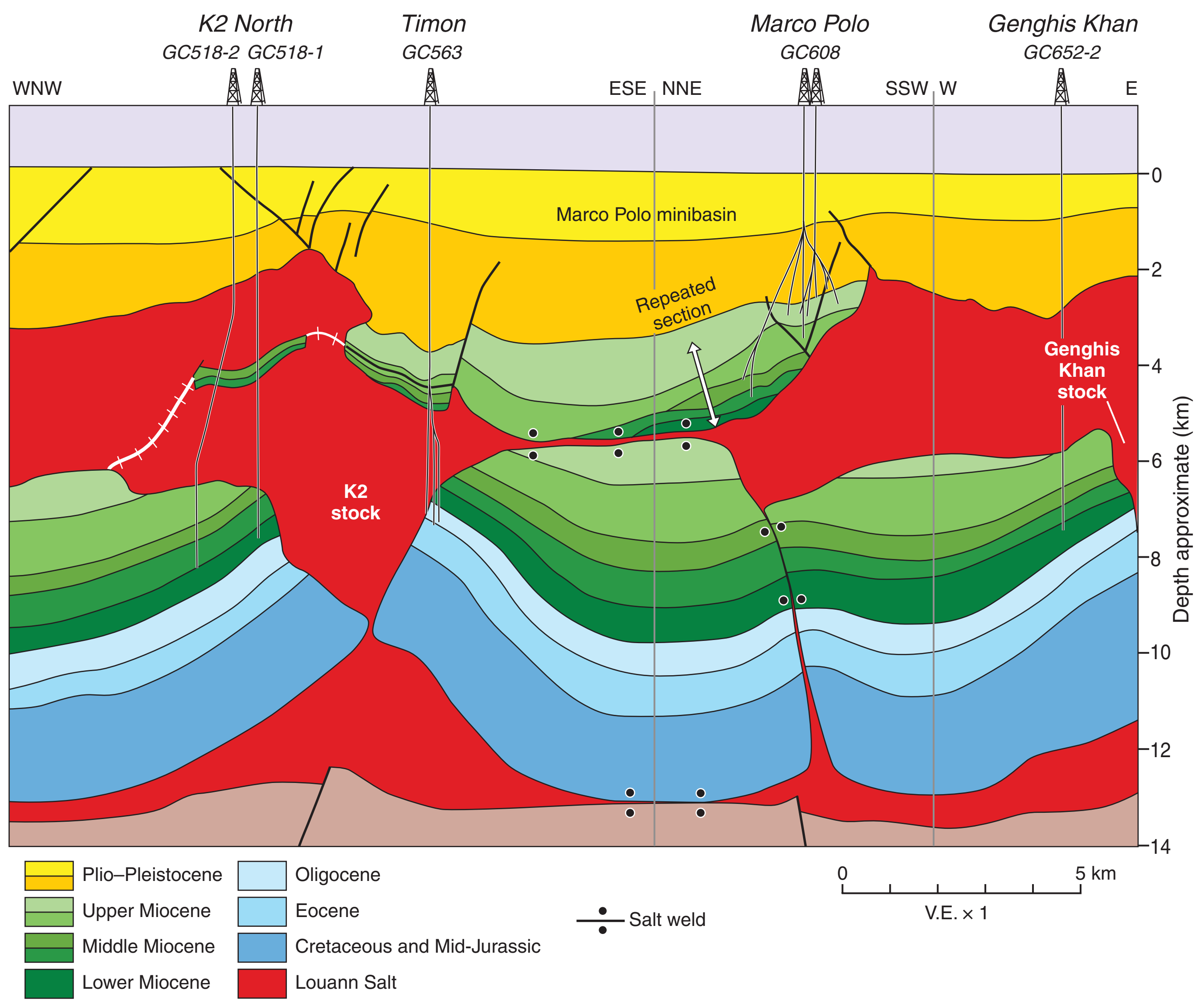

Fig. 19. Suprasalt Miocene strata *c.* 1500 m thick in the Marco Polo minibasin overlie coeval subsalt strata, Green Canyon area, northern Gulf of Mexico. A few kilometres NW of Marco Polo minibasin, condensed Oligocene and Lower Miocene strata are encased within the canopy. Encased strata mark a suture where a salt sheet merged with the K2 stock. After Mount *et al.* (2006).

repeated section suggests the Norton fragment is in place. The carapace fragment is flanked by deeper Pleistocene minibasins.

Besides their unusually shallow depth, some exotic fragments are stratigraphic duplicates. A prime example is the Marco Polo minibasin (Figs 17 & 19). About 1500 m of Oligo-Miocene strata in the minibasin overlie a thinned or welded salt canopy (Mount *et al.* 2006). At the base of the minibasin, condensed Lower Miocene strata represent the formerly elevated roof strata of the canopy. Below the salt canopy are repeated coeval strata. This stratigraphic duplication suggests that from the latest Miocene onwards, basinward-flowing salt carried the exotic fragment laterally over coeval strata.

Such a large exotic fragment can only be carried by a thick salt canopy. The thickness of repeated section in the Marco Polo minibasin is *c.* 1800 m, equivalent to *c.* 2100 m when uncompacted. The spreading salt must have been at least as thick as *c.* 2100 m; perhaps even thicker to overcome basal drag of the entrained minibasin. Is this thickness realistic for spreading salt? Analogy with salt glaciers spreading subaerially in the Zagros Mountains (Talbot & Jarvis 1984; Talbot 1998; Talbot *et al.* 2000) and buried below the Sigsbee Escarpment suggests that an unimpeded salt glacier flows across a flat surface with a thickness of 1000 m or less. That is too thin to carry a 2100 m-thick minibasin, even if its average density was less than that of salt. However, a spreading salt canopy can thicken by ponding against structural and sedimentary buttresses (Fig. 20). In this schematic restoration, by the end of the Pliocene an anticline of the Atwater fold belt formed a structural buttress 2600 m high. Then rapid early Pleistocene aggradation built a sedimentary buttress, which further ponded salt flow. Together both types of buttress allowed the salt canopy to thicken to as much as 5200 m, which would have been enough to entrain a minibasin thicker than the Marco Polo minibasin (Fig. 20).

Where do these exotic fragments originate? Imagine a possible sequence of events, partly shown in Figure 20. Initially, a minibasin sank into a broad diapir, which flared upward into a salt canopy. Next the canopy inflated and carried the minibasin basinward by viscous traction across subsalt strata coeval with the minibasin. As a result, Miocene and Palaeogene stratigraphy became repeated. Left behind was a stratigraphic gap from which the exotic fragment was plucked. The gap must have been at least as wide and as deep as the minibasin that originally nestled within the evacuated diapir. After salt evacuation Plio-Pleistocene strata could fill that Miocene gap.

Where kilometre-scale exotic pieces travel far from their source, stratigraphic prediction in a complexly deformed basin is even more difficult. These exotic pieces create odd stratigraphic repetitions. Stratigraphic gaps remain from where they were plucked, which could be many kilometres away. Despite the challenge, linking the source and destination of an exotic fragment would greatly improve structural restoration. Knowing the breadth and thickness of an exotic fragment provides clues to the size of the source gap and the thickness of the salt canopy that carried it. Knowing the thickness, a restoration can include enough structural and stratigraphic buttresses behind which the canopy can thicken.

Exotic fragments also provide stark evidence of high strains in salt canopies. As a canopy carries exotic slabs, it shears internally. This inherent shear is shown by deformed grids of numerical models or by streaked-out markers in physical models. During shear, former roof strata trapped as sutures within a salt canopy are extremely stretched into thin wisps or blocky boudins, some of which can be recognized on 3D seismic (Liro *et al.* 2004) and in physical models (Dooley *et al.* 2008). Even without exotic fragments, field observations suggest that salt recrystallizes readily,

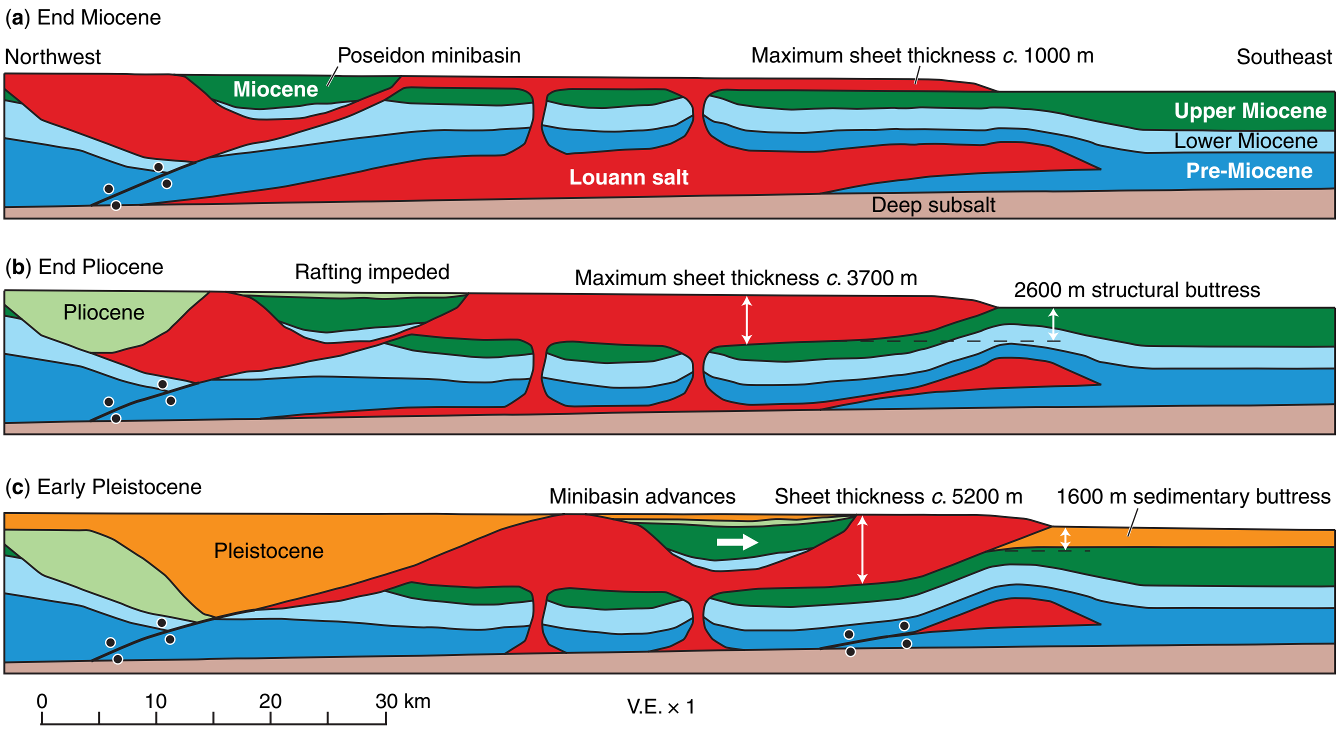

Fig. 20. Schematic restoration showing how a spreading salt canopy can carry an allochthonous minibasin seawards during the Pleistocene. (**a**) The original Miocene location of the minibasin is unknown, but the restoration shows a stratigraphic gap into which the Miocene strata may have fitted. (**b**) The salt canopy thickened by ponding against a late Miocene anticline, but this thickening was still not enough to carry the minibasin. (**c**) Rapid aggradation of lower Pleistocene sediments further thickened the salt canopy enough to transport the minibasin seawards. Vertical scale is only approximate but shows the initial thickness of Louann salt as *c.* 4 km, a thickness used in other restorations (Peel *et al.* 1995). However, the autochthonous salt layer has been variably inflated and deflated, expelled to several canopy levels, and lost to the world ocean, so estimates of the original thickness are highly speculative.

losing its strain memory (Talbot 1979). Even so, shear is likely to create an anisotropic fabric in the salt. This fabric anisotropy may cause an equivalent seismic anisotropy. Seismic anisotropy is poorly understood, but it could affect how accurately the shape and depth of the base of salt is predicted from seismic data.

State of knowledge

The abstract summarizes our current understanding of how diapiric salt can intrude downwards into a source layer, how salt canopies can advance despite being completely buried, how minibasins can form even when loaded by low-density sediments, and how the fragmented remnants of a canopy roof travel laterally to leave gaps and duplicate stratigraphy. Despite these significant advances, it is well to reflect on what we do not understand about these processes.

How much must natural diapirs shorten before they intrude their source layer? Does the outward plume from a squeezed diapir thicken only the nearby source layer? How does thickening affect the temperature of the source-layer salt and influence maturation?

Where buried salt canopies advance by thrusting, does the thrust root into the basal contact of the salt, or into a shear zone within the salt, or into an overpressured rubble zone below the salt? Can we use thrust style to predict overpressure below the salt canopy? Do imbricate wedges form rapidly or slowly? How widespread are thrust structures at the front of spreading canopies other than along the Sigsbee Escarpment?

If minibasins form when loaded by uncompacted sediments, which is the most important mechanism: compression, decay of dynamic bulge, or topographic loading? Are there regional zones where one mechanism dominates? How well do we understand the dynamics of shortening in salt canopies on the lower continental slope?

If exotic fragments of a salt-canopy roof can travel far, what proportion of these pieces have we been able to recognize? In what setting do the pieces originate? What determines whether a fragment is carried? Where and why are allochthonous fragments stranded? Will we be able to restore them all to their original positions in three dimensions? Once restored, can we infer trends and patterns in the distribution of source rocks and reservoirs?

To take a step further, what surprising or puzzling new processes will emerge in another 10 years?

The project was funded by the Applied Geodynamics Laboratory consortium, comprising the following companies: Anadarko, BHP Billiton, BP, CGGVeritas, Chevron, Cobalt, ConocoPhillips, Devon, ENI, ExxonMobil, Fugro, GX Technology, Hess, IMP, Maersk, Marathon, Mariner, Maxus, Murphy, Nexen, Noble, Pemex, Petrobras, PGS, Samson, Saudi Aramco, Shell, StatoilHydro, TGS-NOPEC, Total and Woodside. The authors received additional support from the Jackson School of Geosciences, The University of Texas at Austin. F. Diegel kindly provided his unpublished map of exotic fragments. Robin Pilcher and an anonymous reviewer provided insightful, helpful suggestions to improve the paper. We thank CGGVeritas and BP, BHPBilliton and Unocal for allowing us to reproduce seismic data. GeoLogic provided *LithoTect* software for the restoration in Figure 20. Publication was authorized by the Director, Bureau of Economic Geology, Jackson School of Geosciences, The University of Texas at Austin.

References

Bailey, E. B. 1931. Salt plugs. *Geological Magazine*, **68**, 335–336.

Baldschuhn, R., Binot, F., Frisch, U. & Kockel, F. 2001. Geotektonischer Atlas von Nordwest-Deutschland und dem deutschen Nordsee-Sektor. *Geologisches Jahrbuch*, **A 153**, 3 CD-ROM.

Baldwin, B. & Butler, C. O. 1985. Compaction curves. *American Association of Petroleum Geologists Bulletin*, **69**, 622–626.

Balk, R. 1949. Structure of Grand Saline salt dome, Van Zandt County, Texas. *American Association of Petroleum Geologists Bulletin*, **33**, 1791–1829.

Bryant, W. R. & Liu, J. Y. 2000. *Bathymetry of the Gulf of Mexico (TAMU-SG-00-606)*. Texas Sea Grant, College Station, TX, CD-ROM.

Chemia, Z. & Koyi, H. 2008. The control of salt supply on entrainment of an anhydrite layer within a salt diaper. *Journal of Structural Geology*, **30**, 1192–1200.

Cohen, H. A. & Hardy, S. 1996. Numerical modeling of stratal architecture resulting from differential loading of a mobile substrate. *In*: Alsop, G. I., Blundell, D. J. & Davison, I. (eds) *Salt Tectonics*. Geological Society, London, Special Publications, **100**, 265–273.

Divins, D. L. & Metzger, D. 2007. *NGDC Coastal Relief Model*. World Wide Web Address: http://www.ngdc.noaa.gov/mgg/coastal/coastal.html.

Dixon, J. M. 1975. Finite strain and progressive deformation in models of diapiric structures. *Tectonophysics*, **28**, 89–124.

Dooley, T. P., Jackson, M. P. A. & Hudec, M. R. 2006. Allochthonous salt extrusion, roof dispersion, and intrusive import and export of salt in squeezed stocks (abstract). *American Association of Petroleum Geologists Annual Convention and Exhibition Abstracts Volume*, **15**, 27.

Dooley, T., Monastero, F. C. & McClay, K. R. 2007. Effects of a weak crustal layer in a transtensional pull-apart basin: results from a scaled physical modeling study. *EOS*, **88**, Abstract V53F-04.

Dooley, T., Hudec, M. R. & Jackson, M. P. A. 2008. Dismembered sutures formed during asymmetric salt-sheet collision (abstract). *American Association of Petroleum Geologists 2008 Annual Convention and Exhibition Abstracts Volume*, **17**, 46.

Dooley, T. P., Jackson, M. P. A. & Hudec, M. R. 2009. Inflation and deflation of deeply buried stocks during lateral shortening. *Journal of Structural Geology*, **31**, 582–600.

Escher, B. G. & Kuenen, P. H. 1929. Experiments in connection with salt domes. *Leidsche Geologiese Meddelanden*, **3**, 151–182.

Fletcher, R. C., Hudec, M. R. & Watson, I. A. 1995. Salt glacier and composite sediment-salt glacier models for the emplacement and early burial of allochthonous salt sheets. *In*: Jackson, M. P. A., Roberts, D. G. & Snelson, S. (eds) *Salt Tectonics: A Global Perspective*. American Association of Petroleum Geologists, Tulsa, OK, Memoirs, **65**, 77–108.

Ge, H., Jackson, M. P. A. & Vendeville, B. C. 1997. Kinematics and dynamics of salt tectonics driven by progradation. *American Association of Petroleum Geologists Bulletin*, **81**, 398–423.

Giles, K. A. & Lawton, T. F. 2002. Halokinetic sequence stratigraphy adjacent to the El Papalote diapir, northeastern Mexico. *American Association of Petroleum Geologists Bulletin*, **86**, 823–840.

Hall, S. H. 2002. The role of autochthonous salt inflation and deflation in the northern Gulf of Mexico. *Marine and Petroleum Geology*, **19**, 649–682.

Hart, W. H., Jaminski, J. & Albertin, M. 2004. Recognition and exploration significance of supra-salt stratal carapaces. *24th Bob F. Perkins Research Conference*, Gulf Coast Section, Society for Sedimentary Geology (SEPM), 166–199.

Heard, H. C., Abey, A. E., Bonner, B. P. & Duba, A. 1975. *Stress–strain behavior of polycrystalline NaCl to 3.2 GPa*. Lawrence Livermore Laboratory Report, **UCRL-51743**, 16.

Heyn, T., Jackson, M. P. A. *et al*. 2008. Accretionary-wedge shortening caused by advance of the Sigsbee Escarpment, Alaminos Canyon, Gulf of Mexico (abstract). *American Association of Petroleum Geologists Annual Convention and Exhibition Abstracts Volume*, **17**, 89–90.

Hudec, M. R. 2004. Salt intrusion: time for a comeback? *24th Bob F. Perkins Research Conference*, Gulf Coast Section, Society for Sedimentary Geology (SEPM), 120–132.

Hudec, M. R. & Jackson, M. P. A. 2004. Regional restoration across the Kwanza Basin, Angola: salt tectonics triggered by repeated uplift of a metastable passive margin. *American Association of Petroleum Geologists Bulletin*, **88**, 971–990.

Hudec, M. R. & Jackson, M. P. A. 2009. Interaction between spreading salt canopies and their peripheral thrust systems. *Journal of Structural Geology*, **31**, 1114–1129.

Hudec, M. R., Jackson, M. P. A. & Schultz-Ela, D. D. 2009. The paradox of minibasin subsidence into salt: clues to the evolution of crustal basins. *Geological Society of America Bulletin*, **121**, 201–221.

Jackson, M. P. A. 1995. Retrospective salt tectonics. *In*: Jackson, M. P. A., Roberts, D. G. & Snelson, S. (eds) *Salt Tectonics: a Global Perspective.* American Association of Petroleum Geologists, Tulsa, OK, Memoirs, **65**, 1–28.

Jackson, M. P. A. & Hudec, M. R. 2004. A new mechanism for advance of allochthonous salt sheets. *24th Annual Bob F. Perkins Research Conference*, Gulf Coast Section, Society for Sedimentary Geology (SEPM), 220–242.

Jackson, M. P. A. & Talbot, C. J. 1986. External shapes, strain rates, and dynamics of salt structures. *Geological Society of America Bulletin*, **97**, 305–323.

Jackson, M. P. A. & Talbot, C. J. 1989. Anatomy of mushroom-shaped diapirs. *Journal of Structural Geology*, **11**, 211–230.

Jackson, M. P. A., Hudec, M. R. & Hegarty, K. A. 2005. The great West African Tertiary coastal uplift: fact or fiction? A perspective from the Angolan divergent margin. *Tectonics*, **24**, TC6014; doi: 10.1029/2005TC001836.

Kadri, M. S., Liro, L. M., Lahr, M. J., Hobbs, R. & Montecchi, P. 2000. Occurrence and distribution of seismic reflectors internal to allochthonous salt, Walker Ridge lease area, deepwater Gulf of Mexico (abstract). *American Association of Petroleum Geologists Annual Convention & Exhibition Abstracts Volume*, 75–76.

Kehle, R. O. 1988. The origin of salt structures. *In*: Schreiber, B. C. (ed.) *Evaporites and Hydrocarbons*. Columbia University Press, New York, 345–404.

Kilby, R. E., Diegel, F. A. & Styzen, M. J. 2008. Age of sediments encasing allochthonous salt in the Gulf of Mexico; clues to emplacement history. *American Association of Petroleum Geologists Search and Discovery Article*, **90078**.

Kupfer, D. H. 1974. Boundary shear zones in salt stocks. Fourth Symposium on Salt. *Northern Ohio Geological Society*, **1**, 215–225.

Kupfer, D. H. 1980. Problems associated with anomalous zones in Louisiana salt stocks, USA. Fifth Symposium on Salt. *Northern Ohio Geological Society*, **1**, 119–134.

Lee, G. H., Watkins, J. S. & Bryant, W. R. 1996. Bryant Canyon fan system: an unconfined, large river-sourced system in the northwestern Gulf of Mexico. *American Association of Petroleum Geologists Bulletin*, **80**, 340–358.

Letouzey, J. & Sherkati, S. 2004. Salt movement, tectonic events, and structural style in the central Zagros fold and thrust Belt (Iran). *24th Annual Bob F. Perkins Research Conference*, Gulf Coast Section, Society for Sedimentary Geology (SEPM), 753–778.

Liro, L. M., Murillas, J., Villalobos, L., Gatenby, G. & Mathur, V. 2004. Salt sutures in single- and multi-tiered allochthons, Green Canyon and Walker Ridge areas, deepwater Gulf of Mexico. *24th Annual Bob F. Perkins Research Conference*, Gulf Coast Section, Society for Sedimentary Geology (SEPM), 200–219.

McGuinness, D. B. & Hossack, J. R. 1993. The development of allochthonous salt sheets as controlled by rates of extension, sedimentation, and salt supply. *In*: Armentrout, J. M., Bloch, R., Olson, H. C. & Perkins, B. F. (eds) *Rates of Geological Processes. Fourteenth Annual Research Conference*, Gulf Coast Section, SEPM Foundation, Program with Papers, 127–139.

Mount, V. S., Rodriguez, A., Chauche, A., Crews, S. G., Gamwell, P. & Montoya, P. 2006. Petroleum system observations and interpretation in the vicinity of the K2/K2-North, Genghis Khan, and Marco Polo fields, Green Canyon, Gulf of Mexico. *Gulf Coast Association of Geological Societies Transactions*, **56**, 613–625.

Nelson, T. H. & Fairchild, L. H. 1989. Emplacement and evolution of salt sills in northern Gulf of Mexico. *American Association of Petroleum Geologists Bulletin*, **73**, 395.

Peel, F. J. 2001. Emplacement, inflation and folding of an extensive allochthonous salt sheet in the Late Mesozoic (ultra-deepwater Gulf of Mexico) (abstract). *American Association of Petroleum Geologists Annual Convention Official Program*, **10**, A155.

Peel, F. J. 2003. Styles, mechanisms and hydrocarbon implications of syndepositional folds in deepwater fold belts; examples from Angola and the Gulf of Mexico. Houston Geological Society: HGS International and HGS Dinner Meeting, December 15, 2003.

Peel, F. J., Travis, C. J. & Hossack, J. R. 1995. Genetic structural provinces and salt tectonics of the Cenozoic offshore U.S. Gulf of Mexico: a preliminary analysis. *In*: Jackson, M. P. A., Roberts, D. G. & Snelson, S. (eds) *Salt Tectonics: a Global Perspective*. Association of Petroleum Geologists, Tulsa, OK, Memoirs, **65**, 153–175.

Rowan, M. G. 2002. Salt-related accommodation in the Gulf of Mexico deepwater: withdrawal or inflation, autochthonous or allochthonous? *Gulf Coast Association of Geological Societies Transactions*, **52**, 861–869.

Rowan, M. G., Lawton, T. F., Giles, K. A. & Ratliff, R. A. 2003. Near-salt deformation in La Popa basin, Mexico, and the northern Gulf of Mexico: a general model for passive diapirism. *American Association of Petroleum Geologists Bulletin*, **87**, 733–756.

Sclater, J. G. & Christie, P. A. F. 1980. Continental stretching: an explanation of the post-mid-Cretaceous subsidence of the central North Sea basin. *Journal of Geophysical Research*, **85**, 3711–3739.

Stewart, S. A. 2007. Salt tectonics in the North Sea basin: a structural style template for seismic interpreters. *In*: Ries, A. C., Butler, R. W. H. & Graham, R. H. (eds) *Deformation of the Continental Crust: the Legacy of Mike Coward*. Geological Society, London, Special Publications, **272**, 361–396.

Stewart, S. A. & Clark, A. J. 1999. Impact of salt on the structure of the Central North Sea hydrocarbon fairways. *In*: Fleet, A. J. & Boldy, S. A. R. (eds) *Petroleum Geology of Northwest Europe: Proceedings of the 5th Conference*. Geological Society, London, 179–200; doi: 10.1144/0050179.

Talbot, C. J. 1979. Fold trains in a glacier of salt in southern Iran. *Journal of Structural Geology*, **1**, 5–18.

Talbot, C. J. 1998. Extrusions of Hormuz salt in Iran. *In*: Blundell, D. J. & Scott, A. C. (eds) *Lyell: The Past is the Key to the Present*. Geological Society, London, Special Publications, **143**, 315–334.

Talbot, C. J. & Aftabi, P. 2004. Geology and models of salt extrusion at Qum Kuh, central Iran. *Journal of the Geological Society London*, **161**, 1–14.

Talbot, C. J. & Alavi, M. 1996. The past of a future syntaxis across the Zagros. *In*: Alsop, G. I., Blundell, D. J. & Davison, I. (eds) *Salt Tectonics*. Geological Society, London, Special Publications, **100**, 89–110.

Talbot, C. J. & Jackson, M. P. A. 1987. Internal kinematics of salt diapirs. *American Association of Petroleum Geologists Bulletin*, **71**, 1068–1093.

Talbot, C. J. & Jarvis, R. J. 1984. Age, budget and dynamics of an active salt extrusion in Iran. *Journal of Structural Geology*, **6**, 521–533.

Talbot, C. J., Medvedev, S., Alavi, M., Shahrivar, H. & Heidari, E. 2000. Salt extrusion at Kuh-e-Jahani, Iran, from June 1994 to November 1997. *In*: Vendeville, B., Mart, Y. & Vigneresse, J.-L. (eds) *Salt, Shale and Igneous Diapirs in and around Europe*. Geological Society, London, Special Publications, **174**, 93–110.

Talbot, C. J., Aftabi, P. & Chemia, Z. 2009. Potash in a salt mushroom at Hormoz Island, Hormoz Strait, Iran. *Ore Geology Reviews*, **35**, 317–332.

Velde, B. 1996. Compaction trends of clay-rich deep sea sediments. *Marine Geology*, **133**, 193–201.

Vendeville, B. C. & Jackson, M. P. A. 1992. The fall of diapirs during thin-skinned extension. *Marine and Petroleum Geology*, **9**, 354–371.

Waltham, D. 1997. Why does salt start to move? *Tectonophysics*, **182**, 117–128.

Source-to-sink systems on passive margins: theory and practice with an example from the Norwegian continental margin

O. J. MARTINSEN,[1] T. O. SØMME,[2] J. B. THURMOND,[1] W. HELLAND-HANSEN[2] and I. LUNT[1]

[1]*Statoil Research, PO Box 7200, 5020 Bergen, Norway (e-mail: ojma@statoil.com)*
[2]*Department of Earth Sciences, University of Bergen, 5007 Bergen, Norway*

Abstract: Source-to-sink system analysis involves a complete, earth systems model approach from the ultimate onshore drainage point to the toe of related active deepwater sedimentary systems. Several methods and techniques have evolved in recent years, from experimental and numerical modelling through analysis of modern and recent systems, to analysis of ancient systems. A novel method has been developed, bridging between the previous approaches and dividing and analysing source-to-sink systems based on linked geomorphic segments along the source-to-sink profile. This approach builds on uniformitarian principles. The method is driven by the need to understand ancient, subsurface systems and still has high uncertainty but is an original, first-order approach to source-to-sink system analysis. In modern systems, entire onshore-to-offshore systems can be analysed with a higher degree of confidence than in ancient systems and semi-quantitative relationships can be established. Application in ancient systems is much more challenging but, in some cases, antecedent morphologies have been preserved onshore that can be matched with offshore known occurrences of, for instance, sandy submarine fan systems. Along the Norwegian North Sea and Norwegian Sea margins the Paleocene deep-marine reservoir of the giant Ormen Lange gas field is such an example. There, antecedent onshore drainage patterns which formed the feeder system to the offshore, deepwater fan system can be interpreted and aligned with onshore palaeogeomorphological evidence. Understanding the palaeogeomorphic development of basement regions such as the Fennoscandian shield is of high importance for understanding the offshore presence of deepwater sandstones.

Keywords: source-to-sink, passive margins, Norwegian margin, geomorphology

Source-to-sink analysis is a novel method in sedimentary geology that includes investigating the entire sedimentary system from its ultimate upstream source in the continental realm to the ultimate sediment sink, most commonly on deep basin plains (Fig. 1; Sømme *et al.* 2009*a*, *b*). While the method currently is best applied on margins with a clear division between catchment, shelf, slope and basin plain geomorphic segments, such as on passive margins, there is considerable further potential for application in other basins such as foreland regions.

The concept of source-to-sink analysis was first introduced qualitatively by Meade (1972, 1982) and the relationships between sediment source and basin and the ability to integrate various data sources and geo-disciplines were discussed by Dickinson (1997) and Hovius & Leeder (1998). However, in recent years, utilization of the concept has expanded, not least given the ability provided by new tools and digital elevation data to work with onshore and offshore data sources such as geomorphologic and seismic data in fully integrated, quantitative ways (Sømme *et al.* 2009*a*). Furthermore, the conceptual understanding of the role of onshore drainage systems on sediment sink or basin filling patterns has been widely developed (e.g. Allen 2008). Also both numerical and experimental modelling studies have experienced great development and compare more realistically with natural systems (e.g. Granjeon & Joseph 1999; Paola 2000; Syvitski *et al.* 2003; National Science Foundation Science Plans 2004).

A whole series of methods and techniques can be used to investigate the sedimentary systems, such as palaeoclimatic (deep-time) studies, continental and subaqueous geomorphology, sequence stratigraphy, classic sedimentary analysis, tectonic studies and various basin analysis techniques. Several schools have developed (see Sømme *et al.* 2009*a* for an overview) and these will be briefly reviewed below, from those that are fully quantitative and numerical to experimental flume studies and on to semi-quantitative, geomorphologically based studies. The main advantage for the petroleum industry is that source-to-sink studies potentially allow for prediction of reservoir, source and sealing rocks in basins in deep time from a host of methods and data. Thus, predictive, reliable methods that can reduce uncertainty in basin and inter-basin scale exploration can be developed.

The aim of this paper is to provide a brief overview of available source-to-sink methods and demonstrate their potential by reviewing the study of Sømme *et al.* (2009*b*). This study applies source-to-sink methods to an ancient passive margin, the Paleocene Møre margin of the Mid-Norway Møre Basin, where the giant Ormen Lange gas discovery was made in 1997 (cf. Gjelberg *et al.* 2001).

Significance of the source-to-sink approach

For hydrocarbon exploration, a major challenge is to select the correct basins, plays and sedimentary systems within which to explore. The correct selection of play and complete understanding of reservoir, seal and source rocks depends on the best possible analysis of geological data from complete sedimentary systems. A favoured method to achieve this understanding is to analyse and compare with recent systems, but transfer of this knowledge to ancient systems in which petroleum systems occur is challenging since controls cannot be observed directly in past systems.

The United States National Science Foundation (NSF) has had source-to-sink studies on its science plan since the initiation of the Margins Programme in 2004. The plan states that: ‘Erosion sculpts the landscape, and redistribution of the sediment creates the alluvial plains, coasts, deltas, and continental shelves upon which most of the world’s population lives and derives such of

VINING, B. A. & PICKERING, S. C. (eds) *Petroleum Geology: From Mature Basins to New Frontiers – Proceedings of the 7th Petroleum Geology Conference*, 913–920. DOI: 10.1144/0070913

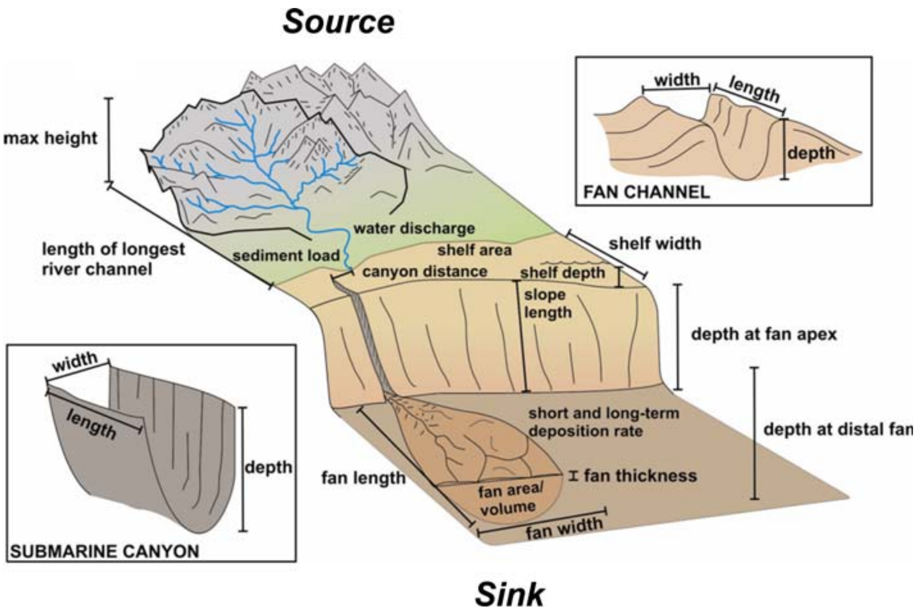

Fig. 1. Overview of key elements of a source-to-sink system developed on a margin with a distinct drainage basin–shelf–slope–basin floor profile. The key elements have quantitative characteristics that can be measured and compared between segments and between individual source-to-sink systems. The quantitative data base forms an empirical data base for application of source-to-sink analysis to ancient systems where segments (see Fig. 2) or elements of segments are preserved or can be measured. Modified from Sømme *et al.* (2009*a*).

its energy and water.' This transfer of sediment and solute mass from source to sink plays a key role in the cycling of elements such as carbon, in ecosystem change caused by global change and sea-level rise, and in resource management of soils, wetlands, groundwater and hydrocarbons. Although the source-to-sink system has been studied in its isolated component parts for more than 100 years, significant advances in our predictive capability require physical and numerical modelling of fluxes and feedbacks based on data from integrated field studies. According to the Margins programme (National Science Foundation Science Plans 2004), the Source-to-Sink Initiative is an attempt to quantify the mass fluxes of sediments and solutes across the Earth's continental margins by answering the following questions:

- How do tectonics, climate, sea-level fluctuations, and other forcing parameters regulate the production, transfer, and storage of sediments and solutes from their sources to their sinks?
- What processes initiate erosion and transfer, and how are these processes linked through feedbacks?
- How do variations in sedimentary processes and fluxes and longer-term variations such as tectonics and sea-level build the stratigraphic record to create a history of global change?

Various oil and energy companies have invested significant effort and research in understanding components of and complete source-to-sink systems, such as recent shallow-marine and deep-water systems in the Gulf of Mexico (e.g. Badalini *et al.* 2000). The competition for new attractive acreage globally will be based not only on access to the best technology and data, but also on access to the best geological methods and minds with the ability to master them. There is now growing recognition that new software tools and access to new quantitative datasets and new ideas facilitate analysis of complete source-to-sink systems and not just components. The depositional realm, where hydrocarbons are generated, migrate and are trapped, is significantly controlled by source area characteristics, climate and tectonics (cf. Sømme *et al.* 2009*a*, *b*). Thus there is a need to step out from the traditional approach of analysing only elements of the complete erosional–depositional system and describe and interpret in a source-to-sink manner.

Methods and technology

In general, four types of approaches have developed which all require different insight and technology to deliver results:

- modern and recent systems analysis;
- ancient systems analysis;
- numerical and experimental modelling;
- source-to-sink segment analysis.

Modern and recent systems analysis

The coupled process–response models of source areas and sediment sinks in basins can best be investigated along margins with recently or presently active source-to-sink systems. Numerous examples exist where particular segments have been analysed, but relatively few workers have investigated the entire source-to-sink systems. An exception is the incipient work of Leeder & Gawthorpe (1987; but followed by numerous other publications) on rift basins, years or even decades ahead in its in-depth understanding of the role of catchment development on resulting deposition. Other examples include the summary by Weaver *et al.* (2006) of the STRATAFORM and EUROSTRATAFORM projects, and the work of Einsele *et al.* (1996) and Goodbred (2003), who both investigated the giant Ganges–Brahmaputra system and showed the relationship of the sink sediments to Himalayan source area tectonic and climatic change. Other workers, such as Blum & Törnqvist (2000) and Blum (2008) have focused mainly on the drainage or source part of the system. Nevertheless, this focus is crucial because the majority of earlier work has been sink focused and much more empirical data needs to be collected and models built on the source system to create predictive models for basin-fill stratigraphy. In a recent paper, Sømme *et al.* (2009*a*; see also below) collected data and showed relationships from 29 modern and recent source-to-sink systems as an empirical data base for application to ancient systems. In general, empirical data is lacking from source-to-sink systems. Using data from

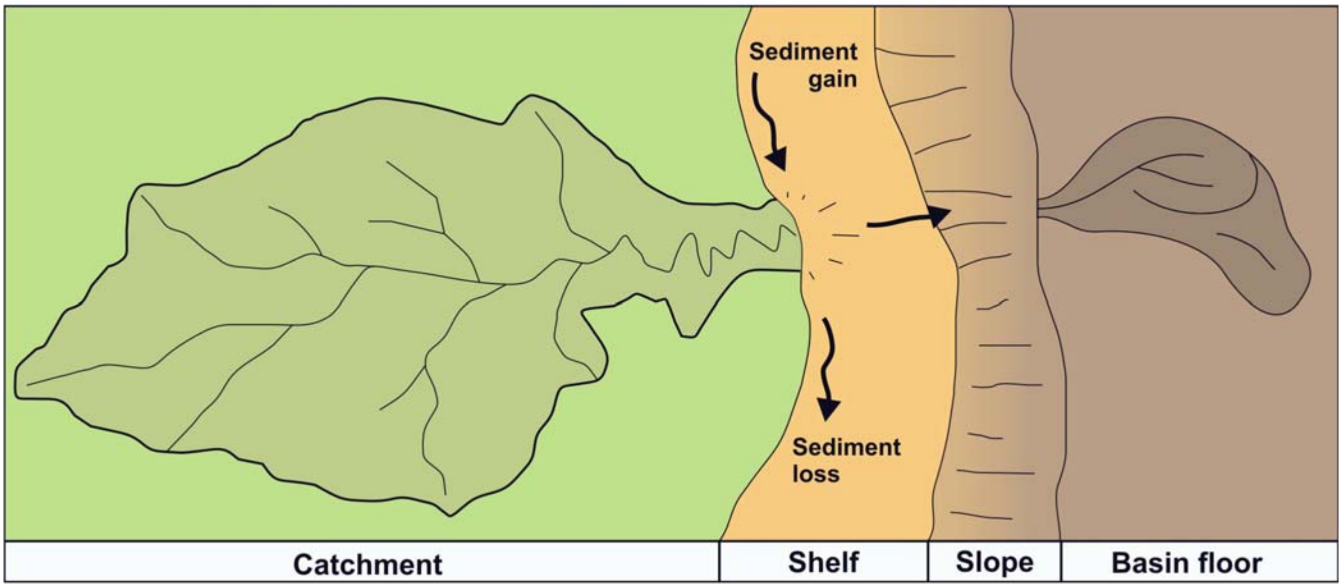

Fig. 2. Overview of the four segments of source-to-sink systems developed on margins with a distinct drainage basin–shelf–slope–basin floor profile. While the size of the individual segments is schematic and not to scale, the relative sizes are realistic, so that catchments are usually several times the area of, for example, basin floor fans (see Sømme *et al.* 2009*a*, *b* for statistics).

modern and recent systems to analyse ancient systems further highlights the principle of uniformitarianism and to what extent this principle can be used in source-to-sink analysis needs to be tested.

Ancient systems analysis

Very few examples of application of source-to-sink analysis (*sensu* the definition applied here; see above) to ancient systems have been published. There are many challenges with such application, not least that in most ancient systems single or several parts of the entire source-to-sink system are not preserved or data cannot be collected from them. In addition, while controlling factors such as climate, slope and sediment supply can be interpreted in modern and recent systems, these factors must be estimated with care in ancient systems (see also Leeder *et al.* 1998). Nevertheless, herein lies the power and potential of the source-to-sink method in its ability to predict the characteristics of segments which cannot be directly observed, and this is illustrated by the Ormen Lange case study (Sømme *et al.* 2009*b*; see below).

Commonly the case is that, the older the prospective source-to-sink system, the higher the uncertainty of data and interpretations, meaning that apparently the application of the method in deep time has severe limitations. Nonetheless, if uniformitarian principles apply and more empirical data are collected, the method has high potential. This will have potential significant impact on exploration in virgin basins and stratigraphy.

Numerical and experimental modelling

Over the last decade, various workers have developed software which deals with sediment delivery from drainage areas and deposition in adjacent basins (e.g. Granjeon & Joseph 1999; Paola 2000; Syvitski & Bahr 2001; Syvitski *et al.* 2003; National Science Foundation Science Plans 2004; Syvitski & Milliman 2007). Syvtiski's group has been working with developing a quantitative approach to source-to-sink studies using focused computer modelling and field investigation of landscape and seascape evolution, sediment transport and accumulation in two primary field areas (Fly River, SE Asia and Waipaoa system, New Zealand) where the complete source-to-sink system can be analysed. To what degree the mathematical and physical approach is fully useful from a petroleum exploration perspective, where there are large uncertainties, is a topic for future discussion.

Forward computer modelling of sedimentary basin filling has been focused on by several workers, including the fundamental work of Granjeon & Joseph (1999) and many later workers. This type of modelling is particularly useful to gain understanding of the physical processes that control basin filling.

Another experimental approach is large flume tank experiments (e.g. Paola 2000). In these experiments, controlling factors such as overall basin shape, basin gradient and sediment supply can be controlled quantitatively and scaled to each other. However, a critical point is whether the flume processes are scaled to natural systems both spatially and temporally. Nevertheless, flume modelling is an integral part of source-to-sink studies to build a quantitative understanding of sedimentary processes and sediment flux.

The linked segment-style approach

A fourth approach to analysing source-to-sink systems is driven by prediction of ancient systems and truly is a synthesis of the other approaches described above. This method (Sømme *et al.* 2009*a*), which relies on dividing the source-to-sink systems into segments (Figs 1 & 2), utilizes a uniformitarian approach where complete modern and recent source-to-sink systems are the key to predicting characteristics of ancient systems. By investigating a series of recent source-to-sink systems, an empirical framework of controlling factors which govern the delivery and distribution of sediments to basins is built. The method relies on a fundamental principle that processes and characteristics in one segment (Fig. 2) are dependent on updip segments and influence processes and characteristics in downdip segments.

In more detail, the method involves carrying out classic geomorphological studies of onshore drainage systems, collection of quantitative parameters of precipitation and river discharge to understand sediment supply and sedimentary processes, investigation of slope gradient across the terrestrial, shallow marine and deepwater parts of depositional systems, and comparison with sediment volumes deposited at the ultimate sink location of the sedimentary systems (Sømme *et al.* 2009*a*). This approach concentrates on the identification and actual measurement of the critical controls for sediment delivery to and deposition in basins. Thus, the method to a large extent avoids the scaling problems of experimental and numerical methods. Its focus is on identifying those parameters which can be used for the analysis of ancient systems, a critical consideration for transfer of knowledge between modern–recent systems and ancient, potentially petroleum-bearing systems. In many ways, numerical and experimental methods are less useful for prediction as it is often uncertain what knowledge is directly transferable from model to application in natural-scale systems. For instance, methods which rely on seismic data are likely to be much more useful for the identification of plays and prospects since this data is such an integral part of the exploration process. Quantitative data can be extracted from seismic data that can be applied directly in source-to-sink analysis (see Sømme *et al.* 2009*b*).

Application of the source-to-sink method to an ancient passive margin case: the Paleocene Ormen Lange system, Norwegian continental shelf

That the onshore geomorphology of particularly the south and central parts of Norway possesses antecedent characteristics formed prior to Neogene glaciations and which has genetic relationships to the offshore stratigraphy is widely accepted (Fig. 3; e.g. Riis 1996; Martinsen *et al.* 1999, 2005, and references therein). Nevertheless, the quantitative relationship between pre-glacial onshore geomorphology and offshore stratigraphy has not been published properly previously. Recently, Sømme *et al.* (2009*b*) investigated in detail the relationship between the latest Maastrichtian–Early Paleocene sediments of the Ormen Lange field and their antecedent source area, partly preserved onshore mainland Norway (Figs 4 & 5). In contrast to forward modelling using the drainage area size and characteristics to predict basinal deposits, inversion was used to test the segment-style approach of Sømme *et al.* (2009*a*). As mentioned previously, the segment-style approach resulted from analysis of 29 modern–recent source-to-sink systems. As such, the application of this database in analysing the Ormen Lange dataset is also a test of the usefulness of uniformitarianism in working with source-to-sink systems.

Critical quantitative aspects addressed by Sømme *et al.* (2009*b*) include: (i) can the volume of the Ormen Lange fan confidently predict the size of the onshore source area using the modern–recent database developed by Sømme *et al.* (2009*b*); (ii) what is the shape of the source and catchment area honouring onshore antecedent geomorphology and tectonics; and (iii) when defined, what other characteristics of the onshore drainage system can be interpreted which are of importance for the supply of reservoir sands to the deepwater basin? The Ormen Lange system has been studied extensively over the last decade, and details of the reservoir units and their formation can be found in Gjelberg *et al.* (2001, 2005) and references therein.

Fan volume v. onshore source area size

Calculations from published subsurface data (Gjelberg *et al.* 2005) show that the fan (Figs 4 & 5) reaches a maximum thickness of *c.* 110 m in the proximal part, from where it gradually thins into heterolithic lobe fringe deposits at its termination, giving a total fan volume of *c.* 104 km^3. This fan volume, compared with the global dataset of Sømme *et al.* (2009*a*), yields an estimated source area of *c.* 22×10^3 km^2, with minimum and maximum values of 1 and 560×10^3 km^2. The large uncertainty, possibly in part related to uncertainty regarding depositional rates, is discussed in detail by Sømme *et al.* 2009*a*, *b*), but the mean estimate is of great interest because it corresponds very closely to the proposed source area inferred purely from onshore geomorphologic and tectonic data (Figs 4 & 5; see also below; cf. Martinsen *et al.* 2002).

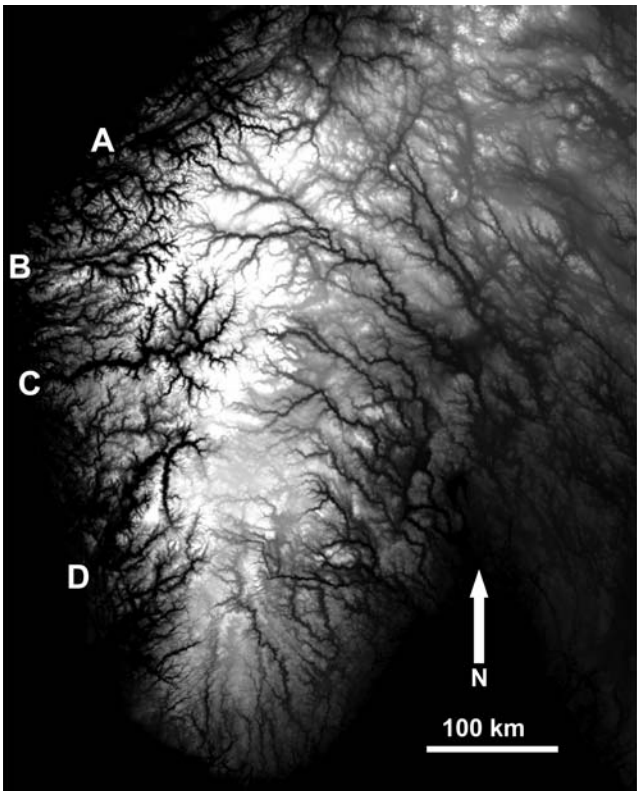

Fig. 3. Satellite image of the south of Norway highlighting major fjords and river valleys. Four fjord systems along the west coast are highlighted: (**a**) fjords of the Møre region, (**b**) Nordfjord, (**c**) Sognefjord and (**d**) Hardangerfjord. It is generally accepted that the fjords developed initially as Cenozoic fluvial drainage systems enhanced by Pleistocene glaciations (cf. Nesje & Whillans 1994 for a review). In terms of palaeomorphic shape, the Møre region fjords take on a rectangular pattern steered by the major faults of the Møre–Trøndelag Fault Complex (cf. Martinsen & Nøttvedt 2008). In contrast, the Nordfjord and Sognefjord examples have generally classic dendritic shapes uninfluenced by major tectonics. The last example, Hardangerfjord, shows a first-order, SW–NE linear shape controlled by a major tectonic lineament, the Hardangerfjord Shear Zone, widely believed to be the easternmost expression of Caledonian extensional collapse in the latest Silurian to early Devonian (cf. Martinsen & Nøttvedt 2008). The four examples, all interpreted to be major palaeodrainage systems to the Norwegian continental shelf, clearly show the importance of basement structure and geomorphology in transporting sediments from catchment to offshore basins.

This provides confidence that the linked segment-style method of Sømme *et al.* (2009*a*) is useful, but the large uncertainty needs to be handled in further work. The likely causes for the uncertainties are considered to be a general lack of empirical data from source-to-sink systems globally coupled with challenges in calculating fan volume correctly.

Shape and size of source area

The source-to-sink modelling inversion of the Ormen Lange fan system yields quantitative values of the size of the source area and catchment. Nevertheless, to be fully valuable, local geological data must be incorporated. The antecedent geomorphology and tectonics of the source area region are strongly influenced by the presence of the Palaeozoic-age Møre–Trøndelag Fault Zone and Cenozoic uplift of southern Scandes (Fennoscandia) (Figs 4 & 5; Riis 1996; Martinsen *et al.* 1999, 2005; Martinsen & Nøttvedt 2008; Sømme *et al.* 2009*b*). The source area did not develop a classic dendritic leaf-shape, as expected on flat, gently inclined surfaces with no tectonic influence. Instead, a rectangular pattern

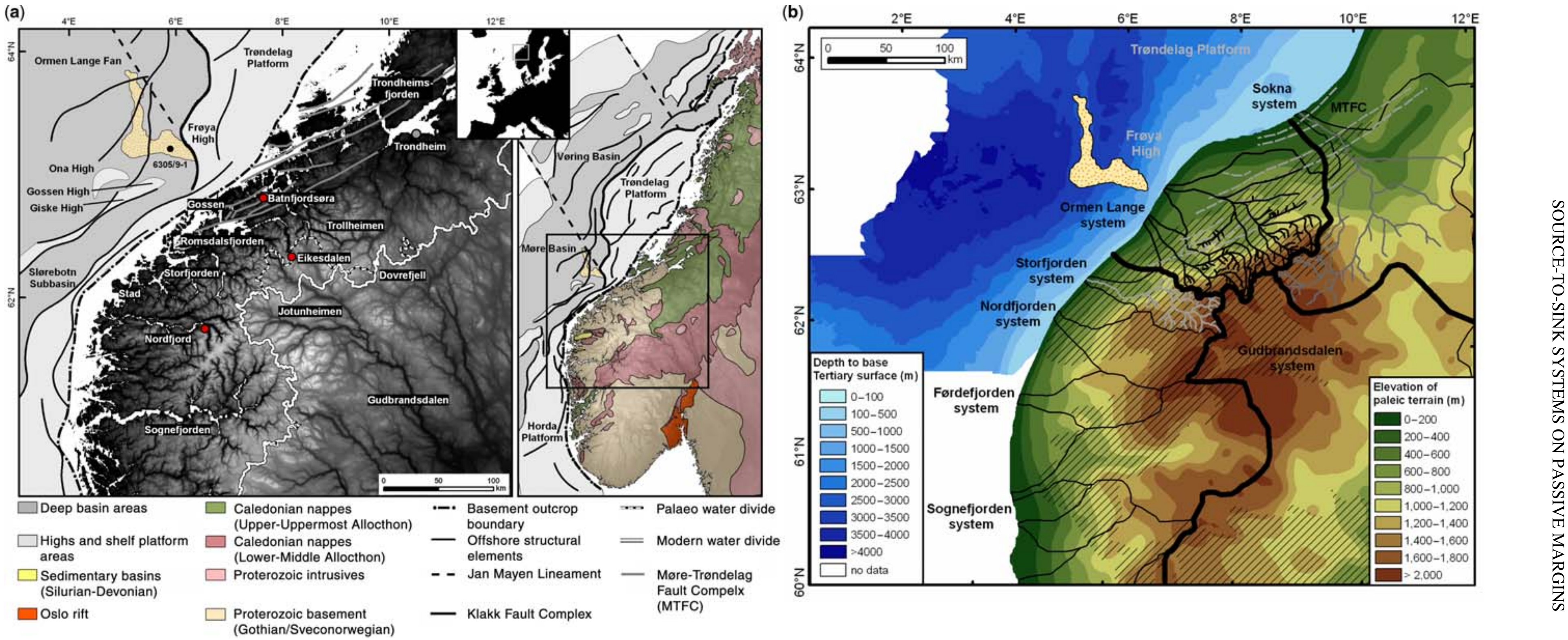

Fig. 4. (**a**) Overview of major geological features in the mid-Norway region and their spatial relation to the Ormen Lange deepwater fan system of latest Maastrichtian–Paleocene age. The white solid line along the highest mountains and oriented south–north–NE is the current drainage divide in Norway, generally interpreted as also roughly representing the pre-glacial Cenozoic drainage divide (Riis 1996; Martinsen *et al.* 2002; Martinsen & Nøttvedt 2008). A significant deviation occurs in the Møre region, shown by the dashed white line, where the palaeodrainage divide occurred further to the NW, and Neogene stream piracy moved the current divide further to the SE (cf. Sømme *et al.* 2009*b* for a discussion). This drainage divide formed an important hinterland constraint on the development of the Ormen Lange catchment, in addition to the Møre–Trøndelag Fault Zone structuring (shown by grey lines oriented in an ENE–WSW direction obliquely to the current coastline). From Sømme *et al.* (2009*b*). (**b**) Semi-quantitative interpretation of the pre-glacial Palaeic landscape and drainage basins in the Møre region. The Ormen Lange catchment is shown NW of the thick black line and to the north of the Gudbrandsdalen system. Note the deviation of drainage towards the SW along the Møre–Trøndelag Fault Zone and skewness towards the ENE. Modified from Sømme *et al.* (2009*b*).

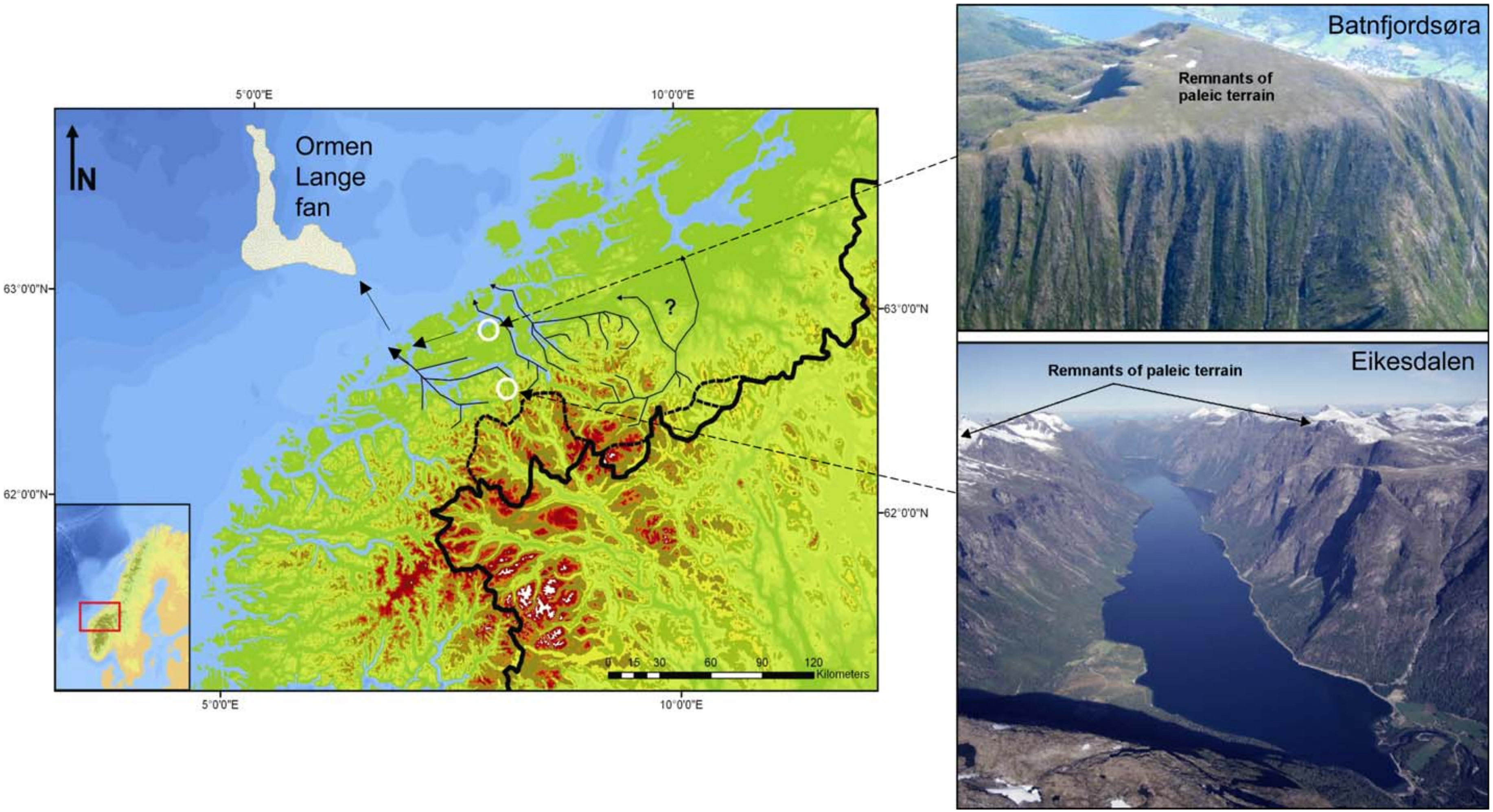

Fig. 5. Remnants of pre-glacial terrain can be observed at many places in the south of Norway. Two examples from the catchment of the Ormen Lange system are shown. The upper example from Batnfjordsøra shows a flat, slightly inclined surface on top of a mountain surrounded by glacial and post-glacial fluvial valleys and recent, steep avalanche-prone valley walls. The lower example from Eikesdalen shows gently inclined high surfaces on the margins of a major glacially cut valley modified by recent rock falls. The high surfaces are interpreted to have formed by fluvial erosion prior to Pleistocene glaciations (modified from Martinsen & Nøttvedt 2008; Sømme *et al.* 2009*b*).

developed, with a preferred drainage axis obliquely oriented in an ENE–WSW direction to the current coastline and steered by the major faults of the Møre–Trøndelag Fault Zone (Figs 3 & 4). The main sub-drainages meet at the apex of the feeder system to the Ormen Lange fan (Fig. 5), thus also explaining the general lack of sand of Paleocene age north of the Ormen Lange fan system, because no major drainage system reached these areas. It is generally believed that the southeastern boundary of this Paleocene drainage system lay at the culmination of the Palaeic surface (see Sømme *et al.* 2009*a*, *b* for a discussion). This culmination corresponds generally with a south–north–NE line drawn through the axis of the highest mountains in Norway (Figs 3–5), and is considered with minor modifications to be inherited from the Palaeogene (Martinsen & Nøttvedt 2008; cf. also Martinsen *et al.* 2002). Therefore, as a result, a drainage area skewed to the ENE developed (Fig. 4).

The skewness of the drainage area is also supported by provenance data from U–Pb isotopes in zircons, showing that the bedrock to the east and NE of the Ormen Lange fan supplied a higher proportion of sediment than the area to the SW, which is immediately inland from the fan system (Fonneland *et al.* 2004).

Other drainage system characteristics

The segment-style source-to-sink method developed by Sømme *et al.* (2009*a*) allows for the prediction of a range of parameters due to its basis in linkage and genetic relationships between segments. Thus, based on fan volume and catchment size calculations, other characteristics of the Ormen Lange system can be inferred. Coupled with the grain size characteristics of the depositional system (variable coarse-to-fine fractions but generally fining in a proximal-distal direction; Gjelberg *et al.* 2001, 2005; Sømme *et al.* 2009*b*), a relatively steep system is predicted with a peak/average discharge ratio of 100–1000, indicative of the frequency-magnitude characteristics of the system, and thus the timing and mode of sediment delivery to the fan.

The number and configurations of catchments feeding the shallow-marine area can also be interpreted, with implications for the spacing of sediment sources in the region (Fig. 4b). Sømme *et al.* (2009*b*) shows that, along the Møre margin, drainage basins were closely spaced (*c.* 40–80 km), implying that several smaller catchments may have fed the Ormen Lange fan.

It is also suggested that the palaeotopography and bathymetry in source-to-sink systems with a distinct shelf–slope–basin floor configuration are generically related. Thus, flattening and uplift of the catchment may occur in conjunction with flattening and deepening of the slope and basin floor as a system develops. For the Ormen Lange system, a catchment height of *c.* 2500 m (ranging between 900–4200 m) and water depths of *c.* 1800 m (ranging between 600–3200 m) are suggested for the Maastrichtian–Danian period (Sømme *et al.* 2009*b*).

A final point concerns to what extent onshore geomorphic evidence in a drainage basin can be used as an indicator and predictor of offshore deposition. Obviously, the deeper the time and age of a particular system, the more the uncertainty in application of source-to-sink analysis increases. Nevertheless, contrary to many people's expectation, many continental regions landward of prospective offshore basins contain strong evidence of the characteristics of the drainage areas that supplied the older, subsurface sediments (see e.g. Leturmy *et al.* 2003 for a thorough deep-time analysis of the West African margin). In the south of Norway, fjords (Fig. 3), perceived by many as generated during the Pleistocene glaciations (cf. discussion in Nesje & Whillans 1994), show a lot of evidence for a pre-glacial origin controlled by fluvial discharge and steered in some regions by major tectonic lineaments (Nesje & Whillans 1994; Martinsen & Nøttvedt 2008). There are numerous remnants of pre-glacial surfaces that relate to the supply of sediments to offshore basins (Fig. 5). These sediments are most commonly reservoirs, but the drainage history in deep time reveals important aspects of source and seal rock formation as well.

Uncertainties for applying source-to-sink methodology in exploration

In general, the older the ancient/subsurface system, the larger the uncertainty is in applying source-to-sink concepts on a particular exploration margin. In the Ormen Lange case, the inversion (i.e. estimation of the catchment area from fan volume) shows the dependency on a correctly interpreted fan volume from seismic. Thus, obviously, the quality of seismic data and the seismic interpretation is a significant factor for the confidence of the interpretation. In the Ormen Lange case, the confidence is relatively high, thus providing estimates of catchment size, shelf width and slope length that are reliable. Nevertheless, using this data in an inversion exercise also warrants calibration towards other regional and independent data such as palaeogeomorphical data (see above; Sømme *et al.* 2009*b*). In regions where such independent data do not exist, the uncertainty of the method grows significantly larger given the still small empirical database that exists for source-to-sink systems (cf. Sømme *et al.* 2009*a*).

The real value for exploration of the source-to-sink approach naturally lies in using it as a predictive tool in regions where little data exist, but also as a test and uncertainty-reduction tool where some data are present. In prospective regions with very low data quality and resolution, such as in sub-salt regions, the value is very high. There is no lower limit to how much quantitative data should be present from, for example, one segment to apply the method as a predictive tool to understand another segment, as the method is of immense value as an idea-generation tool. However, the more data is available, the better the constraints on geological models can be established. The revelation that there is a genetic link, for example, between catchment size, slope length and fan volume as established by Sømme *et al.* (2009*a*) and shown by the Ormen Lange case study, is a major breakthrough. The quest now is to collect more empirical data to reduce the uncertainty, and apply the concept to other basins.

Although the current empirical data base is established for margins with a distinct stepped profile with four segments (i.e. catchment, shelf, slope and basin floor), there is no reason to believe that similar relationships exist in other basin types such as rift and foreland basins. Conceptual relationships can be established in these and other settings, but the time-consuming and tedious work to collect the data must be done to establish similar quantitative relationships to those established by Sømme *et al.* (2009*a*).

Summary

This paper has briefly attempted to illustrate the potential of source-to-sink analysis on continental margins for predicting modern, recent and ancient, subsurface basin fill stratigraphy. Source-to-sink analysis has a wide potential, and the technique is based on experimental and numerical modelling, as well as analysis of modern to ancient systems. Previous methods for predicting basin filling have either been source or sink focused, but now new technology (software, computer processing), new data (such as coupling of high-resolution digital elevation data with seismic) and new insights provide the capability for a potential paradigm shift in how analysis of sedimentary systems and their source areas are analysed.

An approach based on linked segments along the source-to-sink profile is preferred (Sømme *et al.* 2009*a*), which builds on uniformitarian principles. Nevertheless, the validity of a uniformitarian approach needs further testing and more empirical data, not least from ancient systems.

The application of the linked segment-style analysis to the Ormen Lange system offshore mid-Norway is one valid test of the source-to-sink method. In addition, the analysis in this region has shed new light and added credibility to the use of onshore palaeogeomorphic data as predictors of offshore deposition, even in regions traditionally perceived as possessing or having preserved little evidence of antecedent supply systems to the offshore, subsurface stratigraphic record.

References

Allen, P. A. 2008. From landscapes into geological history. *Nature*, **451**, 274–276.

Badalini, G., Kneller, B. & Winker, C. D. 2000. Architecture and processes in Late Pleistocene Brazos-Trinity turbidite system, Gulf of Mexico. *In*: Weimer, P. *et al*. (eds) *Turbidite Reservoirs of the World. 20th Annual Gulf Coast Section SEPM Bob F. Perkins Research Conference Proceedings*, Gulf Coast Section, Society for Sedimentary Geology (SEPM), Houston, TX, 16–34.

Blum, M. 2008. Continental shelves as the lowstand fluvial long profile: possible implications for icehouse vs. greenhouse stratigraphic records. *American Association of Petroleum Geologists Annual Convention Abstracts*, **17**, 20.

Blum, M. D. & Törnqvist, T. E. 2000. Fluvial responses to climate and sea-level change: a review and look forward. *Sedimentology*, **47**, 2–48.

Dickinson, W. 1997. Panel throws down gauntlet. *GSA Today*, **7**, 25.

Einsele, G., Ratschbacher, L. & Wetzel, A. 1996. The Himalaya–Bengal Fan denudation–accumulation system during the last 20 Ma. *Journal of Geology*, **104**, 163–184.

Fonneland, H. C., Lien, T., Martinsen, O. J., Pedersen, R. B. & Kosler, J. 2004. Detrital zircon ages: a key to understanding the deposition of deep marine sandstones in the Norwegian Sea. *Sedimentary Geology*, **164**, 147–159.

Gjelberg, J. G., Enoksen, T., Kjærnes, P., Mangerud, G., Martinsen, O. J., Roe, E. & Vågnes, E. 2001. The Maastrichtian and Danian depositional setting, along the eastern margin of the Møre Basin (mid-Norwegian Shelf): implications for reservoir development of the Ormen Lange Field. *In*: Martinsen, O. J. & Dreyer, T. (eds) *Sedimentary Environments Offshore Norway – Paleozoic to Recent*. Norwegian Petroleum Society, Oslo, Special Publications, **10**, 421–440.

Gjelberg, J. G., Martinsen, O. J., Charnock, M., Møller, N. & Antonsen, P. 2005. The reservoir development of the Late Maastrichtian–Early Paleocene Omen Lange gas field, Møre Basin, Mid-Norwegian Shelf. *In*: Doré, A. G. & Vining, B. A. (eds) *Petroleum Geology: North-West Europe and Global Perspectives: Proceedings of the 6th Petroleum Geology Conference*. Geological Society, London, 1165–1184; doi: 10.1144/0061165.

Goodbred, S. L. 2003. Response of the Ganges dispersal system to climate change: a source-to-sink view since the last interstade. *Sedimentary Geology*, **162**, 83–104.

Granjeon, D. & Joseph, P. 1999. Concepts and applications of a 3-D multiple lithology, diffusive model in stratigraphic modeling. *In*: Harbaugh, J. W., Watney, W. L. *et al*. (eds) *Numerical Experiments in Stratigraphy: Recent Advances in Stratigraphic and Computer Simulations*. Society for Sedimentary Geology, Special Publications, **62**, 197–210.

Hovius, N. & Leeder, M. R. 1998. Clastic sediment supply to basins. *Basin Research*, **10**, 1–5.

Leeder, M. R. & Gawthorpe, R. L. 1987. Sedimentary models for extension in tilt-block/half-graben basins. *In*: Coward, M. P., Dewey, J. F. & Hancock, P. L. (eds) *Extensional Tectonics*. Geological Society, London, Special Publications, **28**, 139–152.

Leeder, M. R., Harris, T. & Kirkby, M. J. 1998. Sediment supply and climate change: implications for basin stratigraphy. *Basin Research*, **10**, 7–18.

Leturmy, P., Lucazeau, F. & Brigaud, F. 2003. Dynamic interactions between the Gulf of Guinea passive margin and the Congo River drainage basin 1: morphology and mass balance. *Journal of Geophysical Research – Solid Earth*, **108**, 1–13.

Martinsen, O. J. & Nøttvedt, A. 2008. Norway rises from the sea. *In*: Ramberg, I., Bryhni, I., Nøttvedt, A. & Rangnes, K. (eds) *The Making of a Land – Geology of Norway*. Norwegian Geological Society, Trondheim, 441–477.

Martinsen, O. J., Bøen, F., Charnock, M. A., Mangerud, G. & Nøttvedt, A. 1999. Cenozoic development of the Norwegian margin 60–64 degrees N: sequences and sedimentary response to variable basin physiography and tectonic setting. *In*: Fleet, A. J., Boldy, S. A. R. & Burley, S. D. (eds) *Petroleum Geology of North-West Europe: Proceedings of the 5th Conference*. Geological Society, London, 293–304; doi: 10.1144/0050293.

Martinsen, O. J., Fonneland, H. C., Lien, T. & Gjelberg, J. G. 2002. On latest Cretaceous–Palaeocene drainage and deep-water sedimentary systems on- and offshore Norway. *In*: Thorsnes, T. (ed.) *Onshore–Offshore Relationships on North Atlantic Margins*. Norwegian Geological Society, Trondheim, Abstracts and Proceedings, 123–124.

Martinsen, O. J., Lien, T. & Jackson, C. 2005. Cretaceous and Palaeogene turbidite systems in the North Sea and Norwegian Sea basins: source, staging area and basin physiography controls on reservoir development. *In*: Doré, A. G. & Vining, B. A. (eds) *Petroleum Geology: North-West Europe and Global Perspectives: Proceedings of the 6th Petroleum Geology Conference*. Geological Society, London, 1147–1164; doi: 10.1144/0061147.

Meade, R. H. 1972. Sources and sinks of suspended matter on continental shelves. *In*: Swift, D. J. P., Duane, D. B. & Pilkey, O. H. (eds) *Shelf Sediment Transport*. Dowden, Hutchinson & Ross, Stroudsburg, 249–262.

Meade, R. H. 1982. Sources, sinks, and storage of river sediment in the Atlantic drainage of the United States. *Journal of Geology*, **90**, 235–252.

National Science Foundation Science Plans. 2004. *Margins*. National Science Foundation, Washington, DC.

Nesje, A. & Whillans, I. M. 1994. Erosion of Sognefjord, Norway. *Geomorphology*, **9**, 33–45.

Paola, C. 2000. Quantitative models of sedimentary basin filling. *Sedimentology*, **47**, 121–178.

Riis, F. 1996. Quantification of Cenozoic vertical movements of Scandinavia by correlation of morphological surfaces with offshore data. *Global and Planetary Change*, **12**, 331–357.

Sømme, T., Helland-Hansen, W., Martinsen, O. J. & Thurmond, J. B. 2009*a*. Relationships between morphological and sedimentological parameters in source-to-sink systems: a basis for predicting semi-quantitative characteristics in subsurface systems. *Basin Research*, **21**, 361–387.

Sømme, T., Martinsen, O. J. & Thurmond, J. B. 2009*b*. Reconstructing morphological and depositional characteristics in subsurface sedimentary systems: an example from the Maastrichtian-Danian Ormen Lange system, Møre Basin, Norwegian Sea. *American Association of Petroleum Geologists Bulletin*, **93**, 1347–1377.

Syvitski, J. P. M. & Bahr, D. B. 2001. Numerical models of marine sediment transport and deposition. *Computers and Geosciences*, **27**, 617–753.

Syvitski, J. P. M. & Milliman, J. D. 2007. Geology, geography and humans battle for dominance over the delivery of fluvial sediment to the coastal ocean. *Journal of Geology*, **115**, 1–19.

Syvitski, J. P. M., Peckham, S. D., Hilberman, R. & Mulder, T. 2003. Predicting the terrestrial flux of sediment to the global ocean: a planetary perspective. *Sedimentary Geology*, **162**, 5–24.

Weaver, P. P. E., Canals, M. & Trincardi, F. (eds) 2006. Source-to-sink sedimentation on the European margin. *Marine Geology*, **234**, 1–292.

An integrated study of Permo-Triassic basins along the North Atlantic passive margin: implication for future exploration

J. REDFERN,[1] P. M. SHANNON,[2] B. P. J. WILLIAMS,[2] S. TYRRELL,[2] S. LELEU,[3] I. FABUEL PEREZ,[1] C. BAUDON,[1] K. ŠTOLFOVÁ,[2] D. HODGETTS,[1] X. VAN LANEN,[1] A. SPEKSNIJDER,[4] P. D. W. HAUGHTON[2] and J. S. DALY[2]

[1]*University of Manchester, North Africa Research Group, School of Earth, Atmospheric and Environmental Sciences, Williamson Building, Oxford Road, Manchester M13 9PL, UK (e-mail: jonathan.redfern@manchester.ac.uk)*
[2]*UCD School of Geological Sciences, University College Dublin, Belfield, Dublin 4, Ireland*
[3]*University of Aberdeen, Geology & Petroleum Geology, School of Geosciences, Meston Building, King's College, Aberdeen AB24 3UE, Scotland, UK*
[4]*Shell International Exploration and Production BV, Kessler Park 1, 2288GS, Rijswijk, Netherlands*

Abstract: Permo-Triassic rift basins offer important hydrocarbon targets along the Atlantic margins. Their fill is dominated by continental red beds, comprising braided fluvial, alluvial fan, aeolian, floodplain and lacustrine facies. These relatively lightly explored basins span both the Atlantic and Tethyan domains and developed above a complex basement with inherited structural fabrics. Sparse data in offshore regions constrain understanding of depositional geometries and sedimentary architecture, further impeded by their deep burial beneath younger strata, combined with the effects of later deformation during continental breakup. This paper provides results from a multidisciplinary analysis of basins along the Atlantic margin. Regional seismic and well data, combined with geochemical provenance analysis from the European North Atlantic margins, are integrated with detailed outcrop studies in Morocco and Nova Scotia. The research provides new insights into regional basin tectonostratigraphic evolution, sediment fill, and reservoir distribution, architecture and quality at a range of scales. Regional seismic profiles, supported by key well data, indicate the presence of post-orogenic collapse basins, focused narrow rifts and low-magnitude multiple extensional depocentres. Significantly, Permo-Triassic basin geometries are different and more varied than the overlying Jurassic and younger basins. Provenance analysis using Pb isotopic composition of detrital K-feldspar yields new and robust controls on the sediment dispersal patterns of Triassic sandstones in the NE Atlantic margin. The evolving sedimentary architecture is characterized by detailed sedimentological studies of key outcrops of age equivalent Permian–Triassic rifts in Morocco and Nova Scotia. The interplay of tectonics and climate is observed to influence sedimentation, which has significant implications for reservoir distribution in analogue basins. New digital outcrop techniques are providing improved reservoir models, and identification of key marker horizons and sequence boundaries offers a potential subsurface correlation tool. Future work will address source and seal distribution within the potentially petroliferous basins.

Keywords: Permian Triassic Atlantic Borderland basins, Morocco, Atlas, Fundy, continental red beds, provenance, rifting

Integrated regional study

The Late Mesozoic and Cenozoic development of basins along the Atlantic margin (Fig. 1) has been documented in a number of regional syntheses (e.g. Blystad *et al.* 1995; Doré *et al.* 1999; Naylor *et al.* 1999; Stoker *et al.* 2005). Seismic and well data from the Northern Atlantic margin show the extensive presence of Permo-Triassic strata, preserved in a suite of elongate, largely fault-bounded basins (Fig. 2). Their depositional extent and regional architecture are generally poorly constrained. This is due to overprinting of later rifting and continental breakup, together with deformation in the thick overlying Jurassic to Cenozoic strata and the effects of early Cenozoic igneous activity in the North Atlantic Igneous Province. However, the frequently sandy nature of the lower part of the Permo-Triassic succession makes it a potentially important reservoir target in petroleum exploration.

Previous studies have focused either on individual basins or plays. This study extends from Norway to Morocco (Fig. 1) and offers a broad perspective that examines the influence of regional as well as local and small-scale controls, investigating the complete spectrum of scales from regional crustal, through outcrop and to the pore scale. The aims of this paper are to (a) present initial results from an interdisciplinary basin analysis of Atlantic Margin Permo-Triassic successions and (b) illustrate how regional basin analysis, using a range of techniques and at scales through orders of magnitude from the basin to the pore throat, can provide an improved understanding of basin development and reservoir architecture, with implications for petroleum prospectivity.

Geological framework

The North Atlantic passive continental margin has a complex history, influenced by the inherited basement framework (Fig. 2). The Caledonian Orogeny, in latest Silurian to earliest Devonian times, resulted in the accretion of terranes with different crustal composition and structural fabrics (Coward 1995). Following the Variscan Orogeny in latest Carboniferous times, further structural fabrics were added to the basement of the newly formed Pangaean Supercontinent. In the region west of mid-Norway through to western Ireland, comprising the Caledonian domain, the major structures strike NE–SW to north–south. Further south in the

VINING, B. A. & PICKERING, S. C. (eds) *Petroleum Geology: From Mature Basins to New Frontiers – Proceedings of the 7th Petroleum Geology Conference*, 921–936. DOI: 10.1144/0070921

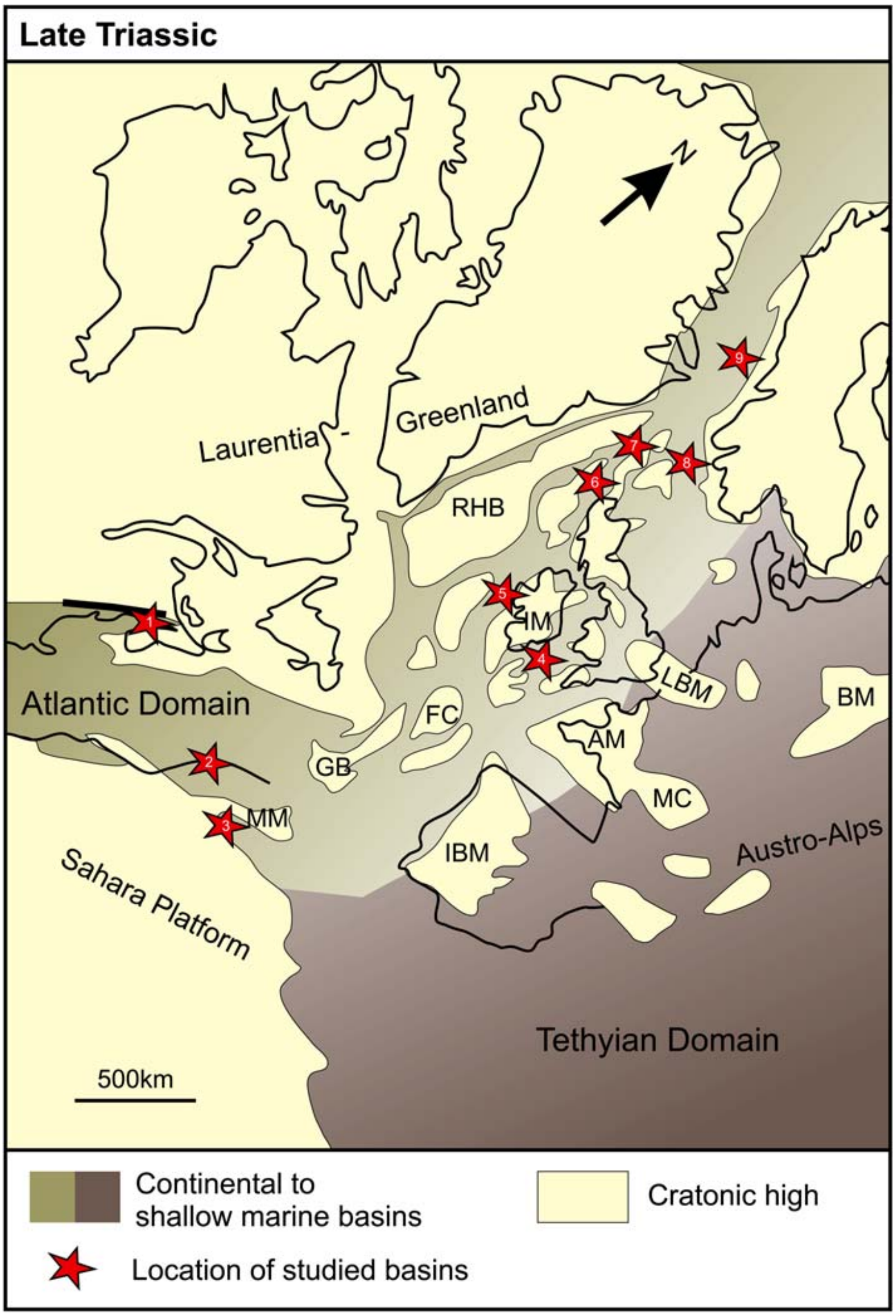

Fig. 1. Location map showing the main Permian–Triassic basins on the northern and central Atlantic borderland. Basins reviewed in this paper are denoted with numbered stars. 1, Fundy Basin; 2, Argana Basin; 3, Central High Atlas Basin; 4, Celtic Sea basins; 5, Slyne and Rockall basins; 6, Solan Bank High; 7, Magnus–East Shetland basins; 8, Horda Platform; 9, Froan Basin. MM, Moroccan Massif; IBM, Iberian Massif; FC, Flemish Cap; AM, Armorican Massif; LBM, London Brabant Massif; GB, Grand Banks; BM, Belgian Massif; MS, Massif Central; IM, Irish Massif; RHB, Rockall High Bank.

Variscan region the orientation of the structures was predominantly east–west. The inherited Caledonian and Variscan fabric provided the structural template that controlled the location, orientation and development of the Permo-Triassic basins (Naylor & Shannon 2009; Štolfová & Shannon 2009). The accreted terranes that constitute the Pangaean Supercontinent have a range of compositions and these exerted a major control on the composition of the Permo-Triassic sediments, and determined their reservoir quality. The basins examined in this study extend from the North Atlantic offshore mid-Norway, west of the major Caledonian Iapetus suture and fold belt, across the Variscan orogenic fold belt and core complex to the Moroccan basins of the central Atlantic. They also include outcrop studies from the conjugate margin basins of offshore Canada (Nova Scotia).

Structural style and evolution: regional seismic analysis

The shapes of the preserved remnant Permo-Triassic basins of the Atlantic margin show a clear association with the underlying structural fabrics (Doré *et al.* 1999). West of Norway, the UK and western Ireland basins developed in a broadly NE–SW to north–south belt, parallel to the Caledonian domain. Further south, basin orientation is dominated by an east–west trend parallel to the Variscan structures, with a similar trend documented in the region of the Innuitian fold belt north of Greenland.

The basins west of mid-Norway, exemplified by the Froan Basin on the Trøndelag Platform (Fig. 3) contain several kilometres of Permo-Triassic strata and the basins are often controlled by eastward-dipping master growth faults. The overall basin trend

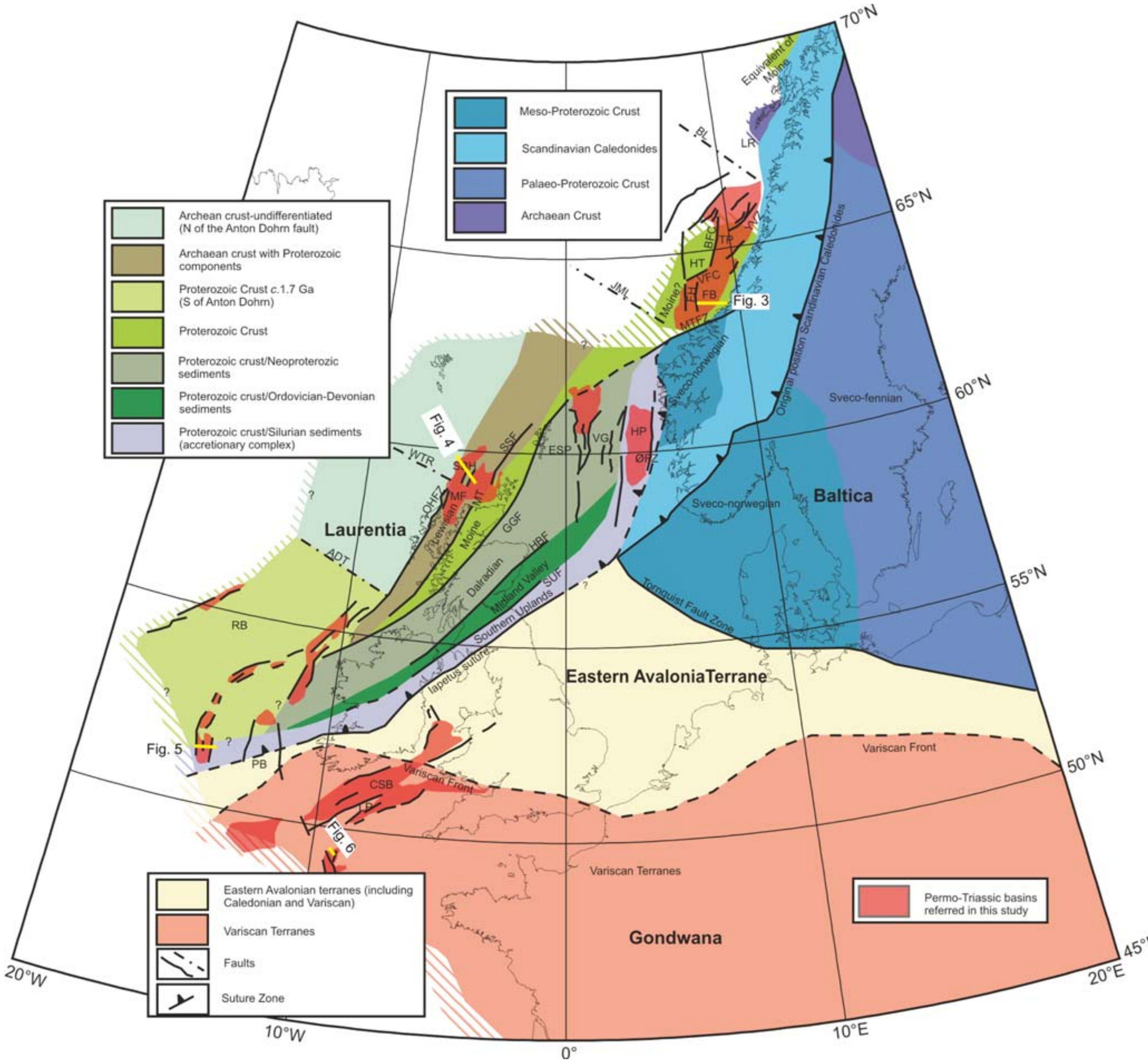

Fig. 2. Simplified structural and terrane map of the Northwest European Atlantic margin. Superimposed on this is the location of the various Permo-Triassic basins involved in the present study. The location of Figures 3–6 is also shown. Abbreviations: ADT, Anton Dohrn Transfer; BFC, Bremstein Fault Complex; BL, Bivrost Lineament; CSB, Celtic Sea basins; ESP, East Shetland Platform; FB, Froan Basin; FH, Frøya High; GGF, Great Glen Fault; HBF, Highland Boundary Fault; HP, Horda Platform; HT, Halten Terrace; JML, Jan Mayen Lineament; LP, Labadie Bank–Pembrokeshire Ridge; LR, Lofoten Ridge; MF, Minch Fault; MTFZ, Møre, Trøndelag Fault Zone; MT, Moine Thrust; ØFZ, Øygarden Fault Zone; OHFZ, Outer Hebrides Fault Zone; PB, Porcupine Basin; RB, Rockall Basin; SBH, Solan Bank High; SSF, Shetland Spine Fault; SUF, Southern Upland Fault; TP, Trøndelag Platform; VFC, Vingleia Fault Complex; VG, Viking Graben; WTR, Wyville–Thompson Ridge; YVZ, Ylvingen Fault Zone. Dashed areas represent uncertain terrane occurrence or boundary. From Štolfová & Shannon (2009).

appears to be influenced by a Caledonian structural fabric (e.g. the Ylvingen Fault Zone). However, no evidence is seen of direct reactivation of individual major Caledonian thrust structures. The basins are therefore interpreted as the product of narrow ‘classical’ rifting (McKenzie 1978; Buck *et al.* 1999).

The Permo-Triassic basins immediately west of the UK show similar pronounced half-graben geometries. The North Minch Basin is interpreted as having developed by strain localization in a narrow rift system, with a slight northwestward migration of strain through time resulting in the progressive movement of active fault systems (Štolfová & Shannon 2009). In the Magnus Basin, where the Permo-Triassic is preserved in a series of rotated fault blocks, initial palaeotopographic infill was followed by late Triassic and younger growth faulting, which also has the characteristic geometry of a narrow rift system (Štolfová & Shannon 2009).

In a number of areas a series of small, Permo-Triassic half-graben basins are controlled directly by growth faults developed along pre-existing Caledonian structures. The West Orkney Basin is probably associated with reactivation along the Caledonian and Precambrian Moine Thrust and Outer Hebrides Fault Zone complex. The Slyne and Erris basins west of Ireland (Naylor *et al.* 1999) and the Magnus Basin NE of Shetlands lie close to the projected offshore extensions of the Great Glen Fault complex, a major strike-slip Caledonian fault system that was reactivated initially in Devonian times and later in Permo-Triassic times.

The Solan Bank High, an elongate fault-bounded basement block running along a Caledonian structural fabric, acted as a barrier to

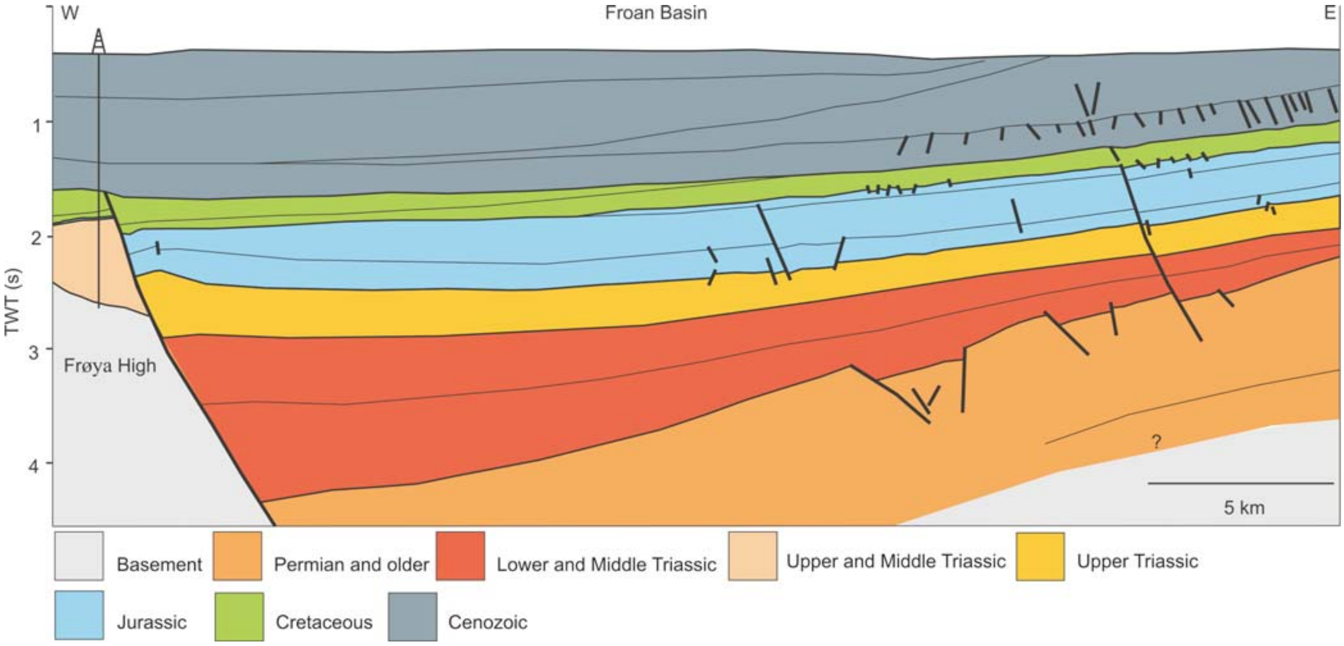

Fig. 3. Geoseismic profile across the Froan Basin showing typical half-graben geometry characteristic of a narrow 'classical' rift. The thick Permo-Triassic succession is subdivided into three seismic packages indicating different structural styles and demonstrating clear growth faulting, especially in the central, second package.

westward progression of the narrow rift system that fringed the west coast of Scotland. To the east, the basins are typical narrow rifts while the large basin to the west has a different style, with thick uniform sediments showing no evidence of major growth faulting, albeit modified and eroded by later tectonism (Fig. 4).

This pattern of uniformly thick sediments, with subtle fault-controlled thickness variations, is seen in much of the Irish Atlantic margin region. This is interpreted to represent wide rift basin development resulting from strain delocalization and lateral migration of the locus of extension (Buck *et al.* 1999; Buiter *et al.* 2008). Wide rift zones, often composed of multiple low-magnitude rifts, are predicted to develop in regions of higher than normal heat flow with relatively thick crust (Buck 1991; Hopper & Buck 1996). The margins of the Irish Rockall Basin exhibit uniformly thick interpreted Permo-Triassic successions, with subtly different internal stratigraphy between adjacent basins, inset by younger faults as a string of north–south trending 'perched' basins (Fig. 5). The overall interpretation is wide basin extension producing a broad region of Permo-Triassic deposition.

The Triassic successions over much of the Celtic Sea region, south of Ireland, are characterized by uniform sediment thickness across wide areas. Subtle internal wedging of individual seismic packages occurs, with fault polarity changes, but the overall succession is not markedly asymmetric. A wide rift basin system above the Variscan basement domain is suggested. Inferred Permian strata lie unconformably beneath the Triassic succession in small, isolated half-grabens with common syn-sedimentary wedging (Fig. 6). These probably developed in response to post-orogenic collapse of thickened, hot Variscan crust. Similar features are observed in the outcrop study of the marginal Moroccan basins.

The overall Permo-Triassic succession in the European North Atlantic margin region thickens northwards from the Celtic Sea region offshore Ireland to the mid-Norwegian basins. In most basins distinct seismic sequences can be identified, reflecting different phases of early post-Pangaean rift development. While these can be mapped through individual basins, correlation between the various basins is only tentative at this stage due largely to limited well control. Nonetheless, regional patterns can be recognized. Permian strata are only locally developed in the south but have a significant thickness in the northern basins. In the south (e.g. Celtic Sea region) interpreted Permian strata occur within small, fault-controlled half-graben basins that are hinged by extensionally reactivated Variscan structures. These are interpreted as early Variscan collapse intermontane basins. Further

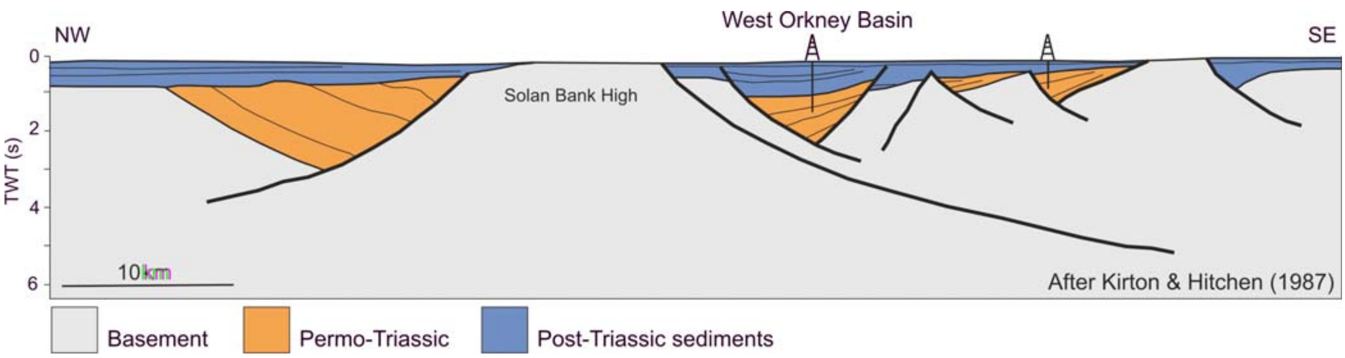

Fig. 4. Geoseismic profile across the Solan Bank High. The basement high compartmentalized the rifting style, with a series of narrow rift half-grabens developed to the SE while the remnants of an eroded and tilted wide-rift system occurs to the NW. This lacks evidence of major growth faulting and probably had a more extensive thick, uniform depositional geometry.

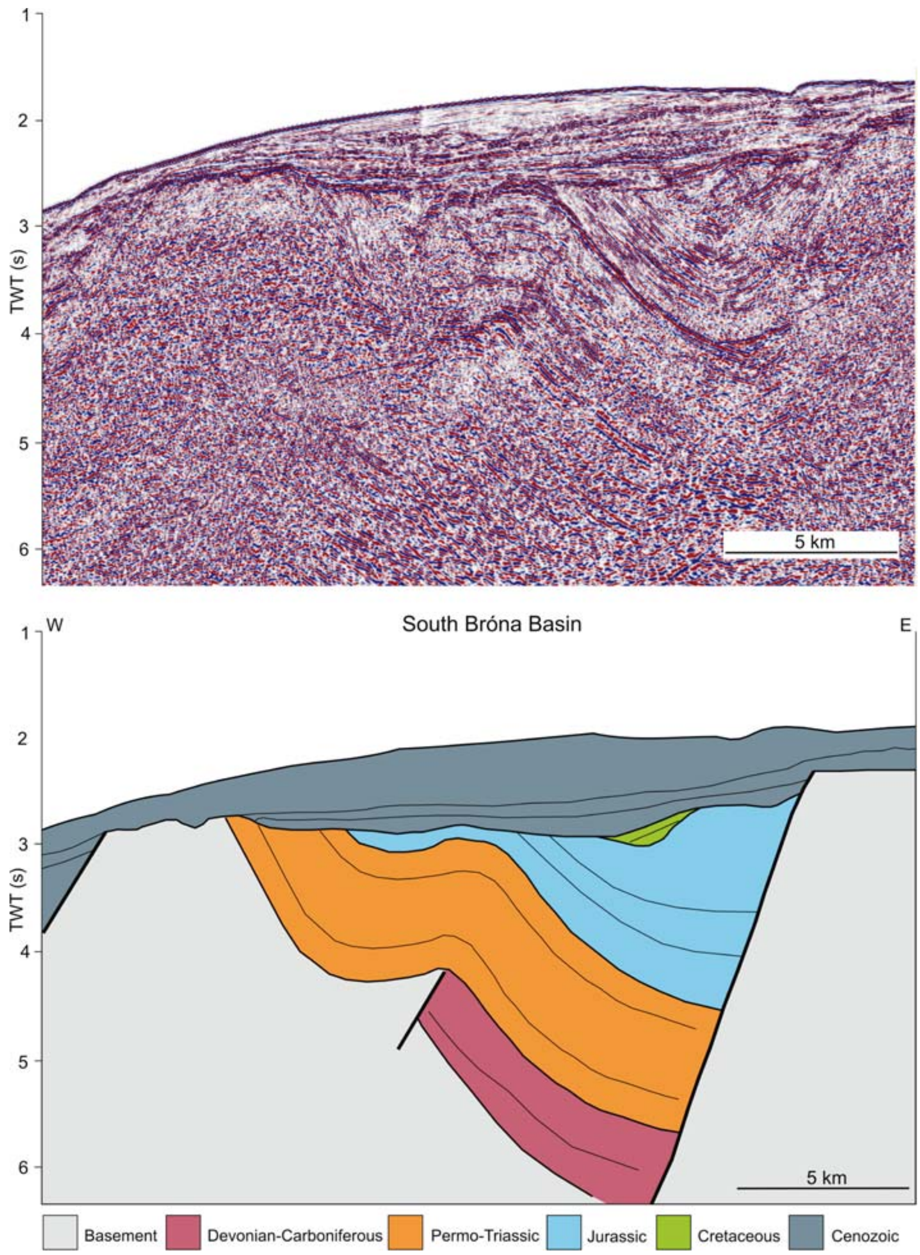

Fig. 5. Seismic profile and geoseismic profile across the South Bróna Basin on the SE flank of the large Rockall Basin. The preserved basin, incised by later faulting and erosion, had a larger depositional extent as evidenced by the absence of any evidence of thickness variations towards the bounding fault to the east or the basement block to the west. It is interpreted as an example of a wide-rift basin.

north, as typified by the Slyne Basin, basins NW of Scotland, and the Froan Basin on the Trøndelag Platform, the Permian succession is significantly thicker. The thin succession resting unconformably upon the interpreted Permian strata in the south of the region is suggested to be of Late Triassic age, while in the Norwegian region a complete Triassic succession is commonly proven by well data. This suggests that rifting commenced in the Norwegian region in Permian times, synchronous with intermontane localized Variscan collapse basins further south. Regional Triassic sedimentation did not take place in the south until later in the Triassic, when deposition was of regional extent, with wide rift processes dominating in this region.

Structural style/evolution: evidence from outcrop: Morocco

The Permo-Triassic Central High Atlas and Argana basins in Morocco (Fig. 7) are 100 km apart, separated by the Palaeozoic and Pre-Cambrian rocks of the 'Massif Ancien'. The exceptional exposures provide information on contrasting structural style, and the geodynamic response to North Atlantic and Tethyan tectonics. The basin types are similar to those documented from regional seismic, and outcrop analysis provides an analogue study to detail the fault geometries and impact of tectonics on local sedimentation and reservoir development. The outcrop evidence builds upon the regional picture and elucidates in more detail the semi-regional to reservoir scale tectonostratigraphic features of the successions.

The Oukaimeden–Ourika Valley, part of the broader Central High Atlas Basin, comprises an ENE-elongated rift basin bounded by extensionally reactivated Variscan structures. Although the present-day outcrop pattern reflects inversion due to the Alpine compression that led to major uplift in the High Atlas and subsequent erosion, it is possible to reconstruct the basin's earlier structural history. Both the ENE–WSW and NNE–SSW striking sets of normal faults show evidence for syn-sedimentary

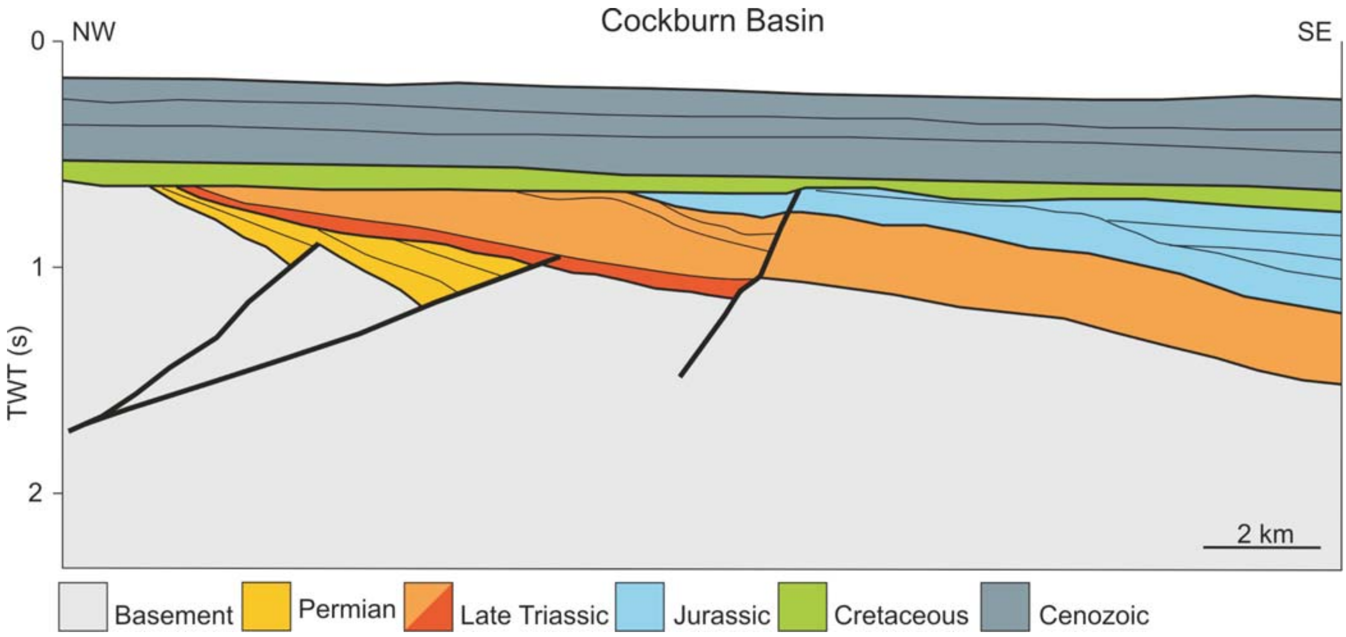

Fig. 6. Geoseismic profile from the Cockburn Basin. Interpreted Permian strata are developed in small half-graben controlled by early extensional collapse of the thick Variscan crust along reactivated thrusts. These sediments are unconformably overlain by late Triassic strata showing as relatively uniform, with subtle thickness variations, interpreted as the product of wide-rift extension. The planar nature of the unconformity, with no evidence of residual topography, suggests a significant hiatus between the two sedimentary sequences.

movement, displaying stratigraphic thickening into growth faults and associated progressive change in dip of the bedding (Fig. 8). The ENE–WSW faults are deep rooted and controlled the geographical extent of the basin, providing the accommodation for sediment deposition within a typical narrow half-graben basin geometry following NW–SE extension during the Late Triassic. The direction of extension is nearly parallel to the dip on NE to NNE striking faults, illustrated by striations. ENE trending structures display left-lateral movement, with a strong normal component.

Close to the bounding fault the main sandstone units have a higher net to gross ratio (N:G), consistent with a tectonic control on reservoir development. Increased accommodation on the downthrown side of the main faults resulted in river capture, and detailed sedimentary logging (Fabuel-Perez & Redfern 2009) shows that the main fluvial system flowed parallel to the controlling faults. More mudstone-rich overbank deposits become the dominant facies as the section thins away from the main fault-controlled depocentres (Fig. 8). The presence of thick locally derived conglomerates adjacent to the main bounding faults, with palaeocurrents oblique to the dominant axial trends for the main fluvial system (Figs 7 & 8), record alluvial fans derived from erosion of the main fault scarp during tectonic activity (Fabuel-Perez & Redfern 2009).

Smaller NE to NNE oriented faults are interpreted to be contemporaneous to the main fault set and are compatible with NW–SE extension. However, these faults have a small throw and are interpreted to have a limited influence on sediment deposition.

The second area of study in the Argana Basin, on the western margin of the High Atlas, contains exceptionally exposed Permian and Triassic red beds. This is the SE extension of the Essaouira Basin (Fig. 7). Permian and Upper Triassic beds strike approximately parallel to the NNE trend of the valley and dip 5–30° towards the NW. The Upper Permian sediments consist predominantly of conglomerates interpreted to be deposited within alluvial fans, grading vertically and laterally into sandstones deposited in fluvial channels and as floodplain deposits. A major unconformity separates the Permian from the overlying Upper Triassic sediments that mainly consist of siltstones and mudstones deposited in floodplain or playa environments, alternating with coarse alluvial conglomerates and continental fluvial or aeolian sandstones (Tixeront 1973; Brown 1980; Mader 2005).

Several models have been proposed to explain the structural evolution of the basin and the structural control on sedimentation (Tixeront 1973; Brown 1980; Medina 1988, 1991; Hofmann *et al.* 2000). Episodic movement of east–west trending fault blocks tilted towards the north was initially suggested to control the deposition of the whole Permo-Triassic sequence (Brown 1980). Other studies recognized two main phases of syn-sedimentary extension characterized by the two sets of normal-faults, striking east–west and NE to NNE (Laville & Petit 1984; Medina 1988, 1991, 1995). Both these interpretations attribute the evolution of Mesozoic basins in the High Atlas of Morocco to pull-apart extensional mechanism along the ENE–WSW trending fractures (Manspeizer 1982; Laville & Petit 1984).

Recently analysed field data as part of this study are modifying this interpretation. It is suggested that the large east–west striking-faults do not significantly influence Triassic deposition. The thick Permian conglomerates, deposited as large alluvial fans, were sourced mainly from the uplifted Ancien Massif (Baudon *et al.* 2009). These conglomeratic units are cut by, but not sourced from, the east–west faults. The Upper Permian sequence was tilted towards the NW prior to Upper Triassic sedimentation producing a marked angular inconformity. Upper Triassic sedimentation in the Argana Valley does not show significant lateral variation in thickness or facies, which suggests the east–west and smaller NNE trending normal faults were not significantly active. The main basin-bounding fault is speculated to be a sub-surface extensional fault located to the west of the valley, now masked by later Jurassic and Cretaceous cover. This is parallel to faults producing similar half-graben structures identified further NW in the Essaouira Basin (Hafid 2000; Le Roy & Pique 2001). This fault probably controlled the regional tilt of the beds. In contrast to the Ourika Basin, deposition in the Argana Basin is interpreted to have been part of the much broader Essaouira Basin, with limited local fault control on sedimentation. This pattern of uniformly thick sediments, with subtle fault-controlled thickness variations, is comparable to that observed in the seismic study from the North Atlantic,

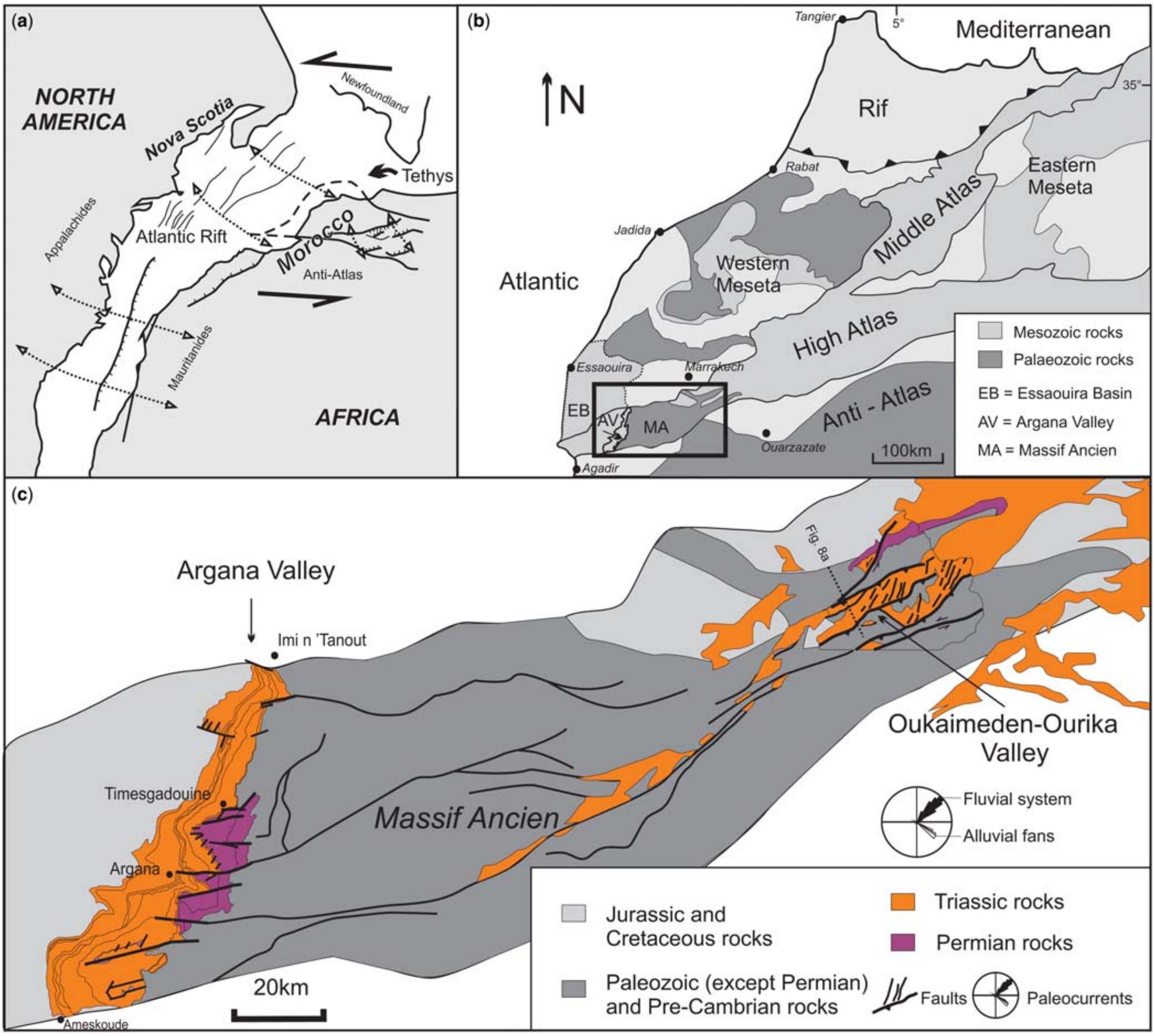

Fig. 7. (**a**) Palaeogeographic map of Morocco at Triassic time (modified from Laville & Piqué 1991). (**b**) Present-day structure summary map of Morocco (modified from Ellouz *et al.* 2003). The box denotes the location of the study area. (**c**) Close-up of study area showing the main structures. The Permian and Triassic outcrops in the Oukaimeden–Ourika Valley (modified after Taj-Eddine & Pignone 2005) and Argana Valley (modified after Tixeront 1973) are highlighted with respect to the Massif Ancien. Palaeocurrents in the Ourika Valley for the F5 Unit from Fabuel-Perez & Redfern (2009).

suggesting this Moroccan section provides a good outcrop analogue for subsurface exploration in the Atlantic borderland area.

Provenance studies: tracking Triassic sand dispersal on the NW European margin

The Moroccan outcrops described in the previous section illustrate the interplay of tectonics and sedimentation at regional and local scale and the resulting complexity of the depositional system. To better understand reservoir sand dispersal within such complex systems a novel provenance tool was utilized as part of the integrated analysis, illustrated by results from the Atlantic Margin basins west of Ireland and the UK.

Recent studies have demonstrated the utility of the Pb isotopic composition of detrital K-feldspar as a sand provenance tool, particularly when applied on a regional scale (Tyrrell *et al.* 2006, 2007; Clift *et al.* 2008). Common Pb isotopes vary in the crust on a sub-orogenic scale and it has been shown that detrital K-feldspar can retain the signature of its source despite erosion, transport and diagenesis (Tyrrell *et al.* 2006). The Pb isotopic signature of individual K-feldspar sand grains can be analysed *in situ* using laser ablation multicollector inductively-coupled plasma mass spectrometry (LA-MC-ICPMS). Imaging prior to analysis highlights heterogeneities which then can be avoided during laser ablation. The use of ion counters to measure Pb ion beams means that data can be retrieved at a spatial resolution (*c.* 20 μm laser spot sizes) similar to that achievable using ion microprobe techniques but with reduced analytical uncertainty (Tyrrell *et al.* 2009).

One of the major advantages of the Pb K-feldspar tool is that, in contrast to provenance approaches that utilize signals in robust grains (e.g. U–Pb zircon), it provides a means of assessing first-cycle sand-grain provenance. As detrital K-feldspar is unlikely to survive more than one sedimentary cycle, these grains can be tracked back directly to their basement source, allowing the scale and geometry of the drainage system to be constrained. These types of insights can aid in more accurate prediction of reservoir sandstone distribution and quality in the subsurface.

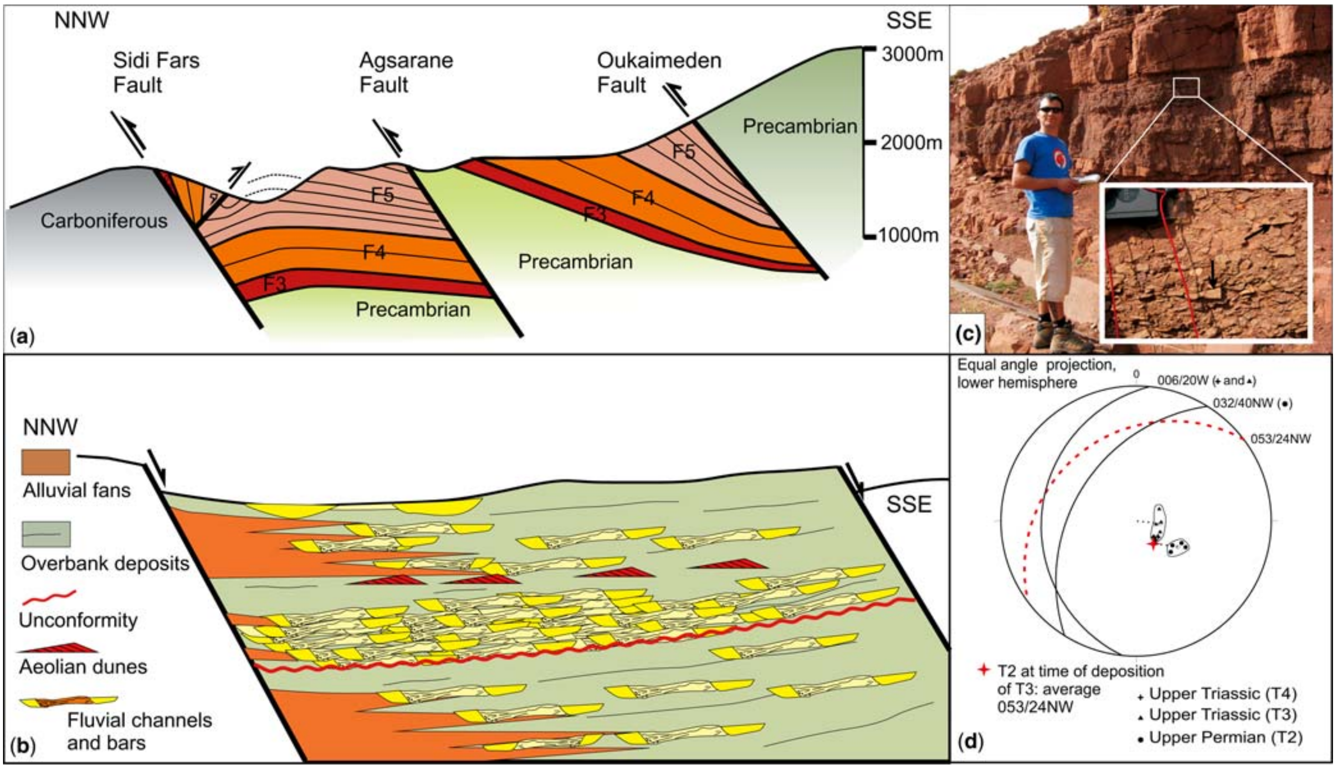

Fig. 8. (**a**) Structural cross-section across the Oukaimeden Valley showing the main ENE striking faults. Location of cross-section shows on Figure 6*c*. (**b**) Schematic model of the structural control on sedimentation, showing alluvial fans shed from the footwall highs, and the axial river system preferentially captured close to the main fault. (**c**) Photograph of the alluvial fan breccias, with close up of clasts. (**d**) Stereonet plot illustrating the angular unconformity between the Permian and Triassic bedding in the Argana Valley.

The Pb K-feldspar provenance tool is particularly appropriate in an investigation of Triassic sand dispersal in the NE Atlantic margin basins, given the abundance of arkosic and sub-arkosic sandstones in these successions. Recently published provenance data have shed new light on the nature and origin of these sandstones. Data from K-feldspar from Lower Triassic sandstones in the Slyne Basin (including the Corrib Gasfield), offshore west of Ireland, define two distinct Pb populations (Fig. 9), which are likely to have been sourced from Archaean and Proterozoic crust to the north and west (Tyrrell *et al.* 2007; McKie & Williams 2009).

Pb K-feldspar data from Permo-Triassic sandstones in the Rockall Basin (Dooish gas condensate discovery, Well 12/2-1z; Fig. 9) appear to have been derived from the north and NE, probably from elements of the Lewisian Complex (Fig. 9; Tyrrell *et al.* 2010). In basins west of Shetland (Fig. 9), new Pb K-feldspar data (Fig. 10; McKie & Williams 2009; Tyrrell *et al.* 2009) from Middle–Upper Triassic Foula Formation sandstones (part of the Strathmore Field) indicate derivation from Archaean– Palaeoproterozoic rocks on the margins of the rift basin (Nagssugtoqidian Mobile Belt of East Greenland and/or the Lewisian Complex of NW Scotland and equivalents), although whether the derivation is from the east- or west-rift margins, or from a northern axial source, cannot be distinguished. Here, the Pb K-feldspar data are in broad agreement with U–Pb detrital zircon geochronology (Morton *et al.* 2007).

The Pb K-feldspar data from Atlantic margin basins consistently preclude Irish Massif, the UK Mainland south of the Moine Thrust and the remnant Variscan Uplands to the far south as sources for Triassic sand (Fig. 10). This indicates no linkage between the drainage systems supplying these Atlantic margin basins and those delivering sand to onshore UK, the East Irish Sea Basin and the Central and Southern North Sea. The sedimentary contribution of non-radiogenic Archaean and Palaeoproterozoic Pb sources appears to increase in basins further to the north. The data indicate that palaeodrainage evolution in these marginal Triassic basins was strongly influenced by uplifted Archaean–Palaeoproterozoic basement highs, and not Variscan Uplands to the south, with consequent implications for potential reservoir sandstone distribution in these areas (e.g. Tyrrell *et al.* 2010). These studies reveal the value and effectiveness of the Pb K-feldspar provenance tool in investigations of both ancient and modern broad-scale drainage systems.

Developing analogue depositional and reservoir models

Building upon the work defining the basin architecture and provenance, detailed sedimentological analysis is improving our understanding of basin development, basin-scale depositional systems and producing analogue reservoir models. Correlations within the Central Atlantic domain have been attempted by Olsen (1997) and Olsen *et al.* (2000) from the Fundy Basin to Morocco. This is based on limited biostratigraphic data and often poorly defined unconformities. Because of the low resolution of biostratigraphy with red bed deposits, the only synchronous marker beds that can confidently be picked are the radiometrically dated CAMP basalt and the palynological turnover of the Rhaetian/Jurassic boundary located a few metres below the basalt. Biostratigraphical correlations across the Triassic basins of Morocco have been assessed recently by El Arabi *et al.* (2006) while the biostratigraphy in the Fundy Basin is still relatively poorly constrained. The stratigraphy from the Fundy Basin, Canada and the Argana and Central High Atlas basins in Morocco is compared in Figure 11. Triassic rift basins along the Central and North Atlantic margins display a similar sedimentary evolution characterized by an initial phase of

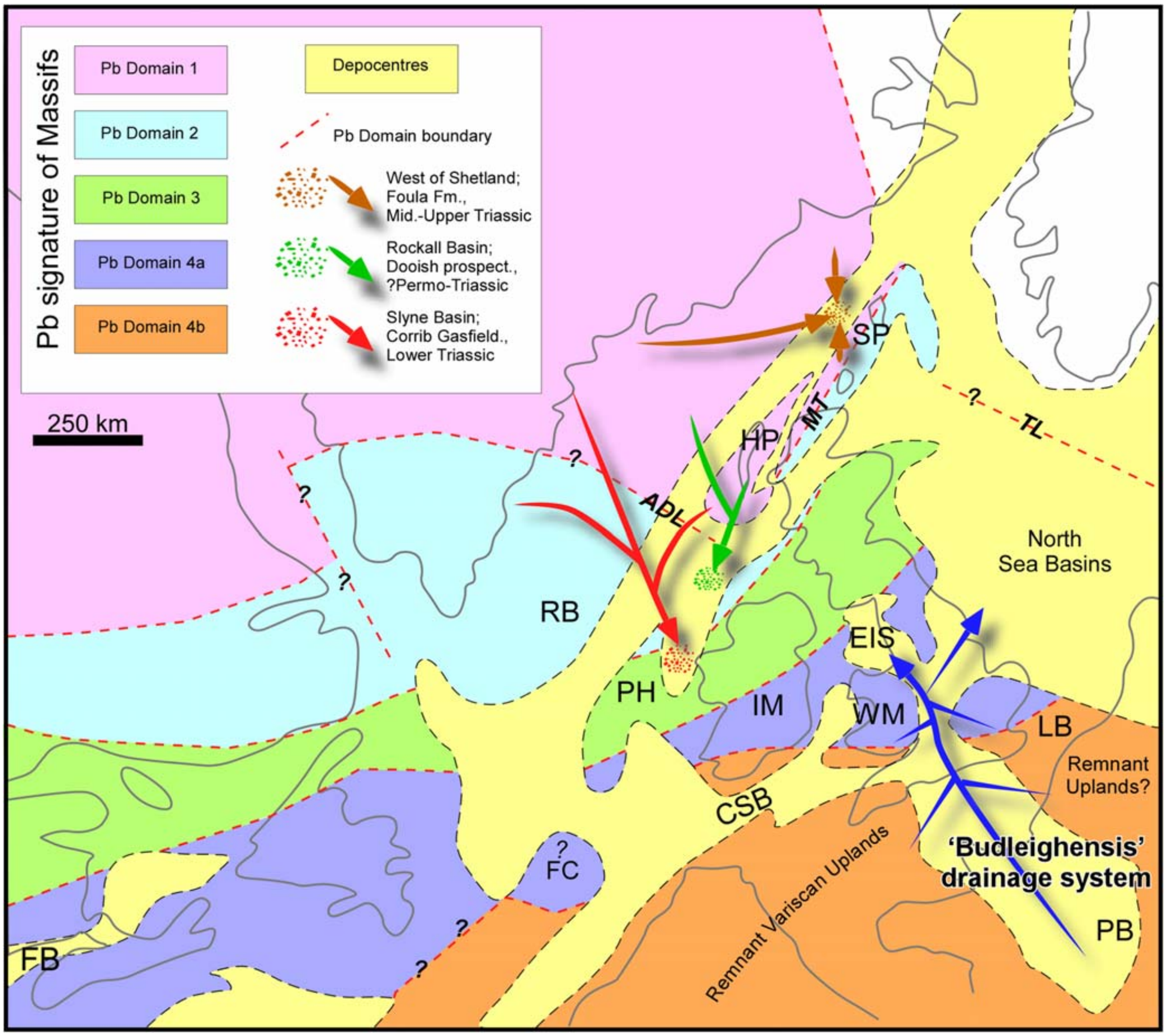

Fig. 9. Schematic Triassic palaeogeographic reconstruction of the circum-North Atlantic region (after Torsvik *et al.* 2001; Eide 2002; Scotese 2002) showing the configuration of massifs and depocentres. The massifs are colour-coded to reflect their broad Pb isotopic signature (after Tyrrell *et al.* 2007 and references therein). The 'Budleighensis' drainage system is also shown (blue). Directional arrows (red, green, brown) show likely derivation directions for sandstones from the marginal basins, based on the Pb isotopic composition of individual K-feldspar sand grains. ADL, Anton Dorhn Lineament; CSB, Celtic Sea basins; EIS, East Irish Sea Basin; FB, Fundy Basin; FC, Flemish Cap; HP, Hebridean Platform; IM, Irish Massif; LB, London–Brabant Massif; MT, Moine Thrust; PB, Paris Basin; PH, Porcupine High; RB, Rockall Bank; SP, Shetlands Platform; TL, Tornqvist Line; WM, Welsh Massif.

alluvial fan and fluvial sedimentation and a later playa/lacustrine dominated phase. Although the sedimentological evolution of these basins is similar, the timing and duration of the phases of fluvial and playa deposition vary within and between the basins. In order to understand the basin-fill evolution, and in particular the depositional systems, the sedimentology of two broadly co-eval Permo-Triassic basins is reviewed in this paper: the Minas Basin (Nova Scotia) and the Central High Atlas Basin (Morocco). These formed at different palaeolatitudes and now lie on different sides of the Atlantic passive margin.

In the Fundy Basin, detailed analysis of laterally extensive coastal outcrops allows definition of basin-scale sedimentary architecture and assessment of basin development. A comparable Moroccan section provides equally extensive sections, offering another analogue for the subsurface basins, and using innovative LiDaR (Laser Detection and Ranging) analysis, detailed sedimentary and reservoir models have been produced (Fabuel-Perez *et al.* 2009).

Fundy Basin, Nova Scotia, Canada

The Fundy Basin, one of a series of early Mesozoic rift basins developed along the NW Atlantic margin, contains 6–12 km of Anisian to basal Hettangian non-marine clastic sediments (Olsen *et al.* 1989; Wade *et al.* 1996; Leleu *et al.* 2009). It represents a large complex Triassic half-graben (Wade *et al.* 1996) with a strike-slip component of movement (Olsen & Schlische 1990; Withjack *et al.* 1995, 2009) and is subdivided into three sub-basins; amongst them the easternmost Minas sub-basin shows the most extensive outcrops and preservation of sequences (Fig. 12).

The Triassic succession in the Minas sub-basin comprises the Wolfville (<800 m) and the overlying Blomidon (<250 m) formations (Fig. 12). The Wolfville Formation is Carnian in age (Olsen *et al.* 1989), and lies unconformably on Carboniferous and older rocks, forming the earliest syn-rift unit in the basin (Wade *et al.* 1996). The Wolfville Formation comprises coarse- and fine-grained fluvial sandstones (Klein 1962; Hubert & Forlenza 1988;

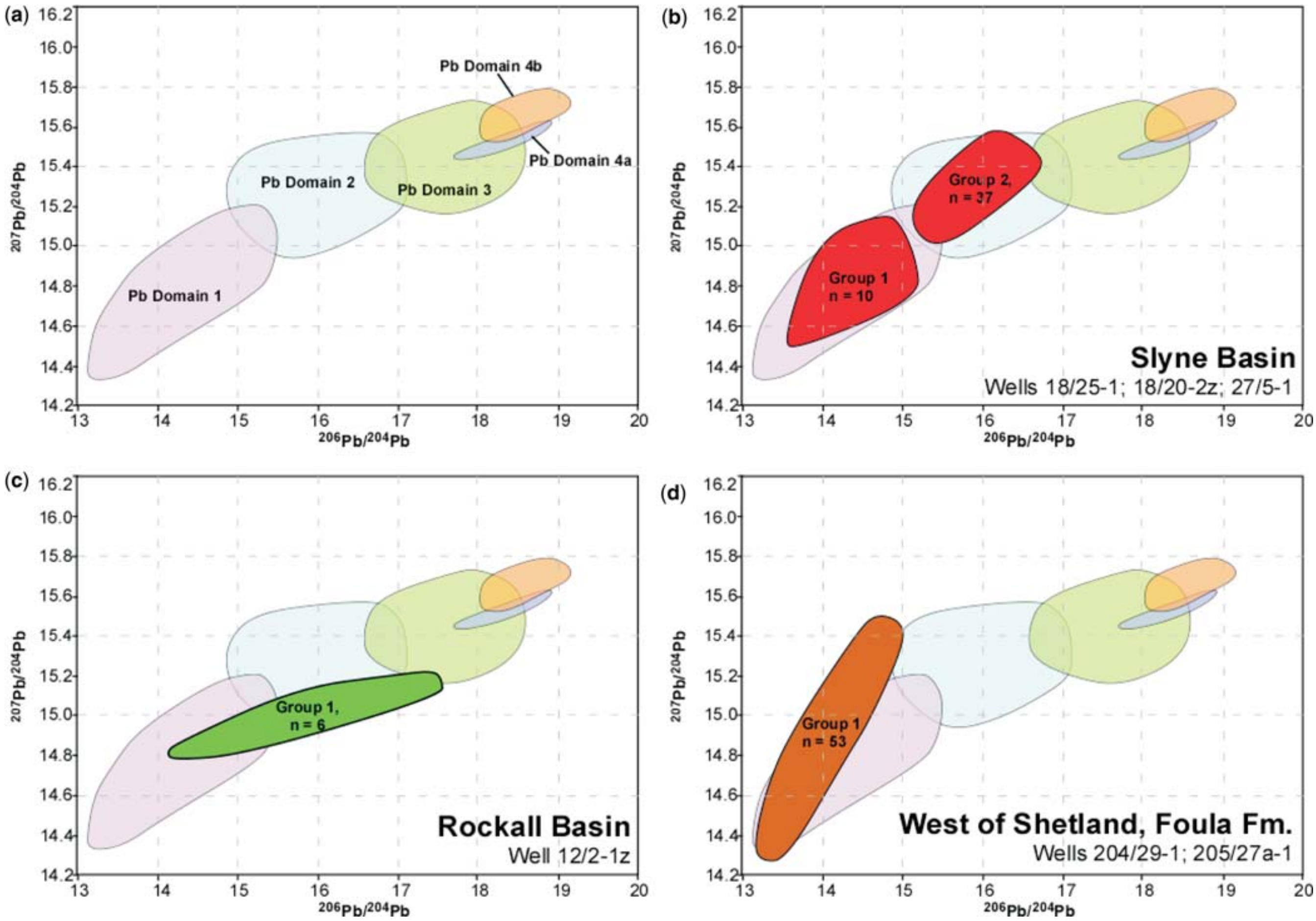

Fig. 10. Plot of $^{206}\mathrm{Pb}/^{204}\mathrm{Pb} - ^{207}\mathrm{Pb}/^{204}\mathrm{Pb}$ lead space (after Tyrrell *et al.* 2007 and references therein) illustrating (**a**) the isotopic composition of Pb basement domains in the circum-North Atlantic (Fig. 8); (**b**) the Pb isotopic range of K-feldspar from Lower Triassic sandstones in the Slyne Basin; (**c**) the Pb isotopic range of K-feldspar from Permo-Triassic sandstones in the Rockall Basin (Dooish gas condensate discovery); (**d**) the Pb isotopic range of K-feldspar in Foula Formation sandstones from basins west of Shetland.

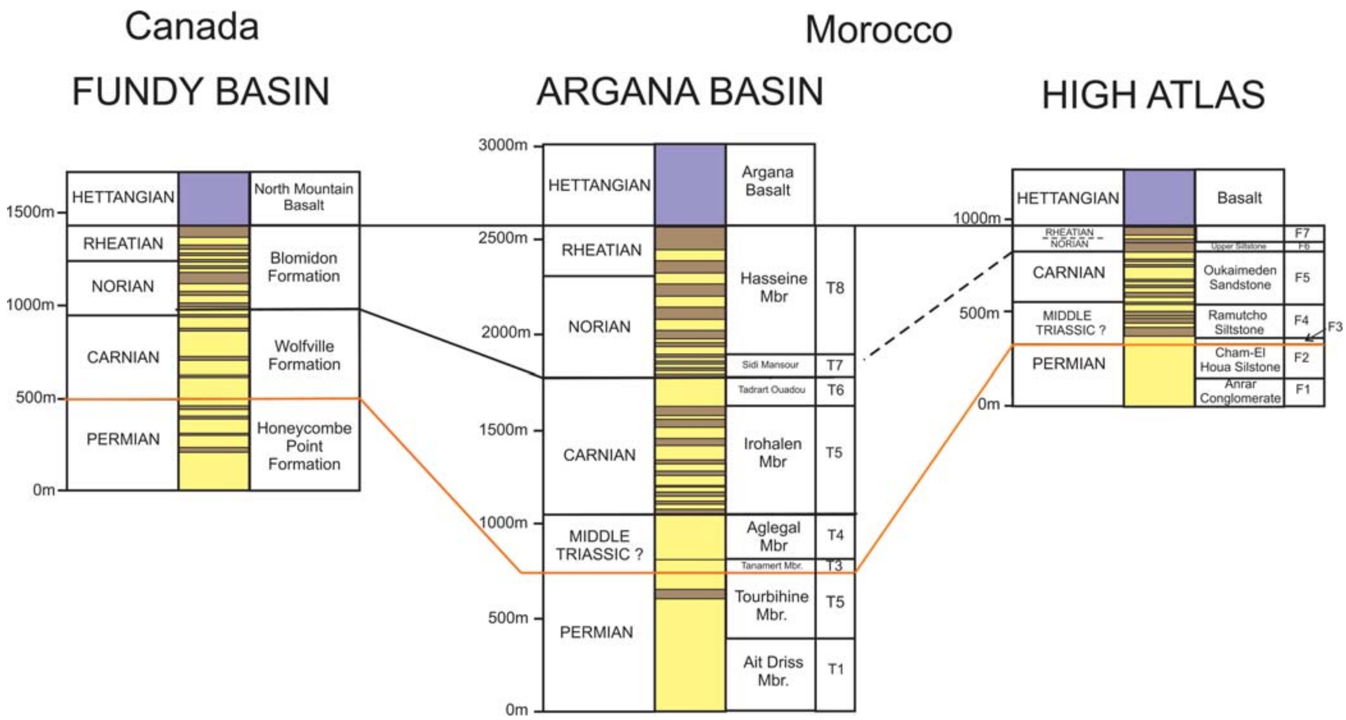

Fig. 11. Simplified stratigraphy comparing the Permian and Triassic sections in the Fundy Basin, Nova Scotia, and the Argana and Central High Atlas basins in Morocco. Modified from Olsen *et al.* (2000).

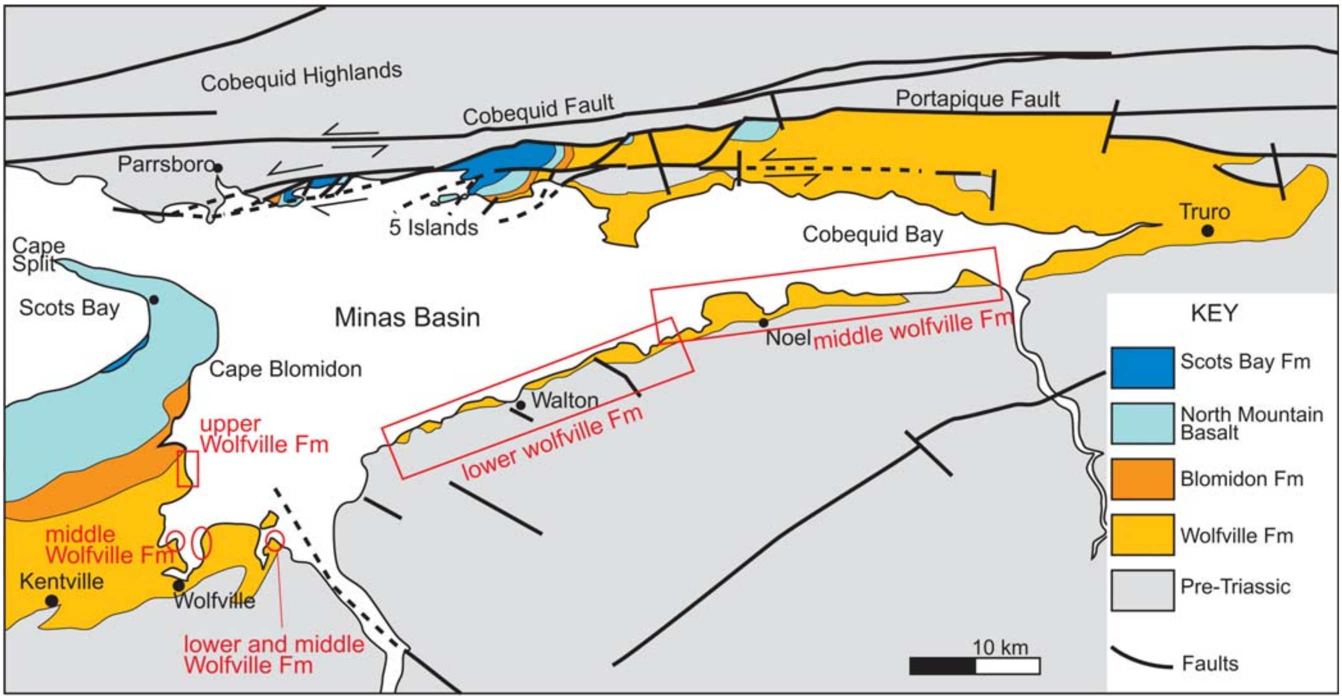

Fig. 12. Location of the Minas Basin in Nova Scotia, Canada, showing the studied Triassic outcrops.

Leleu *et al.* 2009) and subordinate aeolian dune deposits (Hubert & Mertz 1980, 1984) and alluvial fan sediments (Hubert & Mertz 1984). The contact between the formations corresponds to a major change in facies architecture to mud-rich playa margin deposits containing evaporites and ephemeral fluvial sheet-sandstones (Hubert & Hyde 1982; Mertz & Hubert 1990; Gould 2001). The extensive North Mountain Basalt, part of the Central Atlantic Magmatic Province event (McHone 2000), overlies the Blomidon Formation, and straddles the Triassic–Jurassic boundary (Olsen *et al.* 1989; Olsen 1997).

Within the Wolfville fluvial succession three distinguishable packages with very different characteristics of grain size and stacking patterns have been observed. The lower Wolfville Formation (110 m thick) is dominated by coarse-grained fluvial deposits (Fig. 12) which filled remnant palaeotopography. It comprises four mega-units and 13 smaller scale high-resolution fining-upwards cycles of pebbly conglomerates to sandstones (Fig. 13). The bounding surfaces can be correlated regionally over a distance of between 10 and 27 km (Leleu *et al.* 2009), thereby providing effective basin-scale stratigraphic correlation. The overall succession has a sheet-like geometry comprising stacked, erosion-dominated, multi-storey channel bodies with a drainage system that evolves to the north and NE. An individual high-resolution cycle records braid-plain development and is interpreted as a multi-storey channel belt. However, the width of the active channel belt is unknown. Recognition of key surfaces across a 10–20 km section (Fig. 14), provides criteria for correlation of these continental facies, barren of biostratigraphic markers (Leleu *et al.* 2009).

The middle Wolfville Formation abruptly overlies the lower Wolfville Formation (Fig. 12). It is a well sorted sandy bedload fluvial system ($<$ 350 m thick) and consists of 15 repetitive units. These comprise stacked channel bodies forming channel belt complexes that are intercalated with upward thickening floodplain deposits. Application of LiDaR digital outcrop analysis aids the definition of detailed architecture (van Lanen *et al.* 2009). Large-scale sequences have been defined based on grain size evolution that encompasses several channel belt complexes. The grain size variation reveals a climatic control which influences the bedload transport capacity of the river, while smaller scale repetitive channels and channel belt migration/avulsion possibly result from autocyclic processes. The larger scale architectural evolution including the development of the channel belt architecture, channel body dimensions and the increased upwards preservation of greater floodplain units result from allocyclic processes which may reflect a tectonic control producing increased accommodation.

The upper Wolfville Formation (240 m thick) occurs beneath the lacustrine/playa deposits of the Blomidon Formation (Fig. 12). It displays repetitive packages of channelized and unconfined fluvial facies and playa deposits together with occasional aeolian dune deposits. Grain size varies from pebbly coarse sand and medium to coarse sand in the channelized facies to well sorted medium to fine sand in the unconfined facies and aeolian deposits. Development of the playa margin environment in the basin during Blomidon Formation deposition records retrogradation of the fluvial profile within the drainage basin, and the extension of the playa and playa margin towards the catchment. Retrogradation suggests a major decrease in water and sediment supply. This major shift could be interpreted as the result of climate change. However, although all Triassic basins along the Atlantic margins show a similar sedimentological evolution from fluvial to playa depositional phases, the transition occurs at different times and with variable duration. This suggests that basin development governs the large-scale basin-fill and the shift from fluvial to playa depositional phase (Schlische & Olsen 1990; Smoot 1991). In particular, because the transition from fluvial to playa/lacustrine conditions takes place at different times, it indicates that climate may not be the critical controlling factor. The transition is interpreted to be associated with a progressive decrease in source area relief related to a decline in fault-generated topography towards the end of the syn-rift phase of basin development.

The Central High Atlas Basin, Morocco

Previous work in Morocco (Petit & Beauchamp 1986; Mattis 1977; Benaouiss *et al.* 1996; Tourani *et al.* 2000) provided an overview

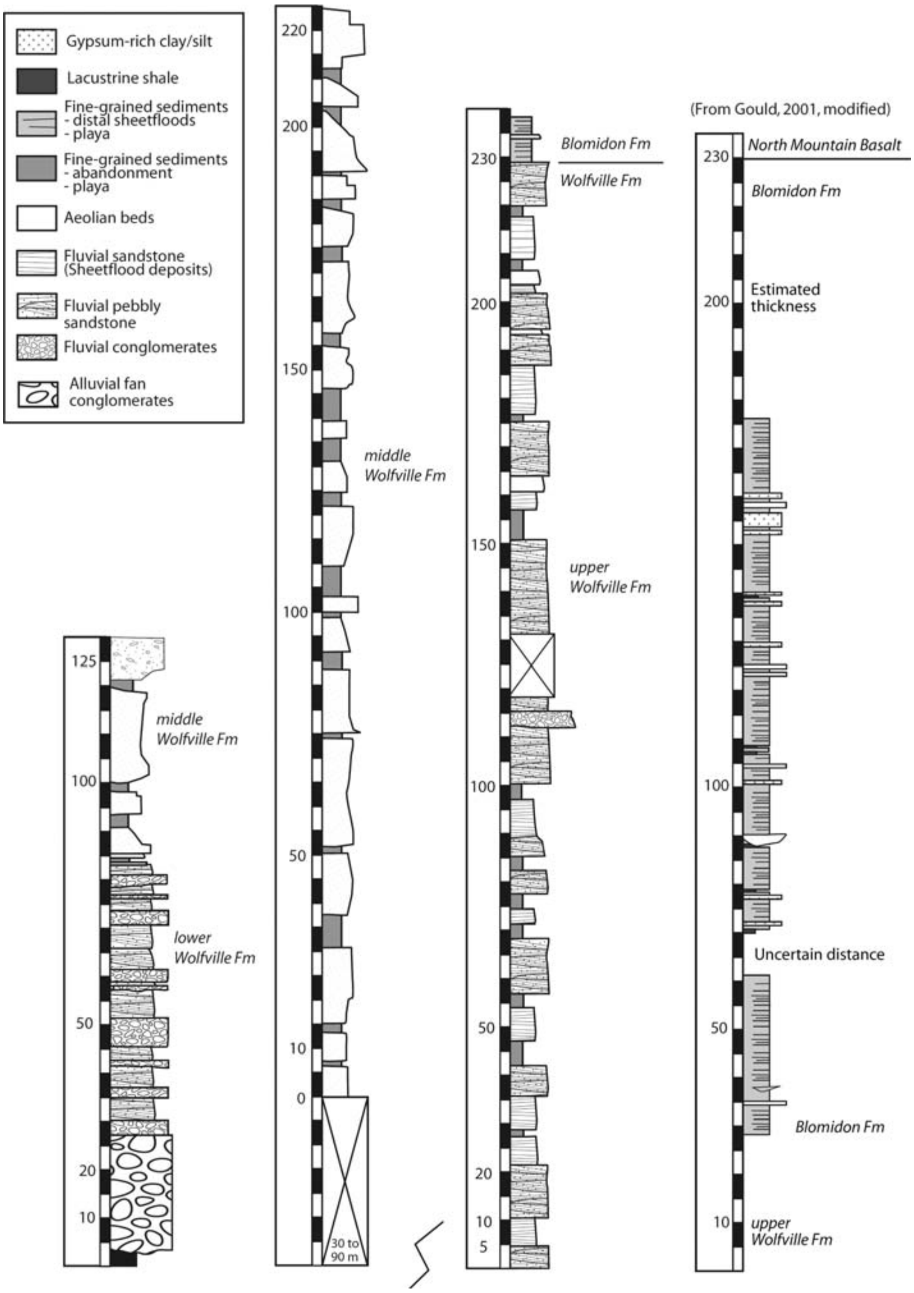

Fig. 13. Two summary sedimentary logs through the Triassic succession in the Minas sub-basin comprising the Wolfville (<800 m) and the overlying Blomidon (<250 m) formations. The Wolfville Formation is Carnian in age (Olsen *et al.* 1989), and lies unconformably on Carboniferous and older rocks.

of the broad depositional setting and stratigraphy for the Permian and Triassic section in the Central High Atlas (Fig. 11). Fabuel-Perez & Redfern (2009), as part of this research project, recently revised the sedimentological interpretation of the Oukaimeden Sandstone Formation in the Oukaimeden–Ourika valley area (Fig. 7). Detailed sedimentary models were produced using LiDaR for digital outcrop analysis, and a reservoir model was developed (Fabuel-Perez & Redfern 2009; Fabuel-Perez *et al.* 2009).

Within the Oukaimeden Sandstone Formation five major facies associations have been identified (Fig. 15). Changes in the distribution of facies associations, identification of key boundaries, surfaces and variation in the architectural style through time have been used to subdivide the Oukaimeden Sandstone Formation into three major members (Fig. 15): (a) a lower member comprising channels and bars (Facies Association 1) alternating with floodplain mudstone units (Facies Association 2); (b) a middle member, characterized by vertically stacked amalgamated channels and bars and a significant decrease in the amount of preserved mudstone units; and (c) an upper member showing a similar style to the one observed in the lower member with the first occurrence of aeolian facies (Facies Association 3) and tidally influenced sandstones (Facies Association 4).

Using a process-based depositional facies model based on genetically related packages (Fabuel-Perez & Redfern 2009), the Lower Oukaimeden Member is interpreted to record deposition from large axial ephemeral river systems. The Middle Oukaimeden displays a change in depositional style to perennial fluvial conditions. This is interpreted to record the rejuvenation of the fluvial regime related to a change in climate to more humid conditions and subsequent increased run-off. The Upper Oukaimeden is interpreted to record a change in fluvial conditions from perennial back to ephemeral combined with the presence of aeolian dunes (Facies Association 3) which reflect climatic variations shifting

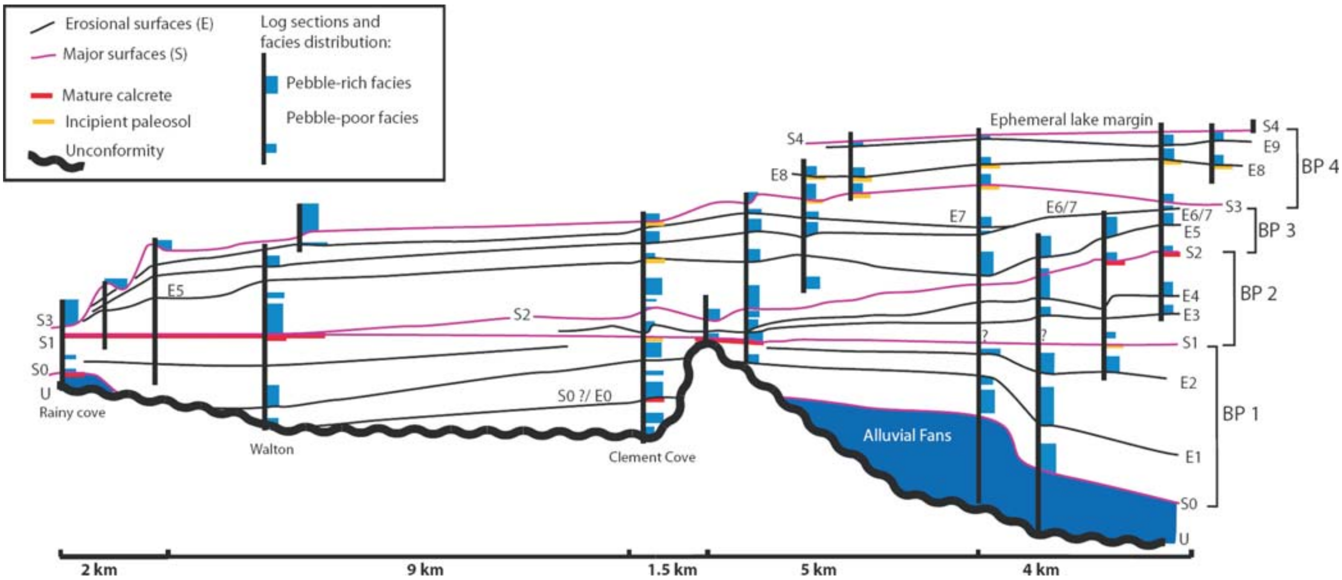

Fig. 14. Summary correlation of the lower Wolfville Formation (110 m thick). It comprises multi-storey channel bodies arranged as four mega-units bounded by 'S' surfaces and 13 smaller scale high-resolution fining-upwards cycles of pebbly conglomerate to sandstone, bounded by 'E' (or 'S') surfaces which can be correlated regionally between 10 and 27 km (Leleu *et al.* 2009).

towards more arid conditions. The top of the Oukaimeden Sandstone is characterized by the presence of tidally influenced facies recording the first marine incursion into the basin.

In the lower and upper member, alluvial fans were deposited in response to footwall uplift erosion of the controlling Sidi Fars fault. These alluvial fans, which pinchout towards the SW, are interpreted to force the axial rivers away from the controlling fault. The lack of alluvial fan deposits in the middle member could be due to 'toe cutting' of the alluvial fan by the axial rivers due to their increased size and switch to perennial conditions of the river system as a consequence of a climatic change (Leeder & Mack 2001).

Evidence is seen of a tectonic control on deposition and changes in architectural style. Preferred orientation of palaeocurrents in Facies Association 1 is towards the ENE. This is interpreted to be related to the palaeogeography of the basin (ENE–WSW orientated), which was tectonically controlled by the orientation of the syn-sedimentary Sidi Fars fault. Alluvial fans have a preferred palaeocurrent orientation towards the SE, normal to the ENE–WSW orientation of the Sidi Fars fault, indicating a sediment source from the uplifted footwall. N:G ratio decreases away from the fault, indicative of capture of the axial river system close in the depocentre. The morphology of the contacts also varies with distance from the controlling fault, with a sharp erosive contact

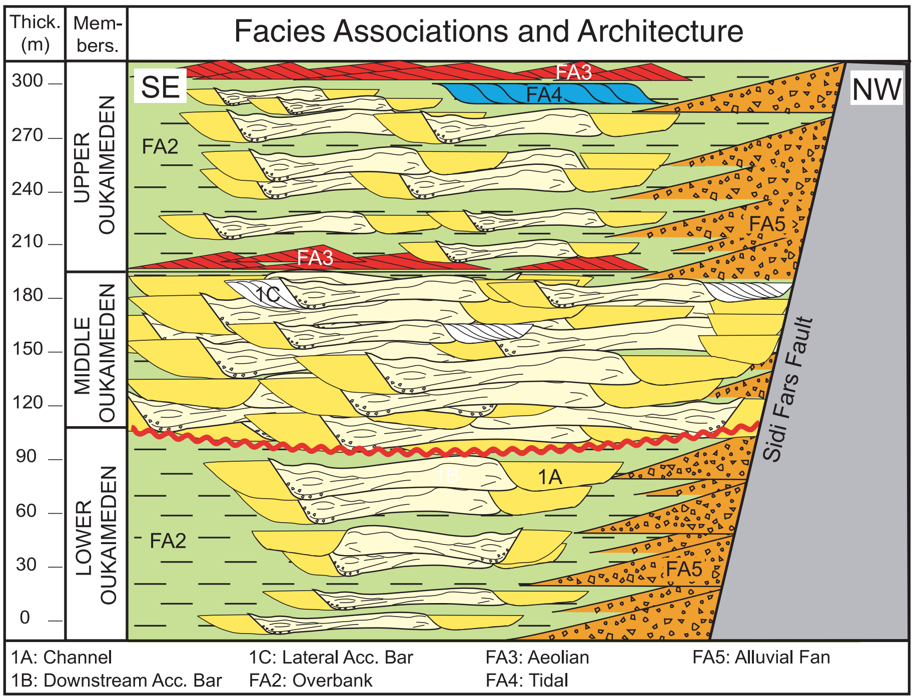

Fig. 15. Composite log summarizing the gross distribution of facies associations in the Ouikamaiden Sandstone, key surfaces used to define the three members and the changing architectural style through time.

near the fault due to successive erosional events by downcutting channels, and more gradation contact on the basin margin.

The sections in Morocco record both the tectonic and climatic influence on depositional architecture and reservoir distribution. The contact between Lower and Middle Oukaimeden is interpreted to record possible tectonic reactivation in the hinterland magnified by a concurrent change in climate towards more humid conditions. Increasing run-off and input of coarse sediment into the basin produced a change in architectural style, and a switch from ephemeral to perennial conditions. In the Upper Oukaimeden, a return to ephemeral conditions, combined with the presence of aeolian facies, suggests a climatic change back towards more arid conditions. Similar gross facies shifts, also interpreted as a response to climatic change, are observed in the Argana Basin. Improved dating and more detailed correlation are required to corroborate these as regionally correlatable events.

Conclusions

(1) An improved understanding of basin and sedimentary evolution, provided by multidisciplinary analysis, is illustrated by this regional study of the Atlantic margin Permo-Triassic basins. This addresses basin and outcrop to pore scales, across three orders of magnitude. Regional seismic scale allows analysis of a number of structurally linked basins, imaging the large-scale structure, in order to understand overall basin architecture and identify mega-sequences. Outcrop analysis provides ground-truth information to refine the seismic-scale structural interpretations and the resolution to model reservoir architecture at sequence scale, with definition of depositional systems and key correlation surfaces. Provenance analysis has the potential to test regional structural models and predict source to sink fairways, improving reservoir characterization by identifying provenance sources and sediment transport directions.

(2) A range of basin geometries are identified in the Permo-Triassic Atlantic margin basins, using both seismic (offshore, NE Atlantic) and outcrop (onshore, Morocco) studies. These include post-orogenic collapse basins, focused narrow rifts and wide, low-magnitude multiple extension depocentres. The shape and evolution of the basins were influenced by both Atlantic and Tethyan tectonic regimes, with significant control from inherited basement structures and structural fabrics.

(3) The basin fill, characterized in detail by examining the onshore Permo-Triassic outcrops in both Morocco and Nova Scotia, is dominated by continental red beds. They comprise braided fluvial, alluvial fan, aeolian, floodplain and lacustrine facies, and display a cyclicity in fluvial deposits from major ephemeral to perennial fluvial systems. Detailed outcrop analysis has identified key marker horizons and sequence boundaries that can be used to provide constraints for the delineation of laterally correlatable cycles. The depositional architecture at high-resolution outcrop scale is complex, controlled by the interplay of local and regional tectonic and climatic factors, as well as autocyclic processes. At basin scale, sedimentation records climatic changes, but the low-resolution basin fill evolution is mainly controlled by tectonically induced basin development. This has implications for reservoir distribution and quality on a regional and field scale.

(4) Application of a new Pb in K-feldspar provenance technique to determine the source of Triassic sandstones offers new and robust controls on sediment dispersal patterns in the North Atlantic. Results indicate that the regional palaeodrainage evolution of the basins was predominantly controlled by uplifted Archaean–Palaeoproterozoic basement highs to the north and NW and not, as hitherto assumed, by the Variscan uplands to the south. In addition to providing information on likely reservoir quality, the technique also has applications as a test for the robustness of large-scale structural basin tectonics and timing.

Funding is acknowledged from a Griffith Geoscience Research Award (Irish Department of Communications, Energy and Natural Resources) under the National Geoscience Programme 2007–2013. Funding from a Science Foundation Ireland Research Frontiers Programme grant (RFP06/GEO029) is also acknowledged. Thanks to K. Souders, P. Sylvester and M. Tubrett (Microanalysis Facility, Memorial University, Newfoundland, Canada) for assistance with ICPMS and A. Kronz (Electron Microprobe Laboratory, Geowissenschaftliches Zentrum, Göttingen, Germany) and to the Petroleum Affairs Division (Ireland), the Petroleum Infrastructure Programme (Ireland) and D. Sutherland (DTI core store, Edinburgh, UK) for facilitating access to core. Shell, EPE Stavanger, Shell EPX, EPTS and the North Africa Research Group (NARG) Consortium – Hess, Conoco, Repsol, Petrocanada, Maersk, Woodside, BG Group, Wintershall, RWE, ConocoPhilips, Pluspetrol, and ONHYM in Morocco – are all gratefully acknowledged for funding and support.

References

Baudon, C., Fabuel-Perez, I. & Redfern, J. 2009. Structural style and evolution of a Late Triassic rift basin in the Central High Atlas, Morocco: controls on sediment deposition. *Geological Journal Special Issue*, **44**, 677–691.

Benaouiss, N., Courel, L. & Beauchamp, J. 1996. Rift-controlled fluvial/tidal transitional series in the Oukaimeden Sandstones, High Atlas of Marrakesh (Morocco). *Sedimentary Geology*, **107**, 21–36.

Blystad, P., Brekke, H., Færseth, R. B., Larsen, B. T., Skogseid, J. & Tørudbakken, B. 1995. *Structural Elements of the Norwegian Continental Shelf, Part II: the Norwegian Sea Region*. Norwegian Petroleum Directorate, Bulletin, **8**.

Brown, R. H. 1980. Triassic rocks of Argana Valley, Southern Morocco, and their regional structural implications. *American Association of Petroleum Geologists Bulletin*, **64**, 988–1003.

Buck, W. R. 1991. Modes of Continental Lithospheric Extension. *Journal of Geophysical Research*, **96**, 20161–20178.

Buck, W. R., Lavier, L. L. & Poliakov, A. N. B. 1999. How to make a rift wide. *Philosophical Transactions of the Royal Society of London*, **357**, 671–693.

Buiter, S. J. H., Huismans, R. S. & Beaumont, Ch. 2008. Dissipation analysis as a guide to mode selection during crustal extension and implications for the styles of sedimentary basins. *Journal of Geophysical Research*, **113**, 1–20.

Clift, P. D., Van Long, H. *et al*. 2008. Evolving east Asian river systems reconstructed by trace element and Pb and Nd isotope variations in modern and ancient Red River–Song Hong sediments. *Geochemistry Geophysics Geosystems*, **9**, Q04039; doi: 10.1029/2007GC001867.

Coward, M. P. 1995. Structural and tectonic setting of the Permo-Triassic basins of northwest Europe. *In*: Boldy, S. A. R. (ed.) *Permian and Triassic Rifting in Northwest Europe*. Geological Society, London, Special Publications, **91**, 7–39.

Doré, A. G., Lundin, E. R., Jensen, L. N., Birkeland, Ø., Eliassen, P. E. & Fichler, C. 1999. Principal tectonic events in the evolution of the northwest European Atlantic margin. *In*: Fleet, A. J. & Boldy, S. A. R. (eds) *Petroleum Geology of Northwest Europe: Proceedings of the 5th Conference*. Geological Society, London, 41–61; doi: 10.1144/0050041.

Eide, E. A. 2002. *BATLAS – Mid Norway Plate Reconstruction Atlas with Global and North Atlantic Perspectives*. Geological Survey of Norway.

El Arabi, E. H., Diez, J. B., Broutin, J. & Essamoud, R. 2006. First palynological characterization of the Middle Triassic; implications for the first Tethysian rifting phase in Morocco. *Comptes Rendus Geosciences*, **338**, 641–649.

Ellouz, N., Patriat, M., Gaulier, J. M., Bouatmani, R. & Sabounji, S. 2003. From rifting to Alpine inversion: Mesozoic and Cenozoic subsidence some Moroccan basins. *Sedimentary Geology*, **156**, 185–212.

Fabuel-Perez, I. & Redfern, J. 2009. Sedimentology of an intra-montane rift-controlled fluvial dominated succession: the Upper Triassic Oukaimeden Sandstone Formation, Central High Atlas, Morocco. *Sedimentary Geology*, **218**, 103–140.

Fabuel-Perez, I., Hodgetts, D. & Redfern, J. 2009. A new approach for outcrop characterization and geostatistical analysis of a low-sinuosity fluvial-dominated succession using digital outcrop models: Upper Triassic Oukaimeden Sandstone Formation, central High Atlas, Morocco. *America Association of Petroleum Geoscience, Bulletin*, **93**, 795–827; doi: 0.1306/02230908102.

Gould, S. 2001. *Integrated sedimentological and whole-rock trace element geochemical correlation of alluvial red-bed sequences at outcrop and in the subsurface*. Unpublished PhD thesis, University of Aberdeen.

Hafid, M. 2000. Triassic–early Liassic extensional systems and their Tertiary inversion, Essaouira Basin (Morocco). *Marine and Petroleum Geology*, **17**, 409–429.

Hofmann, A., Tourani, A. & Gaupp, R. 2000. Cyclicity of Triassic to Lower Jurassic continental red beds of the Argana Valley, Morocco: implications for palaeoclimate and basin evolution. *Palaeogeography, Palaeoclimatology, Palaeoecology*, **161**, 229–266.

Hopper, J. R. & Buck, W. R. 1996. The effect of lower crustal flow on continental extension and passive margin formation. *Journal of Geophysical Research*, **101**, 20175–20194.

Hubert, J. F. & Forlenza, M. F. 1988. Sedimentology of braided-river deposits in Upper Triassic Wolfville redbeds, southern shore of Cobequid Bay, Nova Scotia. *Developments in Geotectonics*, **22**, 231–237.

Hubert, J. F. & Hyde, M. G. 1982. Sheet-flow deposits of graded beds and mudstones on an alluvial sandflat–playa system: Upper Triassic Blomidon redbeds, St. Mary's Bay, Nova Scotia. *Sedimentology*, **29**, 457–474.

Hubert, J. F. & Mertz, K. A. 1980. Eolian dune field of Late Triassic age, Fundy Basin, Nova Scotia. *Geology*, **8**, 516–519.

Hubert, J. F. & Mertz, K. A., Jr. 1984. Eolian sandstones in Upper Triassic–Lower Jurassic red beds of the Fundy Basin, Nova Scotia. *Journal of Sedimentary Petrology*, **54**, 798–810.

Kirton, S. R. & Hitchen, K. 1987. *Timing and Style of Crustal Extension N of the Scottish Mainland*. Geological Society, London, Special Publications, **28**, 501–510; doi: 10.1144/GSL.SP.1987.028.01.32.

Klein, G. D. 1962. Triassic sedimentation, Maritime provinces, Canada. *Geological Society of America Bulletin*, **73**, 1127–1145.

Laville, E. & Petit, J.-P. 1984. Role of synsedimentary strike-slip faults in the formation of Moroccan Triassic basins. *Geology*, **12**, 424–427.

Laville, E. & Piqué, A. 1991. La distension crustale atlantique et atlasique au Maroc au debut du Mésozoïque: le rejeu des structures hercyniennes. *Bulletin Societe Géologique France*, **162**, 1161–1171.

Leeder, M. R. & Mack, G. H. 2001. Lateral erosion ('toe-cutting') of alluvial fans by axial rivers: implications for basin analysis and architecture. *Journal of the Geological Society of London*, **158**, 885–893.

Leleu, S., Hartley, A. J. & Williams, B. P. J. 2009. Large-scale alluvial architecture and correlation in a Triassic pebbly braided river system, lower Wolfville Formation (Fundy Basin, Nova Scotia, Canada). *Journal of Sedimentary Research*, **79**, 265–286.

Le Roy, P. & Pique, A. 2001. Triassic-Liassic Western Moroccan synrift basins in relation to the Central Atlantic opening. *Marine Geology*, **172**, 359–381.

Mader, N. K. 2005. *Sedimentology and sediment distribution of Upper Triassic fluvio-aeolian reservoirs on a regional scale (Central Algeria, SW Morocco, NE Canada): an integrated approach unravelling the influence of climate v. tectonics on reservoir architecture*. PhD Thesis, University of Manchester.

Manspeizer, W. 1982. Triassic–Liassic basins and climate of the Atlantic passive margins. *Geologische Rundschau*, **71**, 895–917.

Mattis, A. F. 1977. Nonmarine Triassic sedimentation, central High Atlas Mountains, Morocco. *Journal of Sedimentary Research*, **47**, 107–119.

McHone, J. G. 2000. Non-plume magmatism and rifting during the opening of the central Atlantic Ocean. *Tectonophysics*, **316**, 287–296.

McKenzie, D. 1978. Some remarks on the development of sedimentary basins. *Earth and Planetary Science Letters*, **40**, 25–32.

McKie, P. & Williams, B. P. J. 2009. Triassic fluvial dispersal across northwest European basins – a north–south divide. *Geological Journal Special Issue*, **44**, 711–741.

Medina, F. 1988. Tilted-blocks pattern, paleostress orientation and amount of extension, related to Triassic early rifting of the central Atlantic in the Amzri area (Argana Basin, Morocco). *Tectonophysics*, **148**, 229–233.

Medina, F. 1991. Superimposed extensional tectonics in the Argana Triassic formations (Morocco), related to the early rifting of the central Atlantic. *Geological Magazine*, **128**, 525–536.

Medina, F. 1995. Syn- and postrift evolution of the El Jadida-Agadir basin (Morocco): constraints for the rifting models of the central Atlantic. *Canadian Journal of Earth Sciences*, **32**, 1273–1291.

Mertz, K. A. & Hubert, J. F. 1990. Cycles of sand-flat sandstone and playa-mudstone in the Triassic–Jurassic Blomidon redbeds, Fundy rift basin, Nova Scotia: implications for tectonic and climatic controls. *Canadian Journal of Earth Sciences*, **27**, 442–451.

Morton, A. C., Herries, R. & Fanning, C. M. 2007. Correlation of Triassic sandstones in the Strathmore Field, west of Shetland, using heavy mineral provenance signatures. *In*: Mange, M. & Wright, D. K. (eds) *Heavy Minerals in Use, Developments in Sedimentology*, **58**, Elsevier, Amsterdam, 1037–1072.

Naylor, D. & Shannon, P. M. 2009. Geology of offshore Ireland. *In*: Holland, C. H. & Sanders, I. S. (eds) *The Geology of Ireland*. Dunedin Academic Press, Edinburgh, 405–460.

Naylor, D., Shannon, P. M. & Murphy, N. 1999. *Irish Rockall Basin Region – a Standard Structural Nomenclature System*. Petroleum Affairs Division, Dublin, Special Publications, **1/99**.

Olsen, P. E. 1997. Stratigraphic record of the early Mesozoic breakup of Pangea in the Laurasia–Gondwana rift system. *Annual Review of Earth and Planetary Sciences*, **25**, 337–401.

Olsen, P. E. & Schlische, R. W. 1990. Transtensional arm of the early Mesozoic Fundy rift basin; penecontemporaneous faulting and sedimentation. *Geology*, **18**, 695–698.

Olsen, P. E., Schlische, R. W. & Gore, P. J. W. 1989. *Newark Basin, Pennsylvania and New Jersey; Stratigraphy (Field Guide): Field Trips for the 28th International Geological Congress*. American Geophysical Union, Washington, DC, 69–152. Seilacher, 1967.

Olsen, P. E., Kent, D. V., Fowell, S. J., Schlische, R. W., Withjack, M. O. & LeTourneau, P. M. 2000. Implications of a comparison of the stratigraphy and depositional environments of the Argana (Morocco) and Fundy (Nova Scotia, Canada) Permian-Jurassic basins. *In*: Oujidi, M. & Et-Touhami, M. (eds) *Le Permien et le Trias du Maroc, Actes de la Premièr Réunion su Groupe Marocain du Permien et du Trias*. Hilal Impression, Oujda, 165–183.

Petit, J. P. & Beauchamp, J. 1986. Synsedimentary faulting and palaeocurrent patterns in the Triassic sandstones of the High-Atlas (Morocco). *Sedimentology*, **33**, 817–829.

Schlische, R. W. & Olsen, P. E. 1990. Quantitative filling models for continental extensional basins with applications to the early Mesozoic rifts of eastern North America. *Journal of Geology*, **98**, 135–155.

Scotese, C. R. 2002. http://www.scotese.com (PALEOMAP website).

Smoot, J. P. 1991. Sedimentary facies and depositional environments of early Mesozoic Newark Supergroup basins, eastern North America. *Palaeogeography, Palaeoclimatology, Palaeoecology*, **84**, 369–423.

Stoker, M. S., Praeg, D. *et al*. 2005. Neogene evolution of the Atlantic continental margin of NW Europe (Lofoten Islands to SW Ireland): anything but passive. *In*: Doré, A. G. & Vining, B. A. (eds) *Petroleum Geology: North-West Europe and Global Perspectives: Proceedings of the 6th Petroleum Geology Conference*. Geological Society, London, 1057–1076; doi: 10.1144/0061057.

Štolfová, K. & Shannon, P. M. 2009. Permo-Triassic development from Ireland to Norway: basin architecture and regional controls. *Geological Journal Special Issue*, **44**, 652–676.

Taj-Eddine, K. & Pignone, R. 2005. *L'Ourika: Haut Atlas-Haouz de Marrakech, Maroc. Un patrimoine geologique, biologique et culturel exceptionnel*. SELCA, Florence, scale 1:60.000, 1 sheet.

Tixeront, M. 1973. Lithostratigraphie et minéralisations cuprifères et uranifères stratiformes syngénétiques et familières des formations détritiques permo-triasiques du couloir d'Argana (Haut-Atlas occidental, Maroc). *Notes et Memoires du Sérvice Géologique du Maroc*, **33**, 147–177.

Torsvik, T. H., Van der Voo, R., Meert, J. G., Mosar, J. & Walderhaug, H. J. 2001. Reconstructions of the continents around the north Atlantic at about the 60th parallel. *Earth and Planetary Science Letters*, **197**, 55–69; doi: 10.1016/S0012-821X(01)00284-9.

Tourani, A., Lund, J. J., Benaouiss, N. & Gaupp, R. 2000. Stratigraphy of Triassic syn-rift deposition in Western Morocco. *Zentralblatt fuer Geologie und Palaeontologie*, **1**, 1193–1215.

Tyrrell, S., Haughton, P. D. W., Daly, J. S., Kokfelt, T. F. & Gagnevin, D. 2006. The use of the common Pb isotope composition of detrital K-feldspar grains as a provenance tool and its application to Upper Carboniferous palaeodrainage, Northern England. *Journal of Sedimentary Research*, **76**, 324–345; doi: 10.2110/jsr.2006.023.

Tyrrell, S., Haughton, P. D. W. & Daly, J. S. 2007. Drainage re-organization during break-up of Pangea revealed by in-situ Pb isotopic analysis of detrital K-feldspar. *Geology*, **35**, 971–974; doi: 10.1130/G4123A.1.

Tyrrell, S., Leleu, S., Souders, A. K., Haughton, P. D. W. & Daly, J. S. 2009. K-feldspar sand-grain provenance in the Triassic, west of Shetland: distinguishing first-cycle and recycled sediment sources? *Geological Journal Special Issue*, **44**, 692–710.

Tyrrell, S., Souders, A. K., Haughton, P. D. W., Daly, J. S. & Shannon, P. M. 2010. Sedimentology, sandstone provenance and palaeodrainage on the eastern Rockall Basin margin: evidence from the Pb isotopic composition of detrital K-feldspar. *In*: Vining, B. A. & Pickering, S. C. (eds) *Petroleum Geology: From Mature Basins to New Frontiers – Proceedings of the 7th Petroleum Geology Conference*. Geological Society, London, 937–952; doi: 10.1144/0070937.

Van Lanen, X. M. T., Hodgetts, D., Redfern, J. & Fabuel-Perez, I. 2009. Applications of digital outcrop models: two fluvial case studies from the Triassic Wolfville Fm., Canada and Oukaimeden Sandstone Fm., Morocco. *Geological Journal*, **44**, 742–760.

Wade, J. A., Brown, D. E., Traverse, A. & Fensome, R. A. 1996. The Triassic–Jurassic Fundy Basin, eastern Canada: regional setting, stratigraphy and hydrocarbon potential. *Atlantic Geology*, **32**, 189–231.

Withjack, M. O., Olsen, P. E. & Schlische, R. W. 1995. Tectonic evolution of the Fundy Rift Basin, Canada – evidence of extension and shortening during passive margin development. *Tectonics*, **14**, 390–405.

Withjack, M. O., Schlische, R. W. & Baum, M. S. 2009. Extensional development of the Fundy rift basin, southeastern Canada. *Geological Journal*, **44**, 631–651.

Sedimentology, sandstone provenance and palaeodrainage on the eastern Rockall Basin margin: evidence from the Pb isotopic composition of detrital K-feldspar

S. TYRRELL,[1] A. K. SOUDERS,[2] P. D. W. HAUGHTON,[1] J. S. DALY[1] and P. M. SHANNON[1]

[1]*Sand Provenance Centre, UCD School of Geological Sciences, University College Dublin, Belfield, Dublin 4, Ireland (e-mail: shane.tyrrell@ucd.ie)*

[2]*MicroAnalysis Facility, INCO Innovation Centre and Department of Earth Sciences, Memorial University, St John's, NL A1B 3X5, Canada*

Abstract: The Rockall Basin, west of Ireland, is a frontier area for hydrocarbon exploration, but currently the age and location of sand fairways through the basin are poorly known. A recently developed provenance approach based on *in-situ* Pb isotopic analysis of single K-feldspar grains by laser ablation multi-collector inductively coupled mass spectrometry (LA-MC-ICPMS) offers advantages over other provenance techniques, particularly when applied to regional palaeodrainage issues. K-feldspar is a relatively common, usually first-cycle framework mineral in sandstones and its origin is typically linked to that of the quartz grains in arkosic and sub-arkosic rocks. Consequently, in contrast to other techniques, the Pb-in-K-feldspar tool characterizes a significant proportion of the framework grains. New Pb isotopic data from K-feldspars in putative Permo-Triassic and Middle Jurassic sandstones in Well 12/2-1z (the Dooish gas condensate discovery) on the eastern margin of the Irish Rockall Basin are reported. These data suggest that three isotopically distinct basement sources supplied the bulk of the K-feldspar in the reservoir sandstones and that the relative contribution of these sources varied through time. Archaean and early Proterozoic rocks (including elements of the Lewisian Complex and its offshore equivalents), to the immediate east, NE and north of the eastern Rockall Margin, are the likely sources. More distal sourcelands to the NW cannot be ruled out but there was no significant input from southern sources, such as the Irish Massif. These data, together with previously published regional Pb isotopic data, highlight the important role played by old, near and far-field Archaean–Proterozoic basement highs in contributing sediment to NE Atlantic margin basins. The Irish Massif appears to have acted as a significant, but inert, drainage divide from the Permo-Triassic to the Late Jurassic and hence younger, Avalonian and Variscan sand sources appear to have been less important on the Irish Atlantic Margin.

Keywords: sedimentology, palaeodrainage, provenance, Pb isotopes, K-feldspar, Mesozoic, Rockall Basin, Dooish

Understanding the provenance of sandstones helps in the reconstruction of palaeogeography and in constraining drainage scales and sediment pathways in sedimentary basins. This helps to predict the source and distribution of sandstones, with implications for reservoir quality in the subsurface. However, there are some inherent shortcomings in provenance analysis. Provenance studies are limited by the ability to geochemically distinguish the wide range of potential sourcelands. Additionally, their specific use in the reconstruction of robust palaeodrainage models is problematic, as there are difficulties in recognizing and quantifying the extent of sedimentary recycling and mixing (Tyrrell *et al.* 2009).

Provenance techniques fall into two broad categories – those that utilize the bulk composition of the sediment or sedimentary rock and those which exploit signals in individual sand grains. Bulk compositional approaches (e.g. petrological techniques, Sm–Nd whole rock) are particularly hampered by problems such as framework grain modification, failure to recognize mixing and recycling, inadequate source characterization and non-unique signals. These issues cannot be easily overcome with a bulk compositional approach. With the increased availability of *in-situ* micro-analytical techniques, provenance studies increasingly utilize geochemical or isotopic signals in single grains of a specific mineral (e.g. Cawood *et al.* 2004; Clift *et al.* 2008). However, although these techniques enable sourcelands to be distinguished, the full transport history experienced by individual framework components often remains unconstrained. Many provenance tools use 'trace' components that may be difficult to relate to the framework grains that determine reservoir characteristics. Robust mineral phases (e.g. zircon) may have been recycled through one or more intermediary sediments or sedimentary rock. In contrast, unstable mineral grains (e.g. K-feldspar) are less likely to survive sedimentary recycling and, therefore, if present, can be regarded as first-cycle components derived directly from source. The identification of first-cycle detritus is key to resolving drainage scales and sediment transport pathways in reservoir sandstone intervals. Recent studies have demonstrated the utility of the Pb isotopic composition of detrital K-feldspar as a sand provenance tool that can be applied on a regional scale (Tyrrell *et al.* 2006, 2007; Clift *et al.* 2008). As detrital K-feldspar is unlikely to survive more than one sedimentary cycle, grains can be tracked back directly to their basement source.

In recent years Pb K-feldspar data have been collected from NW European Margin basins as part of an ongoing study of Permo-Triassic to Early Cretaceous sediment dispersal (Tyrrell *et al.* 2007, 2009). The aims of this regional work are to understand better the large-scale controls on drainage development throughout the Mesozoic, to examine the evolving drainage patterns prior to and during the breakup of Pangaea, to identify potential linkages between basins on the conjugate Atlantic margins, and to consider the implications for regional sand distribution within and across the lightly explored basins west of Ireland.

Detailed investigations of the *c.* 6 km of Mesozoic and Cenozoic stratigraphy in the Rockall Basin have been hampered by the lack of wells drilled in the basin. Until recently, stratigraphic control points were limited to a single DSDP borehole (610) in the SW of the

VINING, B. A. & PICKERING, S. C. (eds) *Petroleum Geology: From Mature Basins to New Frontiers – Proceedings of the 7th Petroleum Geology Conference*, 937–952. DOI: 10.1144/0070937 © Petroleum Geology Conferences Ltd. Published by the Geological Society, London.

basin, which penetrated Miocene and younger sediments, and a small number of boreholes in the NE Rockall Basin within the UK sector. However, a programme of shallow borehole drilling carried out in 1999 (Haughton *et al.* 2005) allowed the Mesozoic stratigraphy of the eastern basin margin to be directly constrained for the first time. The oldest definitively dated rocks penetrated by these boreholes are Late Jurassic (Early Kimmeridgian). More recently, exploration drilling on the eastern Rockall Basin margin, offshore NW Ireland (well 12/2-1 and sidetrack 12/2-1z; Fig. 1), led to the Dooish gas condensate discovery which is hosted in sandstones of Permo-Triassic and Middle Jurassic age (see below). The cores from well 12/2-1z present a unique opportunity to expand our knowledge of evolving drainage in the region. In this paper, new provenance data obtained from both the Permo-Triassic and Middle Jurassic reservoir sandstone intervals in this well are discussed in detail. In addition, these data are incorporated with recently published data from Triassic, Upper Jurassic and Cretaceous sandstones from the Slyne, Porcupine and eastern Rockall basins, respectively, in order to understand better regional sediment dispersal patterns and controls on palaeodrainage development. These impact directly on the prospectivity of the Irish Atlantic margin basins.

The Pb-in-K-feldspar provenance tool: rationale and approach

The Pb-in-K-feldspar provenance tool can provide valuable information on regional sand dispersal in sedimentary basins, especially, as in this case, where the reservoir intervals are feldspathic. The common Pb isotopic signature of K-feldspar has proved to be a powerful method of mapping gross crustal structure (e.g. Connelly & Thrane 2005) and hence potential sand source areas. Systematic regional variations in common Pb composition are seen at sub-orogenic scale (<100 km) in both active mountain belts and ancient orogens (Vitrac *et al.* 1981) reflecting the assembly of basement domains with different ages and U–Th–Pb fractionation histories. Therefore, broad regional patterns in Pb composition can be identified by characterizing a relatively small number of granite feldspars (DeWolf & Mezger 1994; Connelly & Thrane 2005). K-feldspar typically contains between 5 and 150 ppm Pb, and has low U and Th contents (typically <1 ppm), and hence the corrections to the common Pb signature for radioactive decay are negligible.

K-feldspar is a common mineral in many sandstones and a key constituent of arkose, and it has been shown that detrital grains retain the Pb isotopic signature of their source (Tyrrell *et al.* 2006). Importantly, the source of K-feldspar is very likely linked to the source of the majority of the quartz grains. Therefore determining K-feldspar provenance ultimately can constrain the source of the majority of the framework grains. With the advent of *in-situ* techniques (laser ablation inductively coupled plasma mass spectrometry, LA-ICPMS, and secondary ion mass spectrometry, SIMS), it is now possible to measure variations in the Pb composition within individual K-feldspar sand grains so that the extent of intra-grain variation and mixing of different grain populations can be isolated (Tyrrell *et al.* 2006). The rapid, non-destructive, *in-situ* analysis of large numbers of individual grains by laser ablation multi-collector inductively coupled plasma mass spectrometry (LA-MC-ICPMS) within an arkose represents a significant advance in provenance characterization (Tyrrell *et al.* 2006, 2007). The use of ion counter instead of Faraday collectors (see below) allows for the analysis of low Pb and finer grain sizes (Tyrrell *et al.* 2009).

Five principal Pb basement source domains have been distinguished in the North Atlantic region using published Pb data (Fig. 1; Tyrrell *et al.* 2007 and references therein). Spatially, these zones strike NE–SW and correspond to the basement terranes involved in the assembly of Laurentia and Rodinia, the Caledonian collision of Laurentia with Avalonia, and the Variscan Orogen. Although there are variations within each of these zones, there is a broad shift towards more radiogenic Pb values towards the SE, reflecting the history of crustal growth. Pb domain 1 comprises Archaean and Palaeoproterozoic basement and has the least radiogenic Pb. Pb domain 2 corresponds mainly to older basement reworked during late Meso- and Palaeoproterozoic. Pb domain 3 largely comprises Mesoproterozoic basement with Neoproterozoic metasedimentary rocks and younger Caledonian granites. Pb domain 4a corresponds to Avalonian basement and has a large overlap with Pb domain 4b, which corresponds with the Variscan and contains radiogenic Pb remobilized from Avalonian basement during end-Palaeozoic closure of the Rheic Ocean.

Mesozoic sediment dispersal into NE Atlantic margin basins

During the Permian and Triassic, NW Europe lay at low latitudes close to the margins of the Pangaean Supercontinent. Late Permian and Early Triassic sedimentary basins in the region are characterized by non-marine deposits, comprising local alluvial fans, extensive fluvial deposits, playa lakes and aeolian sands in successions in excess of 1 km thick (Warrington & Ivimey-Cooke 1992). The Early Triassic sandstones form reservoirs for hydrocarbons offshore west of Ireland (the Corrib gas field in the Slyne Basin), in the East Irish Sea Basin (the Morecombe gas field), in the Wessex Basin of southern England (the Wytch Farm oil field) and in the North Sea. The Lower Triassic sandy deposits (Sherwood Sandstone and equivalents) are overlain by the Middle–Upper Triassic dominantly mud-prone (but locally sand-rich) successions (Mercia Mudstone). The 'Budleighensis' palaeo-river system drained northward from the Variscan Uplands into the Wessex Basin (Audley-Charles 1970) and extended further north into the Cheshire Basin, and probably as far as the East Irish Sea Basin. However, until recently the extent of drainage systems with this geometry in basins further north and west remained unclear.

In the Slyne Basin west of Ireland (Fig. 1), Sherwood sandstone equivalent Triassic sandstones host the Corrib gas field and comprise fine- to medium-grained arkosic fluvial and alluvial sandstones with subordinate sand-flat and playa mudstone deposits (Dancer *et al.* 2005). Previous palaeodrainage models for these sandstones, based on borehole dipmeter logs and whole-rock geochemistry, suggested derivation from the south and SW (the Variscides) with some input from the uplifted Irish mainland (Dancer *et al.* 2005). Recently published Pb isotopic data for the K-feldspar component suggest a contrasting interpretation: two distinct Pb populations appear to have been sourced from Archaean and Proterozoic crust, suggesting derivation from a potentially wide area to the north and west (Tyrrell *et al.* 2007). Significantly, grains appear to have been dispersed across the subsequent site of the Rockall Basin, with drainage scales likely to have been in excess of 500 km. These data indicate that very few (if any) grains could have been derived from the Irish Massif or, significantly, from the Varisican Uplands. Furthermore, in basins west of Shetland, new Pb K-feldspar data (Tyrrell *et al.* 2009) from Middle–Upper Triassic Foula Formation sandstones (Strathmore Field) indicate local derivation from Archaean–Palaeoproterozoic rocks on the margins of the rift basin (Nagssugtoqidian Mobile Belt of East Greenland and/or the Lewisian Complex of NW Scotland), although an eastern or western source cannot be distinguished. Here, the Pb K-feldspar data is in broad agreement with U–Pb detrital zircon geochronology (Morton *et al.* 2007). Regionally, data from Triassic sandstones suggest that sediment dispersal was at this time controlled by uplifted Archaean and Proterozoic

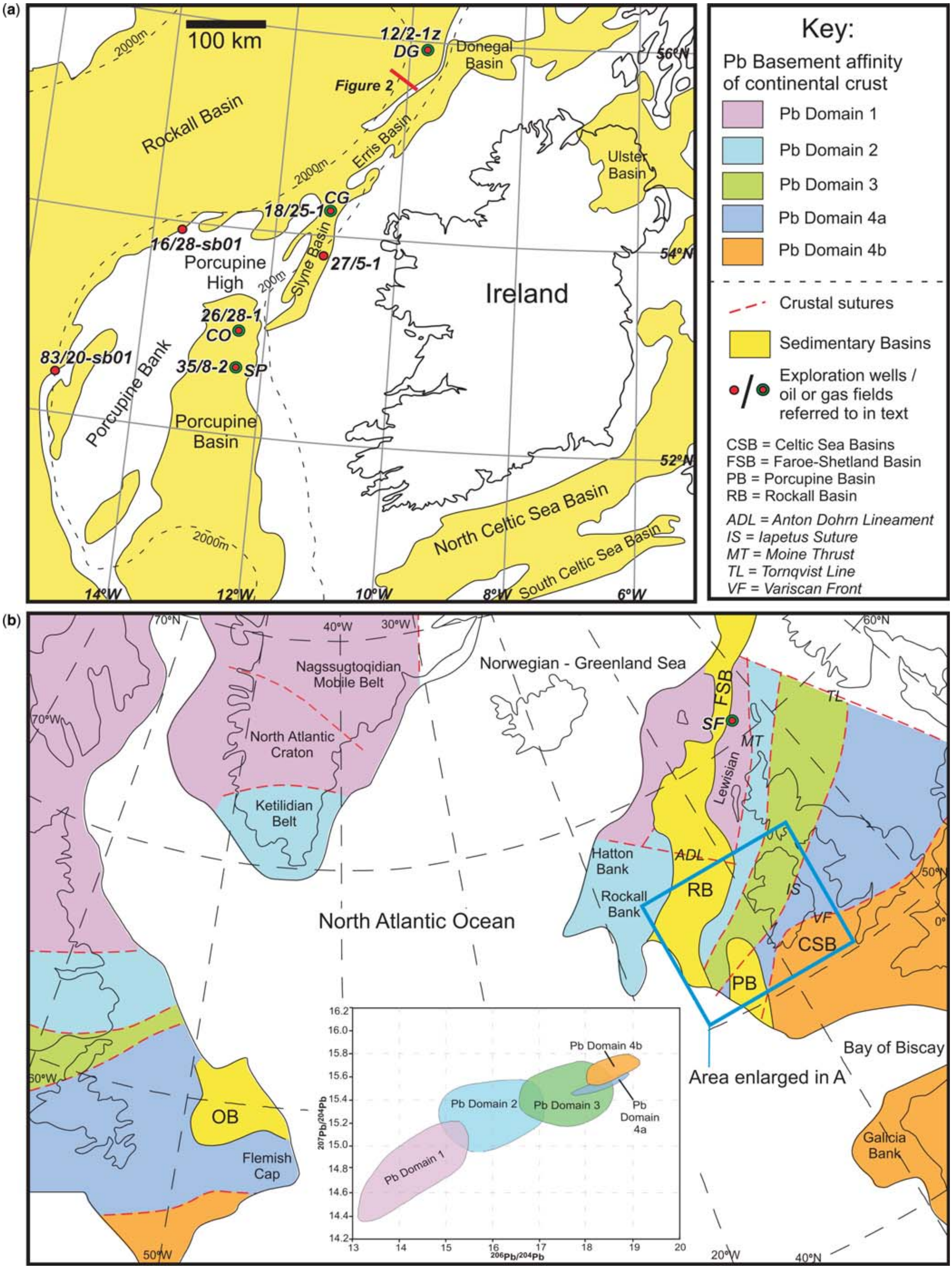

Fig. 1. Maps illustrating (**a**) the basins offshore western Ireland, showing the position of Dooish well 12/2-1z and other regional wells from which K-feldspar provenance data has been retrieved; and (**b**) the broader North Atlantic region showing the distribution of Pb domains (adapted from Tyrrell *et al.* 2007) with a plot showing Pb isotopic composition of these domains. Also shown are the approximate location of the geoseismic section in Figure 2 and the position of hydrocarbon fields and discoveries referred to in text. CG, Corrib gas field; CO, Connemara oil accumulation; DG, Dooish gas condensate discovery; SP, Spanish Point gas condensate discovery; SF, Strathmore field.

basement, with the Irish Massif acting as a drainage divide for south-derived Variscan sediment.

The Porcupine Basin, SW of the Slyne Basin (Fig. 1), includes a Jurassic sequence deposited during a phase of rifting (Croker & Shannon 1987; Naylor & Shannon 2005). In the northern part of the basin, an Upper Jurassic (Kimmeridgian–Tithonian) sequence of low-energy fluvial (meandering river) and marginal marine facies is present. These sandstones are the reservoirs for the Connemara oil accumulation in well 26/28-1 (Fig. 1). These facies are replaced southwards by marine sandstones and deep-water fans (Butterworth *et al.* 1999; Williams *et al.* 1999), which host the Spanish Point gas condensate discovery (35/8-2). Previous work (Butterworth *et al.* 1999) suggested north to south basin-axial flowing drainage in the Upper Jurassic section in the northern Porcupine Basin. Published Pb data from K-feldspars from the Upper Jurassic of the Northern Porcupine basin (Tyrrell *et al.* 2007) define two Pb isotopic populations. Both occur in sandstones from wells 26/28-1 and 35/8-2. These data have been interpreted (Tyrrell *et al.* 2007) to represent axial derivation from a northern source, probably from the uplifted Porcupine High, with possible transverse input from the basin margins. Dispersal distances are envisaged as being *c.* 100 km. These data also indicate that the sandstones in quadrants 26 and 35 share the same source and that the northern fluvial systems may have been linked with the turbiditic fans further south. Grains derived from Archaean and Palaeoproterozoic sources are very rare in this dataset, suggesting that drainage did not extend across the developing Rockall Basin at this time.

Previously published Pb data from detrital K-feldspar grains from Cretaceous sands and sandstones sampled from the western flanks of the Porcupine Bank (eastern Rockall Basin margins; 83/20-sb01 and 16/28-sb01; Fig. 1) show relatively radiogenic compositions. These sediments, sampled from shallow boreholes, are calcareous and appear to have been deposited in a high-energy shelf environment (Haughton *et al.* 2005). The sedimentology of these sands and the Pb isotopic composition of the K-feldspar component suggest they are locally derived directly from the Porcupine High (Tyrrell *et al.* 2007). Transport of K-feldspar sand grains across the Rockall Basin is not indicated.

The Dooish gas condensate discovery, Eastern Rockall Basin

The Dooish gas condensate discovery, on the eastern margins of the Rockall Basin, comprises pre-rift sandstones in a 40 km^2 tilted fault block sealed by post-rift sediments of Late Cretaceous age (Fig. 2). Well 12/2-1, some 125 km NW of Donegal, was drilled in 2002 in order to test the prospect. The target sandstones were presumed to be Middle–Late Jurassic in age, based on seismic jump correlation with the Slyne–Erris Basin to the south, although it was recognized that they could be as old as Permo-Triassic. Well 12/2-1 successfully demonstrated the presence of a working petroleum system in the eastern Rockall Basin, but insufficient biostratigraphic information was retrieved to date precisely the reservoir intervals. Well 12/2-1z, a deviated sidetrack of 12/2-1, was drilled in 2003 in order to determine the vertical extent of the hydrocarbon column

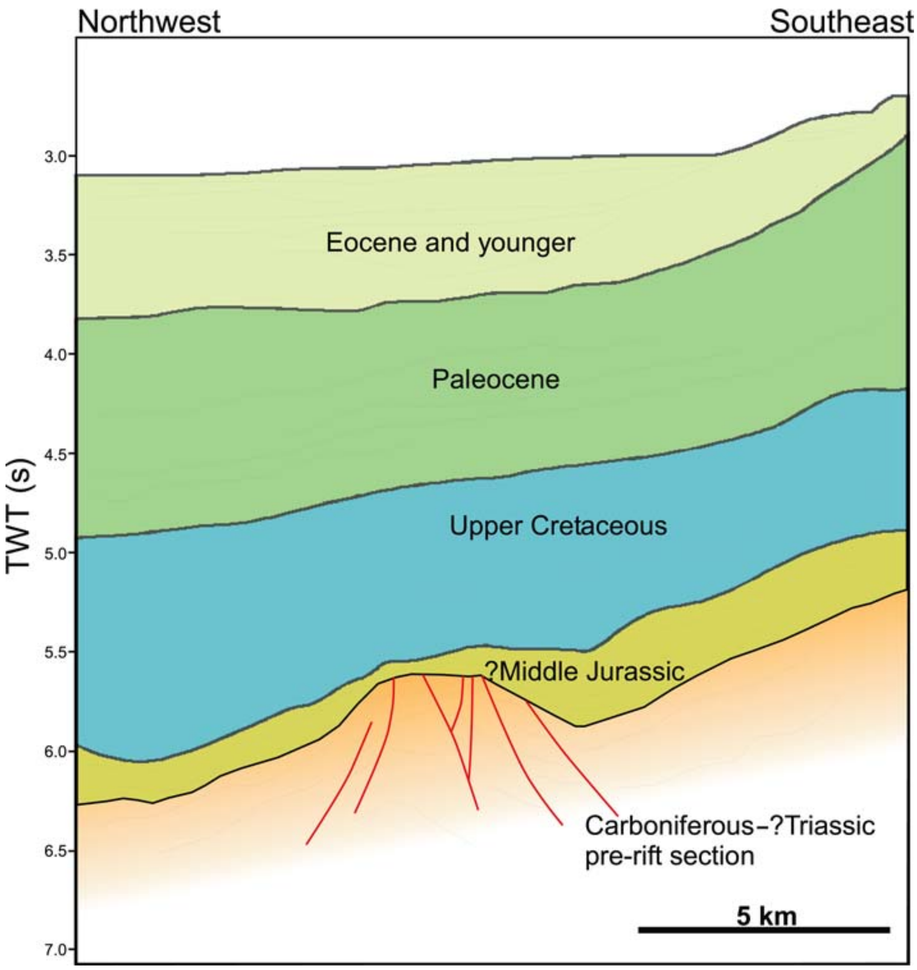

Fig. 2. Representative NW–SE geoseismic section through the NE Rockall Basin margin illustrating the pre-Cretaceous tilted fault block structure of the Dooish trend, offset to the south of well 12/2-1z. Figure is reproduced courtesy of the Petroleum Affairs Division (Ireland) and PGS Geophysical.

penetrated by the earlier well and to investigate the potential of the previously undrilled deeper section.

Well 12/2-1z terminated in Late Carboniferous interbedded sandstones and shales at a depth of *c.* 4.5 km (Fig. 3). Gas condensate was recorded within younger sand-prone intervals that span ages between Permian and Lower Cretaceous (see below). A total of three cores were retrieved from the well. This study utilizes new sedimentological logging of the cored intervals,

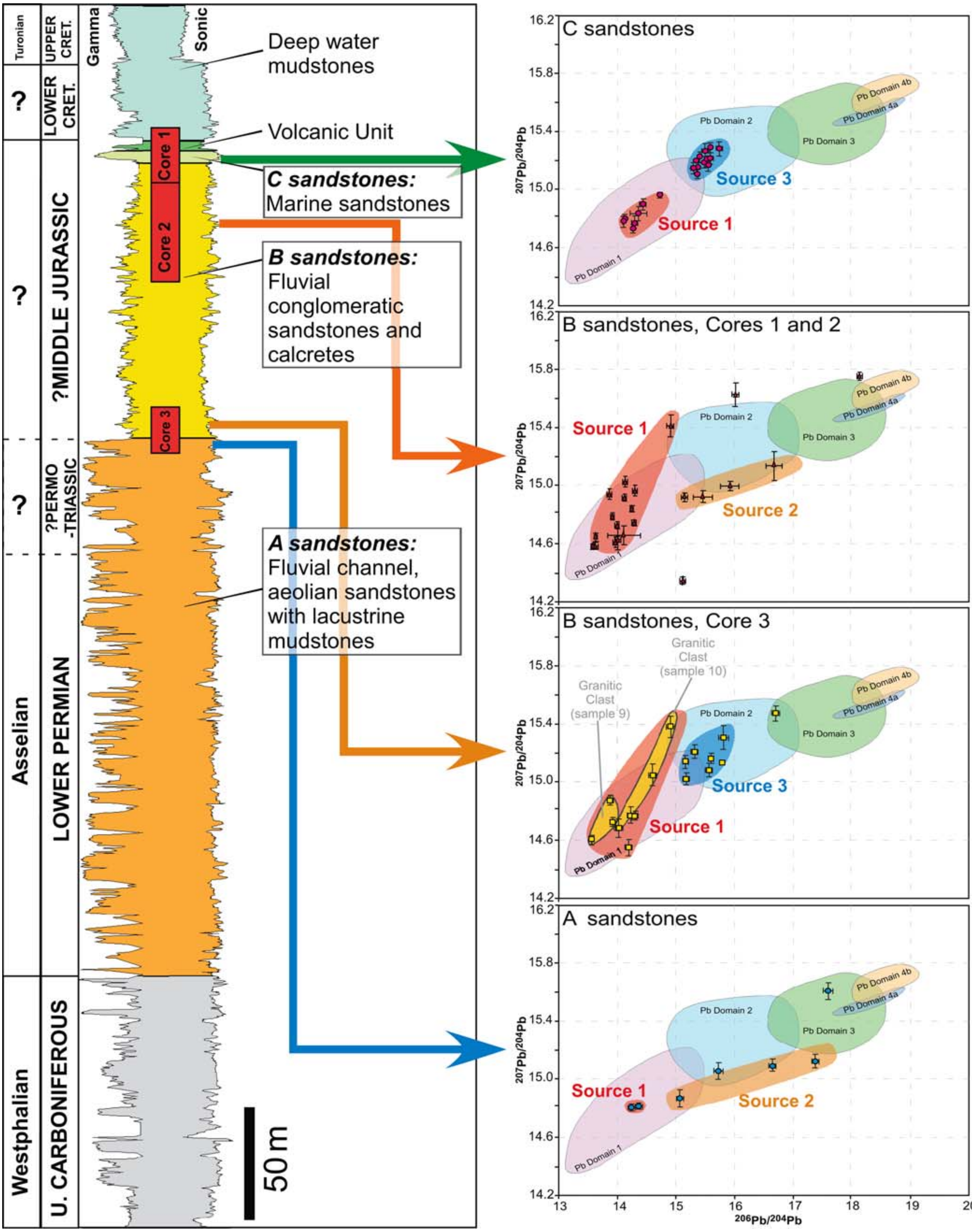

Fig. 3. Simplified gamma and sonic log wireline profiles from well 12/2-1z, illustrating the stratigraphy and contrasting response between the A, B and C sandstones (left) with $^{206}Pb/^{204}Pb$–$^{207}Pb/^{204}Pb$ lead space plots showing the variation of Pb K-feldspar populations with stratigraphy.

together with well reports and completion logs to constrain depositional and stratigraphic context for the provenance analysis.

Methodology

Core logging and sampling

The three cored intervals in well 12/2-1z, comprising a total of 90 m of section, were logged at a scale of 1:50. The cores were sampled at intervals of *c.* 2 m, with sand-rich beds and distinct facies intervals preferentially targeted. Wherever possible, core plug trims were used in preference to sampling the core directly. Thin sections of these samples were prepared, and their petrography assessed optically. On the basis of bulk facies and petrographic assessment, a subset of samples was selected for provenance analysis (see below).

Provenance analysis

Imaging and EMPA analysis. Thin sections of *c.* 300 μm thickness were prepared from which K-feldspar grains were imaged using backscatter electron (BSE) and cathodoluminescence (CL) at the Electron Microprobe Laboratory, Geowissenschaftliches Zentrum, Göttingen, Germany. The majority of the imaged grains were analysed using electron microprobe analysis at the above facility, to constrain bulk composition of the feldspar grains.

Pb analysis. The analytical techniques used are detailed in Tyrrell *et al.* (2009). Data were acquired using a Neptune MC-ICPMS linked to a Geolas 193 nm Excimer laser, at the Microanalysis Facility, InCo Innovation Centre, Memorial University, Newfoundland (MUN). Initially, a Faraday cup array was used to collect the isotopic data. However, grains with low Pb concentration (<30 ppm) produced weak Pb ion beams, resulting in unacceptably poor errors (2 SE >1%) in Pb isotopic ratios. More recently, the technique has been refined such that reliable Pb isotopic measurements can be made on grains smaller than 50 μm long axis or with low (<10 ppm) Pb concentrations. This advancement utilizes ion counters, in preference to Faraday cups, for more accurate measurement of weak Pb ion beams. This technique requires *in-situ* measurement of the Pb concentration in the K-feldspar grains prior to isotopic analysis. This enables the laser spot size to be adjusted during isotopic analysis such that sufficient, but not excessive, Pb is released. Optimizing the Pb ion beam allows for the reduction of analytical error and prevents damage to the ion counter array which can result from strong beams. Pb concentrations were measured using an Element ICPMS in the Microanalysis Facility at MUN. U and Th concentrations of individual K-feldspars, used to constrain potential radiogenic growth, were measured at the same time (Table 1).

In the case of all the analytical approaches, the data can be acquired rapidly and require only a previously imaged, thick

Table 1. Pb concentration, Pb isotopic and bulk feldspar composition data of detrital K-feldspars from sandstones in the Dooish well (12/2-1z)

Sample	Technique	Depth (m)	Grain	Or:Ab:An	Package	Pb (ppm)	$^{206}Pb/^{204}Pb$	2SE	$^{207}Pb/^{204}Pb$	2SE	$^{208}Pb/^{204}Pb$	2SE
1	F	4096.90	6	97.15:2.58:0.26	A	–	15.077	0.063	14.867	0.059	34.303	0.137
	F	4096.90	8	96.53:3.36:0.11	A	–	14.252	0.052	14.813	0.051	34.387	0.122
3	IC	4093.55	1	97.55:2.43:0.02	A	5	14.344	0.039	14.806	0.031	34.255	0.153
	IC	4093.55	2	97.00:3.00:0	A	7	17.360	0.062	15.116	0.043	37.214	0.257
	IC	4093.55	3	97.05:2.95:0	A	19	17.576	0.084	15.605	0.060	38.046	0.353
	IC	4093.55	5	98.31:1.69:0	A	12	16.632	0.057	15.084	0.041	36.520	0.235
	IC	4093.55	7	97.69:2.28:0.03	A	10	15.710	0.076	15.055	0.058	35.417	0.313
4	IC	4091.00	1	98.34:1.64:0.03	B1	34	14.598	0.029	15.042	0.029	34.839	0.162
	IC	4091.00	2	96.23:3.77:0	B1	11	15.314	0.048	15.203	0.047	34.981	0.250
	IC	4091.00	4	97.41:2.59:0	B1	9	15.816	0.083	15.301	0.081	35.442	0.408
	IC	4091.00	5	96.85:3.15:0	B1	8	14.197	0.057	14.540	0.057	33.653	0.297
	IC	4091.00	6	97.88:2.06:0.6	B1	17	15.163	0.042	15.132	0.043	34.880	0.228
5	F	4089.00	2	95.19:4.81:0	B1	–	14.308	0.030	14.760	0.032	34.079	0.072
6	IC	4087.50	2	87.76:11.91:0.33	B1	25	15.575	0.059	15.073	0.048	34.896	0.277
	IC	4087.50	3	83.38:15.18:1.45	B1	16	16.708	0.069	15.467	0.053	35.534	0.300
	IC	4087.50	5	96.15:3.85:0	B1	11	15.175	0.051	15.014	0.041	34.550	0.241
8	F	4084.85	1	90.85:9.15:0	B1	–	15.582	0.036	15.161	0.034	34.980	0.080
9*	IC	4084.00	2	96.44:3.02:0.54	B1	24	13.876	0.029	14.867	0.033	36.160	0.203
	IC	4084.00	3	94.63:5.37:0	B1	13	13.566	0.029	14.592	0.033	35.375	0.206
	IC	4084.00	4	95.34:4.64:0.02	B1	8	13.927	0.030	14.718	0.032	35.858	0.211
10*	IC	4083.10	1	96.21:3.79:0	B1	9	14.598	0.071	15.044	0.075	35.242	0.403
	IC	4083.10	2	95.82:4.18:0	B1	22	14.230	0.055	14.764	0.058	34.653	0.319
	IC	4083.10	3	96.91:3.09:0	B1	10	14.909	0.072	15.373	0.074	36.263	0.408
	IC	4083.10	4	96.04:3.06:0	B1	36	14.028	0.057	14.672	0.061	34.127	0.331

(*Continued*)

Table 1. *Continued*

Sample	Technique	Depth (m)	Grain	Or:Ab:An	Package	Pb (ppm)	$^{206}Pb/^{204}Pb$	2SE	$^{207}Pb/^{204}Pb$	2SE	$^{208}Pb/^{204}Pb$	2SE
12	F	4021.10	1	97.81:2.19:0	B2	–	14.236	0.086	13.903	0.060	32.142	0.161
	F	4021.10	6	96.44:3.50:0.05	B2	–	13.536	0.088	13.020	0.096	30.252	0.211
19	F	4006.00	1	97.03:2.97: 0	B2	–	15.159	0.052	14.920	0.029	34.562	0.080
	F	4006.00	2a	96.40:3.60:0	B2	–	15.463	0.164	14.924	0.040	34.672	0.160
	F	4006.00	2b	96.40:3.60:0	B2	–	15.929	0.158	14.998	0.033	35.006	0.142
20	IC	4004.00	2	97.01:2.99:0	B2		14.140	0.043	15.026	0.036	35.102	0.274
	IC	4004.00	3	–	B2		13.871	0.042	14.942	0.036	34.568	0.265
	IC	4004.00	5	97.33:2.67:0	B2		13.977	0.042	14.611	0.035	33.878	0.264
	IC	4004.00	6	97.24:2.72:0.04	B2		14.306	0.043	14.969	0.036	34.600	0.267
21	IC	3999.70	1	97.38:2.62:0	B2		15.111	0.036	14.347	0.024	33.744	0.095
	IC	3999.70	2	96.06:3.94:0	B2		14.003	0.033	14.726	0.024	34.806	0.096
	IC	3999.70	3	97.47:2.51:0.02	B2		14.296	0.034	14.744	0.024	35.295	0.104
	IC	3999.70	4	97.64:2.36:0	B2		18.142	0.046	15.755	0.027	35.426	0.112
	IC	3999.70	5	96.23:3.77:0	B2		13.923	0.033	14.792	0.024	34.287	0.098
	IC	3999.70	6	97.36:2.64:0	B2		14.127	0.034	14.917	0.024	34.677	0.094
22	IC	3998.50	1	97.53:2.47:0	B2		16.018	0.063	15.627	0.079	35.728	0.323
	IC	3998.50	2	97.21:2.79:0	B2		14.018	0.055	14.630	0.074	33.986	0.297
	IC	3998.50	3	93.75:6.25:0	B2		14.909	0.059	15.412	0.078	36.387	0.322
23	F	3997.25	6	–	B2	–	14.254	0.027	14.840	0.018	34.465	0.044
	F	3997.25	3a	–	B2	–	13.581	0.019	14.578	0.019	33.818	0.046
	F	3997.25	3b	–	B2	–	13.626	0.052	14.585	0.023	33.811	0.066
27	F	3987.60	1	96.96:3.04:0	B2	–	16.683	0.131	15.137	0.100	35.670	0.248
	F	3987.60	5a	95.30:4.68:0.02	B2	–	14.122	0.282	14.656	0.065	34.406	0.222
	F	3987.60	5b	95.30:4.68:0.02	B2	–	13.645	0.030	14.645	0.029	34.163	0.072
30	F	3967.65	1	96.03:3.97:0	C	–	14.295	0.041	14.780	0.044	34.412	0.103
	F	3967.65	6	97.19:2.77:0.05	C	–	14.376	0.140	14.839	0.046	34.636	0.153
	F	3967.65	7	96.20:3.76:0.04	C	–	14.734	0.019	14.966	0.020	34.588	0.047
31	IC	3965.25	1	–	C	38	15.353	0.031	15.193	0.028	34.963	0.154
	IC	3965.25	2	–	C	46	15.527	0.031	15.204	0.028	35.371	0.152
	IC	3965.25	3	–	C	13	15.387	0.031	15.156	0.028	35.160	0.153
	IC	3965.25	4	–	C	25	14.290	0.031	14.733	0.030	34.156	0.161
	IC	3965.25	5	–	C	27	14.132	0.028	14.805	0.027	34.553	0.150
	IC	3965.25	6	–	C	3	15.496	0.031	15.182	0.027	35.187	0.149
	IC	3965.25	7	–	C	36	15.380	0.034	15.110	0.031	34.863	0.166
	IC	3965.25	8	–	C	11	15.593	0.036	15.292	0.034	35.350	0.181
33	IC	3963.83	1	–	C	41	14.443	0.042	14.904	0.041	34.765	0.197
	IC	3963.83	2	–	C	5	15.307	0.041	15.151	0.038	35.067	0.186
	IC	3963.83	3	–	C	38	14.121	0.037	14.783	0.036	34.484	0.174
	IC	3963.83	4	–	C	48	15.594	0.043	15.220	0.040	35.175	0.193
	IC	3963.83	5	–	C	51	15.412	0.040	15.227	0.036	35.219	0.175
	IC	3963.83	6	–	C	39	15.548	0.042	15.167	0.038	35.122	0.185
	IC	3963.83	7	–	C	14	15.509	0.058	15.265	0.056	34.956	0.265
	IC	3963.83	8	–	C	6	15.746	0.050	15.285	0.047	35.121	0.236

Note: Data have been collected using two techniques (F, Faraday collector configuration; IC, ion counter collector configuration), detailed in the text.
*Analysis of K-feldspar crystals in granitic clasts.

(*c.* 300 μm) polished thin section, thereby retaining the grain context within the sedimentary rock sample. The approach also uses minimal core material and can be undertaken on small core chips or plug trims. Previous workers have used multiple- or single-grain leaching techniques coupled with TIMS analysis (Hemming *et al.* 1998), but this approach does not allow for potential intra-grain heterogeneities to be characterized prior to and avoided during analysis. The use of ion microprobe techniques (Clift *et al.* 2001, 2008) allows for *in-situ* high spatial resolution analysis (*c.* 20 μm spot sizes), but produces consistently larger errors on ^{204}Pb dependent ratios than LA-MC-ICPMS analysis. In previous LA-MC-ICPMS Pb K-feldspar work (Tyrrell *et al.* 2006, 2007) data could only be retrieved from grains larger than *c.* 300 μm long axis, but the refinement of the technique has allowed for Pb analysis of very fine-grained sand and even silt grains – with similar levels of spatial resolution to those in ion microprobe analysis now possible (*c.* 20 μm laser spot sizes). Analytical uncertainties (2 SE on ^{206}Pb/^{204}Pb) are typically <0.5% for the Faraday configuration and typically <0.25% with the ion counter collection array. In all cases, ^{204}Pb, ^{206}Pb, ^{207}Pb and ^{208}Pb were measured. ^{202}Hg was also measured during analysis in order to correct for isobaric interference of ^{204}Hg on ^{204}Pb. Standard-sample bracketing, using NIST standard glass 612 (^{206}Pb/^{204}Pb = 17.099), was carried out in order to correct for mass bias fractionation (Tyrrell *et al.* 2009).

Results

Well stratigraphy

Wireline logs from 12/2-1z were used to constrain the well stratigraphy. On the basis of gamma and sonic velocity response, three post-Carboniferous sand-prone packages have been identified and targeted for further investigation (Fig. 3). These form a continuous sand-rich sequence which hosts the hydrocarbon column. The oldest of the three intervals, referred to here as the A sandstones, is *c.* 225 m thick and shows typically low gamma response in sandstones, intercalated with thin high gamma mudstones. The A sandstones are overlain directly by the B sandstones (*c.* 128 m thick). The boundary is marked by a distinct change in the character of the gamma log profile (Fig. 3), with much lower variations, but with an overall higher gamma response within the sandstones. This change is attributed to an increase in K-feldspar modal abundance. The C sandstones are very thin (*c.* 4.5 m) and directly overlie the B sandstones. The C sandstones have a similar low gamma response to the A sandstones.

The deepest core (core 3), from 4098 to 4078 m driller depth (d.d.) RKB, comprises a 20 m interval of well-sorted, medium-coarse-grained, red-buff sandstones with minor mudstones, and includes the boundary between the A and B sandstones (Fig. 3). Cores 1 and 2 represent a near-continuous *c.* 70 m section some 57 m above the top of core 3 (4021.1–3952 m d.d. RKB). These cores, corresponding to the uppermost part of the B sandstones and the entire C sandstone, comprise coarse pebbly to fine-grained sandstones, calcareous sandstones, siltstones and minor mudstones, with a distinctive volcanic horizon toward the top of the core 1.

Given the unfossiliferous nature of the cored intervals, their age has yet to be firmly established. Biostratigraphical results from released well reports suggest an early Permian (Asselian) age for the lowermost, uncored part of the A sandstones and a Middle Jurassic to Earliest Cretaceous age for the B and C sandstones. In the absence of definitive biostratigraphic data, released well reports have assigned a broad Permo-Triassic age for the uppermost and cored part of A sandstones, and B and C sandstones are assigned a tentative Middle Jurassic age. For the purposes of this study, the important issues are the compositional variations between packages and the broad correspondence between this well and others in the region at the level of Permo-Triassic compared to Jurassic–Cretaceous.

Core description

The short section of cored A sandstones (*c.* 4.5 m) comprises well sorted medium- to coarse-grained buff-coloured sandstones with subordinate siltstones and mudstones (Fig. 4). The sandstones are characterized by common low-angle cross-stratification and minor ripple cross-lamination. The top of the package is marked by muddier horizons, with a distinctive red mudstone bed just beneath the contact with the A package. The boundary between the A and B sandstones occurs as an erosion surface at 4092.5 m d.d. RKB. This is directly overlain by a pebbly based, medium-grained buff-coloured sandstone. B sandstones in core 3 are distinguished from the underlying A sandstones by their more abundant coarser sandstones beds, frequently with distinct erosive bases and mud rip-up clasts. The gamma log confirms an abrupt change in character at the A/B contact.

B sandstones in core 2 comprise coarse to pebbly sandstones (Fig. 4) in graded beds with common erosive bases. They tend to be cross-stratified, particularly towards bed tops (Fig. 4). The sandstones contain extraclasts (pebbles of vein quartz, granite and granitic gneiss) and rounded fragments of intraclastic calcareous sandstones. Sandstone beds frequently appear to have been internally remobilized or disrupted during deposition, and there are abundant post-depositional siderite-cemented fractures. Coarser beds become less abundant at higher levels (above *c.* 3991 m d.d. RKB, toward the top of core 1 and base core 2), where there are abundant calcareous bands, marls and siltstone beds. Here, the logged interval is marked by a change from buff to dominantly grey colour. There are several distinct coarsening-upward beds (0.5–1 m scale) which comprise mud-dominated bases with sandy lenses, becoming increasingly sandy toward their tops which contain mud-lenses (e.g. at depth 3976.5–3975.5 m). These heterolithic beds are frequently associated with *in-situ* calcareous horizons.

The boundary between the B and C sandstones occurs toward the top of core 1 (3968 m d.d. RKB) and appears conformable. It is marked by a distinct, green, pebble-based sandstone bed overlying B package muddy siltstones. The C sandstones are *c.* 4.5 m thick and comprise coarse- to medium-grained sandstones with distinct cm-scale pebble-rich bands. There are abundant buff, rounded, intraclastic calcareous sandstone fragments (Fig. 4), which appear to be enveloped by green remobilized sandstones. The green colour is attributed to the presence of fine-grained glauconite. The top of the C sandstone (3963.5 m d.d. RKB) is marked by a dark green, vesicular, volcanic rock.

Depositional environments

A sandstones. In cored A sandstones, the sedimentary structures, the well sorted nature of the sandstones, lack of marine indicators (e.g. fossils, glauconite) and the presence of rounded grain-types are suggestive of a non-marine aeolian or fluvially reworked aeolian facies with possible fluvial unconfined channel sandstones.

B sandstones. The coarse nature of the B sandstones in core 3 and the presence of both trough cross-bedding and low-angle cross-stratification suggest intermittent fluvial shallow channel sandstones and sandflat deposition. The calcareous layers are interpreted as calcretes, indicating a semi-arid environment. The remobilized or disrupted appearance of some beds may be due to modification during pedogenesis.

The coarse sandstone packages toward the base of core 2 are interpreted to be the deposits of a relatively high-energy alluvial/fluvial system, with channel lag deposits and sandy bar-forms interbedded with unconfined sheet sand deposits. The energy of this

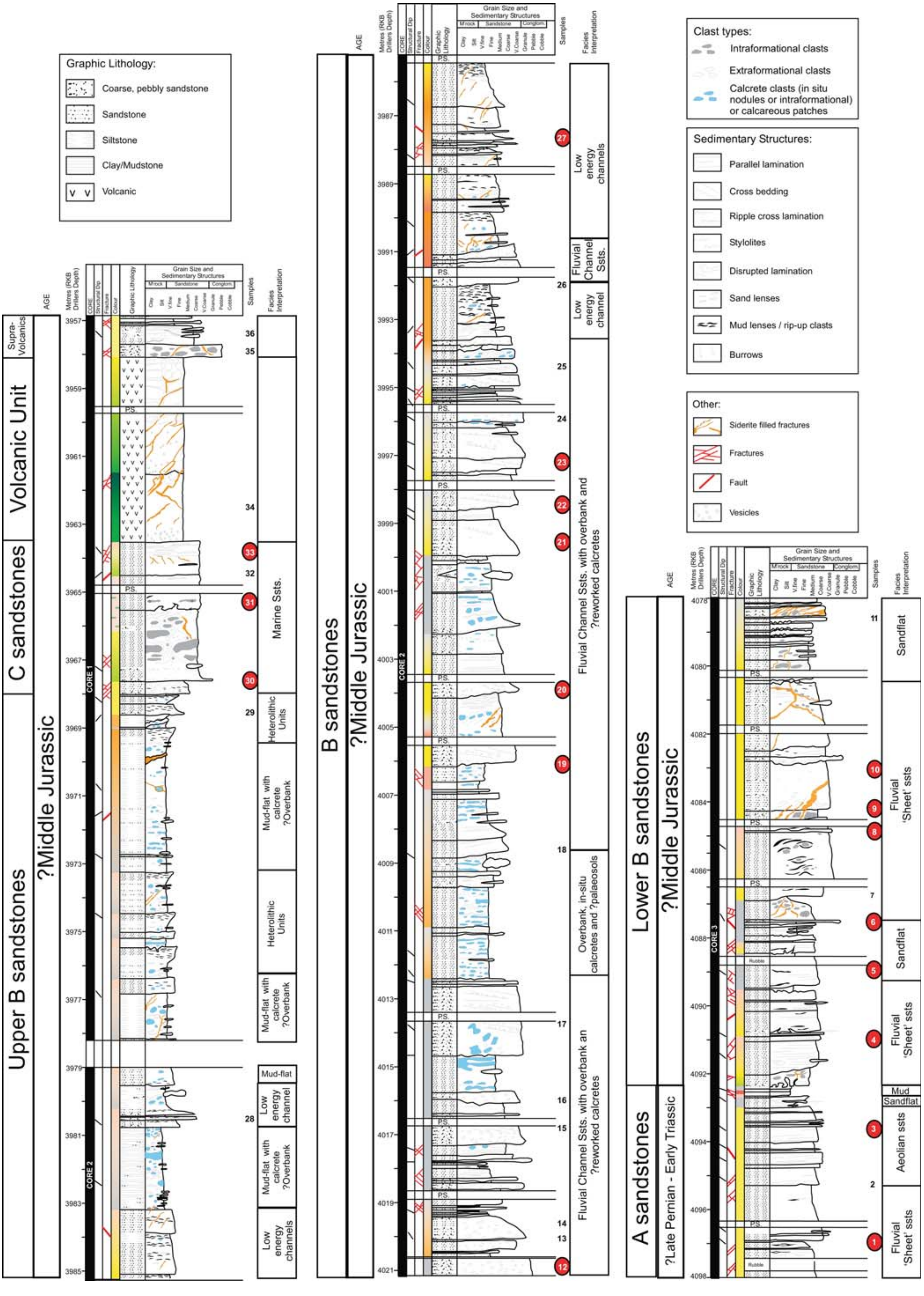

Fig. 4. Sedimentological logs of cores 1–3 in well 12/2-1z, illustrating the character and distribution of facies. Samples from which the Pb composition of K-feldspar have been analysed are highlighted with a red circle.

system wanes upward with more frequent unconfined sheet sand deposits, lower energy channels, and abundant mudstone-lenses.

The finer grained, grey, muddy lithologies observed from the upper part of core 2 appear likely to represent overbank deposits. Calcareous horizons are interpreted as palaeosols, and occur as *in-situ* continuous mature calcrete horizons, *in situ*-nodules (immature calcretes) and possibly reworked intraformational clasts. Disruption of lamination is likely attributed to soil formation processes. The heterolithic beds in core 1 and 2 suggest a tidal influence. The structures in the upper part of core 2 and lower part of core 1 are indicative of the transition from a low-energy floodplain/lacustrine to an estuarine environment with possible tidal influence.

C sandstones. The presence of glauconite in C package sandstones suggests a marine environment, possibly a shoreface setting (Fig. 4). The disrupted appearance of C package sandstones may be caused by de-watering and/or related to deposition on an unstable slope. The volcanic horizon occurring above package C is interpreted as a lava flow as its upper boundary appears blocky and weathered.

Sandstone petrography

A sandstones. Sampled sandstones are well sorted sub-arkosic arenites, with sub-angular to rounded grain shapes (Fig. 5a). Rounded grains may represent an aeolian grain population which has been reworked by fluvial action. K-feldspar is common (*c*. 15% modal abundance), and it has a very fresh appearance, commonly displaying perthitic textures (Fig. 5d). Traces of plagioclase, muscovite mica and detrital clay occur. Minor lithic fragments, dominantly of plutonic igneous origin, also occur. Macroporosities vary between 5 and 15%.

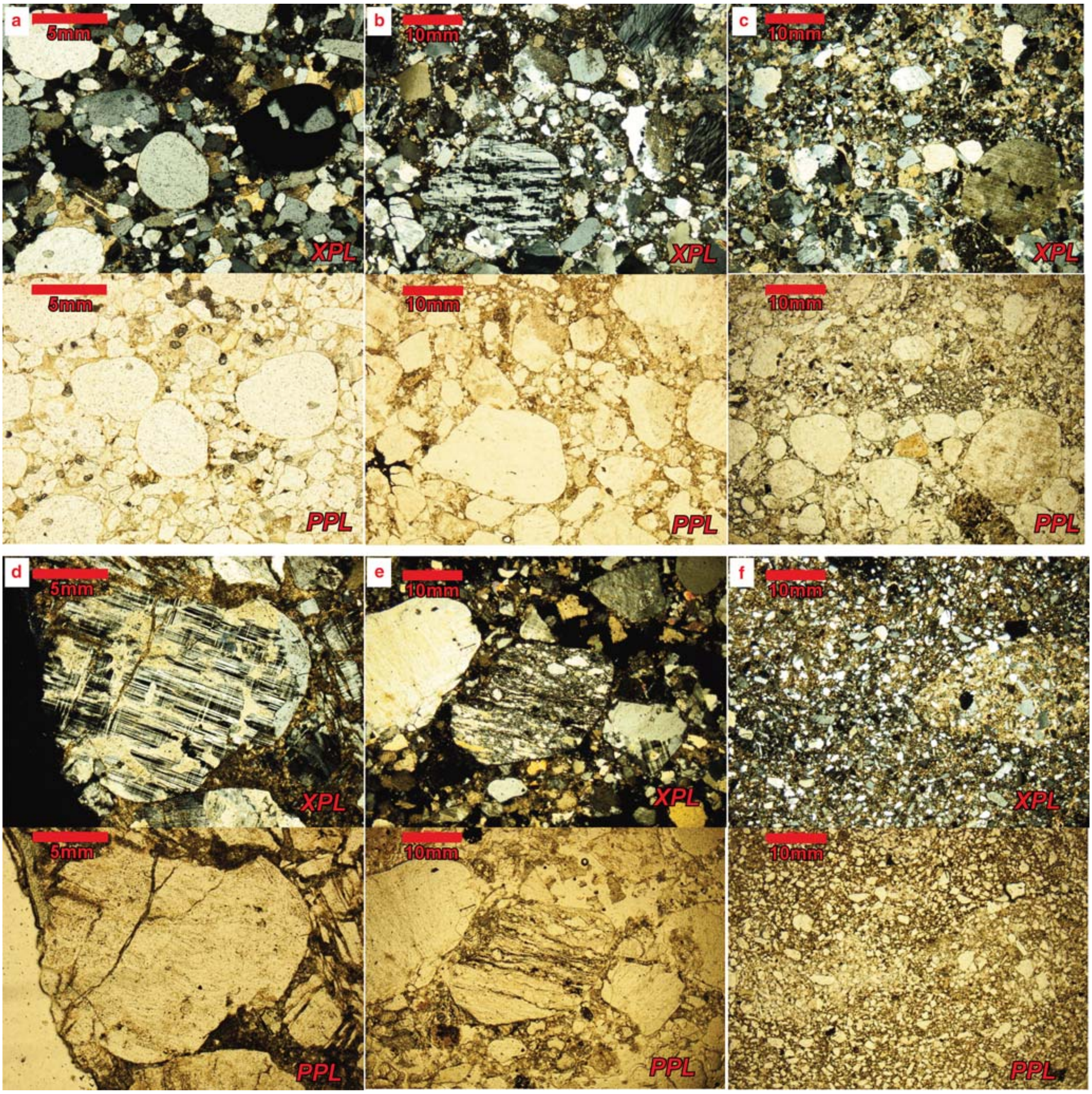

Fig. 5. Photomicrographs (XPL and PPL) of (**a**) A sandstones with typical bimodal grain distribution of rounded and finer, angular grains; (**b**) arkosic, lithic, B sandstones; (**c**) C sandstones with bimodal grain size distribution; (**d**) perthitic microcline K-feldspar grains from A sandstones; (**e**) quartzo-feldspathic gneissic lithic from B sandstones and (**f**) fine-grained calcareous sandstones associated with soil-forming processes from upper B sandstones.

B sandstones. Sampled sandstones are generally texturally more immature than A sandstones and are lithic arkoses. They comprise abundant K-feldspar (up to *c*. 30%) with a significantly higher lithic component than A sandstones. Lithic fragments are dominantly quartzo-feldspathic aggregates of likely plutonic igneous origin, but also including minor gneissic (Fig. 5e) and schistose fragments. Some fine-grained B sandstones are calcareous and contain micritic intraclasts. Trace accessory minerals include albite, muscovite mica and detrital clay. Macroporosities in these sandstones range between 5 and 20%. Calcite occurs as a patchy poikilotopic pore-filling cement in all the sandstones. Minor authigenic illitic clays occur, usually as a grain-rimming cement, and pyrite is present as a late phase.

C sandstones. Sampled sandstones are relatively well sorted and invariably display a bimodal grain size distribution comprising a fine angular grain component and a medium-coarse rounded grain component (Fig. 5c). The sandstones are arkosic, with K-feldspar dominant, and sublithic, with plutonic igneous fragments most common. The sandstones contain glauconite. Macroporosity is less than *c*. 15%.

Analytical results

Sixty-seven Pb isotopic analyses of 64 K-feldspar grains/crystals from sandstone intervals in well 12/2-1z K-feldspar were carried out and the data are presented in Table 1. Of these, 18 were obtained using a Faraday collector configuration with the remaining analysis carried out using the ion counter collector configuration (see above).

Seven grains were analysed from two samples of the A sandstones in core 3, 17 grains from six samples of B package sandstones in core 3, 21 grains from seven samples of B sandstones from cores 1 and 2, and 19 grains from three samples of C sandstones from core 1. The bulk composition of 45 of these grains was constrained using electron microprobe analysis. Results show that feldspars are dominantly orthoclase, with an average composition of Or:Ab:An = 96.08:3.83:0.08. There appears to be no link between the Pb isotopic and the bulk feldspar composition.

Overall, the feldspars largely exhibit relatively unradiogenic Pb isotopic compositions, with $^{206}Pb/^{204}Pb$ ratios varying between 13.53 and 16.70, averaging at 14.92, with only three more radiogenic grains with $^{206}Pb/^{204}Pb$ in excess of 17. Overall, the Pb data form three distinct groupings or trends. These groupings are considered to represent three distinct sources, although it should be noted that geographically different sources may have a shared basement history and thus have the same Pb isotopic composition. Source 1 corresponds to a grouping of the most unradiogenic Pb compositions plotting within Pb domain 1 (see above); source 2 corresponds to a group of data with an apparent linear trend, while source 3 forms a tight grouping of grains, more radiogenic than source 1, and plotting within Pb domain 2 (Fig. 6).

Samples 9 and 10 from B package sandstones in core 3 are granitic clasts from which several K-feldspar crystals were analysed. Pb isotopic analyses of 3 K-feldspar crystals from sample 9 exhibit an unradiogenic composition plotting within a restricted range (Fig. 6), but isotopic analyses of 4 K-feldspars from sample 10 show a significant spread in $^{207}Pb/^{204}Pb$. This illustrates that K-feldspars from the same source rock can, at least in terms of the ^{207}Pb, can have a range of Pb isotopic compositions. This

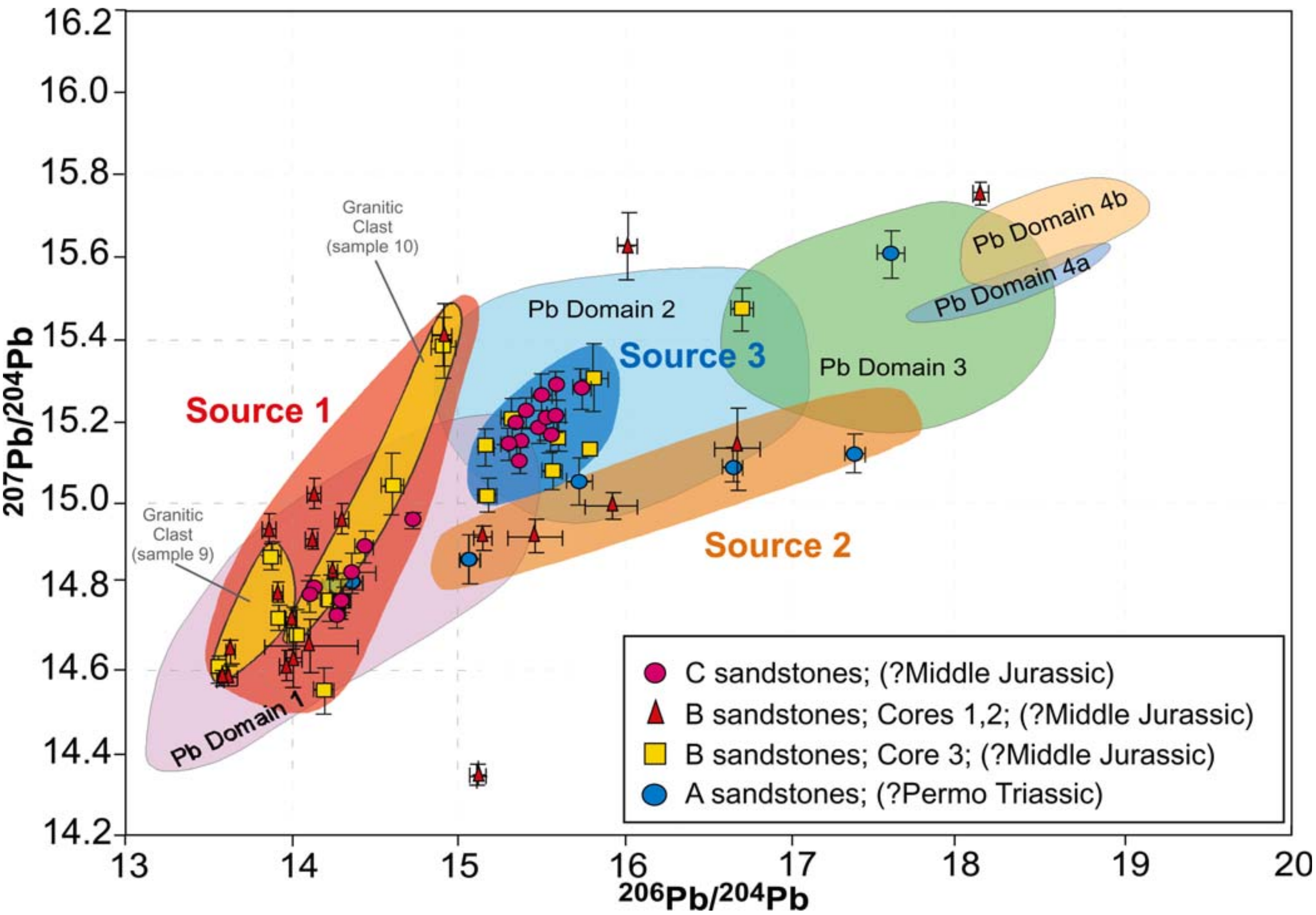

Fig. 6. $^{206}Pb/^{204}Pb$ – $^{207}Pb/^{204}Pb$ lead space plots for all the Dooish sandstones K-feldspar. Data are plotted with reference to Pb domains 1–4 (after Tyrrell *et al.* 2007, Fig. 1b). Three groupings, corresponding to sources 1–3, are highlighted.

characteristic could help explain some of the outlying Pb isotopic compositions, and could be due to small initial variations in Pb, U and Th, either between K-feldspars in the same rock or within individual zoned crystals. However, the differences appear insignificant in terms of the regional variation in Pb, for example, despite the Pb isotopic variation in sample 10, all data vary little in terms of $^{206}Pb/^{204}Pb$ and plot along a steep trend line.

Provenance interpretation

The majority of K-feldspars from A sandstones show a Pb isotopic composition that falls within the range defined by source 2. There is a relatively minor component (two grains) which falls within source 1 (Fig. 3). K-feldspars from lower B sandstones (i.e. those from core 3) show bimodal Pb isotopic populations, attributed to sources 1 and 3, but with no source 2 grains (Fig. 3). K-feldspars from upper B sandstones (i.e. those from cores 1 and 2) also have a bimodal Pb isotopic composition, corresponding to source 1 and 2, but with no source 3 grains. K-feldspars from C sandstones plot within sources 1 and 3, with no source 2 grains, a similar distribution pattern to that seen in lower B sandstones (Fig. 3).

In order to constrain the sourcelands, the three 'source' ranges have been plotted with Pb isotopic data for basement in the region (Fig. 7). There is good correspondence between source 1 and elements of the Lewisian Complex, in particular the offshore Stanton Banks area, but grains with this composition could also have been derived from elements of the Nagssugtoqidian of SE Greenland. Source 2 appears to correspond with the linear data arrays that are manifest in some of the blocks within the Lewisian Complex (e.g. Uist Block).

Source 3 has a more radiogenic Pb composition than source 1, but a less radiogenic composition than other sampled regional basement units (e.g. the Rhinns Complex) and offshore highs (e.g. Rockall Bank, Porcupine High). Reconstructions of the North Atlantic region suggest continuation of orogenic belts across the Atlantic (Tyrrell *et al.* 2007), yet much of the offshore basement remains poorly characterized. Source 3 may correspond to an area of as yet unsampled basement in the region. On the basis of its Pb isotopic composition, this source seems unlikely have an affinity with the oldest basement in the region (Lewisian, Nagssugtoqidian), but could feasibly represent basement of Ketilidian affinity. Ketilidian-affinity crust in the region is likely to display a broader range in Pb isotopic composition than that shown by the limited samples analysed from the Rockall Bank. Such a source could have been available at times during deposition of the Dooish sandstones, but may presently be buried. Naturally, there are problems speculating on the past geographical occurrence and areal extent of such basement but, given its Pb isotopic composition (plotting in the Pb domain 2) it could occur to the immediate east of the Dooish area or, alternatively, within the northern Rockall Bank.

Palaeogeographic reconstructions for the intervals of deposition of the Dooish sandstones and the position of likely source areas are shown in Figure 8. A sandstones have probably been derived directly from the north or from the NW, with drainage scales in the order of 300 km envisaged. More local sources, directly from

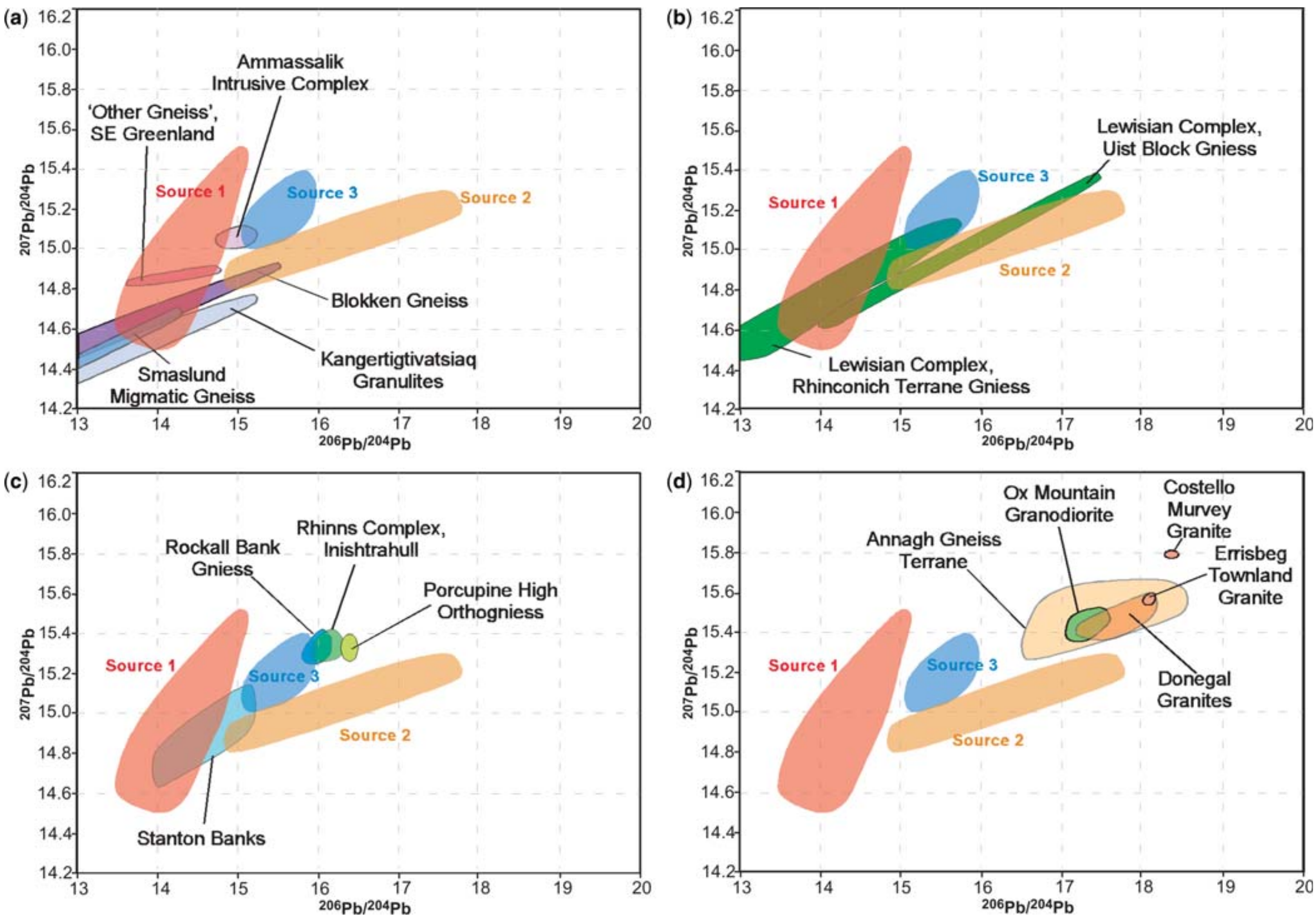

Fig. 7. $^{206}Pb/^{204}Pb$ – $^{207}Pb/^{204}Pb$ lead space plots for the three sources, plotted with Pb data from (**a**) the Nagssugtoqidian Mobile Belt of SE Greenland; (**b**) Lewisian Complex Rocks from NW Scotland; (**c**) offshore crystalline basement blocks from the NW Atlantic and (**d**) crystalline basement from onshore western Ireland. Pb basement data from Tyrrell *et al.* (2007, Fig. 1b and references therein).

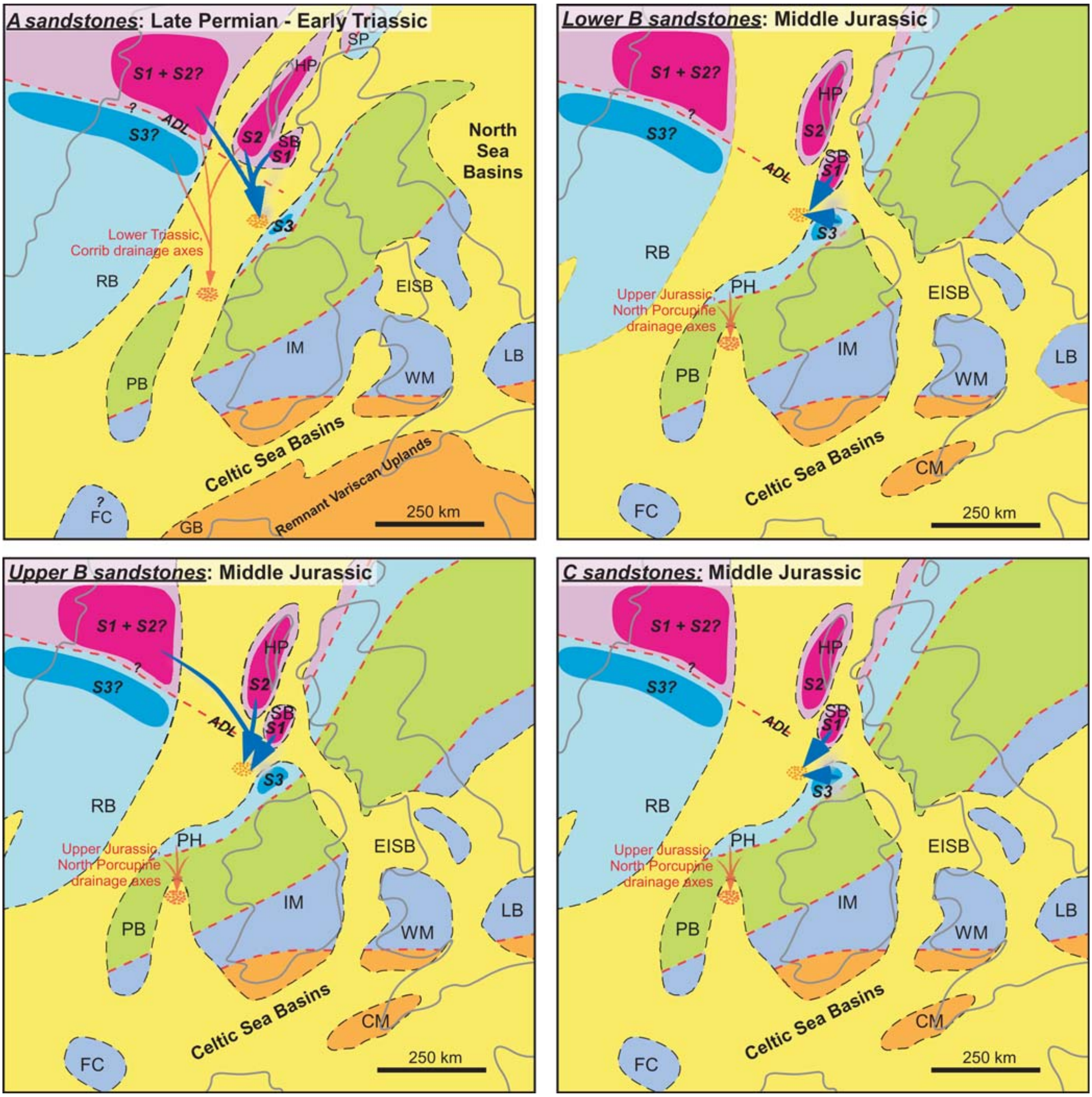

Fig. 8. Palaeogeographic reconstructions of the circum North Atlantic region during the Late Permian–Early Triassic and Middle Jurassic (after Williams *et al.* 1999; Ziegler 1999; Torsvik *et al.* 2001; Eide 2002; Scotese 2002), showing the palaeodrainage directions (arrows) during the deposition of the Dooish sandstones. The land masses are colour coded so as to reflect their bulk Pb signature (Tyrrell *et al.* 2007) with darker colours used to highlight areas that are potential sources. Also shown, for reference, are the orientation of drainage axes supplying the Corrib gas field sandstones (Lower Triassic, Slyne Basin) and Upper Jurassic of the northern Porcupine Basin (from Tyrrell *et al.* 2007). ADL, Anton Dohrn Lineament; CM, Cornubia Massif; EISB, East Irish Sea Basin; FC, Flemish Cap; GB, Galicia Bank; HP, Hebridean Platform; IM, Irish Massif; LH, Labadie Bank High; LB, London–Brabant Massif; PB, Porcupine Bank; PH, Porcupine High; RB, Rockall Bank; SP, Shetland Platform; WM, Welsh Massif.

the east, NE and north are suggested for the lower B sandstones. Data from upper B sandstones suggest dominantly north and NE derivation, while C package sandstones could have been derived from more local sources to the north, NE and east.

There is an abrupt change in source area between A sandstones and overlying lower B sandstones as sampled from core 3, manifesting as a switching off of source 2 and an influx on source 1 and 3 grains. This change of source area corresponds to an abrupt change in the wireline character at the boundary of these units, and is consistent with the apparent prolonged period of non-deposition between the Permo-Triassic and Middle Jurassic. During this hiatus it is possible the palaeo-erosion surface and hinterland geological composition changed considerably.

Upper B sandstones (from cores 1 and 2) have a different provenance character from the lower B sandstones (core 3), with the loss of source 3 grains in the upper B sandstones and the presence of a source 2 population, while source 1 continues to be important. This may reflect a more gradual evolution of drainage/erosion in the hinterland than that suggested by the abrupt change between the A and B sandstones. However, analysis of the intervening B sandstones between the top of core 3 and base of core 2 is required in order to test this hypothesis.

Another rapid change in sourcing occurs between the deposition of B and C sandstones, to the disappearance of source 2 grains and a bimodal distribution of distinct source 1 and 3 grains. This change could be linked to the change in depositional environment, with marine currents influencing the routing of grains and the detrital composition of the sandstones.

It is important to note that, in bulk terms, source 1 appears to have been consistently available as a source during the Permo-Triassic and Middle Jurassic. Also, at every sampled stratigraphic level, either source 2 or 3 is available, but never at the same time. The intermittent delivery to the basin of either source 2 or 3 grains could be caused by the periodic rejuvenation of specific tributary systems, possibly linked to variations in uplift rates in the hinterland, or may be the effect of subtle climatic factors affecting the delivery of grains to the basin. The variation of provenance with stratigraphy in the succession highlights the potential of the Pb-in-K-feldspar provenance technique as a tool in the correlation of sand-prone but unfossiliferous intervals.

Implications for regional sand-sourcing

The three source-types can be compared with Pb isotopic data from K-feldspar grains in (1) Triassic sandstones from Corrib gas field sandstones in the Slyne Basin, (2) Upper Jurassic sandstones from the northern Porcupine Basin and (3) Cretaceous sandstones from the western margin of the Porcupine Bank (Fig. 9).

Sources 1 and 3 show strong correspondence with the two groupings observed in Corrib gas field sandstones. This suggests that Triassic Corrib sandstones share the same provenance as the lower B sandstones and the C sandstones, but have a different provenance to A sandstones in the Dooish area of the Rockall Basin. It is envisaged that grains from the Corrib gas field sandstones were transported across the nascent Rockall Basin (Tyrrell *et al.* 2007; Fig. 8), but more local sourcing within or close to the Slyne Basin could as yet be unrecognized. Although drainage-length scales appear to be shorter in the Permo-Triassic of the eastern Rockall basin, the orientations are similar to those interpreted for the Triassic of the Slyne Basin.

There is no correspondence between the three Dooish source-types and detrital K-feldspar data from Upper Jurassic sandstones in the northern Porcupine Basin, or from Cretaceous sandstones on the margins of the Porcupine Bank. This suggests that Jurassic sandstones deposited to the north and to the south of the Porcupine High have a contrasting provenance, and that the Porcupine High itself could have been uplifted and acted as a barrier to drainage during the Middle to Late Jurassic (Fig. 8). It appears that local sand sourcing dominated during the Middle and Late Jurassic in both the Rockall and Porcupine basins, with drainage scales in both basins interpreted to be *c.* 100 km.

Additionally, in the Upper Jurassic of the Porcupine Basin, recycled Carboniferous sedimentary rocks are suggested to have been an important source (Robinson & Canham 2001). These seem to play a far less important role in the Dooish sandstones, where petrography clearly shows crystalline plutonic igneous and metamorphic basement as the predominant source.

In overall terms, the pattern of detrital Pb isotopic compositions of K-feldspars in Permo-Triassic to Cretaceous sandstones in basins on the NW European margins highlights the important role played by local (often poorly characterized) Archaean and Proterozoic basement blocks as sand sources and drainage divides and, consequently, in controlling reservoir sandstone distribution in the region (Fig. 8). Perhaps unsurprisingly, grains with an Archaean and Palaeoproterozoic signature (Pb Domain 1) are more abundant in basins further north, which is also consistent with provenance data from Triassic sandstones in the Faroe–Shetland region (Tyrrell *et al.* 2009), but become increasingly less so in basins further south.

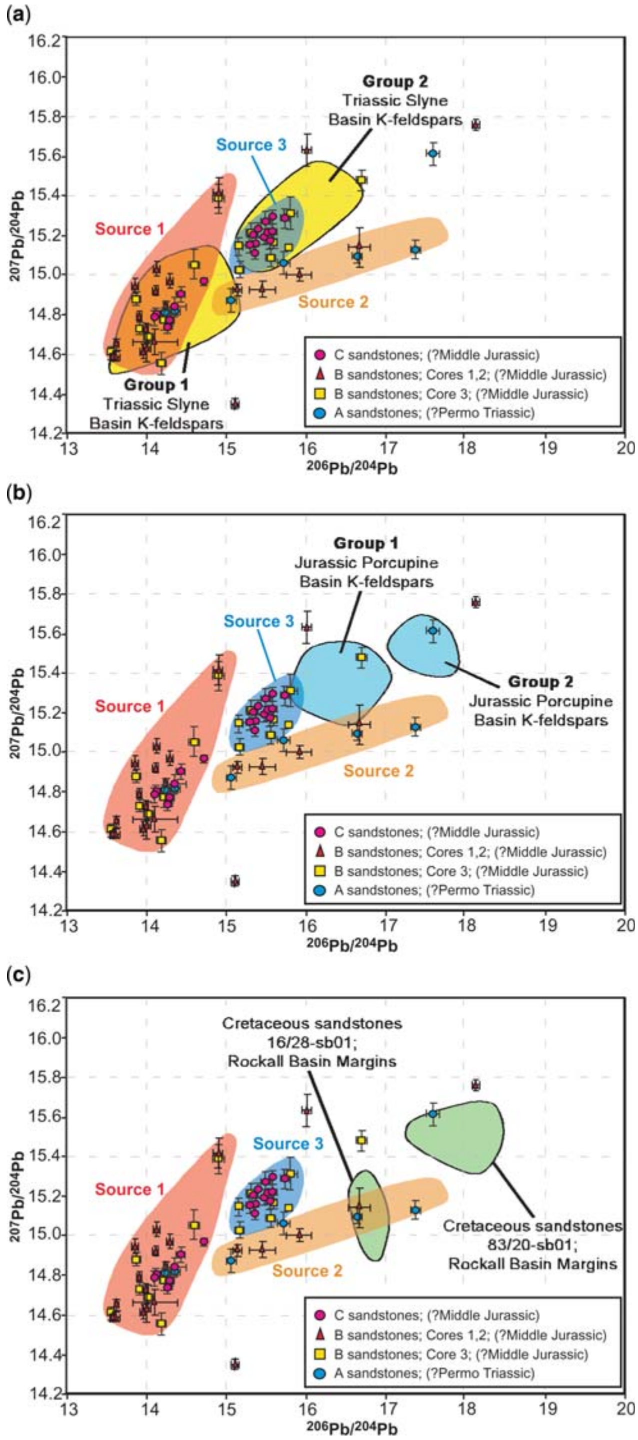

Fig. 9. $^{206}Pb/^{204}Pb-^{207}Pb/^{204}Pb$ lead space plots for (**a**) Dooish K-feldspars compared with populations from Triassic sandstones in the Slyne Basin, including those from the Corrib gas field; (**b**) Dooish K-feldspars compared with populations from Upper Jurassic sandstones in the northern Porcupine Basin (the Connemara field and the Spanish Point gas condensate); and (**c**) Dooish K-feldspars compared with populations from Cretaceous sandstones from shallow boreholes on the eastern Rockall Basin margin. Previously published data is from Tyrrell *et al.* (2007).

Conclusions

(1) The Pb isotopic composition of detrital K-feldspar offers a powerful method of determining the provenance of arkosic

and sub-arkosic sandstones, and prospective source areas are also relatively easily characterized. When applied to Mesozoic sandstones in basins west of Ireland, the technique can place constraints on the scale and pattern of palaeodrainage and constrain the relative contribution of different source areas.

(2) The bulk of K-feldspars in Permo-Triassic and Middle Jurassic sandstones from the eastern Rockall Basin (Dooish; 12/2-1z) appear to have been derived from three isotopically distinct source areas. Elements of the Lewisian Complex, similar to the Stanton Bank, formed an important and persistent source for all the sampled sandstones (source 1), but other Lewisian Complex rocks (such as the Uist Block and its equivalents; source 2) and a currently unidentified, likely Ketilidian, source (source 3) variably provided additional sediment during deposition of the these sandstones. Intriguingly, sources 2 and 3 do not appear to be available at the same time, which may suggest that the grains are being delivered through different tributary systems which are active at different times. There are very few grains that could have been derived from southern sources, such as the Irish Massif and the Variscan Uplands. Although sources from the far north and west (e.g. SE Greenland) cannot be entirely ruled out, there are more proximal terranes that can supply feldspar with the requisite Pb isotopic composition. Similarly, it is difficult to clearly ascertain if grains were transported across the nascent Rockall Basin, although the overall textural immaturity of the sampled sandstones supports local sourcing. The simplest model for palaeodrainage reconcilable with all the Pb data suggests derivation directions from the NW, north, NE or directly from the eastern margin of the basin. North-derived dispersal directions appear to have persisted during deposition of the Permo-Triassic and the Middle Jurassic sequences, but more north-eastern and, potentially local, eastern sources appear to have supplied detritus intermittently.

(3) There are difficulties constraining transport distances both during the Permo-Triassic and the Jurassic in the Dooish area, given the uncertainty associated with the nature and palaeo-position of all the potential sources, but palaeogeographic reconstructions suggest they are unlikely to be in excess of 300 km. It is probable that local sources (transport <100 km) played an important role, especially during the Jurassic. The Irish Massif appears to have acted consistently as a significant and persistent drainage divide or barrier during the Permo-Triassic and into the Late Jurassic. Although this massif prevented the transport of Variscan sand grains into the basins west of Ireland, it does not appear to have supplied significant sediment itself.

(4) Determining the provenance of sandstones provides a first-order control on the distribution of reservoir intervals. The directions of sediment transport derived from the provenance data suggest that more distal equivalents of the sedimentary rocks in 12/2-1z may have been deposited to the south and SW, implying that sandstones with similar bulk characteristics may occur at depth within the Rockall Basin.

(5) The overall dispersal pattern of K-feldspar into basins west of Ireland during the Mesozoic suggests that Archaean and Proterozoic basement blocks played a crucial role in controlling drainage during this prolonged period. It is therefore important to understand the nature, palaeo-position and late uplift history of these crustal blocks.

This work is based on research funded by the Department of Communications, Energy and Natural Resources under the National Geoscience Programme 2007–2013 (Griffiths Geoscience Awards) awarded to the Marine and Petroleum Geology Research Group at UCD, and by a Science Foundation Ireland Research Frontiers Programme grant (RFP06/GEO029) awarded to PDWH. ST acknowledges P. Sylvester and M. Tubrett (Microanalysis Facility, Memorial University, Newfoundland, Canada) for assistance with ICPMS and A. Kronz (Electron Microprobe Laboratory, Geowissenschaftliches Zentrum, Göttingen, Germany). ST thanks Shell International and the Petroleum Affairs Division (Ireland) for facilitating access to core and providing well data. David MacDonald and Tony Doré are thanked for detailed reviews which improved the manuscript.

References

Audley-Charles, M. G. 1970. Triassic palaeogeography of the British Isles. *Quarterly Journal of the Geological Society, London*, **126**, 49–89.

Butterworth, P., Holba, A., Hertig, S., Hughes, W. & Atkinson, C. 1999. Jurassic non-marine source rocks and oils of the Porcupine Basin and other North Atlantic margin basins. *In*: Fleet, A. J. & Boldy, S. A. R. (eds) *Petroleum Geology of Northwest Europe: Proceedings of the 5th Conference*. Geological Society, London, 471–486; doi: 10.1144/0050471.

Cawood, P. A., Nemchin, A. A., Strachan, R. A., Kinny, P. D. & Loewy, S. 2004. Laurentian provenance and an intracratonic tectonic setting for the Moine Supergroup, Scotland, constrained by detrital zircons from the Loch Eil and Glen Urquhart successions. *Journal of the Geological Society, London*, **161**, 861–874.

Connelly, J. N. & Thrane, K. 2005. Rapid determination of Pb isotopes to define Precambrian allochthonous domains: an example from West Greenland. *Geology*, **33**, 953–956.

Clift, P. D., Shimizu, N., Layne, G. D. & Blusztajn, J. 2001. Tracing patterns of erosion and drainage in the Paleogene Himalaya through ion probe Pb isotope analysis of detrital K-feldspars in the Indus Molasse, India. *Earth and Planetary Science Letters*, **188**, 475–491.

Clift, P. D., Van Long, H. *et al*. 2008. Evolving east Asian river systems reconstructed by trace element and Pb and Nd isotope variations in modern and ancient Red River-Song Hong sediments. *Geochemistry Geophysics Geosystems*, **9**, Q04039.

Croker, P. F. & Shannon, P. M. 1987. The evolution and hydrocarbon prospectivity of the Porcupine Basin, Offshore Ireland. *In*: Brooks, J. & Glennie, K. W. (eds) *Petroleum Geology of North West Europe*. Graham and Trotman, London, 633–642.

Dancer, P. N., Kenyon-Roberts, S. M., Downey, J. W., Baillie, J. M., Meadows, N. S. & Maguire, K. 2005. The Corrib gas field, offshore west of Ireland. *In*: Doré, A. G. & Vining, B. A. (eds) *Petroleum Geology: North-West Europe and Global Perspectives: Proceedings of the 6th Petroleum Geology Conference*. Geological Society, London, 1035–1046; doi: 10.1144/0061035.

DeWolf, C. P. & Mezger, K. 1994. Lead isotope analyses of leached feldspars: constraints on the early crustal history of the Grenville Orogen. *Geochimica et Cosmochimica Acta*, **58**, 5537–5550.

Eide, E. A. 2002. *BATLAS – Mid Norway Plate Reconstruction Atlas with Global and North Atlantic Perspectives*. Geological Survey of Norway.

Haughton, P., Praeg, D. *et al*. 2005. First results from shallow stratigraphic boreholes on the eastern flank of the Rockall Basin, offshore western Ireland. *In*: Doré, A. G. & Vining, B. A. (eds) *Petroleum Geology: North-West Europe and Global Perspectives: Proceedings of the 6th Petroleum Geology Conference*. Geological Society, London, 1077–1094; doi: 10.1144/0061077.

Hemming, S. R., Broecker, W. S. *et al*. 1998. Provenance of Heinrich layers in core V28–82, northeastern Atlantic: $^{40}Ar/^{39}Ar$ ages of ice-rafted hornblende, Pb isotopes in feldspar grains, and Nd–Sr–Pb isotopes in the fine sediment fraction. *Earth and Planetary Science Letters*, **164**, 317–333.

Moore, T. E., Hemming, S. R. & Sharp, W. D. 1997. Provenance of the Carboniferous Nuka Formation, Brooks Range Alaska: a multicomponent isotope provenance study with implications for age of cryptic crystalline basement. *In*: Dumoulin, J. A. & Gray, J. E. (eds) *Geologic Studies in Alaska by the U.S Geological Survey, 1995*. US Geological Survey, Professional Papers, **1574**, 173–194.

Morton, A. C., Herries, R. & Fanning, C. M. 2007. Correlation of Triassic sandstones in the Strathmore Field, west of Shetland, using heavy mineral provenance signatures. *In*: Mange, M. & Wright, D. K.

(eds) *Heavy Minerals In Use*. Developments in Sedimentology, Elsevier, Amsterdam, **58**, 1037–1072.

Naylor, D. & Shannon, P. M. 2005. The structural framework of the Irish Atlantic Margin. *In*: Doré, A. G. & Vining, B. A. (eds) *Petroleum Geology: North-West Europe and Global Perspectives: Proceedings of the 6th Petroleum Geology Conference*. Geological Society, London, 1009–1021; doi: 10.1144/0061009.

Robinson, A. J. & Canham, A. C. 2001. Reservoir characteristics of the Upper Jurassic sequence in the 35/8-2 discovery, Porcupine Basin. *In*: Shannon, P. M., Haughton, P. D. W. & Corcoran, D. V. (eds) *The Petroleum Exploration of Ireland's Offshore Basins*. Geological Society, London, Special Publications, **188**, 301–321.

Scotese, C. R. 2002. PALEOMAP website; http://www.scotese.com.

Torsvik, T. H., Van der Voo, R., Meert, J. G., Mosar, J. & Walderhaug, H. J. 2001. Reconstructions of the continents around the north Atlantic at about the 60th parallel. *Earth and Planetary Science Letters*, **197**, 55–69.

Tyrrell, S., Haughton, P. D. W., Daly, J. S., Kokfelt, T. F. & Gagnevin, D. 2006. The use of the common Pb isotope composition of detrital K-feldspar grains as a provenance tool and its application to Upper Carboniferous palaeodrainage, Northern England. *Journal of Sedimentary Research*, **76**, 324–345.

Tyrrell, S., Haughton, P. D. W. & Daly, J. S. 2007. Drainage re-organization during break-up of Pangea revealed by *in-situ* Pb isotopic analysis of detrital K-feldspar. *Geology*, **35**, 971–974.

Tyrrell, S., Leleu, S., Souders, A. K., Haughton, P. D. W. & Daly, J. S. 2009. K-feldspar sand-grain provenance in the Triassic, west of Shetland: a first-cycle sedimentary fingerprint? *Geological Journal*, **44**, 692–710.

Vitrac, A. M., Albarede, F. & Allégre, C. J. 1981. Lead isotopic composition of Hercynian granite K-feldspars constrains continental genesis. *Nature*, **291**, 460–464.

Warrington, G. & Ivimey-Cooke, H. C. 1992. Triassic. *In*: Cope, J. C. W., Ingham, J. K. & Rawson, P. F. (eds) *Atlas of Palaeogeography and Lithofacies*. Geological Society, London, Memoirs, **13**, 97–106.

Williams, B. P. J., Shannon, P. M. & Sinclair, I. K. 1999. Comparative Jurassic and Cretaceous tectono-stratigraphy and reservoir development in the Jeanne d'Arc and Porcupine basins. *In*: Fleet, A. J. & Boldy, S. A. R. (eds) *Petroleum Geology of Northwest Europe: Proceedings of the 5th Petroleum Geology Conference*. Geological Society, London, 487–499; doi: 10.1144/0050487.

Ziegler, P. A. 1991. *Geological Atlas of Western and Central Europe*. Geological Society, London/Shell International Petroleum Maatschappij B.V.

Cretaceous revisited: exploring the syn-rift play of the Faroe–Shetland Basin

M. LARSEN, T. RASMUSSEN and L. HJELM

DONG Energy, E&P, Agern Allé 24-26, DK-2970 Hørsholm, Denmark (e-mail: micla@dongenergy.dk)

Abstract: Improved seismic imaging of the deep structures in the Faroe–Shetland Basin has revealed a complex Mesozoic rift system with shifting block polarity along the West Shetland Platform. Newly acquired seismic data has led to the focus of hydrocarbon exploration on structurally defined Mesozoic traps and has re-opened exploration in the deeper stratigraphic sections beyond the stratigraphic, Paleocene deep-water play. In the study area, rift geometry changes from symmetrical (south) to asymmetrical (north), the latter creating a large-scale seaward-dipping flexure. The polarity shift may link up with deep-seated basement structures (rift-oblique lineaments) segmenting the rift zone. The initial rifting along the West Shetland Platform strongly influenced the depositional setting and lateral distribution of the Lower Cretaceous sediments. During rift initiation in the Early Cretaceous faulting took place along numerous small faults, which eventually linked up, creating a set of basin master faults in the main rift phase. Sand derived from rivers and longshore currents on the West Shetland Platform was transported down the axis of relay ramps and filled the juvenile rift basins. These sediments formed thick onlapping wedges, reflecting the continuous creation of accommodation space and the overall transgressive nature of the syn-rift and early post-rift succession. In this period, rift basins were elongated, which to some extent hindered cross-rift transport of coarse material except at relay ramps and rift-oblique lineaments. As fault movements ceased, the rift topography was levelled out and allowed gravity-driven systems to reach further into the basin, overstepping former cross-rift barriers. Lower Cretaceous syn-rift sediments are well exposed at several localities along the margins of the northern North Atlantic including onshore NE Greenland. The close analogy to the syn-rift structural setting imaged in the west of Shetland seismic succession may provide valuable information on structurally controlled depositional systems, reservoir architecture and properties.

Keywords: Faroe–Shetland Basin, NE Greenland, petroleum geology, syn-rift, Cretaceous, sediments, extensional faulting, relay ramp

Faroe–Shetland exploration history

The presence of deep sedimentary basins on the continental slope west of the Shetland Islands was first recognized by academic and government-sponsored geophysical surveys in the early 1960s and was confirmed by the first petroleum industry deep reflection seismic surveys in the late 1960s. Exploration drilling began in 1972 and more than 30 wells were drilled during the following decade. Early exploration activity primarily targeted potential Mesozoic reservoir sandstones associated with tilted fault block structures, using the highly successful oil plays of the Viking Graben as analogues. Oil and gas shows were encountered in several wells, and in 1977 the giant Clair Field was discovered (Fig. 1). Oil in place was estimated at up to 4.0×10^9 barrels (Lamers & Carmichael 1999), but was retained in poor-quality reservoirs comprising fractured basement and Devonian–Carboniferous sandstones.

Exploration continued at a slower pace through the 1980s, chasing the Clair play concept, but without significant commercial success. Oil was discovered in 1990 in Triassic sandstones (Strathmore) and in 1991 in Jurassic sandstones (Solan), but volumes were relatively small and the fields were considered sub-economic. A number of wells encountered gas in the Paleocene and Cretaceous reservoirs (e.g. Laggan, Laxford, Torridon and Victory), but again field sizes were only small to moderate, and gas development was not considered economically feasible at the time.

The discovery of large volumes of oil in good quality Paleocene sandstone reservoirs in the Foinaven, Schiehallion and nearby fields in the early 1990s represented an important breakthrough in the west of Shetlands area and the new fields were on stream by 1998. Further significant oil and gas discoveries (Tobermory, Cambo, Rosebank, Laggan/Tormore and Glenlivet) have been made in the recent years in the Faroe–Shetland Basin, supporting the future development of a gas infrastructure and the possibilities for commercialization of minor gas discoveries as well.

The initial exploration was focused on the Palaeozoic and Mesozoic pre- and syn-rift plays, whereas the late exploration successes are mostly related to combined structural and stratigraphic traps in the Palaeogene (Lamers & Carmichael 1999). Numerous exploration wells, targeting the deeper structural play, were drilled on the crest of tilted fault blocks identified on poor-quality 2D seismic and encountered fractured crystalline basement, often with oil shows. However, the continued search for the Clair play concept to a large extent neglected the downdip opportunities of a Cretaceous syn-rift play. In this study, we discuss the Cretaceous syn-rift play, using high-quality reprocessed 2D seismic data and play concepts developed on the basis of onshore analogues. The depositional systems are linked to the structural evolution along the West Shetland Platform and it is demonstrated how improved seismic data, structural analysis and extensive use of analogue data may re-open the syn-rift play of the Faroe–Shetland Basin.

Methods

Reflection seismic data

Vintage 2D seismic data in the study area (Fig. 1) are from the 1970s and 1990s and are generally of poor quality. The data are characterized by multiple energy and noise, which heavily mask primary energy and hamper interpretation of the geology and structures below the base Palaeogene horizon (Fig. 2). Most of these vintage data are thus of limited use in imaging of the Mesozoic rift basins along the western edge of the West Shetland Platform.

VINING, B. A. & PICKERING, S. C. (eds) *Petroleum Geology: From Mature Basins to New Frontiers – Proceedings of the 7th Petroleum Geology Conference*, 953–962. DOI: 10.1144/0070953

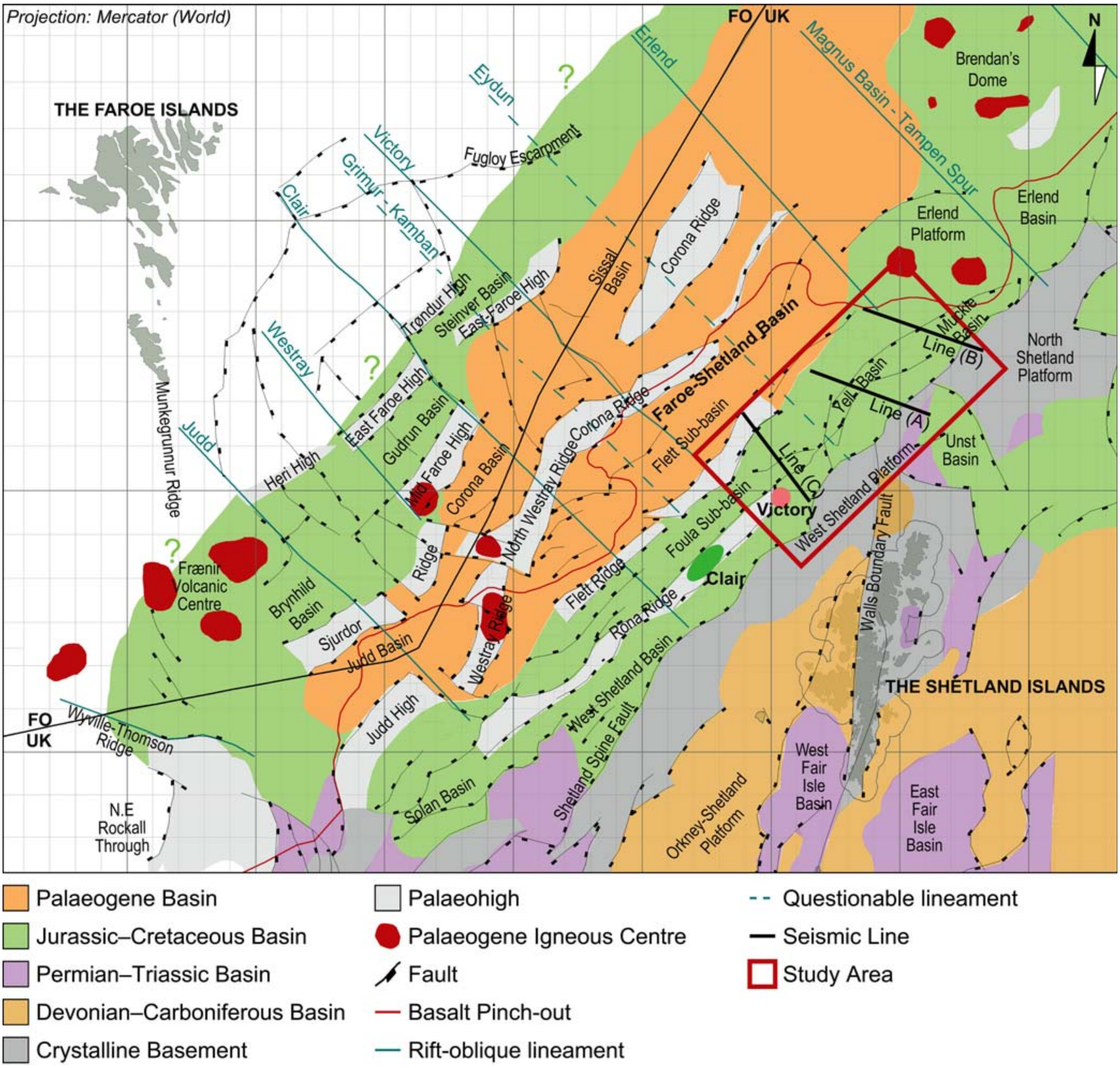

Fig. 1. Generalized structural map of the Faroe–Shetland region with the study area outline. Major Cretaceous depocentres are present along the West Shetland Platform and potentially in the sub-basalt area SE of the Faroes, whereas the Palaeogene depocentres were shifted further towards the rift axis. A series of NE–SW striking half-grabens formed along the margins of the rift in the Early Cretaceous. The sub-basins and intervening ridges (e.g. Rona Ridge) form the key structural elements in the syn-rift play of the basin.

A new 2D data set (long offset) was acquired by TGS-NOPEC in 2005 and 2006 (NSR05 and -06) in a regular grid with approximately 5 km spacing suitable for regional screening and imaging of the deeper targets. These data were successfully reprocessed in 2006 with focus on careful velocity picking and improved imaging of the fault cuts.

The seismic examples (Fig. 2) show the overall improvement from old v. new 2D seismic acquisition, modern processing techniques and the gain in resolution that can be obtained through careful reprocessing of 2D data. The reprocessed data give confidence in the interpretation of the platform–transition–outer basin trend and allow identification of deeper, tilted fault blocks. This may form the key to unlocking the remaining exploration potential along the West Shetland Platform. Regional gravimetric maps and filtered gravity data from the seismic surveys have been utilized for basement trend analysis and act as support for evaluation of the large-scale structural setting, including Caledonian and older structural grains (Kimbell *et al.* 2005).

Wells

The Mesozoic–Palaeozoic structural play of the Faroe–Shetland Basin was targeted during the early exploration phases and most wells of interest are thus released. Control of sedimentary facies and depositional models along the margin of the West Shetland Platform has been achieved from well analysis and onshore analogue studies. Although most of the older wells are situated at the crest of the tilted fault blocks, drilling updip from the syn-rift succession, valuable information on the syn-rift sediments was obtained from the Victory gas discovery situated downdip from the crest of a hanging wall block, east of the Rona Ridge (Goodchild *et al.* 1999; Fig. 1).

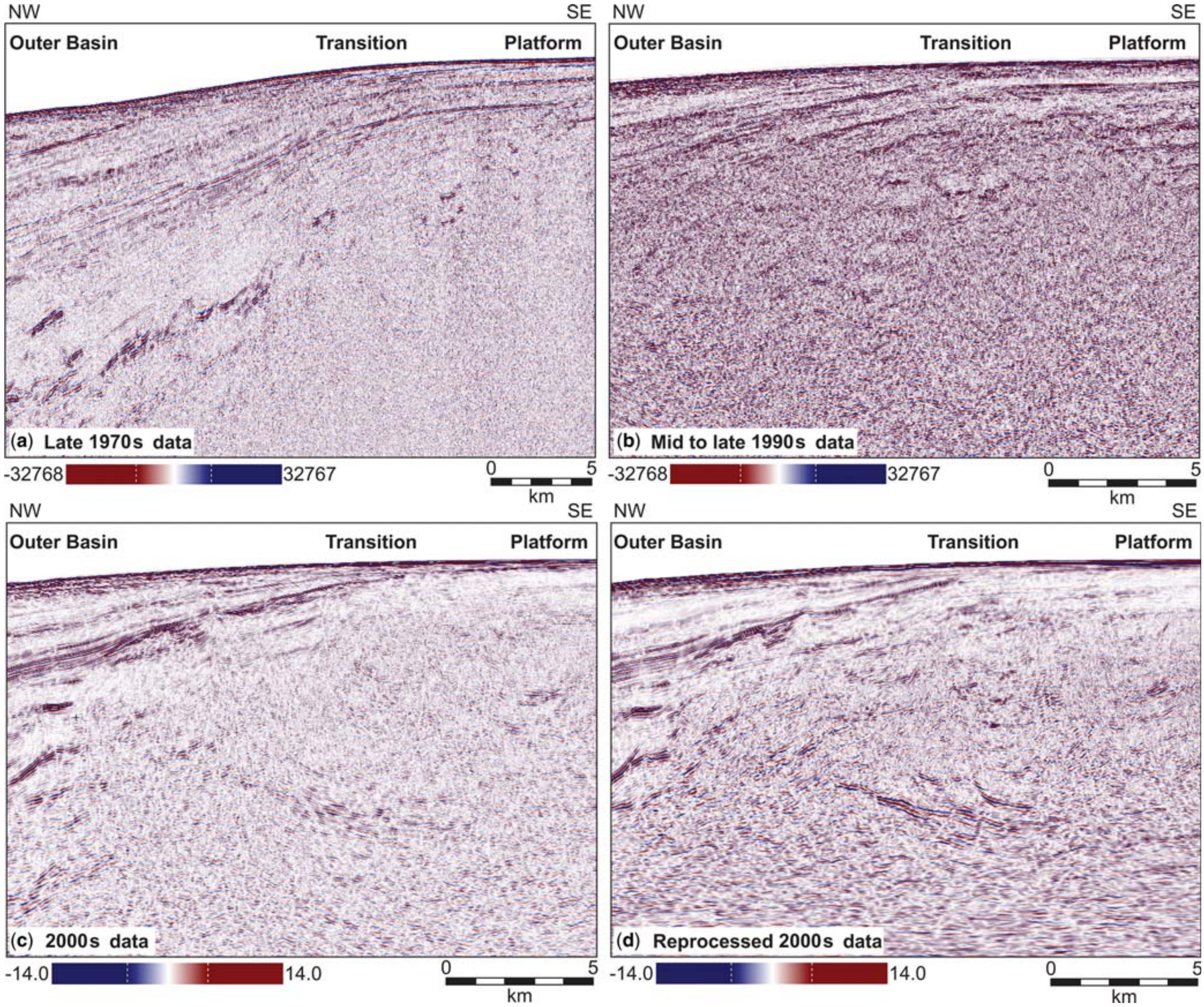

Fig. 2. Four generations of seismic acquisitions/processing showing approximately the same section across the 'Yell' Basin at the western edge of the West Shetland Platform. The differences in the seismic character are related to the acquisition parameters, especially cable length (TGS long offset data) and the processing and re-processing techniques, which have been improved over recent decades (e.g. careful velocity picking and multiple removal).

The key wells used in the present study are 206/3-01, 206/4-01, 207/1-02, 207/1-03, 207/1a-05, 208/24-1A, 208/26-01 and 209/12-01. The data comprise biostratigraphic analysis, petrophysical evaluation, and description and interpretation of relevant core.

Onshore analogues

Lower Cretaceous sandstone-dominated successions are widespread in the northern North Atlantic and excellent outcrop examples occur in southern England (Ruffell & Wach 1998), Svalbard (Gjelberg & Steel 1995) and in East Greenland, for example, Kangerlussuaq (Larsen *et al.* 1999) and Hold with Hope (Kelly *et al.* 1998; Larsen *et al.* 2001). In this study, we compare structural observations and depositional models derived from the seismic interpretation of the Cretaceous rift basins west of Shetlands with a Barremian–Aptian syn-rift succession in northern Hold with Hope, NE Greenland (Larsen *et al.* 2001). It consists of a sandstone-dominated, coarse clastic wedge onlapping a series of rotated Triassic–Jurassic fault blocks. The Cretaceous succession is up to 300 m thick and exposed in coastal cliffs for approximately 18 km.

Structural observations

The West Shetland Platform consists of a deformed high with a core of crystalline basement and pre-Jurassic sediments. The NW margin of the high is defined by a few prominent, NE–SW-striking master faults. These faults are characterized by large offsets and bound a series of asymmetrical half-grabens, approximately 10 km wide. The characteristic expression of rift structures in the Faroe–Shetland Basin is illustrated by the NE–SW-oriented Shetland Spine Fault, with a series of westward down-stepping basement highs and basins (Fig. 1). Important structural trends inherited from the basement fabric are a general NE–SW 'Caledonian' trend although with a marked north–south component in the study area (probably controlled by the Walls Boundary Fault Zone) and a possibly older NW–SE 'Tornquist' trend (Fig. 1). The NW–SE structural trend is also mimicked in the transfer zones (Rump *et al.* 1993) or rift-oblique lineaments (see discussion by Moy & Imber 2009), which may correspond to zones of major changes in structural style along the West Shetland Platform. The basement fabric has frequently been reactivated and appears to have exerted important influence on the Cretaceous rifting and segmentation of the West Shetland

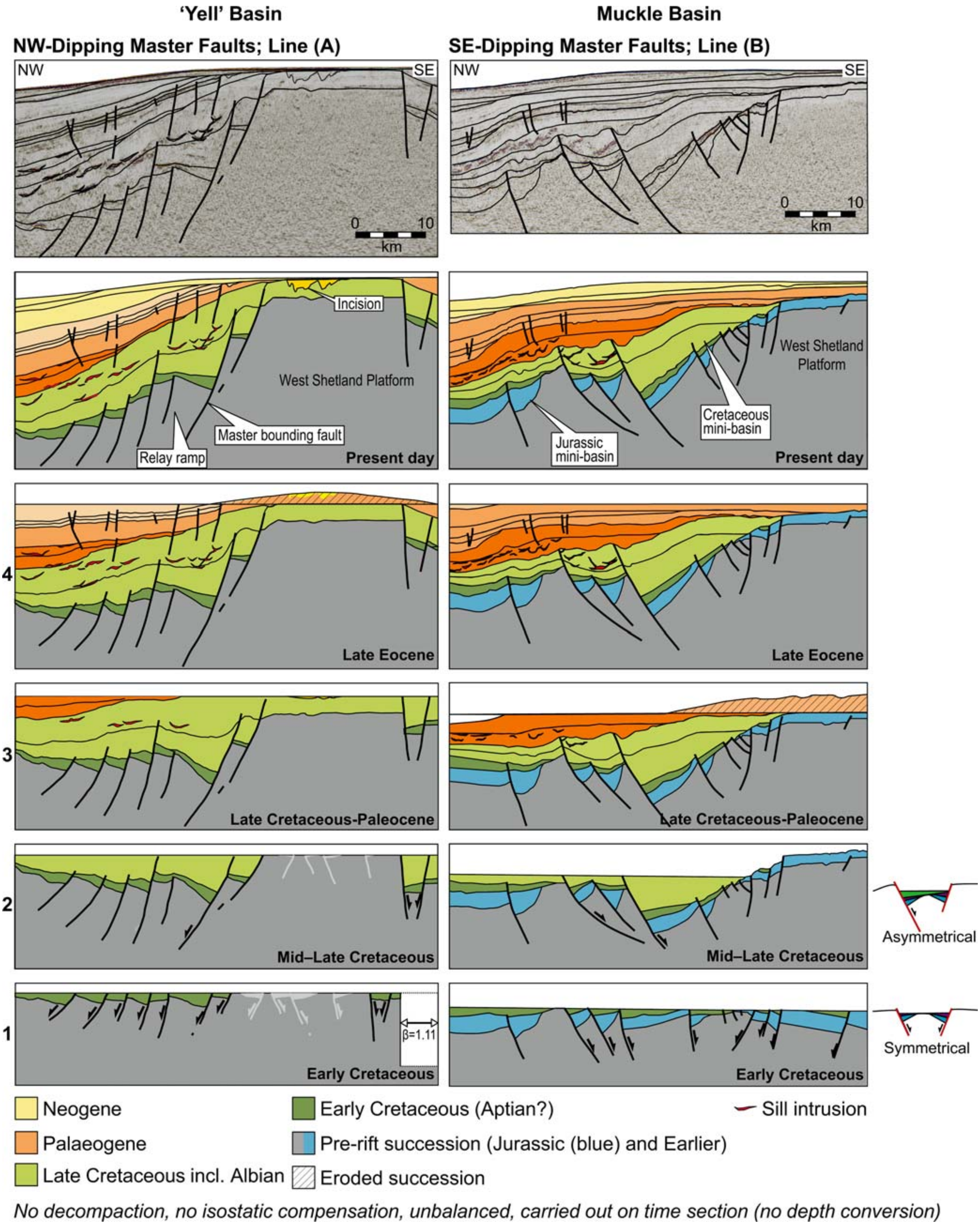

Fig. 3. Structural reconstruction of the 'Yell' and Muckle Basins along the West Shetland Platform based on interpretation of 2D seismic lines and gravimetric maps. (1) The Early Cretaceous was dominated by small, isolated to semi-connected basins formed during the rift initiation. (2) Displacement became focused on a few master faults during the early syn-rift. Because of segmentation of the West Shetland Platform, markedly different basin developments are recognized in the study area. Line A, cross-section of the 'Yell' Basin showing NW-dipping master faults. Line B, cross-section of the Muckle Basin showing SE-dipping master faults giving rise to a marginal rollover. (3–4) The rift climax and late syn-rift were controlled by thermal contraction and subsidence. See Figure 1 for location of seismic lines A and B.

Platform margin and may also have influenced sedimentation in the Palaeogene.

The varied structural configuration along the West Shetland Platform has fundamental importance for the trap configuration of the leads and plays in the area as some may be located in down-faulted, breached relay ramps and other in rotated and tilted fault blocks. The present-day structural setting indicates a highly dynamic structural evolution and the structural configuration varies over small distances in the study area. However, the overall structural evolution in the area is believed to have similar dynamics in spite of the changes in structural configuration observed along the margin. Structural analysis, simple 2D sectional back-stripping and flattening of the geometries are illustrated in Figure 3, seismic lines A and B. Rift terminology and subdivision into rift stages are adapted from Ravnås & Steel (1998).

Although the main structural elements are widely recognized in the Faroe–Shetland Basin, there is currently no standard nomenclature and some confusion exists in the published literature. DONG Energy's current usage is illustrated in Figure 1. In the quadrant 208 area we refer to the basin situated NE of the Unst Basin as the 'Yell' Basin (Fig. 1). The name is taken from one of the northern Shetland Islands. In the quadrant 209 area, the narrow, asymmetrical sub-basin lying between the volcanic extrusives of the Erlend Platform and the shallow basement of the North Shetland Platform is referred to as the Muckle Basin (Fig. 1). This name is taken from the end of well report produced after the drilling of well 209/12-01.

Pre-Early Cretaceous. The pre-Early Cretaceous structural evolution in the 'Yell' and Muckle Basin is poorly documented as seismic data below the BCU only allow identification of poorly defined, wedge-shaped geometries, suggesting the presence of older basins of probable Late Jurassic age. This is in line with regional observations indicating a general onset of the extensional pulses in the Late Jurassic–Early Cretaceous. The Jurassic rifting event decreased in intensity in the earliest Cretaceous and was followed by a period of general uplift with only minor structural modifications due to gravity-driven collapse of over-steepened faults scarps.

Early Cretaceous (rift initiation). The main episode of Cretaceous rifting began in the Valanginian as dated by coarse, clastic sediments in wells from the West Shetland and Solan Basins (Booth *et al.* 1993). Although the presence of older faults is acknowledged in the study area, the recognition of NE–SW oriented faults of Aptian–Albian age is interpreted as a significant and dominating overprint. Back-stripping suggests that several faults were present in scattered arrays across broad parts of the Faroe–Shetland Basin and that growth-faulting initiated the development of several isolated mini-basins. The scatted fault array created accommodation space in minor isolated to semi-connected basins and continental to shallow marine environments were established, leading to erosion of structural highs and deposition in the intervening fault-controlled basins (e.g. Victory Formation). Initially the graben system was probably symmetrical along the entire margin, with half-grabens developing across a wide area. This early rift stage may not have seen great subsidence rates due to the dominance of minor, isolated faults (Fig. 3, stage 1).

Mid-Cretaceous (early syn-rift). During the latest Early Cretaceous–early Late Cretaceous the scattered fault array began to link up. This transition from the initial syn-rift stage to the early syn-rift stage is marked by several faults terminating near the Aptian–Albian horizon and only a few major faults continuing into the Upper Cretaceous succession (Fig. 3, stage 2).

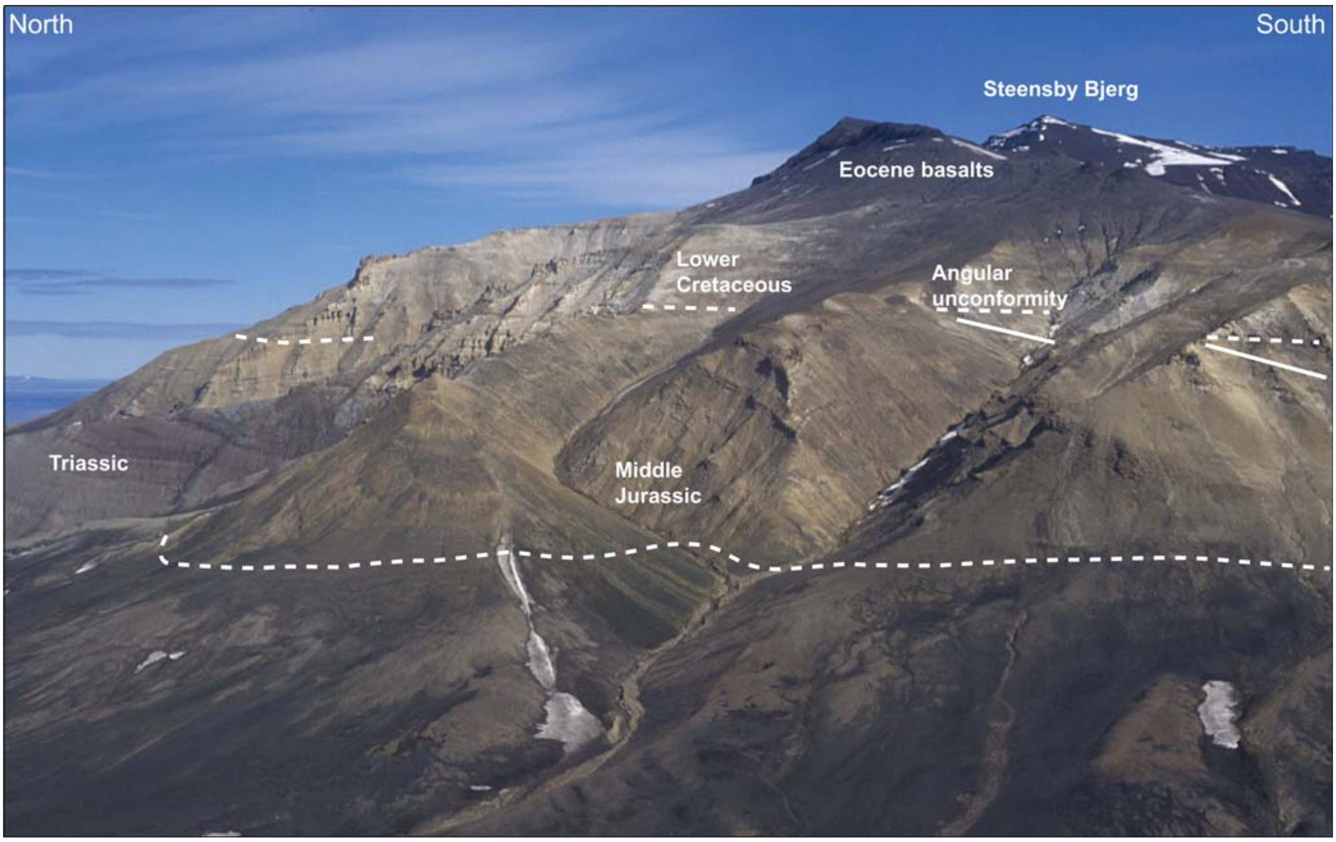

Fig. 4. Triassic/Jurassic pre-rift succession dipping towards SW unconformably overlain by Lower Cretaceous early syn-rift sediments, Hold with Hope, NE Greenland. The succession is overlain by Eocene plateau basalts forming the mountain peaks in the back. Height of succession approximately 800 m.

Displacement was focused on a few major faults and subsidence rates changed dramatically during this rift-stage transition, from scattered fault-related subsidence to a more focused subsidence related to displacement along a few linked master faults. The focused fault displacement resulted in development of major half-grabens and uplifted highs of varied geometry (Fig. 3, stage 2). Fault growth and interaction became increasingly important as faults progressively linked up into major fault segments, thus creating greater subsidence and increased marine influence. Relay ramps between major fault zones may have acted as conduits for sedimentary input, feeding mature sediments into depocentres along the platform–basin margin.

Mid–Late Cretaceous (rift climax)

Maximum subsidence occurred along a few master faults during the rift climax stage and deposition was dominated by thick mud-prone successions. The transfer of fault displacement in this stage also led to segmentation of the West Shetland Platform. In some of the segments, basin geometries changed from being symmetrical full-grabens to asymmetrical half-grabens associated with formation of a gentle marginal rollover dipping towards the Northwest (Fig. 3, stage 2). The observed segmentation and change in fault polarity between the southern 'Yell' Basin and the northern Muckle Basin may relate to interaction between Caledonian north–south structural grain (extension of the Walls Boundary Fault Zone) and Mesozoic NE–SW rifting along the West Shetland Platform (Fig. 1). Both the syn-rift and early post-rift plays are strongly affected by the asymmetrical graben geometry and formation of the marginal rollover, thus experiencing a higher risk on reservoir and trap.

Late Cretaceous (late syn-rift–early post-rift)

Continued rifting resulted in completely linked master faults and increased rotation of the associated half-grabens. This led to a dramatic increase in subsidence of the basins and transgression of the slopes. The marine transgression may have caused reworking of previously deposited sands across structural highs as they subsided and became submerged. Finally, the rift topography was filled in and the coarse-grained, syn-rift successions became capped by Upper Cretaceous marine mudstones (Fig. 3, stages 3 & 4). Post-rift thermal cooling continued in the latest Cretaceous and led to differential subsidence from West Shetland Platform towards the basin and as a result the Palaeogene depocentres became translated towards the rift axis (Fig. 1). The post-rift succession is dominated by thick mudstones, providing an excellent seal for the syn- and early post-rift plays of the Faroe–Shetland Basin. Although the general post-rift tectonic setting was affected by thermal subsidence in the basins, the West Shetland Platform itself experienced relative uplift of 300–800 m during several Eocene and Neogene pulses (e.g. Smallwood 2008).

Cretaceous reservoir formations

The Lower Cretaceous succession in the West Shetland Basin includes fan delta and shallow marine sandstones deposited in narrow half-grabens east of the Rona Ridge (Victory Formation) and submarine fan conglomerates and mass-flow sandstones and mudstones (Royal Sovereign and Cruiser Formations) deposited on the basin-ward side of the platform bounding fault system (Grant *et al.* 1999). Stacked shoreface sandstones, inner shelf mudstones and fan-delta sandstones were ponded in the hanging wall 'back-basin' of the Rona Ridge and other rotated fault blocks, and form the reservoir in the Victory gas discovery (Fig. 1).

The Victory wells (207/1-02, -03 and 207/1a-05) penetrated a succession of Aptian–Albian sandstones more than 200 m thick. Sandstone-dominated, Lower Cretaceous sediments were also penetrated in four neighbouring wells, 207/2-01, 208/23-01, 208/24-01 and 208/27-01. The sands in 208/23-01, 208/24-01 and 208/27-01 were of variable reservoir quality with relatively low porosity and permeability, whereas those in 207/1-02, -03 and 207/1a-05 and 207/2-01 were quite clean, with a high N/G and excellent porosity and permeability. Sedimentological interpretation based on cores from wells 207/1-03 and 207/1a-05 suggests that the conglomerates and sandstones of the Victory area were deposited as fan delta and shoreface sandstones in a shallow marine depositional environment (Goodchild *et al.* 1999). The younger Whiting sandstone described in well 207/1-03 may represent a second phase of sediment input or re-deposition of older sediments in the Victory area.

Greenland analogues

Lower Cretaceous sandstone-dominated successions are widespread in the northern North Atlantic and in East Greenland. In this study we refer to a Barremian–Aptian syn-rift succession in northern Hold with Hope (Larsen *et al.* 2001). The Lower Cretaceous succession, up to 300 m thick, rests with an angular unconformity on Lower Triassic and Middle–Upper Jurassic strata (Fig. 4). The unconformity formed after block faulting and rotation in Late Jurassic–earliest Cretaceous times and it is represented by an erosional surface overlain by a transgressive lag conglomerate.

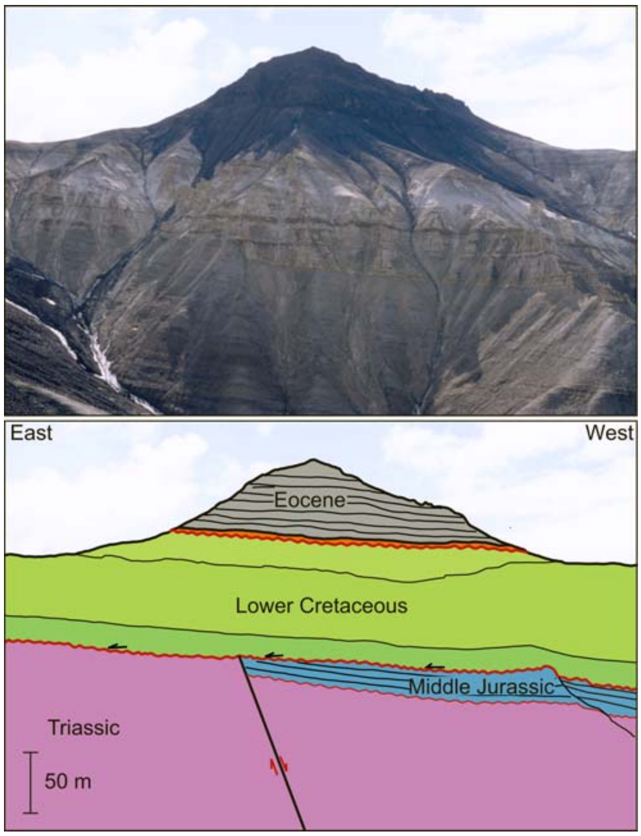

Fig. 5. Close-up photograph of the Lower Cretaceous sandstone-dominated syn-rift succession in Hold with Hope, NE Greenland. Note the minor antithetic fault terminating against the base of the Cretaceous succession corresponding to a change in fault activity, from rift initiation to early syn-rift stage, where extension is concentrated on a few major basin-forming faults and smaller faults become inactive. The Middle Jurassic sandstones form a potential pre-rift reservoir, but are only preserved in the small graben, downdip from the fault crest. The main reservoir unit would be the onlapping Lower Cretaceous syn-rift succession consisting of paralic and shallow marine sandstones.

The succession is interpreted as paralic, tidal and shallow marine, reflecting an overall transgression (Larsen *et al.* 2001).

The structural setting is comparable to the West Shetland Platform/Faroe–Shetland Basin transition and consists of a series of landward rotated half-grabens 10–30 km wide providing accommodation space for coarse-grained syn-rift sediments (Vischer 1943; Surlyk 1990). Hanging wall fan conglomerates are exposed in Wollaston Forland (Surlyk 1978, 1984), whereas sand-rich systems onlapping the more gentle slopes of the footwall blocks are found in eastern Wollaston Forland and Hold with Hope (Larsen *et al.* 2001). Minor faults truncated by the base Cretaceous unconformity (Fig. 5) indicate that the initial faulting along many smaller faults had ceased and that faulting at the time of deposition was focused along a few major faults.

The rift topography had fundamental control of the depositional systems and sediment transport direction feeding sand-rich sediments into the inherited rift topography and cross-rift along major relay ramps. The coarse-grained sediments, which seem to dominate the Lower Cretaceous successions, are a combination of the half-graben morphology, easy access to Jurassic sand-rich sections being exposed in the core of tilted footwall blocks and an overall transgressive regime piling shallow marine sands up against the exhumed fault blocks along the basin margins (Larsen *et al.* 1999).

Based on the outcrops, a number of potential plays can be defined: (1) pre-rift Middle Jurassic sandstones preserved in down-faulted grabens in the hanging wall block (this study, Surlyk 1977); (2) syn-rift coarse-grained submarine fan deposits along footwall blocks (Surlyk 1978, 1984); (3) Lower Cretaceous early syn-rift shallow marine sandstones deposited along the crest of the hanging wall block (Larsen *et al.* 2001); and (4) mass flow and mature turbiditic fans deposited after infilling of the rift topography in the late rift stage (Whitham *et al.* 1999; Surlyk & Noe-Nygaard 2001).

Structural control on sedimentation

Rift basins have strongly variable syn-rift sedimentary geometries because of the accommodation creation and variations in the sediment supply throughout the rift cycle (Ravnås & Steel 1998). Accommodation changes are mainly controlled by local basin-floor

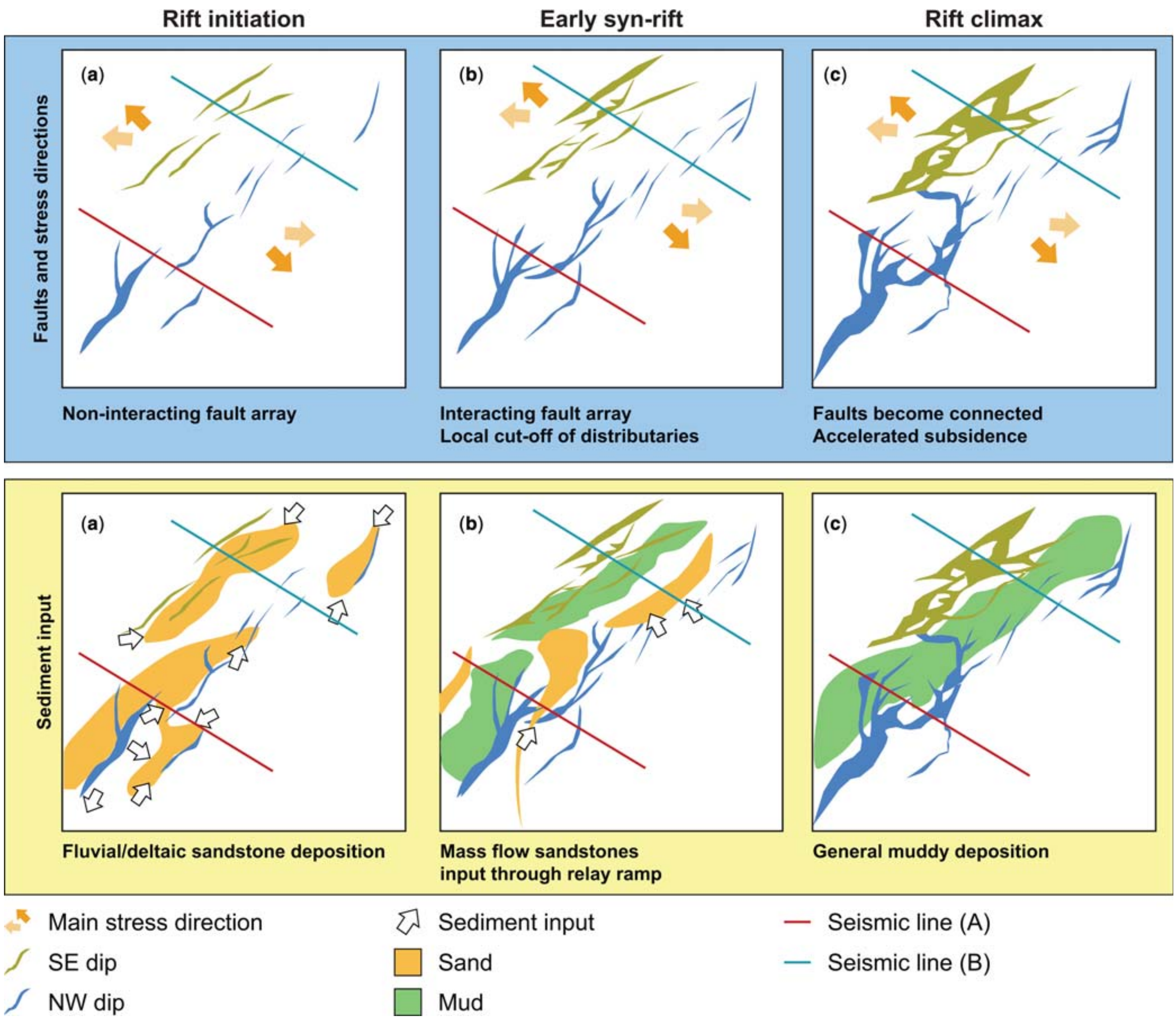

Fig. 6. Conceptual model for the structural evolution, depositional setting and resulting sand/mud distribution. Sedimentation in the Cretaceous syn-rift play is believed to be strongly controlled by structural evolution along the West Shetland Platform. The rift basin is divided into three stages: initial, early syn-rift and rift climax. (**a**) The rift initiation is characterized by non-interacting faults and deposition of fluvial/deltaic and shallow marine sandstones. (**b**) The early syn-rift is characterized by interacting faults and mass-flow sandstones sourced through relay ramp systems. (**c**) The rift climax is characterized by fully connected faults and maximum subsidence rates. Sediments deposited are generally mudstone. (See Fig. 3 for seismic and back-stripped cross-sections.)

rotation and background subsidence. Basically, the sediment supply determines how much of the accommodation is filled and in what manner. It is also controlled by the distance to the main hinterland areas and the size and sediment yield potential of any local fault block source area. Marine siliciclastic syn-rift successions are classified in terms of sediment supply as overfilled, balanced, underfilled and starved (Ravnås & Steel 1998). Sediment-overfilled and sediment-balanced infill types are characterized by a sandstone–mudstone–sandstone infill motif. The sediment-underfilled type is represented by a conglomerate–sandstone–mudstone motif and finally the sediment-starved type is commonly represented by a mudstone motif (Surlyk 1978). The sequential development, linked depositional systems, and stratigraphic signatures of the early syn-rift, the rift climax and the late syn-rift to early post-rift stages vary significantly between the rift basin infill types (Ravnås & Steel 1998).

A model for the structural evolution and sediment dispersal systems in the study area, 'Yell' Basin and Muckle Basin, offshore West Shetlands, has been proposed based on the seismic data and outcrop analogues described in the sections above. The structural evolution and the rift stages are summarized in Figure 6.

Jurassic rift stage. The seismic data suggest that the Middle to Late Jurassic sediments were deposited during an earlier rift episode. However, little is known of the Jurassic sediments as the later main rifting event obscures the seismic imaging of the succession and there is poor well control. In the Muckle and 'Yell' Basins Jurassic sediments are penetrated in wells 209/12-01 (30.5 m Upper Jurassic Rona Sandstone) and 208/24-01A (64.6 m sandstone assigned to the Rona Sandstone, but still undated). The Upper Jurassic succession unconformably overlies crystalline basement or pre-Jurassic sediments.

Rift initiation. During the rift initiation the margin was dominated by minor, scattered and unconnected faults. These faults created accommodation space in minor isolated to more connected basins along the West Shetland Platform. In these fault-bounded basins, shallow marine environments were established and stacked shallow marine shoreface sandstones, inner shelf deposits and fan-delta sandstones became deposited (Fig. 6a). The coarse sediments apparently became trapped in the hanging wall 'back-basin' of the Rona Ridge, being unable to cross the NE–SW elongated rift topography, leading to development of sediment overfilled/balanced basin fill. The onlapping, stacked sandstones form the reservoir in the Victory gas discovery (Goodchild *et al.* 1999). In contrast, immature coarse-grained submarine fans are found adjacent to the major rift controlling faults along the NW-dipping Rona Fault and represent classic syn-rift fan deposits (e.g. Royal Sovereign Formation in wells 206/3-01 and 208/26-01). These fault-related deposits were deposited in completely submerged basins and probably correspond to a sediment-underfilled outer basin fill during the rift initiation stage. This proximal to distal change in basin fill is also recognized in the syn-rift sediment fill model of Ravnås & Steel (1998).

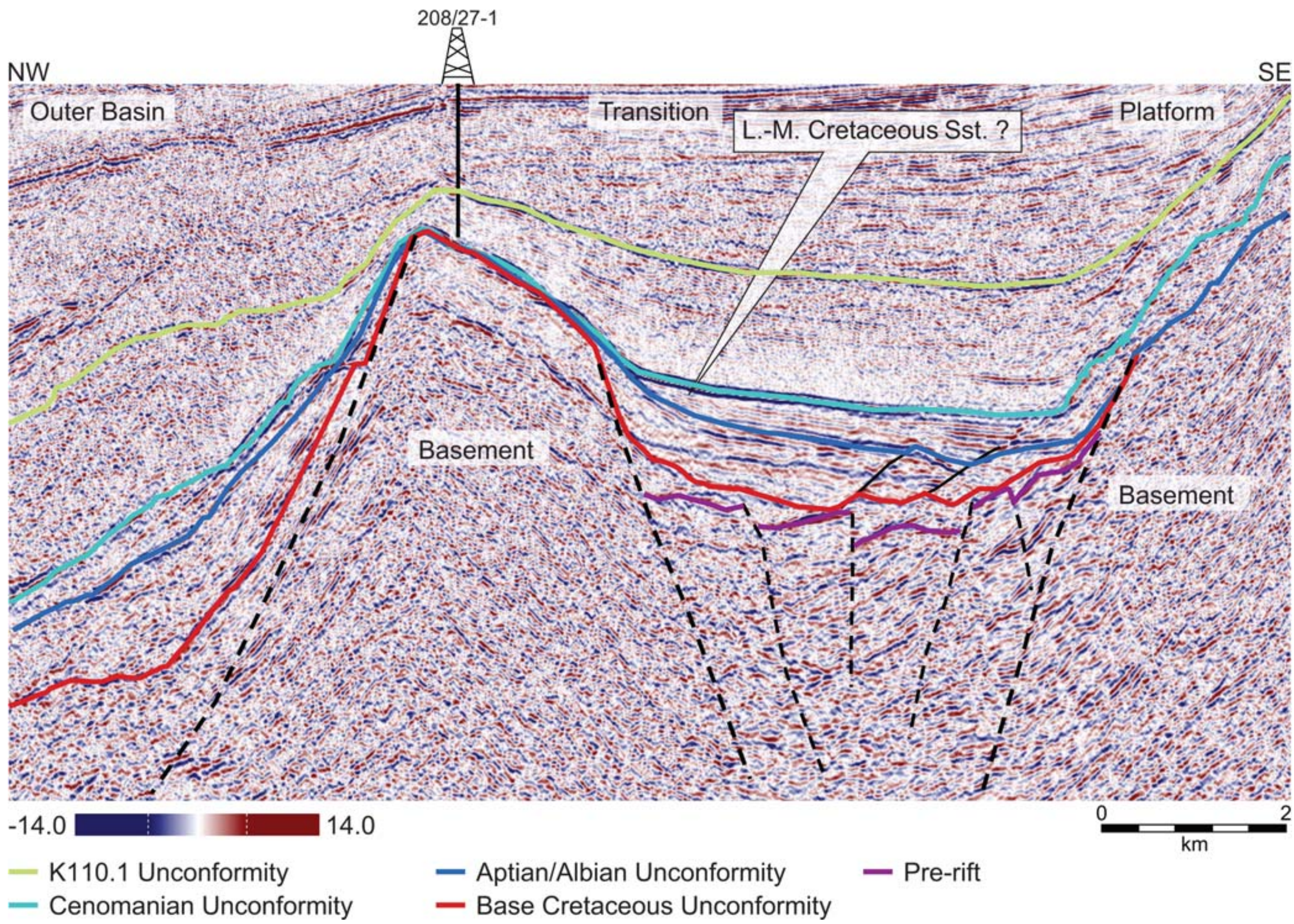

Fig. 7. Two-dimensional seismic example of a classic half-graben characteristic of the rifted margin in the southern part of the 'Yell' Basin. The exploration well targeted the Clair play and was drilled on the crest of the rotated fault block, penetrating crystalline basement and missing out potential Cretaceous syn-rift reservoirs. Despite the poor seismic quality, the data indicate the possibility of a thick Cretaceous succession (with embedded sandstones) downdip on the hanging wall block. See Figure 1 for location of seismic line C.

Lower Cretaceous shallow marine and deltaic sandstones are widespread in the North Atlantic and reflect a phase of overall transgression. The sandstones are associated with the basin margins and intra-basinal highs and are commonly dominated by locally derived material. Reworking of crystalline basement and older sediments (Devonian–Jurassic) provided large quantities of coarse material. Because of the recycled nature of the sands, they commonly show excellent reservoir properties, although weathered crystalline basement may locally source immature and clay-rich (kaolinitic) sandstones and conglomerates as seen in the Victory area (well 207/1-01).

Early syn-rift. In the early syn-rift stage, fault growth and interaction became increasingly important as faults progressively linked up to form major fault zones, thus creating greater subsidence and increased marine influence. Relay ramps connecting major fault zones and rift oblique lineaments segmenting the rift margin may have acted as conduits for sedimentary inputs to the basins (Fig. 6b). The sediments were mainly mass-flow deposited, mature sandstones (e.g. Commodore Formation) as a stable feeding system became established on the West Shetland Platform. Episodic deposition of mass-flow sandstones in the more distally located half-grabens resulted in sediment balanced/underfilled basin fill.

Rift climax. In the rift climax stage a completely linked master fault existed and resulted in a dramatic increase in subsidence of the basin with consequent transgression of the slope (Fig. 6c). Locally the marine transgression led to reworking of earlier sediments and on structural highs a second phase of shallow marine sand deposition became established (e.g. Whiting Sandstone).

Late syn-rift and early post-rift. Rifting waned during the Late Cretaceous and the entire Faroe–Shetland basin experienced thermally induced basin-wide subsidence and a thick succession of homogeneous mudstones with subordinate limestones (e.g. Kyrre Formation) was deposited.

The syn-rift plays

In spite of decades of industry activity, well control of the syn-rift succession is limited as early exploration in the Faroe–Shetland Basin was focused on the successful North Sea structural play with the reservoir forming part of the pre-rift system. Many wells are therefore situated at the crest of the tilted fault blocks, drilling updip from the syn-rift succession and failing due to lack of reservoir (Fig. 7). Improved seismic imaging of the deep structures in the 'Yell' and Muckle Basins along the West Shetland Platform has revealed the presence of a complex Mesozoic rift system with shifting fault polarity. The new seismic data led to a focus of exploration on structurally defined traps and re-opened exploration in the deeper stratigraphic sections. Based on the seismic observations, core data and onshore analogue studies, a revised syn-rift play model for the Faroe–Shetland Basin is proposed.

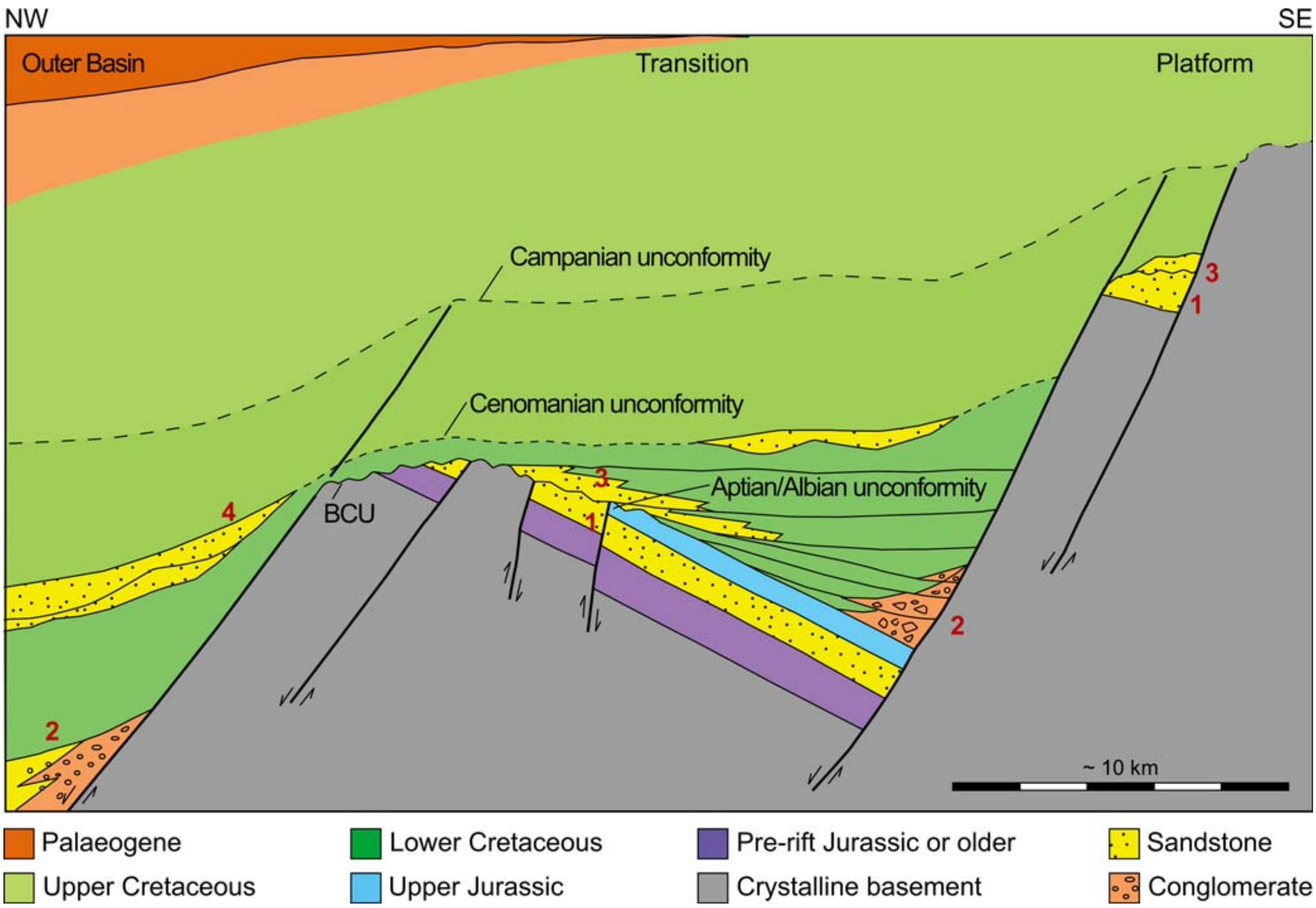

Fig. 8. Conceptual play models along the West Shetland Platform margin showing tectonic stages and possible related deposits. (1) Middle Jurassic pre-rift sandstones preserved in down-faulted grabens. (2) Lower Cretaceous rift initiation (e.g. Royal Sovereign Formation) deposited along major basin-forming faults. (3) Lower Cretaceous early syn-rift shallow marine sandstones (e.g. Victory Formation) onlapping structural highs (fault crests). (4) Mid to Upper Cretaceous early syn-rift, mature, mass-flow sandstones sourced through relay ramps (e.g. Commodore Formation). Play models inspired by Surlyk (1978, 1984), Grant *et al.* (1999) and Ravnås & Steel (1998).

The conceptual play models (Fig. 8) include:

(1) Middle Jurassic pre-rift sandstones preserved in down-faulted grabens. The play may form an interesting target in already drilled tilted fault blocks in quadrant 207 and 208. The play concept is supported by analogues in NE Greenland.
(2) Lower Cretaceous rift initiation and early syn-rift stage conglomerates and sandstones (e.g. Royal Sovereign Formation) deposited along major basin-forming faults. The immature sandstones are proven in quadrant 206 and may form an untested exploration target in the marginal basins.
(3) Lower Cretaceous early syn-rift stage sandstones deposited in shallow marine settings along the crest of structural highs during initial marine transgression (e.g. Victory Formation). The play is proven in the Victory gas discovery in quadrant 207 and probably has a large untested potential in basins along the margin of the West Shetland Platform.
(4) Mid-Cretaceous early syn-rift stage mature, mass-flow deposited sandstones sourced into the marginal basins along relay ramps and rift oblique lineaments (e.g. Commodore Formation). The reservoir unit is proven in quadrant 206, but the play apparently failed due to lack of updip sealing (Grant *et al.* 1999). It may form an attractive exploration target if sediment entry points can be identified along the West Shetland Platform margin.

The key elements for future exploration along the margins of the Faroe–Shetland Basin will be:

- careful reprocessing of existing 2D seismic data (fair to good quality) and acquisition of fit-for-purpose 3D seismic surveys;
- structural reconstructions and improved understanding of the interaction between the Caledonian structural grain, Mesozoic rift related faults and rift oblique lineaments (transfer zones);
- acknowledgement of structural control on depositional systems;
- full implementation of onshore analogues.

The Cretaceous syn-rift play models along the West Shetland Platform evolved from technical input and discussions with numerous persons; however, the presented views and conclusions are the sole responsibility of the authors. The manuscript benefited from critical reviews by Martyn Stoker and Finn Surlyk. We are especially grateful for the support from our licence partners Dana Petroleum Ltd and GDF SUEZ E&P UK Ltd. TGS long offset data are reproduced with the permission of TGS-NOPEC. Field work in East Greenland by Michael Larsen formed part of the project ‘Resources of the sedimentary basins of North and East Greenland’ supported by the Danish Research Councils, and additional mapping was supported by the Geological Survey of Denmark and Greenland (GEUS).

References

Booth, J., Sweicicki, T. & Wilcockson, P. 1993. The tectonostratigraphy of the Solan Basin, West of Shetlands. *In*: Parker, J. R. (ed.) *The Petroleum Geology of Northwest Europe: Proceedings of the 4th Conference*. Geological Society, London, 987–998; doi: 10.1144/0040987.

Gjelberg, J. & Steel, R. J. 1995. Helvetiafjellet Formation (Barremian–Aptian), Spitsbergen: characteristics of a transgressive succession. *In*: Steel, R. J., Felt, V. L., Johannessen, E. P. & Mathieu, C. (eds) *Sequence Stratigraphy on the Northwest European Margin*. Norwegian Petroleum Foundation, Oslo, Special Publications, **5**, 571–593.

Goodchild, M. W., Henry, K. L., Hinkley, R. J. & Imbus, S. W. 1999. The Victory gas field, West of Shetland. *In*: Fleet, A. J. & Boldy, S. A. R. (eds) *Petroleum Geology of Northwest Europe: Proceedings of the 5th Conference*. Geological Society, London, 713–724; doi: 10.1144/0050713.

Grant, N., Bouma, A. & McIntyre, A. 1999. The Turonian play in the Faeroe–Shetland Basin. *In*: Fleet, A. J. & Boldy, S. A. R. (eds) *Petroleum Geology of Northwest Europe: Proceedings of the 5th Conference*. Geological Society, London, 661–673; doi: 10.1144/0050661.

Kelly, S. R. A., Whitham, A. G., Koraini, A. M. & Price, S. M. 1998. Lithostratigraphy of the Cretaceous (Barremian–Santonian) Hold with Hope Group, NE Greenland. *Journal of the Geological Society, London*, **155**, 993–1008.

Kimbell, G. S., Ritchie, J. D., Johnson, H. & Gatliff, R. W. 2005. Controls on the structure and evolution of the NE Atlantic margin revealed by regional potential field imaging and 3D modelling. *In*: Doré, A. G. & Vining, B. (eds) *Petroleum Geology: North-West Europe and Global Perspectives – Proceedings of the 6th Conference*. Geological Society, London, 933–945; doi: 10.1144/0060933.

Lamers, E. & Carmichael, S. M. M. 1999. The Paleocene deepwater sandstone play West of Shetland. *In*: Fleet, A. J. & Boldy, S. A. R. (eds) *Petroleum Geology of Northwest Europe: Proceedings of the 5th Conference*. Geological Society, London, 645–659; doi: 10.1144/0050645.

Larsen, M., Hamberg, L., Olaussen, S., Nørgaard-Pedersen, N. & Stemmerik, L. 1999. Basin evolution in southern East Greenland: an outcrop analogue for Cretaceous–Paleogene basins on the North Atlantic volcanic margins. *Bulletin of the American Association of Petroleum Geologists*, **83**, 1236–1261.

Larsen, M., Nedkvitne, T. & Olaussen, S. 2001. Lower Cretaceous (Barremian–Albian) deltaic and shallow marine sandstones in North-East Greenland – sedimentology, sequence stratigraphy and regional implications. *In*: Martinsen, O. J. & Dreyer, T. (eds) *Sedimentary Environments Offshore Norway – Palaeozoic to Recent*. Norwegian Petroleum Foundation, Oslo, Special Publications, **10**, 259–278.

Moy, D. J. & Imber, J. 2009. A critical analysis of the structure and tectonic significance of rift-oblique lineaments (‘transfer zones’) in the Mesozoic–Cenozoic succession of the Faroe–Shetland Basin, NE Atlantic margin. *Journal of the Geological Society, London*, **166**, 831–844.

Ravnås, R. & Steel, R. J. 1998. Architecture of marine rift-basin successions. *Bulletin of the American Association of Petroleum Geologists*, **82**, 110–146.

Ruffell, A. & Wach, G. 1998. Estuarine/offshore depositional sequences of the Cretaceous Aptian-Albian boundary, England. *In*: de Graciansky, P.-C., Hardenbol, J., Jacquin, T. & Vail, P. (eds) *Mesozoic and Cenozoic Sequence Stratigraphy of European Basins*. SEPM, Special Publications, **60**, 411–421.

Rump, B., Reaves, C. M., Orange, V. G. & Robinson, D. L. 1993. Structuring and transfer zones in the Faroe Basin in a regional tectonic context. *In*: Parker, J. R. (ed.) *The Petroleum Geology of Northwest Europe: Proceedings of the 4th Conference*. Geological Society, London, 7–40; doi: 10.1144/0040007.

Smallwood, J. R. 2008. Uplift, compression and the Cenozoic Faroe–Shetland Basin sediment budget. *In*: Johnson, H., Doré, A. G., Gatliff, R. W., Holdsworth, R., Lundin, E. R. & Ritchie, J. D. (eds) *The Nature and Origin of Compression in Passive Margins*. Geological Society, London, Special Publications, **306**, 137–152.

Surlyk, F. 1977. Stratigraphy, tectonics and palaeography of the Jurassic sediments of the areas north of Kong Oscars Fjord, East Greenland. *Bulletin Grønlands Geologiske Undersøgelse*, **123**.

Surlyk, F. 1978. Submarine fan sedimentation along fault scarps on tilted fault blocks (Jurassic–Cretaceous boundary, East Greenland). *Bulletin Grønlands Geologiske Undersøgelse*, **128**.

Surlyk, F. 1984. Fan delta to submarine fan conglomerates of the Volgian–Valanginian Wollaston Forland Group, East Greenland. *In*: Koster, E. H. & Steel, R. J. (eds) *Sedimentology of Gravels and Conglomerates*. Canadian Society of Petroleum Geologists, Calgary, Memoirs, **10**, 359–382.

Surlyk, F. 1990. Timing, style and sedimentary evolution of Late Palaeozoic–Mesozoic extensional basins of East Greenland. *In*: Hardman, R. F. P. & Brooks, J. (eds) *Tectonic Events Responsible for Britain's Oil and Gas Reserves*. Geological Society, London, Special Publications, **55**, 107–125.

Surlyk, F. & Noe-Nygaard, N. 2001. Cretaceous faulting and associated coarse-grained marine gravity flow sedimentation, Traill Ø, East Greenland. *In*: Martinsen, O. J. & Dreyer, T. (eds) *Sedimentary Environments Offshore Norway – Palaeozoic to Recent*. Norwegian Petroleum Foundation, Oslo, Special Publications, **10**, 293–319.

Vischer, A. 1943. Die Post-Devonische tektonik von Ostgrönland zwischen 74° to 75°N.Br., Kuhn Ø, Wollaston Forland, Clavering Ø und angrenzende gebiete. *Meddelelser om Grønland*, **133**, 1–194.

Whitham, A. G., Price, S. P., Koraini, A. M. & Kelly, S. R. A. 1999. Cretaceous (post-Valanginian) sedimentation and rift events in NE Greenland (71–77°N). *In*: Fleet, A. J. & Boldy, S. A. R. (eds) *Petroleum Geology of Northwest Europe: Proceedings of the 5th Conference*. Geological Society, London, 325–336; doi: 10.1144/0050325.

Timing, controls and consequences of compression in the Rockall–Faroe area of the NE Atlantic Margin

A. TUITT,[1,2] J. R. UNDERHILL,[1] J. D. RITCHIE,[2] H. JOHNSON[2] and K. HITCHEN[2]

[1]*School of GeoSciences, University of Edinburgh, Grant Institute of Earth Science, King's Buildings, West Mains Road, Edinburgh EH9 3JW, UK*

[2]*British Geological Survey, Murchison House, West Mains Road, Edinburgh EH9 3LA, UK (e-mail: jdri@bgs.ac.uk)*

Abstract: The simplest models of passive margins would suggest that they are characterized by tectonic quiescence as they experienced gentle thermal subsidence following the extensional events that originally formed them. Analysis of newly acquired and pre-existing 2D seismic data from the Rockall Plateau to the Faroe Shelf, however, has confirmed that the NE Atlantic Margin was the site of significant active deformation. Seismic data have revealed the presence of numerous compression-related Cenozoic folds, such as the Hatton Bank, Alpin, Ymir Ridge and Wyville–Thomson Ridge Anticlines. The distribution, timing of formation and nature of these structures have provided new insights into the controls and effects of contractional deformation in the region. Growth of these compressional features occurred in five main phases: Thanetian, late Ypresian, late Lutetian, Late Eocene (C30) and Early Oligocene. Compression has been linked to hotspot-influenced ridge push, far-field Alpine and Pyrenean compression, asthenospheric upwelling and associated depth-dependent stretching. Regional studies make it clear that compression can have a profound effect on seabed bathymetry and consequent bottom-water current activity. Bottom-water currents have directly formed the early Late Oligocene, late Early Miocene (C20), Late Miocene–Early Pliocene, and late Early Pliocene (C10) unconformities. The present-day Norwegian Sea Overflow (NSO) from the Faroe–Shetland Channel into the Rockall Trough is restricted by the Wyville–Ymir Ridge Complex, and takes place via the syncline (Auðhumla Basin) between the two ridges. The Auðhumla Basin Syncline is now thought to have controlled the path of the NSO into the Rockall Trough and the resulting unconformity formation and sedimentation therein, no later than the Mid Miocene.

Keywords: NE Atlantic continental margin, Cenozoic, compression, inversion, sedimentary basin, bottom-water currents

Over the past two decades there has been an increasing realization of the general role that compression may have played in the tectonic development of the NE Atlantic passive continental margin (Boldreel & Andersen 1993; Doré & Lundin 1996; Ritchie *et al.* 2003; Johnson *et al.* 2005). Previous studies have revealed Cenozoic compressional structures in the Norwegian Margin (Brekke 2000; Lundin & Doré 2002; Løseth & Henriksen 2005), Faroe–Shetland Basin (Ritchie *et al.* 2003; Smallwood 2004; Ritchie *et al.* 2008) and the Rockall–Faroe area (Boldreel & Andersen 1993, 1994, 1998; Hitchen 2004; Johnson *et al.* 2005; Ritchie *et al.* 2008). These compressional features have been attributed to normal ridge push (Boldreel & Andersen 1993), hotspot-influenced ridge push (Doré & Lundin 1996; Lundin & Doré 2002), Alpine compression (Roberts 1989; Doré & Lundin 1996; Vågnes *et al.* 1998; Brekke 2000), Pyrenean compression (Knott *et al.* 1993), plate reorganization (Boldreel & Andersen 1993; Lundin & Doré 2002) and the Iceland Plateau Body force (Doré *et al.* 2008).

The ages of compression in the Norwegian Margin (Lundin & Doré 2002) and the Faroe–Shetland Basin (Ritchie *et al.* 2003) have been derived from dating unconformities associated with compression and calibrated using well data. The ages of compression in the Rockall–Faroe area (Boldreel & Andersen 1993; Johnson *et al.* 2005), however, were not well constrained hitherto. In addition, there has been relatively little emphasis on the study of compressional structures in the Rockall–Faroe area compared with other areas of the NE Atlantic Margin.

The aim of this paper is to date Cenozoic compressional structures in the Rockall–Faroe area and to link the ages of these structures to regional events. The study area is located on the continental margin to the SE of Iceland (Fig. 1). This study utilizes 40 000 km of 2D seismic data (line-length), acquired over the past 20 years, extending from the north Rockall Plateau to the south Faroe Shelf and covering an area of *c.* 300 000 km^2 (Fig. 2). Well data have been used to date unconformities within the area to constrain the timing of both compressional and non-compressional events. With the quality of seismic data and the number of wells and boreholes available, it is now possible to calibrate and define the specific effects of compression and bottom-water current activity in the Rockall–Faroe area. The better constrained ages for these events have facilitated the linking of compression and bottom-water current activity to regional events affecting the NE Atlantic Margin.

Unconformities

Unconformities are stratigraphic surfaces which represent an interruption in the deposition of sediment (McQuillin *et al.* 1984). Eustasy (changes in sea-level) has long been thought to control unconformity formation in quiescent basins. However, it has been previously recognized in the Rockall Basin that some unconformities and progradational features are not produced by eustatic sea-level changes (Shannon *et al.* 2005). The erosional nature of some unconformities in the Rockall–Faroe area has been previously attributed to bottom-water current activity (Andersen & Boldreel 1995). In this study post-Oligocene unconformities, such as the late Early Miocene (C20) and Late Miocene–Early Pliocene unconformities, have also been ascribed to the actions of bottom-water currents.

Unconformities formed by the onlap of sediments onto tilted strata of anticlines are considered to be the result of folding

VINING, B. A. & PICKERING, S. C. (eds) *Petroleum Geology: From Mature Basins to New Frontiers – Proceedings of the 7th Petroleum Geology Conference*, 963–977. DOI: 10.1144/0070963

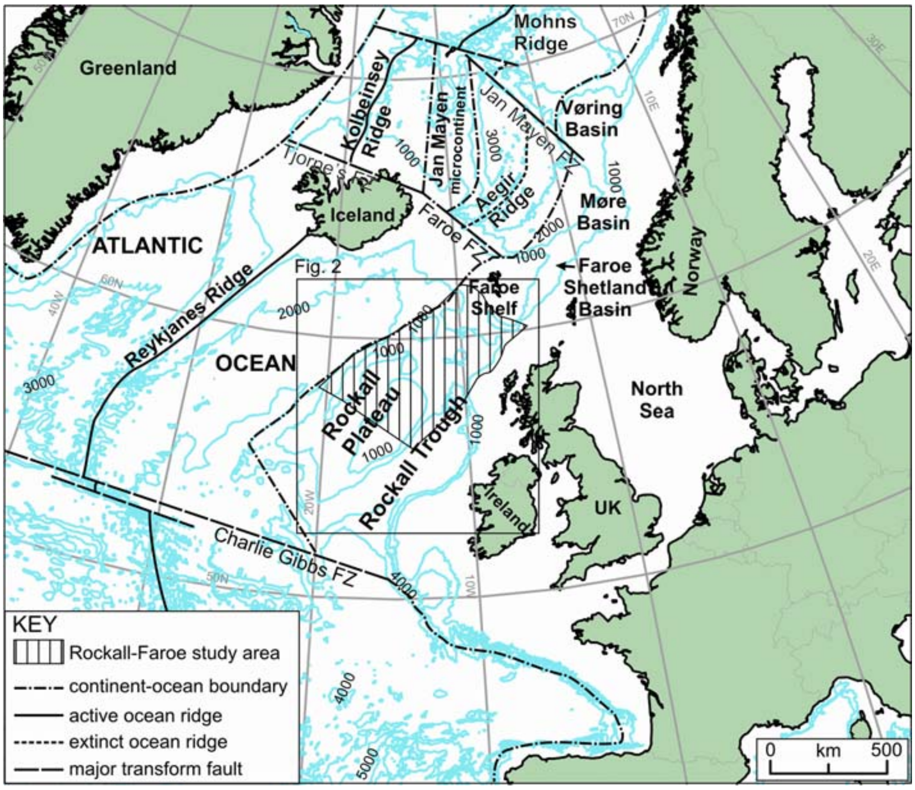

Fig. 1. Bathymetric map of the NE Atlantic Margin and surroundings showing the location of the Rockall–Faroe study area. The bathymetry is reproduced from the GEBCO Digital Atlas published by the British Oceanographic Data Centre on behalf of the IOC, IHO & BODC (2003; www.gebco.net).

(Stoker *et al.* 2005) and can provide important markers for the initiation of compressional events. In the Rockall–Faroe area, the Thanetian, late Ypresian, late Lutetian, Late Eocene (C30) and Early Oligocene unconformities are dated using well information and define distinct compressional episodes. The characteristics of these unconformities and other stratigraphic surfaces are shown in Table 1.

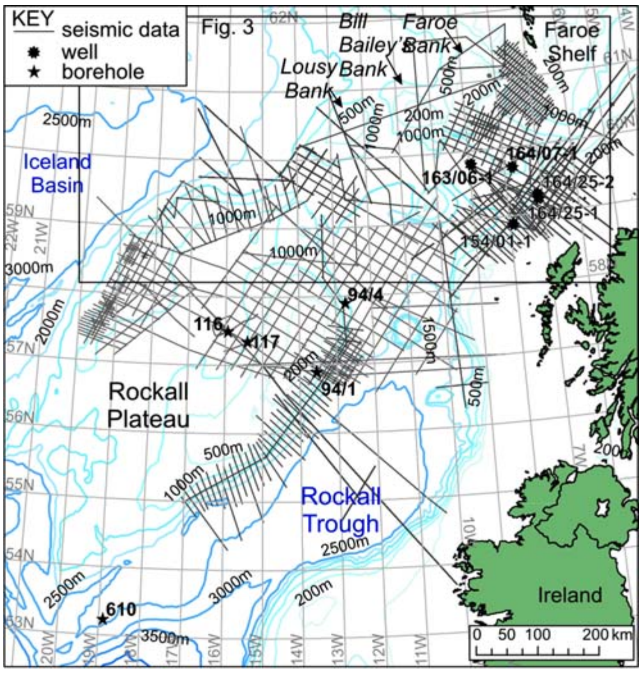

Fig. 2. Location of seismic and well/borehole data used in the Rockall–Faroe study area. Seismic data courtesy of BGS, Fugro Multi Client Services, CGG Veritas and GEUS.

Compressional structures

The NE Atlantic Margin has been affected by horizontal compressional forces during the Cenozoic (Boldreel & Andersen 1993; Doré & Lundin 1996; Lundin & Doré 2002; Doré *et al.* 2008), giving rise to the growth of anticlines, synclines and reverse faults in the Rockall–Faroe area. These anticlines and synclines have defined fold axes (Fig. 3) and have been mapped using reflection seismic data. The compressional structures vary in size, orientation and shape. The folds in the study area have long wavelengths and relatively small amplitudes representing $<1\%$ shortening.

There are three dominant orientations of folds and reverse faults: NE, NW and east–west trends. The axes of the Hatton Bank, Lousy Bank and South Faroe Bank anticlines are parallel to the adjacent NE-trending continent–ocean boundary. The West Lewis reverse faults and the Bridge Anticline are also NE-trending. The NW-trending Bill Bailey's Bank and North Faroe Bank anticlines lie adjacent to the continent–ocean boundary. Other NW-trending structures include the Faroe Bank Channel Syncline, the Vine reverse faults, and the Dawn, Wyville–Thomson Ridge, Ymir Ridge (North, Central and South) and Viera anticlines. The Hatton Bank reverse faults and the Alpin and Judd anticlines exhibit east to west trends.

Hatton Bank Anticline

Hatton Bank Anticline has a positive bathymetric expression (Fig. 3) and is also well expressed by the top-basalt surface (Fig. 4). The axial trace of this NE-trending anticline is *c*. 210 km in length, running parallel to the continent–ocean boundary. The Hatton Bank Anticline (Fig. 5) has an amplitude of 1.1 km (measured from the top-basalt surface) and a wavelength of *c*. 40 km. Marked onlap onto the Intra-Eocene 1, Intra-Eocene 2, C30 (Late Eocene) and Early Oligocene unconformities (Fig. 6) suggests that major phases of compression took place at these

Table 1. The age and characteristics of mapped seismic horizons within the Rockall–Faroe area

Age and name of mapped horizon	Seismic character and nature of mapped horizon	Source of stratigraphic correlation
C10 (late Early Pliocene)	Strong, continuous seismic reflector characterized by erosional truncation in the NE Rockall Trough and the Hatton–Rockall Basin	This unconformity was dated and constrained using wells 154/01-1, 164/25-1 and 164/25-2 in the NE Rockall Trough and borehole 116 in the Hatton–Rockall Basin
Late Miocene–Early Pliocene	Strong seismic reflector characterized by erosional truncation in the North Rockall Trough (see Fig. 10) and the NE Rockall Trough (see Fig. 17)	The age of this unconformity was inferred based on its stratigraphic position between the C20 and C10 horizons. A Pliocene unconformity of this age was mapped in the Faroe–Shetland Basin (Davies & Cartwright 2002)
C20 (late Early Miocene)	Moderately strong seismic reflector marked by onlap and erosional truncation in the North Rockall Trough (see Fig. 10) and the Hatton–Rockall Basin. It is also characterized by an onlapping layer of smectite in the South Rockall Trough (Dolan 1986)	This unconformity was dated using borehole 610 in the South Rockall Trough and borehole 116 in the Hatton–Rockall Basin. Wells 164/25-1 and 164/25-2 were used to constrain the position of the C20 stratigraphic surface in the NE Rockall Trough
Early Late Oligocene	Strong seismic reflector marked by onlap in the NE and North Rockall Trough and onlap and erosional truncation in the Hatton–Rockall Basin (see Fig. 6)	This unconformity was dated by well 164/25-2 and further constrained using well 164/25-1 in the NE Rockall Trough. The early Late Oligocene stratigraphic surface was also constrained by borehole 116 in the Hatton–Rockall Basin. This unconformity is inferred as representing the Top Palaeogene unconformity (TPU) mapped previously in south Faroe–Shetland Channel and the Faroe Bank Channel (Smallwood 2004)
Early Oligocene	Strong seismic reflector marked by onlap and defining folding in the Hatton Bank, Alpin, Mordor, Ymir and Wyville–Thomson Ridge anticlines	The Early Oligocene unconformity was dated using wells 164/25-1 and 164/25-2 in the NE Rockall Trough
C30 (Late Eocene)	Strong seismic reflector marked by onlap. Unconformity represents extensive compression across the Rockall–Faroe area and also coincides with a period of dramatic subsidence in the Rockall Trough	The C30 unconformity was dated using wells 154/01-1, 163/06-1, 164/07-1, 164/25-1 and 164/25-2 in the NE Rockall Trough and borehole 94/01 on the east margin of the Rockall Bank. The unconformity has also been constrained using boreholes 117 and 94/04 in the Hatton–Rockall Basin and the NE margin of the Rockall Bank, respectively
Late Lutetian	Moderately strong seismic reflector dated in the NE Rockall Trough and mapped from this area to the Faroe Bank Channel by jump correlation. The unconformity marks a significant phase of compression in the Mordor, Ymir Ridge (North, Central and South), Wyville–Thomson Ridge, Bridge and Onika anticlines	The late Lutetian stratigraphic surface was dated using wells 154/01-1, 163/06-1, 164/07-1, 164/25-1 and 164/25-2. This unconformity has also been inferred, in this study, in the Hatton–Rockall Basin (Intra-Eocene 2; see Fig. 6) and the South Rockall Trough
Late Ypresian	Strong seismic reflector dated in the NE Rockall Trough and mapped from this area to the Faroe Bank Channel. This unconformity marks compression in the Dawn, Mordor, North Ymir Ridge and Wyville–Thomson Ridge anticlines	The late Ypresian stratigraphic surface was dated using wells 154/01-1, 163/06-1, 164/07-1, 164/25-1 and 164/25-2. This unconformity has also been inferred, in this study, in the Hatton–Rockall Basin (Intra-Eocene 1; see Fig. 6)
Top-basalt	Strong seismic reflector marking the cessation of Palaeogene lava flow extrusion in the Late Paleocene–Early Eocene. It should be noted that the lava flows consist of other volcanic rocks, such as dacite, in addition to basalt	Seismic reflector easily identified throughout the Rockall–Faroe area and has been calibrated using wells 154/01-1, 163/06-1, 164/07-1, 164/25-1 and 164/25-2 in the NE Rockall Trough and borehole 117 in the Hatton–Rockall Basin
Thanetian	Moderately strong seismic reflector marked by onlap. The Thanetian unconformity defines inversion of the West Lewis Basin. Unconformity inferred within basalt lava flows representing initial growth of the North Ymir Ridge and Wyville–Thomson Ridge anticlines and the Faroe Bank Channel Syncline	Unconformity dated by well 164/25-1 over the West Lewis Basin. The unconformity may represent the Base Balder unconformity dated in the south Faroe–Shetland Basin (Smallwood & Gill 2002)

times. There is also some evidence of onlap of Early Eocene sediment onto the top-basalt surface. This suggests that a structural high existed prior to the Early Eocene. Eocene sediment on Hatton Bank Anticline southern limb is cut by east–west-trending reverse faults 15–25 km in length, which dip towards the north and south (Fig. 6). Reverse faulting is inferred as occurring at C30 (Late Eocene) time supported by the onlap of Early Oligocene sediment onto the C30 unconformity on the hanging wall of one of the reverse faults (Fig. 6). A compressional phase in the Late Eocene for the Hatton Bank was also proposed in previous work (Hitchen 2004; Johnson *et al.* 2005). Boldreel & Andersen (1993), however, inferred Mid Miocene reverse faults for the Hatton Bank. The early Late Oligocene, C20 (late Early Miocene) and C10 (late Early Pliocene) unconformities in the Hatton–Rockall Basin, overlying the reverse faults, are marked by onlap and erosional truncation and have been inferred as being related to bottom-water current activity.

Lousy Bank

The Lousy Bank Anticline has a positive expression on the seabed bathymetry (Fig. 3) and the top-basalt surface (Fig. 4). The axial

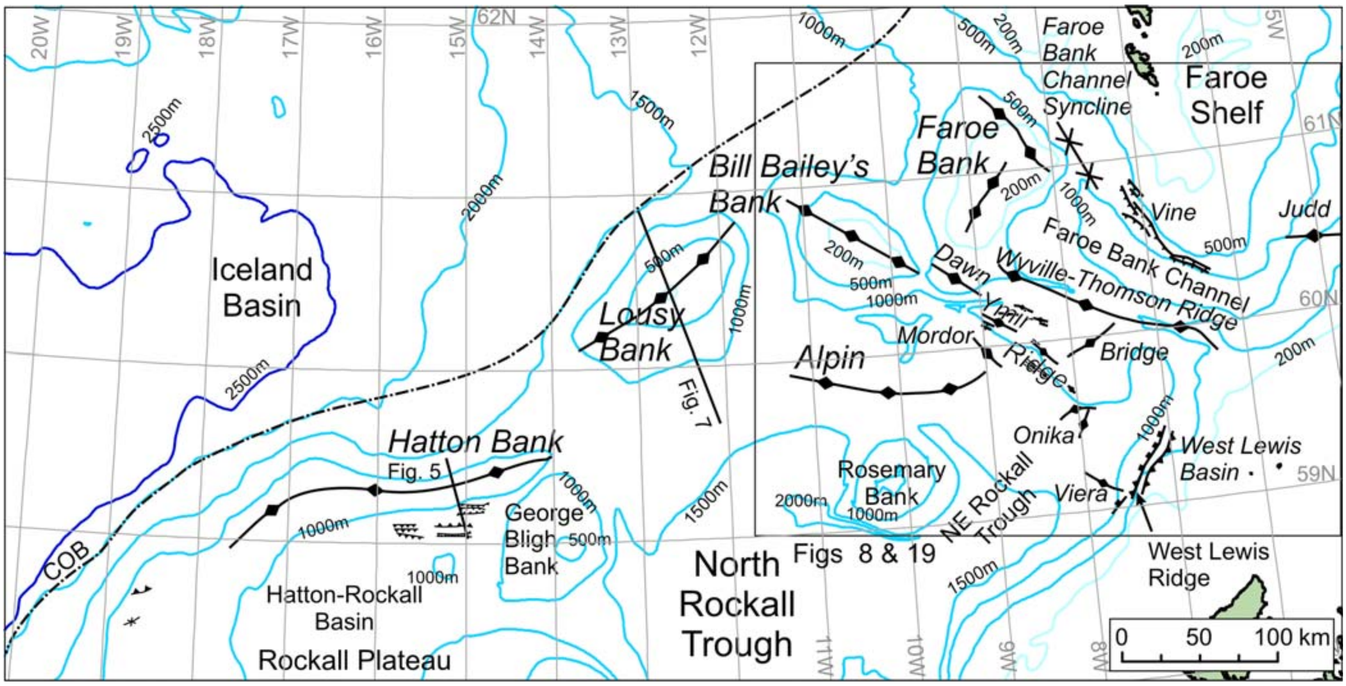

Fig. 3. Location of compressional structures in the Rockall–Faroe study area. Compressional structures are labelled in italics. The locations of seismic illustrations are shown by solid lines.

trace of this NE-trending anticline extends for 125 km, parallel to the continent–ocean boundary and was previously mapped by Boldreel & Andersen (1993, 1994). The anticline has an amplitude of up to 1.9 km (measured from the top-basalt surface) and a wavelength of *c.* 95 km (Fig. 7). On the southeastern limb of the anticline the C30 (Late Eocene) unconformity is marked by onlap and defines a compressional phase for the growth of the Lousy Bank. The lack of deep penetrating and high-resolution seismic data, across the Lousy Bank Anticline, precludes the mapping of any possible earlier compression-related unconformities.

Bill Bailey's Bank

The Bill Bailey's Bank Anticline, like the Lousy Bank Anticline, has a positive expression on the seabed bathymetry (Fig. 3) and the top-basalt surface (Fig. 4). The axial trace of this anticline is NW-trending and extends for 100 km. The anticline has an amplitude of up to 1.7 km (measured from the top-basalt surface) and a wavelength of *c.* 85 km, and was first mapped as a compressional ridge by Boldreel & Andersen (1994). The C30 (Late Eocene) unconformity, in this study, defines a compressional phase of

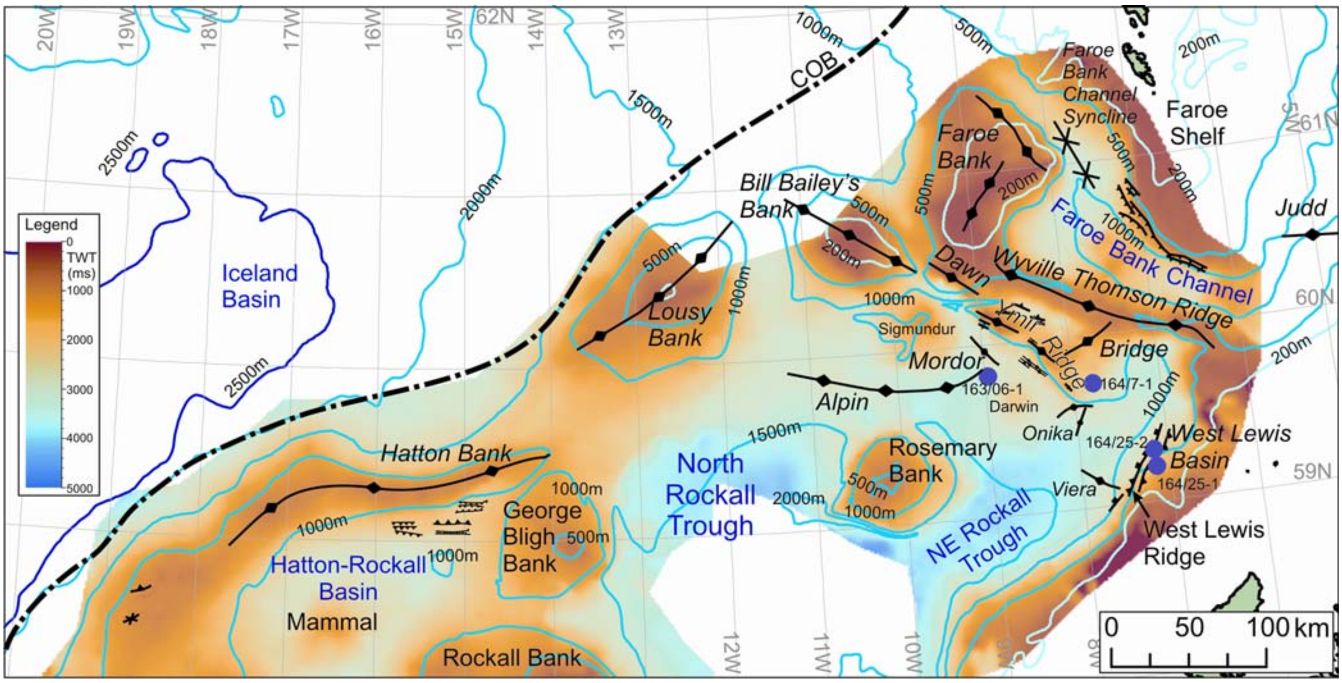

Fig. 4. Top-basalt isochron (time structure) map. Wells used to calibrate the top-basalt surface are delineated by purple circles. The edges of the top-basalt isochron indicate the limit of the data. Compressional structures are labelled in italics.

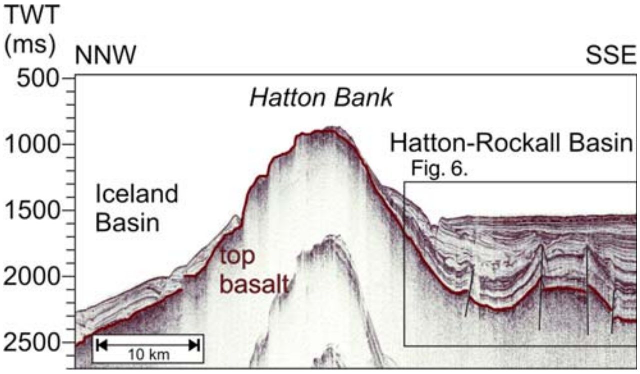

Fig. 5. NNW-trending seismic profile across the Hatton Bank Anticline. For the location of the seismic illustration, see Figure 3. Seismic profile, BGS © NERC 2009. All rights reserved.

growth of the Bill Bailey's Bank Anticline (seismic profile not illustrated).

Faroe Bank Anticlines

The Faroe Bank is well delineated on seabed bathymetry (Fig. 3) and the top-basalt surface (Fig. 4). The bank is interpreted as comprising two anticlines with orthogonal trends. The South Faroe Bank Anticline is NE-trending and has a length of 60 km. The Thanetian, late Ypresian, late Lutetian, C30 (Late Eocene) and Early Oligocene unconformities, on the southeastern limb of the fold, are inferred to mark compressional growth phases of the South Faroe Bank Anticline (seismic profile not illustrated).

The North Faroe Bank Anticline is *c.* 65 km in length and was previously mapped by Boldreel & Andersen (1994). On its northern limb the interpreted late Lutetian and C30 (Late Eocene) unconformities are marked by onlap and are interpreted to have formed as a result of compression. The C10 (late Early Pliocene) unconformity is marked by erosional truncation as a result of bottom-water current activity (seismic profile not illustrated).

Faroe Bank Channel Syncline

The Faroe Bank Channel Syncline is NW-trending and lies between the Faroe Bank and the Faroe Shelf (Fig. 8). It is characterized by the folding of Palaeogene basalt lava flows and Cenozoic sediments (Fig. 9). The syncline has an amplitude of up to 2.2 km (measured at the top-basalt surface) and is 50 km in length. Thinning and onlap onto the Thanetian, late Ypresian, late Lutetian and C30 (Late Eocene) unconformities suggest compression at these times.

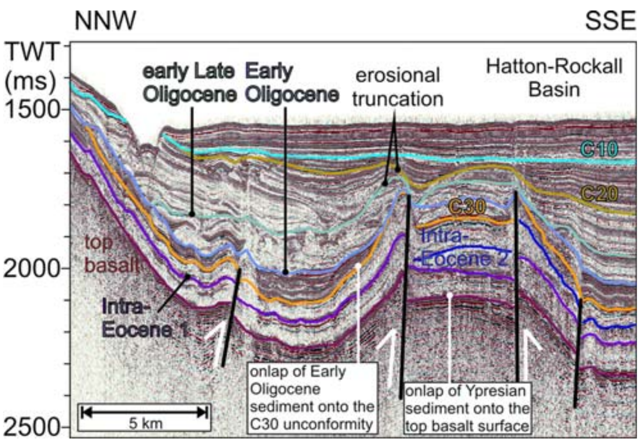

Fig. 6. NNW-trending seismic profile of unconformities and reverse faults on the southern limb of the Hatton Bank Anticline. For the position of the seismic illustration, see Figure 5. Seismic profile, BGS © NERC 2009. All rights reserved.

Alpin Anticline

The Alpin Anticline is east–west trending and lies between Bill Bailey's Bank and Rosemary Bank (Fig. 8). The anticline (Fig. 10) has an amplitude of up to 700 m (measured from the C30 unconformity), a length of *c.* 150 km and a wavelength of 30 km. Thinning and onlap onto the C30 (Late Eocene) and Early Oligocene unconformities suggest compression at these times. Previous work ascribed Late Eocene, Late Oligocene and Mid Miocene compression in the formation of the Alpin Anticline (Stoker *et al.* 2005; Ritchie *et al.* 2008).

The C20 (late Early Miocene) and Late Miocene–Early Pliocene unconformities, over the northern limb of the anticline, are defined by onlap and erosional truncation and are interpreted as being the result of bottom-water current activity. Poor seismic imaging between the top-basalt surface and the C30 (Late Eocene) unconformity, on the western section of the fold, precludes the mapping of any possible Early Eocene unconformities within the Alpin Anticline. The Alpin Anticline comprises relatively thick Eocene sediment bounded by the Sigmundur and Darwin seamounts and the Rosemary Bank (Fig. 11). This suggests that the Alpin Anticline developed from the compression of an Eocene depocentre.

Mordor Anticline

The Mordor Anticline (Fig. 12) is a symmetrical NW-trending fold with an amplitude of 500 m (measured from the late Lutetian unconformity), and is *c.* 25 km in length. The fold has no expression on the seabed as the crest of the anticline is covered by a veneer of Late Pliocene–Recent sediment, 100 m thick. The Mordor Anticline is surrounded by the Sigmundur and Darwin seamounts and the North Ymir Ridge Anticline, and lies partly within a basin bounded by basalt escarpments (Fig. 12). The basin facilitated the accumulation of a relatively thick Early Eocene basin fill (Fig. 13) which has been compressed to form the Mordor Anticline. The Mordor Anticline is characterized by both the folding of basalt lava flows and overlying Cenozoic sediments. Folding of the Mordor Anticline is defined by the late Ypresian, late Lutetian, C30 (Late Eocene) and Early Oligocene unconformities as represented by onlap and thinning onto these stratigraphic surfaces (Fig. 12). The Late Miocene–Early Pliocene unconformity has truncated the Early Oligocene and early Late Oligocene unconformities at the crest of the fold and the C20 (late Early Miocene) unconformity located more distally above the South Ymir Ridge Anticline (Fig. 12). The erosional nature of the Late Miocene–Early Pliocene unconformity is interpreted as being the result of bottom-water current activity.

Dawn Anticline

The Dawn Anticline is a NW-trending linear anticline located on the southern end of the Faroe Bank and is parallel to the Wyville–Thomson Ridge Anticline and the North Ymir Ridge Anticline (Fig. 8). The anticline was previously mapped as part of the Ymir Ridge by Ziska & Varming (2008). In this study, however, a bathymetric gorge separates the Dawn Anticline from the North Ymir Ridge Anticline (Fig. 8). The fold is 30 km in length and has a wavelength of 18 km. The amplitude of the Dawn Anticline (measured from the top-basalt surface) is 2.1 km off the southern limb and 0.34 km off the northern limb of the

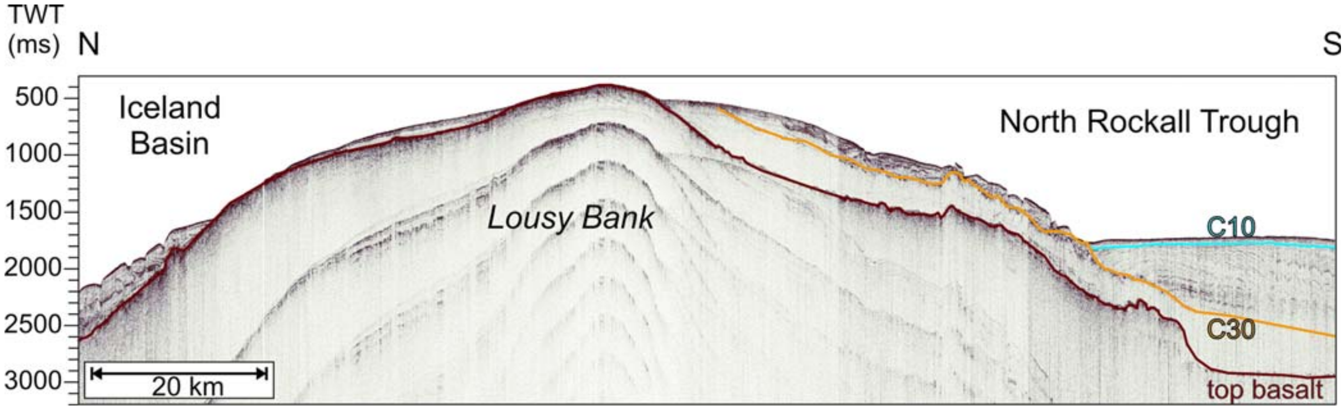

Fig. 7. North–south seismic profile of the Lousy Bank Anticline. For the location of the seismic illustration, see Figure 3. Seismic profile, BGS © NERC 2009. All rights reserved.

fold. The late Ypresian, late Lutetian, C30 (Late Eocene) and the Early Oligocene unconformities are marked by onlap and are interpreted as representing compressional phases forming the Dawn Anticline (seismic profile not illustrated).

Ymir Ridge Complex

The Ymir Ridge is a bathymetric high (Fig. 8) comprising a series of three anticlines – the North, Central and South Ymir Ridge anticlines. Ziska & Varming (2008) also segmented the Ymir Ridge into North, Central and South sections, but these differ from the sections defined in this study. The Ymir Ridge was also previously mapped by Boldreel & Andersen (1993), Johnson *et al.* (2005) and Ritchie *et al.* (2008). However, in these studies there was no attempt to differentiate the Ymir Ridge into separate anticlines.

The North Ymir Ridge Anticline is NW-trending and is 25 km in length. The fold (Fig. 14) has an amplitude of 1.4 km (measured from the top-basalt surface) and a wavelength of up to 28 km. A Thanetian unconformity is defined by thinning and onlap within the basalt lava flows on the southern limb of the North Ymir Ridge Anticline, suggesting folding at this time. The late Ypresian, late Lutetian and C30 (Late Eocene) compression-related unconformities are also marked by onlap.

The Central Ymir Ridge Anticline is NW-trending, 23 km in length and has a wavelength of *c*. 30 km. The fold (Fig. 15) is asymmetrical with the southern limb having a steeper gradient than the northern limb. The amplitude of the fold (measured from the top-basalt surface) is up to 1.24 km. The northern limb of the fold is cut by north-dipping reverse faults. The late Lutetian, C30 (Late Eocene) and the Early Oligocene unconformities areas are marked by onlap on both limbs of the fold and represent the ages of compression for the Central Ymir Ridge Anticline.

The South Ymir Ridge Anticline is NW-trending, and is *c*. 7 km in length. There are no seismic data available showing the full wavelength of the fold, but the fold is assumed to have a wavelength *c*. 26 km (Fig. 12). The late Lutetian, C30 (Late Eocene) and Early Oligocene unconformities area are marked by onlap on the southern limb of the fold and are inferred to represent the ages of compression of the South Ymir Ridge Anticline.

Wyville–Thomson Ridge Anticline

The Wyville–Thomson Ridge Anticline has a positive expression on seabed bathymetry (Fig. 8) and the top-basalt surface (Fig. 4). The axial trace of the fold is NW-trending and 200 km in length. The anticline extends from the Faroe Bank to the Hebrides/West Shetland Shelf, separating the Rockall Trough from the Faroe Shetland Channel. The Wyville–Thomson Ridge Anticline (Figs 14 & 15) has a wavelength of *c*. 28 km and an amplitude of up to 1.7 km (measured from the top-basalt surface). On the northern limb of the

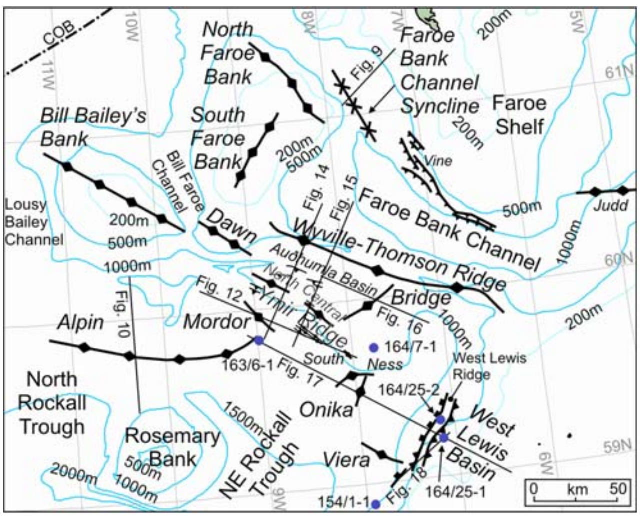

Fig. 8. Compressional structures in the north Rockall–Faroe study area. The locations of seismic illustrations are shown by solid black lines. Compressional structures are labelled in italics. The position of the continent–ocean boundary is based on Kimbell *et al.* (2005). For the location of the area, see Figure 3.

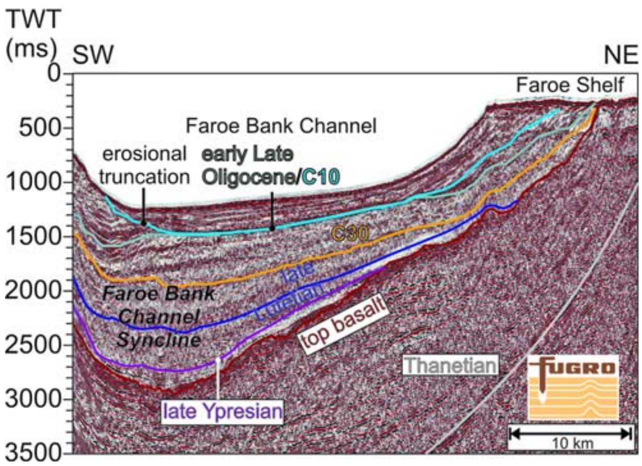

Fig. 9. North–south seismic profile of the Faroe Bank Channel Syncline. Seismic illustration courtesy of Fugro Multi Client Services. For the location of the seismic illustration, see Figure 8.

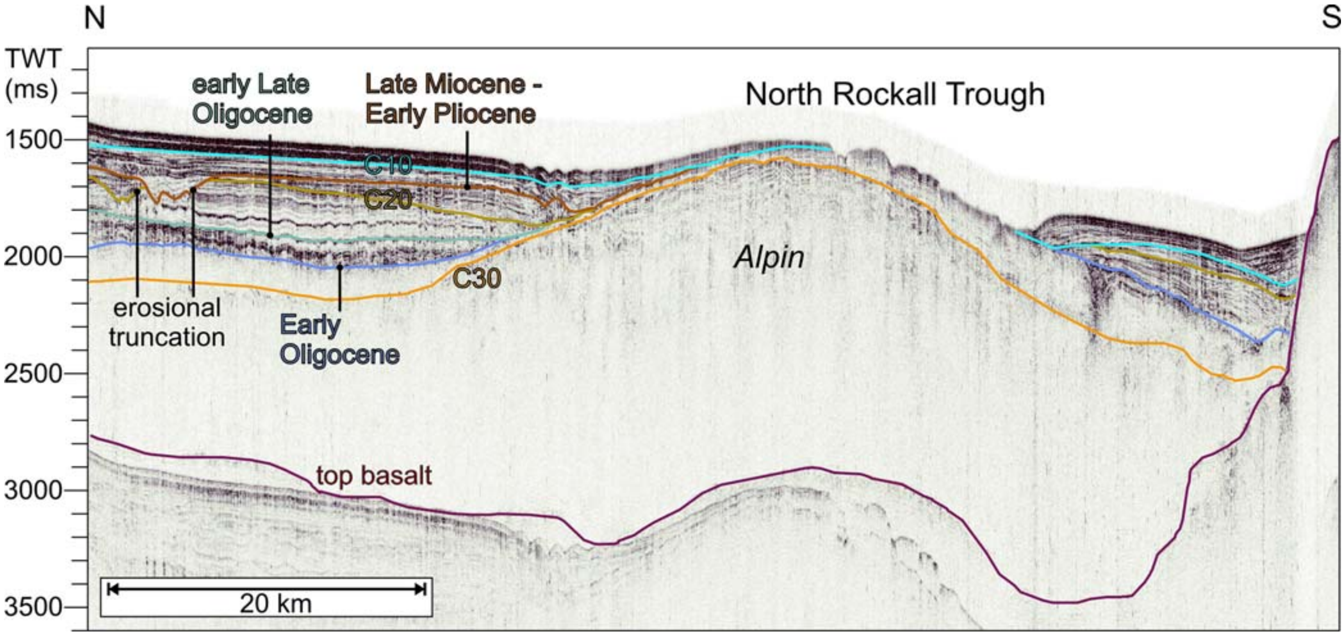

Fig. 10. North–south seismic profile of the Alpin Anticline. For the location of the seismic illustration, see Figure 8. Seismic profile, BGS © NERC 2009. All rights reserved.

Wyville–Thomson Ridge Anticline, the unconformities inferred as being the result of fold growth – Thanetian, late Ypresian, late Lutetian, C30 (Late Eocene) and the Early Oligocene – are marked by thinning and onlap of basaltic or sedimentary successions onto these surfaces. Previous work ascribed Late Paleocene–Early Eocene, Late Eocene, Oligocene and Miocene compression to the growth of the anticline (Boldreel & Andersen 1993; Johnson *et al.* 2005).

The Early Oligocene stratigraphic surface on the northern limb of the Wyville–Thomson Ridge is inferred as forming a composite unconformity with the early Late Oligocene unconformity. The early Late Oligocene unconformity is interpreted as the Top Palaeogene unconformity (TPU) previously mapped in the south Faroe Shetland Channel (Smallwood 2004). The C20 (late Early Miocene) unconformity is marked by onlap on the northern limb of the Wyville–Thomson Ridge. Here, the C10 (late Early Pliocene) unconformity, formed by bottom-water current activity, truncates the late Ypresian, late Lutetian, C30, Early Oligocene/early Late Oligocene and C20 unconformities.

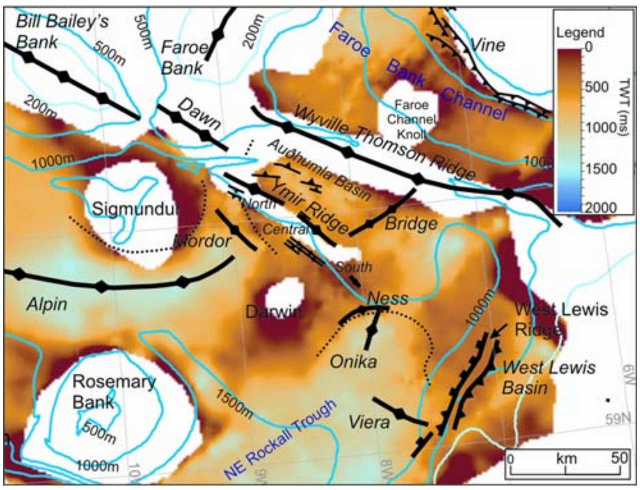

Fig. 11. Top-basalt–C30 (Late Eocene) isochore. Basalt escarpments, representing palaeo-shorelines, are delineated by dotted black lines. Compressional structures are labelled in italics.

Auðhumla Basin Syncline

A syncline, the Auðhumla Basin, is located between the Ymir Ridge (North and Central) and the Wyville–Thomson Ridge anticlines (Figs 14 & 15). Within the Auðhumla Basin there are fault propagation folds (Fig. 15) which run in a NW direction, are 6–12 km in length and their associated reverse faults are northward dipping.

The development of the Auðhumla Basin Syncline is governed by the growth of both the Ymir and Wyville–Thomson Ridge anticlines. The earliest growth phase is inferred as Thanetian based on this unconformity defining growth of both the North Ymir Ridge and the Wyville–Thomson Ridge anticlines. On the northern limb of the Central Ymir Ridge anticline, the late Lutetian unconformity defines the earliest compressional phase, suggesting that the Auðhumla Basin Syncline formed at this time between the Wyville–Thomson Ridge and the Central Ymir Ridge anticlines.

Bridge Anticline

The Bridge Anticline is well expressed on the top-basalt surface (Fig. 4). The anticline is a NE-trending symmetrical fold between the Wyville–Thomson Ridge Anticline and the southern end of the Central Ymir Ridge Anticline and separates the Auðhumla Basin from the NE Rockall Trough (Fig. 8). The Bridge Anticline (Fig. 16) has an amplitude of up to 1.2 km (measured from the top-basalt surface) and a wavelength of 40 km. The fold is characterized by both the folding of basalt lava flows and Cenozoic sediments. On the crest and on the eastern limb of the fold, Middle Eocene sediment, up to 800 m thick, onlaps onto the late Ypresian unconformity. The Middle Eocene succession is interpreted as being sourced from the Wyville–Thomson Ridge to the north. These sediments are themselves onlapped by a wedge of Late Eocene sediment (*c*. 500 m thick). The late Lutetian unconformity, separating the Middle and Late Eocene sediment packages and the C30 (Late Eocene) unconformity on the eastern limb of the fold, are marked by strong onlap. Initial growth of the Bridge Anticline is

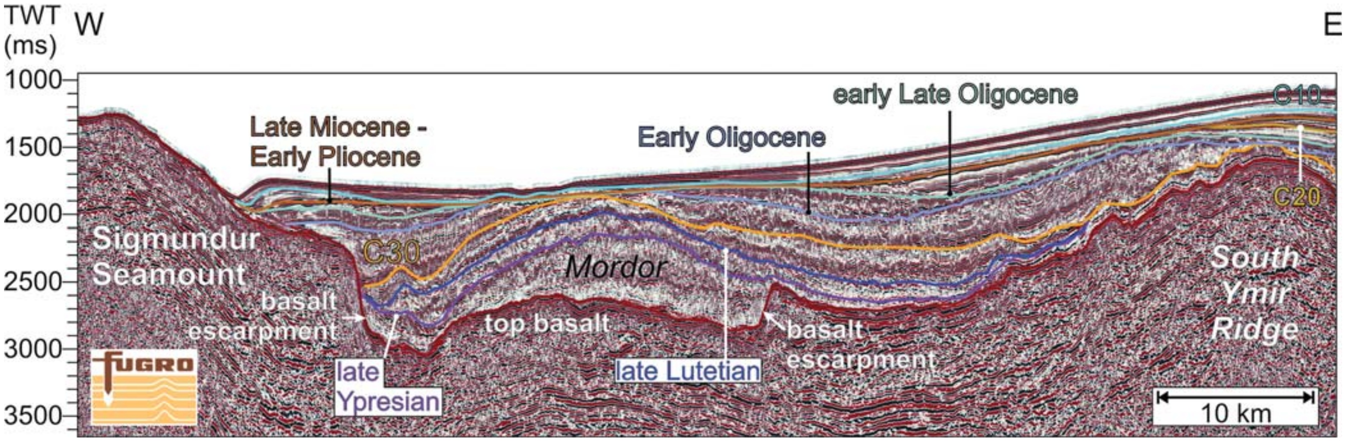

Fig. 12. East–west seismic profile of the Mordor and South Ymir Ridge Anticlines. Seismic illustration courtesy of Fugro Multi Client Services. For the location of the seismic illustration, see Figure 8.

interpreted to have occurred during the late Lutetian. Onlap and thinning onto the top-basalt surface on the eastern limb of the Bridge Anticline is interpreted as being associated with earlier growth of the proximal Wyville–Thomson Ridge Anticline.

Onika Anticline

The Onika Anticline lies between the Darwin seamount and the West Lewis Ridge (Fig. 17). The anticline is NNE-trending, has an amplitude of up to 800 m [measured from the C30 (Late Eocene) unconformity] and is not expressed at the seabed as its crest is covered with *c*. 500 m of post-Early Oligocene sediment. The Onika Anticline has been previously recognized, but not named, by Tate *et al.* (1999), and it appears to be a southeastern extension of the South Ymir Ridge Anticline. However, in this study, the Onika Anticline is considered to be a separate feature which is not linked to the Ymir Ridge. The anticline is located within a basin that is partly bounded by basalt escarpments, which has facilitated the accumulation of relatively thick Early Eocene sediment (Fig. 13). Sediment thickness between the top-basalt surface and the late Lutetian unconformity increases towards the crest of the fold and is consistent with folding of basin sediment. The thinning and onlap onto the late C30 (Late Eocene) unconformity suggest compression at this time.

West Lewis Ridge reverse faults

Reverse faults partially bound the margins of the NE-trending West Lewis Ridge, which is located on the east margin of the NE Rockall Trough (Fig. 8). These reverse faults (Figs 17 & 18) are termed the West Lewis reverse faults and are interpreted as normal faults which have undergone inversion. Along the eastern side of the ridge the reverse fault is 40 km in length, with the West Lewis Basin occurring within the hanging wall of the fault. This reverse fault cuts the late Ypresian and late Lutetian unconformities in the north (Fig. 17), but towards the south, it forms a fault-propagation fold (Fig. 18). The Thanetian unconformity, defined by onlap within the Palaeogene lava flow succession, is located

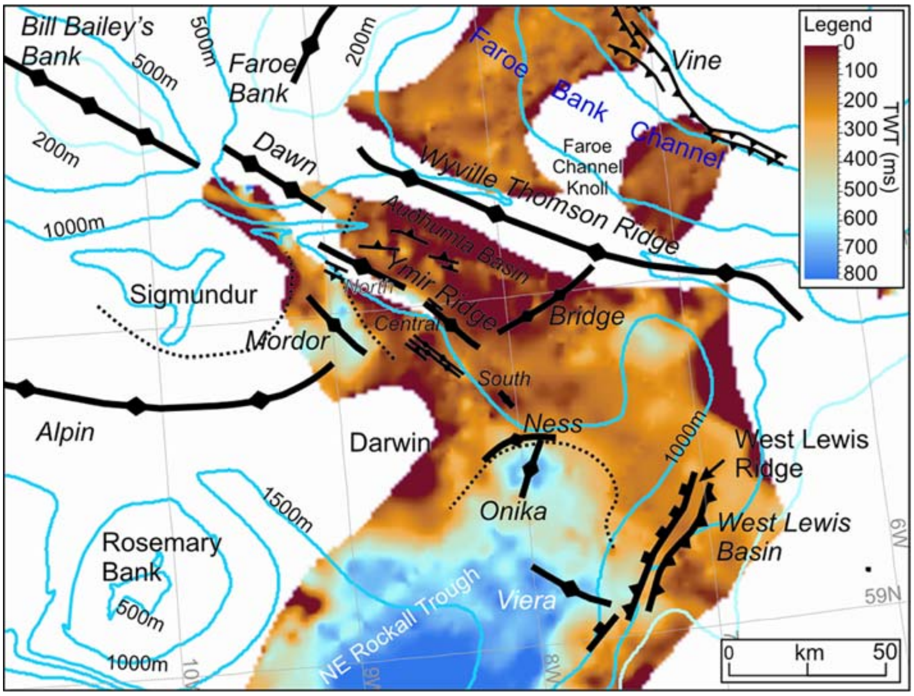

Fig. 13. Top-basalt–late Ypresian isochore. Basalt escarpments, representing palaeo-shorelines, are delineated by dotted black lines. Compressional structures are labelled in italics.

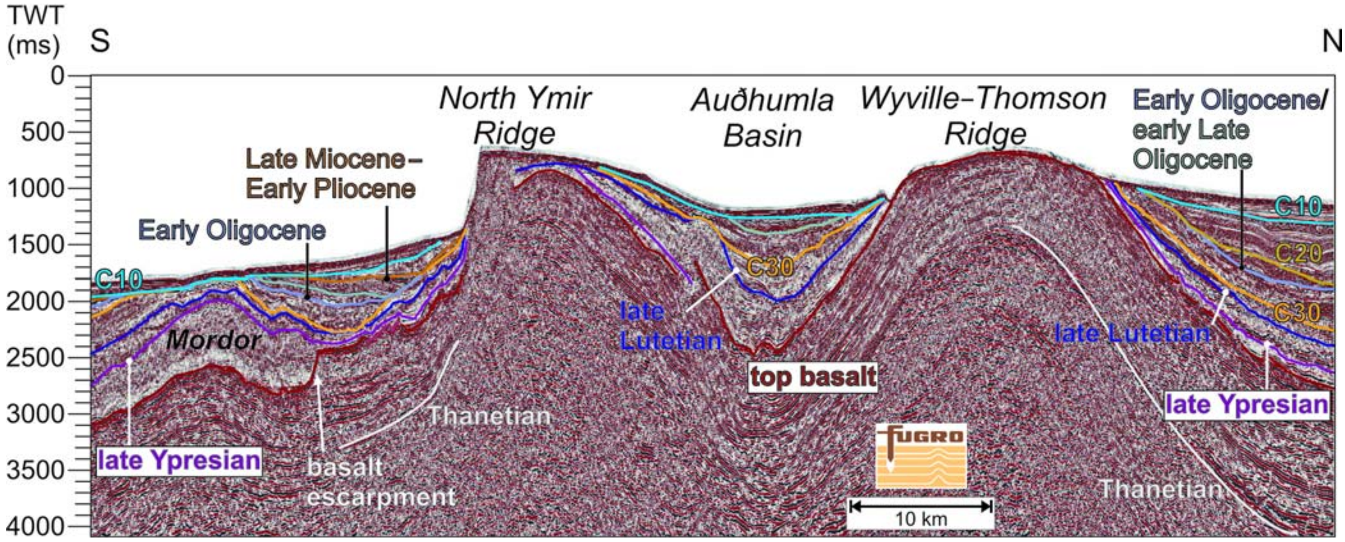

Fig. 14. North–south seismic profile of the Mordor, North Ymir Ridge and Wyville–Thomson Ridge anticlines. Seismic illustration courtesy of Fugro Multi Client Services. For the location of the seismic illustration, see Figure 8.

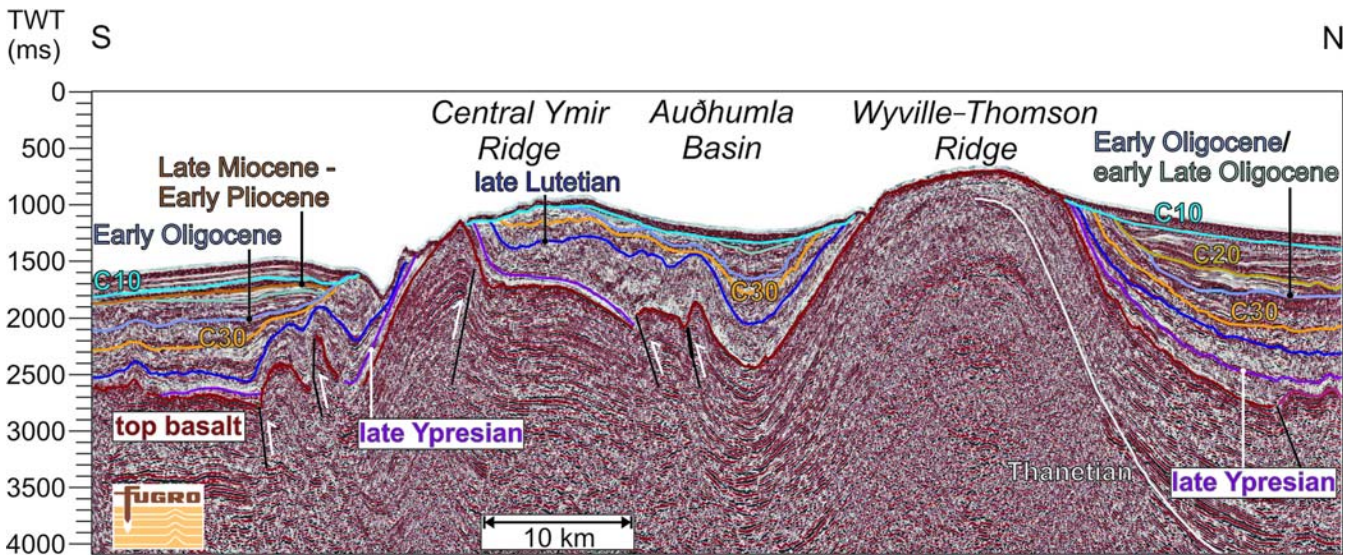

Fig. 15. North–south seismic profile of the Central Ymir Ridge and Wyville–Thomson Ridge anticlines. Seismic illustration courtesy of Fugro Multi Client Services. For the location of the seismic illustration, see Figure 8.

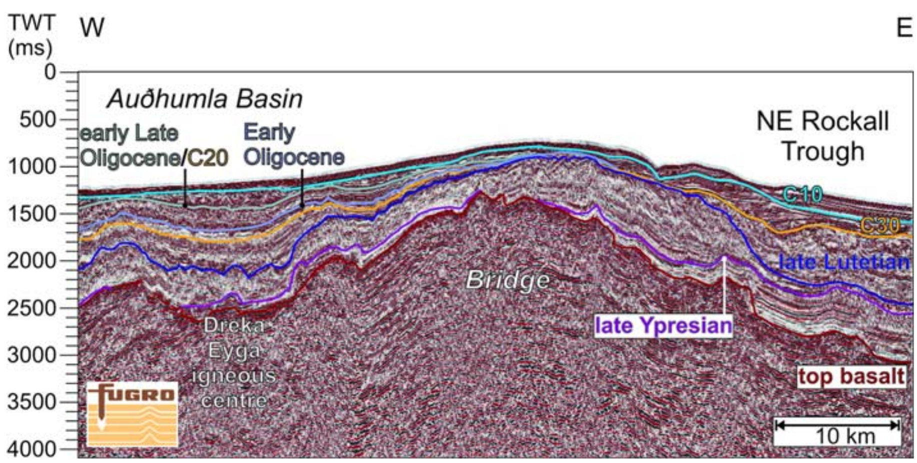

Fig. 16. East–west seismic profile of the Bridge Anticline. Seismic illustration courtesy of Fugro Multi Client Services. For the location of the seismic illustration, see Figure 8.

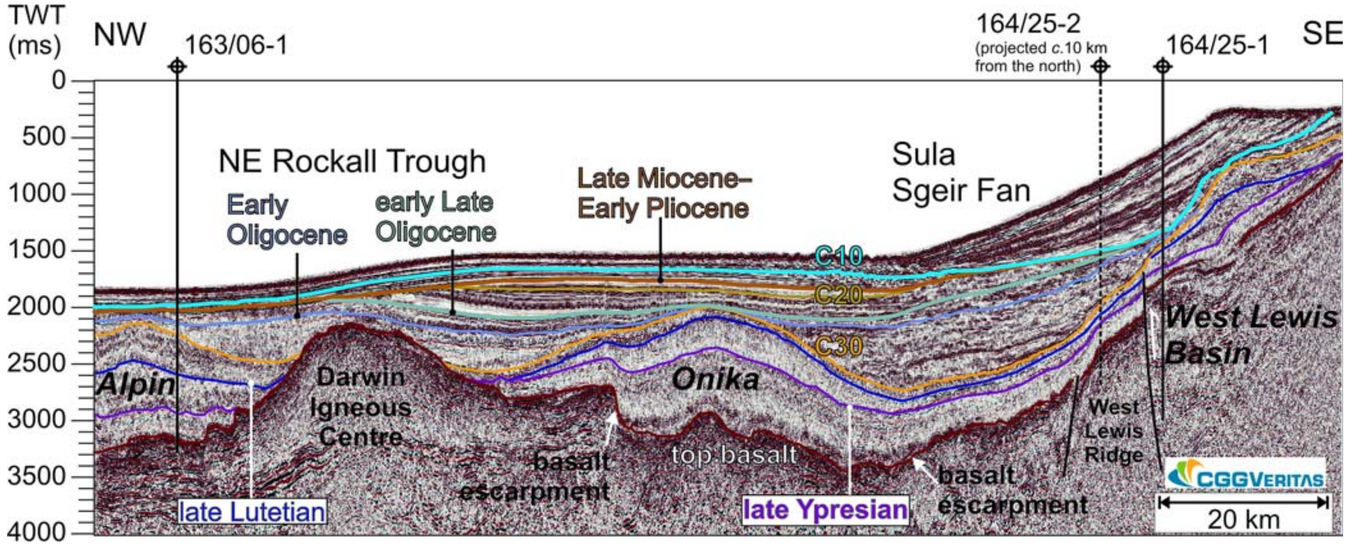

Fig. 17. NW–SE seismic profile of the Alpin Anticline, Onika Anticline and the inverted West Lewis Basin. Seismic illustration courtesy of CGG Veritas. For the location of the seismic illustration, see Figure 8.

in the south West Lewis Basin and defines the initiation of reverse faulting.

Viera Anticline

The Viera Anticline is a NW-trending fold, 30 km in length and located to the SW of the West Lewis Ridge in the NE Rockall Trough (Fig. 8). The amplitude of the anticline (measured from the late Ypresian unconformity) is up to *c*. 700 m (seismic profile not illustrated). The C30 (Late Eocene) unconformity, which is interpreted as marking the initial age of folding, is defined by onlap of Early Oligocene sediment. The Viera Anticline represents the folding of relatively thick Early Eocene sediment (Fig. 13).

Basin control on the orientation of compressional structures

The effects of basin inversion have been described in other areas of the NE Atlantic Margin. On the Norwegian Margin, for example, the Helland–Hansen Arch and other large domes are thought to be due to compressional reactivation of normal faults developed during Cretaceous rifting (Grunnaleite & Gabrielsen 1995; Vågnes *et al.* 1998). The Naglfar Dome, between the Vøring and Møre Basins (Fig. 1), is located within the Hel Graben (Lundin & Doré 2002). In addition, the Balder Graben in the NE Rockall Trough has been mapped beneath the Viera Anticline (Waddams & Cordingley 1999). Lundin & Doré (2002) proposed that Mid to Late Cenozoic compression resulted in basin inversion affecting deep Cretaceous depocentres on the Norwegian–Greenland Sea margins.

Results presented here suggest inversion of the West Lewis Basin from Thanetian to C30 (Late Eocene) time (Figs 17 & 18). In addition, the development of the Alpin, Mordor, Onika and Viera anticlines is considered to be due to the compression of Early Cenozoic depocentres. It has been previously recognized that basins within the NE Atlantic Margin follow the Caledonide (NE–SW) and the Lewisian (NW–SE, north–south and east–west) structural trends (Tate *et al.* 1999). All compressional structures in the Rockall–Faroe area have orientations which fit these trends. The orientation of the folds in the Rockall–Faroe area could, thus, be determined by their underlying basin morphologies. However, seismic masking by Palaeogene lavas largely precludes direct observation of such a relationship.

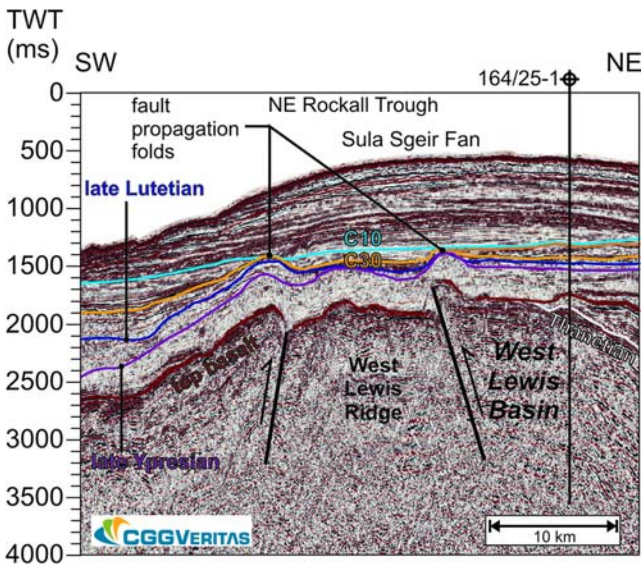

Fig. 18. SW–NE seismic profile of the West Lewis Ridge bounded by reverse faults. Seismic illustration courtesy of CGG Veritas. For the location of the seismic illustration, see Figure 8.

Bottom-water current activity

Post Oligocene unconformities, such as the C20 (late Early Miocene) unconformity (Fig. 10) and the Late Miocene–Early Pliocene unconformities (Figs 10 & 17), are characterized by strong erosional channelling and truncation that are most likely the result of bottom-water current activity rather than onlap onto growth folds. This is in contrast to the well documented Miocene unconformities which mark compression in the Vøring Basin (Blystad *et al.* 1995; Lundin & Doré 2002) and the Faroe–Shetland Basin (Ritchie *et al.* 2003; Johnson *et al.* 2005). In the Rockall–Faroe area, however, well defined reverse faults are observed which do not cut Early Miocene sediment (Fig. 6). This characteristic, and the lack of tighter folding immediately below the C20 (late Early Miocene) unconformity (Fig. 17), suggests that a Miocene compressional event was not as significant in this area.

It has been suggested that compression could alter seabed bathymetry to result in changes in bottom-water current activity

(Laberg *et al.* 2005). The study assesses the possible role of compression in influencing, directly or indirectly, bottom-water current activity.

Compression and C30 subsidence

The Rockall Trough is a basin which formed by rifting in the Early Cretaceous (Musgrove & Mitchener 1996). Sharp subsidence of this basin coincides with a major compressional phase at C30 (Late Eocene) time (Stoker 1997; Stoker *et al.* 2001; Praeg *et al.* 2005). Praeg *et al.* (2005) proposed that the C30 subsidence was the result of a loss of dynamic support by convection in the underlying mantle. However, the onset of this subsidence at the time of compression suggests that these events could be related. Flexural downwarping due to compression has been postulated for the Late Pliocene subsidence in the southern North Sea basin (Kooi *et al.* 1991). Compression-induced downwarping occurs as a result of folding of weak lithosphere of low flexural rigidity (Kooi *et al.* 1991). The Rockall Trough is characterized by weak lithosphere with an elastic thickness of approximately 6 km on the eastern margin near the Porcupine Bank (Daly *et al.* 2004). This is thinner than the 25 km elastic thickness of continental lithosphere (Fowler 2001). The Rockall Trough, having a relatively low elastic thickness, could have been prone to the effects of compression-induced flexural downwarping at C30 time. The deepening of the Rockall Trough facilitated the flow of bottom-water currents and the subsequent deposition of contourites (Stoker 1997; Stoker *et al.* 2001).

Compression and the Norwegian Sea Overflow

The present-day bottom-water currents in the North Rockall Trough stem partly from the Norwegian Sea Overflow (NSO) (Fig. 19; Stow & Holbrook 1984; Stoker 1997; Stoker *et al.* 2001). The NSO flows from the Faroe Bank Channel to the North Rockall Trough via a bathymetric gorge at the west end of the Auðhumla Basin Syncline (Figs 19 & 20). Previous work has proposed that the initiation of the NSO was in the Mid Miocene (Blanc *et al.* 1980; Bohrmann *et al.* 1990; Eldholm 1990; Ramsay *et al.* 1998; Stoker *et al.* 2005). The Auðhumla Basin Syncline would have thus been a major conduit for the passage of the NSO into the North Rockall Trough no later than Mid Miocene times. The location of this compressional feature would have influenced the direction of the NSO, affecting the subsequent distribution of contourites and unconformities within the North Rockall Trough.

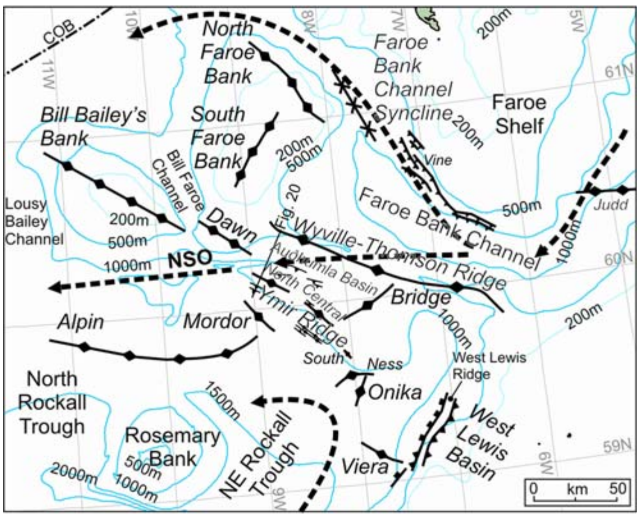

Fig. 19. Present-day circulation of bottom-water currents (dashed lines) in the north Rockall–Faroe study area (Stow & Holbrook 1984; Stoker 1997; Stoker *et al.* 2001). Note the bathymetric gorge between the Dawn and North Ymir Ridge anticlines, within the Auðhumla Basin, through which the Norwegian Sea Overflow passes. For the location of the area, see Figure 3.

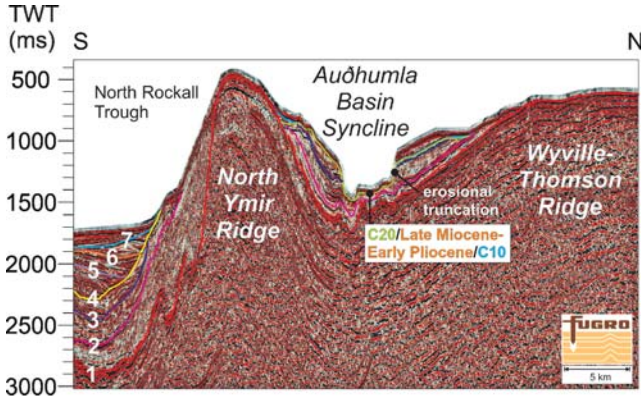

Fig. 20. North–south seismic profile across the west end of the Auðhumla Basin Syncline. Note the erosional truncation of Cenozoic sediment within the syncline. Seismic horizons: 1, top basalt; 2, late Ypresian; 3, late Lutetian; 4, C30 (Late Eocene); 5, Early Oligocene; 6, Late Miocene–Early Pliocene; 7, C10 (late Early Pliocene). Seismic illustration courtesy of Fugro Multi Client Services. For the location of the seismic illustration, see Figure 19.

Driving mechanisms

The formation of compressional features within the NE Atlantic Margin has been attributed to normal ridge push (Boldreel & Andersen 1993; Doré & Lundin 1996), hotspot-influenced ridge push (Lundin & Doré 2002), Alpine compression (Roberts 1989; Doré & Lundin 1996; Vågnes *et al.* 1998; Brekke 2000), Pyrenean compression (Knott *et al.* 1993), plate reorganization (Boldreel & Andersen 1993; Lundin & Doré 2002) and the Iceland Plateau Body force (Doré *et al.* 2008). Uplift and exhumation in the nearby Irish Sea during the early Palaeogene and the Late Palaeogene–Neogene has been partly attributed to Alpine compression and Atlantic continental break-up (Holford *et al.* 2005).

In this study, we attempt to link compressional events in the Rockall–Faroe area to ridge push (normal and hotspot-influenced), Alpine and Pyrenean compression, depth-dependent stretching/asthenospheric upwelling and the Iceland body force (Fig. 21).

The Thanetian compressional event would coincide with the timing of postulated depth-dependent stretching which is thought to occur just prior to continental break-up as a result of asthenospheric upwelling which pushes the adjacent lithosphere towards the continental margin (Withjack *et al.* 1998; Kusznir *et al.* 2005). Depth-dependent stretching is modelled to affect a marginal zone 75–150 km from the continent–ocean boundary (Kusznir *et al.* 2005). The Hatton Bank, Lousy Bank, Bill Bailey's Bank, Faroe Bank anticlines and the Faroe Bank Channel Syncline are all located within such a marginal zone in the Rockall–Faroe area. The Thanetian unconformity defines the Faroe Bank Channel Syncline. Furthermore, onlap of Eocene sediment onto the top basalt lava flows of Hatton Bank suggests a structural high existed in this area prior to the Early Eocene. The North Ymir Ridge Anticline, Wyville–Thomson Ridge Anticline and the inverted West Lewis Basin also underwent Thanetian compressional growth. These structures, however, are located beyond the range of the marginal zone modelled to be affected by depth-dependent stretching. It is, therefore, postulated in this study that

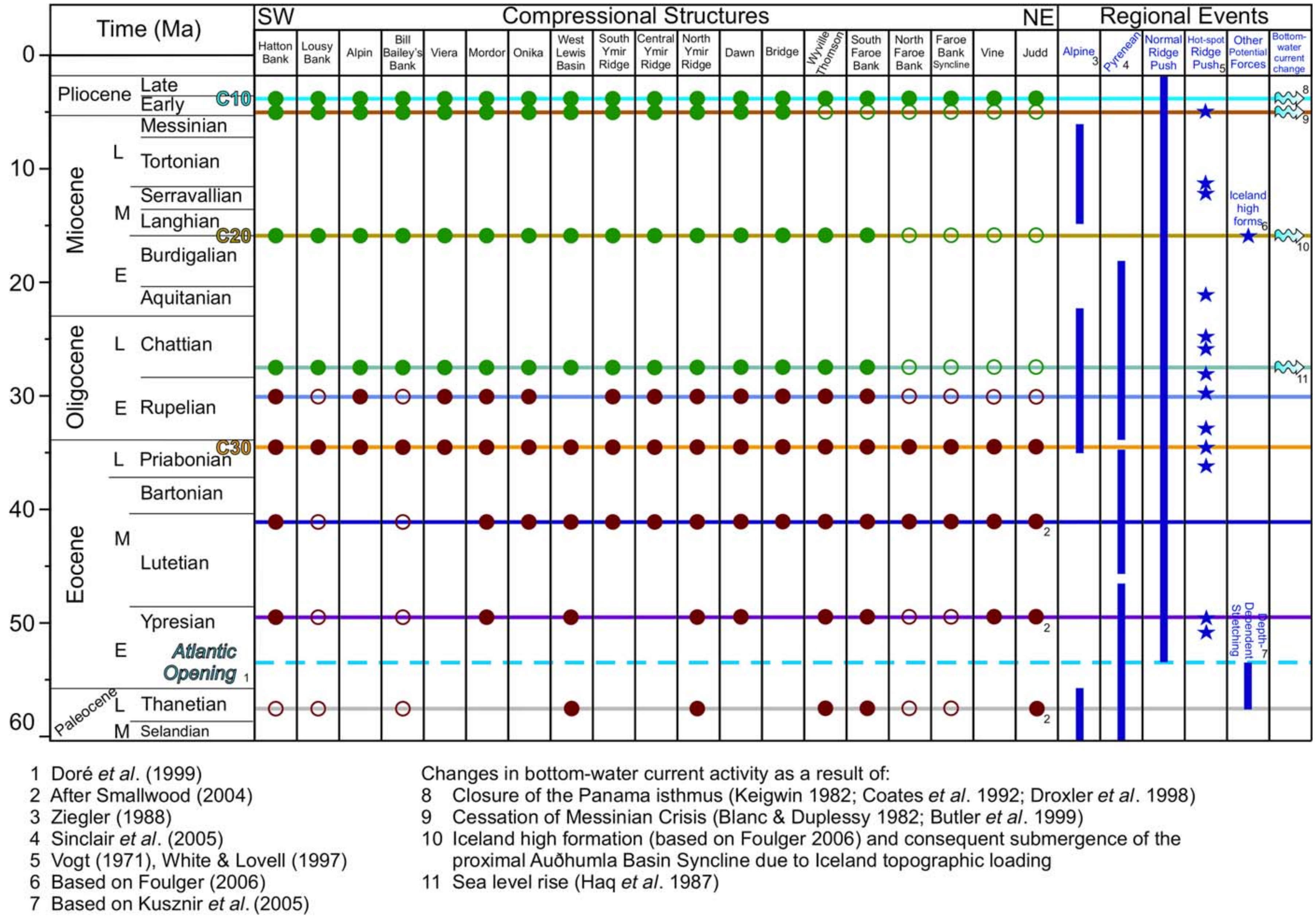

Fig. 21. Cenozoic unconformities within the Rockall–Faroe area and regional events affecting the NE Atlantic Margin. Red circles define the ages of compressional unconformities while green circles define the ages of non-compressional unconformities in the Rockall–Faroe area. Filled circles represent unconformities which have been mapped or dated. Circle outlines represent unconformities inferred to be present but have not been mapped.

these structures are more likely to be the result of compression on the periphery of a region uplifted by asthenospheric upwelling. A hotspot was present prior to NE Atlantic rifting which resulted in considerable uplift as a result of extensive asthenospheric upwelling (Skogseid & Eldholm 1988; White & McKenzie 1989). This uplift produces significant gravitational potential (White & McKenzie 1989) which can release horizontal stresses towards the rim of the uplifted area. Oligocene–Holocene compression of the Kwanza Basin, located in the continental margin off Angola, for example, has been attributed to mantle-driven uplift of the African superswell (Hudec & Jackson 2002). The Base Balder unconformity in the southern Faroe–Shetland Basin is attributed to uplift as a result of 'the introduction of asthenospheric mantle with an anomalously high potential temperature' (Smallwood & Gill 2002). The age of the Base Balder unconformity is modelled at Mid to Late Paleocene (60.5–55.2 Ma) (Jolley *et al.* 2002; cited in Smallwood & Gill 2002). It is the view, in this study, that the Base Balder unconformity in the southern Faroe–Shetland Channel is contemporaneous with the Thanetian (Late Paleocene) unconformity in the Rockall–Faroe area.

The late Ypresian, C30 (Late Eocene) and Early Oligocene compressional events coincide with the timings of hotspot-influenced or plume enhanced ridge push (Fig. 21). These compressional events also take place during times of Alpine and/or Pyrenean compression. Lundin & Doré (2002) negate the effects of Alpine and Pyrenean compression due to the presence of Cenozoic compressional features present on the East Greenland continental margin, indicating that the structures formed due to hotspot-influenced ridge push. The Traill Ø region on the East Greenland margin, for example, experienced compression during the Cenozoic (post-54 Ma) based on the folding of sills *c.* 54 Ma in age (Price *et al.* 1997). Kjelstad *et al.* (2003), however, cast doubt on any far-field stresses resulting in the compression and inversion of underlying basins. According to these authors the horizontal stress required to reverse a basement fault of a basin at 5 km depth, with a dip of 45° and an internal angle of friction of 30°, is 376 MPa based on the Mohr–Coulomb failure criterion. The force exerted onto the continental margin from hotspot-influenced ridge push is lower, modelled at 100 MPa (Bott 1993). However, the effects of hotspot-influenced ridge push could have potentially been amplified by Alpine and Pyrenean compression to result in the inversion of underlying basins in the Rockall–Faroe area. The East Greenland continental margin contains smaller scale deformation in comparison with deformation present in the NE Atlantic Margin, where structures are greater in length, width and amplitude (Tsikalas *et al.* 2005). This is consistent with the lack of contributing forces from the Alpine and Pyrenean compression.

However, the late Lutetian compressional event, which occurs at a time of Pyrenean compression, does not correlate with the timings of hotspot-influenced ridge push (Fig. 21). It remains uncertain in this study whether other factors could have contributed to the growth of compressional structures in the late Lutetian.

It is interesting to note that the uplifts bordering the ocean–continent boundary such as Lousy and Hatton Bank lie in a region shown to be underlain by highly intruded lower crust (White *et al.* 2010) and, where present, this 'underplate' is likely to have resulted in rapid isostatic uplift. However, major growth that we can observe on the anticlines bordering the ocean–continent boundary, such as Hatton Bank, occurred in Eocene and Oligocene times. The compressive strain is not restricted to the flank of the structure, but does mark its overall growth. Consequently, it would appear that growth of the Hatton Bank Anticline occurred millions of years after the 'underplate' is generally considered to have been intruded (Late Paleocene–Early Eocene times). On the basis of this timing of fold development, we prefer to explain the folds bordering the ocean–continent boundary such as Lousy and Hatton Bank as primarily compressional in origin. Of course, this would not preclude the possibility of an earlier phase of uplift associated with underplating.

Implications for prospectivity

Continental margins have often provided ideal settings for petroleum plays. Shale deposited in anoxic conditions during young ocean basin development has the potential to become an ideal source for hydrocarbons (Boillot 1981). As the ocean basin deepens, turbidite sands intercalated with hemipelagic sediments are deposited and can form reservoirs and seals (Boillot 1981). Normal faults formed as a result of rifting can act as conduits for migrating hydrocarbons. The presence of anticlines within continental margins completes the play setting by forming ideal structural traps of four-way dip closure (Doré & Lundin 1996; Doré *et al.* 1997). In the NE Atlantic Margin, gas accumulation in the Ormen Lange Dome in the Vøring Basin is located within such a structural trap (Lundin & Doré 2002; Smith & Møller 2003). The timing of growth of compressional structures is critical in determining their presence at the time of hydrocarbon migration. Uplift as a result of compression can remove potential source rocks from the gas/oil generation window. Thus, there is often a mismatch between the timing of petroleum migration from source rocks and later trap-forming events in structurally inverted basins. Secondary migration, however, can supply these later traps with hydrocarbons. Further understanding of the area's prospective potential will rely upon determining whether there were ever any mature source rocks and if the compressional structures described herein lay on suitable migration pathways as, or after, they formed.

Conclusions

Horizontal forces have resulted in compression within the Rockall–Faroe area to form structures such as the Lousy Bank and Alpin anticlines during Cenozoic times. The orientation and extent of compressional structures were most likely governed by their underlying basin morphologies. The growth of structures in the Thanetian could be linked to depth-dependent stretching and asthenospheric upwelling. Late Ypresian, C30 (Late Eocene) and Early Oligocene compressional phases correlate well with hotspot-influenced ridge push, but were most likely due to the combined effects of this force and the Alpine and Pyrenean stresses. The study suggests evidence for the role of compression in changing seabed bathymetry to result in changes in bottom-water current activity. Subsidence of the Rockall Trough at C30 (Late Eocene), which increased bottom-water current activity in the basin, could have resulted from compression-induced flexural downwarping. The west end of the Auðhumla Basin Syncline is a major conduit for the transport of the NSO from the Faroe Bank Channel to the North Rockall Trough. The growth of the syncline has controlled the distribution of sediments and unconformities within the North Rockall Trough by influencing the direction and existence of the NSO. A full understanding of the timing and distribution of the structures and basin subsidence histories will help unlock the petroleum prospectivity in the area.

This work was carried out jointly between the British Geological Survey and The University of Edinburgh under the auspices of a British University Funding Initiative (BUFI) Grant, which is gratefully acknowledged. The work was carried out at the British Geological Survey. We thank Fugro Multo Client Services and CGG Veritas for kind permission to publish their seismic data. We also thank M. Stoker for helpful discussions. The contributions from J. D. Ritchie, H. Johnson and K. Hitchen are published with permission of the Executive Director, British Geological Survey (NERC).

References

Andersen, M. S. & Boldreel, L. O. 1995. Effect of Eocene–Miocene compression structures on bottom-water currents in the Faeroe-Rockall area. *In*: Scrutton, R. A., Stoker, M. S., Shimmield, G. B. & Tudhope, A. W. (eds) *The Tectonics, Sedimentation and Palaeoceanography of the North Atlantic Region*. Geological Society, London, Special Publications, **90**, 141–143.

Blanc, P. & Duplessy, J. 1982. The deep-water circulation during the Neogene and the impact of the Messinian salinity Crisis. *Deep-Sea Research*, **29**, 12A, 1391–1414.

Blanc, P.-L., Rabussier, D., Vernaud-Grazzini, C. & Duplessy, J.-C. 1980. North Atlantic Deep Water formed by the later middle Miocene. *Nature*, **283**, 553–555.

Blystad, P., Brekke, H., Faerseth, R. B., Larsen, B. T., Skogseid, J. & Tørudbakken, B. 1995. *Structural Elements of the Norwegian Continental Shelf. Part II: The Norwegian Sea Region*. Norwegian Petroleum Directorate Bulletins, **8**.

Bohrmann, G., Henrich, R. & Thiede, J. 1990. Miocene to Quaternary Paleoceanography in the northern North Atlantic: variability in carbonate and biogenic opal accumulation. *In*: Bleie, U. & Thiede, J. (eds) *Geological History of the Polar Ocean*. Kluwer, Dordrecht, 647–675.

Boillot, G. 1981. *Geology of the Continental Margins*. Longman Higher Education, Harlow.

Boldreel, L. O. & Andersen, M. S. 1993. Late Paleocene to Miocene compression in the Faeroe-Rockall area. *In*: Parker, J. R. (ed.) *Petroleum Geology of Northwest Europe: Proceedings of the 4th Conference*. Geological Society, London, 1025–1034; doi: 10.1144/0041025.

Boldreel, L. O. & Andersen, M. S. 1994. Tertiary development of the Faeroe-Rockall Plateau based on reflection seismic data. *Bulletin of the Geological Society of Denmark*, **41**, 162–180.

Boldreel, L. O. & Andersen, M. S. 1998. Tertiary compressional structures on the Faroe–Rockall Plateau in relation to northeast Atlantic ridge-push and Alpine foreland stresses. *Tectonophysics*, **300**, 13–28.

Bott, M. H. P. 1993. Modelling the plate-driving mechanism. *Journal of the Geological Society, London*, **150**, 941–951.

Brekke, H. 2000. The tectonic evolution of the Norwegian Sea Continental Margin with emphasis on the Vøring and Møre Basins. *In*: Nøttvedt, A. *et al.* (eds) *Dynamics of the Norwegian Margin*. Geological Society, London, Special Publications, **167**, 327–378.

Butler, R. W. H., McClelland, E. & Jones, R. E. 1999. Calibrating the duration and timing of the Messinian salinity crisis in the Mediterranean: linked tectonoclimatic signals in thrust-top basins of Sicily. *Journal of the Geological Society, London*, **156**, 827–835.

Coates, A. G., Jackson, J. B. C., Collins, L. S., Cronin, T. M., Dowsett, H. J., Bybell, L. M., Jung, P. & Obando, J. A. 1992. Closure of the Isthmus of Panama: the nearshore marine record of Costa Rica and western Panama. *Geological Society of America Bulletin*, **104**, 814–828.

Daly, E., Brown, C., Stark, C. P. & Ebinger, C. J. 2004. Wavelet and multitaper coherence methods for assessing the elastic thickness of the Irish Atlantic margin. *Geophysical Journal International*, **159**, 445–459.

Davies, R. J. & Cartwright, J. 2002. A fossilized Opal A to Opal C/T transformation on the northeast Atlantic margin: support for a significantly elevated Palaeogeothermal gradient during the Neogene? *Basin Research*, **14**, 467–486.

Dolan, J. F. 1986. The relationship between 'R2' seismic reflector and a zone of abundant detrital and authigenic smectities, Deep Sea Drilling Project Hole 610. Rockall Plateau region, North Atlantic. *In*: Ruddiman, W. F., Kidd, R. B., Thomas, E. *et al.* (eds) *Initial Reports of the Deep Sea Drilling Project*, **94**, 1109–1115.

Doré, A. G. & Lundin, E. R. 1996. Cenozoic compressional structures on the NE Atlantic margin: nature, origin and potential significance for hydrocarbon exploration. *Petroleum Geoscience*, **2**, 299–311.

Doré, A. G., Lundin, E. R., Birkeland, Ø., Eliassen, P. E. & Jensen, L. N. 1997. The NE Atlantic Margin: implications of late Mesozoic and Cenozoic events for hydrocarbon prospectivity. *Petroleum Geoscience*, **3**, 117–131.

Doré, A. G., Lundin, E. R., Jensen, L. N., Birkeland, O., Eliassen, P. E. & Fichler, C. 1999. Principal tectonic events in the evolution of the northwest European Atlantic margin. *In*: Fleet, A. J. & Boldy, S. A. R. (eds) *Petroleum Geology of Northwest Europe: Proceedings of the 5th Conference*. Geological Society, London, 41–61; doi: 10.1144/0050041.

Doré, A. G., Lundin, E. R., Kusznir, N. J. & Pascal, C. 2008. Potential mechanisms for the genesis of Cenozoic domal structures on the NE Atlantic margin: pros, cons and some new ideas. *In*: Johnson, H., Doré, A. G., Gatliff, R. W., Holdsworth, R., Lundin, E. R. & Ritchie, J. D. (eds) *The Nature and Origin of Compression in Passive Margins*. Geological Society, London, Special Publications, **306**, 1–26.

Droxler, A. W., Burke, K. C. *et al.* 1998. Caribbean constraints on circulation between Atlantic and Pacific Oceans over the past 40 million years. *In*: Crowley, T. J. & Burke, K. C. (eds) *Tectonic Boundary Conditions for Climate Reconstructions*. Oxford University Press, New York, 169–191.

Eldholm, O. 1990. Paleogene North Atlantic magmatic–tectonic events: environmental implications. *Memorie Societa Geologica Italiana*, **44**, 13–28.

Foulger, G. R. 2006. Older crust underlies Iceland. *Geophysical Journal International*, **165**, 672–676.

Fowler, C. M. R. 2001. *The Solid Earth; An Introduction to Global Geophysics*. Cambridge University Press, Cambridge.

Grunnaleite, I. & Gabrielsen, R. H. 1995. Structure of the Møre Basin, mid-Norway continental margin. *Tectonophysics*, **252**, 221–251.

Haq, B. U., Hardenbol, J. & Vail, P. R. 1987. Chronology of fluctuating sea levels since the Triassic. *Science*, **235**, 1156–1167.

Hitchen, K. 2004. The geology of the UK Hatton–Rockall margin. *Marine and Petroleum Geology*, **21**, 993–1012.

Holford, S. P., Turner, J. P. & Green, P. F. 2005. Reconstructing the Mesozoic–Cenozoic exhumation history of the Irish Sea basin system using apatite fission track analysis and vitrinite reflectance data. *In*: Doré, A. G. & Vining, B. A. (eds) *Petroleum Geology: North-West Europe and Global Perspectives: Proceedings of the 6th Petroleum Geology Conference*. Geological Society, London, 1095–1107; doi: 10.1144/0061095.

Hudec, M. R. & Jackson, M. P. A. 2002. Structural segmentation, inversion, and salt tectonics on a passive margin: evolution of the Inner Kwanza Basin, Angola. *Geological Society of America Bulletin*, **114**, 1222–1244.

IOC, IHO & BODC. 2003. *Centenary Edition of the GEBCO Digital Atlas*. British Oceanographic Centre, Liverpool.

Johnson, H., Ritchie, J. D., Hitchen, K., McInroy, D. B. & Kimbell, G. S. 2005. Aspects of the Cenozoic deformational history of the Northeast Faroe–Shetland Basin, Wyville–Thomson Ridge and Hatton Bank areas. *In*: Doré, A. G. & Vining, B. A. (eds) *Petroleum Geology: North-West Europe and Global Perspectives: Proceedings of the 6th Petroleum Geology Conference*. Geological Society, London, 993–1007; doi: 10.1144/0060993.

Jolley, D. W., Clarke, B. & Kelley, S. 2002. Paleogene time scale miscalibration: evidence from the dating of the North Atlantic Igneous Province. *Geology*, **30**, 7–10.

Keigwin, L. 1982. Isotopic paleoceanography of the Caribbean and East Pacific: role of Panama uplift in late Neogene time. *Science*, **217**, 350–353.

Kimbell, G. S., Ritchie, J. D., Johnson, H. & Gatliff, R. W. 2005. Controls on the structure and evolution of the NE Atlantic margin revealed by regional potential field imaging and 3D modelling. *In*: Doré, A. G. & Vining, B. A. (eds) *Petroleum Geology: North-West Europe and Global Perspectives: Proceedings of the 6th Petroleum Geology Conference*. Geological Society, London, 933–945; doi: 10.1144/0060933.

Kjelstad, A., Skogseid, J., Langtangen, H. P., Bjørlykke, K. & Høeg, K. 2003. Differential loading by prograding sedimentary wedges on continental margins: an arch-forming mechanism. *Journal of Geophysical Research*, **108**, 2036; doi: 10.1029/2001JB001145.

Knott, S. D., Burchell, M. T., Jolley, E. J. & Fraser, A. J. 1993. Mesozoic to Cenozoic plate reconstructions of the North Atlantic and hydrocarbon plays of the Atlantic margins. *In*: Parker, J. R. (ed.) *Petroleum Geology of Northwest Europe: Proceedings of the 4th Conference*. Geological Society, London, 953–974; doi: 10.1144/0040953.

Kooi, H., Hettema, M. & Cloetingh, S. 1991. Lithospheric dynamics and the rapid Pliocene-Quaternary subsidence phase in the southern North Sea Basin. *Tectonophysics*, **192**, 245–259.

Kusznir, N. J., Hunsdale, R., Roberts, A. M. & iSIMM Team, 2005. Timing and magnitude of depth-dependent lithosphere stretching on the southern Lofoten and northern Vøring continental margins offshore mid-Norway: implication for subsidence and hydrocarbon maturation at volcanic rifted margins. *In*: Doré, A. G. & Vining, B. A. (eds) *Petroleum Geology: North-West Europe and Global Perspectives: Proceedings of the 6th Petroleum Geology Conference*. Geological Society, London, 767–783; doi: 10.1144/0060767.

Laberg, J. S., Stoker, M. S. *et al*. 2005. Cenozoic alongslope processes and sedimentation on the NW European Atlantic Margin. *Marine and Petroleum Geology*, **22**, 1069–1088.

Løseth, H. & Henriksen, S. 2005. A Middle to Late Miocene compression phase along the Norwegian passive margin. *In*: Doré, A. G. & Vining, B. A. (eds) *Petroleum Geology: North-West Europe and Global Perspectives: Proceedings of the 6th Petroleum Geology Conference*. Geological Society, London, 845–859; doi: 10.1144/0060845.

Lundin, E. & Doré, A. G. 2002. Mid-Cenozoic post-breakup deformation in the 'passive' margins bordering the Norwegian-Greenland Sea. *Marine and Petroleum Geology*, **19**, 79–93.

McQuillin, R., Bacon, M. & Barclay, W. 1984. *An Introduction to Seismic Interpretation*. Graham and Trotman, London.

Musgrove, F. W. & Mitchener, B. 1996. Analysis of the pre-Tertiary rifting history of the Rockall Trough. *Petroleum Geoscience*, **2**, 353–360.

Praeg, D., Stoker, M. S., Shannon, P. M., Ceramicola, S., Hjelstuen, B., Laberg, J. S. & Mathiesen, A. 2005. Episodic Cenozoic tectonism and the development of the NW European 'passive' continental margin. *Marine and Petroleum Geology*, **22**, 1007–1030.

Price, S., Brodie, J., Whitham, A. & Kent, R. 1997. Mid-Tertiary rifting and magmatism in the Traill Ø region, East Greenland. *Journal of the Geological Society, London*, **54**, 419–434.

Ramsay, A. T. S., Smart, C. W. & Zachos, J. C. 1998. A model of early to middle Miocene deep ocean circulation for the Atlantic and Indian Oceans. *In*: Cramp, A., MacLeod, C. J., Lee, S. V. & Jones, E. J. W. (eds) *Geological Evolution of Ocean Basins: Results From the Ocean Drilling Program*. Geological Society, London, Special Publications, **131**, 55–70.

Ritchie, J. D., Johnson, H. & Kimbell, G. S. 2003. The nature and age of Cenozoic contractional deformation within the NE Faroe–Shetland Basin. *Marine and Petroleum Geology*, **20**, 399–409.

Ritchie, J. D., Johnson, H., Quinn, M. F. & Gatliff, R. W. 2008. The effects of Cenozoic compression within the Faroe–Shetland Basin and adjacent areas. *In*: Johnson, H., Doré, A. G., Gatliff, R. W., Holdsworth, R., Lundin, E. R. & Ritchie, J. D. (eds) *The Nature and Origin of Compression in Passive Margins*. Geological Society, London, Special Publications, **306**, 121–136.

Roberts, D. G. 1989. Basin inversion in and around the British Isles. *In*: Cooper, M. A. & Williams, G. D. (eds) *Inversion Tectonics*. Geological Society, London, Special Publications, **44**, 131–150.

Shannon, P. M, Stoker, M. S. *et al*. 2005. Sequence stratigraphic analysis in deep-water, underfilled NW European passive margin basins. *Marine and Petroleum Geology*, **22**, 1185–1200.

Sinclair, H. D., Gibson, M., Naylor, M. & Morris, R. G. 2005. Asymmetric growth of the Pyrenees revealed through measurement and modelling of orogenic fluxes. *American Journal of Sciences*, **305**, 369–406.

Skogseid, J. & Eldholm, O. 1988. Early Cainozoic evolution of the Norwegian volcanic passive margin and the formation of marginal highs. *In*: Morton, A. C. & Parson, L. M. (eds) *Early Tertiary Volcanism and the Opening of the NE Atlantic*. Geological Society, London, Special Publications, **39**, 49–56.

Smallwood, J. R. 2004. Tertiary inversion in Faroe–Shetland Channel and the development of major erosional scarps. *In*: Davies, R. J., Stewart, S. A., Cartwright, J. A., Lappin, M. & Underhill, J. R. (eds) *3D Seismic Technology: Application to the Exploration of Sedimentary Basins*. Geological Society, London, Memoirs, **29**, 187–198.

Smallwood, J. R. & Gill, C. E. 2002. The rise and fall of the Faroe–Shetland Basin: evidence from seismic mapping of the Balder Formation. *Journal of the Geological Society, London*, **159**, 627–630.

Smith, R. & Møller, N. 2003. Sedimentology and reservoir modelling of the Ormen Lange field, mid Norway. *Marine and Petroleum Geology*, **20**, 601–613.

Stoker, M. S. 1997. Mid- to late Cenozoic sedimentation on the continental margin off NW Britain. *Journal of the Geological Society, London*, **154**, 509–515.

Stoker, M. S., Van Weering, T. C. E. & Svaerdborg, T. 2001. A Mid- to Late Cenozoic tectonostratigraphic framework for the Rockall Trough. *In*: Shannon, P. M., Haughton, P. D. W. & Cororan, D. V. (eds) *The Petroleum Exploration of Ireland's Offshore Basins*. Geological Society, London, Special Publications, **188**, 411–438.

Stoker, M. S., Praeg, D. *et al*. 2005. Neogene evolution of the Atlantic continental margin of NW Europe (Lofoten Islands to SW Ireland): anything but passive. *In*: Doré, A. G. & Vining, B. A. (eds) *Petroleum Geology: North-West Europe and Global Perspectives: Proceedings of the 6th Petroleum Geology Conference*. Geological Society, London, 1057–1076; doi: 10.1144/0061057.

Stow, D. A. V. & Holbrook, J. A. 1984. North Atlantic contourites: an overview. *In*: Piper, D. J. & Stow, D. A. V. (eds) *Fine Grained Sediments: Deep Water Processes and Fabrics*. Geological Society of America, Boulder, CO, Special Publications, **15**, 245–256.

Tate, M. P., Dodd, C. D. & Grant, N. T. 1999. The Northeast Rockall Basin and its significance in the evolution of the Rockall-Faeroes/East Greenland rift system. *In*: Fleet, A. J. & Boldy, S. A. R. (eds) *Petroleum Geology of Northwest Europe: Proceedings of the 5th Conference*. Geological Society, London, 391–406; doi: 10.1144/0050391.

Tsikalas, F., Faleide, J. I., Eldholm, O. & Wilson, J. 2005. Late Mesozoic–Cenozoic structural and stratigraphic correlations between the conjugate mid-Norway and NE Greenland continental margins. *In*: Doré, A. G. & Vining, B. A. (eds) *Petroleum Geology: North-West Europe and Global Perspectives: Proceedings of the 6th Petroleum Geology Conference*. Geological Society, London, 785–801; doi: 10.1144/0060785.

Vågnes, E., Gabrielsen, R. H. & Haremo, P. 1998. Late Cretaceous–Cenozoic intraplate contractional deformation at the Norwegian continental shelf: timing, magnitude and regional implications. *Tectonophysics*, **300**, 29–46.

Vogt, P. R. 1971. Asthenosphere motion recorded by the ocean floor south of Iceland. *Earth and Planetary Science Letters*, **13**, 153–160.

Waddams, P. & Cordingley, T. 1999. The regional geology and exploration potential of NE Rockall Basin. *In*: Fleet, A. J. & Boldy, S. A. R. (eds) *Petroleum Geology of Northwest Europe: Proceedings of the 5th Conference*. Geological Society, London, 379–390; doi: 10.1144/0050379.

White, R. & McKenzie, D. 1989. Magmatism at rift zone: the generation of volcanic continental margins and flood basalts. *Journal of Geophysical Research*, **94**, 7685–7729.

White, N. & Lovell, B. 1997. Measuring the pulse of a plume with the sedimentary record. *Nature*, **387**, 888–891.

White, R. S., Eccles, J. D. & Roberts, A. W. 2010. Constraints on volcanism, igneous intrusion and stretching on the Rockall Faroe–continental margin. *In*: Vining, B. A. & Pickering, S. C. (eds) *Petroleum Geology: From Mature Basins to New Frontiers – Proceedings of the 7th Petroleum Geology Conference*. Geological Society, London. 831–842; doi: 10.1144/0070831.

Withjack, M. O., Schlische, R. W. & Olsen, P. E. 1998. Diachronous rifting, drifting, and inversion on the passive margin of Central Eastern North America: An analogue for other passive margins. *AAPG Bulletin*, **82**, (5A), 817–835.

Ziegler, P. A. 1988. *Evolution of the Arctic-North Atlantic and the Western Tethys*. AAPG Memoir, **43**.

Ziska, H. & Varming, T. 2008. Palaeogene evolution of the Ymir and Wyville Thomson ridges, European North Atlantic margin. *In*: Johnson, H., Doré, A. G., Gatliff, R. W., Holdsworth, R., Lundin, E. R. & Ritchie, J. D. (eds) *The Nature and Origin of Compression in Passive Margins*. Geological Society, London, Special Publications, **306**, 153–168.

Episodic uplift and exhumation along North Atlantic passive margins: implications for hydrocarbon prospectivity

P. JAPSEN,[1] P. F. GREEN,[2] J. M. BONOW,[1] E. S. RASMUSSEN,[1] J. A. CHALMERS[1] and T. KJENNERUD[3]

[1]*Geological Survey of Denmark and Greenland (GEUS), Øster Voldgade 10, DK-1350 Copenhagen, Denmark (e-mail: pj@geus.dk)*

[2]*Geotrack International, 37 Melville Road, Brunswick West, Victoria 3055, Australia*

[3]*Exploro Geoservices, Stiklestadveien 1, 7041 Trondheim, Norway*

Abstract: We present observations that demonstrate that the elevated passive margins around the North Atlantic were formed by episodic, post-rift uplift movements that are manifest in the high-lying peneplains that characterize the coastal mountains, in the unconformities in the adjacent sedimentary basins and in accelerated subsidence in the basin centres. Results from West Greenland show that subsidence of the rifted margin took place for *c.* 25 Myr after rifting and breakup in the Paleocene, as predicted by classical rift theory, but that this development was reversed by a series of uplift movements (starting at *c.* 35, 10 and 5 Ma) that remain unexplained. East Greenland and Scandinavia seem to have had a similar evolution of post-rift subsidence followed by uplift starting at *c.* 35 Ma. There was no notable fall in sea-level at this time, so the subsiding basins must have been inverted by tectonic forces. We speculate that the forces causing this phase were related to the plate boundary reorganization in the North Atlantic around Chron 13 time. One feature that these areas have in common is that uplift took place along the edges of cratons where the thickness of the crust and lithosphere changes substantially over a short distance. It may be that the lateral contrasts in the properties of the stretched and unstretched lithosphere make the margins of the cratons unstable long after rifting. These vertical movements have profound influence on hydrocarbon systems, not only in frontier areas such as West and East Greenland, where Mesozoic basins are deeply truncated and exposed onshore, but also for the understanding of near-shore hydrocarbon deposits in mature areas such as the North Sea Basin, where low-angular unconformities may represent episodes of deposition and removal of significant sedimentary sections.

Keywords: uplift, landscape, hydrocarbons, Greenland, Scandinavia, North Atlantic, exhumation, erosion

There are mountains along the passive continental margins on both sides of the North Atlantic (north of Charlie–Gibbs Fracture zone; Figs 1 & 2), as along many passive margins around the world. Characteristic features of these mountains are elevated plateaux that are cut by deep river valleys that may have been enlarged by glaciers (e.g. Lidmar-Bergström *et al.* 2000; Bonow 2006*a*, *b*). We have previously shown that the regional peneplain in West Greenland (Fig. 2) was formed as an erosion surface after removal of up to 1 km of additional section starting at *c.* 35 Ma, following kilometre-scale post-rift subsidence after breakup in the Paleocene, and that the present-day mountains are the result of late Neogene uplift and dissection of this erosion surface (Japsen *et al.* 2006, 2009). Peneplains have also been identified at high elevations in Norway, and it has been suggested that these surfaces were formed during the Cenozoic (Lidmar-Bergström *et al.* 2000, 2007). Neogene uplift of the land masses along North Atlantic rift systems has been documented by numerous studies (see Japsen & Chalmers 2000 for a review and also Bonow *et al.* 2007), but it is less widely recognized that such elevated plateaux are evidence of at least two major phases of uplift: one phase to produce the peneplain as an erosion surface that cuts unconformably across rocks of different ages and resistance, and a second phase of uplift to bring the peneplain to its present elevation above sea-level (a.s.l.).

The sedimentary successions in many basins around the North Atlantic also provide evidence for significant vertical movements and deep exhumation during the Neogene and earlier (e.g. Green & Duddy 2010). Pre-Cenozoic rocks are commonly exposed onshore and the pre-Quaternary sediments offshore are generally of Neogene age. Inclined Palaeogene and older beds are truncated by erosional unconformities along many coastlines such as along the western and eastern margins of the North Sea Basin and along Norway (Fig. 1; Japsen & Chalmers 2000). This configuration is consistent with Neogene uplift of the continents, and of the adjacent shelf, which significantly post-dates Palaeogene breakup both in the North Atlantic and between Greenland and Canada. That most of this uplift is unrelated to late Cenozoic glaciations has been documented by several studies, notably Stoker *et al.* (2005), who found that early Pliocene tilting of the Atlantic continental margin of NW Europe pre-dates the onset of widespread glaciation. The sedimentary succession, however, may also include low-angle unconformities that represent deep, regional exhumation that is not easily recognized.

These observations suggest strongly that episodic, post-rift uplift along passive continental margins has formed the present high mountains and affected the adjacent sedimentary basins. Such vertical movements cannot easily be understood in terms of the classical theory of continental stretching that predicts deposition of a thick post-rift sequence overlying both the rift and its margins (e.g. McKenzie 1978; White & McKenzie 1988). The ability to understand and model geological and physical processes in the past is, however, fundamental for our understanding of how hydrocarbon systems have evolved. It is thus essential to have an open-minded approach to such observations that indicates that theories which have proven useful for decades may not be applicable under all circumstances or may not tell the complete story. Recognition of such evidence is essential in order for new theories to be

Vining, B. A. & Pickering, S. C. (eds) *Petroleum Geology: From Mature Basins to New Frontiers – Proceedings of the 7th Petroleum Geology Conference*, 979–1004. DOI: 10.1144/0070979

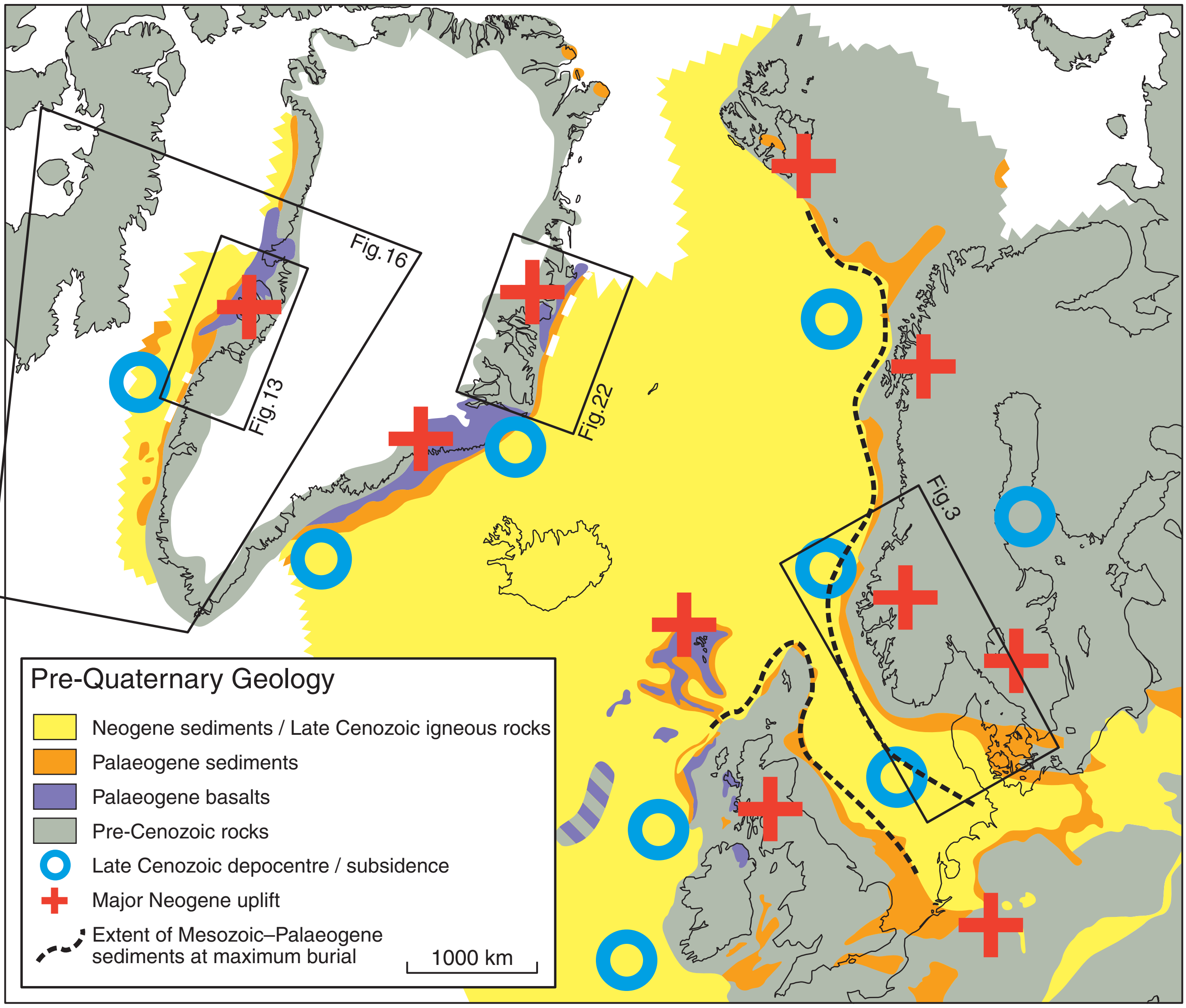

Fig. 1. Pre-Quaternary geology around the North Atlantic, showing centres of Neogene/late Cenozoic uplift and of accelerated subsidence/deposition. Pre-Cenozoic rocks are generally exposed onshore and the pre-Quaternary sediments offshore are generally of Neogene age. Between the two, inclined Palaeogene and older beds are truncated by erosional unconformities along many coastlines. Cenozoic exhumation is not limited to the areas of high topography, but has also affected much if not all of the area where Neogene cover is absent, as well as some regions where Neogene sediments are present. Along the Atlantic margin of NW Europe and Scandinavia, the extent of Mesozoic–Palaeogene sediments at maximum burial is traced (dashed line) based on numerous investigations (e.g. Japsen & Chalmers 2000; Japsen *et al.* 2007*a*; Green & Duddy 2010). Study areas discussed in this paper are indicated. The evidence presented here points to major Neogene uplift of the continents and the nearby basins which significantly post-dates the Palaeogene breakup. Modified after Japsen & Chalmers (2000).

formulated which may allow us to understand the nature of the unknown processes that are apparently driving vertical movements along passive continental margins.

It is thus a fundamental question as to whether a hiatus in the stratigraphic record represents an episode of stability and non-deposition or an event involving deposition and removal of rocks. A hiatus represents not only a gap in the stratigraphic record, but also a gap in our understanding of the geological history. The interpretation of what happened during the formation of a hiatus can thus have a profound influence on our understanding of the hydrocarbon system in an area (cf. Doré *et al.* 2002): when did maximum burial occur? How much section has been removed? How have migration paths been affected? Has a significant amount of hydrocarbon charge been lost from a breached reservoir during uplift? Such questions become very important not only in frontier areas such as West and East Greenland where Mesozoic basins are deeply truncated and exposed onshore, but also for the understanding of near-shore hydrocarbon deposits in mature areas such as the North Sea Basin (e.g. Japsen *et al.* 2007*a*).

Here we summarize results from recent and ongoing studies of burial, uplift and exhumation that are based on the integration of palaeothermal (apatite fission-track analysis, AFTA, and vitrinite reflectance, VR) data, palaeoburial (sonic) data and analysis of large-scale landforms constrained by the geological record. We will thus provide and review evidence for tectonic control of the palaeogeography of the eastern North Sea Basin (Case A), Neogene exhumation offshore south Norway (Case B), formation of the West Greenland mountains long after rifting and breakup (Case C), removal during the Oligocene of a significant cover offshore West Greenland (Case D), deposition and subsequent removal of a thick Ordovician–Triassic cover onshore West Greenland (Case E) and for post-rift burial of the East Greenland margin followed by uplift and exhumation (Case F).

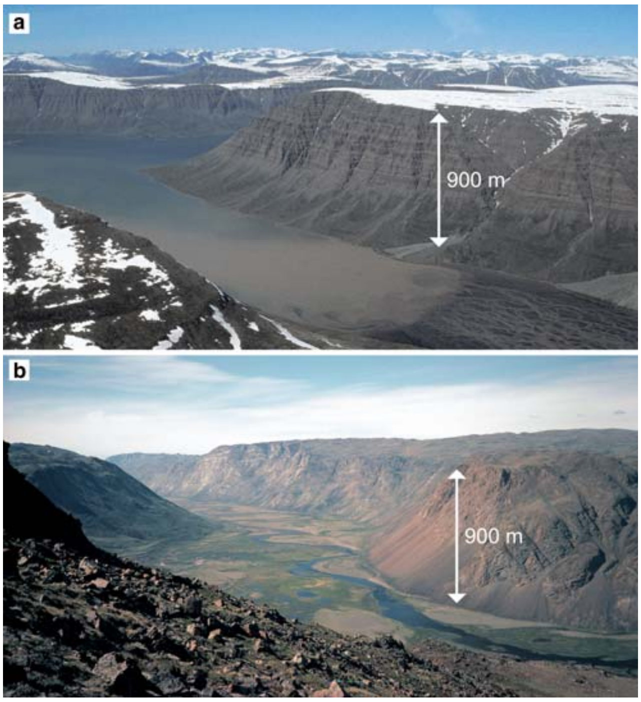

Fig. 2. Photos of the uplifted, regional peneplain in West Greenland (the upper planation surface, UPS) on (**a**) Disko and (**b**) northeast of Sukkertoppen Iskappe, in both cases around 900 m a.s.l. The UPS cuts across Precambrian basement (b), but the erosion surface can be traced northwards, to where it cuts across Palaeogene basalt on Nuussuaq and Disko (a). The peneplain is thus of Cenozoic age across central West Greenland and interpretation of AFTA and VR data has shown that the peneplain is an erosional surface formed after removal of a rock column up to 1 km thick after *c*. 35 Ma (see Fig. 15; Japsen *et al.* 2005*b*, 2009). Photo locations on Figure 13. Photo a, Niels Nielsen; photo b, Karsten Secher. Modified from Japsen *et al.* 2006, 2009.

Methods for estimating timing and magnitude of uplift and exhumation

Corcoran & Doré (2005) presented a review of techniques for estimating the magnitude and timing of exhumation in sedimentary basins and found that they could be categorized into four reference frames: tectonic, thermal, compactional (or rather effective stress) and stratigraphic. To this list we want to add geomorphological analysis that investigates the formation, preservation and destruction of large-scale landforms relative to changes in base level.

Tectonic-based techniques

A framework for the assessment of exhumation in offshore basins is provided by the lithospheric stretching model of McKenzie (1978), which predicts an initial syn-rift (fault related) subsidence followed by an exponentially decreasing post-rift (thermal) subsidence. White & McKenzie (1988) extended this analysis into two dimensions and showed that the post-rift subsidence cover should extend beyond the margins of the actual rift. Deviations of the observed from the predicted subsidence curves may be used to estimate the magnitude and timing of exhumation (e.g. Rowley & White 1998).

Palaeothermal techniques

Since temperature increases with depth within a sedimentary basin, determining the thermal history of a sedimentary unit provides the basis for estimating the depth to which it has been buried. A variety of methods are available which essentially constrain the maximum temperature experienced by a sedimentary unit, the most widely adopted of which is VR (e.g. Tissot & Welte 1984). In contrast, AFTA (Green *et al.* 1989, 2002) not only allows determination of the maximum temperature attained by a sedimentary unit, but also the time at which the sample began to cool from that temperature. In tandem, AFTA and VR in a vertical sequence of samples allow determination of the palaeogeothermal gradient at the palaeothermal maximum and extrapolation to an appropriate surface temperature allows determination of the amount of section that has been removed as a result of uplift and erosion (e.g. Bray *et al.* 1992; Japsen *et al.* 2005*b*, 2007*a*, 2009).

Palaeoburial (effective-stress) techniques

Reduction in sediment porosity takes place during burial due to the increased effective stress (the load of the overburden minus the pore pressure) that causes mechanical compaction and redistribution of mass due to pressure solution at grain contacts (e.g. Sclater & Christie 1980). As porosity reduction is largely irreversible, porosity becomes a proxy for the maximum burial (effective stress) of the sedimentary rock. Sonic velocity of a sedimentary rock may also be used as a proxy for maximum burial. The sonic-velocity method is robust for estimating maximum burial of sedimentary rocks of specific lithological composition because sonic velocities are measured directly in boreholes, they represent bulk properties of the sediment and they are sensitive to changes in burial as porosity is reduced and grain contacts become firmer during diagenesis (cf. Japsen *et al.* 2007*b*).

Palaeostructure techniques

The stratigraphic approach to the quantification of exhumation at an unconformity involves the identification of the maximum preserved section beneath the unconformity (the reference section). A minimum estimate of exhumation is then determined for a particular location by comparing the thickness of the equivalent stratigraphic unit encountered at that location with the reference section (e.g. Holliday 1993). Moreover, the method can be utilized even if the unconformity is at its maximum burial depth today. The technique is, however, difficult to apply over long distances and if an area has been deeply eroded.

Palaeosurface techniques

Extensive low-relief erosion surfaces (peneplains) defined by their geometric basal plane cutting across bedrock of different age and resistance form as erosion surfaces by river systems grading to the prevailing base level (Fig. 2) (cf. Ahlmann 1941; King 1967; Lidmar-Bergström 1996; Bonow *et al.* 2006*a*, *b*; Japsen *et al.* 2006, 2009). Unless the local base level is represented by a resistant rock surface, sea-level is the most likely base level, particularly for locations at or close to continental margins (e.g. in the cases of the coastal areas in Greenland and Scandinavia during the Cenozoic). Where such a surface has risen relative to base level, valleys will be incised into it as a new phase of erosion grades the landscape to the new base level. If a low-relief surface with incised valleys is found at a substantial height above present sea-level, the parsimonious explanation is that such a surface represents an uplifted peneplain. The height difference between the valley floor and the overlying peneplain is thus a proxy for the relative fall in base level (amount of uplift). Over time the valleys below the uplifted peneplain will expand to form a new peneplain graded to the new, lower base level. Erosion surfaces that have been buried and protected by sedimentary deposits and then re-exposed provide evidence of repeated episodes of uplift and erosion, subsidence and burial and renewed uplift. Analysis of the relationship between mapped erosion surfaces (re-exposed and those never buried; horizontal, inclined or in steps) and valleys incised below the surfaces provides a relative chronology for the formation of surfaces and for uplift/incision or subsidence/covering events as well as tilting and offsets by faulting of the surfaces.

Integrated studies of uplift and exhumation

The history of burial and exhumation of a sedimentary basin can be reconstructed most confidently by integrating a variety of independent methods, particularly involving methods based on thermal data (e.g. AFTA and VR) with methods based on palaeoburial (or effective stress, e.g. sonic velocities) and those based on landscape studies. Analysis of large-scale landforms (base-level governed peneplains) is the only method that provides an absolute estimate of the amount of surface uplift, whereas studies of palaeothermal and palaeoburial indicators provide estimates of exhumation (removal of rock column). By combining such studies, it is thus possible to evaluate if exhumation was accompanied by surface uplift (e.g. Japsen *et al.* 2006). Uplift and subsidence may be driven tectonically, but can also be caused by isostatic compensation due to erosional unloading and depositional loading, respectively (e.g. Medvedev *et al.* 2008) and the trigger for the erosion and deposition may be eustatic changes in sea-level. The driving forces behind such vertical movements must thus be assessed in each and every case (see Case A and the discussion at the end of this paper). It is additionally possible to limit the likely range of the palaeothermal gradients during maximum burial by estimating the maximum burial depth independently from sonic data (Case B; cf. Japsen *et al.* 2007*a*). Studies of the Cenozoic thermal and burial history in West Greenland have shown that the regional, elevated peneplain there provides a more useful reference level for evaluating palaeotemperature profiles than present-day sea-level (Cases C and E). Integration of the results from thermochronological studies with even very simple constraints from the geological record will often highlight the episodic nature of the burial and exhumation history along a margin (Case F). Effects related to climate change can also cause cooling in the subsurface and hence potentially cause effects detectable in AFTA data. In a study in the eastern North Sea Basin, Japsen *et al.* (2007*a*) found that the effects of Eocene climate change could be resolved confidently from those of late Neogene burial only by integrating palaeothermal methods with temperature-independent estimates from sonic data.

Case A: tectonic control on Cenozoic stratigraphy and palaeogeography in the eastern North Sea Basin

The eastern North Sea Basin is a key region for studies of the Cenozoic development of Scandinavia because Paleocene to upper Miocene sediments crop out onshore Denmark and because it is possible to correlate these occurrences with the up to 3 km thick Cenozoic succession of the North Sea Basin (cf. Fig. 1). However, the Cenozoic deposits onshore Denmark occur close to the surface only because they have been exhumed from beneath their cover of younger rocks. This implies that a reconstruction of the Cenozoic development in the eastern North Sea Basin, involving both burial and exhumation, must rely on sedimentological and seismostratigraphic studies of preserved sediments as well as on physical parameters that may yield evidence of the post-depositional history of the sediments now at the surface. Only if the burial and exhumation history of the basins can be deciphered is it possible to infer the geological development in the Scandinavian hinterland where Cenozoic sediments are rarely preserved.

In a study using AFTA and VR data from eight Danish wells, Japsen *et al.* (2007*a*, 2008) identified four Mesozoic–Cenozoic palaeothermal events, that is, episodes of heating and subsequent cooling that are not reflected in the preserved rock record. These episodes were interpreted as being caused by burial and subsequent exhumation and one phase reflecting climate change during the Eocene. The study combined thermal history reconstruction with exhumation studies based on palaeoburial (sonic velocity), stratigraphic and seismic data (cf. Japsen & Bidstrup 1999; Green *et al.* 2002; Nielsen 2003; Rasmussen 2004; Japsen *et al.* 2007*b*). Two of the exhumation phases occurred during the mid-Jurassic and the mid-Cretaceous, but here we focus on the Cenozoic development and on the early and late Neogene exhumation phases during which up to 1 km of sediments was removed across much of the eastern North Sea Basin (Fig. 3). The inferred palaeogeographical development of the area during the Cenozoic reflects a complex interaction of subsidence, progradation after tectonic pulses in the Scandinavian hinterland and episodes of uplift and exhumation reaching far into the sedimentary basin (see Fig. 4).

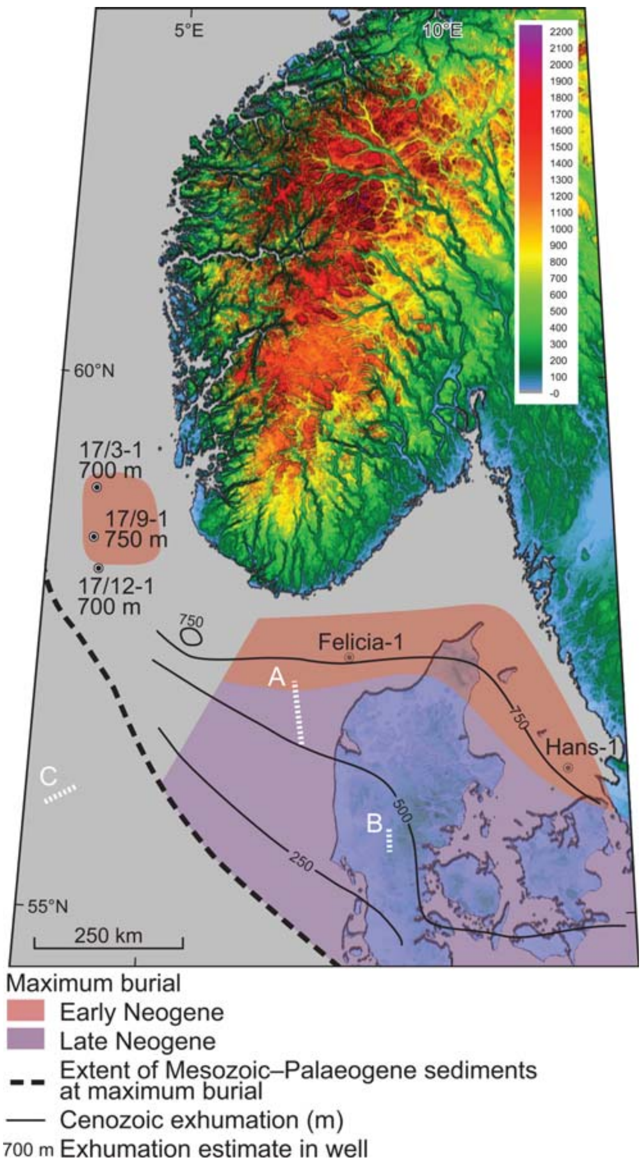

Fig. 3. The eastern North Sea Basin and southern Norway (topographic colour code). Contours of estimated thickness of the section removed during Cenozoic exhumation (modified after Japsen *et al.* 2007*a*). Maximum burial of the Mesozoic sediments took place during the late Neogene in most of the study area. Near the present coasts of Norway and Sweden, however, maximum burial occurred subsequent to deposition of the Oligocene wedges and prior to early Neogene exhumation. Only near the Hans-1 well did maximum burial occur during the Mesozoic. Modified after Globe Task Team (1999) and Japsen *et al.* (2007*a*). Location of map shown in Fig. 1.

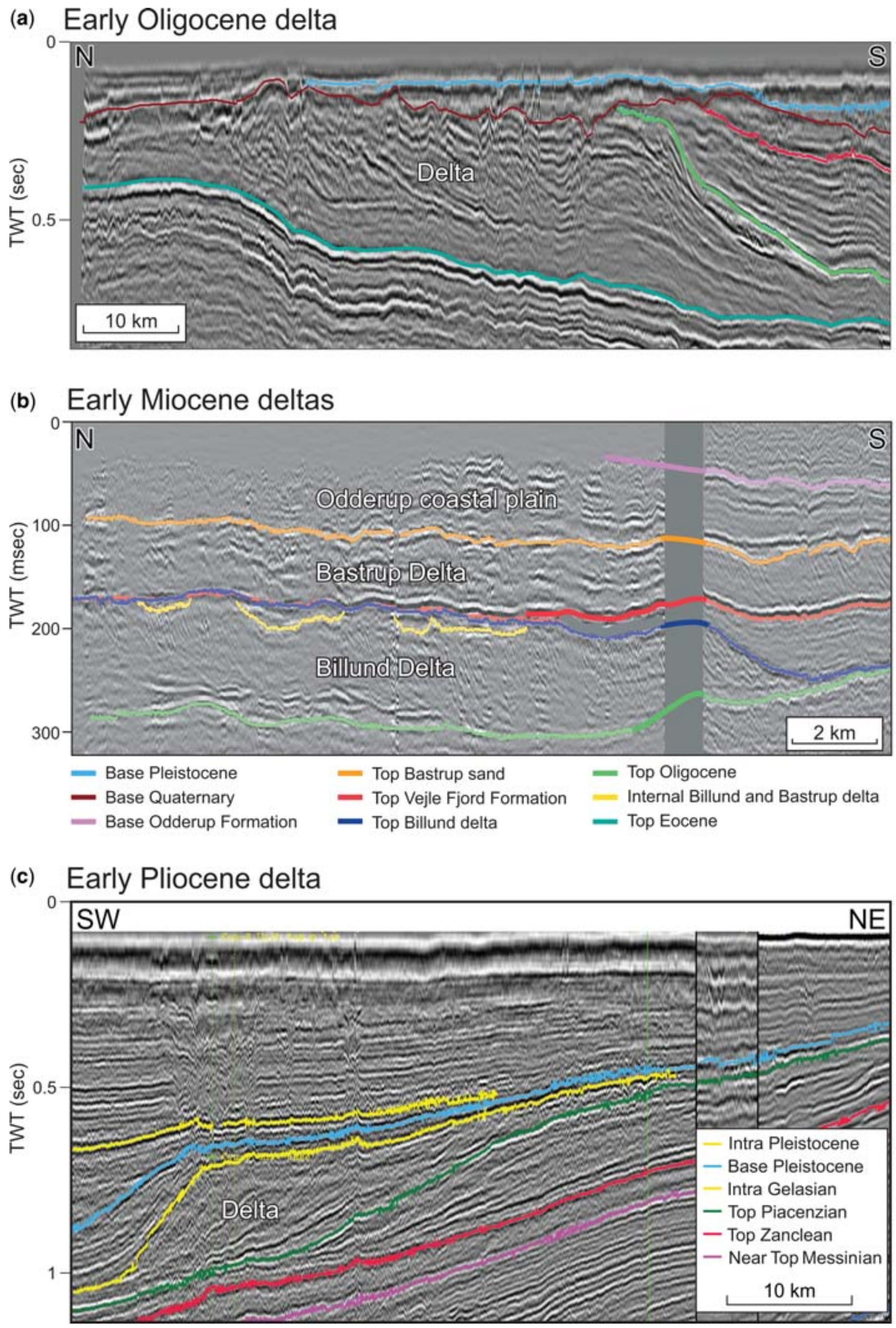

Fig. 4. Seismic sections illustrating deltas prograding in directions away from present-day Norway in response to uplift. (**a**) Early Oligocene delta prograding towards the south. This progradation represents a major change from the deposition of fine-grained hemipelagic marine sediments prior to the progradation. (**b**) Early Miocene deltas prograding southwards (modified from Rasmussen 2009*a*). The Billund delta was characterized by a braided fluvial system while the Bastrup delta was dominantly characterized by a meandering system. This indicates a tectonic influence on the sedimentary pattern in the earliest early Miocene. (**c**) Pliocene delta prograding towards SW (modified from Japsen *et al.* 2007*a*). The progradation after the Zanclean (*c*. 3.6 Ma, red reflector) is followed by renewed subsidence in the central North Sea. Locations in Figure 3.

Early and late Neogene exhumation

A major phase of exhumation of the parts of the eastern North Sea Basin adjacent to the presently exposed basement areas in Norway and Sweden began between 30 and 20 Ma ago according to the AFTA data from wells Felicia-1 and Hans-1 (Fig. 3). Japsen *et al.* (2007*a*) suggested that this phase corresponds to a regional early Neogene unconformity (*c*. 23 Ma at the Oligocene–Miocene boundary, but for simplicity we will refer to this event as early Neogene; see Rasmussen 2009*b*). Prior to this exhumation phase, the Mesozoic sediments in the Felicia-1 well were at maximum burial. The maximum burial of the Mesozoic sediments in the Hans-1 well occurred during the mid-Cretaceous, prior to inversion along the Sorgenfrei–Tornquist Zone, while renewed Cenozoic exhumation began in the early Neogene phase.

AFTA data from several wells (e.g. Felicia-1) suggest that the most recent episode of Neogene exhumation began between 10 and 5 Ma, but Japsen *et al.* (2007*a*) suggested that exhumation probably began in the early Pliocene at *c*. 4 Ma, as suggested by the prominent unconformity of this age (with only one AFTA sample limiting the onset to 5 Ma). A section of 450–850 m was removed over much of Denmark in association with this reshaping of the North Sea Basin (Fig. 3). The exhumation affected extensive regions where Neogene strata are truncated, and a sub-Cretaceous

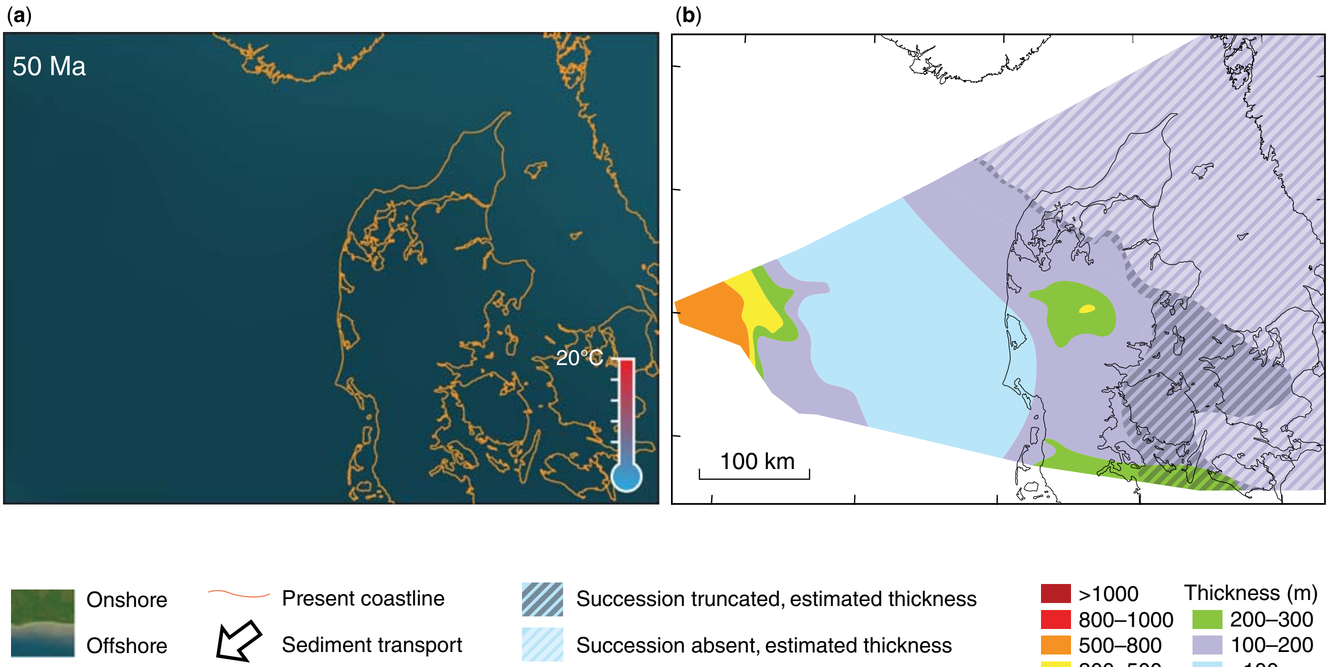

Fig. 5. (**a**) Early Eocene (50 Ma) palaeogeography in the eastern North Sea Basin. Deep sea, no indication of any coastline near the present Scandinavian basement areas. (**b**) Upper Paleocene–Eocene isochore prior to Neogene exhumation. Temperatures indicated are for the coldest month along the southern margin of the North Sea Basin (Utescher *et al.* 2009). Modified after Japsen *et al.* (2007*a*, 2008).

etch surface (ES) was re-exposed along the coasts of southern Norway and Sweden during the late Neogene phase (Lidmar-Bergström *et al.* 2000; Japsen *et al.* 2002).

Cenozoic palaeogeography of the eastern North Sea Basin

We have compiled a series of maps to illustrate the Cenozoic development of the eastern North Sea Basin (Figs 5–9). The isochore maps are based on present thicknesses and estimates of the total amount of section removed by Cenozoic exhumation. The estimates of the removed sections of specific ages are furthermore constrained by the known geology and our interpretation of the depositional pattern. Each isochore map shows the thicknesses prior to the first phase of exhumation that affected the distribution of the unit, that is, prior to early Neogene exhumation (starting at *c.* 23 Ma) in the case of the Palaeogene units and prior to late Neogene exhumation (starting at *c.* 4 Ma) for the Neogene units. The palaeogeographic maps show the distribution of onshore and offshore areas separated by the coastline based on the known geology. In the areas where the deposits of a given age have been removed, the maps have been drawn from an estimate based on our interpretation of the depositional system and on the inferred burial and exhumation history.

The presence of hemipelagic, deep-marine deposits of Eocene age in the eastern North Sea Basin suggests that much of Scandinavia was covered by a deep sea from the early Eocene until latest Eocene times (Fig. 5a; Heilmann-Clausen *et al.* 1985; Michelsen *et al.* 1998): Eocene deposits less than 100 km from basement currently exposed in Sweden contain a deep-marine fauna with no

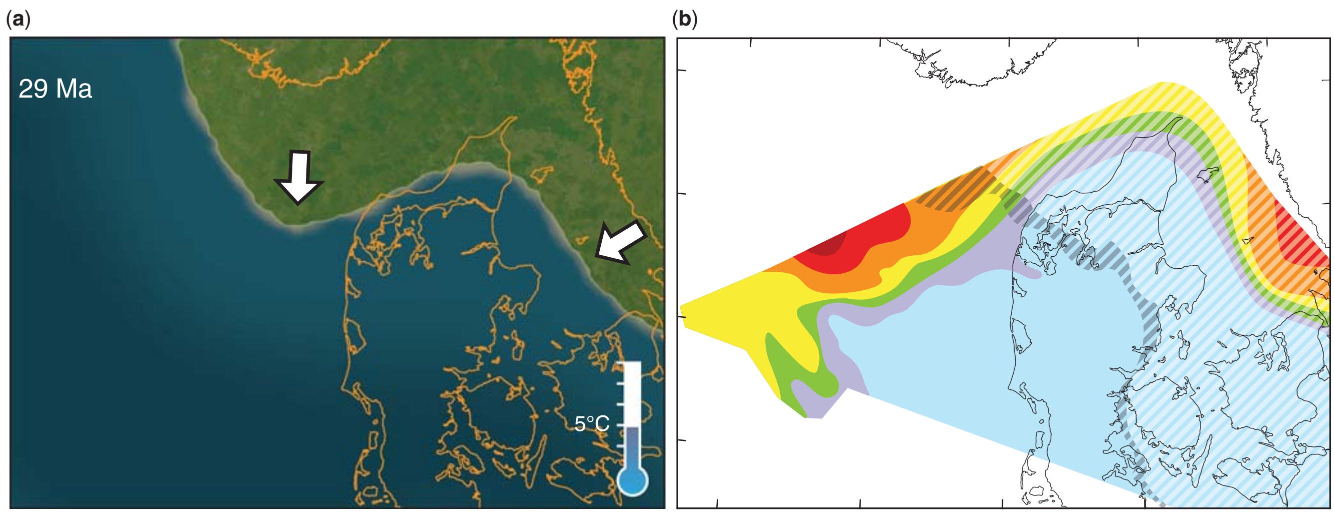

Fig. 6. (**a**) Mid-Oligocene (29 Ma) palaeogeography in the eastern North Sea Basin. Progradation of sedimentary wedges after first Scandinavian uplift phase (*c.* 33 Ma). (**b**) Oligocene isochore prior to Neogene exhumation. Legend in Figure 5. Modified after Japsen *et al.* (2007*a*, 2008), Schiøler *et al.* (2007).

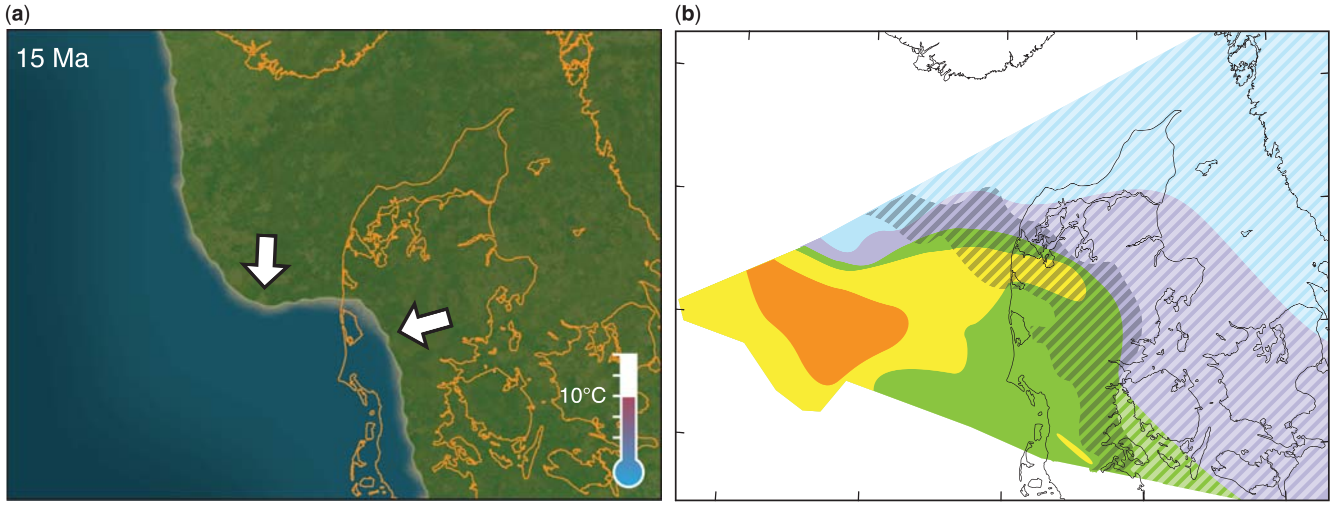

Fig. 7. (**a**) Middle Miocene (15 Ma) palaeogeography in the eastern North Sea Basin. Progradation of sedimentary wedges after second Scandinavian uplift phase (*c*. 23 Ma). (**b**) Lower to lower, middle Miocene isochore prior to late Neogene exhumation. Legend in Figure 5. Modified after Japsen *et al.* (2007*a*, 2008).

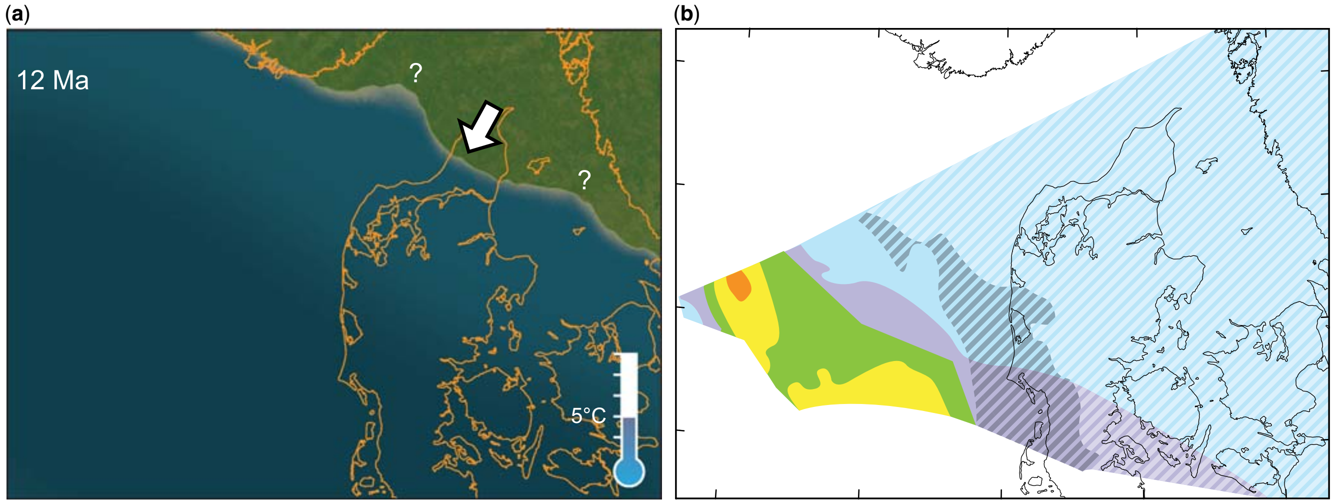

Fig. 8. (**a**) Late Miocene (12 Ma) palaeogeography in the eastern North Sea Basin. Transgression, despite colder climate, due to tectonic subsidence. (**b**) Upper, middle to lower, upper Miocene isochore prior to late Neogene exhumation. Legend in Figure 5. Modified after Japsen *et al.* (2007*a*, 2008).

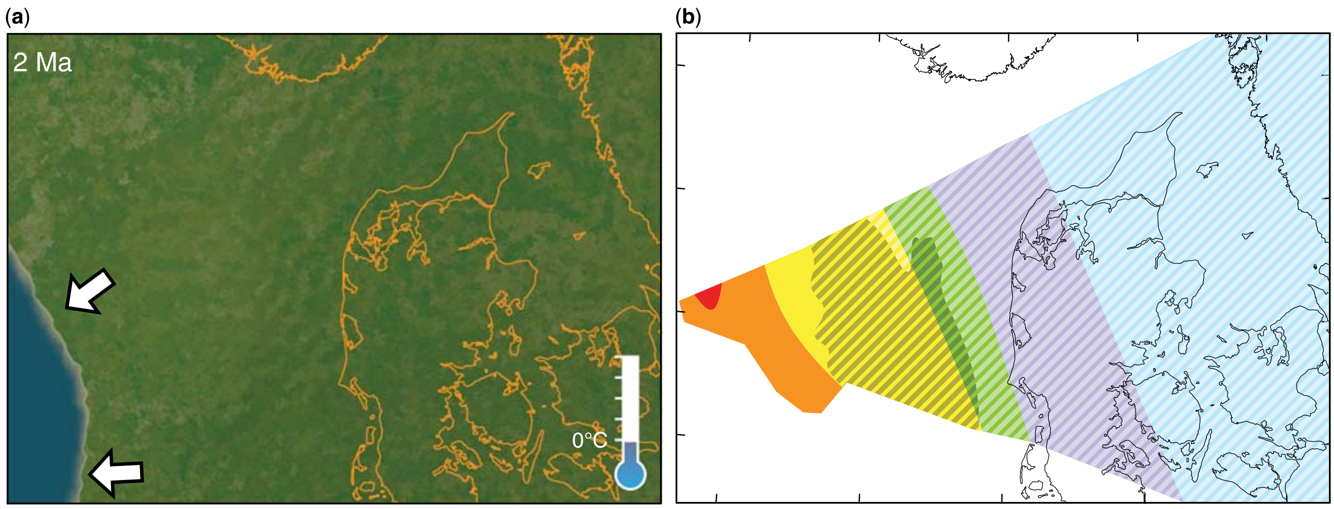

Fig. 9. (**a**) Pliocene (2 Ma) palaeogeography in the eastern North Sea Basin. Progradation and subsidence after third Scandinavian uplift phase (*c*. 4 Ma). (**b**) Upper, upper Miocene–Pliocene isochore prior to late Neogene exhumation. Legend in Figure 5. Modified after Japsen *et al.* (2007*a*, 2008).

signs of a near-shore fauna (Fig. 5a) (C. Heilmann-Clausen, pers. comm. 2005). Reworked Eocene dinocysts and clasts of Eocene muds interbedded with Miocene deltaic sediments in Denmark clearly indicate the presence of marine Eocene deposits in the Scandinavian hinterland that were eroded and redeposited during the Miocene (Rasmussen 2004). The thickness of the upper Paleocene–Eocene sediments that were removed from the study area during the Neogene rise of Scandinavia was probably limited to less than about 200 m (Fig. 5b).

During the early Oligocene, major clastic wedges prograded southwards from present-day Norway and reached their maximum extent at 29 Ma (Figs 4a & 6a) (Schiøler *et al.* 2007). This change in depositional environment from Eocene times indicates a phase of uplift of southern Norway that started a few million years before the maximum extent of the prograding wedges (i.e. *c.* 33 Ma) (e.g. Michelsen *et al.* 1998; Clausen *et al.* 1999; Lidmar-Bergström *et al.* 2000; Faleide *et al.* 2002). Miller *et al.* (2005) show no large fall in eustatic sea-level at any time within the uncertainty of these dates, so the cause of the uplift is presumably tectonic. We suggest that a thick succession of Oligocene shelf and delta sediments that prograded southwards from southern Norway and westwards from southern Sweden made up a substantial part of the section that was removed during the Neogene exhumation beginning at *c.* 23 Ma at the locations of the Felicia-1 and Hans-1 wells (>1 km; Fig. 6b).

During the early Miocene, deltas prograded to the south and SW from present-day Norway and southern Sweden, reaching a thickness of up to 300 m (Figs 4b & 7a). Deposition of coarse-grained sediments extended over much of the present-day Danish onshore area during the Neogene (Rasmussen 2004). These prograding systems reflect partly a redistribution of older sediments and partly erosion of strongly weathered basement. The basinward progradation in the early Neogene was caused by uplift in the Scandinavian hinterland that also resulted in the early Neogene exhumation near the craton. The occurrence of both immature and mature sediments reflects erosion of weathered as well as newly exposed basement. In the Danish area, the early Miocene tectonic activity is demonstrated by coarse-grained, braided fluvial systems and later by a sudden increase in the heavy mineral content at *c.* 17 Ma (Rasmussen 2004). The thickness of the lower to lower-middle Miocene sediments that was removed during late Neogene exhumation was substantial (<500 m) (Fig. 7b). The lowering of relative sea-level implied by this event does not correlate with cooler climate, because the climate was warm temperate and subtropical during both the late Oligocene and early Miocene (Utescher *et al.* 2009), so the lowering of sea-level must have been due to basin-wide inversion tectonism (Rasmussen 2009*b*).

A distinct marine flooding of the area took place after *c.* 15 Ma in the middle Miocene, with maximum transgression of the sea taking place at *c.* 12 Ma (Fig. 8*a*; Rasmussen 2005). Up to 150 m of clayey sediments were deposited in southwestern Denmark during the middle to late Miocene. This flooding occurred at the same time as the mid-Miocene deterioration in climate. Cool climate should correlate with low sea-level due to the formation of land ice, so this flooding must have been caused by increased tectonic subsidence in the eastern North Sea Basin in the late Miocene (Rasmussen 2004). The thickness of the upper-middle to lower-upper Miocene sediments that was removed during late Neogene exhumation was limited (<200 m; Fig. 8b).

Delta progradation resumed from the northeast and in particular the east at the end of the Miocene (Figs 4c & 9a; Rasmussen 2005). The infilling of the North Sea Basin continued during the Pliocene when up to 500 m of sediment were deposited in the central North Sea Basin. Substantial thicknesses (<500 m) of Upper–Upper Miocene–Pliocene sediments were removed during late Neogene exhumation across an extensive region of the eastern North Sea (Fig. 9b).

Phases of post-breakup uplift of southern Scandinavia

These results emphasize that the tectonic development of a region cannot be reconstructed solely on evidence from the preserved sedimentary record. Such reconstructions must also integrate evidence provided by palaeothermal and palaeoburial techniques of geological units that were once present but have now been removed. As described above, we find evidence for three phases of uplift that have affected southern Scandinavia after North Atlantic breakup at the Paleocene–Eocene transition at *c.* 55 Ma (e.g. Eldholm *et al.* 1989; Ziegler 1990; Skogseid *et al.* 2000):

(1) a phase that began at the Eocene–Oligocene transition at *c.* 33 Ma as indicated by the onset of progradation of clastic wedges away from southern Norway and inferred progradation away from southern Sweden;
(2) an early Neogene phase that began at *c.* 23 Ma, as indicated by exhumation of the basins adjacent to the presently exposed basement areas and by early Miocene coarse-grained braided fluvial systems south of Scandinavia;
(3) a late Neogene phase that began at *c.* 4 Ma, as indicated by the widespread exhumation, Pliocene delta progradation off Scandinavia and subsequent tilting of the Neogene succession in the eastern North Sea.

These phases are consistent with the stratigraphy in the NE Atlantic (Stoker *et al.* 2005) and around southern Norway (e.g. Michelsen *et al.* 1998; Faleide *et al.* 2002; Rasmussen 2004). The observations thus suggest that southern Norway, with peaks higher than 2 km a.s.l., emerged during several phases since Eocene times, when a deep sea covered much of the region. This deep Eocene sea may have developed in response to post-rift subsidence after breakup in the North Atlantic. However, the subsequent uplifts are clearly not in agreement with classical theory for the post-rift development of a rifted margin (e.g. McKenzie 1978; White & McKenzie 1988). We discuss this further in the Chapter 'On the origin of post-rift uplift along passive margins'.

The reconstruction of the palaeogeography of the eastern North Sea Basin (Figs 5–9) illustrates that the variations in relative sea-level cannot be explained by climate variations alone: for each palaeogeographic episode, the mean temperature of the coldest month is indicated and this shows that, whereas the high sea-level in the Eocene could reflect the warm climate, the transgression at 12 Ma occurs during a cold period. Consequently, the increased sea-level at that time must be due to tectonic subsidence.

As we have shown here, these events of uplift and erosion affected not only the exposed basement areas onshore, but also adjacent basins that are mainly offshore today. An accurate reconstruction of these events, both with respect to timing and magnitude, is important for understanding the petroleum systems of the marginal basins fringing southern Norway. For example, failure to account for the additional burial offshore can lead to underestimation of likely maturity levels. Similarly, understanding the timing of maximum burial and subsequent exhumation in relation to formation of potential trapping structures is essential to predict migration pathways and possible loss of charge due, for example, to breach of seals and phase changes during uplift. In this connection, the Neogene maximum burial off southern Norway and the resulting late hydrocarbon generation increases the likelihood of charging early-formed structures and the preservation of hydrocarbons to the present day. Early hydrocarbon expulsion can become a critical factor because it involves a long preservation phase for the hydrocarbons in the traps.

Case B: early Neogene exhumation offshore southern Norway

Early Neogene uplift caused the regional inversion of the Norwegian–Danish Basin and of the southern Central Graben (Japsen *et al.* 2007*a*; Rasmussen 2009*b*). A regional unconformity was formed, especially over elevated areas and on top of major prograding Oligocene successions. The style of the early Neogene tectonism contrasts with the pronounced tilting of the sedimentary succession produced during the late Neogene uplift, which resulted in truncated Neogene and older units overlain by flat-lying Quaternary units which makes the late Neogene event easily recognizable on seismic sections. The regional nature of early Neogene uplift and erosion results in a very low-angle unconformity over wide areas and can thus be difficult to identify on seismic sections. In addition, stratigraphic data for the Oligocene–Miocene strata are often sparse, as this section is often drilled prior to the first casing being set and is not sampled, so any base-Neogene unconformity may be difficult to identify. However, the exhumation caused by the event may, as we show here, be identified with palaeoburial (sonic) and palaeothermal (AFTA and VR) methods.

Magnitude of exhumation estimated from palaeoburial data

Basic concepts. Exhumation can be estimated from sonic velocities of sediments measured in boreholes. The basic parameter is the burial anomaly, dZ_B, which is the difference between the present-day burial depth of a rock, z, and the depth, $z_N(V)$, corresponding to normal compaction for the measured velocity, V, and the lithology in question (Japsen 1998):

$$dZ_B = z - z_N(V)$$

The depth corresponding to normal compaction (the effective depth; Japsen *et al.* 2005*a*) may be determined from a normal velocity–depth trend (baseline), which is a function that describes how sonic velocity increases with depth in a relatively homogeneous, brine-saturated sedimentary formation when porosity is reduced during normal compaction (mechanical or by pressure solution). Compaction is ‘normal’ when the fluid pressure of the formation is hydrostatic, and the formation is at maximum burial depth. Normal velocity–depth trends are specific for given lithologies such as marine shale (Japsen 1999, 2000), sandstone (Japsen *et al.* 2007*b*) and chalk (Japsen 1998, 2000).

The burial anomaly is zero for normally compacted sediments, whereas high velocities relative to depth give negative burial anomalies which may be caused by a reduction in overburden thickness when lithology is relatively homogeneous over the study area, and if lateral variations of horizontal stress are minor. A positive burial anomaly may indicate undercompaction due to overpressure. Any post-exhumational burial, B_E, will mask the magnitude of the missing (removed) overburden section, Δz_{miss}:

$$\Delta z_{\text{miss}} = -dZ_B + B_E \qquad (1)$$

where the minus indicates that erosion reduces depth (Hillis 1995; Japsen 1998). The timing of the exhumation events is thus important for understanding the succession of events, their true magnitude and for identifying the age of the eroded succession.

Estimation of burial anomalies in three Norwegian wells. Burial anomalies have been estimated for the Mesozoic–Palaeogene succession in three Norwegian wells from quadrant 17 (Figs 3 & 10). The estimates are primarily based on a comparison between (1) the sonic data for the chalk of the Upper Cretaceous–Danian Shetland Group and the chalk baseline (Japsen 2000), (2) the sonic data for the Palaeogene shales and the shale baseline (Japsen 2000) and (3) the sonic data from below the chalk and the shale baseline. There are ample variations of the sonic data over the latter interval where shale units typically dominate above the Upper Jurassic Tau Formation, which is a local source rock with a characteristic, low sonic velocity that reflects high organic content. Very low velocities in the upper part of the Lower Cretaceous Åsgård Formation and the overlying Sola Formation may have a similar explanation.

Anomalously low velocities are found in the uppermost part of the chalk below high-velocity carbonates in two wells, 17/9-1 and 17/12-1R. There is no correlation between the gamma response and the low velocities in these chalk intervals. A possible explanation is that these low velocities (high porosities) are caused by the presence of hydrocarbons in the chalk at an early stage during the compaction of the chalk. Since 17/12-1R was the discovery well of the Bream Field, leaking from the Jurassic reservoir rocks into the chalk in the overburden is not unlikely and hence the presence of hydrocarbons at some stage during the Cenozoic burial history. The presence of hydrocarbons is known to have a porosity-preserving effect in chalk where the coating of the grains with hydrocarbons prevents pressure solution of the carbonates (e.g. Fabricius *et al.* 2008).

The estimation of the burial anomaly is based on depth-shifting shale and chalk baselines by the same amount until a match is obtained with the data for the intervals of the identified lithologies that are considered most reliable – typically the Upper Cretaceous–Danian chalk and the Palaeogene shale. The match is primarily based on the absolute level of the sonic velocities in these intervals, but also on identification of velocity–depth trends for these intervals. The benefit of this integrated approach is that, whereas the velocity–depth trend for one of the above mentioned intervals may be difficult to identify, the comparison of sonic data for two or more lithologies with their respective baselines effectively limits the range of the possible burial anomalies and also guards against the possible effects of local variations in lithology (Fig. 10).

The timing of the exhumation can only be broadly estimated from the available sonic and stratigraphic data (as being younger than the overcompacted Palaeogene shales), but the available AFTA data for these wells provide good constraints on when maximum burial took place.

Timing and magnitude of exhumation from palaeothermal and palaeoburial data

Thermal history reconstruction, based on AFTA and VR data, has been applied in the three wells to define the onset of cooling, as well as providing independent corroboration of the magnitude of the exhumation revealed from the sonic velocity analysis. The methods employed are described in detail by, for example, Japsen *et al.* (2007*a*). Results from all three wells provide consistent evidence that the pre-Cenozoic section has been hotter in the past. AFTA and VR data in each well provide consistent indications of maximum post-depositional palaeotemperatures, and the combined AFTA dataset from all three wells shows that cooling from the palaeothermal maximum began some time in the interval 30–15 Ma, that is, late Oligocene to middle Miocene.

Palaeotemperatures derived from AFTA and VR data in the three wells are plotted as a function of depth in Figure 11. Results from each well define consistent linear profiles, sub-parallel to the present-day temperature profile derived from corrected borehole temperature (BHT) values in each well, and offset to higher temperatures by around 20–30 °C. The form of these profiles suggests that deeper burial is the most likely explanation of the

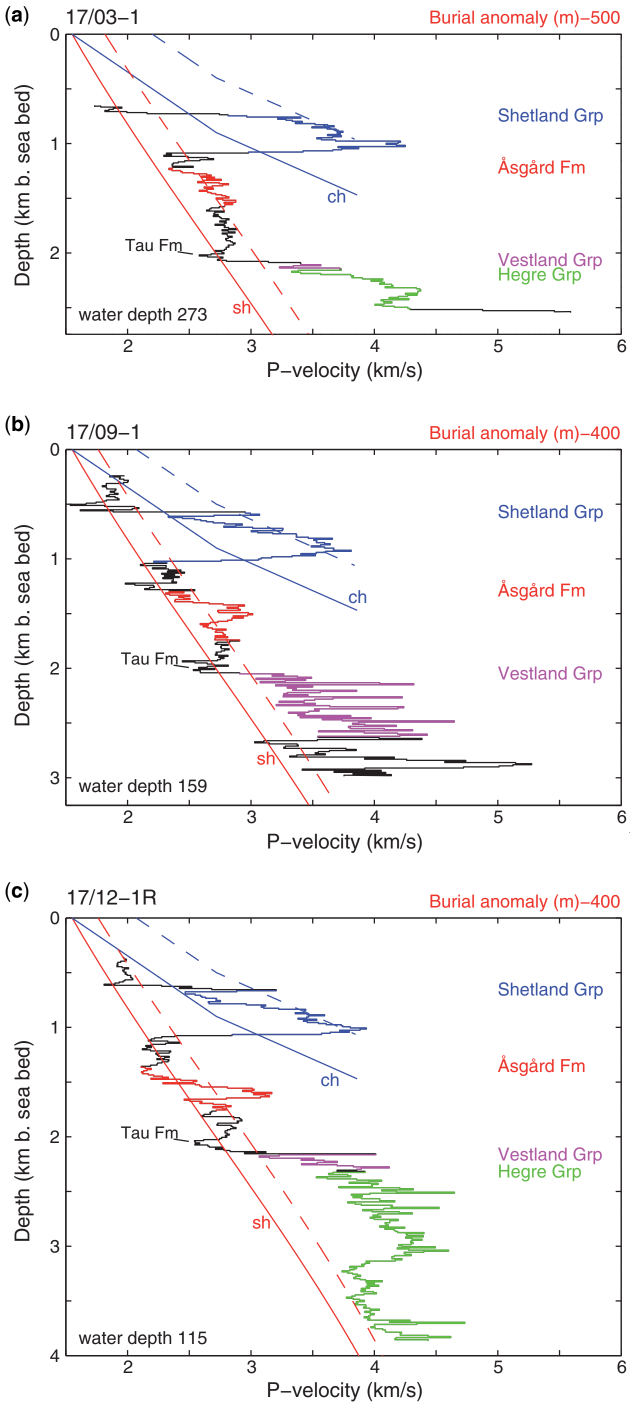

Fig. 10. Plot of sonic logs for three Norwegian wells compared with (1) the baselines for chalk and shale and (2) these baselines shifted by the burial anomaly estimated for the pre-Neogene section in each of the wells: (**a**) 17/3-1 (**b**) 17/9-1 and (**c**) 17/12-1R (location in Fig. 3). The chosen value of the burial anomaly is based on the agreement between the sonic data for the Palaeogene shale, for the chalk of the Shetland Group and for the Lower Cretaceous–Jurassic shale and the depth-shifted baselines for chalk and shale. The match is primarily based on the absolute level of the sonic velocities in these intervals, but also on identification of velocity–depth trends for these intervals. The comparison of sonic data for two lithologies with their respective baselines effectively limits the range of the possible burial anomalies. See Table 1 for details concerning the estimation of the burial anomaly in each well. Selected lithostratigraphic units are indicated in the diagram with a colour corresponding to the colouring of that part of the sonic log (cf. Well Data Summary Sheets at www.npd.no). Legend: ch, baseline for chalk; full blue line (only for velocities less than 3.9 km/s; see Japsen *et al.* 2005*a*); sh, baseline for shale; full red line (Japsen 2000); dashed line, baseline for respective lithology shifted vertically by the burial anomaly to fit the data trend. Burial anomaly <0 indicative of exhumation.

palaeotemperatures derived from AFTA and VR in these wells, supporting the conclusion derived from the sonic velocity analysis that the Palaeogene and older section in these wells has been more deeply buried and subsequently exhumed. The profile of palaeotemperatures derived from VR data in the 17/12-1 well is less well defined than in the other two wells, resulting in broader constraints on allowed palaeogeothermal gradients in this well.

The timing of cooling indicated by AFTA data in these three wells, between 30 and 15 Ma, correlates closely with the 30–20 Ma onset of cooling obtained from AFTA in the Felicia-1 well by Japsen *et al.* (2007*a*), where this cooling was correlated with exhumation corresponding to formation of a regional early Neogene unconformity (as discussed under Case A). We therefore infer that the cooling revealed by AFTA in the three wells from Quad 17 also represents exhumation at this time. Given these timing constraints, we have selected the top-Oligocene horizon identified in these wells as the reference for determining amounts of additional section (Table 1).

Using the methods outlined by Bray *et al.* (1992) and Green *et al.* (2002), we have determined the range of palaeogeothermal gradients allowed by the palaeotemperature constraints derived from AFTA and VR data in each well. Extrapolating the fitted palaeogeothermal gradients from the corresponding unconformity surface to an appropriate palaeosurface temperature allows determination of the amount of additional section that is required to explain the observed palaeotemperatures. This analysis explicitly assumes that the palaeogeothermal gradient was linear at the palaeothermal maximum. Comparison of the amounts of additional section determined from this approach with independent values determined from the sonic velocity analysis provides a check on the validity of this assumption.

Results of this analysis for the three wells are shown in Figure 12. For each well, a hyperbolic region defines the range of correlated values of palaeogeothermal gradient and removed section that can explain the observed palaeotemperatures with 95% confidence limits (see e.g. Green *et al.* 2002, 2004; Japsen *et al.* 2007*a* for further details). Also shown for each well is the range of values of additional burial defined by the sonic velocity analysis, obtained by adding the amounts of post-Oligocene re-burial in each well to the appropriate burial anomaly from Figure 10 [Equation (1)]. In two wells (17/3-1 and 17/9-1), values of additional burial defined from the palaeoburial approach show excellent agreement with the range of values indicated from palaeothermal techniques for a constant heat-flow scenario (i.e. for palaeogeothermal gradients equal to the present-day value in each well). In well 17/12-1, the palaeothermal constraints are wider than in the two other wells (Fig. 11) and comparison with the results of the sonic analysis shows a discrepancy. Based on the consistent results of the sonic data in all three wells, the sonic estimate of exhumation in well 17/12-1 is preferred. Thus, the combination of the two approaches in these wells provides strong evidence for deposition and subsequent erosional removal of around 700 m of additional section on an early Neogene unconformity in the eastern North Sea off southern Norway (Fig. 3).

Multiple episodes of uplift onshore and offshore Norway

The evidence presented here for a major exhumation event between 30 and 15 Ma in Norwegian quadrant 17, which correlates with the early Neogene event (*c.* 23 Ma) identified in Danish wells, supports the conclusion that a regional uplift event affected southern Norway and the adjacent basins at that time, as suggested in Case A. The geological response to this event is the lower Miocene deltas that prograded to the south and SW from mainland Norway and central Sweden with thicknesses of up to 300 m (cf. Figs 4b & 7a).

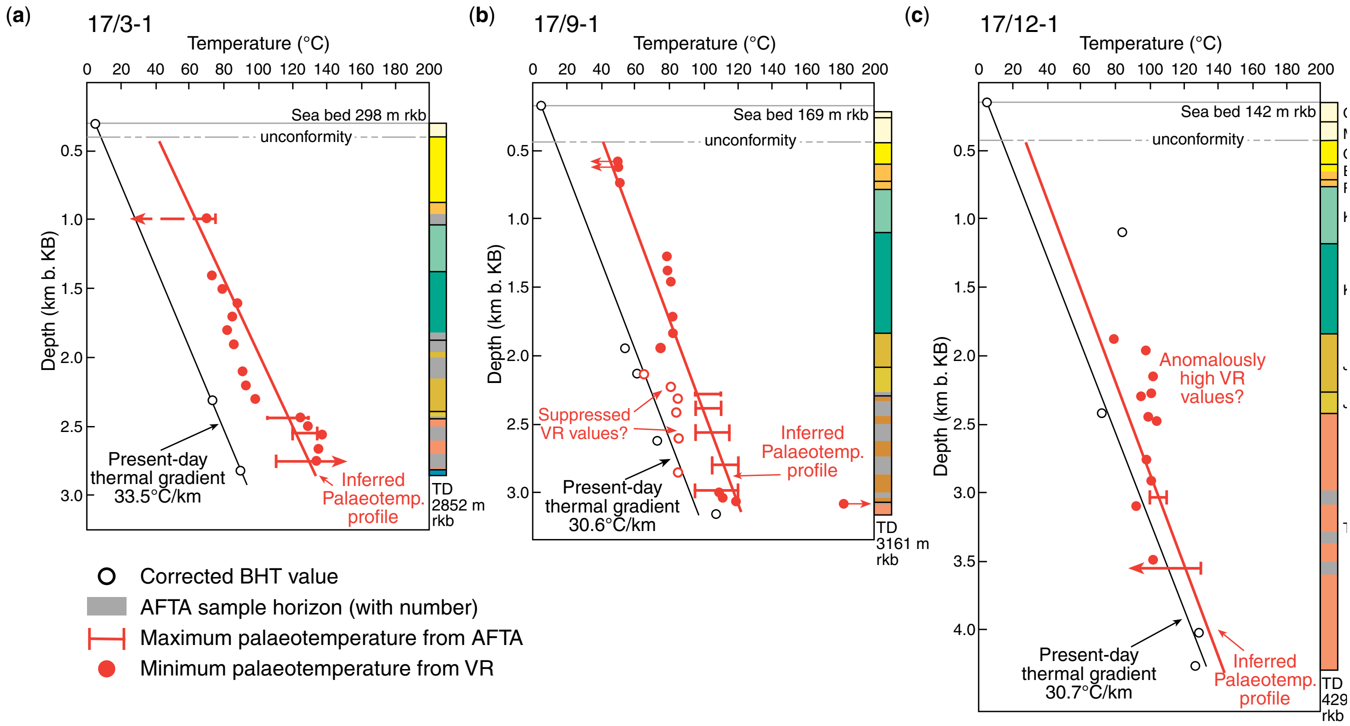

Fig. 11. Thermochronological constraints on the amounts of section removed in three Norwegian wells (location in Fig. 3). AFTA and VR data have been used in each well to determine maximum post-depositional palaeotemperatures, while AFTA have also been used to determine the time at which samples began to cool from those palaeotemperatures. As shown here, palaeotemperatures from both techniques define consistent linear profiles in the 17/3-1 and 17/9-1 wells, although some results from VR data in the 17/9-1 well appear to be anomalously low, probably due to suppression in Jurassic units. Palaeotemperatures derived from VR data in the 17/12-1 well also show excessive scatter, with some values appearing to be much higher than present-day temperatures compared with others. The highest values have not been used in determining palaeogradients and removed section. This uncertainty produces a less consistent match with results from sonic velocity analysis in Figure 12.

As with the example of the Norwegian–Danish Basin in Case A, recognition of the exhumed nature of the sedimentary section offshore southern Norway has major implications not only for hydrocarbon exploration offshore but also for understanding the nature of the tectonic processes involved. In terms of hydrocarbon systems, failure to account for the greater depths of burial prior to exhumation can lead to serious underestimation of maturity levels, while the effects of exhumation on the timing of hydrocarbon generation, changes in migration routes and on any reservoired hydrocarbons also require assessment (e.g. Doré *et al.* 2002). In terms of tectonics, the results presented here show that not only southern Norway but also major portions of the offshore shelf underwent exhumation in the early Neogene, and any attempt to understand the underlying processes must take into account the linkage

Table 1. Estimation of the burial anomaly for the pre-Neogene section based on sonic data (Fig. 10), the post-Oligocene reburial (cf. www.ndp.no) and the amount of exhumation during the early Neogene phase in three Norwegian wells (Eq. 1). Depths below sea bed (bsb)

Well	Burial anomaly (1) Re-burial (2) Exhumation (3) (m)	Estimate based on	Shale	Chalk
17/03-01	-500 ± 100 (1) 100 (2)* 600 (3)	Good agreement between results from chalk and shale data	Shale trend defined below the chalk and above Tau Fm., 1.1–1.9 km bsb, with some scatter. No data above the chalk	Chalk trend well defined by upper bound, 0.7–1.0 km bsb
17/09-01	-400 ± 150 (1) 300 (2) 700 (3)	Good agreement between results from chalk and shale data	Shale trend loosely defined by upper bound for the Palaeogene shales, 0.2–0.5 km bsb, and for the section between the chalk and the Tau Fm., 1.0–2.1 km bsb (disregarding peak velocity for Åsgård Fm.)	Chalk trend broadly defined by upper bound below data for Ekofisk Fm. and high-velocity chalk, 0.7–0.9 km bsb
17/12-1R	-400 ± 150 (1) 300 (2) 700 (3)	Agreement between results from chalk and shale data	Shale trend defined by limited data for the Palaeogene section, 0.4–0.6 km bsb, and by a loosely defined upper bound below the chalk and above the Tau Fm. (disregarding peak velocity for Åsgård Fm.)	Chalk trend defined by upper bound over the deeper part of the chalk, 0.8–1.0 km bsb

*Approximated by the thickness of the Nordland Group.
The burial anomaly is estimated by comparing the normal velocity–depth trends for shale and chalk and sonic log data for the relevant intervals (Fig. 10, Eq. 1). The timing of maximum burial between 30 and 20 Ma is based on AFTA data and this event is interpreted as corresponding to a regional early Neogene unconformity at *c.* 23 Ma (cf. Japsen *et al.* 2007*a*).

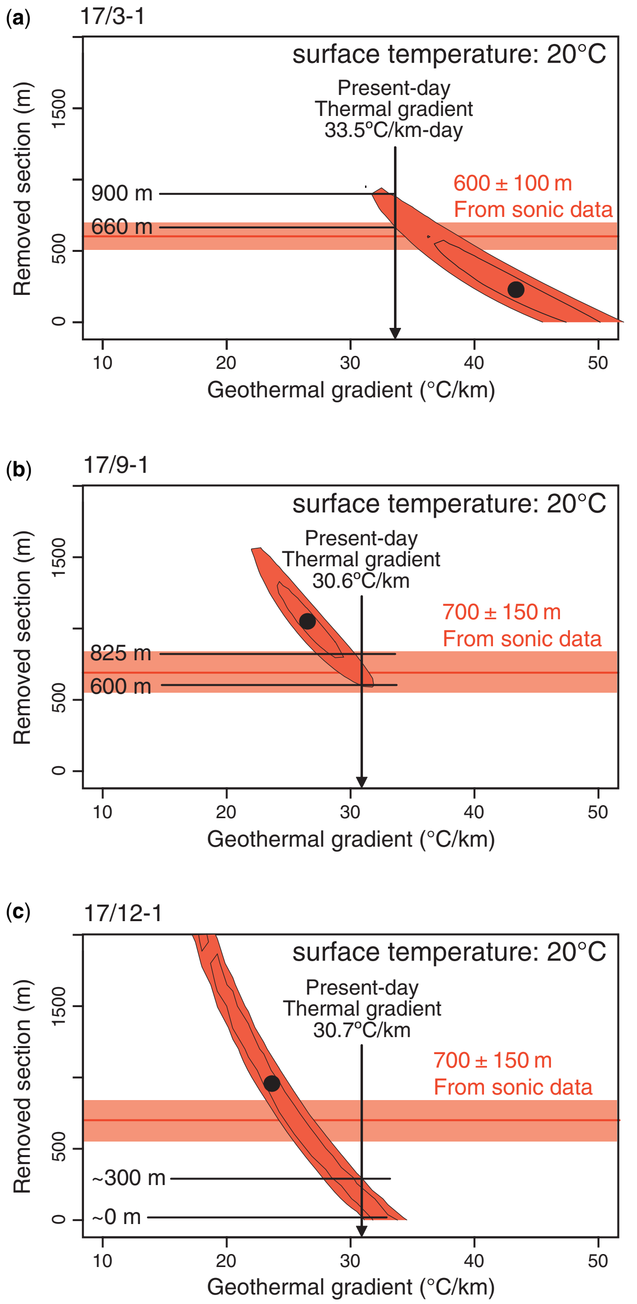

Fig. 12. The range of values of palaeogeothermal gradient and removed section that are allowed by the palaeotemperature constraints from AFTA and VR data in each of the Norwegian wells shown in Figure 11 are shown by the hyperbolic ellipsoid regions (Bray *et al.* 1992; Green *et al.* 2002). These are compared with the estimates of removed section derived from sonic velocities in each well (Table 1). In the 17/3-1 and 17/9-1 wells, the two approaches give highly consistent results for a scenario based on a constant heat flow (palaeogeothermal gradients close to present-day values). In the 17/12-1 well, the agreement is less good, due most likely to the excessive scatter in VR values. Black dots mark maximum likelihood solutions.

between onshore and offshore demonstrated by these results. Similar results from West Greenland are presented below, suggesting that this may be a common phenomenon.

Case C: West Greenland's mountains are surprisingly young

In West Greenland, where rifting occurred during mid-Cretaceous and earliest Paleocene times and seafloor spreading started in the mid-Paleocene, kilometre-thick Palaeogene post-rift volcanic sequences with incursions of marine sediments are exposed in mountains reaching to above 2 km a.s.l. (Figs 2 & 13; Chalmers *et al.* 1999). Japsen *et al.* (2006) analysed these landscapes by combining the cooling history from AFTA data with the denudation history from landscape analysis (Bonow *et al.* 2006*a*, *b*) and the stratigraphic record. These results demonstrate that post-rift subsidence and burial continued until the end of the Eocene when seafloor spreading ceased between Canada and Greenland (Chalmers & Pulvertaft 2001). Maximum burial of the post-rift sequence occurred at the end of the Eocene and was followed by uplift in which up to 1 km of the post-rift sequence was removed, forming a regional, low-relief erosion (or planation) surface (the upper planation surface, UPS) that was graded to sea-level during the Oligocene–Miocene. This erosion surface was uplifted to present-day altitudes of up to 2 km (Fig. 13) and offset by reactivated faults. Broad and uplifted palaeovalleys (the valley floor of these defining the lower planation surface, LPS) incised below the surface demonstrate that the uplift took place in two phases and AFTA data define the onset of these phases to around 10 and 5 Ma.

Episodes of cooling defined by AFTA data

The geomorphological and geological observations in West Greenland have been complemented by AFTA data supported by VR data (Japsen *et al.* 2005*b*, 2006, 2009). Thermal history constraints have been extracted from our AFTA data following the principles established in Green *et al.* (2002). Data in individual samples of both Cretaceous sediments and basement define typically two (rarely three) discrete palaeothermal episodes. Synthesis of the timing constraints for the cooling episodes identified in all samples suggests that at least six discrete episodes of cooling are required to explain all of the AFTA results.

The events identified date back to the latest Proterozoic, but here we focus on the Cenozoic (Cases C and D) and Mesozoic (Case E) episodes. The AFTA data define five cooling episodes that began in the intervals 230–220, 160–150, 36–30, 11–10 and 7–2 Ma (cooling episodes C0–C4; see Fig. 14). Note that these time intervals represent the ranges of uncertainty for the time of onset of cooling in each episode, not the intervals during which all of the cooling took place. The onset of the C1 event is recognized from AFTA in most samples of basement rocks across the area and the C2 event in almost every sample. In contrast, the palaeotemperatures from which most basement samples cooled in the C3 and C4 events are too low in most of the basement outcrop samples for these events to be detected. These late Neogene events are mainly defined from samples of sedimentary rocks from the Nuussuaq Basin because of the higher palaeogeothermal gradients in this region, and they are particularly well defined in AFTA data from the 3 km deep Gro-3 well (Japsen *et al.* 2005*b*).

The C0 cooling event that is defined by many samples from the Precambrian basement areas began in the late Triassic. Palaeotemperatures for this episode estimated from rocks at present-day outcrop increase westwards to above 100 °C near the present-day coast. Rocks of Triassic age are not known from West Greenland, either onshore or offshore, but the increase in palaeotemperatures towards the present-day coast may indicate a relation with the later Mesozoic rift events.

Integration of thermochronological and geomorphological results

A Mesozoic etch or weathering surface, formed subsequent to uplift initiated in the Late Jurassic (C1), has been re-exposed from below Cretaceous–Paleocene cover rocks after Neogene uplift (Bonow 2005). This surface is characterized by an undulating topography and has been mapped on Nuussuaq, Disko and in the

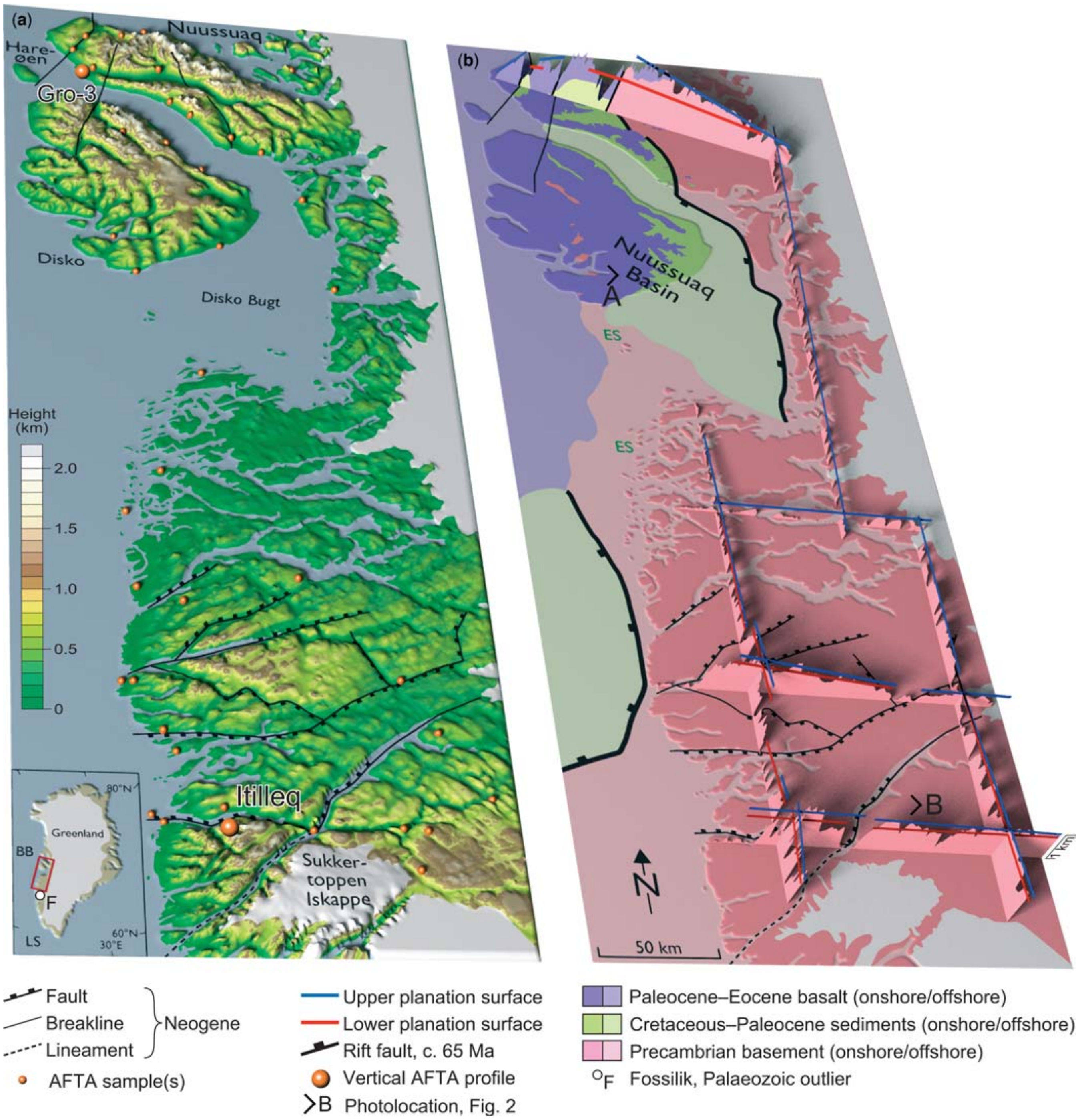

Fig. 13. Three-dimensional maps of central West Greenland. (**a**) Topography. (**b**) Geology with topographical profiles. An elevated plateau is defined by the regional upper and the partially developed lower planation surface that cut across Precambrian basement and Palaeogene volcanic rocks. The formation of the planation surfaces was uniform across the study area and they must be younger than mid-Eocene basalts. The planation surfaces now dip in different directions and are offset by faults that displace them. An ES has been re-exposed from below Cretaceous–Paleocene cover rocks on Nuussuaq, Disko and south of Disko Bugt. Note the Palaeozoic outlier at Fossilik ('F' on the key map, lower left). LS, Labrador Sea; BB, Baffin Bay. Modified from Japsen *et al.* (2006, 2009); based on Chalmers *et al.* (1999); Bonow (2005); Bonow *et al.* (2006*a*, *b*). Location of map shown in Fig. 1.

coastal regions south of Disko Bugt. The ES is cut off by a younger surface in the area south of Disko Bugt. The younger surface is tilted and rises towards the south, where it gradually splits into the UPS and LPS.

The C2 cooling episode that began at the Eocene–Oligocene transition is recognized in AFTA results from almost every sample, both within the Nuussuaq Basin and in the basement areas. The samples recording the C2 event are distributed across an area similar in extent to the UPS that has been dated independently to be post-middle Eocene because it cuts across basalts of that age (Bonow *et al.* 2006*a*; Fig. 13). We therefore consider that both the formation of the UPS and the C2 cooling event are evidence of the same episode of exhumation (Japsen *et al.* 2006). AFTA and VR data from the Gro-3 well show that up to 1 km of rocks were removed during Oligocene–Miocene times before the final formation of the UPS across Cenozoic, Mesozoic and basement rocks (Japsen *et al.* 2005*b*). Similarly, up to 1 km of rocks (most likely including Cretaceous–Palaeogene sediments) were removed before the final formation of the UPS in the basement area north of Sukkertoppen as we shall discuss in Case E (Japsen

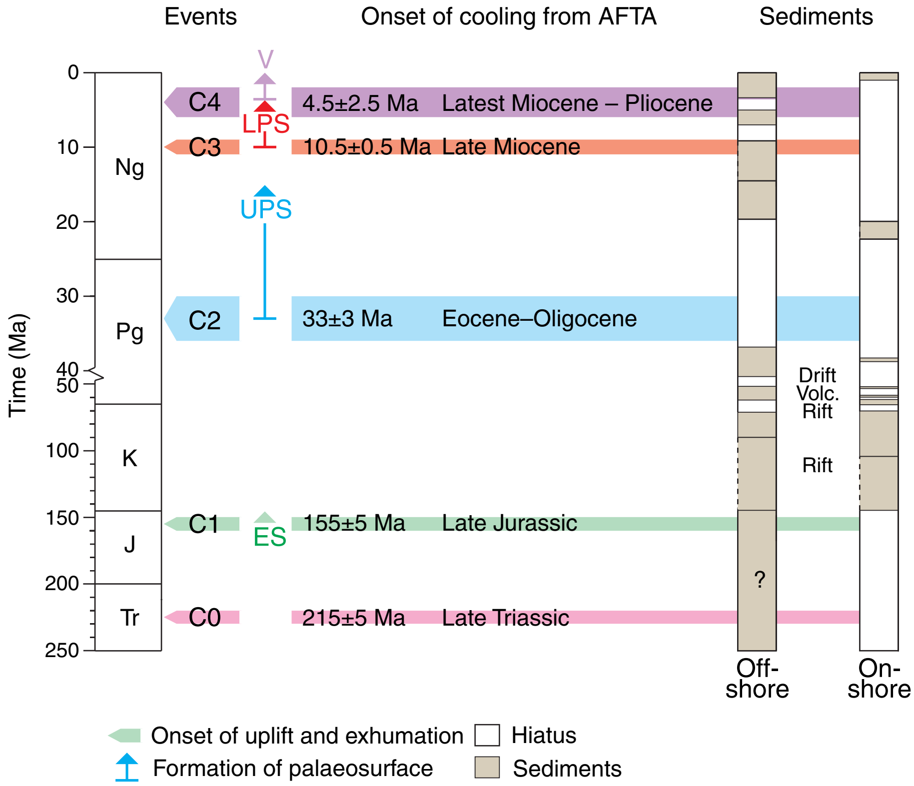

Fig. 14. Chronology of events in West Greenland. Correlation between discrete episodes during which AFTA data indicate onset of cooling (C0–C4), the formation of surfaces and valleys and the age of sediments and main tectonic events. At least six discrete episodes of cooling are required to explain all the AFTA results, but only the five youngest are shown on the figure. Dotted lines: maximum age range of sediments. Renewed development of the ES probably took place prior to Paleocene volcanism. ES, etch surface; UPS, upper planation surface; LPS, lower planation surface; V, deeply incised valleys; Tr, Triassic; J, Jurassic; K, Cretaceous; Pg, Palaeogene; Ng, Neogene; Subs, thermal subsidence; Volc, volcanism. Stratigraphy from Storey *et al.* (1998); Chalmers *et al.* (1999); Nøhr-Hansen (2003); Piasecki (2003); Schmidt *et al.* (2005); Pedersen *et al.* (2006); Sørensen (2006). Modified after Japsen *et al.* (2009).

et al. 2009). Figure 15 shows a possible reconstruction of the landscape development near Sukkertoppen Iskappe.

Uplift to present-day altitudes of up to 2 km took place in two late Neogene events (C3 and C4), resulting in dissection and tilting of the UPS into megablocks. Evidence from AFTA for these cooling events is found in samples from the bottom of valleys that have been incised by rivers subsequent to the uplift (and in subsurface samples below the valley floor, for example, the Gro-3 well). The UPS is well preserved as a low-relief surface in resistant rocks while it has started to be dissected in less resistant rocks. However, the faults offset the UPS so that it now dips in different directions in different fault blocks.

The late Neogene uplift phases post-date the final episode of rifting (in the Maastrichtian–early Danian) by *c.* 50 million years and seafloor spreading west of Greenland by *c.* 30 million years (Chalmers *et al.* 1999; Chalmers & Pulvertaft 2001), after which both the basins and their surrounds continued subsiding until the end of the Eocene. Our analysis shows that uplift started at this time, leading to erosion that led ultimately to formation of a low-relief erosion surface close to sea-level by the late Miocene. Remnants of this low-relief surface are now preserved as plateaux of large extent at elevations up to 2 km a.s.l., forming the UPS (Bonow *et al.* 2006*a*, *b*). The present-day elevated passive continental margin of West Greenland is thus in no way a reflection of the processes acting during the rifting or drifting events but developed much later.

As we will see in the following discussion of Case D, the events identified from the onshore margin discussed here are also expressed in the offshore basins (Fig. 14), where they have important implications for hydrocarbon prospectivity. Thus, integration of onshore and offshore events forms an important component of fully understanding the processes which control hydrocarbon systems in offshore basins.

Case D: the nature of the Oligocene hiatus offshore southern West Greenland

Oligocene sediments are absent on the West Greenland shelf (Sørensen 2006) and, north of about 66°N, upper Eocene sediments are separated from lower Eocene sediments by another pronounced hiatus (Fig. 16; Chalmers 2000). South of about 66°N, the two hiatuses merge into one and upper Miocene sediments lie directly on lower Eocene sediments (cf. Chalmers & Pulvertaft 2001; Nøhr-Hansen 2003; Piasecki 2003; Sønderholm *et al.* 2003; see the offshore stratigraphic column in Fig. 14). The earlier hiatus coincides with the substantial decrease in the speed of seafloor spreading in the Labrador Sea, and the latter hiatus with the final cessation of seafloor spreading between Canada and Greenland (Chalmers & Pulvertaft 2001).

It is not possible to use only reflection seismic data to evaluate whether a hiatus represents a period of non-deposition or if sediments have been deposited and then removed. The Oligocene hiatus is seen as a very low-angle unconformity on seismic data from much of the Greenland shelf and it can thus be difficult to judge if it is a truncational unconformity (Fig. 17). Such low-angle unconformities are conventionally regarded as representing intervals of stability. In the area penetrated by the Qulleq-1 exploration well, however, the middle Miocene hiatus is clearly angular and truncates lower Eocene, Paleocene and Upper Cretaceous strata (Fig. 18; Christiansen *et al.* 2001).

VR data from the Qulleq-1 well suggest that the pre-Neogene succession in the well has been more deeply buried in the past.

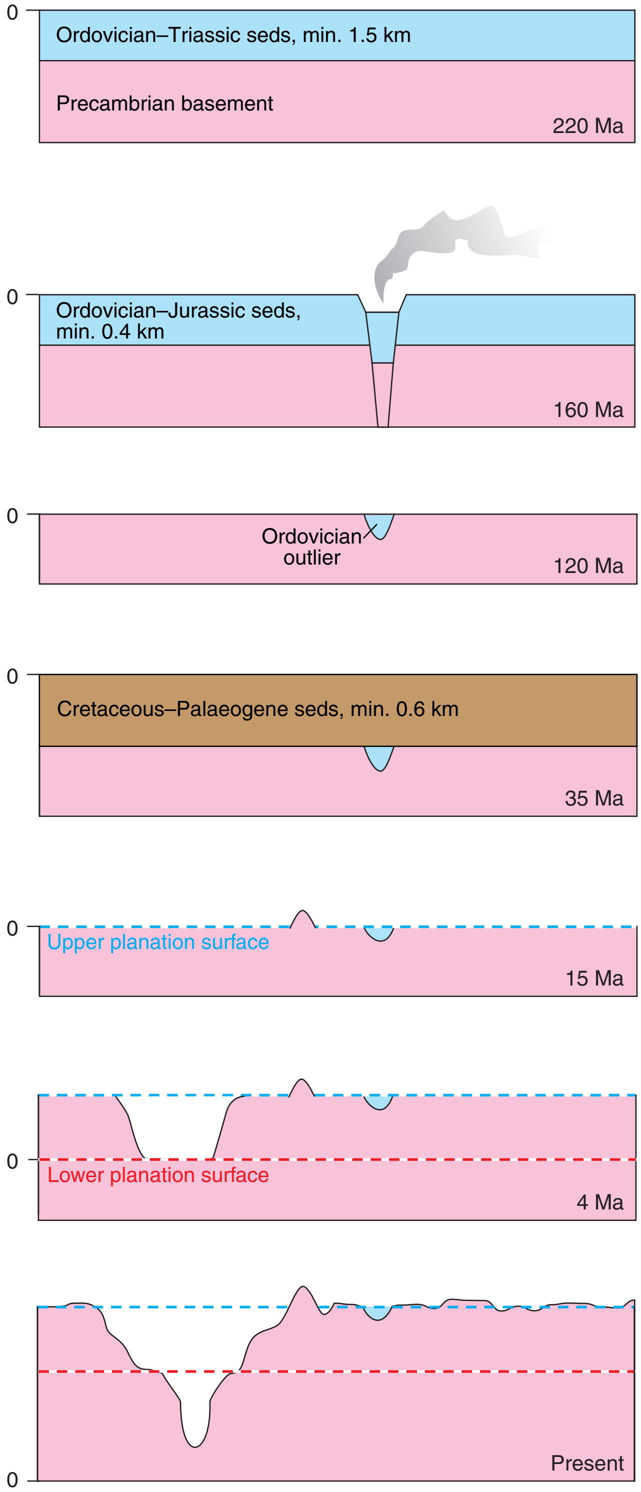

Fig. 15. Idealized profile illustrating the landscape development across the present basement area near Sukkertoppen Iskappe, West Greenland, based on AFTA data from the Itilleq vertical section (Figs 13 & 20). Note the UPS and two levels of valleys incised in the UPS: the wide valleys of the LPS and the present valleys incised in the LPS. We correlate the incision of these valley systems with the two uplift phases that formed the present topography. 220 Ma, Triassic maximum burial before C0 uplift (cooling episode C0 from AFTA data, see Fig. 14); 160 Ma, Jurassic maximum burial before C1 uplift and volcanism preserving Ordovician sediments as fall-back material; 120 Ma, most likely removal of sedimentary cover after C1 uplift and volcanism; 35 Ma, Palaeogene maximum burial after rifting and Palaeogene volcanism, before C2 uplift; 15 Ma, Oligocene–Miocene UPS; 4 Ma, late Neogene LPS after C3 and before C4 uplift; Present, deeply incised valleys after final uplift. Based on Stouge & Peel (1979); Bonow *et al.* (2006*a*, *b*); Japsen *et al.* (2006, 2009); Larsen (2006).

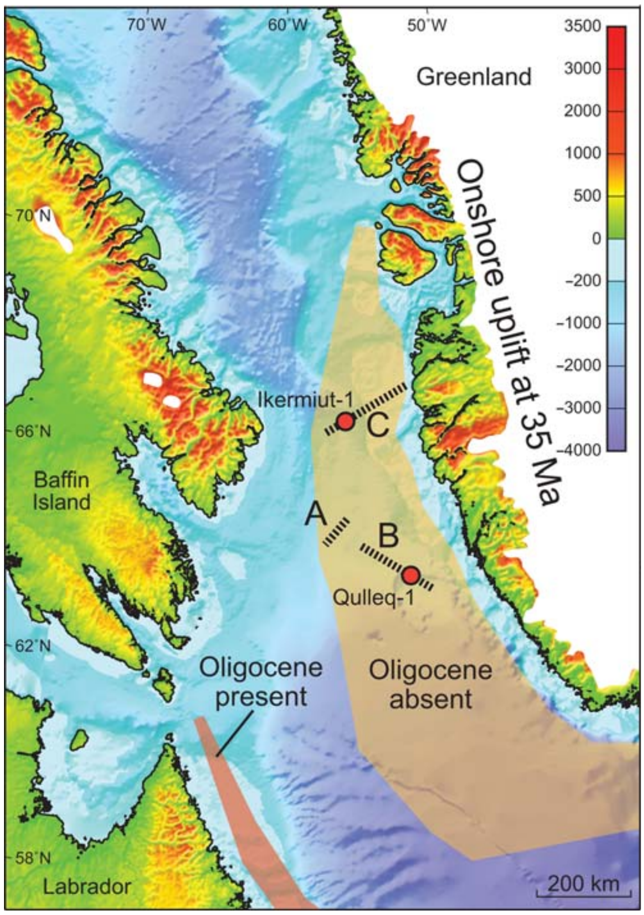

Fig. 16. Outline of the Oligocene hiatus offshore West Greenland based on seismic and well data, for example, profiles A and B, and well Qulleq-1 (Figs 18–20). The area offshore from which Oligocene deposits are known to be absent is marked. Oligocene strata have been encountered east of Labrador, but the presence of these strata in the remaining parts of the offshore area is unknown. Lower Miocene strata are also absent west of Greenland (Sørensen 2006; see the offshore stratigraphic column in Fig. 14). The Oligocene hiatus thus represents the time interval during which the Oligocene–Miocene peneplain, UPS, was graded to sea-level onshore after the C2 uplift event that began *c*. 35 Ma. Bathymetry and bedrock topography in metres. Icecaps indicated as white. Profile C is shown in Figure 21. Map location shown in Fig. 1.

In Figure 19, VR data from the well is seen to plot above curves of predicted VR trends based on the ‘default history’ derived from the preserved stratigraphy and based on a likely range of geothermal gradients between 20 and 30 °C/km (in this history, hiatuses are assumed to represent periods of non-deposition, not erosion). The discrepancy between observed and predicted VR values indicates that the drilled section below the unconformity has been hotter in the past, most likely due to deeper burial below a section that has been removed. This possibility is strengthened by the observation that the VR value for the only Neogene sample matches the default history, indicating that this sample is now at its maximum burial depth.

Further studies, based on palaeothermal (AFTA and VR) data and palaeoburial (sonic) data, constrained by the preserved stratigraphy, are needed to evaluate the timing, magnitude and extent of the exhumation related to the Oligocene hiatus offshore West Greenland. Such studies would provide firm constraints on both the thermal and the burial history of the preserved sedimentary section, allowing definition of those areas where maximum burial was reached during mid-Cenozoic times. This, in turn, would allow identification of areas where hydrocarbon generation ceased prior to exhumation, and conversely those areas where hydrocarbon

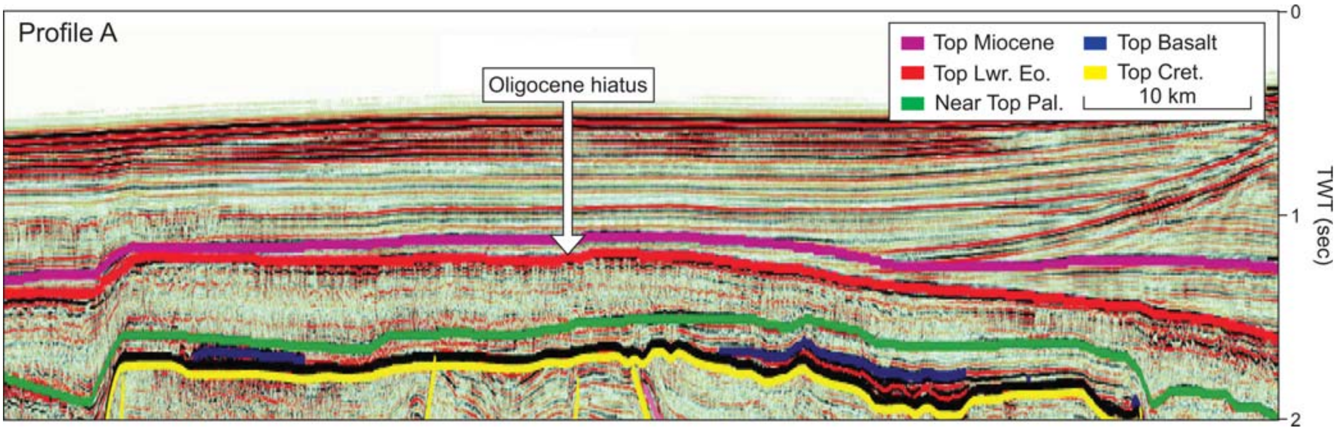

Fig. 17. Seismic profile A showing a low-angle Oligocene unconformity offshore West Greenland with lower Eocene strata below and Miocene strata above the unconformity. It is not possible from the seismic profile to evaluate whether the hiatus represents a period of no deposition or whether sediments have been deposited and then removed during the time interval represented by the unconformity. TWT, seismic two-way-time. Location in Figure 16. Modified after Sørensen (2006).

generation proceeded until the present day, allowing charging of structures formed during the mid-Cenozoic uplift and erosion.

Such studies will also be important for understanding the tectonic evolution of the Arctic during the Cenozoic within a wider context: a hiatus similar to that encountered on the West Greenland shelf is also present in the Sverdrup Basin in the eastern Canadian Arctic (Harrison *et al.* 1999) and a similar stratigraphic break was unexpectedly penetrated on the Lomonosov Ridge (central Arctic Ocean) by the Integrated Ocean Drilling Program (IODP) Expedition 302 (Backman *et al.* 2008). The drilled core documented a 26 Myr hiatus, separating middle Eocene (*c.* 44 Ma) from lower Miocene sediments (*c.* 18 Ma). Sangiorgi *et al.* (2008) were unable to determine whether that hiatus was generated by sediment erosion or by non-deposition, but emphasized that it conflicts with classical post-rift thermal subsidence models for passive margins. The temporal correlation between this Oligocene hiatus and the time interval during which the Oligocene–Miocene peneplain, UPS, was graded to sea-level onshore West Greenland, emphasizes the regional controls on such processes, as was also highlighted by Green & Duddy (2010).

Case E: are there Ordovician source rocks offshore West Greenland?

The thermal and burial history of the Precambrian basement south of the rifted Nuussuaq Basin and east of the rifted basins now offshore (Chalmers & Pulvertaft 2001) has been determined by analysing AFTA data from five samples taken at different heights on an

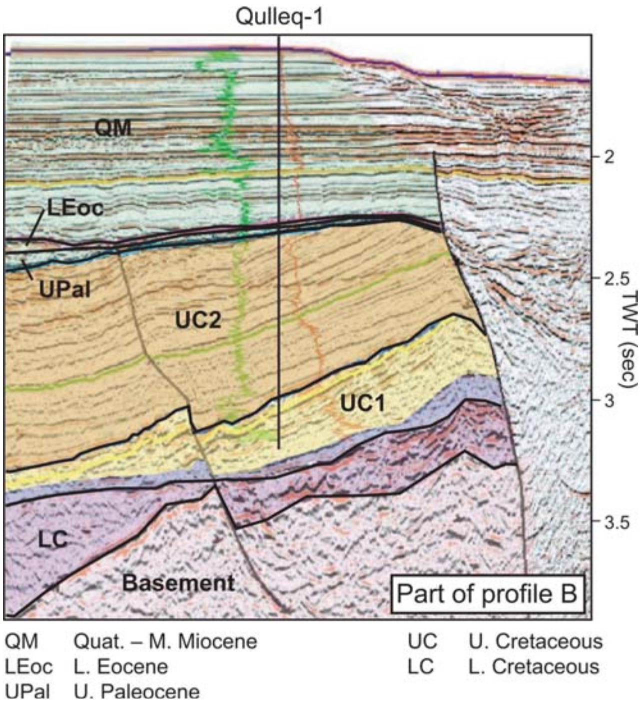

Fig. 18. Seismic line through the Qulleq-1 well, offshore West Greenland. Note the pronounced angular unconformity below the Neogene succession (QM) that truncates lower Eocene, Paleocene and Upper Cretaceous strata. The gamma-ray log from the Qulleq-1 well is shown in green to the left of the well and the acoustic impedance log is shown in red to the right. TWT, seismic two-way-time. Location in Figure 16. Modified after Christiansen *et al.* (2001).

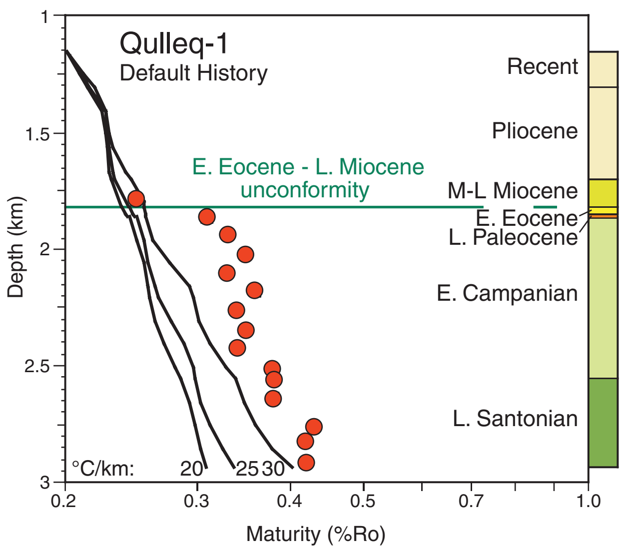

Fig. 19. Plot of VR data v. depth for the Qulleq-1 well, offshore West Greenland. Drilled succession shown on the right-hand side of the plot. Black curves indicate predicted VR trends based on the default history (preserved stratigraphy and geothermal gradients ranging from 20 to 30 °C/km). The discrepancy between observed and predicted VR values indicates that the section has been hotter in the past, possibly due to deeper burial below a section that was subsequently removed. Only the VR value for the sample above the base–Neogene unconformity matches the default history. This suggests that the early Eocene–middle Miocene hiatus represents the removal of sediments of that age. Location in Fig. 16. Modified after Christiansen *et al.* (2001).

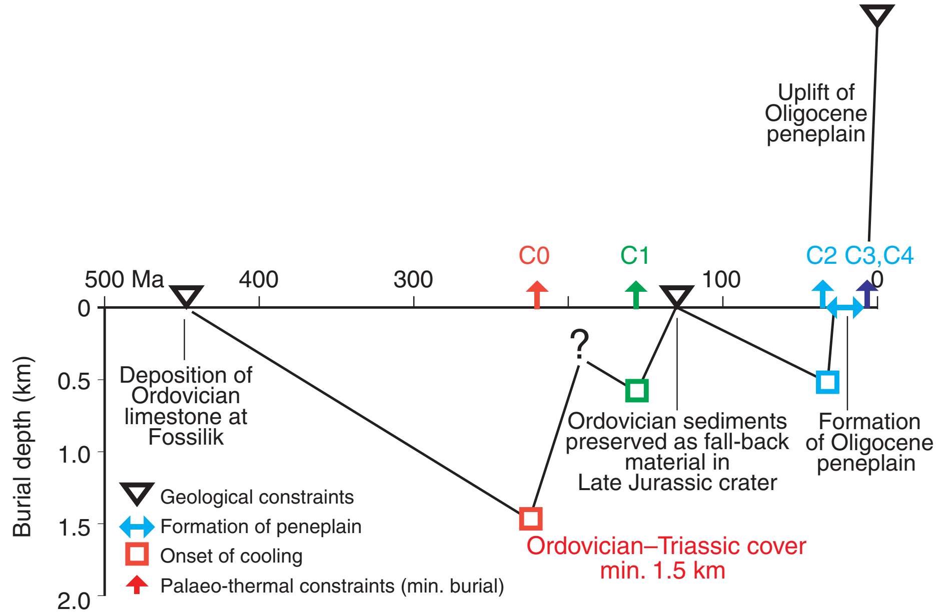

Fig. 20. Diagram illustrating the burial and uplift history of the summit at Sukkertoppen Iskapppe, West Greenland (*c.* 2 km a.s.l., location in Fig. 13). The interpretation is based on AFTA data from the Itilleq vertical section (minimum burial depths prior to exhumational events), interpretation of the landscape development (formation and uplift of the Oligocene peneplain, UPS) and geological constraints (presence of Ordovician sediments as fallback material in Late Jurassic volcanic breccia). The presence of Ordovician sediment at Fossilik within Upper Jurassic rocks shows that the section removed during the Triassic (C0) event must have consisted of Phanerozoic sedimentary rocks and thus that a minimum of 1500 m of Ordovician to Triassic sedimentary rocks must have been present above the basement prior to the C0 event (cf. Fig. 15).

elevation section up to a summit of 1848 m in the Itilleq fjord, NW of Sukkertoppen Iskappe (Fig. 13). The AFTA data, together with the thermal history solutions extracted from individual samples, are presented by Japsen *et al.* (2009), whereas the full details of these analyses and a regional dataset are provided in the online data repository associated with Japsen *et al.* (2006).

Three palaeothermal episodes can be defined from the AFTA data in the Itilleq profile over a range of altitudes and these events correspond well with regional cooling events (C0, C1, C2; see Fig. 14). The range of palaeotemperatures for all events is wide, but the palaeogeothermal gradients must have been less than 40 °C/km during these three events and much of the heating reflected in the observed palaeotemperatures must represent greater depth of burial; that is, the present summit must have been buried below a section with a minimum thickness of 1500 m prior to the Triassic C0 event, a minimum of 400 m prior to the Late Jurassic C1 event and a minimum of 600 m prior to the Cenozoic C2 event corresponding to the maximum allowed palaeogeothermal gradients of 40, 35 and 22.5 °C/km, respectively, during these events (Fig. 20). Lower palaeogeothermal gradients would require larger amounts of additional section.

Implications of the presence of an Ordovician outlier

An Ordovician outlier is known from a Late Jurassic explosion breccia at Fossilik, south of Sukkertoppen Iskappe (Stouge & Peel 1979; see Fig. 13, lower left). These rocks were probably preserved as fall-back deposits into a crater formed by a violent volcanic explosion that shattered the overlying rocks in Late Jurassic times (Larsen 2006). The presence of Palaeozoic sediment at Fossilik in the Late Jurassic shows that the section removed during the Triassic (C0) event must have consisted of Ordovician to Triassic sedimentary rocks because Ordovician sediments were still present after the Triassic erosional event. The AFTA data show that the minimum thickness of the Ordovician–Triassic cover was 1500 m (Fig. 15).

It is likely that the basement around Sukkertoppen Iskappe was exposed following Late Jurassic (C1) exhumation and prior to the Cretaceous rifting. Regional AFTA data show extensive cooling across central West Greenland following the onset of the C1 event and this is likely to have been caused by exhumation because all sedimentary cover around and within the Nuussuaq Basin was stripped at this time prior to the development of the Cretaceous ES (Bonow 2005). This is further supported by the evidence for Late Jurassic removal of cover rocks at Fossilik (Larsen 2006; Steenfelt *et al.* 2006). These observations imply that the C2 palaeothermal peak recognized in AFTA samples from Itilleq represents the culmination of Cretaceous–Palaeogene reburial in this area.

Dalhoff *et al.* (2006) reported that several samples of marine carbonates of late Ordovician age were dredged by seabed sampling west of Greenland where dipping reflectors of unknown age extend to near the seabed. One Ordovician carbonate sample had oil staining. The authors suggested a correlation between these samples and lower Palaeozoic carbonate successions of the SE Arctic Platform and the Hudson Platform in eastern and northeastern Canada (Sanford & Grant 2000) and North Greenland, and those at Fossilik, onshore West Greenland (Stouge & Peel 1979).

Indications of thick successions of pre-Cretaceous strata offshore Greenland are provided by the presence of the so-called 'Deep Sequence' (Chalmers & Pulvertaft 2001), a thick succession of reflections below lower to mid-Cretaceous sequences (Fig. 21). What these reflections represent is unknown, but Ordovician carbonates are not unlikely, although Triassic or even Jurassic sediments cannot be ruled out. If the successions are Ordovician, the oil-stained sample recovered by Dalhoff *et al.* (2006) leads us to suggest that this sequence may contain a source rock horizon which has generated oil. The possibility of thick Palaeozoic deposits being present offshore West Greenland is further strengthened by the documentation here that a significant Ordovician–Triassic cover has been deposited even in the onshore areas.

Case F: post-rift burial of the East Greenland margin

Published thermal history studies in East Greenland have provided important insights into the thermal and tectonic history of both

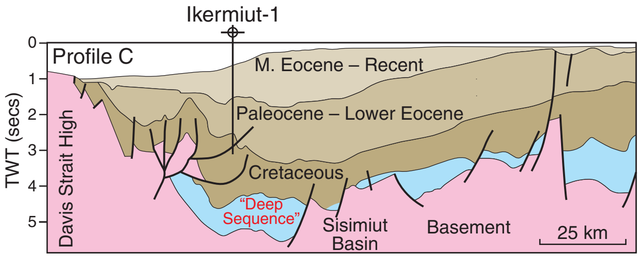

Fig. 21. Interpretation of seismic profile C, offshore West Greenland. The 'Deep Sequence' is defined by sub-horizontal reflections below and truncated by reflections that come from sediments that can be dated as Cretaceous by the Ikermiut-1 well (Chalmers & Pulvertaft 2001). The age and lithology of the 'Deep Sequence' is unknown, but Ordovician carbonates are not unlikely, although Triassic or even Jurassic sediments cannot be ruled out. If these successions are Ordovician, the oil-stained sample recovered by Dalhoff *et al.* (2006) suggests that they could act as a regional source rock. The possibility of thick Palaeozoic deposits being present offshore West Greenland is further strengthened by the documentation that a significant Ordovician–Triassic cover has been deposited onshore (see Figs 15 & 20). TWT, seismic two-way-time. Location in Figure 16.

Palaeozoic–Mesozoic sediments and basement terrains. Early studies revealed considerable Cenozoic cooling of country rock along the margin, usually interpreted in terms of kilometre-scale denudation related in some way to the process of rifting and separation of the North Atlantic Ocean (e.g. Gleadow & Brooks 1979; Hansen 1988, 1992, 1996). Here we will show that the later studies, despite the many uncertainties remaining, point to a quite different interpretation.

Thermal effects of Palaeogene intrusive bodies and of Cenozoic burial and exhumation revealed by AFT data

Thomson *et al.* (1999) published the first results from the sedimentary sequences to the north of Jameson Land (Fig. 22). They reported that AFTA data in a series of outcrop samples from Traill Ø and adjacent regions showed two dominant episodes of Cenozoic cooling, plus an earlier episode of cooling beginning between 225 and 165 Ma, recognized only in samples from westernmost locations. Cooling in the earlier of the two Cenozoic episodes began between 40 and 30 Ma (late Eocene–Oligocene), closely matching the timing of syenite intrusions (*c.* 35 Ma, e.g. Price *et al.* 1997) at the western extremity of Traill Ø. Because of the proximity of many of the samples analysed by Thomson *et al.* (1999) to these intrusions, the origin of the Eocene–Oligocene palaeothermal effects identified in these samples was not clear. The more recent Cenozoic episode, in which cooling began in the interval 10–5 Ma, was interpreted as due to uplift and erosion related to a change in the North Atlantic spreading vector. Several samples cooled from palaeotemperatures as high as 90–100 °C in this late Cenozoic episode, and measured AFT ages less than 20 Ma in several samples testify to the pronounced degree of Neogene cooling that has occurred in this region. Thomson *et al.* (1999) commented specifically that 'No paleo-thermal effects have been identified related to the onset of rifting in the Early Tertiary'.

Subsequently, Johnson & Gallagher (2000) reported AFT data from samples of Carboniferous sandstones from a vertical section on Clavering Ø (Fig. 22). Although this location lies near two samples analysed by Thomson *et al.* (1999), Johnson & Gallagher (2000) made no reference to the earlier study. This is made more surprising by the general consistency in the results of the two studies. Johnson & Gallagher (2000) found that the section began to cool from maximum post-depositional palaeotemperatures at *c.* 274 Ma (early Permian), with subsequent cooling episodes at *c.* 206, 140 and 23 Ma. The *c.* 206 Ma episode correlates closely with the earliest episode identified by Thomson *et al.* (1999), while the *c.* 23 Ma episode falls between the two Cenozoic episodes identified by Thomson *et al.* (1999) and the single Cenozoic episode defined by Johnson & Gallagher (2000) may well represent the unresolved effects of these two. The *c.* 140 Ma cooling episode identified by Johnson & Gallagher (2000) was not recognized in the Thomson *et al.* (1999) study, possibly because of the pronounced effect of Cenozoic events on Traill Ø, which would have masked any Mesozoic effects.

Johnson & Gallagher (2000) interpreted these cooling episodes largely in terms of denudation involving removal of several kilometres of section, while also suggesting that Cenozoic palaeothermal effects could be related to Palaeogene volcanic activity. One notable shortcoming of the Johnson & Gallagher (2000) study is that, despite their sampled section being overlain by Palaeogene sediments and basalts (their Fig. 1, cf. Henriksen *et al.* 2000), their analysis took no note of this basic constraint on the thermal history of the sequence. The thermal history that Johnson & Gallagher (2000) reported for their sampled section shows temperatures of *c.* 60 °C or more during Palaeogene times, and only a minor reheating to the Cenozoic palaeothermal peak around 70 °C at 23 Ma (Fig. 23). The presence of the Palaeogene deposits shows, however, that their uppermost sample must have been at near-surface temperature in the Palaeogene. This implies a major degree of re-burial by Palaeogene volcanics and/or younger sediments prior to the onset of cooling from the mid-Cenozoic palaeothermal peak. Note also that only the palaeothermal peaks are constrained by AFT data, and that it thus remains unknown what degree of cooling and reheating (e.g. exhumation and reburial) may have taken place between the peaks. The Carboniferous rocks studied by Johnson & Gallagher (2000) may thus have been near the surface several times after initial burial in the Carboniferous. As with the Thomson *et al.* (1999) study, Johnson & Gallagher (2000) reported no evidence of Palaeogene palaeothermal effects.

Hansen *et al.* (2001) reported results from the Jameson Land Basin and adjacent regions, based largely on AFT data (Fig. 22*b*). The results presented by Hansen *et al.* (2001) show a very consistent regional pattern, with youngest ages less than 25 Ma restricted to a region around the north and south coasts of Kong Oscar Fjord (Traill Ø and northern Jameson Land, respectively), surrounded by a wider region characterized by ages between 25 and 45 Ma, while older ages are largely restricted to higher elevations and/or locations to the south and west of Jameson Land. Hansen *et al.* (2001) interpreted their results as reflecting a complex interplay between deeper burial prior to Cenozoic exhumation, circulation of hot fluids associated with mid-Cenozoic intrusive activity around the eastern end of Kong Oscar Fjord and also possibly elevated basal heat flow in eastern Traill Ø. Hansen *et al.* (2001) favoured an onset of exhumation at *c.* 55 Ma in the south of the basin, and 'before 25 Ma' in the north, suggesting removal of as much as 4–5 km for palaeogeothermal gradients around 25 °C/km.

A notable feature of the data from Jameson Land presented by Hansen *et al.* (2001) is the erratic variation of fission track age with elevation. Preservation of fission track ages in excess of 200 Ma in SW Jameson Land, in relatively close proximity to much younger ages (Fig. 22b), suggests that regional Cenozoic heating was relatively minor in this region, and that local heating effects dominate the data. In view of these observations, any evidence for Palaeogene exhumation in this dataset is tentative at best, with all evidence suggesting that any Palaeogene palaeothermal effects are localized, due either to contact heating from the widespread minor intrusions of this age or associated hydrothermal effects (or both). In contrast to the erratic variation in heating

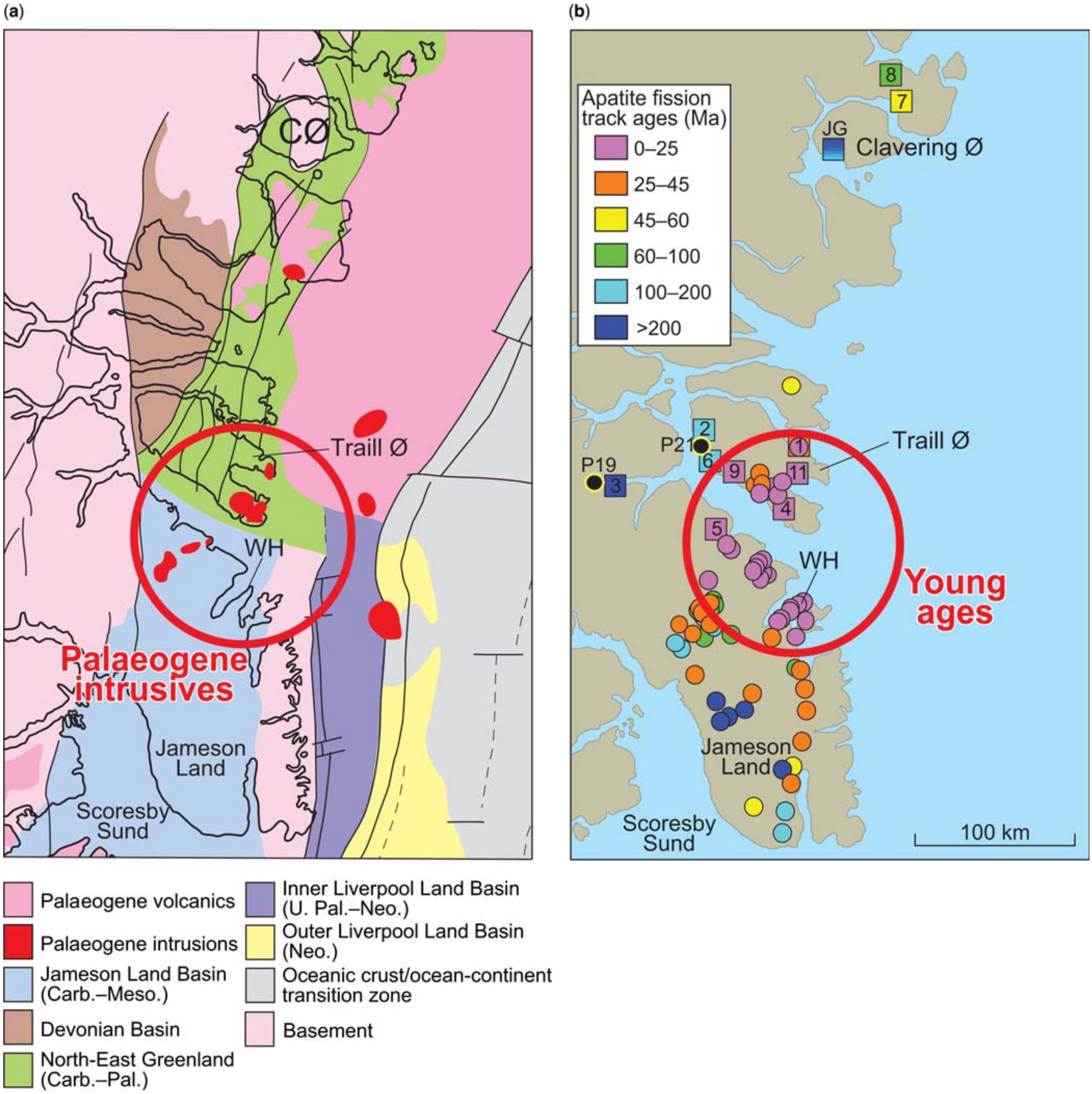

Fig. 22. Maps of central East Greenland. (**a**) Geological map of the East Greenland margin (after Hamann *et al.* 2005). (**b**) Map of AFT ages from Thomson *et al.* (1999; squares with sample numbers) and Hansen *et al.* (2001; circles). The coincidence of the area with Palaeogene intrusives (map A) and the area with young AFT ages (map B) is highlighted with red circles. Vertical profile of samples analysed by Johnson & Gallagher (2000, marked JG) and Swift *et al.* (2008, black circles P19 and P21) is also indicated. JL, Jameson Land; WH, Wegener Halvø. Location of map shown in Fig. 1.

effects in the south of Jameson Land, the pattern of fission track ages in Figure 22b shows that Neogene palaeothermal effects in eastern Traill Ø and NE Jameson Land around Wegener Halvø are more uniform. The correspondence of these younger ages with the presence of late Eocene–Oligocene intrusive bodies suggests a causal relationship.

A number of basin modelling and maturation studies of the Jameson Land Basin have used AFT data to constrain the history of uplift and denudation (Christiansen *et al.* 1990, 1992; Mathiesen *et al.* 1995, 2000). Mathiesen *et al.* (2000) assumed that generation of hydrocarbons was dominated by deeper burial after deposition of the thick volcanic pile during the early Paleocene and prior to denudation beginning in the late Paleocene, with a total of 2–3 km of section removed since that time. Christiansen *et al.* (1992) drew attention to the presence of hydrothermal effects in upper Permian carbonates in Wegener Halvø, which correlates closely with the AFT age 'hot spot' in Figure 22b.

Mismatch between apatite (U–Th)/He dating and AFT results

Swift *et al.* (2008) presented apatite (U–Th)/He dating results from two vertical sections where one profile (number 21) is located close to samples 2 and 6 from the Thomson *et al.* (1999) study (Fig. 22). Apatite (U–Th)/He ages reported from Profile 21 by Swift *et al.* (2008) show erratic variation with elevation, with youngest ages between 23 and 29 Ma in three samples (with uncertainties of ±1 or 2 Ma) while other samples give ages between 56

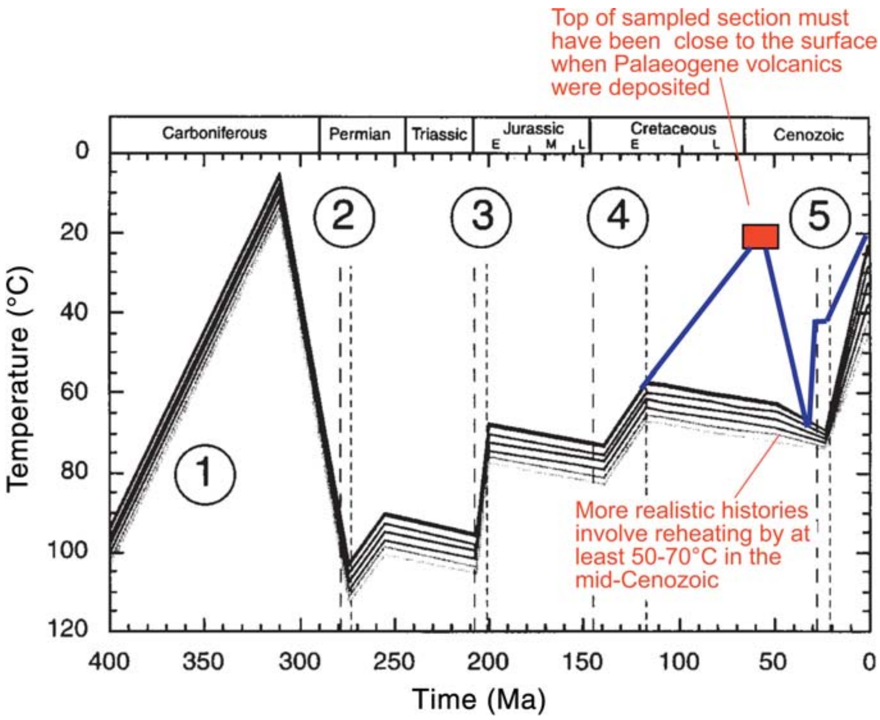

Fig. 23. Thermal history solutions for a vertical section of rocks on Clavering Ø, East Greenland, from Johnson & Gallagher (2000), showing a more realistic interpretation obtained by incorporating basic geological constraints based on the presence of the Palaeogene deposits at the highest elevations above the section sampled by Johnson & Gallagher (2000). These constraints show that the uppermost sample must have been at near surface temperature in the Palaeogene, implying a major degree of re-burial by additional volcanics and/or post-volcanic Palaeogene sediments prior to the onset of cooling from the mid-Cenozoic palaeothermal peak of *c.* 70 °C. The alternative cooling history indicated is based on two episodes of cooling at *c.* 35 and 10 Ma (Thomson *et al.* 1999). Each line represents the temperature history of an individual sample. In section (1), fission tracks are produced and annealed in the source region of the sediment prior to deposition; in section (2), maximum temperatures at 274 Ma mid-Permian; in section (3), cooling at 206 Ma early Jurassic; in section (4), poorly constrained cooling at 140 Ma; and in section (5), Cenozoic reheating and maximum temperatures at 23 Ma. Location on Fig. 22.

and 70 Ma with one older value of 137 ± 8 Ma. Results from Profile 19 show more internal consistency, with two of the samples from low elevations giving reproducible (U–Th)/He-ages around 70–80 Ma. Swift *et al.* (2008) interpreted these results as indicating a phase of rapid denudation which began at 74 ± 15 Ma. This conclusion stands in stark contrast to previous studies in this region which, as reviewed above, showed no evidence of late Cretaceous/Palaeogene cooling (Thomson *et al.* 1999; Johnson & Gallagher 2000). Swift *et al.* (2008) also claimed that 'AFTA data published by Thomson *et al.* (1999) for sea level bedrock samples located near to profiles 19 and 21 are consistent with rapid cooling from temperatures of *c.* 70 °C at *c.* 70 Ma.' This is not correct. For example, Thomson *et al.* (1999) reported that their sample 2 cooled from between 85 and 95 °C in the interval 40–5 Ma.

Swift *et al.* (2008) stated that He ages can be interpreted qualitatively as reflecting the time at which samples cool through 75–35 °C. We should then expect He ages in sample 2 from Thomson *et al.* (1999) of perhaps 30 Ma or younger, in contrast to most of the measured He ages, which are *c.* 60 Ma or older. This mismatch can be understood in terms of the now widely recognized problems with the (U–Th)/He system, in which the He retentivity is enhanced over the 'normal' systematics as a result of the accumulation of radiation damage within the apatite lattice (Green *et al.* 2006; Shuster *et al.* 2006). The apatite (U–Th)/He ages cannot therefore be interpreted simply in terms of cooling below 35–75 °C as stated by Swift *et al.* (2008). Comparison of their (U-Th)/He ages with the interpretations provided by Thomson *et al.* (1999) suggests that the three youngest ages from Profile 21 probably provide a more reliable assessment of the low-temperature history of the sampled rock section, while ages around 60 Ma or older are likely to be spuriously old as a result of the factors discussed above. Unfortunately, the results provided by Swift *et al.* (2008) do not contain sufficient detail to allow assessment in similar terms to the analysis presented by Green *et al.* (2006).

Development of the East Greenland margin

In summary, despite a number of regional, thermal-history studies of the East Greenland margin, resulting in a consistent regional pattern of variation, significant uncertainty remains with regard to the precise time at which individual rock units reached their palaeothermal maximum, how this timing varies across the region, and about the nature of the mechanisms responsible for heating and cooling, including palaeogeothermal gradients and amounts of section removed by uplift and erosion.

Remarkably, no convincing evidence for regional palaeothermal effects related to Palaeogene breakup has been reported; Cenozoic maximum temperatures appear to have occurred in the mid- and late Cenozoic. In particular, results from Clavering Ø show that Palaeogene basalts preserved on the summits there have been heated to peak temperatures of *c.* 70 °C prior to cooling in the late Cenozoic. As there is no Palaeogene intrusive activity reported from this area, a major cause of the post-basalt heating must be due to burial below rocks that have been removed, presumably by uplift and erosion in the Neogene.

The lack of evidence for palaeothermal cooling (which might reflect uplift) related to breakup is supported by evidence from the geological record. The Scoresby Sund area (Fig. 22) was characterized by net subsidence during the eruption of the basalts at the Paleocene–Eocene transition with no evidence for crustal upwarping (Brooks 1985; see also Larsen & Tegner 2006). There are marine incursions in the youngest plateau lavas (see Larsen *et al.* 1989), and outliers of Eocene marine sediments overlie the basalt just south of Scoresby Sund (see Larsen *et al.* 2005). The margin therefore subsided following rifting and breakup, and deposition of this post-rift sequence during thermal subsidence is just what is predicted from the theory of continental stretching (McKenzie 1978; White & McKenzie 1988).

Medvedev *et al.* (2008) investigated the effects of erosional unloading based on geological and topographical observations from the Scoresby Sund area where peaks reach 2.5–3.7 km a.s.l. According to their calculations, erosional unloading due to incision below the highest peaks in the area can account for 1.1 km of uplift, which is comparable with the elevation of Mesozoic marine sediments that are now at an elevation of 1.2 km a.s.l. The authors concluded that 'the active erosion of the region is the first-order feature responsible for significant uplift of the marine sediments and adjacent Fjord Mountains'. Medvedev *et al.* (2008) did not, however, consider that these marine sediments may have been buried below a pile of Upper Cretaceous–Palaeogene sediments, in which case the true amount of uplift of these marine sediments since their maximum burial would be much larger than 1.2 km. Much of the high ground north of Scoresby Sund appears to consist of a dissected plateau similar to those in Norway and West Greenland (Ahlmann 1941; see Henriksen 2008, pp. 22–23). As noted above, formation of such a plateau requires at least two episodes of uplift; a first phase during which an erosion surface is formed near sea-level and a second to uplift it to its present elevations. Medvedev *et al.*'s (2008) calculations may show that a large part of the uplift of the erosion surface in the Scoresby Sund area is due to isostatic response to erosion, but none of the calculations address the reasons for any earlier episode.

In East Greenland, uplift events have led to exhumation of remnants of hydrocarbon accumulations hosted in Jurassic sandstones now at elevations of around 1 km on Traill Ø (Price *et al* 1997; Price & Whitham 1997). The generation of hydrocarbons in the vicinity of eastern Traill Ø from Upper Jurassic source rocks (Price & Whitham 1997; Price *et al.* 1997) was most likely enhanced due to the increased heat flow in this region associated with the intrusions in the late Eocene (combined with the palaeoburial at that time). This suggestion agrees well with the very low organic carbon content of the reservoir rocks (GEUS unpublished data). According to J. Bojesen-Koefoed (pers. comm. 2009) the organic content is much lower than would be expected if the petroleum was degraded through biogeochemical processes upon exhumation of the reservoir, and it is thus more likely explained by destruction of the hydrocarbons by high temperature rather than by leakage and biodegradation. The implication of this is that the presence of these accumulations is likely to be closely associated with the local thermal perturbation caused by the intrusions. Further afield, in areas where heat flow was not enhanced, any source rocks present would have remained at lower maturity levels at the end of the Eocene. Particularly in offshore regions that were not affected by mid-Cenozoic exhumation, such source rocks may then have generated hydrocarbons during later burial in areas of Neogene subsidence. Therefore the presence of these exhumed oil accumulations may be seen as a positive feature for exploration in the region, instead of the more negative impact generally attributed to exhumation. Moreover, uplift of the margin may have created potential traps for these hydrocarbons, suggesting that hydrocarbons may be present in the offshore region. In exploring for these hydrocarbons, detailed mapping of the key uplift events will be crucial in identifying suitable targets in more prospective regions where the timing relationships are most favourable.

Are elevated rift margins formed by processes related to rifting and breakup?

Evidence from West Greenland clearly shows that the present-day elevated continental margin there is not a remnant of the original rifting process, as rifting terminated in the Paleocene (Dam *et al.* 1998), after which kilometre-scale subsidence occurred (Pedersen *et al.* 2002; Japsen *et al.* 2006). Instead the uplift occurred in Oligocene to Recent times (Japsen *et al.* 2005*b*, 2006; Bonow *et al.* 2006*a*, *b*). Observations presented here from the sedimentary basins adjacent to southern Norway similarly indicate that the mountains in that region emerged during several phases of uplift long after North Atlantic breakup at the Paleocene–Eocene transition. The mountains along these passive continental margins are characterized by elevated plains and deeply incised valleys which is also the case for margins in other parts of the world, such as southern Africa and southeastern Australia (see King 1967; Partridge & Maud 1987; Lidmar-Bergström *et al.* 2000). The results from West Greenland and the eastern North Sea Basin therefore lead us to suggest that other elevated rift margins may also have been formed by processes that are related neither to rifting nor to continental breakup (Japsen *et al.* 2009).

Both southern Africa and southeastern Australia have been well studied by both thermochronological and geomorphological standpoints. Partridge & Maud (1987) concluded after a thorough morphological analysis of the South African margin that the regional peneplain that defines the elevated topography in the area (the African Surface; King 1967) was uplifted in the Neogene, thereby agreeing with one of King's (e.g. 1967) major conclusions. In contrast to these results, many of the more recent studies of that area are predicated on the basic assumption that the morphology reflects the processes of rifting (e.g. Ollier 1985; Brown *et al.* 2002; van der Beek *et al.* 2002). However, AFTA ages from outcrop samples across a large area of southern Africa (Gallagher & Brown 1999) post-date rifting by many tens of millions of years, showing that rocks forming the extensive low-relief surface there were at temperatures around 100 °C well after the rift episode. Similar results were reported by Raab *et al.* (2005) from Namibia, where young AFT ages extend several hundreds of kilometres inland, as they also do in southeastern Australia (e.g. O'Sullivan *et al.* 1995; Kohn *et al.* 1999). Along the Brazilian margin, AFTA ages are younger than rifting by up to *c.* 50 Ma (Gallagher *et al.* 1996). None of these observations are consistent with simple models of rift margin development as summarized by, for example, Persano *et al.* (2002), and it seems far from straightforward to infer that these results reflect processes related directly to rifting.

In West Greenland, integration of stratigraphic evidence provided by the sediments and erupted volcanic rocks of the Nuussuaq Basin, objective interpretation of the denudational history from study of the landscape and a detailed thermochronological dataset have provided unique constraints on the development of the margin. In contrast to this setting, the majority of previous thermochronological studies in other regions have been focused on basement terrains and the data have been interpreted by assuming monotonic cooling, presumably because it is assumed that such areas never had a sedimentary cover and have undergone continued emergence. Our results show that these assumptions are false in West Greenland. We have shown that even the basement terrain in this region was buried repeatedly during the Phanerozoic by sedimentary covers that were subsequently removed during episodes of burial and exhumation (Japsen *et al.* 2009). We suggest that similar histories are likely to be appropriate to many other passive continental margins (see Bonow *et al.* 2007). We further suggest that studies designed to investigate the development of passive continental margins should be focused on areas where remnants of the syn- and post-rift sequence are preserved onshore (e.g. Brazil; Cobbold *et al.* 2001) since these areas contain far more information on the history of vertical displacements than those where basement is exposed at the surface. Unfortunately, the high terrain in Norway is an example of a continental margin where only rocks that predate rifting and breakup by hundreds of millions of years are preserved, limiting severely the information that can be obtained on the evolution of this region.

The sedimentary record in the basins adjacent to the elevated passive continental margins of West Greenland and southern Norway also provide evidence for the episodic post-rift uplift and erosion of the offshore shelves along these margins. This evidence comes partly from seismic and stratigraphic data that reveal sedimentary wedges prograding away from the centres of uplift in the present highlands and partly from palaeothermal and palaeoburial data from wells that make it possible to show when a hiatus represents a time interval of burial followed by exhumation. The application of this approach has demonstrated that the Neogene uplift of Scandinavia was accompanied by exhumation that reaches far into the North Sea Basin. The exhumation thus reaches beyond the truncated Palaeogene strata in Figure 1 and also affected areas with a Miocene cover, far from the centre of uplift in the Scandinavian hinterland.

In East Greenland, a major cause of the post-basalt heating reported in several studies (e.g. Thomson *et al.* 1999; Johnson & Gallagher 2000) must be due to burial below rocks that have been removed presumably by uplift and erosion in the Neogene. This interpretation resembles the burial and exhumation history established for West Greenland by Japsen *et al.* (2006) where rifting and breakup was followed by kilometre-scale subsidence and burial over an interval of many millions of years until this trend was reversed by uplift and exhumation during the mid- and late Cenozoic. These interpretations imply that post-rift subsidence of both the West and East Greenland margins, together with burial of the pre- and syn-rift sections, has taken place after rifting and breakup, just as predicted by classical rift theory. Subsequently, this subsidence was reversed by a series of uplift movements (in the West Greenland case at *c.* 35, 10 and 5 Ma) which as yet remain unexplained.

On the origin of post-rift uplift along passive margins

The regional nature of the post-rift uplift movements along passive, continental margins is now well documented (e.g. Japsen & Chalmers 2000; Green & Duddy 2010) and it is instructive to compare these events in the North Atlantic domain.

Post-breakup subsidence seems to have continued on most passive margins around the North Atlantic until the Eocene–Oligocene transition (*c.* 35 Ma), after which it was interrupted. There was no particularly notable fall in sea-level at this time (Miller *et al.* 2005), so it is difficult to see how the change could be due to a fall in eustatic sea-level. It seems instead that the subsiding basins must have been inverted by tectonic forces. We speculate that the forces causing this phase may have been related to the major plate boundary reorganization in the North Atlantic around Chron 13 time at *c.* 33 Ma (Gaina *et al.* 2009). We would also point out that this is also the approximate time at which the Iceland plume started to pulse, as revealed by gravity anomalies and the V-shaped ridges (Poore *et al.* 2009).

The next events of regional exhumation occur at very different times in Greenland and Scandinavia; in the late Miocene in West Greenland at *c.* 10 Ma (most likely at about the same time in East Greenland; cf. Thomson *et al.* 1999) and in the early Neogene at *c.* 23 Ma in southern Scandinavia. The time difference alone rules out the possibility that these events can be explained by eustasy; differential tectonics are needed to explain these movements. West Greenland provides the example where the chronology of events is best understood, and here the fully developed peneplain prior to 10 Ma provided no relief to be eroded. Thus, even if erosion was increased due to climate deterioration, no valley incision could have occurred to initiate late Neogene uplift and, as there was no significant change in eustatic sea-level at this time (Miller *et al.* 2005), a tectonic trigger was required. The early Neogene phase of regional uplift in Scandinavia correlates with the Savian phase of Alpine tectonics in central Europe (Rasmussen 2009*b*).

The third event of post-rift uplift in the region seems to have affected almost all margins beginning around the early Pliocene and, within the accuracy of the methods applied, almost simultaneously (e.g. Green & Duddy 2010): West Greenland between 7 and 2 Ma, Norwegian–Danish Basin *c.* 4 Ma, NE Atlantic margin *c.* 4 Ma and Barents Sea 10–5 Ma. The effects of this event are probably more widespread, but they cannot be resolved in many areas because of the relatively low palaeotemperatures (<60 °C that could equate to deeper burial by up to 1.5 km) of outcrop samples prior to this final phase of Cenozoic exhumation. These movements overlap with the early Pliocene warm period in NE Greenland, and predate the late Pliocene glacial maximum (Funder 1989). In fact this event caused significant surface uplift across the region and this relief, combined with climate deterioration, may thus have had a triggering role in the formation of the Greenland and Scandinavian ice sheets (Letréguilly *et al.* 1991; Japsen *et al.* 2006). Miller *et al.* (2005) show that lowstands of sea-level fell by about 25 m starting at 6 Ma and that there was significant fall in average sea-level after *c.* 2 Ma, during the latest Pliocene and in the Pleistocene. The latter fall must have reduced base levels significantly, leading to increased erosion and consequent enhanced uplift, but we question whether the earlier fall in lowstands alone is enough to trigger the final phase of uplift (cf. Stoker *et al.* 2005). That some tectonic trigger is needed is suggested by there being large negative gravity lows over all of the uplifted areas around the North Atlantic (Sandwell & Smith 1992; Laxon & McAdoo 1998). Such lows would not be produced by only an isostatic response to lowered base level, but need some form of low density or vertical motions in either the lower crust or upper mantle. The early Pliocene phase does not seem to be related to any of the plate reorganizations in the NE Atlantic found by Gaina *et al.* (2009).

The regional synchronicity between these vertical movements (and to some extent also the lack of synchronicity) and the emerging correlation between these events and episodes of plate reorganization (e.g. Gaina *et al.* 2009) and magmatic activity in Iceland (Doré *et al.* 2008; Poore *et al.* 2009) indicates that there have been tectonic triggers to the uplift movements, but does not, however, indicate a direct causal relationship between uplift movements and plate reorganization. The forces produced by the moving plates do not seem to be sufficient alone to produce the regional uplifts with kilometre-scale magnitudes along passive margins discussed in this paper. Doré *et al.* (2008) thus argued that the mild compressional structures that formed mainly between 20 and 15 Ma on the passive margins along NW Europe were generated by horizontal stress from the significant bathymetric–topographic high around Iceland. Doré *et al.* (2008) found that ridge push, generally thought to be the dominant body force acting on passive margins, was able to generate enough stress to cause only mild deformation. However, the regional uplift movements as well as the events of plate reorganization may both be expressions of deep-rooted changes in, for example, the lithosphere–asthenosphere system. The considerable distance between uplift movements along passive margins and active plate boundaries suggests that the causal mechanisms must be located in the deep crust or the upper mantle where the thickness of the crust and lithosphere changes substantially over a short distance (cf. King & Anderson 1998; Praeg *et al.* 2005; Japsen *et al.* 2006). The response to such tectonic movements is then amplified by the isostatic response to resulting erosion and redeposition of mass in the basins (cf. Medvedev *et al.* 2008).

Conclusions

The study of the burial and exhumation history of the eastern North Sea Basin emphasizes that the tectonic development of a region cannot be reconstructed solely on evidence from the preserved sedimentary record. Such reconstructions also need to be based on the record of physical indicators of palaeothermal and palaeoburial events related to the former presence of geological units that are now removed. Many studies of the sedimentary record across Denmark and offshore Norway have been published, but unconformities, particularly the low-angle unconformities, have received less attention and gaps in the sedimentary record have often been considered as periods of non-deposition (e.g. Faleide *et al.* 2002). As we have shown, such unconformities often represent intervals during which significant amounts of previously deposited section have been eroded. Only by considering episodic exhumation as an inherent aspect of the sedimentary record can the tectonic evolution in general, and the history of petroleum systems in particular, be reconstructed.

The study of the eastern North Sea Basin provides evidence for three major uplift episodes that have affected southern Scandinavia during the Cenozoic: starting at the Eocene–Oligocene transition (*c.* 33 Ma), in the early Neogene (*c.* 23 Ma) and in the late Neogene (*c.* 4 Ma). These phases, of which the two youngest involve exhumation of the offshore basin as well as the onshore region, are consistent with the sedimentary record in the NE Atlantic and around southern Norway. The observations indicate that the high mountains of southern Norway have emerged since Eocene times when a deep sea covered much of the area.

The West Greenland case underlines the importance of investigating the development of passive continental margins where sedimentary and volcanic sequences are preserved, since these areas contain far more information on the history of vertical displacements than those where only basement is exposed at the surface. The preservation of evidence of kilometre-scale subsidence within the Palaeogene volcanic–sedimentary succession makes it possible to rule out the assumption that the landscape was already high subsequent to rifting in West Greenland. However, AFTA data from areas where only basement is exposed have allowed us to infer that, even there, Cenozoic maximum burial and subsequent uplift to present elevations occurred well after rifting. We have shown that even basement terrains were covered by a Phanerozoic sedimentary cover that was subsequently removed during several episodes of burial and exhumation and in particular that a cover of at least 1500 m of Ordovician to Triassic sediments must have been deposited and then removed over the present basement high near Sukkertoppen Iskappe. This increases the possibility that the thick 'Deep Sequence' identified on seismic data from west of Greenland below deposits of Cretaceous age may include Palaeozoic sediments and possibly intervals that may act as source rocks for hydrocarbon systems.

Oligocene strata are absent from offshore West Greenland, but seismic data show that over parts of the shelf this hiatus is an erosional unconformity where middle Miocene strata truncate lower Eocene, Paleocene and Upper Cretaceous deposits. Interpretation of VR data from the Qulleq-1 well suggests that the pre-Neogene sediments have been hotter in the past and that it is likely that the Oligocene hiatus represents a period when previously deposited Palaeogene and locally older sediments were removed by erosion. Mesozoic and Cenozoic source rocks in this region are likely to have reached their maximum post-depositional palaeotemperatures as a result of burial by these eroded sediments, and hydrocarbon generation in these areas will therefore have terminated at the onset of uplift and exhumation in mid-Cenozoic times. Any structures formed during this uplift were therefore not available for charging during the main phase of generation and only structures formed earlier are likely to be viable exploration targets. Further definition of areas where timing relationships may be more favourable must await more detailed definition of regional variation in the timing and magnitude of exhumation, based on palaeothermal and palaeoburial indicators together with the regional stratigraphy.

In East Greenland, Cenozoic maximum palaeotemperatures occurred in the mid- and late Cenozoic. In particular, results from Clavering Ø show that Palaeogene basalts preserved on the summits there have been heated to peak temperatures of *c.* 70 °C prior to cooling in the late Cenozoic. As there is no Palaeogene intrusive activity reported from this area, a major cause of the post-basalt heating must be due to burial below rocks that have been removed, presumably by uplift and erosion in the Neogene. The lack of evidence for palaeothermal cooling (which might reflect uplift) related to breakup is supported by evidence from the geological record that indicates net subsidence during the eruption of the basalts at the Paleocene–Eocene transition. The margin therefore subsided following rifting and breakup, and deposition of this post-rift sequence during thermal subsidence is just what is predicted from the theory of continental stretching, whereas uplift in the mid- and late Cenozoic led to the formation of the present-day landscape. The uplift caused exhumation of remnants of hydrocarbon accumulations hosted in Jurassic sandstones on Traill Ø (Price *et al.*, 1997). The generation of hydrocarbons here was most likely enhanced due to the increased heat flow in this region associated with the intrusions in the late Eocene (combined with the palaeo-burial at that time). Further afield, in areas where heat flow was not enhanced, any source rocks present would have remained at lower maturity levels at the end of the Eocene, and Neogene burial may have resulted in generation of significant amounts of hydrocarbons that remain to be discovered.

Our observations demonstrate that elevated passive margins around the North Atlantic were formed by episodic, post-rift uplift movements that are manifest in the high-lying peneplains that characterize the coastal mountains and in the unconformities in the adjacent sedimentary basins. Moreover, the results from West Greenland, supported by observations from East Greenland and Scandinavia, show that post-rift subsidence took place for *c.* 25 Myr (in West Greenland between *c.* 60 and *c.* 35 Ma) after rifting and breakup, as predicted by classical rift theory, but that this development was reversed by a series of uplift movements (in West Greenland starting at *c.* 35, 10 and 5 Ma). These post-rift uplift movements are clearly unexplained by the existing theory of continental stretching and rifting (e.g. McKenzie 1978; White & McKenzie 1988).

The tectonic forces driving the phases of post-rift uplift along passive continental margins are unknown, but the regional nature of these movements, their considerable distance from active plate boundaries and, in some cases, their correlation with phases of plate reorganization (e.g. Gaina *et al.* 2009) and magmatic activity around Iceland (Doré *et al.* 2008) suggest that similar causal mechanisms may be active along many so-called passive continental margins. One feature that all of these areas have in common is that uplift has taken place along the edges of cratons where the thickness of the crust and lithosphere changes substantially over a short distance. It may be that the lateral contrasts in the properties of the stretched and unstretched lithosphere make the margins of the cratons unstable long after rifting, causing uplift movements that form both the present-day mountains, the regional unconformities in the adjacent basins and accelerated subsidence in the basin centres.

We thank Det norske oljeselskap ASA for permission to publish results from a study of exhumation based on sonic data in the southern Norwegian sector and ConocoPhillips for permission to publish AFTA results from three Norwegian wells. We also thank Tony Doré for a complementary, instructive and thoughtful review that improved the paper. The paper is published with permission from the Geological Survey of Denmark and Greenland.

References

Ahlmann, H. W. 1941. Studies in North–East Greenland 1939–1940. *Geografiska Annaler*, **23**, 145–209.

Backman, J., Jakobsson, M. *et al.* 2008. Age model and core-seismic integration for the Cenozoic Arctic Coring Expedition sediments from the Lomonosov Ridge. *Paleoceanography*, **23**, 1–15; doi: 10.1029/2007PA001476.

Bonow, J. M. 2005. Re-exposed basement landforms in the Disko region, West Greenland – disregarded data for estimation of glacial erosion and uplift modelling. *Geomorphology*, **72**, 106–127.

Bonow, J. M., Japsen, P., Lidmar-Bergström, K., Chalmers, J. A. & Pedersen, A. K. 2006*a*. Cenozoic uplift of Nuussuaq and Disko, West Greenland – elevated erosion surfaces as uplift markers of a passive margin. *Geomorphology*, **80**, 325–337.

Bonow, J. M., Lidmar-Bergström, K. & Japsen, P. 2006*b*. Palaeosurfaces in central West Greenland as reference for identification of tectonic movements and estimation of erosion. *Global and Planetary Change*, **50**, 161–183.

Bonow, J. M., Lidmar-Bergström, K., Japsen, P., Chalmers, J. A. & Green, P. F. 2007. Elevated erosion surfaces in southern Norway and West Greenland: their significance in studies of uplift and tectonic events. *Norwegian Journal of Geology*, **87**, 181–196.

Bray, R., Green, P. F. & Duddy, I. R. 1992. Thermal history reconstruction in sedimentary basins using apatite fission track analysis and vitrinite reflectance: a case study from the east Midlands of England and the Southern North Sea. *In*: Hardman, R. F. P. (ed.) *Exploration Britain: Into the Next Decade*. Geological Society, London, Special Publications, **67**, 3–25.

Brooks, C. K. 1985. Vertical crustal movements in the Tertiary of central East Greenland: a continental margin at a hot-spot. *Zeitschrift für Geomorphologie*, **54**, 101–117.

Brown, R., Summerfield, M. A. & Gleadow, A. J. W. 2002. Denudational history along a transect across the Drakensberg Escarpment of southern Africa derived from apatite fission track analysis. *Journal of Geophysical Research*, **107**, 2350–2367.

Chalmers, J. A. 2000. Offshore evidence for Neogene uplift in central West Greenland. *Global and Planetary Change*, **24**, 311–318.

Chalmers, J. A. & Pulvertaft, T. C. R. 2001. Development of the continental margins of the Labrador Sea: a review. *In*: Wilson, R. C. L., Withmarsh, R. B., Taylor, B. & Froitzheim, N. (eds) *Non-volcanic Rifting of Continental Margins: A Comparison of Evidence from Land and Sea*. Geological Society, London, Special Publications, **187**, 77–105.

Chalmers, J. A., Pulvertaft, T. C. R., Marcussen, C. & Pedersen, A. K. 1999. New insight into the structure of the Nuussuaq Basin, central West Greenland. *Marine and Petroleum Geology*, **16**, 197–224.

Christiansen, F. G., Piasecki, S. & Stemmerik, L. 1990. Thermal maturity history of the Upper Permian succession in the Wegener Halvø area, East Greenland. *Rapport Grønlands Geologiske Undersøgelse*, **148**, 109–114.

Christiansen, F. G., Larsen, H. C. *et al*. 1992. Uplift study of the Jameson Land Basin, East Greenland. *Norsk Geologisk Tidsskrift*, **72**, 291–294.

Christiansen, F. G., Bojesen-Koefoed, J. A. *et al*. 2001. Petroleum geological activities in West Greenland in 2000. *Geology of Greenland Survey Bulletin*, **189**, 24–33.

Clausen, O. R., Gregersen, U., Michelsen, O. & Sørensen, J. C. 1999. Factors controlling the Cenozoic sequence development in the eastern parts of the North Sea. *Journal of the Geological Society, London*, **156**, 809–816.

Cobbold, P. R., Meisling, K. E. & Mount, V. S. 2001. Reactivation of an obliquely rifted margin, Campos and Santos basins, southeastern Brazil. *American Association of Petroleum Geologists Bulletin*, **85**, 1925–1944.

Corcoran, D. V. & Doré, A. G. 2005. A review of techniques for the estimation of magnitude and timing of exhumation in offshore basins. *Earth Science Reviews*, **72**, 129–168.

Dalhoff, F., Larsen, L. M. *et al*. 2006. Continental crust in the Davis Strait: new evidence from seabed sampling. *Geological Survey of Denmark and Greenland Survey Bulletin*, **10**, 33–36.

Dam, G., Larsen, M. & Sørensen, J. C. 1998. Sedimentary response to mantle plumes: implications from Paleocene onshore successions, West and East Greenland. *Geology*, **26**, 207–210.

Doré, A. G., Corcoran, D. V. & Scotchman, I. C. 2002. Prediction of the hydrocarbon system in exhumed basins, and application to the NW European margin. *In*: Doré, A. G., Cartwright, J. A., Stoker, M. S., Turner, J. & White, N. (eds) *Exhumation of the North Atlantic Margin: Timing, Mechanisms and Implications for Petroleum Explorations*. Geological Society, London, Special Publications, **196**, 401–429.

Doré, A. G., Lundin, E., Kusznir, N. J. & Pascal, C. 2008. Potential mechanisms for the genesis of Cenozoic domal structures on the NE Atlantic margin: pros and cons and some new ideas. *In*: Johnson, H., Doré, A. G., Gatliff, R. W., Holdsworth, R. E., Lundin, E. & Ritchie, J. D. (eds) *The Nature and Origin of Compression in Passive Margins*. Geological Society, London, Special Publications, **306**, 1–26.

Eldholm, O., Thiede, J. & Taylor, E. 1989. Evolution of the Vøring volcanic margin. *In*: Eldholm, O., Thiede, J. & Taylor, E. (eds) *Proceedings of the Ocean Drilling Program (ODP), Scientific Results*, College Station, TX (Ocean Drilling Program), **104**, 39–68.

Fabricius, I. L., Gommesen, L., Krogsbøll, A. & Olsen, D. 2008. Chalk porosity and sonic velocity versus burial depth: influence of fluid pressure, hydrocarbons, and mineralogy. *American Association of Petroleum Geologists Bulletin*, **92**, 201–223.

Faleide, J. I., Kyrkejbø, R. *et al*. 2002. Tectonic impact on sedimentary processes during Cenozoic evolution of the northern North Sea and surrounding areas. *In*: Doré, A. G., Cartwright, J. A., Stoker, M. S., Turner, J. P. & Whites, N. (eds) *Exhumation of the North Atlantic Margin: Timing, Mechanisms and Implications for Petroleum Exploration*. Geological Society, London, Special Publications, **196**, 235–269.

Funder, S. 1989. Quaternary geology of the icefree areas and adjacent shelves of Greenland. *In*: Fulton, J. R. (ed.) *Quaternary Geology of Canada and Greenland*. The Geology of North America. Geological Society of America, Boulder, CO, 741–792.

Gaina, C., Gernigon, L. & Ball, P. 2009. Palaeocene–Recent plate boundaries in the NE Atlantic and the formation of the Jan Mayen microcontinent. *Journal of the Geological Society, London*, **166**, 601–616.

Gallagher, K. & Brown, R. 1999. The Mesozoic denudation history of the Atlantic margins of southern Africa and southeast Brazil and the relationship to offshore sedimentation. *In*: Cameron, N. R., Bate, R. H. & Clure, V. S. (eds) *The Oil and Gas Habitats of the South Atlantic*. Geological Society, London, Special Publications, **153**, 41–53.

Gallagher, K., Hawkesworth, C. J. & Mantovani, M. 1996. The denudation history of the onshore continental margin of SE Brazil inferred from apatite fission track data. *Journal of Geophysical Research*, **99**, 18117–18145.

Gleadow, A. J. W. & Brooks, C. K. 1979. Fission-track dating, thermal histories and tectonics of igneous intrusions in East Greenland. *Contributions to Mineralogy and Petrology*, **71**, 45–60.

GLOBE Task Team and others (Hastings, D. A., Dunbar, P. K. *et al*., eds) 1999. *The Global Land One-kilometer Base Elevation (GLOBE) Digital Elevation Model, Version 1.0*. National Oceanic and Atmospheric Administration, National Geophysical Data Center, Boulder, CO. Digital database on the World Wide Web http://www.ngdc.noaa.gov/mgg/topo/globe.html and CD-ROMs.

Green, P. F. & Duddy, I. 2010. Synchronous exhumation events around the Arctic including examples from Barents Sea, Alaska North Slope. *In*: Vining, B. A. & Pickering, S. C. (eds) *Petroleum Geology: From Mature Basins to New Frontiers – Proceedings of the 7th Petroleum Geology Conference*. Geological Society, London, Special Publications, 633–644; doi: 10.1144/0070633.

Green, P. F., Duddy, I. R., Gleadow, A. J. W. & Lovering, J. F. 1989. Apatite fission track analysis as a palaeotemperature indicator for hydrocarbon exploration. *In*: Naeser, N. D. & McCulloh, T. (eds) *Thermal History of Sedimentary Basins – Methods and Case Histories*. Springer, New York, 181–195.

Green, P. F., Duddy, I. R. & Hegarty, K. A. 2002. Quantifying exhumation from apatite fission-track analysis and vitrinite reflectance data: precision, accuracy and latest results from the Atlantic margin of NW Europe. *In*: Doré, A. G., Cartwright, J. A., Stoker, M. S., Turner, J. P. & Whites, N. (eds) *Exhumation of the North Atlantic Margin: Timing, Mechanisms and Implications for Petroleum Exploration*. Geological Society, London, Special Publications, **196**, 331–354.

Green, P. F., Crowhurst, P. V. & Duddy, I. R. 2004. Integration of AFTA and (U–Th)/He thermochronology to enhance the resolution and precision of thermal history reconstruction in the Anglesea-1 well, Otway Basin, SE Australia. *In*: Boult, P. J., Johns, D. R. & Lang, S. C. (eds) *Eastern Australian Basins Symposium II*. Petroleum Exploration Society of Australia, 117–131.

Green, P. F., Crowhurst, P. V., Duddy, I. R., Japsen, P. & Holford, S. P. 2006. Conflicting (U–Th)/He and fission track ages in apatite: enhanced He retention, not anomalous annealing behaviour. *Earth and Planetary Science Letters*, **250**, 407–427.

Hamann, N. E., Whittaker, R. C. & Stemmerik, L. 2005. Geological development of the Northeast Greenland Shelf. *In*: Doré, A. G. & Vining, B. A. (eds) *Petroleum Geology: North-West Europe and Global Perspectives: Proceedings of the 6th Petroleum Geology*. Geological Society, London, 887–902; doi: 10.1144/0060887.

Hansen, K. 1988. Preliminary report of fission track studies in the Jameson Land basin, East Greenland. *Rapport Grønlands Geologiske Undersøgelse*, **140**, 85–89.

Hansen, K. 1992. Post-orogenic tectonic and thermal history of a rifted continental: the Scoresby Sund area, east Greenland. *Tectonophysics*, **216**, 309–326.

Hansen, K. 1996. Thermo-tectonic evolution of a rifted continental margin: fission track evidence from the Kangerlussuaq area, SE Greenland. *Terra Nova*, **8**, 458–469.

Hansen, K., Bergman, S. C. & Henk, B. 2001. The Jameson Land basin (east Greenland): a fission track study of the tectonic and thermal evolution in the Cenozoic North Atlantic spreading regime. *Tectonophysics*, **331**, 307–339.

Harrison, J. C., Mayr, U. *et al*. 1999. Correlation of Cenozoic sequences of the Canadian Arctic region and Greenland; implications for the tectonic history of North America. *Bulletin of Canadian Petroleum Geology*, **47**, 223–254.

Heilmann-Clausen, C., Nielsen, O. B. & Gersner, F. 1985. Lithostratigraphy and depositional environments in the upper Palaeocene and Eocene of Denmark. *Bulletin of the Geological Society of Denmark*, **33**, 287–323.

Henriksen, N. 2008. *Geological History of Greenland*. Geological Survey of Denmark and Greenland (GEUS), Copenhagen.

Henriksen, N., Higgins, A. K., Kalsbeek, F. & Pulvertaft, T. C. R. 2000. *Greenland from Archaean to Quaternary. Descriptive Text to the Geological Map of Greenland 1:2 500 000*. Geology of Greenland Survey Bulletins, **185**.

Hillis, R. R. 1995. Quantification of tertiary exhumation in the United Kingdom southern North Sea using sonic velocity data. *American Association of Petroleum Geologists Bulletin*, **79**, 130–152.

Holliday, D. W. 1993. Mesozoic cover over northern England: interpretation of apatite fissiontrack data. *Journal of the Geological Society, London*, **150**, 657–660.

Japsen, P. 1998. Regional velocity–depth anomalies, North Sea Chalk: a record of overpressure and Neogene uplift and erosion. *American Association of Petroleum Geologists Bulletin*, **82**, 2031–2074.

Japsen, P. 1999. Overpressured Cenozoic shale mapped from velocity anomalies relative to a baseline for marine shale, North Sea. *Petroleum Geoscience*, **5**, 321–336.

Japsen, P. 2000. Investigation of multi-phase erosion using reconstructed shale trends based on sonic data. Sole Pit axis, North Sea. *Global and Planetary Change*, **24**, 189–210.

Japsen, P. & Bidstrup, T. 1999. Quantification of late Cenozoic erosion in Denmark based on sonic data and basin modelling. *Bulletin of the Geological Society of Denmark*, **46**, 79–99.

Japsen, P. & Chalmers, J. A. 2000. Neogene uplift and tectonics around the North Atlantic: overview. *Global and Planetary Change*, **24**, 165–173.

Japsen, P., Bidstrup, T. & Lidmar-Bergström, K. 2002. Neogene uplift and erosion of southern Scandinavia induced by the rise of the South Swedish Dome. *In*: Doré, A. G., Cartwright, J., Stoker, M. S., Turner, J. P. & White, N. (eds) *Exhumation of the North Atlantic Margin: Timing, Mechanisms and Implications for Petroleum Exploration*. Geological Society, London, Special Publications, **196**, 183–207.

Japsen, P., Mavko, G. *et al*. 2005*a*. Chalk background velocity: influence of effective stress and texture. *EAGE 67th Conference & Exhibition*, Madrid, 13–16 June.

Japsen, P., Green, P. F. & Chalmers, J. A. 2005*b*. Separation of Palaeogene and Neogene uplift on Nuussuaq, West Greenland. *Journal of the Geological Society, London*, **162**, 299–314.

Japsen, P., Bonow, J. M., Green, P. F., Chalmers, J. A. & Lidmar-Bergström, K. 2006. Elevated, passive continental margins: long-term highs or Neogene uplifts. New evidence from West Greenland. *Earth and Planetary Science Letters*, **248**, 315–324.

Japsen, P., Green, P. F., Nielsen, L. H., Rasmussen, E. S. & Bidstrup, T. 2007*a*. Mesozoic–Cenozoic exhumation in the eastern North Sea Basin: a multi-disciplinary study based on palaeo-thermal, palaeo-burial, stratigraphic and seismic data. *Basin Research*, **19**, 451–490.

Japsen, P., Mukerji, T. & Mavko, G. 2007*b*. Constraints on velocity–depth trends from rock physics models. *Geophysical Prospecting*, **55**, 135–154.

Japsen, P., Rasmussen, E. S., Green, P. F., Nielsen, L. H. & Bidstrup, T. 2008. Cenozoic palaeogeography and isochores before Neogene exhumation in the eastern North Sea Basin. *Geological Survey of Denmark and Greenland Bulletin*, **15**, 25–28.

Japsen, P., Bonow, J. M., Green, P. F., Chalmers, J. A. & Lidmar-Bergström, K. 2009. Formation, uplift and destruction of planation surfaces at passive continental margins. *Earth Surface Processes and Landforms*, **34**, 683–699.

Johnson, K. & Gallagher, K. 2000. A preliminary Mesozoic and Cenozoic denudation history of the North East Greenland onshore margin. *Global and Planetary Change*, **24**, 303–309.

King, L. C. 1967. *The Morphology of the Earth* (2nd edn). Oliver & Boyd, Edinburgh.

King, S. D. & Anderson, D. L. 1998. Edge-driven convection. *Earth Planetary Science Letters*, **160**, 289–296.

Kohn, B. P., Gleadow, A. J. W. & Cox, S. J. D. 1999. Denudation history of the Snowy Mountains: constraints from apatite fission track analysis. *Australian Journal of Earth Science*, **46**, 181–198.

Larsen, L. M. 2006. *Mesozoic to Palaeogene Dyke Swarms in West Greenland and their Significance for the Formation of the Labrador Sea and the Davis Strait*. Danmarks og Grønlands Geologiske Undersøgelse Rapport **2006/34**.

Larsen, R. B. & Tegner, C. 2006. Pressure conditions for the solidification of the Skaergaard intrusion: eruption of East Greenland flood basalts in less than 300 000 years. *Lithos*, **92**, 181–19.

Larsen, L. M., Watt, W. S. & Watt, M. 1989. Geology and petrology of the Lower Tertiary plateau basalts of the Scoresby Sund region, East Greenland. *Grønlands Geologiske Undersøgelse Bulletin*, **157**, 164.

Larsen, M., Heilmann-Clausen, C., Piasecki, S. & Stemmerik, L. 2005. At the edge of a new ocean: post-volcanic evolution of the Palaeogene Kap Dalton Group, East Greenland. *In*: Doré, A. G. & Vining, B. A. (eds) *Petroleum Geology: North-West Europe and Global Perspectives: Proceedings of the 6th Petroleum Geology Conference*. Geological Society, London, 923–932; doi: 10.1144/0060923.

Laxon, S. & McAdoo, D. 1998. Satellites provide new insights into polar geophysics. *EOS Transactions, American Geophysical Union*, **79**, 72–73.

Letréguilly, A., Huybrechts, P. & Reeh, N. 1991. Steady-state characteristics of the Greenland ice sheet under different climates. *Journal of Glaciology*, **37**, 149–157.

Lidmar-Bergström, K. 1996. Long term morphotectonic evolution in Sweden. *Geomorphology*, **16**, 33–59.

Lidmar-Bergström, K., Ollier, C. D. & Sulebak, J. C. 2000. Landforms and uplift history of southern Norway. *Global and Planetary Change*, **24**, 211–231.

Lidmar-Bergström, K., Näslund, J.-O., Ebert, K., Neubeck, T. & Bonow, J. M. 2007. Cenozoic landscape development on the passive margin of northern Scandinavia. *Norwegian Journal of Geology*, **87**, 181–196.

Mathiesen, A., Christiansen, F. G., Bidstrup, T., Marcussen, C., Dam, G., Piasecki, S. & Stemmerik, L. 1995. Modelling of hydrocarbon generation in the Jameson Land Basin, East Greenland. *First Break*, **13**, 329–341.

Mathiesen, A., Bidstrup, T. & Christiansen, F. G. 2000. Denudation and uplift history of the Jameson Land Basin, East Greenland – constrained from maturity and apatite fission track data. *Global and Planetary Change*, **24**, 303–309.

McKenzie, D. 1978. Some remarks on the development of sedimentary basins. *Earth and Planetary Science Letters*, **40**, 25–32.

Medvedev, S., Hartz, E. H. & Podladchikov, Y. Y. 2008. Vertical motions of the fjord regions of central East Greenland: impact of glacial erosion, deposition, and isostasy. *Geology*, **36**, 539–542.

Michelsen, O., Thomsen, E., Danielsen, M., Heilmann-Clausen, C., Jordt, H. & Laursen, G. 1998. Cenozoic sequence stratigraphy in the eastern North Sea. *In*: de Graciansky, P.-C. *et al*. (eds) *Mesozoic and Cenozoic Sequence Stratigraphy of European Basins*. Society of Economic Paleontologists and Mineralogists, Special Publications, **60**, 91–118.

Miller, K. G., Kominz, M. A. *et al*. 2005. The phanerozoic record of global sea-level change. *Science*, **310**, 1293–1298.

Nielsen, L. H. 2003. Late Triassic–Jurassic development of the Danish Basin and Fennoscandian Border Zone, southern Scandinavia. *In*: Ineson, J. & Surlyk, F. (eds) *The Jurassic of Denmark and Greenland. Geological Survey of Denmark and Greenland Bulletin*, **1**, 459–526.

Nøhr-Hansen, H. 2003. Dinoflagellate cyst stratigraphy of the Palaeogene strata from the Hellefisk-1, Ikermiut-1, Kangâmiut-1, Nukik-1, Nukik-2 and Qulleq-1 wells, offshore West Greenland. *Marine and Petroleum Geology*, **20**, 987–1016.

Ollier, C. D. 1985. Morphotectonics of passive continental margins: introduction. *Zeitschrift für Geomorphologie Neue Folge, Suppl.*, **54**, 1–9.

O'Sullivan, P. B., Kohn, B. P., Foster, D. A. & Gleadow, A. J. W. 1995. Fission track data from the Bathurst batholith: evidence for rapid mid-Cretaceous uplift and erosion within the eastern highlands of Australia. *Australian Journal of Earth Sciences*, **42**, 597–607.

Partridge, T. C. & Maud, R. R. 1987. Geomorphic evolution of southern Africa since the Mesozoic. *South African Journal of Geology*, **90**, 179–208.

Pedersen, A. K., Larsen, L. M., Riisager, P. & Dueholm, K. S. 2002. Rates of volcanic deposition, facies changes and movements in a dynamic basin: the Nuussuaq Basin, West Greenland, around the C27n-C26r transition. *In*: Jolley, D. W. & Bell, B. R. (eds) *The North Atlantic Igneous Province. Stratigraphy, Tectonic, Volcanic and Magmatic Processes*. Geological Society, London, Special Publications, **197**, 157–181.

Pedersen, A. K., Pedersen, G. K. & Larsen, L. M. 2006. Geologien. *In*: Bruun, L., Nielsen, N., Pedersen, G. K. & Pedersen, P. M. (eds) *Arktisk Station, 1906–2006*. Arktisk Station, Københavns Universitet with Forlaget Rhodos, Copenhagen, 17–32.

Persano, C., Stuart, F. M., Bishop, P. & Barfod, D. N. 2002. Apatite (U–Th)/He age constraints on the development of the Great Escarpment on the southeastern Australian passive margin. *Earth and Planetary Science Letters*, **219**, 1–12.

Piasecki, S. 2003. Neogene dinoflagellate cysts from Davis Strait, offshore West Greenland. *Marine and Petroleum Geology*, **20**, 1075–1088.

Poore, H. R. N., White, N. & Jones, S. 2009. A Neogene chronology of Iceland plume activity from V-shaped ridges. *Earth & Planetary Science Letters*, **283**, 1–13; doi: 10.1016/j.epsl.2009.02.028.

Praeg, D., Stoker, M. S., Shannon, P. M., Ceramicola, S., Hjelstuen, B. O., Laberg, J. S. & Mathiesen, A. 2005. Episodic Cenozoic tectonism and the development of the NW European 'passive' continental margin. *Marine and Petroleum Geology*, **22**, 977–1005.

Price, S. P. & Whitham, A. G. 1997. Exhumed hydrocarbon traps in east Greenland: analogs for the lower–middle Jurassic play of northwest Europe. *American Association of Petroleum Geologists Bulletin*, **81**, 196–221.

Price, S. P., Brodie, J. A., Whitham, A. G. & Kent, R. 1997. Mid-Tertiary rifting and magmatism in the Traill Ø region, East Greenland. *Journal of the Geological Society, London*, **154**, 419–434.

Raab, M. J., Brown, R. W., Gallagher, K., Webber, K. & Gleadow, A. J. W. 2005. Denudational and thermal history of the Early Cretaceous Brandberg and Okenyenya igneous complexes on Namibia's passive margin. *Tectonics*, **24**, TC3006.

Rasmussen, E. S. 2004. The interplay between true eustatic sea-level changes, tectonics, and climatical changes: what is the dominating factor in sequence formation of the Upper Oligocene–Miocene succession in the eastern North Sea Basin, Denmark? *Global and Planetary Change*, **41**, 15–30.

Rasmussen, E. S. 2005. The geology of the upper Middle–Upper Miocene Gram Formation in the Danish area. *Palaeontos*, **7**, 5–18.

Rasmussen, E. S. 2009*a*. Detailed mapping of marine erosional surfaces and the geometry of clinoforms on seismic data: a tool to identify the thickest reservoir sand. *Basin Research*, **21**, 721–737.

Rasmussen, E. S. 2009*b*. Neogene inversion of the Central Graben and Ringkøbing-Fyn High, Denmark. *Tectonophysics*, **465**, 84–97.

Rowley, R. & White, N. 1998. Inverse modeling of extension and denudation in the East Irish Sea and surrounding areas. *Earth and Planetary Science Letters*, **161**, 57–71.

Sandwell, D. T. & Smith, W. H. E. 1992. *Global Marine Gravity Field from ERS-1, Geosat and Seasat*. Scripps Institute of Oceanography, La Jolla, CA.

Sanford, B. V. & Grant, A. C. 2000. Geological framework of the Ordovician system in the Southeast Arctic Platform, Nunavut. *In*: McCracken, A. D. & Bolton, T. E. (eds) *Geology and Paleontology of the Southeast Arctic Platform and Southern Baffin Island, Nunavut*. Geological Survey of Canada, Bulletins, **557**, 13–38.

Sangiorgi, F., Brumsack, H. J. *et al*. 2008. A 26 million year gap in the central Arctic record at the greenhouse-icehouse transition: looking for clues. *Paleoceanography*, **23**, 1–13; doi: 10.1029/2007PA001477.

Schiøler, P., Andsbjerg, J. *et al*. 2007. *Lithostratigraphy of the Palaeogene – Lower Neogene Succession of the Danish North Sea*. Geological Survey of Denmark and Greenland, Bulletins, **12**.

Schmidt, A. G., Riisager, P., Abrahamsen, N., Riisager, J., Pedersen, A. K. & van der Voe, R. 2005. Palaeomagnetism of Eocene Talerua Member lavas on Hareøen, West Greenland. *Bulletin of the Geological Society of Denmark*, **52**, 27–39.

Sclater, J. G. & Christie, P. A. F. 1980. Continental stretching; an explanation of the post-Mid-Cretaceous subsidence of the central North Sea basin. *Journal of Geophysical Research*, **85**, 3711–3739.

Shuster, D. L., Flowers, R. M. & Farley, K. A. 2006. The influence of natural radiation damage on helium diffusion kinetics in apatite. *Earth and Planetary Science Letters*, **249**, 148–161.

Skogseid, J., Planke, S., Faleide, J. I., Pedersen, T., Eldholm, O. & Neverdal, F. 2000. NE Atlantic continental rifting and volcanic margin formation. *In*: Nøttvedt, A. (ed.) *Dynamics of the Norwegian Margin*. Geological Society, London, Special Publications, **167**, 295–326.

Sønderholm, M., Nøhr-Hansen, H., Bojesen-Koefoed, J. A., Dalhoff, F. & Rasmussen, J. A. 2003. *Regional Correlation of Mesozoic–Palaeogene Sequences across the Greenland–Canada Boundary*. Danmarks og Grønlands Geologiske Undersøgelse Rapport **2003/25**.

Sørensen, A. B. 2006. Stratigraphy, structure and petroleum potential of the Lady Franklin and Maniitsoq Basins, offshore southern West Greenland. *Petroleum Geoscience*, **12**, 221–234.

Steenfelt, A., Hollis, J. A. & Secher, K. 2006. The Tikiusaaq carbonatite: a new Mesozoic intrusive complex in southern West Greenland. *Geological Survey of Denmark and Greenland Bulletin*, **10**, 41–44.

Stoker, M. S., Praeg, D. *et al*. 2005. Neogene evolution of the Atlantic continental margin of NW Europe Lofoten Islands to SW Ireland: anything but passive. *In*: Doré, A. G. & Vining, B. A. (eds) *Petroleum Geology: North-West Europe and Global Perspectives: Proceedings of the 6th Petroleum Geology Conference*. Geological Society, London, 1057–1076; doi: 10.1144/0061057.

Storey, M., Duncan, R. A., Pedersen, A. K., Larsen, L. M. & Larsen, H. C. 1998. $^{40}Ar/^{39}Ar$ geochronology of the West Greenland Tertiary volcanic province. *Earth and Planetary Science Letters*, **160**, 569–586.

Stouge, S. & Peel, J. S. 1979. Ordovician conodonts from the Precambrian shield of southern West Greenland. *Rapport Grønlands Geologiske Undersøgelse*, **91**, 105–109.

Swift, D. A., Persano, C., Stuart, F. M., Gallagher, K. & Whitham, A. 2008. A reassessment of the role of ice sheet glaciation in the long-term evolution of the East Greenland fjord region. *Geomorphology*, **97**, 109–125.

Thomson, K., Green, P. F., Whitham, A. G., Price, S. P. & Underhill, J. R. 1999. New constraints on the thermal history of North-East Greenland from apatite fission-track analysis. *GSA Bulletin*, **111**, 1054–1068.

Tissot, B. P. & Welte, D. H. 1984. *Petroleum Formation and Occurrence*. Springer, Berlin.

Utescher, T., Mosbrugger, V., Ivanov, D. & Dilcher, D. L. 2009. Present-day climatic equivalents of European Cenozoic climates. *Earth and Planetary Science Letters*, **284**, 544–552.

van der Beek, P., Summerfield, M. A., Braun, J., Brown, R. W. & Fleming, A. 2002. Modelling postbreakup landscape development and denudational history across the southeast African (Drakensberg Escarpment) margin. *Journal of Geophysical Research*, **107**, 2351; doi: 10.1029/2001JB000744.

White, N. & McKenzie, D. 1988. Formation of the steers head geometry of sedimentary basins by differential stretching of the crust and the mantle. *Geology*, **16**, 250–253.

Ziegler, P. A. 1990. *Geological Atlas of Western and Central Europe* (2nd edn). Elsevier for Shell Internationale Petroleum Maatschappij, Amsterdam.

New methods of improving seismic data to aid understanding of passive margin evolution: a series of case histories from offshore west of Ireland

R. J. J. HARDY,[1] E. QUERENDEZ,[1] F. BIANCOTTO,[1] S. M. JONES,[1] J. O'SULLIVAN[2] and N. WHITE[3]

[1]*Trinity College Dublin, School of Natural Science, Department of Geology, Dublin 2, Ireland (e-mail: hardyr@tcd.ie)*

[2]*Providence Resources Plc Airfield House, Airfield Park, Donnybrook, Dublin 4, Ireland*

[3]*Bullard Laboratories, Department of Earth Sciences, Madingley Road, Cambridge CB3 0EZ, UK*

Abstract: Deepwater sedimentary basins are attracting increased attention from the hydrocarbon industry and academia as they remain one of the last geological frontiers still to be fully explored and understood. As part of a regional project to understand basin development offshore Ireland, we have developed and tested new ways of improving seismic images, and of incorporating these improvements into geological interpretations. Here we illustrate this methodology using three case histories from the Porcupine, Slyne and Erris Basins. In each case, the first stage of the workflow consists of reprocessing a selection of key seismic data. Processing includes relative amplitude preservation and advanced demultiple and interpretation-driven pre-stack depth imaging. Interpretation of the data is assisted by incorporating products such as multiple models, pre-stack gathers, velocity models and attributes. Finally, we show how a velocity model can be inverted to exhumation estimates. The results and approach developed here can be applied to other deepwater exploration areas.

Keywords: seismic data, seismic data processing, seismic data interpretation, exhumation

Recent technological and modelling advances provide an excellent opportunity to constrain the quantitative temporal and spatial evolution of Irish sedimentary basins and passive margins. Margin formation and growth play an integral role in the Mesozoic and Cenozoic geological history of Ireland (Naylor & Shannon 2005). The deeper reaches of margins are of considerable interest to the hydrocarbon industry since they constitute an important exploration frontier. However, methods are required to reduce exploration risk since drilling costs are high. Despite the large volumes of seismic data acquired offshore Ireland over the last 20 years, considerable improvements in imaging are possible. Here we apply state-of-the-art processing and interpretation technology to legacy seismic reflection datasets and well-log information from the Irish Continental Shelf, concentrating on the Porcupine, Slyne and Erris Basins (Fig. 1).

The first phase of this project was to understand and improve the quality of seismic reflection imaging throughout the sedimentary pile and basement. In collaboration with the project sponsors, we selected regional profiles for reprocessing from field and stacked records for each of the three basins of interest. The purpose of the reprocessing phase was to produce uniform quality depth images for a range of analyses at basin and prospect scales. We used novel pre-stack processing techniques such as deterministic deconvolution, advanced multiple suppression and interpretation driven pre-stack depth imaging. For the Porcupine Basin study area, the new depth images have been calibrated against well-log information to produce uniform quality reinterpretations. Reprocessed and existing legacy datasets have been integrated and carefully interpreted using other available geological and geophysical information in order to constrain basin configuration. The main improvements are in the imaging of syn-rift stratigraphy, but post-rift stratigraphic imaging has also benefited from our approach. Integrated use of pre-stack data, gravity and seismically derived velocity fields has been the key to better mapping. The Cenozoic exhumation history of the Slyne Basin has also been studied using reprocessed depth sections and derived velocity fields utilizing a suite of in-house tools that exploit thermal data (e.g. fission track, vitrinite reflectance), compaction data (e.g. sonic velocities, stacking velocities) and remnant subsidence data.

Porcupine Basin

The Porcupine Basin is generally believed to have formed by lithospheric stretching. However, several aspects of basin evolution are controversial. There is a significant discrepancy between the amount of extension measured across normal faults and that estimated from analysis of subsidence and crustal thinning. Early studies interpreted significant syn-rift igneous activity (Tate *et al.* 1993) while later work cited the basin as a natural laboratory to study the pre-breakup evolution of amagmatic passive margins (Reston *et al.* 2004). Good quality seismic imaging at depth is clearly required in order to resolve these controversies.

Database

Prior to commencement of our study in 2003, no academic digital database existed containing all released well and seismic data for the region. Our initial project requirement was therefore to establish and maintain a local digital database of seismic surveys (field, stacked and migrated 2D and 3D data), well logs (e.g. sonic, density, gamma), seabed mapping (e.g. sidescan sonar surveys) together with potential field information (gravity, magnetic). Our focus was on pre-stack seismic data. Seismic field tapes were required to enable pre-stack analysis of prospect-scale targets, which can be quantitatively compared with similar analysis worldwide. Stacked data, where available, formed an additional resource for this project. For example, investigation of stacked data can facilitate identification of high impedance scatterers (e.g. volcanic packages or salt features) within the stratigraphic section. Furthermore, interpretation of migrated 2D regional lines can be considerably improved by mapping and compensating for out-of-plane effects at line ties using the stack data. Available datasets ranged in vintage from 5 to 20 years and little had been reprocessed using pre-stack imaging or advanced demultiple techniques. No prestack gathers (either time or depth migrated) or depth migrated

VINING, B. A. & PICKERING, S. C. (eds) *Petroleum Geology: From Mature Basins to New Frontiers – Proceedings of the 7th Petroleum Geology Conference*, 1005–1012. DOI: 10.1144/0071005

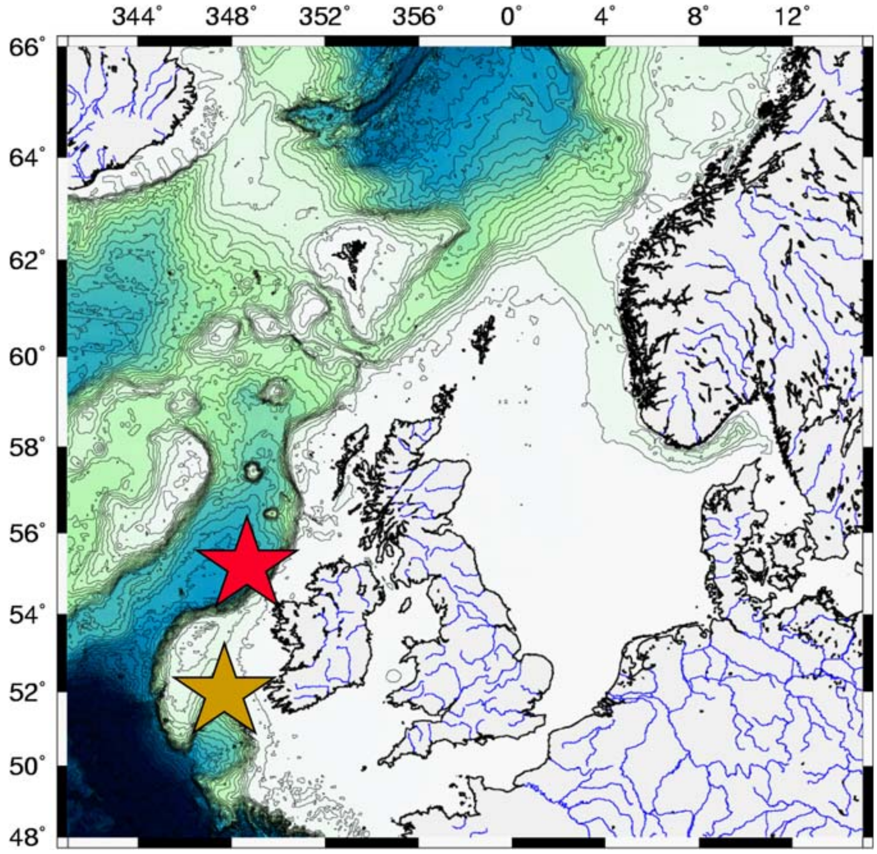

Fig. 1. Location map showing basins of interest. Porcupine Basin (lower star), Slyne–Erris basins (upper star).

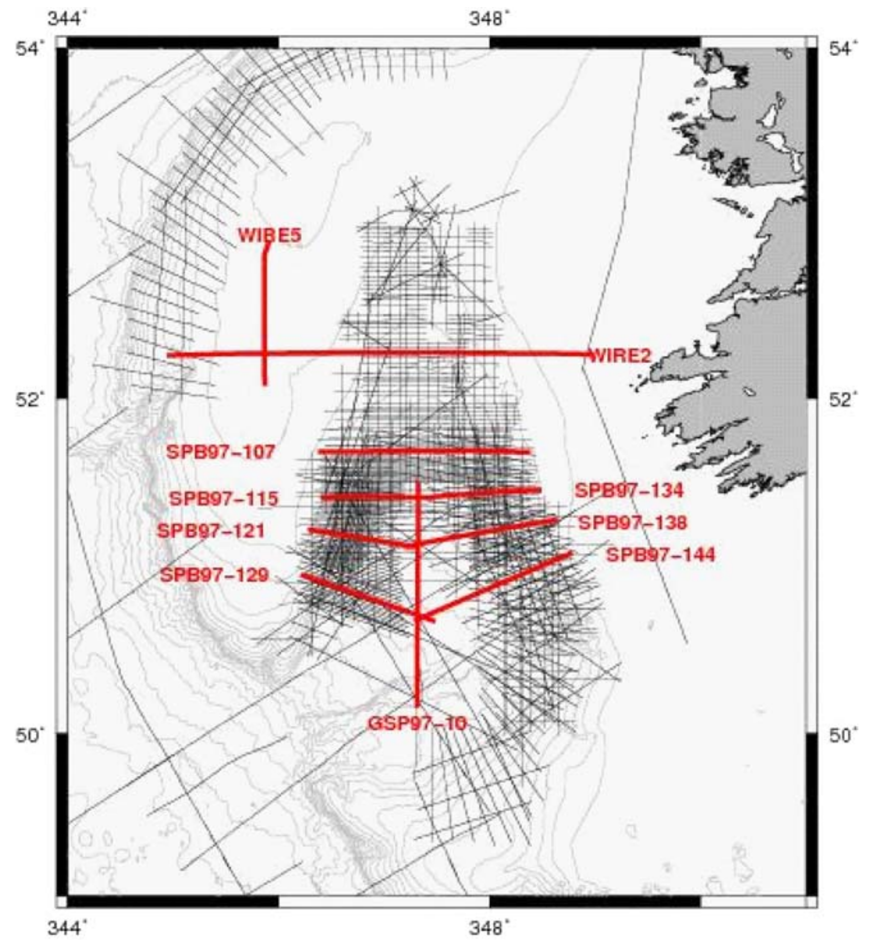

Fig. 2. Basemap of interpretation grid used for Porcupine Basin study. Lines highlighted were used for pre-stack reprocessing studies.

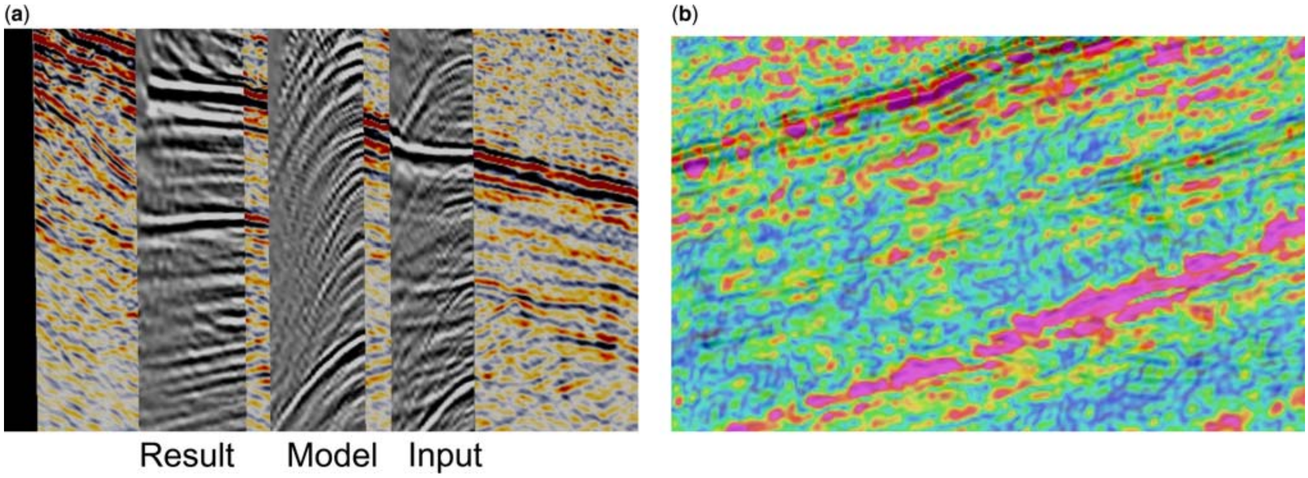

Fig. 3. (**a**) Visualization quality control of surface-related multiple elimination showing pre-stack gathers used during interpretation of deep water offshore seismic data. (**b**) Colour overlay of multiple energy and seismic data for quality control and reduction of interpretation risk.

sections were available. Recently there have been several programmes to acquire long-offset data which can benefit both multiple suppression and pre-stack imaging. However, these data are not yet generally released.

Seismic data reprocessing

An optimal grid of eight lines of released seismic data was selected for test reprocessed from field and stacked records (Fig. 2). Our philosophy is that novel seismic processing is an integral component of seismic interpretation and basin modelling and that data reprocessing (particularly depth imaging) can reduce uncertainty in the basin modelling phases.

In the last 10 years, there has been a revolution in the quality of multiple suppression and seismic imaging. One example is the surface-related multiple elimination (SRME) or inverse scattering approach of Weglein *et al.* (1997). Another example is pre-stack wave-field extrapolation imaging in place of the more limited traditional Kirchhoff approach (O'Brien *et al.* 2001). Both approaches have become economically feasible thanks to the upsurge of commodity PC equipment which can be linked together to provide supercomputer power at minimal cost (Bednar & Bednar 2001). Results of the new processing algorithms are commonly shown for sub-salt imaging of synthetic data, and in these cases the increase in signal-to-noise ratio and image quality, even on 2D data, is often remarkable. We anticipated similar improvements for the Irish Continental Shelf, where the main cause of image degradation is basaltic igneous intrusions (Martini & Bean 2002).

Our processing flow incorporated 2D SRME to suppress multiples. Initially we were disappointed by the SRME results. In particular, considerable residual multiple energy remained following the adaptive subtraction phase. Recent industry demonstrations have indicated that 3D SRME is dramatically better than 2D SRME, and in part this perhaps explains our poor initial 2D SRME results for some areas such as the Slyne Basin. However, we were able to use the 2D SRME multiple prediction to aid geological interpretation. An example is shown in Figure 3, which depicts a modern visualization-based development of methods originally reported by Hardy *et al.* (1990). We then developed an alternative adaptive subtraction technique (Hardy & Mongan

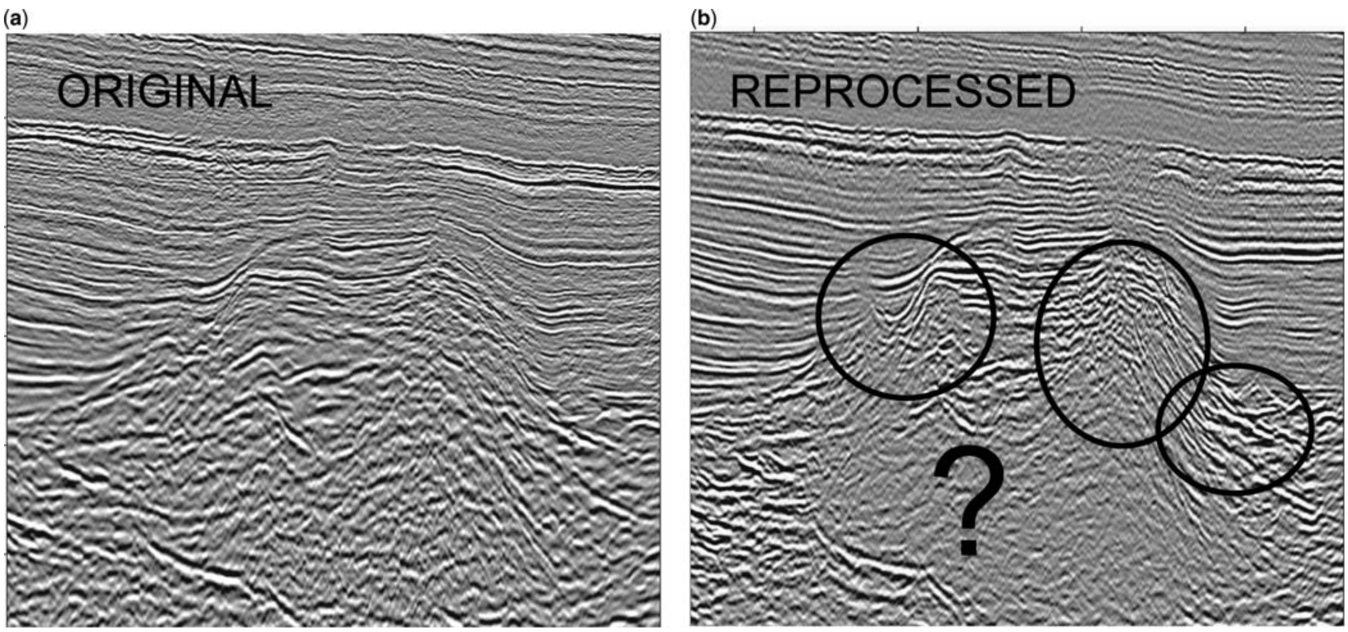

Fig. 4. (**a**) Original and (**b**) reprocessed section from the Porcupine Median Ridge. Circles indicate areas of improvement. '?' represents uncertainty in structure in the core of the ridge.

2006) which is a multichannel approach that preserves primary reflections and can be combined with residual radon transform-based multiple suppression. Additionally we used predictive techniques based on 3D side-scan sonar data to isolate areas where 2D SRME should be effective. Once multiple suppression was resolved, we developed an iterative, interpreter-driven workflow for producing high quality depth images. Each image required around eight iterations of velocity picking and residual moveout analysis. We also incorporated horizon-guided smoothing in order to increase the geological bias of the resulting velocity field. This procedure should improve results when extrapolating interpretation away from existing sparse well locations.

Figure 4 shows a comparison of initial time migration processing (left) with our radon transform multiple suppression and pre-stack time migration processing (right). This structure, part of the Porcupine Median Ridge (PMR) complex, has been interpreted as being of volcanic or serpentinitic origin (Reston *et al.* 2004). The PMR is thought to be capped by a commercially viable carbonate reservoir. Our new imaging of this capping structure shows several areas of improvement (circled), particularly on the steep flanks. The core of the PMR is seismically transparent in the new imaging. We attribute this change to more effective multiple suppression, that is, some of the deep reflections in the original images were residual multiples. More recent long offset data and a revised structural interpretation of this enigmatic structure are currently underway.

In general we have found that many existing vintages of post-stack migrated data from offshore Ireland are under-migrated

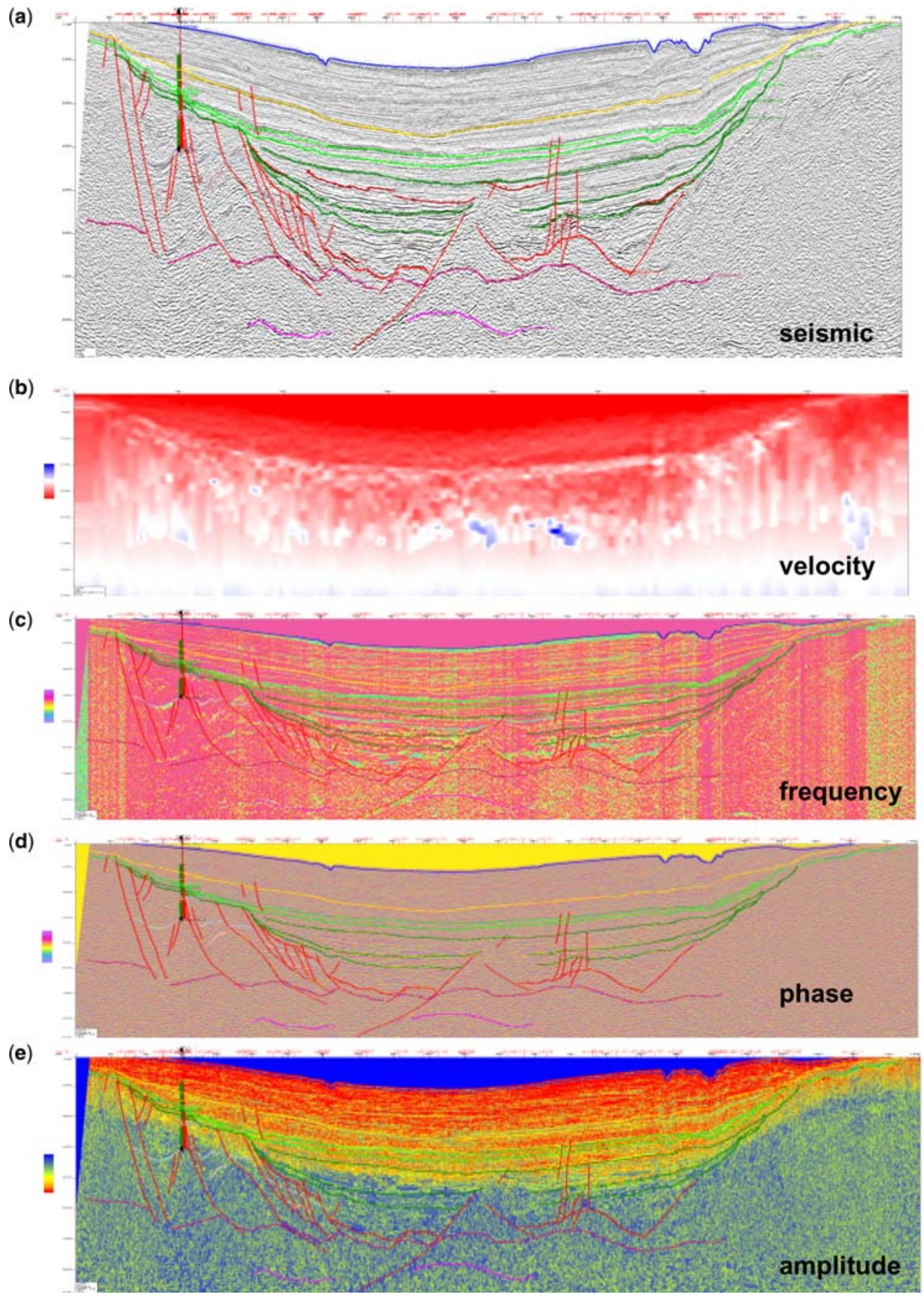

Fig. 5. (**a**) Example of interpretation showing extrapolation of horizons to basin centre from flank well. (**b**) Extrapolation was performed with conventional interpretation aided by interval velocity models; (**c**) instantaneous frequency; (**d**) instantaneous phase; and (**e**) amplitude envelope. Horizons shown (in order of increasing age): Base Oligocene unconformity [brown]; Near Top Danian (Top Chalk) [light green]; Intra-Cenomanian unconformity; Base Albian unconformity; Intra-Aptian unconformity; Base Cretaceous unconformity [dark green]; Top Crystalline Basement [purple]; Seismic Moho [pink].

with residual diffraction energy present. For some surveys where we have not been able to obtain field data, we have been able to demigrate (or diffract) the data using a background velocity field and then re-image it with a modern steep-dip algorithm. This procedure provides a quicker method of producing improved images than full pre-stack reprocessing.

Seismic data interpretation: Porcupine Basin

Over 17 000 line km of digital 2D seismic data, representing seven major surveys and five minor surveys, were incorporated into our interpretation together with all released wells. We used sonic and density logs where available to attempt to extrapolate stratigraphy from the basin margin highs (where most of the wells are drilled) to the deeper undrilled parts of the basin to the south. Standard seismic attributes such as instantaneous amplitude, frequency and phase were used to help extrapolate horizons (Fig. 5). The seismic stacking velocity model was interpolated and converted to SEGY, then loaded as an attribute. In this way the velocities could also be used to extrapolate lithology, where suitable well ties were available.

Figure 6 shows examples of depth maps for two horizons in the post-rift stratigraphy. These are the first published maps to use all released digital data. Depth data and interpretations are currently being utilized in basin modelling and studies of basin formation.

Erris Basin

Data reprocessing

Figure 7 illustrates results of data reprocessing from the Erris Basin. In the main basin itself we improved multiple suppression (using standard Radon demultiple), imaging around and beneath sills, and imaging of fault blocks utilizing the pre-stack imaging techniques described above.

In the deeper water sections we found that residual diffracted multiple energy hampered imaging of key targets. Radon demultiple (applied during the original and reprocessed version) can remove the simple deep water multiples but leaves residual parts of the multiple wave field which subsequently 'overmigrate' into the image and degrade it. We therefore found that better deep imaging was possible when the multiple wave field was retained in the data (Fig. 8) which compares original processing versus a reprocessed line in which the multiples were 'left in' prior to pre-stack imaging. Note the pre-stack imaging has not only improved images of the sill complex, but has also improved the deeper parts of the section, potentially dykes feeding the sill complex. Therefore in deep water it may not be necessary or even optimum to suppress the multiples prior to imaging. Possibilities exist for multiple suppression post-pre-stack imaging; however in this case these are not needed as the interpretation is fairly clear.

Slyne Basin

In this section, we focus on a study from the Slyne Basin, offshore Ireland, which has been affected by rift flank and epeirogenic uplift (Biancotto *et al.* 2007). Measuring uplift directly is generally impossible because reference levels are usually destroyed or at least modified by the processes of erosion. A way to address this problem is to evaluate the magnitude and distribution of exhumation at regional unconformities. The most common methods used exploit the thermal or mechanical properties of rocks, such as apatite fission track, vitrinite reflectance and sonic velocity modelling, but they all have the disadvantage of being restricted to the location of boreholes. In addition, there is often a large scatter in these sparsely distributed measurements. We show in

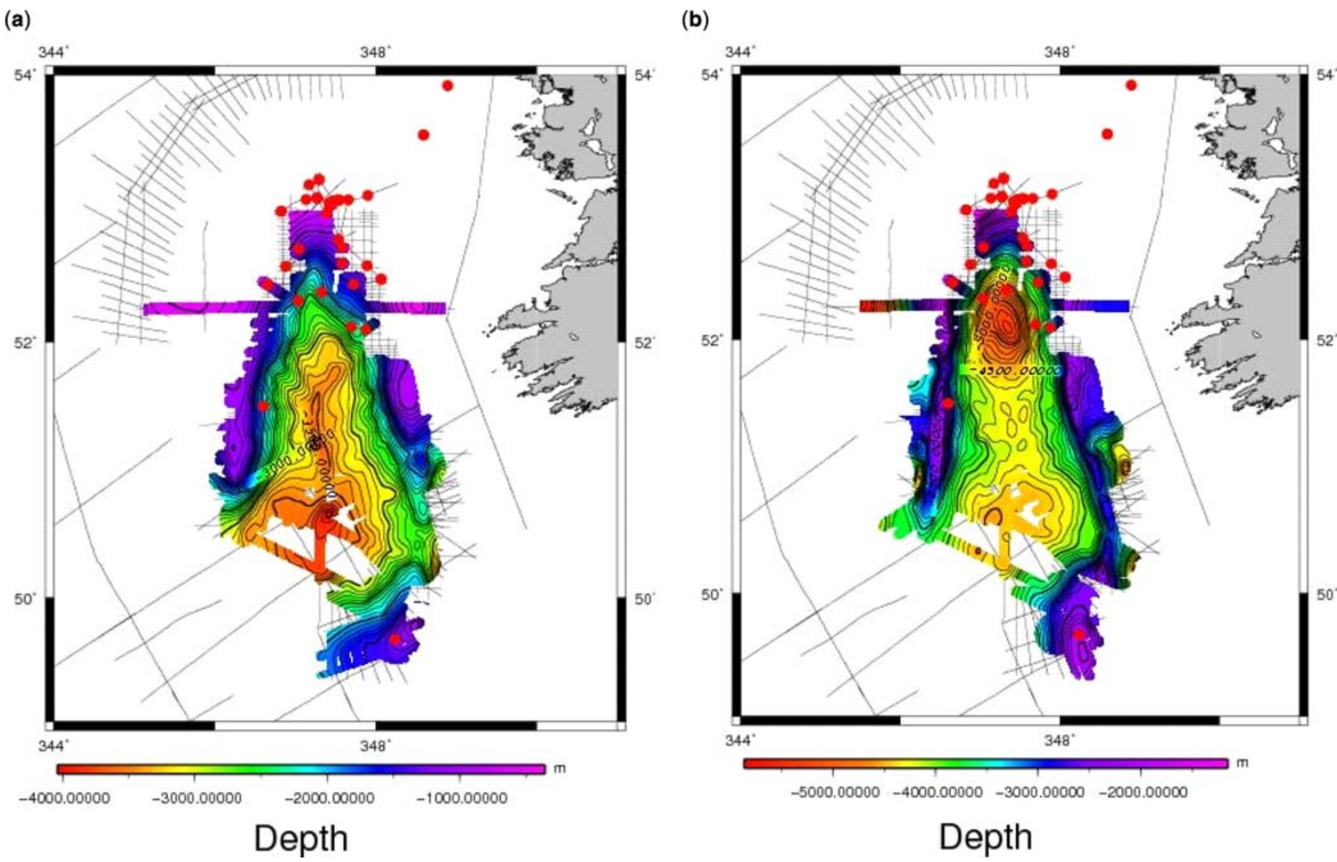

Fig. 6. Example depth maps of (**a**) Top Eocene and (**b**) Top Chalk horizons from integrated interpretation.

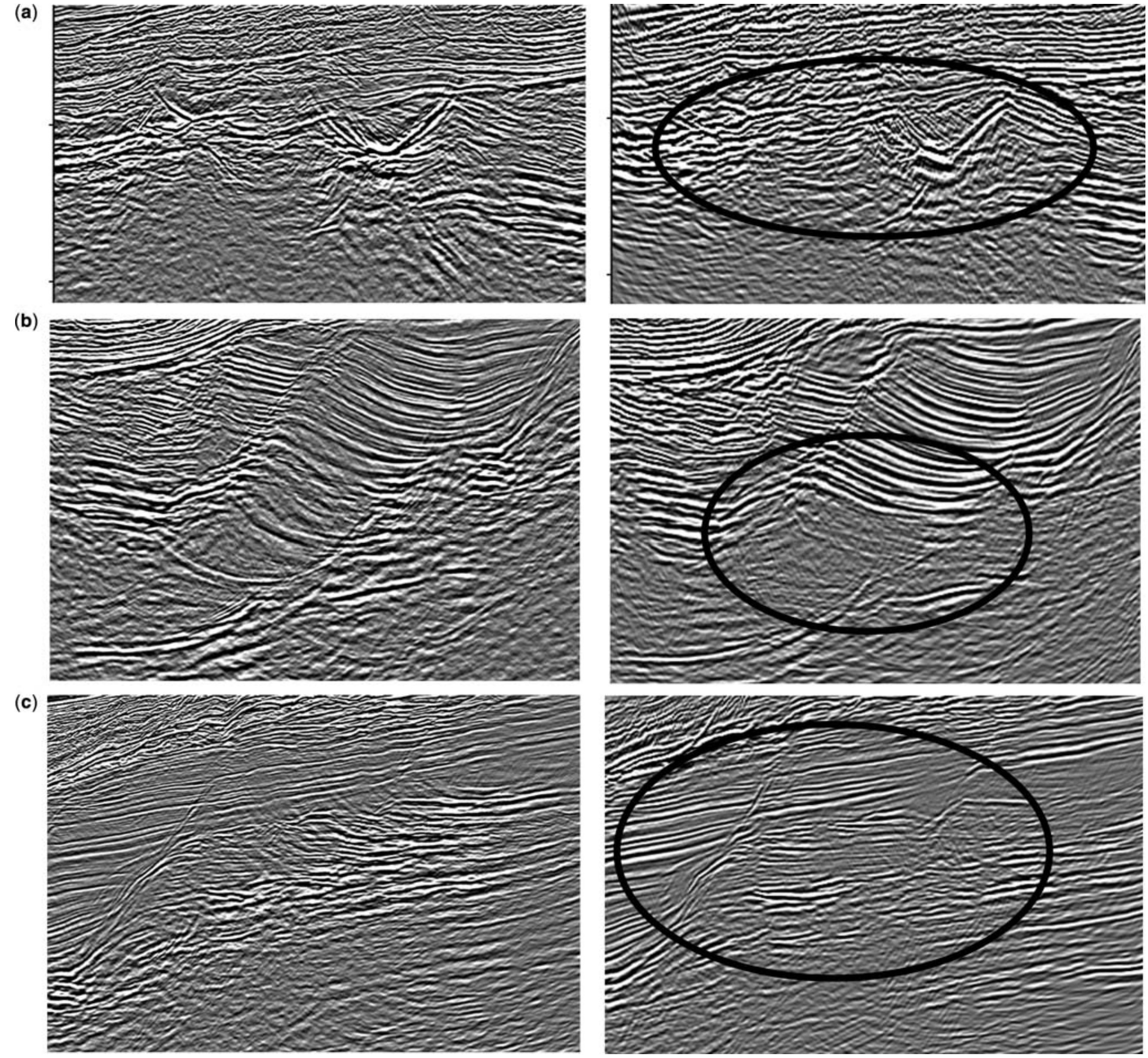

Fig. 7. Examples of reprocessing from the Erris Basin: left (original) and right (reprocessed). (**a**) Improved imaging around intrusive sills. (**b**) Improved multiple suppression and fault plane imaging. (**c**) Improved fault block imaging.

this study that inversion of seismic velocity profiles from seismic reflection datasets can be a useful tool to spatially constrain the distribution and the magnitude of exhumation (Walford & White 2005). The subject is important to oil exploration in the region in order to calibrate maturity models. This is the first such study which attempts to integrate 2D and 3D seismic-based measurements.

The Slyne Basin lies about 60 km off the NW coast of Ireland, with water depth ranging between 150 and 500 m. As part of a series of extensional basins trending NNE–SSW, it is a half-graben cut by transfer faults, dividing it into northern, central and southern parts (Scotchman & Thomas 1995). Dancer *et al.* (1999) have documented the sediment fill of the Slyne Basin from regional well data.

Exhumation estimates from seismic velocity data

Seismic velocity is controlled by the mineralogy, porosity, density, pore fluid composition and properties, pressure and depth of the imaged succession. However, the porosity of the medium is often the primary control factor on the seismic velocity because the sonic velocity of the pore fluid is much lower than that of solid sediment grains. Therefore, by measuring the sonic velocity of a sedimentary rock, we can evaluate its porosity. Similar methods are routinely used by the hydrocarbon industry, for example inverting seismic amplitude to porosity in chalk reservoirs (e.g. Dvorkin & Alkhater 2004). As sediment is buried, it is subjected to higher pressure and higher temperature and cementation begins. These processes of cementation and compaction reduce porosity. The decrease in porosity of sediments with depth of burial is largely irreversible. If a sedimentary rock is subsequently uplifted, it will keep the signature of the porosity reached at the maximum depth of burial.

Thus, by measuring the present-day porosity of a sedimentary rock and estimating the porosity decay trend with the depth of an unexhumed sedimentary column, we can calculate the maximum depth of burial of that sedimentary rock. The difference between present-day and maximum depth indicates the magnitude of exhumation. Here we are ignoring the secondary effects of cementation and diagenesis together with complications such as the presence of gas hydrates and hydrocarbons (Walford & White 2005). Thus,

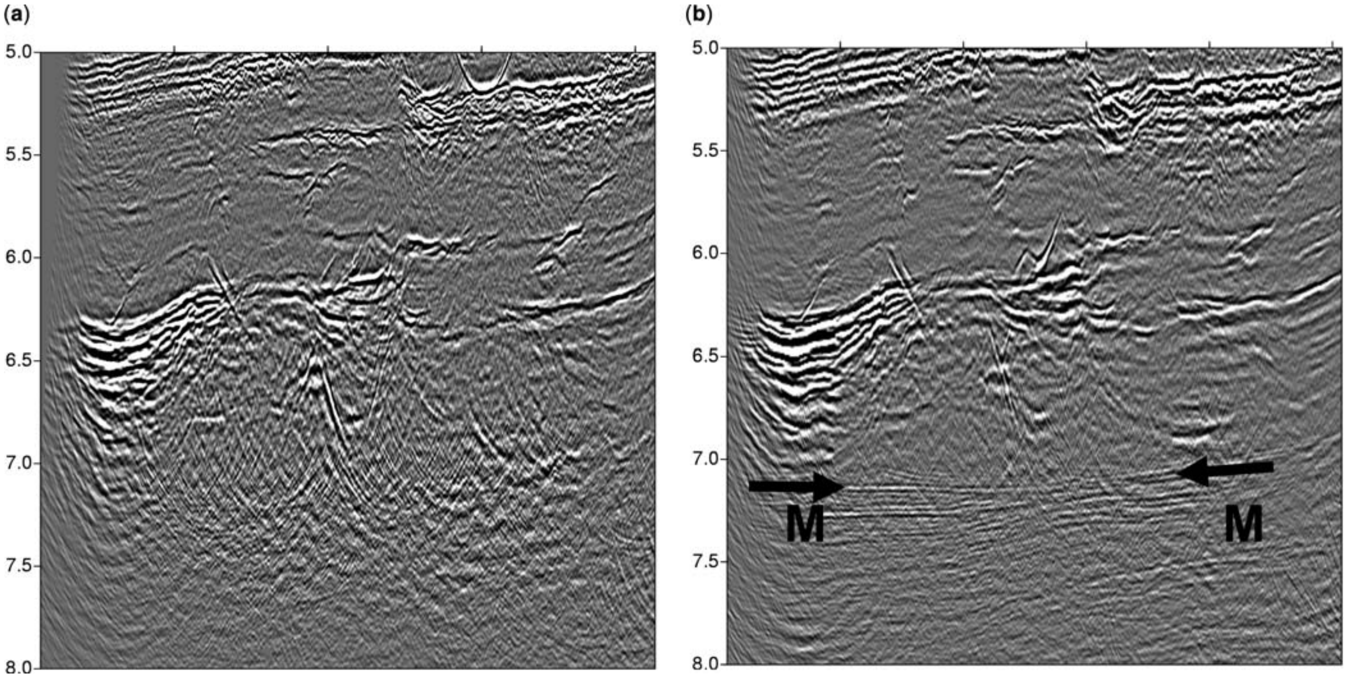

Fig. 8. Example of reprocessing from deeper water areas where multiple suppression is inadequate, particularly peg-leg multiples from instrusions. (**a**) Original processing where residual multiple energy contaminates deeper image. (**b**) Reprocessed pre-stack migration with no multiple suppression. Image is clearer beneath multiple (shown with arrows and 'M' text).

following these assumptions, we can use seismic velocity to estimate the amount of denudation of a sedimentary region. Walford & White (2005) developed an inverse model to determine the magnitude of denudation at the seabed that best fits stacking velocity measurements obtained from individual common midpoint gathers during seismic reflection processing. By building a simple, theoretical, 1D velocity profile and by minimizing the misfit between this simple synthetic profile and the observed profile, the amount of denudation can be constrained.

We have automated the inversion technique to make the method suitable for 2D lines, and by extension, 3D surveys (Biancotto *et al.* 2007). Generally 2D lines are inexpensive to reprocess and provide good quality control of velocities as long as the structures are not too complex and vary strongly out of the 2D plane.

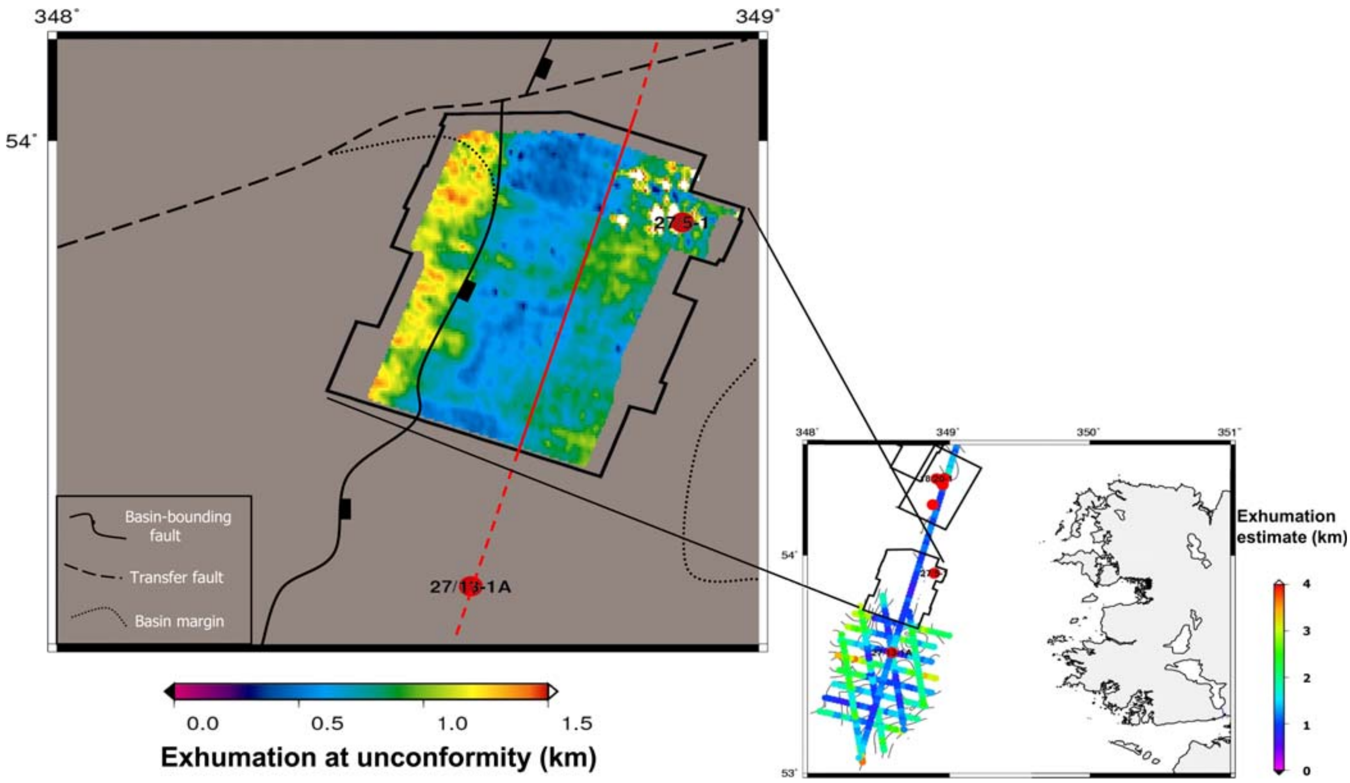

Fig. 9. Exhumation estimates from seismic velocities showing 3D and 2D results in the Slyne Basin. Estimates are in agreement with other 'well-based' methods and can be extrapolated away from wells.

Figure 9 shows the location of a 3D survey and 2D seismic profiles analysed for this study together with exhumation values calculated from seismic velocity around the Oligo-Miocene unconformity. Our estimates at the well location vary from 0.9 to 1.7 km exhumation. Scotchman & Thomas (1995) used several more classic methods of measuring the denudation, on well 27/13-1. They found magnitude of uplift ranging from 0.7 to 1.9 km. With apatite fission track analysis, uplift and erosion of 1.6 km were obtained. Shale sonic log interval velocities suggest a magnitude of denudation between 0.7 and 1.05 km. Biomarker analyses show results indicating denudation between 0.7 and 1.06 km. On these biomarker data, vitrinite reflectance studies and sterane analysis were conducted and respectively indicate 1.9 km of erosion and 1.06 km of denudation. The seismic method therefore gives results which are in good agreement with traditional methods and additionally can be extrapolated away from the well locations.

Conclusions

In this paper we have summarized the results of recent research into Irish offshore basins which utilizes, for the first time in an academic study, all available well and seismic data in a digital interpretation. We have developed a workflow that incorporates a spine of data for seismic data reprocessing and we have shown some reprocessed data comparisons. Even if images are not spectacularly improved, integration of the reprocessed depth images, together with prestack gathers and velocity model, can improve the reliability of a regional interpretation. Finally we demonstrated results of a specific application which can invert seismic velocity to exhumation and compared results from 2D and 3D seismic data with those previously obtained at a well location in the Slyne Basin.

This publication uses data and survey results acquired during a project undertaken on behalf of the Irish Shelf Petroleum Studies Group (ISPSG) of the Irish Petroleum Infrastructure Programme (PIP) Group 4. The ISPSG comprises Chevron Upstream Europe, ENI Ireland BV, ExxonMobil International plc, Island Oil & Gas plc, OMV (Ireland) Exploration GmbH, Providence Resources plc, Serica Energy plc, Shell E&P Ireland Ltd, Sosina Exploration Ltd, Statoil Exploration (Ireland) Ltd, Total E&P UK plc and the Petroleum Affairs Division of the Department of Communications, Energy and Natural Resources. The EOSG (PIP) is thanked for provision of computer equipment. Schlumberger are thanked for donation of software licences (Petrel, Geoframe, Omega). Fugro are thanked for permission to use and show data in Figures 4 and 5. Statoil are thanked for permission to use and show data in Figures 7 and 8. TGS and Spectrum and WesternGeco are thanked for data contributions to this study. Enterprise Ireland are thanked for funding of FB and the exhumation study.

References

Bednar, C. J. & Bednar, J. B. 2001. Whither geophysical technology: a true paradigm shift? *The Leading Edge*, **20**, 550–551.

Biancotto, F., Hardy, R., Jones, S. M., Brennan, D. & White, N. J. 2007. Estimating denudation from seismic velocities offshore northwest Ireland. *SEG Expanded Abstracts*, **26**, 407; doi: 10.1190/1.2792452.

Dancer, P. N., Algar, S. T. & Wilson, I. R. 1999. Structural evolution of the Slyne trough. *In*: Fleet, A. J. & Boldy, S. A. R. (eds) *Petroleum Geology of Northwest Europe: Proceedings of the 5th Conference*. Geological Society, London, 445–453; doi: 10.1144/0050445.

Dvorkin, J. & Alkhater, S. 2004. Pore fluid and porosity mapping from seismic. *First Break*, **22**, 53–57.

Hardy, R. J. J. & Mongan, J. 2006. *Identification, Interpretation and Attenuation of Multiples from West Africa*. 68th EAGE Conference and Exhibition.

Hardy, R. J. J., Hobbs, R. W., Warner, M. R. & Jones, I. F. 1990. The reliability of multiple suppression. *First Break*, **08**, 297–304.

Martini, F. & Bean, C. J. 2002. Interface scattering versus body scattering in subbasalt imaging and application of prestack wave equation datuming. *Geophysics*, **67**, 1593; doi: 10.1190/1.1512750.

Naylor, D. & Shannon, P. M. 2005. The structural framework of the Irish Atlantic margin. *In*: Doré, A. G. & Vining, B. A. (eds) *Petroleum Geology: North-West Europe and Global Perspectives: Proceedings of the 6th Petroleum Geology Conference*. Geological Society, London.

O'Brien, J., Addis, D., Drummond, J., Raney, G., Walraven, D., Weigant, J., Stein, J. & Key, S. 2001. 3-D subsalt wave-equation depth imaging: a case study from the Hickory Field. *SEG Expanded Extracts*, **20**, 957; doi: 10.1190/1.1816798.

Reston, T. J., Gaw, V., Oennell, J., Klaeschen, D., Stubenrauch, A. & Walker, I. 2004. Extreme crustal thinning in the south Porcupine Basin and the nature of the Porcupine Median High: implications for the formation of non-volcanic rifted margins. *Journal of the Geological Society, London*, **161**, 783–798.

Scotchman, I. C. & Thomas, J. R. W. 1995. Maturity and hydrocarbon generation in the Slyne Trough, northwest Ireland. *In*: Croker, P. F. & Shannon, P. M. (eds) *The Petroleum Geology of Ireland's Offshore Basins*. Geological Society, London, Special Publications, **93**, 385–411.

Tate, M., White, N. & Conroy, J. J. 1993. Lithospheric extension and magmatism in the Porcupine Basin, West of Ireland. *Journal of Geophysical Research*, **98**, 13905–13923.

Walford, H. L. & White, N. J. 2005. Constraining uplift and denudation of west African continental margin by inversion of stacking velocity data. *Journal of Geophysics Research*, **110**, B04403; doi: 10.1029/2003JB002893.

Weglein, A. B., Gasparotto, F. A. F., Carvalho, P. M. & Stolt, R. H. 1997. An inverse-scattering series method for attenuating multiples in seismic reflection data. *Geophysics*, **62**, 1975; doi: 10.1190/1.1444298.

WATS it take to image an oil field subsalt offshore Angola?

E. EKSTRAND,[1] G. HICKMAN,[2] R. THOMAS,[3] I. THREADGOLD,[4] D. HARRISON,[2] A. LOS,[2] T. SUMMERS,[2] C. REGONE[5] and M. O'BRIEN[6]

[1]*BP America Inc, 200 Westlake Park Boulevard, Houston, TX 77079, USA (e-mail: ekstraej@bp.com)*
[2]*BP Exploration Operating Company Ltd, Chertsey Road, Sunbury-on-Thames TW16 7LN, UK*
[3]*RT Geophysics Ltd, 108 Kenilworth Avenue, Wimbledon, London SW19 7LR, UK*
[4]*BP America Inc, 501 Westlake Park Boulevard, Houston, TX 77079, USA*
[5]*Consulting Geophysicist, 1650 Shillington Drive, Katy, TX 77450, USA*
[6]*Allied Geophysics Inc, 27891 Man O War Trail, Evergreen, CO 80439, USA*

Abstract: BP's exploration success in deepwater Block 31, offshore Angola, has been driven by conventional narrow-azimuth 3D seismic data coupled with the latest available imaging algorithms. However limitations in these data are now apparent and the data is deemed insufficient for the appraisal and development of the subsalt discoveries in the western part of the block. 3D acoustic finite-difference modelling was applied to Block 31 to evaluate the potential data quality uplift from a wide-azimuth towed streamer (WATS) survey. Results showed that a significant improvement in data quality is possible. The modelling also investigated key acquisition variables (acquisition direction, sail line separation, number of tiles, cable length) to arrive at a solution that optimized both data quality and cost. Acquisition of this survey began in December 2008 and it is expected to complete in August 2009. This is the first WATS seismic survey outside the Gulf of Mexico and the first in Angola.

Keywords: wide-azimuth, WATS, subsalt, 3D finite-difference modelling, deepwater, Angola

Block 31 is located approximately 150 km offshore Angola in 1200–2500 m of water (Fig. 1). The block covers part of the Lower Congo Basin and lies to the south and east of the modern day Zaire fan. The Block 31 licence group consists of BP as operator, ExxonMobil, Sonangol P&P, Statoil, Marathon and Total.

The petroleum geology of Block 31 involves sandstone reservoirs of Oligocene to earliest Miocene age, sealed by overlying deep water mudstones, and sourced from Late Cretaceous to Palaeogene organic-rich marine sediments. The reservoirs are typically deposited in erosional channel complexes within a lower slope depositional environment. The structural evolution of the block is complex and dominated by salt-induced tectonics. Traps are commonly formed through the uplift of turbidite channels on the flanks and crests of salt-cored ridges.

Block 31 exploration activities to date have resulted in 19 discoveries that are currently the focus of appraisal and development activities. Following the acquisition of a block-wide conventional exploration 3D seismic survey in 1999, BP had early success in the block outside and adjacent to salt (referred to as extrasalt), with initial exploration focus in the NE open salt basins (Fig. 1). The majority of the reservoirs in this area are well imaged on seismic data and direct hydrocarbon indicators are present. Exploration activities then moved to the southeastern area, which contains isolated salt canopies and diapirs. Imaging in this part of the block is more complex, consisting of steeply dipping salt flank structures with portions of the trap obscured by salt.

Exploration efforts were then focused in the western area of Block 31, where reservoirs are completely covered by an extensive allochthonous salt canopy (Fig. 1). Seismic imaging in this area is extremely poor compared with the extrasalt regions of the block. A deep-tow, long cable 3D seismic survey was acquired in 2004 prior to the subsalt exploration drilling campaign to optimize the imaging on conventional narrow-azimuth seismic data. The first subsalt discovery in Block 31 and in Angola was made in 2006. There are currently five subsalt discoveries in Block 31, shown as red stars in Figure 1. Approximately 60% of Block 31 is covered by salt, which is characterized by complex 3D geometries (Fig. 2). Subsequent complexities in the velocity model result in significant subsalt imaging challenges for both appraisal and development.

Subsalt imaging challenges

Deepwater Angola is typically associated with excellent seismic imaging, based on shallow-tow, high-resolution 3D seismic surveys which have become the standard for extrasalt developments in Angola over the last decade. The root mean square (RMS) amplitude extraction shown in Figure 3a illustrates the detailed channel complex geometries which are resolvable with high-resolution 3D seismic in the extrasalt areas in Block 31. The RMS amplitude extraction in Figure 3b is from conventional 3D data over a subsalt reservoir interval in Block 31, where only a gross outline of the channel trend is visible. Although the frequency content between shallow and conventional tow-depth data is very different, the key imaging difference between Figure 3a, b is associated with poor illumination, low signal-to-noise and significant residual multiple energy, which is characteristic of the subsalt environment.

Sections through 3D pre-stack depth-migrated seismic data over two Block 31 subsalt discoveries are shown in Figure 4 to illustrate the subsalt imaging challenges for appraisal and development. Imaging is generally good over Well A (Fig. 4a); however the high amplitude reflectors targeted by the well were found to be associated with wet sands. The well encountered hydrocarbons in the updip side-track; therefore the field is actually located in an area of extremely poor imaging. Overall imaging is somewhat better at Well B (Fig. 4b); however poor imaging in the crestal area results in high levels of uncertainty in reservoir extent, container dimension and resource size. Although adequate for exploration, seismic imaging is clearly not sufficient for appraisal and

VINING, B. A. & PICKERING, S. C. (eds) *Petroleum Geology: From Mature Basins to New Frontiers – Proceedings of the 7th Petroleum Geology Conference*, 1013–1024. DOI: 10.1144/0071013

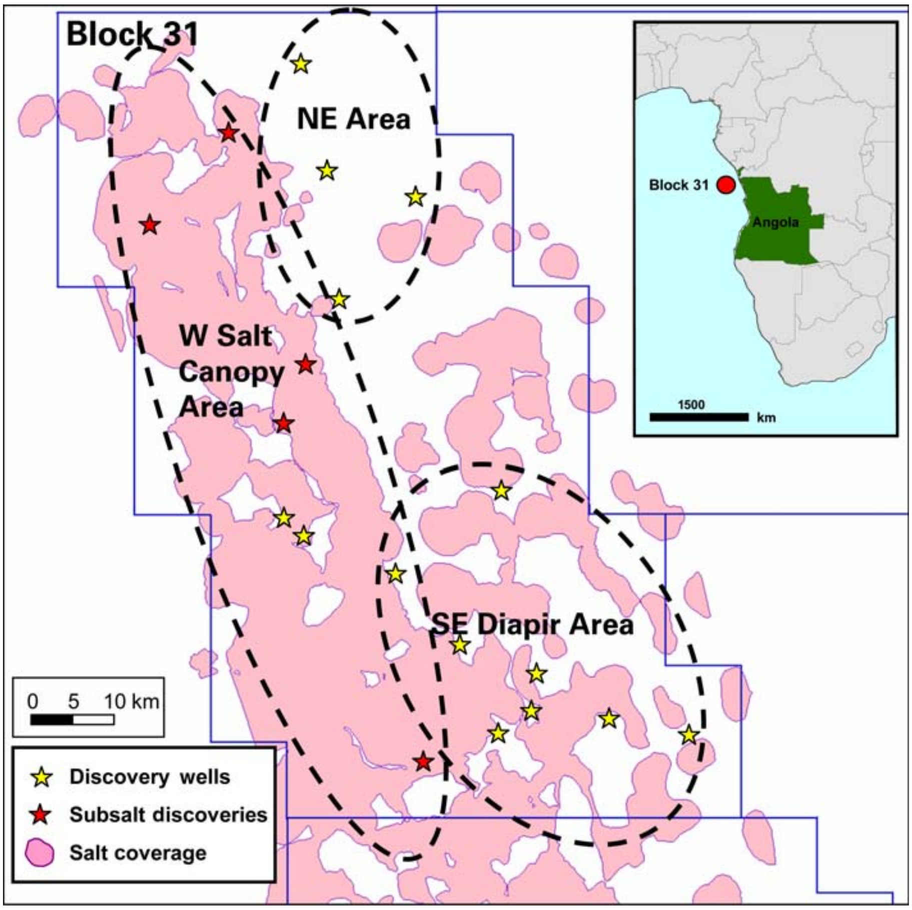

Fig. 1. Location of Block 31, offshore Angola, illustrating discovery wells, salt coverage and exploration focus areas.

development of these subsalt discoveries and requires a step change in quality.

As illustrated in Figure 4, complex salt bodies and associated velocity variations distort the seismic wave field. Historical attempts to image subsalt data in deepwater Angola and the Gulf of Mexico have used conventional narrow-azimuth towed streamer (NATS) seismic technology (shown in Fig. 4). This approach to a very complex 3D problem (using conventional 3D seismic surveys consisting of relatively narrow swathes of data) results in significant gaps in the seismic wave field. BP's subsalt experience in the Gulf of Mexico has shown that processing alone will not overcome limitations in conventional narrow-azimuth seismic acquisition. In order to address these acquisition limitations, BP has developed a portfolio of wide-azimuth solutions over the last decade that is

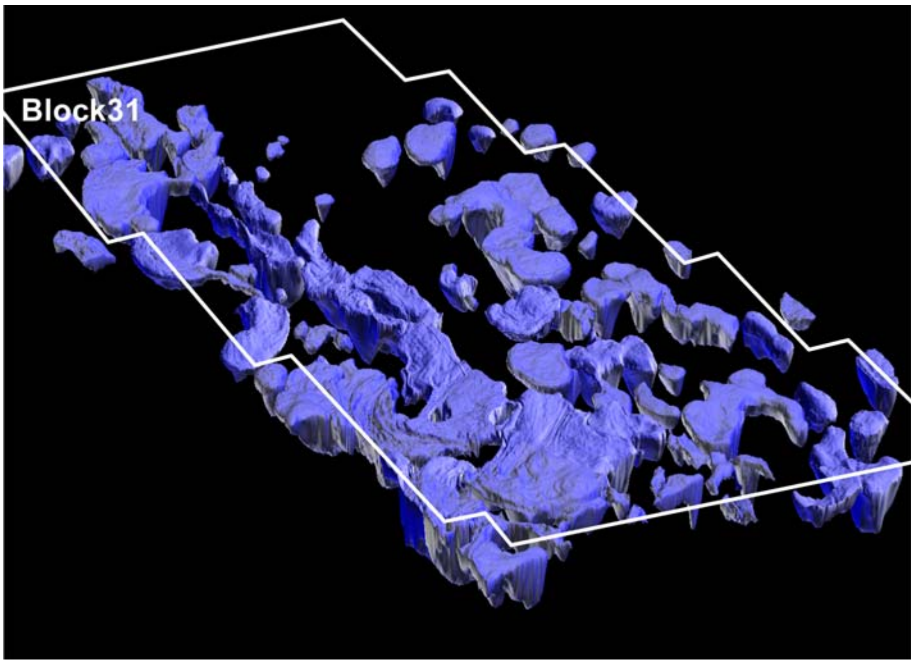

Fig. 2. Block 31 salt geometries.

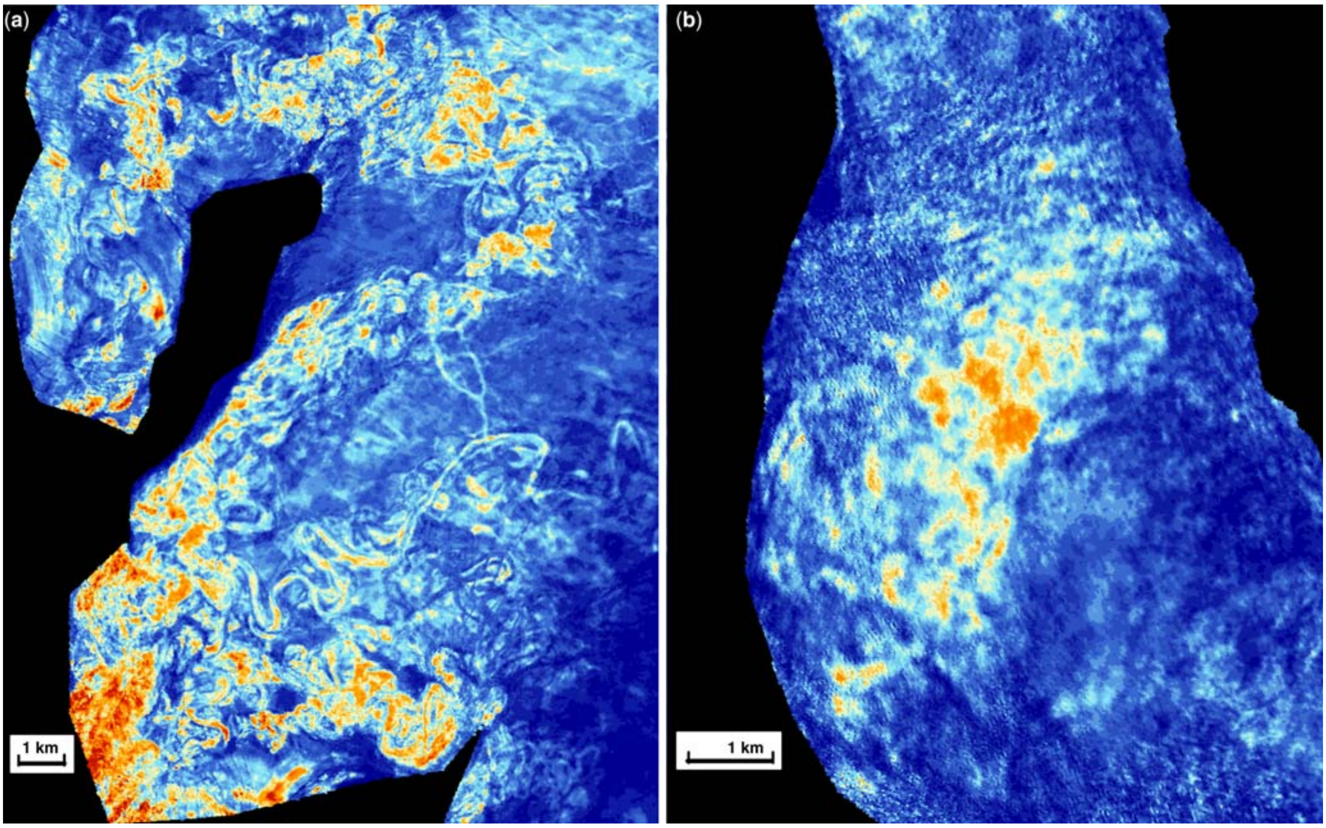

Fig. 3. RMS amplitude extractions over (**a**) extrasalt and (**b**) subsalt areas in Block 31.

showing significant quality improvement over conventional narrow-azimuth data (Barley & Summers 2007). The wide-azimuth towed streamer (WATS) seismic approach is considered by BP as the preferred option for imaging under large salt bodies (characterized by long-wavelength velocity anomalies) across the value chain from exploration through appraisal and development (Barley & Summers 2007).

The wide-azimuth solution: WATS

Michell *et al.* (2004) illustrated the benefits of variable illumination from dual-azimuth imaging over the subsalt Mad Dog Field in the Gulf of Mexico. Analysis in this area, however, highlighted the ineffectiveness of combining a finite number of conventional narrow-azimuth surveys (acquired in different orientations), to sufficiently address imaging challenges below large salt bodies, such as poor illumination, low signal-to-noise and significant multiple energy (Barley & Summers 2007). BP conducted a field trial in 2004 over the Mad Dog Field to acquire a wide range in azimuths with a single towed streamer acquisition (Michell *et al.* 2006; Threadgold *et al.* 2006), utilizing full 3D finite-difference (3DFD) modelling to optimize survey design (Regone 2006). The field trial confirmed the 3DFD modelling and demonstrated that this type of wide-azimuth survey can provide vastly improved imaging below salt. This acquisition method is called wide-azimuth towed streamer, in contrast with conventional NATS acquisition.

A comparison of NATS and WATS acquisition design is illustrated in Figure 5. Conventional NATS acquisition utilizes a single vessel towing both the source and receiver arrays, acquiring

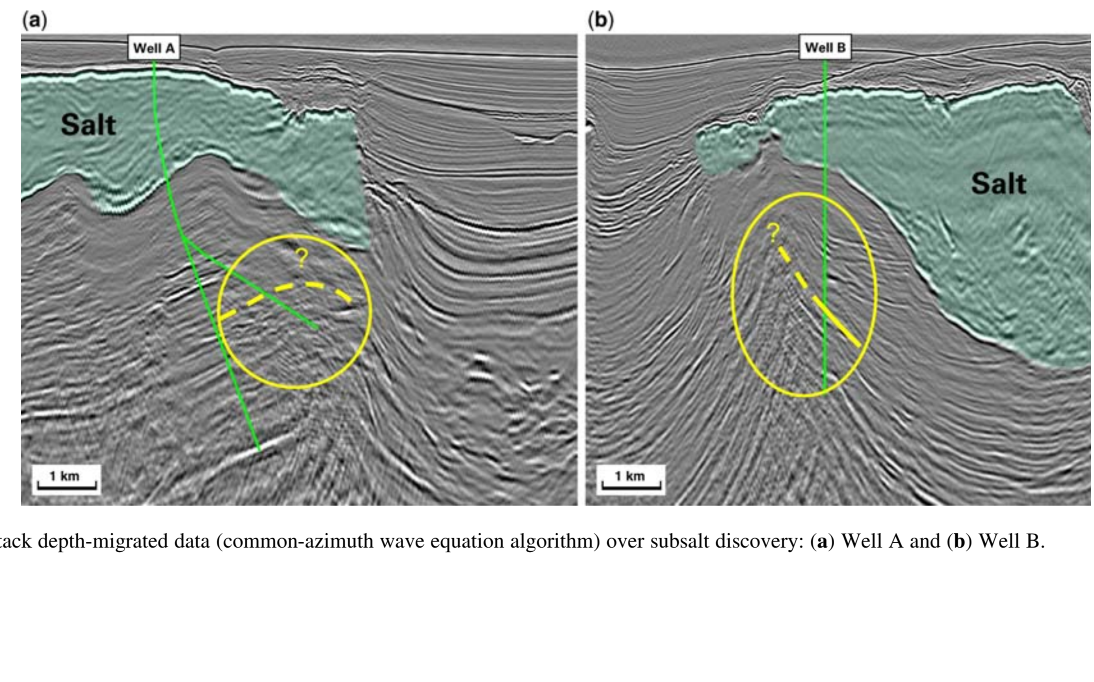

Fig. 4. Pre-stack depth-migrated data (common-azimuth wave equation algorithm) over subsalt discovery: (**a**) Well A and (**b**) Well B.

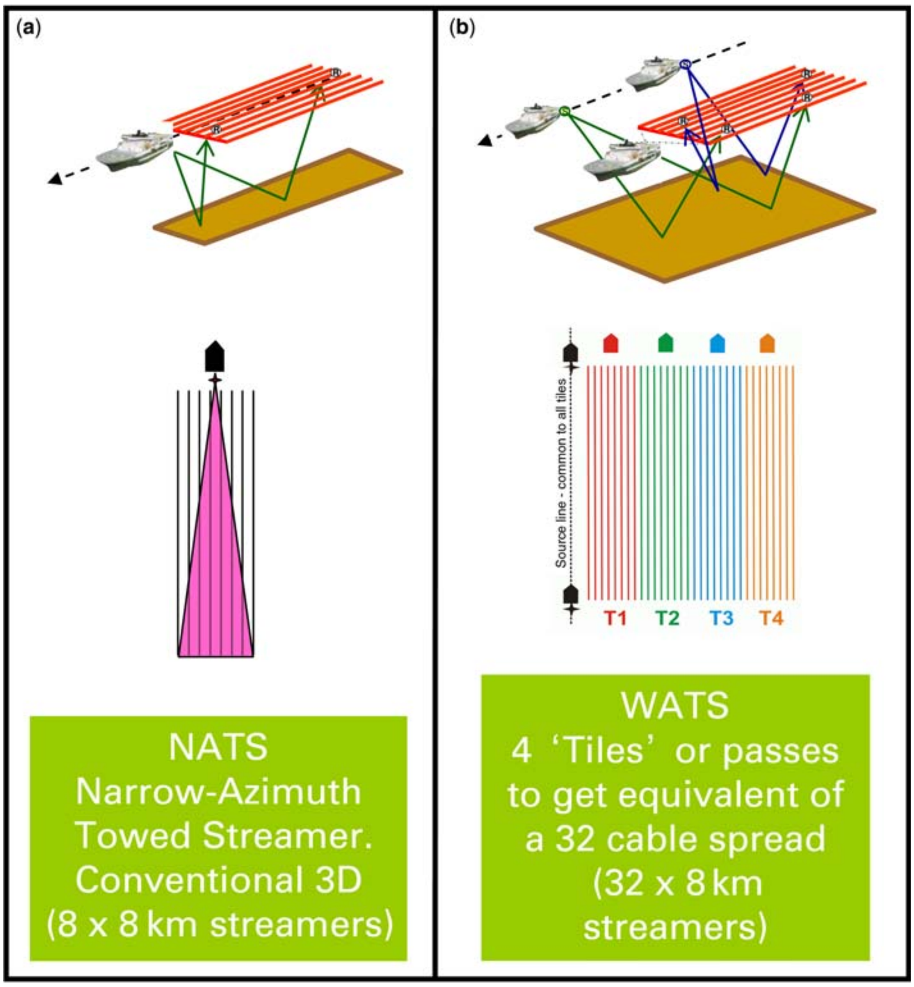

Fig. 5. Acquisition configuration for (**a**) NATS (narrow-azimuth towed streamer) and (**b**) WATS (wide-azimuth towed streamer) data.

a narrow range in azimuths (Fig. 5a). WATS acquisition utilizes two source vessels offset at the head and the tail of the streamer array, which is towed by a separate, third vessel (Fig. 5b). The source/receiver crossline offset is varied by acquiring successive, overlapping passes (Michell *et al.* 2006; Threadgold *et al.* 2006). In the WATS configuration shown in Figure 5b, four passes, or 'tiles' are acquired to build up a 4 × 8 km receiver patch, or the equivalent of a 32-cable spread (32 × 8 km). The basic vessel layout for WATS acquisition is illustrated in Figure 6a. The source and receiver array positions are shown for a four-tile WATS acquisition in Figure 6b. Following the acquisition of all four tiles, in this example, the source line position is offset by 500 m (source line or sail line separation) to acquire the next set of tiles (Fig. 6c). This process is then repeated to cover the entire survey area.

As each tile is an independent 3D survey, the entire WATS survey area is effectively acquired multiple times depending on the number of tiles used in the design. With three vessels required plus support, costs are high for WATS compared with conventional NATS acquisition. WATS acquisition parameters in general order of relative cost impact are shown in Table 1. The challenge in WATS survey design is to optimize these parameters for the specific survey objectives, particularly sail line separation and number of tiles, since they have a linear relationship with cost – in addition to building confidence that imaging uplift will actually be obtained.

3D finite-difference modelling

The key is to build a fit-for-purpose model to demonstrate potential WATS imaging uplift and to determine optimized acquisition parameters. The reservoirs of interest in Block 31 are relatively shallow subsalt channel complexes; therefore modelling needs to contain appropriate detail to demonstrate the potential WATS data uplift in both stratigraphic as well as structural definition. One of the earth models generated in western Block 31 is shown in Figure 7, illustrating the extent of the Miocene channel complexes that were investigated, comprising five individual channels. The geometries modelled were selected to investigate variation in channel wavelength, confinement width, channel body width, sinuosity and direction. The input area of this particular model is approximately 1600 km^2. The surfaces which define the model are based on interpretation of actual NATS data from Block 31 (Fig. 8a). The model is then populated with appropriate densities (Fig. 8b) in order to generate sufficient acoustic impedance contrasts since the velocity field is smooth apart from salt (Fig. 8c). An example of the band-limited reflectivity volume is shown in Figure 8d to illustrate the 'ideal' model image.

A 3DFD model was then generated based on the earth model. This methodology is discussed in detail by Regone (2006), in which 3DFD modelling was used in the Gulf of Mexico to design BP's first WATS survey over the Mad Dog Field in 2004 and an ocean bottom seismic (OBS) nodes survey over the Atlantis Field in 2005. The Block 31 input model area (yellow) is illustrated in Figure 9 with salt coverage shown in pink. Propagating wave fields of individual shots are modelled with a finite-difference (FD) algorithm, generating FD shot records (Fig. 10a). The significant impact of salt on the seismic wave field is illustrated in a comparison of an extrasalt shot v. a subsalt shot shown in Figure 10b, c. Referring back to Figure 9, data are recorded for

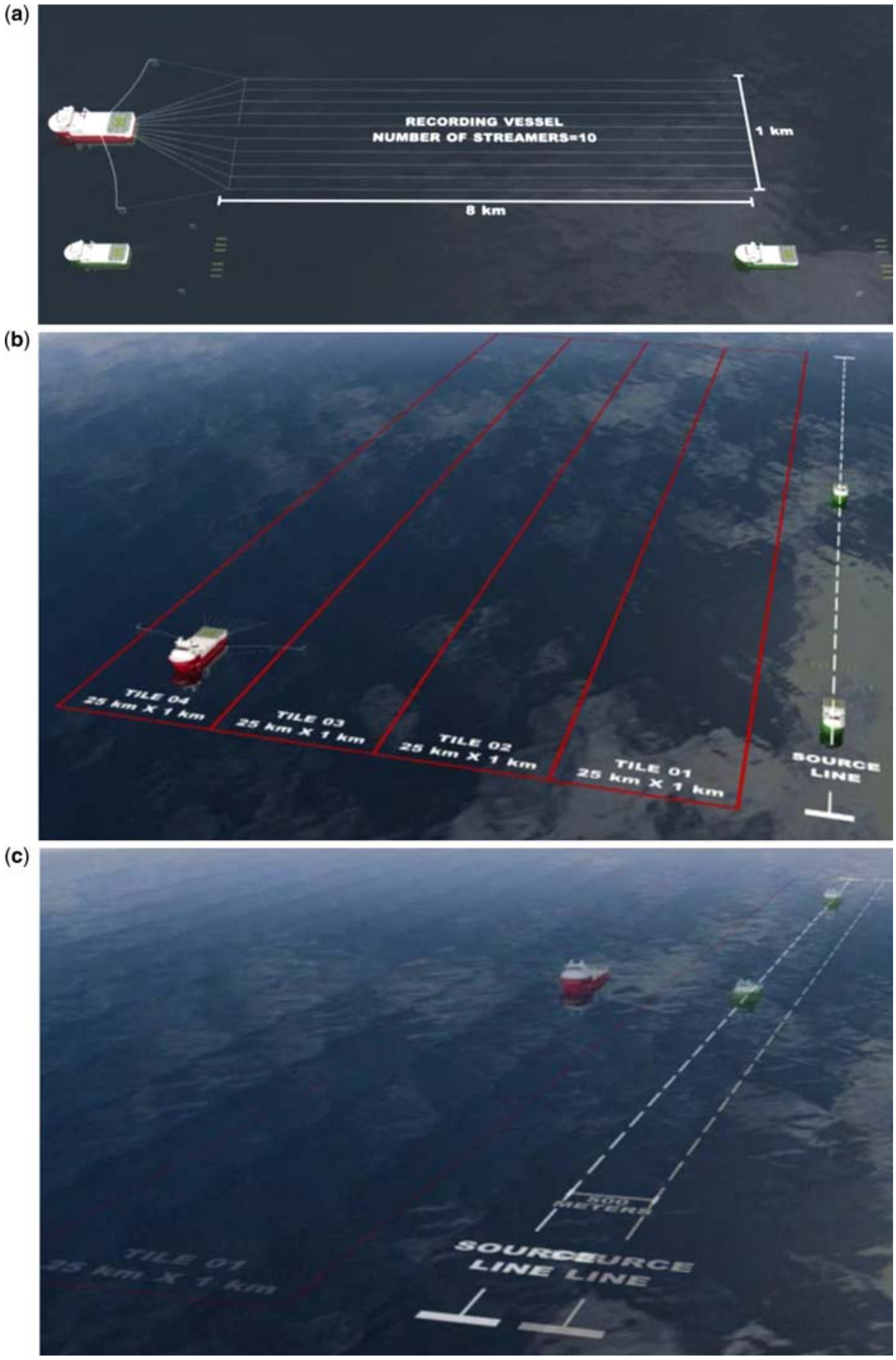

Fig. 6. WATS acquisition details: (**a**) basic vessel layout; (**b**) four-tile acquisition summary; (**c**) 500 m source line (sail line) spacing example.

Table 1. Relative cost impact of WATS acquisition parameters

Parameters	Relative cost impact
Sail line separation (source line)	High
Number of tiles	|
Migration aperture and survey area	|
Acquisition direction (rectangular surveys)	|
Acquisition configuration and streamer length	|
Record length and shotpoint interval	↓
Source and receiver tow depths	Low

each shot in a sub-model receiver spread of 16 × 16 km (blue); the image area (orange) is covered by shots on a 250 m grid. Data is then sorted and migrated with wave-field shot migration with the exact velocity model to create different acquisition geometries (Fig. 11). 3DFD modelling produces realistic simulations of 3D seismic data. Since the velocity model is known, modelling allows the imaging impact of velocity errors, free-surface multiple effects and acquisition geometry to be isolated (Regone 2006). 3DFD modelling is also very computer-intensive, with runtime being proportional to the fourth power of frequency (f^4). Modelled datasets were consequently generated with a maximum frequency of 15 Hz (which is sufficient given modelling parameters).

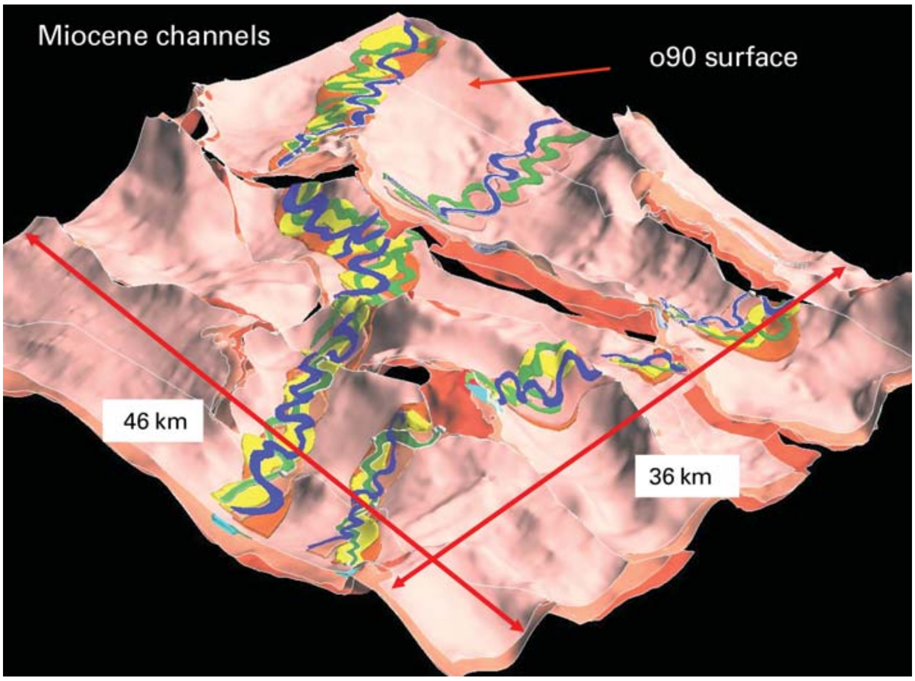

Fig. 7. Earth model incorporating channel complex details.

Model evaluation

A representative cross-section from 3DFD model data is shown in Figure 12 to illustrate the expected imaging uplift from WATS data in western Block 31. Both the NATS (Fig. 12a) and WATS (Fig. 12b) datasets are modelled with free-surface multiples. The density model for this cross-section is shown in Figure 12c to illustrate the structural surfaces and channel body geometries contained in the input model. This specific WATS section is based on 250 m sail line separation, 8 km streamers and four tiles. Model WATS data (Fig. 12b) shows significant improvements in imaging,

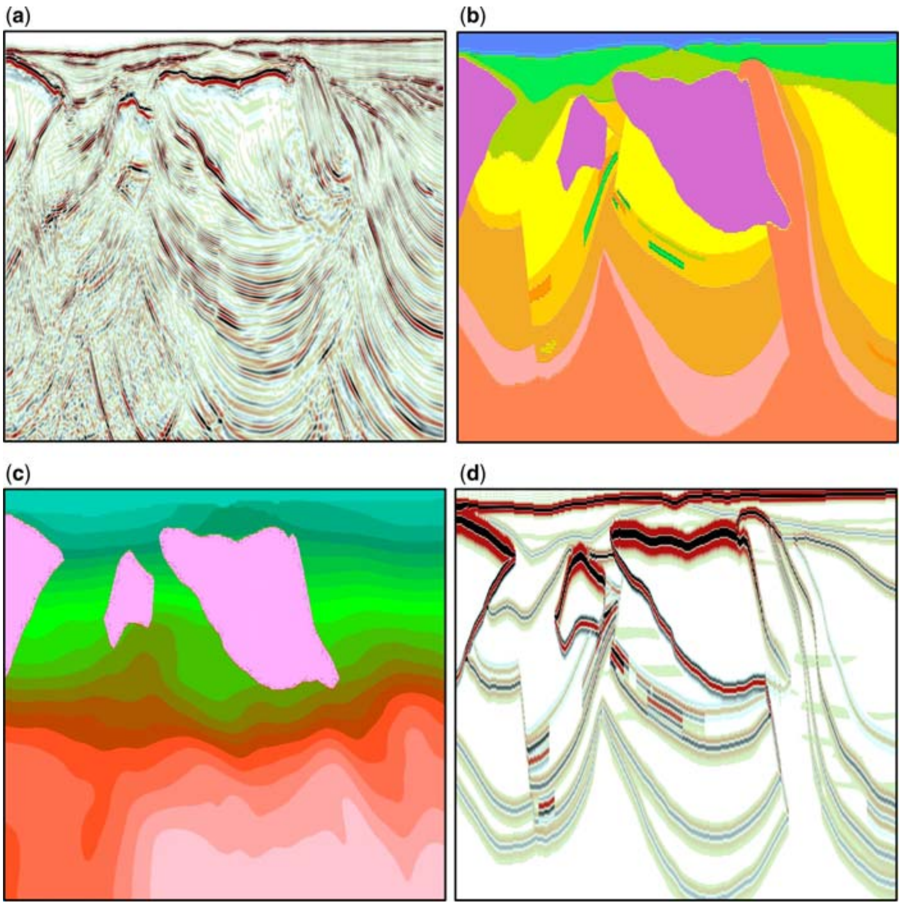

Fig. 8. Earth model construction: (**a**) structural horizons based on actual pre-stack depth-migrated NATS data; (**b**) density model; (**c**) velocity model; (**d**) model-based band-limited reflectivity.

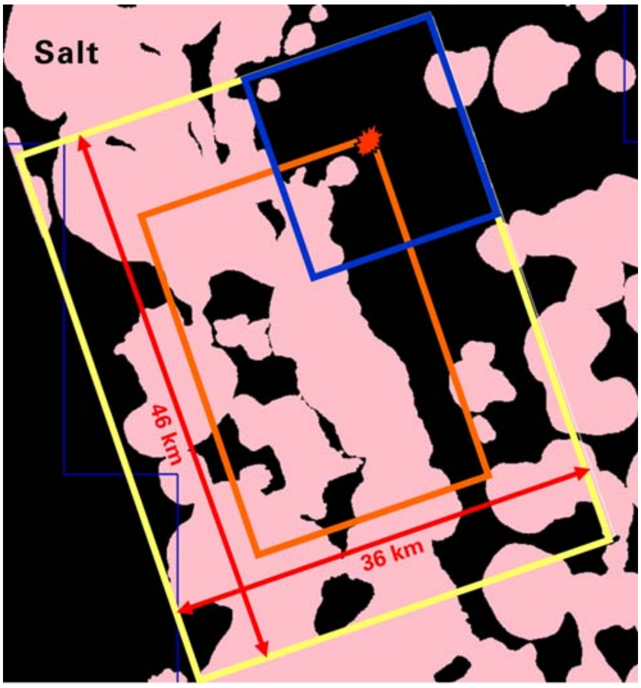

Fig. 9. 3DFD model area – input area, yellow; output area, orange; data area recorded for each shot (sub-model receiver spread), blue.

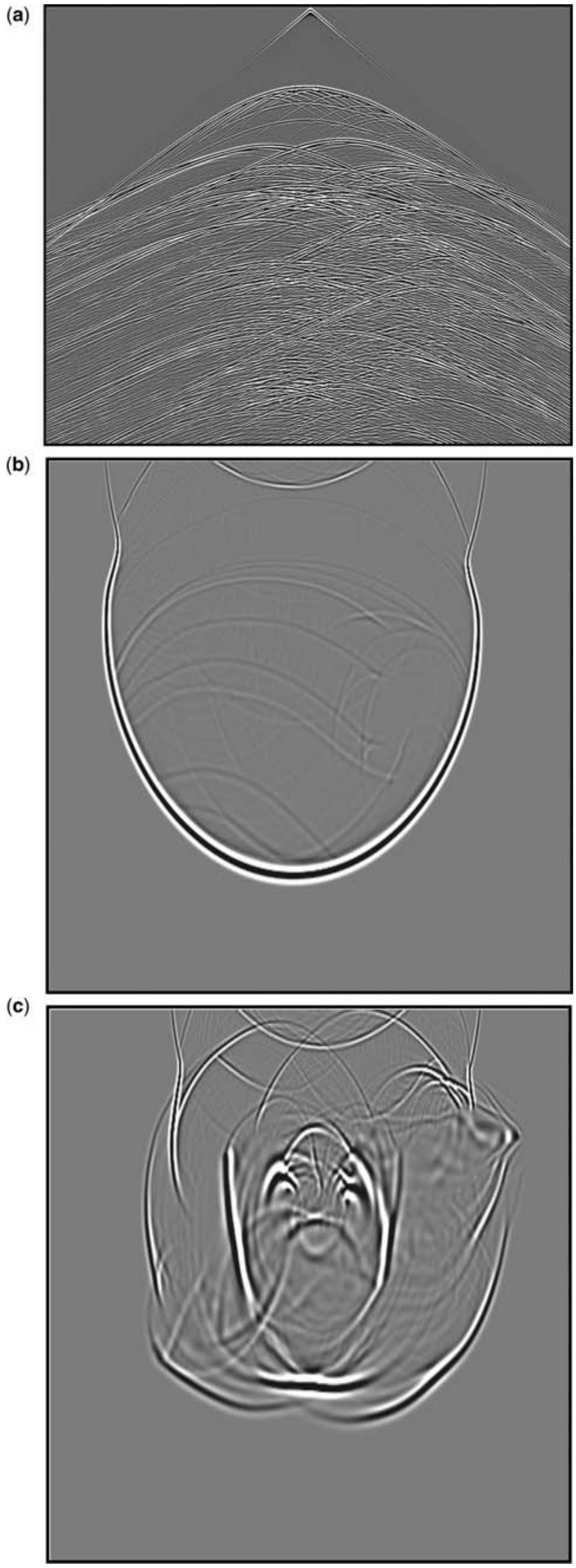

Fig. 10. 3DFD model generation: (**a**) typical shot record; (**b**) extrasalt shot; (**c**) subsalt shot.

reflector continuity and signal-to-noise compared with the model NATS section (Fig. 12a). It is clear on the model WATS data that reflectors either extend up to salt or are offset by faulting prior to reaching the salt interface. Model WATS data also clearly allow more confident horizon correlation across the section, particularly in the deeper parts of the cross-section where multiple energy is very strong on the NATS data. As supported by actual WATS datasets in the Gulf of Mexico, one of the benefits of WATS acquisition is that, owing to acquisition design, specular multiples are significantly reduced simply through the stacking process (the details of this effect are modelled and discussed by VerWest & Lin 2007).

To illustrate the impact of the number of WATS tiles (or the width of the acquisition receiver patch) on imaging improvements, Figure 13 shows RMS amplitude extractions over the deepest, isolated channel interval from Figure 12c. The channel is associated with the red, north–south trending feature on the amplitude maps in Figure 13. A substantial improvement in continuity and signal-to-noise can be seen simply going from NATS to a two-tile WATS case, with progressive improvements up to six-tile WATS. All of the model WATS data in Figure 13 are based on a 500 m sail line separation and 8 km streamer length.

In addition to comparing RMS amplitude extractions and cross-sections through focused areas of interest, a more quantitative analysis of data quality uplift was also done. One approach utilized is based on a coherency attribute which is the first principle component of the data, extracted over appropriate modelled intervals. The area of coherent data from different modelled acquisition volumes can be measured to compare the progressive uplift in data quality with, for example, increasing tile number. The graph shown in Figure 14a plots the normalized area or percentage of 'good' data for the NATS case and increasing tile number WATS cases. As illustrated in the RMS amplitude extraction maps in Figure 13, the most significant uplift in data quality occurs between the NATS and two-tile WATS cases, with smaller incremental improvements in quality with increasing tile number. The curve appears to be flattening around the five-tile case. Although this coherency attribute extraction is from one modelled interval over a large subsalt basin, the trends are considered representative of WATS data uplift overall. The curve can be translated into generic costs using a 2008 cost reference, and acquisition assumptions of 8 × 8 km streamers, 8 km data aperture, 500 m sail line

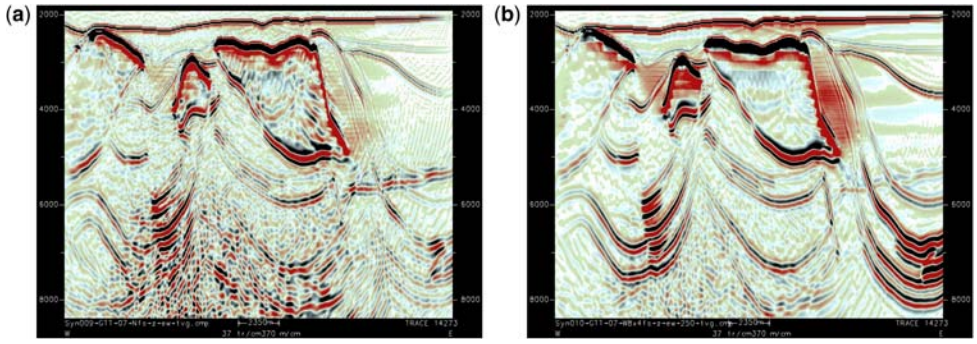

Fig. 11. 3DFD model output examples: (**a**) model NATS data; (**b**) model WATS data.

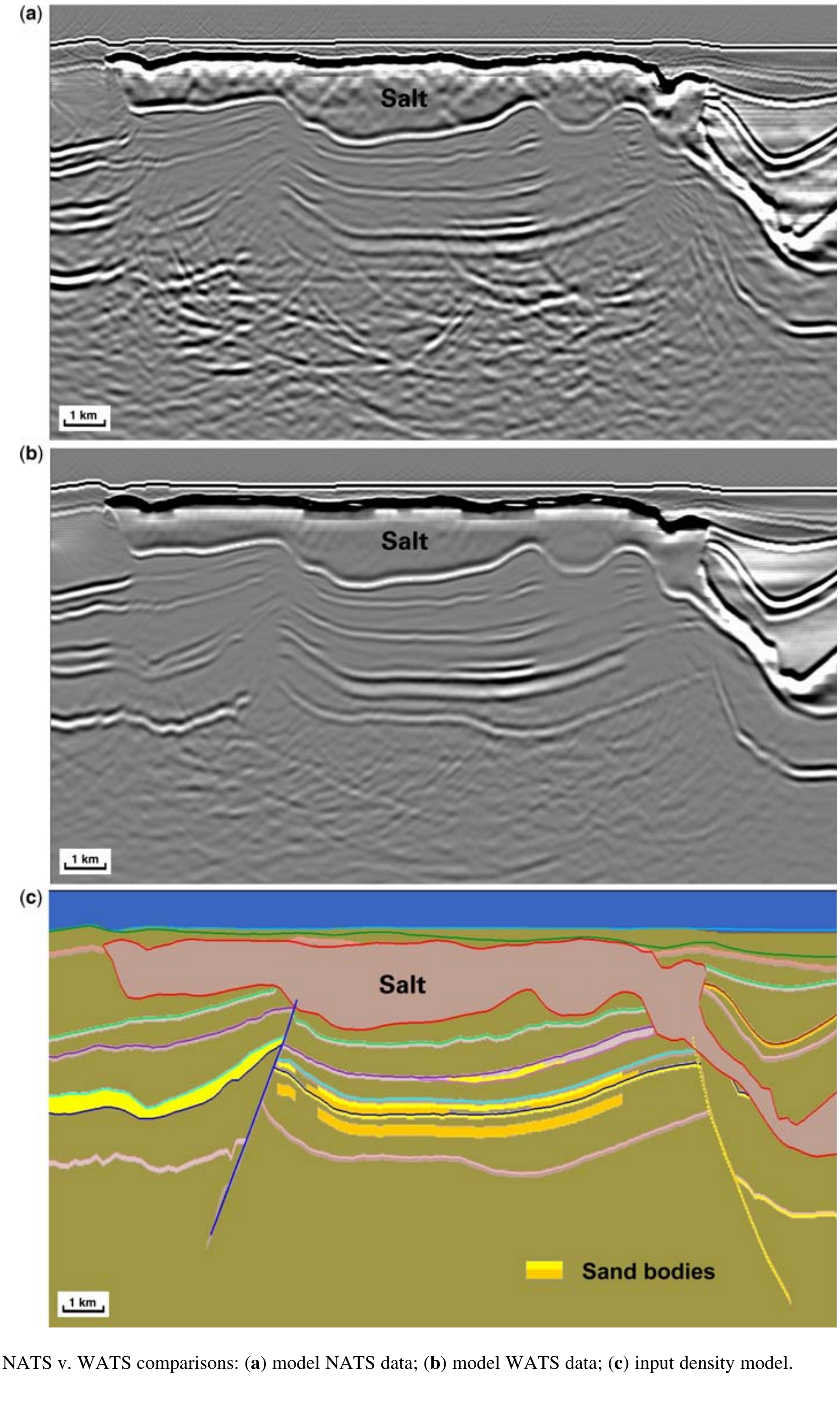

Fig. 12. 3DFD model NATS v. WATS comparisons: (**a**) model NATS data; (**b**) model WATS data; (**c**) input density model.

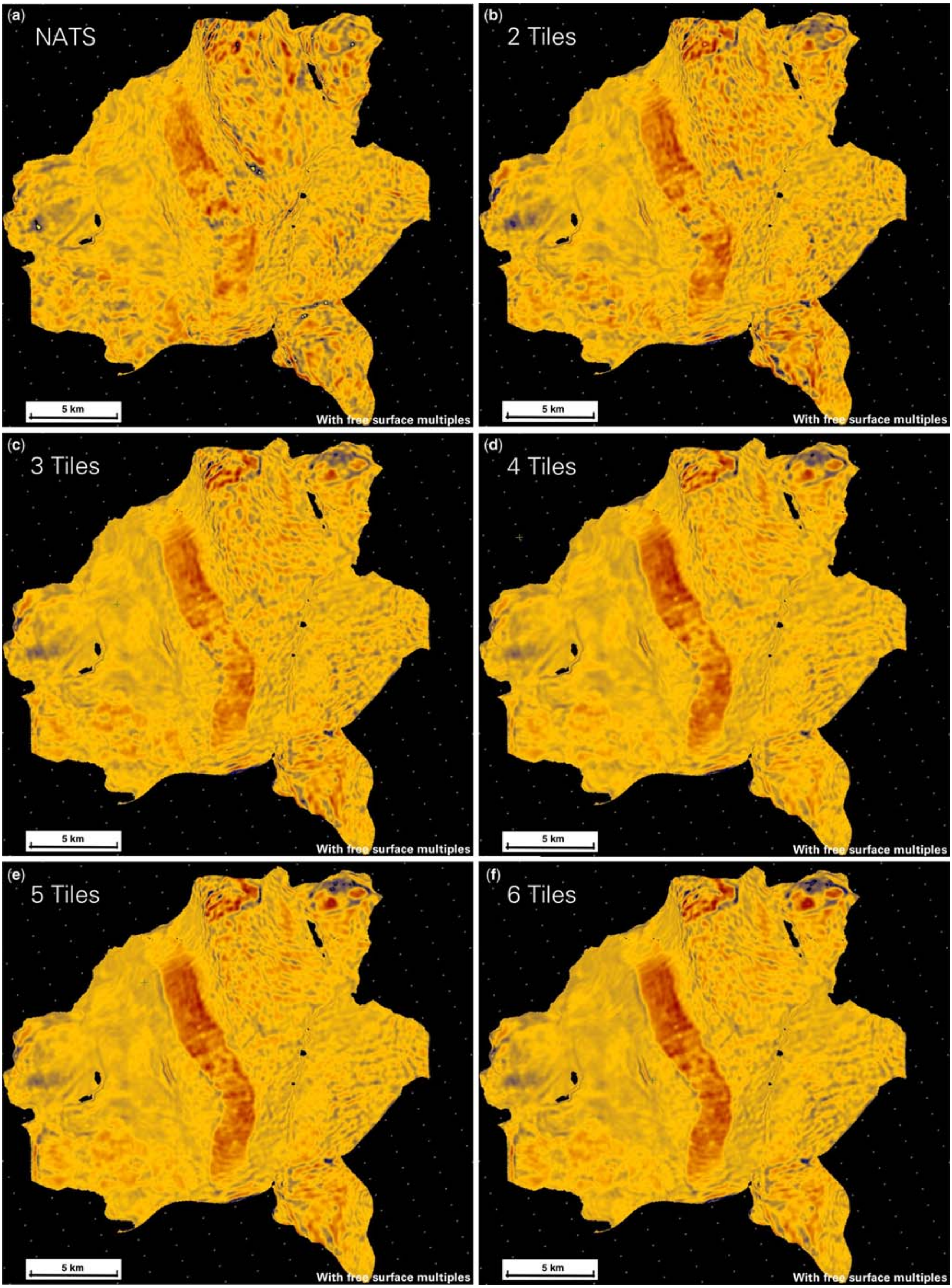

Fig. 13. Model NATS v. WATS tile number comparison: (**a**) NATS; (**b**) two-tile WATS; (**c**) three-tile WATS; (**d**) four-tile WATS; (**e**) five-tile WATS; (**f**) six-tile WATS.

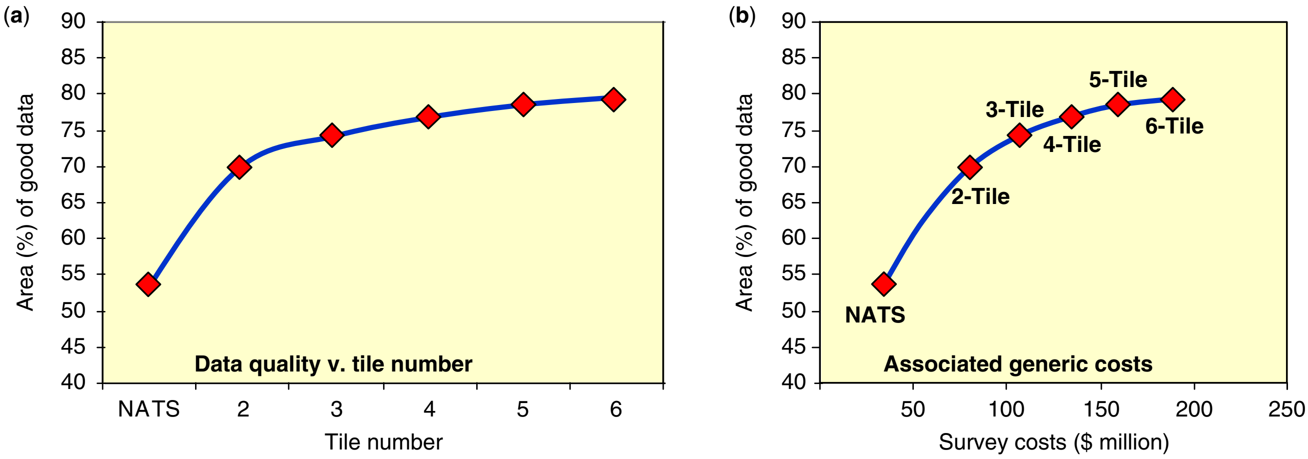

Fig. 14. Quantification of quality and cost: (**a**) data quality v. tile number: area/percentage of 'good' (coherent) model data from different acquisition designs; (**b**) associated generic costs.

separation and full-fold survey area of 1000 km^2. This approach allows both quality and costs to be optimized, consistent with survey objectives. These types of graphs were utilized in conjunction with analysis of targeted cross-sections and RMS amplitude extractions to determine the final recommended survey parameters. As we can see, there are significantly higher costs for WATS acquisition v. conventional NATS. However, the costs of not having better quality data will be significant and probably higher.

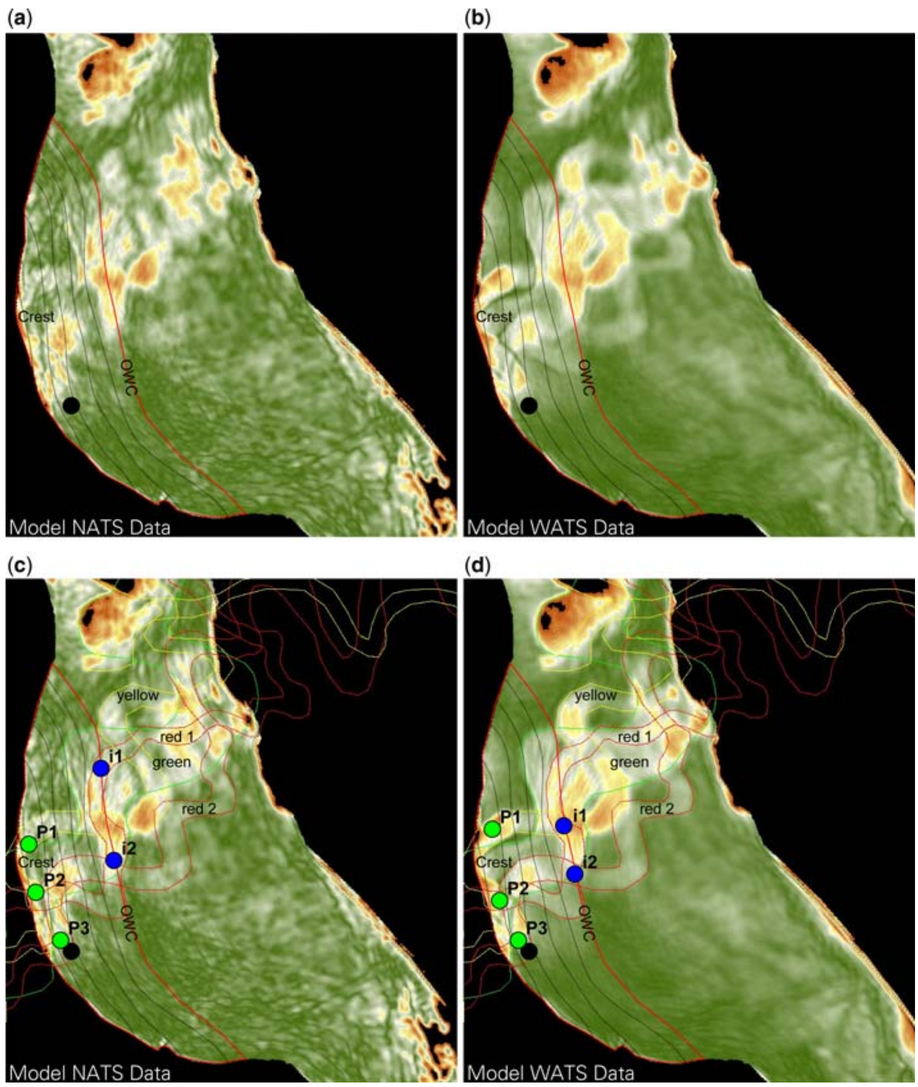

Fig. 15. Well targeting blind test to illustrate business justification: objective was to locate three producer and two water injector wells given (**a**) an RMS attribute map from model NATS data, location of a discovery well and the reservoir container geometry; (**b**) an RMS attribute map from model WATS data was then provided with an opportunity to revise the initial well locations. Input model channel geometries (not provided in the blind test) are shown on the (**c**) RMS attribute map from model NATS data with a representative example of initial NATS-based well locations and on the (**d**) RMS attribute map from model WATS data with the WATS-based revised well locations.

Business case support

Gulf of Mexico WATS experience suggests that benefits in improved imaging of a WATS survey will result in: increased confidence in top reservoir mapping subsalt; definition of reservoir compartments and better description of internal reservoir architecture leading to optimized well locations, improved recovery and potentially reduced well count; greater understanding of potential risks during drilling; and associated cost benefits. Block 31 3DFD model data results were used to test some of these potential business case benefits.

A well targeting blind test was constructed to simulate the development implications of WATS imaging improvements. This blind test was given to a number of subsurface staff, with a representative example illustrated in Figure 15. The objective of the blind test was to locate three producer and two water injector wells given an RMS attribute map from model NATS data, the location of a discovery well and the reservoir container geometry (Fig. 15a). An RMS attribute map from model WATS data (Fig. 15b) was then provided with an opportunity to revise the initial well locations. Input model channel geometries (not provided in the blind test) are shown on the RMS attribute map from model NATS data with a representative example of initial NATS-based well locations (Fig. 15c) and on the RMS attribute map from model WATS data with the WATS-based revised well locations (Fig. 15d). The model WATS data shows significant imaging improvements compared with the model NATS data which is clearly reflected in the updated well locations shown in Figure 15d.

By making some basic assumptions linking recovery factor directly to well targeting efficiency, the example shown in Figure 15 resulted in a 20% increase in recovery based on improved imaging from the model WATS dataset. Although a 20% increase in recovery cannot be guaranteed from actual WATS data, this blind test example demonstrates that better imaging from WATS data will lead to better decision-making in actual appraisal and development.

Recommended WATS survey

The actual WATS survey acquisition for Block 31 based on the 3DFD modelling discussed in this paper is shown in Figure 16. The survey consists of four tiles, acquired in a NW–SE direction, using an 8×8 km cable configuration. The survey area is targeted over key subsalt discoveries and consists of two parts: a 1735 km^2 appraisal quality survey shown in green, and a 295 km^2 development quality over a focused area shown in red. Appraisal quality is defined by a sail line separation of 500 m over the entire survey area (green). The red area will be infilled to a 250 m sail line separation, providing a development-quality WATS dataset around a focused, priority area. Because of the scalability of the WATS acquisition design, surveys can be optimized across the value chain. Should further development opportunities be identified, it will be straightforward to subsequently upgrade the appraisal quality WATS seismic survey to development quality by acquiring additional infill data. Acquisition of this survey began in December 2008 and is expected to complete in August 2009. This is the first WATS seismic survey outside the Gulf of Mexico and the first in Angola.

Summary

Subsalt imaging in Block 31 is significantly poor compared with the extrasalt environment of current Angola developments. Existing narrow-azimuth data is clearly not sufficient for subsalt appraisal and development; experience in the Gulf of Mexico supports the case that WATS will provide a step change in Angola subsalt imaging. 3DFD modelling has been key in developing the technical justification for WATS, optimizing survey design (quality and costs) and building business case support. Modelling is high effort, in both cost and time, but is also high value. Over 100 scenarios (volumes) were generated in the Block 31 modelling project discussed in this paper. However this commitment is small

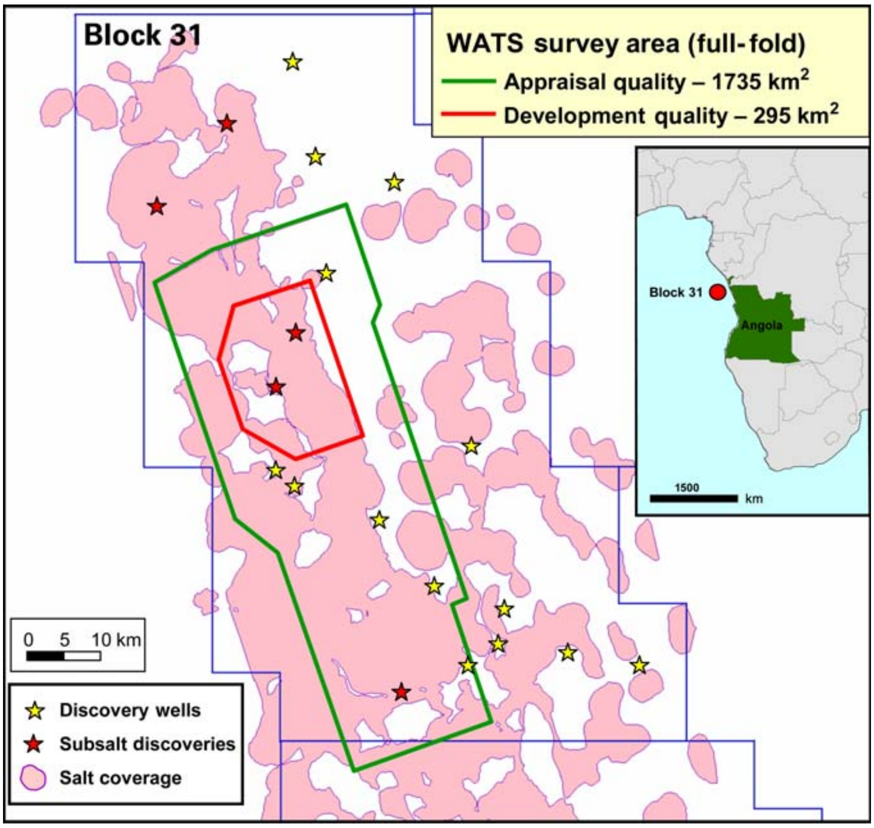

Fig. 16. Block 31 WATS survey acquisition area.

compared with the cost of WATS acquisition and the future cost benefits for appraisal and development.

The authors would like to thank Sonangol, BP, ExxonMobil, Sonangol P&P, Statoil, Marathon and Total for permission to present the data in this paper.

References

Barley, B. & Summers, T. 2007. Multi-azimuth and wide-azimuth seismic: shallow to deep water, exploration to production. *The Leading Edge*, **26**, 450–458.

Michell, S., Billette, F. J., Sharp, J. & Turner, J. 2004. Taking advantage of dual-azimuth analysis for model building and imaging over Mad Dog. *SEG International Exposition and 74th Annual Meeting, Expanded Abstracts*, 410–413.

Michell, S., Shoshitaishvili, E., Chergotis, D., Sharp, J. & Etgen, J. 2006. Wide azimuth streamer imaging of Mad Dog; have we solved the subsalt imaging problem? *SEG International Exposition and 76th Annual Meeting, Expanded Abstracts*, 2905–2909.

Regone, 2006. A modeling approach to wide-azimuth design for subsalt imaging. *The Leading Edge*, **25**, 1467–1475.

Threadgold, I. M., Zembeck-England, K., Aas, P. G., Fontana, P. M., Hite, D. & Boone, W. E. 2006. Implementing a wide azimuth towed streamer field trial: the what, why and mostly how of WATS in Southern Green Canyon. *SEG International Expostion and 76th Annual Meeting, Expanded Abstracts*, 2901–2904.

VerWest, B. J. & Lin, D. 2007. Modeling the impact of wide-azimuth acquisition on subsalt imaging. *Geophysics*, **72**, SM241–SM250.

Sub-basalt hydrocarbon prospectivity in the Rockall, Faroe–Shetland and Møre basins, NE Atlantic

I. DAVISON,[1] S. STASIUK,[2] P. NUTTALL[3] and P. KEANE[3]

[1]*GEO International Ltd, 38–42 Upper Park Road, Camberley, Surrey GU15 2EF, UK (e-mail: i.davison@earthmoves.co.uk)*
[2]*International Geoscience Ltd., Burnham, Slough, Berks SL18AS, UK*
[3]*Ion/GXT, 2105 City West Boulevard, Building III, Suite 900, Houston, TX 77042 USA*

Abstract: The seismic imaging below the basalts in the NE Atlantic basins is generally poor and the thickness of the basalts is difficult to predict. Two recent wells (William, 6005/13-1 and Brugdan, 6104/21-1) drilled in Faroes waters were suspended before reaching the main sub-basalt reservoir targets, because the basalts were thicker than expected. New deep-tow (18 m) seismic reflection data has now allowed more detailed imaging of the sub-basalt Mesozoic strata. The base of the basalt is not always reflective and is probably a transitional contact, with low acoustic impedance. The underlying Mesozoic strata produce coherent reflectivity. Large structural closures produced by Cretaceous rifting and Cenozoic folding have been imaged in the Rockall and Faroe–Shetland basins and these may contain Cretaceous and Paleocene clastic reservoirs at drillable depths of about 4 km. The Rockall Trough contains 4–7 km thickness of Mesozoic strata and appears to be floored by stretched continental crust throughout. The lower section may contain Jurassic source rocks similar to the areas to the south, east and north of the basin. Large Cenozoic age folds are present which produce potential traps at Late Cretaceous level, where sandstones equivalent to the Upper Cretaceous Nise Formation may occur. These folds represent some of the largest undrilled structures in NW Europe.

Keywords: sub-basalt prospecting, sub-basalt imaging, NE Atlantic margin

Basalts of Palaeogene age extend over much of the Faroe–Shetland, Rockall and Møre basins and reach up to approximately 6 km thickness around the Faroe Islands (White *et al.* 2005). The existing seismic data quality is generally very poor below the basalt. Promising oil and gas field discoveries are present in the shallower eastern portions of both the Rockall and Faroes–Shetlands, but no wells drilled through the thick basalts have encountered Cretaceous reservoir targets. The new deep-tow seismic data presented here have imaged the deeper Mesozoic strata, which enhances new play possibilities for oil exploration across this area.

Seismic data acquisition and processing

Various seismic acquisition techniques have been used to try to image below the volcanic rocks in the Faroes–Shetlands area: over–under technique; ocean-bottom seismometer surveys; wide-angle reflection and seismic refraction (e.g. White *et al.* 1999, 2003, 2005; Hobbs & Jakubowicz 2000; England *et al.* 2005; Gallagher & Dromgoole 2007, 2008; Christie & White 2008). However, most of these surveys have been limited to a few lines due to the high cost of acquisition.

New seismic data presented in this paper was shot and processed by ION/GXT in 2008 (see Fig. 1 for line locations). The seismic line acquisition and Pre-Stack Depth Migration (PSDM) processing are all designed to provide optimum seismic imaging below thick (>1 km) Palaeogene basalts, which cover much of the NE Atlantic margin (Fig. 1). This was achieved with:

(1) long receiver offset (10.2 km);
(2) large source size (7440 cu. in.) with 173 barm peak output measure through system filters;
(3) deep-towed airgun (17.5 m);
(4) deep-towed geophone streamer (18 m); and
(5) minimum bubble interference.

The airgun and streamer deep tow provided a maximum energy input at 20–30 Hz frequency. This low-frequency energy penetrates through the basalts more effectively. Another significant data quality benefit of deep tow is the reduced noise caused by near-surface current and wave action.

This acquisition produced more coherent reflections below the basalts which have a high seismic attenuation factor. Data was recorded to 18 s TWT, to image the complete crustal structure (Fig. 2). All the PSDM seismic data was migrated using velocities derived from iterative tomographic velocity modelling. The velocity-modelled depths are within 5% of the depths from several calibration wells in the Faroe–Shetland Basin.

Faroe–Shetland and Møre basins

The Faroe–Shetland and Møre basins were proved to be important new hydrocarbon provinces when the Foinaven, Scheihallion and Ormen Lange fields were discovered in the 1990s. However, subsequent discoveries have been smaller and more difficult to find. Large areas of the UK and Faroes sector are covered by thick Palaeogene volcanics from the Iceland plume eruptions. The Lopra-1 well on the Faroe Islands drilled 3565 m of the lower basalt series (Ziska & Andersen 2005). Their total thickness is not known but seismic data suggest perhaps >6 km of basalt may be present below the Faroe Islands (White *et al.* 2005). Only two wells (6104/21-1 and 6005/13-1) have been drilled in the Faroes continental shelf into thick basalt and the results have not yet been released into the public domain. The volcanics have a high seismic absorption (Q factor, Maresh *et al.* 2006; Shaw *et al.* 2008) caused by interbedded lower velocity sediments, coals and palaeo-sol horizons, which produce a large number of internal reflections. Several seismic lines have been shot with wide aperture arrays or sea-bottom seismometers that have produced encouraging results with sub-basalt imaging (Richardson *et al.* 1999; White *et al.* 2003, 2005). However, until now there have been no

VINING, B. A. & PICKERING, S. C. (eds) *Petroleum Geology: From Mature Basins to New Frontiers – Proceedings of the 7th Petroleum Geology Conference*, 1025–1032. DOI: 10.1144/0071025

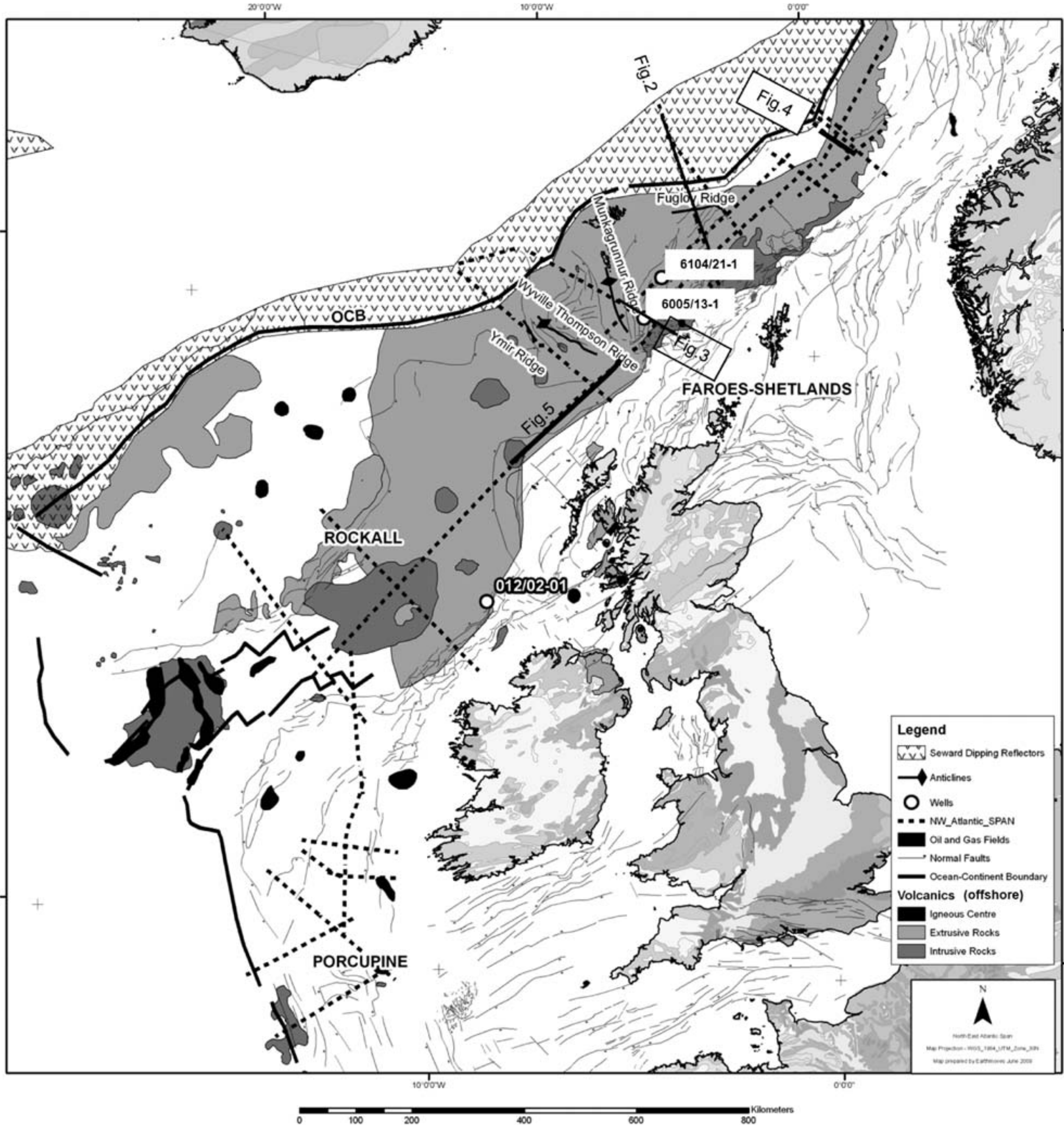

Fig. 1. Map of Faroes and Rockall basins showing location of seismic lines used in this study as well as the distribution of the Palaeogene volcanics. The locations of key wells mentioned in the text are also shown.

basin-wide seismic data sets available which image the whole crustal structure.

The base basalt is interpreted to be a transitional zone of thinly bedded tuffs, lavas and sediments as there is usually no clear seismic event associated with the base (Fig. 3). However, deeper stratal reflections are clearly imaged in many areas below a weakly reflective zone. Large-scale Cenozoic age folds (Munkagrunnur Ridge and Fugloy Ridge; Ritchie *et al.* 2008) and Mesozoic rotated fault blocks constitute major potential traps with Mesozoic reservoirs and Jurassic source rocks present (Lamers & Carmichael 1999; Figs 2–4). The Cenozoic folds are cored by Late Cretaceous strata (well 6004/16-1; Smallwood 2009) and are laterally extensive. More closely spaced seismic lines will be required to properly define structural closures on these long ridges. To our knowledge many of these deeper sub-basalt structures were not visible on previous seismic data. They are located in water depths up to 2 km, at drillable depths, and in the oil window (4–6 km), making them viable exploration plays which have yet to be tested.

The onset of volcanism started at 61–62 Ma (Saunders *et al.* 1997), with the main period of extrusion following at 56–53 Ma, which accompanied seafloor spreading of the North East Atlantic (Chron 24). Magmatism along the North East Atlantic produced a thick seaward dipping reflector (SDR) zone which is oriented parallel to the ocean–continental crust boundary (Spitzer *et al.* 2008; Fig. 1). The individual SDRs extend for some 20 km horizontally in a NW–SE direction orthogonal to the spreading centre. This length of lava run-out is thought to be indicative of sub-aerial volcanism (Fig. 2). This suggests that the mid-ocean ridge was sub-aerial at this time due to the anomalously high mantle potential temperature created by the Iceland plume. The ocean–continent crust boundary is here defined as the seaward end of the last

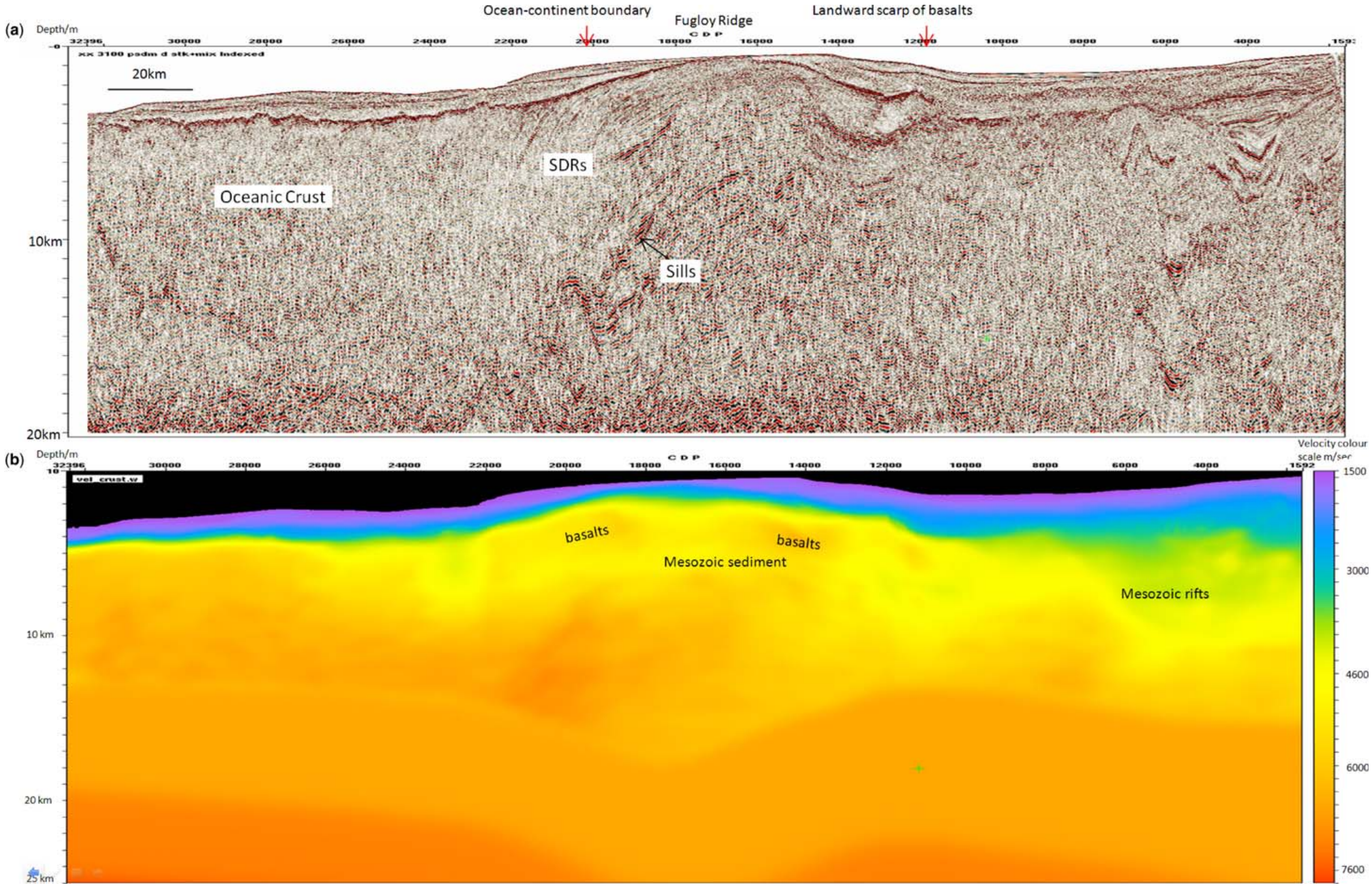

Fig. 2. (**a**) Seismic line across the Faroe–Shetland Basin showing the complete crustal structure. A large anticline is imaged below the basalts which may constitute a large potential trap in Mesozoic strata. This line is shot along the same location as the iSIMM line (White *et al.* 2005). (**b**) Velocity model used to produce the PSDM image in (a).

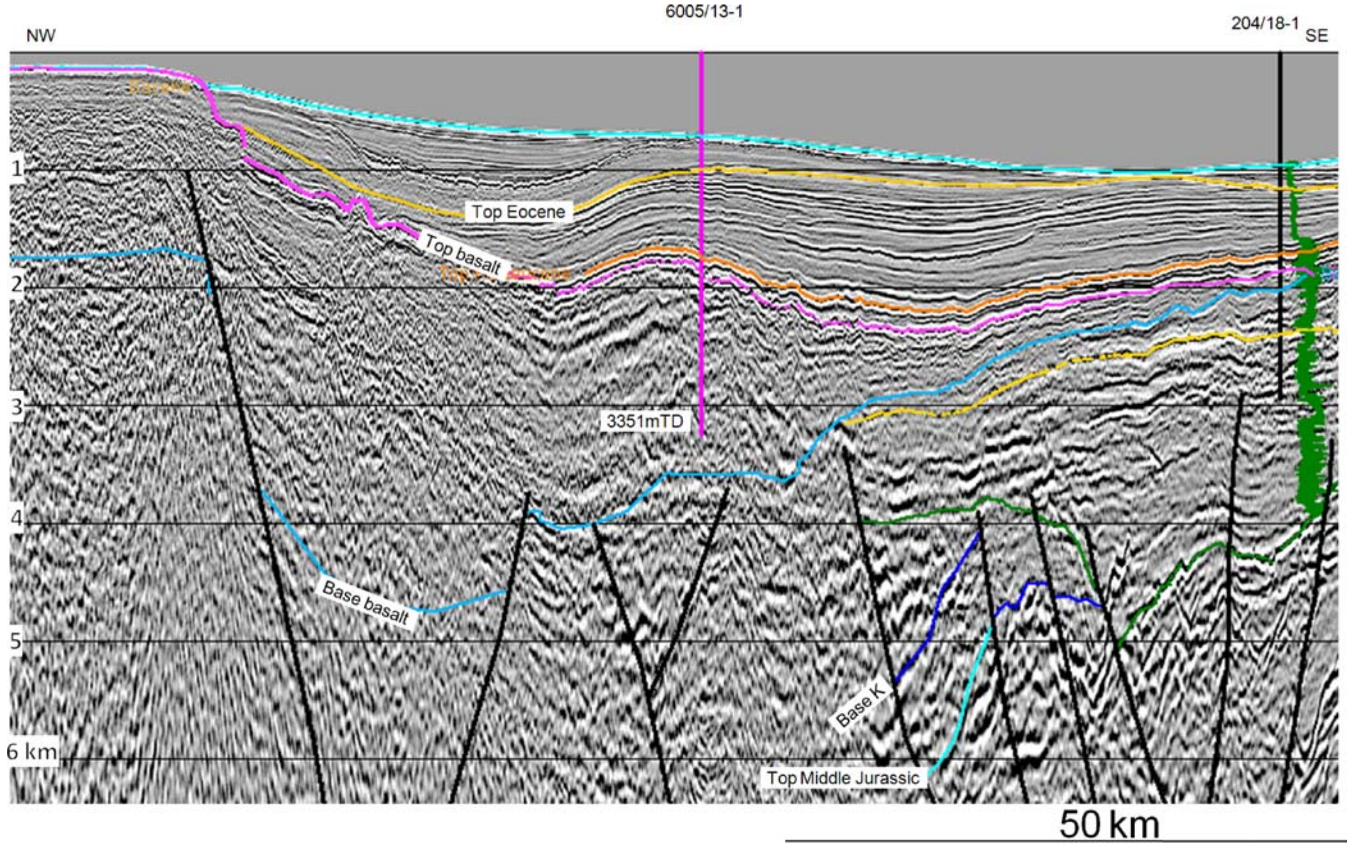

Fig. 3. Seismic section through the 6005/13–1 well illustrating the problem with definition of the base basalt.. The underlying rotated fault blocks are well imaged and may be viable exploration targets situated at >4 km depth. The well log for 204/18-1 is the sonic curve.

visible rotated fault block below the thick basalts (>2 km), which lies close to the landward edge of the main SDR sequence (Fig. 2).

The SDRs reach up to approximately 6–7 km maximum thickness. We interpret this to be new oceanic crust erupted above sea-level when they reach this thickness. The basalts flowed landward from the spreading centre to produce lava deltas, with eastward prograding foresets. These reach up to 1 km in vertical relief, indicating the probable palaeowater depths (Fig. 4). Below the landward (eastern) edge of the basalts, rifted sedimentary strata are clearly imaged which reach up to 5–7 km in thickness. These can be traced for a short distance below the basalts (Figs 2 & 4). Stratal reflections are imaged, even under the thickest sequence of SDRs; however, these are apparently injected by a large number of magmatic sills (Fig. 4). Strong irregular reflections occur at depths of 12–16 km below the SDRs, and are interpreted to be basic intrusions injected into Lewisian basement (Fig. 2). Prominent intrusions are occasionally imaged where there is a strong landward (eastward)-dipping reflection imaged at depths of 10–15 km (Fig. 2).

Many igneous sills were injected into the crust during the Palaeogene (Fig. 4) and 70 such sills have been intersected by the well 164/7-1; these sills range in thickness from 2 to 150 m in thickness (Linnard & Nelson 2005). The sills are mainly injected around 1–3 km below the level of the Paleocene basalts, where the depth of sill injection was determined by the depth at which the magmatic pressure exceeded the prevailing lithostatic pressure. Below this depth, the magmatic pressure was not great enough to overcome the lithostatic pressure and only dyke injection would have occurred. Hence, the deeper Jurassic source rocks may have escaped pervasive heating from sill injection as they are situated at greater depths than 3 km below base basalt.

Rockall

The nature of the crust below Rockall has been suggested to be either oceanic or continental (e.g. England & Hobbs 1995, 1997; O'Reilly *et al.* 1996; Shannon *et al.* 1999, Morewood *et al.* 2004; Chappell & Kusznir 2005; Klingelhoer *et al.* 2005). The presence of rifted continental crust would significantly improve the prospectivity of the basin with the possibility of the occurrence of Jurassic source rocks in deep half-graben. The new data presented here support the presence of continental rifted blocks throughout the basin (Fig. 5).

The Rockall Trough has proven hydrocarbons on the eastern perched rifted margin with gas condensate discovered in the Dooish well. However, the central part of the basin is virtually unexplored with no wells drilled below the basalt and only a sparse 2D seismic grid is available. Basalts cover over two-thirds of this basin (Fig. 1) and a large number of igneous sills are also injected into the Late Cretaceous strata that inhibit seismic penetration in the deepest parts of the basin (Archer *et al.* 2005).

The new seismic data indicate that between 2 and 7 km of sedimentary strata are present throughout the basin, of which up to 4 km may lie below the basalts (Fig. 5). If a Jurassic source rock were present in the area, it is predicted to be in the oil generation window at the present time.

Structural inversion and uplift occurred in the Middle to Upper Eocene when the Wyville–Thompson and Ymir Ridges were formed. These structures were also reactivated in the Miocene (Ritchie *et al.* 2003). These ridges are capped by basalts and it has never been possible to image the sedimentary packages below the basalt. The new data presented here indicate that underlying layered Mesozoic? strata are present and that rotated fault

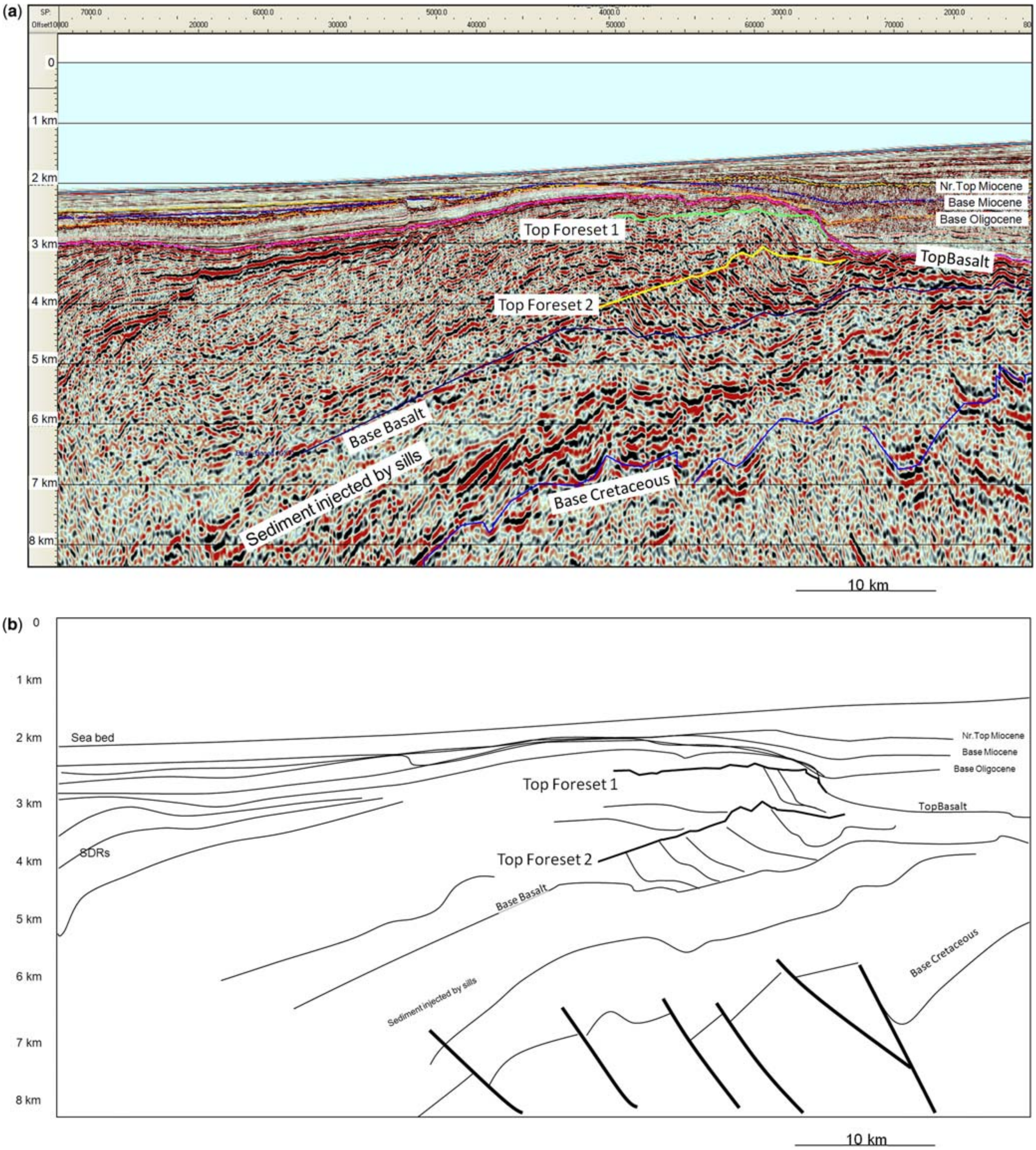

Fig. 4. Seismic section through the Møre Basin showing a lava pile with a landward-dipping scarp edge. Two foreset sequences of lavas are piled one on top of one another. The lavas overlie rifted fault blocks which have been injected by sills (bright reflections). These rifted basins are buried to depths of 5–6 km and reservoir quality is predicted to be poor at these depths.

block geometries are present in the anticlines. Consequently, large structural closures may be expected below the basalts.

The age of rifting in the Rockall Trough is not known, as the deeper section has never been drilled and it is debatable whether a Jurassic source rock will be present within the basin (Shannon *et al.* 1999; Tate *et al.* 1999). However, Jurassic source rocks are present in the Porcupine Basin to the south, in the Slyne–Erris Trough to the east and in the Faroe–Shetland Basin to the north, suggesting the presence of a regional Jurassic source (see Scotchman 2001; Scotchman *et al.* 2006). The Rockall Basin is situated 100–400 km from the British mainland but Late Cretaceous turbidite sandstones may have also been sourced from the Greenland, similar to the Nise Formation in the Vøring Basin farther north (Fig. 6). The large rotated fault blocks in Rockall are located at depths of 3–4 km in water depths of 1000 m, making these viable exploration targets.

Conclusions

New PSDM seismic data along the NE Atlantic margin have successfully imaged the sub-basalt strata and indicate that there are many potentially large structural closures located below

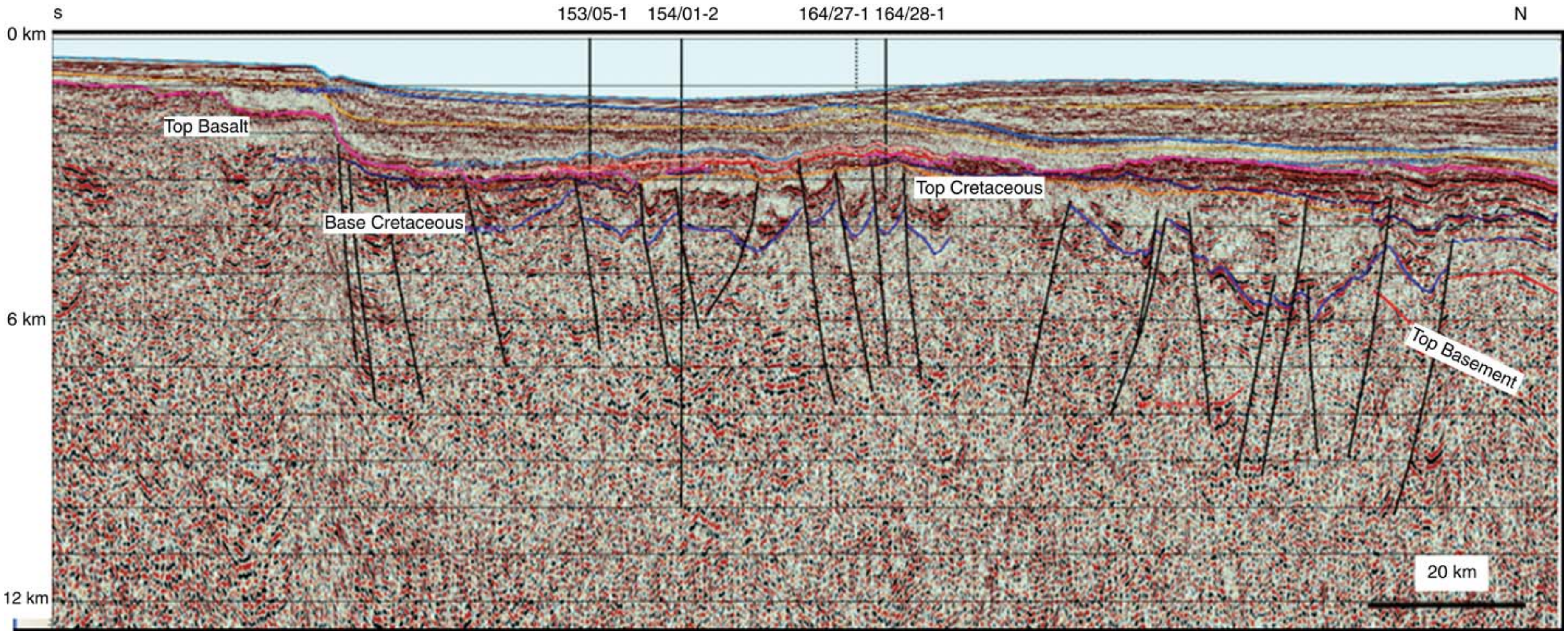

Fig. 5. NE–SW strike line in the northern part of the Rockall Basin showing rotated faults (blocks?) of presumed Jurassic/Cretaceous age with up to 7 km of sedimentary strata in the basin. Rotated fault block crests are potential targets at depths of 4–5 km.

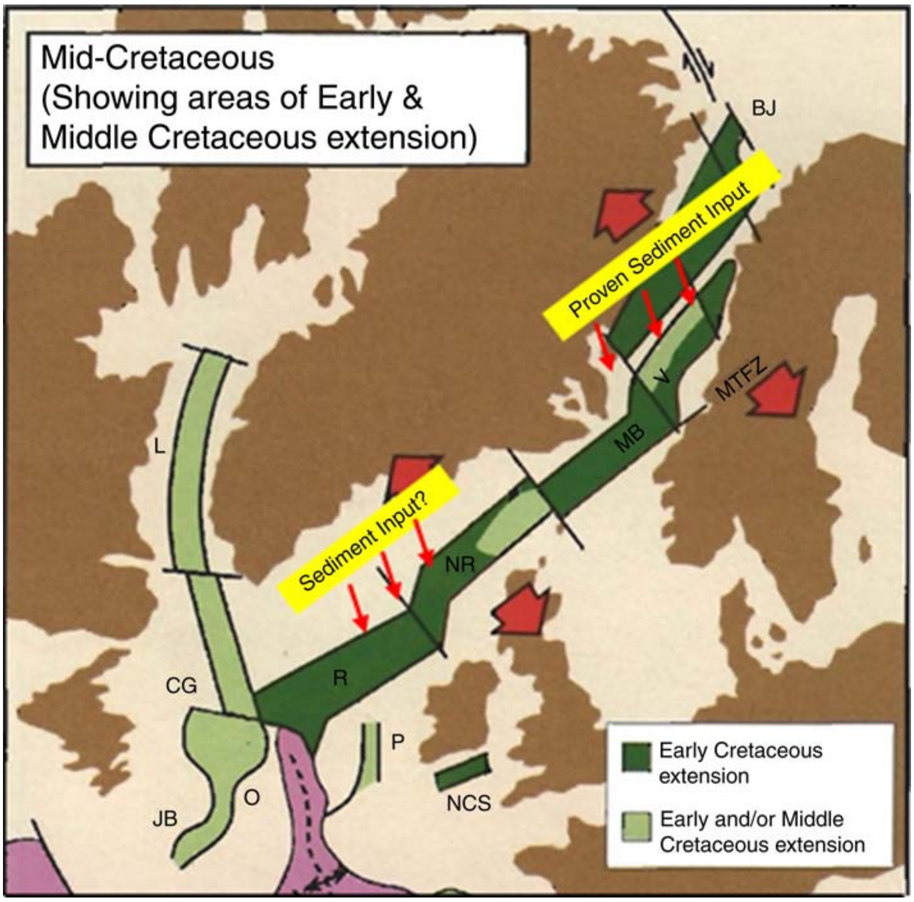

Fig. 6. Map of the NE Atlantic showing a pre-drift reconstruction (Doré *et al.* 1999). Cretaceous strata are derived from Greenland in the Vøring Basin and Paleocene strata were derived from Greenland in the Shetlands area. We suggest here that Late Cretaceous sandstones in the Rockall could also be sourced from west of the basin.

the Palaeogene basalts and sills in the Faroe–Shetland, Rockall and Møre basins. The base of the Palaeogene volcanics is not clearly imaged on the seismic data, probably because this is a transitional contact with little acoustic impedance contrast; the thickness of basalts is therefore very difficult to predict. This increases the risk of exploration targets but this does not preclude exploration as the deeper Mesozoic half-grabens are well-imaged 1–2 km below the presumed base of the volcanics.

The Rockall Trough contains on average 4–7 km of Mesozoic strata which were deposited on rifted continental crust with rotated fault blocks imaged throughout the basin. The presence of Jurassic source rocks and good quality Cretaceous reservoirs is not yet proven but is considered to be the key to successful exploration in the Rockall. The new seismic data presented here have helped to identify many potential structures below the basalts, which are some of the largest undrilled structures in NW Europe. Deep-towed long streamer seismic data have successfully imaged below the basalt province.

We would like to thank ION/GXT BasinSPAN programs for permission to show the seismic data used in this paper. John Smallwood is thanked for a very useful review of this paper.

References

Archer, S. G., Bergman, S. C., Lliffe, J., Murphy, C. M. & Thornton, M. 2005. Palaeogene igneous rocks reveal new insights into the geodynamic evolution and petroleum potential of the Rockall Trough, NE Atlantic Margin. *Basin Research*, **17**, 171–201.

Chappell, A. R. & Kusznir, N. J. 2005. Evidence for slow spreading ocean ridge in the southern Rockall Trough from satellite inversion and seismic data. *EOS Transactions*, *AGU*, **86**, Abstract T53A-05.

Christie, P. A. F. & White, R. S. 2008. Imaging through Atlantic margin basalts: an introduction to the sub-basalt mini-set. *Geophysical Prospecting*, **56**, 1–4.

Doré, A. G., Lundin, E. R., Birkeland, Ø., Eliassen, P. E. & Fischler, C. 1999. Principal tectonic events in the evolution of the northwest European Atlantic margin. *In*: Fleet, A. J. & Boldy, S. A. R. (eds) *Petroleum Geology of Northwest Europe: Proceedings of the 5th Conference*. Geological Society, London, 41–61; doi: 10.1144/0050041.

England, R. W. & Hobbs, R. W. 1995. Westline: a deep near normal incidence reflection profile across the Rockall Trough. *In*: Croker, P. F. & Shannon, P. M. (eds) *The Petroleum Geology of Ireland's Offshore Basins*. Geological Society, London, Special Publications, **93**, 423–427.

England, R. W. & Hobbs, R. W. 1997. The structure of the Rockall Trough imaged by deep seismic reflection profiling. *Journal Geological Society London*, **154**, 497–502.

England, R. W., McBride, J. H. & Hobbs, R. W. 2005. The role of Mesozoic rifting in the opening of the NE Atlantic: evidence from deep seismic profiling across the Faroe-Shetland Trough. *Journal Geological Society London*, **162**, 661–673.

Gallagher, J. W. & Dromgoole, P. W. 2007. Exploring below the basalt, offshore Faroes: a case history of sub-basalt imaging. *Petroleum Geoscience*, **13**, 213–225.

Gallagher, J. W. & Dromgoole, P. W. 2008. Seeing below the basalt – offshore Faroes. *Geophysical Prospecting*, **56**, 33–45.

Hobbs, R. & Jakubowicz, W. 2000. Sub-basalt imaging using low frequencies. *Geophysics*, **56**, 190–201.

Klingelhoer, F., Edwards, R. A., Hobbs, R. W. & England, R.W. 2005. Crustal structure of the NE Rockall Trough from wide-angle seismic data modelling. *Journal of Geophysical Research*, **110**, B11105; doi: 10.1029/2005JB003763.

Lamers, E. & Carmichael, S. M. M. 1999. The Palaeocene deepwater sandstone play west of Shetlands. *In*: Fleet, A. J. & Boldy, S. A. R. (eds) *Petroleum Geology of Northwest Europe: Proceedings of the 5th Conference*. Geological Society, London, 635–644.

Linnard, S. & Nelson, R. 2005. Effects of Tertiary volcanism and later events upon the Faroese hydrocarbon system. *Faroe Islands Exploration Conference Proceedings of the 1st Conference*. Annales Societatis Scientarum Faeroensis, Supplementum, **43**, Torshavn, 44–53.

Maresh, J., White, R. S., Hobbs, R. W. & Smallwood, J. R. 2006. Seismic attenuation of Atlantic margin basalts. *Geophysics*, **56**, 645–653.

Morewood, N. C., Shannon, P. M. & Mackenzie, G. D. 2004. Seismic stratigraphy of the southern Rockall Basin: a comparison between wide-angle seismic and normal incidence reflection data. *Marine and Petroleum Geology*, **21**, 1149–1163.

O'Reilly, B. M., Hauser, F., Jacob, A. W. B. & Shannon, P. M. 1996. The lithosphere below the Rockall Trough: wide-angle seismic evidence for extensive serpentinisation. *Tectonophysics*, **255**, 1–23.

Richardson, K. R., White, R. S., England, R. W. & Fruehn, J. 1999. Crustal structure east of the Faroe Islands: mapping sub-basalt sediments using wide angle seismic data. *Petroleum Geoscience*, **5**, 161–172.

Ritchie, J. D., Johnson, H. & Kimbell, G. S. 2003. The nature and age of Cenozoic contractional deformation within the NE Faroe–Shetland Basin. *Marine and Petroleum Geology*, **20**, 399–409.

Ritchie, J. D., Johnson, H., Quinn, M. F. & Gatliff, R. W. 2008. The effects of Cenozoic compression and the Cenozoic Faroe-Shetland Basin and adjacent areas. *In*: Johnson, H., Dore, T. G., Gatliff, R. W., Holdsworth, R. W., Lundin, E. R. & Ritchie, J. D. (eds) *The Nature and Origin of Compression in Passive Margins*. Geological Society, London, Special Publications, **306**, 121–136.

Saunders, A. D., Fitton, J. G., Kerr, A. C., Norry, M. J. & Kent, R. W. 1997. *In*: Mahoney, J. J. & Coffin, M. F. (eds) *The North Atlantic Igneous Province*. American Geophysical Union, Washington, DC, Geophysical Monographs, **100**, 45–93.

Scotchman, I. C. 2001. *Petroleum Geochemistry of the Lower and Middle Jurassic in Atlantic Margin Basins of Ireland and the UK*. Geological Society, London, Special Publications, **188**, 31–60.

Scotchman, I. C., Carr, A. D. & Parnell, J. 2006. Hydrocarbon generation modelling in a multiple rifted and volcanic basin: a case study in the Foinaven Sub-basin, Faroe–Shetland Basin, UK Atlantic margin. *Scottish Journal of Geology*, **42**, 1–19.

Shannon, P. M., Jacob, A. W. B., O'Reilly, B. M., Hauser, F., Readman, P. W. & Makris, J. 1999. Structural setting, geological development and basin modelling in the Rockall Trough. *In*: Fleet, A. J. & Boldy, S. A. R. (eds) *Petroleum Geology of Northwest Europe: Proceedings of the 5th Conference*. Geological Society, London, 42–43; doi: 10.1144/0050042.

Shaw, F., Worthington, M. H., White, R. S., Andersen, M. S. & Petersen, U. K. 2008. Seismic attenuation in Faroe Islands basalts. *Geophysical Prospecting*, **56**, 5–20.

Smallwood, J. R. 2009. Back-stripped 3D seismic data: a new tool applied to testing sill emplacement models. *Petroleum Geoscience*, **15**, 259–268.

Spitzer, R., White, R. S. & Christie, P. A. F. 2008. Seismic characterisation of basalt flows from the Faroes margin and the Faroe–Shetland Basins. *Geophysical Prospecting*, **56**, 21–31.

Tate, M. P., Dodd, C. D. & Grant, N. T. 1999. The Northeast Rockall Basin and its significance in the evolution of the Rockall–Faeroes/East Greenland rift system. *In*: Fleet, A. J. & Boldy, S. A. R. (eds) *Petroleum Geology of Northwest Europe: Proceedings of the 5th Conference*. Geological Society, London, 391–406; doi: 10.1144/0050391.

White, R. S., Fruehn, J., Richardson, K. R., Cullen, E., Kirk, W., Smallwood, J. R. & Latkiewicz, C. 1999. Faroes Large Aperture Research Experiment (FLARE): imaging through basalt. *In*: Fleet, A. J. & Boldy, S. A. R. (eds) *Petroleum Geology of Northwest Europe: Proceedings of the 5th Conference*, 1243–1252; doi: 10.1144/0051243.

White, R. S., Smallwood, J. R., Fliedner, M. M., Boslaugh, B., Maresh, J. & Fruehn, J. 2003. Imaging and regional distribution of basalt flows in the Faeroe–Shetland Basin. *Geophysical Prospecting*, **51**, 215–231.

White, R. S., Spitzer, R., Christie, P. A. F., Roberts, A., Lunnon, Z., Maresh, J. & iSIMM. 2005. Seismic imaging through basalt flows on the Faroes Shelf. *Proceedings of the 1st Faroe Islands Exploration Conference*. Annales Societatis Scientiarum Færoensis, Supplementum, **43**, Tórshavn, 11–31.

Ziska, A. H. & Andersen, C. 2005. Exploration opportunities in the Faroe Islands. Faroe Tórshavn. *Proceedings of the 1 Faroe Islands Exploration Conference*. Annales Societatis Scientiarum Færoensis, Supplementum, **43**, Tórshavn, 146–162.

Intra-basalt units and base of the volcanic succession east of the Faroe Islands exemplified by interpretation of offshore 3D seismic data

M. ELLEFSEN,[1,2] L. O. BOLDREEL[1] and M. LARSEN[2]

[1]*Department of Geography and Geology, Copenhagen University, Øster Voldgade 10, DK-1250 Copenhagen, Denmark (e-mail: melle@dongenergy.dk)*
[2]*DONG Energy, Exploration, Agern Alle 24-26, DK-2970 Hørsholm, Denmark*

Abstract: Recent exploration activities in the basalt covered part of the offshore Faroe Island region has stressed the need for a better understanding of the volcanic succession, especially the lowermost part and the transition to the underlying non-volcanic succession. Using the proposed interpretation methods, which include careful identification of inclined reflector segments and flattening to various reflectors representing pronounced continuous markers embedded horizontally and 3D visualization, six volcanic units have been identified. The upper three units consist of plane-parallel reflector packages and probably represent subaerially extruded lava flows. The three lower units are characterized by irregular hummocky and inclined reflectors and are interpreted as lava deltas composed mainly of hyaloclastites. Within the data coverage area, the direction of extrusion is inferred from the seismic interpretation and four units originate from the NW and two from the SE. It is believed that the base of the volcanic succession is situated at a deeper level than the base of the parallel bedded units. At the base of the basalt succession and in the lower part of the volcanic succession pronounced reflector segments are ascribed to saucer-shaped sills. Analysing the seismic data using principles of seismic stratigraphy and observing them in a 3D environment, it is possible to obtain a broader understanding of the volcanic succession in the area and thereby divide the volcanic succession into characteristic facies units and separate it from the non-volcanic lithology and sills. The study shows that applying the proposed interpretation technique allows an evolution model to be put forward and it is suggested that the approach used in the study can be of use for hydrocarbon exploration in other basalt-covered areas.

Keywords: Faroe Islands, volcanics, basalts, hyaloclastites, facies interpretation, 3D seismic data

The Faroe Islands consist of 18 islands situated in the North Atlantic Ocean. The islands are mainly composed of layered basaltic rocks of the FIBG (Faroe Island Basalt Group) (Passey 2009). The FIBG is on a regional-scale part of the North Atlantic Palaeogene flood basalt province that is characterized by widespread lava successions extruded subaerially during continental breakup (e.g. Saunders *et al.* 1997; Larsen *et al.* 1999). The province covers an area of more than 2000 km in diameter and the subaerially extruded lavas can be observed onshore in East and West Greenland (e.g. Pedersen & Dueholm 1992; Larsen *et al.* 1999; Hopper *et al.* 2003; Peate *et al.* 2003; Pedersen *et al.* 2006), on the Faroe Islands (Rasmussen & Noe-Nygaard 1970, 1990; Waagstein 1988, 1996; Passey 2007), Baffin Island in northeastern Canada, and in parts of northern Scotland (Ritchie *et al.* 1999). In the Faroe region the extrusion and evolution of the volcanic succession has been treated from a non-geochemical aspect by, for example, Rasmussen & Noe-Nygaard (1969, 1970), Boldreel & Andersen (1994), Ellis *et al.* (2002), Passey (2004, 2009), Passey *et al.* (2006), Passey & Bell (2007) and Ellis *et al.* (2009). There seems to be an agreement that the volcanics spread eastwards into basins and covered the former subaerially exposed landscapes. A regional Paleocene correlation in the Faroe–Shetland area, which includes this idea, was published by Ellis *et al.* (2009).

The thickness of the volcanic successions and whether siliciclastic sediments are present below the basalts and volcanic rocks in the Faroes area have been debated for many years. Results of refraction seismic experiments give the impression that sediments are to be found and that the volcanic succession is 2–7 km thick (Eccles *et al.* 2009). Details of the volcanic and pre-volcanic succession based on reflection seismic methods are difficult to obtain as sub-basalt imaging is difficult. In order to enhance sub-basalt imaging by reflection seismic methods, a large number of studies have been carried out related to acquisition and processing (e.g. Eccles *et al.* 2009; Gallagher & Dromgoole 2009; Leathard *et al.* 2009) and pronounced progress has been obtained. Exploration wells offshore Faroe Islands and west of Shetland have been drilled at the distal edge of the basalt cover where the thickness of the basalt succession is limited and, based on released wells offshore the Faroe Islands, it is clear that the Paleocene/Eocene basalts have been drilled through (Varming 2009). Onshore the Faroe Islands a deep scientific well drilled through the lowermost part of the plane-parallel bedded basaltic succession (Beinisvørð Formation) and had total depth (TD) in a succession of hyaloclastites (The Lopra Formation; Ellis *et al.* 2009). Geological observations and studies have resulted in a better understanding of the architecture of flood basalts and the complexity of volcanic succession (e.g. Nelson & Jones, 1970; Heinesen 1987; Pedersen *et al.* 2006; Passey 2007; Nelson *et al.* 2009). Results from earlier studies have in this study been used in the interpretation of 3D reflection seismics (e.g. Boldreel & Andersen 1994; Planke & Eldholm 1994; Andersen *et al.* 2007).

The aim of our study is to use seismic stratigraphic principles based on facies architecture of volcanic successions (e.g. Pedersen *et al.* 2006; Andersen *et al.* 2007; Nelson *et al.* 2009) and lithostratigraphic interpretation of wireline logs in flood basalt (e.g. Boldreel 2006; Andersen & Boldreel 2009) to carry out interpretation of a sub-basalt 3D digital reflection seismic survey. The interpretation methodology is applied in order to enhance sub-basalt interpretation and investigate the internal structure of the volcanic succession and its base on the scale of resolution based on conventional reflection seismic data. In this paper we describe the strategy and methods used in the offshore study area east of the Faroe Islands.

Vining, B. A. & Pickering, S. C. (eds) *Petroleum Geology: From Mature Basins to New Frontiers – Proceedings of the 7th Petroleum Geology Conference*, 1033–1042. DOI: 10.1144/0071033 © Petroleum Geology Conferences Ltd. Published by the Geological Society, London.

The background of the study

Results from fieldwork on outcrops in West Greenland and the interpretation of the wireline logs in the Lopra-1 well illustrate the problem of locating the base of the volcanic succession. In West Greenland, it is found that the lower part of the volcanic succession consists of lavas extruded into a large lake forming a lava delta showing foreset-bedded hyaloclastites. As the depression of the terrain was filled up, the plane-parallel bedded basalts became embedded (Pedersen *et al.* 2006). A similar scenario is outlined for the transition of hyaloclastites to massive lava flows in the Lopra-1 well (Boldreel 2006). These two examples illustrate that the base of the plane-parallel bedded basalts does not constitute the base of the volcanic succession if the lavas were extruded into water-filled lows where lava deltas developed. Only in the case that the lavas were extruded onto dry land can it be expected that the base of the parallel bedded basalt will actually form the substratum for the volcanic succession. Even under these circumstances it should be expected that the lowest part of the volcanic succession may not be an even surface as the lava filled up topographic depressions and locally developed pyroclastic deposits and lava deltas.

At the distal edge of the basalt-covered region east of the Faroe Islands it seems from the seismic data that steeply dipping foresets indicating lava deltas (hyaloclastites) are absent below the plane-parallel bedded basalts whereas a thick pile of hyaloclastites is found in the Lopra-1 well on the Faroe Islands. This raises the question of how far out from the Faroe Islands the lava deltas extend; that is, where does the base of the plane-parallel bedded basalt form the base of the volcanic succession? This has proved to be a difficult task using 2D reflection seismic data and therefore it was decided to carry out a study in order to investigate if a recently acquired 3D survey of high quality could support the ideas from West Greenland and the Lopra-1 well regarding the base of the volcanic succession. The idea of the project was to investigate the volcanic succession, especially the part found below the parallel bedded basaltic units, by detailed interpretation of the 3D survey using seismic stratigraphy and modern interpretation – viewing – and mapping software.

Data and methods

Multichannel reflection seismic data was acquired in the 1970s by Western Geophysical in the North Atlantic and, based on part of their data, it was found that the surface of the basalt was represented by a pronounced strong positive reflector, that the basalt succession was characterized by parallel bedded reflections and that the eastern limit of the basalt cover is located in the Faroe–Shetland Channel. In the northern part of the Faroe–Shetland Channel an escarpment indicates that the upper part of the plane-parallel bedded unit was extruded into a water-covered basin. In the southern part, the escarpments is absent, thus suggesting that the upper part of the basaltic unit was extruded onto dry land. The interpretation of the data also showed that sediments are present below the outer parts of the basalt covered area and that these sediments extend westwards towards the Faroe Islands for some distance before sub-basalt seismic imaging can no longer be obtained. Western Geophysical was awarded the obligation to acquire new multichannel reflection seismic data using the state of the art in the period 1994–1995 and the seismic data showed pronounced improvement of subsurface and sub-basalt imaging and thus the zone of sub-basalt imaging moved further to the west towards the Faroe Islands. Especially in the eastern part of the Faroes part of the Faroe–Shetland Channel the sub-basalt imaging was improved and pronounced inclined (foresets) and likely basin floor fan configurations were seen below a parallel bedded basalt unit (Boldreel *et al.* 1996). In addition, distinct seismic units could be identified below the foreset bedded units (Boldreel *et al.* 1996). Since 1996 a large number of conventional reflection seismic surveys, both 2D and 3D, have been carried out offshore the Faroe Islands in addition to experiments aimed at improving sub-basalt imaging. This has resulted in improvement of the sub-basalt imaging, but it is still a difficult task to carry out interpretation below the parallel bedded flood basalts in order to locate the base of the volcanic succession.

The data used in this study is 3D offshore reflection seismic data acquired in 2003 in license area 006 on the East Faroe High SE of the Faroe Islands. The survey covers an area of approximately 12×24 km (Fig. 1). A bubble-tuned source on a depth of 15 m was used, together with 8 km-long cables, placed in a depth of 20 m below the sea surface (Gallagher & Dromgoole 2007, 2009). The data was processed as zero phase data and frequencies higher than 38 Hz were removed. Great effort was put into processing the data, as discussed by Gallagher & Dromgoole (2007, 2009), and this resulted in a pronounced improvement in the subsurface imaging of the basaltic unit. The vertical resolution of the data is estimated to be of the order of 50–60 m using an average frequency of 20–25 Hz and 5000 m s^{-1} for the velocity of subaerially extruded basalt as based on the interpretation of subaerially extruded flood basalt in the Lopra-1 well (Boldreel 2006). The thickness of individual basaltic beds (lava flows) on the Faroe Islands differs according to the stratigraphic position (Series) they are part of, but the average in the Beinsisvørd Formation (former Lower Series) is 5–25 m (Hald & Waagstein 1984; Boldreel 2006) and similar thicknesses of basalt flows are noticed by interpreting wireline logs from exploration wells located in the West of Shetland area (Andersen & Boldreel 2009). Similar thickness variations of simple flows from various regions are published by Nelson *et al.* (2009). Thus, it is expected that most individual lava flows in the surveyed area are below seismic resolution, as is also illustrated by Nelson *et al.* (2009). This implies that the reflections observed in the basaltic unit may represent a number of lava flows. A

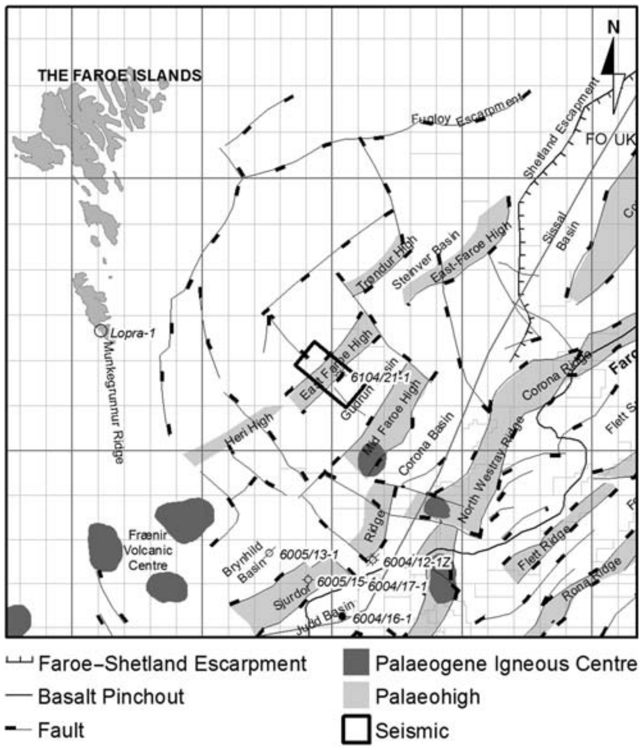

Fig. 1. Regional map showing the geological structures and the location of the study area.

similar problem of resolution has been addressed in a study of flood basalts from West of Shetland area, where it was shown that the reflectors interpreted as lava flows actually are made up of a number of lava flows (Hansen 2007). In another study addressing chalk mounds it was shown that the size of the individual mounds was below seismic resolution but the overall form of the mound and directions of growth could still be determined (Nielsen *et al.* 2004).

In order to estimate the thickness of the basaltic units in metres, a velocity has to be ascribed to the basaltic succession. Several authors have dealt with this subject by measuring the velocity of rock samples, from velocity picking in reflection seismic data, refraction seismic studies and interpreting acoustic wireline logs. It was shown that the velocity of basaltic rock varies according to whether it represents a compound or simple flow, hyaloclastites or intrusions. In addition the internal composition of, for example, a simple flow shows a large variation of velocity in the massive core and porous top and base (Planke 1994; Boldreel 2006; Andersen *et al.* 2007; Andersen & Boldreel 2009). In this study the findings by Planke (1994), Boldreel (2006), Andersen *et al.* (2007) and Andersen & Boldreel (2009) are applied with a velocity of 5000 m s^{-1} for units 1–3 (parallel bedded basalt) and a velocity of 3000 m s^{-1} for units 4–6 (hyaloclastites). Stacking velocities from reflection seismic surveys east of the Faroe Islands reveal a velocity of 5000–6000 m s^{-1} for the parallel bedded basalt unit and a drop in velocity leaving the unit and entering the unit below the parallel bedded basalt is seen.

Seismic interpretation

The basalt has been drilled in various places offshore UK and Faroese and by use of long-distance seismic ties it is believed that the succession which is the focus of the present study in the upper part consists of basalt. This has recently been confirmed by released information from the exploration well 6104/21–1 situated within the study area (Ellis pers. comm. 2009). From the interpretation of 2D seismic profiles in the East Faroe High area and in a westwards direction it is found that pronounced escarpments are located below the parallel bedded basalt, indicating that the palaeo-environment was probably water covered (Boldreel *et al.* 1996). The Lopra-1/1A well encountered the base of the Beinisvørð Formation at some 2489 m depth before entering the Lopra Formation, which consists of hyaloclastites (Boldreel 2006; Ellis *et al.* 2009). Thus it is expected that a hyaloclastite succession could be present below the base of the parallel bedded basalts in the study area.

Previous work has shown that the surface of the subaerial extruded basalt is easily mapped and that the principles of seismic stratigraphy are applicable for interpreting basalt successions (e.g. Gatliff *et al.* 1984; Boldreel & Andersen 1994; Andersen *et al.* 2007). Various studies have dealt with the architecture of flood basalts and their seismic expression on 2D reflection seismic data, for example, Planke *et al.* (1999, 2000), Jerram (2002), Andersen *et al.* (2007), Nelson *et al.* (2009). In this study we have compared the volcanic succession with five seismic facies types (cf. Andersen *et al.* 2007) that are also recognized in the subsurface of the British and Faroe Island continental shelves. The five types are

- The *parallel bedded platform* facies represent subaerially erupted volcanics and have been sampled by drilling or surface sampling.
- The *oblique progradational* facies represent basaltic hyaloclastic rocks tentatively interpreted as foreset breccias of basaltic flows that flowed into a subaqueous environment, and this type has been sampled by drilling or surface sampling.
- The *sigmoid aggradational* facies are believed to represent basaltic lavas that flowed into water. In contrast to the *sigmoid aggradational* facies, the *oblique progradational* facies are characterized by a disconformity above the foresets. It is proposed that this may reflect a relatively larger lava supply during formation of the *oblique progradational* than during formation of the *sigmoidal aggradational* facies. This type has been interpreted by comparison with well exposed volcanic provinces in Antarctica, West Greenland, Hawaii and Iceland.
- The *chaotic hummocky mounded* facies are believed to represent submarine volcanic products representing volcanic material deposited around a single feeder dyke (or stock). This type is inferred by comparison to well exposed volcanic provinces in Antarctica, West Greenland, Hawaii and Iceland.
- The chaotic *hummocky basin floor* facies probably represents submarine volcanic products that have been deposited over wider areas and this type was interpreted by comparison to well exposed volcanic provinces in Antarctica, West Greenland, Hawaii and Iceland.

In the basalt covered region around the Faroe Islands, West of Shetlands and in Norwegian waters, irregular, wavy, very pronounced high-amplitude reflectors of limited extent and often crossing bedding planes are observed. These saucer-shaped reflectors have been interpreted as magmatic intrusions (sills) by Hansen *et al.* (2004), Planke *et al.* (2005), Hansen & Cartwright (2006) and Smallwood & Harding (2009).

The interpretation method used in the present study was first to interpret and map the surface of the basalt followed by interpretation of an intrabasaltic reflector that forms the base of unit 1. In the study area both the surface of the basalt and the lower boundary of unit 1 are regional surfaces that were almost horizontal at the time of formation. Therefore the seismic flattening technique on these boundaries was applied to eliminate the effects of later tectonic events and morphological expression on the lower lying units (Fig. 2). The top basalt reflector was flattened and the interpretation of the base unit 1 reflector was refined. Following this, the base unit 1 reflector was flattened. The flattening technique was used for all of the plane-parallel bedded basalt units. Below the plane-parallel bedded basalt units, the flattening technique was applied to the part of the units that was originally embedded horizontal. In this manner a total of six units were interpreted.

In places it was difficult to identify the base of the lower seismic units from later intruded sills that make up a large proportion of the reflections around the base of the succession (Naylor *et al.* 1999; Ellis *et al.* 2002). Applying the principles of saucer-shaped sills and the facility of working with 3D data, it was possible to carry out a detailed interpretation of the individual sills and thus to separate the intrusions from the background facies (Planke *et al.* 2005; Hansen 2006). Furthermore, working with 3D data it was possible to select optimal orientated seismic profiles for interpreting the individual seismic facies units. The detailed study of the facies units and their reflectors made it possible to establish the direction of foreset dip and thus interpret the local migration direction of lava-flows within the lowermost units, and to recognize and reconstruct the palaeocoastline in the southeastern part of the study area. Finally, the interpreted seismic reflectors were displayed as surfaces in a 3D visualization environment to increase the understanding of the geological evolution of the area.

Description of facies units

A typical seismic profile through the volcanic succession in the study area is found in Figure 2. The succession is divided into seismic facies units numbered from top to base. The thickness and outer shape of the units are illustrated in Figure 3, which shows the outline of the basalt facies units in a 3D perspective.

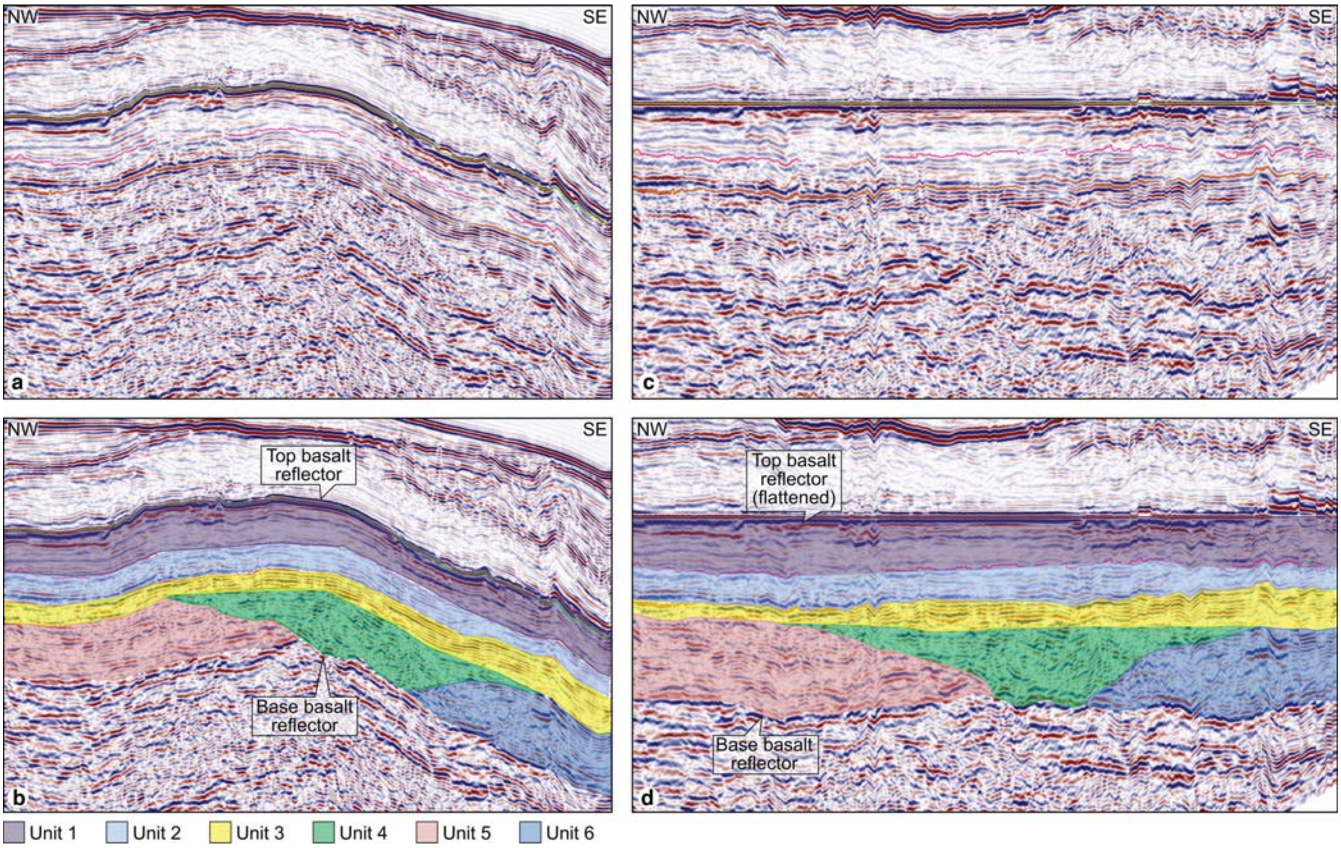

Fig. 2. Representative seismic crossline profile orientated NW–SE. (**a**) Seismic profile. (**b**) Seismic profile with interpreted units and top basalt and base basalt reflector indicated. (**c**) Seismic profile flattened to the surface of the basalt. (**d**) Seismic profile flattened to the surface of the basalt with interpreted units and top basalt and base basalt reflector indicated.

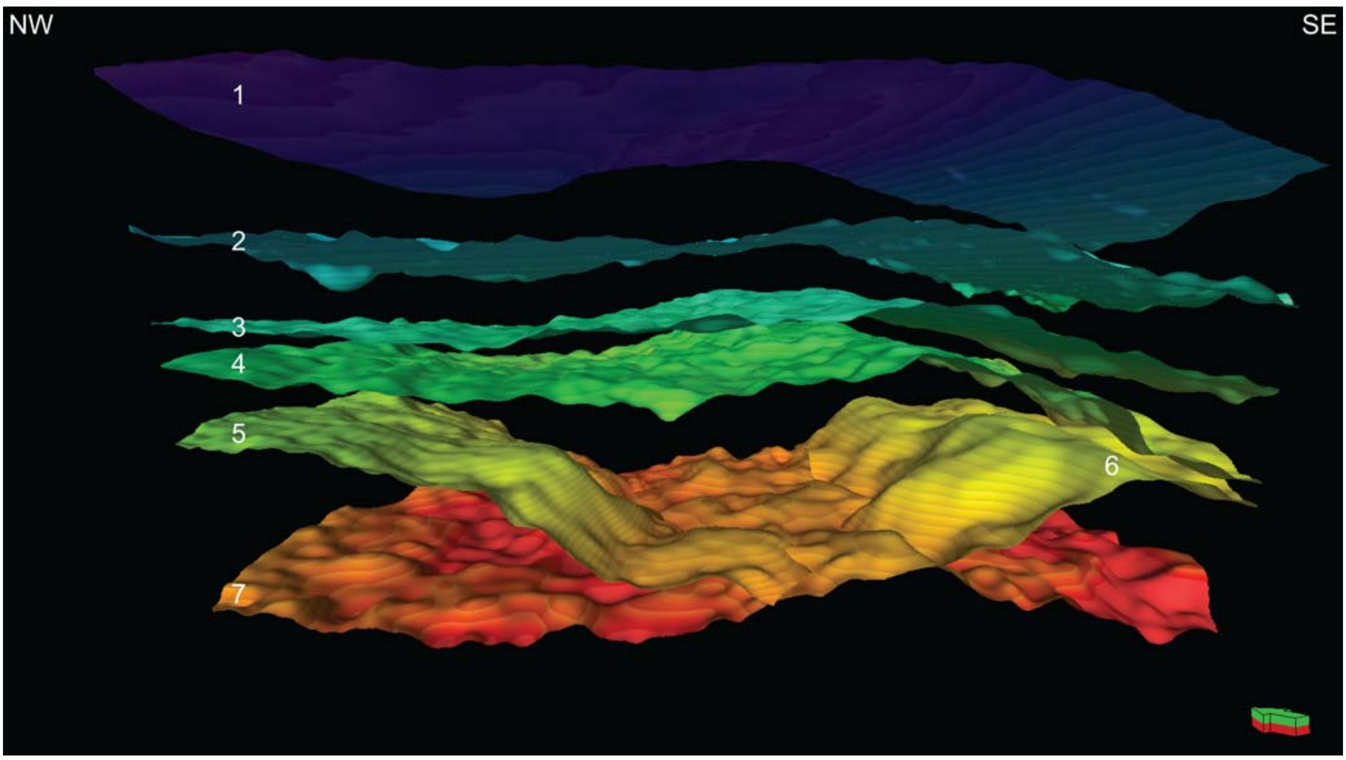

Fig. 3. Three-dimensional perspective of the interpreted unit boundaries including the top basalt and base basalt reflector. Colouring indicates depth. Numbers indicate top surfaces of units and number 7 indicates base basalt surface.

Facies unit 1. The upper boundary of unit 1 is a very distinct continuous reflector characterized by pronounced strong positive (hard kick) high amplitude. The reflector is smooth in appearance and very slightly undulating in the survey area, although the continuity of the reflector is broken at minor geographical places. At the base, unit 1 is defined by a continuous rather smooth, slightly undulating reflector with positive medium amplitude. The reflector parallels the top reflector, although slightly more irregular. The reflector and the internal bedding of unit 1 are broken at the same geographical locations as the top reflector. The internal reflection pattern is continuous with sub-parallel to partly irregular parallel reflections of medium amplitude. The external form of the unit seems to be sheet-like, but the unit extends outside the study area.

The upper boundary of the unit is interpreted as top basalt reflector (Ellis pers. comm. 2009; Fig. 2). Facies unit 1 experiences a rather constant thickness of approximately 800 m (Fig. 3). The unit is interpreted as subaerially parallel bedded platform facies erupted on an almost horizontal surface. In limited areas small changes in the internal pattern may indicate individual lava flows, or groups of lava flows, that stand out. The unit is widespread with the source area situated outside the study area.

Facies unit 2. The base of unit 2 is a positive (hard kick), partly broken reflector of medium to low amplitude (Fig. 2). In the southeastern part of the study area the reflector is smoother and more regular than in the northwestern part of the study area. In limited locations the base of unit 2 is not a pronounced reflector as the lowermost part of the units is almost reflection-free. Here the base of the unit is defined by the change in reflection pattern to unit 3. The internal reflector configuration is somewhat thicker and more faded as compared with unit 1, which could be a result of thinning of layers below seismic resolution. The internal reflection pattern of unit 2 consists of fairly continuous, partly irregular parallel to subparallel reflections of medium amplitude. The external form of the unit is a sheet that continues outside of the study area. The thickness is fairly constant at approximately 500 m (Fig. 3). Facies unit 2 belongs to the subaerially erupted parallel bedded platform facies that is emplaced over a large flat-lying area with the source area outside the study area. Within the upper part of unit 2 individual younger lava flows or groups of flows are seen to build out in limited locations. There is a slight change of the internal reflections pattern of unit 2 as compared with unit 1 that may indicate that unit 2 represents a change in style of eruption and thus there might have been a halt in lava production between units 1 and 2.

Facies unit 3. The base of unit 3 is defined by a low-amplitude negative (soft kick) reflector that in places is non-continuous (Fig. 2). In the southeastern part of the study area the reflector is easily followed. The lowermost part of the unit is nearly reflection-free, especially in the northwestern part of the study area, and here the base of unit 3 is defined by the change in reflection configuration between units 3 and 4. The internal reflection pattern consists of pronounced continuous, closely spaced plane-parallel reflections of medium amplitude in the northeastern part of the area. Gradually the pattern becomes less continuous towards the SW and furthest to the SW the pattern consists of irregular and broken sub-parallel reflections. The unit is cut by a small number of faults, most of which are located in the northwestern part of the study area. The external form of the unit is sheet-like and the unit extends out of the study area. The thickness is approximately 300 m but differs slightly, being thicker where the unit fills small depressions in the underlying surface (Fig. 3). Facies unit 3 belongs to the subaerially erupted parallel bedded platform facies and was extruded onto an almost flat land area. The unit spread out in thinner lava flows as compared with units 1 and 2.

Facies unit 4. The base of unit 4 is made up of three different reflectors as the unit fills in a basin (Fig. 2). In the NW the base of unit 4 is defined by a positive (hard kick) continuous reflector of medium to high amplitude that gradually dips towards the basin. The internal reflector pattern shows downlap onto the base reflector. In the SE the lower boundary of unit 4 is a positive (hard kick) fairly continuous reflector of medium to high amplitude that gradually dips towards the basin. The internal reflector pattern shows downlap towards the lower boundary. In the central part of the study area the lower boundary of unit 4 is defined by a very complex wavy negative (soft kick) reflector. In some locations the reflector is continuous with a high amplitude whereas in other locations the unit is nearly reflection-free and the lower boundary difficult to identify. The internal reflection configuration in unit 4 is mostly characterized by medium to low amplitude reflector segments that have a wavy chaotic pattern with little continuity. Analysing the unit in more detail, a number of smaller internal units are identified. The unit is easily distinguished from the underlying units 5 and 6 except for a few locations. The external form is a basin fill-form. The extent of the upper part of the unit goes beyond the study area. The thickness of unit 4 differs greatly throughout the study area and the maximum thickness is found in the central part of the study area, where it reaches approximately 800 m (Fig. 3). Facies unit 4 is ascribed to a hummocky basin-floor facies. It is suggested that unit 4 is subaquatically extruded and consists of a mixture of lava flows from various directions that have flowed out into a basin and here formed lava deltas (hyaloclastites). The basin extends out of the study area both to the north and south. After emplacement, unit 4 has been heavily influenced by intrusions.

Facies unit 5. Unit 5 is located in the northwestern part of the study area and its lower boundary is a very complex wavy negative (soft kick) reflector (Fig. 2). In places it is a high-amplitude continuous reflector whereas in other places the reflector is hard to distinguish as the unit here is nearly reflection-free. The internal reflection configuration is very complex as in most places the pattern shows downlap toward the lower boundary, whereas in minor areas it appears chaotic or reflection-free. Unit 5 mainly consists of a mixture of minor prograding sigmoid and complex sigmoid-oblique clinoforms, with reflections of medium to high amplitude, that dip from NW towards the SE (Figs 2 & 4). The external form of the unit is a sigmoid/complex sigmoid-oblique prograding clinoform where the northwestern part of the unit extends out of the study area (Fig. 3). The thickness of unit 5 differs between 650 and 1150 m as the unit is thickest in the SW and thins towards the NE. Unit 5 is made up of a large number of smaller units consisting of prograding clinoforms with a low inclination.

Facies unit 6. This unit is found beneath unit 4 in the southeastern part of the study area. The lower boundary is a very complex wavy negative (soft kick) reflector (Fig. 2). In places the reflector is continuous with a high amplitude whereas in other places the unit is nearly reflection-free and the boundary difficult to identify. The internal reflection configuration in unit 6 consists of medium-amplitude S-shaped prograding clinoforms prograding from the SE towards the NW. In some places the configuration is rather chaotic and the S-shaped clinoforms can be difficult to distinguish from one another and it is difficult to see whether the clinoforms are sigmoid, complex sigmoid-oblique or oblique. A careful analysis of the internal reflector configuration reveals that a large number of smaller units can be outlined that mostly dip to the NW, although at the outer parts of unit 6 the flows show various directions (Fig. 4). The external form of unit 6 is a sigmoid-oblique prograding clinoform and the southeastern part of the unit extends beyond

Fig. 4. Facies map of units 5 (purple colour) and 6 (grey colour) showing the locations of main prograding subunits and direction of movement.

the study area. The thickness of unit 6 varies but is largest in the southeastern part of the study area. The internal reflection pattern of the unit is more regular than unit 5 and the maximum thickness of the unit is approximately 800 m (Fig. 3). Breakpoints on the prograding clinoforms are mapped and thus it is possible to construct the extent of a palaeocoastline. Unit 6 shows almost ideal sigmoid-oblique clinoforms as opposed to unit 5 and it is suggested that unit 6 consists of a mixture of lava and sedimentary deposits that alternately prograded across an existing coastline. The unit has been intruded by younger intrusions, for example, sills or dykes.

'Base volcanic reflector' and subvolcanic unit. The 'base volcanic reflector' is interpreted as a composed surface corresponding to the base of volcanic units 4–6. It is a very complex wavy negative (soft kick) reflector that is disrupted by intrusions and faults (Figs 2 & 3). The reflector is generally characterized by downlap of younger reflectors and reflector segments, as illustrated by flattening of the surface of the parallel bedded basalt units (Fig. 2). The reflector is in places distinct and continuous with high amplitude, whereas it is hard to identify the reflector in other locations as the overlying unit is nearly reflection-free. Flattening to the surface of basalt unit 1 reveals that the 'base volcanic reflector' in places undulates as it drapes minor highs and lows. Beneath the 'base volcanic reflector' the reflection pattern changes are pronounced and the internal reflector pattern of the underlying units resembles what is usually interpreted as sedimentary, faulted units (Fig. 2). In the northwestern part of the investigated area below unit 5 the internal reflector pattern consists of reflectors of medium amplitude that show dip to the SE. The reflector pattern between the uppermost of these inclined reflectors and the base basalt onlaps towards an inclined reflector. Beneath unit 6 in the southwestern part of the study area pronounced strong diverging reflectors of slightly wavy appearance are found that originate in the SE and dip to the NW. Below unit 4 the seismic signal is incoherent and this, in addition to the large amount of sills, makes it hard to interpret the geological succession below the basin fill.

Intrusions. On the majority of the seismic profiles intrusions are mainly identified in the level of the base of the volcanic succession. The intrusions are seen as pronounced high-amplitude continuous positive (hard kick) reflectors that on the individual inlines and crosslines are arc shaped and exhibit a limited extent. Using 3D display facility it is seen that the intrusions are individual reflectors that are saucer-shaped and have a characteristic behaviour similar to what was reported by Planke *et al.* (2005) and Hansen (2006). Analysing the intrusions in detail it is found that in places the intrusions are connected and this probably indicates that they have been fed from the same source, similar to the findings of Smallwood & Harding (2009).

Analogues

Onshore analogues to the parallel bedded basalt, inclined basalt flows and hyaloclastites are found at various volcanic provinces around the world. To present an analogue to the seismic study, a comparison with the nearby geographical area of the Faroe Islands and West Greenland, which was extruded within the same time frame, is suggested (Rasmussen & Noe-Nygaard 1970; Pedersen *et al*. 2006; Passey 2007). Based on photogrammetry of the south coast of Nuussuuaq, west Greenland, five detailed geological maps have been constructed (Pedersen *et al.* 2006) that show a similar setting as revealed from the present seismic study. The volcanic succession is more than 2 km thick and consists of plane-parallel bedded basalt flows, hyaloclastites and foreset beds exposed on a scale that is similar to seismic resolution. At Nuussuuaq, plane-parallel basaltic lava-flows in association with sediments can be shown to have prograded into a more than 700 m deep marine basin, creating a basin-fill mixture of hyaloclastites and sediments (Pedersen & Dueholm 1992). Above this succession plane-parallel bedded lava flows are found. On the Faroe Islands the Lopra-1/1A well encountered the transition from subaerial extruded plane-parallel bedded lava flows to the hyaloclastites, and downhole wireline logs measured in the entire hole form an important dataset for studying the plane-parallel bedded basalt in the Beinisvørð Formation and the transition to the hyaloclastites in the Lopra Formation. From the interpretation of the wireline logs it is found that the petrophysical properties of the basalt succession in the borehole change drastically from hyaloclastites to plane-parallel bedded lava flows, especially in relation to P-wave velocity, density and porosity, which make an important contribution to the seismic expression of basalts belonging to the hyaloclastites and plane-parallel bedded facies (Boldreel 2006). This means that the transition from plane-parallel bedded basalt to hyaloclastites is characterized by a negative reflection coefficient (soft kick) which was also seen from the interpretation of the VSP survey of the Lopra-1 well (Kiørboe & Petersen 1995). From the UK part of the Faroe–Shetland Channel, a seismic modelling study was carried out in which results from the interpretation of wireline logs in released wells were used as input and released 2D reflection seismic profiles were used for comparison. The study showed that the overall seismic expression of hyaloclastites and parallel bedded basalt could be produced (Hansen 2007).

Geological development of the area

Findings from the detailed interpretation of a 3D digital reflection seismic survey using principles of seismic stratigraphy, flattening technique to selected reflectors and 3D visualization technique combined with 2D seismic reflection studies in the region and released wells and analogy studies to the Faroe Islands and West Greenland, have proposed the following geological evolution of the study area (Fig. 5a–f).

(a) The oldest identified unit in this study shows a negative reflection coefficient (soft kick) at the transition to the overlying volcanic succession (units 4–6), which means a unit characterized by a predominately lower velocity than the oldest volcanic succession. The unit shows a strong resemblance to a sedimentary succession with indications of highs and basins offset by faults. It is known that sedimentary successions are present below the flood basalts at the edge of the basalt covered region in the Faroe–Shetland Channel and thus it could be concluded that a sedimentary succession is present beneath the volcanic unit in the study area.

(b–d) In the northwestern part of the survey area reflectors show onlap towards older inclined reflectors in the lowermost part of the volcanic succession (unit 5). Further to the SE, the unit that contains the dipping reflectors diminishes and becomes less inclined. Unit 5 is made up of minor prograding sigmoid and complex sigmoid-oblique clinoforms that extend from NW to SE. Unit 5 seems not to be truncated at the upper boundary. The fronts of a large number of prograding subunits within unit 5 have been mapped (Fig. 4) and suggest that the lava flows of unit 5 prograded in a southeastern direction. It is suggested that unit 5 consists of minor basalt flows of northwestern source that gradually build out into a water-covered area. The outer parts of unit 5 gradually build out as a lava delta (hyaloclastite) in the basin and interfinger laterally and vertically with unit 6. The geographic change in the inclination may indicate the outer basinward part of subaerial extruded basalt, and this implies that subaerial extruded plane-parallel bedded basalt or units of basalt foresets are present in the direction towards the Faroe Islands, as suggested by Ellis *et al.* (2002). The lack of truncation at the upper level suggests that the relative sea-level rose following the eruption of unit 5.

In the southeastern part of the study area, part of a lava delta named unit 6 is found. The delta builds out from the SE towards the NW, crossing an existing coastline. The detailed interpretation of the lava delta reveals that unit 6 consists of an alternating sigmoid and oblique prograding facies constructed of subaerially extruded basalt that entered an aquatic environment. It is not possible to judge if unit 6 is truncated at the upper level or whether the uppermost part consists of thin basalt flows below seismic resolution. If truncation has occurred, this would imply that erosion took place before a relative sea-level rise prior to the emplacement of unit 4. If truncation did not take place this probably implies that subsidence took place and that the relative sea-level rose prior to the eruption of unit 4. Within unit 6 the fronts of a large number of prograding subunits have been identified and mapped (Fig. 4) and this shows that the direction of progradation of unit 6 is variable in that the main part of the flows prograded from the SE towards the NW, although flows originating from south, SSE and SW are also identified. The outer parts of unit 6 gradually build out as a lava delta in the basin and interfinger laterally and vertically with unit 5. It is not possible from the data available to this study to judge if units 5 and 6 are of the same origin. The basin between units 5

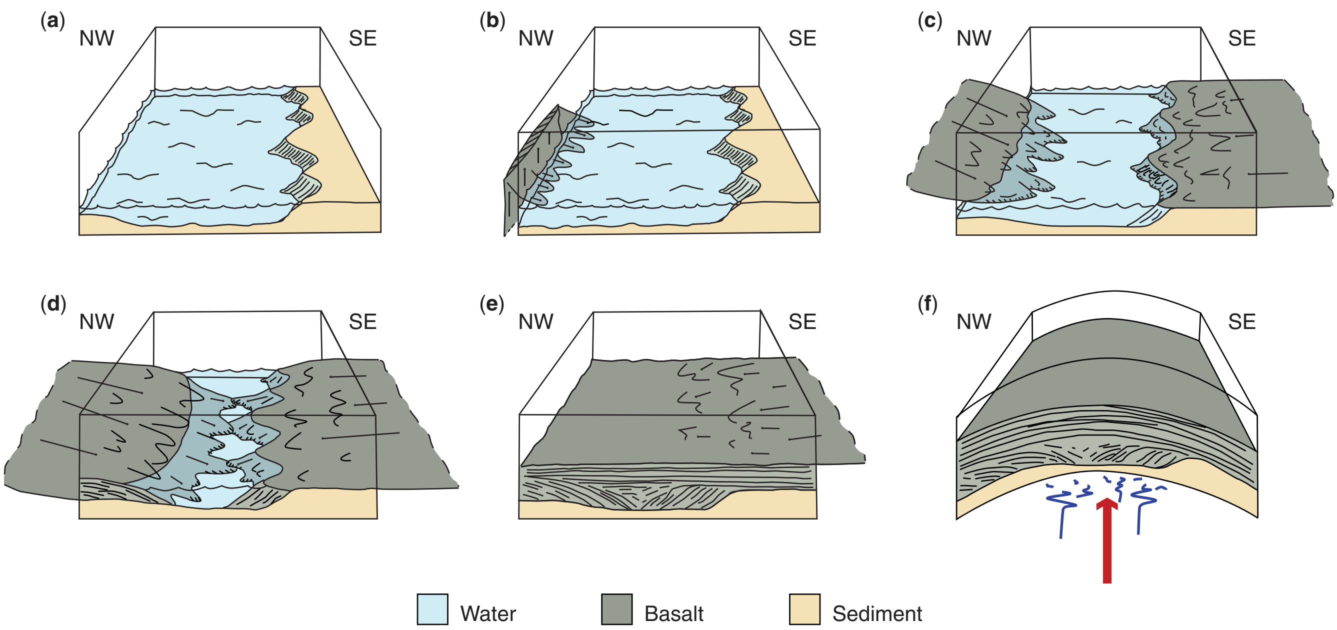

Fig. 5. Geological model for the study area. (**a**) Seismic mapping indicates that there is a basin underneath the volcanic succession in the study area. (**b-d**) At the beginning of volcanism lava flowed into the basin forming two prograding units – one from the NW (interpreted unit 5) and one from the SE (interpreted unit 6). (**e**) After filling up the basin (interpreted unit 4) the volcanism dominantly came from the SE, covering the lava filled basin with plane-parallel bedded basalts (interpreted units 3–5). (**f**) After the volcanism ceased, the area and the volcanic succession underwent differential subsidence and was subject to compression bending the volcanic succession. Blue lines indicate sill intrusions.

and 6 extends outside the data coverage. The time relation between units 5 and 6 cannot be unravelled for sure but, as the tops of units 5 and 6 are at a similar depth interval, it is suggested that units 5 and 6 are within the same time frame.

In the central part of the study area unit 4 is located geographically between units 5 and 6. The internal reflector pattern of unit 4 suggests that it consists of hyaloclastites deposited in a lava delta that entered the basin from various directions and gradually filled the basin.

(e) Unit 3 consists of thin plane-parallel bedded lava flows. The unit is most distinct and well developed in terms of internal configuration in the southeastern part of the studied area and the unit thins towards the NW. Detailed interpretation and visualization technique shows that small internal units prograde from SE to NW and that the lower part of unit 3 fills in minor lows. It is suggested that unit 3 is subaerially extruded onto a dry landscape and that the surface of the underlying unit has been exposed to weathering and erosion, indicating that a pause in eruption to the underlying unit is likely. The thickness variation of the unit and the direction of progradation of the small internal units strongly indicate that unit 3 originated from the SE outside the study area.

The internal reflector pattern in units 1 and 2 is plane-parallel bedded basalt flows and the units are very much alike. The units are separated by a pronounced reflector of positive reflection coefficient (hard kick). The internal configuration of the basalt unit indicates that the lava flows of units 1 and 2 are thicker than those in unit 3 and the thickness of both units decreases towards the SE. In the southeastern part of the study area it is seen that the lowermost part of unit 2 in places onlaps unit 3 towards the SE. It is found that units 1 and 2 are subaerial extruded basalt flows that originated from a (north) western direction and that there seems to have been a pause between the extrusions of the units, represented by the pronounced reflector.

(f) After the volcanism ceased, sedimentation took place first from the east and later on from the west, as is well known from a number of studies. The area and the volcanic succession underwent differential subsidence in the area and was subject to compression that bent the succession (e.g. Boldreel & Andersen 1993). From the use of 3D data it is found that a large number of faults offset the volcanic succession and this further complicates the interpretation of both the lower part of the volcanic succession and the sedimentary succession found below.

Sills are found to have intruded into units 4–6, that is, the lower part of the volcanic succession. The studied area is located close to the main sill complex of likely Early Eocene age where a sill has been dated as Early Eocene (Smallwood & Harding 2009), and as the behaviour of that finding is similar to the sills in the present study, it is suggested that the sills identified in the present study are of Early Eocene age. From the present seismic interpretation it is suggested that the sills were intruded either at a similar time to the eruption of units 4–6 or by later tectonic activity, but according to Smallwood & Harding (2009) it is most likely that the sills were intruded in Early Eocene, which corresponds to the uppermost part of the Beinsvørð Formation or the younger basalt formations (Ellis *et al.* 2009).

From the seismic interpretation it is found that the internal reflector patterns and identified minor escarpments in units 6 and 3 indicate that these two basaltic units originated from a (south) eastern direction within the study area whereas units 5, 4, 2 and 1 mainly originated from a (north) western direction as expected and illustrated from various papers (e.g. Ellis *et al.* 2009). It may seem that units 6 and 3 are sourced from a different area from the remaining basaltic units within the data coverage area as unit 4 fills in a basin area that extends outside the study area. The two units may have been emplaced from fissures or a volcano located further to the east of the study area. From the work of Ellis *et al.* (2009, fig. 3) it is indicated that lava is present on the eastern side of the Faroe–Shetland area but the published literature does not mention fissures or volcanoes located close to the eastern part of the studied area. This seems to indicate that the basin that was filled by unit 4 may have been an embayment and thus the basalt flows originated from a western to northwestern source and part of the flows were directed towards the basin area and part flowed on land to the other side of the embayment, from where the flows thus entered the basin from an easterly direction. From the data used in the present study, the validity of the two scenarios cannot be judged.

Conclusion

A detailed interpretation on a recently acquired 3D reflection seismic survey in a basalt-covered area SE of the Faroe Islands has been carried out. Based on seismic stratigraphic principles, the use of flattening of original horizontally embedded lava flows and 3D visualization software, a new approach to interpreting seismic data in basalt-covered regions is proposed (Fig. 2). In addition, knowledge from onshore exposed volcanic successions from west Greenland and information from the interpretation of wireline log data in basalt covered areas west of Shetland and on the Faroe Islands gives valuable geological information that can be evaluated in view of seismic resolution.

We divided the volcanic succession into six seismic facies units. The lowermost two facies units represent two individual successions building out from the NW and SE, respectively, on a landmass into a water-covered basin where the two volcanic successions form the flanks of the basin. The outer parts of the individual flows within the units interfinger with each other in the basin.

Following the emplacement of the two units the basin was gradually filled up and the following unit was clearly subaerially parallel bedded basalt extruded from the SE. The youngest two units consist of parallel bedded basalt flows that were subaerially extruded from the NE.

It is proposed that the 'base volcanic reflector' is not located at the base of the parallel bedded basalts, but is found at a greater depth where it reflects the base of lava deltas (hyaloclastites) formed in a basin. This implies that only in regions where lavas flowed onto dry land is the base basalt reflector located at the lower boundary of the parallel bedded basalt succession.

Sills have been identified by careful interpretation of the seismic data using the possibility of choosing optimal orientated profiles and inspecting the data in a 3D visualization software. In this manner it was found that the sills are saucer-shaped and often part of a common feeder system.

Below the volcanic succession a sedimentary succession is suggested to be present with indications of highs and basins offset by faults. It is suggested that the proposed interpretation technique is a valuable tool for interpreting reflection seismic data east of the Faroe Islands and in other basalt-covered regions.

We are grateful for the support from 006 Licence partners Statoil, Atlantic Petroleum and Dong Energy for putting the seismic data at our disposal and for the permission to publish part of the study. The manuscript benefited from critical reviews by Simon Passey and an anonymous referee. The interpretations and conclusions expressed, however, are the sole responsibility of the authors and do not necessarily reflect the views of all the Partners.

References

Andersen, M. S., Egerton, P. D., Hitchen, K. & Boldreel, L. O. 2007. Seismic facies analysis of volcanic sequences offshore the British Isles and the Faroes. *Evolution of Basaltic Provinces, 1st Jóannes Rasmussen Conference on the Faroe Islands*, August 2007, Extended Abstract.

Andersen, M. S., Boldreel, L. O. & SeiFaBa Group. 2009. Log responses in basalt successions in 8 wells from the Faroe–Shetland Channel – a classification scheme for interpretation of geophysical logs and case studies. *In*: Varming, T. & Ziska, H. (eds) *Faroe Island Exploration Conference Proceedings of the 2nd Conference*, 364–391. Føroya Fróðskaparefelag, The Faroese Academy of Sciences. *Annales Societatis Scientiarum Færoensis Supplementum*, **50**, Tórshavn.

Boldreel, L. O. 2006. Wire-line log-based stratigraphy of floodbasalts from the Lopra-1/1A well, Faroe Islands. *In*: Chalmers, J. A. & Waagstein, R. (eds) *Scientific Results from the Deepened Lopra-1 Borehole, Faroe Islands*. Geological Survey of Denmark and Greenland Bulletin, **9**, 7–22.

Boldreel, L. O. & Andersen, M. S. 1993. Late Paleocene to Miocene compression in the Faroe-Rockall Area. *In*: Parker, P. J. R. (ed.) *Petroleum Geology of Northwest Europe: Proceedings of the 4th Conference*. Geological Society, London, 1025–1034; doi: 10.1144/0041025.

Boldreel, L. O. & Andersen, M. S. 1994. Tertiary development of the Faroe–Rockall Plateau based on reflection seismic data. *Bulletin of the Geological Society of Denmark*, **41**, 162–180.

Boldreel, L. O., Neish, J. K. & Ziska, H. 1996. Exploration of the Faroes region: seismic images beneath a basalt province. *American Association of Petroleum Geologists Bulletin*, **80**. Abstract; doi: 10.1306/64EDA596-1724-11D7-8645000102C1865D.

Eccles, J. D., White, R. S., Christie, P. A. F., Roberts, A. W. & iSIMM Team. 2009. Insight into sub-basalt lithology from wide-angle converted shear wave analysis. *In*: Varming, T. & Ziska, H. (eds) *Faroe Islands Exploration Conference Proceedings of the 2nd Conference*, **226**, 43–60. Føroya Fróðskaparefelag, The Faroese Academy of Sciences. *Annales Societatis Scientiarum Færoensis Supplementum*, **50**, Tórshavn.

Ellis, D., Bell, B. R., Jolley, D. W. & O'Callaghan, M. 2002. The stratigraphy, environment of eruption and age of the Faroes Lava Group, NE Atlantic Ocean. *In*: Jolley, D. W. & Bell, B. R. (eds) *The North Atlantic Igneous Province: Stratigraphy, Tectonic, Volcanic and Magmatic Processes*. Geological Society, London, Special Publications, **197**, 253–269.

Ellis, D., Passey, S. R., Jolley, D. W. & Bell, B. R. 2009. Transfer zones. The application of new geological information from the Faroe Islands applied to the offshore exploration of intra and sub-basalt strata. *In*: Varming, T. & Ziska, H. (eds) *Faroe Islands Exploration Conference, Proceedings of the 2nd Conference*, 205–226. Føroya Fróðskaparefelag, The Faroese Academy of Sciences. *Annales Societatis Scientiarum Færoensis Supplementum*, **50**, Tórshavn.

Gallagher, J. W. & Dromgoole, P. W. 2007. Exploring below the basalt, offshore Faroes: a case history of sub-basalt imaging. *Petroleum Geoscience*, **13**, 213–225.

Gallagher, J. W. & Dromgoole, P. W. 2009. Sub-basalt seismic imaging-offshore Faroes. *In*: Varming, T. & Ziska, H. (eds) *Faroe Islands Exploration Conference Proceedings of the 2nd Conference*, 319–332. Føroya Fróðskaparefelag, The Faroese Academy of Sciences. *Annales Societatis Scientiarum Færoensis Supplementum*, **50**, Tórshavn.

Gatliff, R. W., Hitchen, K., Ritchie, J. D. & Smythe, D. K. 1984. Internal structure of the Erland Tertiary volcanic complex north of Shetland, revealed by seismic reflection. *Journal of the Geological Society*, **141**, 555–562.

Hald, N. & Waagstein, R. 1984. Lithology and geochemistry of a 2-km sequence of lower Tertiary tholeiitic lavas drilled on Suduroy, Faroe Islands (Lopra-1). *In*: Bertelsen, O., Noe-Nygaard, A. & Rasmussen, J. (eds) *The Deep Drilling Project 1980–1981 in the Faroe Islands*. Føroya Frodskaparfelag, Torshavn, 13–38.

Hansen, D. M. 2006. The morphology of intrusion-related vent structures and their implications for constraining the timing and intrusive events along the NE Atlantic margin. *Journal of the Geophysical Society, London*, **163**, 789–800.

Hansen, T. J. A. 2007. *Investigation of basalts east of the Faroe Islands, using geophysical logs and seismic methods*. Unpublished MSc thesis in Danish (abstract in English), University of Copenhagen, Institute of Geology.

Hansen, D. M. & Cartwright, J. A. 2006. Saucer-shaped sill with lobate morphology revealed by 3D seismic data: implications for resolving a shallow level sill emplacement mechanism. *Journal of the Geological Society*, **163**, 509–523.

Hansen, D. M., Cartwright, J. A. & Thomas, D. 2004. 3D seismic analysis of the geometry of igneous sills and sill junction relationships. *In*: Davis, R. J., Stewart, S. A., Cartwright, J. A., Lappin, M. & Underhill, J. R. (eds) *3D Seismic Technology: Application to the Exploration of Sedimentary Basins*. Geological Society, London, Memoirs, **29**, 199–208.

Heinesen, M. V. 1987. *Nedre tertiære basalt breccier og undervandslavastrømme, sydlige Disko, Vestgrønland. Strukturelle, petrografiske og mineralogiske studier*. Unpublished MSc thesis in Danish. University of Copenhagen, Institute of Geology.

Hopper, J. R., Dahl-Jensen, T. *et al*. 2003. Structure of the SE Greenland margin from seismic reflection and refraction data: implications for nascent spreading center subsidence and asymmetric crustal accretion during North Atlantic opening. *Journal of Geophysical Research*, **108**, 2269.

Jerram, D. A. 2002. Volcanology and facies architecture of flood basalts. *In*: Menzies, M. A., Klemperer, S. L., Ebinger, C. J. & Baker, J. (eds) *Volcanic Rifted Margins*. Geological Society America, Boulder, CO, Special Papers, **362**, 119–132.

Jones, J. G. & Nelson, P. H. H. 1970. The flow of basalt lava from air into water – its structural expression and stratigraphic significance. *Geological Magazine*, **107**, 13–19.

Kiørboe, L. & Petersen, S. A. 1995. *Seismic Investigation of the Faeroe Basalts and their Substratum.* Geological Society, London, Special Publications **90**, 111–123.

Larsen, L. M., Waagstein, R., Pedersen, A. K. & Storey, M. 1999. Trans-Atlantic correlation of the Paleogene volcanic successions in the Faroe Islands and East Greenland. *Journal of the Geological Society, London*, **156**, 1081–1095.

Leathard, M., McHugo, S. & Hoare, R. 2009. Imaging below Faroese Basalts using over/under acquisition. *In*: Varming, T. & Ziska, H. (eds) *Faroe Islands Exploration Conference, Proceedings of the 2nd Conference*, 61–66. Føroya Fróðskaparefelag, The Faroese Academy of Sciences. *Annales Societatis Scientiarum Færoensis Supplementum*, **50**, Tórshavn.

Naylor, P. H., Bell, B. R., Jolley, D. W., Durnall, P. & Fredsted, R. 1999. Paleogene magmatism in the Faroe–Shetland Basin: influences on uplift history and sedimentation. *In*: Fleet, A. J. & Boldy, S. A. R. (eds) *Petroleum Geology of North West Europe: Proceedings of the 5th Conference*, 545–558; doi: 10.1144/0050545.

Nelson, C. E., Jerram, D. A., Single, R. T. & Hobbs, R. W. 2009. Understanding the facies architecture of flood basalts and volcanic rifted margins. *In*: Varming, T. & Ziska, H. (eds) *Faroe Islands Exploration Conference, Proceedings of the 2nd Conference*, 84–103. Føroya Fróðskaparefelag, The Faroese Academy of Sciences. *Annales Societatis Scientiarum Færoensis Supplementum*, **50**, Tórshavn.

Nielsen, L., Boldreel, L. O. & Surlyk, F. 2004. Ground-penetrating radar imaging of carbonate mound structures and implications for interpretation of marine seismic data. *American Association of Petroleum Geologists Bulletin*, **88**, 1069–1082.

Passey, S. R. 2004. *The volcanic and sedimentary evolution of the Faroe Plateau Lava Group, Faroe Islands and the Faroe–Shetland basin, NE Atlantic*. PhD thesis, University of Glasgow.

Passey, S. R. 2007. Geological field guide to the central and north-eastern Islands, Faroe Islands. *Basaltic Plains Volcanism and Sedimentation. 1st Jóannes Rasmussen Conference: Evolution of Basaltic Provinces*, 28 August 2007, Jarðfeingi.

Passey, S. R. 2009. Recognition of a faulted basalt lava flow sequence through the correlation of stratigraphic marker units, Skopunarfjørdur, Faroe Islands. *In*: Varming, T. & Ziska, H. (eds) *Faroe Islands Exploration Conference Proceedings of the 2nd Conference*, 174–204. Føroya Fróðskaparefelag, The Faroese Academy of Sciences. *Annales Societatis Scientiarum Færoensis Supplementum*, **50**, Tórshavn.

Passey, S. R. & Bell, B. R. 2007. Morphologies and emplacement mechanisms of the lava flows of the Faroe Islands Basalt Group, Faroe Islands, NE Atlantic Ocean. *Bulletin of Volcanology*, **70**, 139–156.

Passey, S. R., Jolley, D. W. & Bell, B. R. 2006. Lithostratigraphic framework for the Faroe Islands Basalt Group, NE Atlantic. *A George P. L.*

Walker Symposium on Advances in Volcanology, 12–17 June, Reykholt, Iceland.

Peate, I. U., Larsen, M. & Lesher, C. E. 2003. The transition from sedimentation to flood volcanism in the Kangerlussuaq Basin, East Greenland: basaltic pyroclastic volcanism during initial Paleogene continental break-up. *Journal of the Geological Society, London*, **160**, 759–772.

Pedersen, A. K. & Dueholm, K. S. 1992. New methods for the geological analysis of Tertiary volcanic formations on Nuussuaq and Disko, central West Greenland, using multi-model photogrammetry. *In*: Dueholm, K. S. & Pedersen, A. K. (eds) *Geological Analysis and Mapping Using Multi-model Photogrammetry*. Rapport Grønlands Geologiske Undersøgelse, **156**, 19–34.

Pedersen, A. K., Larsen, L. M., Pedersen, G. K. & Dueholm, K. S. 2006. Five slices through the Nuussuaq Basin, West Greenland. *Geological Survey of Denmark and Greenland Bulletin*, **10**, 53–56.

Planke, S. 1994. Geophysical response of flood basalts from analysis of wire-line logs. Ocean Drilling Program Site 642, Vøring volcanic margin. *Journal of Geophysical Research*, **99**, 9279–9296.

Planke, S. & Eldholm, O. 1994. Seismic response and construction of seaward dipping wedges of flood basalts: Vørring volcanic margin. *Journal of Geophysical Research*, **99**, 9263–9278.

Planke, S., Alvestad, E. & Eldholm, O. 1999. Seismic characteristics of basaltic extrusive and intrusive rocks. *The Leading Edge*, **18**, 342–348.

Planke, S., Symmonds, P. A., Alvestad, E. & Skogseid, J. 2000. Seismic volcanostratigraphy of large-volume basaltic extrusive complexes on rifted margins. *Journal of Geophysical Research*, **105**, 19335–19351.

Planke, S., Rasmussen, T., Rey, S. S. & Myklebust, R. 2005. Seismic characteristics and distribution of volcanic intrusions and hydrothermal vent complexes in the Vøring and Møre basins. *In*: Doré, A. G. & Vining, B. A. (eds) *Petroleum Geology: North-West Europe and Global Perspectives. Proceedings of the 6th Petroleum Geology Conference*, 883–844; doi: 10.1144/0060883.

Rasmussen, J. & Noe-Nygaards, A. 1969. Beskrivelse til geologiske Kort over Færøerne. *Geological Survey of Denmark* I, series 24.

Rasmussen, J. & Noe-Nygaard, A. 1970. Geology of the Faroe Islands. *Danmarks Geologiske Undersøgelser* I, serie 25.

Rasmussen, J. & Noe-Nygaard, A. 1990. The origin of the Faroe Islands. Ministry of the Environment, Geological Survey of Denmark.

Ritchie, J. D., Gatliff, R. W. & Richards, P. C. 1999. Early Tertiary magmatism in the offshore NW UK margin & surrounds. *In*: Fleet, A. J. & Boldy, S. A. R. (eds) *Petroleum Geology of North-West Europe: Proceedings of the 5th Conference*, 573–584; doi: 10.1144/0050573.

Saunders, A. D., Fitton, J. G., Kerr, A. C., Norry, M. J. & Kent, R. W. 1997. The North Atlantic igneous province. *In*: Mahoney, J. J. & Coffin, M. L. (eds) *Large Igneous Provinces: Continental, Oceanic and Planetary Flood Volcanism*. American Geophysical Union, Geophysical Monographs, **100**, 45–93.

Smallwood, J. R. & Harding, A. 2009. New seismic imaging methods, dating, intrusion style and effects of sills: a drilled example from the Faroe-Shetland Basin. *In*: Varming, T. & Ziska, H. (eds) *Faroe Islands Exploration Conference Proceedings of the 2nd Conference*, 104–123. Føroya Fróðskaparefelag, The Faroese Academy of Sciences. *Annales Societatis Scientiarum Færoensis Supplementum*, **50**, Tórshavn.

Varming, T. 2009. Results from drilling of the 1st license round wells in the Faroese part of Judd Basin. *In*: Varming, T. & Ziska, H. (eds) *Faroe Islands Exploration Conference Proceedings of the 2nd Conference*, 346–363. Føroya Fróðskaparefelag, The Faroese Academy of Sciences. *Annales Societatis Scientiarum Færoensis Supplementum*, **50**, Tórshavn.

Waagstein, R. 1988. Structure, composition and age of the Faroe basalt plateau. *In*: Morton, A. C. & Parson, L. M. (eds) *Early Tertiary Volcanism and the Opening of the NE Atlantic*. Geological Society, London, Special Publications, **39**, 225–238.

Waagstein, R. 1996. Early Tertiary volcanism in the Faroe region and the initiation of the North Atlantic mantle plume. *International Lithosphere Programme*, August–September, Tórshavn, Faroe Islands.

Exploring for gas: the future for Angola

C. A. FIGUEIREDO,[1] L. BINGA,[1] J. CASTELHANO[1] and B. A. VINING[2]

[1]*Sonangol Gas Natural, Av. Lenin no. 58, 5/6 Andar, Luanda, Angola (e-mail: carlos.a.figueiredo@sonangol.co.ao)*
[2]*Gaffney, Cline & Associates, Bentley Hall, Blacknest, Alton GU34 4PU, UK*

Abstract: Offshore Angola is a world-class petroleum province with oil production in excess of 2 million barrels per day in 2008. Exploration activity in the offshore commenced in earnest in the early 1990s, with the contractual terms permitting only the production of oil. There is no provision for the production of gas. However, there have been several discoveries of associated and non-associated gas, by accident, in the search for oil. Gas will play a significant role in the future of Angola. A new gas business is emerging. Demand from a new liquefied natural gas (LNG) plant, the emerging Soyo industrial complex and the growing domestic and industrial sectors have created a business environment whereby near-term gas exploration, development and production is a critical need for the future of Angola. What is the gas resource potential of Angola: from mature basins to new frontiers? Is there potential for new giant gas fields? Conceivably, there are multiple petroleum system opportunities. This paper provides some insights into the petroleum geoscience exploration efforts being made by Angola's national gas company, Sonangol Gas Natural. The focus of this paper will be on the exploration for non-associated gas. The associated gas potential of Angola is relatively well known and will not be discussed. Sonangol Gas Natural has an extensive offshore seismic and well database. This is characterized by a series of merged, high-quality 3D seismic surveys that facilitate the application of the most advanced technologies. In excess of 130 offshore wells have encountered gas at multiple stratigraphic levels. However, the interior basins are a truly frontier province and data are limited to a regional gravity and magnetic dataset and surface rock outcrops. The conventional thermogenic petroleum systems of the offshore and the adjacent onshore Lower Congo, Kwanza/Benguela and Namibe basins are relatively well known. These comprise a Late Cretaceous and Cenozoic post-salt petroleum system, and an Early Cretaceous and Late Jurassic pre-salt petroleum system. The primary emphasis of the exploration effort in these basins is to better understand and to delineate the gas kitchens for the known source horizons, for example Malembo, Iabe (post-Aptian salt) and Bucomazi (pre-Aptian salt) formations. Biogenic gas plays constitute an unconventional petroleum system that requires different exploration concepts from those of conventional thermogenic petroleum systems. The principal challenges are to identify palaeo-gas hydrates, reservoired in Miocene clastics, to define the biogenic gas fairway and to evaluate the play elements of reservoir, trap and seal. The geological conditions necessary to establish a biogenic gas play in the deepwater and ultra-deepwater will be examined. The interior Owambo, Okawango and Kassanje Basins have no proven petroleum systems. However, some new play concepts of Neoproterozoic age will be presented using possible analogues worldwide. The future demand for gas will increase globally. New developments in LNG will change the world of gas. Angola will be a key player.

Keywords: gas, biogenic, petroleum systems, Angola

Exploration for gas in Angola is only now commencing in earnest. However, Angola has long been known as a hydrocarbon province. In 1767, 59 barrels of viscous oil were exported to Lisbon. The first exploration well, Dande-1, was drilled in 1915 to a total depth of 602 m, but was a dry hole. There then followed a period of 40 years when 30 exploration wells were drilled in the onshore Kwanza Basin, before the first commercial oil discovery, the Benfica field, close to the capital Luanda, was made in 1955 by Missao de Pesquisa de Petroleos, an affiliate of the Belgian Petrofina group. Subsequently, exploration activity proceeded principally onshore and focused in the Cabinda area. The first offshore well, 96-1X, was drilled in 1966, resulting in the discovery of the Limba field.

The state oil company, Sonangol, was formed in 1978 and actively participated in 2D seismic acquisition and later drilling and oil production. The award of offshore licence blocks commenced in 1980 in the shallow waters (less than 200 m water depth) in the Lower Congo Basin. The contractual terms permitted only the production of oil. There was no provision for the production of gas. Exploration activity in shallow waters continued to increase in pace throughout the 1980s with discoveries in the Cretaceous Albian, Pinda carbonates and Cenomanian clastics. Deepwater exploration (between 200 and 2000 m water depth) commenced in 1993 with the award of Blocks 16 and 17 in the Lower Congo Basin followed by the award of other deepwater blocks in the mid-1990s. The first well in deepwater, Bengo-1 in 1994, resulted in an oil and associated gas discovery that was subcommercial at that time. However, it unveiled the presence of a Cenozoic petroleum system that is characterized by what were known as direct hydrocarbon indicators (DHIs) on seismic data. The discovery of the giant Girassol field in 1996, in a water depth of 1400 m, confirmed Angola as an emerging world-class petroleum province. Other exciting discoveries in the Lower Congo Basin soon followed, including: Kuito (Block 14), Dalia (Block 17) in 1997; Kissanje (Block 15) in 1998; and Platina and Plutonio (Block 18) in 1999. These discoveries enabled Angola to exceed production of 1 million barrels per day of oil (MBPD) in 2001.

Exploration moved into progressively deeper water depths, the first ultra-deepwater (between 2000 and 3000 m water depth) licence awards being made in 1998.

Today, Angola is well recognized as a world-class oil province with oil production exceeding 2 MBPD. It is well positioned to supply gas to countries surrounding the Atlantic basin, notably in Europe and North America. What does the future hold for gas?

VINING, B. A. & PICKERING, S. C. (eds) *Petroleum Geology: From Mature Basins to New Frontiers – Proceedings of the 7th Petroleum Geology Conference*, 1043–1058. DOI: 10.1144/0071043 © Petroleum Geology Conferences Ltd. Published by the Geological Society, London.

Associated gas and some non-associated gas has been discovered, by accident, in the search for oil. Undoubtedly, Angola will continue to develop as a world-class oil province. However, what is the potential for gas? From a global perspective, demand for energy worldwide continues to increase. World consumption of gas is approximately 100×10^{12} SCF/year. Recent advances in liquefied natural gas (LNG) technologies are changing the world of gas, for the first time providing flexibility of supply. It is predicted that world LNG production may double by 2016. Angola will be a key player in the future world gas business. As mentioned above, the current Petroleum Sharing Contracts (PSC) are for oil; there is no provision for gas production. A contractual framework for gas has to be established in the near term. First production of LNG in Angola is scheduled for 2012, supplied solely by associated gas.

This paper provides some insights into the petroleum geoscience efforts being made by Angola's national gas company, Sonangol Gas Natural (Sonagas), in exploring for gas. Recently founded in 2004, Sonagas is charged to explore, develop and produce gas to address the growing demand. This demand comes from a new LNG plant and the emerging Soyo industrial complex in the northern coastal fringe, and the growing number of industrial and domestic consumers.

The focus of this paper is on the challenges facing the effective and efficient exploration for non-associated gas in a world-class prolific oil province. The associated gas potential of Angola is relatively well known and will not be discussed.

The potential for gas throughout Angola, both offshore and onshore, will be reviewed. Following a discussion of the regional tectonostratigraphic framework that underpins play definition, the potential for gas in the conventional thermogenic Pre-Aptian salt and Post-Aptian salt plays will be investigated. These are relatively emerging to mature plays. The possibility of an unconventional biogenic petroleum system, with multiple TCF resource potential in frontier plays, will then be examined in the deep and ultra-deepwater. Finally, the potential for gas in the truly frontier interior basins of Angola, from highly conceptual Neoproterozoic plays, will also be addressed, in the first instance using a global analogue approach.

Regional framework

A location map of the sedimentary basins of Angola is shown in Figure 1. These comprise the predominantly offshore Lower Congo Basin, the Kwanza/Benguela Basin and the Namibe Basin. The Lower Congo Basin is currently considered to be the most prospective. The modern South Atlantic passive margins started their evolution as part of a continental rift system that developed in the southern parts of the Gondwana super-continent at the Jurassic–Cretaceous boundary (Brice *et al.* 1982; Ala & Selley 1997). The interior basins of Angola are also shown in Figure 1. The location of offshore blocks in shallow, deep and ultra-deepwater and onshore blocks is shown.

A Mesozoic and Cenozoic stratigraphic summary of potential gas-prone petroleum systems is shown in Figure 2. The principal gas plays are highlighted by the red gas symbol. The source rocks of the Lower Congo Basin and the Kwanza/Benguela Basin are discussed in Burwood (1999). Thermogenic petroleum systems are proven in the Pre-Aptian salt plays and the Post-Aptian salt plays. An unconventional biogenic gas petroleum system is postulated in deepwater, comprising Middle to Late Miocene and Plio-Pleistocene plays. In addition, a highly conceptual, unproven Neoproterozoic petroleum system is being investigated in the interior basins, principally the Okavango and Owambo Basins.

Sonagas has access to an extensive offshore seismic and well database. This is summarized in Figure 3. Digital seismic databases comprise in excess of 17 000 km of 2D seismic, shown in the central panel of Figure 3, and in excess of 58 000 km^2 of merged

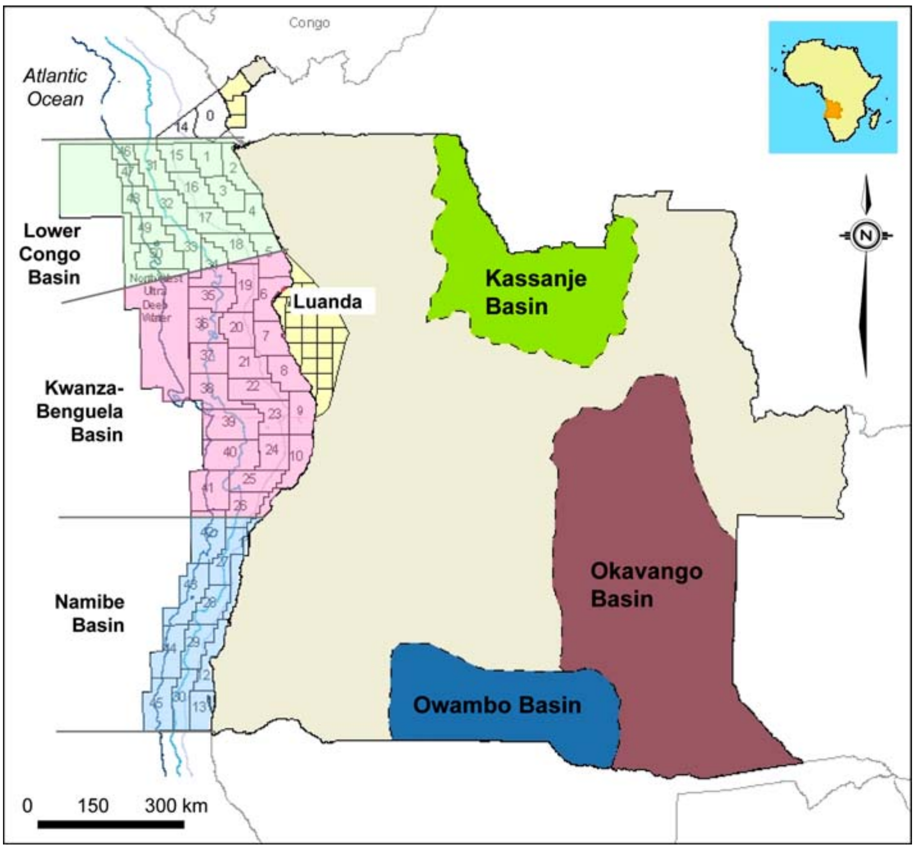

Fig. 1. Location map of the sedimentary basins of Angola.

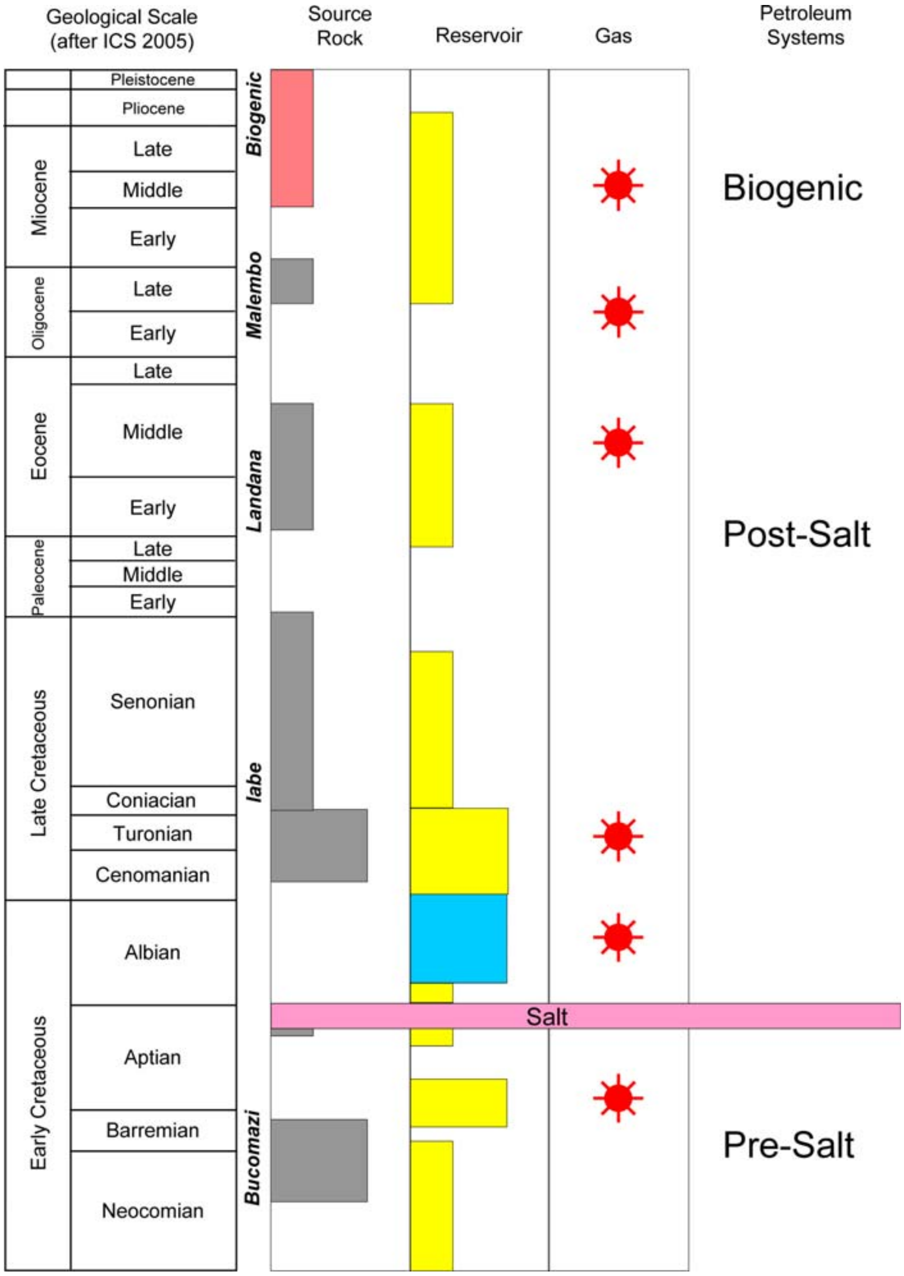

Fig. 2. Stratigraphic summary of potential gas-prone petroleum systems.

3D seismic surveys as shown in the panel on the right of Figure 3. The majority of the merged 3D seismic surveys are located in the Lower Congo Basin and provide an excellent quality dataset, both for regional play synthesis and prospect definition. The seismic datasets are of varying vintages and quality. Overall, seismic data quality in the Post-Aptian salt section is good to excellent. However, seismic data quality in the Pre-Aptian salt section is poor to fair and is a current limitation to prospect generation and maturation efforts. There is access to in excess of 450 wells of which 130 have gas shows, the latter shown in red in Figure 3. The number of gas well discoveries by block and by play are shown in Figure 4. Gas has been encountered in all the principal plays. The shallow water Albian Pinda carbonate play shows the highest number of gas discoveries. These gas wells lie principally in the Lower Congo Basin. Their geographic distribution, in the context of the interpreted limits of their respective plays, is shown in Figure 5. However, it must be remembered that all drilling activity has intentionally avoided the discovery of gas by focusing on predicted oil-prone areas. The discovery of gas has occurred by accident.

The deliberate search for gas, as mentioned above, is focused on three distinctly different types of petroleum system. Firstly, conventional thermogenic petroleum systems, where all the gas discoveries have been made to date, will be reviewed.

Thermogenic petroleum systems

Pre-Aptian salt plays

An understanding of the basin configuration for the Pre-Aptian salt plays, in particular the depth to basement, is somewhat tenuous due to poor seismic imaging. Gravity and magnetic studies are currently underway to better define basin architecture and the depth to crystalline basement. However, the main structural style is believed to be rotated fault block geometries, reflecting a syn-rift lower section of Late Triassic to Jurassic age and an Early Cretaceous sag phase

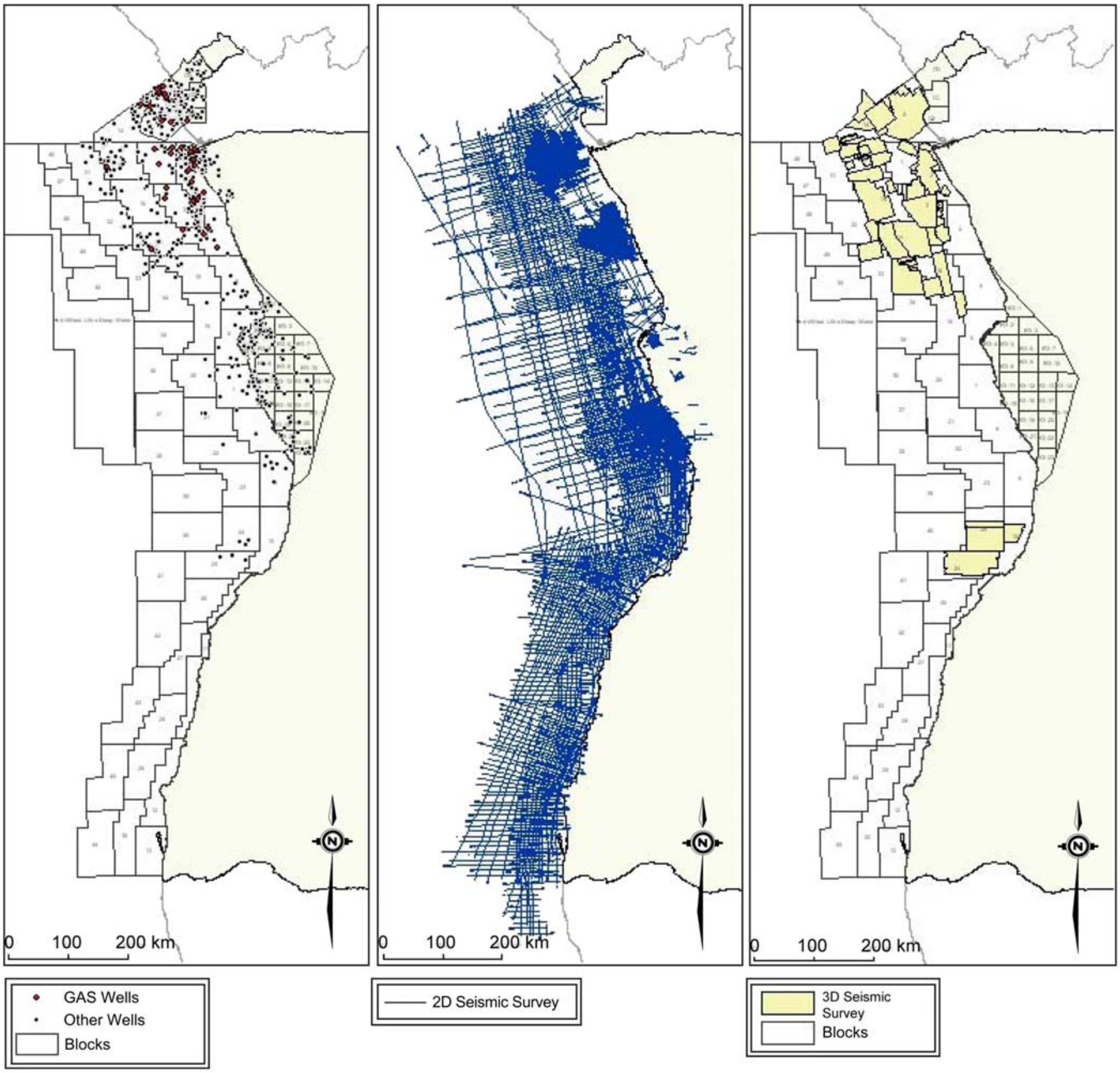

Fig. 3. Well and seismic database.

represented as a sedimentary wedge. The active rifting has been divided into three separate phases: Berriasian, Hauterivian and Late Barremian to Early Aptian (Karner & Driscall 1999). The key facies associations characterizing the syn-rift areas are continental-fluviatile and lacustrine. The sag phase sedimentary wedge has an increasing marine influence with some carbonate deposition. A schematic play cross-section of the Pre-Aptian salt plays in the Kwanza/Benguela Basin is shown in Figure 6.

The principal source rock for the Pre-Aptian salt plays is the Neocomian–Barremian Bucomazi Formation. This is a prolific super source rock that is believed to be areally extensive. However, additional source horizons exist in the syn-rift section that are predominantly lacustrine in facies.

Extensive hydrocarbon maturation studies have been performed, calibrated where possible to well data. A generalized present-day basal heat flow map is shown in Figure 7. Two areas of high heat flow are shown in red. Maturation modelling of the Bucomazi Formation present day delineates gas kitchens corresponding to the two areas of high heat flow (Fig. 7) and a further conjectural area offshore Luanda. These interpreted gas kitchen areas for the Bucomazi Formation present day are shown in Figure 8.

Migration of hydrocarbons from pre-salt source rocks is driven by buoyancy and believed to take place vertically up fault planes and laterally updip where there is an effective stratigraphic conduit. These hydrocarbon migration pathways are shown schematically in Figure 6.

Exploration for pre-salt gas plays is in progress, focused in the vicinity of the predicted gas kitchens (Fig. 8), and encouraged by the exciting recent discoveries in the conjugate margin offshore Brazil. The latter discoveries are used as analogues to aid the interpretation of structural style and reservoir distribution in the Angolan margin.

The leads and prospects identified to date have a variety of structural styles, for example antiformal features, fault-related closures and combination structural and stratigraphic traps. Many of the large leads lie below the Aptian salt. As with sub-salt plays in

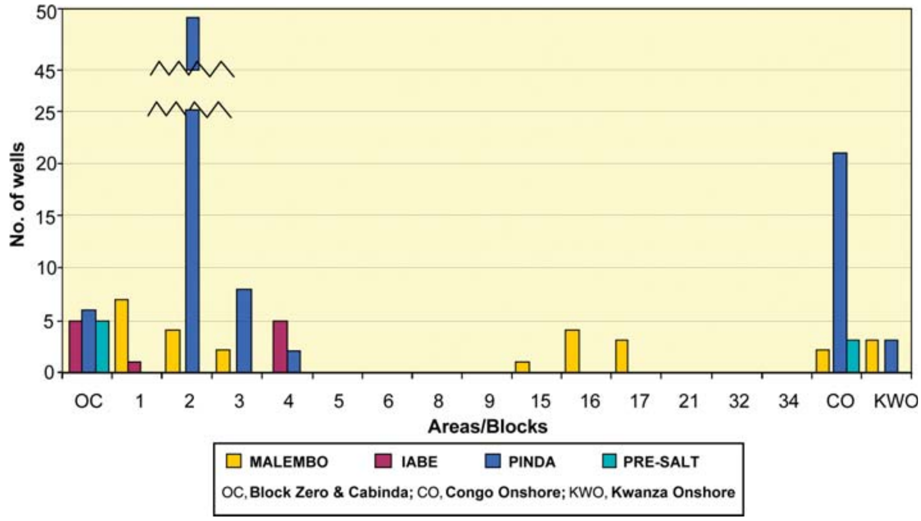

Fig. 4. Gas discoveries by area and play.

other areas of the world, such as the Gulf of Mexico, seismic imaging is challenging. In many of the seismic datasets offshore Angola there is poor seismic imaging beneath salt. Detailed velocity analyses have revealed that, in areas of massive salt, large features identified in the seismic time domain are not present in the depth domain. The effect of salt pullups is critical in lead generation. In this regard, it is imperative to clearly differentiate between massive salt and thin salt sills, below which there is a clastic stratigraphic section, albeit masked by poor seismic data quality. In addition, leads are being generated in the inter-salt structurally high areas, the areas beneath the salt affording the structural lows for trap definition.

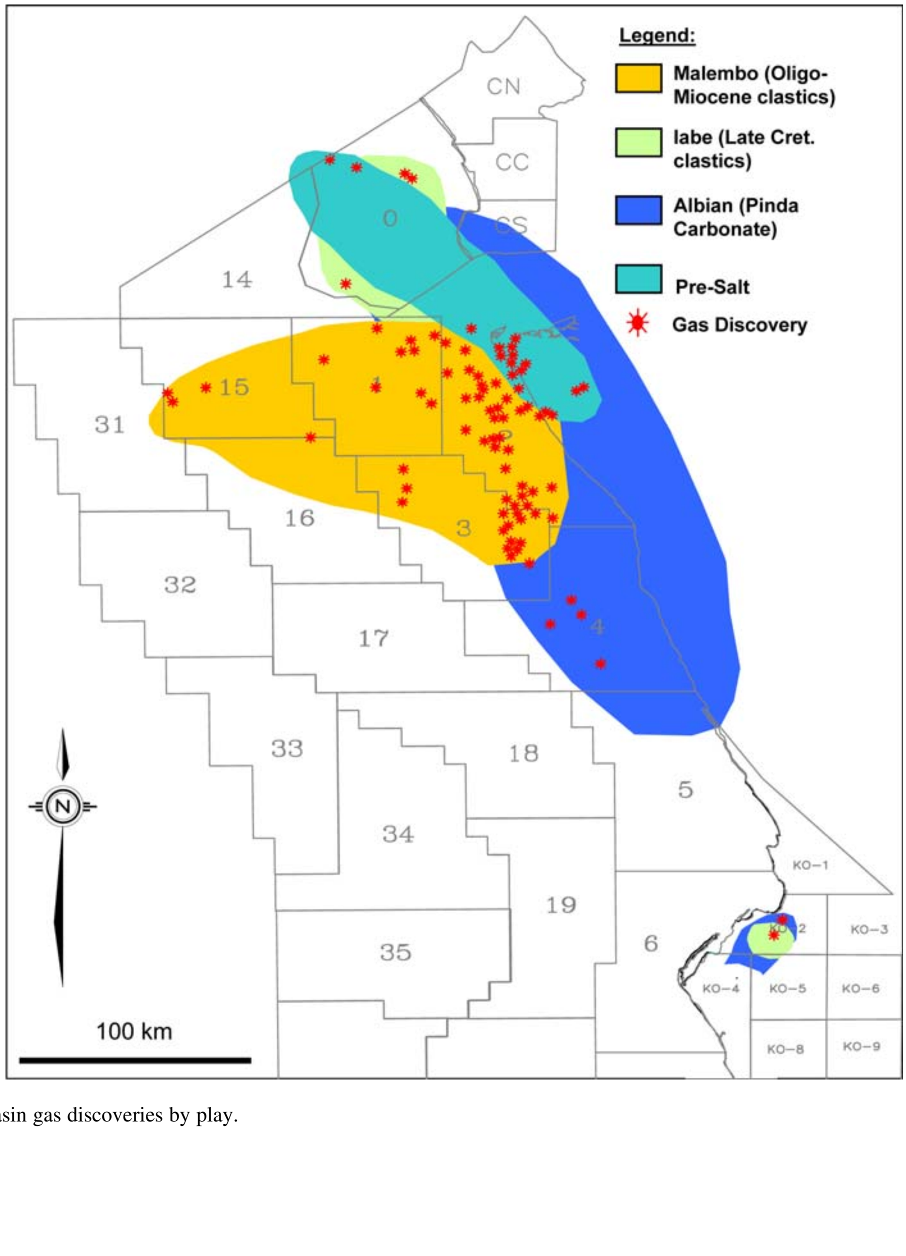

Fig. 5. Lower Congo Basin gas discoveries by play.

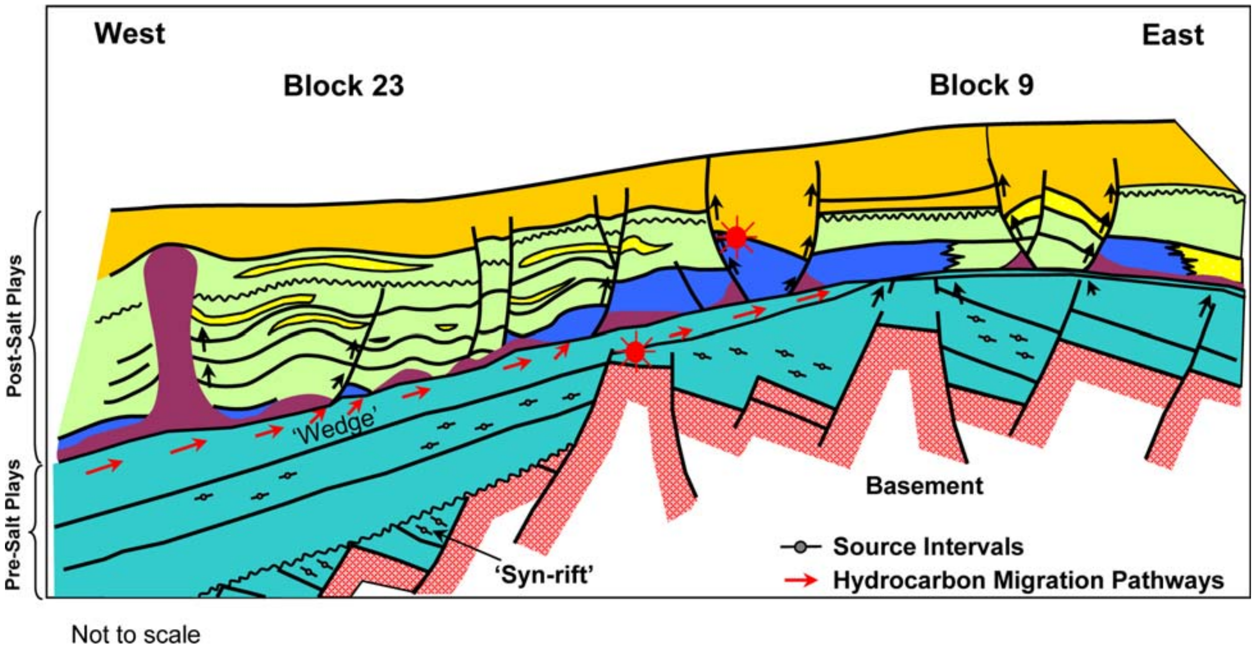

Fig. 6. Schematic play cross-section Kwanza/Benguela basin.

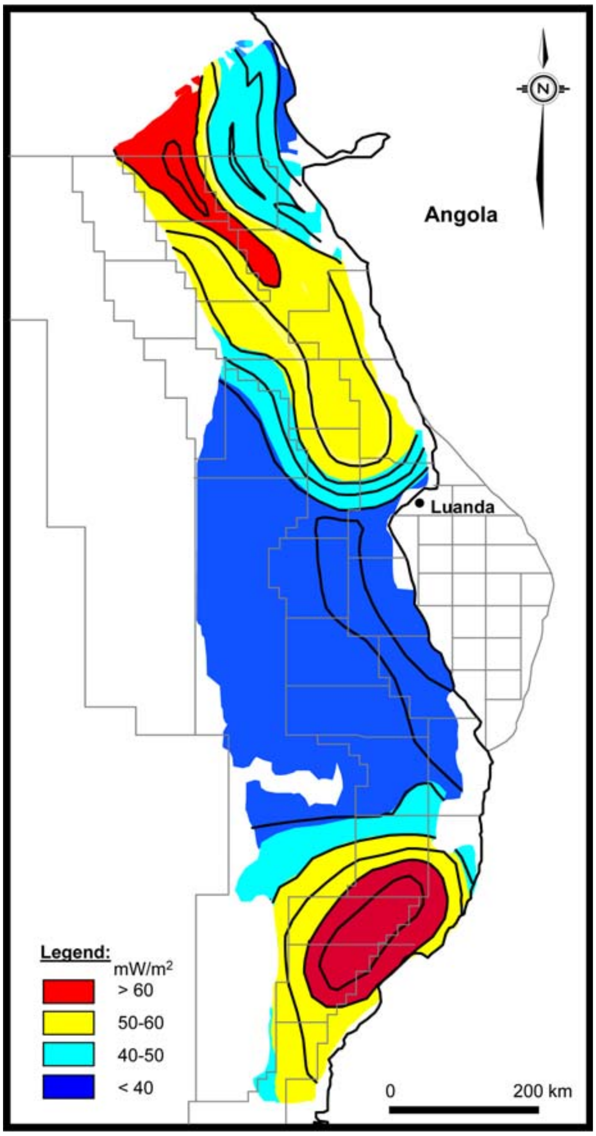

Fig. 7. Generalized basal heat flow.

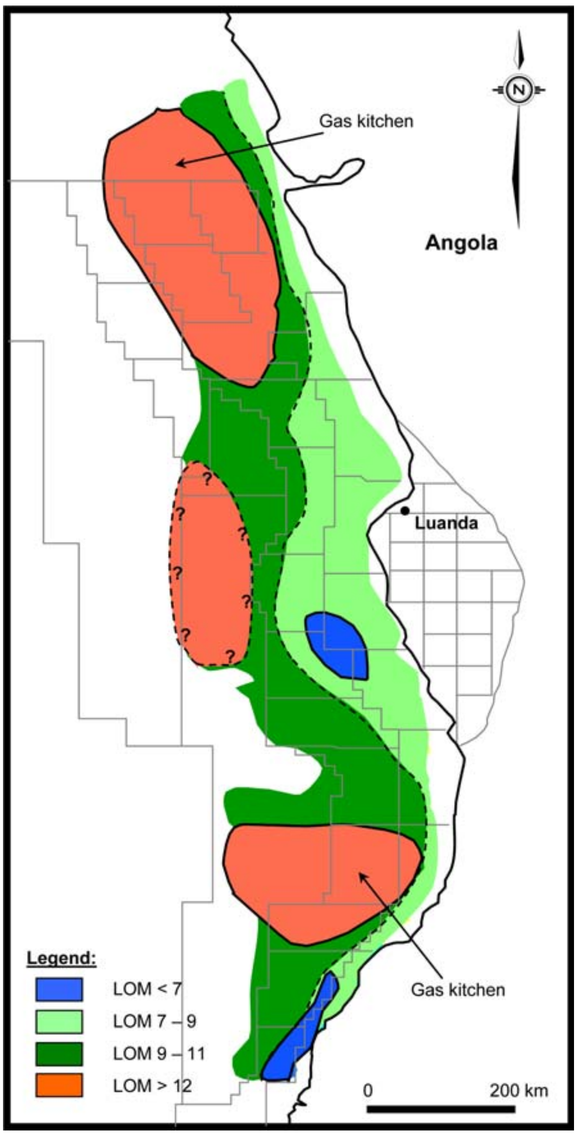

Fig. 8. Generalized base salt (Bucomazi Fm.) maturity present day.

The salt provides a regional super seal. Invariably, a sedimentary wedge, mentioned earlier, directly underlies the salt and is the primary exploration objective. In these areas, a syn-rift section is also sometimes present. An intra-formational seal(s) is therefore required to form stacked objectives. The presence of intra-formational seals may be problematic, particularly in areas of lacustrine facies, where the potential sealing horizon is predicted to be thin and discontinuous. A detailed knowledge of the nature of the depositional systems and facies associations is therefore required to facilitate the distribution of intra-formational seals.

The nature and distribution of the depositional systems for the pre-salt sedimentary wedge and syn-rift sequences, as it relates to seal and reservoir, is highly conceptual and is, in large part, driven by an interpretation of the mega-regional tectono-stratigraphic framework in the Mesozoic at the time of continental breakup. The principal marine influence is from the SW. The reservoir in the syn-rift Jurassic lacustrine facies is believed to be discontinuous and exploration is focused on the prediction of possible fluviatile systems, not identifiable on the current seismic datasets. Reservoir distribution in the Early Cretaceous sedimentary wedge is believed to have a more marine influence and the reservoir intervals are predicted to be better developed and more widespread. Well control in the pre-salt section is limited, primarily to the Lower Congo Basin. Long distance extrapolation of the depositional models is therefore required for pre-salt exploration in the Kwanza/Benguela and Namibe Basins.

Post-Aptian salt plays

Exploration for gas in thermogenic Post-Aptian salt plays is focused on identifying windows in the salt through which gas, derived from Pre-Aptian salt source rocks, enters the Post-Aptian salt petroleum system. Predicted gas migration conduits, as in the pre-salt section, are vertically up faults and laterally updip contingent on a stratigraphic conduit being present (Fig. 6).

Several post-salt source rocks have been identified: the Cenomanian–Senonian Iabe Formation; the Eocene Landana Formation and the Late Oligocene Malembo Formation as shown in Figure 2. A generalized present-day level of maturation map for the Iabe Formation source rocks is shown in Figure 9. A further gas kitchen exists derived from source rocks of the Malembo Formation. This is of limited areal extent and coincident in area with that shown in red in Figure 9. These stacked, areally constrained Post-Aptian salt gas kitchens immediately overlie that of the Pre-Aptian salt source rocks in the Lower Congo Basin (Fig. 8), thereby providing an increased focus area for gas exploration in this region.

Structural trap geometries are largely influenced by salt tectonics. The latter vary in style and intensity in the offshore areas, from low relief salt swells resulting in anticlinal closures in the shallow water areas, to diapirs and sills in the deeper water areas. Raft tectonics, a term first introduced by Burollet (1975) for the Kwanza Basin, are prevalent in the more proximal, listric fault areas (Duval *et al.* 1992; Lundin 1992; Valle *et al.* 2001), extension being taken up in the more distal areas by compressional, thrust features. Examples of the 3D geometry and displacement configuration of fault arrays from a raft system in the Lower Congo Basin are discussed in detail in Dutton *et al.* (2004). The controls on Miocene sand deposition during gravity-driven extension in Block 4 are well documented in Anderson *et al.* (2000). Combination structural/stratigraphic and stratigraphic traps are present; their identification and maturation relying on the application of advanced seismic technologies.

The Post-Aptian salt stratigraphic section, in the most part, possesses the physical properties conducive to the seismic identification of gas. Seismic amplitude anomalies may indicate the

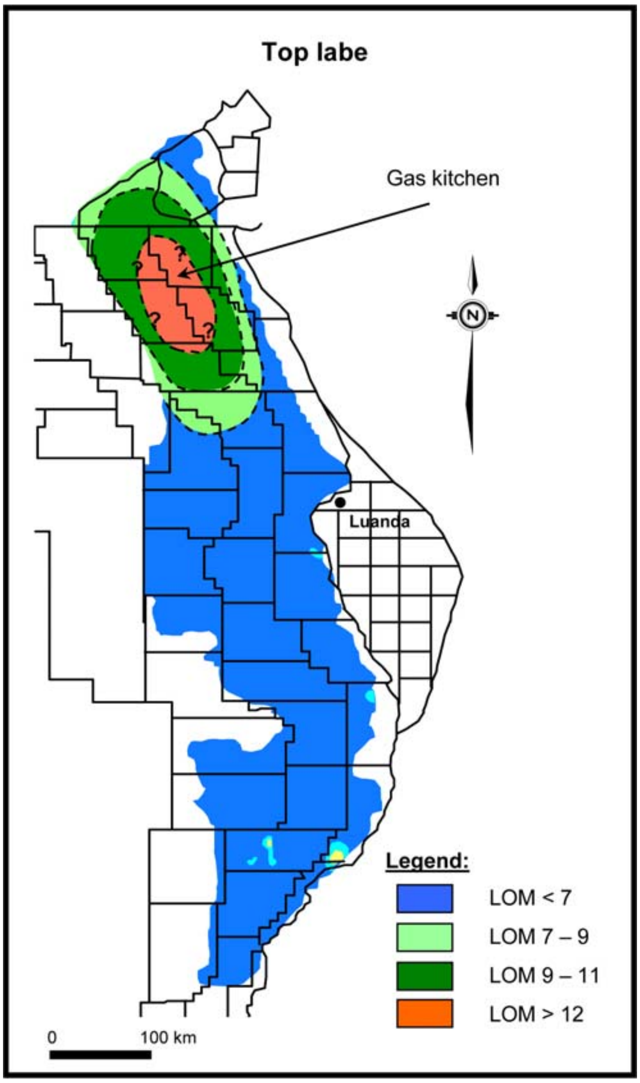

Fig. 9. Generalized present day level of maturity top Tabe formation.

presence of gas in the immediate vicinity of fault planes and in amalgamated channel complexes. For example, this is illustrated in Block 15 by a prospect, defined by high seismic amplitudes, shown on the seismic line A–A′ in Figure 10. A seismic flat spot, indicating a possible gas–water contact and conformable to the structural spill point, may be present. The distribution of this seismic anomaly is delineated by the high amplitude response shown in the time slice in the upper part of Figure 10. The reservoir is interpreted as an amalgamated Miocene channel complex. Gas charge is predicted by migration up a bounding fault from a pre-salt gas kitchen in a structurally high area. There is crestal faulting and possible seismic evidence of a gas migration trail to the seabed resulting in pock marks. Similar seismic indications of gas are observed adjacent to fault planes and as amalgamated channel complexes in Block Zero, as shown within the green ellipses in Figure 11.

Exploration for gas in the Post-Aptian salt section is further focused in areas where there is evidence of the presence of pock marks on the seabed. These latter areas are readily identifiable on the extensive quilt of merged 3D seismic surveys (Fig. 3) Pock marks are primarily the result of escape of gas to the seabed. However, they may also be formed by the escape of fluids, principally water.

A combination of multiple seismic and geological indicators for gas reduces uncertainty and risk in the exploration effort. Current

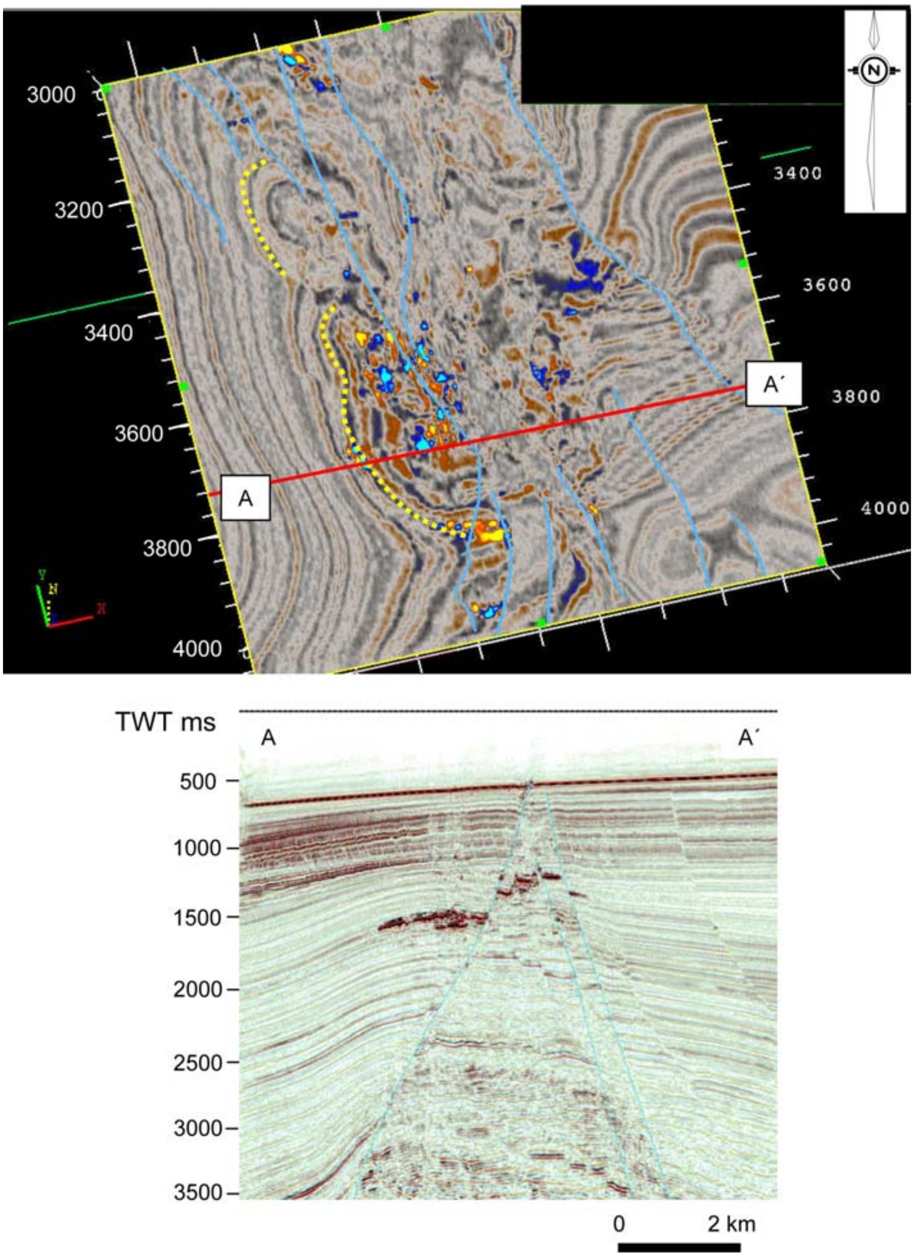

Fig. 10. Block 15 post-salt gas plays.

technologies such as neural networks are currently being applied to the identification and subsequent maturation of Post-Aptian salt thermogenic prospects and unconventional biogenic gas prospects. These technologies are predicated on seismic attribute responses, such as seismic amplitude, being associated with gas-charged sands in a particular area. The neural network technique then searches for similar responses throughout the seismic dataset. Numerous gas migration trails have been identified.

Although exploration focus is in the gas kitchen areas, exploration methodologies use the play as the fundamental unit of analysis. The Post-Aptian salt traps are structural, stratigraphic and combination traps. Reservoir prediction in deepwater depositional systems leverages seismic identification of reservoir facies. Exploration techniques include the reconstruction of seismic geomorphologies at times of large sea-level lowstands, for example Middle Miocene and Middle Oligocene, when large influxes of coarse clastics, principally transported by the Congo and Kwanza rivers, are predicted to dominate the depositional systems. Seismic RMS amplitude and variance displays, derived from 3D seismic datasets, are successful in defining these amalgamated channel complexes and predicting reservoir distribution, architecture and quality. The major amalgamated channel complexes of Middle Miocene and Middle Oligocene age are invariably located off-structure, infilling topographic lows adjacent to the lowside of listric faults, and possess a major stratigraphic trapping component. The geometry and evolution of deepwater submarine channels, particularly in offshore Angola, are described extensively in Kolla *et al.* (1998, 2001), Anderson *et al.* (2000), Mayall & Stewart (2000), Sikkema & Wojcik (2000), Abreu *et al.* (2003), Deptuck *et al.* (2003), Fonnesu (2003) and Gee & Gawthorpe (2007). Further insights into the distribution of these types of depositional systems on the Angolan and Brazilian margins may be obtained from their gravity signatures (Dickson *et al.* 2003). These channel complexes are illustrated by a prospect in Block 2 shown in Figure 12. The dark blue area is a fault plane, juxtaposed to the lowside of which are the

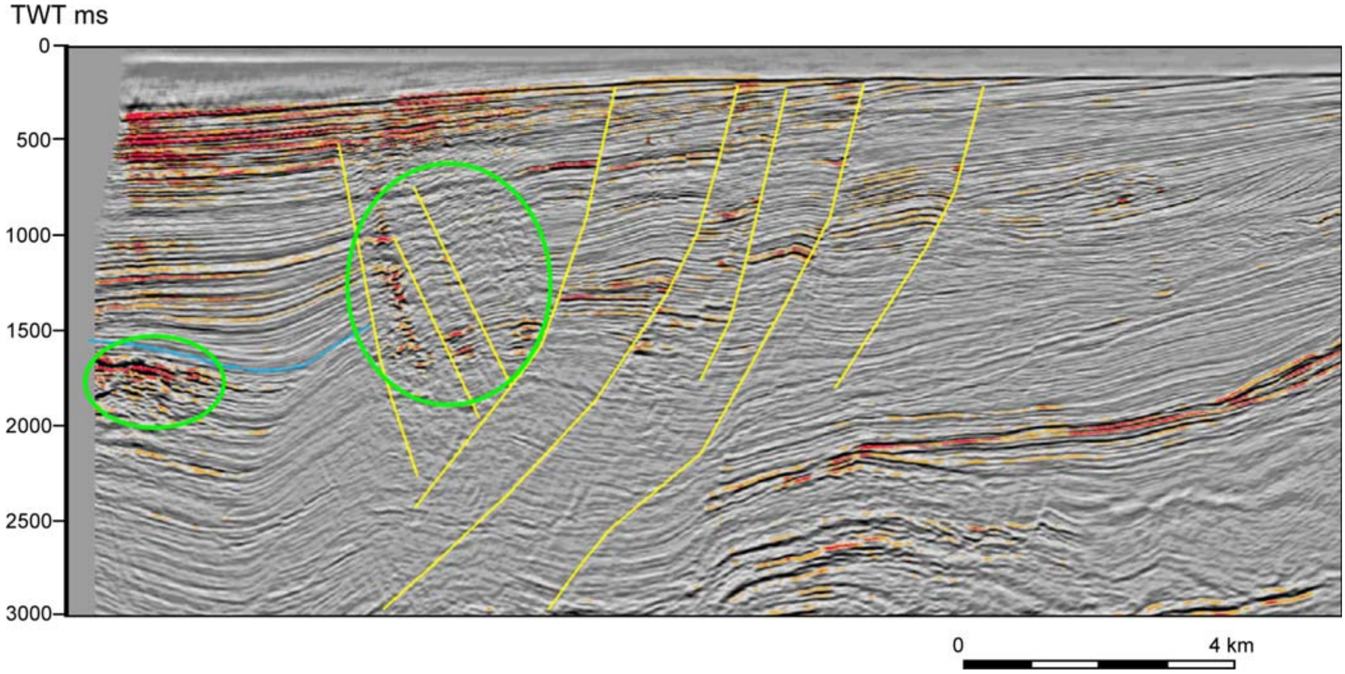

Fig. 11. Block zero seismic amplitude gas indications.

interpreted amalgamated channel complexes of Middle Miocene and Middle Oligocene age, shown as yellow and red seismic amplitudes.

Prospect generation and maturation efforts are therefore focused on placing leads in their regional play context, in particular with respect to the environment of deposition and in proximity to gas kitchens. Risk mitigation in the prospect maturation process comprises the application of amplitude versus offset (AVO) and electromagnetic (EM) techniques.

These exploration techniques for trap definition, reservoir presence, quality and pore-fill are not wholly confined to the search for gas in thermogenic petroleum systems. They can be applied to the search for biogenic gas prospects. However, the search for biogenic gas requires a different exploration approach.

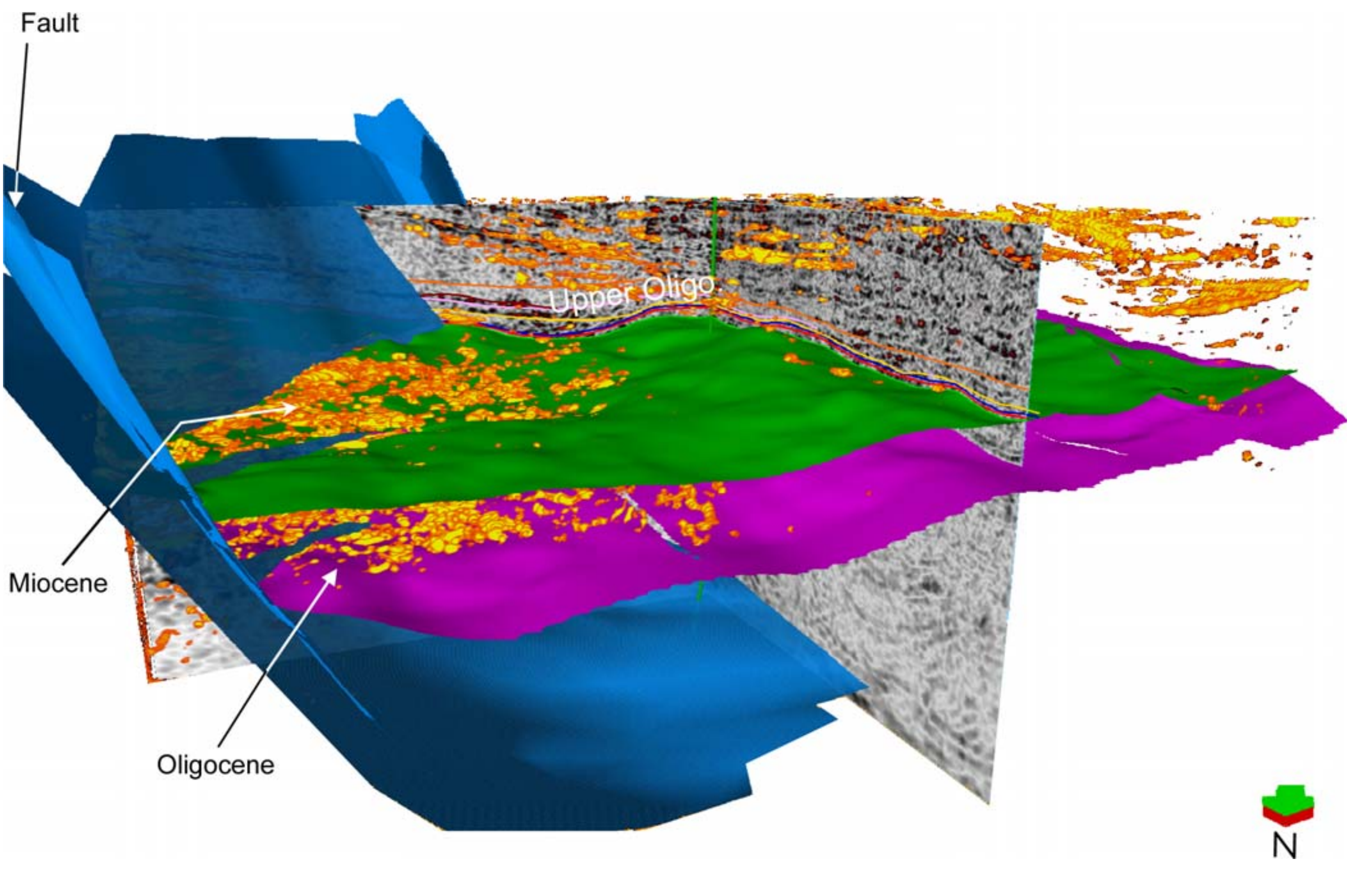

Fig. 12. Block 2 thermogenic petroleum systems: post-salt.

Biogenic gas unconventional petroleum system

The presence of an unconventional biogenic gas petroleum system in deepwater offshore Angola is currently being investigated. A possible analogue is the Reliance Industries Limited giant D1–D3 gas field in the Krishna Godavari Basin, offshore east coast of India, which commenced first production in 2009.

The relative volumes of gas produced by organic source rocks, as an integral of time and temperature, is shown schematically in red in Figure 13 (Rice & Claypool 1981, p. 6, fig. 1). Thermogenic gas, as discussed above, is generated from source rocks in the late mature oil window and in the overmature stage. Biogenic gas can be generated in large quantities in the shallow stratigraphic section in areas immature for thermogenic gas. Exploration for biogenic gas thereby significantly increases the prospective area for gas.

Biogenic gas generation requires a source rock of microbial origin. The microbes produce methane through metabolic activities in the sediment. At low temperatures in deepwater, the resultant methane forms gas hydrates. Seafloor microbes may produce biosurfactants that are concentrated on bubbles which, with upward fluid flow, are disseminated in the sediments. Total organic carbon (TOC) of the biogenic gas source rocks may be low, at 2–3%, disseminated through a shale succession. Alternatively, the TOC may be concentrated in thin, centimetre-scale, condensed zones. Figure 14 (Rice & Claypool 1981, p. 7, fig. 2) shows the vertical microbial ecosystem succession for methane generation. Biogenic methane generation requires anaerobic conditions, immediately below the sulphate reduction zone and only a few metres below the sediment–water interface.

Exploration for biogenic gas in Angola is predicated on identifying palaeo-gas hydrate occurrences in the low temperature conditions found in deepwater. These exploration methodologies are similarly being investigated, as mentioned above, in the Krishna–Godavari Basin, India (Kundu *et al.* 2008).

The present-day stability field for gas hydrates is temperature- and pressure-dependent. The relationship between methane solubility, depth of burial and water depth is illustrated in Figure 15 (Rice & Claypool 1981, p. 10, fig. 6). The line of gas hydrate stability is also shown (Fig. 15) below which gas hydrates break down to release biogenic methane into the surrounding sediments. The base of the gas hydrate zone and the possible top of the free gas zone is characterized seismically by a bottom simulating reflector (BSR). Shallow BSRs on the Angola margin and their relationship to gas and gas hydrates are discussed in detail in Nouze & Baltzer (2003). This biogenic methane free gas is therefore available for migration and subsequent entrapment, contingent on migration conduits transecting this gas hydrate-free gas transition zone. Entrapment is envisaged primarily as stratigraphic traps where an effective updip, base and top seals are present. Reservoir is therefore considered to be the key play element to be investigated. As in exploration in thermogenic petroleum systems, pock marks on the seabed are direct indicators of fluid escape features and particularly gas. Figure 16 graphically shows the dimensions and widespread occurrence of pock marks in Block 31. In this example, it is recognized that the gas may be biogenic, thermogenic or a combination of both. Pock marks, although indicating the presence of gas on the seabed, represent gas leakage from the subsurface. This may indicate a gas accumulation at depth, but could also indicate a gas leakage risk whereby the seismic amplitude response is a

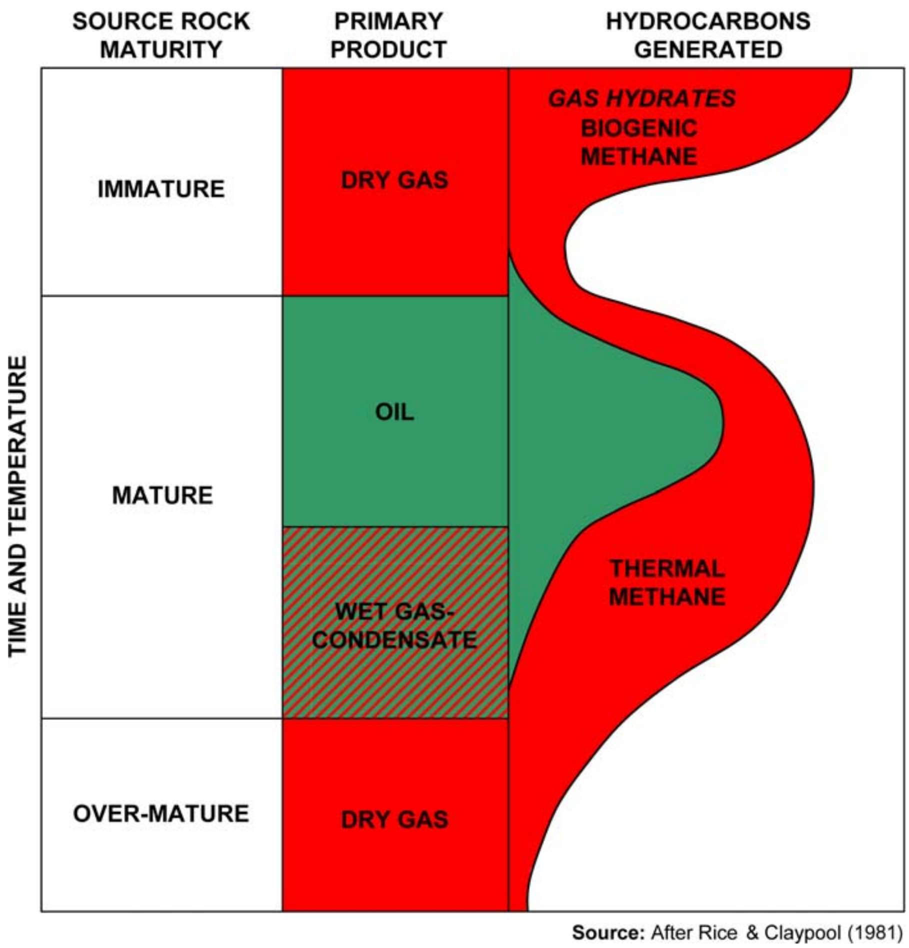

Fig. 13. Gas generation schematic.

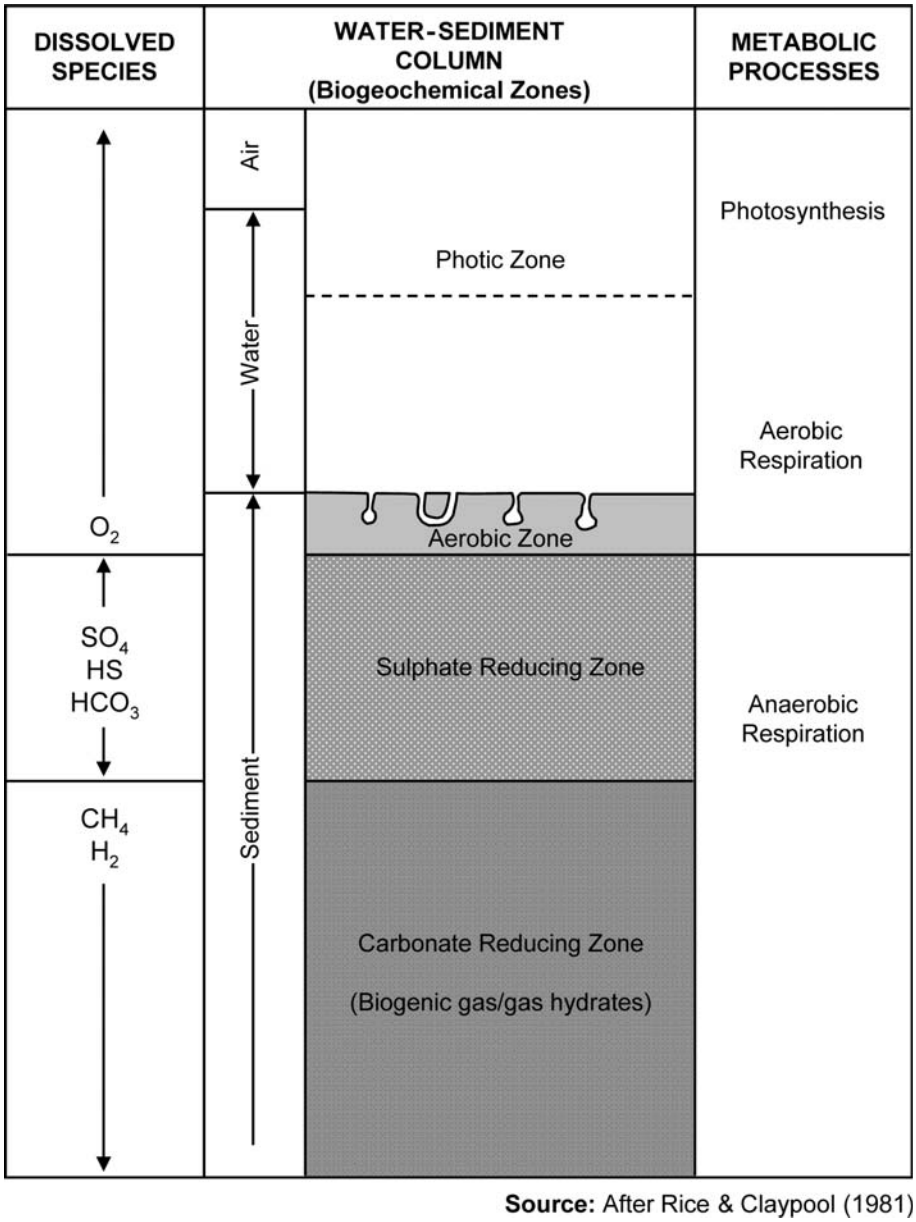

Fig. 14. Microbial ecosystem succession for methane generation.

consequence of residual gas saturations. The seismic line C–C′, highlighted in Figure 16, is shown in cross-section view in Figure 17. The presence of two salt features is shown. The high seismic amplitude events in the shallow section are interpreted to be biogenic gas. Pock marks are seen as perturbations on the seabed.

In this overall context present day, the most favourable conditions for the entrapment of biogenic gas occur in 2000–4000 m water depth at approximately 1000 m below the seabed. In deepwater passive margin settings, such as offshore Angola, similar bathymetric and depth of burial relationships are predicted to have occurred from the Middle Miocene to the present day. Exploration in this unconventional petroleum system is focused in the ultra-deepwater blocks (2000–3000 m water depth) where the Middle to Late Miocene and Plio-Pleistocene sequences are at burial depths in excess of 2000 m. The depth of burial of the trap, as it relates to reservoir pressure, is of paramount importance in controlling the producibility characteristics, flow rates and recovery. The deeper targets, at higher reservoir pressures, will exhibit better flow rates and recovery factors. The sustained long-term production characteristics of these deepwater, shallow depth of burial, gas reservoirs is unknown. Reservoir depressurization resulting in the need for installation of compression facilities in the early life of a field can have a serious adverse effect on the commercial viability of the field.

A biogenic gas play fairway can then be defined both in geographic areal extent and within a vertical depth window. Exploration efforts are focused on the development of a sequence stratigraphic framework for the Middle to Late Miocene and Plio-Pleistocene sequences to determine, through the environment of deposition maps, the distribution of reservoir and seal in each time-stratigraphic equivalent unit. The principal reservoir targets are amalgamated, stacked channel sand complexes.

The identification of leads and prospects is facilitated by the seismic attribute response of some of these gas sands. Simple 2D seismic wedge models and fluid (gas) substitution studies indicate the seismic amplitude response to gas reservoirs of varying thickness and porosity characteristics within the play. Furthermore, seismic AVO and EM methodologies are used as risk mitigation techniques. The optimal methodology for trap definition is through mapping high-amplitude response.

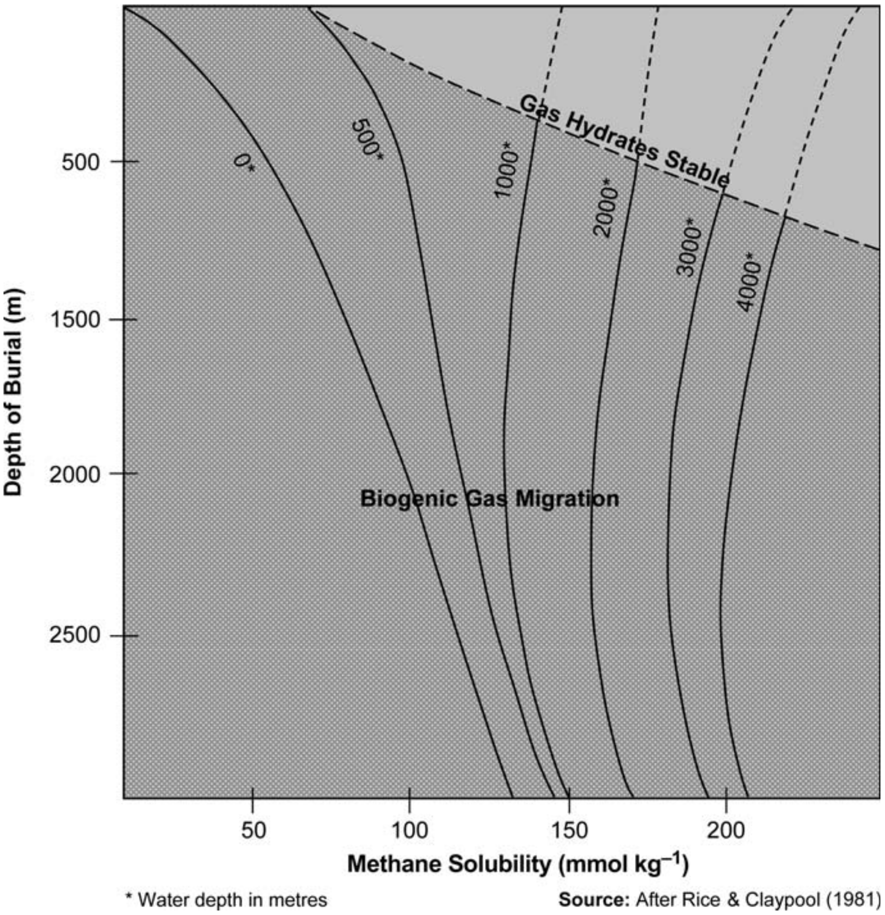

Fig. 15. Estimated methane solubility.

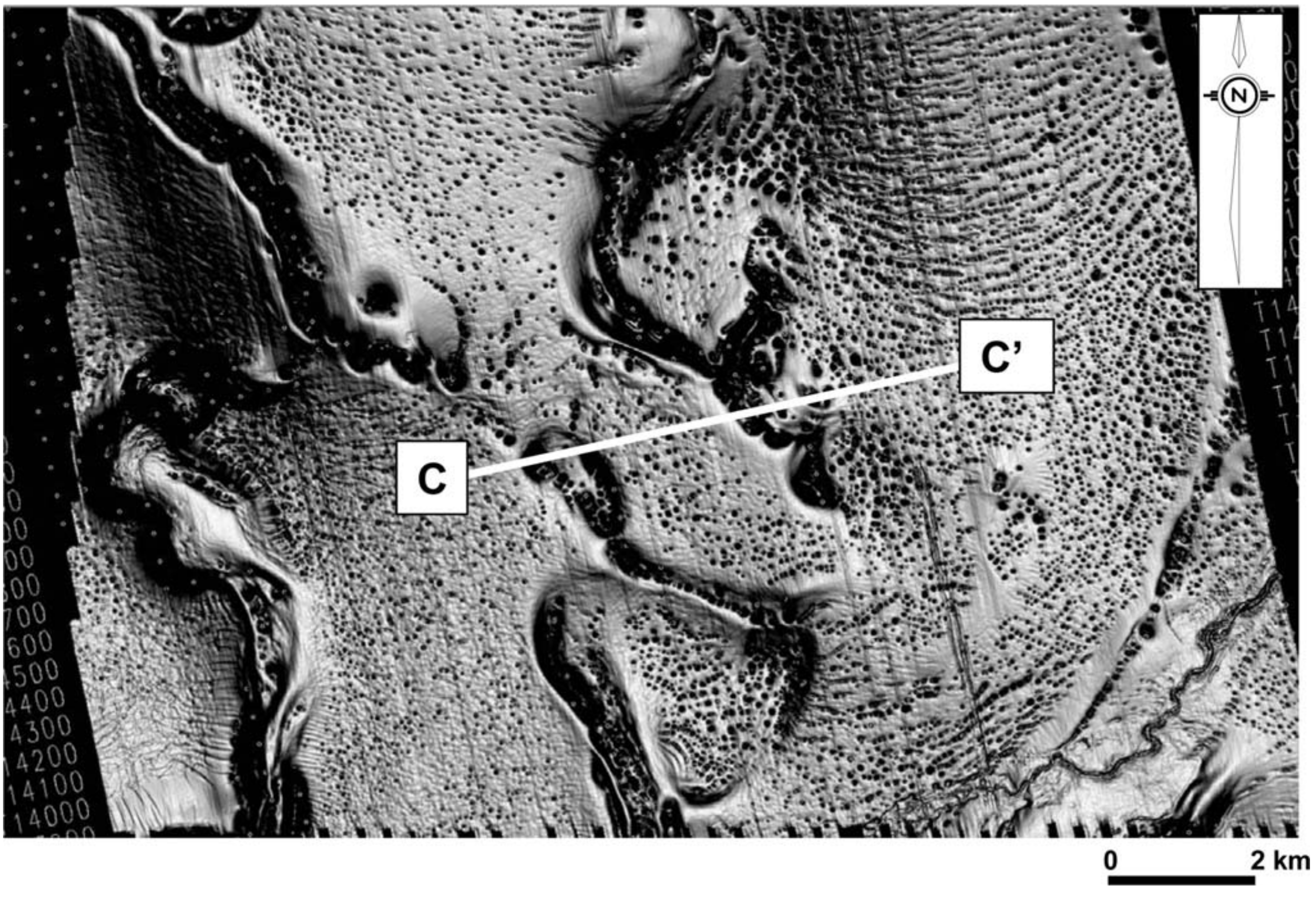

Fig. 16. Direct gas indicators: Block 31.

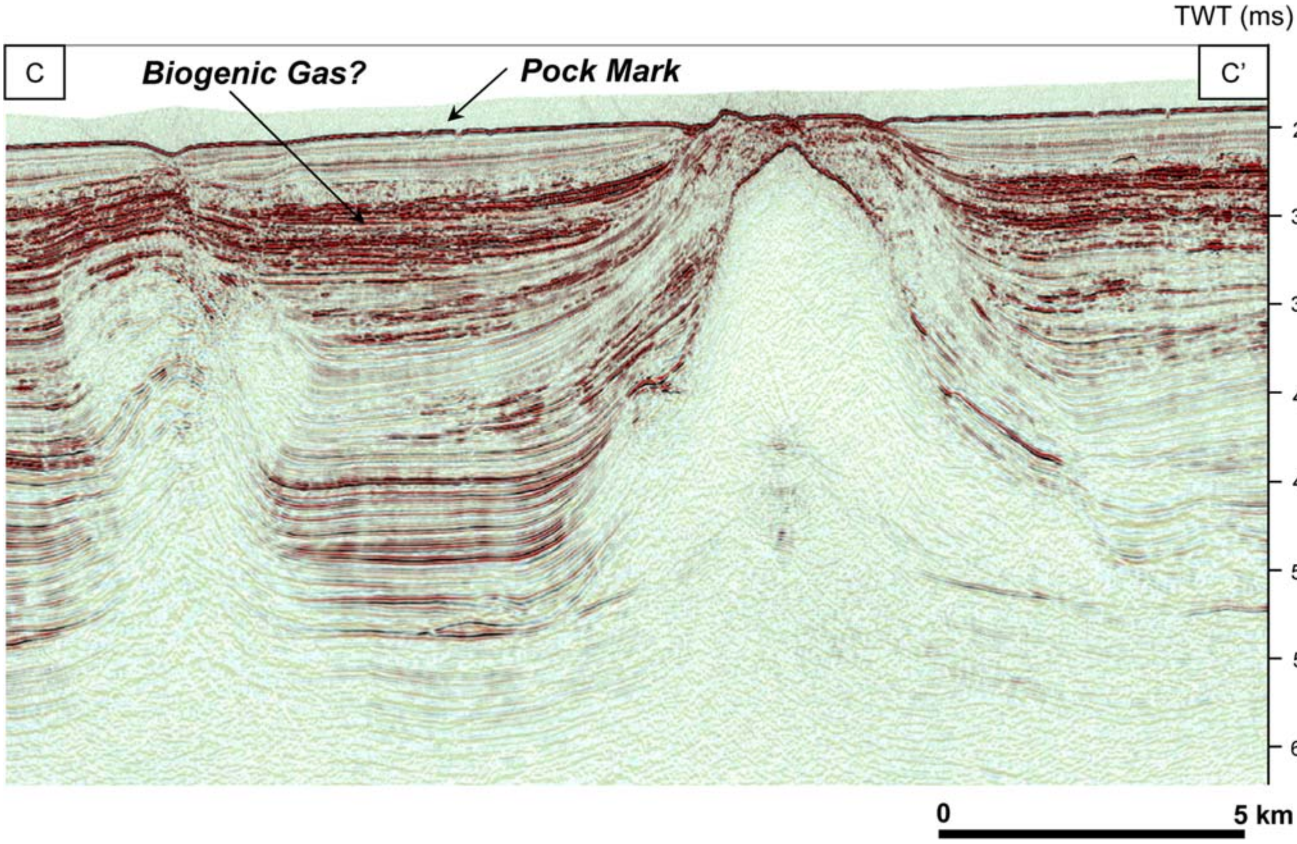

Fig. 17. Possible biogenic gas play: Block 31.

It is envisaged that biogenic gas prospects will be predominantly stratigraphic traps. The field size distribution for biogenic gas stratigraphic traps is expected to be larger than that of the post-salt plays, with structural, stratigraphic and combination traps, in the thermogenic petroleum system.

A third and final petroleum system to be discussed is a conceptual Neoproterozoic petroleum system that may be present in the interior basins of Angola.

Conceptual Neoproterozoic petroleum system

The interior basins of Angola, the Kassanje Basin, Okavango Basin and Owambo Basin cover a significant geographic area, as shown in Figure 1. The geology, as it pertains to possible petroleum systems, is poorly understood. There are no proven petroleum systems. There is a high level of uncertainty and it is high risk. The database to date is limited to gravity and magnetic data and surface geology. There are no seismic or well data.

The exploration approach currently in progress is two-fold. Firstly, an investigation of the plate tectonic setting in the Neoproterozoic, examining the terranes and possible depositional environments in a mega-regional Rodinia super continent context. Rodinia is shown schematically in the lower part of Figure 18. The interior basins of Angola are highlighted by the red star, juxtaposed to similar terranes in the Central Basin of the Democratic Republic of Congo and the Sao Francisco Basin in Brazil. The Neoproterozoic–Early Palaeozoic tectonostratigraphy and palaeogeography of the peri-Gondwanan terranes of West Africa and Brazil are discussed in detail in Murphy *et al.* (2004) and Nance *et al.* (2008). The second approach is the use of possible analogues worldwide. For example, these include the proven glaciogenic petroleum systems of the Infra-cambrian of North Africa, notably Algeria and Mauritania; the Middle East, in particular the Ghaba Salt Basin of Oman; the Volga–Urals and east Siberia Basins in Russia; the Sichuan Basin in China; the Rajasthan Basin in India; and the Amadeus, Officer and McArthur Basins in Australia.

A preliminary sediment thickness map, based on gravity and magnetic data, is shown in the upper part of Figure 18. A more detailed gravity and magnetic study, integrated with crustal structure, remote sensing data and surface geology data is in progress. At the time of publication, it is believed that the definition of the basin boundaries and depth to crystalline basement may change significantly. However, the southern part of the Okavango Basin and the eastern part of the Owambo Basin, located in the SE of Angola, are interpreted to have sediment thicknesses in excess of 8 km. Contingent on the presence of source rocks, this is sufficient sediment thickness to generate hydrocarbons. A schematic play cross-section, located A–A′ on Figure 18, is shown in Figure 19. The crystalline basement is believed to be composed of Proterozoic metasediments. Neoproterozoic depositional systems infill and are influenced by this pre-existing topography. Source rocks are the Neoproterozoic Mulden Black Shales or the equivalent Lagoa de Jacare Formation in the Sao Francisco Basin in Brazil. Basin modelling in the Neoproterozoic is recognized as being problematic. Technological capability and input data are severely limited. For example, source rock kinetics are unknown. A chronostratigraphic framework, as it pertains to burial analysis, is highly conceptual. Age dating relies on geochronology isotope analyses. However, preliminary indications suggest that hydrocarbon charge may have occurred several hundred million years ago. Hydrocarbon retention is therefore considered a major risk. Reservoirs are the glaciogenic sandstones of the Marinoan and Sturtian glaciations, analogous to those cited from the Infra-cambrian above, and the Sansikwa carbonates of the intervening greenhouse periods. This latter carbonate play may comprise reservoirs analogous to the Neoproterozoic microbial–metazoan reefs similar to those found in the Nama Basin of southern Namibia (Wood 2005). These pinnacle reefs and platforms are over 300 m thick, in

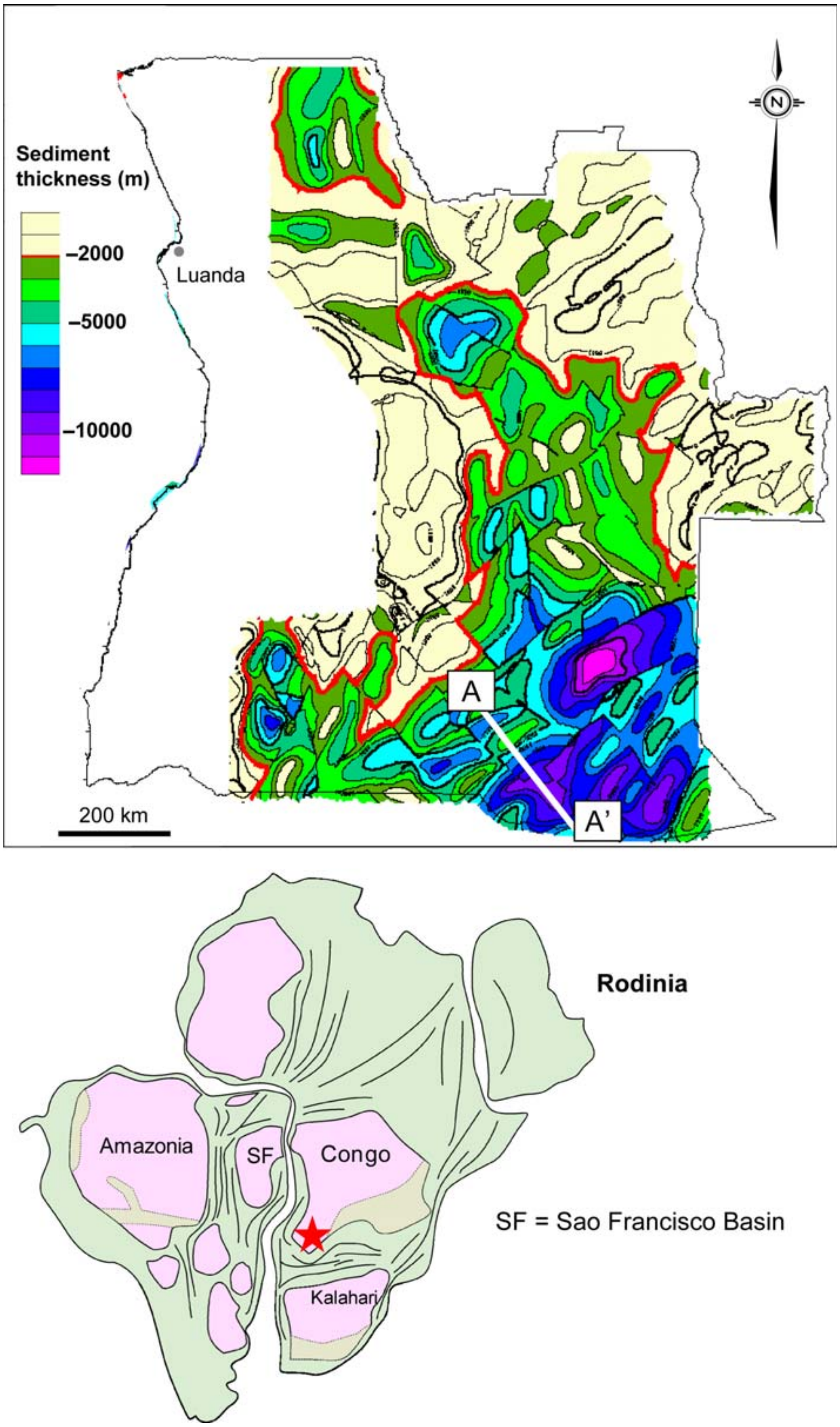

Fig. 18. A conceptual Neoproterozoic petroleum system?

excess of 7 km long and have the potential to be possible future giant fields.

A series of collaborative studies is in progress with NamCor in Namibia to investigate potential analogue petroleum systems and to determine their possible extension northwards into Angola.

Conclusions

In conclusion, energy demand, particularly for gas, is increasing globally. The advent of new technological developments in LNG will, for the first time, provide flexibility in supply. Angola will be a key player supplying this demand.

The exploration and exploitation of gas in Angola is in its infancy. From a petroleum geoscience perspective, there are multiple petroleum system opportunities. These comprise the emerging and mature conventional thermogenic Pre-Aptian salt and Post-Aptian salt petroleum systems of the offshore, renowned as a world-class oil province. Exploration for gas in these areas has the benefit of extensive, high quality seismic and well datasets. An unconventional biogenic gas petroleum system is postulated

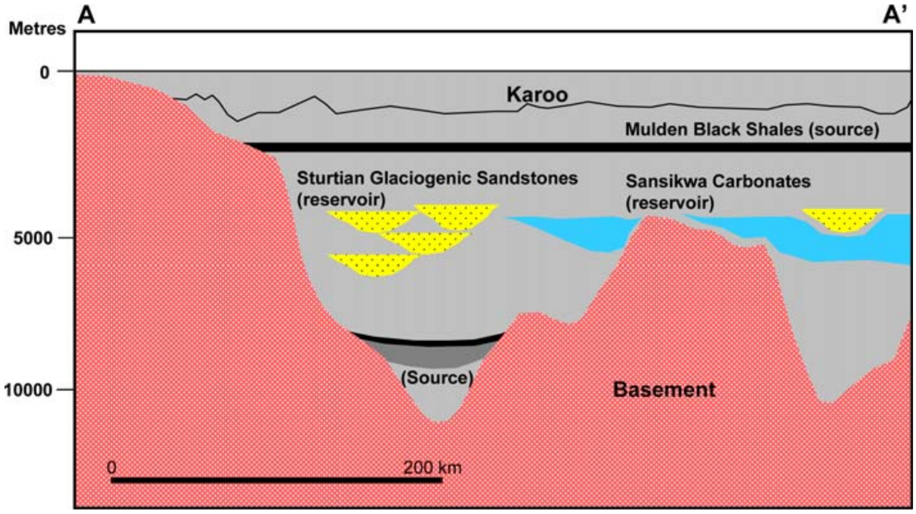

Fig. 19. Schematic Neoproterozoic play cross-section.

in deepwater that may extend beyond the boundaries of the thermogenic gas kitchens. Although unproven, the potential for gas in this frontier is large, principally in giant stratigraphic traps. Finally, the onshore interior Okavango and Owambo basins are vast – a true frontier. Data and knowledge are limited. However, conceptual Neoproterozoic petroleum systems are being developed using possible analogue settings from proven Neoproterozoic petroleum systems worldwide. As in the theme of the conference: '*from Mature Basins to New Frontiers*', Angola has both.

Sonagas has an ambitious discovery targets. This will require exploration for giant fields. A gas resource assessment of Angola is in progress suggesting potential in the tens to hundreds of TCF. The single most important issue to attain this potential is field size; do giant fields exist? Sonagas is confident that success exploring for gas in Angola will be unlocked by a combination of creativity and technology in petroleum geoscience.

The authors wish to thank the following current and former members of the Sonangol Gas Natural Exploration Department: S. Abiodun, A. Lasam, S. Dabeer, J. Gu, R. Rocca, S. Bastiot and A. Setiawan. We thank K. Black (GCA) for the graphics.

Delegate discussion

Question from John Argent (BG Group)

Is the current associated gas volume from the existing oil and serendipitous gas discoveries sufficient for multiple LNG trains? If so, when should we consider the deliberate exploration for gas in Angola?

Answer

The current associated gas volume from existing oil and gas discoveries is sufficient for the first train of LNG. Subsequent trains will rely on the exploration, development and production of new gas discoveries. The Soyo LNG facility is under construction and is due to be commissioned in 2012. It is therefore imperative to fast track the discovery, development and production of new gas volumes in preparation for a second train of LNG. In this regard, Sonangol Gas Natural and its partners are currently pursuing the deliberate exploration for gas in Angola.

References

Abreu, V., Sullivan, M., Pirmez, C. & Mohrig, D. 2003. Lateral accretion packages (LAPS): an important reservoir element in deep-water sinuous channels. *Marine and Petroleum Geology*, **20**, 631–648.

Ala, M. A. & Selley, R. C. 1997. *The West African Coastal Basins*. SADCC Energy Sector Technical and Administrative Unit, TAU, 129–150.

Anderson, J. E., Cartwright, J. A., Drysdall, S. J. & Vivian, N. 2000. Controls on turbidite sand deposition during gravity-driven extension of a passive margin: examples from Miocene sediments in Block 4, Angola. *Marine and Petroleum Geology*, **17**, 1165–1203.

Brice, S. E., Cochran, M. D., Pardo, G. & Edwards, A. D. 1982. Tectonics and sedimentation of the South Atlantic rift sequence; Cabinda, Angola. *Studies in Continental Margin Geology*, **34**, 5–18.

Burollet, P. F. 1975. Tectonique en radeaux en Angola. *Bulletin de la Societe Geologique de France*, **17**, 503–504; Les marge continentales et leur interet economique.

Burwood, R. 1999. Angola: source rock control for Lower Congo Coastal and Kwanza Basin petroleum systems. *In*: Cameron, N. R., Bate, R. H. & Clure, V. S. (eds) *The Oil and Gas Habitats of the South Atlantic*. Geological Society, London, Special Publications, **153**, 181–194.

Deptuck, M. E., Steffens, G. S., Barton, M. D. & Pirmez, C. 2003. Architecture and evolution of upper fan channel belts on the Niger Delta slope and in the Arabian Sea. *Marine and Petroleum Geology*, **20**, 649–676.

Dickson, W. G., Danforth, A. & Odegard, M. 2003. Gravity signatures of sediment systems: predicting reservoir distribution in Angolan and Brazilian basins. *In*: Arthur, T. J., MacGregor, D. S. & Cameron, N. R. (eds) *Petroleum Geology of Africa: New Themes and Developing Technologies*. Geological Society, London, Special Publications, **207**, 241–256.

Dutton, D. M., Lister, D., Trudgill, B. D. & Pedro, K. 2004. Three-dimensional geometry and displacement configuration of a fault array from a raft system, Lower Congo Basin, Offshore Angola: implications for the Neogene turbidite play. *In*: Davies, R. J., Cartwright, J. A., Stewart, S. A., Lappin, M. & Underhill, J. R. (eds) *3D Seismic Technology: Application to the Exploration of Sedimentary Basins*. Geological Society, London, Memoirs, **29**, 133–142.

Duval, B. C., Cramez, C. & Jackson, M. P. A. 1992. Raft tectonics in the Kwanza Basin, Angola. *In*: Jackson, M. P. A. (ed.) *Special Issue; Salt Tectonics. Marine and Petroleum Geology*. Butterworth/Geological Society, London, **9**, 389–404.

Fonnesu, F. 2003. 3D seismic images of a low sinuosity slope channel and related depositional lobe (West Africa deep-offshore). *Marine and Petroleum Geology*, **20**, 615–629.

Gee, M. J. R. & Gawthorpe, R. L. 2007. Early evolution of submarine channels offshore Angola revealed by three-dimensional seismic data. *In*: Davies, R. J., Posamentier, H. W., Wood, L. J. & Cartwright, J. A. (eds) *Seismic Geomorphology: Applications to Hydrocarbon Exploration and Production*. Geological Society, London, Special Publications, **277**, 223–235.

Karner, G. D. & Driscoll, N. W. 1999. Tectonic and stratigraphic development of the west African and eastern Brazilian margins: insights from quantitative basin modelling. *In*: Cameron, N. R., Bate, R. H. & Clure, V. S. (eds) *The Oil and Gas Habitats of the South Atlantic*. Geological Society, London, Special Publications, **153**, 11–40.

Kolla, V., Bourges, P., Urruty, J. M., Claude, D., Morice, M., Durand, J. & Kenyon, N. H. 1998. Reservoir architecture in recent and subsurface deep-water meandering channel and related depositional forms. *European Association of Geoscientists and Engineers/AAPG Third Research Symposium Extended Abstracts*, unpaginated.

Kolla, V., Bourges, P., Urruty, J. M. & Safa, P. 2001. Evolution of deep-water Tertiary sinuous channels offshore Angola (West Africa) and implications for reservoir architecture. *American Association of Petroleum Geologists Bulletin*, **85**, 1373–1405.

Kundu, N., Pal, N., Sinha, N. & Budhiraja, I. L. 2008. Palaeo-hydrate and its role in deep-water Plio-Pleistocene gas reservoirs in Krishna–Godavari Basin, India. *Proceedings of the 6th International Conference on Gas Hydrates (ICGH 2008)*, Vancouver, BC.

Lundin, E. R. 1992. Thin-skinned extensional tectonics on a salt detachment, northern Kwanza Basin, Angola. *In*: Jackson, M. P. A. (ed.) *Special Issue; Salt Tectonics. Marine and Petroleum Geology*. Butterworth/Geological Society, London, **9**, 405–411.

Mayall, M. & Stewart, I. 2000. The architecture of turbidite slope channels. *In*: Weimer, P., Slatt, R. M. *et al*. (eds) *Deep-water Reservoirs of the World: Gulf Coast Section Society of Economic Palaeontologists and Mineralogists Foundation 20th Annual Research Conference*, Houston, TX, 578–586.

Murphy, J. B., Pisarevsky, S. A., Nance, R. D. & Keppie, J. D. 2004. Neoproterozoic–Early Palaeozoic evolution of peri-Gondwanan terranes: implications for Laurentia–Gondwana connections. *International Journal of Earth Sciences*, **93**, 659–682.

Nance, R. D., Murphy, J. B. *et al*. 2008. Neoproterozoic–early Palaeozoic tectonostratigraphy and palaeogeography of the peri-Gondwanan terranes: Amazonian v. West African connections. *In*: Ennih, N. & Liegeois, J.-P. (eds) *The Boundaries of the West African Craton*. Geological Society, London, Special Publications, **297**, 345–383.

Nouze, H. & Baltzer, A. 2003. Shallow bottom-simulating reflectors on the Angola margin, in relation with gas and gas hydrate in the sediments. *In*: Van Rensbergen, P., Hillis, R. R., Maltman, A. J. & Morley, C. K. (eds) *Subsurface Sediment Mobilisation*. Geological Society, London, Special Publications, **216**, 191–206.

Rice, D. D. & Claypool, G. E. 1981. Generation, accumulation and resource potential of biogenic gas. *American Association of Petroleum Geologists Bulletin*, **65**, 5–28.

Sikkema, W. & Wojcik, K. 2000. 3D visualisation of turbidite systems, Lower Congo Basin, offshore Angola. *In*: Weimer, P., Slatt, R. M. *et al*. (eds) *Deep-water Reservoirs of the World: Gulf Coast Section Society of Economic Palaeontologists and Mineralogists Foundation 20th Annual Research Conference*, Houston, TX, 928–939.

Valle, P. J., Gielberg, J. G. & Helland-Hansen, W. 2001. Tectonostratigraphic development in the eastern Lower Congo Basin, offshore Angola, West Africa. *Marine and Petroleum Geology*, **18**, 909–927.

Wood, R. A. 2005. Neoproterozoic microbial-metazoan reefs, Nama Basin, Namibia. *Geological Society of America Abstracts with Programmes*, **37**, No. 7, 484.

Session: Unconventional Hydrocarbons Resources

Unconventional oil and gas resources and the geological storage of carbon dioxide: overview

H. JOHNSON[1] and A. G. DORÉ[2]

[1]*British Geological Survey, Murchison House, West Mains Road, Edinburgh EH9 3LA, UK (e-mail: hj@bgs.ac.uk)*
[2]*Statoil, 2103 CityWest Boulevard, Suite 800, Houston, TX 77042, USA*

Abstract: The 'Unconventional oil and gas resources and the geological storage of carbon dioxide' section of the *Proceedings* is designed to provide new insights from recent research and exploitation within these major growth areas in applied geology. Research and innovation on unconventional oil and gas have been driven by market needs – specifically concerns over oil and gas supply – as well as technological development. A cross-section of this work is highlighted in the current set of papers, covering ultra-heavy oil, shale oil, shale gas, basin-centred gas, tight gas and clathrates. Unsurprisingly, much of this research has been pioneered in North America. This work is complemented herein by some initial studies from Europe. Similarly, the geological storage of CO_2 is not simply a story of technological advance but also a response to an urgent societal imperative. Carbon dioxide sequestration is recognized as an important method for reducing greenhouse gas emissions in the near future, and is expected to have growing relevance to the oil and gas industry and the energy sector. Recent findings from current commercial carbon capture and storage projects in the North Sea and North Africa are presented and are complemented by an overview of major research programmes established in North America.

Keywords: unconventional hydrocarbons, heavy oil, shale gas, shale oil, gas hydrates, CO_2, carbon capture and storage

The Seventh Petroleum Geology Conference, held in London in 2009, reflected the significant interest in the geology of unconventional oil and gas resources that has developed over the past 5–10 years. Market drivers, specifically the concerns over supply, which culminated in wildly inflated oil and gas prices during 2008, probably provided the main impetus for this research. Given this perception, it is no surprise that much research and innovation regarding the exploration and development of unconventional oil and gas resources has been pioneered in North America, where these resources already have a long history of exploitation, contribute significantly to current production, and represent very large future energy sources (e.g. Jarvie *et al.* 2007; Ross & Bustin 2008). Nine of the papers in this section provide a good cross-section of research into the commercial exploration and exploitation of unconventional resources in North America and internationally, including ultra-heavy oil, shale oil, shale gas, basin-centred gas, tight gas and clathrates.

Although there is some history of commercial carbon dioxide (CO_2) injection or reinjection as a means of enhancing oil recovery, the current growth of interest in carbon capture and storage (CCS) is primarily driven by societal imperatives, with concerns about climate change raising the need to stabilize atmospheric concentrations of CO_2. The geological storage of CO_2 is gaining recognition as an important large-scale option for reducing greenhouse gas emissions in the near and foreseeable future. Four papers in this section describe very different approaches to CCS in the North Sea, North Africa and the USA.

Unconventional oil and gas resources

Unconventional oil and gas resources can be characterized by either intractable rock with very low permeability or intractable fluids (or in the case of clathrates, solids) where some form of stimulation is typically required for commercial production. These resources overturn many of the exploration and production paradigms that are applied to conventional hydrocarbons. For example, some unconventional gas resources are found in synclines rather than anticlines. In some cases, oil and gas is reservoired in rocks previously considered sources or seals. In other cases water is encountered updip of gas. In fact, many unconventional hydrocarbon resources lack fluid contacts. Whereas conventional gas resources are buoyancy-driven deposits, which form discrete accumulations in structural and/or stratigraphic traps, unconventional gas resources do not share these characteristics (e.g. Law & Curtis 2002). Unconventional hydrocarbons are commonly described as continuous or regionally pervasive in nature. Although the total in-place resource volume may be large, the overall recovery factor is commonly relatively low (e.g. Schmoker 2002; Sonneberg & Pramudito 2009). Completely dry holes cannot be drilled within the boundaries of such accumulations, but it is very possible to drill wells that are not economic. In other words, these resources are heterogeneous with commercial 'sweet spots', which are controlled by geological parameters such as structure, stratigraphy and diagenesis (e.g. Law 2002; Sonneberg & Pramudito 2009). Economically speaking, unconventional hydrocarbons are usually (but not always) characterized by high break-even product prices and, as such, become the focus of attention as conventional resource supplies diminish or become unavailable to the multinational companies.

Tight oil/shale oil

North America has a long history of producing oil from shales or very tight reservoirs, and considerable interest currently focuses on the Devonian–Mississippian Bakken petroleum system of the Williston Basin in central North America. This formation is generally regarded as a prime example of a continuous, unconventional tight oil exploration play, that is, a petroleum system where the source, seal and reservoir are the same unit, and prospectivity is not constrained by conventional trapping mechanisms. The play is commonly described as self-contained, with short migration

VINING, B. A. & PICKERING, S. C. (eds) *Petroleum Geology: From Mature Basins to New Frontiers – Proceedings of the 7th Petroleum Geology Conference*, 1061–1063. DOI: 10.1144/0071061

distances from mature source rock of the Bakken Formation (Sonneberg & Pramudito 2009). High pressure within the formation has been attributed to the generation of hydrocarbons within the Bakken and only limited fluid expulsion. However, there is some debate regarding the degree of migration of the hydrocarbons generated. Insight into this question is provided by Kuhn *et al.* through careful examination of geochemical parameters. The authors conclude that there is probably more migration within the Bakken Formation than previously assumed, and that the system can in fact be described as partially 'open'.

Shale gas

During the Sixth Petroleum Geology Conference held in 2004, a single paper by Richard Selley drew attention to the use of shale gas in parts of the USA and to the potential for exploitation of this resource in the UK (Selley 2005). Since then there has been an astonishing growth in research on the exploration and exploitation of shale gas plays. Harnessing this resource has converted a local curiosity into a multi-billion dollar international business, and has helped transform the North American market from gas starvation to guaranteed supply for 20 years or more. It is a classic example of market-driven research, whereby both innovation and pre-existing technology are brought together by economic necessity. This significant change was reflected by the high interest in shale gas shown at the Seventh Conference.

As with shale oil, shale gas systems are considered discrete, self-enclosed systems in which the source, seal and reservoir are one and the same. Shale gas is a very important exploration target in North America, where the resource falls into two distinct types: biogenic and thermogenic, although there can also be mixtures of the two gas types (Jarvie *et al.* 2007 and references therein). Known shale gas systems have been characterized by a number of parameters including total organic carbon content, thermal maturity, kerogen transformation, the efficiency of the source rock to retain its generated hydrocarbon products and the nature of the storage system. However, examination of productive shale gas systems indicates that the current parameters used to assess shale gas prospectivity vary greatly and may not provide a strong predictive model. Consequently, additional criteria, such as the clay and mineral content of the shales, the burial history and the precise nature of the gas storage and retention systems are fertile grounds for further research (e.g. Ross & Bustin 2008).

No major economic shale-gas enterprises are currently known from outside of North America, but many parts of Europe contain targets for shale gas exploration and commercial production is considered purely a matter of time. In this volume, Schulz *et al.* provide an overview of black shale successions that may be attractive for shale gas exploration in European basins, where conventional production is declining, underutilized gas gathering infrastructure exists and markets are accessible. Smith *et al.* follow Selley's pioneering work in providing a summary of organic-rich shale successions in the UK that may offer potential for shale gas resources. While no bonanzas equivalent to the Barnett or Marcellus Shales of the USA are envisaged, particular attention is drawn to the potential regional importance of the Mississippian Bowland Shales of northern England.

Basin-centred and tight gas

The basin-centred gas exploration play within the Western Canada Foreland Basin is characterized by a regionally pervasive gas saturated accumulation in low permeability, abnormally pressured reservoirs, with a lack of downdip water contact. Within this unconventional gas play, zones with commercially favourable reservoir producibility characteristics are controlled by a number of geological factors. For commercial success, Boettcher *et al.* highlight the importance of fully understanding the stratigraphy, sedimentology, rock properties and structure. They show that a process of long-term regional migration of undersaturated gas from source rocks into adjacent reservoir rocks, and the associated expulsion of water, is particularly important.

Kiraly *et al.* describe a basin-centred gas exploration play within the Pannonian Basin, Hungary, where thick Upper Miocene shales provide excellent pressure sealing above the significantly overpressured Upper and Middle Miocene formations. Within the overpressured zone, thick and poorly consolidated turbidite sandstones, as well as the shales, form unconventional reservoirs for basin-centred hydrocarbon accumulations.

Gas within unconventional fine-grained reservoirs is commonly extracted using hydraulic fracture treatments. Horizontal wells with multiple fracture stimulations are currently the most economic means of producing gas from tight reservoirs. Such wells are very expensive and typically suffer from a steep early production decline. Natural fractures, which are present in most shale units, act as weak planes that reactivate during hydraulic fracturing. Gale and Holder explain how knowledge of the geometry and intensity of the natural fracture system is therefore necessary for effective hydraulic fracture treatment design. Commonly occurring fracture types are reviewed and evaluated as to whether they are relevant to gas production.

Ultra-heavy oil

Ultra-heavy oil is too heavy or viscous to be produced by conventional flow from a reservoir. Biodegradation is generally responsible for the specific gravity and viscosity. Consequently, such accumulations are often found shallowly buried or even at surface. Again, there has been a resurgence of interest in exploiting ultra-heavy oil driven by the price rises of the mid-2000s. This enterprise is, however, technically and logistically demanding and is characterized by high break-even prices. Concerns also exist over the environmental challenges of exploiting this resource, since such enterprises can be seen as environmentally disruptive and CO_2-intensive. The heavy oil deposits of Canada are a case in point. With an estimated 1.7×10^{12} barrels in place, some assessments rank Canada second behind Saudi Arabia in terms of oil resources. Heavy oil makes up 98% of this resource, with the Athabasca Oil Sands of the Lower Cretaceous McMurray Formation in northern Alberta containing approximately 900×10^9 barrels in place. Depending upon the amount of overburden, the oil sands are developed through either surface mining or thermal *in situ* techniques, including steam-assisted gravity drainage. Like most unconventional resources, the accurate prediction and location of 'sweet spots' is critical. In this volume, Peacock shows how the development of an understanding of the regional distribution of fluvial–estuarine point bars, which comprise the principal reservoir rocks, is critical to maximizing commercial production from the Athabasca Oil Sands. For heavy oil thermal developments, the understanding and prediction of reservoir characteristics is particularly important because mudstone units within the reservoir can have a dramatic effect on steam chamber growth and the subsequent oil recovery.

Gas hydrates (clathrates)

Geoscientists have long speculated that gas hydrate accumulations could eventually be a commercially producible energy resource. The gas hydrates are naturally occurring 'ice-like' combinations of natural gas and water that have the potential to provide an immense resource of natural gas from the world's oceans and polar regions. The amount of gas in the world's gas hydrate accumulations is thought to exceed the volume of known conventional gas resources. However, until recently significant technical and economic hurdles made gas hydrate development seem a distant goal. This view began to change in recent years with the realization that this unconventional resource could possibly be developed with existing conventional oil and gas production technology. In this volume, Collett summarizes the most significant recent developments in this regard, such as gas hydrate production testing conducted during 2002 at the Mallik site in Canada and, more recently, the testing of the 'Mount Elbert Prospect' gas hydrate accumulation on the North Slope of Alaska.

Coal gasification

Coal has commonly been seen as a potential fall-back fossil fuel resource as hydrocarbons become depleted. Younger *et al.* describe how deep-seated coal resources may be exploited by means of underground coal gasification (UCG) with the possibility for coupling the technique to CCS. Significantly for the petroleum industry, the technological requirements for UCG, using directionally drilled boreholes from ground level, are far more akin to those of oil and gas production than they are to those of deep mining.

Geological storage of carbon dioxide

There is a range of options regarding the geological storage of CO_2. One possibility is the use of CO_2 in enhanced oil recovery and this is already commercial in some circumstances. The other main options are storage within depleted oil and gas fields or saline aquifers, while other techniques, such as storage in coals with enhanced coal bed methane, remain at an early stage. A key challenge for wider deployment of CO_2 geological storage is the requirement for the technique to be accepted as safe and verifiably effective. Senior *et al.* describe a commercial project that has been operating at In Salah in Algeria since 2004. CO_2 recovered from the natural gas production of the Krechba Field amounts to 1×10^6 tonnes per year, and this is injected into the water leg of the gas reservoir for the purpose of geological storage.

Injection of CO_2 commenced at the Sleipner Field in the Norwegian sector of the North Sea in 1996, and over 10×10^6 tonnes is currently stored in the late Cenozoic Utsira Sand saline aquifer. As a means of verifying its effectiveness, a comprehensive seismic monitoring programme of the storage site has been implemented, with repeat time-lapse 3D surveys that image the progressive development of the CO_2 plume. The total amount of CO_2 injected is known, and Chadwick and Noy show that independent verification of this amount can be achieved from the seismic data. Encouragingly, their observations of the laterally spreading CO_2 plume at Sleipner seem to confirm the integrity of the topseal to the Utsira Sand. Of equal significance, however, is their observation that history-matching techniques do not adequately predict the flow pathways indicated on the time-lapse 3D seismic, suggesting that our ability to model fluid behaviour in complex reservoirs remains at a simplistic level. Hermanrud *et al.* describe how monitoring of the CO_2 plume at Sleipner provides insights into the processes of subsurface fluid migration, especially with regard to vertical migration.

Esser *et al.* provide an insight into research by one of the seven major Regional Carbon Sequestration Partnerships in the USA and Canada, which aim to establish the best practices for permanently storing CO_2 in different geological formations. The research will help develop regulations and infrastructure requirements for future sequestration deployment and also includes a deep saline test in a structural dome 120 miles south of Salt Lake City, Utah, where deep saline formations are major targets for commercial-scale sequestration associated with the coal-fired power plants currently planned for the area.

References

Jarvie, D. M., Hill, R. J., Ruble, T. E. & Pollastro, R. M. 2007. Unconventional shale-gas systems: the Mississippian Barnett Shale of north-central Texas as one model for thermogenic shale-gas assessment. *American Association of Petroleum Geologists, Bulletin*, **91**, 475–499.

Law, B. E. 2002. Basin-centred gas systems. *American Association of Petroleum Geologists, Bulletin*, **86**, 1891–1919.

Law, B. E. & Curtis, J. B. 2002. Introduction to unconventional petroleum systems. *American Association of Petroleum Geologists, Bulletin*, **86**, 1851–1852.

Ross, D. J. K. & Bustin, R. M. 2008. Characterizing the shale gas resource potential of Devonian-Mississippian strata in the Western Canada sedimentary basin: application of an integrated formation evaluation. *American Association of Petroleum Geologists, Bulletin*, **92**, 87–125.

Schmoker, J. W. 2002. Resource-assessment perspectives for unconventional gas systems. *American Association of Petroleum Geologists, Bulletin*, **86**, 1993–1999.

Selley, R. C. 2005. UK shale-gas resources. *In*: Doré, A. G. & Vining, B. A. (eds) *Petroleum Geology: North-West Europe and Global Perspectives: Proceedings of the 6th Petroleum Geology Conference*. Geological Society, London, 707–714; doi: 10.1144/0060707.

Sonneberg, S. A. & Pramudito, A. 2009. Petroleum geology of the giant Elm Coulee field, Williston Basin. *American Association of Petroleum Geologists, Bulletin*, **93**, 1127–1153.

Bulk composition and phase behaviour of petroleum sourced by the Bakken Formation of the Williston Basin

P. KUHN, R. DI PRIMIO and B. HORSFIELD

Helmholtz-Centre Potsdam, German Research Centre for Geosciences (GFZ), Section 4.3, Organic Geochemistry, Telegrafenberg, D-14473 Potsdam, Germany (e-mail: kuhn@gfz-potsdam.de)

Abstract: The Bakken Formation is currently regarded primarily as a self-contained, unconventional petroleum system. While previously viewed as a source for oil occurring in overlying formations, it is now predicted that resources of more than 3.5 billion barrels of oil are trapped intraformationally. New insights into the formation's open v. closed nature are presented here using the physical properties of natural petroleum, source rock characteristics and the numerical modelling of phase behaviour. In the mature western part of the basin petroleum accumulations have been postulated to be continuous in nature, characterized by very short migration distances of indigenous hydrocarbons. This necessitates that the composition and therefore physical properties of the generated hydrocarbons must be controlled by the maturity of the source rock in the immediate vicinity. This assumption is not supported by the clustering of higher gas–oil ratios and lighter oil gravities along the locations of the anticlines in the basin. We have used open and closed system pyrolysis techniques to predict the bulk composition of the petroleum generated at different transformation stages, both cumulatively and instantaneously. Based on these predictions the Bakken would contain dominantly undersaturated fluids throughout the basin. Differences in predicted GORs of cumulative and instantaneous models support the conclusion that the reported hydrocarbon compositions cannot completely be explained by a tight self-contained petroleum system. The observed variability of in-place hydrocarbon compositions is readily explained by lateral migration of petroleum in the main middle Bakken carrier, and vertical leakage of emplaced hydrocarbons from the fractured reservoir at anticline locations. This has resulted in the loss of the early generated petroleum, and led to a present-day dominance of late generation products. These results reveal that the Bakken Formation is a partly open petroleum system, at least along the major anticlines of the Williston Basin.

Keywords: unconventional resources, shale oil play, North America, geochemistry, phase kinetics, phase behaviour, play assessment

The Devonian–Mississippian Bakken Formation of the Williston Basin in central North America (Fig. 1), recently described as a continuous, unconventional source rock–reservoir formation (Pitman *et al.* 2001; Pollastro *et al.* 2008; Sonnenberg & Pramudito 2009), is experiencing another renaissance as a major hydrocarbon resource. Earliest exploration for Bakken resources was initiated about half a century ago, three years after an unsuccessful well, targeting the overlying Madison Formation, recovered oil on a drill stem test in 1953 (LeFever 2005*b*). In succeeding decades, exploration in the 'Bakken Fairway' along the Nesson anticline proved to be successful. Unfortunately, the volumetric expectations for large amounts of oil based on its high hydrocarbon generation potential were not realized and interest in the Bakken as a reservoir decreased. With improvement of drilling technologies (Fritz 1990) and introduction of horizontal drilling techniques to the Williston Basin, interest returned and the Bakken reservoir potential was again targeted. Focusing on the middle member promised higher yield per well and greater success for this play, but high cost per well and low oil prices left the Bakken in disregard again. It took another 15 years and successful horizontal drilling in the middle member of the Bakken Formation in Elm Coulee and Parshall Field to kick off a new era in Bakken Formation drilling. With a new assessment of undiscovered oil resources (Pollastro *et al.* 2008) and higher oil prices, the Bakken play is back to prominence as an attractive onshore exploration target.

Despite the vast amount of work already performed on the Bakken Formation of the Williston Basin, questions regarding the dynamics of the system with respect to hydrocarbon generation and migration still remain. Here we combine natural data, including petroleum physical properties and geochemistry, with experimental results obtained on a multitude of Bakken source rock samples to provide an integrated understanding of the Bakken petroleum system.

Geological overview

The intracratonic, symmetrical Williston Basin (Hansen 1972) contains sediments of all geological periods from the Cambrian to the Cenozoic (Carlson & Anderson 1965) that amount to a maximum thickness of more than 4800 m sediment (Pitman *et al.* 2001) and multiple oil plays. Prominent source rocks were identified in the three members of the Mississippian Madison Group, the Mississippian–Devonian Bakken Formation, the Devonian Duperow Formation, and the Ordovician Red River and Winnipeg Formations (Jarvie 2001). Additionally, there has been some effort to produce gas from Cretaceous sediments and glacial drifts. The overall structural development of the basin is simple and defined mainly by the Nesson, Billings and Cedar Creek anticlines. While earlier publications described inversion of less than 100 m (Webster 1984), both Sweeney *et al.* (1992) and Osadetz *et al.* (2002) agree on greater inversion of around 550–700 m during the Cenozoic for the US and the Canadian parts of the basin. Additionally, based on apatite fission-track thermochronology, another inversion of *c.* 700 m during the Permian is proposed (Osadetz *et al.* 2002) for at least the Canadian part of the basin.

The low-permeability Bakken petroleum system, which can be found only in the subsurface of the basin, has a maximum thickness of 49 m (Murphy *et al.* 2009). The black shale source rocks have maximum thicknesses of 7 m for the upper and 15.2 m for the lower member (Webster 1984). The lithology in both shale members throughout their extent is invariant and homogenous,

VINING, B. A. & PICKERING, S. C. (eds) *Petroleum Geology: From Mature Basins to New Frontiers – Proceedings of the 7th Petroleum Geology Conference*, 1065–1077. DOI: 10.1144/0071065

Fig. 1. Location of the Williston Basin at the border of the USA and Canada; important structural features are indicated.

consisting of evenly distributed organic material of Type II kerogen, which is mixed with lesser amounts of clay, silt and dolomite grains (Meissner 1978; Webster 1984). Each of the three successively higher members of the Bakken Formation reaches across a wider area than the preceding one as they all pinch out against the older Upper Devonian Three Forks Formation that they overlay unconformably (Fig. 2; Meissner 1978; Webster 1984; LeFever 2008). The Bakken Formation, which extends blanket-like in the subsurface of the Williston Basin, consists of the middle reservoir layer encased by the upper and lower source rocks that are easily correlated through the basin by their high gamma ray signals (Murray 1968; Dembicki & Pirkle 1985; LeFever 2005*a*). Additionally, in some locations in the deeper part of the basin, the Sanish Sands of the Three Forks Formation are hydrologically connected to the Bakken Formation and need to be included when discussing the Bakken Petroleum system (Murray 1968). The total organic carbon (TOC) of the Bakken shales falls between 10 and 15 wt% and is seen petrologically as amorphous sapropelic kerogen (Schmoker & Hester 1983; Price *et al.* 1984; Webster 1984). Hydrogen indices are typically $>$500 mg HC g^{-1} TOC at a maturity below 0.4% vitrinite reflectance (Muscio & Horsfield 1996). Deposition occurred in a marine, euxinic environment in the photic zone (Requejo *et al.* 1992) during sea-level rise (Smith & Bustin 1998) in Devonian to Mississippian times based on conodont dating (Hayes & Holland 1983).

The lithology of the middle Bakken is more variable and changes laterally from dolomitic fine-grained silt to very silty fine-crystalline dolomite (Meissner 1978; Webster 1984). Porosity varies over a wide range from 1 to 16% but is generally low, averaging around 5% (Pitman *et al.* 2001) to 3.7% (Ropertz 1994). While the vertical permeability of the Bakken Formation ranges from 0.01 to 0.001 nd (Burrus *et al.* 1996*a*), the permeability of the middle Bakken is much higher, varying between 0 and 20 mD, and averaging around 0.04 mD (Pitman *et al.* 2001). These variations in the porosity and permeability together with the variability of the lithology of the middle Bakken should be kept in mind in the following, due to their first-order control on Bakken petroleum migration. The Lodgepole Formation conformably overlies the Bakken Formation, and is the basal unit of the Madison Group (Meissner 1978; Webster 1984).

Geochemistry has played a growing role in assessing the vertical and lateral extent of the Bakken petroleum system by addressing one of the most controversial issues, namely the contribution of Bakken sourced petroleum to other reservoir formations, that is, migration from the Bakken into the Madison Group. Williams (1974) proposed a vertical migration of petroleum from the Bakken based on carbon-isotope ratio measurements, gas chromatography, optical-rotation measurements and infrared spectroscopy. This was supported by Dow (1974), who indicated that oils expelled from the Bakken migrated vertically and laterally into Madison Formation traps or would eventually be retained by an evaporite seal of the Charles Salt of the Madison Group. In disagreement with his earlier publication (Price *et al.* 1984), Price & LeFever (1992, 1994) found support for the idea of a closed system without any major migration into overlying formations based on interpretation of reservoir rock extracts analysed by liquid and gas chromatography and mass spectrometry. Based on biomarker

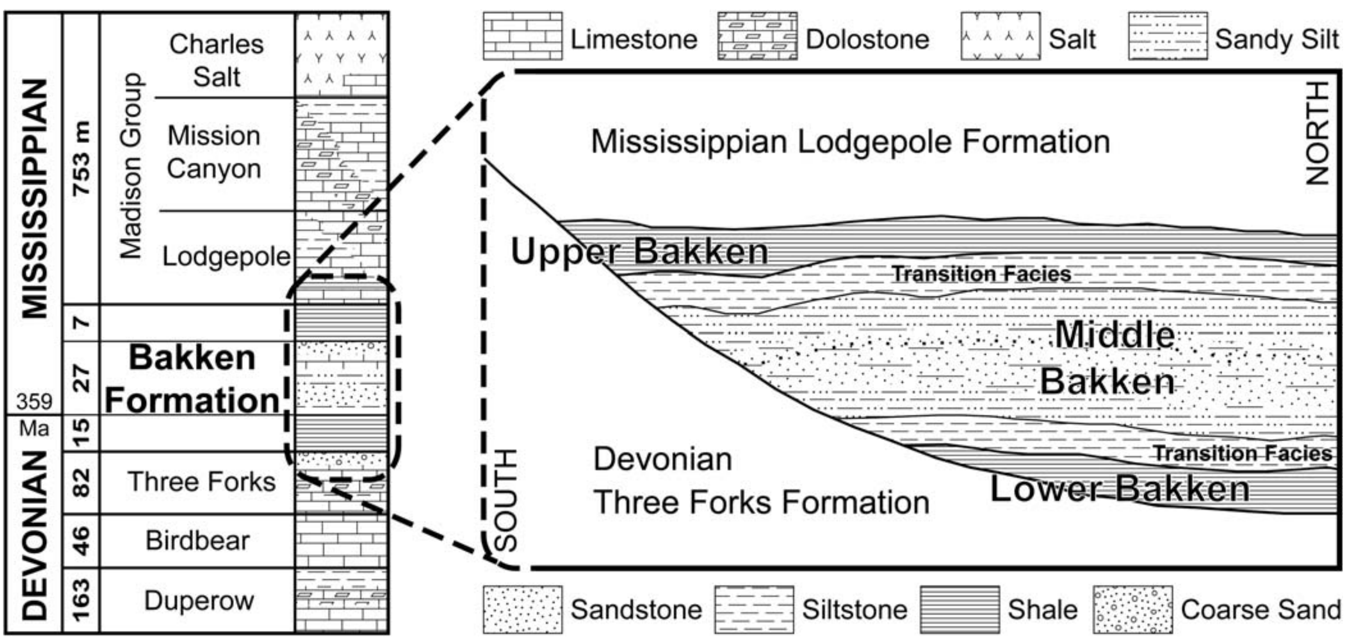

Fig. 2. Stratigraphic column of the Bakken (Webster 1984) and adjacent formations modified after the North Dakota Stratigraphic Column (Murphy *et al.* 2009); schematic profile of the Bakken Formation.

analysis Osadetz *et al.* (1994) agree that the mid-Madison accumulations were not sourced by Bakken-generated petroleum as they, in fact, had a carbonate biomarker signature inconsistent with Bakken biomarkers. This assessment was supported by Jarvie (2001), who used light hydrocarbon data to complement higher molecular weight biomarker data and discounted vertical migration in the US part of the Williston Basin except along major faults. However, Jiang & Li (2002) interpreted their quantitative biomarker analysis to support oil accumulations in the Canadian part of the basin, the Madison Group have significant contribution from Bakken-generated hydrocarbon.

An argument for a limited contribution from other sources to the Bakken petroleum system is provided by high overpressure within the Bakken system (Murray 1968; Finch 1969; Meissner 1978), which is attributed to the generation of hydrocarbons (Spencer 1987; Burrus *et al.* 1996*b*). Further, Pitman *et al.* (2001) discuss the development of small fracture systems in the Bakken Formation as related to hydrocarbon generation. Fractured areas in which the Bakken was exposed to greater stress by either external (structural movement) or internal (overpressure) processes are important, since exploration in these areas resulted in greater economical success, for example, the Bakken fairway along the Nesson anticline (LeFever 2005*b*).

The main result of the intense analysis and discussion of the Bakken Formation over the last four decades is a better understanding of the play associated with a continuous increase in the predicted in-place volume of hydrocarbons (Dow 1974; Williams 1974; Schmoker & Hester 1983; Price *et al.* 1984; Webster 1984; Flannery & Kraus 2006), which currently culminates in estimates of undiscovered resources of 3.65×10^9 BBL of oil and 1.84×10^{12} SCF of associated/dissolved natural gas (Pollastro *et al.* 2008). Further, the Bakken is currently described as an unconventional, continuous tight oil formation that has to be approached with new exploration and production techniques. The *in situ* generated petroleum in this continuous play is commonly found in close proximity to the mature source rock (Sonnenberg & Pramudito 2009), underlining the low impact of intraformation migration (Muscio *et al.* 1994), while stratigraphic (Johnson 2009) and maturity related traps (Coskey & Leonard 2009) are also described.

Goals and approach

Very little has been published on the bulk composition of Bakken petroleums. Therefore, this study integrates production data characterizing the physical properties of Bakken petroleums with geochemical analyses of the source rock including phase-predictive compositional kinetic models of hydrocarbon generation. By comparing these with the petroleum that is actually produced from the Bakken across North Dakota, further information regarding the effectiveness and extent of petroleum migration can be derived.

Data sources

Results of new Rock-Eval measurements were combined with data published by Muscio (1995), Sweeney *et al.* (1992), Webster (1984) and Price *et al.* (1984) to produce newly compiled maps. All newly measured data and model calculations are based on a sample set of more than 250 samples including all members of the Bakken and adjacent formations from 22 wells. The new dataset covers a maturity range from 405 to 453 °C $T_{\max}$, which corresponds to an equivalent vitrinite reflectance of about 0.35–1.10% (Dembicki & Pirkle 1985).

Gas–oil ratios (GOR) and oil gravity data (production API°) were taken from drilling reports and the database of the North Dakota Geological Survey and the Department of Mineral Resources (Oil and Gas Division) of the North Dakota Industrial Commission.

Analytical techniques

TOC was determined using a LECO SC632 analyser. Further, the petroleum generation potential was quantified by Rock-Eval pyrolysis (Espitalié *et al.* 1977) using a Rock-Eval 6 instrument following procedures of *The Norwegian Industry Guide to Organic Geochemical Analyses* (NIGOGA, Weiss *et al.* 2000). For analytical details of published data, please refer to the references cited above.

Open system pyrolysis gas chromatography (Horsfield *et al.* 1989) was used for kerogen-type characterization as well as determination of petroleum-type organofacies. Samples were heated from 300 to 600 °C using a temperature ramp of 50 °C $\min^{-1}$. Pyrolysis products were collected in a cryogenic trap (liquid nitrogen) from which they were liberated by ballistic heating (300 °C held for 10 min). Gas chromatography analysis was made using an Agilent 6890 GC with a HP-Ultra 1, 50 m × 0.32 mm internal diameter, dimethylpolysiloxane-coated (0.52 μm film thickness) column programmed from 30 to 320 °C at 5 °C/min (held for 35 min). Identification of prominent peaks of the chromatogram traces was carried out via retention time correlations with a standard sample and literature data (Horsfield & Dueppenbecker 1991) to determine the composition of generated hydrocarbons at different maturities.

Bulk kinetic parameters for Bakken source rocks were determined using an SR analyser (Humble Instruments). Open system programmed-temperature pyrolysis was performed at four different heating rates (0.7, 2, 5 and 15 °C $\min^{-1}$). The ensuing petroleum formation rate curves were analysed assuming a maximum of 25 first-order parallel reactions and a single frequency factor using Kinetics 2000 software (Lawrence Livermore National Laboratory). The kinetic model thus obtained allows extrapolation to hydrocarbon generation in nature (Braun & Burnham 1990; Ungerer 1990; Schenk *et al.* 1997).

Based on the results from the 0.7 °C $\min^{-1}$ heating rate experiments, laboratory temperatures for conversion stages representing 10, 30, 50, 70 and 90% transformation were determined. In preparation for closed system non-isothermal pyrolysis (MSSV, Horsfield *et al.* 1989), source rock material was sealed in small glass tube aliquots and heated to the five determined temperatures at a heating rate of 0.7 °C $\min^{-1}$. Analysis of the generated products was performed using the same analytical technique as for the open system pyrolysis experiments. This approach enabled insight into the compositional evolution of the generated hydrocarbons and calculated the GOR at different stages of source rock transformation. These results were further tested against natural conditions employing the compositional mass balance approach (Santamaría-Orozco & Horsfield 2003).

The evolving petroleum composition derived from MSSV pyrolysis was further used as input to phase kinetic modelling (di Primio & Horsfield 2006). Based on the composition of generated hydrocarbons and after gas phase compositional tuning, the behaviour of the generated fluid at different pressure and temperature conditions could be determined using PVT simulation software (PVTSim, Calsep, Denmark) to predict phase behaviour, physical properties and single or multiple phase compositions in the subsurface.

Finally, new and available well data were compiled to give an overview of the maturity, petroleum generation potential and physical production parameter distributions across the Bakken Formation. These maps were prepared utilizing a geographical information system (ArcGIS, ESRI Inc.).

Results

Bulk geochemical signature

During the first phase of this evaluation, the individual datasets were checked for consistency. It emerged that vitrinite reflectance data from two different datasets (Dembicki & Pirkle 1985; Muscio 1995) were inconsistent. In lieu of using vitrinite reflectance from the vitrinite-poor Bakken Formation, the Rock-Eval parameter T_{max} was used as a maturity parameter. Data from earlier publications (Price *et al.* 1984; Webster 1984; Sweeney *et al.* 1992; Muscio 1995) and newly derived data were compiled in a maturity map (Fig. 3a). In general the maturity was positively correlated with current burial depth, disregarding differentiation of upper or lower Bakken members. Highest values around 450 °C were measured on samples taken from wells within the deepest area of the basin, while the T_{max} decreased with shallower burial depth, for example, in an eastern direction. Furthermore, the higher T_{max} values in the northern part of the depocentre indicated a higher maturity, while in the southern part the source rock was less mature at similar depth. Therefore slightly increasing maturity from south to north in the western part of North Dakota is evident. Currently, it is not possible to further relate these changes to an increased heat flow or other variations in the temperature history, but the earlier mentioned higher inversion proposed for the Canadian part in contrast to the US part of the basin could have had an impact on this maturity trend.

The distribution of hydrogen index (HI) values, which describe the remaining petroleum generation potential of the Type II kerogen source rocks, conformed to the maturity distribution given by T_{max}. The lowest HI values in western North Dakota clustered around the deeper buried areas, in which the highest T_{max} values were encountered. Also, the shift to higher maturities from south to north in shallower buried areas away from the deeper parts of the basin was evident (Fig. 3b). In general, HI increased almost radially from deeper to shallower depths. While the negative relationship between HI and maturity was consistent with a uniform kerogen type across the area prior to maturation, inconsistencies for HI and T_{max} correlations were nevertheless found. In the shallower, immature part of the Bakken located east of 101°40′W longitude, a decrease of HI was not always accompanied by an increasing T_{max}. These low HI values in the counties of Renville, Ward and further east, which were in a similar range to the HI values in the deeper area, were not related to the catagenetic transformation of the source rocks but instead to either slightly different depositional environments in locations closer to the edge of the accumulation area or effects related to decarboxylation at low mature levels. Concerning the latter, a maximum HI of the Bakken source rocks may not be present in the original immature samples but rather at the end of diagenesis (Boudou *et al.* 1994; Killops *et al.* 1998). In Figure 4 the low maturity samples, which were sampled from a well in Rolette County, North Dakota, have the highest oxygen index (OI) values of all displayed samples, while the HI of more mature samples that are still in the immature range (Baskin 1997) are *c.* 100 mg HC g^{-1} TOC higher. This would indicate that the Bakken kerogen in the eastern part of the basin is also very similar to the composition in the west, but needs to further mature to fall into line with the original trends as they were described for the different kerogen types in the pseudo van Krevelen diagram (Tissot & Welte 1984).

Since neither explanation for the lower HI in the low mature area can be verified on the available sample set, samples from these areas will not be used as a corresponding immature counterpart for the samples in the deeper western part of the basin.

The TOC content of the Bakken Formation in North Dakota supports the thesis of a slight but recognizable facies variation of the source rocks. The reason for the decline of the percentage of organic carbon content in the east of the research area (Fig. 3c) can possibly be related to a slightly different depositional environment with poorer preservation potential due to its location closer to the edge of the basin. In this area changes of TOC related to hydrocarbon generation can be disregarded based on low T_{max} values of the rock samples, indicating immaturity. In contrast to the east, the lower TOC in the western part of the research area can be explained reasonably well by reduction due to hydrocarbon generation.

Quantification of generation and expulsion

Using the algebraic scheme developed by Cooles *et al.* (1986) and underlying assumptions (e.g. fixed amount of inert carbon, which is the part of the kerogen, i.e. not converted to petroleum during maturation), the original TOC in samples of elevated maturity was calculated. Based on the discussion above, samples from shallow areas in the east with lowest maturities were excluded. A sample whose T_{max} (427 °C) is still outside the threshold of hydrocarbon generation (Baskin 1997) with a production index less than 0.1 was selected as a standard representative of the immature source rock of the Bakken.

Following the Cooles *et al.* (1986) approach, the petroleum generation index (PGI) and petroleum expulsion efficiency (PEE) for the natural maturity sample set were calculated. The results show (Fig. 5) that the source rock starts to expel almost half of the generated hydrocarbons at a PGI of less than 0.15, where '0' is immature and '1' indicates the maximum amount of generated hydrocarbons. Further, the PEE (0 = no expulsion, 1 = expulsion of all generated hydrocarbons) increases to 0.9 at a PGI greater 0.4, which shows that 90% of the hydrocarbons generated in the source rock so far do not remain in the rock, but have been expelled into adjacent sediments. This indicates weak hydrocarbon retention in the Bakken source rocks, especially in the higher mature areas.

While Cooles *et al.* (1986) define the inert kerogen as constant throughout the main phase of petroleum generation, during which it undergoes internal rearrangement, publications by Horsfield (1997), Mann *et al.* (1997) and Jarvie *et al.* (2007) consider the formation of additional amounts of 'dead carbon' during petroleum generation. Dead carbon formation during hydrocarbon generation has been described for the Bakken source rocks (Muscio & Horsfield 1996); therefore, all results based on the Cooles approach have to be considered as maxima, since an increasing amount of dead carbon would lead to an overestimation of original immature TOC.

Further, when reviewing the PEE, the light composition of petroleum generated by Bakken source rocks has to be considered. Since some of the core samples were recovered nearly 30 years ago, part of the volatile components could have been lost during sample handling and storage. This would elevate the PEE for individual samples. Still, the majority of heavier hydrocarbons (C_{5+}) should have remained in the low-permeability and -porosity source rock samples that were used to conduct the measurements. The general trend will be the same, although slightly lower PEE values are possible.

Pyrolysis gas chromatography

After assessment of the bulk potential and behaviour of the petroleum generated by the Bakken, more detailed analysis of the hydrocarbon composition was performed. Pyrolysis gas chromatography was conducted on more than 60 source rock samples, representing the entire maturity range of the Bakken up to the end of the oil window between 450 and 460 °C T_{max} (Baskin 1997). Parts of the results are displayed in the petroleum-type organofacies diagram (Horsfield *et al.* 1993) and the kerogen-type sulphur

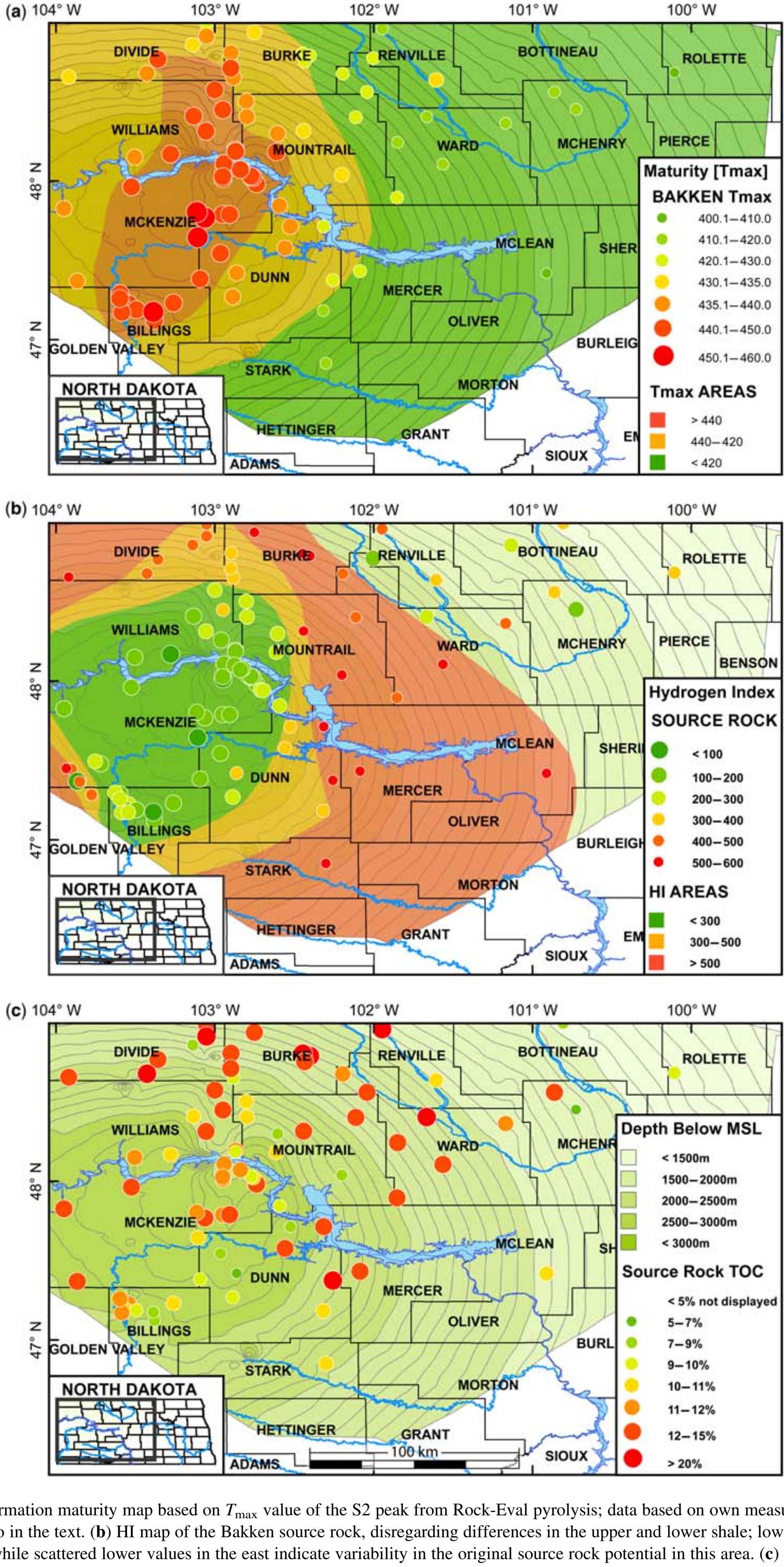

Fig. 3. (**a**) Bakken Formation maturity map based on T_{max} value of the S2 peak from Rock-Eval pyrolysis; data based on own measurements and publications referred to in the text. (**b**) HI map of the Bakken source rock, disregarding differences in the upper and lower shale; lowest values cluster in the deeper western area, while scattered lower values in the east indicate variability in the original source rock potential in this area. (**c**) Map of the weight percentage of TOC measured on source rock samples of several wells; in the background the depth of the top of the Bakken Formation below sea-level in the North Dakota part of the Williston Basin based on LeFever (2008) is displayed.

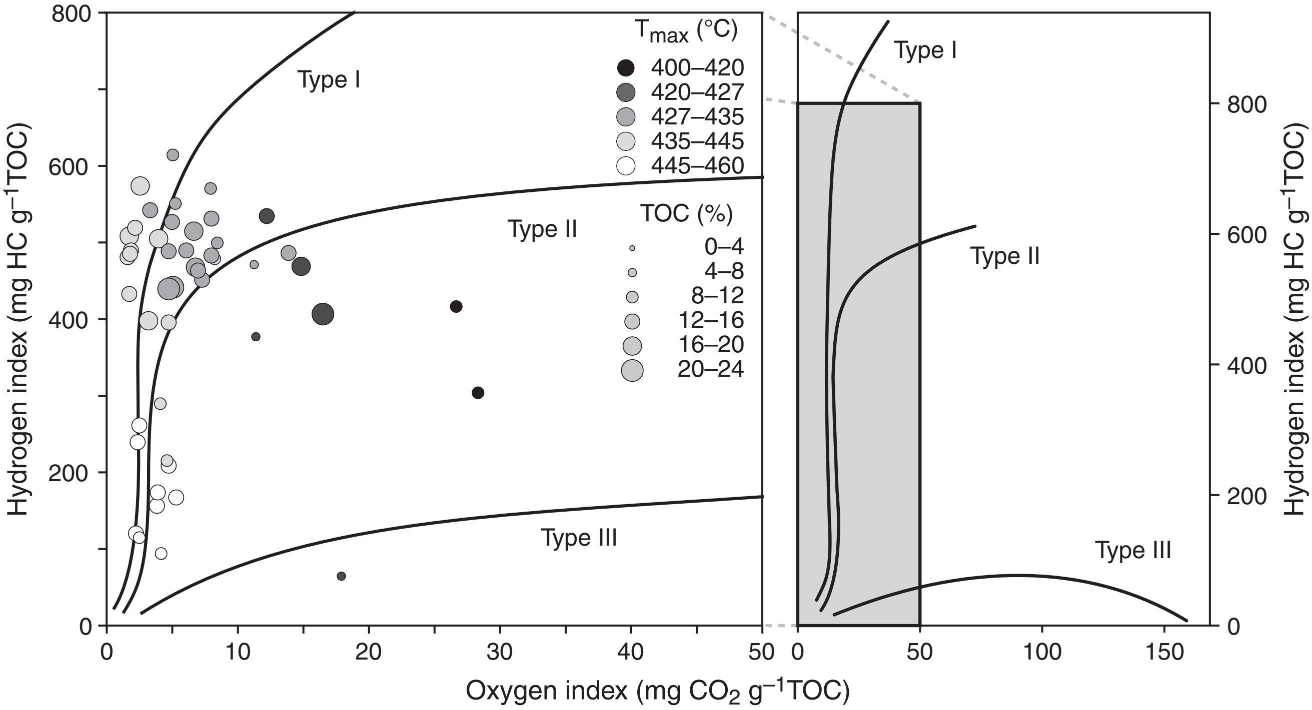

Fig. 4. Pseudo van Krevelen diagram (modified after Tissot & Welte 1984) displaying the HI and OI of samples from the upper Bakken member; maturity (T_{max}) and TOC (weight %) are greyscale- and size-coded.

diagram (Eglinton *et al.* 1990) in Figure 6, which shows clustering of the samples in both diagrams, with no distinction between the upper or lower Bakken member. Based on these results, a low variability of the composition of generated hydrocarbons and therefore a narrow range of variability in the original Bakken kerogen across the North Dakota part of the basin can be inferred.

Further, when comparing the percentage of C_{1-5}/C_{1+} of the bulk pyrolysis to the maturity of the samples (Fig. 7), it is clear that the change in composition is very linear, even including the low mature samples from the eastern part of the basin at $T_{max} < 415$ °C. Especially at the higher mature range, which represents the deeper part of the basin, the petroleum generated by the Bakken has a very low variability and a predictable GOR. Greater variability is only found in the immature interval from 415–428 °C T_{max}. The reasons for this remain unclear, but might be related to some source rock variability in these immature areas from which the samples originate. The significance of these laboratory-based results was further tested against a natural Bakken maturity sequence employing the compositional mass balance approach (Santamaría-Orozco & Horsfield 2003).

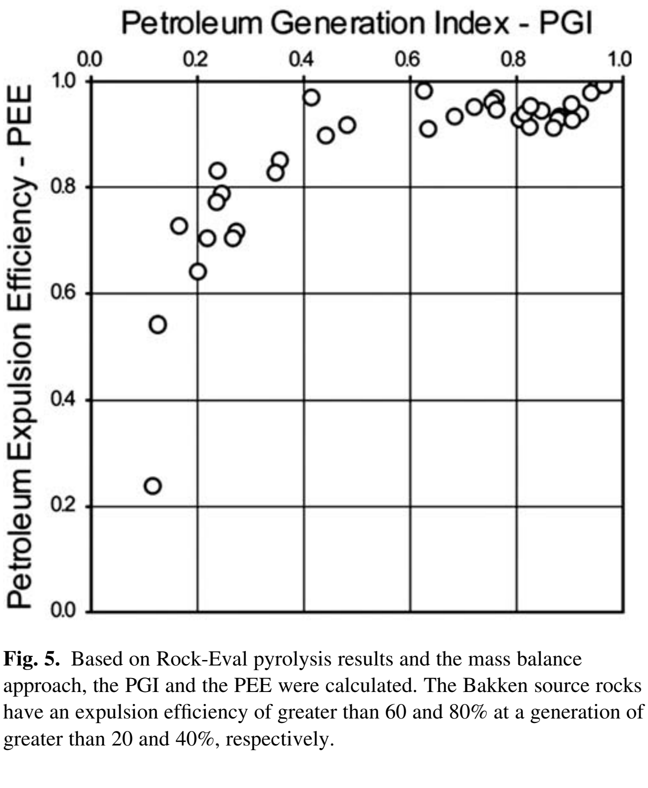

Fig. 5. Based on Rock-Eval pyrolysis results and the mass balance approach, the PGI and the PEE were calculated. The Bakken source rocks have an expulsion efficiency of greater than 60 and 80% at a generation of greater than 20 and 40%, respectively.

Source rock kinetics

Kinetic analyses of 12 low-maturity source rocks of five wells were performed to determine the variability of the petroleum generation behaviour of the Bakken kerogen. The majority of the resulting conversion rates that were calculated for a constant geological heating rate of 3 °C/Ma (Fig. 8) indicate a very narrow range of generation temperatures, disregarding any difference of upper or lower member. The low variability of 13 °C at 50% transformation ratio (TR) implies a very similar response to maturation, which underlines the homogeneity of the Bakken kerogen.

Phase behaviour

Based on analytical procedures described above, the composition of hydrocarbons generated from the Bakken Formation's kerogen at different degrees of transformation was assessed. As displayed in Figure 9 the GOR that is generated at different generation stages ranges from 30 $Sm^3\ Sm^{-3}$ at a TR of 10% to *c.* 220 $Sm^3\ Sm^{-3}$ at a TR of 90%. The higher rate of GOR increase at higher TR stages is related to the almost exponential increase in gas (C_{1-5}) generation. Based on T_{max} the maturity of the Bakken source rocks in the deepest area of the basin did not pass the oil window; there the highest TR was at 96%. This limits the cumulative naturally generated GOR in the Bakken to around 240 $Sm^3\ Sm^{-3}$.

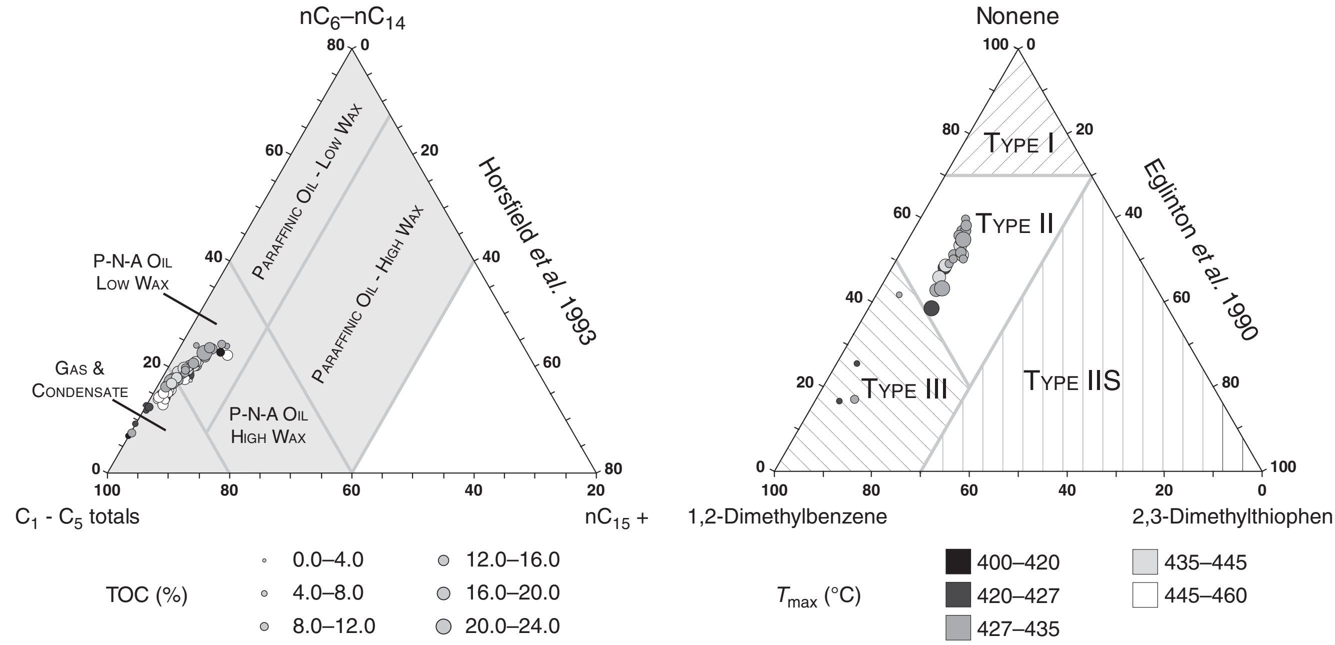

Fig. 6. Ternary plots show chain length distribution (left) and relative abundance of 2,3-dimethylthiophen, *n*-non-1-ene and 1,2-dimethylbenzene based on pyrolysis–gas chromatography; the majority of the samples from the upper and lower Bakken member cluster tightly together, implying a low kerogen variability; maturity (T_{max}) and TOC (weight %) are greyscale- and size-coded; plots are based on Horsfield *et al.* (1993) and Eglinton *et al.* (1990).

Using the phase kinetic approach, the phase behaviour of the generated hydrocarbons at variable pressure and temperature combinations could be defined for Bakken-generated hydrocarbons. Figure 9 displays the phase envelopes of petroleums generated from a selected source rock sample at five transformation stages. The pressure–temperature (PT) conditions within the phase envelopes describe conditions at which the hydrocarbons in the reservoir will occur in a two-phase state. All PT combinations outside the phase envelopes will result in an undersaturated phase of either liquid or gas (di Primio & Horsfield 1996). The temperature and pressure conditions are in general dependent on depth, while in some areas pressure significantly above hydrostatic conditions has been described for the Bakken petroleum system (Murray 1968; Finch 1969; Meissner 1978). Based on regular PT gradients of the area, temperature and minimum pressure conditions for the variable depth in which the Bakken can be found were identified. With these simple assumptions it is possible to determine if a single or a two-phase fluid can be expected at different locations of the Bakken. The phase distribution map (Fig. 10) is based on a Bakken Formation depth map (LeFever 2008), log tops of several wells provided by the North Dakota Geological Survey and average PT gradients. This map indicates that all regions in which the Bakken is currently under exploration and production have PT conditions that result in an undersaturated fluid. Even the elevated areas of the anticlines are not in or near the transition zone where PT conditions are suitable for phase separation.

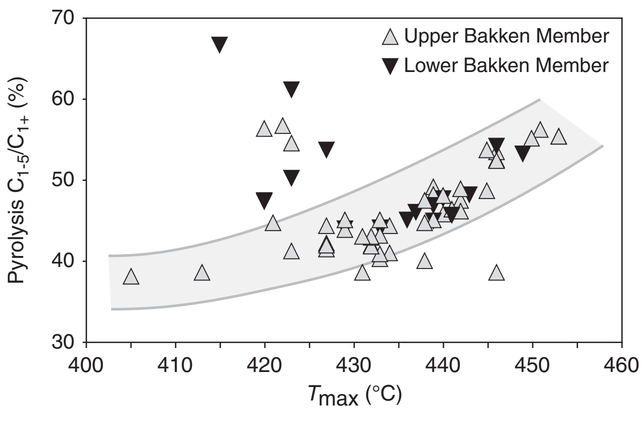

Fig. 7. Percentage of the C_{1-5}-bulk of the total C_{1+}-bulk yield based on pyrolysis–gas chromatography plotted against maturity in T_{max} (°C); in the range above 427 °C, which includes the oil window of the Bakken, a close relation between maturity and hydrocarbon yield composition is visible, irrespective of upper or lower source rock member; a continuation of this trend is also identified for a the maturity interval below 415 °C. Outliers are visible for a few samples that have not yet reached the oil window, the reasons for which remain uncertain.

Gas–oil ratio

After detailed laboratory analysis of the source rocks of the Bakken petroleum system, natural petroleum production data (predominantly surface produced GOR and API gravity) were assessed to be incorporated into a consistent description of the petroleum

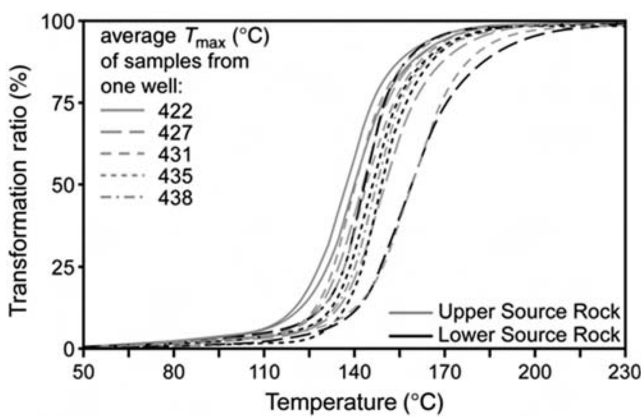

Fig. 8. Computed transformation ratios of 12 different source rock samples from five different wells and both source rock members are displayed for a constant heating rate of 3 °C/Ma; the majority of the curves cluster in a narrow range, which spans across a difference of 13 °C at a transformation of 50%.

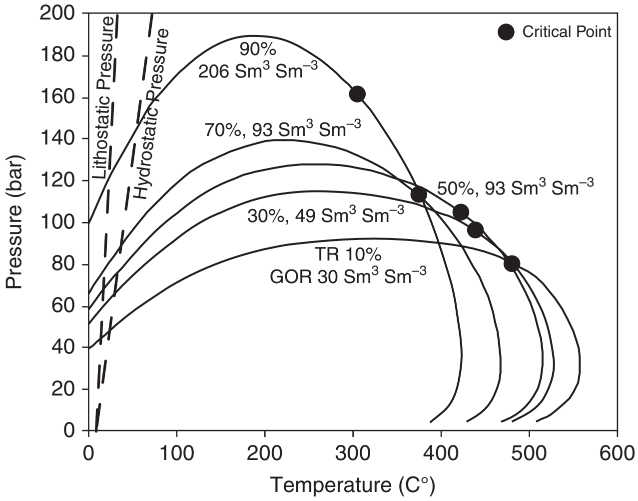

Fig. 9. Phase envelopes of petroleum of increasing maturity generated by MSSV from a Bakken Formation sample. Lithostatic and hydrostatic pressure gradients that can be expected in the Williston Basin are indicated by the dashed lines. GOR are included for the individual transformation stages in $Sm^3\ Sm^{-3}$.

system. As displayed for around 500 wells, which all tested Bakken pools, in Figure 11a, the GOR ranges from <50 to *c*. 900 $Sm^3\ Sm^{-3}$ (<280 to *c*. 5050 ft^3/BBL; in the following to convert to ft^3/BBL multiply values in $Sm^3\ Sm^{-3}$ by a factor of 5.61), with only eight wells showing GORs in excess of 500 $Sm^3\ Sm^{-3}$. While a limited number of values show the presence of gas condensates, the gross production from the Bakken has a GOR below 350 $Sm^3\ Sm^{-3}$, which characterizes the Bakken as a black oil play (McCain 1990).

When GORs are plotted by well location, a correlation with the major structures is visible. In Figure 12a, the highest GORs are situated in the areas of the major anticlines, while oil-dominated fluids are distributed in all other mature areas, regardless of depth. A relationship of GOR to depth could not be identified in the total dataset as displayed in Figure 11b.

Oil density

Similar observations as for the GOR arise from the distribution of oil gravities measured on Bakken pool-producing wells in North Dakota. In the following, the API° gravity scale is used to describe the oil gravity [API° at 15.6 °C = 141.5/density ($g\ cm^{-3}$) − 131.5]. The API° histogram in Figure 11c has a unimodal distribution with a mean around 42° API, implying that more than 600 wells across the state produce a non-degraded high-quality oil. Again, a correlation of API° gravity to areas of structural deformation is evident (Fig. 12b). Furthermore, plotting the oil gravity against depth (Fig. 11d) does not generate any trend and therefore implies a limited API° variability which is independent of source rock maturity.

Even though both parameters – light API° gravity and high GOR – cluster along the same locations, an expected statistical correlation cannot be reported (Fig. 13). This independence becomes obvious when compared with a dataset of the Devonian Exshaw Formation of the neighbouring Western Canadian Basin (Evans *et al.* 1971), which has been added for orientation. Even though the values are in a comparable range in some parts of the datasets, a similar trend is not identifiable.

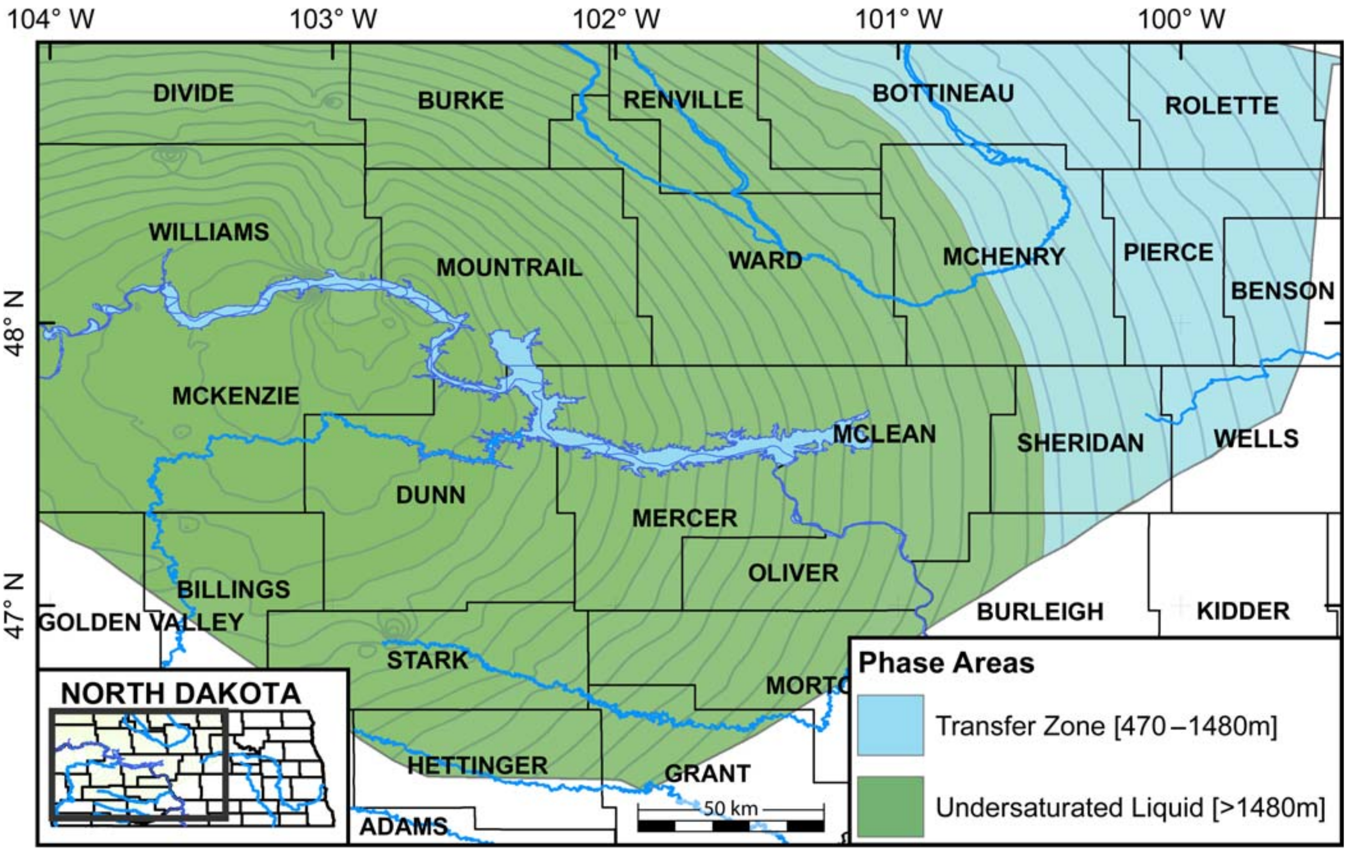

Fig. 10. Areas in which undersaturated liquid should be available are indicated. The whole area where the Bakken reached the threshold of petroleum generation is included in this area; only parts in the still immature shallower east are in the transfer zone in which first evidence of phase separation can be expected. This map is based on a depth map by LeFever (2008).

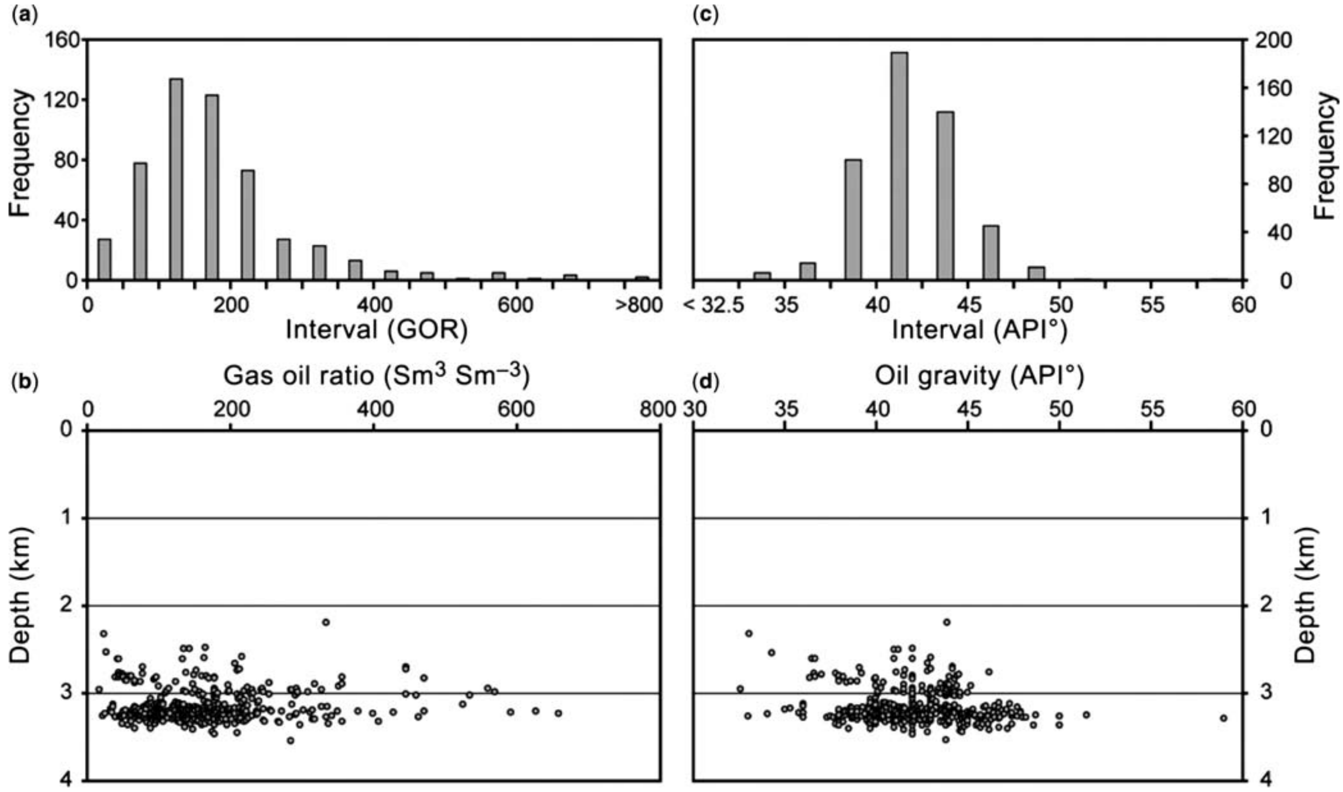

Fig. 11. GOR and oil gravity data of wells testing Bakken hydrocarbon pools from the database of the North Dakota Geological Survey is displayed: the upper left histogram (**a**) shows the GOR measured on *c*. 500 wells in the Williston Basin; most measured GORs are in the range from 50 to 250 $Sm^3\ Sm^{-3}$, while higher values are less frequent; the lower left graph (**b**) displays the same dataset against the depth of the Bakken Formation for their respective location; the right upper histogram (**c**) shows the oil gravity measured on *c*. 600 wells, most measured GORs are in the range from 37.5 to 45 API°, indicating only small variability in the Bakken Formation. In the lower right graph (**d**) the API° dataset is displayed against the depth of the Bakken Formation in their respective locations.

Further, from pyrolysis-gas chromatography and in agreement with Muscio & Horsfield (1996), petroleum compositions generated from the Bakken Formation are considerably lighter as compared with other Type II kerogen-containing source rocks like the Kimmeridge Clay or the Posidonia Formation. However, there are other marine source rocks that yield fairly light oils, for example, the Barnett shale (Hill *et al.* 2007).

Discussion

The abundance of source rock samples as well as production data allows a comprehensive investigation of the processes and mechanisms controlling petroleum generation, migration and accumulation for the Bakken Formation. Based on a collection of geochemical and production data, the variability of the Bakken source rocks is very narrow, concerning appearance, kerogen composition and general composition of the generated hydrocarbons, especially in the deeper buried western part of the Williston Basin in North Dakota. This is deduced based on the observed systematic changes in source rock properties as a function of increasing maturity as exemplified in the mass balance calculations and Figures 3a, b and 6–8. The eastern immature part of the source rock appears more variable with respect to the TOC and HI in the mature areas. The possible inhomogeneities require further investigation but might be related to their position closer to the edge of the basin that could facilitate variability in the source rock's depositional environment. Alternatively very low maturity of these samples may result in the remaining decarboxylation potential being absent in the samples that have gone through the early diagenetic stage. However, for this study their anomalous characteristics eliminate them from the list of potential immature reference samples representative of the mature western Bakken areas.

The upper and lower Bakken are indistinguishable from each other based on appearance and geochemical characteristics; accordingly they most likely both contribute to the hydrocarbon accumulations in the Bakken Formation and associated reservoirs.

The current understanding of the Bakken Formation as expressed by Pollastro *et al.* (2008) is that it is a continuous, unconventional, tight oil play where migration distances are short and accumulations are present throughout the formation, at least where the source rock is mature. Based on this description it should be expected that the in-place hydrocarbons should predominantly reflect the original source rock maturity or degree of transformation in any given location. This statement can be tested based on the data available from our own sampling as well as from the database of the North Dakota Geological Survey.

It is observed that the highest GORs and lightest oil gravities cluster along the locations of the anticlines. Further, the general lack of a depth trend for both GOR and API gravity indicate that source rock maturity, which is dependent on burial depth, does not control the petroleum properties encountered. The results from the mass balance calculations following the methodology of Cooles *et al.* (1986) indicate that, even at low transformation ratios (PGI *c*. 20%), the PEE reaches values above 60%, while PGIs higher than 40% result in PEEs above 90%. These values indicate that the Bakken source rock is an excellent expeller, as observed for a multitude of high-quality source rocks worldwide. In other words, there is no evidence from the available data that the Bakken source rocks have been subject to delayed expulsion due to a low-permeability surrounding environment, where

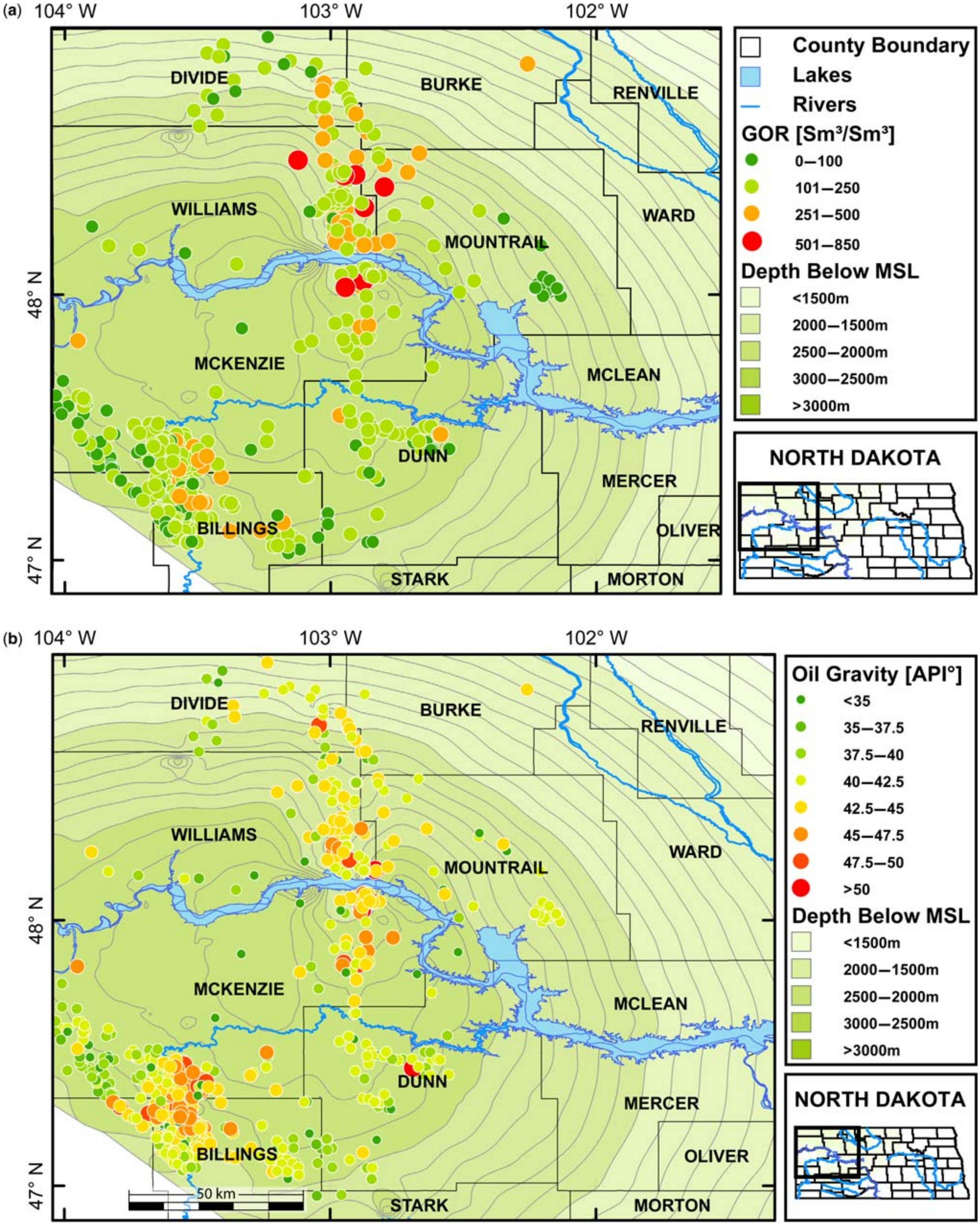

Fig. 12. Maps show the distribution of the wells with GOR (**a**) and oil gravity (**b**) measurements for the Bakken Formation; colours and size of the circles indicate the specific value at a well location.

secondary migration distances are short and a build-up of saturation during expulsion would be expected to have influenced the primary migration from the source. From these observations, the Bakken appears to be a petroleum system where generated hydrocarbons migrate to structural highs or stratigraphic traps and accumulate there. This is, of course, only a simplistic explanation for the distribution of GORs and oil gravities and contradicts current opinion on the Bakken Formation. The concept of an open Bakken petroleum system is, however, not supported by the persistent overpressure observed in the formation, which indicates a relatively tight formation where significant fluid loss has been hindered over geological periods.

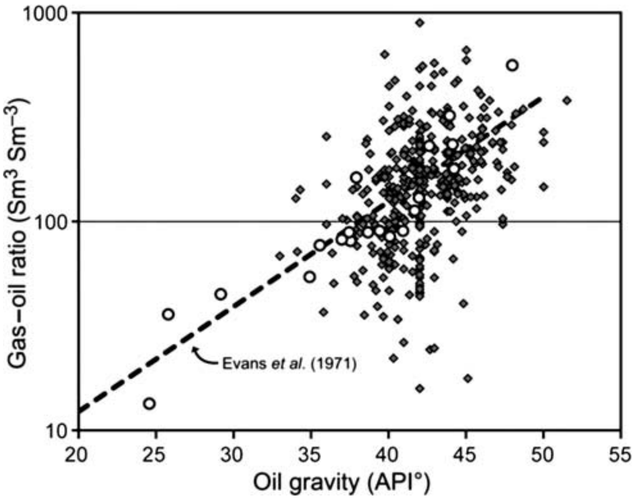

Fig. 13. GOR of the Bakken Formation plotted against the API°. For comparison, data from Evans *et al.* (1971) from the Devonian Exshaw from the neighbouring Western Canada Basin is included.

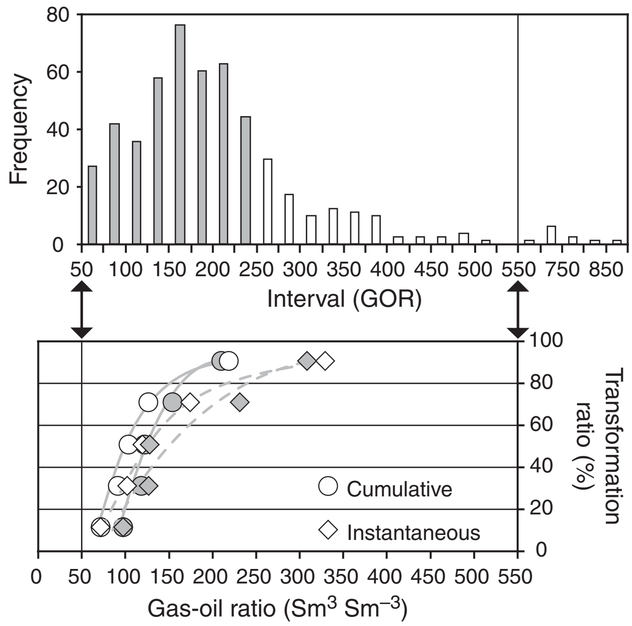

Fig. 14. Comparison of the actual measured GORs from the Bakken Formation with the laboratory based results from the PhaseKinetic approach. In the top histogram GOR values below 250 $Sm^3\ Sm^{-3}$ in grey, while higher values are white. The higher values correspond to the orange and red coloured GOR values in Figure 12a, which cluster primarily along the areas of the anticlines. In the lower graph the cumulative GOR that is generated at different transformation stages from two different immature source rock samples is displayed with circles; hydrocarbons generated at higher thermal maturity are lighter, leading to higher GORs at higher transformation stages. The cumulative generation of GORs can explain the majority of the production GORs. The diamond-shaped data points indicate the change of the GOR of the instantaneous generated petroleum. These reach higher GOR values and can therefore explain the higher GORs in the areas of the anticlines.

Laboratory simulation of hydrocarbon generation following the phase kinetic approach (di Primio & Horsfield 2006) indicates that the span of petroleum GORs generated reaches from roughly 50 $Sm^3\ Sm^{-3}$ at lowest stages of conversion to around 200 $Sm^3\ Sm^{-3}$ at complete conversion for a cumulative system. In a petroleum system characterized by short migration routes and no losses, it would be expected that reservoired petroleum should reflect the cumulative charge and, hence, be directly comparable to the laboratory predictions. This is in fact the case for the majority of the fluids tested in the basin, as is evident from the GOR histogram (Fig. 14). Fluid GORs from 50 to 250 $Sm^3\ Sm^{-3}$ can thus easily be explained. The lack of correlation between GOR and depth (i.e. maturity) indicates that the middle Bakken member petroleum is able to facilitate migration at least over moderate distances, thus erasing a clear relationship of petroleum maturity (as expressed by GOR or API gravity) and depth. The higher GORs observed, however, indicate a different situation. Higher GORs than those predicted experimentally can be explained by:

(1) variation in the source rock facies, which results in more gas-prone products; this is excluded based on the low kerogen variability of the source rock;
(2) influence of secondary cracking, which is unlikely to be dominant based on the present-day maturity of the Bakken; or
(3) dominance of a late stage generation phase, that is, an instantaneous as opposed to a cumulative composition.

The most likely explanation for the observed high GORs in the anticlines appears therefore to be leakage of the early generation stage and accumulation of late stage generation products. This process seems to have dominated only in the structurally influenced, and probably fractured anticlines, since GORs and API gravities are lower in both deeper and shallower structurally less disturbed areas of the Bakken. This observation underlines the relevance of the structural influence on the composition of accumulated hydrocarbons as opposed to the reservoir depth.

Based on the composition of Bakken-generated petroleum, which is inferred from closed system experiments and observed in the natural fluids, the phase behaviour at different pressure and temperature conditions was calculated. The applied average pressure and temperature gradients, which are very conservative since we are dealing with an overpressured formation (Murray 1968; Finch 1969; Meissner 1978), did not reach values that would allow a phase separation at depths at which mature Bakken source rocks are present. Thus, the hydrocarbons that were generated in the Bakken Formation should only exist as a single-phase undersaturated liquid, thus reducing the probability of phase separation and differential migration of oil and gas phases in the basin to a large extent.

Conclusion

Analysis of the geochemical data of a source rock maturity sequence, the GOR and gravity data of more than 600 wells and earlier published rock-evaluation data provided a detailed insight into the development and behaviour of source rock potential and generated petroleum in the Bakken Formation.

The upper and lower members of the Bakken Formation represent excellent source rocks which generate and very efficiently expel high API gravity petroleum. Source rock maturity within the basin is constrained to the oil window, reaching almost total kerogen conversion in the deepest regions of the Williston Basin. Secondary cracking of residual oil to gas, based on source rock maturity, is irrelevant in the Bakken Formation.

The middle Bakken member is a low-permeability carrier in which the generated and expelled petroleum is able to migrate laterally and accumulate in structural or stratigraphic traps.

The continuous nature of the middle Bakken accumulations is not apparent in our data, where fluid properties and source rock maturity do not correlate. In areas where structural deformation has increased the permeability of the Bakken system, hydrocarbon losses to surrounding formations through vertical leakage are assumed to have occurred, resulting in the isolation of a late mature petroleum phase in the reservoir.

We would like to thank the North Dakota Geological Survey, the Wilson M. Laird Core and Sample Library and staff for providing the core samples of the Bakken Formation and database access. Special thanks to J. A. LeFever for assistance and advice with the samples. Further, we would like to acknowledge D. M. Jarvie and an additional reviewer for their constructive and helpful comments and the effort they invested to improve the quality of the manuscript. The research on the Bakken Formation is part of the GFZ Industry Partner Project 'Predicting Petroleum Quality' that is sponsored by Chevron, ConocoPhillips, Devon Energy, Petrobras, and Statoil. This publication is part of a PhD study on the organic geochemistry of the Bakken Formation (P.P.K.).

References

Baskin, D. K. 1997. Atomic H/C ratio of kerogen as an estimate of thermal maturity and organic matter conversion. *American Association of Petroleum Geologists Bulletin*, **81**, 1437–1450.

Boudou, J. P., Espitalie, J., Bimer, J. & Salbut, P. D. 1994. Oxygen groups and oil suppression during coal pyrolysis. *Energy & Fuels*, **8**, 972–977.

Braun, R. L. & Burnham, A. K. 1990. Mathematical model of oil generation, degradation, and expulsion. *Energy & Fuels*, **4**, 132–146.

Burrus, J., Osadetz, K., Wolf, S., Doligez, B., Visser, K. & Dearborn, D. 1996*a*. A two-dimensional regional basin model of Williston Basin hydrocarbon systems. *American Association of Petroleum Geologists Bulletin*, **80**, 265–291.

Burrus, J., Wolf, S., Osadetz, K. & Visser, K. 1996*b*. Physical and numerical modelling constraints on oil expulsion and accumulation in the Bakken and Lodgepole petroleum systems of the Williston Basin (Canada-USA). *Bulletin of Canadian Petroleum Geology*, **44**, 429–445.

Carlson, C. G. & Anderson, S. B. 1965. Sedimentary and tectonic history of North Dakota part of Williston Basin. *American Association of Petroleum Geologists Bulletin*, **49**, 1833–1846.

Cooles, G. P., Mackenzie, A. S. & Quigley, T. M. 1986. Calculation of petroleum masses generated and expelled from source rocks; advances in organic geochemistry, 1985; Part I, Petroleum geochemistry. *Organic Geochemistry*, **10**, 235–245.

Coskey, R. J. & Leonard, J. E. 2009. Bakken oil accumulations – what's the trap? *In*: *American Association of Petroleum Geologists Annual Convention & Exhibition*. American Association of Petroleum Geologists, Denver, CO, 48.

Dembicki, H., Jr. & Pirkle, F. L. 1985. Regional source rock mapping using a source potential rating index. *American Association of Petroleum Geologists Bulletin*, **69**, 567–581.

di Primio, R. & Horsfield, B. 1996. Predicting the generation of heavy oils in carbonate/evaporitic environments using pyrolysis methods. Proceedings of the 17th International Meeting on Organic Chemistry; Part III, Origin of natural gases; petroleum geochemistry, impact of organic geochemistry on exploration; migration and expulsion of oil and gas. *Organic Geochemistry*, **24**, 999–1016.

di Primio, R. & Horsfield, B. 2006. From petroleum-type organofacies to hydrocarbon phase prediction. *American Association of Petroleum Geologists Bulletin*, **90**, 1031–1058.

Dow, W. G. 1974. Application of oil-correlation and source-rock data to exploration in Williston basin. New ideas; origin, migration and entrapment of oil, symposium. *American Association of Petroleum Geologists Bulletin*, **58**, 1253–1262.

Eglinton, T. I, Damste, J. S. S., Kohnen, M. E. L. & Deleeuw, J. W. 1990. Rapid estimation of the organic sulfur-content of kerogens, coals and asphaltenes by pyrolysis-gas chromatography. *Fuel*, **69**, 1394–1404.

Espitalié, J., Laporte, J. L. *et al*. 1977. Methode rapide de caracterisation des roches meres de leur potentiel petrolier et de leur degre d'evolution. *Revue de l'Institute Francais du Petrole*, **32**, 23–42.

Evans, C. R., Rogers, M. A. & Bailey, N. J. L. 1971. Evolution and alteration of petroleum in western Canada. *Chemical Geology*, **8**, 147–170.

Finch, W. C. 1969. Abnormal pressure in the Antelope field, North Dakota. *Journal of Petroleum Technology*, **21**, 821–826.

Flannery, J. & Kraus, J. 2006. *Integrated Analysis of the Bakken Petroleum System, U.S. Williston Basin. American Association of Petroleum Geologists Annual Convention*, 10–12 April 2006. Search and Discovery.

Fritz, M. 1990. Promising play endures. *American Association of Petroleum Geologists Explorer*, **11**, 14–15.

Hansen, A. R. 1972. Petroleum and natural gas; the Williston Basin. *In*: *Geological Atlas of the Rocky Mountain Region*. Rocky Mountain Association of Geologists, Denver, CO.

Hayes, M. D. & Holland, F. D., Jr. 1983. Conodonts of Bakken Formation (Devonian and Mississippian), Williston Basin, North Dakota. *In*: *American Association of Petroleum Geologists Rocky Mountain Section Meeting, 67*, Billings, MT. American Association of Petroleum Geologists, Tulsa, OK, Bulletins, 1341–1342.

Hill, R. J., Jarvie, D. M., Zumberge, J., Henry, M. & Pollastro, R. M. 2007. Oil and gas geochemistry and petroleum systems of the Fort Worth Basin. *American Association of Petroleum Geologists Bulletin*, **91**, 445–473.

Horsfield, B. 1997. The bulk composition of first-formed petroleum in source rocks. *In*: Welte, D. H., Horsfield, B. & Baker, D. R. (eds), *Petroleum and Basin Evolution*. Springer, Berlin, 335–402.

Horsfield, B. & Dueppenbecker, S. J. 1991. The decomposition of Posidonia shale and green river shale kerogens using microscale sealed vessel (MSSV) pyrolysis. *Journal of Analytical and Applied Pyrolysis*, **20**, 107–123.

Horsfield, B., Disko, U. & Leistner, F. 1989. The micro-scale simulation of maturation; outline of a new technique and its potential applications; geological modelling; aspects of integrated basin analysis and numerical simulation. *Geologische Rundschau*, **78**, 361–374.

Horsfield, B., Dueppenbecker, S. J., Schenk, H. J. & Schaefer, R. G. 1993. Kerogen typing concepts designed for the quantitative geochemical evaluation of petroleum potential; basin modelling; advances and applications. *Proceedings of the Norwegian Petroleum Society Conference*. Norwegian Petroleum Society, Trondheim, Special Publications, **3**, 243–249.

Jarvie, D. M. 2001. Williston Basin petroleum systems; inferences from oil geochemistry and geology. *The Mountain Geologist*, **38**, 19–41.

Jarvie, D. M., Hill, R. J., Ruble, T. E. & Pollastro, R. M. 2007. Unconventional shale-gas systems; the Mississippian Barnett Shale of North-Central Texas as one model for thermogenic shale-gas assessment; Special issue; Barnett Shale. *American Association of Petroleum Geologists Bulletin*, **91**, 475–499.

Jiang, C. & Li, M. 2002. Bakken/Madison petroleum systems in the Canadian Williston Basin; Part 3, Geochemical evidence for significant Bakken-derived oils in Madison Group reservoirs. *Organic Geochemistry*, **33**, 761–787.

Johnson, M. S. 2009. Parshall field, North Dakota, discovery of the year for the Rockies and beyond. *In*: *American Association of Petroleum Geologists Annual Convention & Exhibition*, Denver, CO, 109.

Killops, S. D., Funnell, R. H. *et al*. 1998. Predicting generation and expulsion of paraffinic oil from vitrinite-rich coals. *Organic Geochemistry*, **29**, 1–21.

LeFever, J. A. 2005*a*. The Bakken play of Montana and North Dakota. *The Bulletin of the Houston Geological Society*, **47**, 45.

LeFever, J. A. 2005*b*. Oil production from the Bakken Formation; a short history. *NDGS Newsletter*, **32**, 5–10.

LeFever, J. A. 2008. Bakken formation map series. *In*: LeFever, J. A. (ed.) *Geological Investigations*. North Dakota Geological Survey, Bismarck, ND.

Mann, U., Hantschel, T. *et al*. 1997. Petroleum migration; mechanisms, pathways, efficiencies and numerical simulation. *In*: Welte, D. H., Horsfield, B. & Baker, D. R. (eds) *Petroleum and Basin Evolution*. Springer, Berlin, 403–520.

McCain, W. D. 1990. *The Properties of Petroleum Fluids*. Penn Well Books, Tulsa, OK.

Meissner, F. F. 1978. Petroleum geology of the Bakken Formation, Williston Basin, North Dakota and Montana. *In*: *Williston Basin Symposium; 24th Annual Conference*. Montana Geological Society, Billings, MT.

Murphy, E. C., Nordeng, S. H., Juenker, B. J. & Hoganson, J. W. 2009. *In*: Helms, L. D. (ed.) *North Dakota Stratigraphic Column*. Miscellaneous Series 91. North Dakota Geological Survey, Bismarck, ND.

Murray, G. H., Jr. 1968. Quantitative fracture study; Sanish pool, McKenzie County, North Dakota. *American Association of Petroleum Geologists Bulletin*, **52**, 57–65.

Muscio, G. 1995. *The fate of oil and gas in a constrained natural system – implications from the Bakken petroleum system*. PhD thesis, Institut für Chemie und Dynamik der Geosphäre 4: Erdöl und Geochemie, RWTH Aachen University, Jülich.

Muscio, G. P. A. & Horsfield, B. 1996. Neoformation of inert carbon during the natural maturation of a marine source rock: Bakken Shale, Williston Basin. *Energy & Fuels*, **10**, 10–18.

Muscio, G. P. A., Horsfield, B. & Welte, D. H. 1994. Occurrence of thermogenic gas in the immature zone – implications from the Bakken in-source reservoir system. *Organic Geochemistry*, **22**, 461–476.

Osadetz, K. G., Snowdon, L. R. & Brooks, P. W. 1994. Oil families in Canadian Williston Basin (southwestern Saskatchewan). *Bulletin of Canadian Petroleum Geology*, **42**, 155–177.

Osadetz, K. G., Kohn, B. P., Feinstein, S. & O'Sullivan, P. B. 2002. Thermal history of Canadian Williston basin from apatite fission-track thermochronology; implications for petroleum systems and geodynamic history; low temperature thermochronology; from tectonics to landscape evolution. *Tectonophysics*, **349**, 221–249.

Pitman, J. K., Price Leigh, C. & LeFever Julie, A. 2001. *Diagenesis and Fracture Development in the Bakken Formation, Williston Basin; Implications for Reservoir Quality in the Middle Member*. US Geological Survey Professional Paper, **1653**, 19.

Pollastro, R. M., Cook, T. A. *et al*. 2008. *National Assessment of Oil and Gas Fact Sheet: Assessment of Undiscovered Oil Resources in the Devonian–Mississippian Bakken Formation, Williston Basin Province, Montana and North Dakota, 2008*. US Department of the Interior, US Geological Survey, 2.

Price, L. C. & LeFever, J. A. 1992. Does Bakken horizontal drilling imply a huge oil-resource base in fractured shales? *In*: Schmoker, J. W. C., Brown, E. B. & & Charles, A. (eds) *Geological Studies Relevant to Horizontal Drilling; Examples from Western North America*. Rocky Mountain Association of Geologists, Denver, CO, 199–214.

Price, L. C. & LeFever, J. 1994. Dysfunctionalism in the Williston Basin; the Bakken/mid-Madison petroleum system. *Bulletin of Canadian Petroleum Geology*, **42**, 187–218.

Price, L. C., Ging, T., Daws, T. A., Love, A., Pawlewicz, M. J. & Anders, D. E. 1984. Organic metamorphism in the Mississippian-Devonian Bakken Shale, North Dakota portion of the Williston Basin. *In*: Woodward, J., Meissner, F. F. & Clayton, J. L. (eds) *Rocky Mountain Association of Geologists 1984 Symposium; Hydrocarbon Source Rocks of the Greater Rocky Mountain Region*. Rocky Mountain Association of Geologists, Denver, CO, 83–133.

Requejo, A. G., Allan, J., Creaney, S., Gray, N. R. & Cole, K. S. 1992. Aryl isoprenoids and diaromatic carotenoids in Palaeozoic source rocks and oils from the Western Canada and Williston Basins. *Organic Geochemistry*, **19**, 245–264.

Ropertz, B. 1994. *Wege der primären Migration: Eine Untersuchung über Porennetze, Klüfte und Kerogennetzwerke als Leitbahnen für den Kohlenwasserstoff-Transport*. PhD thesis, Institut für Chemie und Dynamik der Geosphäre 4: Erdöl und Geochemie, RWTH Aachen University, Jülich.

Santamaría-Orozco, D. & Horsfield, B. 2003. *Gas Generation Potential of Upper Jurassic (Tithonian) Source Rocks in the Sonda de Campeche, Mexico*. *In*: Bartolini, C., Buffler, R. T. & Blickwede, J. F. (eds) American Association of Petroleum Geologists Memoirs, **79**. American Association of Petroleum Geologists, Tulsa, OK, 349–363.

Schenk, H. J., Di Primio, R. & Horsfield, B. 1997. The conversion of oil into gas in petroleum reservoirs; Part 1, Comparative kinetic investigation of gas generation from crude oils of lacustrine, marine and fluviodeltaic origin by programmed-temperature closed-system pyrolysis. *Organic Geochemistry*, **26**, 467–481.

Schmoker, J. W. & Hester, T. C. 1983. Organic carbon in Bakken Formation, United States portion of Williston Basin. *American Association of Petroleum Geologists Bulletin*, **67**, 2165–2174.

Smith, M. G. & Bustin, R. M. 1998. Production and preservation of organic matter during deposition of the Bakken Formation (Late Devonian and Early Mississippian), Williston Basin. *Palaeogeography, Palaeoclimatology, Palaeoecology*, **142**, 185–200.

Sonnenberg, S. A. & Pramudito, A. 2009. Petroleum geology of the giant Elm Coulee Field, Williston Basin. *American Association of Petroleum Geologists Bulletin*, **93**, 1127–1153.

Spencer, C. W. 1987. Hydrocarbon generation as a mechanism for overpressuring in Rocky Mountain region. *American Association of Petroleum Geologists Bulletin*, **71**, 368–388.

Sweeney, J. J., Gosnold, W. D., Braun, R. L. & Burnham, A. K. 1992. *A Chemical Kinetic Model of Hydrocarbon Generation from the Bakken Formation, Williston Basin North Dakota*. Lawrence Livermore National Laboratory, Livermore, CA, 60.

Tissot, B. P. & Welte, D. H. 1984. *Petroleum Formation and Occurrence*. Springer, Heidelberg.

Ungerer, P. 1990. State of the art of research in kinetic modelling of oil formation and expulsion. *Organic Geochemistry*, **16**, 1–25.

Webster, R. L. 1984. Petroleum source rocks and stratigraphy of the Bakken Formation in North Dakota. *In*: Woodward, J., Meissner, F. F. & Clayton, J. L. (eds) *Rocky Mountain Association of Geologists 1984 Symposium; Hydrocarbon Source Rocks of the Greater Rocky Mountain region*. Rocky Mountain Association of Geologists, Denver, CO, 57–81.

Weiss, H. M., Wilhelms, A. *et al*. 2000. *The Norwegian Industry Guide to Organic Geochemical Analyses*. Norsk Hydro, Statoil, Geolab Nor, SINTEF Petroleum Research, Norwegian Petroleum Directorate.

Williams, J. A. 1974. Characterization of oil types in Williston Basin; new ideas; origin, migration and entrapment of oil; symposium. *American Association of Petroleum Geologists Bulletin*, **58**, 1243–1252.

Shale gas in Europe: a regional overview and current research activities

H.-M. SCHULZ,[1] B. HORSFIELD[1] and R. F. SACHSENHOFER[2]

[1]*GFZ German Research Centre for Geosciences, Telegrafenberg, D-14473 Potsdam, Germany (e-mail: schulzhm@gfz-potsdam.de)*

[2]*University of Leoben, Chair of Petroleum Geology, Peter-Tunner-Straße 5, A-8700 Leoben, Austria*

Abstract: Shale gas is produced from fine-grained siliciclastic sediments that are typically rich in organic carbon. Nearly all shales contain thermal gas generated *in situ* at mature to overmature levels of thermal alteration, although gas of biogenic origin is also produced from some shales. While shale gas production in the USA began in 1821, it is only in the last few years that it has become widely significant (currently about 8% of the domestic gas). In contrast, European shale gas exploration is still in its infancy. In general, European sedimentary basins offer the best potential for shale gas occurrence because thick, organic matter-rich sediments occur in nearly all Phanerozoic strata. Even so, there is little knowledge about the factors controlling shale gas generation and, more importantly, shale gas production in European basins. These factors are not necessarily the same as those that control commercial shale gas production in the USA. Palaeozoic sediments of Cambrian to Ordovician age are currently being tested for their shale gas potential and productivity in Sweden, as are those of Silurian age in Poland. Moreover, Lower and Upper Carboniferous sedimentary successions from England in the west to Poland in the east probably contain shale gas, but their depth, thickness and thermal maturity may be limiting factors for exploration in continental regions. Lower Carboniferous black shales in the Dniepr–Donets Basin of the Ukraine may also hold a significant potential. Moreover, organic-rich sediments of Oligocene/Miocene age in the Paratethyan Basin may offer shale gas potential, for example in the Pannonian Basin. At present, Upper Jurassic black shales are currently being tested for their shale gas potential in the Vienna Basin. European analogues of known biogenic shale gas systems may occur locally in organic-rich Lower Cretaceous sediments in the North German Basin with gas generation being related to Pleistocene glaciation/deglaciation cycles.

Keywords: Shale gas, Europe, sedimentary basin, maturity, organic carbon, geological controls, resource potential

A great many formations with inherent shale gas potential occur throughout the world. Whether these potential targets emerge as economically viable depends not only upon geological characteristics, such as gas-in-place and rock properties, but also upon whether a distribution infrastructure exists and markets are readily accessible. Commercial production of shale gas occurs exclusively in North America to date. Here, shale gas is amongst the most active plays in recent years as a result of relatively high gas prices and the remarkable technological advances that have enabled the shales to be fractured and their gas potential exploited, beginning with the Mississippian Barnett Shale of the Fort Worth Basin (Curtis 2002; Frantz *et al.* 2006).

Annual natural gas production from shale gas reservoirs in the USA is approximately 1.0×10^{12} SCF and comes from more than 40 000 shale gas wells of which nearly half have been drilled in the last 10 years (around 6–10% of total natural gas production in the USA today; numbers vary according to reference). The Energy Information Agency (EIA) forecasts that shale gas production in the USA will more than double by 2020 if advanced exploration technologies are applied, and possibly reach 50% all told. The Haynesville Formation (Upper Jurassic, East Texas–North Louisiana, USA) is the most recent and promising addition to the existing US shale gas plays. Although production data are only preliminary because the basin is underexplored, the potential of the Haynesville is probably many times larger than that of the Barnett Shale. Very promising initial production rates, but steeper decline rates, have been reported (about 80% first year projected declines; Phasis 2008). A very high potential for shale gas has been determined in the Western Canada Basin (estimates are up to 1000×10^{12} SCF; Phasis 2008) and for the Devonian Muskwa Shale of the Horn River Basin, British Columbia, which is showing outstanding initial production rates (D. Jarvie pers. comm.).

A first estimation of global shale gas resources was published by Rogner (1997; $16\,112 \times 10^{12}$ SCF) with North America and China as the regions with the largest potential (both around 3000–4000×10^{12} SCF).

According to this study, Western Europe is a region with a lower potential shale gas resource ($\sim 510 \times 10^{12}$ SCF; Rogner 1997). It is true that Europe's geological setting is strongly compartmentalized and prospective basins of the size of the Fort Worth Basin, in other words roughly the area of Belgium, are therefore unlikely to occur. However, as black shales with gas window thermal maturity occur in almost all European Phanerozoic formations, a significant potential for exploration success exists and Europe is well positioned to buffer local energy demands.

European shale gas exploration is still in its infancy, although the first ideas to search for this unconventional gas resource were published by Selley (1987) about 20 years ago. Today, many companies have included this topic in their portfolios and actively explore for shale gas in Europe. For example, applications for licences to explore and develop shale gas were submitted during the 13th Onshore Round (launched in 2007) by the UK Department for Business Enterprise and Regulatory Reform (BERR). Moreover, the significance of shale gas is visible as, for example, shale gas prospects are available throughout Europe in large acreage positions, e.g. in France.

In recent years high energy prices and advances in fracturing technology and directional drilling have enabled shale gas production to become a lucrative reality in the USA, also because infrastructure is already in place. It is the predictions ahead of drilling

VINING, B. A. & PICKERING, S. C. (eds) *Petroleum Geology: From Mature Basins to New Frontiers – Proceedings of the 7th Petroleum Geology Conference*, 1079–1085. DOI: 10.1144/0071079

of gas-in-place and rock properties that are of paramount importance for reducing risk and identifying 'sweet spots' or fairways. In other words, there is still a lot to learn scientifically about how shale gas systems actually work. Significant advances have been made over the last five years, but there are great opportunities for major advances in science and technology.

The well known shale gas systems in the USA differ from one another as regards the key factors which controlled shale gas formation, and therefore exhibit different shale properties and gas compositions. Thus, the gas shale systems may contain thermogenic (Mississipian Barnett Shale) or biogenic gas (Devonian Antrim Shale), or mixtures of both (Cretaceous Lewis Shale; Fishman & Hill 2008). It is therefore difficult to transfer a single genetic model to potential European systems.

In this short contribution, general geological and shale gas-relevant features of selected onshore European black shales are introduced and analysed for significance. Moreover, known industry activities are presented alongside major basic research activities.

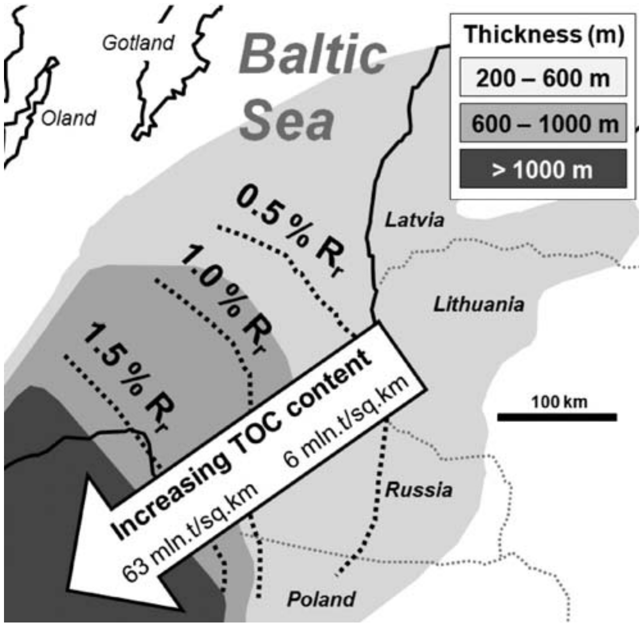

Fig. 1. Maturity, thickness and TOC contents of the Silurian dark-grey argillaceous complex (modified after Zdanaviciute & Lazauskiene 2004).

Stratigraphic overview of selected potential gas shales and case studies

Cambro-Ordovician black shales in northern Europe

A prominent example from northern Europe is the Scandinavian Alum Shale (Upper Cambrian to Lower Ordovician), exploited over the last century and more for heavy metals like uranium and vanadium. Total organic carbon (TOC) contents can exceed 20% (Schovsbo 2003; Nielsen & Schovsbo 2007, and references therein), and the organic matter, albeit of marine origin, has a high intrinsic potential for generating and storing gas at all maturity levels (Horsfield *et al.* 1992). A significant gas potential has also been found by hydrous pyrolysis experiments (Buchardt 1999). In this region the Alum Shale displays organic matter content and type, maturity and thicknesses that are typical of productive shale gas areas (Dyni 2006). Because of deeper burial in a southward direction the Alum Shale exhibits maturities of more than 2% vitrinite reflectance (random reflectance R_r) in the southern Baltic Sea region. Currently, the Alum Shale is being evaluated by Shell for its shale gas potential in southern Sweden, where the sediments are about 100 m thick.

Silurian black shales in Poland

Organic-rich sediments of the Silurian are widespread in Europe and contain intervals with TOC contents of more than 20%. In the Danish–Polish Trough organic-rich sediments can be more than 200 m thick and are proven source rocks for oils in the Baltic region. In general, the maturity of the sedimentary organic matter increases from the NE part of the Baltic Syneclise towards the Teisseyre–Tornquist Zone (Zdanaviciutė & Lazauskiene 2004, 2007; Fig. 1). It is not clear yet whether these sedimentary successions contain shale gas systems. 3Legs Resources plc has secured licences covering over 1 000 000 acres in the Baltic region of Poland to investigate shale gas potential.

Of the Silurian formations outside Poland that may contain shale gas potential, an excellent example is afforded by the Barrandian Basin of the Czech Republic where shales of Llandovery to Ludlow age have TOC contents of up to 8% and graptolite reflectances of up to 1.53% R_r (Volk *et al.* 2002).

Carboniferous black shales of the Variscan Foreland Basin

Investigations of Lower Carboniferous sediments from Ireland in the west to Poland in the east indicate an extended, northern calcareous shelf ('Carboniferous limestone facies') grading into deep basins north of the uprising Variscan orogen. The deep basins were filled by siliciclastic material sourced from the southern mountain chains. Fine-grained sediments of the basinal 'Culm' facies were enriched with organic carbon during periods of high productivity during the deposition of the Tournaisian Alum Shale ('Lower Alum Shale'; Gursky 2006). These sediments have TOC contents of more than 10% in the Rhenish Massif, for example (Siegmund *et al.* 2002). Interestingly, they are also regarded as good magnetotelluric conductors in the North German Basin (Al Duba *et al.* 1988; Hoffmann *et al.* 2001). The palaeogeographic situation during the Upper Visean and Serpukhovian (Early Namurian) is comparable to the Tournaisian situation with black shale deposition in deep basins (e.g. the Serpukhovian 'Upper Alum Shale' with TOC contents up to 3% in Germany; Zimmerle & Stribrny 1992). The belt with similar black shales extends to the west as the Bowland Shale facies (Hoffmann *et al.* 2001).

Locally high maturities (3–7% R_o) along outcrops of Lower Carboniferous sediments in the Rhenish Massif may exclude shale gas prospectivity. On the other hand, maturities of Lower Carboniferous shales below 3% R_o in central Germany (e.g. Harz mountains) as well as in boreholes in NE Germany indicate a potential for the occurrence of productive gas shales (Franke & Neumann 1999).

Gas-prone Westphalian black shales have gas window maturities along the Baltic coast of eastern Germany and Poland. Thicknesses of more than 1 km with frequent shaly intervals represent promising shale gas systems with ongoing gas generation (Hoth 1997). Towards the SW, increasing overburden coupled with increasing maturity and local intrusions during the Carboniferous/Permian transition may restrict shale gas occurrence. Locally high nitrogen contents of conventional gas shows in Namurian intervals might also point to reduced shale gas calorific value.

Both a thermogenic and biogenic shale gas potential is assumed for basinal Lower Carboniferous sediments across England and Wales, and for the Oil Shale Group in the Midland Valley of Scotland (Selley 2005). Details about UK data and their ramifications for shale gas prospectivity are discussed by Smith *et al.* (2010). Moreover, Lower Carboniferous black shales in the Northwest Carboniferous Basin in Ireland (Bundoran Formation; Clayton

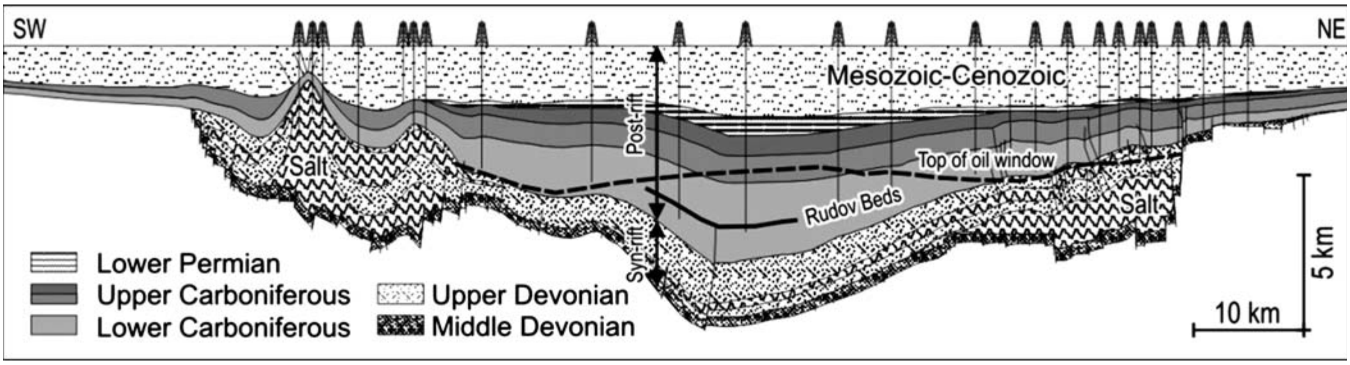

Fig. 2. Cross-section through the northwestern part of the Dniepr–Donets Basin (modified after Kivshik *et al.* 1993). Position of the Rudov Beds at the base of the Upper Visean section is indicated.

& Baily 1999) and in the Pomerian Basin in NW Poland (Lobzonka Shale Formation, Sapolno Calcareous Shale Formation; Matyja 2008) also are promising for shale gas.

Carboniferous black shales of the Dniepr–Donets Basin

The Dniepr–Donets Basin (DDB), a Late Devonian rift structure located within the East European Craton in Ukraine, hosts a large number of conventional gas and oil fields (Kabyshev *et al.* 1998; Ulmishek 2001). The basin fill includes about 4 km of syn-rift deposits and a Carboniferous to Cenozoic post-rift succession (Fig. 2) whose thickness increases towards the SE and reaches 15 km near the transition to the coal-bearing Donbas Foldbelt. Salt activity, tectonic reactivations and erosional events in the Permian and Late Cretaceous/Paleocene occurred during the post-rift stage (Stephenson *et al.* 2006 and references cited therein).

The Lower Carboniferous succession in the DDB is characterized by a high number of transgressive–regressive cycles controlled by tectonics and eustatic sea-level fluctuations (Dvorjanin *et al.* 1996). These cycles include shallow marine organic-rich shaly horizons several tens of metres thick. Typical TOC contents of these horizons range from 2 to 4%, though TOC contents averaging 6% and values as high as 12% occur in the 'Rudov Beds' defining the base of the Upper Visean section. This black shale, up to 70 m thick, is considered to be the main petroleum source rock in the DDB (Gavrish *et al.* 1994; Machulina & Babko 2004). According to Rock-Eval data, the organic matter in Upper Visean shales is mainly of kerogen type III–II (Kabyshev *et al.* 1999). Oil-prone coals with a Serpukhovian age occur mainly along the southern basin margin, whereas highly oil-prone shales with TOC contents above 10% occur locally in the northwestern part of the basin. Pelitic rocks in Bashkirian and Moscovian horizons typically have low TOC contents, but coal seams are widespread in the transition zone to the Donbas Foldbelt.

According to Shpak (1989) and Shymanovskyy *et al.* (2004), vitrinite reflectance at 5 km depth ranges from less than 1% R_o to 2% R_o in the northwestern DDB. Values above 2% R_o occur in the southeastern part of the DDB and the transition zone to the Donbas Foldbelt (Shpak 1989). At least in its northwestern part, the main oil and gas generation in Lower Carboniferous rocks occurred during Late Carboniferous/Permian time (Shymanovskyy & Sachsenhofer 2002).

Based on maturity and TOC contents, Upper Visean rocks (especially Rudov Beds) are considered the most interesting from a shale gas perspective.

Lower Jurassic black shales

Early Toarcian black shales are widespread in Europe (Farrimond *et al.* 1989). Occasionally, the sediments have TOC contents up to 19% and the marine organic matter enrichment is attributed to oceanic anoxic events (Schouten *et al.* 2000). These sediments are proven hydrocarbon source rocks in the South Central Graben in the North Sea, the Paris Basin and the Lower Saxony Basin (for an overview see Dill *et al.* 2008).

Early Toarcian black shales such as the Posidonia Shale display highly variable and locally very high maturity in the areas of Bramsche, Uchte and Vlotho (so-called massifs) in the Lower Saxony Basin. Maturation history is controlled by either deep burial at low, moderate or elevated heat flows or of shallow burial at very high heat flows such as in the vicinity of magmatic intrusions or volcanoes (Petmecky *et al.* 1999). The maturity of the Posidonia Shale with a thickness of several tens of metres increases constantly towards the centre of the massifs and can reach values of more than 4% R_o (Rullkötter *et al.* 1988).

Upper Jurassic shale gas in the Vienna Basin

The Vienna Basin is about 200 km long and 55 km wide, and extends from the Czech and Slovak Republics in the north to Austria in the south. It is of Miocene age, and lies superimposed on the outer allochthonous nappes of the Alpine–Carpathian thrust-belt (Kováč *et al.* 2004). Since conventional gas production started during the 1930s, more than 3000 wells have been drilled. The Vienna Basin is a mature oil and gas province with at least 46 fields. However, there is additional potential for 15×10^{12} SCF of shale gas in the Upper Jurassic Mikulov Marls (Langanger 2008), which is the main source rock for oil and gas in the basin (Ladwein 1988; Picha & Peters 1998; Adámek 2005). The TOC content of the more than 1500 m thick interval can exceed 10% and is composed of a kerogen type II–III (Ladwein *et al.* 1991). Mature gas-containing rocks are found below 5000 m, and cover an area of 500–800 km^2 (Fisher 2008).

Fractured intervals with gas kicks in the Mikulov Marls (Kimmeridgian to Upper Tithonian) have been observed at great depths (7500–8500 m in well Zistersdorf UT 2a; Wessely 1990; Fig. 3). This fracturing is argued to be the result of a pressure increase due to hydrocarbon generation.

The shale gas potential of the Mikulov Marls is currently under investigation by OMV (Vienna), utilizing horizontal drilling, completion and fracture stimulation and using an existing deep well.

Jurassic black shales are locally present also in the Carpathian foreland in Poland and Ukraine, but with less effective shale gas properties (Lafargue *et al.* 1994).

Neogene shale (basin centred) gas in the Makó Trough (Pannonian Basin)

The Makó Trough, located in SE Hungary and extending into Romania, is a 75 km long, NW–SE trending sub-basin of the

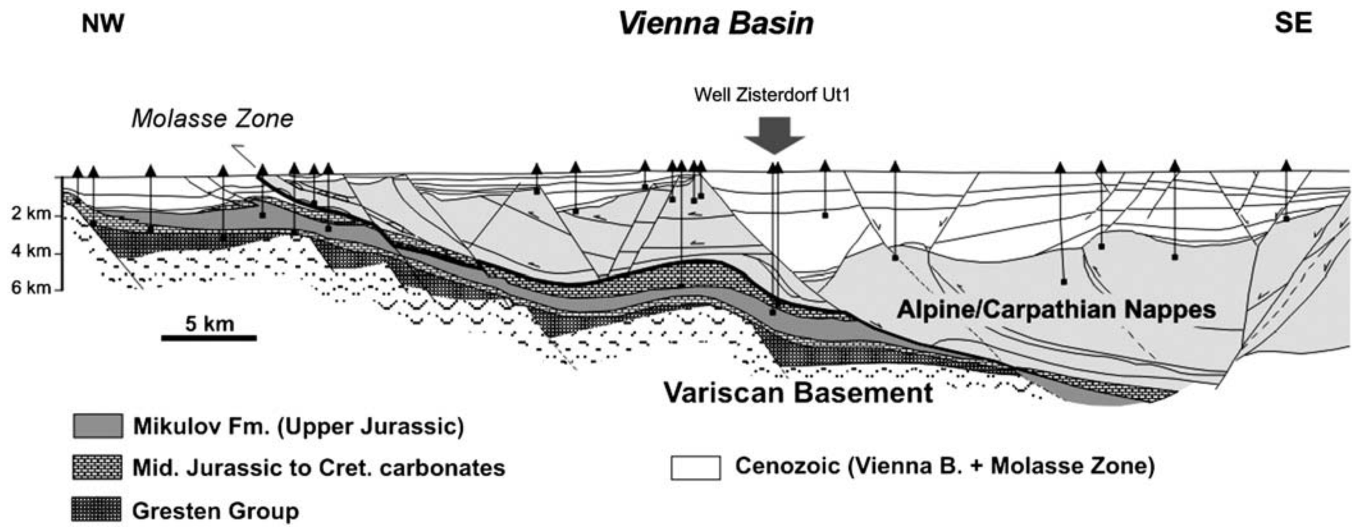

Fig. 3. Geological cross-section of the Vienna Basin highlighting the Mikulov Marl as a potential shale gas system (modified and simplified after Arzmüller *et al.* 2006).

Pannonian Basin System (Fig. 4). The total sediment thickness of Neogene–Quaternary rocks amounts to about 7000 m. Subsidence commenced during late Early Miocene times. Marine transgressions reached the Makó Trough during the Middle Miocene when black shales were deposited in oxygen-depleted deep marine settings (Haas 2001). Maximum water depth was attained during the Early Pannonian. This event is documented by the presence of pelagic fine-grained rocks of the Tótkomlós Member and the overlying turbidite-rich Szolnok Formation. At the end of the Pannonian, subsidence slowed down and the Makó Trough was filled by delta-slope and delta-plain deposits (post-rift phase). Subsidence rates increased again during Late Pliocene times as a result of east–west directed compression (cf. Horváth & Cloetingh 1996).

Middle Miocene basinal rocks (e.g. Makó Formation) and the Late Miocene Tótkomlós Member are considered the main sources of oil and gas (Dolton 2006). TOC contents range up to 5% (Middle Miocene) and 2% (Late Miocene), respectively, and are composed mainly of kerogen type III (and II) (Clayton *et al.* 1994). Minor source rocks occur in the basinal marls of the Szolnok Formation, whereas the delta-plain deposits include excellent source rocks, but are probably immature.

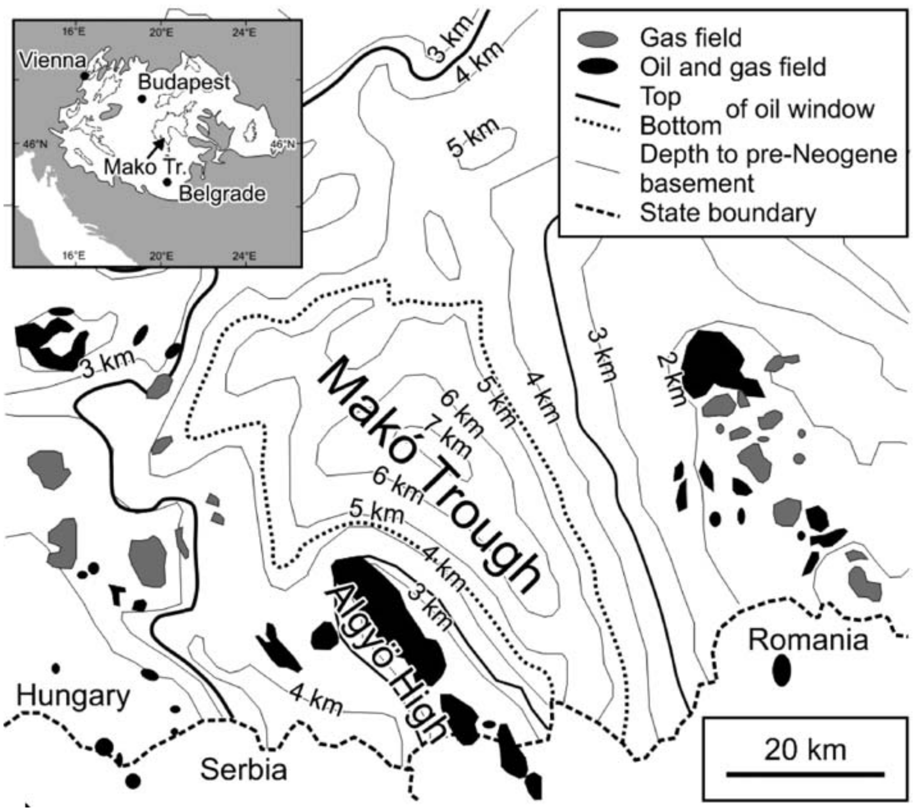

Fig. 4. Map showing depth to pre-Neogene rocks in the Makó Trough. Position of the oil window and of hydrocarbon fields are also shown (after Korosi 2007). Insert illustrates position of the Makó Trough in the Pannonian Basin system.

The oil window in SE Hungary is located in the depth range 2.4–4.3 km (Horváth *et al.* 1988). High heat flows (80–120 mW m^{-2}) and geothermal gradients (4–8 °C/100 m) are associated with lithospheric thinning. Hydrocarbon generation started during the latest Miocene and is still in progress (Magyar *et al.* 2006). The generated hydrocarbons filled major oil and gas fields above the surrounding basement highs (Horváth & Tari 1999; Tari & Horváth 2006), including the giant Algyö field, which produced 31×10^6 tonnes of oil and 70×10^9 m^3 of gas (Magyar *et al.* 2006). However, major resources estimated at about 600×10^9 m^3 of potential recoverable unconventional gas (shale gas and basin centred gas) remain within the Makó Trough (Korosi 2007) and are currently being evaluated by ExxonMobil, MOL and Falcon Oil & Gas.

Is there potential to find Antrim Shale-analogues with biogenic methane in Europe?

Before the Barnett became *the* shale gas system in the USA, shale gas was predominantly produced from the Upper Devonian Antrim Shale along the margins of the Michigan Basin during the 1990s (Curtis 2002). The gas in these areas is predominantly of biogenic origin ($\delta^{13}C$ as low as −56‰) and contains significant amounts of CO_2 (Martini *et al.* 1998; Jenkins & Boyer II 2008). Post-Pleistocene deglaciation resulted in a decrease of hydrostatic pressure. Meteoric water circulating along newly created weak zones diluted the highly saline pore water and enabled microbes to produce biogenic methane (Formolo *et al.* 2008). Is such a scenario applicable to other parts of northern Europe?

Organic matter-rich intervals of Lower Cretaceous age (Wealden, Barremian–Aptian boundary; Littke *et al.* 1998) may have undergone similar geological pathways, e.g. in the Lower Saxony Basin (Germany). This region was glaciated during the Pleistocene and experienced a similar geological history to the Michigan Basin. Intervals of Wealden sediments and along the Barremian/Aptian transition may have a biogenic shale gas potential in this basin. Moreover, some prerequisites for shale gas formation may also exist in the Puchkirchen Formation (Upper Oligocene to Early Miocene) of the Alpine Foreland Basin, which can be more than 1000 m thick (de Ruig 2003). Prominent bacterial methane gas accumulations occur in these clastic deep-water sediments. The gas is sourced from clayey horizons of the formation which contain immature kerogen type III (to II). A detrimental element may be the low level of compaction and therefore ductility of the Puchkirchen Formation.

Shale gas research activities in Europe

There is an urgent need for research concerning different aspects of shale gas formation in Europe. Firstly it must be stated that Europe still lacks a systematic database in which the occurrence of European black shales and their properties (thickness, TOC contents, maturity, brittleness, etc.) are compiled. This situation needs to be rectified. Secondly, the fraccability, gas contents and adsorption/desorption properties have to be analysed for individual gas shales. These characteristics are an indirect result of the complex geological history of the sediments in time and space (palaeogeography and depositional environment, diagenesis, basin history, etc.). In particular, tectonic, geomechanical and basin modelling approaches must be integrated to predict relevant gas shale properties.

Numerous small shale gas research projects have already started in Austria, England, France and Germany. For example, GeoEnergie focuses on the German federal state of Brandenburg and adjacent federal states. In the UK Lower Namurian shale gas prospectivity is being investigated by the University of Leicester. Furthermore, research at the University of Vienna focuses on the Mikulov Marl (Malmian gas shales in the Vienna Basin) and its diagenetic and clay mineralogical changes with depth to enable an optimized hydraulic fracturing. By far the largest effort is the 'Gas Shales in Europe' (GASH) project, coordinated by the German National Research Centre GFZ. This industry-sponsored project is interdisciplinary and run by a multinational expert task force drawn from leading research institutions, geological surveys, universities and consultants. Its overall goal is to predict shale gas formation and occurrence in time and space, and consists of reservoir-scale and regional-scale projects incorporating geophysics, rock mechanics, organic geochemistry, mineralogy and basin modelling. The research consortium focuses on potential gas shales of Europe, but it also integrates proven US gas shales (e.g. Barnett Shale) for calibration of key variables.

Outlook

Shale gas is an unconventional resource in Western Europe with predicted reserves of 510×10^{12} SCF gas (Rogner 1997). The international E&P industry has started to investigate single potential plays. To date, it is not clear whether these plays, e.g. in Poland, Sweden or Austria, can be exploited economically. However, the numerous Phanerozoic black shales in Europe offer promising targets for future exploration campaigns. Basic scientific work conducted as part of GASH and other projects will help to better understand European sedimentary basins in terms of shale gas formation over the coming three years. One major effort will be to compile a black shale database containing key properties of shale gas on a European scale. Moreover, research projects on both regional and reservoir scale aspects (e.g. ability to stimulate, fraccability, gas isotherms) for selected European gas shales will deliver insight into specific processes and properties. In this context, the available knowledge from North American shale gas systems can help to initially categorize potential targets, but detailed research due to different basin histories is required.

European offshore regions like the North or Baltic Seas are not considered here as no current activities are known from these areas. However, the existing infrastructure in such mature offshore hydrocarbon provinces may prove to be an advantage.

The authors thank reviewers N. Smith and D. Jarvie for their constructive reviews that helped to improve the manuscript. Editorial help by H. Johnson and S. Pickering is gratefully acknowledged.

References

Adámek, J. 2005. The Jurassic floor of the Bohemian Massif in Moravia – geology and paleogeography. *Bulletin of Geosciences*, **80**, 291–305.

Al Duba, Huenges, E., Nover, G., Will, G. & Jödicke, H. 1988. Impedance of black shale from Munsterland 1 borehole: an anomalously good conductor? *Geophysical Journal*, **94**, 413–419.

Arzmüller, G., Buchta, S., Ralbovsky, E. & Wessely, G. 2006. The Vienna basin. *In*: Golonka, J. & Picha, F. J. (eds) *The Carpathians and their Foreland: Geology and Hydrocarbon Resources*. AAPG Memoir, **84**, 191–204.

Buchardt, B. 1999. Gas potential of the Cambo-Ordovician Alum Shale in Southern Scandinavia and the Baltic Region. *In*: Whiticar, M. J. & Faber, E. (eds) *The Search for Deep Gas Selected*. Papers presented at the I.E.A./BMFT International Deep Gas Workshop, Hannover. Geologisches Jahrbuch Reihe D, **107**, 9–24.

Clayton, G. & Baily, H. 1999. Organic maturation levels of pre-Westphalian carboniferous rocks in Ireland, and in the Irish offshore. *In*: Whiticar, M. J. & Faber, E. (eds) *The Search for Deep Gas Selected*. Papers presented at the I.E.A./BMFT International Deep Gas Workshop, Hannover. Geologisches Jahrbuch Reihe D, **107**, 25–42.

Clayton, J. L., Koncz, I., King, J. D. & Tatar, E. 1994. Organic geochemistry of crude oils and source rocks, Bekes basin. *In*: Teleki, P. G., Mattick, R. E. & Kokay, J. (eds) *Basin Analysis in Petroleum Exploration. A Case Study from the Bekes Basin, Hungary*. Kluwer Academic, Dordrecht, 161–185.

Curtis, J. B. 2002. Fractured shale–gas systems. *American Association of Petroleum Geologists Bulletin*, **86**, 1921–1938.

De Ruig, M. 2003. Deep marine sedimentation and gas reservoir distribution in Upper Austria. *Oil Gas European Magazine*, **2**, 1–7.

Dill, H. G., Sachsenhofer, R. *et al*. 2008. The origin of mineral and energy resources of Central Europe II. *In*: McCann, T. (ed.) *Geology of Central Europe*. Geological Society, London, Special Publications, 1341–1449.

Dolton, G. L. 2006. *Pannonian Basin Province, Central Europe (Province 4808) – Petroleum Geology, Total Petroleum Systems, and Petroleum Resource Assessment*. US Geological Survey Bulletin, **2204–B**.

Dvorjanin, E. S., Samoyluk, A. P., Egurnova, M. G., Zaykovsky, N. Ya., Podladchikov, Yu. Yu., van den Belt, F. J. G. & de Boer, P. L. 1996. Sedimentary cycles and paleogeography of the Dnieper Donets Basin during the late Visean-Serpukhovian based on multiscale analysis of well logs. *Tectonophysics*, **268**, 169–187.

Dyni, J. R. 2006. Geology and resources of some world oil-shale deposits. US Geological Survey Scientific Investigations Report 2005–5294. World Wide Web Address: http://pubs.usgs.gov/sir/2005/5294/pdf/sir5294_508.pdf.

Farrimond, P., Eglinton, G. & Brassell, S. C. 1989. Toarcian anoxic event in Europe: an organic geochemical study. *Marine and Petroleum Geology*, **6**, 136–147.

Fisher, T. 2008. Austria turns to unconventional, shale gas. *International Gas Report*, **596**, 7–8.

Fishman, N. & Hill, R. 2008. Organic-rich shales as important, potentially prolific unconventional petroleum reservoirs – the US experience. GEP-17 Unconventional gas? Coalbed, shale, and tight gas-sands gases. *33rd International Geol. Congress Oslo, 6–14 August 2008*. World Wide Web Address: http://www.cprm.gov.br/33IGC/1351784.html.

Formolo, M. J., Petsch, S. T., Martini, A. M. & Nüsslein, K. 2008. A new model linking atmospheric methane sources to Pleistocene glaciation via methanogenesis in sedimentary basins. *Geology*, **36**, 139–142.

Franke, D. & Neumann, E. 1999. Geology and hydrocarbon of the pre-Westphalian in the deep underground of the NE German Basin. *In*: Whiticar, M. J. & Faber, E. (eds) *The Search for Deep Gas*. Selected papers presented at the I.E.A./BMFT International Deep Gas Workshop, Hannover. Geologisches Jahrbuch Reihe D, **107**, 43–54.

Frantz Jr, J. H., Jochen, V. & Contributors. 2006. Shale gas. *Schlumberger White Paper*. World Wide Web Address: www.oilfield.slb.com/whitepaper/shalegas.

Gavrish, V. K., Machulina, S. A. & Kurilenko, V. S. 1994. Visean oil-source formation of the Dnieper-Donets basin. *Doklady Akademii Nauk Ukrainy*, **7**, 92–95.

Gursky, H.-J. 2006. Paläogeography, Paläoozeanographie und Fazies. *In*: Deutsche Stratigraphische Kommission (ed.) *Stratigraphie von Deutschland VI. Unterkarbon (Mississippium)*. Schriftenreihe der Deutschen Gesellschaft für Geowissenschaften, **41**, 51–68.

Haas, J. (ed.) 2001. *Geology of Hungary*. Eötvös University Press, Budapest.

Hoffmann, N., Jödicke, H. & Gerling, P. 2001. The distribution of pre-Westphalian source rocks in the North German Basin – evidence from magnetotelluric and geochemical data. *Geologie en Mijnbouw, The Netherlands Journal of Geosciences*, **80**, 71–84.

Horsfield, B., Bharati, S., Larter, S. R., Leistner, F., Littke, R., Schenk, H. J. & Dypvik, H. 1992. On the atypical petroleum-generating characteristics of alginite in the Cambrian Alum Shale. *In*: Schidlowski, M. *et al*. (eds) *Early Organic Evolution: Implications for Mineral and Energy Resources*. Springer, Berlin, 257–266.

Horváth, F. & Cloetingh, S. 1996. Stress-induced late-stage subsidence anomalies in the Pannonian Basin. *Tectonophysics*, **266**, 287–300.

Horváth, F. & Tari, G. 1999. IBS Pannonian Basin project: a review of the main results and their bearings on hydrocarbon exploration. *In*: Durand, B., Jolivet, L., Horváth, F. & Seranne, M. (eds) *The Mediterranean Basins: Tertiary Extension within the Alpine Orogen*. Geological Society, London, Special Publications, **156**, 195–213.

Horváth, F., Dovenyi, P., Szalay, A. & Royden, L. H. 1988. Subsidence, thermal, and maturation history of the Great Hungarian Plain. *In*: Royden, L. & Horváth, F. (eds) *The Pannonian Basin: A Study in Basin Evolution*. American Association of Petroleum Geologists Memoirs, **45**, 355–372.

Hoth, P. 1997. Fazies und Diagenese von Präperm-Sedimenten der Geotraverse Harz – Rügen. *Schriftenreihe für Geowissenschaften*, **4**, 1–139.

Jenkins, C. D. & Boyer II, C. M. 2008. Coalbed- and shale-gas reservoirs. *Journal of Petroleum Technology*, 92–99. SPE paper 103514.

Kabyshev, B., Krivchenkov, B., Stovba, S. & Ziegler, P. A. 1998. Hydrocarbon habitat of the Dniepr–Donets Depression. *Marine and Petroleum Geology*, **15**, 177–190.

Kabyshev, B. P., Kabyshev, Yu. B., Krivosheev, V. T., Prigarina, T. M. & Ulmishek, G. F. 1999. Oil-gas-generating characteristics of Paleozoic rocks of the Dniepr–Donets Basin based on Rock-Eval pyrolysis (in Russian). *Dopovidi Natsionalnoi Akademii Nauk Ukrainy*, 112–117.

Kivshik, M. K., Stovba, S. M., Turchanenko, M. T. & Redkolis, V. A. 1993. *The Regional Seismostratigraphic Investigations in the Dniepr–Donets Depression* (in Russian). Ukrgeofisika, Kiev.

Korosi, T. 2007. *Natural Gas Overview Hungary 2006*. 17th Session of Working Party on Gas, United Nations, Geneva, 23–24 January 2007. World Wide Web Address: http://www.unece.org/energy/se/pdfs/wpgas/session/17_countr/korosi.pdf.

Kováč, M., Baráth, I., Harzhauser, M., Hlavatý, I. & Hudáčková, N. 2004. Miocene depositional systems and sequence stratigraphy of the Vienna Basin. *Courier Forschungsintitut Senckenberg*, **246**, 187–212.

Ladwein, W. 1988. Organic geochemistry of Vienna Basin: model for hydrocarbon generation in overthrust belts. *American Association of Petroleum Geologists Bulletin*, **72**, 586–599.

Ladwein, W., Schmidt, F., Seifert, P. & Wessely, G. 1991. Geodynamics and generation of hydrocarbons in the region of the Vienna basin, Austria. *In*: Spencer, A. M. (ed.) *Generation, Accumulation, and Production of Europe's Hydrocarbons*. Oxford University Press, Oxford, 289–305.

Lafargue, E., Elliouz, N. & Roure, F. 1994. Thrust-controlled exploration plays in the outer Carpathians and their foreland (Poland, Ukraine and Romania). *First Break*, **12**, 69–79.

Langanger, H. 2008. *Exploration and Production*. OMV Capital Markets Day 2008, London. World Wide Web Address: http://www.omv.com/SecurityServlet/secure?cid = 1225986876259&lang = de&swa_site = wps.vp.com&swa_nav = OMV + Holding%7C%7CInvestor + Relations%7C%7CEvents%7C%7CCapital + Markets + Day + 2008%7C%7C&swa_pid = 6_B_QFO + %5BCONTENT_NODE%3A30962 24743844344%5D&swa_lang = de.

Littke, R., Jendrzejewski, L., Lokay, P., Shuangqing, W. & Rullkötter, J. 1998. Organic geochemistry and depositional history of the Barremian–Aptian boundary interval in the Lower Saxony Basin, northern Germany. *Cretaceous Research*, **19**, 581–614.

Machulina, S. A. & Babko, A. K. 2004. On the geology of Visean Domanik-type rocks in the Dniepr-Donetsk Depression (in Ukrainian). *Naftova i gazova promyslovist*, **5**, 3–8.

Magyar, I., Fogarasi, A., Vakarcs, G., Bukó, L. & Tari, G. C. 2006. The largest hydrocarbon field discovered to date in Hungary: Algyo. *In*: Golonka, J. & Picha, F. J. (eds) *The Carpathians and their Foreland: Geology and Hydrocarbon Resources*. American Association of Petroleum Geologists Memoirs, **84**, 619–632.

Martini, A. M., Walter, L. M., Budai, J. M., Ku, T. C. W., Kaiser, C. J. & Schoell, M. 1998. Genetic and temporal relations between formation waters and biogenic methane: Upper Devonian Antrim Shale, Michigan Basin, USA – CO_2 reduction vs. acetate fermentation-isotopic evidence. *Geochimica et Cosmochimica Acta*, **62**, 1699–1720.

Matyja, H. 2008. Pomeranian basin (NW Poland) and its sedimentary evolution during Mississippian times. *Geological Journal*, **43**, 123–150.

Nielsen, A. T. & Schovsbo, N. H. 2007. Cambrian to basal Ordovician lithostratigraphy in southern Scandinavia. *Bulletin of the Geological Society of Denmark*, **53**, 47–92.

Petmecky, S., Meier, L., Reiser, H. & Littke, R. 1999. High thermal maturity in the Lower Saxony Basin: intrusion or deep burial? *Tectonophysics*, **304**, 317–344.

Phasis, 2008. *US Shale Gas Brief September 2008*. World Wide Web Address: http://www.phasis.ca/files/pdf/Phasis_Shale_Gas_Study_Web.pdf.

Picha, F. J. & Peters, K. E. 1998. Biomarker oil-to-source rock correlation in the Western Carpathians and their foreland, Czech Republic. *Petroleum Geoscience*, **4**, 289–302.

Rogner, H.-H. 1997. An assessment of world hydrocarbon resources. *Annual Review of Energy and the Environment*, **22**, 217–262.

Rullkötter, J., Leythaeuser, D. *et al*. 1988. Organic matter maturation under the influence of a deep intrusive heat source: a natural experiment for quantitation of hydrocarbon generation and expulsion from a petroleum source rock. (Toarcian Shale, Northern Germany). *In*: Mattavelli, L. & Novelli, L. (eds) *Advances in Organic Geochemistry 1987*. Pergamon Press, Oxford, 847–856.

Schouten, S., van Kaam-Peters, H. M. E., Rijpstra, W. I. C., Schoell, M. & Sinninghe Damsté, J. S. 2000. Effects of an oceanic anoxic event on the stable carbon isotopic composition of early Toarcian carbon. *American Journal of Science*, **300**, 1–22.

Schovsbo, N. H. 2003. The geochemistry of Lower Palaeozoic sediments deposited on the margins of Baltica. *Bulletin of the Geological Society of Denmark*, **50**, 11–27.

Selley, R. C. 1987. British shale gas potential scrutinized. *Oil & Gas Journal*, **85**, 62–64.

Selley, R. C. 2005. UK shale-gas resources. *In*: Doré, A. G. & Vining, B. A. (eds) *Petroleum Geology: North-West Europe and Global Perspectives: Proceedings of the 6th Petroleum Geology Conference*. Geological Society, London, 707–714. doi: 10.1144/0060707.

Shpak, P.F. (ed.), 1989. *Geology and Petroleum Productivity of the Dniepr-Donetsk Depression – Petroleum Productivity* (in Russian). Naukova Dumka, Kiev.

Shymanovskyy, V. A. & Sachsenhofer, R. F. 2002. Hydrocarbon generation in the NW Dniepr–Donets Basin, Ukraine. *63rd Conference, European Association of Geoscientists & Engineers*, Extended Abstracts, paper 121.

Shymanovskyy, V. A., Sachsenhofer, R. F., Izart, A. & Li, Y. 2004. Numerical modelling of the thermal evolution of the northwestern Dniepr–Donets Basin (Ukraine). *Tectonophysics*, **381**, 61–79.

Siegmund, H., Trappe, J. & Oschmann, W. 2002. Sequence stratigraphic and genetic aspects of the Tournaisian 'Liegender Alaunschiefer' and adjacent beds. *International Journal of Earth Sciences*, **91**, 934–949.

Smith, N., Turner, P. & Williams, G. 2010. UK data and analysis for shale gas prospectivity. *In*: Vining, B. A. & Pickering, S. C. (eds) *Petroleum Geology: From Mature Basins to New Frontiers – Proceedings of the 7th Petroleum Geology Conference*. Geological Society, London, 1087–1098; doi: 10.1144/0071087.

Stephenson, R. A., Yegorova, T. *et al*. 2006. Late Paleozoic intra- and pericratonic basins on the East European Craton and its margins. *In*: Gee, D. G. & Stephenson, R. A. (eds) *European Lithosphere Dynamics*. Geological Society, London, Memoirs, **32**, 463–479.

Tari, G. C. & Horvath, F. 2006. Alpine evolution and hydrocarbon geology of the Pannonian Basin: an overview. *In*: Golonka, J. & Picha, F. J. (eds) *The Carpathians and their Foreland: Geology and Hydrocarbon Resources*. American Association of Petroleum Geologists Memoirs, **84**, 605–618.

Ulmishek, G. F. 2001. *Petroleum Geology and Resources of the Dnieper–Donets Basin, Ukraine and Russia*. U.S. Geological Survey Bulletin 2201-E, US Department of the Interior U.S. Geological Survey. World Wide Web Address: http://geology.cr.usgs.gov/pub/bulletins/b2201-e/.

Volk, H., Horsfield, B., Mann, U. & Suchý, V. 2002. Variability of petroleum inclusions in vein, fossil and vug cements – a geochemical study in the Barrandian Basin (Lower Palaeozoic, Czech Republic). *Organic Geochemistry*, **33**, 1319–1341.

Wessely, G. 1990. Geological results of deep exploration in the Vienna basin. *Geologische Rundschau*, **79**, 513–520.

Zdanaviciutė, O. & Lazauskiene, J. 2004. Hydrocarbon migration and entrapment in the Baltic Syneclise. *Organic Geochemistry*, **35**, 517–527.

Zdanaviciutė, O. & Lazauskiene, J. 2007. The petroleum potential of the Silurian succession in Lithuania. *Journal of Petroleum Geology*, **30**, 325–337.

Zimmerle, W. & Stribrny, B. 1992. Organic carbon rich pelitic sediments in the Federal Republic of Germany. *Courier Senckenbergsche Naturforschende Gesellschaft*, **152**, 1–142.

UK data and analysis for shale gas prospectivity

N. SMITH, P. TURNER and G. WILLIAMS

British Geological Survey, Kingsley Dunham Centre, Nicker Hill, Keyworth NG12 5GG, UK (e-mail: njps@bgs.ac.uk)

Abstract: Organic-rich shale contains significant amounts of gas held within fractures and micropores and adsorbed onto organic matter. In the USA shale gas extracted from regionally extensive units such as the Barnett Shale currently accounts for 6% of gas production and is likely to reach 30% by 2015. Shale gas prospectivity is controlled by the amount and type of organic matter held in the shale, its thermal maturity, burial history, microporosity and fracture spacing and orientation. Potential targets range in age from Cambrian to the late Jurassic, within the main UK organic-rich black shales: younger shales have been excluded because they have not reached the gas window, but they may possess a biogenic gas play. A geographic information system, showing the distribution of potential reservoir units, has been created combining information on hydrocarbon shows, thermal maturity, fracture orientation, gas composition, and isotope data to identify potentially prospective areas for shale gas. Some of these data are shown as graphs and maps, but crucial data is lacking because earlier exploration concentrated on conventional reservoirs. The prospects include Lower Palaeozoic shale basins on the Midland Microcraton (a high risk because no conventional gas has been proved in this play), Mississippian shales in the Pennine Basin (the best prospect associated with conventional fields and high maturity), Pennsylvanian shales in the Stainmore and Northumberland Basin system (high risk because no conventional gas discoveries exist) and Jurassic shales in Wessex and Weald basins (small conventional fields signify potential here).

Keywords: shale, gas, maturity, thickness, source rock and reservoir

Organic-rich shale contains significant amounts of gas held within fractures and micropores and adsorbed onto organic matter. In the USA, shale gas extracted from regionally extensive units such as the Barnett Shale accounts for *c.* 6% of gas production. The success of US shale gas exploitation (over 28 000 wells producing *c.* 380×10^9 SCF per year) has stimulated significant interest in identifying potential reservoirs throughout the world. The depth range of the US shale gas plays extends down to 4500 m at present. Selley (1987, 2005), farsightedly, advocated shale gas exploration in the UK, based on Upper Devonian gas fields of the Appalachian Basin, which have been producing since 1821. However, in the past decade the Mississippian Barnett Shale of the Fort Worth Basin has become the most productive shale gas reservoir in the USA. US shales generally, and the Barnett Shale in particular, provide good analogues for potential shale gas plays in the UK, which has thick Mississippian shales both on and offshore; therefore the geology and geochemistry of the Barnett Shale are discussed briefly below.

The Barnett Shale

The Barnett Shale Formation (354–323 Ma) of the Fort Worth Basin is up to 300 m thick and underlies an area of *c.* 13 000 km^2 (Fig. 1). It contains *c.* 2.5×10^{12} SCF of proven gas reserves held in a low porosity and very low permeability shale matrix. Permeability is in the micro- to nanodarcy range and porosity rarely exceeds 6% (Bowker 2007): consequently the Barnett Shale Formation is slightly overpressured, with formation pressures in excess of 4000 psi (Frantz *et al.* 2005).

The Fort Worth Basin shows a northward-thickening, half-graben-like structure, but is bounded by reverse faults against the Lower Palaeozoic Muenster Arch (part of the Southern Oklahoma Aulacogen; Fig. 1). The Mississippian Barnett Shale unconformably overlies Ordovician strata (Viola Formation limit in Fig. 1) and can be subdivided into two units, the Upper and Lower Barnett, separated by the Forestburg Limestone. The upper shale unit is overlain by the Marble Falls Limestone, also of Mississippian age, which is conformable with a thick succession of overlying Pennsylvanian sediments. Sedimentary structures suggest that the main shale units were deposited by distal turbidity flows in a sediment-starved anoxic basin environment. The Carboniferous sequence is truncated by a Cretaceous supercrop above the Variscan unconformity. The Ouachita (Variscan) fold belt lies at right angles to the Muenster Arch and impinges on the Fort Worth Basin in the SE.

The three main factors controlling prospectivity of the Barnett are the thermal maturity, thickness and total organic carbon (TOC) content of the shale (Zhao *et al.* 2007). Local and regional structures such as joints, folds and faults control fracture porosity and thus influence production potential at a variety of scales. Most natural fractures are sealed but these can potentially be exploited by artificial fracturing techniques (Bowker 2007) to improve flow rates around a well. Siltstone bands and chert nodules can also affect prospectivity locally.

The Newark East shale gas field lies updip west of the depocentre of the Barnett Shale in the wedge between the Muenster Arch and the Ouachita (Variscan) fold belt (Fig. 1; Pollastro *et al.* 2004). The rest of the depocentre lies under the Fort Worth–Dallas conurbation. The Barnett Shale also produces oil from the area to the NW (Fig. 1), where overlying conventional reservoirs are also present.

In a similar tectonic position the Big Sandy shale gas field in eastern Kentucky lies over the thickest part of the Devonian Brown Shale in a foreland basin, which is bounded to the SE by the Pine Mountain thrust (Ray 1976) of the Appalachian (Variscan) fold belt.

The UK's closest tectonic analogue

Satellite basins of the Worcester Graben (Fig. 2) beneath the Bristol Coalfield and in Berkshire to the east (Mississippian strata are thin in the latter area) provide the closest UK tectonic

VINING, B. A. & PICKERING, S. C. (eds) *Petroleum Geology: From Mature Basins to New Frontiers – Proceedings of the 7th Petroleum Geology Conference*, 1087–1098. DOI: 10.1144/0071087 © Petroleum Geology Conferences Ltd. Published by the Geological Society, London.

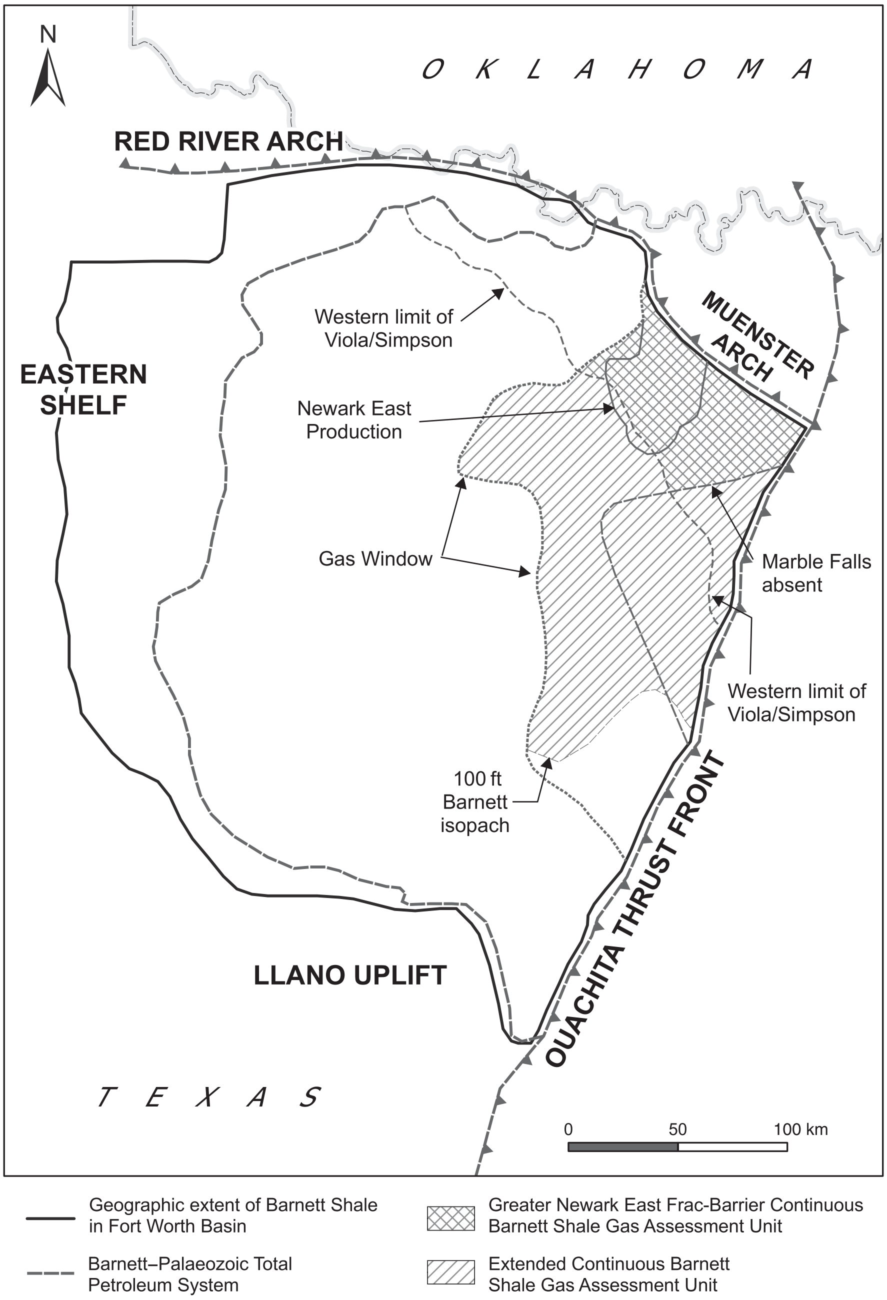

Fig. 1. Barnett Shale of the Fort Worth Basin, Texas, USA. The Muenster Arch and Ouachita Thrust Front form the northern and eastern boundaries of the foreland-type basin (barbed lines). The Barnett Shale lies unconformably on Ordovician strata. The Barnett Shale gas system, the Newark East Gasfield outline, the western limit of the gas window and other geological features relevant to completion fracturing are shown (Montgomery *et al.* 2005).

analogues to the Fort Worth Basin. They are small foreland basins preserved between the Variscides and the Worcester Graben. The latter formed in response to extensional faulting during the Lower Palaeozoic and inverted during the Variscan Orogeny comparable with the Southern Oklahoma Aulacogen (Smith 1993; Smith & Rushton 1993). The Bristol depocentre lacks the acreage of the Fort Worth Basin but contains the Lower Limestone Shale Group, conformably overlying Devonian and of roughly equivalent age (359–327 Ma) to the Barnett Shale Formation. Few wells and no maturity or geochemical data are available though, and seismic is sparse.

It is important to note, however, that there are significant differences between shale gas plays developed in different basins in the USA (age, maturity, tectonic position). So many black shale plays are currently being developed there, that whilst the three main factors (above) are paramount, exact comparisons with US shales are not deemed necessary to confirm or refute potential. Consequently this contribution considers the main generic controls on shale gas prospectivity identified in key US plays (see above) in a regional UK context, before identifying potential exploration targets.

General characteristics of any potential source rocks

Organic-rich sediments have a lower density, lower sonic velocity, higher porosity, higher resistivity and higher gamma ray (GR) values compared with sedimentary units of equal compaction and comparable mineralogy. Potential source rocks can thus be readily identified on well logs, provided they are rich in organic matter. For example, the Arnsbergian Sabden Shale typically exhibits anomalously low sonic velocity and high GR values in

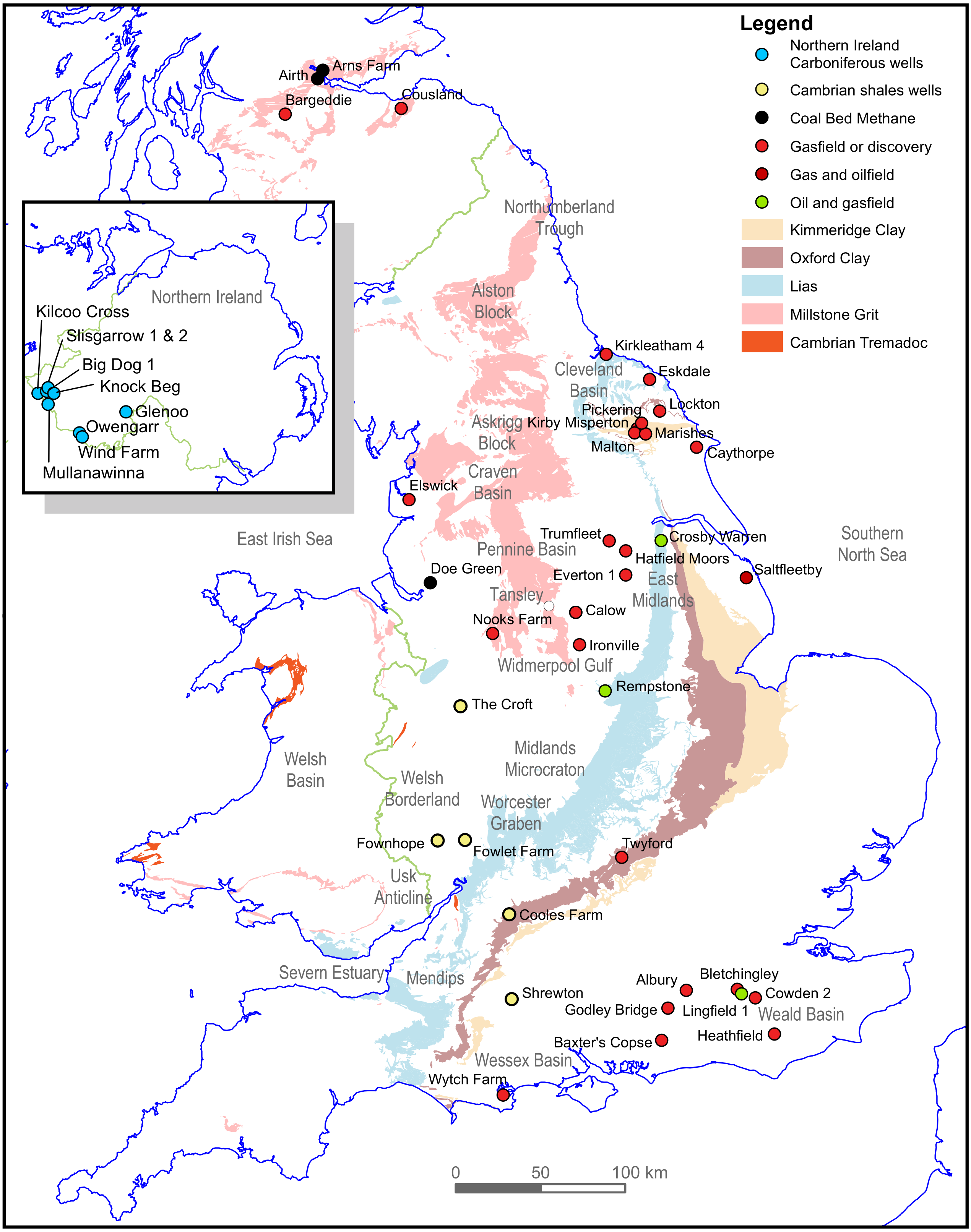

Fig. 2. Outcrops of main potential hydrocarbon source rocks (Lower Carboniferous strata beneath Millstone Grit are not shown). Wells reaching Tremadoc to Cambrian in England indicate the few provings at this level. Gas fields and discoveries indicate that gas window maturity has been reached. Hydrocarbon wells, plotted in inset of Northern Ireland, tested a tight gas Carboniferous play in several phases (Griffith 1983) as recently as 2001. Coalbed methane fields are also shown.

the Pennine Basin (Smith *et al.* 2005). Classification schemes based on wireline logs break down at high water saturations because water and organic material have comparable densities: the specific gravity of organic matter is about 0.95–1.05 g cm^{-3} (Stocks & Lawrence 1990).

The outcrop distribution of key organic-rich shale formations identified on well logs is summarized in Figure 2. In the UK, organic-rich shales can be subdivided into three broad stratigraphic groups belonging to the Lower Palaeozoic (principally Cambrian), Mississippian and Jurassic (of Liassic, Oxfordian and

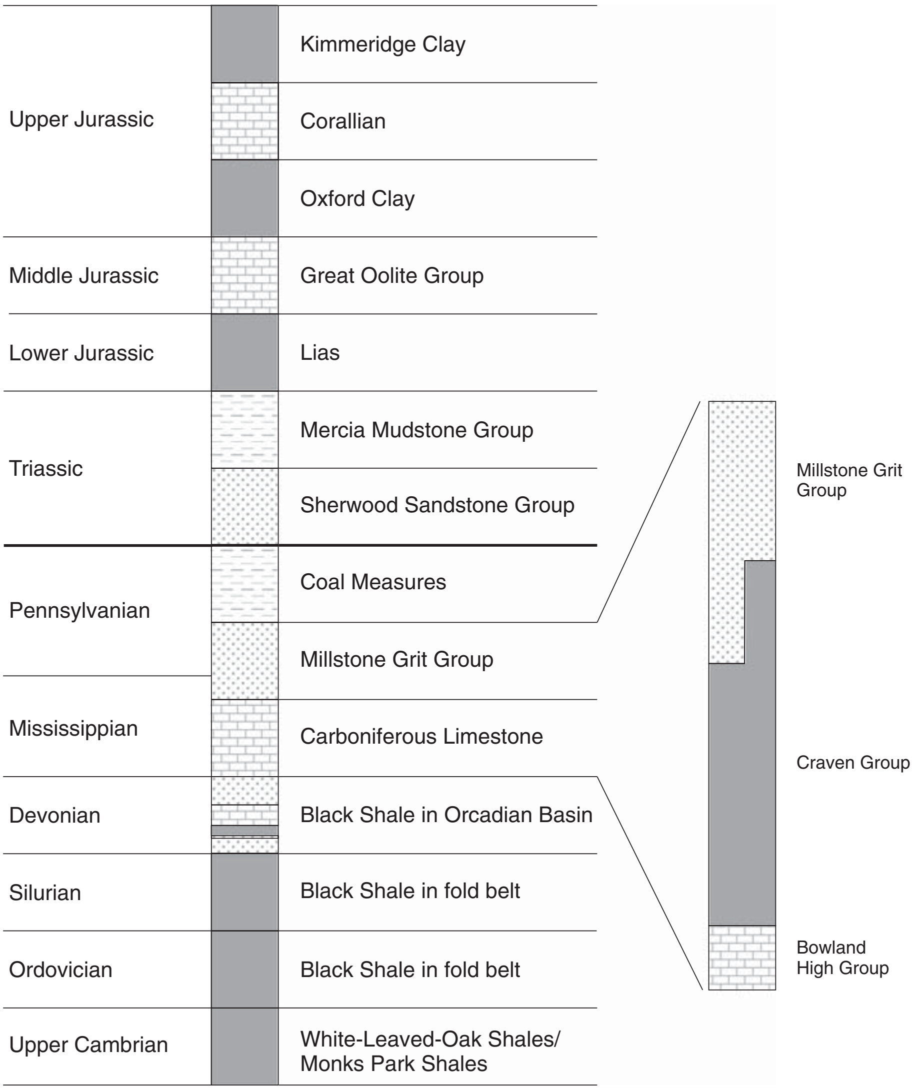

Fig. 3. Generalized stratigraphic column for UK onshore shows the main black shale formations (grey shading) and other representative lithologies in a typical sequence. The Sherwood Sandstone (stipple) lies unconformably on Coal Measures. Some black shales are only found in the Caledonian and Variscan fold belts (e.g. in the Orcadian Basin, Ordovician and Silurian shales in the Caledonides), which have been largely excluded from this study.

Kimmeridgian age), although such shales occur in other periods and groups (Fig. 3).

Pre-Carboniferous black shales

Black shales are developed in the Upper Cambrian, Upper Ordovician and Lower Silurian strata of the UK (Leggett 1980). Ordovician and Silurian shales are largely restricted to deeper basins and deformed in fold belts, while Cambrian black shale deposits are also found on the Midland Microcraton. Unexplained gas shows in the Welsh Borderland and Welsh Caledonides may have been sourced from concealed Lower Palaeozoic black shales. In most US basins conventional gas fields are present above the shale gas being developed. However this is not the case with the Cambrian Conasauga Shale in Alabama, where exploration and some production has been achieved. So-called overmature shales in conventional hydrocarbon terminology, often located in tectonic positions where conventional exploration has therefore been deemed unfavourable, may retain potential for shale gas.

Upper Cambrian black shales outcrop in small inliers close to zones of uplift, but seismic data suggest that they are widespread in the subsurface (Smith *et al.* 2005). Shales of this age were proved by the Fowlet Farm and Fownhope boreholes SW of the Malverns (Fig. 2; Earp & Hains 1971). In these boreholes, *c.* 68 m of black shale has been intruded by dolerite sills; the shales have high GR values and represent a potential source rock. Outcrop measurements of TOC support this interpretation, with values of *c.* 5% recorded by Parnell (1983).

In Shropshire *c.* 5 m of black shales with bituminous limestone concretions are underlain by 20 m of dark grey shale. To the NE at Lilleshall a small outcrop and the Croft borehole (Fig. 2) revealed *c.* 53 m of black, pyrite-rich shale lying unconformably on Lower Cambrian strata (Rushton *et al.* 1988). Unfortunately TOC and thermal maturity analyses were not made in this borehole. The Lilleshall deposits may be the erosional remnants of a tilted fault-block high (Middle Cambrian strata are missing; Smith & Rushton 1993), with a half-graben basin deepening eastwards (Smith *et al.* 2005).

Merevale borehole No. 2 (located on Fig. 5) encountered *c.* 60 m of condensed black mudstone (Monk's Park Shales; Taylor & Rushton 1971). TOC values exceeded 2% and sulphur content reached 10%; phosphate was present in the form of scattered nodules. These deposits may provide some shale gas potential. Conversely, the Cooles Farm borehole tested part of the Worcester Graben (Fig. 2). It was drilled into Cambrian strata but did not record the presence of any Upper Cambrian high gamma shale units. Seismic hereabouts reveals many reflectors beneath the well terminal depth. This play derives encouragement from the Cambrian Conasauga Shale in the Appalachians, where production has been achieved.

Ordovician and Silurian shale units seem to have less potential as a shale gas play, based on limited drilling. In the Fownhope well only a short section of Llandovery-age clay approached GR values indicative of a potential source rock. A borehole drilled at Usk (east of the Usk Anticline in Fig. 2) penetrated no potential source rocks in the Lower Palaeozoic, although minor gas shows occurred in some sandstone units. However this well was drilled on a structural high missing a large section of Llandovery or older sequence where black shales might have formed in the depocentre beneath the Usk Anticline. A black shale facies of Llandovery age is known in the Welsh Caledonides to the west (Leggett 1980).

UK Lower Palaeozoic black shales often show preferential enrichment of various heavy elements including As, Co, Cr, Cu, Mo, Ni, Pb, S, U and V (Leggett 1980; Jones & Plant 1989). This is particularly true of the Upper Cambrian interval and appears to be associated with organic matter. The presence of these minerals may be useful proxies for high TOC shales, where mining exploration data is available.

A few samples from the Withycombe Farm borehole (between Cooles Farm and Twyford; Fig. 2) suggest a porosity of 5–10% survives down to a depth of 1000 m in Lower Cambrian (Poole 1978). In many places these rocks have been subjected to significant compaction, intrusion and tectonism and primary porosity would be expected to be very low. There is, however, scope for induced fracture permeability in these rocks. These few porosity values are comparable with US shales being developed currently.

In contrast to the Appalachian Basin in the USA, there are no Devonian black shale sequences in the Variscan foreland of the UK. Lacustrine shale deposits are present in the Middle Devonian of the Orcadian Basin in Scotland: TOC values typically average *c.* 1.4%. Thermal maturity is variable, but these rocks largely fall within the oil window or are overmature (in the vicinity of underlying intrusions), and offshore they probably helped charge the Beatrice Oilfield (Hillier & Marshall 1992). Two boreholes drilled at Dounreay proved up to 150 m of interbedded high gamma shale beds.

Carboniferous black shales

Mississippian shale units (Fig. 3) offer the best potential for shale gas exploration in the UK because they have sourced hydrocarbons, have high TOCs (Armstrong *et al.* 1997) and were deposited in deep half-graben, within the Pennine Basin in northern England (Fraser *et al.* 1990). The younger (Namurian) of these shales are more widely deposited as the extensional half-graben subsidence was transforming to a more regional thermal subsidence.

Gas content and kerogen type

The gas content of Coal Measures strata was measured by the National Coal Board (Creedy 1989). Carbonaceous mudstones (including marine bands) contained 0.18–0.63 m^3/t (6.3–22.2 SCF/t) gas; whereas non-carbonaceous mudstones contained 0.009–0.1 m^3/t (0.3–3.5 SCF/t). Budge (1932) reported methane adsorption of 1.8 m^3/t (63.6 SCF/t) in carbon-rich Coal Measures mudstone and 0.25 m^3/t (8.8 SCF/t) in black shale from the South Wales Coalfield. These values in Westphalian strata are comparable with the reported values in the Cretaceous Lewis Shale in the USA, which has the lowest values of the US explored shales.

Ferguson (1984) measured methane values of up to 46 000 ppb in the Carboniferous Limestone of northern England, near to mineralized areas on the Alston Block: there also appeared to be an association between base metal vein mineralization in Derbyshire and the adjacent shale-rich Pennine Basin half-graben (Plant & Jones 1989). Ewbank *et al.* (1993) noted that Alportian–Pendleian mudstones exposed at outcrop in the northern part of the Pennine Basin predominantly contained gas-prone type III kerogen, whereas mudstone samples from a Widmerpool Gulf well (Arnsbergian age) and various Visean mudstones were dominated by type II kerogen (gas- and oil-prone).

Total organic carbon

Namurian marine shales have generally higher TOC values (over 4%) compared with non-marine shales (Spears & Amin 1981), which have an average value of around 2% (Fig. 4). Maynard *et al.* (1991) found that two Namurian black shale marine bands had a TOC content of between 10–13%, whereas values within interbedded strata ranged between 2 and 3%. The Namurian Holywell Shale, source rock for the southern East Irish Sea and Formby hydrocarbon fields, has TOC values ranging from 0.7–5%, with an average of 2.1% (Armstrong *et al.* 1997). The lower part of this formation gave an average of 3% TOC and pyrolysate yields of 7 kg/t^{-1}. These values are comparable with US shales.

Thermal maturity

Vitrinite reflectance (%R_o) measurements at outcrop and in boreholes provide a widely accepted proxy for thermal maturity and hydrocarbon generation. These are shown for the nearest value to the basal Namurian (Fig. 5; at Knutsford it is probably within the Westphalian D). Maturity zones can be divided into immature for oil, within the oil window, within the gas window and overmature for hydrocarbons. The oil window is normally considered to fall between 0.6 and 1.3% R_o, although it varies according to kerogen type. There is no agreement on the lower limit of the gas window, which has variously been put at 2% R_o (Landes 1967), 3% R_o (Dow 1977), 3.2% R_o (Dow & Connor 1982) and 5% R_o (Hood *et al.* 1975). In this study a value of 1.1% R_o has been used to differentiate maturity levels above and below the gas window (Fig. 5), because this value defines the limit of the Newark East gas field in the Barnett Shale (Pollastro *et al.* 2004 and see Fig. 1).

Porosity, permeability and fracture porosity

Limited porosity data from BGS boreholes in the southern Midlands suggest that porosities of 5–10% survive to a depth of 1000 m in Upper Palaeozoic shales (Poole 1977, 1978). Coal Measures mudstones, seat-earths and siltstones have measured permeability values in the range 4.34×10^{-6} to 7.1×10^{-3} mD (Oldroyd *et al.* 1971).

Joints, developed in the limestone platforms of Derbyshire and the Askrigg Block (Moseley & Ahmed 1967), are predominantly sub-vertical and perpendicular to bedding. Joint development preceded the main phase of movement on the main fault zones and they are frequently mineralized. Well bedded marine shales tend to have a high joint density, in contrast to mudstones and sand-rich shale units. Minor joints are more difficult to distinguish in argillaceous rocks, but master joints persist strongly with a high fracture density (0.6–3 m spacing).

The predominant NW trend of the main Carboniferous joint sets is coincident with the present-day maximum horizontal stress

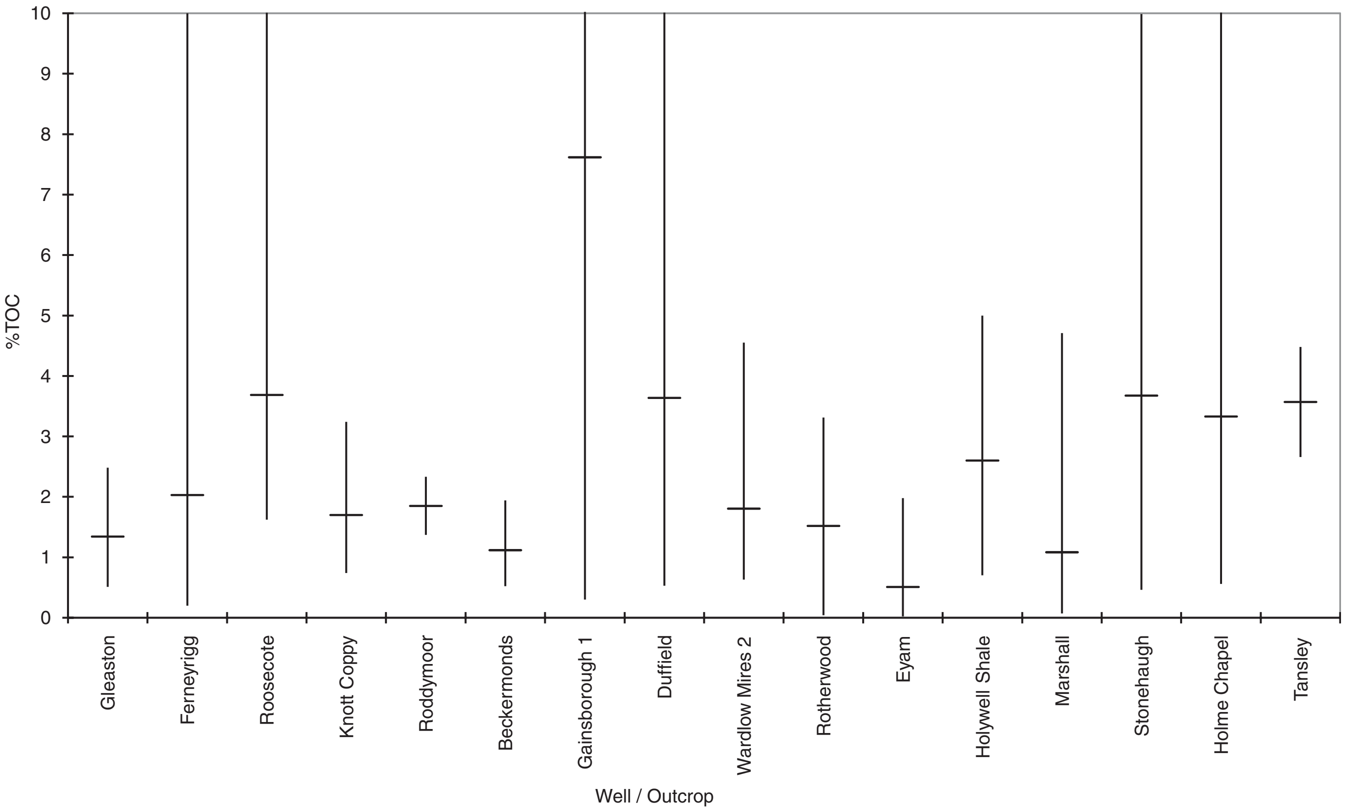

Fig. 4. Variation of TOC contents in the Carboniferous of northern England. Gleaston borehole is in south Cumbria; Ferneyrigg, Stonehaugh and Marshall Meadows are in the Northumberland Trough; Roddymoor is on the Alston Block; and Beckermonds is on the Askrigg Block. The other boreholes are in the Pennine Basin.

direction (145/325°; Evans & Brereton 1990). Rogers (2003) predicted that the stress-induced fracture permeability is likely to be higher along this trend in the current UK stress field.

Mineralogy

The Al_2O_3 content of UK Carboniferous mudstones ranges between 12 and 38%, with an average of around 25% (Ramsbottom *et al.* 1981). Marine and non-marine shales in the Tansley borehole (Fig. 2) have average Al_2O_3 contents of 20.6 and 17.9% respectively, with clay minerals making up 59 and 56% of the shale matrix (Spears & Amin 1981). The Barnett Shale has a relatively low clay content (*c.* 27%; Jarvie *et al.* 2004) compared with other shales. The presence of significant amounts of quartz (45%) and carbonate (10%) in the shale matrix imparts brittleness to the rock, facilitating artificial fracturing.

Gas fields and discoveries

The presence of conventional gas fields in Carboniferous and Jurassic basins (Fig. 2) demonstrates that gas has been generated. In a few cases there is unambiguous evidence of the source being Namurian shales (e.g. the Elswick Gasfield; Fig. 2), because Coal Measures are absent in the subcrop (Fig. 5; Smith 1985). In some gas fields migration could have occurred from either a Coal Measures source or from Namurian strata uplifted in an inverted basin (e.g. Nooks Farm; Fig. 2). Along the southern margin of the Cleveland Basin (Marishes to Malton gas fields; Fig. 2) a third migration direction, along east–west faults, from the Southern North Sea, is also a possibility.

Gas wetness (percentage of non-methane gas) values (Fig. 6) are high when gas is associated with oil in the source rock and lower (<5%) when the gas has been exclusively derived from coal-rich strata, is biogenic or overmature. Jarvie *et al.* (2004) typified two gas samples in the Barnett Shale as overmature dry gas, with gas wetness values of around 5%: in contrast, oil-associated gas had values over 12%. In the Carboniferous of the UK, high values measured at Welbeck Colliery are associated with oil shows, but at nearby Thoresby Colliery (also associated with oil) the gas is rich in methane and was probably sourced from the Coal Measures (Challinor 1990).

Insufficient gas composition and carbon isotope data were available to resolve the migration directions in most gas fields. Carbon and hydrogen isotope data from methane samples accompanying water flows within shallow tunnels in Namurian strata (Fig. 7) suggest that the methane either had a biogenic (modern) origin or formed through CO_2 reduction (Bath *et al.* 1988). The US Antrim Shale and New Albany Shale (Fig. 7; Illinois Quaternary-hosted gas) have late generation biogenic gas systems related to glacial meltwater ingress via fractures (Shurr & Ridgley 2002). US exploration has used stable isotopes to confirm source, maturity and hydrocarbon generation zone (Fig. 7).

Principal source rocks

Two lithostratigraphic units from the Mississippian represent potential shale gas plays in the UK: these are the Craven Group found in the Pennine Basin (Fig. 3) and the Lower Limestone Shale around the Mendips (Fig. 2). The Craven Group comprises a thick sequence of interbedded limestone and shale. The Pennine Basin formed to the north of the Wales–Brabant Massif: this geological and tectonic setting is not a direct tectonic analogue to the Barnett Shale. Conversely the Lower Limestone Shale was deposited in a similar tectonostratigraphic setting to the Barnett,

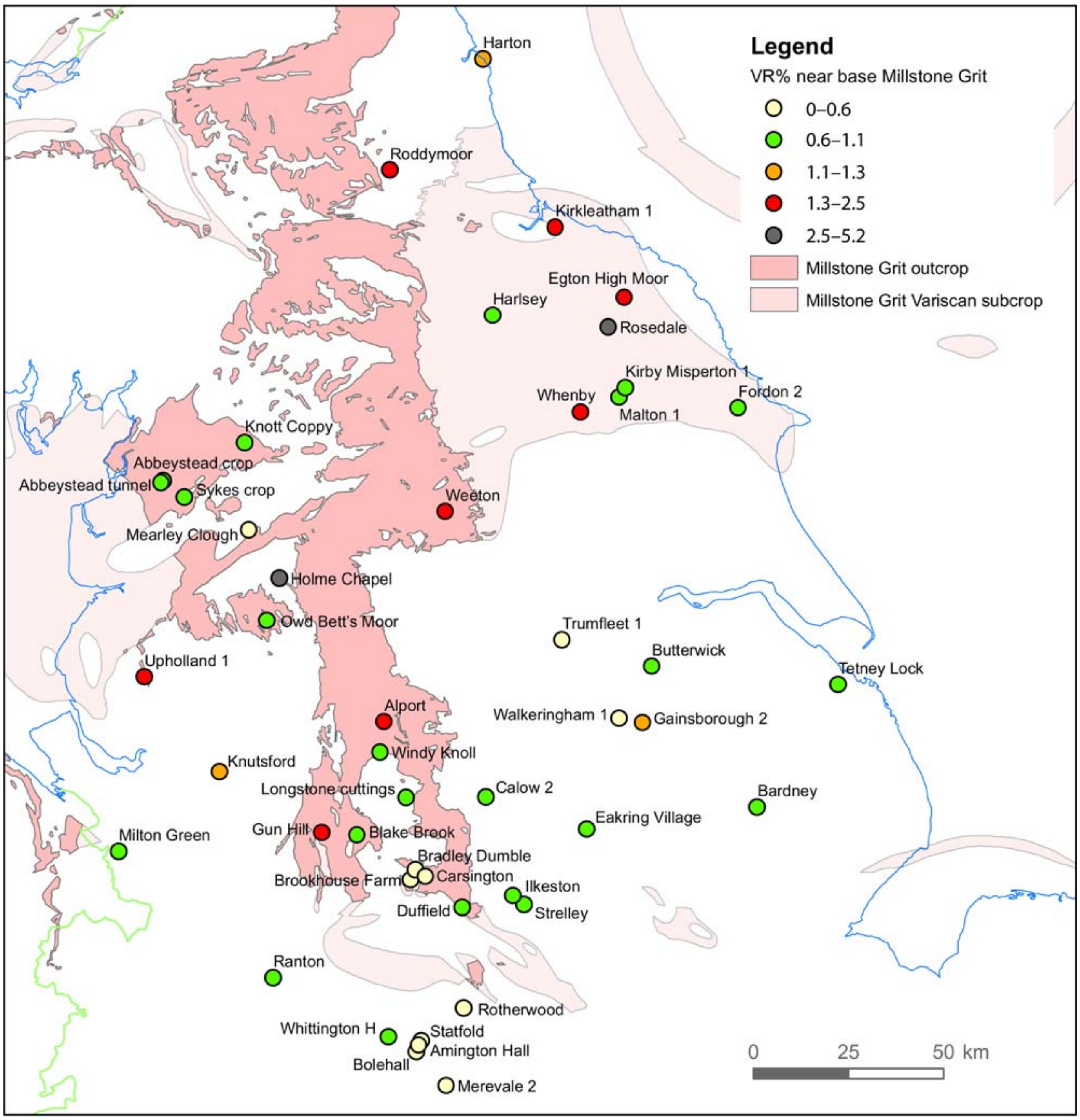

Fig. 5. Vitrinite reflectance percentage values obtained nearest to the base Namurian. Yellow spots are immature for hydrocarbons, green represents early part of oil window, orange late part of oil window (cf. Barnett Shale top of gas window), red the gas window and grey overmature (conventional hydrocarbon zones). The overmature areas should not be ruled unprospective for shale gas. Most existing hydrocarbon wells were drilled on structural highs and are likely to possess lower maturity than the potential source rock.

in the foreland of the Variscan Front, west of the Worcester Graben. It thickens southward from *c.* 35 m north of the Severn Estuary to *c.* 170 m in the Mendips (Kellaway & Welch 1948) and is also present south of the Bristol Channel.

The Pennine Basin has been the focus of extensive coal and hydrocarbon exploration in the past, producing a comprehensive database, available to evaluate shale gas potential in the region. The Craven Group (Mississippian) ranges in thickness from >1450 m in the Craven sub-basin to >5000 m in the Widmerpool Gulf (Waters *et al.* 2007; Fig. 2). The mudstones were deposited in distal slope turbidite and hemi-pelagic environments in relatively narrow, deep depocentres within the Pennine Basin (e.g. Craven and Widmerpool; Fig 2). Individual shale units that might represent potential source rocks include (Table 1) the Worston Shale Group, the Long Eaton Formation and the Widmerpool Formation. The latter has a high TOC content in Duffield borehole (Figs 5 & 8), but the GR values are low (Aitkenhead 1977).

Younger shale gas targets include the Bowland (Edale) Shales and the Sabden Shales (both Namurian). The condensed black Bowland Shale sequence outcropping in the Derbyshire Peak District is thin and immature for hydrocarbon generation, but these units thicken to the east and represent the main source rocks that charged the East Midlands hydrocarbon system. In the Tansley borehole (Fig. 2), TOC content averaged 4.48% in marine bands and 2.66% in non-marine shale sequences (Fig. 4). A GR peak is found close to the base of the Arnsbergian sequence, extending down into the Pendleian. In the nearby Uppertown borehole this interval coincides with phosphatic nodules and collophane, in a sequence of dark grey shale, containing abundant fossilized plants. Ponsford (1955) recorded higher than average

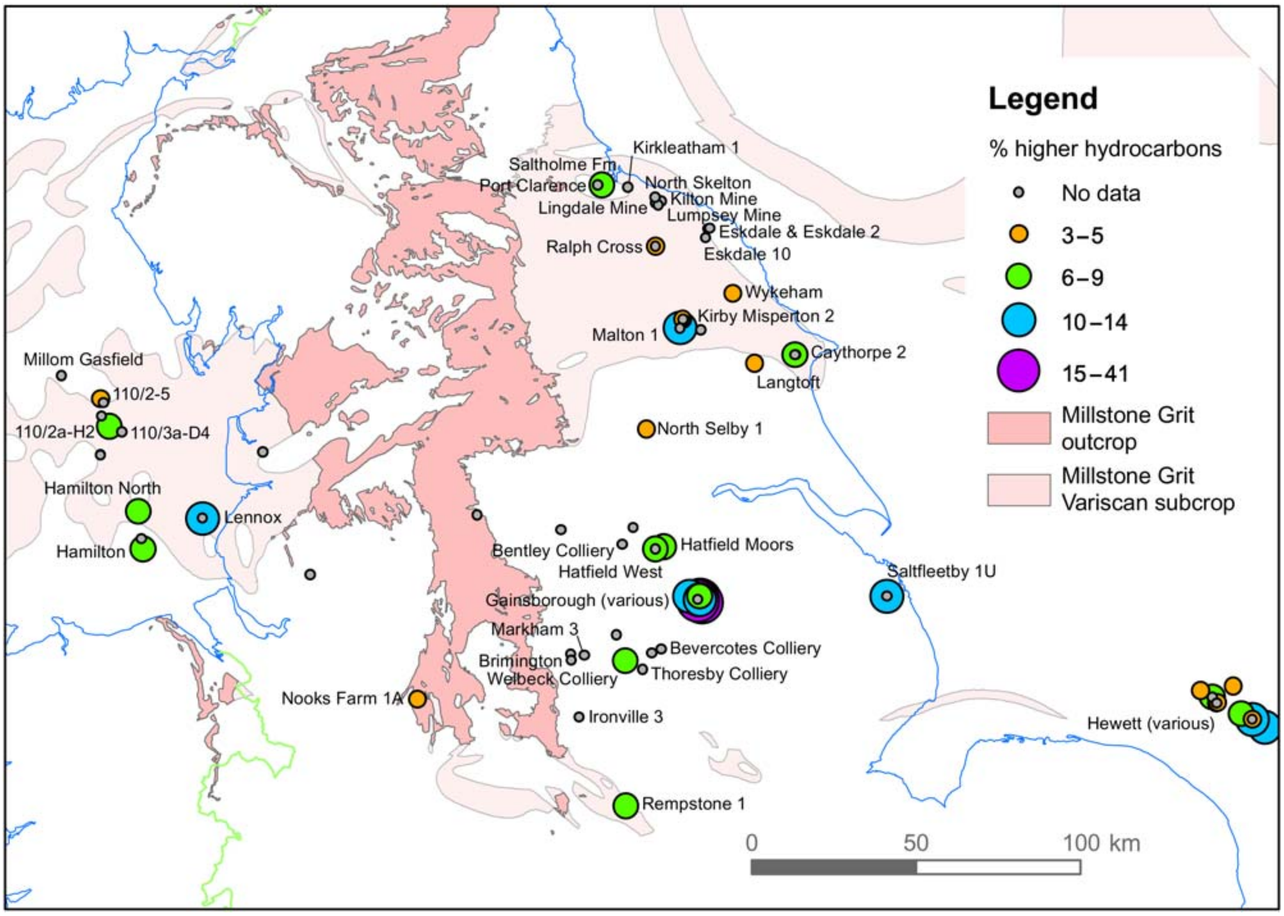

Fig. 6. Gas wetness ratio of analysed gases. The gases associated with oil fields have higher gas wetness values (a greater percentage of higher hydrocarbons). Welbeck Colliery has a high gas wetness, suggesting perhaps some gas from sources other than Coal Measures. These values suggest that source rocks, which have sourced the gas, exist in strata other than Coal Measures. However potential shale gas is likely to be nearer to dry methane within deeper parts of the half-graben.

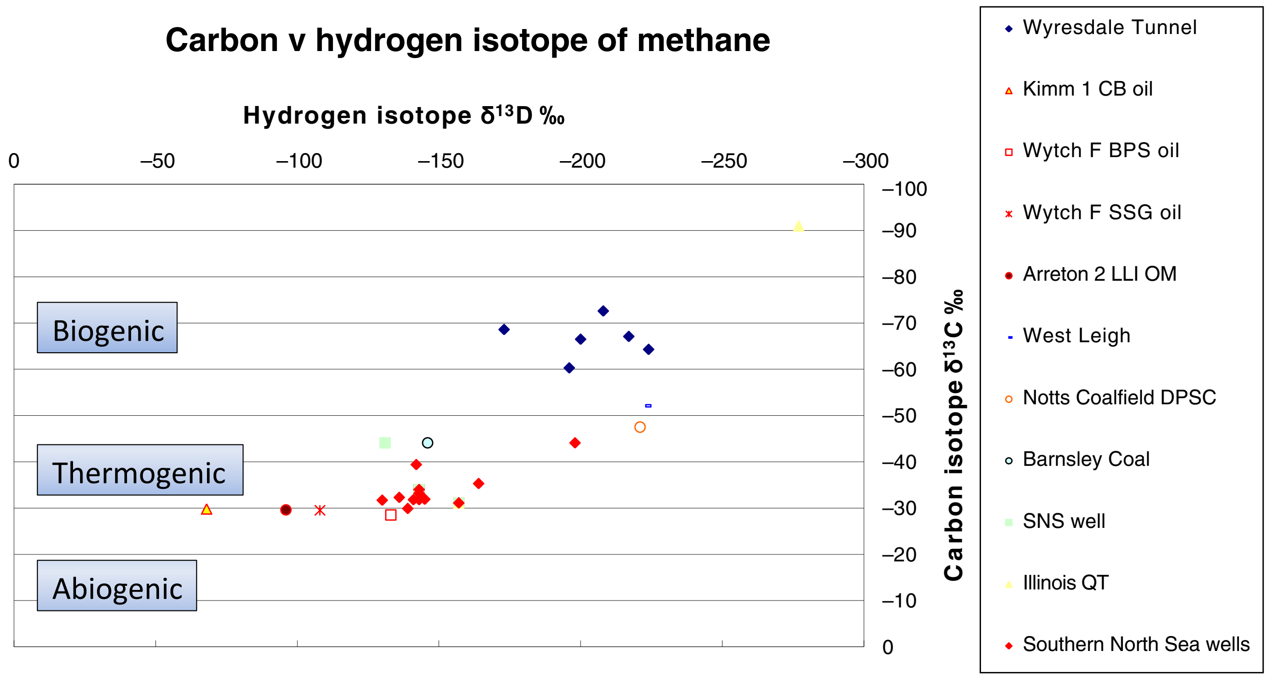

Fig. 7. Carbon and hydrogen isotope ranges in various methane gases. The $\delta^{13}C$ values 0 to −20‰ are probably abiogenically derived (e.g. Fischer–Tropsch reactions with hydrogen). The $\delta^{13}C$ values of −20 to about −55‰ represent thermogenic methane. The gas field methanes (Lokhurst 1998) are migrated gases. Coal field gases (Hitchman *et al.* 1989) might be more depleted than the migrated gases, with biogenic and CO_2-reduced gases (Bath *et al.* 1988) even more depleted. BC, Barnsley Coal; BPS, Bridport Sandstone; CB, Cornbrash; SSG, Sherwood Sandstone Group; LIAS, lower Lias organic matter; Arreton NC, Nottinghamshire Coalfield deep soft coal; SNS, Southern North Sea; WL, West Leigh; WT, Wyresdale Tunnel, Illinois; QT, Quaternary.

Table 1. Names of main black shale formations and their equivalents

Formation	Equivalents	Stages	Basin
Kimmeridge Clay		Kimmeridgian	Weald
Oxford Clay		Callovian–Oxfordian	Weald
Lias		Hettangian–Toarcian	Weald
Sabden Shales		Arnsbergian	Pennine
Upper Bowland Shale	Edale Shale	Pendleian	Pennine
Lower Bowland Shale	Widmerpool Formation	Brigantian	Pennine
Worston Shale	Hodder Mudstone	Chadian–Holkerian	Craven
Long Eaton Formation		Chadian–Asbian	Widmerpool
Other names			
Holywell Shale	Pentre Chert, Bowland Shale	Namurian	NE Wales
Craven Group	All local named formations	Mississippian–Namurian	Pennine

The Craven Group is a new term, extending from Courceyan to Yeadonian stages which has rendered a lot of the local names in the Carboniferous obsolete for stratigraphic purposes (Waters *et al.* 2007).

radioactivity in these shale units in this area. The gross thickness of the Upper Bowland Shale (Namurian), together with the net thickness of high-gamma shale layers, is shown for most of the hydrocarbon wells (Fig. 9). The Upper Bowland Shale typically has a GR profile which shows a higher value basal section, overlying Mississippian limestone: this type of profile is also seen in the Haynesville Shale of Louisiana, USA. The presence of underlying limestone is also similar to the Barnett Shale. In the latter the Ordovician Viola–Simpson provides an impermeable barrier. This is eroded southwards where the Ellenburger Limestone, an aquifer, subcrops (Fig. 1): this latter configuration makes artificial fracturing of the Barnett more difficult.

The Sabden Shales are characterized by anomalously low density and velocity on wireline logs, which might be indicative of high organic matter content. Overpressure caused by disequilibrium compaction or volume expansion related to hydrocarbon generation (Osborne & Swarbrick 1997) can also cause anomalous velocity–density trends. Core samples indicate that the unit predominantly comprises hard, dark grey to black micaceous mudstone with abundant plant fossils. The presence of interbedded coal

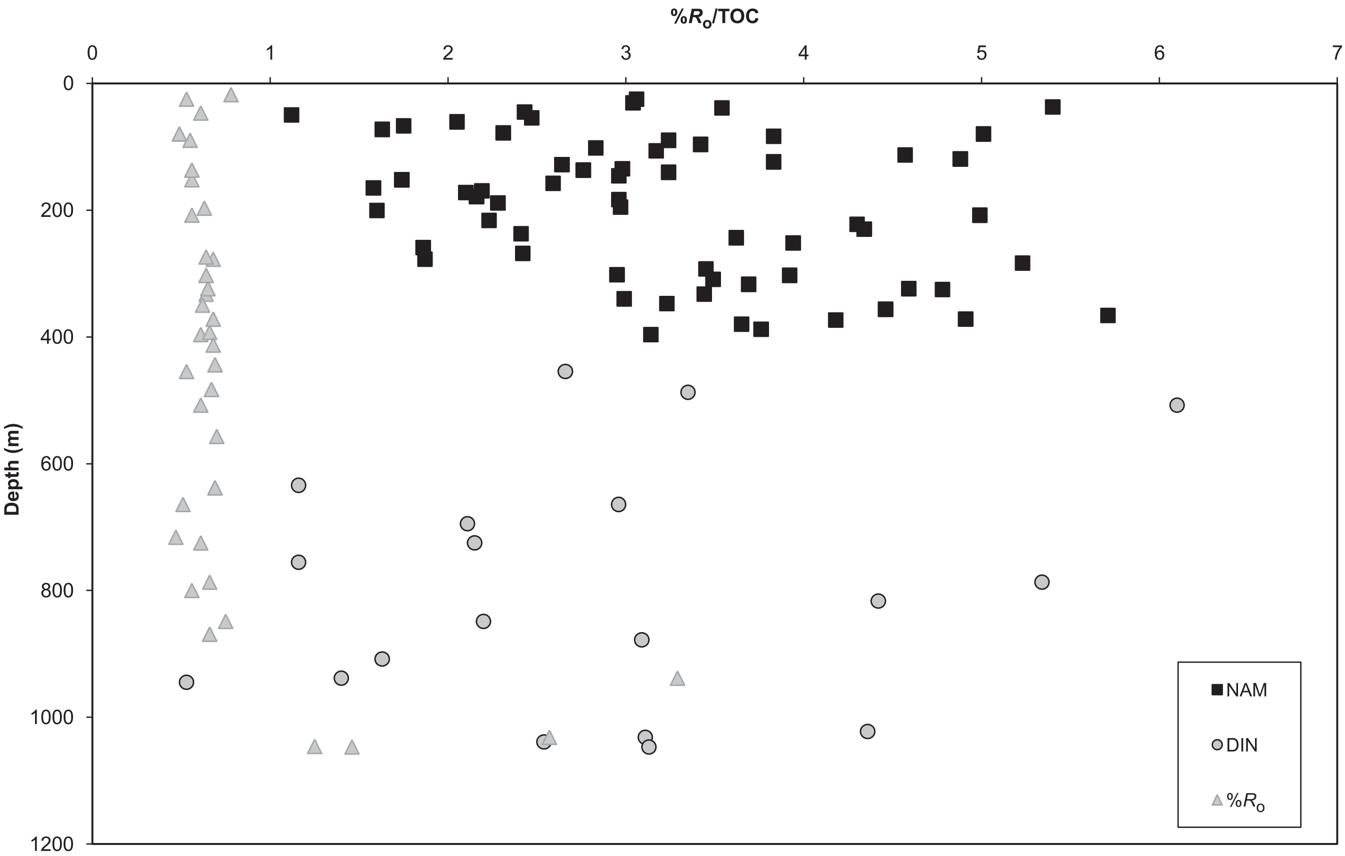

Fig. 8. Range of TOC contents and vitrinite reflectance in the BGS Duffield borehole, Widmerpool Gulf. NAM, Namurian; DIN, Dinantian; R_o%, vitrinite reflectance. The high R_o% near the base is caused by igneous sills but may lead to gas window maturity near or below terminal depth.

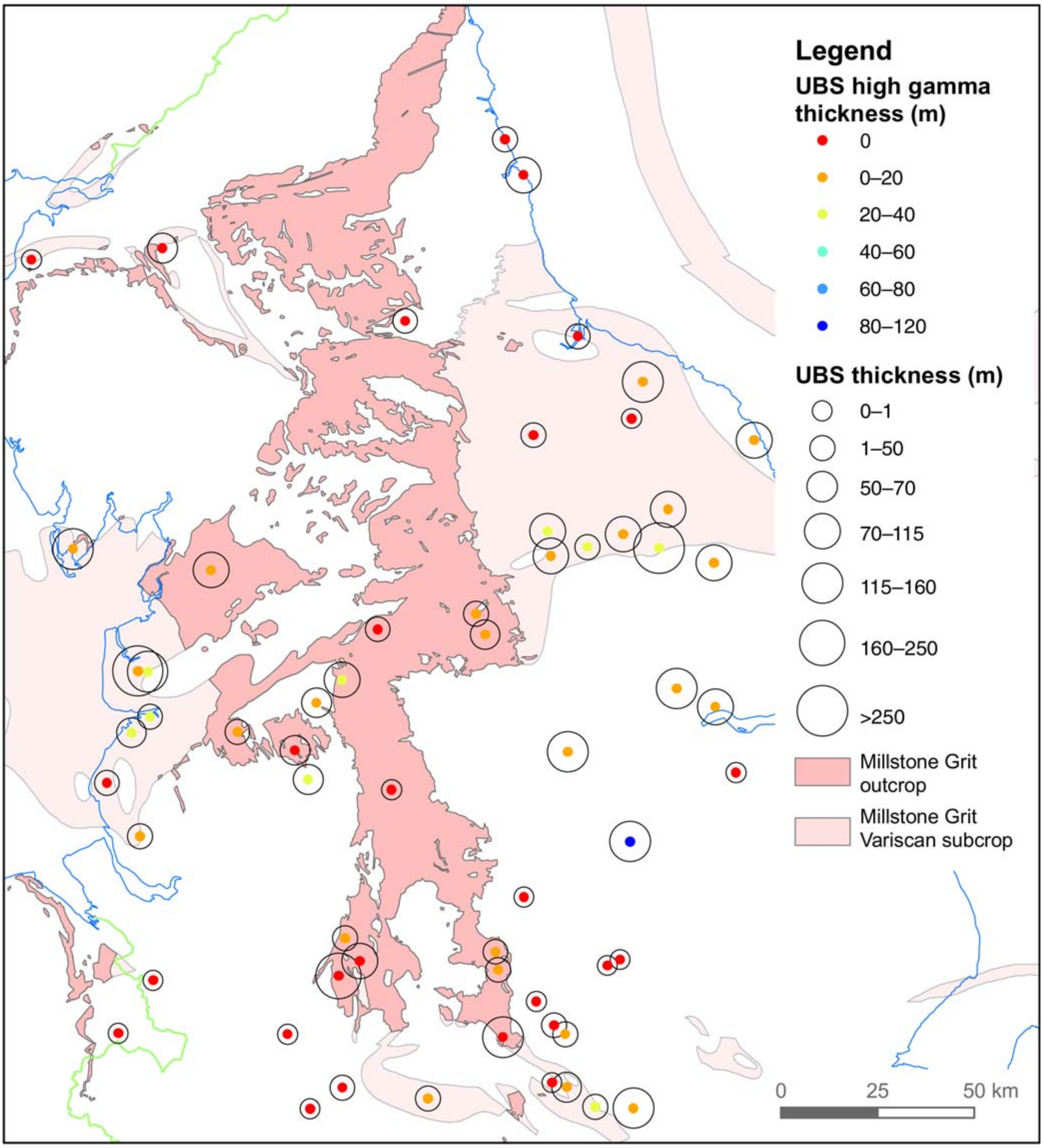

Fig. 9. Upper Bowland Shale (UBS): gross thickness of mudstones and net thickness of high gamma mudstones.

seams in some places suggests that at least part of the sequence may be gas-prone. TOC measurements in the Knott Coppy borehole (Figs 4 & 5) are in the range 1–3%, making these shale units potential hydrocarbon source rocks; however in this borehole TOC-rich shales do not always correspond to high gamma intervals.

Jurassic black shales

Black shales are found in the three main Jurassic mudstone formations: the Lias, Oxford Clay and Kimmeridge Clay (Figs 2 & 3). Liassic shales form the main source rocks for the Wessex and Weald oil fields (Ebukanson & Kinghorn 1986). These shales are mature for gas generation and small gas accumulations (dubbed 'enigmatic' by Butler & Pullan 1990) occur on the margins of the Weald Basin and are associated with oil at Wytch Farm in the Wessex Basin (Fig. 2). In northern England the Lias is within the oil window in the Cleveland Basin. The Oxford and Kimmeridge Clays contain organic-rich formations and might also prove to be potential source rocks in onshore basins, but not for thermogenic gas.

Porosity and permeability values are likely to be higher in Jurassic shale units because they have not been subject to as much compaction as Palaeozoic shale formations. Jurassic mudstones encountered in shallow (<30 m) engineering boreholes have porosities in the range 30–40%. Organic-rich shale units are preferentially enriched in Cu, Ni, V, Ag and Mo (Gad *et al.* 1969) in common with shales of Palaeozoic age. Exploration of a number of Cretaceous and Jurassic shales is underway in the USA, for example the Haynesville Shale of Texas and Louisiana. This formation lies above the concealed Ouachita fold belt in a similar relationship to the Weald Basin Jurassic shales, which overlie the Variscan fold belt.

Conclusions

At the regional scale the Mississippian Bowland Shale Formation provides the most prospective shale gas play. The Bowland Shale is a proven source rock mature for gas production. Those shales, which have not sourced conventional hydrocarbons, need to be carefully evaluated to see if they can make a contribution. Locally, shales of Lower Palaeozoic (principally Upper Cambrian) and Jurassic age might prove suitable targets. The small size of basins and the lack of overpressure, relative to the USA, make it unlikely that a large potential exists onshore UK, unless these older shales are proved to be prospective. However, additional data are required to minimize exploration risk. In particular, isotope studies of gas source provenance and more information on joint and fracture densities are required. Not all the organic-rich shale sections occur where there are high GR values. Shale gas is most likely to occur in the sub-basin depocentres of the Pennine and Weald basins. Previous conventional hydrocarbon exploration wells tested structural highs and fault traps, with the result that some entirely missed source rocks known from other wells or interpreted from seismic. Drilling wells in the depocentres and the greater attention to shales required for this unconventional exploration are likely to lead to a new surge in subsurface geological knowledge of the UK.

This paper is published with the permission of the Executive Director of the British Geological Survey (NERC). We thank S. Holloway, M. Stephenson, H. Johnson and A. Doré for improving drafts and D. Entwisle for providing porosity data.

References

Aitkenhead, N. 1977. The Institute of Geological Sciences Borehole at Duffield, Derbyshire. *Bulletin of the Geological Survey of Great Britain*, **59**, 1–59.

Armstrong, J. P., Smith, J., D'Elia, V. A. A. & Trueblood, S. P. 1997. The occurrence and correlation of oils and Namurian source rocks in the Liverpool Bay–North Wales area. *In*: Meadows, N. S., Trueblood, S. P., Hardman, M. & Cowan, G. (eds) *Petroleum Geology of the Irish Sea and Adjacent Areas*. Geological Society, London, Special Publications, **124**, 195–211.

Bath, A., Darling, W. G. *et al*. 1988. *Chemical and Stable Isotopic Analyses of Dissolved Gases and Groundwater Seepages collected from Wyresdale Tunnel, November 1987*. WE/88/1C.

Bowker, K. A. 2007. Barnett shale gas production, Fort Worth Basin: issues and discussion. *American Association of Petroleum Geologists*, **91**, 523–533.

Budge, G. D. 1932. Methane storage in strata. *Proceedings of the South Wales Institute of Engineers*, **48**, 177–200.

Butler, M. & Pullan, C. P. 1990. Tertiary structures and hydrocarbon entrapment in the Weald Basin of southern England. *In*: Hardman, R. F. P. & Brooks, J. (eds) *Tectonic Events Responsible for Britain's Oil and Gas Reserves*. Geological Society, London, Special Publications, **55**, 371–391.

Challinor, P. J. 1990. Oil ingress into mine workings. *The Mining Engineer*, August, 68–74.

Creedy, D. P. 1989. Geological sources of methane in relation to surface and underground hazards. *Paper 1.4 Methane – Facing the Problems*. Symposium, 26–28 September, Nottingham.

Dow, W. G. 1977. Kerogen studies and geological interpretations. *Journal of Geochemical Exploration*, **7**, 77–79.

Dow, W. G. & O'Connor, D. E. 1982. Kerogen maturity and type by reflected light microscopy applied to petroleum exploration. *In*: Staplin, F. L., Dow, W. G. *et al*. (eds) *How to Assess Maturation and Paleotemperatures. Short Course No. 7*. Society of Economic Paleontologists and Mineralogists, Tulsa, OK, 133–157.

Earp, J. R. & Hains, B. A. 1971. *The Welsh Borderland*. British Geological Survey, London, British Regional Geology Memoirs.

Ebukanson, E. J. & Kinghorn, R. R. F. 1986. Oil and gas accumulations and their possible source rocks in southern England. *Journal of Petroleum Geology*, **9**, 413–428.

Evans, C. J. & Brereton, N. R. 1990. *In situ* crustal stress in the United Kingdom from borehole breakouts. *In*: Hurst, A., Lovell, M. A. & Morton, A. C. (eds) *Geological Applications of Wireline Logs*. Geological Society, London, Special Publications, **48**, 327–338.

Ewbank, G., Manning, D. A. C. & Abbott, G. D. 1993. An organic geochemical study of bitumens and their potential source rocks from the South Pennine Orefield, central England. *Organic Geochemistry*, **20**, 579–598.

Ferguson, J. 1984. The methane content of some Carboniferous limestones from the northern Pennines and its relationship to mineralisation. *Proceedings of the Yorkshire Geological Society*, **45**, 67–69.

Frantz, J. H., Waters, G. A. & Jochen, V. A. 2005. Operators re-discover shale gas value. *E&P*, 1 October 2005.

Fraser, A. J., Nash, A. J., Steele, R. P. & Ebdon, C. C. 1990. A regional assessment of the intra-Carboniferous play of northern England. *In*: Brooks, J. (ed.) *Classic Petroleum Provinces*. Geological Society, London, Special Publications, **50**, 417–440.

Gad, M. A., Gatt, J. A. & Le Riche, H. H. 1969. Geochemistry of the Whitbian (Upper Lias) sediments of the Yorkshire coast. *Proceedings of the Yorkshire Geological Society*, **37**, 105–139.

Griffith, A. E. 1983. The search for petroleum in Northern Ireland. *In*: Brooks, J. (ed.) *Petroleum Geochemistry and Exploration of Europe*. Blackwell Scientific Publications, 213–222.

Hillier, S. & Marshall, J. E. A. 1992. Organic maturation, thermal history and hydrocarbon generation in the Orcadian Basin, Scotland. *Journal of the Geological Society, London*, **149**, 491–502.

Hitchman, S. P., Darling, W. G. & Williams, G. M. 1989. *Stable Isotope Ratios in Methane Containing Gases in the United Kingdom*. BGS Technical Report, WE/89/30.

Hood, A., Gutjahr, C. C. M. & Heacock, R. L. 1975. Organic metamorphism and the generation of petroleum. *American Association of Petroleum Geologists*, **59**, 986–996.

Jarvie, D., Pollastro, R., Hill, R., Bowker, K., Claxton, B. & Burgess, J. 2004. *Evaluation of Hydrocarbon Generation and Storage in the Barnett Shale, Fort Worth Basin, Texas*. World Wide Web Address: www.humble-inc.com.

Jones, D. G. & Plant, J. A. 1989. Geochemistry of shales. *In*: Plant, J. A. & Jones, D. G. (eds) *Metallogenic Models and Exploration Criteria for Buried Carbonate-hosted Ore Deposits – a Multidisciplinary Study in Eastern England*. British Geological Survey, Keyworth, 65–94.

Kellaway, G. A. & Welch, F. B. A. 1948. Bristol and Gloucester district. *British Regional Geology* (2nd edn). British Geological Survey, London.

Landes, K. K. 1967. Eometamorphism, and oil and gas in time and space. *Bulletin of the American Association of Petroleum Geologists*, **51**, 828–841.

Leggett, J. K. 1980. British Lower Palaeozoic black shales and their palaeo-oceanographic significance. *Journal of the Geological Society*, **137**, 139–156.

Lokhurst, A. (ed.) 1998. *The Northwest European Gas Atlas – Composition and Isotope Ratios of Natural Gases in Northwest European Gasfields*. NITG-TNO, Haarlem (CD ROM).

Maynard, J. R., Wignall, P. B. & Varker, W. G. 1991. A hot new shale facies from the Upper Carboniferous of Northern England. *Journal of the Geological Society*, **148**, 805–808.

Montgomery, S. L., Jarvie, D. M., Bowker, K. A. & Pollastro, R. M. 2005. Mississippian Barnett Shale, Fort Worth Basin, north central Texas: gas shale play with multi-trillion cubic foot potential. *American Association of Petroleum Geologists Bulletin*, **89**, 155–175.

Moseley, F. & Ahmed, S. M. 1967. Carboniferous joints in the north of England and their relation to earlier and later structures. *Proceedings of the Yorkshire Geological Society*, **36**, 61–90.

Oldroyd, G. C., McPherson, M. J. & Morris, L. H. 1971. Investigations into sudden abnormal emissions of firedamp from the floor strata of the Silkstone seam at Cortonwood Colliery. *The Mining Engineer*, **130**, 577–593.

Osborne, M. J. & Swarbrick, R. E. 1997. Mechanisms for generating overpressure in sedimentary basins: a reevaluation. *Bulletin of the American Association of Petroleum Geologists*, **81**, 1023–1041.

Parnell, J. 1983. The distribution of hydrocarbon minerals in the Welsh Borderlands and adjacent areas. *Geological Journal*, **18**, 129–139.

Plant, J. A. & Jones, D. G. 1989. *Metallogenic Models and Exploration Criteria for Buried Carbonate-hosted Ore Deposits – a Multidisciplinary Study in Eastern England*. British Geological Survey and the Institution of Mining and Metallurgy, London.

Pollastro, R. M., Hill, R. J. *et al.* 2004. *Assessment of Undiscovered Oil and Gas Resources of the Bend Arch–Fort Worth Basin Province of North-Central Texas and Southwestern Oklahoma, 2003: U.S. Geological Survey Fact Sheet 2004–3022*. World Wide Web Address: http://pubs.usgs.gov/fs/2004/3022/

Ponsford, D. R. A. 1955. Radioactivity studies of some British sedimentary rocks. *Bulletin of the Geological Survey*, **10**, 24–44.

Poole, E. G. 1977. Stratigraphy of the Steeple Aston Borehole, Oxfordshire. *Bulletin of the British Geological Survey*, **57**.

Poole, E. G. 1978. Stratigraphy of the Withycombe Farm Borehole, near Banbury, Oxfordshire. *Bulletin of the British Geological Survey*, **68**.

Ramsbottom, W. H. C., Sabine, P. A., Dangerfield, J. & Sabine, P. W. 1981. Mudrocks in the Carboniferous of Britain. *Quarterly Journal of Engineering Geology*, **14**, 257–262.

Ray, E. O. 1976. Devonian shale development in eastern Kentucky. *In*: *Natural Gas from Unconventional Geologic Sources*. Board on Mineral Resources and Commission on Natural Resources. National Academy of Sciences, Washington, DC, 100–111.

Rogers, S. F. 2003. Critical stress-related permeability in fractured rocks. *In*: Ameen, M. (ed.) *Fracture and In-situ Stress Characterization of Hydrocarbon Reservoirs*. Geological Society, London, Special Publications, **209**, 7–16.

Rushton, A. W. A., Hamblin, R. J. O. & Strong, G. E. 1988. The Croft Borehole in the Lilleshall Inlier of north Shropshire. *Reports of the British Geological Survey*, **19**, 1–14.

Selley, R. C. 1987. British shale gas potential scrutinized. *Oil and Gas Journal*, 15 June, 62–64.

Selley, R. C. 2005. UK shale-gas resources. *In*: Doré, A. G. & Vining, B. A. (eds) *Petroleum Geology: North-west Europe and Global Perspectives: Proceedings of the 6th Petroleum Geology Conference*. Geological Society, London, 707–714; doi: 10.1144/0060707.

Shurr, G. W. & Ridgley, J. L. 2002. Unconventional shallow biogenic gas systems. *Bulletin of the American Association of Petroleum Geologists*, **86**, 1939–1969.

Smith, N. J. P. (Compiler) 1985. *Map 1: Pre-Permian Geology of the United Kingdom (South)*. 1:1,000,000 scale. British Geological Survey.

Smith, N. J. P. 1993. The case for exploration of deep plays in the Variscan fold belt and its foreland. *In*: Parker, J. R. (ed.) *Petroleum Geology of Northwest Europe: Proceedings of the 4th Conference*. Geological Society, London, 667–675; doi; 10.1144/0040667.

Smith, N. J. P. & Rushton, A. W. A. 1993. Cambrian and Ordovician stratigraphy related to structure and seismic profiles in the western part of the English Midlands. *Geological Magazine*, **130**, 665–671.

Smith, N. J. P., Kirby, G. A. & Pharaoh, T. C. 2005. Structure and evolution of the south-west Pennine Basin and adjacent area. British Geological Survey, London, Subsurface Memoirs.

Spears, D. A. & Amin, M. A. 1981. Geochemistry and mineralogy of marine and non-marine Namurian black shales from the Tansley borehole. *Sedimentology*, **28**, 407–417.

Stocks, A. E. & Lawrence, S. R. 1990. Identification of source rocks from wireline logs. *In*: Hurst, A., Lovell, M. A. & Morton, A. C. (eds) *Geological Applications of Wireline Logs*. Geological Society, London, Special Publications, **48**, 241–252.

Taylor, K. & Rushton, A. W. A. 1971. The pre-Westphalian geology of the Warwickshire Coalfield. *Bulletin of the Geological Survey of Great Britain*, **35**, 1–150.

Waters, C. N., Browne, M. A. E., Dean, M. T. & Powell, J. H. 2007. *Lithostratigraphical Framework for Carboniferous Successions of Great Britain (Onshore)*. British Geological Survey, London, **RR/07/01**.

Zhao, H., Givens, N. B. & Curtis, B. 2007. Thermal maturity of the Barnett Shale determined from well-log analysis. *American Association of Petroleum Geologists Bulletin*, **91**, 535–549.

The Western Canada Foreland Basin: a basin-centred gas system

D. J. BOETTCHER,[1] M. THOMAS,[1] M. G. HRUDEY,[2] D. J. LEWIS,[2] C. O'BRIEN,[2] B. OZ,[2] D. REPOL[2] and R. YUAN[2]

[1]*Shell Canada Ltd (Retired)*
[2]*Shell Canada Ltd, 400 4th Avenue SW, PO Box 100, Station M, Calgary, Alberta, Canada T2P 2H5 (e-mail: michael.hrudey@shell.com)*

Abstract: Enormous volumes of gas (>30 Tcf) are contained within the deepest portions of the Western Canada Foreland Basin, where tight gas-saturated Cretaceous sandstones grade updip into porous water-saturated sandstones. Production has occurred from coarse-grained shoreline sands both near the updip gas–water interface, such as those found in the Elmworth Field, and from low-porosity–permeability reservoirs found deeper in the basin. These basin-centred gas (BCG) reservoirs are characterized by regionally pervasive gas-saturated lithologies, abnormal pressures and no downdip water contact, and occur in low-permeability reservoirs. The keys to Shell's exploration success were an understanding of the stratigraphy, sedimentology and rock properties of the basin, the development of structural, petrophysical and geomechanical models, development of an understanding of the desiccation or dewatering process, the distribution of water within the basin and how the pressure regime evolved, interpretation of 3D seismic, and an aggressive land strategy. The evaluation of structural leads was aided when seismic and geomechanical modelling were combined, thereby aiding in the prediction of zones with a higher probability of encountering favourable reservoir producibility characteristics, that is, areas where a well developed, well connected open fracture network is expected. This multidisciplinary approach has resulted in economic success in regions once thought to be non-productive, and where it was once said, 'People go broke chasing the Nikanassin'.

Keywords: basin-centred gas, tight gas sandstones, Canada, Cretaceous, Nikanassin, Cadomin, Falher, Cadotte, desiccated reservoir, fracture modelling, permeability enhancement, geomechanical modelling, updip water

Basin-centred gas systems, as defined by Law (2002), are those characterized by being: regionally gas pervasive, abnormally pressured (high or low), lacking a downdip water contact and occurring in low-permeability reservoirs. Bennion *et al.* (2002) stated that, in order to produce economic volumes of gas from these low-permeability (<0.05 mD) reservoirs, the initial water saturation must be significantly lower than what would be expected from a system in capillary equilibrium where the matrix is in dynamic contact with a free water level. In the past these have been variably referred to as tight gas sands or 'Deep Basin' gas with the latter first used by Masters (1979) to describe the thick, low-permeability, gas-bearing, Cretaceous section of west-central Alberta.

From the initial phases of exploration in this portion of Western Alberta to the mid-1970s, industry concentrated on either deep Palaeozoic objectives or conventional Cretaceous zones where reservoir properties were good and production rates were high. Beginning with the Elmworth discovery in 1976, the focus began to shift to the 'upside down trapping conditions of the Deep Basin' (Masters 1984). Initially the exploration and development concentrated on low-permeability (<0.4 mD) but well sorted shoreline sandstones of the Lower Cretaceous. Prolific drilling continued in the Deep Basin throughout the following decades, such that within the central focus area nearly 18 000 wells have been located and drilled. Of these, nearly 10 000 wells are currently producing a total of 4.92×10^9 SCF/day with a total cumulative gas volume of 23.8×10^{12} SCF. At present, the average well deliverability is approximately 0.5 mmcf/day.

As a relative latecomer to the area, in January 2003, Shell Canada began to investigate opportunities in the Deep Basin of west-central Alberta. The initial area examined (Fig. 1a) ranged from west of Calgary Alberta in the SE, to the NE corner of British Columbia, covering an area of 100 000 km^2. The western boundary was the edge of the Rocky Mountain disturbed belt (Fig. 1) while the eastern boundary was the updip water edge associated with each formation. The formations examined ranged from the Upper Cretaceous Cardium Formation to the Lower Cretaceous/Jurassic Nikanassin Formation (Fig. 3). From this analysis, an area of interest ranging from Township 45 Range 20W5 in the SE to 93-P in northeastern British Columbia (Fig. 2), covering 50 000 km^2, was selected. This region was chosen as all reservoirs of interest are present, principally the Cadotte, Falher, Cadomin and Nikanassin formations (Fig. 3), and pressures (along the basinal axis) are for the most part above hydrostatic (except the Cardium Formation). Within these units, the thickest sandstones occur in the upper Nikanassin Formation, where net reservoir can exceed 100 m. Available petroleum and natural gas rights directed Shell's attention into the deepest portions of the basin, corresponding to the region of lowest matrix permeability, where pressures were highest, where sandstone thickness were highest and where multiple thrust cored structures were evident on Shell's existing 2D seismic data base.

Shell's understanding of data within the study area favoured an exploration strategy for basin-centred gas (BCG) and, in the latter part of 2004, Shell drilled and completed its first BCG well at 15-20-65-13W6. Gas was encountered in the Cadotte (absolute open flow potential, AOFP, of 3.5 mmcf/day from 18.7 m of 5.6%phi), Cadomin (AOFP of 4.8 mmcf/day, 10.0 m at 5.0%phi) and Nikanassin formations (three intervals were tested; two were shut in while still cleaning up but the uppermost zone had a calculated AOFP of 9.0 mmcf/day, 93 m at 4.2%phi) and flowed from sandstones and conglomerates whose matrix permeability is commonly less than 100 μD. Continued exploration and subsequent exploitation has resulted in an understanding of the regional depositional history, rock properties, stratigraphic and

VINING, B. A. & PICKERING, S. C. (eds) *Petroleum Geology: From Mature Basins to New Frontiers – Proceedings of the 7th Petroleum Geology Conference*, 1099–1123. DOI: 10.1144/0071099

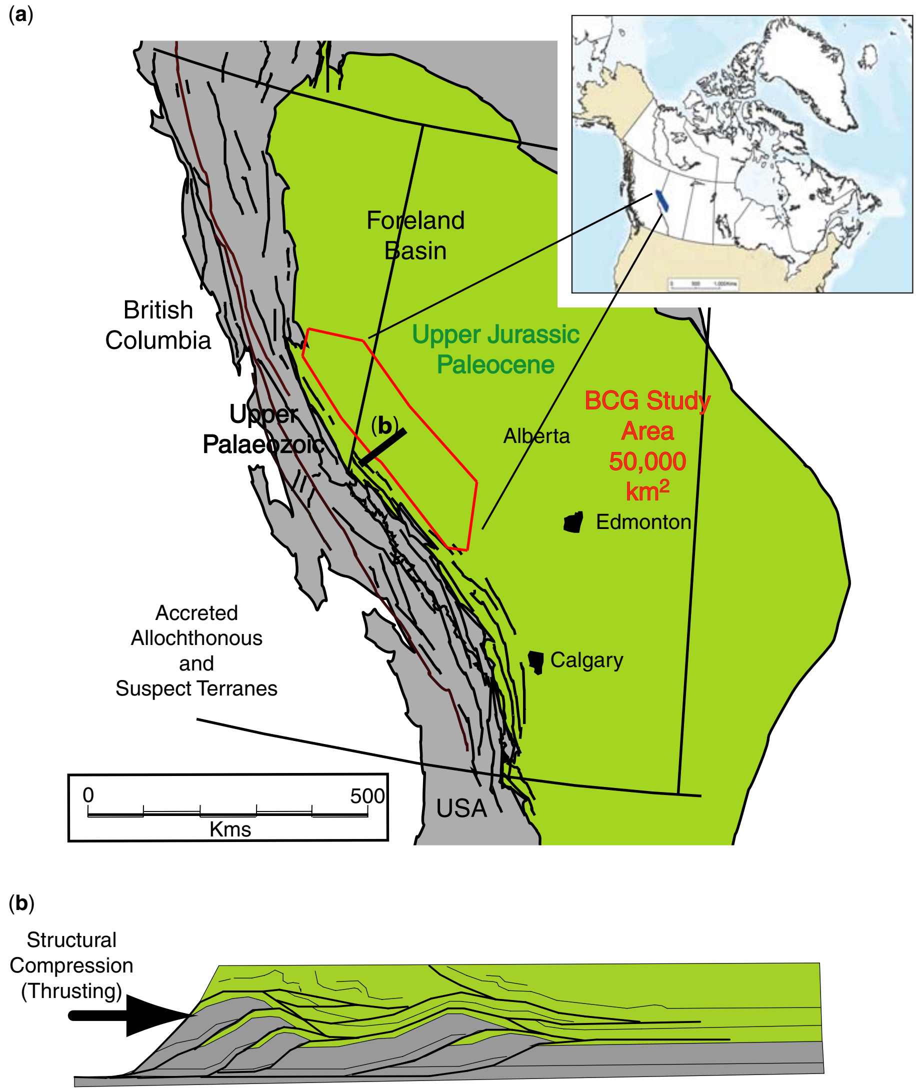

Fig. 1. Schematic regional tectonic map of the Western Canadian Foreland Basin. (**a**) Basin showing the outline of Upper Palaeozoic, Upper Jurassic/Paleocene sediments and faulting. (**b**) Generalized cross-section east of Palaeozoic outcrop.

structural geophysics, reservoir petrophysics (including water saturations, S_w, and updip water line complexities), reservoir desiccation and pressure distributions. These different facets are used in conjunction with geomechanical models to aid in the targeting of wells into features where the probabilities of encountering an effective fracture network and associated enhanced gas productivity have been maximized.

Deep basin stratigraphy, sedimentology and rock properties

During Late Jurassic and Early Cretaceous time, uplift and exhumation associated with the Columbian orogeny (Mossop & Shetsen 1994) provided abundant sediment to the foredeep trough, defined by Leckie & Smith (1992) as a succession of sedimentary rocks deposited in a cratonic region adjacent to an active orogenic belt. Sediments were derived mainly from the orogenic zone and thinned away from it. In Western Canada, this foreland basin was an elongate trough that developed between the eastern flanks of the ancestral Rocky Mountains and the stable interior platform, represented by the North American craton and extending across most of western Alberta and NE British Columbia.

In the Western Canada Foreland Basin (WCFB, also referred to as the Alberta Basin), the amount and rate of subsidence was greatest adjacent to the advancing thrust sheets and it was here that the greatest amount of sediment accumulated, resulting in stacked, eastward-thinning clastic wedges. The asymmetric subsidence of the basin also affected drainage patterns, creating a prevailing drainage system that was largely parallel to the basin axis (i.e. NW–SE).

Leckie & Smith (1992) subdivided the depositional history of the WCFB into five cycles of differing ages, each representing strata bounded by major unconformities or lithological changes. Prospective BCG sandstones are contained within the first two cycles, the first of which extends from Oxfordian (earliest Upper Jurassic) to late Valanginian time (mid Lower Cretaceous) and includes sediments from the base of the Fernie Formation shales to the top of the Nikanassin Formation (Fig. 3). The base of Cycle 1 (Leckie & Smith 1992), in the grey or green beds of the Late Jurassic Fernie Formation, marks the first widespread appearance of sediments that were derived from the rising Cordillera to the west. The top of Cycle 1 is represented by a regional unconformity that separates the Nikanassin Formation or Kootenay Group sediments from the overlying Lower Cretaceous Cadomin Formation (Fig. 4). This unconformity represents a hiatus that may have been in excess of 27 Ma (Leckie & Smith 1992). The second cycle incorporates the majority of the remaining zones of interest ranging from the Cadomin Formation to the Cadotte Formation.

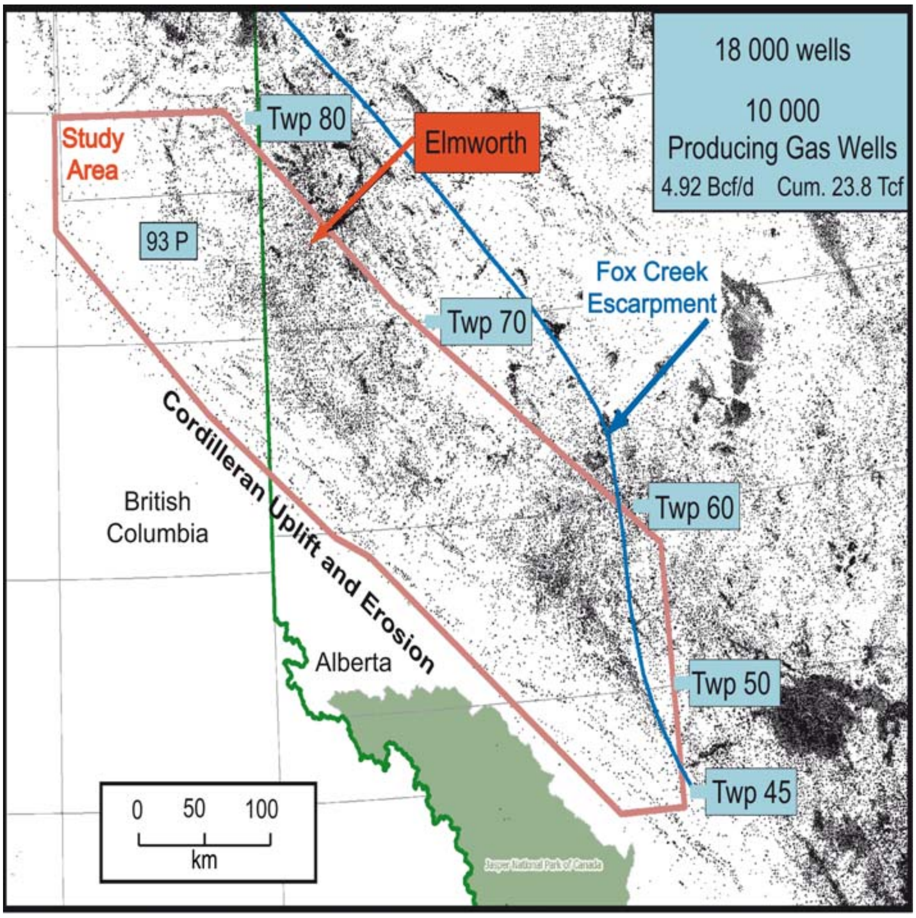

Fig. 2. Well density across study area.

Jurassic to Eocene tectonics produced a series (Fig. 5) of anticlinal structures of decreasing magnitude to the NE across the basinal axis, from structures of high amplitude to updip regions where no structures are evident and the reservoir units are essentially flat lying, dipping at angles of 1–2° to the SW.

Allen (1980) stated that, within the WCFB, hydrocarbons have been found in 20 rock units ranging in age from Permian to Late Cretaceous with the majority of reserves contained within the Lower Cretaceous Spirit River Formation (mainly Falher Member) and in the tight fluvial sandstones of the Upper Jurassic Nikanassin Formation. Each of the principal objective formations are discussed below.

Nikanassin Formation

The name ‘Nikanassin Formation’ (Poulton *et al.* 1990) extends northwards from outcrops into the subsurface in west-central Alberta, although no type section has been formally designated for the Formation. In the outcrop belt of the Rocky Mountain Foothills of northeastern British Columbia the equivalent Upper Jurassic sandstones and associated sediments have been included in the Minnes Group (Fig. 3). Stott (1993) correlated the Minnes Group eastward into the subsurface where the upper zones are absent below the sub-Cadomin Formation unconformity and only the Monteith Formation and parts of the Beattie Peaks Formation are preserved (Fig. 3). These two formations are not easily distinguishable in well logs and together comprise what is more commonly referred to as the Nikanassin Formation.

The Fernie/Nikanassin Formation assemblages form a clastic wedge that represents the earliest orogenic detritus in the foreland basin. The lower units, including the Green Beds, Fernie and Passage Beds, consist of marine deposits that initially filled the foredeep. These marine sediments grade upward into continental clastic deposits of the Kootenay Group and Nikanassin Formation (Barclay & Smith 1992), with basin filling occurring in a northerly direction along the axis of the basin. While the Passage Beds (siltstone and shale) represent marine deposition during the initial stages of basin-fill, sandstones of the Morrissey Formation or basal unit of the Kootenay Group (Fig. 3) were deposited along a northerly to northwesterly prograding high-energy shoreline. In southwestern Alberta, the Morrissey is overlain by fluviodeltaic quartz and chert-rich sandstones, siltstones, shales and coals of the Mist Mountain Formation. North of the North Saskatchewan River (off the south edge of Fig. 2), the coeval Nikanassin Formation is dominated by flood plain deposits in the west, grading to shoreline and estuarine sandstones near its eastern erosional limits. The equivalent Monteith Formation in northeastern British Columbia contains fluviodeltaic lithic sandstones, shales and coals in the west and shoreline to estuarine quartz arenites in the east, suggesting that both western and eastern provenances are represented in preserved strata in this early narrow foredeep trough.

The Minnes Group is interpreted to have been deposited in an entirely fluvial system in northeastern British Columbia, south of the Sukunka River (at the north edge of Fig. 2). Similar to the Kootenay Group of southwestern Alberta, it contains flood plain shales, fluvial channel sandstones and coal in its lower part, which grade upward into upland fluvial sandstones and conglomerates. During the late Jurassic, basin fill apparently occurred from south to north, suggesting that shoreline sequences became progressively younger in the same direction (Mossop & Shetsen 1994). Detailed log evaluation of the Nikanassin Formation, especially from wells in northeastern British Columbia, suggests

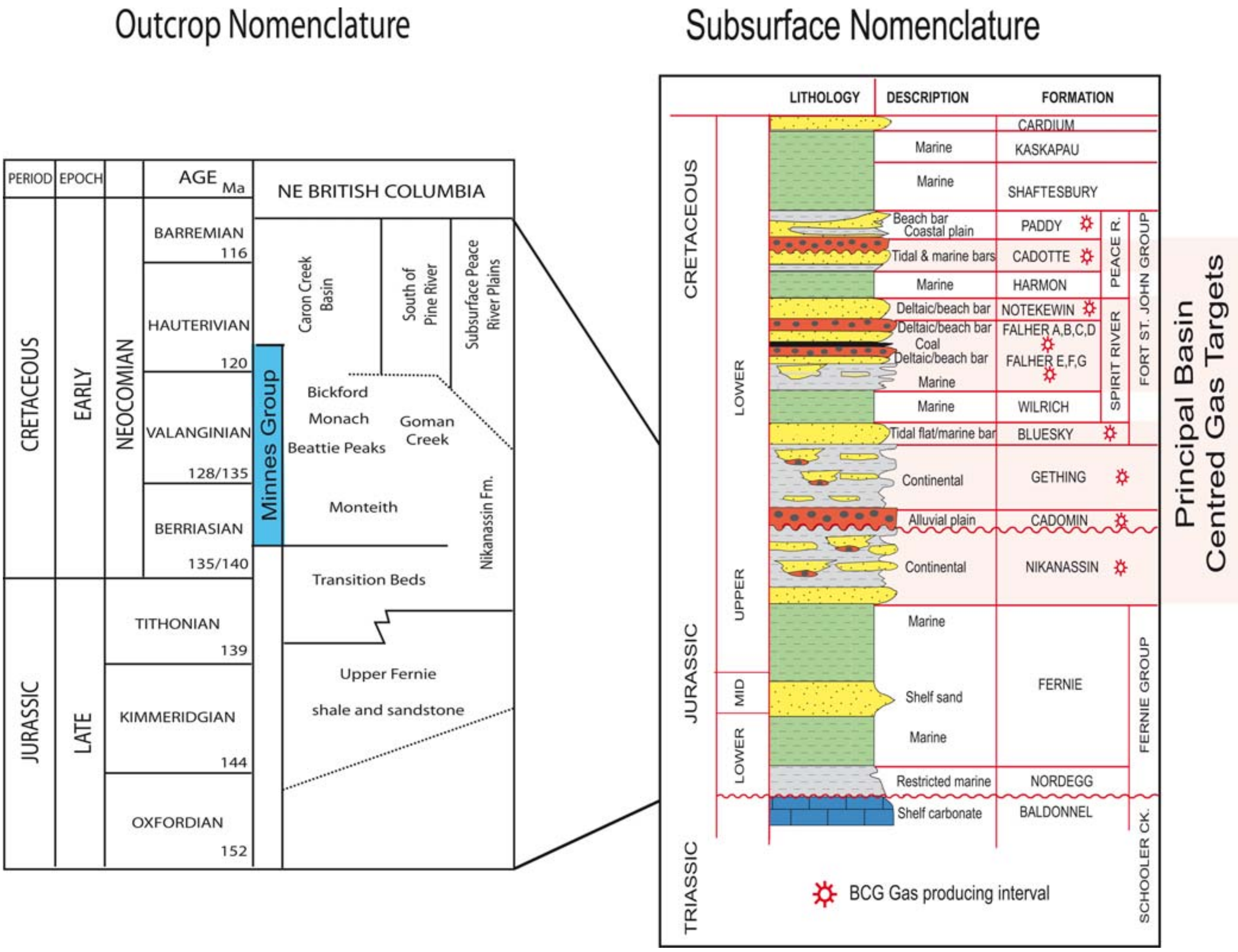

Fig. 3. BCG stratigraphic summary for NE British Columbia and west-central Alberta. Surface and subsurface.

that the lower portions of the formation consist of marine sediments characterized by thin, relatively 'dirty' coarsening upward beach sequences. These grade upward into units composed predominantly of continental (flood plain?) sediments including numerous coals and fluvial sandstones.

Depositional model

As previously indicated, those zones that are correlative with the Nikanassin Formation to the SE in the Kootenay Group and to the NW in the Minnes Group are primarily fluvial in nature. In the central portion of the BCG study area, the Nikanassin Formation can be subdivided into two main units, referred to simply as the Upper and Lower Nikanassin (Fig. 6). Net sand in the Upper Nikanassin can exceed 130 m in thickness along the axis of the trough. This depocentre is approximately 50 km long and can range in width from 10 to 20 km. To the east and NE these sands thin to a zero edge. The basal portion of the Upper Nikanassin (Fig. 6b) consists of discrete point bar and channel sand deposits (as determined from log signatures) separated by siltstones and shales. Moving up in the section, the sands become more continuous, both vertically and laterally, although some irregularly distributed shales are present. Stacked channel sandstones in the Upper Nikanassin can exceed 130 m in thickness (Fig. 6a). In cross-section (Fig. 7) the Upper Nikanassin thins to the east, with the more continuous sands near the top over much of the area.

The Lower Nikanassin consists predominantly of siltstones and shales with some scattered sandstones. Resistivity at the boundary between the two units shows a distinctive shift (Fig. 6). Zaitlin *et al.* (2002) indicated that changes in Basal Quartz deposition (early Cretaceous–southeastern Alberta) from low accommodation braided deposits to higher accommodation meandering deposits were associated with local syn-depositional faulting. Lukie *et al.* (2002) indicated that mudstone-dominated deposits consisting of terrestrial overbank sediments with included isolated channel sandstones are interpreted to reflect a progressive increase in accommodation space that led to successively less amalgamation of the channel deposits.

In the Western Canada Foreland Basin, the amount and rate of subsidence was greatest adjacent to the advancing thrust sheets and it was here that the greatest amount of sediment accumulated (Leckie & Smith 1992). Arnott *et al.* (2002) stated that in basins with increasing accommodation space meander deposits predominate in which irregularly distributed fluvial sands are preserved in thick overbank deposits. Thus, it is interpreted that the continental sediments of the Lower Nikanassin as well as those in the basal portions of the Upper Nikanassin were deposited in meander systems that formed in response to increasing accommodation space resulting from subsidence in the foreland basin. In contrast, it is postulated that the more regionally continuous sheet-like sandstones of the Upper Nikanassin were deposited in a braid plain complex where little overbank sediment is preserved. These braid plain deposits formed when accommodation space decreased (or sediment supply increased) and the sands build laterally as opposed to vertically (as noted for the Cadomin Formation by Johnson & Dalrymple 2005). In northeastern British Columbia the more laterally continuous

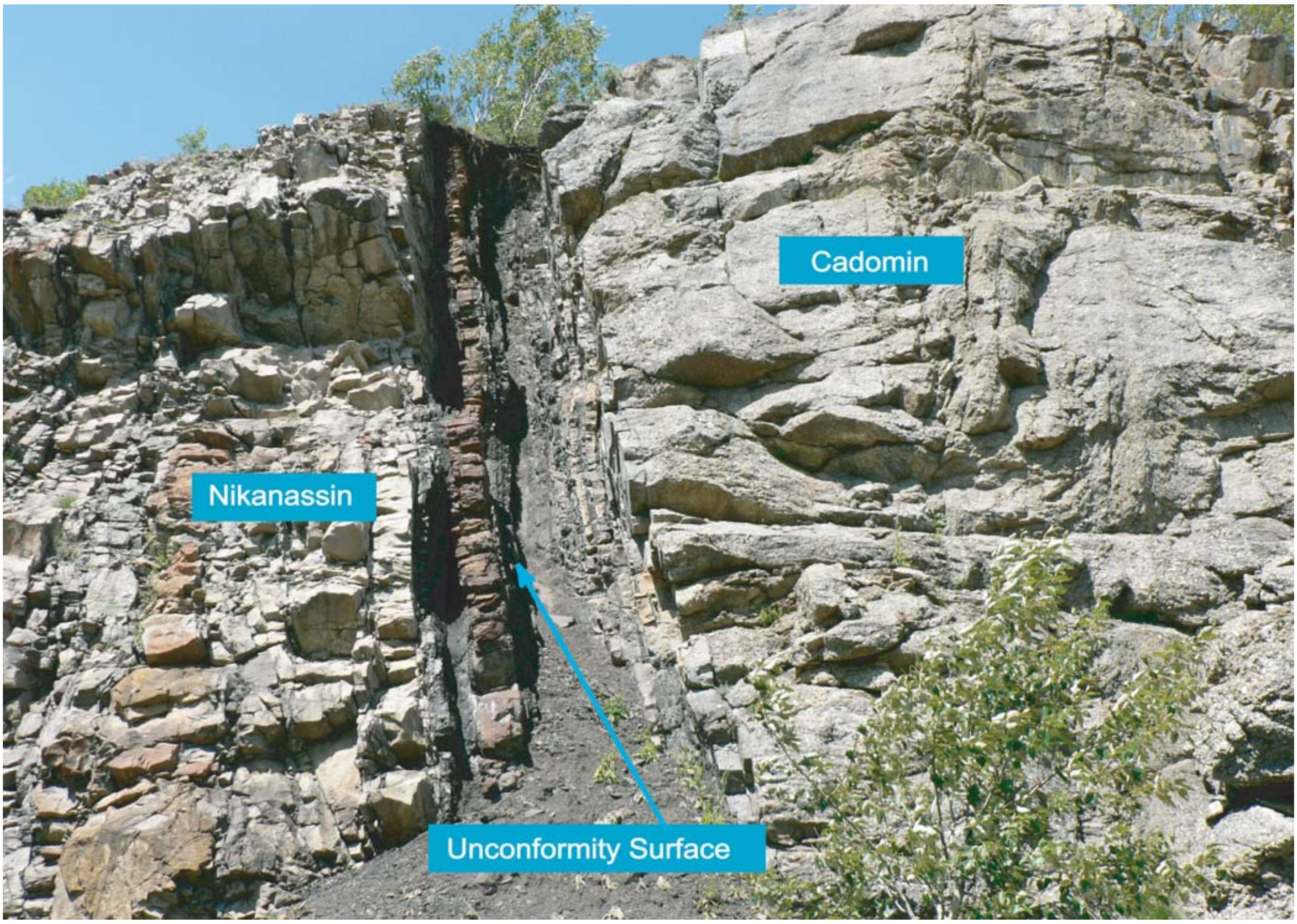

Fig. 4. Outcrop photograph of the Cadomin to Top Nikanassin interval showing the top Nikanassin unconformity. Note the difference in fracture density and patterns in the coarse-grained Nikanassin sandstones v. the conglomerates of the Cadomin.

braid plain sandstones are not evident. Instead the Nikanassin Formation consists predominantly of thick sequences of siltstones, coals and shales with some interbedded channel and point bar sands indicative of deposition in a meander system.

The distribution of the braid plain and meander systems in the Nikanassin Formation can be explained through examination of deeper features in the basin as seen on a seismic strike line (Fig. 8), flattened on the 4th coal in the Falher Member (Spirit River Formation), extending from Township 63 into NE British Columbia. Moving from SE to NW it is apparent that accommodation space is increasing from the 4th coal to the Triassic level. The break in slope where the thickness starts to increase can also be correlated to a Devonian reef edge deeper in the section and a hinge line in the Basement. The braid plain system was developed across the region to the SE, where the seismic 4th coal to Triassic isotime is relatively constant. Northwest of the break in slope, accommodation space increases and the Nikanassin Formation is characterized by sandstones deposited primarily in meander systems. Overall, the Nikanassin Formation represents a significant period of basin fill as the gross isopach ranges from approximately 200 m in the NE to over 1500 m in the centre of the foreland basin adjacent to the disturbed belt in the NW portions of the study area.

Rock properties

The upper portion of the Nikanassin Formation consists primarily of medium- to coarse-grained lithic sandstones in which the principal framework grains are quartz, chert and argillaceous rock fragments. Primary porosity was destroyed by the combined effects of mechanical compaction (physical rearrangement of grains into a closest packing in response to increasing overburden pressure), chemical compaction (suturing or welding of grain boundaries), quartz overgrowth development and the precipitation of kaolinite and late stage ankerite (iron-carbonate) cement (Fig. 9). The current porosity in these sandstones is mainly secondary and resulted from the partial to complete dissolution of chemically unstable argillaceous clasts and chert grains.

In a cross-plot of ambient porosity v. air permeability (Fig. 10a), the dark blue rhombs represent core averages (thickness weighted porosity and geometrically averaged permeability) for individual wells. The magenta squares are ambient whole-core values, from the Nikanassin Formation in Shell's 11-21-65-13W6 well. The green triangles represent ambient values on drill plugs from the same core. All of these values fall within the same general trend except for a few core averages (dark blue rhombs) where the permeability values are near to or greater than 1 mD, the result of an effective fractures network. From the individual well analysis (dark blue rhombs) average ambient porosity and permeability values are 0.05 and 0.14 mD, respectively. When conducting the regional scoping work to assess the thickness and distribution of the Upper Nikanassin Formation sandstones, it was noted that the sonic response is very consistent throughout the interval, averaging about 200 $\mu s\,m^{-1}$. Using a sonic-porosity transform of ([interval transit time − 180]/400 $\mu s\,m^{-1}$) results in a porosity of 5%. Core analysis is consistent with this, giving porosity values in the Upper Nikanassin Formation sandstones of 4–6%.

In situ permeability values tend to be one order of magnitude lower than corresponding ambient values, but the actual reduction

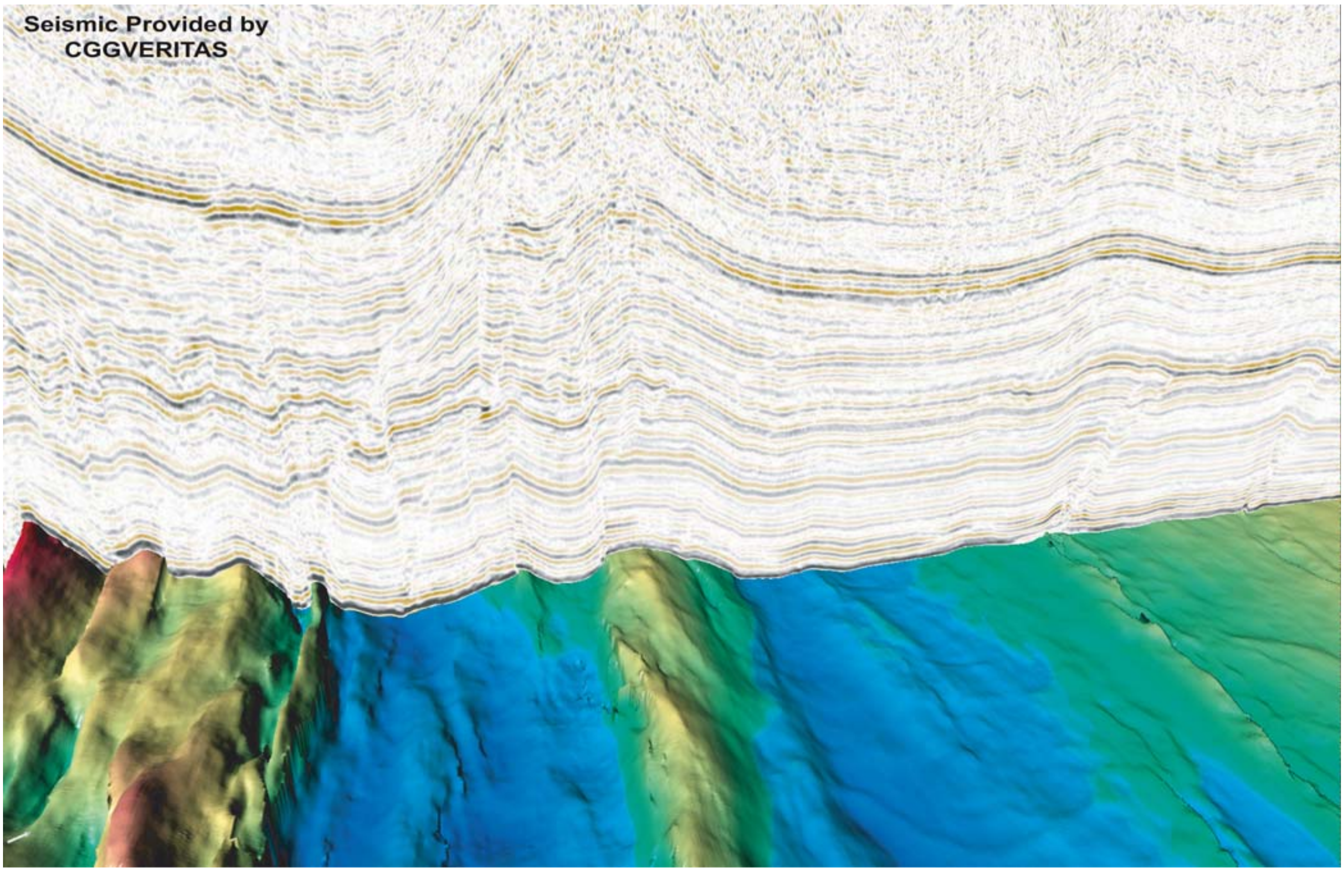

Fig. 5. Seismic and structure example showing a series of anticlinal structures related to a number of fault propagation folds. Seismic runs from SW to NE across the deepest portion of the BCG play area. Displayed horizon is in the lowermost Falher; line is 18 km long, displayed depth 3000 m. Viewed to NW.

is controlled by the fabric, composition and local stress values of the sandstones. More quartz-rich sandstones tend to be less pressure-sensitive than more argillaceous samples. For example, analysis of two core plugs from the Nikanassin Formation (Fig. 10b) in the 11-21-65-13W6 well shows the reduction in permeability is less than one order of magnitude and is more gradual than three samples shown from the low-permeability, illitic Rotliegendes sandstones.

Laboratory measurements conducted on whole-core and drill plugs, measuring matrix properties, showed that small-scale features such as argillaceous laminae, grain size variations and bedding have an impact on permeability. Reservoir performance, however, is controlled by larger scale facies and rock properties variations as well as natural and mechanically induced fractures. In the central portion of the BCG study area understanding such properties as concentration, size and distribution of fractures is key to optimizing reservoir performance, with fracture distribution being controlled by lithology, structural location, degree and effectiveness of the fracture network and tectonic history. Pressure transient analysis (Fig. 10a) shows the effect of fractures, as system permeabilities with values of hundreds of microDarcies are not uncommon.

Cadomin Formation

The Cadomin Formation in west-central Alberta has been documented extensively by Jackson (1984), Gies (1984), and Smith *et al*. (1984). The formation was deposited upon a widespread unconformity at the top of the Nikanassin Formation which formed as a result of uplift associated with the docking of allochthonous terrains along the western margin of the North American craton. Cadomin Formation strata are bounded to the NE by the Fox Creek Escarpment and by the Cut Bank Valley edge in the SE (Hayes *et al.* 1994). East of the topographically high Fox Creek escarpment the formation is absent. Lack of well control results in a poorly defined NW limit and to the SW the regime is breached with moderate to high amplitude foothill structuring.

Cadomin gas production is modest but widespread in the Deep Basin. Low-porosity–permeability sandstones and conglomerates forced Canadian Hunter to write off hundreds of BCF of Cadomin reserves at Elmworth in the late 1990s, as the company could not demonstrate that the gas could be recovered economically.

Depositional model

The conglomerates of the Cadomin Formation are considered to have formed in an alluvial plain environment as sediments were shed in an easterly direction from the rising Cordillera. At various places along the Cordilleran uplift rivers debouched coarse-grained sediment onto the interior plains. Upon emerging from the confines of mountain canyon systems these streams abruptly deposited their bed-load material to build large alluvial fans. With continued water flow and redistribution of sediment, these fans expanded away from their source area and ultimately merged to form a single widespread alluvial plain covering much of Western Alberta, with the eastern limit marked by the Fox Creek Escarpment (Fig. 2). Between the escarpment and the alluvial plain a broad braid-plain was formed by a north-flowing river system called the Spirit River channel. The alluvial plain deposits consist of poorly sorted, sandy, chert pebble conglomerates, while the Spirit River braid plain conglomerates are better sorted and consist of paler coloured finer grained chert pebbles. The main Deep Basin gas accumulation in the Cadomin Formation occurs in a downdip location, in low-permeability

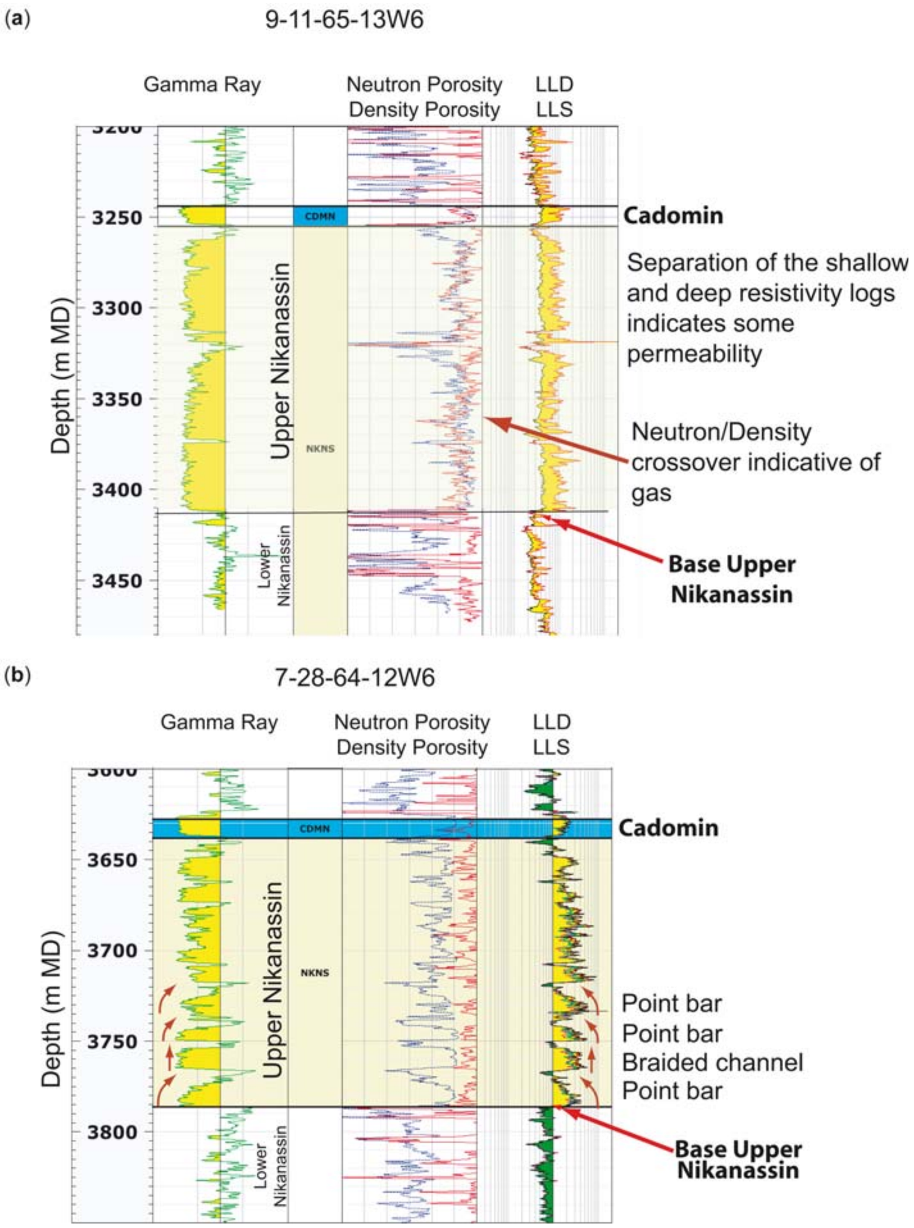

Fig. 6. Well log characteristics of the upper portion of the Nikanassin Formation.

alluvial plain sediments, while the more permeable braided river deposits predominate throughout the updip region near the gas–water contact.

Johnson & Dalrymple (2005) suggest that during Cadomin Formation time there was little accommodation space, which resulted in widespread deposition of the relatively thin Cadomin Formation conglomerates. This is apparent through much of northwestern Alberta where the Cadomin Formation averages about 5–10 m thick (Fig. 11a). Rapid changes in thickness and an irregular distribution of contours suggest deposition on either a peneplained surface or river reworking. In British Columbia (Fig. 11b) a regionally definable 10 m contour exists between Shell's Thunder and Bennett acreage. East of this contour the distribution of Cadomin Formation conglomerates is very similar to that observed in Alberta. Northwest of this contour, however, the Cadomin Formation can thicken to over 40 m with contours following the basin axis, suggesting some degree of subsidence and increased accommodation space in this area. Several relatively narrow zones of increased thickness are observed extending eastward from the disturbed belt, interpreted as alluvial fans feeding sediments into the basin.

Rock properties

In contrast to the Nikanassin Formation (Fig. 10a), there is no correlation between porosity and permeability in the Cadomin Formation (Fig. 12) within the BCG area. This lack of correlation is attributed to changes in rock fabric and the presence of fractures within the analysed core. The overall average ambient porosity (thickness weighted) and permeability (geometric average) values for cores are 5% and 2 mD, respectively. As with the Nikanassin Formation, *in situ* permeabilities are generally an order of magnitude lower.

In the conglomerates, reservoir properties are dependent upon the amount and quality of matrix. Chert pebbles contain variable amounts of microporosity and generally do not contribute to the overall properties of the reservoir. The coarser pebble-supported conglomerates tend to have poorer reservoir quality compared with those rocks where the larger grains are suspended in a 'finer' grained matrix (i.e. matrix supported). The chert pebbles can be very clean, consisting essentially of very finely crystalline silica, while others can contain variable amounts of impurities such as clays and organic matter. In some cases, impurities have

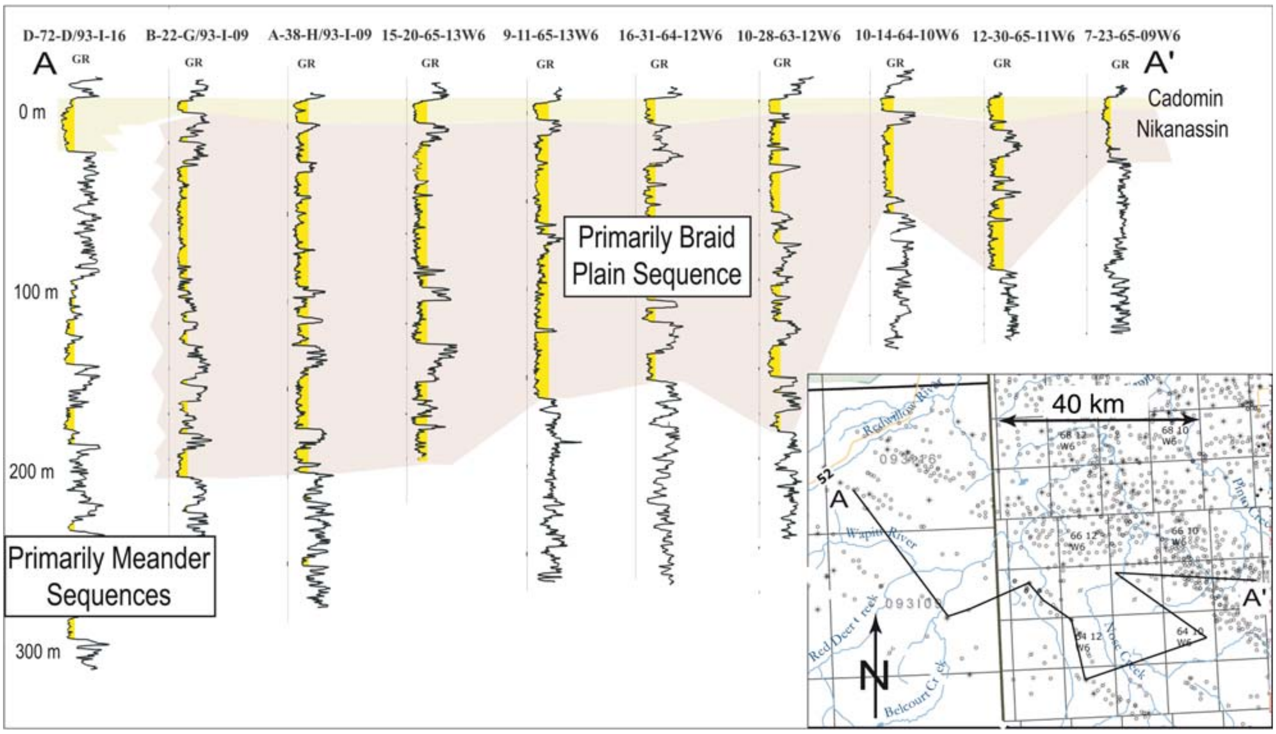

Fig. 7. Cross-section of upper Nikanassin Formation showing distribution of sandstones across the central BCG region.

been leached out, resulting in chert grains containing variable amounts of ineffective microporosity. As chert grains are composed of numerous small silica crystals, each with their own crystallographic *c*-axis, they generally do not develop large equant pore-filling overgrowths; rather a quartz druse will form on the grain surface. Throughout the area of interest, kaolinite is the principal authigenic clay and can infill isolated pores and/or much of the pore network.

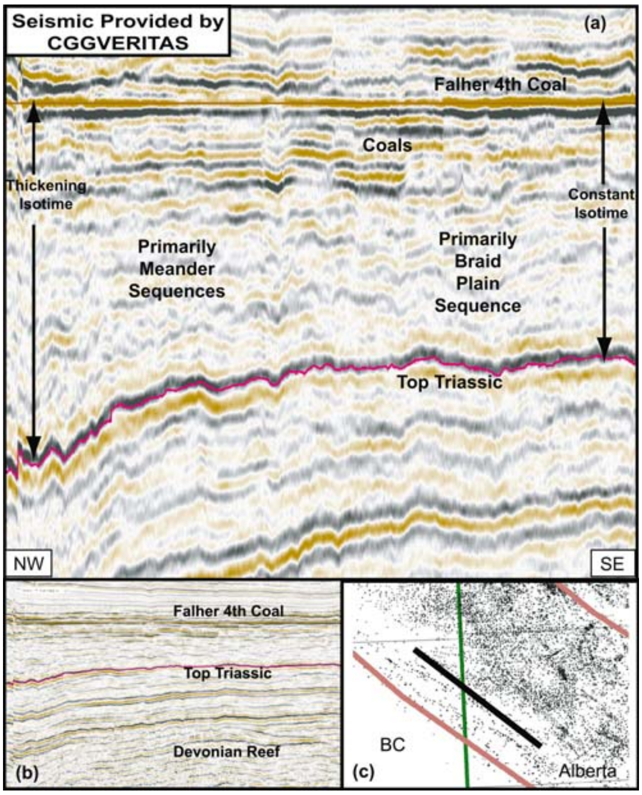

Fig. 8. NW to SE strike seismic line running across the British Columbia–Alberta border from Township 63 to south of Bearhole Lake. Both scales display the degree of changes in accommodation space from the SE to NW in the Nikanassin interval. Both displays (**a** and **b**), different scales, are flattened on the 4th Falher coal and are 70 km (**c**) in length.

Gething Formation

Smith *et al.* (1984) suggest that the Gething Formation is a terrestrial sequence composed of interbedded fine-grained sandstones, siltstones, mudstones and coals. The Gething Formation can best be described as having been deposited on a low relief interior drainage plain on the eastern flanks of the Cordillera. The physiography of this drainage basin was a low-lying swampy plain with numerous lakes and forests (Smith *et al.* 1984). Sandstones in the Gething Formation were deposited in fluvial systems with the main drainage pattern oriented NE from the Cordillera and then switching to the NW along the Spirit River channel system, the same system that affected Cadomin Formation deposition. Johnson & Dalrymple (2005) found that Gething Formation sequence boundaries display little incision, indicating a high rate of subsidence during deposition. Where thin (<5–7 m) vertically isolated Gething Formation sandstones are observed in logs through the study area, they typically have a point bar or channel signature. Given the physiography of the basin at this time and the observed distribution of facies, it is assumed that the sandstones were deposited in meander systems resulting in a lower degree of reservoir predictability from well and/or seismic data.

Spirit River Formation

Falher Member

Sediments associated with the Falher Member of the Spirit River Formation were deposited in an overall regressive cycle. Five distinct cycles have been identified in the Falher Member with each cycle representing a rapid transgression followed by a slow regression as the coastline oscillated (Smith *et al.* 1984).

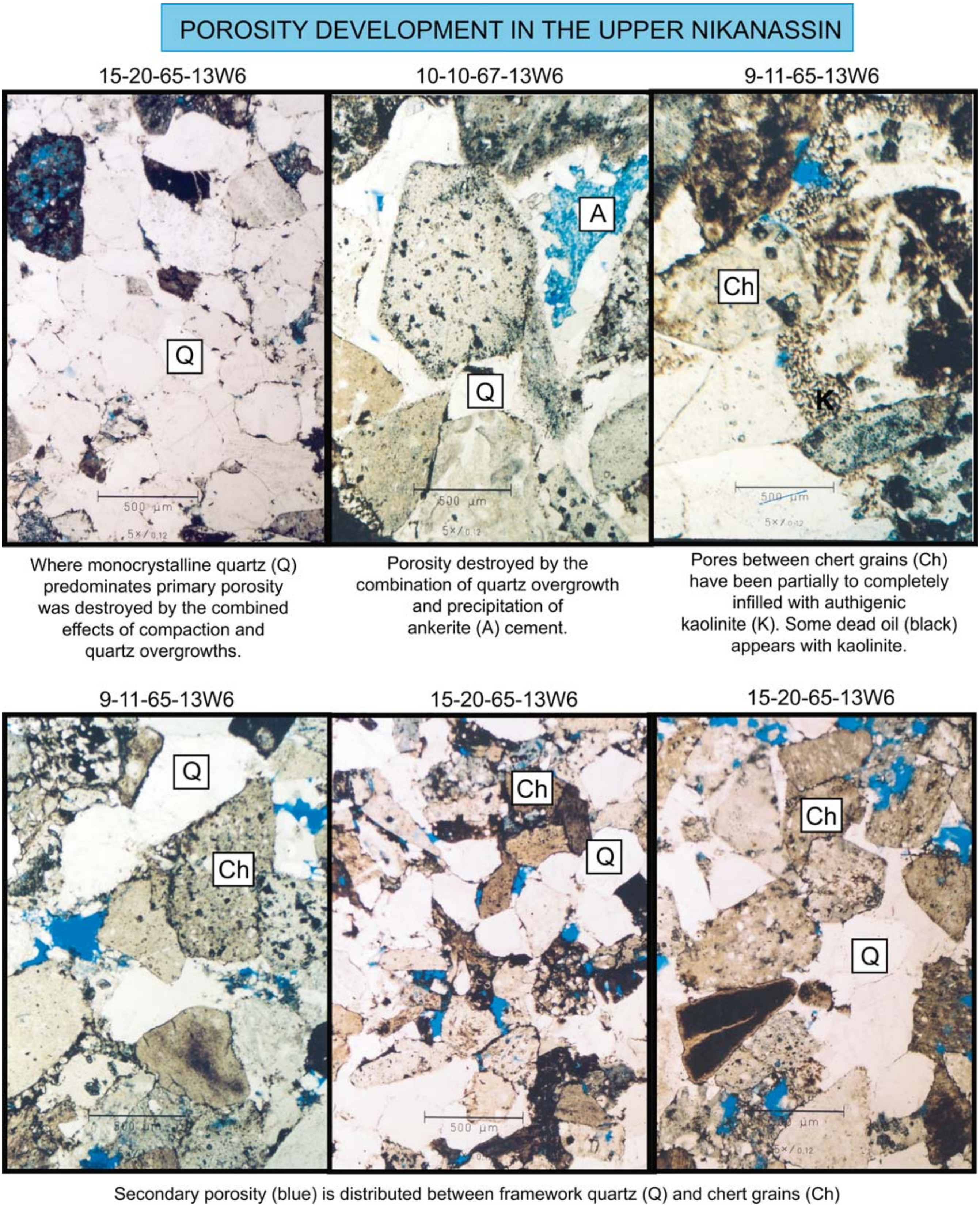

Fig. 9. Upper Nikanassin thin sections showing primarily medium- to coarse-grained lithic quartz rich sandstones. Secondary porosity is blue, and results from the dissolution of unstable argillaceous clasts and chert grains.

Coastal/deltaic sandstones and high-productivity conglomerates are common through the Elmworth Field (Fig. 2). To the south the Falher Member sediments represent deposition in a coastal plain environment and are characterized by shales, siltstones and coals, thus making the subdivision into cycles more difficult. The irregularly distributed Falher Member sandstones in this environment were deposited primarily in fluvial meander systems and consist of channel and point bar deposits.

Continuous coals (some up to 14 m thick) can be mapped over several townships. The thickest coal seam, referred to as the 4th

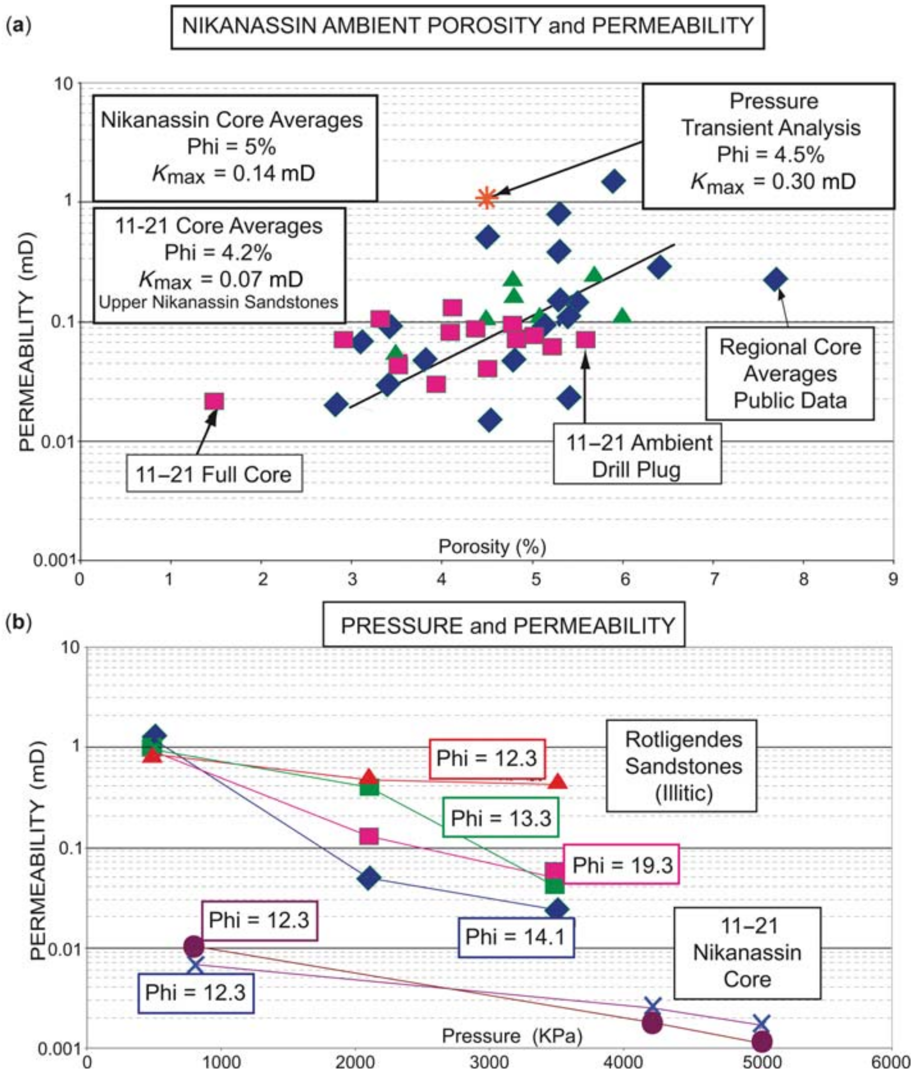

Fig. 10. Cross-plots of data from Nikanassin Formation core plugs. (**a**) Ambient porosity v. permeability. (**b**) Effects of increasing pressure on permeability for Nikanassin Formation and Rotliegendes sandstones.

coal, is found near the bottom of the Falher Member and contains approximately 10×10^{12} SCF of gas-in-place (Wyman 1984). Geochemical analysis of the Elmworth coal seams (Wyman 1984) indicates that the coals and carbonaceous shales were the most prolific source beds for the gas, which is still being expelled today (Michael & Bachu 2001).

Notikewin Member

Schmidt & Pemberton (2004) state that the Notikewin Member is the youngest member of the Spirit River Formation, and is underlain by the Falher and Wilrich Members, respectively. During deposition, the Western Canada Foreland Basin was inundated by the Boreal Sea, resulting in the formation of a shallow epeiric seaway. The Notikewin Member represents a conglomerate-rich shoreline, formed within that seaway, which the aforementioned authors subdivided into four allomembers. The Notikewin Member had previously been described as a barrier island complex that had prograded as much as 150 km, although modern barrier islands generally form in transgressive environments. Schmidt & Pemberton's (2004) work demonstrated, however, that the barrier deposits formed in Notikewin time did not prograde a great distance as a barrier island/lagoon complex; instead sandstones and conglomerates of limited lateral extent were deposited in an orientation that was approximately parallel to the shoreline. The most prolific Notikewin Member wells occur in a narrow east–west trend through Township 67 from ranges 8 to 13W6. In this trend Schmidt & Pemberton (2004) defined a barrier spit that was formed as sediments were introduced into a shoreline as a result of channel avulsion. This barrier had little progradational extent, instead growing longshore, creating a large estuarine/lagoonal complex. The greatest concentration of net sand in the Notikewin Member occurs north of Township 65. To the south, the Notikewin Member consists primarily of coastal plain sediments, including silts, shales and coal.

Cadotte Member

As was observed with the Cadomin Formation, the Cadotte Member of the Peace River Formation can be found throughout the BCG study area in west-central Alberta and northeastern British Columbia. Early in middle Albian time, the Boreal Sea advanced across much of what is now known as the Western Canada Foreland Basin depositing marine shales of the Harmon Formation. This transgressive event occurred during a global rise in sea-level and was the beginning of a major transgression, which intensified during Late Albian time with the spread of the Shaftesbury/Colorado sea across much of western North America (Smith *et al.* 1984). A pause in this overall transgressive event occurred with deposition of the Paddy/Cadotte Members during

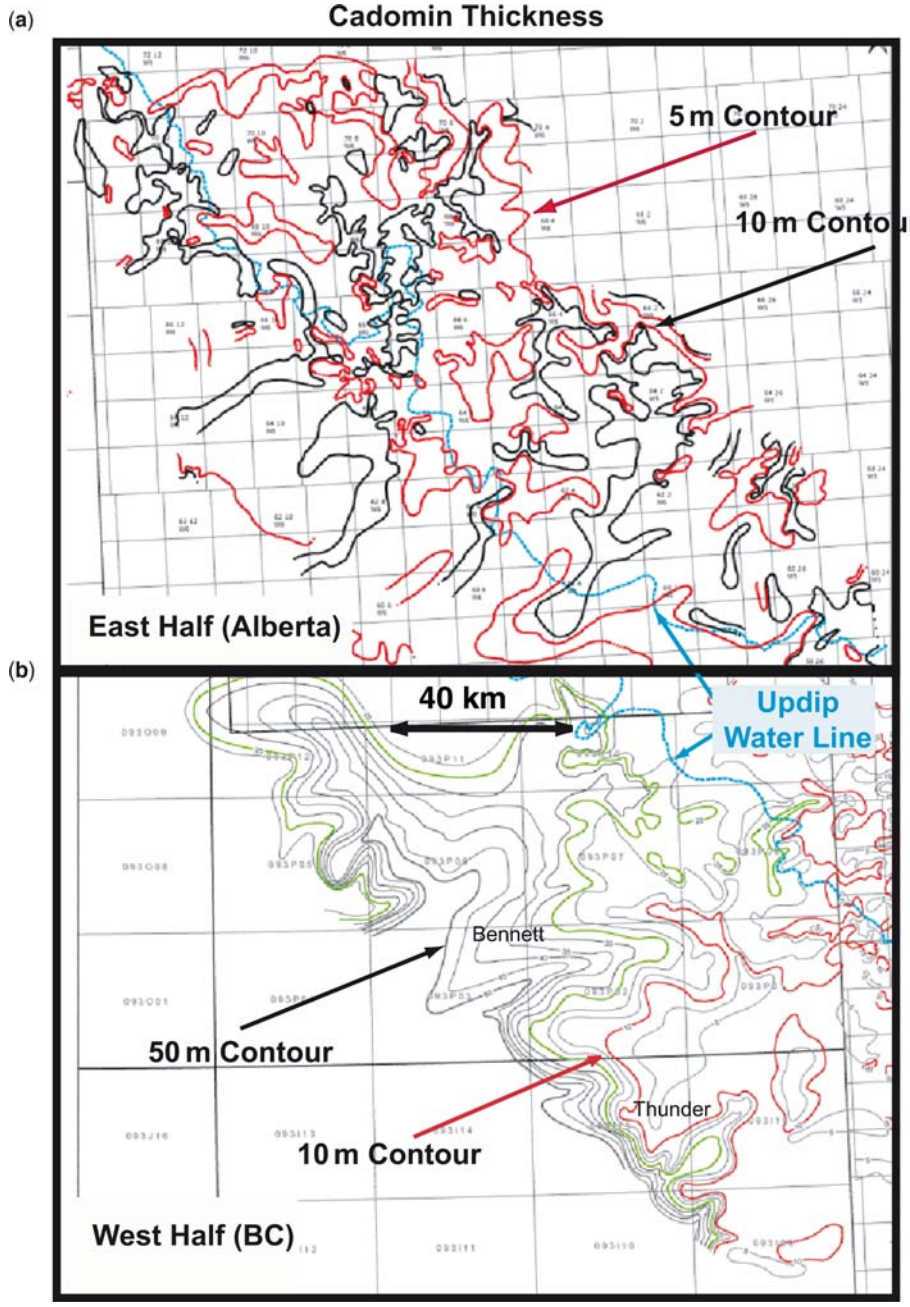

Fig. 11. Cadomin Formation thickness across the central portion of the study area, split into (**a**) eastern and (**b**) western portions. The east shows widespread thin conglomerates and uniformly low accommodation, whereas the west shows thickening from an increase in accommodation space, and the impact of alluvial fans forming from the west.

a regressive phase. Lettley *et al.* (2006) stated that the Cadotte Member forms an extensive shallow-marine complex that spans about 300 km along depositional strike and 150 km alongdip. A sharp, but conformable facies contact is typically seen in the middle of the Cadotte Member and is interpreted as a scour surface, separating the underlying very fine- to fine-grained sandstones of the lower to middle shoreface from the overlying chert-bearing sandstones and conglomerates of the upper shoreface. Lettley *et al.* (2006) observed lateral variations in texture and mineralogy throughout the upper shoreface sequence, which they attributed to the influence of deltaic sources.

To observe reservoir distribution, the thickness of the upper shoreface sands and conglomerates were mapped. Throughout the central portion (Fig. 13) of the study area the thickness of the upper shoreface is generally less than 10 m, with the thicker areas generally having a relatively well defined east–west orientation. This also matches the deviations seen on the updip water edge (blue line, Fig. 13). The exception to this is in the NW corner of the study area in British Columbia where the upper shoreface sediments follow a regular NW–SE oriented contour pattern and are interpreted to be filling a low coincident with the basinal axis. This pattern of basin fill is similar to that observed in the Cadomin Formation (Fig. 11a), although the area covered by the Cadotte Member is smaller, suggesting that between Cadomin and Cadotte time, the basin had progressively filled toward the NW.

Rock properties. Throughout the study area, both in British Columbia and Alberta, a significant scatter occurs on cross-plots of Cadotte Member permeability and porosity (Fig. 14a). The scatter on these data is most likely due to facies variations (i.e. sandstone v. conglomerate). Variability in grain size as well as porosity and permeability occurs in upper shoreface sandstones, where the finer grained rocks have a higher porosity but lower permeability than the coarser grained conglomerates where the pore

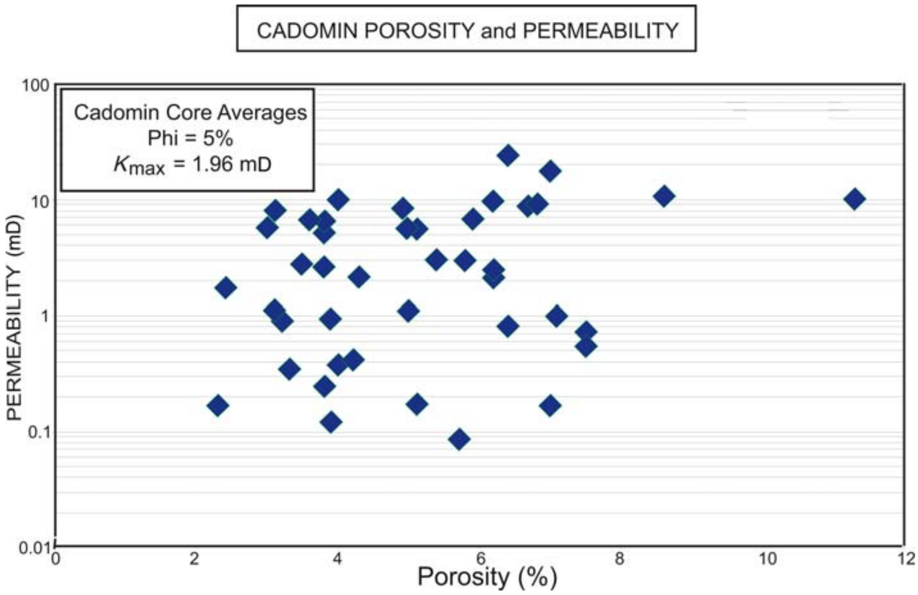

Fig. 12. Cadomin Formation porosity–permeability cross-plot.

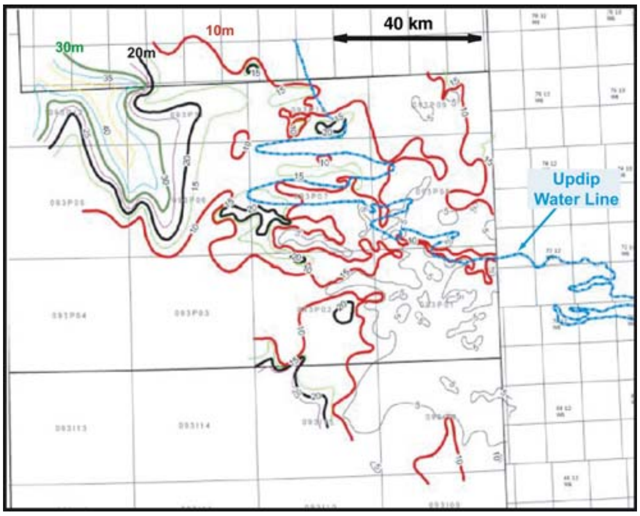

Fig. 13. Isopach of upper shoreface sandstones and conglomerates of the Cadotte Member across the western portion of the study area. Thicknesses are generally less than 10 m, except in the far NW, where up to 40+ m is encountered. Updip water edge outlined in blue.

throats are larger. When comparing the upper shoreface sandstones to those found in the very fine- to fine-grained middle to lower shoreface sandstones (Fig. 14b), a relatively good trend between core measured porosity and permeability is encountered, showing the impact of facies on these parameters. If the entire core is averaged, irrespective of facies, the average porosity and ambient permeability values are 6.5% and 0.68 mD, respectively. When evaluating just the upper shoreface the average porosity is 9.2% while the permeability is 2.32 mD.

In the unstructured regions of the study area, where the reservoir units are relatively flat, production is dependent upon matrix permeability, which in turn is dependent on facies and grain size. To the west in the structured areas, matrix permeability is enhanced by natural fractures.

Western Canadian BCG basin model

An idealized cross-section through the central BCG region (Fig. 15) shows that the deepest part of the basin occurs immediately in front of the disturbed zone with each unit rising gradually to the NE where the updip water contact is encountered. The Shaftesbury Formation shales (top seal) and Fernie Formation shales (bottom seal) encase the main reservoir units that extend from the Cadotte Member to the Nikanassin Formation. Also contained in this interval is an abundance of coals, which Wyman stated (for the Elmworth area, in 1984) were and continue to be the most prolific source beds for gas.

Since maximum burial, the Deep Basin of Western Canada has been uplifted with the loss of from 1500 to 3500 m of overburden (Issler *et al.* 1999). Over geological time, the process of hydrocarbon generation, the expulsion of dry gas, updip migration of these gases and basin exhumation have produced a pressure system in a state of pseudo-equilibrium. Overpressures (Fig. 16) are still maintained in Cretaceous strata in the deepest and most compacted portion of the basin, maintained by the very low-permeability strata. To the west of this pressure high, within the highly deformed structure belt, tectonic complications (blind fault zones) have provided leak points and/or impaired gas migration within structural units. Throughout this region, pressure lows are thought to be produced by breaches in reservoir units and as such some zones are totally water-wet.

To the east and near the updip water line, the BCG portion of the basin is unstructured with only a gentle 1 or 2° western dip. Gas migration continues from deeper regions towards the updip water edge, where permeability and porosities increase. At this point, hydrocarbon loss increases above the migration rate and formation pressures fall. As gas continues to escape from the system, water slumps back into the basin (Fig. 17) along higher permeability streaks, driven by hydrostatic forces. This slumping occurs until the relative permeability inhibits the movement of water and capillary forces become dominant. Further downdip from this, water continues to move deeper into the basin, drawn by capillary pressure, until gas migration and desiccation within the reservoir prevent further slumping. The transition region from gas to water across this interface is observed to have subnormal pressures, whereas further updip, pressures are supported by the hydrostatic gradient. Across this complex horizontal transition zone, variations in the formation permeability produce water-saturated and undersaturated intervals directly next to each other within the same reservoir unit. In the deepest portions of the basin, the pore pressure increases to values above the hydrostatic gradient. High gas gradients across

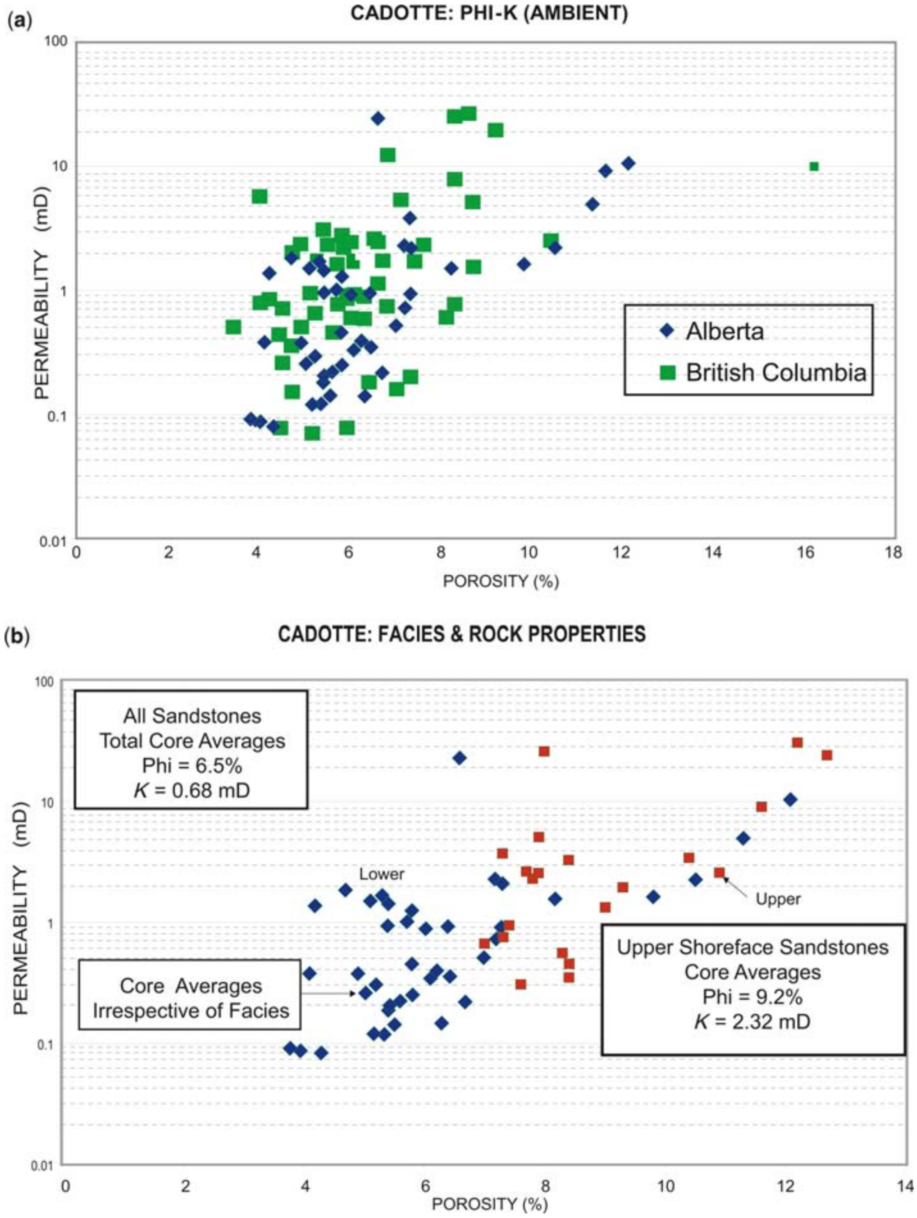

Fig. 14. Cadotte permeability v. porosity cross-plots. (**a**) BC v. Alberta data shows similar scatter of sandstone v. conglomerate. (**b**) Impact of facies on porosity and permeability values.

this area are the result of the burial, maturation, overpressuring, unroofing and expulsion history of the basin and where low leak-off rates maintain dynamic pressures above hydrostatic values.

It has also been found that vertical pressures can be highly variable, depending on the formation permeability. The overall high K_v/K_h results in the location of the recharging aquifer being at a significant distance from and at much lower elevations than the well location, thereby producing further under pressure. The location of the observed water edge is controlled by the magnitude of the capillary pressure and the concurrent hydrodynamic drive. Overall, all of these factors produce a complex and abnormal pressure regime that can range from significantly underpressure to significantly overpressure.

Early in the geological development of the Western Canada Foreland Basin, sedimentation, subsidence and thermal maturation resulted in overpressured source rocks expelling dry gas into 'tight' but higher porosity/permeability lithologies. Local gas pools would have been formed at this time. As time progressed, continued dry gas expulsion removed connate water and, in the process, desiccated the column through which the gas was migrating, although variations in sweep efficiency would have created regions of higher and lower water-saturated zones. The gas with dissolved water migrated updip, to regions where the relative permeability for water allowed the mobile phase to be water, and the situation switched from gas-carrying water to gas in solution in water. With time and unroofing, gas migration rates slowed and capillary and hydrostatic pressures collapsed water back into the basin. This occurred where porosity, permeability and the wetting phase permitted this process to happen. The present state of pseudo-equilibrium is the result of a balance between these pressures, gas expulsion and migration from the basin's source rocks and loss of gas from the system.

Water saturation

In order to produce economic volumes of gas from low-permeability reservoirs, the initial or irreducible water saturation must be less than what would be expected in a reservoir that is in capillary equilibrium with free water. In such a water-wet, tight gas sandstone, with very small pore throats and 'normal' water

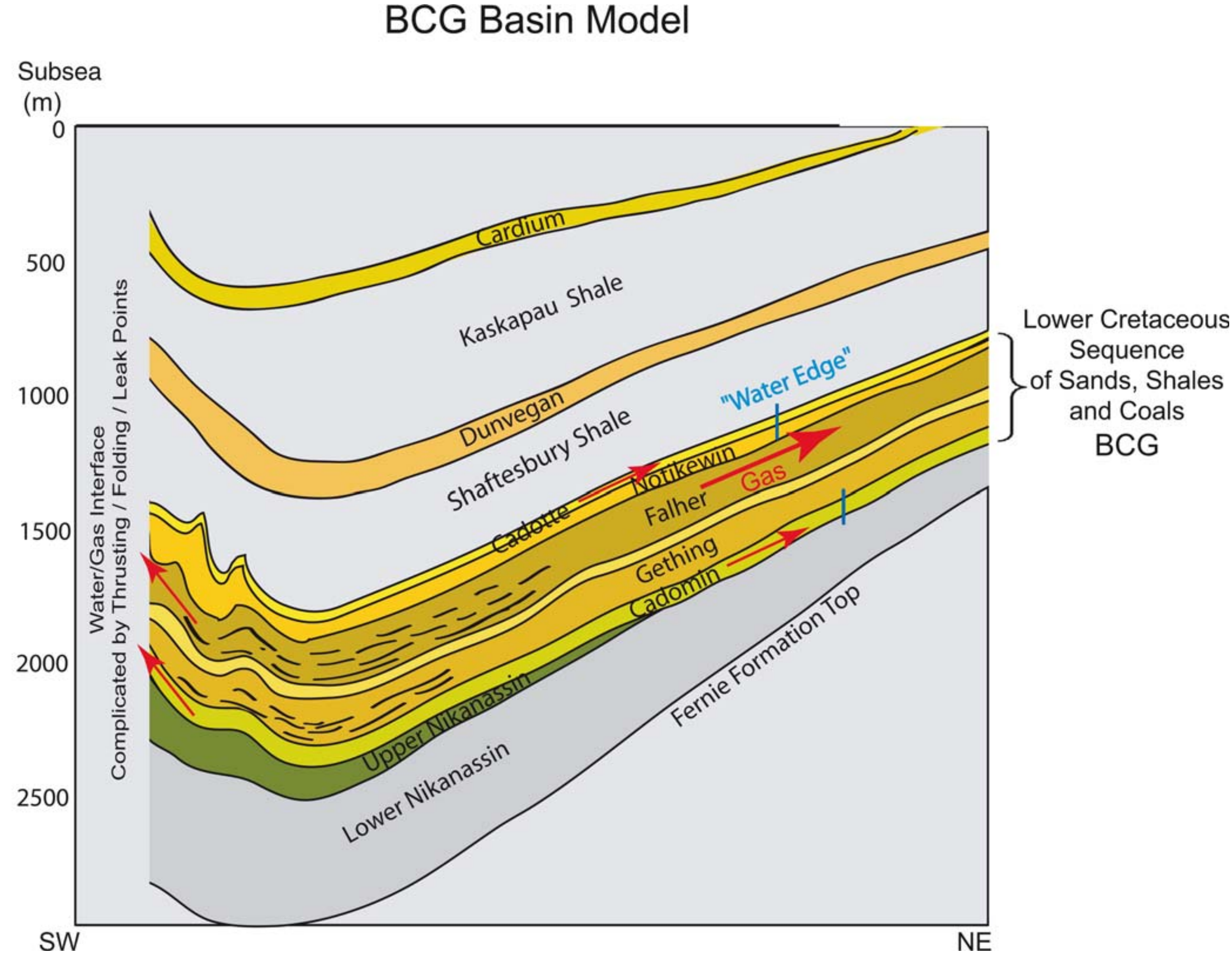

Fig. 15. BCG model of gas expulsion from coals into low porosity and permeability units and migration updip toward higher quality reservoir sandstones with water.

saturation, as determined from capillary pressure (with a transition zone of 250 m, S_w would be 45%, Fig. 18) gas-in-place would be significantly reduced and relative permeabilities would inhibit the flow of gas. However, Bennion *et al.* (2002) point out that economic volumes of gas are produced from these reservoirs on a worldwide basis, with the only water production being fresh water of condensation, generally in the range of 1–2 BBL/MMscf of gas. This is identical to the area within and surrounding the principal BCG region, where the average water production is 1.5–2 BBL/MMscf of gas (Fig. 19). This very low water production and corresponding low water saturation are the result of the removal of water, caused by long-term regional migration of undersaturated gas from source rocks adjacent to the producing interval. Newsham *et al.* (2002) stated that the key element required to remove water effectively is the process of vaporizing connate water into the gas phase. They further suggest that, based on laboratory data, at pressures and temperatures exceeding 10 000 psi and 350 °C, respectively, significant volumes of water vapour may be dissolved in the hydrocarbon gas. Thus, as long as hydrocarbon gas continues to migrate into and through the reservoir, a mechanism exists to continuously vaporize and effectively remove connate water.

In the Bossier sandstones of the East Texas Basin, Bennion *et al.* (2002) found that measured water saturations in the reservoir ($k < 0.01$ mD) averaged 5%. In Nikanassin Formation core from the 11-21-65-13W6 well, where average porosity was 4.5%, averaged core-measured water saturations of 15% and values as low as 6% were recorded. Overall, the desiccation process results in an increase in salinity in the remaining water phase, thereby suppressing the true *in situ* R_w (resistivity of the formation brine). Within the BCG region of Western Canada, the calculation of water saturation is difficult, as no representative sample of formation water can be produced from a desiccated reservoir. As such, R_w cannot been determined, but values for the Archie equation must be low to balance the extremely low water saturations, and as such, caution must be exercised when evaluating S_w in water-desiccated (BCG) systems.

Reservoir and petrophysical summary

The Deep Basin of Western Canada displays all the characteristics of BCG as defined by Law (2002):

- Regionally pervasive gas-saturated accumulations – gas is present in all prospective reservoir intervals examined and deliverability and commerciality is dependent upon reservoir quality (mainly ‘system’ permeability).
- Lack of a downdip water contact – no free water level has been identified in any of the zones of interest. The only water produced is water of condensation at rates of approximately 1.5–2 BBL/MMCF.
- Situated in low-permeability reservoirs – ambient matrix permeability values generally range from 100 to 500 μD with

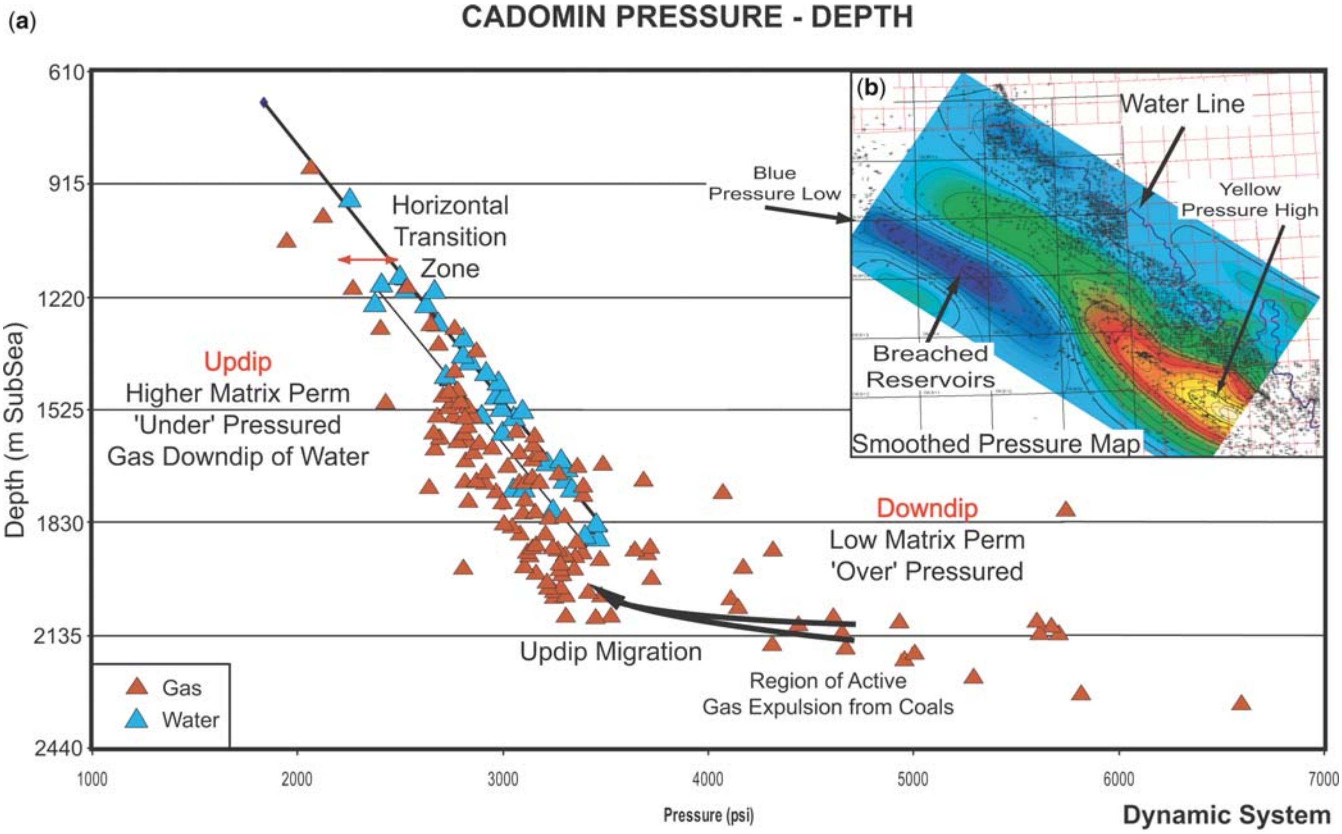

Fig. 16. (**a**) Cadomin Formation pressure–depth plot across the central BCG region showing the continuum of pressure with respect to depth from downdip, low-permeability, high pressure to updip, higher permeability, low pressure. Throughout the area, gas is expelled from coals and migrates updip to more permeable sandstones until, near the water level, relative permeability has the gas escaping into the water zones, lower pressures, but not allowing the water to slide further downdip. (**b**) The smoothed pressure map also shows the low pressures along the southwestern side of the study area, where regional tectonics has produced pressure leaks across faults and along folds.

in situ values about one order of magnitude less. Grain size does influence permeability with conglomerates being more permeable than fine-grained sandstones. Permeability increases updip towards the gas–water contact. In the non-structured areas reservoir performance is dependent primarily upon matrix permeability, while in the structured areas natural fracturing can enhance permeability. In structured fields, 'system' permeability values in excess of 1 mD have been determined from pressure transient analysis.

- Reservoirs are abnormally pressured (high or low) – pressures can range from greater than 40 MPa in the Cadomin/Nikanassin Formation intervals in the deeper portions of the basin to less than 5 MPa in the Cadotte Formation in northeastern British Columbia, just downdip of the water edge. A depth–pressure plot for the Cadomin Formation across the central BCG study area (Fig. 16) shows that, in the deepest portions of the basin, overpressuring is evident as charging occurs from the coals into the low-permeability sandstones. Gas then migrates updip, through these sandstones, to areas where permeability increases and the leaky gas–water interface is encountered and pressures fall as the relative permeability of gas v. water comes into play.

In summary, 'BCG basins' will display a continuum between conventional tight gas and 'true' BCG reservoirs. As dry gas is expelled from source units into low-porosity–permeability reservoir units, water is absorbed and carried updip to the leaky water interface. As geological time progresses, and as continued migration occurs, water saturation drops, until eventually the column is gas-saturated and desiccated of water. At the updip limits of the BCG region, higher porosity–permeability streaks will exhibit a slumping into the basin of higher S_w values, both vertically and laterally (see Fig. 13, Cadotte Formation water level).

Structural style and strain

Reservoir performance in non-structured areas is dependent primarily upon *in situ* matrix permeability which, as stated above, is often less than 50 μD. Pressure-transient analysis, on the other hand, indicates 'system' permeability in the hundreds of milliDarcies, well above matrix values. Many of these 'sweet spots' occur along structures where natural fracture permeability greatly influences the reservoir performance, and locating the best of these sweet spots was a challenge in the early phases of Shell Canada's exploration efforts. As such, much effort has been devoted both to understanding the detailed architecture of the thrust and fold front, and modelling these areas appropriately for the prediction of areas of enhanced fracture permeability.

The Western Canada Foreland Basin forms a shallowly west-dipping panel, tilted toward the Foothills and Foreland Belt (Rocky Mountains) of the Canadian Cordillera, lying between the conventional Foothills gas fields and the unstructured SW-dipping Deep Basin Belt. The deepest portion of this low-permeability BCG system is telescoped into the thrust front wedge or 'Triangle Zone', forming relatively low-displacement fault-transported fold structures (Fig. 5). The folding and thrust faulting of the deepest portion of the BCG system provided an opportunity for Shell Canada to target natural permeability pathways along strain-related fracture sets. Along this structured belt, understanding the geometry and kinematics of the structures was a necessary part of the process of well location and wellbore design. Further to the east, very little structure is evident (Fig. 5) and the reservoir units are

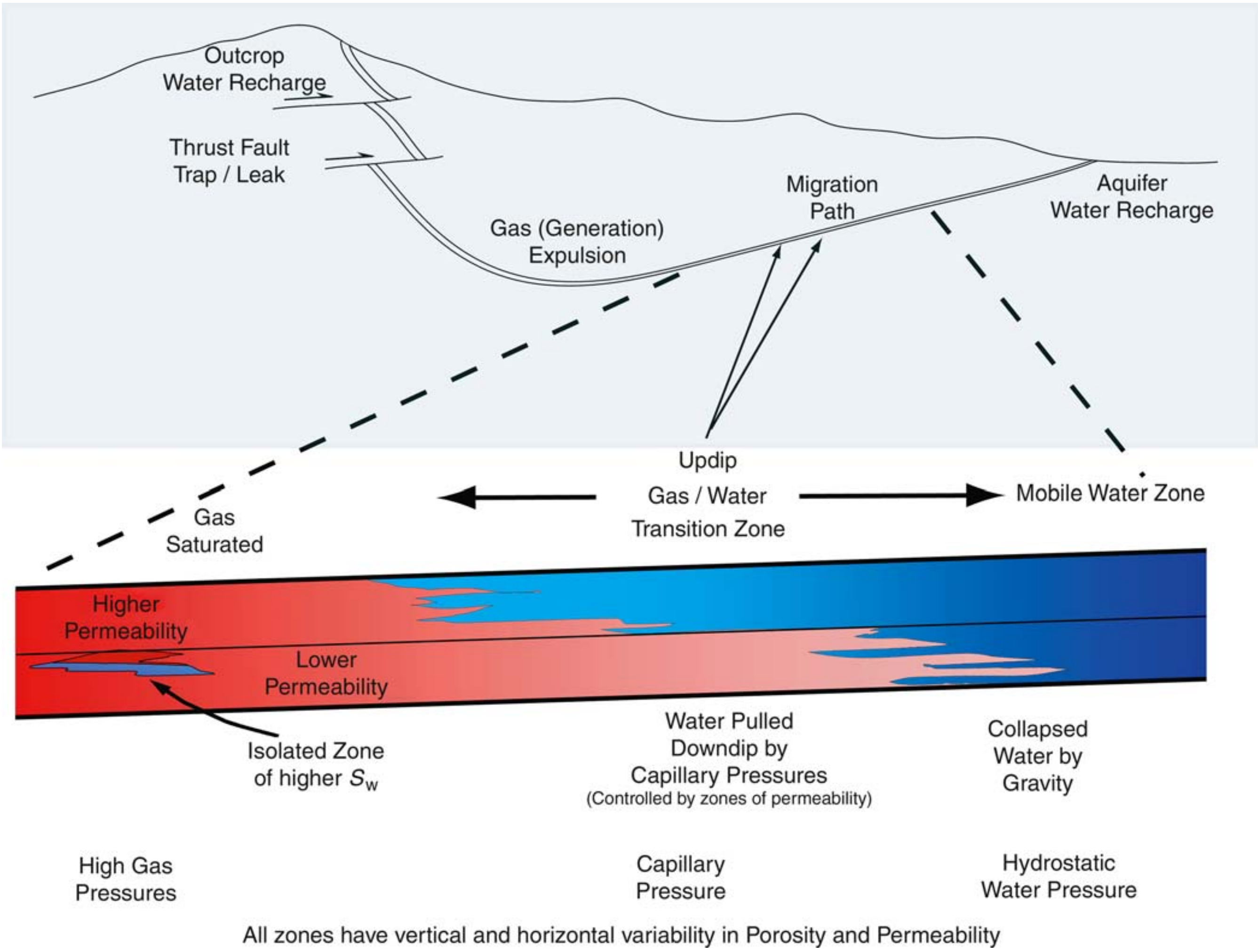

Fig. 17. Schematic of BCG basin pressures and gas–water transition zone.

essentially flat lying. In these areas reservoir performance is dependent primarily on matrix permeability, making facies analysis a more critical part of the evaluation process.

The structural style in the Foothills fold-thrust belt in west-central Alberta to northeastern British Columbia is strongly influenced by the mechanical stratigraphy of the Palaeozoic/Mesozoic succession. The thick Palaeozoic carbonates form thick thrust plates, folded around relatively low-angle thrust ramps. Opposed to this, the Jurassic–Cretaceous section in the study area, comprising relatively thin bedded sandstone–siltstone–shale–coal

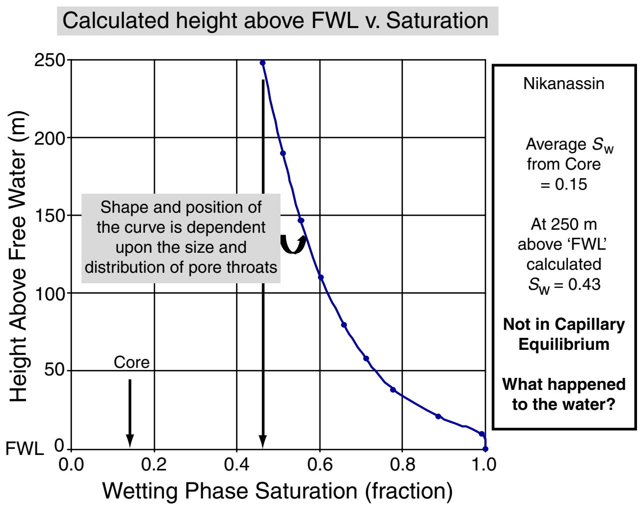

Fig. 18. Normal water saturation, as determined from capillary pressure, with a transition zone of 250 m (2.5% porosity sandstone) would be 45%. At these values, gas will not flow, but in fact, reservoirs do flow at economic rates with only minor volumes of water.

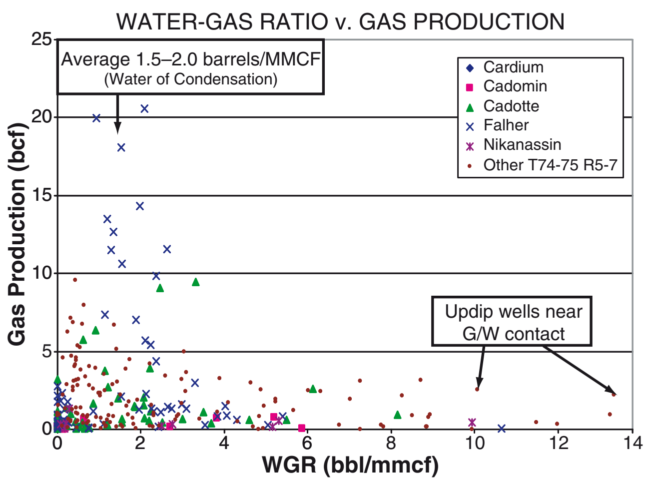

Fig. 19. Distribution of water to gas production across basin. Updip wells show a marked increase in water with respect to gas, whereas downdip wells only produce water at rates consistent with water of condensation.

intervals, appears to be almost completely decoupled from the underlying panels and is deformed more commonly by folding (see also Cooper *et al*. 2004). The detachment between the Palaeozoic thrust panels and overlying Mesozoic fold panels apparently occurs in the lowermost Nikanassin and/or Fernie formations. The thin-skinned fold-and-thrust belt is therefore decoupled into several mechano-stratigraphic wedges (see also Cooper *et al*. 2004). In general the Palaeozoic succession is detached from the Triassic succession, and the Triassic succession is detached from the Jurassic–Cretaceous wedge. This study focuses on the tectonostratigraphic panel above the detachment in the lowermost Nikanassin and/or Fernie formations, and will be referred to here as the Cretaceous wedge. The Cretaceous wedge is then further internally decoupled on detachments of varying regional significance in the Gething, Spirit River and Shaftesbury formations (see also McMechan 1999). Interpretations of regional 3D seismic surveys aided the development of an understanding of the geometry and kinematics of mapped structures, with relevance to the exploitation of high permeability fracture networks and the stress–strain relationships in the deformed portion of the BCG study area.

Megascale structure

The interval between the Dunvegan Formation and Nikanassin Formation, within the Cretaceous wedge, is deformed into fault-bend folds, fault-propagation folds, detachment folds and variations between these end members (e.g. Fig. 5). The structures that define the thrust front, and various BCG target areas, are typically broad anticlines with 1000–1500 m wavelength, and up to approximately 500 m amplitude. These structures vary from ones having more typically planar limbs with tight hinges and flat crests, to ones that are arcuate in shape. The anticlines are generally about 10 km in strike length, with down plunge terminations commonly transferring laterally into en echelon folds.

Folds with tight hinges and relatively steeply dipping limbs are characterized seismically by steeply dipping ‘wash-out’ zones of poor data quality (e.g. Fig. 20a). These kink bands deflect at overlying or underlying fault ramps (Fig. 20b, d), and define fold hinge surfaces through tight hinge zones. These kink band zones could alternately be interpreted as steep fault zones; however, since they fold overlying thrust fault ramps (Fig. 20b, d) rather than offset them, they are generally thought to comprise hinge surfaces rather than fault zones.

The geometry of these structures has been strongly influenced by the mechanical stratigraphy. The highly layered Mesozoic succession, juxtaposing and repeating relatively competent sandstone and siltstone with incompetent shale and coal, leads to structures that have many internal complications produced through flexural slip between the competent beds, and complex fault linkages (Fig. 20; for a photograph see Fig. 21).

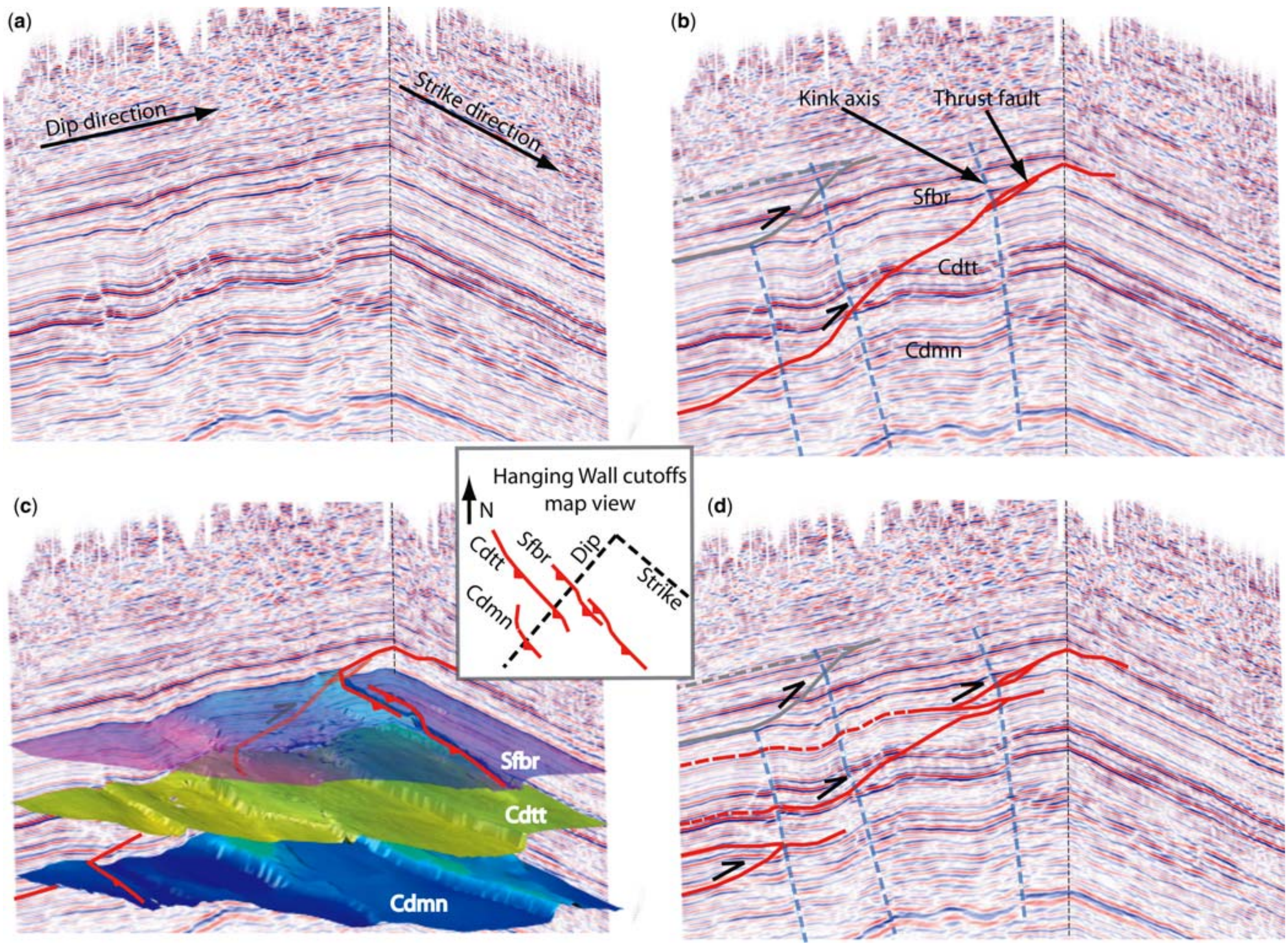

Fig. 20. Dip and strike seismic profile through frontal portion of the thrust front in the BCG system, NE British Columbia. (**a**) Uninterpreted. (**b**) One thrust ramp interpretation, and ‘wash-out’ at kink axes. (**c**) Surfaces added to provide map view of thrust linkages (inset also shows map view of hanging wall cutoffs) showing difficulty in linking thrust ramps. (**d**) Preferred interpretation with several thrust ramps linked by bedding-parallel décollement, and slightly folded at ‘kink axis’ fold hinges. Cdmn, Cadomin Formation; Cdtt, Cadotte member; Sfbr, Shaftesbury Formation.

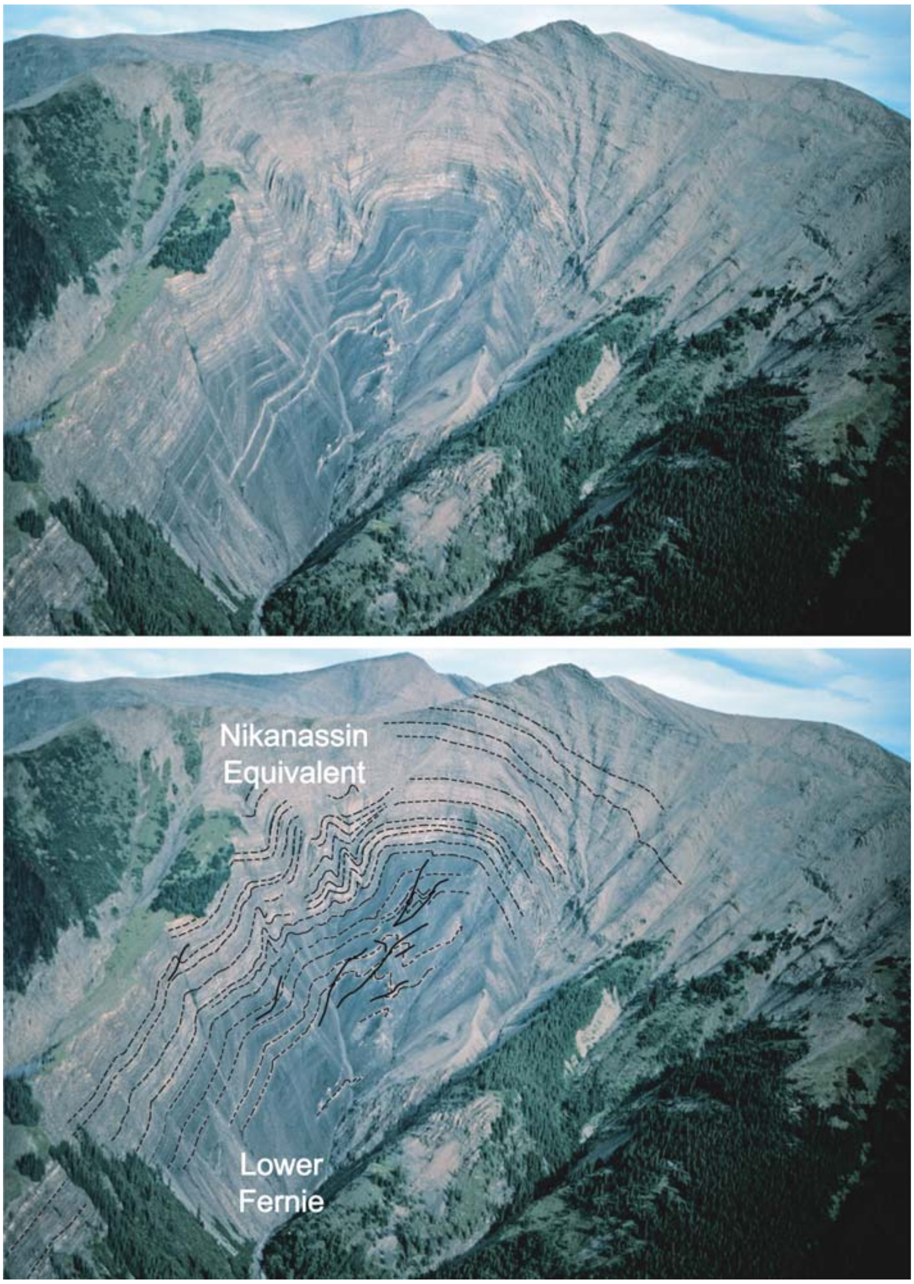

Fig. 21. Interbedded sandstones, siltstones, shales and coals of the Lower Fernie and Nikanassin equivalent formations. The anticlinal structure shows the typical internal complications from flexural slip between competent beds. Photo is looking NW up Davey Creek to the Davey Creek anticline formed in the immediate hanging wall of the Mount Russell thrust. Mountain is unnamed; photo by M. McMechan.

Interpreting internal fold structure

The Cretaceous wedge generally is deformed into folds across the central and northern portions of the study area; however, in detail, stacked low-angle folded thrust faults are visible within these anticlines. A high quality 3D seismic 'dip' profile shows what appears, at first glance, to be an apparent fault ramp between two horizons (e.g. Fig. 20b). Detailed analysis shows this apparent single ramp comprises several stacked fault ramps, linked by bed-parallel décollements. While hanging wall to footwall separation between décollements may be apparent on dip seismic data, imaging commonly precludes precise measurements of fault separation. However, when viewed at map orientation, hanging wall cutoffs with disparate strike lengths and different cutoff orientations between horizons (e.g. Fig. 20c) make it difficult to link the horizontal fault segments that form the hanging wall cutoffs into one surface. If fault surfaces are interpreted by linking segments along only 'dip' seismic profiles, it is possible that one erroneous fault surface will be interpreted where there are actually several linked fault surfaces. Such a mispicked fault surface will have inaccurate cutoff locations, angles and displacement vectors across ramps and, as such, will lead to inaccurate kinematic and geomechanical models and potentially mistargeted well paths.

These low-angle, low-displacement thrust faults commonly define a complex duplex network between stacked bedding-parallel décollements within the fold structures (e.g. Fig. 20d). Generally, the faults are linked only to the floor and roof décollement (lower Fernie or above outcrop in Fig. 21), and not laterally to each other. They do not form horses that would compartmentalize the reservoirs, but rather form en echelon duplexes (Fermor & Price 1987), with distinct lateral fault tips (Figs 22 & 23). These en echelon duplex structures (between décollements) are folded by the broad anticlines of interest, and developed in-sequence (either pre- or syn-folding).

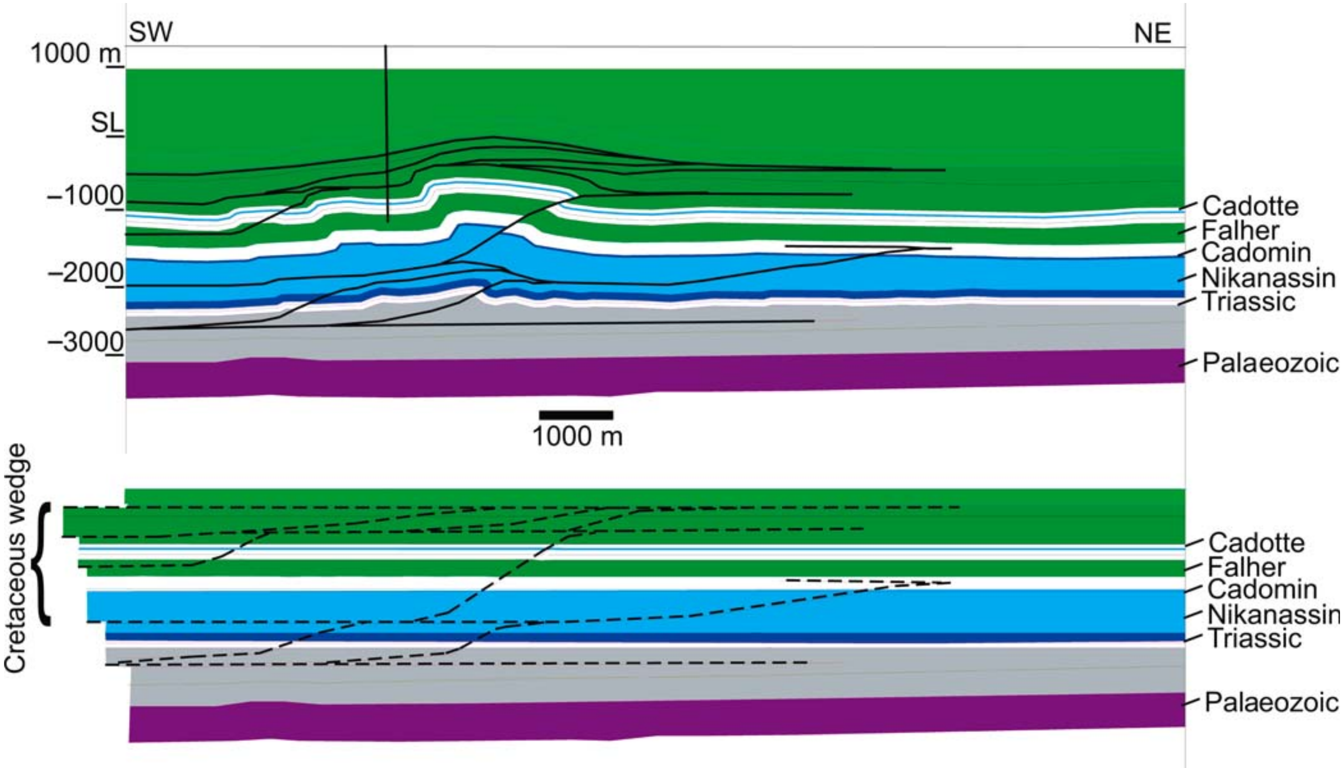

Fig. 22. Typical structural geometry (and restored) at thrust front, in the deepest portion of the BCG system. The thrust front is segmented by bedding-parallel décollement, defining the 'Mesozoic wedge'.

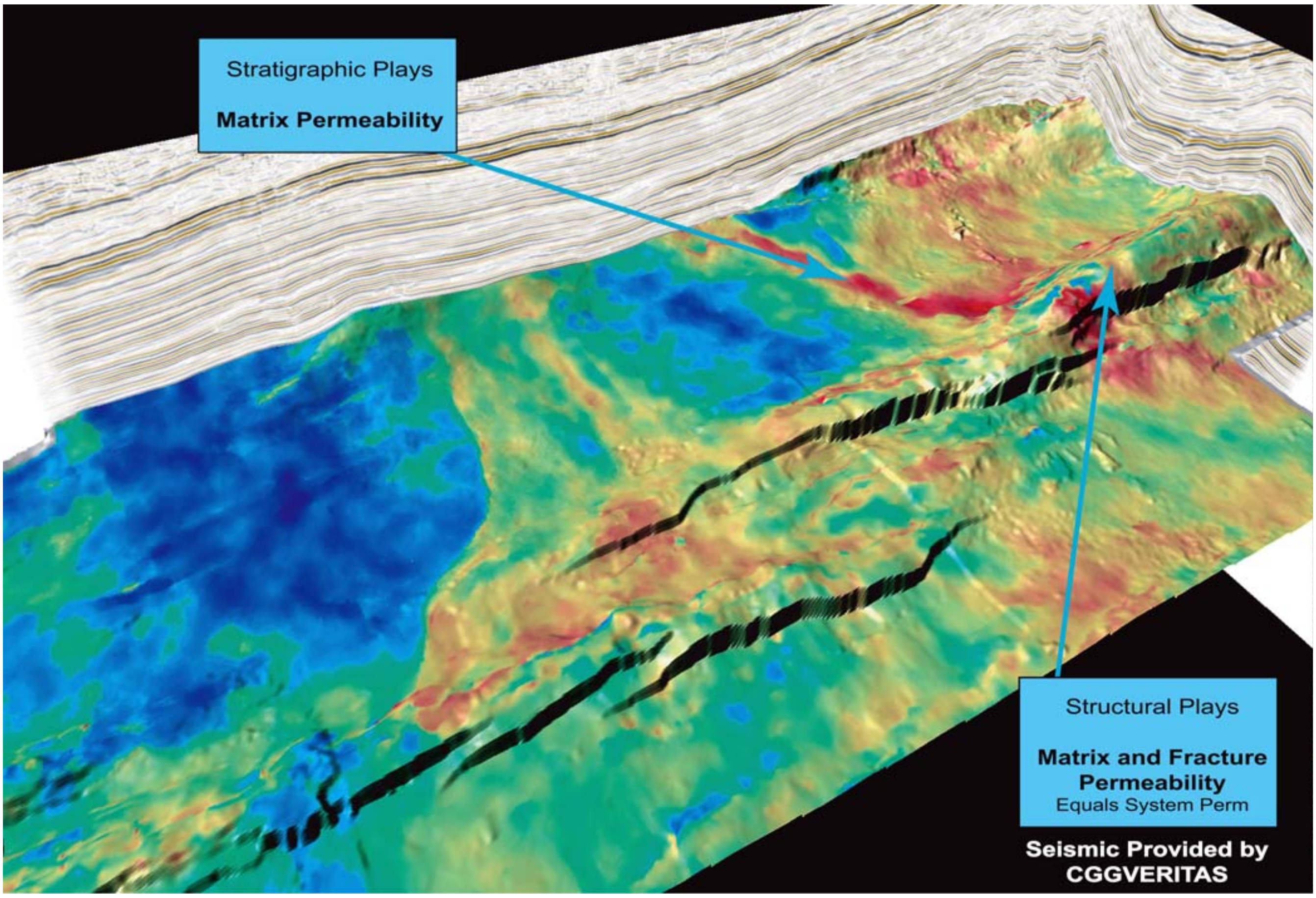

Fig. 23. Three-dimensional structure, stratigraphic and seismic view across the central BCG region. View includes an area of 20 × 40 km, with north to the right.

Fractures, mechanical modelling and structural sweet spot prediction

Unlike the identification of stratigraphic leads (e.g. facies mapping from seismic, Fig. 23), structural sweet spots do not necessarily need closely spaced well data. This especially applies to the structured portion along the west side of the BCG play area where the inherent risks and high costs associated with exploration and development have left the area with a sparse well population. Moreover, since the beginning of the 20th century the search for gas has been mainly focused on the exploration and exploitation of conventional hydrocarbon plays (Palaeozoic and Triassic carbonates). Overall this contributes toward a more sparse sampling of data to characterize the unconventional portion of the intersected gas-prone reservoir sequences (Jurassic/Cretaceous clastics) in this structured domain. In this context, regions where the probability of encountering zones of enhanced permeability through a well developed and/or well connected fracture network need to be identified through a combination of 2D and 3D seismic-based structural modelling and stratigraphic reservoir mapping techniques combined with geometric, kinematic and geomechanical modelling.

There are two types of quantitative approaches in structural modelling, geometric and numerical. In the first, geometric methods are based on either the principle of fixed hinge folding (De Sitter 1956; Biot 1964), or active-hinge-folding-related deformation (Suppe *et al.* 1992; Salvini & Storti 1997, 2001, 2004). Historically, in the principle of fixed hinge folding, the damage zone is calculated by means of layer curvature (Decker *et al.* 1989; Schultz-Ela & Yeh 1992; Lemiszki *et al.* 1994; Lisle 1994; Hennings & Olson 1997; Fischer & Wilkerson 2000; Bergbauer *et al.* 2003) to approximate the strain distribution across a structure. However, while useful in certain tectonic regimes, this method neglects the cumulative effects of strain during progressive deformation. The correct application of the principles of fixed-hinge or active-hinge-migration folding requires a thorough understanding of the kinematic evolution that characterizes each structure. In active-hinge-folding, high-strain areas or damage zones on the deformation panels are

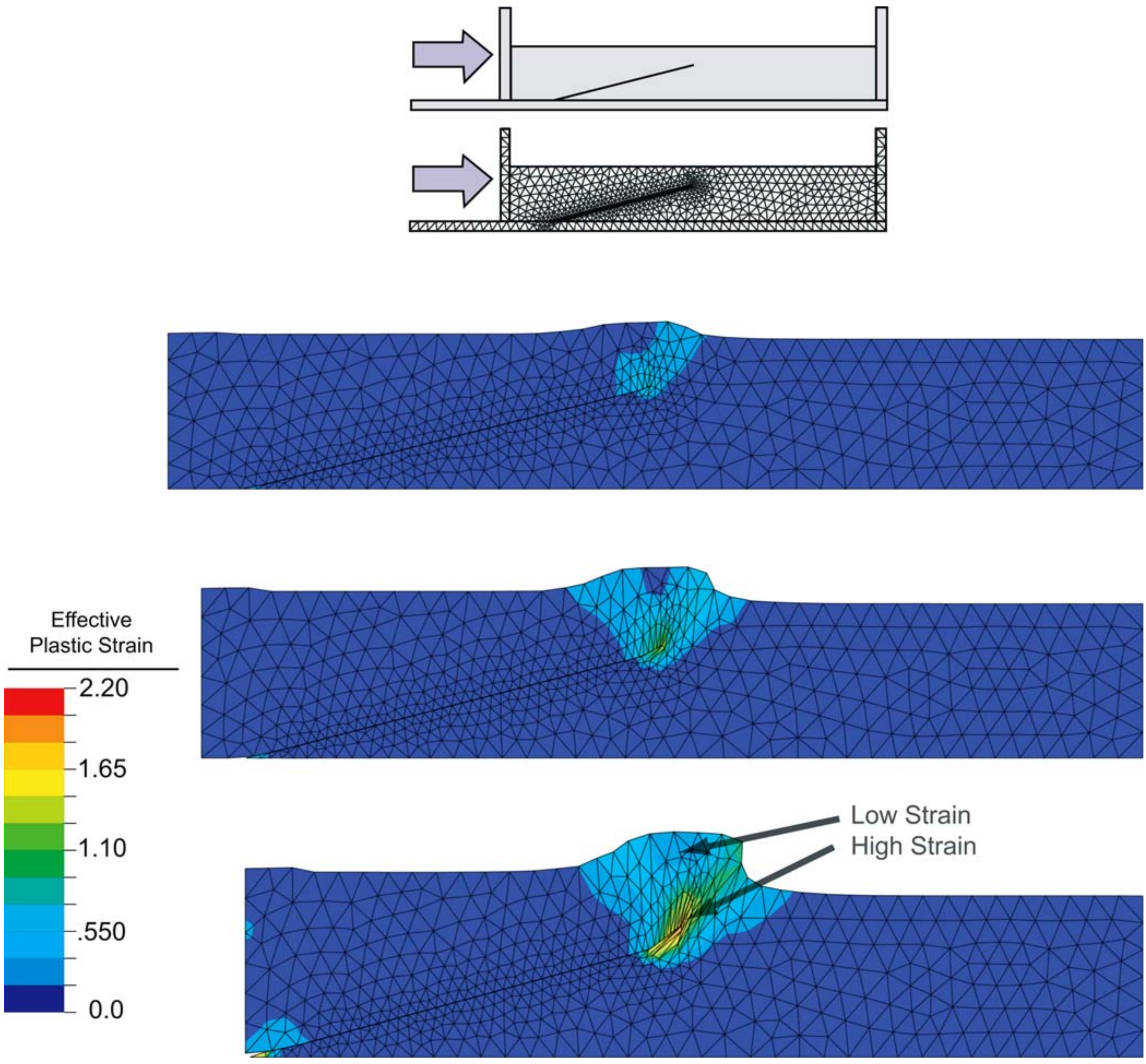

Fig. 24. Example of geomechanical modelling of a fault-related fold under artificial and simplified boundary conditions. (**a**) Model configuration and mesh discretization. (**b**) Evolution of plastic strain during fault-related folding.

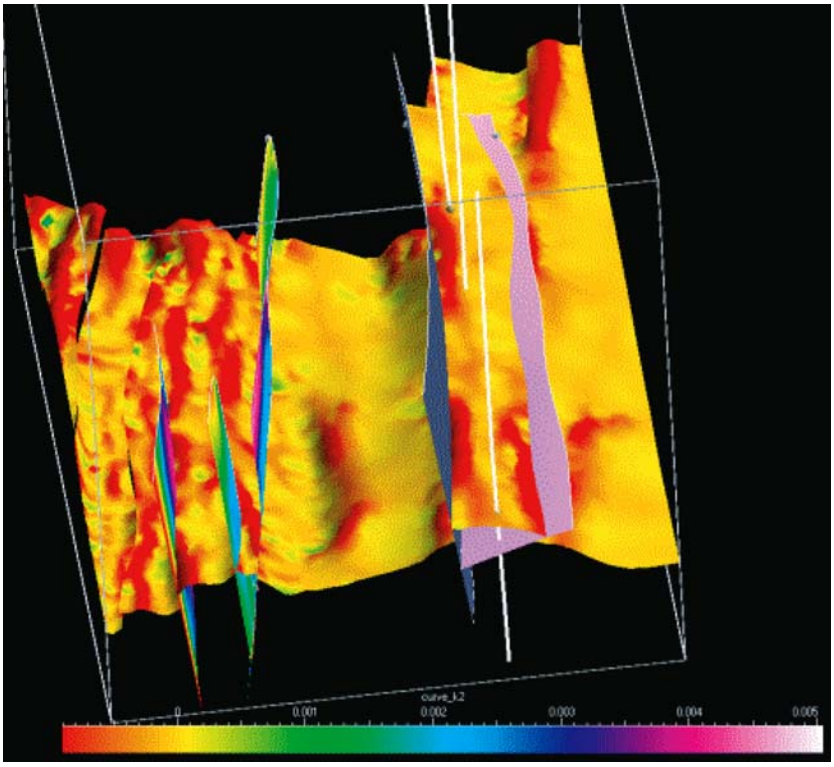

Fig. 25. Three-dimensional output from geomechanical modelling package displays regions of higher (red)/lower (green) probabilities of encountering favourable reservoir producibility characteristics, open fractures. It is in these locations where stress is predicted to be lower and drill targets located.

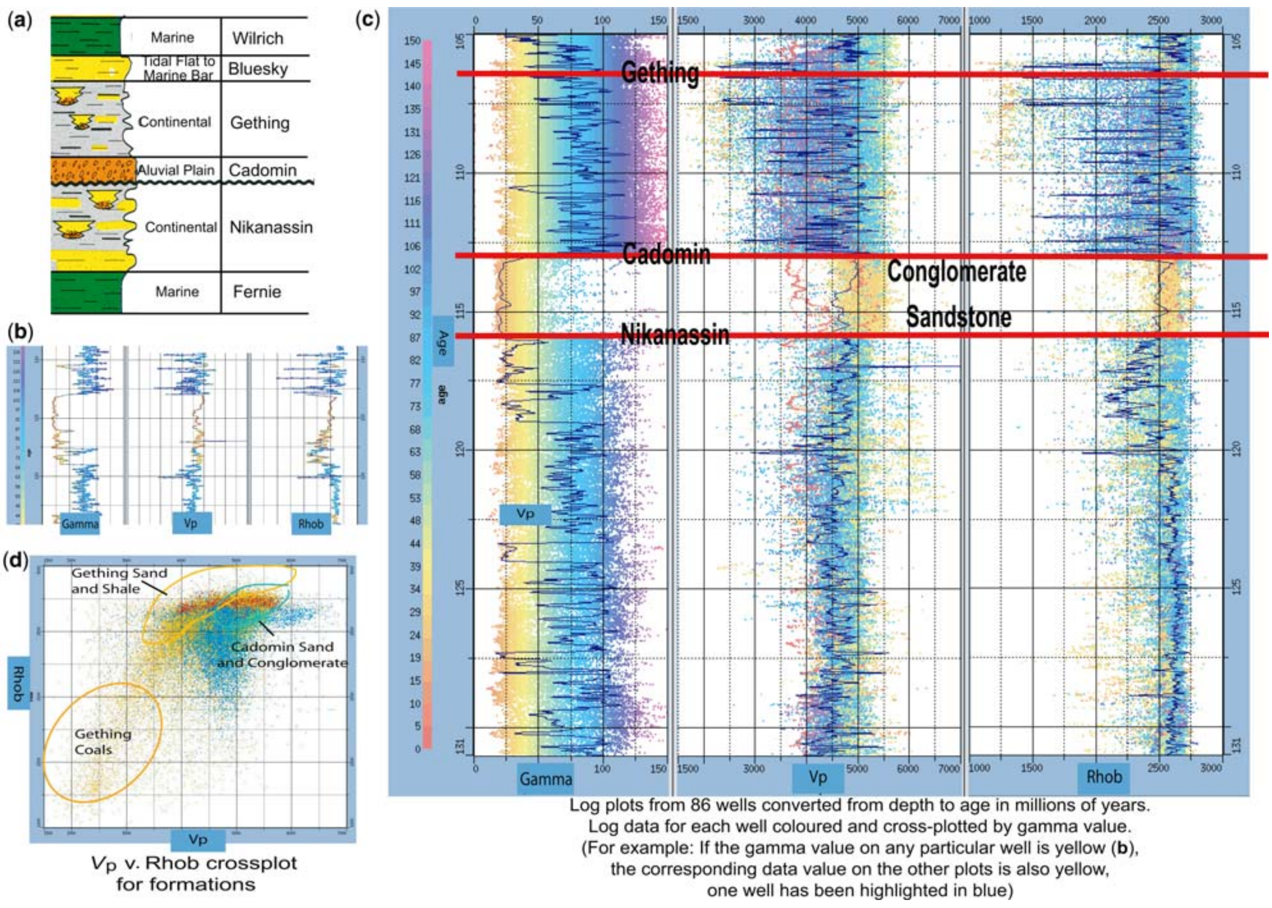

Fig. 26. Acoustic properties across the Gething to Upper Nikanassin (**a**) intervals from (**b**) a single well and (**c**) 86 wells near the BC Alberta border of the study area. The variability of Gething and Nikanassin velocity and density contrasts with the tight cluster of values from the Cadomin and demonstrates the variability of the total seismic response. (**d**) The V_p v. Rhob cross-plot also demonstrates the same issue, the overlapping of P-wave velocity and density of the Gething and Cadomin formations.

the consequence of tectonic interference between these domains, defined by the rock volumes as they migrated through the active axial surface(s) (Mosar & Suppe 1991; Salvini & Storti 1997, 2001, 2004). Overall, this method constitutes a better approach to replicating the consequences of strain accumulation in fault-related folding and/or fold-related faulting which occurred during tectonic transport in thin-skinned fold-and-thrust belts.

A further step in the prediction of damage zones in compressional tectonic settings is obtained through the use of numerical models (Erickson & Jamison 1995; Strayer & Hudleston 1997; Erickson *et al.* 1999; Salvini & Storti 2004), incorporating the evolution of contractional fold-and-thrust structures into the complex process of stress redistribution, strain localization and evolving mechanical properties of the deformed rocks. The use of this class of mechanical analysis requires the introduction of a complete set of equations that include stress equilibrium, strain compatibility, constitutive relations of rock units and appropriate numerical schemes, such as finite element analysis (FEA) or discrete element (DE) methods to solve boundary value problems with complex geometry, initial and boundary conditions, and non-linear mechanical behaviour. The application of such modelling computes the spatial and temporal distribution of damage zones associated with folding and faulting in these contractional regimes. Results show, for example (Fig. 24), that frictional slip along a pre-existing planar fault on a generic fault propagation fold concentrates inelastic strain along limbs, away from the crest.

In a total 3D analysis, output consists of 3D stress and strain envelopes, fault strength distribution, unbalanced strain tensors (equates to plastic deformation) and active deformation boundaries. From this, a non-linear, multiscale point source integration computes the local stress and strain for each point in the reservoir. The final product is a 3D representation of a structure (Fig. 25) with zones of higher and lower probabilities of encountering favourable reservoir producibility characteristics, that is, areas where a well developed and/or well connected open fracture network is expected. Unknown, or poorly understood in the analysis, is the 'detailed' tectonic history, including fault sequencing, the local stress field and the specific lithological failure conditions, all of which complicate the predictions.

Seismic stratigraphic mapping

An analysis of rock physics for 86 wells, both above and below the Cadomin Formation, demonstrates the difficulty in geophysical interpretation of many Cretaceous tight gas sandstones (Fig. 26). The well logs have been aligned based on formation top age and using linear interpolation between picks. The consistency of acoustic and elastic rock properties of the Cadomin Formation can be readily observed (Fig. 26) where little difference occurs between conglomerate and sandstone lithology. The over- and underlying formations, on the other hand, comprise siltstones, shales, coals and sandstones with a large variability in acoustic and elastic impedance. As the geophysical response of the Cadomin Formation is a tuned combination of thickness and a contribution from the surrounding rocks, the seismic reflection from this specific geological interface cannot usually be made, so a nearby tuned reflector is picked, usually caused by the nearest high impedance contrast rocks, often coals. Any stratigraphic interpretation or quantitative

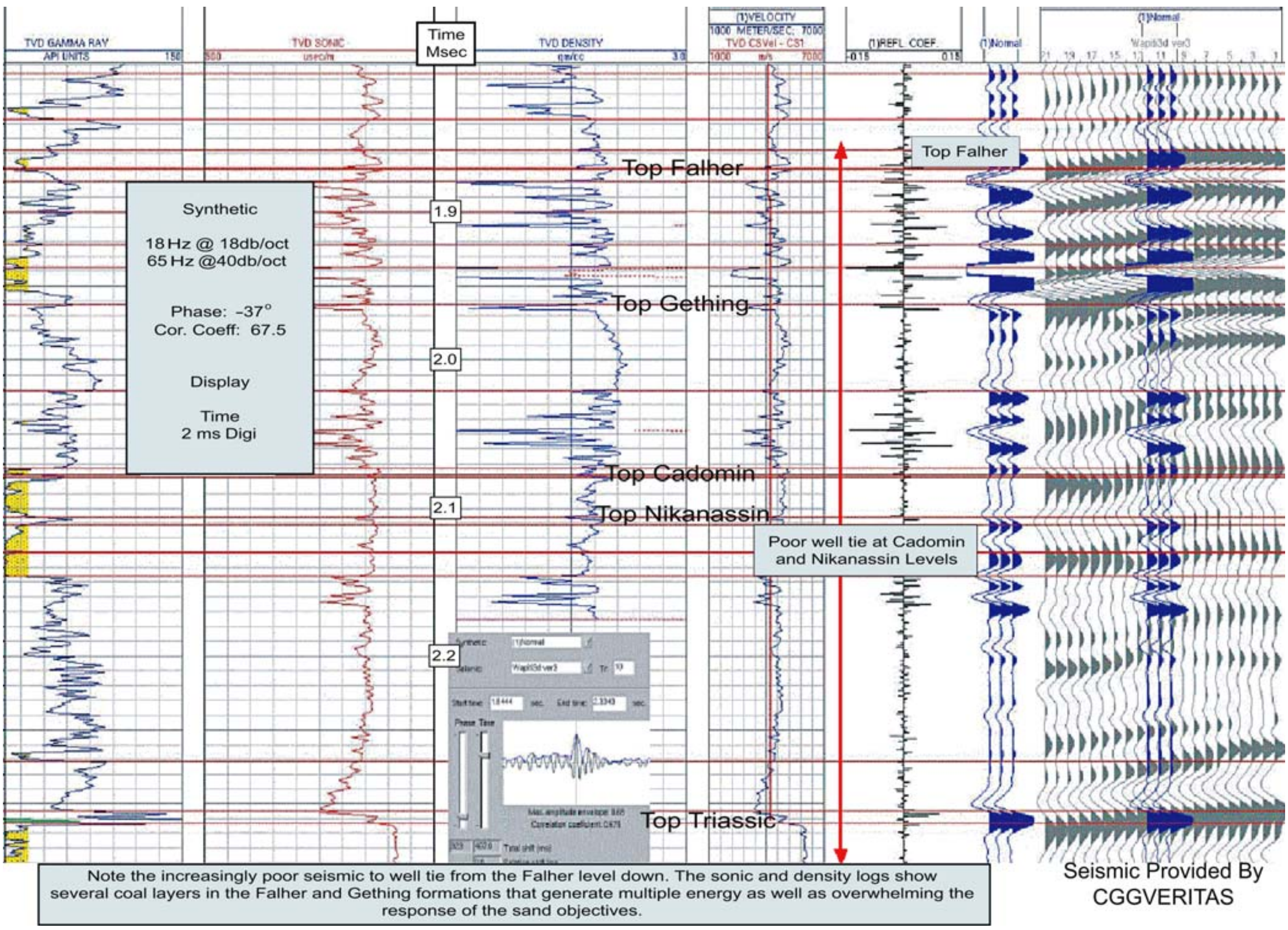

Fig. 27. Seismic to synthetic tie for a typical well.

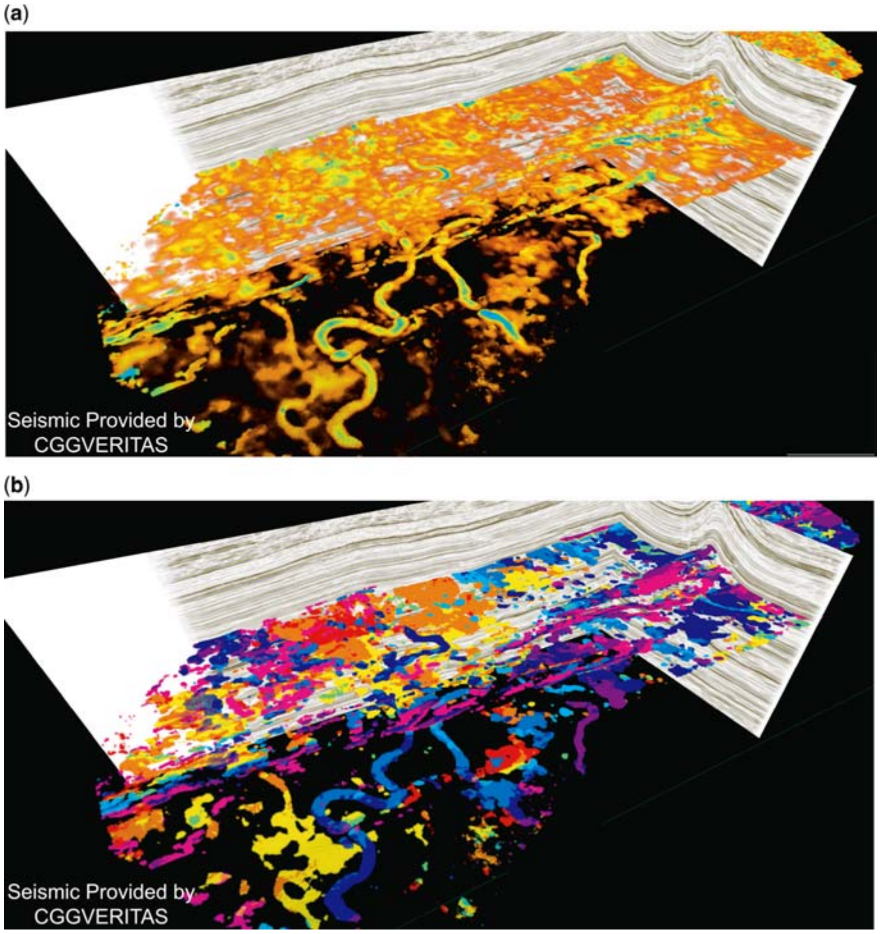

Fig. 28. Mid Cretaceous stratigraphic interpretation from events over an seismic time interval equivalent to 0.8 Ma (60 ms). (**a**) Events coloured by amplitude. (**b**) Events subdivided and coloured by relative age, revealing the stacking of channel systems.

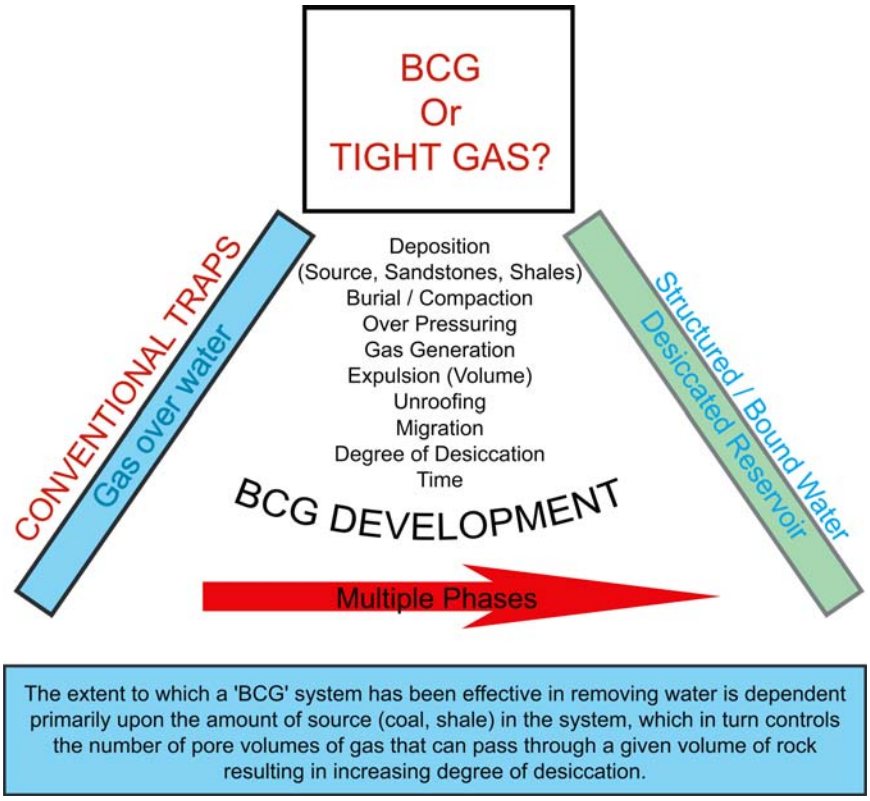

Fig. 29. 'Tight gas' to 'BCG' occurs over time involving amount and quality of source rocks, burial history, gas generation and degree of (over)pressuring, expulsion timing and rate, degree of unroofing, quality of reservoir and gas flow-through.

geophysical measurements are as such not accurate, as it is not known what formation and/or lithology/thickness variations are contributing to the measured response. Gas effects are also not observed or expected, with the low porosities of the sandstones and conglomerates.

A seismic to well tie (Fig. 27) demonstrates an additional problem in events below the coals of the Falher, where intra-bed multiples become dominant. At and above the Falher interval, good ties are evident, but below this level (where the coals begin) ties degrade severely into the Cadomin–Nikanassin formations. Across these deeper BCG units, attribute analysis is meaningless, although structural correlations may still be inferred.

In spite of the above complications, volume-based visualization techniques have still been very useful. Within the Falher Member, regional scale stratigraphic variations have mapped (Fig. 23) channels, valley systems and coaly regions. Above this interval, chronostratigraphic interpretation of seismic events has provided additional insight into depositional environments. In a younger event (Fig. 28), an amplitude extraction over a seismic volume has been age sculpted across an equivalent interval of 0.8 million years (60 ms). The fluvial channels are clearly visible and depositional environments can be interpreted (Fig. 28a). Coloured by relative age (Fig. 28b), the separation and stacking of channel systems is clearly interpretable.

Discussion

Law (2002) defined basin-centred gas regions as those that display four characteristics: regionally pervasive gas, abnormal pressure (high or low), common lack of a downdip water contact and located in low-permeability reservoirs. In general, 'BCG basins' will display all of these characteristics to one degree or another, and lie somewhere between a 'true' conventional tight gas or a 'true' BCG basin (Fig. 29). The complexities or degree of BCG development will be dependent on the basin's history, including lithology, burial, compaction, amount of overpressuring, gas maturation, expulsion, migration, degree of desiccation and gas loss out of the system. As gas is expelled from source units into a basin's low-porosity–permeability reservoir units, water is absorbed by the gas and carried updip, lowering the Deep Basin's water saturation (and R_{w}). That water is removed over time until eventually the entire objective column may be gas-saturated and 'fully' desiccated. Enough gas must flow through the system to remove this volume of water. Eventually, depending on local conditions, a dynamic updip gas–water interface will be established, controlled by a complex relationship between free, capillary and collapsed water, porosity, permeability and hydrostatic and capillary pressures regimes. Both the collapsed and capillary water will be present across each reservoir zone, producing a different geographical 'water line' across formations, often mimicking depositional environments. Capillary pressures acting to wick water along internal reservoir permeability and porosity variations will also produce a complex interfingering of higher and lower water saturations, often within metres of each other. This will in turn lead to a vertical intraformational set of various S_{w} lines, established along lines of common permeability. It is not unexpected for water-wet and gas-bearing zones to be encountered in various combinations within a given borehole, especially near to but also at some distance from the updip water transition zone. Some of the downdip wetter zones could also be by-passed water pools left behind and produced during the basin migration and desiccation process. Basin evolution will dictate the geographical distribution of water and pressure highs and lows across the basin, within the dynamics of an active system.

Conclusions

Western Canada, a mature BCG basin, displays all of Law's (2002) defining points, variable and complex pressures and water saturations within very tight gas-saturated sandstones and conglomerates, downdip of free water. With very low matrix permeabilities, commonly less than 100 μD, structural and geomechanical models were developed by Shell Canada to aid in the prediction of regions where producibility probabilities were highest, thereby increasing the likelihood of encountering areas of enhanced and effective natural fractures within the depositional and structural framework. With the integration of geological, petrophysical, geophysical and geomechanical models, Shell Canada was able to mount a successful exploration, land acquisition and eventual developmental programme. Both structural and stratigraphic leads were mapped and from the initiation of the unconventional gas plays in 2003, through organic and inorganic growth, more than 1000 drill spacing units (square miles) were acquired and more than 100 wells were drilled. In summary, a multidisciplinary approach resulted in economic success in regions once thought to be non-prospective.

M. Minchau is thanked for his directorship throughout the project, from a small study group to a full business unit. A. Cortis is thanked for his insightful review and technical guidance, J. Noad for his generous assistance, and C. Spencer for her assistance in the preparation of many of the figures and diagrams. Thanks are also given to Shell Canada for permission to publish this manuscript. Special thanks go to CGGVERITAS for permission to publish examples of their 3D seismic data.

References

Allen, F. H. 1980. Deep Basin, Alberta. *Annual AAPG-SEPM-EMD Convention*, Denver, 8–11 June 1980, Abstract.

Arnott, R. W. C., Zaitlin, B. A. & Potocki, D. J. 2002. Stratigraphic response to sedimentation in a net-accommodation-limited setting, Lower Cretaceous Basal Quartz, south-central Alberta. *Bulletin of Canadian Petroleum Geology*, **50**, 92–104.

Barclay, J. E. & Smith, D. G. 1992. Western Canada foreland basin oil and gas plays. *In*: Macqueen, R. W. & Leckie, D. A. (eds) *Foreland Basins and Fold Belts*. American Association of Petroleum Geologists, Tulsa, OK, Memoirs, **55**, 191–227.

Bennion, D. B., Thomas, F. B., Schulmeister, B. E. & Rushing, J. 2002. Laboratory and field validation of the mechanism of establishment of very low initial water saturations in ultra-low permeability porous media. *Canadian Institute of Mining, Metallurgy and Petroleum; Petroleum Society's Canadian International Petroleum Conference*, Calgary, Alberta, 11–13 June 2002, paper 2002–063.

Bergbauer, S., Mukerji, T. & Hennings, P. 2003. Improving curvature analyses of deformed horizons using scale-dependent filtering techniques. *American Association of Petroleum Geologist Bulletin*, **87**, 1255–1272.

Biot, M. A. 1964. Theory of internal buckling of a confined multilayered structure. *Geological Society of America Bulletin*, **75**, 563–568.

Cooper, M., Brealey, C., Fermor, P., Green, R. & Morrison, M. 2004. Structural models of subsurface thrust-related folds in the foothills of British Columbia; case studies of sidetracked gas wells. *In*: McClay, K. R. (ed.) *Thrust Tectonics and Hydrocarbon Systems*. American Association of Petroleum Geologists, Tulsa, OK, Memoirs, **82**, 579–597.

Decker, A. D., Close, J. C. & McBane, R. A. 1989. The use of remote sensing, curvature analysis, and coal petrology as indicators of higher coal reservoir permeability. *International Coalbed Methane Symposium Proceedings*, 325–340.

De Sitter, L. U. 1956. Elastic or plastic buckling of the earth's crust. *Leide Geologische Mededelingen*, 171–176.

Erickson, G., Strayer, L. & Suppe, J. 1999. Mechanical modelling of deformation mechanism in folds. *Thrust Tectonics 99*. Royal Holloway University of London, Abstracts, 188.

Erickson, S. G. & Jamison, W. R. 1995. Viscous-plastic finite-element models of fault-bend folds. *Journal Structural Geology*, **17**, 561–573.

Fermor, P. R. & Price, R. A. 1987. Multiduplex structure along the base of the Lewis thrust sheet in the southern Canadian Rockies. *Bulletin of Canadian Petroleum Geology*, **35**, 159–185.

Fischer, M. P. & Wilkerson, M. S. 2000. Predicting the orientation of joints from fold shape, Results of pseudo three-dimensional modeling and curvature analysis. *Geology*, **28**, 15–18.

Gies, R. M. 1984. Case history for a major Alberta Deep Basin gas trap: the Cadomin Formation. *In*: Masters, J. A. (ed.) *Elmworth – Case Study of a Deep Basin Gas Field*. American Association of Petroleum Geologists, Tulsa, OK, Memoirs, **38**, 115–140.

Hayes, B. J. R., Christopher, J. E., Rosenthal, L., Los, G., McKercher, B., Minken, D. F., Tremblay, Y. M., Fennell, J. W. & Smith, D. G. 1994. Cretaceous Manville Group of the western Canada sedimentary basin. *In*: Mossop, G. D. & Shetsen, I. (compilers) *Geological Atlas of the Western Canada Sedimentary Basin*. Canadian Society of Petroleum Geology and Alberta Research Council, 317–334.

Hennings, P. H. & Olson, J. E. 1997. The relationship between bed curvature and fracture occurrence in a fault-propagation fold. AAPG/SEPM Annual Meeting, Abstracts, **6**, 49.

Issler, D. R., Willett, S. D., Beaumont, C., Donelick, R. A. & Griet, A. M. 1999. Paleotemperature history of two transects across the Western Canada Sedimentary Basin: constraints from apatite fission track analysis. *Bulletin of Canadian Petroleum Geology*, **47**, 475–486.

Jackson, P. C. 1984. Paleogeography of the Lower Cretaceous Mannville Group of Western Canada. *In*: Masters, J. A. (ed.) *Elmworth – Case Study of a Deep Basin Gas Field*. American Association of Petroleum Geologists, Tulsa, OK, Memoirs, **38**, 49–77.

Johnson, M. F. & Dalrymple, R. W. 2005. The Early Cretaceous Cadomin and Gething formations of the Deep Basin area, Western Canada: Cordilleran tectonics and alluvial sedimentation in a retroarc foreland basin. *American Association of Petroleum Geologists Annual Convention*, Calgary, Alberta, 22–22 June, Abstract.

Law, B. E. 2002. Basin-centred gas systems. *American Association of Petroleum Geologists Bulletin*, **86**, 1891–1919.

Leckie, D. A. & Smith, D. G. 1992. Regional setting, evolution, and depositional cycles of the Western Canada foreland basin. *In*: Macqueen, R. W. & Leckie, D. A. (eds) *Foreland Basins and Fold Belts*. American Association of Petroleum Geologists, Tulsa, OK, Memoirs, **55**, 9–46.

Lemiszki, P. J., Landes, J. D. & Hatcher, R. D. Jr. 1994. Controls on hinge-parallel extension fracturing in single-layer tangential-longitudinal strain fold. *Journal of Geophysical Research*, **99**, 22027–22041.

Lettley, C. D., Pemberton, S. G., Gingras, M. K. & Saunders, T. 2006. Depositional control of lateral reservoir variability within an extensive shoreline complex: example from the Lower Cretaceous Cadotte Member of Western Canada. *American Association of Petroleum Geologists Bulletin*, **90**, Program Abstracts.

Lisle, R. J. 1994. Detection of zones of abnormal strains in structures using Gaussian curvature analysis. *American Association of Petroleum Geologists Bulletin*, **78**, 1811–1819.

Lukie, T. D., Ardies, G. W., Dalrymple, R. W. & Zaitlin, B. A. 2002. Alluvial architecture of the Horsefly unit (Basal Quartz) in southern Alberta and northern Montana: influence of accommodation changes and contemporaneous faulting. *Bulletin of Canadian Petroleum Geology*, **50**, 73–91.

Masters, J. A. 1979. Deep Basin gas trap, western Canada. *American Association of Petroleum Geologists Bulletin*, **63**, 152–181.

Masters, J. A. 1984. Lower Cretaceous oil and gas in Western Canada. *In*: Masters, J. A. (ed.) *Elmworth – Case Study of a Deep Basin Gas Field*. American Association of Petroleum Geologists, Tulsa, OK, Memoirs, **38**, 1–33.

McMechan, M. E. 1999. Geometry of the structural front in the Kakwa area, foothills of northern Alberta. *Bulletin of Canadian Petroleum Geology*, **47**, 31–42.

Michael, K. & Bachu, S. 2001. Fluids and pressure distributions in the foreland-basin succession in the west-central part of the Alberta basin, Canada: evidence for permeability barriers and hydrocarbon generation and migration. *American Association of Petroleum Geologists Bulletin*, **85**, 1231–1252.

Mosar, J. & Suppe, J. 1992. Role of shear in fault-propagation folds. *In*: McClay, K. R. (ed.) *Thrust Tectonics*. Chapman & Hall, London, 123–132.

Mossop, G. & Shetsen, I. 1994. *Geological Atlas of the Western Canada Sedimentary Basin*. Alberta Geological Survey.

Newsham, K. E., Rushing, J. A., Chaouche, A. & Bennion, D. B. 2002. *Laboratory and Field Observations of an Apparent Sub-capillary Equilibrium Water Saturation Distribution in a Tight Gas Sand Reservoir*. SPE **75710**.

Poulton, T. P., Tittemore, J. & Dolby, G. 1990. Jurassic strata of northwestern Alberta and northeastern British Columbia. *Bulletin of Canadian Petroleum Geology*, **38A**, 159–175.

Salvini, F. & Storti, F. 1997. Spatial and temporal distribution of fractured rock panels from geometric and kinematic models of thrust-related folding (abstract). *American Association of Petroleum Geologists Bulletin*, **81**, 1409.

Salvini, F. & Storti, F. 2001. The distribution of deformation in parallel fault-related folds with migrating axial surfaces: comparison between fault-propagation and fault-bend folding. *Journal of Structural Geology*, **23**, 25–32.

Salvini, F. & Storti, F. 2004. Active-hinge-folding-related deformation and its role in hydrocarbon exploration and development – insights from HCA modeling. *In*: McClay, K. R. (ed.) *Thrust Tectonics and Hydrocarbon Systems*. American Association of Petroleum Geologists, Tulsa, OK, Memoirs, **82**, 453–472.

Schmidt, G. A. & Pemberton, S. G. 2004. Stratigraphy and paleogeography of a conglomeratic shoreline: Notikewin Member of the Spirit River Formation in the Wapiti area of west-central Alberta. *Bulletin of Canadian Petroleum Geology*, **52**, 57–76.

Schultz-Ela, D. D. & Yeh, J. 1992. Predicting fracture permeability from bed curvature. *In*: Tillerson, J. R. & Wawersik, W. R. (eds) *Rock Mechanics; Proceedings of the 33rd US Symposium*, **33**, 579–589.

Smith, D. G., Zorn, C. E. & Sneider, R. M. 1984. The paleogeography of the Lower Cretaceous of western Alberta and northeastern British Columbia in and adjacent to the Deep Basin of the Elmworth area. *In*: Masters, J. A. (ed.) *Elmworth – Case Study of a Deep Basin Gas Field*. American Association of Petroleum Geologists, Tulsa, OK, Memoirs, **38**, 79–114.

Stott, D. F. 1993. *Evolution of Cretaceous foredeeps: a comparative analysis along the length of the Canadian Rocky Mountains*. Geological Association of Canada, Boulder, CO, Special Papers, **39**, 131–150.

Strayer, L. M. & Hudleston, P. J. 1997. Numerical modeling of fold initiation at thrust ramps. *Journal of Structural Geology*, **19**, 551–556.

Suppe, J., Chou, G. T. & Hook, S. C. 1992. Rates of folding and faulting determined from growth strata. *In*: McClay, K. R. (ed.) *Thrust Tectonics*. Chapman & Hall, London, 105–121.

Wyman, R. E. 1984. Gas resources in Elmworth coal seams. *In*: Masters, J. A. (ed.) *Elmworth – Case Study of a Deep Basin Gas Field*. American Association of Petroleum Geologists, Tulsa, OK, Memoirs, **38**, 173–187.

Zaitlin, B. A., Warren, M. J., Potocki, D., Rosenthal, L. & Boyd, R. 2002. Depositional styles in a low accommodation foreland basin setting: an example from the Basal Quartz (Lower Cretaceous), southern Alberta. *Bulletin of Canadian Petroleum Geology*, **50**, 31–72.

Tight gas exploration in the Pannonian Basin

A. KIRÁLY, K. MILOTA, I. MAGYAR and K. KISS

MOL Hungarian Oil and Gas Plc, Budapest, Október 23. u. 18, H-1117, Hungary
(e-mail: Andras.Kiraly@ina.hr)

Abstract: The Pannonian Basin is a mature exploration area where most of the obvious structural features have been tested and the largest conventional accumulations probably have been found. The history of hydrocarbon exploration and production in the central Pannonian Basin, Hungary, is more than 90 years old. The evaluation of unconventional hydrocarbon reserves offers an opportunity to rejuvenate exploration in this young and hot basin.

Keywords: unconventional hydrocarbon, tight gas, basin-centred gas, Pannonian Basin, hydrocarbon system, overpressure

Structural and sedimentary evolution of the Pannonian Basin

Structural evolution

The Pannonian Basin is a Neogene extensional basin located in the east Central European segment of the convergence zone between the European and African plates (Fig. 1). The basin has a complex deformation history with distinct structural episodes (Horváth *et al.* 2006). Extensional tectonics started in the Early Miocene and culminated in the Middle Miocene. Because of strain localization along zones of crustal weakness inherited from the Cretaceous, that is, rejuvenation of thrust planes as low-angle normal faults, the extension was heterogeneous and resulted in a highly irregular basement morphology. Sub-basins of the Pannonian Basin system are thus separated by prominent basement highs, and are often treated as individual basins (e.g. Nagymarosy 2008).

Thinning of the lithosphere caused subsidence starting from the late Middle Miocene or early Late Miocene. This process affected almost the entire area between the Alps, Carpathians and Dinarides, and led to the formation of the geographically separate Pannonian Basin. Short-term local or regional (but not basinwide) compressional events also occurred during this period, the most significant of which caused a prominent unconformity between the Middle and Upper Miocene successions (Horváth 1995).

Subsidence anomalies at about the Miocene–Pliocene boundary mark the onset of structural inversion in the Pannonian Basin. Basin centres continued to subside whereas basin flanks suffered uplift and erosion at this advanced stage of basin evolution (Horváth & Cloetingh 1996; Magyar & Sztanó 2008).

Palaeogeographic evolution and sedimentary environments

Palaeogeographic evolution of the Pannonian Basin was intimately associated with the history of the Paratethys, the northern heir of the Tethys Ocean, which was more or less effectively separated from the Mediterranean Sea by the Alpine Orogen (Popov *et al.* 2004). Tectonic processes and eustasy controlled the palaeogeographic connections of the Pannonian Basin both towards the Mediterranean and towards the neighbouring Paratethyan basins (Vakarcs *et al.* 1999).

In the early, extensional phase of basin evolution, marine connections opened between the Pannonian Basin and the Mediterranean. Marine sedimentary environments first formed in the northern and western sub-basins and then became widespread across the entire intra-Carpathian area by the Middle Miocene. In the late Middle Miocene, however, the basin lost its direct connection to the sea, and became part of a large, closed or semi-closed inland sea, a uniform Paratethys. The marine environments were replaced by marginal marine (brackish to hypersaline) depositional settings and by euxinic environments in the basin centres.

A compressional tectonic phase at the Middle/Late Miocene boundary isolated the Pannonian Basin from the rest of the Paratethys, thus forming a brackish lake in the basin (Lake Pannon). The former archipelago of the Pannonian Basin gradually submerged as regional subsidence became dominant. In the Late Miocene through the Pliocene, sedimentation took place in the several-hundred-metre-deep lake and in the adjacent deltaic and fluvial environments (Magyar *et al.* 1999). Sediment input to the lacustrine basin was most intense from the NW and, in the eastern sub-basins, from the NE. The deep basin was gradually converted into fluvial plains as the shoreline prograded basinward. The lithostratigraphic boundaries within this shoaling-upward sequence are strongly diachronous.

Generalized stratigraphy of the basin fill

The area of the Pannonian Basin system extends over 10 countries. In this paper we focus on the central sub-basins which lie mostly within Hungary. In these basins, the Lower Miocene is dominated by terrestrial and limnic deposits, such as breccias, conglomerates, non-marine sandstones and siltstones, and freshwater clays. Following a transgression, the lower Middle Miocene (Badenian stage in the regional Paratethyan chronostratigraphy) is characterized by marine shales in the deep basins and corallinacean limestones and calcarenites on the highs. The upper Middle Miocene (Sarmatian stage) is represented by marls (often laminated, bituminous, with fish fossils) in the basins, and biogenic limestones, sandstones and evaporites above basement highs and in minor closed basins. There is a difference, however, in the development of these formations between the western and eastern sub-basins. In the west, the Lower and Middle Miocene succession is relatively thick, and generally each unit (Lower Miocene, Badenian, Sarmatian) is well represented in the sequence. In addition, traces of marine ingressions may occur in the Lower Miocene. In contrast, the Lower and Middle Miocene units are significantly thinner in the depocentres of the eastern sub-basins, there are no marine sediments older than Badenian and the separation of the Badenian,

VINING, B. A. & PICKERING, S. C. (eds) *Petroleum Geology: From Mature Basins to New Frontiers – Proceedings of the 7th Petroleum Geology Conference*, 1125–1129. DOI: 10.1144/0071125

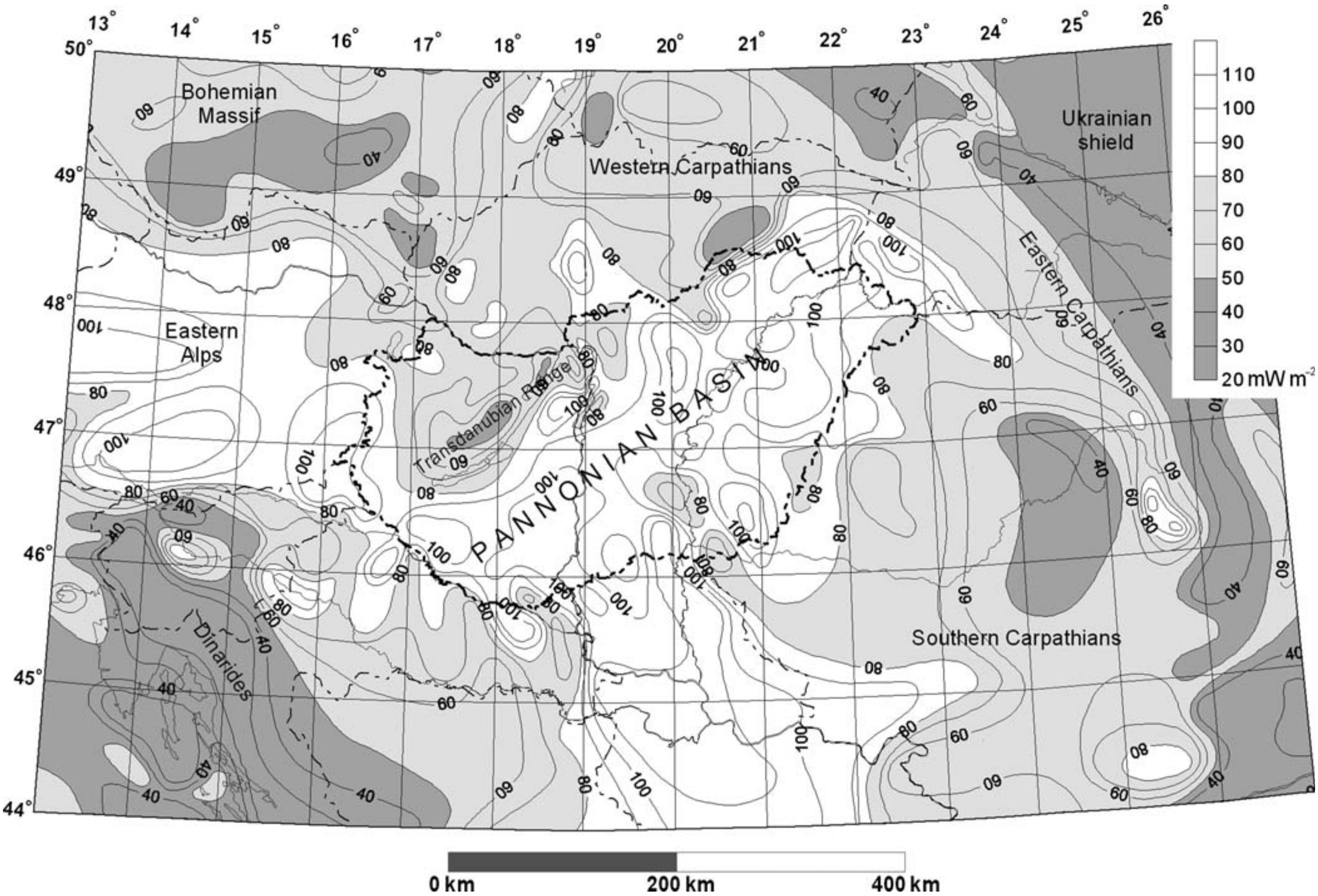

Fig. 1. The Pannonian Basin in Central Europe with the present-day heat flow (Lenkey *et al.* 2009). The borders of Hungary are indicated with a thicker line.

Sarmatian, and Upper Miocene Pannonian stages is often problematic due to condensed sedimentation, effective reworking of fossils and redeposition of sediments at various time intervals during the Neogene (Szuromi-Korecz *et al.* 2004). It remains unclear whether these differences between the western and eastern sub-basins are due to their different geographic positions relative to the sediment source, or to the different timing of the opening of the basins.

The Upper Miocene and Pliocene (together referred to as the 'Pannonian stage' in Hungary) are relatively uniform in the entire basin. Generally, they consist of five, strongly diachronous lithological units (Juhász 1991; Fig. 2). Shales deposited in the several-hundred-metre deep, giant brackish-water lacustrine basin comprise the Endrőd Formation. The Endrőd Formation is overlain by the turbidite-bearing Szolnok Formation. The distribution of this unit was closely controlled by the coeval basin morphology. The overlying shaly slope deposits comprise the Algyő Formation. The sequence is capped by the deltaic Újfalu Formation and by fluvial deposits (Zagyva and Nagyalföld Formations). Finally, much of the Pannonian Basin is covered by Quaternary deposits, which are missing from the inverted areas but can be as thick as 700 m in the subsiding sub-basins.

The Neogene petroleum system of the Pannonian Basin

Source rocks

Three main source units can be distinguished within the Neogene sequence based on their stratigraphic position, depositional environments and organic facies: transgressive marine shales of Badenien age; various Sarmatian sediments; and deep-water marls and deltaic–alluvial deposits of Pannonian age (Fig. 3). The deep water facies are not exposed in the surface, thus their description is based on cores and cutting samples from deep exploration wells.

The deep-water marine shales of the Badenian usually remain unexplored in the deepest parts of the sub-basins. Hydrocarbon shows and well test results, however, often indicate the presence of Badenian source rocks in the central parts of the sub-basins. The present source richness of the investigated samples reflects the maturity phase after migration of generated hydrocarbons: commonly low total organic carbon (TOC) content, low remaining potential and low hydrogen indices (HI) are characteristic. The thickness of the Badenien is highly variable, and 10–30% of the studied samples proved to be fair- to good-quality source rocks based on organic richness (Fig. 4). The kerogen type can hardly be estimated due to the high level of maturity. Low HI values and the relatively low rate of liptinites in the composition of the kerogen can be related to type III, but the biomarker composition of the extracts refers to organic matter of marine or mixed marine/terrigenous origin. The source maturity corresponds to the wet gas or dry gas window, but it is not surprising as all samples came from deeper than 3000 m.

The distribution, thickness and lithology of the Sarmatian sedimentary rocks within the Pannonian Basin reflect both a highly complex basin topography and a complex sedimentary system. The high variety of lithologies and facies compounded with uncertainties of stratigraphic correlation could be the reason why only a limited number of Sarmatian source rocks were geochemically studied. The organic facies of the Sarmatian deposits varies considerably with the depositional environment. It seems to be common that the higher organic content is related to anoxic

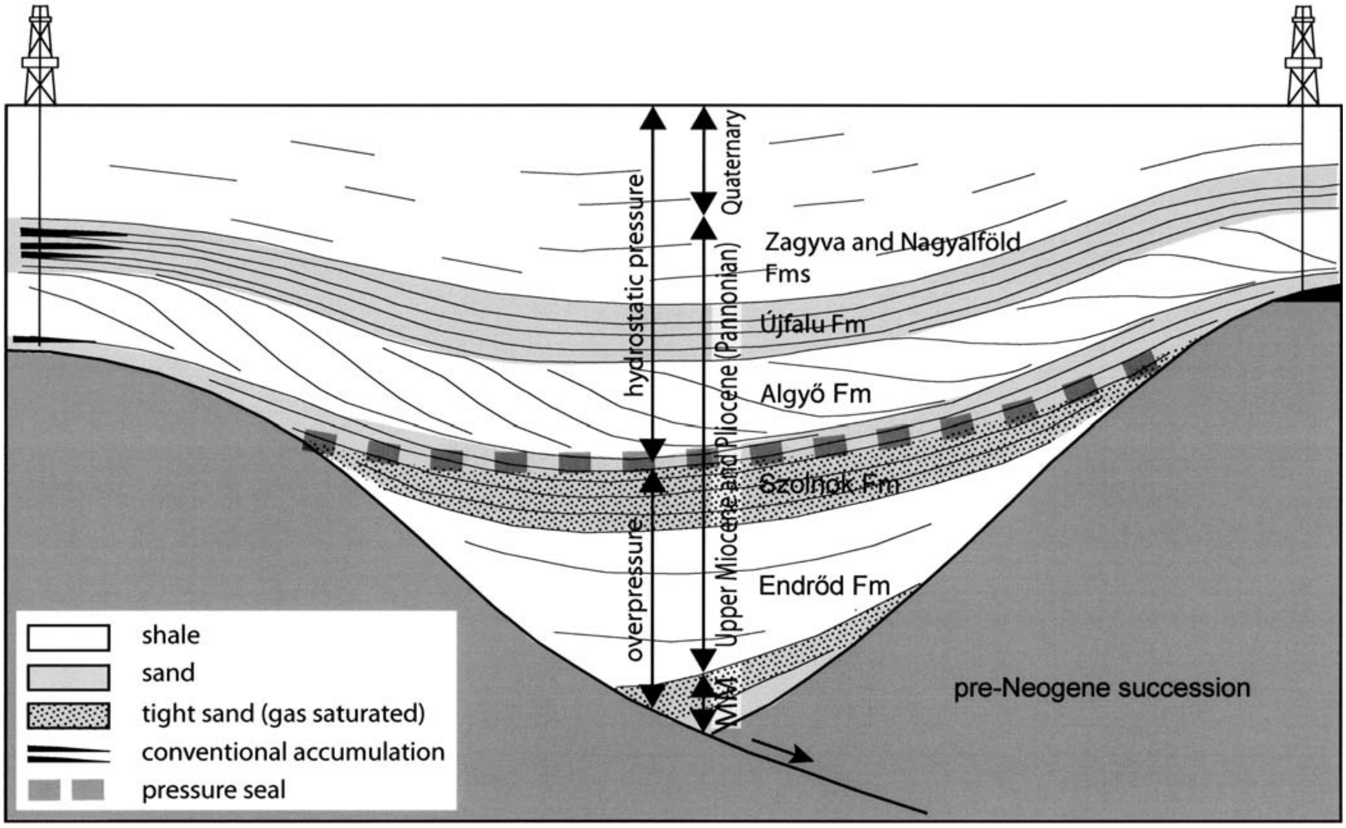

Fig. 2. Cartoon with the major lithostratigraphic units and pressure regimes in a deep sub-basin of the Pannonian basin. Conventional accumulations are known above the structural highs. MM, Middle Miocene.

or dysoxic conditions. NW from the largest Hungarian oil and gas field, Algyő, Sarmatian calcareous marl source rock was found with more than 12% average TOC content. The hydrocarbon yield is higher than 7 kg hydrocarbon/t rock. The kerogen content is dominated by type II. From shaly beds of some deep wells good-quality gas-prone sources of Sarmatian age were identified.

The transgressive basal marls and clays of Late Miocene Pannonian age are the main source rocks of both the conventional and unconventional accumulations. The average TOC is between 1 and 4% and goes up to 10%. The hydrocarbon yield shows great variability from less than 1 kg/t up to 12 kg hydrocarbon/t rock. Kerogen content varies, type II with HI up to 600 and more frequently a mixture of type III and II occur. The shaly beds interlayered between distal turbidites also contain fair-quality effective gas-prone source rocks (Fig. 3). Because of the deep burial and high maturity of these rocks (from onset of the oil window down to dry gas window) the original richness, hydrocarbon potential and kerogen type can only be estimated/calculated. Visual kerogen analysis indicates the organic matter being primarily of type III, terrigenous. In the upper part of the Pannonian sedimentary column coaly shale beds are known within the delta plain sediments; these might be good gas sources but are generally immature.

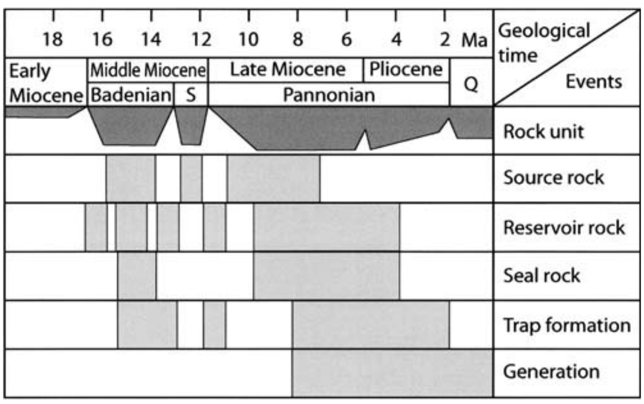

Fig. 3. Generalized events chart for the Neogene hydrocarbon system of the Pannonian Basin. S, Sarmatian.

Maturity

The uppermost limit of the oil window (at 0.6% vitrinite reflectance) lies at about 2300 m or deeper across all sub-basins. The base of the oil or wet gas generation zone is variable and generally at an uncertain depth. Usually it can be characterized only by a calculated value as in most cases the maturity of the penetrated Neogene sequences remains within the oil or wet gas generation phase. In the deep sub-basins the depth zone of peak generation (0.9–1.1% vitrinite reflectance) is between 3900 and 4500 m.

Considering the present geothermal gradient of 44–55 °C/km, the onset of the oil generation is at a formation temperature of at least 100 °C, which is significantly higher than the world average. The oils of the largest Hungarian (conventional oil) field, Algyő, were generated at about 130 °C (Sajgó 1984). It seems to be that the Pannonian Basin was recently subjected to a relatively short but intensive heating event resulting in hydrocarbon generation. As a consequence of the high present-day heat flow (Fig. 1) and high geothermal gradient (Völgyi 1978), the source rocks are still actively generating oil, condensate and natural gas. This dynamic hydrocarbon system makes the Pannonian Basin exceptional.

Reservoirs and seals

Middle Miocene corallinacean limestones and calcarenites, sandstones of the Upper Miocene section, including deep-water turbidites and deltaic deposits (Szolnok and Újfalu Formations,

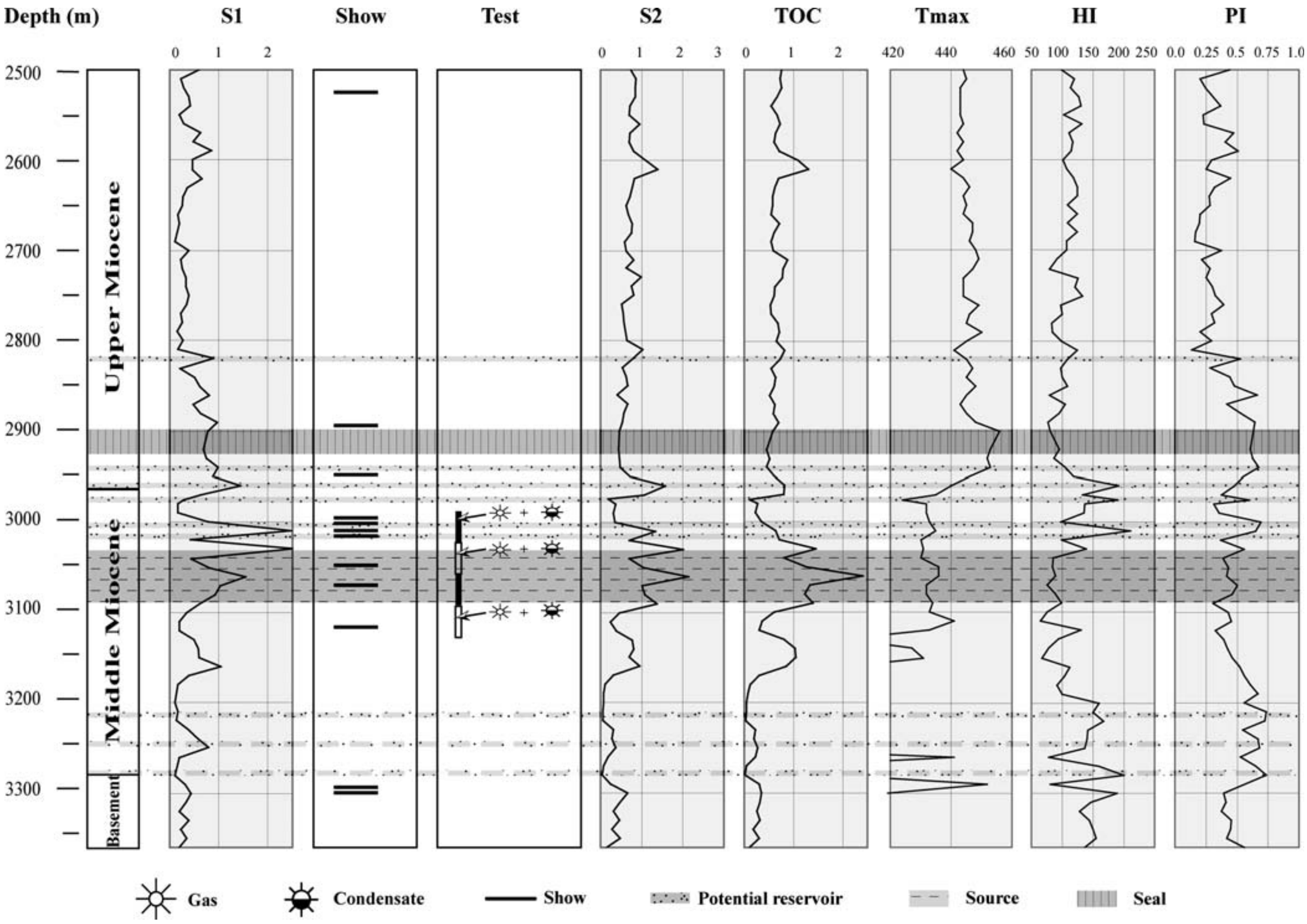

Fig. 4. Geochemical log of a well with Middle Miocene source rocks from eastern Hungary.

respectively), transgressive basal conglomerates of various age and even the weathered basement are confirmed reservoirs for conventional accumulations. These reservoirs are sealed by interbedded shales (Figs 3 & 4).

The thick shaly beds of the Upper Miocene Algyő Formation divide the sedimentary complex into two parts hydrodynamically (Fig. 2). These shales can provide excellent pressure sealing above the significantly overpressured basal shales, marls and turbidite sandstones (Endrőd and Szolnok Formations). The extension of the high pressure zone below the thick shale beds of the Algyő Formation exceeds thousands of square kilometres, and its thickness ranges between a few hundred metres and more than 1000 m. This thick overpressured succession that includes the turbidite sandstones of Szolnok Formation, the shales and marls of the Endrőd Formation and the transgressive middle Miocene sediments encompasses the unconventional reservoirs of the basin centre hydrocarbon accumulations (tight gas in the sand-dominated units and shale gas in the Endrőd Formation; Fig. 2). The sealing has been predicted to be capillary seal developed under high deposition rate and rapid compaction. On the flanks of the deep subbasins producing conventional hydrocarbon fields related to structural highs were also discovered.

Timing

Thermal history simulations show imbalance between the present formation temperature and kerogen maturity expressed as vitrinite reflectance in the Pannonian Basin. The relatively low maturity values do not support an assumption of high palaeo-heat flow. It seems probable that the present-day formation temperature (the gradient is at least twice the world average) relates to a geologically very recent increase in heat flow. In other words, the actual heat flow (Fig. 1) is currently the highest since the beginning of the Neogene.

According to thermal history simulations, the earliest Neogene hydrocarbon generation started about 9–8 million years ago due to the significant subsidence and burial of the pre-Neogene succession (Fig. 3). Later the heat flow increased everywhere in the basin, resulting in intensive cracking of hydrocarbons. In the deep subbasins the rising heat flow was partly balanced by the cooling effect of the huge sediment pile, which can explain the variability in the position of the oil window.

The development of capillary sealing happened within the last 5 Ma, resulting in high petroleum saturation within the fine-grained basal sediments and turbidite sandstones.

Tight gas plays in the Neogene of the Pannonian Basin

Two tight gas reservoirs are known in the Neogene sequence of Hungary: one in the Middle Miocene Badenian sandstones, and one in the Upper Miocene Szolnok Formation (Fig. 2).

Middle Miocene play

Exploratory wells in recent years proved the presence of a working hydrocarbon system in the Middle Miocene. The Badenian tight gas reservoirs are at great depth (deeper than 3000 m). They comprise mostly sandstones with 6–10% porosity and low permeability. The source rocks are probably Middle Miocene marine shales. The discoveries have particularly high pressure and high temperature (HPHT mainly HT) conditions, such as 50–60 MPa reservoir pressure and 180–200 °C. These wells produced mainly dry and/or good-quality wet gas.

The reservoirs showed typical tight gas behaviour under exploration tests and in the early production phase. Production started – without any stimulation – with higher daily rates and pressure, and then declined within some weeks. The original pressure was 10 times higher than the pressure during the tail production. After the pressure drop, production was stabilized at a lower level with limited water production and at a low well head pressure.

Although production has been continuous since the discovery, the commerciality of the accumulation has not been proven yet. Analysis of the reservoir system and fluid quality indicated that rates may be successfully enhanced with reservoir stimulation. The technical and economical analysis of two projects, i.e. drilling highly deviated wells and/or hydraulic fracturing of the reservoir, is in progress.

Upper Miocene play

Exploration for tight gas occurrences are focused on the Upper Miocene fill of the deep sub-basins, especially the turbidites of the Szolnok Formation (Fig. 2). Tight gas may form a continuous basin-centred accumulation in this reservoir. The major source rock is the underlying, highly overpressured Upper Miocene brackish-water shale (Endrőd Fm.), but the shaly beds of the Szolnok Fm. may have also contributed to gas generation. The porosity of the Szolnok sandstones goes up to 5–8%; their permeability is about 1.5 mD or less. The estimated (residual) water saturation varies widely (50–85%). The simulated/calculated (PetroFlow software) gas saturation varies with source richness in the Szolnok Formation and with the vertical distance from the Endrőd source. Reservoir quality also varies depending on the present depth (between 3000 and 4500 m) and on the depositional environment. Intensive exploration programmes are currently evaluating this play.

Summary

Tight gas occurrences in the sub-basins of the Pannonian Basin include a working system in the Middle Miocene (Badenian) and a more voluminous, continuous-type accumulation in the Upper Miocene. The deep Neogene sub-basins are characterized by high heat flow and high geothermal gradient, and the source rocks are actively generating hydrocarbons. The reservoirs are sandstones, characterized by high overpressures and extremely high temperatures. These conditions require special solutions in drilling, completion and stimulation technology.

The authors thank the two reviewers, Robert Gatliff (British Geological Survey, Edinburgh) and Hans-Martin Schulz (Helmholtz Centre, Potsdam) for their useful comments on the manuscript.

References

Horváth, F. 1995. Phases of compression during the evolution of the Pannonian basin and its bearing on hydrocarbon exploration. *Marine and Petroleum Geology*, **12**, 837–844.

Horváth, F. & Cloetingh, S. 1996. Stress-induced late-stage subsidence anomalies in the Pannonian Basin. *Tectonophysics*, **266**, 287–300.

Horváth, F., Bada, G., Szafián, P., Tari, G., Ádám, A. & Cloetingh, S. 2006. Formation and deformation of the Pannonian Basin: constraints from observational data. *In*: Gee, D. G. & Stephenson, R. A. (eds) *European Lithosphere Dynamics*. Geological Society, London, Memoirs, **32**, 191–206.

Juhász, Gy. 1991. Lithostratigraphical and sedimentological framework of the Pannonian (s.l.) sedimentary sequence in the Hungarian Plain (Alföld), Eastern Hungary. *Acta Geologica Hungarica*, **34**, 53–72.

Lenkey, L., Zsemle, F., Mádl-Szőnyi, J., Dövényi, P. & Rybach, L. 2009. Possibilities and limitations in the utilization of the Neogene geothermal reservoirs in the Great Hungarian Plain, Hungary. *Central European Geology*, **51**, 241–252.

Magyar, I. & Sztanó, O. 2008. Is there a Messinian unconformity in the Central Paratethys? *Stratigraphy*, **5**, 247–257.

Magyar, I., Geary, D. H. & Müller, P. 1999. Paleogeographic evolution of the Late Miocene Lake Pannon in Central Europe. *Palaeogeography, Palaeoclimatology, Palaeoecology*, **147**, 151–167.

Nagymarosy, A. 2008. Pannonian basins system. *In*: McCann, T. (ed.) *The Geology of Central Europe*. Geological Society, London, 1070–1074.

Popov, S. V., Rögl, F., Rozanov, A. Y., Steininger, F. R., Shcherba, I. G. & Kovač, M. (eds) 2004. *Lithological–Paleogeographic Maps of Paratethys. 10 Maps Late Eocene to Pliocene*. Courier Forschungsinstitut Senckenberg, **250**. E. Schweizerbart'sche Verlagsbuchhandlung, Stuttgart, 1–46.

Sajgó, Cs. 1984. Organic geochemistry of the crude oils from south-east Hungary. *Organic Geochemistry*, **6**, 569–578.

Szuromi-Korecz, A., Sütő-Szentai, M. & Magyar, I. 2004. Biostratigraphic revision of the Hód-I well: Hungary's deepest borehole failed to reach the base of the Upper Miocene Pannonian stage. *Geologica Carpathica*, **55**, 475–485.

Vakarcs, G., Hardenbol, J., Abreau, V. S., Vail, P. R., Tari, G. & Várnai, P. 1999. Correlation of the Oligocene–Middle Miocene regional stages with depositional sequences, a case study from the Pannonian Basin, Hungary. *In*: Degraciansky, P.-C., Hardenbol, J., Jacquin, T., Vail, P. R. & Farley, M. B. (eds) *Mesozoic–Cenozoic Sequence Stratigraphy of European Basins*. SEPM, Special Publications, **60**, 211–233.

Völgyi, L. 1978. Geothermal inhomogeneity in the Hungarian Great Plain (Pannonian Basin). *Acta Mineralogica–Petrographica*, **24**, 137–147.

Natural fractures in some US shales and their importance for gas production

JULIA F. W. GALE[1] and JON HOLDER[2]

[1]*Bureau of Economic Geology, Jackson School of Geosciences, The University of Texas at Austin, University Station Box X, Austin, TX 78713, USA (e-mail: julia.gale@beg.utexas.edu)*
[2]*Department of Petroleum and Geosystems Engineering, The University of Texas at Austin, 1 University Station C0300, Austin, TX 78712, USA*

Abstract: Shale gas reservoirs are commonly produced using hydraulic fracture treatments. Microseismic monitoring of hydraulically induced fracture growth shows that hydraulic fractures sometimes propagate away from the present-day maximum horizontal stress direction. One likely cause is that natural opening-mode fractures, which are present in most mudrocks, act as weak planes that reactivate during hydraulic fracturing. Knowledge of the geometry and intensity of the natural fracture system and the likelihood of reactivation is therefore necessary for effective hydraulic fracture treatment design. Changing effective stress and concomitant diagenetic evolution of the host-rock controls fracture initiation and key fracture attributes such as intensity, spatial distribution, openness and strength. Thus, a linked structural-diagenesis approach is needed to predict the fracture types likely to be present, their key attributes and an assessment of whether they will impact hydraulic fracture treatments significantly. Steep ($>75^{\circ}$), narrow (<0.05 mm), calcite-sealed fractures are described in the Barnett Shale, north-central Texas, the Woodford Formation, west Texas and the New Albany Shale in the Illinois Basin. These fractures are weak because calcite cement grows mostly over non-carbonate grains and there is no crystal bond between cement and wall rock. In bending tests, samples containing natural fractures have half the tensile strength of those without and always break along the fracture plane. By contrast, samples with quartz-sealed fractures do not break along the fracture plane. The subcritical crack index of Barnett Shale is >100, indicating that the fractures are clustered. These fractures, especially where present in clusters, are likely to divert hydraulic fracture strands. Early, sealed, compacted fractures, fractures associated with deformation around concretions and sealed, bedding-parallel fractures also occur in many mudrocks but are unlikely to impact hydraulic fracture treatments significantly because they are not widely developed. There is no evidence of natural open microfractures in the samples studied.

Keywords: natural fractures, shale gas play, mudrock, hydraulic fracture treatment, reactivation

Shales and mudrocks form a substantial proportion of the sedimentary record and in petroleum exploration have previously been regarded as source or seal rocks. Recognition that mudrocks may also act as gas reservoirs has led to a rapid increase in production from basins across the USA (Fig. 1) and elsewhere. The Barnett Shale of the Fort Worth Basin (FWB; Table 1) in north-central Texas has been one of the most successful plays, where a combination of horizontal wells with staged, slick water hydraulic fracture treatments is the preferred completion strategy (Montgomery *et al.* 2005; Steward 2007). Friction reducers are added to the water (slick water) so that high rates can be pumped. Exploration for other shale gas reservoirs that may be exploited using a similar approach has proceeded rapidly, but it is now understood that most are sufficiently different in some key aspect to require a case-specific approach to drilling and completions. Emerging highly successful plays include the Jurassic (Kimmeridgian) Haynesville Formation in East Texas and Louisiana (Durham 2008), the Devonian Marcellus Shale in the Appalachian Basin (Curtis 2002) and the Devonian Horn River and Muskwa Shales in the Horn River Basin, NE British Columbia (Ross & Bustin 2008). The gas-generation mechanism must also be considered. Barnett Shale gas is thermogenic in origin (Hill *et al.* 2007; Jarvie *et al.* 2007), but some other successful plays, including the Antrim Shale in the Michigan Basin, produce biogenic gas and are not generally subject to hydraulic fracture stimulation (Fig. 1). Rather, the biogenic plays utilize horizontal drilling across open natural fractures in shallow parts of the basin (Curtis 2002). The purpose of this paper is to explain how natural fractures can be important in thermogenic shale gas reservoirs; biogenic gas plays are not considered further. Some commonly occurring fracture types will be reviewed and discussed as to whether they are relevant to gas production.

Montgomery *et al.* (2005) listed key attributes for a successful thermogenic shale gas reservoir on the basis of their knowledge of the Barnett Shale. These include high organic matter content (TOC), high thermal maturity, and sufficiently low clay content so that the rock is brittle enough to allow hydraulic fracture treatment. This last attribute gives rise to a problem with terminology. Many so-called 'shale gas' reservoirs, including the Barnett Shale, are not true shales but are better described as siliceous mudrocks with less than one-third clay minerals (Loucks & Ruppel 2007). Carbonate-rich mudrocks or marls can also fit the brittleness requirement; for example, the Cretaceous Niobrara Formation, a series of chalk-marl couplets, forms gas reservoirs in the Denver–Julesburg Basin (Fig. 1).

Relevance of natural fractures

Montgomery *et al.* (2005) concluded that natural fractures are not important to production in the Barnett Shale and at worst are detrimental. Their understanding was based on observations of opening-mode fractures sealed with calcite cement (Fig. 2), and they concluded, quite reasonably, that these sealed fractures could neither store nor transmit gas. The only observed fractures that are transmissive are large faults, some of which are associated with sag structures due to palaeokarst collapse in the underlying Ellenburger

VINING, B. A. & PICKERING, S. C. (eds) *Petroleum Geology: From Mature Basins to New Frontiers – Proceedings of the 7th Petroleum Geology Conference*, 1131–1140. DOI: 10.1144/0071131

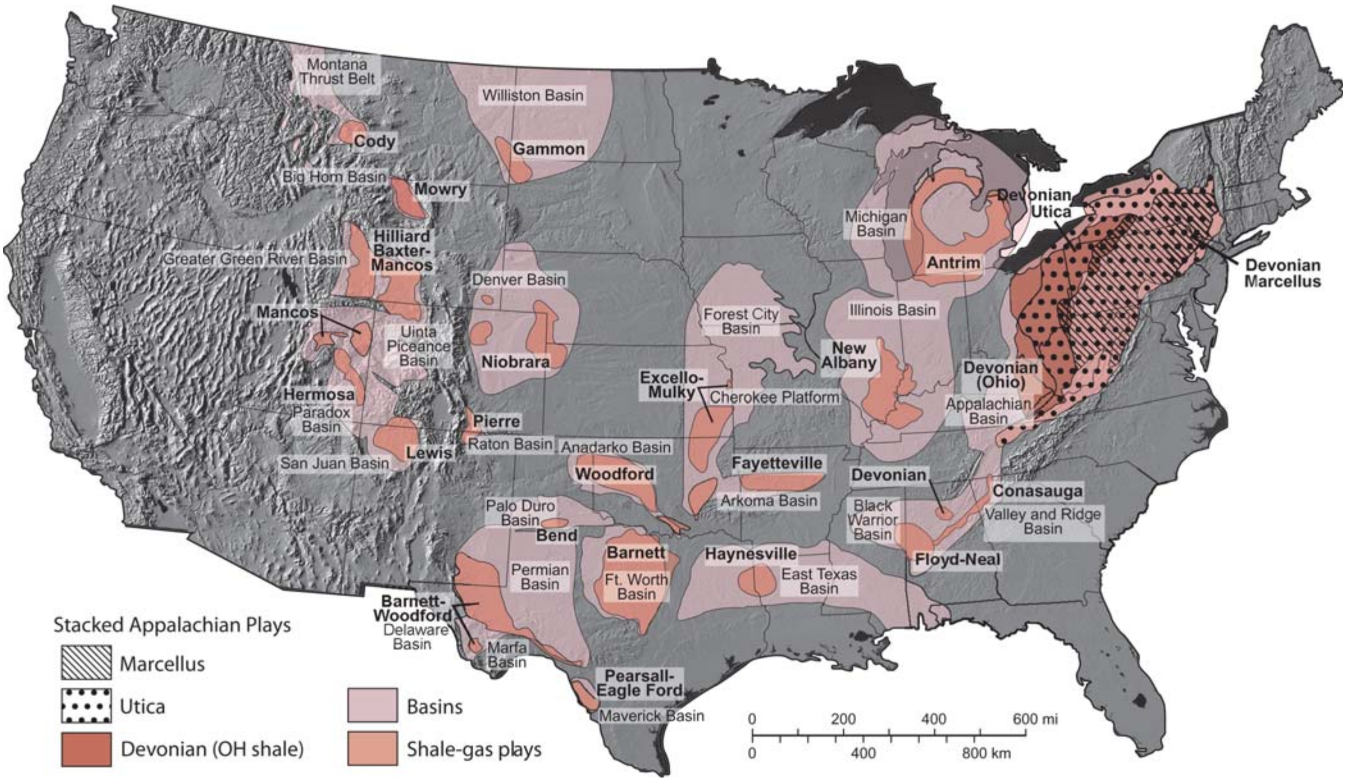

Fig. 1. Map of currently producing shale-gas reservoirs in the USA (after Energy Information Administration Map, March 2009).

Group (McDonnell *et al.* 2007). The Montgomery *et al.* (2005) conclusion that some fractures could be detrimental relates to these faults because they are thought to connect with the water-wet Ellenburger Group.

Warpinski & Teufel (1987) and Zhang *et al.* (2007) showed that mechanical discontinuities, including natural fractures and bedding, can affect hydraulic fracture propagation. On this basis, Gale *et al.* (2007) recognized that sealed fractures in the Barnett Shale might be weak planes that could reactivate in shear or opening-mode during hydraulic fracture treatment (Fig. 3). The natural fracture reactivates as the hydraulic fracture approaches, causing delamination of the cement from the wall rock. Hydraulic fracture fluid enters the opening and possibly causes further opening normal to the walls if treatment fluid pressure continues to increase (Fig. 3a, b). Once fracture reactivation has proceeded to the sealed fracture tip, the hydraulic fracture resumes growth parallel to S_{Hmax}.

Fracture origins

Processes giving rise to natural fracture sets in mudrocks include:

(1) local stress perturbations due to differential compaction and pore fluid during early burial;
(2) regional burial plus oil and gas generation and other diagenetic reactions, for example, smectite to illite conversion;
(3) regional, tectonic palaeostress;
(4) accommodation effects around major faults and folds;
(5) local structures, for example, in the FWB, fault-bounded sag features associated with underlying karst;
(6) stress release during uplift.

A mudrock reservoir may contain fractures generated by all or any subset of the mechanisms listed. Burial conditions and diagenetic alteration of the mudrock may be quite different at the time of

Table 1. Summary of cores and outcrops examined and fracture types observed

Basin	Formation	Age	No. of cores	Approx. total length (m)	Fracture types (opening-mode only)		
					Vertical planar	Vertical deformed	Horizontal sealed
Fort Worth (N)	Barnett Shale	Mississippian	5	187	Many	No	Few, local
Fort Worth (S)	Barnett Shale	Mississippian	2	4 + outcrop	Few	No	No
Delaware	Barnett Shale	Mississippian	1	91	Many	Few	Few
Fort Worth (S)	Smithwick Fm.	Pennsylvanian	2	58	Yes	No	Multiple swarms
Delaware	Woodford Fm.	Devonian	20	171	Some	Few	No
Illinois	New Albany Shale	Devonian	6	210 + outcrop	Many	Some	No
Denver–Julesberg	Niobrara Fm.	Cretaceous	2	105 + outcrop	Many	No	Few
Gulf of Mexico	Austin Chalk	Cretaceous	3	159 + outcrop	Many	Few	No

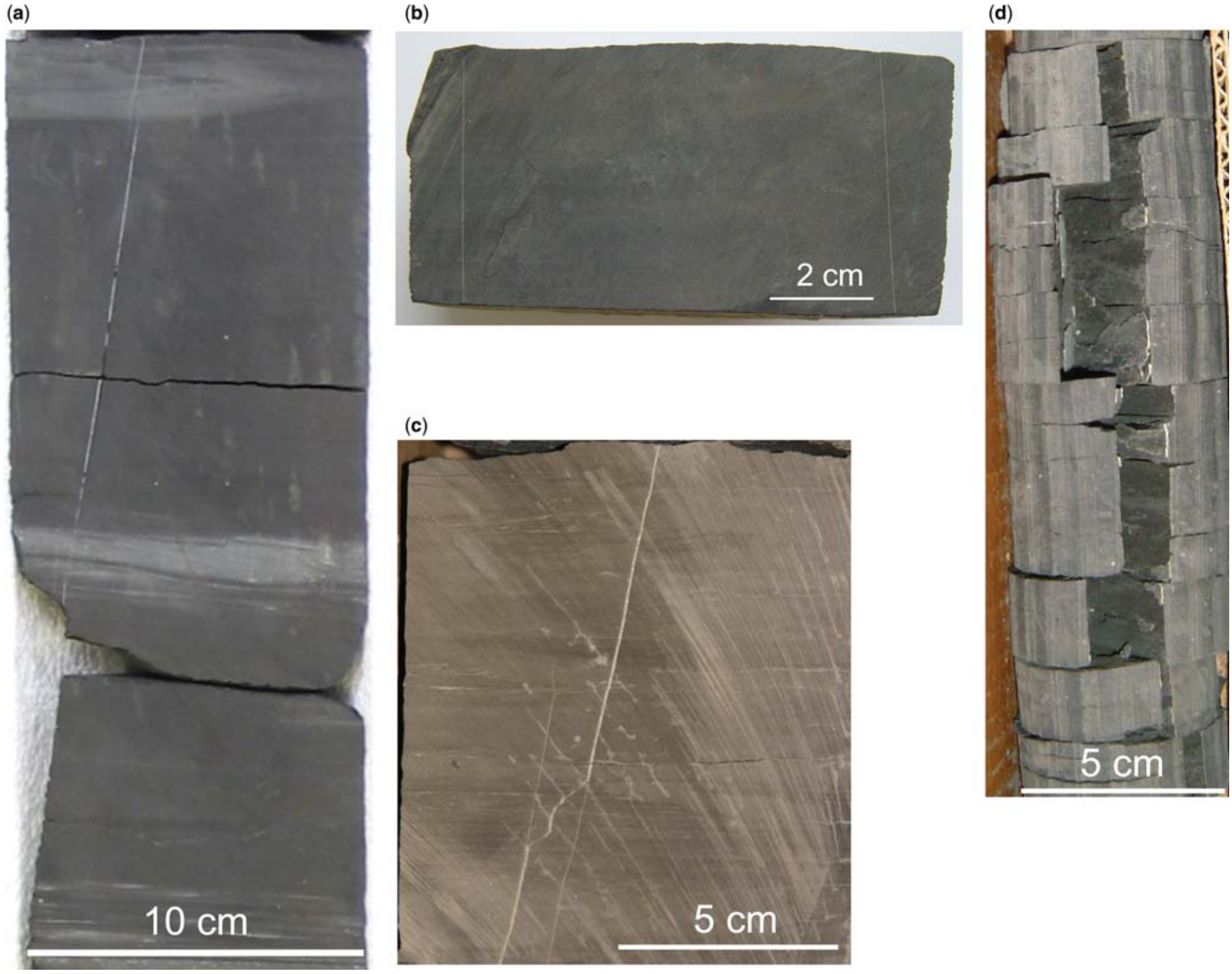

Fig. 2. Tall calcite-sealed fractures: (**a**) Barnett Shale, FWB; (**b**) Woodford Shale, Permian Basin; (**c**) New Albany Shale, Illinois Basin; and (**d**) Smithwick Formation, southern FWB. This type of fracture is prone to reactivation during hydraulic fracture treatments.

formation of each set. The interplay of mechanical and chemical processes during growth of a fracture set, termed *structural diagenesis*, governs propagation and sealing processes (Laubach *et al.* 2004; Olson *et al.* 2007). Difference in ambient conditions and rock properties at the time of formation of each set leads to differences in intensity, geometry and sealing attributes, and spatial arrangement.

Fracture types

Several shale gas reservoirs have been studied using cores and outcrops (Fig. 4; Table 1). The natural fractures observed are grouped into three categories: sub-vertical deformed, bedding parallel and sub-vertical planar. We confine our outcrop observations to cemented fractures.

Although we observed unmineralized joint sets in some outcrops, we did not include these as part of this study. Other authors have associated joint sets with fractures in the subsurface. For example, Lash & Engelder (2008) described joints in the Marcellus Shale, and Carr (1981) and Comer *et al.* (2006) described lineaments, joints and fractures in the New Albany Shale (Table 1). We are of the opinion that unmineralized joints are not representative of structures in the subsurface at depths sufficient for gas thermogenesis. Observations in core indicate that natural fractures at these depths have partial or complete mineralization on their walls, even if the mineralization constitutes only a very thin veneer of cement (Hooker *et al.* 2009). Moreover, where the natural fractures are parallel to present day S_{Hmax}, reactivation of natural fractures during drilling is common, such that the tips are unmineralized whereas the main body of the fracture contains significant cement. There are examples in thermogenic gas shales of microfractures with bituminous fill or coatings and otherwise no cement (Lash & Engelder 2005), but bitumen is known as a cement inhibitor (e.g. Marchand *et al.* 2000). Unmineralized opening-mode fractures (joints) may be important in shallow biogenic shale gas plays such as the Antrim or parts of the New Albany shale, where temperatures are too low for significant cement growth, but here we focus on thermogenic gas shales. Unmineralized opening-mode fractures could also be present in tectonically active regions, for example the Wabash Valley Fault System in the central part of the Illinois basin (New Albany Shale), where there would have been too little time for significant cementation in recently formed fractures. These fractures, if present, would require a separate systematic study to distinguish them from drilling-induced fractures. The fractures we observed in cores from wells near the Wabash Valley Fault System (Figs 2c & 4b) are partly cemented with quartz, pyrite and calcite.

Deformed fractures

Sealed fractures that have been subsequently deformed are present in several mudrock formations. Vertical shortening may be manifested by folding – for example, calcite-sealed fractures in the Woodford Formation in the Permian Basin (Table 1; Fig. 5a) or

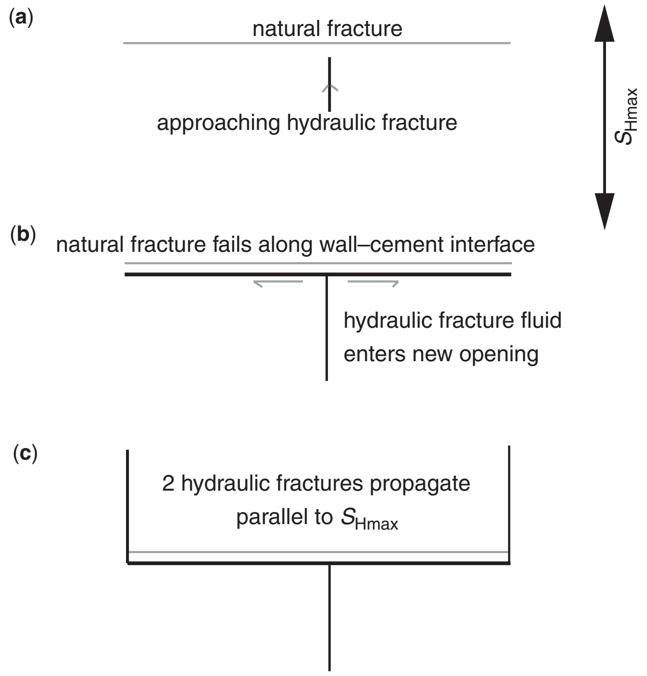

Fig. 3. Simplified, schematic diagram of interaction of a hydraulic fracture with a pre-existing natural fracture. (**a**) The natural fracture (grey) is shown normal to the maximum horizontal stress, S_{Hmax}. The hydraulic fracture (black) grows parallel to S_{Hmax}. (**b**) Natural fracture reactivation causes delamination of the cement from the wall rock. (**c**) Resumption of hydraulic fracture growth parallel to S_{Hmax}. The original single strand in diagram (a) is now two strands.

folding and faulting in dolomite veins in outcrops and cores of the lower part (Blocher Member) of the New Albany Shale in the Illinois Basin (Fig. 5b–d). It is likely that these fractures formed at an early stage of lithification. The rock was brittle enough to fracture, but subsequent compaction shortened the fracture and deformed the host-rock fabric around it. Fractures of this group have irregular walls because they are deformed and are therefore less likely to reactivate. They are commonly confined to mechanical layers on the order of a few centimetres to half a metre. Larger examples in the lower part of the New Albany Shale preserve centimetre-wide bitumen-filled pores, but they lie well below the main reservoir interval, and the bitumen has an origin different from that of the organic matter in the shales (Dumitrescu *et al.* 2004). This fracture type is not likely to be significant for gas production on a reservoir scale but could provide some local enhancement if the fractures coincided with the producing interval.

Bedding-parallel fractures

Bedding-parallel fractures include sealed macrofractures, which we describe here, and sealed microfractures that are observable in thin sections and have been reported in the literature. Speculation about the presence of open, bedding-parallel microfractures is reserved for the Discussion section because no such fractures were observed.

Sealed bedding-parallel macrofractures that can be seen without visual aid in core or outcrop samples are present in many mudrocks, but they vary considerably in intensity and in spatial distribution. They were not seen in the Barnett Shale cores from the FWB that were described by Gale *et al.* (2007). Examples do occur, however, in other FWB Barnett Shale cores, where they are most commonly associated with deformed laminae around the margins of carbonate concretions and short, vertical fractures between the concretions (Fig. 6a) (Gale, unpublished data). Local fractures associated with concretions are most likely formed by mechanism 1. Rare bedding-parallel fractures in the Barnett Shale in the Delaware Basin, west Texas, contain petroleum fluid inclusions in fibrous barite. In the Pennsylvanian Smithwick Formation from the southern FWB, swarms of bedding-parallel fractures are sealed with fibrous calcite (Fig. 6b). These most likely formed by mechanism 2. Cobbold & Rodrigues (2007) interpreted fibrous bedding-parallel veins in the Jurassic 'Shales-with-Beef' of SW England as being formed as a result of *seepage forces* that develop in response to an overpressure gradient.

Bedding-parallel fractures in outcrops of the Barnett Shale in central Texas are sealed with gypsum (Fig. 6c). Gypsum is not present as a fracture-sealing cement in the subsurface so these fractures are not considered to be representative of fractures in the reservoir, highlighting the potential danger in using outcrops as direct analogues to the subsurface. The gypsum-filled fractures probably developed during uplift and exposure of the black, pyrite-bearing mudrocks to oxidizing groundwater. When pyrite is oxidized, sulphuric acid is liberated, and this acid most likely reacted with calcite to produce gypsum. Calcite is present as concretions and discontinuous layers in the Barnett Shale at this location. Reactions are as follows:

$$4FeS_2 + 15O_2 + 14H_2O = 4Fe(OH)_3 + 8H_2SO_4 \quad (1)$$

and

$$H_2SO_4 + CaCO_3 + H_2O = CaSO_4 \cdot 2H_2O + CO_2 \quad (2)$$

Sealed bedding-parallel microfractures have been noted in several mudrocks. For example, Lash & Engelder (2005) observed bedding-parallel, bitumen-filled microfractures within clay laminae in the Upper Devonian Dunkirk Shale, western New York, which they interpreted as being due to overpressure during conversion of kerogen to bitumen (mechanism 2). With respect to their effect on production, because they are typically less abundant than sub-vertical sealed fractures, we contend that the sealed bedding-parallel fractures are of secondary importance.

Sub-vertical sealed planar fractures

The most common fractures observed in mudrock cores are the straight-sided, calcite-sealed planar fractures that were described in the Barnett Shale in the FWB by Gale *et al.* (2007). These are present in many other mudrocks, including the Woodford Formation and New Albany Shale and the Pennsylvanian Smithwick Formation (Fig. 2). These fractures are not deformed and most likely form as a result of mechanism 2 or 3, developing after compaction is complete.

Gale & Holder (2008) conducted bending tests on Barnett Shale samples and found that samples with calcite-sealed natural fractures have approximately half the tensile strength of the host rock. In these tests the sample always failed along the natural fracture. The reason for the weakness is that there is no physical bond between the calcite cement and the siliceous mudrock wall rock; the calcite cement simply grows over the wall rock. Calcite precipitates easily in this manner, unlike quartz and dolomite, which tend to require an existing grain of that mineral on which to precipitate (Lander *et al.* 2008; Gale *et al.* 2009). Although these fractures are dominantly sealed with calcite, some are sealed with other minerals, including quartz, albite, dolomite, barite and pyrite (Gale *et al.* 2007). In the example shown, quartz cement has grown over quartz grains in the wall rock, forming incomplete mineral bridges (Fig. 7). Albite cement makes up most of the rest of the fracture fill. Our hypothesis is that this part of the fracture

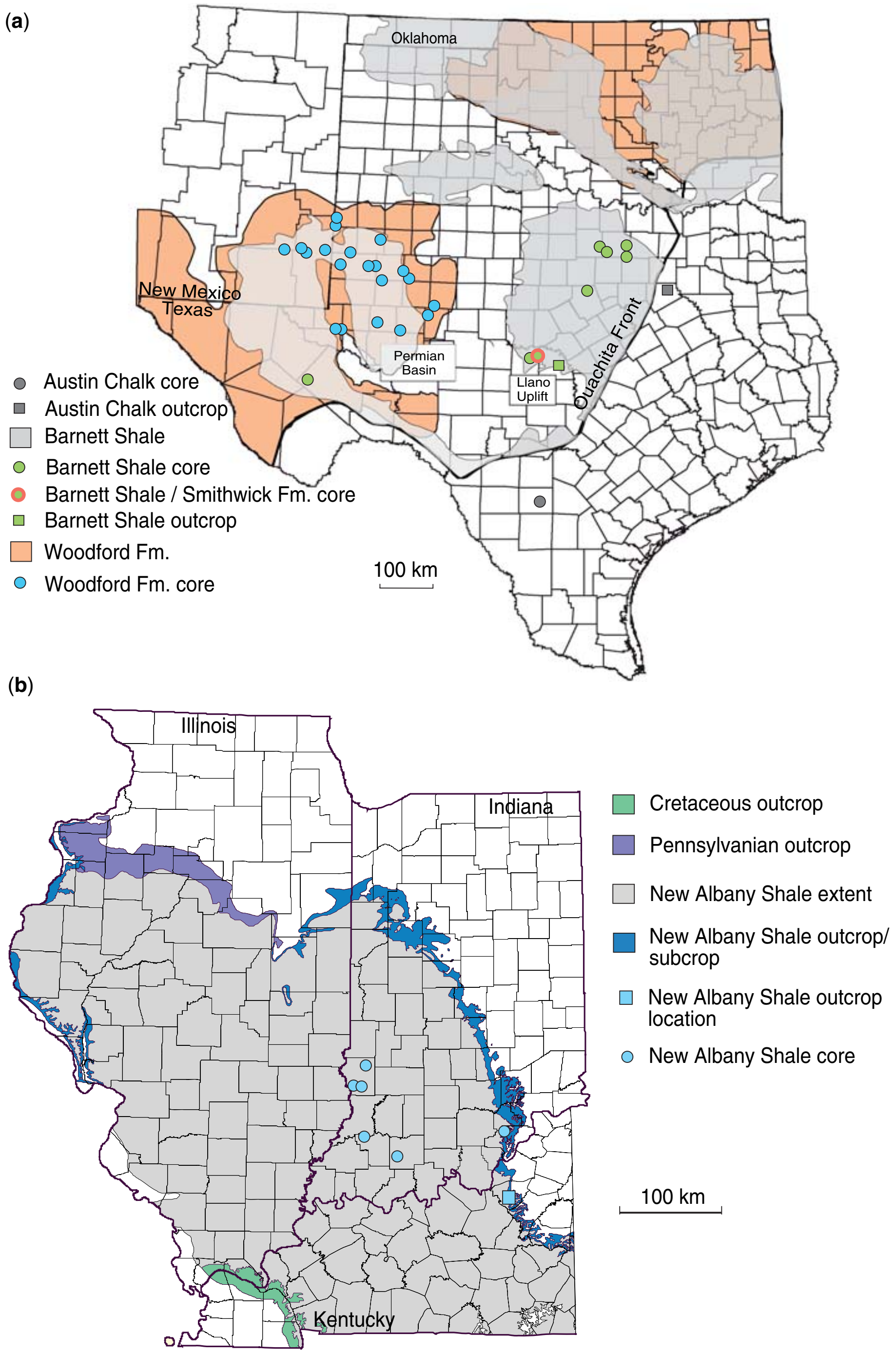

Fig. 4. Maps showing locations of cores and outcrops examined. (**a**) Texas locations; (**b**) New Albany Shale locations.

is stronger than the calcite-filled fractures tested by Gale & Holder (2008) and that, more generally, fractures sealed with cements that template onto grains in the wall rock will be stronger than those that simply precipitate over a surface regardless of composition. We could not test the fracture shown (Fig. 7) because of its small extent, but tests on other samples so far support the hypothesis. For example, in a chert–siliceous mudrock interbedded sequence (Woodford Formation), where the mineral fill is quartz, tested samples did not break along natural fracture planes but broke along planes away from the fracture. By contrast, calcite-sealed fractures in siliceous mudrock are consistently weak. In addition to quantitative bending tests conducted by Gale & Holder (2008), observation of calcite-sealed fractures in cores commonly reveals the cement–wall rock interface to be a weakness, along which the core breaks. In extreme cases the cement may part from both walls, leaving it as a completely detached thin sliver (Fig. 8).

Subcritical crack growth

Subcritical fracturing occurs when fractures propagate, even though the stress intensity at the crack tip is well below the fracture toughness of the material. They propagate at velocities several orders of magnitude slower than the dynamic rupture velocity of critical cracks. The process is assisted by chemical weakening at the crack tip (Lawn 1975; Atkinson & Meredith 1981; Atkinson 1984). Fracture patterns can be predicted from geomechanical models of subcritical fracture growth (Olson 2004). Fracture development and the geometry of the patterns that form are sensitive to mechanical layer thickness, fracture toughness of the rock, Young's

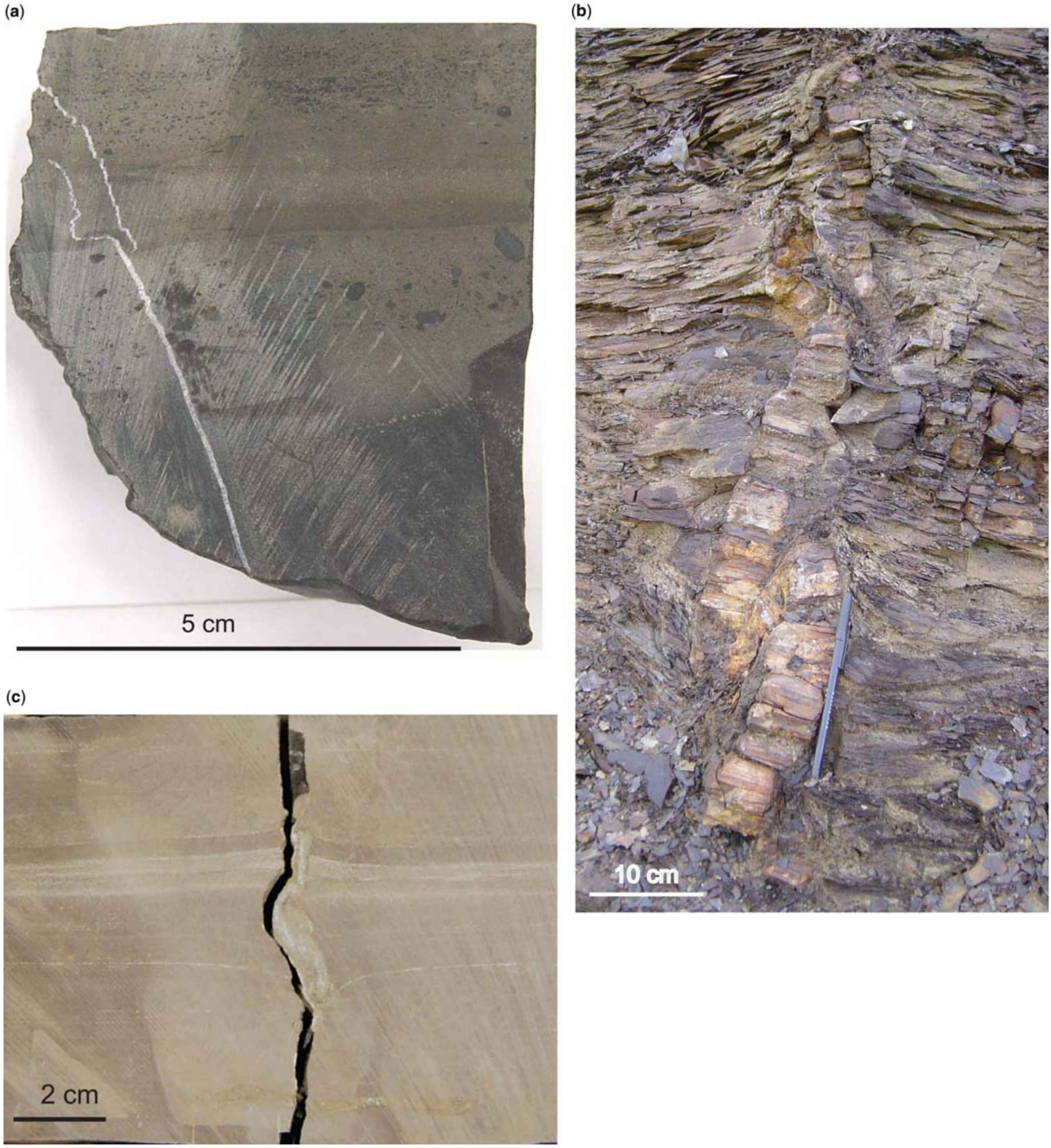

Fig. 5. (**a**) Folded calcite-sealed fracture in core from the Woodford Formation in the Permian Basin. (**b**) Folded dolomite veins in an outcrop of the lower part (Blocher Member) of the New Albany Shale. (**c**) Folded and faulted dolomite vein also with surrounding bedding laminae compaction in New Albany Shale core, Indiana (855 m depth).

modulus, Poisson's ratio, *in situ* stress anisotropy and the subcritical crack index. Values of these parameters at the time of fracturing are the main input to the model. Holder *et al.* (2001) adapted a dual-torsion-beam test apparatus and procedure for measuring subcritical crack index in sedimentary rocks. The subcritical index, *n*, is the slope of a curve on a plot of log load applied in the test v. log crack propagation velocity. We used their test procedure to measure subcritical indices for several shale samples from two Barnett Shale cores. Samples from the Mitchell Energy #2 T. P. Sims core were not distinguished by lithology; they are all dark, laminated mudrock, but there are no compositional data for the samples. Samples from a second core, core A, were selected across a wide range of lithologies, including light, carbonate-rich layers and dark layers (Fig. 2a). Subcritical crack indices for samples from both these Barnett Shale cores are mostly >100 and the range of values for the two cores is similar. The highest values occur in the more carbonate-rich facies in core A (Fig. 9) (Gale *et al.* 2007; Gale & Holder 2008). The range of subcritical index values for the Mitchell Energy #2 T. P. Sims core samples suggests these are of variable composition.

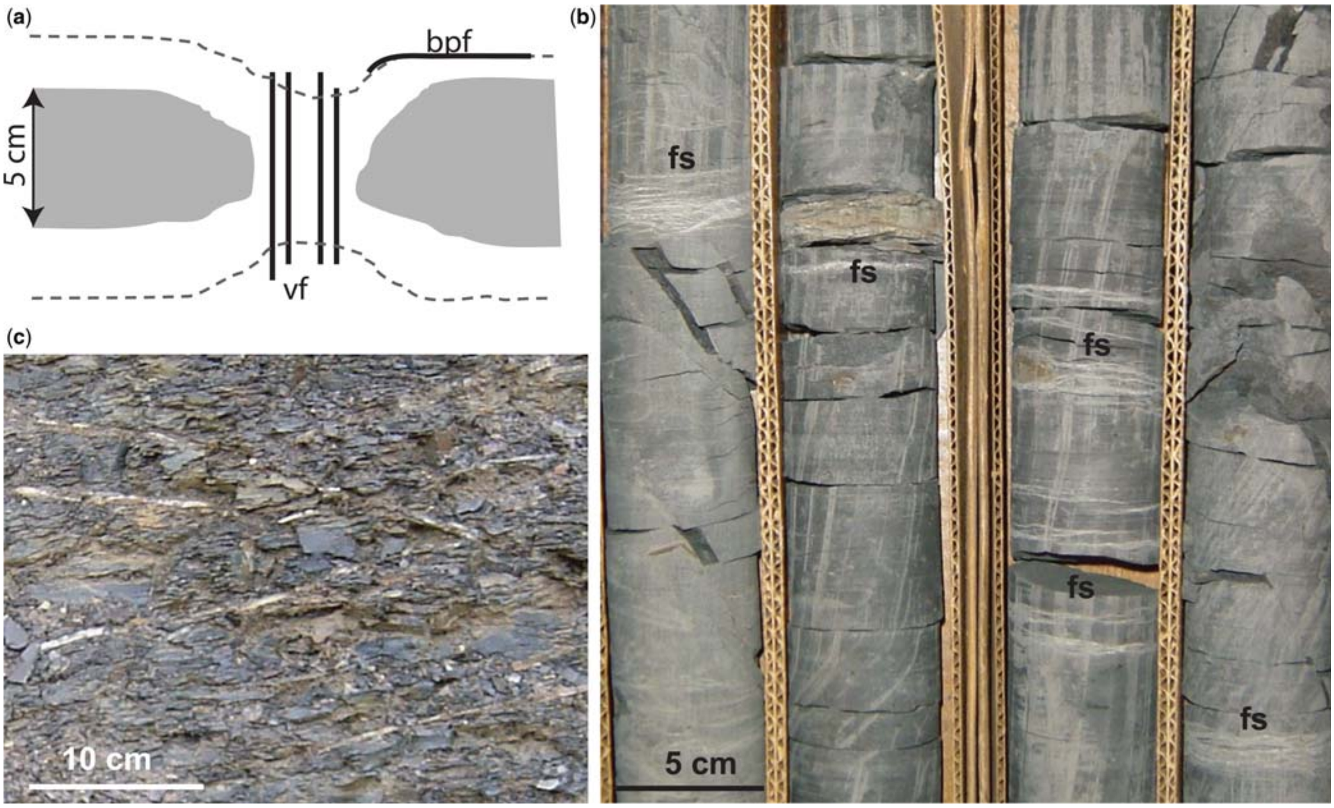

Fig. 6. (**a**) Sketch of bedding-parallel fractures (bpf) associated with carbonate concretions (grey) and sub-vertical fractures (vf) in the zone between the concretions. (**b**) Bedding-parallel fracture swarms (fs) sealed with fibrous calcite in core from the Smithwick Formation, central Texas. (**c**) Bedding-parallel gypsum-filled fractures in Barnett Shale in a quarry in San Saba County, central Texas.

The subcritical index measured from a present-day sample is a fair representation of the subcritical index at the time of formation of tall, planar, calcite-sealed fractures. Because these fractures show no evidence of compaction, they probably formed after the shale was fully compacted, and the host rock has probably not altered much from the time of fracture growth to present day. Geomechanical modelling, using a subcritical index that is >100 as an input parameter, predicts that fractures are clustered, with spaces between large fracture clusters on the order of several times the mechanical layer thickness (Olson 2004). Gale *et al.* (2007) concluded that if the total Barnett Shale thickness of 200 m is taken as the upper boundary to mechanical layer thickness, the distance between large clusters may be several hundred metres. The narrow, sealed fractures observed in core are distributed between clusters, possibly reflecting smaller internal mechanical layers or growth within mechanical layer boundaries. For shales with a

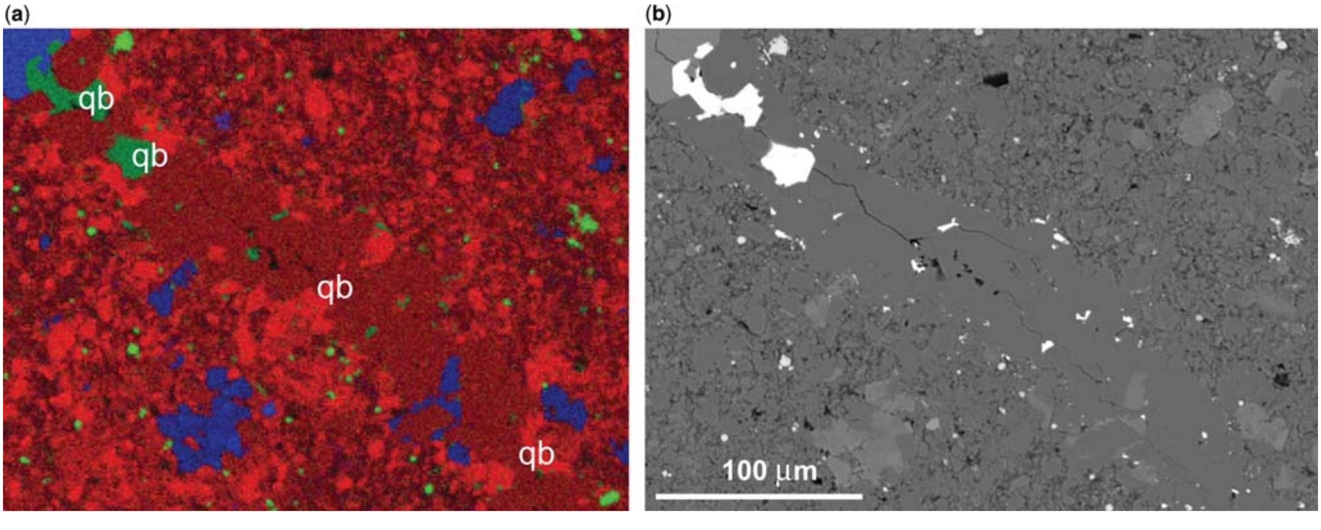

Fig. 7. Quartz and albite fracture fill in a Barnett Shale mudrock sample. (**a**) False colour combination of three greyscale element maps. Quartz is bright red, albite is dull red, barite is green and calcite is blue. Growths of quartz, interpreted as incomplete cement bridges (qb), overgrow groups of quartz grains in the wall rock. (**b**) The fracture wall is best differentiated in the backscattered electron image of the same area shown in (a). The quartz bridges in the fracture are overgrowing areas of quartz grains in the wall rock.

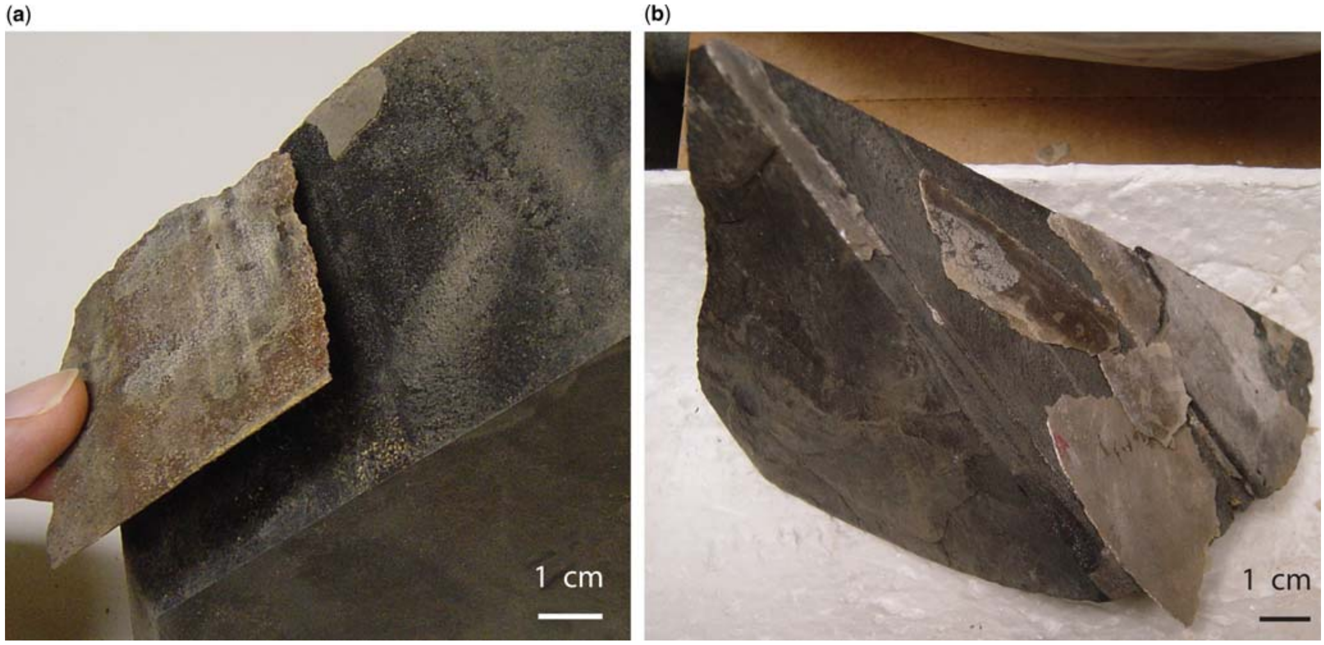

Fig. 8. (**a, b**) Calcite-sealed fractures in a New Albany Shale core where the cement fill has detached from both fracture walls during core handling.

moderate subcritical index, a less strongly clustered pattern would be expected, with dominant fractures spaced closer to the mechanical layer thickness.

Fracture size distributions and open fractures

Although the narrow, steep fractures of the most common type are sealed and probably do not enhance reservoir permeability, their population may follow a power-law size distribution. By analogy with fractured chalks we infer that the largest fractures in this distribution would be open and present in widely spaced clusters, several hundred feet apart. This inference is made on the basis of observed power distributions of opening-mode fractures in the Austin Chalk (Gale 2002), where the largest fractures (>11 mm) are partly open, whereas the smaller fractures (<11 mm wide) are sealed. A similar relationship is seen in the Niobrara Formation, although the crossover size from sealed to partly open is smaller (~3 mm) (Fig. 10). The crossover size of a given population, termed *emergent threshold* by Laubach (2003), depends partly on the composition of the cement. For a fracture to seal, rate of cement growth is in competition with fracture opening rate (Laubach *et al.* 2004). That is, for identical temperatures and opening rates, fracture populations sealed with fast-growing calcite have a larger emergent threshold than those sealing with quartz. Indeed, fractures as narrow as 4 mm in the Barnett Shale in the Delaware Basin retain porosity, being only partly sealed with quartz (Gale 2008), whereas calcite-sealed fractures of this width in the Barnett Shale in the FWB are completely sealed.

Discussion

Effect of natural fractures on hydraulic fracture treatment efficiency

Gale *et al.* (2007) concluded that the effect of natural fracture reactivation would be beneficial to gas production because it would

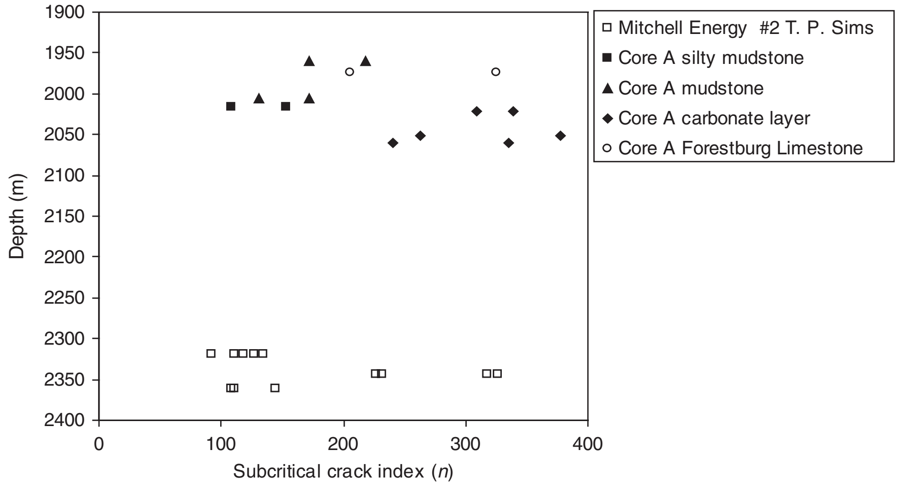

Fig. 9. Plot of subcritical crack index measurements v. depth for samples from two Barnett Shale cores, the Mitchell Energy #2 T. P. Sims and a second core, labelled core A, from the FWB, north-central Texas.

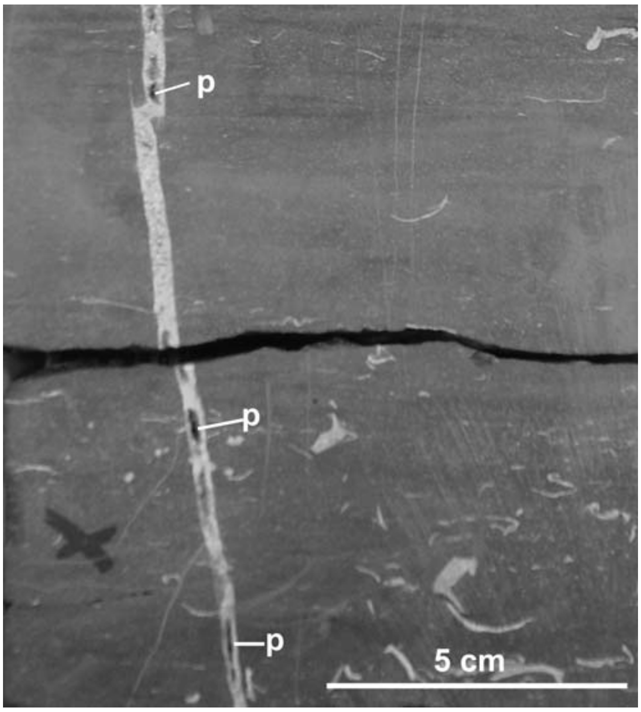

Fig. 10. Fracture porosity (p) in Niobrara Formation core from the Denver–Julesberg Basin (920 m depth). The fracture is otherwise sealed with calcite.

serve to multiply the number of hydraulic fracture strands and, thus, the total surface area, connected to the host rock (Fig. 3). This might not be the case. Doubling of the number of hydraulic fracture strands will not lead to doubling of surface area because increase in the number of strands will be offset by decrease in individual strand length as the fracture treatment energy is dissipated through more fractures. The movement of proppant through such a tortuous fracture network is also problematic. Figure 3 is simplistic because it only considers the case where the natural fracture is opened. Whether hydraulic fractures arrest at, cross over, divert at or reactivate natural fractures is a function of many factors, including relative strength of natural fracture planes and orientation with respect to the stress field (Olson 2008). Spreading the treated zone normal to S_{Hmax} might not be desirable if a staged hydraulic fracture treatment is planned because the rock volume expected to be treated by each successive stage could already have been fractured. New fractures might then link up to old ones, yielding less freshly broken shale surface area than anticipated. Moreover, the volumes of rock between the diverted fracture strands (Fig. 3c) remain unstimulated and represent lost pay. In any case, prediction of the hydraulic fracture geometry resulting from interaction with natural fractures is desirable.

Open microfractures

On the basis of production rates and volumes, some speculate that storage and permeability in mudrocks must be due to an open microfracture network (e.g. Bowker 2003). Most commonly this network is thought to be bedding parallel because of the known bedding-parallel weakness of mudrock. The only open microfractures we have seen are in thin sections and are due to section damage during preparation. Reed & Loucks (2007) examined many samples of Barnett and Woodford Shale using SEM-based techniques, some on argon-ion-milled surfaces, in search of microfractures and/or pores, but they saw no evidence of an open microfracture network in these formations. Rather, gas storage is accommodated partly by micro- to nanosized pores (free gas) and partly by sorption of methane and other molecules in organic matter and clay particles (Ruppel & Loucks 2008; Ross & Bustin 2009). The mechanism by which free or sorbed gas can move from its storage location into a hydraulic fracture network remains a challenging problem. Bedding-parallel weaknesses could allow transient openings, but unless cement or bitumen remains along the fracture, there would be no record of its presence (e.g. Lash & Engelder 2005). Of course it is well known during drilling, especially in the presence of reactive fluids, that shales and mudrocks can fracture, but this fracturing is due to the drilling process rather than a natural event. Drilling and sample preparation commonly cause fractures to form parallel to bedding, and these may be wrongly interpreted as fractures open in the subsurface.

Conclusions

Host-rock and fracture characteristics in shale gas reservoirs are diverse, and the role that natural fractures play must be considered case by case. Some common relationships can, however, be stated as general principles:

(1) Planar, sub-vertical, calcite-sealed fractures in siliceous mudrocks are weak and may reactivate during hydraulic fracture treatments. These form the most common type of natural fracture in many reservoirs. Interaction with hydraulic fracture networks may be beneficial or detrimental.
(2) Planar, sub-vertical fractures completely sealed with quartz can produce strong planes. Hydraulic fractures could arrest at these planes, causing premature screen-out of the fracture treatment.
(3) Early formed fractures are commonly deformed during host-rock compaction. They have irregular shapes and are commonly confined to mechanical layers of the order of a few centimetres to half a metre. These fractures are not likely to be significant for gas production on a reservoir scale, but they could provide some local enhancement if they are open and coincide with the producing interval.
(4) Horizontal fractures are preserved in some mudrocks. They are now sealed with bitumen or mineral cements, some of which have petroleum fluid inclusions in them. These fractures are evidence of fracturing during the hydrocarbon cracking process. Other mudrocks such as the Barnett may have had similar transient fractures during cracking, but they are not preserved.
(5) Large opening-mode natural fractures may be open above the emergent threshold for that fracture set. If the subcritical index is high, which is typical in siliceous mudrocks, then the large fractures are likely to be clustered, with spaces between clusters being several times the mechanical layer thickness.
(6) There is no evidence of open microfracture networks in the mudrocks examined in this study. In thin sections, open microfractures with no cement or hydrocarbon along them, if present, are likely to have been caused by drilling or sample damage and are not representative of structures in the subsurface.

J. F. W. Gale was supported in part by a GDL Foundation Fellowship. The principal funding groups for this work are the Fracture Research and Application Consortium at The University of Texas at Austin, the State of Texas Advanced Resource Recovery program, and the Permian Basin Geological Synthesis Project, the latter two being Bureau of Economic Geology projects. Funding for work on the New Albany Shale is through the Research Partnership to Secure Energy for America. R. Reed provided images for Figure 7. J. Olson and S. Laubach provided insight and discussion of fracture processes and helpful reviews were given by Robert Gatliff and an anonymous reviewer. Publication is authorized by the Director, Bureau of Economic Geology.

References

Atkinson, B. K. 1984. Subcritical crack growth in geologic materials. *Journal of Geophysical Research*, **89**, 4077–4114.

Atkinson, B. K. & Meredith, P. G. 1981. Stress corrosion cracking of quartz. A note on the influence on chemical environment. *Tectonophysics*, **77**, T1–T11.

Bowker, K. A. 2003. Recent development of the Barnett Shale play, Fort Worth Basin. *West Texas Geological Society Bulletin*, **42**, 4–11.

Carr, D. D. 1981. Lineament analysis. *In*: Hasenmueller, N. R. & Woodard, G. S. (eds) *Studies of the New Albany Shale (Devonian and Mississippian) and Equivalent Strata in Indiana*. US Department of Energy, contract number DE-AC 21-76MC 05204, 62–69.

Cobbold, P. R. & Rodrigues, N. 2007. Seepage forces, important factors in the formation of horizontal hydraulic fractures and bedding-parallel fibrous veins ('beef' and 'cone-in-cone'). *Geofluids*, **7**, 313–322.

Comer, J. B., Hasenmueller, N. R., Mastalerz, M. D., Rupp, J. A., Shaffer, N. R. & Zuppann, C. W. 2006. The New Albany Shale gas play in southern Indiana. Program with Abstracts, 2006 Eastern Section. *American Association of Petroleum Geologists 35th Annual Meeting, Buffalo, NY*, 17.

Curtis, J. B. 2002. Fractured shale–gas systems. *American Association of Petroleum Geologists Bulletin*, **86**, 1921–1938.

Dumitrescu, M., Finkelstein, D. B., Lazar, R., Schieber, J. & Brassell, S. C. 2004. Origin and history of bitumen in geodes of the New Albany Shale. *In*: Schieber, J. & Lazar, R. (eds) *Devonian Black Shales of the Eastern U.S.* Field Guide for the 2004 Annual Field Conference of the Great Lakes Section of the Society for Sedimentary Geology, Indiana Geological Survey, 61–67.

Durham, L. 2008. Haynesville, lower Tertiary the latest allures; Gulf Coast still revealing its charms. *American Association of Petroleum Geologists Explorer*, **29**, 9.

Gale, J. F. W. 2002. Specifying lengths of horizontal wells in fractured reservoirs. *Society of Petroleum Engineers Reservoir Evaluation and Engineering*, **5**, 266–272.

Gale, J. F. W. 2008. Natural fractures in the Barnett Shale in the Delaware Basin, Pecos Co., West Texas: comparison with the Barnett Shale in the Fort Worth Basin. *West Texas Geological Society Fall 2008 Symposium, Proceedings Abstracts*. WTGS digital publication 08–120, 13.

Gale, J. F. W. & Holder, J. 2008. Natural fractures in the Barnett Shale: constraints on spatial organization and tensile strength with implications for hydraulic fracture treatment in shale-gas reservoirs. *Proceedings of the 42nd US Rock Mechanics Symposium*. Paper no. ARMA 08-96.

Gale, J. F. W., Reed, R. M. & Holder, J. 2007. Natural fractures in the Barnett Shale and their importance for hydraulic fracture treatments. *American Association of Petroleum Geologists Bulletin*, **91**, 603–622.

Gale, J. F. W., Lander, R. H., Reed, R. M. & Laubach, S. E. 2009. Modeling fracture porosity evolution in dolostone. *Journal of Structural Geology*; doi: 10.1016j.jsg.2009.04.018.

Hill, R. J., Jarvie, D. M., Pollastro, R., Henry, M. & King, J. P. 2007. Geochemistry of oils and gases from the Fort Worth Basin, USA. *American Association of Petroleum Geologists Bulletin*, **91**, 445–473.

Holder, J., Olson, J. E. & Philip, Z. 2001. Experimental determination of subcritical crack growth parameters in sedimentary rock. *Geophysical Research Letters*, **28**, 599–602.

Hooker, J. N., Gale, J. F. W., Gomez, L. A., Laubach, S. E., Marrett, R. & Reed, R. M. 2009. Aperture-size scaling variations in a low-strain opening-mode fracture set, Cozzette Sandstone, Colorado. *Journal of Structural Geology*, **31**, 707–718.

Jarvie, D. M., Hill, R. J., Ruble, T. E. & Pollastro, R. 2007. Unconventional shale-gas systems: the Mississippian Barnett Shale of north-central Texas as one model for thermogenic shale-gas assessment. *American Association of Petroleum Geologists Bulletin*, **91**, 475–499.

Lander, R. H., Larese, R. E. & Bonnell, L. M. 2008. Toward more accurate quartz cement models – the importance of euhedral vs. non-euhedral growth rates. *American Association of Petroleum Geologists Bulletin*, **92**, 1537–1563.

Lash, G. G. & Engelder, T. 2005. An analysis of horizontal microcracking during catagenesis: example from the Catskill delta complex. *American Association of Petroleum Geologists Bulletin*, **89**, 1433–1449.

Lash, G. G. & Engelder, T. 2008. Tracking the burial and tectonic history of Devonian shale of the Appalachian Basin by analysis of joint intersection style. *Geological Society of America Bulletin*, **121**, 265–277.

Laubach, S. E. 2003. Practical approaches to identifying sealed and open fractures. *American Association of Petroleum Geologists Bulletin*, **87**, 561–579.

Laubach, S. E., Reed, R. M., Olson, J. E., Lander, R. H. & Bonnell, L. M. 2004. Coevolution of crack-seal texture and fracture porosity in sedimentary rocks: cathodoluminescence observations of regional fractures. *Journal of Structural Geology*, **26**, 967–982.

Lawn, B. R. 1975. An atomistic model of kinetic crack growth in brittle solids. *Journal of Materials Science*, **10**, 469–480.

Loucks, R. G. & Ruppel, S. C. 2007. Depositional setting and lithofacies of the Mississippian Deepwater Barnett Shale in the Forth Worth Basin, Texas. *American Association of Petroleum Geologists Bulletin*, **91**, 579–601.

Marchand, A. M. E., Haszeldine, R. S., Macaulay, C. I., Swennen, R. & Fallick, A. E. 2000. Quartz cementation inhibited by crestal oil charge; Miller deep water sandstone, UK North Sea. *Clay Minerals*, **35**, 201–210.

McDonnell, A., Loucks, R. G. & Dooley, T. 2007. Quantifying the origin and geometry of circular sag structures in northern Fort Worth Basin, Texas: paleocave collapse, pull-apart fault systems, or hydrothermal alteration? *American Association of Petroleum Geologists Bulletin*, **91**, 1295–1318.

Montgomery, S. L., Jarvie, D. M., Bowker, K. A. & Pollastro, R. M. 2005. Mississippian Barnett Shale, Fort Worth basin, north-central Texas: gas–shale play with multi-trillion cubic foot potential. *American Association of Petroleum Geologists Bulletin*, **89**, 155–175.

Olson, J. E. 2004. Predicting fracture swarms – the influence of subcritical crack growth and the crack-tip process zone on joint spacing in rock. *In*: Cosgrove, J. W. & Engelder, T. (eds) *The Initiation, Propagation, and Arrest of Joints and Other Fractures*. Geological Society, London, Special Publications, **231**, 73–87.

Olson, J. E. 2008. Multi-fracture propagation modeling: applications to hydraulic fracturing in shales and tight gas sands. *Proceedings of the 42nd US Rock Mechanics Symposium*. Paper no. ARMA 08-327.

Olson, J. E., Laubach, S. E. & Lander, R. H. 2007. Combining diagenesis and mechanics to quantify fracture aperture distributions and fracture pattern permeability. *In*: Lonergan, L., Rawnsley, K. & Sanderson, D. (eds) *Fractured Reservoirs*. Geological Society, London, Special Publications, **270**, 97–112.

Reed, R. M. & Loucks, R. G. 2007. Imaging nanoscale pores in the Mississippian Barnett Shale of the northern Fort Worth Basin (abstract). *Abstracts Volume, American Association of Petroleum Geologists Annual Convention*, **16**, 115.

Ross, D. J. K. & Bustin, R. M. 2008. Characterizing the shale gas resource potential of Devonian–Mississippian strata in the Western Canada sedimentary basin: application of an integrated formation evaluation. *American Association of Petroleum Geologists Bulletin*, **92**, 87–125.

Ross, D. J. K. & Bustin, R. M. 2009. The importance of shale composition and pore structure upon gas storage potential of shale gas reservoirs. *Marine and Petroleum Geology*, **26**, 916–927.

Ruppel, S. C. & Loucks, R. G. 2008. Black mudrocks: lessons and questions from the Mississippian Barnett Shale in the southern Midcontinent. *The Sedimentary Record*, **6**, 4–8.

Steward, D. B. 2007. *The Barnett Shale Play, Phoenix of the Fort Worth Basin: A History*. The Fort Worth Geological Society & The North Texas Geological Society.

Warpinski, N. R. & Teufel, L. W. 1987. Influence of geologic discontinuities on hydraulic fracture propagation. *Journal of Petroleum Technology*, **39**, 209–220.

Zhang, X., Jeffrey, R. G. & Thiercelin, M. 2007. Effects of frictional geological discontinuities on hydraulic fracture propagation. *Proceedings of the Society of Petroleum Engineers Hydraulic Fracturing Technology Conference*, Paper SPE 106111.

Athabasca oil sands: reservoir characterization and its impact on thermal and mining opportunities

M. J. PEACOCK

Imperial Oil Resources Limited, 237 4 Avenue SW, Calgary, Alberta, T2P 3M9, Canada (e-mail: mike.j.peacock@esso.ca)

Abstract: The heavy oil deposits of Canada are a large resource with an estimated 1.7×10^{12} barrels of bitumen in place. The Lower Cretaceous McMurray Formation in the Athabasca area of northern Alberta contains about 900×10^{9} barrels of bitumen in place. This resource can be developed through surface mining and thermal *in situ* techniques. This paper examines the size of this resource in a global context and highlights its position relative to the North American market. The regional geology of the Western Canada Sedimentary Basin and the Athabasca area will also be reviewed. Understanding the regional reservoir distribution of the McMurray Formation is critical to understanding oil sands opportunities. Fluvial estuarine point bar reservoirs are a large portion of the resource that can be developed. Examples will be shown from the type outcrop location, where the stratigraphy can be organized into a hierarchy that subdivides channel-fills into bedsets, storeys, bars and barsets. Inclined heterolithic strata (IHS) surfaces can be identified. Considerable resource delineation drilling has occurred in the basin. The regulator for the Athabasca area specifies minimum drilling densities before project approvals are granted. Regional 2D seismic lines and project-specific 3D and 4D seismic datasets have also been acquired, to reduce the reservoir uncertainty and improve resource definition in this complex depositional environment. These techniques provide a unique opportunity to analyse a complex depositional system with abundant well and core control, outcrop data and seismic information.

To determine preliminary deposition environments, software techniques have been successfully used to interpret large datasets quickly. Laser imaging of mine faces has also been used to record stratigraphy and determine the mined volume of ore. The importance of detailed reservoir characterization studies and their impact on thermal *in situ* recovery mechanisms will also be discussed. Understanding reservoir facies distributions and lateral relationships affects any recovery process, but has an even greater significance in a heavy oil reservoir.

Keywords: Athabasca, oil sands, thermal, *in situ*, mining, 2D, 3D, 4D seismic, reservoir, characterization

The heavy oil deposits of Canada are predominantly located in northern Alberta (Fig. 1) and range in age from Upper Devonian to Lower Cretaceous (Fig. 2). This large resource contains *c.* 1.7×10^{12} barrels of bitumen in place. The Energy Resources Conservation Board (ERCB), the regulator for Alberta, quotes a recoverable resource of 175×10^{9} barrels from these deposits (Energy Resources Conservation Board 2008). Canada ranks second behind Saudi Arabia in oil resources, with heavy oil contributing 98% of this resource (Fig. 3). The proximity of these resources to the North American market highlights the strategic importance they will have in supplying the future energy requirements of the North American continent.

Currently, industry extracts about 1.1×10^{6} barrels of bitumen each day, which represents about one-third of the province's total crude oil production. This rate is expected to rise to 2.7×10^{6} barrels a day by 2015 (Energy Resources Conservation Board 2008).

The Lower Cretaceous McMurray Formation in the Athabasca area of northern Alberta contains about 900×10^{6} barrels of bitumen in place. This resource can be developed through surface mining and thermal *in situ* techniques. Generally, where the overburden is less than 70 m thick, the resource is extracted through open-pit mining, with all land being reclaimed at the end of pit life. New regulatory standards are accelerating the reclamation timing of inactive pit areas. In areas where the overburden is greater than 70 m, thermal *in situ* recovery techniques are used. One of the thermal *in situ* recovery techniques used in the Athabasca area is a process called steam-assisted gravity drainage, commonly referred to as SAGD (Fig. 4). In this process, two horizontal wellbores are drilled about 5 m apart. A typical SAGD well length is 1 km. Steam is then continuously injected into the upper wellbore, which reduces the viscosity of the bitumen, allowing continuous production from the lower wellbore through gravity drainage of the bitumen (Fig. 4). These well pairs are typically drilled from a common well pad in a set pattern or configuration. The SAGD process was originally patented by Imperial Oil Limited (Imperial) in 1982. For a detailed description of the process, see Butler (1982). Because the SAGD process relies on gravity drainage to recover the bitumen, the wells must be located in higher energy depositional units with minimal shale interbeds that could act as barriers or baffles to steam movement.

Regional setting

The Western Canada Sedimentary Basin comprises a northeastward thinning wedge of supracrustal rocks overlapping the North American craton (Price 1994). The thickest and stratigraphically the most complete section is in the Rocky Mountain foreland fold-and-thrust belt. Two main stages of development of the basin have been identified (Bally *et al.* 1966; Price and Mountjoy 1970). The first stage is represented by a Late Proterozoic to Late Jurassic miogeosyncline platform, dominated by carbonate, evaporate and shale deposition. This stage has been correlated to the continental rifting and drifting that created the initial continental margin of the North American craton and its adjacent ocean basin. The subsequent continental terrace wedge (miogeocline) prograded outboard from this passive margin. The second stage consisted of a Late Jurassic to Early Eocene foreland basin, bounded to the west by the emerging Cordilleran mountain belt,

VINING, B. A. & PICKERING, S. C. (eds) *Petroleum Geology: From Mature Basins to New Frontiers – Proceedings of the 7th Petroleum Geology Conference*, 1141–1150. DOI: 10.1144/0071141

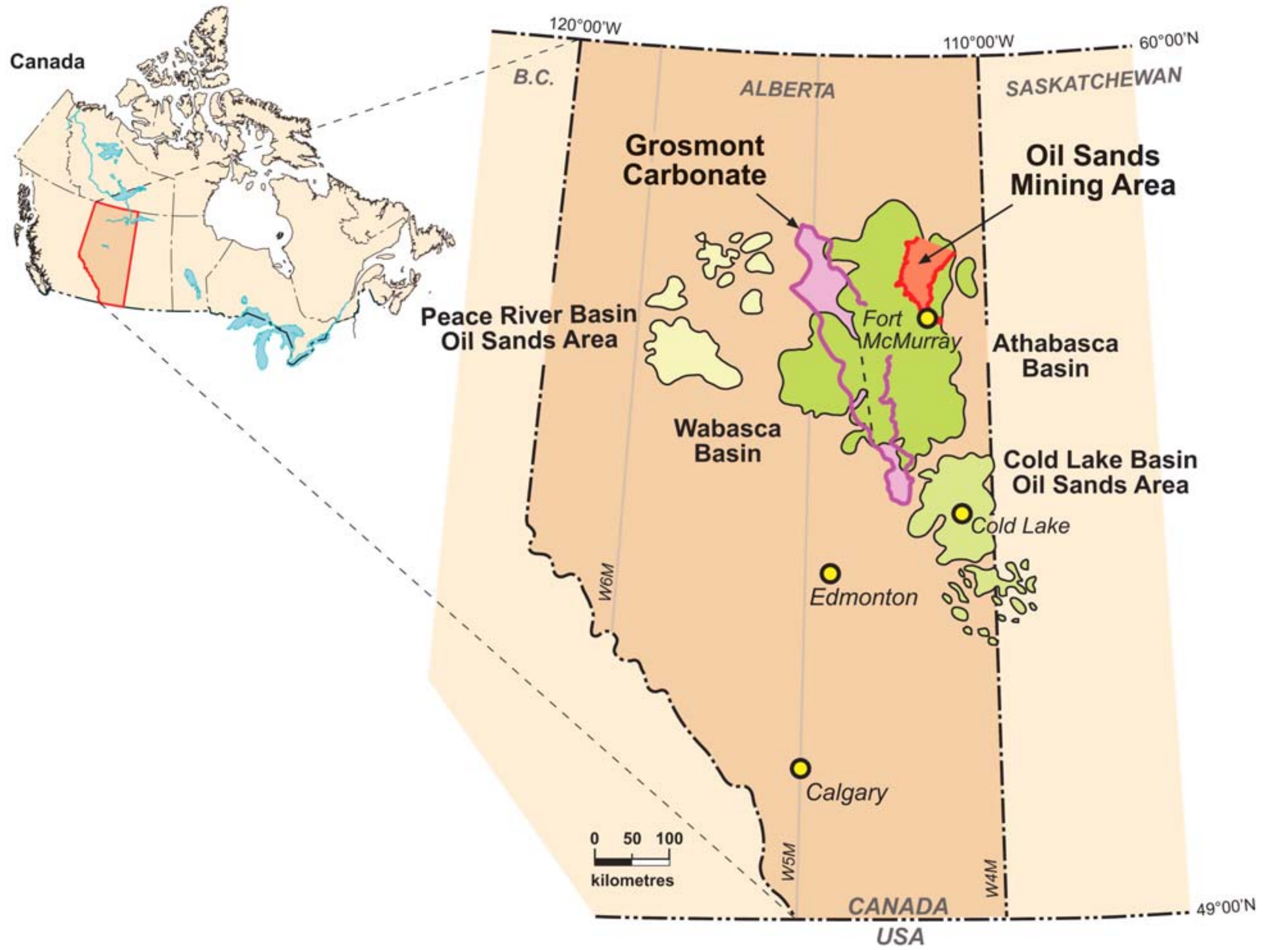

Fig. 1. General location map showing the heavy oil deposits of Alberta.

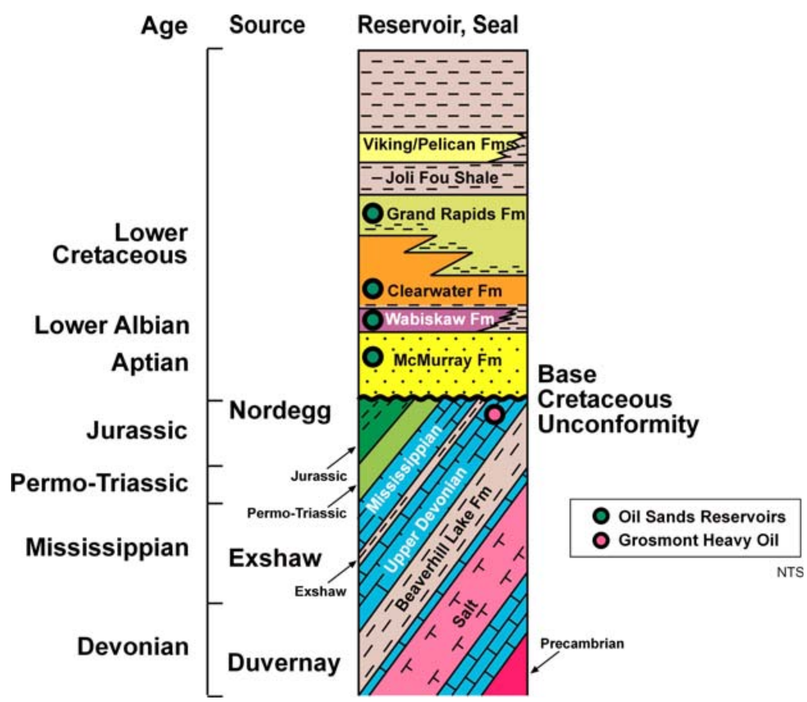

Fig. 2. Generalized stratigraphic column of the Western Canada Sedimentary Basin.

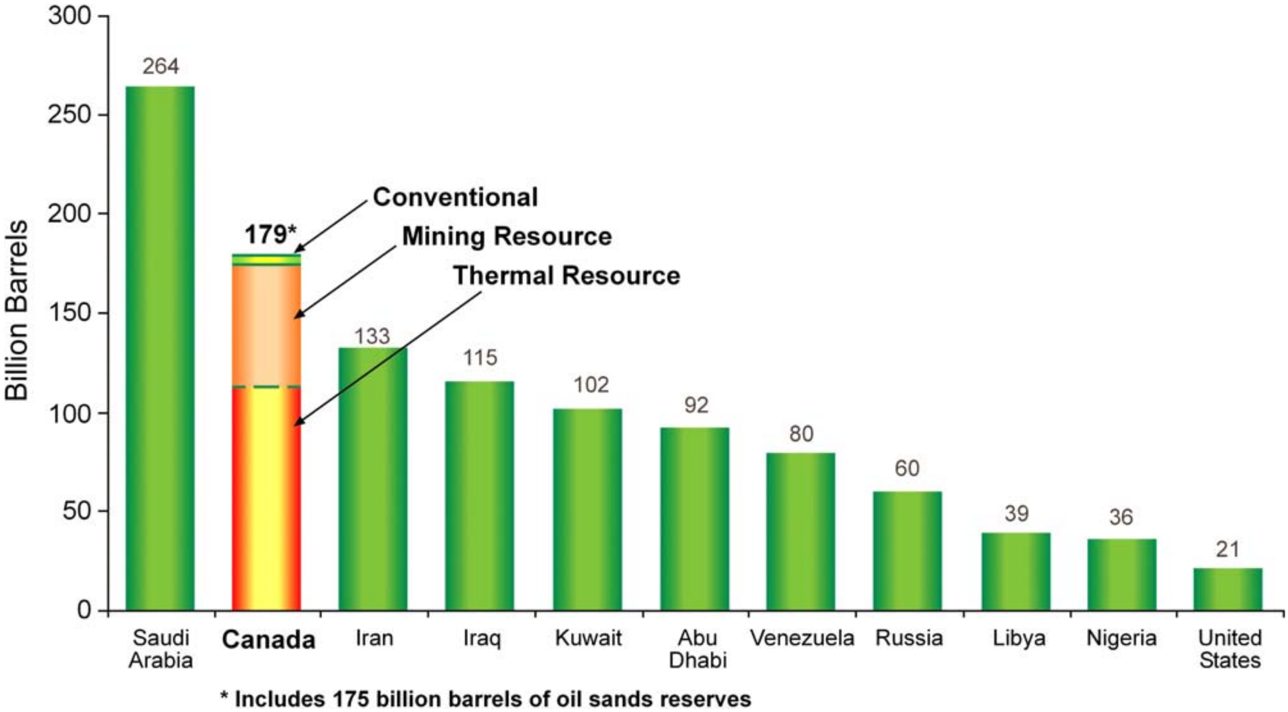

Fig. 3. Global oil resources. *Source*: Oil & Gas Journal, December 2005.

and to the east by the Precambrian (Canadian) Shield. The depositional system was mixed, varying between fluvial and marine. The Cordilleran mountain belt eventually resulted in detachment, thickening and compression of the fold belt, with tectonic thickening and subsidence of the foreland basin (Fig. 5). This compression continued until the Middle Eocene, when it was terminated by a period of crustal extension in the central part of the Cordillera.

In northern Alberta, the large, areally extensive Athabasca Anticline forms the regional trap for the heavy oil accumulations, and was the regional focus for migration. The anticline was the result of one of the final Laramide compressive events associated with the formation of the Cordillera.

Several petroleum source rocks (Fig. 2), ranging in age from Middle Devonian to Lower Cretaceous, have been identified in

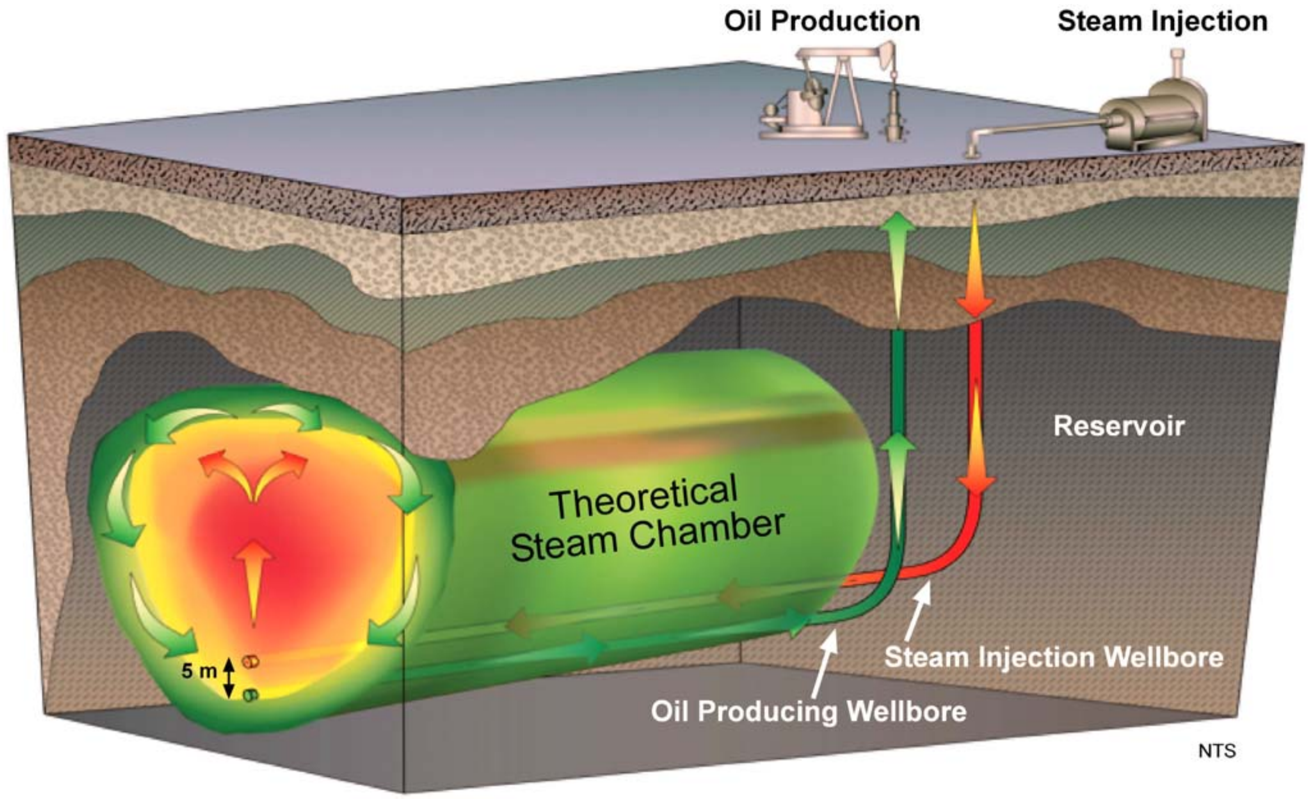

Fig. 4. Steam-assisted gravity drainage (SAGD) process.

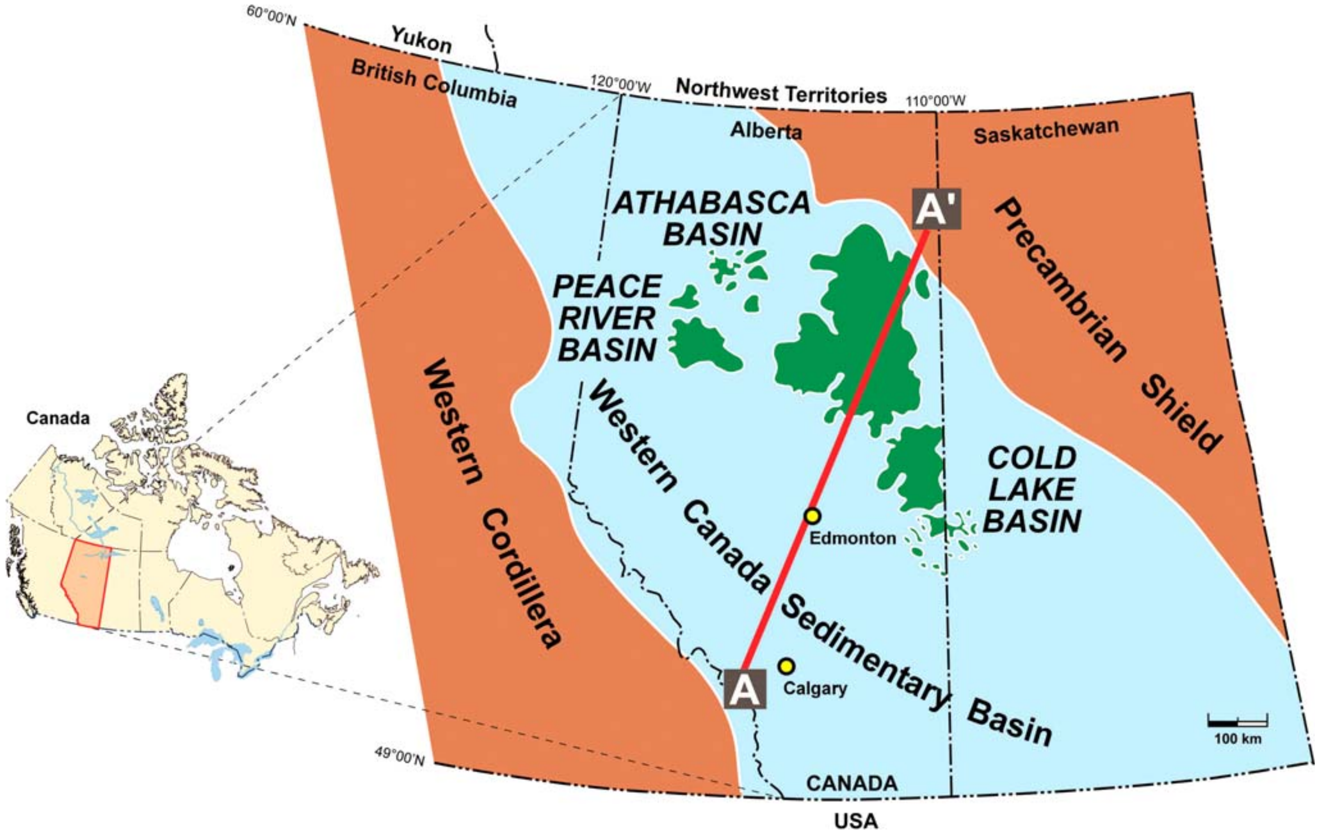

Fig. 5. Tectonic setting of the Western Canada Sedimentary Basin from the Late Jurassic to the Early Eocene.

the Western Canada Sedimentary Basin (Creaney and Allan 1990). A number of these source rocks have world-class source characteristics of high total organic content and hydrogen indices. The development of an effective regional top seal (Joli Fou Shale), combined with simple synclinal foreland basin geometry, enabled a highly efficient migration system to develop (Fig. 6), with migration focused on the Athabasca Anticline. Freshwater meteoric recharge on the eastern edge of the basin, where the major heavy oil reservoirs onlap the Canadian Shield, resulted in conventional oil biodegrading to heavy oil, that is, less than 25° API gravity. The Western Canada Sedimentary Basin contains about 1.75×10^{12} barrels of oil in place, of which an estimated 98% (1.7×10^{12} barrels) is heavy oil (Energy Resources Conservation Board 2008).

Stratigraphy

The Athabasca Basin is located on the eastern margin of the larger Western Canada Sedimentary Basin and, in some places, onlaps the Canadian Shield. During Barremian time, a major drop in relative sea-level occurred, resulting in substantial erosion across the entire foreland basin. The earliest post-unconformity sediments in the Athabasca Basin are the fluvial estuarine deposits of the McMurray Formation (Fig. 2). The McMurray Formation is equivalent to the Aptian age Lower Mannville Group that contains prolific conventional reservoirs in other parts of the basin. A marine transgression followed, resulting in the deposition of the shallow marine sands of the Lower Albian Wabiskaw Formation. These sands formed a secondary reservoir in the Athabasca Basin. Another third-order sea-level drop resulted in the return to fluvial estuarine conditions and the deposition of the Clearwater Formation, also Lower Albian in age. The Clearwater Formation is the main reservoir objective in the Cold Lake Basin to the south of the Athabasca Basin (Fig. 1). However, this formation becomes shaley to the north and is not a reservoir unit in the Athabasca Basin. The transgressive event that followed then deposited the Grand Rapids Formation, which consists of a series of shoreface sands cut by several incised valley-fill units. The Grand Rapids Formation is present in the southern part of the Athabasca Basin and is considered a secondary reservoir target.

The primary heavy oil reservoir target in the Athabasca Basin for both SAGD and mining exploitation is the Aptian McMurray Formation. Regionally, the McMurray Formation is a deepening-upward fluvial estuarine complex deposited within an Early Cretaceous palaeovalley system. The establishment of this palaeovalley system was controlled in part by structure on the Base Cretaceous unconformity and proximity to the Canadian Shield to the east (Fig. 5). The main valley trended north to NW toward the Boreal Sea. The isopach map of the McMurray Formation (Fig. 7) illustrates the size of the depositional system, which extends about 320 km northwards, and in places is up to 160 km wide. The thickness of the McMurray Formation can be greater than 120 m. There is a strong correlation between isopach thickness and a high net-to-gross ratio. The tributary systems are evident on the isopach map, as indicated by the fluvial transport directions. These tributary systems are normally filled with thick deposits of quartz-rich sands that form high-quality reservoirs. As a result of the shallow burial of these reservoirs, the sands are unconsolidated, which allows for open-pit mining in areas of thin overburden cover. Porosity ranges from 30 to 35%, with multidarcy permeability and high oil saturation. East of this water line (Fig. 7), the reservoir is structurally low and water-wet. This water line is controlled by the dissolution of underlying salt in the Palaeozoic section (Fig. 2). Figure 7 shows the location of several of the largest SAGD projects and the major mining developments.

In the Athabasca Basin, the McMurray Formation is characterized by abrupt lithofacies changes, inclined stratal geometry and high-relief unconformities in a complex environment of deposition. To reduce uncertainty in resource description and

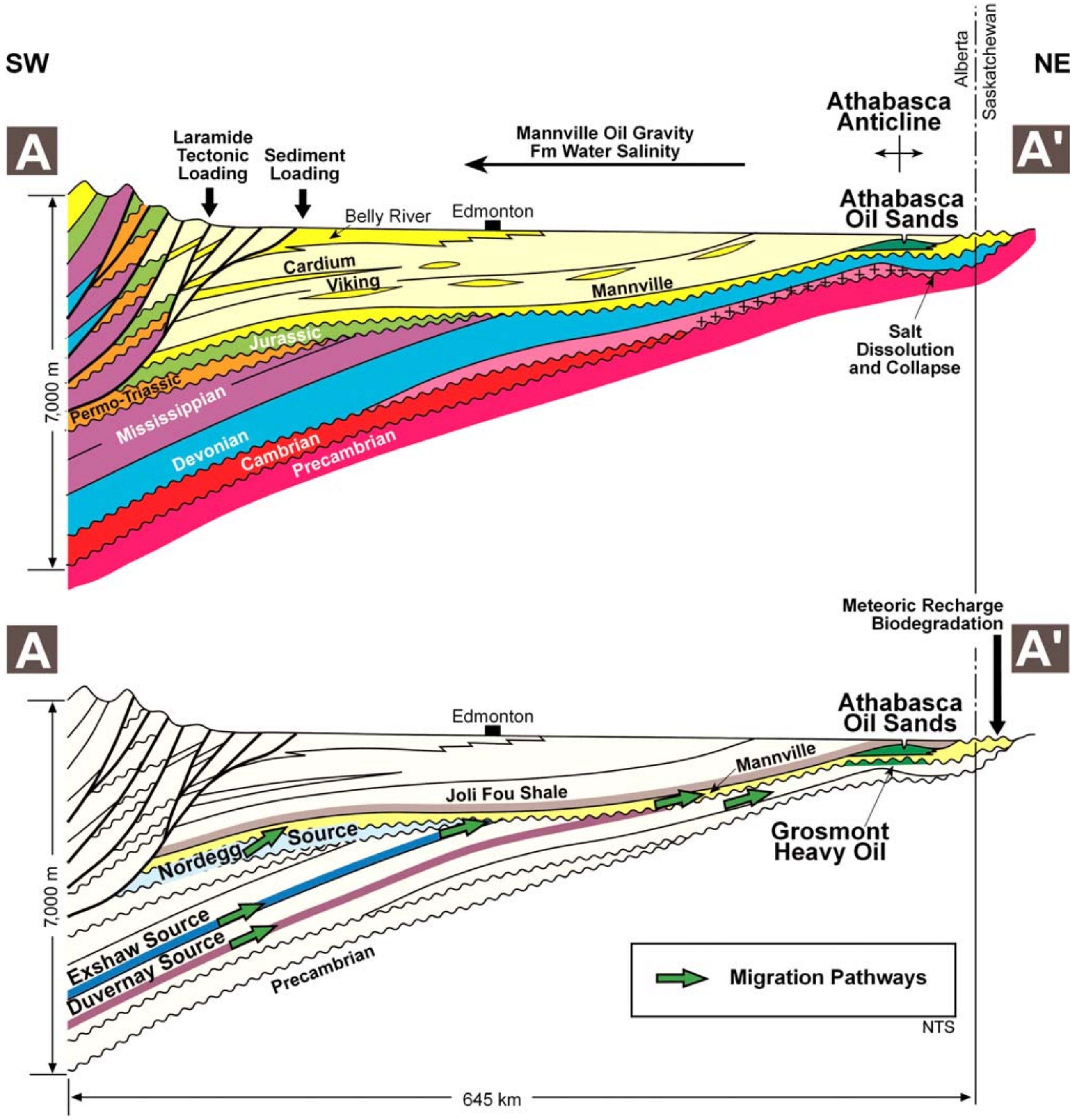

Fig. 6. Regional cross-section through the Western Canada Sedimentary Basin showing location of the Athabasca heavy oil deposits.

assessment, the ERCB stipulates a minimum well spacing before it will approve a project for development. The required well spacing is reduced to 100 m in certain areas. These wells have to be cored and logged. Dipmeter data is critical to understanding palaeodepositional trends. In addition, in the thermal or SAGD areas, baseline 3D seismic is required for 4D monitoring of steam flooding. This, combined with regional 2D seismic type outcrop exposures and mine face exposures, provides world-class datasets for detailed reservoir characterization studies. Fluvial estuarine point bar reservoirs represent a large fraction of the resource that can be developed. Examples will be given of the type of outcrop location where the stratigraphy can be organized into a hierarchy that subdivides channel-fills into bedsets, storeys, bars and barsets. Inclined heterolithic surfaces can be identified.

This complex stratigraphic environment of deposition can be organized within a sequence stratigraphic framework (Nardin *et al.* 2005). Several sequence-keyed facies are identifiable, including thick, amalgamated, braided stream facies, fluvial floodplain and estuarine facies, and large-scale fluvial estuarine point bars. The fluvial estuarine point bar facies are the major reservoir targets for Imperial's mining and SAGD developments. The characteristics of the fluvial estuarine point bar facies will be described in more detail, along with the effect of the facies on thermal reservoir performance.

The fluvial estuarine point bar facies is an upward-fining or thinning succession of stacked beds, bedsets and storeys. An example of a stacked reservoir hierarchy is the Steepbank River outcrop (Fig. 8). The main features of a typical point bar, as described by Thomas *et al.* (1987), includes basal channel sands, inclined heterolithic strata (IHS) and sand-prone inclined strata (IS).

The basal channel sands are typically amalgamated and characterized by trough and tabular cross-bedding (Fig. 9). These are the

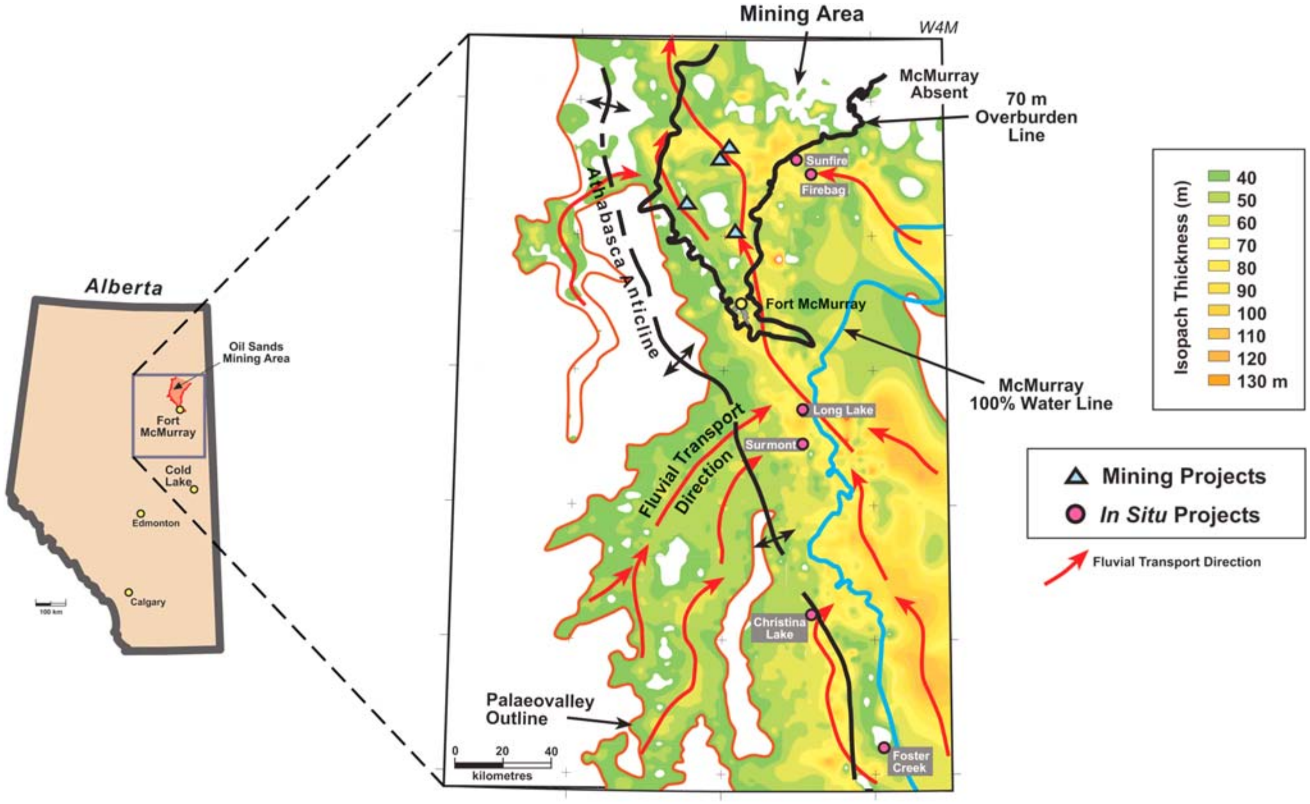

Fig. 7. Isopach map of the Lower Cretaceous McMurray Formation.

highest quality reservoir sands. They are generally overlain in an upward-fining succession by IS sandbodies and IHS sequences. Both IS and IHS are formed by laterally accreting point bars, with IS formed in higher energy, higher discharge depositional periods. Inclined heterolithic strata are dominated by mud, and were deposited in periods of lower energy conditions. In core, they can be recognized by an increase in mudstone bed thickness and frequency, degree of bioturbation and association with mudstone clast facies. The thickness and lateral extent of the mudstone facies can have a considerable impact on thermal reservoir performance. The estuarine conditions can be recognized in core by the brackish water trace fossil assemblage, including *Palaeophycus*, *Cylindrichnus*, *Planolites* and *Skolithos*. Matrix-supported angular mudstone clasts are common in all facies and are derived

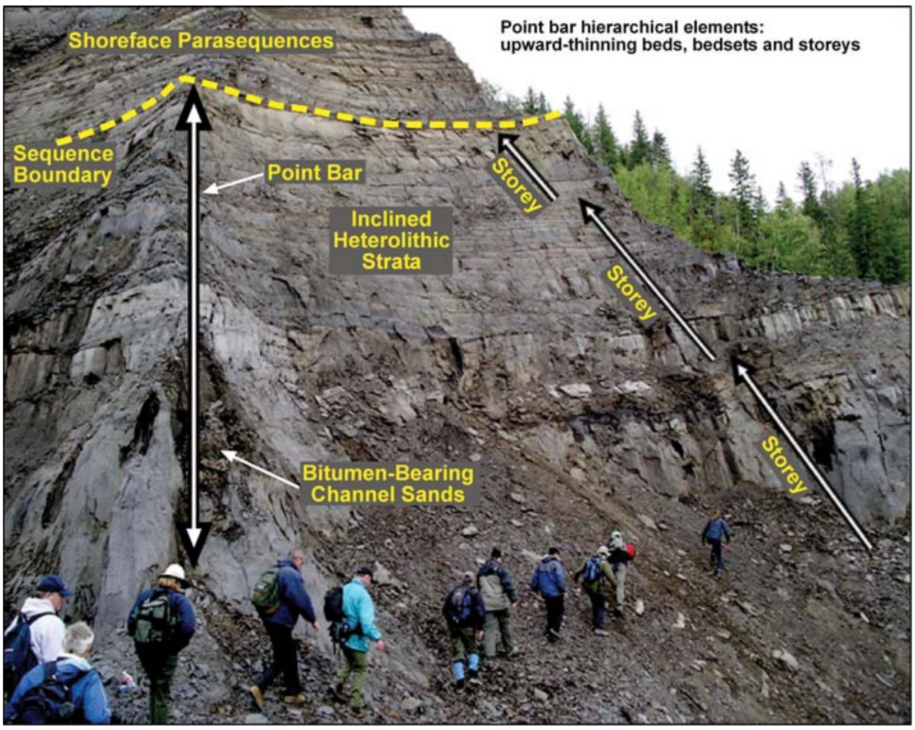

Fig. 8. Steepbank river outcrop, lower McMurray Formation.

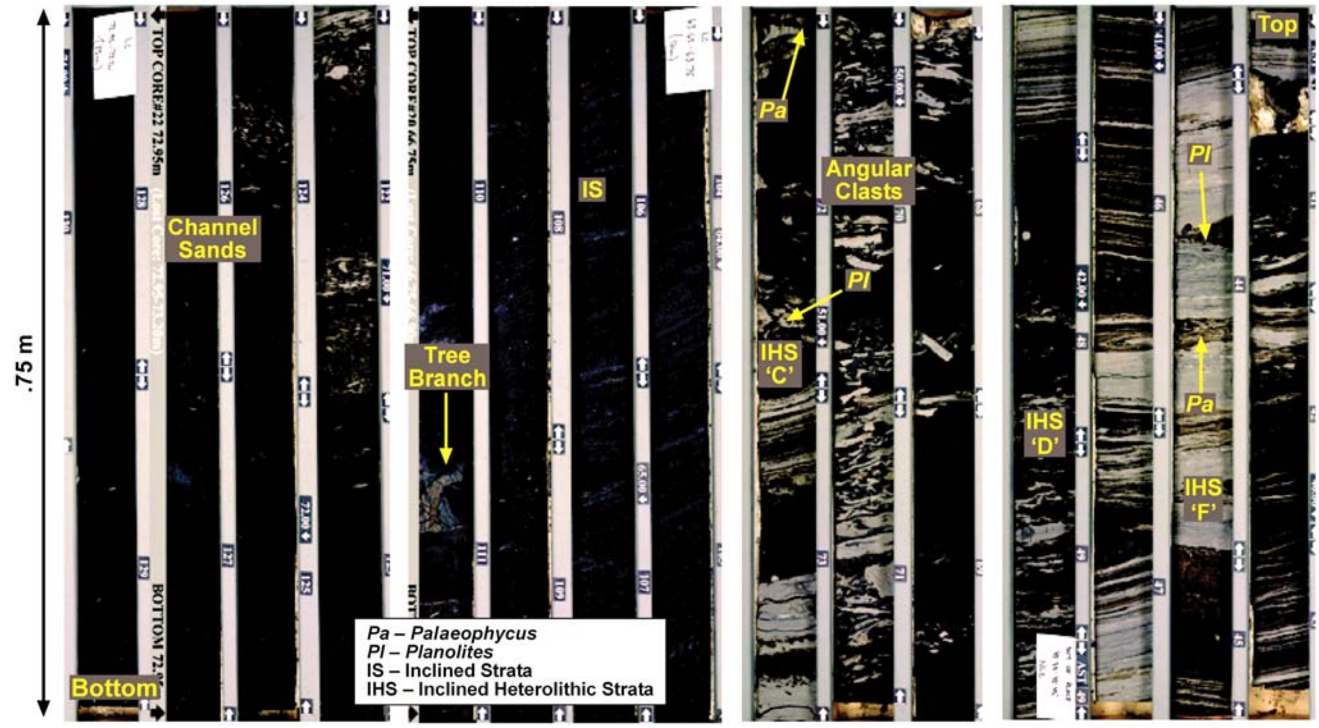

Fig. 9. Core example of a fluvial estuarine point bar sequence of the lower McMurray Formation.

from the erosion associated with the lateral accretion of the point bars (Nardin *et al.* 2005). Being able to differentiate between clasts and more laterally continuous IHS beds is important. On a gamma-ray log, clasts and IHS beds can have the same characteristics, so core is critical for making the ultimate identification. In the thermal recovery process, steam will still be able to move, and a steam chamber will grow within a reservoir section that contains clasts. However, thin mudstone beds can substantially slow and impede steam chamber growth.

The dipmeter is another log that is critical for identifying and interpreting the environment of deposition. Inclined heterolithic strata and IS dips range from 3 to 20°, with an average of about 10°. Typically, azimuths vary, but are generally within 90°. Even with a well spacing of 100 m in places, dips in the range of 10° will have a substantial impact on the ability to correlate surfaces between wells. Imperial has used regional 2D seismic lines to assist in identifying IHS sequences. Inclined heterolithic strata can be recognized on 2D seismic logs, with characteristics of moderate- to high-amplitude, discontinuous reflectors that appear to downlap the underlying sequence boundaries (Nardin *et al.* 2005).

Laser imaging of mine faces is also used for recording stratigraphy and determining the mined volume of ore. Laser images are collected frequently. For a particular mine face, multiple images are collected, capturing the changes in stratigraphy as the mine face migrates through the deposit.

Impact of reservoir heterogeneity on thermal recovery and performance

Thermal recovery efficiency depends on establishing an effective steam chamber within a reservoir unit. Two horizontal wells are drilled 5 m apart, with steam injected into the upper wellbore, and bitumen produced from the lower wellbore. Thermal communication between the two wellbores generally occurs within the first three months of steaming. Once communication has been established, the steam chamber grows like a cone (Fig. 10). The wellbores are positioned to reduce the effect of potential thief zones for the steam. Thief zones, which include top and bottom water and top gas, are zones that significantly reduce the efficiency of establishing a steam chamber. The theoretical recovery efficiency of the process is very high. Typically, theoretical recovery efficiencies are modelled and simulated from reservoirs with minimal mudstone interbeds. However, actual steam chamber growth is much more irregular than the models (Fig. 10), and is heavily affected by reservoir heterogeneity and, in particular, mudstone or shale interbeds. This can be demonstrated by repeatedly running temperature logs in observation wells and acquiring 4D or repeat seismic surveys.

Temperature logs can be used to monitor heat in the reservoir. When integrated with core coverage and detailed facies descriptions, a more accurate interpretation of steam chamber growth is possible. As previously mentioned, identifying clasts v. mudstone or shale interbeds is critical to understanding thermal reservoir performance. In the example from the Athabasca area, shown in Figure 11, the steam injector was located just below the base of the core. Steaming began and the steam chamber rose 4 m in the first 18 months through a section dominated by clasts. Steam chamber growth was then halted for six months by a thin, 1–2 cm mudstone interbed. Eventually, the steam broke through this thin interbed and the growth of the steam chamber continued. The steam chamber then took only six months to grow a further 3 m. The core in Figure 11 shows that this growth occurred in an interval with lower clast content. The steam chamber was then permanently halted by an interval dominated by IHS and more laterally continuous mudstone or shale interbeds.

Seismic monitoring at Imperial's Cold Lake development began in 1985 with the first seismic imaging pilot study. This pilot has evolved into the development of important seismic imaging tools for reservoir monitoring and production optimization (Eastwood *et al.* 1994, 1996), which are currently being used at Imperial's *in situ* heavy oil properties. The ERCB also mandates a baseline 3D seismic survey before approving the development of any SAGD project.

Seismic monitoring of *in situ* heavy oil production relies on the acoustic contrast that results from the introduction of gas within the pore space of the reservoir from both the injection of

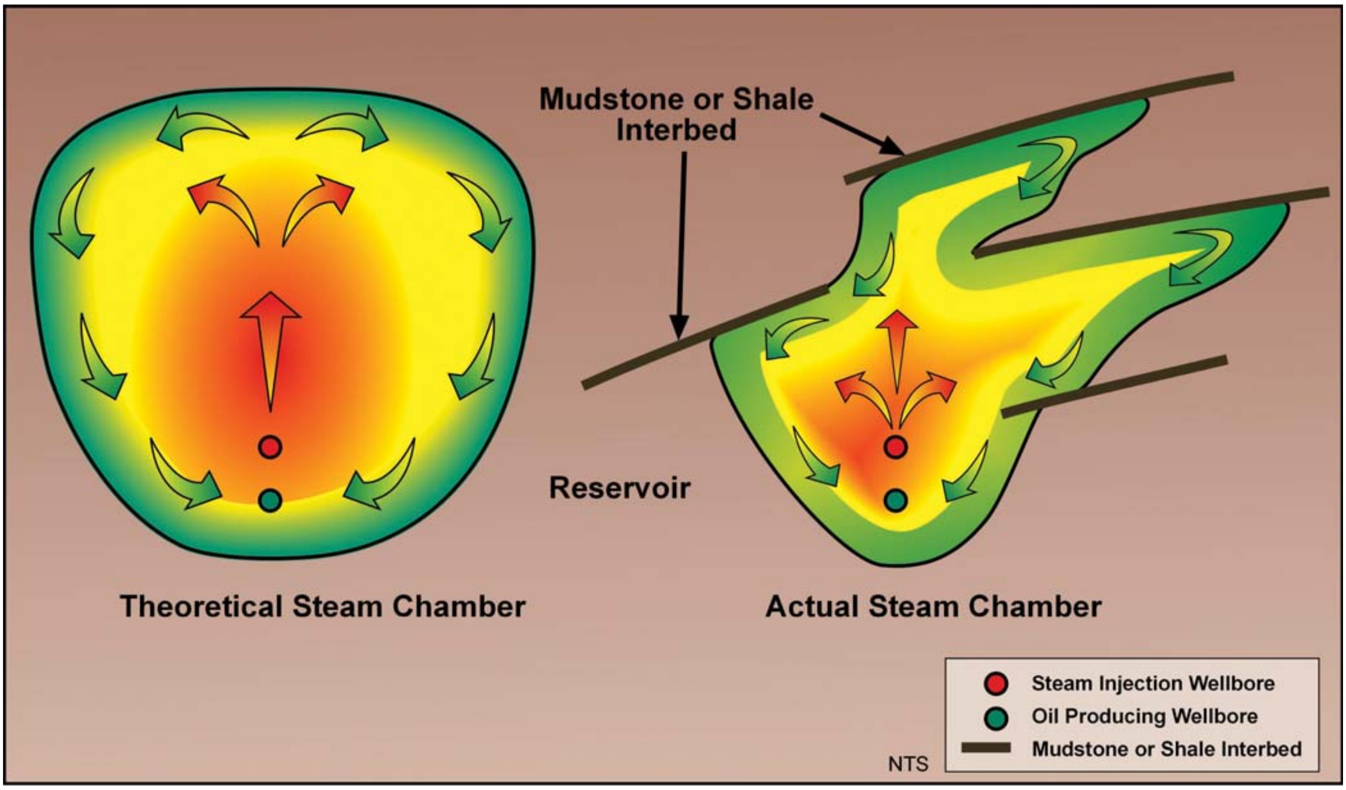

Fig. 10. Steam chamber growth in SAGD process.

steam and the release of gas associated with heating the bitumen. The seismic response associated with the introduction of this gas is a high-amplitude reflection at the top of the gas chamber, a time delay of reflections below the gas chamber because of the decreased seismic velocity within the chamber, and a loss of frequency resulting from the attenuation of the seismic wave through the gas chamber. These attributes can be used to construct areal conformance maps and vertical conformance volumes to monitor the behaviour of the heated region through time (Fig. 12). Conformance maps indicate the efficiency of steam

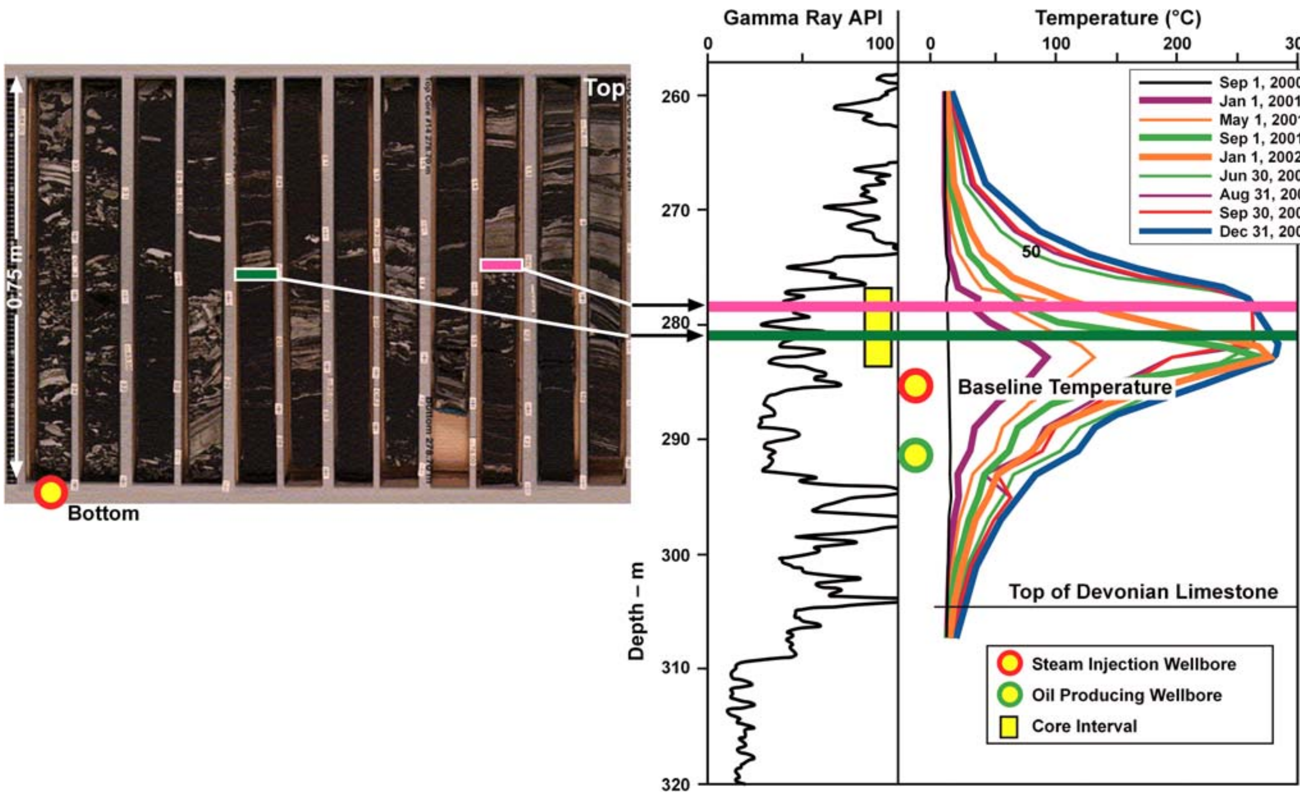

Fig. 11. Integration of core and thermal logging data to monitor steam chamber growth in a vertical observation well.

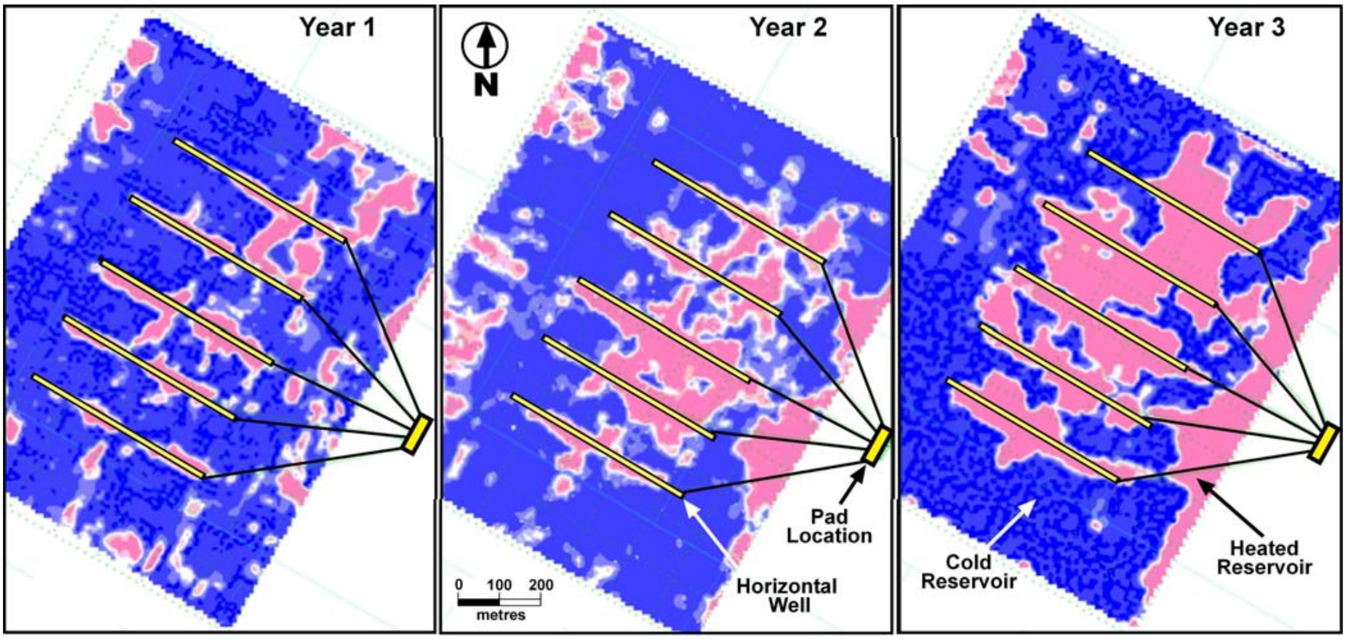

Fig. 12. Steam conformance maps generated from 4D seismic at the Cold Lake Field, Alberta.

chamber growth and areas that have been accessed by the steam injection. The integration of seismic monitoring surveys with the detailed sequence stratigraphy of the reservoir from logs, core and baseline seismic surveys can be used to show the influence of the stratigraphy on the distribution of steam within the reservoir. This understanding allows future well placement and infill drilling to be planned in a way that optimizes bitumen recovery.

The Cold Lake example (Fig. 12) shows the steam conformance mapping of a single five-horizontal-well pad. Through time, the steam front can be mapped. The steam front does not move or build up regularly, but is heavily influenced by the heterogeneity of the reservoir in which that particular well is positioned. The complex environment of deposition of these fluvial estuarine deposits and the relatively steep dips of the beds, averaging 10°, result in high variability of the reservoir along any particular wellbore. During the pre-development phase, vertical pilot holes are used to help determine the best placement of the horizontal wellbores.

Managing large well datasets

In the Athabasca Basin areas where bitumen is recovered through open-pit mining, well density is high (Fig. 13). In places, the well spacing is reduced to 100 m in compliance with regulatory requirements. All wells are cored and logged, providing a large and detailed database to analyse. In a typical mining development, a single pit might have as many as 10 000 core holes drilled before the end of pit development. This provides a large amount of data that conventional 3D geological modelling software is unable to accommodate. Consequently, mining software is used because it can manage the large datasets. However, mining software is not

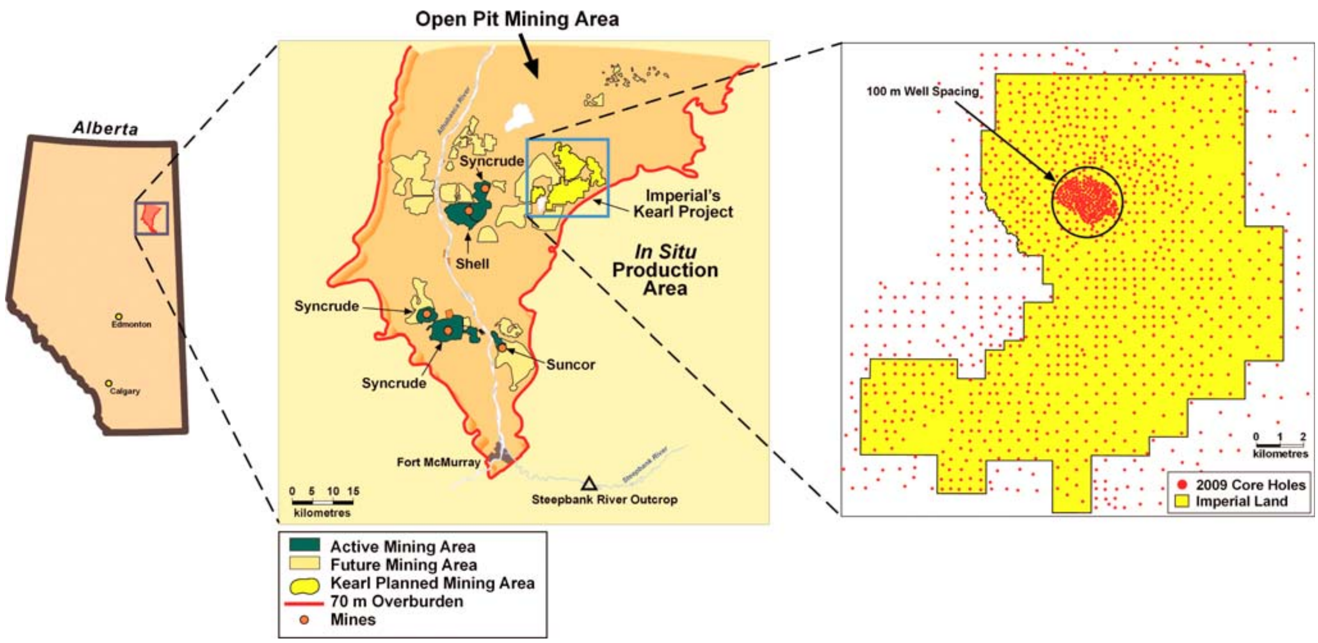

Fig. 13. Map of the Athabasca Basin that can be developed through surface mining.

as sophisticated as geological modelling software in its manipulative capabilities.

Conclusions

The Athabasca oil sands represent a substantial hydrocarbon resource located in a stable, accessible environment. The ERCB, the regulator for Alberta, estimates a recoverable resource of 175×10^9 barrels from these deposits (Energy Resources Conservation Board 2008). The proximity of these resources to the North American market highlights the strategic importance they will have in supplying the future energy requirements of the continent. Thermal processes are still in the early stages of development, but will play an increasing role in Canadian oil production. Lessons learned about recovery performance from new projects will greatly enhance the optimization of these projects. The integration of reservoir characterization studies will be a critical component of interpreting performance. Currently, industry extracts around 1.1×10^6 barrels of bitumen each day, a rate expected to rise to 2.7×10^6 barrels a day by 2015 (Energy Resources Conservation Board 2008).

Detailed reservoir characterization studies are important for any type of reservoir, be it a conventional or heavy oil field development. For heavy oil thermal developments, understanding reservoir characteristics is especially important, because shale interbeds have such a dramatic effect on steam chamber growth and, ultimately, on reservoir performance. Constructing a predictive stratigraphic model will reduce the risk associated with well placement. Horizontal well pairs, typically 1 km in length, will encounter varying stratigraphy along the wellbore.

Monitoring the effective steam chamber growth is critical to understanding reservoir performance and, ultimately, to optimizing the reservoir development plan. The reservoir development plan can be optimized by integrating reservoir description with temperature monitoring techniques, including temperature logs and 4D seismic conformance mapping. The detailed integration of these tools results in an increased improvement in field development management. In Alberta, the ERCB mandates baseline 3D seismic surveys before a project is approved. The incremental cost of repeat surveys is competitive when compared with the cost of misplacing an infill well, drilled to optimize production and improve reservoir conformance.

Reservoir characterization is also essential for mining developments. Mining facilities are designed to process the average parameters of the deposit. To achieve this, the different facies are required to be blended. Depending upon the facies being mined, lower quality facies (facies with an increased content of IHS beds) may be mixed with higher quality facies to produce an average blend for the facilities to process. This is managed on a daily basis, so a comprehensive understanding of the volume of a particular facies to be mined allows an improved predictive capability and increased facility efficiency.

In the Athabasca Basin, the unique combination of abundant well control, core and log data, 2D, 3D and 4D seismic data, mine exposures and outcrops, provides world-class datasets available for detailed reservoir characterization studies of a complex fluvial estuarine depositional environment. Laser images of mine faces are collected frequently to record stratigraphy and to determine the mined volume of ore. Multiple images are collected for each mine face to capture the stratigraphic changes as the mine face migrates through the deposit.

The author wishes to thank Imperial Oil Resources Limited for permission to publish this paper.

References

Bally, A. W., Gordy, P. L. & Stewart, G. A. 1966. Structure, seismic data and orogenic evolution of the southern Canadian Rockies. *Bulletin of Canadian Petroleum Geology*, **14**, 337–381.

Butler, R. M. 1982. *Method for continuously producing viscous hydrocarbons by gravity drainage while injecting heated fluids*. Canadian Patent CA1130201.

Creaney, S. & Allan, J. 1990. Hydrocarbon generation and migration in the Western Canada Sedimentary Basin. *In*: Brooks, J. (ed.) *Classic Petroleum Provinces*. Geological Society, London, Special Publications, **50**, 189–202.

Eastwood, J., Lebel, P., Dilay, A. & Blakeslee, S. 1994. Seismic monitoring of steam-based recovery of bitumen. *The Leading Edge*, **13**, 242–251.

Eastwood, J., Anderson, D. & Boone, T. 1996. 3D seismic monitoring for enhancing thermal recovery. *Canadian Society of Exploration Geophysicists, Recorder*, **21**, 3–5.

Energy Resources Conservation Board. 2008. *Alberta's Energy Reserves 2007 and Supply/Demand Outlook 2008–2017*. Energy Resources Conservation Board, Edmonton, **ST98-2008**.

Nardin, T. R., Carter, B. J. *et al*. 2005. Sequence stratigraphic and depositional facies framework of the Lower Cretaceous McMurray Formation, Kearl Oil Sands Project, Alberta. *Core Workshop 2005*. Canadian Society of Petroleum Geologists, Calgary.

Price, R. A. 1994. Cordilleran tectonics and the evolution of the Western Canada Basin. *In*: Mossop, G. D. & Shetsen, I. (comps.) *Geological Atlas of the Western Canada Sedimentary Basin*. Canadian Society of Petroleum Geologists and Alberta Research Council, Calgary, 13–24.

Price, R. A. & Mountjoy, E. W. 1970. Geologic structure of the Canadian Rocky Mountains between the Bow and Athabasca Rivers: a progress report. *In*: Wheeler, J. O. (ed.) *Structure of the Southern Canadian Cordillera*. Geological Association of Canada, St John's, Special Publications, **6**, 7–25.

Thomas, R. G., Smith, D. G., Wood, J. M., Visser, J., Calverly-Range, E. A. & Koster, E. H. 1987. Inclined heterolithic stratification – terminology, description, interpretation and significance. *Sedimentary Geology*, **53**, 123–179.

Resource potential of gas hydrates: recent contributions from international research and development projects

T. S. COLLETT

US Geological Survey, Denver Federal Center, MS-939, Box 25046, Denver, CO 80225, USA (e-mail: tcollett@usgs.gov)

Abstract: It is generally accepted that the amount of gas in the world's gas hydrate accumulations exceeds the volume of known conventional gas resources. Researchers have long speculated that gas hydrates could eventually be a commercial producible energy resource yet technical and economic hurdles have historically made gas hydrate development a distant goal rather than a near-term possibility. This view began to change in recent years with the realization that this unconventional resource could possibly be developed with existing conventional oil and gas production technology. The most significant development has been gas hydrate production testing conducted at the Mallik site in Canada's Mackenzie Delta. The Mallik Gas Hydrate Production Research Well Program has yielded the first modern, fully integrated field study and production test of a natural gas hydrate accumulation. More recently, BP Exploration (Alaska) Inc. with the US Department of Energy and the US Geological Survey have successfully cored, logged and tested a gas hydrate accumulation on the North Slope of Alaska known as the Mount Elbert Prospect. The Mallik project along with the Mount Elbert effort has for the first time allowed the rational assessment of the production response of a gas hydrate accumulation. In addition to the gas hydrate production tests in Canada and the USA, marine gas hydrate research drilling, coring and logging expeditions launched by the national gas hydrate programmes in Japan, India, China and South Korea have also contributed significantly to our understanding of how gas hydrates occur in nature and have provided a much deeper appreciation of the geological controls on the occurrence of gas hydrates. With an increasing number of highly successful gas hydrate field studies, significant progress has been made in addressing some of the key issues on the formation, occurrence and stability of gas hydrates in nature.

Keywords: gas hydrate, natural gas, resources, energy, Alaska, Mackenzie Delta

Gas hydrates are naturally occurring 'ice-like' combinations of natural gas and water that have the potential to provide an immense resource of natural gas from the world's oceans and polar regions. Gas hydrates are known to be widespread in permafrost regions and beneath the sea in sediments of outer continental margins. It is generally accepted that the volume of natural gas contained in the world's gas hydrate accumulations greatly exceeds that of known gas reserves. There is also growing evidence that natural gas can be produced from gas hydrates with existing conventional oil and gas production technology (Dallimore *et al.* 2008; Moridis *et al.* 2008; Yamamoto & Dallimore 2008). This review of natural gas hydrates is intended to provide an up-to-date analysis of the geological controls on the occurrence of gas hydrates in nature with a focus on understanding the energy resource potential of gas hydrates. The results of some of the more important international gas hydrate research projects are discussed.

Occurrence of gas hydrates

As shown in Figure 1, gas hydrates have been recovered at about 40 locations throughout the world. However, only a limited number of gas hydrate accumulations have been examined and delineated with data collected by deep scientific drilling operations. Included in the following discussion are descriptions of several of the best known drilled marine and onshore permafrost-associated gas hydrate accumulations in the world.

Gulf of Mexico, USA

The occurrence of gas hydrates in the Gulf of Mexico was confirmed during DSDP Leg 96 when numerous gas hydrate samples were recovered from sub-bottom depths ranging from 20 to 40 mbsf in the Orca Basin (Sites 618 and 618A), which is located about 300 km south of Louisiana beneath about 2000 m of water. Near-surface (0–5 m) marine sediment coring has also recovered numerous gas hydrate samples on the Louisiana continental slope.

In 2005, the Chevron-led Gulf of Mexico Gas Hydrate Joint Industry Project (JIP) conducted scientific drilling, coring and downhole logging to assess hydrate-related hazards in fine-grained sediments with low concentrations of gas hydrate (Claypool 2006). This expedition targeted two deep-water locations in the Atwater Valley and Keathley Canyon areas of the Gulf of Mexico. Although gas hydrate was not physically recovered from the Keathley Canyon core hole, other indicators of gas hydrate, such as elevated downhole measured electrical resistivities, suggest the probable occurrence of gas hydrate in the KC151-2 well. Analysis of downhole measured resistivities and resistivity-at-the-bit (RAB) images from the KC151-2 hole revealed the occurrence of fracture filling gas hydrate at relatively high concentrations. The analysis of downhole well log data from the two JIP Atwater Valley wells shows little evidence of significant gas hydrate occurrences, other than several thin, possibly stratigraphically controlled gas-hydrate-bearing intervals. The next phase of the Gulf of Mexico JIP is being extended to coarser grained sediments with much higher expected gas hydrate concentrations. In the spring of 2009, the Gulf of Mexico JIP expects to conduct exploratory drilling and logging to better understand gas hydrate-bearing sands in the deep-water Gulf of Mexico.

Also in the Gulf of Mexico, at the Alaminos Canyon 818 site (AC818), gas hydrate is interpreted to occur within the Oligocene Frio volcaniclastic sand at the crest of a fold that is shallow enough to be in the hydrate stability zone (Smith *et al.* 2006). Examination of the well log data obtained from the Frio section of the Chevron Tiger Shark well drilled in AC818 indicates

VINING, B. A. & PICKERING, S. C. (eds) *Petroleum Geology: From Mature Basins to New Frontiers – Proceedings of the 7th Petroleum Geology Conference*, 1151–1154. DOI: 10.1144/0071151

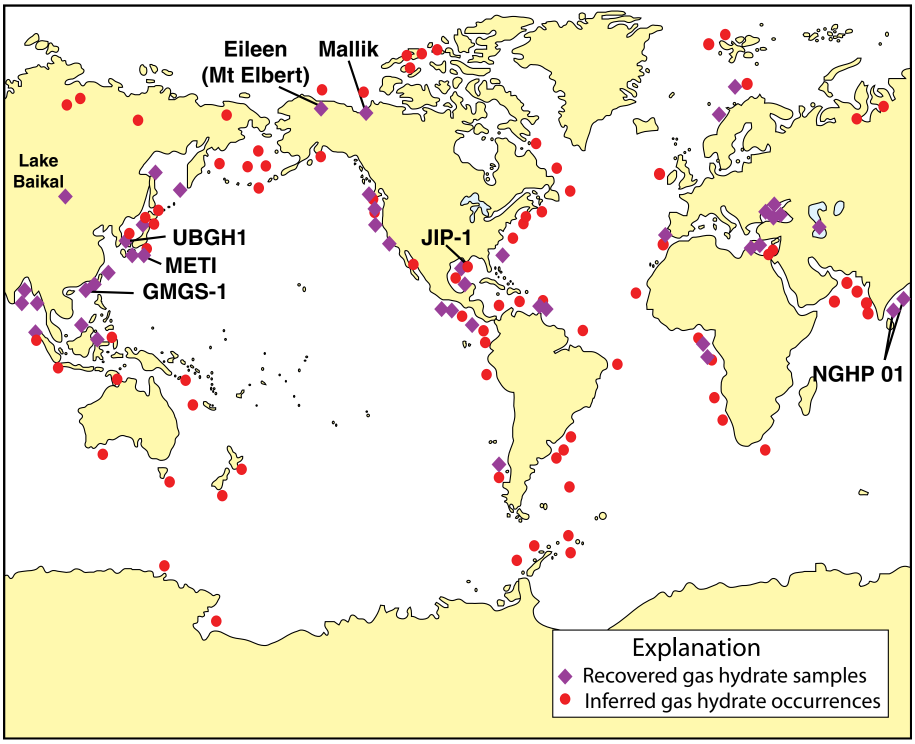

Fig. 1. Locations of sampled and inferred gas hydrate occurrences in oceanic sediment of outer continental margins and permafrost regions. Most of the recovered gas hydrate samples have been obtained during deep coring projects or shallow seabed coring operations. Most of the inferred gas hydrate occurrences are sites at which bottom-simulating reflectors (BSRs) have been observed on available seismic profiles. The gas hydrate occurrences reviewed in this report have also been highlighted on this map.

approximately 18 m of sand (3209–3227 m drilling depth) with porosity of about 30% and downhole measured resistivity in the range 30–40 Ω m. Initial volumetrics derived from downhole log data show very high gas hydrate saturations (up to 80% of available pore volume).

Alaska North Slope, Alaska, USA

Before the recently completed coring and downhole-logging operations in the BP Exploration (Alaska) Mount Elbert well in Milne Point, the only direct confirmation of gas hydrate on the North Slope was obtained in 1972 with data from the Northwest Eileen State-2 well located in the northwestern part of the Prudhoe Bay Field. Gas hydrates are also inferred to occur in an additional 50 exploratory and production wells in northern Alaska based on downhole log responses calibrated to the known gas hydrate occurrences in the Northwest Eileen State-2 well. Most of the well-log inferred gas hydrates occur in six laterally continuous sandstone units; all are geographically restricted to the area overlying the eastern part of the Kuparuk River Field and the western part of the Prudhoe Bay Field. The volume of gas within the gas hydrates of the Prudhoe Bay–Kuparuk River area, which has come to be known as the Eileen Gas Hydrate Accumulation, is estimated to be about $1.0–1.2 \times 10^{12}$ m^3

Under the Methane Hydrate Research and Development Act of 2000 (renewed in 2005), the Department of Energy (DOE) has funded field research on both Arctic and marine gas hydrates. Among the current Arctic studies, BP Exploration (Alaska) Inc. (BPXA) and the DOE have undertaken a project to characterize the commercial viability of gas hydrate resources in the Prudhoe Bay, Kuparuk River and Milne Point field areas on the Alaska North Slope. As part of this effort, the Mount Elbert Gas Hydrate Stratigraphic Test Well was completed in February 2007 and yielded one of the most comprehensive datasets yet compiled on naturally occurring gas hydrates (Boswell *et al.* 2008). In 2005, extensive analysis of BPXA's proprietary 3D seismic data and the integration of that data with existing well log data (enabled by collaborations with the US Geological Survey (USGS) and the Bureau of Land Management), resulted in the identification of more than a dozen discrete and mappable gas hydrate prospects within the Milne Point area. Because the most favourable of those targets was a previously undrilled, fault-bounded accumulation, BPXA and the DOE decided to drill a vertical stratigraphic test well at that location (named the 'Mount Elbert' prospect) to acquire critical reservoir data needed to develop a longer term production testing programme. Gas hydrates were expected and found in two stratigraphic sections. An upper zone, (Unit D) contained *c.* 14 m of gas hydrate-bearing reservoir-quality sandstone. A lower zone (Unit C), contained *c.* 16 m of gas hydrate-bearing reservoir. Both zones displayed gas hydrate saturations that varied with reservoir quality as expected, with typical values between 60 and 75%. The Mount Elbert gas hydrate stratigraphic test well project included the acquisition of pressure transient data from four short-duration pressure-drawdown tests with Schlumberger's wireline MDT (Boswell *et al.* 2008). These tests were conducted in open-hole, and were designed to build upon the knowledge gained from cased-hole MDT tests conducted during the Mallik 2002 testing programme. The MDT and NMR log data from the Mount Elbert well also confirmed the presence of a mobile pore-water phase even in the most highly gas hydrate-saturated intervals. Gas hydrate dissociation and production was confirmed in the later stages of each test in which the pressure was drawn down below gas hydrate equilibrium conditions. Additional work anticipated within this effort includes a long-term production testing programme designed to determine reservoir deliverability under a variety of production/completion scenarios.

Mackenzie River Delta, Mallik, Canada

The JAPEX/JNOC/GSC Mallik 2L-38 gas hydrate research well, drilled in 1998 near the site of the Mallik L-38 well, included extensive scientific studies designed to investigate the occurrence of *in situ* natural gas hydrate in the Mallik field area (Dallimore *et al.* 1999). Approximately 37 m of core was recovered from the gas hydrate interval (878–944 m) in the Mallik 2L-38 well. Pore-space gas hydrate and several forms of visible gas hydrate were observed in a variety of unconsolidated sands and gravels interbedded with non-hydrate-bearing silts. Because of the success of the 1998 Mallik 2L-38 gas hydrate research well programme, the Mallik site was elevated as an important gas hydrate production test site with the execution of two additional gas hydrate production research programmes: (1) the Mallik 2002 Gas Hydrate Production Research Well Program; and (2) the 2006–2008 JOGMEC/NRCan Mallik Gas Hydrate Production Research Program.

In June of 2005, the partners in the Mallik 2002 Gas Hydrate Production Research Well Program publicly released the results of the first modern, fully integrated field study and production test of a natural gas hydrate accumulation (Dallimore & Collett 2005). During the Mallik 2002 testing programme, the response of gas hydrates to heating and depressurization was evaluated. The results of three short-duration gas hydrate tests demonstrate that gas can be produced from gas hydrates exclusively through pressure stimulation. Thermal stimulation experiments were designed to destabilize gas hydrates by using circulated hot water to increase the *in situ* temperature. Gas was continuously produced throughout the test at varying rates with maximum flow rate reaching 360 m^3 per day (Dallimore & Collett 2005). The total volume of gas flowed was small, reflecting that the test was a controlled production experiment rather than a long-duration well test. It also demonstrated the difficulty of heating a relatively large rock mass by conductive heat flow alone.

As described by Dallimore *et al.* (2008) and Yamamoto & Dallimore (2008), the 2006–2008 JOGMEC/NRCan Mallik Gas Hydrate Production Research Program was designed to build on the results of the Mallik 2002 project with the main goal of monitoring long-term production behaviour of gas hydrates. The primary objective of the winter 2006–2007 field activities was to install equipment and instruments to allow for long-term production gas hydrate testing during the winter of 2007–2008. After completing drilling operations, a short pressure drawdown test was conducted to evaluate equipment performance and assess the short-term 'producibility' of the gas hydrate-bearing section. During the most successful 12.5 h of the test, at least 830 m^3 of gas were produced. The test results verified the effectiveness of the depressurization method even for such a short duration. The following winter (2007/2008), the team returned to the site to undertake a longer term production test with the implementation of countermeasures to overcome the problems encountered in the previous year's programme. The 2007/2008 field operations consisted of a six-day pressure drawdown test, during which 'stable' gas flow was measured at the surface. The 2007/2008 testing programme at Mallik established a continuous gas flow ranging from 2000 to 4000 m^3/day.

Nankai Trough, Japan

The presence of extensive bottom-simulating reflectors (BSRs) in the Nankai Trough was confirmed with seismic surveys carried out as a part of METI's domestic geophysical survey programme. The 1999/2000 Nankai Trough drilling and coring programme targeted an area of a prominent BSR located about 50 km from the mouth of the Tenryu River in central Japan at a water depth of 945 m (Takahashi & Tsuji 2005). This drilling project, consisting of a pilot well and three post-survey wells, confirmed the existence of gas hydrate in the intergranular pores of turbiditic sands based on the analysis of downhole-logging data, and observations from both conventional and pressure cores. Gas hydrate was determined to fill the pore spaces in these deposits, reaching saturations up to 80% in some layers. Individual hydrate-bearing sand layers were less than 1 m thick, with the cumulative thickness of the hydrate-bearing sands totalling about 12–14 m.

A multi-well drilling programme titled 'METI Toaki-oki to Kumano-nada' was successfully carried out in early 2004 (Takahashi & Tsuji 2005). A total of 16 sites were drilled at water depths ranging from 720 to 2030 m. Based on the analysis of both the available downhole log data and core observations, three different types of gas hydrate occurrences were identified: (1) sand with pore-filling hydrate; (2) silt with pore-filling hydrate; and (3) nodular or fracture-filling massive hydrate in fine-grain sediments. Analysis of pressure cores and downhole log data indicates that average gas hydrate saturations in the cored sand layers ranged from 55 to 68%, with the average sediment porosities ranging from 39 to 41%.

NGHP Expedition 01, India

NGHP Expedition 01 was designed to study the occurrence of gas hydrate off the Indian Peninsula and along the Andaman convergent margin with special emphasis on understanding the geological and geochemical controls on the occurrence of gas hydrate in these two diverse settings. During its 113.5-day voyage (28 April to 19 August 2006), the research drill ship *JOIDES Resolution* (*JR*) cored or drilled 39 holes at 21 sites (one site in Kerala-Konkan, 15 sites in Krishna–Godavari, four sites in Mahanadi and one site in Andaman deep offshore areas), penetrated more than 9250 m of sedimentary section and recovered nearly 2850 m of core. Twelve holes were logged with logging-while-drilling tools and an additional 13 holes were wireline logged. NGHP Expedition 01 was among the most complex and comprehensive methane hydrates field ventures yet conducted. All of the primary data collected during NGHP Expedition 01 are included in either the NGHP Expedition 01 Initial Reports (Collett *et al.* 2008*a*) or the NGHP Expedition 01 Downhole Log Data Report (Collett *et al.* 2008*b*), which were prepared by the USGS and published by the DGH on behalf of the MOP&NG.

NGHP Expedition 01 established the presence of gas hydrates in Krishna–Godavari, Mahanadi and Andaman basins. The expedition discovered one of the richest gas hydrate accumulations yet documented (Site 10 in the Krishna-Godavari Basin), documented the thickest and deepest gas hydrate stability zone yet known (Site 17 in Andaman Sea), and established the existence of a fully developed gas hydrate system in the Mahanadi Basin (Site 19). For the most part, the interpretation of downhole-logging data and linked imaging of recovered cores, analyses of interstitial water from cores and pressure core imaging from the sites drilled during NGHP Expedition 01 indicate that the occurrence of gas hydrate is mostly controlled by the presence of fractures and/or coarser grained (mostly sand-rich) sediments (Collett *et al.* 2008*a*).

Drilling Expedition GMGS-1, China

In June of 2007, a deep-water gas hydrate drilling and coring programme was successfully completed by the Guangzhou Marine Geological Survey (GMGS), China Geological Survey (CGS) and the Ministry of Land and Resources of P. R. China (Wu *et al.* 2008). Drilling expedition GMGS-1 was carried out from April to June 2007 in the Shenhu Area on the north slope of the South China Sea. During Expedition GMGS-1, eight sites were drilled in water depths of up to 1500 m. Each site was wireline logged to depths of up to 300 mbsf with a set of high-resolution slim wireline tools. Five of the eight sites occupied during the expedition were cored. Gas hydrate was detected at three of the five core sites. The sediments were predominantly clay, with a variable amount of silt-sized particles including foraminifera. The sediment layers rich in gas hydrate were about 10–25 m thick and were found just above the base of the predicted gas hydrate stability zone (BGHSZ) at all three sites. Analysis of pressure cores confirmed that the gas hydrate occurred within fine-grained foraminifera-rich clay sediments, with gas hydrate saturations ranging from 20 to 40%.

Drilling Expedition UBGH1, South Korea

In November of 2007 South Korea completed its first large-scale gas hydrate exploration and drilling expedition in the East Sea: Ulleung Basin Gas Hydrate Expedition 1 (UBGH1). Leg 1 of UBGH1 included the drilling of five logging-while-drilling holes in the Ulleung Basin, which was used to select a sub-set of three sites that were more likely to contain gas hydrate for Leg 2 drilling and coring operations. Coring during Leg 2, at water depths between 1800 and 2100 m, confirmed the presence of gas hydrate-bearing reservoirs up to 150 mbsf (Park 2008). Gas hydrate was recovered at all three core sites, occurring as veins and layers in clay-rich sediments, and as pore-filling material within the silty/sandy layers. At one site, a 130 m thick hydrate-bearing sedimentary section of interbedded sands and clays was penetrated. Analysis of pore-water freshening revealed average gas hydrate saturations of about 30% for the hydrate-bearing sand layers.

Summary

There are numerous research projects under way to investigate the geological origin of gas hydrates, their natural occurrence, the factors that affect their stability and the possibility of using this vast resource in the world energy mix. We have seen highly successful cooperative research projects, such as various phases of the Mallik effort that has for the first time tested the technology needed to produce gas hydrates. We have also seen other highly successful co-operative gas hydrate research studies in India, northern Alaska and the Gulf of Mexico. In most cases, the co-operative nature of these efforts directly contributed to their success. It is also not surprising that the most aggressive and well funded gas hydrate research programmes are in countries highly dependent on imported energy resources, such as Japan and India.

References

Boswell, R., Hunter, R., Collett, T. S., Digert, S., Hancock, S., Weeks, M. & Mount Elbert Science Team 2008. Investigation of gas hydrate bearing sandstone reservoirs at the Mount Elbert stratigraphic test well, Milne Point, Alaska. *Proceedings of the 6th International Conference on Gas Hydrates* (ICGH 2008), Vancouver, British Columbia, 6–10 July.

Claypool, G. E. 2006. The Gulf of Mexico Gas Hydrate Joint Industry Project; covering the cruise of the Drilling Vessel Uncle John; Mobile, Alabama to Galveston, Texas; Atwater Valley Blocks 13/14 and Keathley Canyon Block 151; 17 April to 22 May, 2005. World Wide Web Address: http://www.netl.doe.gov/technologies/oil-gas/publications/Hydrates/reports/GOMJIPCruise05.pdf.

Collett, T., Riedel, M. *et al.* & The NGHP Expedition 01 Scientific Party, 2008*a*. *Indian National Gas Hydrate Program Expedition 01 Initial Reports*. US Geological Survey/Directorate General of Hydrocarbons. Ministry of Petroleum & Natural Gas (India), 1 DVD.

Collett, T., Riedel, M. *et al.* & The NGHP Expedition 01 Scientific Party, 2008*b*. *Indian National Gas Hydrate Program Expedition 01 Downhole Log Data Report*. US Geological Survey/Directorate General of Hydrocarbons. Ministry of Petroleum & Natural Gas (India), 2 DVD set.

Dallimore, S. R. & Collett, T. S. (eds) 2005. *Scientific results from the Mallik 2002 gas hydrate production research well program.* Mackenzie Delta, Northwest Territories, Canada. Geological Survey of Canada Bulletin, **585**, two CD-ROM set.

Dallimore, S. R., Uchida, T. & Collett, T. S. 1999. Scientific results from JAPEX/JNOC/GSC Mallik 2L-38 gas hydrate research well. Mackenzie Delta, Northwest Territories, Canada. *Geological Survey of Canada Bulletin*, **544**.

Dallimore, S. R., Wright, J. F. *et al.* 2008. Geologic and porous media factors affecting the 2007 production response characteristics of the JOGMEC/NRCAN/AURORA Mallik Gas Hydrate Production Research Well. *Proceedings of the 6th International Conference on Gas Hydrates* (ICGH 2008), Vancouver, British Columbia, 6–10 July.

Moridis, G. J., Collett, T. S. *et al.* 2008. Toward production from gas hydrates: assessment of resources and technology and the role of numerical simulation. *Proceedings of the 2008 SPE Unconventional Reservoirs Conference, Keystone, Colorado, 10–12 February*, SPE 114163.

Park, K.-P. 2008. Gas hydrate exploration activities in Korea. *Proceedings of the 6th International Conference on Gas Hydrates* (ICGH 2008), Vancouver, British Columbia, 6–10 July.

Smith, S., Boswell, R., Collett, T. S., Lee, M. W. & Jones, E., 2006. Alaminos Canyon Block 818: documented example of gas hydrate saturated sand in the Gulf of Mexico: Fire in the ice. *Methane Hydrate Newsletter*. US Department of Energy, Office of Fossil Energy, National Energy Technology Laboratory, Fall Issue, 12–13.

Takahashi, H. & Tsuji, Y. 2005. Multi-Well Exploration Program in 2004 for natural hydrate in the Nankai-Trough Offshore Japan. *Proceedings of 2005 Offshore Technology Conference, Houston, Texas, 2–3 May* (OTC17162).

Wu, N., Yang, S., Zhang, H., Liang, J., Wang, H., Su, X. & Fu, S. 2008. Preliminary discussion on gas hydrate reservoir system of Shenhu area, North Slope of South China Sea. *Proceedings of the 6th International Conference on Gas Hydrates* (ICGH 2008), 6–10 July.

Yamamoto, K. & Dallimore, S. 2008. Aurora-JOGMEC-NRCan Mallik 2006–2008. Gas Hydrate Research Project progress. DOE-NETL Fire In the Ice. *Methane Hydrate Newsletter*, Summer, 1–5. World Wide Web Address: http://www.netl.doe.gov/technologies/oil-gas/publications/Hydrates/Newsletter/HMNewsSummer08.pdf#Page=1.

King coal: restoring the monarchy by underground gasification coupled to CCS

P. L. YOUNGER, D. J. RODDY and G. GONZÁLEZ

Sir Joseph Swan Institute for Energy Research, Newcastle University, NE1 7RU, UK (email: p.l.younger@ncl.ac.uk)

Abstract: Coal has hitherto been seen as a potential fall-back resource as hydrocarbons become depleted. However, amidst anxieties over peak oil and gas, some recent studies have painted a picture almost as gloomy about the longer term prospects for coal. Such evaluations are misleading, as they identify as reserves only that coal accessible at reasonable cost by means of conventional mining, which are increasingly modest compared with deeper-seated coal reserves amenable to underground coal gasification (UCG) using directionally drilled boreholes from the surface. Significantly for the petroleum industry, the technological requirements for UCG are far more akin to those of oil and gas production than they are to those of deep mining. A number of projects around the world are revealing the feasibility of UCG. We highlight preliminary findings from a recent investigation of the potential for UCG in NE England, which has the longest history of conventional coal mining at industrial scale anywhere in the world. Despite this history, fully 75% of the coal resources in NE England remain in place. A significant proportion of these is likely to move to the 'reserves' register as underground gasification technology begins to be deployed. A particular attraction of UCG lies in its suitability for coupling to CCS: we can use our long-standing knowledge of the response of incumbent strata to longwall coal mining to predict substantial increases in permeability in and immediately above the voids created by gasification. As these engineered zones of high permeability will already be connected to surface power plants by the wells and pipelines used to produce synthesis gas during gasification, they represent ideal prospects for permanent sequestration of a large proportion of the carbon dioxide arising. Stored CO_2 will be kept in place by cap rocks higher up in the sequence.

Keywords: carbon dioxide, CCS, coal, gasification, *in situ*, reserves, UK, underground, wells

Most forecasters are now confident that 'Hubbert's Peak' – the global peak in oil production – will occur some time in the five years from 2017 to 2021 (e.g. Strahan 2008). The global peak in natural gas will follow a few decades thereafter. As Hubbert's Peak looms into view, the economics of petroleum production are finally shifting in favour of long-known but as yet little-exploited unconventional resources, such as the Athabascan tar sands, oil shales, shale gas and its close relative coalbed methane. Exploitation of coal itself, rather than the methane it contains, has often been identified as the best long-term prospect for maintaining global energy supplies beyond the maximum 50-year horizon offered by nuclear (Trainer 2006). However, atmospheric CO_2 emissions associated with conventional use of coal are the worst of all the fossil fuel categories, so that (outside of the developing world at least) strong resistance to increased coal use is now being experienced, due to concerns over runaway climate change. Opponents of increased use of coal rightly point to the ultimate need to move to a wholly renewable energy economy. Even in the absence of a need to combat climate change, this would still be the only option eventually, once all energy minerals have been exhausted. However, as Trainer (2006) has shown, all available renewable energy resources, exploited using all known or reasonably anticipatable conversion technologies, are insufficient to meet the extravagant demands of a modern consumer society, and will thus be very far from sufficient for a larger global population, especially if the developing countries aspire to levels of consumption already typical of the Global North. Furthermore, no-one has yet devised a renewable energy technology that does not require industrial-scale manufacturing to produce its component parts – and many of these manufacturing processes (e.g. production of steel) rely on continued use of coal. It is therefore likely that coal use will continue, and indeed expand worldwide in coming decades, not only while we develop better renewable technologies, but also while macro-economic adjustments take place (by design or disaster) to lower energy demand per capita in wasteful consumer societies.

Many commentators have complacently assumed that coal reserves are sufficient to support several centuries of exploitation without exhaustion. More recently, concerns have been expressed about some of the assumptions on which the more optimistic projections have been based (e.g. Strahan 2008). However, the pessimistic downgrading of likely reserve estimates is based on a fundamental assumption which cannot be left unchallenged: namely, that coal will only be exploited using conventional mining, which has depth limits of about 1500 m (because of severe floor heave issues), and is usually not economic below depths of a few hundred metres. If the possibility of underground coal gasification (UCG) is taken into account, the world's usable coal reserves are increased by a factor of at least three (McCracken 2008), and this increase will be achieved without the risk to life and limb posed by deep mining. Coupled with carbon capture and storage (CCS), UCG also offers a highly attractive carbon management option whereby most of the CO_2 arising can be permanently sequestered back in deep subsurface voids produced by the UCG process itself. If implemented at commercial scale, UCG with CCS (UCG–CCS) offers mankind's last, best 'bridging technology' to the inevitable renewable energy economy of the future.

A brief history of UCG

Although briefly postulated by Lord Kelvin in the late 19th century, the first UCG experiments were actually carried out by Sir William Ramsay (the discoverer of the noble gases), in 1912 in County Durham, NE England. Although these experiments were successful, further progress was halted by the First World War. Relatively

VINING, B. A. & PICKERING, S. C. (eds) *Petroleum Geology: From Mature Basins to New Frontiers – Proceedings of the 7th Petroleum Geology Conference*, 1155–1163. DOI: 10.1144/0071155 © Petroleum Geology Conferences Ltd. Published by the Geological Society, London.

low prices for oil and gas meant that for many years there was limited interest in further development of the technology. Nevertheless, a number of countries around the world have developed UCG operations. Most notably these have included the former Soviet Union and China, where commercial-scale operations have been conducted. Feasibility studies or trial operations have also been conducted in Australia, the USA, Spain, South Africa, India and the UK. The Underground Coal Gasification Partnership (UCGP) has estimated that around 20×10^9 m^3 of syngas have been produced to date from UCG activities across the world, equivalent to about 15×10^6 tonnes of coal. To date, the largest power generation plant based on UCG is a 100 MW steam turbine plant at Angren in Uzbekistan.

The focus of early trials such as those carried out in the former Soviet Union from 1930 and in China was on finding ways of controlling the underground gasification process, developing effective ways of drilling the injection and production wells, and of linking the two wells as a precursor to gasifying the coal. Most of this work can only be done at a significant scale in real coal seams, so trials tended to be expensive. In time the trials became bigger and longer in duration up to a point where it became sensible to build power generation facilities to run off the syngas being produced from an ongoing programme of coal seam gasification. Europe started to look at UCG during the 1950s and 1960s. Meanwhile, trials in the USA developed new variants on UCG technology and also explored more carefully the potential environmental impacts (Burton 2007). During the 1970s and 1980s, 32 separate tests were carried out along with a large supporting development programme. The main centre of interest was the Powder River Basin in Wyoming. One outcome from all of this was the development of a new control technique called ‘moveable injection’ (Friedmann 2008). Some work was also done on routes to chemicals production from syngas as an alternative to power generation. India started looking at UCG in the 1980s.

By the early 1990s, UCG was considered to be largely technically proven, but unfortunately that coincided with the start of the era of low-cost natural gas. Consequently, interest in UCG diminished and much of the development activity stalled except in China and also in Europe, where UCG came to be seen as an alternative to mining in respect of deeper, thinner coal seams. Between 1992 and 1998, trials were carried out at depths in excess of 500 m by a European consortium (UK, Spain and Belgium) on a site at Teruel in Spain (DTI 1999). These trials demonstrated the efficacy of a new technology termed ‘CRIP’ (controlled retractable injection point) in which the nozzle releasing the steam and oxygen into the coal is gradually drawn back out of a horizontal stretch of borehole as the coal surrounding it is gasified. The trials demonstrated that UCG in deep seams is feasible with minimal environmental impact at surface level. They also found that the gas produced had a calorific value similar to that achievable with surface-level gasification of coal, and showed that, at the higher operating pressure involved, there were significant volumes of methane produced in addition to the normal syngas components. Following on from these trials, a review of the feasibility of UCG in the UK was carried out, leading to proposals for a trial under the Firth of Forth in Scotland (DTI 2006).

The costs of performing UCG using a CRIP are dominated by the costs of geological exploration and drilling. However, parallel developments in the oil and gas industry over the last few decades have led to the opportunity to use effective forms of directional drilling (first used in the Spanish trial) to access coal for UCG. Many countries with indigenous coal resources are now re-examining the opportunities offered by UCG, including South Africa and Australia. The driving forces include security of energy supply, the cost of syngas relative to natural gas and crude oil, and the option of using the syngas for power generation in a combined-cycle power plant.

To date there are no examples of integrated UCG–CCS projects being constructed anywhere in the world. This is because storage of CO_2 as a supercritical fluid (i.e. a fluid with the density of a liquid but the compressibility, viscosity and diffusivity of a gas) requires depths of at least 750 m (and probably more than 800 m for impure CO_2 recovered from flue gas), whereas UCG projects around the world to date have targeted coal seams which are shallower than this ($\leq$600 m).

The UCG process

UCG involves gasifying coal *in situ* by means of directionally drilled wells, using drilling technology developed by the oil and gas industry. The sequence of events involved in UCG is shown in Figure 1. Gasification means ‘partial oxidation’, and in the case of coal, about 80% of the original calorific value of the solid coal will be present in the resultant gas. Gasification is achieved by an exothermic reaction, which is initiated by reaction with hot steam and oxygen introduced via injection boreholes. As the operator controls the availability of oxygen, so the degree of oxidation is under the operator’s control. The resultant hot gas mixture – known as synthesis gas or ‘syngas’ – contains hydrogen, methane and carbon monoxide, all of which have significant calorific value. Depending on precise gasification conditions, varying proportions of CO_2 and hydrogen sulphide may also be present in the syngas, although hydrogen sulphide is mobilized to a far lesser degree than in conventional coal combustion (NCC 2008). The precise proportions of the various component gases in any particular syngas mixture is a function of depth (since gasification is more efficient at high pressure), oxygen injection rate and coal seam quality. Examples of typical UCG syngas compositions from a variety of coals are reported by Galli *et al.* (1983), Pirard *et al.* (2000), Perkins & Sahajwalla (2006), Khadse *et al.* (2007) and Yang (2008). These sources reveal component gas fractions in the following ranges:

- H_2, 11–35%;
- CO, 2–16%;
- CH_4, 1–8%;
- CO_2, 12–28%;
- H_2S, 0.03–3.5%.

The syngas is drawn to the surface via neighbouring production boreholes, whence it can be transported by pipeline for use in a wide range of applications, such as driving turbines to generate electricity or for manufacturing products ranging from plastics to gas and liquid transport fuels. Pre- and/or post-combustion cleanup to minimize emissions of SO_x and NO_x is typically not required for UCG applications, due to the paucity of H_2S and NH_3 in the raw syngas (NH_3 is usually entirely absent because of the strongly exothermic nature of the nitrogen oxidation reaction, which at high temperatures and pressures favours the persistence of nitrogen gas). Gaseous emissions of toxic metals are also generally negligible, as the ash present in the coal remains below ground, and largely avoids fusion (NCC 2008). Given that most UCG processes are oxygen fuelled, CO_2 and water vapour are the only gaseous exhaust streams produced after gasification, thus making separation and capture of the CO_2 relatively simple and cheap. The process is, therefore, particularly compatible with CCS.

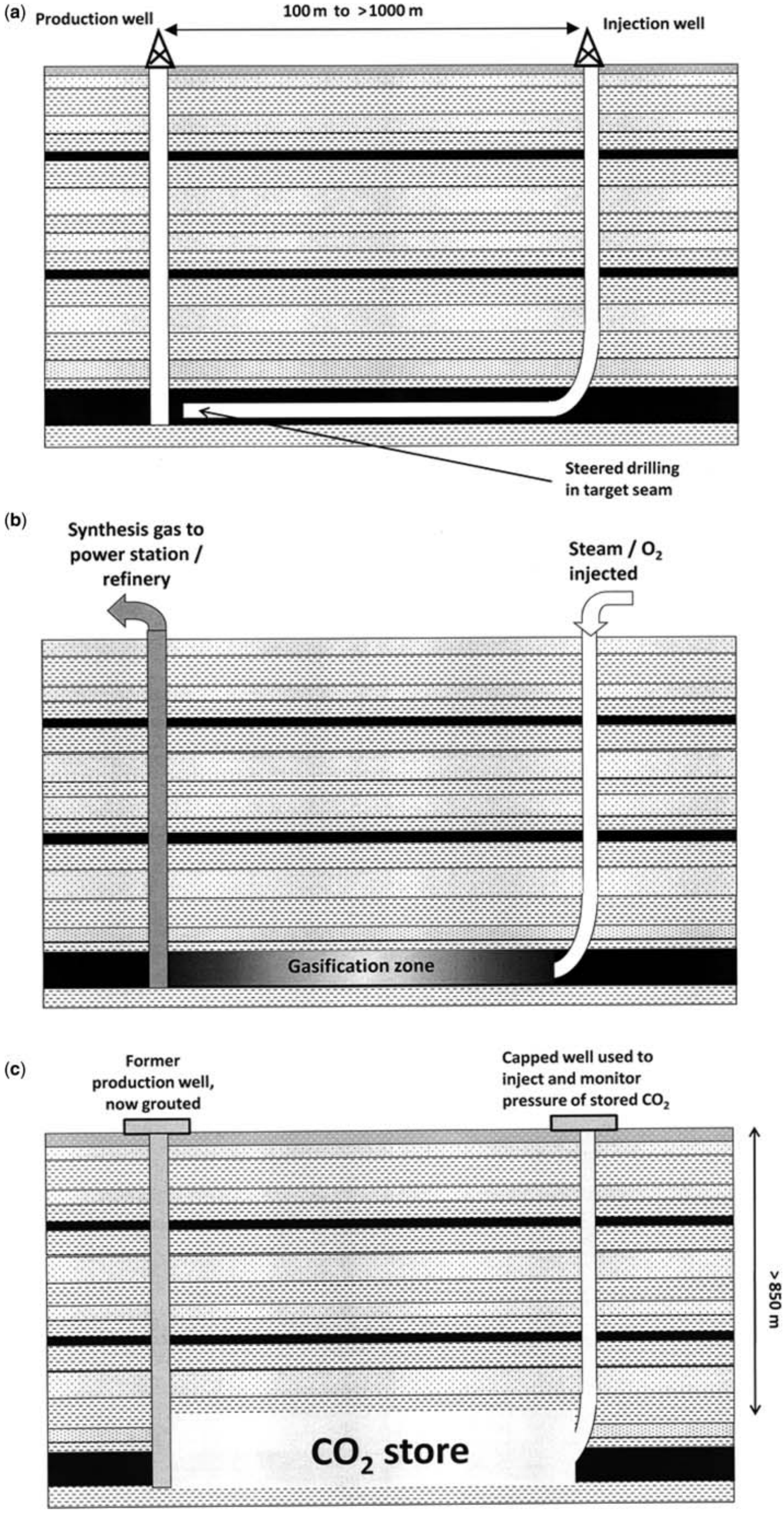

Fig. 1. Three stages in UCG–CCS. (**a**) Directional drilling of injection and production wells; the two wells do not coalesce, but a small pillar of coal is left between them which is amongst the first coal to gasify. (**b**) Creation of void by gasification to produce syngas; the gasification zone develops from left to right, progressively consuming coal closer and closer to the injection well as the controlled injection point is retracted from the end of the lateral bore. (**c**) Sealing of injected CO_2 in goaf produced by collapse of void in former gasification zone.

Prospects for CO_2 storage in UCG goaf

The UCG process creates voids deep underground following gasification of the coal. These voids will inevitably collapse, just as voids produced by longwall coal mining do, leaving high-permeability zones of artificial breccias – known as 'goaf' (from the Welsh word *ogof*, meaning a cave) – which are almost invariably isolated from the surface by low-permeability superincumbent strata (Younger *et al.* 2002). Where UCG has taken place at depths in excess of about 700–800 m, storage of CO_2 in these artificial high-permeability zones is a very attractive proposition. A combined UCG–CCS project could achieve a reduction in CO_2 emissions of as much as 85% compared with conventional coal-fired power generation. Such a project therefore offers a very attractive solution and is the only process yet devised that offers integrated energy recovery from coal and storage of CO_2 at the same site. In principle, UCG–CCS can also sit happily alongside some other CCS approaches: where CO_2 collection and transmission pipelines can be linked together, new degrees of freedom for carbon management emerge (Roddy 2008).

Subsurface injection of gases is being successfully accomplished worldwide for different purposes and in different scenarios. This includes oil and gas operations, temporary storage and permanent disposal. As some examples of this, since the 1970s, the oil industry has been practising enhanced oil recovery (EOR), which involves the injection of CO_2 into the oil reservoir, and more recently enhanced gas recovery (EGR) for gas reservoirs, including coalbed methane systems (e.g. Ross *et al.* 2009). For almost 100 years natural gas storage in salt caverns has been practised to allow supply flexibility against a fluctuating demand, and acid gas has been injected underground since the 1990s as waste in Canada.

With regard to CO_2 geological sequestration, the Intergovernmental Panel on Climate Change (Metz *et al.* 2005) proposed the following main scenarios for underground storage of CO_2: active and depleted oil and gas fields, deep saline aquifers, deep unmineable coal seams and (marginally) caverns or basalts. Based on the expected storage capacity and current experience, most of the efforts in research and all of the commercial-scale operations have been directed to storage in oil and gas operations, depleted hydrocarbon fields and associated deep saline aquifers. That is the case with Sleipner, Weyburn, In-Salah and more recently, Snohvit. Their individual annual injection rates are in a range of $0.7–2 \times 10^6$ tonnes of CO_2 and their total storage will amount to $17–20 \times 10^6$ tonnes of CO_2 each. Injection into deep unmineable coal seams has been tested in laboratory and field, with disparate results. The Recopol project in Poland found major problems in the injection of the CO_2 due to the plasticization and swelling of coal when the CO_2 is adsorbed in the coal matrix and displaces the methane. However, one option that has not been widely considered yet and could be of great interest due to a combination of economic and technical aspects is the storage of the CO_2 in the voids created by UCG.

The prospects for carbon sequestration in a UCG operation arise from a serendipitous association of a source of CO_2 and a viable long-term storage site. As with the other major CCS options, UCG–CCS takes place in a sedimentary basin with specific geological features that are particularly appropriate for geological storage. The general requirements of a site for carbon geological storage are (Metz *et al.* 2005):

- proximity to a source of CO_2, to guarantee the supply of CO_2 and improve the economics of the operation by avoiding long transportation routes;
- injectivity – the formation needs a high enough permeability to allow the injection of the fluid;
- storage capacity – sufficient to store the CO_2 produced during the plant lifetime;
- containment – some trapping mechanism has to guarantee the permanence of the CO_2 store for a considerable amount of time, *c.* 1000 years.

In addition to the generic site requirements, it is important to note the effect of the characteristics of the CO_2 stream in the constraints set on the storage site. The first of the four requirements is fully achieved by the UCG–CCS configuration. The plant and CO_2 injection infrastructures, geological and geophysical studies will have already been developed for the UCG operation when the time comes for CCS. Although capture is the main component of the cost of CCS (70–80%), the cost reduction in the remaining 20–30% is very significant.

For the other three requirements, extensive experience and knowledge in underground coal mining, especially caving methods of mining (longwall and its derivatives), provides the insights for the assessment and preliminary prediction of CO_2 storage capability. In a longwall panel, all of the coal is progressively removed from a rectangular area, and the roof is allowed to collapse, forming goaf. Typical longwall panels are usually about 1 km long, 150–250 m wide and 1–3 m high. Although there are different possible layouts for a UCG operation, one configuration is a chamber with a length of 500–600 m, 30–40 m wide and with the height equal to the thickness of the coal seam. A longitudinal pillar would separate the gasification chambers. A gasification chamber of the above dimensions corresponds to the 'shortwall' variant of collapse-based coal mining, a configuration which is well understood, as it is widely used in conventional mining to achieve rapid face movement with minimal disturbance of overlying aquifers.

Regarding the second requirement, injectivity, the absolute rock permeability is the most significant parameter to consider, the injection pressure is the second most significant parameter, and porosity is not as relevant. Thus, the injected amount varies almost linearly with permeability, while a 20% increase in injection pressure results in a 50% increase in injected CO_2 and a 100% increase in porosity shows only a 7% increase in injected CO_2. It is also important to note that the existence of a high-permeability area (or 'sweet zone') close to the injection point and a high contrast with the regional permeability acts as an enhancing factor for injectivity (Law & Bachu 1996).

Permeability changes in the surrounding strata of underground coal mining operations have been thoroughly studied in the past to inform engineering design for safe operations which avoid inducing large water inflows or gas outbursts (e.g. Younger *et al.* 2002; Esterhuizen & Karacan 2005). The process of goaf formation behind a longwall shearer track induces the formation of four distinct 'layers' above the cavity (Younger & Adams 1999):

- A caved zone, with broken blocks that have come off the roof – this is the broken material referred to as 'goaf'. The zone extends vertically to between three and six times the coal seam thickness. The final permeability of this zone will depend on the grade of re-compaction of the goaf. In the case of longitudinal pillars along the cavity, these would help to decrease the compaction, resulting in a higher permeability of the goaf. Direct measurements of saturated goaf are rather rare, but reported values are in the range of 1–20 Da (Younger *et al.* 2002), while values inferred from the hydrological behaviour of large systems of flooded panels range up to several hundred Da.
- A fractured zone with continuous fractures, joint opening and low stress. It extends to between 15 and 60 times the extraction height. Water and gas can drain directly to the void, as

Table 1. Comparison of typical permeabilities (in Da) of oil/gas reservoirs (and thus of deep saline aquifers) (after Levorsen 1967) and goaf formed by total collapse of extracted voids in coal (from literature sources and modelling results collated by Younger & Adams 1999)

Permeabilities (Da) of oil and gas reservoirs (and of deep saline aquifers)		Permeabilities (Da) of goaf from longwall mining (analogues for those formed by UCG)	
Poor reservoir	0.001–0.01	With mudstone roof strata	1–10
Good reservoir	0.01–0.1	With thinly interbedded silt–sand–mud–stone roof strata	10–50
Excellent reservoir	0.1–1	With strong sandstone/limestone roof strata	20–500

permeability in this zone can be up to 40 times the original permeability.

- A bending zone where horizontal bed separation and joint opening takes place, increasing horizontal hydraulic conductivity. This can extend to 60 m ahead of the longwall face.
- A zone of intact rock, often subject to compression beneath a final carapace of mildly extensionally disturbed rock, at or below the ground surface.

In longwall mining under the North Sea, changes in permeability of three orders of magnitude due to mining have been reported in the fractured zones above goaf (Neate & Whittaker 1979). The usual figures assumed are an increase of 100 mDa in vertical permeability and 50 mDa in horizontal. Predictions with improved modelling techniques show increases of up to 35 times in vertical permeability and 1000–2000 in horizontal permeability up to 50 m above the mining void (Guo *et al.* 2009).

In contrast, the permeabilities of oil and gas reservoirs (and thus of deep saline aquifers generally) have long been known to range from about 0.001 up to 1 Da (Levorsen 1967). As summarized in Table 1, UCG goaf and the relaxed roof strata above this will typically have permeabilities one to three orders of magnitude greater than the high end of this range. Therefore, it can be concluded that the UCG goaf and the zones of enhanced permeability above them represent a highly attractive prospect for CO_2 injection. UCG voids can be expected to cool rapidly due to goaf formation and groundwater ingress, so that even rapid subsequent CO_2 injection would be into pre-quenched zones. However, there are still some gaps in knowledge on the thermal effects on the overlying strata of the cavity, the presence of ashes and coal which can swell, and the effect of the injection pressure if it takes place before collapse.

The third requirement to consider is the storage capacity. Obviously, a remarkable advantage of UCG is the creation of a void that was not previously present. However, a rough estimation shows that the volume needed at 800 m depth to store the CO_2 produced from the syngas can be four or five times the volume occupied by the extracted coal. As with depleted hydrocarbon fields and deep saline aquifers, the storage capacity will depend on the specific storage, that is, the compressibility of the strata without exceeding the fracturing limit of the rock. Regulations for subsurface injection of waste gases in Alberta set the injection pressure limit at 90% of the rock fracturing pressure (Law & Bachu 1996).

The last requirement of a site for CO_2 geological sequestration is that it can provide containment for a considerable period of (say) 1000 years. The trapping mechanisms have been described in detail for deep saline aquifers and depleted hydrocarbon fields (Hitchon *et al.* 1999; Metz *et al.* 2005; Bradshaw *et al.* 2007). First of all a caprock is required which acts as a structural seal for the buoyant supercritical CO_2. Then, with increasing temporal and spatial scale, the rest of the mechanisms start to work: hydrodynamic trapping, residual gas dissolution in formation water and mineral precipitation. All these processes will occur according to the physical and chemical characteristics of the site and the CO_2 stream. In addition, in the case of UCG, the organic and inorganic by-products will certainly be mobilized with the CO_2 due to its solvent power, which is a key consideration in planning to avoid any pollution of adjoining aquifers in the event of contaminant migration. This will affect the chemical reactions in the water and the rock. It is also possible that the CO_2 is adsorbed in the coal matrix due to its higher affinity compared with other elements. In such a case, any resulting methane emissions would need to be factored into the overall greenhouse gas sequestration calculation.

As with permeability issues, the experience of underground coal mining is helpful in the quantification of containment in a coal basin. For more than a century, underground coal mining has been carried out under the sea in NE England using longwall methods, with workings extending as far as 14 km from shore; yet no incident of sea water in-rush ever occurred (Bičer 1987). Coal mining regulations in Britain state that the minimum distance from the seabed to mine works is 105 m, 60 m of which has to be within Coal Measures strata. Given that the viscosity of water is higher than that of supercritical CO_2, further comfort might be sought. In a more closely analogous case, Whittles *et al.* (2006) simulated the leakage of methane (with a viscosity of 1.75×10^{-5} Ns m^{-2}) into the mine workings in a UK colliery. They found that potential sources beyond 20 m of the working face would not leak into the roadway due to the reduced permeability resulting from increased confining stress.

In conclusion, it can be expected that the trapping mechanisms described in the literature will work in the case of UCG, and that specific sites which meet the requirements can provide the necessary confinement. However, caution has to be exercised, as there is no experience of the large scale that CO_2 storage would imply. The cumulative effects of multiseam extraction could also be important.

Another critical aspect which influences the mechanisms and requirements for the CO_2 storage site is the characteristic of the CO_2 stream to be injected. Anthropogenic CO_2 contains impurities which depend on the combustion process and the capture method. Some of these impurities are H_2O, SO_2, NO, H_2S, O_2, CH_4, HCN, Ar, N_2, H_2 and particulates (Anheden *et al.* 2005) and they will affect the thermodynamics (density, viscosity, critical point) compared with pure CO_2 (Li *et al.* 2009). In general, the presence of impurities decreases the critical temperature and increases the critical pressure (Seevam *et al.* 2008) at which CO_2 enters its supercritical state – which is essential for geological storage without further reaction. A stream emanating from a post-combustion process shows the smallest difference compared with pure CO_2, but in the case of pre-combustion or oxyfuel processes, the supercritical pressure can reach 83 or 93 bar while the critical temperature decreases to 29 or 27 °C respectively (Seevam *et al.* 2008). For typical northern Europe conditions, this would imply minimum depths in the order of 800 m for CCS to work (it could be deeper than 900 m if an oxyfuel combustion flue gas is to be stored).

Remaining technical challenges for UCG–CCS implementation

UCG–CCS faces the same challenges as any other comparable industrial operation, in relation to issues such as pollution prevention (e.g. WS Atkins Consultants Ltd 2004; Liu *et al.* 2007), landscape protection, nature conservation, etc. As UCG involves total extraction of coal in certain areas, it has the potential to induce land subsidence in a manner similar to longwall coal mining, albeit at the depths appropriate for UCG–CCS, surface lowering would be barely detectable. Long-established procedures for dealing with coal mining subsidence (e.g. NCB 1975) can be readily transferred across to UCG–CCS operations.

Nevertheless, a number of open questions remain, which will only be settled as UCG–CCS is more widely implemented at full scale and refined in the light of experience. These include the following issues:

- optimal layouts for injection and production boreholes, and strategies for managing simultaneous multiple-seam UCG–CCS development;
- borehole integrity, especially in view of the extremes of heat which are experienced by production boreholes, and the extremes of chilling which can be expected during CO_2 injection;
- the feasibility of adapting existing offshore platform technology to accommodate the full range of high-temperature operations required for UCG–CCS implementation;
- lack of precise process control in comparison to conventional (surface) gasifiers – it is not possible to fully predict or control rates of groundwater ingress, heterogeneity in reactant availability within gasification zones, or the precise limits and rates of expansion of voids and the concomitant formation of goaf and, because of this, and because of the lack of any equivalent of stockpiling fuel, it is difficult to get UCG to proceed as a steady-state process (in terms of both gas yields and heating values) unless a large number of auxiliary boreholes are installed (cf. NCC 2008);
- the response of strata to coal removal under non-isothermal conditions – in conventional coal mining, thermal effects can be ignored in geomechanical modelling, but it is unlikely that this approach will remain valid in situations of extreme temperature gradients as expected during UCG.

Active research on all of these topics is currently under way at a number of centres worldwide, and early indications are that all of these difficulties are surmountable.

The economic case for UCG–CCS

As with all commodities, the economic case for UCG–CCS amounts to a balance of credits and debits. On the credit side, UCG–CCS offers a low-cost route to emissions reduction; the cost is lower than for surface gasification plants because there is no need to mine, store or transport coal, there are no solid residues to dispose of, and there is no need to purchase a gasifier; it converts an abundant natural resource into a secure, economic supply of gas; it enables stranded coal resources (e.g. deep or offshore) to be converted into commercial reserves; there is a range of potential end uses and markets, for example, power generation, heating, synthetic fuels, chemicals and hydrogen; it is largely immune to crude oil price swings (unlike conventional coal mining which relies on diesel-fuelled equipment and transportation); it is cheaper than natural gas for power generation; and finally, as has been explained in greater detail above, UCG creates conditions for deep geological storage of CO_2 which are orders of magnitude more favourable than natural saline aquifers or depleted hydrocarbon reservoirs.

On the debit side of the balance sheet for UCG–CCS are: technical and commercial uncertainties (e.g. lack of economies of scale) since the technology has not yet been widely deployed; syngas production rates and composition are variable compared with pipeline-delivered natural gas; open-cast coal mining (where acceptable) is cheaper; ground subsidence must be managed, and there is some risk of aquifer contamination; trials and prospective site evaluation are expensive; there can be significant costs in transporting the syngas to the point of use; carbon capture technology for high-temperature pre-combustion applications is not yet a commercial reality (though capture post-combustion is); and planning approval processes (not only for UCG but also for CCS) are still under development in the majority of countries.

Wide-scale proliferation of commercial UCG projects has thus far been inhibited by the availability of comparatively cheap supplies of crude oil and natural gas. Looking at 2008 data, against a natural gas price (in the USA) of \$9 per million Btu, raw syngas can be produced via UCG in the onshore USA for \$1.8 per million Btu based on air gasification (Green 2008). Using oxygen-blown UCG in onshore Europe, the cost of syngas becomes \$3.8 per million Btu. These figures are now sufficiently low for UCG to look commercially attractive whenever oil and gas prices are reasonably high.

The economic case for UCG syngas displacing natural gas or coal for power generation is relatively straightforward. Alternative uses such as conversion of syngas into liquid fuels, chemical intermediates or hydrogen are more difficult because, whilst the added value is well known (and much higher than for power generation), there is a tighter requirement for syngas cleanup. Technologies for cleaning up UCG syngas to chemical feedstock standard are still under development and so the costs are less well known. There are several such projects under way at present, which should help elucidate the figures in due course.

Other factors beyond straight economics then come into play to tip the balance. The main considerations are: CO_2 emissions and climate change; air quality and power station emissions; a desire for some protection against volatile and rising oil and gas prices; and considerations of national energy and fuel security in a politically unstable world – after all, the distribution of coal around the world is different from the distribution of oil and gas.

There is an additional factor to consider – and one that is difficult to place a value on in economic terms. More than 5000 deaths a year occur in the coal mines of China: four deaths for every million tonnes of coal mined. In Ukraine, the death rate is even worse: seven deaths per million tonnes. To put these figures into perspective, the last time death rates in UK coal mines were as high as they currently are in China was back in the 1920s; in the case of Ukraine the parallel figures occur way back in the 1880s. Much of this mining is linked to energy provision in support of the manufacture of goods for export to Western countries. UCG could provide an ethically acceptable way of enabling this economically driven low-cost manufacturing activity to continue.

Approaches to environmental risk assessment for UCG–CCS

An Environmental Risk Assessment (ERA) should answer four questions: what can occur that causes adverse consequences; what is the probability of occurrence of these consequences; how severe can they be; and how can they be reduced? This last issue is often referred to as risk management, though it differs from the more general risk management which takes into account economic and social considerations. The steps in performing an ERA to address these questions are:

- hazard identification, to reveal the contaminants and adverse situations that can be expected;
- exposure assessment, to describe the intensity, frequency and duration of exposure, routes of exposure and the nature of the population exposed;
- effect assessment, to describe the response of the receptors;
- risk characterization, to provide an estimate of the likelihood for adverse impacts, with endpoints definition and a qualitative or quantitative approach;
- risk management, which includes monitoring and mitigation options.

The ERA is a critical aspect in the development of both UCG and CCS and so far the two processes have been addressed separately. However, they share substantial common ground. Usually, when the ERAs are undertaken for UCG and for CCS, each is split into surface operations and what happens underground. The handling of gases like syngas from UCG or CO_2 is common practice in industry, and environmental, health and safety and other standards and regulations are well established. Also the engineering design is controlled, resulting in low failure rates. For example, CO_2 pipeline failures in the USA in the period of 1990–2001 had a frequency of 3.2×10^{-4} incidents per kilometre per year and the frequency of oil well blowouts in the Gulf of Mexico and the North Sea was of 10^{-4} incidents per well per year (IEA 2004). However, when it comes to the underground dimension, lack of previous experience and large uncertainties in geology and in hydrogeological, chemical and geomechanical behaviour appear.

The environmental risks associated with UCG were one of the reasons why UCG was not further developed in the 1970s and 1980s in the USA. Despite its indisputable benefits, initial trials at shallow depth (less than 200 m below surface), which produced groundwater contamination and even severe surface subsidence (as in Hoe Creek), discouraged pursuit of new experiments. Nevertheless, more recent projects (like Chinchilla in Australia) have proved that with good site selection and operation control, groundwater contamination can be avoided.

The main risks to be considered in UCG are groundwater depletion, groundwater contamination, gas leakage and subsidence. Set against these, its environmental advantages compared with conventional coal mining and surface combustion include the elimination of coal transport, stockpiles and much of the disturbance at surface, low dust and noise levels, the absence of health and safety concerns relating to underground workers, the avoidance of ash handling at power stations, and the virtual elimination of SO_x and NO_x emissions. Most of the contaminants produced in coal gasification are included in List I of the Water Framework Directive (2000/60/EC), which forbids release into a water body. Consequently, for a UCG operation to be permitted in the EU, any potential water contamination would almost certainly have to be restricted to water which had been previously classified as Permanently Unusable. The potential contaminants have been described and are well known (Humenick & Mattox 1978; Liu *et al.* 2007). They include organic compounds (phenols, benzene, PAHs and heterocyclics) and inorganics (calcium, sodium, sulphate, bicarbonate, aluminium, arsenic, boron, iron, zinc, selenium, hydroxide and uranium).

The approach that is proposed for environmental assessment of UCG is a risk-based approach with a source–pathway–receptor scheme (WS Atkins Consultants 2004). For CO_2 storage, the main risks identified are divided into three groups (Chadwick *et al.* 2008): leakage, dissolution in formation water and displacement. At a local scale, leakage into the atmosphere or the shallow subsurface can cause asphyxiation to animals or humans, or affect plants and underground ecosystems. If the leakage is offshore, it can affect the living organisms in the water column and the seabed and interfere with other legitimate uses of the sea. It is also important to make a distinction between sudden large releases and continuous small ones. Large releases from the storage site, however, are not expected unless there is a secondary accumulation close to the surface. The CO_2 injection could also initiate the mobilization of methane which is potentially explosive. On a global scale, the leakage of CO_2 or methane would hinder the ultimate aim of the sequestration, which is to reduce the concentration of greenhouse gases in the atmosphere. If a leak contains some other contaminants, they can pose an additional threat if exposure times and concentrations are toxic or carcinogenic. Regarding the risks resulting from dissolution in other fluids, the variation in pH of water caused by CO_2 can lead to the mobilization of metals. As CO_2 is a very good solvent, it can also transport other organic contaminants and contaminate potable water. The displacement of the CO_2 plume can induce seismicity or ground heave or subsidence. The brines pushed away can contact and contaminate potable aquifers or damage other mineral or energetic resources. It is also important to note that, although a single specific site should not pose a high risk, there is a cumulative effect as the number of storage sites increases in response to the large-scale opportunity for global warming mitigation.

The coupling of UCG–CCS alters the hazards and the risks inherent in UCG or CCS on its own (Burton 2007). On the one hand, the operation takes place at a much greater depth than conventional UCG (so that the conditions for CO_2 in its supercritical state are met). This certainly decreases the risk of potable aquifer contamination and of subsidence effects on the surface. In addition, the physical response of the surrounding coal to the CO_2 injection can help reduce the migration pathways by swelling. On the other hand, the pressurization of the cavity with the injection of the CO_2 can increase the risk of fracture propagation. Under these circumstances, the organic and inorganic by-products of gasification are forced out of the reaction chamber as the CO_2 is injected and pressurized in the void. The transport of organic and inorganic contaminants dissolved in the CO_2 through a fractured and porous medium is an area that has not been studied yet. Their concentration in the CO_2 plume and the changes in flow and chemical reactions between the CO_2, tars, ash, coal, brine and the formation rocks are unknown.

Although it is desirable to have a quantitative risk assessment, this has not always been possible in the ERAs performed for CO_2 storage projects. The reason for this is the lack of available data at this stage. Consequently, some studies have been performed using a deterministic analysis based on well proven numerical simulation tools and examining different scenarios (Espie *et al.* 2005). There have been various projects around the world to perform the ERA of CO_2 geological storage using several methodologies to characterize risk (Damen *et al.* 2006). From these projects, it seems likely that the most effective approach for UCG–CCS risk characterization in the future will have to combine deterministic numerical models with probabilistic analysis. These models will have to be able to couple thermal, geomechanical, transport and chemical processes.

Monitoring is especially important at the local scale, to be able to detect and mitigate any threat to safety. On a global scale, monitoring is important for dealing with issues related to credits for emissions reduction. Monitoring of the UCG operation is based on measurement of temperature, pressure and mass balance, as well as water chemistry and water level in monitoring wells. In the CO_2 injection phase, CO_2 stream injection rates, composition, temperature and pressure have to be monitored. The migration of the CO_2 can be checked with periodic sampling of air, water and soil, with pressure and logs in wells, with CO_2 flux chambers or using eddy covariance and indirect techniques such as geophysics or remote sensing. Since sealed wells represent the preferential pathway for leakage, their integrity has to be assured. That can be done with cement bond logs (Metz *et al.* 2005; Burton 2007; Chadwick *et al.* 2008). The mitigation options in the event of leakage are: recapping of leaking wells, reducing injection pressure, stopping injection, sealing the fracture or transferring the CO_2 (Anonymous 2006).

Northeast England case study

Despite the long history of industrial coal mining in the region (starting in 1585), huge reserves of coal remain in NE England. Only about 25% of the total coal resources have been extracted. There is coal in abandoned mines that is technically mineable – perhaps in excess of 500×10^6 tonnes. Some of this coal lies under land: most under the sea. However, because the mines have not been maintained there would be expensive problems to overcome. Typically it is found that roadways deteriorate, and electrical and mechanical equipment is destroyed as a result of flooding once water pumping operations cease. There is also the possibility of trapped water leading to sudden in-rushes, which would present a risk to personnel in the event of underground mining being re-established (Younger *et al.* 2002).

Then there is the coal that lies at depths considered uneconomic for conventional mining – both under the land and under the sea. This is particularly attractive for UCG when linked to CCS for the reasons given above, and could easily exceed another 500×10^6 tonnes. Previous estimates for the UK have suggested that between 7 and 16×10^9 tonnes of coal suitable for UCG could be available – and that ignores all coal below a depth of 1200 m (Green 2008).

Project Ramsay (named after Sir William Ramsay) was established to assess the opportunity for UCG–CCS in NE England. As part of the project, specialists were commissioned to undertake a thorough review of all available data to determine the quantity and accessibility of coal suitable for UCG and for UCG–CCS in nearshore areas of the NE coast. The study examined available data from a number of sources including the Coal Authority, the British Geological Survey and BERR as well as data held by others, including Newcastle University.

Suitability of the area was considered for UCG and UCG–CCS taking into account coal seam thickness, depth of cover between the top of target coal seams and the seabed where relevant, permeability of the pertinent strata and, where relevant, stand-off distances from old workings. For UCG a depth of 100 m or greater was used, and for UCG–CCS the minimum depth was increased to 800 m to achieve the storage pressures necessary for CO_2 in its supercritical state.

The project considered both nearshore coal seams (<2 km) and offshore coal seams (up to 10 km) at a few locations. The primary difference in approach between nearshore areas and further offshore is in the ability to reach the coal reserves from a wholly shore-based enterprise using directional drilling v. the need to utilize offshore rigs. Cost analysis has shown that there is not a significant cost advantage in one approach over the other for the coal reserves under consideration. The initial high cost of offshore rigs is broadly offset by the more expensive long-reach drilling costs associated with a nearshore project. The project found some very interesting coal seams and concluded that previous estimates of UCG-compatible coal resource had been conservative.

However, generating syngas from coal is only part of Project Ramsay: the region also provides ready energy and chemicals markets for syngas and its derivatives, and therefore offers a genuine prospect for a commercial UCG–CCS operation. Geography is important: these markets need to be sufficiently close to the chosen UCG base to be serviceable economically. The siting of a UCG production operation in NE England allows ready access to the process industry markets on Teesside for syngas and for derived gas products of methane and hydrogen. Equally, there are a number of existing power users and potential new investments in power generation plant at a scale that could make syngas a viable fuel. These options were all reviewed as part of the feasibility study.

From its inception, Project Ramsay always considered CCS as being an essential element of a successful UCG project. Consequently, detailed consideration has been given to those coal targets that are at sufficient depth to provide the option for CO_2 storage and where significant revenues can be generated by providing a long-term storage site for CO_2. Note, however, that CO_2 is also generated in large quantities by the same process and power industries that provide a potential market for the syngas and its derivatives. Increasingly there is a business opportunity in CO_2 collection, transmission and storage. There is therefore the option of extending the envelope to take in CO_2 from other industrial sources and offer additional storage capacity. The voids created through the UCG process in deep coal seams provide a storage option for CO_2 whether that CO_2 was produced through use of UCG syngas or from other industrial activities.

The study took account of specific local factors such as: the location of the most suitable coal seams relative to existing power plants and potential new power plants; the existence of pipeline corridors; the location of the most suitable coal seams relative to large industrial users of syngas and hydrogen; the potential for linking into other sources of CO_2 and CO_2 collection systems; the potential for connecting the UCG facility to the proposed new CO_2 pipeline linking the Eston Grange IGCC/CCS plant to storage locations under the North Sea, and so on.

The broad conclusions were that: previous estimates for UCG-compatible coal had been conservative; there are coal seams that appear to be usable for CO_2 storage following UCG; and some of the end uses for syngas are potentially attractive. The most attractive options in financial terms are (1) to sell syngas, take back captured CO_2 and store it for a fee, and (2) to sell decarbonized hydrogen and methane. It was concluded that a project could be done in three phases, ramping up the scale over time in order to minimize technical risk and investor exposure. Such a project could deliver a profit before year 10 and therefore might warrant follow-on discussion on a more commercial basis with interested parties. If developed on a broader scale, it could act as a source of investment funds for the renewable energy sector and thereby go beyond the ambition of being a bridging technology on the road to a sustainable energy future.

Conclusion

Estimates of the total global coal resource are in the order of thousands of billions of tonnes, whereas figures usually quoted for accessible coal reserves are typically tens of billions of tonnes. There is thus a huge gap between reserves and resources. UCG offers the tantalizing prospect of closing that gap quite considerably. If the UCG opportunity can be linked successfully to emerging CCS technology, then the implications for addressing the twin challenges of climate change and finite fossil fuel reserves is truly game-changing. There are particular attractions in developing a ‘self-contained’ solution whereby clean use of coal and CO_2 sequestration are combined in the same location without a need for material transfer. From a different perspective, there is an attraction in extending the envelope to include syngas export and CO_2 import/export. The former opens up the prospect of linking into lucrative opportunities beyond the power generation sector: the latter offers contingency plans on a number of fronts. The main environmental challenges lie in guarding against (1) aquifer contamination which can impact on potable water supplies and (2) land subsidence. Well established techniques exist for dealing with both of these. The main economic challenges relate to the up-front costs associated with evaluating specific sites from a commercial perspective and from an environmental perspective, largely because of the drilling costs associated with characterizing deep coal seams. The pace is tending to be set by those countries and regions that are blessed with significant coal resources and are concerned about the greenhouse gas emissions agenda.

We are grateful for funding from One NorthEast, HSBC Partnership for Environmental Innovation and Newcastle University. Project management by Stephen Price is greatly appreciated. Principal contractors on the North East case study were IMC Geophysics, PB Power and UCG Engineering Ltd.

References

Anheden, M., Andersson, A. *et al*. 2005. CO_2 quality requirement for a system with CO_2 capture, transport and storage. *In*: *Greenhouse Gas Control Technologies 7*. Elsevier Science, Oxford, 2559–2564.

Anonymous. 2006. Risk assessment and management framework for CO_2 sequestration in sub-seabed geological structures. *28th Consultative Meeting of Contracting Parties under the London Convention and 1st Meeting of Contracting Parties under the London Protocol*.

Bičer, N. 1987. *The inflow of water into mine workings*. PhD Thesis, Department of Mining Engineering, Newcastle University.

Bradshaw, J., Bachu, S. *et al*. 2007. CO_2 storage capacity estimation: issues and development of standards. *International Journal of Greenhouse Gas Control*, **1**, 62–68.

Burton, E. 2007. *Best Practice in Underground Coal Gasification*. Lawrence Livermore National Laboratories, contract no. W-7405-Eng-48.

Chadwick, A., Arts, R. *et al*. 2008. *Best Practice for the Storage of CO_2 in Saline Aquifers: Observations and Guidelines from the SACS and CO2STORE Projects*. British Geological Survey, Keyworth.

Damen, K., Faaij, A. *et al*. 2006. Health, safety and environmental risks of underground CO2 storage – overview of mechanisms and current knowledge. *Climatic Change*, **74**, 289–318.

DTI. 1999. *Underground Coal Gasification – Joint European Field Trial in Spain*. Project Summary, DTI Publication no. 017-1999.

DTI. 2006. *The feasibility of UCG under the Firth of Forth*. Project Summary 382, DTI Publication, URN 06/885.

Espie, T., Rubin, E. S. *et al*. 2005. Understanding risk for the long term storage of CO_2 in geologic formations. *In*: *Greenhouse Gas Control Technologies 7*. Elsevier Science, Oxford, 1277–1282.

Esterhuizen, G. S. & Karacan, C. O. 2005. Development of numerical models to investigate permeability changes and gas emissions around longwall mining panels. *40th US Rock Mechanics Symposium*, 25–29 June 2005, Anchorage.

Friedmann, J. 2008. North American prospects for UCG in a carbon constrained world. *Proceedings of the International Coal Conference*, October, Pittsburgh, PA.

Galli, R. D., Jones, G. E. & Kiviat, F. E. 1983. Simple field test model for underground coal gasification. *Industrial Engineering and Chemical Process Design and Development*, **22**, 538–544.

Green, M. 2008. The future prospects for underground coal gasification. *Proceedings of the International Coal Conference*, October, Pittsburgh, PA.

Guo, H., Adhikary, D. P. *et al*. 2009. Simulation of mine water inflow and gas emission during longwall mining. *Rock Mechanics and Rock Engineering* **42**, 25–51.

Hitchon, B., Gunter, W. D. *et al*. 1999. Sedimentary basins and greenhouse gases: a serendipitous association. *Energy Conversion and Management*, **40**, 825–843.

Humenick, M. J. & Mattox, C. F. 1978. Groundwater pollutants from underground coal gasification. *Water Research*, **12**, 463–469.

IEA. 2004. *Risk Assessment Workshop*. Report PH4/31. London, IEA GHG R&D Programme.

Khadse, A., Qayyumi, M., Mahajani, S. & Aghalayam, P. 2007. Underground coal gasification: a new clean coal utilization technique for India. *Energy*, **32**, 2061–2071.

Law, D. H. S. & Bachu, S. 1996. Hydrogeological and numerical analysis of CO_2 disposal in deep aquifers in the Alberta sedimentary basin. *Energy Conversion and Management*, **37**, 1167–1174.

Levorsen, A. I. 1967. *Geology of Petroleum*. W H Freeman, New York.

Li, H., Yan, J. *et al*. 2009. Impurity impacts on the purification process in oxy-fuel combustion based CO_2 capture and storage system. *Applied Energy*, **86**, 202–213.

Liu, S.-Q., Li, J.-G. *et al*. 2007. Groundwater pollution from underground coal gasification. *Journal of China University of Mining and Technology*, **17**, 467–472.

McCracken, R. 2008. Mining without mines: UCG. *Energy Economist*, **31**, 216.

Metz, B., Davidson, O., de Coninck, H. C., Loos, M. & Meyer, L. A. (eds) 2005. *IPCC Special Report on Carbon Dioxide Capture and Storage*. Prepared by Working Group III of the Intergovernmental Panel on Climate Change. Cambridge University Press, Cambridge.

NCB. 1975. *The Subsidence Engineers' Handbook*. National Coal Board, London.

NCC. 2008. *Underground Coal Gasification*. National Coal Council, Washington, DC. World Wide Web Address: www.nationalcoalcouncil.org/Documents/Underground_Coal_Gasification.pdf (accessed 13 January 2010).

Neate, C. J. & Whittaker, B. N. 1979. Influence of proximity of longwall mining on strata permeability and ground water. *U.S. Symposium on Rock Mechanics*. Austin, TX, 3rd June, 217–224.

Perkins, G. & Sahajwalla, V. 2006. A numerical study of the effects of operating conditions and coal properties on cavity growth in underground coal gasification. *Energy & Fuels*, **20**, 596–608.

Pirard, J. P., Brasseur, A., Coëme, A., Mostade, M. & Pirlot, P. 2000. Results of the tracer tests during the El Tremedal underground coal gasification at great depth. *Fuel*, **79**, 471–478.

Roddy, D. J. 2008. Linking underground coal gasification to CCS and the downstream opportunities. *Proceedings of the International Coal Conference*, October, Pittsburgh, PA.

Ross, H. E., Hagin, P. & Zoback, M. D. 2009. CO_2 storage and enhanced coalbed methane recovery: reservoir characterization and fluid flow simulations of the Big George Coal, Powder River Basin, Wyoming, USA. *International Journal of Greenhouse Gas Control*, **3**, 773–786.

Seevam, P. N., Race, J. M. *et al*. 2008. Transporting the next generation of CO_2 for carbon capture and storage: the impact of impurities on supercritical CO_2 pipelines. *7th International Pipeline Conference*, Calgary, Alberta. ASME, New York.

Strahan, D. 2008. Coaled comfort. *Geoscientist*, March, 18–21.

Trainer, T. 2006. *Renewable Energy Cannot Sustain A Consumer Society*. Springer, Heidelberg.

Whittles, D. N., Lowndes, I. S. *et al*. 2006. Influence of geotechnical factors on gas flow experienced in a UK longwall coal mine panel. *International Journal of Rock Mechanics and Mining Sciences*, **43**, 369–387.

WS Atkins Consultants Ltd. 2004. *Review of Environmental Issues of Underground Coal Gasification – Best Practice Guide*. DTI Cleaner Coal Technology Transfer Programme. DTI, Birmingham.

Yang, L. 2008. Coal properties and system operating parameters for underground coal gasification. *Energy Sources, Part A: Recovery, Utilization, and Environmental Effects*, **30**, 516–528.

Younger, P. L. & Adams, R. 1999. *Predicting Mine Water Rebound*. R&D Technical Report W179. Environment Agency, Bristol, UK.

Younger, P. L., Banwart, S. A. & Hedin, R. S. 2002. *Mine Water: Hydrology, Pollution, Remediation*. Kluwer Academic Publishers, Dordrecht.

Geological storage of carbon dioxide: an emerging opportunity

W. J. SENIOR,[1] J. D. KANTOROWICZ[2] and I. W. WRIGHT[2]

[1]*Senior CCS Solutions Ltd, Mt Pleasant Cottage, Sly Corner, Bucks HP16 9LD, UK (e-mail: bill@senior-ccs.co.uk)*

[2]*BP Alternative Energy, Chertsey Road, Sunbury-on-Thames, Middlesex TW16 7LN, UK*

Abstract: Concerns about climate change and the need to stabilize atmospheric CO_2 concentrations are driving the development of a lower carbon future. Within this context, carbon dioxide capture and storage (CCS) is gaining momentum as a large-scale option to reduce greenhouse gas emissions. This paper reviews the rationale and potential scale of CCS, the status of geological storage options and lessons from the operating In Salah project. CCS is expected to have applications in the oil and gas industry, and other industries, particularly the coal and power sectors. CO_2-enhanced oil recovery, depleted oil and gas fields and saline formations are considered the most important geological storage options. Experience with geological storage is being gained at the In Salah project in Algeria. Operating since 2004, it is the world's first industrial-scale project storing CO_2 in the water leg of a gas reservoir. A key challenge for wider deployment is for geological storage to be accepted as a safe and effective option, providing long-term CO_2 containment, with high integrity. This has several associated technical and regulatory challenges, including site characterization and selection, geological and well integrity risk assessment, performance prediction, the design of appropriate monitoring schemes and handling the closure and post-closure phases. The petroleum industry has the capabilities and know-how to deploy CCS and to manage the associated risks. This lends confidence that CCS will be a viable option and that deployment will help enable a low-carbon future.

Keywords: carbon dioxide, capture, storage, sequestration

Carbon dioxide capture and storage (CCS) consists of the separation, capture and compression of CO_2 from industrial and power sources, transportation to storage sites and injection of CO_2 into geological formations enabling long-term isolation from the atmosphere (IPCC 2005). This paper reviews the rationale for CCS, the major geological storage options and the operating In Salah CO_2 storage project in Algeria, and summarizes the main challenges for geological storage.

Rationale for carbon capture and storage

Concerns about climate change are driving the need to stabilize atmospheric CO_2 concentrations and to develop a low-carbon energy future. Within this context, CCS is gaining momentum as an important large-scale option to reduce greenhouse gas emissions. By enabling 80–90% reductions in CO_2 emissions from fossil fuels from large industrial sources, CCS can be considered a win–win solution to enable global energy supply, energy security and mitigation of climate change.

Many components of the technologies have been demonstrated at scale and are ready for commercial deployment. Further innovation and technology development should broaden application and reduce costs. CCS can be economically competitive with other low-carbon options such as renewables, especially where used with enhanced oil recovery (EOR). A key challenge for CCS is the urgent need to move ahead with large-scale integrated demonstration projects and commercial deployment, which will require policy and financial support. This requirement is similar to other sustainable low-carbon energy options such as wind power. CCS implementation will also involve creation of value chains which are technically and commercially complex, although analogous to the complex value chains that are involved in the Liquefied Natural Gas business.

The oil and gas industry will have a key role to play in CCS development and deployment. Given existing capabilities, stakeholders are looking to the industry to take a lead on transportation and storage. At the strategic level CCS can be an enabler for cleaner fossil fuels in a low-carbon world. The technology will also be required to manage oil and gas industry emissions. Early applications are expected to be high-CO_2 gas clean-up, concentrated emissions from hydrogen plants, and feedstock conversion including applications in refining, heavy oil, gas-to-liquids and coal-to-liquids, particularly to reduce the carbon footprint of heavier feed stocks. The oil and gas industry could play a leading role in geological storage, and new business models are emerging, for example providing storage solutions to third parties such as power utilities, and for decarbonized energy providers. CCS will be vital in other energy sectors, notably coal and power. Coal is the most carbon-intensive fuel, responsible for 39% of global energy-related CO_2 emissions. It is a low-cost, secure primary energy source that dominates the energy system in several leading economies, notably China and the USA. Resource holders are unlikely to forego the use of coal and thus CCS is vital to control emissions. CCS is also recognized as a key option for the power sector, which generates about 40% of world energy-related CO_2 emissions. Linked to hybrid and electric vehicles, decarbonization of power could also help address transport sector emissions.

Potential scale of CCS

Future energy and emissions models can be used to predict the timing and scale of potential CCS deployment. The scale is linked to emissions trajectories, which are dependent on the climate change objectives and requirement for stabilization of atmospheric greenhouse gas concentrations. The potential for global deployment of CCS could be up to 9000×10^6 tonnes/year of CO_2 by 2050, around 19% of projected business-as-usual CO_2 emissions (International Energy Authority 2008). These figures equate to equipping 15–17 GW of coal-fired power plant

VINING, B. A. & PICKERING, S. C. (eds) *Petroleum Geology: From Mature Basins to New Frontiers – Proceedings of the 7th Petroleum Geology Conference*, 1165–1169. DOI: 10.1144/0071165

with CCS each year, implying that it will become the technology standard, and to an industry handling *c.* 82.5×10^6 BOE/day equivalent of CO_2, comparable to today's oil industry.

Geological storage options

There are a range of options for geological storage of CO_2 in the subsurface. It is generally assumed that CO_2 will be injected and stored in supercritical phase at depths greater than 800 m, assuming normal geothermal gradients. The single most important challenge for wider deployment is for geological storage to be accepted as safe and effective in containing CO_2 underground. The main technical issues relate to the geological integrity of the site: the long-term integrity of any wells and potential pathways creating risks of leakage to atmosphere. There are several associated technical and regulatory challenges, including site characterization and selection, geological and well integrity risk assessment, performance prediction, the design of fit-for-purpose monitoring schemes and handling the closure and post-closure phases, including the transfer of liabilities to the nation.

We consider three large-scale storage options: CO_2 EOR, depleted oil and gas fields, and saline aquifer formations, each of which is reviewed below. These are already being deployed at demonstration scale for CCS, and offer potential for commercial-scale storage. We consider other options to be lower priority. The potential for storage in coals during enhanced coal bed methane production has been piloted in USA, Canada, Poland and China; however technical and economic viability at larger scale is to be confirmed. Research stage options include basalts, salt caverns, disused mines and carbonation of ultramafic rocks.

Storage with CO_2 EOR

CO_2 has been used for EOR since the 1980s (Jarrell *et al.* 2002). Over 120 reservoirs use CO_2 EOR, with total worldwide production of nearly 1×10^6 BOPD, and an average 11% increase in recovery. Many current projects are in the USA, where about 45×10^6 tonnes per year of mostly natural CO_2 is transported by pipeline and injected. The technology is sufficiently well understood for full-field development to be implemented with confidence. Conceptually, the use of CO_2 to enhance recovery could be expanded into other areas of conventional oil and gas development. Firstly, CO_2 could replace natural gas in miscible gas floods. Secondly, under the right circumstances, CO_2 flooding could enhance recovery from condensate reservoirs. Finally, it is theoretically possible to use CO_2 to displace and so enhance recovery of natural gas, which is being piloted at two locations.

Deploying CCS with CO_2 EOR is an important option given the potential benefit of increased revenues. In existing CO_2 EOR projects in North America, the field operators usually purchase CO_2 at prices equivalent to \$11–32/tonne CO_2 at oil prices of \$15–50/barrel (Jarrell et al. 2002). Geological integrity is not a concern, although well integrity risks should be addressed. An advantage over other storage options is that CO_2 EOR is usually permissible within the petroleum licensing agreements. There is commercial experience of CCS with EOR at the Weyburn field in Canada, using CO_2 captured from lignite gasification in North Dakota and which has operated a storage demonstration and monitoring project since 2000 (Wilson & Monea 2004). EOR is being, or has been, considered in CCS project proposals in the North Sea, USA, Canada and the Middle East.

Challenges. If fiscal policy encourages storage of greenhouse gases, then CO_2 EOR projects may also benefit from carbon credits for storage. This opens up the possibility that field development may be optimized to store CO_2 rather than to maximize oil recovery. This will be a function of the relative price of carbon credits and hydrocarbons, and regulatory developments. There are no major obstacles to CCS with EOR, although a number of issues may constrain it from becoming volumetrically significant for storage. These include geography (transportation cost), impact on existing infrastructure (cost), volumetrics, timing, well integrity, storage assurance and individual field viability, which are discussed in turn below.

Geography is important because some major oil provinces are remote from sources of CO_2. Economics may not justify the pipeline cost. The potentially corrosive impact of CO_2 is a consideration for fields that have been developed with metallurgy that will be affected by produced CO_2. This has not been an issue onshore, or where associated gas contains CO_2; however it was cited by Statoil and Shell as a contributing factor at the Draugen field, offshore Norway (Provan 1992), where an offshore CO_2 EOR scheme integrated as part of a value chain to capture carbon at an onshore gas power plant was evaluated. The high cost and one-year shut-down requirement for major modifications to the offshore platform were cited as issues contributing to the unfavourable economics of EOR along with the low extra oil volumes. As a consequence the integrated project and value chain was considered uneconomic (Statoil 2007).

Volumetrics are a consideration given that the amount of CO_2 to be injected may be considerably greater than the available pore space. Larger current EOR projects such as the Rangely field in Wyoming inject up to 3×10^6 tonnes per year CO_2, only equivalent to the emissions of small coal power plants. Time-scales are important in two respects. Firstly, many EOR developments will not require a continuous stream of CO_2, rather after an initial peak, a declining rate is required as the produced CO_2 is recycled. Secondly, whilst the cessation of production is a function of oil price, some oil fields may not continue producing long enough to provide a sustainable storage option. In view of these issues, CO_2 EOR may need to be used in conjunction with other storage options. Well integrity is a key issue, which will be field-specific and which needs to consider longer term risks in a CO_2-rich environment. This is linked to storage assurance: if carbon credits require monitoring and verification to assure storage, then the associated costs need to be offset by the value of the credits to provide sufficient incentive for EOR with storage. The CO_2 produced from additional oil production v. baseline scenario and other options will also need to be factored in. Finally the viability of CO_2 EOR is field specific, and is a key consideration for integrated projects.

Storage in depleted oil and gas fields

Oil and gas fields at or close to the end of production are potentially attractive sites for CO_2 storage. They benefit from data and knowledge from the hydrocarbon life cycle, which should provide high confidence in geological storage integrity and potential capacity, together with opportunities to re-use wells and facilities. This method is being demonstrated in the Dutch sector of the North Sea, where Gaz de France is injecting 20,000/tonnes per year into a mature Rotliegendes gas field in the K12 block. The potential for enhanced gas recovery is still under investigation (Van der Meer *et al.* 2006). Other demonstrations are taking place in Australia (Otway) and Germany (Altmark) and new projects are planned in several areas. In addition, the In Salah project described below is ultimately intended to store CO_2 in a depleted gas reservoir.

Storage in depleted fields will not necessarily involve any attempt to enhance recovery in late field life. It is principally an opportunity to take advantage of a well understood reservoir with facilities and wells that could have their life extended, deferring decommissioning. Clearly, this option will have easier application in depleted fields, as opposed to fields with strong natural aquifers, or that have been water-flooded to maintain pressure.

Challenges. There are no insurmountable technical obstacles to storage in depleted fields. Geographic constraints are the limitations of field distribution, in a similar way to EOR, although more widespread. Perhaps the simplest is size: the 200 000 SCF/day CO_2 output from a 500 MW coal fired power station equates to $>1 \times 10^{12}$ SCF over 20 years. Larger fields may be able to store such volumes; smaller fields could be part of a portfolio. Timing may be a constraint as the optimal timing would involve cessation of production coinciding with the start of injection for storage. If not, the value of early curtailment (reserve loss) would have to be outweighed by the value of carbon credits. Conversely, if cessation of production is too early, then costs may be incurred to maintain facilities to await CO_2 supply. The availability of the fields for storage may also conflict with other possible uses. In some areas depleted gas fields have commercial value as natural gas storage sites.

Well integrity is a key issue for both depleted fields and EOR projects. This needs to take account of the risk of leakage in a CO_2-rich environment over the longer term from both pre-existing and newly drilled wells. With older fields that are approaching the end of design life there may also be costs associated with maintenance and integrity issues. It is also possible that the metallurgy used on old infrastructure and wells may be incompatible with impurities in the CO_2 stream, or not resistant to the corrosion that would result if water entered the system. The field history should also allow inferences regarding direct and indirect communication between the reservoir formations and the surrounding formations, upon which to base any risk assessment on the impact of injection on other users of pore space in the area. The latter is important as the surrounding aquifer system may have repressurized a field over time, reducing the amount of pore space that can readily be used for storage. With higher pressure, injection will cause a pressure pulse and may displace fluids out of the field. Compartmentalization of the reservoir and artificial pressure maintenance of the reservoir during production will limit the amount of CO_2 that can be injected without increasing the pressure to unacceptable levels.

Storage in saline formations

Formations where the pore water is unsuitable for human use or agriculture are expected to be a major geological storage option because of their occurrence in all the world's sedimentary basins. Their existence outside oil and gas provinces will be important in providing storage options in regions such as Europe, China and NE USA. Worldwide capacity is expected to be large and the Intergovernmental Panel on Climate Change (IPCC) provided a lower estimate of 1000 Gtonnes CO_2, with an upper estimate being an order of magnitude greater (IPCC 2005). However the methodology and validity of the estimates has been the subject of considerable debate (Bradshaw *et al.* 2007). This will require further development as storage is commercialized with similarities to oil and gas reserves reporting.

The option is at the early commercial stage overall. There is operating experience of CO_2 injection and storage in a saline aquifer at the commercial Sleipner project in the Norwegian sector of the North Sea since 1996 at a scale of 1×10^6 tonnes CO_2 per year. This scheme involves injection into saline aquifers of the Tertiary Utsira Formation at a depth of around 800 m subsea (Torp & Gale 2003). There has been extensive data acquisition, monitoring and modelling of the project as a demonstration of CO_2 storage. Seismic imaging from repeat 3D seismic surveys has been particularly effective here in understanding plume migration and demonstrates effective underground containment (Holloway *et al.* 2004). Additional experience has been gained at In Salah in Algeria (see below) and from other smaller projects in USA, Germany, Japan and Australia. Scale-up is planned for the Gorgon project in Australia to *c.* 3×10^6 tonnes CO_2 per year.

Challenges. The single most important issue for saline formations is storage integrity, a prerequisite for stakeholders' acceptance that this is a safe option. Confidence that secure sites are selected and that injection performance and integrity can be monitored and managed over the life cycle of the project and after injection ceases will be vital. The main underlying geological considerations are the trapping mechanisms for CO_2 within the aquifers, potential leakage paths and the risk of leakage to surface. At the pore scale a range of trapping mechanisms are expected to secure the CO_2 over differing time-scales: residual saturation trapping, dissolution, buoyancy trapping, mineralization and adsorption. At the field scale different trap types are being considered: structural trapping, stratigraphic trapping and 'migration' traps. These are closely related to potential leakage mechanisms and risk, which are not detailed in this paper. The initial industry focus is on sites involving structural traps, which are considered lowest risk by analogy with oil and gas fields. Recent work has highlighted concerns about the pressure building up in the storage site, together with its potential impacts such as fracturing of the seal and reduction of storage capacity, and how best to manage pressure regimes. Another key research area is how to optimize storage which will need to bring together both subsurface processes and injection strategy in a similar manner to reservoir management. Researchers are reviewing different strategies to manage the tradeoffs with integrity, i.e. whether to inject CO_2, or alternate water and CO_2, or even to dissolve CO_2 in water at the surface. These strategies may provide opportunities to enhance trapping, and gain wider acceptance and thereby reduce monitoring requirements and duration.

In general there is less seismic and well data available for saline formations at the outset of assessment. Therefore resources and lead time may be required for seismic and drilling data acquisition. However, even after these efforts, it is also likely that there will be greater uncertainties in predicting integrity and storage performance than for hydrocarbon fields, because there may be no proof of trap integrity or production data prior to the start of injection. One of the key challenges is that there may be no proof of integrity of aquifer sites until after the injection has ceased and CO_2 has stabilized in the subsurface. This is a risk that will need to be managed, through appropriate monitoring and performance assessment.

The licensing and regulatory frameworks are being developed to provide assurance around these issues. The key elements of these include proposals for site characterization protocols, risk assessment, performance prediction, licensing frameworks, monitoring programmes, remediation options, closure and transfer of longer term liabilities to the nation. The case study presented for In Salah illustrates the importance of demonstration projects to inform these issues.

Storage experience at the In Salah project

In Salah Gas is a BP, Sonatrach and Statoil Joint Venture that operates a number of gas fields in Algeria (Fig. 1). The gas contains up to 10% CO_2, higher than the sales specification, and so 1×10^6 tonnes per year CO_2 is separated from the gas stream. Rather than venting, it is injected into the Krechba C-10 reservoir via three (1500 m long) horizontal wells at a depth of 1900 m subsurface. CO_2 injection started in August 2004, and to date 3×10^6 tonnes have been injected (of the planned 17×10^6 tonnes that will be injected over the project life). This is an industrial-scale

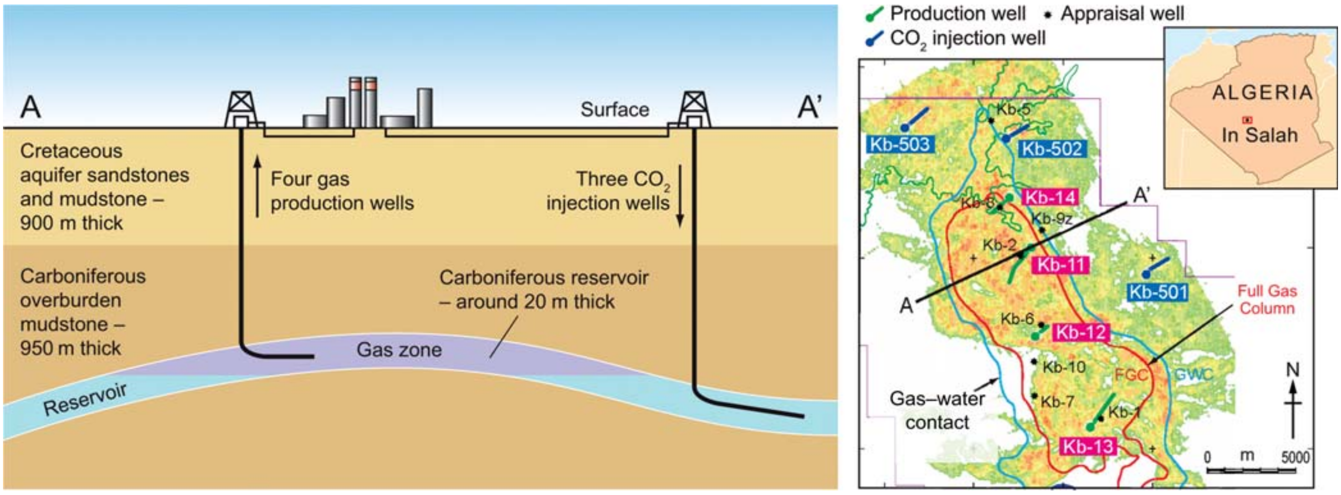

Fig. 1. Schematic cross-section through the Krechba field at In Salah, showing the general geology and well positions. Inset is a map of the field and location within Algeria.

demonstration of CO_2 geological storage in a deep saline formation and is the first such project in the world to store CO_2 in the water leg of a gas reservoir.

The C-10 Carboniferous storage reservoir in Krechba is a sandstone unit which is interpreted as a tidally influenced estuarine deposit of Tournaisian age, within an elongate NW–SE trending anticline (Riddiford *et al.* 2003). The reservoir is 20 m thick, naturally fractured, with porosities of 11–20% and permeability around 10 millidarcies. The reservoir sandstones are sealed by 950 m of Carboniferous mudstones, overlain unconformably by a further 900 m of Cretaceous clastics that contain a regional potable water aquifer (Fig. 1). The field is being produced by NE–SW horizontal wells along the crest of the structure, designed to intersect the expected natural fracture system.

Monitoring demonstration

Separately from the production operation, a joint industry project (JIP) was formed in 2004 to evaluate technologies for long-term monitoring of CO_2 geological storage. The project is a 5 year $30 million JIP involving the European Commission and US Department of Energy. The objective is to identify appropriate monitoring technology to deploy during 15 years of injection that will provide assurance of secure storage for the next 1000 years. This monitoring is also intended to show that underground CO_2 storage is a viable greenhouse gas mitigation option, and to support development of frameworks for the regulation of injection and monitoring for storage.

Prior to injection, a risk assessment concluded that the key risks to permanent storage were well bore integrity (within pre-existing wells) and the direction of CO_2 movement in the subsurface (depth conversion uncertainty). Available monitoring techniques were then assessed to identify specific tools to deploy to monitor the movement of CO_2 in the subsurface.

The technologies were assessed in terms of potential benefit and information gained v. cost (Fig. 2*a*). In some cases assessment was limited by the immaturity of the technology or not being proven in the operating conditions. These technologies had to be evaluated and tested to confirm deployment or rejection. For example, the water table is 100 m below the surface, and there is sparse surface vegetation, potentially diminishing the value of soil gas monitoring. The current and planned programme following this assessment is shown in Figure 2*b*. The aim of the programme is to end up with a cost-effective portfolio of technologies in the bottom left 'Deploy' quadrant. Note that technologies such as repeat 3D (4D) seismic (which are higher cost), may not be required. Satellite imagery has moved into the bottom left since the programme started as it has returned unexpectedly useful results. Technologies shown in blue are in the programme; those in pink are subject to further evaluation.

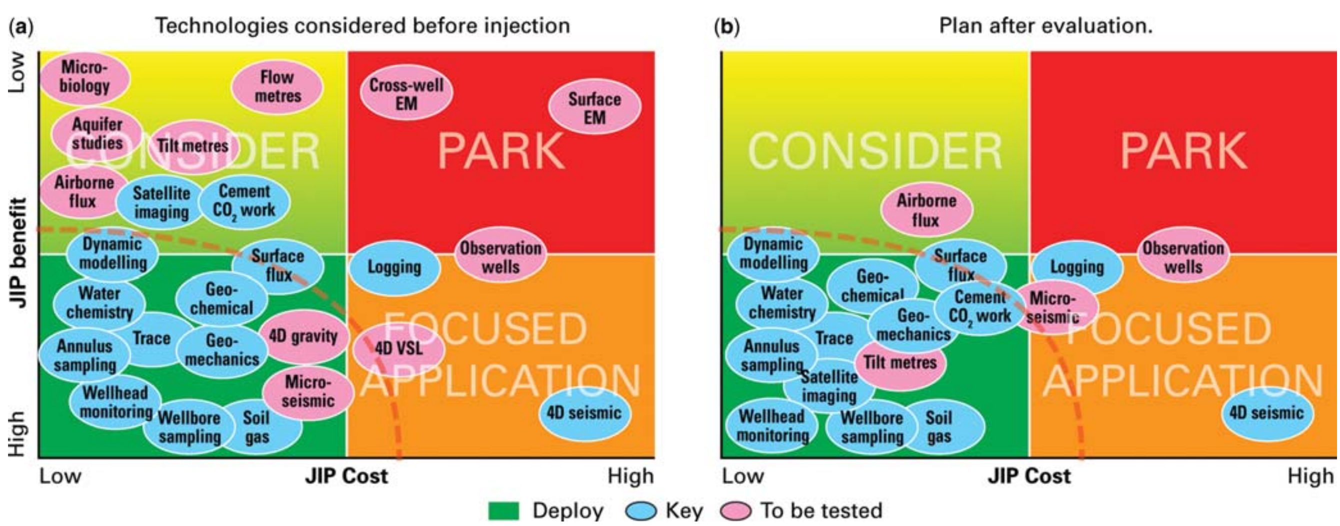

Fig. 2. A comparison of technologies considered by In Salah. (**a**) Technologies considered before injection. (**b**) Plan after evaluation.

The In Salah project receives no commercial credit for the CO_2 storage, but if the site was being regulated, then the monitoring programme would have to be agreed with the regulators and verification agencies. The dashed red line on Figure 2 depicts an envelope that should provide fit-for-purpose site-specific and cost-effective monitoring.

Satellite imagery

Calibrated INSAR satellite images after four years of injection show deformation patterns around producers and injectors, and at natural features (Mathieson *et al.* 2008). These are consistent with the (CO_2) re-pressurization and (natural gas) depletion history of the reservoir as well as surface erosion (Fig. 3). Natural features provide calibration that the induced deformation is being imaged correctly. These images suggest that the injected CO_2 is moving away from the wells along NW–SE trends, inferred to be the natural fracture systems, consistent with the original reservoir models. The surface is moving up to 5 mm per year in response to the reservoir level injection. Pressure changes caused by CO_2 movement have been tracked by satellite since injection commenced. The satellite imagery was recently calibrated by the arrival of CO_2 at a monitoring well 1.5 km from the KB502 injector. The sampled CO_2 contained a tracer, which was added to the CO_2 injected at KB502.

Further work is planned, including images from now higher frequency satellite passes, as well as micro-seismic and tilt-metres to provide accurate ground-level calibration, to interpret these results. This work will address how the reservoir injection pressure is transmitted to the overburden and provide a basis for determining how effectively satellite imagery can be used as a monitoring tool at this and other locations.

Conclusions

Carbon capture and geological storage is emerging as a major option to reduce CO_2 emissions from fossil fuels as part of a lower-carbon future. Progressing geological storage is part of the urgent need to move ahead with CCS. Implementing a wide range of projects is an urgent priority to gain operating experience and deeper understanding for risk and performance optimization. This will meet the key challenge for CCS: gaining public acceptance that geological storage is a safe and effective mitigation option.

The three major geological storage options, EOR, storage in depleted fields and saline aquifer formations, are ready for wider deployment at commercial scale, although learning from demonstration and deployment and further research and development will be needed in parallel.

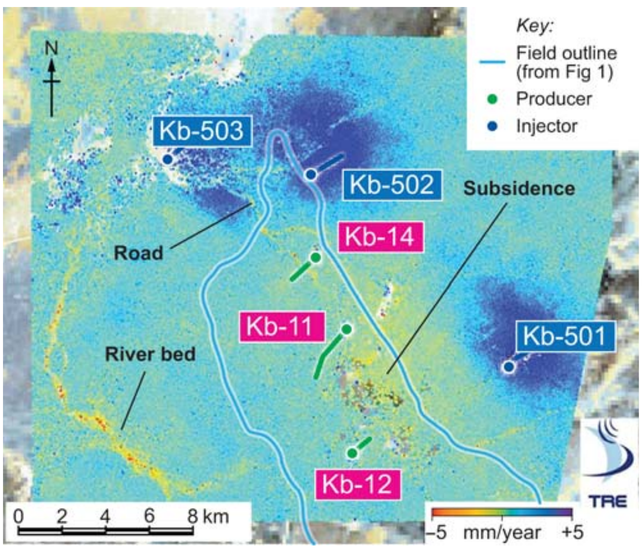

Fig. 3. INSAR satellite image of the northern end of the field showing changes in surface elevation.

CO_2 EOR will be an important early option as it can provide economic benefits and can reduce the cost of CCS demonstration and deployment. In future there may be a gradual transition from commercial EOR to CO_2 storage with EOR, with increasing value for carbon mitigation and the goal of maximizing CO_2 storage. Important issues to be addressed are how to maximize CO_2 storage, safe re-use of wells and infrastructure and well integrity in CO_2-rich conditions over the longer term. Similar challenges will exist for re-use of depleted oil and gas fields for CO_2 storage.

Aquifers are seen as a major long-term option, with a greater need for research and development than oil and gas fields. Further work is required in many areas, including characterization, resource assessment methodology, storage mechanisms and capacities, together with injection strategies to optimize storage efficiency and monitoring approaches.

The In Salah project shows the viability of storage, and the importance of practical experience in developing the storage option. It is a test bed for CO_2 storage which will assist in designing fit-for-purpose monitoring programmes. Projects like this will be essential to develop appropriate regulatory frameworks and policy instruments that will be essential for wider commercial deployment.

This paper is based on work by the authors at BP Alternative Energy, work with BP's partners on In Salah (Sonatrach and Statoil) and independent work by the lead author since leaving BP. We acknowledge these companies and colleagues within them.

References

Bradshaw, J., Bachu, S., Bonijoly, D., Burruss, R., Holloway, S., Christensen, N. P. & Mathiassen, O. M. 2007. CO_2 storage capacity estimation: issues and development of standards. *International Journal of Greenhouse Gas Control*, **1**, 62–68.

Holloway, S. *et al*. 2004, *Saline Aquifer CO_2 Storage Project (SACS) – Best Practice Manual*. IEA Greenhouse Gas & D Programme.

Intergovernmental Panel on Climate Change (IPCC). 2005. *Carbon Dioxide Capture and Storage*. IPCC Special Report. Cambridge University Press, New York.

International Energy Authority (IEA). 2008. *CO_2 Capture and Storage – a Key Carbon Abatement Option*. IEA Report. IEA, Paris.

Jarrell, P. M., Fox, C. E., Stein, M. H. & Webb, S. E. 2002. *Practical Aspects of CO_2 Flooding*. SPE Monograph **22**.

Mathieson, A., Wright, I. W., Roberts, D. M. & Ringrose, P. 2008. Satellite imaging to monitor CO_2 movement at Krechba, Algeria. *In*: *Proceedings of the 9th International Conference on Greenhouse Gas Control Technologies*, November, Washington, DC.

Provan, D. 1992. Draugen Oil Field, Haltenbanken Province, Offshore Norway. In: *Giant Oil and Gas Fields of the Decade 1978–1988*. American Association of Petroleum Geologists, Memoirs, **54**, 371–381.

Riddiford, F. A., Tourqui, A., Bishop, C. D., Taylor, B. & Smith, M. 2003. A cleaner development: the In Salah gas project, Algeria. *In*: *Proceedings of the 6th International Conference on Greenhouse Gas Control Technologies*, October, Kyoto.

Statoil, 2007. Halten CO_2 value chain: technically feasible, but not commercially viable. Press release.

Torp, T. A. & Gale, J. 2003. Demonstrating storage of CO_2 in geological reservoirs: the Sleipner and SACS projects. *In*: *Proceedings of the 6th International Conference on Greenhouse Gas Control Technologies*, October, Kyoto.

Van der Meer, L. G. H., Kreft, E., Geel, C. R., D'Hoore, D. & Hartman, J. 2006. Enhanced gas recovery testing in the K12-B reservoir by CO2 injection, a reservoir engineering study. *In*: *Proceedings of the 8th International Conference on Greenhouse Gas Control Technologies*, June, Trondheim.

Wilson, M & Monea, M. (eds) 2004. IEA GHG Weyburn CO_2 monitoring and storage project summary report 2000–2004. *In*: *Proceedings of the 7th International Conference on Greenhouse Gas Control Technologies*, September, Vancouver.

History-matching flow simulations and time-lapse seismic data from the Sleipner CO_2 plume

R. A. CHADWICK and D. J. NOY

British Geological Survey, Keyworth, Nottingham NG12 5GG, UK (e-mail: rach@bgs.ac.uk)

Abstract: Since its inception in 1996, the CO_2 injection operation at Sleipner has been monitored by 3D time-lapse seismic surveys. Striking images of the CO_2 plume have been obtained showing a multi-tier feature of high reflectivity. In the medium to longer term, the topmost layer of CO_2, accumulating and migrating directly beneath the topseal, is the main determinant of storage site performance. Fortunately it is this topmost layer that can be most accurately characterized, its rate of growth quantified, and CO_2 flux arriving at the reservoir top estimated. The latter is mostly controlled by pathway flow through thin intra-reservoir mudstones. This has increased steadily with time, suggesting either that pathway transmissivities are increasing with time and/or the pathways are becoming more numerous. Detailed 3D history-matching of the topmost layer cannot easily match the observed rate of spreading. Isotropic permeabilities result in a stronger radial component than observed and a degree of anisotropic permeability, higher in a north–south direction, is possible. The main contributor to the mismatch, however, is likely to be small but significant uncertainty in the depth conversion. Irrespective of uncertainty, the observed rate of lateral migration seems to require very high permeabilities, and is, moreover, suggestive of a topseal which behaves like a 'hard' impermeable flow barrier. Detailed studies such as this will provide important constraints on longer term predictive models of plume evolution and storage performance which are key regulatory requirements.

Keywords: Sleipner, Utsira Sand, CO_2 plume, seismic monitoring, time-lapse seismic, reservoir flow simulation, history-matching

Large-scale underground storage of industrially produced carbon dioxide has the potential to play a key role in reducing man-made emissions of greenhouse gases (IPCC 2005). The CO_2 injection operation at Sleipner, in the central North Sea between the UK and Norway, commenced in 1996 and is the world's longest running industrial-scale storage project. It is also, so far, the only example of underground CO_2 storage arising as a direct response to environmental legislation (Baklid *et al.* 1996).

Carbon dioxide separated from natural gas produced at Sleipner is injected into the Utsira Sand, a major saline aquifer of late Cenozoic age (Fig. 1a). Well logs (Fig. 1b) show the Utsira Sand to have a sharply defined top and base, and gamma-ray (GR) values typically around 25 API units compared with 90 API units in the overlying caprock. GR and resistivity peaks within the sand are interpreted as thin intra-reservoir mudstones, mostly around 1 m thick (Zweigel *et al.* 2004).

The injection point is at a depth of about 1012 m below sea-level, some 200 m below the reservoir top, with around 12 million tonnes (Mt) of CO_2 currently stored. A comprehensive monitoring programme has been carried out, with multiple time-lapse 3D seismic surveys, augmented by high-resolution 2D seismic, sea-bottom gravity, controlled-source electromagnetic and seabed imaging surveys. This paper describes analysis of the time-lapse 3D seismic datasets acquired up to 2006, comprising the 1994 (baseline), 1999 (cumulative 2.35 Mt of CO_2 injected), 2001 (cumulative 4.26 Mt injected), 2002 (cumulative 4.97 Mt injected), 2004 (cumulative 6.84 Mt injected) and 2006 (cumulative 8.4 Mt injected) surveys.

The time-lapse seismic data clearly image the progressive development of the CO_2 plume, around 200 m in height and elliptical in plan view (Fig. 2). By 2006 the NNE-trending long axis of the plume spanned 3.6 km with a short axis of around 1 km. The plume forms a prominent multi-tier feature comprising a number of bright sub-horizontal reflections, interpreted as arising from discrete layers of CO_2, each up to a few metres thick, and mostly accumulating beneath the intra-reservoir mudstones (Fig. 1b). The CO_2 layers formed early in plume evolution (by 1999) and have remained identifiable ever since. The upper layers continue to spread laterally and generally increase in brightness, whereas the lower layers have stabilized in size and are growing progressively dimmer. Vertical linear features within the plume characterized by reduced reflection amplitudes and localized velocity pushdown are interpreted as 'chimneys' of moderate or high CO_2 saturation (Chadwick *et al.* 2004). The most prominent of these is located roughly above the injection point (Fig. 2), and is interpreted as the main conduit for CO_2 upward transport through the reservoir and the main feeder of the laterally spreading thin layers. Within the reservoir overburden, there is no evidence of systematic changes in seismic signature, indicating that CO_2 is being contained within the storage reservoir.

Quantitative analysis (Chadwick *et al.* 2004, 2005) has shown that, while the seismic images are consistent with the known injected amounts of CO_2, they do not provide a unique verification of injected mass. Significant uncertainties remain, particularly regarding seismic properties of CO_2-saturated rock, and the fine-scale distribution of dispersed CO_2 in between the reflective layers. Similarly, reservoir flow simulations (Lindeberg *et al.* 2001; Chadwick *et al.* 2008) have reproduced the current observed development of the CO_2 plume as a multi-tier layered structure. However, because the structural geometry of the sealing intra-reservoir mudstones is not precisely known, simulated layer thicknesses are not tightly constrained and have not yet been robustly matched to thicknesses obtained directly from the seismic data.

The objective of this paper is to look at key aspects of the seismic data that constrain models of CO_2 migration through the reservoir, and to assess whether flow processes in the reservoir are understood to the extent that predictions and simulations of future, longer-term, plume behaviour are likely to be robust.

VINING, B. A. & PICKERING, S. C. (eds) *Petroleum Geology: From Mature Basins to New Frontiers – Proceedings of the 7th Petroleum Geology Conference*, 1171–1182. DOI: 10.1144/0071171

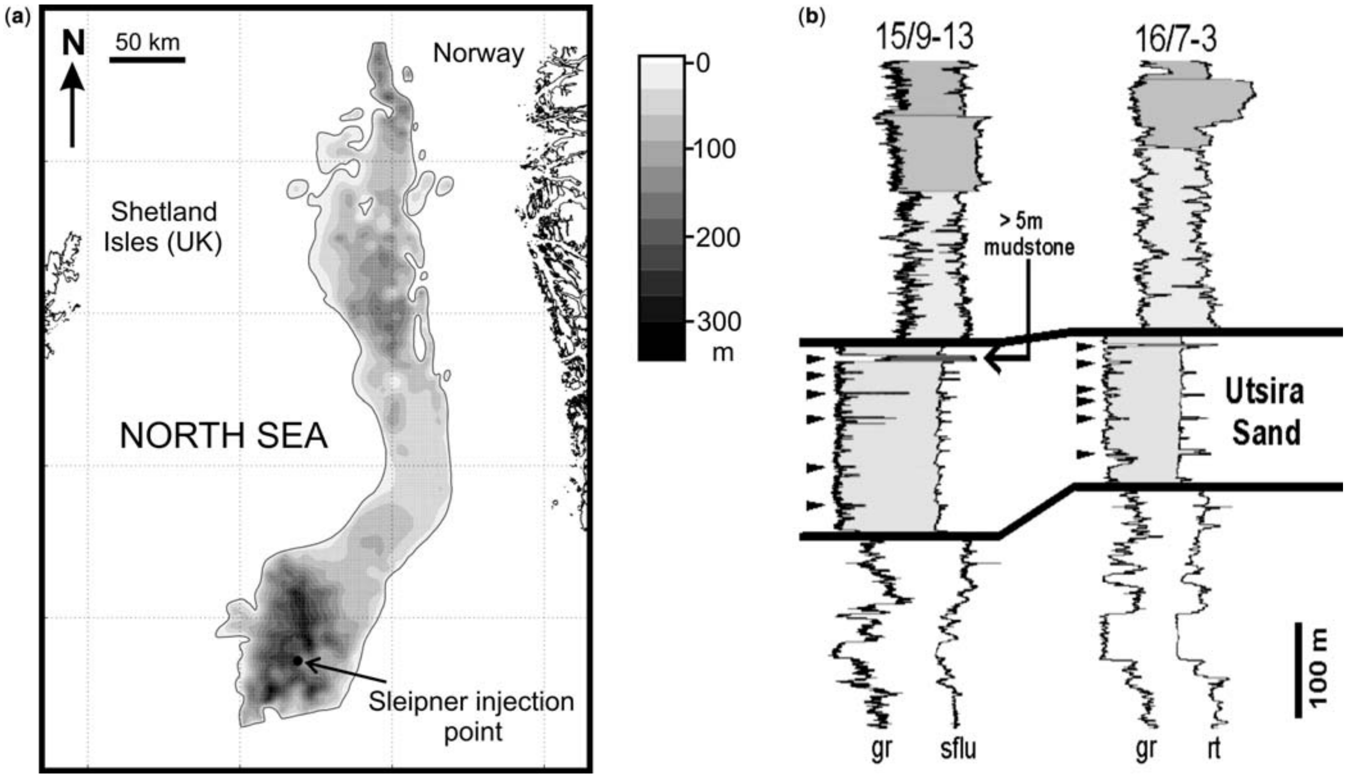

Fig. 1. (**a**) Location of the Sleipner injection operation showing distribution and thickness of the Utsira Sand. (**b**) Geophysical logs through the Utsira Sand showing GR and resistivity peaks corresponding to thin intra-reservoir mudstones. Note thicker (>5 m) mudstone near reservoir top. Wells 15/9-13 and 16/7-3 lie around 1 km WSW and 12 km ENE of the injection point respectively. Log types: gr, gamma ray; rt, deep resistivity; sflu, spherical-focused resistivity.

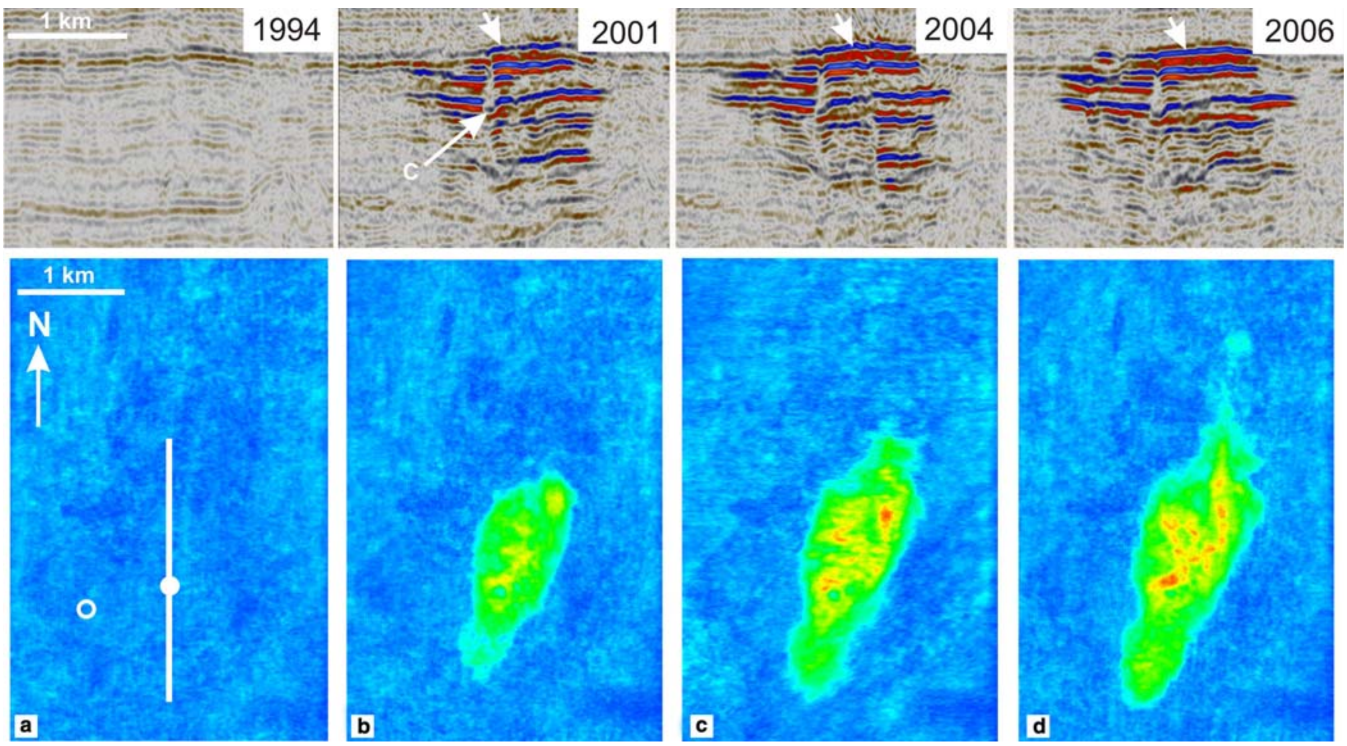

Fig. 2. Seismic images of the Sleipner plume showing its development from 1994 (pre-injection) through to 2006. Top panels show a north–south seismic section through the plume; bottom panels show plan views of the plume displayed as total reflection amplitude. C (on 2001 section) denotes the main feeder chimney in the plume. White arrow denotes topmost CO_2 layer. Location of north–south seismic section, injection point (solid circle) and well 15/9-13 (open circle) also shown.

Analysis of the topmost CO_2 layer

Although up to nine individual CO_2 layers have been identified in the plume (Chadwick *et al.* 2004), from the viewpoint of determining medium- to long-term storage site performance, understanding the topmost layer is of paramount importance. Long-term flow simulations of the Sleipner plume (Erik Lindeberg, pers. comm. 2007) show that within a few decades of ceasing injection most of the CO_2 will have migrated to the top of the reservoir as a buoyant fluid phase. Here, trapped beneath the undulating caprock, it will migrate laterally over significant distances. Over the succeeding centuries, dissolution of CO_2 at the base of the migrating layer, and convective sinking of CO_2 in solution, will gradually 'erode' the CO_2 layer and progressively reduce its mobility. Ultimately, after a few thousand years, most of the CO_2 will be fixed in a gravitationally stable dissolved form. Risk assessment therefore requires robust prediction of how the CO_2 will migrate in the free phase for a protracted period after site closure.

Fortunately, of all the layers in the plume, the topmost is imaged most clearly by the time-lapse monitoring data. Currently its lateral spread can be tracked in detail and its progressive increase in thickness and volume quantified with a degree of accuracy. The latter parameters allow the total upward flux of CO_2 through the reservoir to be calculated, which provides insights into reservoir flow behaviour and how this changes with time.

Quantitative analysis of the 2006 time-lapse processing ensemble, comprising the 1994, 2001, 2004 and 2006 surveys, forms the basis of this paper. Reflection amplitude changes at the top of the Utsira Sand correspond to the development of the topmost CO_2 layer and show how it has grown through time (Fig. 3). A north-trending linear prolongation of the layer is particularly prominent and corresponds to CO_2 migrating northwards along a linear ridge at the reservoir top (Fig. 3d). The CO_2–water contacts (CWC) correspond to the outer edges of the CO_2 layers, defined as the outer limit of detectable amplitude change.

Amplitude maps of the topmost layer from the full time-lapse dataset (Fig. 4) show how CO_2 first reached the reservoir top in 1999 (just prior to the first time-lapse repeat survey), as two small separate accumulations. By 2001 these had coalesced into a single accumulation which continued to expand thereafter.

Layer thicknesses from seismic amplitudes

Earlier work (Arts *et al.* 2003; Chadwick *et al.* 2005) has shown that layer reflectivity for the most part follows a thin-layer tuning relationship, with reflection amplitudes directly related to layer thicknesses. Rock physics properties were calculated for a range of CO_2 saturations in the Utsira Sand using the Gassman fluid substitution equation (Mavko *et al.* 2003), calibrated by P- and S-wave velocity and density data from well logs (Fig. 5a). For uniform fluid mixing (likely in the high saturation CO_2 layers), substitution of water by CO_2 reduces V_p from 2050 to around 1420 m s^{-1} for CO_2 saturations above 0.2. A synthetic wedge model was constructed using the calculated seismic properties and from this an amplitude–thickness relationship was derived (Fig. 5b). The amplitude–thickness relationship for the observed data was then obtained by scaling the maximum tuning amplitude of the synthetic data to the maximum seismic amplitudes observed in the plume. Two simplifying assumptions were made in this analysis. Firstly the CO_2 wedge model incorporated a uniformly high CO_2 saturation. In terms of the calculated seismic response this is acceptable given the characteristic Gassman fluid response with rapid velocity decrease even at low CO_2 saturations and the fact that low CO_2 saturations are likely to be restricted to the very lowermost part of the layer (Fig. 5c). Secondly, rock properties were assumed to be laterally uniform. This is also reasonable given the absence of data to the contrary and the very large changes induced by the CO_2 compared with likely lithological effects.

The amplitude–thickness relationship was used to transform observed amplitudes to layer thicknesses (Fig. 6a–c). CO_2 saturations within the layer were then calculated from a capillary pressure–saturation relationship determined by centrifuge experiments on core material from the Utsira Sand (Erik Lindeberg, pers. comm.). The capillary pressure, p_c, between the formation brine and the injected CO_2 will cause the CO_2 saturation, S_{CO_2}, to vary with height, h, in each CO_2 layer. The saturation can be computed by balancing the buoyancy, $\Delta\rho \cdot g \cdot h$, with the capillary pressure.

In SI units:

$$\Delta\rho \cdot g \cdot h = p_c = 810.35(1 - S_{CO_2})^{-0.948}. \quad (1)$$

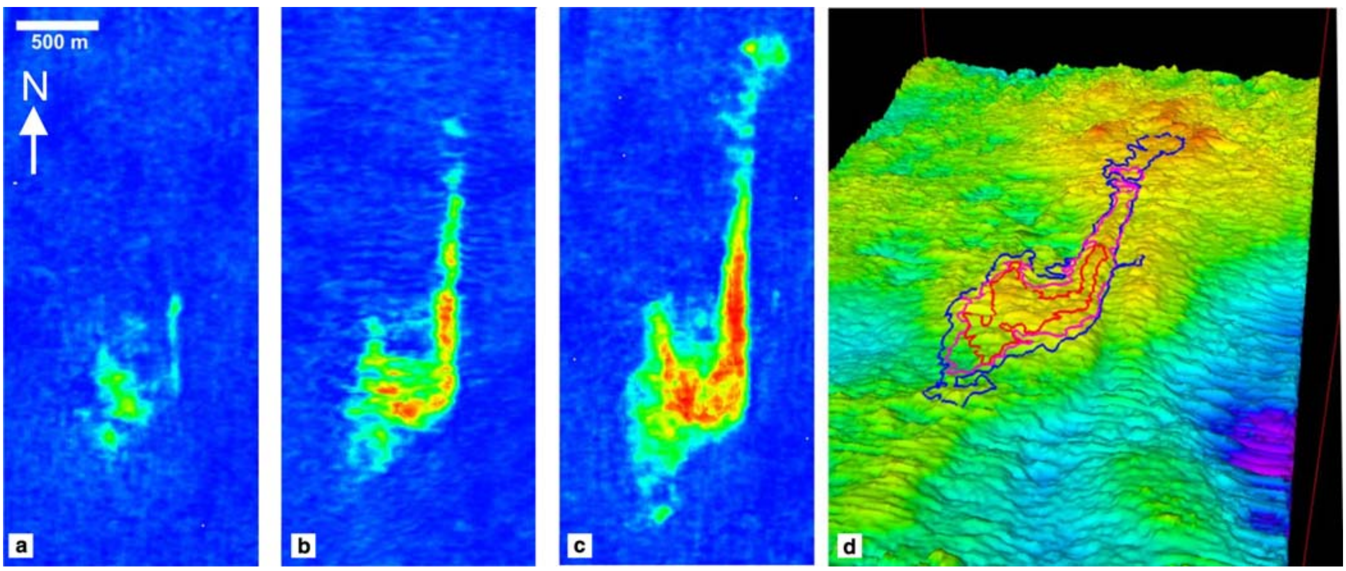

Fig. 3. Growth of the topmost CO_2 layer mapped as amplitude changes at the top of the Utsira Sand: (**a**) 2001–1994 difference; (**b**) 2004–1994 difference; (**c**) 2006–1994 difference; (**d**) 3D view (looking north) of the top Utsira Sand surface (mapped on the baseline 1994 dataset) showing the CWC in 2001 (red), 2004 (purple) and 2006 (blue). RMS amplitudes were extracted from a 4 ms window centred on the trough event corresponding to the negative acoustic impedance change at the top of the CO_2 layer.

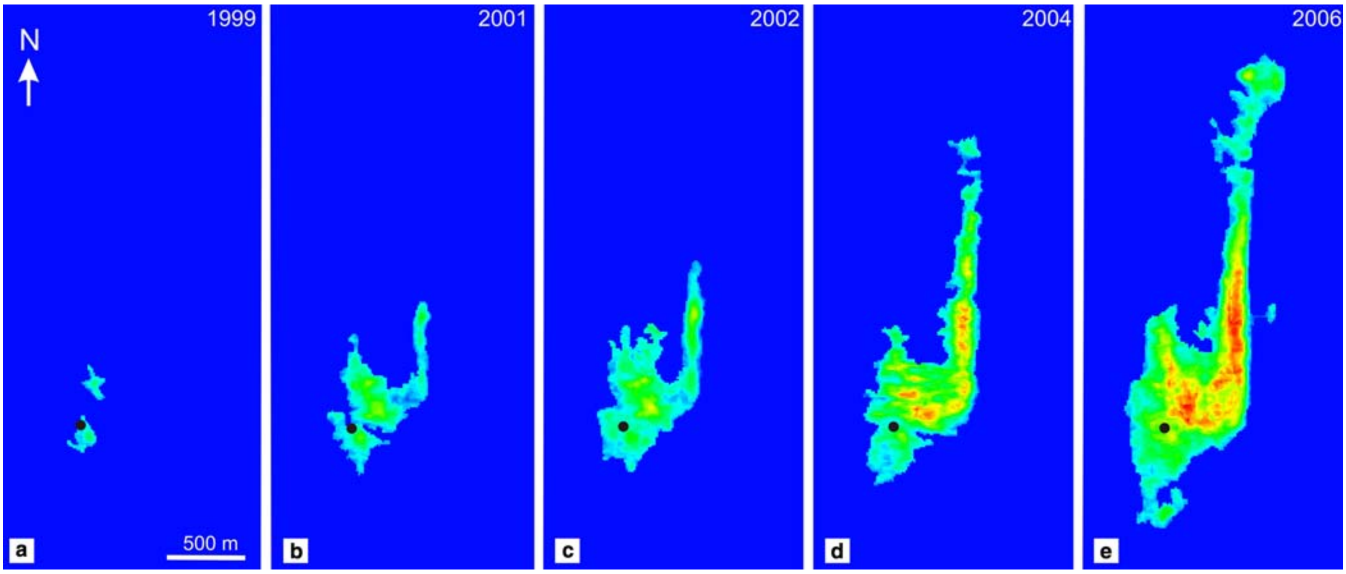

Fig. 4. Amplitude maps of the topmost layer through time. Black spot denotes the location of the injection point for reference. (Note however that the injection point lies roughly 200 m beneath the topmost layer so does not directly control its growth.)

The variation of S_{CO_2} with h was thereby computed and also the average value of S_{CO_2} for a range of layer thicknesses (Fig. 5c). This relationship was used to compute average saturations for the topmost layer (Fig. 6d–f).

Layer thicknesses from structural analysis

An alternative, wholly independent way of obtaining layer thicknesses is by topographic analysis of the reservoir top (Fig. 7). In map view (Fig. 3d), the outer limit of CO_2 reflectivity at this level corresponds to the CWC. The 3D form of the fluid contact at the base of the topmost layer was constructed by fitting a smooth sub-horizontal surface through the elevations of the CWC (note this surface is not truly horizontal because it is constructed in two-way time, not depth, and also because of significant fluid dynamic effects – see below). The two-way time thickness of the topmost layer was then calculated by subtracting the elevations of the reservoir top from the corresponding elevations of the CWC. These were then converted to true (depth) thicknesses (Fig. 8) using a simple velocity model for the overburden, based on well velocity data. Finally, as above, layer saturations were calculated (equation 1).

Evaluation of the thickness maps produced by the two methods shows that structurally derived layer thicknesses have a clear correlation with layer reflectivity (Fig. 3), supporting the general assumption of thin layer tuning. However, it is also clear that the structurally derived thicknesses are in places significantly larger than the thicknesses derived from reflectivity. The main reason for this is probably the non-linearity of the amplitude–thickness relationship whereby amplitude change is quite small for layer thicknesses above about 5 m (Fig. 5b). Application of the tuning assumption will generally tend to progressively underestimate layer thicknesses around and, especially, above the tuning thickness. Other uncertainties in the reflectivity-derived thicknesses include estimation of the maximum tuning amplitude and also the layer velocity. The structurally derived thicknesses are therefore considered to be generally the more reliable. On the other hand, it is clear that layer reflectivity extends into localized areas where the structurally derived layer does not, for example in the southern part of the layer (compare Figs 6 & 8). This is because the structural analysis does not allow CO_2 to be present wherever the constructed CWC is shallower than the topseal (Fig. 7). In reality the CO_2 layer is a dynamic entity with significant horizontal flow and perhaps supplied from below by a number of feeders, some of which may lie

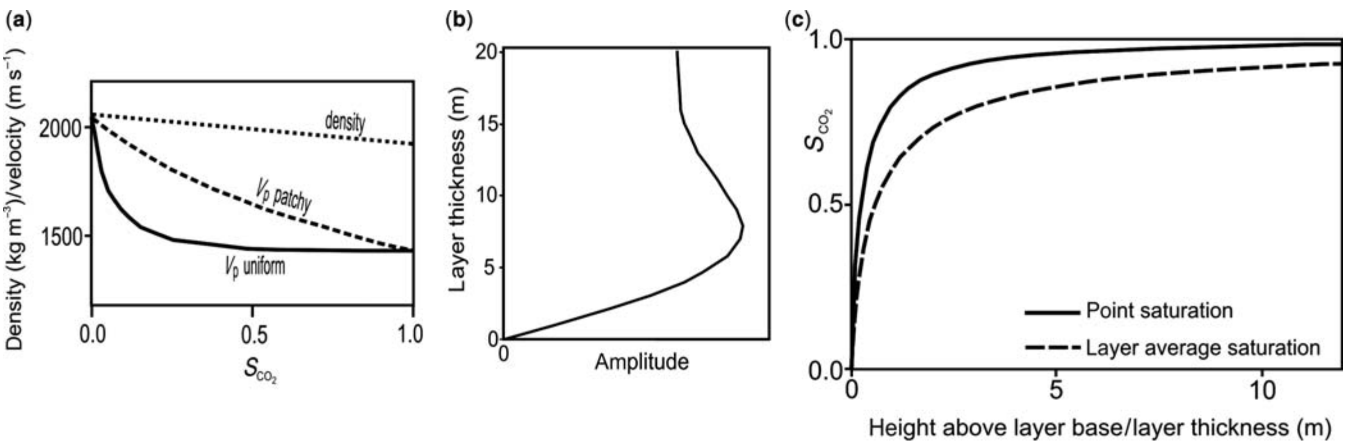

Fig. 5. (**a**) Variation of seismic velocity in the Utsira Sand with CO_2 saturation, calculated for uniform (Reuss bound) and patchy (Hill bound) fluid mixing. (**b**) Amplitude–thickness relationship from a synthetic wedge model of a CO_2-saturated layer within water-saturated sand. (**c**) Layer thickness–saturation function based on capillary pressure data from Utsira core.

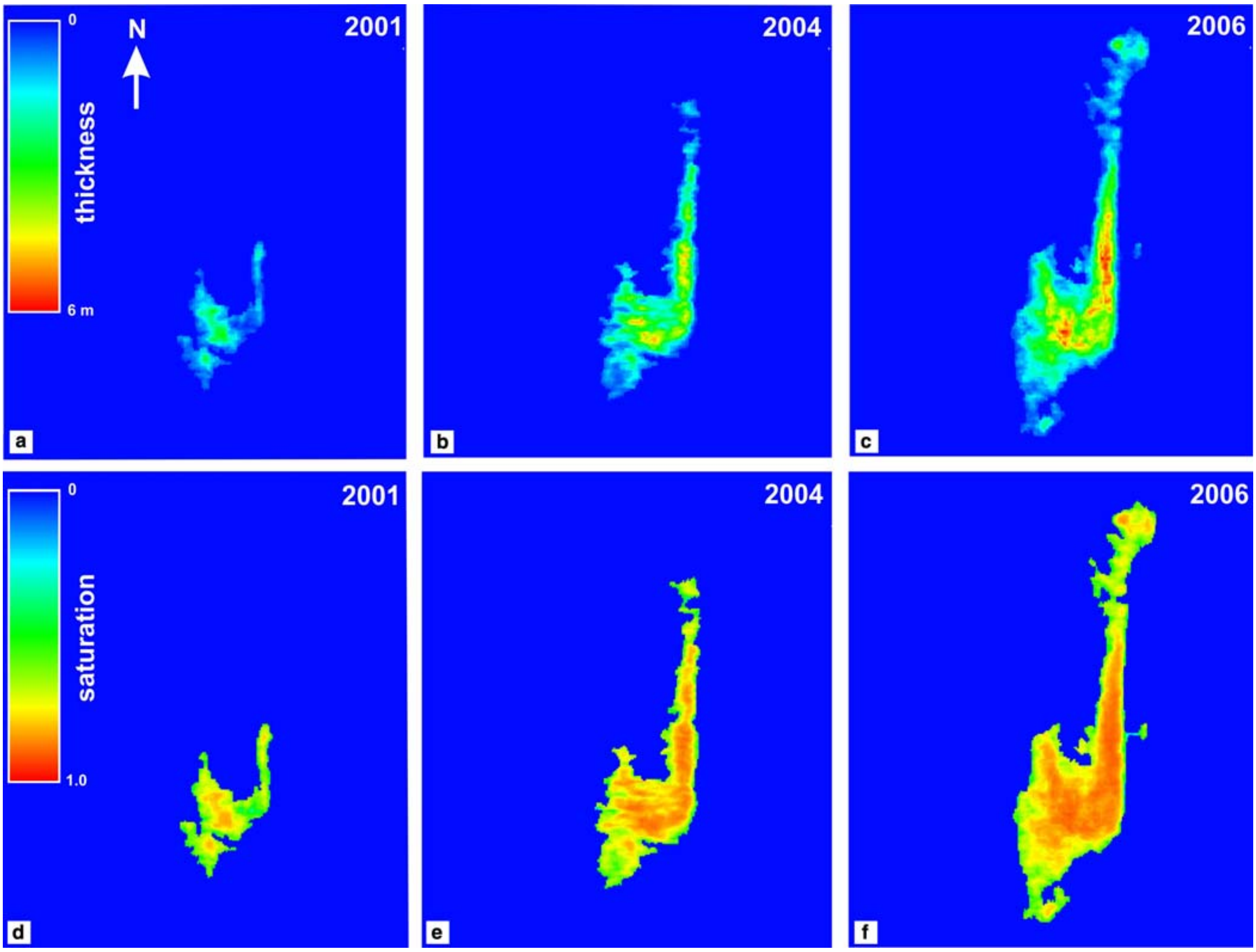

Fig. 6. Topmost CO_2 layer properties: (**a–c**) thicknesses derived from reflection amplitudes; (**d–f**) average saturations determined from capillary pressure data.

beneath topographic depressions in the topseal. These processes will lead to general layer thickening and allow locally 'overdeepened' areas of caprock topography to be underlain by CO_2.

The volume of CO_2 within the topmost layer was computed for the two methods of thickness determination using calculated average saturations and an assumed mean sand porosity of 0.38 (Table 1). As discussed above, volumes derived from the structural analysis are rather higher than those derived from the reflectivity, and, overall are considered to be more reliable.

From the topmost layer volumes, the rate at which CO_2 has arrived at the top of the reservoir can be estimated, bearing in mind that CO_2 first arrived at the reservoir top in 1999, just prior to the first seismic repeat survey when just two small patches of CO_2 had accumulated (Fig. 4a). Taking the structurally derived volumes, an estimated 1.07×10^5 m^3 of CO_2 had arrived at the reservoir top between 1999 and the time of the 2001 survey, an average flux of *c*. 135 m^3 per day. Between the 2001 and 2004 surveys *c*. 3.22×10^5 m^3 of CO_2 arrived at the reservoir top, an average flux of *c*. 316 m^3 per day. Between the 2004 and 2006 surveys a further *c*. 3.76×10^5 m^3 of CO_2 arrived at the reservoir top, averaging *c*. 540 m^3 per day. This marked increase in flux arriving at the reservoir top occurred despite a relatively uniform rate of CO_2 input at the injection point.

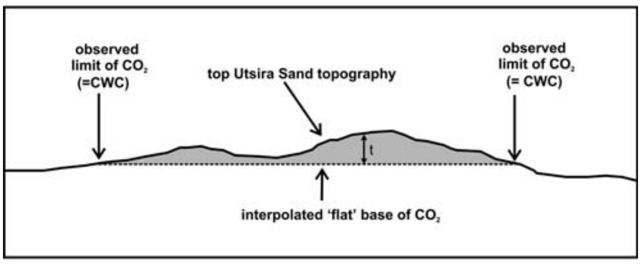

Fig. 7. Schematic cross-section through the topmost CO_2 layer, showing top reservoir topography and a nominally flat CWC. Thickness of the CO_2 layer (t) is the difference in elevation between the top reservoir and the CWC.

2D flow simulation of the whole plume flux

A simple TOUGH2 flow model was set up to simulate the observed growth of the CO_2 plume (Fig. 9). The modelled reservoir geometry was axisymmetrical (radial), with a flat reservoir top and horizontal intra-reservoir mudstones. The latter were all 1 m thick except for the uppermost, which was 5 m thick (Fig. 1b). These deliberately minimal assumptions are justified by the lack of detailed information on internal reservoir structure.

The vertical spacing of the mudstones was set to match the relative spacing of the seismic reflections (Fig. 2). The temperature of the reservoir top was set at 29 °C and the injection point at 36 °C, values in line with available information (see discussion below). Sand properties were based on laboratory core measurements. Mudstones were assumed to be uniformly semi-permeable with relative permeability to CO_2 increasing with CO_2 saturation. The flow properties of the mudstones, permeability and capillary

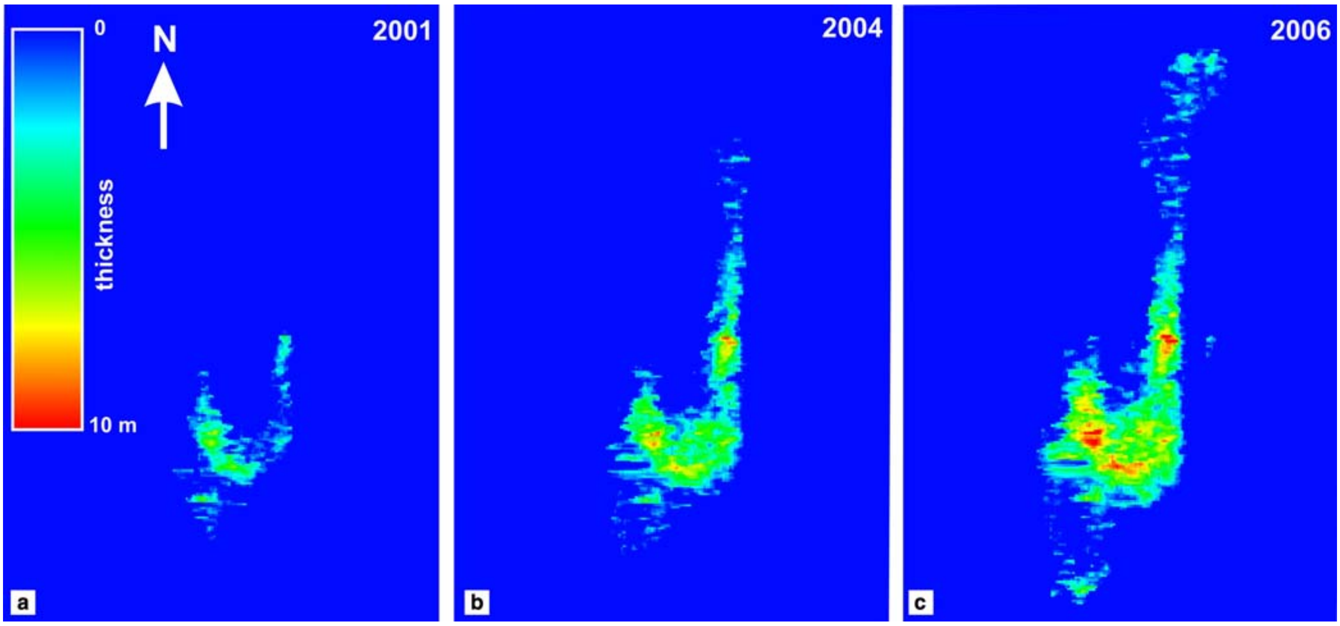

Fig. 8. Topmost CO_2 layer thicknesses derived from structural analysis.

Table 1. Observed volumes of CO_2 in the topmost layer computed from the two different methods

Date	Volume from amplitudes (m^3)	Volume from structural analysis (m^3)
1999	Very small	Very small
2002	66 684	107 380
2004	320 219	429 341
2006	615 876	805 409

entry pressure (Table 2) are the dominant factors in determining the rate of upward migration through the reservoir, and were adjusted such that the simulation matched the observed arrival of CO_2 at the top of the reservoir in 1999. This occurred just prior to the first repeat survey (Fig. 4a) and is a very well constrained key calibrating observation.

The flow simulation (Fig. 9) reproduces the key properties of the CO_2 plume, in particular the characteristic tiered 'Christmas-tree' profile caused by the accumulation of thin layers of CO_2 spreading laterally beneath each intra-reservoir mudstone. It also predicts that the uppermost CO_2 layer shows very rapid lateral spread (Fig. 9). This is driven by a progressive increase in the modelled rate of CO_2 arriving at the topmost layer from 1999 onwards (Fig. 10). This is despite the relatively uniform CO_2 input at the injection point and is largely due to increased effective permeabilities within the central part of the plume as the intra-reservoir mudstones become progressively more saturated with CO_2 and relative permeability to CO_2 increases.

Fluxes predicted by the flow simulation are, therefore, consistent with observed fluxes derived from the seismic data, showing a steady increase in the rate of CO_2 flowing into the topmost layer. The simulation, however, assumes Darcy flow through semi-permeable intra-reservoir mudstones with capillary entry pressures much lower than measured values from the caprock (Table 2), which laboratory testing shows to be a very low permeability capillary seal (Harrington *et al.* 2010). These modified values are required for the CO_2 to reach the top of the reservoir in the observed time-span (immediately prior to the 1999 survey). Even allowing for the simplified geometry of the axisymmetrical model, this is paradoxical, because the well logs (Fig. 1b) suggest that the thin mudstones are lithologically similar to the caprock and would, at least when intact, form capillary seals. It seems likely therefore that CO_2 migration through these mudstones is actually not by Darcy flow but via some form of pathway flow, the pathways becoming more effective, or more numerous with time. This is also consistent with measured pressure distributions in laboratory samples during long-term flow testing, which suggest pathway rather than Darcy flow (Harrington *et al.* 2010). The nature of these pathways is uncertain however. Small faults have been identified in the Utsira Sand, probably related to differential compaction during burial. More radically, Hermanrud *et al.* (2007) have suggested that fluidization effects within the main feeder chimney may have induced minor collapse and faulting of the layers within the reservoir. Whether natural or induced, small faults displacing the intra-reservoir mudstones are plausible candidates for providing the permeability enhancement required to explain the observed upward flow. A number of alternative explanations may be considered. Zweigel *et al.* (2004) showed that most of the individual

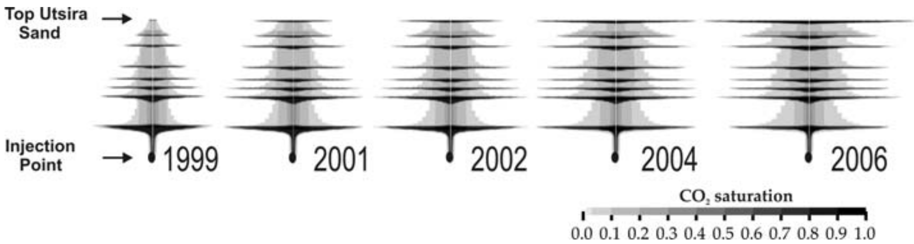

Fig. 9. Simulated growth of the CO_2 plume from 1999 to 2006 from the TOUGH2 axisymmetrical flow model.

Table 2. Flow properties of intra-reservoir mudstones in the flow model, compared with core measurements from caprock (0.9869×10^{12} m^2 equates to 1 Darcy)

	Intra-reservoir mudstones in TOUGH2 model	Laboratory caprock core
Capillary entry pressure (Pa)	1.6×10^4	$1.6 - 1.9 \times 10^6$
Permeability (m^2)	9×10^{-14}	4×10^{-19}

intra-reservoir mudstones are not correlatable from well to well, indicating lateral impersistence and/or the presence of 'holes'. Holes in the mudstones could be due to erosive removal, possibly by channelling, or soft sedimentary processes such as sand mobilization. Alternatively, geochemical processes may play a part. In the short-term, evaporation of residual water into the CO_2 could cause dehydration and possible shrinkage of the mudstones. Mineralogical changes are thought unlikely to occur significantly in the short time-scales considered here. Moreover experimental work on the reactivity of CO_2–caprock systems at reservoir conditions (summarized in Chadwick *et al.* 2008) indicates that mineralogical changes would tend to reduce porosity (and by implication permeability) in mudstone lithologies. Finally, recent experimental work has suggested that in CO_2–water systems in argillaceous rocks (i.e. sealing strata), CO_2 may show intermediate wetting properties, thereby reducing capillary entry pressures to CO_2 (e.g. Chiquet *et al.* 2005). However, by itself this process cannot explain the observed rate of migration of CO_2 to the top of the reservoir because the intrinsic permeability of the mudstones is still much too low.

3D flow simulation of the topmost layer spreading

The growth of the topmost layer between 1999 and 2006 is quite striking (Fig. 4), and has involved rapid lateral spreading of free CO_2 controlled by top reservoir topography. The CO_2 initially impacted the topseal within a local topographic dome, then spilled northwards along a prominent north-trending linear ridge before entering a more vaguely defined northerly topographic high (Fig. 3). Lateral migration was particularly rapid along the linear ridge where the CO_2 front advanced northwards at about 1 m per day between 2001 and 2004. In order to examine layer evolution more closely, a 3D flow model was set up. The top reservoir surface was mapped from the baseline (1994) seismic dataset and depth-converted using a layer-cake, laterally uniform velocity model (available wells constrain regional velocities but are not sufficiently closely spaced to constrain local velocity variation). The nature of the CO_2 supply to the topmost layer depends on the transport properties of the relatively thick (>5 m) mudstone immediately beneath (Fig. 1b). As discussed above, pathway flow is considered most likely, but the number of individual pathways is uncertain. In 1999, initial development of the topmost layer was as two seemingly distinct small accumulations (Fig. 4a), of which the southerly appears to have been fed directly by the main feeder chimney (Fig. 2). The simplest interpretation of the northerly accumulation is that it was supplied laterally from the southerly one, but a second smaller feeder, supplying from directly below, cannot be ruled out. For simplicity, the flow modelling assumed a single feeder, located between the two initial accumulations, with modelled CO_2 flux into the layer matched to the structurally derived volumes (Table 1). A minor adjustment to the model was also made to allow for the fact that the CO_2 injected at Sleipner contains up to about 2% methane, lowering density and increasing buoyancy. The TOUGH2 version used for modelling does not have an option for CO_2–methane mixtures, so to account for this, the top reservoir temperature in the model was raised to 31.5 °C, giving a pure CO_2 density comparable with that of a CO_2–methane (2%) mixture at 29 °C.

Permeability effects

Permeability values for the Utsira Sand range from laboratory determinations of 2–3 Darcy (with no evidence of horizontal/vertical anisotropy), to more regional estimates of up to 8 Darcy from large-scale water production (Zweigel *et al.* 2004).

An initial flow simulation was run using an isotropic reservoir permeability of 3 Darcy (Fig. 11), in accordance with the core measurements. The spread and lateral migration of the simulated layer are much slower than that of the real layer, the modelled CO_2 front barely reaching the southern end of the north-trending ridge. The modelled migration is also more obviously radial from

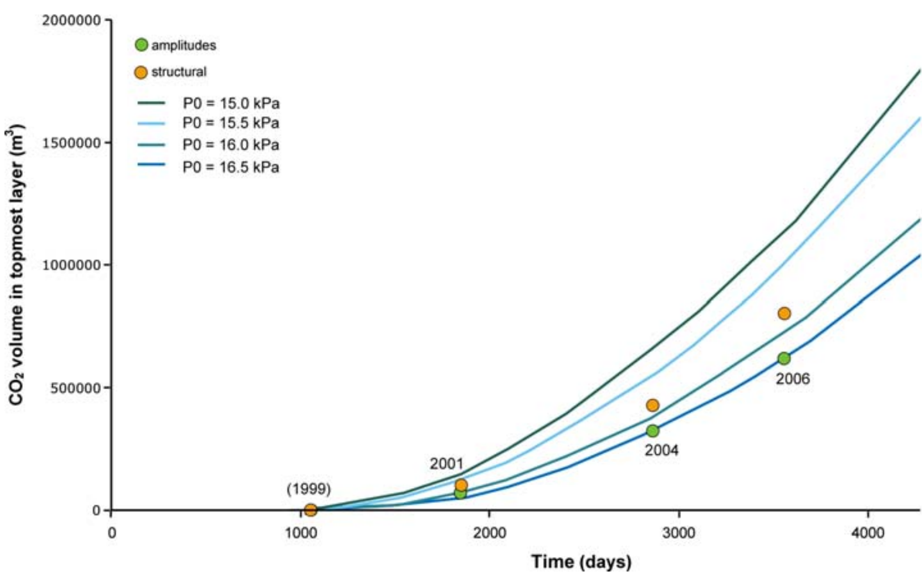

Fig. 10. Growth of the topmost CO_2 layer. Green and orange circles denote observed volumes derived from the seismic amplitudes and from structural analysis of the CWC respectively (Table 1). Solid lines show TOUGH2 flow simulation with semi-permeable intra-reservoir mudstones and a range of capillary entry pressure.

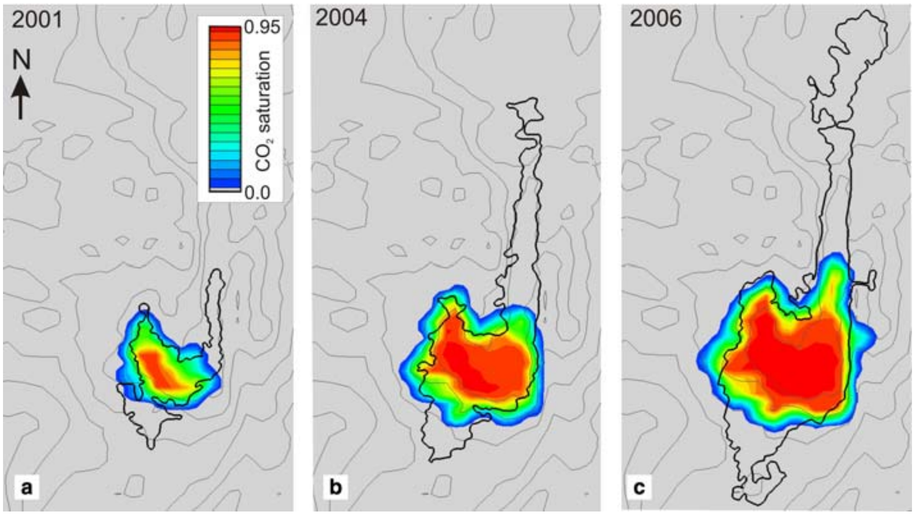

Fig. 11. Modelling topmost layer spreading from 2001 to 2006 assuming a reservoir permeability of 3 Darcy. Polygons denote observed CWC.

the feeder point than the observed spreading, with a greater tendency to spread east–west.

In order to increase the slow simulated spreading rates, a number of flow simulations were run with higher permeability values (Fig. 12). Permeabilities of 6 Darcy (Fig. 12b) and also 10 Darcy, produced more pronounced lateral spreading, but were still insufficient to match the observations. The modelled migration also remained more radial about the feeder point. In order to address this, permeability anisotropy was introduced: 3 Darcy east–west and 10 Darcy north–south. Specific geological justification of this is not obvious, though the assumption is qualitatively consistent with the generally north-trending depositional geometry of the Utsira Sand (Gregersen *et al.* 1997). With anisotropic permeability the match is improved somewhat (Fig. 12c), but migration along the north-trending ridge is still much slower than actually observed. It is clearly difficult to match the observed spreading of the topmost layer by adjusting permeability alone. Even simulations with improbably extreme values of anisotropic permeability, 40 Darcy north–south and 10 Darcy east–west, failed to match the observed northward spreading.

Buoyancy effects

Lateral migration of the topmost layer is driven by buoyancy forces arising from the relatively low density of the injected CO_2 relative to the reservoir pore-water. To test whether enhanced buoyancy could contribute to better history-matching, the top reservoir temperature in the model was increased to 36 °C, reducing the density of the CO_2 by about 300 kg m^{-3} and also its viscosity. A simulation was then run at this higher temperature but with the same injected volumes and with 3/10 Darcy anisotropic permeabilities (Fig. 12d). This simulation shows a better match than the lower temperature models but still fails to reproduce both the northward and southward extents of the observed layer. The justification for reducing plume density via increased temperatures is in any case questionable. The reservoir temperature at Sleipner is believed to

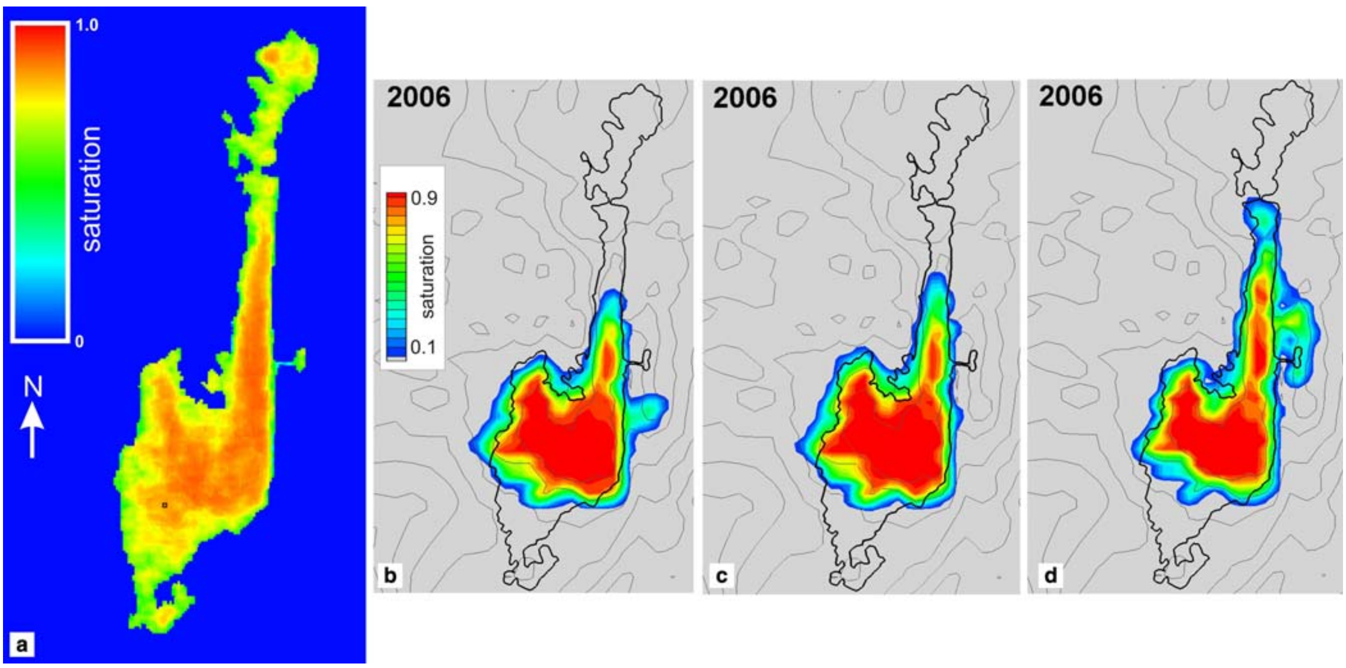

Fig. 12. The topmost layer in 2006. (**a**) Observed extents; (**b**) TOUGH2 simulation with $k = 6$ Darcy; (**c**) TOUGH2 simulation with $k = 3$ Darcy east–west and 10 Darcy north–south; (**d**) TOUGH2 simulation with $k = 3$ Darcy east–west, 10 Darcy north–south and higher reservoir temperature.

be well constrained: a temperature measurement from a Sleipner well has been recently confirmed by downhole measurements from the nearby Volve Field where water is being produced from the Utsira Sand (Ola Eiken, pers. comm.). Nevertheless some doubt remains: interpolation between the seabed and measured temperatures in the much deeper Sleipner East gas field (Christian Hermanrud, pers. comm. 2007) would suggest temperatures in the Utsira Sand up to a few degrees higher than the measured values.

Topographic effects

It is clear that neither adjusting reservoir permeability nor injected fluid properties can satisfactorily match the simulations with the observed spread of the topmost CO_2 layer, in terms of either its northerly or southerly extents. The lack of southerly spreading can partly be explained by the model simplification of a single CO_2 feeder located between the two 1999 patches. Placing a feeder directly beneath the southerly patch would produce much more southward spread. Additional feeders to the south may also be developing as the layer grows. The lack of northward spread in the model is more problematical. Additional feeders beneath the north–south trending tongue of CO_2 can probably be discounted due to the lack of a CO_2 source layer beneath. In addition, specific details of migration which also do not match the observations, such as the simulated spillage eastward from the north-trending linear ridge (Fig. 12d), require explanation. It is likely that slight inaccuracies in the depth topography of the top reservoir surface may explain these discrepancies.

A detailed cross-section through the topmost layer (Fig. 13a) shows that its observed northward progression involved rapid migration along an apparently near-horizontal ridge crest. Top reservoir depths were calculated using a laterally uniform 'layer-cake' overburden velocity model based on average velocities from a number of wells in the vicinity; depths are, in consequence, a simple transform of seismic two-way travel-time. Apparently paradoxical migration trends could therefore be explained by errors in the topography of the topseal produced by lateral velocity variations which have not been accounted for in the depth-conversion.

An initial test of this hypothesis is to examine the overall dip of the topseal. The feeder chimney impacts the topseal at point A1 at a two-way travel-time of 873 ms (Fig. 13). A local topographic culmination north of the linear ridge, point A2, lies at a two-way travel-time of 856 ms. The travel-time difference between A1 and A2 converts to a depth difference of 18.5 m, which over a horizontal spacing of 2249 m gives an average gradient of 0.0082. A more conservative estimate of topseal dip may be obtained by comparing the relative elevations of the southernmost and northernmost extremities of the layer, points B1 and B2 respectively. These two points have an elevation difference of 17.4 m over a distance of 2895 m, giving an average gradient of 0.0058.

In order to test potential CO_2 migration rates along dips of this order, a simple synthetic surface model was constructed. This has two circular domes whose relief and separation match the observed topseal surface, joined by a linear ridge of similar geometry to that observed. Two surface options were examined, one with a uniform

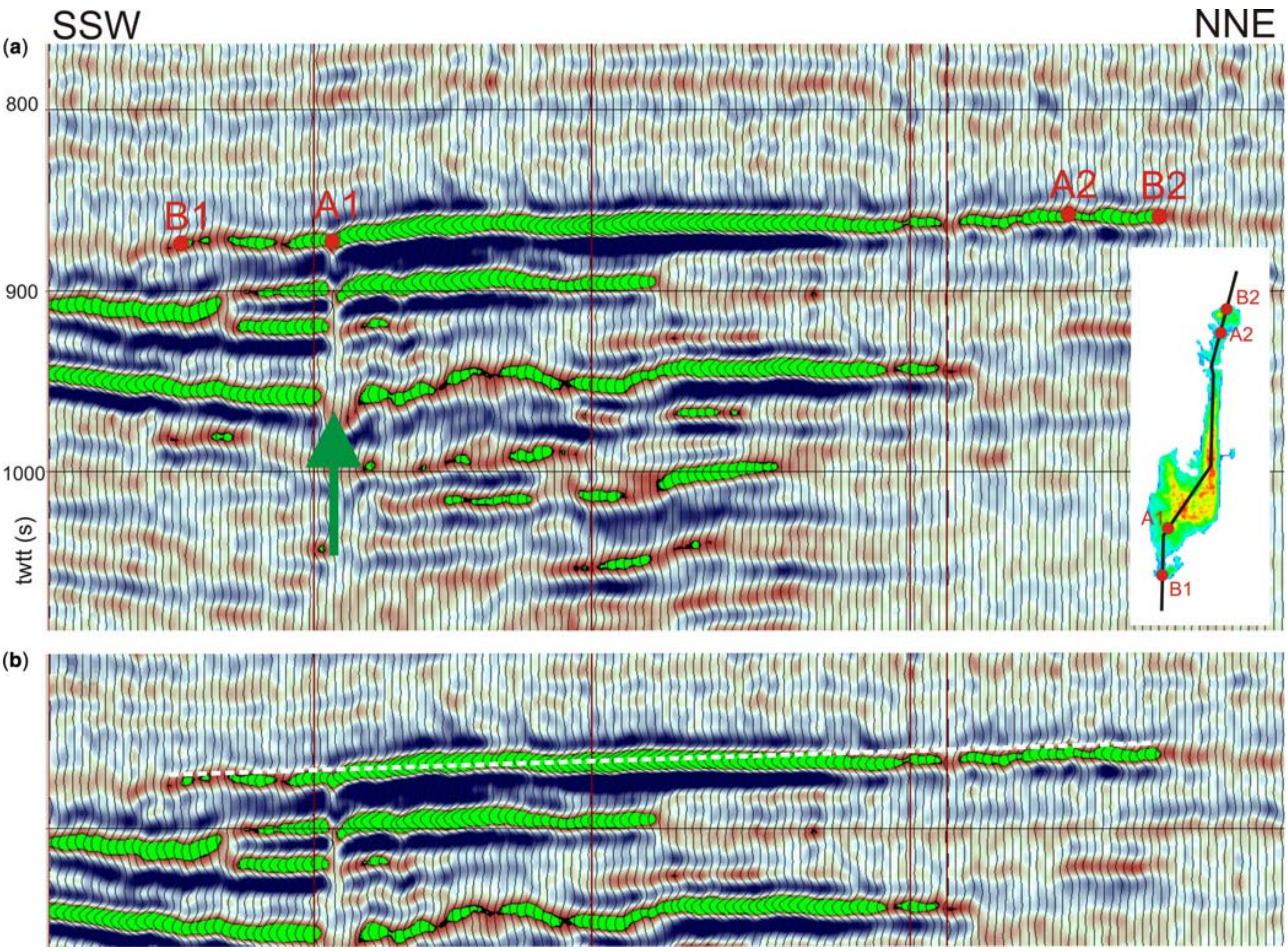

Fig. 13. Seismic line through the CO_2 plume. (**a**) Detailed geometry of the topmost layer in two-way travel-time. The main feeder chimney (arrowed) supplies the layer at point A1. (**b**) Deviation of the topmost layer from planar geometry (white dots). Reflective CO_2 layers in green.

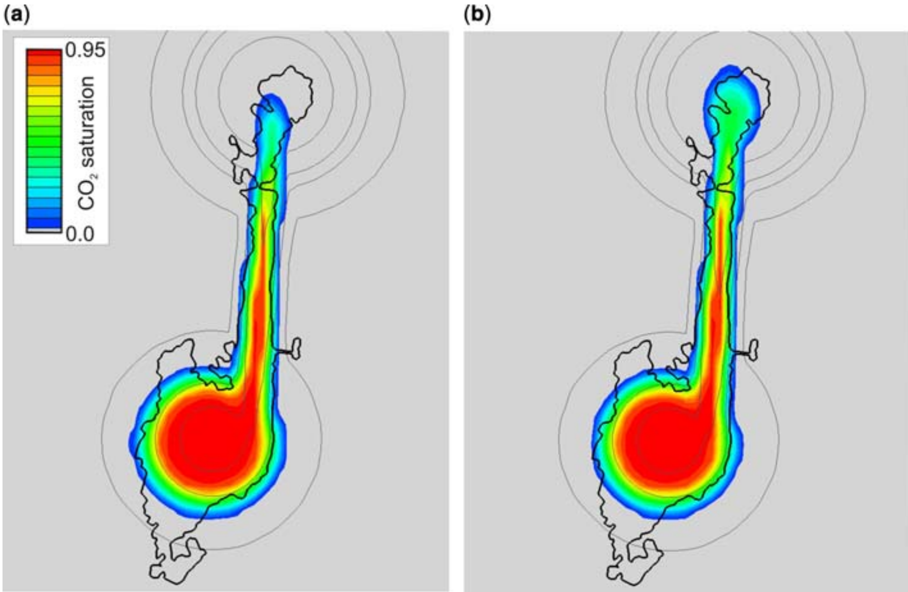

Fig. 14. Flow simulation of synthetic surface with sand permeability of 10 Darcy: (**a**) average gradient of 0.0058; (**b**) average gradient of 0.0082.

gradient along the ridge of 0.0058 and one with a gradient of 0.0082 (Fig. 14).

The simulations show that a synthetic surface with a smooth, uninterrupted dip in the observed range can produce the required rate of lateral migration, albeit requiring a high modelled permeability. A key property of the synthetic surface is that a uniform dip is maintained along the linear ridge. Close inspection of the real data (Fig. 13b) shows local perturbations of up to 5 ms two-way travel-time along the ridge with respect to a uniform gradient. The downwarp towards the northern end of the ridge effectively retards northward migration of the CO_2 in the flow simulations. If, however, this downwarp were not real, but just a localized time shift (pushdown) due to lateral velocity variation, then the discrepancy between the observed and simulated migration patterns could be explained.

There are a number of wells in the vicinity with velocity data, but these are too spatially scattered (typically more than 2 km apart), to explicitly map local velocity variations. Average velocities to the top of the Utsira Sand were calculated for these wells. Well pairs were selected, their spacing noted, and the difference in velocity between them calculated. Velocity difference against well spacing was then plotted for all well pairs (Fig. 15). Significant velocity variation is evident, with differences up to more than 50 m s^{-1}, but these are not clearly related to well spacing with velocity differences up to 30 m s^{-1} between wells only 2–3 km apart. This suggests that the velocity field is characterized by rapid local velocity changes which are not being properly spatially sampled by the widely spaced wells. Velocity difference is readily converted to two-way travel-time difference. Two-way travel-time differences of 10 ms or so are common at well spacings of 2–3 km. The linear best fit, albeit very poorly correlated, suggests that similar time differences could well occur over even smaller distances. It is clear therefore that the postulated time shifts noted on the cross-section (Fig. 13b) – up to 5 ms over a distances of about 1 km – are fully compatible with observed lateral velocity changes between the wells.

Accurate mapping of local velocity variation is required to resolve this issue but this is not possible with the widely spaced well data. Seismic stacking velocities are currently being assessed, but do not appear to be sufficiently precise. Another possibility is interpretive use of the seismic data itself. Bright spots in the overburden are clustered at certain stratigraphical levels and are probably related to natural accumulations of shallow gas which would lower seismic velocity. By mapping integrated bright-spot amplitudes it may be possible to scale these to relative velocity-induced time shifts. This is currently under investigation.

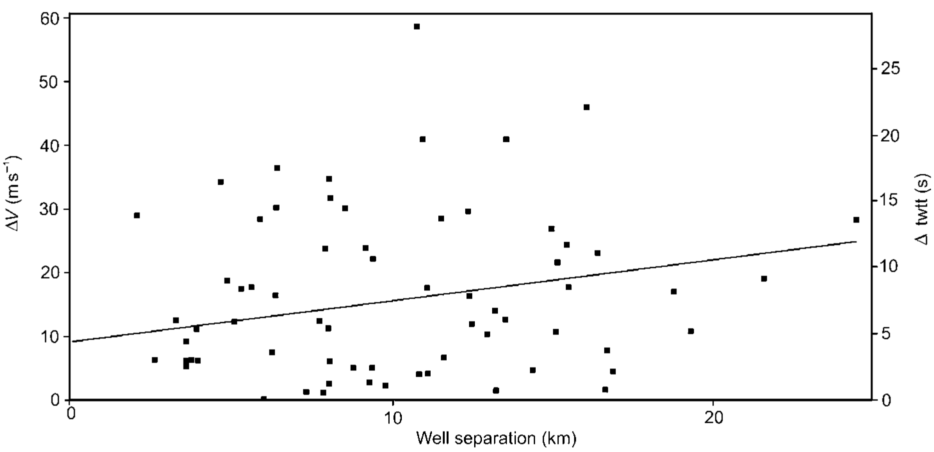

Fig. 15. Average velocity variation to top Utsira Sand showing velocity difference between pairs of wells and corresponding time shifts. Linear best fit also shown.

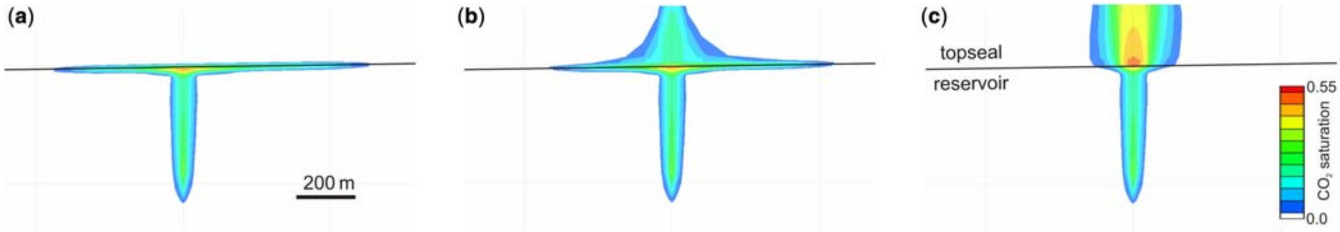

Fig. 16. Flow simulations (after six years) beneath a planar dipping topseal of variable flow properties: (**a**) $k = 4 \times 10^{-19}$ m^2; $P_c = 2$ MPa; (**b**) $k = 9 \times 10^{-14}$ m^2; $P_c = 40$ kPa; (**c**) $k = 9 \times 10^{-14}$ m^2; $P_c = 17$ kPa. Note figure has vertical exaggeration.

To summarize, the well data show that local velocity variations are present which induce significant localized time shifts. Time shift corrections applied to the topseal surface prior to depth conversion could produce a smoother depth surface which would allow simulated layer spreading to more closely match the observed data. Explicit mapping of these time shifts has not currently been achieved, however.

Topseal properties

The flow simulations have all assumed an impermeable reservoir topseal. This is consistent with laboratory testing on caprock core samples which measured capillary entry pressures of around 2 MPa, considerably higher than any credible reservoir pressure increase. However, although they seem to have similar geophysical log properties to the caprock, the thin intra-reservoir mudstones are required to be effectively semi-permeable for the whole plume reservoir simulation to match the observed arrival of CO_2 at the reservoir top (Fig. 4a). The question arises therefore as to whether the basal layers of the caprock might show similar flow properties to the intra-reservoir mudstones. There is no evidence of changes in the seismic signature of the caprock that might indicate migration of CO_2 through the topseal, but this is subject to finite detection capability and so does not unequivocally prove seal integrity, particularly as diffuse migration into the caprock might be difficult to detect seismically.

In order to investigate this, a simple 3D flow model was set up, with a planar dipping topseal of gradient 0.0082 (comparable to the real dips discussed above) and a reservoir permeability of 3 Darcy. CO_2 was input beneath the topseal, at the volumes calculated above, for a range of topseal flow properties and the simulation run for six years (Fig. 16). With topseal properties identical to the core measurements (Harrington *et al.* 2010) the CO_2 migrates updip more than 600 m (Fig. 16a). Modifying the topseal permeability to the modelled permeability of the intra-reservoir mudstones, but maintaining a higher capillary entry pressure, allows limited migration into the caprock and reduces the updip migration to about 550 m (Fig. 16b). With topseal flow properties set identical to the modelled properties of the intra-reservoir mudstones (Fig. 16c), there is major ingress into the topseal with negligible updip migration. It is clear that migration into the caprock would significantly retard lateral migration and is not consistent with the observed very rapid lateral migration of the topmost layer. The high observed migration rates, and the very high reservoir permeabilities that are required to simulate these, suggest therefore that the topseal is behaving as a very 'hard' flow barrier exerting negligible 'drag' on the flowing layer beneath.

Discussion

The type of analysis described above provides an interesting pointer to how the regulatory requirements of future large-scale underground storage may be addressed. For example, the European Storage Directive has three key requirements which have to be satisfied before liability for the storage site can revert to the licensing authority:

- actual behaviour of the injected CO_2 conforms with the modelled behaviour;
- there is no detectable leakage;
- the storage site is evolving towards a situation of long-term stability.

Because the topmost CO_2 layer represents the ultimate trapping level for mobile free CO_2 in the reservoir, understanding its behaviour is key to demonstrating both conformance and constraining future plume behaviour. Results so far suggest that the main processes governing lateral spreading of the topmost layer are quite well understood and its actual behaviour conforms reasonably well with the modelling. Regarding leakage detection, the lack of seismic changes in the caprock, together with the apparent lack of fluid transport into the caprock as deduced above, together make a strong case for no leakage. The third requirement clearly will involve much longer term predictive modelling than the short-term history matching described here; nevertheless, the latter does provide an essential starting point on which to base longer term prediction.

Conclusions

The topmost CO_2 layer in the Sleipner plume represents the ultimate trapping level for mobile free CO_2 in the reservoir. As such it can provide useful insights into key elements of reservoir performance, both in the short and longer term.

Volumetric analysis of the layer closely constrains total upward CO_2 flux through the reservoir. This allows assessment of bulk reservoir flow properties and how these change with time. The thin intra-reservoir mudstones exert the main control on reservoir flow. Laboratory measurements suggest that, in intact form, these should act as capillary seals, so it is inferred that transport is via pathway flow rather than Darcy flow, possibly associated with networks of small faults or other 'holes' perhaps of sedimentary origin. Calculated CO_2 fluxes to the topmost layer have steadily increased with time, suggesting that the feeder pathways are evolving, becoming either more transmissive with time and/or increasing in number.

Detailed 3D history-matching of the topmost layer is challenging, most likely because of uncertainties in exact topseal topography. It nevertheless provides insights into the flow properties of both the topmost reservoir sand and also the integrity of the seal. High observed lateral spreading rates are consistent with very high permeabilities, possibly with some anisotropy. They also suggest that the topseal presents a very 'hard' flow barrier which exerts minimal 'drag' on the lateral flow beneath.

Studies such as this, concentrating on defining the process and performance of the storage system, within and immediately around the reservoir, can provide a robust basis for meeting the regulatory requirements for the large-scale deployment of CCS.

We thank the CO2ReMoVe consortium for permission to publish this work. CO2ReMoVe is funded by the EU 6th Framework Programme and by industry partners BP, ConocoPhillips, ExxonMobil, Statoil, Schlumberger, Total, Vattenfall and Wintershall. R&D partners are BGR, BGS, BRGM, CMI, DNV, ECN, GFZ, GEUS, IFP, IMPERIAL, OGS, SINTEF, TNO and URS. This paper is published with permission of the Executive Director, BGS (NERC).

References

Arts, R., Eiken, O., Chadwick, R. A., Zweigel, P., van Der Meer, L. & Zinszner, B. 2003. Monitoring of CO_2 injected at Sleipner using time lapse seismic data. *In*: Gale, J. & Kaya, Y. (eds) *Greenhouse Gas Control Technologies*. Elsevier Science, Oxford, 347–52.

Baklid, A., Korbol, R. & Owren, G.. 1996. Sleipner vest CO_2 disposal, CO_2 injection into a shallow underground aquifer. *SPE Annual Technical Conference and Exhibition*, Denver, CO, SPE Paper 36600, 1–9.

Chadwick, R. A., Arts, R., Eiken, O., Kirby, G. A., Lindeberg, E. & Zweigel, P. 2004. 4D seismic imaging of a CO_2 bubble at the Sleipner Field, central North Sea. *In*: Davies, R. J., Cartwright, J. A., Stewart, S. A., Lappin, M. & Underhill, J. R. (eds) *3-D Seismic Technology: Application to the Exploration of Sedimentary Basins*. Geological Society, London, Memoirs, **29**, 311–320.

Chadwick, R. A., Arts, R. & Eiken, O. 2005. 4D seismic quantification of a CO_2 plume at Sleipner, North Sea. *In*: Doré, A. G. & Vining, B. A. (eds) *Petroleum Geology: North-West Europe and Global Perspectives: Proceedings of the 6th Petroleum Geology Conference*. Geological Society, London, 1385–1399; doi: 10.1144/0061385.

Chadwick, R. A., Arts, R., Bernstone, C., May, F., Thibeau, S. & Zweigel, P. 2008. *Best Practice for the Storage of CO_2 in Saline Aquifers*. British Geological Survey, Keyworth, Occasional Publications, **14**.

Chiquet, P., Broseta, D. & Thibeau, S. 2005. *Capillary Alteration of Shaly Caprocks by Carbon Dioxide*. Society of Petroleum Engineers Paper SPE 94183.

Gregersen, U., Michelsen, O. & Sorensen, J. C. 1997. Stratigraphy and facies distribution of the Utsira formation and the Pliocene sequences in the northern North Sea. *Marine and Petroleum Geology*, **14**, 893–914.

Harrington, J. F., Noy, D. J., Horseman, S. T., Birchall, D. J. & Chadwick, R. A. 2010. Laboratory study of gas and water flow in the Nordland Shale, Sleipner, North Sea. *In*: Grobe, M., Pashin, J. & Dodge, R. (eds) *Carbon Dioxide Sequestration in Geological Media – State of the Science*. American Association of Petroleum Geologists, Tulsa, OK, Studies in Geology, **59**, 521–543.

Hermanrud, C., Zweigel, P., Eiken, O., Lippard, J. & Andresen, T. 2007. CO_2 flow in the Utsira formation: inferences made from 4D seismic analysis in the Sleipner area. *European Conference of the American Association of Petroleum Geologists*, Athens, Abstract.

IPCC, 2005. Metz, B., Davidson, O., de Coninck, H. C., Loos, M., Meyer, L. A. (eds) *IPCC Special Report on Carbon Dioxide Capture and Storage. Prepared by Working Group III of the Intergovernmental Panel on Climate Change*. Cambridge University Press, Cambridge.

Lindeberg, E., Zweigel, P., Bergmo, P., Ghaderi, A. & Lothe, A. 2001. Prediction of CO_2 distribution pattern by geology and reservoir simulation and verified by time-lapse seismic. *In*: Williams, D. J., Durie, R. A., McMullen, P., Paulson, C. A. J., Mavko, G., Mukerji, T. & Dvorkin, J. 2003. *The Rock Physics Handbook*, 2nd edn. Cambridge University Press, Cambridge, 329.

Mavko, G., Mukerji, T. & Dvorkin, J. 2003. *The Rock Physics Handbook: Tools for Seismic Analysis in Porous Media*. Cambridge University Press, Cambridge.

Zweigel, P., Arts, R., Lothe, A. E. & Lindeberg, E. 2004. Reservoir geology of the Utsira Formation at the first industrial-scale underground CO_2 storage site (Sleipner area, North Sea). *In*: Baines, S. & Worden, R. H. (eds) *Geological Storage for CO_2 Emissions Reduction*. Geological Society, London, Special Publications, **233**, 165–180.

Differences between flow of injected CO_2 and hydrocarbon migration

CHRISTIAN HERMANRUD,[1,2] GUNN MARI GRIMSMO TEIGE,[1] MARTIN IDING,[1] OLA EIKEN,[1] LARS RENNAN[1] and SVEND ØSTMO[1]

[1]*Statoil ASA, 7005 Trondheim, Norway (e-mail: che@statoil.com)*
[2]*University of Bergen, Faculty of Mathematics and Natural Sciences, 2020 Bergen, Norway*

Abstract: Knowledge of fluid flow processes in the subsurface is important for CO_2 storage operations as well as for hydrocarbon exploration. Repeated seismic surveys for more than 10 years of CO_2 injection into the Utsira Formation, in the Sleipner area, offer a unique dataset. This dataset holds information on fluid migration processes that can be analysed for the benefit of hydrocarbon exploration and CO_2 storage considerations alike. Thorough analyses of these datasets reveal several features that give useful information of subsurface fluid flow processes. The CO_2 in the Utsira Formation has flowed laterally beneath thin, intra-formational shales. At the same time, CO_2 has flowed vertically through shaly horizons that would normally be considered as barriers to fluid flow. This flow has apparently taken place through vertically stacked flow conduits through the shales. These conduits may to some extent have existed prior to the start of CO_2 injection, but may also have been augmented by the CO_2 injection process. The calculated pushdown of seismic reflectors below the CO_2 plume is less than that observed, which may point to the presence of hitherto unrecognized flow paths for the CO_2. Hydrocarbon migration pathways are in general not recognizable in seismic data. This implies that such avenues are significantly thinner than those of the CO_2 migration in the Utsira Formation. This result points to the presence of mixed-wet migration pathways, in which capillary flow resistance may not control the (sub-horizontal) flow path thickness. A circular depression at the top of the Utsira Formation that existed prior to the injection may be interpreted as a result of a deeper seated sand remobilization feature. Such features will also promote vertical hydrocarbon migration where they are present. A more widespread occurrence of such features may explain why hydrocarbons are generally found beneath thick shales, but are less likely to be found below thin intra-formational shales below the structural spillpoint of the top seal. These observations suggest that seal thickness is an important parameter, even if the capillary entry pressure of the sealing rock is sufficiently high to preserve significant hydrocarbon columns.

Keywords: CO_2 injection, CO_2 flow, hydrocarbon migration, Utsira Formation, top seal, intra-formational shales

Knowledge of hydrocarbon migration processes is important for predictions of oil and gas occurrence in the subsurface. Direct field observations of hydrocarbon migration are rare and seismic identification of migration routes carries significant uncertainties. As a result, important aspects of hydrocarbon migration remain elusive.

The CO_2 injection that has been carried out in the Utsira Formation above the Sleipner West Field in the Norwegian North Sea has been monitored by a set of repeated seismic surveys (Arts *et al.* 2003; Chadwick *et al.* 2005). These surveys reveal how CO_2 has migrated in the Utsira Formation from 1996 to 2008, and give unique observations of fluid migration in a porous medium.

The conditions of hydrocarbon migration and CO_2 injection differ in many respects. Such differences are partly due to different fluid properties between hydrocarbons and CO_2, including interfacial tensions, solubilities, densities, viscosities, and interactions with pore water (and consequences for the pH). Also, significant differences exist between the injection rate of CO_2 and the much slower hydrocarbon migration velocity. These differences would be expected to significantly influence the flow paths of the migrating fluids.

Nevertheless, the physical parameters that control hydrocarbon migration and the flow of injected CO_2 in the subsurface are the same. Thus, knowledge of hydrocarbon migration processes should be helpful in predicting the short- and medium-term movements of injected CO_2. Likewise, the insight that has been gained from monitoring of the CO_2 flow in the Utsira Formation can give knowledge of fluid dynamics in the subsurface that will aid the understanding of petroleum migration.

The purpose of this paper is to examine the main characteristics of the CO_2 flow in the Utsira Formation, and compare it with the behaviour of hydrocarbon migration. Emphasis will be put on understanding the processes (or realization of the lack of such understanding) that emerges from investigations of the CO_2 flow, and the implication of these findings for analyses of hydrocarbon migration.

CO_2 injection in the Utsira Formation

The Sleipner West Field is situated in the northern North Sea. The field produces gas from a Jurassic structural trap. CO_2 is separated from this gas offshore, and is then reinjected into the Utsira Formation of late Middle Miocene to earliest Late Pliocene age. The CO_2 injector was drilled as a very shallowly inclined well from the Sleipner A platform. This well does not penetrate the caprocks above the Utsira Formation at the position where the CO_2 is being injected.

Only a limited section (7 m) of core material has been retrieved from the Utsira Formation. This core consists of clean, unconsolidated sand with 3% carbonate content (Holloway *et al.* 2004). Also wireline log data suggest that the Utsira Formation in this region (Fig. 1) consists of clean sands. At the injection site, the average porosity is 35–40%, the vertical and horizontal permeabilities are around 2 D, and the net/gross ratio is 0.90–0.97 (Zweigel *et al.* 2004). The formation has been described as a lower shoreface deposit, heavily influenced by longshore currents after deposition (Galloway 2002). The Cenozoic strata below the Utsira Formation contain abundant sand injection features at the Tampen Spur, 300 km north of the injection site (Rodrigues *et al.* 2009), and sand injection phenomena may have affected rocks of similar age as the Utsira Formation in this area (H. Løseth, pers. comm.). Injected sands in the Utsira Formation in the Sleipner area have not been documented.

VINING, B. A. & PICKERING, S. C. (eds) *Petroleum Geology: From Mature Basins to New Frontiers – Proceedings of the 7th Petroleum Geology Conference*, 1183–1188. DOI: 10.1144/0071183

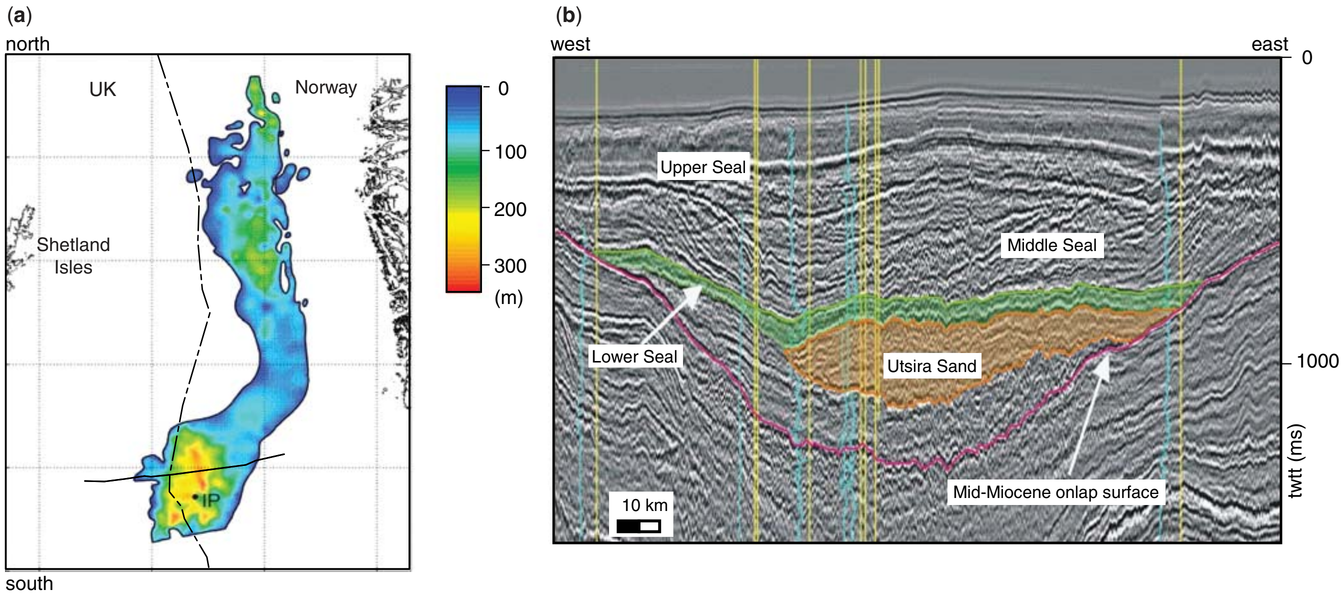

Fig. 1. (**a**) Location and extent of the Utsira Formation in the North Sea. Colours refer to formation thickness (metres); (**b**) a West–East cross-section of the Sleipner area. The location of the line is marked with a black solid line in (a). IP, injection point; twtt (ms), two-way travel time in milliseconds. From Holloway *et al.* (2004), and Schlumberger (courtesy of Schlumberger).

More than 12×10^6 tons of CO_2 have been injected into the Utsira Formation at Sleipner Field since 1996. A seismic survey was shot prior to the injection (1994), and six repeated seismic surveys have been acquired since then to monitor the CO_2 flow in the Utsira Formation. The repeated seismic surveys show how the CO_2 plume has grown with time (Fig. 2). The seismic data also reveal that the CO_2 has been distributed in nine individual layers (Fig. 3), that several of these have grown laterally with time, and that at the same time the CO_2 has moved through (as opposed to around) the intra-formational shaly layers on its way towards the top seal (Fig. 4). The shale beds that cap the individual CO_2 layers are typically 1–1.5 m thick, judging from well data in neighbouring wells (Zweigel *et al.* 2004). By assuming that the brightest amplitudes correspond to the maximum constructive interference between top and bottom of a thin CO_2-filled layer, a corresponding thickness of about 7–8 m has been suggested (Arts *et al.* 2003). Figure 5 shows how the CO_2 is envisaged to be distributed in the Utsira Formation from this assumption. The eight deepest CO_2 layers are trapped by intra-reservoir shales. Only the shallowest of these can be identified seismically; the others are inferred from the trapping of CO_2 and from log responses within the Utsira Formation in nearby wells (Zweigel *et al.* 2004).

CO_2 flow characteristics inferred from seismic data

The seismic data reveal that the injected CO_2 has followed flow paths that differ from those that would be inferred from knowledge of hydrocarbon migration processes alone:

(1) CO_2 is moving laterally in layers that are clearly visible on seismic data.
(2) The pushdown of the seismic reflectors below the CO_2 plume is larger than what would be expected from CO_2 in the nine

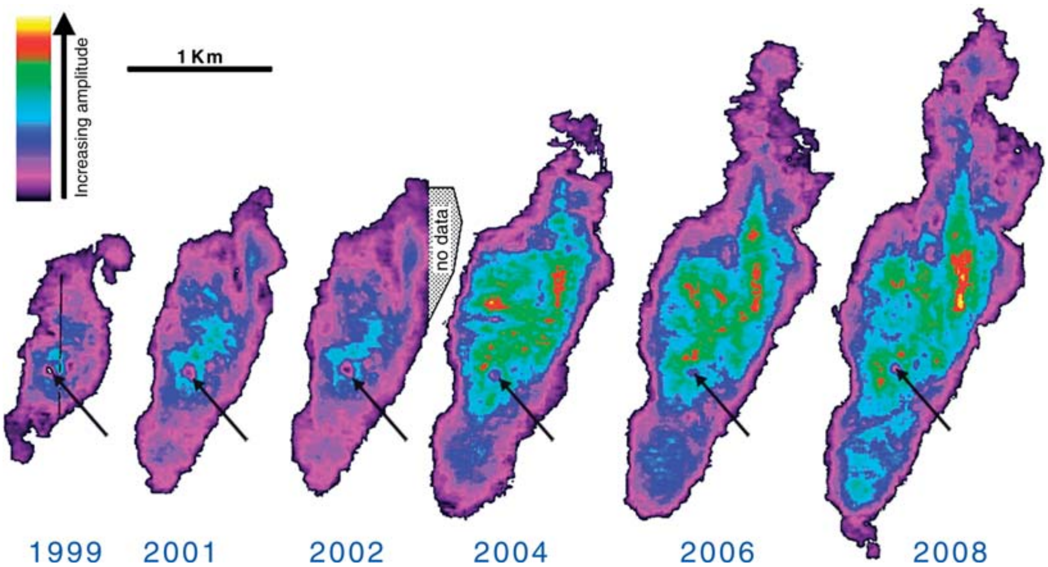

Fig. 2. Cumulative total reflection strength for all nine layers of the Sleipner CO_2 plume as seen on different vintage seismic surveys. Arrows show seismic chimney.

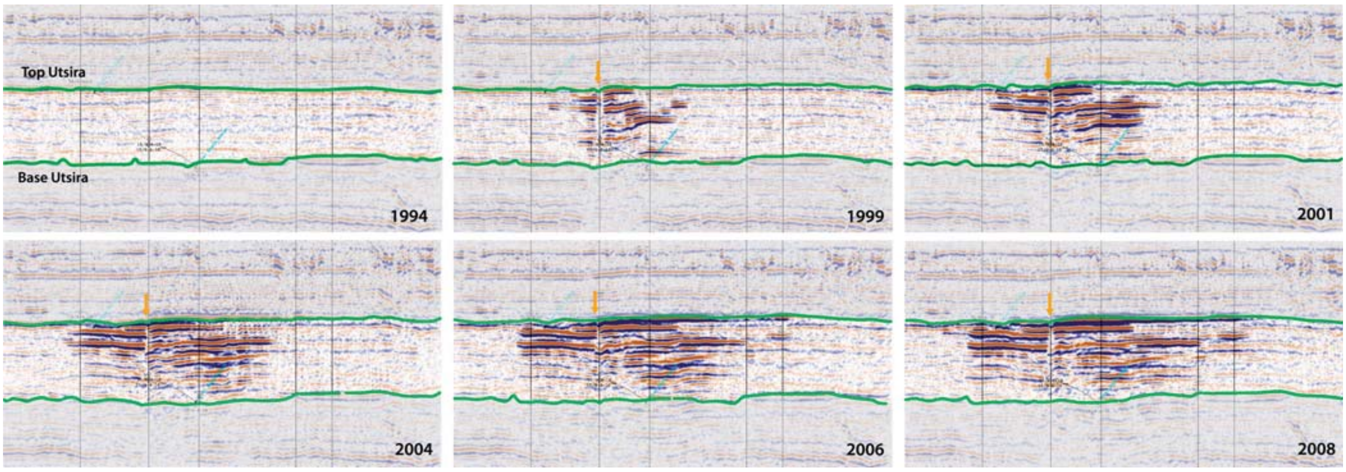

Fig. 3. Seismic signatures of the CO_2 plume in the Utsira Formation in different time-lapse seismic data. All lines are displayed at the same location, oriented north–south, and pass through the injection point. Arrows show seismic chimney.

layers alone. Chadwick *et al.* (2005) noted that a diffuse (low saturation) distribution of about 20% of the CO_2 is required to derive a satisfactory match between seismic amplitudes and pushdown, provided that the influence of gas saturation on seismic data follows the Gassman equation (Gassmann 1951). No flow model that explains how such diffuse gas saturation could have developed has to our knowledge been proposed.

(3) The vertical flow paths that have been exploited by the CO_2 are intriguing. The CO_2 in the individual layers is trapped by seals, yet the CO_2 flowed through all of these and reached the top layer within a three-year period (from injection started in 1996 to shooting of the first post-injection seismic survey in 1999). The vertical permeability of clays is typically at least six orders of magnitude below the horizontal permeability of the Utsira Formation sands (Katsube & Coyner 1994; Schlömer & Krooss 1997), which implies that the flow of CO_2 in the pore network would give a vertical CO_2 displacement of 1 mm or less during the time the CO_2 migrated 1 km horizontally. Clearly, the CO_2 did not flow vertically through continuous and unbroken shale horizons.

The seismic imaging of the CO_2 reveals a central area (chimney) with no coherent signals. This area emerges as a circular feature on the amplitude maps for all layers combined (Fig. 2), but does not show up in the amplitude maps of the uppermost layer. This circular feature is positioned approximately above the position of the CO_2 injection, and is included in the 95% confidence ellipsoid of this position.

The coincidence of the position of the central chimney approximately above the injector and the circular expression of the chimney on the amplitude maps renders the possibility that the chimney displays an image of a vertical flow path that was created by the injection process. A laboratory experiment was carried out to evaluate this hypothesis. In this experiment, a Plexiglas cylinder was filled with water. First sand then kaolin were added to the water and were allowed to settle for several weeks. Thereafter, the cylinder was tilted, and then shaken to promote sand compaction (Fig. 6). The tilting was made to ensure that the water flow velocity was sufficiently large to result in fluidization as the compact-derived excess water rose to the surface along the upper slope of the cylinder. The left picture was taken during fluidized water flow, when compaction-derived water broke the sand layering along the upper

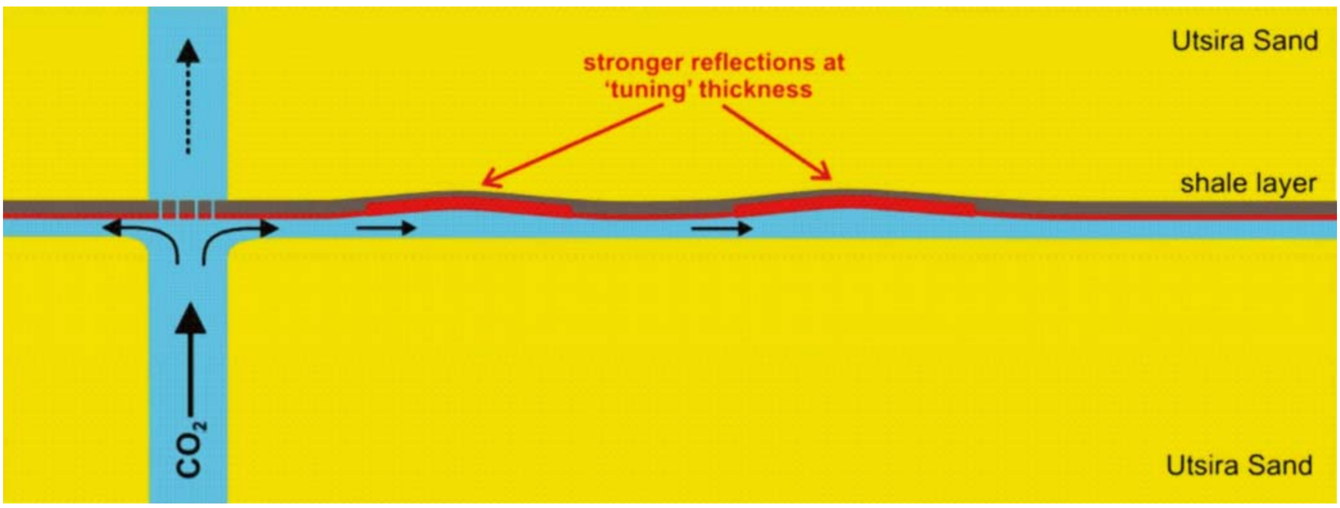

Fig. 4. Flow model of CO_2 from the injection point towards the top of the Utsira Formation and into discrete layers. From Arts *et al.* (2003), reproduced courtesy of Elsevier.

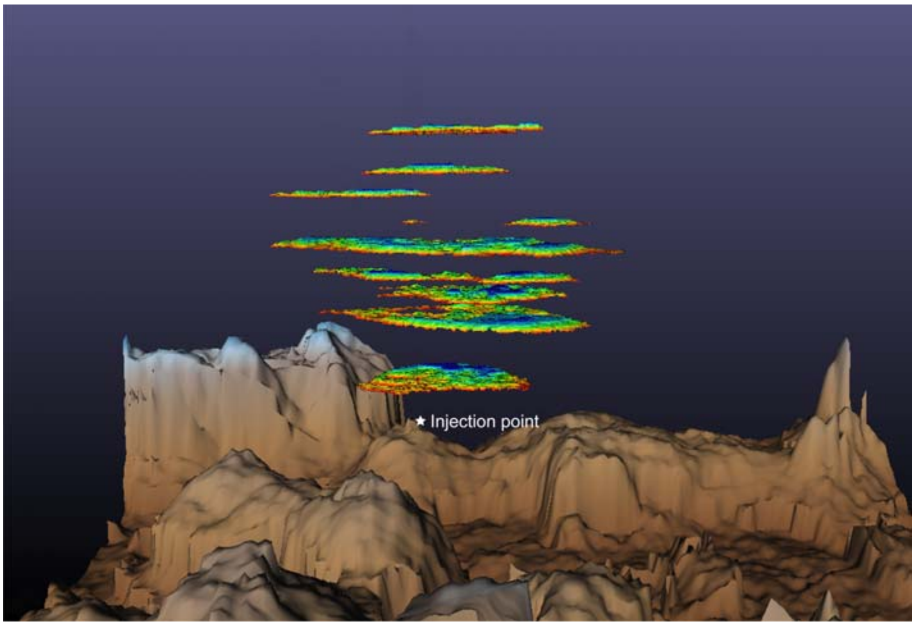

Fig. 5. Modelled 3D CO_2 distribution in the Utsira Formation, with layer thicknesses calculated from tuning thicknesses of seismic amplitudes. Flat CO_2–water contacts were applied for the construction of this figure. Courtesy of Permedia Inc.

slope of the tilted cylinder and erupted into the kaolin (Fig. 6, inserted picture). The right picture was taken after the fluidized flow had ceased, approximately half a minute after the first picture. At this stage, the porosity in the flow path is being reduced, and kaolin sinks into the vacant space at the top of the sand layer.

A vertical flow path through the shaly beds of the Utsira Formation might have resulted from fluidization of the unconsolidated sand, and could have been triggered by localized sand matrix collapse resulting, for example, from the dissolution of carbonate material in coquina beds. Calcite dissolution would be expected to take place as CO_2-saturated water is slightly acidic (pH = 5). An increasingly large portion of the injected CO_2 has found its way to the shallowest layer as the injection has progressed (Chadwick *et al.* 2009). This observation is consistent with an injection-made flow path that becomes more effective as injection proceeds.

However, a comparison of the seismic signatures from the (pre-injection) 1994 survey with that of later surveys demonstrates that a circular depression existed above layer 8 even before the injection started (Fig. 7). The seismic data quality precludes identification of possible circular features at deeper levels. The circular feature was thus not caused by the injection, although it could have been augmented by it. One could speculate that this feature is a collapse feature from a sand injection deeper in the Utsira Formation, created by processes similar to that of the laboratory experiment displayed in Figure 6.

Implications for the understanding of hydrocarbon migration

The seismic data acquired before and during the CO_2 injection at Sleipner Field give unique images of fluid migration within the subsurface. As such they also reveal information on hydrocarbon migration processes. We see several aspects of the migrating CO_2 that give such information, although the interpretation of this information may be ambiguous.

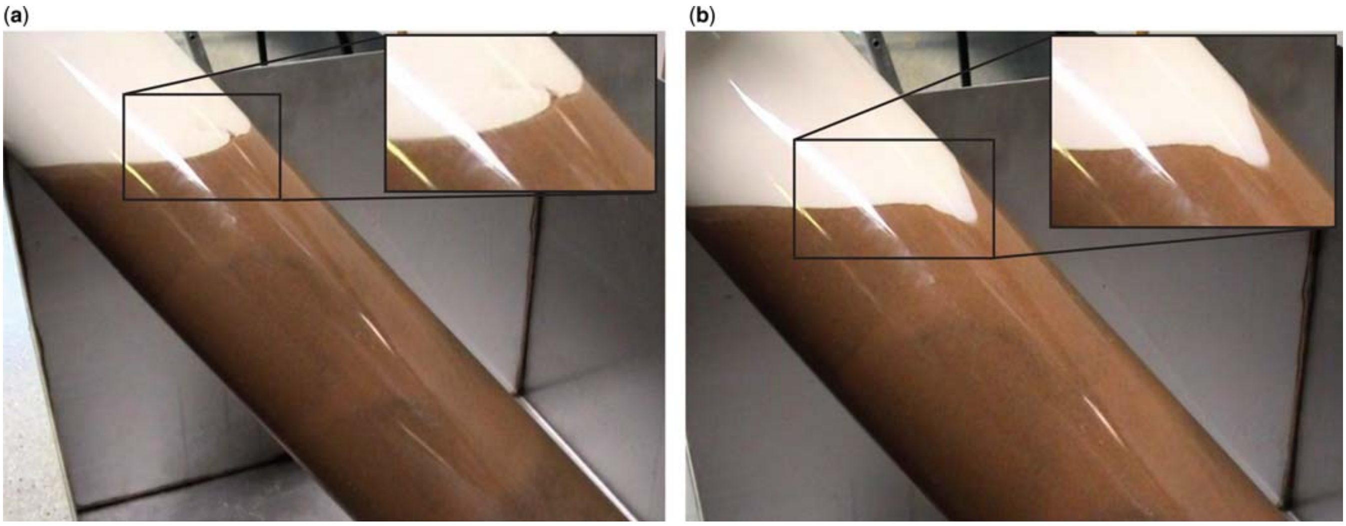

Fig. 6. Laboratory experiment demonstrating the implications of sand fluidization on overlying strata: (**a**) water eruption into kaolin layer; (**b**) kaolin sinks into sand layer. See text for further explanations.

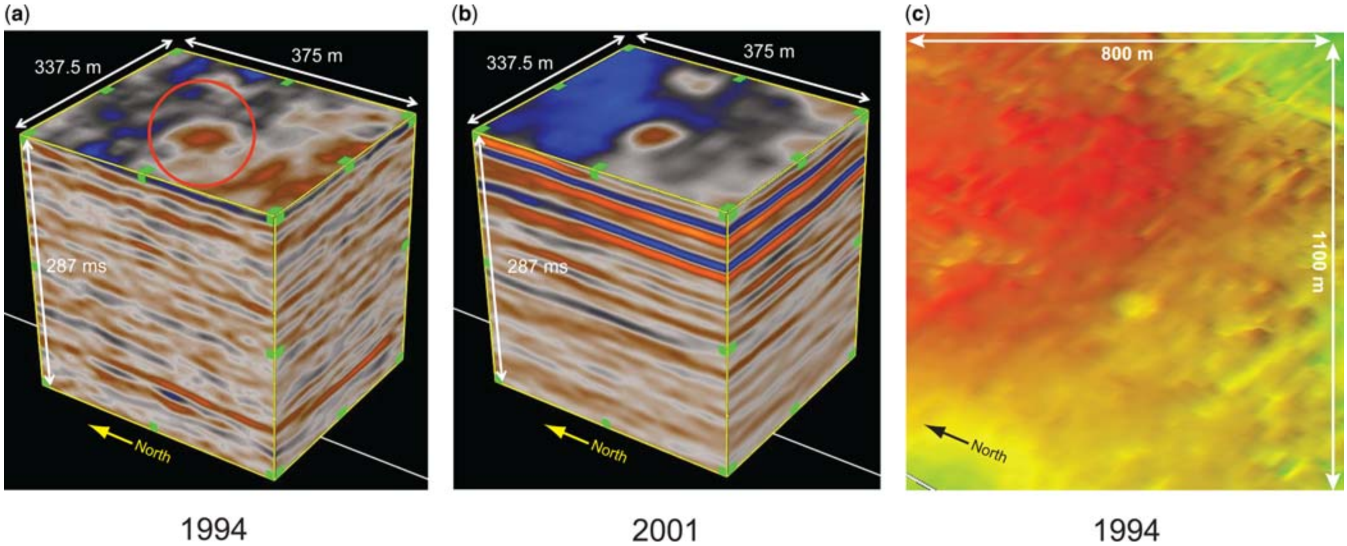

Fig. 7. Seismic signatures of the base of the top seal above CO_2 layer 8. Note the circular feature that is present above the chimney in time slices in both the (**a**) 1994 and (**b**) 2001 data. This circular feature emerges as a depression when the reflector that defines the base of the top seal is mapped (**c**).

The calculations of reflector pushdown by the Gassmann equation with all the CO_2 in layers of high CO_2 saturation give less pushdown than that observed in the seismic data. These calculations involve several parameters that carry some uncertainty. Also, documentations of the accuracy of Gassman-calculated pushdown variations due to fluid substitutions in the subsurface are sparse. Nevertheless, the mismatch between observed and calculated pushdown may hold information on CO_2 distributions and flow paths that are presently unrecognized. Resolving this would be beneficial for both CO_2 monitoring and for hydrocarbon migration and production studies.

Only trapping below the top seals would be considered in hydrocarbon exploration in reservoirs with properties similar to those of the Utsira Formation in the Sleipner area. Intra-reservoir shales of metre thickness would not be expected from exploration experience to result in multiple reservoirs. However, even thin but laterally continuous shale beds should in theory trap hydrocarbons at deeper levels and prevent them from reaching the top seal. That hydrocarbons in most cases find pathways through sequences with interfingering shale beds demonstrates that vertical flow paths are more prevalent than one would infer if thin intra-reservoir shales were thought of as unbroken and laterally continuous. Vertical seal bypass systems have recently attained significant attention (Cartwright *et al.* 2007). The effective vertical seal bypass apparent at Sleipner Field is the first dataset that we are aware of that images vertical flow through heterogeneous sandstones in (almost) real time. The observation of an effective seal bypass system in these data opens the possibility that such bypass systems are relatively common, and that their presence may explain why hydrocarbons so frequently find pathways to the shallowest positions in clastic reservoir traps. Whatever causes the migration to bypass the internal seals (such as water escape structures, sand injections, erosional features), they are probably more likely to disrupt thin than thick seal rock intervals. The practical implication of this assumption is that seal rock thickness is an important parameter in hydrocarbon sealing, even if mercury injection measurements should conclude that the capillary entry pressure of the seal has not been overcome by the buoyancy of the hydrocarbon column.

Migrating CO_2 is clearly visible in the seismic images of the Utsira Formation in the Sleipner area. With these clear images in mind, why do we not observe hydrocarbon migration pathways in seismic data?

The thickness of a sub-horizontally migrating fluid layer can in general be calculated by assuming that the buoyancy in this layer must overcome the capillary entry pressure for *lateral* flow in the top of the migrating layer. This entry pressure is overcome when

$$(\rho_w - \rho_g)gh > 2\gamma/r_t \tag{1}$$

where ρ_w is the density of formation water, ρ_g is the density of the migrating, non-wetting fluid, g is the acceleration of gravity, h is the column height of the migrating fluid, γ is the interfacial tension and r_t is the largest pore throat radius in contact with the non-wetting fluid. The minimum thickness of a migrating body of a non-wetting fluid should thus be controlled by

$$h > 2\gamma/r_t(\rho_w - \rho_g)g \tag{2}$$

The density difference between water and that of migrating CH_4 and CO_2, respectively, may be about 2:1 (Nordgård Bolås *et al.* 2005; Nooner *et al.* 2007). On the other hand, the interfacial tension of CH_4–water is approximately twice that of CO_2–water in the Utsira Formation in the Sleipner area (Nordgård Bolås *et al.* 2005; Chalbaud *et al.* 2009). Thus, the minimum thickness of laterally migrating CO_2 should be approximately equal to the thickness of migrating CH_4.

One could calculate this minimum thickness if the critical pore-throat size of the Utsira Formation sands was known. Such knowledge has not been published. The critical pore-throats can nevertheless be calculated from the rock permeability. Unfortunately, such calculations carry significant uncertainties, and the deviation between calculations by the methods of Pittman (1992) and Berg & Avery (1995) give an order-of-magnitude difference in the calculated height (from 7 to 70 cm by assuming a density contrast between migrating CO_2 and water of 0.3 g cm^{-3}, and an interfacial tension of 30 mN between CO_2 and water; Chalbaud *et al.* 2009).

The highest seismic amplitudes are assumed to correspond to the maximum tuning of the CO_2-saturated layers. The amplitude of a CO_2 layer at 1 m thickness would be expected to be 15% of this, which approximately corresponds to the detection limit on the time-lapse difference cubes. The thickness of migrating CO_2 is at or possibly below the seismic detection limit at saddle points (such as to the north in the 2004 data of Fig. 2). This observation may suggest that migration pathways of less than a metre are in fact what one should expect in both CO_2 flow and CH_4 migration.

The greater thicknesses of the CO_2 layers close to the injection point are mainly a result of the large injection rate, and thus the build-up of slightly inclined gas–water contacts, below the intra-formational shale beds (Bickle *et al.* 2007).

The above calculations and observations suggest that capillary trapping may well determine the retention of both CO_2 and CH_4 in the subsurface, and yet result in migration paths that are too thin for seismic detection in rocks with permeability of 2 D. However, the thickness of migrating CH_4 and CO_2 stringers alike should be ten times the thickness observed in the Utsira Formation in less permeable carrier beds with permeabilities of 20 mD instead of 2 D. This follows from the permeability v. pore throat relationships of both Pittman (1992) and Berg & Avery (1995). Gas migration in water-wet, low-permeable carrier beds should thus be visible in seismic data, due to their high capillary entry pressures. The observation that gas migration routes have not been identified as continuous stringers of bright seismic amplitudes may suggest that such migration routes are not controlled by capillary trapping over geological time, which would imply that the carrier bed rocks have a mixed wettability. Mixed-wetted rocks would result in less trapping of residual hydrocarbons in the carrier beds, and would also result in less storage capacity of CO_2 below or outside structural spill points, especially since wettabilities may change with time in the presence of both hydrocarbons (Teige 2008) and CO_2 (Chiquet *et al.* 2005). Further examinations of the CO_2 flow paths in the Utsira Formation can possibly result in more accurate knowledge of the role of capillary trapping, and thereby of the subsurface wettability distribution.

Summary and conclusions

The CO_2 that has been injected into the Utsira Formation in the Sleipner area has been distributed in nine different layers, most of which are capped by metre-thick shales. The injected CO_2 penetrated these layers and migrated to the top layer during the three year period between the start of injection and the first repeat seismic survey. The CO_2 has migrated several kilometres laterally in layers of *c*. 8 m thickness.

Inferences of hydrocarbon migration processes are based on indirect evidence. As migration pathways are not in general identified in seismic data, they are by inference significantly thinner than what is observed as typical thicknesses of flowing CO_2 in the Sleipner Field data. Observations of minimum CO_2 migration thicknesses close to the *c*. 1 m detection limit at spill points are consistent with calculated values, and so do not preclude that capillary trapping plays an important role in controlling the subsurface flow of CO_2 and CH_4. The importance of such trapping depends on the wettability of the carrier beds and possible change of wetting characteristics with time, a topic that needs further investigations.

In theory, hydrocarbons would not be expected to migrate vertically through shale beds, yet vertical migration of hydrocarbons is an efficient process in clastic rocks, which in the large majority of cases contain shale layers of significant lateral extents. It is suggested that vertical migration of hydrocarbons is frequently enhanced by the presence of vertical sand conduits, created by dewatering and/or injection of deeper sands. Wettability changes in the presence of migrating hydrocarbons may also play a significant role in explaining the efficiency of vertical hydrocarbon migration.

Thanks are due to Andrew Cavanagh for preparing Figure 5 and to Elin Storsten for drafting the figures. M. C. Akhurst and an anonymous referee are thanked for constructive comments to an earlier version of the manuscript. We are thankful for Statoil's permission to publish this paper.

References

Arts, R., Eiken, O., Chadwick, A., Zweigel, P., van der Meer, B. & Zinszner, B. 2003. Monitoring of CO_2 injected at Sleipner using time-lapse seismic data. *In*: Gale, J. & Kaya, Y. (eds) *Greenhouse Gas Control Technologies*. Elsevier, Oxford, 347–352.

Berg, R. R. & Avery, A. H. 1995. Sealing properties of Tertiary growth faults, Texas Gulf Coast. *American Association of Petroleum Geologists Bulletin*, **79**, 375–393.

Bickle, M., Chadwick, A., Huppert, H. E., Hallworth, M. & Lyle, S. 2007. Modelling carbon dipoxide accumulation at Sleipner: implications for underground carbon storage. *Earth and Planetary Science Letters*, **225**, 164–176.

Cartwright, J., Huuse, M. & Aplin, A. 2007. Seal bypass systems. *American Association of Petroleum Geologists Bulletin*, **91**, 1141–1166.

Chadwick, A., Arts, R. & Eiken, O. 2005. 4D seismic quantification of a growing CO_2 plume at Sleipner, North Sea. *In*: Dore, A. G. & Vining, B. A. (eds) *Petroleum Geology: North-west Europe and Global Perspectives: Proceedings of the 6th Petroleum Geology Conference*. Geological Society, London, 1–15. doi: 10.11440060001.

Chadwick, A., Noy, D., Arts, R. & Eiken, O. 2009. Latest time-lapse seismic data from Sleipner yield new insights into CO2 plume development. *Energy Procedia* **1**, 2103–2110.

Chalbaud, C., Robin, M., Lombard, J-M., Martin, J-M., Egermann, P. & Bertin, H. 2009. Interfacial tension measurements and wettability evaluation for geological storage. *Advances in Water Resources*, **32**, 98–109.

Chiquet, P., Broseta, D. & Thibeau, S. 2005. *Capillary Alteration of Shaly Caprocks by Carbon Dioxide*. Presented at the 14th Europec Biennial Conference, Madrid, 13–16 June 2005. SPE **94183**.

Galloway, W. E. 2002. Paleogeographic setting and depositional architecture of a sand-dominated shelf depositional system, Miocene Utsira Formation, North Sea Basin. *Journal of Sedimentary Research*, **72**, 476–490.

Gassmann, F. 1951. Über die Elastizität poröser Medien. *Vierteljahrsschrift der Naturforschenden Gesellschaft*, **96**, 1–23.

Holloway, S., Chadwick, A., Lindeberg, E., Czernichowski-Lauriol, I. & Arts, R. 2004. *Best Practice Manual*. Saline Aquifer CO_2 storage (SACS) project.

Katsube, T. J. & Coyner, K. 1994. Determination of permeability–compaction relationship from interpretation of permeability-stress data for shales from eastern and northern Canada. Geological Survey of Canada, *Current Research*, **1994-D**, 169–177.

Nooner, S. L., Eiken, O., Hermanrud, C., Sasagawa, G. S., Stenvold, T. & Zumberge, M. A. 2007. Constraints on the *in situ* density of CO_2-within the Utsira formation from time-lapse seafloor gravity measurements. *International Journal of Greenhouse Gas Control*, **1**, 198–214.

Nordgård Bolås, H., Hermanrud, C. & Teige, G. M. G. 2005. Seal capacity estimation from subsurface pore pressures. *Basin Research*, **17**, 583–599.

Pittman, E. D. 1992. Relationship of porosity and permeability to various parameters derived from mercury injection-capillary pressure curves for sandstone. *American Association of Petroleum Geologists Bulletin*, **76**, 191–198.

Rodrigues, N., Cobbold, P. R. & Løseth, H. 2009. Physical modelling of sand injectites. *Tectonophysics*, **474**, 610–632.

Schlömer, S. & Krooss, B. M. 1997. Experimental characterization of the hydrocarbon sealing efficiency of cap rocks. *Marine and Petroleum Geology*, **4**, 565–80.

Teige, G. M. G. 2008. *Sealing mechanisms at pore scale, and consequences for hydrocarbon exploration*. Ph.D. thesis, University of Oslo, Norway.

Zweigel, P., Arts, R., Lothe, A. E. & Lindeberg, E. B. G. 2004. Reservoir geology of the Utsira Formation at the first industrial-scale underground CO_2 storage site (Sleipner area, North Sea). *In*: Baines, S. J. & Worden, R. H. (eds) *Geological Storage of Carbon Dioxide*. Geological Society, London, Special Publications, **23**, 165–180.

Preparing for a carbon constrained world; overview of the United States regional carbon sequestration partnerships programme and its Southwest Regional Partnership

R. ESSER,[1] R. LEVEY,[1] B. MCPHERSON,[1,2] W. O'DOWD,[3] J. LITYNSKI[3] and S. PLASYNSKI[3]

[1]*Energy & Geoscience Institute, 423 Wakara Way, Suite 300, University of Utah, Salt Lake City, UT 84108, USA (e-mail: resser@egi.utah.edu)*

[2]*Department of Civil and Environmental Engineering, University of Utah, Salt Lake City, UT 84112, USA*

[3]*National Energy Technology Laboratory, PO Box 1094, US Department of Energy, Pittsburgh, PA 15236, USA*

Abstract: The Southwest Carbon Partnership (SWP), one of seven United States Department of Energy-funded Regional Carbon Sequestration Partnerships, has been tasked with assessing the CO_2 sequestration potential within the southwestern United States. Carbon dioxide is considered a 'greenhouse' gas and is emitted, in large volumes, by the burning of fossil fuels and other industrial processes. CO_2 capture from point source emitters and subsequent geological sequestration is being considered as a viable short- to intermediate-range mitigation option to combat the phenomena of global warming. Significant fossil fuel reserves and consumers exist within the seven member states of the SWP and, as such, the Partnership is dedicating a large amount of resources to the challenges posed by large-scale CO_2 sequestration. Three distinct phases of work have been or will be performed by the SWP: a Characterization Phase to identify carbon capture and sequestration potential; a Validation Phase to test small-scale field injection of CO_2; and a Deployment Phase to test commercial-scale field injection of CO_2. Each phase presents challenges and opportunities to the refinement of the best approach to safe and efficient geological storage of CO_2 within the SW region of the United States.

Keywords: CO_2, sequestration, EOR, ECBM, geological storage, saline aquifer, fossil fuel, global warming, greenhouse gas

Preliminary reports by the United State Federal Energy Information Administration (EIA) indicate that total US energy-related carbon dioxide emissions have grown by 19.4% since 1990. More than 80% of US greenhouse gas emissions are energy-related carbon dioxide emissions. In 2007 US carbon dioxide emissions from fossil fuel consumption increased by 1.6%, from 5888×10^6 metric tons of carbon dioxide ($MMTCO_2$) in 2006 to 5984 $MMTCO_2$ in 2007 (United States EIA 2008).

The United States Department of Energy designated an initiative of partnerships throughout the USA and Canada to help develop the best practices for permanently storing carbon dioxide in geological formations. The seven Regional Carbon Sequestration Partnerships (RCSPs) include over 350 organizations in 42 states and four Canadian provinces (Litynski *et al.* 2008). It is anticipated that the outcomes of studies and tests will help develop regulations and infrastructure requirements for future sequestration deployment. These seven RCSPs represent regions with elements that are geologically representative of all the sequestration site variability in the USA. They encompass 97% of coal-fired CO_2 emissions, and 97% of industrial CO_2 emissions. The RCSPs initiative is being implemented in three phases:

- Phase I – the Characterization Phase (2003–2005), which characterized opportunities for carbon capture and sequestration;
- Phase II – the Validation Phase (2005–2010), in which small-scale field tests are being concluded;
- Phase III – the Deployment Phase (2010–2017), which will conduct large-volume CO_2 storage tests.

The Southwest Regional Partnership (SWP) includes all or part of eight states (Arizona, Colorado, Kansas, Nevada, New Mexico, Oklahoma, Texas, Utah and Wyoming) that represent vast opportunities for carbon storage, spanning enhanced oil recovery, saline reservoir sequestration, enhanced coalbed methane production and terrestrial carbon sequestration.

In the SW region, over 95% of anthropogenic CO_2 emissions result from fossil fuel combustion, with approximately half of these emissions from power plants (National Energy Technology Laboratory 2008). Geological storage options include coal seams (1×10^9 metric tons of minimum storage potential), natural gas and depleted and marginal oil fields (23×10^9 metric tons minimum storage potential), and deep saline formations (82×10^9 metric tons minimum storage potential). The SWP is also exploring the viability of supplanting the CO_2 currently produced from natural CO_2 reservoirs, used for enhanced oil and natural gas recovery, with anthropogenic CO_2 from power plants. The presence of CO_2 pipelines that bridge CO_2 sources and potential CO_2 sinks improves the viability of this possibility. Although terrestrial CO_2 sequestration appears to be a viable alternative in several parts of the SW region, low rainfall in some areas decreases the relative terrestrial storage capacity, limiting the applications of this option.

This paper summarizes the breadth of the RCSPs and focuses on the current results of field injection tests conducted by the SWP. The SWP has completed one pilot injection test, is in the active injection phase of two additional tests, and the results of all three are providing the basis for a commercial-scale test (exceeding 1×10^6 tons injection). This large-scale injection deployment is planned for the Gordon Creek Field, near Price, Utah, 120 miles south of Salt Lake City. The target storage reservoirs are Jurassic sandstones, present throughout the region from Wyoming to Northern New Mexico. We will inject over 1×10^6 tons of CO_2 over 4 years (up to 500 000 tons per year) from a natural CO_2 deposit and monitor migration and storage efficacy. The project will evaluate state-of-the-art monitoring techniques to determine the impact of injection operations and the integrity of the storage

VINING, B. A. & PICKERING, S. C. (eds) *Petroleum Geology: From Mature Basins to New Frontiers – Proceedings of the 7th Petroleum Geology Conference*, 1189–1195. DOI: 10.1144/0071189

reservoirs. The area provides an excellent deployment test opportunity for analysis of high injection rates and high-resolution monitoring of CO_2 in multiple geological horizons. These deep saline formations are major targets for commercial-scale CO_2 sequestration associated with future coal-fired power plants planned for the area.

Overview of completed and ongoing validation tests

During 2010, the SWP will conclude five separate field tests, including the three geological tests mentioned previously as well as two terrestrial analyses, each designed to validate the most promising carbon sequestration technologies and infrastructure concepts. The field tests represent a variety of carbon sink targets, including enhanced oil recovery (EOR) with carbon sequestration, enhanced coal bed methane (ECBM) production with carbon sequestration and geological sequestration combined with terrestrial (surface) sequestration.

The primary project goal of these tests is to develop an optimum sequestration strategy for the southwestern United States, subject to the constraints unique to the region (such as water availability). Development of this sequestration 'framework' will incorporate best practices for (1) permitting and regulatory requirements, (2) comprehensive geological characterization, (3) risk mitigation, (4) monitoring, verification and accounting (MVA) protocols and (5) effective outreach and communication to stakeholders and the general public.

The SW region contains a large number and volume of geological sinks, including depleted oil and natural gas fields, saline formations and coal beds. EOR using CO_2 has been conducted in the region since the early 1970s. Several hundred miles of CO_2 pipelines through the region provide access to CO_2 near many candidate geological sequestration sites. McElmo Dome, Colorado is the major source of CO_2 for many of the EOR/ECBM operations located within the SWP region. Ideally, these sources would be supplanted by the abundant anthropogenic CO_2 sources in the region, such as coal-fired power plants.

Paradox Basin, Utah: Aneth EOR-sequestration test

Since August 2007, the SWP has conducted EOR and concomitant CO_2 sequestration in the Aneth oil field in San Juan County, Utah. Discovered in 1956, the Aneth Field is currently owned and operated by Resolute Natural Resources Company and the Navajo Nation Oil and Gas Company, and has produced greater than 149×10^6 barrels of oil (of an estimated 421×10^6 barrels of oil in place). The pilot test site is centrally located within the Paradox Basin in the Aneth mound complex (Fig. 1). The primary oil-producing zones and CO_2 sequestration targets are the Desert Creek and overlying Ismay carbonate members of the Pennsylvanian Paradox Formation. The oil and injected CO_2 are accommodated within a stratigraphic trap that is sealed by the overlying Gothic Shale and underlying Chimney Rock Shale. The approximate depth of the Desert Creek/Ismay Members is 5600 ft with a cumulative thickness of less than 200 ft. Average porosity and permeability for the CO_2 injection zone are 10% and 20 mD, respectively. Porosity and permeability measurements for the overlying Gothic Shale (thickness *c.* 15 ft) yield *c.* 3% and less than 0.01 mD, respectively.

Beginning in late 2005, we conducted pre-injection geological characterization, model development and simulations. The majority of data used for the baseline characterization of the Aneth site was obtained from geophysical well logs made available by the Utah Division of Oil, Gas and Mining (DOGM). Approximately 460 digitized well logs from 1077 Aneth area wells yielded direct and indirect data pertaining to formation depth, thickness, temperature, porosity, permeability and lithology. The digitized well logs were used to construct a 3D model of the injection site (Petrel® software by Schlumberger) from which various simulations were conducted to assess CO_2 capacity, migration of reservoir fluids and forces (CO_2, oil, groundwater, tracers, pressure, stress), as well as short- and long-term CO_2 trapping phenomena (structural, residual, solubility and mineral).

Between August 2007 and January 2010, an average of 29 000 MCF (1700 tons) per day was injected into 16 wells within the Aneth Field for a total of *c.* 1.5×10^6 tons of injected CO_2. Monitoring activities at Aneth are ongoing, and include periodic surface CO_2 flux surveys, downhole sampling (water, pressure, temperature, natural and artificial tracers), vertical seismic profiling, time-lapse 2D seismic, self-potential and geodetic surveys (tilt, GPS, InSar). Final analyses of each monitoring technique are anticipated by mid-2010. To date, no unanticipated migration of the injected CO_2 at Aneth, either within or beyond the injection zone, has been detected.

Permian Basin, Texas: SACROC EOR sequestration test

The SACROC Unit in the Texas Permian Basin is the oldest CO_2-EOR operation in the USA, with CO_2 injection dating from 1972; only the CO_2-EOR project in Hungary is older, dating from *c.* 1969 (Kane 1979). The Kinder–Morgan-operated SACROC Field/Unit lies along a trend of fields described by Galloway *et al.* (1983) as the Horseshoe Atoll Play (Fig. 2). The major

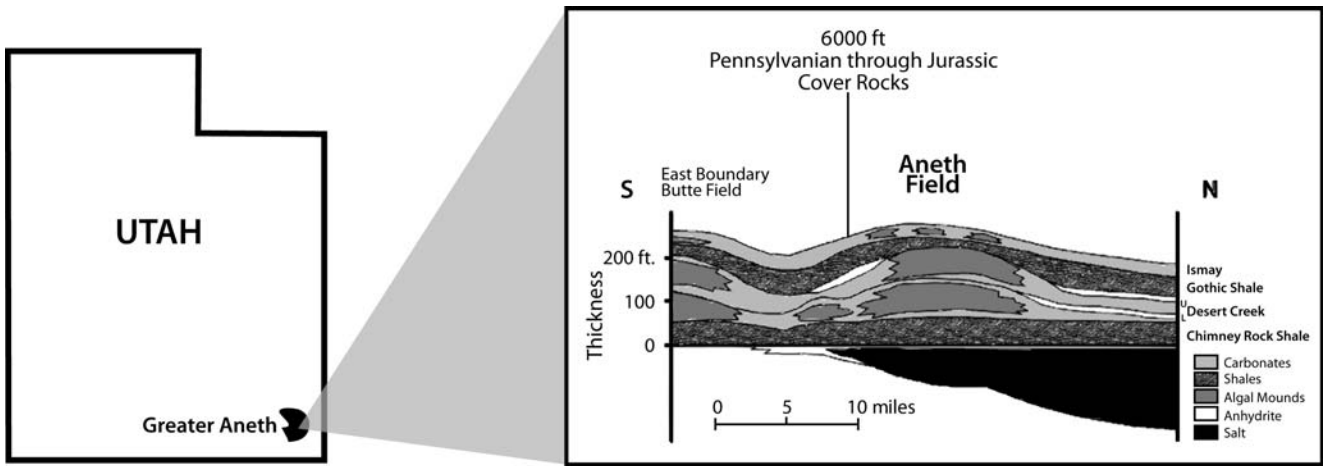

Fig. 1. Location map of Aneth Field and pilot site (left) and representative cross-section (right).

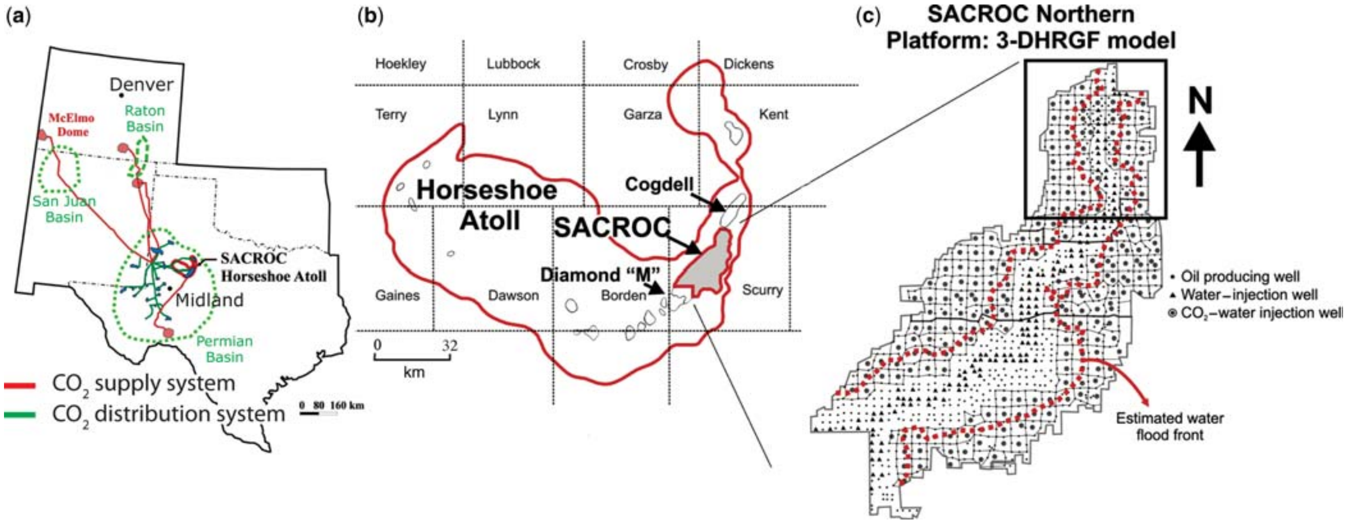

Fig. 2. Regional location map for the SACROC EOR Field, Texas.

oil-bearing and CO_2 injection zones are carbonates of the Pennsylvanian Cisco and Canyon Group formations. Lithologies of the Cisco and Canyon Group formations vary in observed facies, from interbedded pellet, crinoid, algal, to intraclast grainstones and boundstones with an average porosity and permeability of 8% and 20 mD. The oil-bearing zones are overlain by the low-permeability, Permian Wolfcamp Formation (shale). The depth of the CO_2 injection zone ranges from 6300 to 7100 ft.

The SACROC Field has an extensive dataset for evaluating virtually all aspects of the oil production and CO_2 injection since operations began in the 1950s. The SWP has gained access to much of this historical data to build comprehensive geological models and perform detailed simulations to evaluate capacity, injectivity, migration and storage of the CO_2, not only for current field tests but also to evaluate potential impacts of long-term EOR operations. The SACROC pilot represents an opportunity to match, in tandem with large-scale monitoring operations, injection of greater than 1.5×10^6 tons of CO_2. Early, fully parameterized simulations of historical CO_2 injection and multiphase flow of oil, CO_2 and brine at SACROC focused on determining the various trapping mechanisms, short and long term (Fig. 3; Han *et al.* 2010). An important outcome of this project is the efficiency with which CO_2 is trapped within saline aquifers that are immediately overlain by oil.

The total volume of CO_2 injected at the SACROC oil field between 1972 and January 2010 is greater than 175×10^6 metric tons (Fig. 3). At the end of the current injection test, CO_2 injection will exceed 18×10^6 metric tons per year total. Like Aneth, the monitoring activities at SACROC are ongoing and include periodic surface CO_2 flux surveys, downhole sampling (water, pressure, temperature, natural and artificial tracers), vertical seismic profiling, time-lapse 2D/3D seismic, self-potential and geodetic surveys (tilt, GPS, InSar). Some early monitoring analyses resulted in the identification of shallow groundwater flow paths, regional trends in groundwater chemistry and impacts to shallow groundwater from pre-1975 produced water evaporation pits. Additional monitoring results are not expected until mid-2010. Currently, no unanticipated migration of the injected CO_2 at SACROC, either within or beyond the injection zone, has been detected.

Because of the relatively large dataset at SACROC, encompassing a greater number of years of CO_2 injection, the pilot will be an initial high-resolution analysis of the potential for CO_2 storage in the broader carbonate Horseshoe Atoll system. Given that most of the western side of the atoll is below the oil–water contact, it is particularly agreeable for large-scale sequestration.

San Juan Basin, New Mexico: ECBM sequestration test

The San Juan basin (SJB) is one of the top ranked basins in the world for CO_2 coalbed sequestration because it has: (1) advantageous geology and coals with high methane content; (2) abundant anthropogenic CO_2 from nearby power plants; (3) low capital and operating costs; (4) well developed natural gas and CO_2 pipeline systems; and (5) local companies, for example, ConocoPhillips, with coalbed methane (CBM) and ECBM expertise. The geology consists of the thick (>200 ft) coal-bearing Fruitland Formation with an average porosity and permeability of >10% and >200 mD, respectively. The Fruitland coal is saturated with methane (and variable quantities of low total dissolved solids (TDS) groundwater) that is contained structurally and stratigraphically by the low-permeability Kirtland Shale.

ConocoPhillips has operated the SJB project in collaboration with the SWP, specifically to examine ECBM efficacy with CO_2 sequestration. Pilot CO_2 injection began in July 2008, and

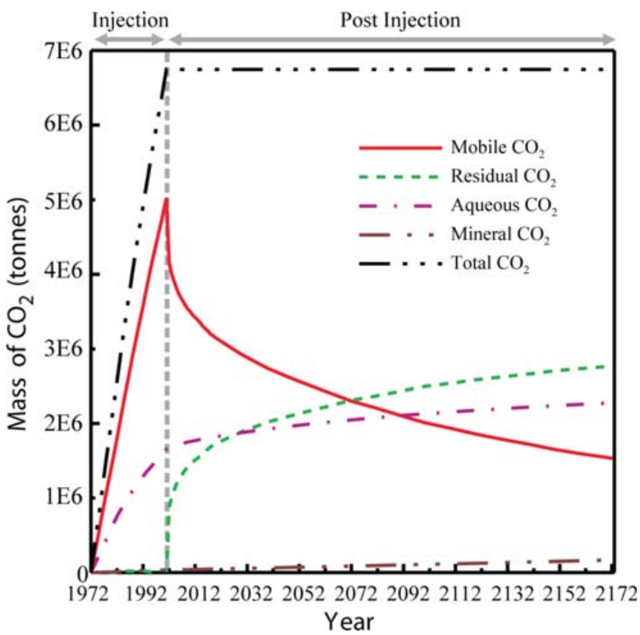

Fig. 3. Results of an extensive history-match analysis to evaluate trapping mechanisms at SACROC for 100 years starting in 1972.

continued for *c.* 1 year; the total amount of CO_2 injected is *c.* 18 000 tons. The SJB pilot has tested a suite of monitoring approaches tailored for its unique geology (e.g. increased geodetic surveys to assess swelling of coalbeds) and value-added benefit (methane production). Early monitoring results suggest differential transport rates between natural (N_2) and man-made (perfluoroocarbon) tracers and the injected CO_2, although a full analysis awaits. Likewise, tilt-meter and GPS stations indicate no significant swelling of the CO_2-saturated coals. No unanticipated migration of the injected CO_2 at the SJB has been detected.

SWP terrestrial pilot test and terrestrial Riparian Restoration Project

Terrestrial carbon capacity in the SW region is limited by low average annual precipitation and yearly variability in precipitation. Even in systems managed for carbon storage, wet years followed by a series of dry years may result in a net carbon flux out of the system. Limited opportunities exist for increasing carbon storage on rangelands because most areas are at a relatively stable equilibrium with respect to land use history and management. Much of the desert grassland and shrubland areas with less than 12 inches of annual precipitation are subject to loss of cover and exposure to wind and water erosion. Retaining soil carbon levels in these ecosystems will require active restoration practices that are challenging given current technologies. Two demonstration projects are nearing completion: a regional-scale terrestrial analysis of land-use trends and a local-scale arid-land restoration project.

The regional analysis includes a detailed reporting and monitoring system that functions consistently across hierarchical scales and is compatible with the existing technology underlying the DOE's Energy Information Administration Voluntary Reporting of Greenhouse Gases (1605b) Program. Within this system, the project has: (1) developed improved technologies and systems for direct measurement of soil and vegetation carbon at reference sites selected within the region; (2) developed remote sensing and classification protocols to improve mesoscale (km^2) soil and vegetation carbon estimates; (3) constructed ecological process (state and transition) models that reflect soil/vegetation changes resulting from current land use and land use associated with implementation of programs to sequester carbon or reduce carbon losses; and (4) developed a regional inventory and decision

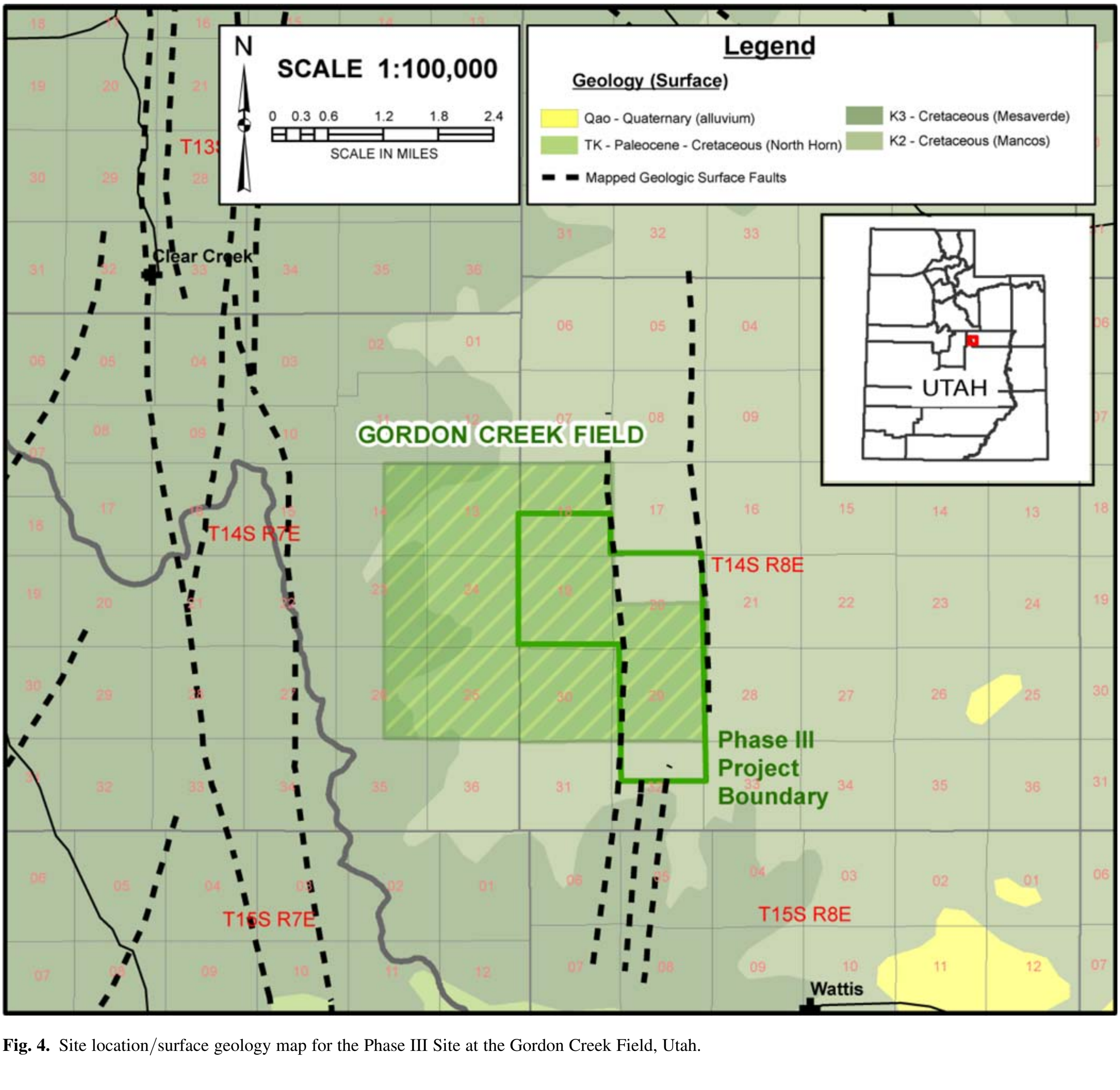

Fig. 4. Site location/surface geology map for the Phase III Site at the Gordon Creek Field, Utah.

support tool. The value-added products of the test include new carbon credits and increased land productivity.

The local-scale arid-land restoration project entailed desalination of small quantities of produced water from the SJB ECBM pilot (described previously in this paper). This water was utilized for irrigating a tract of arid land, with carbon soil content measured before and after irrigation. Preliminary results suggest over 10% increases in soil carbon uptake resulting from this irrigation. The test site is the San Juan Basin Coal Fairway, near Navajo City, New Mexico, and involves such value-added products as new carbon credits, improved water quality and improved ecological conditions.

Medium-scale validation project impacts

The SWP medium-scale validation tests will impact the USA by providing a comprehensive assessment of the sources and potential sinks for CO_2 in the SW region. These data are being integrated with the data from other partnerships to provide a database covering the entire nation. The data generated by these field tests are providing information to evaluate potential commercial-scale sequestration projects in the southwestern USA and other regions of the country. Some value-added benefits of the project include enhanced recovery of oil, natural gas and coalbed methane. Part of the value-added benefits for oil, natural gas and methane recovery is that revenue from sale of the recovered hydrocarbons mitigates some of the cost of CO_2 storage. Currently, all such enhanced resource recovery operations use CO_2 drawn from natural CO_2 reservoirs. If all enhanced recovery operations in the southwestern USA were to use powerplant-generated CO_2 (from fossil fuels) rather than natural CO_2, it is estimated that the region would see at least a 10% reduction in greenhouse gas intensity.

Commercial-scale deployment project overview

Gordon Creek Field, Utah: commercial-scale injection test

The SWP will accomplish a major sequestration deployment in the Gordon Creek Field, located 120 miles SE of Salt Lake City in central Utah (Fig. 4). This test will follow an injection schedule over four years, leading up to 500 000 tonnes (551 000 US tons) of CO_2 per year, and a total injection amount exceeding 1 000 000 tonnes. The target formations for this deployment are several deep Jurassic sandstones. These formations are also targets of potential commercial sequestration throughout the western USA. The SWP plans include a possible 'dual completion' with injection in two different formations at the same time. By carrying out two tests in two different formations within the same stratigraphy, portability of science and engineering results can begin to be evaluated.

Gordon Creek sits on an elongated surface anticline located along the northern plunge of the San Rafael uplift. Drilling at Gordon Creek in the 1950s–1970s resulted in the discovery of significant deposits of CO_2 in the Jurassic–Triassic Sinbad Member of the Moenkopi Formation and Permian White Rim Sandstone. Also, CO_2 shows have occurred in a number of other Triassic, Permian and Pennsylvanian reservoirs. The most significant and consistent shows have been in the White Rim Sandstone. The area provides an excellent deployment test opportunity for analysis of high injection rates and high-resolution monitoring of CO_2 in multiple reservoirs. These deep saline formations are major targets for commercial-scale sequestration associated with future coal-fired power plants and CBM (coalbed methane) development planned for the area. For this research project, no profits will be earned, and no CO_2 will leave the site. Much of the Gordon Creek site falls under the jurisdiction of the state government of Utah.

For the sequestration deployment test at the Gordon Creek Field, the primary target formation is the Jurassic Navajo Formation Sandstone. The Navajo Formation lies within a true 'stacked' system of alternating reservoirs and seals (Fig. 5), and possesses ample storage capacity for a commercial-scale sequestration demonstration (>1 000 000 tons of CO_2).

The Gordon Creek Field is a methane-producing field located on the eastern flank of the Wasatch Plateau, which has produced *c.* 4 MMcf of methane from the Cretaceous Ferron Sandstone since 2002 (Utah DoGM, pers. comm.). Additionally, the Permian White Rim Sandstone hosts an untapped source of >98% pure CO_2 (Morgan & Chidsey 1991). A 9 mile long by 5 mile wide anticline serves as the structural trap for the Ferron Sandstone methane and possibly the White Rim Sandstone CO_2 (Fig. 5; estimated from existing data by T. C. Morgan). The anticline itself is obliquely divided by north–south normal faults that terminate in the middle Jurassic evaporite deposits of the Carmel Formation. The entire sedimentary package at the Gordon Creek Field is in excess of 15 000 ft thick, although wells within the field only penetrate the Permian White Rim Sandstone (Fig. 5). The thick (>4000 ft) Cretaceous Mancos Shale is exposed at the surface of the Gordon Creek Field. Beneath the Mancos Shale, from the

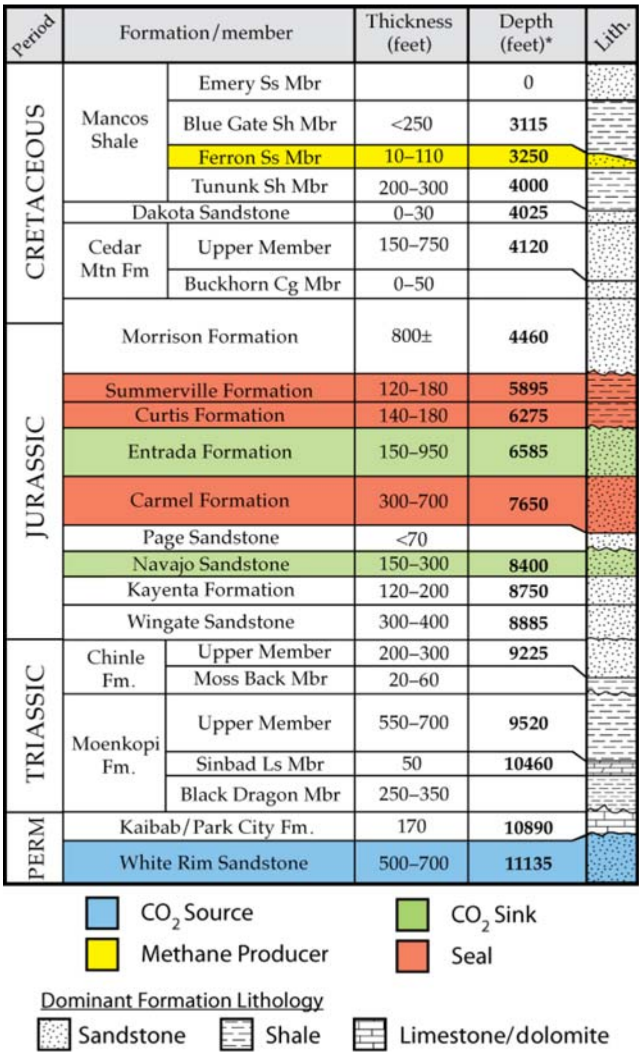

Fig. 5. Stratigraphy of the Gorden Creek area (modified from Hintze 1992); Ss, sandstone; Sh, shale; Ls, limestone; Cg, conglomerate; Fm., formation; Mbr, member.

mid Cretaceous to the Mississippian, are a series of interbedded sandstones, shales and limestones. Potential CO_2 sinks in the section include the Dakota, Morrison, Entrada, Navajo, Wingate and White Rim sandstones, although the Navajo Sandstone is the preferred candidate due to its intermediate depth and proven injectivity; the Navajo is currently being utilized as a salt water disposal zone for waste waters from the methane production in the Ferron Sandstone. Assuming an average depth of 8400 ft and an average thickness of 215 ft, the Navajo Sandstone within the 45 square mile anticlinal structure of the Gordon Creek Field has a CO_2 capacity of 5.9 MMtons (10% porosity with only 1% of the porosity occupied with CO_2). The Entrada Sandstone may have additional capacity of about three times this volume. The primary seal stratigraphically above the Navajo Sandstone is the Carmel Formation, a series of interbedded, low-porosity, low-permeability limestones, shales and sandstones. Additional stratigraphic seals include the Curtis and Summerville formations (shales and low permeability sandstones) and the thick Mancos Shale.

The project will require extensive monitoring and simulation to determine if storage operations are effective with respect to

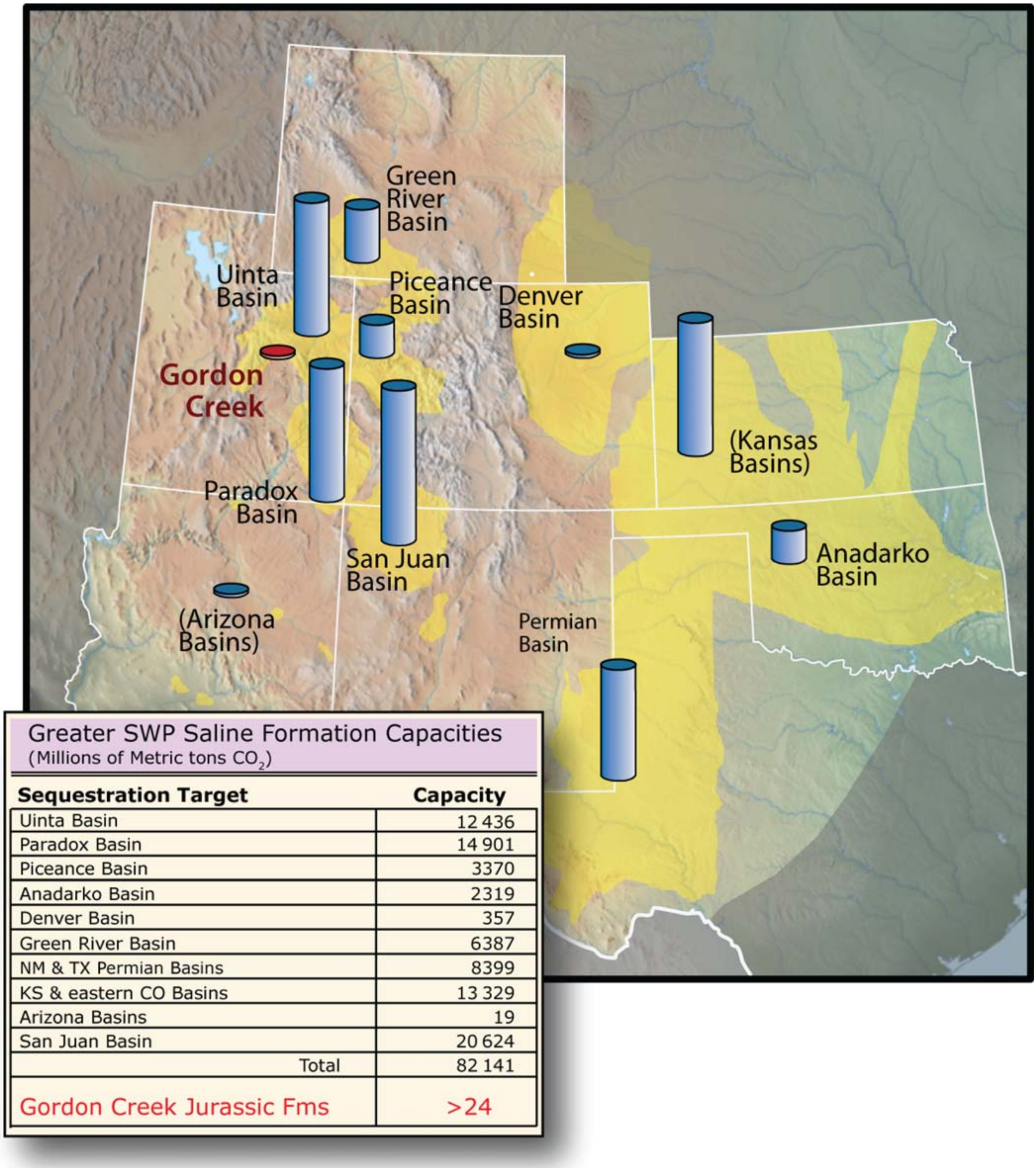

Sequestration Target	Capacity
Uinta Basin	12 436
Paradox Basin	14 901
Piceance Basin	3370
Anadarko Basin	2319
Denver Basin	357
Green River Basin	6387
NM & TX Permian Basins	8399
KS & eastern CO Basins	13 329
Arizona Basins	19
San Juan Basin	20 624
Total	82 141
Gordon Creek Jurassic Fms	>24

Fig. 6. SWP CO_2 sequestration capacities for deep saline formations. Size of column for each site represents relative CO_2 storage capacity.

trapping injected CO_2. Vertical seismic profiling and other geophysical methods will be particularly utilized, given their proven ability to resolve CO_2 plumes (Hovorka *et al.* 2006). Monitoring techniques that will be used include repeat 3D (4D) seismic surveys, pressure monitoring, groundwater chemistry monitoring, pressure and fluid sample monitoring from other locations, soil gas sampling, and other methods. A variety of software code created and modified by SWP organizations as well as commercial/public simulation model tools are in use for this project.

Anticipated carbon storage capacity

The SWP determined that the region's point sources emit *c.* 335×10^6 tonnes (369×10^6 US tons) of CO_2 per year (National Energy Technology Laboratory 2008); over 100 years, assuming no change in emissions rate, these emissions translate to *c.* 3.4×10^9 tonnes (*c.* 3.7×10^9 short tons) of total storage capacity needed. Preliminary geological characterization by the SWP provides an initial estimate of capacity of the deep Jurassic and older saline formations in the SWP region to exceed 82×10^9 tonnes (*c.* 90×10^9 short tons; National Energy Technology Laboratory 2008). The Gordon Creek Field site, in comparison, is projected to store at least 24×10^6 metric tons of CO_2 in formations that are Jurassic in age (Fig. 6). During continued project activities, the SWP and collaborators at the National Energy Technology Laboratory will continue to refine capacity estimates and evaluate injectivity and other critical factors relevant to regional storage goals.

Conclusions

The Southwest Regional Partnership has been charged by the US Department of Energy, along with six other regional partnerships, with providing a framework for the safe and efficient storage of CO_2 within geological sinks. To that end, the SWP has successfully completed two of the three phases of the DOE mandate: (1) assess the major point sources of anthropogenic CO_2 and potential sinks within the southwestern USA; and (2) utilize small pilot CO_2 injection operations to evaluate the steps necessary for larger scale ($>1 \times 10^6$ metric tons of CO_2 injected per year). The third phase of the SWP operations, commercial-scale CO_2 injection, will be commencing in mid to late 2010.

Within the SWP, annual emissions from fossil fuel burning electrical generation as well as cement and fertilizer plants exceed 335×10^6 metric tons of CO_2. With a conservative estimate of 82×10^9 metric tons of storage in deep saline aquifers alone, the SWP can potentially sequester over 100 years of anthropogenic CO_2, at current emission rates. Additional geological storage potential within depleted oil reservoirs (EOR) and unmineable coal seams (ECBM) has been successfully assessed by SWP organizations at sites in Texas, Utah and New Mexico. Detailed regulatory observance, geological characterization, simulations and surface/subsurface monitoring have been utilized at each site in order to determine the best approach to CO_2 sequestration elsewhere.

The third phase of the SWP project is the large-scale injection of CO_2 within a deep saline aquifer in the Gordon Creek Field of central Utah. Up to 1×10^6 metric tons of CO_2 will be injected into the Jurassic Navajo Formation over a four year period beginning in 2010. The lessons learned from the pilot-scale injection operations in Texas, Utah and New Mexico will be applied to the project at the Gordon Creek site, although it is anticipated that deep saline CO_2 sequestration will have a unique set of challenges when compared with previous EOR or ECBM studies. Ultimately, the lessons learned from all phases of the SWP and other regional partnership programs will populate DOE/NETL databases so that future CO_2 sequestration operators can achieve maximum efficiency while minimizing risk.

References

Galloway, W. E., Ewing, T. E., Garrett, C. M., Tyler, N. & Bebout, D. G. 1983. *Atlas of Major Texas Oil Reservoirs*. The University of Texas at Austin, Bureau of Economic Geology, Austin, TX.

Han, W. S., McPherson, B. J., Lichtner, P. C. & Wang, F. P. 2010. Evaluation of trapping mechanisms in geologic CO_2 sequestration: case study of SACROC northern platform, a 35-year CO_2 injection site. *American Journal of Science*, **310**, 282–324; doi: 10.2475/04.2010.03.

Hintze, L. F. 1992. *Geologic History of Utah*. Brigham Young University, Provo, UT. Geology Studies Special Publications, **7**.

Hovorka, S. D., Benson, S. M. *et al*. 2006. Measuring permanence of CO_2 storage in saline formations: the Frio experiment. *Environmental Geosciences*, **13**, 1–17.

Kane, A. 1979. Performance review of a large-scale CO_2-WAG Enhanced Recovery Project, SACROC Unit Kelly–Snyder Field. *Journal of Petroleum Technology*, **31**, 217–231.

Litynski, J. T., Plasynski, S., McIlvried, H. G., Mahoney, C. & Srivastava, R. D. 2008. The United States Department of Energy's Regional Carbon Sequestration Partnerships Program Validation Phase. *Environment International*, **34**, 127–138; doi: 10.1016/j.envint.2007.07.005

Morgan, T. C. & Chidsey, T. 1991. Gordon Creek, Farnham Dome and Woodside fields, Carbon and Emery Counties, Utah. *In*: Chidsey, T. C., Jr (ed.) *Geology of East-central Utah*. Utah Geological Association, Salt Lake City, UT, **19**, 301–309.

National Energy Technology Laboratory. 2008. *Carbon Sequestration Atlas of United States and Canada*. NETL, Washington, DC.

United States EIA. 2008. *US energy-related carbon dioxide emissions rose by 1.6 percent in 2007*. Press Release. Retrieved May 20, 2008. World Wide Web Address: http://www.eia.doe.gov/neic/press/press298.html.

Index

Page numbers in *italic* denote figures. Page numbers in **bold** denote tables.